Can. J. Chem. Downloaded from www.nrcresearchpress.com by 210.87.254.42 on 09/05/12
For personal use only.

Canadian Journal of Chemistry

Published by
THE NATIONAL RESEARCH COUNCIL OF CANADA

Journal canadien de chimie

Publié par
LE CONSEIL NATIONAL DE RECHERCHES DU CANADA

Volume 54 Number 1 January 1, 1976 Volume 54 numéro 1 1 janvier 1976

The heat of formation of N_2H_2 and the proton affinity of N_2[1]

C. WILLIS, F. P. LOSSING, AND R. A. BACK
Division of Chemistry, National Research Council of Canada, Ottawa, Canada K1A 0R6

Received September 5, 1975

C. WILLIS, F. P. LOSSING, and R. A. BACK. Can. J. Chem. **54**, 1 (1976).

Measurements of the heat of formation of N_2H_2 from the appearance potential for m/e 30 ion from N_2H_4 give irreproducible results. Using N_2H_2, reproducible values for the appearance potentials of m/e 30, 29, and 28 ions were obtained. These values yield an ionization potential of N_2H_2, $IP(N_2H_2) = 9.7 \pm 0.1$ V, a heat of formation of N_2H_2, $\Delta H_f(N_2H_2) = 36 \pm 2$ kcal/mol and a proton affinity of N_2, $PA(N_2) = 5.6$ eV. An estimate of the ionization potential of N_2H radical, $IP(N_2H) = 7.6$ V, was also obtained.

C. WILLIS, F. P. LOSSING et R. A. BACK. Can. J. Chem. **54**, 1 (1976).

La mesure de la chaleur de formation de N_2H_2, à partir du potentiel d'apparition de l'ion de $m/e = 30$ provenant de N_2H_4, donne des résultats non-reproductibles. Utilisant du N_2H_2, on peut obtenir des valeurs reproductibles pour les potentiels d'apparition des ions de m/e 30, 29 et 28. Ces valeurs permettent d'évaluer le potentiel d'ionisation de N_2H_2, $IP(N_2H_2) = 9.7 \pm 0.1$ V, la chaleur de formation de N_2H_2, $\Delta H_f(N_2H_2) = 36 \pm 2$ kcal/mol et l'affinité du proton par N_2, $PA(N_2) = 5.6$ eV. On a aussi obtenu un estimé du potentiel d'ionisation du radical N_2H, $IP(N_2H) = 7.6$ V.

[Traduit par le journal]

Introduction

The gas-phase heat of formation of diimide, N_2H_2, is not well established. The ionization potential, 9.59 V, has recently been obtained from its photoelectron spectrum (1), and in principle this can be combined with the appearance potential (AP) of $N_2H_2^+$ (m/e 30) fragment ion from hydrazine to obtain the heat of formation, according to the reaction

[1] $$N_2H_4 + e \rightarrow N_2H_2^+ + H_2 + 2e$$

Unfortunately the appearance potential for this process is rather uncertain, and values for $\Delta H_f(N_2H_2)$ obtained in this way range from 55 to 80 kcal/mol (2). Similar estimates based on m/e 30 ion from methyl substituted hydrazines show even wider variations (2). Because of the current interest in diimide and its reactions, new measurements of the $AP(N_2H_2^+)$ from hydrazine and of the AP's for the m/e 28, 29, and 30 peaks from diimide were undertaken in order to obtain more reliable thermochemical information.

Experimental

Ionization efficiency curves were obtained as described earlier (3) using an energy-resolved electron beam from a double-hemispherical electrostatic energy selector, coupled to a quadrupole mass filter. *trans*-Diimide was prepared by passing anhydrous hydrazine vapor (Matheson, Coleman, and Bell) through a weakly-coupled microwave discharge (4). Small samples were collected at −196 °C and then vaporized into a 5 l bulb connected to the mass spectrometer inlet. Since the half-life of diimide in this system was only about 3 min, it was necessary to scan the appearance potential curve over the initial portion at a rapid repetition rate. Using a mini-computer to provide a staircase voltage and to record the ion currents (5), repetitive scans of an 0.8 V electron energy range were

[1]NRCC No. 14961.

made, with ion current readings at 0.02 V intervals. Each scan required about 6 s, and forty scans were found to give a satisfactory signal-to-noise ratio. The energy scale was calibrated against krypton.

The diimide prepared in the way described was always mixed with about a five-fold excess of ammonia (4), which, however, caused no serious interference. The amount of hydrazine impurity was negligible.

Results

Measurements with N_2H_4

Attempts to obtain a reliable appearance potential for $N_2H_2^+$ from hydrazine were unsuccessful. Freshly-introduced samples of hydrazine gave an AP(*m/e* 30) of about 10.5 V. This value decreased with time in an irreproducible manner, perhaps as the result of formation of N_2H_2 by decomposition of hydrazine on metal surfaces in the ion source. This method for estimating $\Delta H_f(N_2H_2^+)$ was therefore abandoned.

Measurements with N_2H_2

The following reproducible appearance potentials were obtained from diimide

m/e	Ion	AP (V)
30	$N_2H_2^+$	9.7 ± 0.1
29	N_2H^+	10.98 ± 0.05
28	N_2^+	14.00 ± 0.05

Discussion

The appearance potential found in this work for the parent ion of diimide, *m/e* 30, lies between the ionization potential 9.59 V recently measured by photoelectron spectroscopy (1) and the earlier electron impact value of 9.85 V (6). Because of low ionization cross-section at the threshold it must be considered to be a less accurate measurement than the PES value.

Assuming that the AP for *m/e* 28 corresponds to the process

[2] $$N_2H_2 + e \rightarrow N_2^+ + H_2 + 2e$$

and assuming no excitation of the products, we obtain

$$\Delta H_f(N_2H_2) = IP(N_2) - AP(N_2^+) = 36 \text{ kcal/mol}$$

with an estimated uncertainty of ± 2 kcal/mol. This is in fair agreement with group additivity estimates based on the heats of formation of NH_3, alkyl amines, and azoalkanes which give 32–38 kcal/mol.[2] From our value, a mean N—H bond energy of 68 kcal/mol is obtained. This rather low value offers an explanation of the high reactivity of diimide in concerted hydrogenation reactions (7). Taking $D(N_2—H) = -9$ kcal/mol from a recent theoretical estimate (8), $\Delta H_f(N_2H_2) = 36$ kcal/mol leads to $D(HNN—H) = 77$ kcal/mol, which is close to $D(H_2NNH—H) = 78$ kcal/mol in hydrazine. A rather weak bond in diimide is in accord with recent observations of very fast abstraction of H from diimide and methyl diimide in their photochemical decompositions (9, 10).

For the process

[3] $$N_2H_2 + e \rightarrow N_2H^+ + H + 2e$$

the AP (*m/e* 29) of 10.98 V leads to $\Delta H_f(N_2H^+) = 237$ kcal/mol. This corresponds to a proton affinity $PA(N_2) = 5.6$ V. From relative reaction rates in flowing afterglow experiments, Roche *et al.* (11) found that the $PA(N_2)$ lies in the sequence $4.9 \text{ V} < PA(N_2) < 5.5$ V. The lower limit comes from the observation that the reaction

[4] $$CD_4^+ + N_2 \rightarrow N_2D^+ + CD_3$$

is fast, and hence exothermic. From this, Shannon and Harrison (12) calculated $\Delta H_f(N_2H^+) \leq 253$ kcal/mol, giving $PA(N_2) = 4.9$ V. Recalculating the exothermic limit for the heat of this reaction, using more recent heat of formation data $\Delta H_f(CH_4^+) = 274$ kcal/mol (2) and $\Delta H_f(CH_3) = 34$ kcal/mol (13), gives $\Delta H_f(N_2H^+) \leq 240$ kcal/mol and hence $PA(N_2) \geq 5.46$ V, in close agreement with the present result. The upper limit of 5.5 V proposed by Roche *et al.* (11) is derived from the ionization potential of DNO obtained in a conventional electron impact source (14). Measurements of this kind are typically too high by a few tenths of a volt as a result of low energy-resolution in the electron beam. If this were the case, the result would be to lower Kohout and Lampe's (14) value for $\Delta H_f(DNO^+)$ and to increase PA(NO) correspondingly above 5.5 V. It would seem therefore that our value of $PA(N_2) = 5.6$ V is compatible with the rate data of Roche *et al.*

Finally, from $D(N_2—H) = -9$ kcal/mol (8) one can derive $\Delta H_f(N_2H) = 61.1$ kcal/mol.

[2]This form of estimation of heat of formation was suggested to us by N. C. Baird, via private communication.

Can. J. Chem. Downloaded from www.nrcresearchpress.com by 210.87.254.42 on 09/05/12
For personal use only.

From this, and our value of $\Delta H_f(N_2H^+) = 237$ kcal/mol, the ionization potential of the N_2H radical would be 7.6 V.

1. D. C. Frost, S. T. Lee, C. A. McDowell, and N. P. C. Westwood. Chem. Phys. Lett. **30**, 26 (1975).
2. J. L. Franklin, J. G. Dillard, H. M. Rosenstock, J. T. Herron, K. Draxl, and F. H. Field. Ionization potentials, appearance potentials, and heats of formation of gaseous positive ions. Nat. Stand. Ref. Data Ser. NBS-26, National Bureau of Standards, Washington, 1969.
3. F. P. Lossing and G. P. Semeluk. Can. J. Chem. **48**, 955 (1970).
4. C. Willis and R. A. Back. Can. J. Chem. **51**, 3605 (1973).
5. F. P. Lossing and J. C. Traeger. Int. J. Mass Spectrom. Ion Phys. In press.
6. S. N. Foner and R. L. Hudson. J. Chem. Phys. **28**, 719 (1958).
7. E. M. Kosower. Accounts Chem. Res. **4**, 193 (1971).
8. N. C. Baird. J. Chem. Phys. **62**, 300 (1975).
9. C. Willis, J. R. Parsons, and R. A. Back. To be published.
10. S. K. Vidyarthi, C. Willis, and R. A. Back. J. Phys. Chem. Submitted for publication.
11. A. E. Roche, M. M. Sutton, D. K. Bohme, and H. I. Schiff, J. Chem. Phys. **55**, 5480 (1971).
12. T. W. Shannon and A. G. Harrison. J. Chem. Phys. **43**, 4201 (1965).
13. D. M. Golden, R. Walsh, and S. W. Benson. J. Am. Chem. Soc. **87**, 4053 (1965).
14. F. C. Kohout and F. W. Lampe, J. Chem. Phys. **45**, 1074 (1966).

Can. J. Chem. Downloaded from www.nrcresearchpress.com by 210.87.254.42 on 09/05/12
For personal use only.

Kinetic study of the spin orbit states of atomic germanium, Ge($4^3P_{0,1,2}$), by time-resolved attenuation of atomic resonance radiation

ADAM BROWN AND DAVID HUSAIN

Department of Physical Chemistry, University of Cambridge, Lensfield Road, Cambridge CB2 1EP, England

Received April 30, 1975

ADAM BROWN and DAVID HUSAIN. Can. J. Chem. **54**, 4 (1976).

Germanium atoms in all the three spin orbit states arising from the $4p^2$ ground state configuration, 4^3P_0, 4^3P_1 (557 cm^{-1}), and 4^3P_2 (1410 cm^{-1}), have been generated by the pulsed irradiation of $GeBr_4$ and monitored photoelectrically in absorption by time-resolved attenuation of atomic resonance radiation derived from a microwave discharge. The decays have been monitored in the presence of added gases and absolute second order rate constants for the removal of all three atomic states reported for the collision partners, He, Xe, O_2, CO, NO, and $GeBr_4$. These rate constants constitute the first detailed rate data for germanium atoms in any specific quantum state.

ADAM BROWN et DAVID HUSAIN. Can. J. Chem. **54**, 4 (1976).

On a généré par irradiation pulsée du $GeBr_4$, des atomes de germanium dans les trois états de spin orbitalaire (4^3P_0, 4^3P_1 à 557 cm^{-1} et 4^3P_2 à 1410 cm^{-1}) dérivant de la configuration $4p^2$ de l'état fondamental; on les a aussi enregistré photoélectriquement en absorption par une atténuation résolue en fonction du temps de radiation de résonance atomique dérivée d'une d'écharge à micro-ondes. On a aussi enregistré les affaiblissements en présence de gas additionnés et on rapporte les constantes absolues de vitesse du deuxième ordre pour l'élimination des trois états atomiques par les partenaires de collision He, Xe, O_2, CO, NO et $GeBr_4$. Ces constantes de vitesse sont les premières données détaillées de vitesse impliquant des atomes de germanium et ce quel que soit leur état quantique spécifique.

[Traduit par le journal]

Introduction

The kinetic study of spin orbit states arising from the gross electronic structure of the ground state configuration constitutes part of a wider growing development in recent years, designed to reach a general understanding of the relationship between electronic structure and atomic reactivity (1–4). A major experimental objective in such a general approach is to obtain collisional rate data on *all* the low lying states from the ground state configuration for *all* the atoms within a given group of the periodic table. One purpose of such an approach is to investigate how the change in kinetic behavior with increasing atomic weight can be explained by a change of dominance from weak spin orbit coupling effects for light atoms (4, 5) to (J,Ω) coupling for heavy atoms (4).

With particular regard to the spin orbit states of Group IV elements (np^2), detailed kinetic investigations have been carried out on Sn($5^3P_{0,1,2}$) (6) and Pb($6^3P_{0,1,2}$) (7–11). The resulting rate data, together with those for the more energized low lying $^1S_0$ and $^1D_2$ states of tin (12–15) and lead (16–19), have been found to be in accord with correlations based on (J,Ω) coupling (4, 15). Whilst the ^3P_J states of germanium have been detected photographically by Callear and Oldman (20) following flash photolysis, detailed collisional rate data have not been reported. In this paper, we describe a method for monitoring the individual states, Ge($4p^2\ ^3P_{0,1,2}$), photoelectrically and report the first detailed collisional rate data for atomic germanium in specific electronic states.

Experimental

The experimental arrangement was similar to that employed in previous studies of tin atoms in the Sn(5^1D_2) (12, 13) and Sn(5^1S_0) (14, 15) states. Germanium atoms in the $4p^2\ ^3P_0$, $^3P_1$, and $^3P_2$ states ($^3P_0$, 0; $^3P_1$, 557; $^3P_2$, 1410 cm^{-1}) (21) were generated by the pulsed irradiation of low pressures of $GeBr_4$ in a coaxial lamp and vessel assembly (E = 500 J, p_{Kr} = 1.3 kN m^{-2}), the common wall being constructed of high purity quartz (Spectrosil) which allowed photolysis at $\lambda > 165$ nm. An excess of helium buffer gas (*ca.* 50 000 : 1) was always employed in order to ensure no significant temperature rise on irradiation. The $^3P_1$ and $^3P_2$ states are highly metastable with respect to spontaneous emission (22). The Einstein coefficients for magnetic dipole emission, those for quadrupole emission being negligible, (22) have been calculated to be 0.0031 and 0.0082 s^{-1} for the $^3P_1$

Can. J. Chem. Downloaded from www.nrcresearchpress.com by 210.87.254.40 on 09/05/12
For personal use only.

TABLE 1. Atomic resonance transitions employed

Atomic transition	λ (nm)*	$10^{-8}gA$ (s^{-1})*	γ-value
$5s(^3P_1{}^0) \leftarrow 4p^2(^3P_2)$	275.5	9.8	0.58 ± 0.02
$5s(^3P_2{}^0) \leftarrow 4p^2(^3P_1)$	259.3	11	0.68 ± 0.04
$5s(^1P_1{}^0) \leftarrow 4p^2(^3P_0)$	249.8	2.4	0.75 ± 0.06

*Reference 23.

and $^3P_2$ levels. Hence, all the three states in the $4p^2\ ^3P_J$ manifold could be monitored by the time-resolved absorption of the atomic resonance transitions at the wavelengths listed in Table 1. Concentrations of all three transient atomic species that were produced were sufficiently high to permit kinetic analyses in the single-shot mode.

An intense atomic emission spectroscopic source was provided by a microwave discharge through a flow system of $GeCl_4$ in helium ($p_{GeCl_4} = 4.0$ N m^{-2}, $p_{\text{total with He}} = 400$ N m^{-2}). As the strength of the $^3P_0$ transition was lower than that of the other two transitions (Table 1), a higher incident microwave power ($^3P_2$, $^3P_1$, 100 W; $^3P_0$, 140 W) was used to produce this line at an intensity suitable for kinetic measurements. The atomic lines were optically separated with a grating monochromator (Hilger and Watts, Monospek 1000) and the resonance absorption monitored by means of a photomultiplier (E.M.I. 9783 B) mounted on the exit slit of the instrument. The output was fed to a current-to-voltage converter employing a fast settling operational amplifier (24) and then to a rapid response precision logarithmic amplifier (25, 26). The advantages of this system, even in the single-shot mode, have been discussed previously (27). The resulting signals of ln (I_0/I_{tr}), where the symbols have their usual meaning within the context of the modified Beer–Lambert law (28)

$$[1] \qquad I_{tr} = I_0 \exp(-\epsilon(cl)^\gamma)$$

were subsequently stored in a transient recorder (Biomation Model 610B), displayed on an oscilloscope for inspection, and transferred to an XY recorder (Bryans Ltd.) for kinetic analysis. The scattered light from the photolysis pulse, even after considerable narrowing of the slits which was permitted by the high intensity of the spectroscopic source, prevented kinetic measurements being made during the first 80–100 μs following pulsed irradiation.

Materials

$GeBr_4$ (Koch-Light) was thoroughly degassed, redistilled *in vacuo*, and then fractionally distilled from an ice-bath (0 °C) to liquid nitrogen temperature (−196 °C). $GeCl_4$ (Koch-Light) was simply degassed and redistilled *in vacuo* before use in the atomic flow lamp. He, Xe, O_2, CO, and NO were prepared as described previously (12, 13).

Results and Discussion

Figure 1 shows typical transient recorder traces for the decay of Ge(4^3P_2, 4^3P_1, and 4^3P_0) following the pulsed irradiation of $GeBr_4$. Standard

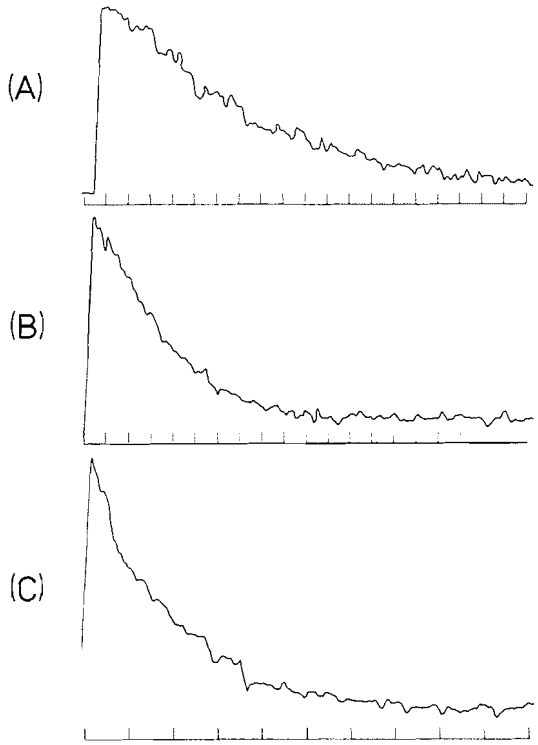

FIG. 1. Typical transient recorder traces for the decay of (*A*) Ge(4^3P_0) (λ = 249.8 nm); (*B*) Ge(4^3P_1) (λ = 259.3 nm); (*C*) Ge(4^3P_2) (λ = 275.5 nm) in the presence of excess helium; $p_{\text{total with He}} = 3.33$ kN m^{-2}; $E = 500$ J; time scale = 100 μs per division for all traces starting at $t = 50$ μs; p_{GeBr_4} (N m^{-2}): (*A*) 0.033; (*B*) 0.058; (*C*) 0.11 (leading edge = scattered light from photolysis pulse).

plots (28) (ln (ln (I_0/I_{tr}))$_{t=0}$ *vs.* ln p_{GeBr_4}) yielding γ-values (eq. 1) for the three atomic transitions employed (Table 1) are given in Fig. 2. Figure 3 gives an example of first order kinetic plots for the decay of Ge(4^3P_2) in the presence of molecular oxygen. Similar sets of plots were obtained for Ge(4^3P_1) and Ge(4^3P_0) with this added gas. These first-order plots, in particular, those for the $^3P_1$ and $^3P_0$ levels, are not sufficiently sensitive with the present technique to permit signifi-

Can. J. Chem. Downloaded from www.nrcresearchpress.com by 210.87.254.40 on 09/05/12
For personal use only.

Can. J. Chem. Downloaded from www.nrcresearchpress.com by 210.87.254.40 on 09/05/12
For personal use only.

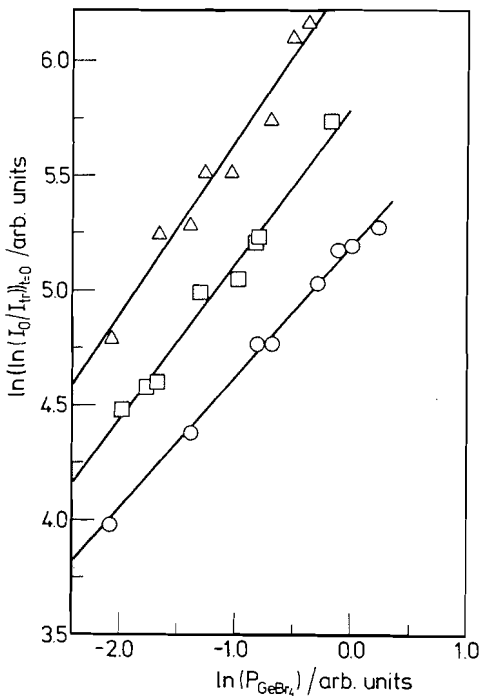

FIG. 2. Beer–Lambert plots for light absorption by the individual spin orbit states of Ge(4^3P_J), ($p_{\text{total with He}}$ = 3.33 kN m^{-2}). △, $5s(^1P_1{}^0 \leftarrow 4p^2(^3P_0)$ (λ = 249.8 nm); □, $5s(^3P_2) \leftarrow 4p^2(^3P_1)$ (λ = 259.3 nm); ○, $5s(^3P_1) \leftarrow 4p^2(^3P_2)$ (λ = 275.5 nm).

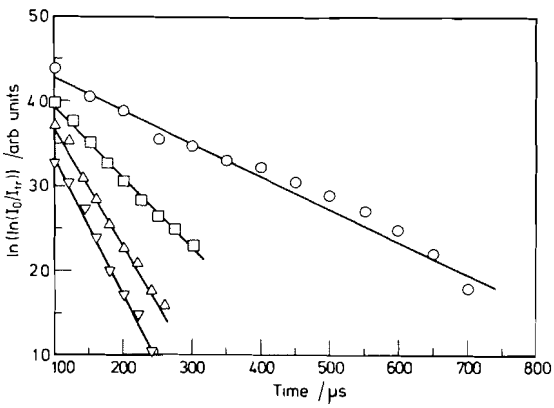

FIG. 3. Pseudo first-order plots for the decay of Ge(4^3P_2) in the presence of oxygen; p_{GeBr_4} = 0.05 N m^{-2}, $p_{\text{total with He}}$ = 3.33 kN m^{-2}; E = 500 J. p_{O_2}(N m^{-2}); ○, 0.0; □, 0.27; △, 0.38; ▽, 0.42.

cant detection of contributions to growth arising from relaxation from higher spin orbit states. Further, no significant yields of either Ge(4^1D_2) or Ge(4^1S_0) were detected using the resonance absorption technique applied to these states at times during which decays of the spin orbit states were investigated ($t > 80$–$100\ \mu$s), and hence relaxation of the singlet states into the 4^3P_J manifold will have no significant effect on the kinetics, particularly for the $^3P_2$ level. Further the longer observed life time of the $^3P_0$ level, resulting from its higher absolute concentration, at least permits some rate measurements on this state by the time in which the other atomic states have relaxed. Hence the data for the $^3P_1$ level is most sensitive to error. In general, the observed decays for the individual 4^3P_J states are treated as processes first order overall in kinetics, as supported by plots such as those in Fig. 3.

The slopes of the first order plots ($-\gamma k'$) can, with the appropriate γ-values (Table 1), be expressed in the form

$$k' = k_M[M] + K \qquad [2]$$

where k' is the observed first order decay coefficient and k_M is the absolute second order rate constant for removal of the particular spin orbit state by an added gas, M. K may be taken as constant for a given series of kinetic experiments in which [M] is varied and will include first order contributions to losses by diffusion, weak spontaneous emission (22), and collisional quenching by the parent molecule, products of photolysis, and impurities. The variation of k' ($\gamma k'$) with O_2 for Ge($4^3P_{0,1,2}$) are given in Fig. 4. Linear plots similar to those given in Fig. 4 were obtained for the decays of Ge(4^3P_2), Ge(4^3P_1), and Ge(4^3P_0) in the presence of CO, NO, and $GeBr_4$, the values of k_M for the different states clearly being derived from the slopes of such plots. Decays of all three J states were investigated in the presence of both H_2 and D_2 but simple kinetics were not observed. This complex behavior presumably arises, in part, from a chain reaction between products of photolysis, say, Br($4^2P_{1/2}$) and Br($4^2P_{3/2}$) with the hydrogen isotopes. The resulting absolute collisional rate constants (k_M) obtained in this investigation are given in Table 2. The quoted errors in k_M are simply derived from weighted least squares analyses of plots of the type given in Fig. 4. The upper limits representing removal of the atomic states by helium and xenon are derived from the intercepts of plots of the type given in Fig. 4, after correction due to removal by the parent molecule, $GeBr_4$.

The low efficiency for electronic-to-translational (E–T) transfer between Ge(4^3P_J) + He

TABLE 2. Second order rate constants (k_M, cm^3 molecule^{-1} s^{-1}, 300 K) for the collisional removal of Ge(4^3P_2), Ge(4^3P_1), and Ge(4^3P_0) by added gases, M

M	k_M		
	4^3P_2	4^3P_1	4^3P_0
He	$<5\times10^{-15}$	$<5\times10^{-16}$	$<10^{-15}$
Xe	$<10^{-14}$	$<2\times10^{-16}$	$<10^{-16}$
O_2	$1.5\pm0.3\times10^{-10}$	$1.3\pm0.1\times10^{-10}$	$1.2\pm0.1\times10^{-10}$
CO	$3.6\pm0.3\times10^{-13}$	$4.0\pm0.4\times10^{-13}$	$3.6\pm0.4\times10^{-13}$
NO	$2.1\pm0.2\times10^{-12}$	$2.5\pm0.2\times10^{-12}$	$3.8\pm0.6\times10^{-12}$
$GeBr_4$	$2.1\pm0.2\times10^{-10}$	$2.9\pm0.3\times10^{-10}$	$1.5\pm0.1\times10^{-10}$

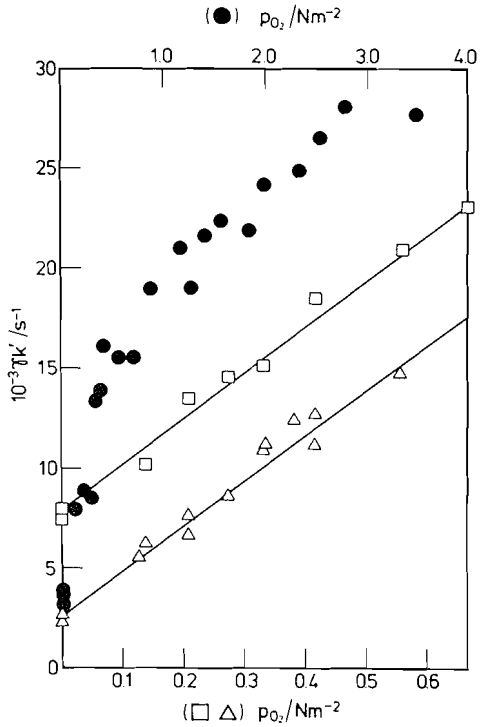

FIG. 4. Pseudo first order rate coefficients ($\gamma k'$) for the decay of Ge(4^3P_J) in the presence of oxygen; p_{GeBr_4} = 0.05 N m^{-2}, $p_{total\ with\ He}$ = 3.33 kN m^{-2}; E = 500 J. ●, Ge(4^3P_2); □, Ge(4^3P_1); △, Ge(4^3P_0).

and Xe (Table 2) is expected in view of the presumed repulsive nature of the interaction. The transfer of large quantities of electronic energy to translation can only occur if the potential curves describing the initial and final states either cross or approach sufficiently closely for quantum mechanical tunnelling to be of high probability. This may even occur with transfer from light atoms, as in the case in this group, of the highly efficient quenching of C(2^1D_2) by xenon (29) where states, which would cross in Hund's coupling cases (*a*) or (*b*) would mix in case (*c*). The effect of such a mechanism is clearly not significant here (Table 2). Discussion of the collisional behavior with molecules of individual spin atomic orbit states in terms of potential energy surfaces must, of necessity, employ (J,Ω) coupling as J splittings are neglected in the weak spin orbit coupling approximation. At the same time, we may expect, by analogy with the chemistry of the atomic states of arsenic (27), that that of germanium will be intermediate between the weak (*e.g.* as for C(2^3P_J, 2^1D_2, 2^1S_0) (30, 31) and strong spin orbit (*e.g.* Sn and Pb ^3P_J) (6–11) coupling cases.

Preliminary inspection of the rate data, in particular, the closeness to equality observed for the various rate constants of the atomic states with a given collision partner (Table 2) might lead one initially to conclude the presence of equilibrium between the three J levels. Experiment does not support this. Firstly, a formal kinetic analysis on this basis, similar to that given hitherto for Sn(4^3P_J) and Pb(6^3P_J) (6) shows that this should yield equality in the measured first order decay coefficients (k') for the J levels in a given experiment. This was not generally observed. Secondly, in such an analysis, low and high pressure limits for, say, O_2, CO, or NO, should yield decay rates which are determined solely by $GeBr_4$. This is the principal purpose for determining rate data for the parent molecule. Neither is this borne out by experiment.

In the absence of any dramatic difference in the quenching rate data for the three spin orbit states with a given molecule (Table 2), there is clearly a limit to the scope for detailed discussion in most individual cases. Chemical reaction of Ge(4^3P_J) + CO or NO would be endothermic. Hence removal of both the $^3P_2$ and $^3P_1$ levels

Can. J. Chem. Downloaded from www.nrcresearchpress.com by 210.87.254.40 on 09/05/12
For personal use only.

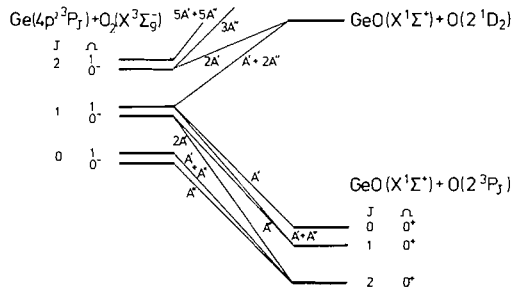

FIG. 5. Correlation diagram connecting the states of Ge + O_2 and GeO + O using (J,Ω) coupling for reactants and products (not drawn to scale).

must involve crossings of the appropriate A' and A'' surfaces (in (J,Ω) coupling) for CO or the $E_{1/2}$ surfaces for NO leading to physical relaxation via nonadiabatic conditions. In the case of Ge(4^3P_2) with CO or NO, considerations of the relevant energetics, including the appropriate Boltzmann fractions of collisions providing the energy defect from translation, indicate that the data is not inconsistent with $E \rightarrow V$ ($v'' = 0 \rightarrow 1$) transfer. Surprisingly, in the case of O_2, where k_{O_2} is taken from the initial slope of Fig. 4, for experimental reasons given above, a near-resonance E–V transfer process

$$[3] \quad \mathrm{Ge}(4^3P_2) + \mathrm{O_2}(v'' = 0) \underset{}{\overset{K}{\rightleftharpoons}} \mathrm{Ge}(4^3P_0) + \mathrm{O_2}(v'' = 1)$$

where $\Delta E = +146\ \mathrm{cm^{-1}}$, does *not* cause an equilibrium ($K = 9.9 \times 10^{-2}$) to be rapidly established for processes [3] and [−3]. The curvature in Fig. 4 may arise from some role played by $O_2(v'' = 1)$ at higher P_{O_2}. On the basis of (J,Ω) coupling, we would clearly expect kinetic differences between Ge(4^3P_2) and Ge(4^3P_1) as seen from the appropriate correlation diagram (Fig. 5). The absence of such differences demonstrates the limitation of what is, at present, the *general* vehicle for considering the collisional behavior of spin orbit states. When dealing with relatively small J splittings, as in the third row of the periodic table, coupled with the large number of surfaces and surface crossings arising from the loss of spin degeneracy, correlations resulting from (J,Ω) coupling are not seen to be highly restrictive.

Acknowledgments

We thank the Science Research Council of Great Britain for a research grant and for a maintenance grant to one of us (A.B.) during the tenure of which this work was carried out.

1. R. J. DONOVAN and D. HUSAIN. Ann. Rep. Prog. Chem. Sect. A, **68**, 124 (1972).
2. R. J. DONOVAN, D. HUSAIN, and L. J. KIRSCH. Ann. Rep. Prog. Chem. Sect. A, **69**, 19 (1973).
3. D. HUSAIN and R. J. DONOVAN. Adv. Photochem. **8**, 1 (1970).
4. D. HUSAIN. Acc. Chem. Res. In preparation.
5. R. J. DONOVAN and D. HUSAIN. Chem. Rev. **70**, 489 (1970).
6. P. D. FOO, J. R. WIESENFELD, and D. HUSAIN. Chem. Phys. Lett. **32**, 443 (1975).
7. D. HUSAIN and J. G. F. LITTLER. J. Photochem. **2**, 247 (1973/74).
8. D. HUSAIN and J. G. F. LITTLER. Combust. Flame, **22**, 295 (1974).
9. D. HUSAIN and J. G. F. LITTLER. Int. J. Chem. Kinet. **VI**, 61 (1974).
10. J. J. EWING, D. M. TRAINOR, and S. YATSIV. J. Chem. Phys. **61**, 4433 (1974).
11. J. J. EWING. Chem. Phys. Lett. **29**, 50 (1974).
12. A. BROWN and D. HUSAIN. J. Photochem. **3**, 37 (1974/75).
13. A. BROWN and D. HUSAIN. Int. J. Chem. Kinet. **VII**, 77 (1975).
14. A. BROWN and D. HUSAIN. J. Photochem. **3**, 305 (1974/75).
15. A. BROWN and D. HUSAIN. J. Chem. Soc. Faraday Trans. II, **71**, 699 (1975).
16. D. HUSAIN and J. G. F. LITTLER. Chem. Phys. Lett. **16**, 145 (1972).
17. D. HUSAIN and J. G. F. LITTLER. J. Chem. Soc. Faraday Trans. II, **68**, 2110 (1972).
18. D. HUSAIN and J. G. F. LITTLER. J. Photochem. **1**, 327 (1972/73).
19. D. HUSAIN and J. G. F. LITTLER. J. Chem. Soc. Faraday Trans. II, **69**, 842 (1973).
20. A. B. CALLEAR and R. J. OLDMAN. Spectrosc. Lett. **1**, 149 (1968).
21. C. E. MOORE (*Editor*). Atomic energy levels. Vols. I–III. Natl. Bur. Stand. Circular 467, U.S. Government Printing Office, Washington, D.C. 1958.
22. R. H. GARSTANG. J. Res. Natl. Bur. Stand. **68A**, 61 (1964).
23. C. H. CORLISS and W. R. BOZMAN. Experimental transition probabilities of spectral lines of seventy elements. Natl. Bur. Stand. Monograph 53, U.S. Government Printing Office, Washington, D.C. 1962.
24. W. H. WING and J. M. SANDERS. Rev. Sci. Instrum. **38**, 1341 (1967).
25. D. HUSAIN, S. K. MITRA, and A. N. YOUNG. J. Chem. Soc. Faraday Trans. II, **70**, 1721 (1974).
26. D. HUSAIN and A. N. YOUNG. J. Chem. Soc. Faraday Trans. II, **71**, 525 (1975).
27. M. J. BEVAN and D. HUSAIN. Int. J. Chem. Kinet. **VII**, 63 (1975).
28. R. J. DONOVAN, D. HUSAIN, and L. J. KIRSCH. Trans. Faraday Soc. **66**, 2551 (1970).
29. D. HUSAIN and L. J. KIRSCH. Trans. Faraday Soc. **67**, 2886 (1971).
30. D. HUSAIN and L. J. KIRSCH. Trans. Faraday Soc. **67**, 3166 (1971).
31. D. HUSAIN and L. J. KIRSCH. J. Photochem. **2**, 297 (1974).

Can. J. Chem. Downloaded from www.nrcresearchpress.com by 210.87.254.40 on 09/05/12
For personal use only.

A simplified form of Stokes–Robinson equation

CHAI-FU PAN
Department of Chemistry, Alabama State University, Montgomery, Alabama 36101

Received March 24, 1975

CHAI-FU PAN. Can. J. Chem. **54**, 9 (1976).

In non-associated dilute aqueous electrolyte solutions, the deviation from ideality is principally attributed to the interionic interactions and hydration of ions. Stokes and Robinson combined Bjerrum's thermodynamic treatment of ion–solvent interactions with Debye–Hückel treatment of interionic interactions to obtain a two-parameter equation. In very dilute regions, the Stokes and Robinson's equation reduces to a much simpler form, *i.e.*

$$\log \gamma_{\pm} = \log f_{\pm} + 0.0156m(h - v/2)$$

Activity coefficients of an electrolyte at lower concentrations, say up to 0.1 *m*, can be calculated from the equation provided suitable values of $\mathring{a}$ and *h* are available. Solutions of hydrogen chloride and sodium chloride were chosen as examples. The results agree with the existing data very satisfactorily.

CHAI-FU PAN. Can. J. Chem. **54**, 9 (1976).

Dans des solutions aqueuses diluées et non-associées d'électrolytes, on attribue la déviation de l'idéalité principalement à des interactions interioniques et à l'hydratation des ions. Stokes et Robinson ont combiné le traitement thermodynamique de Bjerrum des interactions ion–solvant avec le traitement de Debye–Hückel des interactions interioniques et ont ainsi obtenu une équation à deux paramètres. Dans les régions très diluées, l'équation de Stokes et de Robinson se réduit à une forme beaucoup plus simple, *i.e.*

$$\log \gamma_{\pm} = \log f_{\pm} + 0.0156m(h - v/2)$$

On peut calculer les coefficients d'activité d'un électrolyte à basse concentration, par exemple jusqu'à 0.1 *m*, à partir de l'équation, à condition que des valeurs appropriées de $\mathring{a}$ et *h* soient disponibles. On a choisi des solutions de HCl et de NaCl comme exemples. Les résultats obtenus sont en très bon accord avec les données existantes.

[Traduit par le journal]

The modern theories of electrolytes date from the theory of Debye and Hückel (1) in 1923. However, the theory is valid only for solutions of electrolyte at infinite dilutions. There are now no theories easily applicable to any real solutions of given concentration since their behavior is influenced by several inseparable factors. The thermodynamic properties of these solutions are mainly obtained by experimental measurements.

The concept of hydration is one of the simplest and most effective modifications of the Debye–Hückel theory. Stokes and Robinson (2, 3) employed an empirical approach based on Bjerrum's ideas of ion solvation (4) and the Debye–Hückel treatment of interionic interactions. By taking the Debye–Hückel equation to account for the mean rational activity coefficient of the solvated ions, they were able to derive a two-parameter equation. Their equation in dilute solutions takes the form (3)

$$[1] \quad \log \gamma_{\pm} = \log f_{\pm} - \frac{h}{v} \log a_w - \log [1 - 0.018(h - v)m]$$

in which $\gamma_{\pm}$ is the mean molal activity coefficient, $f_{\pm}$ is the mean rational activity coefficient calculated from the Debye–Hückel equation, *h* is the hydration number, *v* is the stoichiometric ion number of the electrolyte, a_w is the activity of water, and *m* is the molality of the solution. The Debye–Hückel equation (3) is

$$[2] \quad \log f_{\pm} = -\frac{A|z_+z_-|\sqrt{I}}{1 + B\mathring{a}\sqrt{I}}$$

where *I* is the molar ionic strength of the solution, z_+ and z_- are charge numbers on cation and anion, respectively, and *A* and *B* are constants. For aqueous solutions at 25 °C, $A = 0.5115$, and $B = 0.3291 \times 10^8$ (3).

Can. J. Chem. Downloaded from www.nrcresearchpress.com by 210.87.254.105 on 09/05/12
For personal use only.

Can. J. Chem. Downloaded from www.nrcresearchpress.com by 210.87.254.105 on 09/05/12
For personal use only.

TABLE 1. Mean activity coefficients in dilute hydrochloric acid solutions at 25 °C ($\mathring{a}$ = 4.47 Å, h = 8.0)

			$\gamma_\pm$		
m	$-\log f_\pm$	$0.0156m(h-v/2)$	Eq. [6]	Reference 6	Reference 7
0.0001	0.00503	0.00001	0.9885	0.9891	—
0.0002	0.00708	0.00002	0.9839	0.9842	—
0.0005	0.01106	0.00005	0.9750	0.9752	—
0.001	0.01543	0.00011	0.9653	0.9656	0.965
0.002	0.02143	0.00022	0.9523	0.9521	0.952
0.005	0.03271	0.00055	0.9286	0.9285	0.929
0.01	0.04453	0.00109	0.9048	0.9048	0.905
0.02	0.05979	0.00218	0.8758	0.8755	0.876
0.03	0.07049	0.00328	0.8566	—	—
0.04	0.07891	0.00437	0.8423	—	—
0.05	0.08591	0.00546	0.8309	0.8304	0.832
0.06	0.09193	0.00655	0.8215	—	—
0.07	0.09722	0.00764	0.8136	—	—
0.08	0.10195	0.00874	0.8068	—	—
0.09	0.10623	0.00983	0.8009	—	—
0.1	0.11015	0.01092	0.7957	0.7964	0.797

TABLE 2. Mean activity coefficients in dilute aqueous sodium chloride solutions at 25 °C ($\mathring{a}$ = 3.97 Å, h = 3.5)

			$\gamma_\pm$		
m	$-\log f_\pm$	$0.0156m(h-v/2)$	Eq. [6]	Reference 5*	Reference 7
0.001	0.01551	0.00004	0.9650	—	0.965
0.002	0.02158	0.00008	0.9517	—	0.952
0.005	0.03306	0.00020	0.9271	0.9281	0.928
0.007	0.03852	0.00027	0.9157	0.9169	—
0.01	0.04517	0.00039	0.9020	0.9029	0.903
0.02	0.06095	0.00078	0.8706	0.8720	0.872
0.03	0.07211	0.00117	0.8493	0.8504	—
0.04	0.08094	0.00156	0.8330	0.8342	—
0.05	0.08831	0.00195	0.8197	0.8207	0.822
0.06	0.09468	0.00234	0.8085	0.8101	—
0.07	0.10031	0.00273	0.7988	—	—
0.08	0.10534	0.00312	0.7903	0.7917	—
0.09	0.10992	0.00351	0.7827	—	—
0.1	0.11411	0.00390	0.7759	0.7768	0.779

*The original data were mean rational activity coefficients ($f_\pm$) which are related to mean molal activity coefficients ($\gamma_\pm$) by the equation (3):

$$f_\pm = \gamma_\pm(1 + 0.018\nu m)$$

If we wish to use molal concentrations to calculate $f_\pm$ at non-vanishing concentrations we use (3)

$$[3] \qquad I = \tfrac{1}{2}|z_+z_-|\nu M = \tfrac{1}{2}|z_+z_-|\nu\left(\frac{md}{1+0.001mW_2}\right)$$

in which W_2 is the molecular weight of solute, M is the molarity, and d is the solution density.

In most cases, in dilute solutions of concentrations below 0.1 m, it causes negligible errors in calculating $\gamma_\pm$ from [1] by putting $\phi = 1$ in the following

$$[4] \qquad \log a_w = \frac{-\nu m\phi}{2.303 \times 55.508} \approx \frac{-\nu m}{2.303 \times 55.508}$$

Also

$$[5] \qquad \log[1 - 0.018(h-\nu)m] \approx -\frac{0.018}{2.303}(h-\nu)m$$

By substituting [4] and [5] into [1], we obtain

$$[6] \quad \log \gamma_{\pm} = \log f_{\pm} + 0.0156m(h - \nu/2)$$

Therefore, in dilute solutions the Stokes–Robinson two-parameter equation may be reduced to a simpler form, [6]. In applying the derived equation to calculate the mean molal activity coefficients of electrolytes in dilute regions, aqueous solutions of hydrogen chloride and sodium chloride were chosen as examples. The molar ionic strength in [2] is calculated from [3], but the density of water (d_0) is used for d; at 25 °C, d_0 = 0.99707 g/ml (3). Values of $\mathring{a}$ and h for these electrolytes were taken from Robinson and Stokes (3). The calculated values of $\gamma_{\pm}$ agree very satisfactorily with the values obtained or compiled by Brown and MacInnes (5), Harned and Owen (6), and Hamer and Wu (7) throughout the concentration range studied (Tables 1 and 2).

Acknowledgment

The author is grateful to one of the referees who provided the particular derivation of [6] given here. He also demonstrated that the derivation of a slightly different equation given in earlier versions of this paper was inaccurate.

1. P. DEBYE and E. HÜCKEL. Phys. Z. **24**, 185 (1923); **24**, 305 (1923).
2. R. H. STOKES and R. A. ROBINSON. J. Am. Chem. Soc. **70**, 1870 (1948).
3. R. A. ROBINSON and R. H. STOKES. Electrolyte solutions. Revised 2nd ed. Butterworths, London. 1965. pp. 31–32, 229, 245–248, 457, 468.
4. N. BJERRUM. Kgl. Danske Videnskab Selskab. Mat-Fys. Medd. **7**, No. 9 (1926).
5. A. S. BROWN and D. A. MACINNES. J. Am. Chem. Soc. **57**, 1356 (1935).
6. H. S. HARNED and B. B. OWEN. Physical chemistry of electrolytic solutions. 3rd ed. Reinhold, New York. 1958. p. 716.
7. W. J. HAMER and Y. C. WU. J. Phys. Chem. Ref. Data. **1**, 1047 (1972).

Can. J. Chem. Downloaded from www.nrcresearchpress.com by 210.87.254.105 on 09/05/12
For personal use only.

The formation of cycloheptenone and cycloheptadienones from bicyclo[3.2.0]heptanone derivatives. An acid-catalyzed, two carbon ring expansion reaction[1]

KENNETH E. HINE[2] AND RONALD F. CHILDS
Department of Chemistry, McMaster University, Hamilton, Ontario L8S 4M1

Received August 1, 1975

KENNETH E. HINE and RONALD F. CHILDS. Can. J. Chem. **54**, 12 (1976).

In strong acids, such as FSO_3H and 96% H_2SO_4, bicyclo[3.2.0]heptan-6-one and bicyclo-[3.2.0]hept-2-en-7-one undergo a clean isomerization to form protonated cyclohept-2-enone and cyclohepta-2,4-dienone, respectively. Substituted derivatives undergo comparable ring expansions when dissolved in these strong acids. The seven-membered ring ketones can be recovered on quenching the acid solutions with a $NaHCO_3$–ether mixture. In contrast, bicyclo-[3.2.0]hept-2-en-6-one when dissolved in FSO_3H rearranged to give protonated 1-acetylcyclo-pentadiene. The mechanism and synthetic utility of these reactions is discussed.

KENNETH E. HINE et RONALD F. CHILDS. Can. J. Chem. **54**, 12 (1976).

Dans les acides forts comme FSO_3H et H_2SO_4 96% la bicyclo[3.2.0]heptanone-6 et la bicyclo[3.2.0]heptène-2 one-7 subissent des isomérisations propres conduisant respectivement aux formes protonées de la cycloheptène-2 one et de la cycloheptadiène-2,4 one. Des dérivés portant des substituants subissent des extensions de cycle comparables lorsque dissous dans ces acides forts. On peut récupérer les cétones cycliques à sept chaînons en traitant les solutions acides par un mélange $NaHCO_3$–éther. Par ailleurs le traitement de la bicyclo[3.2.0]heptène-2 one-6 par FSO_3H conduit à la forme protonée de l'acétyl-1 cyclopentadiène. On discute du mécanisme et de l'utilité en synthèse de ces réactions.

[Traduit par le journal]

There are numerous examples of fused bicyclic ring systems in which one of the rings is a cyclobutanone moiety. Indeed, one common and facile synthetic entry into this type of ring system involves the cycloaddition of a ketene to a cycloalkene (1). If a means could be found of inducing cleavage of the cyclobutanone bond that is common to both rings, then combined with this ketene addition, we would have a route to functionalized monocyclic systems possessing a ring two carbons larger than that of the alkene used in the original cycloaddition. A viable two carbon ring expansion reaction would be of value in general syntheses of medium size rings (2).

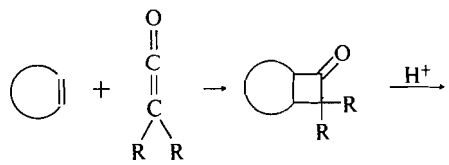

Ring expanded products

The well known interconversion of cyclobutyl, cyclopropylcarbinyl, and open chain cationic systems (3) suggested to us that one method of inducing the desired cleavage of the cyclobutanone bond would be to react this carbonyl function with an electrophile. There are several reports of the isomerization of cyclobutanones upon protonation and it would appear that in many of these rearrangements the carbon–carbon bond β to the carbonyl group is cleaved (4). In view of our interest in the chemistry of the monocyclic, unsaturated, seven-membered ring ketones (5), we have examined the effect of protonation on several bicyclo[3.2.0]heptan-6-ones and bicyclo[3.2.0]heptenones and report here the results of this study.

Results

Careful solution of bicyclo[3.2.0]heptan-6-one, **1**, in FSO_3H at $-78\,^{\circ}C$ yielded a clear yellow solution whose pmr spectrum at $+20\,^{\circ}C$ (Table 1) was completely consistent with the formation of the hydroxycyclobutyl cation **1H**. On allowing the solution to stand at room temperature for several hours, **1H** cleanly rearranged to a further

[1]The Chemistry of Cycloheptadienones, Part VIII.

[2]Present address: Central Research Laboratories, Canadian Industries Limited, McMasterville, Quebec J3G 1T9.

Can. J. Chem. Downloaded from www.nrcresearchpress.com by 210.87.254.105 on 09/05/12
For personal use only.

TABLE 1. Proton chemical shifts of neutral and protonated ketones*

Compound	Position			
	Vinyl H			Other H's
1				3.50(1),3.08(1),2.82(1),2.34(1),2.0–1.6(6)
1H				4.1(1),3.7(1),3.4–3.1(2),2.4–1.9(6)
2	6.40^{dt}(1)	(J=12&5.5Hz)	5.80^{d}(1)	2.4–2.5(4),1.90(4)
2H	8.36^{dt}(1)	(J=12&5.0 Hz)	6.89^{d}(1)	3.28(2),3.05(2),2.06(4)
3	5.87(1)		5.60(1)	4.21(1),3.40–2.20(4)
3H†	6.32(1)		5.56(1)	4.70(1),4.0–2.6(4)
5	5.53(1)		5.32(1)	3.06(1),2.72(1),2.08(1),1.25^{s}(3),1.14^{s}(3),1.23^{s}(3)
5H	6.16(1)		5.66(1)	3.55(1),3.10(1),2.62(1),1.74^{s}(3),1.30^{s}(6)
6	6.27^{d}(1)	(J=9 Hz)	5.58^{d}(1)	2.72(2),2.22(1),1.93^{s}(3),1.88^{s}(3),0.98^{d}(3)
6H	6.24^{d}(1)	(J=5.5 Hz)	5.77^{d}(1)	3.50^{d}(2),2.68^{t}(1),1.82^{s}(3),1.30^{s}(6)
8	7.13(1)		6.60(2)	3.20(2),2.27^{s}(3)

*Ketones in CCl_4, TMS internal standard; protonated ketones in FSO_3H at −50 °C, CH_2Cl_2 taken as 5.30 δ as internal standard (s, singlet; d, doublet; t, triplet; integrations given in parentheses).
†In FSO_3H–SO_2ClF (1:3) at −80 °C.

cation, whose pmr spectrum at +20 °C displayed resonances at 8.39, 6.92, 3.31, 3.08, and 2.09 δ with relative areas of 1:1:2:2:4, respectively. The two low field signals were mutually coupled (J = 12 Hz) and are typical in both position and magnitude of their mutual coupling to that found for the vinyl proton resonances of protonated, α,β-unsaturated ketones (6). Double resonance experiments showed further that the resonance at 8.39 δ was coupled to the resonance at 3.08 δ (J = 5 Hz). This evidence, taken together with the positions and integrations of the remaining resonances, suggested that the cation produced on isomerization of **1H** was protonated cyclohept-2-enone, **2H**. The pmr spectrum of protonated cycloheptenone, reported by Olah and Liang (7) was similar to that of **2H**.

On neutralization of the acid solution of the rearranged product, a pale yellow oil was obtained whose pmr and ir spectra were virtually identical to those reported for **2** (8). Gas–liquid partition chromatography (glpc) analysis of this oil showed it to consist of **2**, 92%, **1**, 4%, and an unidentified minor product, 4%. In separate reactions, the amount of residual **1** detected by glpc was reduced still further by allowing the isomerization to proceed for a longer period of time. The half-life for rearrangement of **1H** to **2H** at 20 °C was found to be *ca.* 25 min.

When **1** was dissolved in FSO_3D and the cation produced, **1D**, allowed to rearrange to give **2D**, no incorporation of deuterium (other than on the oxygen) could be detected by pmr.

An analogous type of reaction was observed

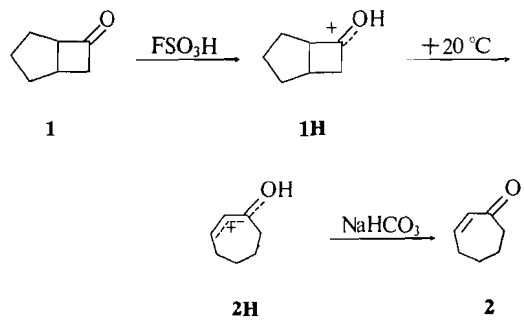

with the cyclobutanone **3** except that the thermal isomerization of **3H** occurred at very much lower temperatures. In order to observe a pmr spectrum of **3H** it was necessary to protonate **3** by extracting it from CD_2Cl_2 into a FSO_3H–SO_2ClF mixture (1:3 v/v) at −100 °C. The pmr spectrum of the solution so obtained, recorded at temperatures below −80 °C, was consistent with the formation of **3H** (Table 1). At −75 °C, **3H** isomerized, with a half-life of *ca.* 25 min., to give protonated cyclohepta-2,4-dienone, **4H**. The pmr spectrum of the rearranged product, **4H**, was identical in all respects to that obtained by protonation of authentic **4** (5). Cyclohepta-2,4-dienone, **4**, was obtained on careful neutralization of the acid solution and this was identical in all respects to an authentic sample (5, 9). Other acids, such as FSO_3H or H_2SO_4, could be used to effect this isomerization; however, with H_2SO_4 some charring occurred on the initial dissolution. In these reactions no other product could be detected in the pmr spectra of the acid solutions

Can. J. Chem. Downloaded from www.nrcresearchpress.com by 210.87.254.105 on 09/05/12
For personal use only.

Can. J. Chem. Downloaded from www.nrcresearchpress.com by 210.87.254.105 on 09/05/12
For personal use only.

even when the amplitude of the instrument was adjusted to obtain the maximum possible sensitivity.

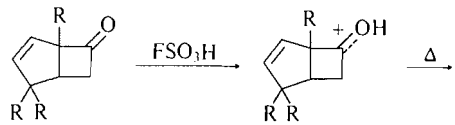

3 R = H **3H** R = H
5 R = Me **5H** R = Me

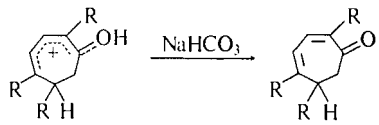

4H R = H **4** R = H
6H R = Me **6** R = Me

The trimethyl derivative **5** dissolved in FSO_3H to form **5H**. At −55 °C, **5H** isomerized, with a half-life of 15 min, to give a protonated trimethylcycloheptadienone, identified as **6H**. The structural assignments of **6H** and **6**, the product obtained on quenching the acid solution of **6H**, are based upon the spectral properties of these materials and an elemental analysis of **6**. In the pmr spectrum of **6H**, the H_3 and H_4 proton resonances displayed an AB pattern, J = 9.0 Hz. The C_2 and C_5 methyl signals were sharp singlets whereas the C_6 methyl signal was a doublet, J = 7.2 Hz. All the resonances of **6H** occurred in the regions of the spectrum expected for a protonated cyclohepta-2,4-dienone (5).

The infrared spectrum of **6** exhibited a carbonyl absorption at 1655 cm^{-1} and the uv spectrum, λ_{max} (MeOH) 318 nm, are again both typical of a conjugated cycloheptadienone. The resonance position and coupling patterns found in the pmr spectrum of **6** are fully consistent with its assigned structure.

When a solution of **7** in CD_2Cl_2–SO_2ClF was mixed with FSO_3H–SO_2ClF (1:3 v/v) at −130 °C, a clear, yellow solution was obtained. The pmr spectrum of this solution, obtained in less than five minutes at −117 °C, could not be understood in terms of a cation such as **7H**. Three one proton multiplets were observed at 9.04, 8.08 and 7.25 δ, together with a two proton multiplet at 3.78 δ and a sharp three proton singlet at 2.94 δ. The spectrum was temperature invariant up to −30 °C. In separate experiments, the same protonation was carried out using FSO_3H or H_2SO_4 as solvents and once more very similar pmr spectra were observed, even when the samples were kept at +20 °C for several hours. Protonation of the 7,7-dideuterio derivative of **7** in FSO_3H gave a product with a pmr spectrum which only differed from that described above for the protonation product of **7** in the relative intensities of the various resonances. The signal at 2.94 δ was now found by integration to have an area corresponding to slightly more than one proton.

The product arising from the protonation of **7** has been assigned the structure **8H**. The positions of the various proton resonances and coupling constants, derived from double resonance experiments are in full accord with this structure.

Careful, low-temperature neutralization of the acid solution containing **8H** followed by a rapid work up procedure, gave an unstable oil. To obtain the pmr and ir spectra of this product it was necessary to work rapidly and use dilute CCl_4 solutions. The ir spectrum displayed a strong absorption at 1670 cm^{-1}, suggesting a conjugated carbonyl group. Moreover, this ir spectrum was very similar to that reported for 1-acetylcyclopentadiene, **8**, by Hafner *et al.* (10). The pmr spectrum contained a singlet at 2.27 δ and multiplets at 3.20, 6.60, and 7.13 δ in relative areas of 3:2:2:1, corresponding to methyl, methylene, and vinyl protons respectively. The

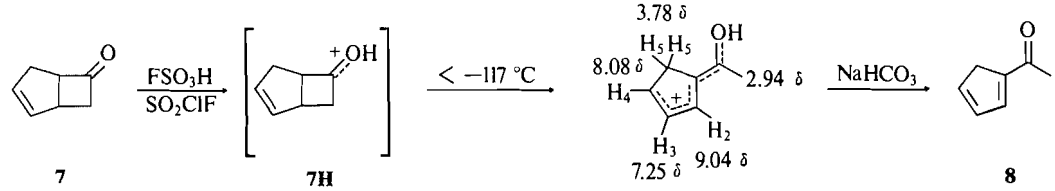

7 **7H** **8**

$J_{2,3}$ = 2.5 Hz
$J_{3,4}$ = 5.0 Hz

8H

Can. J. Chem. Downloaded from www.nrcresearchpress.com by 210.87.254.105 on 09/05/12
For personal use only.

positions of these resonances agree well with those reported for **8** and other similar cyclopentadienes (10, 11).

Dissolution of **7** in $DFSO_3$ at −78 °C gave the cation **8D**, the pmr spectrum of which indicated that a deuterium atom had been incorporated into the methyl group. Careful integration of the signal at 2.94 δ showed that it corresponded to only two protons. No further reduction in the intensity of this resonance could be detected upon standing of a $DFSO_3$ solution of **8D** at room temperature for several hours.

Discussion

The results presented above leave two questions to be answered, namely what determines whether a five- or seven-membered ring product is formed and why do the rates of these isomerizations vary.

The chemistry of the cyclobutyl cation is intimately linked with that of the closely related cyclopropylcarbinyl and allylcarbinyl cations (3). Indeed the products obtained upon solvolysis of a cyclobutyl ester can be understood in terms of the interconversion and nucleophilic capture of these three types of cations.

The equilibrium position between these three types of cations is determined by the nature and position of any substituents. Thus the charge stabilizing ability of a hydroxy or methoxy group situated on C_1 of a cyclobutyl cation has been found to be sufficient to make this the predominant form present (12). Similarly in this work, where the initial product of protonation could be observed, the cations existed predominantly as their cyclobutyl valence tautomers. Thus, for example, the pmr spectrum of **3** in FSO_3H showed that **3H** was the major species present and not **9**, **10**, **11**, or **12**. It is interesting that the vinyl proton resonances of both **3** and **5** are substantially deshielded on protonation (Table 1), indicating some homoconjugative participation of the double bond in charge delocalization (13). Such a downfield shift is of a much greater magnitude than can be accounted for with just an inductive effect.

The rearrangement of these protonated bicyclic ketones would most reasonably involve cyclopropylcarbinyl and allylcarbinyl intermediates, there being ample precedent for this in the products that have resulted from the ionization of related bicyclic systems in nucleophilic media (3, 14). As is shown for **3H** there are two ways in which the rearrangement of this cation could proceed that differ in the cyclobutane bond involved. In practice only **4H** was found as a product and no cation such as **13** could be detected.

The question of which of the cyclobutane bonds will be involved in this type of rearrangement has been considered extensively in the solvolysis of related bicyclic systems (3, 14) and it has been shown that the stereochemistry of the leaving group plays a major role in determining which bond is broken. However, with these long lived hydroxy cations such considerations have little meaning and additional factors must be examined.

One possible reaction scheme that can account for the selectivity in the rearrangements of these bicyclic ketones is shown for **3H** in Scheme 1.[3] This involves an equilibrium between the various cyclopropylcarbinyl and allylcarbinyl cations and **3H**, the latter predominating as was discussed earlier, and a rate determining final step or steps in which the product is formed. Evidence to suggest that the hydride shift involved in the formation of **4H** is rate determining comes from a comparison of the rates of rearrangement of **3H** and **5H**. With the latter system a methyl migration is required and as would be expected if this occurs during the rate determining step, the rate of the overall transformation of **5H** to **6H** is substantially less than that of **3H** to **4H** (15). The overall rate would also, of course, be dependent on the equilibrium concentrations of the various intermediary cations; however, the additional methyl substituents involved with **5H** would not be expected to change the populations by a large factor as compared to those encountered with **3H**.

The transformation of **10** to **4H** can be considered to be a [1,2], or [1,6] suprafacial shift, a type of rearrangement that occurs very readily in related cationic systems (15). However no such ready isomerization of allylcarbinyl species such as **12** to **13** can be envisaged but rather a series of protonation and deprotonation steps would be

[3]Homoconjugative interactions and cyclopropyl participation have not been indicated on the diagrams in this or other schemes solely for reasons of clarity. Such interactions would undoubtedly be expected with these ions.

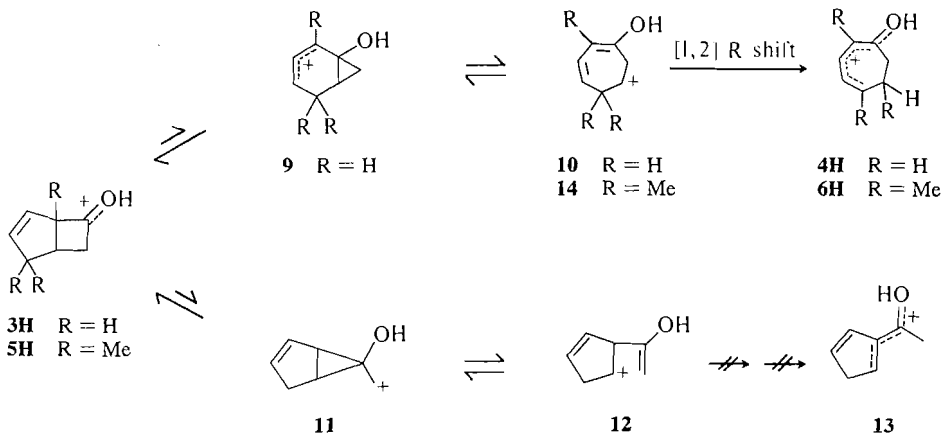

SCHEME 1

required. Not only are such steps unlikely to compete with a concerted intramolecular hydride shift involved in the transformation of **10** to **4H** but it could well be expected that cations such as **11** and **12** might be less stable than **9** and **10** and thus be present to a smaller extent in equilibrium with **3H**.

The rearrangement of **1H** to **2H** can be considered in a similar manner to that outlined for **3H** above and the same preference for the formation of a seven-membered ring would be expected. The lack of deuterium incorporation when the isomerization was carried out in FSO_3D would suggest that the final step in the reaction sequence is an intramolecular 1,4 hydride shift (16). Such a transannular hydrogen shift is well precedented (17).

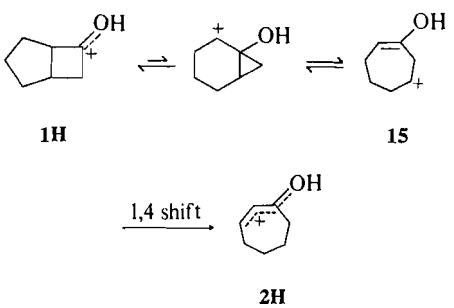

The rearrangement of **7H** to **8H** is of interest in that in this case the external cyclobutane bond is broken. From a consideration of the same type of equilibria (Scheme 2) it is apparent that the transformation of **16** to **4H** would be expected to be difficult. Thus if this isomerization were to be an intramolecular process, then the presence of the extra double bond in **16** as compared to **15** necessitates that orbital symmetry by considered. Such a suprafacial [1,4] hydride shift is symmetry forbidden in the ground state and would thus be expected to involve a high activation energy (18). The alternate route for the transformation of **16** to **4H** would involve a protonation–deprotonation mechanism and while the dication which would result from carbon protonation of the enol has been implicated in the rearrangement of protonated cyclohepta-3,5-dienone to **4H**, it was formed only at much higher temperatures than are encountered for the rearrangement of **7H**.

The observed isomerization of **7H** and **8H** must also involve a protonation–deprotonation sequence as is evidenced by the incorporation of deuterium when FSO_3D is used as the acid medium. Evidence has recently been presented to show that dications related to **17** can be formed at low temperatures in FSO_3H (19) and it is possible that such a species is involved in the isomerization of **7H**. It might well be expected that a dication such as **17** which could adopt a conformation whereby interaction between the two positive centres is minimized, would be preferred over a more rigid one derived by protonation of **16**. The alternative deprotonation–protonation sequence is of course also possible with this system; however, with related ketones it has been found that, in FSO_3H, proton removal from carbon is a slow process and that diprotonated species are frequently involved (5).

The observed rates of isomerization of **1H**, **3H**, and **7H** can also be accounted for on the basis of the type of reaction sequence suggested here. The presence of the 'extra' double bond in **3H** as

Can. J. Chem. Downloaded from www.nrcresearchpress.com by 210.87.254.105 on 09/05/12
For personal use only.

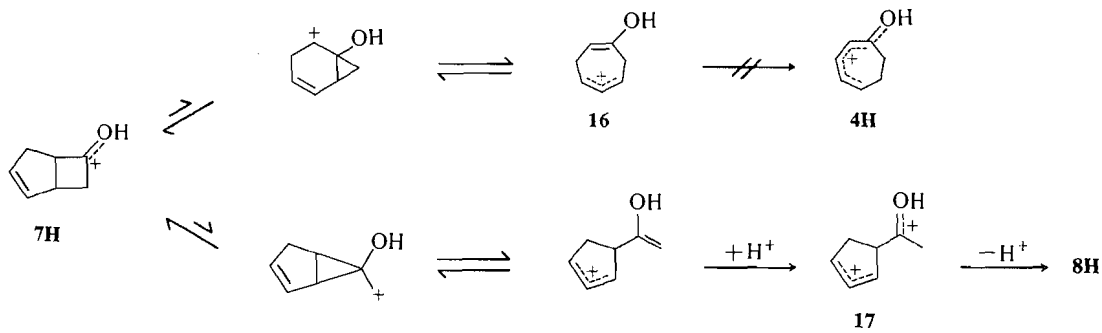

SCHEME 2

compared to **1H** would be expected to stabilize intermediates such as **9** and **10**, so increasing their relative concentrations, and possibly, moreover, facilitate the rate determining hydride shift (20). The difference in the rate of isomerization of **3H** and **7H** could possibly result from a difference in their relative ground state energies. As has already been pointed out, there is spectral evidence that **3H** is stabilized by a homoallylic interaction of the ketone carbon with the double bond in the five-membered ring. Such a stabilization would not appear to be possible with **7H** (13).

Conclusion

In an earlier paper in this series we described (5) a synthesis of cyclohepta-2,4-dienone which although effective for the parent system, was of limited value for the preparation of substituted cycloheptadienones. The acid-catalyzed ring opening reaction of bicyclo[3.2.0]hept-3-en-6-ones described in this present paper can potentially be used as a basis for the preparation of a variety of substituted systems.

The synthesis of cyclohept-2-enone **2** has been approached by others in a variety of different ways most of which involve a fairly difficult separation of **2** from related byproducts (8*a*, 21). The ring expansion route described here can routinely give **2** in 96% purity and eliminates the problems of the separation of isomeric mixtures.

Before the general applicability of this two carbon ring expansion can be claimed, it will be necessary to extend these studies to other ring systems so as to assess more completely the factors determining the observed mode of rearrangement.

Experimental

General

Proton magnetic resonance spectra were recorded on Varian HA100 or T60 spectrometers using TMS as internal reference standard. Probe temperatures were measured with a methanol sample or a thermocouple inserted at the appropriate depth in a nonspinning pmr tube. Infrared spectra were recorded on a Perkin-Elmer Model 521 grating spectrometer and uv spectra on a Cary 14 instrument. An Aerograph A90-P3 preparative gas chromatograph equipped with a Carbowax 2000 M column was used for all glpc work described.

Fluorosulphuric acid (Allied Chemicals) was treated as previously described (5). All other solvents were used as supplied.

The following compounds were prepared by literature procedures: bicyclo[3.2.0]hept-3-en-6-one (22), bicyclo-[3.2.0]hept-2-en-6-one (23), and cyclohepta-2,4-dienone (5) and 2,2,5-trimethylbicyclo[3.2.0]hept-3-en-6-one (13*a*). Bicyclo[3.2.0]heptan-6-one was prepared by hydrogenation of **3** (23 °C, 1 atm) in absolute ethanol; ir (thin film) 2960, 2865, 1775, 1315, 1285, 1237, 1195, 1078, 788, 760, and 730 cm^{-1}. 7,7-Dideuteriobicyclo[3.2.0]hept-2-en-6-one was prepared from the 7,7-dichloro derivative by the method of Grieco (23) using deuteroacetic acid. Mass spectral analysis of **3** so prepared showed it to be a mixture of 89% d_2, 7% d_1, and 4% d_0 species. All compounds were purified by glpc and had spectroscopic properties which agreed with those reported in the literature.

*Reaction of **1** in FSO_3H*

A solution of **1** (50 mg) in CD_2Cl_2 (0.25 ml) was added slowly to FSO_3H (0.5 ml) at −78 °C in an nmr tube. The pmr spectrum of the resulting solution (Table 1) remained unchanged up to +20 °C when an isomerization to **2H** was detected. After isomerization was complete as judged by pmr analysis, the acid solution was neutralized by adding it dropwise to a stirred suspension of excess $NaHCO_3$ in diethylether (10 ml) at −65 °C. The resultant mixture was allowed to warm up to 0 °C and poured into 5% aqueous $NaHCO_3$ solution at 0 °C. The ether layer was separated, dried ($MgSO_4$) and the ether evaporated *in vacuo* to give an oil (39 mg) identified as **2**; ir (CCl_4) 3035, 2950, 1665, 1450, 1420, 1390, 1245, and 864 cm^{-1}.

*Reaction of **3** in FSO_3H*

Compound **3** was protonated in a FSO_3H–SO_2ClF

Can. J. Chem. Downloaded from www.nrcresearchpress.com by 210.87.254.105 on 09/05/12
For personal use only.

(1:3 v/v) mixture at −130 °C and the pmr spectrum observed at temperatures below −75 °C. Rearrangement of **3H** to **4H** occurred at −75 °C and the resulting solution was quenched in a similar manner to that described above to give **4** with identical properties to those previously described (5).

Reaction of 5 in FSO_3H

Compound **5** was protonated, the pmr spectrum observed before and after rearrangement, and the solution quenched as outlined for **3** above. The resulting oil was identified as **6**; ir (CCl_4) 2965, 2930, 1655, 1455, 1378, 1260, 1250, 1208, 1090, 1000, and 865 cm^{-1}, pmr spectra given in Table 1. *Anal.* Calcd. for $C_{10}H_{14}O$: C 79.96; H 9.39; found: C 79.83; H 9.35.

Reaction of 7 in FSO_3H

Compound **7** was protonated in FSO_3H–SO_2ClF (1:3) at −130 °C in a comparable manner to that described above for **3**. Observation of the pmr spectrum at −117 °C five minutes after sample preparation showed that the material had completely rearranged to **8H**. The acid solution was quenched as described before, all manipulations being carried out rapidly and keeping the solutions as cold as possible. The resulting ether solution of **8** was evaporated under reduced pressure keeping the temperature below 0 °C and the resulting oil was immediately dissolved in CCl_4 for spectral characterization. Infrared (CCl_4) 1670, 1515, and 1510 cm^{-1}.

Acknowledgments

The authors gratefully acknowledge the financial assistance of the National Research Council of Canada and the technical assistance of Mr. Brian Sayer.

1. L. Ghossez, R. Montaigre, A. Roussel, H. Vanleide, and P. Mallet. Tetrahedron, **27**, 615 (1971); W. T. Brady and E. F. Hoff, Jr. J. Org. Chem. **35**, 3733 (1970).
2. P. R. Story and P. Busch. Adv. Org. Chem. **8**, 67 (1972); C. D. Gutsche, Org. React. **8**, 364 (1954); G. Wilke. Pure Appl. Chem. **7**, 179 (1968).
3. K. B. Wiberg, B. A. Hess, Jr., and A. J. Ashe III. *In* Carbonium ions. Vol. 3. *Edited by* G. A. Olah and P. von R. Schleyer. Wiley-Interscience, New York. 1972. p. 1295.
4. F. Bourelle-Wargnier. Tetrahedron Lett. 1589 (1974); E. Lee-Ruff. Can. J. Chem. **50**, 952 (1972); W. F. Erman, R. S. Treptow, P. Bakuzis, and E. Wenkert. J. Am. Chem. Soc. **93**, 657 (1971); W. F. Erman, W. Wenkert, and W. P. Jeffs. J. Org. Chem. **34**, 2196 (1969); J. Beereboom. J. Org. Chem. **30**, 4230 (1965); K. Wiberg and S. W. Kleine. Tetrahedron Lett. 1043 (1963); J. M. Conia and J. R. Salem. Acc. Chem. Res. **5**, 33 (1972); R. L. Cargill, T. E. Jackson, N. P. Peet, and D. M. Pond. Acc. Chem. Res. **7**, 106 (1974).
5. K. E. Hine and R. F. Childs. J. Am. Chem. Soc. **95**, 3289 (1973), and references cited therein.
6. D. M. Brouwer. Tetrahedron Lett. 453 (1968); G. A. Olah, Y. Halpern, Y. K. Mo, and G. Liang. J. Am. Chem. Soc. **94**, 3554 (1972); N. C. Deno, C. U. Pittman, Jr., and M. J. Wisotsky. J. Am. Chem. Soc. **86**, 4370 (1964).
7. G. A. Olah and G. Liang. J. Am. Chem. Soc. **94**, 6434 (1972).
8. (*a*) G. Stork, M. Nussim, and B. August. Tetrahedron Suppl. **8**, 105 (1966); (*b*) N. Heap and G. H. Whitman. J. Chem. Soc. B, 164 (1966).
9. D. J. Bertelli, T. G. Andrews, Jr., and A. D. Crews. J. Am. Chem. Soc. **91**, 5286 (1969); A. P. ter Borg and H. Kloosterziel. Recl. Trav. Chim. Pays-Bas, **82**, 1189 (1963).
10. K. Hafner, H. E. A. Kramer, H. Musso, G. Ploss, and G. Schulz. Ber. **97** 2066 (1964).
11. V. A. Korenevsky and N. M. Sergeyev. J. Am. Chem. Soc. **94**, 8586 (1972).
12. G. A. Olah and M. Calin. J. Am. Chem. Soc. **90**, 938 (1968); E. M. Arnett, R. P. Quirk, and J. W. Larsen. J. Am. Chem. Soc. **92**, 3977 (1970); Ch. H. V. Dusseau, S. E. Schaafsma, and Th. J. De Boer. Recl. Trav. Chim. Pays-Bas, **89**, 535 (1970).
13. (*a*) H. Hart and T. Takino. J. Am. Chem. Soc. **93**, 720 (1971); (*b*) D. E. Bays and R. C. Cookson. J. Chem. Soc. B, 226 (1967); R. C. Cookson and N. S. Wariyar. J. Chem. Soc. B, 215 (1967); J. B. Stothers, Can. J. Chem. **47**, 3602 (1969).
14. H. L. Dryden, Jr. J. Am. Chem. Soc. **76**, 2841 (1954); J. Alberti, R. Siegfried, and W. Kirmse. Ann. 1605 (1974); and H. L. Goering and F. F. Nelson. Unpublished results quoted by Wiberg *et al.* in reference 3.
15. D. M. Brouwer, C. MacLean, and E. L. Mackor. Discuss. Faraday Soc. **39**, 121 (1965); V. A. Koptyug, V. G. Shubin, A. I. Rezvukhin, D. V. Korchagina, V. P. Tret'yakov, and E. S. Rudakor. Dokl. Acad. Nauk, SSSR **171**, 1109 (1966); D. M. Brouwer, E. L. Mackor, and C. MacLean. *In* Carbonium ions Vol. 2 *Edited by* G. A. Olah and P. von R. Schleyer. Wiley-Interscience, New York. 1970. p. 837.
16. J. M. Shepherd, D. Singh, and P. Wilder, Jr. Tetrahedron Lett. 2743 (1974); M. Saunders and J. J. Stofko, Jr. J. Am. Chem. Soc. **95**, 252 (1973).
17. A. C. Cope, M. M. Martin, and M. A. McKervey. Q. Rev. (London) **20**, 119 (1966).
18. R. B. Woodward and R. Hoffmann. The conservation of orbital symmetry. Verlag Chemie, GmbH, Weinheim/Bergstr. 1970.
19. R. F. Childs and M. Zeya. Can. J. Chem. **53**, 3425 (1975).
20. J. L. Fry and G. J. Karabatsos. *In* Carbonium ions, Vol. 2. *Edited by* G. A. Olah and P. von R. Schleyer. Wiley-Interscience, New York. 1970. p. 521.
21. W. E. Parham, F. M. Parham, J. F. Dooley, and M. K. Meslahn. J. Org. Chem. **33**, 3615 (1968); E. A. Braude and E. A. Evans. J. Chem. Soc. 607 (1954); E. Garbisch. J. Org. Chem. **30**, 2109 (1965); J. MacLean and R. P. A. Sneeden. Tetrahedron, **21**, 31 (1965).
22. D. I. Schuster, M. Axelrod, and J. Auerbach. Tetrahedron Lett. 1911 (1963).
23. D. A. Grieco. J. Org. Chem. **37**, 2363 (1972).

Can. J. Chem. Downloaded from www.nrcresearchpress.com by 210.87.254.105 on 09/05/12
For personal use only.

Effets des cations alcalins et pseudo-alcalins sur quelques équilibres et en particulier sur l'équilibre d'extraction de l'acide thiocyanique par la méthylisobutylcétone

LOUISE SCHRIVER

Laboratoire de Chimie XIII, Université Pierre et Marie Curie, 8, Rue Cuvier - 75005 Paris

Reçu le 15 janvier 1975

LOUISE SCHRIVER. Can. J. Chem. **54**, 19 (1976).

La constante de l'équilibre d'extraction de l'acide thiocyanique par la méthylisobutylcétone varie à force ionique constante avec la nature des cation alcalins présents en phase aqueuse. Tout se passe comme s'il existait des paires d'ions thiocyanate cation pour lesquelles on pourrait calculer une constante d'association K_p. Cependant, l'étude d'autres équilibres ne vérifie pas cette hypothèse: l'extraction du thiocyanate de chlorpromazinium par le même solvant, la formation du complexe mono-thiocyanate de zirconium IV, ne sont pas modifiés par la nature des électrolytes. Le phénomène observé dans le cas de l'acide thiocyanique qui existe également lors de l'extraction des acides chlorhydrique et perchlorique par la méthylisobutylcétone apparait donc du aux variations d'activité des différentes espèces sous l'effet des cations.

LOUISE SCHRIVER. Can. J. Chem. **54**, 19 (1976).

The equilibrium constant for the extraction of thiocyanic acid by methylisobutyl ketone at constant ionic strength, depends on the nature of alkaline cations present in the aqueous phase. The phenomenon could be explained by the existence of ion pairs for which the association constant K_p is derivable. However the extraction of chlorpromazinium thiocyanate by the same solvent and the formation of the monothiocyanate complex of zirconium in aqueous phase are both independent of the nature of the electrolyte. The observed variations for the extraction of thiocyanic acid which exist also for the extraction of hydrochloric and perchloric acids by methylisobutyl ketone, result from the variation of species activities with a change in the identity of the cations.

Can. J. Chem. Downloaded from www.nrcresearchpress.com by 210.87.254.105 on 09/05/12
For personal use only.

L'extraction par solvant d'espèces chimiques varie dans certains cas, en fonction de l'électrolyte dissout en phase aqueuse (1). Ainsi, l'étude qualitative de l'extraction d'acide forts contenant de gros anions, par des solvants organiques de faible constante diélectrique, a permis à Diamond (2) en s'appuyant sur les travaux de Némethy et Schéraga (3) de supposer l'existence de nouvelles "paires d'ions" en phase aqueuse par renforcement des liaisons eau–eau entre un anion et un cation assez volumineux et peu chargés.

Nous nous sommes proposés d'étudier quantitativement les variations apportées par différents cations alcalins ou pseudo-alcalins sur l'équilibre d'extraction de l'acide thiocyanique par la méthylisobutylcétone et d'étendre cette étude à d'autres équilibres où interviennent soit des ions thiocyanate, soit des protons.

Extraction de l'acide thiocyanique par la méthylisobutylcétone

La méthylisobutylcétone solvant de faible constante diélectrique (ϵ 13.11) et de moment dipolaire 2.79 D, extrait fortement l'acide thiocyanique de solutions aqueuses contenant un thiocyanate alcalin et un acide minéral fort (4). Pour des concentrations en thiocyanate inférieures à 10^{-1} *M* et pour une acidité totale telle que l'acide thiocyanique soit totalement dissocié en phase aqueuse, on peut définir une constante de partage (4, 5)

$$K_{\overline{HSCN}} = \frac{[\overline{HSCN}]}{[H^+][SCN^-]}$$

L'acide thiocyanique est en fait extrait avec une molécule d'eau, sous forme d'un complexe tétramoléculaire:

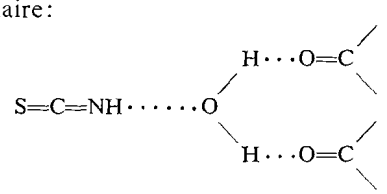

comme nous l'avons précédemment montré par spectroscopie infrarouge (6).

La constante d'extraction K_{HSCN} a été mesurée avec des solutions aqueuses: (*i*) HCl, LiSCN,

Can. J. Chem. Downloaded from www.nrcresearchpress.com by 210.87.254.105 on 09/05/12
For personal use only.

TABLEAU 1. Valeurs des constantes K_{HSCN}

Cation alcalin M^+	$I = 1.5$	$I = 3$	$I = 4.5$
Li^+	11.5	36	105
Na^+	10.5	23.5	50
K^+	8.5	14.5	—
NH_4^+	8	13	18

LiCl, (*ii*) HCl, NaSCN, NaCl, (*iii*) HCl, KSCN, KCl et (*iv*) HCl, NH_4SCN, NH_4Cl.

La force ionique I est maintenue constante à l'équilibre; la concentration en thiocyanate est très inférieure à 10^{-1} M pour éviter sa dimérisation (5) et l'acidité totale est de l'ordre de 0.1 M. L'extraction des chlorure et thiocyanate alcalins comme celle de l'acide chlorhydrique est négligeable devant celle de HSCN, aux conditions expérimentales choisies.

Tous les réactifs utilisés dans le cadre de cette étude sont de qualité analytique. Le thiocyanate de lithium a été préparé à partir de solutions aqueuses de lithine et d'acide thiocyanique puis recristallisé deux fois. La méthylisobutylcétone a été distillée avant son utilisation.

L'extraction est réalisée par agitation de volumes égaux de solution aqueuse et de solvant. L'équilibre est très rapidement atteint et après quelques essais préliminaires le temps d'agitation a été choisi de 5 min. Les deux phases sont séparées par centrifugation. Toutes les expériences ont été effectuées dans une pièce thermostatée à 20 ± 1 °C.

En dose à l'équilibre le thiocyanate dans les deux phases par spectrométrie avec Fe(III). L'acidité totale en phase aqueuse à l'équilibre est connue par dosage avec de la soude en présence de rouge de méthyle. L'écart entre les valeurs de K_{HSCN} obtenues pour cinq à huit expériences dans chaque mélange considéré est inférieur à 1%. L'ensemble des résultats à différentes forces ioniques est indiqué tableau I. La constante d'extraction K_{HSCN} croît avec la force ionique mais à une force ionique déterminée, diminue quand la taille du cation augmente, cette dernière variation étant d'autant plus sensible que la force ionique est élevée.

A force ionique constante 1.5, nous avons fait varier la concentration des ions ammonium, en remplaçant le cation NH_4^+ par le proton ceci jusqu'à $[H^+] = 0.6$ M, la formation de HSCN n'étant plus négligeable pour une acidité supérieure (7, 8). Nous avons ainsi vérifié que l'extraction augmente quand la concentration en NH_4^+ diminue.

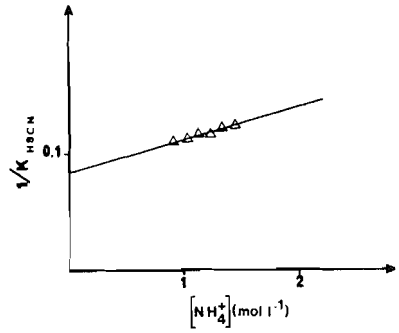

FIG. 1. Variation de $1/K_{HSCN}$ en fonction de la concentration en $[NH_4^+]$ à force ionique 1.5.

D'autre part, nous constatons que la variation de $1/K_{HSCN}$ est une fonction linéaire de la concentration du cation ammonium comme le montre la figure 1. Le traitement des données $1/K_{HSCN}$, $[NH_4^+]$ par une méthode des moindres carrés linéaires pondérés et extrapolation à $[NH_4^+] = 0$ donne la valeur théorique K^0_{HSCN} à influence nulle des cations alcalins soit pour $I = 1.5$, $K^0_{HSCN} = 11.70$ valeur très proche de K_{HSCN} obtenue en milieu lithium. Pour une force ionique respectivement de 3 et de 4.5 la variation de $1/K_{HSCN} = f(M^+)$ conduit à $K^0_{HSCN} = 41$ et $K^0_{HSCN} = 140$.

Une partie du thiocyanate semble donc ne plus être libre en présence de Li^+, Na^+, K^+, NH_4^+ et ceci pourrait nous conduire à supposer l'existence de paires d'ions thiocyanate cation d'autant plus stables que le rayon du cation est grand (9). Cependant, avant d'interpréter quantitativement nos résultats, nous avons choisi d'examiner d'autres équilibres où interviennent, soit des ions thiocyanate, soit des ions H^+ en présence des différents cations alcalins utilisés.

Extraction du thiocyanate de chlorpromazinium par la méthylisobutylcétone

Nous avons utilisé en milieu chlorure, l'équilibre d'extraction du thiocyanate de chlorpromazinium

$$\overline{HPCl} + SCN^- \leftrightharpoons \overline{HPSCN} + Cl^-$$

le cation chlorpromazinium:

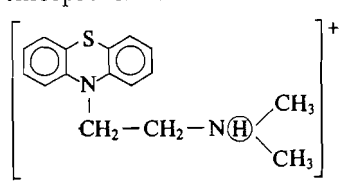

Can. J. Chem. Downloaded from www.nrcresearchpress.com by 210.87.254.105 on 09/05/12
For personal use only.

TABLEAU 2

Cation	[HPCl] total ($M \times 10^2$)	$[\overline{HPSCN}]$ à l'équilibre ($M \times 10^3$)	$[\overline{HPCl}]$ à l'équilibre ($M \times 10^3$)	$[SCN^-]_{aq}$ à l'équilibre ($M \times 10^3$)	$K = \frac{[\overline{HPSCN}][Cl^-]}{[\overline{HPCl}][SCN^-]}$
Li^+	1.0064	3.375	6.69	1.312_5	1152
Na^+	0.938	3.1875	6.19	1.400	1102
NH_4^+	0.948	3.600	5.88	1.650	1113

en abrégé HP^+ a déjà été utilisé par S. Tribalat et A. Jamard pour l'étude de la séparation des ions perrhénates et des ions rhénihexachlorure (10, 11).

Dans toutes nos séries d'extraction, nous avons des conditions expérimentales telle que tout le chlorpromazinium soit totalement extrait par le solvant organique ([HP] total = $[\overline{HPCl}] + [\overline{HPSCN}]$); les concentrations initiales des réactifs sont alors: (*i*) [HPCl] total $\sim 10^{-2}$ *M*, (*ii*) [MSCN] $\sim 5 \times 10^{-3}$ *M* et (*iii*) [HCl] $\sim 5 \times 10^{-3}$ *M*; la force ionique étant maintenue constante à 3 par un sel alcalin MCl (M^+ étant successivement Li^+, Na^+, NH_4^+). L'acide chlorhydrique ajouté évite qu'en milieu neutre le cation HP^+ se transforme en sa base conjuguée P. On dose SCN^- dans les deux phases par spectrophotométrie avec Fe(III) après une double extraction par la méthylisobutylcétone en milieu basique de façon à éliminer HPCl. La concentration de $\overline{HPCl}$ est connue par différence entre [HPCl] total et $[\overline{HPSCN}]$ formé. Les résultats indiqués dans le tableau 2 montrent que la constante *K*,

$$K = \frac{[\overline{HPSCN}]\,[Cl^-]}{[\overline{HPCl}]\,[SCN^-]}$$

est la même à 5% près en milieu Li^+, Na^+, NH_4^+. On pourrait supposer ici que les ions thiocyanate et chlorure présentent le même degré d'association pour chaque cation considéré, or il a été montré que la constante de l'équilibre $HP^+ + Cl^- \rightleftharpoons HPCl$ ne varie pas en fonction de la nature des cations alcalins.[1]

Equilibre de formation du thiocyanate de zirconium en phase aqueuse

Nous avons déjà montré que le zirconium(IV) formait avec les ions thiocyanate en solution aqueuse acide un complexe 1–1 (12):

$$Zr(OH)^{3+} + SCN^- \rightleftharpoons Zr(OH)(SCN)^{2+}$$

[1] C. Piolet, observation non publiée.

TABLEAU 3

Cation	$[H^+]_{aq}$ à l'équilibre ($M \times 10$)	$[\overline{HClO_4}]$ ($M \times 10$)	$D = \frac{[\overline{HClO_4}]}{[H^+]}$
Li^+	1.55	0.46	0.297 ± 0.005
Na^+	1.675	0.34	0.202
NH_4^+	1.75	0.27	0.154

ce complexe absorbe dans l'uv, sa constante de stabilité est égale à 11.5 à force ionique 3.5. Pour [HCl] = 2 *M*, [Zr] = 10^{-4} *M*, [SCN^-] = 10^{-2}*M* et [MCl] = 3 *M* (M^+ étant successivement Li^+, Na^+, NH_4^+), nous avons mesuré l'absorption du complexe formé, et n'avons trouvé aucune variation. La concentration du complexe est donc la même quel que soit le cation il n'y a pas variation de la concentration en thiocyanate libre.

Par ailleurs, la constante β' de formation du complexe à une acidité donnée varie avec l'acidité selon

$$\beta' = \beta \times \frac{1}{1 + \frac{[H^+]}{K_A}}$$

(K_A constante d'acidité de l'acide thiocyanique). L'étude de cette variation qui revient, à force ionique constante, à remplacer H^+ par un cation alcalin, nous donne une droite, ce qui est incompatible avec l'existence de paires d'ions thiocyanate cation.

Extraction de l'acide perchlorique par la méthylisobutylcétone

Nous avons déterminé le coefficient de partage

$$D = \frac{[\overline{HClO_4}]}{[H^+]}$$

à force ionique maintenue égale à 1.5 par $MClO_4$ (M^+ étant successivement Li^+, Na^+, NH_4^+); la concentration initiale d'acide est de l'ordre de 2×10^{-1} *M* afin de pouvoir négliger la dissociation de l'acide dans la méthylisobutylcétone dont la constante est de l'ordre de 3×10^{-4} (13). Les résultats sont indiqués dans le tableau 3.

Can. J. Chem. Downloaded from www.nrcresearchpress.com by 210.87.254.105 on 09/05/12
For personal use only.

Nous constatons ici que dela même façon que pour HSCN, l'extraction diminue quand la taille du cation augmente et la différence observée dans le cas de l'acide perchlorique est encore plus importante que dans le cas de l'acide thiocyanique.

Extraction de l'acide chlorhydrique par la méthylisobutylcétone

L'acide chlorhydrique est très faiblement extrait par la méthylisobutylcétone. S. Tribalat et A. Jamard ont étudié son extraction dans ce solvant à force ionique 5 (HCl + NaCl) en fonction de la concentration d'acide (HCl de 0.5 à 5 *M*) (11). Ils ont constaté que la variation du coefficient de partage *D*:

$$D = \frac{\overline{[HCl]} + \overline{[H^+]}}{[H^+]}$$

$$= Ke[Cl^-] + \sqrt{Ki}\frac{\sqrt{[Cl^-]}}{\sqrt{[H^+]}}$$

$$Ke = \frac{\overline{[HCl]}}{[H^+]\,[Cl^-]}$$

$$Ki = \frac{\overline{[H^+]}\,\overline{[Cl^-]}}{[H^+]\,[Cl^-]}$$

qui devrait être une fonction linéaire de $[H^+]^{-1/2}$ ne l'est plus pour des concentrations de H^+ supérieures à 2 *M*.

Nous avons repris l'extraction de l'acide chlorhydrique par la méthylisobutylcétone dans les mêmes conditions expérimentales mais successivement avec LiCl, NaCl, NH_4Cl pour maintenir la force ionique. L'acidité totale en phase solvant est dosée par une base forte après avoir réagité la méthylisobutylcétone avec un petit volume d'eau. Les courbes $D = f[H^+]^{-1/2}$ obtenues sont représentées figure 2.

On constate, comme pour HSCN et $HClO_4$: (*i*) d'une part, que toutes autres conditions égales, le coefficient de partage diminue quand la taille du cation augmente; (*ii*) d'autre part, que pour un même cation, *D* diminue avec la concentration en cation, cette variation n'étant sensible que lorsque $1/[H^+]$ varie très peu (de $[H^+]$ 5 *M* à 2 *M*).

Conclusion

L'extraction de l'acide thiocyanique par la méthylisobutylcétone comme celle des acides perchlorique et chlorhydrique varie sensiblement quand on modifie la nature de la concentration des cations alcalins de la phase aqueuse. La variation linéaire de $1/K_{HSCN}$ en fonction de la concentration du cation à force ionique constante, pourrait laisser supposer l'existence de paires d'ions thiocyanate cation pour lesquelles il serait possible de calculer une constante d'association

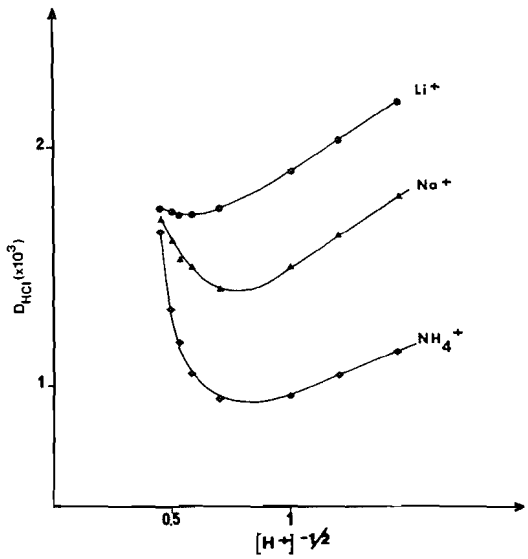

FIG. 2. Variation de D_{HCl} en fonction de $[H^+]^{-1/2}$ à force ionique 5 (HCl + M^+Cl^- = 5; M^+ = Li^+, Na^+, NH_4^+).

$$K_p = \frac{[SCNM]}{[SCN^-]\,[M^+]}$$

à l'aide de l'équation:

$$\frac{1}{K_{HSCN}} = \frac{K_p}{K^0_{HSCN}}[M^+] + \frac{1}{K_0}$$

K_{HSCN} et K^0_{HSCN} étant connus.

Cependant, l'étude d'autres équilibres-extraction du thiocyanate de chlorpromazinium par la méthylisobutylcétone, formation de thiocyanate de zirconium, montre que cette hypothèse aussi séduisante soit-elle, ne peut être retenue: pour ces équilibres, aucune variation du thiocyanate libre n'est observée quand on modifie la nature des cations.

Les variations observées pour les trois acides considérés apparaissent donc dues essentielle-

ment aux variations d'activité des ions H^+ et des anions correspondants en phase aqueuse, quand aux forces ioniques importantes choisies, on modifie la nature du cation. En milieu potassium, les coefficients d'activité de H^+ et de SCN^- sont plus faibles qu'en milieu lithium, cation plus hydraté, et l'extraction est moins bonne. Par ailleurs, les effets des électrolytes sur la tension de surface des deux phases eau–méthylisobutylcétone peuvent également contribuer à modifier la distribution des acides.

1. Y. MARCUS et A. S. KERTES. Ion exchange and solvent extraction of metal complexs. Wiley Interscience, London. 1969.
2. R. M. DIAMOND. J. Phys. Chem. **67**, 2513 (1963).
3. G. NÉMEHY et H. A. SCHÉRAGA. J. Chem. Phys. **36**, 3382 (1963); **36**, 3401 (1963).
4. S. TRIBALAT. C.R. Acad. Sci. **256**, 5586 (1963).
5. L. SCHRIVER. Bull. Soc. Chim. Fr. **6**, 1882 (1973); **6**, 1884 (1973).
6. L. SCHRIVER et J. CORSET. J. Chim. Phys. Fr. **10**, 1463 (1973).
7. T. D. E. MORGAN, G. STEDMANN et P. A. E. WHINCUP. J. Chem. Soc. 4813 (1965).
8. S. TRIBALAT et J. M. CALDERO. Bull. Soc. Chim. Fr. 774 (1966).
9. R. BURY, M. C. JUSTICE et J. C. JUSTICE. J. Chim. Phys. Fr. **67**, 2045 (1970).
10. S. TRIBALAT et A. JAMARD. Ann. Chim. **8**, 87 (1973).
11. S. TRIBALAT et A. JAMARD. Ann. Chim. **8**, 230 (1973).
12. L. SCHRIVER. C.R. Acad. Sci. **274**, 849 (1972).
13. D. DELAFOSSE. Thèse Paris 1956.

Can. J. Chem. Downloaded from www.nrcresearchpress.com by 210.87.254.105 on 09/05/12
For personal use only.

Carbamates and 2-oxazolidinones from tertiary alcohols and isocyanates

THOMAS FRANCIS[1] AND MELANIE P. THORNE[2]
Ontario Research Foundation, Sheridan Park, Ontario L5K 1B3

Received July 22, 1975

THOMAS FRANCIS and MELANIE P. THORNE. Can. J. Chem. **54**, 24 (1976).

Organo-tin catalysts have been used to prepare a large number of new carbamates of tertiary alcohols. Cyclization of carbamates of unsaturated tertiary alcohols leads to the formation of 2-oxazolidinones, and provides a new synthetic route for some of these compounds.

THOMAS FRANCIS et MELANIE P. THORNE. Can. J. Chem. **54**, 24 (1976).

On a utilisé des catalyseurs organostanniques pour préparer un grand nombre de nouveaux carbamates d'alcools tertiaires. La cyclisation des carbamates d'alcools tertiaires non-saturés conduit à la formation d'oxazolidinones-2 et fournit ainsi une nouvelle méthode de synthèse pour quelques-uns de ces composés.

[Traduit par le journal]

Can. J. Chem. Downloaded from www.nrcresearchpress.com by 210.87.254.40 on 09/05/12
For personal use only.

Preparation of Carbamates using Organo-tin Catalysts

N-Substituted carbamates of primary and secondary alcohols have been widely used in organic chemistry as a means of characterizing alcohols and, industrially, in the medical and agricultural fields. In contrast the carbamates of tertiary alcohols have received scant attention due, presumably, to the difficulties encountered in their preparation. Reaction of an organic isocyanate with a tertiary alcohol often leads to dehydration of the alcohol in addition to or instead of carbamate formation, [1]. For the most part, even in the presence of basic catalysts such as amines or sodium acetate (1) yields of carbamates are low when R'OH = *tert*-alcohol. *tert*-Ethynyl carbinols provide the exception by reacting stoichiometrically with phenyl isocyanate in the presence of *N*-methylpyrolidinone (2) and with alkyl isocyanates in the presence of sodium or potassium acetate and triethylamine (3) to yield the expected carbamates.

$$[1] \qquad RNCO + R'OH \rightarrow RNHCOOR'$$

Griffith (4) has reported that the lithium alkoxide of the *tert*-alcohol will catalyze the reaction 1 for R = phenyl or 1-naphthyl. He obtained yields of about 75% for catalyst concentrations of up to 14 mol%.

We have found that yields of up to 90% can be obtained using the organo-tin catalysts which are well known, particularly in the polyurethane industry, as catalysts for the isocyanate and primary or secondary alcohol reactions. There are no literature reports that these catalysts have been used before to prepare carbamates from *tert*-alcohols and we report here the preparation of a number of new carbamates from saturated and unsaturated *tert*-alcohols and aryl- or alkyl-isocyanates.

As a measure of the catalytic efficiency of three organo-tin compounds, *tert*-butyl alcohol was treated with phenyl isocyanate in refluxing benzene in the presence of stannous octoate (stannous-2-ethylhexanoate), stannous oleate, dibutyltin dilaurate, an amine catalyst (*N*-methylmorpholine) and in the absence of added catalyst. The percentage yields of *tert*-butyl-*N*-phenylcarbamate were 94, 96, 80, 55, and 46 respectively. Stannous octoate and oleate also proved to be efficient catalysts for the *tert*-butyl alcohol–2,4-tolylene diisocyanate reaction in contrast to *N*-methylmorpholine, *N*,*N*-dimethylaniline, and triethylamine all of which failed to effect condensation. In the preparations reported in Tables 1 and 2 stannous octoate was used exclusively as the catalyst; the reaction medium was usually refluxing benzene.

For carbamates of 1,1-diphenylethanol and of 2-methyl-2-hydroxy-3-butanone large quantities of diphenylurea were obtained when preparations were done in refluxing benzene. Carbamate yields were improved by carrying out the reactions at room temperature. Similarly stannous octoate in

[1]Present address: Faculty of Food Science, University of Toronto, Toronto, Ontario M5S 1A1.
[2]Present address: Chemistry Department, University of Keele, Keele, Staffs., England ST5 5BG.

Can. J. Chem. Downloaded from www.nrcresearchpress.com by 210.87.254.40 on 09/05/12
For personal use only.

TABLE 1. Carbamates from tertiary alcohols and monoisocyanates, $R_1-NH-C(=O)-O-C(R_2)(R_2)-R_3$

R_1	R_2	R_3	mp (bp) (°C)	Yield (%)	Crystallization solvent	C (%) Calcd.	C (%) Obsvd.	H (%) Calcd.	H (%) Obsvd.	N (%) Calcd.	N (%) Obsvd.
n-C_4H_9	CH_3	CH_3	32 °C/0.04 Torr	92	—	62.40	62.48	10.98	11.15	8.09	8.15
	CH_3	C_2H_5	44 °C/0.04 Torr	82	—	64.20	64.20	11.23	11.07	7.48	7.83
	CH_3	$C{\equiv}CH$	50	92	Heptane	65.57	65.52	9.29	9.56	7.65	7.65
	CH_3	$CH{=}CH_2$	60–65 °C/0.3 Torr	92	—	64.86	64.76	10.27	10.41	7.57	7.38
	C_6H_5	C_6H_5	167	82	Benzene–heptane	80.22	80.19	6.96	7.00	3.90	4.07
C_6H_5	CH_3	C_2H_5	42.5–43	90	Heptane	69.53	69.76	8.27	8.12	6.76	6.81[a]
	CH_3	$CH{=}CH_2$	61–62	90	Heptane	70.24	70.30	7.30	7.19	6.83	6.90
	CH_3	$C{\equiv}CH$	103.5	95	Benzene–heptane	70.90	70.50	6.41	6.56	6.90	6.90[b]
	CH_3	$COCH_3$	80.5	95	Petroleum ether[d]	65.43	65.60	6.80	7.00	6.35	6.40
	C_6H_5	CH_3	123–124	78	Petroleum ether[d]	79.47	79.90	6.03	6.13	4.50	4.40[c]
	C_6H_5	C_6H_5	175–178	95	Benzene–heptane	82.32	82.30	5.54	5.66	3.69	3.92
p-$CH_3C_6H_4$	CH_3	C_2H_5	74–75	80	Heptane	70.59	70.52	8.60	8.41	6.33	6.15
m-$CH_3C_6H_4$			31–32	85	Heptane (sublimed)	70.59	70.84	8.60	8.72	6.33	6.42
p-ClC_6H_4			76.5–77	95	Heptane	59.64	60.07	6.62	6.59	5.80	5.99
m-ClC_6H_4			60–61	85	Heptane (sublimed)	59.63	60.09	6.62	6.49	5.80	5.93
p-$NO_2C_6H_4$			66.5–67.5	90	Toluene–heptane	56.90	56.80	6.70	6.52	11.10	11.10
p-$C_2H_5OC_6H_4$	CH_3	CH_3	111	94	Heptane	65.82	65.97	8.02	7.98	5.91	5.77
o-ClC_6H_4	CH_3	$C{\equiv}CH$	48.5	92	THF–benzene	60.63	60.91	5.05	5.18	5.89	5.91
m-ClC_6H_4			93	88	THF–benzene	60.63	60.40	5.05	4.95	5.89	6.00
p-ClC_6H_4			117–118.5	91	THF–benzene	60.63	60.79	5.05	5.16	5.89	5.72
p-$CH_3C_6H_4$			87	90	Petroleum ether[d]	71.89	71.71	6.91	6.86	6.45	6.26
p-$CH_3C_6H_4$	CH_3	$C(=O)CH_3$	84	76	Petroleum ether[d]	66.38	66.73	7.23	7.38	5.95	5.96
p-ClC_6H_4			64	70	Petroleum ether[d]	56.36	56.20	5.52	5.50	5.48	5.30
p-ClC_6H_4	CH_3	$CH{=}CH_2$	70	75	Petroleum ether[d]	60.13	60.34	5.85	5.98	5.85	5.82
p-$CH_3C_6H_4$			58	75	Petroleum ether[d]	71.23	71.36	7.76	7.87	6.39	6.43

[a]Lit. mp 42 °C (ref. 16).
[b]Lit. mp 102–103 °C (ref. 2).
[c]Lit. mp 124–125 °C (ref. 3).
[d]Petroleum ether bp 60–80 °C.

Can. J. Chem. Downloaded from www.nrcresearchpress.com by 210.87.254.40 on 09/05/12
For personal use only.

TABLE 2. Dicarbamates from *tert*-alcohols and diisocyanates

Isocyanate	Tertiary alcohol	Dicarbamate mp (°C)	Yield (%)	Crystallization solvent	C (%)		H (%)		N (%)	
					Calcd.	Obsvd.	Calcd.	Obsvd.	Calcd.	Obsvd.
3,3′-Dimethoxy-4,4-diphenylene diisocyanate	*tert*-Butyl	175–177	87	Ethyl acetate	64.84	64.64	7.25	7.42	6.30	6.11
3,3′-Dimethoxy-4,4-diphenylene diisocyanate	*tert*-Pentyl	116.5–118.5	86	Heptane	66.08	66.26	7.68	7.41	5.93	5.75
3,3′-Dimethyl-4,4′-diphenylene diisocyanate	*tert*-Butyl	192–193	95	Benzene	69.87	70.18	7.82	7.95	6.79	6.73
3,3′-Dimethyl-4,4′-diphenylene diisocyanate	*tert*-Pentyl	164.5–166	63	Heptane	70.87	70.92	8.24	8.36	6.36	6.41
1,6-Hexane diisocyanate	*tert*-Butyl	102.5–103.5	98	Heptane	60.74	60.92	10.20	10.37	8.86	8.92
1,6-Hexane diisocyanate	*tert*-Pentyl	64.5–66	77	Heptane	62.77	62.57	10.56	10.50	8.13	8.02
m-Phenylene diisocyanate	*tert*-Butyl	142–144	90	Benzene–heptane	62.54	62.53	7.87	8.07	9.12	9.02
m-Phenylene diisocyanate	*tert*-Pentyl	72–74.5	90	Heptane	64.47	64.57	8.42	8.53	8.36	8.20
2,4-Tolylene diisocyanate	*tert*-Butyl	159–161	83	Ethyl acetate–heptane	63.33	63.03	8.13	8.19	8.69	8.80
2,4-Tolylene diisocyanate	*tert*-Pentyl	122–123	81	Benzene–heptane	65.11	65.42	8.63	8.78	7.99	8.06
Diphenylmethane-4,4′-diisocyanate	*tert*-Butyl	192–193	98	Ethyl acetate	69.32	69.50	7.59	7.82	7.03	6.88
Diphenylmethane-4,4′-diisocyanate	*tert*-Pentyl	144.5–145.5	92	Ethyl acetate–heptane	70.39	70.14	8.03	8.04	6.57	6.82
3,3′-Dimethyldiphenylmethane-4,4′-diisocyanate	*tert*-Butyl	183–185	99	Ethyl acetate–heptane	70.40	70.39	8.04	8.10	6.57	6.80
3,3′-Dimethyldiphenylmethane-4,4′-diisocyanate	*tert*-Pentyl	131–132.5	97	Heptane	71.33	71.54	8.43	8.42	6.16	6.08

Can. J. Chem. Downloaded from www.nrcresearchpress.com by 210.87.254.40 on 09/05/12
For personal use only.

cold benzene catalyzed the formation, in 95% yield, of triphenylmethyl *N*-phenylcarbamate from triphenyl carbinol and phenyl isocyanate, but in refluxing benzene the product was *N*-triphenylmethyl aniline [2].

[2] $PhNCO + (C_6H_5)_3COH \rightarrow PhNHC(C_6H_5)_3 + CO_2$

The products were identified by elemental microanalysis, by ir and nmr spectra, and, for known compounds, by melting point. Infrared absorption bands (C=O) were observed in the regions 1740–1750 cm^{-1} for solutions in CCl_4 and 1680–1700 cm^{-1} for KBr pellets. A similar shift in C=O absorption on going from solution to solid has been noted by Chen and Benson (5). Bands at 3300–3440 cm^{-1} are attributed to N—H and, in the ethynyl carbamates, at 2120 cm^{-1} to C≡C stretching vibrations. These absorptions agree well with those reported for other *N*-substituted carbamates (3, 5–7). The proton chemical shifts for the nmr spectra of the *tert*-butyl carbamates have already been reported (9). Structural variations in the other carbamates gave the expected variations in the nmr spectra In all cases the H—N absorption appeared at about $\delta = 6.5$ ppm; frequently as a broad band.

The carbamates are thermally stable up to about 150–200 °C when they decompose to yield olefins, amines, and carbon dioxide. Thus they can provide useful intermediates in the preparation from tertiary alcohols of olefins which rearrange under acid-catalyzed dehydration conditions. Their lower decomposition temperatures and ease of preparation offer advantages over acetates and xanthates which have been used previously (8). A kinetic study of the thermal degradation of the monocarbamates has already been reported (9, 10).

Olefins are not produced in two cases. The triphenylmethyl carbamates having no β-hydrogens decompose thermally to yield a secondary amine and the ketonic carbamates cyclize on heating to yield 4-hydroxy-2-oxazolidinones (see below).

Cyclization of Acetylenic Carbamates

That *N*-arylcarbamates of propargyl alcohols can be cyclized to give 4-alkylidene-2-oxazolidinones is well established (3, 11, 12); the nmr spectra of the products having been shown (3, 12, 13) to be in agreement with the structure containing a five-membered ring and an exocyclic double bond [3]. The conditions necessary for

[3] 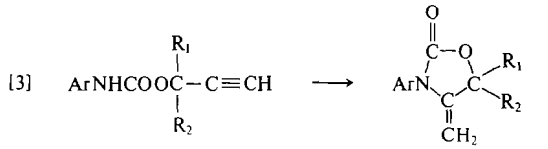

the reaction vary from heating to 140 °C (for $R_1 = R_2 = H$; Ar = phenyl) to use of basic catalysts such as sodium acetate or pyridine ($R_1 = R_2$ = alkyl; Ar = dichlorophenyl) or sodium methoxide ($R_1 = R_2$ = alkyl; Ar = phenyl).

The 3-aryl-4-methylene-5,5-dimethyl-2-oxazolidinones reported in Table 3 were prepared by heating the carbamates in boiling pyridine; sodium acetate in refluxing dioxan failed to bring about cyclization. Interestingly, however, sodium acetate would catalyze the formation of the oxazolidinones directly from the isocyanate and acetylenic alcohols without prior isolation of the carbamate.

The aliphatic isocyanate, *n*-butyl isocyanate also reacted with the acetylenic alcohol, in the presence of stannous octoate, to give the desired carbamate, which was not cyclized after boiling in pyridine for 8 h. In the presence of the sodium salt of the acetylenic alcohol, however, the *N*-alkylcarbamate did rearrange to give the oxazolidinone.

Carbamates of the olefinic alcohol, 3-methylbut-1-en-3-ol have not previously been reported and consequently cyclization of these compounds to yield 4-alkyl-2-oxazolidinones [4] is also reported here for the first time.

[4] 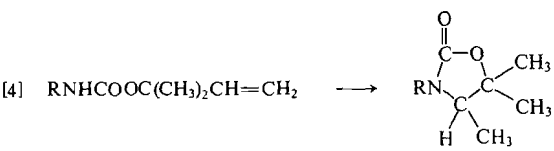

A strong base, such as the sodium salt of the olefinic alcohol was required to bring about the cyclization reaction, which then occurred in good yield.

This reaction provides a much simpler and more convenient method of preparation of 4-alkyl-2-oxazolidinones than the catalytic hydrogenation under pressure of 4-alkylidene-2-oxazolidinones previously used.

When the carbamates of the ketonic alcohol, 2-methyl-2-hydroxy-3-butanone are heated in boiling water, crystalline compounds having melting points different from those of the carba-

Can. J. Chem. Downloaded from www.nrcresearchpress.com by 210.87.254.40 on 09/05/12
For personal use only.

TABLE 3. Oxazolidinones from cyclization of carbamates

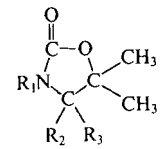

R_1	R_2	R_3	mp (bp) (°C)	Yield (%)	Crystallization solvent	C (%) Calcd.	C (%) Obsvd.	H (%) Calcd.	H (%) Obsvd.	N (%) Calcd.	N (%) Obsvd.
C_6H_5			130.5	68	Ethanol–H_2O	70.90	70.91	6.41	6.48	6.90	6.94[a]
p-ClC_6H_5			130	70	Ethanol	60.63	60.75	5.05	4.82	5.89	5.84[b]
m-ClC_6H_5			100	80	Petroleum ether (60–80)	60.63	60.96	5.05	5.11	5.89	5.94
o-ClC_6H_5		$=CH_2$	108	83	Benzene	60.63	60.48	5.05	5.03	5.89	6.07
p-$CH_3C_6H_5$			139	86	Petroleum ether (60–80)	71.89	71.72	6.91	7.11	6.45	6.48
n-C_4H_9			80–82 °C/0.3 Torr	95	—	65.57	65.53	9.29	9.56	7.65	7.69
C_6H_5			102–103	70	Benzene–heptane	70.24	70.42	7.30	7.51	6.83	7.08
p-ClC_6H_5			56	65	Petroleum ether (40–60)	60.15	60.13	5.85	5.95	5.85	5.85
p-$CH_3C_6H_5$	H	CH_3	66	50	Petroleum ether (60–80)	71.23	71.23	7.76	7.93	6.39	6.22
n-C_4H_9			72–74 °C/0.3 Torr	100	—	64.86	64.76	10.27	10.41	7.57	7.38
C_6H_5			129.5	100	Water	65.16	65.00	6.79	6.97	6.33	6.37[c]
p-ClC_6H_4	OH	CH_3	133.0	100	Water	56.25	56.31	5.47	5.53	5.47	5.55
p-$CH_3C_6H_4$			139.0	100	Water	66.38	66.32	7.23	7.32	5.96	6.13

[a]Lit. mp 130–133 °C (ref. 2).
[b]Reported mp 98–99 °C believed to be in error (ref. 11).
[c]Lit. mp 133–135 °C (ref. 14).

Can. J. Chem. Downloaded from www.nrcresearchpress.com by 210.87.254.40 on 09/05/12
For personal use only.

mates are formed in theoretical quantities. These products were identified by nmr spectra as 4-hydroxy-4-methyl-2-oxazolidinones [5]. Easton

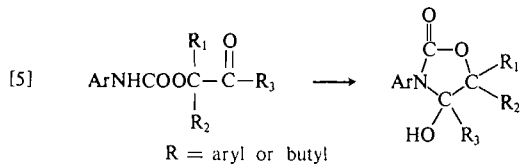

et al. (12) mentioned the formation of a compound of this type ($R_1 = R_2 = R_3 = CH_3$; Ar = *p*-chlorophenyl) as an intermediate in the preparation of 4-alkylidene-2-oxazolidinones, but they did not isolate it. Saettone (14) cyclized phenacyl *N*-benzylcarbamate (R_3 = phenyl; $R_1 = R_2$ = H; Ar = benzyl) in the presence of a base, but found that the corresponding *N*-phenylcarbamate would not cyclize. Saettone attributed this to the lower nucleophilicity of the anion intermediate. In a later publication Nutti and Saettone reported the preparation of 3-phenyl-4-hydroxy-4-methyl-2-oxazolidinones by hydrolysis of the 4-alkylidene-2-oxazolidinones in dilute acid at room temperature (15).

The ease with which [5] occurs does depend on the nature of the aryl group. Thus for $R_1 = R_2 = R_3 = CH_3$, the *N*-(*p*-chlorophenyl)carbamate is completely cyclized at room temperature after a few weeks storage, the *N*-phenylcarbamate is converted more slowly and the *N*-*p*-tolylcarbamate is storage stable for at least two years.

When phenylisocyanate and 2-methyl-2-hydroxy-3-butanone were heated in pyridine, both the 4-hydroxy-4-methyl- and the 4-alkylidene-2-oxazolidinones were formed. No carbamate intermediate was isolated. The two products were easily separated by dissolution of the hydroxy compound in water.

Conversion of the 4-hydroxy-4-methyl-oxazolidinone into the unsaturated 4-alkylidene oxazolidinone [6] can be achieved by refluxing in glacial acetic acid, or in xylene in the presence of *p*-toluenesulphonic acid.

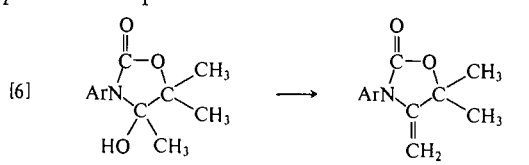

Cyclization of the carbamates of ketonic alcohols thus represents a simple route to the 4-hydroxy-2-oxazolidinones.

Experimental

Reagent grade materials obtained from the usual commercial suppliers were used in the preparation of the compounds. The solvents were dried over sodium, redistilled from sodium, and stored over sodium. Stannous octoate was obtained from Metal and Termit Corporation as catalyst T9, and from Albright and Wilson. Infrared spectra were done in carbon tetrachloride solution or as KBr pellets using a Perkin-Elmer model 137 or a Unicam 200G spectrophotometer. Nuclear magnetic resonance spectra were obtained in deuteriochloroform solution on a Varian A-60 spectrometer using trimethylsilane as the internal standard.

tert-Butyl and tert-Pentylcarbamates

A solution of the isocyanate (0.20 mol) in dry benzene (150 ml) was added dropwise over a 15–30 min period to a stirred refluxing solution of the alcohol (0.40 mol) in dry benzene (150 ml) containing about 0.1 g of catalyst, after which time a further 0.1 g of catalyst was added and the mixture was refluxed for 2 h. If the reaction product failed to crystallize on cooling the solution, the solvent was evaporated under reduced pressure and the residue recrystallized from a suitable solvent (see Tables 1 and 2). The lower boiling *tert*-pentyl carbamates were often obtained as oils from which pure crystalline compounds were obtained by vacuum sublimation. For *m*- and *p*-nitrophenyl derivatives, the commercially available samples of the isocyanates were not sufficiently pure to dissolve completely in the solvent. Thus for carbamates from these compounds the isocyanate solutions were obtained by heating the crushed commercial material in boiling benzene for 1 h and filtering off the insoluble impurities. *tert*-Pentyl-*N*-(*p*-nitrophenyl)carbamate decomposed on attempted sublimation and was purified by recrystallization from a well cooled 5:1 petroleum ether (60–80) – toluene mixture after treatment of a toluene solution with activated charcoal.

1,1-Diphenylethyl- and Triphenylmethylcarbamates

A similar procedure using stoichiometric quantities of the alcohol and isocyanate was employed. The reaction mixture was stirred at room temperature for 48 h.

Carbamates of Unsaturated Alcohols

A similar method was employed using a 10% excess of alcohol. For the 2-methyl-2-hydroxy-3-butanone condensations, the solvent was cold toluene and the reaction time 24 h; a nitrogen atmosphere was used to prevent coloration of the products. Crystallization solvents are reported in Table 2.

4-Alkylidene-2-oxazolidinones

4-Alkylidene-2-oxazolidinones were prepared by cyclization of the appropriate carbamates of 3-methylbut-1-yn-3-ol. For the 3-aryl derivatives the *N*-arylcarbamates (20 g) were heated in boiling pyridine (100 ml) for several hours. The solvent was evaporated under reduced pressure and the product recrystallized from a suitable solvent and identified by nmr.

For the 3-*n*-butyl derivative a solution of the *N*-butylcarbamate (10 g) in 10 ml of 3-methylbut-1-yn-3-ol was added slowly to a refluxing solution of sodium (0.05 g) in methylbutynol (20 ml). A vigorous reaction took place.

After the addition was complete the mixture was refluxed for 30 min, cooled and diluted with ether (200 ml). The solution was washed with water, dried over sodium sulphate and evaporated. Vacuum distillation of the residual oil yielded a fraction boiling at 79–82 °C/0.3 Torr which was shown by nmr to be the desired 3-butyl-4-methylene-2-oxazolidinone.

4-Alkyl-2-oxazolidinones

The carbamates of 3-methylbut-1-en-3-ol were cyclized in the presence of the sodium salt of the alcohol by the method described above. The 3-aryl-oxazolidinones were recrystallized from a benzene–heptane mixture and the 3-butyl-oxazolidinone was purified by vacuum distillation (bp 70–74 °C/0.3 Torr). The products were identified by nmr.

4-Hydroxy-2-oxazolidinones

The *N*-arylcarbamates of 2-methyl-2-hydroxy-3-butanone were heated in boiling water for 15 min, during which time a clear solution was formed from which the oxazolidinone (identified by nmr) crystallized out in 100% yield on cooling.

Dehydration of 4-Hydroxy-2-oxazolidinones

The compounds (1 g) were refluxed in glacial acetic acid (10 ml) for 2 h. The acetic acid was evaporated off under vacuum and the solid product washed with 10% sodium carbamate and with water. The 4-alkylidene-2-oxazolidinones thus formed were recrystallized and identified by nmr.

Acknowledgments

This work was initiated at the Ontario Research Foundation and financed by a grant from the Province of Ontario. Subsequent work was carried out at Memorial University, Newfoundland under a grant from the National Research Council of Canada, and at Keele University. The authors wish to thank Dr. M. H. Jones of the Ontario Research Foundation for his encouragement and support. We wish also to acknowledge technical assistance from Mr. D. Cobb (O.R.F.), Miss Carol Cronsberry (summer student, O.R.F.), Dr. M. Sole (summer student, O.R.F.), Dr. H. Pushie (summer student, Memorial University), Mr. M. Ball (B.A. student, Keele University), and Mrs. B. Cooper (technician, Keele).

1. H. Ensslin and K. Meier. Brit. Patent No. 740, 990 (to CIBA Ltd.) (November, 1957); Chem. Abstr. **51**, 467d (1957).
2. D. S. Tarbell, R. C. Mallatt, and J. W. Wilson. J. Am. Chem. Soc. **64**, 2229 (1942).
3. N. Shachat and J. J. Bagnall, Jr. J. Org. Chem. **28**, 991 (1963).
4. J. R. Griffith. (*a*) U.S. Patent No. 3,007,494 (February, 1963); Chem. Abstr. **58**, 13843h (1963) (*b*) Doctoral Thesis, University of Maryland, College Park, Maryland. 1964.
5. J. Y. T. Chen and W. R. Benson. J. Assoc. Off. Anal. Chem. **49**, 412 (1966).
6. T. Tanaka, T. Yokohama, Y. Yamaguchi, S. Naganuma, and M. Furukawa. Kogykayaku Zasshi, **74**, 171 (1972); Chem. Abstr. **74**, 142400g (1971).
7. V. V. Zharkov and N. K. Rudenevskii. Tr. Khim. Khim. Tekhnol. 91 (1966); Chem. Abstr. **67**, 6240h (1967).
8. D. V. Banthorpe. *In* Elimination reactions. Elsevier Pub. Co. London. 1963. p. 167; W. H. Saunders, Jr. and A. F. Cockerill. *In* Mechanisms of elimination reactions. John Wiley & Sons, New York. 1973. pp. 381, 406.
9. M. P. Thorne. Can. J. Chem. **45**, 2537 (1967).
10. S. J. Ashcroft and M. P. Thorne. Can J. Chem. **50**, 3478 (1972).
11. M. D. Cameron. U.S. Patent No. 2,844,590 (1958); Chem. Abstr. **53**, 2254f (1959).
12. N. R. Easton, D. R. Cassady, and R. D. Dillard. J. Org. Chem. **27**, 2927 (1962).
13. P. J. Stoffel and A. J. Speziale. J. Org. Chem. **28**, 2814 (1963).
14. M. F. Saettone. J. Org. Chem. **31**, 1959 (1966).
15. V. Nutti and M. F. Saettone. Tetrahedron, **26**, 3875 (1970).
16. P. Lambling. Bull. Soc. Chim. Fr. [3], **19**, 777 (1898).

Can. J. Chem. Downloaded from www.nrcresearchpress.com by 210.87.254.40 on 09/05/12
For personal use only.

The ν_{CO} absorption of ketones in cooled solution

J. WEINMAN, M. MAILLOUX, AND S. WEINMAN

Laboratoire associé au C.N.R.S. N° 87, U.E.R. Biomédicale des Saints-Pères, 45, rue des Saints-Pères, 75270 Paris, Cedex 06, France

Received April 22, 1975

J. WEINMAN, M. MAILLOUX, and S. WEINMAN. Can. J. Chem. **54**, 31 (1976).

The infrared spectra of diluted solutions of acetone, acetone-d_6, cyclopentanone, cyclopentanone-d_4, and cyclohexanone have been measured in the C=O stretching region from 290 to 90 K. As the solutions are cooled, several new bands appear at lower and lower frequencies. An interpretation of these spectra is given in terms of molecular association and anharmonic resonances.

J. WEINMAN, M. MAILLOUX et S. WEINMAN. Can. J. Chem. **54**, 31 (1976).

Les spectres infrarouge de l'acétone, de l'acétone-d_6, de la cyclopentanone, de la cyclopentanone-d_4 et de la cyclohexanone ont été enregistrés dans la région de la vibration de valence ν_{CO}, à l'état dissous, de 290 à 90 K. L'abaissement de la température provoque l'apparition de nouvelles bandes à des fréquences de plus en plus basses. L'interprétation des spectres est basée sur les rôles respectifs des associations moléculaires et de la résonance anharmonique.

Introduction

The infrared absorption of the ketonic carbonyl group in different physical states has been extensively investigated. However, no study has been made of the influence of temperature on the C=O stretch fundamental of ketones in solution. We have undertaken this for some aliphatic and alicyclic ketones.

Experimental

Most of the ketones are commercially available compounds: acetone (Merck, Uvasol), acetone-d_6 (C.E.A., France, 99% deuterium), cyclopentanone (Eastman-Kodak) purified by distillation, cyclohexanone (Merck, reference substance for GC). We prepared cyclopentanone-$\alpha\alpha\alpha'\alpha'$-$d_4$ as Kartha *et al.* (1); the amount of d_4-compound was near 90%, d_3 being the major impurity. Prior to use, each substance was dried by contact with molecular sieve for 48 h and stored in a sealed Pyrex tube.

The ketones were dissolved in the mixture isopentane–methylcyclopentane 2:1 at an average concentration of 2.5×10^{-2} *M*.

A variable low temperature unit RIIC was used for the measurements; the sample thickness was 0.2 mm.

Infrared spectra were recorded on a Perkin-Elmer model 180 spectrophotometer flushed with dry nitrogen produced by boiling off liquid nitrogen; in the spectrum of the residual water vapor, in single beam mode, the od was 0.010 at 1751.4 cm^{-1} and 0.020 at 1695.9 cm^{-1}. The spectra of the solvent and solutions were recorded in double beam mode between 1820 and 1660 cm^{-1} with a real resolution of 2 cm^{-1}, at 290, 180, 140, 120, and 90 K. Solvent and solutions remain transparent in this range of temperatures with formation of a glass near 115 K. The spectra were retraced point by point, plotting log I_0/I *vs.* frequency. Graphic deconvolutions using a Lorentzian profile were effected in some favorable cases.

Results

The spectra are shown in Figs. 1, 2, and 3 and the frequencies listed in Tables 1, 2, and 3.

At 290 K two broad bands are observed in the spectra of acetone and acetone-d_6, while cyclopentanone, cyclopentanone-d_4, and cyclohexanone exhibit one wide band ($\Delta\nu_{1/2} \sim 11$ to 13 cm^{-1}) which is very asymmetric. As the temperature is lowered the absorption becomes

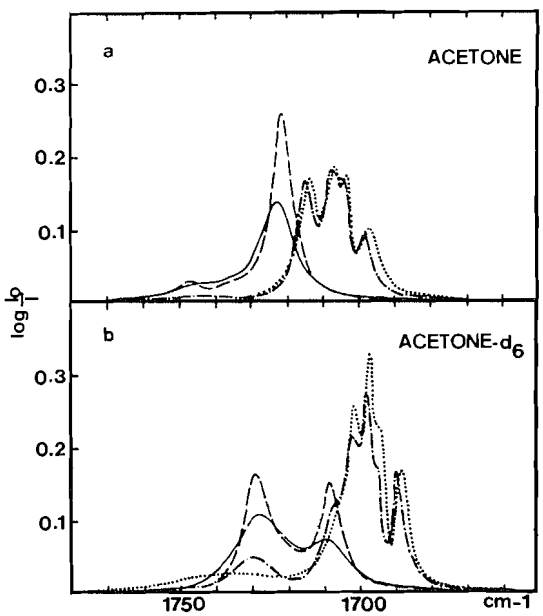

FIG. 1. The ν_{CO} absorption of acetone and acetone-d_6. —, 290; ---, 180; -·-·-, 148; and ···, 90 K.

Can. J. Chem. Downloaded from www.nrcresearchpress.com by 210.87.254.5 on 09/05/12
For personal use only.

TABLE 1. ν_{CO} frequencies of acetone and acetone-d_6

(*a*) Infrared frequencies (cm^{-1}) in liquid state at 300 K from ref. 2

Acetone	Acetone-d_6
1747w	1726s
1720s	1703s

(*b*) Infrared frequencies (cm^{-1}) in solution

T (K)	Acetone						Acetone-d_6					
			ν_1	ν_2	ν_3	ν_4			ν_1	ν_2	ν_3	ν_4
290	1746w	1722s					1728s	1708m				
180	1747w	1721vs					1728s	1708s				
148	1740vw	1717m*	1714.5s	1707s	1704s*	1698m	1729m	1708m*	1702s	1697.5vs	1695.5m*	1689s
90		1716.5w*	1714s	1707s	1704s*	1697.5m	1737w	1706.5m*	1701s	1697vs	1694.5m*	1688.5s

*Obtained by decomposition of the experimental curve.

(*c*) Infrared and Raman frequencies (cm^{-1}) in solid state at 84 K from ref. 3

Acetone		Acetone-d_6	
Infrared	Raman	Infrared	Raman
1761m		1732w	
1745m		1701s	
1718m		1697s	
1714s		1688s	1692vs
1706s	1706w		
1697s	1699vs		

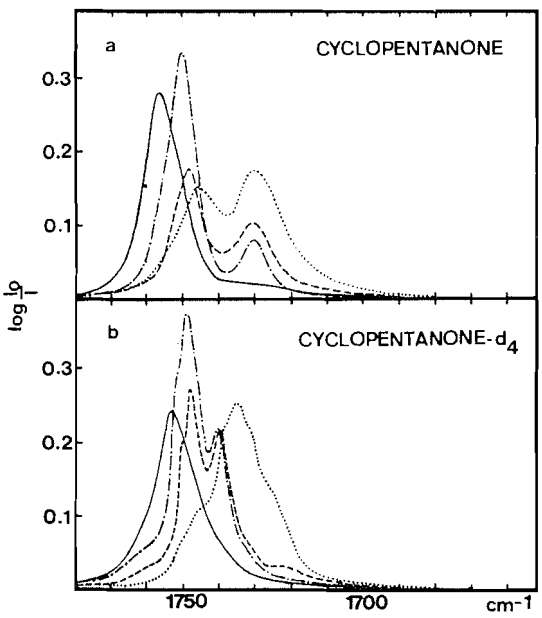

FIG. 2. The ν_{CO} absorption of cyclopentanone and cyclopentanone-d_4. —, 290; -·-·-, 140; ---, 120; and ···, 90 K.

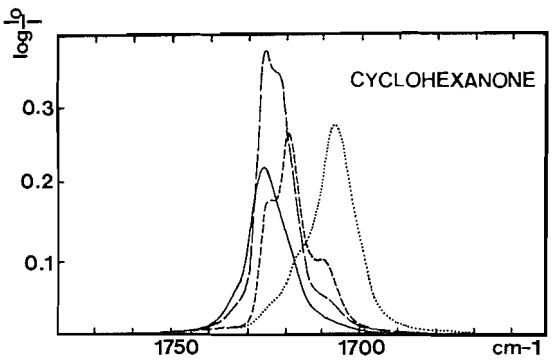

FIG. 3. The ν_{CO} absorption of cyclohexanone. —, 290; – – –, 180; ---, 120; and ···, 90 K.

more complex with additional bands and shoulders appearing in the spectra and there is an overall shift to lower frequency. At 90 K the absorption profile is significantly different from that at 290 K and a major part of the change takes place over a narrow temperature range. For the cyclic ketones the major change occurs with glass formation of the solution at ~115 K,

Can. J. Chem. Downloaded from www.nrcresearchpress.com by 210.87.254.5 on 09/05/12
For personal use only.

TABLE 2. ν_{CO} frequencies of cyclopentanone and cyclopentanone-d_4

(*a*) Raman frequencies (cm^{-1}) in liquid state at 300 K from ref. 4

Cyclopentanone	Cyclopentanone-d_4
1741s	1744m*
1726s	1731s

*The graphic decomposition by which these frequencies are obtained is justified by the shift of asymmetry between 290 and 140 K.

(*b*) Infrared frequencies (cm^{-1}) in solution

T (K)	Cyclopentanone				Cyclopentanone-d_4					
	ν_1	ν_2	ν_3	ν_4	ν_1	ν_2	ν_3	ν_4	ν_5	ν_6
290	1756s	1752m*		1728vw	1757m*	1752s	1747m*			
180		1752.5vs		1728w	1757w*	1750.5vs	1747m*	1740m		
140		1753m*	1749vs	1730m	1759w	1750m*	1747s	1739.5s		
120			1748s	1730.5s	1760w	1750m	1747s	1739s	1732w	1722w
90			1747s	1730s			1746m	1736s	1732s	1724m

*See footnote to (*a*).

(*c*) Infrared frequencies (cm^{-1}) in solid state at 84 K from ref. 4

Cyclopentanone	Cyclopentanone-d_4
1754m	1753m
1743s	1742s
1738m	1731s
1732s	1723s
1725s	

TABLE 3. Infrared ν_{CO} frequencies (cm^{-1}) of cyclohexanone

(*a*) In solid and liquid state from ref. 3

Physical state	T (K)	Frequency (cm^{-1})		
Liquid	300	1718vs	1707vs	
Solid	84	1724m	1716m	1708s
		1702vs	1698s	

(*b*) In solution state

T (K)	Frequency (cm^{-1})			
	ν_1	ν_2	ν_3	ν_4
290	1725s	1722m*		
180	1724.5vs	1720s	1708m	
140	1724.5s	1719s	1708m	
120	1724m	1718.5s	1709m	
90	1723.5w*	1717m	1706vs	~1697w

*Obtained by decomposition.

but for acetone and acetone-d_6 the major change occurs at ~150 K, well above the temperature for glass formation.

Discussion

In the search for an explanation of the splitting of the absorption and the changes observed upon lowering the temperature, several phenomena can be eliminated: (*i*) Overlapping of overtones or combinations; these bands are much too weak to be seen at the concentrations used. (*ii*) Interactions between ketonic and enolic forms; the stabilization of an appreciable amount of enol is unlikely at the given temperatures. (*iii*) Coexistence of conformers; very little is known about the conformer equilibrium of ketones, but it is improbable that such small structural differences could result in such great perturbations of the ν_{CO} vibration.

Can. J. Chem. Downloaded from www.nrcresearchpress.com by 210.87.254.5 on 09/05/12
For personal use only.

Can. J. Chem. Downloaded from www.nrcresearchpress.com by 210.87.254.5 on 09/05/12
For personal use only.

However, two phenomena could produce the modifications seen in the spectra: molecular association and anharmonic resonances.

Molecular Association

In a solution, cooling causes local fluctuations of concentration which induce the formation of molecular groups with different stoichiometry (5); the number, size, and rate of formation of these groups increase as the temperature is lowered. The process ends with either crystallization or glass formation. In glasses, zones of relatively high order are separated from one another by zones of less order (6). We identify the major change observed in the absorption profile with the appearance of a high percentage of the solute molecules in a state of 'semi order' which lies somewhere between the rigid crystalline structure and the 'free' molecule in solution.

The similarity between some frequencies of the low-temperature solutions and those of the crystalline solid is striking (Tables 1–3). Given this similarity, the possibility of microcrystallization must be considered. However, differential thermal analysis of the solvent and ketone solutions has shown that below 10^{-1} M no crystallization takes place during a slow controlled cooling; only a second order transition attributable to glass formation is observed in the range 118–113 K (7).[1]

In the solutions of acetone and acetone-d_6, a definitive ordering is indicated at 150 K. This occurs at a much higher temperature than the glass formation; moreover, it is also observed in isopentane, a nonglass-forming solvent.

For cyclic ketones, the transformation is more gradual than for the acetones. The solution vitrifies before all of the molecules have been converted to a semi-ordered state. Thus, at 90 K, in addition to the bands of the semi-ordered molecules which resemble the bands of the crystalline solid, there remain weak shoulders at frequencies which correspond to bands that have been prominent earlier in the cooling process. We propose that some of these weak bands can be attributed to the existence of a small percentage of the molecules which remain in a nonordered or free state even in the glass at 90 K. It is significant that this heterogeneity agrees exactly with the structure of glass as described by Valenkov and Porai-Koshits (6).

These considerations lead us to postulate that the transition which occurs in the spectrum can be attributed to the appearance in solution of a semi-ordered state. Comparison of the frequencies observed in solution and in the solid state supports the idea that, in cooled solutions, interactions similar to those existing in the crystalline solid may occur. This is consistent with the fact that dipolar interactions arise because of the higher concentration of the polar molecules in the groups formed at low temperatures. Such ordering occurs at different temperatures depending on the nature of the solute molecule and the concentration of the original solution.

Anharmonic Resonances

Le Corff (8) was the first to have used Fermi resonances to explain the splitting of the band of liquid cyclopentanone and the strong asymmetry of this same band in cyclohexanone. In the case of cyclopentanone this hypothesis was confirmed by many subsequent studies (9–15). Recently, Kidd and Jones (4) showed that, contrary to previous assumptions, a weak anharmonic resonance was present in the ν_{CO} band of liquid cyclopentanone-d_4; they attributed the complex ν_{CO} solid spectra of these two compounds to multiple resonance. Forel and Fouassier (16) also explained the splitting of acetone and acetone-d_6 by an anharmonic resonance between ν_{CO} and the combination $\nu_{CC} + \delta_{CO}$. With these interpretations in mind, we examine our results below, in order to determine the eventual role of the anharmonic resonance in the splitting of the absorption in ketone solutions.

The existence of strong and weak anharmonic resonances in the region of the C=O stretching fundamental is, then, a factor which contributes to the complexity of the carbonyl absorption. The C=O stretching frequency is sensitive to solvent effects, and with cooling it can be anticipated that the unperturbed frequency of 'free' molecules in the liquid solution will change with changing conditions. Even if the anharmonic force field remains unchanged this will lead to changes in the nature of the frequency coincidences between perturbing levels, and accompanying changes in the observed intensities of the transitions.

[1]The glass transition is essentially caused by a relaxation effect which prevents the ready attainment of the internal equilibrium of the material.

TABLE 4. Calculated frequencies for acetone and acetone-d_6 at 90 K

	Acetone				Acetone-d_6			
Doublets*	Δ†	R‡	W_{nt}§	Unperturbed levels (cm^{-1})	Δ†	R‡	W_{nt}§	Unperturbed levels (cm^{-1})
$\nu_1\nu_2$	7	1	3.5	1710.5–1710.5	4	0.62	1.9	1699.5–1698.5
$\nu_2\nu_3$‖	3	0.84	1.5	1705.5–1705.5	2.5	0.52	1.2	1696.2–1695.3
$\nu_2\nu_4$	9.5	0.62	4	1703.4–1701.1	8.5	0.51	4	1694.2–1691.3
Overtone or combination levels								1701, 1690–1695?

*Frequencies are given in Table 1; the strongest band is commonly associated with the C=O stretching fundamental. Frequencies calculated from $\nu_1\nu_3$, $\nu_1\nu_4$, and $\nu_3\nu_4$ are similar to either $\nu_1\nu_2$ or $\nu_2\nu_3$.
†Δ is the separation in cm^{-1} of the observed bands.
‡R is the ratio of the intensities of the two bands as checked after graphic deconvolution.
§W_{nt} is the value of the matrix element of the perturbation term as calculated from Δ and R (12).
‖Note the theoretical incompatibility between the weak W_{nt} and the close perturbing levels.

We have proposed that the observed spectrum is the summation of several individual spectra, each of which corresponds to the various degrees of order in the solution. Now it is necessary to recognize the added complication that each individual spectrum consists of a multiplet produced by anharmonic resonance. The band widths in these multiplets decrease with lower temperature, and weak perturbations which could not be observed at room temperature become resolved.

If we assume that the strong bands of the spectra in the glass at 90 K can be attributed to molecules in a single state of order we can attempt an analysis of the multiplet structure in terms of anharmonic resonance. Bertran *et al.* (12) have detailed a method for evaluating anharmonic constants for a Fermi-doublet from the ratio of the intensities of the pair. If we assume that the multiplet band system consists of the C=O stretching fundamental in pair-wise resonance with a number of overtone or combination bands then we can carry out the analysis given in Table 4 for acetone. The values obtained for the cubic force constants all fall within an acceptable range (4) but the assumptions are rather too simplistic for such a complex problem.

It is preferable to limit the discussion to a qualitative consideration of the possible existence of overtone or combination bands which have frequency coincidence with the C=O stretch. The strong absorption of the mixture isopentane–methylcyclopentane prevents the recording of fingerprint bands for the ketones diluted in this solvent. The frequencies of the ketones in other physical states can be used since there are only small shifts in the spectrum in this range.

The overtones or combinations must have the same symmetry as the carbonyl stretching fundamental; however, there are some ambiguities in the vibrational assignment; furthermore, one does not know if the molecular structure remains unchanged during cooling and, therefore, whether the ketone always belongs to the same symmetry group.

In spite of these reservations, we suggest some perturbing levels.

Using the results of Cossee and Schachtschneider (17), Dellepiane and Overend (18), Forel and Fouassier (19), and Harris and Levin (20), we have found no suitable levels for acetone; for acetone-d_6 two combinations are possible:

$$\delta_{CD_3}(1033) + r_{CD_3}(668) = 1701\ cm^{-1}\ (20)$$

and

$$2\nu_{CCC}(2 \times 690 - \nu_x) + \delta_{CCC}(324) = 1704 - \nu_x\ cm^{-1}\ (19)$$

where ν_x whose value is unknown represents the anharmonicity.

Based on the results of Howard-Lock and King (21) and Kartha *et al.* (1), we confirm the possibility of perturbation by the combinations proposed by Kidd and Jones (4) for the interpretation of the spectrum of the cyclopentanones in the solid state.

In the case of cyclohexanone, the vibrational analyses of Rey-Lafon and Forel (22) and Fuhrer *et al.* (23) suggest as perturbing levels:

$$2\delta_{HCC}(2 \times 861) = 1722 - \nu_x\ cm^{-1}\ (22, 23)$$

$$\delta_{HCC}(1263) + \delta_{CCC}(460) = 1723\ cm^{-1}\ (23)$$

$$\delta_{HCC}(1220) + \delta_{CCC,HCC}(490) = 1710\ cm^{-1}\ (23)$$

$$\delta_{HCC}(861) + \nu_{CC}(838) = 1699\ cm^{-1}\ (22, 23)$$

Can. J. Chem. Downloaded from www.nrcresearchpress.com by 210.87.254.5 on 09/05/12
For personal use only.

Thus, in all the cases studied, anharmonic resonances seem to be possible.

In summary, at least two mechanisms cause the complexity of the ν_{CO} absorption in the ketone solutions.

Through cooling, molecules tend to form more or less ordered groups because of dipolar interactions. The occurrence of these interactions can explain the presence of several ν_{CO} bands at lower and lower frequencies in the same spectrum.

However, anharmonic resonances taking place simultaneously could be another possible cause of the splitting of the ν_{CO} absorption: the more complex the absorbing molecule, the more numerous the possibilities of anharmonic resonances.

Acknowledgments

We are indebted to the Directors of the D.R.A., C.E.N.-Saclay (France) who permit us to use the PEC 180 spectrophotometer; we wish to thank particularly Dr. Ceccaldi, Dr. Leicknam, and Dr. Majoube for helpful assistance and comments during the experimental work.

1. V. B. KARTHA, H. H. MANTSCH, and R. N. JONES. Can. J. Chem. **51**, 1749 (1973).
2. M. FOUASSIER. Thesis, Bordeaux. 1968.
3. D. ROCHE. D.E.S. Univ. Paris VI (1974); A. MARCOU and D. ROCHE. C. R. Acad. Sci. Ser. B, **276**, 599 (1973).
4. K. G. KIDD and R. N. JONES. Acta Phys. Acad. Sci. Hung. **35**, 261 (1974).
5. A. P. ROLLET and R. BOUAZIZ. L'analyse thermique. Gauthier-Villars, Paris. 1972. Chapt. 7. p. 338.
6. J. D. MACKENZIE. Modern aspects of the vitreous state. Butterworth, London. 1960. p. 17.
7. J. WEINMAN and D. ROCHE. J. Chim. Phys. **72**, 972 (1975).
8. R. LE CORFF. Thesis, Poitiers. 1954.
9. R. N. JONES and C. SANDORFY. Techniques of organic chemistry. Vol. IX. *Edited by* A. Weissberger. Interscience, New York. 1956. Chapt. 4. p. 487.
10. C. L. ANGELL, P. J. KRUEGER, R. LAUZON, L. C. LEITCH, K. NOACK, R. J. D. SMITH, and R. N. JONES. Spectrochim. Acta, **11**, 926 (1959).
11. G. ALLEN, P. S. ELLINGTON, and G. D. MEAKINS. J. Chem. Soc. 1909 (1960).
12. J. F. BERTRAN, L. BALLESTER, L. DOBRIHALOVA, N. SANCHEZ, and R. ARRIETA. Spectrochim. Acta, Part A, **24**, 1765 (1967).
13. R. CATALIOTTI and R. N. JONES. Spectrochim. Acta, Part A, **27**, 2011 (1971).
14. I. M. GINZBURG and V. S. KHLEVNYUK. Opt. Spectrosc. **31**, 169 (1971).
15. R. E. DAVIS and K. S. KIM. Theor. Chim. Acta, **25**, 89 (1972).
16. M. T. FOREL and M. FOUASSIER. Spectrochim. Acta, Part A, **23**, 1977 (1967).
17. P. COSSEE and J. H. SCHACHTSCHNEIDER. J. Chem. Phys. **44**, 97 (1966).
18. G. DELLEPIANE and J. OVEREND. Spectrochim. Acta, **22**, 593 (1966).
19. M. T. FOREL and M. FOUASSIER. J. Chim. Phys. **67**, 1132 (1970).
20. W. C. HARRIS and I. W. LEVIN. J. Mol. Spectrosc. **43**, 117 (1972).
21. H. E. HOWARD-LOCK and G. W. KING. J. Mol. Spectrosc. **35**, 393 (1970).
22. M. REY-LAFON and M. T. FOREL. J. Chim. Phys. **68**, 384 (1971).
23. H. FUHRER, V. B. KARTHA, P. J. KRUEGER, H. H. MANTSCH, and R. N. JONES. Chem. Rev. **72**, 439 (1972).

Can. J. Chem. Downloaded from www.nrcresearchpress.com by 210.87.254.5 on 09/05/12
For personal use only.

Heterocyclic compounds. VIII. Studies on oxazolophenoxazines[1]

A. M. OSMAN, S. A. M. METWALLY,[2] AND M. S. K. YOUSSEF
Department of Chemistry, Assiut University, Assiut, Egypt

Received June 6, 1975

A. M. OSMAN, S. A. M. METWALLY, and M. S. K. YOUSSEF. Can. J. Chem. **54**, 37 (1976).

5*H*-Oxazolo[4,5-*b*]phenoxazine (**5**) was synthesized by the reaction of 3-amino-2-hydroxyphenoxazine hydrochloride (**2**) with formamide. A series of styryl-oxazolophenoxazines (**9**) were prepared by condensation of 2-methyl-5-acetyloxazolo[4,5-*b*]phenoxazine methiodide (**8**) with aromatic aldehydes. By contrast, 2-aryl-oxazolophenoxazines (**14**) were synthesized by reaction of 3-aminophenoxaz-2-one (**1**) with the appropriate aldehydes in the presence of an acid–base catalyst. The biological activities of some of these compounds were tested.

A. M. OSMAN, S. A. M. METWALLY et M. S. K. YOUSSEF. Can. J. Chem. **54**, 37 (1976).

On a synthétisé la 5*H*-oxazolo[4,5-*b*]phénoxazine (**5**) par réaction du chlorhydrate de l'amino-3 hydroxy-2 phénoxazine (**2**) avec de la formamide. On a préparé une série de styryl-oxazolophénoxazines (**9**) par condensation du méthiodure de la méthyl-2 acétyl-5 oxazolo-[4,5-*b*]phénoxazine (**8**) avec des aldéhydes aromatiques. D'autre part, on a synthétisé des aryl-2 oxazolophénoxazines (**14**) par interaction de l'amino-3 phénoxazone-2 (**1**) avec les aldéhydes appropriés en présence de catalyseurs acides ou basiques. On a vérifié les activités biologiques de quelques-uns de ces composés.

[Traduit par le journal]

Oxazolophenoxazines, as polycondensed diheterocyclic compounds, may be of considerable importance in the fields of dyes, optical brighteners, photographic sensitizers, or as reagents in biological assays.

The parent compound, 5*H*-oxazolo[4,5-*b*]-phenoxazine (**5**) was successfully prepared by heating 3-amino-2-hydroxyphenoxazine hydrochloride (**2**) with formamide in the presence of hydrogen chloride gas as a catalyst. Other methods described for similar cases in the literature (1), such as using formic acid–sodium formate instead of formamide, were not successful. The reaction with formamide was smooth and it could be stopped at intermediate stages, namely the formation of mono- and diformyl derivatives (**3** and **4** respectively) by conducting the reaction for short periods at a moderate temperature (100 °C) and separating the products by thin layer chromatography. This clarifies the mechanism of the reaction which is represented in Scheme 1.

3-Amino-2-hydroxyphenoxazine hydrochloride (**2**), a very unstable amine salt, was prepared by acidic reduction of 3-aminophenoxaz-2-one. This salt is easily reoxidized in the presence of oxygen to the aminoquinone (**1**). The chemical structure of 5*H*-oxazolo[4,5-*b*]phenoxazine (**5**) was deduced from its analytical data, in conjunction with other chemical and physical properties. The ir absorption spectrum indicated the absence of carbonyl or primary amino groups, but showed a strong absorption band at 3260 cm^{-1} characteristic of a secondary amino group (2). The bands at 1590, 1220, and 1200 cm^{-1} indicated the presence of an oxazole ring structure (3). This assignment is further supported by the nmr spectrum which showed a singlet at τ 1.96 due to the oxazole proton (4). The mass spectrum of (**5**) showed a molecular ion at m/e 224, thus confirming the above findings.

It is of interest to point out that the hydrogen atom of the oxazole ring in **5** is quite active and this is shown by the coupling reaction of **5** with benzene diazonium chloride in neutral medium. The resulting azo dye was found to lack the oxazole proton as indicated by nmr spectra.

Attempts to prepare 2-methyl-5*H*-oxazolo-[4,5-*b*]phenoxazine by fusion of **2** with acetamide were not successful. Instead, 2-methyl-5-acetyl-oxazolo[4,5-*b*]phenoxazine (**7**) was obtained by heating 5-acetyl-3-diacetylamino-2-acetoxy-phenoxazine (**6**) above its melting point (190 °C) where it lost the equivalent of an acetic anhydride fragment giving the corresponding oxazolophe-

[1]For part VII see ref. 14.

[2]Author to whom all correspondence should be addressed.

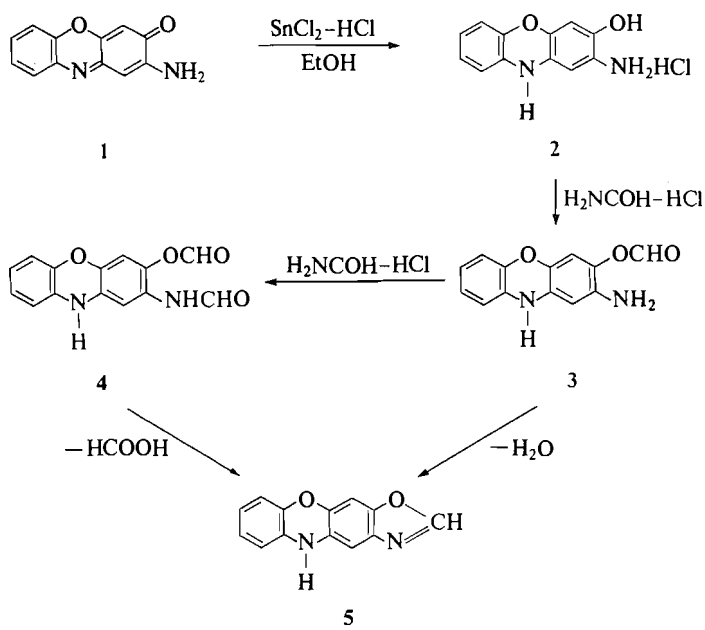

SCHEME 1

noxazine (**7**). The tetraacetate **6** was prepared by reductive acetylation of 3-aminophenoxaz-2-one (**1**). The structure of **6** was elucidated by elemental analysis, ir, uv, and mass spectroscopy which indicated a molecular weight of 382.

2-Methyl-5-acetyloxazolo[4,5-*b*]phenoxazine (**7**), though stable under normal conditions, is cleaved by hot dilute hydrochloric acid to give 3-acetylaminophenoxaz-2-one (**10**). On the other hand, attempted condensation of **7** with aromatic aldehydes to form the corresponding styryl base was not successful. However, the methyl group of **7** could be activated by quaternization using methyl iodide and the active methyl derivative, **8**, reacted easily with aromatic aldehydes in the presence of anhydrous zinc chloride to give the corresponding styryl-oxazolophenoxazines (**9**). The above reactions can be represented by Scheme 2.

The styryl-oxazolophenoxazines (**9**) are brown to reddish-violet in color with high melting points and exhibited strong violet fluorescence in organic solvents. The absorption spectra of the compounds studied ranged between 400 and 450 nm, in general with one single broad band. These properties may be considered as quite satisfactory for a photosensitizer (5). Spectral and analytical data are given in Table 1.

The investigation was carried further to prepare 2-aryl-oxazolo[4,5-*b*]phenoxazines (**14**) which form the basis for the preparation of different dyes and which may be of use as medicinal components. The preparation was accomplished by the reaction of aromatic aldehydes and 3-aminophenoxaz-2-one (**1**) in the presence of glacial acetic acid as a solvent and a suitable catalyst. Usually such reactions are conducted in the presence of either acidic (6) or basic catalysts (7) depending on the type of molecules used, but from our thorough investigation in this area, we have found that the best results are obtained by using acid–base catalysts such as ammonium or amine salts of organic acids. Also, the weakly basic compound acetamide was found to be an effective catalyst in these condensations.

The mechanism of formation of such oxazole derivatives apparently involves an amino-aldehyde addition reaction forming an intermediate hydroxy derivative, **11**. This intermediate is expected to undergo a hydride shift to give the unstable dihydroxy Schiff's base **13**. At this stage the molecule attains its stability by the loss of a water molecule with the formation of oxazolophenoxazines (**14**). The course of the reaction may be represented by Scheme 3.

The elemental analyses, uv, ir, and the strong

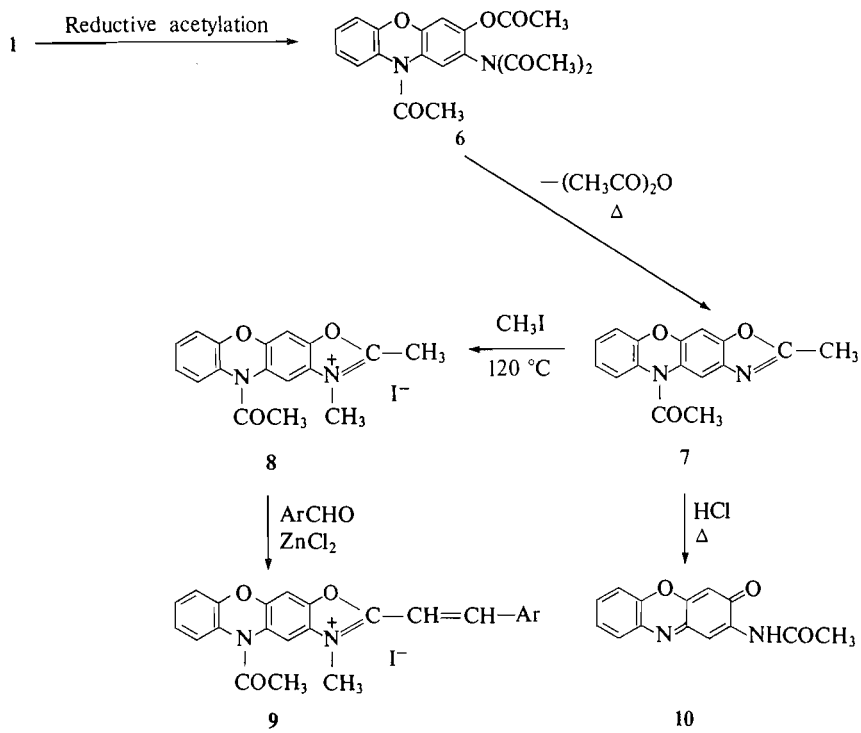

SCHEME 2

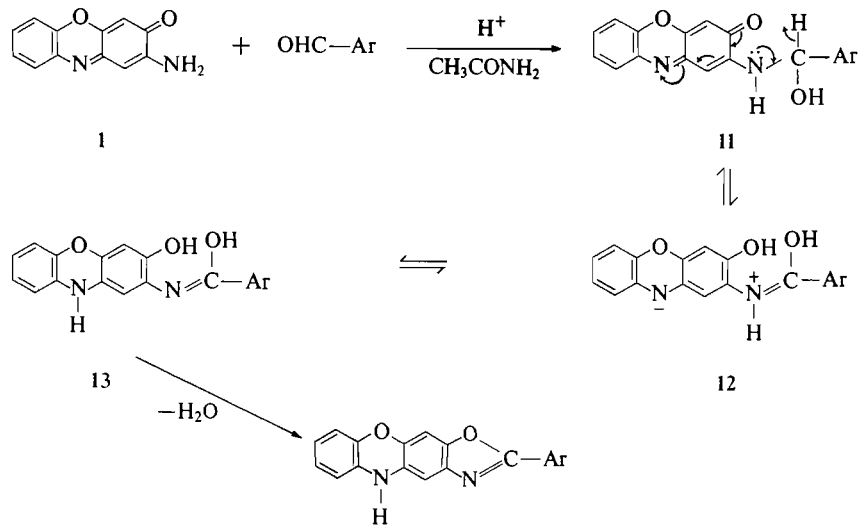

SCHEME 3

fluorescence of these products in solutions (8) are in agreement with the oxazolophenoxazine structure **14**. Chemical evidence for such a structure was obtained by mild hydrolysis with dilute hydrochloric acid yielding 3-aminophenoxaz-2-one (**1**) via autoxidation of the intermediate aminophenol **2**.

The fluorescence spectra of the oxazolo-

TABLE 1. Spectral and analytical data

Aldehyde used in preparation of styryl cyanines	Solvent of crystallization*	λ_{max}† (nm)	ν (ir) (cm^{-1})		Analytical data: Calculated (%) C	H	N	I	Observed (%) C	H	N	I
Benzaldehyde	A	580 420	C═N C═O C—O—C	1580 1640 1185	56.47	3.73	5.49	24.49	56.70	3.91	5.34	24.29
Anisaldehyde	B	475 355	C═N C═O C—O—C	1610 1700 1880	55.56	3.89	5.19	23.52	55.83	4.02	5.12	23.89
Salicylaldehyde	C	420 335 345	OH C═N C═O C—O—C	3350 1580 1640 1170	54.75	3.61	5.32	24.14	54.58	3.83	5.50	23.60
Cinnamaldehyde	D	630 470 335	C═O C═N	1680 1600	58.21	3.92	5.22	23.68	57.79	4.24	5.59	24.0
N-Dimethyl-*p*-aminobenzaldehyde	B	390 325	$N(CH_3)_2$ C═O C═N	1360 1640 1590	56.42	4.34	7.59	22.97	56.16	4.62	7.95	23.30
m-Chlorobenzaldehyde‡	E	448 340	C═N C═O	1580 1620	52.81	3.31	5.14	23.32	53.0	2.96	5.48	22.72
p-Nitrobenzaldehyde	B	435 325	NO_2 C═O C═N	1520 1670 1610	51.89	3.24	7.57	22.88	52.35	3.13	7.24	23.33
m-Nitrobenzaldehyde	B	455 345	NO_2 C═N C═O	1536 1620 1680	51.89	3.24	7.57	22.88	51.75	3.46	7.58	23.43
2,4-Dihydroxybenzaldehyde	D	428 325	—		53.28	3.51	5.18	22.34	53.39	3.62	5.23	22.95

*A, glacial AcOH; B, pyridine–water; C, pyridine–ethanol; D, pyridine–methanol; E, methanol–ether.
†λ_{max} in pyridine.
‡Analysis for Cl: calcd. 6.5%; found 6.6%.

phenoxazines (**14**) were found to be a mirror image of their ultraviolet spectra (9). It was found that the salt-forming groups such as NH_2, OH, and OCH_3 increase the fluorescence of **14** to a marked extent. On the other hand, the electron-attracting groups diminish the fluorescence of such compounds.

The mass spectra of oxazolophenoxazines (**14**) were determined. As expected from such stable cyclic structures, the molecular ions are the base peaks (10). The spectra are characterized by the presence of doubly charged ions of considerable intensity. The general feature of the fragmentation patterns of these compounds under electron impact is the formation of a stable ion with the structure $C_{11}H_7NO$ (*m/e* 169). This ion has exceptional stability as indicated by a doubly charged ion at *m/e* 84.5 (11).

To test the validity of oxazolophenoxazines (**14**) as optical brightners especially for synthetic fibres, derivatives containing the triazine nucleus were prepared (12). This was achieved by reaction of cyanuric chloride or its amino derivatives with **14**.

Some of the hitherto prepared oxazolophenoxazines (**14**) were tested *in vitro* for their biological activities on some fungi, yeasts, and bacteria. The best results were obtained with 2-(*o*-anisyl)- and 2-(*o*-nitrophenyl)-5*H*-oxazolo-[4,5-*b*]phenoxazines, respectively, and at concentrations of 10^{-3} *M* gave 100% inhibition.

Experimental

Melting points were taken on a Mel-Temp electrically heated melting point unit and are uncorrected. Infrared spectra were measured on a Perkin-Elmer Model 21 Spectrophotometer. Ultraviolet and visible spectra were measured on a No. 2 Hardy General Electric spectrophotometer in benzene. Emission spectra were measured on an HΦM Fluorimeter. Nuclear magnetic resonance spectra were obtained on a Varian A-60 spectrophotometer in deuterated chloroform. Mass spectra were obtained using an AEI MS 9 mass spectrometer operating at 70 eV. Samples were introduced through a heated inlet system.

3-Amino-2-hydroxyphenoxazine Hydrochloride, 2

Five grams of 3-aminophenoxaz-2-one (**1**) (13) were dissolved in a mixture of 150 ml ethyl alcohol and 20 ml of concentrated hydrochloric acid. A solution of 3 g stannous chloride dissolved in 30 ml dilute HCl was added to the previous solution. The mixture was heated under reflux until the red color changed to pale yellow. The solution was cooled and the product was collected and crystallized from dilute HCl to give colorless clusters mp 164 °C (dec.). This salt is unstable and it is easily oxidized by air oxygen to give the aminoquinone **1**. ν_{max} 3430 cm^{-1} (OH), 3265, and 1599 cm^{-1} (NH). *Anal.* Calcd. for $C_{12}H_{10}N_2O_2HCl$: C, 57.48; H, 3.99; Cl, 14.17; N, 11.17; found: C, 57.64; H, 4.12; Cl, 14.35; N, 11.37.

5H-Oxazolo[4,5-b]phenoxazine, 5

3-Amino-2-hydroxyphenoxazine hydrochloride (**2**) (0.5 g) was dissolved in formamide (30 ml) and heated at 120 °C for 2 h in the presence of dry HCl gas. The greenish brown mixture was cooled, diluted with water, and neutralized with dilute sodium bicarbonate. The product was collected and crystallized from petroleum ether (bp 60–95 °C) to give pale green needles, mp 207 °C, yield 0.3 g. *Anal.* Calcd. for $C_{13}H_8N_2O_2$: C, 69.64; H, 3.57; N, 12.5; found: C, 69.51; H, 3.53; N, 12.54. Spectral data: τ 1.96 (oxazole proton); ν_{max} 1535 and 1680 cm^{-1} (oxazole ring) (3); uv λ_{max} 325 nm, log ϵ 3.99. When the reaction was carried out at about 100 °C, interrupted after 45 min and the reaction mixture diluted with water, a precipitate formed. It was collected and chromatographed using a plate coated with a thin layer of Kieselgel and a toluene–acetone 5:1 mixture used as eluent. Three products were identified. The first product with an R_f value of 0.71 was identified as the oxazole **5**. The second product with an R_f value of 0.54 was separated and identified as the monoformyl derivative **3**: colorless needles recrystallized from ethanol mp 215 °C. *Anal.* Calcd. for $C_{13}H_{10}N_2O_3$: C, 64.46; H, 4.12; N, 11.57; found: C, 64.62; H, 4.51; N, 11.31. The third product with an R_f value of 0.33, was characterized as the diformyl compound **4**: colorless needles crystallized from benzene, mp 241 °C. *Anal.* Calcd. for $C_{14}H_{10}N_2O_4$: C, 62.22; H, 3.7; N, 10.37; found: C, 62.53; H, 4.11; N, 10.45.

Coupling of 5H-Oxazolo[4,5-b]phenoxazine, 5, with Benzene Diazonium Chloride

Aniline (0.05 g) was dissolved in dilute HCl (20 ml) and cooled to 0 °C; sodium nitrite (0.12 g) was added and the diazonium salt was kept in ice for 15 min. This mixture was combined with 0.1 g of **5** dissolved in methanol (20 ml). The mixture was neutralized with dilute sodium carbonate, and a brown dye separated. It was collected and crystallized from ethanol to give fine brown needles, mp 267 °C. *Anal.* Calcd. for $C_{19}H_{12}N_4O_2$: C, 69.51; H, 3.65; N, 14.02; found: C, 69.73; H, 3.82; N, 14.11. Spectral data: ν_{max} 3252 and 1592 cm^{-1} (NH); visible λ_{max} 455 nm, log ϵ 3.98. The nmr indicated the absence of the oxazole ring proton at τ 1.96.

5-Acetyl-3-diacetylamino-2-acetoxyphenoxazine, 6

3-Aminophenoxaz-2-one (0.5 g) was dissolved in acetic anhydride (10 ml), zinc dust (2 g) was added to the hot solution, and the mixture was heated for a few minutes, whereby it acquired a yellowish color. Excess zinc dust was removed by filtration and the filtrate was allowed to reflux for 20 min in the presence of fused sodium acetate (5 g). Glacial acetic acid (5 ml) was added and heating was continued for 10 min after which the reaction mixture was added to ice-cold water and the precipitate filtered, washed thoroughly with water, and dried. It was crystallized from ethyl alcohol into colorless needles, mp 185 °C, yield quantitative. *Anal.* Calcd. for $C_{20}H_{18}O_6N_2$: C, 62.82; H, 4.71; N, 7.2; found: C, 62.61; H, 4.80; N, 7.31.

TABLE 2. Analytical and spectral data of 2-aryl-5*H*-oxazolo[4,5-*b*]phenoxazines

Aryl group of 2-aryl-5*H*-oxazolo-[4,5-*b*]phenoxazine	mp (°C)	Solvent of crystal-lization*	λ_{max}† (nm)	log ϵ	λ_{max} (nm) (emission spectra)	ν (ir) (cm^{-1})	Analytical data: Calculated (%) C	H	N	Cl	Observed (%) C	H	N	Cl
2-Phenyl-	298–300	A	372	4.15	473	—NH 3280 C=N 1600 C—O—C 1065	76.0	4.0	9.33	—	76.22	4.17	9.30	—
2-Anisyl-	265–267	A	376	4.25	498	NH— 3400 C=N 1600	72.73	4.24	9.30	—	72.60	4.63	8.58	—
2-(*o*-Hydroxyphenyl)-	310–312	P	385	4.20	485	OH 3360 C=N 1600	72.15	3.80	8.86	—	72.34	3.82	8.79	—
2-(*p*-Hydroxyphenyl)-	320–323	B	378 288	4.23 4.46	—	CH 3400 C=N 1590 C—O—C 1100	72.15	3.80	8.86	—	72.0	3.82	8.75	—
2-(*m*-Hydroxyphenyl)-	—	—	—	—			72.15	3.79	8.86	—	—	—	—	—
2-(*o*-Chlorophenyl)-	245–247	A	385	4.09	482	NH— 3305 C=N 1595 C—O—C 1090	68.16	3.29	8.37	10.61	68.42	3.34	8.35	10.69
2-(*p*-Chlorophenyl)-	238.5	A	385	4.13	—		68.16	3.29	8.37	10.61	68.25	3.61	8.57	10.51
2-(*m*-Chlorophenyl)-	241	A	382	4.37	—		68.16	3.29	8.37	10.61	68.51	3.52	8.61	10.70
2-(*o*-Methylphenyl)-	311	A	375	4.21	394		76.43	4.46	8.92	—	76.83	4.72	9.14	—
2-(*p*-Methylphenyl)-	284	A	378	4.18	491		76.43	4.46	8.92	—	76.91	4.83	9.24	—
2-(*m*-Methylphenyl)-	292	A	374	4.32	482		76.43	4.46	8.92	—	76.67	4.9	9.38	—
2-(*o*-Nitrophenyl)-	210–212	C	415	4.39		NH— 3320 C=N 1600 NO_2 1540	66.09	3.19	12.17	—	66.04	2.94	11.02	—
2-(*p*-Nitrophenyl)-	330–333	D	448 288	4.22 4.55		NH— 3260 C=N 1598 NO_2 1550	66.09	3.19	12.17	—	65.80	3.12	12.08	—
2-(*m*-Nitrophenyl)-	290–292	E	298	4.39		C—N 1600 NH 3400 NO_2 1540	66.09	3.19	12.17	—	66.20	3.23	12.22	—
2-(*o*-Aminophenyl)-	298	F	387	4.27		C=N 1615 NH_2 3410 3470	72.38	4.13	13.33	—	72.62	4.54	13.51	—
2-(*p*-Aminophenyl)-	285	F	376 302	4.23 4.38	491		72.38	4.13	13.33	—	72.52	4.43	13.61	—
2-(*m*-Aminophenyl)-	292	F	382	4.13	479		72.38	4.13	13.33	—	72.76	4.62	13.40	—

*A, benzene; B, *n*-butanol; P, pyridine; C, ethanol–water; D, dilute AcOH; E, isoamyl alcohol; F, benzene – petroleum ether.
†λ_{max} in benzene.

2-Methyl-5-acetyl-oxazole[4,5-b]phenoxazine, 7

A pure sample of the tetraacetate **6** (5 g) was heated in a porcelain dish at 190 °C until no more acetic anhydride was evolved. The dark brown melt was cooled, extracted with ethyl alcohol, then diluted with water to yield a precipitate after 2 h. The product was collected and crystallized from dilute ethyl alcohol to give colorless needles, mp 130–132 °C. *Anal.* Calcd. for $C_{16}H_{12}O_3N_2$: C, 68.57; H, 4.28; N, 10.0; found: C, 68.66; H, 4.30; N, 9.93.

2-Methyl-5-acetyl-oxazolo[4,5-b]phenoxazine-3-methiodide, 8

A pure sample of the methyloxazolophenoxazine **7** (5 g) was suspended in excess methyl iodide (50 ml) and heated in a sealed tube in an electric furnace at 120 °C for 3 h. The reactants dissolved at 110 °C, giving a yellowish orange color to the mixture and the quaternary salt was precipitated at 120 °C in the course of 30 min. The product was collected, washed with ether, and dried. It was crystallized from acetone to give yellow needles, mp 260–261 °C, yield, quantitative. *Anal.* Calcd. for $C_{17}H_{15}N_2O_3I$: C, 48.34; H, 3.55; N, 6.64; I, 30.1; found: C, 48.57; H, 3.61; N, 6.48; I, 29.89.

Styryl Bases of Oxazolophenozaxines, 9

2-Methyl-5-acetyl-oxazolo[4,5-*b*]phenoxazine-3-methiodide (**8**) was mixed with the aromatic aldehyde, then refluxed for 5–10 min in the presence of a small amount of anhydrous zinc chloride. The reaction mixture was cooled, triturated with few ml of alcohol, the solid product was collected and washed several times with ethyl alcohol, then recrystallized from the proper solvent. The results are listed in Table 1.

2-Aryl-5H-oxazolo[4,5-b]phenoxazines, 14

The aminophenoxazone **1** (1 mol) was mixed with the aromatic aldehyde (1 mol) and the mixture was dissolved in 99.8% glacial acetic acid (240 ml) in the presence of acetamide (0.5 mol). The solution was placed in a modified Claisen flask and distilled slowly for 4 h, heating being regulated so that the temperature of the vapor remained between 105 and 115 °C. The reaction mixture was cooled and the solid product was collected, washed thoroughly with water, and dried. The spectral and analytical data are listed in Table 2.

2-Aryl-5-(3′,5′-dichlorotriazinyl)-oxazolo[4,5-b]phenoxazine

2-Aryl-5*H*-oxazolo[4,5-*b*]phenoxazine (0.1 mol) was dissolved in acetone (50 ml) and the solution was cooled to 0 °C. Cyanuric chloride (0.1 mol) was added, while the solution was stirred and 0.1 *N* sodium hydroxide added until just alkaline. The buff precipitate was collected and dried.

The following compounds were prepared. (*a*) 2-Phenyl-5-(3′,5′-dichlorotriazinyl)-oxazolo[4,5-*b*]phenoxazine: pale brown plates from benzene, mp 289 °C. *Anal.* Calcd. for $C_{22}H_{11}O_2N_5Cl_2$: N, 15.63; Cl, 15.85; found: N, 15.40, Cl, 15.64. (*b*) 2-*o*-Anisyl-5-(3′,5′-dichlorotriazinyl)-oxazolo[4,5-*b*]phenoxazine: pale brown plates from benzene, mp 315–317 °C. *Anal.* Calcd. for $C_{23}H_{13}O_3N_5Cl_2$: N, 14.64; Cl, 14.85; found: N, 14.47; Cl, 15.40.

1. E. BAMBERGER. Ber. **36**, 2042 (1903).
2. L. J. BELLAMY. The infrared spectra of complex molecules. 2nd ed. Methuen and Co. Ltd., London. 1958. p. 249.
3. P. BASSIGNANA, C. COGROSSI, and M. GANDINO. Spectrochim. Acta, **19**, 1885 (1963).
4. N. S. BHACCA, L. F. JOHNSON, and J. N. SHOOLERY. NMR spectra catalog. Varian Associates, Palo Alto, California. 1962. Spectrum No. 147.
5. O. BLOCK and F. M. HAMER. Photogr. J. **70**, 374 (1930).
6. A. M. OSMAN and S. A. M. METWALLY. Indian J. Chem. **11**, 868 (1973).
7. A. M. OSMAN. J. Am. Chem. Soc. **79**, 966 (1957).
8. S. G. LEVINE and M. C. WANI. J. Org. Chem. **30**, 3185 (1965).
9. M. PESTEMER, A. BERGER, and A. WAGNER. Textilveredlung, **19**, 420 (1964).
10. J. H. BEYNON. Mass spectrometry and its applications to organic chemistry. Elsevier, Amsterdam. 1960. p. 241.
11. R. E. FOX. J. Chem. Phys. **32**, 385 (1960).
12. D. A. W. ADAMS. J. Soc. Dyers and Colour. **75**, 22 (1959).
13. A. M. OSMAN and I. BASSIONI. J. Am. Chem. Soc. **82**, 1607 (1960).
14. A. M. OSMAN and S. A. M. METWALLY. Aust. J. Chem. In press.

1,3-Dipolar cycloadditions with diazomethylphosphonates. Double pyrazolines derived from norbornadiene

HUGUETTE COHEN AND CLAUDE BENEZRA[1]

Department of Chemistry, University of Ottawa, Ottawa, Canada K1N 6N5

Received July 24, 1975

HUGUETTE COHEN and CLAUDE BENEZRA. Can. J. Chem. **54**, 44 (1976).

Four new *exo*- double pyrazolines **3–5** have been prepared from norbornadiene and dimethyl phenyldiazomethylphosphonate; their structures have been proven by nmr spectroscopy. There is a strong predominance of the isomers with the two aryl groups *syn* to the bridge. When the two aryl groups were different no electronic interaction between them could be detected by uv spectroscopy. Direct photolysis of the double pyrazolines leads to the corresponding double cyclopropanes with retention of configuration.

HUGUETTE COHEN et CLAUDE BENEZRA. Can. J. Chem. **54**, 44 (1976).

Quatre nouvelles doubles pyrazolines *exo* **3–5** ont été préparées à partir du norbornadiène et du phényldiazométhylphosphonate de diméthyle; leur structure est déduite des spectres de rmn. Il y a une forte prédominance des isomères dans lesquels les deux noyaux aryles sont *syn* par rapport au pont. Quand les deux groupes aryles sont différents il n'a été détecté aucune interaction électronique entre les noyaux aromatiques par spectroscopie uv. La photolyse directe des doubles pyrazolines conduit aux doubles cyclopropanes correspondants, avec rétention de configuration.

Norbornadiene provides a good model for studying 1,3-dipolar cycloadditions (1) with dimethyl aryl- and alkyldiazomethylphosphonates $RC(N_2)P(O)(OMe)_2$ (2). The adducts (Δ^1-pyrazolines) have a defined geometry which can be deduced mostly from nmr spectra making use of the reported vicinal $^{31}P—C—C—^1H$ couplings (3) and of stereospecific *homoallylic* $^5J_{PH}$ couplings (4). The stereochemical results with R = alkyl are in agreement with Huisgen's theory for a concerted mechanism (2, 5) since steric factors are mainly responsible for the *anti*:*syn*[2] ratio of pyrazolines **1** and **2**, but other

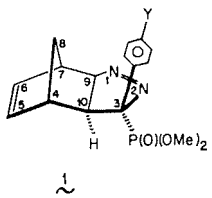

1

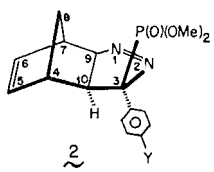

2

effects seem to operate when an *aryl* (R = Aryl) diazo compound is being used (2). Usually the reaction was carried out with a large excess of norbornadiene with methylene chloride as a solvent: under those conditions, only *mono* adducts were detected. Nevertheless, if an equimolar amount of norbornadiene and diazo compound was used *double* pyrazolines were also formed.

In this paper, we report the preparation of several double pyrazolines obtained either from norbornadiene or from the *anti*-pyrazoline **1**. In the latter case, it was deemed interesting to look for a possible electronic interaction (6, 7) between aryl nuclei with different substituents.

Results and Discussion

Double Pyrazolines from Dimethyl Phenyldiazomethylphosphonate

When norbornadiene was heated for two weeks with phenyldiazomethylphosphonate in benzene at 55–60 °C, it was possible to detect the formation of mono-pyrazolines **1** and **2**. These partly disappeared and four double pyrazolines were formed, as shown by tlc monitoring and column chromatography separation on silica gel.

Monoaddition to norbornadiene resulted in the exclusive formation of *exo*-pyrazolines (2). If the assumption is made that only *exo*-adducts are formed (as it was shown), there are, in

[1]To whom all correspondence concerning this and related work should be directed. New address: Institut de Chimie, Université Louis Pasteur de Strasbourg, 1 Rue Blaise Pascal, 67008 - Strasbourg, France.

[2]The prefixes *anti* and *syn* refer to the relative position of the bridge (C_8) and the dimethylphosphono group.

Can. J. Chem. Downloaded from www.nrcresearchpress.com by 210.87.254.40 on 09/05/12
For personal use only.

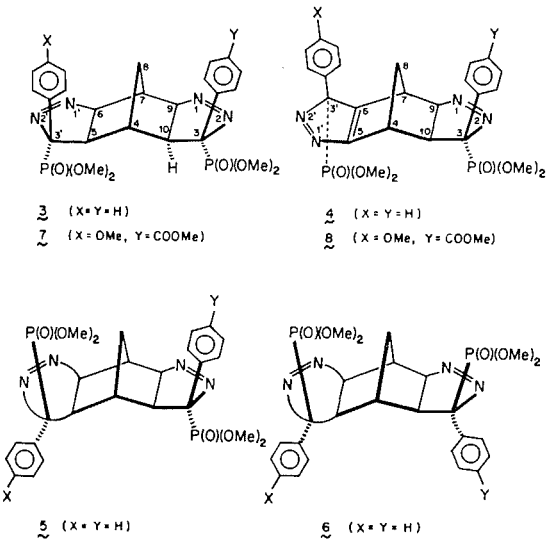

principle, six double pyrazolines which can be formed **3–6** (X = Y = H). Two are called *anti,anti* using the convention mentioned in note 2 (**3** and **4**): one, **3**, has a σ-plane of symmetry, it will be called the *σ-anti,anti* double pyrazoline, the other, **4**, has a C_2 axis of symmetry, it will be called the *C_2-anti,anti* double pyrazoline. Two have the *anti,syn* geometry (two **5** differing one from the other by the attachment of the azo group either to the 6 or to the 5 carbon atom and finally there can be two *syn,syn* **6** derivatives (attachment of N=N either to the 5 or 6 position).

In fact, besides the *mono*-pyrazolines **1** and **2** (R=phenyl), only *four* double pyrazolines were formed, namely **3**, **4**, **5** (two pyrazolines) in the approximate ratio of 1:1:1. The pyrazolines **3** and **4** were actually separated (see Experimental) while **5** was analyzed as a mixture of two *anti,syn* pyrazolines. The structure assignment rests, besides analytical and spectral (ir, uv) data, on the nmr spectra. All of the pyrazolines isolated had the *exo* attachment as commonly found in radical (8), ionic (9), and cycloaddition reactions (10) in bicyclo[2.2.1]heptene systems and also in 1,3-dipolar cycloadditions with diazoalkylphosphonates (2). This was shown by the clear absence of coupling between the bridgehead hydrogens 4,7 and the hydrogens 5,6,9, and 10 ($\sim$90° angle, see ref. 11).

The *anti* attachment is shown by a large (19–20 Hz) $^{31}P—C—C—^{1}H$ coupling (2, 3) compared with a small (6–8 Hz) $^{31}P—C—C—^{1}H$ coupling in the *syn* arrangement, in accordance with a Karplus-type behavior of vicinal *PCCH* coupling in phosphonates (3). Differentiation between the *σ-anti,anti* and the *C_2-anti,anti* derivatives is mainly based on the presence of only one bridgehead signal in the C_2 isomer **4** (hydrogens 4 and 7 are made equivalent by the C_2 symmetry) at δ 2.61 and only *one* signal for hydrogens 9 and 5 α to the N=N group at δ 4.96. In the case of the *σ-anti-anti* derivative **3**, there are *two* bridgehead signals at δ 1.69 and 3.67 and *two* signals for the hydrogens 9 and 6 α to the azo group. All nmr chemical shifts of the double pyrazolines are assembled in Table 1, the coupling constants in Table 2. Interesting to note is the dramatic shift of the bridge hydrogens which appear at higher field than the TMS signal. Compared to the same hydrogens in the *mono*-pyrazoline **1** (2), this represents a *ca.* 1 ppm upfield shift. This dramatic shift is probably due to the diamagnetic anisotropy of the phenyl ring with the simultaneous presence of the π systems of the two azo groups. This probably corresponds to a preferred orientation of the phenyl ring which, as shown on Dreiding models, corresponds to the minimum steric interaction.

Structures **5** can also be deduced from nmr. The two pyrazolines were isolated as a mixture (with one isomer preponderant). The signal for H_{10} was a four line signal with a 20.0 Hz, P,H_{10} coupling and that for H_5 (or H_6) showed a 5.8 Hz coupling corresponding to a *ca.* 120° dihedral P,H angle (3).

There was no trace of the *syn,syn* isomers **6**. This was not unexpected in view of the known 95:5 ratio of *anti:syn* mono-pyrazolines **1** and **2** (2), the likelihood for having double *syn* addition being therefore extremely small.

The same four pyrazolines **3** to **5** were also obtained from the addition of $C_6H_5C(N_2)P(O)(OMe)_2$ to the *anti*-mono-pyrazoline **1**, but *not in the same proportions*. There was much less *anti,syn* double pyrazoline **5**: while this represented 29% of the total double adducts in the direct addition to norbornadiene, there was only 12% isolated from the mono-pyrazoline **1**. This is not surprising in view of the fact that the mono-pyrazolines **1** and **2** are intermediates in the double cycloaddition (as shown by tlc monitoring) and part of the *anti,syn* double pyrazolines **5** are formed from the *syn* pyrazoline **2**.

Can. J. Chem. Downloaded from www.nrcresearchpress.com by 210.87.254.40 on 09/05/12
For personal use only.

TABLE 1. Nuclear magnetic resonance of double pyrazolines

Hydrogens	Chemical shifts[a] 3(σ) X = Y = H	4(C_2) X = Y = H	5(mixt.) X = Y = H	7(ψ-σ) X = OCH_3 Y = $COOCH_3$	8(ψ-C_2) X = OCH_3 Y = $COOCH_3$
8	−0.33(s)	−0.24(s)	0.34 (AB q; $\Delta\delta = 0.48$ $\delta_A = 0.58$ $\delta_B = 0.10$)	−0.39(s)	−0.27(s) 0.16(s)
10	2.64(dd)	2.86(dd)	2.61(dd)	2.60(dd) or 2.64(dd)	2.82(dd) or 2.86(dd)
5	2.64(dd)	4.96(dd)	2.23(dd)[b]	2.60(dd) or 2.64	4.97(m)
4	1.69 or 3.67(s)	2.61(s)	2.47(s)	1.69 or 3.69(s)	2.54 or 2.60(s)
7	3.67 or 1.69(s)	2.61(s)	nm[c]	3.69 or 1.69(s)	2.60 or 2.54(s)
6	5.23(dd)	2.86(dd)	4.86(dd)[b]	5.21(m)	2.86(dd) or 2.82
9	5.23(dd)	4.96(dd)	5.12(dd)	5.21(m)	4.97(m)
$POCH_3$	3.45(d) 3.67(d)	3.48(d) 3.70(d)	3.44;3.68(2d)[c] 3.38;3.35(2d)[c]	3.46;3.49(2d) 3.66;3.69(2d)	3.50;3.51(2d) 3.69;3.72(2d)
Aromatic	7.1–7.6(m)	7.3–7.8(m)	7.2–7.9(m)	2 AA'BB'XY[d] 6.71,6.80 7.36*,7.45* 7.57*,7.66* 7.88,7.97	2 AA'BB'XY[d] 6.86,6.94 7.54*/,7.62*, 7.72*,7.81*, 8.01,8.10
Aromatic OCH_3	—	—	—	3.71(s), 3.78(s)	3.91(s), 3.73(s)

[a]Expressed in δ ppm units with TMS as internal standard, in $CDCl_3$ solutions; s, singlet, d, doublet; t, triplet, q, quartet, m, multiplet.
[b]Appears as a triplet (^1H-^{31}P decoupling causes it to collapse into a d).
[c]There is clearly a predominant isomer.
[d]X = Y = P; only main peaks are given.
[e]Hidden under the OCH_3's signals.
[f]Peaks with asterisks are further coupled with phosphorus.

TABLE 2. Nuclear magnetic resonance of double pyrazolines

Couplings	Coupling constants in Hz 3(σ) X = H Y = H	4(C_2) X = H Y = H	5(mixt.) X = H Y = H	7(ψ-σ) X = OCH_3 Y = $COOCH_3$	8(ψ-C_2) X = OCH_3 Y = $COOCH_3$
9,10 = 5,6	5.6	6.5	5.8	7.0	7.0
P,10	19.5	19.5	20.0	19.5[a]	19.0[a]
P,5	19.5	4.0	5.8	19.5	19.0
P,6	3.9	19.5	5.8	nm[b]	4.0
P,9	3.9	4.0	3.5	nm[b]	4.0
$POCH_3$	10.5	10.5	10.4	10.5	10.8
P,H_{ar}	—	—	—	~1.5	~1.5

[a]±0.5 Hz. Since the signals are broad it was not possible to measure the coupling constants more accurately.
[b]Not measurable; appears as five equidistant lines collapsing into a dd by $^1H(^{31}P)$ irradiation.

Double Pyrazolines with Phenyl Substituted Diazomethylphosphonates

Aryl groups located closely in space can show electronic interaction (6, 7). In view of the fact that, in Dreiding models, the phenyl ring of the *anti,anti* pyrazolines **3** and **4** are less than 5 Å

Can. J. Chem. Downloaded from www.nrcresearchpress.com by 210.87.254.40 on 09/05/12
For personal use only.

Can. J. Chem. Downloaded from www.nrcresearchpress.com by 210.87.254.40 on 09/05/12
For personal use only.

apart from each other, it was thought interesting to make pyrazolines with different X and Y substitutents. The starting material was a mono-pyrazoline **1** (R = *p*-Y-C_6H_4) to which was added an aryldiazomethylphosphonate $RC(N_2)P(O)(OMe)_2$ (R = *p*-X-C_6H_4). Only *two* double pyrazolines were formed and separated by fractional crystallization, the *anti,anti* derivatives **7** and **8**: there was no trace of an *anti,syn* isomer such as **5** formed. This result is quite interesting and might indicate some sort of acceptor–donor interactions between the aryl rings in the transition state, favoring the isomers where both aryl rings are *syn* to the CH_2 bridge.

Structures **7** and **8** which are called respectively ψ-σ-*anti,anti* and ψ-C_2-*anti,anti* by analogy with **3** and **4** (see above) are deduced from combustion analysis, ir and uv data (see below) and essentially by consideration of the nmr spectra (results are collected in Tables 1 and 2). The *anti,anti* configuration in both compounds is secured by the large vicinal P,H coupling: 19.5 Hz in **7**, 19.0 Hz in **8**. The evidence for the 'ψ-C_2' and 'ψ-σ' assignment is the appearance of the signals for the bridgehead protons in both compounds: in one of them, the chemical shifts of H_4 and H_7 are very close (δ 2.54 and 2.60) while in the other one, they are far apart from each other. (δ 1.69 and 3.69). It has been shown above that bridgeheads were equivalent in the C_2-*anti,anti* derivatives (for symmetry reasons) and far apart (1.69 and 3.67) in the σ-*anti,anti* double adduct. For these reasons, we assign structure **8** ('ψ-C_2') to the double pyrazoline, where H_4 and H_7 are nearly equivalent and consequently, structure **7** to the one remaining. Consistently, in the addition of dimethyl *p*-methoxyphenyldiazomethylphosphonate to the mono-pyrazoline **1** (Y = COOMe),[3] decomposition products of the diazo compound were isolated but their structure could not be determined.

In order to allow comparison between the double pyrazolines and the 'isolated' chromophores which constitute them, we prepared saturated pyrazolines **9** (Y = OMe) and **10** (X = COOMe) from the unsaturated ones **1** (2) by catalytic hydrogenation. These were also photolyzed (as described previously for X = Y = H, ref. 12) to give compounds **11**. The *syn*-cyclopropane **12** was also prepared from the *syn* saturated pyrazolines (12). The nmr data on these mono-adducts are summarized in Table 3.

Photolysis of the Adducts

When the double pyrazolines *anti,anti* **3** and **4** dissolved in benzene were separately irradiated at 350 nm in a Rayonet apparatus, using a Pyrex filter, the same double cyclopropane **13** was obtained with the *anti,anti* structure as shown by a large $^{31}PCC^{1}H_{10}$ coupling of 15.0 Hz (12), and an extremely simple nmr spectra indicating a

[3]Also in some other addition with this diazophosphonate as will be described later (H. Cohen and C. Benezra, unpublished results).

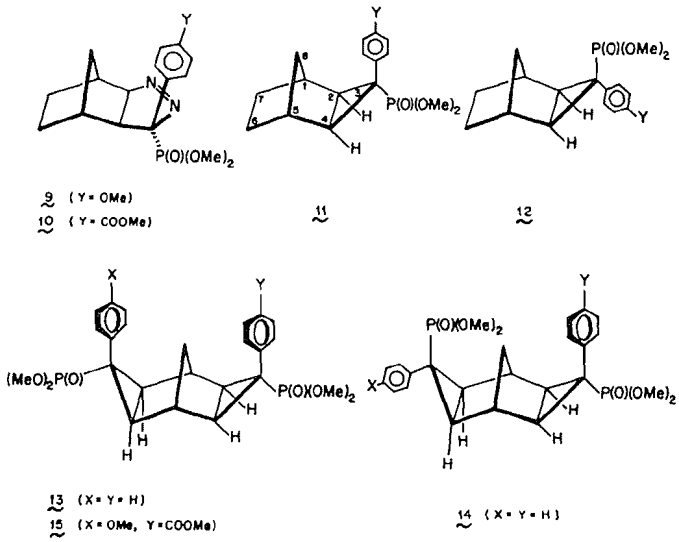

TABLE 3. Nuclear magnetic resonance of monoadduct derivatives

Hydrogens	Chemical shift (couplings in Hz)			
	10 Y = COOMe	**9** Y = OMe	**11** Y = COOMe	**11** Y = OMe
8	0.43(AB q) $\Delta\delta = 0.44$ $\delta_A = 0.21$ $\delta_B = 0.64$ ($J_{AB} = 11.0$)	0.47 $\Delta\delta = 0.47$ $\delta_A = 0.27$ $\delta_B = 0.67$ ($J_{AB} = 11.0$)	0.24(AB q) $\Delta\delta = 0.34$ $\delta_A = 0.06$ $\delta_B = 0.41$ ($J_{AB} = 12.0$)	0.31(s)
4	1.82[a] or 2.97(s)	1.82 or 2.97(s)	1.75[f](d) ($J_{P,4} = 15.0$)	1.66(d)[b] ($J_{P,4} = 15.0$)
10	2.56(dd)[b] ($J_{9,10} = 7.0$) ($J_{P,10} = 20.0$)	2.50(dd)[b] ($J_{9,10} = 7.0$) ($J_{P,10} = 20.0$)	— —	— —
7	2.97 or 1.82(s)	2.92 or 1.82(s)	—	—
$POCH_3$	3.49(d) 3.67(d) ($J_{PH} = 10.5$)	3.48(d) 3.66(d) ($J_{PH} = 10.5$)	3.60(d) ($J_{PH} = 10.5$)	3.59(d) ($J_{PH} = 10.0$)
Aromatic OCH_3	3.89(s)	3.80(s)	3.88(s)	3.76(s)
9	4.90(dd)[c] ($J_{P,9} = 4.0$)	4.86(dd)[c] ($J_{P,9} = 4.0$)	—	—
Aromatic hydrogens	7.73[d,e]7.82[e] 7.99,8.08	6.94[d],6.86, 7.64[e],7.56[e]	7.30[d],7.38 7.92,8.00	6.77[d],6.86 7.11[e],7.21[e]

[a]Because this signal is strongly affected when one goes from the *anti*-derivative to the *syn*-derivative ($\Delta\delta > 1$ ppm) it seems reasonable to assign it to H_5, the bridgehead hydrogen closer to the epimeric center C_3; also the irradiation of the lower field signal (2.97 ppm) has some effect on H_9 (unpublished works from this laboratory).

[b]Further doubled by long range H_8,H_{10} coupling (1.5 Hz).

[c]Appears actually as a ddt because of long range coupling H_8,H_9 and also some coupling with the *bridgehead* H_7: irradiation of the signal at 2.97 causes this *apparent* ddt (in actual fact a dddd) to collapse into a ddd.

[d]AA'BB'X(X = ^{31}P) m: only the main peaks are given.

[e]Further coupled to ^{31}P ($^4J_{PH}$ coupling = 2.0 Hz).

[f]H_2 and H_4 are equivalent as a consequence of the presence of a plane of symmetry through the bridge and cyclopropane.

high symmetry. This high stereoselectivity for 'direct' photolysis (13) has already been shown in the mono-pyrazoline series. This can be interpreted as indicating the formation of a singlet diradical (from each pyrazoline part) short-lived enough not to allow any rotation of the C_{10}—C_3 bond (14). In the same way, the *anti,syn* mixture led to a single compound, the *anti,syn*-biscyclopropane **14**: only apparent couplings of 6.0 Hz and 11.5 Hz were measured on the nmr spectra. In the 100 MHz spectrum, protons 2,4 and 6,7 respectively were accidently equivalent and P,H coupling could not be deduced directly from the splitting.

A 1:1 mixture of the *anti,anti*-pyrazolines **7** and **8** was irradiated under the same conditions as above, leading to the double cyclopropane **15** which also has the *anti,anti* configuration (large PCCH coupling).

All these photolysis results confirm previous findings from this laboratory that non-sensitized (or direct) photolysis lead to complete retention of configuration of the cyclopropanes. Attempts to perform the photolysis in the presence of benzophenone with compounds **3**, **4**, **5**, **7**, or **8** led to intractable mixtures of biscyclopropanes and the sensitized reaction was not studied any further. Nuclear magnetic resonance results are summarized in Table 4.

Ultraviolet Spectra

In order to detect a possible electronic interaction between close aromatic rings, uv spectra of all the compounds described above were taken and the results are summarized in Table 5. There was no evidence of any special effect due to an electronic interaction of the donor–acceptor (6, 7) type. Comparison spectra were taken by using the double adducts **7** or **8** in one cell and an equimolecular mixture of the saturated com-

Can. J. Chem. Downloaded from www.nrcresearchpress.com by 210.87.254.40 on 09/05/12
For personal use only.

TABLE 4. Nuclear magnetic resonance data for the double cyclopropanes

Hydrogens	Chemical shifts (couplings in Hz)[a]		
	13	**14**	**15**
8	−0.13(s)	−0.15(AB q) $\Delta\delta = 0.85$ $\delta_A = 0.27$ $\delta_B = -0.57$ $(J_{AB} = 14.0)$	−0.15(AB q) $\Delta\delta = 0.19$ $\delta_A = 0.037$ $\delta_B = -0.34$ $(J_{AB} = 13.0)$
2,4	2.06(d) $(J_{PH} = 15.0)$	1.89(d) $('J_{PH}' = 11.5)$	2.00 or 2.08(d) $(J_{PH} = 15.0)$
6,7	2.06(d) $(J_{PH} = 15.0)$	1.89(d) $('J_{PH}' = 6.0)$	2.08 or 2.00(d) $(J_{PH} = 15.0)$
1,5	2.69(s)	2.92(s)	2.70(s)
$POCH_3$	3.53(d) $(J_{PH} = 10.5)$	3.55(d) 3.35(d) $(J_{PH} = 10.5)$	3.56(d) 3.57(d) $(J_{PH} = 10.5)$
Aromatic	7.15(s)	7.28(s) 7.24(s)	2 AA'BB'XY systems main lines at 7.90, 7.82, 7.28[b], 7.20[b], 7.10[b], 7.02[b], 6.76 and 6.68
X or Y	—	—	3.68 3.83

[a]Spectra in $CDCl_3$ solutions, chemical shifts in δ ppm units, couplings in Hz.
[b]Further coupled to phosphorus (~1.0 Hz).

TABLE 5. Ultraviolet spectra in methanol solution

Compound	λ_{max} in nm (log ϵ)				
3[a] (X = Y = H)	222(3.8)				337(2.5)
4[b] (X = Y = H)	223(3.1)				340(1.9)
5 (X = Y = H)	215(4.2)				336(2.8)
7 (X = OCH_3, Y = $COOCH_3$)	234(4.3)				339(2.5)
8 (X = OCH_3, Y = $COOCH_3$)	234(4.2)				339(2.8)
9 (Y = H)	208(4.1)				338(2.4)
9 (Y = OCH_3)	206(3.4)	230(4.3)	278(3.0)	286(3.0)	337(2.4)
10 (Y = $COOCH_3$)	210(4.0)	243(4.2)			337(2.5)
11 (Y = OCH_3)	207(3.3)	235(4.1)	281(3.1)	288(3.0)	
11 (Y = $COOCH_3$)	212(3.0)	254(3.5)			
12 (Y = H)	214(3.1)				337(2.3)
13 (X = Y = H)[c]	224(4.1)				
14 (X = Y = H)	212(3.8)	223(3.9)	249(2.0)	254(2.1)	260(2.2) 267(2.0)
15 (X = OCH_3, Y = $COOCH_3$)	211(3.9)	238(4.4)	252(3.5)		

[a]Shoulders, characteristic of aromatic derivatives at 260, 266, 274.
[b]Shoulders at 257, 263, 269, and 274.
[c]Shoulders at 258, 264, 271, and 280.

ponents **9** (Y = OMe) and **10** (Y = COOMe). A straight line was observed. The same was true for the comparative uv spectra of compound **15** on the one hand and an equimolecular mixture **11** (Y = OMe) + **11** (Y = COOMe) on the other hand. This lack of interaction is surprising in view of the proximity of the aryl rings (~3.6 Å in the 'ψ-σ' isomer **7**, almost the van der Waals contact (15), 4.5 Å in the dicyclopropane **15**).[4]

[4]These distances were measured approximately on Dreiding models. It was not possible to measure emission spectra because the pyrazolines are photoreactive (Dr. Szabo, personal communication).

Can. J. Chem. Downloaded from www.nrcresearchpress.com by 210.87.254.40 on 09/05/12
For personal use only.

Can. J. Chem. Downloaded from www.nrcresearchpress.com by 210.87.254.40 on 09/05/12
For personal use only.

Conclusion

It has been shown that the trend observed for 1,3-dipolar cycloadditions with dimethyl aryldiazomethylphosphonates (2), namely the predominant formation of the *anti*-isomer, was a quite general one. Aryl derivatives give mainly the stereoisomer corresponding to the less sterically favorable transition state. A possible interpretation that this might be due to a favored phenyl, azo *cis* relationship such as **16** in the transition state has found recent support in CNDO/2 calculations performed on model compounds: phenyldiazomethane and diazoethane.[5] This work has also confirmed that direct photolysis of Δ^1-pyrazolines was stereospecific.

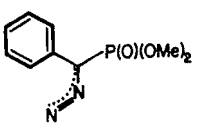

16

Experimental

The diazophosphonates were prepared as described previously (2, 16). Melting points (mp) are uncorrected. Silicic acid from Merck (0.05–0.20 mm) was used for column chromatography. The ir spectra were recorded on a Beckman-20 ir spectrometer either in chloroform solution or as Nujol mulls. The nmr spectra were run on a HA-100 Varian Spectrometer in $CDCl_3$ solutions; δ in ppm relative to TMS. Analyses were performed in Chemalytics Laboratories, Tempe, Arizona.

*Reaction of Dimethyl Phenyldiazomethylphosphonate with Norbornadiene. Isolation of Compounds **1**, **2**, **3**, **4**, and **5***

A solution of diazophosphonate $C_6H_5C(N_2)P(O)(OCH_3)_2$ (15.0 g, 66 mmol) and norbornadiene (4.0 g, 43 mmol) in benzene (80 ml) was heated for 8 days in an oil bath whose temperature was kept at 55–60 °C. The reaction mixture was poured as such on a 410 g silica gel column prepared with ether. Elution was done with ether and ether–methanol mixtures.

Successively eluted were (weight, millimoles, and eluent): (*i*) unreacted diazophosphonate (7.10 g, ether); (*ii*) a 95:5 mixture of *anti–syn* mono-pyrazoline **1** and **2** (2.33 g, 8.10 mmol, 95:5 ether–methanol), identified with authentic samples (2) by tlc, nmr; (*iii*) decomposition products (0.53 g); (*iv*) *syn–anti* double pyrazolines **5** (mixture of the two; 2.18 g, 4.00 mmol, 90:10 ether–methanol); (*v*) the *anti–anti* double pyrazolines **3** and **4** (5.33 g, 9.78 mmol, 80:20 ether–methanol); the nmr showed clearly a 1:1 mixture of 'σ' and 'C_2'.

No attempt was made to separate further the *syn,anti* double pyrazoline **5**. The 100 MHz nmr spectrum clearly showed that one isomer was strongly predominant (attachment of the *azo* group at C_5 or C_6) but it could not be decided which was which. The mixture melted at 216–218 °C. *Anal.* Calcd. for $C_{25}H_{30}N_4O_6P_2$ (mw 544.74): C, 55.11; H, 5.55; N, 10.28; P, 11.38; found: C, 55.19; H, 5.42; N, 10.55; P, 11.54. The nmr data are reported in Tables 1 and 2; ir 1595 (arom.), 1545 (N=N), 1240 (P=O), and ~1000–1100 (POC).

Further separation of the 'C_2' and 'σ' *anti,anti*-pyrazolines **3** and **4** was effected as follows. The 5.33 g mixture from the above chromatography was recrystallized in hot ether–methanol; after cooling, 1.70 g crystals precipitated out and were shown by nmr to be pure σ-*anti,anti* isomer **3** (see theoretical part); mp 196–198 °C. *Anal.* Calcd. for $C_{25}H_{30}N_4O_6P_2$ (mw 544.74): C, 55.15; H, 5.55; N, 10.28; P, 11.12 (11.38); found: C, 55.11; H, 5.47; N, 10.57; P, 11.12. Nuclear magnetic resonance data are reported in Tables 1 and 2; ir 1595 (arom.), 1550 (N=N), 1240 (P=O), and 1000–1100 (POC).

The mother liquors of the above are evaporated to dryness and recrystallized in acetone which, after cooling yielded 2.56 g of pure C_2-*anti,anti* isomer **4** as shown by 100 MHz nmr (see theoretical part); mp 152–153 °C. *Anal.* Calcd. for $C_{25}H_{30}N_4O_6P_2$ (mw 544.74): N, 10.28; P, 11.38; found: N, 9.80; P, 11.66; ir 1600 (arom.), 1550 (N=N), 1250 (P=O), and ~1000–1100 (POC).

*Reaction of Dimethyl Phenyldiazomethylphosphonate with the anti-Mono-pyrazoline **1** (X = Y = H)*

A solution of the *anti*-mono-pyrazoline **1** (6.00 g, 19.0 mmol) and dimethyl phenyldiazomethylphosphonate (6.00 g, 26.5 mmol) in benzene (40 ml) was heated in an oil bath maintained at 55–60 °C for 8 days. Chromatographic separation was effected as above on a 400 g silica gel column. In order of elution, the successive fractions were (in brackets weight, millimoles and eluent): (*i*) unreacted diazophosphonate (4.19 g, 18.5 mmol, ether); (*ii*) unreacted pyrazoline **1** (3.40 g, 10.7 mmol, ether–MeOH 95:5); (*iii*) mixture of double pyrazolines **3**, **4**, and **5** (3.15 g, 5.8 mmol, ether–MeOH 90:10); (*iv*) unidentified decomposition products (0.420 g).

The above mixture of **3**, **4**, and **5** was further chromatographed on a 200 g silica gel column using an ether–methanol solution. Eluted first is the *syn,anti*-pyrazoline **5** (0.370 g, mmol, ether–methanol 9:1), then a mixture of the *anti,anti*-pyrazolines **3** and **4** (2.75 g, 5.0 mmol, ether–methanol 8:2). This mixture (shown by nmr to be a ~50:50 mixture of σ and C_2) is separated as described above, by recrystallization during which some decomposition occurs. Thus it was obtained: 0.970 g of the σ-*anti,anti*-derivative **3** (crystallization solvent ether–methanol), 0.960 g of the C_2-*anti,anti*-derivative **4** (with acetone) and evaporation of the mother liquors gave 0.420 g of unidentified decomposition products.

*Addition of Dimethyl p-Methoxyphenyldiazomethylphosphonate to the anti-p-Carbomethylphenyl Pyrazoline **1** (Y = $COOCH_3$)*

A solution of the diazophosphonate (8.0 g, 23 mmol) and of the pyrazoline **1** (Y = $COOCH_3$, 8.10 g, 21.5 mmol) in methylene chloride (80 ml) was heated for 15 days at 55–60 °C in an oil bath. The reaction mixture was poured as such on a 400 g silica gel column prepared with ether. Eluted were, successively, (*i*) unreacted diazo com-

[5] J. Bastide, H. Cohen, and C. Benezra, unpublished results.

Can. J. Chem. Downloaded from www.nrcresearchpress.com by 210.87.254.40 on 09/05/12
For personal use only.

pound (4.20 g, 12.1 mmol, ether); (*ii*) unreacted *anti*-pyrazoline **1** (4.28 g, 11.3 mmol, ether–MeOH 95:5); (*iii*) diazo decomposition products (~1.24 g, nmr: only aromatic protons, and OCH_3 and $POCH_3$); (*iv*) double pyrazolines (5.16 g, 7.1 mmol, ether–MeOH 80:20). The nmr showed the mixture to be a 1:1 mixture of 'ψ-σ' and 'ψ-C_2' *anti,anti*-pyrazolines **7** and **8**. (*v*) unidentified decomposition products (0.520 g).

Compounds **6** and **7** were analyzed as a 1:1 mixture after further chromatography on a short silica gel column. *Anal.* Calcd. for $C_{28}H_{34}N_4O_9P_2$: C, 53.17; H, 5.42; N, 8.86; P, 9.79; found: C, 53.16; H, 5.48; N, 8.89; P, 9.42.

Separation of the 'ψ-σ' and the 'ψ-C_2' isomers was effected as follows. Fraction 4 (mixture of **6** and **7**, 5.16 g) was suspended in ether (120 ml) and enough methanol was added to the warm solution to solubilize the products). After 24 h at room temperature and filtration, 1.05 g of crystals were isolated and shown to be pure 'ψ-σ'-*anti,anti*-pyrazoline **7**; mp 210 °C; ir and nmr data are shown in Tables 1 and 2 the uv data in Table 5.

After concentrating the resulting solution, letting it stand overnight at room temperature, a second precipitate was formed and filtered (1.50 g, crystals); it was shown by nmr to be pure 'ψ-C_2' derivative; mp 183–184 °C; ir 1710, 1595, 1550, 1270, 1230, and 1000–1100; nmr data are collected in Tables 1 and 2; uv data in Table 5.

Preparation of the Saturated Pyrazolines ***9*** *(Y = OCH_3) and* ***10*** *(Y = $COOCH_3$)*

The *anti*-pyrazoline **1** (Y = $COOCH_3$, 1.70 g) prepared from norbornadiene (2) was dissolved in methanol (50 ml), 150 mg of Pd/C catalyst was added and hydrogenation was conducted in a Parr apparatus (~3 atm pressure) for 1 h 15 min. After filtration and chromatography on a silica gel column (100 g), 1.35 g of pure saturated pyrazoline **10** (Y = $COOCH_3$) was obtained; mp 128–129 °C. *Anal.* Calcd. for $C_{18}H_{23}N_2O_5P$ (mw 379.37): C, 56.99; H, 6.11; N, 7.30; P, 8.16; found: C, 56.88; H, 6.11; N, 7.41; P, 8.20; nmr data in Table 3, uv data in Table 5.

The same procedure was followed for pyrazoline **1** (X = OCH_3) obtained from previous work. From 1.79 g starting pyrazoline (same amount of solvent, catalyst) were obtained 1.45 g of saturated pyrazoline **9** (Y = OCH_3); mp 146–147 °C. *Anal.* Calcd. for $C_{17}H_{23}N_2O_4P$ (mw 351.36): C, 58.11; H, 6.60; N, 7.97; P, 8.81; found: C, 58.11; H, 6.62; N, 8.05; P, 8.95; ir 1610, 1560, 1250, and ~1000–1100; nmr data in Table 3, uv data in Table 5.

Direct Photolysis of Mono-pyrazoline ***10*** *(Y = $COOCH_3$) and* ***9*** *(Y = OCH_3)*

The pyrazoline **10** (2.83 g, 7.46 mmol) dissolved in spectrograde benzene (100 ml) was irradiated in a Rayonet apparatus, at 350 nm, using a Pyrex filter, for 5 h 15 min. Evaporation of the benzene, chromatography on a 150 g silica gel column and elution with ether–methanol 8:2 mixture, afforded 2.07 g of the cyclopropane **11** (Y = $COOCH_3$); mp 150–151 °C. *Anal.* Calcd. for $C_{18}H_{23}O_5P$ (mw 350.42): C, 61.71; H, 6.62; P, 8.82; found: C, 61.92; H, 6.59; P, 8.40; ir 1710, 1600, 1270, and ~1000–1100; uv data in Table 5.

The same procedure was followed for pyrazoline **9** (X = OCH_3) (1.05 g, 3.00 mmol), irradiation was conducted for 4 h 30 min. Chromatography as above afforded the cyclopropane **11** (Y = OCH_3, 0.910 g) mp 98–99 °C. *Anal.* Calcd. for $C_{17}H_{23}O_4P$ (mw 322.17): C, 63.33; H, 7.20; P, 9.61; found: C, 63.16; H, 7.20; P, 9.68; ir 1600, 1500, 1230, and ~1000–1100; for uv data see Table 5.

Direct Photolysis of the Double Pyrazolines: Isolation of Compounds ***13***, ***14***, *and* ***15***

(*a*) A solution of the *σ-anti,anti* double pyrazoline **3** (X = Y = H; 0.750 g, 1.4 mmol) in 100 ml benzene was irradiated for 8 h in a Rayonet apparatus with a 350 nm monochromatic lamp, using a Pyrex filter. The crude product was chromatographed on a silica gel column giving 0.654 g (1.3 mmol) of the double cyclopropane **13** (X = Y = H) mp 199 °C. *Anal.* Calcd. for $C_{25}H_{30}O_6P_2$ (mw 488.46): C, 61.47; H, 6.19; P, 12.68; found: C, 61.11; H, 6.15; P, 12.58; ir 1590, 1440, 1230, and ~1000–1100; nmr data collected in Table 4; uv data in Table 5.

(*b*) The same experiment carried out on the C_2-*anti,anti*-derivative (0.240 g, 0.40 mmol) in 100 ml benzene for 8 h under identical conditions led, after chromatography to pure double cyclopropane **13** (X = Y = H, 0.190 g, 0.40 mmol), identical in all respects with the double cyclopropane from (*a*) (tlc, nmr, ir).

(*c*) The mixture of *anti,syn*-pyrazolines **5** (X = Y = H; 0.180 g, 0.3 mmol) dissolved in 75 ml benzene and irradiated for 8 h gave, after chromatography on a 60 g silica gel column the *anti,syn* double cyclopropane **14** (X = Y = H, 0.135 g, 0.28 mmol); mp 214–215 °C. *Anal.* Calcd. for $C_{25}H_{30}O_6P_2$ (mw 488.46): C, 61.47; H, 6.19; P, 12.68; found: C, 61.79; H, 6.18; P, 12.61; ir 1590, 1440, 1230, and ~1000–1100; uv data in Table 5; nmr data in Table 4.

Direct Photolysis of the 'ψ-σ' and 'ψ-C_2' Double Pyrazolines ***7*** *and* ***8*** *(X = OCH_3, Y = $COOCH_3$): Formation of Cyclopropane* ***15***

A 1:1 mixture of the two pyrazolines **7** and **8** (0.620 mg) dissolved in anhydrous benzene (110 ml) was irradiated in a Rayonet apparatus at 350 nm, using a Pyrex filter, during 16 h. Most of the solvent is then evaporated and the remaining concentrated solution is poured on a 120 g silica gel column prepared with ether. The double cyclopropane **15** (0.510 mg) is eluted with an 8:2 ether–methanol mixture, mp 208–209 °C. *Anal.* Calcd. for $C_{28}H_{34}O_9P_2$ (mw 576.52): C, 58.33; H, 5.94; found: C, 58.12; H, 5.90; ir 1700, 1590, 1490, 1220 and 1260, and ~1000–1100; uv data in Table 5, nmr data in Table 3.

Acknowledgments

The authors wish to thank the National Research Council of Canada for financial support (Grant A-5496) of this work. Thanks are due to Dr. Szabo from NRCC Ottawa, for helpful discussions on both emission and absorption spectra.

1. R. Huisgen. Angew. Chem. Inter. Ed. Engl. **2**, 565 (1963); **2**, 633 (1963).
2. H. Cohen and C. Benezra. Can. J. Chem. **52**, 66 (1974).

3. C. BENEZRA. J. Am. Chem. Soc. **95**, 6890 (1973).
4. H. COHEN and C. BENEZRA. Org. Magn. Reson. **5**, 205 (1973).
5. R. HUISGEN. J. Org. Chem. **33**, 2291 (1968).
6. D. S. C. CHANG and N. FILIPESCU. J. Am. Chem. Soc. **94**, 4170 (1972).
7. S. A. LATT, H. T. CHEUNG, and E. R. BLOUT. J. Am. Chem. Soc. **87**, 995 (1965).
8. S. J. CRISTOL, G. D. BRINDELL, and J. A. REEDER. J. Am. Chem. Soc. **80**, 635 (1958); H. J. CALLOT and C. BENEZRA. Can. J. Chem. **49**, 500 (1971); H. C. BROWN and J. H. KAWAKAMI. J. Am. Chem. Soc. **92**, 201 (1970).
9. C. W. JEFFORD and F. DELAY. J. Am. Chem. Soc. **94**, 4794 (1972) and references therein.
10. R. HUISGEN, G. GROSHEY, and J. SAUER. Cycloaddition reactions of alkenes. *In* The chemistry of alkenes. *Edited by* S. Patai. Interscience Publishers, London. 1964; N. FILIPESCU and J. R. DEMEMBER. Tetrahedron, **24**, 5181 (1968).
11. M. KARPLUS. J. Chem. Phys. **30**, 11 (1959).
12. H. J. CALLOT and C. BENEZRA. Can. J. Chem. **50**, 1087 (1972).
13. C. BENEZRA and N. D. THO. Tetrahedron Lett. 4437 (1974).
14. P. S. ENGEL and P. D. BARTLETT. J. Am. Chem. Soc. **92**, 5883 (1970).
15. R. C. WEAST. (*Editor*). Handbook of Chemistry and Physics. 49th ed. Chemical Rubber Co., Cleveland. 1968. p. D107.
16. N. GURUDATA, C. BENEZRA, and H. COHEN. Can. J. Chem. **51**, 1142 (1973).

Can. J. Chem. Downloaded from www.nrcresearchpress.com by 210.87.254.40 on 09/05/12
For personal use only.

Heavy transition metal complexes of biologically important molecules. I. The crystal and molecular structure of *trans*-dichloro(bis(isopropyl)-sulfoxide-*S*)(1-methylcytosine-*N*)platinum(II)

COLIN JAMES LYNE LOCK[1] AND ROBERT ANTHONY SPERANZINI
Institute for Materials Research, McMaster University, Hamilton, Ontario L8S 4M1
AND
JOHN POWELL
Lash Miller Chemical Laboratories, University of Toronto, Toronto, Ontario M5S 1A1

Received June 18, 1975

COLIN JAMES LYNE LOCK, ROBERT ANTHONY SPERANZINI, and JOHN POWELL. Can. J. Chem. **54**, 53 (1976).

The crystal and molecular structure of *trans*-dichloro(bis(isopropyl)sulfoxide-*S*)(1-methylcytosine-*N*)platinum(II) has been determined by single crystal X-ray diffraction. The crystals are triclinic with $a = 16.205(5)$, $b = 8.078(2)$, $c = 6.776(2)$ Å, $\alpha = 106.53(2)$, $\beta = 96.35(2)$, $\gamma = 98.54(2)°$. The space group is $P\bar{1}$ and there are two molecules per unit cell. A total of 2294 independent reflections, of which 2023 were observed, were examined on a Syntex $P\bar{1}$ diffractometer. The structure was refined by full matrix least squares analysis to an R_2 value of 0.0427. The ligands form a rough square around the platinum atom with Pt—Cl(1), 2.304(3), Pt—Cl(2), 2.287(4), Pt—S, 2.232(2), Pt—N, 2.058(7). Distances within the ligands are normal. The plane of the cytosine ring is at 84.4° to the plane formed by the ligands around platinum.

COLIN JAMES LYNE LOCK, ROBERT ANTHONY SPERANZINI et JOHN POWELL. Can. J. Chem. **54**, 53 (1976).

On a déterminé, par diffraction de rayons-X sur un cristal unique, la structure cristalline et moléculaire du *trans*-dichloro(bis(isopropyl)sulfoxide *S*) (méthyl-1 cytosine *N*) de platine(II). Les cristaux sont tricliniques avec $a = 16.205(5)$, $b = 8.078(2)$ $c = 6.776(2)$ Å, $\alpha = 106.53(2)$, $\beta = 96.35(2)$, $\gamma = 98.54(2)°$. Le groupe d'espace est $P\bar{1}$ et il y a deux molécules par maille. On a examiné un total de 2294 réflexions indépendantes à partir desquels 2023 ont été observées à l'aide d'un diffractomètre Syntex $P\bar{1}$. On a affiné la structure par la méthode des moindres carrées (matrice complète) jusqu'à une valeur de R_2 de 0.0427. Les ligands forment approximativement un carré autour de l'atome de platine avec Pt—Cl(1), 2.304(3), Pt—Cl(2), 2.287(4), Pt—S, 2.232(2), Pt—N, 2.058(7). Les distances internales des ligands sont normales. Le plan du cycle de la cytosine est à 84.4° avec le plan formé par les ligands autour du platine.
[Traduit par le journal]

Introduction

It is possible to 'see' heavy transition metal atoms using the electron microscope (1) and the formation of heavy metal atom complexes with DNA might allow sequencing of the bases on a DNA strand, if one can design compounds which form complexes preferentially with a particular base.[2] In addition some heavy transition metal complexes, particularly those of platinum, show potent anti-tumor activity (2–4). This activity is postulated to be caused by the formation of complexes between molecules of the type *cis*-$Pt(NH_3)_2Cl_2$ and the DNA strands. The formation of the complex is supposed to prevent the unwinding of the two strands of the double helix and thus prevent replication (4). While in both cases above specificity is postulated to depend primarily on kinetic factors (4),[3] clearly structural effects may be important. In order to obtain structural information which may be used in modelling the nature of the metal–DNA interaction, we are undertaking a series of X-ray structural studies of heavy transition metal complexes of DNA bases. We report here the structure of *trans*-dichloro(bis(isopropyl)sulfoxide-*S*)(1-methylcytosine-*N*)platinum(II).

[1]To whom correspondence should be addressed.
[2]DNA is deoxoribonucleic acid.
[3]J. Powell, unpublished results.

Can. J. Chem. Downloaded from www.nrcresearchpress.com by 210.87.254.6 on 09/05/12
For personal use only.

Can. J. Chem. Downloaded from www.nrcresearchpress.com by 210.87.254.6 on 09/05/12
For personal use only.

Experiments

Preparation of trans-Dichloro(bis(isopropyl)sulfoxide-S)-(1-methylcytosine-N)platinum(II),

$PtCl_2((CH_3)_2CH)_2SO(OC.N.C(NH_2).(CH)_2.NCH_3)$

Potassium trichloro(bis(isopropyl)sulfoxide)platinate-(II) was prepared according to the method of Kukushlan *et al.* (5) for potassium trichloro(dimethylsulfoxide)-platinate(II). To an aqueous solution of potassium trichloro(bis(isopropyl)sulfoxide)platinate(II) (0.36 g in 10 ml) was added an aqueous solution of 1-methylcytosine (0.115 g in 15 ml) and the mixture stirred for 0.5 h. The mixture was then evaporated to dryness and the residue washed with a little water to remove excess HCl. Recrystallization of the residue from an isoproponal–water mixture gave the required product as yellow prisms (70%), mp 220–224° (dec.). *Anal.* Calcd. for $C_{11}H_{21}Cl_2N_3O_2SPt$: C 25.2, H 4.03; found: C 25.2, H 4.0.

Collection of the Diffraction Data

A yellow crystal of the title compound, selected after examination on a polarizing microscope was bounded by the $(1\bar{1}0)$, $(\bar{1}10)$ faces, 0.13 mm apart and by {100}, 0.10 mm apart, and {001}, 0.18 mm apart.

Weissenberg and precession photographs using MoKα radiation revealed no lattice symmetry, nor did a Delaunay reduction show any hidden symmetry. The possible space groups were thus $P1[C_1^1$, No. 1] or $P\bar{1}[C_i^1$, No. 2]. The second space group was assumed and confirmed by the successful refinement of the structure in this space group.

The crystal was transferred to a Syntex $P\bar{1}$ diffractometer and accurate unit cell parameters were obtained by least squares refinement from 15 centered medium angle reflections. The density of a few crystals was measured by flotation in a degassed methylene iodide – carbon tetrachloride mixture. Crystal data were

$C_{11}H_{21}Cl_2N_3O_2PtS$ fw = 525.0

Triclinic, $a = 16.205(5)$, $b = 8.078(2)$, $c = 6.776(2)$ Å, $\alpha = 106.53(2)$, $\beta = 96.35(2)$, $\gamma = 98.54(2)°$, $V = 834(1)$ Å^3, $P\bar{1}(C_i^1$, No. 2), $\rho_o = 2.08(2)$, $Z = 2$, $\rho_c = 2.09$ (22 °C, $\lambda = 0.71069$ Å, $\mu = 68.9$ cm^{-1}).

Intensity data were recorded on the Syntex $P\bar{1}$ diffractometer using graphite monochromatized MoKα radiation for the hemisphere defined by h, $\pm k$, $\pm l$, up to $2\theta = 50°$. Data were collected by executing a coupled θ(crystal)–2θ(counter) scan 1° on either side of the peak, scan rates varying from 8 to 24 deg min^{-1}. The stability of the system was monitored by measuring a standard reflection after each 50 reflections. The counting esd of the standard peak was 1.2% and an analysis of the standard counts showed an overall esd of 1.4% with no systematic variation with time. The intensity of a reflection, I, and its esd, σ_I, were calculated as outlined previously (6). A total of 2294 symmetry-independent reflections were measured and 95 were rejected, 94 because they were 'not significantly above background' and one because it was so intense that significant errors would have arisen from counter dead time. A further 176 reflections had $I < 3\sigma_I$ and were called unobserved. Such reflections were only used in the refinement if $F_c > F_o$ for the reflections. In the final refinement 81 unobserved reflections were used with the 2023 observed reflections. Corrections were made for absorption[4] assuming the crystal had the dimensions listed above.

Unscaled structure factor amplitudes, F, and their standard deviations, σ_F, were calculated from the expression $F = (I/L_P)^{1/2}$,

$$\sigma_F = \frac{1}{2}\frac{1}{\sqrt{L_P}}\sqrt{\frac{\sigma_I^2}{I}}$$

L_P, the Lorentz-polarization factor is $(1 + \cos^2 2\theta)/(2 \sin 2\theta)$.

Solution of the Structure

The coordinates of the platinum atom were found from a three-dimensional Patterson synthesis and three-dimensional electron density and difference maps revealed the two chlorine atoms, the sulfur atom, and the nitrogen atom. Least squares refinement of these atom positions followed by further three-dimensional electron density synthesis and difference calculations, and calculations of the likely geometries of the ligands revealed all the remaining nonhydrogen atoms. At this stage the temperature factors which were isotropic for all atoms in the initial stages of the structure solution, were made anisotropic for the Pt Cl, and S atoms. Further refinement, using a Cruickshank weighting scheme with weights equal to

$$(23.0 - 0.558|F_o| + 0.00457F_o^2)^{-1}$$

and full matrix least square refinement, minimizing $\Sigma\omega(|F_o| - |F_c|)^2$ was terminated at $R_1 = 0.0459$, $R_2 = 0.0464$.[5] In the last cycle of refinement no parameter shifted by more than 1/20 of its esd. Examination of the data showed correction for secondary extinction was not required.

The final difference map revealed a number of peaks between 0.6 and 1.0 e/Å^3 near probable hydrogen positions and attempts were made to locate hydrogen atom positions. Only small improvement was made in the structure and the errors in hydrogen bond lengths and angles were so large that we have not reported the results here. Other than the peaks near hydrogen atom positions the largest peaks were 0.60 e/Å^3 (0.33, 0.04, 0.10) between Pt and Cl(1) and 0.55 e/Å^3 (0.21, 0.13, 0.21) between Pt and Cl(2). The deepest valleys were -0.65 e/Å^3 (0.21, -0.04, 0.08) between Pt and S and -0.60 e/Å^3 (0.31, 0.21, 0.21) between Pt and N(1).

Throughout the refinement the scattering curves used were those from the *International Tables for X-ray Crystallography* (8) and the anomalous dispersion correc-

[4]All calculations were carried out on a CDC 6400 computer. The programs DATCO3, ABSORB, and DATRDN from the X-RAY 71 package were used for preliminary treatment of data. The full matrix least squares program CUDLS and Fourier program SYMFOU were written locally by J. S. Stephens and J. S. Rutherford, respectively. Least square planes were calculated by the local program PALS by P. G. Ashmore and diagrams were prepared by the program ORTEP by C. K. Johnson (7).

[5]$R_1 = \dfrac{\Sigma||F_o| - |F_c||}{\Sigma|F_o|}$; $R_2 = \left\{\dfrac{\Sigma\omega(|F_o| - |F_c|)^2}{\Sigma\omega F_o^2}\right\}^{1/2}$.

Can. J. Chem. Downloaded from www.nrcresearchpress.com by 210.87.254.6 on 09/05/12
For personal use only.

TABLE 1
(*a*) Atom parameters for $PtCl_2((i\text{-pr})_2SO)$(1-methylcytosine) ($\times 10^3$)*

Atom	*x*	*y*	*z*	*U* (Å²)
Pt	272.66(3)	92.57(6)	156.11(7)	
Cl(1)	399.6(2)	31.8(4)	61.4(5)	
Cl(2)	153.4(2)	164.7(5)	283.7(6)	
S	205.4(2)	−138.2(4)	−111.0(4)	
O(1)	239.5(5)	−162(1)	−307(1)	41(2)
O(2)	341.8(5)	461(1)	164(1)	47(2)
N(1)	339.9(6)	305(1)	396(1)	28(2)
N(2)	403.8(6)	607(1)	496(1)	34(2)
N(3)	335.2(8)	159(1)	639(2)	52(3)
C(1)	360.4(7)	459(1)	344(2)	26(2)
C(2)	426(1)	605(2)	694(2)	45(3)
C(3)	407(1)	457(2)	749(2)	41(3)
C(4)	360.4(7)	306(1)	592(2)	31(3)
C(5)	423(1)	772(2)	443(2)	58(4)
C(6)	211(1)	−332(2)	−28(2)	40(3)
C(7)	193(1)	−499(2)	−210(2)	50(3)
C(8)	158(1)	−338(2)	147(3)	62(4)
C(9)	94(1)	−130(2)	−174(2)	42(3)
C(10)	48(1)	−293(2)	−339(2)	52(4)
C(11)	92(1)	36(2)	−243(2)	61(4)

(*b*) Anisotropic temperature factors U_{ij} ($\times 10^3$)†

	U_{11}	U_{22}	U_{33}	U_{12}	U_{13}	U_{23}
Pt	27.8(3)	22.0(2)	24.6(2)	−2.5(2)	0.9(2)	0.4(1)
Cl(1)	27(2)	40(2)	42(2)	3(1)	1(1)	−1(1)
Cl(2)	35(2)	64(2)	50(2)	6(2)	10(2)	−15(2)
S	32(2)	27(1)	28(1)	−2(1)	3(1)	1(1)

*Estimated standard deviations from the least squares programs are given in parentheses.
†The temperature factor parameters U_{ij} were obtained from $\beta_{ij} = 2\pi^2 b_i b_j U_{ij}$ where β_{ij}'s appear as a temperature effect through $\exp[-(\beta_{11}h^2 + \ldots + 2\beta_{12}hk + \ldots)]$ in the structure factor expression and $\boldsymbol{b}_i$ are the reciprocal lattice vectors.

tions from the *International Tables for X-ray Crystallography* (9) were applied to the curves for Pt, Cl, and S. The atom parameters from the final refinement without hydrogen atoms are listed in Table 1, and the corresponding moduli of F_o and F_c are listed in Table 2.[6]

Discussion

Selected bond lengths and angles are given in Table 3 and the molecule is illustrated in Fig. 1. It can be seen that the platinum is in rough square planar coordination with the chlorine atoms *trans*. The bis(isopropyl)sulfoxide molecule is bonded to the platinum atom through the sulfur atom and the 1-methylcytosine[7] ring is

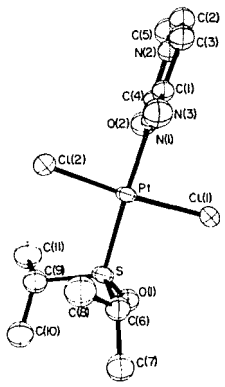

FIG. 1. The molecular structure of the title compound showing the plane of the cytosine ring almost perpendicular to the plane defined by the atoms bonded to platinum. The labelling of the atoms is as in Table 1.

[6]Table 2 is available, at a nominal charge, from the Depository of Unpublished Data, CISTI, National Research Council of Canada, Ottawa, Canada K1A 0S2.

[7]The ring numbering follows the IUPAC definitive rules B-2, 11, example 17, ref. 10. The equivalence between the conventional numbering of the atoms and our numbering of the atoms in the structure is N1, N(2); C2, C(1); O2, O(2); N3, N(1); C4, C(4); N4, N(3); C5, C(3); C6, C(2).

Can. J. Chem. Downloaded from www.nrcresearchpress.com by 210.87.254.6 on 09/05/12
For personal use only.

TABLE 3. Selected distances and angles for $PtCl_2(i\text{-pr})_2SO$)(1-methylcytosine) (esd's are given in parentheses in terms of the least significant figure)

Atoms	Distance (Å)	Atoms	Distance (Å)
	Bonded distances		
Pt—Cl(1)	2.302(3)	Pt—N(1)	2.058(7)
Pt—Cl(2)	2.288(4)	N(1)—C(1)	1.39(2)
Pt—S	2.231(2)	C(1)—N(2)	1.37(1)
S—O(1)	1.46(1)	C(1)—O(2)	1.23(2)
S—C(6)	1.82(2)	N(2)—C(2)	1.35(2)
S—C(9)	1.83(1)	N(2)—C(5)	1.47(2)
C(6)—C(7)	1.51(2)	C(2)—C(3)	1.35(2)
C(6)—C(8)	1.54(2)	C(3)—C(4)	1.42(1)
C(9)—C(10)	1.50(2)	C(4)—N(1)	1.33(2)
C(9)—C(11)	1.54(2)	C(4)—N(3)	1.33(2)
	Nonbonded distances		
Cl(1)—S	3.19(1)	Cl(1)—N(1)	3.04(1)
Cl(2)—S	3.35(1)	Cl(2)—N(1)	3.00(1)

Atoms	Angle (deg)	Atoms	Angle (deg)
Cl(1)—Pt—Cl(2)	174.3(1)	C(3)—C(4)—N(1)	122(1)
Cl(1)—Pt—S	89.3(1)	C(3)—C(4)—N(3)	120(1)
Cl(2)—Pt—S	95.7(1)	N(3)—C(4)—N(1)	118(1)
Cl(1)—Pt—N(1)	88.1(3)	C(4)—N(1)—C(1)	120(1)
Cl(2)—Pt—N(1)	87.0(3)	Pt—S—O(1)	116.0(3)
S—Pt—N(1)	177.2(3)	Pt—S—C(6)	106.6(4)
Pt—N(1)—C(1)	115.3(7)	Pt—S—C(9)	111.9(4)
Pt—N(1)—C(4)	125.1(8)	O(1)—S—C(6)	108.5(6)
N(1)—C(1)—O(2)	121(1)	O(1)—S—C(9)	106.1(6)
N(1)—C(1)—N(2)	119(1)	C(6)—S—C(9)	107.5(6)
N(2)—C(1)—O(2)	120(1)	S—C(6)—C(7)	112(1)
C(1)—N(2)—C(5)	119(1)	S—C(6)—C(8)	112(1)
C(1)—N(2)—C(2)	121(1)	C(7)—C(6)—C(8)	114(1)
C(2)—N(2)—C(5)	120(1)	S—C(9)—C(10)	111(1)
N(2)—C(2)—C(3)	122(1)	S—C(9)—C(11)	106(1)
C(2)—C(3)—C(4)	117(1)	C(10)—C(9)—C(11)	112(1)

attached to the platinum atom through the other ring nitrogen atom. The four nearest neighbor ligand atoms are close to planar although there is a slight distortion towards the tetrahedral arrangement. Cl(1) and Cl(2) lie 0.035(4) and 0.034(4) Å below the best plane through the four atoms while S and N(1) lie 0.032(3) and 0.037(7) Å above the plane. The platinum atom lies 0.022(1) Å above the plane. The 1-methylcytosine ring is planar (within the errors) and lies almost at right angles to the Cl(1)Cl(2)SN(1) plane (84.4°), as is shown clearly in Fig. 1.

There are some deviations from the ideal square planar angular arrangement. Cl(1)—Pt—Cl(2) is only 174.3(1)°, such that the chlorine atoms bend away from the bulky bis(isopropyl)-sulfoxide group with Cl(2)—Pt—S being 95.7(1)°, apparently because of the Cl(2)—C(11)(methyl) repulsion. The S—Pt—N(1) angle of 177.2(3) Å is much closer to the ideal angle.

The Pt—Cl bond lengths are normal (the range 2.289(7)–2.361(5) Å was observed in refs. 11–19), and the Pt—S bond length agrees well with the values (2.244(2), 2.229(2) Å) found by Melanson and Rochon (19) for *cis*-$PtCl_2(dmso)_2$. The distances and angles found in the bis(isopropyl)sulfoxide group agree fairly well with equivalent values found by Melanson and Rochon (19), (S—O, 1.469(6), 1.454(9); S—C 1.786(11), 1.767(11), 1.783(11), 1.790(12); Pt—S—O, 112.4(3), 117.3(3); Pt—S—C, 111.8(4), 113.5(4), 111.4(4), 108.2(4); O—S—C, 110.3(5), 108.5(5), 107.6(5), 107.9(5); C—S—C, 99.5(5), 103.3(5)), although the S—C distances in our compound may be slightly longer. The bis(isopropyl)sulfoxide group is arranged to minimize interaction

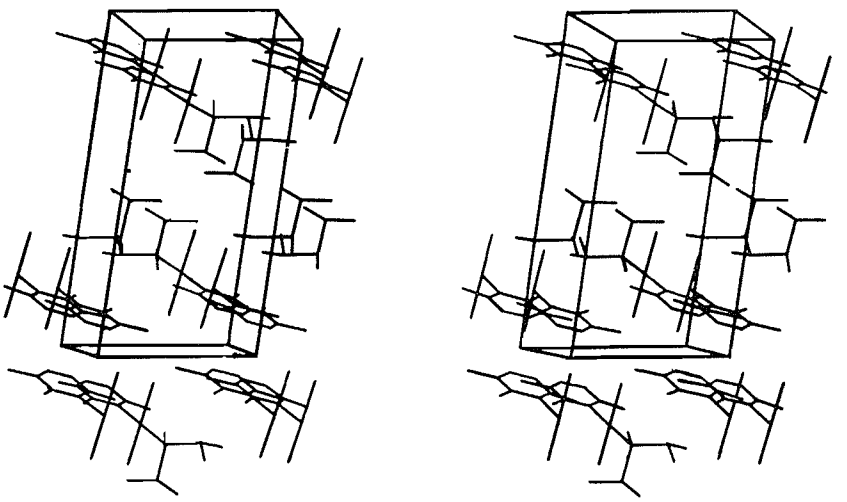

FIG. 2. Stereogram (stereoscopic pair of perspective projections) of $PtCl_2(i\text{-}Pr_2SO)$(1-methylcytosine). The contents of one unit cell are shown plus portions of other molecules to show the packing. ***b*** and ***a**** are parallel to the top and side of the page respectively, and the view is down ***c****. The cell outline shown is shifted by $\frac{1}{2},\frac{1}{2},\frac{1}{2}$ from the cell used in the structure determination.

with the chlorine atoms, the Pt—S—O(1) plane making an angle of about 40° with the Cl(1)-Cl(2)SN(1) plane. This means the biggest interaction is between Cl(2) and the groups attached to C(9), as noted above.

The Pt—N distance of 2.058(7) Å is about the expected value. *S*-bonded sulfoxides have a relatively low *trans*-influence (15), about equal to Cl^-. Although we have found no structures in which there is an aromatic system bonded to Pt(II) through nitrogen and in which the aromatic group is *trans* to a ligand with small *trans*-influence, typical values for other nitrogen ligands bonded to Pt(II) and subjected to a weak *trans*-influence are 2.04(1)–2.10(1) Å (13–18, 20–27).

An excellent and very comprehensive review has been made of bond lengths and bond angles found in cytosine rings, hemiprotonated cytosine rings, and fully protonated cytosine rings (29), and we shall not repeat the data here. Comparison of the bond lengths within the 1-methylcytosine ring in our compound with those reported for 1-methylcytosine hydrobromide (28) and those in ref. 29 shows there are no significant differences. Comparison of bond angles, however, suggests that the 1-methylcytosine ring in our compound is more like that in various neutral cytosines, rather than the protonated species. Thus, there are significant differences between the angles C(1)N(1)C(4), (C2N3C4); N(1)C(4)-C(3), (N3C4C5); C(3)C(2)N(2), (C5C6N1) in our compound and those in 1-methylcytosine hydrobromide (127(1), 117(1), 127.5(6) respectively) and the angles N(2)C(1)N(1), (N1C2N3); C(1)N(1)C(4), (C2N3C4); N(1)C(4)C(3), (N3C4-C5) in our compound are probably different from the average values for protonated cytosines (113.7(4), 125.3(11), 118.4(1) respectively) (29). Although an electrophile, the $PtCl_2((i\text{-}Pr)_2SO)$ group clearly has very little effect on the structure of the cytosine ring, unlike the proton. Finally, the bond lengths and angles in our compound are in relatively good agreement with those predicted by Spencer (30) and favor the Spencer model over that of Pauling (31), where there are significant differences.

The packing of the molecules is shown in Fig. 2. In the ***a*** direction there are two main types of contact. Near $x = 0.5$ contact is primarily between the cytosine rings, which lie parallel to each other, and which are interspersed with Cl(1) atoms. At $x = 0$ contact is primarily between the C(10) and C(11) methyl groups interspersed with Cl(2) atoms. In the ***b*** direction contact is primarily between the Cl(1) on one molecule and O(2) and the C(5) methyl group on the next. In the ***c*** direction packing is primarily between pairs of cytosine rings on adjacent molecules. All contact distances mentioned above

Can. J. Chem. Downloaded from www.nrcresearchpress.com by 210.87.254.6 on 09/05/12
For personal use only.

are at or greater than the van der Waals contact distance. There are no short distances to N(3), suggesting no intermolecular hydrogen bonding.

Acknowledgments

We thank the National Research Council of Canada for financial support of this work and Dr. Rochon for permission to use her structural results before publication.

1. F. P. Ottensmeyer, E. E. Schmidt, T. Jack, and J. Powell. J. Ultrastruct. Res. **40**, 546 (1972).
2. B. Rosenberg. Platinum Met. Rev. **15**, 42 (1971).
3. M. J. Cleare and J. D. Hoeschele. Platinum Met. Rev. **17**, 2 (1973).
4. M. J. Cleare. Coord. Chem. Rev. **12**, 349 (1974).
5. Y. N. Kukushkin, Y. E. Vyaz'menskii, and L. I. Zorina. Russ. J. Inorg. Chem. **13**, 1573 (1968).
6. R. P. Hughes, N. Krishnamachari, C. J. L. Lock, and J. Powell. To be published.
7. C. K. Johnson. U.S. Atomic Energy Commission Report, ORNL-3794. Revised June, 1965.
8. D. T. Cromer and J. A. Waber. International tables for X-ray crystallography. Vol. IV. *Edited by* J. A. Ibers and W. C. Hamilton. Kynoch Press, Birmingham. 1974. Table 2.2A, p. 72ff.
9. D. T. Cromer. International tables for X-ray crystallography. Vol. IV. *Edited by* J. A. Ibers and W. C. Hamilton. Kynoch Press, Birmingham. 1974. Table 2.3.1, pp. 149–150.
10. J. Am. Chem. Soc. **82**, 5545 (1960).
11. J. A. Jarvis, B. T. Kilbourn, and P. G. Owston. Acta Crystallogr. Sect. B, **27**, 366 (1971).
12. R. H. B. Mais, P. G. Owston, and A. M. Wood. Acta Crystallogr. Sect. B, **28**, 393 (1972).
13. G. R. Davies, W. Hewertson, R. H. B. Mais, P. G. Owston, and C. G. Patel. J. Chem. Soc. 1873 (1970).
14. E. Benedetti, P. Corradini, and C. Pedone. J. Organomet. Chem. **18**, 203 (1969).
15. S. Merlino, R. Lazzaroni, and G. Montagnoli. J. Organomet. Chem. **30**, C93 (1971).
16. C. Pedone and E. Benedetti. J. Organomet. Chem. **29**, 443 (1971).
17. D. B. Brown, R. D. Burbank, and M. B. Robin. J. Am. Chem. Soc. **91**, 2895 (1969).
18. R. T. Kops, E. Van Aken, and H. Schenk. Acta Crystallogr. Sect. B, **29**, 913 (1973).
19. R. Melanson and F. D. Rochon. Can. J. Chem. **53**, 2371 (1975).
20. T. G. Appleton, H. C. Clark, and L. E. Manzer. Coord. Chem. Rev. **10**, 335 (1973).
21. L. Gastaldi and P. Porta. Cryst. Struct. Commun. **1**, 353 (1972).
22. R. Graziani, G. Bombieri, and E. Forsellini. Inorg. Nucl. Chem. Lett. **8**, 701 (1972).
23. J. W. Carmichael, N. Chan, A. W. Cordes, C. K. Fair, and D. A. Johnson. Inorg. Chem. **11**, 1117 (1972).
24. S. D. Ittel and J. A. Ibers. Inorg. Chem. **12**, 2290 (1973).
25. H. C. Freeman and M. L. Golomb. Acta Crystallogr. Sect. B, **25**, 1203 (1969).
26. J. S. Anderson, J. W. Carmichael, and A. W. Cordes. Inorg. Chem. **9**, 143 (1970).
27. C. F. Liu and J. A. Ibers. Inorg. Chem. **9**, 773 (1970).
28. R. F. Bryan and K. I. Tomita. Acta Crystallogr. **15**, 1174 (1962).
29. D. Voet and A. Rich. Prog. Nucl. Acid Res. Mol. Biol. **10**, 183 (1970).
30. M. Spencer. Acta Crystallogr. **12**, 59 (1959).
31. L. Pauling and R. B. Corey. Arch. Biochem. Biophys. **65**, 164 (1956).

Can. J. Chem. Downloaded from www.nrcresearchpress.com by 210.87.254.6 on 09/05/12
For personal use only.

Donor–acceptor interactions in biomolecules. II. Spectroscopic and molecular orbital studies of amino acid – nicotinamide adenine dinucleotide complexes

JAYANTI NAGCHAUDHURI AND RASHMI SURI

Department of Chemistry, University of Delhi, Delhi-110007 India

Received May 5, 1975

JAYANTI NAGCHAUDHURI and RASHMI SURI. Can. J. Chem. **54**, 59 (1976).

The nature of complex formation between aromatic amino acids and some of their components with NAD^+ (nicotinamide adenine dinucleotide) have been studied by spectrophotometric methods. A comparison of the stability of these complexes with that of the complexes of the same donors with a model compound of NAD^+ *i.e.* *N*-methyl-3-carboxamide pyridinium chloride (MCP) has been carried out by examining the type of complexes formed and their geometry. Simple molecular orbital calculations have been done to determine the quantity of charge transfer δQ and stabilization energy δE and to show the significance of mutual orientation of donor and acceptor in determining the stability. The enhanced stability of tryptophan–NAD^+ complex in comparison to indole–NAD^+ complex has also been explained.

JAYANTI NAGCHAUDHURI et RASHMI SURI. Can. J. Chem. **54**, 59 (1976).

On a étudié, par des méthodes spectrophotométriques, la nature de la formation de complexes entre des acides aminés aromatiques et quelques-uns de leurs composants avec la NAD^+ (nicotinamide adénine dinucléotide). On a fait, à partir de considérations sur le type de complexe formé et de leur géométrie, une comparaison de la stabilité de ces complexes avec celle de complexes des mêmes donneurs avec le composé modèle de NAD^+ soit le chlorure du *N*-méthyl carboxamide-3 pyridinium (MCP). On a fait des calculs simples d'orbitales moléculaires pour déterminer la quantité de transfert de charge δQ et l'énergie de stabilisation δE et pour montrer l'importance de l'orientation mutuelle du donneur et de l'accepteur en vue de déterminer la stabilité. On explique la stabilité accrue du complexe tryptophane–NAD^+ par comparaison avec celle du complexe indole–NAD^+.

[Traduit par le journal]

Introduction

In a previous paper (1), a systematic and complete study of the characteristics of the interactions of some enzyme–coenzyme models (*e.g.* aromatic amino acids and *N*-methyl-3-carboxamide pyridinium chloride (MCP)) was reported. Since MCP is a model compound for the pyridine coenzyme nicotinamide adenine dinucleotide, NAD^+, it was felt that we should next investigate the nature of the complex formation of NAD^+ itself with the same aromatic amino acids under similar experimental conditions and compare these results with those obtained for the model compound MCP as acceptor. Such studies are necessary to be able to draw any conclusion regarding the nature of enzyme–coenzyme (NAD^+) interactions from the observations made in simple systems.

Cilento and co-workers (2, 3) have reported the spectral changes when NAD^+ is added to some indole derivatives and have attributed these changes to charge–transfer interaction. They also have mentioned complex formation of tyrosine with NAD^+ (4). Fulton and Lyons (5) found evidence of such interaction between indole and NAD^+ and have roughly estimated the charge–transfer (C–T) absorption maximum at 310 nm. A more detailed study of non-enzymatic interactions of various indoles with NAD^+ has been carried out by Alivisitos *et al.* (6). Their spectral data indicate a 1:1 stoichiometry for the complexes, and the association constants for indoles with a side chain at the 3-position are found to be 3 to 4 times larger than those obtained for the indole–NAD^+ complex. This prompted them to suggest that the ethylamine side chain of indole may enhance the association and also that the groups associated with the nicotinamide moiety of NAD^+ may play an important role. Recently, Boers and Verhoeven (7) observed a difference in the relative intensities of two absorption bands obtained by resolution of the C–T band due to addition of MCP and NAD^+ respectively to

Can. J. Chem. Downloaded from www.nrcresearchpress.com by 210.87.254.42 on 09/05/12
For personal use only.

Can. J. Chem. Downloaded from www.nrcresearchpress.com by 210.87.254.42 on 09/05/12
For personal use only.

rabbit muscle glyceraldehyde phosphate dehydrogenase and have attributed this difference to dissimilarities in the relative orientation of the nicotinamide ion of MCP and NAD^+ respectively, with respect to the tryptophan molecule. In any of these observations however, no systematic studies have been made to correlate and compare the nature of interaction of all aromatic amino acids with MCP and that of the same donors with NAD^+. The significance of the amino acid chain in modifying the association strength of NAD^+ as well as possible effects of the adenosine portion of NAD^+ in such interactions have also not been further investigated except for a recent paper by Umeyama *et al.* (8) in which MO studies of the interaction of indole with the adenine and nicotinamide moieties of NAD^+ have been reported.

In the present study therefore, we have investigated all the above mentioned points from both experimental and molecular orbital approaches.

Experimental

Materials

The amino acids were purchased from B.D.H. or E. Merck and the NAD^+ used was an imported chemical purchased from V.P. Chest Institute, Delhi. These were used without further purification. All spectral studies were made in aqueous medium except in the case of the tyrosine–NAD^+ system, where 2 *M* HCl was used. The solutions were prepared just prior to the experiment and measurements were made with a Beckman DU2 spectrophotometer at room temperature using a matched pair of 10 mm quartz cells.

Methods

The calculations for association constants, *K*, and molar extinction coefficients, ϵ, were done using the equation of Foster *et al.* (9), corrected by a least-squares procedure and also by the Rose and Drago method (10). The details of these equations and their significance for evaluation of *K* and ϵ have been discussed in a previous report (1). In order to ensure the accuracy of these parameters, they were also calculated using Scatchard's equation (11). In all these experiments the concentration of NAD^+ was kept constant and at a much lower value than the varying concentration of the donor. The Foster equation could not be applied in the study of the indole–NAD^+ system as the extremely low solubility of indole in water prevented any appreciable concentration variation, which was necessary for such measurements. Hence the $K\epsilon$ value was calculated by measuring the net absorbance of the complex, ΔOD ($OD_{obs} - OD_A - OD_D$), for a series of equimolar solutions "*a*" of indole and NAD^+, at two different wavelengths and plotting $\Delta OD/a$ versus *a* according to the equation,

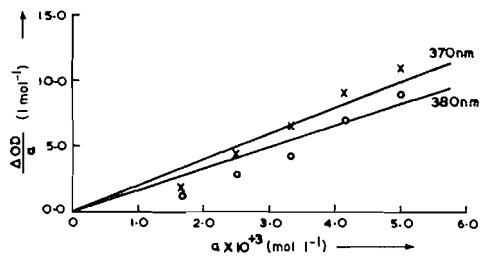

FIG. 1. Ratio of the absorbance, ΔOD, to concentration, *a*, plotted against concentration *a* when the concentration of both reactants, indole and NAD^+ were varied (0.83×10^{-3} *M* to 5×10^{-3} *M*).

$$[1] \qquad \frac{\Delta OD}{a} = K\epsilon a$$

for $a \gg C$, where *C* is the concentration of the complex.

This plot is found to be a straight line (Fig. 1) proving 1:1 stoichiometry of the complex. Then *K* was estimated from the slope, substituting the value of ϵ from the Alivisitos *et al.* (6) data at 380 nm.

Molecular Orbital Calculations

The MO calculations have been done by the Hückel molecular orbital method including hyperconjugation. The Pullman (12) parameters were used in calculations except that the value of δH_3 was taken to be -0.2 and that of δC_{aliph} 0.0. The HMO calculations were done only on the *N*-methyl-3-carboxamide pyridinium moiety of NAD^+. The stabilization energies δE and the quantities of charge-transfer δQ of various complexes have been calculated using the following equations as given by Nagata *et al.* (13),

$$[2] \quad \delta E = -2\left[\sum_j^{occ}\sum_k^{vac} - \sum_j^{vac}\sum_k^{occ}\right] \times \frac{(C^j{}_r C^k{}_s l_1 + C^j{}_t C^k{}_u l_2\text{--})^2 \beta'^2}{(\epsilon_{1j} - \epsilon_{2k})}$$

$$[3] \quad \delta Q = +2\left[\sum_j^{occ}\sum_k^{vac} - \sum_j^{vac}\sum_k^{occ}\right] \times \frac{(C^j{}_r C^k{}_s l_1 + C^j{}_t C^k{}_u l_2\text{--})^2 \beta'^2}{(\epsilon_{1j} - \epsilon_{2k})^2}$$

where $C^j{}_{r,t}$--- are the coefficients of the *r*th, *t*th, ----- atomic orbitals in the *j*th molecular orbital and ϵ_{1j} is the energy of the *j*th molecular orbital of molecule 1; $C^k{}_{s,u}$---- are the coefficients of the *s*th, *u*th, ---- atomic orbitals in the *k*th molecular orbital and ϵ_{2k} is the energy of the *k*th molecular orbital of the molecule 2 and

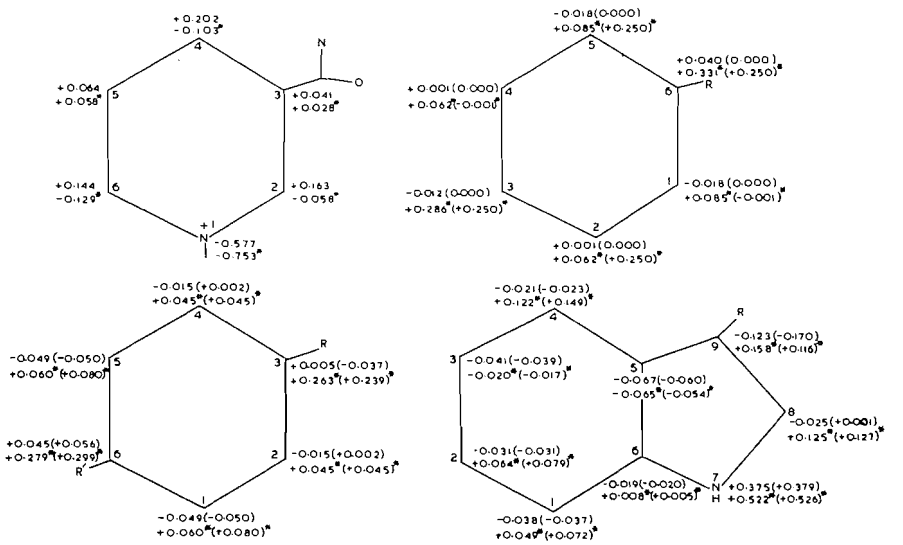

FIG. 2. The net charges at various positions (1,2,3----) of MCP, phenylalanine, tyrosine, and tryptophan molecules. The values marked with asterisk are net charges for the ions. The values within parentheses are net charges for the respective compounds without the amino acid chain, R.

$$R = -H_2C-\underset{\displaystyle NH_2}{\underset{|}{CH}}-COOH, \quad R' = -OH$$

$\sum^{occ}$ and $\sum^{vac}$ are respectively the summation of the occupied and vacant orbitals, assuming the molecules are in parallel planes, 3 Å apart. $l_1\beta'$ is the resonance integral between the orbital at the rth atom of molecule 1 and sth atom of the molecule 2 and β' is the magnitude of resonance integral between the atomic orbitals of carbon atoms of the charge-transfer complex. The respective values of $lx - y/lc - c$, as estimated by Nagata *et al.* (13) from the consideration of the table of overlap integrals of Mulliken *et al.* (14) have been used in our calculations. All calculations were done using an I.B.M. 360 (model 44) computer.

The calculations of δE and δQ were done taking Karreman's (15) view into consideration that the relative orientation of donor and acceptor, and hence the structure of the complex, would be governed to a large extent by the complimentarity of electronic charges so as to maximize electrostatic or dipole attraction. The net charges on the molecules concerned are given in Fig. 2 and the various points of overlap between *N*-methyl-3-carboxamide pyridinium chloride and various donors for the most electrostatically favorable orientations are given in Table 1 (part *i*).

Results and Discussion

The difference spectra of the complexes between various donors and NAD^+ have been measured between 285 and 360 nm (the concentration of NAD^+ is $\sim 1\text{–}2 \times 10^{-3}$ *M* and the concentration of donors $\sim 1\text{–}50 \times 10^{-3}$ *M*). These measurements were always repeated at least twice keeping the concentration the same and the reproducibility of λ_{max} was found to be within ± 3 nm. These λ_{max} values as well as the association constants, *K*, and the molar extinction coefficients, ϵ, of the complexes, as calculated by the Foster, Scatchard, and Rose–Drago equations at several wavelengths are given in Table 2 (high absorbances of the components as well as of the C–T complex prevented such measurements to be made at λ_{max}). The data within parentheses in each column denotes the corresponding parameters for that donor and MCP complex (1). Figures 3 and 4 represent characteristic plots of data for the phenylalanine–NAD^+ system by application of the Foster equation, Scatchard equation, and by the Rose and Drago method respectively, indicating 1:1 complex formation. The close correspondence of *K* and ϵ values obtained by different methods shows the accuracy and reliability of these param-

Can. J. Chem. Downloaded from www.nrcresearchpress.com by 210.87.254.42 on 09/05/12
For personal use only.

TABLE 1. Atomic location of MCP where overlap of molecular orbitals is assumed to occur

	Atomic location of MCP (X)					
(*i*) Compound	1	2	3	4	5	6
Phenylalanine (benzene)	6	1	2	3	4	5
Tyrosine (phenol)	6	1	2	3	4	5
Tryptophan (indole)	6	5	4	3	2	1
(*ii*) Ions	Points of charge, complimentarity in ion orientations					
Phenylalanine (benzene)	3	2	1	6	5	4
Tyrosine (phenol)	6	1	2	3	4	5
Tryptophan (indole)	1	6	5	4	3	2

TABLE 2. The absorption maximum λ_{max}, association constants K and molar extinction coefficients ϵ of charge–transfer complexes of respective donors with NAD^+

Donor	λ_{max} (nm)	$K_\lambda{}^a$ (l mol^{-1})	$\epsilon_\lambda{}^a$ (l mol^{-1} cm^{-1})	$K_\lambda{}^b$ (l mol^{-1})	$\epsilon_\lambda{}^b$ (l mol^{-1} cm^{-1})
L-Phenylalanine	296.0(287.0)	$13.71_{310}(0.25)$	$106.66_{310}(106.60)$	13.51_{310}	110.00_{310}
		13.84_{320},14.05[d]	74.97_{320},72.69[d]	14.29_{320}	72.00_{320}
		15.38_{330}	49.83_{330}	15.38_{330}	50.00_{330}
		12.00_{340}	37.18_{340}	13.33_{340}	36.00_{340}
L-Tyrosine	296.0(293.0)	1.80_{315}	324.56_{315}	1.72_{315}	330.00_{315}
		$2.05_{330}(1.18)$	$194.50_{330}(169.60)$	$2.13_{330}(1.20)$	$190.00_{330}(170)$
		1.47_{340},1.61[d]	178.84_{340},169.51[d]	1.61_{340}	170.00_{340}
		2.73_{350}	82.45_{350}	2.86_{350}	80.00_{350}
Indole	301.0(300.0)	$3.87_{380}(2.77)$	534.18_{370}	—	—
			430.00_{380}[c](686.67)		
L-Tryptophan	308.0(305.0)	16.66_{330}	449.80_{330}	17.80_{330}	450.00_{330}
		17.64_{340}	362.08_{340}	18.18_{340}	360.00_{340}
		$18.51_{350}(3.33)$	293.88_{350}	$18.18_{350}(3.24)$	$295.00_{350}(760)$
		17.46_{370},17.33[d]	217.97_{370},224.13[d]	17.86_{370}	220.00_{370}

[a]Foster plot.
[b]Rose–Drago plot.
[c]Taken from ref. 6.
[d]Scatchard plot.

eters. It is evident from Table 2, that the association constants for phenylalanine–NAD^+ and tryptophan–NAD^+ complexes are of much higher order than those of corresponding MCP complexes, while K values for tyrosine–NAD^+, although larger, are comparable with those of the tyrosine–MCP complex. Indole also shows slightly enhanced complexing capacity with respect to NAD^+ than with MCP. Alivisitos *el al.* (6) have also observed the difference in magnitude of K between indole–NAD^+ and some indole derivative–NAD^+ complexes, although no definite explanation has been drawn by them regarding the origin of such differences. In order to arrive at a more definite conclusion, we have not only studied the complex formation between the three aromatic amino acids and indole with MCP and NAD^+ respectively by spectrophotometric methods but also have done molecular orbital calculations on the system. The assumption was made that the differences between these two sets of complexes are similar to those between the weak outer complexes with partial charge–transfer and strong inner charge–transfer complexes in which charge–transfer is almost complete and stabilization is due to electrostatic attraction between the NAD^+ free radical (assuming that the odd electron is not localized on any particular atom, but is distributed over the whole molecule. *cf.* ref. 12, p. 526) and the donor cation (16). One set of calculations has, therefore, been done for donor–MCP complexes where the quantity of charge–transfer δQ and the stabilization energy δE due to charge–transfer have been calculated according to the principle described in the pre-

Can. J. Chem. Downloaded from www.nrcresearchpress.com by 210.87.254.42 on 09/05/12
For personal use only.

TABLE 3. The frequency of charge-transfer maxima (ν_{max}), the energies of HOMO, quantities of charge-transfer (δQ) and stabilization energies (δE) of some complexes of amino acids and their components with *N*-methyl-3-carboxamide pyridinium chloride (MCP)

Donor	ν_{max} (cm^{-1})	HOMO (β units)	δQ $+\beta'^2/\beta^2$	δE $-\beta'^2/\beta$
Benzene	35398.20[a]	1.000	0.225	0.355
Phenol	33726.81[a]	0.790	0.410	0.519
Indole	33333.33[b]	0.534	0.515	0.649
Phenylalanine	34843.20[b]	0.908	0.289	0.416
Tyrosine	34129.69[b]	0.727	0.405	0.513
Tryptophan	32786.88[b]	0.479	0.547	0.668

[a]Ref. 17.
[b]Ref. 1.

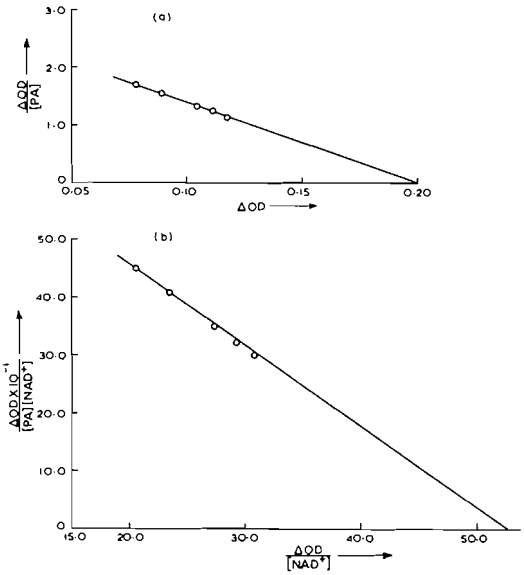

FIG. 3. (*a*) Foster plot for the phenylalanine–NAD^+ complex in water at 320 nm. The concentration of phenylalanine is varied from 1.5×10^{-2} *M* to 10.5×10^{-2} *M*. The concentration of NAD^+ is 3.80×10^{-3} *M*. (*b*) Scatchard plot for the above system.

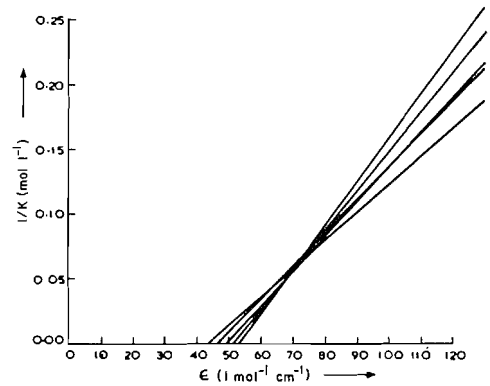

FIG. 4. Rose–Drago plot for the phenylalanine–NAD^+ complex at 320 nm.

vious section. These values along with the experimentally observed ν_{max} (cm^{-1}) for the C–T complex (1) and HOMO (highest occupied molecular orbital) of donors are given in Table 3. The ν_{max} (cm^{-1}) for benzene and phenol are that of the intramolecular complex, *i.e.*, *N*-(β-X-phenylethyl)-3-carboxamide pyridinium chloride, where X is H and OH respectively (17). The variation of δQ and δE with ν_{max} (cm^{-1}) for complexes and also with the HOMO of donors as shown in Fig. 5, proves their charge–transfer nature to be consistent with weak outer type complexing. The much stronger complexing ability shown by aromatic amino acids with respect to NAD^+ on the other hand, is attributed to strong inner complex formation with complete transfer of charge. Another set of calculations for the net charges for donor cations and NAD^+ free radicals have, therefore, been done. These data, denoted in Fig. 2 with asterisks, clearly show that the enhanced stability of these complexes is due to greater charge complimentarity between donor cations and the NAD^+ free radical when these are in juxstaposition according to the atomic locations given in section (*ii*) of Table 1. It should be noted that the orientations of the donors with respect to MCP as shown in section (*i*) are different than those of donor cations and NAD^+ free radical shown in section (*ii*). This is assumed to be the case in NAD^+ complexes, except in the case of tyrosine, where the orientation is the same in both cases. This is significant in the sense that experimentally the stability of tyrosine–MCP complex and tyrosine–NAD^+ complex have also

Can. J. Chem. Downloaded from www.nrcresearchpress.com by 210.87.254.42 on 09/05/12
For personal use only.

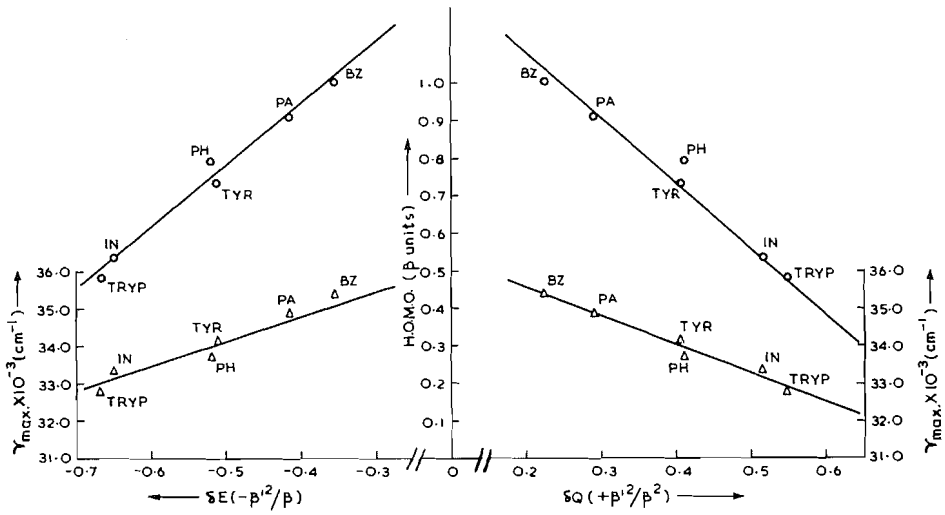

FIG. 5. A plot of ν_{max} (cm^{-1}) *vs.* $\delta E(\Delta)$ and $\delta Q(\Delta)$ respectively and HOMO *vs.* $\delta E(0)$ and $\delta Q(0)$ respectively for donor–MCP complexes.

been found to be comparable. Boers and Verhoeven (7), in their study of the binding of NAD$^+$ and MCP respectively, with rabbit-muscle glyceraldehyde phosphate dehydrogenase have predicted such differences in the relative orientation of nicotinamidium ion of NAD$^+$ and MPC with respect to tryptophan.

It is thus evident from these simple molecular orbital calculations that MCP, being unhindered by any side groups, has more mobility in its complexing with amino acids and forms comparatively loose complexes due to partial transfer of charge from donor to acceptor. In fact, we have also calculated δE and δQ values for several other orientations of MCP and each of the donors, and have found that these quantities do have significant values, although the largest δQ and lowest δE are those corresponding to the orientation given in Table 1. The nicotinamidium moiety of NAD$^+$, however, has a large side group (adenosine part) and is known to exist in a stacked conformation. It is therefore possible that only a very specific orientation of the nicotinamidium moiety of NAD$^+$ with respect to donors would cause complexing and when this occurs, the more specific and rigid orientation of components will lead to almost complete transfer of charge from donor to acceptor (an interesting discussion by Herriott *et al.* (18) about the importance of coulombic forces and of specific geometry between the components in such complexes is worth noting in this connection). Recently, Umeyama *et al.* (8) have studied the interaction of NAD$^+$ with indole by a more sophisticated MO method for several orientations of indole and MCP and have reported the calculated wavelengths for the C–T absorption from 298.1 to 316.7 nm. They have chosen a preferred orientation that gives calculated wavelengths in close correspondence to the experimentally observed values by previous workers. In our simple calculation scheme we have estimated δQ and δE for the orientation which is very similar to their preferred orientation and have found $\delta Q = +0.188$ and $\delta E = -0.686$. It is interesting to note that our experimentally observed value, λ_{max} of 300 ± 3 nm is in good agreement with that obtained by them for an orientation very similar to the one chosen by us (Table 1, part *i*). These workers have also predicted the C–T wavelengths of 344.6 and 302 nm for the adenine-nicotinamidium moiety (3.4 Å apart) in the stacked conformation of NAD$^+$, the oscillator strength of the former band being extremely small. We have studied the charge–transfer complex formation of adenine and MCP in aqueous medium and have found the value of K to be ~ 4.0 l mol^{-1} (both for a Foster as well as for a Rose–Drago plot), ϵ, ~ 73.0 l mol^{-1} cm^{-1} and λ_{max} as 300 ± 3.0 nm. This complex although fairly strong in isolated molecules, apparently, according to the calculations of the

Can. J. Chem. Downloaded from www.nrcresearchpress.com by 210.87.254.42 on 09/05/12
For personal use only.

above mentioned workers, would affect only slightly the indole–nicotinamidium complexing when NAD^+ is the acceptor (C–T maximum of indole–nicotinamidium has been predicted to be red shifted by 1.3 nm only by stacking of adenine).

The fact that the indole–NAD^+ complex has a K value much smaller than tryptophan–NAD^+, shows that the amino acid chain also has an effect in determining complexing ability. This effect can be visualized by noting the changes in net charge at the carbon atom to which the side chain is attached. This carbon which is a high negative center in indole and tryptophan molecules becomes a fairly strong electron deficient center (net charge being positive) in ions, tryptophan having the more positive carbon. In the case of tryptophan it can be shown, by steric models for the orientation chosen by us, that this carbon is quite close to the negative carbonyl oxygen of $CONH_2$ group of the nicotinamidium moiety and this causes an extra center of charge complimentarity and hence enhanced stabilization. No experimental data are available for K values for phenol–NAD^+ or benzene–NAD^+ complexes to make a comparison with corresponding tyrosine–NAD^+ or phenylalanine–NAD^+ complexes but similar considerations show that, for the chosen orientations of these complexes, the carbon atom having the side chain, although a positive center in both amino acid ions, is sterically not in close proximity to the carbonyl oxygen.

In conclusion, we have shown that simple MO calculations can provide a reasonable explanation of the nature of complex formation of amino acids with MCP and NAD^+ respectively, and also of the role of the amino acid chain of tryptophan in complexing with NAD^+. Such information will enhance a better understanding of enzyme–NAD^+ interaction and of the role of MCP, when it is used as a probe for conformational studies of proteins.

A more detailed study involving the calculations of oscillator strengths from the charge–transfer bands is in progress, not only for these complexes but also for various protein–NAD^+ systems and will be reported in a future communication.

Acknowledgments

One of us (R.S.) wishes to thank University Grants Commission, India, for a Junior Research Fellowship. We thank Dr. N. K. Ray for helping us in computer programming. The technical assistance of Mr. J. S. Garcha is gratefully acknowledged.

1. J. NAGCHAUDHURI and R. SURI. Indian J. Chem. **13**, 1032 (1975) and references therein; Indian J. Chem. **13** (12) 1975.
2. G. CILENTO and P. GUISTI. J. Am. Chem. Soc. **81**, 3801 (1959).
3. G. CILENTO and P. TEDESCHI. J. Biol. Chem. **236**, 907 (1961).
4. G. CILENTO and M. BERENHOLC. Biochim. Biophys. Acta, **94**, 271 (1965).
5. A. FULTON and L. E. LYONS. Aust. J. Chem. **20**, 2267 (1967).
6. S. G. A. ALIVISTOS, F. UNGAR, A. JIBRIL, and G. A. MOURKIDES. Biochim. Biophys. Acta, **51**, 361 (1961).
7. W. BOERS and J. W. VERHOEVEN. Biochim. Biophys. Acta, **328**, 1 (1973).
8. H. UMEYAMA, A. IMAMURA, and C. NAGATA. J. Theor. Biol. **46**, 1 (1974).
9. R. FOSTER, D. LL. HAMMICK, and A. A. WARDLEY. J. Chem. Soc. 3817 (1953).
10. N. J. ROSE and R. S. DRAGO. J. Am. Chem. Soc. **81**, 6138 (1959).
11. G. SCATCHARD. Ann. N.Y. Acad. Sci. **51**, 660 (1949).
12. B. PULLMAN and A. PULLMAN. *In* Quantum biochemistry. Interscience, New York and London. 1963.
13. C. NAGATA, A. IMAMURA, K. FUKUI, and H. SAITO. Gann, **54**, 401 (1963).
14. R. S. MULLIKEN, C. A. RIEKE, and H. ORLOFF. J. Chem. Phys. **17**, 1248 (1949).
15. G. KARREMAN. Ann. N.Y. Acad. Sci. **96**, 1029 (1962).
16. R. S. MULLIKEN and W. B. PERSON. *In* Molecular complexes. Wiley Interscience, New York. 1969. Chapt. 14–16.
17. S. SHIFRIN. *In* Molecular association in biology. *Edited by* B. Pullman. Academic Press, New York and London. 1968. p. 323.
18. J. R. HERRIOTT, A. CAMERMAN, and D. A. DERANLEAU. J. Am. Chem. Soc. **96**, 1585 (1974).

Can. J. Chem. Downloaded from www.nrcresearchpress.com by 210.87.254.42 on 09/05/12
For personal use only.

Decomposition of butyl dixanthogen in the presence of cationic micelles

LUIS SEPULVEDA AND SERGIO CONTRERAS[1]

Department of Chemistry, Faculty of Sciences, University of Chile, Santiago, Chile

Received January 20, 1975

LUIS SEPULVEDA and SERGIO CONTRERAS. Can. J. Chem. **54**, 66 (1976).

The decomposition of butyl dixanthogen in the presence of cetyl trimethylammonium bromide (CTA) at p*H* 10.5 is studied. CTA micelles strongly catalyze the decomposition. A great difference is also found between freshly prepared dixanthogen and that stored pure or dissolved in dioxane for more than one month. A general mechanism is proposed to account for the results obtained.

LUIS SEPULVEDA et SERGIO CONTRERAS. Can. J. Chem. **54**, 66 (1976).

On a étudié, à un p*H* de 10.5, la décomposition du dixanthogène de butyle en présence de bromure de cétyltriméthylammonium (CTA). Les micelles de CTA agissent comme un puissant catalyseur pour la décomposition. On trouve aussi une grande différence entre un dixanthrogène fraîchement préparé et d'autres conservés à l'état pur ou en solution dans le dioxanne pour plus d'un mois. On propose un mécanisme général pour expliquer les résultats obtenus.
[Traduit par le journal]

Introduction

The problem of the chemical stability of dixanthogen is of interest not only in organic chemistry but also in surface physical chemistry in its application to mineral flotation. In this process the hydrophobic qualities exhibited by the minerals are attributed to the adsorption of dixanthogen formed at the expense of the xanthate added as collecting agent. For this reason the xanthate–dixanthogen system has been the subject of several investigations during recent years. Pomianowski and Leja (1), for example, arrived at the conclusion that dixanthogen is spontaneously reduced to xanthate according to the scheme:

[1] $$2R{-}O{-}\overset{\overset{S}{\|}}{C}{-}S{-}S{-}\overset{\overset{S}{\|}}{C}{-}O{-}R + 4OH^- \rightarrow 2R{-}O{-}\overset{\overset{S}{\|}}{C}{-}S^- + 2H_2O + O_2$$

Tipman (2), on the other hand, has postulated that dixanthogen decomposes as follows:

[2] $$R{-}O{-}\overset{\overset{S}{\|}}{C}{-}S{-}S{-}\overset{\overset{S}{\|}}{C}{-}O{-}R + OH^- \rightarrow R{-}O{-}\overset{\overset{S}{\|}}{C}{-}S{-}OH + R{-}O{-}\overset{\overset{S}{\|}}{C}{-}S^-$$

In this work we intend to demonstrate that the spontaneous decomposition of dixanthogen in aqueous solution is far more complex than the mechanism proposed by both Pomianowski and Tipman.

One of the main difficulties encountered when dealing with aqueous solutions of dixanthogen is its high insolubility in water. We have solved this problem by adding cetyl trimethylammonium bromide (CTA) to the system. This cationic detergent in its micellar form can solubilize dixanthogen or any other hydrophobic compound. One also would expect the CTA micelles to be capable of inhibiting the chemical decomposition of dixanthogen as a result of the solubilization phenomenon.

Experimental

Aged butyl dixanthogen, $(BuX)_2^a$, was prepared by oxidizing an aqueous solution of potassium butyl xanthate with iodine (1). The product was extracted with ether, the ether evaporated off, and the yellowish oily liquid obtained was stored in a closed tube for more than one month before using it. Dixanthogen thus prepared was dissolved in dioxane and 0.01 ml of this solution was added to a cell of 1 cm path length containing 3 ml of solution at the given p*H* and CTA concentration. The solutions were buffered with 0.01 *M* sodium borate and the p*H* adjusted by adding NaOH or HCl. The reaction was followed at 25 °C and at 350 nm in a Beckman DU-2 spectrophotometer and the spectra were obtained either on this instrument operated manually (Figs. 3 and 4) or on a Zeiss PM QII spectrophotometer (Fig. 1).

Fresh butyl dixanthogen, $(BuX)_2^f$, was prepared in exactly the same way as the $(BuX)_2^a$ but it was used no more than 1 h after its preparation. We shall also give

[1]Present address: Université Libre de Bruxelles, Faculté des Sciences, Brussels, Belgium.

Can. J. Chem. Downloaded from www.nrcresearchpress.com by 210.87.254.42 on 09/05/12
For personal use only.

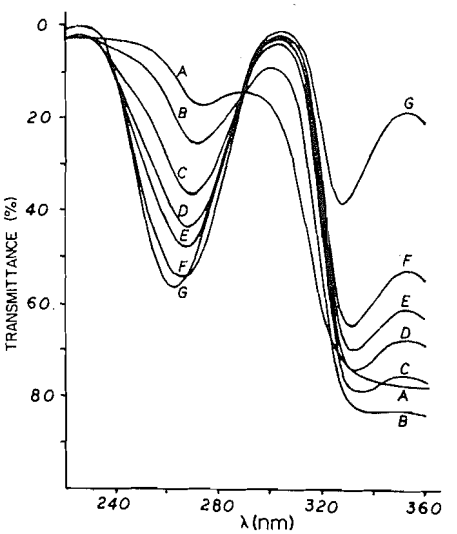

FIG. 1. Spectra after the addition of $(BuX)_2^a$ dissolved in dioxane to a 0.01 *M* CTA solution at p*H* 10.5. Curve A: spectrum immediately after the mixing. Curves B,C,D,E,F, and G, spectra at 3,5,7,11,17, and 25 min after the mixing.

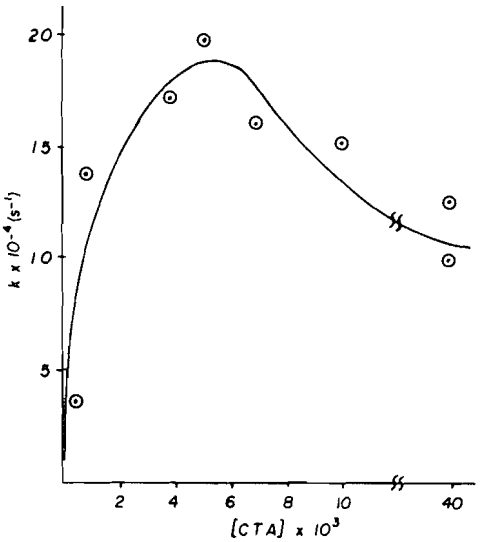

FIG. 2. First-order rate constants for the decomposition of $(BuX)_2^a$ as a function of the concentration of CTA at p*H* 10.5.

the name $(BuX)_2^f$ to the reagent prepared *in situ* in the spectrophotometer cell as will be described below.

CTA was purified by recrystallization from ethanol–ether solutions. Unless otherwise stated all the experiments were carried out in 0.01 *M* CTA solution at p*H* 10.5.

Results and Discussion

Figure 1 shows several spectra obtained at different times after the addition of $(BuX)_2^a$ to a solution of CTA. An unexpected band at 350 nm is observed which increases in intensity from Curve A to G. No mechanism known for the decomposition of dixanthogen can explain the appearance of this band. The first order rate constants for the appearance of the compound absorbing at 350 nm are shown in Fig. 2 as a function of the concentration of CTA. It is observed that CTA catalyzes the reaction from concentrations near to its CMC (8×10^{-4} *M*). The decrease of the rate beyond certain concentrations of micelles has been interpreted as a characteristic behavior of bimolecular reactions due to the decrease in the surface concentration of reactants as the concentration of micelles increase (3). It is interesting to note that CTA micelles enhance the rate of the reaction rather than depress it. Dixanthogen is highly hydrophobic and one would have expected that it would be incorporated inside the micelle to avoid the attack of water or hydroxyl ions.

When $(BuX)_2^f$ was added to a CTA solution it was found that the rate of appearance of the band at 350 nm was about 500 fold less than for $(BuX)_2^a$ (a half life of 51 h as compared to 6 min). This difference was more obvious when enough iodine was added to a xanthate–CTA solution contained in the spectrophotometer cell to oxidize all the xanthate. The spectra of this solution at different times after the addition of iodine were very similar to those shown in Fig. 1 in the region below 320 nm. However no band was observed at 350 nm even after 4 h.

One further difference between $(BuX)_2^a$ and $(BuX)_2^f$ was found when the spectra of their reaction products were compared before and after acidification with a drop of concentrated HCl (Fig. 3). The spectra of the products differ mainly by the band at 350 nm presented by the products of $(BuX)_2^a$ (curve A and A′). This band disappeared after acidification giving in turn a band at about 300 nm (curve B′). The big band at 300 nm of both dixanthogen products also disappeared after acidification. On the other hand, the acid solution of $(BuX)_2^f$ gave no band at about 300 nm (curve B). This behavior could be interpreted by assuming that the compound absorbing at 350 nm gave, after decomposition in acid media, a new one absorbing at 300 nm. This hypothesis was confirmed after measuring the absorbances of samples withdrawn at differ-

Can. J. Chem. Downloaded from www.nrcresearchpress.com by 210.87.254.42 on 09/05/12
For personal use only.

Can. J. Chem. Downloaded from www.nrcresearchpress.com by 210.87.254.42 on 09/05/12
For personal use only.

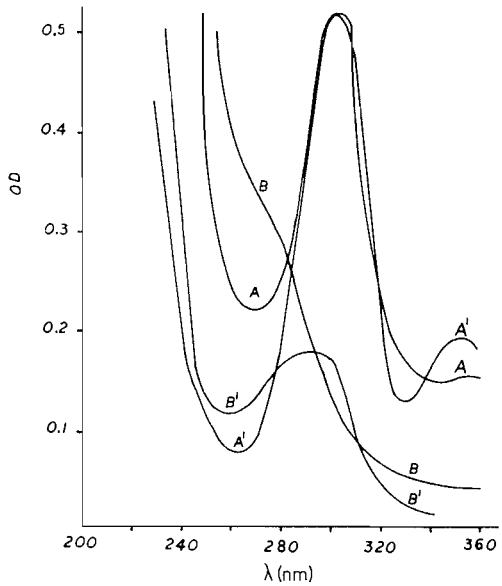

FIG. 3. Spectra of decomposed butyl dixanthogen in a 0.01 *M* CTA solution at p*H* 10.5. Curves A and A': spectra of decomposed $(BuX)_2^f$ and $(BuX)_2^a$. Curves B and B': spectra of decomposed $(BuX)_2^f$ and $(BuX)_2^a$ after acidification.

ent times from a $(BuX)_2^f$–CTA solution. Each sample was read at 350 nm before acidification and at 300 nm after acidification. The plot of one absorbance against the other gave a straight line suggesting a close correspondence between the compound absorbing at 350 nm and the one appearing in acid media. No xanthate can be present in acid solution (4) so decomposition of butyl dixanthogen gives products which are not necessarily xanthates. A similar conclusion was achieved when a portion of a solution containing the products of the reaction of $(BuX)_2^a$ was extracted with chloroform and the other portion acidified with concentrated HCl. The spectra of the chloroform phase, its aqueous residue and the acidified portion are shown in Fig. 4. Almost all the absorbing products are extracted by chloroform, with the aqueous fraction exhibiting only a small absorption at 350 nm. If butyl xanthate were a product of the reaction it would be present in the aqueous phase with its characteristic band at 301 nm. In the acidified portion we found, as before (Fig. 3), that the compound absorbing at 350 nm disappeared yielding the one stable in acid media with a band at about 300 nm.

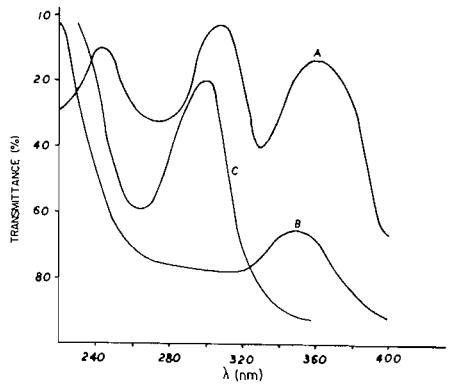

FIG. 4. Spectra of decomposed $(BuX)_2^a$ in a 0.01 *M* CTA solution at p*H* 10.5 after extraction with chloroform. Curve A: chloroform phase. Curve B: aqueous phase. Curve C: acidified portion of the decomposed solution.

One of the probable mechanisms that can be proposed in order to account for the present results is the following:

[3] $(BuX)_2 \xrightarrow{k_1} Y$ (non aqueous solvent or micellar phase)

[4] $(BuX)_2 \xrightarrow{k_2}$ 300 nm band plus deep minima at 270 nm (aqueous detergent solution)

[5] $Y \xrightarrow{k_3}$ 350 nm band $\xrightarrow[H^+]{k_4}$ 300 nm band (aqueous detergent solution)

where Y would be a compound that would be formed slowly at a rate k_1 while dixanthogen is stored pure or dissolved in a non polar solvent. Y also would be formed in the interior of micelles at the rate k_1; its decomposition, to give the 350 nm absorbing compound, would be strongly catalyzed by CTA micelles and highly p*H* dependent. It would also be required that $k_2 \gg k_1$, $k_3 \approx k_2$, and $k_3 \gg k_1$. According to this scheme the rates shown in Fig. 2 correspond to k_3, and the rate which we have referred to as having a half life of $\sim$51 h corresponds to k_1 because this would be the rate determining step when reactions 3 and 5 are occurring simultaneously, *i.e.* when fresh butyl dixanthogen is added to the aqueous CTA solution.

Finally, we can conclude that (*a*) decomposition of dixanthogen begins just after its prepara-

tion, and (*b*) under the conditions studied, xanthate is not a product of the decomposition of dixanthogen. Other compounds are formed.

Acknowledgment

Support of this work by the Oficina Técnica de Desarrollo Científico y Creación Artística de la Universidad de Chile and The Fund for Overseas Research Grant Education is gratefully acknowledged.

1. A. POMIANOWSKI and J. LEJA. Can. J. Chem. **41**, 2219 (1963).
2. N. R. TIPMAN. Ph.D. Thesis. The University of British Columbia, Vancouver, B.C. 1970.
3. C. A. BUNTON. Reaction kinetics in micelles. *Edited by* E. Cordes. Plenum Press, New York. 1973.
4. C. A. BUNTON, P. NG, and L. SEPULVEDA. J. Org. Chem. **39**, 1130 (1974).

Can. J. Chem. Downloaded from www.nrcresearchpress.com by 210.87.254.42 on 09/05/12
For personal use only.

Linear oligopeptides. XXVII.[1] Contribution to the circular dichroism of internal peptide chromophores

CLAUDIO TONIOLO AND GIAN MARIA BONORA

Institute of Organic Chemistry, University of Padova, 35100 Padova, Italy, and Center for the Study of Biopolymers, C.N.R., 35100 Padova, Italy

Received June 5, 1975

CLAUDIO TONIOLO and GIAN MARIA BONORA. Can. J. Chem. **54**, 70 (1976).

The contribution to the circular dichroism of L-Ala-L-Ala, L-Nva-L-Nva, L-Val-L-Val, L-Leu-L-Leu, L-Ile-L-Ile, L-Cys(Me)-L-Cys(Me), L-Met-L-Met, and L-Phe-L-Phe internal peptide chromophores in 1,1,1,3,3,3-hexafluoropropan-2-ol were calculated by subtracting the total molar ellipticity values of N- and C-protected homo-trimers from those of the pertinent protected homo-tetramers.

The circular dichroism of the internal peptide chromophore of aliphatic hydrocarbon- and sulfur-containing peptides, each of the L-configuration, show a negative band at 215–230 nm accompanied by a more intense negative band near 200 nm. A structured weak and negative band near 260 nm along with bands at 240 nm (negative), 222 nm (positive), and 210.5 nm (negative) of progressively increasing intensity are apparent in the circular dichroic spectrum of L-Phe-L-Phe internal peptide chromophore. The effect of solvent polarity is discussed in the case of L-Val-L-Val and L-Ala-L-Ala internal peptide chromophores.

Among the protected homo-trimers and tetramers only those of L-alanine are soluble in aqueous solution; consequently, the effect of water as a function of temperature, urea, and guanidinium chloride on the L-Ala-L-Ala internal peptide chromophore circular dichroism was established.

CLAUDIO TONIOLO et GIAN MARIA BONORA. Can. J. Chem. **54**, 70 (1976).

On a calculé la contribution des chromophores peptidiques internes au dichroïsme circulaire de L-Ala-L-Ala, L-Nva-L-Nva, L-Val-L-Val, L-Leu-L-Leu, L-Ile-L-Ile, L-Cys(Me)-L-Cys(Me), L-Met-L-Met et L-Phe-L-Phe dans l'hexafluoro-1,1,1,3,3,3 propanol-2 en soustrayant les valeurs de l'ellipticité molaire totale des homo trimères N- et C-protégés de celles des homo tétramères protégés appropriés.

Le dichroism circulaire des chromophores peptidiques internes de peptides, chacun de configuration L, contenant un hydrocarbure aliphatique ou de soufre montre une bande négative plus intense près de 200 nm. Une faible bande structurée et négative près de 260 nm de même que des bandes à 240 nm (négative), 222 nm (positive) et 210.5 nm (négative) d'intensité croissant progressivement sont apparentes dans le spectre de dichroïsme circulaire du chromophore peptidique interne de la L-Phe-L-Phe. On discute de l'effet de la polarité du solvant dans le cas des chromophores peptidiques internes des L-Val-L-Val et L-Ala-L-Ala.

Parmi les homo trimères et tétramères protégés seulement ceux de la L-alanine sont solubles dans des solutions aqueuses; par conséquent l'effet de l'eau en fonction de la température, l'effet de l'urée et du chlorure de guanidinium sur le dichroïsme circulaire du chromophore peptidique interne du L-Ala-L-Ala a pu être établi.

[Traduit par le journal]

Introduction

Recently, work has been carried out with the explicit purpose of determining the circular dichroism (cd) spectra to 190 nm of amino acid residues (2) or peptide chromophores[2] occupying an internal position in a randomly coiled polypeptide chain.[3]

The present work represents an extension of this approach in which we describe the cd contribution to 190 nm of L-Ala-L-Ala, L-Nva-L-Nva, L-Val-L-Val, L-Leu-L-Leu, L-Ile-L-Ile, L-Cys(Me)-L-Cys(Me), L-Met-L-Met, and L-Phe-

[1]For the previous paper in this series see ref. 1.

[2]W. L. Mattice and W. H. Harrison III, personal communication to one of us (C.T.).

[3]The following abbreviations were used in the text: cd, circular dichroism; ord, optical rotatory dispersion; BOC, *tert*-butyloxycarbonyl; MEEA, 2-methoxy-[2-ethoxy-(2-ethoxy)]-acetyl; Ac, acetyl; OMe, methyl ester; Mo, morpholine amide; HFIP, 1,1,1,3,3,3-hexafluoropropan-2-ol; TFE, 2,2,2-trifluoroethanol; MeOH, methanol; EtOH, ethanol; PrOH, *n*-propanol; BuOH, *n*-butanol; TFA, trifluoroacetic acid; GuHCl, guanidinium chloride; Gly, glycine; Ala, alanine; Nva, norvaline; Val, valine; Leu, leucine; Ile, isoleucine; Cys(Me), *S*-methylcysteine; Met, methionine; Phe, phenylalanine.

Can. J. Chem. Downloaded from www.nrcresearchpress.com by 210.87.254.5 on 09/05/12
For personal use only.

Can. J. Chem. Downloaded from www.nrcresearchpress.com by 210.87.254.5 on 09/05/12
For personal use only.

L-Phe internal peptide chromophores. Temperature and solvent effects were also examined.

Experimental

Synthesis of Peptides

The BOC—(L—X)$_3$—OMe were synthesized from BOC—L—X—OH and H—(L—X)$_2$—OMe by the dicyclohexylcarbodiimide method (4, 5); the BOC—(L—X)$_4$—OMe were synthesized from BOC—(L—X)$_2$—$NHNH_2$ and H—(L—X)$_2$—OMe by the modified acid azide method (6). The detailed description of the various preparations, along with the elemental analytical data and physical properties of all trimers and tetramers, were reported in previous papers (7–14). The characterization of these compounds gave evidence of their chemical and optical purities.

Measurements of Circular Dichroism

Circular dichroism spectra were recorded using a Cary Model 61 circular dichroic spectrophotometer. The spectra were obtained using cylindrical fused quartz cells of 0.5 mm, 1 mm, and 10 mm path-lengths. Dry prepurified nitrogen was employed to keep the instrument oxygen-free during the experiments. A complete base line was recorded for every measurement using the same cell in which the sample had been replaced with solvent. The calibration was based upon $[\theta]_{290} = 7.840$ deg·cm^2 dmol^{-1} for a purified sample at *d*-10-camphorsulfonic acid (Fluka, Buchs) in 0.1% aqueous solution (15). The temperature was controlled by circulating water from a constant temperature bath through a hollow metal cell holder. The temperature in the cell was determined using a Philips thermistor. No thermal degradation of the sample occurred, as shown by regeneration of the original spectra upon cooling. Solutions of 10^{-2} to 10^{-3} *M* peptide were prepared by placing the weighed peptide in a volumetric flask and adding the appropriate solvent. Whenever a solution was diluted, the spectra of the concentrated and dilute solutions were measured in overlapping regions of the spectrum. The cd properties were independent of peptide concentration in every case. The cd data employed in the computations represent average values from at least four recordings. The values for each oligomer were calculated on a total molar ellipticity basis (the molecular weight of each compound was used for the computations, not that of the constituent amino acid residue). Then, the total molar ellipticity values of BOC—(L—X)$_3$—OMe were subtracted from those of the pertinent BOC—(L—X)$_4$—OMe giving the ellipticity/mol of peptide chromophore, $[\theta]_R$:

$$[\theta]_R = [\theta]_{\text{BOC-(X)}_4\text{-OMe}} - [\theta]_{\text{BOC-(X)}_3\text{-OMe}}$$

where

$$[\theta]_{\text{BOC-(X)}_n\text{-OMe}} = \frac{100 \times \text{measured ellipticity (deg)}}{\text{cell path (cm)} \times \text{molar concentration of BOC—(X)}_n\text{—OMe}}$$

The Lorentz refractive index correction was not applied (15).

The solvents used for the cd measurements were TFE (Fluka, Buchs), HFIP (Du Pont and Company, Wilmington, Del.), MeOH (Merck A.G., Darmstad), EtOH, *n*-PrOH, and *n*-BuOH (Erba, Milan), and double distilled water. All solvents were of the highest purity commercially available and were used without further purification. Urea (16) and GuHCl (17) were purchased from Fluka (Buchs) and purified in the standard conditions.

Results and Discussion

Brand and Erlanger in 1950 first suggested that each kind of amino acid residue in a polypeptide chain should have a characteristic residue optical activity at any wavelength, and that the molar optical activity of a randomly coiled polypeptide chain should just be the sum of the intrinsic residue optical activities of the constituent amino acids (18). They also made the first systematic study of D-line rotations of various series of oligopeptides (19). Later on, Tanford and co-workers were able to demonstrate that the amino acid composition affects the ord properties from unordered regions of protein chains (20). The approach of Brand and co-workers (18, 19) was extended by Beacham *et al.* (21), Schechter and Berger (22) and Beecham (23).

It should be stressed that studies in this area have dealt almost exclusively with ord. Also, usually the measurements did not penetrate in the region of $\pi \rightarrow \pi^*$ peptide transition (24). Notwithstanding the well-established superiority of cd over ord and the relevant amount of information which one can obtain from the spectral region below 220 nm (24) only two papers have appeared with the explicit purpose of determining the cd spectra to 190 nm of amino acid residues (2) or peptide chromophores[2] occupying an internal position in a randomly coiled polypeptide chain.

As correctly pointed out by Schechter and Berger (22), although the Brand and co-workers treatment (18, 19) describes the situation fairly well, it clearly represents an oversimplification of the problem. In fact, it introduces an artificial concept, namely a residue optical activity as an additive parameter assigned to an asymmetric carbon atom. Since the chirospectroscopic properties of peptide molecules derive mainly from the contribution of their amide (peptide) chromophores, it is more correct to assign additive optical activity parameters to these chromo-

Can. J. Chem. Downloaded from www.nrcresearchpress.com by 210.87.254.5 on 09/05/12
For personal use only.

phores. Therefore, the concept of a 'peptide chromophore parameter' should be introduced as defined by the two amino acid residues forming the peptide bond.

Thus, in a cd study the total molar ellipticity of a randomly coiled polypeptide chain must be represented at any wavelength by an equation of the form.

$$[\theta]_T = \sum_i n_i[\theta]_R$$

where n_i is the number of peptide chromophores of type i, and $[\theta]_R$ the intrinsic (internal and terminal) peptide chromophore ellipticity.

In this paper we illustrate the intrinsic cd to 190 nm for L-Ala-L-Ala, L-Nva-L-Nva, L-Val-L-Val, L-Leu-L-Leu, L-Ile-L-Ile, L-Cys(Me)-L-Cys(Me), L-Met-L-Met, and L-Phe-L-Phe internal peptide chromophores. To calculate the internal $[\theta]_R$ values we subtracted the total molar ellipticity values of N- and C-blocked homo-tripeptides from those of corresponding homotetrapeptides. This approach is analogous to that described by Schechter and Berger (22) (see their β_3 parameter). For this study we used the *tert*-butyloxycarbonyl as the N-protecting group and the methyl ester as the C-protecting group for practical reasons connected with the synthesis of peptides. The contribution to cd of the urethane and ester chromophores was eliminated in using our treatment. The influence of charged terminal groups, which are known to affect the environment of a peptide chromophore at some distance into the chain (2), was also removed.

The present method of analysis, which makes use of tripeptides and tetrapeptides, can be considered as the simplest method giving $[\theta]_R$ values of internal peptide chromophores. In this connection it should be recalled that terminal peptide chromophores of a chain are solvated differently from internal peptide chromophores and consequently may have different cd properties (20, 25).

The cd contribution of internal peptide chromophores can be influenced, even in a statistically unordered conformation, by the nature of the residues immediately adjacent to them (2, 20). Thus, the cd patterns of the various internal peptide chromophores described in this paper represent rigorously only those of the corresponding homo-polypeptides in a randomly coiled conformation (usually expressed as mean residue ellipticity), provided solvent and temperature are the same. Consequently, the extension of our results to protein chains should be considered as an approximation.

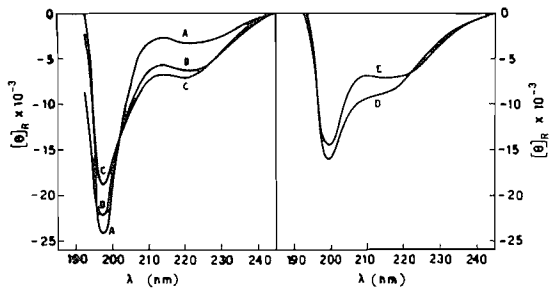

FIG. 1. Circular dichroism of L-Ala-L-Ala (*A*), L-Leu-L-Leu (*B*), L-Nva-L-Nva (*C*), L-Val-L-Val (*D*), and L-Ile-L-Ile (*E*) internal peptide chromophores in HFIP at 21 °C.

Our approach has also the disadvantage that the $[\theta]_R$ values of the internal peptide chromophores studied here, with the only exception of L-Ala-L-Ala, could not be obtained in water solution because of the poor solubility of the various homotrimers and homo-tetramers in this solvent.

A summary of the pertinent data which we have been able to find is given in Figs. I–4 and discussed below.

A. Studies in HFIP

HFIP, a highly fluorinated alcohol, is a weak acid with a pK_a of 9.30 (26). This solvent does not support ordered secondary structures in short oligopeptides (1, 9–11, 27–29). Clearly, protonation of the peptide backbone is ruled out in HFIP; but the competitive hydrogen bonding of this structure-disrupting solvent to the receptive sites of amide groups of peptide molecules largely determines its solvent power. Therefore the conformation of oligopeptides in HFIP is assumed to be a solvated unordered coil. For this reason and because of its transparency in the ultraviolet region to 190 nm (30, 31) it was employed in our cd study.

Internal Peptide Chromophore Circular Dichroism of Peptides Containing Aliphatic Hydrocarbon Side Chains

The cd spectra of L-Ala-L-Ala, L-Nva-L-Nva, and L-Leu-L-Leu internal peptide chromophores are characterized by two negative bands of different intensities centered at about 220 nm ($n \rightarrow \pi^*$ amide transition) (24) and 198 nm ($\pi \rightarrow \pi^*$ amide transition) (24), respectively (Fig. 1). The $[\theta]_{220}/[\theta]_{197.5}$ ratios range from 0.13

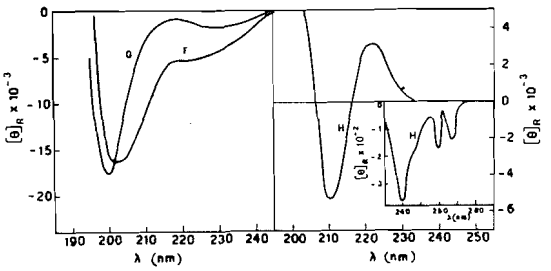

FIG. 2. Circular dichroism of L-Cys(Me)-L-Cys(Me) (*F*), L-Met-L-Met (*G*), and L-Phe-L-Phe (*H*) internal peptide chromophores in HFIP at 21 °C.

for L-Ala-L-Ala to 0.38 for L-Nva-L-Nva. In all cases the ellipticity is negative from 250 to 192 nm.

A similar general trend is observed for the cd of internal peptide chromophores of β-branched aliphatic hydrocarbon peptides (Fig. 1). However, in these cases the two dichroic bands are located near 215 nm and at 200 nm, respectively. Also, the $[\theta]_{215}/[\theta]_{200}$ ratios are considerably higher than those above reported for L-Ala-L-Ala, L-Nva-L-Nva, and L-Leu-L-Leu, being situated in the range 0.50–0.60. This latter finding is mainly due to the fact that the negative $\pi \rightarrow \pi^*$ cd band is much less intense for L-Val-L-Val and L-Ile-L-Ile.

It is also of interest that the L-Ala-L-Ala cd above 195 nm is definitely the least negative among those shown in Fig. 1.

Internal Peptide Chromophore Circular Dichroism of Sulfur-containing Peptides

The cd curves of L-Met-L-Met and L-Cys(Me)-L-Cys(Me) internal peptide chromophores are illustrated in Fig. 2. The L-Met-L-Met cd closely resembles those of aliphatic hydrocarbon peptides discussed above. Two negative bands are visible at 228 nm and 200 nm, respectively. The $[\theta]_{228}/[\theta]_{200}$ ratio (0.10) is near that of L-Ala-L-Ala.

Also the cd spectrum of L-Cys(Me)-L-Cys(Me) is always negative above 196 nm. But, its pattern presents a distinctive mark in the pronounced broadness of the $\pi \rightarrow \pi^*$ band. The $[\theta]_{220}/[\theta]_{203}$ ratio (0.34) approximates that of isosteric L-Nva-L-Nva.

In discussing the cd of sulfur-containing peptides attention should be drawn to the fact that the thioether chromophore also absorbs in the 190–250 nm region. Actually, a number of uv absorption bands have been reported for this chromophoric group and their assignments discussed (32). Furthermore, several bands are present in the cd spectrum of *S*-methylcysteine, whereas the curve of methionine is much simpler (32). In particular, the strong 220 nm band of *S*-methylcysteine, assigned to a transition of the sulfur atom dissymmetrically perturbed by the centre at C-2, is not observed in the spectrum of methionine. In this context it is significant that in methionine the sulfur chromophore is separate from the asymmetric carbon atom by one more methylene groups than in *S*-methylcysteine.

L-Phe-L-Phe Internal Peptide Chromophore Circular Dichroism

Among the internal peptide chromophores of aromatic peptides, we have investigated L-Phe-L-Phe which contains benzylic side chains (Fig. 2).

In the 280–235 nm region a structured weak and negative band at about 260 nm is apparent in the L-Phe-L-Phe internal peptide chromophore cd (24, 33, 34), corresponding to the $^1B_{2u} \leftarrow {}^1A_{1g}$ benzene transition in the Platt notation (35). The negative band at approximately 240 nm, which does not have any counterpart in the uv absorption spectrum of phenylalanine peptides (8), is assigned to an overlapping of the two more intense short-wavelength bands of opposite sign. These latter Cotton effects are both associated with contributions from peptide and benzyl chromophores.

The most interesting feature of L-Phe-L-Phe internal peptide chromophore cd resides undoubtedly in the strong *positive* dichroism exhibited in the 230–217 nm region and below 207 nm (2, 20). Consequently, the cd curve of a peptide molecule abundant in L-Phe-L-Phe bonds will reflect these properties and exhibit a pattern below 230 nm much less negative than those of polypeptides devoid of this aromatic sequence.

B. Studies in Various Alcohols

The effect of solvent polarity was examined in some detail in the case of L-Val-L-Val, and a number of alcohols, the polarity of which ranges from BuOH to HFIP, were used for this investigation. The resulting composite internal peptide chromophore cd is shown in Fig. 3. As for HFIP (Fig. 1) the cd pattern is characterized by a pronounced negative shoulder at approximately 215 nm followed by a more intense maximum of the same sign near 200 nm. In the spectral region examined (250–195 nm) the ellip-

Can. J. Chem. Downloaded from www.nrcresearchpress.com by 210.87.254.5 on 09/05/12
For personal use only.

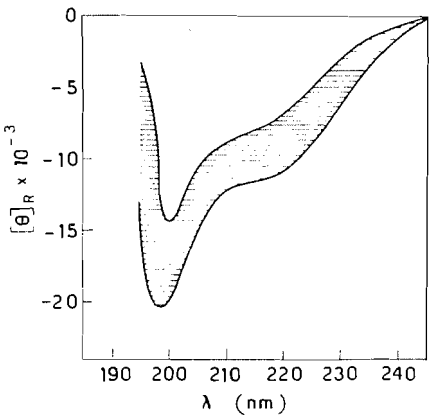

FIG. 3. Composite circular dichroism curves of L-Val-L-Val internal peptide chromophore in HFIP, TFE, MeOH, EtOH, PrOH, BuOH at 21 °C.

ticity is always largely negative. We were not able to observe any distinct trend on gradually changing the solvent polarity.

C. Studies in Aqueous Solution

Norvaline, valine, leucine, isoleucine, methionine, *S*-methylcysteine, and phenylalanine homo-trimers and homo-tetramers exhibit poor solubility in water, so that we were forced to confine our cd study in aqueous solution exclusively to the L-Ala-L-Ala internal peptide chromophore (Fig. 4).

The L-Ala-L-Ala cd curve in water at ambient temperature presents a large negative maximum at 195 nm accompanied by a less intense *positive* maximum at 219 nm. An additional extremely small Cotton effect (negative) is visible near 235 nm. The differences between this spectrum and the corresponding one in HFIP are marked above 210 nm. In particular, the main feature distinguishing the cd in water is represented by the *positive* dichroism in the 212–230 nm region.

The temperature effect on L-Ala-L-Ala internal peptide chromophore cd is also illustrated in Fig. 4. At 65 °C the spectral region of *positive* dichroism disappears and the cd above 230 nm also becomes more negative. Interestingly enough, these findings do not seem to be associated with an increase in the negative ellipticity of the high-energy $\pi \rightarrow \pi^*$ band with increasing temperature. Actually, just the opposite was observed.

At variance with the behavior as a function of temperature, the gross features of L-Ala-L-Ala cd at 21 °C are essentially unaffected in 8 *M* urea or 6 *M* GuHCl (Fig. 4).

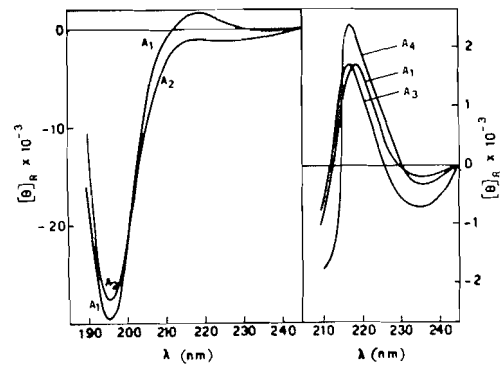

FIG. 4. Circular dichroism of L-Ala-L-Ala internal peptide chromophore in water at 21 °C (A_1), in water at 65 °C (A_2), in 8 *M* urea at 21 °C (A_3), and in 6 *M* GuHCl at 21 °C (A_4).

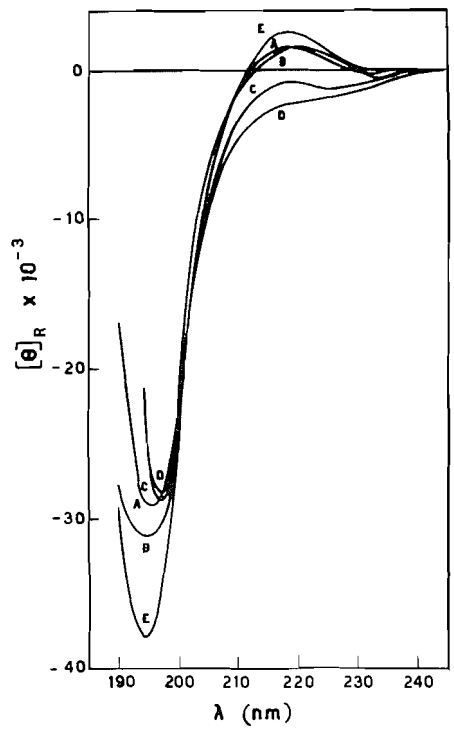

FIG. 5. Circular dichroism of L-Ala-L-Ala internal peptide chromophore in water at room temperature: *A*, this work; *B*, calculated from Fig. 11 in ref. 36; *C*, from Gly_2-Ala_2-Gly_2 (ref. 2); *D*, from Gly_2-Ala-Gly_2 (ref. 2); *E*, from Ac—$(Ala)_{3-4}$—OMe.[2] The various curves are not directly comparable (see text for a discussion).

Figure 5 compares the L-Ala-L-Ala internal peptide chromophore cd in water shown in Fig. 4 with those reported by Lord and Cox (2) and Mattice and Harrison,[2] and with that calculated by us from Fig. 11 in ref. 36.

Can. J. Chem. Downloaded from www.nrcresearchpress.com by 210.87.254.5 on 09/05/12
For personal use only.

Can. J. Chem. Downloaded from www.nrcresearchpress.com by 210.87.254.5 on 09/05/12
For personal use only.

It should be noted that Mattice and Harrison[2] measured the cd properties of the series Ac—(Ala)$_n$—OMe, while Goodman and coworkers (36) examined a similar series, namely MEEA—(Ala)$_n$—Mo. Also, the approach used by Mattice and Harrison[2] is strictly analogous to that employed by us in the calculation of L-Ala-L-Ala cd from BOC—(Ala)$_n$—OMe (this paper) and MEEA—(Ala)$_n$—Mo (36). Thus, it is not surprising that the cd patterns reported in Fig. 5 (curves *A*, *B*, and *E*) are quite similar. In particular, the *positive* Cotton effect at 216–219 nm and the large negative Cotton effect at 194–196 nm are present in all cases. The 20% difference in ellipticity found below 200 nm could be reasonably ascribed to the relatively low signal to noise ratios exhibited by the oligopeptides in that spectral region.

The method employed by Lord and Cox (2) is different in the sense that they calculate the cd of an internal L-alanine residue (not of an L-Ala-L-Ala internal peptide chromophore) by measuring the cd curves of the unblocked Gly_2-L-Ala-Gly_2 and Gly_2-L-Ala_2-Gly_2 (in the latter case the experimental values were divided by the number of optically active residues in the peptide). In fact, according to Lord and Cox (2), two glycyl residues are required to remove charge effects of α-carboxyl or α-amino groups. Their data are shown in Fig. 5 (curves *C* and *D*). It is noteworthy that in both cases the dichroism is always negative; however, the spectrum from Gly_2-L-Ala_2-Gly_2 is different from that of Gly_2-L-Ala-Gly_2 in the sense that in the former the ellipticity above 205 nm is clearly less negative, thereby approaching more closely that of curves *A*, *B*, and *E*. This latter finding illustrates well the fact that the intrinsic peptide chromophore cd can be influenced, even in a statistical coil conformation, by the nature of the amino acid residues immediately adjacent to it. In addition, it is of interest that if one subtracts the spectrum of Gly_2-L-Ala-Gly_2 from that of Gly_2-L-Ala_2-Gly_2 a *positive* dichroism is apparent in that region around 215–220 nm (2).

We believe that at the present stage of the research in this area it is impossible to indicate conclusively the origin of the *positive* dichroism. In fact, *inter alia* the assignment of the electronic transition responsible is still a matter of controversy (37). In any case our cd results on short, unionized alanine derivatives substantiate previous findings (2, 37)[2] that it is definitely not essential to claim the occurrence of ordered secondary structures for explaining the onset of a *positive* ellipticity near 215–220 nm (38–40).

As far as the temperature dependence of the L-Ala-L-Ala cd is concerned, in accordance with Mattice (37)[2] we assign it to the increasing population of the higher energy rotamers of the conformational map as the temperature increases. Also, our results, indicating a very small effect of 8 *M* urea and 6 *M* GuHCl on the chirospectroscopic properties of oligopeptides without charged side chains, parallel previous findings reported by Hooker (41). In this context it should be recalled that little difference is apparent in the cd of rigid bicyclic lactams in water and in 8 *M* urea (42). In addition, these data exclude a change in association as a factor responsible for the observed temperature effect.

The cd spectrum of poly-L-alanine in the solvated randomly coiled conformation in 100% TFA is always negative in the 190–250 nm region (3, 43), closely resembling that of L-Ala-L-Ala internal peptide chromophore in HFIP shown in Fig. 1. On the contrary, the cd spectrum of L-Ala-L-Ala internal peptide chromophore in water exhibits *positive* ellipticity around 215–220 nm (Fig. 4). We interpret this solvent dependence as arising from simultaneous conformational and solvation processes; however, invoking the occurrence of preferred conformations (38–40) is absolutely not required by the above statement.

Finally, it is of interest to note that a *positive* dichroism around 215 nm is also exhibited by an internal L-glutamyl residue (2) and an L-Lys-L-Lys internal peptide chromophore[2] in water, but only in the p*H* regions where the side chains are ionized.

1. C. Toniolo and G. M. Bonora. J. Polym. Sci. C. In press.
2. R. S. Lord and D. J. Cox. Biopolymers, **12**, 2359 (1973).
3. G. P. Lorenzi, G. Greco, and R. Mona. Biopolymers, **14**, 237 (1975).
4. J. C. Sheehan and G. P. Hess. J. Am. Chem. Soc. **77**, 1067 (1955).
5. H. G. Khorana. Chem. Ind. (London), 1087 (1955).
6. J. Honzl and J. Rudinger. Collec. Czech. Chem. Commun. **26**, 2333 (1961).
7. C. Toniolo. Biopolymers, **10**, 1707 (1971).
8. C. Toniolo and G. M. Bonora. Bioorg. Chem. **3**, 114 (1974).

9. C. TONIOLO, G. M. BONORA, and A. FONTANA. Int. J. Pept. Protein Res. **6**, 371 (1974).
10. G. M. BONORA and C. TONIOLO. Biopolymers, **13**, 2179 (1974).
11. G. M. BONORA, A. MAGLIONE, and C. TONIOLO. Polymer, **15**, 767 (1974).
12. G. M. BONORA, D. NISATO, and C. TONIOLO. Makromol. Chem. In press.
13. G. M. BONORA, A. MAGLIONE, A. FONTANA, and C. TONIOLO. Bull. Soc. Chim. Belges, **84**, 299 (1975).
14. G. M. BONORA, A. MAGLIONE, and C. TONIOLO. Gazz. Chim. Ital. **176**, 2535 (1975).
15. A. J. ADLER, N. J. GREENFIELD, and G. D. FASMAN. *In* Methods in enzymology. Vol. XXVII, part D. *Edited by* C. H. W. Hirs and S. N. Timasheff. Academic Press, New York. 1973. p. 675.
16. Y. SCHECHTER, A. PATCHORNIK, and Y. BURSTEIN. Biochemistry, **12**, 3407 (1973).
17. Y. NOZAKI and C. TANFORD. J. Am. Chem. Soc. **89**, 736 (1967).
18. E. BRAND and B. F. ERLANGER. J. Am. Chem. Soc. **72**, 3314 (1950).
19. E. BRAND, B. F. ERLANGER, J. POLATNICK, H. SACHS, and D. KIRSCHENBAUM. J. Am. Chem. Soc. **73**, 4027 (1951), and previous papers in this series.
20. C. TANFORD, K. KAWAHARA, S. LAPANJE, T. M. HOOKER, JR., M. H. ZARLENGO, A. SALAHUDDIN, K. C. AUNE, and T. TAKAGI. J. Am. Chem. Soc. **89**, 5023 (1967).
21. J. BEACHAM, V. T. IVANOV, P. M. SCOPES, and D. R. SPARROW. J. Chem. Soc. C, 1449 (1966).
22. I. SCHECHTER and A. BERGER. Biochemistry, **5**, 3362 (1966).
23. A. F. BEECHAM. Tetrahedron Lett. 211 (1967), and previous papers in this series.
24. M. GOODMAN and C. TONIOLO. Biopolymers, **6**, 1673 (1968).
25. M. LEGRAND and R. VIENNET. C. R. Acad. Sci. **262**, 943 (1966).
26. W. J. MIDDLETON and R. V. LINDSEY, JR. J. Am. Chem. Soc. **86**, 4948 (1964).
27. C. TONIOLO and G. M. BONORA. Makromol. Chem. **176**, 2547 (1975).
28. C. TONIOLO, G. M. BONORA, and A. FONTANA. Bull. Soc. Chim. Belges, **84**, 305 (1975).
29. C. TONIOLO, G. M. BONORA, and A. SCATTURIN. Gazz. Chim. Ital. In press.
30. J. R. PARRISH, JR. and E. R. BLOUT. Biopolymers, **10**, 1491 (1971).
31. J. R. PARRISH, JR. and E. R. BLOUT. Biopolymers, **11**, 1001 (1972).
32. C. TONIOLO and A. FONTANA. *In* The chemistry of the thiol group. *Edited by* S. Patai. J. Wiley and Sons, New York. 1974. p. 355.
33. E. PEGGION, M. PALUMBO, G. M. BONORA, and C. TONIOLO. Bioorg. Chem. **3**, 125 (1974).
34. C. TONIOLO and G. M. BONORA. Gazz. Chim. Ital. **104**, 843 (1974).
35. J. R. PLATT. J. Chem. Phys. **16**, 832 (1948).
36. M. GOODMAN, F. NAIDER, and R. RUPP. Bioorg. Chem. **1**, 310 (1971).
37. W. L. MATTICE. Biopolymers, **13**, 169 (1974).
38. S. KRIMM and M. L. TIFFANY. Isr. J. Chem. **12**, 189 (1974).
39. Y. P. MYER. Macromolecules, **2**, 264 (1969).
40. D. G. DEARBORN and D. B. WETLAUFER. Biochim. Biophys. Res. Commun. **39**, 314 (1970).
41. T. M. HOOKER, JR. Ph.D. Thesis, Duke University. 1966.
42. M. GOODMAN, C. TONIOLO, and J. FALCETTA. J. Am. Chem. Soc. **91**, 1816 (1969).
43. M. GOODMAN, F. TODA, and N. UEYAMA. Proc. Nat. Acad. Sci. USA **70**, 331 (1973).

Can. J. Chem. Downloaded from www.nrcresearchpress.com by 210.87.254.5 on 09/05/12
For personal use only.

Photosensitization by Cd($^3P_{0,1}$) atoms. III. Gas phase decomposition of cyclopentane[1]

BANSI L. KALRA AND ARTHUR R. KNIGHT
Department of Chemistry and Chemical Engineering, University of Saskatchewan, Saskatoon, Saskatchewan S7N 0W0

Received November 16, 1973[2]

BANSI L. KALRA and ARTHUR R. KNIGHT. Can. J. Chem. **54**, 77 (1976).

The triplet cadmium photosensitized decomposition of cyclopentane in the vapor phase has been studied at 355 °C and has been shown to give rise to cyclopentyl radicals and hydrogen atoms with close to unit efficiency in the primary process. Subsequent reactions of these species, including an important contribution from unimolecular decomposition of cyclopentyl radicals, yield the observed volatile products, hydrogen, methane, ethylene, ethane, propylene, and cyclopentene. As a result of significant olefin scavenging of H-atoms product yields are strongly time dependent. The system has been shown to be unaffected by addends. The temperature dependence of the rate of product formation is consistent with the known energetics of cyclopentyl radical decomposition.

BANSI L. KALRA et ARTHUR R. KNIGHT. Can. J. Chem. **54**, 77 (1976).

On a étudié, à 355 °C, la décomposition, photosensibilisée par le cadmium à l'état triplet, du cyclopentane en phase vapeur et on a montré qu'elle conduit à des radicaux cyclopentyles et des atomes d'hydrogène avec une efficacité proche de l'unité pour le processus primaire. Des réactions subséquentes de ces espèces, y compris une contribution importante de la décomposition unimoléculaire des radicaux cyclopentyles, conduisent aux produits volatiles observés soit l'hydrogène, le méthane, l'éthylène, l'éthane, le propylène et le cyclopentène. Il résulte d'une élimination importante des atomes d'hydrogène par les oléfines que les rendements en produits dépendent fortement du temps. On a montré que le système n'est pas affecté par des adduits. La dépendance sur la température des vitesses de formation des produits est en accord avec les énergies connues pour la décomposition du radical cyclopentyle.
[Traduit par le journal]

Introduction

In a previous paper (1) it was shown that the decomposition of cyclohexane by triplet cadmium atoms at 3261 Å generally exhibited the same characteristics as the analogous triplet mercury sensitized system. Very few cadmium sensitized systems have been examined, however, and it is important to establish whether this similarity extends to other cyclic hydrocarbons, as well as to examine the cyclopentane system in its own right. In the present investigation, therefore, we have studied the triplet cadmium sensitized decomposition of cyclopentane vapor at 3261 Å.

In an attempt to elucidate more fully the role of olefinic products from this reaction, experiments with added propylene were conducted. These necessitated a correction to the observed product yields for competitive quenching of the sensitizer. There are, however, significant difficulties in such computations because of the dearth of meaningful cross-section data. It has been shown recently (2, 3), in studies of cadmium atoms produced in the flash photolysis of dimethyl cadmium, that there is very rapid equilibration of Cd($^3P_0$) and Cd($^3P_1$) atoms. Thus quenching cross sections determined on the basis of fluorescence measurements at 3261 Å are likely significantly in error. Furthermore, the quenching efficiencies of hydrocarbons in general for triplet cadmium atoms is quite small, and the quenching rate constants in most cases are either effectively zero or too minute to be determined by any presently available technique. In the absence of definitive data we have carried out a brief series of experiments to determine the approximate relative quenching cross section of cyclopentane by competitive quenching measurements to allow a tentative correction of product yields in the added propylene experiments.

No previous investigations of the triplet cadmium–cyclopentane system have been reported. The mercury photosensitized reaction has been investigated, both at room temperature (4–7) and

[1]From the Ph.D. thesis of B. L. Kalra, University of Saskatchewan, Saskatoon, 1973.

[2]Revision received August 21, 1975.

Can. J. Chem. Downloaded from www.nrcresearchpress.com by 210.87.254.42 on 09/05/12
For personal use only.

Can. J. Chem. Downloaded from www.nrcresearchpress.com by 210.87.254.42 on 09/05/12
For personal use only.

at temperatures up to 400 °C (8, 9). Cyclopentyl radicals and H-atoms are formed in the primary process, leading to molecular hydrogen, cyclopentene, and bycyclopentyl. Above 250 °C, the cyclic radical undergoes unimolecular decomposition and various other products, including ethylene, propylene, and propane can be detected.

Experimental

The apparatus and procedures have been described previously (1). The cadmium-containing reservoir attached to the reaction cell was maintained at 315 °C, while the cell itself was at 355 ± 2 °C in the experiments at fixed temperature.

The absorbed light intensity was determined to be $4.0 \pm 0.4 \times 10^{-3}$ μeinstein min^{-1} by measuring the initial rate of *cis–trans* isomerization of butene-2 (10), taking $\Phi = 0.50$ for that process (11, 12).

The cyclopentane (BDH) was subjected to low temperature distillation in the vacuum line and was purified prior to each experiment by preparative scale gc using a 25 ft dimethylsulfolane column.

A number of relatively non-volatile products, notably bicyclopentyl and allyl cyclopentane, which have been determined in the Hg-sensitized systems using an *in situ* gc sampling technique (8), would not have been detected here.

No detectable dark reactions were observed when thermal blanks were run with cyclopentane and with the various cyclopentane–addend mixtures studied.

Results

The decomposition of cyclopentane vapor photosensitized by triplet cadmium atoms at 3261 Å and 355 °C yields the following products that could be detected in this system: hydrogen, methane, ethylene, ethane, propylene, cyclopentene, and a product tentatively identified from its mass spectrum as cyclopentadiene. Propane was detected in trace quantities but was not analyzed for, quantitatively.

Figures 1 and 2 show the pressure dependence of product yields. The methane quantum yields are not shown, $\Phi(CH_4)$ remaining constant at 0.010 ± 0.003 over the pressure range investigated. Because of the low absorbed intensity, exposure times of 3 h were required to give at small cyclopentane pressures sufficiently large product yields for accurate analysis. However, at the highest pressure studied, the amount of hydrogen formed corresponds to only 0.3% of the starting material decomposed. On the basis of the variation in the hydrogen and cyclopentene quantum yields, it would appear that quenching is complete at around 150–200 Torr and that additional influences are operative at higher pressures.

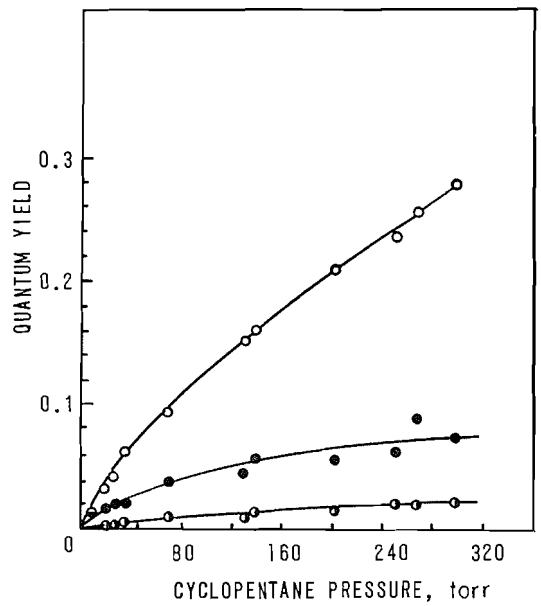

FIG. 1. Quantum yield of C_2H_4, ○; C_3H_6, ●; and C_2H_6, ◑; as a function of reactant pressure in the Cd-photosensitized decomposition of cyclopentane vapor at 355 °C and 3261 Å for 36 h.

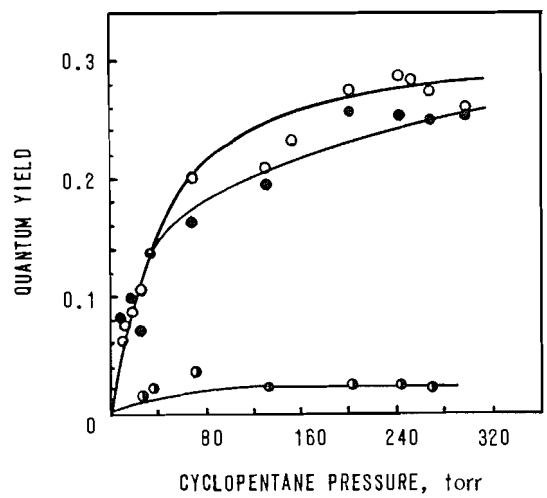

FIG. 2. Quantum yield of H_2, ●; cyclo-C_5H_8, ○; and cyclo-C_5H_6, ◑; as a function of reactant pressure in the Cd-photosensitized decomposition of cyclopentane vapor at 355 °C and 3261 Å for 36 h.

The effect of the extent of reaction was examined in two series of runs. Figure 3 shows the quantum yields observed in the limited product

Can. J. Chem. Downloaded from www.nrcresearchpress.com by 210.87.254.42 on 09/05/12
For personal use only.

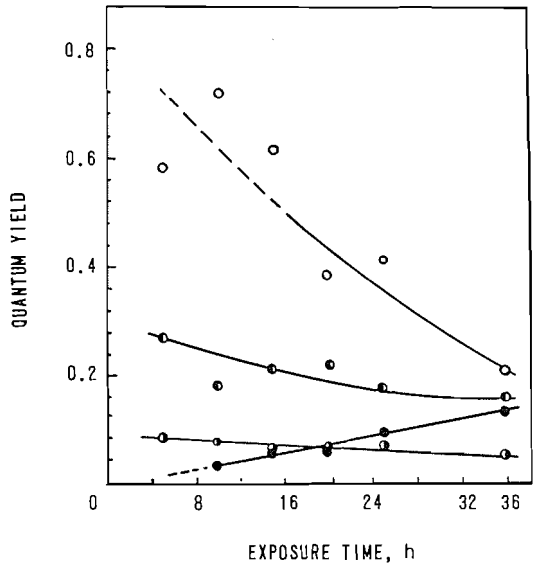

FIG. 3. Quantum yield of H_2, ○; C_2H_4, ◐; C_2H_6, ●; and C_3H_6, ◑; as a function of exposure time in the Cd-photosensitized decomposition of 139 Torr cyclopentane vapor at 355 °C and 3261 Å.

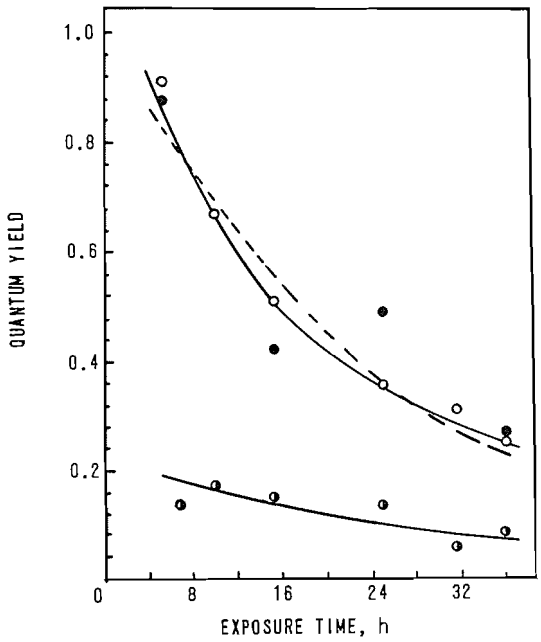

FIG. 4. Quantum yield of cyclo-C_5H_8, ●; C_2H_4, ○; and C_3H_6, ◑; as a function of exposure time in the Cd-photosensitized decomposition of 269 Torr cyclopentane vapor at 355 °C and 3261 Å.

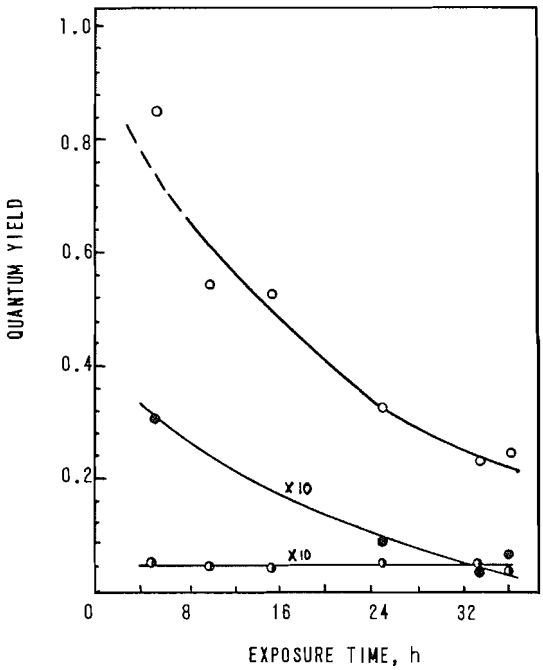

FIG. 5. Quantum yield of H_2, ○; C_2H_6, ◑; and cyclo-C_5H_6, ●; as a function of exposure time in the Cd-photosensitized decomposition of 269 Torr cyclopentane vapor at 355 °C and 3261 Å.

analysis in a series of runs at various exposure times using 139 Torr cyclopentane. A similar series of experiments wherein a more complete analysis was carried out was conducted at 269 Torr cyclopentane and the product yields therefrom are displayed in Figs. 4 and 5. Because of the minute amounts of products formed at the shorter exposure times the scatter in the observed values is considerable for those experiments. The largest uncertainty is associated with the quantum yields for cyclopentene at 269 Torr substrate, because of the difficulty in separating this product quantitatively from the large quantity of unreacted cyclopentane. These experiments definitively establish the very strong time (extent of reaction) dependence of hydrogen and cyclic olefin yields.

To establish the effect in general of inert gases to assist in the interpretation of the competitive quenching experiments, a series of runs was carried out wherein CF_4 was added to the reaction cell. Carbon tetrafluoride has an effective quenching cross section of zero for triplet mercury atoms (13) and was shown previously (1) not to influence the rates of product forma-

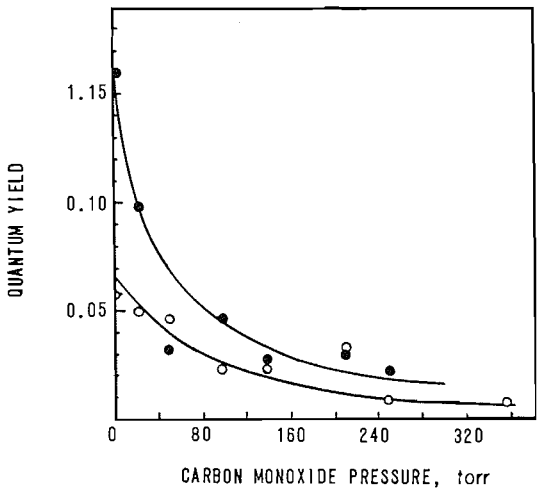

FIG. 6. Quantum yield of C_2H_4, ●; and C_3H_6, ○; as a function of CO pressure in the Cd-photosensitized decomposition of 139 Torr cyclopentane vapor at 355 °C and 3261 Å.

tion in the Cd-sensitized cyclohexane decomposition.

Here 139 Torr of cyclopentane was photolyzed in the presence of CF_4 at pressures from 50 to 530 Torr and the yields of C_3H_6 and cyclo-C_5H_8 as representative products measured. In these and subsequent quenching experiments, 139 Torr cyclopentane was employed. This pressure is likely just below the complete quenching region, but unfortunately, higher pressures of the substrate would not have allowed for accurate analysis of the cyclopentene product. Considering the other uncertainties in these measurements, however, the potential error introduced by the possible small amount of incomplete quenching is not significant. As with cyclohexane, the yields remained constant within experimental error.

Having thus demonstrated that an inert gas does not decrease product yields by deactivation of excited molecules or radicals, the decreases in yields observed when another addend is present can appropriately be ascribed to competitive quenching of the sensitizer.

Carbon monoxide was chosen for such experiments. Figure 6 shows yields of ethylene and propylene as a function of CO pressure for the decomposition of 139 Torr cyclopentane. Ascribing the decrease observed to competitive quenching, a ratio of the quenching cross sections, σ_1^2 for cyclopentane and σ_2^2 for carbon monoxide, of the two quenchers can be obtained from the relation:

$$[1]\quad \Phi/\Phi_0 = p_1\sigma_1^2 \Big/ \left[p_1\sigma_1^2 + p_2\sigma_2^2 \left(\frac{M_1}{M_2} \frac{M_2 + M_{Cd}}{M_1 + M_{Cd}} \right)^{1/2} \right]$$

where Φ and Φ_0 are the quantum yields of ethylene or propylene in the presence and absence of CO respectively, p_1 and σ_1^2 are the pressure and cross section of cyclopentane and p_2 and σ_2^2 refer to CO. On the basis of the Φ/Φ_0 values observed for the two products analyzed, $\sigma_1^2/\sigma_2^2 = 1.4$. On the basis of the literature values for the quenching cross section of CO for triplet cadmium atoms, 0.14 Å^2 (14) and for propylene, 29 Å^2 (14), the ratio of the quenching cross sections of cyclopentane and propylene would be $\Phi_{cyclopentane}/\Phi_{propylene} = 0.0069$. In conjunction with [1] then these values can be used to correct yields observed in the presence of propylene for competitive quenching. Because of the comments indicated earlier with respect to the considerable uncertainties in the absolute values of these quenching cross sections, it would appear inappropriate to quote the values that could be calculated from the data available here but rather to restrict the use of the data to determine relative values to correct yields observed in the presence of propylene.

Table 1 lists the observed product quantum yields in a series of experiments in which the decomposition of 139 Torr cyclopentane was studied in the presence of propylene. The hydrogen quantum yields corrected for competitive quenching on the basis of the above approach and [1] have also been included. These corrected values show a trend quite different from the analogous data reported for the cyclohexane system (Table 3 of ref. 1). In that case, however, a much larger value for the quenching cross section of the hydrocarbon was used, and it would appear on the basis of the results here that the smaller, by a factor of about 10, relative value determined here by actual quenching experiments is more appropriate. Among the other reaction products observed in the cyclopentane system and listed in Table 1, the appearance of significant yields of propane, even before any corrections might be applied, is consistent with

Can. J. Chem. Downloaded from www.nrcresearchpress.com by 210.87.254.42 on 09/05/12
For personal use only.

TABLE 1. Effect of propylene on the cadmium sensitized photodecomposition of 139 Torr cyclohexane vapor for 36 h at 355 °C and 3261 Å

$P(C_3H_6)$ (Torr)	Quantum yield				
	H_2[a]	H_2[b]	C_2H_4[a]	C_2H_6[a]	C_3H_8[a]
0	0.21	0.21	0.16	0.014	—
0.45	0.048	0.075	0.023	0.005	—
0.58	0.071	0.12	0.052	0.004	0.010
1.00	0.053	0.12	0.043	0.003	0.013
1.00	0.076	0.17	0.048	0.004	0.014
2.50	0.047	0.19	0.016	0.008	0.012
6.00	0.031	0.26	0.004	0.004	0.027

[a]Uncorrected.
[b]Corrected for competitive quenching of Cd* by propylene, see text.

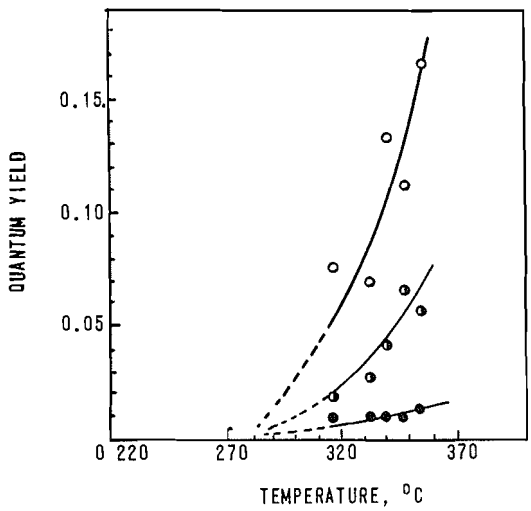

FIG. 7. Quantum yield of C_2H_4, ○; C_3H_6, ◑; and C_2H_6, ●; as a function of reaction temperature in the Cd-photosensitized decomposition of 139 Torr cyclopentane vapor for 36 h at 3261 Å.

the importance of hydrogen atom scavenging by the olefin in this system.

In an effort to determine the apparent overall activation energy for the decomposition of cyclopentyl radicals, the effect of temperature on the production of ethylene, propylene, and ethane was examined and the results are shown in Fig. 7. The temperature range that can be examined in this system is quite restricted because of the necessity of using temperatures high enough to give sufficient cadmium vapor pressure but low enough to prevent significant thermal decomposition.

Discussion

The primary process in this system is undoubtedly reaction 2,

[2] $Cd(^3P) +$ $\rightarrow CdH +$

followed by unimolecular decomposition of the cadmium hydride. The formation of CdH in a number of hydride systems has been confirmed spectroscopically (2, 15–17). The alternative, a process involving the direct production of H-atoms and cyclopentyl radicals is certainly less favorable energetically, having an activation energy of at least 15 kcal/mol. The lack of dependence of the quantum yields on the pressure of added CF_4 would indicate that any type of 'excited molecule' mechanism can be ruled out.

Hydrogen atoms formed in the initial decomposition abstract from cyclopentane to form the observed product, molecular hydrogen, in reaction 3,

[3] $H +$ 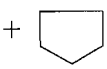 $\rightarrow H_2 +$

which also provides an additional source of cyclopentyl radicals. Thus the net result of the energy transfer process is the formation of one molecule of hydrogen and two cyclopentyl radicals for each molecule of cyclopentane initially decomposed.

It is thus apparent that the major features of this system are similar to those observed in the Hg-sensitized decomposition of this compound and our previously reported behavior of the Cd-sensitized decomposition of cyclohexane vapor to which reference has been made previously.

To explain the nature and relative yields of the final products of the decomposition here, a variety of reactions must be considered in order to demonstrate that our observations are con-

Can. J. Chem. Downloaded from www.nrcresearchpress.com by 210.87.254.42 on 09/05/12
For personal use only.

Can. J. Chem. Downloaded from www.nrcresearchpress.com by 210.87.254.42 on 09/05/12
For personal use only.

sistent with the proposed initial radical producing steps in the mechanism and with the known behavior of the reactive species that are important in this decomposition. The fact that the reaction is taking place at 355 °C requires consideration of a number of reactions with relatively high activation energies that nevertheless would be expected to be important at elevated temperatures. It is instructive to consider initially the reactions of the cyclopentyl radical.

In addition to decomposition modes of the cyclo-C_5H_9 radical to be enumerated presently, one must also consider those reactions which would be expected to be important at all temperatures, namely recombination and disproportionation, both mutual and with H-atoms.

[4] 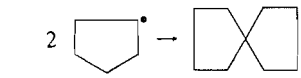

[5] 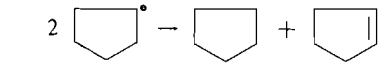

[6] 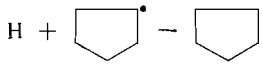

[7] 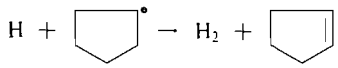

In this system reaction 5 is the most important source of cyclopentene. In the mercury photosensitized reaction the bicyclic product from reaction 4, a product that would not have been detected in this system, amounts to 20–40% of the cyclopentene yield depending on conditions (6).

It is not possible to gauge the contribution from reactions 6 and 7. Although the overall observable decomposition quantum yield would appear to approach unity at short exposure times,[3] the uncertainty is such that reaction 6 could be responsible for some diminution of the overall efficiency of the decomposition. There is no way in this system of distinguishing between the molecular hydrogen that may be formed in process 7 from that arising via other routes, and the reaction must be included as a possible source of H_2.

[3]The quantum yield of hydrogen approaches 0.8 (Fig. 3) at 139 Torr and it is apparent from Fig. 2 that this yield would be larger at higher cyclopentane pressures.

Three unimolecular decomposition reactions of the cyclopentyl radical must be considered, namely:

[8] 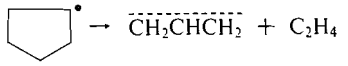

[9] 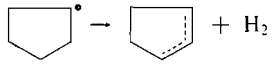

[10] 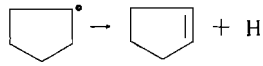

In his study of the decomposition of this species, Gordon (18) obtained evidence for all three processes. Reaction 8 was reported to have $E_a = 37.7$ kcal mol^{-1} and log $A = 14.5$. Data on the other two reactions are less definitive; Gordon suggests that the activation energy for process 10 has a minimum value of 38 kcal mol^{-1}, while for process 9, E_a is 35–40 kcal with a preexponential about 0.1 that of reaction 8. Thus in this system, where the nature of the products indicates that reaction 8 is occurring to an appreciable extent, processes 9 and 10 must also be considered as contributing to the mechanism as well. On the other hand, the relative rates of the various reactions of the products of reactions 8–10 would be expected to be appreciably different in this system, where initially H-atoms and cyclopentyl radicals are formed at the same time, as opposed to Gordon's investigation where cyclopentyl radicals are formed by methyl radical abstraction and the only source of H-atoms is reaction 10.

For the allyl radicals formed in reaction 8 there are several possibilities.

[11] $$2C_3H_5 \rightarrow C_3H_4 + C_3H_6$$

[12] $$2C_3H_5 \rightarrow C_6H_{10}$$

[13] $$C_3H_5 + H \rightarrow C_3H_6$$

Data obtained by Laidler and Wojciechowski (19) indicate that reaction 13 would be the most important. These authors report that $k_{13}/k_{12} = 10$ and $k_{13}/k_{11} = 3.2 \times 10^{10}$ at 600 K and the three processes should not have a strong temperature dependence. The absence of allene as a product indicates that reaction 11 does not occur to a significant extent here. The product 1,3-hexadiene from process 12 would not have been detected in this system. However, the reaction likely does occur to some extent; the diene

originating in this fashion was found by Gordon (18). The occurrence of significant yields of propylene in the system requires that reaction 13 be invoked. The alternative route to propylene, abstractions by allyl radicals from cyclopentane,

[14] $C_3H_5 +$ $\rightarrow C_3H_6 +$

would lead to a chain reaction with cyclopentyl radicals as carrier and therefore to decomposition quantum yields far in excess of those observed.

The pronounced time dependence of the olefinic products indicates that olefinic scavenging of H-atoms via reaction 15

[15] $\qquad H + \text{olefin} \rightarrow R\cdot$

is an important influence on the decomposition. Subsequent reactions of the R· radicals formed in reaction 15 readily account for the minor hydrocarbon products. The importance of reaction 15 is also evidenced by the results obtained when propylene is added. Even without competitive quenching corrections, the yield of propane originating with the radical formed in reaction 15 is observed to increase significantly with propylene pressure.

The relative importance of the various possible reactions of H-atoms is not quantitatively evident. In addition to reactions 5, 6, 7, and 15, two other abstractive processes,

[16] $H +$ $\rightarrow H_2 +$

[17] $H +$ $\rightarrow H_2 +$

cannot be excluded.

The cyclopentenyl radicals formed in reactions 9 or 17 can, according to evidence adduced by Gordon (18), undergo a further decomposition to yield cyclopentadiene, one of the minor products observed here, in a process that provides yet another, if minor, source of H-atoms.

The hydrogen yields observed in the presence of propylene are somewhat difficult to interpret because of the uncertainties in the quenching corrections. Although the formation of propane is evidently the result of H-atom scavenging, the apparent constancy of $\Phi(H_2)$ within the large uncertainty here, would suggest that reactions 16 and 17 may be involved. A further difficulty in interpretation of these particular results is that they were obtained at relatively large extents of decomposition where the relative yields are not necessarily indicative of the initial quantum yields. Hirokami and Sato (20), report no hydrogen from the Cd-sensitized decomposition of pure propylene, but in view of the very small absolute H_2 yields, a relatively small contribution from such a process would have an inordinately large effect on the corrected H_2 yields calculated here.

Finally, the temperature dependence data for the C_2 products shown in Fig. 7 may be used to make a comparison with the apparent activation energy for reaction 8, reported by Gordon. An Arrhenius plot of the total quantum yield of C_2H_4 and C_2H_6 from the data in the figure is linear, except for the point at 317 °C where the very small difference in temperature between the cell and cadmium reservoir may have led to changes in the cadmium vapor pressure. However, there is appreciable scatter in the points and although the graph can be drawn within experimental error so that the line yields a slope giving a value of 37 kcal mol^{-1} for the activation energy, the data provide only a tentative confirmation of that value. These data also support the proposal that the C_2 and C_3 products originate with the radical decomposition step whose importance would be expected to increase with temperature.

In conclusion, perhaps the most important feature of the data obtained in this system, and that reported earlier for cyclohexane, is with respect to their implications for the technique of cadmium sensitization as a method of determining the effect of sensitizer energy. There are no really significant differences in the two cyclic hydrocarbons under cadmium and mercury photosensitization. Evidently any potential differences in the two cases arising from the change in sensitizer energy (one would not anticipate any alterations in the mechanism of the primary sensitizer – acceptor interaction) are outweighed by the higher temperature, and consequent larger energy input, in the case of the cadmium systems, and therefore at which the mercury system must be examined for comparison. On the basis of these two investigations, at least, it would appear that investigations of the effect of triplet sensitizer energy on gas phase hydrocarbon decompositions could be more profitably carried out by making use of sensitizers whose reactions could

Can. J. Chem. Downloaded from www.nrcresearchpress.com by 210.87.254.42 on 09/05/12
For personal use only.

be compared at lower temperatures. The situation is further complicated by the difficulties in obtaining in cadmium-sensitized systems, results of sufficient accuracy to make detailed and quantitative comparisons.

For the cyclopentane system itself, however, it has been demonstrated that the sensitized decomposition initiated by triplet cadmium atoms proceeds with such high quantum efficiency, likely unity, that the energy transfer gives rise to H-atoms and cyclopentyl radicals, the latter undergoing unimolecular decomposition along with other reactions, these processes giving rise to products whose relative importance and occurrence are entirely consistent with the reactions known to be associated with these reactive species.

Acknowledgment

The authors acknowledge the financial support of the National Research Council of Canada and the University of Saskatchewan for a graduate scholarship to B.L.K.

1. B. L. KALRA and A. R. KNIGHT. Can. J. Chem. **50**, 2010 (1972).
2. P. J. YOUNG, G. GREIG, and O. P. STRAUSZ. J. Am. Chem. Soc. **92**, 413 (1970).
3. P. J. Young, E. HARDWIDGE, S. TSUNASHIMA, G. GREIG, and O. P. STRAUSZ. J. Am. Chem. Soc. **96**, 1946 (1974).
4. G. A. ALLEN, D. L. KANTRO, and H. E. GUNNING. J. Am. Chem. Soc. **72**, 3588 (1954).
5. P. W. BECK, D. V. KNIEBES, and H. E. GUNNING. J. Chem. Phys. **22**, 678 (1954).
6. R. L. STOCK and H. E. GUNNING. Can. J. Chem. **38**, 2295 (1960).
7. R. A. HOLYROYD and G. W. KLEIN. J. Phys. Chem. **67**, 2273 (1963).
8. H. E. GUNNING and R. L. STOCK. Can. J. Chem. **42**, 357 (1964).
9. S. ARAI and S. SHIDA. Kogyo Kagaku Zasshi, **64**, 454 (1961), *cf.* Chem. Abstr. **57**, 2088b (1962).
10. S. TSUNASHIMA, S. SATOH, and S. SATO. Bull. Chem. Soc. Jpn. **42**, 1531 (1969).
11. S. TSUNASHIMA and S. SATO. Bull. Chem. Soc. Jpn. **41**, 284 (1968).
12. H. E. HUNZIKER. J. Chem. Phys. **50**, 1294 (1969).
13. R. J. CVETANOVIC. Prog. React. Kinet. **2**, 39 (1964).
14. E. W. R. STEACIE and D. J. LEROY. J. Chem. Phys. **11**, 164 (1943).
15. W. H. BRECKENRIDGE and A. B. CALLEAR. Chem. Phys. Lett. **5**, 17 (1970).
16. W. H. BRECKENRIDGE and A. B. CALLEAR. Trans. Faraday Soc. **67**, 2009 (1971).
17. A. B. CALLEAR and J. G. MCGURK. Nature, **226**, 844 (1970).
18. A. S. GORDON. Can. J. Chem. **43**, 570 (1965).
19. K. J. LAIDLER and B. W. WOJCIECHOWSKI. Proc. R. Soc. London, Ser. A, **259**, 257 (1960).
20. S. HIROKAMI and S. SATO. Bull. Chem. Soc. Jpn. **43**, 2389 (1970).

Can. J. Chem. Downloaded from www.nrcresearchpress.com by 210.87.254.42 on 09/05/12
For personal use only.

Spectroscopic studies of benzoxazole-2-thione complexes. Derivatives of cobalt(II) and nickel(II) halides

CARLO PRETI AND GIUSEPPE TOSI
Istituto di Chimica Generale ed Inorganica, University of Modena, 41100 Modena, Italy

Received July 21, 1975

CARLO PRETI and GIUSEPPE TOSI. Can. J. Chem. **54**, 85 (1976).

The preparation of some complexes of benzoxazole-2-thione with halides of cobalt(II) and nickel(II) is reported. The complexes of cobalt(II) and nickel(II) are tetrahedral of the type ML_2X_2 with the exception of $NiLBr_2$. The complexes have been studied by means of magnetic susceptibility measurements, infrared and far ir spectra, electronic spectra, and conductivity measurements. The ligand behaves as monodentate *N*-bonded. The various ligand field parameters, Dq, B', and β show about 60 and 80% of covalency in the cobalt(II) and nickel(II) complexes respectively and suggest a medium strong ligand field. The spectroscopy parameters of cobalt and nickel derivatives confirm the presence of CoN_2X_2 and NiN_2X_2 chromophores.

CARLO PRETI et GIUSEPPE TOSI. Can. J. Chem. **54**, 85 (1976).

On rapporte la préparation de quelques complexes de la benzoxazolethione-2 avec des halogénures de cobalt(II) et de nickel(II). Les complexes du cobalt(II) et du nickel(II) sont tétraédriques et du type ML_2X_2 à l'exception de $NiLBr_2$. On a étudié les complexes à l'aide de mesures de susceptibilité magnétique, de spectres infrarouges et infrarouges lointoins, de spectres électroniques et de mesures de conductivité. Les ligands se comportent comme des ligands liés à l'azote et monodentates. Les divers paramètres de champ de ligands, Dq, B' et β montrent qu'il y a approximativement 60 et 80% de covalence respectivement dans les complexes de cobalt(II) et de nickel(II) et suggèrent un champ de ligand moyennement fort. Les paramètres spectroscopiques des dérivés du cobalt et du nickel confirment la présence des chromophores du CoN_2X_2 et du NiN_2X_2.

[Traduit par le journal]

In view of the importance of the oxazole group in biological systems, we have begun a study of the coordination behavior of benzoxazole-2-thione. This molecule has a marked bacteriostatic and fungicidal activity and is very important as a regulator for plant growth and development. Furthermore this heterocyclic base is very important as a stabilizing or antifogging agent in photographic emulsions adsorbed on silver bromide (1, 2).

The benzoxazole-2-thione forms a variety of interesting complexes with transition metal ions; complexation potentially could occur through either the nitrogen or the oxygen atom of the oxazole ring or via the sulfur atom. The interactions of several oxazole or isoxazole containing ligands with metal ions are being studied in these laboratories. We report here an investigation of the complexes formed by this ligand with cobalt(II) and nickel(II) halides. The nature of bonding has been ascertained by ir studies and electronic spectral measurements.

The ligand exhibits thiol-thione isomerism involving —N=C—SH and —NH—C=S

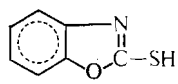

Thiol form

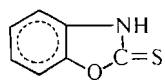

Thione form

It has been demonstrated from the ir spectra that this ligand exists in the solid state as a hydrogen-bonded thioamide complex, which partially breaks down in carbon tetrachloride solution (3). The ir spectra do not show a ν(SH) peak in the region of 2500 cm^{-1} but a strong absorption around 3400 cm^{-1} corresponding to the ν(NH) stretch. Thione compounds containing the H—N—C=S skeleton give rise to four thioamide bands: around 1550, 1300–1200, 1000, and 750–800 cm^{-1} (4–7). The presence of ir bands in such regions indicates that our ligand exists in the thione form in the solid state. It is possible that in the ligand molecule only two atoms could act as bonding sites, *i.e.* the thiocarbonyl sulfur atom and the nitrogen atom. Since the lone pairs on the oxygen atom present in the skeleton of the ring are involved in the resonating structures of the molecule, it is

Can. J. Chem. Downloaded from www.nrcresearchpress.com by 210.87.254.105 on 09/05/12
For personal use only.

TABLE 1. Analytical data and other physical properties

Compound	Color	Found (%)			Calculated (%)			μ (B.M.)	Melting point (°C)
		C	H	N	C	H	N		
$[Cobot_2Cl_2]\cdot H_2O$	Green	37.6	2.7	6.2	37.4	2.7	6.2	4.5	160–162
$[Cobot_2Br_2]$	Bright green	32.1	2.1	5.3	32.3	1.9	5.4	4.5	164–166
$[Cobot_2I_2]\cdot H_2O$	Dark green	26.5	1.6	4.3	26.6	1.9	4.4	4.6	170–172
$[Nibot_2Cl_2]\cdot 3H_2O$	Dark brown	34.7	3.2	5.9	34.6	3.3	5.8	3.5	202–204
$[NibotBr_2]$	Green–grey	22.7	1.4	3.6	22.7	1.4	3.8	3.6	>350
$[Nibot_2I_2]\cdot 6H_2O$	Dark brown	23.4	2.9	3.7	23.3	3.1	3.9	3.6	>350

TABLE 2. Solid state electronic spectra (cm^{-1})

Compound	Absorption bands*
$[Cobot_2Cl_2]\cdot H_2O$	26315sh, 16670, 15455, 9090, 4385
$[Cobot_2Br_2]$	25640sh, 16130, 15270, 12900, 8660, 4395
$[Cobot_2I_2]\cdot H_2O$	22300sh, 15150, 14390, 7935, 4350
$[Nibot_2Cl_2]\cdot 3H_2O$	15270, 7490, 4705, 4545
$[NibotBr_2]$	14820, 11100, 7410, 4695
$[Nibot_2I_2]\cdot 6H_2O$	14535, 7280, 4740, 4610

*sh = shoulder.

TABLE 3. Most important visible peaks and crystal field parameters (cm^{-1})*

Compound	ν_3	ν_2	ν_1†	Dq	B'	β
	$^4A_2(F) \rightarrow {}^4T_1(P)$	$^4A_2(F) \rightarrow {}^4T_1(F)$	$^4A_2(F) \rightarrow {}^4T_2(F)$			
$[Cobot_2Cl_2]\cdot H_2O$	16000	9090	5490	549	575	0.59
$[Cobot_2Br_2]$	15550	8660	5200	520	574	0.59
$[Cobot_2I_2]\cdot H_2O$	14815	7935	4720	472	572	0.59
	$^3T_1(F) \rightarrow {}^3T_1(P)$	$^3T_1(F) \rightarrow {}^3A_2(F)$	$^3T_1(F) \rightarrow {}^3T_2(F)$			
$[Nibot_2Cl_2]\cdot 3H_2O$	15270	7490	3430	406	831	0.80
$[NibotBr_2]$	14820	7410	3400	401	802	0.77
$[Nibot_2I_2]\cdot 6H_2O$	14535	7280	3330	395	788	0.76

*B is taken to be 967 cm^{-1} for the Co^{2+} free ion and 1041 cm^{-1} for the Ni^{2+} free ion.
†Calculated values.

expected that it should have very weak coordinating ability (8).

Results and Discussion

The complexes obtained, analytical data, room temperature magnetic moments, and other physical properties are reported in Table 1. The electronic spectra are listed in Tables 2 and 3. The most important ir bands are given in Tables 5 and 6. The compounds are microcrystalline, soluble in nitromethane, *N,N'*-dimethylformamide, less soluble in nonpolar solvents. All the complexes are paramagnetic.

Electronic Spectral Study

The spectral data and the values chosen for the energies ν_2 and ν_3, from which the values of the parameters Dq, B', and β have been derived, are presented in Tables 2 and 3 respectively. With the cobalt and nickel halides, complexes of essentially tetrahedral geometry are formed; their magnetic moments and solid state electronic spectra are in accord with those expected for this stereochemistry.

The Dq values (Table 3) for the complexes suggest the order

$$Cl > Br > I$$

for the halides in the spectrochemical series and this order is consistent with the generally accepted sequence. In order to determine the position of the ligand in the spectrochemical series, the Dq values of the complexes were compared with the Dq values of known tetrahedral

Can. J. Chem. Downloaded from www.nrcresearchpress.com by 210.87.254.105 on 09/05/12
For personal use only.

TABLE 4. Comparison of Dq and B' values

	CoL_2Cl_2		CoL_2Br_2		CoL_2I_2		
L*	Dq	B'	Dq	B'	Dq	B'	Reference
btt	559	586	523	612	504	616	9
bot	549	575	520	574	472	572	This work
2-Mebi	529	588	524	572	514	526	10
3-Me-5-Phisox	520	511	523	470	588	387	11
abi	492	643	452	669	435	637	12
ts	467	722	451	670	430	643	13
ttz	460	660	410	710	360	710	14
3,5-diMeisox	454	632	440	647	426	623	15
tzse	400	737	387	732	382	719	13

*btt = benzothiazole, bot = benzoxazole-2-thione, 2-Mebi = 2-methylbenzimidazole, 3-Me-5-Phisox = 3-methyl-5-phenylisoxazole, abi = 2-aminobenzimidazole, ts = thiomorpholin-3-thione, ttz = thiazolidine-2-thione, 3,5-diMeisox = 3,5-dimethylisoxazole, tzse = thiazolidine-2-selenone.

halide complexes of cobalt(II). Table 4, which lists the Dq and B' values of the complexes suggests the following order for the ligands (9–15):

benzothiazole > benzoxazole-2-thione > 2-methylbenzimidazole > 3-methyl-5-phenylisoxazole > 2-aminobenzimidazole > thiomorpholin-3-thione > thiazolidine-2-thione ≃ 3,5-dimethylisoxazole > thiazolidine-2-selenone

Table 3 shows that the B' values for all the complexes here studied are of the order of 59–80% of the free ions values (967 cm^{-1} for Co(II) and 1041 cm^{-1} for Ni(II)), which suggests that there is a considerable orbital overlap in the metal–ligand σ bond. The ligands can be placed in the nephelauxetic series in the order

thiazolidine - 2 - selenone > thiomorpholin - 3 - thione > thiazolidine - 2 - thione > 2 - aminobenzimidazole > 3,5 - dimethylisoxazole > 2-methylbenzimidazole > benzoxazole-2-thione > 3-methyl-5-phenylisoxazole

It should be noted that our ligand is at the beginning of the spectrochemical series and at the end of the nephelauxetic series. This fact can be explained as the former is a measure of the electrical field produced by the ligand while the latter is a measure of the covalency of the metal–ligand bond.

In the cobalt derivatives the bands at 16 670–14 390 cm^{-1} may be assigned as the $^4A_2(F) \rightarrow {}^4T_1(P)$ transition, the second at 9090–7935 cm^{-1} as the $^4A_2(F) \rightarrow {}^4T_1(F)$ transition. These bands passing from the chloro- to iodo-derivative are shifted towards lower energies. The ν_3 transition is split because of the distorted tetrahedral structure of the complexes and this splitting decreases from chloride to iodide. We have calculated the ligand field parameters using only the ν_2 transition and the visually estimated frequencies of the centers of gravity of the split bands corresponding to ν_3 using the equations proposed by Underhill and Billing (16). The assignment of ν_1 is made difficult by the presence of vibrational modes in the range where this transition should be expected. The calculated ν_1 wave numbers are reported in Table 3.

From the analysis of the electronic spectra we could determine the mode of bonding of the ligand by comparison of Dq values reported for CoL_2X_2 complexes and CoL_4^{2+} and CoX_4^{2-} ions (17, 18).

Tables 3 and 4 show that Dq values are in good agreement with the literature data for CoL_2X_2 derivatives containing cobalt–nitrogen bonds.

A pseudo-tetrahedral stereochemistry has been assigned to the nickel-derivatives on the basis of their electronic spectra (14, 16, 19, 20). The medium strong band in the range 7490–7280 cm^{-1} can be attributed to the $^3T_1(F) \rightarrow {}^3A_2(F)$ transition (ν_2), while the band present at 15 270–14 535 cm^{-1} may be assigned to the ν_3 transition $^3T_1(F) \rightarrow {}^3T_1(P)$. The values of Dq and B' have been calculated using ν_2 and ν_3 only, the assignment of ν_1 very often being ambiguous because of the presence of vibrations due to the ligand itself in the region near 4000 cm^{-1}; the calculated ν_1 values are listed in Table 3. Comparison of the electronic spectra of our complexes with those of derivatives involving Ni—S bonds and Ni—N bonds confirms that these derivatives are *N*-bonded as the band energies are at higher values than in *S*-bonded derivatives (17, 21).

Can. J. Chem. Downloaded from www.nrcresearchpress.com by 210.87.254.105 on 09/05/12
For personal use only.

Can. J. Chem. Downloaded from www.nrcresearchpress.com by 210.87.254.105 on 09/05/12
For personal use only.

TABLE 5. Most important infrared bands (cm^{-1})

Compound	Infrared (cm^{-1})							
	ν(NH)	Thioamide I*	ν(C═S) + δ(NCS)	Thioamide II†	$\nu(COC)_{asym}$	Thioamide III‡	$\nu(COC)_{sym}$	Thioamide IV§
bot Solid	3250s	1505vs	1282s	1245ms	1095vs	1010s	820ms	745vs
bot $CHCl_3$	3450s	—	1285s	—	1100s	1013s	—	—
$[Cobot_2Cl_2]\cdot H_2O$	3220s	1510s	1285s	1245ms	1098s	1011ms	818m	747vs
$[Cobot_2Br_2]$	3210s	1510s	1290s	1248ms	1100ms	1013ms	820m	749vs
$[Cobot_2I_2]\cdot H_2O$	3200ms	1510s	1289s	1242m	1100ms	1012m	817m	749vs
$[Nibot_2Cl_2]\cdot 3H_2O$	3130vs	1505mw	1289m	1242ms	1095m	1010m	818m	745vs
$[NibotBr_2]$	3240vs	1510s	1282s	1250ms	1100s	1012m	820m	745vs
$[Nibot_2I_2]\cdot 6H_2O$	3140m	1505m	1285m	1240m	1098m	1010m	815m	745vs

*Thioamide I has contribution from δ(NH) + δ(C—H) + ν(C═N).
†Thioamide II has contribution from ν(C═N) + δ(NH) + δ(C—H) + ν(C═S).
‡Thioamide III has contribution from ν(C═N) + ν(C═S).
§Thioamide IV has contribution from ν(C═S).

TABLE 6. Far infrared spectra (400–120 cm^{-1})

Compound	ν(M—X)	ν(M—L)	Other bands
bot	—	—	425ms, 264m, 237m
$[Cobot_2Cl_2]\cdot H_2O$	329m, 307mw	226m	425ms, 260mw, 235m
$[Cobot_2Br_2]$	248m, 219m	225m	422ms, 256m, 240sh
$[Cobot_2I_2]\cdot H_2O$	212m, 206m	222ms	424ms, 258m, 230sh
$[Nibot_2Cl_2]\cdot 3H_2O$	309m, 286m	221ms	427ms, 265m, 236mw
$[NibotBr_2]$	199s t, 166vs b, 143m b	219ms	428ms, 264m, 236mw
$[Nibot_2I_2]\cdot 6H_2O$	202ms	220ms	428sh, 265w, 238w

Magnetic and Conductivity Studies

The magnetic susceptibility results, 4.5–4.6 B.M., of the cobalt complexes fall within the normal range for tetrahedral high-spin complexes of divalent cobalt. The μ values of the nickel derivatives, in the range 3.5–3.6 B.M., are as expected for nickel(II) high-spin pseudo-tetrahedral complexes.

The molar conductances suggest that these complexes are not conducting in *N,N'*-dimethylformamide solution (Λ lying below 30 ohm^{-1} cm^2 mol^{-1} for all compounds) and are true molecular addition compounds.

Infrared Spectral Studies

The spectra of the ligand in the solid state and in chloroform solution show a noticeable difference in the position of ν(NH) stretching frequency, clearly indicating intermolecular hydrogen bonding between the hydrogen of the NH group and the sulfur of the thioketo group. The ν(NH) in the complexes is shifted towards lower wave numbers by about 300 cm^{-1} using as reference the value of 3450 cm^{-1} for ν(NH) for the free ligand in chloroform solution, or by about 100 cm^{-1} using the 3250 cm^{-1} value obtained from the solid phase spectrum of the free ligand. The extensive hydrogen bonding disappears after dissolution in chloroform and after complexation.

According to Singh and Rivest (22) a sharp NH band in the metal derivatives is indicative of the absence of hydrogen bonding and a comparison of these values with the ν(NH) solution frequency of the ligand could be used to suggest a coordination through the nitrogen atom. In our complexes sharp bands are present in the range 3240–3130 cm^{-1} and a comparison with the ν(NH) value of 3450 cm^{-1} would indicate a M–N coordination.

This negative shift in the NH stretching frequency clearly suggests a coordination through the nitrogen atom both in the cobalt and in the nickel complexes. The coordination mode can be distinguished by an analysis of the positions and intensities of the thioamide bands, Table 5. The directions of the shifts in the position of all the bands in the spectra of the complexes are the same. This fact indicates that the bonding pattern in the complexes must be similar.

The band at 1505 cm^{-1}, assigned to thioamide I, shows in the complexes small positive shifts and there is ample evidence that this band shifts to higher wave numbers whenever the coordination takes place through the nitrogen atom (22). Coordination via the thiocarbonyl sulfur atom can be excluded because the thioamide II band, having major contribution from ν(C=N), is at the same wave number as in the free ligand while it undergoes a red shift in the case of a sulfur coordination. Furthermore the thioamide bands III and IV, having their main contribution from ν(C=S), are not shifted towards lower energies while a red shift should be present if the sulfur atom were involved in the coordination to the metal (14, 23–26).

The bands at 1095 and 820 cm^{-1}, attributed to the prevailing contribution of ν(COC) sym and asym, are at the same wave numbers or show small blue shifts, thus excluding the possibility of coordination through the oxygen atom of the oxazole ring.

Further confirmation of this assumption of coordination through the nitrogen atom comes out from the far infrared spectra. No bands are present in the ranges where ν(M—S) and ν(M—O) usually lie for cobalt and nickel derivatives, but new halogen independent bands are present in the ranges expected for ν(Co—N) and ν(Ni—N) respectively, Table 6, in very good agreement with the literature data (13, 27).

These assignments are strongly supported by the above discussed results reported in Table 4. We can see that the Dq and B' values for cobalt

Can. J. Chem. Downloaded from www.nrcresearchpress.com by 210.87.254.105 on 09/05/12
For personal use only.

Can. J. Chem. Downloaded from www.nrcresearchpress.com by 210.87.254.105 on 09/05/12
For personal use only.

derivatives are in the expected range and agree very well with the other data reported for tetrahedral CoL_2X_2 complexes containing Co—N bonds. The same conclusion may be reached from the inspection of Table 3 for nickel complexes.

As for the metal–halogen stretching modes, Table 6, they are in accord with the literature data for tetrahedral monomeric compounds for the complexes having a 1:2 metal:ligand ratio. In the complex [NibotBr$_2$] the values found at 166 and 143 cm^{-1} are typical for halide bridged nickel(II) complexes; the stretching mode at 199 cm^{-1} is due to terminal bromide (28, 29). We can therefore assign to this last complex a tetrahedral dimeric structure involving terminal ligands and terminal and bridging halide atoms.

The medium strong bands present in the range 3440–3460 cm^{-1}, ν(OH), and around 1630 cm^{-1}, δ(HOH), in all the water containing complexes, (Table 1) clearly confirm the presence of water of crystallization, which is purely lattice and not coordination water as confirmed by the absence of wagging, twisting, and rocking modes typical of coordinated water.

Experimental

The ligand bot, supplied by Fluka, was purified by recrystallization from ethanol: mp 192–194 °C (lit. (30) 193 °C).

All compounds were obtained by reaction of the corresponding metal salt in molten ligand in the required stoichiometrical ratio. The complexes have been purified by means of repeated washing with ethyl ether and dried over P_4O_{10}.

The ir spectra have been recorded in the range 4000–120 cm^{-1} with Perkin–Elmer 457 and 225 and Hitachi–Perkin–Elmer FIS3 spectrophotometers. The spectra in the range 4000–400 cm^{-1} were measured for KBr discs or $CHCl_3$ solution. Far ir spectra were measured for Nujol mulls supported between polyethylene sheets. Atmospheric water was removed from the spectrophotometer housing by flushing with dry nitrogen. The electronic spectra have been recorded with a Shimadzu MPS-50L spectrophotometer in the solid state in the range 4000–27 000 cm^{-1}.

Magnetic susceptibility measurements were carried out by Gouy's method at room temperature. Molecular susceptibilities were corrected for diamagnetism of the component atoms using Pascal's constants. Conductivity measurements were carried out with a WTW LBR type conductivity bridge at 25 °C for 10^{-3} M solutions in N,N'-dimethylformamide.

Acknowledgments

We thank Dr. R. Grani for his experimental work and the National Research Council (C.N.R.) of Italy for financial support.

1. P. Bassignana, C. Cogrossi, and M. Gandino. Spectrochim. Acta, **19**, 1885 (1963).
2. M. Tamura, H. Hada, J. Noguchi, and S. Hayashi. J. Phys. Chem. **66**, 559 (1962) and references therein.
3. M. St. C. Flett. J. Chem. Soc. 347 (1953).
4. E. Lieber, C. N. R. Rao, C. N. Pillai, and R. D. Hites. Can. J. Chem. **36**, 801 (1958).
5. L. J. Bellamy. The infrared spectra of complex molecules. J. Wiley, New York. 1966.
6. C. N. R. Rao and R. Venkataraghavan. Spectrochim. Acta, **18**, 541 (1962).
7. C. N. R. Rao, R. Venkataraghavan, and T. R. Kasturi. Can. J. Chem. **42**, 36 (1964).
8. R. T. Morrison and R. N. Boyd. Organic chemistry. Allyn and Bacon Inc., Boston. 1963.
9. N. N. Y. Chan, M. Goodgame, and M. J. Weeks. J. Chem. Soc. A, 2499 (1968).
10. D. M. L. Goodgame, M. Goodgame, and G. W. Rayner-Canham. Inorg. Chim. Acta, **6**, 245 (1972).
11. M. Massacesi, G. Ponticelli, and C. Preti. J. Inorg. Nucl. Chem. **37**, 1641 (1975).
12. M. J. M. Campbell, D. W. Card, R. Grzeskowiak, and M. Goldstein. J. Chem. Soc. A, 1687 (1972).
13. C. Preti, G. Tosi, D. De Filippo, and G. Verani. Can. J. Chem. **52**, 2021 (1974).
14. D. De Filippo and C. Preti. J Chem. Soc. A, 1904 (1970).
15. G. Devoto, G. Ponticelli, and C. Preti. J. Inorg. Nucl. Chem. **37**, 1635 (1975).
16. A. E. Underhill and D. E. Billing. Nature, **210**, 834 (1966).
17. A. B. P. Lever. Inorganic electronic spectroscopy. *Edited by* M. F. Lappert. Elsevier, Amsterdam. 1968.
18. B. P. Kennedy and A. B. P. Lever. Can. J. Chem. **50**, 3488 (1972).
19. W. J. Eilbeck, F. Holmes, C. E. Taylor, and A. E. Underhill. J. Chem. Soc. A, 1189 (1968).
20. S. L. Holt and R. L. Carlin. J. Am. Chem. Soc. **86**, 3017 (1964).
21. J. R. Allan, D. H. Brown, and M. Lappin. J. Inorg. Nucl. Chem. **32**, 2287 (1970).
22. P. P. Singh and R. Rivest. Can. J. Chem. **46**, 2361 (1968).
23. U. Agarwala, V. A. Narayan, and S. K. Dikshit. Can. J. Chem. **45**, 1057 (1967).
24. U. Agarwala and S. K. Dikshit. J. Inorg. Nucl. Chem. **30**, 1248 (1968).
25. B. Singh and R. Singh. J. Inorg. Nucl. Chem. **34**, 3449 (1972).
26. B. Singh and K. P. Thakur. J. Inorg. Nucl. Chem. **36**, 1735 (1974).
27. I. S. Ahuja. J. Inorg. Nucl. Chem. **29**, 2091 (1967).
28. C. Postmus, J. R. Ferraro, A. Quattrochi, K. Shobatake, and K. Nakamoto. Inorg. Chem. **8**, 1851 (1969).
29. M. Goldstein and W. D. Unsworth. Spectrochim. Acta Part A, **28**, 1107 (1972).
30. R. C. Weast (*Editor*). Handbook of Chemistry and Physics, 49th ed. The Chemical Rubber Co., Cleveland, Ohio. 1968–1969. p. C204.

Photoamidation of 2,3,4,6-tetra-*O*-acetyl-1-deoxy-D-*arabino*-hex-1-enopyranose and of (*Z*)-3-deoxy-3-*C*-(methoxycarbonyl)methylene-1,2:5,6-di-*O*-isopropylidene-α-D-*ribo*-hexofuranose

ALEX ROSENTHAL AND M. RATCLIFFE

Department of Chemistry, The University of British Columbia, Vancouver, British Columbia V6T 1W5

Received July 7, 1975

ALEX ROSENTHAL and M. RATCLIFFE. Can. J. Chem. **54**, 91 (1976).

The acetone-initiated photochemical addition of formamide to 2,3,4,6-tetra-*O*-acetyl-1-deoxy-D-*arabino*-hex-1-enopyranose (**1**) afforded 3,4,5,7-tetra-*O*-acetyl-2,6-anhydro-D-*glycero*-D-*ido*-heptonamide (**2**), 3,4,5,7-tetra-*O*-acetyl-2,6-anhydro-D-*glycero*-D-*talo*-heptonamide (**3**), and 4,5,6,8-tetra-*O*-acetyl-3,7-anhydro-1-deoxy-2-methyl-D-*glycero*-D-*talo*-octitol (**4**), in 55, 7, and 23% yields, respectively. Reduction of **2** with diborane followed by acetylation yielded 1-acetamido-3,4,5,7-tetra-*O*-acetyl-2,6-anhydro-1-deoxy-D-*glycero*-D-*ido*-heptitol (**7**) in 70% yield. Deacetylation of **2** and **3** with sodium methoxide yielded the unsubstituted heptonamides **5** and **6**.

Photoamidation of (*Z*)-3-deoxy-3-*C*-(methoxycarbonyl)methylene-1,2:5,6,-di-*O*-isopropylidene-α-D-*ribo*-hexofuranose (**8**) yielded 3-*C*-[*R* and *S*-carbamoyl(methoxycarbonyl)methyl]-3-deoxy-1,2:5,6-di-*O*-isopropylidene-α-D-allofuranose (**9**) and (**10**).

ALEX ROSENTHAL et M. RATCLIFFE. Can. J. Chem. **54**, 91 (1976).

L'addition photochimique, initiée par l'acétone, de la formamide au tétra-*O*-acétyl-2,3,4,6 déoxy-1 D-*arabino*-hexèno-1 pyrannose (**1**) conduit au tétra-*O*-acétyl-3,4,5,7 anhydro-2,6 D-*glycéro*-D-*ido*-heptonamide (**2**), au tétra-*O*-acétyl-3,4,5,7 anhydro-2,6 D-*glycéro*-D-*talo*-heptonamide (**3**) et au tétra-*O*-acétyl-4,5,6,8 anhydro-3,7 déoxy-1 méthyl-2 D-*glycéro*-D-*talo*-octitol (**4**) avec des rendements respectifs de 55, 7 et 23%. La réduction de **2** par le diborane, suivie par une acétylation, conduit à l'acétamido-1 tétra-*O*-acétyl-3,4,5,7 anhydro-2,6 déoxy-1 D-*glycéro*-D-*ido*-heptitol (**7**) avec un rendement de 70%. La déacétylation de **2** et de **3** par le méthylate de sodium conduit aux heptonamides **5** et **6** non-substitués.

La photoamidation du (*Z*) déoxy-3 (méthoxycarbonyl)méthylène-3-*C* di-*O*-isopropylidène-1,2:5,6 α-D-*ribo*-hexofurannose (**8**) conduit aux [*R* et *S*-carbamoyl(méthoxycarbonyl)méthyl]-3-*C* déoxy-3 di-*O*-isopropylidène-1,2:5,6 α-D-allofuranoses (**9**) et (**10**).

[Traduit par le journal]

The photoamidation (1, 2) of unsaturated carbohydrates provides a facile procedure for achieving anti-Markovnikov hydrocarbamoylation (hydrogen and carbamoyl (O=Ċ—NH_2)) of carbon–carbon double bonds. Thus, application of this reaction to 3-deoxy-1,2:5,6-di-*O*-isopropylidene-α-D-*erythro*-hex-3-enofuranose (3) afforded branched-chain products in which the carbamoyl group had added exclusively to C-3, and *trans* addition of the addends occurred. Similarly, photoamidation of 1,2,4,6-tetra-*O*-acetyl-3-deoxy-α-D-*erythro*-hex-2-enopyranose (4) yielded anti-Markovnikov products exclusively, but both *trans* and *cis* addition of the addends took place (the major product occurred via *cis* addition). When both carbon atoms of the unsaturated group bear hydrogen, the addition is non-selective (5).

Irradiation of 2,3,4,6-tetra-*O*-acetyl-1-deoxy-D-*arabino*-hex-1-enopyranose (**1**) in the presence of 1,3-dioxolane gave only *endo cis*-addition products (6). It therefore appeared to be interesting to extend the photoamidation reaction to **1** to determine if there exists any generalizations of the stereochemistry of the addition of different addends to the same starting compound.

When a solution of compound **1** in acetone containing formamide and *tert*-butyl alcohol was irradiated through a Pyrex filter for 24 h according to the previously published procedure (3, 5), a mixture of three products, **2**, **3**, and **4** was formed (Scheme 1) in 55, 7, and 23% yields, respectively. The principal product **2** was readily obtained pure by fractional crystallization of the product mixture from ethanol – petroleum ether (bp 30–60 °C). Column chromatography of the mother liquors on silica gel with 10:5:1 benzene – ethyl ether – ethanol afforded the remaining components in pure form.

The structures of the photoproducts were

Can. J. Chem. Downloaded from www.nrcresearchpress.com by 210.87.254.5 on 09/05/12
For personal use only.

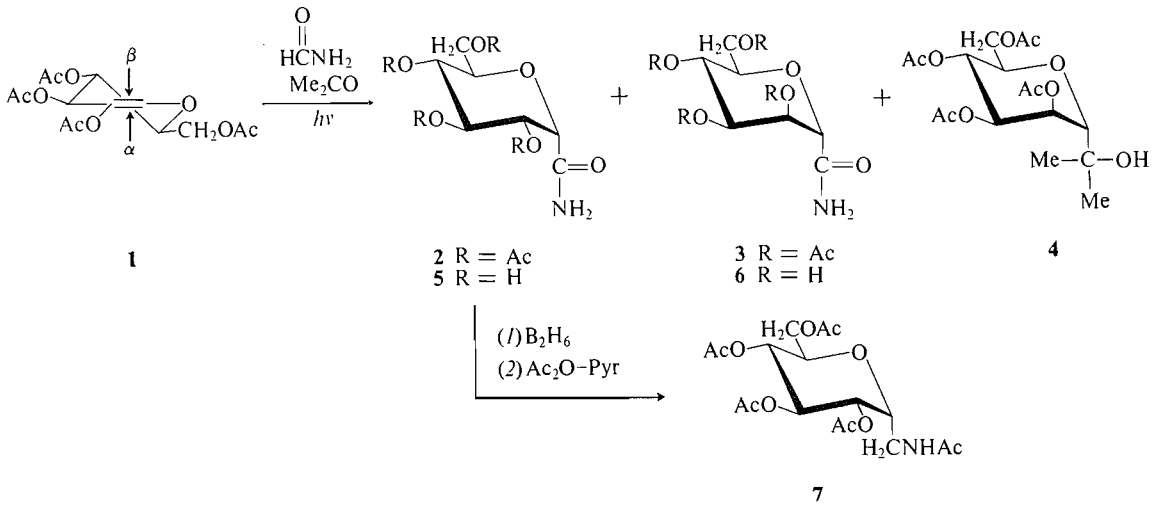

1 2 R = Ac, 5 R = H 3 R = Ac, 6 R = H 4 7

SCHEME 1

TABLE 1. Nuclear magnetic resonance spectral data of **2**, **3**, **4**, and **7**

Protons	Chemical shifts in τ value[a]			
	2	**3**	**4**	**7**
H-1				6.36–6.65 (m)
H-2	5.48 (d)	5.51 (d)		5.5–6.0 (overlapping)
H-3	4.93 (q)	4.18 (q)	6.63 (d)	4.90 (q)
H-4	4.38 (t)	4.64–4.8 (m)	4.4 (q)	4.70 (t)
H-5	5.19 (t)		5.02 (q)	5.0 (t)
H-6	5.32–5.6 (m)	6.01	4.75 (t)	5.50–6.0
H-7,7[b]	5.65–5.95 (o)	5.6–5.91 (m)	6.37 (m)	
H-8,8[b]			5.8 (m)	
CH_3			8.79 (s)	
$OCOCH_3$	7.94, 7.95	7.88, 7.94, 8.0, 8.04	7.89, 7.90, 7.96, 8.04	7.9, 7.92, 7.96, 8.0
NH_2 or NH	2.9 and 3.3 (s)	3.14, 3.46 (s)		4.15 (s)
OH			7.78 (s)	
	Coupling constants in Hz			
H-2e–H-3a	5.2			5
H-2e–H-3e		2		
H-3a–H-4a	7.5			8
H-3e–H-4a		4.4		
H-3e–H-4e			0.8	
H-4e–H-5			3	
H-4a–H-5	7.5			8
H-5–H-6			10	7.8
H-6–H-7				
H-7–H-7[b]				

[a]s, singlet; d, doublet; t, triplet; m, multiplet; o, octet.
[b]These data were obtained in $CDCl_3$ and in $((CD_3)_2CO)^*$ by the use of tetramethylsilane as the internal standard.

readily deduced by analysis of their ir and pmr spectra. Compounds **2** and **3** showed amide peaks at 3575, 3450, and 1700 cm^{-1}, whereas **4** exhibited a hydroxyl peak at 3600 cm^{-1} and no amide peaks. The pmr spectra of **2**, **3**, and **4** (see Table 1) clearly showed doublets which were attributed to a single methine hydrogen, thus establishing that the carbamoyl and ketyl radical

Can. J. Chem. Downloaded from www.nrcresearchpress.com by 210.87.254.5 on 09/05/12
For personal use only.

Can. J. Chem. Downloaded from www.nrcresearchpress.com by 210.87.254.5 on 09/05/12
For personal use only.

($(CH_3)_2\dot{C}OH$) had added exclusively to C-1 of **1**. Irradiation of the doublets in the pmr spectra of the heptonamides **2** and **3** led to a collapse of the H-3 quartets to doublets having $J_{3,4}$ = 7.5 and 4.4 Hz, respectively. Therefore, H-3 of **2** must be in the axial orientation and H-3 of **3** must be in the equatorial orientation. The much larger $J_{2,3}$ of compound **2** (5.2 Hz) than of compound **3** (2 Hz) suggests that H-2 of **2** probably exists in the equatorial orientation and H-2 of **3** undoubtedly is in the equatorial orientation. Corroboration that the configuration of C-2 of both compounds was the same was provided by the fact that compounds **5** and **6** (deacetylated **2** and **3**) exhibited positive Cotton effects in their circular dichroism spectra. Furthermore, reduction of **2** followed by acetylation afforded an acetamido derivative **7** which was different from the known 1-acetamido-3,4,5,7-tetra-*O*-acetyl-2,6-anhydro-1-deoxy-D-*glycero*-D-*gulo*-heptitol (C-2 epimer of **7**) previously reported (7). A first-order analysis of the pmr spectrum of **7** showed that it had the D-*glycero*-D-*ido*-configuration. Thus compound **2** must be 3,4,5,7-tetra-*O*-acetyl-2,6-anhydro-D-*glycero*-D-*ido*-heptonamide and compound **3** is 3,4,5,7-tetra-*O*-acetyl-2,6-anhydro-D-*glycero*-D-*talo*-heptonamide.

A first-order analysis of the pmr spectrum of the hydroxyalkylation photoproduct **4** readily showed that it had approximately the same $J_{3,4}$ (0.8 Hz) and $J_{4,5}$ (5 Hz) values as the $J_{2,3}$ and $J_{3,4}$ values of compound **3**. Thus, the configuration of C-3 and C-4 of **4** must be the same as the configuration of C-2 and C-3 of **3** and compound **4** must be 4,5,6,8-tetra-*O*-acetyl-3,7-anhydro-1-deoxy-2-methyl-D-*glycero*-D-*talo*-octitol. It is interesting to note that the carbamoyl and ketyl radicals have added to C-1 of the 2-hydroxy-1-enopyranosyl ring from the α-side exclusively whereas the 1,3-dioxolan-2-yl radical was found to add from both the α- and β-side of the ring (6). Although *cis* addition of the ketyl and hydrogen addends occurred to yield **4** (similar *cis* addition of the 1,3-dioxolan-2-yl and hydrogen radicals to **1** took place (6)), both *cis* and *trans* addition of the carbamoyl and hydrogen radicals occurred.

The crystalline unblocked heptonamides **5** and **6** were obtained by treatment of **2** and **3** with sodium methoxide in anhydrous methanol followed by deionization with Amberlite IR-120 (H^+), filtration, and removal of the solvent.

Irradiation of (*Z*)-(or of *Z*,*E*)-3-deoxy-3-*C*-(methoxycarbonyl)-methylene-1,2:5,6-di-*O*-isopropylidene-α-D-*ribo*-hexofuranose (8) afforded a mixture of two amides **9** and **10** and an hydroxyalkyl product. Chromatographic separation of the products on silica afforded amides **9** and **10** in about equal yield (45% combined). The hydroxyalkyl product could not be obtained in pure form. The pmr spectra of **9** and **10** showed triplets at τ 5.08. and 5.13 which were attributed to H-2, thus establishing that the carbamoyl radical had added exclusively to the α-carbon near the ester group. The large coupling constants of 3.7 and 4.0 Hz for $J_{2,3}$ established that the sugar had the *allo* configuration. Thus compounds **9** and **10** are 3-*C*-[*R* and *S*-carbamoyl-(methoxycarbonyl)methyl]-3-deoxy-1,2:5,6-di-*O*-isopropylidene-α-D-allofuranose. In order to establish the chirality of the branched-chain moiety of **9** and **10**, the amides were subjected to Hofmann rearrangement reactions to afford the glycos-3-yl amino acids **11** which were expected to be similar to those previously synthesized. Because these reactions were unsuccessful, the amide **10** was partially unblocked and the diol then acetylated to yield a 5,6-di-*O*-acetate. Acetolysis of the latter compound with trifluoroacetic acid followed by acetylation afforded two γ-lactones **12** and **13** which were separated by chromatography. Compound **12** was readily established, by ir and pmr, to possess the ester and lactone functionalities, whereas **13** possessed the amide and lactone groupings. A first-order analysis of the pmr spectrum of **12** showed that H-3 had a large $J_{2,3}$ = 6 Hz and a small $J_{3,1'}$ = 2 Hz. Thus, the α-carbon of the lactone must possess *R* chirality and compound **12** is tentatively assigned the structure depicted. This deduction is corroborated by the fact that $J_{3,1'}$ of the lactone **13** was much larger (4 Hz) as expected and thus the chirality of the exocyclic carbon of **13** is *S*. Therefore compound **10** is 3-*C*-[*S*-carbamoyl(methoxycarbonyl)methyl]-3-deoxy-1,2:5,6-di-*O*-isopropylidine-α-D-allofuranose.

Surprisingly, the orientation of addition of the carbamoyl radical was exclusively toward the α-carbon atom of the α,β-unsaturated ester side chain. With aliphatic α,β-unsaturated esters the mode of addition of the carbamoyl radical is toward the β-carbon atom, except for the cinnamate, where the orientation is toward the α-carbon (2).

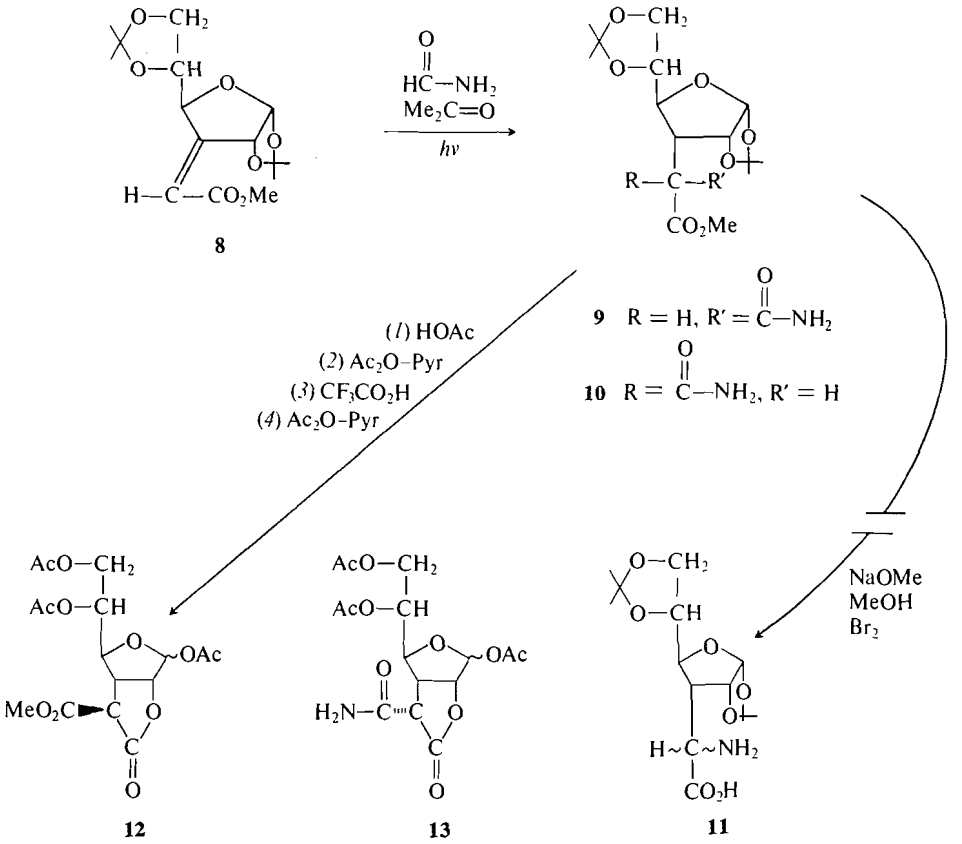

SCHEME 2

Experimental

General Conditions

These have been described previously (5).

Irradiation of 2,3,4,6-Tetra-O-acetyl-1-deoxy-D-arabino-hex-1-enopyranose, 1

Following an established procedure (4, 5), a mixture of compound **1** (2 g), formamide (30 ml), *tert*-butyl alcohol (15 ml), and acetone (15 ml) was added dropwise to a mixture of formamide (200 ml), *tert*-butyl alcohol (10 ml), and acetone contained in the photolysis cell. Irradiation was continued during the addition and prolonged for 24 h. After the solution had been concentrated to remove *tert*-butyl alcohol and acetone by evaporation (30 Torr at 50 °C), the resulting mixture was diluted with saturated aqueous sodium chloride (200 ml). The resulting solution was then extracted with dichloromethane (4 × 200 ml). The combined dichloromethane extract was concentrated to 100 ml and the resulting solution was washed with saturated aqueous sodium chloride (50 ml), dried over anhydrous sodium sulfate, filtered, and evaporated under diminished pressure to a syrup (2.1 g). The main product **2** (0.4 g, 18%) was obtained by fractional crystallization from ethanol – petroleum ether (bp 30–60 °C). A second recrystallization of **2** from the same solvent mixture afforded analytically pure 3,4,5,7-tetra-*O*-acetyl-2,6-anhydro-D-*glycero*-D-*ido*-heptonamide, mp 158–159 °C, $[\alpha]_D^{26}$ +16.5° (*c* 0.38, chloroform); ν_{max} (Nujol) 3570, 3450, and 1700 cm^{-1} ($CONH_2$). *Anal.* Calcd. for **2**, $C_{15}H_{21}NO_{10}$: C, 48.00; H, 5.64; N, 3.73; found: C, 47.80; H, 5.53; N, 3.53.

After product **2** had been removed from the recrystallization solvents, the mother liquor was evaporated to a syrup (1.6 g). This syrup was chromatographed on tlc silica gel (24.5 × 6.5 cm), with 10:5:1 benzene – ethyl ether – ethanol as a developer to afford the amide **2** (0.8 g, 36%), the amide **3** (0.16 g, 7%), and the alcohol **4** (0.540 g, 23%).

Compound **3** was recrystallized from ethyl ether – ethanol to yield pure 3,4,5,7-tetra-*O*-acetyl-2-6-anhydro-D-*glycero*-D-*talo*-heptonamide, mp 150.5–152 °C; $[\alpha]_D^{26}$ +3.0° (*c* 0.37, chloroform); ν_{max} (Nujol), 3595, 3460, and 1700 cm^{-1} ($CONH_2$). *Anal.* Calcd. for **3**, $C_{15}H_{21}NO_{10}$: C, 48.00; H, 5.64; N, 3.73; found: C, 47.88; H, 5.70; N, 3.50.

Compound **4** was recrystallized from ethanol – petroleum ether (bp 30–60 °C), mp 139–140 °C; $[\alpha]_D^{26}$ −18.5° (*c* 0.2, chloroform); ν_{max} (Nujol) 3600–3400 cm^{-1} (OH). *Anal.* Calcd. for **4**, $C_{17}H_{26}O_{10}$: C, 52.30; H, 6.71; found: C, 52.16; H, 6.76.

Can. J. Chem. Downloaded from www.nrcresearchpress.com by 210.87.254.5 on 09/05/12
For personal use only.

Can. J. Chem. Downloaded from www.nrcresearchpress.com by 210.87.254.5 on 09/05/12
For personal use only.

*2,6-Anhydro-D-glycero-D-ido-heptonamide, **5**, and 2,6-Anhydro-D-glycero-D-talo-heptonamide, **6***

To a solution of compound **2** (0.04 g) in 2 ml of anhydrous methanol was added a catalytic amount of sodium methoxide. After the resulting solution was stirred for 10 min, the sodium ions were removed with Amberlite IR-120 (H^+) resin. After filtering off the resin, removal of the solvent left a syrup (0.027 g). An analytical sample of **5** was crystallized from methanol–water, mp 219.5–221 °C; $[\alpha]_D^{26}$ +128° (*c* 0.34, water); τ (D_2O), 5.33 (d, 1H, H-2, $J_{2,3}$ = 1.5); cd $\Delta\epsilon$ +0.48 (ν_{max} 223 nm, water), $[\theta]_{223}^{30}$ +1585. *Anal.* Calcd. for **5**, $C_7H_{13}NO_6$: C, 40.58; H, 6.32; N, 6.76; found: C, 40.86; H, 6.43; N, 6.45.

Compound **3** (0.021 g) was deacetylated as described above for the preparation of **5** to afford compound **6** (0.011 g), mp 212–214 °C; $[\alpha]_D^{26}$ +11.7° (*c* 0.17, water); cd $\Delta\epsilon$ +500 (ν_{max} 208 nm, water), $[\theta]_{208}^{30}$ +500; τ ($(CD_3)_2CO$), 5.86 (t, 1H, H-3, $J_{2,3}$ = 1.5), 6.02 (d, 1H, H-2, $J_{2,3}$ = 1), 6.1–6.6 (overlapping peaks, 5H).

*1-Acetamido-3,4,5,7-tetra-O-acetyl-2,6-anhydro-1-deoxy-D-glycero-D-ido-heptitol, **7***

A solution of compound **2** (0.5 g) in 15 ml of anhydrous tetrahydrofuran was added dropwise to a cooled solution (0 °C) of diborane (9) in tetrahydrofuran (10 ml, 0.5 molar in BH_3) under dry nitrogen. After the resulting solution was refluxed for 3 h, a 0.1 *M* HCl aqueous solution (10 ml) was added dropwise to the cooled solution (~5 °C) with stirring. After 30 min, the solution was heated to evaporate most of the remaining tetrahydrofuran and to complete hydrolysis. After the resulting aqueous solution was evaporated to near dryness, the residue was diluted with methanol (4 × 50 ml) and the solvent removed *in vacuo*. The resulting residue (0.175 g) was thoroughly dried under reduced pressure, dissolved in pyridine (5 ml) and acetic anhydride (2 ml), and stirred at ambient temperature for 24 h. The solution was then evaporated to dryness and the residue taken up in water (10 ml) and extracted with dichloromethane (2 × 50 ml). The combined organic extracts were dried over anhydrous sodium sulfate, filtered, and the filtrate evaporated to dryness to yield a syrup (0.375 g, 70% yield) which was crystallized from ethyl ether, mp 124.5–125 °C; $[\alpha]_D^{26}$ +56.3° (*c* 0.19, chloroform); ν_{max} (Nujol) 3370, 3300, and 1690 cm^{-1} (—CONH—). *Anal.* Calcd. for $C_{17}H_{25}NO_{10}\cdot\frac{1}{2}H_2O$: C, 49.51; H, 6.33; N, 3.39; found: C, 49.56; H, 6.33; N, 3.32.

*Irradiation of (Z)-(or of Z,E)-3-Deoxy-3-C-(methoxycarbonyl)methylene-1,2:5,6-di-O-isopropylidene-α-D-ribo-hexofuranose, **8** to Yield Amides **9** and **10***

Compound **8** (10) (1 g) was irradiated and the products separated following the same procedure already described above. The three products were an acetone addition product (0.24 g, 21%), and two formamide products **9** and **10** in about equal yields (0.5 g, 45%). Compound **9** was crystallized from ethyl ether – petroleum ether (bp 30–60 °C), mp 105–107 °C; $[\alpha]_D^{30}$ +82° (*c* 0.15, chloroform); ν_{max} ($CHCl_3$) 1750 cm^{-1} (CO_2Me), 3520, 3420, and 1700 cm^{-1} ($CONH_2$); nmr data ($CDCl_3$) τ 3.90 (broad s, 2H, NH_2, exchanges with D_2O), 4.25 (d, 1H, H-1, $J_{1,2}$ = 3.7), 5.08 (t, 1H, H-2, $J_{2,3}$ = 3.7), 6.22 (s, 3H, CH_3), 6.47 (d, 1H, H-1′, $J_{1',3}$ = 10) 7.22 (q, 1H, H-3), 8.48, 8.6, 8.65 (3s, 12H, CH_3). Irradiation at τ 4.25 changed the signal at τ 5.08 to a doublet. Irradiation at τ 5.08 produced a singlet at τ 4.25 and a doublet at τ 7.22. Irradiation at τ 7.22 produced a doublet at τ 5.08 and a singlet at τ 6.47. *Anal.* Calcd. for $C_{16}H_{25}NO_8$: C, 53.48; H, 7.01; N, 3.90; found: C, 53.29; H, 7.01; N, 3.60.

Compound **10** was recrystallized from ethyl ether – petroleum ether (bp 30–60 °C), mp 75–77 °C; $[\alpha]_D^{28}$ + 25.2° (*c* 0.6, chloroform); ν_{max} ($CHCl_3$), 3510, 3420, 1700 cm^{-1} ($CONH_2$), 1750 cm^{-1} (CO_2Me); nmr data ($CDCl_3$) τ 3.8 (broad s, 2H, exchanges with D_2O), 4.2 (d, 1H, H-1, $J_{1,2}$ = 4), 5.16 (t, 1H, H-2, $J_{2,3}$ = 4), 6.22 (s, 3H, CH_3), 6.36 (d, 1H, H-1′, $J_{1',3}$ = 8), 7.3 (q, 1H, H-3), 8.45, 8.57, 8.68 (3s, 12H, CH_3). Irradiation at τ 4.2 produced a doublet at τ 5.16. Irradiation at τ 5.16 produced a singlet at τ 4.2 and a doublet at τ 7.3. Irradiation at τ 7.3 produced a doublet at τ 5.16 and a singlet at 6.36.

The acetone addition product was not characterized.

*Attempted Conversion of Amides **9** and **10** into Glycosyl Amino Acids **11***

The glycosyl amides **9** and **10** were unaffected by treatment with (*1*) 6% aqueous sodium hypochlorite, (*2*) bromine and sodium methoxide in methanol, (*3*) lead tetraacetate in anhydrous *N*,*N*-dimethylformamide.

*Formation of 2,3-γ-Lactones from Amide **10***

The pure amide **10** (0.015 g) was dissolved in 66% aqueous acetic acid (1 ml) and left at room temperature for 12 h. The solvent was removed under diminished pressure and the resulting residue was dissolved in chloroform (3 ml) and the organic solution was washed with water (1 ml). After drying the organic solution with anhydrous sodium sulfate, filtering and removal of the solvent under diminished pressure, the residue was dissolved in pyridine (1 ml) and acetic anhydride (0.1 ml). After the solution was left standing for 30 min at room temperature, the solvent was removed under diminished pressure. The residue was dried by co-distillation with toluene (1 ml) and the resulting syrup (0.01 g) was then dissolved in 80% trifluoroacetic acid at 0 °C. After allowing the solution to warm to room temperature, the solvent was removed under diminished pressure and any remaining trifluoroacetic acid removed by successive co-distillation with toluene (2 × 1 ml) under reduced pressure. The resulting syrup (0.008 g) was acetylated as described above to give two compounds which were separated by chromatography on tlc silica (10 × 1 cm) using 1:1 benzene – ethyl acetate as developer. The major component was tentatively assigned the structure 1,5,6-tri-*O*-acetyl-3-deoxy-3-*C*-[(*R*)-acetoxy(methoxycarbonyl)methyl]-2,3-γ-lactone-β-D-allofuranose (**12**) (0.005 g); $[\alpha]_D^{28}$ −2.7° (*c* 0.4 chloroform); ν_{max} ($CHCl_3$) 1795 cm^{-1} (γ-lactone) and 1742 cm^{-1} (OAc); nmr data ($COCl_3$) τ 3.60 (s, 1H, H-1), 4.93 (d, 1H, H-2, $J_{2,3}$ = 6), 6.27 (s, 3H, CH_3) 6.4 (q, 1H, H-3, $J_{3,1'}$ = 2) 7.36, 7.87, 7.94 (3s, 9H, OAc).

The minor component was tentatively assigned the structure of 1,5,6-tri-*O*-acetyl-3-deoxy-3-*C*-[(*S*)-carboxy-(carbamoyl)methyl]-2,3-γ-lactone-α(and β)-D-allofuranose (**13**) (0.003 g); $[\alpha]_D^{28}$ −42° (*c* 0.1, chloroform); ν_{max} ($CHCl_3$) 3480, 3270, and 1700 cm^{-1} ($CONH_2$), 1780 cm^{-1} (γ-lactone), 1745 cm^{-1} (OAc); nmr data ($CDCl_3$) τ 3.48 (d, 1H, H-1, $J_{1\alpha,\beta}$ = 4), 3.6 (s, 1H, H-1β), 4.35 (broad s,

2H, NH_2), 6.18 (d, 1, H-1′β, $J_{1',3} = 4$), 6.44 (q, 1H, H-3β, $J_{2,3} = 10$), 7.86, 7.92 (2s, 9H, OAc).

Acknowledgments

The authors wish to acknowledge the financial support of the National Research Council of Canada.

1. D. ELAD and J. ROKACH. J. Org. Chem. **29**, 1855 (1964); D. ELAD and J. ROKACH. J. Chem. Soc. 800 (1965).
2. D. ELAD and J. ROKACH. J. Org. Chem. **30**, 3361 (1965); J. ROKACH and D. ELAD. J. Org. Chem. **31**, 4210 (1966).
3. A. ROSENTHAL and K. SHUDO. J. Org. Chem. **37**, 1608 (1972).
4. A. ROSENTHAL and M. RATCLIFFE. Carbohydr. Res. **39**, 79 (1973).
5. A. ROSENTHAL and A. ZANLUNGO. Can. J. Chem. **50**, 1192 (1972).
6. K. MATSUURA, K. NISHIYAMA, K. YAMADA, Y. ARAKI, and Y. ISHIDO. Bull. Chem. Soc. Jpn. **46**, 2538 (1973).
7. B. COXON and H. G. FLETCHER, JR. J. Am. Chem. Soc. **85**, 2637 (1963).
8. R. J. FERRIER and G. H. SANKEY. J. Chem. Soc. 2345 (1966).
9. H. C. BROWN and P. HEIM. J. Org. Chem. **38**, 912 (1973).
10. A. ROSENTHAL and L. NGUYEN. J. Org. Chem. **34**, 1029 (1969).

Can. J. Chem. Downloaded from www.nrcresearchpress.com by 210.87.254.5 on 09/05/12
For personal use only.

Ormosia alkaloids. VII. Total synthesis of ormosanine, piptanthine, 18-epiormosanine, and *d,l*-panamine[1]

HSING-JANG LIU, YASUHIKO SATO, ZDENEK VALENTA, JEROME SUTHERLAND WILSON, AND TERRY TA-JEN YU

Department of Chemistry, University of New Brunswick, Fredericton, New Brunswick E3B 5A3

Received July 17, 1975

HSING-JANG LIU, YASUHIKO SATO, ZDENEK VALENTA, JEROME SUTHERLAND WILSON, and TERRY TA-JEN YU. Can. J. Chem. **54**, 97 (1976).

A stereoselective synthesis of ormosanine (**1**), identical in all respects with the naturally occurring racemic alkaloid of *O. jamaicensis*, has been accomplished. Subsequent transformation of synthetic ormosanine into racemic piptanthine (**2**) and into *d,l*-panamine (**3**) is described. 18-Epiormosanine (**22**) has also been prepared by total synthesis. Some unusual stereochemical effects allowing the control of configuration at C_6, C_{11}, and C_{18} are discussed.

HSING-JANG LIU, YASUHIKO SATO, ZDENEK VALENTA, JEROME SUTHERLAND WILSON et TERRY TA-JEN YU. Can. J. Chem. **54**, 97 (1976).

On a réalisé une synthèse stéréosélective d'une ormosanine (**1**) identique en tous points à l'alcaloïde racémique que l'on retrouve dans l'*O. jamaicensis*. On décrit aussi la transformation subséquente de l'ormosanine de synthèse en pipthantine racémique (**2**) et en *d,l*-panamine (**3**). On a aussi préparé par synthèse totale l'épi-18 ormosanine (**22**). On discute de quelques effets stéréochimiques inusités permettant de contrôler la configuration au niveau des carbones C_6, C_{11} et C_{18}.

[Traduit par le journal]

Introduction

We wish to report an eleven-step total synthesis of ormosanine (**1**) (2–6), a widely occurring C_{20} *Ormosia* alkaloid,[2] using ethyl 2-pyridineacetate as starting material. No relays were used in the synthesis and the correct configuration of all relevant asymmetric centers was achieved either exclusively or in strong preference. Since naturally occurring ormosanine is racemic (5), no resolution was required. Subsequent transformation of synthetic ormosanine into natural racemic piptanthine (**2**) (7–10, 13–15) and *d,l*-panamine (**3**) (2, 5, 9–11) has also been performed.[3] The work, hence, also represents the total syntheses of these two additional *Ormosia* bases.

Our choice of synthetic design was strongly influenced by the following considerations.

(*a*) The presence of three basic groups in ormosanine and related alkaloids makes the compounds relatively unstable. It was therefore decided to carry the nitrogen atoms through most of the synthesis in the form of lactams and/or pyridines.

(*b*) The azabicyclo[3.3.1]nonane system represents a special feature of the *Ormosia* alkaloid skeleton. It appeared desirable to form it in an efficient way in the early stages of the synthesis, keeping in mind that the C_9—C_{18} bond must be preformed and that the formation of the C_{15}—C_{16} bond could present special difficulties.

(*c*) Stereochemical control is obviously crucial in the synthesis of a compound with six asymmetric carbons allowing 16 geometrically possible diastereoisomers. The stereochemical problem is, however, significantly simplified by previous work on the structure, interconversion, and configuration of *Ormosia* alkaloids. Some time ago, we have been able to achieve a catalytic epimerization at C_6 which converted ormosanine into the alkaloid piptanthine (**2**) (10). Thus, the preparation of compounds with C_6—H *trans* to the C_7–C_9 bridge would lead to the synthesis of

[1]For part VI in this series, see ref. 1.

[2]A part of this work has been reported in preliminary form (1).

[3]It is interesting to note that, until recently, racemic piptanthine had not been reported as a naturally occurring base. (Natural piptanthine from *P. nanus* is *levo*-rotatory (8).) Recently, racemic piptanthine was found in *O. semicastrata* (13, 14) and later in traces in *Templetonia retusa* (Vent.) (15). An exchange of samples with Professor S. McLean, University of Toronto, established the identity of the natural and synthetic racemic base. Only *levo*-rotatory panamine has been isolated from nature up to date (5); its absolute configuration is now known (15).

Can. J. Chem. Downloaded from www.nrcresearchpress.com by 210.87.254.105 on 09/05/12
For personal use only.

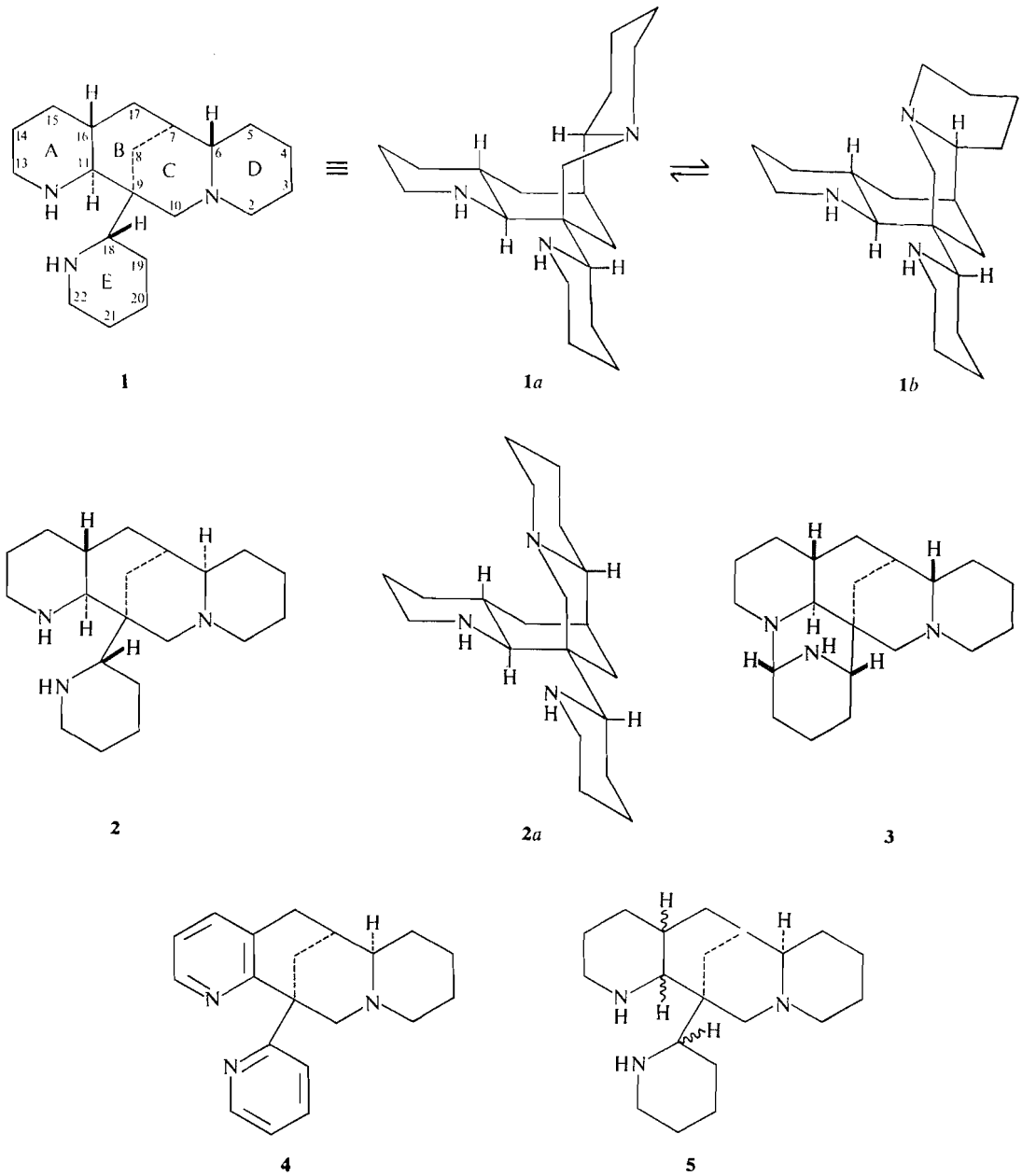

1 1*a* 1*b*

2 2*a* 3

4 5

both ormosanine (**1**) and piptanthine (**2**), while the less favorable exclusive formation of compounds with C_6—H *cis* to the C_7–C_9 bridge could at least allow the synthesis of piptanthine (**2**). Furthermore, the dipyridine **4** obtained by a mild catalytic dehydrogenation of ormosanine (**1**) (16) and related alkaloids (6), had previously been converted in our laboratory into five of the eight theoretically possible diastereoisomers of the general formula **5** (10). This reduction study encouraged us to expect that the configuration at centers C_{11}, C_{16}, and C_{18} could be controlled at the appropriate later stages of the total synthesis through a proper choice of reagents.

Can. J. Chem. Downloaded from www.nrcresearchpress.com by 210.87.254.105 on 09/05/12
For personal use only.

Can. J. Chem. Downloaded from www.nrcresearchpress.com by 210.87.254.105 on 09/05/12
For personal use only.

Synthesis of the Skeleton

An efficient construction of four of the five rings of ormosanine (**1**) was achieved in three synthetic steps. Following Clemo *et al.* (17), ethyl 2-pyridineacetate was treated with ethyl orthoformate in boiling acetic anhydride to give an 86% yield of the yellow crystalline ester **6**.[4] Selective hydrogenation with palladium-on-charcoal in ethanol then efficiently converted **6** into a mixture of isomers represented by the general formula **7**. Intermediate **7** contains rings C, D, and E of ormosanine with the two nitrogen atoms suitably protected; furthermore, the doubly activated hydrogen atom at C_9 and the ester grouping at C_7 provide functionalities suitable in principle for the attachment of rings A and B. Before the synthetic elaboration of **7** is described, its stereochemistry and purity deserve comment.

An extensive chromatographic analysis of **7** revealed the presence of two major isomers (out of the theoretically possible four) which proved difficult to separate efficiently.[5] One was characterized as the corresponding picrate.[4] Since all isomers of **7** should be interconvertible under conditions which allow equilibration at C_7 and C_9, crude oily **7** was used in further synthesis. Treatment of **7** with sodium hydride and ethyl acrylate in *N*,*N*-dimethyl formamide gave the crystalline enol ester **8**;[6] no detectable trace of the C_6-epimer could be found in the mother liquors. The overall yield of the two step conversion **6** → **8** was 42% of pure crystalline material. The structure of **8** follows unambiguously from its analysis and from its spectral properties; a sharp singlet corresponding to one hydrogen atom at τ −2.2 in its nuclear magnetic resonance (nmr) spectrum is characteristic of the chelated hydroxyl group (18), while the presence of infrared maxima at 1640 (lactam) and 1660 cm^{-1} (enol ester) and the complete absence of carbonyl absorption above 1700 cm^{-1} show that, interestingly, the keto ester grouping is fully enolized (19). The ultraviolet spectrum showing a maximum at 254 nm (log ϵ 4.1) shifting in base to 280 nm is also in full agreement with the proposed structure (20).

As far as stereochemistry is concerned, the conversion of **8** into ormosanine and several of its isomers together with the physical properties of these pentacyclic compounds rigorously establishes that the C_6-hydrogen atom in **8** is *trans* to the C_7–C_9 bridge. Details of this assignment are described in the stereochemistry section. It should be noted that we originally made an incorrect stereochemical assignment for the C_6-proton in a preliminary communication written before the synthesis of pentacyclic triamines was achieved (21). The reason for this error is interesting. Ester **8** was subjected to acid hydrolysis to give in 80% yield the crystalline ketone **9** which on subsequent vigorous reduction with lithium aluminum hydride gave an oily mixture of hydroxy amine epimers **10**. This mixture shows strong bands in the 2800 cm^{-1} region of its infrared (ir) spectrum taken in chloroform, characteristic of at least two hydrogen atoms situated α to the tertiary nitrogen and antiparallel to the nitrogen electron pair (22). Since, in the pentacyclic alkaloid series, all bases containing the C_6-hydrogen atom *cis* to the C_7–C_9 bridge show these strong bands in solution while the corresponding bases with a *trans* arrangement do not (10), and since **10** does not differ greatly from the alkaloids in the proximity of the tertiary nitrogen atom, we felt that an extrapolation to the tetracyclic series was justified. The completion of the ormosanine synthesis and the ir study of all synthetic pentacyclic bases described below now not only rigorously establishes the stereochemistry of **8** at C_6, but shows that the ir bands in the 2800 cm^{-1} region must be interpreted with caution, particularly in systems possessing configurational and conformational instability. Based on the now established stereochemistry, the ir result shows that **10** is present in solution in form **10***a* (or the corresponding boat-form cyclohexanol) rather than **10***b* or **10***c*.

Our evidence does not lead to an unique explanation of the fact that the formation of **8** is stereospecific with ethyl acrylate adding to C_9 exclusively from a direction *cis* to the C_6-hydrogen atom. One possible rationalization is provided by the assumption that the two reduction products **7** are epimeric only at C_9, that the

[4]All analytical data are recorded in the experimental section; only those of special relevance are discussed.

[5]Although the present evidence cannot be considered rigorous, we believe that our inability to prepare a pure isomer **7** arises from equilibration at C_9 during chromatographic purification. Attempts to prepare the C_6-epimer of **8** by vigorous base treatment of **7** before acrylate addition have so far proved unsuccessful.

[6]All synthetic compounds described in this paper are racemic. One absolute configuration is arbitrarily chosen for illustrations.

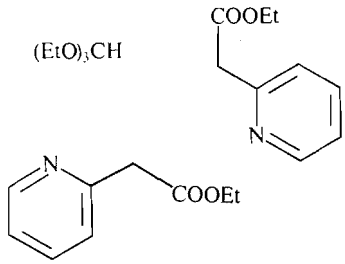

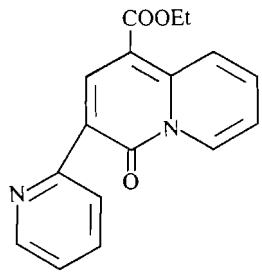

6

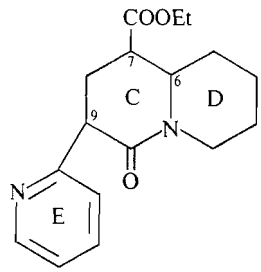

7

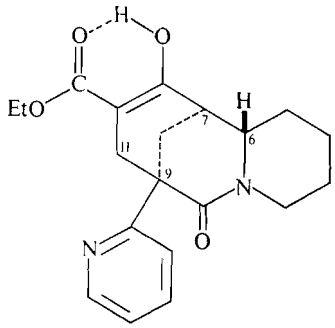

8

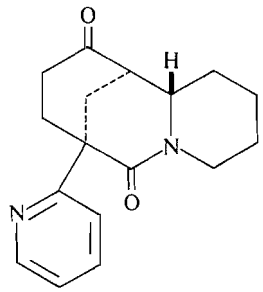

9

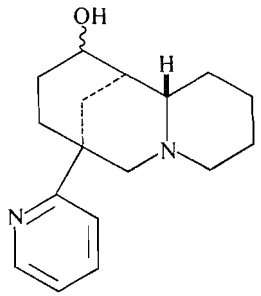

10

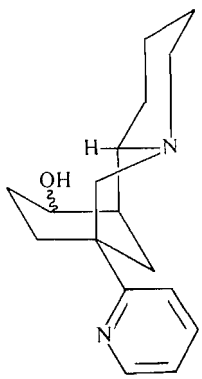

10*a*

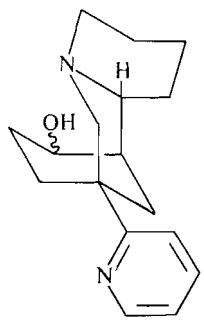

10*b*

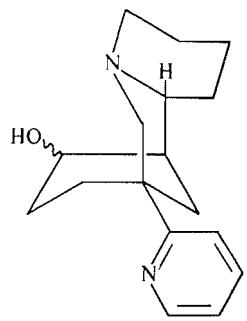

10*c*

hydrogen atoms at C_6 and C_7 in both esters **7** are *cis* as a result of hydrogenation, and that the ester group at C_7 does not epimerize before ethyl acrylate adds to C_9. The enolate **11***a* ⇌ **11***b* might well add acrylate exclusively from the observed direction and this addition could then be followed by epimerization at C_7 and cyclization.[5]

The ease of the three-step conversion of ethyl 2-pyridineacetate into tetracyclic compounds suitable for the synthesis of *Ormosia* alkaloids encouraged us to study the condensation step in more detail. The possibility of condensing **7** with compounds of the type **12** (R = Me, H, or Ac) appeared particularly tempting. However, no condensation of a preformed ring A with lactam **7** could be achieved. It was found that methyl and ethyl vinyl ketone could be used instead of ethyl acrylate in the condensation step, but the products, formed in low yield, did not offer the synthetic versatility of enol ester **8**.

With the synthesis of the tetracyclic intermediates **8** and **9** completed, it now remained to annelate ring A and, finally, to perform several reduction steps under stereochemical control.

Can. J. Chem. Downloaded from www.nrcresearchpress.com by 210.87.254.105 on 09/05/12
For personal use only.

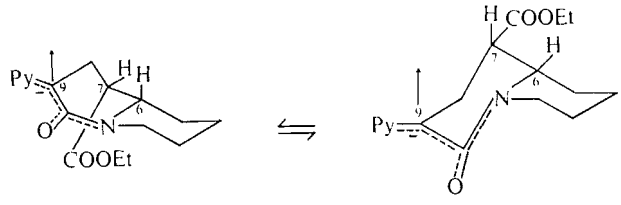

11*a* **11***b*

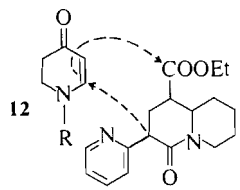

12 **7**

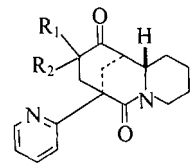

13 R_1 = H, R_2 = CH_2CH_2COOEt
14 R_1 = R_2 = CH_2CH_2COOEt
15 R_1 = Br, R_2 = CH_2CH_2COOEt

After extensive initial difficulties, two methods were developed leading to the complete skeleton. The preparatively simpler one will be described here and used for the completion of ormosanine synthesis. The second method, involving a photo-addition fragmentation sequence (21, 23), will be described in detail in a separate communication.

Michael addition of **9** to ethyl acrylate with sodium hydride in benzene at 70 °C gave the desired oily keto ester **13** in good yield. A small amount of the crystalline dialkylation product **14** was also obtained. Ester **13** was purified and characterized via the corresponding crystalline acid. Bromination of **13** with bromine in carbon tetrachloride gave the crystalline bromo ketone **15** which was subjected to dehydrobromination with boiling pyridine. The resulting crystalline olefin **16** was obtained in 70% yield for the last three steps. The endocyclic nature of the double bond in **16** follows rigorously from the sharpness of the nmr signal for the vinyl hydrogen atom, from the fact that **16** is also obtained (21) in an entirely different synthetic sequence in which the double bond position at C_{11}—C_{16} is unambiguous, and from subsequent transformations.

It can now be seen that ester **16** contains all the carbon atoms of ormosanine and that, in order to complete the synthesis of the required skeleton, a nitrogen atom has to be incorporated at C_{11}. This incorporation could be achieved simply by a prolonged passing of ammonia gas through an ethanolic solution of ester **16** which led to crystalline keto dilactam **17**, mp 245–247 °C, in a 70% yield. The structure (but not stereochemistry) of dilactam **17** follows rigorously from spectral and analytical data and from its subsequent transformations.

Thus, ethyl 2-pyridineacetate has been converted into keto dilactam **17** containing the complete skeleton of C_{20} *Ormosia* alkaloids in eight synthetic steps and a 14% overall yield. The synthesis involves essentially the condensation of two molecules of ethyl 2-pyridineacetate, one molecule of ethyl orthoformate, two molecules of ethyl acrylate and one molecule of ammonia.

The stereochemistry at C_{11} and at C_{16} in dilactam **17** must now be discussed. The following considerations strongly favor the configuration at C_{11} indicated in formula **17**. Firstly, inspection of stereoformula **16***a* (corresponding to **16**), shows that the addition of ammonia

Can. J. Chem. Downloaded from www.nrcresearchpress.com by 210.87.254.105 on 09/05/12
For personal use only.

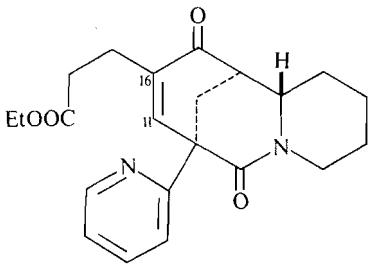

16

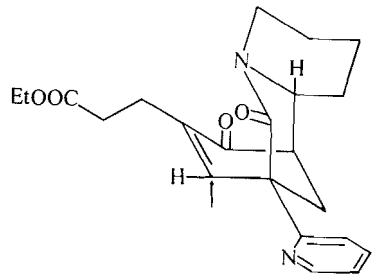

16*a*

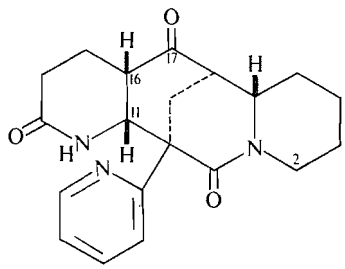

17

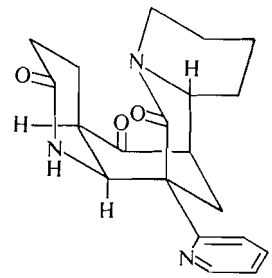

18

should be expected to proceed axially from the less hindered *exo* side.[7] If this assignment is correct, the configuration at C_{16} follows: the coupling constant of C_{11}—H in the nmr spectrum of **17** (4 Hz) only agrees with a cisoid attachment of ring A. Secondly, keto dilactam **17** proved stable to attempted epimerization at C_{16} by mild acid or base. This is expected for stereochemistry **17** (see stereoformula **17***a*). A similar stability order at C_{16} had previously been observed for the epimeric pair tetrahydro-ormojanine – iso-tetrahydro-ormojanine (10). The only other possible isomer with a cisoid attachment of ring A, **18**, could clearly be expected to epimerize to **19** (10). Finally, a mild reduction sequence in which the keto group of dilactam **17** was removed by treatment with sodium borohydride, dehydration of the resulting alcohol and hydrogenation did not lead to ormosanine (**1**), piptanthine (**2**), or any other known $C_{20}H_{35}N_3$ base (10) containing the C_{11}-H atom *cis* to the C_7–C_9 bridge.[8]

Reduction to Ormosanine

The above stereochemical arguments constitute, in our opinion, strong evidence that the configuration of dilactam **17** at C_{11} is opposite to that of ormosanine (**1**). Rather remarkably, however, this 'incorrect' configuration proved no obstacle to a preparatively simple three-step conversion of **17** into ormosanine. Wolff–Kishner reduction of **17** using the Huang-Minlon modification (24) resulted in the removal of the ketone carbonyl giving a crystalline dilactam **20**, mp 268–270 °C, in a 42% yield. Catalytic hydrogenation of this compound with Adams' catalyst in glacial acetic acid gave, in 87% yield after chromatography, an oily mixture of two C_{18} isomers of dilactam **21**. The estimated ratio of these two isomers is 30:1. The major isomer could be crystallized and melted at 181–181.5 °C. On reduction with diborane in tetrahydrofuran at room temperature (25), the mixture of isomers furnished two products. *The major product, obtained in 45% yield, was found to be identical with natural racemic ormosanine (1) by melting point, mixed melting point, thin layer chromatography, and by infrared, nuclear magnetic resonance, and mass spectra.* Epimerization of synthetic ormosanine (**1**) at C_6 was performed under the reported conditions (10) and gave racemic piptanthine (**2**), identical in solution spectra with natural optically active piptanthine

[7]It should be noted that ammonia must be added to the double bond directly since the primary amide corresponding to ester **16** was found not to form dilactam **17** under the reaction conditions.

[8]Unpublished results in this department.

Can. J. Chem. Downloaded from www.nrcresearchpress.com by 210.87.254.105 on 09/05/12
For personal use only.

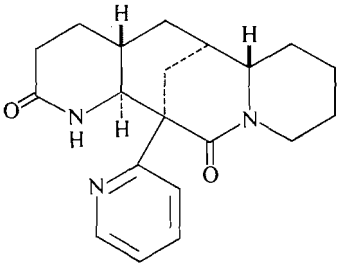

20

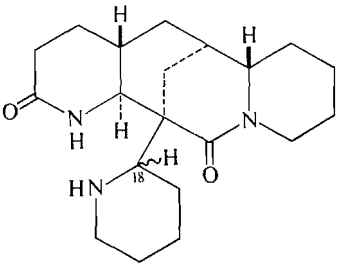

21

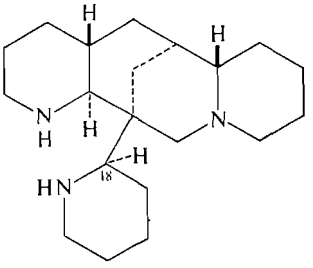

22

(8) and in all respects with natural racemic piptanthine (14). The structure of the two synthetic bases was further confirmed by their conversion to the corresponding cyclic ureas, homoxyormosanine, and homoxypiptanthine (10).

The minor diborane reduction product was obtained in 1.3% yield. Since it originates, together with ormosanine, from the pure, configurationally homogeneous, crystalline dilactam **20**, this additional synthetic $C_{20}H_{35}N_3$ base could readily be assigned the 18-epiormosanine structure (**22**). This assignment is fully confirmed by correlation of **22** with other *Ormosia* bases of known configuration.[8] As this synthesis was being completed, a new $C_{20}H_{35}N_3$ base was isolated from *O. semicastrata* by S. McLean *et al.* (13). Its identity with synthetic 18-epiormosanine (**22**) could be established by direct comparison of the natural and synthetic bases and their homoxy derivatives.

Stereochemistry

With the synthesis of ormosanine (**1**), piptanthine (**2**), and 18-epiormosanine (**22**) completed, it is now necessary to discuss some stereochemical aspects of the reported synthesis in more detail.

Obviously, the most serious remaining problem is the fate of C_{11} during the conversion **17** → **20** → ormosanine (**1**). This sequence, involving a Wolff–Kishner reduction, gave exclusively the configuration at C_{11} and at C_{16} required for ormosanine and piptanthine; the eleven-step conversion of ethyl 2-pyridineacetate into ormosanine is therefore highly stereoselective and proceeds in a 2.3% overall yield. The fact remains, however, that our evidence clearly indicates that keto dilactam (**17**) has a configuration at C_{11} opposite to that of ormosanine (*vide supra*); it follows that an inversion of configuration must take place at C_{11} during the conversion of **17** into ormosanine. Of the three reactions involved in this sequence, only the Wolff–Kishner reduction can reasonably be implicated in this inversion. Such an efficient inversion during the catalytic reduction of the pyridine ring (**20** → **21**) or during the diborane reduction of the lactam groups (**21** → **1**) is not chemically reasonable, nor has it been observed during similar reactions of isomeric compounds (10).[8]

It must thus be assumed that, under the Wolff–Kishner reduction conditions, keto dilactam (**17** ≡ **17***a*) first undergoes an efficient conversion into **19** (or the corresponding hydrazone) and

Can. J. Chem. Downloaded from www.nrcresearchpress.com by 210.87.254.105 on 09/05/12
For personal use only.

Can. J. Chem. Downloaded from www.nrcresearchpress.com by 210.87.254.105 on 09/05/12
For personal use only.

that this is then followed by a normal reduction to dilactam **20** (stereoformula **20***a*). The postulated initial conversion **17** → **19** is clearly plausible from the thermodynamic standpoint. Concerning a possible mechanism, there are, in addition to the unlikely simple abstraction of the C_{11}-H atom and reprotonation after inversion, four 'fragmentation' – cyclization pathways available: (*a*) breakage of the C_{11}—N bond by β-elimination followed by recyclization of the resulting primary amide enone;[9] (*b*) breakage of the C_{11}—C_{16} bond by a reverse Mannich reaction with an electron flow towards the keto group; (*c*) and (*d*) breakage of the C_9—C_{11} bond by an electron flow towards the α-picoline carbon (C_9) by elimination β to the keto group or in a reverse Mannich reaction. When all possible conformations of **17** and its corresponding enolate ion and amide anion are considered, pathways *a*[9] and *b* appear particularly plausible on stereo-electronic grounds.

Clearly, from a purely structural standpoint, these events are sufficiently complicated as to render the synthesis of little value for the confirmation of ormosanine stereochemistry at C_{11} and C_{16}. From the synthetic standpoint, however, the favorable fact remains that keto dilactam **17** can, at least in principle, be used as a starting material for the preparation of *Ormosia* bases of either configuration at C_{11}.

The configuration at C_6 in enol ester **8** and all subsequent synthetic compounds follows unambiguously from three lines of evidence. The alkaloids synthesized (ormosanine and 18-epiormosanine) are known to contain the C_6-H atom *trans* to the C_7–C_9 bridge. Two catalytic inversions at C_6, previously done with natural alkaloids (10) (ormosanine → piptanthine; dasycarpine → isotetrahydro-ormojanine) are known to lead unambiguously to products containing a C_6-H atom *cis* to the C_7–C_9 bridge (10). Finally, and most importantly, ir analysis of all pentacyclic *Ormosia* bases shows that, without exception, any pair of compounds in this series differing only in the configuration at C_6 can be distinguished by bands in the 2800 cm^{-1} region (22) of the solution spectra, the compound with the C_6-H atom *cis* to the C_7–C_9 bridge (*e.g.* piptanthine **2***a*) showing prominent bands and the C_6-epimer (*e.g.* ormosanine **1***a* ⇌ **1***b*) showing no bands or bands of greatly reduced intensity. All our synthetic pentacyclic bases, before their subsequent epimerization at C_6, were found to belong to the latter category.

It now remains to comment on the pronounced stereoselectivity observed during the catalytic reduction of the pyridine ring of the dilactam **20**. Since, after subsequent diborane reduction, ormosanine (**1**) is obtained in a 45% yield and 18-epiormosanine (**22**) in a 1.3% yield, it follows that the major product of the catalytic reduction has the configuration **21***a* and that a very efficient conformational control must be involved in the process.

Model inspection of dilactam **20***a* clearly shows that a hydrogen bond between the pyridine nitrogen and the NH-group present in ring A would lead to a conformation of the molecule which, on catalytic reduction from the less hindered (bottom) side, would give a C_{18}-configuration opposite to the one actually obtained. The observed stereoselectivity can, however, be explained in the following simple way. Since the hydrogenation is carried out in acidic medium, a pyridinium ion can be postulated as the reactive species; a hydrogen bond between the protonated pyridine nitrogen and the tertiary lactam oxygen as indicated in stereoformula **20***b* then leads to a molecular conformation which can be expected to reduce from the direction shown by arrows in **20***b* and to lead preferentially to the observed product.

Clearly, this postulate could be tested by simply reversing the last two reduction steps of the synthesis. Treatment of dilactam **20***a* with diborane in tetrahydrofuran gave the diamino pyridine **23** isolated in the form of its hydrochloride. Hydrogenation of the crude hydrochloride with platinum oxide in glacial acetic acid followed by treatment with phosgene to prepare the corresponding cyclic ureas (10) gave, after purification, two crystalline compounds in a

[9]The involvement of this isomerization pathway is, however, now made improbable by our finding that the primary amide corresponding to ester **16** is completely destroyed under the Huang-Minlon conditions. No dilactam **20** is produced. An attempt to achieve the **17** → **19** conversion under the drastic conditions in the absence of hydrazine also led to complete destruction of material. We are now preparing a large amount of keto dilactam **17** in order to study this reduction in greater detail. We hope, in particular, that it will be possible to find critical (milder) Wolff–Kishner conditions under which the keto group will be removed without epimerization at C_{11}.

Can. J. Chem. Downloaded from www.nrcresearchpress.com by 210.87.254.105 on 09/05/12
For personal use only.

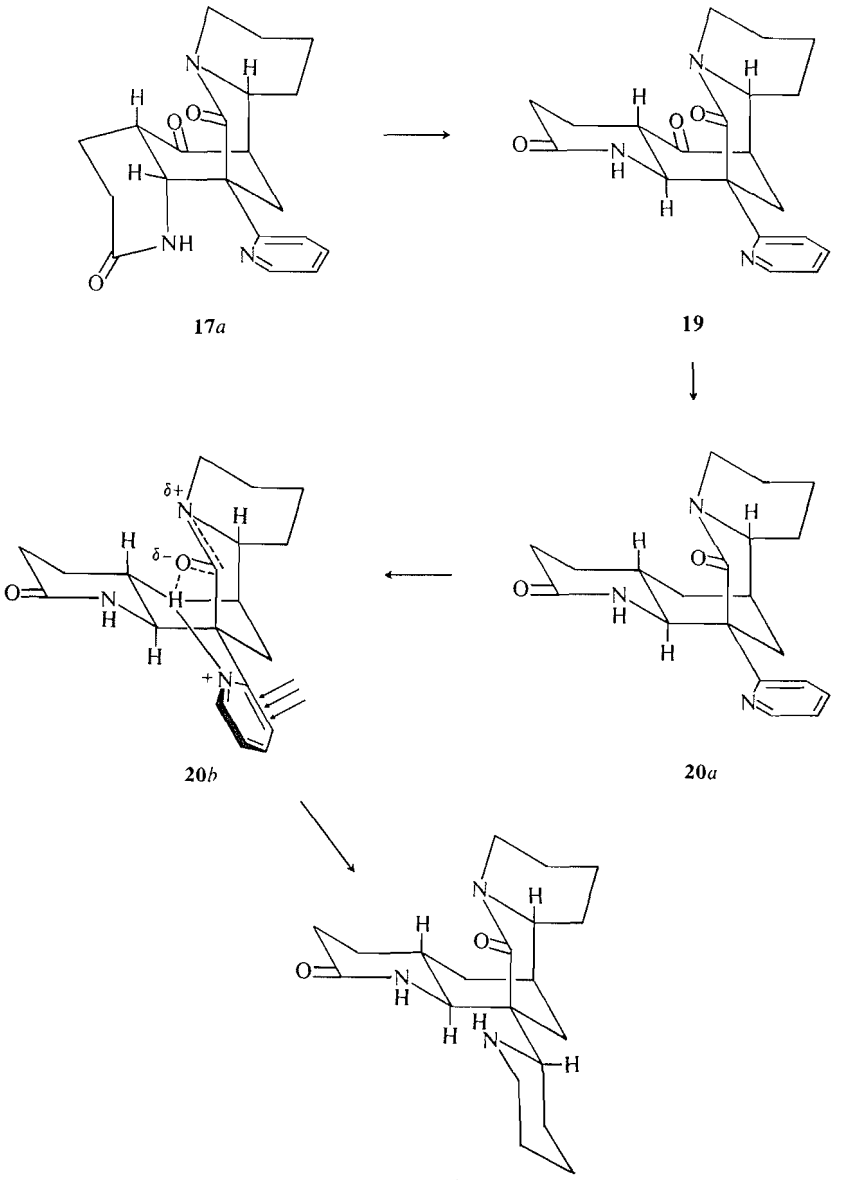

5:3 ratio. The major one was identified as homoxy-18-epiormosanine **24** and the minor one as homoxyormosanine (10). Thus, the selectivity at C_{18} has in fact been reversed and the involvement of the tertiary lactam group during the catalytic reduction of dilactam **20***a* is made more plausible. It seems reasonable to assume that the preferential formation of 18-epiormosanine (**22**) during the catalytic reduction of **23** can be explained by a slightly preferred conformation indicated in stereoformula **23***a*.

Synthesis of d,l-Panamine

With the synthesis of ormosanine completed, it became desirable to study its possible oxidative conversion into panamine (**3**) (10–12). It has now been found (1) that this could be accomplished simply by reacting ormosanine (**1**) with *N*-chlorosuccinimide in methylene chloride. The racemic panamine (**3**) thus obtained in a 74% yield was identified by comparison of ir, nmr, and mass spectra, as well as by thin layer chromatography, with the natural *levo*-rotatory alkaloid.

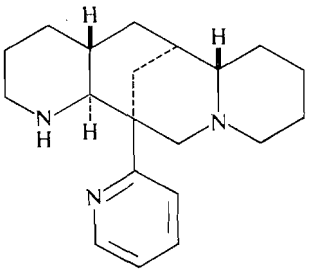

23

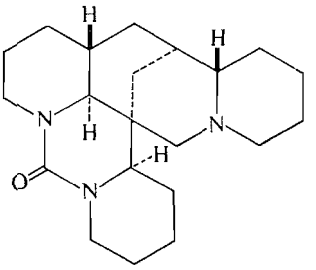

24

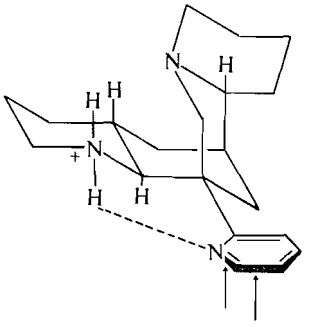

23*a*

Since, as noted briefly above, ormosanine (**1**) was dehydrogenated to dipyridine (**4**) (6, 16) and the latter was converted reductively to four ormosanine stereoisomers in addition to piptanthine (**2**) (10), the present work also represents a formal total synthesis of these four unnatural $C_{20}H_{35}N_3$ bases.

Experimental

General

Melting points were determined on a Kofler hot stage apparatus and are uncorrected. The ir spectra were recorded on Perkin-Elmer spectrophotometers, Models 137B and 237B; chloroform was used for all solution spectra. The uv spectra were taken in 95% ethanol solution using a Beckman double-beam spectrophotometer, Model DK-2. The nmr spectra were recorded on Varian HR-60 and T-60 instruments using tetramethylsilane as internal standard and chloroform-D as solvent. The mass spectra (ms) were determined on a Hitachi–Perkin-Elmer Model RMU-6D Spectrometer and an A.E.I. Model MS-2 Spectrometer. The abbreviations s, d, t, q, and m refer to singlet, doublet, triplet, quartet, and multiplet, respectively.

Ethyl 4-Oxo-3-(2'-pyridyl)-pyridocoline-1-carboxylate, 6

As described by Clemo *et al.* (17), ethyl 2-pyridineacetate (320 g, 1.94 mol), ethyl orthoformate (300 g, 2.02 mol), and acetic anhydride (360 ml) were heated on a steam bath for 20 h under N_2 atmosphere. The product was poured into a solution of potassium carbonate (400 g) in warm water (500 ml) and extracted with chloroform. The extract after drying ($MgSO_4$), filtration, and concentration gave a viscous oil (325 g) which crystallized from ethanol to give yellow crystalline **6** (245 g, 86.0%), mp 126–127 °C; uv λ_{max} 265 nm (log ϵ 4.3); ir 1715 (unsaturated ester), 1660 (lactam), 1640 (double bonds), and 1590 cm^{-1} (pyridine); nmr τ 0.52–2.83 (9H, aromatic), 5.65 (q, 2H, —COOCH_2CH$_3$), and 8.64 (t, 3H, —COOCH$_2$$CH_3$).

Hydrogenation of 6

Crystalline **6** (45 g, 0.15 mol) in ethanol (750 ml) was hydrogenated over 10% Pd–C (15 g; pre-saturated with hydrogen) at room temperature and normal pressure. The reaction was stopped after 4 mol of hydrogen had been taken up. The catalyst was filtered and washed thoroughly with ethanol. The filtrate was evaporated *in vacuo* to dryness to give an oil (45 g) which was chromatographed on neutral alumina (Grade III). Elution with ether gave the configurationally impure ester lactam **7** (36.5 g, 79.0%) which showed two spots of about equal intensity on tlc analysis, but no other impurities. Extensive tlc, column, and short column chromatography failed to resolve the mixture cleanly. *Mol. Wt.* Calcd. for $C_{17}H_{22}N_2O_3$: 302.1630; found (high resolution ms): 302.1630.

Picrate: mp 162–163 °C (recrystallized from ethanol, yellow feather plates). *Anal.* Calcd. for $C_{17}H_{22}N_2O_4 \cdot C_6H_3N_3O_7$: C, 51.97; H, 4.73; N, 13.17; found: C, 51.88; H, 4.68; N, 13.23.

Preparation of Keto Ester 8

To a solution of chromatographed **7** (17.35 g, 57.4

Can. J. Chem. Downloaded from www.nrcresearchpress.com by 210.87.254.105 on 09/05/12
For personal use only.

Can. J. Chem. Downloaded from www.nrcresearchpress.com by 210.87.254.105 on 09/05/12
For personal use only.

mmol) in anhydrous *N,N*-dimethyl formamide (120 ml), was added sodium hydride (4.90 g, 114.1 mmol, 56% dispersion in mineral oil). After the vigorous evolution of hydrogen ceased, ethyl acrylate (11.54 g, 115.4 mmol) was added dropwise over a 5 min period. The resulting mixture was heated at 110 °C under N_2 atmosphere for 15 h, cooled to room temperature, poured into water containing chopped ice, and extracted with ether to remove mineral oil and impurities. The aqueous layer was then extracted with chloroform. The chloroform solution after drying ($MgSO_4$), filtration, and concentration *in vacuo* gave a viscous oil (17.26 g) which was chromatographed on silica gel. Elution with ether afforded the crystalline keto ester **8** (10.84 g, 52.8%), mp 155–156 °C (recrystallized from isopropyl ether, colorless prisms). *Mol. Wt.* Calcd. for $C_{20}H_{24}N_2O_4$: 356.1736; found (high resolution ms): 356.1733. Ultraviolet λ_{max} 254 nm (log ϵ 4.1); ir 1660 (hydrogen-bonded unsaturated ester), 1640 (lactam and double bond), and 1590 and 1580 cm^{-1} (pyridine); nmr τ −2.20 (s, 1H, enolic), 1.56 (d, 1H, aromatic), 2.54 (m, 2H, aromatic), 2.93 (m, 1H, aromatic), 5.40 (m, 1H, C_2-eq.-H), 5.83 (q, 2H, —COO*CH*$_2$CH$_3$), and 8.77 (t, 3H, —COOCH$_2$*CH*$_3$). *Anal.* Calcd. for $C_{20}H_{24}N_2O_4$: C, 67.39; H, 6.78; N, 7.85; O, 17.95; found: C, 67.44; H, 6.65; N, 7.83; O, 18.15.

Decarbethoxylation of Keto Ester ***8***

The keto ester **8** (20 g, 56.1 mmol) was refluxed with stirring in 10% aqueous sulfuric acid (400 ml) for 15 h. After cooling to room temperature, the solution was made basic with ice-cold 4 *N* aqueous sodium hydroxide and extracted with chloroform. Removal of the solvent, after drying the extract over magnesium sulfate and filtration, gave a solid (14.35 g). Recrystallization from ethyl acetate gave the pure ketone **9** (12.76 g, 80.5%), mp 174–175 °C, colorless prisms. *Mol. Wt.* Calcd. for $C_{17}H_{20}N_2O_2$: 284.1525; found (high resolution ms): 284.1517. Infrared 1715 (ketone), 1630 (lactam), and 1590 and 1580 cm^{-1} (pyridine); nmr τ 1.47 (d, 1H, aromatic), 2.20–2.97 (m, 3H, aromatic), and 5.20 (m, 1H, C_2-equatorial). *Anal.* Calcd. for $C_{17}H_{20}N_2O_2$: C, 71.80; H, 7.08; N, 9.85; O, 11.25; found: C, 71.75; H, 6.91; N, 9.77; O, 11.51.

Alkylation of Ketone ***9***

The ketone **9** (2.0 g, 7.04 mmol) and sodium hydride (314 mg, 7.33 mmol, 56% dispersion in mineral oil) were reacted in boiling anhydrous benzene for 15 h under N_2 atmosphere. A solution of ethyl acrylate (705 mg, 7.04 mmol) in anhydrous benzene (5 ml) was then added, the resultant mixture was heated at 70 °C for 0.5 h, cooled to room temperature, poured into ice-cold water, and extracted with chloroform. Removal of the solvent after drying the extract over magnesium sulfate and filtration gave an oily mixture (2.62 g). Chromatography on silica gel gave, on elution with ether, the dialkylated ketone **14** (98 mg, 10.5%); mp 100–101 °C (recrystallized from cyclohexane or cyclohexane – ethyl acetate, colorless prisms). *Mol. Wt.* Calcd. for $C_{27}H_{36}N_2O_6$: 484.2573; found (high resolution ms) 484.2566. Infrared 1725 (two esters), 1700 (ketone), 1640 (lactam), and 1590 and 1580 cm^{-1} (pyridine); nmr τ 1.41 (d, 1H, aromatic), 2.60 (m, 3H, aromatic), 5.28 (m, 1H, C_2-equatorial), 5.84 (q, 4H, —COO*CH*$_2$CH$_3$), 8.77 (t, 3H, —COOCH$_2$*CH*$_3$), and 8.84 (t, 3H, —COOCH$_2$*CH*$_3$). *Anal.* Calcd. for $C_{27}H_{36}N_2O_6 \cdot \frac{1}{2}C_6H_{12}$(cyclohexane): C, 68.41; H, 8.07; N, 5.31; found: C, 68.37; H, 8.09; N, 5.28. Further elution with ether gave the keto ester **13** (621 mg, 84.0%). *Mol. Wt.* Calcd. for $C_{22}H_{28}N_2O_4$: 384.2049; found (high resolution ms): 384.2056. Infrared 1710 (broad, ketone and ester), 1625 (lactam), and 1590 and 1575 cm^{-1} (pyridine); nmr τ 1.41 (d, 1H, aromatic), 2.14–2.90 (m, 3H, aromatic), 5.14 (m, 1H, C_2-equatorial), 5.84 (q, 2H, —COO*CH*$_2$CH$_3$) and 8.74 (t, 3H, —COOCH$_2$*CH*$_3$). Unchanged starting material (1.453 g) was the final ether eluate.

The acid derivative of compound **13** had mp 216–217 °C (recrystallized from ethanol, colorless prisms). *Mol. Wt.* Calcd. for $C_{20}H_{24}N_2O_4$: 356.1736; found (high resolution ms): 356.1744. *Anal.* Calcd. for $C_{20}H_{24}N_2O_4$: C, 67.39; H, 6.78; N, 7.86; found: C, 67.13; H, 6.85; N, 7.72.

Bromination of Keto Ester ***13***

A solution of **13** (1.10 g, 2.86 mmol) and bromine (0.9 g, 5.62 mmol) in carbon tetrachloride (25 ml), was stirred at room temperature for 1 h. It was then made basic with saturated sodium bicarbonate, extracted with chloroform, washed with brine, and dried over sodium sulfate. Removal of solvent gave a powder, **15** (1.32 g, 100%), mp 146–147 °C (recrystallized from ethyl acetate, colorless prisms). *Mol. Wt.* Calcd. for $C_{22}H_{27}N_2O_4Br$: 462.1145; found (high resolution ms): 462.1145. Infrared 1727 (broad, ketone and ester), 1635 (lactam), and 1590 and 1575 cm^{-1} (pyridine); nmr τ 1.47 (d, 1H, aromatic), 2.20–3.00 (m, 3H, aromatic), 5.24 (m, 1H, C_2-equatorial), 5.84 (q, 2H, —COO*CH*$_2$CH$_3$), and 8.84 (t, 3H, —COOCH$_2$*CH*$_3$). *Anal.* Calcd. for $C_{22}H_{27}N_2O_4Br$: C, 57.02; H, 5.87; N, 6.05; found: C, 56.97; H, 5.79; N, 5.94.

Dehydrobromination of Bromo Ketone ***15***

The above bromide **15** (1.32 g, 2.85 mmol) was refluxed with stirring in anhydrous pyridine (25 ml) for 4 h. The solution was evaporated to dryness under reduced pressure and saturated aqueous sodium bicarbonate was added. Extraction with chloroform followed by the usual work-up gave an oil (1.16 g). Chromatography on silica gel afforded, on elution with ether, the keto ester **16** (904 mg, 83.0%), mp 97–98 °C (recrystallized from ether–cyclohexane, colorless prisms). *Mol. Wt.* Calcd. for $C_{22}H_{26}N_2O_4$: 382.1893; found (high resolution ms): 382.1887. Infrared 1725 (ester), 1675 (unsaturated ketone), 1635 (lactam and double bond), and 1590 and 1580 cm^{-1} (pyridine); nmr τ 1.44 (d, 1H, aromatic), 2.13–2.90 (m, 4H, 1 vinyl and 3 aromatic), 5.34 (d of t, 1H, C_2-equatorial), 5.89 (q, 2H, —COO*CH*$_2$CH$_3$), and 8.78 (t, 3H —COOCH$_2$*CH*$_3$). *Anal.* Calcd. for $C_{22}H_{26}N_2O_4$: C, 69.08; H, 6.85; N, 7.32; found: C, 69.04; H, 6.87; N, 7.32.

Preparation of Keto Dilactam ***17***

Compound **16** (7.0 g, 18.32 mmol) was dissolved in absolute ethanol (500 ml) in a flask fitted with a gas-inlet tube and a KOH drying tube as gas outlet. At room temperature, a stream of anhydrous ammonia gas (dried by passing through a KOH tower) was allowed to pass through the solution for one week. Removal of the solvent afforded an oil (7.32 g). Chromatography on silica gel with ether as eluent resulted in partial recovery of starting material (1.05 g). Elution with methanol–ether

Can. J. Chem. Downloaded from www.nrcresearchpress.com by 210.87.254.105 on 09/05/12
For personal use only.

(1:20), gave the keto dilactam **17** (3.85 g, 70.1%), mp 245–247 °C (recrystallized from ethanol, colorless prisms). *Mol. Wt.* Calcd. for $C_{20}H_{23}N_3O_3$: 353.1739; found (high resolution ms): 353.1727. Infrared 3400–3250 (lactam NH), 1710 (ketone), 1635 (lactam carbonyls), and 1593 and 1575 (pyridine); nmr τ 1.40 (d, 1H, aromatic), 2.10–2.87 (m, 3H, aromatic), 5.04 (C_{11}-H, J = 4 Hz), and 5.10 (m, 1H, C_2-equatorial). *Anal.* Calcd. for $C_{20}H_{23}N_3O_3$: C, 67.96; H, 6.51; N, 11.87; O, 13.60; found: C, 67.77; H, 6.50; N, 11.97; O, 13.68.

Wolff–Kishner Reduction of Keto Dilactam ***17***

A solution of **17** (100 mg, 0.283 mmol), powdered KOH (20 mg, 0.511 mmol) and 99–100% hydrazine hydrate (0.2 ml, 4.00 mmol) in triethylene glycol (2 ml) was heated at 190 °C for 2 h. The solution, after cooling to room temperature, was poured into water and extracted with chloroform. Drying ($MgSO_4$), filtration, and evaporation gave a foam (73 mg). Chromatography on alumina (type G) afforded, on elution with 20% ethanol in isopropyl ether, dilactam **20** (40 mg, 41.6%), mp 268–270 °C (crystallized from ethyl acetate, colorless prisms). *Mol. Wt.* Calcd. for $C_{20}H_{25}N_3O_2$: 339.1947; found (high resolution ms): 339.1951. Infrared 3415 (NH), 1640 (lactams), and 1585 and 1575 cm^{-1} (pyridine); nmr τ 1.62 (d, 1H, aromatic), 2.78 (m, 3H, aromatic), 3.66 (s, 1H, NH), 5.10 (m, 1H, C_2-equatorial), and 5.75 (broad, 1H, C_{11}-H). *Anal.* Calcd. for $C_{20}H_{25}N_3O_2$: C, 70.77; H, 7.42; N, 12.37; found: C, 70.80; H, 7.30; N, 12.16.

Catalytic Hydrogenation of Dilactam ***20***

Dilactam **20** (270 mg, 0.796 mmol) in glacial acetic acid (10 ml) was hydrogenated over platinum oxide (280 mg, 1.230 mmol) at room temperature and normal pressure for 20 h. The solution was filtered, concentrated, and made basic with saturated sodium bicarbonate. Extraction with chloroform gave, after work-up of the extract in the usual manner, dilactam **21** (240 mg, 87.2%), mp 181–181.5 °C (recrystallized from ethyl acetate, colorless prisms). *Mol. Wt.* Calcd. for $C_{20}H_{31}N_3O_2$: 345.2416; found (high resolution ms): 345.2421. Infrared 3400, 3300 (NH's), and 1625 cm^{-1} (lactams); nmr no signal for aromatic protons. Thin layer chromatography and the following experiment showed crude **21** to be a mixture of two C_{18}-epimers in a ratio of about 30:1.

Diborane Reduction of Dilactam ***21***

The mixture of **21** (240 mg, 0.696 mmol) was treated with a solution of diborane in tetrahydrofuran (15 ml, 15 mmol) at room temperature under N_2 atmosphere for three days. An excess of methanolic HCl was then added. After further stirring for 4 h, the reaction mixture was concentrated under reduced pressure, made basic with 4 *N* aqueous NaOH, and extracted continuously with ether. Removal of the solvent gave a foam (150 mg) consisting of two products whose separation was performed by preparative tlc on alumina, using 20% methanol in ether as eluent. The faster-moving fraction (R_f 0.7; 100 mg, 45.4%) crystallized from benzene–ether, melted at 179–180 °C and was found to be identical with natural ormosanine (**1**) in tlc, mp, mixture mp, ir, nmr, and ms.

The slower-moving fraction (3 mg, 1.3%) was C_{18}-epiormosanine (**22**); ms M^+ 317; ir 3200 cm^{-1} (NH's), no carbonyl and pyridine absorption bands.

Isomerization of Synthetic Ormosanine, ***1****, to Piptanthine,* ***2***

Synthetic ormosanine (**1**) (20 mg) was isomerized under the reported conditions (10) to crystalline piptanthine (8 mg, 40.0%), mp 217–218 °C, identical with natural optically active base in tlc, ir, nmr, and ms and with the natural racemate in mp.

Preparation of Urea Derivatives of Synthetic Ormosanine, ***1****, Piptanthine,* ***2****, and 18-Epiormosanine,* ***22***

The urea derivatives were prepared by the procedures used for the natural alkaloids (10). Thus, after the phosgene treatment, synthetic ormosanine (**1**) (100 mg) gave crystalline homoxyormosanine (10) (50 mg, 46.3%), mp 171–173 °C. Synthetic piptanthine (**2**) (8 mg) afforded homoxypiptanthine (10, 13) (5 mg, 58.1%), mp 153–154 °C and synthetic 18-epiormosanine (**22**) (8 mg) gave rise to homoxy-18-epiormosanine (**24**) (4 mg, 46.5%), mp 218–220 °C (crystallized from ether); ms M^+ 343; ir 1610 cm^{-1} (urea).

Diborane Reduction of Dilactam ***20***

Dilactam **20** (97 mg, 0.286 mmol) was treated with a solution of diborane in tetrahydrofuran (5 ml, 5 mmol) under N_2 atmosphere at room temperature for three days. The reaction mixture was evaporated under reduced pressure to dryness. An excess of methanolic HCl was added to the residue and the resultant solution was stirred for 4 h. Removal of the solvent *in vacuo* gave the hydrochloride of diamino pyridine **23** which without purification was subjected to hydrogenation.

Preparation of Homoxyormosanine and Homoxy-18-epiormosanine, ***24****, from Diamino Pyridine,* ***23***

A solution of the above hydrochloride of **23** in glacial acetic acid (5 ml) was hydrogenated with platinum oxide (50 mg) at room temperature and normal pressure for one day. The solution was filtered, concentrated, made basic with aqueous NaOH and continuously extracted with ether for 24 h. Removal of the solvent gave a residue (75 mg) which was dissolved in benzene (50 ml). Triethylamine (5 ml) was added, phosgene was bubbled through for 10 min, and the solution was then allowed to stand at room temperature for 24 h. The reaction mixture was diluted with benzene and extracted with aqueous HCl. The aqueous solution was made basic with ammonium hydroxide and extracted with chloroform. Work-up of the extract in the usual manner gave a foam (50 mg). Preparative tlc on silica gel, using 20% methanol in ether as eluent, resulted in the separation of homoxyormosanine (6 mg, 6%) and homoxy-18-epiormosanine, **24** (10 mg, 10%).

Conversion of Ormosanine, ***1****, into Panamine,* ***3***

A solution of ormosanine (**1**) (2 g, 6.31 mmol) and *N*-chlorosuccinimide (840 mg, 6.31 mmol) in methylene chloride (100 ml) was stirred at room temperature for 2 h. The solvent was removed under reduced pressure and aqueous sodium bicarbonate was added to the residue. Extraction with chloroform gave, after drying over sodium sulfate, filtration and evaporation, a foam (2.1 g) which was chromatographed on silica gel. Elution with 3% diethylamine in petroleum ether gave starting material (1.165 g). Elution with 5% diethylamine in petroleum

ether afforded oily *d,l*-panamine (**3**) (622 mg, 74.4%), identified by comparison of tlc, ir, nmr, and ms with the natural alkaloid.

Acknowledgments

Support of this work by the National Research Council of Canada in the form of an operating grant and of scholarships to H.J.L. and J.S.W. is gratefully acknowledged. We thank Dr. W. D. Jamieson, N.R.C.C., Halifax, for some of the high resolution mass spectral measurements. Special thanks are due to Professor S. McLean for providing us with the unusual opportunity of completing the synthesis of *d,l*-piptanthine and 18-epiormosanine concurrently with their first isolation from natural sources and for many useful discussions.

1. H. J. Liu, Z. Valenta, and T. T. J. Yu. Chem. Commun. 1116 (1970).
2. H. A. Lloyd and E. C. Horning. J. Am. Chem. Soc. **80**, 1506 (1958).
3. C. H. Hassall and E. M. Wilson. Chem. Ind. (London), 1358 (1961).
4. I. L. Karle and J. Karle. Tetrahedron Lett. 2065 (1963).
5. P. Naegeli, W. C. Wildman, and H. A. Lloyd. Tetrahedron Lett. 2069 (1963).
6. Z. Valenta, P. Deslongchamps, M. H. Rashid, R. H. Wightman, and J. S. Wilson. Can. J. Chem. **44**, 2525 (1966).
7. U. Eisner and F. Šorm. Coll. Czech. Chem. Commun. **24**, 2348 (1959).
8. R. A. Konovalova, B. S. Diskina, and M. S. Rabinovich. Zh. Obshch. Khim. **21**, 773 (1951).
9. P. Deslongchamps, J. S. Wilson, and Z. Valenta. Tetrahedron Lett. 3893 (1964).
10. P. Deslongchamps, Z. Valenta, and J. S. Wilson. Can. J. Chem. **44**, 2539 (1966).
11. E. M. Wilson. Tetrahedron, **21**, 2561 (1965).
12. I. L. Karle and J. Karle. Tetrahedron Lett. 1659 (1966).
13. S. McLean, P. K. Lau, S. K. Cheng, and D. G. Murray. Can. J. Chem. **49**, 1976 (1971).
14. S. McLean, M. L. Roy, H. J. Liu, and D. T. Chu. Can. J. Chem. **50**, 1639 (1972).
15. J. R. Cannon, J. R. Williams, J. F. Blount, and A. Brossi. Tetrahedron Lett. 1683 (1974).
16. P. Naegeli, R. Naegeli, W. C. Wildman, and R. J. Highet. Tetrahedron Lett. 2075 (1963).
17. G. Clemo, W. Morgan, and R. Raper. J. Chem. Soc. 1025 (1936).
18. R. Hay and P. Williams. J. Chem. Soc. 2270 (1964).
19. S. J. Rhoads, J. C. Gibert, A. W. Decora, T. R. Garland, R. J. Spangler, and M. J. Urbigkit. Tetrahedron, **19**, 1625 (1963).
20. E. Levin. Bull. Acad. Sci. SSR, Ser. Phys. **11**, 413 (1947); C.A. **42**, 3261i (1948).
21. H. J. Liu, Z. Valenta, J. S. Wilson, and T. T. J. Yu. Can. J. Chem. **47**, 509 (1969).
22. F. Bohlmann. Ber. **91**, 2157 (1958).
23. N. R. Hunter, G. A. MacAlpine, H. J. Liu, and Z. Valenta. Can. J. Chem. **48**, 1436 (1970).
24. Huang-Minlon. J. Am. Chem. Soc. **68**, 2487 (1946).
25. H. C. Brown and P. Hein. J. Am. Chem. Soc. **86**, 3566 (1964).

Can. J. Chem. Downloaded from www.nrcresearchpress.com by 210.87.254.105 on 09/05/12
For personal use only.

Vibrational spectra of η^5-cyclopentadienyldicarbonyl(thiocarbonyl)-manganese(I) and η^5-cyclopentadienylcarbonyl(dithiocarbonyl)-manganese(I)[1,2]

G. G. BARNA,[3] I. S. BUTLER, AND K. R. PLOWMAN
Department of Chemistry, McGill University, P.O. Box 6070, Station A, Montreal, Quebec H3C 3G1

Received August 11, 1975

G. G. BARNA, I. S. BUTLER, and K. R. PLOWMAN. Can. J. Chem. **54**, 110 (1976).

The ir and laser Raman spectra of η^5-$C_5H_5Mn(CO)_2(CS)$ and η^5-$C_5H_5Mn(CO)(CS)_2$ have been investigated. In the case of the monothiocarbonyl complex, vapor phase, solution, and solid-state measurements were made, while for the dithiocarbonyl, only solid-state data were obtained. The vibrational spectra of both complexes have been assigned satisfactorily in terms of the C_{5v} and C_s local symmetries of the η^5-C_5H_5—Mn and $Mn(CO)_2(CS)$ (or $Mn(CO)(CS)_2$) moieties, respectively. The effect of change of state on the spectra of the monothiocarbonyl complex is discussed.

G. G. BARNA, I. S. BUTLER et K. R. PLOWMAN. Can. J. Chem. **54**, 110 (1976).

On a étudié les spectres ir et Raman laser des η^5-$C_5H_5Mn(CO)_2(CS)$ et η^5-$C_5H_5Mn(CO)(CS)_2$. Dans le cas du complexe du monothiocarbonyle, on a fait des mesures en phase vapeur, en solution et à l'état solide alors qu'avec le complexe dithiocarbonyle, on n'a obtenu que des données à l'état solide. On a attribué d'une façon satisfaisante les spectres vibrationnels des deux complexes en termes de symétrie locale C_{5v} du η^5-C_5H_5—Mn et C_s du $Mn(CO)_2(CS)$ (ou $Mn(CO)(CS)_2$). On discute de l'effet de changement d'état sur le spectre du complexe du monothiocarbonyle.

[Traduit par le journal]

Introduction

The first transition metal thiocarbonyl complexes were discovered in 1966 (1). Since then, over one hundred of these complexes containing terminal CS groups have been synthesized encompassing essentially all the transition metals (3–19, for a review on the chemistry of transition metal thiocarbonyls, up to March 1973, see ref. 2). Whereas the vibrational spectra of the related transition metal carbonyls have been widely studied (20), little attention has been paid to the spectra of the thiocarbonyls apart from the assignment of the ir-active CS stretching fundamentals. To date, a detailed study of the vibrational spectra of a metal thiocarbonyl complex has not been reported, although a recent preliminary communication indicates that an analysis of the complete vibrational spectra of $(\eta^6$-$C_6H_5CO_2Me)Cr(CO)_2(CS)$ is forthcoming (21).

Several years ago, we discovered the manganese carbonylthiocarbonyls, η^5-$C_5H_5Mn(CO)_2(CS)$ and η^5-$C_5H_5Mn(CO)(CS)_2$, and reported ir data for the ν(CO) and ν(CS) modes (22, 23). We have now investigated the complete ir and laser Raman spectra of these complexes in various phases and present here our proposed assignments for the spectra.

Experimental

The yellow, crystalline thiocarbonyl complexes were prepared from η^5-$C_5H_5Mn(CO)_3$ (a generous gift from Ethyl Corp.) by the methods described in the literature (9) and were sublimed (25 °C/0.01 Torr) immediately prior to recording their spectra. Spectrograde solvents, freshly distilled under nitrogen, were used for all the solution spectra.

The ir spectra in the 4000–350 cm^{-1} region were recorded on a Perkin-Elmer 521 grating spectrophotometer using the 1653.3 cm^{-1} band of water vapor and the 667.3 cm^{-1} band of CO_2 as calibrations. The accuracy of the measurements is ± 2 cm^{-1} (4000–2000 cm^{-1} region) and ± 1 cm^{-1} (2000–350 cm^{-1} region). The far-ir spectra (400–33 cm^{-1}) were recorded on a Perkin-Elmer FIS-3 spectrometer. The observed bands were calibrated against the low frequency bands of water vapor (accuracy ± 2 cm^{-1}). The sample handling conditions employed for

[1]This paper is dedicated to Professor C. A. Winkler of McGill University on the occasion of his sixty-fifth birthday by one of his colleagues (I.S.B.).

[2]Taken in part from the Ph.D. Thesis of G.G.B., McGill University, 1973. Presented in part at the 165th National Meeting of the American Chemical Society, Dallas, Texas, April, 1973.

[3]Present address: Texas Instruments Inc., Dallas, Texas.

Can. J. Chem. Downloaded from www.nrcresearchpress.com by 210.87.254.42 on 09/05/12
For personal use only.

Can. J. Chem. Downloaded from www.nrcresearchpress.com by 210.87.254.42 on 09/05/12
For personal use only.

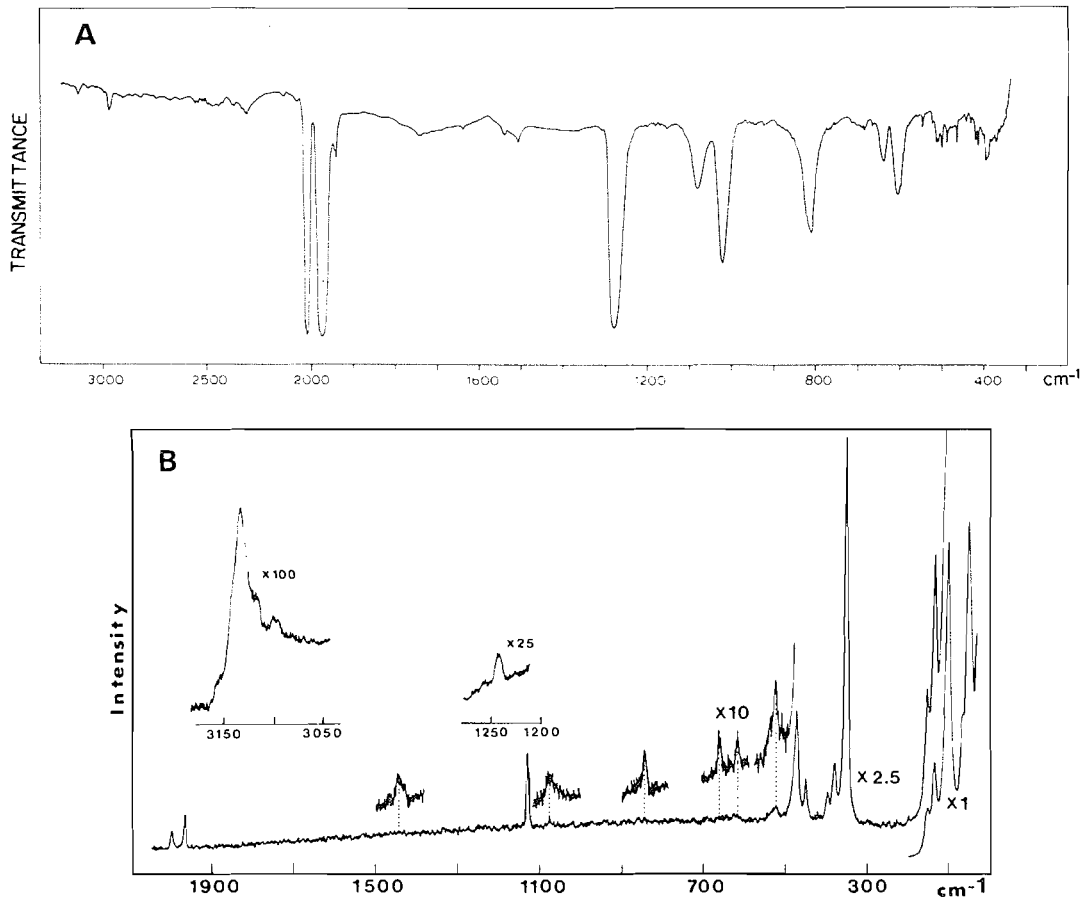

FIG. 1. Vibrational spectra of η^5-$C_5H_5Mn(CO)_2(CS)$. (*A*) Infrared spectrum of vapor at ~100 °C. (*B*) Raman spectrum of solid (Kr^+ excitation, 647.1 nm (~50 mW)). Conditions (× 2.5 scale): slit widths, 5.0 cm^{-1}; time constant, 2 s; scan speed, 50 cm^{-1} min^{-1}.

the various ir spectra are indicated in the tables.

The solid-state Raman spectra were recorded at room temperature for powdered samples in a spinning cell (η^5-$C_5H_5Mn(CO)_2(CS)$) or in a capillary tube (η^5-$C_5H_5Mn(CO)(CS)_2$) on a Jarrell-Ash 25-300 spectrometer equipped with a Coherent Radiation Ltd. Kr^+ laser (model 52K) using 647.1 nm excitation (~50 mW). Unfortunately, solution data were difficult to obtain (even with the laser beam drastically detuned) owing to rapid decomposition of the complexes at high laser powers and the relatively low concentrations which had to be employed. Nevertheless, the frequencies and polarizations of the major bands in the CS_2 solution Raman spectrum of the monothiocarbonyl complex could be determined. The observed Raman spectra were calibrated against either the 730.1 and 533.7 cm^{-1} peaks of indene or the emission lines from a neon lamp (accuracy ±1–2 cm^{-1}).

Results and Discussion

The vibrational spectra of numerous η^5-cyclopentadienylmetal carbonyl complexes have been analyzed quite successfully by the local symmetry approach (24, 25, and their references). Therefore, we will initially examine the spectra of the two manganese carbonylthiocarbonyls in terms of the vibrations of the C_{5v} η^5-C_5H_5—Mn and C_s $Mn(CO)_2(CS)$ or $Mn(CO)(CS)_2$ moieties. As examples of typical spectra, the vapor phase ir and solid-state Raman spectra of η^5-$C_5H_5Mn(CO)_2(CS)$ are shown in Fig. 1. The actual frequencies and the proposed assignments for all the spectra recorded are collected together in Table 1.[4]

[4]The table shown here contains only data for the fundamental vibrations. A complete listing of all the observed frequencies, including the binary overtones and combinations, is available at a nominal charge from the Depository of Unpublished Data, CISTI, National Research Council of Canada, Ottawa, Canada K1A 0S2.

TABLE 1. Vibrational spectra (cm^{-1}) of η^5-$C_5H_5Mn(CO)_2(CS)$ and η^5-$C_5H_5Mn(CO)(CS)_2$[a]

η^5-$C_5H_5Mn(CO)_2(CS)$				η^5-$C_5H_5Mn(CO)(CS)_2$		
Infrared						
Vapor	CS_2 solution	Solid-state (KBr disk)	Raman (solid-state)[d]	Infrared (solid-state, KBr disk)	Raman (solid-state)	Assignment
			3130 s			
3119 vw	3121 s	3120 w	3115 m, sh	3110 vw	3115	a_1 CH str. (ν_1) e_1 CH str. (ν_5) e_2 CH str. (ν_9)
			3095 w			
2025 vs	2007 vs	2009 vs	1990 m (2012 p)	1997 1989 1980 } vs[e]	1987 1981 } w	a' CO str.
1979 vvs	1956 vs	1933 vs	1958 m (1954 dp)			a'' CO str.
	1425 vvs[b]		1440 vw	1424 w		e_1 CC str. (ν_8)
	1359 w, sh[b]					e_2 CC str. (ν_{12})
1279 vs	1266 vs	1260 vs	1242 vw	1298 1289 sh } vs[e]		a' CS str.
				1230 sh 1220 } vs[e]		a'' CS str.
	1113 w	1115 w	1120 s (1123 p)		1113 m	a_1 ring breath. (ν_3)
1084 m	1061 m	1064 m	1075 vw	1060 vw		e_2 CH bend ($\perp$) (ν_{11})
1025 s	1006 s	1005 w		1011 vw		e_1 CH bend ($\parallel$) (ν_6)
	917 m			923 vw		e_2 ring dist. ($\parallel$) (ν_{13})
				845 vw, sh	840 w, sh	e_1 CH bend ($\perp$) (ν_7)
818 s	825 vs	835 s	854 vw	832 m	834 w	a_1 CH bend ($\perp$) (ν_2)
643 w	645 vs	645 vs	651 vw	625 w		MnCO and MnCS bends
610 m	612 605 } vs	607 s	615 vw	590 m		
515 509 } vw	519 513 } vs	516 s	515 w	570 m		
		473 vw	475 w, sh	499 w	500 494 } w	
				479 w	478 mw	
		458 vw	462 s (463 p)			a' Mn—CO str.
423 417 } vvw	430 w	437 vw	441 m (438 dp)	429 vw	437 sh 428 } s	a'' Mn—CO str.
					404 m	a'' Mn—CS str.
	360 w	364 w	373 m		359 m	a' Mn—CS str.
397 w	399 sh	382 w	390 m		350 vw, sh	e_1 ring tilt
	330[c]	339 w	342 vs (337 p)		321 vvs	a_1 ring–Mn str.

[a]Some of the lists of frequencies have been divided into sections and the intensities given are relative to the most intense peak within each section.
[b]In CCl_4 solution.
[c]In benzene solution.
[d]CS_2 solution data are shown in parentheses.
[e]From ref. 9: ν(CO) 1991 s, ν(CS) 1305 s and 1235 vs (in CS_2 solution); ν(CO) 1996 s, ν(CS) 1308 s and 1240 s cm^{-1} (in Nujol mull).

η^5-*Cyclopentadienyl Ring Vibrations*

The molecular vibrations for a η^5-C_5H_5—Mn moiety on the basis of C_{5v} local symmetry are distributed as $4a_1$ (ir/Raman) + a_2(inactive) + $5e_1$ (ir/Raman) + $6e_2$(Raman) (20). Two of these modes are the a_1 ring – Mn stretch and the e_1 ring tilt, while the other fourteen modes are all associated with the vibrations of the η^5-C_5H_5 ring itself.

The vibrational spectra of the closely related tricarbonyl complex, η^5-$C_5H_5Mn(CO)_3$, have been the subject of several investigations (24, 26–29) culminating in the recent extensive study by Parker (30). In Table 2, we have compared our assignments for the ring vibrations of the monothiocarbonyl complex with those of Parker for η^5-$C_5H_5Mn(CO)_3$. It is immediately evident that η^5-$C_5H_5Mn(CO)_2(CS)$ vapor obeys the C_{5v} selection rules reasonably well with four (ν_1, ν_2, ν_5, ν_6) of the seven expected ir-active modes and only one (ν_{11}) of the seven formally ir-inactive modes being observed. On the other hand, like

Can. J. Chem. Downloaded from www.nrcresearchpress.com by 210.87.254.42 on 09/05/12
For personal use only.

TABLE 2. Comparison of the η^5-cyclopentadienyl ring vibrations (cm^{-1}) or η^5-$C_5H_5Mn(CO)_3$ and η^5-$C_5H_5Mn(CO)_2(CS)$

Vibrational mode	η^5-$C_5H_5Mn(CO)_3$[a]				η^5-$C_5H_5Mn(CO)_2(CS)$			
	Infrared			Raman of solid[e]	Infrared			Raman of solid[e]
	Vapor	Solution[b]	Solid[d]		Vapor[g]	Solution[c]	Solid[h]	
ν_1 (a_1)			3132?	3132[f]	3119	3121	3120	3130
ν_2 (a_1)	830	831[c]	837	833	818	825	835	854
ν_3 (a_1)	1110	1114	1114	1114		1113	1115	1120
ν_4 (a_2)	1256	1267	1265					
ν_5 (e_1)	3105	3122	3124	3121[f]	3119	3121	3120	3115
ν_6 (e_1)	1003	1007	1012 1007	1012 1005	1025	1006	1005	
ν_7 (e_1)		842[c]	848	844				
ν_8 (e_1)	1418	1425	1426 1421	1426 1421		1425[b]		1440
ν_9 (e_2)			3104	3109[f] 3098[f]				3095
ν_{10} (e_2)?		1200	1205	1218				
ν_{11} (e_2)	1038	1062 1051	1064 1058	1065 1059	1084	1061	1064	1075
ν_{12} (e_2)			1360	1360		1359[b]		
ν_{13} (e_2)		922	938	938 931		917		
ν_{14} (e_2)			609	608				

[a]Data from ref. 30.
[b]In CCl_4 solution.
[c]In CS_2 solution.
[d]At room temperature (CsI disk).
[e]Using Kr^+ 647.1 nm excitation.
[f]Using Kr^+ 568.2 nm excitation.
[g]In a 10-cm pathlength Beckman gas cell heated to ~100 °C.
[h]At room temperature (KBr disk).

η^5-$C_5H_5Mn(CO)_3$, the solution ir data clearly indicate that C_{5v} local symmetry may only be regarded as an approximation because bands attributable to several of the strictly ir-inactive e_2 modes (ν_9–ν_{14}) were detected. Surprisingly, the solid-state ir and Raman data evidence only a slight breakdown of C_{5v} selection rules, but this may well be due to the broadness of some of the bands and the weak spectral activity of certain of the modes.

The assignments proposed for the ring vibrations of the dithiocarbonyl complex (Table 1) follow directly from those given for η^5-$C_5H_5Mn(CO)_3$ and η^5-$C_5H_5Mn(CO)_2(CS)$. The solid-state data are indicative of little relaxation in the C_{5v} selection rules, but this might also be attributable to accidental degeneracies and the weak spectral activity of some modes.

A few comments on the assignments of the η^5-C_5H_5 ring modes of the thiocarbonyls are now in order. First, it is possible that the a_2 mode (ν_4) of η^5-$C_5H_5Mn(CO)_2(CS)$ is masked by the intense ν(CS) absorption in the ir spectra at ~1270 cm^{-1}. However, this seems unlikely because ν_4 is definitely not observed in the solid-state ir spectrum of the dithiocarbonyl. Second, in an earlier study on the vibrational spectra of various structurally related η^5-cyclopentadienyl-metal carbonyl complexes, Parker and Stiddard (24) constructed a series for the order of decreasing local symmetry of the η^5-C_5H_5–metal moiety on the basis of solid-state ir data. The thiocarbonyls would fit in this series at about the same place as η^5-$C_5H_5V(CO)_4$. Consequently, we consider it unlikely that any of the bands at ~600 cm^{-1} are due to ν_{14}, the $e_2 \perp$ ring distortion (observed for the tricarbonyl at 609 cm^{-1} (30)), because this mode only becomes ir-active much further down the series.

Again, by analogy with the previous results for η^5-$C_5H_5Mn(CO)_3$ (29, 30), we have assigned the a_1 ring – Mn stretching modes of the thiocarbonyls to the extremely intense bands in the solid-state Raman spectra at ~330 cm^{-1}. In the case of the monothiocarbonyl, the corresponding band in the CS_2 solution Raman spectrum (at

Can. J. Chem. Downloaded from www.nrcresearchpress.com by 210.87.254.42 on 09/05/12
For personal use only.

Can. J. Chem. Downloaded from www.nrcresearchpress.com by 210.87.254.42 on 09/05/12
For personal use only.

TABLE 3. Spectral predictions for the fundamentals of the C_s local symmetry $Mn(CO)_2(CS)$ and $Mn(CO)(CS)_2$ moieties

Type (and No.) of fundamentals for $Mn(CO)_2(CS)$ moiety[a]		Symmetry[b]
ν(CO)	(2)	$a'+a''$
ν(CS)	(1)	a'
ν(Mn—C(O))	(2)	$a'+a''$
ν(Mn—C(S))	(1)	a'
δ(MnCO)	(4)	$2a'+2a''$
δ(MnCS)	(2)	$a'+a'$
δ((O)CMnC(O))	(1)[c]	a'
δ((O)CMnC(S))	(2)[c]	$a'+a''$

[a]For the modes of the $Mn(CO)(CS)_2$ moiety, interchange the O and S atoms.
[b]Activities for C_s symmetry: a' and a'' (ir/Raman).
[c]These modes are expected in the region below 150 cm^{-1}. However, because of the complexity of the spectra in this region, no attempt has been made to assign the observed bands although the bands are reported in the complete version of Table 1.

337 cm^{-1}) is strongly polarized, thus confirming the a_1 symmetry. Also, we have attributed the weak ir/Raman band at ~390 cm^{-1} for the monothiocarbonyl and the very weak shoulder at 350 cm^{-1} in the solid-state Raman spectrum of the dithiocarbonyl to the e_1 ring tilt modes. Parker's values (30) for the corresponding modes of η^5-$C_5H_5Mn(CO)_3$ are: a_1 ring – Mn stretch, ~350 cm^{-1}; e_1 ring tilt, ~370 cm^{-1}.

Mn—C—O and Mn—C—S Vibrations

The fundamentals predicted for the $Mn(CO)_2$-(CS) and $Mn(CO)(CS)_2$ moieties on the basis of C_s local symmetry are shown in Table 3.

In all the ir and Raman spectra of η^5-C_5H_5Mn-$(CO)_2(CS)$, there are two bands in the CO stretching region (2150–1900 cm^{-1}). We have assigned these, in order of decreasing energy, to the a' and a'' ν(CO) modes, respectively. These assignments follow directly from the CS_2 solution Raman polarization measurements and from our previous approximate force field calculations using ir data from the uv-light induced CO exchange reaction of the monothiocarbonyl complex with $C^{18}O$ (25). The a' ν(CO) mode of the dithiocarbonyl (at ~1990 cm^{-1}) is split into a triplet in the solid-state ir spectrum and a doublet in the solid-state Raman spectrum; these splittings almost certainly arise from factor group effects.

The ν(CS) modes have been assigned by analogy with the ν(CO) modes. For the solid-state ir spectra, these assignments are: η^5-C_5H_5-$Mn(CO)_2(CS)$, 1260 vs (a'); η^5-$C_5H_5Mn(CO)$-$(CS)_2$, 1298 vs/1289 sh (a') and 1220 vs cm^{-1} (a''). One band of very low intensity was observed in the ν(CS) region (at 1242 cm^{-1}) in the solid-state Raman spectrum of the monothiocarbonyl complex using the spinning cell technique. We have attributed this band to the a' ν(CS) mode, but it could possibly be due to the $e_2 \parallel$ CH bend (ν_{10}) (observed for the tricarbonyl at 1218 vvw cm^{-1} (30)). No bands were detected in the ν(CS) region for either complex using the capillary tube method, even at −78 °C; there was insufficient sample available to use the spinning cell for the dithiocarbonyl complex.

From both physical (31, 32) and chemical evidence (*e.g.*, 2, 3, 14), CS appears to be a better σ-donor and π-acceptor ligand than CO. The ν(CS) modes of metal thiocarbonyls seem to reflect the well-known 'synergistic effect' (33) of the ν(CO) modes of metal carbonyls. Thus, the ν(CO) and ν(CS) modes of η^5-$C_5H_5Mn(CO)_2$-(CS) (2009 vs, 1933 vs, 1260 vs (ir spectrum, KBr disk)) occur at appreciably lower wavenumbers than the identical modes of the isoelectronic, cationic species $(\eta^5$-$C_5H_5Fe(CO)_2$-$(CS))^+$, under the same conditions (2092 vs, 2058 vs, 1347 vs (34)).

The π-acid character of the CS ligand is presumably responsible for the gradual increase in the primary Cotton–Kraihanzel CO force constants down the series η^5-$C_5H_5Mn(CO)_3$ (15.61), η^5-$C_5H_5Mn(CO)_2(CS)$ (15.83), and η^5-$C_5H_5Mn(CO)(CS)_2$ (16.00 mdyn $Å^{-1}$) (35). Furthermore, since no CS force constants have yet been reported for metal thiocarbonyls, it is worth mentioning here that the Cotton–Kraihanzel values (provided that the assumption of energy factoring still holds for bands at ~1300 cm^{-1}) for the following species are: η^5-$C_5H_5Mn(CO)_2(CS)$ (8.24), η^5-$C_5H_5Mn(CO)$-$(CS)_2$ (8.30), and η^5-$C_5H_5Mn(CS)_3$ (8.33 mdyn $Å^{-1}$) (35). It seems that increasing the extent of CS substitution has relatively little effect on the primary CS force constants in contrast to the significant changes in the primary CO force constants.

It is difficult to make definitive assignments for the spectra below 750 cm^{-1} in the absence of isotopic data or complete force field calculations. However, we feel that we can make the tentative assignments shown in Table 1 following a comparison of the spectra of the thiocarbonyls with those of η^5-$C_5H_5Mn(CO)_3$ and keeping in mind

Can. J. Chem. Downloaded from www.nrcresearchpress.com by 210.87.254.42 on 09/05/12
For personal use only.

the three points below. (*a*) From our previous work on η^5-$C_5H_5Mn(CS)$(Polyphosphine) complexes, it appears that the δ(MnCS) modes lie in the 550–530 cm^{-1} region, some 60 cm^{-1} lower than the δ(MnCO) modes in the corresponding metal carbonyl complexes (11). (*b*) In general, δ(MCO) fundamentals of metal carbonyls are at higher energies than the ν(M—C) modes. Also, the bending modes are more intense in the ir, while the reverse is true in the Raman (36, 37). (*c*) The heavier mass of sulfur compared to oxygen should result in ν(M—C(S)) modes appearing at somewhat lower frequencies than ν(M—C(O)) modes.

There are three bands in the 465–340 cm^{-1} region of the solid-state Raman spectra of the thiocarbonyls which have yet to be assigned. This is the region where we expect to find the ν(Mn—C) modes. From Table 3, there should be one ν(Mn—C(S)) (a') and two ν(Mn—C(O)) ($a' + a''$) modes for η^5-$C_5H_5Mn(CO)_2(CS)$. Owing to the mass effect discussed above, we have assigned the lowest energy band at 373 cm^{-1} to the a' ν(Mn—C(S)) fundamental. Since totally symmetric vibrations are usually more intense in the Raman than antisymmetric vibrations, we have attributed the 462 and 441 cm^{-1} bands to the a' and a'' ν(Mn—C(O)) modes, respectively. The CS_2 solution Raman polarization measurements are in accord with these assignments. Following similar arguments, the proposed assignments for the dithiocarbonyl complex are: ν(Mn—C(O)), 428 (a'); ν(Mn—C(S)), 404 (a'') and 359 cm^{-1} (a').

In the higher energy region usually associated with δ(MCO) modes, there are four bands in the solid-state ir spectrum of η^5-$C_5H_5Mn(CO)_2(CS)$ and six bands in that of η^5-$C_5H_5Mn(CO)(CS)_2$. Reference to Table 3 shows that there should be four ($2a' + 2a''$) and two ($a' + a''$) δ(MnCO) modes for these complexes, respectively. We suspect that the four extra bands in the case of the dithiocarbonyl are most probably due to the four expected δ(MnCS) modes ($2a' + 2a''$). There should also be two δ(MnCS) modes ($a' + a''$) for the monothiocarbonyl, meaning that in all there should be six bands observed for this complex as well. From the data given in Table 1, it is clear that while there are only four bands observed in the vapor phase ir and solid-state ir, and Raman spectra, these are not always the same four bands. There are five very strong bands in the CS_2 solution ir spectrum but the sixth band expected at ~470 cm^{-1} was apparently too weak to be detected. In any event, it seems reasonable to conclude that the six predicted δ(MnCO) and δ(MnCS) fundamentals for the thiocarbonyls fall in the following ranges: η^5-$C_5H_5Mn(CO)_2(CS)$, 651–473 cm^{-1}; η^5-$C_5H_5Mn(CO)(CS)_2$, 625–448 cm^{-1}. More specific assignments for these spectral ranges are unwarranted at this time.

Binary Overtones and Combinations

The binary overtone and combination regions of the CS_2 solution ir spectrum of η^5-$C_5H_5Mn(CO)_2(CS)$ have also been investigated. The observed frequencies and the proposed assignments are given in the complete Table which is lodged in the Depository of Unpublished Data (*vide supra*).[4] With only one exception, all the overtone and combination bands can be assigned without requiring combinations between fundamentals associated with the η^5-C_5H_5 ring and the $Mn(CO)_2(CS)$ moiety. On the other hand, the a_1 ring – Mn stretch and the e_1 ring tilt do apparently combine with vibrations of both the η^5-C_5H_5 ring and the $Mn(CO)_2(CS)$ fragment. These observations provide some support for the applicability of the method of local symmetry in interpreting the vibrational spectra of η^5-$C_5H_5Mn(CO)_2(CS)$.

Solvent Effects

A solvent shift study on the ir-active fundamentals of the monothiocarbonyl complex was also carried out. The solvents employed were CS_2, C_6H_{12}, CCl_4, C_6H_6, CH_2Cl_2, $CHCl_3$, CH_3I. CH_3CN, and CH_3NO_2. While none of the shifts observed with respect to the vapor phase data were really appreciable, the largest shift (24 cm^{-1}) was for the $a_1 \perp$ CH bending mode (ν_2). Neither the ν(CS) nor the ν(CO) modes were particularly solvent sensitive indicating little interaction with the solvents and thereby implying low bond polarities for these groupings.

Conclusions

The vapor phase ir data for η^5-$C_5H_5Mn(CO)_2(CS)$ indicate that there is hardly any coupling between the modes of the η^5-C_5H_5—Mn and $Mn(CO)_2(CS)$ moieties. The partial breakdown in C_{5v} selection rules for the ring modes of this complex in solution may be explained by weak solute–solvent interactions. Since solid-state vi-

brational spectra are usually more complex than solution or vapor phase spectra, the apparent simplicity of the solid-state spectra of η^5-$C_5H_5Mn(CO)_2(CS)$ (and also those of η^5-$C_5H_5Mn(CO)(CS)_2$) most probably results from accidental degeneracies and the weak spectral activity of certain of the fundamentals.

Overall, the method of local symmetry works quite well in explaining the vibrational spectra of the two η^5-cyclopentadienylmanganese carbonyl–thiocarbonyls. In addition, we have satisfied our original objective by providing reasonable assignments for the ν(CS) and ν(Mn—C(S)) modes and by locating the δ(MnCS) region. It is also worth pointing out here that, as is the case for metal carbonyls in general, the δ(MnCS) modes appear to be strong in the ir and weak in the Raman, while the converse applies to the ν(Mn—C(S)) modes.

On the basis of absolute integrated ir intensity measurements, we have shown earlier (38) that the intensities of the ν(CO) and ν(CS) modes in η^5-$C_5H_5Mn(CO)_2(CS)$ are comparable. The same appears to be qualitatively true for the corresponding modes in the ir spectra of the dithiocarbonyl reported here. However, in the Raman, the ν(CS) modes are decidedly weaker than the ν(CO) modes; in fact, no ν(CS) peaks could even be detected for the dithiocarbonyl complex. These results are particularly surprising because sulfur is generally considered to be a more polarizable atom than oxygen and so CS vibrations would be expected to be at least as intense as CO stretching vibrations in the Raman, provided, of course, that the bonding in these groupings is similar. For (η^6-$C_6H_5CO_2Me$)-$Cr(CO)_2(CS)$, a medium-intense Raman band at 1205 cm^{-1} (with a corresponding very strong band in the ir at 1215 cm^{-1}) was assigned to the CS stretching vibration (21). However, from our work on approximately twenty thiocarbonyl complexes of several different transition metals, extremely weak or non-existent Raman activity seems to be a general property of the ν(CS) modes in metal thiocarbonyls. We will discuss this phenomenon more fully in a forthcoming paper on the complete vibrational spectra of the Group VIB complexes, $M(CO)_5(CS)$ (M = Cr, W) and *trans*-$W(CO)_4(^{13}CO)(CS)$ (39).

Acknowledgments

We thank Miss S. R. Desjardins and Dr. A. E. Fenster for providing samples of the thiocarbonyl complexes. This research was supported by the National Research Council of Canada and, in part, by the Quebec Department of Education.

1. M. C. Baird and G. Wilkinson. Chem. Commun. 267 (1966).
2. I. S. Butler and A. E. Fenster. J. Organomet. Chem. **66**, 161 (1974).
3. B. D. Dombek and R. J. Angelici. J. Am. Chem. Soc. **95**, 7516 (1973).
4. J. M. Lisy, E. D. Dobrzynski, R. J. Angelici, and J. Clardy. J. Am. Chem. Soc. **97**, 656 (1975).
5. B. D. Dombek and R. J. Angelici. J. Am. Chem. Soc. **97**, 1261 (1975).
6. L. Ruiz-Ramirez, T. A. Stephenson, and E. S. Switkes. J. Chem. Soc. Dalton Trans. 1770 (1973).
7. T. A. Stephenson, E. S. Switkes, and P. W. Armit. J. Chem. Soc. Dalton Trans. 1134 (1974).
8. P. W. Armit and T. A. Stephenson. J. Organomet. Chem. **73**, C33 (1974).
9. A. E. Fenster and I. S. Butler. Inorg. Chem. **13**, 915 (1974).
10. N. J. Coville and I. S. Butler. J. Organomet. Chem. **64**, 101 (1974).
11. I. S. Butler and N. J. Coville. J. Organomet. Chem. **80**, 235 (1974).
12. G. Jaouen. Tetrahedron Lett. 5159 (1973).
13. G. Simonneaux, A. Meyer, and G. Jaouen. Tetrahedron Lett. 5163 (1973).
14. G. Jaouen and R. Dabard. J. Organomet. Chem. **72**, 377 (1974).
15. G. Simonneaux, A. Meyer, and G. Jaouen. J. Chem. Soc. Chem. Commun. 69 (1975).
16. L. W. Yarbrough, G. V. Calder, and J. G. Verkade. J. Chem. Soc. Chem. Commun. 705 (1973).
17. M. Kubota and C. J. Curtis. Inorg. Chem. **13**, 2277 (1974).
18. K. R. Grundy, R. O. Harris, and W. R. Roper. J. Organomet. Chem. **90**, C34 (1975).
19. A. Efraty, R. Arneri, and J. Sikora. J. Organomet. Chem. **91**, 65 (1975).
20. D. M. Adams. Metal–ligand and related vibrations. Arnold, London. 1967.
21. P. Caillet and G. Jaouen. J. Organomet. Chem. **91**, C53 (1975).
22. I. S. Butler and A. E. Fenster. Chem. Commun. 933 (1970).
23. A. E. Fenster and I. S. Butler. Can. J. Chem. **50**, 598 (1972).
24. D. J. Parker and M. H. B. Stiddard. J. Chem. Soc. A, 480 (1970).
25. I. S. Butler and A. E. Fenster. J. Organomet. Chem. **51**, 307 (1973).
26. I. J. Hyams, R. T. Bailey, and E. R. Lippincott. Spectrochim. Acta, **23A**, 273 (1967).
27. D. J. Parker. J. Chem. Soc. A, 1382 (1970).
28. H. J. Buttery, S. F. A. Kettle, G. Keeling, P. J. Stamper, and I. Paul. J. Chem. Soc. A, 3148 (1971).
29. D. M. Adams and A. Squire. J. Organomet. Chem. **63**, 381 (1973).
30. D. J. Parker. J. Chem. Soc. Dalton Trans. 155 (1974).

Can. J. Chem. Downloaded from www.nrcresearchpress.com by 210.87.254.42 on 09/05/12
For personal use only.

31. W. G. RICHARDS. Trans. Faraday Soc. **63**, 257 (1967).
32. N. JONATHAN, A. MORRIS, M. O'KADA, D. J. SMITH, and K. J. ROSS. Chem. Phys. Lett. **13**, 324 (1972).
33. F. A. COTTON and G. WILKINSON. Advanced inorganic chemistry. 3rd. ed. Wiley Interscience, New York. 1972. p. 684.
34. G. G. BARNA. Ph.D. Thesis, McGill University, Montreal, Quebec. 1973.
35. A. E. FENSTER. Ph.D. Thesis, McGill University, Montreal, Quebec. 1973.
36. G. DAVIDSON. Inorg. Chim. Acta, **3**, 596 (1969).
37. D. M. ADAMS and A. SQUIRE. J. Chem. Soc. A, 814 (1970).
38. I. S. BUTLER and D. A. JOHANSSON. Inorg. Chem. **14**, 701 (1975).
39. I. S. BUTLER, A. GARCIA-RODRIQUEZ, C. F. SHAW III, and K. R. PLOWMAN. To be published.

Can. J. Chem. Downloaded from www.nrcresearchpress.com by 210.87.254.42 on 09/05/12
For personal use only.

Structure électronique de dérivés sulfures. XVIII. Influence de l'environnement sur la réactivité nucléophile du groupement thiocarbonyle

DANIELLE GONBEAU[1] ET GENEVIÈVE PFISTER-GUILLOUZO

Laboratoire de Chimie Organique Physique, Institut Universitaire de Recherche Scientifique, Avenue Philippon, 64016 Pau, France

Reçu le 12 juin 1975

DANIELLE GONBEAU et GENEVIÈVE PFISTER-GUILLOUZO. Can. J. Chem. **54**, 118 (1976).

Les effets d'hétéroatomes différents en α sur le caractère nucléophile du groupement thiocarbonyle ont été examinés. Trois types d'environnements symétriques ont été considérés: environnement par des atomes d'azote, de soufre et d'oxygène.

L'analyse de données théoriques déduites de calculs CNDO/2 ainsi que l'examen des interactions orbitalaires mises en jeu ont permis de vérifier pour cette réaction le caractère de contrôle par les orbitales frontières.

DANIELLE GONBEAU and GENEVIÈVE PFISTER-GUILLOUZO. Can. J. Chem. **54**, 118 (1976).

The effects of different heteroatoms in the α position to the thiocarbonyl group on nucleophilic behavior of sulfur atom have been studied. Three symmetrical environments have been considered: nitrogen, sulfur, and oxygen atoms.

The theoretical treatment by the CNDO/2 method and the analysis of orbitals interactions show a frontier orbital control for the reaction studied.

Introduction

Ce travail se place dans le cadre d'une étude d'ensemble sur la réactivité nucléophile du groupement thiocarbonyle (1).

Dans un article précédent nous avons pu, par une approche théorique, d'une part vérifier que le mécanisme de *S*-méthylation était de type S_N2, et d'autre part examiner l'influence de la nature du réactif attaquant CH_3X (1).

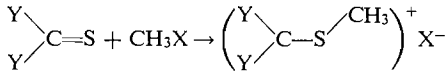

Nous nous proposons d'analyser l'influence des effets électroniques sur ce mécanisme. Ceux ci peuvent être envisagés comme seuls facteurs à l'origine des différences de réactivité, dans la mesure où les effets stériques sont du même ordre.

Dans ce but, nous avons choisi des substrats aussi comparables que possible; nous avons ainsi examiné l'approche de CH_3Cl sur la diméthylthiourée (Y = $NHCH_3$), le trithiocarbonate de méthyle (Y = SCH_3) et le thionocarbonate de méthyle (Y = OCH_3).

Expérimentalement par une étude cinétique des réactions de méthylation de différents composés thiocarbonylés, par l'iodure de méthyle en milieu acétonique, Arbelot *et coll.* (2) ont mis en évidence que la nucléophilie des thiones varie selon la nature de l'atome en α dans l'ordre suivant: N > C > S > O.

Par ailleurs, l'une d'entre nous a montré l'existence d'une corrélation entre les potentiels d'ionisation des orbitales de type n déterminés par spectroscopie photoélectronique et les constantes de vitesse de *S*-méthylation de ces mêmes composés (3). Il nous a paru par là même intéressant à côté des données théoriques recueillies d'analyser la nature des interactions orbitalaires mises en jeu pour les trois environnements considérés.

Analyse des donnees theoriques

Nous avons travaillé dans le cadre de la méthode CNDO/2, la paramétrisation utilisée étant celle adoptée lors des études antérieures (1, 4). Nous avons dans tous les cas, aussi bien en ce qui concerne les molécules isolées que les 'modèles d'approche', minimisé l'énergie totale des systèmes par rapport à l'ensemble des paramètres géométriques (longeurs et angles).

Produits initiaux, produits finaux

En premier lieu nous avons examiné la topologie privilégiée des réactifs.

[1]Ce travail fait partie de la thèse de Doctorat ès-Sciences de D. Gonbeau enregistrée au C.N.R.S. sous le n° AO 9786.

Can. J. Chem. Downloaded from www.nrcresearchpress.com by 210.87.254.6 on 09/05/12
For personal use only.

Can. J. Chem. Downloaded from www.nrcresearchpress.com by 210.87.254.6 on 09/05/12
For personal use only.

En ce qui concerne la diméthyl thiourée la conformation la plus stable correspond à un environnement symétrique (forme A) (fig. 1), Toutefois, la différence énergétique entre les deux conformations (A et B) est faible et compatible avec la présence de deux formes en équilibre en solution. Ce résultat est en accord avec les résultats expérimentaux obtenus en résonance magnétique nucléaire sur la diméthyl thiourée (5).

Dans le cas du trithiocarbonate de méthyle et du thionocarbonate de méthyle, nous avons constaté que la forme B était énergétiquement nettement privilégiée. Par contre, au niveau du produit final de méthylation nous trouvons une disposition privilégiée des groupements alkyles identique pour les trois composés examinés (forme B).

Ayant fait l'hypothèse d'une planéité des systèmes étudiés et d'une géométrie fixe des groupements méthyles nous avons procédé à une minimisation des énergies totales des réactifs (Y = $NHCH_3$, SCH_3, OCH_3) et des produits finaux par variation indépendante des paramètres structuraux ($d(C_2—S_1)$, $d(C_2—Y_3)$, $d(C_2—Y_4)$, $d(C_5—Y_3)$, $d(C_6—Y_4)$, $d(S_1—C_{13})$, $\angle S_1C_2Y_3$, $\angle S_1C_2Y_4$, $\angle C_2Y_3C_5$, $\angle C_2Y_4C_6$, $\angle \alpha C_2S_1C_{13}$, $\angle \beta S_1C_{13}H$). Les géométries ainsi optimisées ont été reportées dans le tableau 1.

L'examen de ce tableau ne fait apparaître aucune corrélation possible entre les paramètres géometriques ou leur évolution entre le réactif initial et le produit final et la différence de réactivité entre les trois composés examinés.

De même l'analyse des termes des matrices densité en particulier des charges obtenues au niveau de l'atome de soufre ne permet aucune interprétation des données expérimentales et montre par là même qu'il est difficile d'appréhender de façon simple la réactivité de ces composés.

Chemin de reaction

Afin d'analyser de manière plus précise les effets électroniques dus à la nature des hétéroatomes en α du groupement thiocarbonyle, nous avons examiné l'allure des chemins réactionnels pour les trois composés étudiés lors de l'approche de l'halogénure d'alcoyle.

Selon le procédé utilisé antérieurement (1) en prenant en considération les effets de solvant par application du formalisme de Born selon la relation de Jano (6) nous avons obtenu les variations d'énergie depuis l'état initial jusqu'à

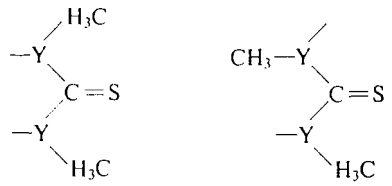

Forme A Forme B

FIG. 1. Conformations envisagées pour les réactifs.

l'état final et observé l'apparition de barrières pour les trois réactions examinées.

Lors de l'approche lointaine du chlorure de méthyle vers la fonction thiocarbonyle nous avons constaté un gain de stabilité par rapport aux réactifs initiaux; il existe ainsi une disposition privilégiée des deux molécules qui correspond à un puits de potentiel atteint par minimisation des paramètres suivants: $d(C_2—S_1)$, $d(C_2—Y_3)$, $d(C_2—Y_4)$, $d(S_1—C_{13})$, $d(C_{13}—Cl_{17})$, $\angle Y_3C_2S_1$, $\angle Y_4C_2S_1$, $\angle \alpha C_2S_1C_{13}$, $\angle \beta S_1C_{13}H$) (géométrie a).

Pour décrire ensuite le chemin de réaction et atteindre le produit final nous avons imposé un allongement à la longueur C—Cl et minimisé les autres paramètres: $d(C_2—S_1)$, $d(C_2—Y_3)$, $d(C_2—Y_4)$, $d(S_1—C_{13})$, $\angle Y_3C_2S_1$, $\angle Y_4C_2S_1$, $\angle \alpha C_2S_1C_{13}$, $\angle \beta S_1C_{13}H$.

Configurations géométriques optimales obtenues

Les géométries optimisées en différents points du chemin de réaction ont été reportées dans le tableau 2.

Après une approche privilégiée de CH_3Cl dans le plan de la molécule et selon l'axe de la liaison C=S (puits de potentiel, géométrie a) on constate en imposant un allongement à la longueur C—Cl une réorganisation structurale très importante au voisinage de l'état de transition concernant en particulier les angles α et β.

On observe ainsi une inversion du groupement méthyle avec passage par un état d'hybridation sp^2 au niveau de l'état de transition.

On peut noter que dans le cas de la diméthyl thiourée le passage par l'état de transition s'accompagne d'une rotation du groupement méthyle autour de la liaison C—N, l'édifice moléculaire adoptant ainsi la conformation privilégiée du produit final.

Bien que les principaux paramètres géométriques prennent des valeurs très voisines dans les trois états de transition, on peut remarquer quelques points intéressants.

Can. J. Chem. Downloaded from www.nrcresearchpress.com by 210.87.254.6 on 09/05/12
For personal use only.

TABLEAU 1. Géométries minimisées des réactifs et des produits finaux

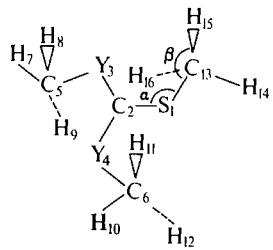

Etat	Longueur de lien (Å)						Angle (deg)					
	C_2—S_1	C_2—Y_3	C_2—Y_4	C_5—Y_3	C_6—Y_4	C_{13}—S_1	$Y_3C_2S_1$	$Y_4C_2S_1$	$C_2Y_3C_5$	$C_2Y_4C_6$	$\alpha C_2S_1C_{13}$	$\beta S_1C_{13}H_{15}$
Initial Y = $NHCH_3$	1.785	1.351	1.351	1.410	1.410		120.7	120.7	122.1	122.1		
Initial Y = SCH_3	1.691	1.758	1.756	1.821	1.819		125.1	131.6	98.9	99.7		
Initial Y = OCH_3	1.756	1.332	1.333	1.387	1.377		121.2	122.5	107	108.3		
Final Y = $NHCH_3$	1.802	1.340	1.339	1.410	1.410	1.812	123.3	110	122.1	122.1	100.2	108.8
Final Y = SCH_3	1.733	1.743	1.736	1.821	1.819	1.810	129.2	128.2	98.9	99.7	100.1	108.8
Final Y = OCH_3	1.785	1.321	1.319	1.387	1.377	1.811	121	120	107	108.3	100	108.7

Can. J. Chem. Downloaded from www.nrcresearchpress.com by 210.87.254.6 on 09/05/12
For personal use only.

TABLEAU 2. Géométries optimisées en différents points du chemin de réaction

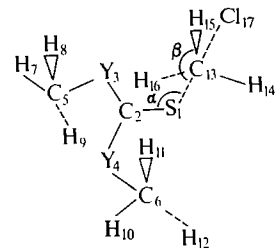

Y		Etat	Longueur de lien (Å)					Angle (deg)			
			C_2—S_1	C_2—Y_3	C_2—Y_4	S_1—C_{13}	C_{13}—Cl_{17}	$Y_3C_2S_1$	$Y_4C_2S_1$	α	β
$NHCH_3$		Géométrie a	1.807	1.351	1.351	2.186	1.754	119.8	119.8	180	75.3
	Etat de transition	C—Cl = 2.05 Å	1.796	1.350	1.346	2.020	2.050	120.2	119.6	110.2	88.6
		C—Cl = 2.15 Å	1.800	1.348	1.346	1.965	2.150	119.9	119.4	109.6	92.6
		C—Cl = 2.2 Å	1.798	1.349	1.345	1.929	2.2	119.9	119.4	109.4	94.6
SCH_3		Géométrie a	1.725	1.759	1.755	2.186	1.754	125.2	134.5	180	75.3
	Etat de transition	C—Cl = 2.1 Å	1.701	1.757	1.751	2.017	2.100	125.3	133.2	110.4	89.5
		C—Cl = 2.2 Å	1.704	1.759	1.750	1.965	2.200	125.1	133	110.3	93.1
		C—Cl = 2.3 Å	1.707	1.754	1.746	1.919	2.300	125.1	133	110.4	97.2
OCH_3		Géométrie a	1.776	1.331	1.333	2.166	1.753	121	122.6	180	75.4
	Etat de transition	C—Cl = 2.1 Å	1.770	1.326	1.330	2.011	2.100	120.2	121.5	120.3	89.1
		C—Cl = 2.2 Å	1.772	1.326	1.329	1.967	2.200	120.6	122	119.5	92.6
		C—Cl = 2.3 Å	1.770	1.325	1.326	1.928	2.300	120.1	121.6	116.1	96.4

Can. J. Chem. Downloaded from www.nrcresearchpress.com by 210.87.254.6 on 09/05/12
For personal use only.

En examinant la liaison qui se coupe C—Cl, on note que le déplacement de l'atome de chlore par rapport à sa position initiale dans CH_3Cl est moins important dans le cas de la dimethyl thiourée que pour les deux autres composés. Ceci est en accord avec les règles d'Haberfield (7) et les conclusions déduites des travaux expérimentaux sur les basicités relatives des trois dérivés. En effet, selon Haberfield un accroissement dans la basicité du nucléophile conduit à un état de transition plus proche des réactifs initiaux.

Par ailleurs on constate par rapport à l'état initial des perturbations au niveau des liaisons C—Y et des angles $\angle YCS$. On peut noter que ces modifications sont du même type pour $Y = NHCH_3$ et $Y = OCH_3$ (raccourcissement des liaisons, diminutions des angles); par contre dans le cas où $Y = SCH_3$ les variations des mêmes paramètres géométriques sont nettement différentes.

Enfin les structures géométriques obtenues pour l'état de transition paraissent nettement plus proches des produits finaux que des réactifs; il apparaît si l'on observe la liaison qui se forme S—C que l'on se trouve plus proche du produit final dans le cas d'un environnement par des atomes d'azote que dans celui d'un environnement par des atomes de soufre ou d'oxygène, l'édifice moléculaire correspondant à $Y = OCH_3$ s'en trouvant le plus éloigné.

Structures électroniques

Pour les trois environnements dans l'état de transition la distribution électronique parait correspondre au schéma $X^{\delta-}\ldots Y^{\delta 2+}\ldots Z^{\delta-}$. On remarque que la charge négative sur l'atome de Cl suit l'ordre de réactivité

$$q_{Cl}\left(\begin{matrix}N\\ \\N\end{matrix}\!\!>\!C{=}S\right) > q_{Cl}\left(\begin{matrix}S\\ \\S\end{matrix}\!\!>\!C{=}S\right) > q_{Cl}\left(\begin{matrix}O\\ \\O\end{matrix}\!\!>\!C{=}S\right)$$

Une analyse détaillée des modifications dans la répartition électronique des systèmes depuis l'état initial jusqu'à l'état de transition, nous a permis de constater le rôle trés différent suivant leur nature des hétéroatomes en α du groupement thiocarbonyle.

Dans le cas de la diméthyl thiourée et du thionocarbonate de méthyle l'atome de chlore acquiert une charge négative aux dépens de l'atome de soufre et du groupement méthyle, la charge totale des atomes d'azote et d'oxygène n'étant que très peu modifiée.

Par contre, dans le trithiocarbonate de méthyle, on observe une intervention très nette des atomes de soufre placés en α du groupement thiocarbonyle. Ainsi l'atome de chlore voit sa charge négative s'accroître en passant de l'état initial à l'état de transition aux dépens du groupement méthyle, du soufre thiocarbonyle mais également des deux atomes de soufre divalents, la participation globale de ces derniers étant équivalente à celle de l'atome de soufre du groupement thiocarbonyle.

On note que les modifications essentielles sont localisées au niveau σ (paires libres dans le plan $\begin{matrix}Y\\ \\Y\end{matrix}\!\!>\!C{=}S$).

Par ailleurs un examen des indices de Wiberg des liaisons $S_1—C_{13}$ et $C_{13}—Cl_{17}$ reportés dans le tableau 3 permet de voir que les valeurs de ces indices sont les plus voisines dans le cas où $Y = NHCH_3$ et les plus différentes quand $X = OCH_3$.

Cette remarque est en accord avec la règle de symbiose (8) selon laquelle un édifice moléculaire est d'autant plus stable que les liaisons mises en jeu autour de l'atome central ont un caractère voisin. L'état de transition le plus stabilisé correspondrait ainsi à celui où $Y = NHCH_3$.

Résultats énérgétiques

L'examen des valeurs des barrières calculées (tableau 4) (définies comme les différences entre le point le plus bas du chemin de réaction et l'état de transition) conduit au classement suivant quant à l'ordre de réactivité de ces dérivés

$$\begin{matrix}N\\ \\N\end{matrix}\!\!>\!C{=}S > \begin{matrix}S\\ \\S\end{matrix}\!\!>\!C{=}S > \begin{matrix}O\\ \\O\end{matrix}\!\!>\!C{=}S$$

Ces résultats sont en parfait accord avec l'échelle de nucléophilie établie expérimentalement. Par un examen de la partition de l'énergie totale (selon le formalisme de Fischer et Kollmar (9)) nous avons cherché à préciser à quel niveau se traduisait cette différence de réactivité entre les trois composés.

Can. J. Chem. Downloaded from www.nrcresearchpress.com by 210.87.254.6 on 09/05/12
For personal use only.

TABLEAU 3. Indices de Wiberg des liaisons S...C et C...Cl

Liaison	Indices		
	$NHCH_3$	SCH_3	OCH_3
$S_1—C_{13}$	0.4981	0.4768	0.4617
$C_{13}—Cl_{17}$	0.5474	0.5652	0.5802

Nous avons ainsi pu constater que le terme qui permettait d'interpréter les variations de l'énergie totale, et par suite les différences de barrières d'activation, était celui qui représentait la somme des énergies associées aux liaisons $S_1 \ldots C_{13}$ et $C_{13} \ldots Cl_{17}$.

Plus précisément alors que la destabilisation de la liaison $C_{13} \ldots Cl_{17}$ est du même ordre pour les trois dérivés on constate que dans l'état de transition le caractère liant de la liaison qui se forme $S_1 \ldots C_{13}$ est plus important pour Y = $NHCH_3$ que pour Y = SCH_3 ou Y = OCH_3, ce dernier environnement correspondant au caractère liant le plus faible. L'influence d'hétéroatomes différents en α du soufre thiocarbonyle se traduit donc par la seule stabilisation de la liaison $S_1 \ldots C_{13}$ qui se forme dans l'état de transition.

Analyse des interactions orbitalaires

L'étude théorique réalisée ayant mis en évidence que la stabilisation plus ou moins grande de la liaison covalente $S_1 \ldots C_{13}$ qui se formait était à l'origine de la réactivité différente des composés nous avons cherché à préciser les principales interactions orbitalaires stabilisantes et destabilisantes mises en jeu lors de la formation de cette liaison.

Pour une fonction thiocarbonyle isolée les énergies des paires libres de l'atome de soufre sont nettement différenciées.

Ainsi pour le thioformaldehyde d'après les données de spectroscopie photoélectronique (10) les énergies des paires n_S et π_S sont respectivement de 9.33 et 11.90 eV.

Par ailleurs, l'étude des spectres photoélectroniques de différents composés thiocarbonylés (11–14) a mis en évidence la très grande sensibilité de ces premières bandes à la nature des hétéroatomes en α du groupement thiocarbonyle. Ainsi les potentiels d'ionisation relatifs aux orbitales n_S et π_S pour les trois environnements considérés sont les suivants:

Composé	Potentiels d'ionization (eV)	
	n_S	π_S
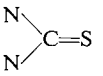	8.08	8.08
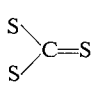	8.50	8.97
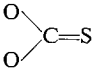	8.99	9.52

Par rapport au thioformaldehyde ces valeurs peuvent s'interpréter par une analyse des interactions entre les paires de l'atome de soufre et celles des hétéroatomes Y (fig. 2).

En ce qui concerne les orbitales n_S et π_S les interactions destabilisantes suivantes sont à envisager: intéraction de type 1 de l'orbitale n_S avec la combinaison antisymétrique des orbitales p_x des hétéroatomes Y principalement localisées sur les liaisons σ_{C-Y}; interaction de type 2 de l'orbitale π_S avec la combinaison symétrique des orbitales π_Y.

Compte tenu des énergies associées aux orbitales σ_{C-Y} et π_Y, les interactions les plus importantes interviennent pour Y = SCH_3 et les plus faibles pour Y = OCH_3. On s'attendrait donc, en ce qui concerne les potentiels d'ionisation relatifs aux orbitales n_S et π_S à obtenir l'ordre suivant:

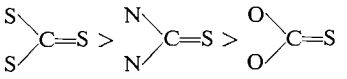

Toutefois des interactions supplémentaires de nature stabilisantes sont susceptibles d'intervenir: la combinaison antiliante issue de l'interaction de type 1 peut interréagir avec les combinaisons antisymétriques des orbitales p_x^* et p_y^* des hétéroatomes Y; la combinaison antiliante issue de l'interaction de type 2 peut interréagir avec la combinaison symétrique des orbitales π_Y^*.

Ces interactions seront les plus importantes dans le cas d'un environnement par des atomes de soufre et sensiblement du même ordre dans le cas d'environnements par des atomes d'azote ou d'oxygène.

Cette analyse qualitative des interactions orbitalaires permet d'interpréter le classement observé expérimentalement, ordre d'ailleurs retrouvé théoriquement.

TABLEAU 4. Données énergétiques

Système	Etat	E_{totale} (u.a.)	$E_{solv.}$ (u.a.)	Barrière (kcal/mol)
Diméthyl thiourée + CH_3Cl		−87.1222	−87.1640	
	Géométrie a	−87.1578	−87.1999	
	Etat de transition C−Cl = 2.05 Å	−87.0885	−87.1575	
	Etat de transition C−Cl = 2.15 Å	−87.0665	−87.1543	28.6
	Etat de transition C−Cl = 2.20 Å	−87.0565	−87.1564	
	Etat final	−86.8652	−87.2481	
Trithiocarbonate de méthyle + CH_3Cl		−83.6231	−83.6326	
	Géométrie a	−83.6564	−83.6697	
	Etat de transition C−Cl = 2.10 Å	−83.5676	−83.6104	
	Etat de transition C−Cl = 2.20 Å	−83.5432	−83.6047	40.7
	Etat de transition C−Cl = 2.30 Å	−83.5226	−83.6079	
	Etat final	−83.3375	−83.7045	
Thionocarbonate de méthyle + CH_3Cl		−99.0669	−99.1091	
	Géométrie a	−99.1031	−99.1463	
	Etat de transition C—Cl = 2.10 Å	−99.0139	−99.0832	
	Etat de transition C—Cl = 2.20 Å	−98.9888	−99.0732	45.8
	Etat de transition C—Cl = 2.30 Å	−98.9678	−99.0754	
	Etat final	−98.7795	−99.1781	

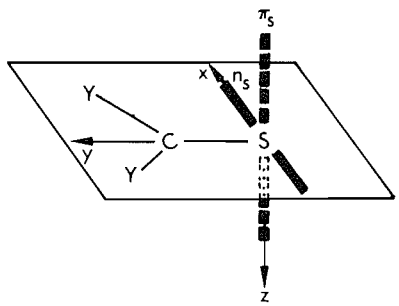

FIG. 2. Définition des paires libres de l'atome de soufre.

Nous avons ensuite examiné lors de l'approche du chlorure de méthyle vers le groupement thiocarbonyle les interactions intervenant entre l'atome de soufre de la fonction thiocarbonyle et CH_3Cl.

L'interaction prépondérante destabilisante concerne l'orbitale fortement localisée sur la paire n de l'atome de soufre et celle σ_{C-Cl} de CH_3Cl; elle peut être évaluée sensiblement de la même importance pour les trois composés; compte tenu des positions énergétiques de la paire n de soufre dans les trois environnements et de σ_{C-Cl} cette interaction a été schématisée sur la fig. 3.

Toutefois une interaction de nature stabilisante intervient entre la combinaison antiliante ainsi

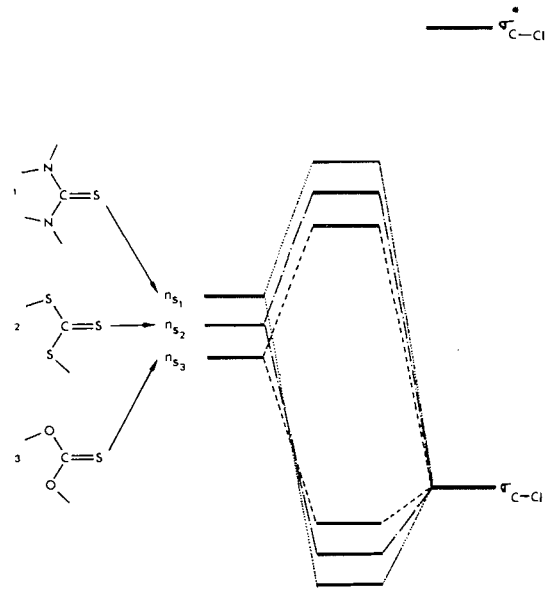

FIG. 3. Interactions orbitalaires déstabilisantes mises en jeu.

formée et la première orbitale vacante σ_{C-Cl}^* de CH_3Cl; son importance selon la nature de l'hétéroatome en α du thiocarbonyle variera de la manière suivante: N > S > O, reflétant ainsi les différences de barrières d'activation observées expérimentalement.

Can. J. Chem. Downloaded from www.nrcresearchpress.com by 210.87.254.6 on 09/05/12
For personal use only.

Une illustration de l'importance de cette interaction peut être trouvée dans l'élément $S_{\mu\nu}P_{\mu\nu}$ entre le soufre thiocarbonyle et le carbone du groupement méthyle.

D'après les valeurs de ces indices pour les trois ensembles moléculaires à 0.1 Å de l'état de transition nous avons l'ordre suivant:

Composé	$S_{\mu\nu}$	$P_{\mu\nu}$
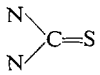	−0.2419	−0.4628
	−0.2418	−0.4440
	−0.1897	−0.3807

Conclusions

L'étude théorique des facteurs à l'origine de la différence de réactivité nucléophile du groupement thiocarbonyle selon l'environnement menée conjointement à une analyse qualitative des interactions orbitalaires intervenant au cours de l'approche ont mis en évidence que ce type de réaction était essentiellement controlé par la plus ou moins grande stabilisation énergétique de la liaison covalente S . . . C formée.

Cette stabilisation est en relation directe avec l'énergie des paires n de l'atome de soufre du groupement thiocarbonyle, conclusion en accord avec la corrélation établie antérieurement à partir des données de la spectroscopie photoélectronique.

1. D. GONBEAU et G. PFISTER-GUILLOUZO. Tetrahedron, **31**, 459 (1975).
2. M. ARBELOT et Coll. Int. J. Sulfur Chem. A paraître.
3. M. ARBELOT, J. METZGER, M. CHANON, C. GUIMON et G. PFISTER-GUILLOUZO. J. Am. Chem. Soc. **96**, 6217 (1974).
4. C. GUIMON, D. GONBEAU et G. PFISTER-GUILLOUZO. J. Mol. Struct. **16**, 271 (1973).
5. W. WALTER et K. P. RUESS. Annalen, **746**, 54 (1971).
6. I. JANO. C.R. Acad. Sci. **261**, 103 (1965).
7. P. HABERFIELD. J. Am. Chem. Soc. **93**, 2091 (1971).
8. R. G. PEARSON et J. SONGSTAD. J. Org. Chem. **32**, 2899 (1967).
9. H. FISCHER et H. KOLLMAR. Theoret. Chim. Acta, **16**, 163 (1970).
10. H. W. KROTO et R. J. SUFFOLK. Chem. Phys. Lett. **15**, 545 (1972).
11. C. GUIMON, G. PFISTER-GUILLOUZO, M. ARBELOT et M. CHANON. Tetrahedron, **30**, 3831 (1974).
12. C. GUIMON, D. GONBEAU, G. PFISTER-GUILLOUZO, L. ASBRINK et J. SANDSTROM. J. Electron Spectrosc. Relat. Phenom. **4**, 49 (1974).
13. D. GONBEAU, C. GUIMON, J. DESCHAMPS et G. PFISTER-GUILLOUZO. J. Electron Spectrosc. Relat. Phenom. **6**, 99 (1975).
14. C. GUIMON, M. ARBELOT et G. PFISTER-GUILLOUZO. Spectrochim. Acta, **31A**, 985 (1975).

Can. J. Chem. Downloaded from www.nrcresearchpress.com by 210.87.254.6 on 09/05/12
For personal use only.

Morpholines: stereochemistry and preferred steric course of quaternization

ALAN J. JONES,[1] C. P. BEEMAN, AND M. U. HASAN
Department of Chemistry, University of Alberta, Edmonton, Alberta T6G 2G2
AND
A. F. CASY[2] AND M. M. A. HASSAN
Faculty of Pharmacy and Pharmaceutical Sciences, University of Alberta, Edmonton, Alberta T6G 2G2

Received June 24, 1975

ALAN J. JONES, C. P. BEEMAN, M. U. HASAN, A. F. CASY, and M. M. A. HASSAN. Can. J. Chem. **54**, 126 (1976).

The ^{13}C magnetic resonance spectra of a series of methyl and phenyl substituted morpholines, their hydrochlorides, and methiodides have been determined. The effects of methyl substitution adjacent to oxygen and nitrogen are reasonably equivalent and substituent induced chemical shift parameters derived for the series show favorable agreement with those previously observed in both alicyclic and heterocyclic systems. Results for the *cis* and *trans* isomers of phendimetrazine (3,4-dimethyl-2-phenylmorpholine), confirm the preferred chair conformations and configurations *cis*-3-CH_3, *cis*-2-phenyl (*cis*) and *trans*-3-CH_3, *cis*-2-phenyl (*trans*) for these isomers. The preferred course of quaternization of nitrogen in these systems was determined as axial, using deuteriomethyliodide as a label. This ^{13}C–^{2}H technique relies on the observation of the γ-*syn*-axial effect and is clearly unambiguous and superior to other methods used in evaluating this mechanism. Product ratios and consequently free energies of this reaction were measured from proton and deuterium nmr spectra.

ALAN J. JONES, C. P. BEEMAN, M. U. HASAN, A. F. CASY et M. M. A. HASSAN. Can. J. Chem. **54**, 126 (1976).

On a déterminé les spectres rmn du ^{13}C d'une série de morpholines méthylées et phénylées ainsi que de leurs chlorhydrates et de leurs méthiodures. Les effets de substitution par un méthyle adjacent de l'oxygène et de l'azote sont assez équivalents et les paramètres de déplacements chimiques induits par les substituants dérivés de la série sont en bon accord avec ceux observés antérieurement dans des systèmes alicycliques et hétérocycliques. Les résultats obtenus avec les isomères *cis* et *trans* de la phèndimétrazine (diméthyl-3,4 phényl-2 morpholine) confirment les conformations chaises préférées et les configurations au niveau *cis*-CH_3(3), *cis*-phényl(2) (*cis*) et *trans*-CH_3(3), *cis*-phényl(2) (*trans*) de ces isomères. Utilisant l'iodure de deutériométhyle comme marqueur, on a déterminé que le sens préféré pour la quaternisation de l'azote dans ces systèmes est la face axiale. Cette technique ^{13}C–^{2}H se base sur l'observation de l'effet γ-*syn*-axial; elle est non ambigue et supérieure à d'autres méthodes utilisées pour évaluer ce mécanisme. Utilisant les spectres rmn du proton et du deutérium, on a mesuré les quantités relatives de produits desquelles on peut déduire les énergies libres de cette réaction.
[Traduit par le journal]

In our continuing interest concerning the application of ^{13}C magnetic resonance techniques to conformational analysis (1) we have investigated a series of pharmacologically active compounds (2) and their precursors (3) and have illustrated the use of substituent-induced chemical shift additivity relationships in establishing stereochemistry.

We now report the investigation of a series of substituted morpholines in which the heterocyclic ring contains both oxygen and nitrogen. Additivity parameters derived from this data confirm the preferred conformation, in solution of the isomers of the pharmacologically active phendimetrazine (3,4-dimethyl-2-phenylmorpholine), **6**. These results supplement our initial efforts to demonstrate the potential of the ^{13}C nmr technique for conformational analysis of molecules in which there exists a stereo-structural activity relationship (2, 3). The morpholines **1–6**, their hydrochlorides and methiodides form the basis of this study.

[1]Address correspondence to this author: National NMR Centre, Australian National University, Canberra, 2601, Australia.
[2]Present address: Norfolk and Norwich Hospital, St. Stephens Rd., Norwich, U.K. NR1 3SR.

Can. J. Chem. Downloaded from www.nrcresearchpress.com by 210.87.254.105 on 09/05/12
For personal use only.

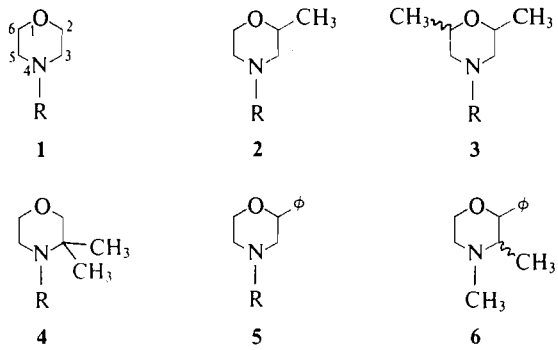

1 **2** **3**

4 **5** **6**

(*a*) R = H (*b*) R = CH_3

There has been considerable controversy concerning the preferred course of quaternization of *N*-heterocyclic compounds (4–6). In the present paper we describe an isotopic labelling experiment using deuteriomethyliodide which relies on the well-established observation (1, 2, 7) that an axial methyl group ^{13}C resonance will be shifted to high field due to the γ-gauche interactions. We have applied this method to a series of piperidines, tropinones, and the morpholines in order to demonstrate its general validity in resolving the assignment of configuration to pairs of diastereoisomeric quaternary salts. The method is clearly unambiguous and is superior to other methods (5) used in resolving configurational assignments. During the course of this work Wenkert (8) briefly reported a similar study on a series of tropane derivatives.

Experimental

Carbon-13 and deuterium spectra were obtained in the Fourier mode using a Bruker HFX-90 spectrometer operating at 22.63 and 13.81 MHz, respectively, as described in previous papers (2, 9). Spectra were obtained for solutions in either deuteriochloroform or deuterium oxide with 2–5% tetramethylsilane (TMS) or dioxane–TMS mixture respectively added as internal reference. In the variable temperature studies deuteriochloroform and carbon disulphide were employed as mixed solvents in order to enhance the effective low temperature range. In the case of the deuterium nmr studies deuterium oxide was used as reference. Commercially available morpholine (Fisher Scientific Co.) and 2,6-dimethylmorpholine (Aldrich Chemical Co.) were used without further purification. 2-Phenylmorpholine was prepared according to the method of Bailey *et al.*, (10) and exhibited identical physical characteristics to those reported (10). 2-Methyl- and 3,3-dimethylmorpholine were prepared following Cottle *et al.* (11), 2-methylmorpholine, bp 130–131 °C, 705 Torr (lit. (11) bp 135–136 °C, atmospheric pressure); 3,3-dimethylmorpholine bp. 52 °C, 30 Torr (lit. (11) bp 143–144 °C, atmospheric pressure). Pure *cis*-2,4,6-trimethylmorpholine was obtained by the method of Booth and Gidley (12). 4-*tert*-butyl-*N*-methylpiperidine was kindly donated by Dr. M. L. Stein (13). All piperidines and tropines were obtained from commercial sources as bases and were treated with methyl iodide in ether to obtain the appropriate salt.

Results

The observed ^{13}C chemical shifts in the morpholines **1**–**6**, their hydrochlorides and respective methiodides are presented in Table 1. The conventional labelling system (see **1**) for the morpholine ring is employed throughout this discussion. Prime numbers refer to methyl substituents at the respective ring carbons. To avoid ambiguity, the 1-position in the phenyl ring is designated C-*q* and the remaining phenyl carbons C-*o*, C-*m* and C-*p*.

The ^{13}C spectrum of morpholine exhibits lines of equal intensity at 68.0_9 ppm and 46.7_4 ppm downfield from internal TMS, which are assigned to carbons C-2,6 and C-3,5, respectively, on the basis of comparison with shifts for 1,4-dioxane (67.1 ppm) and the α-carbons in piperidine (48 ppm) (14). Subsequent assignments were made using conventional techniques (15). Data for 2,6-dimethyl- , **3***a*, and 2,4-6-trimethylmorpholine, **3***b*, were obtained for mixtures of *cis*- and *trans*-isomers. In all cases the resonances due to both isomers were clearly distinguishable on the basis of chemical shift separation and relative intensities. Comparison with data for pure *cis*-2,4,6-trimethylmorpholine identified the *cis*-isomer as the major component of the mixtures as also indicated in earlier pmr studies (12). Low temperature (−80 °C) conditions were employed to resolve the rapidly equilibrating 3,3-dimethylmorpholine, **5**, and its derivatives, and consequently distinguish the axial and equatorial 3-methyl groups. Assignment of the carbons C-3 and C-5 in 2-phenyl-, **5***a*, and 4-methyl-2-phenylmorpholine, **5***b*, were confirmed by comparison of the observed chemical shifts with those predicted using the *N*-methylation parameters derived in this work. The assignments for aromatic carbons C-*o* and C-*m* in **5** and **6** are based on the pattern of shifts generally observed in substituted benzenes (16) but are not unequivocal.

Can. J. Chem. Downloaded from www.nrcresearchpress.com by 210.87.254.105 on 09/05/12
For personal use only.

Can. J. Chem. Downloaded from www.nrcresearchpress.com by 210.87.254.105 on 09/05/12
For personal use only.

TABLE 1. Carbon-13 chemical shifts in substituted morpholines[a]

Structure	Solvent	C-2	C-3	C-5	C-6	N—CH_3	C-2′,6′	C-3′,3″	C-*q*	C-*o*	C-*m*	C-*p*
1*a*	$CDCl_3$	68.09	46.74	46.74	68.09	—	—	—	—	—	—	—
	D_2O	67.33	45.10	45.10	67.33	—	—	—	—	—	—	—
HCl	D_2O	63.72	43.38	43.38	63.72	—	—	—	—	—	—	—
1*b*	$CDCl_3$	67.07	55.68	55.68	67.07	46.56	—	—	—	—	—	—
	D_2O	66.36	54.22	54.22	66.36	45.00	—	—	—	—	—	—
HCl	D_2O	63.99	53.41	53.41	63.99	43.43	—	—	—	—	—	—
MeI	D_2O	60.80	61.29[n]	61.29[n]	60.80	52.17[n]	—	—	—	—	—	—
2*a*	$CDCl_3$	72.99	53.03	45.85	68.13	—	19.10	—	—	—	—	—
	D_2O	73.00	51.15	44.14	67.23	—	18.30	—	—	—	—	—
HCl	$CDCl_3$	69.38	48.39	42.56	63.44	—	18.72	—	—	—	—	—
	D_2O	70.03	48.07	42.57	63.45	—	17.86	—	—	—	—	—
2*b*	$CDCl_3$	71.70	62.15	54.86	66.68	46.23	19.10	—	—	—	—	—
HCl	$CDCl_3$	69.38	58.32	52.60	63.44	43.64	18.45	—	—	—	—	—
	D_2O	70.52	58.11	52.71	63.83	43.60	17.65	—	—	—	—	—
MeI	D_2O	66.74	65.88	60.70	60.70	[b]	17.49	—	—	—	—	—
3*a*(*cis*)	$CDCl_3$	73.18	52.24	52.24	73.18	—	19.16	—	—	—	—	—
	D_2O	73.27	50.34	50.34	73.27	—	18.25	—	—	—	—	—
HCl	$CDCl_3$	69.26	47.90	47.90	69.26	—	18.72	—	—	—	—	—
	D_2O	70.03	47.48	47.48	70.03	—	17.82	—	—	—	—	—
3*a*(*trans*)	$CDCl_3$	66.53	51.35	51.35	66.53	—	17.63	—	—	—	—	—
	D_2O	66.74	49.26	49.26	66.74	—	16.79	—	—	—	—	—
HCl	$CDCl_3$	63.81	47.04	47.04	63.81	—	17.85	—	—	—	—	—
	D_2O	64.15	46.78	46.78	64.15	—	16.57	—	—	—	—	—
3*b*(*cis*)	$CDCl_3$	71.65	61.46	61.46	71.65	45.96	19.14	—	—	—	—	—
HCl	$CDCl_3$	69.10	57.83	57.83	69.10	43.80	18.39	—	—	—	—	—
MeI	D_2O	66.74	65.23[p]	65.23[p]	66.74	[c,p]	17.44	—	—	—	—	—
3*b*(*trans*)[d]	$CDCl_3$	66.50	60.81	60.81	66.50	46.61	18.22	—	—	—	—	—
HCl	$CDCl_3$	64.64	57.71	57.71	64.64	44.96	18.01	—	—	—	—	—
4*a*	$CDCl_3$	77.25	48.93	41.48	67.97	—	—	24.92[e]	—	—	—	—
	D_2O	75.91	48.24	39.77	66.74	—	—	23.48	—	—	—	—
HCl	$CDCl_3$	73.42	54.22	39.06	63.66	—	—	21.68[f]	—	—	—	—
	D_2O	72.94	54.22	39.12	63.61	—	—	21.05	—	—	—	—

Can. J. Chem. Downloaded from www.nrcresearchpress.com by 210.87.254.105 on 09/05/12
For personal use only.

TABLE 1 (*Concluded*)

Structure	Solvent	C-2	C-3	C-5	C-6	N—CH_3	C-2′,6′	C-3′,3″	C-*q*	C-*o*	C-*m*	C-*p*
4*b*	$CDCl_3$	77.84	53.02	50.00	67.86	37.38	—	18.29[g]	—	—	—	—
HCl	$CDCl_3$	73.90	60.20	49.79	64.41	36.68	—	[h]	—	—	—	—
	D_2O	73.97	60.86	49.37	64.58	36.31	—	[i]	—	—	—	—
MeI	D_2O	70.30	68.41	59.24	61.40	47.86	—	18.84	—	—	—	—
5*a*	$CDCl_3$	79.38	53.32	45.80	68.44	—	—	—	140.57	(126.02)	(128.28)[q]	127.61
HCl	$CDCl_3$	75.29	48.47	42.81	63.99	—	—	—	137.15	(126.04)	(128.79)	(128.79)
5*b*	$CDCl_3$	78.11	62.30	54.80	67.05	46.17	—	—	140.52	(126.12)	(128.22)	127.63
HCl	$CDCl_3$	75.09	58.31	52.70	63.87	43.75	—	—	136.80	(126.17)	(128.81)	(128.81)
MeI	D_2O	72.35	65.01	60.48	61.08	[j]	—	—	135.89	(127.15)	(129.31)	129.80
6(*cis*)	$CDCl_3$	81.84	58.82	47.14	67.39	42.80	—	2.43	140.41	(125.56)	(127.98)	126.80
HCl	$CDCl_3$	77.74	59.95	46.69	64.29	41.11	—	4.66	136.64	(125.29)	(128.52)	128.04
MeI	D_2O	74.24	68.95	55.14	61.62	[k]	—	7.83	136.87	(125.65)	(129.05)	128.62
6(*trans*)	$CDCl_3$	85.14	63.61	56.22	67.12	43.16	—	15.00	140.34	(128.09)	(128.30)	[l]
HCl	$CDCl_3$	81.69	64.80	54.60	63.88	41.49	—	12.52	137.05	(127.77)	(129.01)	129.44
MeI	D_2O	78.23	70.46	63.61	60.91	[m]	—	9.99	136.32	(128.02)	(129.42)	130.01

[a]Given in ppm downfield relative to TMS.
[b]Nonequivalent *N*-methyl carbons at 48.02 ppm (axial) and 57.19 ppm (equatorial).
[c]Nonequivalent *N*-methyl carbons at 48.83 ppm (axial) and 57.14 ppm (equatorial).
[d]Only the *cis*-methiodide was isolated.
[e]Chemical shifts at 193 K: 76.77, 48.90, 41.11, 67.81, and 21.90 ppm (axial) and 27.24 ppm (equatorial).
[f]Chemical shifts at 198 K: 72.88, 54.00, 38.57, 63.44, and 19.69 ppm (axial) and 22.98 ppm (equatorial).
[g]Chemical shifts at 193 K: 77.84, 52.87, 49.36, 67.70, 37.28, and 12.02 ppm (axial) and 24.22 ppm (equatorial).
[h]Broadened, nonequivalent methyl carbons at ambient temperature: 16.83 ppm (axial) and 21.04 ppm (equatorial).
[i]Nonequivalent methyl carbons at ambient temperature: 15.28 ppm (axial) and 20.40 ppm (equatorial).
[j]Nonequivalent *N*-methyl carbons at 48.08 ppm (axial) and 57.25 ppm (equatorial).
[k]Nonequivalent *N*-methyl carbons at 50.12 ppm (axial) and 54.33 ppm (equatorial).
[l]*para*-Carbon resonance unresolved.
[m]Nonequivalent *N*-methyl carbons at 42.52 ppm (axial) and 54.71 ppm (equatorial).
[n]Observed resonance split due to nitrogen coupling ($J_{^{14}N-^{13}C_3}$ = 2.7 Hz, $J_{^{14}N-^{13}CH_3}$ = 3.9 Hz).
[p]Broadening of resonance observed.
[q]Parentheses indicate that unequivocal assignments were not made.

TABLE 2. Substituent parameters in substituted morpholines[a]

Substituent	α_e	α_a	β_e	β_a	γ_e	γ_a
N—CH_3			9.13		−1.24[b]	
C—CH_3(O)	5.09	−2.31	5.50	3.72		(−5.9)[c]
C—CH_3(N)	4.41	1.50	6.78	3.48		−5.98[d]
C—ϕ(O)	11.29		6.58			

[a]In ppm. A negative sign indicates an upfield shift. (O) Substitution adjacent to oxygen. (N) Substitution adjacent to nitrogen.
[b]Does not include the negligible shift observed in *trans*-2,4,6-trimethylmorpholine.
[c]Reference 7*b*.
[d]The value −8.54 ppm occurs in *cis*-**6** where additional steric compression factors contribute to the shifts.

Discussion

It is necessary that the stereochemistry of selected compounds be well established if they are to serve as valid models for studying conformational features. It is well established that the heterocyclic ring in morpholine bases exists predominantly in the chair form (17–20). However, there is considerable disagreement concerning the configuration of the N—R group (R = H or CH_3) (17–21). While we do not presume to assess this configuration in the hydrides (R = H), it is clear from the evidence in the following section that the *N*-methyl group prefers the equatorial configuration.

(*a*) *Substituent Effects*

All substituent parameters derived in this study are summarized in Table 2.

N-Methyl substituent γ- and β-effects are observed at C-2,6 (−1.0 ppm) and C-3,5 (9 ppm) in *N*-methylmorpholine, compared with morpholine. These values are almost identical to those observed in the *N*-methylpiperidines (−1.2 and 8.9 ppm) (3) and *N*-methylpiperazines (−1.0 and 9.1 ppm) (22). The magnitude of the γ-parameter emphasizes the predominantly equatorial configuration of the *N*-methyl group, since larger γ-effects (−6.4 ppm) (7) are observed in cases where γ-gauche (1,3-steric) interactions occur between diaxial groups. The generally observed γ- and β-*N*-methyl induced shifts throughout the series **1**–**6** are −1.2 and 9.1 ppm, respectively. In addition, the observed chemical shifts for the *N*-methyl carbons occur over a narrow range (0.6 ppm), further indicating the equatorial *N*-methyl configuration throughout the series.

The effects of methyl substitution at ring carbons are observed in compounds **2**–**4**. In 2-methylmorpholine, **2***a*, in which the methyl group is expected to be predominantly equatorial, induced downfield shifts are observed for carbons C-2 (4.90 ppm) and C-3 (6.29 ppm) relative to morpholine. Small induced shifts (less than 1.0 ppm) are observed for the remaining ring carbons, C-5 and C-6. The *cis*-isomer of 2,6-dimethylmorpholine, **3***a*, in which both methyl groups are established as equatorial (12), exhibits downfield shifts, relative to morpholine, for carbons C-2,6 (5.09 ppm) and C-3,5 (5.50 ppm). The α-parameter obtained from this data (5.00 ppm downfield) compares with that observed for methylcyclohexanes (5.96 ppm) (7*a*) methylpiperidines (5.4 ppm) (3), and methylpiperazines (5.7 ppm) (22). The magnitude of the induced shift (β-parameter) at the β-carbons (5.90 ppm) might be considered anomalous in view of this parameter (9.1 ppm) derived from the *N*-methylation data. However, a similarly attenuated parameter was observed in 2-*tert*-butyl-5-methyl-1,3-dioxane (1*a*) and 2-methylpiperazine (22) and it is clear that the substituent effect at β-carbons is reduced (compared to methylcyclohexanes) when these carbons are adjacent to oxygen or nitrogen.

The *trans*-2,6-dimethylmorpholine isomer, **3***a*, is a mixture of rapidly inverting and energetically equivalent chair forms as shown by the occurrence of only one methyl resonance in the ^{13}C spectrum. Therefore, the shifts at C-2,6 (−1.56 ppm) and C-3,5 (4.61 ppm), compared to morpholine, are the average of axial and equatorial methyl contributions. The α- and β-axial methyl substituent parameters derived from these data are −2.31 and 3.72 ppm, respectively. The shifts at C-2,6 in *trans*-**3***a* must include an effect from γ-gauche 1,3-steric interactions, which is assumed to be of the order of −5.9 ppm, by analogy with this contribution in 3,5-dimethyltetrahydropyran (7*b*). The uncertainties involved

Can. J. Chem. Downloaded from www.nrcresearchpress.com by 210.87.254.105 on 09/05/12
For personal use only.

Can. J. Chem. Downloaded from www.nrcresearchpress.com by 210.87.254.105 on 09/05/12
For personal use only.

in the derivation of the axial α-methyl parameter preclude further discussion, though the β-term may be reasonably compared to that observed in the methylcyclohexanes (7*a*).[3]

The *gem*-dimethyl effect (2.19 ppm) observed at C-3 in 3,3-dimethylmorpholine (**4***a*) is attenuated, though reasonably characteristic of similar effects observed in the methylcyclohexanes (2.9 ppm) (7) and 1,3-dioxanes (3.5 ppm) (1*a*). Lowering the temperature of the solutions of the 3,3-dimethylmorpholine series (**4***a*, *b*) froze out the chair conformation (−80 °C) which characterized the axial and equatorial methyl groups and provided the average, and typical (7*b*) γ-gauche parameter of −5.98 ppm at C-5 in **4***a*, *b*.

A phenyl substituent on a morpholine ring is expected to adopt the equatorial configuration. The observed chemical shifts in 2-phenyl-, (**5***a*), and 4-methyl-2-phenylmorpholine, **5***b*, are consistent with this configuration since substituent induced shifts in these compounds are negligible except at the sites α- and β- to the substituent. The downfield shifts for carbons C-2 (11.29 ppm) and C-3 (6.58 ppm) in **5***a* are taken as equatorial α- and β-phenyl substituent effects and may be compared with those observed in 1-methyl-4-phenylpiperidine (17.7 and 6.7 ppm) (2). Presumably, the smaller α-effect in the 2-phenylmorpholine is due to the higher degree of substitution at the β-positions (23) in **5***a* compared with 1-methyl-4-phenylpiperidine.

(*b*) *The Phendimetrazines*

The chemical shifts for the phendimetrazine isomers, **6**, their hydrochlorides, and methiodides are also given in Table 1. The isomers of **6** are suggested to differ only in the configuration of the 3-methyl group, *cis* (axial methyl) or *trans* (equatorial methyl) (24). Proton (24) and ^{13}C magnetic resonance data, to be discussed, confirm these configurations.

Two features in the data for **6** should be noted: (*i*) the observed chemical shifts for the phenyl carbon, C-*q*, are identical in the two isomers and, moreover, are identical to those observed for the equatorial phenyl groups in **5**; and (*ii*) the large upfield shifts at C-5 (9 ppm) and C-3′ (12 ppm) in the *cis*- compared to the *trans*-isomer are indicative of a change in configuration at C-3. The identical shifts for the phenyl substituents in the phendimetrazines confirm their equatorial configuration and may be contrasted with those in α- and β-1,2-dimethyl-4-phenylpiperidin-4-ol (2*a*) in which an upfield shift of approximately 5 ppm was observed at C-*q* in the α-isomer (axial phenyl) relative to the β-isomer (equatorial phenyl). The second feature clearly establishes the axial 3-methyl configuration in the *cis*-isomer. The magnitudes of the steric shifts (compare the characteristic 5–6 ppm (7*b*) and −5.98 ppm, Table 2) suggest a greater interaction between the 3-methyl group and the C-5 axial proton probably due to additional steric compression induced by the adjacent phenyl group. The lower stability[4] of the *cis*- compared with the *trans*-isomer has been attributed to the destabilizing nonbonded interaction between the phenyl and 3-methyl groups (24). Further evidence of this interaction is apparent in the observed upfield shifts in the phenyl ring (1.4 ppm average for C-*o* and C-*m* in the *cis*- compared with the *trans*-isomer).

Establishment of the configurations for the phendimetrazine isomers permits derivation of parameters for equatorial and axial methyl substitution adjacent to nitrogen in the morpholines. Thus, for the *trans*-isomer, the shift at C-2 (18.07 ppm downfield) comprises contributions from equatorial α-phenyl and β-methyl substituents. Taking the α-phenyl parameter (11.29 ppm), derived previously, the calculated β-methyl parameter is 6.78 ppm. Upfield shifts of the *N*-methyl (3.40 ppm) and C-3′ methyl (4.16 ppm relative to *cis*-2,4,6-trimethylmorpholine) carbons may be attributed to their diequatorial interactions. The average upfield shifts of the two methyl carbons (3.52 ppm) compares favorably with that in 1,3-dimethylpiperidine (3.78 ppm) (3), 1,2-dimethyl-4-piperidone (3.55 ppm) (3), and methylcyclohexanes (2.82 ppm) (7). This steric interaction also influences the shift at C-3. Assuming the same proportional decrease

[3]It would be interesting to compare this data with its equivalent *trans*-isomer of 2,6-dimethylpiperazine. Unfortunately, Ellis and Jones (22) reported the observation of only a three line spectrum for this compound and for a solution of a *cis–trans* mixture of 2,5-dimethylpiperazine and made no distinction between axial or equatorial substituents.

[4]Treatment of the *cis*-isomer with strong acid causes inversion at the benzylic carbon to form the more stable *trans*-isomer (24).

Can. J. Chem. Downloaded from www.nrcresearchpress.com by 210.87.254.105 on 09/05/12
For personal use only.

in magnitude for the induced shift at C-3 relative to C-3′, as observed in methylcyclohexanes (2.82 to 2.45 ppm), then the modified shift parameter (3.06 ppm upfield) is obtained. This value and the β-phenyl parameter permit calculation of the equatorial α-methyl parameter (4.41 ppm downfield) for substitution adjacent to nitrogen.

From the data for *cis*-phendimetrazine an axial β-methyl substituent effect (3.48 ppm downfield) is derived in an analogous manner. The upfield shift at C-5 (8.54 ppm) in this isomer results from 1,3-*syn* axial interactions with the C-3′ methyl group and this steric effect compares with that in 4-phenylpiperidine (7.9 ppm) (2*a*). The upfield shift at C-3′ (13.67 ppm relative to the axial methyl in *trans*-2,4,6-trimethylmorpholine) comprises this same effect and the additional steric compression from the adjacent phenyl group. The magnitude of the latter parameter (5.13 ppm upfield) is surprisingly similar to other steric parameters (7). The *N*-methyl shift (3.81 ppm upfield relative to *trans*-2,4,6-trimethylmorpholine) is slightly larger than that in the *trans*-isomer reflecting an increased steric interaction for equatorial–axial methyl relative to equatorial–equatorial methyl (7). Assuming that the induced shift for the two interactions increases proportionally to the same extent as in methylcyclohexanes (2.45 to 3.43 ppm) (7) the axial α-methyl substituent parameter is calculated to be 1.50 ppm downfield.

The observed chemical shifts in the phendimetrazines are consistent with the application of the parameters given in Table 2 thus confirming the predominantly chair conformations and configurations *cis*-3-CH_3, *cis*-2-phenyl (*cis*) and *trans*-3-CH_3, *cis*-2-phenyl (*trans*) in these isomers.

(*c*) *Solvent Effects and Hydrochlorides*

The presence of two electronegative centers with nonbonded electrons in the morpholines is expected to be manifested in solubility behavior and solvent induced chemical shifts. In the case of morpholine a change of solvent from deuteriochloroform to deuterium oxide results in chemical shift differences at carbons C-2,6 (0.76 ppm, upfield) and C-3,5 (1.64 ppm upfield). *N*-Methylation of morpholine has little effect on the observed solvent behavior (Table 1) and the highly polar nature of the corresponding hydrochloride is evidenced by its insolubility in the weakly polar deuteriochloroform. In 2,6-dimethylmorpholine it is apparent that the methyl groups sterically hinder polar solvent association at the oxygen since only small changes are induced in the shifts at C-2,6 (0.15 ppm) while large changes occur at C-3,5 (2.00 ppm), with change of solvent. The removal of one site of solvent association is further indicated by the solubility of the hydrochloride in both deuteriochloroform and deuterium oxide.

Since the changes in observed chemical shift appear to parallel the solubility behavior it is assumed that they are true solvent induced shifts rather than the result of changes in conformation. To obviate the possibility of large solvent contributions to chemical shifts between the bases and hydrochlorides solutions in the two solvents were compared where possible. The additivity parameters derived in this work, therefore, suffer no loss of validity in those cases (most notably the nitrogen quaternization data, Section *d*) in which solvent shifts are unavoidably incorporated.

Characteristic upfield shifts of 2.3 and 3.28 ppm are observed at the carbon atoms C-2,6 and C-3,5, respectively, on protonation of the nitrogen atom in this series. The usual exceptions of deshielding occur when the positions adjacent (C-3,5) to the nitrogen atom are substituted (as in **4** and **6**), presumably the consequence of additional steric compression. In the 2-phenyl substituted systems **5** and **6** it is noteworthy that the shielding effects at C-2 are marginally larger than the average and furthermore that the quaternary carbons C-*q* shift upfield by 3.55 ppm. Only small upfield shifts (av. 0.48 ppm) occur at the methyl carbon atoms in the same position. All of these values appear consistent with the charge polarization interpretation recently discussed by Morishima, *et al.* (25).

(*d*) *The Preferred Steric Course of Quaternization*

The effects of quaternization of the morpholines studied using methyl iodide are given in Table 1. First, it is observed that the resonances of the carbon atoms bonded directly to nitrogen exhibit splitting and/or broadening due to coupling between the ^{13}C and ^{14}N nuclei. Similar effects have been reported in the spectrum of choline (26) in which the quaternized nitrogen is bonded only to carbon. Second, the trends in the chemical shifts of the ring carbons induced upon

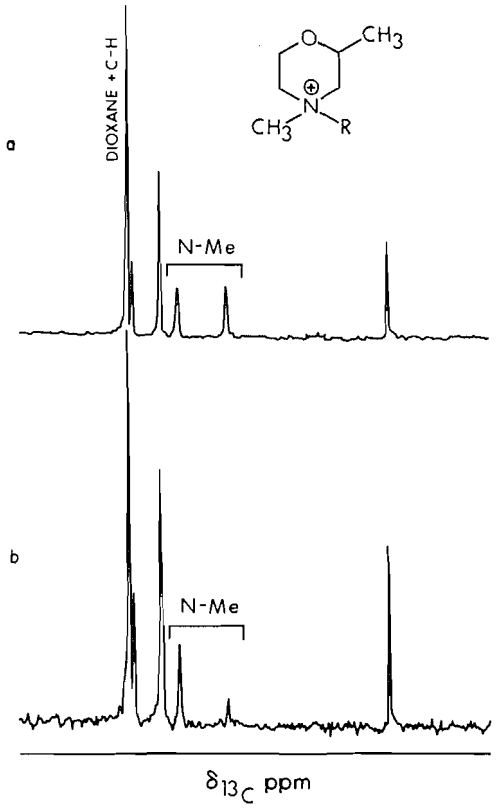

FIG. 1. The ^{13}C spectrum of 2,4-dimethylmorpholine quaternized by (*a*) methyl iodide (*b*) deuteriomethyl iodide.

quaternization are quite consistent with additivity trends described for other nitrogen monocycles (3). Thus, the induced shifts at C-2 and C-6 are upfield in the range 4.9–6.3 ppm and those at C-3 and C-5 are downfield 2.7–5.7 ppm (β-methyl axial effect). Furthermore, the *N*-methyl shifts, relative to the respective bases, in 4-piperidone methiodides (11.2 and 2.1 ppm) (3) are in close agreement with those reported here (11.1 and 2.4 ppm). The smaller *N*-methyl shift (5.6 ppm) observed in *N*-methylmorpholine methiodide clearly is the average value produced by rapid interconversion of the contributing conformers.

Of much greater significance is the preferred course of quaternization of the morpholines and other *N*-heterocyclic compounds. Figure 1 contrasts the observed ^{13}C spectra of **2***b* obtained after quaternization with methyl iodide (Fig. 1*a*) and trideuteriomethyl iodide (Fig. 1*b*). Clearly

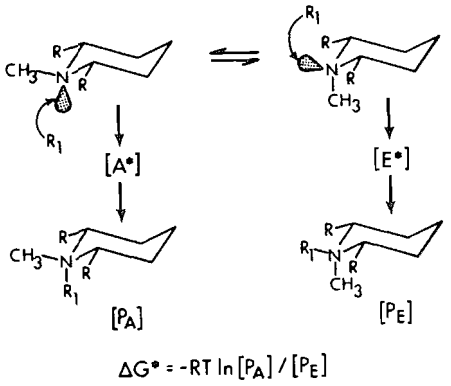

FIG. 2. Free energy difference at the transition state shown in relation to the mode of methylation.

the C^2H_3 signal is much reduced in intensity (washed out) as a result of ^{13}C–^2H coupling. In addition, the large chemical shift difference between *axial* (steric compression) and *equatorial* methyl groups (1, 2, 7) enables clear assignment of these resonances. In the corresponding proton spectra of these C^2H_3 quaternized species, where 2-isomers are produced in differing amounts, the *N*-methyl signal of reduced intensity must be the one replaced (preferentially) by NC^2H_3. The position (axial or equatorial) that this occupies is clear from the ^{13}C spectrum and hence accurate proton assignments can be made and the relative distributions of the isomers determined by integration of the two proton *N*-methyl signals. Corresponding isomer ratios may be obtained in an analogous manner from the deuterium spectra which as anticipated were not as well resolved.

Table 3 summarizes proton, deuterium, and ^{13}C chemical shifts in a series of selected *N*-heterocycles including the morpholines. The product ratios, obtained from integration of their proton and deuterium resonances, were analyzed following the Curtin–Hammett principle (6). That is, the free energy differences at the transition state were obtained using the scheme shown in Fig. 2. These energy differences (Table 3) clearly indicate the preferred course of the reaction in the systems studied. Thus, in the selected piperidines the ^{13}C results corroborate the earlier proton studies showing that axial attack of the incoming methyl iodide preponderates and the higher field position of the axial *N*-methyl (^1H) is proved. In the tropines the

Can. J. Chem. Downloaded from www.nrcresearchpress.com by 210.87.254.105 on 09/05/12
For personal use only.

TABLE 3. Proton, deuterium, and ^{13}C chemical shifts, the ratios of the epimeric products and the free energy differences at the transition states (a/e) obtained from quaternization of cyclic six-membered bases

Compound	δ ppm a,e[a]			Product ratios		$-\Delta G^*$
	^1H	^2H	^{13}C	P_a	P_e	cal/mol
4-*tert*-Butyl-*N*-methylpiperidine	3.44,3.54	—	47.04,56.27	78	22	745
1,2-Dimethylpiperidine	3.02,3.20	1.81,1.63	42.1,53.6	62 65	38 35[b]	326
1,3-Dimethylpiperidine	3.34,3.49	1.66	48.1,56.6	80	20	815
1,4-Dimethylpiperidine	3.34,3.49	1.73	47.9,55.7	75	25	647
Tropine	3.52,3.48	1.69	44.25,50.99	20	80	−815
2-Tropinone	3.51,3.54	1.66	46.02,50.72	10	90	−1291
3-Tropinone	3.81,3.63	1.58,1.38	45.1,51.5	45 36	55 64[b]	−231
2,4-Dimethylmorpholine	3.66[c]	1.45	48.02,57.19	—	—	—
2,4,6-Trimethylmorpholine	3.69,3.71	1.45	47.97,57.1	80	20	815
3,3,4-Trimethylmorpholine	3.22[c]	1.56	47·1[d]	—	—	—
2-Phenylmorpholine	3.46,3.35	1.45	48.08,57.3	80	20	815
cis-Phendimetrazine	3.92,3.55	1.27	50.1,54.3	90	10	1291
trans-Phendimetrazine	3.28,3.32	1.59	42.36,54.7	68	32	443

[a] ^1H and ^{13}C chemical shifts given relative to TMS. ^2H relative to D_2O and shielded.
[b] Determined using ^2H spectra.
[c] Only one broad ^1H signal prevented determination of isomer ratio.
[d] Not resolved.

negative value of ΔG indicates that equatorial attack is preferred. Again these results corroborate earlier findings (4). In the morpholines axial attack preponderates and the otherwise confusing order of the proton *N*-methyl signals is resolved.

The type of analysis described above is clearly applicable to quaternary salts derived from other base systems. In general it can be stated that the configuration of pairs of diastereoisomeric quaternary salts may be readily and unambiguously determined by the above method.

Conclusions

The results for the phendimetrazine isomers further demonstrate the value of ^{13}C magnetic resonance spectroscopy for conformational analysis of pharmacologically active compounds. The particular sensitivity of the carbon nucleus to sterically induced charge polarization makes it especially useful for observing non-bonded interactions in these molecules, especially in the quaternized derivatives. The substituent parameters derived from the morpholine series support the view that ^{13}C substituent effects in alicyclic and heterocyclic compounds are generally equivalent.

Acknowledgments

We thank Dr. D. Dvornik, Ayerst Research Laboratories, for supplying the *trans*-phendimetrazine base. We also thank the National Research Council of Canada for financial support.

1. (*a*) A. J. JONES, E. L. ELIEL, D. M. GRANT, SR., M. C. KNOEBER, and W. F. BAILEY. J. Am. Chem. Soc. **93**, 4772 (1971); (*b*) A. J. JONES, A. F. CASY, and K. M. J. MCERLANE. Tetrahedron Lett. 1727 (1972).
2. (*a*) A. J. JONES, A. F. CASY, and K. M. J. MCERLANE. Can. J. Chem. **51**, 1782 (1973); (*b*) A. J. JONES, C. P. BEEMAN, A. F. CASY, and K. M. J. MCERLANE. Can. J. Chem. **51**, 1790 (1973); (*c*) A. J. JONES, A. F. CASY, and K. M. J. MCERLANE. J. Chem. Soc. Perkin Trans. 1, 2576 (1973).
3. A. J. JONES and M. M. A. HASSAN. J. Org. Chem. **37**, 2332 (1972).
4. G. FODOR, J. D. MEDINA, and N. MANDAVA. Chem. Commun. 581 (1968); G. FODOR, R. V. CHASTAIN, D. FREHEL, M. J. COOPER, N. MANDAVA, and E. L. GOODEN. J. Am. Chem. Soc. **93**, 403 (1971).
5. D. R. BROWN, R. LYGO, M. MCKENNA, J. M. MCKENNA, and B. G. HUTLEY. J. Chem. Soc. (B), 1184 (1967); J. MCKENNA. *In* Topics in stereochemistry. Vol. 5. *Edited by* E. L. Eliel and N. L. Allinger. Wiley, New York. 1970.
6. Y. KAWAZOE and M. TSUDA. Chem. Pharm. Bull. **15**, 1405 (1967).
7. (*a*) D. K. DALLING and D. M. GRANT. J. Am. Chem. Soc. **89**, 6612 (1967); **94**, 5318 (1972); D. M. GRANT and B. V. CHENEY. J. Am. Chem. Soc. **89**, 5315 (1967); (*b*) E. L. ELIEL, W. F. BAILEY, L. D. KOPP, R. L. WILLER, D. M. GRANT, R. BERTRAND, K. A. CHRISTENSEN, D. K. DALLING, M. W. DUCH, E. WENKERT, F. M. SCHELL, and D. W. COCHRAN. J. Am. Chem. Soc. **97**, 322 (1975).

Can. J. Chem. Downloaded from www.nrcresearchpress.com by 210.87.254.105 on 09/05/12
For personal use only.

8. G. FODOR. *In* The alkaloids. Vol. XIII. *Edited by* R. H. F. Manske. Academic Press, New York. 1973.
9. A. J. JONES and M. H. BENN. Can. J. Chem. **51**, 486 (1973).
10. T. BAILEY, T. P. SEDEN, and R. W. TURNER. J. Heterocycl. Chem. **6**, 751 (1969).
11. D. L. COTTLE, A. E. JELTSCH, T. H. STOUDT, and D. R. WALTERS. J. Org. Chem. **11**, 286 (1946).
12. H. BOOTH and G. C. GIDLEY. Tetrahedron, **21**, 3429 (1965).
13. M. L. STEIN, R. OTTINGER, J. REISSE, and G. CHIWDOGLU. Tetrahedron Lett. 1521 (1968).
14. W. O. CRAIN, JR., W. C. WILDMANN, and J. D. ROBERTS. J. Am. Chem. Soc. **93**, 990 (1971).
15. A. J. JONES, D. M. GRANT, and K. F. KUHLMANN. J. Am. Chem. Soc. **91**, 5013 (1969), and references therein.
16. H. SPIESECKE and W. G. SCHNEIDER. J. Chem. Phys. **35**, 731 (1969).
17. M. ARONEY and R. J. W. LE FEVRE. Proc. Chem. Soc. 82 (1958).
18. M. J. ARONEY, C.-Y. CHEN., R. J. W. LE FEVRE, and J. D. SAXBY. J. Chem. Soc. 4269 (1964).
19. R. W. BALDOCK and A. R. KATRITZKY. J. Chem. Soc. **13**, 1470 (1968).
20. R. K. HARRIS and R. A. SPRAGG. J. Chem. Soc. **13**, 684 (1968).
21. J. J. SLOAN and R. KEWLEY. Can J. Chem. **47**, 3453 (1969).
22. G. ELLIS and R. G. JONES. J. Chem. Soc. Perkin Trans. 2, 437 (1972).
23. J. B. GRUTZNER, M. JAUTELAT, J. B. DANCE, R. A. SMITH, and J. D. ROBERTS. J. Am. Chem. Soc. **92**, 7107 (1970).
24. D. DVORNIK and G. SCHILLING. J. Med. Chem. **8**, 466 (1965), and references therein.
25. I. MORISHIMA, K. YOSHIKAWA, K. OKADA, T. YONEZAWA, and K. GOTO. J. Am. Chem. Soc. **95**, 165 (1973).
26. J. FEENEY. First Rocky Mountain Regional Meeting, A.C.S., Colorado State University, Fort Collins. June 30, 1972.

Can. J. Chem. Downloaded from www.nrcresearchpress.com by 210.87.254.105 on 09/05/12
For personal use only.

A convenient synthesis of the flavor and scent material (±)-γ-(*Z*)-6-dodecenolactone and some analogs via *N*-chloroamide thermolysis

MICHAEL BENN AND KANWAL NAIN VOHRA
Chemistry Department, The University of Calgary, Calgary, Alberta T2N 1N4

Received July 22, 1975

MICHAEL BENN and KANWAL NAIN VOHRA. Can. J. Chem. **54**, 136 (1976).

N-Chloro-*N*-propyl-*threo*-6,7-dibromododecanamide, prepared by the successive bromination and *N*-chlorination of *N*-propyl-(*Z*)-6-dodecenamide, was subjected to thermolytic homolysis in aqueous dioxane to yield a mixture of products from which, after zinc debromination, γ-6-(*Z*)-dodecenolactone was isolated. Some analogs of this lactone were similarly prepared.

MICHAEL BENN et KANWAL NAIN VOHRA. Can. J. Chem. **54**, 136 (1976).

On a soumis le *N*-chloro *N*-propyl *thréo*-dibromo-6,7 dodécanamide, préparé par une bromuration suivie du *N*-chloruration du *N*-propyl (*Z*)-dodécène-6 amide, à une thermolyse homolytique dans le dioxanne aqueux; cette réaction conduit à un mélange de produits à partir duquel on a pu isoler, après débromuration par le zinc, la γ-(*Z*)-dodécèno-6 lactone. On a préparé, de la même manière, quelques analogues de cette lactone.

[Traduit par le journal]

Dihydro-5-[(*Z*)-2′-octenyl]-2(3*H*)-furanone ('γ-(*Z*)-6-dodecenolactone'), **1**, and the side-chain saturated derivative ('γ-dodecanolactone'), **2**, are two odiferously interesting natural products[1] which we needed in connection with some studies of olfaction in animal behavior. In contrast to **2**, **1** is commercially unavailable, and not readily obtainable. Only a single synthesis of **1** appears to have been described, and in this, the key coupling of methyl-4-oxobutanoate with 1-bromo-2-octyne, via a Grignard reaction yielded a mixture from which, after semi-hydrogenation and lactonization, **1** was isolated by preparative glc as a minor product with **3** predominating (77:22) (6).

There are a multitude of routes to γ-lactones but, serendipitously, during a study of the cyclization of some *N*-chlorolactams, we had noted that the thermolytic homolysis of *N*-chloro-*N*-methylvaleramide in aqueous dioxane, containing suspended calcium carbonate, gave a fair yield of γ-valerolactone (7). This reaction is analogous to the photochemical cyclization of *N*-haloamides to iminolactone lactone salts, followed by hydrolysis (8), and presumably follows the same sequence of steps (7)[2] (see Scheme 1).

The simplicity of the *N*-chloramide thermolysis procedure attracted us and we decided to explore the utility of this approach by applying it to the synthesis of **1**, and the analogs **2** and **4**.

Under our usual thermolysis conditions (7) decomposition of *N*-chloro-*N*-methyllauramide, **6**, was complete within 1 h, when glc analysis revealed that the reaction products contained the desired **2** (42%), accompanied by the amide **7** (50%).[3] Pure **2** was isolated from the mixture by column chromatography.

Before attempting the synthesis of **1** we first examined the synthesis of its analog **4** from oleic acid. The *N*-propyl amide **8** was prepared in high yield by the mixed anhydride procedure,

[1]Very recently it has been reported that the butterfat of cows fed a special lipid diet, high in linoleic acid, is enriched in **1** and **2** (1), while the taint to the meat of lambs fed a similar diet has been attributed to **1** (2). Apart from the occurrence of **1** and **2** as normal trace-components of butterfat (3), **1** has been reported to be the major pheromonal component of the tarsal-tuft scent of blacktailed deer (4), and **2** has been identified in the pygidial secretion of a rove-beetle, where it may play a role in defence against predators, or as a regulator of the algal colonies which these beetles maintain (5).

[2]However, in contrast to the photolytic route to γ-lactones (**8**), we found (for *N*-alkyl-*N*-chlorovaleramides) no significant advantage to employing *N*-*tert*-butyl amides.

[3]A small amount (*ca* 8%) of δ-dodecalactone was also present, arising by abstraction of a hydrogen atom from the δ-carbon atom by the amidyl radical: a process disfavored with respect to abstraction from the γ-carbon atoms at C-9 or C-10. However, the carbonyl region of the is quasi seven-membered rather than six, *cf.* ref 8*b* and references therein.

Can. J. Chem. Downloaded from www.nrcresearchpress.com by 210.87.254.42 on 09/05/12
For personal use only.

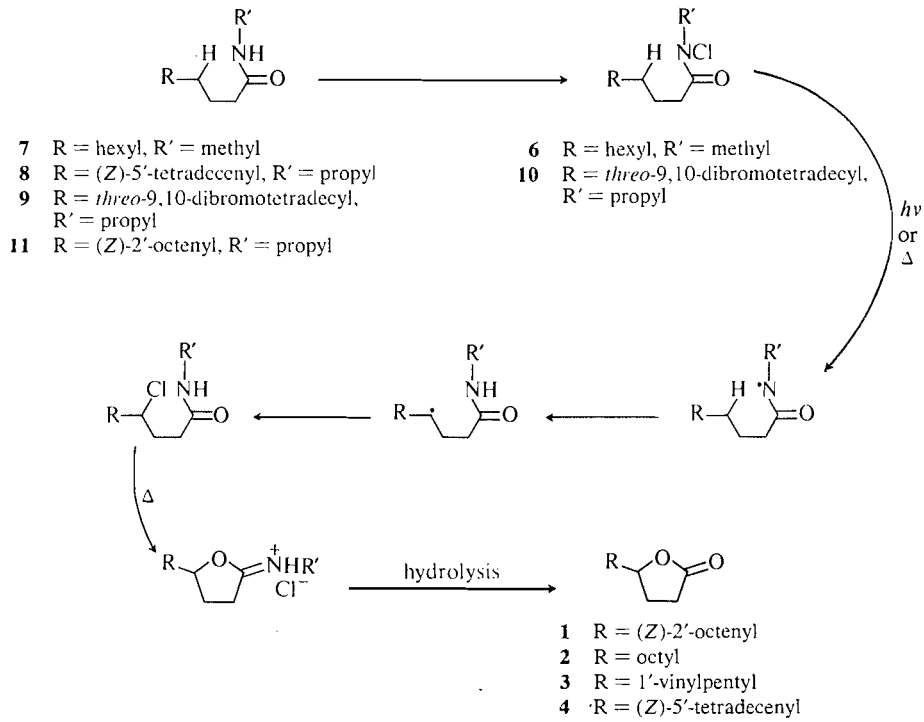

SCHEME 1. Lactone synthesis via chloroamide homolysis.

but attempts to convert it to the corresponding *N*-chloro derivative using a variety of reagents, including sodium hypochlorite and *tert*-butyl hypochlorite, gave complex mixtures. Presumably these complications arose from olefinic function, and possibly allylic chlorination, since after conversion of **8** to the *threo*-dibromo derivative **9** the *N*-chloro derivative **10** could be prepared without trouble. Thermolysis of **10** gave a mixture of products[4] which was debrominated with zinc dust, and then subjected to preparative tlc, by which means two products were isolated in approximately equal amount. On the basis of spectroscopic evidence one of these (46%) was identified as the amide **8**, while the other (41%) was the desired γ-lactone **4**, dihydro-5-[(*Z*)-5′-hexadecenyl]-2(3*H*)-furanone.

Following this experience, the synthesis of **1** was straightforward. 6-Dodecynoic acid was prepared by a sequence of reactions similar to that used to prepare 6-hendecynoic acid (9). After conversion of the acetylenic acid to its *N*-methyl amide, semi-hydrogenation gave *N*-methyl-(*Z*)-6-dodecenoamide, **11**. By the procedure used to convert oleic acid to **4**, **11** yielded **1** (21%), the parent amide being the major (and thus recyclable) side-product.

As the success in achieving the synthesis of our target compounds reveals, the thermolysis of *N*-chloroamides merits attention as a preparatively convenient route to aliphatic γ-lactones.

Experimental

Melting points were determined on a Kofler hot-stage and are, like the boiling points, uncorrected. Infrared spectra were measured on a Perkin-Elmer Model 337 spectrometer using solutions in chloroform in a 0.1 mm path-length cell, unless otherwise stated.

The pmr spectra were obtained using Varian A-60 or HA-100 spectrometers and deuteriochloroform solutions. Tetramethylsilane was used as an internal reference and chemical shifts are reported on the δ scale in ppm. Mass spectra were recorded on a Varian-MAT CH5 spectrom-

[4]In principle in this situation macrocyclic lactones might arise: if the amide carbonyl displaced the bromine atoms at C-9 or C-10. However, the carbonyl region of the infrared spectrum of the crude thermolysis products from **10**, and its analog from **11**, contained only a weak absorption at 1730 cm^{-1} (δ-, and macrocyclic lactones, or esters), together with strong absorptions at 1770 (γ-lactone) and 1630 cm^{-1} (amide).

Can. J. Chem. Downloaded from www.nrcresearchpress.com by 210.87.254.42 on 09/05/12
For personal use only.

Can. J. Chem. Downloaded from www.nrcresearchpress.com by 210.87.254.42 on 09/05/12
For personal use only.

eter with a direct inlet, at 70 eV ionization potential. Significant ions are quoted as *m/e* values in amu, with their approximate relative abundance in parentheses. Gas–liquid chromatographic analyses were carried out with a Bendix Model 2500 instrument, using 6 ft × ¼ in. glass columns containing 5% Versamid 900 on HMDS treated Chromosorb W, at 200 °C. Preparative glc separations were performed with a Varian-Aerograph A-700 unit and 8 ft × ⅜ in. columns of 30% SE-30 on Chromosorb W, at a flow rate of *ca.* 50 ml/min. Thin layer chromatography was done with silica gel GPF_{254}, and spots detected with iodine vapour. The dioxane was distilled from sodium, and final traces of peroxide were removed by percolation through Woelm Grade I neutral alumina before use, however this final purification can be omitted.

N-Methyllauramide, **7**

This compound was prepared from methylamine and lauric acid by the mixed anhydride method (*cf.* preparation of **8**) and obtained as a colorless solid (90%) mp 69 °C (lit. (10) mp 68.4 °C); ν_{max} 3300 and 1650 cm^{-1}, δ 6.0 (1H broad, N—H), 2.8 (3H, d, J = 5 Hz, CH_3—N), 2.2 (2H, t, J = 6 Hz, H-2), 1.3 (18H, m, CH_2), and 0.9 (3H, distorted t, J = 6 Hz, CH_3); *m/e* 213 (28) and 73 (100).

γ-Dodecalactone, **2**

The amide **7** (5 g, 0.023 mol) in carbon tetrachloride (50 ml) was treated, at 0 °C and in the dark, with *tert*-butyl hypochlorite (2.8 g, 0.024 mol). After 4 h tlc revealed that conversion was complete, and after removing the solvent under reduced pressure, titrimetric assay corresponded to a 98% yield of **6**. The chloroamide was dissolved in dioxane–water (4:1 v/v) containing suspended calcium carbonate (5 g), and benzoyl peroxide (50 mg), and heated to 85 °C under an atmosphere of nitrogen. After 2 h titrimetry revealed that all of **6** had been destroyed. The mixture was then filtered, and the filtrate evaporated under reduced pressure to a residual oil (4.6 g) which partially crystallized on standing: ν_{max} (film) 1780(s), 1740(sh), and 1650(s) cm^{-1}. Gas–liquid chromatography using authentic specimens of **7**, **2**, and δ-dodecalactone revealed the product to be a mixture of these three compounds in *ca.* 50:42:8 ratio.

When kept at −5 °C for 30 min, a pentane solution of the crude product deposited white crystals, mp 68 °C, of the amide (1.5 g), and evaporation of the filtrate then yielded an oil (3.1 g). This oil was chromatographed on a column of silica gel, from which benzene and ether eluted material corresponding to the γ-lactone (2.6 g). Distillation with a micro-spinning band column gave γ-dodecalactone (2.1 g 45%) bp 84–88 °C; ν_{max} (film) 1775 cm^{-1}; glc > 98% pure, with the same retention time as authentic **2**; *m/e* 198 and 85 (100).

N-Propyloleamide, **8**

Ethyl chloroformate (1.86 g; 0.017 mol) was added dropwise to a stirred solution of oleic acid (4.9 g, 0.017 mol) and triethylamine (1.72 g, 0.017 mol) in THF (100 ml) cooled to −5 °C. The mixture was stirred for 30 min and then *n*-propylamine (1.08 g, 0.018 mol) was added at 0–5 °C. After having kept the reaction for 2 h at room temperature, the triethylamine hydrochloride was removed by filtration and the filtrate evaporated under reduced pressure. An ethereal solution of the residue was washed with aqueous sodium hydroxide (5%) (2 × 40 ml), then with dilute hydrochloric acid (10%, 20 ml) and finally with water (50 ml). The dried ($MgSO_4$) ether solution on evaporation gave an oil which solidified on cooling; mp 30–32 °C, (lit. (11) mp 32 °C); yield 4.438 g (96%), ν_{max} (film), 3300, 3080, and 1650 cm^{-1}, δ 6.4 (1H, br, NH), 5.10 (2H, t, J = 4 Hz), 3.0 (2H, q, J = 7 Hz, N—CH_2), 2.0 (6H, m, H-2, H-8, and H-11), 1.3 (24H, br m, CH_2), and 0.8 (6H, br t, J = *ca.* 7 Hz, CH_3).

N-Propyl-threo-9,10-dibromoöleamide, **9**

To a solution of oleamide **8** (225 mg, 7 mmol) in carbon tetrachloride (25 ml) was added bromine (115 mg, 7.1 mmol) in carbon tetrachloride (5 ml). After stirring for 15 min the orange solution was concentrated *in vacuo* to give dibromo amide **9** (310 mg, 97%) as an oil: ν_{max} (film) 3300 and 1650 cm^{-1}; δ 6.75 (1H, br, NH), 4.20 (2H, d, J = 10 Hz, H-9,10), 3.15 (2H, q, J = 6 Hz, NCH_2), 2.2–1.30 (30H, m, CH_2), and 0.95 (6H, distorted t, J = 6 Hz, CH_3). *Anal.* Calcd. for $C_{21}H_{41}Br_2NO$: N 2.90; found: N 2.77.

γ-Z-Octadecenolactone ***(4)***

The dibromoöleamide **9** (300 mg, 0.6 mmol) was treated with 72 mg (0.66 mmol) of *tert*-butyl hypochlorite in carbon tetrachloride and the mixture left in the dark for 1 h. Removal of solvent gave an oil (320 mg); ν_{max} (neat) 1680 cm^{-1}, and no NH absorption. Thiosulfate titration indicated 79% conversion to the *N*-chloroderivative. This product was taken up in aqueous dioxane (1:4, v/v, 50 ml) containing calcium carbonate (3 g) and benzoyl peroxide (20 mg, 0.01 mmol) and thermolyzed at 80 °C under nitrogen. The reaction was titrimetrically complete after 105 min. Work up of the reaction gave an oil (280 mg): ν_{max} (film) 3350, 1770, 1730, and 1650 cm^{-1}. The crude thermolysis product (275 mg) was dissolved in absolute ethanol (25 ml) and heated under reflux with zinc dust (500 mg) for 1 h. Filtration followed by evaporation of the alcohol gave an oil (191 mg, 70%). Thin layer chromatography (ethyl formate – benzene 1:1 v/v) examination showed two major components (R_f *ca.* 0.75 and 0.50) and these were separated by plc (with the same eluant system).

The higher R_f component was obtained as an oil (80 mg, 41%), ν_{max} (film), 1780(s), and 1650(w). It was still impure as judged by tlc and was therefore rechromatographed on a silica gel plate to yield 52 mg (26%) of an oil, homogeneous on tlc: ν_{max} (film) 1775 cm^{-1}; δ 5.3 (2H, seeming t, J = 5 Hz, H-9, H-10), 4.35 (1H, m, H-4), 2.30 (2H, t, J = 6 Hz, H-2), 2.0 (4H, br, m, H-8, H-11), *ca.* 1.2 (20H, m, CH_2), and 0.85 (3H, distorted triplet, J = 6 Hz, CH_3); *m/e* 280 (25) and 85 (100). This data is consistent with the assignment of structure **4** to this product.

The lower R_f component was also obtained as an impure oil (92 mg) from which, on repeated plc, was isolated pure **8** (54 mg) (ir spectrum superimposable on that of the authentic amide).

Preparation of 6-Dodecynoic Acid

In a 3 l, three-neck round bottom flask fitted with a stirrer, dropping funnel, gas inlet tube and solid CO_2 condenser cooled with a chloroform – dry ice mixture, was placed liquid ammonia (1500 ml). While stirring, ferric nitrate (0.3 g) and sodium (1 g) were added. Dry air

Can. J. Chem. Downloaded from www.nrcresearchpress.com by 210.87.254.42 on 09/05/12
For personal use only.

was bubbled through the solution for a few minutes until the blue color was discharged, after which an additional amount of sodium (14.6 g, 0.68 g atom total) was added slowly in small portions. After the reaction had been in progress for 30 min, sodium peroxide (1 g) was added. After 2½ h the reaction mixture turned grey and the conversion of the sodium to sodamide was complete. To this solution was added 1-heptyne (Chemical Samples Co., 48 g, 0.50 mol), dropwise with stirring, over a period of 2 h and, after an additional interval of 3 h, 1-chloro-4-iodobutane (117 g 0.54 mol) was added over 4 h. Stirring was continued 4 h longer, and the mixture was then allowed to stand at room temperature until the ammonia had evaporated. Water (100 ml) was added cautiously, and the organic layer collected in ether. The ether solution was washed free from inorganic halides with water, then dried ($MgSO_4$) and evaporated. Distillation of the residual oil on a Nester–Faust spinning band column resulted in fractionation to give a main fraction of 1-chloro-5-undecyne, (37.6 g 40%) bp 114 °C/12 Torr δ 3.5 (2H, t, J = 6 Hz, H-1), 2.15 (4H, m, H-4, H-6), *ca.* 1.6 (10H, m, CH_2), and 0.95 (3H, t, J = 6 Hz, CH_3); *m/e* 188 (0.2), 186 (0.5), 159 (2), 157 (5), 95 (35), and 41 (100).

To a solution of sodium cyanide (16 g, 0.33 mol) in water (125 ml) was added 95% ethanol (115 ml) and 1-chloro-5-undecyne (28 g, 0.15 mol). The mixture was refluxed until the bulk of the chloride had been converted to the inorganic form (20 h), after which sodium hydroxide (20.5 g, 0.5 mol) was added, and the refluxing continued overnight. Most of the alcohol was then distilled off, water added, and the alkaline solution extracted with ether (2 × 100 ml). Acidification of the aqueous solution caused the separation of an oily liquid which was taken up in ether, and fractionated to give 6-decynoic acid, bp 130–132 °C/0.1 Torr; 20 g (67%); n_D^{25} 1.4585; ν_{max} (film) 3150 (broad), 1705 together with broad absorption in the region 2800–2500 cm^{-1}; δ 2.3 (2H, t, J = 7 Hz, H-2), 2.1 (4H, m, H-5, H-8), *ca.* 1.5 (10H, m, CH_2), and 0.95 (3H, t, J = 6 Hz, CH_3); *m/e* 196 (2), 179 (2), 140 (81), 95 (50), 81 (100), and 67 (95). *Anal.* Calcd. for $C_{12}H_{20}O_2$: C 73.45, H 10.28; found: C 73.72, H 10.39.

The identity of the acid was further confirmed by its conversion with diazomethane to a methyl ester, bp 95 °C/0.1 Torr; ν_{max} (film) 1740 cm^{-1}; nmr δ 3.6 (3H, s, OCH_3), 2.2 (6H, m, H-2, H-5, H-7) 1.5 (10H, m, CH_2) and 0.95 (3H, t, J = 6 Hz, CH_3). *Anal.* Calcd. for $C_{13}H_{22}O_2$: C 74.24, H 10.54; found: C 73.82, H 10.61.

N-Propyl-6-dodecynamide

Ethyl chloroformate (1.2 g, 0.011 mol) was added to a stirred solution of the acetylenic acid (1.96 g, 0.01 mol) and triethylamine (1.12 g, 0.011 mol) in 50 ml of THF at −2 °C. After the addition was complete the reaction mixture was stirred for another 30 min, then *n*-propylamine (0.66 g, 0.11 mol) was added, in one portion. After being kept overnight, the reaction was worked up, as for **8**, giving an oil (2.21 g, 93%), bp 130 °C/0.01 Torr; ν_{max} (film) 3300, 3075, 1650, and 1550 cm^{-1}; δ 7.85 (1H, br, s, NH), 3.15 (2H, q, J = 6 Hz, NCH_2), 2.10 (6H, m, H-2, H-5, H-8), *ca.* 1.45 (12H, m, CH_2), and 0.95 (6H, t, J = 7 Hz, CH_3); *m/e* 237 (20), 194 (14), 180 (38), 166 (20), 152 (14), 128 (27), 114 (46), 102 (41), 95 (68), 79 (75), 67 (100), and 60 (70). *Anal.* Calcd. for $C_{15}H_{27}NO$: C 75.97, H 11.40, N 5.90; found: C 75.85, H 11.96, N 5.74.

N-Propyl-6-dodecenamide, ***11***

The acetylenic amide (1.2 g, 0.005 mol) was hydrogenated using Lindlar's catalyst (40 mg) and quinoline (95 mg) in methanol (100 ml). The hydrogenation ceased after 25 min, exactly one equiv. of hydrogen having been taken up. The catalyst was removed by filtration and, after distilling off the solvent and quinoline, *N*-propyl-6-dodecenamide, **11**, was obtained, bp 140 °C/0.01 Torr, 1.1 g (91%), homogeneous by glc; δ 5.31 (2H, apparent t, J = 4 Hz, H-6, H-7), 3.15 (2H, q, J = 6 Hz, NCH_2), 2.10 (6H, m, H-2, H-5, H-8), *ca.* 1.5 (12H, m, CH_2), and 0.9 (6H, t, J = 6 Hz, CH_3); *m/e* 239 (16), 114 (64), 101 (100), 86 (40), and 55 (27). *Anal.* Calcd. for $C_{15}H_{29}NO$: C 75.26, H 12.21, N 5.85; found: C 75.11, H 12.56, N 6.15.

N-Propyl-threo-6,7-dibromododecanamide, ***10***

A solution of bromine (700 mg, 4.4 *M*) in carbon tetrachloride (10 ml) was added to a solution of **11** (1.0 g, 4.2 mmol) in the same solvent (10 ml). Removal of solvent left a colorless viscous liquid (1.55 g, 90%): ν_{max} (film) 3300, 1655, and 1560 cm^{-1}; δ 7.5 (1H, broad s, NH), 4.25 (2H, m, H-6, H-7), 2.23 (2H, q, J = 7 Hz, NCH_2), 2.20–1.2 (18H, m, CH_2), and 0.95, (6H, distorted t, CH_3); *m/e* 401 (1), 399 (2), 397 (1), 320 (18), 318 (20), 238 (60), and 114 (100).

(Z)-6-Dodecenolactone, ***1***

The dibromoamide **10** (1.5 g) was chlorinated with *tert*-butyl hypochlorite, as described for **9**. The oily product (1.8 g) which gave a titrimetric assay corresponding to 95% *N*-chloroamide was dissolved in aqueous dioxane (1:4 v/v) (40 ml) containing calcium carbonate (5 g), and benzoyl peroxide (25 mg) and thermolyzed under a nitrogen atmosphere at 85 °C until all the *N*-chloro compound had been consumed. Work-up as before (*cf.* for **2**) gave an oil (1.3 g), ν_{max} (film) 3300, 1780, 1740, 1650, and 1550 cm^{-1}. This material was boiled under reflux with zinc dust (200 mg) in absolute ethanol (40 ml) for 2 h. Removal of ethanol afforded an oily mixture (0.82 g) of γ-lactone and amide, as revealed by characteristic absorptions at 1770 and 1640 cm^{-1} respectively. Gas–liquid chromatographic analysis on SE30 revealed two components, the faster corresponding to γ-lactone and the slower one to the amide. The mixture was separated by thick layer chromatography (silica gel PF_{254}, ethyl acetate – benzene 1:1 v/v) to yield the two components.

The amide **11** (360 mg, 36%) was recovered from the band R_f *ca.* 0.60, and the γ-lactone (175 mg, 21%) from the band R_f *ca.* 0.08. The lactone had bp 85 °C/0.01 Torr; ν_{max} (film) 1775 cm^{-1}; δ 5.47 (2H, m, H-6, H-7), 4.45 (1H, apparent t, J = 6 Hz, H-4), 2.4 (4H, m, H-5, H-8), 2.10 (2H, m, H-2), 1.35 (8H, m, CH_2), and 0.90 (3H, distorted t, J = 6 Hz, CH_3); *m/e* 196 (17) (M^+), and 85 (100); all consistent with structure **1**.

A small sample of the above lactone (15 mg) in methanol (10 ml) was hydrogenated over palladium–charcoal at atmospheric pressure. The product had an infrared spectrum, and retention time on gas chromatographic analysis, identical with those of authentic γ-dodecalactone.

Acknowledgment

The work described here was supported by an

operating grant from the National Research Council of Canada.

1. R. J. PARK, K. E. MURRAY, and G. STANLEY. Chem. Ind. 380 (1974).
2. W. STARK, and G. URBACH. Chem. Ind. 413 (1974).
3. A. S. M. VAN DER ZIJDEN, K. DE JONG, D. SLOOT, J. CLIFFORD, and R. J. TAYLOR. Rev. Fr. Corps Gras, **13**, 731 (1966).
4. R. G. BROWNLEE, R. M. SILVERSTEIN, D. MILLER-SCHWARTZE, and A. G. SINGER. Nature (London), **221**, 284 (1969).
5. J. W. WHEELER, G. M. HAPP, and J. M. PASTEELS. Tetrahedron Lett. 4635 (1972).
6. P. H. BEGEMANN, V. LAMBERTI, and W. T. WELLER. Rec. Trav. Chim. Pays Bas, **86**, 1335 (1967).
7. O. E. EDWARDS, J. M. PATON, M. H. BENN, R. E. MITCHELL, C. WATANATADA, and K. N. VOHRA. Can. J. Chem. **49**, 1648 (1971).
8. (*a*) R. S. NEALE, N. L. MARCUS, and R. G. SCHEPERS. J. Am. Chem. Soc. **88**, 3051 (1966); (*b*) R. S. NEALE. Synthesis, **1**, 1 (1971).
9. K. AHMED, and F. M. STRONG. J. Am. Chem. Soc. **70**, 1948 (1699).
10. G. F. D'ALELIO and E. E. REID. J. Am. Chem. Soc. **59**, 109 (1937).
11. E. T. ROE, J. T. SCANLAN, and D. SWERN. J. Am. Chem. Soc. **71**, 2215 (1949).

Can. J. Chem. Downloaded from www.nrcresearchpress.com by 210.87.254.42 on 09/05/12
For personal use only.

A synthesis of methyl lambertianate

RUSSELL A. BELL[1]
Department of Chemistry, McMaster University, Hamilton, Ontario L8S 4M1
AND
MARCEL FÉTIZON
Laboratoire de Stéréochemie, Faculté des Sciences d'Orsay, Orsay 91, France

Received August 7, 1975

RUSSELL A. BELL and MARCEL FÉTIZON. Can. J. Chem. **54**, 141 (1976).

A partial synthesis of methyl lambertianate from the 13-keto-degradation product **1** from methyl agathate is described. The furan ring is synthesized by the method of Burness, and involves hydroxymethyleneation of methyl ketone **1**, acetal formation, glycidic ester condensation, and final pyrolysis of the glycidic ester-acetal **5** to give methyl 16-carboxylambertianate. Methyl lambertianate was obtained in moderate yield by copper-quinoline decarboxylation.

RUSSELL A. BELL et MARCEL FÉTIZON. Can. J. Chem. **54**, 141 (1976).

On décrit une synthèse partielle du lambertianate de méthyle à partir du produit de dégradation **1** contenant un groupement cétonique en position 13 et provenant de l'agathate de méthyle. On synthétise le noyau furannique par la méthode de Burness; ceci implique une hydroxyméthylénation de la méthyle cétone **1**, la formation d'un acétal, une condensation glycidique et une pyrolyse finale de l'ester glycidique-acétal **5** pour conduire au carboxy-16 lambertianate de méthyle. On obtient le lambertianate de méthyle, avec un rendement modéré, par une décarboxylation en présence de cuivre et de quinoléine.

[Traduit par le journal]

The naturally occurring furano-diterpenoids are an interesting group of compounds of which vinhaticoic acid (1), vouacapenic acid (2), polyalthic acid (3), marrubiin (4), and lambertianic acid[2] *7b* (5) have been synthesized, either totally or via formal total syntheses. The general methodology of the syntheses has been to incorporate the furan ring either as an intact, preformed unit (3–5) or to generate the ring from carbons already present in the forming diterpenoid skeleton (1, 2).[3] We wish to report here a novel alternative partial synthesis of methyl lambertianate *7a* which uses the latter mode of furan ring construction.

The general method of attack was patterned after the sequence used by Burness (8) for the synthesis of 3-methylfuran, and the intermediates employed for the present synthesis are shown in Scheme 1. The starting material was the bicyclic keto-ester[4] **1** which was itself readily available by the carefully controlled selective oxidation of methyl agathate with $KMnO_4$.[5] The hydroxymethylene derivative **2** of keto-ester **1**, obtained in routine fashion (10) and in 95% yield by the action of sodium hydride – ethyl formate on the ketoester in anhydrous benzene, was treated with thionyl chloride – pyridine in anhydrous methanol (11) at room temperature to afford a mixture of the ketone-acetal **3** (proton magnetic resonance (pmr) spectrum: δ 4.64 ppm, t, $J_{14,15}$ = 5.5 Hz, H-15) and the enol-ether **4** (pmr spectrum: δ = 5.40 ppm, d, $J_{14,15}$ = 12.0 Hz, H-14; 7.41 ppm, d, H-15). The relative proportions of the acetal and enol-ether varied depending on the concentration of pyridine used, and although this latter base was not required for the acetalization reaction, it was included in

[1]Recipient of a Canada–France Scientific Exchange Award.

[2]Lambertianic acid (6) is the optical enantiomer of daniellic acid (7).

[3]The method of Garst and Spencer (13) for the formation of furans from *n*-butylthiomethylene derivatives of ketones and dimethylsulphonium methylide has been applied to the synthesis of perillene and dendrolasin but has not yet been reported for the synthesis of a diterpenoid. The method has most attractive possibilities for the synthesis of compounds such as lambertianic acid. We thank a referee for drawing our attention to reference 13.

[4]Keto-ester **1** has not been totally synthesized, but the corresponding 19-methyl compound has been totally synthesized by Bigley *et al.* (9) and via a novel photochemical route by Fétizon (unpublished results).

[5]M. Fétizon, N. Moreau, C. Mayer, and K. Man Duc Do, unpublished results.

Can. J. Chem. Downloaded from www.nrcresearchpress.com by 210.87.254.5 on 09/05/12
For personal use only.

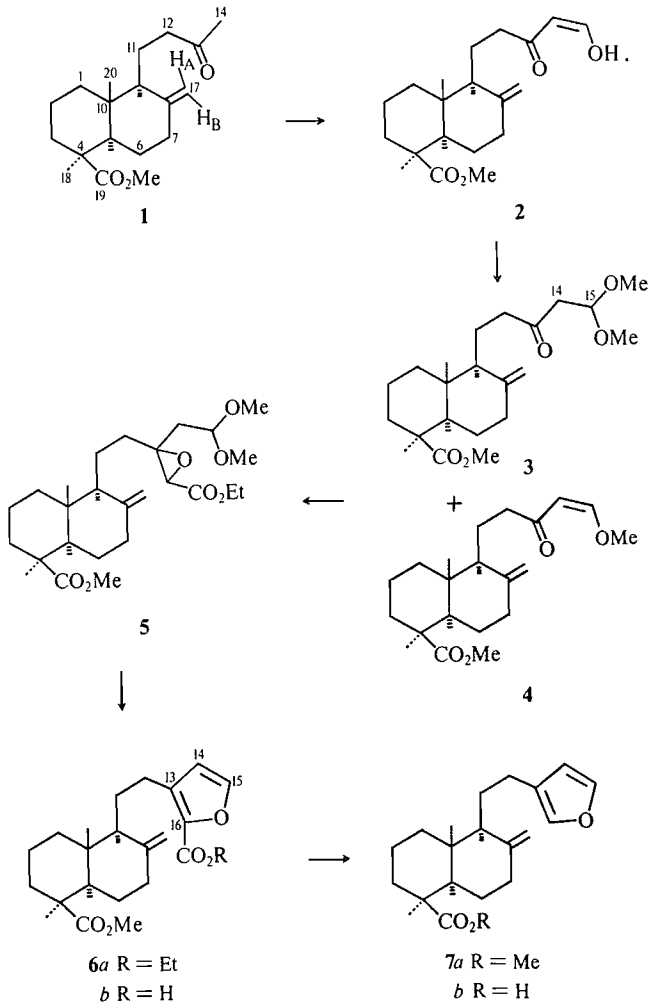

SCHEME 1

order to buffer the reaction mixture to prevent acid-catalyzed isomerization of the exocyclic 8,17-double bond (9, 12). Since the following reaction was intended to be a Darzens glycidic ester condensation with sodium methoxide as base, the enol-ether **4** would be interconvertible with acetal **3** via a Michael addition of methoxide ion, and therefore no attempt was made to separate the two species. Instead, the mixture of **3** and **4** was submitted to the Darzens glycidic ester condensation with sodium methoxide–ethyl chloroacetate in ether–dimethoxyethane (10:3) as solvent. The crude glycidic ester showed no low field olefinic absorptions in its pmr spectrum, indicating that enol-ether **4** had indeed undergone Michael addition with methoxide ion prior to its condensation with chloroacetate anion. Repeated attempts to purify the glycidic ester **5** resulted in excessive decomposition and it was therefore subjected to pyrolytic cyclization by heating at 160 °C for 10 min under reduced pressure to produce the furan-ester ***6a***. A possible pathway for this reaction is shown in Scheme 2 where the first step is depicted as methanol elimination from the acetal to give the enol-ether-epoxide **8**. Acid-catalyzed opening of the epoxide ring is plausibly followed by closure to the cyclic acetal **10** via the stabilized allyl-oxy

Can. J. Chem. Downloaded from www.nrcresearchpress.com by 210.87.254.5 on 09/05/12
For personal use only.

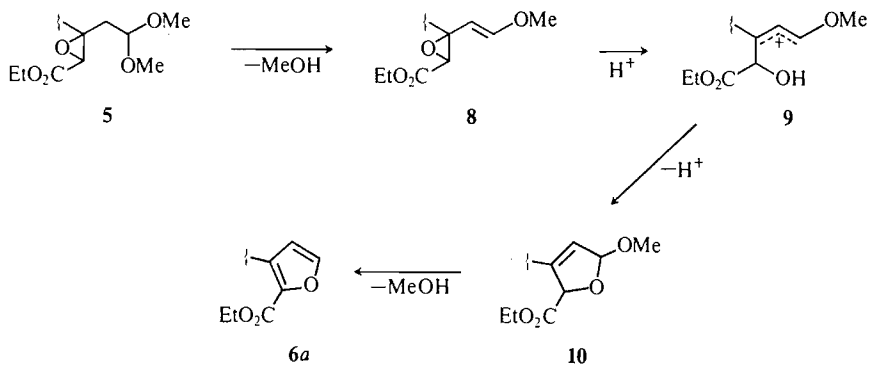

SCHEME 2

cation **9**, and a final 1,4-elimination of methanol then leads to the furan ring. The methanol formed during the reaction had a deleterious effect on the purity of the furan product **6***a* since some 10–15% of the C-16 ethyl ester was transformed by acid-catalyzed exchange into the corresponding methyl ester. In the event, mild base hydrolysis of **6***a* produced the mono-acid **6***b* in 65% overall yield from the keto-acetal **3**. Removal of the 16-carboxyl group was carried out in the normal manner (2) using copper powder and quinoline at 220 °C under nitrogen, and gave a 63% yield of methyl lambertianate **7** which was identical in its infrared, pmr and mass spectrum with a sample of **7** prepared from natural lambertianic acid.[6]

Summary

A novel method for the synthesis of methyl lambertianate **7***a* from the 13-ketone **1** has been carried out following the Burness (8) approach to the synthesis of 3-substituted furans. Formation of the 13-keto-15-dimethylacetal **3** from the hydroxymethylene **2** allowed a glycidic ester condensation to take place at the 13-position. Mild pyrolysis of the glycidic esteracetal resulted in the formation of methyl 16-carboxylambertianate **6***b* in good yield. Methyl lambertianate was obtained in moderate yield by copper–quinoline catalyzed decarboxylation of **6***b*.

[6]We thank Professor W. G. Dauben for supplying this sample of lambertianic acid. The synthetic methyl lambertianate prepared here (diazomethane treatment) also showed identical spectroscopic properties with another sample of methyl lambertianate prepared by an alternative synthetic sequence (5).

Experimental

Spectra were recorded in the following solvents and instruments: ir ($CHCl_3$) Perkin-Elmer 337; pmr ($CDCl_3$, CCl_4) Varian Associates T-60 and HA-100, and Jelco 60C, tetramethylsilane (TMS) as internal standard; cmr Bruker WH-90 Fourier transform spectrometer, TMS as internal standard; mass spectra, C.E.C. 21-110. In the experimental descriptions to follow, the organic substrates were isolated by extraction with the appropriate solvent (2×) followed by washing of the combined solvent layer with water, saturated brine, and finally drying with anhydrous Na_2SO_4. The solvents were removed by evaporation at reduced pressure on a Buchi Rotavapor.

Methyl 15-Hydroxy-16-norlabda-8(17),14-dien-13-one-19-oate, **2**

A modification of the method of Ireland and Schiess (10*b*) was used. Sodium hydride (0.190 g, 7.92 mmol, 50% oil dispersion) was washed with three 3 ml portions of dry benzene and then 10 ml of dry benzene, 2.5 ml of dry (from CaH_2) dimethoxyethane, and 1.554 g (5.08 mmol) of methyl 15,16-norlabd-8(17)-en-13-one-19-oate **1** added under a nitrogen atmosphere. The whole was heated to reflux for 30 min, cooled, and 1.180 g (13.7 mmol) of freshly distilled ethyl formate added, and the mixture allowed to stir at room temperature under nitrogen for 36 h. The small excess of NaH was decomposed with ice, and after dilution with ether the aqueous layer separated and the organic layer further washed (2×) with 1 *M* NaOH. The aqueous layers were combined, cooled with the addition of ice, and acidified with 1 *M* HCl. Extraction of the acidified mixture with ether–benzene and the usual work-up gave 1.652 g (97%) of the hydroxymethylene derivative **2** as a colorless waxy solid, mp 73–77 °C. Crystallization from ethyl acetate – pentane gave **2** as colorless microprisms, mp 76–78 °C; ir ν_{max} 3375 (OH), 3040 (=CH), 1725 (ester C=O), 1690 (unsaturated CO), 1650 (C=C), 1230, 1160, and 910 cm^{-1}; pmr δ ($CDCl_3$) 0.532 (s, 20-CH_3), 1.187 (s, 18-CH_3), 3.605 (s, ester CH_3), 4.50 (s, brd, 17-H_A), 4.87 (s, brd, 17-H_B), 5.48 (d, $J_{14,15}$ = 4.0 Hz, 14-H), 7.87 ppm (d, $J_{14,15}$ = 4.0 Hz, 15-H); cmr δ_{TMS} 12.4 (20-CH_3), 19.3 (6-CH_2), 19.9 (2-CH_2), 26.2 (11-CH_2), 28.6 (18-CH_3), 38.1 (7-CH_2), 38.4 (12-

Can. J. Chem. Downloaded from www.nrcresearchpress.com by 210.87.254.5 on 09/05/12
For personal use only.

Can. J. Chem. Downloaded from www.nrcresearchpress.com by 210.87.254.5 on 09/05/12
For personal use only.

CH_2), 38.6 (1-CH_2), 39.0 (3-CH_2), 40.3 (10-C), 44.2 (4-C), 50.8 (19 ester CH_3), 55.4 (5-CH), 56.2 (9-CH), 101.5 (14-CH), 106.2 (17-CH_2), 147.1 (8-C), 174.5 (15-CH), 176.9 (19-CO), and 199.3 ppm (13-CO); mass spectrum, *m/e* 334 (M^+, calcd. for: $C_{20}H_{30}O_4$, 334.21439; found: 334.21619).

Methyl 15,15-Dimethoxy-16-norlabd-8(17)-en-13-one-19-oate, **3**, *and Methyl 15-Methoxy-16-norlabda-8(17),14-dien-13-one-19-oate*, **4**

A modification of the method of Hata *et al.* (11) was used. To a solution of 1.650 g (4.94 mmol) of dry (benzene azeotroped) hydroxymethylene ketone **2** in 10 ml of anhydrous methanol (from $Mg(OMe)_2$) was added 0.5 g anhydrous pyridine and 0.25 g thionyl chloride, and the whole stirred at room temperature under a nitrogen atmosphere for 18 h. The bulk of the methanol was removed by evaporation at reduced pressure (bath temperature 40 °C), and the residue taken up in benzene, washed with 1 *M* NaOH, saturated $NaHCO_3$, water (3×), and dried in the usual manner. Evaporation of the organic solvent afforded 1.50 g (80% based on **3**) of a colorless oil which from its pmr spectrum was a mixture of approximately 30% acetal **3** and 70% enol-ether **4**. A sample of 0.075 g of the reaction mixture was taken up in anhydrous methanol (3 ml) containing 0.1 g of sodium methoxide and the whole allowed to stand at room temperature overnight under an atmosphere of nitrogen. Work-up via extraction with ether gave 0.072 g of **3** as a light tan oil which appeared greater than 95% pure from its pmr spectrum. The nmr absorptions assigned to **3** were: pmr δ ($CDCl_3$) 0.533 (s, 3H, 20-CH_3), 1.167 (s, 3H, 18-CH_3), 2.80 (d, 2H, $J_{14,15}$ = 5.3 Hz, 14-CH_2), 3.30 (s, 6H, 15-OCH_3), 3.58 (s, 3H, C-19 ester OCH_3), 4.43 (s, brd, 1H, 17-H_A), 4.75 (t, 1H, $J_{14,15}$ = 5.3 Hz, 15-H), and 4.85 ppm (s, brd, 1H, 17-H_B); cmr δ ($CDCl_3$) 12.51 (20-CH_3), 17.39 (C-6), 20.08 (C-2), 26.38 (C-11), 28.92 (C-18), 38.34 (C-7), 38.83 (C-1), 39.18 (C-3), 40.49 (C-10), 42.93 (C-12), 44.39 (C-4), 46.70 (C-14), 51.08 (19-ester CH_3), 53.75 (15-acetal CH_3), 55.56 (C-5), 56.47 (C-9), 101.9 (C-15), 106.55 (C-17), 147.85 (C-8), 177.6 (C-16 ester CO), and 207.76 ppm (C-13 ketone CO).

The enol-ether **4** was never obtained in greater than 70% purity as a colorless oil. The pmr absorptions assigned to **4** were: δ (CCl_4) 0.487 (s, 20-CH_3), 1.15 (s, 18-CH_3), 3.56 (s, 19-ester CH_3), 3.65 (s, 15-OCH_3), 4.46 (s, brd, 17-H_A), 4.81 (s, brd, 17-H_B), 5.40 (d, $J_{14,15}$ = 12.0 Hz, 14-H), and 7.41 ppm (d, $J_{14,15}$ = 12.0 Hz, 15-H). In other experiments carried out for differing reaction times and containing variable quantities of $SOCl_2$, the ratio of **3** to **4** changed from 9:1 to 1:3. Since all ratios of **3** to **4** gave the same reaction product upon subjection to the Darzens glycidic ester condensation, no attempt was normally made to separate **3** and **4**.

Methyl 16-Carboethoxy-13,16-epoxy-15,16-dimethoxylabd-8(17), 13(16),14-trien-19-oate, **5**

To a cooled (ice–salt bath) slurry of NaH (0.084 g, 3.49 mmol) in 7 ml of dry ether and 3 ml of dry dimethoxyethane (from CaH_2) was added a solution of 0.500 g (1.32 mmol) of the mixed keto-acetal **3** and enol-ether **4** in 3 ml of dry ether. A mixture of 0.490 g (4.0 mmol) of ethyl chloroacetate and 0.085 g (2.68 mmol) of dry methanol was then added dropwise via a syringe over a period of 2 min, and the whole stirred at the ice–salt bath temperature under a nitrogen atmosphere for 5 h. The reaction mixture was then allowed to slowly warm to room temperature and stirred for a further 12 h. Excess benzene (50 ml) was then added and the reaction mixture decomposed by the addition of 7% aqueous acetic acid. The organic layer was washed with dilute $NaHCO_3$ and the reaction products, isolated in the usual way, afforded 0.520 g (84%) of **5** as a light tan oil. The crude glycidic ester **5** appeared particularly susceptible to decomposition and resisted attempts at purification by either column or thin layer chromatography. A small sample of **5** showed: pmr δ (CCl_4) 0.475 (s, 3H, 20-CH_3), 1.15 (s, 3H, 18-CH_3), 1.30 (t, 3H, J = 7.5 Hz, ester CH_3), 3.24 (s, 6H, acetal OCH_3), 3.40 (s, 1H, epoxide H-16), 3.562 (s, 3H, C-19 ester CH_3), 4.69 (q, 2H, J = 7.5 Hz, ester CH_2), 4.425 (t, 1H, $J_{14,15}$ = 4.0 Hz, H-15), 4.50 (s, brd, 1H, H_B-17), and 4.825 ppm (s, brd, 1H, H_A-17).

Methyl 16-Carboxylambertianate, **6***b*

A sample of 0.500 g (1.07 mmol) of the crude glycidic ester **5** was heated at 160–165 °C under a water pump vacuum for 20 min. At this point all apparent decomposition and gas evolution (CH_3OH) had ceased. The residue was cooled and the crude 16-carboethoxylambertianate, **6***a*, hydrolyzed by dissolution in 7 ml of 2 *M* KOH in CH_3OH, careful degassing, and heating at reflux for 4 h under a nitrogen atmosphere. After cooling the dark solution was taken up in 100 ml of 1:1 ether-benzene and extracted with 5% NaOH (3×). The combined base layer was acidified to p*H* 2 with 10% HCl and the 16-carboxylambertianate **6***b* isolated via benzene extraction giving 0.470 g of the crude acid as a dark gum. Chromatography on 10 g silica gel and elution with CH_2Cl_2 gave 0.121 g of non-furan containing material, and elution with 1:1 methylene chloride – ethyl acetate gave 0.314 g (78%) of the acid **6***b* as a viscous oil. The acid showed: pmr δ ($CDCl_3$) 0.571 (s, 3H, 20-CH_3), 1.18 (s, 3H, 18-CH_3), 3.605 (s, 3H, 19-ester OCH_3), 4.55 (s, brd, 1H, 17-H_A), 4.88 (s, brd, 1H, 17-H_B), 6.09 (s, brd, 1H, 14-H), and 6.84 ppm (s, brd, 1H, 15-H); cmr δ ($CDCl_3$) 12.58 (20-CH_3), 19.96 (C-2), 21.78 (C-6), 24.43 (C-12), 26.23 (C-11), 28.80 (18-CH_3), 38.20 (C-7), 38.65 (C-1), 39.17 (C-3), 40.31 (C-10), 44.37 (C-4), 51.20 (19-ester CH_3), 55.78 (C-5), 56.30 (C-9), 97.07 (C-14), 106.69 (C-17), 138.40 (C-13), 143.66 (C-15), 147.46 (C-8), 172.26 (16-CO_2H), 175.74 (C-16), and 177.95 ppm (C-19 ester CO); mass spectrum, *m/e* 374 (M^+, calcd. for $C_{22}H_{30}O_5$: 374.20931; found: 374.20781).

Methyl Lambertianate **7**

A sample of 0.045 g (0.12 mmol) of chromatographed 16-carboxylambertianate **6***b* was mixed with 0.150 g distilled, dry quinoline and 0.034 g copper powder. The whole was heated at 225 °C under a nitrogen atmosphere for 25 min, cooled to room temperature and placed under vacuum (10^{-2} Torr) for 3 h to remove the bulk of the quinoline. The residue was then heated at 220 °C under 10^{-4} Torr in a micro sublimation apparatus. In this way a sample of 0.025 g of methyl lambertianate **7** (63%) was obtained as a colorless oil. The sample showed: ν_{max} (film) 1724 (C=O), 1642 (C=C), 1153, 1070, 1028, 889, and 875 cm^{-1}; pmr δ ($CDCl_3$) 0.50 (s, 3H, 20-CH_3), 1.18

(s, 3H, 18-CH_3), 3.62 (s, 3H, 19-ester CH_3), 4.58 (s, brd, 1H, H_A-17), 4.89 (s, brd, 1H, H_B-17), 6.25 (s, brd, 1H, H-14), 7.20 (s, brd, 1H, H-16), and 7.34 ppm (s, brd, 1H, H-15); mass spectrum *m/e* 330 (M^+, calcd. for $C_{21}H_{30}O_3$: 330.21948; found: 330.21873), 271 ($M - CO_2CH_3$, calcd. for $C_{19}H_{27}O$: 271.20617; found: 271.20593), 249 ($M - C_5H_4O$ (furan ring plus C-12 methylene), calcd. for $C_{16}H_{25}O_2$: 249.18544; found: 249.18587).

The spectral properties of synthetic **7** were identical in all respects with a sample of authentic methyl lambertianate prepared by the action of diazomethane on lambertianic acid **7***b*.

In another experiment the quinoline was omitted and although a high yield (>80%) of decarboxylated product was obtained the pmr spectrum showed the presence of *ca.* 40% of the $\Delta^{7,8}$-double bond isomer (δ ($CDCl_3$), 0.77 (20-CH_3), 1.26 (18-CH_3), 2.64 (19-ester CH_3), and 5.42 ppm (H-7 alkene) (12)).

Acknowledgments

Acknowledgment is gratefully made to the French and Canadian Governments for financial support in the form of a Canada-France Scientific Exchange Award (R.A.B.). One of us (R.A.B.) thanks Professor Fétizon for his gracious and enlivening hospitality.

1. T. A. Spencer, R. M. Villarica, D. L. Storm, T. D. Weaver, R. J. Friary, J. Posler, and R. P. Schafer. J. Am. Chem. Soc. **89**, 5497 (1967).
2. T. A. Spencer, R. A. J. Smith, D. L. Storm, and R. M. Villarica. J. Am. Chem. Soc. **93**, 4856 (1971).
3. A. Ogiso and S. W. Pelletier. Chem. Commun. 94 (1967); S. W. Pelletier, L. B. Hawley, Jr., and K. W. Gopinth. Chem. Commun. 96 (1967).
4. L. Mangoni, M. Adinolfi, G. Laonigro, and R. Caputo. Tetrahedron, **28**, 611 (1972).
5. R. A. Bell, M. B. Gravestock, and V. Y. Taguchi. Can. J. Chem. **50**, 3749 (1972).
6. W. G. Dauben and V. F. German. Tetrahedron, **22**, 679 (1966).
7. J. Haeuser, R. Lombard, F. Lederer, and G. Ourisson. Tetrahedron, **12**, 205 (1961).
8. D. M. Burness. Organic Syn. Coll. Vol. 4, 649 (1963).
9. D. B. Bigley, N. A. J. Rogers, and J. A. Barltrop. J. Chem. Soc. 4613 (1960).
10. (*a*) W. S. Johnson and H. Posvic. J. Am. Chem. Soc. **69**, 1361 (1947); (*b*) R. E. Ireland and P. W. Schiess. J. Org. Chem. **28**, 6 (1963).
11. J. Hata, S. Yamada, J. Jwao, N. Kato, N. Sugimoto, and R. Inouye. J. Pharm. Soc. Jpn. **69**, 477 (1949).
12. V. Y. Taguchi. Ph.D. Thesis, McMaster University, Hamilton, Ontario. 1973.
13. M. E. Garst and T. A. Spencer. J. Am. Chem. Soc. **95**, 250 (1973).

Can. J. Chem. Downloaded from www.nrcresearchpress.com by 210.87.254.5 on 09/05/12
For personal use only.

Analyse conformationnelle de trithiolannes-1,2,4[1]

M. F. GUIMON, C. GUIMON, F. METRAS et G. PFISTER-GUILLOUZO

Laboratoire de Chimie Organique Physique, Institut Universitaire de Recherche Scientifique, Avenue Philippon, 64016 PAU, France

Reçu le 25 avril 1975

M. F. GUIMON, C. GUIMON, F. METRAS et G. PFISTER-GUILLOUZO. Can. J. Chem. **54**, 146 (1976).

L'étude conformationnelle du trithiolanne-1,2,4 et de son dérivé tétraméthylé a pu être réalisée à l'aide des spectroscopies de vibration et photoélectronique uv (HeI). L'analyse des spectres de vibration montre l'existence d'une forme unique possédant une symétrie C_2 ou C_s (forme demi-chaise ou enveloppe). A partir des données des spectres photoélectroniques, on peut conclure que la forme préférentielle à l'état gazeux est la forme demi-chaise (C_2).

M. F. GUIMON, C. GUIMON, F. METRAS, and G. PFISTER-GUILLOUZO. Can. J. Chem. **54**, 146 (1976).

A conformational study of 1,2,4-trithiolane and its tetramethyl derivative was carried out by vibrational and uv photoelectron spectroscopy (HeI). Analysis of the vibrational spectra shows the existence of a single form with C_2 or C_s symmetry (half chair or envelope form). From the photoelectron data, we can conclude that the preferential form in the vapor phase is the half chair (C_2).

L'analyse conformationnelle d'hétérocycles à cinq chaînons se révèle très souvent fort délicate compte tenu des barrières de pseudo-rotation très faibles que présentent ces composés. En particulier, les possibilités actuelles de la résonance magnétique nucléaire ne permettent pas d'atteindre les barrières d'interconversion et par suite d'identifier la nature des formes préférentielles.

Ainsi dans le cas de trithiolannes-1,2,4, cette technique a permis antérieurement à S. B. Tjan *et al.* (2) de mettre en évidence l'existence vraisemblable d'une pseudo-rotation rapide mais ces auteurs n'ont pu déterminer par cette technique la ou les formes en équilibre.

Par analogie avec les formes proposées pour le cyclopentane, on peut en effet envisager pour le trithiolanne-1,2,4 différentes formes que l'on peut classer suivant les groupes de symétrie auxquels elles appartiennent (fig. 1): (*A*) la forme plane de symétrie C_{2v}; (*B*) une forme enveloppe, de symétrie C_s, dans laquelle l'atome de soufre S_4 serait hors du plan défini par les quatre autres atomes du cycle; (*C*) une forme demi-chaise de symétrie C_2 dans laquelle les atomes S_1 et S_2 se trouvent de part et d'autre du plan défini par les atomes C_3, S_4 et C_5; (*D*) d'autres formes enveloppe ou demi-chaise ne présentant pas d'élément de symétrie et par conséquent appartenant au groupe C_1.

[1]Partie XX de Structure électronique de dérivés sulfurés; partie XIX, réf. 1.

Nous nous proposons d'examiner ce problème par l'utilisation conjointe de la spectroscopie de vibration et de la spectroscopie photoélectronique en examinant le trithiolanne-1,2,4 lui-même et son dérivé tétraméthylé.

Etude par spectroscopies infrarouge et Raman

Le trithiolanne-1,2,4 possède 21 vibrations fondamentales et le tétraméthyl-3,3,5,5 trithiolanne-1,2,4, 57 vibrations. Nous avons reporté dans le tableau 1, pour les différentes formes possibles, leur activité théorique en spectroscopies infrarouge et Raman. Les fréquences observées à l'état liquide sont reportées dans le tableau 2.

On remarque que le nombre de bandes relativement faible laisse présumer de la présence d'une seule forme pour chaque composé. Cette hypothèse est d'ailleurs confirmée par l'examen des spectres infrarouges des composés à l'état solide (−180 °C) pour lesquels le nombre de bandes est identique à celui des composés à l'état liquide. On n'observe en effet aucune disparition de bandes mais seulement quelques variations d'intensité qui peuvent être attribuées au changement d'état.

Admettant l'existence des trithiolannes étudiés sous une seule conformation, nous allons tenter par l'analyse comparative des données infrarouge et Raman d'éliminer certaines des formes possibles, compte tenu de leur symétrie.

Si l'on envisage une forme plane, on peut attendre quatre vibrations actives seulement en

Can. J. Chem. Downloaded from www.nrcresearchpress.com by 210.87.254.6 on 09/05/12
For personal use only.

Can. J. Chem. Downloaded from www.nrcresearchpress.com by 210.87.254.6 on 09/05/12
For personal use only.

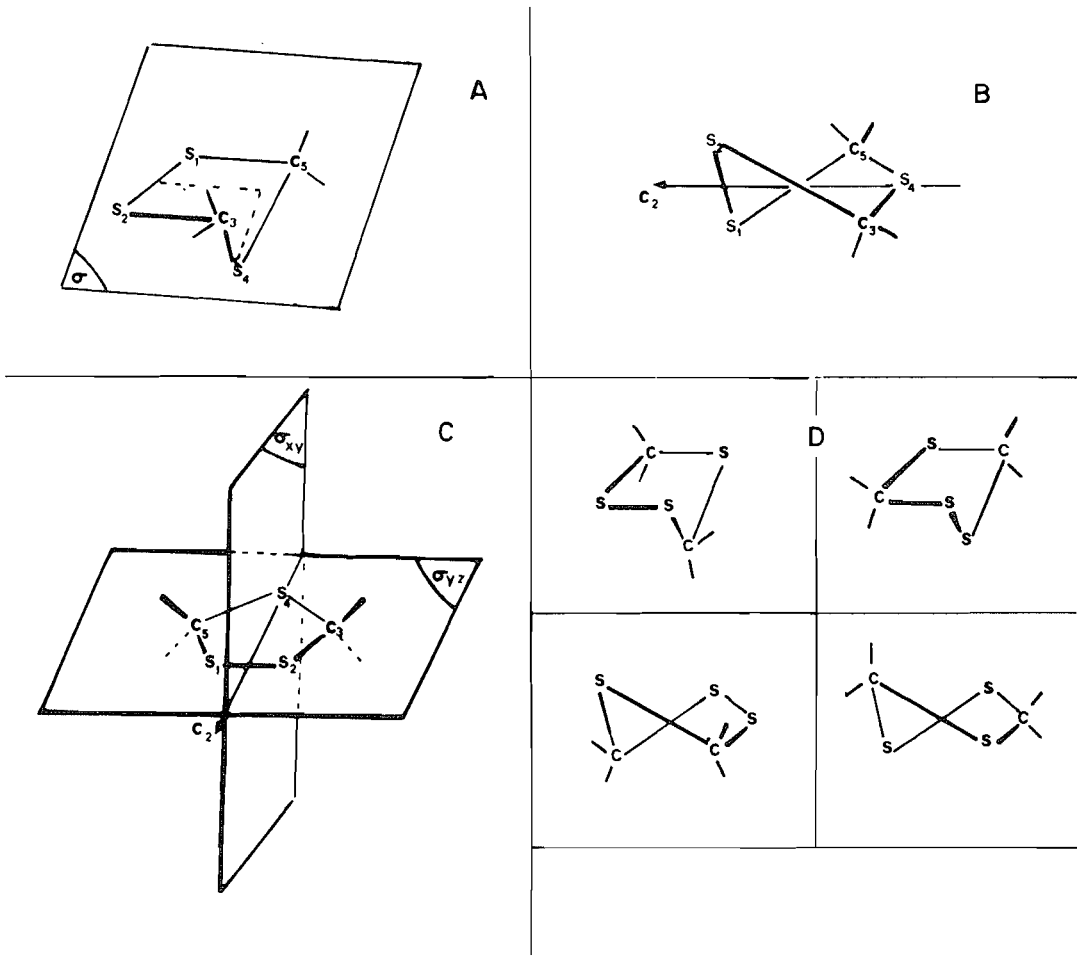

FIG. 1. Différentes formes envisagées pour les trithiolannes-1,2,4. *A*, forme enveloppe (C_s); *B*, forme demi-chaise (C_2); *C*, forme plane (C_{2v}); *D*, formes asymmétriques (C_1).

TABLEAU 1. Classement et activité des vibrations du trithiolanne-1,2,4 et du tétraméthyl-3,3,5,5 trithiolanne-1,2,4

Formes	Trithiolanne-1,2,4	Tétraméthyl-3,3,5,5 trithiolanne-1,2,4
Plane C_{2v}	$\Gamma_{C_{2v}} = 7A_1[\text{IR,R(p)}] + 4A_2[\text{R(dp)}] + 6B_1[\text{IR,R(dp)}] + 4B_2[\text{IR,R(dp)}]$	$\Gamma_{C_{2v}} = 16A_1[\text{IR,R(p)}] + 13A_2[\text{R(dp)}] + 13B_1[\text{IR,R(dp)}] + 15B_2[\text{IR,R(dp)}]$
Enveloppe C_s	$\Gamma_{C_s} = 11A'[\text{IR,R(p)}] + 10A''[\text{IR,R(dp)}]$	$\Gamma_{C_s} = 29A'[\text{IR,R(p)}] + 28A''[\text{IR,R(dp)}]$
Demi-chaise C_2	$\Gamma_{C_2} = 11A[\text{IR,R(p)}] + 10B[\text{IR,R(dp)}]$	$\Gamma_{C_2} = 29A[\text{IR,R(p)}] + 28B[\text{IR,R(dp)}]$
Asymétriques C_1	$\Gamma_{C_1} = 21A[\text{IR,R(p)}]$	$\Gamma_{C_1} = 57A[\text{IR,R(p)}]$

Raman (et non polarisées) pour le trithiolanne-1,2,4 et 13 pour le dérivé tétraméthylé. Il apparaît (tableau 2) que toutes les vibrations sont actives en Raman et en infrarouge à l'exception de la bande à 529 cm^{-1} pour le tétraméthyl-3,3,5,5 trithiolanne-1,2,4 active seulement en Raman et que nous attribuons à une vibration ν_{S-S} toujours d'intensité très faible en infrarouge. Cette forme ne peut donc être retenue.

TABLEAU 2. Fréquences des vibrations du trithiolanne-1,2,4 et du tétraméthyl-3,3,5,5 trithiolanne-1,2,4 (état liquide)*

Trithiolanne-1,2,4				Tétraméthyl-3,3,5,5 trithiolanne-1,2,4			
Fréquences ir (cm^{-1})	Fréquences Raman (cm^{-1})		Attribution	Fréquences ir (cm^{-1})	Fréquences Raman (cm^{-1})		Attribution
					164(m)	DP	
?	254(m)	DP	Vibrations de squelette	221(f)	226(f)	DP	
				270(f)	275(F)	DP	Vibrations
				313(f)			
				323 (ép)	317(F)	DP	de
					345(m)	DP	
				362(f)	364(F)	P	squelette
360(f)	355(F)	DP		374(f)			
	389(F)	P		409(f)	412(m)	DP	
				430(tf)	430(m)	DP	
505(f)	507(TF)	DP	ν(S—S)		529(TF)	P	ν(S—S)
				554(m)	542(TF)	P	
	638(tf)	P		646(m)	648(F)	DP	ν(C—S)
668(m)	668(F)	P	ν(C—S)	691(m)	694(f)	DP	ν(C—S)
680(m)	680(ép)		ν(C—S)	896(f)	902(m)	DP	
700(F)	699(m)	DP		943(f)	943(f)	DP	
725(F)	728(m)	P		1002(f)	1003(TF)	P	
838(TF)	838(TF)	DP		1090(m)	1080(f)	DP	
855(m)	856(TF)	P		1125(F)			
1070(m)	1070(f)	DP		1137(ép)	1129(f)	DP	
1085(F)	1087(f)	DP	r(CH_2)	1146(ép)	1158(m)	DP	r(CH_3)
1160(m)	1143(ép)		t(CH_2)	1153(F)			
1175(m)	1164(f)	DP	w(CH_2)	1363(F)	1365(f)	DP	
1195(F)	1198(f)	DP		1380(F)	1382(f)	P	
	1370(ép)			1434(F)			δ(CH_3)
1392(TF)	1397(m)	DP	δ(CH_2)	1438(ép)	1437(m)	DP	
				1448(F)			
				1455(ép)	1452(m)	DP	
				2851(F)	2849(m)	P	
				2883(ép)	2889(m)	P	ν(CH)
2910(TF)	2912(F)	P	ν(CH)	2918(F)	2920(F)	P	
				2958(F)	2959(m)	DP	
2960(TF)	2967(F)	DP		2978(F)	2980(m)	DP	

*Abréviations utilisées: P, polarisée; DP, dépolarisée; TF, très fort; F, fort; m, moyen; f, faible; tf, très faible; ép, épaulement; ν, vibration de valence; δ, vibration de cisaillement (scissoring); t, vibration de torsion (twisting); r, vibration de balancement dans le plan (rocking); w, vibration de balancement perpendiculaire au plan (wagging).

D'autre part, si le trithiolanne-1,2,4 appartenait au groupe C_1 (formes enveloppe et demi-chaise ne présentant pas d'éléments de symétrie), toutes les bandes devraient être polarisées en Raman. Or, tant pour le trithiolanne-1,2,4 que pour son dérivé tétraméthylé, les vibrations se répartissent en nombre à peu près égal en vibrations polarisées et vibrations non polarisées.

Il semble donc compte tenu des données du tableau 1 que la seule hypothèse envisageable soit que le cycle trithiolanne-1,2,4 existe sous une forme de symétrie C_s (forme enveloppe) ou une forme de symétrie C_2 (forme demi-chaise).

Etude par spectroscopie photoélectronique

Les deux formes envisagées (C_2 et C_s) diffèrent entre autres par l'angle dièdre formé par les paires libres des atomes S_1 et S_2 ($\theta = 0°$ pour la forme enveloppe et $\theta \neq 0$ pour la forme demi-chaise); la spectroscopie photoélectronique semblait particulièrement bien adaptée pour leur différenciation. On sait, en effet, que l'interaction entre les orbitales atomiques associées aux paires libres de deux hétéroatomes contigus est liée directement à l'angle dièdre existant entre ces paires (3–12). L'éclatement entre les deux composantes antiliante et liante résultant de cette interaction est minimum

Can. J. Chem. Downloaded from www.nrcresearchpress.com by 210.87.254.6 on 09/05/12
For personal use only.

Can. J. Chem. Downloaded from www.nrcresearchpress.com by 210.87.254.6 on 09/05/12
For personal use only.

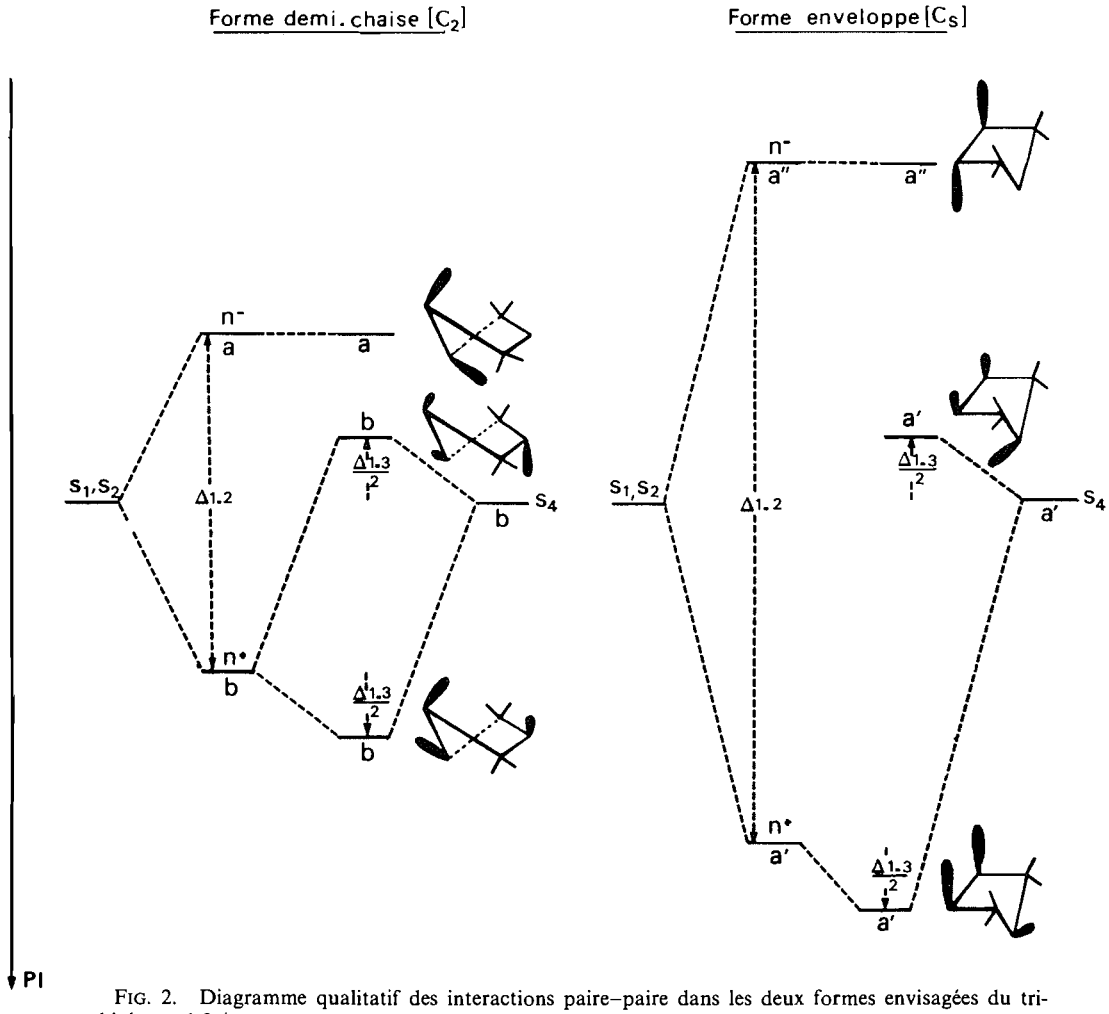

FIG. 2. Diagramme qualitatif des interactions paire–paire dans les deux formes envisagées du trithiolanne-1,2,4.

pour un angle voisin de 90°. Expérimentalement, pour la liaison disulfure les valeurs de ΔE_{1-2} sont voisines de 0.3 eV pour un angle de 84.7° et de 1.80 eV pour un angle de 30° (acide lipoïque) (12).

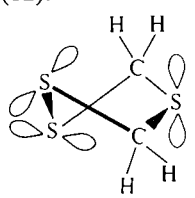

Forme demi-chaise

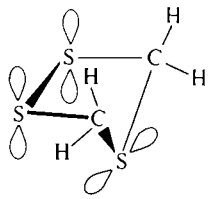

Forme enveloppe

A côté de ces interactions de type 1–2, on peut envisager une interaction de type 1–3 entre les atomes du groupement disulfure et l'atome de soufre S_4. Comme précédemment l'éclatement résultant dépend du recouvrement des orbitales associées aux paires libres. Ici encore l'orbitale la plus stable correspondra à la combinaison liante (4, 13, 14). De par la symétrie des deux conformères, l'orbitale atomique non liante de l'atome S_4 ne pourra interéagir qu'avec la combinaison liante des deux orbitales atomiques considérées de S_1 et S_2. Ces deux types d'interaction sont schématisés dans la fig. 2. Dans ces schémas, nous n'avons considéré qu'une perturbation du premier ordre, c'est-à-dire le cas où le barycentre des orbitales non perturbées (paires libres des atomes isolés) est à la même position que celui des orbitales après interaction. Ceci est une approximation

Can. J. Chem. Downloaded from www.nrcresearchpress.com by 210.87.254.6 on 09/05/12
For personal use only.

(7) qui permet de traduire qualitativement l'importance de ces interactions. Pour être plus précis et obtenir des résultats quantitatifs, il faudrait considérer la perturbation du second ordre qui introduit le recouvrement entre les orbitales (5, 15).

A ces interactions s'ajoute une contribution du squelette carboné. Dans le cas du dimercapto méthane (14) pour lequel la conformation privilégiée est non plane, nous avons pu mettre en évidence que l'interaction spatiale (1.07 eV) était très supérieure à l'interaction par les liaisons (~0.1 eV). Pour les deux conformères envisagés du trithiolanne-1,2,4 l'angle dièdre formé par les paires libres des atomes de soufre S_1 et S_4 est certainement inférieur à celui présenté par le dimercapto méthane. Il s'en suit que l'interaction spatiale est moins importante et que l'interaction par les liaisons n'est plus négligeable. Toutefois, il faut remarquer que les interactions entre les orbitales $n^-_{(S_1S_2)}$ et $n^+_{(S_1S_2)}$ et les combinaisons antisymétriques et symétriques des orbitales pseudo π localisées sur les groupements méthylènes (16) doivent être sensiblement du même ordre. Il en résulte une légère destabilisation des trois orbitales considérées (fig. 3). Par ailleurs, le recouvrement et par suite l'interaction entre les paires libres π des atomes de soufre et les liaisons σ_{C-S} sont pour les deux conformations examinées suffisamment faibles pour pouvoir, en première approximation, être négligés.

Cette évaluation qualitative des interactions mises en jeu est d'ailleurs confirmée par les données théoriques d'un calcul CNDO/S (17). Cette paramétrisation s'est révélée en effet beaucoup plus satisfaisante pour traduire, dans le cadre du théorème de Koopmans l'ordre des potentiels d'ionisation observés expérimentalement.

Les spectres photoélectroniques des deux composés étudiés présentent, entre 8 eV et 11 eV, quatre bandes fines bien résolues (tableau 3 et fig. 4). A l'état gazeux, comme en solution ces composés n'existent donc que sous une seule forme; un équilibre conformationnel conduirait en effet à un dédoublement de ces bandes (14, 18). Pour les deux composés les trois premières bandes peuvent être attribuées aux trois orbitales moléculaires résultant des interactions entre paires libres des atomes de soufre; la quatrième bande provient de l'ionisation d'un

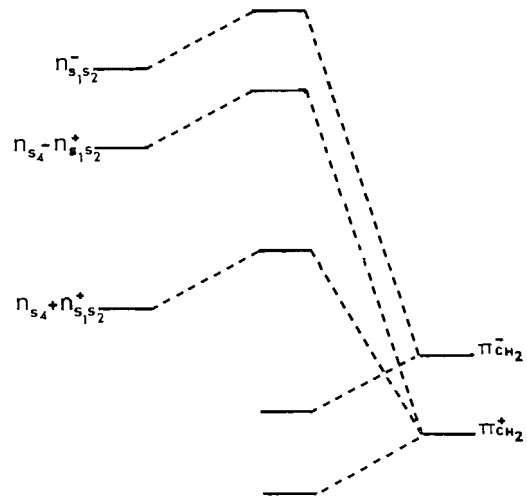

FIG. 3. Diagramme qualitatif des interactions entre les paires libres π des soufres et les pseudo-orbitales π des groupements méthylène dans le trithiolanne-1,2,4.

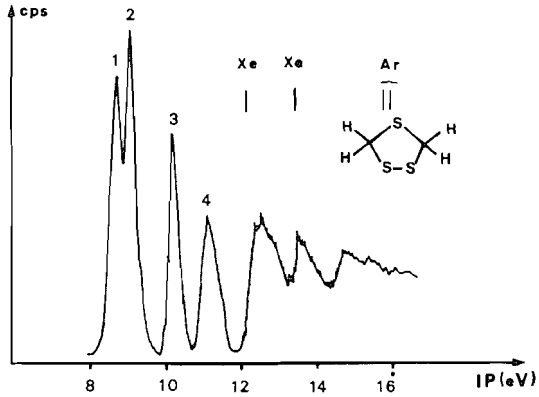

FIG. 4. Spectre photoélectronique du trithiolanne-1,2,4.

électron σ des liaisons C—S. Les valeurs des potentiels d'ionisation observés pour cette bande (10.36 eV et 11.06 eV) sont en effet à rapprocher de celles obtenues pour le dithia-2,4 pentane (10.95 eV et 12.14 eV) et le dimercapto méthane (11.90 eV et 13.40 eV).

On remarque ainsi que l'écart entre la première et la troisième bande est respectivement de 1.47 eV pour le trithiolanne-1,2,4 et 1.66 eV pour le tétraméthyl-3,3,5,5 trithiolanne-1,2,4. On peut essayer d'évaluer grossièrement l'importance des deux types d'interaction d'après la position des trois premières bandes toujours dans l'approximation d'une perturbation au premier ordre. Un calcul élémentaire conduit aux valeurs de 1.23 eV (interaction 1–2) et 0.48 eV

TABLEAU 3. Potentiels d'ionisation théoriques (CNDO/S) et expérimentaux (verticaux)

P.I. calculés (eV)*		P.I. observés (eV)		
Forme enveloppe	Forme demi-chaise	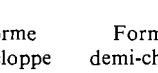	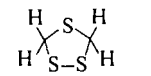	Attribution
8.52	9.25	8.72	8.12	$n^{-}_{(S_1S_2)}$
9.51	9.80	9.10	8.48	$n^{+}_{(S_1S_2)} - n_{(S_4)}$
12.91	10.99	10.19	9.78	$n^{+}_{(S_1S_2)} + n_{(S_4)}$
11.80	11.87	11.06	10.36	σ_{C-S}

*Les valeurs sont calculées pour le trithiolanne-1,2,4.

(interaction 1–3) pour le trithiolanne et 1.35 eV (interaction 1–2) et 0.63 eV (interaction 1–3) pour le tétraméthyl-3,3,5,5 trithiolanne. Ces deux valeurs de ΔE_{1-2} (1.23 eV et 1.35 eV) inférieures à celle observée pour l'acide lipoïque ne peuvent correspondre qu'à la conformation demi-chaise du trithiolanne-1,2,4. D'après la courbe de corrélation établie antérieurement entre la valeur de l'éclatement ΔE_{1-2} et l'angle dièdre θ formé par les paires libres des deux atomes liés la valeur approximative de cet angle serait d'environ 50° pour les trithiolannes-1,2,4.[2]

Conditions expérimentales

Spectrométrie d'absorption infrarouge

Les spectres ont été enregistrés à l'aide d'un spectromètre Perkin-Elmer modèle 521 équipé de deux réseaux. L'incertitude sur les fréquences est de ± 2 cm^{-1}.

Les spectres à l'état solide ont été étudiés sous forme de film cristallin obtenu par refroidissement du composé liquide par un mélange acétone–carboglace puis par l'azote liquide.

Spectrométrie de diffusion Rayleigh

Les spectres ont été réalisés à l'aide d'un spectromètre de marque Coderg "type Physique" équipé d'un laser "rouge" à gaz (Hélium–Néon) de marque OIP modèle 18/E émettant à 6328 Å avec une puissance de 150 mW.

Spectrométrie photoélectronique

L'appareil utilisé est un spectromètre Perkin Elmer PS_{18} muni d'une source à Hélium I (21.21 eV). La résolution est d'environ 20 m eV. Les spectres ont été étalonnés avec les pics $^2P_{1/2}$ et $^2P_{3/2}$ du Xénon (12.127 eV et 13.427 eV) et de l'Argon (15.755 eV et 15.943 eV).

Calculs theoriques

Les P.I. théoriques ont été calculés à l'aide de la méthode CNDO/S (17). Les paramètres géométriques utilisés ont, pour chaque forme, été déterminés par optimisation énergétique par la méthode de plus grande pente (CNDO/2) (19) et sont reportés ci-dessous

Paramètres géométriques de		
Paramètre	Forme enveloppe	Forme demi-chaise
d_{12}	2.041 Å	2.034 Å
d_{23}	1.799 Å	1.805 Å
d_{34}	1.801 Å	1.805 Å
∠123	101.2°	92.1°
∠234	103.3°	106.3°
∠345	99.0°	101.9°

Remerciements

Les auteurs remercient la "Société Nationale des Pétroles d'Aquitaine" pour leur aide financière.

1. D. GONBEAU et G. PFISTER-GUILLOUZO. A paraître.
2. S. B. TJAN, J. C. HAAKMAN, C. J. TEUNIS et H. G. PEER. Tetrahedron, **28**, 3489 (1972).
3. D. A. SWEIGART et D. W. TURNER. J. Am. Chem. Soc. **94**, 5599 (1971).
4. H. BOCK et G. WAGNER. Angew. Chem. Int. Ed. Engl. **11**, 150 (1972).
5. R. F. HUDSON. Angew. Chem. Int. Ed. Engl. **12**, 36 (1973).
6. P. RADEMACHER. Angew. Chem. Int. Ed. Engl. **12**, 408 (1973).
7. R. G. JESAITIS. Theor. Chim. Acta. **32**, 71 (1973).
8. S. F. NELSEN et J. M. BUSCHEK. J. Am. Chem. Soc. **96**, 2392 (1974).
9. G. WAGNER et H. BOCK. Chem. Ber. **197**, 68 (1974).
10. A. D. BAKER, M. BRISK et M. GELLENDER. J. Elect. Spect. **3**, 227 (1974).
11. C. BATICH et W. ADAM. Tetrahedron Lett. 1470 (1974).

[2]Cette valeur est légèrement différente de cette avancée dans une publication précédente (12) où l'on n'avait pas tenu compte de l'interaction du type 1–3.

Can. J. Chem. Downloaded from www.nrcresearchpress.com by 210.87.254.6 on 09/05/12
For personal use only.

12. M. F. GUIMON, C. GUIMON et G. PFISTER-GUILLOUZO. Tetrahedron Lett. 441 (1975).
13. R. HOFFMANN, A. IMAMURA et W. HEHRE. J. Am. Chem. Soc. **90**, 1499 (1968).
14. C. GUIMON, M. F. GUIMON et G. PFISTER-GUILLOUZO. Tetrahedron Lett. 1413 (1975)
15. L. LIBIT et R. HOFFMANN. J. Am. Chem. Soc. **96**, 1370 (1974).
16. W. L. JORGENSEN et L. SALEM. The organic chemist's book of orbitals. Academic Press, New York. 1973.
17. C. GUIMON, D. GONBEAU et G. PFISTER-GUILLOUZO. Tetrahedron, **29**, 3399 (1973).
18. A. H. COWLEY, M. J. S. DEWAR, D. W. GOODMAN et M. C. PADOLINA. J. Am. Chem. Soc. **96**, 2648 (1974).
19. A. DARGELOS, D. LIOTARD et M. CHAILLET. Tetrahedron, **28**, 5595 (1972).

Can. J. Chem. Downloaded from www.nrcresearchpress.com by 210.87.254.6 on 09/05/12
For personal use only.

Etude comparée du rapport isomérique du ^{84m,f}Rb produit dans une cible d'yttrium 89 par des protons et des particules α

JEAN-CLAUDE KRUPA

Division de Radiochimie, Institut de Physique Nucléaire, B.P. N° 1, 91406 Orsay, France

Reçu le 16 mai 1975

JEAN-CLAUDE KRUPA. Can. J. Chem. **54**, 153 (1976).

Une méthode de séparation physique des éléments alcalins s'effectuant à l'intérieur de la source d'ions à effet de thermoionisation d'un séparateur d'isotopes a permis de mesurer le rapport des sections efficaces de formation des états isomériques de ^{84m,f}Rb produits par réactions nucléaires dans des cibles de ^{89}Y par des protons et des particules α. Le domaine d'énergie exploré s'étend de 40 à 160 MeV environ.

L'examen de la variation de ce rapport en fonction de l'énergie des projectiles incidents a permis dans un premier temps de dégager parmi les nombreux mécanismes possibles, les processus prépondérants. Ensuite, les prévisions du modèle statistique du gaz de Fermi et du modèle "Independent Pairing", lorsque ces réactions procèdent par formation du noyau composé, ont pu être testées en confrontant les valeurs du paramètre de "spin cut off σ" estimées à partir de l'expérience à celles déduites des calculs effectués sur la base de ces modèles avec le formalisme de Huizenga et Vandenbosch. Enfin, l'effet du moment cinétique a pu être mis en évidence en comparant les réactions induites par les protons à celles induites par les particules α auxquelles sont toujours associées des quantités de mouvement plus importantes.

JEAN-CLAUDE KRUPA. Can. J. Chem. **54**, 153 (1976).

A physical method for separation of alkali metals, carried out inside a surface ionization ion source of an electromagnetic isotope separator, was used to determine the isomeric ratio of ^{84m,f}Rb produced in ^{89}Y targets bombarded by protons and α-particles of energies between 40 and approximately 160 MeV.

The variation of isomeric ratio with energy of the incident particles enabled the principal reaction to be differentiated from other possible mechanisms. With compound nucleus formation as the mechanism and the use of a statistical Fermi-gas model, the spin cut-off parameters were deduced, based on the Huizenga–Vandenbosch formalism. The kinetic momentum effect was investigated by a comparison of the proton and α-particle induced reactions.

Introduction

Un des principaux intérêts des réactions induites par des particules α réside dans l'importance relative de moment cinétique pouvant être transféré au cours de l'interaction. Lorsque le paramètre d'impact est égal au rayon du noyau cible, le moment angulaire maximal du noyau de fusion peut s'exprimer par la relation:

$$[1] \qquad l_{max}\hbar = (R_1 + R_2)[2\mu(\varepsilon - B)]^{1/2}$$

dans laquelle R_1 est le rayon du noyau cible, R_2 le rayon du projectile, μ la masse réduite du système, ε l'énergie de la particule incidente et B la barrière coulombienne.

A l'inverse, les réactions induites par des protons sont caractérisées par de très faibles moments angulaires résultants ce qui permet en première approximation de négliger les effets de ce facteur. Aussi, afin d'en apprécier l'influence, il nous a semblé intéressant de comparer les rapports des sections efficaces de formation des états isomériques d'un même noyau produit par ces deux types de particules. En effet, la valeur du rapport isomérique est en premier lieu conditionnée par la loi de conservation de moment angulaire. Ceci résulte du fait que deux états isomériques sont toujours caractérisés par une différence importante de moment angulaire alors qu'il présente une faible différence d'énergie. Le problème consiste donc à savoir pourquoi un niveau est peuplé préférentiellement à l'autre. Le formalisme développé par Huizenga et Vandenbosch (1) répond en partie à cette question. Il est basé sur le modèle statistique du noyau composé et traîte la désexcitation en termes de moment angulaire en calculant à chaque étape du processus la distribution des moments angulaires des noyaux résiduels. Le peuplement préférentiel de chacun des deux niveaux finaux est alors supposé s'effectuer lors de l'émission du dernier photon selon la règle empirique de la variation la plus faible de moment angulaire.

Can. J. Chem. Downloaded from www.nrcresearchpress.com by 210.87.254.42 on 09/05/12
For personal use only.

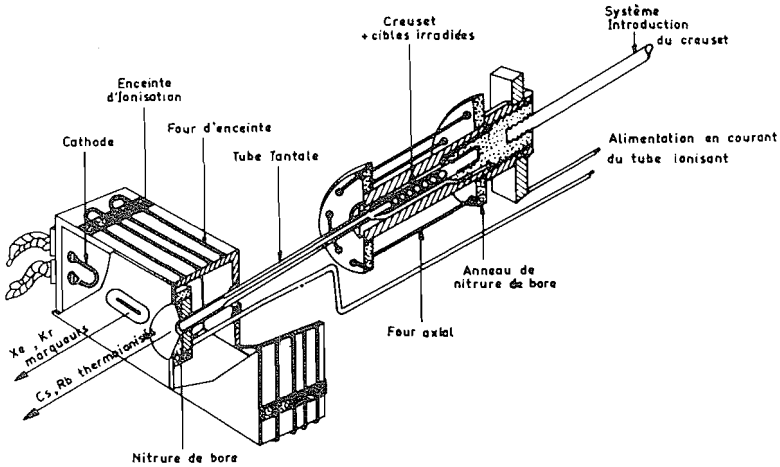

FIG. 1. Schéma de la source d'ions du séparateur d'isotopes.

C'est ce mode de traitement que nous avons adopté pour interpréter les rapports isomériques de ^{84m,f}Rb produit par réactions du type (X, Xαn) induites dans des cibles de ^{89}Y par des protons et des particules α, dans un domaine d'énergie allant de 40 à 160 MeV environ. Il est évident que son domaine d'application est réduit à la région des faibles énergies où le mécanisme de formation du noyau composé est prépondérant. Dans cette région, la comparaison des résultats expérimentaux et calculés permet d'approfondir la relation qui existe entre densité de niveaux et moments angulaires J (2):

$$[2] \quad \rho(J) = \rho_0(2J + 1) \exp[-J + \tfrac{1}{2})^2/2\sigma^2]$$

en rendant possible une estimation du paramètre σ de "spin cut off".

De plus, et d'une façon générale, la valeur du rapport isométrique est très sensible à la nature des mécanismes mis en jeu; l'étude de sa variation en fonction de l'énergie des projectiles incidents permet donc de dégager les principaux processus régissant les réactions étudiées.

Techniques expérimentales

Les irradiations ont été effectuées au synchrocyclotron de l'Institut de Physique Nucléaire à Orsay. La séparation du rubidium produit en très faible quantité dans les cibles d'yttrium a été réalisée à l'intérieur de la source d'ions à émission thermoionique d'un séparateur d'isotopes (fig. 1). La séparation est basée sur la grande volatilité et le faible potentiel d'ionisation de cet élément (3). Elle s'effectue en mettant à profit successivement ces deux propriétés. Dans un premier temps, la cible est portée à haute température et les éléments les plus volatils produits en son sein diffusent préférentiellement vers les faces. Ils sont alors dirigés vers une surface métallique incandescente choisie telle que le travail d'extraction d'un électron de cette surface soit supérieur au potentiel d'ionisation du rubidium (ϕ = 4.16 eV) et inférieur à celui des autres éléments volatilisés: une sélection s'opère ainsi au niveau du métal où seuls les atomes alcalins sont ionisés de façon prépondérante. Les ions alcalins formés sont extraits et accélérés par un champ électrique intense et analysés en masse par une induction magnétique.

Le rubidium 84 séparé est collecté sur des feuilles d'aluminium de 5μm. L'activité des deux états isomériques est ensuite mesurée à l'aide d'un détecteur NaI(Tl) de 3 × 3 "inches" associé à une chaîne électronique conventionnelle.

L'état métastable 6^+ ($T_{1/2}$ = 20 min) est caractérisé par trois pics photoélectriques respectivement d'énergie 216, 248 et 464 keV. Les mesures sont effectuées avec une géométrie voisine de 1% sur le pic de 464 keV qui correspond à 35% de l'activité total (4). L'activité de l'état fondamental 2^- ($T_{1/2}$ = 33 jours) est mesurée à l'aide du rayonnement de 880 keV du krypton 84 associé à 73.4% des désintégrations du niveau fondamental du ^{84}Rb (5).

Résultats expérimentaux. Incertitudes

Les figs 2 et 3 représentent la variation du rapport isomérique du ^{84m,f}Rb produit dans des cibles de ^{89}Y en fonction respectivement de l'énergie des protons et des particules α incidents.

La principale erreur commise dans la détermination du rapport isomérique est inhérente aux schémas de désintégrations. Cependant, c'est là une erreur systématique qui n'a pas été prise en considération dans le calcul. Seules ont été retenues l'erreur statistique introduite lors du comptage des activités et l'erreur affectant la valeur de l'efficacité du détecteur. L'ensemble de ces deux erreurs peut conduire à une incertitude maximum sur la valeur du rapport isomérique d'environ 10%.

Can. J. Chem. Downloaded from www.nrcresearchpress.com by 210.87.254.42 on 09/05/12
For personal use only.

Can. J. Chem. Downloaded from www.nrcresearchpress.com by 210.87.254.42 on 09/05/12
For personal use only.

Calcul du rapport isomérique. Discussion

A partir du seuil de la réaction, la valeur du rapport isomérique croît lorsque l'énergie des particules incidentes augmente. Ceci est en accord avec un schéma de formation du noyau composé et les prévisions du modèle statistique. En effet, des particules de grande quantité de mouvement peuvent transférer des moments angulaires importants ($mv \times d$) permettant ainsi d'atteindre préférentiellement l'état de haut spin.

Lors de l'interaction, la distribution des moments angulaires, J_B, des noyaux composés d'énergie E_B peut être calculée à partir de l'expression suivante (6):

$$[3] \quad \sigma(J_B, E_B) = \Pi\lambda^2 \frac{2J_B + 1}{(2s + 1)(2J_A + 1)} \times \sum_{S=|J_A - s|}^{J_A + s} \sum_{l=|J_B - S|}^{J_B + S} T_l(\varepsilon_i)$$

dans laquelle: $\lambda = (\hbar^2/2\mu\varepsilon_i)^{1/2}$ est la longueur d'onde de la particule incidente d'énergie ε_i et de spin s; S, le module du vecteur spin du canal d'entrée $\boldsymbol{S} = \boldsymbol{J}_A + \boldsymbol{s}$; J_A, le spin du noyau cible; et $T_l(\varepsilon_i)$, le coefficient de transmission de l'onde partielle d'ordre l associée à la particule incidente.

Les noyaux composés ainsi formés possèdent une énergie d'excitation uniforme, mais une variété de moments angulaires. Les barycentres des configurations (E^*, J) étant loin de la ligne "Yrast", la désexcitation va s'opérer par émission préférentielle de particules suivie de l'émission de rayonnements électromagnétiques; le dernier photon peuplant soit l'état métastable, soit l'état fondamental. Suivant Hafner *et al.* (7), le rapport isomérique est alors donné par la relation suivante dans laquelle $P[J_{f(N_i-1)}]$ est la distribution normalisée des moments angulaires des noyaux résiduels avant l'émission du dernier photon:

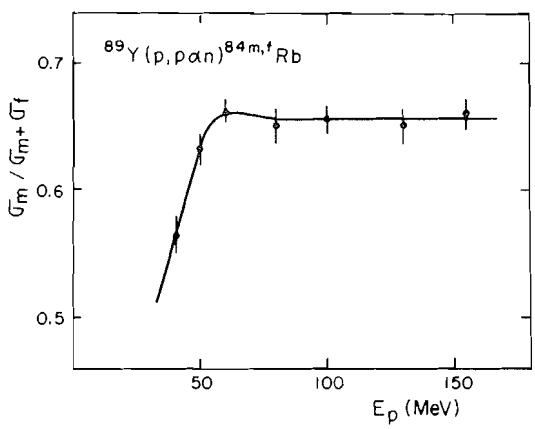

FIG. 2. Variation du rapport isomérique en fonction de l'énergie des protons incidents.

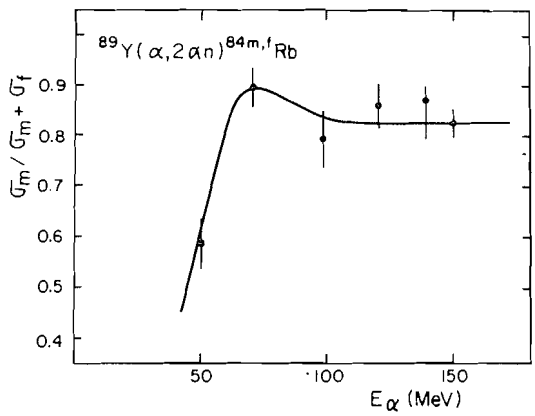

FIG. 3. Variation du rapport isomérique en fonction de l'énergie des particules α incidentes.

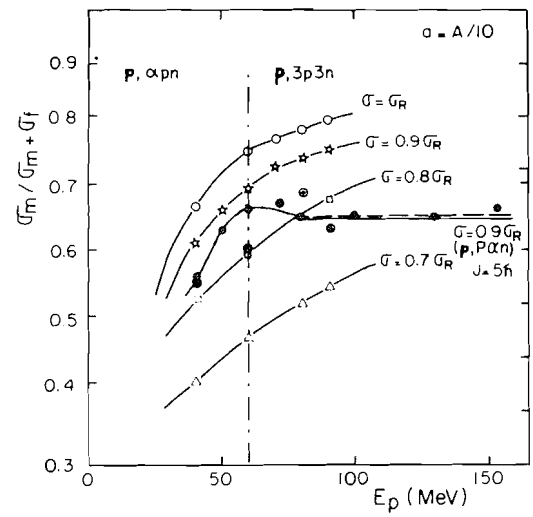

FIG. 4. Variation du rapport isomérique pour la réaction ^{89}Y(p, pαn)^{84m,f}Rb en fonction de l'énergie des protons incidents. Les points (○, △, □, ★) représentent les valeurs calculées sur la base d'un mécanisme de formation du noyau composé et modèle du gaz de Fermi, les points (⊙) sur la base de IPM; les points (●), les valeurs expérimentales. La droite en pointillé est la droite théorique représentative de la réaction de diffusion quasi-élastique (p, pαn).

$$[4]\qquad \frac{\sigma_m}{\sigma_m + \sigma_f} = \begin{cases} \displaystyle\sum_{J_f + \frac{J_m - J_f + 1}{2}}^{J_{max}} P[J_{f(N_\lambda - 1)}] & \text{pour } J_m - J_f \text{ impair} \\ \frac{1}{2}P\left[J_f + \frac{J_m - J_f}{2}\right] + \displaystyle\sum_{J_f + \frac{J_m - J_f}{2} + 1}^{J_{max}} P[J_{f(N_\lambda - 1)}] & \text{pour } J_m - J_f \text{ pair} \end{cases}$$

J_m et J_f étant respectivement les spins des états métastable et fondamental.

C'est à l'aide de ce formalisme que les calculs ont été tentés pour exploiter les résultats expérimentaux obtenus. Il fait appel à de nombreux paramètres pour lesquels nous avons adopté les valeurs suivantes.

Paramètre de densité de niveaux

Conformément aux valeurs nécessaires pour interpréter les densités de niveaux dans les noyaux magiques ou voisins de la magicité des valeurs de a comprises entre $A/8$ et $A/12\,\text{MeV}^{-1}$ ont été adoptées dans le calcul.

Energie des particules évaporées

En accord avec Bishop (8), nous avons supposé d'une part que le neutron était émis avec une énergie cinétique moyenne égale à deux fois la température nucléaire et d'autre part que l'énergie des particules chargées satisfaisait à la relation:

$$[5]\qquad \bar{\varepsilon}_i = 2T + B_{i_{eff}}$$

dans laquelle B_{eff} est la barrière coulombienne efficace. Nous avons adopté pour celle-ci les valeurs proposées par Williams et Thomas (9) représentées par une fonction croissante de l'énergie d'excitation.

Ce mode d'évaluation de l'énergie de la particule évaporée a été utilisé chaque fois que le bilan énergétique $E^* = \sum_i(\varepsilon_i + B_i + S_i)$ est respecté (S_i étant l'énergie de séparation de la particule i). Mais pour des énergies d'excitation telles que ce bilan ne peut être satisfait, seule la partie du spectre en énergie conduisant à la réaction envisagée a été retenue. Ce calcul suppose l'équilibre statistique obtenu et ne tient donc pas compte des phénomènes précomposés pendant lesquels l'émission de particules de grande énergie peut intervenir. Ils représentent au maximum 10% de la section efficace totale (10).

Coefficients de transmission

Les coefficients de transmission ont été calculés à partir du modèle optique en utilisant une version du programme ABACUS-2 (11). Pour les neutrons et les protons, nous avons adopté pour la partie réelle du potentiel nucléaire une répartition de la matière nucléaire en forme de puits arrondi de Saxon–Wood et pour la partie imaginaire une forme gaussienne. Pour les particules α nous les avons supposés toutes deux de forme identique représentées par un puits de Saxon–Wood.

Nombre et multipolarité des photons émis

Nous faisons l'hypothèse selon laquelle l'émission de photons intervient toujours lorsque l'évaporation de particules devient énergétiquement impossible. Ceci est justifié par le fait que dans les chaînes de désexcitation des noyaux considérés, le barycentre des configurations (E^*, J) se déplace toujours bien au-dessus de la courbe Yrast, diminuant ainsi la probabilité relative d'émission γ.

Dans ces conditions, le nombre de photons émis est fonction de l'énergie d'excitation du noyau résiduel issu de la dernière étape d'évaporation de particule. Il peut être déterminé en calculant l'énergie moyenne emportée par chaque photon selon l'expression (12):

$$[6]\qquad \bar{E}_\gamma = 4\left[\frac{E}{a} - \frac{5}{a^2}\right]^{1/2}$$

ou plus directement, en utilisant l'expression proposée par Strutinski *et al.* (13):

$$[7]\qquad \bar{N}_\gamma = (aE^*)^{1/2}/(l_p + 1)$$

dans laquelle l_p est la multipolarité du photon et $\bar{N}_\gamma$ le nombre moyen de photons émis.

Dans les réactions considérées, les moments angulaires mis en jeu étant relativement faibles, nous avons considéré que les photons émis sont tous dipolaires ($l_p = 1$).

Can. J. Chem. Downloaded from www.nrcresearchpress.com by 210.87.254.42 on 09/05/12
For personal use only.

Can. J. Chem. Downloaded from www.nrcresearchpress.com by 210.87.254.42 on 09/05/12
For personal use only.

Paramètre de "spin cut off" σ

C'est le paramètre le plus important et le plus sensible dans l'évaluation du rapport isomérique. Dans le cadre le plus simple du gaz de Fermi, il est exprimé par la relation suivante:

$$[8] \qquad \sigma^2 = ct$$

t étant la température thermodynamique satisfaisant à l'équation d'état: $E^* = at^2 - t$; c étant défini à travers $c\hbar^2$ qui a les dimensions d'un moment d'inertie (14) I, donc:

$$[9] \qquad \sigma^2 = \frac{It}{\hbar^2}$$

Pour des nucléons se déplaçant librement dans un puits de potentiel carré et de profondeur infinie, le modèle prévoit que I est égal au moment d'inertie d'une sphère rigide:

$$[10] \qquad I_{rig} = \tfrac{2}{5} mAR^2$$

m étant la masse du nucléon, A le nombre de masse et R le rayon du noyau calculé à partir de la relation $R = r_o A^{1/3}$, avec $r_o = 1.25$ fermi. Cependant, des travaux antérieurs (15, 16) et nos résultats expérimentaux montrent que des écarts importants peuvent apparaître avec la théorie. Pour minimiser ces écarts, il convient alors de considérer des valeurs réduites de σ, donc une fraction réduite du moment d'inertie:

$$[11] \qquad I_{eff} = kI_{rig}$$

Cette réduction du moment d'inertie est généralement attribuée aux forces d'appariement. C'est ainsi que Lang et Le Couteur (17) ont élaboré pour les noyaux déformés et par extension pour les noyaux sphériques, un modèle (IPM) dans lequel les nucléons sont organisés en paires de même nature. L'énergie d'excitation est alors mesurée à partir d'un niveau de référence situé sous le fondamental, même pour les noyaux Pair–Pair. Elle est donnée par les relations suivantes:

$$[12] \quad \begin{aligned} E^* &= U + \tfrac{1}{12}g(2\delta)^2 \rightarrow \text{Pair–Pair} \\ E^* &= U + \tfrac{1}{12}g(2\delta)^2 + \delta \rightarrow \text{Impair–Pair} \\ E^* &= U + \tfrac{1}{12}g(2\delta)^2 + 2\delta \rightarrow \text{Impair–Impair} \end{aligned}$$

avec $g = 6a/\pi^2$ et $2\delta = 3.36 - 0.0084A$ (MeV) pour $A > 40$ (18). Dans ce modèle σ s'exprime par la relation:

$$[13] \qquad \sigma^2 = ct \exp\left[-\frac{0.437 \times 2\delta}{t}\right]$$

avec toujours $E^* = at^2 - t$.

C'est à l'aide de ces deux modèles que le calcul a été mené pour la réaction induite par les protons.

Réactions induites par les protons: $^{89}Y(p, p\alpha n)^{84m,f}Rb$

Mécanismes d'interaction

Aux faibles énergies, à partir du seuil de la réaction jusqu'à environ 60 MeV (fig. 4), l'augmentation du rapport isomérique avec l'énergie des protons incidents est la conséquence de la formation du noyau composé avec en particulier l'évaporation d'une particule α. La courbe passe ensuite par un maximum et tend vers un palier. Nous attribuons le maximum à un phénomène de compétition entre les mécanismes de formation du noyau composé et d'interaction directe mettant en jeu plusiers nucléons de cascade dont la particule α émise. Ce dernier processus devient prépondérant à partir de 70 MeV. Dès lors, l'indépendance du rapport $\sigma_m/(\sigma_m + \sigma_f)$ en fonction de l'énergie laisse supposer un mécanisme de diffusion quasi-élastique sur une sous-structure α considérée comme libre dans le potentiel nucléaire. L'éjection de la particule α est suivie de l'évaporation d'un neutron. Ce mécanisme aboutit à une répartition des moments angulaires résiduels J_B indépendante de l'énergie de la particule incidente:

$$[14] \qquad |J_A - J| \leq J_B \leq J_A + J$$

si J_A est le spin du noyau cible et J le moment angulaire de la particule α éjectée.

Valeur du rapport isomérique

Dans la région d'énergie où prédomine la formation du noyau composé, un système de paramètres $a = A/10$ MeV^{-1} et $\delta = 0.9\sigma_{rig}$ (fig. 4) conduit à des valeurs compatibles avec les résultats expérimentaux. Cette dernière valeur à laquelle correspond $I_{eff} = 0.8I_{rig}$ est comparable à celle rapportée par Kanda (19) et par Esterlund et Pate (20) pour des noyaux de nombre de masse voisin.

Ce même jeu de paramètres appliqué à la réaction de diffusion quasi-élastique (p, Pαn) fait apparaître une valeur $J = 5\hbar$ pour le moment angulaire orbital de la particule α éjectée lors de cette interaction de "knock out". De plus, afin de tester les prévisions du modèle

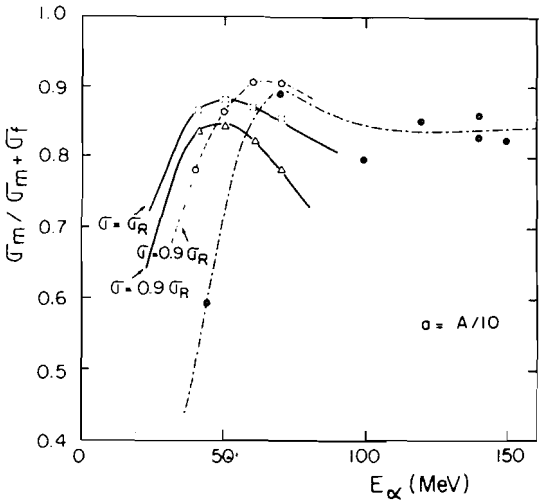

FIG. 5. Variation du rapport isomérique pour la réaction $^{89}Y(\alpha, 2\alpha n)^{84m,f}Rb$ en fonction de l'énergie des α incidents. Les courbes en trait plein représentent les valeurs calculées sur la base d'un mécanisme de formation du noyau composé sans tenir compte de l'énergie de rotation; la courbe en pointillé (○) est issue du même calcul avec introduction de E_{rot}. Les points (●) sont les résultats expérimentaux.

"Independent Pairing" (IPM) une série de calculs a été entreprise avec les valeurs de σ définies dans ce modèle [eqs 12 et 13] pour les noyaux possédant une énergie d'excitation élevée alors qu'en fin de chaîne de désexcitation, au voisinage de l'énergie de liaison du neutron, les valeurs moyennes proposées par Gilbert et Cameron (21) ont été adoptées. Les points calculés ont été reportés sur la fig. 4.

Réactions induites par α: $^{89}Y(\alpha, 2\alpha n)^{84m,f}Rb$

L'analyse comparative de la variation du rapport isomérique en fonction de l'énergie des protons et des particules α incidents conduit à deux remarques: d'une part, l'allure générale de la courbe (fig. 5) permet de supposer que les mécanismes prépondérants sont identiques à ceux envisagés pour la réaction $^{89}Y(p, p\alpha n)^{84m,f}Rb$ et d'autre part, conformément à la quantité de moment angulaire transféré, le rapport isomérique est en moyenne plus élevé pour la réaction induite par le projectile le plus lourd.

Afin d'apprécier quantitativement cet effet, nous avons reporté sur la fig. 6 la répartition des moments angulaires des noyaux composés formés par des captures respectives de protons et de particules α de même énergie (40 MeV dans le laboratoire) par des noyaux de ^{89}Y.

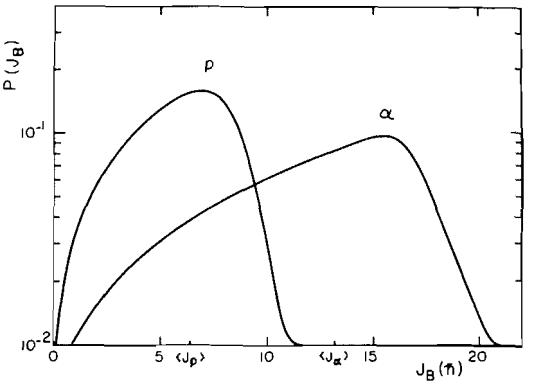

FIG. 6. Distribution normalisée des moments angulaires des noyaux composés ^{89}Y + (40 MeV)p et ^{89}Y + (40 MeV)α.

Il apparaît une différence d'environ $7\hbar$ entre les moments angulaires moyens alors mis en jeu. Cet écart dans le modèle simple du corps rigide, correspond à une différence d'énergie de rotation de plusieurs MeV. Cette différence augmente lorsque le moment d'inertie efficace, I_{eff} n'est plus qu'une fraction du moment d'inertie rigide conformément à la relation:

$$[15] \qquad E_{rot} = \frac{\hbar^2(J + \frac{1}{2})^2}{2I_{eff}}$$

Calcul du rapport isomérique

Deux séries de calcul ont été tentées pour expliciter les résultats expérimentaux obtenus. Dans un premier temps, les calculs ont été menés sans tenir compte des effets dûs à la rotation du noyau. Ils ont été effectués dans le domaine des basses énergies sur la base d'un mécanisme de formation du noyau composé suivi de l'évaporation de deux α et d'un neutron; ce processus pouvant être favorisé par des moments angulaires importants.

Pour $a = A/10$ MeV^{-1} et $\sigma = \sigma_{rig}$, un désaccord d'environ 20 MeV apparaît entre les maxima des courbes calculées et expérimentales (fig. 5). Cet écart important nous a conduit à prendre en considération les effets dûs à la rotation du noyau en recalculant d'une part l'énergie d'excitation efficace (22):

$$[16] \qquad E_{eff}^* = E^* - E_{rot}$$

et d'autre part, l'énergie cinétique moyenne effective des particules évaporées (9):

$$[17] \qquad \varepsilon_{i_{eff}} = B_{eff} + 2T_{eff} + \frac{2}{3}\frac{\mu R^2}{I} E_{rot}$$

Can. J. Chem. Downloaded from www.nrcresearchpress.com by 210.87.254.42 on 09/05/12
For personal use only.

T_{eff} étant défini par la relation:

$$[18] \qquad \frac{1}{T_{\text{eff}}} = \frac{\delta \log \omega(E_{\text{eff}}^*, J)}{\delta E}$$

avec $\omega(E_{\text{eff}}^*, J) = (2J + 1)\rho(E_{\text{eff}}^*, J)$ et μ étant la masse réduite du système.

Dans ces conditions un jeu de paramètres $\sigma = 0.9\sigma_{\text{rig}}$ et $A = A/10$ MeV^{-1} conduit à un accord plus satisfaisant entre les valeurs théoriques et expérimentales.

Conclusion

Au vu de cet accord, nous pouvons conclure que l'effet du moment angulaire dans le cas des réactions induites par des particules α n'est plus négligeable, même aux basses énergies, alors qu'il l'est pour les réactions induites par les protons. De plus, l'ensemble des résultats est assez parfaitement reproduit en utilisant les prévisions du modèle du gaz de Fermi simple compte tenu des approximations utilisées.

Remerciements

Je remercie Monsieur le Professeur G. Bouissières pour l'intérêt qu'il a porté à ce travail ainsi que l'équipe du séparateur d'isotopes.

1. J. R. Huizenga et R. Vandenbosch. Phys. Rev. **120**, 1305 (1960); R. Vandenbosch et J. R. Huizenga. Phys. Rev. **120**, 1313 (1960).
2. C. Bloch. Phys. Rev. **93**, 1094 (1954).
3. L. D. Nguyen. C.R. Acad. Sci. **261**, 5465 (1965).
4. L. Cohen. Phys. Rev. **111**, 587 (1958).
5. Nuclear Data Sheets. Academic Press, New York.
6. J. Blatt et V. F. Weisskopf. Theoretical nuclear physics. John Wiley and Sons, New York, 1962.
7. W. L. Hafner, J. R. Huizenga et R. Vandenbosch. ANL-6662. 1962.
8. C. T. Bishop. Isomeric cross-section ratios for some (n, γ) and (α, xn) reactions. ANL-6405. 1961.
9. D. C. Williams et T. D. Thomas. Nucl. Phys. A, **92**, 1 (1967).
10. C. K. Cline et M. Blann. Nucl. Phys. A, **172**, 225 (1971).
11. E. H. Auerbach. ABACUS-2 (revised form). BNL 6562. 1962.
12. R. Vandenbosch, L. Haskin et J. C. Norman. Phys. Rev. **137**, 1134 (1965).
13. V. N. Strutinski, L. V. Groshev et M. K. Akimova. Nucl. Phys. **16**, 657 (1960).
14. D. W. Lang. Nucl. Phys. **77**, 545 (1966).
15. J. H. Carver, G. E. Gooth et T. R. Sherwood. Nucl. Phys. **37**, 449 (1967).
16. D. R. Sachdev et L. Yaffe. Can. J. Chem. **45**, 2711 (1967).
17. D. W. Lang et K. J. Le Couteur. Nucl. Phys. **14**, 21 (1959).
18. A. Stolovy et J. A. Harvey. Phys. Rev. **108**, 353 (1957).
19. Y. Kanda. Nucl. Phys. A, **185**, 177 (1972).
20. R. A. Esterlund et B. D. Pate. Nucl. Phys. **69**, 401 (1965).
21. A. Gilbert et A. G. W. Cameron. Can. J. Phys. **43**, 1446 (1965).
22. T. Ericson et V. N. Strutinski. Nucl. Phys. **8**, 284 (1958).

Can. J. Chem. Downloaded from www.nrcresearchpress.com by 210.87.254.42 on 09/05/12
For personal use only.

Isotope effect on the thermodynamic quantities of gaseous uranium hexafluoride

JAN BRON
University of Natal, Department of Chemistry, Durban, South Africa

Received June 6, 1975

JAN BRON. Can. J. Chem. **54**, 160 (1976).

For gaseous UF_6 changes in the thermodynamic quantities $\Delta G (= \Delta A), \Delta H (= \Delta U), \Delta C_p (= \Delta C_v)$, and ΔS upon isotopic substitution can be determined by using the spectroscopically determined geometry and force field. The differences ΔG etc. are defined as $(G_{238} - G_x)$, where 238 and x (x = 235, 234, 233, and 232) are the masses of the central uranium atom. The changes in the thermodynamic quantities are related to the logarithm of the partition function ratio of the UF_6 species compared. The logarithm of the partition function ratio can be conveniently expressed as a series in temperature and hence, by using statistical mechanical relationships, the changes in thermodynamic quantities can be expressed as a series in temperature.

Since these changes form examples of heavy isotope effects the validity and utility of the first quantum correction can be investigated. Uncertainties and trends in the magnitudes of the differences in the thermodynamic quantities due to uncertainties or changes in spectroscopic parameters are discussed by means of the first quantum correction. It has been found that the first quantum correction has little quantitative value in the lower temperature region, but it can be used in that range to explain some observed trends in the isotope effects. Some of the conclusions can also be applied to kinetic and equilibrium heavy isotope effects.

JAN BRON. Can. J. Chem. **54**, 160 (1976).

Pour le UF_6 à l'état gaseux, on peut déterminer, en faisant appel aux géométries et aux forces de champs évaluées spectroscopiquement, les changements dans les quantités thermodynamiques $\Delta G (= \Delta A)$, $\Delta H (= \Delta U)$, $\Delta C_p (= \Delta C_v)$ et ΔS qui se produisent par substitutions isotopiques. On définit les différences ΔG etc. comme $(G_{238} - G_x)$ où 238 et x (x = 235, 234, 233 et 232) sont les masses de l'atome d'uranium central. On relie les changements dans les quantités thermodynamiques avec le logarithme du rapport des fonctions de partition des espèces UF_6 comparées. On peut exprimer facilement le logarithme du rapport des fonctions de partition comme une série en température et ainsi, utilisant les relations de la mécanique statistique, ces changements dans les quantités thermodynamiques peuvent être exprimées comme une série en température.

Comme ces changements correspondent à des effets isotopiques lourds, on peut étudier la validité et l'utilité de la première correction quantique. On discute, en faisant appel à la première correction quantique, des incertitudes et des tendances dans les grandeurs des différences dans les quantités thermodynamiques dues à des incertitudes et des changements dans la paramètres spectroscopiques. On a trouvé que la première correction quantique a peu de valeur quantitative dans la région des basses températures mais qu'elle peut être utilisée dans cette zone pour expliquer quelques tendances observées dans les effets isotopiques. Quelques-unes des conclusions peuvent aussi s'appliquer aux effets isotopiques lourds cinétiques et d'équilibre.

[Traduit par le journal]

Introduction

Many processes involving molecules only differing in isotopic substitution are determined by the partition function ratio of the species concerned. Examples, may be isotope exchange equilibria (1) and vapor pressure isotope effects (2). Because of the practical importance of UF_6 it is worthwhile to determine the partition function ratios for various UF_6 molecules containing different isotopes of uranium. Differences in thermodynamic quantities of isotopically different molecules, which, depending upon the process, determine the ease of isotope separation, can all be expressed in terms of the logarithm of the partition function ratio (3).

If the logarithm of the partition function ratio of two molecules differing in isotopic substitution is defined as

$$[1] \qquad \Gamma = \ln (q_2/q_1)$$

where q is the molecular partition function (4) and the subscript 2 refers to the heavier isotope, then the equations for the differences in thermodynamic quantities are

$$[2] \qquad \Delta G = G_2 - G_1 = -RT\Gamma = \Delta A$$

Can. J. Chem. Downloaded from www.nrcresearchpress.com by 210.87.254.5 on 09/05/12
For personal use only.

Can. J. Chem. Downloaded from www.nrcresearchpress.com by 210.87.254.5 on 09/05/12
For personal use only.

$$[3] \quad \Delta H = H_2 - H_1 = RT^2\frac{\partial \Gamma}{\partial T} = \Delta U$$

$$[4] \quad \Delta S = S_2 - S_1 = R\left[T\frac{\partial \Gamma}{\partial T} + \Gamma\right]$$

and

$$[5] \quad \Delta C_p = (C_p)_2 - (C_p)_1 = R\left[T^2\frac{\partial^2 \Gamma}{\partial T^2} + 2T\frac{\partial \Gamma}{\partial T}\right] = \Delta C_v$$

In order to evaluate Γ at various temperatures for UF_6, the geometry and force field of this species must be known (5). Recently a reliable force field for UF_6 has become available (ref. 6 and references quoted therein). Since many other force fields for UF_6 have been published previously the effects of uncertainties or variations in the force field and geometry of UF_6 on Γ and the thermodynamic quantities will be investigated.

General Considerations

The expression for Γ within the framework of the harmonic approximation (1, 7) is

$$[6] \quad \Gamma = \sum_{i=1}^{3N-6} \ln\left[\frac{(\frac{1}{2}u_i)_1^{-1}\sinh(\frac{1}{2}u_i)_1}{(\frac{1}{2}u_i)_2^{-1}\sinh(\frac{1}{2}u_i)_2}\right] + \tfrac{3}{2}\sum_{j=1}^{N}\ln\left(\frac{m_{2j}}{m_{1j}}\right)$$

In this expression $u_1 = (hc/kT)\omega_i$. The Planck constant is h, the Boltzmann constant is k, the velocity of light is c, the harmonic frequency of vibration of normal mode i is ω_i, and m_{ij} is the atomic mass of the jth atom of species i.

Although [6] is readily evaluated if the vibrational frequencies are known, its expansion in terms of u_i in connection with kinetic isotope effects (8) has been discussed in great detail. If u_i is small compared to unity the first term in u_i in the expansion is

$$[7] \quad \Gamma - \beta \simeq \ln(1 + \tfrac{1}{24}\sum_i[(u_i)_1^2 - (u_i)_2^2]) \simeq \tfrac{1}{24}\sum_i[(u_i)_1^2 - (u_i)_2^2] = \alpha$$

The sum $\frac{3}{2}\sum \ln(m_{2j}/m_{1j})$ has been replaced by the symbol β. The quantity α is called the first quantum correction since classically $(\Gamma - \beta)$ is equal to zero. It may be anticipated that the first quantum correction α will have little quantitative value since the condition that u_i is small compared to unity will be seldom met in the temperature range of chemical interest. However, as will be discussed below, α may be used to explain or predict trends and changes in Γ caused by uncertainties or changes in spectroscopically determined parameters.

By means of the matrix equation (5)

$$[8] \quad \mathbf{GFL} = \mathbf{L\Lambda} \quad (\lambda_i = 4\pi^2c^2\omega_i^2)$$

where **G** and **F** are matrices defined by Wilson and $\mathbf{\Lambda}$ is the eigenvalue matrix, the theorem that the trace of a matrix is invariant under a transformation (9)

$$[9] \quad \sum_i \lambda_i = \sum_i\sum_j G_{ij}F_{ij}$$

and the assumption that the force field of a molecule does not change upon isotopic substitution [7] can be written as

$$[10] \quad \Gamma - \beta \simeq \alpha = \kappa T^{-2}\sum_i\sum_j F_{ij}(G_{ij}^{(1)} - G_{ij}^{(2)})$$

The constant κ is equal to $(h/2\pi k)^2(24)^{-1}$. This last equation is more useful to explain changes in $(\Gamma - \beta)$ caused by changes or uncertainties in geometry and force field than [6], although it is only a poor approximation of $(\Gamma - \beta)$. Since for UF_6 deviations of certain quantities from their classical values are examples of heavy isotope effects for which [10] may be more applicable, an opportunity is presented to investigate the value of the first quantum correction.

Calculations and Results

The frequencies of vibration have been calculated by means of Wilson's **FG** matrix method (5). The harmonic force field and geometry for UF_6 have been taken from a paper by McDowell *et al.* (6). The symmetry coordinates used are the ones listed by Pistorius (10). Only two triply degenerate frequencies (F_{1u}) ω_3 and ω_4, are isotope dependent. The values of these isotope dependent frequencies for the $^xUF_6$ (x = 238, 235, 234, 233, 232) molecules have been listed in Table 1. The other computed isotope independent frequencies are (6)

$$[11] \quad \begin{aligned} \omega_1(A_{1g}) &= 671.70\ \text{cm}^{-1} \\ \omega_2(E_g) &= 539.68\ \text{cm}^{-1} \\ \omega_5(F_{2g}) &= 200.06\ \text{cm}^{-1} \\ \omega_6(F_{2u}) &= 142.72\ \text{cm}^{-1} \end{aligned}$$

Can. J. Chem. Downloaded from www.nrcresearchpress.com by 210.87.254.5 on 09/05/12
For personal use only.

TABLE 1. Isotope dependent, triply degenerate harmonic frequencies of vibration of $^{x}UF_6$ molecules in units of cm^{-1}

x	ω_3	ω_4
238	633.850	186.161
235	634.453	186.369
234	634.657	186.439
233	634.863	186.510
232	635.071	186.581

By means of [6] and the frequencies in Table 1, Γ can be evaluated at different temperatures. To avoid long listings of Γ at various equally spaced temperatures, a curve of the equation (3)

$$[12] \quad \Gamma = c_1 \ln \tau + c_2\tau^{-1} + c_3 + c_4\tau + c_5\tau^2$$

where $\tau = T/500$, has been fitted to the values of Γ between 200 and 1000 K by the method of the least squares. The quantity Γ for UF_6 is defined as

$$[13] \quad \Gamma = \ln [q(^{238}UF_6)/q(^{x}UF_6)]$$

It may be observed that β in this case is equal to $\frac{3}{2} \ln (238/x)$. The coefficients in the expansion, c_i, are listed in Table 2 for $x = 232$, 233, 234, and 235. Equation 12 reproduces Γ as calculated by [6] with a mean deviation of less than 0.001% in the temperature range of 200 to 1000 K.

ΔG, ΔH, ΔS, and ΔC_p for $^{238}UF_6$ *vs.* $^{235}UF_6$, computed by means of [1]–[6], are listed in Table 3. Another way of calculating the thermodynamic quantities is by expressing them in terms of the coefficients c_i (3). The use of [12] and [2]–[5] leads to the results (R is the gas constant)

$$[14] \quad \Delta G = -RT(c_1 \ln \tau + c_2\tau^{-1} + c_3 + c_4\tau + c_5\tau^2)$$

$$[15] \quad \Delta H = RT(c_1 - c_2\tau^{-1} + c_4\tau + 2c_5\tau^2)$$

$$[16] \quad \Delta S = R(c_1 + c_1 \ln \tau + c_3 + 2c_4\tau + 3c_5\tau^2)$$

$$[17] \quad \Delta C_p = R(c_1 + 2c_4\tau + 6c_5\tau^2)$$

Hence the differences ΔG, ΔH, ΔS, and ΔC_p, to the accuracy implied in Table 3, can also be computed by using [14]–[17] and the coefficients in Table 2.

Discussion

As $^{238}UF_6$ and $^{235}UF_6$ are the most important uranium hexafluorides only the differences between these two fluorides will be discussed unless stated otherwise. As an approximation of $(\Gamma - \beta)$ the first quantum correction, α, is inadequate for all cases especially at low temperatures. The equality $\alpha = (\Gamma - \beta)$ should be expected to be a better approximation at very high temperatures. In the temperature range considered (200–1000 K) the value of $\alpha(^{238}UF_6; ^{235}UF_6)$ is always larger than $(\Gamma - \beta)$. For example, at 200 K α is 25% greater than $(\Gamma - \beta)$ and only 1% greater at 1000 K. Similar differences are obtained for the other isotopes. Hence, the quantitative value of α seems to be limited.

The magnitude of Γ is always small. It varies from 0.023 (200 K) to 0.019 (1000 K). This smallness is expected on the basis of the relatively small change in mass, when ^{238}U is replaced by ^{235}U in UF_6. Since quite a few force fields for UF_6 have appeared (6), it is useful to analyze how Γ is affected by changes or uncertainties in the force constants. Equation 10 is more useful for the purpose of discussion of variations in Γ with respect to changes in force constants. A change in Γ with respect to F_{ij} can be written by means of the first quantum correction, [10], as

$$[18] \quad \delta\Gamma = \frac{\partial\Gamma}{\partial F_{ij}}\delta F_{ij} = \kappa T^{-2}(2 - \delta_{ij})(G_{ij}^{(1)} - G_{ij}^{(2)})\delta F_{ij}$$

In this equation the superscript (1) refers to lighter isotope as mentioned above and δ_{ij} is the Kronecker δ symbol. Hence, within the

TABLE 2. Coefficients of the expansion $\ln [q(^{238}UF_6)/q(^{x}UF_6)] = c_1 \ln \tau + c_2\tau^{-1} + c_3 + c_4\tau + c_5\tau^2$

x	$c_1 \times 10^3$	$c_2 \times 10^3$	$c_3 \times 10^2$	$c_4 \times 10^3$	$c_5 \times 10^4$
232	8.67312	8.51850	3.52758	−4.10015	3.67275
233	7.20011	7.06987	2.93396	−3.40477	3.05075
234	5.73954	5.63424	2.34315	−2.71486	2.43328
235	4.28767	4.20790	1.75368	−2.02868	1.81879

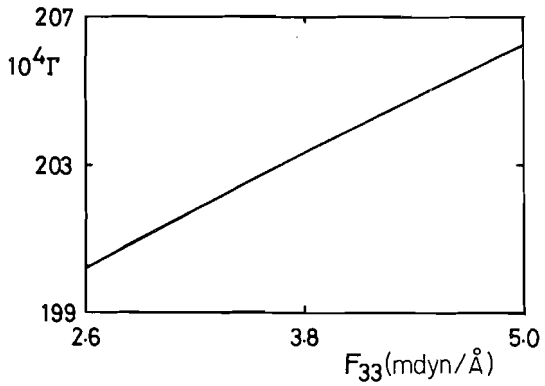

FIG. 1. The dependence of the logarithm of the partition function ratio, Γ of $^{238}UF_6$ and $^{235}UF_6$ on F_{33}. Γ has been calculated by means of [1] and [6] at 401 K. The literature value (ref. 6) for F_{33} is 3.84 mdyn/Å.

TABLE 3. Differences* in thermodynamic properties $^{238}UF_6$ and $^{235}UF_6$

T(K)	$-\Delta G$†	$-\Delta H$	ΔS	$\Delta C_p \times 10^3$
200	38.8	11.6	0.136	21.0
267	48.2	10.2	0.142	20.2
334	57.8	8.9	0.147	17.5
401	67.8	7.8	0.149	14.5
468	77.9	7.0	0.152	11.9
535	88.1	6.2	0.153	9.8
602	98.3	5.6	0.154	8.2
669	108.7	5.1	0.155	6.9
736	119.1	4.7	0.155	5.8
803	129.5	4.3	0.156	5.0
870	140.0	4.0	0.156	4.3
937	150.5	3.8	0.157	3.8
1004	161.0	3.5	0.157	3.3

*Differences are for example defined as $\Delta G = G(^{238}UF_6) - G(^{235}UF_6)$.

†Units are for ΔG (= ΔA) and ΔH (= ΔU), J mol^{-1}; ΔS and ΔC_p (= ΔC_v), J mol^{-1} K^{-1}.

framework of the first quantum correction a plot of F_{ij} *vs.* Γ should give (approximately) a straight line, the change in Γ should only depend on the magnitude of δF_{ij} and changes should be additive. Since the magnitude of stretching force constants are always larger than bending force constants, a 10% uncertainty in a stretching force constant should introduce a larger error than a 10% uncertainty in a bending force constant, if the difference $(G_{ij}^{(1)} - G_{ij}^{(2)})$ is about the same for the particular stretching and bending modes.

By using

$$[19] \qquad \mathbf{G} = \mathbf{B}\mathbf{M}^{-1}\mathbf{B}^{t}$$
$$\mathbf{S} = \mathbf{B}\mathbf{X}$$

and [18], it can be seen that a plot of diagonal force constant, F_{ii}, *vs.* Γ should give a positive slope, since in [18]

$$[20] \quad [G_{ii}^{(1)} - G_{ii}^{(2)}] = (\mu_k^{(1)} - \mu_k^{(2)}) \sum_{\alpha} (B_{ik}^{(\alpha)})^2 \geqslant 0$$

$\mu_k^{(i)}$ is the reciprocal mass of the kth atom and α is either x, y, or z. The **B** matrix defines the transformation from internal (**S**) to Cartesian coordinates (**X**). Figure 1 is a plot of Γ, calculated by means of the 'exact' eq. 6, *vs.* F_{33}. The relationship is *almost* linear, which is encouraging since [18] should be only approximately true. It can also be seen in Fig. 1 that a 10% change in F_{33} results only in a 0.5% change in Γ, which is in good agreement with a calculation based on [18]. For off-diagonal force constants the relationship between Γ and F_{ij} is more difficult to predict. However, off-diagonal force constants are usually much smaller than diagonal ones and less important in determining isotope effects.

The change or uncertainty in Γ caused by a change or uncertainty in a geometrical parameter, δR, can be written by means of [10] as

$$[21] \quad \delta\Gamma = \frac{\delta\Gamma}{\delta R}\delta R = \kappa T^{-2} \sum_{i \leqslant j} \sum F_{ij}(2 - \delta_{ij}) \frac{\delta(G_{ij}^{(1)} - G_{ij}^{(2)})}{\delta R} \delta R$$

Equation 21 is not easy to interpret, but it may be anticipated that $\delta\Gamma$ will vary slowly with R since $\delta\Gamma$ is proportional to the derivative of the *difference* of the two matrix elements $G_{ij}^{(1)}$ and $G_{ij}^{(2)}$. This prediction is consistent with the observation that isotope effects are not very sensitive towards geometry (11, 12). Figure 2 shows the dependence of Γ (eq. 6) upon the bond lengths of the *six* U—F bond distances. It can be seen that even for very large changes Γ does not change appreciably and therefore, say, a 1% uncertainty in the U—F bond distance will have almost no effect on Γ.

Equation 10 can be written by means of [19] as

$$[22] \quad \Gamma = \kappa T^{-2}(\mu_k^{(1)} - \mu_k^{(2)}) \times \sum_i \sum_j F_{ij} \sum_{\alpha} B_{ik}^{(\alpha)} B_{jk}^{(\alpha)} + \beta$$

It is assumed that only the kth atom differs in

Can. J. Chem. Downloaded from www.nrcresearchpress.com by 210.87.254.5 on 09/05/12
For personal use only.

Can. J. Chem. Downloaded from www.nrcresearchpress.com by 210.87.254.5 on 09/05/12
For personal use only.

isotopic substitution. Then for a given geometry, force field, and temperature, Γ is proportional to the difference of the reciprocal masses of the atoms differing in isotopic substitution.[1] Figure 3 is a plot of $\mu_k^{(x)} - \mu_k^{(238)}$, where (left to right in Fig. 3) x is equal to 238, 235, 234, 233, and 232 respectively, *vs.* Γ calculated by means of [6]. It may be observed that the relationship is linear on the scale used.

Table 3 lists the differences in thermodynamic quantities between $^{238}UF_6$ and $^{235}UF_6$. As expected these differences are small. The differences between the thermodynamic quantities for the molecules $^{238}UF_6$ and $^{x}UF_6$ can be calculated by means of the coefficients as listed in Table 2. But [17] for ΔC_p holds only for temperatures below 600 K. Since ΔG, ΔH, ΔS, and ΔC_p are related to Γ via [2]–[5] a similar mass relationship (eq. 22) exists for these quantities. For example, if M_x is defined as

$$[23] \quad M_x = \mu^{(x)} - \mu^{(238)} = (238 - x)(238x)^{-1}$$

then the value of M_x is 5.374×10^{-5} for $x = 235$ and 10.887×10^{-5} for $x = 232$. By using the exact value at 200 K for $\Delta G(238,235)$ from Table 3 a magnitude of -77.7 J/mol is obtained for $\Delta G(238,232)$ by the simple proportionality of ΔG to M_x. This compares well with the exact value of -77.3 J/mol for $\Delta G(238,232)$ and the error amounts to only 0.5%. For the calculation of $\Delta C_p(238,x)$ the mass relationship gives better values for ΔC_p than [17] over the whole temperature range of 800 K. More specifically the values computed for ΔG, ΔH, ΔS, and ΔC_p from the linear mass relationship agree to well within 1% with the exact values for these quantities.

If [10] is substituted in [2] and [3], then it can be shown that the change in ΔH, caused by a change in F_{ij}, is twice as large as the change in ΔG at the same temperature. Calculations show that this is only true at 1000 K. Similarly to Γ, relatively large uncertainties or changes in the geometry or force field of UF_6 result in much smaller changes or uncertainties in ΔG, ΔH, ΔS, and ΔC_p. It is estimated on these grounds that the error in the thermodynamic quantities, calculated by means of [2]–[6], should be less than 10%.

Equation 6 has been referred to as 'exact', while in fact many assumptions and simplifications are implicit in this equation. These have been discussed in detail (1) and in analogy with these findings and the fact that the effect discussed in this paper is a heavy isotope effect, the corrections for Γ and the thermodynamic quantities, due to these approximations, will be quite small. The smallness of the correction factors for Γ, say the corrections due to anharmonicity of vibration, is the result of cancellation. This is reasonable, since the isotope effect on the correction factors for the partition functions of the UF_6 species that define Γ

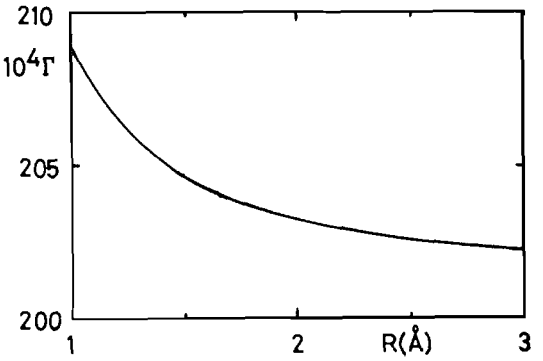

FIG. 2. The variation of $\Gamma(^{238}UF_6, ^{235}UF_6)$ as a function of the UF_6 bond distance. Γ has been calculated by means of [1] and [6] at 401 K. The equilibrium bond distance for UF_6 is 1.999 ± 0.003 Å (ref. 6).

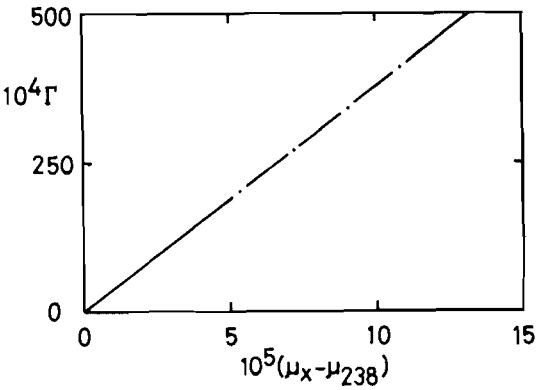

FIG. 3. A plot of $\Gamma(401\text{ K})$ *vs.* $(\mu_x - \mu_{238})$, where x is equal to 238 ($\Gamma = 0$), 235, 234, 233, and 232. Left to right in the figure, the dots represent the values of Γ, which increase with decreasing x.

[1]It may not be immediately obvious why the relationship between $\frac{3}{2}\ln(m_{2j}/m_{1j})$ and $(m_{1j}^{-1} - m_{2j}^{-1})$ should be linear. This may be seen as follows. In the case of $^{238}UF_6$ and $^{x}UF_6$, β is equal to $\frac{3}{2}\ln(238/x) = \frac{3}{2}\ln[1 + (238 - x)/x] \simeq \frac{3}{2}(238 - x)/x$. Hence a plot of $\frac{3}{2}\ln(238/x)$ *vs.* $(x^{-1} - 238^{-1})$ will be *approximately* a straight line with slope $\frac{3}{2} \times 238$.

should be small. The small isotope effect on the correction factors is caused by the relatively small difference in mass between the various uranium isotopes. More quantitative arguments are not possible since the required data have not been published yet.

From the above discussion it may be concluded that the first quantum correction has a limited quantitative value in the lower temperature region. It is, however, of use to explain or predict trends in isotope effects. Some of the methods used in this paper to explain trends in Γ and the differences in thermodynamic quantities can also be applied, after only minor modifications, to equilibrium and kinetic isotope effects.

1. M. WOLFSBERG, CHEN FEE CHANG, and J. BRON. Z. Naturforsch. **28**a, 129 (1973).
2. G. JANSCO and W. A. VAN HOOK. Chem. Rev. **74**, 689 (1974).
3. J. BRON and S. O. PAUL. J. Chem. Soc. Faraday Trans. 2, 1294 (1974).
4. T. L. HILL. An introduction to statistical thermodynamics. Addison-Wesley Publishing Company Inc., Reading, Massachusetts. 1960.
5. E. B. WILSON, J. C. DECIUS, and P. C. CROSS. Molecular vibrations. McGraw-Hill Book Company, Toronto, Ontario. 1955.
6. R. S. MCDOWELL, L. B. ASPREY, and R. T. PAINE. J. Chem. Phys. **61**, 3571 (1974).
7. J. BRON and M. WOLFSBERG. J. Chem. Phys. **57**, 2862 (1972).
8. J. BIGELEISEN and T. ISHIDA. J. Chem. Phys. **62**, 80 (1975).
9. J. IRVING and N. MULLINEUX. Mathematics in physics and engineering. Academic Press, New York. 1959.
10. C.W.F.T. PISTORIUS. J. Chem. Phys. **29**, 1328 (1958).
11. M. J. STERN and M. WOLFSBERG. J. Pharm. Sci. **54**, 849 (1965).
12. M. WOLFSBERG and M. J. STERN. Pure Appl. Chem. **8**, 325 (1964).

Can. J. Chem. Downloaded from www.nrcresearchpress.com by 210.87.254.5 on 09/05/12
For personal use only.

Mercury(I) chemistry. Part I. Complexes of the mercurous ion with some arenes

PHILIP A. W. DEAN, DAVID G. IBBOTT, AND J. B. STOTHERS

Department of Chemistry, University of Western Ontario, London, Ontario N6A 5B7

Received July 29, 1975

PHILIP A. W. DEAN, DAVID G. IBBOTT, and J. B. STOTHERS. Can. J. Chem. **54**, 166 (1976).

A wide range of arene complexes of the mercurous ion has been prepared from mercurous hexafluoroarsenate and the appropriate arene in liquid sulfur dioxide. Raman spectroscopy confirmed the integrity of the dimeric Hg_2^{2+} cation in these complexes. ^{13}C nuclear magnetic resonance spectroscopy showed that Hg_2^{2+}–arene complexes exist in sulfur dioxide solution. The ^{13}C data allowed the estimation of formation constants for the hexamethylbenzene, *p*-xylene, and *p*-dichlorobenzene complexes together with the ^{13}C chemical shifts for the bound substrates in these cases. The ^{13}C chemical shift changes (relative to the free substrate) on addition of Hg_2^{2+} to SO_2 solutions of various methylated benzenes are compared with those occurring on complexation of the same arenes by the argentous ion and the $Cr(CO)_3$ moiety. In mercurous ion–arene complexes, it is concluded that the cation is involved in a localized interaction with the arene and that there are preferred binding sites. These sites may be identified by the complexation shifts for the Ag^+– and Hg_2^{2+}–arene complexes.

PHILIP A. W. DEAN, DAVID G. IBBOTT et J. B. STOTHERS. Can. J. Chem. **54**, 166 (1976).

On a préparé une grande variété de complexes d'arènes avec des ions mercureux en faisant réagir de l'hexafluoroarsénate mercureux et des arènes appropriés dans l'anhydride sulfureux liquide. La spectroscopie Raman a confirmé l'intégrité du cation dimère Hg_2^{2+} dans ces complexes. La rmn du ^{13}C montre que des complexes Hg_2^{2+}–arène existent en solution dans l'anhydride sulfureux. Les données ^{13}C permettent d'estimer les constantes de formation des complexes avec l'hexaméthylbenzène, le *p*-xylène et le *p*-dichlorobenzène de même que les déplacements chimiques ^{13}C pour les substrats liés dans ces cas. Les changements dans les déplacements chimiques ^{13}C (par rapport au substrat libre) par addition de Hg_2^{2+} aux solutions dans le SO_2 pour les divers benzènes méthylés sont comparés avec ceux qui se produisent lors de la complexation des mêmes arènes avec des ions argenteux et des moitiés $Cr(CO)_3$. Dans les complexes ion mercureux – arène, on en conclut que le cation est impliqué dans une interaction localisée avec l'arène et qu'il y a des sites de liaisons préférées. On a identifié ces sites par les déplacements de complexation pour des complexes Ag^+– et Hg_2^{2+}–arène.

[Traduit par le journal]

Introduction

The paucity of organometallic compounds of mercury(I) contrasts markedly with the very extensive organometallic chemistry of mercury(II). Until recently only the subvalent organomercurials, $(RHg)_n$, of unknown structure (1) and a few arene complexes of the mercurous ion had been reported. The arene complex "$C_6H_6 \cdot AlCl_3 \cdot HgCl$" (now recognized as containing the dimeric mercurous ion, Hg_2^{2+}) was apparently first prepared by Gulewitsch (2) who used a reducing Friedel–Crafts synthesis, a method also shown to be suitable for preparing similar complexes of toluene and the xylenes. Turner and Amma (3) offered an alternative route to $(C_6H_6)_2Hg_2(AlCl_4)_2$, gave preliminary X-ray diffraction data for this compound, and considered three possible ideal bonding geometries for the Hg_2^{2+}–arene complex. Briefly, the bonding models considered are: (*i*) central bonding of the arene to one of the mercury atoms, a geometry most commonly found for transition metals (4) but also known for some ns^2 metal ions (ref. 5 and references therein); (*ii*) localized bonding, where one C—C linkage of the arene is bound to one mercury atom, an arrangement similar to that found for both cuprous (6) and argentous (7) complexes with arenes, and (*iii*) the unique bonding geometry found in the bis(benzene)dipalladium chloroaluminates (8) where both metal ions of the dimeric cation are equally associated with each arene molecule. While the preliminary X-ray data did not allow distinction between these possibilities, the authors rejected the type (*i*) geometry on the grounds that the lowest-lying, $6s\sigma_u$, acceptor orbital of the Hg_2^{2+} ion is incompatible in symmetry with the highest energy, e_1, filled orbital of benzene. Recently (9) we reported a synthetic route appropriate for a

Can. J. Chem. Downloaded from www.nrcresearchpress.com by 210.87.254.105 on 09/05/12
For personal use only.

Can. J. Chem. Downloaded from www.nrcresearchpress.com by 210.87.254.105 on 09/05/12
For personal use only.

wide range of mercurous ion–arene complexes and demonstrated the utility of ^{13}C nmr spectroscopy for solution studies of this type of complex; on the basis of our preliminary data, we favored the type (*iii*) bonding geometry for the mercurous complexes. Our completed study, which we now present, provides evidence that the Hg_2^{2+}–arene interaction is, in fact, of type (*ii*).

Results and Discussion

Preparation of the Complexes

The complexes were synthesized by mixing solutions of the hydrocarbon and mercurous hexafluoroarsenate (10) in liquid sulfur dioxide:

$$m\mathrm{Hg_2(AsF_6)_2} + n\mathrm{Arene} \xrightarrow{SO_2} m\mathrm{Hg_2(AsF_6)_2 \cdot} n\mathrm{Arene}$$

In many cases the complexes precipitated immediately on mixing and most of the materials isolated in this way had 1:1 arene:Hg_2^{2+} stoichiometries (arene = benzene, biphenyl, naphthalene, 2-methyl- and 2,6-dimethylnaphthalene, acenaphthene, fluoranthene, fluorene, phenanthrene, anthracene, 9,10-dimethylanthracene, and *m*-dinitrobenzene). In some cases (arene = benzene, biphenyl, fluorene, fluoranthene, and naphthalene and its derivatives) more soluble *n*:1 complexes seemed to form with excess arene but these are, as yet, uncharacterized. With the anthracenes decomposition occurs if the preparations are attempted using excess hydrocarbon. No 1:1 complex was found with 9,10-benzophenanthrene; instead 1:2 and 3:1 complexes form.

Several arene complexes were soluble in liquid SO_2; these were studied using ^{13}C nmr.

Raman Spectra

Most of the complexes isolated decomposed in the beam of both He–Ne and Ar^+ lasers, but the mercury–mercury stretching region of the Raman spectrum could be obtained for a few examples; the results are given in Table 1. These spectra all exhibited at least one intense Raman line attributable to the mercurous ion, showing that the dimeric metal cation is intact in the arene complexes. The infrared spectrum of the *m*-dinitrobenzene complex indicated that the nitro groups are involved in bonding to the Hg_2^{2+} ion. The asymmetric stretching mode of the NO_2 groups decreases on complexation, from 1542 to 1512 cm^{-1} with a 1525 cm^{-1} shoulder, whereas the symmetric stretching mode, at 1347 cm^{-1}, is unaffected by complexation. The infrared spectra of carboxylato complexes (ref. 11 and references therein) and of nitrobenzene solvates of divalent metal ions (12) suggest that behavior of the NO_2 groups in a monodentate *O*-bonded manner should cause an increase in $\nu_{as}(NO_2)$, if anything. The decrease observed in $\nu_{as}(NO_2)$ thus rules out the monodentate bonding mode, indicating the presence of either chelate or bidentate bridging nitro groups in the *m*-dinitrobenzene complex. The bonding of the NO_2 groups could be additional to, or instead of, bonding to the aromatic ring.

TABLE 1. Mercury–mercury stretching frequencies in the Raman spectra of some mercurous ion – arene complexes

Compound	ν(Hg—Hg) (cm^{-1})[a,b]
$Hg_2(AsF_6)_2 \cdot$ benzene	166
$Hg_2(AsF_6)_2 \cdot$ biphenyl	169, 157
$Hg_2(AsF_6)_2 \cdot$ naphthalene	134
$Hg_2(AsF_6)_2 \cdot$ phenanthrene	124
$Hg_2(AsF_6)_2 \cdot$ *m*-dinitrobenzene[c]	200, 184

[a] ± 2 cm^{-1}.
[b] In $Hg_2(AsF_6)_2$, ν(Hg—Hg) = 180 cm^{-1}.
[c] For discussion of this compound see text.

The value of ν(Hg—Hg) in the other complexes is arene-dependent, demonstrating that the mercurous ion is bound to the hydrocarbon. ν(Hg—Hg) appears to decrease as the electron-donating ability of the arene (as measured, for instance, by anodic half-wave potentials)[1] increases. This is the expected trend if there is significant electron transfer from the arene into the σ^* orbital of the mercurous ion.

^{13}C Nuclear Magnetic Resonance Spectra

If no precipitation occurs on mixing SO_2 solutions of $Hg_2(AsF_6)_2$ and an arene, ^{13}C n.m.r. can be used to demonstrate Hg_2^{2+}–arene complexation. Typically, shifts, relative to the free arene, are observed in arene solutions containing the mercurous ion. In no case could separate signals for free and complexed arene be observed at ambient probe temperature. The observed exchange-averaged ^{13}C shift, $\Delta\delta_c (= \delta_c^{obsd} - \delta_c^{arene})$ of any resonance in a given system is dependent on the arene:Hg_2^{2+} ratio, as well as on the reactant concentrations. The variation of $\Delta\delta_c$ with reactant ratio pro-

[1] For a review see ref. 13.

Can. J. Chem. Downloaded from www.nrcresearchpress.com by 210.87.254.105 on 09/05/12
For personal use only.

vides information about the stoichiometry and stability of the complexes formed, while the signs and relative magnitudes of $\Delta\delta_c$ for the different carbon nuclei in an arene give structural information.

Formation Constants and Stoichiometries of Some Typical Complexes

The variation of $\Delta\delta_c$ with arene:Hg_2^{2+} ratio was studied in detail for hexamethylbenzene (HMB), *p*-xylene (*p*-X), and *p*-dichlorobenzene (*p*-DCB). Figure 1*a* shows the results for the resonance of the quaternary carbon nuclei in the system HMB–$Hg_2(AsF_6)_2$. A shift to lower field occurs as HMB:Hg_2^{2+} decreases but $\Delta\delta_c$ does not change monotonically.[2] The shape of the curve is inexplicable in terms of a single complex having arene:Hg_2^{2+} of either 1:1 or 2:1. However, using the program LISA (14), the data in Fig. 1*a* were analyzed statistically in terms of two labile equilibria:

$$[1] \qquad Hg_2^{2+} + \text{arene} \overset{K_1}{\rightleftharpoons} Hg_2(\text{arene})^{2+}$$

$$[2] \qquad Hg_2(\text{arene})^{2+} + \text{arene} \overset{K_2}{\rightleftharpoons} Hg_2(\text{arene})_2^{2+}$$

Both the formation constants, K_1 and K_2, and the bound shifts[3] in the 1:1 and 2:1 complexes Δ_1 and Δ_2, were obtained and are given in Table 2. Shapiro and co-workers (ref. 15 and references therein) have discussed the accuracy of the parameters derived from statistical analyses using LISA: if, as in the HMB system, K_2 is $\gtrsim 500$, K_1/K_2 is well-determined and the bound shifts are accurate, but both K_1 and K_2 are ill-determined. Thus the values of the stability constants must be regarded as semiquantitative at best. This is especially true since we have been unable to take account of either (*a*) changes in activity as the concentration of $Hg_2(AsF_6)_2$ changed or (*b*) equilibria involving ion-pairing or specific solvation of the arene by SO_2.[4] Despite these cautions it is clear that HMB complexes of the mercurous ion have considerable stability in liquid SO_2.

[2]The methyl carbon resonance also moved downfield, but the maximum shift of only 1.8 ppm precluded meaningful statistical analysis.

[3]The bound shift in a complex is the incremental shift which would be found if the arene was present entirely as that complex.

[4]We note, however, that according to the work of Andrews and Keefer (16) the solvation must be virtually complete in liquid SO_2.

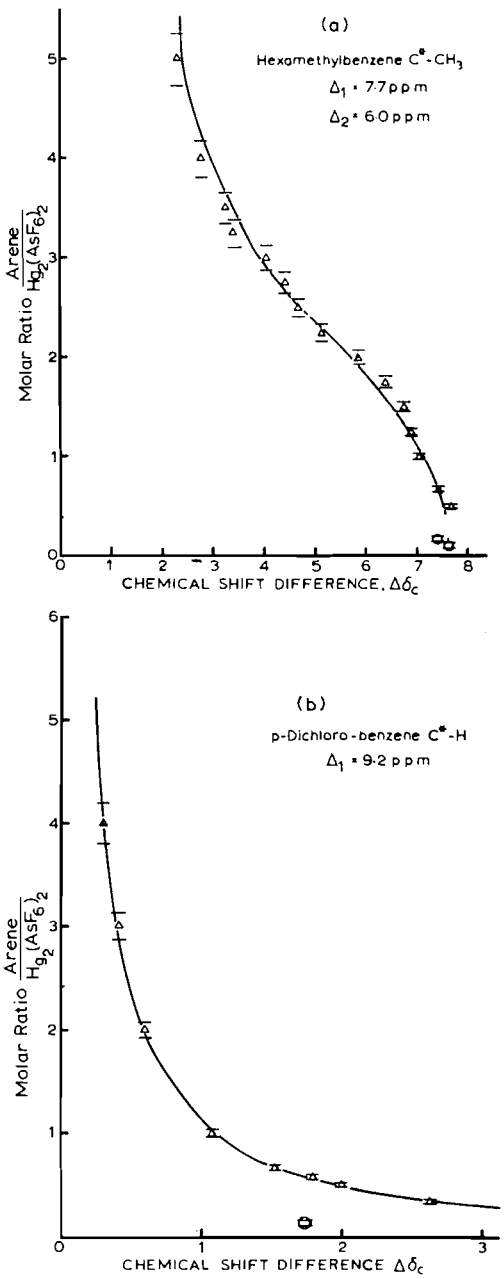

FIG. 1. Dependence of the downfield shift, $\Delta\delta_c$, of (*a*) the aryl carbon of HMB, and (*b*) the unsubstituted carbon of *p*-DCB, on the Arene:Hg_2^{2+} ratio in SO_2 solution at 32 °C. The best statistical fit in each case is represented by a solid line (see text). (Arene concentrations are: △, 0.75 *M*; ○, 0.15 *M*.)

For the system *p*-xylene–$Hg_2(AsF_6)_2$ the $\Delta\delta_c$ titration curves for both C—H and C—Me were similar in overall shape to the curve found for

TABLE 2. Bound shifts and formation constants for some arene complexes of mercury(I) in SO_2

Arene	^{13}C resonance	K_1 (M^{-1})	K_2 (M^{-1})	Δ_1 (ppm)	Δ_2 (ppm)
Hexamethylbenzene	C_{1-6}[a]	9.4×10^4	3.5×10^3	7.7	6.0
p-Xylene[b]	$C_{1,4}$[c]	2.9×10^3	1.5×10^2	12.6[b]	10.0[b]
	$C_{2,3,5,6}$[d]			2.4[b]	1.9[b]
p-Dichlorobenzene[e]	$C_{1,4}$[f]	0.22		20.7	
	$C_{2,3,5,6}$[f]			9.2	

[a]Standard deviation of fit to titration curve = 0.15 ppm.
[b]The formation constants given are the averages weighted by the standard deviations for the two curves. The bound shifts are calculated using the weighted average formation constants.
[c]Analysis of the curve for $C_{1,4}$ gives $K_1 = 6.7 \times 10^3\ M^{-1}$, $K_1/K_2 = 19$, $\Delta_1 = 12.6$ ppm, and $\Delta_2 = 9.9$ ppm. The standard deviation of the fit was 0.18 ppm.
[d]Analysis of the curve for $C_{2,3,5,6}$ gives $K_1 = 1.5 \times 10^3\ M^{-1}$, $K_1/K_2 = 19$, $\Delta_1 = 2.4$ ppm, and $\Delta_2 = 2.0$ ppm. The standard deviation of the fit was 0.07 ppm.
[e]Both curves can be fit to a one step process. Both analyses give $K_1 = 0.22\ M^{-1}$.
[f]The standard deviation of the fit was 0.03 and 0.08 ppm for $C_{1,4}$ and $C_{2,3,5,6}$, respectively.

the HMB system. Analysis in terms of the formation, but again the maximum shift (1.1 ppm) parameters listed in Table 2. The methyl resonance moved to lower field on complexation, but again the maximum shift (1.1 ppm) was too small to allow meaningful analysis.

Titration curves for both C—Cl and C—H in the *p*-DCB–$Hg_2(AsF_6)_2$ system were quite dissimilar from those for the aryl carbons of either HMB or *p*-X, since $\Delta\delta_c$ changed smoothly with the *p*-DCB:Hg_2^{2+} ratio as shown in Fig. 1*b* for the C—H resonance. The smooth curves are readily interpreted in terms of the formation of a 1:1 complex only (*i.e.* equilibrium (1) above); the results of the analysis are given in Table 2.

The relative sizes of the formation constants, *i.e.* HMB > *p*-X > *p*-DCB for K_1, are in the expected order, assuming that the extent of complexation depends on the π-electron donor ability of the arene. It is not completely certain that the Hg_2^{2+} is bound to the aromatic ring and not the chlorine in the *p*-DCB complexes. However, for chlorobenzene, at least, both argentation (17) and protonation (18) occur on the aromatic ring, and this seems the more likely site for Hg_2^{2+} binding to *p*-DCB also. The interaction of the mercurous ion with various other halogenated substrates is currently under investigation.

The Structure of the Mercurous Ion – Arene Complexes

Our thesis is that the variation of the ^{13}C shifts in an arene upon complexation should be dependent on the type of metal–arene interaction involved. Accordingly we have determined shifts occurring on complexation of a representative range of arenes by Hg_2^{2+}, and have compared these with the shifts produced for arenes bound to Cr(0), in (arene)$Cr(CO)_3$, and to Ag^+ (from $AgAsF_6$), in argentous complexes. The chromium complexes, chosen to typify type (*i*) bonding,[5] have been well-studied by ^{13}C nmr (19, 20); the arene in this type of complex is nonlabile and many bound shifts are known. For the labile silver complexes, chosen to typify type (*ii*) bonding, only the exchange-averaged shifts, (*i.e.* $\Delta\delta_c$) have been reported (21, 22); the present study confirms the rapid exchange of free and complexed ligands in Ag^+–arene complexes at ambient temperatures. The bis(benzene)dipalladium complexes are apparently known only in the solid state (8) so no nmr data are available; it seems reasonable to invoke bonding of type (*iii*) only if the data for the mercurous complexes cannot be reconciled with either of the two much better-known types, (*i*) and (*ii*).

Except for the HMB, *p*-X, and *p*-DCB complexes we have not determined the bound shifts for the mercurous complexes. Instead, we have used the more economically obtained values of $\Delta\delta_c$ to give the relative shifts occurring at different carbon nuclei of the same substrate upon complexation.[6] Values of $\Delta\delta_c$ for some

[5]There have apparently been no reports of the shifts induced by centrally-bound ns^2 metal cations.

[6]When both 1:1 and 2:1 complexes form in solution, the value(s) of $\Delta\delta_c$ will, of course, depend on the different bound shifts in these two complexes as well as on the values of the formation constants. However, our data for the *p*-X complexes (Table 2) show that the relative shifts for different carbons are the same in both complexes, *i.e.* Δ(C—H) < Δ(C—Me) and so the correct relative order will be given by $\Delta\delta_c$.

Can. J. Chem. Downloaded from www.nrcresearchpress.com by 210.87.254.105 on 09/05/12
For personal use only.

Can. J. Chem. Downloaded from www.nrcresearchpress.com by 210.87.254.105 on 09/05/12
For personal use only.

TABLE 3. ^{13}C chemical shifts, $\Delta\delta_c$, induced in substituted benzenes by $Hg_2(AsF_6)_2$ and $AgAsF_6$[a]

Substituent(s)	Metal cation	Arene:salt ratio[b]	$\Delta\delta_c$ (ppm)[c]						
			C_1	C_2	C_3	C_4	C_5	C_6	CH_3
Hexamethyl	Hg_2^{2+}	2[d,e]	[5.87]	[5.87]	[5.87]	[5.87]	[5.87]	[5.87]	1.19
	Ag^+	2	[−0.83]	[−0.83]	[−0.83]	[−0.83]	[−0.83]	[−0.83]	0.56
1,2,4,5-Tetramethyl	Hg_2^{2+}	2	[6.98]	[6.98]	−0.95	[6.98]	[6.98]	−0.95	0.56
(Durene)	Ag^+	2	[1.19]	[1.19]	−6.26	[1.19]	[1.19]	−6.26	0.28
1,3,5-Trimethyl	Hg_2^{2+}	2[d,f]	[13.73]	−2.14	[13.73]	−2.14	[13.73]	−2.14	0.95
(Mesitylene)	Ag^+	2	[1.90]	−3.89	[1.90]	−3.89	[1.90]	−3.89	0.36
1,2-Dimethyl	Hg_2^{2+}	5	[3.97]	[3.97]	1.19	−0.83	−0.83	1.19	0.36
(*o*-Xylene)	Ag^+	5	[2.22]	[2.22]	−1.39	−4.01	−4.01	−1.39	0.20
1,3-Dimethyl	Hg_2^{2+}	5	[4.92]	2.02	[4.92]	−0.95	0.79	−0.95	0.32
(*m*-Xylene)[g]	Ag^+	5	[1.75]	0.67	[1.75]	−2.46	−4.33	−2.46	0.08
1,4-Dimethyl	Hg_2^{2+}	2[d,h]	[9.44]	1.83	1.83	[9.44]	1.83	1.83	0.40
(*p*-Xylene)	Ag^+	2	[2.46]	−3.13	−3.13	[2.46]	−3.13	−3.13	0.08
1-Methyl	Hg_2^{2+}	5	[3.93]	1.43	1.15	−0.91	1.15	1.43	0.40
(Toluene)	Ag^+	5	[2.10]	−0.36	−1.98	−2.78	−1.98	−0.36	0.08
1-Trifluoromethyl	Hg_2^{2+}	5	Not observed	2.50	0.24	−0.16	0.24	2.50	
(Benzotrifluoride)	Ag^+	5	Not observed	0.32	−0.56	−0.99	−0.56	0.32	

[a]SO_2 solutions with [arene] = 0.75 *M*; $\Delta\delta_c = \delta_c^{obsd} - \delta_c^{arene}$; spectra measured at 32 °C except where noted.
[b]Choice of one of the two common ratios was made on the basis of solubility.
[c]Chemical shifts of the free arenes are given in the Experimental section. Square brackets denote substituted carbons. Estimated error due to spectral measurement ±0.06 ppm. Van Dongen and Beverwijk (21) have reported $\Delta\delta_c$ extrapolated to a 1:1 ratio for benzene, toluene, and the xylenes with $AgBF_4$ in $CDCl_3$.
[d]Incremented shifts were also measured with Arene:salt = 5.
[e]At 5:1, C_{1-6} = [2.30]; CH_3 = 0.40 ppm.
[f]At 5:1, $C_{1,3,5}$ = [5.40]; $C_{2,4,6}$ = −0.87; CH_3 = 0.40 ppm.
[g]*m*-Xylene spectra measured at 38 °C.
[h]At 5:1, $C_{1,4}$ = [3.81]; $C_{2,3,5,6}$ = 0.79; CH_3 = 0.16 ppm.

Can. J. Chem. Downloaded from www.nrcresearchpress.com by 210.87.254.105 on 09/05/12
For personal use only.

Hg_2^{2+}–arene systems are given in Table 3 together with data for the corresponding silver-containing systems.

A comparison of the data in Table 3 with those reported (19, 20) for (arene)$Cr(CO)_3$ shows little similarity. Complexation of an arene by the $Cr(CO)_3$ moiety produces upfield shifts of all carbon nuclei relative to the free substrate, whereas for the Hg_2^{2+} and Ag^+ complexes both upfield and downfield shifts are observed when series of substrates are considered. The results support the conclusion of Turner and Amma (3), that the mercurous ion is not centrally bound to the arene.

A comparison of the data for mercurous and argentous complexes is more fruitful. The apparently dissimilar shifts produced when HMB is coordinated to the mercurous ion (a downfield shift) and to the argentous ion (an upfield shift) have been noted earlier (9). However, a pattern clearly emerges from the results for a series of less symmetrically substituted benzenes complexed with the Hg_2^{2+} and Ag^+ cations. With arenes for which internal comparison is possible, methyl-substituted carbons display the most positive $\Delta\delta_c$ values (*i.e.* downfield complexation shifts) for both systems. Also, with one exception, ordering the carbons according to their $\Delta\delta_c$ values produces the same sequence for both Hg_2^{2+} and Ag^+ complexes, *e.g.* for toluene, $\Delta\delta_c^{C_1} > \Delta\delta_c^{C_2} > \Delta\delta_c^{C_3} > \Delta\delta_c^{C_4}$. The single exception occurs for the *m*-xylene complexes for which the positions of $\Delta\delta_c^{C_4}$ and $\Delta\delta_c^{C_5}$ are reversed; in all other respects the data for the *m*-xylene complexes fit in well. The similarity of the $\Delta\delta_c$ patterns in the mercurous and argentous complexes provides good evidence for a fundamental parallelism between Hg_2^{2+} and Ag^+ complexes of arenes. Accordingly it seems that localized, type (*ii*) bonding, represented diagrammatically in **1**, must occur in the mercurous complexes, as it does in argentous complexes.

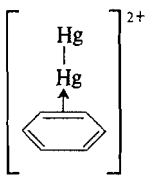

1

Features of the data in Table 3 which warrant further discussion include the dissimilarities in $\Delta\delta_c$ for the HMB complexes of Hg_2^{2+} and Ag^+, the related observation that the values of $\Delta\delta_c$ for the silver complexes are less positive than those for the analogous mercurous complexes, and the origins of the $\Delta\delta_c$ patterns observed for the various arenes studied. Any discussion of the data must recognize that the bound shifts, either measured directly or inferred from $\Delta\delta_c$ values, are themselves averages. Facile exchange of free and coordinated arenes ensures the ready equilibration of both chemically equivalent and isomeric complexes:

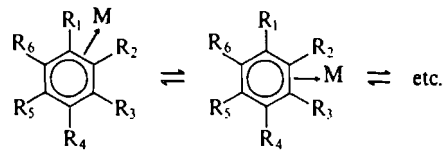

2a **2b**

The observed bound shifts will thus depend on the shifts in each of the entities in equilibrium and on the distribution of the various species.

Interestingly, our data show that at a constant arene: Hg_2^{2+} ratio the weighted average value of $\Delta\delta_c$, $\Delta\delta_c^{ave}(=\frac{1}{6}\sum_i \Delta\delta_{c,i}$, with the summation for all aromatic carbon nuclei) for the various methylated benzenes is of the same sign and order of magnitude. For instance, with arene: $Hg_2^{2+} = 2$, $\Delta\delta_c^{ave}$ is 5.9, 4.3, 5.8, and 4.3 ppm for HMB, durene, mesitylene, and *p*-X, respectively, and the total range of $\Delta\delta_c$ in these complexes is 15.8 ppm, while with arene: $Hg_2^{2+} = 5$, $\Delta\delta_c^{ave}$ is 2.3, 2.3, 1.4, 1.8, 1.8, and 1.3 ppm for HMB, mesitylene, *o*-, *m*-, and *p*-xylene, and toluene, respectively, and the total range is 6.3 ppm. In the latter sequence the *m*-xylene complex clearly behaves regularly. A corresponding situation holds for the silver complexes; the values of $\Delta\delta_c$ for all of the silver complexes are similar, though different from the values for the mercurous complexes, *e.g.* with arene: $Ag^+ = 2$, $\Delta\delta_c^{ave}$ is -0.8, -2.3, -1.0, and -1.2 ppm for HMB, durene, mesitylene, and *p*-X respectively,[7] and the range of $\Delta\delta_c$ is 8.8 ppm, and with arene: $Ag^+ = 5$, $\Delta\delta_c^{ave}$ is 1.0, 0.9, and 0.9 ppm for *o*- and *m*-xylene, and toluene respectively, the total range being

[7]In addition, Crist *et al.* (22) found $\Delta\delta_c^{ave} = -1.0$ ppm for benzene: $AgBF_4 = 1$ in CH_2Cl_2.

Can. J. Chem. Downloaded from www.nrcresearchpress.com by 210.87.254.105 on 09/05/12
For personal use only.

6.5 ppm. As in the mercurous complexes, the *m*-xylene complex is regular in its $\Delta\delta_c^{ave}$ value. The similarity of the $\Delta\delta_c^{ave}$ values for complexes of a given metal ion is particularly remarkable as the various $\Delta\delta_c$ values take no account of the (presumably) different formation constants of complexes with different hydrocarbons. However, for the mercurous complexes at least, $\Delta\delta_c^{ave}$ reflects the weighted average bound shifts fairly accurately, *e.g.* the weighted average bound shifts are 7.7 and 5.8 ppm for the 1:1 complexes of HMB and *p*-X, respectively (from Table 2).

Though in HMB (and benzene) complexes with type (*ii*) bonding the metal ion may be attached to any C—C linkage with equal probability, not all C—C bonds can be equally probable binding sites for complexes of a less symmetrically substituted benzene. Since $\Delta\delta_c^{ave}$ is similar for complexes of various methylated benzenes with a given metal ion, this must mean that complexation with that cation produces approximately the same weighted average shift for all equilibrating isomers. This strongly implies that roughly the same *range* of complexation shifts occurs in any isomer of any methylated benzene, *i.e.* the complexation shift for a carbon resonance depends primarily on the position of that particular carbon nucleus relative to the metal cation.[8] Clearly the dissimilarities in $\Delta\delta_c$ for HMB complexes of Hg_2^{2+} and Ag^+ are but one example of the different $\Delta\delta_c^{ave}$ values found for Hg_2^{2+} and Ag^+ in general, and according to the preceding arguments, the differences in $\Delta\delta_c^{ave}$ have as their root the difference in the ways an arene is perturbed when involved in a localized bond to one or the other of the two metal cations.

To assess the effect of a localized interaction on the ^{13}C resonances of an arene it seems plausible to regard the bound arene as a combination of a bound olefin and a perturbed diene. According to this model either greater deshielding of the 'dienic' carbons, or greater deshielding of the 'olefinic' carbons, or both, in the mercurous complexes than in the argentous complexes could result in the observed $\Delta\delta_c^{ave}$ differences. Silver(I) is thought to act mainly as a σ-acceptor in its complexes with olefins (ref. 24 and references therein), and a variety of physicochemical evidence suggests that Hg_2^{2+} is also primarily a σ-acceptor, Hg_2^{2+} being a stronger Lewis acid than Ag^+ if the two cations are compared as the hexafluoroarsenate salts (25). A consideration of the contributing structures

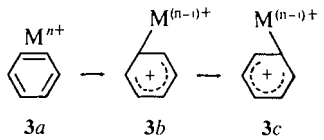

3a *3b* *3c*

leads to the conclusion that, on complexation, charge will be withdrawn from the π-system of the diene, more charge being withdrawn by the better Lewis acid, Hg_2^{2+}. As the accumulation of positive charge in a π-system of sp^2 carbons causes downfield shifts (26), the 'dienic' carbons in both the Hg_2^{2+} and the Ag^+ complexes should be deshielded, relative to the free substrate, but this effect should be larger for the mercurous complexes.

Generally, complexation of a symmetrically alkyl-substituted olefin by Ag(I) produces shielding of the olefinic carbons[9] (27). With asymmetrically alkyl-substituted olefins, silver complexation causes deshielding of the more highly substituted carbon and shielding of the less substituted carbon, but, on balance, there is a net shielding effect (27). $\Delta\delta_c^{ave}$ for the arene complexes of silver(I) is negative and, thus, according to the proposed model, the shielding of the 'olefinic' carbons in these complexes more than offsets the deshielding of the 'dienic' carbons. The effect of the Hg_2^{2+} on the shielding of the 'olefinic' carbons is more difficult to judge *a priori*. However, since some carbons in the series of methylated benzenes are shielded on complexation (see Table 3), whereas the model suggests that carbons remote from the site of complexation are deshielded, the 'olefinic' carbons in the mercurous–arene complexes must be shielded. The deshielding of the 'dienic'

[8]This is also true for protonated methylbenzenes. In the case of toluene, mesitylene, and HMB, proton exchange can be stopped at low temperatures and the ^{13}C nmr spectra of the static σ-complexes observed (ref. 23 and references therein). These three arenes and benzene share an approximately constant weighted average complexation shift: 17, 18.2, 19.3, and 20.3 ppm for benzene, toluene, mesitylene, and HMB, respectively (calculated from the data of ref. 23), the total range of complexation shifts being *ca.* 130 ppm for each case in which this could be determined.

[9]The sole reported exception appears to be C_2Me_4 for which the olefinic carbon resonance moves downfield on complexation (27).

Can. J. Chem. Downloaded from www.nrcresearchpress.com by 210.87.254.105 on 09/05/12
For personal use only.

carbons appears to more than compensate for the shielding of the bound carbons; the net effect, reflected by the positive value of $\Delta\delta_c^{ave}$ for the Hg_2^{2+} complexes, is deshielding. Thus the difference in the Lewis acidity of Hg_2^{2+} and Ag^+, with the resultant differing effect on the shieldings of the 'dienic' carbons, is at least partly responsible for the dissimilarities between $\Delta\delta_c^{ave}$ in the two series of complexes.

These arguments imply that when complexes of a given arene with either Hg_2^{2+} or Ag^+ equilibrate rapidly, as in **2**, those carbons most closely associated with the metal ion (on a time-average) will be shielded most. Furthermore, the $\Delta\delta_c$ *pattern* observed for a given arene must reflect the preference of the metal ion for the various possible chemically different binding sites. Since the patterns observed for complexes of Hg_2^{2+} and Ag^+ are so similar, it can be concluded that the two metal ions have similar preferences, a not unexpected result if the bonding is of the same type for each. It seems reasonable to expect that the binding site for the mercurous ion in the insoluble complexes obtained in this study will, in most cases, be the same as those for silver in the corresponding silver complexes, which have been more extensively studied (7).

It is of particular interest to try and determine the preferred binding sites where chemically distinct[10] C—C bonds occur. Our results for toluene and the xylenes suggest the following preferred binding sites (indicated by the thick lines):

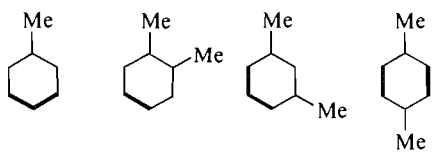

Significantly, these are just the sites predicted by the well-supported (7) theoretical study made by Fukui *et al.* (28) for argentous–arene complexes. ^{13}C nmr therefore seems to offer a viable alternative to X-ray crystallography for determining points of attachment in arene complexes of both Hg_2^{2+} and Ag^+.

[10]In HMB and mesitylene complexes all C—C bonds are equivalent, but the data for mesitylene suggest that given a choice the metal ions prefer the unsubstituted end of the C—C bonds.

Experimental

Reagents

Sulfur dioxide (Matheson) was stored in the gas phase over Linde 3A Molecular Sieves at least 12 h prior to use. All arenes were obtained commercially and purified by standard methods. Mercurous hexafluoroarsenate, $Hg_2(AsF_6)_2$, was prepared by reaction of elemental mercury with an excess of arsenic pentafluoride in liquid sulfur dioxide as described previously (10). Satisfactorily pure silver hexafluoroarsenate, $AgAsF_6$, was prepared in a directly analogous manner which was somewhat simpler than an alternative method of preparation (29) involving reaction of arsenous oxide with bromine trifluoride and silver metal. *Anal.* Calcd. for $AgAsF_6$: Ag 36.35; found (by standard Volhard titration): 36.19.

Preparation of Complexes Insoluble in SO_2

Reactions were carried out in baked-out (140 °C) glass vessels similar to that described previously for the reactions of tin(II) fluoride with Lewis acid fluorides (30). Solid reagents and products were handled in a nitrogen-filled glove box, the atmosphere of which was circulated through liquid nitrogen traps. Liquid reagents were added by volume via a syringe through rubber serum caps. Transfer of solvent was carried out on a glass–Teflon vacuum line using standard techniques. All of the products are exceedingly moisture-sensitive. A typical preparation is described below for the 1:1 biphenyl: $Hg_2(AsF_6)_2$ complex.

$Hg_2(AsF_6)_2$ (0.779 g, 1 mmol) was added to the side arm of the reaction vessel containing the magnetic stirrer, and biphenyl (0.231 g, 1.5 mmol) was added to the other arm. The apparatus was attached to the vacuum line via Swagelok fittings and a suitable amount of SO_2 (~15 ml) was condensed in before both side arms were sealed off. The reaction vessel was allowed to warm up to room temperature and the SO_2 solution of biphenyl was added to the SO_2 solution of the mercurous salt. The pale yellow precipitate was washed repeatedly with SO_2 and the product, $Hg_2(C_{12}H_{10})(AsF_6)_2$, isolated. *Anal.* Calcd. for $As_2C_{12}H_{10}F_{12}Hg_2$: C 15.45, H 107, Hg 42.92; found: C 15.34, H 1.22, Hg 42.62.

In general, preparation of other complexes was similar. However, for the preparation of the 1:1 anthracene: $Hg_2(AsF_6)_2$ complex, an excess of $Hg_2(AsF_6)_2$ was essential to avoid decomposition of the arene, probably by oxidation. (An SO_2 solution of $Hg_2(AsF_6)_2$.Anthracene showed, on standing, the characteristic esr spectrum of the anthracene cation, $C_{14}H_{10}^+$ (31).) In order to isolate the 3:1 9,10-benzophenanthrene: $Hg_2(AsF_6)_2$ complex in a pure form it was essential that the arene be in excess at all times during mixing of reactants and similarly it was essential that the mercurous ion be in excess at all times during preparation of the 1:2 9,10-benzophenanthrene: $Hg_2(AsF_6)_2$ complex. The complexes prepared and results of analyses are given in Table 4.

Raman Spectra

The Raman spectra of the solids were obtained at McMaster University on a Spex Industries Model 1400 Spectrometer with He–Ne (6328 Å) and/or Ar^+ (5145 Å) laser excitation. The solids were contained in glass capillary (melting point) tubes.

Preparation of ^{13}C Nuclear Magnetic Resonance Samples

The samples for chemical shift titrations (see text) and for some of the earlier single measurements of $\Delta\delta_c$ were

Can. J. Chem. Downloaded from www.nrcresearchpress.com by 210.87.254.105 on 09/05/12
For personal use only.

TABLE 4. Analyses of some prepared complexes

Complex	Formula	Color	Analysis (%) Theoretical C	Theoretical H	Theoretical Hg	Found C	Found H	Found Hg
$Hg_2(AsF_6)_2 \cdot$ benzene	$As_2C_6H_6F_{12}Hg_2$	White	8.41	0.70		7.84	0.80	
$Hg_2(AsF_6)_2 \cdot$ naphthalene	$As_2C_{10}H_8F_{12}Hg_2$	Yellow	13.24	0.88	44.23	13.08	1.01	44.40
$Hg_2(AsF_6)_2 \cdot$ 2-methylnaphthalene	$As_2C_{11}H_{10}F_{12}Hg_2$	Yellow	14.35	1.09		14.23	1.18	
$Hg_2(AsF_6)_2 \cdot$ 2,6-dimethylnaphthalene	$As_2C_{12}H_{12}F_{12}Hg_2$	Yellow	15.41	1.29		15.22	1.43	
$Hg_2(AsF_6)_2 \cdot$ acenaphthene	$As_2C_{12}H_{10}F_{12}Hg_2$	Yellow	15.44	1.08		14.72	1.27	
$Hg_2(AsF_6)_2 \cdot$ fluoranthene	$As_2C_{16}H_{10}F_{12}Hg_2$	Yellow	19.58	1.02	40.80	19.66	1.22	40.78
$Hg_2(AsF_6)_2 \cdot$ fluorene	$As_2C_{13}H_{12}F_{12}Hg_2$	Yellow	16.53	1.06	42.37	16.34	1.25	44.28
$Hg_2(AsF_6)_2 \cdot$ phenanthrene	$As_2C_{14}H_{10}F_{12}Hg_2$	Yellow	17.57	1.05		16.66	1.06	
$Hg_2(AsF_6)_2 \cdot$ anthracene	$As_2C_{14}H_{10}F_{12}Hg_2$	Red	17.57	1.05	41.84	17.81	1.28	41.64
$Hg_2(AsF_6)_2 \cdot$ 9,10-dimethylanthracene	$As_2C_{16}H_{14}F_{12}Hg_2$	Red	19.51	1.42	40.65	19.61	1.55	40.96
$Hg_2(AsF_6)_2 \cdot m$-dinitrobenzene	$As_2C_6H_4F_{12}N_2O_4Hg_2$	White	7.61	0.42	42.28	7.67	0.63	42.49
$Hg_2(AsF_6)_2 \cdot$ 3(9,10-benzophenanthrene)	$As_2C_{54}H_{36}F_{12}Hg_2$	Red	44.31	2.46		44.46	2.56	
$2(Hg_2(AsF_6)_2) \cdot$ 9,10-benzophenanthrene	$As_4C_{18}H_{12}F_{24}Hg_4$	Yellow	12.11	0.67	44.84	12.29	0.84	45.17

TABLE 5. ^{13}C chemical shifts of free arenes[a]

Arene	Chemical shifts (ppm)						
	C_1	C_2	C_3	C_4	C_5	C_6	CH_3
Hexamethylbenzene	[134.3]	[134.3]	[134.3]	[134.3]	[134.3]	[134.3]	16.5
Durene	[134.9]	[134.9]	132.6	[134.9]	[134.9]	132.6	18.7
Mesitylene	[138.9]	128.0	[138.9]	128.0	[138.9]	128.0	20.7
o-Xylene	[137.6]	[137.6]	130.7	126.8	126.8	130.7	19.3
m-Xylene	[138.9]	130.9	[138.9]	127.1	129.2	127.1	20.9
p-Xylene	[135.7]	129.9	129.9	[135.7]	129.9	129.9	20.5
Toluene	[138.9]	130.0	129.2	126.2	129.2	130.0	21.1
Benzotrifluoride	Not observed	125.5	129.3	132.5	129.3	125.5	
p-Dichlorobenzene	[132.7]	130.3	130.3	[132.7]	130.3	130.3	

[a]Square brackets denote substituted carbons. Assignments are those used in ref. 32.

prepared in custom-made (Wilmad Glass Co. Inc.) nmr tubes (10.00 mm o.d. and 7.99 mm i.d.), each fused, initially to a Rotaflo stopcock. The large amounts of solutes required for these samples reduced the percentage error arising from the difficulty of weighing in a very dry atmosphere (estimated at ± 5 mg).

Typical weights of reagents are illustrated for the hexamethylbenzene (HMB) system wherein 0.195 g of HMB was used together with 0.934 to 0.187 g of $Hg_2(AsF_6)_2$. Solid reagents were added in the dry box and then attached to the vacuum line via the attached Rotaflo stopcock. Sulfur dioxide was condensed into the tube at -196 °C. The tube was allowed to warm up to room temperature. The molarity of the arene was held constant by adjusting the solution level to a constant height in the tube before freezing the solution using liquid N_2 and separating the tube from the stopcock by sealing off.

In later single measurements of $\Delta\delta_c$ it was found more economical and convenient to use coaxial nmr tubes with the inner, sample-containing tube made of 4 mm o.d. tubing, the outer tube being a standard 5 mm nmr tube. Arene concentrations were held constant at 0.75 *M* by adjusting the solution height as before.

^{13}C Nuclear Magnetic Resonance Spectra

The proton-decoupled ^{13}C spectra were obtained using a Varian XL-100-15 system operating in the Fourier transform mode. All measurements were taken with a probe temperature of 32 °C except for the *m*-xylene system for which the temperature was 38 °C. The 10-mm sample tubes were placed coaxially in a 12-mm sample tube; the annulus contained a dioxane–D_2O solution (10/90% v/v). The D_2O signal was used as the lock while the dioxane signal was used as the external reference. With [arene] = 0.75 *M*, good spectra were obtained in approximately 1 h for samples in 10-mm o.d. tubes, while samples in 4-mm o.d. tubes typically required about 5 h. Peak positions are estimated to be accurate to ± 0.06 ppm. The major source of error in peak positions in the mixtures is considered to arise from weighing errors in sample preparation. Assignments were made either by a comparison of the intensities with those of the free substrate or by extrapolating incremental shifts back to Hg_2^{2+}:arene = 0. The chemical shifts of the free arenes were converted to the TMS scale using δ_c(TMS in SO_2, int) = δ_c(dioxane in D_2O, ext) + 67.8 and are given in Table 5.

Analysis of ^{13}C Nuclear Magnetic Resonance Data

The exchange-averaged shifts observed were fit to the appropriate form of the fast-exchange equation,

$$\Delta\delta_c = S_0^{-1} \sum_{i=1}^{N} n_i c_i \Delta_i$$

where S_0 is the total arene concentration, N is the number of different complexes in solution, n_i is the number of arene molecules in the particular complexes, c_i is the concentration of the particular complexes, and Δ_i is the bound shift of the particular complexes. Iterative fits were made to the appropriate form of the above equation using the program LISA (14), the best agreement (in the least-squares sense) between observed and calculated $\Delta\delta_c$ values giving values of equilibrium constants and bound shifts (Δ).

Analyses

Microanalyses were carried out by Alfred Bernhardt, Mikroanalytisches Laboratorium, Mülheim, West Germany or by Chemalytics, Inc., Tempe, Arizona.

Acknowledgments

We thank the donors of the Petroleum Research Fund, administered by the American Chemical Society, and the National Research Council of Canada for financial support of this research.

1. B. H. M. BILLINGE and B. G. GOWENLOCK. J. Chem. Soc. 1201 (1962) and references therein; J. Casanova and H. R. Rogers. J. Am. Chem. Soc. **96**, 1942 (1974).
2. W. GULEWITSCH. Ber. **37**, 1560 (1904).
3. R. W. TURNER and E. L. AMMA. J. Inorg. Nucl. Chem. **28**, 2411 (1966).
4. G. E. COATES, M. L. H. GREEN, and K. WADE. Organometallic compounds, 3rd ed. Vol. 2. Methuen, London, 1968. p. 165.
5. M. S. WEININGER, P. F. RODESILER, A. G. GASH, and E. L. AMMA. J. Am. Chem. Soc. **94**, 2135 (1972).
6. R. W. TURNER and E. L. AMMA. J. Am. Chem. Soc. **88**, 1877 (1966).

Can. J. Chem. Downloaded from www.nrcresearchpress.com by 210.87.254.105 on 09/05/12
For personal use only.

7. E. A. H. GRIFFITH and E. L. AMMA. J. Am. Chem. Soc. **96**, 5407 (1974).
8. G. ALLEGRA, G. T. CASAGRANDE, A. IMMURZA, L. PORRI, and G. VITULLI. J. Am. Chem. Soc. **91**, 5745 (1969).
9. P. A. W. DEAN, D. G. IBBOTT, and J. B. STOTHERS. J. Chem. Soc. Chem. Commun. 626 (1973).
10. B. D. CUTFORTH, C. G. DAVIES, P. A. W. DEAN, R. J. GILLESPIE, P. R. IRELAND, and P. K. UMMAT. Inorg. Chem. **12**, 1343 (1973).
11. K. NAKAMOTO. Infrared spectra of inorganic and coordination compounds. 2nd ed. Wiley-Interscience, New York. 1970. p. 222.
12. W. L. DRIESSEN, L. M. VAN GELDROP, and W. L. GROENEVELD. Recl. Trav. Chim. Pays-Bas, **89**, 1271 (1970).
13. N. L. WEINBERG and H. R. WEINBERG. Chem. Rev. **68**, 449 (1968).
14. B. L. SHAPIRO and M. D. JOHNSTON, JR. J. Am. Chem. Soc. **94**, 8185 (1972).
15. M. D. JOHNSTON, JR., B. L. SHAPIRO, M. J. SHAPIRO, T. W. PROULX, A. D. GODWIN, and H. L. PEARCE. J. Am. Chem. Soc. **97**, 542 (1975).
16. L. J. ANDREWS and R. M. KEEFER. J. Am. Chem. Soc. **73**, 4169 (1951).
17. L. J. ANDREWS and R. M. KEEFER. J. Am. Chem. Soc. **72**, 3113 (1950).
18. G. A. OLAH, Y. YAMADA, and R. J. SPEAR. J. Am. Chem. Soc. **97**, 680 (1975).
19. B. E. MANN. J. Chem. Soc. Dalton Trans. 2012 (1973).
20. G. M. BODNER and L. J. TODD. Inorg. Chem. **13**, 360 (1974).
21. J. P. C. M. VAN DONGEN and C. D. M. BEVERWIJK. J. Organomet. Chem. **51**, C36 (1973).
22. D. R. CRIST, Z-H. HSIEH, G. J. JORDAN, F. B. SCHINCO, and C. MACIOROWSKI. J. Am. Chem. Soc. **96**, 4932 (1974).
23. G. A. OLAH, H. C. LIN, and D. A. FORSYTH. J. Am. Chem. Soc. **96**, 6908 (1974).
24. R. G. SALOMON and J. K. KOCHI. J. Am. Chem. Soc. **95**, 1889 (1973).
25. P. A. W. DEAN and D. G. IBBOTT. Can. J. Chem. This issue.
26. H. SPIESECKE and W. G. SCHNEIDER. Tetrahedron Lett. 468 (1961).
27. C. D. M. BEVERWIJK and J. P. C. M. VAN DONGEN. Tetrahedron Lett. 4291 (1972).
28. K. FUKUI, A. IMAMURA, T. YONEZAWA, and C. NAGATA. Bull. Chem. Soc. Jpn. **34**, 1076 (1961).
29. D. W. A. SHARP and A. G. SHARPE. J. Chem. Soc. 1855 (1956).
30. T. BIRCHALL, P. A. W. DEAN, and R. J. GILLESPIE. J. Chem. Soc. A, 1777 (1971).
31. A. CARRINGTON, F. DRAVNIEKS, and M. C. R. SYMONS. J. Chem. Soc. 947 (1959).
32. J. B. STOTHERS. Carbon-13 nmr spectroscopy. Academic Press, New York. 1972. p. 95.

Can. J. Chem. Downloaded from www.nrcresearchpress.com by 210.87.254.105 on 09/05/12
For personal use only.

Mercury(I) chemistry. Part II. Reactions of the mercurous ion with some ligands having the heavier Group VA or VIA elements as donor atoms

PHILIP A. W. DEAN AND DAVID G. IBBOTT

Department of Chemistry, University of Western Ontario, London, Ontario N6A 5B7

Received July 29, 1975

PHILIP A. W. DEAN and DAVID G. IBBOTT. Can. J. Chem. **54**, 177 (1976).

The reactions of $Hg_2(AsF_6)_2$ with $P(CF_3)_3$, PF_3, PCl_3, $P(CF_3)Ph_2$, $PClPh_2$, PPh_3, $P(OMe)_3$, $AsPh_3$, $SbPh_3$, $SPPh_3$, $SP(p\text{-}C_6H_4F)_3$, and $SePPh_3$ in liquid sulfur dioxide have been studied. The last five ligands form insoluble 1:1 complexes, $Hg_2(AsF_6)_2 \cdot L$, if $L:Hg_2^{2+} \leqslant 1$, but disproportionation of the mercurous ion occurs if $L:Hg_2^{2+} > 1$; the 1:1 mercurous complexes have been characterized by analysis and vibrational spectroscopy. There is no evidence for complexation of $P(CF_3)_3$. PPh_3 and $P(OMe)_3$ cause disproportionation of the mercurous ion under all conditions; $Hg(PPh_3)_2^{2+}$ and $Hg(P(OMe)_3)_2^{2+}$ have been characterized by ^{13}C and ^1H nmr respectively. When $P(CF_3)Ph_2:Hg_2^{2+} \leqslant 1$ soluble $Hg_2(P(CF_3)Ph_2)^{2+}$ is formed; the ^{19}F and ^{13}C nmr spectra of this complex are reported, as are those of $Hg(P(CF_3)Ph_2)_2^{2+}$. In the system PF_3–$Hg_2(AsF_6)_2$–SO_2 no disproportionation occurs; ^{19}F nmr provides evidence that $Hg_2PF_3^{2+}$ and, probably, $Hg_2(PF_3)_2^{2+}$ are formed. $^1J(P-F)$ in mercurous and silver(I) complexes of PF_3 is of unusually large magnitude. The ^{13}C nmr spectra of $Hg(PPh_3)_2^{2+}$, $Hg_2(P(CF_3)PPh_2)^{2+}$, and $Hg(P(CF_3)Ph_2)_2^{2+}$, are consistent with the occurrence of little metal-to-phosphorus back-bonding in these phosphine complexes. The relationship between the net electron donating ability of a phosphine and the nature of its interaction with the mercurous ion is discussed.

PHILIP A. W. DEAN et DAVID G. IBBOTT. Can. J. Chem. **54**, 177 (1976).

On a étudié les réactions, dans l'anhydride sulfureux liquide, du $Hg_2(AsF_6)_2$ avec $P(CF_3)_3$, PF_3, PCl_3, $P(CF_3)Ph_2$, $PClPh_2$, PPh_3, $P(OMe)_3$, $AsPh_3$, $SbPh_3$, $SPPh_3$, $SP(p\text{-}C_6H_4F)_3$ et du $SePPh_3$. Les cinq derniers ligands forment des complexes 1:1 insolubles, $Hg_2(AsF_6)_2 \cdot L$, si $L:Hg_2^{2+} \leqslant 1$, mais une disproportionation de l'ion mercureux se produit si $L:Hg_2^{2+} > 1$; on a caractérisé les complexes mercureux 1:1 par analyse et spectroscopie vibrationnelle. Il n'y a aucune évidence indiquant qu'il y a une complexation avec du $P(CF_3)_3$. PPh_3 et $P(OMe)_3$ causent une disproportionation de l'ion mercureux dans toutes les conditions; on a caractérisé les ions $Hg(PPh_3)_2^{2+}$ et $Hg(P(OMe)_3)_2^{2+}$ respectivement par rmn du ^{13}C et du ^1H. Quand $P(CF_3)Ph_2:Hg_2^{2+} \leqslant 1$, il se forme du $Hg_2(P(CF_3)Ph_2)^{2+}$. On rapporté les spectres rmn du ^{19}F et du ^{13}C de ce complexe de même que ceux du $Hg(P(CF_3)Ph_2)_2^{2+}$. Dans le système PF_3–$Hg_2(AsF_6)_2$–SO, aucune disproportionation ne se produit. La rmn du ^{19}F fournit une preuve qu'il y a formation de $Hg_2PF_3^{2+}$ et probablement de $Hg_2(PF_3)_2^{2+}$. La constante $^1J(P-F)$ dans les complexes mercureux et de l'argent(I) avec PF_3 est très grande. Les spectres rmn du ^{13}C du $Hg(PPh_3)_2^{2+}$, $Hg_2(P(CF_3)PPh_2)^{2+}$ et $Hg(CF_3)$-$Ph_2)_2^{2+}$, sont en accord avec l'existence d'une faible quantité rétro de liaison métal à phosphore dans ces complexes de phosphine. On discute de la relation qui existe entre l'habilité nette à donner des électrons pour une phosphine et de la nature de son interaction avec l'ion mercureux.

[Traduit par le journal]

Introduction

The complex chemistry of the mercurous ion, Hg_2^{2+}, is restricted by the ease with which disproportionation occurs in the presence of ligands strongly complexed by the mercuric ion. Prior to the present work, mercurous complexes with group VA and VIA donors were limited to those with nitrogen and oxygen donors (1–5); previous attempts to prepare complexes with a variety of heavier donor atoms were unsuccessful (5). We have recently shown that arene complexes of the mercurous ion are preparable in liquid sulfur dioxide, a very weak donor solvent, though they disproportionate in the more common donor solvents (6). It was therefore of interest to determine whether, using liquid SO_2 as a solvent, we could obtain evidence for mercurous complexes with ligands containing the heavier group VA and VIA elements as donor atoms. Part of this work has been reported in a preliminary communication (7).

Results and Discussion

Reactions of $Hg_2(AsF_6)_2$ with Phosphines in Liquid Sulfur Dioxide

Triphenylphosphine

When SO_2 solutions of triphenylphosphine and mercurous hexafluoroarsenate (8) are mixed, finely divided (black) mercury is formed at the

Can. J. Chem. Downloaded from www.nrcresearchpress.com by 210.87.254.40 on 09/05/12
For personal use only.

Can. J. Chem. Downloaded from www.nrcresearchpress.com by 210.87.254.40 on 09/05/12
For personal use only.

point of mixing. Provided that $PPh_3 : Hg_2^{2+} \leqslant 1$, the mercury disappears on shaking leaving a clear yellow solution. However, when $PPh_3 : Hg_2^{2+} > 1$ the mercury remains permanently. When the reactant ratio is greater than unity, it is clear that disproportionation has occurred. The overall reaction can be represented by [1] ($n \geqslant 2$)

[1] $Hg_2^{2+} + n\text{Phosphine} \rightleftarrows Hg(\text{Phosphine})_n^{2+} + Hg\downarrow$

In the region $1 < PPh_3 : Hg_2^{2+} < 2$, $n = 2$ (see below), but higher coordination numbers may occur with a greater excess of ligand.

The absence of metallic mercury in the solutions where $PPh_3 : Hg_2^{2+} \leqslant 1$ cannot be used to show the absence of disproportionation, since mercury is known to react with $Hg_2(AsF_6)_2$ in SO_2 to give the yellow Hg_3^{2+} cation (8) and other polynuclear mercury cations (9, 10). Thus one or both of the following reactions could have occurred in the yellow phosphine solutions:

[2] $Hg_2^{2+} + \text{Phosphine} \rightleftarrows Hg_2(\text{Phosphine})^{2+}$

[3] $Hg_2^{2+} + \text{Phosphine} \rightleftarrows \frac{1}{2}Hg(\text{Phosphine})_2^{2+} + Hg_3^{2+}$

Reaction 4 would result in permanent disproportionation at

[4] $Hg_2^{2+} + \text{Phosphine} \rightleftarrows Hg(\text{Phosphine})^{2+} + Hg\downarrow$

$PPh_3 : Hg_2^{2+} > 0.5$ and thus does not occur. In an attempt to distinguish between [2] and [3] we have obtained the ^{13}C nmr spectrum of a solution with $PPh_3 : Hg_2^{2+} = 0.667$ as shown in Fig. 1*a*. In this spectrum the resonances due to C_1, $C_{2,6}$, and $C_{3,5}$ are 'triplets'. This type of 'triplet' fine structure is characteristic of a 'virtually-coupled' bis(phosphine) complex; the ^{13}C nmr spectrum is of the AA'X (A = A' = ^{31}P; X = ^{13}C) or $[A]_2X$ (11) type. We therefore assign the ^{13}C nmr spectrum to $Hg(PPh_3)_2^{2+}$ with, presumably, linear coordination about mercury. This assignment is confirmed by the identity of the spectrum with that of an authentic sample of $[Hg(PPh_3)_2](AsF_6)_2$ produced by the reaction

[5] $HgI_2 + 2AgAsF_6 + 2\text{Phosphine} \xrightarrow{SO_2} [Hg(\text{Phosphine})_2](AsF_6)_2 + 2AgI\downarrow$

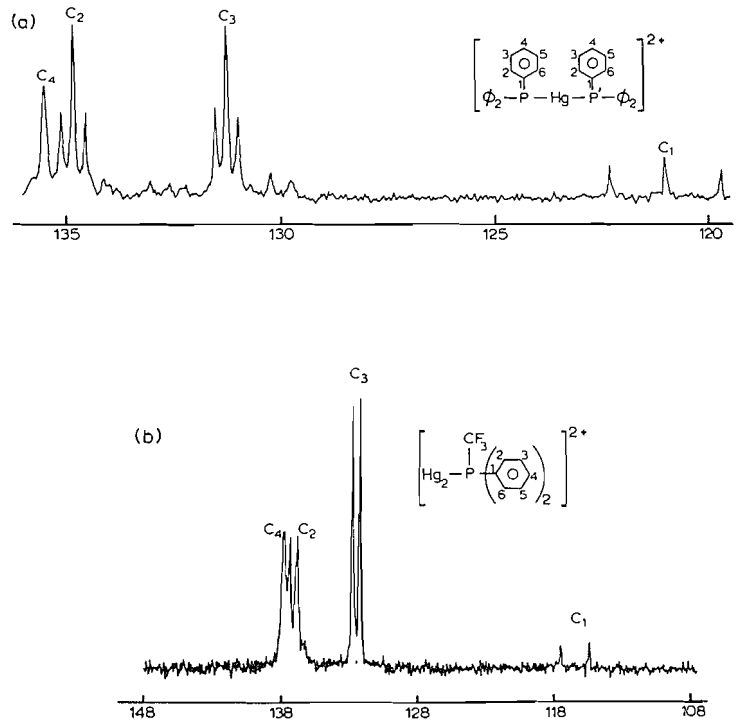

FIG. 1. The 32 °C 25.2 MHz ^{13}C nmr spectra of SO_2 solutions in which (*a*) $PPh_3/Hg_2(AsF_6)_2 = 0.667$, (*b*) $CF_3PPh_2/Hg_2(AsF_6)_2 = 0.83$.

TABLE 1. Aryl carbon chemical shifts for PPh_3, $P(CF_3)Ph_2$, and some of their compounds and complexes[a]

Compound (solvent)	Chemical shift (ppm)			
	C_1	C_2	C_3	C_4
PPh_3 (CS_2 + $(CD_3)_2CO$)[b]	137.8[c]	134.1[c]	128.9[c]	129.1[c]
PPh_3 (SO_2)	134.9[d]	134.1[d]	129.5[d]	130.2[d]
$[Hg(PPh_3)_2][AsF_6]_2$ (SO_2)	121.1[d]	134.9[d]	131.3[d]	135.5[d]
$(OC)_5MoPPh_3$[e,f]	136.4	133.7	129.3	130.7
$O{=}PPh_3$ ($CDCl_3$)[g]	135.6	132.3	128.8	132.3
$H_2C{=}PPh_3$ (C_6D_6 + Et_2O)[h]	132.3	133.1	128.6	131.3
$[MePPh_3]I$ ($CDCl_3$)[i]	118.8	133.7	130.5	135.2
$P(CF_3)Ph_2$ ($CDCl_3$)[j]	138.4	135.1	130.0	131.6
$P(CF_3)Ph_2$ (SO_2)[j]	137.9[d]	134.6[d]	129.6[d]	131.3[d]
$[Hg{-}Hg{-}P(CF_3)Ph_2][AsF_6]_2$ (SO_2)[j]	116.2[d]	137.4[d]	132.1[d]	137.5[d]
$[Hg(P(CF_3)Ph_2)_2][AsF_6]_2$ (SO_2)[j]	~113.0[d]	135.6[d]	131.8[d]	137.6[d]

[a]Relative to internal TMS; increasing frequency is taken as positive. This work unless otherwise specified.
[b]Reference 25.
[c]Data converted to internal TMS scale using δ_c(TMS,int) = δ_c(CS_2,int) + 192.8 (26).
[d]Spectra initially referenced to external 1:9 dioxane:D_2O and converted to internal TMS using δ_c(TMS in SO_2,int) = δ_c(dioxane in D_2O,ext) + 67.8.
[e]Reference 22.
[f]Solvent not specified.
[g]Reference 27.
[h]Reference 28.
[i]Reference 29.
[j]The ^{13}C resonance of CF_3 was not observed.

TABLE 2. Aromatic $^{13}C{-}^{31}P$ nuclear spin coupling constants in PPh_3, $P(CF_3)Ph_2$, and some of their complexes[a]

Compound (solvent)	Coupling constant			
	C_1	C_2	C_3	C_4
PPh_3 (CS_2 + $(CD_3)_2CO$)[b]	−12.51	19.65	6.80	0.33
PPh_3 (SO_2)	2.9	16.7	7.6	<1.5[c]
$[Hg(PPh_3)_2][AsF_6]_2$ (SO_2)	65.6[d]	13.7[d]	12.8[d]	<4.7[c,d]
$(OC)_5MoPPh_3$[e]	36	13	9	<2
$P(CF_3)Ph_2$ ($CDCl_3$)[f]	30.1	20.6	7.9	<1.5[c]
$P(CF_3)Ph_2$ (SO_2)[f]	30.6	20.8	7.7	<1.5[c]
$[Hg{-}Hg{-}P(CF_3)Ph_2][AsF_6]_2$ (SO_2)[f]	53.7	20.0	13.2	<5[c]
$[Hg(P(CF_3)Ph_2)_2][AsF_6]_2$ (SO_2)[f]	[g]	13[h,i]	13[h,i]	8[c,h]

[a]In Hz. This work unless otherwise specified. Estimated error in new data ±1.0 Hz.
[b]Reference 25.
[c]Not resolved.
[d]$|J(P{-}C) + J(P'{-}C)|$.
[e]Reference 27.
[f]The ^{13}C resonance of CF_3 was not observed.
[g]Could not be determined with certainty due to weakness of signal.
[h]Width at half-height.
[i]Incompletely resolved fine structure.

Evidently [3] has occurred in the solution with $PPh_3:Hg_2^{2+}$ = 0.667. The $Hg(PPh_3)_2^{2+}$ cation persists when a greater than equimolar amount of PPh_3 is present; the ^{13}C nmr spectrum of the supernatant liquor from a mixture where $PPh_3:Hg_2^{2+}$ = 1.33 is identical to Fig. 1*a*. The ^{13}C nmr parameters for the $Hg(PPh_3)_2^{2+}$ cation are given in Tables 1 and 2.

The ^{13}C nmr spectrum of a yellow solution of PPh_3 itself in SO_2 deserves further comment. Both the chemical shift of C_1, and $J(^{31}P{-}C_1)$, are dissimilar from the values in other solvents.

Can. J. Chem. Downloaded from www.nrcresearchpress.com by 210.87.254.40 on 09/05/12
For personal use only.

Can. J. Chem. Downloaded from www.nrcresearchpress.com by 210.87.254.40 on 09/05/12
For personal use only.

For instance, the resonance due to C_1 occurs at higher applied field in SO_2 than in CS_2 (Table 1), and $J(^{31}P-C_1)$ is much smaller in SO_2 than in CS_2 (Table 2). $\delta_c(C_1)$ of PPh_3 is known to decrease to a greater or lesser extent on coordination, as demonstrated by the data in Table 1 and discussed further below. In addition, the sign of $J(^{31}P-C_1)$ has been shown to change on coordination (12). Our data for PPh_3 in SO_2 suggest that the PPh_3 is coordinated to the SO_2, the sulfur presumably acting as an acceptor as it does in various SO_2 (amine) complexes (ref. 13 and references cited therein). In $O_2S \leftarrow PPh_3$ $J(^{31}P-C_1)$ must be close to the crossover in sign. The PPh_3-SO_2 complex is evidently not very strong; in a mixture of composition $4CS_2:4SO_2:PPh_3$, $\delta_c(C_1)$ and $J(^{31}P-C_1)$ do not have the values found in pure SO_2 but rather are 137.3 ppm and 9.5 Hz, respectively.

Diphenyltrifluoromethylphosphine

When CF_3PPh_2 is added to Hg_2^{2+} in excess of an equimolar ratio disproportionation occurs, metallic mercury being formed. Clearly [1] is occurring. However, when $CF_3PPh_2:Hg_2^{2+} \leqslant 1$ no permanent deposit of mercury occurs but rather a clear yellow solution is formed. The ^{13}C nmr spectrum of a solution with $CF_3PPh_2:Hg_2^{2+} = 0.83$ is shown in Fig. 1*b*; ^{13}C spectral parameters are given in Tables 1 and 2. The chemical shift of C_1 in Fig. 1*b* relative to the corresponding value in the free phosphine (Table 1) shows the presence of a coordinated phosphine in the mercury-containing solution. The signals due to C_1, $C_{2,6}$, and $C_{3,5}$, in Fig. 1*b* are doublets suggesting the occurrence of a species containing a single coordinated phosphine, though doublet splitting is also possible in a bis(phosphine) species if $J(P-P') = J(P'-C) = 0$ (14). The latter possibility can be ruled out in the present instance by comparison of the spectrum in Fig. 1*b* with the spectrum of an authentic sample of the $Hg(CF_3PPh_2)_2^{2+}$ cation. Such a sample can be produced via [5], and its ^{19}F nmr spectrum (Fig. 2*a*), being of the classic $X_3AA'X_3'$ (or $[AX_3]_2$ (11)) type (15) readily confirms the presence of the desired cation. The fluorine spectrum can be analyzed by well-established methods (15) to give the nmr parameters listed in Table 3. The phenyl region in the ^{13}C nmr spectrum of $Hg(CF_3PPh_2)_2^{2+}$ is unfortunately

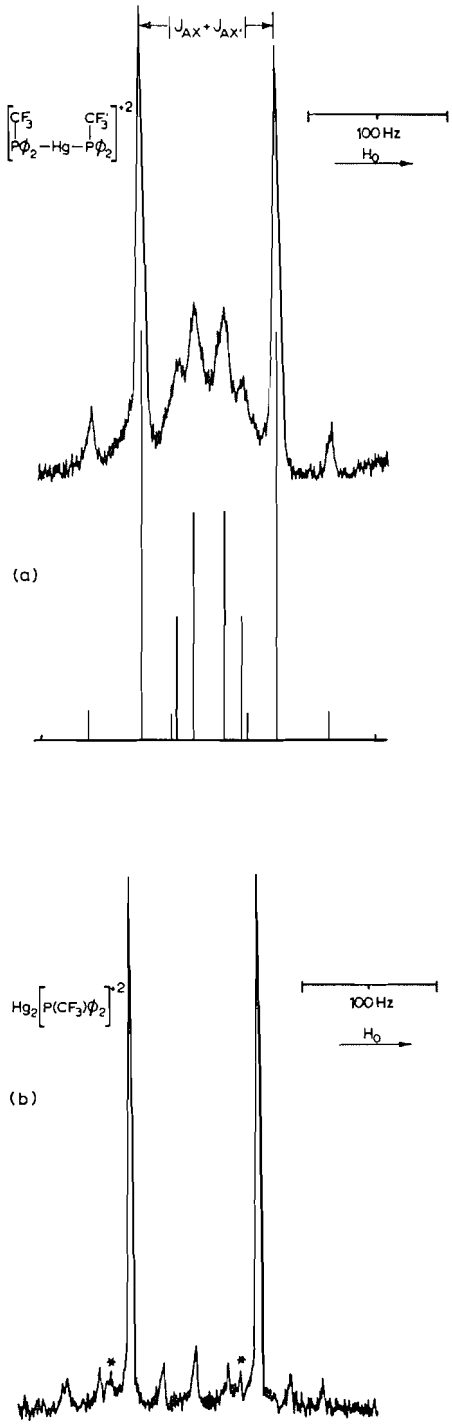

FIG. 2. The 32 °C 94.1 MHz ^{19}F nmr spectra of SO_2 solutions of (*a*) the $Hg(P(CF_3)Ph_2)_2^{2+}$ cation, with theoretical spectrum below, (*b*) the $Hg_2(P(CF_3)Ph_2)^{2+}$ cation. (* = impurity.)

Can. J. Chem. Downloaded from www.nrcresearchpress.com by 210.87.254.40 on 09/05/12
For personal use only.

TABLE 3. ^{19}F nmr parameters for CF_3PPh_2, $Hg_2(CF_3PPh_2)^{2+}$ and $Hg(CF_3PPh_2)_2^{2+}$ in liquid SO_2

Compound	^{19}F chemical shift (ppm)[a]	Nuclear spin coupling constants (Hz)
CF_3PPh_2	54.6	^2J(P–F) = 73
$Hg_2(CF_3PPh_2)^{2+}$	53.7	^2J(P–F) = 93 ^3J(Hg–F) = 94[b] ^4J(Hg–F) = 46[b]
$Hg(CF_3PPh_2)_2^{2+}$	53.3	^2J(P–F) = 77 ^5J(P–F) = 18 J(P–P′) = 74

[a]Relative to $CFCl_3$; upfield shifts are taken as positive. Spectra were initially referenced to the high field component of the CF_3H signal and converted using $\delta(CFCl_3) = \delta(CF_3H) + 78.2$.
[b]These assignments are tentative.

not well resolved, even when the ^{19}F nmr spectrum is, but the ^{13}C chemical shifts of the cation (Table 1) differ significantly from those of the spectrum in Fig. 1*b*. The species giving rise to the spectrum in Fig. 1*b* is therefore not $Hg(CF_3PPh_2)_2^{2+}$ and so must be **1**, a phosphine complex of mercury(I). This conclusion is

$$[Hg—Hg—P(CF_3)Ph_2]^{2+}$$
1

confirmed by the ^{19}F nmr spectrum, shown in Fig. 2*b*, of the solution which gives rise to the ^{13}C spectrum in Fig. 1*b*. In Fig. 2*b* can be seen a doublet, each component of which is symmetrically flanked by *two* pairs of satellites. The *total* satellite intensity is 17.2%, close to the 16.9% expected if the satellites arise from coupling to ^{199}Hg ($I = \frac{1}{2}$; 16.86% abundant). Thus the CF_3 group is coupled to two chemically distinct ^{199}Hg nuclei as it must be in **1**. The nmr parameters derived from Fig. 2*b* are given in Table 3. The larger value of $J(^{199}Hg–F)$ is tentatively assigned to the short-range coupling, ^3J(Hg–F), while the smaller is assigned to ^4J(Hg–F).

The data in Table 3 show that ^2J(P–F) in **1** is larger than the corresponding coupling in the free phosphine in contrast to previously reported CF_3PPh_2 complexes (16) where ^2J(P–F) is smaller in magnitude in the coordinated phosphine than in the free. We find that the magnitude of ^2J(P–F) also increases in the system $AgAsF_6$–CF_3PPh_2–SO_2, the maximum value observed in this rapidly-exchanging system being 86 Hz. Because ^2J(P–F) in the silver(I) system increases continuously up to its limiting value, there can be no change in the sign of this coupling on coordination of CF_3PPh_2 to Ag^+, and the same is presumably true in the mercurous complex. An earlier explanation of the effect of coordination on ^2J(P–F) of CF_3PPh_2 appears to preclude the possibility of $|^2J(P–F)|$ increasing except in the unlikely event that ^2J(P–F) changes sign on coordination (16). Our results show that this explanation is not general; further theoretical study of the phenomenon appears desirable.

Trifluorophosphine

PF_3 dissolves in liquid SO_2 giving colorless solutions stable for long periods at room temperature. The 0 °C ^{19}F nmr spectrum of PF_3 in SO_2 is a doublet, $^1J(P–F) = 1403 \pm 2$ Hz, centered at 35.6 ϕ. Mixtures of colorless $Hg_2(AsF_6)_2$ and PF_3 in SO_2 are yellow; they are unstable at room temperature, decomposing[1] over a period of a few hours to give PF_5 and AsF_3 (identified by ^{19}F nmr as a doublet, $J = 944 \pm 2$ Hz, at 68.0 ϕ, and a broad line at 47.8 ϕ, respectively) as well as reduced mercury species including, eventually, the visually identifiable $Hg_{2.86}AsF_6$(10). The mixtures could, however, be studied by ^{19}F nmr at 0 °C, at which temperature they are stable. When $PF_3:Hg_2(AsF_6) < 1$, ^1J(P–F) is 1555 ± 2 and the chemical shift is 47.7 ϕ. Little change in these values occurs up to equimolarity, after which both ^1J(P–F) and the chemical shift decrease, moving closer to the value for free PF_3. The variation of ^1J(P–F) is shown in Fig. 3. Clearly PF_3 and Hg_2^{2+} initially combine in a 1:1 ratio, which is consistent with the occurrence of either (or both) of [2] and [3]. As no metallic mercury is formed when $PF_3:Hg_2^{2+} > 1$ this rules out [3],[2] leading to the conclusion that the solutions initially contain Hg—Hg—PF_3^{2+}. The PF_3 complex must be involved in rapid exchange of PF_3 with free PF_3, as an averaged signal is seen after the 1:1 ratio even down to −80 °C, the lowest temperature attainable. The presence of rapid exchange

[1]Colorless mixtures of $^nBu_4NAsF_6$ and PF_3 are stable indefinitely. The decomposition in the mercurous ion solutions may involve oxidation by the Hg_2^{2+} cation directly, or metal ion catalyzed reduction of the AsF_6^- anion by PF_3 followed by disproportionation of the Hg_2^{2+} and then reduction of the mercuric ion by PF_3.

[2]In addition we find that Hg^{2+}, as $HgF(AsF_6)$, immediately oxidizes PF_3.

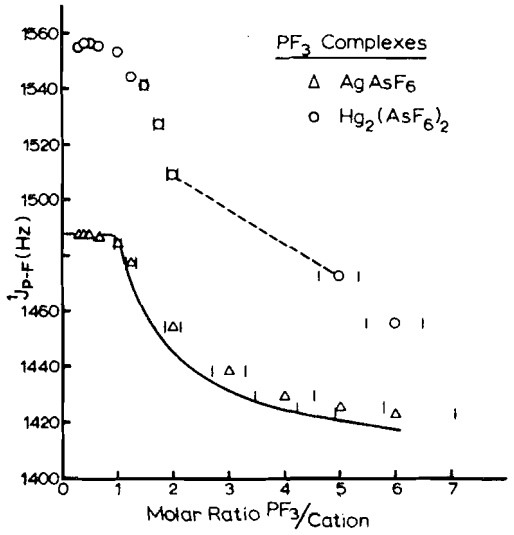

FIG. 3. The variation in ^1J(P–F) with change in the PF_3:cation ratio for the systems $Hg_2(AsF_6)_2$–PF_3–SO_2 (○) and $AgAsF_6$–PF_3–SO_2 (△) at 0 °C. In all cases SO_2:PF_3 = 17.2. Solid material was present in the region represented by the dashed line. The solid line is the variation expected if a single stable but labile 1:1 complex, $AgPF_3^+$, with ^1J(P–F) = 1487 Hz is formed in the silver(I) system.

accounts for the absence of observable three- and four-bond mercury–fluorine couplings which might be expected for static $Hg_2PF_3^{2+}$.

At the PF_3 concentrations used (SO_2:PF_3 = 17.2) a white precipitate forms when $2 < PF_3:Hg_2^{2+} < 4$. It seems that a second, probably 2:1 $PF_3:Hg_2^{2+}$ complex, occurs in the system; the discontinuity seen in Fig. 3 at $PF_3:Hg_2^{2+}$ = 2 or thereabouts is support for this proposal. After $PF_3:Hg_2^{2+} \gtrsim 4$, ^1J(P–F) and the chemical shift continue to decrease with increasing molar ratio, providing evidence that the 2:1 $PF_3:Hg_2^{2+}$ complex also undergoes facile PF_3 exchange. Even at large values of $PF_3:Hg_2^{2+}$ ^1J(P–F) remains greater than that of free PF_3, showing that the 2:1 complex also has a larger value of ^1J(P–F) than PF_3 itself.

The 2:1 complex could not be isolated. When the volatiles are allowed to escape *in vacuo* from a precipitate-bearing sample in which, initially, $2 < PF_3:Hg_2^{2+} < 4$, we firstly observe dissolution of the precipitate yielding a clear yellow solution. Further removal of volatiles from this solution under gentle conditions yields a pale yellow moisture-sensitive material which slowly loses further PF_3. In SO_2 solution this yellow material has a ^{19}F nmr spectrum with ^1J(P–F) = 1553 Hz and it thus contains $Hg_2PF_3^{2+}$, possibly solvated. The impure $Hg_2PF_3^{2+}$ salt has a Raman band at 138 cm^{-1} attributable to ν(Hg—Hg), and bands at 968 and 936 cm^{-1} in the infrared spectrum (Nujol mull) which we tentatively assign to P—F stretching. If the $Hg_2PF_3^{2+}$ salt is pumped for an extended period at room temperature all of the PF_3 is lost (as indicated by the infrared spectrum) and the Raman spectrum shows only the 180 cm^{-1} mercury–mercury stretching frequency of $Hg_2(AsF_6)_2$ itself (8). The PF_3–Hg_2^{2+} system in SO_2 can clearly be described by reaction 6:

$$[6] \quad Hg_2^{2+} \underset{-PF_3}{\overset{+PF_3}{\rightleftharpoons}} Hg_2(PF_3)^{2+} \underset{-PF_3}{\overset{+PF_3}{\rightleftharpoons}} Hg_2(PF_3)_2^{2+}$$

The increase in $|^1J$(P–F)| when PF_3 coordinates to Hg_2^{2+} is most unusual and gives rise to what is, to our knowledge, a uniquely large one-bond phosphorus–fluorine coupling. Generally $|^1J$(P–F)| decreases when PF_3 becomes coordinated (17, 18). The increase in $|^1J$(P–F)| in the mercurous complexes cannot, however, be associated with the unusual dimeric nature of Hg_2^{2+}, since we have observed a similar increase (to a maximum value of 1487 Hz) in the system PF_3–$AgAsF_6$–SO_2 as shown in Fig. 3. (As can be seen by the full line in Fig. 3,[3] the behavior of the silver(I) system is close to that expected if a single stable but labile silver complex $AgPF_3^+$ is formed in the system and is involved in rapid PF_3 exchange with free PF_3.)[4]

Evidence presented below suggests that little mercury-to-phosphorus back-bonding occurs in $Hg_2(CF_3PPh_2)_2^{2+}$, and this is probably true for $Hg_2PF_3^{2+}$ also. Similarly, proton nmr studies of argentous–olefin complexes have been interpreted as meaning that Ag^+ is a good σ-acceptor but a poor π-donor (ref. 19 and references cited therein). It may well be then that the large values of ^1J(P–F) in the PF_3 complexes of Hg_2^{2+} and Ag^+ are to be associated with the occurrence of very little π-backbonding in the metal–phosphorus bonds of these complexes.

[3]In calculating the full line no allowance has been made for the PF_3 in the gas phase in the sealed nmr tube.

[4]$[AgPF_3][AsF_6]$ can be isolated, impure, by gently removing volatiles from an SO_2 solution in which $PF_3/Ag^+ > 1$. It is characterized by P—F stretching frequencies of 932 and 907 cm^{-1} and a ^{19}F chemical shift of 38.5 ϕ.

Can. J. Chem. Downloaded from www.nrcresearchpress.com by 210.87.254.40 on 09/05/12
For personal use only.

Can. J. Chem. Downloaded from www.nrcresearchpress.com by 210.87.254.40 on 09/05/12
For personal use only.

Trimethylphosphite

The behavior of the trimethylphosphite–$Hg_2(AsF_6)_2$ system in SO_2 resembles that of the corresponding PPh_3 and CF_3PPh_2 systems; no permanent deposit of mercury is observed until $P(OMe)_3 : Hg_2^{2+} > 1$. The proton nmr spectrum of a freshly-prepared SO_2 solution of $P(OMe)_3$ consists of a doublet $J \approx 12$ Hz, $\delta \approx 3.5$ ppm.[5] However in mercurous ion-containing solutions the free phosphine resonances are absent, being replaced by a 'triplet' at $\delta = 4.10$ with apparent coupling 12.8 Hz. Such 'triplet' fine structure is diagnostic of a virtually-coupled bis(trimethylphosphite) complex (see, for instance, ref. 20). The presence of $Hg(P(OMe)_3)_2^{2+}$ is thus indicated, and is confirmed by comparison with the identical spectrum of a solution of $Hg(P(OMe)_3)_2^{2+}$ prepared by [5]. Evidently the mercurous ion in SO_2 disproportionates in the presence of trimethylphosphite even when $P(OMe)_3 : Hg_2^{2+} \leqslant 1$.

Other Phosphines

Tris(trifluoromethyl)phosphine, $P(CF_3)_3$, in SO_2 has a ^{19}F nmr spectrum consisting of a doublet, $J = 83$ Hz, at 52.2 ϕ. This spectrum is insensitive to the addition of $Hg_2(AsF_6)_2$, and the mercurous ion is not decomposed by excess $P(CF_3)_3$. It seems highly unlikely that complexation would produce no change in the fluorine spectrum of $P(CF_3)_3$, and it must be concluded that this phosphine is too poor a ligand to complex the mercurous ion under the experimental conditions used.

Both trichlorophosphine and chlorodiphenylphosphine undergo halogen exchange on treatment with $Hg_2(AsF_6)_2$ in SO_2 solution. The reactions of the $Hg_2(AsF_6)_2$ with a variety of halogenated substrates will be the subject of a later paper in this series.

The Relationship Between the Net Electron Donor Abilities of the Phosphines and Disproportionation of the Mercurous Ion

Our results show [1] to be important for the phosphines PPh_3, CF_3PPh_2, and $P(OMe)_3$ when phosphine: $Hg_2^{2+} > 1$, though no disproportionation occurs with excess PF_3, and no complexation with $P(CF_3)_3$ in excess or otherwise. When phosphine: $Hg_2^{2+} \leqslant 1$, however, disproportionation according to [3] still occurs with PPh_3 and $P(OMe)_3$, but mercurous complexes of CF_3PPh_2 and PF_3 are stable. Tolman (21) has shown that, towards the $Ni(CO)_3$ moiety at least, the 'electron donor–acceptor properties' (*i.e.* the net electron donating abilities) of the phosphines are in the order $P(CF_3)_3 < PF_3 \ll CF_3PPh_2 < P(OMe)_3 < PPh_3$, the values of $\sum\lambda_i$ (21) being 58.8, 54.6, 28.2, 23.1, and 12.9 cm^{-1}, respectively, for these phosphines. It appears that those ligands ($P(OMe)_3$ and PPh_3) which are relatively good donors always cause disproportionation of Hg_2^{2+}, while those which are weaker donors (CF_3PPh_2 and PF_3) cause disproportionation only when present in excess, if at all. Judging by the $\sum\lambda_i$ values, there appears to be quite a fine line between phosphines exhibiting these alternate behaviors (*cf.* CF_3PPh_2 *vs.* $P(OMe)_3$) and an equally fine line between those phosphines which coordinate to Hg_2^{2+} and those which do not (*cf.* $P(CF_3)_3$ *vs.* PF_3).

^{13}C Nuclear Magnetic Resonance Spectra and the Question of Mercury-to-phosphorus Backbonding in Mercurous and Mercuric Complexes with Phenyl Phosphines

In addition to ^{13}C chemical shift data for PPh_3, CF_3PPh_2, and some of their mercury complexes, Table 1 includes data for a variety of other compounds and complexes of PPh_3 for comparison. Of particular interest are the chemical shifts of C_1 and C_4 in the various species; no readily discernible trends occur in the data for C_2 and C_3. Of all the triphenylphosphine compounds listed, PPh_3 itself, in the inert solvent CS_2, has the largest value for $\delta_c(C_1)$, and also the smallest value of $\delta_c(C_4)$. Increasing the coordination number of phosphorus causes $\delta_c(C_1)$ to decrease and $\delta_c(C_4)$ to increase relative to free PPh_3. The changes in the case of $(Ph_3P)Mo(CO)_5$ have been remarked upon previously (22).

Both Lauterbur (23) and Spiesecke and Schneider (24) have examined the ^{13}C spectra of a variety of monosubstituted benzenes. These authors concur in attributing changes in the *para* carbon shielding to changes in the π-effects of the substituents; π-donors cause increased shielding and π-acceptors decreased shielding.

[5] $P(OMe)_3$ is unstable in SO_2 solution and decomposes completely in *ca.* 30 min at room temperature. The nmr spectrum of the decomposition products partly overlaps that of $P(OMe)_3$. SO_2 solutions of $Hg(P(OMe)_3)_2^{2+}$ are stable for much longer periods.

Can. J. Chem. Downloaded from www.nrcresearchpress.com by 210.87.254.40 on 09/05/12
For personal use only.

It is thus apparent that, for all the PPh_3 compounds in Table 1, the π-density in the phenyl rings is reduced when PPh_3 becomes coordinated. Notably large effects are seen in $MePPh_3^+$ and $Hg(PPh_3)_2^{2+}$.

In monosubstituted benzenes, changes in $\delta_c(C_1)$ have been shown to depend upon both the effects of magnetic anisotropy occurring in the region of the carbon-substituent bond and the electronegativity of the substituent, increased electronegativity causing decreased shielding of C_1 (24). Clearly the changes observed in the various PPh_3 compounds (Table 1) are in the wrong direction to be ascribable to the increased electronegativity of phosphorus occurring with increased coordination. The changes must reflect changes in local magnetic anisotropy. If the magnetic anisotropy of the phosphorus is reduced on coordination, an upfield shift is expected, as observed. The shielding in this case reflects the difference in the magnetic anisotropies of the phosphorus 'lone pair' and the phosphorus-substituent bond (24).

The triphenylphosphine compounds in Table 1 fall into two groups: those ($(OC)_5MoPPh_3$, $O{=}PPh_3$, $H_2C{=}PPh_3$) for which the change in $\delta_c(C_1)$ upon coordination is $\lesssim 6$ ppm, and those ($MePPh_3^+$ and $Hg(PPh_3)_2^{2+}$) for which $\Delta\delta_c(C_1)$ is $\gtrsim 14$ ppm. Partial back-bonding between the substituent and phosphorus is expected in $O{=}PPh_3$ and $H_2C{=}PPh_3$ and, from the data in Table 1, seems to occur in $(OC)_5MoPPh_3$ also. In contrast, only a σ-bond between the phosphorus and the methyl group is expected in the phosphonium cation, and the great similarity between the spectrum of this and the mercuric cation speaks strongly for the absence of multiple Hg—P bonding in the latter cation also. This explanation is consistent with observed changes in the shielding of C_4 (see above); the positive charge on phosphorus will most likely be larger in those compounds where no back-bonding to phosphorus occurs and this should lead to greater polarization of the aromatic π-density, as reflected by $\delta_c(C_4)$.

The shielding of C_1 and deshielding of C_4 which occur when either the mercuric or mercurous complex of CF_3PPh_2 is formed, are of comparable magnitude to the changes accompanying formation of $Hg(PPh_3)_2^{2+}$. Accordingly, the interpretation of the previous paragraph holds, *i.e.* little, if any, Hg-to-P back-bonding occurs in either the mercurous or mercuric complexes of CF_3PPh_2.

Reactions of $Hg_2(AsF_6)_2$ with Triphenyl- and Tris(p-fluorophenyl)phosphine Sulfides, Triphenylphosphine Selenide, Triphenylarsine, and Triphenylstibine in Liquid Sulfur Dioxide

When a greater than equimolar amount of Ph_3PS, $(p\text{-}FC_6H_4)_3PS$, Ph_3PSe, Ph_3As, or Ph_3Sb is added to $Hg_2(AsF_6)_2$ in SO_2, permanent disproportionation is observed to occur. With an excess of $Hg_2(AsF_6)_2$, however, the reaction with each ligand proceeds as follows: mercury is formed at the point of contact of the two solutions but readily dissolves on shaking to give a clear yellow solution from which, on standing for a few minutes, a white or pale yellow solid precipitates. The products all have the stoichiometry $Hg_2(AsF_6)_2 \cdot L$. Addition of traces of water or other strong donor solvent to the 1:1 complexes causes decomposition, metallic mercury being observed. This disproportionation is good evidence that the products contain the mercurous ion. The Raman spectra of the adducts (Table 4) provide further evidence for the integrity of the mercury–mercury bond; in each spectrum a very intense band is observed in the mercury–mercury stretching region. Though this band is almost certainly not due to a pure Hg—Hg stretching vibration, it does signify the presence of the dimeric cation.

TABLE 4. Partial Raman and infrared spectra of some new mercurous complexes, $Hg_2(AsF_6)_2 \cdot L$ (cm^{-1})

L	Raman	Infrared	
	ν(Hg—Hg)[a]	ν(P—S(Se))[b]	$\Delta\nu$(P—S(Se))[c]
PF_3	138		
CF_3PPh_2[d]	135		
$SPPh_3$	170	552	83
$SP(p\text{-}C_6H_4F)_3$	173	[e]	
$SePPh_3$	145	525	36
$AsPh_3$	120		
$SbPh_3$	110		

[a] Probably not a pure vibration; ± 2 cm^{-1}.
[b] ± 2 cm^{-1}.
[c] $\nu(P{-}S(Se))_{free\ ligand} - \nu(P{-}S(Se))_{complex}$; ± 3 cm^{-1}.
[d] Sample prepared by removing solvent from an equimolar mixture of $Hg_2(AsF_6)_2$ and CF_3PPh_2 in SO_2.
[e] Could not be assigned with certainty.

Can. J. Chem. Downloaded from www.nrcresearchpress.com by 210.87.254.40 on 09/05/12
For personal use only.

The sensitivity of ν(Hg—Hg) (Table 4) to the group VA or VIA donor atom present in the ligand is good evidence that this donor atom is indeed coordinated to the mercurous ion; the lowering of ν(P—S(Se)) in the infrared spectra of the phosphine chalcogenide adducts (Table 4) provides corroboration of this for these complexes. The infrared spectra, in the phenyl region, of all the adducts (see Experimental section) bear great resemblance to those of the uncoordinated ligands, ruling out the possibility of phenyl coordination in addition to coordination by the more normal donor atom. All the evidence is consistent with Ph_3M (M = As, Sb) acting as monodentate ligands in their mercurous complexes, which presumably have structures analogous to **1**. The phosphine chalcogenides very probably act in a similar monodentate manner through the chalcogen. If so, the relatively large values of $\Delta\nu$(P—S(Se)) can reasonably be ascribed to a combination of the 'mass effect' and the pronounced Lewis acidity of the mercurous ion (30). However, chalcogen-bridged structures for the $Ph_3PS(Se)$ adducts cannot be ruled out with certainty; the magnitude of the changes in ν(P—S(Se)) are not inconsistent with this possibility (30, 31).

The adducts prepared here are clearly true mercurous complexes, apparently the first reported with sulfur, selenium, arsenic, or antimony as donor atoms. The complexes may be stable in solution, but it is also possible that they owe their existence to their insolubility in SO_2 which would force equilibrium [2] to the right and hence equilibrium [3] towards the left (*cf.* the stability of very insoluble mercurous compounds in water (1–3)).

Experimental

Reagents

Sulfur dioxide (Matheson) was stored in the gas phase over Linde 3A Molecular Sieves at least 12 h prior to use. Triphenylphosphine, -arsine, -stibine (Eastman) were recrystallized from ethanol before use, while phosphorus trifluoride (Matheson) and trimethylphosphate (Alfa) were used as obtained commercially, as was tris(4-fluorophenyl)-phosphine (Maybridge Research Chemicals), the melting point and infrared and ^{19}F nmr spectra of which showed the absence of the phosphine oxide. Triphenylphosphine sulfide, tris(4-fluorophenyl)phosphine sulfide, and triphenylphosphine selenide were prepared by literature methods (ref. 32 and references cited therein). Diphenyltrifluoromethylphosphine was prepared by the reaction of diphenylchlorophosphine with trifluoroiodomethane (33). Tris(trifluoromethyl)phosphine was the gift of C. J. Willis of this department. Mercurous hexafluoroarsenate and silver hexafluoroarsenate were synthesized as described previously (6, 8). Tetramethylammonium hexafluoroarsenate, Me_4NAsF_6, was obtained by reaction of tetramethylammonium chloride with arsenic pentafluoride in anhydrous hydrogen fluoride. The product, sparingly soluble in SO_2, showed a single resonance in the ^1H nmr spectrum at 3.16 ppm relative to internal TMS. Fluoroform (Matheson) was used as obtained.

Preparation of Complexes Insoluble in SO_2

The preparative technique was identical to that described previously for the preparation of insoluble arene complexes of $Hg_2(AsF_6)_2$ (6) except that the molar ratio of ligand to metal salt was kept below unity. Analyses and partial infrared spectra of the new complexes are given in Table 5.

Preparation of ^{19}F and ^{13}C Nuclear Magnetic Resonance Samples

The samples for ^{19}F nmr studies of PF_3 and $Hg_2(AsF_6)_2$ or $AgAsF_6$ were prepared in 5 mm o.d. thick-walled nmr tubes, each fused initially to a small length of $\frac{1}{4}$ in. medium-wall glass tubing. Amounts of metal salt used ranged from 1.5 to 0.08 g of $Hg_2(AsF_6)_2$ and 0.57 to 0.03 g of $AgAsF_6$. The metal salts were added in the dry box from which the tubes were removed after capping with rubber serum caps. The ^{19}F nmr reference material, hexafluorobenzene (^{19}F chemical shift = 164.9 ϕ), was added via a syringe and the tube attached to the vacuum line. Sulfur dioxide and PF_3 were condensed into the tube at −196 °C and the nmr tube separated from the $\frac{1}{4}$ in. tubing by flame-sealing. The molality of PF_3 was held constant by adding the same volume of PF_3 and SO_2 each time. Preparation of ^{19}F nmr samples of the systems CF_3PPh_2–$Hg_2(AsF_6)_2$–SO_2 and CF_3PPh_2–$AgAsF_6$–SO_2 was essentially identical, the phosphine being added by weight from a syringe, and fluoroform, CHF_3 (^{19}F chemical shift = 78.2 ϕ, $^2J_{HF}$ = 79.5 Hz), being used as internal reference. Samples of $(MeO)_3P$–$Hg_2(AsF_6)_2$–SO_2 for proton nmr were prepared similarly, using Me_4NAsF_6 (δ = 3.16 ppm) as internal reference.

For ^{13}C nmr, samples of PPh_3 in SO_2[6] or in CS_2 or in CS_2–SO_2 mixtures, and samples containing $Hg_2(AsF_6)_2$–PPh_3 mixtures in SO_2, were prepared in 10 mm o.d. sample tubes. ^{13}C nmr samples of CF_3PPh_2 or $Hg_2(AsF_6)_2$–CF_3PPh_2 were prepared and run in 4 mm o.d. coaxial nmr tubes as described previously (6).

The apparatus used for [5] (see text) consisted of a glass tube reaction chamber separated from the appropriate nmr tube by a fine sinter. In the dry box, all necessary solids were added to the glass tube which was then capped, removed from the box, and attached to the vacuum line. Following addition of SO_2 (and CHF_3 for ^{19}F nmr samples), the reaction vessel was flame-sealed and allowed to warm up to room temperature. After reaction the solution was filtered through the sinter into the attached nmr tube and frozen down to allow flame-sealing and separation of the nmr tube.

[6] PPh_3 was found to react with liquid SO_2 at a rate dependent on the PPh_3 concentration; a 0.25 *M* solution was decomposed slightly after *ca.* 12 h but a 2.5 *M* solution was extensively decomposed after *ca.* 1 h at 32 °C. PPh_3 has been shown previously to react with SO_2 at elevated temperatures yielding $OPPh_3$ and $SPPh_3$ (34).

Can. J. Chem. Downloaded from www.nrcresearchpress.com by 210.87.254.40 on 09/05/12
For personal use only.

TABLE 5. Analyses and infrared spectra of complexes prepared[a]

Complex	Formula	Color	Analysis (%) Theoretical C	H	X	Found C	H	X	Infrared spectra[a]
$Hg_2(AsF_6)_2$.triphenylarsine	$As_3C_{18}H_{15}F_{12}Hg_2$	White	19.92	1.39		20.06	1.55		1579w, 1570w, 1445s, 1435m, 1335w, 1321w, 1316sh, 1307sh, 1277w, 1193m, 1162w, 1079m, 1025w, 1017m, 1003m, 999m, 994m, 990m, 945m, 790s, 786s, 760s, 755s, 735m, 699m, 687sh, 615vw, 473m, 467s (ν_{as}C—As), 456w.
$Hg_2(AsF_6)_2$.triphenylstibine	$As_2C_{18}H_{15}F_{12}Hg_2Sb$	Yellow	19.09	1.34	10.75(Sb) 35.44(Hg)	19.23	1.42	11.01(Sb) 35.58(Hg)	1574s, 1478m,sh, 1440s, 1426s, 1337w, 1331w, 1319vw, 1193w, 1066m, 1050m, 1019m, 998m, 990s, 940w, 924vw, 784m,sh, 779m, 750m, 735m,sh, 689m,sh, 613m, 460m,sh, 447s.
$Hg_2(AsF_6)_2$.triphenylphosphine sulfide	$As_2C_{18}H_{15}F_{12}Hg_2PS$	White	20.14	1.41	2.99(S)	20.28	1.34	2.93(S)	1483m,sh, 1445s, 1338w, 1310w, 1199w, 1186w, 1164w, 1124w, 1102s, 1022vw,sh, 995m, 751m,sh, 740m,sh, 723m, 710m, 615w, 580w, 552s (νP═S), 515s (ν_{as}C—P), 445w,sh, 430vw, sh (ν_sC—P).
$Hg_2(AsF_6)_2$.triphenylphosphine selenide	$As_2C_{18}H_{15}F_{12}Hg_2PSe$	Yellow	19.30	1.34	7.05(Se)	19.04	1.39	7.21(Se)	1479m,sh, 1442m, 1333w, 1310w, 1194w, 1186w,sh, 1164w, 1124w, 1095s, 1022w, 1016w, 994m, 747w, 739w, 720m, 704m,sh, 609vw, 525s (νP═Se), 512s (ν_{as}C—P), 444w,sh, 429w,sh (ν_sC—P).
$Hg_2(AsF_6)_2$.tris(4-fluorophenyl)-phosphine sulfide	$As_2C_{18}H_{12}F_{15}Hg_2PS$	White	19.18	1.07	2.84(S)	19.29	1.23	2.97(S)	1493m, 1401w, 1307w, 1294vw, 1261m, 1250s, 1162s, 1102s, 1002w, 947vw, 844m, 830m, 714m,sh, 690m, 634m, 613w, 540s, 533m,sh, 524m,sh, 510w, 464m, 452m.

[a]1600–300 cm^{-1} region; bands attributable to the anion have been omitted.

Spectroscopic Measurements

The ^{19}F nmr spectra were obtained using a modified Varian HA-100 nmr spectrometer operating at 94.1 MHz. Measurements were taken with a probe temperature of 32 °C except for measurements on PF_3 samples which were made at 0 °C.

^{1}H nmr spectra were recorded on a Varian T-60 with a probe temperature of 32 °C.

The 32 °C proton-decoupled ^{13}C spectra were obtained using a Varian XL-100-15 system operating in the Fourier transform mode. Both the 10 and 4 mm sample tubes were placed coaxially in appropriate tubes. The external reference and deuterium lock were contained in a dioxane–D_2O solution (10/90% v/v) in the annulus.

Raman spectra were obtained on a Cary 82 Raman spectrometer with Ar^+ (5145 Å) laser excitation. The solids were contained in glass capillary (melting point) tubes.

Infrared spectra were obtained using Nujol mulls between potassium bromide plates on a Perkin–Elmer 621 grating infrared spectrometer and/or on a Beckman IR-20A spectrometer.

Acknowledgments

Acknowledgement is made to the donors of the Petroleum Research Fund, administered by the American Chemical Society, and to the National Research Council of Canada for financial support of this research. We thank Professor J. B. Stothers for obtaining many of the ^{13}C nmr spectra and for helpful discussions, and Mrs. H. Schroeder for technical assistance with the ^{19}F nmr spectra.

1. D. J. Cardin. *In* MTP international review of science. Inorganic chemistry, Series 1, Volume 1. *Edited by* M. F. Lappert. Butterworth and Co., Ltd., London. 1972. p. 45 *et seq.*
2. B. J. Aylett. *In* Comprehensive inorganic chemistry. Vol. 3. Pergamon Press Ltd., Oxford. 1973. p. 286.
3. F. A. Cotton and G. Wilkinson. Advanced inorganic chemistry. 3rd ed. Interscience Publishers, New York. 1972. p. 510.
4. D. L. Kepert and D. Taylor. Aust. J. Chem. **27**, 1199 (1974) and references cited therein.
5. R. A. Potts and A. L. Allred. Inorg. Chem. **5**, 1066 (1966).
6. P. A. W. Dean, D. G. Ibbott, and J. B. Stothers. Can. J. Chem. This issue.
7. P. A. W. Dean and D. G. Ibbott. Inorg. Nucl. Chem. Lett. **11**, 119 (1975).
8. B. D. Cutforth, C. G. Davies, P. A. W. Dean, R. J. Gillespie, P. R. Ireland, and P. K. Ummat. Inorg. Chem. **12**, 1343 (1973).
9. B. D. Cutforth, R. J. Gillespie, and P. R. Ireland. J. Chem. Soc. Chem. Commun. 723 (1973).
10. I. D. Brown, B. D. Cutforth, C. G. Davies, R. J. Gillespie, P. R. Ireland, and J. E. Vekris. Can. J. Chem. **52**, 791 (1974).
11. C. W. Haigh. J. Chem. Soc. A, 1682 (1970).
12. W. McFarlane. Proc. R. Soc. London, Ser. A, **306**, 185 (1968).
13. D. van der Helm, J. D. Childs, and S. D. Christian. Chem. Commun. 887 (1969).
14. D. A. Redfield, J. H. Nelson, and L. W. Cary. Inorg. Nucl. Chem. Lett. **10**, 727 (1974).
15. F. A. L. Anet. J. Am. Chem. Soc. **84**, 747 (1962); R. K. Harris. Can. J. Chem. **42**, 2275 (1964).
16. A. J. Rest. J. Chem. Soc. A, 2212 (1968).
17. J. F. Nixon. Adv. Inorg. Chem. Radiochem. **13**, 452 (1970).
18. E. R. Alton, R. G. Montemayor, and R. W. Parry. Inorg. Chem. **13**, 2267 (1974).
19. R. G. Salomon and J. K. Kochi. J. Am. Chem. Soc. **95**, 1889 (1973).
20. G. M. Bancroft and E. T. Libbey. Can. J. Chem. **51**, 1482 (1973).
21. C. A. Tolman. J. Am. Chem. Soc. **92**, 2953 (1970).
22. O. A. Gansow and B. Y. Kimura. Chem. Commun. 1621 (1970).
23. P. C. Lauterbur. J. Am. Chem. Soc. **83**, 1846 (1961).
24. H. Spiesecke and W. G. Schneider. J. Chem. Phys. **35**, 731 (1961).
25. T. Bundgaard and H. J. Jacobsen. Acta Chem. Scand. **26**, 2548 (1972).
26. J. B. Stothers. Carbon-13 N.M.R. spectroscopy. Academic Press, New York. 1972. p. 49.
27. G. A. Gray. J. Am. Chem. Soc. **95**, 7736 (1973).
28. T. A. Albright, W. J. Freeman, and E. E. Schweizer. J. Am. Chem. Soc. **97**, 940 (1975).
29. T. A. Albright, W. J. Freeman, and E. E. Schweizer. J. Am. Chem. Soc. **97**, 2942 (1975).
30. P. M. Boorman and D. Potts. Can. J. Chem. **52**, 2016 (1974).
31. P. M. Boorman and K. J. Reimer. Can. J. Chem. **49**, 2926 (1971).
32. G. M. Kosolapoff. Organophosphorus compounds. J. Wiley and Sons, Inc., New York. 1950. p. 99.
33. M. A. A. Beg and H. C. Clark. Can. J. Chem. **40**, 283 (1962).
34. B. C. Smith and G. H. Smith. J. Chem. Soc. 5516 (1965).

Can. J. Chem. Downloaded from www.nrcresearchpress.com by 210.87.254.40 on 09/05/12
For personal use only.

ERRATUM

Erratum: A photoelectron investigation of acyl silanes: the photoelectron spectra of trimethylsilyl phenyl ketone and phenyl *tert*-butyl ketone

R. S. BROWN
Department of Chemistry, University of Alberta, Edmonton, Alberta T6G 2E1
Received October 3, 1975

(Ref.: Can. J. Chem. **53**, 2446 (1975))

The correct structure **3** is that given below and not as shown in the article.

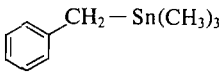

Erratum: Synthesis and characterization of some dibasic tridentate Schiff base ligands

ELMER C. ALYEA AND ABDUL MALEK
Department of Chemistry, University of Guelph, Guelph, Ontario N1G 2W1
Received October 30, 1975
(Ref.: Can. J. Chem. **53**, 2809 (1975))

The name of Professor J. M. Fresco was spelled incorrectly in the text of the original erratum.

Can. J. Chem. Downloaded from www.nrcresearchpress.com by 210.87.254.105 on 09/05/12
For personal use only.

COMMUNICATIONS

The environment of tertiary alcohols from nuclear magnetic resonance spectral shifts on formation of trichloroacetylcarbamates

DAVID R. TAYLOR
Chemistry Department, University of Alberta, Edmonton, Alberta T6G 2G2

Received August 29, 1975

DAVID R. TAYLOR. Can. J. Chem. **54**, 189 (1976).

Reaction of tertiary alcohols with trichloroacetylisocyanate causes a marked downfield shift of the nmr signals of protons β to the hydroxyl group. This can be used to reveal the presence of methyl groups adjacent to a tertiary hydroxyl group and of other β protons which are sufficiently deshielded to be observed. This method has also been used to assign the geometry of the double bond of an allylic alcohol.

DAVID R. TAYLOR. Can. J. Chem. **54**, 189 (1976).

La réaction des alcools tertiaires avec l'isocyanate de trichloroacétyle produit un déplacement important vers les bas champs des signaux rmn des protons en β du groupe hydroxyle. On peut utiliser cette propriété pour mettre en évidence la présence de groupes méthyles adjacents au groupe hydroxyle tertiaire et d'autres protons en β qui sont suffisamment déblindées pour être observés. On a aussi utilisé cette méthode pour attribuer la géométrie de la double liaison d'un alcool allylique.

[Traduit par le journal]

The facile reaction of alcohols with trichloroacetylisocyanate (TAI) to yield carbamates in which the N*H* signal in the nmr spectrum appears at δ 8–9 has been used by Goodlett (1) and Bose and co-workers (2) to determine the number and type of hydroxyl groups in a molecule by the number of N*H* signals formed and by observing the downfield shifts of the α protons. Mak and Rogers (3) have recently reported the use of this reagent for determining chain branching in epoxy resins. We now report that the nmr signals of protons β to tertiary alcohols undergo significant downfield shifts on reaction of the alcohol with TAI. These shifts can be useful in defining the environment of tertiary alcohols and can thus aid in structure determination.

Trichloroacetylcarbamates are particularly attractive derivatives for nmr study because, as has been pointed out (1, 2), they are readily formed in minutes from even hindered secondary and tertiary alcohols on adding TAI to a solution of the alcohol in the nmr tube, and because TAI is devoid of protons. Conversion of *tert*-butyl alcohol into its trichloroacetylcarbamate in this way causes the signal for the methyl protons (δ ($CDCl_3$) 1.28) to shift to δ 1.56, a downfield shift of 0.28 ppm. In all the other tertiary alcohols examined (see Fig. 1), the signals of the methyl groups adjacent to the tertiary alcohol shifted by more than this amount, the range found being 0.29–0.44 ppm. Other methyl groups shift considerably less (*cf.* **1** and **5**). This method allowed us to decide readily between the alternative structures, **8** and **9**, for the monomethyl ether of **7**. Reaction of the monomethyl ether of **7** with TAI caused only negligible shifts in the signals for the methyl groups and this is only consistent with the structure **8**. As shown in Fig. 1, the signal for the tertiary methyl group in **7** shifts downfield by 0.37 ppm and **9** would be expected to show a similar shift.

Other protons β to a tertiary hydroxyl group also show large downfield shifts on formation of trichloroacetylcarbamates. Thus H-24 in sapelin A diacetate, **6** (4), is shifted downfield by 0.70 ppm on reaction with TAI. Even larger shifts are shown by the methine hydrogen of the isopropyl group in **7** and **8**[1] (see Fig. 1). The C-7 proton (H_a) in cedrol, **4**, is hidden under the methylene envelope. On reaction with TAI, however, H_a can be seen as a broadened doublet at δ 2.50 (J = 4.5 Hz). The C-9 protons, H_b and H_c, also become visible but form too complex a pattern

[1]The shifts are given as a range in Fig. 1 since the methine hydrogens in **7** and **8** are obscured by other absorption.

Can. J. Chem. Downloaded from www.nrcresearchpress.com by 210.87.254.6 on 09/05/12
For personal use only.

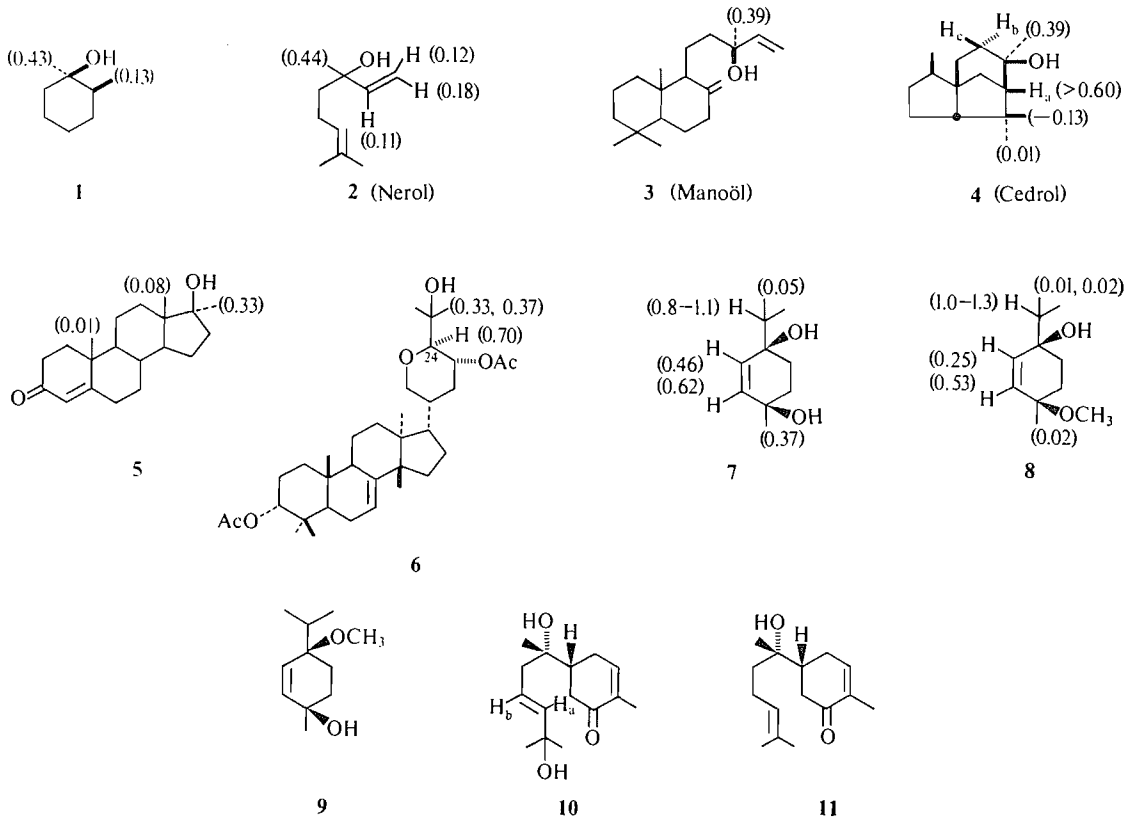

FIG. 1. Positive numbers in parentheses represent downfield shifts (in ppm) of the protons indicated on addition of TAI to solutions in $CDCl_3$.

to reveal chemical shifts. The downfield shifts of similar protons in some dammarane triterpenes on addition of TAI have been recently reported without comment by Lavie and co-workers (5).

Bose and co-workers (2) have made the generalization that reaction of allylic alcohols with TAI causes a downfield shift of vinyl protons β to the hydroxyl group of 0.08–0.17 ppm[2] while α vinyl protons are largely unaffected. Our results on nerol, **2**, manoöl, **3**,[3] and **8**[4] indicate that this does not hold for all allylic alcohols. Although the shifts of the vinylic protons in allylic alcohols are variable, the simplification of the spectrum on adding TAI can be useful in cases where α and β vinylic protons have the same or almost the same chemical shifts. Thus, in the allylic alcohol **10**,[5] H_a and H_b form a complex pattern from which J_{ab} is not easily obtained. On addition of TAI to **10**, the chemical shifts of H_a and H_b became sufficiently different for J_{ab} to be observed (15.5 Hz) and the *trans* geometry assigned. In many similar allylic alcohols, the geometry of the double bond was either assumed or proven by more laborious methods (7). The magnitude of the downfield shifts of H_a and H_b could not be reliably obtained, but, interestingly, H_a (the α vinylic proton) underwent a slightly larger shift than did H_b (the β vinylic proton). These results show the danger of using TAI shifts for determining the substitution of the double bond in allylic alcohols.

[2]In ref. 2, the range given was 10–15 Hz while the one case cited showed a shift of 9 Hz. However, the frequency of the spectrometer was not specified. In a later paper (6), the range of 5–10 Hz (at 60 MHz) was given, and an example of a 5 Hz shift was quoted.

[3]Not surprisingly, manoöl, **3**, showed virtually the same shifts of the corresponding vinyl protons as nerol, **2**.

[4]We could not distinguish between the two vinylic protons in **8**.

[5]**10** was formed from (−)-delobanone, **11**, (W. R. Chan and D. R. Taylor, unpublished results) via singlet oxygen oxidation.

Can. J. Chem. Downloaded from www.nrcresearchpress.com by 210.87.254.6 on 09/05/12
For personal use only.

The observation of nmr acylation shifts of protons β to a tertiary alcohol is not new. Formylation shifts of methyl groups (8) and acetylation shifts of methyl groups and other β protons (9) have been recently reported. However, *in situ* formation of trichloroacetylcarbamates would appear to be the method of choice since derivatization is so simple and the shifts obtained are larger. For those compounds that were available only in small amounts, the data were obtained by FT nmr using samples of 1 mg or less. This can be done routinely by adding one drop of TAI since even such a large excess of the reagent does not affect the chemical shifts.

Acknowledgments

The author thanks Dr. W. A. Ayer for compounds **1**–**5**, and Dr. R. S. Brown for **7** and **8**.

1. V. W. Goodlett. Anal. Chem. **37**, 431 (1965).
2. I. R. Trehan, C. Monder, and A. K. Bose. Tetrahedron Lett. 67 (1968).
3. H. D. Mak and M. G. Rogers. Anal. Chem. **44**, 837 (1972).
4. W. R. Chan, D. R. Taylor, and T. Yee. J. Chem. Soc. C, 311 (1970).
5. M. M. Rao, H. Meshulam, R. Zelnik, and D. Lavie. Tetrahedron, **31**, 333 (1975).
6. O. N. Devgan, M. M. Bokadia, A. K. Bose, M. S. Tibbetts, G. K. Trivedi, and K. K. Chakravarti. Tetrahedron Lett. 5337 (1967).
7. C. D. Snyder and H. Rapoport. J. Am. Chem. Soc. **91**, 731 (1969); J. L. Fourrey, J. Rondest, and J. Polonsky. Tetrahedron, **26**, 3839 (1970); G. W. K. Cavill and I. M. Coggiola. Aust. J. Chem. **24**, 135 (1971).
8. R. Misra and S. Dev. Tetrahedron Lett. 4865 (1972).
9. A. Bianco, M. Guiso, C. Iavarone, and C. Trogolo. Gazz. Chim. Ital. **105**, 185 (1975); C. R. Narayanan and M. R. Sarma. Tetrahedron Lett. 1553 (1968).

Can. J. Chem. Downloaded from www.nrcresearchpress.com by 210.87.254.6 on 09/05/12
For personal use only.

Can. J. Chem. Downloaded from www.nrcresearchpress.com by 210.87.254.6 on 09/05/12
For personal use only.

Canadian Journal of Chemistry

Published by
THE NATIONAL RESEARCH COUNCIL OF CANADA

Journal canadien de chimie

Publié par
LE CONSEIL NATIONAL DE RECHERCHES DU CANADA

Volume 54 Number 2 January 15, 1976

Volume 54 numéro 2 15 janvier 1976

Asymmetric induction in the Sommelet rearrangement of chiral benzyl sulfonium salts

STEWART JOHN CAMPBELL[1] AND DAVID DARWISH[2]

Department of Chemistry, University of Alberta, Edmonton, Alberta T6G 2G2

Received January 15, 1975[3]

STEWART JOHN CAMPBELL and DAVID DARWISH. Can. J. Chem. **54**, 193 (1976).

The Sommelet rearrangement of (+)-ethylmethyl-*p*-nitrobenzylsulfonium perchlorate, (+)-**1**, and (+)-ethylmethyl-*p*-chlorobenzylsulfonium perchlorate, (+)-**2**, are described. Elution of (+)-**1** through an hydroxide exchange resin generated ethylmethylsulfonium *p*-nitrobenzylide (+)-**3** which decomposed in methanol at room temperature to ethyl 2-methyl-5-nitrobenzyl sulfide, **6**, and (+)-methyl α-(2-methyl-5-nitrophenyl)ethyl sulfide, (+)-**7**, with 18 to 20.3% asymmetric induction. Decomposition of (+)-**2** in sodium methoxide solution at 70 °C for 2 h produced ethyl 2-methyl-5-chlorobenzyl sulfide, **8**, and (+)-methyl α-(2-methyl-5-nitrophenyl)ethyl sulfide, (+)-**9**, with 21 to 25.5% asymmetric induction. The lower estimates of asymmetric induction for each sulfide were made by comparison with specific rotations of authentic samples obtained by synthesis and resolution. The higher estimates were obtained by the use of a chiral lanthanide shift reagent Eu(hfbc)$_3$ with the sulfone derivatives of these chiral sulfides. The ylide (+)-**3** reacted with aldehydes in high yield to produce oxiranes with no induction of asymmetry.

STEWART JOHN CAMPBELL et DAVID DARWISH. Can. J. Chem. **54**, 193 (1976).

On décrit le réarrangement de Sommelet du perchlorate du (+) éthylméthyl *p*-nitrobenzylsulfonium, (+)-**1** et du (+)-éthylméthyl *p*-chlorobenzylsulfonium, (+)-**2**. L'élution de (+)-**1** à travers une colonne échangeuse d'ions contenant des groupes OH génère le *p*-nitrobenzylide d'éthylméthylsulfonium, (+)-**3**, qui se décompose dans le méthanol à température de la pièce pour fournir le sulfure d'éthyle et de méthyl-2 nitro-5 benzyle, **6**, et le (+) sulfure de méthyle et d'α(méthyl-2 nitro-5 phényl) éthyle, (+)-**7**, avec des inductions asymétriques de 18 à 20.3%. La décomposition de (+)-**2** dans une solution de méthylate de sodium à 70 °C pendant 2 h conduit au sulfure d'éthyle et de méthyl-2 chloro-5 benzyle, **8**, et au (+) sulfure de méthyle et d'α(méthyl-2 nitro-5 phényl) éthyle, (+)-**9** avec une induction asymétrique de 21 à 25.5%. Les estimés les plus bas pour l'induction asymétrique pour chaque sulfure ont été faits par comparaison des indices spécifiques de rotation avec des échantillons authentiques obtenus par synthèse et résolution. Les estimés les plus hauts ont été obtenus par l'utilisation d'un réactif de déplacement chimique impliquant des lanthanides chiraux, Eu(hfbc)$_3$, avec les dérivés sulfoniques des sulfures chiraux. L'ylide (+)-**3** réagit avec les aldéhydes avec de bons rendements pour conduire, sans induction d'asymétrie, à des oxirannes.

[Traduit par le journal]

The general utility of the reaction of sulfonium ylides with aldehydes and ketones to yield the corresponding oxiranes is well known (1–3). Sulfonium ylides, in possessing a pyramidal sulfur (4, 5), might serve as asymmetric transfer

[1]National Research Council of Canada Scholarship holder, 1972, 1973. Current address: Oilseeds Research, Agriculture Canada Research Station, Saskatoon, Saskatchewan.

[2]Deceased, April 15, 1973.

[3]Revision received August 26, 1975.

TABLE 1. Reactions of ethylmethylsulfonium *p*-nitrobenzylide with carbonyl compounds

Added reagent with (±)-**3**	Reaction time† (h)	Product*	Melting point (°C)	Yield (%)
Benzaldehyde	1	Oxirane **4***a*	124	65.5
p-Chlorobenzaldehyde	1	Oxirane **4***b*	125	77.3
p-Nitrobenzaldehyde	1	Oxirane **4***c*	200	77.3
Acetaldehyde	0.5	Oxirane **4***d*	86	66.0
Chalcone	2	**5**	104	16.0‡§
p-Nitroacetophenone	7–9	No oxirane‡		
Acetone	7–9	No oxirane‡		
Benzophenone	7–9	No oxirane‡		
Cyclohexanone	7–9	No oxirane‡		

*Products:

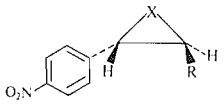

trans-**4***a* R = C_6H_5—, X = O
trans-**4***b* R = *p*-ClC_6H_4—, X = O
trans-**4***c* R = *p*-$NO_2C_6H_4$—, X = O
trans-**4***d* R = CH_3—, X = O
5 R = C_6H_5CO—, X = C_6H_5CH—

†Time for the wine-red colour of the effluent to disappear with equimolar ratio of reactants.
‡Sulfide decomposition products and oxirane **4***c* observed.
§Stereochemistry not assigned.

agents. However, the synthetic potential of the known carbonyl-stabilized chiral sulfonium ylides is severely limited by facile racemization ($t_{1/2}$ *ca.* 12–30 min at 50 °C in benzene) and reduced reactivity (6).

Trost and Hammen reported that the highly reactive (+)-1-adamantylethylsulfonium methylide failed to induce asymmetry in the products from reaction with benzaldehyde (7). However, a highly efficient asymmetric transfer (>94%) was discovered in the base-catalyzed rearrangement at −33 °C of (+)-1-adamantylallylethylsulfonium tetrafluoroborate to (*R*)-(−)-1-adamantyl-2-pent-4-enyl sulfide (7).

We also have failed to observe asymmetry in the products from reactions of several chiral sulfonium methylides with aldehydes and ketones. During these studies, a second example of an asymmetric transfer reaction similar to the allyl rearrangement was discovered. In this article, the asymmetric induction in the products of the Sommelet rearrangement of two chiral benzyl sulfonium salts will be described.

Chiral Benzylsulfonium Salts

(±)-Ethylmethyl-*p*-nitrobenzylsulfonium perchlorate, (±)-**1**, and (±)-ethylmethyl-*p*-chlorobenzylsulfonium perchlorate, (±)-**2**, were prepared and resolved utilizing the hydroxide exchange methods described previously for the synthesis and resolution of sulfonium salts via their (2*R*,3*R*)-hydrogen 2,3-dibenzoyltartrate salts (6, 8, 9). Precautionary measures similar to those employed for synthesizing chiral sulfonium ylides (6) were followed in obtaining the resolved salts with high specific rotations. The rate constants for the racemization of (+)-**1** and (+)-**2** in methanol at 70 °C are (9.15 ± 0.13) × 10^{-5} s^{-1} (8) and (9.66 ± 0.06) × 10^{-5} s^{-1} respectively (9). As with many other chiral sulfonium salts, (+)-**1** and (+)-**2** racemize via pyramidal inversion (8, 9).

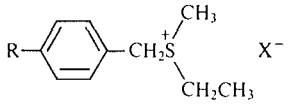

(+)-**1** R = NO_2, X = ClO_4
(+)-**2** R = Cl, X = ClO_4

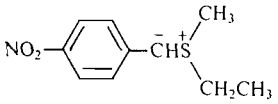

(±)-**3**

Can. J. Chem. Downloaded from www.nrcresearchpress.com by 210.87.254.6 on 09/05/12
For personal use only.

Can. J. Chem. Downloaded from www.nrcresearchpress.com by 210.87.254.6 on 09/05/12
For personal use only.

The Sommelet Rearrangements

Upon elution of a methanol solution of (+)-**1** through a Dowex 1-X8 hydroxide exchange column, a deep wine-red colour develops which is ascribed to the ylide (±)-**3** in equilibrium with its sulfonium hydroxide. Neutralization of the basic effluent with perchloric acid, with concomitant loss of colour, regenerates the perchlorate. Addition of aldehydes to the effluent results in the formation of the corresponding oxiranes **4** in high yields, Table 1. The ylide (±)-**3**, however, fails to react with ketones and reacts in very low yield with chalcone to give the cyclopropane product **5**. In failing to react with ketones, the ylide (±)-**3** decomposes via the Sommelet rearrangement to ethyl 2-methyl-5-nitrobenzyl sulfide, **6**, and (±)-methyl α-(2-methyl-5-nitrophenyl)ethyl sulfide, (±)-**7**. *trans*-4,4-Dinitrostilbene oxide, **4***c*, and other nitroaromatic compounds are also formed during this decomposition by complex radical-anion decomposition pathways (10, 11).

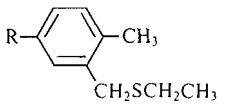

6 R = NO_2
8 R = Cl

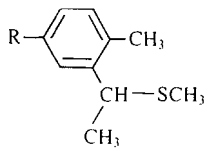

(±)-**7** R = NO_2
(±)-**9** R = Cl

Treatment of the optically active ylide, prepared by eluting (+)- or (−)-**1** through an hydroxide exchange column, with 1 equiv. of several aldehydes or an excess of acetaldehyde to effect an immediate reaction with the chiral ylide produced racemic oxiranes. Decomposition of the wine-red effluent from the hydroxide exchange of (+)-**1** for 17 h at room temperature in the absence of added electrophile yields **6** and the non-fractionally crystallized (+)-**7**, $[\alpha]_{436}^{r.t.}$ +54.2° (*c* 0.51, CH_2Cl_2) in 12 and 30% yields respectively.

This observation of induction of asymmetry in the products of the Sommelet rearrangement was extended to the more general literature procedure for the base-catalyzed rearrangement of benzyl sulfonium salts (12). The *p*-chloro salt, (+)-**2**, was heated for 2 h at 70 °C in the presence of 10 equiv. of a 24% sodium methoxide solution to produce the corresponding chloro Sommelet sulfides, **8** and (+)-**9**, $[\alpha]_{436}^{r.t.}$ +70.8° (*c* 0.26, benzene) and methyl *p*-chlorobenzyl ether in relative yields of 1:4:2 respectively. Under similar conditions, (+)-**3** would be expected to undergo complex radical-anion reactions (10, 11).

The racemic Sommelet sulfides isolated from the rearrangements and their sulfone derivatives, **10**–**13**, were identical in all respects with synthetic materials. Resolved sulfides and sulfones of highest optical rotation were prepared from resolved precursors. The enantiomeric purities (%e.p.) of the resolved sulfones were determined from the relative integrations of the differential downfield shifts (l.i.s.) of the enantiotopic *S*-methyl group of the sulfones in the presence of the chiral shift reagent, tris[3-heptafluorobutyryl-*d*-camphorato]-europium(III), Eu(hfbc)$_3$ (13, 14). No spectral shifts were observed for the Sommelet sulfides in the presence of Eu(hfbc)$_3$. The effect of added Eu(hfbc)$_3$ on the nmr spectra of the Sommelet sulfones is summarized in Tables 2 and 3.

Resolution of (±)-(2-methyl-5-nitrophenyl)-ethyl alcohol, (±)-**14**, the synthetic precursor of (±)-**7**, was achieved as its hydrogen phthalate with (+) or (−)-α-phenylethylamine (15). Recovery of the optically pure alcohol, tosylation, and displacement with methanethiolate afforded the resolved sulfide (+)-**7**. Oxidation of the sulfide with H_2O_2 in acetic acid provided the resolved sulfone, (+)-**11** (86.0 ± 1.0% e.p.). As was expected, a small portion (7%) of the methanethiolate displacement proceeded by an S_N1 mechanism. Comparison of the specific rotation of the sulfone (+)-**11**, obtained via the rearrangement with that of the resolved sulfone corrected for the 86% e.p., indicated the rearrangement in the nitro series proceeded with 18% asymmetric induction.

Resolution of (±)-(α-methyl-5-chlorophenyl)-ethyl alcohol, (±)-**15**, is readily achieved similarly as for the nitro analogue. However, the tosylate of (±)-**15** could not be isolated due to a subsequent chloride displacement reaction under the reaction conditions. Partial resolution of (±)-α-(2-methyl-5-chlorophenyl)ethane thiol, (±)-**16**, was achieved by a chromatographic separation of the diastereoisomers of *O*-menthyl α-(2-methyl-5-chlorophenyl)ethyl thiolcarbonate, (±)-**17**, on alumina (16). Recovery of the thiol from the faster eluting diastereoisomer, alkylation to the methyl sulfide (−)-**9**, and oxidation

TABLE 2. Effect of added $Eu(hfbc)_3$ on the nmr spectra of the chiral Sommelet sulfones (±)-**11*** and (±)-**13**† in $CDCl_3$

		Chemical shifts (ppm)			
		R = NO_2		R = Cl	
	Proton	l.i.s.	Δδ	l.i.s.	Δδ
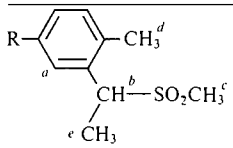	*a*	0.62	0.13	0.71	0.14
	b	1.01	0.12	1.13	0.12
	c	0.73	0.12	0.76	0.09
	d	0.17	0.12	0.20	0.02
	e	0.60	0.13	0.71	0.15

(±)-**11** R = NO_2
(±)-**13** R = Cl

*0.034 *M* $Eu(hfbc)_3$; 0.25 *M* sulfone (±)-**11**; molar ratio 0.14.
†0.057 *M* $Eu(hfbc)_3$; 0.17 *M* sulfone (±)-**13**; molar ratio 0.34.

TABLE 3. Effect of added $Eu(hfbc)_3$ on the nmr spectra of the achiral Sommelet sulfones **10*** and **12**†

		Chemical shifts (ppm)			
		R = NO_2		R = Cl	
	Proton	l.i.s.	Δδ	l.i.s.	Δδ
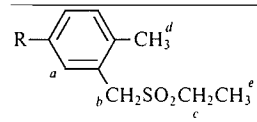	*a*	0.70	0	1.09	0
	b‡	2.37	0.02	2.59	0.05
	c‡	2.52	0.02	2.41	0.05
	d	0.42	0	0.71	0
	e	0.90	0	1.42	0

10 R = NO_2
12 R = Cl

*0.039 *M* $Eu(hfbc)_3$; 0.11 *M* sulfone **10**; molar ratio 0.35.
†0.039 *M* $Eu(hfbc)_3$; 0.11 *M* sulfone **12**; molar ratio 0.35.
‡Become diastereotopic in the presence of $Eu(hfbc)_3$.

afforded the partially resolved sulfone (−)-**13**. Recrystallization of this sulfone from $CHCl_3$ – Skellysolve B gave the racemic (±)-**13**. The evaporation residue was recrystallized twice from benzene – Skellysolve B to give resolved (−)-**13** (100% e.p.). Comparison of the specific rotation of the sulfone (−)-**13**, obtained via the rearrangement with that of the resolved (−)-**13** indicated the rearrangement proceeded with 21% asymmetric induction.

Estimates of asymmetric induction using $Eu(hfbc)_3$ were made directly on the crude oxidized reaction product mixtures without prior isolation of the sulfides. The relative amount of $Eu(hfbc)_3$ added to the oxidized mixture was adjusted such that resonances from reaction by-products such as the achiral sulfones **10** or **12**, ethers and others did not interfere with the resonances of the enantiotopic methyl groups of the chiral sulfones. By this method, enantiomeric purity for the *p*-nitro system was 20.3 ± 0.7% and for the *p*-chloro system was 25.5 ± 0.4%.

The estimates of the asymmetric induction by the two methods are in close agreement. One limit of the classical method of direct comparison of specific rotations with synthetically resolved materials was that, despite considerable effort, optically pure sulfide (+)-**7**, was not obtained. On the other hand, the chiral shift method could not be applied to the sulfides. Fortunately, the sulfides were easily converted to sulfones which experienced differential downfield shifts in the presence of $Eu(hfbc)_3$.

Discussion

The condensation reactions with aldehydes and chalcone gave oxiranes and cyclopropanes

Can. J. Chem. Downloaded from www.nrcresearchpress.com by 210.87.254.6 on 09/05/12
For personal use only.

Can. J. Chem. Downloaded from www.nrcresearchpress.com by 210.87.254.6 on 09/05/12
For personal use only.

derived from ylide formation at the benzyl position. The acidifying effect of the *p*-nitrophenyl substituent resulted in the benzylide formed from the sulfonium hydroxide having sufficient concentration to permit facile condensation. That the *p*-nitrobenzylide and its hydroxide were also in equilibrium with the alkylides formed at the methyl and ethyl substituents was evidenced by the isolation of the Sommelet sulfides in the absence of reactive electrophiles.

The failure to obtain significant optical yields in the asymmetric induction reactions of the *p*-nitrobenzylide with aldehydes was disappointing. By comparison, chiral oxosulfonium ylides are efficient asymmetric transfer agents in reaction with aldehydes (17). Racemization of the *p*-nitrobenzylide is not primarily responsible for the low optical yields as conditions set to minimize racemization by increasing the molar ratio of acetaldehyde results in the production of racemic oxirane. In the same time, neutralization with $HClO_4$ regenerated the chiral sulfonium salt. The ability to transfer asymmetry to the oxirane products may be more dependent in the transition state upon the additional steric and electronic requirements of the oxygen ligand of the oxosulfonium ylides than those of the lone pair of electrons of sulfonium ylides.

The lower efficiency of asymmetric induction in the products of the Sommelet rearrangements, 20–25% compared with 94% for the allyl rearrangement, is anticipated because of the greater opportunity for racemization of the inducing sulfonium centre under the reaction conditions. The much higher temperatures and longer reaction times of the Sommelet rearrangements are necessary to compensate for the loss of resonance stabilization in the aromatic ring in proceeding from the ylide.

The lower efficiency in the Sommelet rearrangement may also be due to inherent differences in the two rearrangements independent of racemization. The initial products of the Sommelet rearrangement consist of a pair of diastereoisomers and their enantiomers, **18**, rather than a single pair of enantiomers as for the allyl rearrangement. Following the rearrangement,

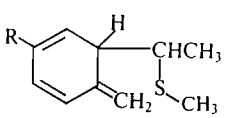

rearomatization removes one asymmetric centre and reduces the products to the enantiomeric pair of sulfides isolated. For the allyl rearrangement, the enantiomeric ratio of products can be attributed to the energy differences of the diastereomeric transition states leading to each enantiomer as there are no energy differences in enantiomeric products. The case is more complex for the Sommelet rearrangement because of the possibility of four diastereomeric transition states leading to a pair of diastereomers and their enantiomers. Energy differences between transition states, reactants and the initial diastereomeric products could be less distinct and result in a lower efficiency of asymmetric induction in the isolated product, the Sommelet sulfides.

Experimental

All melting points (uncorrected) were obtained using a Hershberg type melting point apparatus with a set of Anschutz thermometers. Nuclear magnetic resonance spectra were recorded on Varian Analytical Spectrometers, Models A-60, A-56-60, or HA-100. Chemical shifts are reported in δ units from internal TMS. Infrared spectra were recorded on a Perkin-Elmer Grating Infrared Spectrometer, Model 421. Optical rotations were obtained using a Perkin-Elmer Polarimeter, Model 141.

For enantiomeric purity estimates, stock solutions of $Eu(hfbc)_3$ (Willow Brook Laboratories, Inc.) in $CDCl_3$ were added to solutions of the compounds in the test. Using the HA-100 Spectrometer, %e.p. was determined from the average ± average deviation of six integrations of enantiotopic resonances at expanded sweep widths of 50 or 100 Hz in 100 or 250 s sweep times.

The exchange of counterions of sulfonium salts using Dowex 1-X8 hydroxide exchange resins and resolution techniques using (2*R*,3*R*)-2,3-dibenzyltartaric acid monohydrate, HDBT (18), were as described previously (6). Isolation procedures for new compounds, except where noted, routinely involved diluting the reaction mixture with water and extraction with ether, benzene, or $CHCl_3$. The extracts were washed with H_2O, dried over $MgSO_4$ and concentrated. Solids were crystallized from benzene – Skellysolve B or $CHCl_3$ – Skellysolve B. Liquids were distilled under reduced pressure.

(+)-Ethylmethyl-p-nitrobenzylsulfonium Perchlorate, (+)-1

p-Nitrobenzyl ethyl sulfide (19) was treated with excess $(CH_3)_2SO_4$ in acetone overnight. The solvent was removed and the residue crystallized from methanol–ether to yield (±)-ethylmethyl-*p*-nitrobenzylsulfoniummethylsulfate, mp 102 °C; nmr (DMSO-d_6), δ 8.42 (d, J = 9.0 Hz, 2H), 7.89 (d, J = 9.0 Hz, 2H), 4.96 (s, 2H), 3.52 (s, 3H), 3.44 (q, J = 7.5 Hz, 2H), 2.95 (s, 3H), and 1.40 (t, J = 7.5 Hz, 3H); ir (Nujol), 1610 (m), 1520 (s), 1460 (s), and 1230 (s) cm^{-1}.

Can. J. Chem. Downloaded from www.nrcresearchpress.com by 210.87.254.6 on 09/05/12
For personal use only.

The methylsulfate was converted to a diastereomeric mixture of DBT salts by eluting a methanol solution of the salt through Dowex 1-X8 hydroxide exchange resin and neutralizing the eluate with HDBT. The DBT salts were fractionally crystallized from methanol–ether into the less soluble diastereoisomer, mp 150 °C; $[\alpha]_{436}^{r.t.}$ −172° (*c* 0.27, methanol) and the more soluble diastereoisomer, mp 141 °C; $[\alpha]_{436}^{r.t.}$ −207° (*c* 0.25, methanol). The less soluble diastereoisomer was converted by anion exchange to (+)-**1**, mp 80 °C; $[\alpha]_{436}^{r.t.}$ +41.4° (*c* 0.46, methanol); nmr (DMSO-d_6), δ 8.25 (d, J = 8.0 Hz, 2H), 7.72 (d, J = 8.0 Hz, 2H), 4.80 (s, 2H), 3.33 (q, J = 7.5 Hz, 2H), 2.84 (s, 3H), and 1.36 (t, J = 7.5 Hz, 3H); ir (Nujol), 1610 (s), 1500 (s), 1430 (s), and 1100 (broad) cm^{-1}. The specific rotation reported is the highest obtained for several preparations. *Anal.* Calcd. for $C_{10}H_{14}ClNO_6S$: C 38.53, H 4.53, Cl 11.37, N 4.50, S 10.29; found: C 38.40, 38.08, H 4.39, 4.48, Cl 11.57, 11.17, N 4.51, 4.74, S 10.45, 10.38.

(±)-p-Chlorobenzylethylmethylsulfonium Perchlorate, (±)-2

p-Chlorobenzyl bromide was treated with ethyl methyl sulfide in acetone overnight. The solvent was removed and the residue crystallized from methanol–ether to give the unstable bromide salt. This salt was converted immediately by anion exchange to (±)-**2**, mp 88–89 °C; nmr (DMSO-d_6), δ 7.44 (s, 4H), 4.68 (s, 2H), 3.28 (q, J = 7.5 Hz, 2H), 2.79 (s, 3H), and 1.32 (t, J = 7.5 Hz, 3H); ir ($CHCl_3$), 1585 (w), 1480 (m), 1085 (s), and 610 (m) cm^{-1}. Analyses for carbon and hydrogen were variable due to the sample exploding during analysis with accompanying sample loss.

(+)-Ethylmethyl-p-chlorobenzylsulfonium Perchlorate, (+)-2

The DBT salts of (±)-**2** obtained by anion exchange were fractionally crystallized from methanol–ether into the less soluble diastereoisomer, mp 150–151 °C; $[\alpha]_{436}^{r.t.}$ −174° (*c* 1.5, methanol) and the more soluble diastereoisomer, mp 150 °C; $[\alpha]_{436}^{r.t.}$ −198° (*c* 1.4, methanol). The less soluble diastereoisomer was converted by anion exchange to (+)-**2**, mp 80–81 °C; $[\alpha]_{365}^{r.t.}$ +62.2° (*c* 0.60, methanol). The ir and nmr spectra were superimposable upon those of racemic material.

Reactions of (±)- and (+)-Ethylmethylsulfonium p-nitrobenzylide, (±)-3 and (+)-3

The wine-red solutions of (±)-**3** were prepared by eluting solutions containing 1 g (±)-**1** through hydroxide exchange resin. Treatment of the effluent with equimolar $HClO_4$ generated the perchlorate. Treatment of the effluent with benzaldehyde, *p*-chlorobenzaldehyde, *p*-nitrobenzaldehyde, acetaldehyde, or chalcone afforded the oxiranes **4***a–d* and cyclopropane **5** (Table 1). The effluent left to stand 17 h at room temperature lost the wine-red colour and produced the sulfides **6** and (±)-**7**.

Solutions of (+)-**3** were prepared by eluting (+)-**1**, $[\alpha]_{436}^{r.t.}$ +40.3° (*c* 0.94, methanol) through hydroxide exchange resin. Racemic oxiranes were obtained from reactions of aldehydes with the chiral ylide. Decomposition of (+)-**3** in 17 h at 22 °C produced **6** and (+)-**7**, $[\alpha]_{436}^{r.t.}$ +54.2° (*c* 0.51, CH_2Cl_2) in 12 and 30% yield respectively. Yields were estimated by nmr with benzhydrol as internal standard. A portion of the product mixture was concentrated and the residue heated in excess 30% H_2O_2 in acetic acid for 3 h at 100 °C. Enantiomeric purity of (+)-**7** was 20.3 ± 0.7% as determined on the sulfone in the crude oxidized product mixture. The remaining mixture was chromatographed on alumina with Skellysolve B to separate sulfides **6** and (+)-**7**. The nonfractionally crystallized (+)-**7** was heated in excess 30% H_2O_2 in acetic acid at 100 °C for 3 h to provide the sulfone (+)-**11**, $[\alpha]_{436}^{r.t.}$ +31.6° (*c* 0.57, chloroform) (19.5 ± 0.7% e.p.).

Sommelet Rearrangement of (+)-p-Chlorobenzylethylmethylsulfonium Perchlorate, (+)-2

A 0.5 g (1.65 mmol) quantity of (+)-**2**, $[\alpha]_{365}^{r.t.}$ +62.2° (*c* 0.56, methanol) was heated for 2 h at 70 °C in 10 equiv. of a 24% sodium methoxide solution (0.38 g Na, 16.5 mmol, in 3.42 g methanol). The reaction mixture was poured into water and the mixture extracted with ether. The extracts were dried and concentrated. The evaporation residue was transferred to a 5-ml volumetric flask with benzene. A 1-ml aliquot was added to a known quantity of 2-methylnaphthalene in benzene and the product balance determined by glc. Conditions were: 6 ft by $\frac{3}{8}$ in. 20% Carbowax 1500 on 60–80 Chromosorb W column at 174 °C; helium 60 ml/min. Relative yields of **8**, (+)-**9**, and methyl *p*-chlorobenzyl ether were 1:4:2 respectively, product balance, 94%. A second 1-ml aliquot was concentrated and the residue heated in excess 30% H_2O_2 in acetic acid at 100 °C for 3 h. Enantiomeric purity of (+)-**13** was 25.5 ± 0.4% as determined directly on the sulfone in the crude oxidized product mixture. The remaining 3-ml portion was chromatographed by glc and the sulfide (+)-**9**, $[\alpha]_{436}^{r.t.}$ +70.8° (*c* 0.26, benzene) condensed at the collection port. The sulfide was oxidized with H_2O_2 to yield the sulfone (+)-**13**, $[\alpha]_{365}^{r.t.}$ +26.9° (*c* 0.29, benzene) (27.0 ± 1.2% e.p.).

Ethyl 2-Methyl-5-nitrobenzyl Sulfide, 6

2-Chloromethyl-4-nitrotoluene (12 g, 64.5 mmol) (20) in methanol was added slowly to a methanol solution containing excess sodium and ethane thiol. The resulting solution stirred 30 min at 22 °C to provide **6** (10.5 g, 50.0 mmol, 77%), bp 167–169 °C (5 Torr): η_D^{25} 1.5812; nmr (CD_2Cl_2), δ 7.94 (m, 2H), 7.27 (d, J = 8.0 Hz, 1H), 3.77 (s, 2H), 2.51 (q, J = 7.5 Hz, 2H), 2.48 (s, 3H), and 1.25 (t, J = 7.5 Hz, 3H); ir (neat), 2980 (m), 2940 (m), 1615 (w), 1590 (m), 1520 (s), 1455 (m), 1350 (s), 1085 (m), 815 (s), and 740 (s) cm^{-1}. *Anal.* Calcd. for $C_{10}H_{13}NO_2S$: C 56.83, H 6.20, N 6.66, S 15.17; found: C 56.56, 57.11, H 6.16, 6.33, N 6.77, 6.86, S 15.16, 15.16.

Ethyl 2-Methyl-5-nitrobenzyl Sulfone, 10

The sulfide **6** (0.317 g, 1.50 mmol) was heated for 3 h at 100 °C in the presence of excess of 30% H_2O_2 (0.383 g, 3.26 mmol) in acetic acid (5 ml) to provide **10** (0.291, 1.21 mmol, 80.0%), mp 139–140 °C; nmr ($CDCl_3$), δ 8.21–8.14 (m, 2H), 7.42 (d, J = 7.5 Hz, 1H), 4.38 (s, 2H), 3.09 (q, J = 7.0 Hz, 2H), 2.57 (s, 3H), and 1.45 (t, J = 7.0 Hz, 3H); ir ($CHCl_3$), 1605 (w), 1580 (w), 1510 (m), 1345 (s), 1310 (s), 1270 (m), 1130 (s), 1110 (s), 1080 (w), 1040 (m), 905 (m), and 875 (w) cm^{-1}. *Anal.* Calcd. for $C_{10}H_{13}NO_4S$: C 49.37, H 5.39, N 5.76, S 13.18; found: C 48.91, 49.11, H 5.51, 5.46, N 5.69, 5.58, S 13.09, 13.17.

Can. J. Chem. Downloaded from www.nrcresearchpress.com by 210.87.254.6 on 09/05/12
For personal use only.

*(±)-α-(2-Methyl-5-nitrophenyl)ethyl Alcohol, (±)-**14***

An aqueous solution of $NaBH_4$ (0.60 g, 15.9 mmol) was added to 2-methyl-5-nitroacetophenone (5.41 g, 30.2 mmol) (21) in methanol to provide (±)-**14** (3.29 g, 18.2 mmol, 60.4%), mp 90–91 °C; nmr (CD_2Cl_2), δ 8.26 (d, J = 2.5 Hz, 1H), 7.87 (q, 1H), 7.22 (d, J = 8.0 Hz, 1H), 5.11 (q, J = 6.5 Hz, 1H), 3.13 (s, 1H), 2.36 (s, 3H), and 1.42 (d, J = 6.5 Hz, 3H); ir ($CHCl_3$), 3600 (m), 1585 (m), 1520 (s), 1450 (m), 1345 (s), 1105 (m), and 1065 (m) cm^{-1}. *Anal.* Calcd. for $C_9H_{11}NO_3$: C 59.64, H 6.12, N 7.76; found: C 59.57, 59.62, H 6.35, 6.26, N 7.72, 7.60.

*(±)-α-(2-Methyl-5-nitrophenyl)ethyl Bromide, (±)-**19***

Gaseous HBr was bubbled through benzene (30 ml) containing (±)-**14** (1.27 g, 6.98 mmol) for 30 min to provide (±)-**19** (1.56 g, 6.37 mmol, 91.2%), mp 53–54 °C; nmr ($CDCl_3$), δ 8.39 (d, J = 2.5 Hz, 1H), 8.03 (q, 1H), 7.32 (d, J = 8.4 Hz, 1H), 5.38 (q, J = 2.5 Hz, 1H), 2.52 (s, 3H), and 2.12 (t, J = 7.0 Hz, 3H); ir ($CHCl_3$), 1605 (w), 1580 (m), 1510 (m), 1240 (s), 1050 (m), and 900 (m) cm^{-1}. *Anal.* Calcd. for $C_9H_{10}BrNO_2$: C 44.28, H 4.13, Br 32.73, N 5.76; found: C 44.33, 44.07, H 4.29, 4.21, Br 32.73, 32.56, N 5.90, 5.49.

*(±)-Methyl α-(2-Methyl-5-nitrophenyl)ethyl Sulfide, (±)-**7***

The bromide (±)-**19** (1.49 g, 6.10 mmol) in methanol (25 ml) was added to a methanol solution containing an excess of sodium metal and methane thiol. The resulting solution was stirred 30 min at 22 °C to provide, after isolation and crystallization from Skellysolve B, (±)-**7** (1.09 g, 5.13 mmol, 84%), mp 49.5–50.5 °C; nmr (CD_2Cl_2), δ 8.24 (d, J = 2.4 Hz, 1H), 7.96 (q, 1H), 7.25 (d, J = 8.5 Hz, 1H), 4.17 (q, J = 7.0 Hz, 1H), 2.47 (s, 3H), 1.94 (s, 3H), and 1.58 (d, J = 7.0 Hz, 1H); ir ($CHCl_3$), 1605 (m), 1580 (s), 1500 (s), 1440 (s), 1100 (s), and 910 (s) cm^{-1}. *Anal.* Calcd. for $C_{10}H_{12}NO_2S$: C 56.83, H 6.20, N 6.66, S 15.17; found: C 56.90, 56.59, H 6.04, 6.23, N 6.37, 6.54, S 15.09, 15.06.

*(±)-Methyl α-(2-Methyl-5-nitrophenyl)ethyl Sulfone, (±)-**11***

The sulfide (±)-**7** was heated in H_2O_2 in acetic acid for 3 h at 100 °C to provide (±)-**11** in 85% isolated yield, mp 150–151 °C; nmr ($CDCl_3$), δ 8.38 (d, J = 2.5 Hz, 1H), 8.14 (q, 1H), 7.45 (d, J = 8.0 Hz, 1H), 4.64 (q, J = 7.0 Hz, 1H), 2.85 (s, 3H), 2.59 (s, 3H), and 1.87 (d, J = 7.0 Hz, 3H); ir ($CHCl_3$), 1605 (w), 1580 (w), 1510 (m), 1345 (s), 1310 (s), 1280 (w), 1265 (w), 1135 (s), 1115 (s), 945 (s), and 900 (m) cm^{-1}. *Anal.* Calcd. for $C_{10}H_{13}NO_4S$: C 49.37, H 5.39, N 5.76, S 13.18; found: C 49.20, 49.86, H 5.44, 5.69, N 5.35, S 13.02.

*2-Methyl-5-chlorobenzyl Alcohol, **20***

2-Methyl-5-chlorobenzaldehyde (13.3 g, 0.0862 mol) (22) in methanol (50 ml) was reduced after addition of an aqueous solution of $NaBH_4$ (1.70 g, 0.045 mol) to provide **20** (11.5 g, 0.0735 mol, 85.4%), mp 44 °C; nmr ($CDCl_3$), δ 7.26 (s, 1H), 7.08 (d, J = 8.0 Hz, 1H), 6.99 (d, J = 9.0 Hz, 1H), 4.49 (s, 2H), 2.96 (s, 1H), and 2.18 (s, 3H); ir ($CHCl_3$), 3600 (m), 1600 (m), 1490 (s), 1100 (m), and 880 (m) cm^{-1}. *Anal.* Calcd. for C_8H_9ClO: C 61.35, H 5.79, Cl 22.64; found: C 61.66, 61.54, H 5.57, 6.10, Cl 22.18, 22.90.

*2-Methyl-5-chlorobenzyl Bromide, **21***

Gaseous HBr was bubbled through a 50-ml benzene solution containing **20** (11.3 g, 0.0723 mol) until no further water separated to provide **21** (13.9 g, 0.0632 mol, 87.5%), mp 31–32 °C; nmr ($CDCl_3$), δ 7.26 (s, 1H), 7.18 (d, J = 7.5 Hz, 1H), 7.08 (d, J = 7.5 Hz, 1H), 4.41 (s, 2H), and 2.35 (s, 3H); ir ($CHCl_3$), 1600 (m), 1575 (w), 1145 (w), 1110 (s), and 900 (s) cm^{-1}.

*Ethyl 2-Methyl-5-chlorobenzyl Sulfide, **8***

The bromide **21**, (12.9 g, 0.0587 mol) in methanol (100 ml) was added slowly to a methanol solution containing an excess of sodium and ethane thiol. The resulting solution was stirred for 1 h to provide **8** (8.00 g, 0.0399 mol, 68.2%), bp 117–118 °C (6 Torr); η_D^{30} 1.5611; nmr ($CDCl_3$), δ 7.24–6.99 (m, 3H), 3.64 (s, 2H), 2.46 (q, J = 7.5 Hz, 2H), 2.34 (s, 3H), and 1.23 (t, J = 7.5 Hz, 3H); ir (neat), 2985 (s), 2965 (s), 1595 (m), 1485 (s), 1400 (m), 1265 (m), 1115 (m), 900 (m), 885 (m), and 815 (s) cm^{-1}. *Anal.* Calcd. for $C_{10}H_{13}ClS$: C 59.84, H 6.53; found: C 59.97, 59.68, H 6.79, 6.64.

*Ethyl 2-Methyl-5-chlorobenzyl Sulfone, **11***

The sulfide **8**, was heated in H_2O_2 in acetic acid for 3 h at 100 °C to provide **12**, mp 116–117 °C; nmr ($CDCl_3$), δ 7.28 (m, 3H), 4.23 (s, 2H), 3.00 (q, J = 7.5 Hz, 1H), 2.42 (s, 3H), and 1.41 (t, J = 7.5 Hz, 3H); ir ($CHCl_3$), 2970 (w), 1590 (w), 1475 (m), 1310 (s), 1120 (s), and 890 (m) cm^{-1}. *Anal.* Calcd. for $C_{10}H_{13}ClO_2S$: C 51.61, H 5.63, Cl 15.23, S 13.78; found: C 51.77, 51.31, H 5.68, 5.57, Cl 15.46, 15.35, S 13.93, 13.81.

*(±)-α-(2-Methyl-5-chlorophenyl)ethyl Alcohol, (±)-**15***

2-Methyl-5-chloroacetophenone (6.82 g, 0.0405 mol) (23) in methanol (50 ml) was reduced, after addition of an aqueous solution of $NaBH_4$ (0.746 g, 0.0197 mol), to provide (±)-**15** (5.66 g, 0.0332 mol, 82.2%), bp 97–98 °C (3.5 Torr); η_D^{30} 1.5457; nmr ($CDCl_3$), δ 7.48 (d, J = 1.5 Hz, 1H), 7.08 (m, 2H), 5.04 (q, J = 6.5 Hz, 2H), 2.66 (s, 3H), 2.12 (s, 1H), and 1.38 (d, J = 6.5 Hz, 3H); ir ($CHCl_3$), 3600 (m), 1595 (m), 1400 (m), 1375 (m), 1105 (s), and 1075 (s) cm^{-1}. *Anal.* Calcd. for $C_9H_{11}ClO$: C 63.35, H 6.50, Cl 20.78; found: C 63.16, 63.63, H 6.42, 6.64, Cl 21.01, 21.27.

*(±)-α-(2-Methyl-5-chlorophenyl)ethyl Bromide, (±)-**22***

Gaseous HBr was bubbled through a 10-ml benzene solution containing (±)-**15** (1.62 g, 9.52 mmol) until no further water separated to provide (±)-**22** (1.59 g, 6.78 mmol, 71.3%), bp 94 °C (3.5 Torr); η_D^{30} 1.5720; nmr ($CDCl_3$), δ 7.49 (d, J = 1.4 Hz, 1H), 7.10 (m, 2H), 5.31 (q, J = 6.5 Hz, 1H), 2.35 (s, 3H), and 2.03 (d, J = 6.5 Hz, 3H); ir (neat), 2980 (m), 1590 (m), 1480 (s), 1450 (m), 1185 (s), 860 (s), and 810 (s) cm^{-1}.

*(±)-Methyl α-(2-Methyl-5-chlorophenyl)ethyl Sulfide (±)-**9***

The bromide (±)-**22** (1.63 g, 6.93 mmol) in methanol was added slowly to a methanol solution containing an excess of sodium and methane thiol. The resulting solution was stirred for 30 min to provide (±)-**9** (1.02 g, 5.08 mmol, 73.5%), bp 108–110 °C (5 Torr); η_D^{25} 1.5640; nmr ($CDCl_3$), δ 7.42 (s, 1H), 7.05 (m, 2H), 4.08 (q, J = 6.5 Hz, 1H), 2.33 (s, 3H), 1.94 (s, 3H), and 1.55 (d, J = 6.5 Hz, 3H); ir (neat), 2985 (m), 2920 (m), 1595 (m), 1484

Can. J. Chem. Downloaded from www.nrcresearchpress.com by 210.87.254.6 on 09/05/12
For personal use only.

(s), 1125 (m), 865 (s), and 810 (s) cm^{-1}. *Anal.* Calcd. for $C_{10}H_{13}ClS$: C 59.83, H 6.52, Cl 17.66, S 15.97; found: C 59.90, 59.92, H 6.69, 6.59, Cl 17.37, 17.86, S 15.89, 15.79.

(±)-Methyl α-(2-Methyl-5-chlorophenyl)ethyl Sulfone, (±)-13

The sulfide (±)-**9** was heated in H_2O_2 in acetic acid for 3 h at 100 °C to provide (±)-**13**, mp 143–144 °C; nmr ($CDCl_3$), δ 7.70 (s, 1H), 7.36 (s, 2H), 4.58 (q, J = 7.0 Hz, 1H), 2.78 (s, 3H), 2.46 (s, 3H), and 1.78 (d, J = 7.0 Hz, 3H); ir ($CHCl_3$), 2900 (w), 1590 (w), 1480 (m), 1300 (s), 1130 (s), 945 (s), and 860 (m) cm^{-1}. *Anal.* Calcd. for $C_{10}H_{13}ClO_2S$: C 51.61, H 5.63, Cl 15.23, S 13.78; found: C 51.70, 51.53, H 5.75, 5.61, Cl 14.95, 15.11, S 13.97, 13.91.

(±)-α-(2-Methyl-5-nitrophenyl)ethyl Hydrogen Phthalate, (±)-23

Synthesis

(±)-**14** (0.535 g, 2.96 mmol) and phthalic anhydride (0.437 g, 2.96 mmol) were heated in dry pyridine (5 ml) for 1 h at 100 °C. The solution was cooled, diluted with acetone (5 ml), and neutralized with cold concentrated HCl. The precipitate was recrystallized from $CHCl_3$ – Skellysolve B to yield (±)-**23** (0.777 g, 2.36 mmol, 79.7%), mp 145 °C; nmr ($CDCl_3$), δ 11.87 (s, 1H), 8.32 (d, J = 2.0 Hz, 1H), 8.15–7.50 (m, 5H), 7.30 (d, J = 8.4 Hz, 1H), 6.36 (q, J = 6.5 Hz, 1H), 2.55 (s, 3H), and 1.66 (d, J = 6.5 Hz, 3H); ir ($CDCl_3$), 3000 (broad), 1718 (s), 1695 (s), 1520 (s), 1345 (s), 1055 (m), and 905 (w) cm^{-1}. *Anal.* Calcd. for $C_{17}H_{15}NO_6$: C 62.01, H 4.59, N 4.25; found: C 62.06, 61.74, H 4.75, 4.47, N 4.40, 4.47.

Resolution

(±)-**23** (0.543 g, 1.65 mmol) and (−)-α-phenylethylamine (0.200 g, 1.65 mmol) were dissolved in methanol (5 ml). Ether (75 ml) was added and the resulting solution cooled 18 h at −10 °C to yield a precipitate. Two recrystallizations from methanol–ether gave the less soluble diastereoisomer, mp 167 °C; $[\alpha]_{436}^{r.t.}$ −15.0° (*c* 1.0, CH_3OH). This was dissolved in CH_3OH and the solution acidified with dilute HCl. The mixture was extracted with ether. The ether extracts were washed with water, dried, and concentrated. The residue was crystallized from benzene – Skellysolve B to yield (−)-**23**, mp 75 °C; $[\alpha]_{436}^{r.t.}$ −165° (*c* 0.932, $CHCl_3$). The optically impure (+)-**23** was recovered from the mother liquors of the resolution and resolved using (+)-α-phenylethylamine to provide (+)-**23**, mp 74 °C; $[\alpha]_{436}^{r.t.}$ +164° (*c* 0.956, $CHCl_3$).

(−)- and (+)-α-(2-Methyl-5-nitrophenyl)ethyl Alcohol, (−)- and (+)-14

Optically pure (−)-**23** (0.125 g, 0.381 mmol) was hydrolyzed for 5 min at 100 °C in 9.1 ml 1.25 *N* NaOH to free (−)-**14**. Following extraction with ether, the crude (−)-**14** was chromatographed on a short alumina column with 1:1 benzene–ether to remove red impurities. The eluate was concentrated and the residue crystallized from benzene – Skellysolve B to yield (−)-**14** (0.047 g, 0.26 mmol, 68.3%), mp 67 °C; $[\alpha]_{436}^{r.t.}$ −150° (*c* 0.47, $CHCl_3$). Similarly, (+)-**20** was hydrolyzed to (+)-**14**, mp 67 °C; $[\alpha]_{436}^{r.t.}$ +150° (*c* 0.86, $CHCl_3$), %e.p. 100%.

(−)-α-(2-Methyl-5-nitrophenyl)ethyl Tosylate, (−)-24

Enantiomerically pure (−)-**14** (0.167 g, 0.92 mmol) and *p*-toluenesulfonyl chloride (0.184 g, 0.966 mmol) were dissolved in 0.85 ml dry pyridine and the solution cooled at −10 °C for 3 days. The reaction mixture containing crystallized pyridinium hydrochloride was poured into cold dilute HCl and the resulting mixture extracted with ether. The ether extracts were washed with 5% $NaHCO_3$, water, dried over $MgSO_4$, and concentrated. Two crystallizations of the evaporation residue from benzene – Skellysolve B gave (−)-**24** (0.124 g, 0.369 mmol, 40%), mp 103–104 °C; $[\alpha]_{436}^{r.t.}$ −350° (*c* 1.24, benzene); nmr ($CDCl_3$), δ 8.24–7.05 (m, 7H), 5.92 (q, J = 7.0 Hz, 1H), 2.42 (s, 3H), 2.36 (s, 3H), and 1.61 (d, J = 7.0 Hz, 3H).

(+)-α-(2-Methyl-5-nitrophenyl)ethyl Sulfide, (+)-8

To a flask fitted with a dry ice cold-finger condenser, a sodium ethoxide solution (from 0.0706 g, 3.07 mmol, Na), 95% ethanol (10 ml) at 0 °C, methane thiol (2 ml) and (−)-**24** (0.164 g, 0.49 mmol) in CH_2Cl_2 (2 ml) were added sequentially. After 4 h stirring at 0 °C, the mixture was diluted with H_2O and extracted with CH_2Cl_2. The extracts were dried and concentrated to yield crude (+)-**7** (0.0963 g, 0.46 mmol, 93%); $[\alpha]_{436}^{r.t.}$ +242° (*c* 0.96, CH_2Cl_2). The crude product was crystallized from Skellysolve B to yield (+)-**7** (0.0656 g), mp 29–30 °C; $[\alpha]_{436}^{r.t.}$ +266° (*c* 0.66, CH_2Cl_2). The crystalline (+)-**7** was heated in H_2O_2 in acetic acid at 100 °C for 3 h to yield (+)-**11**, $[\alpha]_{436}^{22}$ +149° (*c* 0.72, $CHCl_3$), mp 165–166 °C; 86.0 ± 1.0% e.p.

(±)-α-(2-Methyl-5-chlorophenyl)ethanethiol, (±)-16

The bromide (±)-**22** (5.0 g, 0.0214 mol) was added to 1.3 *N* KOH (50 ml) saturated with H_2S. The solution was stirred for 90 min at 22 °C, diluted with H_2O and the resulting mixture extracted with ether. The extracts were washed with H_2O, dried and concentrated. The residue was distilled under reduced pressure to yield (±)-**16** (2.56 g, 0.0137 mol, 64%), bp 105–107 °C (6 Torr); η_D^{20} 1.5736; nmr ($CDCl_3$), δ 7.43 (s, 1H), 7.07 (m, 2H), 4.33 (pentet, J = 6.0 Hz, 1H), 2.34 (s, 3H), 1.87 (d, J = 6.0 Hz, 1H), and 1.64 (d, J = 7.0 Hz, 3H); ir (neat), 2975 (m), 2550 (w), 1595 (m), 1490 (s), 1450 (m), and 810 (s) cm^{-1}. *Anal.* Calcd. for $C_9H_{11}ClS$: C 57.90, H 5.94, Cl 18.99, S 17.17; found: C 57.90, 58.36, H 6.00, 6.09, Cl 19.15, 19.32, S 16.81, 16.72.

O-(−)-Menthyl α-(2-Methyl-5-chlorophenyl)ethyl Thiolcarbonate, 17

Synthesis

(±)-**16** (5.55 g, 0.0298 mol) was slowly added to a suspension of 1.27 g (0.0322 mol) 57% NaH in 50 ml ether. After H_2 evolution ceased, this solution was added slowly to a stirred solution of (−)-menthyl chloroformate (24) in ether (50 ml). After 1 h, the mixture was filtered by gravity and the precipitate washed several times. The mother liquor was concentrated and traces of solvent removed under reduced pressure to yield the oily **17**, $[\alpha]_{365}^{r.t.}$ −147° (*c* 1.0, benzene); nmr ($CDCl_3$), δ 7.37 (s, 1H), 7.10 (m, 2H), 4.82 (broad, 1H), 4.75 (q, 7.5 Hz, 1H), 2.39 (s, 3H), 1.67 (d, J = 7.5 Hz, 3H), 1.00–0.65 (m, 9H), and 1.26 (s, impurity); ir ($CHCl_3$), 1760 (m), 1680 (s), 1600 (w), 1170 (s), and 1150 (s) cm^{-1}.

Can. J. Chem. Downloaded from www.nrcresearchpress.com by 210.87.254.6 on 09/05/12
For personal use only.

Resolution

Partial resolution was achieved by chromatography of 5-g quantities alumina oxide (88 g) (Woelm neutral, activity 1). While collecting 50-ml fractions, 700 ml Skellysolve B was eluted through the column. The first fraction contained the oil impurity from the 57% NaH. Subsequent fractions contained the faster-eluting diastereomer with rotations decreasing from $[\alpha]_{365}^{r.t.}$ $-370°$ to $-227°$ (*c* 1.0, benzene). Eluting with 700 ml benzene removed oils with rotations $[\alpha]_{365}^{r.t.}$ $-143°$ to $-50.8°$ (*c* 1.0, benzene). Finally, the column was flushed with 500 ml ether to give the slower-eluting diastereomer $[\alpha]_{365}^{r.t.}$ $-13.5°$ (*c* 1.34, benzene).

The faster-eluting **17** (0.222 g, 0.60 mol), $[\alpha]_{365}^{r.t.}$ $-281°$ (*c* 2.2, benzene) was transesterified upon heating in 5-ml 0.5 *N* $NaOCH_3$ at reflux for 90 min to liberate (−)-**16**. The reaction mixture was cooled, poured into dilute NaOH and extracted with ether several times. The aqueous phase was acidified with HCl, extracted with ether and the latter ether extracts washed with H_2O, dried and concentrated to yield partially resolved (−)-**16** (0.070 g, 0.375 mmol, 63%), $[\alpha]_{365}^{r.t.}$ $-61.7°$ (*c* 0.7, $CHCl_3$). Concentration of the original ether extracts gave menthol.

(−)-Methyl α-(2-Methyl-5-chlorophenyl)ethyl Sulfone, (−)-13

Partially resolved thiol (−)-**16** (0.315 g, 1.69 mmol), $[\alpha]_{436}^{r.t.}$ 51.5° (*c* 3.15, $CHCl_3$) was alkylated with CH_3I in 0.5 *N* $NaOCH_3$ (5 ml) for 1 h to provide (−)-**9** (0.307 g, 1.53 mmol, 90.8%), $[\alpha]_{436}^{r.t.}$ $-75.4°$ (*c* 3.07, benzene). This crude sulfide was heated with excess 30% H_2O_2 in HOAc (5 ml) for 3 h at 100 °C to yield the crude (−)-**13**, $[\alpha]_{365}^{r.t.}$ $-31.3°$ (*c* 3.46, $CHCl_3$). Fractional crystallization from $CHCl_3$ – Skellysolve B gave (±)-**13**. The evaporation residue of the mother liquor was crystallized from benzene – Skellysolve B to give (−)-**13**, mp 99–100 °C, $[\alpha]_{365}^{r.t.}$ $-127°$ (*c* 0.60, benzene or $CHCl_3$), 100% e.p.

1. E. J. Corey and M. Chaykovsky. J. Am. Chem. Soc. **87**, 1353 (1965).
2. A. W. Johnson, V. J. Hruby, and J. L. Williams. J. Am. Chem. Soc. **86**, 918 (1964).
3. V. Franzen and H. E. Driessen. Tetrahedron Lett. 661 (1962).
4. H. Nozaki, D. Tunemoto, K. Nakamura, K. Watanabe, M. Takaku, and K. Kondo. Tetrahedron, **23**, 4279 (1967).
5. A. F. Cook and J. C. Moffat. J. Am. Chem. Soc. **90**, 740 (1968).
6. S. J. Campbell and D. Darwish. Can. J. Chem. **52**, 2953 (1974)
7. B. M. Trost and R. F. Hammen. J. Am. Chem. Soc. **95**, 962 (1973).
8. D. Darwish, S. H. Hui, and R. Tomilson. J. Am. Chem. Soc. **90**, 5631 (1968); D. Darwish and S. H. Hui. Unpublished results presented in part before the Division of Organic Chemistry at the 154th National Meeting of the American Chemical Society, Chicago, September, 1967. Abstract S20.
9. A. Po. Ph.D. Dissertation, University of Alberta Edmonton, Alberta. 1970.
10. G. L. Closs and S. H. Goh. J. Chem. Soc. Perkin Trans. 2, 1473 (1972).
11. U. Schulz. Ph.D. Dissertation, University of Alberta, Edmonton, Alberta. 1968.
12. Y. Hayashi and R. Oda. Tetrahedron Lett. **51**, 5381 (1968).
13. R. R. Fraser, M. A. Petit, and J. K. Saunders. Chem. Commun. 1450 (1971).
14. H. L. Goering, J. N. Eikenberry, G. S. Koermer, and C. J. Lattimer. J. Am. Chem. Soc. **96**, 1493 (1974).
15. A. Ault. Org. Syn. **49**, 93 (1969).
16. J. Westley and B. Halpern. J. Org. Chem. **33**, 3978 (1968).
17. C. R. Johnson and C. W. Schroeck. J. Am. Chem. Soc. **95**, 7418 (1973).
18. C. L. Butler and L. H. Cretcher. J. Am. Chem. Soc. **55**, 2605 (1933).
19. H. Hellmann and D. Eberle. Ann. **662**, 188 (1963).
20. V. M. Berozovskii, V. A. Kurdyukova, and N. A. Proebrazhenskii. Zh. Obschch. Khim. **21**, 1163 (1951).
21. B. B. Day and P. Lakshmi Kantam. J. Indian Chem. Soc. **14**, 149 (1937).
22. S. D. Jolad and S. Rajagopal. Chimia, **16**, 196 (1962).
23. V. Baliah and K. Aparajithan. Tetrahedron, **19**, 2177 (1963).
24. V. Einforn and L. Rothlauf. Ann. **382**, 237 (1911).

Thermodynamics of ester and orthoester formation from trifluoroacetic acid

J. PETER GUTHRIE
Department of Chemistry, University of Western Ontario, London, Ontario N6A 3K7

Received November 18, 1974[1]

J. PETER GUTHRIE. Can. J. Chem. **54**, 202 (1976).

The equilibrium constant for the addition of sodium methoxide to methyl trifluoroacetate, in methanol as solvent, has been measured by ^{19}F nmr, and is 7 M^{-1}. From this was calculated an equilibrium constant, 2×10^{-4} M^{-1}, for addition of methanol to the ester. The equilibrium constant for formation of methyl trifluoroacetate in aqueous solutions is 0.06 M^{-1}. These results, with literature data, permit calculation of the free energies of formation in aqueous solution of orthotrifluoroacetic acid and its mono-, di-, and trimethyl esters. These in turn permit calculation of the standard free energy changes for addition of water and methanol to trifluoroacetic acid and its methyl ester. These combined with the analogous values for formic and acetic acids permit evaluation of ρ^* values for these addition reactions. Linear plots are obtained if correction is made for steric effects, and the ρ^* values are somewhat larger, 2.1–2.9, than was observed for the analogous carbonyl addition reactions.

J. PETER GUTHRIE. Can. J. Chem. **54**, 202 (1976).

Utilisant la rmn du ^{19}F, on a mesuré la constante d'équilibre pour l'addition du méthylate de sodium au trifluoroacétate de méthyle dans le méthanol comme solvant et trouvé que cette constante à une valeur de 7 M^{-1}. A partir de cette valeur, on a calculé une constante d'équilibre de 2×10^{-4} M^{-1}, pour l'addition du méthanol à l'ester. La constante d'équilibre pour la formation du trifluoroacétate de méthyle en solution aqueuse est de 0.06 M^{-1}. Ces résultats, avec des données de la littérature, permettent de calculer les énergies libres de formation, en solution aqueuse, de l'acide orthotrifluoroacétique et de ses esters mono-, di- et triméthylés. Ces valeurs permettent à leur tour de calculer les changements d'énergies libres standards pour l'addition de l'eau et du méthanol à l'acide trifluoroacétique et à son ester méthylique. Ces valeurs combinées avec des valeurs analogues pour l'acide formique et l'acide acétique permet une évaluation des valeurs ρ^* pour ces réactions d'addition. Des relations linéaires sont obtenues si une correction est faite pour les effets stériques et les valeurs de ρ^* sont un peu plus grandes (2.1 à 2.9) que celles observées pour les réactions analogues d'addition sur les carbonyles.

[Traduit par le journal]

Introduction

It has recently been shown that from the free energies of formation of orthoesters, one can calculate the free energies of formation of the corresponding orthoacids and their monoesters (1). These in turn are extremely useful for detailed interpretation of the mechanism of ester hydrolysis, since they permit calculation of equilibrium constants for the formation of the tetrahedral intermediates which are normally unobservable for noncyclic systems (2–4). It would clearly be very useful to map out the sensitivity of the equilibrium constants for addition to esters and acids to electronic effects of the R group

$$RCOOR' + HOR'' \rightleftarrows R{-}\underset{\displaystyle OR''}{\overset{\displaystyle OH}{\overset{|}{\underset{|}{C}}}}{-}OR'$$

The most accessible cases were for R = H or CH_3; consideration of electron-withdrawing ability of commonly encountered R groups suggests that CH_3 is about the most electron-supplying group which can be present without changing the nature of the ester, and CF_3 is about the most electron-withdrawing group. It would then be extremely interesting to determine the free energies for addition reactions of trifluoroacetic acid and its esters. Trimethyl orthotrifluoroacetate is a known compound (5), but its rate of hydrolysis is so slow (unpublished observations) as to preclude measurement of the heat of hydrolysis using the usual apparatus. Although sodium diethyl orthotrifluoroacetate is a known compound (6), it has been reported that addition of methoxide ion to methyltrifluoroacetate occurs to a negligible extent in methanol (7). There is clearly an apparent contradiction in the literature, since it has also been reported that methyl-

[1]Revision received September 5, 1975.

TABLE 1. Rate and equilibrium constants for addition of methoxide ions to methyl trifluoroacetate[a]

$[MeO^-]_0$[b] (M)	ν_{TFA}[c] (Hz)	I_{TFA}[d]	ν_{obs}[e] (Hz)	I_{obs}[d]	$\Delta\nu_{\frac{1}{2}}$[f] (Hz)	$[H_2O]_0$[g] (M) nmr[h]	$[H_2O]_0$[g] (M) K.F.[i]	K[j] (M^{-1})	k_{-1}[k] ($\times 10^2$)(s^{-1})
3.16	7277	5.2±0.1	7912	5.3±0.1	4	0.118	0.107	—	
2.12	7269	7.6±0.2	7912	5.5±0.2	3	0.139	0.108	—	
1.08	7263	3.4±0.2	7862	6.7±0.3	3	0.082	—	13.1±4.5	
0.644	7260	2.8±0.1	7777	5.5±0.4	10	0.082	0.073	8.6±2.3	7.2±3.0
0.319	7261	2.8±0.1	7581	4.4±0.4	42	0.094	0.033	6.6±2.5	4.5±0.4
0.209	7261	2.3±0.1	7482	7.5±0.3	50	0.055	0.033	6.1±1.6	4.4±0.4
0.104	7261	2.0±0.1	7353	7.5±0.3	28	0.050	0.029	7.3±3.9	6.1±0.6
0.062	7259	—[l]	7277	—[l]	12	(0.050)[m]	0.029	14.0±4.5	5.7±2.3
0.0302	7259	1.8±0.1	7251	11.0±0.2	3	0.034	0.026	—	
0.00885	7259	0.9±0.1	7251	11.0±0.1	3	0.019	0.027	—	
Average values[n]								7.3±1.1	4.8±0.2

[a] In methanol, at 25 °C; nmr spectra recorded at 94.1 MHz: reference standard is $CFCl_3$ in a coaxial capillary.
[b] Concentration of methoxide determined by titration of the stock methoxide solutions.
[c] Position of the signal due to trifluoroacetate ion.
[d] Intensity, determined by electronic integration; limits are standard deviations about the mean of repeated (4–7) integrations.
[e] Position of the signal due to the equilibrium mixture of methyl trifluoroacetate and its methoxide adduct.
[f] Width at half height of the signal due to the equilibrium mixture of methyl trifluoroacetate and its methoxide adduct.
[g] Concentration of water in the solvent.
[h] Determined from the ratio $I_{TFA}/(I_{TFA} + I_{obs})$.
[i] Determined by Karl Fischer titration of the methoxide stock solutions.
[j] K = (adduct)/(free ester) (free methoxide).
[k] First order rate constant for breakdown of the adduct to give ester and methoxide ion.
[l] Undetermined: the signals were not adequately resolved.
[m] Estimated: since Karl Fischer titration gave the same initial water content for the 0.062 and 0.104 M methoxide solutions, the final water contents were also assumed to be the same.
[n] Weighted average values.

trifluoroacetate can be titrated conductimetrically by methanolic potassium methoxide (8).

I wish to report a determination of the equilibrium constant for the addition of sodium methoxide to methyltrifluoroacetate in methanol as well as the equilibrium constant for the formation of methyltrifluoroacetate from trifluoroacetic acid and methanol in aqueous solution. These values permit a reasonably precise evaluation of the thermodynamic parameters for the methanol – water – trifluoroacetic acid system, and the evaluation of ρ^*'s for addition of water and methanol to carboxylic acids, RCOOH, and esters R—COOMe.

Results

Addition of Methoxide to Methyltrifluoroacetate

Solutions of methyltrifluoroacetate in methanol show a ^{19}F nmr signal at 77.1 δ (relative to $CFCl_3$ in a coaxial capillary). When increasing concentrations of sodium methoxide are also present there is a shift to higher field, accompanied at first by a broadening and then by a sharpening of the signal. In solutions with $[NaOCH_3] \geq 2\ M$, the ^{19}F nmr signal is at 84.1 δ. This behavior is interpreted in terms of [1]:

[1] $$CF_3COOMe + {}^-OMe \underset{k_{-1}}{\overset{k_1}{\rightleftarrows}} CF_3{-}\underset{\displaystyle OMe}{\overset{\displaystyle O}{\overset{|}{\underset{|}{C}}}}{-}OMe$$

Traces of water present in the solvent are consumed by saponification of the ester, leading to trifluoroacetate ion. Integration of the nmr signals due to trifluoroacetate and to the ester and its adduct permitted calculation of the amount of water which was initially present, since the total concentration of ester initially present is known. The concentrations of ester and methoxide could then be corrected for the losses due to saponification. From the position of the signal due to the ester and its adduct, the portion of the total ester present as the adduct (corrected for saponification) could be calculated, assuming that the signals observed for the two lowest and two highest concentrations of sodium methoxide represented the free ester and the adduct respectively. Concentrations of adduct, free ester, and free methoxide could then be calculated, and finally the equilibrium constant for adduct formation could be obtained; see Table 1. The results reported here lead to an equilibrium constant of 7 M^{-1} at 25 °C.

The origins of the apparent conflict in the

literature are now somewhat clearer. In his study of the reactions of alkoxides with esters of trifluoroacetic acid, Bender (7) apparently utilized 0.1 *M* ester and at most 0.1 *M* alkoxide. Using the equilibrium constant reported above it can be seen that only *ca.* 30% of the ester would be converted to the adduct; this might be expected to be detectable by the infrared spectroscopic method used, but is near the lower limit for the technique. A possible resolution of the dilemma arises from the fact that the addition of sodium methoxide to methyltrifluoroacetate in diethyl ether is vigorously exothermic (unpublished observations). If the temperature of the solution in Bender's ir cell were above room temperature, as it might well be through absorption of energy from the ir beam, the equilibrium would become less favorable; if K shifted to 1.2 M^{-1}, there would have been only a 10% decrease in ester concentration, which might well have been undetectable.

From the observed line broadening, estimates can be made of the rate constant for adduct formation and decomposition (9). Since the widths at half height of the signals from trifluoroacetate ion (all samples) methyltrifluoroacetate (two lowest methoxide concentrations) and the adduct (two highest methoxide concentrations) are all 3 ± 1 Hz, it is assumed that for all of the samples this would be the effective half width in the absence of exchange broadening. Now the corresponding relaxation time, T_2 is given by

$$\frac{1}{T_2} = \pi\Delta\nu_{1/2}$$

and the exchange broadening contribution to T_2 will be:

$$\frac{1}{T_2'} = \pi(\Delta\nu_{1/2} - 3)$$

$$= P_E^2 P_A^2(\delta_A - \delta_E)^2(\tau_E + \tau_A)$$

where P_E is the fraction of free ester, P_A is the fraction of adduct, $(\delta_A - \delta_E)$ is the chemical shift difference in Hz, and τ_E and τ_A are the mean lifetimes of ester and adduct. It may be shown that

$$\frac{1}{T_2'} = P_E^2 P_A(\delta_A - \delta_E)^2/k_{-1}$$

and hence that

$$k_{-1} = P_E^2 P_A(\delta_A - \delta_E)^2/\pi(\Delta\nu_{1/2} - 3)$$

The values found in these experiments lead (Table 1) to a value of 4.8×10^2 s^{-1} for k_{-1} and hence to a value of 3.5×10^3 M^{-1} s^{-1} for k_1.

Although the measureable equilibrium constant is that for [1] in methanol, the interesting process is reaction 2 in water. It is assumed that the major effect of changing solvent upon the equilibrium constant is that due to solvent polarity which is reflected in the pK_a values of the adduct and methanol. This is equivalent to assuming that the equilibrium constants for [2] will be the same in water or methanol.[2]

For oxygen acids the change in pK_a upon transfer from methanol to water is expected to be principally determined by the solvent polarity, but will also be influenced by the greater dispersion interaction between organic compounds and methanol than between organic compounds and water (11). This latter effect is likely to be important when the conjugate base of the organic acid is strongly delocalized and hence highly polarizable. For a set of nine oxygen acids[3] which are not expected to show marked dispersion effects the average ΔpK_a is 4.9 ± 0.2. The acids used range in pK_a from 0.22 to 9.95 (in water); all are carboxylic acids except phenol. The pK_a (in water) for $CF_3C(OMe)_2OH$ may be estimated as *ca.* 8.8 (see Appendix); in methanol the pK_a is estimated to be *ca.* 13.7. The pK_a of methanol in methanol as solvent is 18.3 (13). Thus the equilibrium constant for [2] in methanol or water may be calculated to be 1.8×10^{-4} ($\Delta G^0 = +5.1 \pm 1.1$).

[2] $CF_3-\overset{\overset{O}{\|}}{C}-OMe + MeOH = CF_3-\overset{\overset{OH}{|}}{\underset{\underset{OMe}{|}}{C}}-OMe$

Formation of Methyl Trifluoroacetate

^{19}F nmr spectra of solution of trifluoroacetic

[2]Variations in the equilibrium constant for addition of alcohols to carbonyl compounds have been observed (28) as the solvent is changed from water to pure alcohol, but the variation is usually small. The equilibrium constant for addition of methanol to acetaldehyde at 25 °C is 0.70 M^{-1} in water (1) and 0.74 M^{-1} in methanol (10).

[3]The acids used were: acid, pK_a in methanol, ΔpK_a; $Cl_3C-COOH$, 4.90, 4.68 (12*a*); $Cl_2CH-COOH$, 6.33, 5.03, (12*b*); $NC-CH_2-COOH$, 7.50, 5.05 (12*b*); $Cl-CH_2-COOH$, 7.84, 4.98 (12*b*); $C_6H_5-CH_2-COOH$, 9.17, 4.87 (12*a*); C_6H_5-COOH, 9.40, 5.20 (12*b*); CH_3-COOH, 9.42, 4.66 (12*a*); CH_3CH_2-COOH, 9.61, 4.75 (12*a*); C_6H_5-OH, 14.46, 4.51 (12*c*).

acid in aqueous methanol show an additional peak not present for aqueous trifluoroacetic acid. This peak increases with increasing concentration of methanol and is attributed to the methyl ester. The concentration of undissociated acid was calculated using a value for the degree of dissociation interpolated from the data of Covington *et al.* (15). It was assumed that 1 *M* methanol did not perturb the degree of ionization.[4] In this way the equilibrium constant[5] for [3] was determined

[3] $CF_3COOH + HOMe = CF_3COOMe + H_2O$

to be $0.062 \pm 0.024\ M^{-1}$ ($\Delta G^0 = +1.65 \pm 0.23$). It is striking to note that this value is very similar to the equilibrium constant for the formation of methyl acetate: $K = 0.057\ M^{-1}$ ($\Delta G^0 = +1.70$) (14).

Thermodynamics of Aqueous Trifluoroacetic Acid

Zarakhani and Vorob'eva (19) have reported activity data for monomeric (and dimeric) gaseous trifluoroacetic acid over aqueous trifluoroacetic acid solutions. From their results the partial pressure of monomeric acid over an 18.2 wt.% solution (1.6 *M*) was 1.4% of that of the monomeric acid over pure trifluoroacetic acid. The dimerization constant for gaseous trifluoroacetic acid was determined by Lundin *et al.* (18) and is 3.58 $Torr^{-1}$ at 25 °C. This, plus the vapor pressure of pure trifluoroacetic acid at 25 °C estimated from the boiling point as 112 Torr, leads to a value of 5.5 Torr for the partial pressure of monomeric acid over liquid trifluoroacetic acid, and so to a partial pressure of 0.077 Torr for 1.6 *M* aqueous acid. When one allows for partial dissociation, 1.6 *M* aqueous acid really contains 0.37 *M* undissociated trifluoroacetic acid. There will be an activity coefficient effect because of the presence of 1.2 *M* trifluoroacetate anion. The magnitude of this effect can be estimated using Setchenow constants; these are not available for trifluoroacetic acid, but values for acetic acid can be used as an approximation. From data on the effects of salts upon the partition coefficients for acetic acid between water and 1-pentanol (19) the Setchenow constant is $\simeq 0.079$. This will lead to a difference of 0.13 kcal mol^{-1} in ΔG_t. Finally, one can calculate the free energy of transfer from the monomeric gas (standard state the ideal gas at 1 atm) to aqueous solution (standard state the undissociated acid, at a concentration of 1 *M* with an infinitely dilute reference state) as -4.75 kcal mol^{-1}.

For liquid trifluoroacetic acid $\Delta H_f^0(l) = -253.0 \pm 0.8$ kcal mol^{-1} (20). The heat of vaporization appears not to have been measured but an approximate value can be estimated as follows. Konicek and Wadsö (21) have measured heats of vaporization for the process liquid to monomeric gas, for a series of aliphatic carboxylic acids. Within experimental error these heats of vaporization are linearly related to the boiling points of the acids, according to the equation (determined by a weighted least squares fit for Wadsö's data[6]):

$$\Delta H_v = (6.4 \pm 0.3) + (0.047 \pm 0.008)t_b$$

(ΔH_v in kcal mol^{-1}, t_b is the normal boiling point in °C). From the boiling point of trifluoroacetic acid, one can estimate that $\Delta H_v = 9.8 \pm 0.7$ kcal mol^{-1}. This leads to a value for the heat of formation of gaseous trifluoroacetic acid of -243.2 ± 1.1 kcal mol^{-1}. No entropy data are available for trifluoroacetic acid, but a value for the standard entropy can be estimated, after Benson (22), as 79.6 ± 1.5 e.u. This leads to $\Delta G_f^0(g)[CF_3COOH] = -225.2 \pm 1.1$ kcal mol^{-1}. From the free energy of formation of the gaseous acid, and the free energy of transfer evaluated above, the free energy of formation of aqueous trifluoroacetic acid can be calculated as -230.0 ± 1.2 kcal mol^{-1}.

Thermodynamics of Methyl Trifluoroacetate

From the equilibrium constant for ester formation, and the standard free energy of formation for aqueous trifluoroacetic acid calculated above, one may calculate that the free energy of formation of aqueous methyl trifluoroacetate is -213.6 ± 1.2 kcal mol^{-1}.

[4]This is not strictly correct: Grunwald and co-workers (16) have studied the effect on the ionization of various organic acids of increasing concentrations of methanol. Using their values for formic, acetic, and benzoic acids, one can estimate by interpolation that the pK_a of trifluoroacetic acid would be perturbed by 0.04 log units. The effect of this correction is much less than the experimental error in *K*.

[5]Here and throughout this paper the standard state for water is the pure liquid with unit activity.

[6]The heats of vaporization to the monomeric gas are significantly less precise than the heats of vaporization to the equilibrium vapor, which, as Wadsö showed, define a smooth, but nonlinear, curve. Though less precise, the heats of vaporization to the monomeric gas are more useful and more readily extrapolated.

The solubility of methyl trifluoroacetate is not readily determinable, since the half life at 25 °C is 85 s (23); however, the solubility can be estimated from that of methyl acetate using the linear free energy relationship of Hansch *et al.* (24) as 0.16 *M*.[7] The vapor pressure at 25 °C can be estimated from the boiling point by the method of Has and Newton (26) as 470 Torr. The free energy of transfer from the gas phase to aqueous solution is therefore +0.80 kcal mol^{-1} and ΔG_f^0(g)[CF_3COOCH_3] = −214.4 ± 1.2 kcal mol^{-1}.

The standard entropy can be estimated after Benson (22) as 96.0 ± 1.5 e.u. This value, combined with ΔG_f^0(g), implies that ΔH_f^0[CF_3COOCH_3] = −237.3 ± 1.3. The heat of vaporization can be estimated after Hine and Klueppel (27) as 6.6 ± 0.7 kcal mol^{-1}; therefore ΔH_f^0(l)[CF_3COOCH_3] = −243.9 ± 1.4 kcal mol.

Thermodynamics of Orthotrifluoroacetic Acid and its Esters

From the equilibrium constant for [2] and the free energies evaluated above, one can calculate that ΔG_f^0(aq)[$CF_3C(OH)(OCH_3)_2$] = −250.4 ± 1.2 kcal mol^{-1}.

For [4], the free energy change can be calculated (28) as +4.59 kcal mol^{-1}.

[4] $CF_3C(OH)(OCH_3)_2(aq) + HOCH_3(aq) \rightleftarrows CF_3{-}C(OCH_3)_3(aq) + H_2O(l)$

Then ΔG_f^0(aq)[$CF_3C(OCH_3)_3$] = −231.0 ± 1.3 kcal mol^{-1}. The solubility of $CF_3C(OCH_3)_3$ in water is 0.0089 ± 0.0015 *M*; the vapor pressure is estimated from the boiling point (26) to be 40 Torr; the value for ΔG_t is then +1.1 ± 0.1 and ΔG_f^0(g)[$CF_3C(OCH_3)_3$] = −232.1 ± 1.3 kcal mol^{-1}.

A value for S^0(g) for the orthoester may be estimated (15) as 117.9 e.u.; ΔH_f^0(g) is then −284.5 ± 1.4 kcal mol^{-1}. ΔH_{vap} is estimated after Hine and Klueppel (27) as 9.2 kcal mol^{-1}, so that ΔH_f^0(l)[$CF_3C(OMe)_3$] = −293.7 ± 1.7 kcal mol^{-1}. From this value the heat of hydrolysis for the process [5] can be calculated as −6.3 ± 1.5 kcal mol^{-1}.

[5] $CF_3C(OCH_3)_3(l) + 2H_2O(l) = CF_3COOH(l) + 3HOCH_3(l)$

For [6], the free energy change can be calculated (28) as −3.77 kcal mol^{-1}.

[6] $CF_3C(OH)(OCH_3)_2(aq) + H_2O(l) \rightleftarrows CF_3C(OH)_2(OCH_2)(aq) + CH_3OH(aq)$

This leads to ΔG_f^0(aq)[$CF_3C(OH)_2(OCH_3)$] = −269.0 ± 1.3 kcal mol^{-1}.

Finally, for [7], the free energy change can be calculated (28) as −1.94 kcal mol^{-1}.

[7] $CF_3C(OH)_2(OCH_3)(aq) + H_2O(l) = CF_3C(OH)_3(aq) + CH_3OH(aq)$

This leads to ΔG_f^0(aq)[$CF_3C(OH)_3$] = −285.7 ± 1.3 kcal mol^{-1}. The thermodynamic quantities calculated above, and all others used in this paper are collected in Table 2.

In Table 3 are collected the standard free energies for the addition reactions of water and methanol with RCOOH and $RCOOCH_3$ as well as for the analogous addition reactions of water and methanol with $RCOCH_3$. Plots of ΔG^0 *vs.* σ_R^* for the addition of H_2O or CH_3OH to RCOOH or $RCOOCH_3$ are satisfactorily linear; the ρ^* values for additions to acyl compounds are somewhat larger than for additions to simple carbonyl compounds; see Fig. 1. The plot of ΔG^0 *vs.* σ_R^* for the addition of CH_3OH to $RCOOCH_3$ shows the most deviations, but they are in the sense expected from the steric interactions introduced when R is CH_3 or CF_3 and two methoxyls are present in the adduct. It is interesting that the points for R = H are close to the lines which would be expected from the points for R = CH_3 and CF_3, since Greenzaid *et al.* (29) found that logarithms of the equilibrium constants for hydration of carbonyl compounds, RCOR′, were linearly dependent upon $\sum\sigma^*$, provided that a correction term for compounds with aldehydic hydrogens was introduced. The effect amounted to the hydrations being more favorable by 2.03 log units per aldehydic hydrogen. The logarithms of the hemiacetal formation constants do not depend in any simple way upon σ^*, *unless* both the correction term for aldehydic hydrogens *and* corrections for steric interactions between R and OCH_3 are introduced (28). Since addition reactions of both carboxyl and carbonyl reactions can be related to σ^* it necessarily follows that ΔG^0 values for hydration of RCOOH and $RCOCH_3$

[7] π values are altered for groups attached to electron-withdrawing substituents; the π values used for methyl and trifluoromethyl are derived from acetamide derivatives (25).

TABLE 2. Thermodynamic quantities used in this paper[a]

Compounds	ΔH_f^0(g) (kcal mol^{-1})	S^0(g) (cal deg^{-1} mol^{-1})	ΔG_f^0(g) (kcal mol^{-1})	ΔH_f^0(l) (kcal mol^{-1})	ΔG_t^b (kcal mol^{-1})	ΔG_f^0(aq) (kcal mol^{-1})
H_2O	−57.80[c]	45.11[c]	−54.68[c]	−68.32[c]		−56.69[c,d]
CH_3OH	−48.08[c]	56.8[c]	−38.09[c]	−57.02[c]		−41.88[e]
HCOOH	−90.49[f]	59.45[f]	−83.89[f]	−101.60[g]	−4.94[e]	−88.83[e]
$HCOOCH_3$	−84.97[h]	72.0[f]	−72.40[i]	−92.28[h]	−0.98[e]	−73.38[i]
$HC(OH)_3$						−137[j]
$HC(OH)_2(OCH_3)$						−121[j]
$HC(OH)(OCH_3)_2$						−105[j]
$HC(OCH_3)_3$	−126.58[k]	94.57[e]	−84.70[i]	−135.71[k]	−2.52[e]	−87.22[i]
CH_3•COOH	−103.26[g]	67.52[f]	−89.36[i]	−115.75[g]	−4.85[e]	−94.21[e]
CH_3•$COOCH_3$	−98.00[h]	76.45[e]	−77.05[i]	−106.57[h]	−1.38[e]	−78.43[i]
CH_3•$C(OH)_3$						−140[j]
$CH_3C(OH)_2(OCH_3)$						−124[j]
$CH_3C(OH)(OCH_3)_2$						−107[j]
$CH_3C(OCH_3)_3$	−136.63[k]	99.70[e]	−86.57[i]	−146.00[k]	−2.48[e]	−89.05[i]
CF_3COOH	−243[l]	79.6[l]	−225[i]	−253[m]	−4.88[l]	−230[l]
CF_3COOCH_3	−237[l]	96.0[l]	−214[l]	−244[l]	+0.80[l]	−214[l]
$CF_3C(OH)_3$						−286[l]
$CF_3C(OH)_2(OCH_3)$						−269[l]
$CF_3C(OH)(OCH_3)_2$						−250[l]
$CF_3C(OCH_3)_3$	285[l]	117.9[l]	−232[l]	−294[l]	+1.1[l]	−231[l]

[a]At 25 °C; standard states are ideal gas at 1 atm, pure liquid, and 1 *M* aqueous solutions with an infinitely dilute reference state, unless otherwise specified.
[b]Free energy of transfer from gas to aqueous solution.
[c]Reference 34.
[d]Standard state is the pure liquid.
[e]Reference 1.
[f]Reference 35.
[g]Reference 20.
[h]Reference 36.
[i]Calculated from other values in this table.
[j]Calculated from ΔG_f^0 for the orthoester by the method of ref. 28.
[k]Calculated from heats of hydrolysis and vaporization given in ref. 27.
[l]Calculated as described in the text.
[m]Reference 37.

TABLE 3. Standard free energy changes for addition reactions of carboxyl and carbonyl compounds[a]

Reaction	ΔG^0 (kcal mol^{-1}) R = CH_3	R = H	R = CF_3
R—COOH + H_2O	11	9	1
RCOOH + CH_3OH	12	10	4
R—$COOCH_3$ + H_2O	11	9	3
R—$COOCH_3$ + CH_3OH	13	10	6
R—CO—CH_3 + H_2O	3.90[b]	−0.03[b](2.75)[c]	−2.11[d]
R—CO—CH_3 + CH_3OH	5.01[b]	+0.21[b](2.98)[c]	0.08[d]

[a]In aqueous solution at 25 °C; standard states for reactants is 1 *M* solution with an infinitely dilute reference state except for water, for which the standard state is the pure liquid.
[b]Reference 1.
[c]Corrected for the effect of one aldehydic hydrogen; see text.
[d]Reference 28.

are linearly related. Here again linear correlations result from the use of ΔG values corrected for steric effects, and, in the case of carbonyl compounds, for the presence of an aldehydic hydrogen. Why an aldehydic hydrogen should have a major effect upon hydration of carbonyl

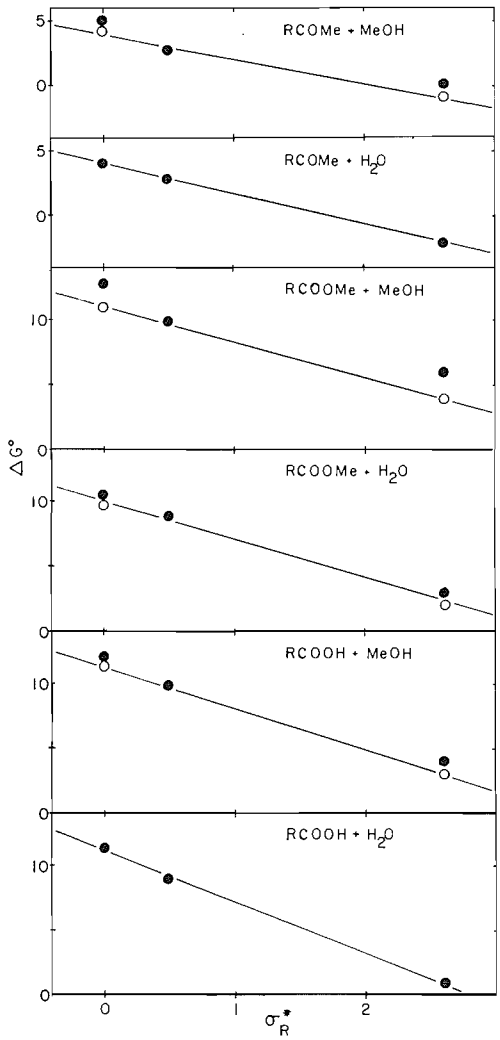

FIG. 1 ΔG^0 for addition reactions of RCOOH or $RCOOCH_3$ as a function of σ_R^*. ●, uncorrected ΔG^0 values (except that for reactions of RCOMe the aldehydic hydrogen correction has been made); ○, ΔG^0 values corrected for steric effects after ref. 28. The slopes of the lines correspond to the following ρ^* values: RCOMe + MeOH, 1.4; RCOMe + H_2O, 1.7; RCOOMe + MeOH, 2.0; RCOOMe + H_2O, 2.1; RCOOH + MeOH, 2.4; RCOOH + H_2O, 2.9.

compounds but a negligible effect upon hydration of carboxyl compounds is quite mysterious.

The linear free energy relations discussed above show that the completely thermochemical approach utilized for the evaluation of free energies of addition to acetic and formic acids and their methyl esters is at least consistent with the more directly evaluated free energies of addition to trifluoroacetic acid and its methyl ester. Furthermore it appears possible that there may be a general linear free energy relationship between addition reactions of acids and the corresponding ketones. This would be extremely useful if true since it would permit the estimation of free energies of addition to carboxyl derivatives based upon the more accessible free energies of addition to carbonyl derivatives.

Experimental

Materials

Trifluoroacetic acid (reagent grade) was used without further purification; no spurious peaks were detectable in the ^{19}F nmr. Methanol (reagent grade) was dried over 3A molecular sieves. Methyl trifluoroacetate was prepared by slow distillation from an equimolar mixture of methanol and trifluoroacetic acid. The fraction boiling below 39 °C was redistilled; bp 38 °C (lit. (30) bp 43 °C). Trimethyl orthotrifluoroacetate was prepared after Holm (5) and had bp 102 °C (lit. (5) bp 106 °C).

Equilibrium Constant for Addition of Methoxide to Methyl Trifluoroacetate

Sodium methoxide (*ca.* 3 *M* solution) was prepared from freshly cut sodium metal and dry methanol, under a nitrogen atmosphere, and was stored in a serum stoppered flask. The fine precipitate of sodium carbonate was allowed to settle out before any samples were withdrawn. Less concentrated solutions were prepared by dilution, using syringes to transfer solutions between serum capped containers. Concentrations of methoxide were determined by titration of 1 ml samples with standard *N*/10 or *N*/100 HCl. Concentrations of water were determined by Karl Fischer titrations using a Photovolt Aquatest meter. Portions (1 ml) of each methoxide solution were placed in stoppered small vials and then 25 μl (Hamilton syringe) of methyltrifluoroacetate was added to each, injecting the ester below the surface of the solvent. Preliminary experiments had shown that dropping the volatile ester onto methoxide solutions resulted in substantial loss of ester. Replicate injections of the ester into methanol in a stoppered, tared vial, showed that 25 μl was 30.65 ± 0.33 mg (mean and standard deviation for eight trials). The sample solutions were transferred to clean nmr tubes (cleaned, rinsed first with aqueous ammonia, then with methanol, and dried) and fitted with coaxial capillary tubes containing $CFCl_3$ as reference standard. ^{19}F nmr spectra were recorded on a Varian HA100 spectrometer at 94.1 MHz with a 1000 Hz sweep width. The probe temperature was held at 25 °C. From these spectra the peak positions, relative areas (electronic integration), and widths at half height were determined.

Equilibrium Constant for Methyl Trifluoroacetate Formation

A stock solution of trifluoroacetic acid in water was prepared (5.60 g in 25.0 ml, 1.93 mol l^{-1}). To 1.0 ml of this solution in a vial was added 28.3 mg of methanol. A portion of the solution was transferred to an nmr tube, and the ^{19}F nmr spectrum was recorded at a probe

temperature of 25 °C, with a coaxial capillary of $CFCl_3$ as reference. At high amplitude the signal due to ester could be seen, close to the signal for trifluoroacetic acid. (The assignment is based upon the absence of this signal when no methanol was present, and the linear dependence of the intensity of this signal upon the concentration of methanol.) The intensity of the signal from CF_3COOCH_3 was determined by electronic integration relative to that of the ^{13}C satellite signal for CF_3COOH.

Solubility of Trimethyl Orthotrifluoroacetate

A drop of trimethyl orthotrifluoroacetate was added to a vial containing 2 ml of water 0.059 *M* in *tert*-butyl alcohol. The vial was stoppered and shaken thoroughly for several minutes, then let stand until the undissolved ester had settled to the bottom of the vial. All operations were at room temperature, *ca.* 25 °C. A sample of the solution was taken and placed in an nmr tube; the sequence of shaking, letting stand, and sampling was repeated. Integration of ^1H nmr spectra (Varian HA 100 spectrometer) gave relative concentrations of $CF_3C(OCH_3)_3$ and $HOC(CH_3)_3$.

1. J. P. GUTHRIE. J. Am. Chem. Soc. **95**, 6999 (1973).
2. S. L. JOHNSON. Adv. Phys. Org. Chem. **5**, 237 (1967).
3. W. P. JENCKS. Catalysis in chemistry and enzymology. McGraw-Hill, New York, New York 1968. pp. 463–554.
4. T. C. BRUICE and S. J. BENKOVIC. Bioorganic mechanisms. Vol. 1. W. A. Benjamin, New York, New York 1966. pp. 1–211.
5. T. HOLM. U.S. Patent No. 2,611,787 (1952). Chem. Abstr. **47**, 9997 (1953).
6. F. SWARTS. Bull. Soc. Chim. Belg. **35**, 414 (1926).
7. M. L. BENDER. J. Am. Chem. Soc. **75**, 5986 (1953).
8. C. J. LUDMAN and T. C. WADDINGTON. J. Chem. Soc. A, 1816 (1966).
9. J. A. POPLE, W. J. SCHNEIDER, and K. J. BERNSTEIN. High resolution nuclear magnetic resonance. McGraw-Hill, New York, New York 1959. Chapt. 10.
10. P. LE HÉNAFF. Bull. Soc. Chim. Fr. 4687 (1968).
11. E. GRUNWALD and E. PRICE. J. Am. Chem. Soc. **86**, 4517 (1964).
12. (*a*) E. J. KING. *In* Physical chemistry of organic solvent systems. *Edited by* A. K. Covington and T. Dickenson. Plenum, London, 1973. p. 398; (*b*) N. A. IZMAILOV, V. S. CHERNYI, and L. L. SPIVAK. Russ. J. Phys. Chem. **37**, 427 (1963); (*c*) C. H. ROCHESTER and B. ROSSALL. J. Chem. Soc. B, 743 (1967).
13. C. D. RITCHIE, G. A. SKINNER, and V. G. BADDING. J. Am. Chem. Soc. **89**, 2063 (1967).
14. A. R. FERSHT and W. P. JENCKS. J. Am. Chem. Soc. **92**, 5442 (1970).
15. A. K. COVINGTON, J. G. FREEMAN, and T. H. LILLEY. J. Phys. Chem. **74**, 3773 (1970).
16. A. BACARELLA, E. GRUNWALD, E. L. PURLEE, and H. P. MARSHALL. J. Org. Chem. **20**, 747 (1955).
17. N. G. ZARAKHANI and N. P. VOROB'EVA. Russ. J. Phys. Chem. **45**, 369 (1971).
18. R. E. LUNDIN, F. E. HARRIS, and L. K. NASH. J. Am. Chem. Soc. **74**, 4654 (1952).
19. J. N. SUGDEN. J. Chem. Soc. **129**, 174 (1926).
20. J. D. COX and G. PILCHER. Thermochemistry of organic and organometallic compounds. Academic Press, New York, New York. 1970.
21. J. KONICEK and I. WADSÖ. Acta Chem. Scand. **24**, 2612 (1970).
22. S. W. BENSON. Thermochemical kinetics. Wiley, New York, New York 1968.
23. J. G. WINTER and J. M. W. SCOTT. Can. J. Chem. **46**, 2887 (1968).
24. C. HANSCH, J. E. QUINLAN, and G. L. LAWRENCE. J. Org. Chem. **33**, 347 (1968).
25. C. HANSCH and N. CORNELL. Arch. Biochem. Biophys. **151**, 351 (1972).
26. H. B. HAS and R. F. NEWTON. *In* Handbook of chemistry and physics. 48th ed. Chemical Rubber Publishing Co., Cleveland, Ohio. 1967. p. D-106.
27. J. HINE and A. W. KLUEPPEL. J. Am. Chem. Soc. **96**, 2924 (1974).
28. J. P. GUTHRIE. Can. J. Chem. **53**, 898 (1975).
29. P. GREENZAID, Z. LUZ, and D. SAMUEL. J. Am. Chem. Soc. **89**, 749 (1967).
30. E. GRYSZKIEWYCZ-TROCHIMOWSKI, A. SPROZYNSKI, and J. WNUK. Recl. Trav. Chim. Pays-Bas, **66**, 4251 (1947).
31. S. TAKAHASHI, L. A. COHEN, H. K. MILLER, and E. G. PEAKE. J. Org. Chem. **36**, 1205 (1971).
32. J. HINE and G. F. KOSER. J. Org. Chem. **36**, 1348 (1971).
33. G. B. BARLIN and D. D. PERRIN. Q. Rev. Chem. Soc. **20**, 75 (1966).
34. F. D. ROSSINI, D. D. NAGMAN, W. H. EVANS, S. LEVINE, and I. JAFFE. Natl. Bur. Stand. (U.S.) Circ. No-500 (1952).
35. D. R. STULL, E. F. WESTRUM, JR., and G. C. SINKE. The chemical thermodynamics of organic compounds. Wiley, New York, New York 1967.
36. H. K. HALL, JR. and J. H. BALDT. J. Am. Chem. Soc. **93**, 140 (1971).

Appendix

The pK_a's of aliphatic alcohols, $R—CH_2—OH$, are described by the empirical relationship (31)

$$pK_a = 15.74 - 1.32\sigma^*$$

Assuming that ρ^* would be the same for $R_1R_2R_3C—OH$ (ρ^* is known to be the same for $R_1R_2C(OH)_2$ (32)), this corresponds to

$$pK_a = 17.03 - 1.32\sum\sigma^*$$

The pK_a of $CF_3(CH_3O)_2C—OH$ can now be estimated as 8.8 (using $\sigma_{CF_3}^* = 2.61$ and $\sigma_{CH_3O}^* = 1.81$ (33)).

Stereomutation of a 1,2,3-triketone: an example of an asymmetric reaction

SAUL WOLFE, JAMES EDWARD BERRY, AND MICHAEL R. PETERSON
Department of Chemistry, Queen's University, Kingston, Ontario K7L 3N6

Received June 25, 1975

SAUL WOLFE, JAMES EDWARD BERRY, and MICHAEL R. PETERSON. Can. J. Chem. **54**, 210 (1976).

The 1,2,3-triketone $PhC(Me)_2COCOCOPh$ has been synthesized from mandelic acid in seven steps. Its proton magnetic resonance spectrum features a sharp six-proton methyl singlet at room temperature which broadens considerably at low temperatures but is not resolved into two peaks at 173 K. Similar dynamic behaviour is observed for the monoketone $PhC(Me)_2COPh$. It is concluded that the barrier to interconversion of enantiomeric tricarbonyl helical conformations is significantly less than 7 kcal/mol. The rotation–rotation surface of the ketodialdehyde HCO—CO—CHO has been computed by the CNDO/2 method; the barrier to stereomutation of enantiomeric helical conformations of this tricarbonyl system is found to be 3.9 kcal/mol. The dynamics of this process are discussed in terms of a recently proposed definition of symmetric and asymmetric reactions.

SAUL WOLFE, JAMES EDWARD BERRY et MICHAEL R. PETERSON. Can. J. Chem. **54**, 210 (1976).

On a synthétisé la tricétone-1,2,3 $PhC(Me)_2COCOCOPh$ en sept étapes à partir de l'acide mandélique. A température de la pièce, son spectre de résonance magnétique du proton présente un singulet bien défini pour les six protons du méthyle; ce signal s'élargit considérablement à basse température mais n'est pas résolu en deux pics à 173 K. On observe un comportement dynamique semblable pour la monocétone $PhC(Me)_2COPh$. On en conclut que la barrière pour l'interconversion des conformations hélicoïdales des tricarbonyles énantiomères est de beaucoup moindre que 7 kcal/mol. On a calculé la surface de rotation–rotation du cétodialdéhyde HCO—CO—CHO par la méthode CNDO/2. On a trouvé que la barrière de stéréomutation des conformations hélicoïdales énantiomères de ce système tricarbonylé est de 3.9 kcal/mol. On discute de la dynamique de ces processus en terme d'une définition proposée récemment pour les réactions symétriques et asymétriques.

[Traduit par le journal]

Introduction

A recent publication from this laboratory presented a theoretical analysis of symmetric and asymmetric reactions (1). By these terms are meant reactions characterized, respectively, by the presence or absence of a plane of symmetry on the reaction coordinate. For a process in which reagents and products are separated by one transition state, it was found that all reaction paths are indistinguishable, *i.e.*, that symmetric and enantiomeric asymmetric reactions proceed at the same rate under all experimental conditions. However, when reagent is converted to product via a stable intermediate, it was predicted that distinguishable enantiomeric reactions should be observable under non-equilibrium experimental conditions.

An experimental test of this prediction requires a four component system consisting of two pairs of enantiomers that are interconvertible by an appropriate sequence of conformational events (stereomutation). In addition, stereomutation must be sufficiently slow on the chemical time scale to permit a physical separation of the components, because the experiment must be initiated with a predominance of a single compound. Scheme 1 illustrates the kinetic model

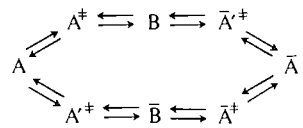

SCHEME 1

which is then operative. In this scheme, A and $\bar{A}$ are enantiomers, as are B and $\bar{B}$, but B and $\bar{B}$ are diastereomers of A and $\bar{A}$. Transition states $A^{\ddagger}$ and $A'^{\ddagger}$ are diastereomeric, as are $\bar{A}^{\ddagger}$ and $\bar{A}'^{\ddagger}$, which are mirror images of $A^{\ddagger}$ and $A'^{\ddagger}$, respectively.

Can. J. Chem. Downloaded from www.nrcresearchpress.com by 210.87.254.5 on 09/05/12
For personal use only.

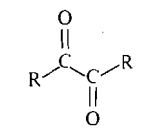

1 (R = H, CH_3)

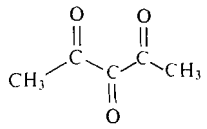

2

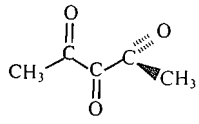

3

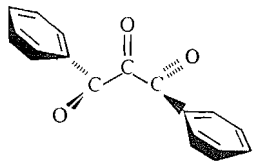

4

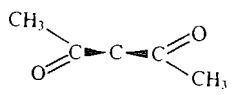

5

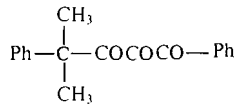

6

The purpose of the present manuscript is to describe a compound whose dynamic conformational behaviour has the experimental features of Scheme 1. However, as will be seen, the particular compound selected for the investigation has been found to undergo stereomutation too rapidly to permit direct observation of an asymmetric reaction.

The *N*-bromosuccinimide (NBS)-promoted dimethyl sulfoxide (DMSO) oxidation of polyacetylenes (2, 3) provides access to polyketones, until recently (4) a relatively little known class of compounds. A particularly interesting property of such compounds is their conformation in solution. It is well-known (5) that glyoxal and butanedione have the *anti*-coplanar conformation **1**, but the introduction of bulky substituents R can cause the carbonyl groups to move out of the plane (6). In the case of pentanetrione (**2**), Calvin and Wood suggested some time ago (7), on the basis of uv spectral observations, that one of the terminal carbonyl groups is orthogonal to the other two (**3**). More recent studies on diphenyltriketone have led Horner and Maurer (8) to propose conformation **4** for this compound in solution. In this conformation, the central carbonyl group is perpendicular to the other two, and the molecule is helical. The helical conformation of this compound is also observed in the solid state.[1]

Elucidation of the helicity of pentanetrione has been attempted by Kroner and Strack (9). These workers reported geometry optimization of the planar *trans-trans* (**2**) and helical (**5**) conformations using CNDO/2 and MINDO/2 SCF–MO computations, and found the helical conformation to be more stable by 21.8 kcal/mol. This result means that, if **2** is the transition state for the interconversion of the two enantiomeric forms of the cylindrical helix, optically active pentanetrione could have a finite lifetime on the chemical time scale.

Because of the many experimental consequences of such behaviour, and to assess the possibility of resolution of a tri- or polycarbonyl system, we undertook the synthesis of the nonenolizable triketone **6**, which was expected to exist in solution as a conical helix. The presence of a chiral axis in this compound would be manifested by magnetic anisochrony of the diastereotopic methyl groups; and the temperature dependence of the methyl signals in the nmr could be employed to study the kinetics of stereomutation of the system. On the assumption that the tricarbonyl moiety of **6** is indeed helical, the results of the work indicated that the *trans-trans* conformation is not the transition state for the interconversion of enantiomeric conformations. Rather, such interconversion must proceed by an asymmetric reaction, as will be discussed below.

Experimental

Melting points were obtained on Fisher-Johns or Meltemp equipment, and are uncorrected. Nuclear magnetic resonance (nmr) spectra were recorded on Varian T60 or Bruker HX60 spectrometers; TMS was employed as an internal standard, and all spectra were obtained in $CDCl_3$, except for the spectra of **6**, which were recorded in 1:1 $CDCl_3$:CD_2Cl_2. Chemical shifts are reported as ppm downfield from the internal standard. Infrared (ir) spectra were recorded on Beckman 5A or

[1]M. B. Rubin, personal communication.

Can. J. Chem. Downloaded from www.nrcresearchpress.com by 210.87.254.5 on 09/05/12
For personal use only.

Can. J. Chem. Downloaded from www.nrcresearchpress.com by 210.87.254.5 on 09/05/12
For personal use only.

Perkin-Elmer 180 spectrometers; data from the Beckman instrument are reported in microns, and those from the Perkin-Elmer instrument are given in cm^{-1}. Column chromatography was performed on silica gel 60, obtained from Brinkmann Instruments. High resolution mass spectra were obtained on a JEOL JMS-O1SC spectrometer.

2-Methyl-2-phenylpropanal, ***9*** *(10)*

To mandelic acid (22.0 g, 0.145 mol), in ether (150 ml), was added at 0 °C a solution of freshly prepared ethereal diazomethane (from 45 g of Diazald) until the yellow colour of diazomethane persisted. Removal of the solvent afforded the methyl ester as a colourless oil (23.8 g, 0.143 mol): nmr; 7.35 (5H), 5.20 (1H), 3.80 (1H), and 3.70 (3H).

A solution of this methyl ester (23.8 g, 0.143 mol) was added dropwise to an excess of methylmagnesium iodide, prepared from methyl iodide (74 g, 0.52 mol) and magnesium turnings (12 g, 0.5 g atom). After the addition was complete, the mixture was refluxed for 1 h, and then poured onto a mixture of 4 *N* H_2SO_4 (50 ml) and crushed ice (200 g). The ether layer was separated and the aqueous layer was extracted three times with 50 ml portions of ether. The combined ether extracts were washed with 10% bicarbonate, dried ($MgSO_4$), and evaporated to yield the diol as a pale yellow oil (18.0 g, 0.109 mol): nmr; 7.35 (5H), 4.40 (1H), 2.70 (2H), 1.20 (3H), and 1.08 (3H).

The diol (17.0 g, 0.102 mol) was added to a mixture of glacial acetic acid (75 ml) and 10 *N* H_2SO_4 (20 ml). After addition of one crystal of iodine, the mixture was refluxed for 10 min. The mixture was then cooled and extracted with three 100 ml portions of ether. The ether extracts were washed with 10% bicarbonate, dried, and evaporated to a dark oil. Distillation afforded material boiling at 52–54 °C/1 Torr (lit. (10): 105 °C/14 Torr): nmr; 9.60 (1H), 7.20 (5H), and 1.45 (6H). An impurity having nmr peaks at 1.20 and 1.30 distilled at the same temperature as the aldehyde and could not be separated from it. The impurity represented 15% of the material.

1,4-Diphenyl-3-hydroxy-4-methylpentane-1-one, ***10***

To a solution of sodium hydroxide (2.18 g, 0.055 mol) in water (20 ml) and ethanol (10 ml) was added acetophenone (5.2 g, 0.043 mol). 2-Methyl-2-phenylpropanal (6.4 g, 0.043 mol) was then added with vigorous stirring, the temperature being maintained at 20 °C. Stirring was continued for 2 h at this temperature, and the mixture was then extracted with ether (3 × 50 ml). The ether extracts were dried and evaporated to give a light yellow oil (11.5 g). Thin layer chromatography showed the presence of unreacted aldehyde, acetophenone, and a third component. Half of the oil was chromatographed on silica gel. Elution with 95:5 petroleum ether – ethyl acetate afforded aldehyde and acetophenone in the first fractions, followed by the third component, which crystallized. Recrystallization from petroleum ether gave white needles (1.1 g) mp 92.0–93.0 °C: nmr; 7.40 (10H, m), 4.40 (1H, t, 3 Hz), 2.90 (1H), 2.87 (2H, d, 3 Hz), and 1.45 (6H). *Anal.* Calcd. for $C_{18}H_{20}O_2$: C 80.50, H 7.65.

1,4-Diphenyl-4-methylpentane-1,3-dione, ***11***

Chromium trioxide (0.60 g, 6 mmol) was added to a magnetically stirred solution of pyridine (0.95 g, 120 mmol) and methylene chloride (15 ml). The flask was fitted with a calcium chloride drying tube and the mixture stirred at 0 °C for 15 min. 1,4-Diphenyl-3-hydroxy-4-methylpentane-1-one (0.268 g, 1 mmol) was then added in one portion, and the mixture was allowed to warm to room temperature during a period of 15 min. The solvent was decanted and the black residue was triturated several times with additional portions of methylene chloride. The combined methylene chloride extracts were washed successively with 10% sodium hydroxide, brine, and 5% HCl, and then dried and evaporated to give a yellow oil (0.128 g): nmr; 12.4 (1H), 7.30 (10H, m), 6.00 (1H), and 1.60 (6H).

2-Bromo-1,4-diphenyl-4-methylpentane-1,3-dione, ***12***

To pyrrolidone hydrotribromide (11) (4.15 g, 8.3 mmol), in tetrahydrofuran (60 ml), was added 1,4-diphenyl-4-methylpentane-1,3-dione (1.11 g, 4.15 mmol). The mixture was stirred at 25 °C for 0.5 h, and the precipitated pyrrolidone hydrobromide was then removed by filtration. The mother liquor was evaporated and the residue, in ether, was washed with water, dried, and evaporated to give 1.20 g of a yellow oil which quickly crystallized. Recrystallization from hot 95% ethanol afforded white needles, mp 137–139 °C: nmr; 7.30 (10H, m), 5.70 (1H), 1.65 (3H), and 1.55 (3H).

1,4-Diphenyl-4-methylpentanetrione, ***6***

2-Bromo-1,4-diphenyl-4-methylpentane-1,3-dione (160 mg, 0.46 mmol) was dissolved in DMSO (1.5 ml) (12), and the solution was heated on the steam bath for 12 h. The mixture was then cooled, diluted with water (5 ml), and extracted with ether (3 × 10 ml). Drying and evaporation of the solvent left an orange oil (123 mg). The ir spectrum showed three carbonyl peaks, at 1675, 1705, and 1720 cm^{-1}: nmr; 7.40 (10H, m) and 1.75 (6H, s). *Mol. Wt.* Calcd. for $C_{18}H_{16}O_3$: (M^+) 280.1099; found: (M^+) 280.1137.

2,2-Dibromo-1,4-diphenyl-4-methylpentane-1,3-dione, ***14***

To 1,4-diphenyl-4-methylpentane-1,3-dione (130 mg, 0.46 mmol), in chloroform (1 ml), was added at 0 °C 0.05 ml (1 mmol) of bromine. After 45 min, the solution was evaporated to dryness to give the dibromo compound as white needles, mp 135–136 °C; 132 mg: nmr; 7.25 (10H, m) and 1.60 (6H)

2-Acetoxy-1,4-diphenyl-4-methylpentane-1,3-dione, ***15***

The above dibromo compound (360 mg, 0.70 mmol) was added to a solution of fused sodium acetate (164 mg, 2.0 mmol) in glacial acetic acid (1 ml). The mixture was refluxed for 2 h, during which time sodium bromide precipitated. After cooling and dilution with water, the mixture was extracted with ether and the ether extract was dried and evaporated to give an orange oil (210 mg). Preparative layer chromatography on silica gel and elution with 9:1 petroleum ether – ethyl acetate separated this oil into an upper band of unreacted dibromo compound and a lower band (136 mg) of material identified as 2-acetoxy-1,4-diphenyl-4-methylpentane-1,3-dione on the basis of its nmr spectrum: 7.30 (10H, m), 6.45 (1H, s), 1.90 (3H, s), 1.70 (3H, s), and 1.55 (3H, s).

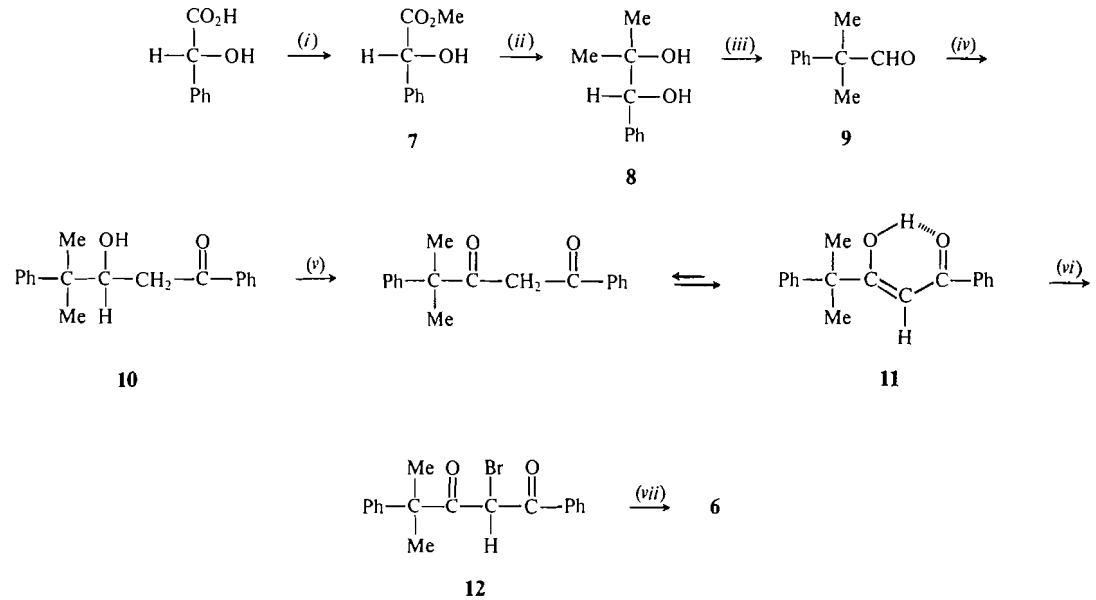

SCHEME 2. Reagents: (*i*) CH_2N_2; (*ii*) CH_3MgI; (*iii*) $AcOH–H_2SO_4–I_2$; (*iv*) $PhCOCH_3$–NaOH; (*v*) CrO_3–pyridine; (*vi*) PHT; (*vii*) DMSO.

*1,2-Diphenyl-2-methylpropanone, **18***

A solution of 2-methyl-2-phenylpropanal (2.5 g, 16 mmol), in ether (10 ml), was added to phenylmagnesium bromide, prepared from magnesium turnings (0.49 g, 20 mg atoms) and bromobenzene (3.14 g, 20 mmol). After refluxing for 1 h, the mixture was poured onto crushed ice (20 g) containing 4 *N* H_2SO_4 (10 ml). The ether layer was separated and the organic layer washed with ether (3 × 10 ml). The combined ether extracts were dried and evaporated to give 1,2-diphenyl-2-methylpropanol as a pale yellow oil (3.39 g): nmr; 7.3 (10H, m), 4.65 (1H), 2.40 (1H), and 1.35 (6H).

Chromium trioxide (1.62 g, 16.2 mmol) was added to a magnetically stirred solution of pyridine (2.56 g, 32.4 mmol) and methylene chloride (30 ml). The flask was then fitted with a calcium chloride drying tube and the contents stirred at 0 °C for 15 min. After addition of the alcohol (570 mg, 2.7 mmol), stirring was continued while the solution was allowed to warm to room temperature during 15 min. The solvent was decanted and the black residue triturated several times with 5 ml portions of methylene chloride. The combined methylene chloride extracts were then washed successively with 10% sodium hydroxide, brine, and dilute HCl, dried, and evaporated to give the ketone (513 mg) as a pale yellow oil: nmr; 7.35 (10H, m) and 1.60 (6H, s).

Results and Discussion

Synthesis of the Triketone

The synthesis of the triketone **6** was achieved in seven steps beginning with mandelic acid, and is summarized in Scheme 2. Methylation afforded the ester **7**, which was converted to the pinacol **8** with excess methylmagnesium iodide and then rearranged to the aldehyde **9** by brief refluxing in a mixture of glacial acetic acid and sulfuric acid (10). Condensation with acetophenone produced the aldol **10**.

The formation of **10** was found to depend critically upon the experimental conditions, and was successful only when performed in a two-phase system containing 10% sodium hydroxide and some ethanol. In this system equilibrium was reached in approximately 2 h, and the aldol, mp 92.0–93.0 °C could be isolated from the equilibrium mixture in yields of 20%. Oxidation of **10** with chromium trioxide – pyridine complex (13) gave the enolic β-diketone **11**. Bromination with pyrrolidone hydrotribromide (11) led to the crystalline bromodiketone **12**, mp 137–139 °C. This compound was found to exist in the diketo form. Its ir spectrum showed carbonyl peaks at 1650 and 1710 cm^{-1}; the most significant feature of the nmr spectrum was the presence of non-equivalent methyl groups, at 1.55 and 1.65. The anisochrony results from the presence of a chiral centre in the diketo structure. Similar behaviour was exhibited by the acetoxydiketone

Can. J. Chem. Downloaded from www.nrcresearchpress.com by 210.87.254.5 on 09/05/12
For personal use only.

Can. J. Chem. Downloaded from www.nrcresearchpress.com by 210.87.254.5 on 09/05/12
For personal use only.

15, which was isolated following an unsuccessful attempt to hydrolyze the dibromo compound **14** with fused sodium acetate. Evidently, in this system, the enol **16** is stable when X = H but, when X = Br or OAc, steric effects in the enol cause the diketo structure to be more stable.

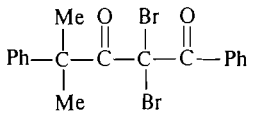

14

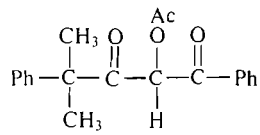

15

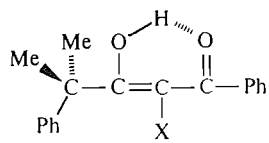

16

Kornblum oxidation of **12** (12) afforded the desired triketone **6**. This compound was obtained as a viscous orange oil which showed no tendency to hydrate. Its infrared spectrum featured three carbonyl peaks, at 1675, 1705, and 1720 cm^{-1}, and the high resolution mass spectrum[2] displayed a molecular ion at 280.1137, corresponding to $C_{18}H_{16}O_3$. At room temperature in 1:1 CD_2Cl_2:$CDCl_3$ or 1:1 CH_2Cl_2:$CFCl_3$ the nmr spectrum showed a sharp six-proton singlet at 1.75 ppm.

Dynamic Nuclear Magnetic Resonance Behaviour of the Triketone[3]

The observation of anisochronous methyl groups in **12** and **15** suggested that diastereotopism of the methyl groups of the triketone ought to be observable by nmr. Consequently, the presence of a sharp six-proton singlet in the nmr at room temperature demonstrated immediately that, either the tricarbonyl system in this compound is achiral, *i.e.*, planar, or that stereomutation of chiral conformations is fast at this temperature on the nmr time scale.[4] The evidence cited in the Introduction and in ref. 4 suggests that the latter explanation is the more plausible.

At low temperatures, the methyl singlet of **6** broadened considerably until, at 173 K, the half band width was 8.50 Hz, as compared to a 0.90 Hz half band width for internal TMS. However, even at this temperature, no separation of the methyl signal into two peaks was observed. Therefore, the process responsible for the line broadening must have a $\Delta G^{\ddagger}$ less than 7 kcal/mol.[5] Such a barrier is in the range observed (14) for rotation about certain carbon–carbon and carbon–nitrogen single bonds.

The results of the dnmr study therefore suggested that a slowing of the rotational process depicted in **17**, and not stereomutation of a

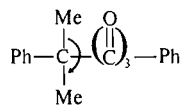

17

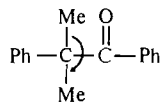

18

helical tricarbonyl system, might be responsible for the experimental observations. To check this point, the aldehyde **9** was converted into the monoketone **18**, by reaction with phenylmagnesium bromide followed by oxidation of the resulting alcohol, and the dnmr spectrum of **18** was examined. The monoketone, like the triketone, showed a sharp six-proton singlet at room temperature, which broadened at low temperature in the same manner as observed for the triketone. The dnmr data on **6** and **18** are summarized in Table 1.

We may conclude that the barrier to interconversion of enantiomeric helical conformations of the triketone is significantly less than

[2]We thank Mr. Peter M. Kazmaier for this determination.

[3]We thank Professor B. K. Hunter and Mr. David Groves for these experiments.

[4]The possibility that this observation is the result of accidental isochrony seems to be ruled out by the finding that a sharp six-proton singlet is also observed at room temperature in a number of other solvents, *e.g.*, benzene, pyridine, DMSO. Loss of chirality of a helical conformation by hydration (4) of the central carbonyl group may also be ruled out from the absence of hydroxyl absorption in the ir spectrum of **6**, our inability to prepare a hydrate, and the failure of pyridine to add to the central carbonyl group. In this latter case, such addition would have generated a chiral centre and, by analogy with **12** and **15**, would have been expected to lead to anisochronous methyl groups.

[5]This is calculated by assuming a coalescence temperature of 150 K, and a limiting chemical shift difference between the methyl groups of 3 Hz, the value observed in **12**.

Can. J. Chem. Downloaded from www.nrcresearchpress.com by 210.87.254.5 on 09/05/12
For personal use only.

TABLE 1. Dynamic nmr data for 1,4-diphenyl-4-methylpentanetrione (**6**) and 1,2-diphenyl-2-methylpropanone (**18**)

Compound	Temperature (K)	TMS line width[a] (Hz)	Methyl line width[a] (Hz)
6	293	0.35	0.50
6	243	0.50	1.40
6	213	0.55	2.20
6	193	0.65	3.80
6	183	0.70	5.00
6	173[b]	0.90	8.50
18	293	0.35	0.50
18	233	0.40	1.60
18	203	0.75	4.30
18	173[b]	1.45	14.70

[a]Line widths were measured at a point at half of the peak height.
[b]Temperatures below 173 K caused the sample to freeze to a glass.

7 kcal/mol. Assuming the validity of Kroner and Strack's computations (9), the *trans-trans* planar conformation **19** can therefore be ruled out as the transition state for the process **20** $\rightleftarrows$ $\overline{\mathbf{20}}$. An alternative to the sequence **20** $\rightleftarrows$ **19** $\rightleftarrows$ $\overline{\mathbf{20}}$ is the sequence **20** $\rightleftarrows$ **21** $\rightleftarrows$ $\overline{\mathbf{20}}$, in which the enantiomers **20** and $\overline{\mathbf{20}}$ interconvert, by sequential rotation about the CC bonds, via **21** or its mirror image, which are stable intermediates on the reaction coordinate and thus diastereomers of **20** and $\overline{\mathbf{20}}$. These various processes are shown in Scheme 3, from which it is evident that the stereomutation of the tricarbonyl moiety of the triketone is an asymmetric reaction of the type depicted in Scheme 1.

Although the asymmetric reaction shown in Scheme 3 is experimentally unobservable because of the low barrier separating **20** ($\overline{\mathbf{20}}$) from **21** ($\overline{\mathbf{21}}$), it was of interest to test theoretically the conclusions just reached. A molecular orbital examination of the rotation–rotation surface of the ketodialdehyde HCO—CO—CHO (**22**) was, therefore, undertaken.

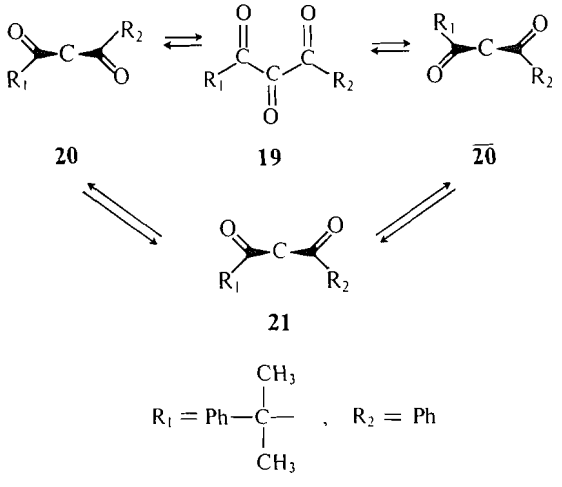

SCHEME 3

Theoretical Rotation–Rotation Surface of a 1,2,3-Tricarbonyl System

Computations were performed, as a function of the dihedral angles ω_1 and ω_2 (see **23**, the 0,0

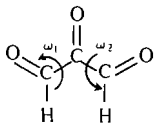

23

conformation), using the standard CNDO/2 programme system,[6] as modified for the Burroughs B6700 computer at Queen's University. All other geometrical parameters were held constant, as follows: C—H, 1.116 Å (15); C=O, 1.20 Å (9); C—C, 1.47 Å (9); ∠CCO, 123.0° (9); ∠HCO, 122.5° (9). Variation of ω_1 and ω_2 was made in 45° increments for all possible combinations of these parameters, so that a total of 21 independent points were obtained. Table 2 summarizes the results. As expected, the helical (90,90) conformation was found to be the most stable, and the third column of Table 2 shows the energy differences of the various conformations relative to the (90,90) conformation.

The stereomutation of **22** can be depicted most conveniently in terms of a rotation–rotation surface $E(\omega_1,\omega_2)$. This surface was generated in two stages. In the first, an analytical expression having the form shown in Eq. 1 was fitted to the data of Table 2. The coefficients of Eq. 1 are found in Table 3. Then, with the aid of this equation a 41 × 41 grid was plotted,[7] and is presented in Fig. 1.

[6]The programme CNINDO (P.A. Dobosh) received from the Quantum Chemistry Program Exchange, Bloomington, Ind. was modified for use in the present work.

[7]These operations are achieved by a series of computer programmes SURFPLOT, which may be obtained from the authors. Additional illustrations of the use of this programme are summarized in ref. 16.

Can. J. Chem. Downloaded from www.nrcresearchpress.com by 210.87.254.5 on 09/05/12
For personal use only.

TABLE 2. The computed (CNDO/2) total energy of HCO—CO—CHO as a function of ω_1 and ω_2

ω_1 (deg)	ω_2 (deg)	E (hartree)	ΔE (kcal/mol)
0	0	−77.65928	8.36
45	0	−77.66266	6.25
90	0	−77.66554	4.44
135	0	−77.66299	6.03
180	0	−77.66086	7.37
45	45	−77.66532	4.57
90	45	−77.66878	2.40
135	45	−77.66701	3.52
180	45	−77.66369	5.60
−135	45	−77.66562	4.38
−90	45	−77.66879	2.40
−45	45	−77.66601	4.15
90	90	−77.67261	0.00
135	90	−77.66972	1.81
180	90	−77.66640	3.90
−135	90	−77.66887	2.35
−90	90	−77.67190	0.45
135	135	−77.66616	4.05
180	135	−77.66373	5.57
−135	135	−77.66633	3.94
180	180	−77.66101	7.28

TABLE 3. The parameters of Eq. 1, employed in the generation of the rotation–rotation surface of HCO—CO—CHO

Parameter	Value
C_0	4.05099
C_1	0.20547
C_2	0.14747
C_3	0.08276
C_4	−0.13194
C_5	−0.22930
C_6	0.08277
C_7	0.27123
C_8	1.83351
C_9	0.06755

$$[1]\quad E(\omega_1,\omega_2)\,(\text{kcal/mol}) = C_0 + C_1(\cos\omega_1 + \cos\omega_2) + C_2\cos\omega_1\cos\omega_2 + C_3\cos 3\omega_1\cos 3\omega_2 + C_4\cos 2\omega_1\cos 2\omega_2 + C_5\sin\omega_1\sin\omega_2 + C_6(\sin\omega_1\sin 2\omega_2 + \sin 2\omega_1\sin\omega_2) + C_7\sin 2\omega_1\sin 2\omega_2 + C_8(\cos 2\omega_1 + \cos 2\omega_2) + C_9(\cos 3\omega_1 + \cos 3\omega_2)$$

There are three kinds of maxima on the rotation–inversion surface, corresponding to the all-planar conformations **23** (0,0), **24** (0,180) and **25** (180,180); and the surface has two kinds of minima, corresponding to the helical conformation **26** and a diastereomeric conformation

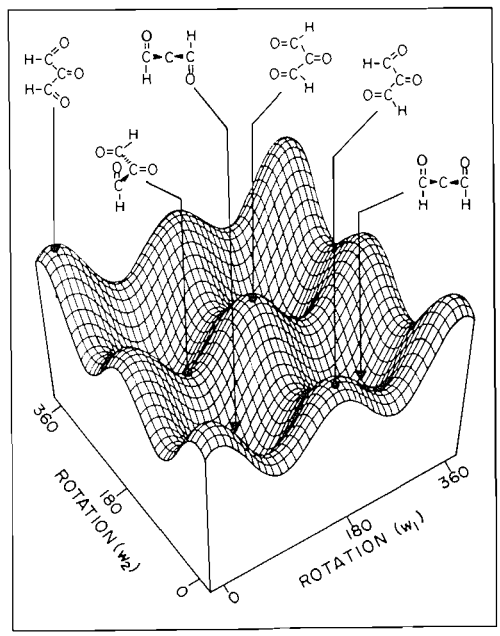

FIG. 1. The rotation–rotation surface of HCO—CO—CHO.

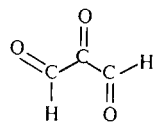

24

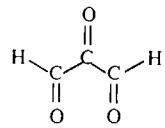

25

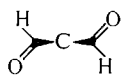

26

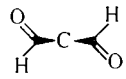

$\overline{\mathbf{26}}$

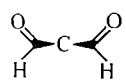

27

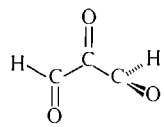

28

27 (−90,90), which is slightly less stable. The interconversion of **26** and its mirror image $\overline{\mathbf{26}}$ by a symmetric reaction will involve **23** (ΔE = 8.36 kcal/mol), **24** (ΔE = 7.37 kcal/mol) or **25** (ΔE = 7.28 kcal/mol) as transition states. These are clearly disfavoured with respect to an asymmetric reaction in which **26** is converted to $\overline{\mathbf{26}}$ via **27**. The transition state for this process is the (180,90) conformation $\overline{\mathbf{28}}$ and its equivalents,

which are found at the saddle points of the surface.

The conclusion derived from the CNDO/2 computations is thus entirely consistent with that reached in the experimental study of the triketone **6**. Stereomutation of the tricarbonyl system proceeds by an asymmetric path, but the transition states are too low in energy to be observed experimentally.

Acknowledgments

We thank the National Research Council of Canada for financial support of this work, and Mr. H. B. Schlegel for helpful discussions.

1. S. Wolfe, H. B. Schlegel, I. G. Csizmadia, and F. Bernardi. J. Am. Chem. Soc. **97**, 2020 (1975).
2. S. Wolfe, W. R. Pilgrim, T. F. Garrard, and P. Chamberlain. Can. J. Chem. **49**, 1099 (1971).
3. J. E. Berry. M.Sc. Thesis, Queen's University, Kingston, Ontario. 1975.
4. M. B. Rubin. Chem. Rev. **75**, 177 (1975).
5. J. E. Luvalle and V. Schumaker. J. Am. Chem. Soc. **61**, 3521 (1939).
6. N. J. Leonard and E. R. Blout. J. Am. Chem. Soc. **62**, 3152 (1940).
7. M. Calvin and C. L. Wood. J. Am. Chem. Soc. **62**, 3152 (1940).
8. L. Horner and F. Maurer. Chem. Ber. **101**, 1783 (1968).
9. J. Kroner and W. Strack. Angew. Chem. Int. Ed. Engl. **11**, 220 (1972).
10. M. Tiffeneau and H. Dorlencourt. C. R. Acad. Sci. **143**, 1242 (1906).
11. D. V. C. Awang and S. Wolfe. Can. J. Chem. **47**, 706 (1969).
12. N. Kornblum, J. W. Powers, and G. J. Anderson. J. Am. Chem. Soc. **79**, 6562 (1957).
13. G. I. Poos, G. E. Arth, R. E. Bayler, and L. H. Sarett. J. Am. Chem. Soc. **75**, 422 (1953).
14. C. H. Bushweller, W. G. Anderson, P. E. Stevenson, D. L. Burkey, and J. W. O'Neil. J. Am. Chem. Soc. **96**, 3892 (1974).
15. J. Pancir. Theor. Chim. Acta, **29**, 21 (1973).
16. F. Bernardi, I. G. Csizmadia, H. B. Schlegel, M. Tiecco, M. H. Whangbo, and S. Wolfe. Gazz. Chim. Ital. **104**, 1101 (1974); F. Bernardi, I. G. Csizmadia, A. Mangini, H. B. Schlegel, M. H. Whangbo, and S. Wolfe. J. Am. Chem. Soc. **97**, 2209 (1975); F. Bernardi, N. D. Epiotis, W. Cherry, H. B. Schlegel, M. H. Whangbo, and S. Wolfe, J. Am. Chem. Soc. In press; S. Wolfe, H. B. Schlegel, I. G. Csizmadia, and F. Bernardi. Can. J. Chem. In press; see also ref. 1.

Can. J. Chem. Downloaded from www.nrcresearchpress.com by 210.87.254.5 on 09/05/12
For personal use only.

Cycloaddition (2 + 3) d'aziridines avec les perfluoroalcènes. Synthèse de pyrroles fluorés

J. Leroy et C. Wakselman
C.N.R.S.-C.E.R.C.O.A., 2 rue Henri Dunant, Thiais 94320 France

Reçu le 4 juin 1975

J. Leroy et C. Wakselman. Can. J. Chem. **54**, 218 (1976).

La condensation thermique de carbométhoxy-2 et de cyano-2 aziridines avec le perfluorobutène et le perfluoropropène produit des pyrrolidines polyfluorées. Ces composés, traités par le méthylate de sodium, conduisent à des pyrroles fluorés en position 3,4. Dans le cas du perfluoropropène, la cycloaddition (2 + 3) n'est pas totalement régiospécifique.

J. Leroy and C. Wakselman. Can. J. Chem. **54**, 218 (1976).

Thermal condensation of 2-carbomethoxy and 2-cyano-aziridines with perfluorobutene and perfluoropropene produces polyfluorinated pyrrolidines. These compounds, treated with sodium methoxide, lead to 3,4-fluorinated pyrroles. In the case of perfluoropropene, the (2 + 3) cycloaddition is not completely regiospecific.

Can. J. Chem. Downloaded from www.nrcresearchpress.com by 210.87.254.40 on 09/05/12
For personal use only.

L'une des propriétés caractéristiques des aziridines est leur ouverture thermique ou photochimique en ylures d'azométhine qui, par cycloaddition (3 + 2) avec les oléfines activées, conduisent à des pyrrolidines substituées (pour une revue voir réf. 1):

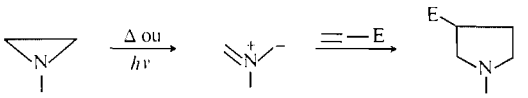

Ces cycloadditions ont, jusqu'à présent, été effectuées dans le cas de substituants activant la liaison éthylénique par effet attracteur mésomère (E = ester, nitrile). Les oléfines perfluorées sont activées d'une manière différente, essentiellement par effet inductif électroattracteur. Ayant observé récemment des réactions de cycloaddition (2 + 2) avec ces perfluoroalcènes (2), nous avons examiné leur réactivité vis-à-vis d'ylures d'azométhine produits thermiquement. Les pyrrolidines fluorées obtenues conduisent par élimination d'acide fluorhydrique à des pyrroles fluorés en positions 3,4 qui peuvent présenter un intérêt pharmacologique. A notre connaissance, ces pyrroles fluorés n'ont pas été décrits, à l'exception du méthyl-1 bis (trifluorométhyl)-3,4 pyrrole que nous avions obtenu comme produit secondaire dans la condensation thermique du méthyl-1 pyrrole avec le perfluorobutyne (3). Par ailleurs, la condensation de ce perfluoroalcyne avec les aziridines produit des pyrrolines-3 (4).[1] Enfin, la fluoration du méthyl-1 pyrrole conduisant à des pyrrolidines perfluorées a été décrite récemment (5).

Dans le cas général, la suite des réactions est montrée dans la schéma 1.

Nous avons particulièrement étudié la condensation du perfluoropropène qui présente l'intérêt d'aboutir à des pyrroles dont l'un des substituants est un atome de fluor. Cet exemple permet de déterminer également le degré de régiosélectivité de la réaction de cycloaddition.

Condensation avec le perfluorobutène-2

(i)—A = $COOCH_3$. Le perfluorobutène-2 étant un mélange d'isomères *cis* (23%) et *trans* (77%), on obtient deux couples de diastéréoisomères que nous avons séparés par chromatographie en phase vapeur préparative (cpvp). La stéréochimie de ces isomères n'a pu être déterminée sans ambiguité à partir de leurs spectres de rmn du proton et du fluor (tableau 1). Cependant, on relève deux types de constantes de couplage ^3J(H–F) dans le motif —*CF*—*CH*($COOCH_3$)—, de l'ordre de 26.5 et 6.5 Hz. Si l'on se base sur la dépendance de la constante de couplage vicinale proton–fluor en fonction de l'angle

[1]De la même façon, nous avons obtenu la *tert*-butyl-1 carbométhoxy-2 bis (trifluorométhyl)-3,4 pyrroline-3 par condensation thermique de la *tert*-butyl-1 carbométhoxy-2 aziridine sur le perfluorobutyne.

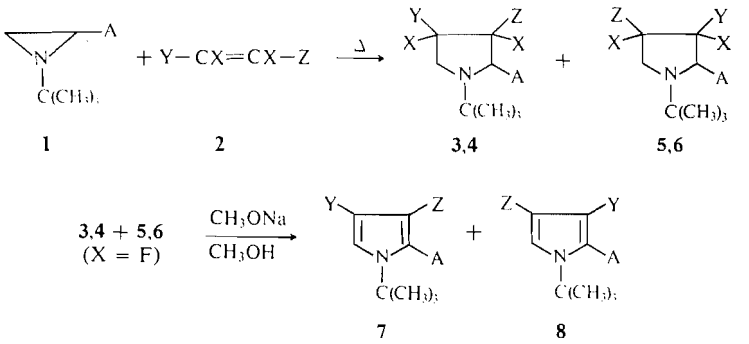

1 **2** **3,4** **5,6**

7 **8**

(**3,4**) et (**5,6**): couples de diastéréoisomères

A = $COOCH_3$ { *a* : X = F, Y = Z = CF_3 ; *b* : X = F, Y = CF_3, Z = F ; *c* : X = H, Y = CF_3, Z = H }

A = CN { *c* : X = F, Y = Z = CF_3 ; *d* : X = F, Y = CF_3, Z = F }

SCHÉMA I

TABLEAU 1. Propriétés spectroscopiques des pyrrolidines *a*

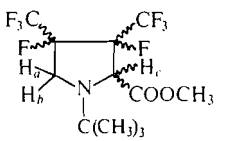

N°	^{1}H rmn ($CDCl_3$) δ	^{19}F rmn ($CDCl_3$) ϕ
3*a*	1.14 (9H, s, $C(CH_3)_3$), 3.7 (3H, s, $COOCH_3$), 4.4 (1H, d, H_c, ^3J(H–F) 6.8), système *ABX*^{a} centré à 3.51 et 4.22 (2H, oct, H_a et H_b, ^2J (H_a–H_b) 11.6, ^3J(H_a–F) 27.8, ^3J(H_b–F) 23.2).	77.1 (d(sext), CF_3, ^3J(CF_3–F) 17.6, ^4J(CF_3–F) 4.9, ^5J(CF_3–CF_3) 2.8), 78.2 (d(sext), CF_3, ^3J (CF_3–F) 19.4, ^4J(CF_3–F) 5.3, ^5J(CF_3–CF_3) 2.8), 175.4 (m, CF, $\simeq$18 raies, $\Sigma J \simeq 128$, ^3J(F–F)$\simeq$0), 182.0 (m, CF, 14 raies, $\Sigma J = 80$).
4*a*	1.13 (9H, s, $C(CH_3)_3$), 3.72 (3H, s, $COOCH_3$), 4.16 (1H, d, H_c, ^3J(H–F) 26.3), système *AB* MX^a de 3.2 à 4.0 (2H, m, H_a et H_b, ^2J(H_a–H_b) 11.0^b, *J* 3.5(H_b)^b).	73.8 (sept, CF_3, ^3J(CF_3–F) 13.4, $J \simeq 6.7$ (d), ^5J(CF_3–CF_3)$\simeq$6.7), 76.6 (oct, CF_3, ^3J(CF_3–F) 19.0, $J \simeq 6.7$(d), ^5J(CF_3–CF_3)$\simeq$6.7), 166.3 (m, CF, $\simeq$13 raies, $\Sigma J \simeq 107$), 178.8 (m, CF, $\simeq$14 raies, $\Sigma J \simeq 104$).
5*a*	1.08 (9H, s, $C(CH_3)_3$), 3.75 (3H, s, $COOCH_3$), 4.18 (1H, d, H_c, ^3J (H–F) 6.4), système *ABX*^{a} de 2.78 à 4.0 (2H, m, H_a et H_b, ^2J(H_a–H_b) 12.0^b).	79.6 (sext, CF_3, ^3J(CF_3–F) 19.7, ^5J(CF_3–CF_3) 9.9), 80.0 (quint, CF_3, ^3J(CF_3–F) 9.9, ^5J(CF_3–CF_3) 9.9), 178.0 (m, CF, $W_{1/2} = 68$), 186 (m, CF, $W_{1/2} = 23$).
6*a*	1.08 (9H, s, $C(CH_3)_3$), 3.73 (3H, s, $COOCH_3$), 4.16 (1H, d(d), H_c, ^3J(H–F) 26.6, *J* 4.5), système *AB*MX^{a,b} centré à 3.30 et 3.62 (2H, doct, H_a et H_b, ^2J(H_a–H_b) 13.0, ^3J(H_a–F) 29.0, ^3J(H_b–F) 25.0, *J* 4.5 (H_b)).	75.8 (quint, CF_3, ^3J(CF_3–F) 9.2, ^5J(CF_3–CF_3) 9.2), 77.3 (sext, CF_3, ^3J(CF_3–F) 18.4, ^5J(CF_3–CF_3) 9.2), 174.0 (m, CF, $W_{1/2} = 56.4$), 178.8 (t, CF, $J \simeq 23$).

[a] H_b est situé à champ fort par rapport à H_a.
[b] Analyse à 240 MHz.

Can. J. Chem. Downloaded from www.nrcresearchpress.com by 210.87.254.40 on 09/05/12
For personal use only.

dièdre (6), la plus grande constante correspond à une situation où H et F sont en position *cis*. Ainsi, avec le *trans*-perfluorobutène-2, il se forme de façon largement prépondérante l'isomère **3***a* (^3J(H–F) = 6.8 Hz).

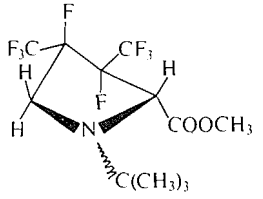

3*a*

Celui-ci, traité par le méthylate de sodium, conduit quantitativement au pyrrole **7***a*. Après saponification, l'acide pyrrole-2-carboxylique **9***a* (Y = Z = CF_3), obtenu avec un bon rendement, est décarboxylé difficilement au reflux du xylène en **10***a* (non isolé).

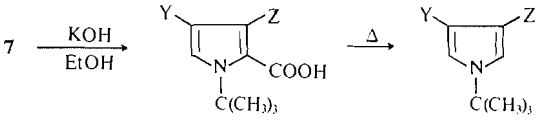

9 **10**

La condensation thermique étant conduite en autoclave d'acier inoxydable, on observe la formation directe des pyrroles **7**, en quantité variable lorsque l'on augmente la durée de la réaction, la température ou le volume de l'enceinte. Curieusement, dans une des réactions de condensation entre le perfluorobutène-2 et la *tert*-butyl-1 carbométhoxy-2 aziridine, nous avons isolé uniquement le pyrrole **11**.

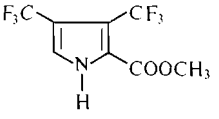

11

(ii)—A = CN. Dans ce cas, nous avons obtenu directement et uniquement le pyrrole **7***c* (Rdt. 20%) par réaction du perfluorobutène-2 sur la *tert*-butyl-1 cyano-2 aziridine.

Condensation avec le perfluoropropène

Avec ce dipolarophile se pose le problème de l'orientation de son addition au dipôle 1,3 formé. En principe, le centre anionique de l'ylure d'azométhine, confiné sur le carbone en α du groupe attracteur (ester ou nitrile) doit se porter sur le groupe difluorométhylène du perfluoropropène, site le plus réactif envers les nucléophiles (7).

En fait, nous observons que l'addition se produit également en sens inverse, dans la proportion de 10 à 15% pour A = $COOCH_3$ et 20 à 25% pour A = CN. De plus, pour chaque sens d'addition, le dipolarophile peut se présenter de façon *syn* ou *anti* (position du groupe trifluorométhyle par rapport au groupe attracteur ester ou nitrile) dans l'état de transition. Par exemple:

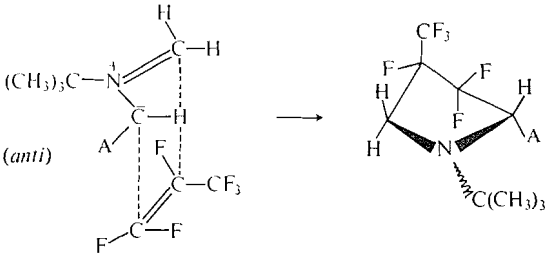

Il peut donc se former en tout deux couples de diastéréoisomères.

(i)—A = $COOCH_3$. Les quatre cycloadduits sont mis en évidence dans le produit brut, à côté d'une proportion variable (jusqu'à 10% environ) de pyrroles **7***b* et **8***b* provenant de la déhydrofluoration des pyrrolidines. Ces pyrroles permettent de déterminer sans ambiguité le sens d'addition du perfluoropropène. La stéréochimie des pyrrolidines diastéréoisomères est beaucoup plus difficile à déterminer en raison de la complexité des spectres de rmn (couplages multiples H–F et F–F).

Les deux pyrrolidines **5***b* et **6***b*, résultant de l'addition inverse ont été isolées par cpvp, dans les proportions 5:2. Les cycloadduits **3***b* et **4***b*, formés en quantité pratiquement égales sont inséparables par cette méthode.

Lorsque l'on traite par le méthylate de sodium un mélange de ces quatre isomères, on obtient toujours deux pyrroles isomères **7***b* et **8***b* dans les proportions (**3***b* + **4***b*):(**5***b* + **6***b*) soit environ 85:15. La stéréochimie attendue du pyrrole **7***b*, correspondant à l'addition normale est contrôlée principalement par l'examen de son spectre de rmn ^{13}C. Le couplage éventuel $^2J(C_1–F)$, de l'ordre de 20 Hz, normalement attendu dans une structure de type **8***b* n'est, en effet, pas observé dans son spectre découplé des protons (8).

Can. J. Chem. Downloaded from www.nrcresearchpress.com by 210.87.254.40 on 09/05/12
For personal use only.

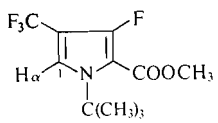

7*b*

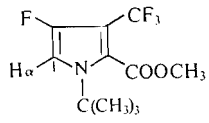

8*b*

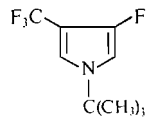

10*b*

La valeur des constantes de couplage H-F n'est pas aussi probante puisque $^3J(H\alpha\text{–}F)$ = 2.5 Hz dans **8***b* tandis que $^4J(H\alpha\text{–}F)$ = 5.2 Hz dans **7***b*. Dans le 3,4,5-trifluorofuranne, la constante *ortho* est supérieure à la constante *méta* de 0.7 Hz (9). En contrepartie, le couplage $J(H\alpha\text{–}CF_3)$ est plus grand dans **7***b* que dans **8***b* (tableau 2).

Les spectres de rmn du fluor des deux pyrrolidines diastéréoisomères **3***b* et **4***b* sont très différents d'aspect. Les signaux dûs au fluor situé au pied du groupe trifluorométhyle sont bien séparés dans $CDCl_3$ (et imbriqués dans C_6D_6): ce sont un triplet sans structure fine et à champ plus fort un dodécuplet très bien résolu. A 56.4 MHz, les groupes difluorométhylène apparaissent comme une partie AB d'un spectre à couplages multiples ($\Delta\nu$ = 773 Hz, $^2J(FF) \simeq$ 250 Hz dans $CDCl_3$) dûe à **3***b*, dans laquelle s'intercale un multiplet complexe dû à **4***b*. En l'absence de solvant, deux satellites apparaissent à $\pm {}^2J(FF)$.

A 240 MHz, ce multiplet est résolu en une autre partie AB ($^2J(F\text{–}F)$ 248 Hz, $\Delta\nu$ 341 Hz à cette fréquence). Les deux spectres ayant une tendance AM, les constantes de couplage autres que $^2J(F\text{–}F)$ sont déterminées au 1er ordre à 56.4 MHz et à 240 MHz. A cette fréquence une double ou triple irradiation homonucléaire est utilisée.

Une fois les pyrroles **7***b* et **8***b* obtenus, la saponification permet de passer aux acides correspondants[2] puis la décarboxylation thermique au pyrrole **10***b*. Ses caractéristiques rmn ont été déterminées par double irradiation hétéronucléaire du groupe trifluorométhyle et du fluor directement lié au cycle et l'identification des protons du cycle est faite sur la base des constantes de couplage. Ainsi un proton en α de l'azote résonne-t-il à champ plus faible lorsqu'il est en *ortho* d'un groupe trifluorométhyle plutôt que d'un atome de fluor (tableau 2).

[2]Seul l'acide **9***b* issu du pyrrole majoritaire **7***b* a été isolé pur et identifié totalement. Son isomère a été détecté seulement par rmn du fluor.

(ii)—A = CN. La condensation conduit à un mélange de trois pyrrolidines cyanées isomères **3***d*, **4***d* (diastéréoisomères inséparables) et **5***d*, ainsi qu'aux deux pyrroles isomères **7***d* et **8***d*. Les proportions des divers constituants varient suivant les conditions opératoires, les pyrrolidines α-cyanées étant plus fragiles que leurs homologues α-ester. La quasi identité des spectres rmn ^{19}F de ces deux classes de pyrrolidines ainsi que le passage aux pyrroles α-cyanés **7***d* et **8***d* (par CH_3ONa) permet de définir le sens d'addition majoritaire qui est celui normalement attendu.

Un propriété particulière des pyrrolidines α-cyanées que nous avons préparées est l'absence totale de bande d'absorption infrarouge du groupe nitrile. Une bande d'absorption intense $\nu(C{\equiv}N)$ réapparaît dans le spectre infrarouge des pyrroles.

Condensation avec le trifluoro-3,3,3 propène

Nous avons donc constaté que dans le cas du perfluoropropène, l'addition de l'ylure n'est pas régiospécifique. Cette oléfine présentant plusieurs substituants électroattracteurs, l'influence du groupe trifluorométhyle pouvait être perturbée par celle des fluors vinyliques. Pour déterminer l'influence exacte de ceux-ci, nous avons examiné la régiosélectivité de l'addition de l'ylure d'azométhine sur le trifluoro-3,3,3 propène, analogue du perfluoropropène dépourvu de fluors vinyliques.

Dans cette réaction, trois cycloadduits sont obtenus et séparés par cpvp et chromatographie en couche mince préparative. Nous les avons identifiés aux pyrrolidines **3***e* (56%), **4***e* (22%) et **5***e* (22%). La structure **3***e* est établie sans ambiguité par rmn du proton à 250 MHz, son spectre étant alors particulièrement clair et analysable au 1er ordre. La double irradiation homonucléaire des protons H_i et H_h confirme l'attribution. Cependant, les constantes de couplage proton-proton vicinales étant du même ordre de grandeur, il n'est pas possible de déterminer avec certitude la configuration relative des carbones portant le groupe trifluorométhyle et le groupe ester. Le spectre de rmn ^1H

Can. J. Chem. Downloaded from www.nrcresearchpress.com by 210.87.254.40 on 09/05/12
For personal use only.

Can. J. Chem. Downloaded from www.nrcresearchpress.com by 210.87.254.40 on 09/05/12
For personal use only.

TABLEAU 2. Propriétés spectroscopiques (rmn) des pyrroles

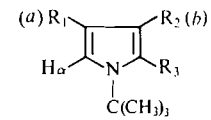

N°	R_1	R_2	R_3	^{1}H rmn	^{19}F rmn
7*a*	CF_3	CF_3	$COOCH_3$	δ ($CDCl_3$), 1.6(9H, s, $C(CH_3)_3$), 3.86(3H, s, $COOCH_3$), 7.21(1H, s, H du cycle, $W_{1/2}=2.85$).	ϕ ($CDCl_3$), 56.3(q, $CF_3(b)$, $^5J(CF_3$–$CF_3)$6.35), 57.8(q, $CF_3(a)$, $^5J(CF_3$–$CF_3)$6.35).
9*a*	CF_3	CF_3	COOH	δ (CD_3COCD_3), 1.71(9H, s, $C(CH_3)_3$), 7.52(1H, s, H du cycle), $\simeq$10.5(1H, COOH).	ϕ (CD_3COCD_3), 55.4(q, $CF_3(b)$, $^5J(CF_3$–$CF_3)$6.7), 57.3 (q(d), $CF_3(a)$, $^5J(CF_3$–$CF_3)$6.7, $^4J(CF_3$–$H)\simeq 1$).
7*b*	CF_3	F	$COOCH_3$	δ ($CDCl_3$), 1.70(9H, s, $C(CH_3)_3$), 3.83(3H, s, $COOCH_3$), 7.13(1H, d(q), H du cycle, ^4J(H–F)5.2, $^4J(H$–$CF_3)\simeq 1$).	ϕ ($CDCl_3$), 57.9(d(d), CF_3, $^4J(CF_3$–F)6.5, $J(CF_3$–$H)\simeq 1$), 142.3(quint, CF, $^4J(F$–$CF_3)$6.5, ^4J(F–H)5.2).
8*b*	F	CF_3	$COOCH_3$	δ ($CDCl_3$), 1.59(9H, s, $C(CH_3)_3$), 3.84(3H, s, $COOCH_3$), 6.68(1H, d(q), H du cycle, ^3J(H–F)2.5, $^5J(H$–$CF_3)\simeq 0.5$).	ϕ ($CDCl_3$), 56.0(d, CF_3, $^4J(CF_3$–F)11.5), 166.0(q(d), CF, $^4J(F$–$CF_3)$11.5, ^3J(F–H)2.5).
9*b*	CF_3	F	COOH	δ (CD_3COCD_3), 1.73(9H, s, $C(CH_3)_3$), 7.29(1H, d(q), H du cycle, ^4J(H–F)5.3, $^4J(H$–$CF_3)$1.0),$\simeq$10(1H, COOH).	ϕ (CD_3COCD_3), 57.5(d(d), CF_3, $^4J(CF_3$–F)6.6, $^4J(CF_3$–H) 1.0), 143(q(d), CF, $^4J(F$–$CF_3)$6.6, ^4J(F–H)5.3).
10*b*	CF_3	F	H(α')	δ ($CDCl_3$), 6.61(1H, t(q), Hα', J(Hα'–Hα)3.0, ^5J(Hα'–CF_3)0.6, ^3J(Hα'–F)3.0), 6.9(1H, t(q), Hα, J(Hα–Hα')3.0, $^4J(H\alpha$–$CF_3)$1.2, ^4J(Hα–F)3.9).	ϕ ($CDCl_3$), 57.9(d($\simeq$q), CF_3, $^4J(CF_3$–F)5.6), 167.9(m, CF).
7*c*	CF_3	CF_3	CN	δ ($CDCl_3$), 1.78(9H, s, $C(CH_3)_3$), 7.28(1H, s, H du cycle, $W_{1/2}=2.6$).	ϕ ($CDCl_3$), 57.5(q, $CF_3(b)$, $^5J(CF_3$–$CF_3)$6.0), 58.2(q, CF_3 (a), $^5J(CF_3$–$CF_3)$6.0).
7*d*	CF_3	F	CN	δ ($CDCl_3$), 1.70(9H, s, $C(CH_3)_3$), 7.05(1H, d(q), H du cycle, ^4J(H–F)5.0, $^4J(H$–$CF_3)$0.9).	ϕ ($CDCl_3$), 59.2 (d, CF_3, $^4J(CF_3$–F)6.3), 148.3 (quint, CF, $^4J(F$–$CF_3)$6.3, ^4J(F–H)5.0).
8*d*	F	CF_3	CN	δ ($CDCl_3$), 1.73(9H, s, $C(CH_3)_3$), 6.8(1H, d(q), H du cycle, ^3J(H–F)2.6, $^5J(H$–$CF_3)$0.6).	ϕ ($CDCl_3$), 58.0(d, CF_3, $^4J(CF_3$–F)8.7), 163.0(q, CF, $^4J(F$–$CF_3)$8.7, ^3J(F–H)2.6).
11[a]	CF_3	CF_3	$COOCH_3$	δ (CD_3COCD_3), 3.9(3H, s, $COOCH_3$), 7.52(1H, s, H du cycle, $W_{1/2}\simeq 3$).	ϕ (CD_3COCD_3), 55.0(q, $CF_3(b)$, $^5J(CF_3$–$CF_3)$8.2), 57.4(q, $CF_3(a)$, $^5J(CF_3$–$CF_3)$8.2).

[a]N-substituant = H.

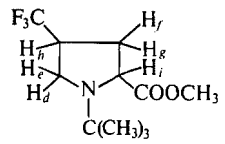

3e, 4e
(diastéréoisomères)

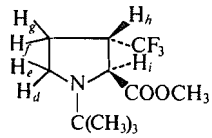

5e

de **4e** est moins clair. Malgré tout, sa similitude avec celui de **3e**, notamment en ce qui concerne les signaux de H_e, H_d et H_h et l'utilisation de la double irradiation homonucléaire des protons H_i et H_h permet une attribution non ambigüe.

L'isomère **5e** résulte alors nécessairement de l'addition inverse. A 250 MHz, le signal dû au proton H_i (la même notation que précédemment est utilisée) est un doublet : $J(H_i\text{–}H_h) = 4.3$ Hz. Un singulet est obtenu par irradiation de H_h. De même, les signaux de H_f et H_g sont fortement modifiés par irradiation de H_d et H_e, sans être toutefois interprétables. De plus, la faible valeur de la constante de couplage $^3J(H_i\text{–}H_h)$ indique que les protons H_i et H_h sont probablement en position *trans* (10).

Ainsi, dans l'exemple du trifluoro-3,3,3 propène, la condensation n'est pas régiospécifique, l'attaque du centre anionique de l'ylure s'effectuant à environ 78% sur le groupe méthylène. Ce résultat, peu différent de celui observé avec le perfluoropropène, montre que l'influence des fluors vinyliques est faible et que l'orientation de l'addition est gouvernée principalement par le groupe trifluorométhyle très électroattracteur.

D'une manière générale, il est à remarquer que si les cycloadditions (2 + 2) et (2 + 4) des perfluoroalcènes ont été intensivement étudiées (11), les cycloadditions (2 + 3) sont peu connues (12).

Dans le cas de la condensation des nitrones sur le perfluoropropène, la formation d'isoxazolidines perfluorées est régiospécifique (13). Par contre, avec les ylures d'azométhine, cette condensation est simplement régiosélective. Elle permet, par là même, d'accéder aux différents hétérocycles polyfluorés fonctionnels isomères, en particulier aux pyrroles substitués directement par un atome de fluor.

Partie expérimentale

Les appareils suivants ont été utilisés pour les mesures physiques: spectres de résonance magnétique nucléaire (rmn) ^1H et ^{19}F (60 et 56.4 MHz), JEOL C-60 HL équipé d'un découpleur hétéronucléaire JEOL JNM-SD-HC. Références internes TMS et $CFCl_3$. La résonance magnétique nucléaire ^{13}C (20 MHz), Varian CFT-20, référence interne TMS. Les spectres rmn ^1H et ^{19}F à 240 MHz ont été enregistrés à l'Institut d'Electronique Fondamentale, Université de Paris XI, Orsay. Les spectres rmn ^1H à 250 MHz ont été enregistrés sur un appareil Cameca au Service de Chimie Physique, C.E.N. de Saclay par Monsieur Forchioni que nous remercions vivement. Les déplacements chimiques sont exprimés en ppm par rapport aux références indiquées et les couplages en Hz. Les spectres infrarouge (ir) (solutions dans CCl_4) ont été enregistrés sur un appareil Perkin-Elmer modèle 457 et les spectres de masse sur un appareil AEI type MS 30 à double faisceau à 70 ev.

Les chromatographies ont été effectuées sur un appareil Varian Aerograph modèle 920 avec les colonnes préparatives suivantes: 30% SE 30 sur Chromosorb PAW 45/60, 10 pieds × ⅜ po; 20% FFAP sur Chromosorb A 45/60, 8 pieds × ⅜ po; 15% EGS sur Chromosorb WAW 60/80, 7 pieds × ⅜ po.

Dans les tableaux des données de rmn, les abréviations suivantes sont utilisées: s, singulet; d, doublet; t, triplet; q, quadruplet; quint, quintuplet; sext, sextuplet; sept, septuplet; oct, octet; doct, dodécuplet; m, multiplet; $W_{1/2}$, largeur à mi-hauteur en Hz; ΣJ, largeur entre raies extrêmes en Hz.

Les *tert*-butyl-1 méthoxycarbonyl-2 et *tert*-butyl-1 cyano-2 aziridines ont été préparées selon des méthodes déjà décrites (14) et (15).

Réaction du perfluorobutène-2 sur la tert-butyl-1 méthoxycarbonyl-2 aziridine

Un mélange de 2 g (13 mmol) d'aziridine fraîchement distillée, 7 g (35 mmol) de perfluorobutène-2 et 3 ml de benzène anhydre est chauffé 12 h à 180 °C dans un autoclave d'acier inoxydable de 50 ml. Après refroidissement, dégazage et évaporation du benzène, le résidu liquide est distillé "bulbe-à-bulbe" entre 50 et 100 °C sous 0.05 Torr. L'huile obtenue est analysée par cpvp sur colonne FFAP (four 108 °C). On recueille, dans l'ordre des temps de rétention croissants les cycloadduits **3a** (1.87 g, 5.2 mmol), **4a** (0.48 g, 1.4 mmol), **5a** (0.12 g, 0.35 mmol) et **6a** (0.10 g, 0.28 mmol). Rdt. total: 56%. *Anal.* Calc. pour $C_{12}H_{15}NO_2F_8$: C 40.34, H 4.24, N 3.92, F 42.54; trouvé: **3a**: C 40.06, H 4.22, N 3.79, F 42.61; **4a**: C 40.58, H 4.23, N 3.94 F 41.87. Spectres de masse: **3a**, **4a**, **5a**, **6a**: *m/e* 357 (M); ir: **3a**, ν (C=O) 1758^{-1}; rmn ^1H et ^{19}F, tableau 1.

Note: dans une autre expérience, portant sur 6 g (40 mmol) d'aziridine, 11.4 g (57 mmol) de perfluorobutène-2, dans 25 ml de benzène anhydre (autoclave de 125 ml), on a obtenu, après 12 h de chauffage à 180 °C une mixture dégageant de l'acide fluorhydrique. Après neutralisation au carbonate de sodium et extraction à l'éther diéthylique, on recueille un semi-solide repris au benzène et additionné de pentane. Un solide floconneux précipite. Celui-ci est recristallisé trois fois dans un mélange benzène–pentane puis sublimé à 120 °C/0.07 Torr. On recueille 2 g (1.3 mmol) de pyrrole **11** (p.f. 105–106 °C). *Anal.* Calc. pour $C_8H_5NO_2F_6$: C 36.79, H 1.93, N 5.36, F 43.66; trouvé: C 36.68, H 2.01, N 5.36, F 43.77. Spectre de masse: *m/e* 261 (M); ir: ν (C=O) 1718 cm^{-1}; rmn ^1H et ^{19}F, tableau 2.

Réaction du perfluorobutène-2 sur la tert-butyl-1 cyano-2 aziridine

2 g (16 mmol) d'aziridine, 6.4 g (32 mmol) de perfluoro-

Can. J. Chem. Downloaded from www.nrcresearchpress.com by 210.87.254.40 on 09/05/12
For personal use only.

Can. J. Chem. Downloaded from www.nrcresearchpress.com by 210.87.254.40 on 09/05/12
For personal use only.

butène-2 et 8 ml de benzène anhydre chauffés 19 h à 200 °C en autoclave d'acier inoxydable de 50 ml conduisent, après évaporation du solvant à un solide marron qui est repris au benzène. La mixture obtenue est passée sur colonne de gel de silice 0.05–0.2 mm, avec le benzène pour éluant. On recueille en tête 1 g (3.5 mmol) de pyrrole **7***c*. Rdt. 22%. Un échantillon analytique est obtenu par sublimation à 80 °C/0.05 Torr. (p.f. 106–108 °C en tube capillaire scellé). *Anal.* Calc. pour $C_{11}H_{10}N_2F_6$: C 46.49, H 3.54, N 9.86, F 40.11; trouvé: C 46.50, H 3.60, N 9.61, F 39.80. Spectre de masse: *m/e* 284 (M); ir: ν (C≡N) 2240 cm^{-1} (intense); rmn ^{1}H et ^{19}F, tableau 2.

Réaction du perfluoropropène sur la tert-butyl-1 méthoxycarbonyl-2 aziridine

(*a*) Un mélange de 3 g (19 mmol) d'aziridine fraîchement distillée, 5 g (33 mmol) de perfluoropropène et 6 ml de benzène anhydre est chauffé en autoclave d'acier inoxydable de 50 ml à 180 °C pendant 12 h. Après refroidissement et dégazage, le benzène est évaporé et le résidu distillé "bulbe à bulbe" entre 50 et 100 °C/0.05 Torr. On recueille 4 g d'une huile dont les constituants sont séparés difficilement (recouvrement) par cpvp sur colonne FFAP (four 110 °C). Dans l'ordre croissant des temps de rétention, on isole **5***b*, (**3***b* + **4***b*) et **6***b*.

(*b*) Dans une autre expérience 7.85 g (50 mmol) d'aziridine, 12 g de perfluoropropène et 25 ml de benzène anhydre sont chauffés 18 h à 190 °C en autoclave de 125 ml. Après distillation "bulbe-à-bulbe", une nouvelle distillation sur colonne Vigreux conduit à 6.4 g d'un mélange des cycloadduits **3***b*, **4***b* (85%), **5***b* (11%), **6***b* (4%); p.éb.$_{0.02}$ ≃ 43 °C. Rdt. 42%.

Cycloadduits (3b + 4b)

Anal. Calc. pour $C_{11}H_{15}NO_2F_6$: C 43.00, H 4.92, N 4.55, F 37.10; trouvé: C 42.89, H 4.91, N 4.31, F 37.09. Spectre de masse: *m/e* 307 (M); ir: ν (C=O) 1749–1756–1778 cm^{-1}; rmn ^{1}H, δ ($CDCl_3$) 1.1 (9 H, singulet, $C(CH_3)_3$, 3.75 (1.5 H, singulet, $COOCH_3$), 3.75 + (0.75 Hz) (1.5 H, singulet, $COOCH_3$)), 2.9–4.4 (3 H, multiplet, protons du cycle): δ (C_6D_6), 0.75 (4.5 H, singulet, $C(CH_3)_3$), 0.75 + (1.43 Hz) (4.5 H, singulet, $C(CH_3)_3$), 3.29 (3 H, singulet, $COOCH_3$), 2.6–4.6 (3 H, multiplet, protons du cycle).

Cycloadduits 5b et 6b

^{1}H rmn: **5***b*: δ ($CDCl_3$) 1.09 (9 H, singulet, $C(CH_3)_3$), 3.74 (3 H, singulet, $COOCH_3$), 2.9–4.4 (3 H, multiplet, protons du cycle).

6*b*: δ ($CDCl_3$) 1.08 (9 H, singulet, $C(CH_3)_3$), 3.71 (3 H, singulet, $COOCH_3$).

La résonance magnétique nucléaire ^{19}F

La notation des noyaux, valable pour les homologues α-cyanés, est la suivante: les lettres *a* et *b* désignent les noyaux géminés H et F portés directement par le cycle, la lettre *c* les noyaux H et F isolés, également liés directement au cycle. Les valeurs notées * sont tirées de l'analyse à 240 MHz. Les $\Delta\nu$ sont rapportés à 56.4 MHz.

3*b*: ϕ ($CDCl_3$) ≃ 76.7 (multiplet, CF_3), système AB centré à 113.4 ($\Delta\nu$ 773.0 $^2J(F_a$–$F_b)$ 249.6, F_a, sextuplet dédoublé, $^3J(F_a$–$H_c)$ 23.3, $^4J(F_a$–$CF_3)$ 14.4, $^4J(F_a$–$H_{a,b})$ 3.5, $^3J(F_a$–$F_c)$ ≃ 0, F_b, multiplet, $W_{1/2}$ 14.0, $^3J(F_b$–$H_c)$ ≃ 7.8, $^3J(F_b$–$F_c)$ ≃ 0, $^4J(F_b$–$CF_3)$ très faible), 179.7 (multiplet, F_c, $^3J(F_c$–$H_{a,b})$ 27.5 et 20.5, $^3J(F_c$–$CF_3)$ 7.0).

4*b*: ϕ ($CDCl_3$) ≃ 76.7 (multiplet, CF_3), système AB centré à ≃ 117.5 ($\Delta\nu$ 80.0*, $^2J(F_a$–$F_b)$ 248.0*, F_a, décuplet ΣJ 35.6, $^3J(F_a$–$H_c)$ 12.5, F_b, quintuplet, $^3J(F_b$–$H_c)$ 15.2, $^4J(F_b$–$CF_3)$ 12.0, $^3J(F_b$–$F_c)$ ≃ 0), 177.1 (triplet (multiplet), F_c, $^3J(F_c$–$H_{a,b})$ 32.0).

5*b*: ϕ ($CDCl_3$) 77.8 (doublet (triplets), CF_3, *J* 12.7 (6.4)), système AB centré à 115 ($\Delta\nu$ 167*, $^2J(F_a$–$F_b)$ 248*, F_a, multiplet, F_b, quadruplet, *J* ≃ 13.4), 183.0 (quintuplet, F_c, *J* ≃ 8.5).

6*b*: ϕ ($CDCl_3$) 74.8 (quintuplet, CF_3, ΣJ 25.4), système AB centré à 120 ($\Delta\nu$ 383, $^2J(F_a$–$F_b)$ 247, F_a, F_b).

Réaction du perfluoropropène sur la tert-butyl-1 cyano-2 aziridine

L'aziridine (1.5 g, 8.1 mmol), 4 g (27 mmol) de perfluoropropène et 8 ml de benzène anhydre sont chauffés 5 h à 175 °C en autoclave d'acier inoxydable de 50 ml. Après refroidissement et dégazage, le benzène est évaporé et le liquide résiduel distillé "bulbe à bulbe" vers 80 °C/0.05 Torr. Le liquide obtenu est chromatographié sur colonne préparative SE 30 (four 120 °C). Dans l'ordre croissant des temps de rétention, on recueille 0.8 g (3 mmol Rdt. 37%) du mélange **3***d* (≃43%), **4***d* (≃43%), **5***d* (14%), 0.18 g (0.7 mmol) de pyrrole **7***d* et 0.15 g (0.5 mmol) de pyrrole **8***d*.

Cycloadduits (3d + 4d + 5d)

Spectre de masse: *m/e* 274 (M); ir: ν (C≡N) invisible; rmn ^{1}H: δ ($CDCl_3$) ≃ 1.23 et 1.29 (9 H, $C(CH_3)_3$), 3.1–4.6 (3 H, multiplet, H du cycle); δ (C_6D_6) 0.73 et 0.87 ($C(CH_3)_3$ **3***d* et **4***d*), 0.93 ($C(CH_3)_3$ **5***d*), 2.6–4.4 (multiplet, H du cycle).

^{19}F rmn: **3***d*: ϕ ($CDCl_3$) ≃ 77 (multiplet, CF_3), système AB centré à 115.0 ($\Delta\nu$ 265.0, $^2J(F_a$–$F_b)$ 243.0, F_a, quintuplet, $J(F_a$–H_c et $CF_3)$ ≃ 13.4, F_b, multiplet, $W_{1/2}$ = 11.3, $^4J(F_b$–$CF_3)$ ≃ 3.5), 178.0 (triplet (≃quintuplets), F_c, *J* 26.8 (triplet), $^3J(F_c$–$CF_3)$ 7, *J* ≃ 7).

4*d*: ϕ ($CDCl_3$) ≃ 77 (multiplet, CF_3), ≃ 113.5 (multiplet, F_a, F_b), 175.0 (triplet (multiplets), F_c, *J* 13.4 (triplet)).

5*d*: ϕ ($CDCl_3$) ≃ 77 (multiplet, CF_3), ≃ 112.5 (multiplet, F_a, F_b), 177.0 (quintuplet, F_c, $^3J(F_c$–$CF_3)$ 7.0, *J* 7.0 (doublet)).

Préparation des pyrroles fonctionnels à partir des pyrrolidines

Dans une expérience type, 6 mmol de pyrrolidine des séries *a*, *b* ou *d*, sont ajoutées goutte à goutte à 17 mmol de méthylate de sodium dans 3 ml de méthanol anhydre. Après agitation pendant quelques heures, le mélange réactionnel est additionné d'eau distillée, de chlorure de sodium et extrait quatre fois à l'éther diéthylique. Après séchage sur $MgSO_4$, les pyrroles isomères sont séparés par cpv préparative: **7***b* (p.f. 43 °C) et **8***b* (p.éb.$_{760}$ 243 °C) sur colonne EGS (four 120 °C); **7***d* (p.f. 45 °C) et **8***d* (p.f. ≃ 35 °C) sur colonne SE 30 (four 120 °C). Le pyrrole **3***a* (p.f. 43 °C) est purifié par cpvp sur colonne SE 30 (four 170 °C). Les rendements de la déhydrofluoration sont quantitatifs. *Anal.* (**7***b* + **8***b*) Calc. pour $C_{11}H_{13}NO_2F_4$: C 49.44, H 4.87, N 5.24, F 28.46; trouvé: C 49.55, H 4.81, N 5.34, F 28.58. Spectres de masse: **7***a*, *m/e* 317 (M); **7***b* et **8***b*, *m/e* 267 (M); **7***d* et **8***d*, *m/e* 234 (M); ir: **7***a* ν (C=O) 1745 cm^{-1}; **7***b* ν (C=O) 1726 cm^{-1}; **8***b* ν (C=O) 1736 cm^{-1}; **7***d* et **8***d* ν (C≡N) 2230 cm^{-1} (intense); rmn ^{1}H et ^{19}F: tableau 2. ^{13}C rmn (découplé des protons) (Cc = carbone du cycle): **7***b*, δ ($CDCl_3$) 30.07 (singulet, $C(CH_3)_3$), 51.84 (singulet, OCH_3), 60.84 (singulet, $C(CH_3)_3$), 106.33 (doublet, $-Cc$=CF–, ^2J(Cc–F) 27.1), 109.15 (quadruplet,

Can. J. Chem. Downloaded from www.nrcresearchpress.com by 210.87.254.40 on 09/05/12
For personal use only.

CF_3, J(C–F) 265.3), 120.78 (singulet, Cc–H), 137.74 (doublet, Cc–F, J(Cc–F) 349.5), 160.21 (doublet, $COOCH_3$, ^3J(C–F) 17.6). **8***b*, δ ($CDCl_3$) 30.55 (singulet, $C(CH_3)_3$), 52.92 (singulet, OCH_3), 60.04 (singulet, $C(CH_3)_3$), 110.81 (doublet, Cc–H, ^2J(Cc–F) 15.5).

Passage aux acides pyrrole-2 carboxyliques **9***a et* **9***b*

Les pyrroles **7***a* et **7***b* sont traités au reflux pendant 3 h par un excès de potasse éthanolique 5 *N*. Après évaporation d'une partie de l'alcool, on acidifie par HCl dilué vers 0 °C. La solution est filtrée et le précipité rincé à l'éther diéthylique. Le filtrat est extrait à l'éther et la solution obtenue séchée sur $MgSO_4$. Après évaporation du solvant, les acides **9***a* et **9***b* sont recristallisés deux fois dans un mélange eau–éthanol. Un échantillon analytique de **9***b* est obtenu par sublimation à 130 °C (15 Torr).

9*a*: pas de point de fusion net. **9***b*: p.f. 158 °C (tube capillaire scellé). *Anal.* Calc. pour **9***a*, $C_{11}H_{11}NO_2F_6$: C 43.56, H 3.63, N 4.62, F 37.62, trouvé: C 43.55, H 3.60, N 4.61, F 36.99; *Anal.* Calc. pour **9***b*, $C_{10}H_{11}NO_2F_4$: C 47.43, H 4.34, N 5.53, F 29.25; trouvé: C 47.59, H 4.24, N 5.50, F 30.15. Spectres de masse: **9***a*, *m/e* 303 (M); **9***b*, *m/e* 253 (M); ir: **9***a* ν (C=O) 1715 et 1740 cm^{-1}; **9***b* ν (C=O) 1690 et 1730 cm^{-1}; rmn ^1H et ^{19}F: tableau 2.

Décarboxylation des acides pyrrole-2 carboxyliques

La pyrrole **9***b* (2 g, 8 mmol) sont portés progressivement à 160 °C, dans un bain d'huile. Il y a alors fusion et évolution de gaz carbonique. Au bout de 1 h, on laisse refroidir. Le liquide obtenu est purifié par cpvp sur colonne FFAP (four 150 °C). On recueille 1.6 g (7.6 mmol) de pyrrole **10***b*; p.éb.$_{15}$ 92 °C. *Anal.* Calc. pour $C_9H_{11}NF_4$: C 51.67, H 5.31, N 6.70, F 36.33; trouvé: C 51.63, H 5.32, N 6.52, F 36.41. Spectre de masse: *m/e* 209 (M); rmn ^1H et ^{19}F: tableau 2; rmn ^{13}C (découplé des protons) (Cc = carbone du cycle): δ ($CDCl_3$) 30.13 (singulet, $C(CH_3)_3$), 56.59 (singulet, $C(CH_3)_3$), 102.15 (quadruplet dédoublé, *Cc*–CF_3, ^2J(Cc–*C*F_3) 37.3, ^2J(Cc–F) 12.05), 103.6 (doublet, –*Cc*=CF–, ^2J(Cc–F) 26.3, 114.58 (singulet large, –*Cc*=C(CF_3)–), 123.33 (quadruplet dédoublé, CF_3, J(C–F) 265.4, ^3J(C–F) 2.7), 148.02 (doublet, Cc–F, J(Cc–F) 245.1).

Le pyrrole **9***a*, chauffé 48 h à reflux de l'ortho-xylène est décarboxylé en partie (30%) en pyrrole **10***a* qui n'a pas été isolé mais décelé par son spectre rmn ^{19}F: ϕ CF_3, 58.0 (singulet). Pour l'homologue N–CH_3, ϕ CF_3, 58.3 (singulet) (3).

Réaction du trifluoro-3,3,3 propène sur la tert-butyl-1 méthoxycarbonyl-2 aziridine

Un mélange de 2 g (12.7 mmol) d'aziridine, 3 g (31 mmol) d'oléfine et 4 ml de benzène anhydre sont chauffés 5 h à 175 °C en autoclave de 50 ml. Après le traitement habituel, on recueille une huile dont les constituants sont en partie séparés par cpvp sur colonne EGS (four 120 °C). Dans l'ordre croissant des temps de rétention, deux fractions principales sont isolées: **4***e* et **5***e* mélangés (0.42 g 1.7 mmol) et **3***e* (0.53 g, 2.1 mmol, p.f. $\simeq$ 25 °C). **4***e et* **5***e* sont séparés ensuite par chromatographie en couche mince préparative sur gel de silice Merck. Type 60 PF. Eluant: benzène – éther diéthylique (6:4). L'isomère **5***e*, le moins élué, est obtenu en proportion égale à **4***e*. *Anal.* Calc. pour $C_{11}H_{18}O_2F_3N$: C 52.17, H 7.16, N 5.53; trouvé: **3***e*, C 52.24, H 7.02, N 5.27. Spectres de masse: **3***e*, **4***e*, **5***e*, *m/e* 253 (M); rmn ^1H (250 MHz): **3***e*, δ ($CDCl_3$) 1.07 (9 H, singulet, $C(CH_3)_3$), 2.07 (1 H, doublet ($\simeq$triplets), H_f, $^2J(H_f–H_g)$ 12.5, $^3J(H_f–H_i)$ 8.75, $^3J(H_f–H_h)$ 9.5), 2.36 (1 H, doublet (triplets), H_g, $^2J(H_g–H_f)$ 12.5, $^3J(H_g–H_i)$ 7.5, $^3J(H_g–H_h)$ 7.5), 2.72 (1 H, octet, H_h, ΣJ = 60.8), 3.12 (1 H, doublet (doublets), H_d, $^2J(H_d–H_e)$ 10.5, $^3J(H_d–H_h)$ 8.75), 3.24 (1 H, doublet (doublets), H_e, $^2J(H_e–H_d)$ 10.5, $^3J(H_e–H_h)$ 8.5), 3.70 et 3.73 (4 H), 3.70 (singulet, $COOCH_3$), 3.73 ($\simeq$triplet, H_i, $^3J(H_i–H_f)$ 8.75, $^3J(H_i–H_g)$ 7.5). **4***e*: δ ($CDCl_3$) 1.08 (9 H, singulet, $C(CH_3)_3$), $\simeq$2.0 à 2.13 (2 H, multiplet, H_f et H_g), 2.83 (1 H, triplet, H_d, $^2J(H_d–H_e)$ 9.0, $^3J(H_d–H_h)$ 9.0), 3.13 (1 H, octet, H_h, ΣJ = 60), 3.30 (1 H, $\simeq$triplet, $^2J(H_e–H_d)$ 9.0, $^3J(H_e–H_h)$ 7.25), 3.71 (4 H, H_i et $COOCH_3$). **5***e*: δ ($CDCl_3$) 1.08 (9 H, singulet, $C(CH_3)_3$), $\simeq$1.96 (1 H, multiplet, H_f, ΣJ = 27), $\simeq$2.19 (1 H, multiplet, H_g, ΣJ = 41), $\simeq$2.81 (2 H, multiplet, H_h et H_d), 3.14 (1 H, $\simeq$triplet (multiplets), H_e, $J \simeq 8$); 3.67 (1 H, doublet, H_i, $^3J(H_i–H_h)$ 4.3), 3.71 (3 H, singulet, $COOCH_3$). ^{19}F rmn: **3***e*: ϕ ($CDCl_3$), 72.3 (doublet, ^3J(F–H_h) 7.5); **4***e*: ϕ ($CDCl_3$), 71.2 (doublet, ^3J(F–H_h) 7.6); **5***e*: ϕ ($CDCl_3$), 71.0 (doublet, ^3J(F–H_h) 9.9).

Remerciements

Nous remercions Madame Ginette Gordon de sa collaboration pour une partie de ce travail.

1. J. W. Lown. *Dans* Record of chemical progress. *Editeur* W. H. Powers. Vol. 32 (2). Plenum Press, New York and London. 1971. p. 51.
2. J. C. Blazejewski, D. Cantacuzene et C. Wakselman. Tetrahedron Lett. 2055 (1974).
3. J. C. Blazejewski, D. Cantacuzene et C. Wakselman. Tetrahedron Lett. 363 (1975).
4. H. W. Heine, R. Peavy et A. J. Durbetaki. J. Org. Chem. **31**, 3924 (1966).
5. P. L. Coe, P. Smith, J. C. Tatlow et M. Wyatt. J. Chem. Soc. Perkin Trans. 1, 781 (1975).
6. K. L. Williamson, Y. F. Li, F. H. Hall et S. Swager. J. Am. Chem. Soc. **88**, 5678 (1966).
7. R. D. Chambers et R. H. Mobbs. Adv. Fluorine Chem. **4**, 50 (1966).
8. J. B. Stothers. Carbon-13 NMR spectroscopy. Academic Press, New York. 1972. p. 367.
9. E. F. Mooney. An introduction to ^{19}F NMR spectroscopy. Heyden/Sadtler. 1970. p. 56.
10. Y. Gelas-Mialhe, R. Hierle et R. Vessiere. Bull. Soc. Chim. Fr. 709 (1974).
11. W. A. Sheppard et C. M. Sharts. Organic fluorine chemistry. W. A. Benjamin, Inc., New York. 1969. p. 330.
12. R. E. Banks et M. G. Barlow. Fluorocarbon and related chemistry. Vol. 2. The Chemical Society, London. 1974. p. 84.
13. I. L. Knunyants, E. G. Bykhovskaya, V. N. Frosin, I. V. Galakhov et L. I. Regulin. Zh. Vses. Khim. Ova. **17**, 356 (1972); Chem. Abstr. **77**, 101432n (1972).
14. (*a*) L. Wartski, C. Wakselman et A. Sierra-Escudero. Tetrahedron Lett. 4193 (1970); Bull. Soc. Chim. Fr. 1478 (1972). (*b*) J. A. Deyrup et C. L. Moyer. J. Org. Chem. **35**, 3424 (1970).
15. K. D. Gundermann, K. Burzin, F. J. Sprenger et H. Schulze. Chem. Ber. **105**, 312 (1972).

Molecular conformations of *ortho*-substituted benzophenones

FELICE ZUCCARELLO, SALVATORE MILLEFIORI, AND SALVATORE TROVATO
Istituto di Chimica Fisica, Università di Catania, 95125 Catania, Italy

Received April 17, 1975

FELICE ZUCCARELLO, SALVATORE MILLEFIORI, and SALVATORE TROVATO. Can. J. Chem. **54**, 226 (1976).

The minimum energy conformations of some mono- and di-substituted benzophenones were determined from contour maps of potential energy calculated by a semiempirical approach. The electrostatic interactions play a relevant role in the relative stabilities when different minima are possible. Comparison with the available experimental data reveals a good agreement with geometrical data, and a poorer agreement with energies in highly strained conformations.

FELICE ZUCCARELLO, SALVATORE MILLEFIORI et SALVATORE TROVATO. Can. J. Chem. **54**, 226 (1976).

On a déterminé les conformations d'énergie minimum de benzophénones mono- et di-substituées à partir de cartes de contour d'énergie potentielle calculée par une méthode semi-empirique. Les interactions électrostatiques jouent un rôle important sur les stabilités relatives quand différents minima sont possibles. Une comparaison avec des données expérimentales disponibles révèle une bonne concordance avec les données géométriques et une concordance moins bonne pour les énergies impliquant des conformations très tendues.

[Traduit par le journal]

Introduction

The conformational preferences of substituted benzophenones have been investigated by a variety of experimental techniques: uv (1, 2), ir (2, 3), and nmr spectroscopy (4–6) and dipole moments (3, 7). Theoretical studies have been reported on benzophenone (8, 9) and on some of its *meta*- and *para*-derivatives (10). Results from different techniques are often not in agreement. The difficulty in assigning the preferred conformation by using the nmr technique has been pointed out (6). On the other hand the simple vector analysis in the dipole moment approach may lead to incorrect results since many rigid molecular conformations, as well as the calculated dipole moments of many conformations (including a freely rotating molecule), may satisfy the experimental dipole moment. Also possible are oscillations over a large angle when the minimum in the potential energy curve is shallow. We think that the building of potential energy maps, by a semiempirical method, may be useful for relative comparisons of molecular conformations and for interconversion pathways within a class of compounds. This approach is followed here on some *ortho*-substituted benzophenones, where the molecular conformations result from a delicate balance of conjugative and large steric and electrostatic effects.

Calculations

The preferred conformations for the compounds studied were determined by a simple semiempirical method of calculation, which gave good results on benzophenone (9), comparable with those obtained by more sophisticated and expensive methods (8). The total energy (E_T) of the molecule was evaluated as a function of the two rotational angles φ and φ' (Fig. 1); individual E_T energy values for each pair of φ and φ' angles were minimized with respect to the variation in the valence angle Ph—C—Ph, α. E_T was approximated by the sum of the π-electron energy (E_π), the non-bonded interactions (E_{NB}), the Ph—C—Ph angular deformation energy (E_D), and the dipole–dipole interaction energy (E_{DD}). E_π (in the HMO approximation) and E_D were evaluated by utilizing the calculation scheme previously described (9, 10). Non-bonded

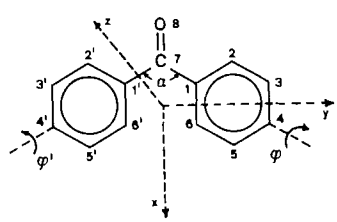

FIG. 1. Benzophenone. The arrows show the positive sense of rotation.

TABLE 1. Minimum energy conformations and relative energy contributions (kcal/mol) for *ortho*-substituted benzophenones

Substituent	Conformation	α^0	φ^0	φ'^0	E_π	E_D	E_{NB}	E_{DD}	ΔE^*
2-Me	*a*	120	40	−15	−416.80	0	1.73	−2.43	0
	b	120	142	28	−415.98	0	0.97	−2.25	0.24
2-F	*a*	121	151	27	−452.44	0.03	0.72	−0.53	0
	b	120	40	−15	−452.20	0	0.62	0.96	1.59
2-Cl	*a*	121	145	28	−416.72	0.03	0.80	−0.36	0
	b	120	45	−11	−416.86	0	0.92	0.91	1.22
2-Br	*a*	120	143	28	−411.63	0	0.79	−0.38	0
	b	120	46	−10	−411.92	0	1.09	0.73	1.13
2,6-Me		120	50	−17	−455.48	0	1.46	−2.42	0
2,6-F		120	44	−15	−527.08	0	0.52	2.50	0
2,6-Cl		120	53	−13	−456.20	0	0.75	2.47	0
2,6-Br		120	56	−12	−446.21	0	0.81	2.23	0
2,2′-Me	*a*	120	47	157	−455.36	0	1.64	−2.38	0
	b	120	141.5	−141.5	−454.73	0	1.08	−2.20	0.25
	c	118	29	−29	−456.77	0.14	3.92	−2.64	0.75
2,2′-F	*a*	120	152.5	−152.5	−527.87	0	1.25	−1.54	0
	b	120	44	164	−527.03	0	0.54	2.04	3.70
	c	119	28.5	−28.5	−527.68	0.03	0.67	5.50	6.69
2,2′-Cl	*a*	121	146	−146	−456.54	0.03	1.14	0.18	0
	b	120	58	166	−455.67	0	0.66	1.77	1.95
	c	119	30	−30	−457.38	0.03	2.04	5.70	5.58
2,2′-Br	*a*	120	144.5	−144.5	−446.49	0	1.07	0.58	0
	b	120	62	167	−445.63	0	0.74	1.59	1.54
	c	119	31	−31	−447.45	0.03	2.71	5.19	5.32

*Relative to the minimum energy conformation.

and dipole–dipole interactions were restricted to substituents in the 2, 6, 2′, and 6′ positions and to carbonyl oxygen. E_{DD} for the interacting dipole vectors was calculated in the usual way (10) by taking $\mu_{C-C=O} = 2.7$ D, $\mu_{C-Cl} = 1.58$ D, $\mu_{C-F} = 1.39$ D, $\mu_{C-Br} = 1.57$ D, $\mu_{CH_3-C} = 0.54$ D, and $\mu_{H-C} = 0.4$ D. The van der Waals interactions between non-bonded atoms were evaluated by means of the Hill equation (11) limited to the repulsive term, following Fournier and Waegell's suggestions (12):

$$E_{NB} = 0.1 \sum_{i<j} \exp\left(\frac{d_{ij} - r_{ij}}{0.0736 d_{ij}}\right)$$

where d_{ij} is the sum of the van der Waals radii for atoms i and j. The validity of this function was also tested for interactions between small atoms (H···H, H···F, and F···F). It was found that the potential energy curves for F···F and H···F interactions are very close to those calculated by means of the functions (including also the attractive term) derived by Heublein *et al.* (13) following Scott and Scheraga's suggestions (14). Moreover we have recalculated, utilizing the new non-bonded H···H function, the minimum energy conformation and activation energies for the interconversion pathways in benzophenone, and have found the same conformation and only slight variations in the activation energies as in ref. 1.

Calculations were performed on a CDC 6600 computer, for which a Fortran IV program was written.

Results and Discussion

In Table 1 the calculated minimum energy conformations and the various energy contributions are reported; in Figs. 2, 3, and 4 the contour maps of potential energy surfaces relative to the minima are reported only for chloro-derivatives; the trends in the energy surfaces are similar to those of other derivatives.

Mono-substituted Benzophenones

Two stable conformations are evident, which are defined by the position of the substituent relative to the carbonyl group (*syn* or *anti*).[1]

The *syn* conformers are characterized by a greater rotation of the substituted ring and a

[1]Alternatively some workers use the prefixes 'proximal' or 'distal' to distinguish the two conformers.

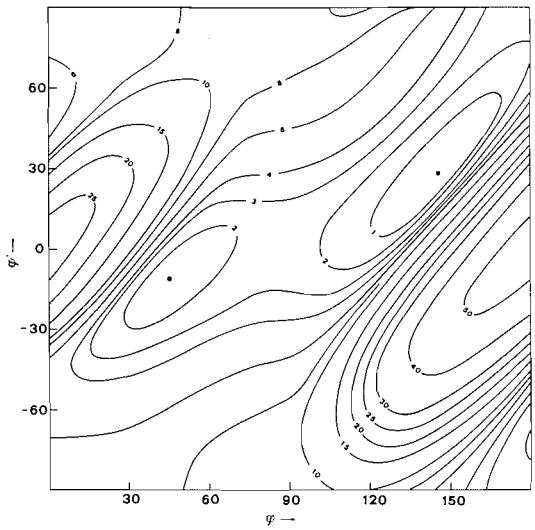

FIG. 2. Contour diagram of the potential energy (kcal/mol) surface for 2-chlorobenzophenone.

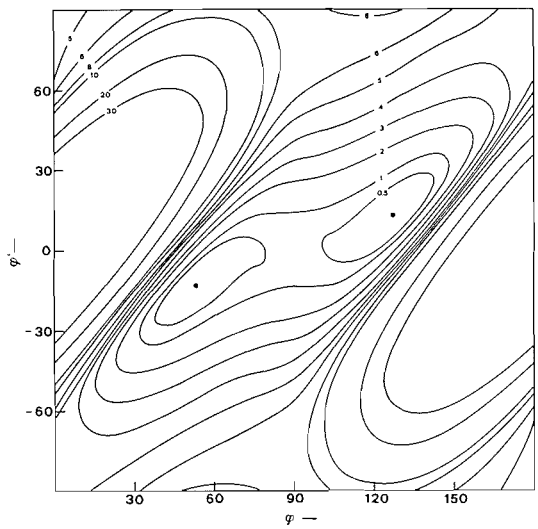

FIG. 3. Contour diagram of the potential energy (kcal/mol) surface for 2,6-dichlorobenzophenone.

smaller rotation of the unsubstituted one with respect to benzophenone (where $\varphi = -\varphi' = 25°$) while the *anti*-conformers retain a geometry similar to benzophenone. For the methyl derivative the most stable conformation is the *cis* one although the difference between the *syn* and *anti* conformers is smaller than *RT*. Our results are comparable with the spectroscopic findings of Rekker and Nauta (1) ($\varphi = 40°$ and $\varphi' = 0°$) and with those obtained by means of non-bonded interaction evaluations ($\varphi = 55°$ and $\varphi' = -5°$) (5). For the halogen derivatives the most stable conformation is *anti* by more than 1 kcal/mol, while the geometrical parameters, φ and φ', are almost unchanged.

In mono-substituted benzophenones the relative stability of the two conformers is determined essentially by the dipole–dipole interactions, the conjugative energy being nearly balanced by the non-bonded interactions.

The most favored pathway from one minimum to the other proceeds through the conformation defined by $\varphi = 90°$ and $\varphi' = 0°$, to which is associated an activation energy (Table 2) lower than that for benzophenone ($\Delta E = 3.46$ kcal/mol). On the other hand the path through the 0–90 barrier leads to an enhanced activation energy, relative to that for benzophenone, as pointed out by Hoffmann and Swenson (8).

Di-substituted Benzophenones

In 2,6-derivatives the two equivalent minima are characterized by a quasi-planar conformation of the unsubstituted phenyl ring and by a greater rotation of the substituted one than in the mono-substituted derivatives. It is apparent also from ir and uv spectra (2) that the unsubstituted benzene ring is more coplanar with the carbonyl group.

The present geometrical results for the 2,6-dimethyl derivative (Table 1) are in good agreement with data reported by Rekker and Nauta ($\varphi = 56°$, $\varphi' = 0°$); the preferred interconversion pathway goes through the 90–0 conformation with an activation energy of the same order of magnitude as *RT*, so that a large libration can occur about the two minima, according to the results of Buchanan *et al.* (5). On these grounds, they report an average conformation with $\varphi = 90°$ and $\varphi' = 0°$.

The enantiomerization through the 90–90 barrier (topomerization) requires an activation energy ≤ 10 kcal/mol, to be compared with the barrier found (17.2 kcal/mol) by Lauer and Staab for 3,5-dimethyl-2′,4′,6′-tri-*tert*-butyl benzophenone (4).

For the 2,2′-halogen derivatives we observe three conformations with a minimum in energy; the most stable conformer has both the substituents in *anti* position, the next one has a *syn*, *anti* conformation, but the minimum is not well defined, and the less stable conformer has both

TABLE 2. Rotational barriers in *ortho*-substituted benzophenones. ΔE, kcal/mol, is relative to the minimum energy conformation

Substituent	φ^0	φ'^0	ΔE
2-Me	0	90	5.03
	90	0	2.02
	90	90	10.37
	180	90	2.07
2-F	0	90	6.12
	90	0	3.02
	90	90	9.83
	180	90	2.85
2-Cl	0	90	6.68
	90	0	2.31
	90	90	9.44
	180	90	2.16
2-Br	0	90	6.96
	90	0	2.14
	90	90	9.72
	180	90	2.03
2,6-Me	0	90	4.16
	90	0	0.97
	90	90	10.21
2,6-F	0	90	4.13
	90	0	1.17
	90	90	7.36
2,6-Cl	0	90	4.87
	90	0	0.58
	90	90	7.40
2,6-Br	0	90	5.30
	90	0	0.48
	90	90	8.17
2,2′-Me	90	0	2.87
	60	60	8.47
	90	−90	9.12
2,2′-F	90	0	8.47
	60	60	13.85
	90	−90	11.39
2,2′-Cl	90	0	7.35
	60	60	11.93
	90	−90	9.62
2,2′-Br	90	0	7.20
	60	60	11.60
	90	−90	9.87

substituents in a *syn* position. There are two possible interconversion pathways between the *anti,anti* and *syn,syn* conformations; the first goes through the (−90)–90, the other through the 90–0 conformation. This latter seems to be the preferred pathway.

For the 2,2′-dimethyl derivative the relative stability of the *syn,anti* and the *anti,anti* conformers is reversed with respect to the halogen derivatives. Rekker and Nauta report for 2,2′-dimethylbenzophenone $\varphi = 41°$ and $\varphi' = 142°$. However, the differenee in the total energies and the value of the activation energy for their

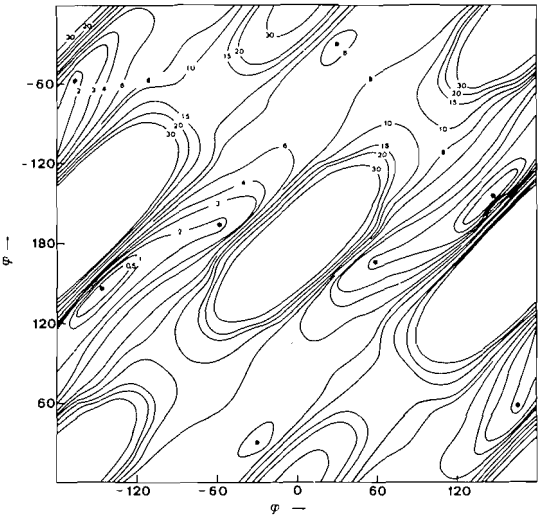

FIG. 4. Contour diagram of the potential energy (kcal/mol) surface for 2,2′-dichlorobenzophenone.

interconversion are so small that we may consider both conformers in the same potential 'valley'. As in the mono-substituted derivatives, the relative stabilities are determined essentially by the dipolar interactions. In these compounds, the *syn–anti* enantiomerization goes through a 60–60 barrier (and not through the 'usual' 90–90 barrier) as can be seen from Fig. 4. The resolution of the various conformers of *o*-substituted benzophenones in the nmr time-scale has been recently discussed (15).

Dipole Moments

In Table 3 are reported the values of dipole moments calculated for various minimum energy conformations and the average moments, which are obtained if we take into account the Boltzmann populations relative to the calculated energies; for comparison the available experimental values are also reported.

A fair agreement is achieved for mono-substituted benzophenones and the 2,2′-dimethyl derivative. The disagreement between $\bar{\mu}$ and μ_{exp} for the two 2,2′-dihalogen derivatives is evident, but if we look at the μ_T's we may observe that the values obtained for the *syn,anti* conformations are close to the experimental ones. In this respect we observe that the actual ΔE values are given by ΔH, while the position of the equilibrium is determined by the ΔG values; so left to be determined is the weight of the ΔS contribution, which depends on the differences

TABLE 3. Theoretical and experimental dipole moments for *ortho*-substituted benzophenones

Substituent	Conformation	μ_π	μ_T	Population (%)	$\bar{\mu}$	μ_{exp}*
2-CH_3	*a*	0.51	2.68	60	2.89	2.77, 2.69
	b	0.84	3.17	40		
2-F	*a*	0.94	2.78	94	2.89	
	b	0.48	4.27	6		
2-Cl	*a*	0.97	2.83	89	3.03	3.32, 3.44
	b	0.48	4.33	11		
2-Br	*a*	0.97	2.86	87	3.08	3.32, 3.42
	b	0.48	4.29	13		
2,6-Me		0.64	2.82	—		
2,6-F		0.67	3.93	—		
2,6-Cl		0.68	3.97	—		
2,6-Br		0.69	3.94	—		
2,2′-Me	*a*	0.69	2.91	67	2.94	2.51, 2.67
	b	0.88	3.27	23		
	c	0.24	2.28	10		
2,2′-F	*a*	1.10	1.91	100	1.91	
	b	0.74	3.89	0		
	c	0.11	5.67	0		
2,2′-Cl	*a*	1.08	1.89	96	2.00	3.34, 3.64
	b	0.78	3.79	4		
	c	0.02	5.84	0		
2,2′-Br	*a*	1.07	1.95	92	2.14	3.57, 3.78
	b	0.80	3.71	8		
	c	0.05	5.77	0		

*The first values refer to cyclohexane, the second to benzene solutions. See refs. 9, 10.

in the curvatures of the potential energy minima.

For this purpose we have calculated the entropy energy term relative to the two energy minima for the 2,2′-dichloro derivative according to ref. 16. The value 0.42 kcal/mol at 25 °C obtained for $T\Delta S$ gives $\Delta G = 1.53$ kcal/mol which does not cause appreciable changes in the equilibrium position already evaluated from the ΔH value. Therefore we conclude that the poor agreement between calculated and experimental dipole moments is due to the approximations inherent in the method. It gives good information about the stable conformations, but in highly strained molecules, where the approximations involved are exaggerated, it gives only rough estimates of relative energies of the various conformations, and hence the relative populations.

Acknowledgments

This work was partially supported by Consiglio Nazionale delle Ricerche, Italy.

1. R. F. REKKER and W. TH. NAUTA. Recl. Trav. Chim. Pays Bas, **73**, 969 (1954); **80**, 747 (1961); **80**, 764 (1961).
2. E. J. MORICONI, W. F. O'CONNOR, and W. F. FORBES. J. Am. Chem. Soc. **84**, 3928 (1962).
3. G. PFISTER-GUILLOUZO, M. GRIMAUD, and J. DESCHAMPS. Bull. Soc. Chim. Fr. 1203 (1969); 1212 (1969).
4. D. LAUER and H. A. STAAB. Chem. Ber. **102**, 1631 (1969).
5. G. W. BUCHANAN, G. MONTAUDO, and P. FINOCCHIARO. Can. J. Chem. **51**, 1053 (1973).
6. H. BENJAMINS and W. D. CHANDLER. Can. J. Chem. **52**, 597 (1974).
7. C. W. N. CUMPER and A. P. THURSTON. J. Chem. Soc. Perkin Trans. 2, 106 (1972).
8. R. HOFFMANN and J. R. SWENSON. J. Phys. Chem. **74**, 415 (1970).
9. F. ZUCCARELLO, S. TROVATO, and S. MILLEFIORI. Z. Phys. Chem. Neue Folge, **79**, 103 (1972).
10. S. TROVATO, F. ZUCCARELLO, and S. MILLEFIORI. Z. Phys. Chem. Neue Folge, **86**, 27 (1973).
11. T. L. HILL. J. Chem. Phys. **16**, 399 (1948).
12. J. FOURNIER and B. WAEGELL. Tetrahedron, **26**, 3195 (1970).
13. G. HEUBLEIN, R. KUHMSTEDT, P. KADURA, and H. DAWCZYNSKI. Tetrahedron, **26**, 81 (1970).
14. R. A. SCOTT and H. A. SCHERAGA. J. Chem. Phys. **42**, 2209 (1965); **44**, 3054 (1966); **45**, 2091 (1966); **46**, 4410 (1967).
15. P. FINOCCHIARO, D. GUST, and K. MISLOW. J. Am. Chem. Soc. **96**, 3198 (1974).
16. A. J. HOPFINGER. Conformational properties of macromolecules. Academic Press, New York. 1973. p. 124.

Stereochemical dependence of ^{13}C shieldings and ^{13}C–^{31}P couplings in phosphonates of known geometry. Is there a Karplus-type relationship for P–C–C–C coupling?[1]

GERALD W. BUCHANAN
Department of Chemistry, Carleton University, Ottawa, Canada K1S 5B6
AND
CLAUDE BENEZRA[2]
Department of Chemistry, University of Ottawa, Ottawa, Canada K1N 6N5

Received August 6, 1975

GERALD W. BUCHANAN and CLAUDE BENEZRA. Can. J. Chem. **54**, 231 (1976).

^{13}C nmr chemical shifts and ^{13}C–^{31}P couplings through one to five bonds are reported for seven dimethylphosphono compounds of known geometry. Vicinal couplings are maximal for a dihedral angle of 180° and are severely attenuated by OH substitution, particularly when the OH is *trans*-coplanar to the carbon terminus of the coupling path. When a cyclopropyl system is part of the C–C–C–P path the J values are much less than those predicted on the basis of dinedral angle. A highly asymmetric dihedral dependence of vicinal J's is suggested. Some 'non-W' long range C–P couplings through saturated networks are found. The '*gauche*-γ' shift of the $-P(O)(OCH_3)_2$ group is about 2 ppm.

GERALD W. BUCHANAN et CLAUDE BENEZRA. Can. J. Chem. **54**, 231 (1976).

On rapporte les déplacements chimiques en rmn du ^{13}C et les constantes de couplage ^{13}C–^{31}P à travers un jusqu'à cinq liens dans sept composés diméthylphosphono de géométrie connue. Les constantes de couplage vicinales sont les plus grandes lorsque l'angle dièdre est de 180°; ces constantes sont très atténuées par une substitution par un groupe hydroxyle particulièrement quand le groupe OH est *trans* et coplanaire avec le carbone terminal du chemin de couplage. Quand un système cyclopropanique fait partie du chemin C–C–C–P, les valeurs de J sont beaucoup plus faibles que celles prédites sur la base de l'angle dièdre. On suggère qu'il existe une dépendance hautement asymétrique sur l'angle dièdre pour les constantes de couplage J vicinales. On a trouvé quelques couplages C–P à longue distance du type 'non-W' à travers des systèmes saturés. Le déplacement '*gauche*-γ' du groupe $P(O)(OCH_3)_2$ est approximativement 2 ppm.

[Traduit par le journal]

Introduction

In recent years, a considerable amount of data has been accumulated regarding coupling between ^{13}C and ^{31}P and the application of such data to stereochemical determinations. For example, the existence of an angular dependence of P–O–C–C coupling has been clearly demonstrated in cyclic nucleotides (1), cyclic phosphites (2), and phosphates (3). Also, a nearly symmetrical Karplus curve has been generated for P–C–C–C coupling in phosphine oxides (4–6).[3]

For acyclic organic phosphonates, a large series of $^1J_{CP}$ values have been obtained (7–9) and finite perturbation calculations have been successful in reproducing the magnitudes of substituent effects (10). Herein we report a determination of ^{13}C chemical shifts and ^{13}C–^{31}P coupling through one to five bonds in a series of seven phosphonates in which the phosphorus is directly bonded to monocyclic, bicyclic, and tricyclic skeletons of well defined geometry. A discussion of factors influencing the magnitude of vicinal couplings is incorporated showing that considerable caution must be used in correlation of vicinal P–C–C–C coupling with dihedral angle. Some comments on the geometrical requirements for long range ^{31}P–^{13}C couplings are made.

Results and Discussion

(a) Spectral Assignments

Routinely, the ^{13}C Fourier transform spectra

[1]Part VII of the series NMR of Phosphonates; for part VI see ref. 28.

[2]Present address: Institut de Chimie, Université Louis Pasteur, 1 Rue Blaise Pascal, 67008-Strassbourg, France.

[3]G. A. Gray, personal communication.

Can. J. Chem. Downloaded from www.nrcresearchpress.com by 210.87.254.105 on 09/05/12
For personal use only.

TABLE 1. ^{13}C chemical shifts for phosphonates **1** → **7** (δ_c from TMS ± 0.1)*

Compound	Position 1	2	3	4	5	6	7	8	9	10	1′	2′	3′	4′	OCH_3
1	36.2	37.5	28.4	37.9	31.7	31.6	36.9								52.4
2	34.0	77.3	34.0	32.2	(27.2)	32.2	33.8	(26.7)	33.8	38.2					53.6
3	71.1	32.1	20.8	47.5	20.8	32.1	32.5	27.5							53.3
4	72.3	32.4	23.5	46.8	23.5	32.4	32.3	27.6							53.4
5	36.4	26.6	27.5	26.6	36.4	29.7	29.7	30.1			135.6	130.5	128.4	126.7	53.4
6	36.9	34.8	29.4	34.8	36.9	29.4	29.4	31.4			135.6	130.6	128.1	126.7	52.4
7		86.6	83.8	48.2	79.7	28.3	23.7	(31.6)	(32.2)						54.0

*0.2–0.3 *M* solutions in $CDCl_3$.

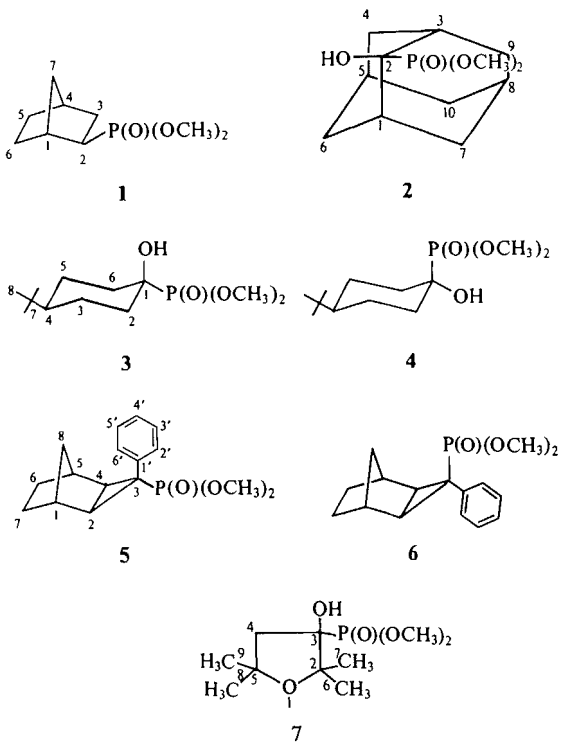

FIG. 1. Structures and numbering scheme for phosphonates.

were recorded with complete ^1H noise decoupling. To aid assignments, the single frequency off resonance decoupling procedure (SFORD) was employed for identification of CH_3, CH_2, CH, and quaternary centres. In cases where the ^1H spectra were unambiguous, selective ^1H irradiation was valuable. Occasionally the lanthanide shift reagent $Pr(FOD)_3$ was employed to distinguish between small chemical shift differences and P–C coupling phenomena. Interpretations were based on the results for

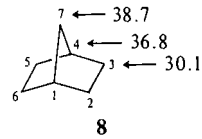

cyclic phosphonates (2-oxo-1,3,2-dioxaphosphorinanes) in which the lanthanide is deemed to coordinate at the phosphoryl oxygen (11). In addition, appropriate model compounds were used throughout.

(b) Chemical Shifts

The ^{13}C shieldings for phosphonates **1–7** are presented in Table 1, and the structures and numbering schemes in Fig. 1. For *exo*-2-dimethylphosphononorbornane **1**, it is interesting to compare the shifts with norbornane (12) and other *exo*-2-substituted cases (13). The norbornane shieldings are shown below (**8**). Selective ^1H decoupling of protons at C-1 and C-4 was carried out using the published assignments (14) for **1**. $Pr(FOD)_3$ was used to distinguish between the small chemical shift difference and P–C coupling interactions involving C-5 and C-6 of **1**.

Replacement of a hydrogen by the dimethylphosphono function deshields C-2 of **1** by 7.4 ppm relative to 8, as a consequence of the well documented α and β substituent effects (12, 13). In contrast to all previously studied *exo*-2-substituted norbornanes, C-1 and C-3 are shielded in **1** relative to **8**. This is likely due to the *gauche* interactions between the P—O bonds and the C-1 and C-3 positions (below) *i.e.* the γ upfield shift (15) which offsets the expected β deshielding effect. Recently, substantial γ shielding effects have been noted for carbons *gauche* to S—O functions (16, 17).

The minor deshielding (1.1 ppm) observed at

Can. J. Chem. Downloaded from www.nrcresearchpress.com by 210.87.254.105 on 09/05/12
For personal use only.

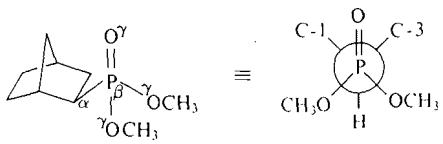

C-4 of **1** relative to **8** may be a consequence of a δ interaction between C-4 and one of the oxygen atoms (18). The 1.8 ppm upfield shift at C-7 of **1** relative to **8** can be attributed to the γ effect of the phosphorus atom, and appears to be a general feature of *exo*-2-substituted norbornanes (13). By contrast, the deshielding at C-6 of **1** compared to **8** is the first reported example in which an *exo*-2-substituent deshields the C-6 position. This result may cast some doubt on the validity of the model for the earlier results which involves substituent electronegativity and back lobe interaction of C-2 and C-6 orbitals (13).

For 2-dimethylphosphono-2-hydroxy adamantane **2**, the carbon shifts of adamantane **9** can be used as a starting point for discussion. Lippmaa *et al.* (19) reported shifts of 28.7 and 38.2 ppm for the bridgehead and methylene carbons of **9** respectively. Since **2** possesses a plane of symmetry there are only seven unique ring carbon positions. Off resonance decoupling experiments and consideration of ^{13}C–^{31}P couplings made assignments unambiguous except for C-5 *vs.* C-8. The most interesting chemical shift changes are seen at the C-4,6 and C-7,9 positions. For C-4,6, which have a dihedral angle of 180° to phosphorus, upfield shifts of 6.0 ppm relative to **9** are apparent. These results are expected since the C-4,6 positions are *gauche* to the 2-OH function, and it is known from epimeric 4-*tert*-butylcyclohexanols, (20) that such interactions shield the *gauche* carbons by *ca.* 5 ppm. The C-7,9 carbons bearing a dihedral angle of 60° to phosphorus, are also shielded considerably (4.4 ppm) relative to the methylene carbons of adamantane. No doubt this is due in part to the *gauche* interaction with the 2-dimethylphosphono group. For C-10 of **2**, the position most remote from the site of substitution, a shift identical to that for the CH_2 groups of **9** is found.

Results for the epimeric 4-*tert*-butylcyclohexyl hydroxyphosphonates **3** and **4** are consistent with the assignments for C-4,6 and C-7,9 of **2**. For **3** having the axial OH, the C-3,5 carbons are shielded by *ca.* 2.7 ppm relative to **4** in which the dimethylphosphono group is axial. Also,

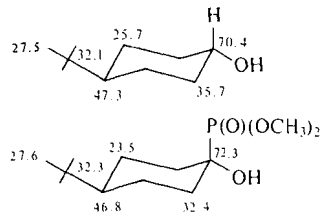

C-1 of **3** is shielded by *ca.* 1 ppm relative to **4**. These findings indicate that the 'γ' effect of the $-P(O)(OCH_3)_2$ group is considerably smaller than that of the OH function. Employing shifts for *trans*-4-*tert*-butylcyclohexanol as a model, and comparing with **4**, the 'γ' shift for the $-P(O)(OCH_3)_2$ function is estimated to be *ca.* 2 ppm.

Carbon shifts for the more remote positions *i.e.* C-4,7 and 8 are remarkably similar in the alcohols (20) and the hydroxylphosphonates **3** and **4**.

In discussing the results for *exo*-3-dimethylphosphono-*endo*-3-phenyl-tricyclo[3.2.1.$0^{2,4exo}$] octane **5** and its epimer **6** it is useful to examine a closely related model system for which ^{13}C data have been published. Tori *et al.* (21) have compared shieldings for norbornene **10**, with tricyclo[3.2.1.$0^{2,4exo}$]oct-6-ene **11** to determine the influence of cyclopropyl substitution. The most dramatic effect of the cyclopropyl ring is the

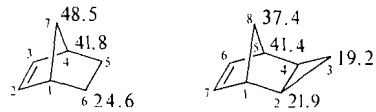

10 **11**

11.1 ppm upfield shift induced at C-8 of **11** *vs.* C-7 of **10**, an example of a remarkably large γ shift. No appreciable effect is observed at the C-1,5 bridgehead positions of **11** *vs.* C-1,4 of **10**, and a shielding effect of *ca.* 3 ppm is noted at C-2,4 of **11** *vs.* C-5,6 of **10**.

Comparing the data for **5** with norbornane **8** some similar trends can be discerned. For example C-8 of **5** is shielded by 8.6 ppm relative to C-7 of norbornane indicative of the γ effect of the cyclopropane ring and perhaps some small (*ca.* 1 ppm) anisotropic shielding effect of the benzene function. Anisotropic effects of similar magnitude have been noted in the ^1H spectrum (22). For **6**, C-8 is slightly deshielded compared to **5** (by 1.3 ppm) in support of a minor anisotropic shielding of C-8 in **5** by the aromatic ring.

Can. J. Chem. Downloaded from www.nrcresearchpress.com by 210.87.254.105 on 09/05/12
For personal use only.

Can. J. Chem. Downloaded from www.nrcresearchpress.com by 210.87.254.105 on 09/05/12
For personal use only.

For both **5** and **6** the resonance positions for C-1,5 are remarkably close to that for C-1,4 of norbornane in accord with the results for **10** and **11**. Also, the positions most remote from the site of substitution *i.e.* C-6,7 of **5** and **6** exhibit chemical shifts close to the value for C-2,3,5,6 of norbornane.

A striking difference in the carbon shifts for the epimers **5** and **6**, however, is present at the C-2,4 positions *i.e.* isomer **5** is shielded by *ca.* 8 ppm relative to **6**. Consideration of the most likely conformations of **5** and **6** aids in the interpretation of this result. For **5**, the conformers **5***a* and **5***b* are most likely.

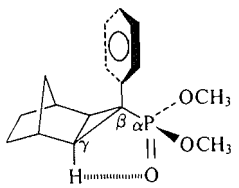

5a

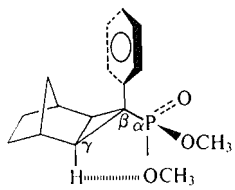

5b

In **5***a* there is a relationship between the P=O group and the *endo* H's at C-2,4 which is closely analogous to a 1,3 diaxial interaction in the chair conformation of a six-membered ring. Recently, such interactions involving the S=O group have been shown to shield the γ carbons by 7–10 ppm (16, 17) relative to cases which lack this interaction. Similarly in **5***b* the γ interaction between the OCH_3 and the C-2,4 positions can, by analogy with an axially substituted cyclohexane, be expected to lead to increased shielding at C-2,4 (20, 23, 24).

For the epimeric compound **6** the molecule will likely adopt a conformation such as that depicted below, in which there is no appreciable nonbonded interaction between the phenyl hydrogens and the *endo* H's at C-2,4. Also, there is no possibility of steric interference between the P—O groups and the *endo* C-2,4 H's which appears to be necessary (25) for a γ shift to be observed.

No remarkable shift differences are present for the aromatic carbons of **5** and **6**.

For compound **7**, the X-ray crystallographic

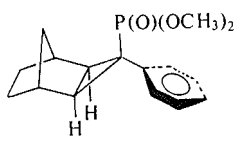

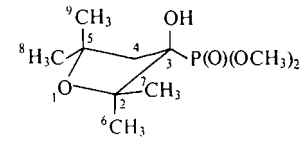

7

structure has been published (26) which corresponds well with the solution geometry as inferred from consideration of vicinal ^{31}P–^{1}H couplings (27, 28). In discussing the ^{13}C chemical shifts of **7** earlier results for methyl cyclopentanols (28, 29, 30) can be usefully examined. On this basis, C-2 of **7** is expected to be more deshielded than C-5 of **7**, a finding which is further confirmed by the large vicinal coupling from C-5 to ^{31}P (dihedral angle *ca.* 160°) (26). The resonance for C-3 is clearly distinguished due to its direct coupling to ^{31}P. Concerning the CH_3 resonances of **7** it is known in the 2-methyl cyclopentanols that a *cis*-OH shields the CH_3 by *ca.* 4 ppm relative to a *trans* configuration. The shift difference between C-6 and C-7 of **7** (as numbered above) is close to that of the simpler model and permits a clear designation for the resonances at δ = 23.7 and 28.3 respectively.

For *cis* and *trans*-CH_3 groups in isomeric 3-methyl cyclopentanols, the CH_3 resonances are deshielded relative to the 2-CH_3 compounds, but there is little effect (0.4 ppm) of OH configuration (28, 29, 30). Accordingly we assign resonances at δ = 31.6 and 32.2 to the methyls bonded to C-5 of **7**, but, at present no distinction can be made between them. Unfortunately, no resolvable coupling is present for any of the methyls of **7** to ^{31}P.

Chemical shifts for the OCH_3 groups of **1**–**7** are all near δ = 53. In compounds **1** and **7** the lack of symmetry should render the OCH_3's nonequivalent. The small splitting observed in these resonances (*ca.* 7 Hz) was in no case, however, affected by the addition of $Pr(FOD)_3$. Thus we conclude in **1** and **7** that the diastereotopic OCH_3 groups have accidentally equivalent chemical shifts, and the observed splitting in each case arises from P–O–C coupling.

(c) Coupling Constants

(1) One Bond Couplings

The direct ^{13}C–^{31}P couplings are shown in Table 2, and from earlier work (7) the sign is assumed to be positive. Couplings in the hydroxy

Can. J. Chem. Downloaded from www.nrcresearchpress.com by 210.87.254.105 on 09/05/12
For personal use only.

TABLE 2. One bond $^{13}C-^{31}P$ couplings (± 0.2 Hz)

Compound	J (Hz)*
1	143.1
2	158.8
3	164.6
4	156.8
5	176.3
6	182.2
7	166.9

*Sign assumed to be positive (7).

TABLE 3. Geminal $^{13}C-^{31}P$ couplings in **1–7** (± 0.2 Hz)

Compound	Path	$\|J\|$ (Hz)†
1	$^{1}C-^{2}C-P$	3.8
	$^{3}C-^{2}C-P$	1.0
	CH_3-O-P	−6.6*
2	$^{1,3}C-^{2}C-P$	4.4
	CH_3-O-P	−7.2*
3	$^{2,6}C-^{1}C-P$	3.1
	CH_3-O-P	−7.4*
4	$^{2,6}C-^{1}C-P$	1.5
	CH_3-O-P	−7.4*
5	$^{2,4}C-^{3}C-P$	1.1
	$^{1'}C-^{3}C-P$	N.R.
	CH_3-O-P	−5.9*
6	$^{2,4}C-^{3}C-P$	1.2
	$^{1'}C-^{3}C-P$	N.R.
	CH_3-O-P	−7.3*
7	$^{2}C-^{3}C-P$	16.9
	$^{4}C-^{3}C-P$	5.9
	CH_3-O-P	−7.4*

*From ref. 7.
†N.R. ≡ not resolvable (less than 0.6 Hz).

phosphonates **2**, **3**, **4**, and **7** are considerably larger than for the simpler phosphonate **1**. This observation is consistent with the results of Gray (10) who reported an increase of *ca.* 20 Hz in the $^{13}C-^{31}P$ coupling in phosphonates in which a hydrogen bonded to the carbon of interest is replaced by a methoxyl group. The enhanced $^{13}C-^{31}P$ coupling of *ca.* 180 Hz in **5** and **6** in which the carbon is part of a cyclopropane ring, is reminiscent of the increased $^{13}C-^{1}H$ couplings observed for cyclopropyl carbons (31).

(2) Geminal Couplings

In Table 3 are presented the two bond $^{13}C-^{31}P$ couplings found in **1–7**. For the P–O–C J's, the range of 5.9–7.4 Hz is similar to that found in cyclic phosphates (3) and in acyclic phosphonates (10). The sign is assigned as being negative based on results for $(CH_3O)_2P(O)CH_3$ (7). Regarding the C–C–P couplings it has been noted that the sign can change, at least for P(III) systems (32) and accordingly absolute values only are quoted. Although there is a substantial range of values *i.e.* less than 0.6 to 16.9 Hz, specific trends are difficult to elucidate. The need for a systematic examination of C–C–P coupling in a series of closely related phosphonates is apparent.

TABLE 4. Vicinal $^{13}C-^{31}P$ couplings (± 0.2 Hz)

Compound	Path	Dihedral angle θ (deg)	J (Hz)*†
1	$^{4}C-C-C-P$	120	1.8
	$^{6}C-C-C-P$	180	18.4
	$^{7}C-C-C-P$	90	N.R.
2	$^{4,6}C-C-C-P$	180	11.8
	$^{7,9}C-C-C-P$	60	0.7
3	$^{3,5}C-C-C-P$	180	12.6
4	$^{3,5}C-C-C-P$	60	N.R.
5	$^{1,5}C-C-C-P$	170	6.1
	$^{2',6'}C-C-C-P$	?	4.9
6	$^{1,5}C-C-C-P$	10	1.1
	$^{2',6'}C-C-C-P$	?	2.5
7	$^{5}C-C-C-P$	160	15.4
	$^{6}CH_3-C-C-P$	30	N.R.
	$^{7}CH_3-C-C-P$	90	N.R.

*Sign taken as positive (7).
†N.R. ≡ nonresolvable (less than 0.6 Hz).

(3) Vicinal Couplings

An examination of the data collected in Table 4 shows the gross features of dihedral dependence of vicinal coupling, however, it is clear that substituents markedly affect the magnitude of C–C–C–P coupling for a given dihedral angle θ. For example in **1**, **2**, and **3** for $\theta = 180°$, $^3J_{CP}$ values are 18.4, 11.8, and 12.6 Hz respectively, suggesting a significant perturbing effect of the OH group in **2** and **3**. It is well known for vicinal H–H coupling (33–35) that electronegative groups decrease the magnitude of ^3J and a similar effect appears to be operative for the C–C–C–P interaction. Also it is known (36, 37) in H–H coupling that the *orientation* of the electronegative group affects ^3J. In ring A of steroids, J_{ae} of structure **12** (below) is 5.5 ± 1 Hz for R = OH or OAc, while for **13** J_{ea} is in the range of 2.5–3.2 Hz,

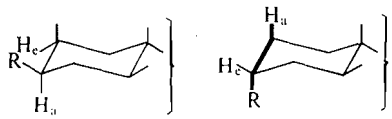

12 13

i.e. the electronegative group exerts its maximum effect (minimum J) when it is *trans*-coplanar to a terminus of the coupling path (as in **13**).

In **2** the OH is *gauche* relative to C-4,6 but nevertheless the coupling is reduced relative to **1** by *ca.* 6.5 Hz. The small magnitudes (less than 1 Hz) for the ^{7,9}C–C–C–P coupling in **2** ($\theta = 60°$) and ^{3,5}C–C–C–P in **4** are thus attributed to the *trans* relation of the OH to carbon terminus of the C–C–C–P path in each case.

In **7** there is no resolvable coupling between P and $^{6}CH_3$, although $\theta = 30°$ (26). In this case the OH is *trans* periplanar to $^{6}CH_3$ which may again be a manifestation of the orientational effect of the electronegative group. Interestingly, C-5 of **7** is nearly orthogonal to the OH and a large vicinal coupling to P is observed (15.4 Hz) for $\theta \approx 160°$.

In the case of $\theta = 90°$ there are two models; ^{7}C–C–C–P in **1** and $^{7}CH_3$–C–C–P in **7**. For both instances the ^{3}J values are less than 0.6 Hz suggesting minimal vicinal coupling for this geometry, in accord with results for other magnetic nuclei.

The small coupling of 6.1 Hz for ^{1,5}C–C–C–P in **5** where $\theta = 170°$ is noteworthy. Apparently the cyclopropyl moiety is a relatively poor transmitter of vicinal coupling information. A similar trend has been noted for vicinal ^{1}H–^{31}P coupling (28). For a given dihedral angle, the coupling in the cyclopropyl system is *ca.* 5 Hz less than for a five-membered ring. In compound **6** the small (1.1 Hz) coupling in the case of $\theta = 10°$ is indicative of a highly asymmetric Karplus type curve for vicinal J's in phosphonates, by contrast to the results for phosphine oxides (4–6)[3] in which an essentially symmetrical curve has been generated.

(4) Long Range Couplings

The resolvable long range ^{31}P–^{13}C couplings are presented in Table 5 with absolute values only being specified. For four bond coupling through a saturated network, a planar W geometry has been shown to be most favourable for ^{1}H–^{1}H J's (38) although many examples of resolvable non W ^{1}H–^{1}H coupling are now known (39).

TABLE 5. Long range ^{13}C–^{31}P couplings ($\pm$0.2 Hz)

Compound	Path	$\lvert J\rvert$ (Hz)
1	^{5}C–C–C–C–P	5.9
2	^{5}C–C–C–C–P	1.5
5	^{8}C–C–C–C–P	2.2
	$^{3',5'}$C–C–C–C–P	1.9
	$^{4'}$C–C–C–C–C–P	3.4
6	$^{3',5'}$C–C–C–C–P	1.5
	$^{4'}$C–C–C–C–C–P	3.4

In the present work, resolvable four bond couplings through saturated networks are found for phosphonates **1**, **2**, and **5**. The geometry in each case is essentially as shown below, with the terminal carbon being nearly perpendicular to the plane of the other four atoms.

For **1**, in which two such paths exist, the largest four bond J (5.9 Hz) is observed. It is interesting to note that in **5**, the path P–^{3}C–^{2}C–^{1}C–^{6}C is very close to a planar W and no resolvable coupling is apparent, indicating $\lvert J\rvert$ is less than 0.6 Hz. In **6**, a 'fork' type arrangement (U) involving P–^{3}C–^{2}C–^{1}C–^{8}C exists and again $\lvert J\rvert < 0.6$ Hz. Also, when a 'sickle' type geometry (⌒) is present *i.e.* P–^{3}C–^{2}C–^{1}C–^{7}C in **6** there is no resolvable coupling.

It is well known that π systems facilitate the transmission of long range coupling information (38) and therefore it is not surprising that substantial four and five bond couplings from phosphorus to the aromatic carbons of **5** and **6** are present. Furthermore there is precedent[3] for situations in which the five bond J's are larger than those through four bonds.

In conclusion, it is apparent from this work that considerable care must be exercised in attempting to relate vicinal ^{13}C–^{31}P couplings with dihedral angle. Also, the geometrical requirements for long range ^{13}C–^{31}P coupling appear to differ from those of ^{1}H–^{1}H coupling. Work is in progress using an extensive series of phosphonates to more clearly define the angular effects.

Can. J. Chem. Downloaded from www.nrcresearchpress.com by 210.87.254.105 on 09/05/12
For personal use only.

Can. J. Chem. Downloaded from www.nrcresearchpress.com by 210.87.254.105 on 09/05/12
For personal use only.

Experimental

Spectra

^{13}C spectra were obtained using the pulsed Fourier transform method at 25.16 MHz on a Varian XL-100-12 nmr spectrometer. The free induction decays were stored in a Nicolet BNC-12 computer (20K memory) and were transformed after a sufficient number had been accumulated. Normally 8192 data points were used in the interferogram accumulation and spectral widths of 5000 and 1000 Hz were employed.

All samples were examined as 0.2–0.3 *M* solutions in $CDCl_3$ containing 4% TMS as an internal standard. Tube size was 8 mm outer diameter. Normally spectra were recorded with complete proton noise decoupling. For the selective decoupling experiments irradiation was performed at low decoupler power in the absence of noise modulation.

Materials

Compounds **1** (40), **5** and **6** (22), and **7** (27) were available from previous work. Compound **2** was prepared as follows:

2-Adamantanone (1.50 g, 9.9 mmol, Aldrich) was dissolved in a minimum amount of benzene (8 ml). To this, dimethyl hydrogen phosphonate, $HP(O)(OCH_3)_2$, (1.20 g, 10.9 mmol, Aldrich) was added, followed by 10 drops of a freshly prepared solution of $NaOCH_3$ in CH_3OH. The reaction was exothermic and crystals were formed within an hour at room temperature. A yield of 1.54 g (60%) of crude product was obtained. The compound was recrystallized from ethyl acetate to yield **2**, mp 138–139 °C. *Anal.* Calcd. for $C_{12}H_{21}O_4P$: C 55.38, H 8.13, P 11.90; found: C 55.19, H 8.25, P 11.71.

A similar procedure starting with 4-*tert*-butylcyclohexanone, yielded a mixture of **3** and **4**, which were separated by column chromatography (alumina, $CHCl_3$–ether). Compound **3**, mp 152–154 °C and compound **4**, mp 117.5–118.5 °C. *Anal.* Calcd. for $C_{12}H_{25}O_4P$: C 54.40, H 9.59, P 11.75; found: C 54.22, H 9.72, P 12.09.

1. R. D. Lapper, H. H. Mantsch, and I. C. P. Smith. J. Am. Chem. Soc. **94**, 6243 (1972).
2. M. Haemers, R. Ottinger, D. Zimmerman, and J. Reisse. Tetrahedron Lett. 2241 (1973).
3. A. A. Borisenko, N. M. Sergeyev, E. Y. Nifantev, and Y. A. Ustynyuk. Chem. Commun. 406 (1972).
4. R. B. Wetzel and G. L. Kenyon. J. Am. Chem. Soc. **94**, 9230 (1972).
5. G. A. Gray and S. E. Cremer, J. Org. Chem. **37**, 3458 (1972).
6. R. B. Wetzel and G. L. Kenyon. J. Chem. Soc. Chem. Commun. 287 (1973).
7. W. McFarlane. Proc. R. Soc. London, Ser. A, **306**, 185 (1968).
8. H. J. Jakobsen, T. Bundaard, and R. S. Hansen. Mol. Phys. **23**, 197 (1972).
9. G. Mavel and M. J. Green. Chem. Commun. 742 (1968).
10. G. A. Gray. J. Am. Chem. Soc. **93**, 2132 (1971).
11. K. C. Yee and W. G. Bentrude. Tetrahedron Lett. 2775 (1971).
12. J. B. Stothers. Carbon-13 NMR spectroscopy. Academic Press, New York, New York. 1972.
13. J. B. Grutzner, M. Jautelat, J. B. Dence, R. A. Smith, and J. D. Roberts. J. Am. Chem. Soc. **92**. 7107 (1970).
14. H. J. Callot and C. Benezra. Can. J. Chem. **48**, 3382 (1970).
15. W. R. Woolfenden and D. M. Grant. J. Am. Chem. Soc. **88**, 1496 (1966).
16. G. W. Buchanan, J. B. Stothers, and G. Wood. Can. J. Chem. **51**, 3746 (1973).
17. G. W. Buchanan and T. Durst. Tetrahedron Lett. 1683 (1975).
18. S. H. Grover, J. P. Guthrie, J. B. Stothers, and C. T. Tan. J. Magn. Reson. **10**, 227 (1973).
19. E. Lippmaa, T. Pehk, and J. Past. Eesti NSV Tead. Akad. Toim. Fuus. Mat. **16**, 345 (1967).
20. J. D. Roberts, F. J. Weigert, J. I. Kroschwitz, and H. J. Reich. J. Am. Chem. Soc. **92**, 1338 (1970).
21. K. Tori, M. Ueyama, T. Tsuji, H. Matsumura, H. Tanida, H. Iwamura, K. Kushida, T. Nishida, and S. Satoh. Tetrahedron Lett. 327 (1974).
22. H. J. Callot and C. Benezra. Can. J. Chem. **50**, 1078 (1972).
23. G. W. Buchanan, D. A. Ross, and J. B. Stothers. J. Am. Chem. Soc. **88**, 4301 (1966).
24. H. J. Reich, M. Jautelat, M. T. Messe, F. J. Weigert, and J. D. Roberts. J. Am. Chem. Soc. **91**, 7445 (1969).
25. H. Beierbeck and J. K. Saunders. Can. J. Chem. **53**, 1307 (1975).
26. S. Samuel and R. Weiss. Tetrahedron, **26**, 2995 (1970).
27. C. Benezra and G. Ourisson. Bull. Soc. Chim. Fr. 1825 (1966).
28. C. Benezra. J. Am. Chem. Soc. **95**, 6890 (1973).
29. M. Christle, H. J. Reich, and J. D. Roberts. J. Am. Chem. Soc. **93**, 3463 (1971).
30. R. G. S. Ritchie, N. Cyr, B. Karsch, H. J. Koch, and A. S. Perlin. Can. J. Chem. **53**, 1424 (1975).
31. V. S. Watts and J. H. Goldstein. J. Chem. Phys. **46**, 4165 (1967).
32. S. Sorensen, R. S. Hansen, and H. J. Jakobsen. J. Am. Chem. Soc. **94**, 5900 (1972).
33. J. S. Waugh and S. Castellano. J. Chem. Phys. **35**, 1900 (1961).
34. C. N. Banwell and N. Sheppard. Discuss. Faraday Soc. **34**, 115 (1962).
35. L. M. Jackman and S. Sternhell. Applications of nuclear magnetic resonance spectroscopy in organic chemistry. 2nd ed. Pergamon Press, London. 1969.
36. D. H. Williams, and N. S. Bhacca. J. Am. Chem. Soc. **86**, 2742 (1964).
37. H. Booth. Tetrahedron Lett. 411 (1965).
38. S. Sternhell. Q. Rev. **23**, 236 (1969).
39. V. Mark. Tetrahedron Lett. 299 (1974).
40. H. J. Callot and C. Benezra. Can. J. Chem. **49**, 500 (1971).

2,3,12,13-Tetraselena[4,4]metacyclophane. A disparity with the literature

REGINALD H. MITCHELL

Department of Chemistry, University of Victoria, Victoria, British Columbia V8W 2Y2

Received August 25, 1975

REGINALD H. MITCHELL. Can. J. Chem. **54**, 238 (1976).

The synthesis of 2,3,12,13-tetraselena[4,4]metacyclophane (**1**) by alkaline hydrolysis of *meta*-xylylene selenocyanate (**3***a*) in 8% yield is described and is shown to have different properties to those described for **1** by Günther and Salzmann. The variable temperature pmr spectra of **1** is described as is its conversion to 2,11-diselena[3,3]metacyclophane (**4**) by tris(diethylamino)-phosphine.

REGINALD H. MITCHELL. Can. J. Chem. **54**, 238 (1976).

On décrit la synthèse du tétraséléna-2,3,12,13[4,4] *méta*-cyclophane (**1**) par hydrolyse alcaline du sélénocyanate du *méta*-xylylène (**3***a*); on montre que ce produit, obtenu avec un rendement de 8%, a des propriétés différentes de celles décrites pour **1** par Günther et Salzmann. On décrit le spectre rmp de **1** à des températures variables de même que sa conversion en diséléna-2,11[3,3] *méta*-cyclophane (**4**) par l'intermédiaire la tris(diéthylamino)phosphine.

[Traduit par le journal]

Introduction

Günther and Salzmann have reported (1) that 2,3,12,13-tetraselena[4,4]metacyclophane, **1**, (the dimer of α,α'-diseleno-*meta*-xylene) is obtainable on cooling a 1,1,2,2-tetrachloroethane (TCE) solution of the polymeric diselenide **2**. To my knowledge such a reaction to prepare a cyclophane is without precedent and especially important in light of the recent advances of both selenium chemistry (2) and thiacyclophane chemistry (3) to remove the heteroatom and generate the parent cyclophanes.

I thus re-investigated this reaction with the goal of a simple synthesis of cyclophanes. No such thermal equilibration of **2** to **1** was found and authentic cyclophane **1** was prepared by alkaline hydrolysis of selenocyanate **3***a* under high dilution conditions.

Results and Discussion

Thiacyclophanes can be prepared in high yield by allowing a dilute solution of mercaptan and halide to interact with base (3*a*). Such a reaction to prepare selenaphanes in reasonable yield has failed (4) mainly due to the extreme difficulty in isolating selenols. The approach of Boekelheide and Mondt (5) in which the analogous tetrathia-**1** was prepared from *meta*-xylylene dithiol is thus not very feasible for application to **1** itself. Klayman (6) lists a number of approaches to diselenide synthesis and of these, hydrolysis of a selenocyanate appeared to be most promising for application to cyclophane synthesis, since the intermediate selenocyanate is readily purified and the hydrolysis can be carried out under high dilution.

Reaction of *meta*-xylylene bromide with KSeCN (readily prepared from KCN and elemental Se (7)) in acetone gave an 87% yield of the bis-selenocyanate **3***a*. This could be hydrolyzed by KOH in methanol under high dilution conditions to yield an oily residue containing the cyclic dimer **1** (in *ca.* 8% yield) as well as much insoluble polymer **2**.

A pure sample of the cyclophane **1** was isolated by chromatography of the reaction mixture on silica gel and crystallization from cyclohexane, when **1** was obtained as pale yellow crystals mp (dec.) *ca.* 110 °C (lit. (1) mp claimed for **1**, 136–138 °C).

The structure of authentic **1** follows from its analysis and mass (M^+ at *m/e* 528 with isotope peaks corresponding to Se_4) and pmr spectra. The latter (Fig. 1) shows the methylene bridges at 4.00 δ deshielded by 0.19 ppm from those of the polymer **2** and the internal aromatic protons at 6.67 δ shielded by 0.36 ppm from those of polymer **2**. This is analogous to the case of the known diselenacyclophane **4** in which the bridges are deshielded by 0.24 ppm and the internal aromatic protons shielded by 0.58 ppm.

Can. J. Chem. Downloaded from www.nrcresearchpress.com by 210.87.254.5 on 09/05/12
For personal use only.

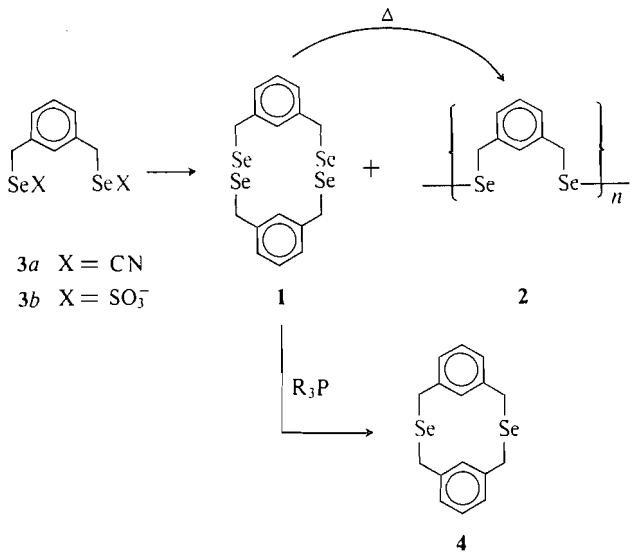

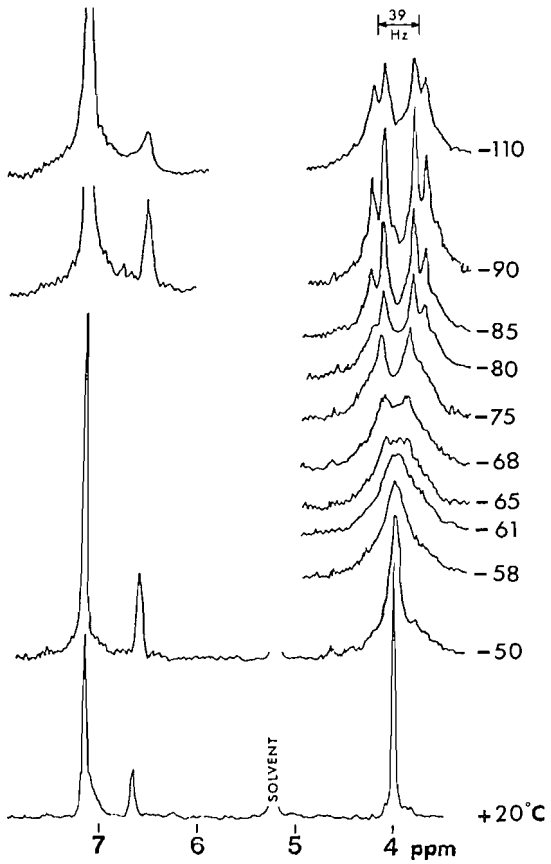

FIG. 1. Proton magnetic resonance spectra of **1** in CD_2Cl_2–$CDCl_3$ (3:1) recorded on a Perkin-Elmer R32-90 MHz spectrometer.

The smaller shifts observed for **1** are consistent for a [4,4] rather than a [3,3] cyclophane. Further evidence for the structure of **1** was obtained by its conversion to **4** (independently prepared from sodium selenide and *meta*-xylylene bromide (4)) by tris(diethylamino)-phosphine in benzene at reflux in excellent yield.

A compound identical in all respects to **1** after extensive purification was obtained in much lower yield (~0.2%) by hydrolysis of the selenosulfate **3***b* as essentially described by Günther and Salzmann (1) along with the polymer **2**.

When solutions of **1** from either route were allowed to stand, polymer **2** precipitated. No difference could be detected, analytically or spectrally (ir, pmr) between samples of polymer prepared by either route, or by decomposition of the dimer.

Samples of the polymer from both sources were equilibrated in TCE at 100 °C as described by Günther and Salzmann (1) and also in an nmr tube and examined spectrally, however, no evidence could be obtained for the conversion of polymer **2** into cyclophane **1**. I therefore conclude that it is likely that the crystalline product obtained from hot solutions of polymer **2** in TCE is not **1** as claimed by Günther and Salzmann but a crystalline modification of **2**.

The pmr spectrum of authentic **1** indicates that at room temperature it consists of conforma-

Can. J. Chem. Downloaded from www.nrcresearchpress.com by 210.87.254.5 on 09/05/12
For personal use only.

Can. J. Chem. Downloaded from www.nrcresearchpress.com by 210.87.254.5 on 09/05/12
For personal use only.

tionally flipping *anti* and *syn* forms. Unlike the case (4) of **4**, however, an *anti*-conformer has not yet frozen out at −110 °C, rather, restricted rotation of the methylene bridges occurs, having $\Delta G^{\pm} = 10.2$ kcal/mol ($T_c = -65$ °C, $\Delta\nu = 39$ Hz, method of calculation of Calder and Garratt (8)). This is interesting in that the analogous tetrathia compound is still mobile at −90 °C (4, 9) and must reflect the slightly larger size of selenium over sulfur.

The synthesis of **4** by this route provides an alternative to that (4) using expensive sodium selenide.

Experimental

All melting points were determined on a Kofler hot stage and are uncorrected. The pmr spectra were determined on a Perkin-Elmer R32-90 MHz spectrometer using tetramethylsilane as internal standard. The mass spectra were recorded on a Hitachi–Perkin-Elmer RMU-7 mass spectrometer at 70 eV. Microanalyses were performed by D. McGillivray. All evaporations were carried out under reduced pressure on the rotary evaporator at *ca.* 40 °C. Extracts were dried with anhydrous sodium sulfate.

meta-Xylylene bis-Selenocyanate, 3a

A solution of α,α'-dibromo-*meta*-xylene (Aldrich, 13.2 g, 50 mmol) in acetone (200 ml) was added with stirring to a solution of KSeCN (7) (16 g, 111 mmol) also in acetone (200 ml). An immediate white precipitate formed. The mixture was heated under reflux for 10 min and then cooled. The precipitate of KBr was removed and the filtrate evaporated to dryness. The resulting residue was dissolved in hot benzene (any remaining KBr being removed by filtration), and then cyclohexane added and cooled. The product **3a**, 13.7 g, 87% yield was collected by filtration as colorless crystals, mp 103–105 °C; pmr ($CDCl_3$) δ 7.38 (4H, s, ArH), 4.25 (4H, s, $—CH_2—$); ms *m/e* (relative intensity) (M^+) 314 ($^{80}Se_2$, 10, correct (10) isotope pattern), 210 ($^{80}Se_1$, 97, correct isotope pattern), 116 (98) 104 (100). *Anal.* Calcd. for $C_{10}H_8N_2Se_2$: C 38.24, H 2.57, N 8.92; found: C 38.09, H 2.60, N 8.96.

2,3,12,13-Tetraselena[4,4]metacyclophane, 1

A solution of the bis-selenocyanate **3a** (6.28 g, 20 mmol) in methanol (500 ml) was added dropwise over 70 h under N_2 to a vigorously stirred solution of KOH (3 g, excess) in methanol (1 litre) at room temperature. The solvent was evaporated and the residue extracted with dichloromethane. The extract was washed with water, dried, and evaporated. An immediate pmr spectrum in $CDCl_3$ indicated that 36% of the oily residue (1.65 g) was product **1**, a yield of 8%. Solutions of this residue gradually deposited yellow polymer and became less concentrated in product.

Addition of the selenocyanate more rapidly, or through one funnel while the KOH solution was added through a second funnel (11), reduced the yield of the cyclic product **1** and gave more polymer.

For characterization purposes a portion of the oily residue from the above reaction was chromatographed on silica gel (using preabsorption) and eluted with benzene – pentane (1:9). Recrystallization from cyclohexane gave **1** as pale yellow crystals; mp (dec.) *ca.* 110 °C, which sintered on standing at room temperature, and slowly deposited polymer from solution; pmr ($CDCl_3$) δ 7.17 (6H, bs, ArH), 6.67 (2H, bs, internal ArH), 4.00 (7H, s, $—CH_2—$); ms *m/e* 528 ($^{80}Se_4$) 448 ($^{80}Se_3$) 368 ($^{80}Se_2$, base peak) each surrounded by isotope peaks. The approximate intensity ratios of these three peaks were 3:45:100. *Anal.* Calcd. for $C_{16}H_{16}Se_4$: C 36.67, H 3.08; found: C 36.62, H 2.74.

Poly(α,α'-diseleno-meta-xylene), 2

This was obtained as a yellow powder, almost insoluble in chloroform, by allowing benzene, cyclohexane, chloroform, or dichloromethane solutions of the cyclic tetraselenide **1** to stand at room temperature. Such samples proved identical by mp, ir, and pmr spectra to that scraped from the walls of the reaction vessel in the above experiment, and to that obtained by adding rapidly a concentrated solution of the bis-selenocyanate **3a** to KOH solution.

As obtained the polymer was a yellow powder, mp 115–118 °C (some softening at ~112 °C) (lit. (1) mp 112–115 °C); pmr ($CDCl_3$) δ 7.16 (4H, bs, ArH), 3.81 (4H, s, $—CH_2—$); no molecular ion in mass spectrum. *Anal.* Calcd. for $(C_8H_8Se_2)_n$: C 36.67, H 3.08; found: C 37.02, H 3.09.

Recrystallization from *sym*-tetrachloroethane at 100 °C gave a sample mp 136–140 °C (dec.) (lit. (1) mp 136–138 °C, with identical pmr and ir spectrum to the unrecrystallized sample.

Cyclic Tetraselenide 1 and Polymer 2 by Hydrolysis of the Selenosulfate 3b

Following the procedure of Günther and Salzmann (1) the product was obtained as a yellow powder, mp *ca.* 115 °C; *Anal.* Calcd. for $(C_8H_8Se_2)_n$: C 36.67, H 3.08; found: C 35.99, H 3.06. Proton magnetic resonance spectroscopy indicated this to contain a small amount of the cyclic selenide **1** which could be separated by extensive chromatography on silica gel as described above. The polymer gave identical pmr and ir spectra to those obtained from the samples from the hydrolysis of selenocyanate **3a**.

Adapting the procedure such that the hydrolysis of the selenosulfate was carried out under high dilution as described for the selenocyanate, did not give a significantly better yield of the dimer **1**.

Thermal Equilibration of the Polymer 2 in TCE

Bulk

The polymer **2** (10 g) from either the selenocyanate or selenosulfate hydrolyses was stirred in *sym*-tetrachloroethane (100 ml) at 95–100 °C for 1 h. The solution was then cooled slowly with scratching. Crystals formed overnight which were collected and dried under vacuum, 4 g, mp 136–140 °C (lit. (1) mp 136–138 °C). These crystals were virtually insoluble in chloroform, and gave identical pmr and ir spectra to starting polymer **2**.

In a Nuclear Magnetic Resonance Tube

A sample of polymer **2** was dissolved in *sym*-tetra-

chloroethane in an nmr tube and held at 100 °C in the spectrometer. No change in the signals could be detected even after several hours. No evidence could be found for the appearance of the cyclic dimer **1** whose methylene bridges appear shielded by 0.19 ppm from those of the polymer.

*Deselenisation of the Cyclic Tetraselenide **1** to the Cyclic Diselenide **4***

The oily residue from the hydrolysis of the selenocyanate above (1.65 g, containing *ca.* 36% dimer) was stirred in benzene (50 ml) and tris(diethylamino)phosphine (also called hexaethylphosphorous triamide) (5 g, excess) was added. The mixture was heated under reflux for 3 h, cooled, and poured into water. The product was extracted with dichloromethane, washed with water, dried, and evaporated. The residue was chromatographed on silica gel using benzene – pentane (1:9) as eluant. The yield of pale yellow product was 152 mg, about 8% from the selenocyanate, almost quantitative from the tetraselenide. Recrystallization from cyclohexane–hexane gave very pale yellow fluffy needles of **4**, mp 120–122 °C (lit. (4) mp 121–122 °C), identical to an authentic sample.

Acknowledgments

I thank the University of Victoria and the National Research Council of Canada for support of this investigation.

1. W. H. H. GÜNTHER and M. N. SALZMANN. Ann. N.Y. Acad. Sci. **192**, 25 (1972).
2. K B. SHARPLESS and R. F. LAUER. J. Am. Chem. Soc. **95**, 2697 (1973); H. J. REICH, I. L. REICH, and M. J. RENGA. J. Am. Chem. Soc. **95**, 5813 (1973); J. Org. Chem. **39**, 2133 (1974); K. B. SHARPLESS, M. W. YOUNG, and R. F. LAUER. Tetrahedron Lett. 1979 (1973); K. B. SHARPLESS, R. F. LAUER, and A. Y. TERANISHI. J. Am. Chem. Soc. **95**, 6137 (1973); D. L. J. CLIVE. J. Chem. Soc. Chem. Commun. 695 (1973); 100 (1974); R. H. MITCHELL. J. Chem Soc. Chem. Commun. 991 (1974).
3. (*a*) R. H. MITCHELL, T. OTSUBO, and V. BOEKELHEIDE. Tetrahedron Lett. 219 (1975) and references quoted therein; (*b*) V. BOEKELHEIDE, I. D. REINGOLD, and M. TUTTLE. J. Chem. Soc. Chem. Commun. 406 (1973); F. VÖGTLE. Angew. Chem. **81**, 258 (1969).
4. R. H. MITCHELL. Tetrahedron Lett. 1363 (1975).
5. V. BOEKELHEIDE and J. F. MONDT. Tetrahedron Lett. 1203 (1970).
6. D. L. KLAYMAN. *In* Organic selenium compounds: their chemistry and biology. *Edited by* D. L. Klayman and W. H. H. Günther. Wiley-Interscience, New York. 1973. Chapt. IV.
7. Inorganic Syntheses, Vol. II. *Edited by* W. C. Fernelius. McGraw-Hill, New York. 1946. p. 186.
8. I. C. CALDER and P. J. GARRATT. J. Chem. Soc. B, 660 (1967).
9. T. SATO, M. WAKABAYASHI, K. HATA, and M. KAINOSHO. Tetrahedron, **27**, 2737 (1971).
10. L. B. AGENÄS. *In* Organic selenium compounds: their chemistry and biology. *Edited by* D. L. Klayman and W. H. H. Günther. Wiley-Interscience, New York. 1973. p. 964.
11. R. H. MITCHELL and V. BOEKELHEIDE. J. Am. Chem. Soc. **96**, 1553 (1974).

Can. J. Chem. Downloaded from www.nrcresearchpress.com by 210.87.254.5 on 09/05/12
For personal use only.

Cysteine-sensitised formation and repair of mixed disulfide in the oxidation of papain by H_2O_2 and OH radicals[1]

WEN SHU LIN, G. MAURICE GAUCHER, AND DAVID A. ARMSTRONG
Department of Chemistry, University of Calgary, Calgary Alberta T2N 1N4
AND
MANOHAR LAL
Bhabha Atomic Research Centre, Trombay, Bombay, India

Received May 27, 1975

WEN SHU LIN, G. MAURICE GAUCHER, DAVID A. ARMSTRONG, and MANOHAR LAL. Can. J. Chem. **54**, 242 (1976).

The inactivation of the proteolytic enzyme papain by hydrogen peroxide produces a sulfenic acid by oxidation of the essential SH of cysteine 25 at the enzyme active site:

[3] $$\text{papainCys}_{25}\text{S}^- + \text{H}_2\text{O}_2 \rightarrow \text{papainCys}_{25}\text{SOH} + \text{OH}^-$$

The kinetics of repair of this entity by cysteine were consistent with the two reactions:

[4] $$\text{papainCys}_{25}\text{SOH} + \text{CysSH} \rightarrow \text{papainCys}_{25}\text{SSCys} + \text{H}_2\text{O}$$

[5] $$\text{papainCys}_{25}\text{SSCys} + \text{CysSH} \rightarrow \text{papainCys}_{25}\text{SH} + \text{CysSSCys}$$

Reaction 4 was the faster with $k_4 \geq 800\ M^{-1}\ s^{-1}$, and $k_5 = 11.3 \pm 0.5\ M^{-1}\ s^{-1}$. A computer program was developed to evaluate the contributions of peroxide-inactivation and cysteine-repair when they occur simultaneously in N_2O-saturated solutions in the absence of catalase. The yields predicted by this program agreed well with the inactivation caused by peroxide in irradiated systems.

The effect of cysteine on the inactivation of papain by OH radicals produced by radiolysis of N_2O-saturated solutions containing catalase was also investigated. Protection against permanent inactivation was much more efficient than expected on the basis of a simple competition between cysteine and papain for OH radicals, but there was a marked increase in the yield of repairable damage which was not due to hydrogen peroxide. These observations can be qualitatively accounted for by the reactions:

[15] $$\text{papainCys}_{25}\text{S}^- + \text{OH} \rightarrow \text{papainCys}_{25}\text{S}\bullet + \text{OH}^-$$

[16] $$\text{papainCys}_{25}\text{S}\bullet \rightarrow \text{(nonrepairable loss of SH)}$$

[18] $$\text{papainCys}_{25}\text{S}\bullet + \text{CysS}\bullet \rightarrow \text{papainCys}_{25}\text{SSCys}$$

The same rate constant was obtained for the repair of $\text{PapainCys}_{25}\text{SSCys}$ from this source as from the peroxide inactivation and treatment with cysteine. However, there was also evidence for additional cysteine-sensitized production of mixed disulfide and this probably occurs through reactions of CysS• radicals:

[22] $$\text{papainCys}_{25}\text{S}^- + \text{CysS}\bullet \rightleftarrows \text{papainCys}_{25}\text{S.S}^-\text{Cys}$$

[20] $$\text{papainCys}_{25}\text{S.S}^-\text{Cys} + \text{CysS}\bullet \rightarrow \text{papainCys}_{25}\text{SSCys} + \text{CysS}^-$$

WEN SHU LIN, G. MAURICE GAUCHER, DAVID A. ARMSTRONG et MANOHAR LAL. Can. J. Chem. **54**, 242 (1976).

L'inactivation de l'enzyme protéolytique de la papaine par le peroxyde d'hydrogène conduit à la formation d'un acide sulfénique par oxydation du SH essentiel de la cystéine 25 au niveau du site actif de l'enzyme:

[1]Issued as publication No. 7507 of the Biopolymer Research Group, University of Calgary. This paper is dedicated to Professor C. A. Winkler of McGill University on the occasion of his sixty-fifth birthday by one of his former students (D.A.A.).

Can. J. Chem. Downloaded from www.nrcresearchpress.com by 210.87.254.42 on 09/05/12
For personal use only.

[3] $$\text{papaineCys}_{25}\text{S}^- + \text{H}_2\text{O}_2 \rightarrow \text{papaineCys}_{25}\text{SOH} + \text{OH}^-$$

La cinétique de la réparation de cette entité par la cystéine est en accord avec deux réactions:

[4] $$\text{papaineCys}_{25}\text{SOH} + \text{CysSH} \rightarrow \text{papaineCys}_{25}\text{SSCys} + \text{H}_2\text{O}$$

[5] $$\text{papaineCys}_{25}\text{SSCys} + \text{CysSH} \rightarrow \text{papaineCys}_{25}\text{SH} + \text{CysSSCys}$$

La réaction 4 est plus rapide avec $k_4 \geq 800\ M^{-1}\ s^{-1}$ et $k_5 = 11.3 \pm 0.5\ M^{-1}\ s^{-1}$. On a développé un programme pour ordinateur afin d'évaluer les contributions de l'inactivation par le peroxyde et la réparation par la cystéine quand elle se produit simultanément dans une solution saturée de N_2O en l'absence de catalase. Les rendements prédits par ce programme sont en bon accord avec l'inactivation causée par le peroxyde dans des systèmes irradiés.

On a aussi étudié l'effet de la cystéine sur l'inactivation de la papaine par les radicaux OH produits par la radiolyse de solutions saturées de N_2O contenant la catalase. La protection contre une inactivation permanente est beaucoup plus efficace qu'attendue sur la base d'une simple compétition entre la cystéine et la papaine pour les radicaux OH, mais il y avait une augmentation marquée dans le rendement de dommage réparable qui n'était pas dû au peroxyde d'hydrogène. On peut tenir compte qualitativement de ces observations par les réactions:

[15] $$\text{papaineCys}_{25}\text{S}^- + \text{OH} \rightarrow \text{papaineCys}_{25}\text{S}\bullet + \text{OH}^-$$

[16] $$\text{papaineCys}_{25}\text{S}\bullet \rightarrow \text{(donne des pertes de SH non-réparables)}$$

[18] $$\text{papaineCys}_{25}\text{S}\bullet + \text{CysS}\bullet \rightarrow \text{papaineCys}_{25}\text{SSCys}$$

On a obtenu les mêmes constantes de vitesse pour la réparation de la papaineCys$_{25}$SSCys à partir de cette source et aussi à partir d'une inactivation par le peroxyde et le traitement avec la cystéine. Toutefois, il y a aussi des indiquations pour la production sensibilisée par la cystéine du disulfure mixte et ceci se produit vraisemblablement par des réactions des radicaux CysS•:

[22] $$\text{papaineCys}_{25}\text{S}^- + \text{CysS}\bullet \rightleftarrows \text{papaineCys}_{25}\text{S.S}^-\text{Cys}$$

[20] $$\text{papaineCys}_{25}\text{S.S}^-\text{Cys} + \text{CysS}\bullet \rightarrow \text{papaineCys}_{25}\text{SSCys} + \text{CysS}^-$$

[Traduit par le journal]

Introduction

The protection of biological systems against the effects of ionizing radiation has been a subject of interest for over 20 years and the *in vivo* protective ability of many low-molecular weight sulfhydryl molecules is well established (1, 2). Although the mechanism of sulfhydryl protection is not fully understood, the high reactivity of the SH group towards free radicals is generally accepted as a particularly important factor (2, 3). This reactivity allows OH, e_{aq}^-, and O_2^- and other radical species to be scavenged before they damage critical cellular targets. Thiols are also capable of repairing the biological damage produced by the abstraction of hydrogen atoms (3, 4). For example, taking BH as a biological target molecule and cysteine as the repairing sulfhydryl, the reactions would be:

[1] $$\bullet\text{OH} + \text{BH} \rightarrow \text{H}_2\text{O} + \text{B}\bullet$$

[2] $$\text{B}\bullet + \text{CysSH} \rightarrow \text{BH} + \text{CysS}\bullet$$

In addition to contributing to the high protective efficiency of small sulfhydryl molecules, the reactivity of the sulfhydryl group is likely to enhance the sensitivity of many cellular macromolecules to free radical damage. For example, DNA polymerase from bacteria and animals (5) and the membrane transport protein, β-galactoside permease (6), possess reactive, functionally important sulfhydryl groups. For these reasons *in vitro* studies of the protection of protein SH groups is important.

Previous work (7) on the sulfhydryl protease papain has shown that the loss of activity due to OH attack is accompanied by, if not solely due to, destruction of the essential Cys$_{25}$SH. Molecular hydrogen peroxide, which is produced in irradiated aqueous systems also inactivates the enzyme by attacking Cys$_{25}$SH. However, in contrast to the nonrepairable damage observed with OH, the product of the papainCys$_{25}$SH and H_2O_2 reaction can be restored to the sulfhydryl form (*i.e.* repaired) by treatment with an excess of a low molecular weight sulfhydryl compound. The following reactions are con-

Can. J. Chem. Downloaded from www.nrcresearchpress.com by 210.87.254.42 on 09/05/12
For personal use only.

Can. J. Chem. Downloaded from www.nrcresearchpress.com by 210.87.254.42 on 09/05/12
For personal use only.

sidered to be responsible for the inactivation by H_2O_2 and the repair by, for example, cysteine.

[3] $\text{papainCys}_{25}\text{SH} + H_2O_2 \rightarrow \text{papainCys}_{25}\text{SOH} + H_2O$

[4] $\text{papainCys}_{25}\text{SOH} + \text{CysSH} \rightarrow \text{papainCys}_{25}\text{SSCys} + H_2O$

[5] $\text{papainCys}_{25}\text{SSCys} + \text{CysSH} \rightarrow \text{papainCys}_{25}\text{SH} + \text{CysSSCys}$

The protection obtained when cysteine is present during irradiation in a [cysteine]:[papain] ratio of 10:1 has been reported previously (8). However at low [cysteine]:[papain] ratios, cysteine was found to increase the amount of repairable damage (9). The purpose of the present work was to investigate the mechanism and efficiency of cysteine protection of papain from inactivation by OH and H_2O_2. It was also of interest to ascertain the reason for the sensitisation observed at low cysteine concentrations.

Experimental

Materials

Papain (crude type II), catalase (product number C-40), *N*-CBZ-glycine-*p*-nitrophenyl ester, DTNB, and cysteine were purchased from the Sigma Chemical Company. All other chemicals were of analytical grade. Oxygen-free nitrogen from Canadian Liquid Air Ltd. and nitrous oxide from Matheson of Canada Ltd. were purified according to the methods described earlier (7). Dilute ($\sim 10^{-4}$ *M*) solutions of hydrogen peroxide were prepared by the ^{60}Co-γ radiolysis of triply distilled water (10).

Procedures

All solutions were prepared using triply distilled water. Crude papain was purified by the previously described methods of fractional precipitation (11) and affinity chromatography (12, 13).

The procedure adopted for the deaeration of N_2O saturation of papain solutions was essentially the same as described in ref. 7, except that all operations were carried out in a glove box through which purified nitrogen gas was continuously passing. This was done in order to avoid the introduction of atmospheric oxygen into the tips of the syringes which were used as irradiation cells. Before bubbling with N_2O, unbuffered papain solutions ($\sim 2 \times 10^{-5}$ *M*, p*H* = 6) were mixed with the desired concentration of cysteine in ratios to papain of 2:1, 5:1, 10:1, or 100:1. When required, catalase at a concentration of 10 μg/ml (*i.e.* 4×10^{-8} *M*) was also added. After 20 min of N_2O bubbling ~4 ml aliquots were withdrawn from each solution using a 10 ml glass syringe and a number 18 needle. After replacing the needle with a plastic cap in the glove box, the syringes were irradiated with an AECL ^{60}Co-γ cell-220 at a dose rate $\sim 0.41 \times 10^{17}$ eV ml^{-1} min^{-1}. Irradiations were normally performed with the solutions at 25 °C, but in some cases, which will be noted in the text, the irradiations were carried out at 1 ± 1 °C. After irradiation the papain-containing syringes were kept at the irradiation temperature for a controlled period (30 min unless otherwise stated) before 0.3 ml aliquots were removed for a preassay treatment designated as 'postirradiation repair' or 'nonrepair'. The repair treatment consisted of diluting the aliquots to 31.1 ml with a solution containing 0.021 *M* phosphate buffer (p*H* = 6.9), 10^{-3} *M* EDTA, and 3.6×10^{-4} *M* cysteine, and incubating at 30 °C for ~30 min. The papain concentration in the mixture was 2×10^{-7} *M* and with the 1000-fold excess of cysteine repair is complete in ~10 min (8). The nonrepair treatment was identical except that no cysteine was present in the incubation mixture other than that from the diluted papain solution. Experiments involving nonrepair treatment for various periods of time showed that these cysteine concentrations (*e.g.* 10^{-6} *M* for the 10:1 [CysSH]:[papain]) were too low to effect significant repair in 30 min at 30 °C.

After the repair or nonrepair treatment the enzyme solutions were assayed for enzyme activity using *N*-CBZ-glycine-*p*-nitrophenyl ester as substrate (8). Losses in activity were calculated from the difference between the activity of an unirradiated but otherwise identically treated control and the activity of the irradiated solution. The activity loss measured after the nonrepair treatment is referred to as the 'total activity loss' and the usually smaller activity loss observed after the repair treatment is the 'nonrepairable activity loss'. The difference between them is referred to as the 'repairable activity loss' and all are normally expressed as a percentage of the activity of the unirradiated control.

The loss of SH groups was determined using DTNB in the presence of urea as previously described (13).

Results and Discussion

I. Repair of Papain Inactivated by Hydrogen Peroxide

(*i*) Reactions 4 and 5 normally proceed to completion at 30 °C in the post-inactivation repair assay due to the 30 min treatment with a 1000-fold excess of cysteine (8). This repair may also occur to some extent at 25 °C with lower cysteine concentrations. The presence of cysteine during the peroxide inactivation of papain (reaction 3) would therefore reduce the normally observed repairable inactivation. To determine the extent of repair expected under these circumstances, the overall rate of the repair process represented by [4] and [5] was determined under a variety of conditions using cysteine as the repair agent. All solutions were purged with nitrous oxide as for the radiolysis experiments to be described later. Mixtures of papain and hydrogen peroxide in equimolar concentrations of $\sim 2 \times 10^{-5}$ *M* were prepared and allowed to stand for 30 min. From previous (13) and present

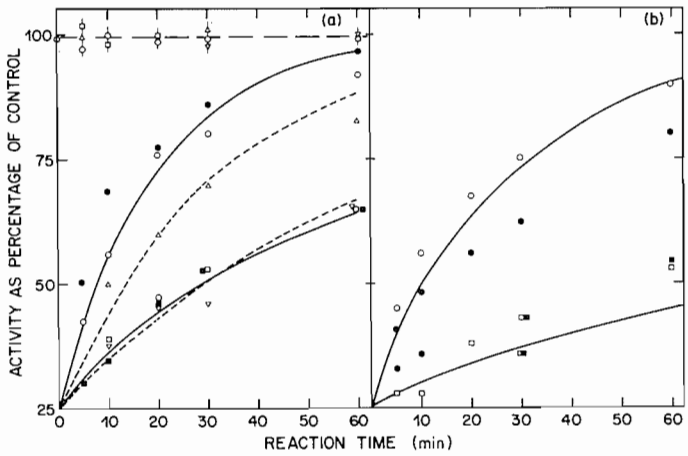

FIG. 1. Cysteine repair of 2×10^{-5} *M* papain after treatment for 30 min with 2×10^{-5} *M* H_2O_2. (*a*) Residual H_2O_2 consumed by adding catalase (4×10^{-8} *M*) before the cysteine: ○, ●, duplicate experiments at 25 ± 2 °C with [CysSH] = 10^{-4} *M*; □, ■, duplicate experiments at 25 ± 2 °C with [CysSH] = 4×10^{-5} *M*; △, ▽, experiments at 1 ± 1 °C with [CysSH] = 2×10^{-4} and 1×10^{-4} *M* respectively. The points on the uppermost dashed line are those obtained after the standard repair assay (*i.e.* after treatment of the reaction mixture with a 1000-fold excess of cysteine at 30 °C for 30 min). The remaining solid and dashed lines were calculated by the computer. (*b*) No catalase added, otherwise as for (*a*).

work this corresponds to a 75 ± 5% consumption of papain and H_2O_2 in [3] at 25 °C. At this point, 0.25 ml of a 4×10^{-6} *M* stock catalase solution was added to the 25 ml papain–H_2O_2 mixture in order to consume the residual H_2O_2 (13). To 5 ml aliquots of this solution 0.05 ml of cysteine solutions of different concentrations were added to yield final cysteine concentrations of 4×10^{-5} and 10×10^{-5} *M* (*i.e.* [cysteine]:[papain] ratios of 2:1 and 5:1) without significantly altering the papain concentration. Each cysteine–papain solution was held at 25 °C, and at various times after the addition of cysteine two aliquots were removed. For one set of aliquots the activity was measured after non-repair treatment (see Procedures in Experimental). For the second set the activity was determined after the repair treatment. The experiment was repeated with [cysteine]:[papain] ratios of 5:1 and 10:1 at 1 °C and the results for all four solutions are presented in Fig. 1*a*. It can be seen that the rate of repair depends on temperature and concentration. At 25 °C and 5:1 [cysteine]:[papain] complete repair was not approached until a reaction time of 60 min had elapsed. Samples obtained at any time were completely repaired if treated with a 1000-fold excess of cysteine at 30 °C for 30 min, the standard post irradiation repair treatment.

From studies of the repair of papain$Cys_{25}SOH$ with a number of different sulfhydryl molecules (14) it is concluded that [4] is much faster than [5]. The present data for cysteine also agree best with this interpretation and give $k_5 = 11.3 \pm 0.3$ M^{-1} s^{-1} and 3.0 ± 0.3 M^{-1} s^{-1} at 25 and 1 °C respectively. The lines in Fig. 1*a* were calculated with a computer program to be described later. The above values of k_5 were used, and k_4 was taken as 800 M^{-1} s^{-1}, since lower values gave a noticeable induction period in the repair and there was no experimental evidence for this. The present data do not give the actual value of k_4 which may be higher than 800 M^{-1} s^{-1}.

Our value of $k_5 = 11.3$ M^{-1} s^{-1} agrees well with a previous one of ~9.2 M^{-1} s^{-1} (15) from experiments in which the mixed disulfide was prepared by disulfide exchange with cystine.

(*ii*) When cysteine and papain are both present with H_2O_2 it is possible that the cysteine may mediate the damage to papain by itself reacting with H_2O_2:

$$[6] \qquad 2CysSH + H_2O_2 \rightarrow CysSSCys + 2H_2O$$

In order to check this, the rate of [6] at p*H* 6 was determined. Cysteine at concentrations similar to those used above was mixed with H_2O_2 in the nitrous oxide atmosphere and the concentration of sulfhydryl was followed as a function of time.

Can. J. Chem. Downloaded from www.nrcresearchpress.com by 210.87.254.42 on 09/05/12
For personal use only.

Can. J. Chem. Downloaded from www.nrcresearchpress.com by 210.87.254.42 on 09/05/12
For personal use only.

The rate constant (k_6) was found to be $\sim 0.5 \pm 0.2\ M^{-1}\ s^{-1}$, which is very small compared to that of [3] ($k_3 = 62\ M^{-1}\ s^{-1}$ (13)). Hence [6] would not be important in the mediation of peroxide inactivation of papain until [CysSH]:[papain] ratios of 100:1 or larger were used.

(*iii*) In a further series of experiments papain and H_2O_2 in the same concentrations as in (*i*) were mixed and again kept for 30 min at 25 °C. Cysteine was added to 5 ml aliquots of this mixture to yield [cysteine]:[papain] ratios of 2:1 and 5:1 and the mixtures were assayed for activity at various time intervals after this. These mixtures differ from those under (*i*) above, in that no catalase was added and residual peroxide would have continued to react with papain-$Cys_{25}SH$ while the repair of papain$Cys_{25}SOH$ was in progress. The results of two such experiments presented in Fig. 1*b* agree well with computer calculated curves based on the above rate constants. As expected the reaction of the residual H_2O_2 with papain leads to lower percentage activities than in Fig. 1*a*.

(*iv*) As a final simulation of the H_2O_2-initiated reactions anticipated in an irradiated system, H_2O_2 was added to mixtures of cysteine and $2 \times 10^{-5}\ M$ papain to give *initial* [cysteine]:[papain]:[H_2O_2] concentration ratios of 5:1:1 and 10:1:1. After a period of 30 min at 25 °C the percentage activity of the enzyme remaining in the two mixtures was assayed. The observed percentages of 60 and 79 respectively are much higher than the 25 ± 5% obtained when H_2O_2 reacts with papain in the absence of cysteine. This confirms that the repair of papain$Cys_{25}SOH$ by cysteine is not inhibited by peroxide and occurs to a significant extent during the time period of [3]. The experimental percentage activities noted above again compare favorably with computer calculated percentages of 67 and 87 for the 5:1:1 and 10:1:1 mixtures respectively.

II. Protection of Papain against Nonrepairable Inactivation by OH

The reactive species formed in the ^{60}Co-γ radiolysis of water are OH, H, the solvated electron (e_{aq}^-), and molecular hydrogen peroxide (16). In nitrous oxide-saturated solutions the electrons are quantitatively converted to OH:

[7] $$e_{aq}^- + N_2O + H_2O \rightarrow N_2 + OH^- + OH$$

giving a total OH yield, g_{OH}, of 5.6 per 100 eV of radiation energy absorbed (17). The yield of H atoms is comparatively small ($g_H = 0.55$ per 100 eV (16)) and their contribution to the inactivation of papain is considered to be negligible (7, 18, 19). The effects caused by OH *per se* can be observed in the presence of $4 \times 10^{-8}\ M$ catalase which removes H_2O_2 and gives no evidence of complicating side effects involving papain (7, 20).

In the present work the total sulfhydryl content and the enzyme activity of nitrous oxide-saturated $2.2 \pm 0.2 \times 10^{-5}\ M$ papain solutions containing catalase and various concentrations of cysteine were measured after different periods of irradiation. From plots of the decrease in SH content *vs.* dose in the range $0\text{–}3 \times 10^{17}$ eV g^{-1} the yields of SH loss in molecules per 100 eV (*i.e.* $G(-SH)$) were calculated for solutions with [CysSH]/[papain] ratios of 2, 5, and 10. The change in $G(-SH)$ with [CysSH]/[papain] ratio is presented in Fig. 2*a*. For the doses used here the percentage change in total SH was too small for a determination of $G(-SH)$ for [CysSH]/[papain] = 100. However, activity losses for such solutions were determined (see below).

Previous work (7) has shown that approximately 90% of OH radical attacks on papain fail to cause inactivation, presumably because they involve reactions at nonessential residues. However, the value of $G(-SH) = 0.5$ per 100 eV for [CysSH]/[papain] = 0 with added catalase in Fig. 2*a* is due to the nonrepairable destruction of the papain$Cys_{25}SH$ group, which is the sole important mechanism of inactivation by the effective 10% of OH attacks. That is for OH radicals $G(-\text{papainSH}) = G(\text{nonrepairable inactivation})$ (7).

Reference to Fig. 2*a* also shows that, with increasing [CysSH]/[papain], $G(-SH)$ rises well above 0.5 and then tends to level off. To explain this one must first consider the processes which occur in nitrous oxide-saturated cysteine solutions without papain (3, 21–25). At pH = 6 the main reactions are [8] and [9]:

[8] $$\cdot OH + CysSH \rightarrow H_2O + CysS\cdot$$

[9] $$CysS\cdot + CysS\cdot \rightarrow CysSSCys$$

with minor contributions from [10] to [13]:

[10] $$CysSH \rightleftarrows CysS^- + H^+$$

[11] $$CysS\cdot + CysS^- \rightleftarrows CysS.S^-Cys$$

[12] $$CysS\cdot + CysS.S^-Cys \rightarrow CysS^- + CysSSCys$$

[13] $$CysSH + \cdot H \rightarrow CysS\cdot + H_2$$

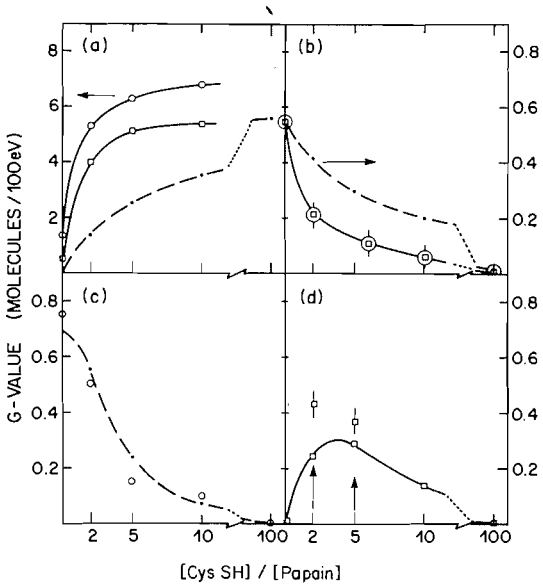

FIG. 2. Plots of G-values (molecules/100 eV) against [CysSH]/[papain]. (*a*) Sulfhydryl losses: ○, G(—SH) without added catalase; □, G(—SH) with added catalase; - - -, G(—SH) calculated from the competition of papain and cysteine for OH. (*b*) Initial nonrepairable yields, G_0^{nr}. ○, without catalase; □, with catalase; - - -, G_0^{nr} calculated from the competition of papain and cysteine for OH. (*c*) ○, G_{30} (inactivation via H_2O_2); the repairable inactivation caused by H_2O_2 obtained by subtracting G_{30}^{t} for catalase containing solutions from G_{30}^{t} for those without it; - - -, derived from computer calculations (see text). (*d*) Repairable yields in the presence of catalase: □, measured 30 min after irradiation, G_{30}^{r}; ⊡, calculated from the percentage repairable activity loss extrapolated to the midpoint of the irradiation period using [21]. The arrows at [CysSH]/[papain] = 2 and 5 are the difference between the calculated and experimental values of G^{nr} in Fig. 2*b* and represent the expected repairable yield from [18], [19], and [20].

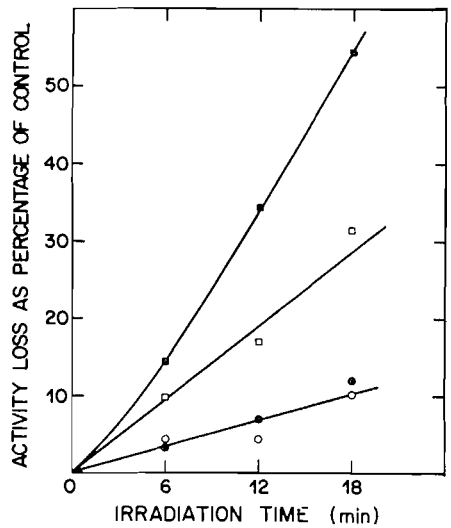

FIG. 3. Loss in activity as a percentage of activity of the unirradiated control for N_2O-saturated 2.2×10^{-5} M papain solutions containing 4×10^{-5} M cysteine. Irradiations were performed at 25 ± 2 °C and solutions were stored for 30 min prior to assay for: □, ■, total activity loss; ○, ●, activity loss after standard repair assay at 30 °C. Open symbols are for solutions containing 4×10^{-8} M catalase and solid symbols for solutions without it.

Taking $G_{OH} = 5.6$ (16) and $G_H = 0.5$ the total radical yield is 6.1 per 100 eV and when all radicals are scavenged there should be an equivalent net loss in cysteine SH (25). If one assumes that the same reactions occur in the presence of papain, the fraction of OH reacting with cysteine would be $\{1 + k_{14}[\text{papain}]/k_8[\text{CysSH}]\}^{-1}$ and the expected loss in cysteine SH, G(—CysSH), would be the product of this quantity and G_{OH}. Here k_{14} is the rate constant for all OH reactions with papain:

[14] OH + papain → •(papain–OH intermediate)

and includes the formation of intermediates at nonessential residues as well as inactivating attacks on papainCys$_{25}$SH. Similarly the small loss of papainCys$_{25}$SH (G(—papainSH)) would be $0.5\{1 + k_8[\text{CysSH}]/k_{14}[\text{papain}]\}^{-1}$. The dashed line in Fig. 2*a* shows the expected total SH loss calculated from these expressions with $k_8 = 8 \times 10^9$ M^{-1} s^{-1} (mean of two values in ref. 26) and $k_{14} = 4.7 \times 10^{10}$ M^{-1} s^{-1} (27). The experimental SH losses for catalase-containing solutions rise far more steeply than predicted and at [CysSH]/[papain] = 10 are already within 12% of the total radical yield of 6.1 per 100 eV. The differences are much greater than the small SH loss ($\lesssim$0.5 per 100 eV) which could derive from H atom reactions and must be attributed to the occurrence of [2], where B is in this instance a papain–OH radical intermediate. Spectral evidence shows that there will be a variety of such intermediates, but phenoxyl radicals formed from tyrosyl side chains will be dominant (27).

The type of plot obtained for percentage loss in activity *vs.* irradiation time is illustrated by the data for [CysSH]/[papain] = 2 in Fig. 3. The activity assays were performed 30 min after the end of the irradiation periods. Total and nonrepairable activity losses with and without catalase are plotted in this figure. Each point is the average of values from three or more experiments, and these usually gave a mean deviation

Can. J. Chem. Downloaded from www.nrcresearchpress.com by 210.87.254.42 on 09/05/12
For personal use only.

TABLE 1. Initial G values* for inactivation of N_2O-saturated 2×10^{-5} M papain irradiated at 25 °C in the presence and absence of catalase and with various concentrations of cysteine

	No catalase			With 4×10^{-8} M catalase		
[CysSH]/[papain]	G^{nr}	$G_{30}{}^{t}$	$G_{30}{}^{r}$	G^{nr}	$G_{30}{}^{t}$	$G_{30}{}^{r}$
0	0.55	1.30	0.75	0.55	0.55	0.00
2	0.21	0.95	0.74	0.21	0.45	0.24
5	0.11	0.55	0.44	0.11	0.40	0.29
10	0.06	0.30	0.24	0.06	0.20	0.14
100	0.00	0.00	0.00	0.00	0.00	0.00

*The superscripts used refer to nonrepairable (nr), total (t), and repairable (r) G values, while the subscript 30 refers to the 30 min post-irradiation period which samples were subjected to before the enzyme assay. The symbol G^{nr} indicates that this nonrepairable initial G value was the same for a post-irradiation period of 0 to 30 min. Estimated uncertainties are ±0.05 molecule per 100 eV for values less than 0.6 molecule per 100 eV and ±10% for others.

of 2 to 3% of the activity of the control. Nonrepairable activity losses were independent of the time elapsed between the end of the radiation and the time of enzyme assay. The nonrepairable inactivation yields in molecules per 100 eV calculated from the linear slopes of plots like that in Fig. 3 are referred to as G^{nr} and presented in Table 1.

The values of G^{nr} are plotted as a function of [CysSH]/[papain] in Fig. 2*b*. It can be shown that, if there is a straightforward competition for OH radicals between cysteine and papain, then G^{nr} in the presence of cysteine should be equal to G^{nr} in the absence of cysteine multiplied by $\{1 + k_8[\text{CysSH}]/k_{14}[\text{papain}]\}^{-1}$. In Fig. 2*b* the dashed line calculated from this relation lies far above the experimental yields. Laying aside the unlikely possibility that the magnitude k_8/k_{14} used here is seriously in error (it would have to be 0.8 instead of 0.17) one must conclude that there are additional reactions responsible for the reduction of G^{nr}. If nonrepairable inactivation by OH is the result of [15] and [16],

[15] $\text{papainCys}_{25}\text{SH} + \cdot\text{OH} \rightarrow \text{papainCys}_{25}\text{S}\cdot + \text{H}_2\text{O}$

[16] $\text{papainCys}_{25}\text{S}\cdot \rightarrow$ nonrepairable product

then the following processes may contribute to the reduction of G^{nr}:

[17] $\text{papainCys}_{25}\text{S}\cdot + \text{CysSH} \rightarrow \text{papainCys}_{25}\text{SH} + \text{CysS}\cdot$

[18] $\text{papainCys}_{25}\text{S}\cdot + \text{CysS}\cdot \rightarrow \text{papainCys}_{25}\text{SSCys}$

[19] $\text{papainCys}_{25}\text{S}\cdot + \text{CysSH} \rightarrow \text{papainCys}_{25}\text{S.S}^{-}\text{Cys} + \text{H}^{+}$

[20] $\text{papainCys}_{25}\text{S.S}^{-}\text{Cys} + \text{CysS}\cdot \rightarrow \text{papainCys}_{25}\text{SSCys} + \text{CysS}^{-}$

Reactions 18, 19, and 20 all lead to the formation of the repairable mixed disulfide and evidence for this is given below. Support for [17], which directly restores the papain activity, is at present lacking.

In previous work (7) with nitrous oxide-saturated solutions containing catalase and no cysteine, only nonrepairable damage was observed and this was confirmed in the present work. However, significant yields of a repairable product were found when cysteine as well as catalase was present, as is illustrated by the differences between the percentage total and nonrepairable activity losses (*i.e.* the open squares and circles respectively) in Fig. 3. To examine the kinetics of the repair, a number of nitrous oxide-saturated solutions containing 4×10^{-8} M catalase and with a cysteine:papain concentration ratio of 2:1 were irradiated for 12 min and allowed to stand for various times after the radiation ended. Aliquots were then taken and assayed by the nonrepair assay which quenches all repair and gives the concentration of active enzyme, E_t, present at that time. For several of these samples aliquots were also taken and subjected to the standard repair with a 1000-fold excess of cysteine at 30 °C to give E_∞, the total concentration of active enzyme after the repair had gone to completion. The concentrations of the repairable product and repairing sulfhydryl at time t are then $(E_\infty - E_t)$ and $(S - E_t)$ respectively, S being the total sulfhydryl concentration (*i.e.* $\text{papainCys}_{25}\text{SH} + \text{CysSH}$) determined after irradiation as discussed under Experimental and above. The values of E_t and

Can. J. Chem. Downloaded from www.nrcresearchpress.com by 210.87.254.42 on 09/05/12
For personal use only.

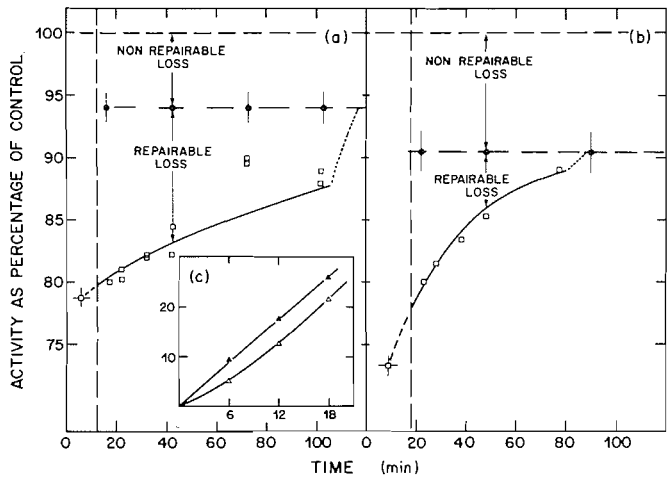

FIG. 4. Percentage activity as a function of time after irradiation for N_2O-saturated 2×10^{-5} *M* papain solutions containing 4×10^{-8} *M* catalase and cysteine. (*a*) Irradiation period = 12 min (see dashed vertical line), [CysSH] = 4×10^{-5} *M*. (*b*) Irradiation period = 18 min, [CysSH] = 10^{-4} *M*. □, percent activity determined by nonrepair assay ($= 100E_t/E_0$); ●, percent activity by repair assay ($= 100E_\infty/E_0$). The ⊹ points show the percentage activity at the radiation half time ($= 100E_{1/2}/E_0$) derived from [21] (see text). The solid lines were calculated using this expression. (*c*) Percentage repairable activity loss as a function of irradiation time for solutions with [CysSH] = 4×10^{-5} *M*. △, measured 30 min after irradiation; ▲, calculated for the midpoints of the radiation periods (*i.e.*, the radiation half times) using [21].

E_∞ for these experiments and similar ones performed with 5:1 cysteine:papain solutions irradiated for 18 min were expressed as a percentage of E_0, the initial enzyme concentration, and are presented in Fig. 4 *a* and *b* respectively.

By substituting $(E_\infty - E_t) = (a - x)$ and $(S - E_t) = (b - x)$ in the standard second order equation $k = \{t(a - b)\}^{-1} \; x \; \ln \; \{b(a - x)/a(b - x)\}$ (28), the data were used to calculate a second order rate constant for the repair reaction and gave a value of $11.5 \pm 1.3 \; M^{-1} \; s^{-1}$. The fact that this is identical within experimental error to the magnitude of k_5 found from the experiments on the repair of peroxide inactivated papain is consistent with the formation of papain-$Cys_{25}SSCys$ in the catalase-containing solutions with cysteine present.

Reference to Fig. 4 *a* and *b* shows that significant repair of the repairable product (papain-$Cys_{25}SSCys$) occurs during the radiation period. In order to obtain an estimate of the total yield of this product the above integrated second order rate law may be rearranged to the form $a = [b(a - x)/(b - x) \exp \{kt(a - b)\}]$. If *a* is taken as the concentration of repairable product at the half time of the radiation period and $E_{1/2}$ the concentration of active enzyme at that time, then $a = (E_\infty - E_{1/2})$ and $b = (S - E_{1/2})$.[2] Making these substitutions and setting $(a - x) = (E_\infty - E_t)$, $(b - x) = (S - E_t)$, and $(a - b) = (E_\infty - S_t)$ one can derive expression 21:

$$[21] \quad E_{1/2} = \frac{(E_\infty - S)}{\dfrac{(S - E_t)}{(E_\infty - E_t)} e^{-k_5 t(S - E_\infty)} - 1} + E_\infty$$

This was used to evaluate $E_{1/2}$ by inserting $k_5 = 11.3 \; M^{-1} \; s^{-1}$, the experimentally obtained values of E_∞ and *S*, and the values of E_t for the times corresponding to the experimental points in Fig. 4 *a* and *b*. The points showing the percentage activity at the radiation half times in Fig. 4 *a* and *b* are derived from the averages of the calculated $E_{1/2}$ values. The curves were calculated from them using [21] and show good fits to the experimental points for both solutions. The same procedure was applied to the percentage repairable activity losses obtained from the

[2] $(E_{1/2} - E_\infty)$ is effectively the concentration of repairable product which would have existed at the midpoint of the radiation period, if it had all been formed instantaneously at that time. This treatment is similar to the extrapolation of yields of intermediates to mid-pulse times in pulse experiments.

Can. J. Chem. Downloaded from www.nrcresearchpress.com by 210.87.254.42 on 09/05/12
For personal use only.

Can. J. Chem. Downloaded from www.nrcresearchpress.com by 210.87.254.42 on 09/05/12
For personal use only.

differences between the open squares and circles in Fig. 3 for solutions in which [CysSH]/[papain] = 2. These percentages of repairable loss, which were observed 30 min after the radiation ended, are shown by the points on the lower curve in Fig. 4*c*. The upper points are the corresponding repairable activity losses calculated for the midpoint in the radiation period. It is significant that this calculated plot is linear with radiation time while the plot for the experimental points obtained 30 min later exhibits an upward curvature. This feature was observed with other [CysSH]/[papain] ratios and appears to be due to the depletion of the cysteine by [2] and [8] to [13], which lowers the rate of the repair as the radiation dose increases.

From the percentage repairable activity losses for the midpoints of the radiation periods a value of the total repairable yield in the absence of a post-irradiation period, G_0^r, of 0.43 ± 0.05 molecules per 100 eV was found for the solutions with [CysSH]/[papain] = 2 at 25 °C. A similar treatment of the results for solutions with [CysSH]/[papain] = 5 at 25 °C gave G_0^r = 0.37 ± 0.05 molecules per 100 eV. As expected these values are larger than the G_{30}^r values given for catalase containing solutions in Table 1.

Since the experiments on repair of peroxide-inactivated papain showed that cysteine repair via [5] has a significant activation energy, less repair of papainCys_{25}SSCys should occur in catalase-containing solutions with [CysSH]/[papain] = 2 and 5 when they are irradiated at 1 °C and stored at this temperature prior to assay. Experiments in fact showed that the repair with 30 min post-irradiation periods at this temperature was negligible and without any corrections gave G^r values similar to those calculated as explained above from the room temperature results.

No attempt was made to estimate G_0^r for solutions with [CysSH]/[papain] = 10 or 100 as the repair rates are very rapid. However, for purposes of future comparisons yields in molecules per 100 eV were calculated from the percentage total and repairable activity losses measured after 12 min irradiation plus 30 min post irradiation for all [cysteine]:[papain] ratios. The vertical arrows in Fig. 4*a* illustrate the total (*i.e.* nonrepairable + repairable) and repairable activity losses for these times with [CysSH]/[papain] = 2. Initial G values (*i.e.* values from initial slopes of percent activity – dose plots) thus obtained are reported as G_{30}^t and G_{30}^r in Table 1.

Figure 2*d* shows the dependence of G_{30}^r and the two available values of G_0^r on [CysSH]/[papain]. If [18] and [19]–[20] are the only processes producing the repairable papainCys_{25}SSCys in the catalase containing solutions then for each [CysSH]:[papain] ratio G_0^r should be equal to the difference, Q, between the yield of papain-$Cys_{25}S\cdot$ radicals actually produced per 100 eV and the observed nonrepairable yield, G^{nr}. The actual yields of papain$Cys_{25}S\cdot$ cannot be measured, but the yields expected on the basis of a competition between [8] and [14] are given by the dashed line in Fig. 2*b*. The values of Q for [CysSH]/[papain] = 2 and 5 are indicated by the arrows in Fig. 2*d*. In each case they are about a factor of two smaller than G_0^r, showing that additional reactions are required to explain the magnitude of the repairable yield in the catalase-containing solutions. Since the papain SH group is considered to be predominantly in the papain$Cys_{25}S^-$ form at pH 6 because of the presence of a neighboring histidine (29, 30), at low cysteine concentrations [22]

[22] papain$Cys_{25}S^- + CysS\cdot \rightarrow$ papain$Cys_{25}S.S^-Cys$

may compete favorably with [9] and [11], and provide an additional route for the production of the repairable mixed disulfide. When taken at face value the results in Fig. 2*b* suggest that this route is at least as important as [18], [19], and [20]. However, further work will be required to establish the exact contribution of $CysS\cdot$ and papain$CysS\cdot$ radicals to the repairable yield.

III. Protection against Concurrent Inactivation by OH and H_2O_2

Protection of essential SH groups against concurrent reactions with OH radicals and H_2O_2 is of interest, and clearly should occur in papain solutions with no catalase. Total and nonrepairable activity losses for such solutions were therefore measured and the values of G^{nr}, G_{30}^t, and G_{30}^r in Table 1 were calculated as described above for the catalase-containing solutions. The magnitudes of G_{30}^t and G_{30}^r are slightly lower than those of 1.6 and 1.0 in ref. 7 and this is probably due to the further elimination of oxygen achieved by the use of a glove box (see Experimental). Sulfhydryl yields were also de-

Can. J. Chem. Downloaded from www.nrcresearchpress.com by 210.87.254.42 on 09/05/12
For personal use only.

termined and the values of G(—SH) are plotted as circles in Fig. 2*a*.

Reference to Fig. 2*a* shows that without cysteine, G(—SH) rises from 0.5 per 100 eV in solutions with catalase to 1.35 per 100 eV without it. The increase is caused by the molecular hydrogen peroxide undergoing reaction 3. When cysteine is present there is a roughly constant difference of about 1.3 molecules per 100 eV between G(—SH) in the absence and in the presence of catalase. This is approximately twice the molecular hydrogen peroxide yield, $G_{H_2O_2}{}^{M}$ = 0.7 (16) molecules per 100 eV, and shows that [3] and [4] must go almost to completion for the present dose rate and 30 min post-radiation treatment.

The filled squares and circles in Fig. 3 illustrate the percentage activity losses observed in the absence of catalase. As shown by the open and filled circles the nonrepairable activity losses are, within experimental error, the same in the presence and absence of catalase. As indicated by the G^{nr} values in Table 1 and Fig. 2*b* this was true for all ratios of [CysSH]-to-[papain] and it is consistent with the view that H_2O_2 damage is completely repairable under the conditions used here.

Since catalase eliminates H_2O_2 without affecting the free radical reactions, the yield of H_2O_2-initiated damage remaining after the standard 30 min post-irradiation period, G_{30}(inactivation via H_2O_2), can be estimated to a good approximation by subtracting $G_{30}{}^{t}$ for catalase-containing solutions from $G_{30}{}^{t}$ for those without it (see Table 1 for $G_{30}{}^{t}$ with and without catalase). Yields obtained by this means are shown in Fig. 2*c*. Since [6] is very slow the marked fall off in G_{30}(inactivation via H_2O_2) for the [CysSH]/[papain] range of 2 to 10 is due solely to the occurrence of [5] during the radiation and post irradiation periods. Indeed the highly reactive SH of papain serves as a catalyst to oxidise cysteine to cystine via [3], [4], and [5].

As a quantitative guide to assist in the interpretation of results when simultaneous free radical and H_2O_2 inactivation and repair of damage by cysteine were occurring a computer program, based on [2] to [6], [8], [14], and [15], was developed as outlined in Appendix 1. This program was used to calculate G_{30}(inactivation via H_2O_2) for conditions corresponding to those for the experimental points in Fig. 2*c*. The calculated yields are shown by the dashed line and they agree well with the experimental points.

Summary and Conclusions

The present study has shown that the protection of an activated sulfhydryl group, such as that of papain, against radiation damage can be a relatively complex phenomenon. In the first place a large part of the reduction in enzyme inactivation by cysteine is really due to the repair of papain$Cys_{25}SOH$ formed from H_2O_2, and this may take place in the post irradiation period, particularly if the dose is delivered in a relatively short period of time. Secondly, the fact that nonrepairable damage is reduced more efficiently than would be expected on the basis of a competition for OH between cysteine and papain supports the view that an intermediate in the OH inactivation mechanism is either directly repaired by cysteine or is converted to a repairable form. The simplest scheme for explaining this includes [15] to [20] and there is clear evidence for the formation of a repairable mixed disulfide. However the yield of it is twice as large as could be accounted for by reactions of papain$Cys_{25}S\cdot$ radicals alone. This shows that there is probably a contribution to papain$Cys_{25}SSCys$ production from [22], and this may be of a similar magnitude to that coming from [18] to [20]. It could be even larger, since papain$Cys_{25}S\cdot$ radicals may be repaired to a significant extent in [17], which reduces G^{nr} without contributing to G^{r}.

Reactions 18 to 20 and 22 may be of considerable importance in living systems, since sulfhydryl radicals are likely to be frequent end products when free radicals are produced. In addition activated SH groups like that of papain will often have a lower than normal pK (29, 30) and hence a high probability of serving as RS$\cdot$ sinks. They may be permanently inactivated via [22] and [20], if the structure of the R group is such that the mixed disulfide cannot readily be repaired. Further studies with different RSH molecules are being undertaken to determine the effect of RSH structure on the relative importance of [17], [18] to [20], and [22] and on the repairability of the mixed disulfides formed.

Acknowledgments

This work was supported by the Defence Research Board of Canada Grant No. 957004

and the National Research Council of Canada Grant No. A 3571.

1. (*a*) Panel on Radiation Damage to the Biological Molecular Information System with Special Regard to the Role of SH groups, I.A.E.A. Vienna, 1969; (*b*) A. PIHL and T. SANNER. *In* Radiation protection and sensitisation. *Edited by* H. L. Moroson and M. Quintiliani. Taylor and Francis Ltd., London. 1970. p. 43.
2. G. E. ADAMS. *In* Radiation protection and sensitisation. *Edited by* H. L. Moroson and M. Quintiliani. Taylor and Francis Ltd., London. 1970. p. 3.
3. G. E. ADAMS, G. S. MCNAUGHTON, and B. D. MICHAEL. Trans. Faraday Soc. **64**, 902 (1968).
4. P. ALEXANDER and A. CHARLESBY. *In* Radiobiology symposium. Butterworths, London. 1954. p. 49.
5. A. KORNBERG. DNA synthesis. W. H. Freeman and Co., San Francisco. 1974. pp. 127, 161.
6. E. P. KENNEDY. *In* The lactose operon. *Edited by* J. R. Beckwith and D. Zipser. Cold Spring Harbor Laboratory, New York. 1970. p. 49.
7. W. S. LIN, J. R. CLEMENT, G. M. GAUCHER, and D. A. ARMSTRONG. Radiat. Res. **62**, 438 (1975).
8. G. M. GAUCHER, B. L. MAINMAN, G. P. THOMPSON, and D. A. ARMSTRONG. Radiat. Res. **46**, 457 (1971).
9. G. M. GAUCHER, B. L. MAINMAN, and D. A. ARMSTRONG. Can. J. Chem. **51**, 2443 (1973).
10. C. J. HOCHANADEL. J. Phys. Chem. **56**, 587 (1952).
11. R. ARNON. Methods Enzymol. **19**, 226 (1970).
12. S. BLUMBERG, I. SCHECHTER, and A. BERGER. Eur. J. Biochem. **15**, 97 (1970).
13. W. S. LIN, D. A. ARMSTRONG, and G. M. GAUCHER. Can. J. Biochem. **53**, 298 (1975).
14. MANOHAR LAL, W. S. LIN, G. M. GAUCHER, and D. A. ARMSTRONG. Int. J. Radiat. Biol. In press.
15. L. A. Æ. SLUYTERMAN. Biochem. Biophys. Acta, **113**, 577 (1966).
16. I. G. DRAGANIC and Z. D. DRAGANIC. The radiation chemistry of water. Academic Press, New York. 1971.
17. G. E. ADAMS, J. W. BOAG, J. CURRANT, and B. D. MICHAEL. *In* Pulse radiolysis. *Edited by* M. Ebert, J. P. Keene, A. J. Swallow, and J. H. Baxendale. Academic Press, London. 1965. p. 117.
18. J. L. REDPATH. Int. J. Radiat. Biol. **22**, 99 (1972).
19. G. E. ADAMS and J. L. REDPATH. Int. J. Radiat. Biol. **25**, 124 (1974).
20. A. PIHL and T. SANNER. Radiat. Res. **19**, 27 (1963).
21. A. AL-THANON, R. M. PETERSON, and C. N. TRUMBORE. J. Phys. Chem. **72**, 2395 (1968).
22. V. G. WILKENING, MANOHAR LAL, M. ARENDS, and D. A. ARMSTRONG. J. Phys. Chem. **72**, 185 (1968).
23. J. P. BARTON and J. E. PACKER. Int. J. Radiat. Phys. Chem. **2**, 159 (1970).
24. M. Z. HOFFMAN and E. HAYON. J. Phys. Chem. **77**, 990 (1973).
25. G. C. GOYAL and D. A. ARMSTRONG. Can. J. Chem. **53**, 1475 (1975).
26. L. M. DORFMAN and G. E. ADAMS. Reactivity of hydroxyl radicals in aqueous solutions. U.S. Department of Commerce, N.B.S. #46, Washington, D.C. 1973.
27. J. R. CLEMENT, D. A. ARMSTRONG, N. V. KLASSEN, and H. A. GILLIS. Can. J. Chem. **50**, 2833 (1972).
28. E. A. MOELWYN-HUGHES. Physical chemistry. Pergamon, New York. 1957.
29. L. POLGAR. Eur. J. Biochem. **33**, 104 (1973).
30. K. BROCKLEHURST and G. LITTLE. Biochem. J. **133**, 67 (1973).
31. T. SANNER and A. PIHL. Radiat. Res. **19**, 12 (1963).

Appendix

The computer program was based on [3] to [9] and [14] to [15] and was designed to calculate the loss of cysteine and the repairable inactivation of the enzyme. The radiation and postirradiation periods were divided into time intervals of 0.0625 min. This is short with respect to the half lives of [3] to [6] and doubling the size of these intervals made no significant difference to the results. The average concentrations of cysteine, [RAV], and the active enzyme, [EAV], were calculated for these intervals, making allowance for the fast radical reactions 2, 7 to 9, and 14 and 15. These average concentrations were then used to calculate the consumption of the enzyme in [3] and of cysteine in [4] and [5] over the same time interval. The repair of the enzyme in [4] and [5] was also calculated and the resultant net concentrations of active enzyme and cysteine at the end of the interval were used as the initial concentration $[E]_i$ and $[CysSH]_i$ respectively for the next interval. All e_{aq}^- were assumed to undergo reaction 7.

From eq. 15 of ref. 31 reaction 15 will reduce the concentration of active enzyme during a 0.0625 min interval from $[E]_i$ to $[E]_i \exp(-0.0625k_{15} \times 10g_{OH}DN^{-1}/(k_{14}[E]_0 + k_8[CysSH]_i))$. Here D is the dose rate in eV cm^{-3} min^{-1}, N is Avogradro's number, and $[E]_0$ the total enzyme concentration (*i.e.* active + inactive). Taking k_{15}/k_{14} as being equal to the ratio of G^{ir}/g_{OH} observed in the absence of cysteine, one can show that

$$[EAV] = \frac{[E]_i}{2}\{1 + \exp(-0.0625GR/([E]_0 + b[CysSH]_i))\}$$

where $b = k_8/k_{14}$ and $GR = 10G^{ir}D/N$.

Can. J. Chem. Downloaded from www.nrcresearchpress.com by 210.87.254.42 on 09/05/12
For personal use only.

For reasons of convenience, repairable inactivation by H_2O_2 was taken care of by two expressions: (*i*) For the H_2O_2 present at the start of the interval at concentration $[H_2O_2]_i$, the concentration, DER, of enzyme and of H_2O_2 reacting = $[H_2O_2]_i$ − H2R, the amount not reacting = ([EAV] − $[H_2O_2]_i$)/([EAV] exp (k_3{[EAV] − $[H_2O_2]_i$}0.0625)/$[H_2O_2]_i$ − 1). (*ii*) For the H_2O_2 produced and reacting during the interval the consumption, DEP = $\rho \times 0.0625$ − H2P, where $\rho = 10G_{H_2O_2}{}^{M}D/N$ and H2P, the peroxide produced that does not react = ρ[1 − exp (−k_3[EAV](0.0625))]/k_3[EAV].

Consumption of H_2O_2 by cysteine during the interval is a very slow process and was taken care of by H2S = $k_6[H_2O_2]_i$[CysSH] × 0.0625. The H_2O_2 concentration at the end of the interval is H2R + H2P − H2S.

The loss of CysSH in molecules per 100 eV due to reactions with OH radicals and to [2] was taken as equal to the observed G(—SH) for catalase-containing solutions. The average cysteine concentration during an interval is then given by [RAV] = $[CysSH]_i$ − H2S − 5G(—SH) × D/N.

The concentration of papain$Cys_{25}SOH$ at the end of an interval, $[PO]_f$, is equal to POR + DEP + DER, where POR = ([RAV] − $[PO]_i$)/{[RAV](exp (k_4x{[RAV] − $[PO]_i$}0.0625))/$[PO]_i$ − 1}, and $[PO]_i$ is the concentration at the start of the interval.

Similarly for the mixed disulfide concentrations $[SS]_i$ and $[SS]_f$ one can write: $[SS]_f$ = $[PO]_i$ − POR − DSS, using DSS = $[SS]_i$ − {[RAV] − $[SS]_i$}/{[RAV] exp (k_5[RAV] − $[SS]_i$}0.0625)/$[SS]_i$ − 1}.

Finally at the end of the interval $[CysSH]_f$ = $[CysSH]_i$ + POR − $[PO]_i$ − DSS, $[E]_f$ = $[E]_i$ exp {− 0.0625GR/($[E]_0$ + b[CysSH]$_i$)} − DEP − DER + DSS where $b = k_8/k_{14}$ and the combined concentrations of repairable sulfenic acid and mixed disulfide = {$[SS]_f$ + $[PO]_f$}.

For radiolysis experiments the initial peroxide concentration was given a very small value (= 10^{-8} M). The program was set to run for a particular radiation period with the required value of D and for a subsequent post irradiation period (usually 30 min) with D = 0. At the end of the latter period $[SS]_f$ and $[PO]_f$ were obtained. The program also yields an expected nonrepairable yield, but this does not take [17] to [20] and [22] into account.

For experiments on peroxide inactivation D is set equal to zero from the start and the initial H_2O_2, cysteine, and enzyme concentrations are given the desired values.

Can. J. Chem. Downloaded from www.nrcresearchpress.com by 210.87.254.42 on 09/05/12
For personal use only.

Intermolecular interactions in nuclear magnetic resonance. X. A site-specific continuum model for the gas-to-liquid shifts of nonpolar solutes. Applications to proton medium shifts and the determination of cavity radii

FRANS H. A. RUMMENS

Department of Chemistry, University of Regina, Regina, Saskatchewan S4S 0A2

Received June 10, 1975

FRANS H. A. RUMMENS. Can. J. Chem. **54**, 254 (1976).

Based on the Onsager reaction field theory of the dielectric polarization of a continuum, a model has been developed to calculate the Van der Waals contribution σ_w to the gas-to-liquid medium shifts of nonpolar solutes. The addition of a site factor correction, to account for the off-center location of the measured nucleus in the solute molecule, provides a marked improvement. The agreement between experimental and calculated σ_w's is good (± 0.05 ppm), but a separate scale factor is required for each solute. This nonuniversality is shown to be related to the Onsager approximation for the solute cavity radius; $a^3 = 3V_1/4\pi N_A$. It is shown that Van der Waals shifts can be used for the determination of the Onsager cavity radii; for a number of molecules these cavity radii are given. It is claimed that this method is as precise, but much easier to apply, than the Böttcher–Onsager optical method.

No evidence could be found for the existence of a σ_{E^2} contribution to the medium shifts due to permanent electric dipoles of solvent molecules. Combination of experimental medium shifts in anisotropic solvents with calculated σ_w contributions allows the evaluation of the neighbor anisotropy contribution σ_a. The σ_a effect is found to be solute dependent; there is a $V_1^{-1/6}$ proportionality related to the molar volume V_1 of the solute and in addition there are site effects with site factors both greater and less than unity, depending on molecular shape. The solvent dependence of σ_a includes not only the magnetic susceptibility anisotropy $\Delta\chi_2$ and the molar volume ($V_2^{-1/3}$) but also a term corresponding to the geometric anisotropy of the solvent molecule.

The solvent CS_2 is found to behave as an isotropic molecule.

FRANS H. A. RUMMENS. Can. J. Chem. **54**, 254 (1976).

Fondé sur la théorie du champ de réaction d'Onsager, un modèle a été développé permettant le calcul de la contribution Van der Waals σ_w sur les déplacements chimiques des solutés nonpolaires en passant de l'état gazeux à l'état liquide. L'inclusion d'un facteur de correction de site, tenant compte de la position non-centrale du noyeau considéré, apporte une amélioration sensible. L'accord entre les σ_w calculés et les σ_w observés est bon (± 0.05 ppm), mais une constante de multiplication, differente pour chaque soluté, est nécessaire. Il a été démontré que ce manque d'universalité est causé par l'approximation d'Onsager pour le rayon de la cavité du soluté; $a^3 = 3V_1/4\pi N_A$. Il est démontré de plus que les déplacements chimiques Van der Waals peuvent être utilisés pour la détermination des rayons de cavité Onsager; ces rayons de cavité ont été donnés pour un certain nombre de molécules. Il est tenu pour certain que cette méthode est aussi précise, mais plus facile à utiliser, que la méthode optique de Böttcher–Onsager.

Il n'a pas été possible de trouver une preuve quelconque en faveur ou contre l'existence d'une contribution σ_{E^2} aux déplacements chimiques de milieu due aux moments électriques permanents des molécules de solvant. En combinant les déplacements chimiques de milieu dans des solvants magnétiquement anisotropes avec des contributions σ_w calculées, il est possible de trouver la contribution anisotropique σ_a. Il est démontré que l'effet σ_a dépend de la molécule de soluté; il existe une relation proportionnelle entre σ_a et $V_1^{-1/6}$ (ou V_1 est le volume molaire de la soluté) et en outre il y a des effets de site, avec des facteurs de site soit plus grands, soit plus petits que l'unité, selon la forme moléculaire. L'effet du solvant sur σ_a n'inclut pas seulement l'anisotropie de la susceptibilité $\Delta\chi_2$ et le volume molaire du solvant ($V_2^{-1/3}$), mais également un facteur correspondant à l'anisotropie géometrique de la molécule de solvant.

Il est démontré que le solvant CS_2 se comporte comme un solvant isotropique.

Introduction

The shielding σ_l of a solute in a liquid state is different from its value σ_0 in the gas phase at zero pressure. Part of this difference is due to sample geometry; for a cylindrical sample perpendicular to the main magnetic field the change

Can. J. Chem. Downloaded from www.nrcresearchpress.com by 210.87.254.42 on 09/05/12
For personal use only.

Can. J. Chem. Downloaded from www.nrcresearchpress.com by 210.87.254.42 on 09/05/12
For personal use only.

in effective field strength can be written in the form of a shielding contribution $\sigma_b = 2\pi\chi_v/3$, where χ_v is the volume bulk susceptibility of the sample. After subtraction of this correction the remaining gas-to-liquid shielding $\sigma_m = \sigma_l - \sigma_0 - \sigma_b$ is a true medium shielding effect. In general one can write

$$[1] \qquad \sigma_m = \sigma_l - \sigma_0 - \sigma_b = \sigma_w + \sigma_a + \sigma_{E^2} + \sigma_E + \ldots$$

Of the various terms in [1] only σ_w, the Van der Waals term, σ_a, the neighbor anisotropy term, and σ_{E^2}, the term due to permanent electric dipoles in the solvent molecules will be discussed in this paper, since all other terms are zero or negligible for nonpolar solutes.

The presently existing models for nmr medium shifts fall in two distinct groups; the statistical mechanical and the continuum models. The former, originally proposed by Raynes *et al.* (1), is in principle superior in its ability to predict with reasonable accuracy the medium shifts of a large range of solute–solvent systems. In practice its applications have been limited, primarily because it requires accurate values for the Lennard–Jones (6–12) potential parameters r_0 and ϵ/k for the solute and the solvent molecules, data which are often difficult to obtain or to estimate. Continuum models offer the prospect of only requiring data on macroscopic properties such as density and refractive index. Such models have been proposed by Linder and coworkers (2, 3) and by De Montgolfier (4). When experimental medium shifts for a particular solute molecule are plotted against medium shifts calculated with either of these continuum models, relations are found which are only approximately linear; in addition the 'best' straight lines do not in general pass through the origin. The models also lack universality; each solute appears to require its own calibration line. (For an extensive review of both types of models see ref. 5.)

In an earlier communication, we reported (6) that much improved results can be obtained with the following relation:

$$[2] \qquad \sigma_w = -C\left(\frac{n_2^2 - 1}{2n_2^2 + 1}\right)^2 = -Cf(n_2)$$

where n_2 is the refractive index of the solvent and C is a solute dependent constant. It was shown that the experimental medium shifts of CH_4 in eleven halomethanes as solvents plotted against $f(n_2)$ of [2] results in a straight line through the origin ($C = 9.62$ ppm, standard deviation $s = \pm 0.021$ ppm).

In a subsequent paper (7) a formal derivation of [2] was given, based on the assumption that the reaction field of a spontaneously oscillating solute molecule is the sole cause for the Van der Waals shift. The result is reproduced below:

$$[3] \qquad \sigma_w = \frac{-6KB\alpha_l I_l}{a^6}\left(\frac{n_2^2 - 1}{2n_2^2 + 1}\right)^2$$

where B is the proportionality factor relating σ_w to the average squared electrical fields at the solute ($\sigma_w = -B\overline{F^2}$ and $B = 0.72 \times 10^{-18}$ esu for protons (8)), α_l and I_l are the polarizability and ionization potential respectively of the solute, and a is the cavity radius of the employed Onsager reaction field model. If one takes the approximate relation

$$[4] \qquad a^3 = \frac{3V_l}{4\pi N_A}$$

where V_l is the molar volume of the solute (since a is a temperature independent parameter (*vide infra*), V_l should be taken at a fixed temperature, for which we have chosen 30 °C), eq. 3 then becomes

$$[5] \qquad \sigma_w = -\frac{32\pi^2 N_A^2 KB\alpha_l I_l}{3(V_l^{30})^2}\left(\frac{n_2^2 - 1}{2n_2^2 + 1}\right)^2$$

Equation 5 was tested for the solutes CH_4, cyclohexane, neopentane, and tetramethyllead (7). Although [5] was shown to constitute a major improvement over previous continuum models, it was also noted that the scale factor K was somewhat different for each solute and that for some solutes the best straight line σ_w(exp) *vs.* σ_w(calcd) did not quite go through the origin. As a tentative and qualitative explanation of these deviations the absence of a site factor in [5] was cited.

Site factors, as introduced by Rummens *et al.* (8, 9) pretend to correct for the fact that the nuclei measured are not normally located at the center of mass of the solute molecule. These nuclei may therefore be expected to experience an average squared electric field different from that calculated at the center of mass. In a reac-

Can. J. Chem. Downloaded from www.nrcresearchpress.com by 210.87.254.42 on 09/05/12
For personal use only.

tion field model where the region outside the cavity is considered as a continuum such a site factor appears to have no place; the reaction field vector is constant over the cavity.

In this paper a site factor for a continuum model will be developed and the validity of the modified model will be investigated. This model for the Van der Waals effect σ_w, together with experimental medium shifts σ_m will then be used to extract information on the neighbor anisotropy effect σ_a and on the electrical field effect σ_{E^2}.

Theory

The Site Factor

As indicated above, the reaction field in an Onsager cavity is constant in magnitude and direction. The direct reason for this is the implicit assumption that the wall of the cavity can be the carrier of any desired charge density (for an ideal dipole in the center of a spherical cavity, for example, the charge density distribution on the cavity wall is given by the first order Legendre function of the first kind). However, the molecules of the first solvent layer around the solute molecule are anything but a continuous dielectric. It can also be estimated from Kirkwood's statistical mechanical theory of dielectrics (10) that one has to form a cavity with a radius at least one order of magnitude larger than that of the solute molecule in order to have an approximately homogeneous cavity wall in the sense of producing a constant reaction field vector over the solute molecule at the center of the cavity. For nmr medium shifts, and in particular for the Van der Waals effect with its inherent r^{-6} dependence, it is the first layer of solvent molecules which carries the larger fraction of the total effect. It seems therefore a justifiable procedure to use $\langle R^{-6}\rangle$ rather than r^{-6} for the interaction of a nucleus at distance d from the solute's mass center, at least for nearby solvent molecules (see Fig. 1). The site factor S_{shell} for the interaction with a continuum spherical shell bounded by distances r and $r + dr$ as defined by $\langle R^{-6}\rangle = S_{shell} r^{-6}$ can be found to be

$$[6] \qquad S_{shell} = \frac{1 + q^2}{(1 - q^2)^4}$$

where q is defined by $q = d/r$. (Note that this calculation is isomorphous to that of calculating the $\langle R^{-6}\rangle$ from all points on a sphere to a chosen point *outside* that sphere. Therefore, S_{shell} will be equal to S_{pair} of previous site factor calculations (9).) To find the total site factor the result of [6] needs to be integrated.

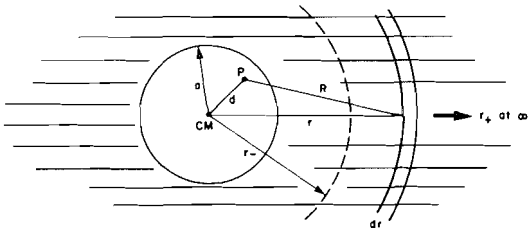

FIG. 1. Solute with center of mass (CM) in center of an Onsager cavity with radius a and with nucleus P at distance d from CM. A concentric shell with radius r has a distance R to the nuclear site P.

$$[7] \qquad S_{cont} = \frac{\int_{r_-}^{r_+} r^{-6} S_{shell} r^2 \, dr}{\int_{r_-}^{r_+} r^{-6} r^2 \, dr}$$

For the lower limit a measure of the distance from the solute center to the centers of the molecules of the first solvent layer should be taken. Therefore r_- is not the cavity radius but rather $r_- = r_{12} = r_1 + r_2$ where r_1 and r_2 are the molecular radii. For the upper limit r_+ a distance $10a$ could be taken but in practice it is permissible to take $r_+ = \infty$; the difference will be negligibly small. The result is as follows:

$$[8] \qquad S_{cont} = \frac{1}{(1 - q^2)^3}$$

with

$$q = d/r_{12}$$

Multiplication of [8] with either [3] or [5] then gives the site-corrected expressions for σ_w (see eq. 12).

The Cavity Radius

It might be argued that the continuum begins where the centers of mass of the nearest neighbor solvent molecules are. If that were so, the cavity radius would be a function of the size of solute *and* solvent molecules, similar to the parameter r_{12} discussed above. This hypothesis can be tested, but as our results will indicate (see next section) the evidence is negative; the cavity radius appears to be independent of the size of the solvent molecules. On the other hand, a

Can. J. Chem. Downloaded from www.nrcresearchpress.com by 210.87.254.42 on 09/05/12
For personal use only.

simple proportionality between a^3 and V_1 (eq. 4) is not very satisfactory either. It causes the σ_w model to be excessively temperature dependent (*vide infra*). In fact, perhaps the best method of determining cavity radii of nonpolar molecules is based on the assumption that a^3 is temperature independent and to interpret the temperature dependence of density and refractive index according to the Böttcher–Onsager method (10). The criteria for success of this method are, (*i*) finding a linear relation between $12\pi N_A n^2/(n^2 - 1)(2n^2 + 1)$ and $(2n^2 - 2)/(2n^2 + 1)$ for all wavelengths, (*ii*) slopes corresponding to $1/a^3$, constant and independent of wavelength, and (*iii*) intercepts of $1/\alpha$ which show a wavelength dependency according to dispersion theory. Such extensive and successful studies have only been done by Pijpers (11), who reported values for a^3 of 30.5, 34.4, and 38.9 Å^3 for benzene, CCl_4, and cyclohexane respectively. The general impression (10) is that a^3 corresponds to the molar volume at absolute zero, or at least to a molar volume in the solid state; extensive studies on cavity radii of simple ions (10) show that these are numerically very close to the ionic radii in crystals. Solid state molar volumes of organic molecules are not available in any number, but one might try other solute parameters which, apart from having the dimension of a volume, also express the 'hardness' of these molecules. For example, the Onsager cavity model implies a potential which is constant (negative) over the continuum, with a jump to infinite repulsion at the cavity wall. Such a potential function resembles *binary* potential functions such as the Lennard–Jones (6–12) potential. The cavity diameter $2a$ could therefore be related to the Lennard–Jones diameter r_{01}. One might therefore use as a trial function $a^3 = Cr_{01}{}^{3-p} V_1{}^{p/3}$, where C is a proportionality constant and p is an adjustable parameter between 0 and 3. Lennard–Jones potential parameters can be estimated with good accuracy from critical point data (12, 13) while the latter, if no experimental data are available, can be estimated from the boiling point, the density at some temperature, and the temperature at which the vapor pressure is 100 mm (14). A detailed account of this method of estimating potential parameters can be found in chapt. 16 of ref. 5. Other possibilities would be to relate a^3 directly to critical parameters, such as a proportionality with the critical molar volume V_c or with $Z_c{}^p V_c$ where $Z_c = P_c V_c/RT_c$. Finally, the effective electron density, as described by the polarization α might be related to a^3. For example, for a macroscopic conducting sphere $a^3 = \alpha$ and for a macroscopic dielectric sphere $a^3 = \alpha(n^2 + 2)/(n^2 - 1)$ (10). Organic molecules are neither conducting nor dielectric spheres, but probably have some characteristics of both. One might therefore expect a proportionality between a^3 and the product of α and some function of the refractive index.

The Medium Effect Contributions σ_{E^2} and σ_a

In the statistical model of Raynes *et al.* (1) the electric field at the solute is not a reaction field of the solute, but a direct field of the spontaneously oscillating solvent molecules. Apart from the Van der Waals fields $\overline{F^2}$, there is then also a contribution E^2 due to the *permanent* solvent dipoles. This contribution can be given by (1):

$$[9] \qquad \sigma_{E^2} = \sigma_w \frac{2\mu_2{}^2}{3\alpha_2 I_2}$$

This contribution is usually small, but it may be substantial ($0.2\sigma_w$ to $0.5\sigma_w$) for small solvent molecules with large permanent dipoles. In the continuum model under discussion, σ_{E^2} does not exist, since the only field recognized is the reaction field of the solute. The permanent dipoles cannot relax fast enough to follow the high frequency fluctuating moments of the solute, so their contribution to the reaction field will be zero. In the present paper, both polar and nonpolar solvents are discussed in the hope of finding evidence for the existence or nonexistence of σ_{E^2}.

The present study also contains data referring to anisotropic solvents. Clearly, if a universally valid model for σ_w is developed, subtracting this from the medium shift will lead to good values for the anisotropic contribution σ_a (or $\sigma_a + \sigma_{E^2}$). For certain solvents such as aromatics, the existence of σ_a is beyond doubt; for others such as acetone, acetonitrile, nitromethane, DMSO, and CS_2 the evidence so far has not been clear. If the solvent aspects of [3] or [5] (combined with [7] are correct, consistent values for the σ_a of these solvents should follow, largely independent of the solute probe molecule. It has been proposed, however (15), that σ_a does have

TABLE 1. Index numbers of solvent and solute molecules

Index number	Molecule	Index number	Molecule	Index number	Molecule
1	CH_3Br	**22**	$Sn(CH_3)_4$	**44**	$C_2H_5NO_2$
2	CH_3I	**23**	$Pb(CH_3)_4$	**45**	$C(NO_2)_4$
3	CH_2Cl_2	**24**	*cyclo*-C_5H_{10}	**46**	CH_3CN
4	CH_2Br_2	**25**	*cyclo*-C_6H_{12}	**47**	C_6H_6
5	CH_2I_2	**26**	*n*-C_5H_{12}	**48**	Toluene
6	CH_2ClBr	**27**	*n*-C_6H_{14}	**49**	*p*-Xylene
7	$CHCl_3$	**28**	*n*-C_7H_{16}	**50**	Mesitylene
8	$CHClBr_2$	**29**	*n*-C_8H_{18}	**51**	C_6H_5Cl
9	$CHBr_3$	**30**	$C(CH_2CH_3)_4$	**52**	$C_6H_5NO_2$
10	CCl_4	**31**	$Si(CH_2CH_3)_4$	**53**	*N*-Methylaniline
11	CCl_3Br	**32**	$Sn(CH_2CH_3)_4$	**54**	Pyrrole
12	CBr_4	**33**	$(C_2H_5)_2O$	**55**	CH_4
13	CS_2	**34**	$(CH_3OCH_2)_2$	**56**	C_2H_6
14	$SiCl_4$	**35**	$Si(OMe)_4$	**57**	C_2H_4
15	$SnCl_4$	**36**	$Si(OEt)_4$	**58**	Cyclopropane
16	$SiBr_4$	**37**	1,4-Dioxane	**59**	*iso*-C_4H_{10}
17	Br_2	**38**	Tetrahydrofuran	**60**	*trans*-Butene-2
18	Freon 112 ($CFCl_2$—$CFCl_2$)	**39**	$(C_2H_5)_3N$	**61**	2-Butyne
		40	Ethyl acetate	**62**	2,3-Pentadiene
19	$C(CH_3)_4$	**41**	DMSO	**63**	3-Hexyne
20	$Si(CH_3)_4$	**42**	Acetone		
21	$Ge(CH_3)_4$	**43**	CH_3NO_2		

a slight solute dependence according to

$$[10] \qquad \sigma_a = C\frac{\Delta\chi(r_{2\parallel}^{-3/2} - r_{2\perp}^{-3/2})}{V_1^{1/6}V_2^{1/3}}$$

Where $\Delta\chi$ is the anisotropy of the susceptibility of the (axially symmetric) solvent molecule and $r_{2\parallel}$ and $r_{2\perp}$ are the solvent molecular radii parallel and perpendicular to the molecular axis.

This point is of some importance because in all factor analysis treatments of nmr solvent effects (16, 17), it has been taken that σ_a is independent of the solute.

It could finally be argued that the simultaneous separation of σ_{E^2} and σ_a is in principle impossible because all molecules that have a permanent dipole thereby must also be anisotropic. However, the magnetic anisotropy of σ bonds is so small that the neglect of σ_a in saturated molecules is permissible.

Experimental

The physical properties of all solutes and solvents to be discussed are given in Table A.[1] Table 1 provides an index to the compounds discussed; throughout this paper these compounds will be referred to by their index numbers alone.

Data on gas-to-liquid medium shifts were taken from the literature; where necessary the bulk susceptibility term σ_b was adjusted using the χ_M and density data of Table A. To all the methane gas-to-solution medium shifts reported by Buckingham *et al.* (18) 0.025 ppm was added to correct for the medium shift of the 10 atm of CH_4 which was taken as the zero point in the original paper. For the datum of CH_4 in CBr_4 (measured at 100 °C) an additional correction was made for the temperature dependence of the shift of $CHCl_3$, the latter having been used as an intermediate reference. Other data used included those reported by Rummens *et al.* (8), Bernstein (17), Louman (19), Rummens and Louman (20), Chenon (21), Lumbroso *et al.* (22), Raynes and Raza (23), Raza and Raynes (24), and Bothner-By (25).

All temperature dependent parameters, such as σ_b, V_2, n_2, r_1, r_2, and q were calculated at the temperature of the experiment. The radii r_1 and r_2 have been calculated according to eq. 11 (8)

$$[11] \qquad r^3\ (\text{Å}^3) = 0.293V\ (\text{ml})$$

For CH_4 a value of $r_1 = 2.068$ Å was adopted which was obtained by interpolation from a graph of r_0^3 *vs.* V for the halomethanes.

Results and Discussion

Van der Waals Shifts According to [5] and [8]

Combination of [5] and [8] results in

[1]Copies of Table A are available, at a nominal charge, from the Depository of Unpublished Data, CISTI, National Research Council of Canada, Ottawa, Canada K1A 0S2.

Can. J. Chem. Downloaded from www.nrcresearchpress.com by 210.87.254.42 on 09/05/12
For personal use only.

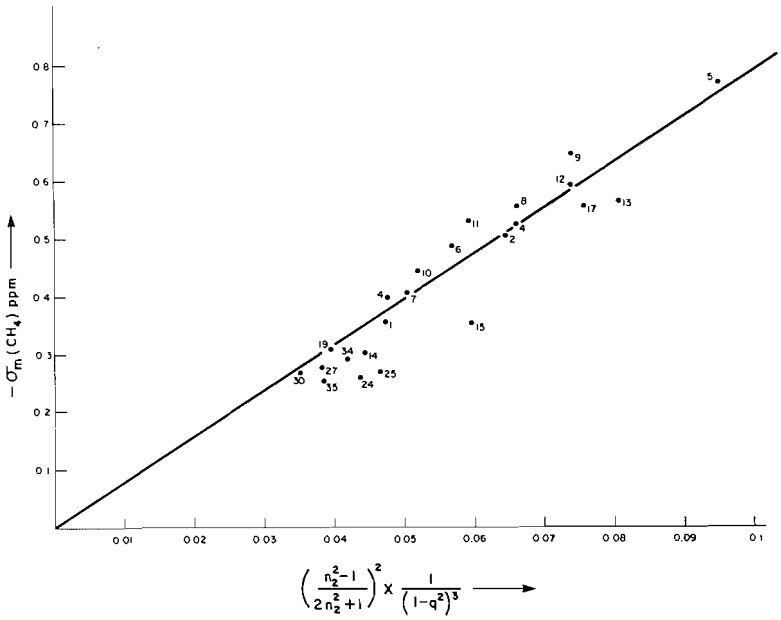

FIG. 2. Experimental medium shifts of CH_4 as function of the solvent terms of [12]. Full line corresponds to slope = 7.89. Numbering of solvents is according to Table 1.

$$[12] \quad \sigma_w = -\frac{32\pi^2 N_A{}^2 K B \alpha_1 I_1}{3(V_1{}^{30})^2}\left(\frac{n_2^2-1}{2n_2^2+1}\right)^2 \times \left(\frac{1}{(1-q^2)^3}\right)$$

This equation can be tested by plotting the medium shifts of nonpolar solutes *vs.* $(n_2^2 - 1)^2/(2n_2^2 + 1)^2(1 - q^2)^3$. The results for CH_4 as a solute are given in Fig. 2. The least-squares slope (= 7.80) of this graph was then used to recalculate σ_w as indicated in Table 2. This calculation was also performed for those solvents (aromatics, acetone, acetonitrile, nitro compounds) which were not included in Fig. 2. The correlation coefficient of the regression analysis was, for the best line forced through the origin, 0.997; the standard deviation is ± 0.038 ppm. The addition of the site factor produces a notable improvement in comparison to plotting σ_m against the refractive index function of eq. 2 (6, 7). All points referring to nonhalomethane solvents are now much closer to the best line through the origin. This is particularly true for Br_2, $SiCl_4$, $SnCl_4$, CMe_4, $(C_2H_5)_2O$, and CH_3COOCH_3. The points corresponding to cyclopentane and cyclohexane are still somewhat off; this may be due to experimental error, since with other solutes this aberrant behavior for C_5H_{10} and C_6H_{12} is not found. Figure 2 and Table 2 also show rather clearly that the solvent aspects of [12] are essentially correct and that specifically the cavity radius cannot be a function of solvent. The range of molar volumes $V_2{}^{30}$ of the solvents employed spans a factor of three. For example, $V^{30}(Br_2) = 51.8$ and $V^{30}(CBr_4) = 112.3$ ml; yet these two points are very close in Fig. 2. A similar pair is triethylamine (**34**) with $V^{30} = 140.7$ and CH_3Br (**1**) with $V^{30} = 57.3$ ml. An inclusion of even a fractional power of V_2 in the cavity radius would destroy the linear relation presently found.

With CH_4, it is difficult to test the solute aspects of [12] because of the uncertainty as to what to take for $V_1{}^{30}$. Such a test can be made, however, with solutes for which α_1, I_1, and V_1 are known. From these parameters, together with the numerical factor $32\pi^2/3$ of [12] and the slope of the regression line through the origin of $-\sigma_w$ *vs.* $(n_2^2 - 1)^2/(2n_2^2 + 1)^2(1 - q^2)^3$ the combined parameter KB can be extracted. Table 3 shows the results for cyclohexane (C_6H_{12}) with a best value of $KB = 6.19 \times 10^{-18}$ esu. The correlation coefficient is 0.991 and the standard deviation is $s = \pm 0.028$ ppm. These results are

Can. J. Chem. Downloaded from www.nrcresearchpress.com by 210.87.254.42 on 09/05/12
For personal use only.

Can. J. Chem. Downloaded from www.nrcresearchpress.com by 210.87.254.42 on 09/05/12
For personal use only.

TABLE 2. Proton gas-to-solvent shifts of CH_4 at 30 °C, corrected for bulk susceptibility[a]

Solvent	Index number	$-\sigma_m$(exp) (ppm)	$-\sigma_w$(calcd) (ppm)
CH_3Br	**1**	0.355	0.370
CH_3I	**2**	0.505	0.503
CH_2Cl_2	**3**	0.398	0.371
CH_2Br_2	**4**	0.523	0.515
CH_2I_2	**5**	0.769	0.741
CH_2ClBr	**6**	0.486	0.444
$CHCl_3$	**7**	0.407	0.393
$CHClBr_2$	**8**	0.556	0.516
$CHBr_3$	**9**	0.646	0.575
CCl_4	**10**	0.443	0.406
CCl_3Br	**11**	0.533	0.462
CBr_4	**12**	0.594	0.575
CS_2	**13**	0.564	0.628
$SiCl_4$	**14**	0.301	0.347
$SnCl_4$	**15**	0.353	0.464
Br_2	**17**	0.556	0.590
$C(CH_3)_4$	**19**	0.307	0.309
cyclo-C_5H_{10}	**24**	0.259	0.342
cyclo-C_6H_{12}	**25**	0.270	0.363
n-C_6H_{14}	**27**	0.275	0.298
$(C_2H_5)_2O$	**33**	0.267	0.276
$(C_2H_5)_3N$	**39**	0.290	0.328
$CH_3COOC_2H_5$	**40**	0.254	0.302
CH_3COCH_3	**42**	0.209	0.289
CH_3NO_2	**43**	0.241	0.330
$C_2H_5NO_2$	**44**	0.213	0.331
CH_3CN	**46**	0.416	0.278
C_6H_6	**47**	−0.124	0.457
$C_6H_5CH_3$	**48**	−0.074	0.449
C_6H_5Cl	**51**	−0.028	0.483
$C_6H_5NO_2$	**52**	−0.251	0.517

[a]Experimental data from Buckingham *et al.* (18). For corrections to these shifts, see text. Calculated data are from Fig. 2, with a best slope of 7.89.

somewhat better than those of a previous study (7) where no site factor was used. The improvement can be traced to the site factors although in the present case they ranged only between 1.39 and 1.61.

A more convincing test of the validity of the site factor is formed by a study of the solutes XMe_4 (X = C, Si, Ge, Sn, and Pb). Without site factors, plots of experimental Van der Waals shifts *vs.* $(n_2^2 - 1)/(2n_2^2 + 1)^2$ result in approximately parallel straight lines, none of which goes through the origin (7). Introduction of the site factor makes these plots go through the origin, all with correlation coefficients of about 0.993. The results of the calculations, together with the extracted *KB* parameters are given in Table 4. The *KB* parameters for these five solutes are almost equal (except possibly for $PbMe_4$), a fact which is also demonstrated by Fig. 3. Solutes with two different kinds of protons can also be used to test the site factor. For example, the CH_2 and CH_3 protons of tetraethyl compounds XEt_4 have different gas-to-liquid shifts. As Table 4 and Fig. 4 show, the slopes and hence the *KB* parameters are virtually the same for the CH_2 and CH_3 protons of $C(C_2H_5)_4$, although the experimental medium shifts are different by 30–50%. The site factor correction appears to be quantitatively correct in this case. Similar results were obtained with $Si(C_2H_5)_4$ although a slightly smaller *KB* parameter results for the CH_3 protons, indicating a small overestimate of the site factor. This trend is continued by the results on $Sn(C_2H_5)_4$; here the site factor correction is clearly too large for the CH_3 protons, resulting in $KB(CH_3)$, substantially larger than $KB(CH_2)$. A similar effect was observed for the CH_3 protons of *p*-xylene (see Table 4). These results are parallel to those obtained by site factor corrections in the binary collision model (20); outer protons of very large or of strongly nonspherical solutes have calculated site factors which are too large. It may be noted, however, that in the present continuum model, these discrepancies are much smaller than with the binary collision model. Furthermore, the use of different *KB* parameters for different proton sites in the same solute molecule still allows the prediction of Van der Waals shifts even for 'outer' protons without loss of precision.

Finally, Table 4 gives *KB* parameters for cyclopentane (C_5H_{10}) and benzene.

Onsager Cavity Radii

Whereas the solvent aspects of [12] seem to be rather universally valid, Table 4 also indicates that the solute part of [12] is not universal; *KB* parameters ranging over a factor of two are found. Yet there is nothing in the nature of the parameters *K* and *B* that would allow such a large variation. To gain a clearer insight into the dependence of σ_w on solute, it is preferable to look at the σ_w's of a variety of solutes in one and the same solvent. This has been done using CCl_4 as a solvent and results are given in Table 5. It is seen that the correlation between σ_w and $\alpha_1 I_1 S/(V_1^{30})^2$ is poor. The correlation coefficient is actually 0.97; if a best slope (= 0.0153) were used to recalculate σ_w's from the solute factors,

Can. J. Chem. Downloaded from www.nrcresearchpress.com by 210.87.254.42 on 09/05/12
For personal use only.

TABLE 3. Proton gas-to-liquid shifts of cyclohexane, corrected for bulk susceptibility[a]

Solvent	Number	Reference	$-\sigma_m$(exp) (ppm)	$-\sigma_w$(calcd) $KB = 6.45 \times 10^{-18}$
$CHCl_3$	**7**	17	0.250	0.240
CCl_4	**10**	21	0.277	0.238
CCl_4	**10**	17	0.267	0.243
CS_2	**13**	17	0.398	0.393
$SiCl_4$	**14**	17	0.185	0.205
$CFCl_2CFCl_2$	**18**	21	0.164	0.201
$C(CH_3)_4$	**19**	17	0.187	0.145
$Si(CH_3)_4$	**20**	17	0.182	0.161
C_6H_{12}	**25**	21	0.192	0.210
C_6H_{12}	**25**	17	0.202	0.222
n-C_5H_{12}	**26**	21	0.156	0.161
n-C_6H_{14}	**27**	21	0.162	0.170
n-C_7H_{16}	**28**	21	0.174	0.176
n-C_7H_{16}	**28**	17	0.170	0.180
n-C_8H_{18}	**29**	21	0.182	0.181
$(CH_3—OCH_2)_2$	**34**	21	0.195	0.180
1,4-Dioxane	**37**	21	0.203	0.217
Tetrahydrofuran	**38**	21	0.182	0.217
DMSO	**41**	21	0.278	0.265
CH_3COCH_3	**42**	21	0.090	0.172
CH_3COCH_3	**42**	17	0.098	0.177
CH_3NO_2	**43**	21	0.075	0.200
CH_3CN	**46**	17	0.285	0.176
C_6H_6	**47**	21	−0.263	0.270
C_6H_6	**47**	17	−0.272	0.276
$C_6H_5NO_2$	**52**	17	−0.403	0.309
N-Methylaniline	**53**	21	−0.067[b]	0.319
Pyrrole	**54**	21	0.013[c]	0.302

[a]Experimental data from Chenon (21) at 41 °C and Bernstein (17) at 30 °C.
[b]At t = 29 °C.
[c]At t = 15 °C.

TABLE 4. Results of comparisons between experimental and calculated (eq. 12) Van der Waals shifts

Solute	Reference to experimental data and solvent numbers		Correlation coefficient	Standard deviation (ppm)	$KB \times 10^{18}$ (esu)
CH_4	(18); **1–15, 17, 19, 24, 25, 27, 33, 39, 40.** (23); **10, 13, 14**		0.997	0.038	$3.77 \times 10^{-3} V_i^2$
C_6H_{12}	(17); **7, 10, 13, 14, 19, 20, 25, 28.** (21); **10, 18, 25, 26, 27, 28, 29, 34, 37, 38, 41.** (24); **10, 14, 22, 24, 25, 31, 35, 36**		0.991	0.029	6.19
CMe_4	(8); **19–23.** (17); **7, 10, 13, 14, 25.** (25); **3, 24**		0.993	0.033	11.47
$SiMe_4$	(8); **19–23.** (17); **7, 10, 13, 14, 25**		0.994	0.034	11.28
$GeMe_4$	(8); **19–23**		0.993	0.034	11.77
$SnMe_4$	(8); **19–23**		0.993	0.040	11.75
$PbMe_4$	(8); **19–23**		0.993	0.038	9.91
CEt_4	(19); **10, 13, 16, 20, 25, 30**	CH_3	0.995	0.021	6.40
		CH_2	0.978	0.036	6.34
$SiEt_4$	(20); **10, 13, 16, 20, 25, 31**	CH_3	0.997	0.019	7.12
		CH_2	0.989	0.030	7.85
$SnEt_4$	(19); **10, 13, 16, 20, 25, 32**	CH_3	0.998	0.018	7.76
		CH_2	0.996	0.023	9.55
C_5H_{10}	(24); **10, 14, 22, 31, 32, 35, 36.** (25); **3, 10, 19, 24, 25**		0.985	0.044	6.31
C_6H_6	(24); **10, 13, 14, 22, 24, 25, 31, 32, 35, 36.** (17); **10, 13, 14, 19, 20, 25, 28**		0.986	0.055	5.68
p-Xylene	(19); **10, 13, 16, 20, 25**	CH_3	0.989	0.050	5.35
	(24); **10, 13, 14, 22, 31, 32**	CH_2	0.995	0.030	7.79

Can. J. Chem. Downloaded from www.nrcresearchpress.com by 210.87.254.42 on 09/05/12
For personal use only.

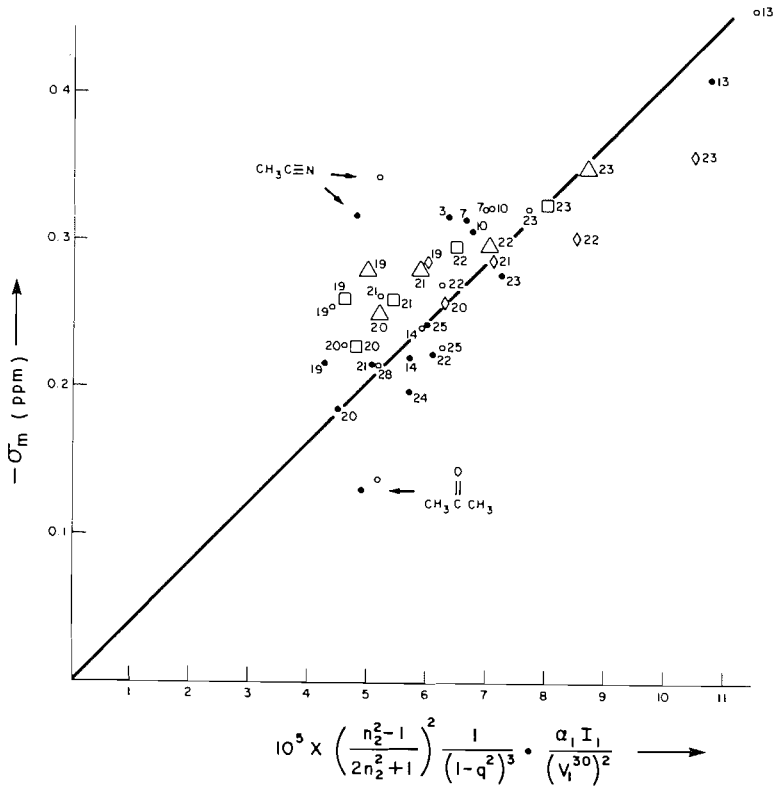

FIG. 3. Experimental medium shifts of CMe_4 (●), $SiMe_4$ (○), $GeMe_4$ (□), $SnMe_4$ (△), and $PbMe_4$ (▽) *vs.* theoretical expression for σ_w of eq. 12. Numbers refer to solvents of Table 1.

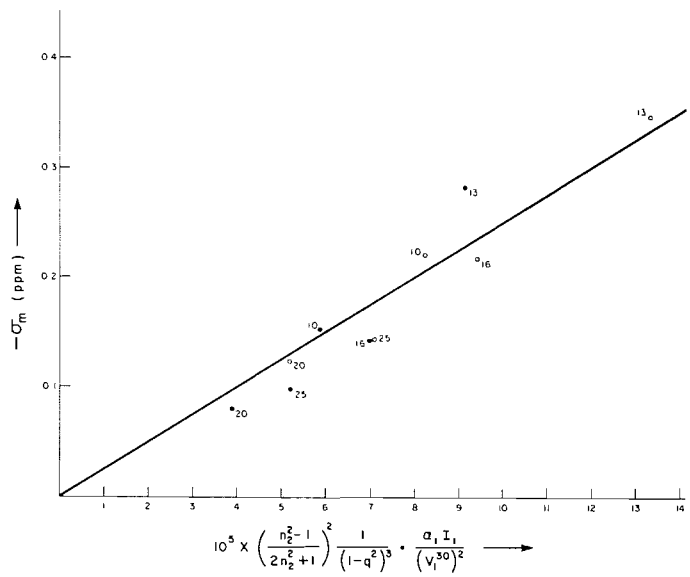

FIG. 4. Experimental medium shifts of CEt_4 (○, CH_3; ●, CH_2) *vs.* σ_w as per eq. 12. Numbers refer to solvents of Table 1.

TABLE 5. Experimental gas-to-CCl_4 solution shifts σ_w and solute factors for a number of solutes

Solute	Reference	$-\sigma_w$(exp) (ppm)	$\frac{\alpha_1 I_1 S}{(V_1^{30})^2} \times 10^{39}$
$C(CH_2CH_3)_4$	19	0.153	13.0
$Si(CH_2CH_3)_4$	20	0.190	12.4
$C(CH_2CH_3)_4$	19	0.220	17.9
$Sn(CH_2CH_3)_4$	19	0.222	12.1
n-C_7H_{16} (CH_2)	8	0.225	15.0
n-C_6H_{14} (CH_2)	21	0.248	14.8
$Si(CH_2CH_3)_4$	20, 24	0.249[a]	17.0
trans-Butene (CH)	19	0.255	15.3
C_6H_{12}	8, 21, 24	0.269[a]	21.4
Mesitylene (CH)	20, 24	0.272[a]	17.0
C_5H_{10}	24, 25	0.297[a]	23.1
i-C_4H_{10} (CH_3)	19	0.298	16.4
i-C_4H_{10} (CH)	19	0.302	13.8
C_2H_6	22	0.31	22.5
$C(CH_3)_4$	8, 22, 24, 25	0.320[a]	14.3
p-Xylene (CH)	19, 24	0.320[a]	19.6
$C(=CHCH_3)_2$	19	0.328	21.5
$(\equiv CCH_2CH_3)_2$	19	0.338	22.5
C_2H_4	22	0.37	30.2
trans-Butene (CH_3)	19	0.372	22.0
$Si(CH_3)_4$	8, 22, 23, 25	0.373[a]	15.7
Cyclopropane	22	0.38	23.8
CH_4	18, 22, 23	0.416[a]	21.7
C_6H_6	8, 24	0.420[a]	32.5
$Sn(CH_3)_4$	23	0.433	17.7
$(\equiv CCH_3)_2$	19, 24	0.468[a]	34.9

[a]Averaged value.

major deviations of up to 0.2 ppm would be found. Although the site factor is more sensitive to the nature of the solute than that of the solvent (because of the d parameter), the evidence of the previous paragraph suggests that the poor correlation is not due to the site factor. (Note that all potential entries in Table 5 of solutes for which $S \doteq 1/(1 - q^2)^3$ might lead to an overestimate of S were deliberately omitted.) There are also indications that the factor $\alpha_1 I_1$ is basically correct. Consider, for example, the five solutes $X(CH_3)_4$. These compounds have very similar V_1^{30} parameters; since these molecules are rather alike, it seems reasonable to assume that they have a very similar relation between a^3 and V_1^{30}. Since, in going from X = C → Pb the polarizability increases strongly and the ionization potential *decreases* strongly in that same direction, the observed constancy of the KB parameters (see Table 4) can be interpreted to mean that α_1 and I_1, if at all relevant to σ_w, must enter the σ_w model as the product $\alpha_1 I_1$ or some power thereof. The KB parameters on the $X(C_2H_5)_4$ solutes give the same indication; the decrease in I_1 is the same as for the $X(CH_3)_4$ molecules, but the relative increase in α_1 is somewhat less, because of the large and constant contribution of the extra CH_2 groups. Consequently, since the V_1^{30} parameters are again constant in this series, KB parameters increasing in the direction X = C → Sn are required as is indeed observed. Another example of chemically similar molecules where the same relation between a^3 and V_1^{30} could be presumed, is formed by the series benzene, *p*-xylene, and mesitylene. As Table 5 shows these solutes have roughly the same correlation between σ_w and $\alpha_1 I_1 S/(V_1^{30})^2$. There are, on the other hand, many examples of pairs of solutes having about the same $\alpha_1 I_1$ product and yet very different KB parameters (for example cyclopentane and neopentane or $Sn(CH_3)_4$ and *p*-xylene in Table 4) or different ratios σ_w to $\alpha_1 I_1 S/(V_1^{30})^2$ (such as $Sn(CH_3)_4$ and C_6H_6 or 2,3-pentadiene and neopentane in Table 5).

In spite of the indirectness of the above evi-

Can. J. Chem. Downloaded from www.nrcresearchpress.com by 210.87.254.42 on 09/05/12
For personal use only.

Can. J. Chem. Downloaded from www.nrcresearchpress.com by 210.87.254.42 on 09/05/12
For personal use only.

TABLE 6. Values of cavity radii cubed based on [3] with $KB = 4.71 \times 10^{-18}$ esu for the solutes of Table 4[a]

	$a^3 \times 10^{24}$ (cm^3)	V_1^{30} (cm^3)	$(r_{01}/2)^3 \times 10^{24}$ (cm^3)
C_5H_{10}	32.1	95.2	21.7
C_6H_6	32.5	90.1	22.7
CH_4	34.3	—	27.3
$C(CH_3)_4$	34.5	131.4	27.8
$Ge(CH_3)_4$	34.6	138.2	33.9
$Sn(CH_3)_4$	35.0	139.5	36.3
$Si(CH_3)_4$	35.8	139.6	30.4
$Pb(CH_3)_4$	37.1	135.9	37.3
C_6H_{12}	37.7	109.3	26.8
p-Xylene	38.4	124.5	40.2
$Sn(CH_2CH_3)_4$	55.1	198.1	58.2
$C(CH_2CH_3)_4$	57.5	171.9	60.5
$Si(CH_2CH_3)_4$	58.5	190.4	61.2

[a]Note: values of V_1^{30} and of $(r_{01}/2)^3$ given for comparison. Values of r_{01} calculated via critical constants (12–14).

TABLE 7. Estimated contributions to σ_{E^2} according to [9] of CH_4 medium shifts

Solvent	$\frac{2\mu_2^2}{3\alpha_2 I_2}$	$\frac{-2\mu_2^2\sigma_w^{CH_4}}{3\alpha_2 I_2}$ (ppm)
CH_3Br	0.023	0.008
CH_3I	0.015	0.008
CH_2Cl_2	0.013	0.005
CH_2Br_2	0.008	0.001
$CHCl_3$	0.005	0.002
$(C_2H_5)_2O$	0.009	0.002
$(C_2H_5)_3N$	0.003	0.001
Ethyl acetate	0.015	0.004
Acetone	0.055	0.016
CH_3NO_2	0.090	0.030
CH_3CN	0.115	0.032
$C_6H_5NO_2$	0.049	0.026
C_6H_5Cl	0.009	0.004
Pyrrole	0.019	0.006

dence, it is surmised that the nonuniversality of [12] as indicated by the results of Tables 4 and 5 is caused by the nonexistence of a unique and universal relation between a^3 and V_1^{30}. Attempts to correlate a^3 with other parameters having a volume-per-molecule dimension (see Theory) all failed to produce any improvement. Also, the three accurately known a^3 parameters (C_6H_6, C_6H_{12}, and CCl_4, see Theory) do not relate simply to any of the investigated volume parameters. It is therefore postulated that [3], modified with the site factor of [8], is essentially correct, including a universal constant for KB for all C—H protons. This postulate can be partly tested by using the data of Pijpers (11) for a^3 of C_6H_6 and C_6H_{12} in combination with the experimental slopes of σ_w *vs.* $\alpha_1 I_1 (n_2^2 - 1)^2/(2n_2^2 + 1)^2(1 - q^2)^3$ to arrive at the KB parameters. The results were $KB(C_6H_6) = 4.41$ and $KB(C_6H_{12}) = 5.02 \times 10^{-18}$ esu. These two values are satisfactorily close. With an average value of $KB = (4.71 \pm 0.3) \times 10^{-18}$, it is now possible to derive values for a^3 of the solutes of Table 4. The results have been tabulated in Table 6, together with values of V_1^{30} and $(r_{01}/2)^3$ for comparison. It may be seen that there is no simple relation between a^3 and V_1^{30} or $(r_{01}/2)^3$; the ratio $(V_1^{30})/a^3$, for example, varies from 2.77 (C_6H_6) to 4.0 ($SnMe_4$). All possible correlations suggested in the Theory section were tried; none of these yielded any useful results. The relatively large value for a^3 of CH_4 can perhaps be understood since the temperature of the measurements (30 °C) is far above the critical temperature of CH_4; it is conceivable that the high collision rate of the CH_4 molecules at 30 °C creates a cavity considerably larger than its 'hard' volume. In principle, any single σ_w measurement, such as those given in Table 5, could be used to determine a^3 of the solute in question. To eliminate at least part of the experimental errors and of the model errors, it is better to use a series of solvents, however. A recommended set would be *n*-C_7H_{16}, $SiCl_4$, $CHCl_3$, CH_3I, and CS_2; Van der Waals shifts in these solvents consistently showed only small and random variations with the shifts calculated from [12] and the KB parameters of Table 4. The presently proposed method of determining the cavity radius is felt to be as precise as the Böttcher method employing refractive indices ($\pm 10\%$ in a^3) but is considerably easier to use. One disadvantage is that this method is only applicable to molecules having a C—H moiety close to its center of gravity; the added assumption that KB is a universal parameter for all C—H bonds is a further possible limitation.

The σ_{E^2} Effect

In Table 7, the factor $2\mu_2^2/3\alpha_2 I_2$ of [9] has been calculated for a number of strongly polar solvents. It is seen that the calculated σ_{E^2} is always smaller than 0.01 ppm for those polar solvents used in the previous sections on σ_w. This justifies the use of polar solvents for the determination of KB or a^3, but it also means that if

Can. J. Chem. Downloaded from www.nrcresearchpress.com by 210.87.254.42 on 09/05/12
For personal use only.

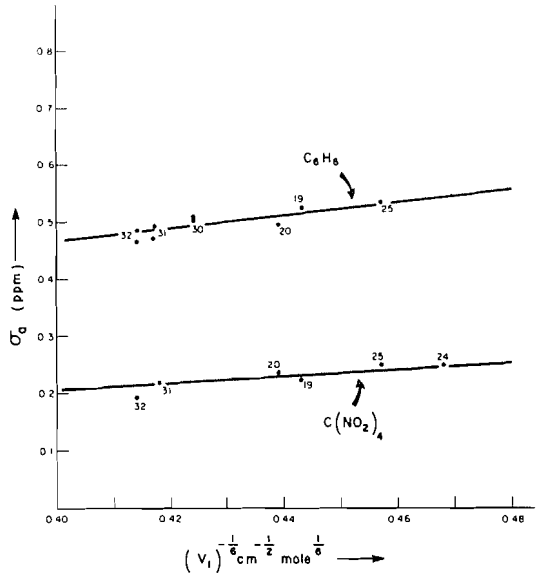

FIG. 5. Neighbor anisotropy shift σ_a of C_6H_6 and $C(NO_2)_4$ *vs.* $(V_l)^{-1/6}$. Data from Table 8. Solvent numbers refer to Table 1.

the σ_{E^2} term were to exist it could not possibly be detected. Among the solvents which are magnetically anisotropic (lower half of Table 7) there are several with potentially detectable σ_{E^2} effects, but if existent this is obscured by the much larger σ_a effects. It is therefore found impossible to employ the σ_{E^2} effect as a means of judging the validity of the present reaction field approach *vs.* the direct field approach of Raynes *et al.* (1).

The Neighbor Anisotropy Contribution σ_a

The calculation of σ_w via [12] and the *KB* parameters for each solute obtained from their medium shifts in isotropic solvents can also be used to calculate the σ_w contribution to the total medium shifts for those solutes in anisotropic solvents. If the possible σ_{E^2} is neglected then one has for nonpolar solvents that $\sigma_a = \sigma_m(\text{exp}) - \sigma_w(\text{calcd})$. This has been done for a number of solutes and anisotropic solvents as given in Table 8. For the more or less spherical solutes (*i.e.* all except benzene and *p*-xylene), a number of trends can be discovered. Acetone and acetonitrile appear to have virtually constant σ_a contributions of $\sigma_a = +0.078 \pm 0.005$ and $\sigma_a = -0.122 \pm 0.006$ ppm respectively. Such a constancy of σ_a has often been noted; it is also consistent with the theoretical result that the site factor for σ_a is unity for spherical solutes (26, 27). It is interesting to note that ethylacetate (solute CH_4) and dimethyl sulfoxide (solute C_6H_{12}) do not show any σ_a effect although they have anisotropic groups, quite similar to the carbonyl group of acetone. However, this observation is based on only one medium shift of each of these solvents; more experimental data would be needed to justify any conclusion.

With the other anisotropic solvents, which produce somewhat larger σ_a effects, it is clear that σ_a is not quite independent of solute. It is seen from Table 8 that σ_a for any given solvent increases slightly with decreasing molar volume of the solutes, as is predicted by [10]. In Fig. 5 it is demonstrated for the solvents C_6H_6 and $C(NO_2)_4$ that there is a good proportionality between σ_a and $(V_l)^{-1/6}$. The results can be written as

$$\sigma_a(C_6H_6) = 1.166/(V_l)^{1/6}$$

$$\sigma_a(C(NO_2)_4) = 0.522/(V_l)^{1/6} \text{ ppm}$$

The proportionality factor for C_6H_6 is close to that reported earlier (1.08; see ref. 15), although in that study the binary collision model was used for the calculation of σ_w.

Table 8 also shows that for the near-spherical bi-site solutes XEt_4, the σ_a for the inner (CH_2) protons is consistently larger than for the outer (CH_3) protons, whereas for the nonspherical *p*-xylene molecule the opposite is observed. These are probably real effects because (*i*) in *intra*-molecular comparisons any systematic experimental errors cancel out, (*ii*) the possible systematic errors in the site effect model used to calculate the σ_w term are eliminated by determining separate *KB* parameters for each proton type, calibrated on the same isotropic solvents, (*iii*) very similar effects were noted by Rummens and Louman (19, 20) in a study on the same solutes and solvents but employing the binary collision model for σ_w. Therefore it appears clear that the σ_a effect exhibits a site effect, with a site factor which may be greater or less than unity, depending on solute geometry. This finding is at least in qualitative accord with Becconsall's model for σ_a of nonspherical solutes (30); the above then forms proof that the XEt_4 solutes are effectively nonspherical, which in turn may explain some of the anomalies found for σ_w of

Can. J. Chem. Downloaded from www.nrcresearchpress.com by 210.87.254.42 on 09/05/12
For personal use only.

TABLE 8. Neighbor anisotropy shifts σ_a(ppm) for nonpolar solutes in anisotropic solvents (Van der Waals shifts σ_w calculated according to [12] with the *KB* parameters of Table 4)

Solute	V_I[30]	Parameter	Value in solvent = C_6H_6	*p*-Xylene	Mesitylene	$C_6H_5NO_2$	CH_3NO_2	$C(NO_2)_4$	Acetone	CH_3CN
$Sn(CH_2CH_3)_4$	198.1	σ_m	0.205[a]	0.132[a]	0.182[a]			−0.008[c]		
		σ_w	−0.261	−0.240	−0.232			−0.202		
		σ_a	+0.466	+0.372	+0.414			+0.194		
$Sn(CH_2CH_3)_4$	198.1	σ_m	0.257[a]	0.190[a]	0.245[a]					
		σ_w	−0.229	−0.218	−0.214					
		σ_a	+0.486	+0.408	+0.459					
$Si(CH_2CH_3)_4$	190.4	σ_m	0.230[a]	0.188[a]	0.208[a]			0.032[c]		
		σ_w	−0.241	−0.224	−0.218			−0.189		
		σ_a	+0.471	+0.412	+0.426			+0.221		
$Si(CH_2CH_3)_4$	190.4	σ_m	0.302[a]	0.268[a]	0.305[a]					
		σ_w	−0.192	−0.185	−0.182					
		σ_a	+0.494	+0.453	+0.487					
$C(CH_2CH_3)_4$	171.9	σ_m	0.278[a]	0.225[a]	0.263[a]					
		σ_w	−0.228	−0.214	−0.209					
		σ_a	+0.506	+0.439	+0.472					
$C(CH_2CH_3)_4$	171.9	σ_m	0.342[a]	0.308[a]	0.347[a]					
		σ_w	−0.162	−0.158	−0.156					
		σ_a	+0.504	+0.466	+0.503					
$Si(CH_3)_4$	139.6	σ_m	0.151[b]			0.273[b]		−0.035[d]	−0.138[b]	−0.343[b]
		σ_w	−0.345			−0.385		−0.272	−0.222	−0.222
		σ_a	+0.496			+0.658		+0.237	+0.084	−0.121

Can. J. Chem. Downloaded from www.nrcresearchpress.com by 210.87.254.42 on 09/05/12
For personal use only.

TABLE 8 (*Concluded*)

Solute	V_I^{30}	Parameter	Value in solvent = C_6H_6	*p*-Xylene	Mesitylene	$C_6H_5NO_2$	CH_3NO_2	$C(NO_2)_4$	Acetone	CH_3CN
$C(CH_3)_4$	131.4	σ_m	0.213[b]			0.343[b]		−0.028[c]	−0.130[b]	−0.317[b]
		σ_w	−0.314			−0.352		−0.251	−0.201	−0.197
		σ_a	+0.527			+0.695		+0.223	+0.071	−0.120
p-Xylene (CH_3)	124.5	σ_m	0.237[a]	0.162[a]	0.208[a]			−0.118[c]		
		σ_w	−0.377	−0.333	−0.319			−0.282		
		σ_a	+0.618	+0.495	+0.527			+0.164		
p-Xylene (CH)	124.5	σ_m	0.162[a]	0.167[a]	0.212[a]			−0.058[c]		
		σ_w	−0.302	−0.288	−0.283			−0.242		
		σ_a	+0.464	+0.455	+0.495			+0.184		
Cyclohexane	109.3	σ_m	0.272[b]			0.403[b]	−0.075[d]	0.043[c]	−0.098[b]	−0.285[b]
		σ_w	−0.265			−0.297	−0.192	−0.207	−0.170	−0.169
		σ_a	+0.537			+0.700	+0.117	+0.250	+0.072	−0.116
Cyclopentane	95.2	σ_m						0.023[c]	−0.100[c]	
		σ_w						−0.227	−0.181	
		σ_a						+0.250	+0.081	
Benzene	90.1	σ_m	0.235[b]			0.093[b]		−0.120[c]	−0.312[b]	−0.452[b]
		σ_w	−0.367			−0.407		−0.285	−0.238	−0.242
		σ_a	+0.602			+0.500		+0.165	−0.074	−0.210
CH_4		σ_m	0.124[f]			0.251[f]	−0.203[e]	−0.053[g]	−0.209[f]	−0.416[f]
		σ_w	−0.464			−0.525	−0.334	−0.377	−0.293	−0.282
		σ_a	+0.588			+0.776	+0.131	+0.322	+0.084	−0.134

[a]Data from Rummens and Louman at 38 °C (19, 20).
[b]Data from Bernstein at 30 °C (17).
[c]Data from Raza and Raynes at 35 °C (24).
[d]Data from Chenon at 41 °C (21).
[e]Data from Bothner-By at 30 °C (25).
[f]Data of Buckingham *et al.* at 30 °C (18).
[g]Data of Raynes and Raza at 35 °C (23).

TABLE 9. Solvent dependence of σ_a

Solvent	V_2[38] (ml)	$\Delta\chi \times 10^6$[b] (emu/mol)	$r_{2\parallel}$[c] (Å)	$r_{2\perp}$[c] (Å)	$\frac{\Delta\chi(r_{2\parallel}^{-3/2} - r_{2\perp}^{-3/2})}{V_2^{1/3}}$[d]
C_6H_6	90.9	59.7	1.90	3.52	1.00
p-Xylene	125.6	61.2	2.14	3.92	0.76
Mesitylene	141.3	61.9	2.14	4.12	0.78
Nitrobenzene	103.2[a]	68	1.90	3.72	1.15

[a]At 30 °C.
[b]Estimated from experimental $\Delta\chi$ data on C_6H_6, 1,2,4,5-tetramethylbenzene, hexamethylbenzene, and 1,4-dinitrobenzene, reference page of Table A; χ data are averaged.
[c]Estimated according to procedure outlined in ref. 15.
[d]Relative value.

these solutes. Both this σ_a site factor and the V_1 dependence of σ_a noted here are of importance for the application of factor analysis on nmr medium shift, where so far it has been maintained (16, 17) that σ_a is independent of solute.

From Table 8, a systematic solvent dependence of σ_a can be noted. For example, the σ_a ratios of C_6H_6, *p*-xylene, mesitylene, and nitrobenzene are 1:0.88:0.95:1.32, almost independent of solute. According to [10], σ_a depends on the diamagnetic anisotropy $\Delta\chi$, the molar volume, and the geometric anisotropy of the solvent. As Table 9 shows, all three factors play a determining role; the expression of eq. 10 is capable of predicting the correct relative magnitudes of σ_a as a function of solvent. It should be remembered, however, that both σ_w and σ_a are in principle dependent on the shape of the *solute* molecule as well, but that the theory presented here (eqs. 5 and 10) assumes spherical solute geometry.

The solvent CS_2 has been said repeatedly (18, 16, 17, 28, 29) to be anisotropic with a negative σ_a. Yet, the present study indicates clearly that there is no experimental evidence for this. For nearly all solutes reported in Table 4, CS_2 was included as a solvent, together with the isotropic solvents. In all these cases, the point corresponding to CS_2 was very close to the 'best' line; the average deviation is ± 0.004 ppm which is negligibly small compared to the standard deviation. Although CS_2 is geometrically anisotropic and has probably a sizeable molecular magnetic anisotropy, this is not necessarily sufficient to produce a σ_a effect. CS_2 has a rather small moment of inertia; its rotation in the liquid phase might therefore well be in the inertial limit rather than in the diffusional limit, the latter which is a prerequisite to producing a nonzero average for the magnetic dipole field of the anisotropic molecule at the solute.

Acknowledgments

Financial support of this work by the National Research Council of Canada is gratefully acknowledged.

1. W. T. RAYNES, A. D. BUCKINGHAM, and H. J. BERNSTEIN. J. Phys. Chem. **36**, 3481 (1962).
2. B. LINDER. J. Chem. Phys. **33**, 668 (1960); **37**, 963 (1962).
3. B. B. Howard, B. LINDER, and M. T. EMERSON. J. Chem. Phys. **36**, 485 (1962).
4. PH. DE MONTGOLFIER. J. Chim. Phys. **64**, 639 (1967); **65**, 1618 (1968); **66**, 685 (1969).
5. F. H. A. RUMMENS. Van der Waals forces in NMR intermolecular shielding. Vol. 10 of NMR, Basic Principles and Progress. *Edited by* P. Diehl, E. Fluck, and R. Kosfeld. Springer Verlag, Heidelberg. 1976.
6. F. H. A. RUMMENS. Chem. Phys. Lett. **31**, 596 (1975).
7. F. H. A. RUMMENS. J. Chim. Phys. **72**, 448 (1975).
8. F. H. A. RUMMENS, W. T. RAYNES, and H. J. BERNSTEIN. J. Phys. Chem. **72**, 2111 (1968).
9. F. H. A. RUMMENS and H. J. BERNSTEIN. J. Chem. Phys. **43**, 2971 (1965).
10. C. J. F. BÖTTCHER. Theory of electric polarisation. Elsevier Publishing Co., Amsterdam. 1952.
11. F. W. PIJPERS. Ph.D. Thesis, University of Leiden, 1958.
12. L. I. STIEL and G. THODOS. J. Chem. Eng. Data, **7**, 234 (1962).
13. L. I. STIEL and G. THODOS. J. Am. Inst. Chem. Eng. **10**, 266 (1964).
14. R. F. CURL and K. S. PITZER. Ind. Eng. Chem. **50**, 265 (1958).
15. F. H. A. RUMMENS. J. Am. Chem. Soc. **92**, 3214 (1970).
16. E. R. MALINOWSKI and P. H. WEINER. J. Am. Chem. Soc. **92**, 4193 (1970); P. H. WEINER, E. R. MALINOWSKI, and A. R. LEVINSTONE. J. Phys. Chem. **74**, 4537 (1970); P. H. WEINER and E. R. MALINOWSKI. J. Phys. Chem. **75**, 1207 (1971).
17. H. J. BERNSTEIN. Pure Appl. Chem. **32**, 79 (1972).
18. A. D. BUCKINGHAM, T. SCHAEFER, and W. G. SCHNEIDER. J. Chem. Phys. **32**, 1227 (1960).
19. F. J. A. LOUMAN. Ph.D. Thesis, University of Saskatchewan, Regina, Saskatchewan. 1972.
20. F. H. A. RUMMENS and F. J. A. LOUMAN. J. Magn. Reson. **8**, 332 (1972).

Can. J. Chem. Downloaded from www.nrcresearchpress.com by 210.87.254.42 on 09/05/12
For personal use only.

21. M. T. CHENON. Thèse doctorat d'état, Faculté des Sciences, Université de Paris. 1970; M. T. CHENON, J. BOUQUANT and N. LUMBROSO-BADER. J. Chim. Phys. **67**, 1252 (1970).
22. N. LUMBROSO, T. K. WU, and B. P. DAILEY. J. Phys. Chem. **67**, 2469 (1963).
23. W. T. RAYNES and M. A. RAZA. Mol. Phys. **17**, 157 (1969).
24. M. A. RAZA and W. T. RAYNES. Mol. Phys. **19**, 199 (1970).
25. A. A. BOTHNER-BY. J. Mol. Spectrosc. **5**, 52 (1960).
26. J. K. BECCONSALL. Mol. Phys. **15**, 129 (1968).
27. F. H. A. RUMMENS. Mol. Phys. **19**, 423 (1970).
28. J. C. SCHUG. J. Phys. Chem. **70**, 1816 (1966).
29. R. J. ABRAHAM. Mol. Phys. **4**, 369 (1961).
30. J. K. BECCONSALL. Mol. Phys. **18**. 337 (1970).

Can. J. Chem. Downloaded from www.nrcresearchpress.com by 210.87.254.42 on 09/05/12
For personal use only.

Reactions of 4-hydroxy-6-methyl-2-pyridone with aldehydes

JOHN A. FINDLAY, JIRI KREPINSKY, FOO YU SHUM, AND WAH HUNG JOHN TAM
Department of Chemistry, University of New Brunswick, Fredericton, New Brunswick E3B 5A3

Received June 16, 1975

JOHN A. FINDLAY, JIRI KREPINSKY, FOO YU SHUM, and WAH HUNG JOHN TAM. Can. J. Chem. **54**, 270 (1976).

A novel condensation reaction of 4-hydroxy-6-methyl-2-pyridone with aldehydes giving **4** has been explored. A number of by-products are accounted for. The mass spectra of the major condensation products are discussed.

JOHN A. FINDLAY, JIRI KREPINSKY, FOO YU SHUM et WAH HUNG JOHN TAM. Can. J. Chem. **54**, 270 (1976).

On a exploré une nouvelle réaction, conduisant à **4**, de condensation de l'hydroxy-4 méthyl-6 pyridone-2 avec des aldéhydes. On explique la formation d'un certain nombre de sous-produits. On discute des spectres de masse des principaux produits de condensation.
[Traduit par le journal]

Can. J. Chem. Downloaded from www.nrcresearchpress.com by 210.87.254.5 on 09/05/12
For personal use only.

In the course of studies directed at the synthesis of the antibiotic flavipucine (1) we encountered a novel base-catalysed condensation reaction of 4-hydroxy-6-methyl-2-pyridone **1** with aldehydes which affords high yields of adducts of structure **4**.

In our preliminary report (2) it was noted that anticipated adducts of the types **2** and **3** had not been detected under the reaction conditions employed. We now present our findings following a more comprehensive study of this new reaction.

In exploring alternative catalysts we have found that employment of β-alanine–pyridine or diethylamine–pyridine offers no advantage over the piperidine–pyridine system used initially, thus **4***h* (R = C_6H_5) was recovered in ~85% yield with any of these catalyst systems when **1** (2 equiv.) was treated with benzaldehyde and the rates of formation of product did not vary significantly.

The optimum solvent system in the cases studied was found to be a 1:1 methanol–ethanol mixture which allowed ready dissolution of starting materials and direct separation in crystalline form of the condensation product **4** in a high state of purity.

In a few cases it was necessary to concentrate the mixture following the reaction to induce crystallization. Table 1 summarizes results obtained when the molar ratio of aldehyde to 4-hydroxy-6-methyl-2-pyridone was 1:2 in a mixture of ethanol–methanol (1:1) in an overnight reaction. All the compounds in Table 1 are fully characterized and show spectroscopic properties consistent with their assigned structures.

No substantial difference in the rate of reaction of aliphatic and aromatic aldehydes was noted; however, formaldehyde underwent complete reaction in less than 2 h at the reflux temperature of the mixture.

In accounting for the ready and often exclusive formation of products of type **4** we visualize the operative mechanism to be that outlined in Scheme 1. Thus the anion **1***a* condenses with an aldehyde molecule to furnish a transient secondary alcohol **2** whose dehydration product **3** is rapidly attacked by the anion **1***a* leading to the adduct **4**. Only in the case of benzaldehyde has it proved possible to isolate the intermediate alcohol **2** (R = phenyl) by adjusting molar ratios in favour of a large excess of aldehyde. The spectral characteristics of this alcohol **2** (R = phenyl) are in accord with expectations; thus its nmr (DMSO-d_6) spectrum displays signals at δ7.4 (broad singlet, 5H) ppm due to aromatic protons, δ5.6 (s, 1H) and δ4.6 (s, 1H) ppm ascribed to the olefinic and benzylic protons, respectively, while the methyl group gives rise to a signal at δ2.0 (s, 3H) ppm.

Reactions carried out with a large excess of aldehyde (*e.g. n*-hexanal) gave, in addition to adduct **4***d* (R = pentyl), small quantities (~20%) of **6***b* (R = pentyl, R′ = butyl). This type of product can readily be accounted for via aldol type condensation of the aldehyde anion with **3** giving **5** which undergoes hemiacetal ring

TABLE 1. Adducts from 4-hydroxy-6-methyl-2-pyridone and aldehydes

Aldehyde	Product **4**	Yield (%)	Melting point
Formaldehyde	(*a*) R = H	70	>370
Acetaldehyde	(*b*) R = CH_3	93	>370
n-Butanal	(*c*) R = $CH_3(CH_2)_2$	61	295–297
n-Hexanal	(*d*) R = $CH_3(CH_2)_4$	48	285–289
n-Nonanal	(*e*) R = $CH_3(CH_2)_7$	50	265–266
n-Decanal	(*f*) R = $CH_3(CH_2)_8$	66	254–256
Isovaleraldehyde	(*g*) R = $(CH_3)_2CHCH_2$	80	308–310
Benzaldehyde	(*h*) R = C_6H_5	84	354–356
Vanillin	(*i*) R = 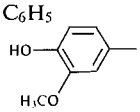	68	297–300
Furfural	(*j*) R =	65	>370
Acrolein	(*k*) R = CH_2=CH	45	>370
Crotonal	(*b*) R = CH_3	55	>370

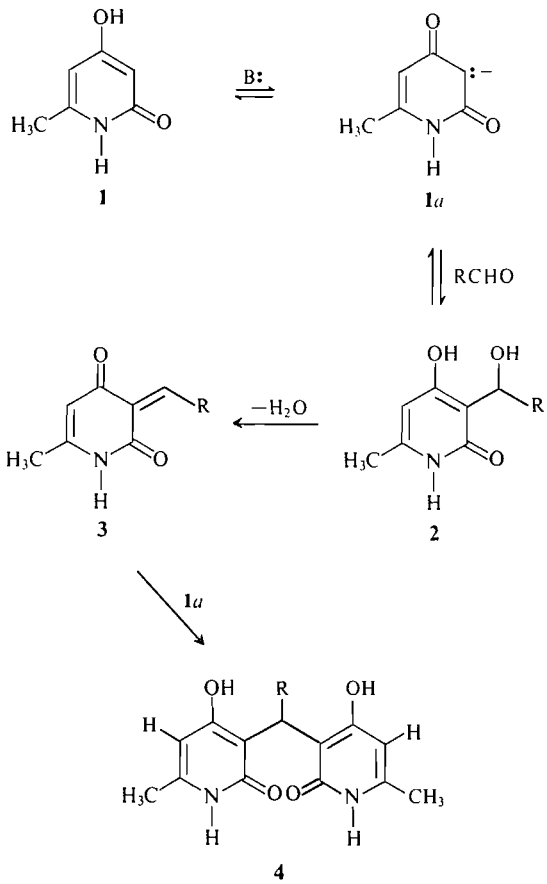

SCHEME 1

formation to **6** as depicted in Scheme 2. The nmr spectrum (DMSO-d_6) of **6***b* shows two low field deuterium exchangeable signals, one centred at δ11.1 ppm (NH) and the other at δ7.2 (OH) while a singlet at δ5.6 ppm accounts for the olefinic proton and a broad singlet at δ5.3 ppm is assigned to the hemiacetal proton. The vinylic methyl signal is located at δ2.1 ppm. The mass spectra of products of the type **6** are characterized by molecular ions and $(M - R'CHCHO)^+$ ions possibly corresponding to **8**.

Reaction of equimolar quantities of crotonaldehyde and 4-hydroxy-6-methyl-2-pyridone, **1**, took an unexpected course and gave a 45% yield of **4** (R = CH_3) identical with the product obtained by condensation of **1** with acetaldehyde. Presumably the crotonaldehyde affords acetaldehyde via hydration and reverse aldolization. The major product (55%), however, proved to have structure **7**.

Attempted condensation of 4-hydroxy-6-methyl-2-pyridone with a variety of ketones under conditions which produced adducts of type **4** from aldehydes resulted in quantitative recovery of starting materials. Thus acetophenone, propiophenone, benzophenone, and acetone all proved to be unreactive. Presumably a combination of electronic and steric factors conspire to prevent the formation of the necessary tertiary alcohol intermediate corresponding to **2**.

It was also ascertained that alkyl halides are unreactive towards 4-hydroxy-6-methyl-2-pyri-

Can. J. Chem. Downloaded from www.nrcresearchpress.com by 210.87.254.5 on 09/05/12
For personal use only.

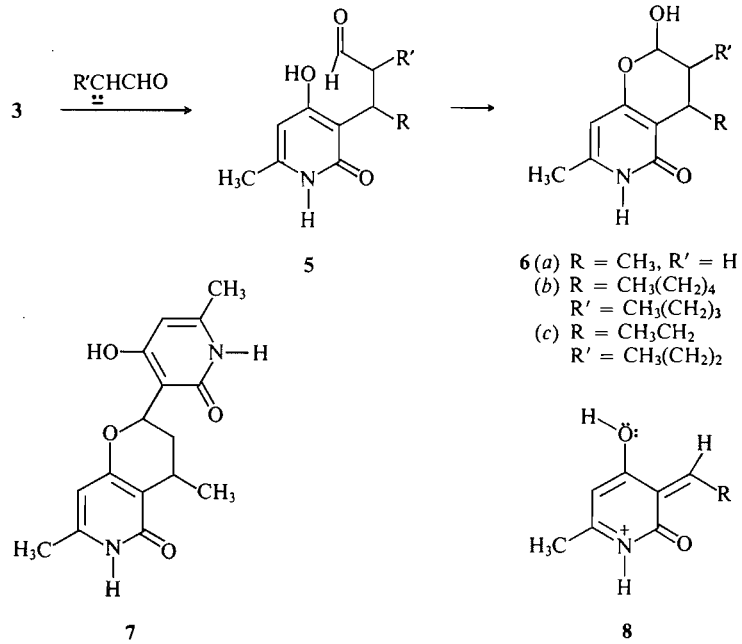

SCHEME 2

done under parallel conditions. Thus methyl iodide, ethyl iodide, benzyl bromide, and alkyl bromide could not be induced to condense with **1** in refluxing methanol–ethanol (1:1) solutions containing catalytic amounts of piperidine and pyridine.

The mass spectra of all the compounds **4** display molecular ions and distinctive ions at *m/e* 125 and 84, the latter being characteristic of 4-hydroxy-6-methyl-2-pyridones (3). Those compounds **4** possessing simple alkyl side chains (R = $CH_3CH_2CH_2$— or larger) show prominent ions at *m/e* 275, 262, 261, 178, 162, 150, 139, and 138. Possible explanations for the major fragmentations are contained in Scheme 3. For the compound **4***c* the *m/e* 178 ion is weak and dominated by the *m/e* 179 ion. The presence in many spectra of a metastable peak at 81.8 ($150^2/275$) lends support to the suggested decomposition of the ion *m/e* 275 to *m/e* 150 by extrusion of a component 4-hydroxy-6-methyl-2-pyridone moiety. The mass spectra of the compounds **4***h*, **4***i*, and **4***j* derived from aromatic aldehydes are less distinctive and besides M^+, *m/e* 125, and *m/e* 84 ions they contain the common feature $(M - 125)^+$ also observed for all other compounds in the series except **4***k* (R = CH_2=CH—).

Experimental

Melting points were determined on a Kofler hot stage apparatus and are uncorrected. Mass spectra were obtained with an Hitachi–Perkin-Elmer RMU-6D spectrometer. The nmr spectra were recorded with a Varian T-60 instrument employing tetramethylsilane as internal standard. Line positions are reported in ppm from this standard. The ir spectra were recorded with a Perkin-Elmer 457 Grating Infrared Spectrophotometer.

Compound **2** *(R = C_6H_5)*

4-Hydroxy-6-methyl-2-pyridone (0.25 g) in 99% ethanol (100 ml) containing piperidine (0.1 ml) and pyridine (0.8 ml) was treated with freshly distilled benzaldehyde (0.6 ml) and the mixture refluxed for 38 h. After evaporation to dryness the oily residue was diluted with ether (20 ml) and a crystalline product **4***h* (mp 345–354 °C) separated and was filtered off and washed with ether. The ethereal mother liquor and washings were combined and evaporated to ~3 ml. After 48 h crystalline **2** (R = C_6H_5) separated from the oily residue and after washing with ether had mp 215–220 °C (120 mg), and after recrystallization from methanol–ether exhibited mp 223–225 °C. Mass spectrum:213.0787 ($M^+ - H_2O$, calcd. 213.0790)$^+$, 212, 184, 156, 115, and 102.

The nmr spectrum: δ_{TMS} (DMSO-d_6) 2.0 (s, 3H, CH_3—C=), 4.6 (s, 1H, —CH—O), 5.6 (s, 1H, —CH=), and 7.4 (bs, 5H, aromatic). The ir spectrum (KBr): 1620 cm^{-1} (conjugated lactam).

Adduct **4***g (R = —$CH_2CH(CH_3)_2$)*

4-Hydroxy-6-methyl-2-pyridone (1.9 g) was dissolved in a mixture of methanol (100 ml) and 96% ethanol (100 ml), and piperidine (0.15 ml) and pyridine (0.45 ml) were

Can. J. Chem. Downloaded from www.nrcresearchpress.com by 210.87.254.5 on 09/05/12
For personal use only.

Can. J. Chem. Downloaded from www.nrcresearchpress.com by 210.87.254.5 on 09/05/12
For personal use only.

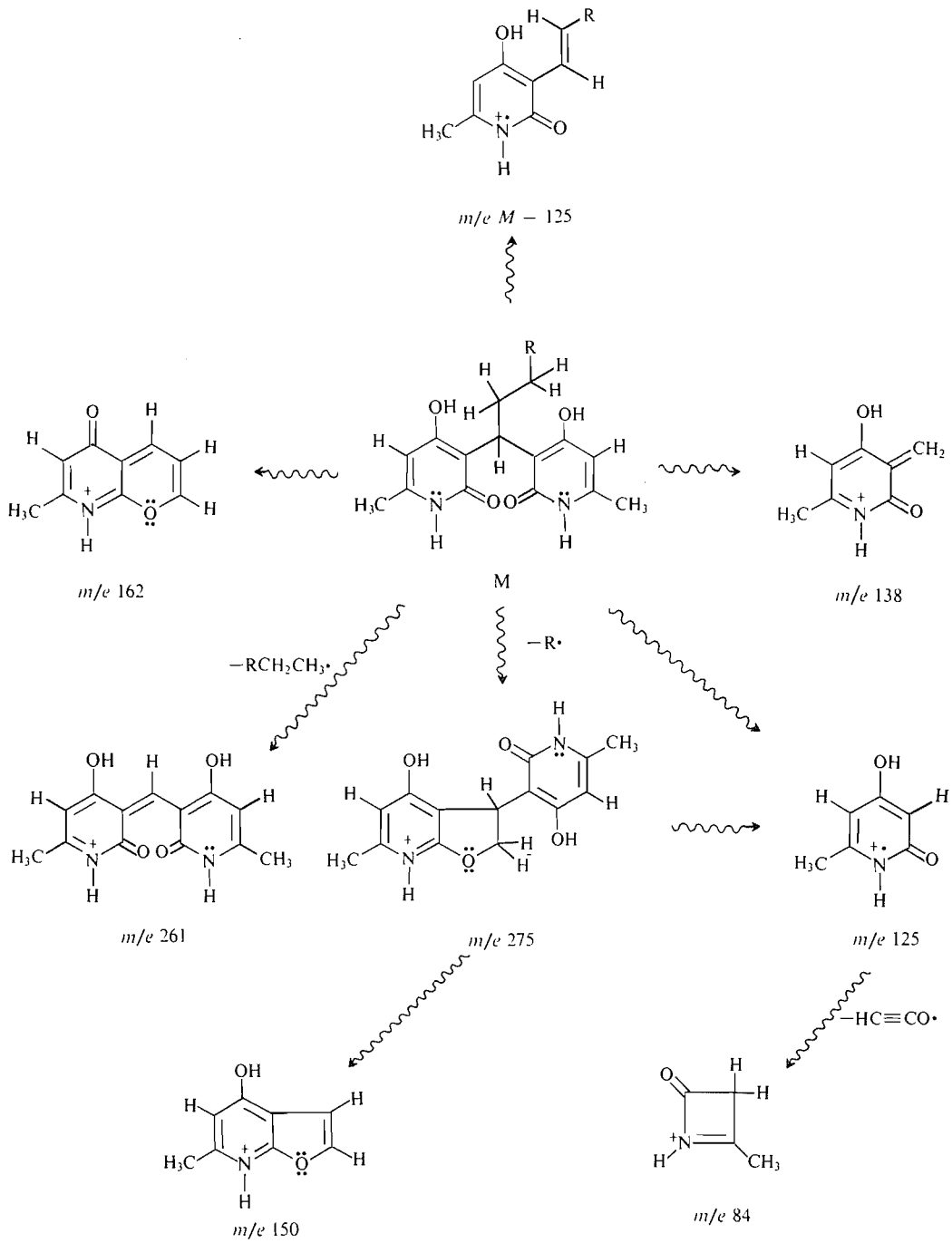

SCHEME 3

added under stirring at room temperature. After 5 min freshly distilled isovaleraldehyde (0.70 g) was added dropwise over 3 min and the mixture was refluxed for 16 h. After cooling, the product **4***g* crystallized out and was washed with methanol and ether and dried *in vacuo* yielding 1.8 g of crystalline compound, mp 308–310 °C, which could be recrystallized from ethanol or methanol, mp 308–310 °C. *Anal.* Calcd. for $C_{17}H_{22}N_2O_4$: C 63.03,

H 6.61, N 8.70; found: C 63.13, H 6.97, N 8.80. *Mol. Wt.* Calcd. for $C_{17}H_{22}N_2O_4$ (M^+): 318.1580; found (mass spectrum): 318.1567. Mass spectrum: 275, 262, 261, 193 ($M - 125$), 178, 162, 150, 138, 125, and 84.

The nmr spectrum δ_{TMS} (DMSO-d_6): 0.9 (m, 6H, $(CH_3)_2CH$—), 1.6 (m, 2H, —CH_2—), 2.1 (s, 6H, $2CH_3$—C═), 4.4 (t, J = 7 Hz, 1H, allylic), 5.8 (s, 2H, 2H—C═), and ~11.0 (b, 2H, 2NH). The ir spectrum ν_{max} (KBr): 1630 cm^{-1} (conjugated lactam).

Adduct 6a (R′ = H, R = CH_3)

4-Hydroxy-6-methyl-2-pyridone (0.2 g) was dissolved in 95% aqueous ethanol (80 ml) and piperidine (0.1 ml) and pyridine (0.6 ml) were added at room temperature under nitrogen. After 5 min crotonaldehyde (0.5 ml) was added and the mixture refluxed for 18 h, evaporated to dryness, and the oily residue was diluted with ether (10 ml). The precipitate was filtered off and subjected to silica gel (100 g) chromatography. Elution with $CHCl_3$–CH_3OH (97:3) gave **6** (R′ = H, R = CH_3) (0.15 g), mp 218–220 °C. *Anal.* Calcd. for $C_{10}H_{13}O_3N$: C 61.84, H 6.58, N 7.09; found: C 61.52, H 6.71, N 7.18. Mass spectrum: *m/e* 195 (M^+), 180 ($M - CH_3$), 166, 152, 150, 139, 138, 125, and 84.

The nmr spectrum δ_{TMS} (DMSO-d_6): 1.3 (d, J = 6 Hz, 3H, CH_3—CH), 1.9 (m, 2H, —CH_2—), 2.2 (s, 3H, CH_3—C═), 2.9 (bm, 1H, allylic —CH—), 5.4 (complex multiplet after D_2O addition, 1H, O—CH—O), 5.7 (s, 1H, —CH═), 7.3 (bs, 1H, —OH), and 11.1 (bs, 1H, NH). The ir spectrum ν_{max} (KBr): 1620 cm^{-1} (conjugated lactam).

Adduct 6b (R′ = butyl, R = pentyl)

4-Hydroxy-6-methyl-2-pyridone (0.25 g) in 99% ethanol (100 ml) containing piperidine (0.1 ml) and pyridine (0.7 ml) was treated with hexanal (0.5 ml) and the mixture refluxed for 18 h. After evaporation to dryness the oily residue was subjected to column chromatography on silica gel (150 g). Elution with $CHCl_3$–CH_3OH (96:4) furnished **6b** (R′ = butyl, R = pentyl) (150 mg), mp 200–202 °C which could be recrystallized from CH_3OH–$(C_2H_5)_2O$. (Similarly **6c** (R′ = ethyl, R = propyl), mp 175–177 °C was prepared by a parallel procedure using butanal.) *Mol. Wt.* Calcd. for **6b** (M^+) 307.2147; found (mass spectrum): 307.2147. Mass spectrum: *m/e* 290, 276, 264, 262, 250, 237, 236, 208, 207, 194, 192, 180, 178, 162, 150, 139, 138, and 84.

The nmr spectrum δ_{TMS} (DMSO-d_6): 0.9 (m, 6H, 2 × CH_3—), 1.3 (b, 15H, —CH_2—), 2.1 (s, 3H, CH_3—C═), 5.3 (bs, 1H, O—CH—O), 5.6 (s, 1H, —CH═), 7.2 (bm, 1H, —OH), and 11.1 (bs, 1H, NH). The ir spectrum ν_{max} (KBr): 1620 cm^{-1} (conjugated lactam).

Adduct 7

4-Hydroxy-6-methyl-2-pyridone (0.9 g) in a mixture of methanol (50 ml) and 96% ethanol (50 ml) containing piperidine (0.1 ml) and pyridine (0.3 ml) was stirred at room temperature for 10 min and then treated with freshly distilled crotonaldehyde (0.28 g) added dropwise over 3 min under a nitrogen atmosphere. This mixture was stirred for 16 h at reflux temperature, then evaporated to dryness and subjected to chromatography on a silica gel (200 g) column. Elution with $CHCl_3$–CH_3OH (98:2) afforded **4b**, mp 322–324 °C (from methanol) (0.52 g). Fractions eluted with $CHCl_3$–CH_3OH (96:4) yielded **7**, mp 254–255 °C (from ethanol) (0.63 g). *Anal.* Calcd. for $C_{16}H_{18}O_4N_2 \cdot H_2O$: C 59.99, H 6.29, N 8.75; found: C 59.60, H 6.26, N 8.39. Mass spectrum: *m/e* 302 (M^+), 177, 164, 162, 151, 150, 139, 125, and 84.

The nmr spectrum δ_{TMS} (DMSO-d_6): 1.2 (d, 3H, $J \simeq 7$ Hz CH_3—CH) superimposed on 1.2–1.6 (m, 2H, —CH_2—), 2.8 (m, 1H, allylic —CH—), 5.5 (bd, 1H, $J \simeq 13$ Hz, —CH—O), 5.65 (s, 1H, —CH═), 5.8 (s, 1H, —CH═), 11 (bs, 2H, —NHCO). The ir spectrum ν_{max} (KBr): 1650, 1610, and 1580 cm^{-1} (conjugated amides).

1. J. A. Findlay and L. Radics. J. Chem. Soc. Perkin Trans. 1, 2071 (1972).
2. J. A. Findlay and F. Y. Shum. Synth. Commun. **3**, 355 (1973).
3. A. M. Duffield, C. Djerassi, G. Schroll, and S. O. Lawesson. Acta Chem. Scand. **20**, 361 (1966).

Can. J. Chem. Downloaded from www.nrcresearchpress.com by 210.87.254.5 on 09/05/12
For personal use only.

Spin trapping of radicals formed during radiolysis of aqueous solutions. Direct electron spin resonance observations[1]

FREDERICK PETER SARGENT AND EDWARD MICHAEL GARDY
Research Chemistry Branch, Atomic Energy of Canada Limited, Whiteshell Nuclear Research Establishment, Pinawa, Manitoba R0E 1L0

Received August 13, 1975

FREDERICK PETER SARGENT and EDWARD MICHAEL GARDY. Can. J. Chem. **54**, 275 (1976).

It is shown that e_{solv}, H•, and OH formed by the radiolysis of water by 3 MeV electrons are trapped by nitroso and nitrone compounds to give nitroxides with well defined esr spectra. Three spin trapping agents were used, nitroso-*t*-butane, phenyl-*t*-butyl nitrone, and 5,5′-dimethyl pyrroline-1-oxide. The latter was shown to be an excellent compound for these studies. Complications due to the instability of some of the nitroxides were overcome by coupling the electron accelerator to the esr spectrometer to permit direct observation of the spectra.

FREDERICK PETER SARGENT et EDWARD MICHAEL GARDY. Can. J. Chem. **54**, 275 (1976).

On a montré que les e_{solv}, H•, et OH formés par radiolyse de l'eau par des électrons à 3 MeV sont captés par des composés nitroso et nitrone et conduisent à des nitroxydes avec des spectres rpe bien définis. On a utilisé trois agents de piégeage; le nitroso *t*-butane, la phényl *t*-butyl nitrone et la diméthyl-5,5′ pyrroline oxyde-1. On a montré que ce dernier composé est excellent pour ces études. On a éliminé les complications dues à l'instabilité de quelques nitroxydes en couplant directement l'accélérateur d'électron au spectromètre de rpe pour permettre une observation directe du spectre.

[Traduit par le journal]

Introduction

Although the spin trapping technique has been used to investigate the radiolysis of alcohols (1–4) and alkanes (5, 6), there has been only limited application to aqueous solutions. These have involved the use of the nitromethane *aci* anion, $CH_2{=}NO_2^-$, and were therefore restricted to alkaline aqueous solutions (7). Here we describe the use of 5,5′-dimethyl pyrroline·1-oxide (DMPO), phenyl-*t*-butyl nitrone (PBN), and 2-nitroso-2-methylpropane (nitroso-*t*-butane), to trap the primary radicals formed during the radiolysis of water with 3 MeV electrons. This was undertaken as part of a wider study using spin trapping to measure electron spin polarisation effects in radiation chemical systems. The spin trapping method involves the use of a nitrone or a nitroso compound which reacts with the radical, R, produced during radiolysis to give nitroxides (reactions 1–3).

[1] 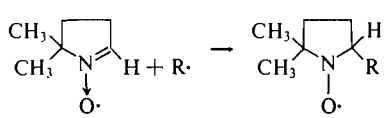

[2] 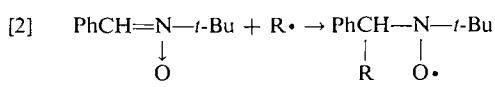

[3] 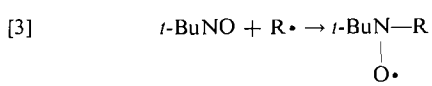

In each case the resulting nitroxide has an esr spectrum characteristic of R. However, some nitroxides are unstable and decay before the sample can be removed from the radiation source and examined by esr spectroscopy. We have overcome this problem by coupling an electron accelerator to an esr spectrometer. This permits direct observation of the esr spectra while the sample is being irradiated. By this means we have successfully trapped and identified OH radicals, electrons, and hydrogen atoms formed during the radiolysis of aqueous solutions. The effect of OH and electron scavengers is also described.

Experimental

The electron beam flight tube from a nominally 4 MeV Van de Graaff electron accelerator was extended axially through 25 mm holes in the esr magnet yoke and pole pieces and finally through a 9 mm hole in the pole cap. The pole caps were fitted with field compensating devices

[1]AECL No. 5220.

Can. J. Chem. Downloaded from www.nrcresearchpress.com by 210.87.254.6 on 09/05/12
For personal use only.

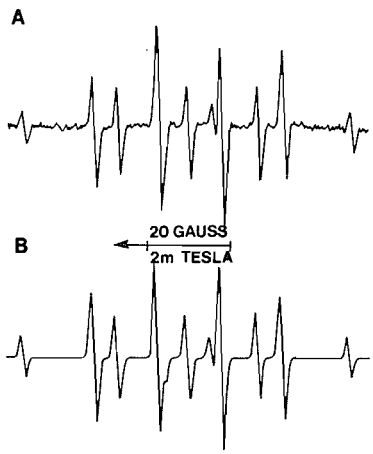

FIG. 1. (*A*) Electron spin resonance spectrum observed during irradiation of argon-saturated aqueous solution of 1.0 mol/m^3 (0.001 *M*) DMPO. (*B*) Computer simulated spectrum.

to give a magnetic field homogeneity of better than 5 μT (50 mG) over the esr sample volume. The conventional T102 rectangular sample cavity was modified to permit irradiation of samples by using thin stainless steel or brass walls. The stainless steel was annealed to remove the ferromagnetic phase and then gold plated whereas the brass walls were silver and gold plated. The solution to be irradiated was bubbled with 99.999% argon to remove oxygen, flowed through the esr sample cavity and irradiated with 3 MeV electrons. For some solutions, 0.5 mm "Suprasil" quartz flat cells were used but the signal from the radiation-induced color centers in the quartz blanked out parts of the esr spectra. However, most of the spectra were recorded while using special sample tubes made of cerium-doped glass which does not give an appreciable esr signal on irradiation (8, 9).

The 2-methyl-2-nitroso-propane, *t*-BuNO, was prepared by oxidation of *t*-butylamine using the method of Stowell (10), recrystallised from *n*-pentane, and stored in a refrigerator. 5,5′-Dimethyl pyrroline-1-oxide, DMPO, was prepared by the method outlined by Iwamura and Inamoto (11) using the detailed notes of Chen (12). Phenyl *t*-butyl nitrone, PBN, was supplied by Fisher.

The water used in this work was at least doubly distilled and for most of the experiments it was triply distilled.

Results and Discussion

Spin Trapping with DMPO

Direct radiolysis of argon-saturated aqueous solution of DMPO gave spectra similar to that shown in Fig. 1. This is derived from two nitroxides, referred to as **1** and **2**. Nitroxide **1** has an esr spectrum resulting from a nitrogen coupling of 1.67 mT (16.7 G) and two equivalent protons of 2.26 mT (22.4 G). Nitroxide **2** shows an equal coupling of 1.5 mT (15.0 G) from one nitrogen and one proton. The simulation of the resulting spectrum, shown in Fig. 1(*B*), was computed with $\Delta g = 0.0002$, and a Gaussian peak-to-peak linewidth of 0.12 mT (1.2 G). The good agreement between the observed and computed spectrum suggests that only two nitroxides are present. Since nitroxide **1** has a coupling to two equivalent protons it must arise from the trapping of hydrogen atoms (reaction 4) or electrons followed by protonation as in [5] and [6]. It will be shown later that most of **1** originates from electrons.

[4] 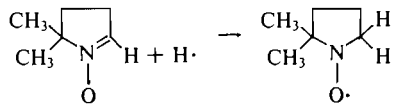

1

[5] $\mathrm{DMPO} + e \rightarrow [\mathrm{DMPO}]^-$

[6] $[\mathrm{DMPO}]^- + H_2 \rightarrow [\mathrm{DMPO}]H + OH^-$

1

Our coupling constants for **1** in water are somewhat higher than the 1.44 mT (14.4 G) and 1.89 mT (18.9 G) observed by Janzen and Liu in benzene for the nitrogen and proton couplings respectively (13). However, this increase of nitroxide coupling constants with solvent polarity is quite normal. For example, di-*t*-butyl nitroxide has a nitrogen coupling of 1.48 mT (14.8 G) in *n*-hexane whereas it increases to 1.697 mT (16.97 G) in water (14). The assignment and origin of **1** were confirmed by using solutions of DMPO in deuterium oxide, which gave the spectrum in Fig. 2. This shows that one of the protons of **1** has been replaced by a deuteron coupling of 0.33 mT (3.3 G). Nitroxide **2** is unaffected by the change to D_2O. Bubbling nitrous oxide through the aqueous solutions significantly decreases the intensity of **1** and enhances that of **2** (Fig. 3). Since nitrous oxide reacts rapidly with electrons to produce OH radicals, this confirms that **1** originates from electrons and suggests that **2** is derived from the trapping of OH radicals.

[7] $e + N_2O + H_2O \rightarrow \cdot OH + N_2 + OH^-$

Nitroxide **2** has also been observed recently in the photolysis of aqueous solutions of hydrogen peroxide containing DMPO (15). Further confirmation that **2** arises from trapping OH is that it is replaced by another nitroxide, **3**, when methanol is present in the irradiated solutions (Fig. 4). This has nitrogen and proton couplings

Can. J. Chem. Downloaded from www.nrcresearchpress.com by 210.87.254.6 on 09/05/12
For personal use only.

Can. J. Chem. Downloaded from www.nrcresearchpress.com by 210.87.254.6 on 09/05/12
For personal use only.

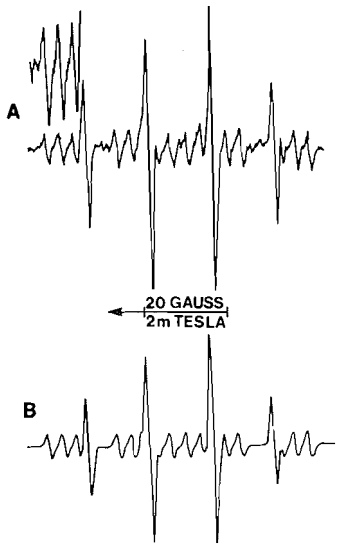

FIG. 2. (*A*) Electron spin resonance spectrum observed during irradiation of argon-saturated solution of 1.0 mol/m^3 (0.001 *M*) DMPO in D_2O. (*B*) Computer simulated spectrum.

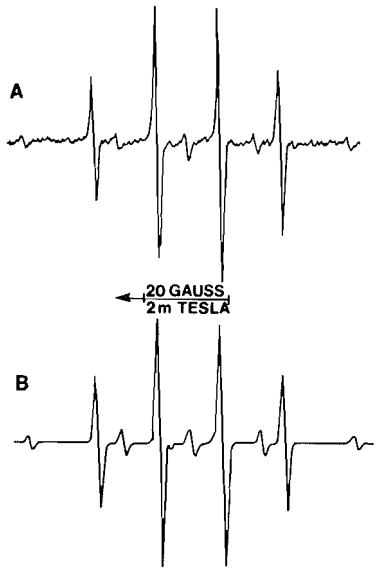

FIG. 3. *(A)* Electron spin resonance spectrum observed during radiolysis of nitrous oxide-saturated aqueous solution of 1.0 mol/m^3 (0.001 *M*) DMPO. *(B)* Computer simulated spectrum.

of 1.6 mT (16 G) and 2.27 mT (22.7 G) respectively and arises from the trapping of $\cdot CH_2OH$ formed by reaction

[8] $$\cdot OH + CH_3OH \rightarrow \cdot CH_2OH + H_2O$$

The observed coupling costants compared favorably with the values 1.466 mT (14.66 G) and 2.07 mT (20.7 G) for the nitrogen and proton couplings for **3** in benzene (13), when the solvent effect is taken into account. Methanol does not completely remove nitroxide **2** and a small amount is included in the simulated spectrum of Fig. 4(*B*).

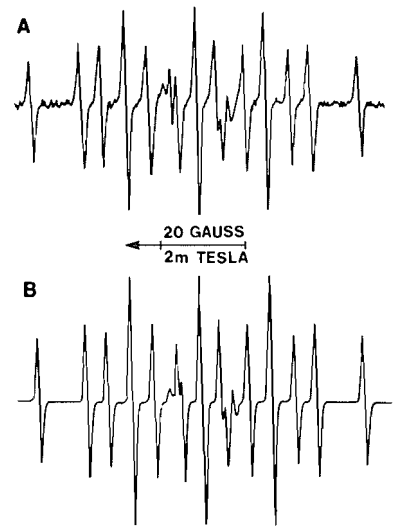

FIG. 4. (*A*) Electron spin resonance spectrum observed during radiolysis of an argon-saturated solution of 10 mol/m^3 (0.01 *M*) DMPO containing 500 mol/m^3 (0.5 *M*) methanol. (*B*) Computer simulated spectrum.

Prebubbling the solutions of DMPO with nitrous oxide does not completely remove nitroxide **1** even at DMPO concentrations as low as 0.05 mol/m^3 (50 μM). Since the solubility of nitrous oxide in water is 16 m*M* and its rate constant for reaction with electrons is almost at the diffusion-controlled limit, the residual **1** cannot be from electrons and must be due to the trapping of H-atoms, the rate of reaction 9 being comparatively slow (16).

[9] $$H\cdot + N_2O \rightarrow N_2 + \cdot OH$$

Spin-Trapping with Phenyl-t-butyl Nitrone

Irradiation of aqueous solutions of PBN gave results similar to those observed with DMPO, namely the trapping of electrons and OH radicals. An argon-saturated solution gave the spectrum shown in Fig. 5. This consists of nitroxide **4**, with coupling to one nitrogen of 1.68 mT (16.8 G) and two equivalent protons of 1.09 mT (10.9 G), and nitroxide **5** with a nitrogen coupling of 1.56 mT (15.6 G) and a proton coupling of 0.27 mT (2.7 G). When the solution was pre-

Can. J. Chem. Downloaded from www.nrcresearchpress.com by 210.87.254.6 on 09/05/12
For personal use only.

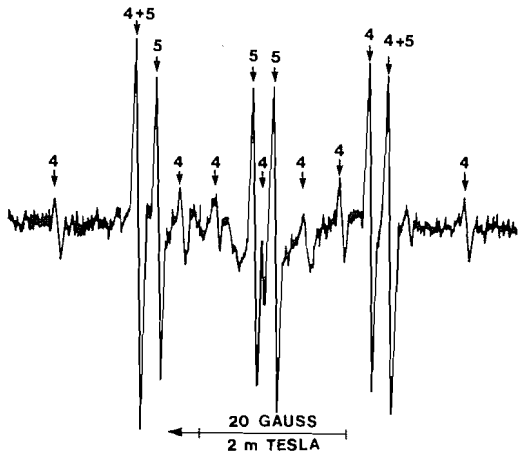

FIG. 5. Electron spin resonance spectrum observed during irradiation of an argon-saturated solution of 10 mol/m³ (0.01 *M*) PBN.

saturated with nitrous oxide, the intensity of nitroxide **4** decreased and that of **5** increased. Since nitrous oxide removes electrons to produce OH radicals, this shows that **4** is formed by trapping of electrons and **5** by trapping of OH radicals.

[10] $PhCH{=}N{-}t\text{-}Bu + e + H_2O \rightarrow PhCH_2{-}N(O\cdot){-}t\text{-}Bu + OH^-$ (**4**)

[11] $PhCH{=}N{-}t\text{-}Bu + {\cdot}OH \rightarrow PhCH(OH){-}N(O\cdot){-}t\text{-}Bu$ (**5**)

The observed coupling constants compare favorably with those observed in benzene (17, 18) when account is taken of the solvent effect. The values for **5** are in good agreement with those observed by Harbour *et al.* (15) during the photolysis of aqueous hydrogen peroxide solutions of PBN.

Spin Trapping with Nitroso-t-butane

Nitroso-*t*-butane is a less satisfactory trapping agent because of its limited solubility and the ease with which it was stripped by the bubbling technique used to deaerate the solutions. However, the results obtained are consistent with those from DMPO and PBN. Irradiation of an argon-saturated aqueous solution of *t*-BuNO gave the spectrum shown in Fig. 6. This is a composite of spectra from three nitroxides, **6**, **7**, and **8**. Nitroxide **6** has a nitrogen coupling of 2.8 mT (28.0 G) and a single proton of 0.44 mT (4.4 G), **7** has equal coupling to one nitrogen nucleus and one proton of 1.44 mT (14.4 G) whereas **8** shows only a nitrogen coupling of 1.7 mT (17.0 G). Nitroxide **7** arises from the trapping of electrons followed by protonation.

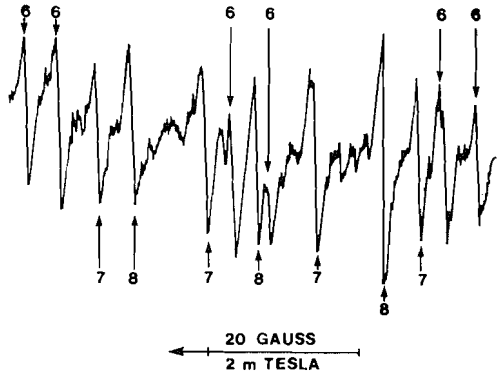

FIG 6. Electron spin resonance spectrum observed during irradiation of an argon-saturated solution of *t*-BuNO.

[12] $e + t\text{-}BuNO + H_2O \rightarrow t\text{-}BuNHO\cdot + OH^-$ (**7**)

The coupling constants for **7** are in reasonable agreement with those previously observed for *t*-BuNHO· (2, 19) when the effect of solvent is allowed for. Nitroxide **8** is almost certainly di-*t*-butyl nitroxide but the identity of **6** is less certain. The nitrogen coupling constant is in the range usually associated with radicals of the type RNO_2R' (1–3). *In situ* irradiation of an aqueous solution of 2-nitro-2-methyl propane, *t*-$BuNO_2$, gave an esr spectrum similar to a composite of **6** and **8**. Therefore we suggest **6** is *t*-$BuNO_2H$ formed by the scavenging of OH by *t*-BuNO and electrons by *t*-$BuNO_2$.

[13] $t\text{-}BuNO + OH \rightarrow t\text{-}BuNO_2H$

[14] $t\text{-}BuNO_2 + e + H_2O \rightarrow t\text{-}BuNO_2H + OH^-$ (**6**)

The origin of the di-*t*-butyl nitroxide, **8**, is obscure. However, it is known to be formed in the reactions of *t*-$BuNO_2$ with sodium metal (20) or with organo-alkali compounds (21) and also in its electrochemical reduction (22). These all involve the radical anion of *t*-$BuNO_2$ which is assumed to be unstable leading to the formation of **8**. This may also be the mechanism in the radiation chemical system. The nitroxides of the

Can. J. Chem. Downloaded from www.nrcresearchpress.com by 210.87.254.6 on 09/05/12
For personal use only.

type, t-$BuNO_2R$, formed by the trapping of alkoxy radicals by t-BuNO (2, 3), are known to be unstable. Perkins and Roberts (23) have shown that at least part of the decomposition proceeds via reaction 15 which generates t-Bu radicals.

[15] $$t\text{-BuN(O}\cdot\text{)—OR} \rightarrow t\text{-Bu}\cdot + \text{RONO}$$

It is possible that t-$BuNO_2H$ decomposes by a similar process and the resulting t-Bu· radicals are scavenged by the t-BuNO present to give **8**.

[16] $$t\text{-BuNO}_2\text{H} \rightarrow t\text{-Bu}\cdot + \text{HONO}$$

[17] $$t\text{-Bu}\cdot + t\text{-BuNO} \rightarrow t\text{-BuN(O}\cdot\text{)—}t\text{-Bu}$$

8

Confirmation that **6** and **8** arise from trapping OH is provided by the results when methanol is present. This removes **6** and **8** since it reacts with OH via reaction 8 to give $\cdot CH_2OH$ radicals which are trapped to give another nitroxide **9**. This has a nitrogen coupling of 1.56 mT (15.6 G) and two equivalent protons of 0.61 mT (6.1 G).

[18] $$t\text{-BuNO} + \cdot CH_2OH \rightarrow t\text{-BuN(O}\cdot\text{)—CH}_2\text{OH}$$

9

Conclusions

The spin trapping studies described here show that the products of the radiolysis of water, OH, H, and electrons, are trapped by DMPO, PBN and t-BuNO to give nitroxides with very distinctive esr spectra. It should be noted that it is most unlikely that OH will ever be seen directly with esr in liquid water. This is because the orbitally degenerate ground state of this radical leads to considerable spin–orbit coupling of the unpaired electron's angular momentum. This in turn leads to g values ranging from 0 to 4 and very short spin relaxation times. These factors make the esr lines too broad to be detected. Therefore spin trapping is one of the few ways by which the presence of OH radicals may be positively demonstrated.

Acknowledgments

It is with pleasure that we acknowledge the discussions held with Carl Lagercrantz following his paper (24) presented at the Second Symposium on ESR held at the University of Georgia, December 1970, which led to our application of spin trapping techniques to radiation chemistry.

We thank Howard Falle for preparing some of the trapping compounds.

1. J. A. Wargon and F. Williams. J. Am. Chem. Soc. **94**, 7919 (1972).
2. F. P. Sargent, E. M. Gardy, and H. R. Falle. Chem. Phys. Lett. **24**, 120 (1974).
3. F. P. Sargent and E. M. Gardy. Can. J. Chem. **52**, 3645 (1974).
4. S. W. Mao and L. Kevan. Chem. Phys. Lett. **24**, 505 (1974).
5. S. W. Mao and L. Kevan. J. Phys. Chem. **78**, 91 (1974).
6. F. P. Sargent and E. M. Gardy. To be published.
7. K. Eiben and R. W. Fessenden. J. Phys. Chem. **72**, 3387 (1968); D. Behar and R. W. Fessenden. J. Phys. Chem. **76**, 1710 (1972).
8. B. Smaller, J. R. Remko, and E. C. Avery. J. Chem. Phys. **48**, 5174 (1968).
9. B. Smaller, E. C. Avery, and J. R. Remko. J. Chem. Phys. **55**, 2414 (1971).
10. J. C. Stowell. J. Org. Chem. **36**, 3055 (1971).
11. M. Iwamura and N. Inamoto. Bull. Chem. Soc. Jpn. **40**, 702 (1967); Bull. Chem. Soc. Jpn. **43**, 856 (1970).
12. K. S. Chen. Private communication.
13. E. G. Janzen and J. I-P. Liu. J. Magn. Reson. **9**, 510 (1973).
14. (*a*) T. Kawamura, S. Matsunami, and T. Yonezawa. Bull. Chem. Soc. Jpn. **40**, 1111 (1967); (*b*) S. Forschult and C. Lagercrantz. Acta Chem. Scand. **23**, 524 (1969).
15. J. R. Harbour, V. Chow, and J. R. Bolton. Can. J. Chem. **52**, 3549 (1974).
16. M. Anbar and P. Neta. Int. J. Appl. Radiat. Isot. **18**, 493 (1967).
17. E. G. Janzen and B. J. Blackburn. J. Am. Chem. Soc. **92**, 4481 (1969).
18. E. G. Janzen, T. Kasai, and K. Kuwata. Bull. Chem. Soc. Jpn. **46**, 2061 (1973).
19. M. J. Perkins, P. Ward, and A. Horsfield. J. Chem. Soc. (B), 395 (1970).
20. A. K. Hoffmann, A. M. Feldman, E. Gelblum, and W. G. Hodgson. J. Am. Chem. Soc. **86**, 639 (1964).
21. A. K. Hoffmann, A. M. Feldman, and E. Gelblum. J. Am. Chem. Soc. **86**, 646 (1964).
22. A. K. Hoffmann, W. G. Hodgson, D. L. Maricle, and W. H. Jura. J. Am. Chem. Soc. **86**, 631 (1964).
23. M. J. Perkins and B. P. Roberts. J. Chem. Soc. Perkins Trans. II, 297 (1974).
24. C. Lagercrantz. J. Phys. Chem. **75**, 3466 (1971).

Carbon-13 nuclear magnetic resonance spectra of organic sulfur compounds.[1] Comparison of chemical shifts for carbonyl and thiocarbonyl compounds in the pyrone, thiopyrone, and pyridone series

I. W. J. STILL[2] AND N. PLAVAC
Department of Chemistry, University of Toronto, Toronto, Ontario M5S 1A1
AND
D. M. MCKINNON AND M. S. CHAUHAN
Department of Chemistry, University of Manitoba, Winnipeg, Manitoba R3T 2N2

Received August 18, 1975

I. W. J. STILL, N. PLAVAC, D. M. MCKINNON, and M. S. CHAUHAN. Can. J. Chem. **54**, 280 (1976).

^{13}C nmr data have been obtained for a series of 2- and 4-pyrones and pyridones, and their sulfur-containing analogues. Correlations have been observed between the nature of the ring hetero-atom and the chemical shift difference ($\Delta\delta$) for the C_α and C_β carbons in these conjugated systems. No significant correlation, however, appears to exist between the chemical shifts of the C=O and C=S groups. Substituent chemical shift (s.c.s.) effects for various simple substituents are compared with those in related series of compounds.

I. W. J. STILL, N. PLAVAC, D. M. MCKINNON et M. S. CHAUHAN. Can. J. Chem. **54**, 280 (1976).

On a obtenu des données rmn du ^{13}C pour une série de pyrone-2 et -4, de pyridones et de leurs analogues contenant du soufre. On a observé des corrélations entre la nature de l'hétéroatome du cycle et les différences de déplacements chimiques ($\Delta\delta$) pour les carbones C_α et C_β de ces systèmes conjugués. Il ne semble pas y avoir de corrélations importantes entre les déplacements chimiques des groupes C=O et C=S. On compare les effets de déplacements chimiques des substituants pour divers substituants simples avec ceux dans des séries de composés apparentés.
[Traduit par le journal]

Introduction

As part of our continuing investigation of ^{13}C nmr spectra of sulfur-containing organic compounds we wish to report a study of a series of 2- and 4-pyrones and of their thione analogues. Turner and Pirkle (1) have recently published some ^{13}C nmr data for a number of monocyclic derivatives of 2-pyrone and pyran-2-thione as well as the analogous 2-thiopyran derivatives. These authors and at least two other investigators have also reported ^{13}C nmr data for the bicyclic coumarin system (2, 3). Our attention in the present investigation has been focussed on a comparison of chemical shifts in such systems, as they are affected by the replacement of the C=O group by C=S, while by including the corresponding 2-pyridone and 2-pyridinethione counterparts we have also been able to examine the effect of the heterocyclic atom (O,N,S) on chemical shifts. In the case of the pyridones we were able to compare our findings with those reported by Vögeli and von Philipsborn (4) in a ^1H and ^{13}C nmr study of the structures of *N*-methyl-3-pyridone and 3-hydroxypyridine and discussed more recently by Paoloni *et al.* (5).

The 4-pyrone analogues seem to have been less intensively examined so far by ^{13}C nmr, perhaps rather surprising in the light of the existence of detailed ^1H nmr data for chromones and xanthones (6) and the obvious importance of chromones and flavones in natural products. Kingsbury and Looker (7) have very recently reported ^{13}C nmr data for chromone, flavone, and a series of methoxyflavones and their chemical shift data for the parent chromone and flavone systems are in good agreement with those observed earlier by us (8). In this series, also, we have included 4-pyridone and 4-pyridinethione as well as their *N*-methyl analogues in our comparison.

The extensive collection of chemical shifts for the carbonyl and thiocarbonyl derivatives in these series of compounds has been used to

[1]Part III of a series. For part II see ref. 10.
[2]Author to whom correspondence should be addressed.

Can. J. Chem. Downloaded from www.nrcresearchpress.com by 210.87.254.6 on 09/05/12
For personal use only.

Can. J. Chem. Downloaded from www.nrcresearchpress.com by 210.87.254.6 on 09/05/12
For personal use only.

reexamine the question of a possible correlation between C=O and C=S chemical shifts for similar types of compounds first put forward by Kalinowski and Kessler (9) and later discussed in our previous paper on this subject (10).

The assignment of the spectra was usually made by a combination of multiplicity arguments applied to the partially coupled spectra and substituent chemical shift (s.c.s.) effects. The s.c.s. effects were obtained from compounds in the series studied if this was possible, and if not, from carefully chosen model systems. In the case of 2-pyridinethione, where considerable ambiguity remained, the final assignment was made by utilizing variations in $^1J_{CH}$ coupling constants for the unsubstituted ring positions involved (*q.v.*).

Experimental

Natural abundance proton decoupled ^{13}C nmr spectra were obtained on a Varian XL-100-15 spectrometer operating at 25.16 MHz in the pulsed Fourier transform mode. The temperature of the probe was 32 ± 3 °C. Spectral widths of 6000 Hz, acquisition times of 0.666 s, and pulse widths of 10 μs (90° pulse = 55 μs) were routinely used. In some cases, pulse delays of 1–10 s were used to intensify quaternary carbons, and in other cases, paramagnetic chromium trisacetylacetonate[3] was used for the same purpose. The spectra were transformed using a Varian 16K-620i computer giving 4096 real points with an accuracy of ±0.1 ppm. Off-resonance proton decoupled spectra were obtained where deemed necessary. The deuterium of the solvent (chloroform-*d* or dimethyl sulfoxide-d_6) was used as lock and primary reference in all cases, and all chemical shifts are measured from TMS (5%) added as internal reference.

The compounds coumarin, 2,6-dimethyl-4-pyrone, xanthone, thioxanthone, 2-pyridinethione, and 4-pyridinethione were available commercially (Aldrich Chemical Co.) and were used without further purification. Literature references for the preparation of the other compounds used in this study, with the exception of dibenzothiopyran-2-one (below), are cited in Tables 1, 3, and 5.

Preparation of (2,3;4,5)-Dibenzothiopyran-2-one

Mercuric oxide (2.0 g) was dissolved in acetic acid (10 ml) and to the solution was added portion-wise dibenzothiopyran-2-thione (2.28 g) (24) with stirring. The solution became yellow and was diluted with water. Work-up, using benzene extraction, gave the required product (95%) as yellow needles, mp 130–131 °C from benzene (lit. (24) mp 130–131 °C).

Results and Discussion

Chemical shift data for a number of phenyl-substituted 2-pyrones and pyran-2-thiones, as well as their thiopyran analogues are collected in Table 1, along with data for some simple bi- and tricyclic analogues. In the case of the monocyclic series, Turner and Pirkle (1) have recently reported ^{13}C nmr data for all four parent compounds of type **1**. As is usually the case, substitution on the ring produces relatively little effect on the chemical shift of the C=O or C=S group. It is, however, of interest to note that the difference in chemical shift ($\Delta\delta$) between the two kinds of carbonyl group is considerably greater (25.0 *vs.* 7.7 ppm) than for the two kinds of thiocarbonyl compound, probably because the contribution from the dipolar canonical structure **2** is greatest in the case where X and Y are both oxygen.

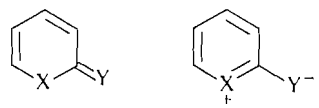

1 (X, Y = O or S) **2** (X, Y = O or S)

Also noteworthy in Table 1 are the effects of phenyl substitution on the monocyclic systems. Using Turner and Pirkle's data for the parent compounds as the reference, phenyl substitution at C-6 produces a deshielding (α) effect at C-6 of from +9.5 to +17.3 ppm, and a shielding (β) effect at C-5 of from −0.5 to −5.6 ppm. The α-effect at C-6 is approximately twice as large when the ring hetero-atom is sulfur and, conversely, the β-effect at C-5 is largest when the ring hetero-atom is oxygen, again probably the result of the greater influence of polar resonance contributors in the latter case. In the two compounds where 3-phenyl substitution is involved the α-effects at C-3 are +7.4 and +11.3 ppm for the C=S and C=O cases respectively and the β-effects are small, both being less than −2 ppm. For 4-phenyl substitution the α-effects are grouped between +11.2 and +14.6 ppm. Interestingly the β-effects produced at C-3, ranging from −4.0 to −7.6 ppm are in each case greater than the shielding effects at C-5 (−0.5 to −5.6 ppm) even though the latter are a combination of effects arising from C-4 and C-6 phenyl substitution. Since the effect at C-5 is probably attributable (as we have earlier assumed) mainly to C-6 phenyl substitution, these findings lend support to Turner and

[3] $[Cr(AcAc)_3] \approx 17$ mg/2.5 ml of solution.

Can. J. Chem. Downloaded from www.nrcresearchpress.com by 210.87.254.6 on 09/05/12
For personal use only.

TABLE 1. Carbon-13 chemical shift data* for 2-pyrones and their thio analogues

Compound	CO/CS	C-3	C-4	C-5	C-6	C-4a	C-8a	Other	Reference
3,6-Diphenylthiopyran-2-one	184.3	133.9	140.7	116.5	152.4	—	—	126.6, 128.3, 128.9, 129.2, 130.2, 135.6,† 136.2†	(18)
3,6-Diphenylthiopyran-2-thione	203.7	146.7	130.8	121.0	159.6	—	—	126.4, 128.1, 128.4, 129.1, 129.4, 134.8,† 135.4, 138.4†	(18)
4,6-Diphenyl-2-pyrone	160.3	109.1	155.5	101.2	162.5	—	—	125.7, 126.7, 128.9, 129.2, 130.7, 130.9, 131.5,† 135.9†	(19)
4,6-Diphenylpyran-2-thione	196.7	125.4	148.2	104.8	165.1	—	—	125.9, 126.9, 129.1, 129.4, 130.7,† 131.2, 131.5, 134.8†	(19)
4,6-Diphenylthiopyran-2-one	185.3	120.0	152.7	118.2	154.7	—	—	126.9, 127.2, 129.2, 129.9, 130.3, 136.9,† 139.6†	(20)
4,6-Diphenylthiopyran-2-thione	204.4	135.3	147.2	121.9	157.9	—	—	126.7, 127.3, 129.3, 129.5, 130.3, 130.9, 135.5,† 138.6†	(21)
Coumarin‡	160.4	116.4§	143.4	127.9	124.3	118.7	153.8	116.5(C-8),§ 131.7(C-7)	—
Benzopyran-2-thione‖	198.0	129.7	134.5	127.8	125.5	120.5	156.7	116.8(C-8), 132.2(C-7)	(22)
Benzothiopyran-2-one	185.4	126.0§	143.7	130.0	124.2	126.2	137.7	126.5(C-8),§ 131.6(C-7)	(23)
Benzothiopyran-2-thione	209.0	136.0	131.4	130.3	123.4	128.0	140.3	127.7(C-8), 134.4(C-7)	(24)
3,8-Dimethylbenzothiopyran-2-thione	208.7	141.0§	130.5	129.0	126.9	129.3	140.8§	131.3(C-8), 135.0(C-7), 18.8(C-3Me), 22.4(C-8Me)	(24)
Naphtho[1,2-*e*]thiopyran-2-thione¶	206.4	136.6	131.3	—	—	130.9	141.9	121.3, 124.2,† 127.4, 128.6, 128.8, 129.3, 132.4†	(24)
Dibenzothiopyran-2-one¶	186.2	127.0	132.2	—	—	128.5	136.0	124.4, 125.3, 126.1, 126.3, 126.7, 128.4, 128.5, 133.9	(see Experimental)
Dibenzothiopyran-2-thione¶	212.5	134.6	130.2	—	—	127.9	135.0	122.9, 124.4, 125.2, 127.6, 128.4, 128.5, 128.9, 133.8	(24)

*All shifts quoted in ppm relative to TMS, in $CDCl_3$.
†Quaternary carbon signals.
‡This compound is included for reference purposes; *cf.* refs. 1–3.
§These assignments may be reversed.
‖^{13}C nmr data have been reported previously for this compound by Turner and Pirkle (1).
¶For simplicity in comparing spectra, the carbon atoms in the heterocyclic ring have been numbered as though they were part of a coumarin-like system.

TABLE 2. Differences in chemical shifts ($\Delta\delta$) between C_α and C_β in heterocycles of type,

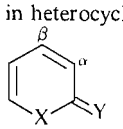

Series	X = O	X = NH	X = S
Y = O	27.6*	21.0†	16.0*
Y = S	2.6*	4.5‡	−6.7*
		$\Delta\Delta\delta$	
Change from C=O to C=S	25.0	16.5	22.7

*Reference 1.
†Reference 4.
‡Our work.

Pirkle's conclusion, based on a comparison of the β-effect of methyl and methoxyl substitution at C-4, that there is a considerable degree of bond localization in these 2-pyrone systems.

Taking the four monocyclic parent compounds reported by Turner and Pirkle (or the four bicyclic coumarin analogues with approximately the same results) we have calculated the differences in chemical shift ($\Delta\delta$) between the C-3 (α) and C-4 (β) carbon atoms (Table 2). Other workers have attempted to quantitatively correlate such differences with electron densities (11), but even on a qualitative basis the trends seem well defined, and one can also include the analogous 2- and 4-pyridone derivatives and their thione counterparts in this comparison. Thus for each ring hetero-atom, there is a somewhat similar reduction in $\Delta\delta$ for C_α and C_β, ranging from 16.5 to 25.0 ppm, involved in replacing C=O in each case by C=S. In fact, this has the interesting effect of reversing the polarities of C_α and C_β for the case where X = S = Y, although whether this can be accounted for solely on electronic grounds or involves anisotropy considerations, at least in part, is arguable.

One of the main reasons for studying the 2-pyrone series of compounds was to obtain evidence for any empirical correlation between the chemical shifts of carbonyl and thiocarbonyl carbon atoms in compounds of similar structure. This question will be discussed toward the end of the paper in the light of the data collected for the 4-pyrone type systems and the pyridones and pyridinethiones.

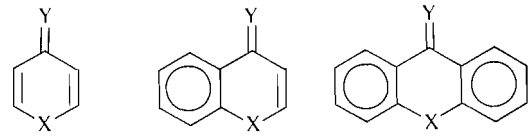

3 (X, Y = O or S) **4** (X, Y = O or S) **5** (X, Y = O or S)

In Table 3, comparable ^{13}C nmr data for a series of 4-pyrone derivatives are collected. In part A of the table a series of monocyclic derivatives **3** are listed, followed by some chromone and thiochromone derivatives **4** in part B and the four simple isomeric xanthone **5** derivatives in part C. Turning first to the question of the chemical shift of the carbonyl and thiocarbonyl carbons in part A, one is immediately struck by the fact that, irrespective of the nature of the hetero-atom in the ring (O or S) the chemical shifts of both carbonyl, in the range 178.7–182.3 ppm, and thiocarbonyl, in the range 200.8-203.1 ppm, remain remarkably constant. This is in sharp contrast to the 2-pyrone series as we have already seen, where the nature of the ring hetero-atom plays a much more significant role. This effect will clearly influence attempts to correlate C=O and C=S chemical shifts and we will return to this point later. Before leaving the question of the carbonyl and thiocarbonyl shifts it should be noted in passing that they also remain largely independent of the electronic effects of ring substitution, at least at C-2 and C-6.

Although we have not included the unsubstituted members of the monocyclic series in this study, we can obtain a fairly good approximation of the parent C_α and C_β chemical shifts in 4-pyrone type systems from an examination of the data for C-3 and C-2 in the bicyclic compounds of part B. Turner and Pirkle (1) also observed very close agreement between the shifts of C_α and C_β carbons in their monocyclic and bicyclic 2-pyrone series. As a check on this assumption in our own series of 4-pyrones in Table 3, it may be noted that the chemical shifts of C-2 in chromone and C-6 in 2-phenyl-4-pyrone, and of C-3 in chromone and C-5 in the same monocyclic pyrone closely approximate one another. Thus, making this assumption, it can be seen that the introduction of methyl at C-2 in the monocyclic systems has a deshielding effect at C-2 of (+)10.5 to 13.1 ppm, and a

Can. J. Chem. Downloaded from www.nrcresearchpress.com by 210.87.254.6 on 09/05/12
For personal use only.

Can. J. Chem. Downloaded from www.nrcresearchpress.com by 210.87.254.6 on 09/05/12
For personal use only.

TABLE 3. Carbon-13 chemical shift data* for 4-pyrones and their thio analogues

Compound	CO/CS	C-2,6	C-3,5	C_6H_5 C-1	*o*-	*m*-	*p*-	Other	Reference
A.									
2,6-Dimethyl-4-pyrone	179.9	165.6	113.6	—	—	—	—	19.7(CH_3)	—
2,6-Dimethylpyran-4-thione	201.8	159.1	124.5	—	—	—	—	19.3(CH_3)	(25)
2,6-Diphenyl-4-pyrone	180.0	163.2	111.2	131.3	125.8	129.1	131.4	—	(26)
2,6-Diphenylpyran-4-thione	200.8	155.7	121.8	130.5	126.0	129.2	131.7	—	(25)
2,6-Diphenylthiopyran-4-one	182.3	153.2	127.1	136.1	126.9	129.3	130.7	—	(27)
2,6-Diphenylthiopyran-4-thione	202.2	145.8	137.3	135.7	126.9	129.4	130.9	—	(27)
2,6-Dicarbomethoxy-4-pyrone	178.7	152.7	120.1	—	—	—	—	53.5(OCH_3), 159.7(COOMe)	(28)
2,6-Dicarbomethoxypyran-4-thione	203.1	144.3	130.1	—	—	—	—	53.8(OCH_3), 160.6(COOMe)	(29)
2-Phenyl-4-pyrone	179.2	164.0(C-2) 155.1(C-6)	112.2(C-3) 117.0(C-5)	130.9	125.7	129.0	131.5	—	(30)
2-Phenyl-4-pyrone-6-carboxylic acid†	178.9	162.7(C-2) 153.1(C-6)	111.9(C-3) 117.8(C-5)	130.4	126.0	129.1	131.8	161.0(COOH)	(30)
Ethyl 2-phenyl-4-pyrone-6-carboxylate	179.4	163.7(C-2) 152.4(C-6)	112.4(C-3) 119.0(C-5)	130.5	126.1	129.1	131.9	14.1(CH_3), 62.9(CH_2), 160.0(COOEt)	(30)
B.									
Chromone 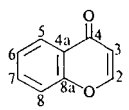	177.6	155.6(C-2) 156.6(C-8a)	113.0(C-3) 125.0(C-4a)	—	—	—	—	118.3(C-8) 125.3(C-6), 125.8(C-5), 133.8(C-7)	(8)
Benzopyran-4-thione	202.8	146.0(C-2) 151.4(C-8a)	126.2(C-3) 130.9(C-4a)	—	—	—	—	118.6(C-8), 124.8(C-6), 128.6(C-5), 134.2(C-7)	(8)
Thiochromone	179.4	137.9(C-2) 137.5(C-8a)	126.6(C-3) 132.2(C-4a)	—	—	—	—	125.5(C-6), 127.7(C-8) 128.5(C-5), 131.4(C-7)	(8)
Benzothiopyran-4-thione	204.4	131.4(C-2) 132.5(C-8a)	137.6(C-3) 138.4(C-4a)	—	—	—	—	127.3(C-6),‡ 127.9(C-8),‡ 129.0(C-5), 132.0(C-7)	(8)

Can. J. Chem. Downloaded from www.nrcresearchpress.com by 210.87.254.6 on 09/05/12
For personal use only.

TABLE 3 (*Concluded*)

Compound	CO/CS	C-2,6	C-3,5	C_6H_5 C-1	*o*-	*m*-	*p*-	Other	Reference
2-Phenylchromone (flavone)	178.3	163.3(C-2) 156.3(C-8a)	107.6(C-3) 124.0(C-4a)	131.8	126.3	129.0	131.6	118.1(C-8), 125.2(C-6), 125.7(C-5), 133.7(C-7)	(8)
2-Phenylbenzopyran-4-thione	201.8	153.8(C-2) 151.3(C-8a)	120.1(C-3) 130.8(C-4a)‡	129.7‡	126.3	129.0	131.7	118.3(C-8), 126.0(C-6), 128.4(C-5), 133.9(C-7)	(8)
2-Phenylthiochromone	180.7	152.9(C-2) 137.6(C-8a)	123.3(C-3) 132.4(C-4a)	136.5	126.9	129.2	130.8	126.5(C-6), 127.7(C-8), 128.5(C-5), 131.5(C-7)	(20)
2-Phenylbenzothiopyran-4-thione	204.7	143.0(C-2) 133.3(C-8a)	135.9(C-3) 137.1(C-4a)	136.1	127.0	129.3	130.9	127.0(C-6), 128.9(C-8), 131.4(C-5), 132.0(C-7)	(31)
C. Xanthone 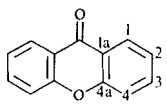	177.0	156.0(C-4a)§	121.7(C-1a)§	—	—	—	—	117.9(C-4), 123.8(C-2), 126.6(C-1), 134.7(C-3)	—
Dibenzopyran-4-thione	204.8	150.5(C-4a)§	129.0(C-1a)§	—	—	—	—	118.2(C-4), 124.7(C-2), 129.8(C-1), 134.8(C-3)	(32)
Thioxanthone	180.1	137.5(C-4a)§	129.4(C-1a)§	—	—	—	—	126.2(C-2), 126.5(C-4), 130.0(C-1), 132.4(C-3)	—
Dibenzothiopyran-4-thione	211.6	131.9(C-4a)§	137.5(C-1a)§	—	—	—	—	125.9(C-2), 126.9(C-4) 131.6(C-1), 133.3(C-3)	(33)

*All shifts quoted in ppm relative to TMS, in $CDCl_3$.
†In DMSO-d_6.
‡These assignments may be reversed.
§For simplicity in comparison these signals are regarded as the counterpart of the C-2,6 and C-3,5 carbons in monocyclic 4-pyrones.

Can. J. Chem. Downloaded from www.nrcresearchpress.com by 210.87.254.6 on 09/05/12
For personal use only.

shielding effect at C-3 of (−)1.7 to 3.4 ppm. For 2-phenyl substitution the corresponding effects range from (+)8.9 to 15.3 ppm, and from (+)0.5 to (−)4.8 ppm. As was noted earlier in the 2-pyrone series, the deshielding (α) effect of phenyl substitution is much greater when the ring hetero-atom is sulfur but the shielding (β) effect is almost negligible compared to the oxygen heterocycles. For the electron-withdrawing ester group at C-2 there is a relatively small (α) shielding effect ($\sim$3 ppm) and also a (β) deshielding effect of like amount. This contrasts with the deshielding effect of an ester group on both the α and β carbons of a simple alkene (12).

The other signals observed in part A of the table are for the most part unremarkable although it should be noted that the position of the C-1 carbon of the phenyl substituent at C-2 is very sensitive to the nature of the adjacent hetero-atom. If the hetero-atom is oxygen the value observed for C-1 is in the narrow range 130.4 to 131.3 ppm, but for the two cases where the ring hetero-atom is sulfur C-1 is considerably downfield at about 136 ppm. Similar values were found by Lapper (13) for the C-1 carbon atoms of phenyl rings in a series of phenyl-substituted 6A-thiathiophthenes. The reason for this relatively large effect is not clear, but it is obvious that it may have considerable value in structure determination

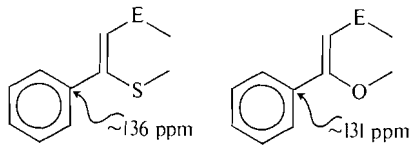

(where E is an electron-withdrawing group)

Turning to part B of Table 3, we have included, for ease of comparison, the ^{13}C nmr data for the parent chromone and thiochromone systems and their thione counterparts, although we have previously reported these compounds in an earlier study (8), while ^{13}C nmr data for chromone and flavone were also included in a recent paper by Kingsbury and Looker (7). The data reported by these authors are in very good agreement with our own assignments. Because of the relation between chemical shifts of C_α and C_β carbons and the nature of the hetero-atoms present, first detected in the 2-pyrone series (*cf.* Table 2, and related discussion), we have now reversed the previous assignments for C-2 and C-3, and for C-8a and C-4a in benzothiopyran-4-thione. The correctness of the new assignments, which again place the C-2 (β) carbon in this system *upfield* of the C-3 (α) carbon, is supported by examination of the 2-phenyl substituted series of compounds in Table 3. By utilizing the expected deshielding and shielding parameters for 2-phenyl substitution derived earlier, one finds excellent agreement between the observed and calculated data.

A small deshielding effect (<2 ppm) on the C=O or C=S chemical shift is observed on replacing the ring oxygen atom by sulfur. The absence of any appreciable effect of phenyl substitution on the chemical shifts of the benzo-ring carbons made the assignments relatively straightforward. As is usually the case for a β-phenyl substituent on an α,β-unsaturated carbonyl or thiocarbonyl system, the *ortho*-carbons are slightly shielded (2–3 ppm) and the *para*-carbon is deshielded by a like amount. On the other hand the C-7 carbon, *para* to the C=O or C=S group experiences a stronger deshielding effect, ranging from (+)2.8 to 5.6 ppm. The effect, already discussed, of the ring sulfur atom in deshielding C-1 of the phenyl ring is also observed here for the two sulfur heterocycles.

The final group of compounds in part C of Table 3 are the symmetrical dibenzo derivatives of the 4-pyrones. Although the general pattern is much the same, the significantly lower field position of the C=S carbon in dibenzothiopyran-4-thione at 211.6 ppm is noteworthy. There appears also to be a definite trend for the C-1 carbon to move to lower field by about 5 ppm as one proceeds through the series from xanthone to the dithio analogue. This effect is also observable, although to a lesser degree, in the chromone series.

The $\Delta\delta$ values for C_α and C_β in the 4-pyrone, 4-thiopyrone, and 4-pyridone compounds and their C=S analogues are collected in Table 4. The differences in chemical shift (and presumably, electron density) for C_α and C_β in this series of compounds are generally of the same order as those for the 2-pyrone series (Table 2). This time, however, there is a more regular progression in the $\Delta\delta$ values as one proceeds through the series of ring hetero-atoms from O to N to S. Since inductive and other proximate effects of the hetero-atoms are presumably much less important for the 4-pyrone type compounds,

TABLE 4. Differences in chemical shifts ($\Delta\delta$) between C_α and C_β in heterocycles of type,

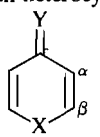

Series	X = O	X = NH	X = S
Y = O	42.6*†	23.9‡	11.3*†
Y = S	19.8*†	3.8*	(−)6.2*†
	$\Delta\Delta\delta$		
Change from C=O to C=S	22.8	20.1	17.5

*Our work.
†Based on chromone and thiochromone parent systems.
‡From ref. 4.

it seems likely that a truer picture of π-electron density distributions is given by the data in Table 4. The reduction in $\Delta\delta$ for each hereroatom as one replaces the C=O group by the C=S group is again approximately 20 ppm.

The last group of heterocyclic compounds for which we present ^{13}C nmr data in Table 5 are the 2- and 4-pyridinethiones and their *N*- and *S*-methylated derivatives **6–9**. Data for the analogous pyridone derivatives have been reported recently by at least two groups of workers. Vögeli and von Philipsborn (4) reported an extensive ^1H and ^{13}C nmr study of the three pyridones (or hydroxypyridines) and their *N*- and *O*-methyl derivatives in an attempt to establish the electronic structure of 3-pyridone.

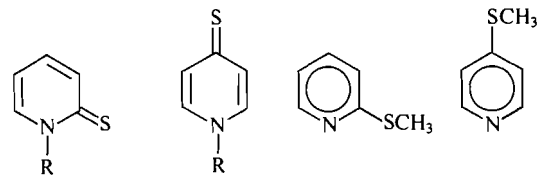

6 (R = H, CH_3) **7** (R = H, CH_3) **8** **9**

Turner and Cheeseman (14) more recently reported similar data for some monosubstituted pyridine and pyrazine derivatives, although they make no reference to the work of the previous authors. Data from these two papers and for pyridine itself (15) are included in Table 5 to simplify comparisons.

The compounds in Table 5 fall conveniently into three subgroups (*a*) the 2-pyridones, (*b*) the 4-pyridones, and (*c*) the methylthio derivatives of pyridine.

In the 2-pyridones, the position of the C=O carbon is virtually unaffected by replacing N—H by N—CH_3, but in the analogous thiones a deshielding effect of +3.8 ppm is observed. Otherwise, the most significant effect on the ring carbons of *N*-methylation is at C-6, where deshielding effects of +4.3 and +2.9 ppm are observed for the carbonyl and thiocarbonyl series, respectively. The N—CH_3 carbon is deshielded by 4.2 ppm in *N*-methyl-2-pyridinethione compared to its carbonyl counterpart. Unlike previous authors (14), we have resisted the temptation to compare substituent chemical shift effects for these compounds with phenol

TABLE 5. Carbon-13 chemical shift data* for 2- and 4-pyridinethiones and their *N*- and *S*-methylated derivatives

Compound	C=S (C=O)	C-2	C-3	C-4	C-5	C-6	Other	Reference
2-Pyridone†	162.3	—	119.8	140.8	104.8	135.2	—	(4, 14)
N-Methyl-2-pyridone†	161.8	—	119.1	139.5	104.8	139.5	41.8(N-CH_3)	(4)
2-Pyridinethione	176.4	—	133.6‡	138.1‡	114.2 ‡	137.0‡	—	—
N-Methyl-2-pyridinethione	180.2	—	134.1	135.8	113.4	141.0	46.0(N-CH_3)	(34)
4-Pyridone†	175.7	139.8	115.9	—	115.9	139.8	—	(4, 14)
N-Methyl-4-pyridone†	176.6	141.4	117.2	—	117.2	141.4	42.6(N-CH_3)	(4)
4-Pyridinethione§	189.8	133.2	129.4	—	129.4	133.2	—	—
N-Methyl-4-pyridinethione	190.5	135.3	131.4	—	131.4	135.3	44.4(N-CH_3)	(35)
Pyridine†	—	150.6	124.5	136.4	124.5	150.6	—	(15)
2-Methylthiopyridine	—	159.9	121.4	135.7	119.0	149.3	13.2(S-CH_3)	(36)
4-Methylthiopyridine	—	149.0	119.8	150.2	119.8	149.0	13.5(S-CH_3)	(37)

*All shifts in ppm relative to TMS, in $CDCl_3$.
†Data for these compounds have previously been reported but they are included for comparison.
‡Assignments confirmed by $^1J_{CH}$ measurements of 172, 166, 175, and 183 Hz for C-3, C-4, C-5, and C-6 respectively.
§In DMSO-d_6.

Can. J. Chem. Downloaded from www.nrcresearchpress.com by 210.87.254.6 on 09/05/12
For personal use only.

Can. J. Chem. Downloaded from www.nrcresearchpress.com by 210.87.254.6 on 09/05/12
For personal use only.

and benzenethiol, since earlier work by Katrizky and Lagowski (16) has shown unambiguously that the hydroxy- and mercaptopyridines exist almost exclusively in the amide and thioamide forms respectively.

It may be noted in passing that the chemical shifts of C-3, C-4, and C-6 in 2-pyridinethione (and its *N*-methyl derivative) are fairly closely spaced, in the range 133.6 to 138.1 ppm. The assignments made were finally confirmed by comparing the $^1J_{C-H}$ coupling constants for these atoms in 2-pyridinethione with those in 2-pyridone. The largest value of $^1J_{C-H}$ (183 Hz) is expected for C-6 because of the proximity of the electronegative nitrogen atom (15), while the results of the previous authors (4, 14) would suggest that the smallest value of $^1J_{CH}$ (166 Hz) should be associated with C-4.

In the 4-pyridone and 4-pyridinethione analogues, the C=O and C=S carbons appear at significantly lower field, the deshielding effect being +13.4 ppm for both the carbonyl and thiocarbonyl systems. This time *N*-methylation has very little influence, the deshielding effect being less than 1 ppm for both the C=O and the C=S compounds. This suggests that the deshielding effect of +3.8 ppm observed in *N*-methyl-2-pyridinethione may be through space, rather than inductive or mesomeric in origin. The differences ($\Delta\delta$) between the chemical shifts of the α (C-3,5) and β (C-2,6) carbons are given in Table 4 and are similar to those for the 2-substituted analogues. In both the C=O and C=S series, *N*-methylation produces shielding effects at both C-2 and C-3 of approximately 2 ppm. Once again, the *N*-methyl carbon appears at lower field in the C=S compound but the deshielding effect this time is much smaller (+1.8 ppm).

For the 2-methylthio- and 4-methylthiopyridines the α-, β-, γ-, and δ-effects of CH_3S-substitution are compared in Table 6 with those in thioanisole (17). As noted by Turner and Cheeseman (14) for their monosubstituted pyridines, the α-deshielding effect of SCH_3 is significantly greater at C-4 than C-2, while the β- and γ-shielding effects of the 4-SCH_3 are also somewhat greater than expected from a comparison with thioanisole.

Returning to the question of a possible correlation between the chemical shifts of C=O and C=S in otherwise identical structures, our experience leads us to the conclusion that no real correlation of this type exists. Data for the three different kinds of heterocyclic systems studied (O,N,S,) have been plotted separately in Fig. 1. (No distinction is made in the graph between the 2-pyrone and the 4-pyrone type systems since, once again, no simple correlation even of this sort was observed.) The respective slopes of the lines obtained by a computer fit for the O, N and S systems were 0.31, 0.84, and −0.08, with intercepts of 147.5, 43.0, and 219.7 respectively. Standard deviations in slope were 0.047 (30.3% error), 0.149 (35.8% error), and 0.049 (124.4% error), respectively. Standard deviations in the intercept were 7.96 (10.8% error), 25.28 (117.6% error), and 8.53 (7.8% error), respectively. The wide variations observed with the different hetero-atoms, and the variation also from the relation claimed by Kalinowski and Kessler (9) ($\sigma_{C=S} = 1.45\delta_{C=O} - 46.5$), strongly suggest that, at best, such a correlation is useful only for obtaining approximate estimates of the chemical shift of the thione functionality in cases where

TABLE 6. Substituent chemical shift effects* of SCH_3 group

Compound	Substituent chemical shift effects			
	α	β	γ	δ
Thioanisole†	+9.8	−2.1	0.0	−3.8
2-Methylthiopyridine	+9.3	−3.1	−0.7 −1.3	−5.5
4-Methylthiopyridine	+13.8	−4.7	−1.6	—

*In ppm; positive values denote deshielding effects.
†*Cf.* ref. 17.

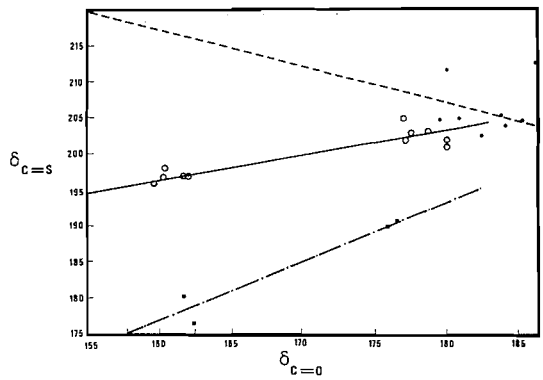

FIG. 1. Relative shifts of the C=O and C=S carbons of the heterocyclic systems studied: O-heterocycles (○) ————; N-heterocycles (■) —•—•—; S-heterocycles (●) — — — —.

data are available for a relatively large number of structurally similar ketones. The absence of a general correlation of the above type for these heterocyclic systems is still evident when the data for the 2-pyrone and 2-pyridone type structures (where proximity effects are maximal) are neglected, although in part this is a reflection of the smaller number of points.

Acknowledgments

We are grateful for the invaluable assistance of Professor J. M. Deckers in processing some of the data. We acknowledge generous financial support of this work by Erindale College and the Department of Chemistry, University of Toronto.

1. W. V. TURNER and W. H. PIRKLE. J. Org. Chem. **39**, 1935 (1974).
2. R. D. LAPPER. Tetrahedron Lett. 4293 (1974).
3. S. A. SOJKA. J. Org. Chem. **40**, 1175 (1975).
4. U. VÖGELI and W. VON PHILIPSBORN. Org. Magn. Reson. **5**, 551 (1973).
5. L. PAOLONI, M. CIGNITTI, and M. L. TOSATO. Org. Magn. Reson. **6**, 469 (1974).
6. R. H. MARTIN, N. DEFAY, F. GEERTS-EVRARD, P. H. GIVEN, J. R. JONES, and R. W. WEDEL. Tetrahedron, **21**, 1833 (1965).
7. C. A. KINGSBURY and J. H. LOOKER. J. Org. Chem. **40**, 1120 (1975).
8. M. S. CHAUHAN and I. W. J. STILL. Can. J. Chem. **53**, 2880 (1975).
9. H.-O. KALINOWSKI and H. KESSLER. Angew. Chem. Int. Ed. Engl. **13**, 90 (1974).
10. N. PLAVAC, I. W. J. STILL, M. S. CHAUHAN, and D. M. MCKINNON. Can. J. Chem. **53**, 836 (1975).
11. R. H. LEVIN and L. WEINGARTEN. Tetrahedron Lett. 611 (1975).
12. G. MIYAJIMA, K. TAKAHASHI, and K. NISHIMOTO. Org. Magn. Reson. **6**, 413 (1974).
13. R. D. LAPPER and A. J. POOLE. Tetrahedron Lett. 2783 (1974).
14. C. J. TURNER and G. W. H. CHEESEMAN. Org. Magn. Reson. **6**, 663 (1974).
15. G. C. LEVY and G. L. NELSON. Carbon-13 nuclear magnetic resonance for organic chemists. John Wiley and Sons, Inc., New York. 1972.
16. R. A. ABRAMOVITCH (*Editor*). The chemistry of heterocyclic compounds. Vol. 14 (Supplement) Part 4. Wiley-Interscience, New York. 1975. p. 198.
17. L. F. JOHNSON and W. G. JANKOWSKI. Carbon-13 n.m.r. spectra. Wiley-Interscience, New York. 1972. p. 249.
18. G. LABAN and R. MAYER. Z. Chem. **7**, 227 (1967).
19. F. ARNDT and B. EISTERT. Ber. **58**, 2318 (1925).
20. D. M. MCKINNON. Can. J. Chem. **48**, 3388 (1970).
21. D. LEAVER, D. M. MCKINNON, and W. A. H. ROBERTSON. J. Chem. Soc. 32 (1965).
22. H. KITAGAWA. J. Pharm. Soc. Jpn. **70**, 730 (1950).
23. G. PFISTER-GUILLOUZO and N. LOZACH'H. Bull Soc. Chim. Fr. 1624 (1962).
24. J. L. CHARLTON, S. M. LOOSMORE, and D. M. MCKINNON. Can. J. Chem. **52**, 3021 (1974).
25. F. ARNDT, E. SCHOLZ, and P. NACHTWEY. Ber. **57**, 1903 (1924).
26. R. J. LIGHT and C. R. HAUSER. J. Org. Chem. **25**, 538 (1960).
27. F. ARNDT, P. NACHTWEY, and J. PUSCH. Ber. **58**, 1633 (1925).
28. R. WILLSTÄTTER and R. PUMMERER. Ber. **37**, 3740 (1904).
29. F. ARNDT and P. NACHTWEY. Ber. **56**, 2406 (1923).
30. W. BORSCHE and W. PETER. Justus Liebig's Ann. Chem. **453**, 148 (1927).
31. F. ARNDT, P. NACHTWEY, and J. PUSCH. Ber. **58**, 1644 (1925).
32. C. GRAEBE and P. RÖDER. Ber. **32**, 1688 (1899).
33. F. ARNDT and L. LORENZ. Ber. **63**, 3121 (1930).
34. J. RENAULT. Bull. Soc. Chim. Fr. 1001 (1953).
35. R. A. JONES and A. R. KATRITZKY. J. Chem. Soc. 3610 (1958).
36. W. MARCKWALD, W. KLEMM, and H. TRABERT. Ber. **33**, 1556 (1900).
37. H. KING and L. L. WARE. J. Chem. Soc. 873 (1939).

Can. J. Chem. Downloaded from www.nrcresearchpress.com by 210.87.254.6 on 09/05/12
For personal use only.

Approaches to the synthesis of quinazolino[1,2,3]benzotriazinones

T. PATRICK AHERN, HANDRICK FONG, AND KEITH VAUGHAN
Department of Chemistry, Saint Mary's University, Halifax, Nova Scotia B3H 3C3

Received July 24, 1975

T. PATRICK AHERN, HANDRICK FONG, and KEITH VAUGHAN. Can. J. Chem. **54**, 290 (1976).

The synthesis of 1-(*o*-carboxamidophenyl)-3-aryl triazenes **12** and **15** (X = $CONH_2$ and H) is described. Reaction of 3-(*o*-carboxamidophenyl)-1-(*o*-methoxycarbonylphenyl)-triazene (**12**) with piperidine in ethanol affords 2-[2-(piperidin-1-ylazo)phenyl]quinazolin-4(3*H*)-one (**18**); the formation of **18** in this reaction can only arise via the unstable quinazolino[1,2-*c*][1,2,3]-benzotriazinone **8** by triazine ring cleavage under the influence of piperidine. Attempted synthesis of the 4-iminotriazine **17**, an isomer of the quinazolone **18**, from the *o*-cyanophenyltriazene **20**, resulted only in the formation of quinazolino[3,2-*c*][1,2,3]benzotriazin-8-one (**6**), an isomer of **8**. The *o*-cyanophenyltriazene **20** undergoes spontaneous cyclisation, rearrangement, and further cyclisation.

T. PATRICK AHERN, HANDRICK FONG et KEITH VAUGHAN. Can. J. Chem. **54**, 290 (1976)

On décrit la synthèse des (*o*-carboxamidophényle)-1 aryl-3 triazènes **12** et **15** (X = $CONH_2$ et H). La réaction du (*o*-carboxamidophényl)-3 (*o*-méthoxycarbonylphényl)-1 triazène (**12**) avec la pipéridine dans l'éthanol conduit à la [(pipéridine-1 ylazo)-2 phényl]-2 quinazoline(3*H*) one-4 (**18**); la formation de **18** dans cette réaction ne peut provenir que de la quinazolino[1,2-*c*][1,2,3]-benzotriazinone **8** instable par une rupture du noyau triazine sous l'influence de la pipéridine. Des essais de synthèse de l'imino-4 triazine **17**, un isomère de la quinazolone **18**, ont été tentés à partir de l'*o*-cyanophényltriazène **20**; on n'a pu isoler de cette réaction que la quinazolino[3,2-*c*]-[1,2,3]benzotriazinone-8 (**6**), un isomère de **8**. L'*o*-cyanophényltriazène **20** subit une cyclisation spontanée, un réarrangement et une autre cyclisation.

[Traduit par le journal]

Introduction

8-Iminoquinazolino[3,2-*c*][1,2,3]benzotriazine, **3**, has been postulated as an intermediate in the conversion of 1,3-di-*o*-cyanophenyltriazene, **1**, to 4-amino-2-phenylquinazoline, **4**, in boiling aqueous ethanol (1). The formation of the quinazolinobenzotriazine **3** was accounted for by rearrangement and cyclisation of the 4-imino-3-aryl-1,2,3-benzotriazine **2** (Scheme 1); this behaviour has since been shown to be typical of 4-imino-3-aryl-1,2,3-benzotriazines (2). The oxo-analogue of **3**, quinazolino[3,2-*c*][1,2,3]benzotriazine-8-one, **6**, has been synthesised by thermolysis of 1,2,3-benzotriazin-4(3*H*)-one, **5** (3). The structure of the quinazolinobenzotriazinone (**6**) was confirmed in an independent synthesis by diazotisation of 2-(*o*-aminophenyl)-quinazolin-4(3*H*)-one, **7** (3), and in its degradation reactions (3), which distinguish the quinazolino[3,2-*c*][1,2,3]benzotriazinone **6** from its isomer, the quinazolino-[1,2-*c*][1,2,3]benzotriazinone **8**. The latter has not previously been isolated or observed as an intermediate.

1-(*o*-Cyanophenyl)-3-(*o*-carbalkoxyphenyl)-triazene, **9**, represents a potential entry to the quinazolino[1,2-*c*][1,2,3]benzotriazine ring system through the conversion **9** → **10** → **8** (route *i*, Scheme 2). However, in a previous study (4), cyclisation of the nitrile-ester **9** afforded the quinazolino[3,2-*c*][1,2,3]benzotriazinone **6** and not the isomer **8**. The formation of **6** from the nitrile-ester **9** was accounted for by rearrangement of the 4-iminobenzotriazine **10** followed by cyclisation of the 4-aryliminobenzotriazine **11** (route *ii*, Scheme 2). Although this sequence was not unexpected in light of the known chemistry of 4-imino-3-aryl-1,2,3-benzotriazines (2), the failure to synthesise the quinazolino[1,2-*c*]-[1,2,3]benzotriazinone **8** was somewhat disappointing. Thus, the possible synthesis of quinazolino[1,2-*c*][1,2,3]benzotriazines from *o*-cyanophenyltriazenes (*e.g.* **1** and **9**) is precluded by the general rearrangement of the intermediate 4-iminobenzotriazines (**2** and **10**).

A more hopeful starting point for the synthesis of a quinazolino[1,2-*c*][1,2,3]benzotriazine was seen to be the amide-ester, **12**, in which the carboxamido group would act as the source of the N-3 nitrogen for the quinazoline moiety but should not be inclined to afford a 4-iminobenzo-

Can. J. Chem. Downloaded from www.nrcresearchpress.com by 210.87.254.5 on 09/05/12
For personal use only.

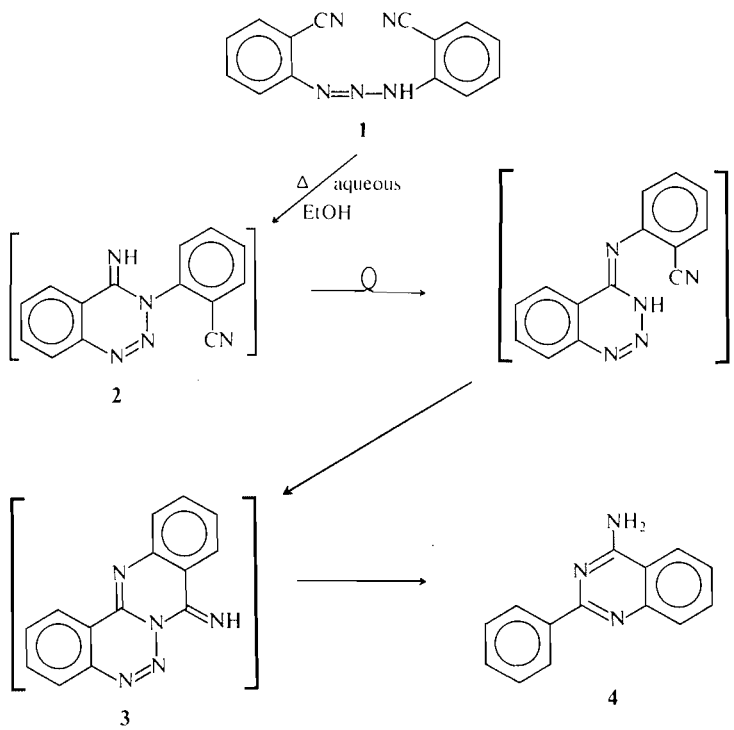

SCHEME 1

triazine. By virtue of the greater reactivity of the ester group over that of the amide group, cyclisation of the amide-ester **12** would be expected to give rise initially to the benzotriazinone **13**. Rearrangement of **13** is not possible and cyclisation of **13**, if achieved, could lead only to the quinazolino[1,2-*c*][1,2,3]benzotriazinone **8**. This paper describes the preparation and study of the amide-ester **12** and some related *o*-carboxamidophenyltriazenes, which had not previously been reported.

Discussion

The synthesis of the unsymmetrical diaryl triazene Ar·N=N·NHAr′ can usually be approached from either of two essentially equivalent directions, which both give the same tautomeric mixture [1]:

[1] $ArN_2^+ + Ar'NH_2 \rightarrow$
$Ar\cdot N{=}N\cdot NHAr' \rightleftarrows ArNH\cdot N{=}N\cdot Ar'$

or

$ArNH_2 + Ar'N_2^+ \rightarrow$
$ArNH\cdot N{=}N\cdot Ar' \rightleftarrows Ar\cdot N{=}N\cdot NHAr'$

However, the synthesis of the 1-(*o*-carboxamidophenyl)-3-aryltriazenes, **15**, via diazotisation of anthranilamide is complicated by the ease with which the *o*-carboxamidobenzenediazonium ion **14** undergoes cyclisation to 1,2,3-benzotriazin-4(3*H*)-one, **5** (5). Consequently, 1-(*o*-carboxamidophenyl)-3-phenyltriazene **15** (X = H) was obtained (in good yield) by coupling benzene diazonium ion with anthranilamide. Similarly, diazotisation of methyl anthranilate **16** (X = CO_2Me), followed by coupling with anthranilamide, afforded 3-(*o*-carboxamidophenyl)-1-(*o*-methoxycarbonylphenyl)-triazene, **12**. Successful coupling of anthranilamide diazonium salt **14** with anthranilamide was achieved by diazotisation of anthranilamide, in the presence of sodium acetate, with $\frac{1}{2}$ equiv. of sodium nitrite, which gave a 50% yield of 1,3-di-(*o*-carboxamidophenyl)-triazene, **15** (X = $CONH_2$). Evidently the diazonium salt **14** is sufficiently stable in acetate buffer to allow coupling only when the amine to be coupled is present in the diazotisation medium; this condition can only be met for the symmetrical di-(carboxamidophenyl)-triazene **15** (X = $CONH_2$).

The spectroscopic characteristics of the amides

Can. J. Chem. Downloaded from www.nrcresearchpress.com by 210.87.254.5 on 09/05/12
For personal use only.

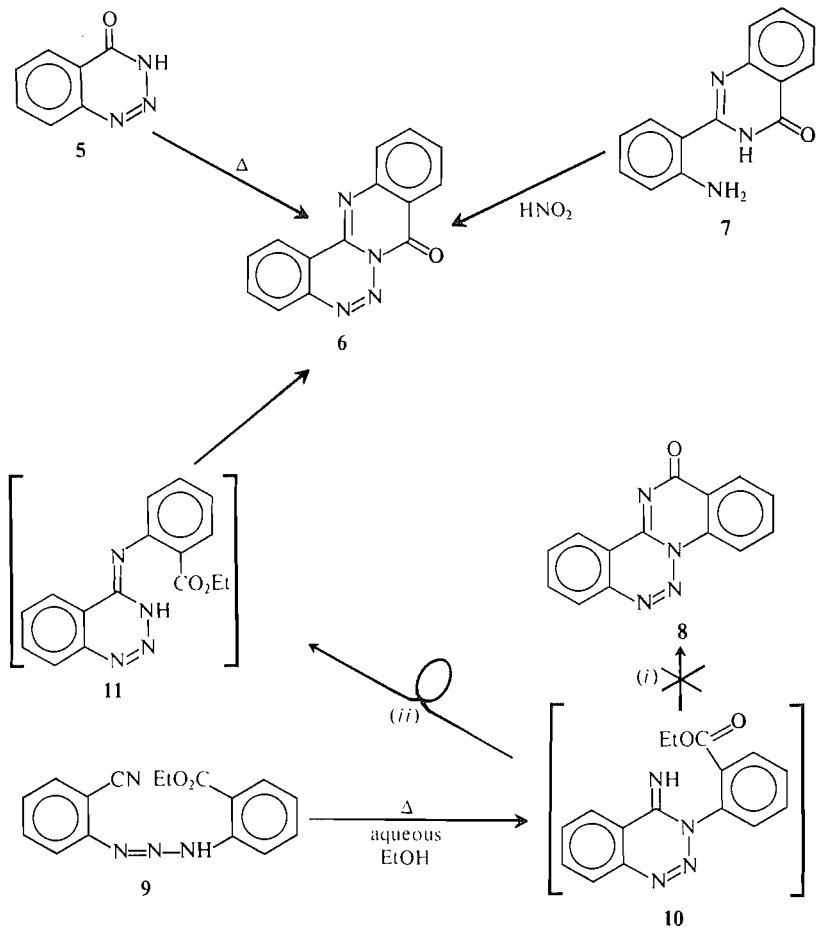

SCHEME 2

12 and **15** (X = H and $CONH_2$) are in accord with their assigned structures, and are consistent with the general characteristics of diaryl triazenes. The infrared spectra all display amide-carbonyl absorption in the range 1640–1660 cm^{-1} and NH absorption of variable multiplicity in the range 3140–3410 cm^{-1}. The amide-ester **12** also shows ester-carbonyl absorption at 1680 cm^{-1}.

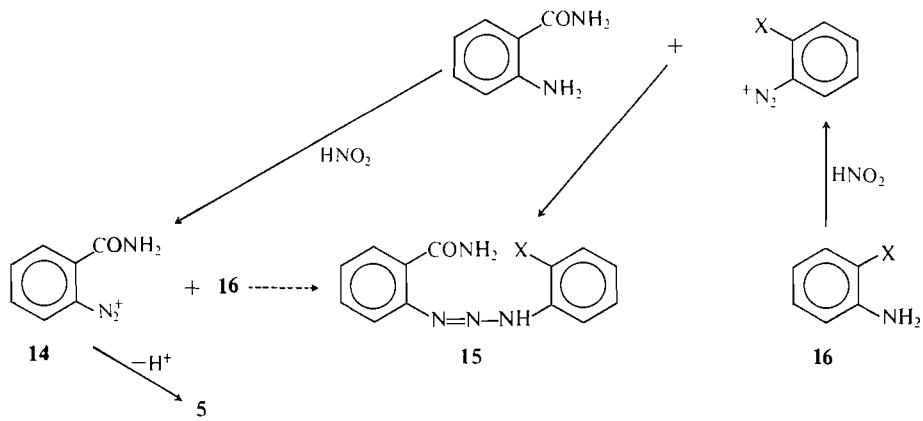

Can. J. Chem. Downloaded from www.nrcresearchpress.com by 210.87.254.5 on 09/05/12
For personal use only.

Can. J. Chem. Downloaded from www.nrcresearchpress.com by 210.87.254.5 on 09/05/12
For personal use only.

The mass spectra of the amide **15** (X = H) and amide-ester **12** exhibit weak molecular ions at *m/e* 240 and 298 respectively; fragmentation by loss of N_2 in the mass spectra of both compounds was indicated by intense peaks at *m/e* 212 and 270 respectively. Likewise the mass spectrum of the diamide **15** (X = $CONH_2$) displayed an intense peak at *m/e* 255 ($M^+ - N_2$), but in this case the molecular ion was not observed. The structures of the amides **12** and **15** (X = H and $CONH_2$) are also confirmed by their nmr spectra.

Attempts to cyclise 1-(*o*-carboxamidophenyl)-3-phenyltriazene **15** (X = H) to a 1,2,3-benzotriazine did not succeed. For example, prolonged refluxing of this amide in 70% aqueous ethanol afforded only anthranilamide, indicating the course of reaction to be protonation and fragmentation of the triazene moiety [2]:

$$[2]\quad Ar\cdot N{=}N\cdot NHPh \rightleftarrows ArNH\cdot N{=}N\cdot Ph \xrightleftharpoons{H^+} \overset{+}{Ar}NH_2\cdot N{=}N\cdot Ph \rightleftarrows ArNH_2 + PhN_2^+$$

(Ar = *o*-$H_2N\cdot CO\cdot C_6H_4$—)

Similar fragmentation was apparent when the amide-ester **12** was boiled in aqueous ethanol, the observed product being 1,2,3-benzotriazin-4(3*H*)-one, **5**. The formation of **5** in this reaction is readily accounted for by protolytic fragmentation of the amide-ester, giving rise to the diazonium ion **14**, which is known (5) to cyclise to the triazinone **5**. Formation of the 3-arylbenzotriazinone **13** was not evident in this reaction. However, these results indicate that the triazenes **12** and **15** (X = H) protonate preferentially on the nitrogen atom adjacent to the aryl group bearing the stronger electron-withdrawing group.

1-(*o*-Carboxamidophenyl)-3-phenyltriazene, **15** (X = H), was recovered unchanged after treatment with piperidine in refluxing ethanol; the diamide **15** (X = $CONH_2$) was also found to be stable under these conditions. The observed unreactivity of the *o*-carboxamidophenyltriazenes towards cyclisation is in marked contrast to the facility of cyclisation of *o*-cyanophenyltriazenes (1) and of *o*-carboalkoxyphenyltriazenes (4, 6). The reluctance of the amide-ester **12** to undergo cyclisation at the ester group in aqueous ethanol is unusual, but is somewhat analogous to the reactivity of the nitrile-ester **9**, which was found to be very slow to react in aqueous ethanol and cyclised preferentially at the cyano group (4). In both cases it would appear that steric interaction between *ortho*-substituents prevents or hinders formation of the required configuration for cyclisation in aqueous ethanol.

The amide-ester **12** was not completely inert towards cyclisation and, indeed, was observed to react with unexpected facility in ethanol containing piperidine, either under reflux or at lower temperatures for longer periods. The product of this reaction was a stable crystalline solid, which surprisingly had a molecular weight (mass spectrum) of 333. The presence of a piperidyl group in this compound was clearly indicated by the initial loss of a fragment of 84 mass units in the mass spectrum, and was corroborated by the nmr spectrum. The infrared spectrum exhibited absorption due to NH (3060 cm^{-1}) and carbonyl (1675 cm^{-1}) groups. The spectral data are in accord with two possible structures for this product, *i.e.* the 4-imino-3-aryltriazine, **17**, and the 2-(*o*-triazenophenyl)-quinazolone, **18**, although the latter is favoured somewhat on the basis of the frequency of carbonyl and NH absorption in the ir spectrum.

The formation of either **17** or **18** from the amide-ester **12** must involve cyclisation, initially at the ester group (Scheme 3), to give the 3-aryltriazinone **13**, followed by ring closure via the amide group to give the quinazolino[1,2-*c*]-[1,2,3]benzotriazinone, **8**, which then might have two possible modes of reaction with piperidine. Nucleophilic displacement at the 4-position of the quinazolone ring (7) would afford the iminotriazine **17** directly. Alternatively, reaction at N-2 of the triazine ring with the nucleophilic piperidine would result in triazine ring cleavage and afford the quinazolone **18**; this mode of reaction has recently been demonstrated for a number of fused 1,2,3-benzotriazine heterocycles (8). Coincidentally, the quinazolone **18** has recently been prepared by reaction of quinazolino[3,2-*c*]-[1,2,3]benzotriazin-8-one, **6**, with piperidine (8), although under more vigorous conditions than employed here. In the present work, the quinazolino[3,2-*c*][1,2,3]benzotriazinone, **6**, reacted with refluxing ethanolic piperidine to afford the quinazolone **18**, which was found to be identical with the product obtained by reaction of the amide-ester **12** with piperidine under the same conditions.

Thus it is possible that the quinazolino[1,2-*c*]-benzotriazine, **8**, formed from the amide-ester **12**, undergoes rearrangement to the quinazolino-

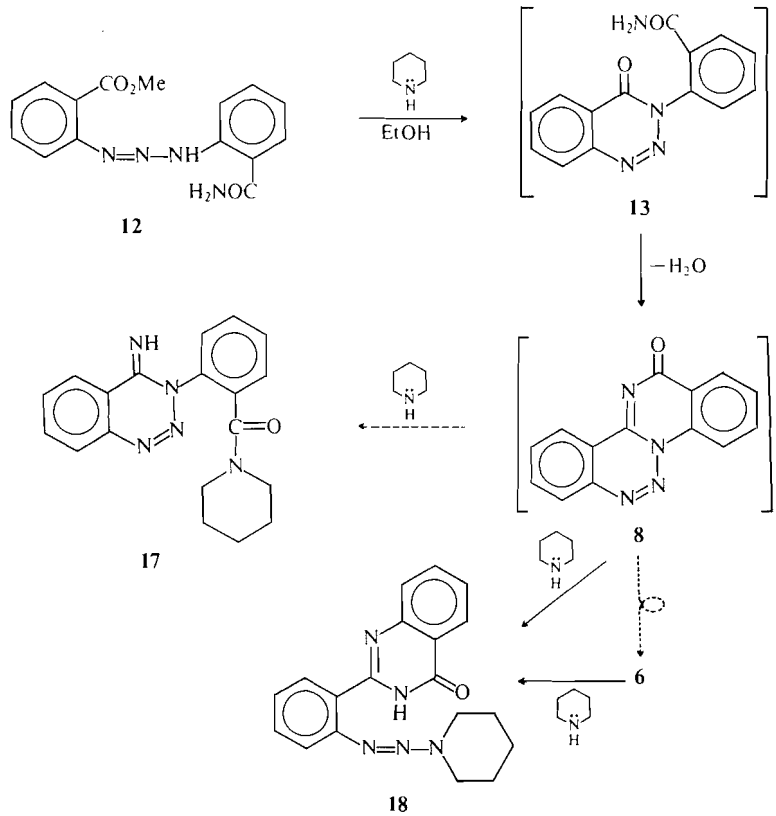

SCHEME 3

[3,2-*c*]benzotriazine, **6**, prior to reaction with piperidine. However, the fact that the yield of **18** is less when obtained directly from **6** than when obtained from the amide-ester **12**, suggests that the conversion **12** → **13** → **8** → **18** is the most likely route. Attempts to isolate the intermediates **13** and **8** by moderation of reaction conditions with piperidine did not succeed.

The elucidation of the structure of the quinazolone **18** led us to try to synthesise the isomeric 4-iminotriazine **17** by an alternate route. 4-Imino-3-aryl-1,2,3-benzotriazines can generally be obtained by cyclisation of *o*-cyanophenyltriazenes (1) and, by analogy, **17** should be available from 1-(*o*-cyanophenyl)-3-(*o*-piperidinocarbonylphenyl)-triazene, **20**. However, the *o*-cyanophenyltriazene **20** whether approached by diazotisation of anthranilonitrile coupled with *N*-(*o*-aminobenzoyl)-piperidine, **19**, or vice versa, proved to be unstable. Both diazonium coupling reactions gave resinous materials, which afforded low to moderate yields of quinazolino[3,2-*c*][1,2,3]benzotriazin-8-one, **6**. The formation of **6** doubtless proceeds by cyclisation of the triazene **20** to the desired 4-iminotriazine **17**, which must rearrange (2) to the 4-aryliminotriazine **21** and cyclise to the quinazolinotriazine **6**. The ease with which the piperidyl group is displaced in the last step indicates surprising reactivity associated with the amide group in **21**, but possibly arises by acid catalysis in the diazotisation medium. The instability of the *o*-cyanophenyltriazene **20** is not without precedent; 1-*o*-cyanophenyl-3-*o*-nitrophenyltriazene likewise cannot be isolated and rearranges spontaneously to a 4-anilinobenzotriazine (9).

In conclusion, the isolation of the quinazolone **18** from the reaction of the amide-ester **12** with piperidine in ethanol provides unequivocal evidence for the intermediate formation and subsequent decomposition of the quinazolino-[1,2-*c*][1,2,3]benzotriazinone, **8**. However, the quinazolinotriazinone **8** is, apparently, unstable under the conditions required to initiate the cyclisation of the amide-ester **12**, the mode of decomposition of **8** being analogous to that of

Can. J. Chem. Downloaded from www.nrcresearchpress.com by 210.87.254.5 on 09/05/12
For personal use only.

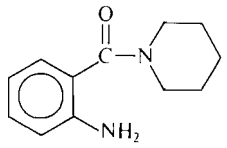

19

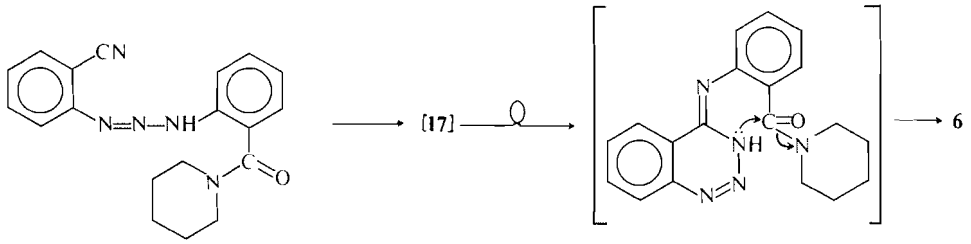

20 21

the isomeric quinazolino[3,2-*c*][1,2,3]benzotriazinone, **6**.

Experimental

Melting points were obtained on a hot-stage apparatus and are corrected. Infrared spectra were recorded with liquid paraffin mulls on a Perkin-Elmer Model 467 grating spectrophotometer, and nmr spectra were recorded, using tetramethylsilane as internal standard, with a Varian EM360 60 MHz spectrometer. Mass spectral data were obtained with a Dupont-C.E.C. Model 21-491 spectrometer.

*1-(o-Carboxamidophenyl)-3-phenyltriazene, **15** (X = H)*

Aniline (1.37 ml) was diazotised at 0 °C in concentrated hydrochloric acid (4.0 ml) and water (7.5 ml) with sodium nitrite (1.04 g), and the diazonium salt solution was treated slowly with a solution of anthranilamide (2.24 g) in a minimum volume of 2 *M* hydrochloric acid. The resulting solution was stirred at 0 °C for 1.5 h and then neutralised with an excess of sodium acetate. After stirring for a further 2 h, the precipitate was filtered; the mother liquor afforded a further batch of the same solid after the addition of more sodium acetate and being set aside overnight. Recrystallisation of the combined solids from ethanol afforded 1-(*o*-carboxamidophenyl)-3-phenyltriazene (2.47 g, 62%), mp 179–181 °C (dec.); ν_{max} 3350, 3220, 3150, and 1655 cm^{-1}; M^+ 240 ($C_{13}H_{12}N_4O$), *m/e* 212 ($M^+ - N_2$); δ (dimethylsulfoxide) 3.4 (s, NH_2), 7.0–8.5 (m, aromatic), and 13.1 (s, NH).

*3-(o-Carboxamidophenyl)-1-(o-methoxycarbonylphenyl)-triazene, **12***

Methyl anthranilate (2.6 g) was diazotised and treated with anthranilamide (2.24 g) by exactly the same procedure as above to afford 1-(*o*-carboxamidophenyl)-3-(*o*-methoxycarbonylphenyl)-triazene (4.5 g, 88%), mp 190–191 °C (dec.) (from ethanol); ν_{max} 3410, 3225, 3190, 1690, and 1640 cm^{-1}; δ (dimethylsulfoxide) 3.4 (s, NH_2), 3.95 (s, CH_3), 7.4–8.5 (m, aromatic), and 12.6 (s, NH); M^+ 298 ($C_{15}H_{14}N_4O_3$), *m/e* 270 ($M^+ - N_2$).

*1,3-Di-(o-carboxamidophenyl)-triazene, **15** (X = CONH$_2$)*

Anthranilamide (2.04 g) was diazotised at 0 °C in concentrated hydrochloric acid (4.0 ml) and water (12.5 ml), containing sodium acetate (5.0 g) as buffer, with ½ equiv. of sodium nitrite (0.52 g). The resulting mixture was stirred below 5 °C for 1 h and the precipitate filtered to afford the diamide, **15** (X = $CONH_2$) (1.06 g, 50%), mp 209–211 °C (dec.) (from ethanol); ν_{max} 3380, 3350 (sh), 3185, 3140 (sh), 1660, and 1650 (sh) cm^{-1}; δ (dimethylsulfoxide) 3.4 (s, NH_2), 7.0–8.4 (m, aromatic), and 13.5 (s, NH); *m/e* 255 ($M^+ - N_2$).

*Attempted Cyclisation of 1-(o-Carboxamidophenyl)-3-phenyltriazene **15** (X = H)*

(*a*) The amide **15** (X = H) (0.25 g) was refluxed in 70% aqueous ethanol (25 ml) for 40 h. Evaporation to dryness and trituration of the residue with benzene afforded a buff-coloured solid, identified as anthranilamide (0.076 g, 56%) mp and mixture mp 105–107 °C; identical ir spectrum with an authentic sample. Evaporation of the benzene mother liquor afforded a brown gum which remained intractable.

(*b*) The amide **15** (X = H) (0.25 g) was refluxed in ethanol (25 ml) containing piperidine (0.25 ml) for 4.0 h. The resulting solution was cooled to afford yellow needles (0.12 g), mp 180 °C (dec.); identical (ir spectrum) with starting material. Evaporation of the mother liquor afforded a solid residue, which was also identical with the starting material.

Likewise, refluxing the diamide **15** (X = $CONH_2$) (0.34 g) in ethanol (70 ml) containing 2% piperidine for 4.5 h resulted in recovery of unchanged starting material.

*Reaction of the Amide-ester **12** in Aqueous Ethanol*

3-(*o*-Carboxamidophenyl)-1-(*o*-methoxycarbonylphenyl)-triazene, **12** (0.276 g), was refluxed for 18.5 h in 70% aqueous ethanol (25 ml). Evaporation of the solution afforded a yellow gummy solid. Trituration of this residue with benzene gave a white solid, which afforded 1,2,3-benzotriazin-4(3*H*)-one, **5** (0.076 g, 56%), identical (ir spectrum) with an authentic sample obtained by diazotisation of anthranilamide.

*2-[2-(Piperidin-1-ylazo)phenyl]quinazolin-4(3H)-one, **18***

(*a*) The amide-ester **12** (0.24 g) was treated with ethanol (25 ml) containing 2% piperidine and was stirred at room

Can. J. Chem. Downloaded from www.nrcresearchpress.com by 210.87.254.5 on 09/05/12
For personal use only.

Can. J. Chem. Downloaded from www.nrcresearchpress.com by 210.87.254.5 on 09/05/12
For personal use only.

temperature for 2 h. Since the amide-ester showed no tendency to dissolve (or react) under these conditions, the mixture was refluxed for just long enough to produce a clear solution (after a few minutes). The resulting solution was kept warm for 5 h and then set aside at room temperature for 2 days. Evaporation of the solution under vacuum left an oily residue which solidified on standing and recrystallised from ethanol to afford 2-[2-(piperidin-1-ylazo)phenyl]quinazolin-4(3*H*)-one, **18**, 0.186 g, 70%, mp 141–142 °C; ν_{max} 3060 (broad) and 1675 cm^{-1}; δ ($CDCl_3$) 1.7 (6H, m, $(CH_2)_3$), 3.85 (4H, m, CH_2—N—CH_2), 7.1–8.7 (8H, m, aromatic), and 13.2 (1H, broad singlet, NH); M^+ 333 ($C_{19}H_{19}N_5O$), *m/e* 249 ($M - C_5H_{10}N$), 221 ($M - C_5H_{10}N_3$).

(*b*) The amide-ester **12** (1.05 g) was refluxed in ethanol containing 1% piperidine for 1.0 h and afforded the same quinazolone **18** (0.9 g, 77%).

(*c*) The same quinazolone **18** (yield 0.45 g, 36%) was obtained when the amide-ester **12** (1.1 g) was stirred at 55–60 °C for 5 h in ethanol containing 1% piperidine and the solution concentrated. The residue from the mother liquor contained starting material.

(*d*) Quinazolino[3,2-*c*][1,2,3]benzotriazin-8-one, **6**, (3) (0.1 g) was refluxed in ethanol (15 ml) with piperidine (0.3 ml) for 1.0 h. Evaporation to dryness and trituration of the residue with petroleum ether gave a solid, which, when recrystallised from ethanol–water, with charcoal treatment, afforded the quinazolone **18** (0.08 g, 60%), identical in all respects with the product obtained from the reaction of the amide-ester **12** with piperidine.

N-(o-Aminobenzoyl)-piperidine, ***19***

(*a*) Piperidine (42.6 g) was dissolved in water (500 ml) and isatoic anhydride (28.9 g) was added. The resulting mixture was stirred at room temperature for 0.5 h, acidified with concentrated hydrochloric acid, and extracted thoroughly with ether. This fraction contained the ureidobenzoic acid by-product, which was not isolated. The acidic aqueous layer was neutralised with sodium bicarbonate and extracted with ether. Evaporation of the dried ($MgSO_4$) ether extracts afforded *N*-(*o*-aminobenzoyl)-piperidine (11.7 g, 32%), mp 82–84 °C (benzene – petroleum ether) (lit. (7) 77.5–79 °C).

(*b*) Reaction of 1,2,3-benzotriazin-4(3*H*)-one, **5**, with neat piperidine, according to the method of Stevens (8), afforded the same *o*-aminobenzoylpiperidine, **19**, yield 72%.

Quinazolino[3,2-c][1,2,3]benzotriazine-8-one, ***6***

(*a*) Anthranilonitrile (2.36 g) was diazotised in concentrated hydrochloric acid (30 ml) at 0 °C with sodium nitrite (1.38 g), and sodium acetate trihydrate (75 g) was added to the clear solution. *N*-(*o*-Aminobenzoyl)-piperidine (4.08 g) was dissolved in 2 *M* hydrochloric acid (10 ml) and was added slowly to the diazonium salt solution. The mixture was stirred for 0.5 h and filtered, to afford an orange-red resin which was taken up in benzene. The benzene solution was chromatographed on a column of alumina and an orange band eluted with benzene. Evaporation of the benzene fraction afforded a red oil, which solidified on standing. Trituration of the residue with ethanol afforded the quinazolinobenzotriazinone **6** (0.8 g, 15%), mp 213–214 °C (from ethanol), mixed mp 213–214 °C; identical (ir spectrum) with a sample prepared by thermolysis of 1,2,3-benzotriazin-4(3*H*)-one (3). Evaporation of the ethanol mother liquor afforded intractable gum.

(*b*) *N*-(*o*-Aminobenzoyl)-piperidine (1.02 g) was diazotised in 2 *M* hydrochloric acid (10 ml) at 0 °C with sodium nitrite (0.4 g) and stirred for 10 min. Anthranilonitrile (0.59 g), dissolved in 2 *M* hydrochloric acid (5 ml) and water (50 ml), was added slowly to the diazonium salt solution, whereupon a pale yellow precipitate separated slowly. After stirring for 1 h the mixture was filtered and the filtrate was treated with sodium acetate (5 g), left at room temperature for 2 h and the orange gum, which had formed, extracted into benzene. Evaporation of the dried ($MgSO_4$) benzene extract, and trituration of the orange residue with benzene afforded the same quinazolino-[3,2-*c*][1,2,3]benzotriazin-8-one (0.44 g, 33%). Evaporation of the benzene mother liquor afforded a dark red intractable tar.

Acknowledgment

The financial assistance of the National Research Council of Canada is gratefully acknowledged.

1. M. W. Partridge and M. F. G. Stevens. J. Chem. Soc. 3663 (1964).
2. M. F. G. Stevens. J. Chem. Soc. (C), 1096 (1967); J. Chem. Soc. (C), 765 (1970).
3. A. W. Murray and K. Vaughan. J. Chem. Soc. (C), 2070 (1970).
4. K. Vaughan. Can. J. Chem. **50**, 1775 (1972).
5. A. Weddige and H. Finger. J. Prakt. Chem. **35**, 262 (1887).
6. H. Mehner. J. Prakt. Chem. **63**, 241 (1901); F. D. Chattaway and A. J. Walker. J. Chem. Soc. 329 (1927).
7. N. J. Leonard, W. V. Ruyle, and L. C. Bannister. J. Org. Chem. **13**, 617 (1948).
8. M. S. S. Siddiqui and M. F. G. Stevens. J. Chem. Soc. Perkin Trans. 1, 611 (1974).
9. M. S. S. Siddiqui and M. F. G. Stevens. J. Chem. Soc. Perkin Trans. 1, 609 (1974).

Composés carbonylés aromatiques: traitement semi-empirique des influences structurales sur leur basicité

D. BEAUPÈRE, J. P. SÉGUIN ET R. UZAN
Laboratoire de Chimie Organique Physique, Université de Picardie, 80039 Amiens Cédex, France
ET
J. P. DOUCET
Laboratoire de Chimie Organique Physique, Université de Paris VII, 75005 Paris, France

Reçu le 27 juin 1975

D. BEAUPÈRE, J. P. SÉGUIN, R. UZAN et J. P. DOUCET. Can. J. Chem. **54**, 297 (1976).

Pour 25 composés du type X—ϕ—CO—R avec X = NO_2, Cl, H, CH_3, OMe et R = H, Me, ϕ—Y et CH=CH—ϕ—Y, nous avons calculé la population électronique totale q_t^0 au niveau de l'atome d'oxygène par la méthode CNDO II. La variation linéaire du pK en fonction de q_t^0 se traduit par l'obtention de quatre droites sensiblement parallèles dont le décalage serait en grande partie attribuable à des modifications d'effets de solvatation dépendant de la nature de R. Un traitement plus général de l'ensemble des résultats permet, à l'aide d'une équation unique $\Delta pK = 154\Delta q_t^0 + 0.1$, d'évaluer l'effet de structure sur la modification de basicité d'un composé carbonylé quelles que soient la nature de X et de R.

D. BEAUPÈRE, J. P. SÉGUIN, R. UZAN, and J. P. DOUCET. Can. J. Chem. **54**, 297 (1976).

We have calculated the total electron density q_t^0 at the oxygen atom, to the CNDO II approximation, for twenty-five compounds of the type X—ϕ—CO—R where X = NO_2, Cl, H, CH_3, OMe, and R = H, Me, ϕ—Y, and CH = OH—ϕ—Y. A linear variation of pK as a function of q_t^0 is shown by a set of four essentially parallel lines; the separation of the lines could be attributed to variations in the solvent effect which depend on the nature of R. A more general treatment of all the results, using a single equation $\Delta pK = 154\Delta q_t^0 + 0.1$, allows an evaluation of the effect of structure on the basicity of a carbonyl compound whatever might be the nature of X or R.

[Journal translation]

Introduction

L'étude de la basicité de composés carbonylés conjugués du type X—ϕ—CO—R a permis de montrer, à partir de différents résultats de la littérature, que pour chaque série de structures caractérisées par un radical R constant et un substituant X variable, il existe une relation linéaire entre pK_{BH^+} et σ_X^+ correspondant (1–5). La variation des pentes des droites ainsi obtenues traduit des réponses différentes à une même perturbation structurale due à une modification de X et cela en fonction de la nature de R. Faute de ne pouvoir estimer dans une même échelle de valeur les effets de X et de R, le caractère prévisionnel de cette approche s'en trouve limité. Des résultats similaires sont obtenus lorsque le paramètre caractérisant la basicité du groupement fonctionnel est l'aptitude du carbonyle à donner des associations avec le phénol (6–9).

Le paramètre expérimental utilisé (pK_{BH^+}) rendant compte du pouvoir du carbonyle à fixer un proton, nous retiendrons dans la recherche d'un modèle semi-empirique exploitable quelle que soit la nature des radicaux X—ϕ et R—, la densité de charge sur l'atome d'oxygène parmi les différents indices de réactivités proposés dans la littérature (10). Des modèles semblables ont été retenus par quelques auteurs qui relient les densités électroniques π sur l'oxygène (densités calculées par l'approximation de Huckel) à différents paramètres physico-chimiques caractéristiques du groupe carbonyle (11–14). Mais dans ces études, les modifications structurales sont limitées, soit à un changement de la chaîne hydrocarbonée (11), soit à un changement de substituant sur une chaîne hydrocarbonée unique (12–14). C'est donc dans un cadre plus général que nous avons abordé cette étude en considérant aussi bien des modifications de substituants que des modifications de la chaîne hydrocarbonée.

Can. J. Chem. Downloaded from www.nrcresearchpress.com by 210.87.254.40 on 09/05/12
For personal use only.

TABLEAU 1. Populations électroniques localisées sur l'oxygène du carbonyle de benzaldéhydes substitués. X—ϕ—CO—H

X (X—ϕ—CO—H)	pK_{BH^+}*	q_t^0
H	−7.5	6.2348
Me-4	−6.6	6.2395
OMe-4	−5.7	6.2434
NO_2-4	−9.1	6.2141
Cl-4	−7.7	6.2271
Me-3	−7.4	6.2343
Cl-3	−8.2	6.2279

*Valeurs des pK_{BH^+} de la réf. 1 calculées dans l'échelle d'acidité de Jorgenson et Hartter.

TABLEAU 2. Populations électroniques localisées sur l'oxygène du carbonyle d'acétophénones substituées. X—ϕ—CO—CH_3

X (X—ϕ—CO—CH_3)	pK_{BH^+}*	q_t^0
H	−6.4	6.2668
Me-4	−5.6	6.2708
OMe-4	−4.8	6.2760
NO_2-4	−8.5	6.2497
Cl-4	−6.8	6.2601
Me-3	−6.2	6.2663
OMe-3	−7.0	6.2634
Cl-3	−7.4	6.2607

*Valeurs des pK_{BH^+} de la réf. 2 calculées dans l'échelle d'acidité de Jorgenson et Hartter.

Resultats

Parmi les 81 aldéhydes et cétones dont l'aptitude à donner des associations avec le phénol a été mesurée (6–9), nous avons retenu un échantillonage de structures représentatives des quatre familles de composés carbonylés définies par R. = H, Me, ϕ—Y et CH=CH—ϕ—Y (tableaux 1–4).

Les équilibres de protonation de ces composés sont mesurés dans des milieux eau–acide sulfurique à 20 °C et dans le calcul des pK_{BH^+}, c'est la fonction d'acidité de Jorgenson et Hartter (15) qui est utilisée. Dans le cas de composés étudiés dans la littérature, les valeurs des pK_{BH^+} ont été recalculées dans cette même échelle d'acidité.

Les populations électroniques totales q_t^0 localisées sur l'atome d'oxygène sont calculées pour tous ces composés dans leur état fondamental tandis que pour un nombre plus limité de structures, la description du modèle est faite à partir de la molécule protonée. Ces calculs font appel à la méthode CNDO II de Pople et Beveridge (16) avec des valeurs standard pour les longueurs et angles de liaisons. Le choix de paramètres standard permet de préciser l'influence de la conformation moléculaire sur la densité de charge sur l'atome d'oxygène (17). Pour les benzaldéhydes (tableau 1), la géométrie moléculaire retenue est plane. Cette même géométrie est appliquée aux acétophénones (tableau 2). Avec les benzophénones (tableau 3), nous avons retenu une torsion de chaque noyau benzénique de 25° par rapport au plan du carbonyle bien que de nombreuses valeurs divergentes aient été proposées dans la littérature (18–20). Pour connaître l'influence de la géométrie sur la valeur de q_t^0, nous avons effectué les calculs avec un angle de torsion de 40° (tableau 5). Enfin dans le cas des chalcones (tableau 4) la géométrie retenue est la conformation *s-cis* plane. Les valeurs de q_t^0 obtenues avec de faibles angles de

TABLEAU 3. Populations électroniques totales localisées sur l'oxygène du carbonyle de benzophénones substituées. X—ϕ—CO—ϕ—Y

X—ϕ—CO—ϕ—Y					
X	Y	pK_{BH^+}†	q_t^0	q_t^+ *cis**	q_t^+ *trans*
H	H	−6.4	6.2752	6.1564	6.1564
Me-4	H	−6.0	6.2784	6.1590	6.1592
OMe-4	H	−5.3	6.2818	6.1608	6.1611
NO_2-4	H	−7.7	6.2611	6.1529	6.1509
Cl-3	H	−7.2	6.2686	—	—
Me-4	Me-4	−5.6	6.2815	6.1615	6.1615
OMe-4	OMe-4	−4.5	6.2873	6.1650	6.1650
OMe-4	NO_2-4	−6.3	—	6.1577	6.1560
Me-4	NO_2-4	−7.2	—	6.1561	6.1539

**Cis* par rapport à X.
†Valeurs des pK_{BH^+} de la réf. 3.

Can. J. Chem. Downloaded from www.nrcresearchpress.com by 210.87.254.40 on 09/05/12
For personal use only.

TABLEAU 4. Populations électroniques localisées sur l'oxygène du carbonyle de chalcones substituées. X—ϕ—CO—CH=CH—ϕ—Y

X—ϕ—CO—CH=CH—ϕ—Y			
Y	X	pK_{BH^+}	q_t^0
H	H	−5.1*	6.2752
H	Me-4	−4.4	6.2803
H	OMe-4	−3.7	6.2859
Me-4	H	−4.6*	6.2786
OMe-4	H	−4.1*	6.2804
NO_2-4	H	−6.3*	6.2680
Me-4	NO_2-4	−6.6	6.2659
Me-4	Me-4	−4.1†	6.2815
OMe-4	OMe-4	−2.8†	6.2870
NO_2-4	OMe-4	−4.7	6.2748
Me-4	OMe-4	−3.2†	6.2857

*Valeurs de pK_{BH^+} calculées dans l'échelle d'acidité de Jorgenson et Hartter, en accord avec les résultats de la réf. 5.
†Valeurs de pK_{BH^+} en accord avec les résultats de la réf. 8.

TABLEAU 5. Influence de la torsion moléculaire sur la population électronique totale localisée au niveau de l'oxygène du carbonyle de benzophénones substituées

	q_t^0 25°	q_t^0 40°	Δq_t^0
H	6.2752	6.2785	33×10^{-4}
Me-4	6.2784	6.2811	27×10^{-4}
MeO-4	6.2818	6.2824	6×10^{-4}
di-MeO-4,4′	6.2873	6.2879	3×10^{-4}

torsion, angles donnés dans la littérature (21) et déterminés en phase cristalline sont pratiquement identiques à 2×10^{-4} électron près à celles calculées pour la forme plane; de plus, la variation de l'équilibre conformationnel *s-cis* ⇄ *s-trans* avec prédominance de l'isomère *s-cis* se traduit également par un décalage faible des valeurs q_t^0.

Discussion

La basicité des aldéhydes et des cétones étant mesurées par leur pK_{BH^+} qui rend compte d'un équilibre thermodynamique, il faudrait relier ce paramètre aux énergies de l'état initial et de l'état final ainsi qu'à l'énergie de solvatation (22). Bien qu'une telle voie d'approche soit a priori, la mieux adaptée (23), les nombreux exemples d'application d'indices statiques (24) d'une part, et la grande taille des molécules étudiées dans ce travail d'autre part, nous ont incités dans un premier temps à retenir la seule description du modèle dans l'état initial. Parmi les différents paramètres de densités de charges obtenus dans nos calculs, le paramètre q_σ est peu sensible aux effets structuraux tandis que q_π et q_t ont des variations plus importantes et du même ordre de grandeur (tableau 6).

TABLEAU 6. Populations électroniques localisées sur l'atome d'oxygène d'acétophénones substituées. X—ϕ—CO—CH_3

X (X—ϕ—CO—CH_3)	q_t^0	q_π	q_σ*
H	6.2668	1.2297	5.0371
Me-4	6.2708	1.2352	5.0356
OMe-4	6.2760	1.2426	5.0334
Cl-4	6.2601	1.2222	5.0379
NO_2-4	6.2497	1.2094	5.0403
Me-3	6.2663	1.2282	5.0381
OMe-3	6.2634	1.2239	5.0395
Cl-3	6.2607	1.2243	5.0364

*$q_\sigma = q_t^0 - q_\pi$

Pour l'ensemble des sept benzaldéhydes du type X—ϕ—CHO, la représentation graphique des pK_{BH^+} en fonction des q_t^0 correspondants montre une nette tendance à la corrélation linéaire. Cette corrélation est définie par l'équation

$$pK_{BH^+} = 107q_t^0 - 677$$

avec un coefficient de corrélation de 0.95 et un écart type moyen de 0.27. La qualité moyenne de cette corrélation est imputable au comportement particulier du nitro-4 benzaldéhyde et du chloro-4 benzaldéhyde (fig. 1). Si l'on exclut ces deux composés, l'équation précédente devient

$$pK_{BH^+} = 160q_t^0 - 1009$$

coefficient de corrélation 0.98 et écart moyen 0.14.

L'écart des points représentatifs des dérivés nitrés et chlorés peut être attribué à une estimation moins précise des effets de substituants sur la densité de charge. De tels écarts ont déjà été observés par ailleurs (25) mais le fait d'observer une telle corrélation semble indiquer que les phénomènes de solvatation varient linéairement avec les paramètres calculés.

Dans le cas des acétophénones, on observe également une tendance à la corrélation à l'exception encore des dérivés nitrés et chlorés (fig. 1). Mis à part ces deux composés, on obtient avec les acétophénones une nouvelle équation entre pK_{BH^+} et q_t^0

$$pK_{BH^+} = 171q_t^0 - 1083$$

Can. J. Chem. Downloaded from www.nrcresearchpress.com by 210.87.254.40 on 09/05/12
For personal use only.

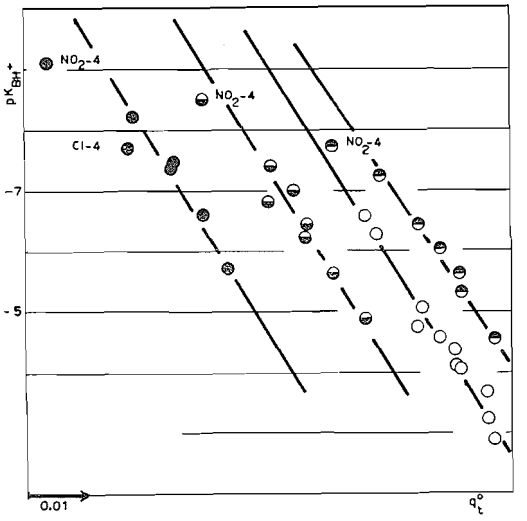

FIG. 1. Corrélations entre basicité et densité de charge pour 4 familles de composés carbonylés aromatiques: ● benzaldehydes; ◒ acetophenones; ◓ benzophenones; ○ chalcones.

coefficient de corrélation 0.99, écart moyen 0.08. La pente de la droite relative aux acétophénones est donc très voisine de celle des benzaldéhydes. Si les deux droites ne sont pas confondues, cela ne peut être attribué à une influence du facteur géométrie moléculaire dans l'évaluation de q_t^0 puisqu'on a vérifié que de petites torsions moléculaires entraînent de faibles modifications de q_t^0. Il est donc probable que ce décalage soit imputable en grande partie à des solvatations différentes des benzaldéhydes et des acétophénones.

Pour les benzophénones substituées, si on admet un angle de torsion de 25° de chaque noyau benzénique par rapport au plan du carbonyle, la corrélation basicité–densité de charge vérifie l'équation

$$pK_{BH^+} = 143q_t^0 - 909$$

coefficient de corrélation 0.99 et écart moyen 0.10.

Pour mettre en évidence le rôle de la géométrie moléculaire sur la variation de la densité électronique au niveau de l'oxygène, nous avons calculé quelques valeurs de q_t^0 en partant de l'hypothèse que l'angle de torsion n'est plus 25° mais 40° comme certains auteurs l'affirment (18). Avec ces nouvelles valeurs de q_t^0, la pente de la corrélation est voisine de 200. Cette valeur plus élevée serait due à une modification de charge plus faible que dans le cas où la torsion moléculaire est inférieure et montre ainsi l'importance de la géométrie sur le calcul de q_t^0.

Enfin les chalcones vérifient l'équation

$$pK_{BH^+} = 175q_t^0 - 1150$$

coefficient de corrélation 0.96, écart moyen 0.15.

Ces différents résultats montrent que pour tous les composés du type X—ϕ—CHO, X—ϕ—CO—CH_3 et ϕ—CH=CH—CO—ϕ—Y, une même modification de la densité de charge au niveau de l'oxygène du carbonyle (Δq_t^0) est exprimée par une même modification de la basicité (ΔpK_{BH^+}). Pour les benzophénones, au même ΔpK_{BH^+}, correspond une variation légèrement inférieure du q_t^0 lorsque l'angle de torsion des deux cycles est de 25°.

Dans son ensemble, cette méthode d'approche de l'influence structurale sur la basicité de composés carbonylés aussi différents que ceux étudiés, est plus générale que celle qui consiste à relier le pK aux constantes de substituant σ_X^+. En effet un tel traitement conduit à l'obtention de quatre corrélations linéaires, caractérisées par des pentes ρ variables avec la structure du composé de référence.

Pour les benzaldéhydes et les acétophénones (un noyau aromatique) les valeurs de ρ sont respectivement égales à -2.2 et -2.4 tandis que pour les benzophénones (deux noyaux aromatiques) et les chalcones (X—ϕ—CO—CH=CH—ϕ), ces valeurs indiquent une diminution des pentes des corrélations ($\rho = -1.6$ et -1.8). Ces résultats permettent de vérifier en première approximation qu'une extension du domaine de la conjugaison se traduit par une diminution de la sensibilité aux effets de structures. En plus de ce paramètre, intervient aussi le facteur géométrique qui favorise ou défavorise la transmission des effets de substituants au niveau du groupe fonctionnel. La diversité des pentes obtenues réduit donc le caractère prévisionnel de cette approche. Par contre, l'utilisation du paramètre densité de charge dans l'estimation des effets de structure sur la basicité conduit pour les quatre composés de références (X = H) et les 21 dérivés correspondants, à une corrélation unique entre le ΔpK_{BH^+} et le Δq_t^0 correspondant. Son équation est

$$\Delta pK_{BH^+} = 154\Delta q_t^0 + 0.1$$

avec un coefficient de corrélation de 0.98 et un écart moyen de 0.16 unité pK. La bonne qualité

Can. J. Chem. Downloaded from www.nrcresearchpress.com by 210.87.254.40 on 09/05/12
For personal use only.

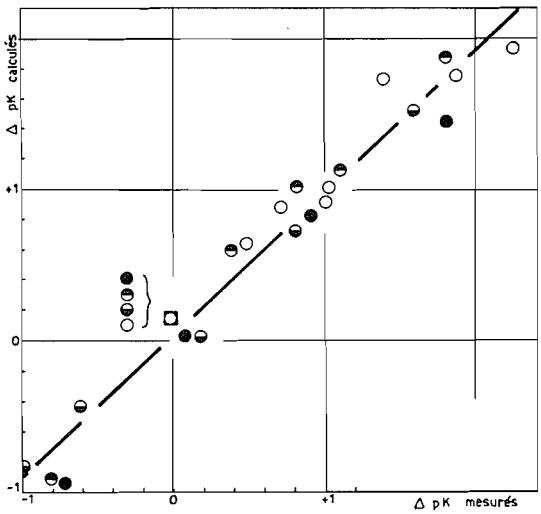

FIG. 2. Corrélation générale pour l'ensemble des quatre familles de composés carbonylés entre les influences structurales mesurées et calculées, représentées par leur ΔpK: ● benzaldehydes; ◓ benzophenones; ◒ acetophenones; ○ chalcones.

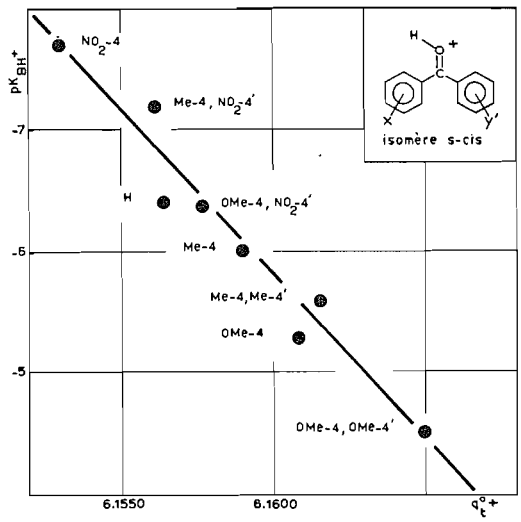

FIG. 3. Variations de la basicité de benzophénones substituées en fonction de la densité de charge calculée à partir de ces composés à l'état protoné.

de cette corrélation est observée sur la fig. 2 dans laquelle ΔpK_{BH^+} calculé est porté en fonction de ΔpK_{BH^+} mesuré. La pente de cette droite, égale à 0.956, est très voisine de 1.

Dans une seconde approche, nous avons cherché à déterminer la densité de charge sur l'oxygène lorsque le composé carbonylé est à l'état protoné. Pour réduire le temps de calcul, nous avons limité cette étude à quelques benzophénones car dans le cas des composés moins symétriques se pose le problème des deux conformères possibles dans la molécule protonée. On peut constater alors (fig. 3) que la *para*-nitrobenzophénone se situe convenablement sur la droite d'équation $pK = f(q_t^{0+})$. Nous avons pu vérifier que l'influence du groupe nitro au niveau du carbonyle était plus précise dans le cas de l'estimation de q_t^0 à partir du modèle protoné. Cependant, il faut noter que ce traitement n'améliore pas de façon sensible la qualité des résultats précédant obtenus par simple description des molécules dans leur état fondamental.

Partie expérimentale

Les chalcones utilisées sont préparées par condensation de Claisen–Schmidt (26) de benzaldéhydes et acétophénones appropriées. L'identification et la pureté de ces composés ont été déterminées par spectroscopie infrarouge, ultra-violette et de résonance magnétique nucléaire. Les valeurs des constantes de couplage du système éthylénique permettent de préciser que tous ces composés sont des isomères *trans*. Les caractéristiques physiques correspondantes sont en accord avec la littérature.

Les mesures des pK_{BH^+} des chalcones sont effectuées par spectrophotométrie ultra-violette, sur un spectrophotomètre Bausch et Lomb spectronic 600 E, dans des milieux eau acide sulfurique à 20 °C selon la méthode classique (27).

1. K. YATES et R. STEWART. Can. J. Chem. **37**, 64 (1959).
2. R. STEWART et K. YATES. J. Am. Chem. Soc. **80**, 6355 (1958).
3. G. GOETHALS, J. P. DOUCET, P. BAUER et R. UZAN. Spectrochim. Acta, **31A**, 1501 (1975).
4. R. STEWART, R. B. MOODIE, M. R. GRANCER, et L. J. MUENSTER. Can. J. Chem. **41**, 1065 (1963).
5. D. S. NOYCE et M. J. JORGENSON. J. Am. Chem. Soc. **84**, 4312 (1962).
6. J. P. SÉGUIN, D. BEAUPÈRE, P. BAUER et R. UZAN. Bull. Soc. Chim. Fr. **1–2**, 167 (1972).
7. D. BEAUPÈRE, R. UZAN et J. P. DOUCET. C. R. Acad. Sci. **278**, 187 (1974).
8. D. BEAUPÈRE, J. P. SÉGUIN et J. P. DOUCET. C. R. Acad. Sci. **276**, 1123 (1973).
9. D. BEAUPÈRE, J. P. SÉGUIN, R. UZAN et J. P. DOUCET. A paraître.
10. M. J. S. DEWAR. Adv. Chem. Phys. **8**, 133 (1963).
11. H.P. FIGEYS et J. NASIELSKI. Spectrochim. Acta, **23A**, 465 (1967).
12. K. S. SPAARGAREN, C. KRUK, T. A. MOLENAAR-LANGEVELD, P. K. KORVER, P. J. VAN DER HAAK et TH. J DE BOER. Spectrochim. Acta, **28A**, 965 (1972).
13. A. GROUILLER, P. THOMASSERY, H. PACHECO, C. DECORET et B. TINLAND. Bull. Soc. Chim. Fr. **12**, 3454 (1973).

Can. J. Chem. Downloaded from www.nrcresearchpress.com by 210.87.254.40 on 09/05/12
For personal use only.

14. P. ZAHRADNIK et J. LESKA. Coll. Czech. Chem. Commun. 36, (1974).
15. M. J. JORGENSON et D. R. HARTTER. J. Am. Chem. Soc. **85**, 878 (1963).
16. J. A. POPLE et D. L. BEVERIDGE. Approximate molecular orbital theory. McGraw-Hill, New-York. 1970.
17. M. GRAFFEUIL, J. F. LABARRE et C. LEIBOVICI. J. Mol. Struct. **22**, 97 (1974); **23**, 65 (1974).
18. P. H. GORE, J. A. HOSKINS, R. J. W. LE FEVRE, L. RADOM et G. L. D. RITCHIE. J. Chem. Soc. B, 741 (1967).
19. M. GRIMAUD, M. LOUDET, R. ROYER et G. PFISTER-GUILLOUZO. Bull. Soc. Chim. Fr. **5–6**, 1161 (1974).
20. R. N. JONES. J. Am. Chem. Soc. **67**, 2227 (1945).
21. D. RABINOWICH. J. Chem. Soc. B, 11 (1970).
22. A. BOTREL et C. R. GUERILLOT. J. Chim. Phys. **71**, 974 (1974).
23. L. ALTSCHULER et E. BERLINER. J. Am. Chem. Soc. **88**, 5837 (1966).
24. A. STREITWIESER. Molecular orbital theory for organic chemists. John Wiley and Sons, New York. 1966.
25. E. GEY. Z. Chem. **11**, 392 (1971).
26. Organic syntheses. **1**, 78 (1967), John Wiley and Sons, New York.
27. M. A. PAUL et F. A. LONG. Chem. Rev. **57**, 1 (1957).

Can. J. Chem. Downloaded from www.nrcresearchpress.com by 210.87.254.40 on 09/05/12
For personal use only.

Etude des complexes aqueux d'uranium(IV) en milieu acide par résonance magnétique nucléaire

C. KIENER, G. FOLCHER, P. RIGNY et J. VIRLET

C.E.N.—Saclay, Division de Chimie, B.P. N° 2, 91190 Gif-sur-Yvette, France

Reçu le 30 juin 1975

C. KIENER, G. FOLCHER, P. RIGNY et J. VIRLET. Can. J. Chem. **54**, 303 (1976).

L'hydratation de l'uranium tétravalent en milieu acide a été étudiée par résonance magnétique du proton. Les vitesses de relaxation longitudinale et transversale de l'eau sont décrites en fonction de la température, de l'acidité et des ions ajoutés. En milieu perchlorique, elles sont gouvernées à haute température, par l'échange des molécules d'eau entre la sphère interne de coordination de l'uranium(IV) et le solvant libre. Le temps de résidence des protons liés τ_M évolue entre 10 ms et 1 s. La vitesse d'échange dépend de l'acidité suivant la loi $1/\tau_M \approx A + B/[H^+]$, à $pH > 0$ et varie linéairement avec l'activité de l'eau, aux fortes concentrations en ions diamagnétiques. A basse température, un effet de sphère externe limite les vitesses de relaxation, ce qui permet de chiffrer le temps de relaxation électronique de l'uranium(IV) à 10^{-13} s environ. Aucun signal de protons dû aux ligands de la première sphère, liés fermement à l'uranium(IV) et soumis à une relaxation rapide, n'est observé. Le déplacement chimique du signal d'absorption des protons en milieu chlorhydrique est causé par les couplages paramagnétiques entre l'uranium(IV) et les ligands dans une seconde sphère en échange rapide avec les molécules du solvant libre. Au-dessus d'une concentration en chlore de 6 *M*, des complexes monochlorés d'uranium(IV) contribuent au déplacement chimique.

C. KIENER, G. FOLCHER, P. RIGNY, and J. VIRLET. Can. J. Chem. **54**, 303 (1976).

The hydration of tetravalent uranium in acid solutions has been studied by proton magnetic resonance. Longitudinal and transversal relaxation rates of water are reported as a function of temperature, acidity, and added ions. The relaxation rates observed in perchloric solutions at high temperature are governed by the exchange process of water molecules between the inner coordination sphere of uranium(IV) and the bulk water. The bound proton's lifetime τ_M lies between 10 ms and 1 s. At $pH > 0$, the exchange rate depends upon acidity according to the law $1/\tau_M \approx A + B/[H^+]$. At high concentrations of diamagnetic ions the exchange rate depends linearly upon water activity. At low temperature, the proton relaxation rates are dominated by an outer sphere effect and the electronic relaxation time of uranium(IV) is found to be about 10^{-13} s. No signal is observed from protons of the water molecules in the first sphere, firmly bound to uranium(IV), which undergo rapid relaxation. The chemical shift of the proton absorption signal in hydrochloric solutions arise from tightly bound water molecules in paramagnetic interaction with uranium(IV) in a second sphere, and in fast exchange with the bulk water. Above a chlorine concentration of 6 *M*, the monochloro complex of uranium(IV) contributes to the chemical shift.

(I) Introduction

Si depuis plusieurs années, des études ont été menées sur les aquo-complexes d'uranium(IV) en solution, ni leur structure, ni leur stabilité ne sont bien connues. Par des travaux spectroscopiques (rayons X, absorption visible, infrarouge, diffusion Raman, etc. . . .) on a tenté d'établir la coordinence et la symétrie de ces complexes (1–5).[1] Les résultats obtenus semblent montrer que l'entourage de l'uranium(IV) en solution aqueuse est constitué par 8 ou 9 molécules d'eau suivant une symétrie élevée. Il existe peu de données (6) dans la littérature sur la cinétique d'échange des coordinats; d'autre part la nature des liaisons chimiques entre l'uranium(IV) et les molécules d'eau solvatantes étant mal définie, il est difficile de préciser si tous les coordinats sont équivalents ou non.

Nous présentons ici une étude de la solvatation de l'uranium(IV) en milieu acide par résonance magnétique nucléaire.

L'effet des ions paramagnétiques sur les vitesses de relaxation et sur les déplacements chimiques des noyaux du solvant se comprend en général, sur la base d'un modèle simple (7) où les coordinats peuvent se trouver dans deux environnements, le solvant libre, site indicé $\langle 0 \rangle$ et la sphère de coordination de l'ion

[1]Laboratoire de Chimie de l'Uranium, D. Ch., S.E.P.C.P., C.E.N. Saclay (communications privées).

Can. J. Chem. Downloaded from www.nrcresearchpress.com by 210.87.254.6 on 09/05/12
For personal use only.

Can. J. Chem. Downloaded from www.nrcresearchpress.com by 210.87.254.6 on 09/05/12
For personal use only.

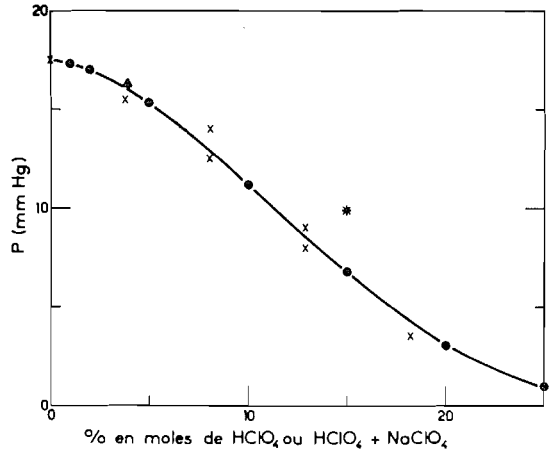

FIG. 1. Tension de vapeur des solutions d'acide perchlorique (×[1] et ● (6)) et des solutions mixtes d'acide perchlorique et de perchlorate de sodium (*,[1] 1.35 *M* $HClO_4$ et 5.0 *M* $NaClO_4$; ▲,[1] 1.0 *M* $HClO_4$ et 1.0 *M* $NaClO_4$) mesurée à 20 °C, en fonction du pourcentage molaire d'acide ou d'acide et de sel.

paramagnétique, site indicé ⟨M⟩. Dans ce dernier environnement ⟨M⟩, les couplages dipolaires et scalaires entre les spins nucléaires des molécules solvatantes et le moment magnétique électronique de l'ion solvaté conduisent à une relaxation nucléaire rapide et à des déplacements chimiques importants. L'effet de l'échange des coordinats entre les deux environnements sur la résonance magnétique des noyaux du solvant va dépendre de la vitesse d'échange.

(II) Partie expérimentale

Les mesures des temps de relaxation des protons ont été faites sur des solutions aqueuses de perchlorate d'uranium(IV) à 0.25 *M*, en présence d'acide perchlorique.

Les solutions de perchlorate d'uranium(IV) ont été préparées par réduction du perchlorate d'uranyle à la cathode de mercure:[1]

$$[1] \qquad UO_2^{2+} + 4H^+ + e^- \rightarrow U^{4+} + 2H_2O$$

Un dosage par le bichromate de potassium a permis de déterminer la concentration en uranium(IV). L'acidité de la solution est titrée par un dosage à la soude après avoir fait précipiter l'uranium(IV) avec du fluorure de sodium.

La gamme des solutions étudiées comprend d'une part des solutions faiblement acides ($[HClO_4] \approx 0.2, 0.48, 1.0, 2.0$ *M*) pour lesquelles la force ionique est maintenue constante par addition de perchlorate de sodium ($[NaClO_4] \approx 1.8, 1.52, 1.0$ *M*), d'autre part deux solutions fortement concentrées en ions diamagnétiques ($[HClO_4] \approx 1.35$ *M* + $[NaClO_4] \approx 5.0$ *M*, $[HClO_4] \approx 8.0$ *M*) et enfin une solution aqueuse de chlorure d'uranium(IV) à 0.25 *M*, en présence d'acide chlorhydrique ($[HCl] \approx 2.0$ *M*).

Des mesures de tension de vapeur ont été effectuées sur les solutions perchloriques en absence d'uranium(IV), afin de déterminer l'activité du solvant. Les résultats sont portés sur la fig. 1.

L'oxygène moléculaire dissous est éliminé des solutions par un barbotage d'azote; les tubes rmn sont ensuite scellés.

On a mesuré les temps de relaxation des protons à des fréquences comprises entre 4 et 30 MHz, sur des spectromètres de rmn par impulsions, cohérents, construits au laboratoire. Le temps de relaxation de l'aimantation longitudinale, T_1, se mesure par la séquence usuelle de deux impulsions $\pi-\pi/2$. Le temps de relaxation de l'aimantation transversale, T_2, est déterminé à l'aide de la séquence de Meiboom et Gill (9). La précision des mesures est de 5% pour le temps de relaxation longitudinale et de 15% pour le temps de relaxation transversale.

Les déplacements chimiques du signal de résonance des protons dans des solutions aqueuses de chlorure d'uranium(IV) en milieu acide chlorhydrique, ont été mesurés sur un spectromètre de rmn haute-résolution DA-60. Le (triméthyl silyl)$_3$ propane sulfonate de sodium ou TMPS de formule $Si(CH_3)_3(CH_2)_3SO_3^-Na^+$ a servi de référence interne.[2]

(III) Relaxation des protons du solvant par les ions paramagnétiques U^{4+}

Aux mécanismes de relaxation dipolaire proton–proton qui existent même dans les solutions acides pures, se superposent les mécanismes de relaxation paramagnétique dus aux ions U^{4+}. La contribution paramagnétique des ions U^{4+} à la vitesse de relaxation, $1/T_1^{(U(IV))}$, s'obtient par différence entre les mesures effectuées dans la solution acide pure et dans la solution contenant de l'uranium(IV). L'effet diamagnétique des ions U^{4+} sur la relaxation des protons peut être négligé tant que la concentration du sel d'uranium reste faible. On écrit donc:

$$[2] \qquad \frac{1}{T_1^{(U(IV))}} = \frac{1}{T_1^{(U(IV)+HClO_4)}} - \frac{1}{T_1^{(HClO_4)}}$$

Dans une solution acide perchlorique ($[HClO_4] = 2.0$ *M*), contenant 0.25 *M* de $U(ClO_4)_4$, on a mesuré le temps de relaxation longitudinale T_1, de −5 à 95 °C. Les résultats sont portés sur la fig. 2. De −5 à +40 °C environ, la vitesse de relaxation $1/T_1^{(U(IV))}$ varie

[2]On a vérifié que la position du signal de résonance du TMPS n'était pas affectée par la présence de l'uranium(IV), en comparant les déplacements chimiques du TMPS et du cation $N(CH_3)_4^+$ dans une solution acide. Lorsque du chlorure d'uranium(IV) est ajouté à la solution, la différence de déplacement chimique entre le TMPS et le cation $N(CH_3)_4^+$ ne varie pas.

Can. J. Chem. Downloaded from www.nrcresearchpress.com by 210.87.254.6 on 09/05/12
For personal use only.

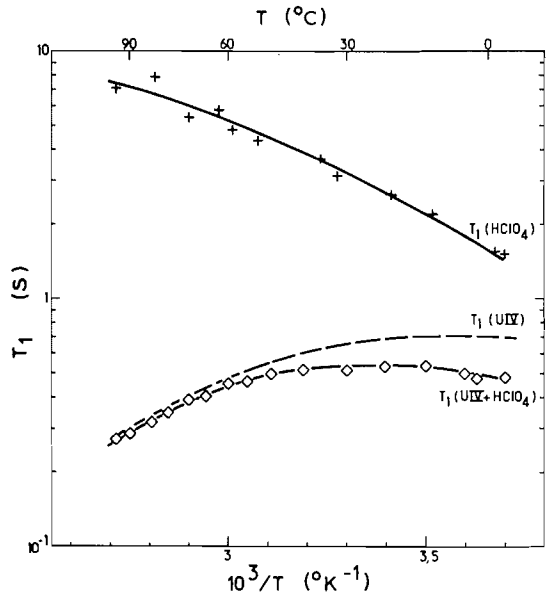

FIG. 2. Temps de relaxation longitudinale des protons mesuré dans des solutions acides avec et sans uranium(IV) (+, $T_1^{(HClO_4)}$ (2.0 *M* $HClO_4$), ◇, $T_1^{(HClO_4+U(IV))}$ (2.0 *M* $HClO_4$, 0.25 *M* $U(ClO_4)_4$)) en fonction de la température. La contribution des ions U^{4+} au temps de relaxation longitudinale des protons $T_1^{(U(IV))}$, est figurée en tirets.

peu avec la température puis elle croît avec elle au-dessus de 40 °C. Nous avons vérifié que cette vitesse $1/T_1^{(U(IV))}$ ne dépendait pas de la fréquence de Larmor, $4 \lesssim \nu_0 \lesssim 30$ MHz et qu'il n'existait pas de différence observable entre les vitesses de relaxation longitudinale $1/T_1^{(U(IV))}$ et transversale $1/T_2^{(U(IV))}$, quelle que soit la température ou la fréquence.

Dans le cadre d'un modèle d'échange des protons entre deux sites (la sphère de coordination de l'uranium(IV), $\langle M \rangle$ et le solvant libre, $\langle 0 \rangle$) où les populations en protons sont très différentes

$$P_M = \frac{n_{int}[U(IV)]}{[H_2O]_{tot} + \frac{1}{2}[HClO_4]} << 1$$

et $$P_0 = 1 - P_M \approx 1$$

où n_{int} est le nombre de molécules d'eau fermement liées à l'uranium(IV), la contribution paramagnétique aux vitesses de relaxation a pour expression (7, 10, 11).

$$[3] \qquad \frac{1}{T_1^{(U(IV))}} \approx \frac{P_M}{P_0(T_{1M} + \tau_M)}$$

$$[4] \qquad \frac{1}{T_2^{(U(IV))}} \approx \frac{P_M}{P_0\tau_M} \times \left[\frac{1/T_{2M}^2 + 1/(T_{2M}\tau_M) + \Delta\omega_M^2}{(1/T_{2M} + 1/\tau_M)^2 + \Delta\omega_M^2}\right]$$

où T_{1M}, T_{2M}, $\Delta\omega_M$ et τ_M sont respectivement les temps de relaxation longitudinale et transversale, le déplacement chimique et le temps de résidence des protons dans la sphère de coordination de l'uranium(IV).

L'identité des vitesses de relaxation $1/T_1^{(U(IV))}$ et $1/T_2^{(U(IV))}$, sachant que le déplacement chimique $\Delta\omega_M$ est important,[1] implique que la relaxation des protons situés dans la sphère interne d'hydratation est rapide devant le processus d'échange (T_{1M}, $T_{2M} < \tau_M$). Dans ce cas on obtient:

$$[5] \qquad \frac{1}{T_{i=1,2}^{(U(IV))}} \approx \frac{P_M}{P_0\tau_M} = \frac{1}{\tau_0}$$

où τ_0 est le temps de résidence des protons dans le solvant libre. A haute température ($T > 40$ °C), la variation thermique de la vitesse de relaxation $1/T_{i=1,2}^{(U(IV))}$ peut se décrire dans un tel modèle, par un mécanisme d'échange thermiquement activé:

$$[6] \qquad \tau_0 \approx \tau_0^{\infty} \exp\left(\frac{V_0}{RT}\right)$$

Aux molarités $[HClO_4] \approx 2$ *M* et $[U(IV)] \approx 0.25$ *M*, on a $\tau_0^{\infty} \approx 6.35 \times 10^{-5}$ s et $V_0 \approx 7 \pm 1$ kcal/mol soit $\tau_0 \approx 3.26$ s à 20 °C et $\tau_0 \approx 0.36$ s à 95 °C. Le temps de résidence τ_M des protons de l'eau dans la sphère d'hydratation vaut par exemple 0.15 s à 20 °C si l'on prend la valeur raisonnable $n_{int} = 9$.

A basse température ($T < 40$ °C), la variation thermique de la vitesse de relaxation $1/T_{i=1,2}^{(U(IV))}$ s'inverse. Ce comportement ne peut pas être attribué à l'échange, mais il est dû à l'existence d'un second mécanisme de relaxation thermiquement désactivé que l'on peut décrire par une loi de la forme

$$[7] \qquad \left(T_i^{(U(IV))}\right)^{(b)} \approx K \exp\left(\frac{-E_b}{RT}\right)$$

avec $E_b \approx 0.9$ kcal/mol. On admet ainsi que:

$$[8] \qquad \frac{1}{T_{i=1,2}^{(U(IV))}} \approx \left(\frac{P_M}{P_0\tau_M}\right)^{(a)} + \left(\frac{1}{T_i^{(U(IV))}}\right)^{(b)}$$

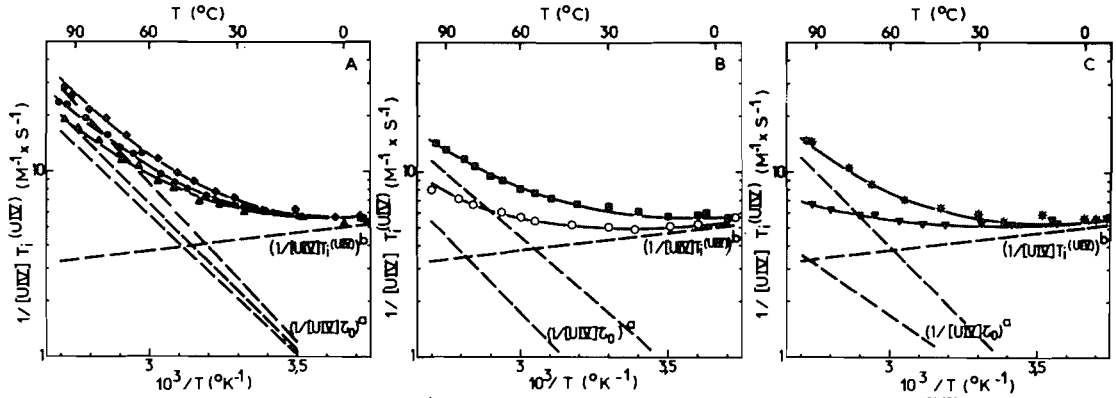

FIG. 3. Contribution des ions U^{4+} à la vitesse de relaxation des protons, $1/[U(IV)]\ T_i^{(U(IV))}$, déduite des mesures effectuées dans des solutions acides d'uranium(IV), en fonction de la température: *A*, à 0.25 *M* $U(ClO_4)_4$ et à faible acidité: (◆, 0.2 *M* $HClO_4$ et 1.8 *M* $NaClO_4$; ●, 0.48 *M* $HClO_4$ et 1.52 *M* $NaClO_4$; ▲, 1.0 *M* $HClO_4$ et 1.0 *M* $NaClO_4$). *B*, en milieu perchlorique: (■, 2.0 *M* $HClO_4$ et 0.25 *M* $U(ClO_4)_4$) et en milieu chlorhydrique: (○, 2.0 *M* HCl et 0.25 *M* UCl_4). *C*, à 0.25 *M* $U(ClO_4)_4$ et à forte concentration en ions diamagnétiques: (*, 1.35 *M* $HClO_4$ et 5.0 *M* $NaClO_4$; ▼, 8.0 *M* $HClO_4$). On a indiqué en tirets la décomposition des courbes en une partie (*a*) thermiquement activée due à l'échange $(1/[U(IV)]\tau_0)^a$ et en une partie (*b*) thermiquement désactivée, $(1/[U(IV)]T_i^{(U(IV))})^b$.

Le mécanisme (b) qui sera analysé au Paragraphe III-2, est un mécanisme de "sphère externe" qui met en jeu des molécules d'eau labiles situées hors de la sphère de coordination et/ou quelques coordinats [1, 2, 3] occupants alors des sites privilégiés plus labiles dans la sphère interne d'hydratation.

(1) Effet des ions diamagnétiques sur la relaxation des protons du solvant

La vitesse d'échange $P_M/(P_0\tau_M)^{(a)} \approx 1/\tau_0^{(a)}$ varie avec l'acidité $[H^+]$ ou la concentration des autres espèces diamagnétiques contenues dans la solution, soient ClO_4^- ou Cl^- et Na^+. L'ensemble des résultats expérimentaux $1/([U(IV)]T_i^{(U(IV))}) = f(1/T)$ pour diverses valeurs de $[H^+]$, $[Na^+]$, $[ClO_4^-]$ ou $[Cl^-]$ est représenté sur la fig. 3. On peut toujours décomposer ces courbes selon la relation 8 en une partie (a) thermiquement activée, due à l'échange et en une partie (b) thermiquement désactivée. La composante (b) qui est unique, est indépendante de la concentration et de la nature des ions diamagnétiques du milieu. A l'opposé, la vitesse d'échange $1/([U(IV)]\tau_0)^{(a)}$ décroît lorsque l'acidité ou la concentration en ions ClO_4^- et Na^+ augmente; elle est légèrement plus rapide par un facteur 2.5 en milieu perchlorique qu'en milieu chlorhydrique.

Nous avons porté sur la fig. 4, l'évolution de la vitesse d'échange $1/([U(IV)]\tau_0) \approx P_M/(P_0[U(IV)]\tau_M)$ en fonction de l'inverse de l'acidité

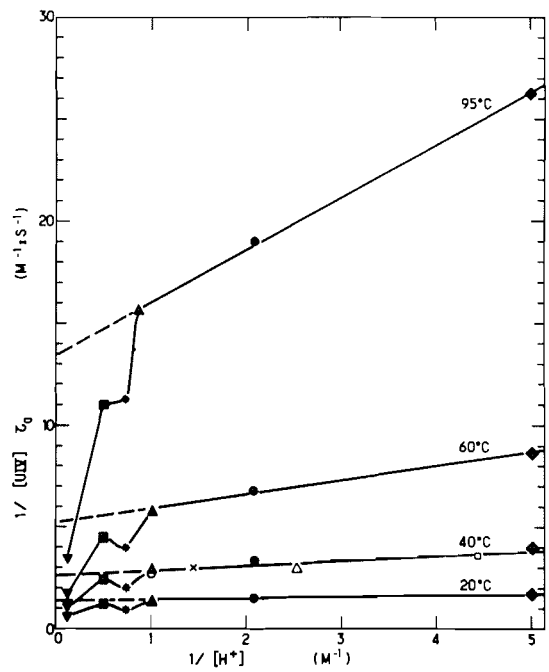

FIG. 4. Comportement de la vitesse d'échange $1/[U(IV)]\ \tau_0 \approx (1/[U(IV)]\tau_M)(P_M/P_0)$ en fonction de l'acidité pour des solutions aqueuses de perchlorate d'uranium(IV), à 0.25 *M* $U(ClO_4)_4$, à différentes températures: (◆, 0.2 *M* $HClO_4$ et 1.8 *M* $NaClO_4$; ●, 0.48 *M* $HClO_4$ et 1.52 *M* $NaClO_4$; ▲, 1.0 *M* $HClO_4$ et 1.0 *M* $NaClO_4$; ■, 2.0 *M* $HClO_4$; ▼, 8.0 *M* $HClO_4$; *, 1.35 *M* $HClO_4$ et 5.0 *M* $NaClO_4$) et pour des solutions aqueuses de perchlorate d'uranium(IV), réfs 4 et 10 à 0.08 *M* $U(ClO_4)_4$, vers 40 °C: (◇, 1.0 *M* $HClO_4$; ×, 0.69 *M* $HClO_4$; △, 0.4 *M* $HClO_4$; □, 0.225 *M* $HClO_4$).

Can. J. Chem. Downloaded from www.nrcresearchpress.com by 210.87.254.6 on 09/05/12
For personal use only.

Can. J. Chem. Downloaded from www.nrcresearchpress.com by 210.87.254.6 on 09/05/12
For personal use only.

pour quelques températures. Nous avons aussi indiqué certains résultats obtenus par Glébov *et al.* (6, 12), en l'absence de cations Na^+, à différentes concentrations en uranium(IV) et en milieu perchlorique, vers 40 °C.

(A) Dans le domaine dilué et faiblement acide ($[H^+] \lesssim 1.0$ *M*, $[ClO_4^-] \lesssim 3.0$ *M*, $[Na^+] \lesssim 1.8$ *M*), la variation de la vitesse d'échange avec l'acidité portée sur la fig. 4, est correctement décrite par une loi empirique de la forme

$$[9] \qquad \frac{1}{[U(IV)]\tau_0} \approx A + \frac{B}{[H^+]}$$

Les coefficients *A* et *B* de l'expression 9 croissent avec la température et sont indépendants de la concentration en ions U^{4+}, ClO_4^- et Na^+. On sait qu'à faible acidité, des complexes monohydroxylés $U(OH)(H_2O)_m^{3+}$ se forment par hydrolyse (12, 13).

$$[10] \quad U(H_2O)_n^{4+} + H_2O \overset{K_{hyd}}{\rightleftharpoons} U(OH)(H_2O)_m^{3+} + H^+$$

L'augmentation de la vitesse d'échange $1/[U(IV)]\tau_0$ lorsque l'acidité décroît, peut s'expliquer qualitativement si la cinétique d'échange des protons est plus rapide pour les complexes monohydroxylés que pour les complexes aqueux. Ce résultat corrobore celui de Glébov *et al.* (12). Mais tant que nous ne connaissons pas les étapes élémentaires de la cinétique (réaction d'hydrolyse, échange par proton seul ou par molécule d'eau entière pour chaque catégorie de complexes, etc. . . .), une interprétation quantitative de la vitesse d'échange reste impossible.

(B) A plus forte concentration en acide $[H^+] > 1.0$ *M*, l'échange se ralentit plus vite qu'à faible acidité, alors que la loi 9 prédit une vitesse d'échange $1/[U(IV)]\tau_0$ presque constante dans ce domaine. Ainsi, lorsque $[H^+]$ croît de 2.0 à 8.0 *M* et $[ClO_4^-]$ de 3.0 à 9.0 *M*, la vitesse d'échange $1/[U(IV)]\tau_0$ devient trois fois plus faible pour des températures comprises entre 95 et 60 °C.

Pour essayer de comprendre si ce ralentissement est imputable à la forte acidité, $[H^+] > 1.0$ *M* ou en partie à la présence des anions ClO_4^- on peut examiner le comportement de l'échange dans une solution peu acide $[H^+] \approx 1.35$ *M*, contenant un excès d'anions, $[ClO_4^-] \approx 7.35$ *M* et de cations, $[Na^+] \approx 5.0$ *M*. Lorsque $[Na^+]$ augmente de 1.0 à 5.0 *M*, $[ClO_4^-]$ de 3.0 à 7.35 *M* et $[H^+]$ de 1.0 à 1.35 *M*, la vitesse d'échange $1/[U(IV)]\tau_0$ devient 1.4 fois plus faible pour des températures comprises entre 95 et 60 °C. La fig. 4 illustre le ralentissement de l'échange dans ces solutions électrolytiques concentrées. L'effet du sel $NaClO_4$ semble être du même ordre de grandeur que celui de l'acide $HClO_4$.

Pour des solutions concentrées, les modèles quantitatifs sont difficiles à établir et les effets combinés des ions ClO_4^- et H^+ ou ClO_4^- et Na^+ sur l'échange ne peuvent pas être séparés. La valeur de l'activité de l'eau, a_{H_2O}, donne cependant une mesure globale des modifications microscopiques qui interviennent dans le solvant lors de la dissolution d'une forte quantité d'ions diamagnétiques. A partir de nos mesures de tension de vapeur P_{sol}^{vap} (Paragraphe II) et celles de Mascherpa (8), on a déterminé l'activité a_{H_2O} du solvant dans les solutions perchloriques, d'après la relation 11:

$$[11] \quad a_{H_2O}^{sol} = \gamma_{H_2O}^{sol} x_{H_2O} = \frac{P_{H_2O}^{vap}}{P_{H_2O\ pure}^{vap}} \approx \frac{P_{sol}^{vap}}{P_{H_2O\ pure}^{vap}}$$

où $\gamma_{H_2O}^{sol}$ et x_{H_2O} sont respectivement le coefficient d'activité et la fraction molaire de l'eau dans la solution. On constate une chute très rapide de l'activité a_{H_2O} à partir de l'eau pure lorsque l'on ajoute de l'acide perchlorique ou du perchlorate de sodium. Ceci peut être interprété en assimilant l'activité a_{H_2O} à la fraction molaire en eau vraiment libre et en admettant que seule l'eau non ionisée et non liée admet une tension de vapeur. L'effet du sel $U(ClO_4)_4$ sur l'activité a_{H_2O} du solvant peut être négligé tant que la concentration du sel reste faible ($[U(ClO_4)_4] \approx 0.25$ *M*). On a porté sur la fig. 5, la vitesse d'échange $1/[U(IV)]\tau_0$ en fonction de l'activité du solvant, pour différentes températures. Les valeurs de l'activité a_{H_2O} du solvant (H_2O + $HClO_4$) ont été extrapolées à 60 °C ainsi que celles des solutions mixtes (H_2O + $NaClO_4$ + $HClO_4$) à 40 et 60 °C. On constate que la vitesse d'échange $1/[U(IV)]\tau_0$ pour les solutions fortement concentrées en espèces diamagnétiques, varie linéairement avec l'activité a_{H_2O} du solvant et donc semble-t-il, avec la proportion d'eau libre non solvatante et non ionisée; ce qui est compatible avec un processus

Can. J. Chem. Downloaded from www.nrcresearchpress.com by 210.87.254.6 on 09/05/12
For personal use only.

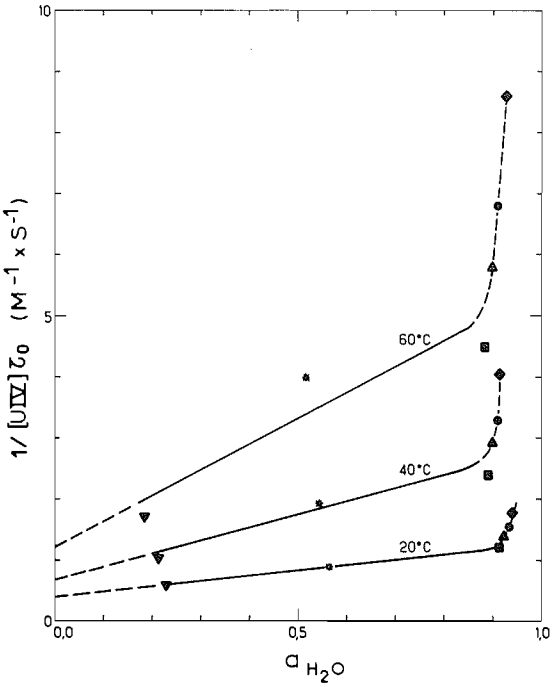

FIG. 5. Evolution de la vitesse d'échange $1/[U(IV)]\tau_0$ en fonction de l'activité de l'eau, a_{H_2O}, des solutions aqueuses de perchlorate d'uranium(IV), à 0.25 *M* $U(ClO_4)_4$, à différentes températures: (◆, 0.2 *M* $HClO_4$ et 1.8 *M* $NaClO_4$; ●, 0.48 *M* $HClO_4$ et 1.52 *M* $NaClO_4$; ▲, 1.0 *M* $HClO_4$ et 1.0 *M* $NaClO_4$; ■, 2.0 *M* $HClO_4$; *, 1.35 *M* $HClO_4$ et 5.0 *M* $NaClO_4$; ▼, 8.0 *M* $HClO_4$).

d'échange dont l'étape élémentaire la plus lente est:

[12] $$U(H_2O)_n^{4+} + H_2O \rightarrow U(H_2O)_{n+1}^{4+}$$

(2) Effet de sphère externe sur la relaxation des protons du solvant

Entre 40 et −5 °C, l'échange des protons devient suffisamment lent pour ne plus être le mécanisme dominant de la vitesse de relaxation $1/T_{i=1,2}^{(U(IV))}$ et le mécanisme (b) qui devient prépondérant, correspond à un effet de "sphère externe". La relaxation est alors déterminée par la modulation des couplages dipolaires entre le moment magnétique de l'ion U^{4+} et les spins des protons situés hors de la sphère interne d'hydratation. La composante (b) de la vitesse de relaxation, $(1/T_i^{(U(IV))})^{(b)}$, n'est pas influencée par la présence des ions diamagnétiques et reste indépendante de la viscosité macroscopique du milieu. L'énergie d'activation apparente, $E_b \approx 0.9$ kcal/mol, est trop faible pour être attribuée à un mécanisme de diffusion moléculaire qui serait de l'ordre de 3 kcal/mol, comme on peut l'observer dans les solutions diamagnétiques. Ces deux éléments conduisent à admettre que la seule cause de variation du champ magnétique produit par les ions U^{4+} à l'emplacement des protons est la relaxation du moment magnétique électronique caractérisée par un temps $\tau_{1\,spin}$.

Considérons d'abord l'effet de la relaxation électronique de l'uranium(IV) sur les protons du solvant libre; une évaluation correcte de l'importance de cette contribution dipolaire à la relaxation peut être obtenue en effectuant une moyenne sur l'interaction de la distance d_{min} de plus courte approche à une distance infinie (11).

$$[13] \quad \left(\frac{1}{T_i^{(U(IV))}}\right)^{(b)} \approx \frac{4n_U\gamma_H{}^2\langle\mu_{eff}{}^2\rangle\tau_{1spin}}{3} \times \int_{d_{min}}^{\infty} \frac{4\pi r^2\,dr}{r^6} = \frac{16\pi n_U\gamma_H{}^2\langle\mu_{eff}{}^2\rangle\tau_{1spin}}{9d_{min}{}^3}$$

où $n_U = [U(IV)]\ N\ 10^{-3}$ est le nombre d'ions paramagnétiques par cm^3, N le nombre d'Avogadro, γ_H le rapport gyromagnétique du proton et $\langle\mu_{eff}\rangle$ le moment magnétique du perchlorate d'uranium(IV) en solution aqueuse. Connaissant les distances moyennes uranium–oxygène des premières couches d'hydratation (3) ($d_{(U-O)_1} \approx 2.5$ Å, $d_{(U-O)_2} \approx 4.5$ Å), on estime la distance minimale d'approche égale à la distance uranium–proton de la seconde couche d'hydratation, soit $d_{min} \approx 5.15$ Å. D'après des mesures de susceptibilité magnétique, (14),[1] le moment magnétique $\langle\mu_{eff}\rangle$ équivaut à $3.6 \pm 0.4\ \beta_{Bohr}$. De la valeur expérimentale $(T_i^{(U(IV))})^{(b)} \approx 0.885$ s à 20 °C, on déduit à partir de la relation 13, l'ordre de grandeur du temps de relaxation $\tau_{1\,spin}$, soit 2.3×10^{-13} s.

S'il existe d'autre part, quelques sites privilégiés dans la sphère interne d'hydratation où les coordinats sont plus labiles, on doit considérer également l'effet de la relaxation électronique de l'uranium(IV) sur les protons de cette catégorie de coordinats. Le temps de relaxation $\tau_{1\,spin}$ moyennera les couplages dipolaires et scalaires entre le moment magnétique de l'ion U^{4+} et les spins des protons considérés. Un terme tenant compte de cet effet s'ajoute à

Can. J. Chem. Downloaded from www.nrcresearchpress.com by 210.87.254.6 on 09/05/12
For personal use only.

l'expression 13 qui devient:

$$[14]\quad \left(\frac{1}{T_i^{(U(IV))}}\right)^{(b)} \approx \frac{16\pi n_U \gamma_H{}^2 \langle \mu_{eff}{}^2 \rangle \tau_{1\ spin}}{9 d_{min}{}^3} + \frac{P_L}{P_0}\left(\frac{4\gamma_H{}^2 \langle \mu_{eff}{}^2 \rangle}{3 r_{(U-H)_L}{}^6} + \frac{2}{3} J(J+1)\left(\frac{A}{\hbar}\right)^2\right)\tau_{1\ spin}$$

où J est le moment angulaire total de l'ion U^{4+} et P_L, $r_{(U-H)_L}$, $(A/\hbar)^2$ sont respectivement la proportion en protons, la distance uranium–proton et l'interaction scalaire pour les coordinats qui s'échangent rapidement avec les protons du solvant. On déduit de la relation 14 un temps de relaxation $\tau_{1\ spin}$ du même ordre de grandeur, 10^{-13} s, en prenant des valeurs raisonnables pour les paramètres $n_L \approx 2$, $r_{(U-H)_L} \approx 4$ Å, $|A/h| \lesssim 1$ MHz. Cette estimation de la limite supérieure de la constante d'interaction superhyperfine semble raisonnable si l'on considère les aquo-ions des terres rares (15) [$A/h(H^1) \approx -33.2$ KHz pour $Pr(H_2O)_n{}^{3+}$] ou les aquo-ions du groupe du fer (16), où $A/h(H^1)$ est typiquement de quelques centaines de KHz. Ainsi l'évaluation du temps de relaxation $\tau_{1\ spin}$ dans les solutions aqueuses de perchlorate d'uranium(IV), est peu sensible à l'existence (ou non) de molécules plus labiles en sphère interne de coordination.

La valeur très faible obtenue ici pour ce temps, $\tau_{1\ spin} \approx 2.3 \times 10^{-13}$ s, est comparable à la limite supérieure du temps de relaxation électronique des ions de terre rare Tm^{3+}, Er^{3+}, Ho^{3+}, Dy^{3+}, Tb^{3+} que Reuben et Fiat (17) ont située entre 2.8 et 5.0×10^{-13} s pour les solutions aqueuses de perchlorate de lanthanides correspondantes.

En utilisant ces résultats, on peut estimer la vitesse de relaxation des protons en sphère interne. Puisque la relaxation électronique de l'uranium(IV) est rapide, c'est elle qui assure la relaxation des coordinats peu labiles. On a

$$[15]\quad \frac{1}{T_{2M}} \lesssim \frac{1}{T_{1M}} \approx \left[\frac{4}{3}\frac{\gamma_H{}^2 \langle \mu_{eff}{}^2 \rangle}{r_{(U-H)_1}{}^6} + \frac{2}{3} J(J+1)\left(\frac{A}{\hbar}\right)^2\right]\tau_{1\ spin}$$

et l'on trouve alors comme limite supérieure du temps de relaxation T_{iM} des protons en sphère interne une valeur de 10^{-3} s. Ce temps est bien plus court que le temps d'échange; typiquement τ_M varie de 0.15 à 0.02 s quand la température croît de 20 à 95 °C, à $[HClO_4] \approx 2$ *M*. Ainsi les coordinats restent fixés à l'ion U^{4+} un temps suffisamment long pour subir la relaxation par l'uranium(IV) avant que l'échange ait lieu, comme le montrait l'identité des vitesses de relaxation transversale $1/T_2{}^{(U(IV))}$ et longitudinale $1/T_1{}^{(U(IV))}$ au Paragraphe III. Dans ces conditions ($T_{iM} \approx 10^{-3}$ s) on devrait pouvoir observer séparément le signal de l'eau libre et celui de l'eau liée dans une solution assez concentrée en uranium(IV). Jusqu'à présent, cependant, nous ne sommes pas parvenus à observer le signal de résonance des protons liés sur le spectre haute-résolution, à 60 MHZ. Il est raisonnable de penser que s'il existe 8 ou 9 coordinats peu labiles en sphère interne, leurs liaisons avec l'uranium(IV) ne sont pas identiques sauf si un réarrangement dynamique dans la sphère de coordination les rend équivalentes. S'il n'existe pas de réarrangement rapide, le spectre des protons liés est constitué par plusieurs signaux de résonance larges ($\Delta_{1/2} \approx 1/(\pi T_{2M}) \approx 3.10^2$ Hz). Si au contraire un réarrangement rapide a lieu, ces différents signaux collapsent en un seul signal très élargi. Dans ces deux cas, le (ou les) signaux de résonance des protons liés deviennent inobservables.

(IV) Déplacement chimique de la raie d'absorption des protons du solvant

Le spectre d'absorption des protons des solutions aqueuses d'acide chlorhydrique avec ou sans tétrachlorure d'uranium(IV) présente un seul signal de résonance. Ce signal se rapproche de celui du TMPS vers les champs décroissants quand on augmente la concentration en uranium(IV). Par contre, le comportement du signal en acidité et en température dépend peu de la concentration en uranium(IV): le signal se rapproche de celui du TMPS quand l'acidité décroît et quand la température croît. Les résultats sont portés sur la fig. 6.

L'évolution du déplacement chimique $\delta^{(UCl_4+HCl)}$ en fonction de la concentration en uranium(IV), n'est pas due aux coordinats peu labiles que nous avons mis en évidence au Paragraphe III. En effet, la relaxation en sphère interne d'hydratation est comme nous l'avons montré au Paragraphe III-2, plus rapide que la vitesse d'échange; le déplacement chimique $\Delta\omega_0'$ que ces coordinats peuvent induire, est

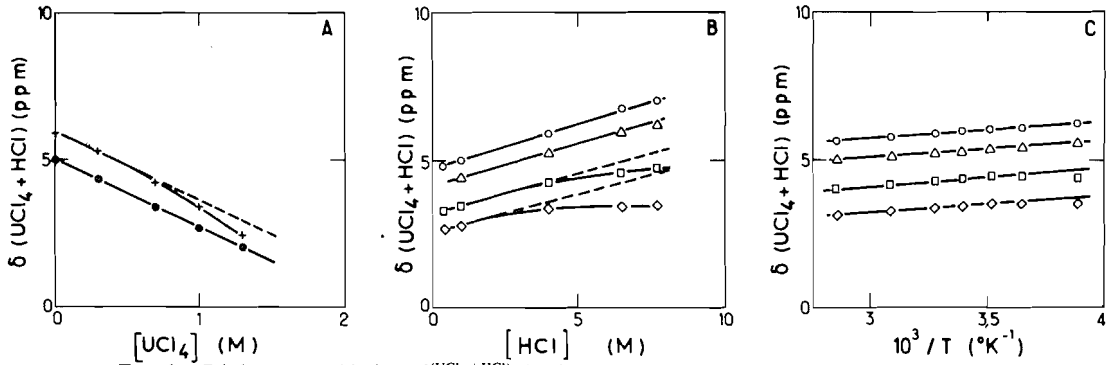

FIG. 6. Déplacement chimique $\delta^{(UCl_4+HCl)}$ du signal d'absorption des protons mesuré dans des solutions acides de chlorure d'uranium(IV) par rapport à celui du TMPS: *A*, à 32.5 °C et à différentes acidités (●, 1.0 *M* HCl; +, 4.0 *M* HCl), en fonction de la concentration en sel UCl_4; *B*, à 32.5 °C et à différentes molarités en sel UCl_4: (○, 0.0 *M* UCl_4; △, 0.3 *M* UCl_4; □, 0.7 *M* UCl_4; ◇, 1.0 *M* UCl_4) en fonction de l'acidité; *C*, à 4.0 *M* HCl et aux molarités en sel UCl_4 indiquées en *B*, en fonction de la température.

alors négligeable devant celui qui est observé. Ainsi, on a (7, 10):

$$[16]\quad \Delta\omega_0' \approx \frac{-P_M\Delta\omega_M}{[(1/T_{2M} + 1/\tau_M)^2 + \Delta\omega_M^2]\tau_M^2} \qquad \text{pour } P_M < P_0$$

qui devient lorsque la condition $\tau_M > T_{2M}$ est vérifiée

$$[17]\quad \Delta\omega_0' \approx -P_M\Delta\omega_M\left(\frac{T_{2M}}{\tau_M}\right)^2\frac{1}{(1 + T_{2M}^2\Delta\omega_M^2)} \lesssim -P_M\Delta\omega_M\left(\frac{T_{2M}}{\tau_M}\right)^2$$

En prenant des valeurs typiques pour $n_{int} \approx 9$, $\tau_M \approx 0.1$ s à 20 °C, $T_{2M} \lesssim 10^{-3}$ s et une valeur maximum du déplacement chimique des protons liés, soit $\Delta\omega_M \sim 3.8 \times 10^4$ rad s^{-1}. On trouve un déplacement induit $\Delta\omega_0' \lesssim 0.2$ rad s^{-1} bien plus petit que celui observé

$$[18]\quad \Delta\omega_0 = 2\pi[\delta^{(UCl_4+HCl)} - \delta^{(HCl)}] = 2\pi\delta^{(UCl_4)} \approx -48 \text{ rad s}^{-1}$$

aux molarités suivantes $[UCl_4] \approx 0.3$ *M* et $[HCl] \approx 4$ *M*, vers 20 °C. La variation du déplacement chimique $\delta^{(UCl_4+HCl)}$ avec la concentration en uranium(IV) doit donc être attribuée à une autre catégorie de protons liés à l'uranium(IV) sur des sites plus labiles que l'on désignera par "deuxième sphère" et qui s'échangent rapidement avec ceux du solvant libre.

L'effet des ions U^{4+} sur les protons de "deuxième sphère" n'est pas non plus d'origine diamagnétique, comme on peut le montrer en comparant leur déplacement chimique molaire $\delta_M^{(UCl_4)}$, aux déplacements chimiques molaires déterminés (18) dans des solutions aqueuses de sels diamagnétiques $Th(NO_3)_4$, $Al(NO_3)_3$, vers 24 °C:

$$\delta_M^{(UCl_4)} \approx 2.5 \text{ ppm } M^{-1} \text{ à } [HCl] \approx 4\ M$$
$$\delta_M^{Th(NO_3)_4} \approx 0.61 \text{ ppm } M^{-1} \text{ à } pK_a \approx 4$$
$$\delta_M^{Al(NO_3)_3} \approx 0.64 \text{ ppm } M^{-1} \text{ à } pK_a \approx 5$$

On constate que l'effet purement diamagnétique des ions Th^{4+} ou Al^{3+} sur les protons situés en sphère interne d'hydratation est faible devant celui observé pour l'uranium(IV); à fortiori, comme il s'agit d'un effet des ions U^{4+} sur les protons plus éloignés de "deuxième sphère", cet effet n'est pas d'origine diamagnétique et ne peut donc être que d'origine paramagnétique: ce sont les interactions de contact et/ou de pseudo-contact entre les protons de la "deuxième sphère" et les électrons non appariés de l'uranium(IV) qui créent le déplacement chimique $\delta^{(UCl_4)}$.

Soit n_L le nombre de sites labiles en "deuxième sphère" et δ^L le déplacement chimique des protons dans cet environnement. On a:

$$[19]\quad \delta^{(UCl_4+HCl)} = (1 - P_L)\delta^{(HCl)} + P_L\delta^L$$

soit

$$[20]\quad \delta^{(UCl_4)} = \delta^{(UCl_4+HCl)} - \delta^{(HCl)} = P_L(\delta^L - \delta^{(HCl)})$$

Can. J. Chem. Downloaded from www.nrcresearchpress.com by 210.87.254.6 on 09/05/12
For personal use only.

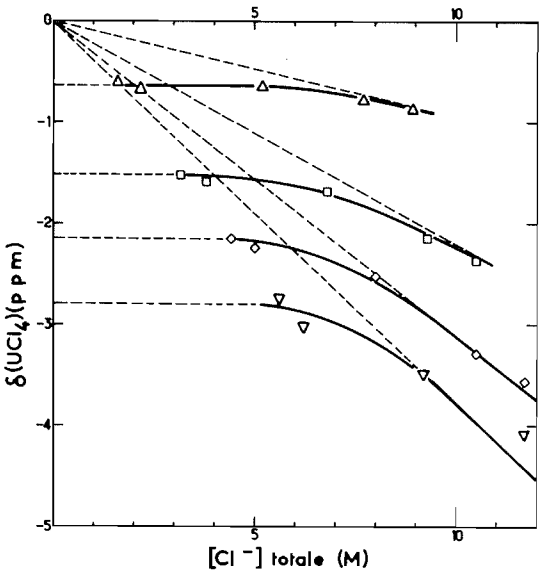

FIG. 7. Variation de la contribution des ions U^{4+} au déplacement chimique des protons, $\delta^{(UCl_4)}$, à 32.5 °C, à différentes molarités en sel UCl_4: (△, 0.3 *M* UCl_4; □, 0.7 *M* UCl_4; ◇, 1.0 *M* UCl_4; ▽, 1.3 *M* UCl_4) en fonction de la concentration totale en chlore.

où

$$P_L = \frac{n_L[U(IV)]}{[H_2O]_{tot} + \frac{1}{2}[HCl] - n_{int}[U(IV)]}$$

est la proportion en protons labiles. La condition d'échange rapide fixe une limite inférieure de la vitesse d'échange:

$$[21] \quad \frac{1}{\tau_L} > \frac{2\pi|\delta^{(UCl_4)}|}{P_L} \approx 2\pi|\delta^L - \delta^{(HCl)}|$$

L'évaluation du déplacement chimique $\delta^L - \delta^{(HCl)}$ dépend du nombre de sites peu labiles et de sites labiles, c'est-à-dire du choix d'un modèle d'aquo-complexe.

Sur la fig. 6, on remarque des déviations à la linéarité lorsque la concentration en anions Cl^- devient forte. Afin de préciser cette évolution, on a porté sur la fig. 7, le déplacement chimique $\delta^{(UCl_4)}$ en fonction de la concentration totale en chlore. Au-dessous de la molarité $[Cl^-] \approx 6.0$ *M*, le déplacement chimique $\delta^{(UCl_4)}$ n'est pas influencé par la présence des chlores en solution, mais au-dessus de cette molarité, il varie linéairement avec la concentration en chlore. Or, on sait[1] que la complexation de l'uranium(IV) par les chlores apparaît à partir de la molarité $[Cl^-] \approx 5.0$ *M* et qu'il se forme principalement des complexes monochlorés UCl^{3+} dans la gamme de concentrations étudiées:

$$[22] \quad U^{4+} + Cl^- \underset{\longleftarrow}{\overset{K_{éq}}{\longrightarrow}} UCl^{3+}$$

L'échange des protons labiles s'effectue alors, entre trois sites: le solvant libre, la "deuxième sphère" des complexes aqueux $U(H_2O)_n^{4+}$ indicé ⟨4⟩ et la première ou la deuxième sphère des complexes monochlorés $U(Cl)(H_2O)_m^{3+}$ indicé ⟨3⟩. L'expression 20 devient

$$[23] \quad \delta^{(UCl_4)} = \delta^{(UCl_4+HCl)} - \delta^{(HCl)} = P_L^4(\delta_4^L - \delta^{(HCl)}) + P_L^3(\delta_3^L - \delta^{(HCl)})$$

où

$$P_L^4 = \frac{n_L^4[U^{4+}]}{[H_2O]_{tot} + \frac{1}{2}[HCl] - n_{int}[U(IV)]}$$

$$P_L^3 = \frac{n_L^3[UCl^{3+}]}{[H_2O]_{tot} + \frac{1}{2}[HCl] - n_{int}[U(IV)]}$$

sont les proportions en protons labiles dans les environnements ⟨3⟩ et ⟨4⟩ et δ_4^L, δ_3^L sont les déplacements chimiques dans ces environnements, avec

$$[U(IV)] = [U^{4+}] + [UCl^{3+}]$$

et

$$K_{éq} = [UCl^{3+}]/([Cl^-][U^{4+}])$$

d'après l'équilibre 22.

D'après l'estimation du pourcentage en complexes $U(H_2O)_n^{4+}$ et $U(Cl)(H_2O)_m^{3+}$ en fonction de la concentration totale en chlore[1] et à partir des résultats expérimentaux portés sur la fig. 7, on a déterminé par la méthode des moindres carrés, à 32.5 °C, les produits suivants:

$$n_L^4(\delta_4^L - \delta^{(HCl)}) = -96 \pm 9 \text{ ppm}$$

et

$$n_L^3(\delta_3^L - \delta^{(HCl)}) = -198 \pm 24 \text{ ppm}$$

où rappelons-le, n_L^4 et n_L^3 sont les nombres de sites labiles dans les complexes $U(H_2O)_n^{4+}$ et $U(Cl)(H_2O)_m^{3+}$. A nouveau, le choix d'un modèle de complexe aqueux est nécessaire pour évaluer les déplacements chimiques $\delta_4^L - \delta^{(HCl)}$ et $\delta_3^L - \delta^{(HCl)}$. Mais l'étude des spectres haute-résolution du proton dans les solutions aqueuses de tétrachlorure d'uranium(IV) ne permet pas de choisir un modèle précis: le nombre de sites labiles n_L^4 peut varier de 2 ou 3 molécules d'eau dans le cadre d'un modèle d'aquo-complexe $U(H_2O)_n^{4+}$ tel que Glébov l'a proposé (4), où

Can. J. Chem. Downloaded from www.nrcresearchpress.com by 210.87.254.6 on 09/05/12
For personal use only.

Can. J. Chem. Downloaded from www.nrcresearchpress.com by 210.87.254.6 on 09/05/12
For personal use only.

les coordinats en sphère interne sont inéquivalents, à 11 ou 12 molécules d'eau appartenant à la seconde sphère d'hydratation dans le cadre d'un modèle d'aquo-complexe $U(H_2O)_n^{4+}$ où les coordinats en sphère interne sont équivalents et peu labiles. La vitesse d'échange de ces coordinats labiles $1/\tau_4{}^L$ est supérieure à $10^4\ s^{-1}$ ou $3 \times 10^3\ s^{-1}$ selon le modèle choisi.

(V) Conclusion

L'étude de la résonance magnétique des protons dans les solutions aqueuses de perchlorate d'uranium(IV) nous a renseigné sur la cinétique d'échange des protons de l'eau solvatante et sur la relaxation du moment magnétique de l'ion solvaté U^{4+}.

Nous avons montré que la relaxation longitudinale et transversale des protons est limitée par le temps de résidence τ_M des protons des molécules d'eau situées dans la sphère interne d'hydratation des ions U^{4+}, qui varie entre 10 ms et 1 s.

La présence des ions diamagnétiques dans la solution modifie de façon assez sensible la cinétique d'échange. Lorsqu'ils sont en faible concentration et pour des $pH > 0$, la vitesse d'échange $1/\tau_M$ croît quand l'acidité diminue. Ceci est attribué au processus d'hydrolyse qui intervient, lorsque le nombre de complexes monohydroxylés $U(OH)(H_2O)_m^{3+}$ augmente et que la cinétique d'échange de leurs protons est plus rapide que celle correspondant aux complexes aqueux $U(H_2O)_n^{4+}$. Aux fortes concentrations en espèces diamagnétiques, on a montré que la vitesse d'échange $1/\tau_M$ varie linéairement avec l'activité a_{H_2O} de l'eau, qui donne une mesure de la fraction molaire des molécules d'eau libres, non ionisées et non solvatantes dans la solution.

Les molécules d'eau de la sphère interne de coordination qui sont peu labiles et à relaxation trop rapide ($\tau_M > T_{iM}$), n'apparaissent pas sur le spectre haute-résolution des protons. Cependant, on met en évidence un déplacement chimique $\delta^{(UCl_4)}$ d'origine paramagnétique dans les solutions aqueuses de chlorure d'uranium(IV). Ceci indique l'existence de molécules d'eau solvatantes, occupant des sites labiles en "deuxième sphère". Ces protons en interaction de contact et/ou de pseudacontact avec l'uranium(IV), s'échangent rapidement avec ceux du solvant libre.

A forte concentration en chlore, $[Cl^-] \gtrsim 6.0\ M$ des aquo-complexes monochlorés, $U(Cl)(H_2O)_m^{3+}$, se forment et donnent naissance à un terme nouveau dans le déplacement chimique $\delta^{(UCl_4)}$.

Enfin, le comportement de la vitesse de relaxation $1/T_i^{(U(IV))}$ à basse température, s'explique par un effet de sphère externe qui nous a permis de chiffrer le temps de relaxation électronique de l'uranium(IV), $\tau_{1\,spin} \approx 10^{-13}$ s, ce dernier restant inaccessible aux autres techniques [rpe, etc. . . .].

L'investigation des complexes aqueux d'uranium(IV) par la résonance magnétique nucléaire nous a permis de décrire essentiellement l'aspect cinétique de l'hydratation. Une interprétation plus fine de ces résultats nécessitera une connaissance plus précise de la structure et de la coordinence des complexes, information que la résonance magnétique nucléaire ne peut pas fournir dans ce cas, mais que l'on peut, peut-être, obtenir par d'autres techniques.

(VI) Remerciements

Nous tenons à remercier nos collègues du laboratoire de chimie de l'uranium et tout particulièrement Monsieur J. Mougin pour leur indispensable concours durant ce travail. Par ailleurs Monsieur J. Reynes a contribué au début de cette étude et nous l'en remercions.

1. I. I. Chernyaev. Complex compounds of uranium. Israel program for scientific translations, Jerusalem. 1966. Chapt. 19.
2. L. M. Toth. J. Phys. Chem. **75**, 631 (1971).
3. S. Pocev et G. Johansson. Acta Chem. Scand. **27**, 2146 (1973).
4. G. Folcher, J. Paris, P. Plurien, P. Rigny et E. Soulie. J. Chem. Soc. Chem. Commun. 3 (1974).
5. J. Paris et G. Folcher. Can. J. Chem. A paraître.
6. V. A. Glebov, Yu. D. Knyazev, V. A. Lekae et N. N. Borodina. Russ. J. Inorg. Chem. **15**, 683 (1970).
7. T. J. Swift et R. E. Connick. J. Chem. Phys. **37**, 307 (1962).
8. G. Mascherpa. Rev. Chim. Miner. **2**, 379 (1965).
9. S. Meiboom et D. Gill. Rev. Sci. Instrum. **28**, 688 (1958).
10. T. J. Swift. *Dans* NMR of paramagnetic molecules. *Edité par* G. N. Lamar, W. de W. Horrocks, Jr. et R. H. Holm. Academic Press, New York. 1973. Chap. 2.
11. Z. Luz et S. Meiboom. J. Chem. Phys. **40**, 2686 (1964).
12. V. A. Glebov, A. E. Klygin, I. D. Smirnova et N. S. Kolyada. Russ. J. Inorg. Chem. **17**, 1740 (1972).
13. K. A. Kraus et F. Nelson. J. Am. Chem. Soc. **72**, 3901 (1950).
14. R. W. Lawrence. J. Am. Chem. Soc. **56**, 776 (1934).
15. J. Reuben et D. Fiat. J. Chem. Phys. **51**, 4909 (1969).
16. Z. Luz et R. G. Shulman. J. Chem. Phys. **43**, 3750 (1965).
17. J. Reuben et D. Fiat. J. Chem. Phys. **51**, 4918 (1969).
18. R. C. Axtman. J. Chem. Phys. **30**, 340 (1959).

Aqueous solutions of bromorhodate(III) complexes. Their use as catalysts for homogeneous hydrogenation, and their reactivity toward carbon monoxide[1]

BRIAN R. JAMES AND GEORGE ROSENBERG

Department of Chemistry, University of British Columbia, Vancouver, British Columbia V6T 1W5

Received July 16, 1975

BRIAN R. JAMES and GEORGE ROSENBERG. Can. J. Chem. **54**, 313 (1976).

Under mild conditions, aqueous acid bromide solutions likely containing principally $RhBr_4(H_2O)_2^-$ catalyze the hydrogen reduction of iron(III), and react with carbon monoxide to give *cis*-$Rh(CO)_2Br_2^-$. The kinetics of these reactions were studied, and were found similar to those previously reported for corresponding systems using $RhCl_5(H_2O)^{2-}$, although the bromo complex is some thirty times more reactive than the chloro complex toward both H_2 and CO. Plausible mechanisms are discussed, and some comparisons made between the two halide systems; the chloride system shows a much more marked inverse dependence on acid concentration. The reductive carbonylation process in a direct reaction step of CO with rhodium(III), and in a autocatalytic step involving formation of a mixed valence Rh^{III} . . . Br . . . Rh^{I} intermediate, appears to involve coordinated and not external water.

BRIAN R. JAMES et GEORGE ROSENBERG. Can. J. Chem. **54**, 313 (1976).

Dans des conditions douces, des solutions aqueuses et acides de bromure contenant vraisemblablement principalement du $RhBr_4(H_2O)_2^-$ catalysent la réduction par l'hydrogène du Fe(III) et réagissent avec le monoxyde de carbone pour fournir le *cis*-$Rh(CO)_2Br_2^-$. On a étudié la cinétique de cette réaction et on a trouvé qu'elle est semblable à celle rapportée antérieurement pour des systèmes correspondants utilisant le $RhCl_5(H_2O)^{2-}$; le complexe bromé est toutefois environ trente fois plus réactif que le complexe chloré vis-à-vis le H_2 et le CO. On discute des mécanismes possibles et on fait quelques comparaisons entre les deux systèmes halogénés; le système chloré présente une dépendance inverse beaucoup plus marquée sur la concentration en acide. Il semble que le processus de carbonylation réductrice par réaction directe du CO avec le Rh(III), et par une réaction autocatalytique impliquant la formation d'un complexe intermédiaire Rh^{III} . . . Br . . . Rh^{I} de valence mixte, implique de l'eau coordonnée et non extérieure.

[Traduit par le journal]

Introduction

Studies from this laboratory (1) have reported previously on the use of chlororhodate(III) species for catalytic hydrogen reduction of inorganic substrates such as ferric in aqueous acid solutions. Other work (2) has described the reaction of the chlororhodate(III) species in hydrochloric acid solutions with carbon monoxide to give initially chlorocarbonylrhodate(III) and then the *cis*-dichlorodicarbonylrhodate(I) anion, $Rh(CO)_2Cl_2^-$. This latter complex has been found to catalyze the carbon monoxide reduction of ferric ion (2), molecular oxygen (3, 4), and nitric oxide (5), as well as catalyze the important carbonylation of methanol to give acetic acid (6).

In view of the potential catalytic properties of other rhodium halides and halogenocarbonyl species, we decided to extend our studies to the bromide and iodide systems. However, corresponding studies on the iodide system were found to be impossible since aqueous acid solutions of rhodium(III) and iodide undergo a redox reaction with the liberation of iodine; iodocarbonyl-rhodate(I) and -rhodate(III) complexes may be made, however, by other routes (7). This paper then summarizes our findings on the reactivity of bromorhodate(III) species in aqueous acid solutions toward both H_2 and CO. The species present in 0.5 *M* HBr solutions (thought to be mainly $RhBr_4(H_2O)_2^-$) is found to be some thirty times more active than the $RhCl_5(H_2O)^{2-}$ anion, under comparable conditions.

Experimental

Rhodium(III) tribromide was obtained as the dihydrate from Platinum Chemicals. Concentrated HBr was diluted and standardized. $Fe(ClO_4)_3 \cdot 6H_2O$ (Alpha Inorganics, reagent grade) and NaBr (B.D.H., C.P. grade) were used as such. Other materials used, and the procedure used for following H_2 or CO uptake at constant pressure have

[1]Taken from the Ph.D. thesis of G. Rosenberg, University of British Columbia, Vancouver, British Columbia, 1974.

Can. J. Chem. Downloaded from www.nrcresearchpress.com by 210.87.254.5 on 09/05/12
For personal use only.

Can. J. Chem. Downloaded from www.nrcresearchpress.com by 210.87.254.5 on 09/05/12
For personal use only.

been described previously (1, 2). The complexes $[Rh(H_2O)_{6-n}Br_n]^{(n-3)-}$ are not as well-characterized in solution as the corresponding chloro complexes (8), but *ca.* 10^{-2} *M* solutions of $RhBr_3 \cdot 2H_2O$ in 0.5 *M* HBr, thermally equilibrated for 20 h at 80 °C, are thought to contain mainly the 4:1 complex $RhBr_4(H_2O)_2^-$. Stability constant data evaluated by Cozzi and Pantani using polarographic and spectrophotometric techniques (9) suggest that such solutions should contain about 75% $RhBr_4(H_2O)_2^-$ and 25% $RhBr_3(H_2O)_3$. The equilibrated red solutions have an absorption maximum at 537 nm (ε = 175 M^{-1} cm^{-1}) and an absorption minimum at 505 nm (ε = 150) which appear consistent with such a mixture using the spectral data reported for the tri- and tetrabromo species (9). During the course of our work Robb and Bekker (10) reported on the aquobromorhodium complexes; the spectrum of the synthesized $K_2[RhBr_5(H_2O)]$ complex *in ice-cold water* showed a λ_{max} at 542 nm (ε = 150), close to that of our equilibrated solutions, but data on the lability of this species were not given. The tri- and tetrabromo species were also said to be characterized in solution after chromatographic separation, but unfortunately the spectra were not recorded. Nevertheless the established trend of the shift of the absorption maxima to lower wavelengths with decreasing number of coordinated halides (8–10) would again indicate that our solutions contain mainly $RhBr_4(H_2O)_2^-$. The added problem of possible geometrical isomers has not been resolved (10).

The solubility of H_2 in 0.5 *M* HBr at 40 °C (7.1×10^{-4} *M* atm^{-1}) was calculated from data of Wiebe and Gaddy (11) correcting for the effect of HBr (12); the CO solubility at 40 °C was taken as 7.9×10^{-4} *M* atm^{-1}, the value in pure water (13).

Results

Hydrogenation of Iron(III)

The equilibrated 0.5 *M* HBr rhodium(III) solutions ($\sim 10^{-2}$ *M*) were found to be effective catalysts for the H_2 reduction of Fe(III) under mild conditions (40–60 °C, up to 1 atm H_2). In the presence of excess Fe(III) substrate, linear hydrogen uptake plots were recorded as a function of time; the plots were linear up to complete reduction of the ferric ion (H_2:Fe = 1:2), and were independent of the $[Fe^{III}]$. Simultaneous spectrophotometric measurements confirmed that the H_2 uptake was consumed in the reduction of Fe(III) to Fe(II) and that the concentration of Rh(III) remained constant. The system is entirely analogous to the $RhCl_5(H_2O)^{2-}$ system studied earlier (1), and the kinetic data for the linear rates again obeyed the simple rate law $k_1^H[Rh^{III}][H_2]$, which gives the pseudo zero-order kinetics at the constant pressure maintained in any given set of conditions. The k_1^H value at 40 °C was 0.17 ± 0.01 M^{-1} s^{-1}; using corresponding values at 45 °C (0.30), 50 °C (0.40), and 55 °C (0.92 M^{-1} s^{-1}), a reasonable Arrhenius plot yields the activation parameters $\Delta H^{\ddagger} = 94.9 \pm 7.1$ kJ mol^{-1}, $\Delta S^{\ddagger} = 44 \pm 21$ J K^{-1} mol^{-1} (14).

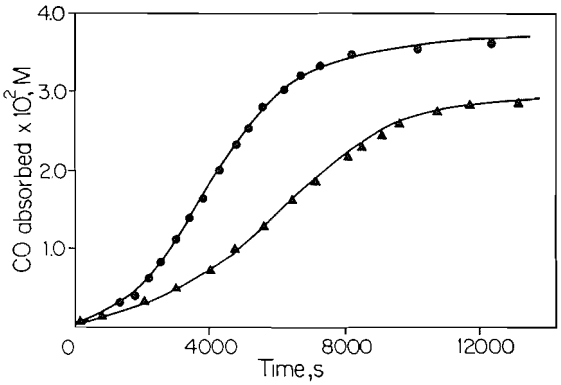

FIG. 1. Rate plot for carbonylation of $RhBr_4(H_2O)_2^-$ at 40 °C, 759 mm Hg CO in 0.5 *M* HBr; ●, 0.02 *M* Rh; ▲, 0.015, *M* Rh.

Carbonylation Reactions

The equilibrated 0.5 *M* HBr rhodium(III) solutions absorbed CO at conveniently measureable rates between 40–55 °C and gave autocatalytic uptake plots of the type shown in Fig. 1. The net measurable uptake corresponded to a 2:1 mole ratio of gas:Rh, and experiments in the presence of a sodalime tube (to absorb CO_2) resulted in a 3:1 uptake. The original red solution becomes yellow (λ_{max} 326 nm, ε = 3700 M^{-1} cm^{-1}) and contains the dibromodicarbonylrhodate(I) anion which may be readily precipitated as the tetrabutylammonium salt. The properties of the isolated solid, ν_{CO} = 2058, 1983 cm^{-1}, correspond to those reported by Vallarino (15) for $[(n\text{-}C_4H_9)_4N][Rh(CO)_2Br_2]$. The overall reaction is:

$$[1] \qquad Rh^{III} + 3CO \xrightarrow{H_2O} Rh^{I}(CO)_2 + CO_2 + 2H^+$$

The system corresponds very closely to the $RhCl_5(H_2O)^{2-}$ system studied previously at higher temperatures (2). Reactions were carried out over a range of rhodium concentrations and CO pressures up to 1 atm, and by analysis of the initial and maximum rates of the uptake plots (Fig. 1), the rate law was shown to be:

$$[2] \qquad -d[CO]/dt = k_1^{CO}[Rh^{III}][CO] + k_2[Rh^{III}][Rh^{I}]$$

The first term is concerned with the initial rate, and the second term the autocatalytic reaction which is the major contribution to the maximum

Can. J. Chem. Downloaded from www.nrcresearchpress.com by 210.87.254.5 on 09/05/12
For personal use only.

TABLE 1. Rate constant data for the CO reaction with bromorhodate(III) species in 0.5 *M* HBr at 40 °C (eq. 2)

Method*	k_1^{CO} (M^{-1} s^{-1})	k_2 (M^{-1} s^{-1})
Initial rates	0.15±0.01	—
(*a*)	—	0.058
(*b*)	0.16	0.047
(*c*)	—	0.047±0.03
(*d*)	—	0.048

*See text.

TABLE 2. Temperature dependence data for the CO reaction (eq. 2)*

Temperature (°C)	k_1^{CO} (M^{-1} s^{-1})	k_2 (M^{-1} s^{-1})
40	0.14	0.050
45	0.39	0.065
50	0.57	0.109
55	1.23	0.157

*$\Delta H_1^{\ddagger} = 112.4 \pm 8.4$; $\Delta H_2^{\ddagger} = 63.1 \pm 4.2$ kJ mol^{-1}; $\Delta S_1^{\ddagger} = 98 \pm 25$; $\Delta S_2^{\ddagger} = -69 \pm 13$ J K^{-1} mol^{-1}.

rate at the 50% reaction point. The analysis of the second term was carried out in the four methods (*a*) to (*d*) described in detail earlier (2): (*a*) involves plotting the maximum rate against $[Rh^{III}][Rh^{I}]$ at constant CO pressure, (*b*) involves plotting maximum rates *vs.* [CO] at a constant $[Rh^{III}]$, (*c*) involves measuring the ratio of maximum to initial rate, and (*d*) involves direct integration of rate law [2]. Table 1 summarizes the evaluated rate constants obtained using these analytical methods on the raw data (14); method (*b*) also yields a k_1 value. Table 2 summarizes the temperature dependence data, where k_2 was evaluated using method (*c*); the activation parameters are given in Table 2.

Variation of the bromide concentration from 0.50–0.25 *M* at a constant acidity of 0.5 *M*, maintained by using HBr and $HClO_4$ mixtures, did not significantly affect the spectrum of the initial rhodium(III) solutions. Thus observed slight increases in initial rate with decreasing $[Br^-]$ at 40 °C are likely attributed to increase in CO solubility (2). An increase in k_2 values from 0.05 to 0.09 M^{-1} as the $[Br^-]$ decreased from 0.50–0.25 *M* is thought significant since the k_2 step is independent of the [CO]; at a $[Br^-] = 0.1$ *M*, k_2 was 0.062 M^{-1} s^{-1}, but at these conditions the initial rhodium(III) spectrum now had an absorption maximum at 515 nm ($\varepsilon = 195$) indicating the presence of an increased amount of lower bromo species, probably $RhBr_3(H_2O)_3$ [λ_{max} 510 nm, $\varepsilon = 320$ (9)]. The effect of acid on k_1^{CO} and k_2 was studied by variation of an HBr:NaBr composition at a total $[Br^-]$ of 0.50 *M*. A slight inverse acid dependence is observed for the autocatalytic reaction (k_2) and possibly for the initial one (k_1^{CO}) (Table 3).

Discussion

The hydrogenation system is thought to involve a rate-determining heterolytic splitting of H_2 by the catalyst to give a hydride, which reduces the iron(III) in a subsequent fast step (1), for example:

$$[3]\quad RhBr_4(H_2O)_2^- + H_2 \overset{k_1^H}{\rightleftharpoons} HRhBr_3(H_2O)_2^- + H^+ + Br^-$$

$$[4]\quad HRhBr_3(H_2O)_2^- + 2FeBr_3 \xrightarrow{fast} RhBr_4(H_2O)_2^- + H^+ + Br^- + 2FeBr_2$$

Direct evidence for an equilibrium such as [3] has been obtained for a corresponding chlororuthenate(III) system by deuterium exchange experiments (16). For certain metal ion complexes, the net hydrogen splitting results via oxidative addition of H_2 to give dihydride, followed by reductive elimination (17), for example:

$$[5]\quad M^{II}X + H_2 \rightleftharpoons M^{IV}H_2X \rightleftharpoons M^{II}H + HX$$

However, such a process seems unlikely for coordinatively saturated Rh(III) complexes. In view of the known interconvertibility of a rhodium(III) hydride to rhodium(I) plus a proton (18), the fast step [4] could alternatively involve rhodium(I), which is known (2) to readily reduce iron(III).

The summarized data in Table 4 show that the bromo species, probably $RhBr_4(H_2O)_2^-$ is some thirty times more reactive than $RhCl_5(H_2O)^{2-}$ toward H_2 in a reaction such as [3], and the activation parameter data indicate that this is primarily reflected in a lower $\Delta H^{\ddagger}$ value.

Following Halpern (19), the net substitution of hydride for bromide in reaction 3 likely involves a transition state such as **1**. Differences

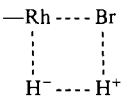

1

Can. J. Chem. Downloaded from www.nrcresearchpress.com by 210.87.254.5 on 09/05/12
For personal use only.

TABLE 3. Effect of acidity on the CO reaction at 40 °C, $[Br^-] = 0.50\ M$, $[Rh] = 0.02\ M$, $[CO] = 7.9 \times 10^{-4}\ M$

$[H^+]$ (M)	k_1^{CO} ($M^{-1}\ s^{-1}$)	k_2 ($M^{-1}\ s^{-1}$)
0.50	0.15	0.048
0.40	0.14	0.051
0.25	0.16	0.054
0.10	0.25	0.059

between the chloride and bromide systems will depend on the strengths of the Rh—X, H—X, and Rh—H bonds, and all of these will vary with the halide X. It is clearly difficult to draw any definite conclusions especially in view of some uncertainty in the nature of the bromo species; a weaker Rh—Br bond will be significant, and a charge difference could be important.

In the carbonylation reaction, the k_1^{CO} step to give the autocatalytic species $Rh(CO)_2Br_2^-$ involves a reductive carbonylation process which has been discussed in detail previously (2). Scheme 1, incorporating a CO insertion reaction to give a carboxylate intermediate, summarizes that discussion.

$$\begin{array}{ccccc} Rh^{III}(H_2O) & \overset{K_a}{\rightleftharpoons} & Rh^{III}(OH) + H^+ & & \\ k \downarrow CO & & k' \downarrow CO & & \\ Rh^{III}(CO)(H_2O) & \rightleftharpoons & Rh^{III}(CO)(OH) & \rightarrow & Rh^{III}(CO_2H) \\ & & & & \downarrow \\ & & Rh^{I}(CO)_2 & \xleftarrow{2CO} & Rh^{I}(+CO_2 + H^+) \end{array}$$

SCHEME 1

Reaction via both hydroxy and aquo species equates k_1^{CO} with $(K_a k'[H^+]^{-1} + k)$. The acid dependence data at 40 °C (Table 3, Fig. 2) would give $k \approx 0.12\ M^{-1}\ s^{-1}$ and $K_a k' \approx 0.01\ s^{-1}$. This analysis assumes that a *coordinated* water (or hydroxide) is involved in the reaction, the H_2O (or OH^-) then migrating to a *cis* carbonyl; such a mechanism follows from that established for many CO insertion reactions (20), and that usually postulated for the related olefin oxidation using palladium(II), the "oxypalladation" reaction (21):

$$[6] \quad \begin{array}{c} | \\ -Pd^{II}- \\ | \\ HO \end{array} \begin{array}{c} CH_2 \\ \| \\ CH_2 \end{array} \rightarrow -Pd-CH_2CH_2OH \rightarrow Pd^0 + CH_3CHO + H^+$$

However, the more well-characterized oxymercuration and oxythallation of olefins are

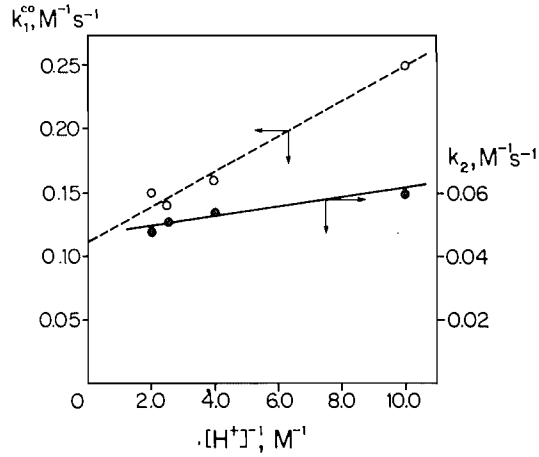

FIG. 2 Inverse acid dependence of k_1^{CO} and k_2 (eq. 2, Table 3); 0.02 M Rh, 0.5 M Br^-, 759 mm HgCO.

stereochemically *trans* reactions involving *external* H_2O or OH^- (22), and reactions involving nucleophilic attack of alcohols on coordinately saturated carbonyls to give esters must also involve external attack of the alcohol (23). Thus the water or hydroxide required for the k_1^{CO} step could involve external attack; this would imply, for example, that the acid dependent contribution to k_1^{CO} (Fig. 2) is of the form (constant)$[Rh^{III}][CO][OH^-]$, and it would be necessary to invoke a preequilibrium reaction with CO (not detected) followed by a rate determining hydroxide attack to account for such kinetics. Since there is no significant inverse bromide dependence, the alternative mechanism with external $H_2O(OH^-)$ attack would then be written, for example:

$$[7] \quad RhBr_4(H_2O)_2^- + CO \overset{K}{\rightleftharpoons} RhBr_4(H_2O)(CO)^- + H_2O$$

$$[8] \quad RhBr_4(H_2O)(CO)^- \xrightarrow[H_2O \text{ or } OH^-]{\text{slow}} RhBr_4(H_2O)(COOH)^- + (H^+)$$

We intuitively consider this less likely than reaction with the coordinated H_2O, although for an aquopentabromo (or chloro) complex, decomposition of an intermediate $RhX_5(CO)^{2-}$ species via external attack seems more feasible. It should be noted, however, that in the oxidation of ethylene to acetaldehyde using $[RhCl_n(H_2O)_{6-n}]^{(n-3)-}$ complexes, the hexachloro species is inactive, giving convincing evidence that a coordinated water is essential in this case (24).

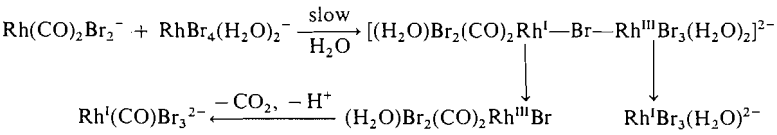

SCHEME 2

The concentration of free hydroxide or hydroxy complexes in the acid media is extremely small. Using acid dissociation constant data for the aquochlororhodate(III) complexes (25) suggests that a hydroxy species would be more reactive than an aquo species (see Scheme 1) by factors of $\sim 10^5$, and such labilizing effects of the order of 10^4 have been noted for substitution reactions of cobalt(III) complexes (26). To account for the observed initial rates of $\sim 10^{-6}$ M s^{-1} (Fig. 1), the mechanism of [7] and [8] would necessitate a rate constant of $\sim 10^{10}$ M^{-1} s^{-1} for reaction 8 which is of the order of diffusion-controlled reactions in solution (27).

The autocatalytic k_2 step involves formation of a mixed valence halide-bridged intermediate, followed by an internal two-electron transfer and decomposition via breaking of the newly-formed labile Rh^I—halide bond (2). The process for diaquotetrabromorhodate(III) is outlined in Scheme 2; the initial rhodium(I) products are then converted rapidly to $Rh(CO)_2Br_2^-$. The small inverse acid effect on k_2 (Table 3, Fig. 2) perhaps suggests some slight contribution via a rhodium(III) hydroxy complex with

$$k_2 = k_{H_2O} + K_a k_{OH}[H^+]^{-1}$$

where

$$k_{H_2O} \approx 0.047\ M^{-1}\ s^{-1}$$

and

$$K_a k_{OH} \approx 0.001\ s^{-1} \text{ at } 40\ °C$$

This again implies that k_{OH} is orders of magnitude greater than k_{H_2O}. The inverse bromide effect could be due to inhibited formation of the bridged intermediate or occupancy of the axial Rh^I ligand position by bromide (*trans* to the bridging bromide).

The data in Table 4 show that the bromide system is some thirty times more reactive than the chloride system toward both CO and H_2. However, as regards CO substitution (Scheme 1), the bromide system appears to proceed mainly via an acid independent path, while the chloride system involves mainly hydroxide species, and the data indicate somewhat greater lability for $RhBr_4(H_2O)_2^-$ compared to $RhCl_5(H_2O)^{2-}$. The positive ΔS^* values could reflect a spreading out of charge in the transition state (1).

The bromide system is more reactive by a factor of about ten in the autocatalytic step of the carbonylation reactions (Table 5), and again, in contrast to the chloride system, hydroxy species play a negligible role. The k_2 values could refer to step (*a*) of [9], or could be a composite constant Kk^* with K small:

[9] $Rh^{III}X + Rh^I \underset{K}{\overset{(a)}{\rightleftharpoons}} Rh^{III}—X—Rh^I \xrightarrow[k^*]{(b)} Rh^I + XRh^{III}$

The reactivity trend will be influenced by the greater ability of the more polarizable Br^- to transmit electrons, and possibly by more favorable electrostatic factors for the bromide system;

TABLE 4. Summary of kinetic data for reaction of rhodium(III) halide complexes with CO and H_2

System	k_1^H or k_1^{CO} (M^{-1} s^{-1}) 40 °C	80 °C	ΔH^* (kJ mol^{-1})	ΔS^* (J K^{-1} mol^{-1})
$RhBr_4(H_2O)_2^-/H_2$*	0.17		94.9	44
$RhCl_5(H_2O)^{2-}/H_2$†	0.005‡	0.56	102.8	37
$RhBr_4(H_2O)_2^-/CO$*	0.14§		112.4	98
$RhCl_5(H_2O)^{2-}/CO$†	0.005‡	0.54§	108	55

*In 0.5 M HBr.
†In 3.0 M HCl.
‡Estimated from activation parameters.
§$k_1^{CO} = k + K_a k'[H^+]^{-1}$: for $RhBr_4(H_2O)_2^-$ at 40 °C, $k = 0.12\ M^{-1}\ s^{-1}$, $K_a k' = 0.01\ s^{-1}$; for $RhCl_5(H_2O)^{2-}$ at 80 °C, $k = 0.2\ M^{-1}\ s^{-1}$, $K_a k' = 1$.

Can. J. Chem. Downloaded from www.nrcresearchpress.com by 210.87.254.5 on 09/05/12
For personal use only.

TABLE 5. Summary of kinetic data for the autocatalytic step

System	k_2 (M^{-1} s^{-1})	$\Delta H_2^{\ddagger}$ (kJ mol^{-1})	$\Delta S_2^{\ddagger}$ (J K^{-1} mol^{-1})
$RhBr_4(H_2O)_2^-/Rh(CO)_2Br_2^-$*	0.05 (40°)‡	63.1	−69
$RhCl_5(H_2O)^{2-}/Rh(CO)_2Cl_2^-$†	0.005 (40°)§		
	0.07 (80°)‡	52.2	−120

*In 0.5 *M* HBr.
†In 3.0 *M* HCl.
‡$k_2 = k_{H_2O} + K_a k_{OH}[H^+]^{-1}$; for the bromide system at 40 °C, $k_{H_2O} = 0.047\ M^{-1}$ s^{-1}, $K_a k_{OH} \approx 0.001$ s^{-1}; for the chloride system at 80 °C, $k_{H_2O} = 0.05\ M^{-1}$ s^{-1}, $K_a k_{OH} = 0.07$ s^{-1}.
§Estimated from activation parameters.

the more negative $\Delta S_2^{\ddagger}$ value for the chloride system could result from greater charge and solvation of the bridged intermediate or activated complex.

An interesting observation is that the second order rate constants and activation parameters for reactions of the bromide and chloride systems with H_2 are quite similar to those found for the corresponding reactions with CO (Table 4), and offers indirect evidence that both the hydrogenation and carbonylation reactions involve substitution via similar mechanisms, for example, an interchange process (28) with transition states similar to **1**:

[10] $$Rh^{III}X^- + CO \rightarrow Rh^{III}(CO) + X^-$$

[11] $$Rh^{III}X^- + H_2 \rightarrow Rh^{III}H^- + H^+ + X^-$$

Such similarities tend to argue against external $H_2O(OH^-)$ attack in the carbonylation system exemplified by reaction 7 and 8.

In view of the decomposition of the $Rh^{III}(CO)$ by water to Rh^I (Scheme 1; *cf.* the $Rh^{III}H^- \rightleftharpoons Rh^I + H^+$ process mentioned earlier), a rhodium(III)–carbon monoxide system ([10]) may also be used for catalytic reduction of iron(III); such studies have been completed (4, 14) and will be reported in detail later.

Acknowledgments

We thank the National Research Council of Canada for support of this research, and Johnson, Matthey Ltd. for the loan of $RhCl_3 \cdot 3H_2O$.

1. J. F. HARROD and J. HALPERN. Can. J. Chem. **37**, 1933 (1959); B. R. JAMES and G. L. REMPEL. Can. J. Chem. **44**, 233 (1966).
2. B. R. JAMES and G. L. REMPEL. J. Chem. Soc. A, 78 (1969).
3. J. A. STANKO, G. PETROV, and C. K. THOMAS. Chem. Commun. 1100 (1969).
4. B. R. JAMES and G. ROSENBERG. Proc. XVIth Intern. Conf. on Coordin. Chem. Dublin, 1974, Abstract 4.33.
5. J. REED and R. EISENBERG. Science, **184**, 568 (1974).
6. J. F. ROTH, J. H. CRADDOCK, A. HERSHMAN, and F. E. PAULIK. Chem. Tech. 600 (1971).
7. D. Forster. Inorg. Chem. **8**, 2556 (1969); Inorg. Chem. **11**, 1686 (1972); M. J. CLEARE and W. P. GRIFFITH. J. Chem. Soc. A, 372 (1969); J. J. DALY, F. SANZ, and D. FORSTER. J. Am. Chem. Soc. **97**, 2551 (1975).
8. W. C. WOLSEY, C. A. REYNOLDS, and J. KLEINBERG. Inorg. Chem. **2**, 463 (1963); W. ROBB and M. M. De V. STEYN. Inorg. Chem. **6**, 616 (1967); K. L. BRIDGES and J. C. CHANG. Inorg. Chem. **6**, 619 (1967); D. A. PALMER and G. M. HARRIS. Inorg. Chem. **14**, 1316 (1975).
9. D. COZZI and F. PANTANI. J. Electroanal. Chem. **2**, 72 (1961).
10. W. ROBB and P. VAN Z. BEKKER. Inorg. Chim. Acta, **7**, 626 (1973).
11. R. WIEBE and V. L. GADDY. J. Am. Chem. Soc. **56**, 76 (1934).
12. A. SEIDELL. Solubilities of inorganic and metal organic compounds. Vol. 1. 3rd ed. Van Nostrand, New York. 1940. p. 557.
13. A. SEIDELL. Solubilities of inorganic and metal organic compounds. Vol. 1. 4th ed. Van Nostrand, New York. 1958. p. 453.
14. G. ROSENBERG. Ph.D. Thesis. University of British Columbia, Vancouver, British Columbia. 1974.
15. L. M. VALLARINO. Inorg. Chem. **4**, 161 (1965).
16. J. HALPERN and B. R. JAMES. Can. J. Chem. **44**, 671 (1966).
17. J. F. HARROD, D. F. R. GILSON, and R. CHARLES. Can. J. Chem. **47**, 1431 (1969); U. BELLUCO, M. GIUSTINIANI, and M. GRAZIANI. J. Am. Chem. Soc. **89**, 6494 (1967); G. STRATHDEE and R. GIVEN. Can. J. Chem. **53**, 106 (1975).
18. R. D. GILLARD, B. T. HEATON, and D. H. VAUGHAN. J. Chem. Soc. A, 3126 (1970).
19. J. HALPERN. J. Phys. Chem. **63**, 398 (1959).
20. K. NOACK and F. CALDERAZZO. J. Organomet. Chem. **10**, 101 (1967).
21. A. AGUILO. Adv. Organomet. Chem. **5**, 321 (1967).
22. P. ABLEY, J. F. BYRD, and J. HALPERN. J. Am. Chem. Soc. **95**, 2591 (1973), and references therein.

Can. J. Chem. Downloaded from www.nrcresearchpress.com by 210.87.254.5 on 09/05/12
For personal use only.

23. A. J. DEEMING and B. L. SHAW. J. Chem. Soc. A, 443 (1969).
24. B. R. JAMES and M. KASTNER. Can. J. Chem. **50**, 1698 (1972); **50**, 1708 (1972).
25. A. V. BELYAEV and B. V. PTITSYN. Zh. Neorg. Khim. **11**, 1345 (1966).
26. F. BASOLO and R. G. PEARSON. Mechanisms of inorganic reactions. 2nd ed. Wiley, New York. 1967. p. 170.
27. A. A. FROST and R. G. PEARSON. Kinetics and mechanism. 2nd ed. Wiley, New York. 1961. Chapt. 11.
28. C. H. LANGFORD and H. B. GRAY. Ligand substitution processes. Benjamin, New York. 1965.

Can. J. Chem. Downloaded from www.nrcresearchpress.com by 210.87.254.5 on 09/05/12
For personal use only.

Reactions of sodium tetrahydroborate and cyanotrihydroborate with ruthenium(II) and (III) systems in the presence of tertiary phosphines

DAVID G. HOLAH, ALAN N. HUGHES, AND BENJAMIN C. HUI

Department of Chemistry, Lakehead University, Thunder Bay, Ontario P7B 5E1

Received July 7, 1975

DAVID G. HOLAH, ALAN N. HUGHES, and BENJAMIN C. HUI. Can. J. Chem. **54**, 320 (1976).

The first tetrahydroborato–phosphine complexes of Ru(II) are reported and a number of new cyanotrihydroborato and hydrido complexes of Ru(II) are also recorded. Among the more interesting complexes prepared are $RuH(BH_4)(PPh_3)_3$, $RuH(BH_4)(CO)(PPh_3)_3$, $RuH(BH_4)(CO)_2[P(C_6H_{11})_3]_2$, and $RuH(BH_3CN)(CO)_2(DBP)_2$ (DBP is the ligand 5-phenyl-5*H*-dibenzophosphole). It is shown that unlike Rh(III), Ru(III) is not stabilized by phosphine complex formation towards reduction by tetrahydroborate ion although Ru(II) is not reduced further by this reagent. A stepwise mechanism is proposed for the reduction of phosphine–dichloro Ru(II) systems to hydrido–tetrahydroborato and dihydro complexes. Nuclear magnetic resonance studies show that certain of the products are mixtures of geometrical isomers and, in several cases, detailed nmr assignments are made.

DAVID G. HOLAH, ALAN N. HUGHES et BENJAMIN C. HUI. Can. J. Chem. **54**, 320 (1976).

On rapporte la préparation des premiers complexes tétrahydroborato–phosphine du Ru(II) ainsi que celle d'un certain nombre de nouveaux complexes cyanotrihydroborato et hydrido du Ru(II). Parmi les complexes les plus intéressants qui ont été préparés, on retrouve $RuH(BH_4)(PPh_3)_3$, $RuH(BH_4)(CO)(PPh_3)_3$, $RuH(BH_4)(CO)_2[P(C_6H_{11})_3]_2$ et $RuH(BH_3CN)(CO)_2(DBP)_2$ (DBP est le ligand phényl-5 5*H*-dibenzophosphole). On montre que le Ru(III), par opposition au Rh(III), n'est pas stabilisé, par formation d'un complexe de phosphine, vis-à-vis de la réduction par l'ion tétrahydroborato et ce même si le Ru(II) n'est pas réduit plus loin par ce réactif. On propose un mécanisme par étapes pour la réduction des systèmes phosphine–dichloro Ru(II) en complexes hydridotétrahydroborato et dihydro. Des études rmn montrent que certain de ces produits sont des mélanges d'isomères géométriques et, dans plusieurs cas, on fait des attributions détaillées des bandes rmn.

[Traduit par le journal]

Introduction

In a series of previous papers (1–3) we have reported that a variety of phosphine–metal(I) chloro, tetrahydroborato, and cyanotrihydroborato complexes may be obtained by treatment of Co(II), Ni(II), or Cu(II) halides with $NaBH_4$ or $NaBH_3CN$ in the presence of tertiary phosphines under carefully controlled conditions. In addition, a mechanism was proposed (2, 3) for the reduction of metal(II) halides to the range of metal(I) complexes of the type mentioned above. The results of this investigation have been summarized more fully elsewhere (4) and, in the same paper, the investigation has also been extended to Rh(I), Rh(II), and Rh(III) systems.

With these rhodium systems, it was shown (4) that both Rh(I) and Rh(II)–tetrahydroborato complexes such as $Rh(BH_4)(PPh_3)_2$ (highly unstable) and $RhH(BH_4)(o\text{-tolyl}_3P)$ could be obtained whereas with Rh(III), the only Rh(III) complexes which could be obtained were hydrido–chloro (*e.g.* RhH_2ClL_3 where L is a phosphine ligand) or hydrido–cyanotrihydroborato (*e.g.* $RhH_2(BH_3CN)L_3$) complexes. In this work, it also became clear that Rh(I) halide complexes such as $RhCl(PPh_3)_3$ react with tetrahydroborate ion in the same way as similar Ni(I) complexes to give first a tetrahydroborato complex which then decomposes to an Rh(I) hydrido complex. Furthermore, it was shown that Rh(I), Rh(II), and Rh(III) are all normally stabilized by complexing phosphine ligands towards reduction by tetrahydroborate ion to lower oxidation states of rhodium. However, certain puzzling features were apparent from these reactions. For example, it was found that the Rh(III) complex $RhCl_3(DBP)_3$ (DBP = the dibenzophosphole ligand 5-phenyl-5*H*-dibenzophosphole previously discussed (4)) reacts with tetrahydroborate ion to give $RhH_2Cl(DBP)_3$ whereas with the milder reducing agent $NaBH_3CN$, an Rh(I)–BH_3CN complex was obtained. Possible mechanisms for the forma-

Can. J. Chem. Downloaded from www.nrcresearchpress.com by 210.87.254.105 on 09/05/12
For personal use only.

Can. J. Chem. Downloaded from www.nrcresearchpress.com by 210.87.254.105 on 09/05/12
For personal use only.

tion of these products were briefly discussed but it was apparent that further work on the tetrahydroborate and cyanotrihydroborate reductions of transition metal halides was essential.

We therefore report here our findings obtained by extending the studies discussed above to ruthenium(II) and (III) systems. Relatively little work has been done on these systems and the only known (5) ruthenium complexes related to the rhodium complexes mentioned above are the ionic species $[Ru(NH_3)_5(BH_3CN)]Br$ and $[Ru(NH_3)_5(BH_3CN)]Br_2$ in which the BH_3CN groups are bound to the metal in the same manner as in the corresponding CH_3CN complexes. However, as reported below, a wide variety of $Ru-BH_4$ and $Ru-BH_3CN$ complexes may be obtained if conditions are carefully controlled.

Results and Discussion

Reactions of Ru(II) and Ru(III) Chlorides in the Presence of Phosphines

Since Co(II) and Ni(II) have been found (3) to react with $NaBH_4$ in ethanol solution in the presence of an excess of PPh_3 to give a variety of univalent complexes, it was considered possible that the well-known (6) blue ruthenium(II) chloride solution, which contains the $[Ru_5Cl_{12}]^{2-}$ species, may behave similarly. However, Ru(II) cannot be reduced to Ru(I) with tetrahydroborate ion under similar conditions. For example, in the presence of a sixfold excess of PPh_3 and with a 1:1 molar ratio of $NaBH_4$ to Ru in ethanol, the known (7) $RuHCl(PPh_3)_3$ is the sole product. On the other hand, addition of a large excess (over 10 times) of $NaBH_4$ to the mixture of Ru(II) (as the above blue solution) and PPh_3 causes the precipitation of a yellow, diamagnetic hydrido–tetrahydroborato complex analyzing well for $RuH(BH_4)(PPh_3)_3$, *i.e.* although reduction of Ru(II) to Ru(I) does not occur, a reasonably stable tetrahydroborato complex is obtained. This compound is only stable under an inert atmosphere and slowly decomposes in air. Prolonged stirring of the reaction mixture (~25 h) without isolating the $RuH(BH_4)(PPh_3)_3$ results in its decomposition and the known (8) $RuH_2(PPh_3)_4$ is formed.

The presence of the tetrahydroborate grouping in the complex formulated as $RuH(BH_4)(PPh_3)_3$ is demonstrated by the infrared spectrum which shows absorptions at 1119, 2340, and 2382 cm^{-1} assignable to the bending and stretching modes respectively of the terminal B—H bonds. The Ru—H bond appears in the infrared spectrum as a weak absorption at 2080 cm^{-1}. This Ru—H linkage can also be identified as a typical metal hydride band in the nmr spectrum as a broad (~35 Hz) signal at 16.87 τ. Further confirmation of this structure is given by the fact that with $NaBD_4$, the corresponding deuterated product has been isolated and, as expected, the bands due to the stretching frequencies of the terminal B—D bonds shift to 1792 and 1810 cm^{-1}. It has also been found that this hydrido–tetrahydroborato complex can also be prepared by using commercial $RuCl_3$ hydrate (presumably because Ru(III) is readily reduced by PPh_3(9)) instead of the blue Ru(II) chloride solution.

On the basis of the infrared and nmr spectra already discussed, and from the fact that $RuHCl(PPh_3)_3$ can be isolated as an intermediate product, a distorted trigonal bipyramidal (similar to $RuHCl(PPh_3)_3$) structure (**1**) is proposed for $RuH(BH_4)(PPh_3)_3$.

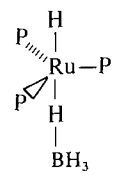

1

A structure involving double hydrogen bridges, and therefore an octahedral Ru(II) species, seems rather unlikely due to the absence of the ring breathing modes of

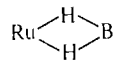

in the ir spectrum. The broad nature of the metal–hydride nmr signal may suggest extensive dissociation of PPh_3.

As mentioned in the introduction, no tetrahydroborato complex of ruthenium has previously been reported although the reactions of $NaBH_4$ and $RuCl_3$ in the presence of PPh_3 in boiling ethanol have been thoroughly investigated (8, 10). Hydrido complexes, such as $RuH_2(PPh_3)_4$ (8), $RuH_2(PPh_3)_3$ (8), and $RuH_4(PPh_3)_3$ (10) are conveniently prepared by this method. Our results therefore indicate that these previously reported reactions involve

Can. J. Chem. Downloaded from www.nrcresearchpress.com by 210.87.254.105 on 09/05/12
For personal use only.

unisolated M–BH_4 intermediate complexes. Some support for this comes from the fact that the tetrahydroborato complex $RuH(BH_4)(PPh_3)_3$ in ethanol under reflux decomposes to the known (7) $RuH_2(CO)(PPh_3)_3$. Decomposition of the hydrido–tetrahydroborato complex is apparently accompanied by abstraction of CO from ethanol. However, in the presence of free PPh_3, $RuH(BH_4)(PPh_3)_3$ decomposes to $RuH_2(PPh_3)_4$.

Thus, from our observations, the action of $NaBH_4$ on Ru(II) complexes in the presence of PPh_3 seems to proceed according to Scheme 1.

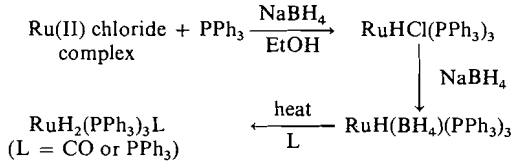

SCHEME 1

Ru(II) therefore behaves quite differently as compared with Co(II), Ni(II), or Cu(II) which have been found (3) to form, as summarized in the introduction, M(I)–chloro or tetrahydroborato complexes. As will be seen in the concluding paragraphs of this paper, further evidence allows the skeleton Scheme 1 to be amplified somewhat.

The formation of the tetrahydroborato complex appears to be very sensitive to the electronic and steric effects operating in the ligand. For example, with Ru(II) or Ru(III) chloride in the presence of $NaBH_4$ under conditions similar to those already outlined, $AsPh_3$ forms only $RuHCl(AsPh_3)_3$ (nmr shows an Ru—H singlet at 21.9 τ), while the rigid bulky DBP gives the known (11) $RuHCl(DBP)_3$ although under more rigorous conditions, $RuH_2(DBP)_4$ (11) is the only product. Furthermore, we have failed to isolate any appreciable amount of solid product when 1,2-bis(diphenylphosphino)ethane (diphos), 1,3- or 1,5-cyclooctadiene, 1,10-phenanthroline, $PEtPh_2$, or $P(C_6H_{11})_3$ is used as ligand.

With regard to similar cyanotrihydroborate reactions, although $NaBH_3CN$ reacts with the Ru(II) blue chloride solutions in the presence of PPh_3 or DBP to give brown solutions, we were unable to isolate any identifiable product. Addition of $Ph_4As^+Cl^-$ or $Na^+Ph_4B^-$ to these brown solutions does not precipitate any salts.

Reactions of $RuCl_2(PPh_3)_3$ and $RuCl_3(DBP)_3$

Although $RuCl_2(PPh_3)_3$ (7) also reacts with $NaBH_4$ in the same manner as the Ru(II) blue solution in the presence of Ph_3P, in ethanol at room temperature to form $RuH(BH_4)(PPh_3)_3$, the product is always contaminated with varying amounts of the known (10, 12) tetrahydrido complex $RuH_4(PPh_3)_3$ which can be identified from both the ir and nmr spectra of the product. Prolonged stirring of $RuCl_2(PPh_3)_3$ with $NaBH_4$ always results in the tetrahydride. Therefore, it appears that in the presence of a large excess of $NaBH_4$, the intermediate $RuH(BH_4)(PPh_3)_3$ tends to decompose quickly and also oxidatively add dihydrogen. Recrystallization of this tetrahydrido complex from N_2-saturated solvent results in the formation of some $RuH_2(N_2)(PPh_3)_3$ (10).

In related experiments, the reaction of $NaBH_4$ with $RuCl_2(PPh_3)_3$ in C_6H_6–ethanol has been reported by Harris *et al.* (12) to give $RuH_4(PPh_3)_3$. However, no intermediate tetrahydroborato complex can be isolated under these conditions. $NaBH_4$ also reacts with $RuCl_2(PPh_3)_3$ in ethanol under reflux to form the already known (7) $RuH_2(CO)(PPh_3)_3$. This reaction seems likely to involve the hydrido–tetrahydroborato complex and the product is probably formed from the intermediate $RuH(BH_4)(PPh_3)_3$ in the same manner as reported in the previous section.

We have noticed that in these reactions, the formation of $RuH_4(PPh_3)_3$ can be suppressed if a 3–6 *M* ratio of PPh_3 is suspended with $RuCl_2(PPh_3)_3$ in ethanol before addition of $NaBH_4$. Thus, if $RuCl_2(PPh_3)_3$ is treated with $NaBH_4$ in ethanol in the presence of an excess of PPh_3 and the reaction time is reduced, $RuH(BH_4)(PPh_3)_3$ can be obtained in a relatively pure state.

In reactions of related DBP complexes, the Ru(III) phosphine complex, $RuCl_3(DBP)_3$ (11) only reacts very slowly with $NaBH_4$ in ethanol, but rapidly in C_6H_6–EtOH to form in both cases either the dihydride $RuH_2(DBP)_3$ or the tetrahydride $RuH_4(DBP)_3$. Since the procedure is very similar to that used by Harris *et al.* (12) for $RuH_4(PPh_3)_3$ we prefer the tetrahydrido formulation for the product. The Ru—H bonds are clearly identifiable in the ir spectrum as broad bands at 1917 and 1945 cm^{-1} (stretching) and at 800 cm^{-1} (bending) but, unfortunately,

Can. J. Chem. Downloaded from www.nrcresearchpress.com by 210.87.254.105 on 09/05/12
For personal use only.

this complex is not sufficiently soluble for high-field nmr studies.

Reactions of Ru(II) Carbonyl Chloride Solutions in the Presence of Phosphines

Since Ru(II) forms a wide class of stable complexes containing carbonyl and phosphine ligands, it was expected that the presence of a carbonyl group could stabilize the tetrahydroborato complex further so that such complexes including phosphines other than PPh_3 could be synthesized. However, as outlined below, only PPh_3 and tricyclohexylphosphine, $P(C_6H_{11})_3$, are effective in this respect although, with $NaBH_3CN$, DBP is also effective.

Reaction of a sixfold excess of PPh_3 with the well-known (9) red Ru(II) carbonyl ethanolic solution and $NaBH_4$ produces a yellow solid, which can be recrystallized from toluene–EtOH to give the tetrahydroborato species $RuH(BH_4)(CO)(PPh_3)_3$. That this species is octahedral involving a monodentate BH_4 ligand is indicated by both the ir and nmr spectra. The infrared bands at 1110 cm^{-1}, 2350 and 2380 cm^{-1} correspond respectively to the bending and stretching frequencies of terminal B—H bonds. The carbonyl group has a very intense band at 1950 cm^{-1} while the Ru—H stretching frequency is at 1970 cm^{-1}. The absence of any ring breathing RuH_2B modes and the close resemblance of the frequencies of the Ru—H and C=O bands to those of $RuH_2(CO)(PPh_3)_3$ (7) (ν_{CO} = 1940 cm^{-1} and ν_{Ru-H} = 1960 and 1900 cm^{-1}) strongly suggest a linkage of the type Ru—H—BH_3. The stretching frequencies for the terminal B—H bonds are relatively low in $RuH(BH_4)(CO)(PPh_3)_3$ as compared with those of the analogous Rh(I) complexes (see Table 1 in ref. 4) which occur at >2400 cm^{-1}, and involve double hydrogen bridges (13, 14). Compounds containing monodentate BH_4 have been shown (15) to have ir bands at ~2400–2250 cm^{-1} and bands at ~2380 cm^{-1} have been observed (3) in the tetrahedral complex $Co(BH_4)(PPh_3)_3$.

The nmr spectrum of $RuH(BH_4)(CO)(PPh_3)_3$ clearly indicates the presence of two geometrical isomers in that two distinct Ru—H signals are seen. The first of these appears as a doublet of doublets of triplets centered on 17.06 τ with the three coupling constants with values of 32, 16, and 6 Hz respectively. The first of these is too high to be anything but J_{P-H} while the second is also probably a phosphorus–hydrogen coupling. The second signal is centered at 18.95 τ and it is also a doublet of doublets of triplets with the three coupling constants having values of 73, 28, and 6 Hz. Again, clearly the first two of these couplings are too large to be anything but phosphorus–hydrogen interactions.

A comparison of this spectrum with the nmr spectrum (7) of $RuH_2(CO)(PPh_3)_3$, which has the geometry shown in **2** and which exhibits Ru—H signals at 18.67 τ and 16.69 τ, suggests that, in solution, the complex $RuH(BH_4)(CO)(PPh_3)_3$ is a mixture of the isomeric structures **3** and **4**.

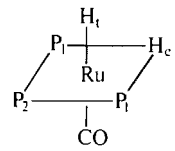

2

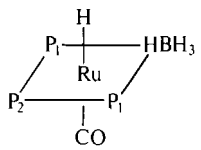

3

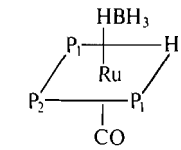

4

The signal at 17.06 τ in the nmr spectrum of $RuH(BH_4)(CO)(PPh_3)_3$ is probably due to structure **3** in which all phosphine ligands are *cis* to the hydrogen atom and, by analogy with the spectrum of **2** (7), the coupling constants (tentatively assigned as J_{P_1-H} = 32 Hz, J_{P_2-H} = 16 Hz, and J_{H-BH_4} = 6 Hz) are consistent with this structure. Similarly, in the other isomer **4** (18.95 τ) the probable coupling assignments are J_{P_1-H} = 28 Hz, J_{P_2-H} = 73 Hz, and J_{H-BH_4} = 6 Hz. Again the assigned J_{P_2-H} value is consistent with the magnitude of that given (7) for $J_{P_2-H_c}$ in **2**. Values of J_{H-BH_4} of 6 Hz have also been reported in tetrahydroborato complexes of Ni(II) (16).

Similar reactions with tri(cyclohexyl)phosphine as ligand produce $RuH(BH_4)(CO)_2[P(C_6H_{11})_3]_2$ which has infrared bands at 2430 and 2480 cm^{-1} assignable to the terminal ν_{B-H}. The carbonyl groups have ir bands at 1935, 1952, and 2020 cm^{-1} and the Ru—H bond stretching frequencies occur at 1912 and 1982

Can. J. Chem. Downloaded from www.nrcresearchpress.com by 210.87.254.105 on 09/05/12
For personal use only.

cm^{-1}. The infrared spectrum alone suggests the presence of more than one species. This is again confirmed by the high field nmr signals of the Ru—H grouping which shows a triplet at 14.82 τ (J_{P-H} = 20 Hz) and another triplet at 24.03 τ (J_{P-H} = 18 Hz). The closely related compound $RuH_2(CO)_2(PPh_3)_2$ (17) has been reported to have signals at 16.9 τ (triplet, J_{P-H} = 23 Hz) in the high field nmr spectrum, and a structure as shown in **5**.

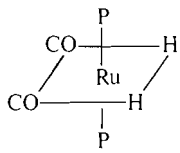

5

The complex ir and nmr spectra of the adduct $RuH(BH_4)(CO)_2[P(C_6H_{11})_3]_2$ can be explained if the complex exists as two isomers (**6** and either **7** or **8**) with the phosphines being *cis* to the hydride group in all cases.

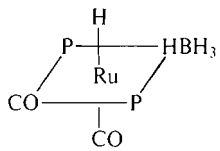

6
(Ru—H at 14.82 τ)

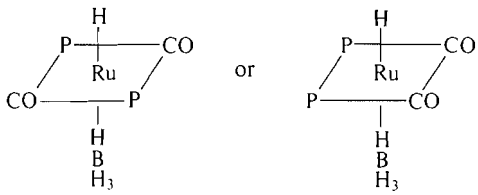

7 **8**
(Ru—H at 24.03 τ)

Even the presence of carbonyl groups does not lead to the formation of tetrahydroborato complexes when other phosphines are used as complexing ligands. For example, under similar reaction conditions, DBP yields $RuH_2(CO)_2(DBP)_2$ (ν_{CO} = 2010, 1955, and 1938 cm^{-1}, ν_{Ru-H} = 2050 and 1860 cm^{-1}) while $PEtPh_2$ forms $RuH_2(CO)(PEtPh_2)_3$ (ν_{CO} = 1895, 1940 cm^{-1}; ν_{Ru-H} = 1830 cm^{-1}). Only the $PEtPh_2$ complex is soluble enough for nmr studies, and a doublet of triplets at 17.07 τ (tentative assignments based on structure **9**, $J_{P_1-H_1}$ = 25 Hz, $J_{P_2-H_1}$ = 19 Hz, $J_{H_1-H_2}$ = 7 Hz) together with another doublet of doublets of triplets at 18.43 τ ($J_{P_1-H_2}$ = 28 Hz, $J_{P_2-H_2}$ = 73 Hz) have been observed. These highly complex signals can be accounted for if structure **9** is assigned to the complex with the coupling constants assigned by analogy with **2**, **3**, and **4**.

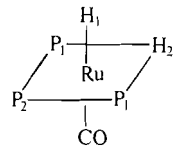

9

Turning to reactions of $NaBH_4$ with Ru(II)–chloro–carbonyl–phosphine complexes rather than the similar reactions with the red ethanolic Ru(II)–carbonyl solution (9) in the presence of phosphines already described above, several differences between the two systems emerge. In this connection, it has been found (14) in the reactions of $NaBH_4$ with the Rh(I) system $RhCl(CO)L_2$ to give $Rh(BH_4)(CO)L_2$ that in the presence of an excess of phosphine, only $RhH(CO)L_3$ can be isolated with no trace of the expected tetrahydroborato intermediate. We have found in related reactions (with no excess of ligand present) between sodium tetrahydroborate and the known Ru(II)–carbonyl–chloro–phosphine systems $RuCl_2(CO)_2(PPh_3)_2$ (18), $RuCl_2(CO)(DBP)_3$ (11), and $RuCl_2(CO)_2$(diphos) (18) where, by analogy with the Ru(II) studies described above and the Rh(I) studies (14) already mentioned, hydrido or tetrahydroborato complexes might be expected, that neither $RuCl_2(CO)_2(PPh_3)_2$ nor $RuCl_2(CO)(DBP)_3$ will react with $NaBH_4$ (~20-fold excess) even after prolonged (~20 h) stirring. On the other hand, the diphos complex forms $RuH_2(CO)_2$(diphos) (ν_{CO}, 1935 and 1965 cm^{-1}; ν_{Ru-H}, 2050 cm^{-1}) although no intermediate tetrahydroborato compound could be obtained. No really satisfactory explanation can be offered for this behavior at this stage although the comparative inertness of these complexes is probably at least partly a result of steric interactions.

The reactions of $NaBH_3CN$ with Ru(II) carbonyl solutions in the presence of phosphines do not generally produce solid products. Only with DBP as the phosphine ligand can a pale

Can. J. Chem. Downloaded from www.nrcresearchpress.com by 210.87.254.105 on 09/05/12
For personal use only.

TABLE 1. Analyses and ir spectra of complexes prepared

Compound	Color	Analyses*			Infrared spectra (cm^{-1})				
		C	H	N	δ_{B-H}	ν_{B-H}	ν_{CO}	ν_{M-H}	Other
$RuH(BH_4)(PPh_3)_3$	Yellow	72.1 71.8	5.6 5.6	— —	1119m	2382s 2340sh		2080w	
$RuHCl(AsPh_3)_3$	Light brown	62.1 61.4	4.4 4.4	—				2030w	
$RuH_4(DBP)_3$	Yellow	73.0 73.2	4.6 4.9	— —				1945mb 1917mb	800 (δ_{Ru-H})
$RuH(BH_4)(CO)(PPh_3)_3$	Yellow	71.6 70.9	5.3 5.4	— —	1105m	2382m 2350w	1950s	2150w (?) 1970m	765 (δ_{Ru-H})
$RuH(BH_4)(CO)_2[P(C_6H_{11})_3]_2$	Yellow	62.1 62.2	9.9 9.8	— —		2480m 2430m	2220s 1952s 1935s	1982m 1912m	
$RuH_2(CO)_2(DBP)_2$	Orange	67.5 67.2	4.3 4.1	— —			2010s 1955s 1938s	2050w 1860w	
$RuH_2(CO)(PEtPh_2)_3$	Yellow	65.9 66.7	6.4 6.1	— —			1940s 1895s	1830w	
$RuH_2(CO)_2$(diphos)	Yellow	60.0 60.3	4.9 4.7	— —			1965s 1935s	2050m	820m (δ_{Ru-H})
$RuH(BH_3CN)(CO)_2(DBP)_2$	Yellow	64.7 65.2	4.8 4.2	1.6 1.9	1120	2340s	2020s 1985s 1965s	1845	2010s (ν_{CN})

*Calculated values below found.

Can. J. Chem. Downloaded from www.nrcresearchpress.com by 210.87.254.105 on 09/05/12
For personal use only.

yellow solid be obtained. This solid analyzes well for $RuH(BH_3CN)(CO)_2(DBP)_2$ and a shift in the intense CN stretching frequency (Table 1) from 2180 cm^{-1} in uncoordinated BH_3CN^- to 2210 cm^{-1} in the complex indicates a strong bonding of the CN group to the Ru atom through the nitrogen. Similar shifts have been observed (3) with *N*-bonded $Cu-BH_3CN$ complexes. The complex carbonyl absorptions in the ir spectrum (2020, 1985, 1965 cm^{-1}) suggest the presence of more than one isomer.

In conclusion, several observations may be made. First no Ru(III)–BH_4 or Ru(III)–BH_3CN phosphine complexes may be prepared from Ru(III) chloride, presumably because in most cases the reduction of Ru(III) to Ru(II) by phosphines is normally very rapid. In the case of the reaction of the $RuCl_3$–PPh_3 system with $NaBH_4$, the hydrido–tetrahydroborato complex $RuH(BH_4)(PPh_3)_3$ is formed. This is the first Ru–BH_4 complex reported. Second, unlike the divalent 3*d* systems previously reported (3), Ru(II) is not reduced to Ru(I) even with very large excesses of $NaBH_4$ and with extended reaction times. Thus, as with Rh(II) systems discussed elsewhere (4), complexation stabilizes Ru(II) towards reduction. However, it is interesting to note that complexation in the complex $RuCl_3(DBP)_3$ does not protect the Ru(III) and a tetrahydrido complex, $RuH_4(DBP)_3$, is formed. This is apparently different from the behavior of complexed Rh(III) (4), as for example in the case of the analogous $RhCl_3(DBP)_3$.

Another observation is that it appears that, as with Rh systems (4), the presence of additional CO ligands lends greater stability to Ru–BH_4–phosphine or Ru–BH_3CN–phosphine complexes since $RuH(BH_4)(CO)(PPh_3)_3$ and $RuH(BH_3CN)(CO)_2(DBP)_2$ are relatively easy to prepare.

Finally, it appears to be very difficult, if not impossible, to prepare Ru–BH_4 complexes of any type which contain more than one BH_4 ligand regardless of the presence or absence of CO ligands. This is in contrast to zirconium systems in which both monotetrahydroborato (19) and bistetrahydroborato (20) complexes such as $ZrH(BH_4)(h^5\text{-}C_5H_5)_2$ and $Zr(BH_4)_2(h^5\text{-}C_5H_5)_2$ may be formed. It is possible, therefore, that the various Ru–hydrido–tetrahydroborato and cyanotrihydroborato complexes described in this paper and summarized in Table 1 are formed by a reaction sequence in which a dichloro–Ru(II) system interacts first with molecular hydrogen (generated presumably by reaction of $NaBH_4$ or $NaBH_3CN$ with the solvent ethanol) to give a chlorohydrido–Ru(II) system. In the second stage, the chloro-grouping is displaced by a tetrahydroborato or cyanotrihydroborato grouping to give the hydrido–tetrahydroborato or hydrido–cyanotrihydroborato complex.

There are two pieces of evidence which lend support to this suggested mechanism. First, it is known (7) that $RuCl_2L_3$ (L = phosphine ligand) will react with molecular hydrogen to give $RuHClL_3$. Second, in the reactions of uncomplexed $[Ru_5Cl_{12}]^{2-}$ or $RuCl_3$ with $NaBH_4$ in the presence of $AsPh_3$ or DBP, the intermediate $RuHClL_3$ (L = $AsPh_3$ or DBP) may be isolated; indeed, these are the only isolable products in these reactions. Similarly, if $[Ru_5Cl_{12}]^{2-}$ is treated with only 1 mol $NaBH_4$ in the presence of Ph_3P, $RuHCl(PPh_3)_3$ is produced.

Apparently, the final step in the proposed sequence

Ru(II)–dichloro → Ru(II)–hydrido chloro → Ru(II)–hydrido–tetrahydroborato complex

is the decomposition of the Ru(II)–hydrido–tetrahydroborato complex to a dihydro–complex and, as mentioned earlier, this may be observed with $RuH(BH_4)(PPh_3)_3$ although, in this case decomposition to a dihydride is accompanied by uptake of CO from the solvent ethanol. Occasionally, the dihydride may react further by oxidative addition of H_2 or by addition of N_2 to give compounds of the type $RuH_4(PPh_3)_3$ or $RuH_2(N_2)(PPh_3)_3$.

It is likely that all the dihydrides listed in Table 1 are formed by this process. It should also be noted that similar decompositions of tetrahydroborato complexes to hydrido complexes have been postulated with Rh(I) systems such as $Rh(BH_4)(PPh_3)_2$ (4) and this type of decomposition has been suggested (3) as one stage in the reaction sequence for the interaction of M(II) systems (M = 3*d* metal) with tetrahydroborate ion.

In conclusion, it should be emphasized that in the cases of $RuH(BH_4)(PPh_3)_3$, $RuH(BH_4)$-

Can. J. Chem. Downloaded from www.nrcresearchpress.com by 210.87.254.105 on 09/05/12
For personal use only.

$(CO)(PPh_3)_3$, and $RuH(BH_4)(CO)_2[P(C_6H_{11})_3]_2$, the BH_4 grouping apparently acts as a monodentate ligand although bidentate ligation is more normal (see discussion in refs. 3, 4, and 15). The evidence for this is very strong. Thus, the ir spectra show no trace of the typical

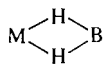

bridging B—H mode which normally occurs (4, 15) in the range 1850–2150 cm^{-1}. Neither is the bridge expansion band which normally occurs (15) at 1300–1500 cm^{-1} in the spectra of bidentate BH_4 complexes present in any of the spectra unless it is unusually sharp and lies directly under one of the Nujol peaks. Furthermore, the nmr spectra can only be satisfactorily interpreted on the basis of a monodentate BH_4 ligand and, indeed, this type of linkage is also strongly suggested by the fact that in $RuH(BH_4)(CO)(PPh_3)_3$ and $RuH(BH_4)(CO)_2[P(C_6H_{11})_3]_2$, the usual octahedral arrangement about the Ru atom would require a monodentate BH_4 grouping. Although monodentate BH_4 complexes are rare, they are not unknown. For example, the paramagnetic, tetrahedral Co(I) complex $Co(BH_4)(PPh_3)_3$ is known (3) to involve a monodentate BH_4 ligand.

Experimental

Materials

$RuCl_2(PPh_3)_3$ (7), the red Ru(II)–carbonyl solution (9), the blue Ru(II)–chloride solution (6), $RuCl_2(CO)_2(PPh_3)_2$ (18), $RuCl_2(CO)_2$(diphos) (18), $RuCl_2(CO)(DBP)_3$ (11), and $RuCl_3(DBP)_3$ (11) were prepared according to literature methods. $RuCl_3$ was purchased from Engelhard Industries and used without further purification. Solvents were purified in the usual manner, degassed, and stored over molecular sieves (type 4A).

Physical Measurements

Infrared spectra were recorded using a Beckman IR12 spectrophotometer calibrated with polystyrene while nmr measurements were made using a Varian Associates model A60-A spectrometer with benzene as solvent and using the benzene peak to calibrate the spectra. Microanalytical data were obtained with a Perkin–Elmer model 240 Elemental Analyzer and the results are recorded in Table 1.

Syntheses

Reactions were carried out under nitrogen in a glove box using degassed solvents. Except where otherwise stated, crude products were purified by washing successively with ethanol, water, ethanol, and either *n*-hexane or diethyl ether. Yields were in the range 50–70%. All of the products are stable as solids indefinitely under nitrogen but decompose in air over several hours at room temperature. The products are thermally unstable (particularly in solution) and decompose in the solid state slowly over a wide temperature range. Melting points are therefore not recorded.

$RuH(BH_4)(PPh_3)_3$

$RuCl_3$ hydrate (0.21 g, 0.87 mmol Ru) was dissolved in ethanol (~15 ml) to which PPh_3 (1.38 g, 5.26 mmol) was then added. $NaBH_4$ (0.33 g, 8.7 mmol) suspended in ethanol (7 ml) was then added dropwise to the vigorously stirred mixture. This vigorous stirring is essential. The mixture went through a series of color changes from reddish brown to green, then blue, and finally became brown with deposition of a yellow–brown solid. The mixture was left stirring for 10 min before the product was separated by filtration, washed in the manner outlined above, and dried by pumping under reduced pressure.

The same product was synthesized by using the blue Ru(II)–chloride solution (prepared from 0.16 g $RuCl_3$ hydrate, 0.66 mmol Ru), PPh_3 (1.3 g, 4.95 mmol), and an excess of $NaBH_4$ (0.25 g, 6.6 mmol) in ethanol (~7 ml). Alternatively, addition of $NaBH_4$ (~0.06 g, 1.5 mmol) to a mixture of $RuCl_2(PPh_3)_3$ (0.15 g, 0.15 mmol) and PPh_3 (0.24 g, 0.91 mmol) in ethanol (~15 ml) also yielded the same product.

$RuHCl(AsPh_3)_3$

This complex was prepared in the same way as $RuH(BH_4)(PPh_3)_3$ starting from the blue Ru(II)–chloride solution (prepared from 0.15 g $RuCl_3$ hydrate, 0.62 mmol Ru) and $AsPh_3$ (0.94 g, 3.06 mmol) with $NaBH_4$ (0.23 g, 6.2 mmol).

$RuH_4(DBP)_3$

$RuCl_3(DBP)_3$ (~0.3 g, 0.3 mmol) was suspended in the minimum amount of benzene to which a suspension of $NaBH_4$ (0.12 g, 3 mmol) in ethanol (~5 ml) was then added. The solution became clear yellow after 0.5 h, and was left stirring for a further 2–3 h before the solvent was removed under reduced pressure. Addition of ethanol precipitated the yellow product which was collected by filtration, washed, and dried in the usual manner.

$RuH(BH_4)(CO)(PPh_3)_3$, $RuH(BH_4)(CO)_2[P(C_6H_{11})_3]_2$, $RuH_2(CO)_2(DBP)_2$, $RuH_2(CO)(PEtPh_2)_3$, and $RuH(BH_3CN)(CO)_2(DBP)_2$

These complexes were prepared by the reactions of the red Ru(II)–carbonyl solution with the appropriate ligand (in a 6 *M* excess) and with a 10-fold excess of $NaBH_4$ (or $NaBH_3CN$ where appropriate) in ethanol. Again the solid products were collected by filtration of the reaction mixture after a suitable time interval and washed and dried in the usual manner.

Typically, PPh_3 (0.92 g, 3.5 mmol) was added to 15 ml of an ethanolic Ru(II)–carbonyl solution (prepared from 0.15 g $RuCl_3$ hydrate, 0.62 mmol of Ru) and this was followed by addition of $NaBH_4$ (0.23 g, 6.2 mmol) in ethanol (5 ml). A yellow solid formed and the mixture was left stirring for 0.5 h before the product was separated by filtration. In this instance, purification was effected by recrystallization from toluene–ethanol followed by low pressure pumping.

$RuH_2(CO)_2$(diphos)

A 10-fold excess of $NaBH_4$ (0.15 g, 3.9 mmol) was allowed to react with $RuCl_2(CO)_2$(diphos) (0.25 g, 0.39

mmol) in ethanol (20 ml) for ~15 h. The precipitated solid product was removed by filtration and purified by washing and drying in the manner outlined above.

Acknowledgments

We thank the National Research Council of Canada for generous financial support of this work. We also thank the Ventron Corporation, Beverly, Massachusetts, in particular Mr. Robert Wade, for a gift of chemicals.

1. D. G. HOLAH, A. N. HUGHES, B. C. HUI, and K. WRIGHT. Inorg. Nucl. Chem. Lett. **9**, 835 (1973).
2. D. G. HOLAH, A. N. HUGHES, and B. C. HUI. Inorg. Nucl. Chem. Lett. **10**, 427 (1974).
3. D. G. HOLAH, A. N. HUGHES, B. C. HUI, and K. WRIGHT. Can. J. Chem. **52**, 2990 (1974).
4. D. G. HOLAH, A. N. HUGHES, and B. C. HUI. Can. J. Chem. **53**, 3669 (1975).
5. P. C. FORD. Chem. Commun. 7 (1971).
6. D. ROSE and G. WILKINSON. J. Chem. Soc. A, 1791 (1970).
7. P. S. HALLMAN, B. R. MCGARVEY, and G. WILKINSON. J. Chem. Soc. A, 3143 (1968).
8. J. LEVISON and S. D. ROBINSON. J. Chem. Soc. A, 2947 (1970).
9. T. A. STEPHENSON and G. WILKINSON. J. Inorg. Nucl. Chem. **28**, 945 (1966).
10. W. K. KNOTH. J. Am. Chem. Soc. **94**, 104 (1972).
11. D. G. HOLAH, A. N. HUGHES, B. C. HUI, N. KRUPA, and K. WRIGHT. Phosphorus, **5**, 145 (1975).
12. R. O. HARRIS, N. K. HOTA, L. SADAVOY, and J. M. C. YUEN. J. Organomet. Chem. **54**, 259 (1973).
13. L. VASKA, W. V. MILLER, and B. R. FLYNN. Chem. Commun. 1615 (1971).
14. A. T. T. HSIEH, J. D. RUDDICK, and G. WILKINSON. J. Chem. Soc. Dalton Trans. 1966 (1972).
15. T. J. MARKS, W. J. KENNELLY, J. R. KOLB, and L. A. SHIMP. Inorg. Chem. **11**, 2540 (1972).
16. M. L. H. GREEN and H. MUNAKATA. J. Chem. Soc. Dalton Trans. 269 (1974).
17. F. L'EPLATTENIER and F. CALDERAZZO. Inorg. Chem. **7**, 1290 (1968).
18. M. I. BRUCE and F. G. A. STONE. J. Chem. Soc. A, 1238 (1967).
19. B. D. JAMES, R. K. NANDA, and M. G. H. WALLBRIDGE. Inorg. Chem. **6**, 1979 (1967).
20. R. K. NANDA and M. G. H. WALLBRIDGE. Inorg. Chem. **3**, 1798 (1964).

Can. J. Chem. Downloaded from www.nrcresearchpress.com by 210.87.254.105 on 09/05/12
For personal use only.

On the interpretation of measured rotational and vibrational relaxation times. I. Sound dispersion experiments

HUW O. PRITCHARD and NABIL I. LABIB

Centre for Research in Experimental Space Science, York University, Downsview, Ontario M3J 1P3

Received July 21, 1975

HUW O. PRITCHARD and NABIL I. LABIB. Can. J. Chem. **54**, 329 (1976).

The simultaneous relaxation to equilibrium of both rotational and vibrational populations is considered for a diatomic molecule immersed in a heat bath of inert-gas atoms. The relaxation is analyzed in terms of normal modes of relaxation, and it is shown that each mode, having its own distinct relaxation time, in general has both rotational and vibrational components. The qualitative form of these modes is very persistent, and survives considerable variations in the assumed temperature and the assumed set of transition probabilities. Using these modes of relaxation, an approximate treatment is given of the contribution made by the diatomic gas to the sound dispersion of the mixture, and conditions under which modes of relaxation may or may not be resolved from each other, or may be characterized as either 'rotational' or 'vibrational' are examined.

HUW O. PRITCHARD et NABIL I. LABIB. Can. J. Chem. **54**, 329 (1976).

On considère la relaxation simultanée vers l'équilibre des populations rotationnelles et vibrationnelles d'une molécule diatomique immersée dans un bain chaud formé d'atomes de gaz inertes. On analyse la relaxation en termes de modes normaux de relaxation et on montre que chaque mode ayant son temps de relaxation propre possède en général les composantes rotationnelles et vibrationnelles. La forme qualitatif de ces modes est très persistante et survit à des variations considérables de la température choisie et de l'ensemble choisi pour les probabilités de transition. Utilisant ces modes de relaxation, on donne un traitement approximatif de la contribution faite par le gaz diatomique à la dispersion du son du mélange et on examine les conditions sous lesquelles des modes de relaxation pourraient ou non être résolus les uns des autres ou pourraient être caractérisés comme "rotationnels" ou "vibrationnels".

[Traduit par le journal]

Can. J. Chem. Downloaded from www.nrcresearchpress.com by 210.87.254.6 on 09/05/12
For personal use only.

Introduction

It is becoming apparent from both experimental and theoretical developments that existing concepts of rotational and vibrational relaxation as separable processes must be inadequate. The difficulties arise because in general (*i*) vibrational and rotational transitions corresponding to both single quantum jumps ($\Delta v = \pm 1$, $\Delta J = \pm 1$) and multiple quantum jumps ($|\Delta v| \geq 2$, $|\Delta J| \geq 2$) are in principle allowed; (*ii*) for an anharmonic oscillator with rotation–vibration coupling, there are no simple relationships between the transition probabilities of successive transitions of the same Δv or ΔJ, nor is there any simple dependence on number of quanta transferred if $|\Delta v|$ or $|\Delta J|$ are greater than one; (*iii*) when any change in vibrational quantum number is considered, there will usually be alternative processes with small values of ΔJ having commensurate transition rates; (*iv*) if large values of ΔJ are permitted, they will be least-discriminated against when there is a roughly equal and opposite change in vibrational energy occurring at the same time. Under these conditions it is obvious that a simple factoring of a relaxation process into a rotational component and a vibrational component could only occur in very special circumstances, and recent theoretical indications are that 'rotational' and 'vibrational' relaxations are actually very complex processes (1–3). Thus it is not surprising that difficulties have arisen recently in the interpretation of relaxation experiments, which are typified by the following two quotations: (*i*) " . . . it is suggested that the process being observed is . . . a coupled relaxation of rotational and vibrational energy" (4); (*ii*) "The probability of energy transfer . . . almost certainly contains contributions from several energy-transfer paths making comparison between theory and experiment difficult" (5).

The purpose of the present work is to try to establish a theoretical framework which will be

Can. J. Chem. Downloaded from www.nrcresearchpress.com by 210.87.254.6 on 09/05/12
For personal use only.

useful in understanding exactly what is being measured in any particular relaxation experiment, and to try to foresee the kinds of behavior which might conceivably arise. To do this, we consider a model molecule with a (fairly) realistic array of rotation–vibration energy levels, sufficient in number to avoid any undesirable truncation effects (3); we then consider how the simplest possible relaxation process, *viz.*

$$[1] \qquad M + X_2(v,J) \rightleftarrows M + X_2(v',J')$$

will take place. This requires a knowledge of the transition rate coefficients connecting every pair of energy levels at the temperature of interest; these are not generally known, and we will proceed by assuming what we regard to be a reasonable set of transition probabilities, and then subjecting the calculation to wide variations in those probabilities to see which resultant properties are likely to persist, and which are likely to be dependent on the particular choice of the transition probability set. (In fact, for M = He and $X_2 = H_2$, it may not be too long before an acceptable set of transition probabilities (6) for such a calculation could be generated.) The rotation–vibration energy-level set used in this work is shown in Fig. 1 of ref. 3, the energy levels of H_2 molecules of odd J; this choice reinforces the notion that our calculations refer to a model molecule, and are not intended to be an attempt to reproduce the observed behavior of the hydrogen molecule!

This paper will present an approximate treatment of the velocity of sound in a gas having an arbitrary number of rotation–vibration levels with numerical transition probabilities connecting *every* pair of levels in the system. This treatment of sound dispersion contains several significant approximations which are unimportant for the present discussion, but which could be relatively easily removed to construct an exact treatment should the need ever arise. The present approximate treatment will then be used to explore the conditions under which it is likely that rotational and vibrational relaxations may be coupled or uncoupled in an ultrasonic dispersion experiment, and in a subsequent paper, we will explore the same problems as they apply to the interpretation of observed relaxation times in shock-wave excitation experiments, and decay times for selectively overpopulated levels produced in laser excitation experiments.

Normal Modes of Relaxation

We begin by considering the relaxation process [1] taking place isothermally; we have N rotation–vibration levels partaking in the relaxation, governed by an Nth order transition rate matrix **A** where

$$[2] \quad [A_{ij}] \equiv [M]Z[(1 - \delta_{ij})P_{ji} - \delta_{ij}\sum_{k=0}^{N-1}(1 - \delta_{ki})P_{ki}]$$

Following the normal convention P_{ij} is the probability per collision for a transition *from* state j *to* state i at the temperature in question, and [M] and Z are respectively the concentration of inert species and the collision number. The temperature is considered to be sufficiently low that dissociation cannot take place. If the initial population distribution is $n_0(0), n_1(0), \ldots, n_{N-1}(0)$ and the equilibrium population distribution is $\tilde{n}_0, \tilde{n}_1, \ldots, \tilde{n}_{N-1}$, the standard procedure is to write the time evolution of the population distribution vector in the form

$$[3] \qquad n_i(t) = \tilde{n}_i^{1/2}\sum_j S_{ij}e^{\lambda_j t}\sum_k S_{kj}\tilde{n}_k^{-1/2}n_k(0)$$

where $i, j, k = 0, 1, 2 \ldots, (N - 1)$, the λ_j are the eigenvalues (in s^{-1}) of **A**, t is the time in seconds, and the S_{ij} are related by a simple transformation to the corresponding eigenvectors of **A** (3). Since there is no dissociation, the last eigenvalue λ_{N-1} is zero to ensure the conservation of particles (7). We can define a set of *normal modes* of relaxation by separating out of [3] the component of each population associated with a particular time constant λ_j, *viz.*

$$[4] \qquad n_i(j,t) = \tilde{n}_i^{1/2}S_{ij}e^{\lambda_j t}\sum_k S_{kj}\tilde{n}_k^{-1/2}n_k(0)$$

where $i, j, k = 0, 1, 2 \ldots, (N - 1)$. Equation 4 has the well-known property that as $t \to \infty$, all the $e^{\lambda_j t}$ terms vanish leaving only those terms associated with the zero eigenvalue and $n_i(N - 1, t) = \tilde{n}_i$, the Boltzmann distribution (7). Thus, in fact, the set of N equations

over i in [4] can be rewritten as

[5]
$$\begin{array}{lcl} n_0(t) = \tilde{n}_0 + m_0(N-2)e^{\lambda_{N-2}t} + m_0(N-3)e^{\lambda_{N-3}t} + \dots \\ \vdots \quad \vdots \quad \vdots \quad \vdots \\ n_i(t) = \tilde{n}_i + m_i(N-2)e^{\lambda_{N-2}t} + m_i(N-3)e^{\lambda_{N-3}t} + \dots \\ \vdots \quad \vdots \quad \vdots \quad \vdots \\ \sum_i n_i(t) = \sum_i \tilde{n}_i + 0 + 0 + \dots \end{array}$$

where

[6] $$m_i(j) = \tilde{n}_i^{1/2} S_{ij} \sum_k S_{kj} \tilde{n}_k^{-1/2} n_k(0)$$

and in the special case of $j = N - 1$, *i.e.* $\lambda_j = 0$

[7] $$m_i(N-1) = \tilde{n}_i$$

for all i and for any $n_k(0)$. Since there is no loss of particles, *i.e.* $\sum_i n_i(t) = \sum_i \tilde{n}_i$, each of the $(N-1)$ remaining modes of relaxation $\sum_i m_i(j)$ is conservative, and consists simply of removing molecules from some levels and transferring them to other levels with a characteristic time λ_j^{-1}. These modes as they are written in [6] are functions of the initial distribution, but in fact it can easily be shown that for a given set of transition probabilities and energy levels, the ratios of the individual terms $m_0(j)$, $m_1(j)$ . . ., etc. are always the same *i.e.*

[8] $$m_i(j) = F_j(0) M_i(j)$$

where the $M_i(j)$ are the elements of the jth mode of relaxation and $F_j(0)$ defines the total flux which uses mode j in the relaxation in question; $F_j(0)$ is obviously a function of the starting distribution $n_0(0)$, $n_1(0)$ . . . .

Figure 1 shows in diagrammatic form a set of normal modes for the relaxation of the lowest 15 levels of the *ortho*-H_2 at 500 K, using a set of transition probabilities defined by eq. 16 of ref. 8; a representative selection of these transition probabilities is given in Table 1 to illustrate their general behavior, which will be discussed in more detail later in the paper. The diagram is made up as follows: the leftmost box gives a representation of the initial population distribution (population displayed horizontally) for the relaxation under consideration, and the rightmost box gives an equivalent representation of the Boltzmann distribution for the temperature of the experi-

TABLE 1. Selected values of deactivation probabilities, per collision, for the standard set of assumed transition probabilities (eq. 16, ref. 8)

Process	Deactivation probability		
	100 K	500 K	2000 K
$v=0; J=3 \rightarrow J=1$	1.1×10^{-3}	1.2×10^{-3}	1.3×10^{-3}
$v=1; J=3 \rightarrow J=1$	1.2×10^{-3}	1.3×10^{-3}	1.4×10^{-3}
$v=0; J=5 \rightarrow J=3$	6.1×10^{-4}	8.0×10^{-4}	1.0×10^{-3}
$v=1; J=5 \rightarrow J=3$	6.9×10^{-4}	8.9×10^{-4}	1.1×10^{-3}
$v=0; J=7 \rightarrow J=5$	2.3×10^{-4}	3.9×10^{-4}	6.2×10^{-4}
$v=0; J=5 \rightarrow J=1$	3.4×10^{-7}	6.7×10^{-7}	1.2×10^{-6}
$v=0; J=7 \rightarrow J=1$	5.6×10^{-12}	6.1×10^{-11}	4.2×10^{-10}
$J=1; v=1 \rightarrow v=0$	2.7×10^{-7}	2.1×10^{-5}	9.0×10^{-4}
$J=3; v=1 \rightarrow v=0$	3.2×10^{-7}	2.3×10^{-5}	9.5×10^{-4}
$J=1; v=2 \rightarrow v=1$	1.1×10^{-6}	5.1×10^{-5}	1.5×10^{-3}
$J=1; v=2 \rightarrow v=0$	1.6×10^{-14}	1.4×10^{-10}	3.7×10^{-7}
$(v=1, J=1) \rightarrow (v=0, J=7)$	1.9×10^{-7}	2.6×10^{-7}	3.3×10^{-7}
$(v=0, J=9) \rightarrow (v=1, J=1)$	9.4×10^{-11}	1.1×10^{-10}	1.2×10^{-10}

Can. J. Chem. Downloaded from www.nrcresearchpress.com by 210.87.254.6 on 09/05/12
For personal use only.

Can. J. Chem. Downloaded from www.nrcresearchpress.com by 210.87.254.6 on 09/05/12
For personal use only.

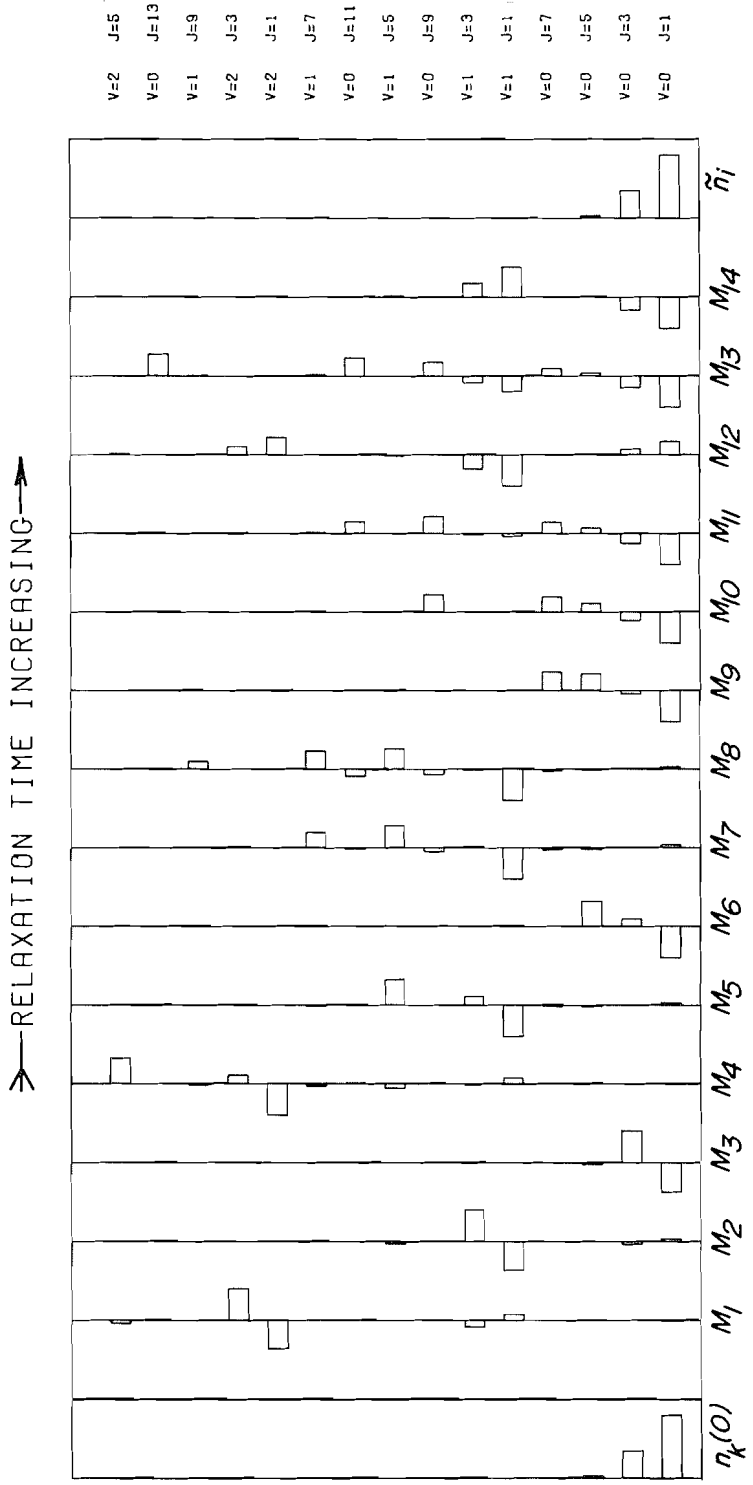

FIG. 1. Normal modes of relaxation: standard set of assumed transition probabilities; $N = 15$, $T = 500$ K.

Can. J. Chem. Downloaded from www.nrcresearchpress.com by 210.87.254.6 on 09/05/12
For personal use only.

ment; (in this particular diagram the initial distribution is that for $T = 499.5$ K and the final distribution is for $T = 500$ K, for reasons which will become obvious later). The energy levels are labelled by their v and J values at the right-hand side of the diagram. The modes themselves are set out in order of *increasing relaxation from left to right*: each mode is normalized so that the largest element is either $+1$ or -1. These modes should be interpreted as follows: mode 3 consists of putting molecules into ($v = 0$, $J = 3$), most of them being taken from ($v = 0$, $J = 1$) and a few from ($v = 0$, $J = 5$); mode 14 consists of taking molecules principally from ($v = 0$, $J = 1$) together with some from ($v = 0$, $J = 3$) and transferring them to ($v = 1$, $J = 1$) and ($v = 1$, $J = 3$) simultaneously. These are essentially what we would characterize as 'rotational' and 'vibrational' relaxations, respectively. Clearly the overall sign associated with each mode is arbitrary; the flow of molecules can be in either direction depending upon whether we are considering a net excitation or a net deexcitation, and this is taken care of in the computational scheme because the initial distribution determines both the sign and numerical magnitude of each $F_j(0)$, eqs. 6 and 8.

It will be noticed that these normal modes (and others reproduced later in this paper) appear to be rather complicated: they have to be, for they have to be able to reduce *any conceivable initial distribution* to a Boltzmann distribution in a time defined by the last eigenvalue (λ_{N-2}), typically 10^{-6} s at 1 atm total pressure.

Heat Capacity Associated with each Normal Mode

As we have argued before (3), the gross observed relaxation behavior of the gas will be determined by those modes which present to the disturbance, *i.e.* sound wave or shock wave, the largest instantaneous values of the heat capacity. Since the energy levels are all known for our model molecule, it is an easy matter to write down the net energy change E_j associated with each mode $M_j = \sum_i M_i(j)$, whence the total amount of energy which is relaxed with a characteristic time λ_j^{-1} is simply

$$[9] \qquad \xi_j = E_j F_j(0)$$

More formally, from [6]

$$[10] \quad \xi_j = \sum_i \tilde{n}_i^{1/2} S_{ij} \sum_k S_{kj} \tilde{n}_k^{-1/2} n_k(0) [\varepsilon_i - \varepsilon_k]$$

and the analog of [5] is now that the evolution of the total internal energy of the molecules is

$$[11] \quad E(t) - E_{\text{initial}} = \xi_{N-1} + \xi_{N-2} e^{\lambda_{N-2} t} + \xi_{N-3} e^{\lambda_{N-3} t} + \ldots .$$

where

$$[12] \quad \xi_{N-1} = -\sum_{j=0}^{N-2} \xi_j = -(E_{\text{initial}} - E_{\text{Boltzmann}})$$

The Velocity of Sound

The treatment of isothermal relaxation given so far is exact, and has been found numerically to be so to the last significant digit in each calculation, (provided, as we have noted before (9), due respect is paid to conservation and detailed balancing in setting up the matrix **A**). We now develop an approximate treatment of the velocity of sound in a relaxing gas, using isothermal relaxation times and modes rather than adiabatic relaxation times and modes (10, 11). There is no fundamental reason why a correct numerical treatment should not be constructed, but it would involve the use of rather more computer time (12); the present approximate treatment will be in error principally by an undetermined scale factor (connecting τ_{pT} with τ_{pS}), but so far as elucidating whether or not particular modes of relaxation can be resolved in an ultrasonic experiment, or if they are not resolved, whether they are just simply unresolved or whether they are coupled, this treatment must be adequate.

Standard treatments of ultrasonic dispersion (13, 14) have been limited to a rather small number of relaxation modes in a relaxing gas: the whole manifold of modes is usually condensed into groups identified as either 'rotational' or 'vibrational', and then it is a fairly easy matter to associate with each composite mode an appropriate value of the specific heat for that mode, leading eventually to well-known formulae for the (velocity)^2 and the dispersion. To extend these ideas to the simultaneous relaxation of an arbitrary number of modes, we have to be able to associate a heat capacity with each individual mode, and we do this

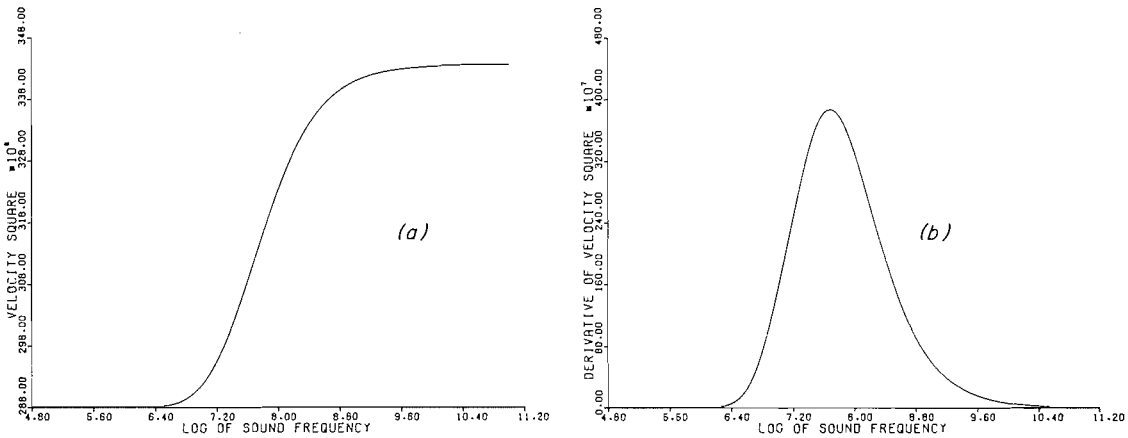

FIG. 2. (*a*) Dispersion in the velocity of sound at 500 K; (*b*) derivative of curve (*a*) with respect to log ω.

using [11]. In each individual term of [11] having the form $\xi_j e^{\lambda_j t}$, ξ_j is the amount of energy relaxed through mode j from the given starting distribution to equilibrium. Thus, if we are interested in a particular temperature T K, then if we choose an initial distribution corresponding to $(T + 0.5)$ K, thereby generating a series of values $\xi_j(T + 0.5)$, and then a second initial distribution corresponding to $(T - 0.5)$ K giving a second set $\xi_j(T - 0.5)$, the individual ('isothermal') heat capacities per degree associated with each mode are simply

$$[13] \quad C_j(T) = \xi_j(T + 0.5) - \xi_j(T - 0.5)$$

(hence the point made earlier about the left-hand distribution depicted in Fig. 1). In fact, the mathematical procedures already exist in molecular wave-function perturbation theory to calculate $C_j(T)$ exactly, but since in all our calculations $\xi_i(T + 0.5)$ was always equal to $-\xi_j(T - 0.5)$ to three decimal places for all significant modes, this refinement is not necessary at the moment.

Consistent with the idea of using isothermal relaxation times is the idea of using a square-wave temperature variation to describe the sound wave, again an approximation capable of considerable refinement. If we focus on one particular mode and make an instantaneous change from some neighboring $(T - \delta T)$ to the reference temperature T, then the amount of energy $C_j(T)\delta T$ will relax through mode j to reach equilibrium; if however the temperature jump is reversed after a time t, then only

$$[14] \quad C_j(T)\delta T(1 - e^{\lambda_j t})$$

will have entered the molecule in that time through mode j. Thus, the total energy entering the molecule by all modes in time t is

$$[15] \quad \delta T \sum_{j=0}^{N-2} C_j(T)(1 - e^{\lambda_j t})$$

which by [12] is the same as

$$[16] \quad -\delta T \sum_{j=0}^{N-1} C_j(T)e^{\lambda_j t}$$

Thus, the time-dependent averaged heat capacity is simply

$$[17] \quad \sum_{j=0}^{N-1} C_j(T)e^{\lambda_j t}$$

Taking t as $1/\omega$ where ω is the angular frequency associated with the sound wave, we can write

$$[18] \quad V_\omega^2 = \gamma\frac{RT}{M} = \frac{C_p}{C_V}\cdot\frac{RT}{M}$$

$$= \frac{C_\omega(T) + 2.5R}{C_\omega(T) + 1.5R}\cdot\frac{RT}{M}$$

$$= \frac{\sum C_j(T)e^{\lambda_j/\omega} + 2.5R}{\sum C_j(T)e^{\lambda_j/\omega} + 1.5R}\cdot\frac{RT}{M}$$

$$= \frac{RT}{M}\left\{1 + R\left(\sum_{j=0}^{N-1} C_j(T)e^{\lambda_j/\omega} + 1.5R\right)^{-1}\right\}$$

analogous to eq. 2.42 of ref. 14. This function is plotted in Fig. 2*a* for the set of modes depicted in Fig. 1, and is relatively featureless; likewise, Fig. 2*b* which is the derivative of Fig. 2*a* with respect to log ω (*analogous* to the absorption curve) is featureless. Equation 18 ignores the

Can. J. Chem. Downloaded from www.nrcresearchpress.com by 210.87.254.6 on 09/05/12
For personal use only.

TABLE 2. Contributions to the sound-velocity dispersion at 500 K for the model molecule (*ortho*-H_2) using the standard set of assumed transition probabilities (eq. 16, ref. 8)

M_j	λ_j (s^{-1})	$C_j(T)$ (erg molecule^{-1} deg^{-1})	Nature of M_j
M_3	4.7×10^7	5.5×10^{-17}	($v=0$, $J=1$ and 5) ↔ ($v=0$, $J=3$)
M_6	2.0×10^7	7.4×10^{-17}	($v=0$, $J=1$) ↔ ($v=0$, $J=3$ and 5)
M_9	1.0×10^7	1.1×10^{-17}	($v=0$, $J=1$ and 3) ↔ ($v=0$, $J=5$ and 7)
M_{10}	4.7×10^6	2.5×10^{-19}	($v=0$, $J=1$ and 3) ↔ ($v=0$, $J=5$, 7 and 9)
M_{14}	1.4×10^6	1.4×10^{-19}	($v=0$, $J=1$ and 3) ↔ ($v=1$, $J=1$ and 3)

contribution to γ due to the presence of the inert gas; in other words [18] represents only that part of eq. 2.118 of ref. 14 which is usually called τ_{AB}, and its true contribution to the dispersion of the mixture would cause the effects shown in Fig. 2 to be reduced by a factor which is the mole fraction of X_2 in M.

The Resolution of Mathematically Distinct Relaxations in an Ultrasonic Dispersion Experiment

Examination of the values of $C_j(T)$ which give rise to the velocity dispersion shown in Fig. 2 reveals that three eigenvalues make a significant contribution, and two others a relatively minor contribution, as shown in Table 2. For the temperature and energy-level scheme assumed, the modes which have significant contributions are not unreasonable, nor are the relative magnitudes of the individual contributions; after all there are relatively major changes in the populations of $J = 1$, 3, and 5, a lesser change in $J = 7$, and relatively small changes in $J = 9$ and $v = 1$. What is significant is that the experiment cannot resolve the two major components M_3 and M_6 which differ in relaxation time by more than a factor of two, and that they appear as one relaxation with a characteristic time intermediate between the two correct values. It is of course well recognized that in dispersion measurements on H_2 and D_2 several distinct processes are involved (10, 13–16), but it is generally accepted (10, 14) that at most temperatures the experimental results can be fitted to curves corresponding to one simple relaxation. We will just note in passing and reserve for later discussion the point that if and when two relaxations are satisfactorily resolved, they will not in general correspond to two consecutive simple excitations but to mixed processes like those depicted by M_3 and M_6 in Fig. 1 and Table 2.

Consequently, we undertook a series of numerical experiments to determine how far apart two relaxations had to be before an ultrasonic dispersion experiment would clearly resolve them. We assigned equal values to the heat capacities associated with two modes ($C_j(T) = C_l(T) = 7 \times 10^{-17}$ erg molecule^{-1} deg^{-1}) and, remembering that $C_{N-1}(T) = -(C_j(T) + C_l(T))$ from [12], investigated the derivative with respect to log ω of [18] for a series of ratios of λ_j/λ_l. Some of these results are displayed in Fig. 3. The first signs of any resolution occur in the derivative (curve *a*) when $\lambda_j = 4.7 \times 10^7$ s^{-1} and $\lambda_l = 1.0 \times 10^7$ s^{-1} although at this stage there are no visual signs of any resolution in the dispersion curve itself. Curve *b* shows a much better resolution when $\lambda_l = 4.7 \times 10^6$ s^{-1}, and in this case one can just see the presence of the second process as a slight 'scree slope' at the foot of the velocity dispersion curve; curve *c*, with $\lambda_l = 1.4 \times 10^6$ s^{-1}, shows a much more definite resolution, which is also quite obvious as a distinct step in the velocity dispersion plot. At the same time, the frequency

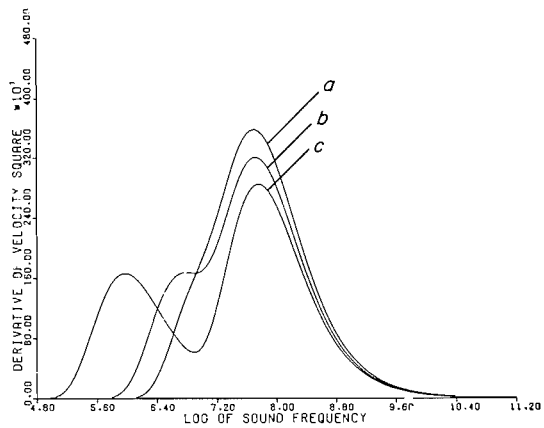

FIG. 3. Resolution of pairs of relaxations of equal strength as a function of eigenvalue ratio.

Can. J. Chem. Downloaded from www.nrcresearchpress.com by 210.87.254.6 on 09/05/12
For personal use only.

Can. J. Chem. Downloaded from www.nrcresearchpress.com by 210.87.254.6 on 09/05/12
For personal use only.

at which the derivative curve has its maximum has reverted to the original position corresponding to $\lambda_j = 4.7 \times 10^{-7}$ s^{-1}, whereas in the unresolved cases, it was displaced to lower frequencies by as much as $\delta \log \omega = 0.2$; the smallness of this displacement is of course associated with the decreasing magnitude of these effects as ω becomes smaller. Thus, we conclude that for *two relaxations of equal strength*, an ultrasonic dispersion *experiment* will only resolve them with difficulty if $\lambda_j/\lambda_l \approx 10$; if $\lambda_j/\lambda_l < 10$, the dispersion will appear to be that caused by a single relaxation, with a time constant nearer to that of the faster process.

Effect of Truncation of Energy-level Scheme on the Form of the Normal Modes

We have mentioned before (2, 3) that truncation of the relaxing system can lead in some circumstances to spurious effects. It is obvious for example that if we remove the topmost level ($v = 2$, $J = 5$) from the relaxation scheme depicted in Fig. 1, M_1 and M_4 (at least) must change because they connect that level to other levels, and that in the contraction from 14 modes to 13, small changes will occur in the forms of all the modes; the dominant modes however, persist. For example, we examined in detail the difference in behavior between 12 relaxing levels and the original 15 relaxing levels. Table 2 showed that for the 15-level scheme, the dominant modes are M_3, M_6, M_9, M_{10}, and M_{14}, which can all be found in the 12-level scheme renumbered as M_3, M_5, M_7, M_8, and M_{11} respectively: moreover, the computed eigenvalues $C_j(T)$ and sound dispersion behavior at 500 K match for both schemes. This still remains true if we truncate the scheme to 7 levels, when the key modes still persist, now labelled M_2, M_3, M_4, M_5, and M_6. Thus, truncation of the set of levels to include only those levels whose populations change appreciably during the passage of the sound wave is quite permissible. Where spurious effects may occur is in selective excitation experiments: for example M_2 of Fig. 1 for the 15-level scheme is virtually unchanged on truncation to 12 levels, but on truncation to 7 levels, it now appears as M_1 with (because of orthogonality constraints) enlarged components for ($v = 1$, $J = 1$) and ($v = 1$, $J = 3$); hence the 7-level scheme would give somewhat different answers from the 12-level or 15-level schemes for an experiment in which the ratio of the populations of ($v = 1$, $J = 1$) and ($v = 1$, $J = 3$) was disturbed.

Persistence of the Normal Modes with Varying Temperature

Since the variation with temperature of the probabilities (Table 1) is assumed to be fairly weak, it is not surprising to find that successive reductions in temperature to 300, 200, and 100 K give rise to a regular progression in the modes; the time constants change somewhat, especially for the essentially vibrational modes (*e.g.* M_{12} and M_{14}), but each mode shown in Fig. 1 persists with very little change, and is clearly recognizable as the same mode at all temperatures down to 100 K. There are quantitative changes, however, in the sense that the very small elements in each mode have a tendency to become smaller. Thus, the $J = 5$ component of M_3 becomes almost imperceptible ($\sim 10^{-6}$ at 100 K) so that M_3 becomes a pure $J = 1 \leftrightarrow J = 3$ relaxation; (at the same time, of course, the heat capacities associated with all the other modes fall off, so that the dispersion behavior also becomes that of the pure $J = 1 \leftrightarrow J = 3$ relaxation). The same thing seems to happen to M_{14}, but the details are a little more subtle. In Fig. 1, the ratios of the $J = 1$ and $J = 3$ components of M_{14} for both $v = 0$ and $v = 1$, are approximately the same (within 10%) as the Boltzmann distribution ratio for $J = 1$ and $J = 3$, and this remains so down to 200 K; thus, we have a simultaneous relaxation persisting, essentially ($v = 1$, $J = 1$ *and* 3) $\leftrightarrow$ ($v = 0$, $J = 1$ *and* 3). Hence the rotational character is preserved in the vibrational transition, more or less. However, at 100 K, the ($v = 0$, $J = 3$) component becomes very small indeed ($\sim 2 \times 10^{-5}$) so that M_{14} has now become a pure vibrational transition; this means that at these very low temperatures the system is tending to two consecutive relaxations, rotation (M_3) followed by vibration (M_{14}), the traditional picture!

Going to higher temperatures, one has to consider more levels to avoid truncation effects, and Fig. 4 shows the set of normal modes at 1500 K for the standard set of transition probabilities, using 20 levels. Notice the matching of M_3 (500 K) with M_4 (1500 K), and a

Can. J. Chem. Downloaded from www.nrcresearchpress.com by 210.87.254.6 on 09/05/12
For personal use only.

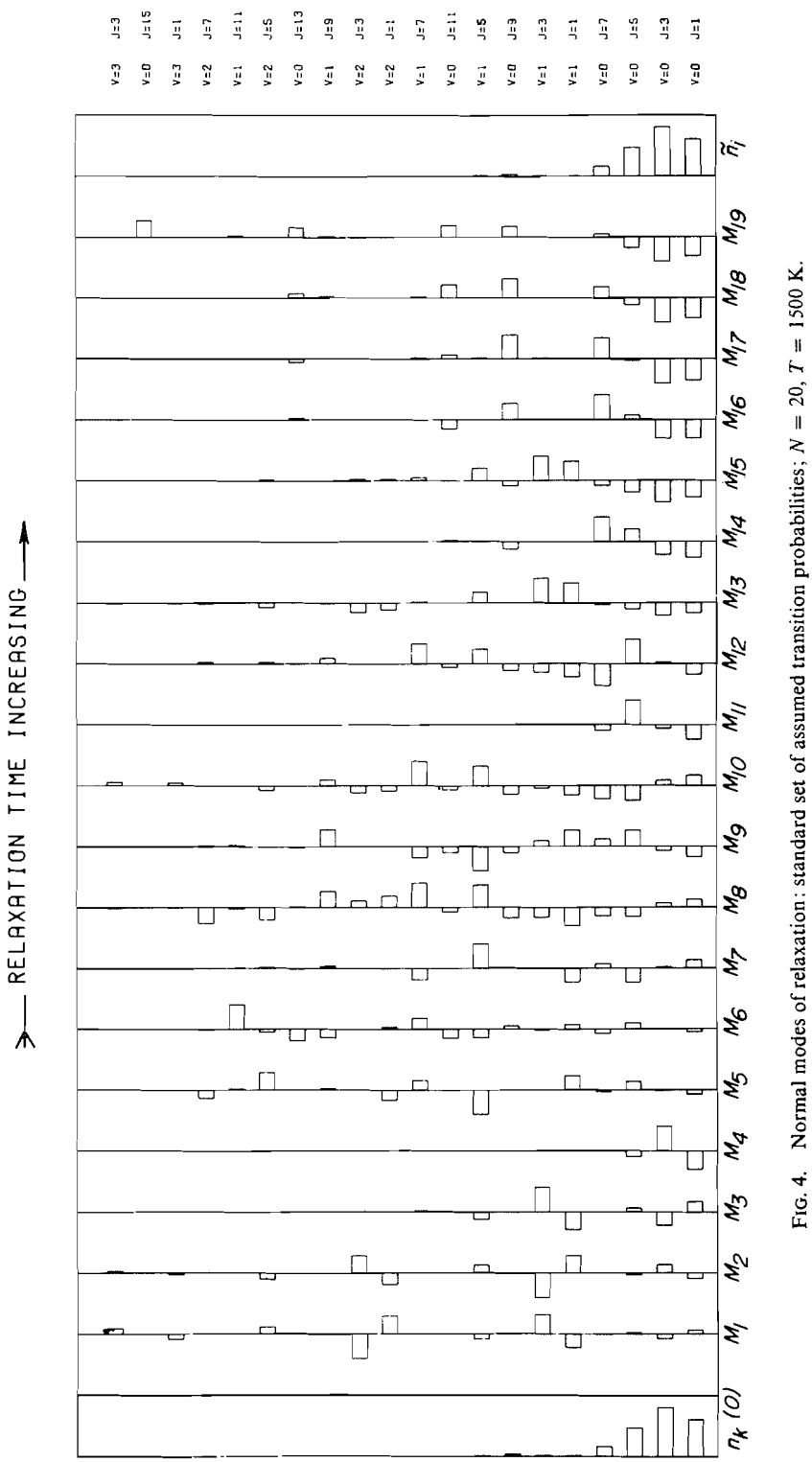

FIG. 4. Normal modes of relaxation: standard set of assumed transition probabilities; $N = 20$, $T = 1500$ K.

Can. J. Chem. Downloaded from www.nrcresearchpress.com by 210.87.254.6 on 09/05/12
For personal use only.

rough and ready matching of M_5 (500 K) with M_{11} (1500 K), and so on. Also notice the transformation of M_{14} (500 K) into M_{15} (1500 K) with the $J = 1$, 3, 5, and 7 components for both $v = 0$ and $v = 1$ matching approximately the Boltzmann distribution ratios, *i.e.* an essentially simultaneous relaxation of all rotational states of $v = 1$ to $v = 0$. The most interesting feature of Fig. 4, however, is that *the four slowest relaxations* M_{16}, M_{17}, M_{18}, and M_{19} *are all rotational relaxations* of $v = 0$, and in the velocity of sound calculations, these four modes together contain 75% of the relaxation strength, most of the remainder being in M_{15}, the 'vibrational' relaxation. Thus, the dominant relaxation for this model molecule at 1500 K is *rotational* in character, and it is the slowest because rotational transition rates decrease markedly as J increases (2, 17, 18), even for $|\Delta J| = 2$. This observation is qualitatively consistent with the experiments of Dove *et al.* (4) who find that the relaxation of hydrogen above 1300 K appears to contain significant rotational character; probably, in fact, it is a mainly rotational relaxation!

Sensitivity of the Normal Modes to the Assumed Transition Probabilities

The standard set of transition probabilities shown in Table 1 and used so far in this paper derive from very old distorted wave calculations (19), but they are probably not wildly wrong in their relative magnitude although they all may well be subject to a shift due to arbitrary normalization. They have fairly unexceptionable properties: (*i*) transition rates fall off with increasing $|\Delta v|$ or $|\Delta J|$; (*ii*) the rotational transition rates for $|\Delta J| = 2$ are faster than the vibrational transition rates for $|\Delta v| = 1$, and vary less strongly with temperature.

Nor do the energy levels of *ortho*-H_2 constitute a particularly good model for a typical diatomic molecule because there are only four rotational levels in the first vibrational gap: typical molecules (*e.g.* O_2, N_2) have more than 30 rotational levels within the first vibrational gap, Cl_2 has over 40, and I_2 over 70. Thus, numerical experiment of the kind described here would be prohibitive in computing costs at the present time for 'typical' molecules; consequently, we have explored a number of variations in our assumed set of transition probabilities designed to test whether or not the results described so far are likely to be general or not.

The major fault with our assumed probabilities is that, for a typical molecule, there is not a large enough difference between the rotational and the vibrational transition rates. We have tried to mimic the typical behavior by multiplying the probabilities for all transitions in which only J changes by 10 and for all transitions in which v changes (whether J changes or not) by 0.1. This has remarkably little effect on the *form* of the modes: those which are essentially rotational in character become 10 times faster and those which are essentially vibrational in character become 10 times slower; thus the diagram for this set of modes would be almost indistinguishable from Fig. 1, *except* that M_{13} and M_{12} are interchanged! At higher temperatures (1500 K), three vibrational modes emerge as the slowest processes (M_{15} and M_{13} of Fig. 4, together with a third one, not present before, connecting $v = 1$, 2, and 3 simultaneously), having changed places because of the factor of 100 scaling with the slower of the rotational modes (M_{16}–M_{19} of Fig. 4); the rotational relaxations however, remain intact, and are clearly recognizable. At the same time the two groups become nicely resolved in the velocity dispersion curve and its derivative.

A second fault from which our probabilities might suffer is that they do not fall off quickly enough for large ΔJ: we checked this by scaling all transition rates for $|\Delta J| > 4$ by 0.1, again with imperceptible effect on the form of the modes, but a very slight depression of the rate of the slower and more complex rotational modes. Another modification one can try is to restrict transitions to Δv *or* ΔJ *only*, but again the form of the modes changes very little from those displayed so far. Thus, it seems that, given a set of energy levels, the form of the modes is rather persistent, although the ordering can be changed by varying the temperature or the transition rates.

It has been suggested recently by several authors (2, 3, 8, 20, 21) that there could be a relatively easy transition between ($v = 0$, $J = 8$) and ($v = 1$, $J = 0$) or between ($v = 0$, $J = 7$) and ($v = 1$, $J = 1$) because the energy separations of these pairs of states are not large;

Can. J. Chem. Downloaded from www.nrcresearchpress.com by 210.87.254.6 on 09/05/12
For personal use only.

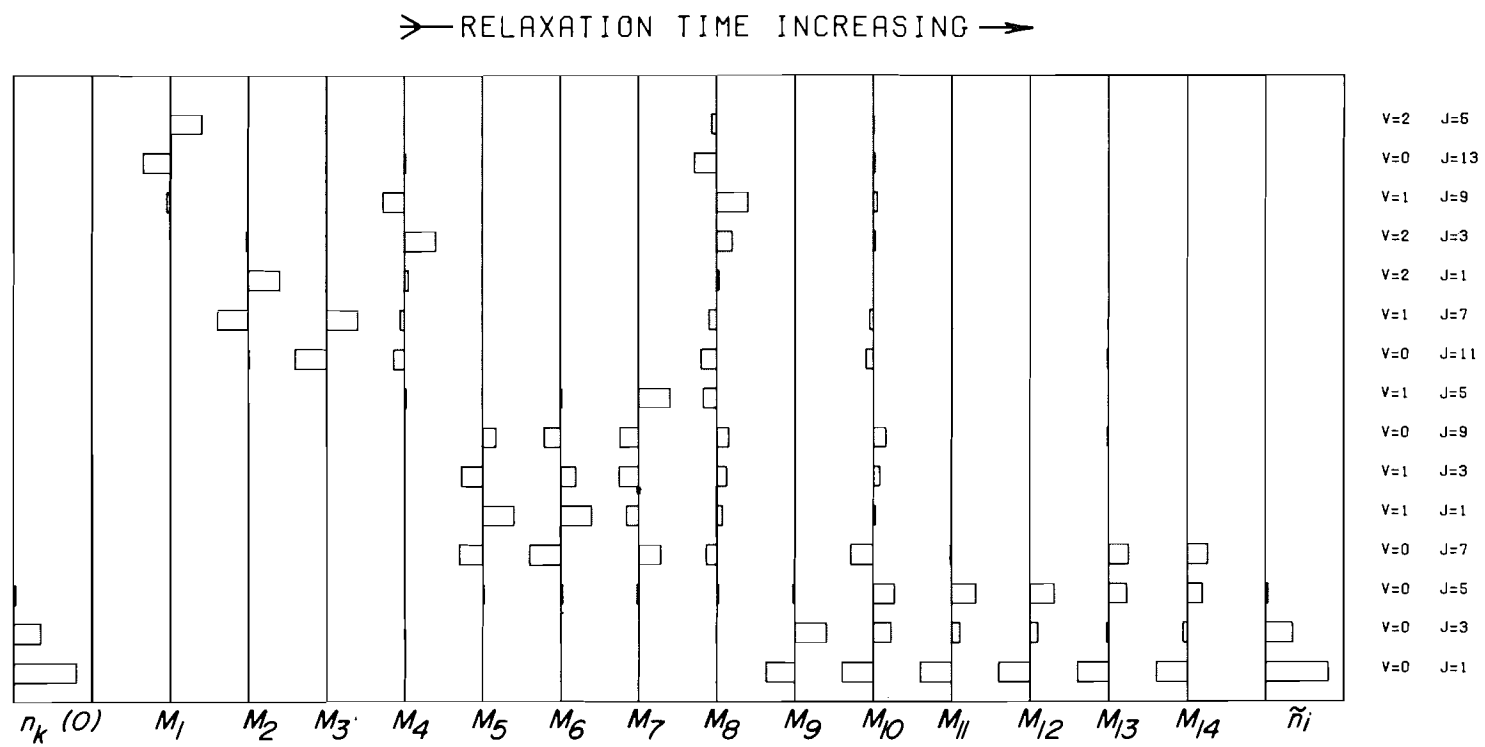

FIG. 5. Normal modes of relaxation: modified set of assumed transition probabilities; $N = 15$, $T = 500$ K (modification: probabilities determined by energy deficit only, irrespective of ΔJ).

Can. J. Chem. Downloaded from www.nrcresearchpress.com by 210.87.254.6 on 09/05/12
For personal use only.

clearly in the context of acoustic measurements, such transitions need not be considered at low temperatures, but very recent experiments suggest that they are not very important in laser-excited relaxations at low temperatures either (22). We have investigated the form the normal modes would have if such processes were strongly allowed, using eq. 16*a* of ref. 8. With these probabilities, almost all entries in Table 1 remain unchanged, but the last two rows of probabilities become about the same as rows 1 and 3 respectively; there are also similar enhancements in probability wherever two levels of disparate J and v are close together in energy. These assumptions have a drastic effect on the form of the modes, and at first sight give the appearance of simplifying them considerably (see also ref. 3). Closer inspection, however, reveals that there are now no such things as 'vibrational' relaxations. In their place, we now have (Fig. 5) a series of very fast relaxations connecting ($v = 2, J = 5$) with ($v = 0, J = 13$), ($v = 2, J = 1$) with ($v = 1, J = 7$), down through all analogous processes to the slowest one which connects ($v = 1$, $J = 1$, 3, and 5) with ($v = 0$, $J = 7$ and 9), and all of these are faster than the fastest 'rotational' process connecting $J = 1$, 3, and 5 of $v = 0$; then follow with increasing time constant the usual succession of more complicated rotational modes.

Conclusions

We conclude that the normal modes are determined by two principal parameters: (*i*) the spacing of the energy levels and (*ii*) the strength of the rotation–vibration coupling. In all those cases (*i.e.* except the last one) where we have discriminated more or less strongly against large changes in J in a collision, and therefore rotation–vibration coupling is by definition weak, the form of the modes depicted in Figs. 1 or 4 is very reproducible; one can manipulate the ordering in speed of the modes somewhat by changing the assumed probabilities or the temperature, but the same modes persist and are recognizable despite these variations. On the other hand, the last variation we investigated upsets the whole pattern, eliminating anything recognizable as a vibrational relaxation time, and giving rise to a progression of rotational processes as the slowest modes of relaxation. It would be reasonable to suppose, since we have come a long way in our understanding of relaxations on the assumption that vibrational and rotational relaxations are separable, that most molecules fall into the weak rotation–vibration coupling regime, with modes of relaxation qualitatively similar to those shown in Figs. 1 and 4. We could not have reached our present level of understanding of such processes making the assumption of separability if the appropriate modes were even remotely like those shown in Fig. 5.

In a subsequent paper we intend to explore what difficulties may be encountered in the implicit assumption of complete separability of rotational and vibrational relaxation in the interpretation of shock-wave and laser selective overpopulation experiments.

Acknowledgments

This work was supported by the National Research Council of Canada.

1. H. RABITZ and G. ZARUR. J. Chem. Phys. **62**, 1425 (1975).
2. H. O. PRITCHARD. Specialist periodical reports, reaction kinetics. Vol. 1. The Chemical Society, London. 1975. p. 243.
3. E. KAMARATOS and H. O. PRITCHARD. Can. J. Chem. **51**, 1923 (1973).
4. J. E. DOVE, D. G. JONES, and H. TEITELBAUM. Fourteenth Symposium (International) on Combustion. The Combustion Institute, Pittsburgh, Pa. 1973. p. 177.
5. J. T. KNUDSTON and G. W. FLYNN. J. Chem. Phys. **58**, 1467 (1973).
6. M. H. ALEXANDER. J. Chem. Phys. **61**, 5167 (1974).
7. E. W. MONTROLL and K. E. SHULER. Adv. Chem. Phys. **1**, 361 (1958).
8. T. ASHTON, D. L. S. MCELWAIN, and H. O. PRITCHARD. Can. J. Chem. **51**, 237 (1973).
9. D. L. S. MCELWAIN and H. O. PRITCHARD. J. Am. Chem. Soc. **91**, 7693 (1969).
10. H. O. KNESER. *In* Physical acoustics. Vol. 2, Part A. *Edited by* W. P. Mason. Academic Press, London. 1965. pp. 133–202.
11. J. L. STRETTON. *In* Transfer and storage of energy by molecules. Vol. 2. *Edited by* G. M. Burnett and A. M. North. J. Wiley and Sons, London. 1969. pp. 1–179.
12. H.-J. BAUER. *In* Physical acoustics. Vol. 2, Part A. *Edited by* W. P. Mason. Academic Press, London. 1965. pp. 47–131.
13. K. F. HERZFELD and T. A. LITOVITZ. Absorption and dispersion of ultrasonic waves. Academic Press, New York. 1959.
14. T. L. COTTRELL and J. C. MCCOUBREY. Molecular energy transfer in gases. Butterworths, London. 1961.
15. C. G. SLUIJTER, H. F. P. KNAAP, and J. J. M. BEENAKKER. Physica, **31**, 915 (1965).
16. J. E. RHODES. Phys. Rev. **70**, 932 (1946).
17. J. C. POLANYI and K. B. WOODALL. J. Chem. Phys. **56**, 1563 (1972).

18. R. B. BERNSTEIN. J. Chem. Phys. **62**, 4570 (1975).
19. H. O. PRITCHARD. J. Phys. Chem. **65**, 504 (1961).
20. R. J. GALLAGHER and J. B. FENN. J. Chem. Phys. **60**, 3492 (1974).
21. M. M. AUDIBERT, C. JOFFRIN, and J. DUCUING. Chem. Phys. Lett. **25**, 158 (1974).
22. M. M. AUDIBERT, R. VILASECA, J. LUKASIK, and J. DUCUING. Chem. Phys. Lett. **31**, 232 (1975).

Can. J. Chem. Downloaded from www.nrcresearchpress.com by 210.87.254.6 on 09/05/12
For personal use only.

Can. J. Chem. Downloaded from www.nrcresearchpress.com by 210.87.254.40 on 09/05/12
For personal use only.

Canadian Journal of Chemistry

Published by
THE NATIONAL RESEARCH COUNCIL OF CANADA

Journal canadien de chimie

Publié par
LE CONSEIL NATIONAL DE RECHERCHES DU CANADA

Volume 54 Number 3 February 1, 1976

Volume 54 numéro 3 1 février 1976

Synthesis, physical properties, and crystal and molecular structure of a binuclear copper(II) complex incorporating 3-methylpyrazolylgallate ligands

RALPH T. BAKER, STEVEN J. RETTIG, ALAN STORR, AND JAMES TROTTER

Department of Chemistry, University of British Columbia, Vancouver, British Columbia V6T 1W5

Received August 5, 1975

RALPH T. BAKER, STEVEN J. RETTIG, ALAN STORR, and JAMES TROTTER. Can. J. Chem. **54**, 343 (1976).

Crystals of $[Me_3Ga_2(N_2C_4H_5)_3CuO]_2$ are monoclinic, $a = 10.766(1)$, $b = 14.419(2)$, $c = 15.174(1)$ Å, $\beta = 115.923(6)°$, $Z = 2$, space group $P2_1/c$. The structure was solved by Patterson and Fourier syntheses and was refined by full-matrix least-squares procedures to a final R of 0.047 and R_w of 0.060 for 3042 reflections with $I \geq 3\sigma(I)$. Details of the preparation and physical properties of the compound are given. The centrosymmetric binuclear complex features copper atoms having distorted square-pyramidal geometry, bonded to four nitrogen atoms and one oxygen atom. Bond distances in the molecule are: Cu—O, 1.923(3), Cu—N, 1.964(4)–2.874(4), Ga—O, 1.825(4) and 1.881(3), Ga—N, 1.952(4)–1.978(5), Ga—C, 1.950(7)–1.979(8), N—N, 1.358(6)–1.385(6), N—C, 1.326(7)–1.352(6), C—C(pyrazolyl), 1.342(9)–1.386(8), C—CH_3, 1.487(9)–1.500(10), and C—H, 0.81(10)–1.06(12) Å.

RALPH T. BAKER, STEVEN J. RETTIG, ALAN STORR et JAMES TROTTER. Can. J. Chem. **54**, 343 (1976).

Les cristaux du $[Me_3Ga_2(N_2C_4H_5)_3CuO]_2$ sont monocliniques, $a = 10.766(1)$, $b = 14.419(2)$, $c = 15.174(1)$ Å, $\beta = 115.923(6)°$, $Z = 2$, groupe d'espace $P2_1/c$. On a résolu la structure par les synthèses de Patterson et de Fourier et on l'a affinée par la méthode des moindres carrés (matrice complète) jusqu'à une valeur finale de R de 0.047 et R_w de 0.060 pour 3042 réflexions avec $I \geq 3\sigma(I)$. On donne les détails pour la préparation et les propriétés physiques du composé. Le complexe binucléaire centrosymétrique comprends les atomes de cuivre ayant une géométrie pyramidale carrée déformée, liée à quatre atomes d'azote et un atome d'oxygène. Les distances des liaisons dans la molécule sont: Cu—O, 1.923(3), Cu—N, 1.964(4)–2.874(4), Ga—O, 1.825(4) et 1.881(3), Ga—N, 1.952(4)–1.978(5), Ga—C, 1.950(7)–1.979(8), N—N, 1.358(6)–1.385(6), N—C, 1.326(7)–1.352(6), C—C(pyrazolyl), 1.342(9)–1.386(8), C—CH_3, 1.487(9)–1.500(10) et C—H, 0.81(10)–1.06(12) Å.

[Traduit par le journal]

Introduction

As part of a general investigation into pyrazolyl and related derivatives of gallium and aluminum (1–4), anionic chelating ligands have been synthesized and a number of their transition metal complexes characterized (5, 6). In addition, confirmation of the structures predicted for a number of the complexes has been forthcoming in crystal structure determinations (7, 8). The importance of steric interactions in determining the geometry of the central CuN_4 moiety in the two bis-chelate Cu(II) complexes, $[Me_2Ga(N_2C_3H_3)_2]_2Cu$ and $[Me_2Ga(N_2C_5H_7)_2]_2Cu$, was clearly illustrated in that the complex incorporating unsubstituted 'pyrazolyl' groups has a square-planar arrangement of four nitrogen

Can. J. Chem. Downloaded from www.nrcresearchpress.com by 210.87.254.40 on 09/05/12
For personal use only.

atoms about the central copper atom, whereas the complex incorporating the '3,5-dimethylpyrazolyl' groups displays a pseudotetrahedral environment for the copper atom (8). The present investigation extends our studies in this area to include the anionic dimethyl bis(3-methylpyrazolyl)gallate ligand, $Me_2Ga(N_2C_4H_5)_2^-$. The reaction of the sodium salt of this ligand with copper(II) bromide in THF did not, however, yield the expected bis-chelate copper(II) complex, $[Me_2Ga(N_2C_4H_5)_2]_2Cu$, but rather, a novel binuclear copper(II) complex, $[Me_3Ga_2(N_2C_4H_5)_3CuO]_2$, incorporating trigonal planar oxygen atoms and '$Me_2Ga(N_2C_4H_5)$' and '$MeGa(N_2C_4H_5)_2$' moieties.

Experimental

Starting Materials

Tetrahydrofuran was refluxed over lithium aluminum hydride and then used immediately following distillation. 3-Methylpyrazole (Aldrich Chemical Co.) and sodium hydride (Alfa Inorganics) were used as purchased. Trimethyl gallium was prepared as previously described (9).

Preparative Details

Sodium Dimethyl Bis(3-methyl-1-pyrazolyl)gallate, $Na^+Me_2Ga(N_2C_4H_5)_2^-$

$$[1]\quad NaH + N_2C_4H_6 \xrightarrow[N_2\ atm]{THF} Na^+N_2C_4H_5^- + H_2$$

$$[2]\quad Na^+N_2C_4H_5^- + Me_3Ga \xrightarrow[N_2\ atm,\ reflux]{THF} Na^+Me_3Ga(N_2C_4H_5)^-$$

$$[3]\quad Na^+Me_3Ga(N_2C_4H_5)^- + N_2C_4H_6 \xrightarrow[N_2\ atm,\ reflux]{THF} Na^+Me_2Ga(N_2C_4H_5)_2^- + CH_4$$

Trimethyl gallium (4.020 g, 35.0 mmol) in THF was added to sodium 3-methylpyrazolide (35.0 mmol) (made from sodium hydride (0.840 g, 35.0 mmol) and 3-methylpyrazole (2.870 g, 35.0 mmol) in THF solution) in the same solvent and the mixture refluxed gently. The solution was cooled to room temperature and a solution of 3-methylpyrazole (2.870 g, 35.0 mmol) in THF was added slowly and the reaction mixture refluxed. The progress of step 3 in the synthesis was followed by monitoring the ^1H nmr spectrum of the THF solution in the Ga—Me region of the spectrum. The two species, $Na^+Me_3Ga(N_2C_4H_5)^-$ and $Na^+Me_2Ga(N_2C_4H_5)_2^-$, gave sharp Ga—Me signals separated by about 0.5 ppm from each other and, consequently, completion of the reaction could be ascertained. The ^1H nmr spectrum of the product in THF solution showed *one* sharp Ga—Me singlet (area 6) and *two* doublet signals (each of area 2 and $J \approx 2$ Hz) due to pyrazolyl ring protons. (The signal due to the 3-Me groups on the pyrazolyl moieties was masked by solvent peaks.) The simplicity of this spectrum suggests the presence of one isomer in the THF solution since a mixture of isomers would give a more complicated ^1H nmr pattern. Upon completion of the reaction, the solution was cooled and the solvent removed under vacuum to give a white hygroscopic solid as product. This ligand salt was used without further purification in the following preparation.

Attempted Preparation of Bis[dimethylbis(3-methyl-1-pyrazolyl)gallato]copper(II)

$$2Na^+Me_2Ga(N_2C_4H_5)_2^- + CuBr_2 \xrightarrow[r.t.]{THF} [Me_2Ga(N_2C_4H_5)_2]_2Cu + 2NaBr$$

The ligand salt (1.249 g, 4.39 mmol) was dissolved in THF and a solution of copper(II) bromide (0.489 g, 2.19 mmol), in the same solvent, added. The reaction mixture was stirred under a dry nitrogen atmosphere for a few hours and the precipitated sodium bromide was then removed by centrifuging. The resultant dark green solution was flash evaporated to yield a dark green oil from which crystals of the expected bis-chelate complex could not be obtained despite numerous attempts. (In a similar reaction with cobalt(II) chloride the same ligand salt had yielded the bis-chelate cobalt complex $[Me_2Ga(N_2C_4H_5)_2]_2Co$.) Interestingly, however, on exposure to the atmosphere, the green oil produced small amounts of a purple crystalline solid which proved insoluble in common organic solvents and also was of high molecular weight (>1000) as evidenced by its mass spectrum. The purple solid was easily separated from the green oil by dissolving the latter in acetone to leave behind the insoluble crystals. Slow evaporation of the resulting green acetone solution in the open air yielded more purple crystals, and eventually quite sizeable crystals suitable for X-ray study were obtained. (Analysis of purple solid. *Anal.* Calcd. for $[Me_3Ga_2(N_2C_4H_5)_3CuO]_2$: C 35.50, H 4.73, N 16.57; found: C 35.36, H 4.62, N 16.30.)

The purple solid melted sharply at 187 °C, with decomposition, and gave a μ_{eff} value of 1.98 B.M. per copper ion at 298 K (corrected for ligand and metal diamagnetism). The reflectance spectrum of the complex exhibited one broad asymmetric absorption band in the 13 500 – 28 600 cm^{-1} range with ν_{max} at 17 465 cm^{-1} and a hexachlorobutadiene mull spectrum displayed no additional bands in the range 4 000 – 28 600 cm^{-1}. The low frequency infrared spectrum (recorded on a Nujol mull) of the complex displayed a number of absorptions attributed to ν_{Ga-C} and 'M—N' and 'M—O' (where M = Ga or Cu) modes. The bands occurred at 585(vs), 565(s), 530(m), 405(m), and 395(m) cm^{-1}. The strongest bands at 585 and 565 cm^{-1} are in the region characteristic of Ga—C stretching frequencies, whilst the remaining bands listed may be tentatively assigned to 'M—N' and 'M—O' ring modes.

Spectra

The mass spectrum was recorded on a Varian MAT CH4-B mass spectrometer at 70 eV with the probe temperature at 140 °C. The magnetic susceptibility was measured on a Gouy balance, the reflectance spectrum on a Spectronic 600 instrument with reflectance attachment, and the mull spectrum on a Cary 14 spectrometer. The infrared spectrum was recorded on a Perkin-Elmer 457 spectrometer and the ^1H nmr spectra were recorded on a Varian T60 instrument.

Can. J. Chem. Downloaded from www.nrcresearchpress.com by 210.87.254.40 on 09/05/12
For personal use only.

X-Ray Crystallographic Study of
$[Me_3Ga_2(N_2C_4H_5)_3CuO]_2$

The crystal chosen for study was mounted with a^* parallel to the goniostat axis and had dimensions of *ca.* 0.15 × 0.40 × 0.45 mm. Unit-cell and space group data were obtained from film and diffractometer measurements. The unit-cell parameters were refined by a least-squares treatment of $\sin^2\theta$ values for 26 reflections measured on a diffractometer with Cu K_α radiation. Crystal data are:

$C_{30}H_{48}Cu_2Ga_4N_{12}O_2$ fw = 1014.8
Monoclinic, a = 10.766(1), b = 14.419(2), c = 15.174(1) Å, β = 115.923(6)°, V = 2118.5(4) Å^3, Z = 2, ρ_c = 1.5906(3) g cm^{-3}, $F(000)$ = 1020 (21 °C, Cu K_α, λ = 1.5418 Å, μ = 30.5 cm^{-1}). Absent reflections: $0k0$, $k \neq 2n$ and $h0l$, $l \neq 2n$ define uniquely the space group $P2_1/c$ (C_{2h}^5, No. 14).

Intensities were measured on a Datex-automated General Electric XRD 6 diffractometer, with a scintillation counter, Cu K_α (nickel filter and pulse height analyser), and a θ–2θ scan at 2 deg min^{-1} over a range of (1.80 + 0.86 tan θ) deg in 2θ, with 10 s background counts being measured at each end of the scan. Data were measured to 2θ = 145° (minimum interplanar spacing 0.81 Å). A check reflection was monitored every 40 reflections throughout the data collection. The intensity of the check reflection decreased slowly to a final value 17% lower than the starting value. Lorentz and polarization corrections and check reflection scaling were applied, and the structure amplitudes were derived. No absorption correction was made due to irregularity of the crystal surface. Of the 4202 independent reflections measured, 1135 had intensities less than $3\sigma(I)$ above background where $\sigma^2(I) = S + B + (0.06S)^2$ with S = scan count and B = time averaged background count. These reflections were given zero weight in the refinement but were included in the structure factor calculations.

The positions of the copper and two gallium atoms were determined from the three-dimensional Patterson function. Two cycles of full-matrix least-squares refinement of the positional and isotropic thermal parameters of the Cu and Ga atoms gave R = 0.41. A difference map at this point gave the positions of the C, N, and O atoms. Isotropic followed by anisotropic refinement of the non-hydrogen atoms reduced R to 0.057; 22 of the 24 hydrogen atoms were located from a subsequent difference map and the two remaining positions were calculated. (Both hydrogen atoms not located from the difference map were associated with the C(12) methyl group.) The entire structure (including hydrogen atoms with isotropic thermal parameters) was refined for five more cycles giving a final R of 0.047 and R_w of 0.060 for 3042 reflections with $I \geq 3\sigma(I)$ (25 reflections which had $|F_o| - |F_c| > 3\sigma(F)$ were removed from the data set in the final stages of refinement).

The least-squares refinement was based on the minimization of $\Sigma w[|F_o| - |F_c/(1 + gI)|]^2$ where g is the extinction parameter and I the uncorrected intensity. The final value of g was 2.0(2) × 10^{-7}. The scattering factors of ref. 10 were used for the nonhydrogen atoms and those of ref. 11 for the hydrogen atoms. Anomalous scattering factors from ref. 12 were used for the Ga, Cu, O, and N atoms. The anisotropic thermal parameters employed in the refinement are U_{ij} in the expression:

$$f = f^0 \exp[-2\pi^2(U_{11}h^2a^{*2} + U_{22}k^2b^{*2} + U_{33}l^2c^{*2} + 2U_{12}hka^*b^* + 2U_{13}hla^*c^* + 2U_{23}klb^*c^*)]$$

where f^0 is the tabulated scattering factor and f is that corrected for thermal motion. The weighting scheme:

TABLE 1. Final positional parameters (fractional × 10^4, Ga and Cu × 10^5, H × 10^3) with estimated standard deviations in parentheses

Atom	x	y	z
Ga(1)	33843(6)	17484(5)	39802(5)
Ga(2)	21840(6)	3976(5)	20703(5)
Cu	51637(7)	−181(5)	39410(5)
O	3536(3)	733(2)	3319(2)
N(1)	5340(4)	1798(3)	4887(3)
N(2)	6024(4)	971(3)	4949(3)
N(3)	3066(4)	−819(3)	2147(3)
N(4)	4350(4)	−951(3)	2904(3)
N(5)	6964(4)	−677(3)	4454(3)
N(6)	7470(4)	−1318(3)	5181(3)
C(1)	6236(6)	2410(4)	5504(4)
C(2)	7496(7)	1980(5)	5963(5)
C(3)	7328(6)	1109(4)	5620(4)
C(4)	2756(6)	−1554(4)	1557(4)
C(5)	3817(8)	−2178(5)	1924(5)
C(6)	4793(7)	−1768(4)	2759(5)
C(7)	7884(5)	−555(4)	4086(4)
C(8)	9010(6)	−1123(5)	4595(5)
C(9)	8719(6)	−1581(4)	5260(5)
C(10)	2416(11)	2852(6)	3270(8)
C(11)	2455(10)	1109(7)	1061(6)
C(12)	352(9)	273(10)	2068(8)
C(13)	5804(12)	3378(6)	5576(9)
C(14)	1405(10)	−1594(9)	657(7)
C(15)	7624(9)	105(6)	3273(6)
H(2)	815(8)	219(5)	643(5)
H(3)	790(6)	53(4)	583(4)
H(5)	377(7)	−278(5)	154(5)
H(6)	551(5)	−205(3)	319(3)
H(8)	979(7)	−104(4)	454(4)
H(9)	923(6)	−207(4)	579(4)
H(10*a*)	227(9)	289(6)	265(7)
H(10*b*)	302(11)	328(7)	315(8)
H(10*c*)	245(10)	336(6)	367(7)
H(11*a*)	329(10)	152(6)	142(6)
H(11*b*)	198(13)	172(9)	84(9)
H(11*c*)	219(7)	89(5)	52(5)
H(12*a*)	16(10)	84(7)	232(7)
H(12*b*)	33(11)	−34(7)	221(8)
H(12*c*)	−42(15)	14(9)	155(10)
H(13*a*)	548(11)	390(9)	503(8)
H(13*b*)	645(11)	360(7)	605(7)
H(13*c*)	487(13)	336(7)	557(8)
H(14*a*)	146(11)	−215(8)	37(8)
H(14*b*)	53(9)	−129(6)	62(6)
H(14*c*)	153(8)	−112(5)	19(5)
H(15*a*)	760(8)	77(6)	348(5)
H(15*b*)	818(15)	18(9)	300(9)
H(15*c*)	657(9)	17(5)	282(6)

TABLE 2. Final thermal parameters and their estimated standard deviations

(*a*) Anisotropic thermal parameters ($U_{ij} \times 100$ Å^2)

Atom	U_{11}	U_{22}	U_{33}	U_{12}	U_{13}	U_{23}
Ga(1)	4.54(4)	5.26(4)	5.44(4)	1.22(3)	2.37(3)	0.57(3)
Ga(2)	3.39(3)	7.21(5)	4.80(4)	−0.05(3)	1.26(3)	0.22(3)
Cu	3.22(4)	5.13(4)	4.26(4)	0.46(3)	1.65(3)	−0.00(3)
O	4.0(2)	6.5(2)	4.6(2)	1.0(2)	1.3(2)	−0.2(2)
N(1)	4.8(2)	5.6(2)	5.8(3)	−0.3(2)	2.9(2)	−0.7(2)
N(2)	3.9(2)	5.6(2)	5.1(2)	−0.2(2)	2.2(2)	−0.1(2)
N(3)	3.9(2)	6.5(3)	4.9(2)	−0.9(2)	1.7(2)	−0.5(2)
N(4)	4.5(2)	6.0(3)	4.9(2)	0.1(2)	2.1(2)	−0.6(2)
N(5)	3.9(2)	5.2(2)	5.7(2)	0.3(2)	2.3(2)	−0.1(2)
N(6)	3.4(2)	5.3(2)	6.0(2)	1.0(2)	2.3(2)	−0.1(2)
C(1)	6.4(4)	6.0(3)	6.4(3)	−1.7(3)	3.5(3)	−1.3(3)
C(2)	5.0(4)	8.1(4)	6.8(4)	−2.3(3)	2.3(3)	−1.7(3)
C(3)	4.0(3)	6.8(4)	6.0(3)	−0.9(3)	1.9(3)	−0.5(3)
C(4)	5.8(4)	7.3(4)	6.5(3)	−2.0(3)	3.3(3)	−2.0(3)
C(5)	8.8(5)	6.0(4)	7.5(4)	−1.1(3)	4.3(4)	−1.7(3)
C(6)	6.3(4)	6.4(4)	6.9(4)	1.0(3)	3.6(3)	−0.5(3)
C(7)	3.8(3)	5.9(3)	6.1(3)	−0.1(2)	2.8(2)	−0.3(2)
C(8)	4.1(3)	7.9(4)	9.0(4)	0.7(3)	3.9(3)	0.3(3)
C(9)	4.3(3)	6.9(4)	8.9(4)	1.9(3)	3.3(3)	0.3(3)
C(10)	11.3(7)	7.4(5)	9.7(6)	3.9(5)	5.6(5)	3.1(5)
C(11)	9.4(6)	10.6(6)	5.9(5)	−1.8(5)	2.1(4)	2.5(4)
C(12)	4.8(4)	13.5(9)	8.6(6)	0.3(5)	2.8(4)	−0.4(6)
C(13)	9.8(7)	6.8(5)	12.9(8)	−1.5(4)	5.0(6)	−3.7(5)
C(14)	6.6(5)	12.9(8)	8.5(6)	−3.5(5)	1.8(4)	−4.3(6)
C(15)	6.7(5)	9.5(6)	8.5(5)	−0.2(4)	4.7(4)	1.6(4)

(*b*) Isotropic thermal parameters ($U \times 100$)

Atom	U (Å^2)	Atom	U (Å^2)	Atom	U (Å^2)
H(2)	10(2)	H(10*c*)	15(4)	H(13*b*)	11(4)
H(3)	6(1)	H(11*a*)	15(3)	H(13*c*)	17(4)
H(5)	10(2)	H(11*b*)	20(5)	H(14*a*)	17(4)
H(6)	4(1)	H(11*c*)	9(2)	H(14*b*)	12(3)
H(8)	9(2)	H(12*a*)	13(4)	H(14*c*)	10(3)
H(9)	6(1)	H(12*b*)	14(4)	H(15*a*)	11(3)
H(10*a*)	12(3)	H(12*c*)	22(6)	H(15*b*)	19(6)
H(10*b*)	13(4)	H(13*a*)	18(5)	H(15*c*)	11(3)

$w = 1/\sigma^2(F)$ where $\sigma^2(F)$ is derived from the previously defined $\sigma^2(I)$ gave uniform average values of $w(|F_o| - |F_c|)^2$ over ranges of $|F_o|$ and was employed in the final stages of refinement. The mean error in an observation of unit weight was 1.35. On the final cycle of refinement the mean parameter shift was 0.25σ, the largest shift corresponded to 1.4σ. The final positional and thermal parameters appear in Tables 1 and 2 respectively. Measured and calculated structure factors have been placed in the Depository of Unpublished Data.[1]

The thermal motion of $[Me_3Ga_2(N_2C_4H_5)_3CuO]_2$ has been analysed in terms of the rigid-body modes of translation and libration (13) using the computer program MGTLS. The rigid-body motion of all atoms in the dimer except the methyl carbon atoms was adequately described by the derived rigid-body parameters (rms $\Delta U_{ij} = 0.0054$ and rms $\sigma U_{ij} = 0.0032$ Å^2). The appropriate bond distances have been corrected for libration (14, 15) and appear along with the uncorrected distances in Table 3. The distances involving methyl carbon atoms have been corrected for riding motion based on the ΔU_{ij} (16, 17).

[1]The structure factor table is available, at a nominal charge, from the Depository of Unpublished Data, CISTI, National Research Council of Canada, Ottawa, Canada K1A 0S2.

Results and Discussion

Mass Spectrum of $[Me_3Ga_2(N_2C_4H_5)_3CuO]_2$

The mass spectrum of the binuclear copper(II) complex, $[Me_3Ga_2(N_2C_4H_5)_3CuO]_2$, did not display a parent ion cluster but did give as its strongest signals groupings corresponding to the

Can. J. Chem. Downloaded from www.nrcresearchpress.com by 210.87.254.40 on 09/05/12
For personal use only.

TABLE 3. Bond lengths (Å) with estimated standard deviations in parentheses

(*a*) Nonhydrogen atoms

Bond	Distance		Bond	Distance	
	Uncorrected	Corrected		Uncorrected	Corrected
Ga(1)—O	1.823(4)	1.825	N(1)—C(1)	1.340(7)	1.342
Ga(2)—O	1.879(3)	1.881	N(2)—C(3)	1.341(7)	1.343
Ga(1)—N(1)	1.949(4)	1.952	N(3)—C(4)	1.333(7)	1.334
Ga(1)—N(6)′	1.968(4)	1.969	N(4)—C(6)	1.325(7)	1.326
Ga(1)—N(3)	1.975(5)	1.978	N(5)—C(7)	1.345(6)	1.346
Ga(1)—C(10)	1.950(7)	1.950	N(6)—C(9)	1.352(6)	1.352
Ga(2)—C(11)	1.968(7)	1.970	C(1)—C(2)	1.372(9)	1.374
Ga(2)—C(12)	1.978(8)	1.979	C(2)—C(3)	1.341(9)	1.342
Cu—O	1.920(3)	1.923	C(4)—C(5)	1.367(9)	1.368
Cu—N(2)	1.999(4)	2.001	C(5)—C(6)	1.376(9)	1.377
Cu—N(4)	1.962(4)	1.964	C(7)—C(8)	1.385(8)	1.386
Cu—N(5)	1.987(4)	1.990	C(8)—C(9)	1.352(9)	1.352
Cu—N(2)′	2.871(4)	2.874	C(1)—C(13)	1.490(10)	1.491
N(1)—N(2)	1.383(6)	1.385	C(4)—C(14)	1.499(10)	1.500
N(3)—N(4)	1.371(6)	1.372	C(7)—C(15)	1.485(9)	1.487
N(5)—N(6)	1.357(6)	1.358			

(*b*) Bonds involving hydrogen atoms

Bond	Distance	Bond	Distance
C(2)—H(2)	0.81(7)	C(12)—H(12*a*)	0.96(10)
C(3)—H(3)	1.00(5)	C(12)—H(12*b*)	0.93(10)
C(5)—H(5)	1.04(7)	C(12)—H(12*c*)	0.88(14)
C(6)—H(6)	0.87(5)	C(13)—H(13*a*)	1.06(12)
C(8)—H(8)	0.89(6)	C(13)—H(13*b*)	0.81(10)
C(9)—H(9)	1.03(5)	C(13)—H(13*c*)	1.00(12)
C(10)—H(10*a*)	0.89(9)	C(14)—H(14*a*)	0.94(11)
C(10)—H(10*b*)	0.97(10)	C(14)—H(14*b*)	1.01(8)
C(10)—H(10*c*)	0.94(9)	C(14)—H(14*c*)	1.03(8)
C(11)—H(11*a*)	1.02(9)	C(15)—H(15*a*)	1.01(8)
C(11)—H(11*b*)	1.00(13)	C(15)—H(15*b*)	0.87(14)
C(11)—H(11*c*)	0.82(7)	C(15)—H(15*c*)	1.04(8)

loss of one, two, and three methyl groups respectively from the parent ion, thus confirming a similar molecular constitution in the gas phase as in the solid. (A similar absence of parent ions in the mass spectrum of organogallium and organoaluminum compounds has been reported previously (1, 18, 19).) These strong signals, corresponding to fragments containing four gallium and two copper atoms, occurred as characteristic septets with individual peaks at separations of two mass units, (*e.g.* $Me_5Ga_4(N_2C_4H_5)_6Cu_2O_2^+$, 995–1007; $Me_4Ga_4(N_2C_4H_5)_6Cu_2O_2^+$, 980–992) the relative intensities of which agreed well with those predicted from the isotopic abundances of the metal atoms (^{69}Ga, 60%; ^{71}Ga, 40%; ^{63}Cu, 69%; ^{65}Cu, 31%). Other strong signals in the spectrum corresponded to the loss of one and two methyl groups from the monomer ion. These signals occurred as characteristic quartets ($Me_2Ga_2(N_2C_4H_5)_3CuO^+$, 490–496; $MeGa_2(N_2C_4H_5)_3CuO^+$, 475–481) with close to predicted relative intensities for the individual peaks. Only one other ion gave a signal of comparable strength to those listed above and that was the $Me_2Ga_2(N_2C_4H_5)O^+$ ion which occurred as a triplet signal at 265–269. Numerous other lower intensity signals were also observed and these were readily assigned to various ion fragments on the basis of predicted relative intensity patterns for the various Ga–Cu ratios involved.

Crystal Structure

Figure 1 shows the molecule viewed into *b* with the atom numbering scheme and 50% probability thermal ellipsoids and Fig. 2 shows

Can. J. Chem. Downloaded from www.nrcresearchpress.com by 210.87.254.40 on 09/05/12
For personal use only.

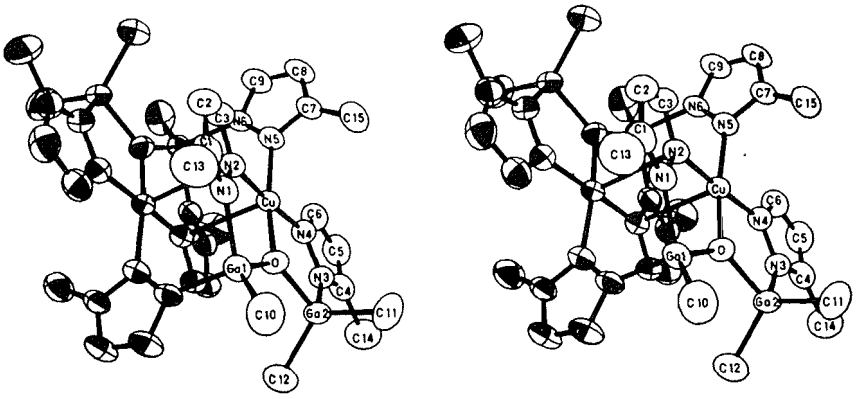

FIG. 1. A stereo view of the molecule; 50% ellipsoids are shown for the nonhydrogen atoms. The atoms labelled in the diagram are related to those in Table 1 by the centre of inversion at (1/2, 0, 1/2).

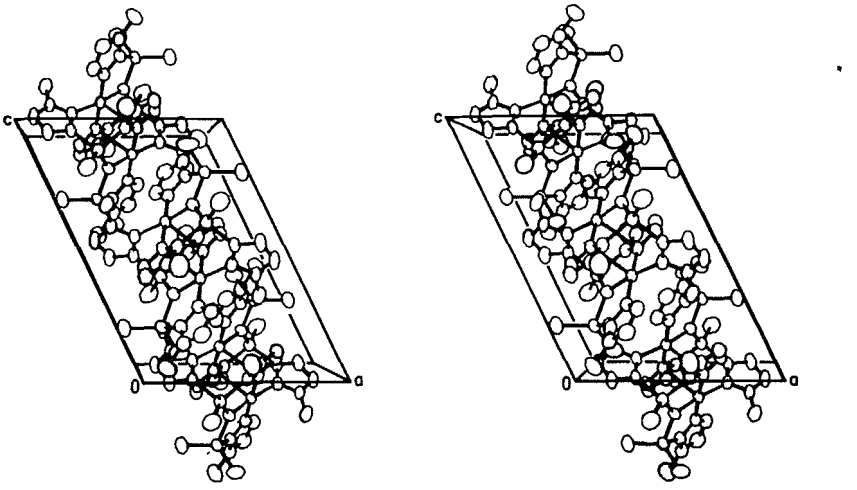

FIG. 2. The crystal structure viewed along *b*.

the packing arrangement viewed along the crystallographic *b* axis. Bond angles are given in Table 4 and torsion angles in Table 5. Deviations of relevant atoms from weighted least-squares mean planes through the molecule are given in Table 6 and selected nonbonded contacts in Table 7. Primed atoms are related to those in Table 1 by inversion through the molecular center of symmetry at $(\frac{1}{2},0,\frac{1}{2})$.

The crystal structures of numerous poly(1-pyrazolyl)borate mononuclear transition metal complexes have been reported (see ref. 8) and representative structures of transition metal complexes incorporating dimethyl bis(1-pyrazolyl)gallate and dimethylbis(3,5-dimethyl-1-pyrazolyl)gallate ligands have recently appeared (7, 8). The structure of a binuclear copper(I) complex incorporating hydrotris(1-pyrazolyl)-borate ligands *viz.* $[HB(N_2C_3H_3)_3Cu]_2$ represents the first reported example of a binuclear transition metal species involving this type of ligand (20). The present structure is the first example of a binuclear copper(II) complex involving 'pyrazolyl–gallate' ligands, and features an unusual arrangement which is probably derived from an attack by water on the initially formed bis-chelate complex $[Me_2Ga(N_2C_4H_5)_2]_2Cu$ (see Experimental section). The overall reaction with atmospheric moisture may be summarized as:

$$2[Me_2Ga(N_2C_4H_5)_2]_2Cu + 2H_2O \rightarrow [Me_3Ga_2(N_2C_4H_5)_3CuO]_2 + 2CH_4 + 2N_2C_4H_6$$

The resulting centrosymmetric dimer is depicted in Fig. 1, and displays the two copper

Can. J. Chem. Downloaded from www.nrcresearchpress.com by 210.87.254.40 on 09/05/12
For personal use only.

Can. J. Chem. Downloaded from www.nrcresearchpress.com by 210.87.254.40 on 09/05/12
For personal use only.

TABLE 4. Bond angles (deg) with estimated standard deviations in parentheses

(*a*) Nonhydrogen atoms

Bonds	Angle (deg)	Bonds	Angle (deg)
O—Ga(1)—N(1)	95.1(2)	Cu—N(2)—C(3)	131.9(4)
O—Ga(1)—N(6)′	106.4(2)	Cu′—N(2)—N(1)	95.3(3)
O—Ga(1)—C(10)	120.4(4)	Cu′—N(2)—C(3)	102.3(3)
N(1)—Ga(1)—N(6)′	102.8(2)	N(1)—N(2)—C(3)	105.9(4)
N(1)—Ga(1)—C(10)	120.8(4)	Ga(2)—N(3)—N(4)	117.1(3)
N(6)′—Ga(1)—C(10)	109.0(3)	Ga(2)—N(3)—C(4)	134.0(4)
O—Ga(2)—N(3)	91.6(2)	N(4)—N(3)—C(4)	108.5(5)
O—Ga(2)—C(11)	109.7(3)	Cu—N(4)—N(3)	120.6(3)
O—Ga(2)—C(12)	111.0(3)	Cu—N(4)—C(6)	132.6(4)
N(3)—Ga(2)—C(11)	106.2(4)	N(3)—N(4)—C(6)	106.8(5)
N(3)—Ga(2)—C(12)	111.8(4)	Cu—N(5)—N(6)	128.4(3)
C(11)—Ga(2)—C(12)	122.2(5)	Cu—N(5)—C(7)	122.9(4)
O—Cu—N(2)	89.5(2)	N(6)—N(5)—C(7)	108.7(4)
O—Cu—N(4)	90.1(2)	Ga(1)′—N(6)—N(5)	127.2(3)
O—Cu—N(5)	170.7(2)	Ga(1)′—N(6)—C(9)	125.7(4)
O—Cu—N(2)′	90.8(1)	N(5)—N(6)—C(9)	107.0(4)
N(2)—Cu—N(4)	176.9(2)	N(1)—C(1)—C(2)	107.9(5)
N(2)—Cu—N(5)	89.8(2)	N(1)—C(1)—C(13)	121.0(7)
N(2)—Cu—N(2)′	94.0(1)	C(2)—C(1)—C(13)	131.1(7)
N(4)—Cu—N(5)	90.1(2)	C(1)—C(2)—C(3)	106.9(6)
N(4)—Cu—N(2)′	89.1(1)	N(2)—C(3)—C(2)	110.6(6)
N(5)—Cu—N(2)′	98.6(2)	N(3)—C(4)—C(5)	109.6(6)
Ga(1)—O—Ga(2)	123.0(2)	N(3)—C(4)—C(14)	120.1(7)
Ga(1)—O—Cu	117.7(2)	C(5)—C(4)—C(14)	130.7(7)
Ga(2)—O—Cu	119.3(2)	C(4)—C(5)—C(6)	105.0(6)
Ga(1)—N(1)—N(2)	113.3(3)	N(4)—C(6)—C(5)	110.4(6)
Ga(1)—N(1)—C(1)	138.0(4)	N(5)—C(7)—C(8)	108.3(5)
N(2)—N(1)—C(1)	108.7(4)	N(5)—C(7)—C(15)	121.6(5)
Cu—N(2)—Cu′	86.0(1)	C(8)—C(7)—C(15)	130.1(6)
Cu—N(2)—N(1)	120.6(3)	C(7)—C(8)—C(9)	105.9(5)
		N(6)—C(9)—C(8)	110.6(6)

(*b*) Angles involving hydrogen atoms

Bonds	Angle (deg)	Bonds	Angle (deg)
C(1)—C(2)—H(2)	127(5)	Ga(2)—C(12)—H(12*a*)	108(6)
C(3)—C(2)—H(2)	125(5)	Ga(2)—C(12)—H(12*b*)	103(6)
N(2)—C(3)—H(3)	114(3)	Ga(2)—C(12)—H(12*c*)	126(9)
C(2)—C(3)—H(3)	134(3)	H(12*a*)—C(12)—H(12*b*)	134(9)
C(4)—C(5)—H(5)	120(4)	H(12*a*)—C(12)—H(12*c*)	104(10)
C(6)—C(5)—H(5)	135(4)	H(12*b*)—C(12)—H(12*c*)	83(10)
N(4)—C(6)—H(6)	125(3)	C(1)—C(13)—H(13*a*)	128(6)
C(5)—C(6)—H(6)	124(3)	C(1)—C(13)—H(13*b*)	105(7)
C(7)—C(8)—H(8)	120(4)	C(1)—C(13)—H(13*c*)	109(6)
C(9)—C(8)—H(8)	132(4)	H(13*a*)—C(13)—H(13*b*)	106(9)
N(6)—C(9)—H(9)	116(3)	H(13*a*)—C(13)—H(13*c*)	91(8)
C(8)—C(9)—H(9)	134(3)	H(13*b*)—C(13)—H(13*c*)	119(9)
Ga(1)—C(10)—H(10*a*)	116(6)	C(4)—C(14)—H(14*a*)	103(7)
Ga(1)—C(10)—H(10*b*)	112(6)	C(4)—C(14)—H(14*b*)	123(5)
Ga(1)—C(10)—H(10*c*)	115(5)	C(4)—C(14)—H(14*c*)	104(4)
H(10*a*)—C(10)—H(10*b*)	65(7)	H(14*a*)—C(14)—H(14*b*)	126(8)
H(10*a*)—C(10)—H(10*c*)	125(8)	H(14*a*)—C(14)—H(14*c*)	101(7)
H(10*b*)—C(10)—H(10*c*)	78(7)	H(14*b*)—C(14)—H(14*c*)	95(7)
Ga(2)—C(11)—H(11*a*)	107(4)	C(7)—C(15)—H(15*a*)	112(4)
Ga(2)—C(11)—H(11*b*)	119(7)	C(7)—C(15)—H(15*b*)	124(9)
Ga(2)—C(11)—H(11*c*)	119(5)	C(7)—C(15)—H(15*c*)	111(4)
H(11*a*)—C(11)—H(11*b*)	83(8)	H(15*a*)—C(15)—H(15*b*)	98(9)
H(11*a*)—C(11)—H(11*c*)	127(7)	H(15*a*)—C(15)—H(15*c*)	88(5)
H(11*b*)—C(11)—H(11*c*)	96(8)	H(15*b*)—C(15)—H(15*c*)	117(9)

TABLE 5. Intraannular torsion angles (deg)

Bond	Angle	Bond	Angle
	Five-membered rings		
Cu—O	11.4(2)	Cu—O	8.4(2)
O—Ga(1)	−17.8(2)	O—Ga(2)	−11.0(2)
Ga(1)—N(1)	19.3(3)	Ga(2)—N(3)	10.4(3)
N(1)—N(2)	−15.1(3)	N(3)—N(4)	−6.8(3)
N(2)—Cu	3.1(3)	N(4)—Cu	−0.6(3)
	Seven-membered rings		
Ga(1)—O	87.1(2)	Ga(1)—O	87.1(2)
O—Cu	−82.6(1)	O—Cu	11.4(2)
Cu—N(2)′	89.6(2)	Cu—N(2)	−90.7(1)
N(2)′—Cu′	−98.6(2)	N(2)—Cu′	90.4(2)
Cu′—N(5)′	88.5(3)	Cu′—N(5)′	−5.4(3)
N(5)′—N(6)′	−4.0(4)	N(5)′—N(6)′	−4.0(4)
N(6)′—Ga(1)	−60.9(3)	N(6)′—Ga(1)	−60.9(3)
	Six-membered ring		
Ga(1)—N(1)	−88.9(3)		
N(1)—N(2)	73.4(3)		
N(2)—Cu′	−30.0(3)		
Cu′—N(5)′	−5.4(3)		
N(5)′—N(6)′	−4.0(4)		
N(6)′—Ga(1)	38.5(3)		
Unique angles in the 10-membered ring:			
	Ga(1)—O—Cu—N(5)	97.0(7)	
	O—Cu—N(5)—N(6)	−174.1(6)	

atoms at a distance of 3.383(1) Å from each other. The complex is magnetically dilute (21) (μ_{eff} = 1.98 B.M. per copper atom at 298 K) with no major detectable intramolecular magnetic coupling interaction between the two copper atoms either directly or via the ligand system. Usually, for such magnetic coupling to occur the Cu. . .Cu distance is $\leq$3.0 Å, and typical binuclear copper(II) complexes showing such magnetic coupling interactions are the copper carboxylate monoadducts $[Cu(RCO_2)_2.L]_2$, (ref. 22 and references therein), the recently reported 7-azaindole copper(II) complexes (23), and a binuclear triketonate copper(II) complex (24).

The individual arrangement about each copper atom is approximately square-planar with three nitrogen atoms and one oxygen atom coordinated to the copper. Within this same general plane there are two gallium atoms and two pyrazolyl rings, giving a system of four fused five-membered

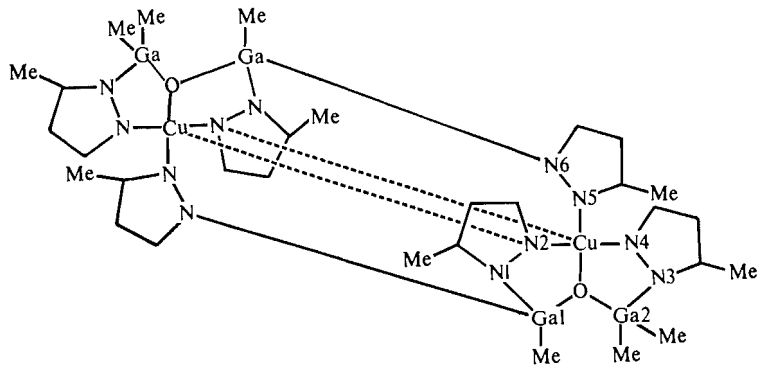

1

Can. J. Chem. Downloaded from www.nrcresearchpress.com by 210.87.254.40 on 09/05/12
For personal use only.

Can. J. Chem. Downloaded from www.nrcresearchpress.com by 210.87.254.40 on 09/05/12
For personal use only.

TABLE 6

(*a*) Equations of weighted least-squares planes in the form $lX + mY + nZ = p$ where X, Y, and Z are orthogonal Å coordinates with respect to a, b, and c^*

Plane	Atoms in plane	χ^2	Equation of plane	Atom	Deviation from plane (Å)	Atom	Deviation from plane (Å)	Atom	Deviation from plane (Å)
1	N(1), N(2), C(1)–C(3)	3.1	$0.6183X+0.3041Y-0.7247Z = -2.4917$	N(1)	−0.002(5)	N(2)	0.003(4)	C(1)	−0.000(7)
				C(2)	0.007(7)	C(3)	−0.007(6)	C(13)	0.035(13)
				H(2)	−0.13(8)	H(3)	−0.17(6)	Ga(1)	−0.0577(7)
				Cu	0.4071(7)				
2	N(3), N(4), C(4)–C(6)	1.8	$0.7230X+0.4385Y-0.5338Z = -0.7243$	N(3)	−0.002(5)	N(4)	0.000(5)	C(4)	0.006(7)
				C(5)	−0.007(8)	C(6)	0.004(8)	C(14)	0.016(11)
				H(5)	0.03(8)	H(6)	−0.14(5)	Ga(2)	0.1746(7)
				Cu	0.0289(7)				
3	N(5), N(6), C(7)–C(9)	1.2	$-0.1616X-0.7294Y-0.6647Z = -4.0588$	N(5)	−0.003(4)	N(6)	0.002(4)	C(7)	0.003(5)
				C(8)	−0.002(7)	C(9)	−0.002(7)	C(15)	0.003(9)
				H(8)	−0.18(6)	H(9)	0.01(5)	Ga(1)	−0.0691(7)
				Cu	0.0269(7)				

*$\chi^2 = \Sigma(d_m/\sigma(d_m))^2$, where d_m is the deviation of atom m from the mean plane.

(*b*) Dihedral angles between planes

Planes	Angle (deg)
1–2	14.7
1–3	80.8
2–3	94.7

TABLE 7. Selected intra- and intermolecular contacts

Intramolecular		Intermolecular*	
Atoms	Distance (Å)	Atoms	Distance (Å)
Ga(1) . . . Ga(2)	3.254(1)	H(1) . . . H(5)^{1}	2.79(7)
Ga(1) . . . Cu	3.203(1)	H(6) . . . H(11*a*)^{2}	2.35(10)
Ga(2) . . . Cu	3.278(1)		
Cu . . . Cu′	3.383(1)		
N(5) . . . C(6)	3.049(8)		
N(5) . . . C(3)	3.053(7)		
Cu . . . H(15*c*)	2.74(8)		
N(5) . . . H(3)	2.56(5)		
C(2) . . . H(13*b*)	2.62(10)		
C(5) . . . H(14*a*)	2.60(11)		

*Superscripts refer to atoms at positions: $^{1}1 - x, 1/2 + y, 1/2 - z$; $^{2}1 - x, y - 1/2, 1/2 - z$.

rings in each of the two polycyclic planar systems. The two 'planes' making up the centrosymmetric dimer are held together primarily by two straddling 'pyrazolyl' moieties which provide a Ga—N—N—Cu link-up between the planes. This is shown diagrammatically in **1**. In addition there is the possibility of a long axial interaction between a nitrogen atom in one plane, N(2), and the copper atom directly below in the other plane, Cu′, thus forming a planar centrosymmetric Cu_2N_2 ring. The distance involved, Cu′–N(2), is 2.874(4) Å and although too long to represent a strong bonding interaction may constitute a "semi-coordination" effect between the two atoms (25–27). The copper atom is displaced slightly (0.111 Å) from the mean plane of the four atoms within normal bonding distance towards the axial nitrogen atom, consistent with some type of weak interaction. The four atoms with normal bonds to the copper are not coplanar, N(2) and N(4) are both displaced 0.06 Å from the mean plane of N(2), N(4), N(5), and O toward Cu′ while N(5) and O are displaced 0.06 and 0.04 Å in the opposite direction, presumably a result of steric forces. As a consequence, some of the bond angles at the copper atom (89.1(1)–98.6(2), 170.7(2), and 176.9(2)°) deviate significantly from their 'ideal' values of 90 and 180°. The Cu—O distance of 1.923(3) Å is normal and the mean Cu—N distance of 1.985 Å for the three N atoms with normal bonds to copper agrees well with the mean distance of 1.987 Å in the related square-planar complex $[Me_2Ga(N_2C_3H_3)_2]_2Cu$ (8). The significant difference between the Cu—N(4) and Cu—N(5) distances (1.964(4) and 1.990(4) Å respectively) is believed to arise from the *trans* effect while the lengthening of Cu—N(2) to 2.001(4) Å relative to Cu—N(4) must result from the weak interaction between N(2) and Cu′.

There are two types of four-coordinate tetrahedral gallium atoms: one bound to oxygen, two 'pyrazolyl' nitrogens, and a methyl group; the other to oxygen, two methyl groups, and one 'pyrazolyl' nitrogen. Of interest is the fact that some of the 3-methylpyrazolyl groups exhibit their methyl groups away from the gallium atoms, as expected, whilst others (the majority) exhibit them toward the gallium atoms. Some ligand scrambling must have taken place during the formation of the binuclear copper(II) complex and steric effects were probably responsible. A noteworthy point is the unprecedented loss of a methyl group from a 'Me_2Ga' unit under such mild conditions, whereas usually such 'Me_2Ga' moieties are quite stable (1, 28).

The gallium tetrahedra are both considerably distorted with valence angles ranging from 95.1(2) to 120.8(4)° at Ga(1) and from 91.6(2) to 122.2(5)° at Ga(2). The two Ga—O distances, 1.825(4) and 1.881(3) Å, are both in the range of 1.80–1.99 Å reported for tetrahedral Ga—O bonds (ref. 29 and references therein). The highly significant difference between the two distances probably results primarily from σ-hybridization effects (30). The Ga—C bonds in related 'pyrazolyl–gallate' structures (2–4, 7, 8) range from 1.90–1.98 Å with a weighted mean value of 1.953(4) Å. The three Ga—C distances in the present structure (Ga(1)—C(10), 1.950(7), Ga(2)—C(11), 1.970(7), and Ga(2)—C(12), 1.979(8) Å) all lie within this range. The Ga—N bond

Can. J. Chem. Downloaded from www.nrcresearchpress.com by 210.87.254.40 on 09/05/12
For personal use only.

Can. J. Chem. Downloaded from www.nrcresearchpress.com by 210.87.254.40 on 09/05/12
For personal use only.

lengths in the related structures range from 1.971 to 2.006 Å and show a bimodal distribution, the mean values for the 'short' and 'long' Ga—N bonds being 1.979(1) and 1.998(1) Å respectively. The three Ga—N bonds in the present structure are Ga(1)—N(1), 1.952(4), Ga(1)—N(6)′, 1.969(4), and Ga(2)—N(3), 1.978(5) Å. The first of these bonds is significantly shorter than any previously observed in the 'pyrazolyl–gallate' structures while the latter two are both in the range of the 'short' Ga—N distances.

Incorporated into the polycyclic structure are ten independent rings. The central four-membered Cu_2N_2 ring is centrosymmetric (and thus planar) with angles of 94.0(1)° at Cu and 86.0° at N. The three 3-methylpyrazolyl rings are planar within experimental error (see Table 6). Torsion angles in the remaining rings ($2CuN_2GaO$, $GaCuN_4$, $2GaCu_2ON_3$, and $Cu_2Ga_2O_2N_4$) are listed in Table 5. The oxygen atom has trigonal planar geometry (displacement −0.0009(37) Å from the Ga(1)Ga(2)Cu plane).

The means and ranges for bond lengths in the 3-methylpyrazolyl groups are: N—N, 1.372 (1.358–1.385), N—C, 1.341 (1.326–1.352), C—C, 1.367 (1.342–1.386), and C—C(Me), 1.493 (1.487–1.500 Å). These values compare well with those observed in related 'pyrazolyl–gallate' structures (2–4, 7, 8): N—N(bimodal) 1.351(5) and 1.372(2) (1.33–1.380), N—C, 1.345 (1.322–1.361), C—C, 1.373 (1.340–1.40), and C—C(Me), 1.498(3) (1.488–1.513 Å). The geometry involving hydrogen atoms is also as expected: mean C(pz)—H. 0.94(4), mean C(Me)—H, 0.96(2) Å, and angles range from 114–135(3–5)° for 'pyrazolyl' hydrogens and from 65–134(4–10)° for methyl hydrogen atoms.

The crystal structure (Fig. 2) consists of well-separated binuclear units, the closest intermolecular contact (H(6)...H(11*a*), 2.35(10) Å) corresponding to a normal van der Waals contract. Intramolecular nonbonded contacts are listed in Table 6. The N(5)...H(3) distance of 2.56(5) Å is less than the sum of van der Waals radii and there may be a weak interaction between H(3) and the $p\pi$ bonding orbital of N(5). The angle C(3)—H(3)...N(5) is 111°.

Acknowledgments

We thank Mr. P. Borda for C, H, and N analyses, Mr. R. Morrison for the magnetic susceptibility measurement, Mr. J. Nip for recording the mass spectrum, and Mr. W. Lee for the ^1H nmr spectra. We are indebted to the National Research Council of Canada for financial support and to the University of British Columbia Computing Centre for assistance.

1. A. Arduini and A. Storr. J. Chem. Soc. Dalton Trans. 503 (1974).
2. D. F. Rendle, A. Storr, and J. Trotter. J. Chem. Soc. Dalton Trans. 2252 (1973).
3. D. F. Rendle, A. Storr, and J. Trotter. Can. J. Chem. **53**, 2930 (1975).
4. D. F. Rendle, A. Storr, and J. Trotter. Can. J. Chem. **53**, 2944 (1975).
5. K. R. Breakell, D. J. Patmore, and A. Storr. J. Chem. Soc. Dalton Trans. 749 (1975).
6. F. G. Herring, D. J. Patmore, and A. Storr. J. Chem. Soc. Dalton Trans. 711 (1975).
7. D. F. Rendle, A. Storr, and J. Trotter. J. Chem. Soc. Dalton Trans. 176 (1975).
8. D. J. Patmore, D. F. Rendle, A. Storr, and J. Trotter. J. Chem. Soc. Dalton Trans. 718 (1975).
9. A. Storr and B. S. Thomas. Can. J. Chem. **48**, 3667 (1970).
10. D. T. Cromer and J. B. Mann. Acta Crystallogr. Sect. A, **24**, 321 (1968).
11. R. F. Stewart, E. R. Davidson, and W. T. Simpson. J. Chem. Phys. **42**, 3175 (1965).
12. D. T. Cromer and D. Liberman. J. Chem. Phys. **53**, 1891 (1970).
13. V. Schomaker and K. N. Trueblood. Acta Crystallogr. Sect. B, **24**, 63 (1969).
14. D. W. J. Cruickshank. Acta Crystallogr. **9**, 747 (1956); **9**, 754 (1956).
15. D. W. J. Cruickshank. Acta Crystallogr. **14**, 896 (1961).
16. W. R. Busing and H. A. Levy. Acta Crystallogr. **17**, 142 (1964).
17. C. K. Johnson. *In* Crystallographic computing. Munksgaard, Copenhagen. 1970. pp. 207–226.
18. B. D. Chambers, G. E. Coates, F. Glockling, and M. Weston. J. Chem. Soc. A. 1712 (1969).
19. K. J. Alford, K. Gosling, and J. D. Smith. J. Chem. Soc. Dalton Trans. 2203 (1972).
20. C. S. Arcus, J. L. Wilkinson, C. Mealli, T. J. Marks, and J. A. Ibers. J. Am. Chem. Soc. **96**, 7564 (1974).
21. B. J. Hathaway. J. Chem. Soc. Dalton Trans. 1196 (1972).
22. J. A. Moreland and R. J. Doedens. J. Am. Chem. Soc. **97**, 508 (1975).
23. R. W. Brooks and R. L. Martin. Inorg. Chem. **14**, 528 (1975).
24. A. B. Blake and L. R. Fraser. J. Chem. Soc. Dalton Trans. 2554 (1974).
25. D. S. Brown, J. D. Lee, B. G. A. Melson, B. J. Hathaway, I. M. Procter, and A. A. G. Tomlinson. J. Chem. Soc. Chem. Commun. 369 (1967).
26. I. M. Procter, B. J. Hathaway, and P. Nicholls. J. Chem. Soc. A, 1678 (1968).

27. A. A. G. TOMLINSON and B. J. HATHAWAY. J. Chem. Soc. A, 65 (1969).
28. G. E. COATES and K. WADE. Organometallic compounds: Vol. 1. The main group elements. 3rd ed. Methuen, London. 1967. Chapt. 3.
29. S. J. RETTIG, A. STORR, and J. TROTTER. Can. J. Chem. **53**, 753 (1975).
30. S. J. RETTIG. Ph.D. Thesis. University of British Columbia, Vancouver, British Columbia. 1974.

Can. J. Chem. Downloaded from www.nrcresearchpress.com by 210.87.254.40 on 09/05/12
For personal use only.

Concentration fluctuations in water–methanol mixtures as studied by ultrasonic absorption

WILLIAM D. T. DALE,[1] PETER A. FLAVELLE,[2] AND PEETER KRUUS
Department of Chemistry, Carleton University, Ottawa, Canada K1S 5B6

Received July 3, 1975

WILLIAM D. T. DALE, PETER A. FLAVELLE, and PEETER KRUUS. Can. J. Chem. **54**, 355 (1976).

Measurements of the ultrasonic absorption and velocity, and viscosity have been carried out in the system methanol–water at 0, 15, and 25 °C at frequencies from 10 to 50 MHz. The data show the existence of two maxima in the excess absorption as a function of composition. The existence of the two maxima are predicted by the Romanov–Solovyev theory relating the absorption to concentration fluctuations. The magnitude of the excess absorption is calculated at 25 and 0 °C from density, vapour pressure, and diffusion data. New experimental data on density and vapour pressure are presented for this system at 0 °C. The calculated excess absorption is in reasonable agreement with the measured. This indicates that any specific localized intermolecular interactions present in this system could be responsible for at best a smaller portion of the excess ultrasonic absorption, as longer range concentration fluctuations account for essentially all of the excess. Ultrasonic data on the systems methanol–octanol and *n*-propanol –water are also presented in the course of examining the generality of these phenomena.

WILLIAM D. T. DALE, PETER A. FLAVELLE et PEETER KRUUS. Can. J. Chem. **54**, 355 (1976).

On a effectué des mesures d'absorption et de vitesse ultrasonique et de viscosité dans le système méthanol–eau à 0, 15 et 25 °C à des fréquences allant de 10 à 50 MHz. Les données montrent l'existence de deux maxima dans l'absorption en excès en fonction de la composition. L'existence des deux maxima est prédite par la théorie de Romanov–Solovyev en reliant l'absorption avec les fluctuations de la concentration. On a calculé l'amplitude de l'excès d'absorption à 25 et à 0 °C à partir des données de densité, de pression de vapeur et de diffusion. On présente de nouvelles données expérimentales pour la densité et la pression de vapeur de ce système à 0 °C. Les absorptions en excès calculées sont en bon accord avec les valeurs mesurées. Ce résultat indique que les interactions intermoléculaires localisées spécifiques présentes dans ce système peuvent être responsables pour au plus une petite portion de l'absorption ultrasonique en excès puisque des fluctuations de concentration sur des grandes étendues tiennent compte pratiquement de tous les excès. On présente aussi des données ultrasoniques pour le système méthanol–octanol et *n*-propanol–eau dans le cadre d'un examen de la généralité de ce phénomène.

[Traduit par le journal]

Introduction

The first ultrasonic measurements in methanol–water mixtures were reported in 1946 by Mikhailov and Gourevitch (1). They found a maximum in the absorption as a function of concentration. Later studies by Burton (2) did not show a maximum. Since that time, many ultrasonic studies of alcohol–water systems have been carried out (3–9), but only one additional study (10) has been reported on methanol–water. A more complete summary of ultrasonic absorption studies for alcohol–water solutions can be found in ref. 11.

An explanation of the absorption in several alcohol–water mixtures (7, 12) has been given in terms of the Romanov–Solovyev theory (12, 13). This theory postulates the excess absorption to be due to the presence of concentration fluctuations in the system and relates it to the free energy of mixing (G^{mix}), the volume of mixing (V^{mix}), and the mutual diffusion constant. Lack of sufficiently accurate thermodynamic data makes quantitative comparison of experiment and theory difficult. Other studies have interpreted the results in terms of specific relaxation times (3–5, 8, 9, 14), postulating the formation of specific intermolecular complexes to be responsible for these relaxations (3, 8, 9, 14). These approaches give a possible explanation of the excess absorption, but do not exclude other explanations.

[1]Present address: Department of Chemistry, State University of New York, Stony Brook, New York 11794.

[2]Present address: Inland Waters Branch, Department of Environment, 562 Booth Street, Ottawa, Canada K1A 0E7.

Can. J. Chem. Downloaded from www.nrcresearchpress.com by 210.87.254.6 on 09/05/12
For personal use only.

TABLE 1. Ultrasonic and viscosity data for methanol–water at 25.0 °C, 31.6 MHz

Mole fraction methanol X_M	Measured absorption α/f^2 (10^{-17} cm^{-1} s^2)	Measured velocity v (10^5 cm s^{-1})	Kinematic viscosity η/ρ (10^{-2} st)	Classical absorption α_c/f^2 (10^{-17} cm^{-1} s^2)
0.0000	22.1	1.500	0.892	7.0
0.0472	23.6_5	1.533	1.113	8.1
0.1002	23.9	1.560	1.327	9.2
0.1603	25.8	1.570	1.403	9.5_5
0.2290	28.9	1.560	1.464	10.2
0.3082	33.7_5	1.525	1.518	11.3
0.4005	36.3	1.466	1.548	12.9
0.5096	35.4_5	1.395	1.388	13.5
0.6404	32.6	1.312	1.159	13.5
0.8003	30.8	1.214	0.946	13.9
1.0000	30.7	1.103	0.770	15.1

This study of methanol–water was initiated to see if the Romanov–Solovyev theory accounts essentially for all the excess absorption, or whether it is necessary to postulate the existence of specific intermolecular complexes in methanol–water. The simplest possible alcohol–water system was chosen to avoid interferences from other possible absorption processes, *e.g.* the proximity of a miscibility gap (6).

This system was examined in considerably greater detail with regard to its concentration and temperature dependence than other systems examined previously. The volume, free energy, and diffusion data necessary for analysis of ultrasonic absorption in terms of concentration-fluctuation theory have not been available for some of the previously examined systems. Such data for the methanol–water system were made complete at both 0 and 25 °C making density and vapour pressure measurements where data were not available in the literature.

Experimental

The *n*-propanol and *n*-octanol used in the studies were Fisher certified grade. The methanol was Fisher spectranalyzed. Density and refractive index measurements confirmed the quoted purity as better than 99.95%. The alcohols were all used without further purification. Deionized water from a Milli-Q3 water purifier (Millipore Corporation) was used. All solutions were made up gravimetrically with a precision in the composition values of better than 0.06%.

The apparatus and method used for the ultrasonic absorption and velocity measurements are described in ref. 6. Although the standard deviation of attenuation *vs.* distance plots suggest the precision of α/f^2 to be better than 0.2%, the absolute accuracy of the data is considerably poorer. In ref. 6 it is estimated to be 3%. The relative accuracy in a series of runs taken on a single day was better than this, but for some reason the reproducibility over long periods was not as good. The reason cannot be variation in thermostat temperature, as the temperature was controlled to better than 0.2° at 0 °C, with better control at 15 and 25 °C. The accuracy of the velocity measurement was estimated to be better than 0.3%.

Kinematic viscosity was measured with a Cannon–Fenske viscometer thermostated in the same bath used for the ultrasonic apparatus. Calibration was with water. The measured viscosities are estimated to have an accuracy of better than 0.7%.

The density measurements were done on a Precision Density Meter DMA 02C (Anton Paar) described in ref. 15. Calibration for operation at 0 °C was accomplished using samples of hexane and methanol obtained from the National Research Council of Canada, and two samples of methanol–water solutions, the densities of which had been determined by a pycnometer. Temperature control was better than 0.01 deg, and the precision of density measurements was estimated to be better than 0.01%.

Vapour pressure measurements were done using a mercury manometer installed in a vacuum apparatus equipped with a single-stage mercury diffusion pump. An equilibration period of at least 20 h was allowed for each sample, during which it was stirred by a magnetic stirrer immersed in the thermostat bath. Pressure measurements were taken against atmospheric pressure using a cathetometer. The refractive index of the samples was taken at the end to check for changes in composition during the measurements. The precision of the vapour pressure measurements is estimated to be better than 4%.

Experimental Results

Tables 1, 2, and 3 give the basic ultrasonic

Can. J. Chem. Downloaded from www.nrcresearchpress.com by 210.87.254.6 on 09/05/12
For personal use only.

TABLE 2. Ultrasonic and viscosity data for methanol–water at 15.0 °C, 31.6 MHz

Mole fraction methanol X_M	Measured absorption α/f^2 (10^{-17} cm^{-1} s^2)	Measured velocity v (10^5 cm s^{-1})	Kinematic viscosity η/ρ (10^{-2} st)	Classical absorption α_c/f^2 (10^{-17} cm^{-1} s^2)
0.0000	30.6	1.492	1.140	9.0
0.0276	31.1	1.495	1.327	10.6
0.0373	32.2	1.507	1.384	10.6
0.0472	32.2	1.508	1.458	11.0
0.0573	32.7	1.523	1.490	11.1
0.0782	32.1	1.537	1.612	11.7
0.1002	33.0	1.556	1.759	12.3
0.1603	34.5	1.576	1.994	13.4
0.2290	39.5	1.573	2.197	14.9
0.3082	44.8	1.544	2.222	15.9
0.4005	46.3	1.488	2.079	16.6
0.5096	44.8	1.421	1.878	17.2
0.6404	38.8	1.347	1.539	16.6
0.8003	33.8	1.246	1.065	14.5
1.0000	32.3	1.137	0.8321	14.9

TABLE 3. Ultrasonic data for methanol–water at 0.0 °C, 31.6 MHz

Mole fraction methanol X_M	Measured absorption α/f^2 (10^{-17} cm^{-1} s^2)	Measured velocity v (10^5 cm s^{-1})	Classical absorption α_c/f^2 (10^{-17} cm^{-1} s^2)
0.0000	57.9	1.413	16.0
0.0087	58.8	1.428	16.7
0.0145	59.6	—	17.1
0.0219	59.8	—	17.6_5
0.0291	60.7	1.456	18.2_5
0.0395	61.7	1.473	18.8
0.0482	61.5_5	1.485_5	19.4
0.0554	60.8	—	19.8
0.0795	60.3	1.518	21.0_5
0.1203	59.3	1.559	22.7
0.1643	61.3	1.588	23.9
0.2077	64.4	1.594	24.6
0.2475	68.1	1.590	24.9
0.3011	71.2	1.581	24.9
0.4115	72.1	1.556	23.9
0.5167	60.9	1.475_5	22.4
0.6365	50.7	1.408	20.9
0.7237	42.3	1.348_5	20.0_5
0.8405	37.1	1.292_5	18.2
0.9082	34.0	1.251	16.5
1.0000	29.5	1.194	15.9

absorption, ultrasonic velocity, and (in Tables 1 and 2) kinematic viscosity data at 25, 15, and 0 °C for methanol–water. The ultrasonic measurements are all for $f = 31.6$ MHz. The variation of α/f^2 with frequency (10.6 to 52.8 MHz) was examined for the peak sound absorption composition ($X_M = 0.229$) at 25 and 0 °C. The values of α/f^2 were found to be independent of f to within the accuracy of the apparatus in both cases. The classical absorption due to viscosity (α_c/f^2) is also given as calculated from the experimental data through ref. 16.

Can. J. Chem. Downloaded from www.nrcresearchpress.com by 210.87.254.6 on 09/05/12
For personal use only.

Can. J. Chem. Downloaded from www.nrcresearchpress.com by 210.87.254.6 on 09/05/12
For personal use only.

TABLE 4. Ultrasonic and viscosity data for methanol–octanol at 25.0 °C

Mole fraction methanol X_M	Measured absorption α/f^2 (10^{-17} cm^{-1} s^2)	Measured velocity v (10^5 cm s^{-1})	Kinematic viscosity η/ρ (10^{-2} st)	Classical absorption α_c/f^2 (10^{-17} cm^{-1} s^2)
0.0000	162.3	1.347	7.58	81.6
0.1432	142.0	1.331	6.39	71.3
0.2608	116.8	1.318	4.92	56.6
0.4426	91.3	1.287	3.39	41.9
0.5765	74.0	1.258	2.46	32.5
0.6792	63.9	1.229	1.80	25.5
0.7605	55.5	1.204	1.51	22.8
0.8265	50.6	1.180	1.24	19.9
0.8811	45.5	1.156	1.04$_5$	17.8
0.9270	38.4	1.135	0.930	16.7
0.9662	34.8	1.118	0.814	15.3
1.0000	30.7	1.103	0.770	15.1

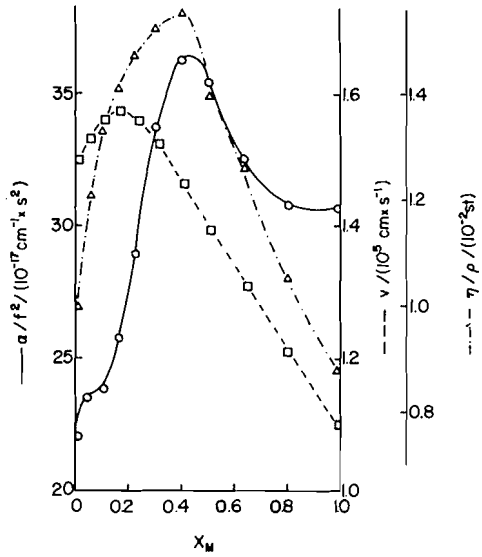

FIG. 1. Ultrasonic absorption, velocity, and viscosity in methanol–water at 25.0 °C, 31.6 MHz. —, Ultrasonic absorption; - - -, ultrasonic velocity; - · - · - kinematic viscosity.

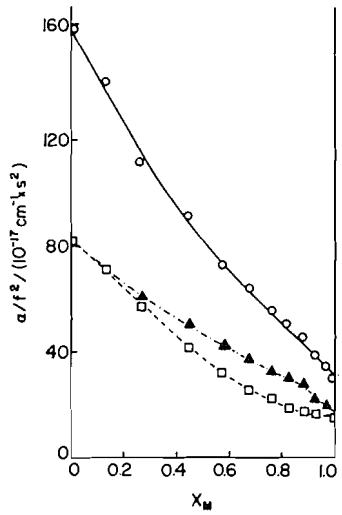

FIG. 2. Experimental, classical, and excess ultrasonic absorption in methanol–*n*-octanol at 25.0 °C, 31.6 MHz. —, Experimental absorption; - - -, classical absorption; - · - · -, excess absorption.

$$[1] \qquad \frac{\alpha_c}{f^2} = \frac{8\pi^2\eta}{3v^3\rho}$$

Table 4 gives the corresponding data for methanol–octanol.

Figure I shows a plot of the 25 °C methanol–water data from Table I, illustrating the composition variation of three of the four quantities listed. The plots of α/f^2 and α_c/f^2 for methanol–octanol are shown in Fig. 2 to illustrate the qualitative difference in the results for the two systems. It was decided to study this system as accurate and complete thermodynamic data is available for it (17).

Figure 3 shows the α/f^2 of methanol–water at the three temperatures. The low X_M absorption is most apparent at 0 °C. In addition to the data listed in Table 3, Fig. 3 shows the results of two additional independent determinations of α/f^2 *vs.* X_M at low X_M made by different experimenters on different dates. These determinations were thought desirable to increase the credibility of the existence of the low X_M maximum due to

Can. J. Chem. Downloaded from www.nrcresearchpress.com by 210.87.254.6 on 09/05/12
For personal use only.

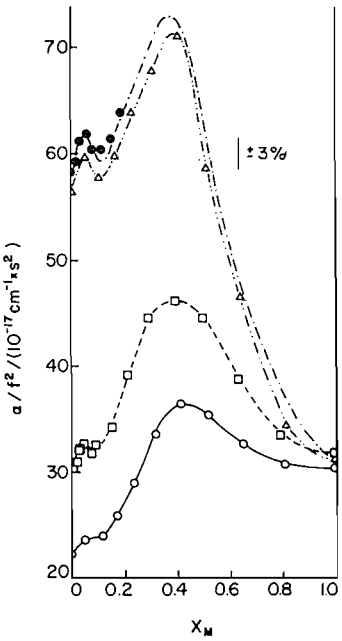

FIG. 3. Experimental ultrasonic absorption in methanol–water at 31.6 MHz. ○, 25.0 °C; □, 15.0 °C; ·-·-·, 0.0 °C, Set 1 (Table 3); △ ·-·-·, 0.0 °C, Set 2; ●, 0.0 °C, Set 3.

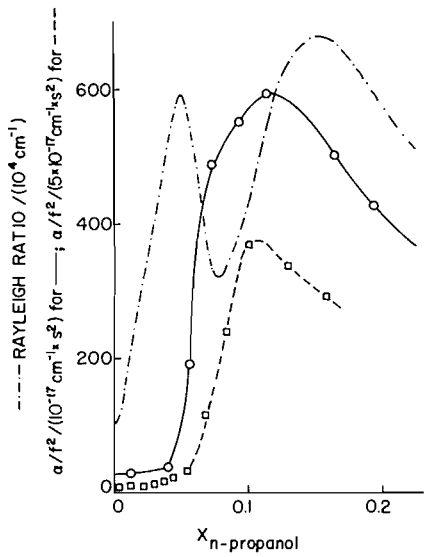

FIG. 4. Ultrasonic absorption at 31.6 MHz and light scattering in *n*-propanol–water. —, Ultrasonic absorption at 25.0 °C; - - -, ultrasonic absorption at 0.0 °C on a scale 0.2 times that for 25.0 °C; ·-·-·, Rayleigh ratio at 22 °C after ref. 17.

its relatively moderate size in comparison to experimental uncertainties. The estimated 3% range of accuracy is shown by bars in Fig. 3. It should be noted that this is the absolute accuracy range estimated. Points taken within the same set, *i.e.* with the same apparatus settings, have a relative accuracy better than this.

The presence of such a double maximum phenomenon in other alcohol–water systems was investigated by measuring α/f^2 for *tert*-butyl alcohol – water at 25 °C and *n*-propanol–water at 25.0 and 0.0 °C. These systems were chosen as they both show a double maximum in their light scattering Rayleigh ratio as a function of composition. A detailed study of α/f^2 *vs.* composition was carried out at low alcohol concentrations for all three cases. Only the results for the *n*-propanol mixtures is presented here, in Fig. 4, where it is plotted together with light-scattering data (18). The results are consistent with the 70 MHz ultrasonic absorption data shown in ref. 5, but are somewhat higher (about 10%) than data interpolated from ref. 9. The detailed *tert*-butyl alcohol – water study gave essentially the same results as in ref. 4, *i.e.* the α/f^2 *vs.* X curve is of the same general shape as those in Fig. 4, and no sign of double maximum is observed.

Tables 5 and 6 show a tabulation of values of viscosity, vapour pressure, and density data for methanol–water at 0.0 °C. This is the basic data used for the calculations at 0.0 °C described in later sections. All other data were taken from the literature.

Application of Concentration-fluctuation Theory

Determination of $(\alpha/f^2)_{CF}$ *from Experimental Values of* α/f^2

The total absorption in the alcohol–water mixtures can be considered to be made up of three contributions,

$$[2] \qquad \alpha/f^2 = \alpha_c/f^2 + \alpha_B/f^2 = \alpha_c/f^2 + \alpha_S/f^2 + \alpha_{CF}/f^2$$

Here α_c/f^2 is the classical absorption due to shear viscosity as expressed in [1]. Both α_S and α_{CF} can be considered to be due to the presence of a bulk or volume viscosity in addition to a shear viscosity.

The contribution α_S/f^2 can be thought to be due to structural reorganizations, causing changes in density independent of concentration changes. Thus it is present in pure liquids as well as in

Can. J. Chem. Downloaded from www.nrcresearchpress.com by 210.87.254.6 on 09/05/12
For personal use only.

TABLE 5. Viscosity and vapour pressure data for methanol–water at 0.0 °C

Mole fraction methanol X_M	Kinematic viscosity η/ρ (10^{-2} st)	Vapour pressure		p (Torr) (Ref. 28)	p_M/p_W (Experimental)
		Experimental	Raoult's law		
0	1.798	4.54	4.54	4.55	—
0.0089	1.887	—	—	—	—
0.0180	1.946	—	—	—	—
0.0264	2.103	—	—	—	—
0.0343	2.211	—	—	—	—
0.0425	2.307	—	—	—	—
0.0538	2.432	—	—	—	—
0.0622	2.643	—	—	—	—
0.0988	3.053	6.03	6.67	6.98	0.46
0.1976	3.745	7.76	8.80	9.47	1.03
0.2494	3.750	8.70	9.91	10.7	1.38
0.3405	3.704	10.3	11.9	12.7	2.11
0.3959	3.374	11.2	13.1	13.9	2.66
0.4974	2.868	12.6	15.3	15.9	3.95
0.5962	2.407	14.1	17.4	17.8	5.80
0.6961	1.968	16.2	19.5	19.7	8.87
0.7990	1.611	19.5	21.8	21.9	15.2
0.8980	1.280	22.8	23.9	24.0	33.0
1.000	1.022	26.1	26.1	26.0	—

TABLE 6. Density data for methanol–water at 0.0 °C

Mole fraction methanol X_M	Density ρ (g cm^{-3})	Mole fraction methanol X_M	Density ρ (g cm^{-3})
0.0064	0.99721	0.1015	0.97523
0.0125	0.99529	0.1083	0.97470
0.0180	0.99362	0.1158	0.97273
0.0234	0.99199	0.1248	0.97137
0.0284	0.99071	0.1350	0.96958
0.0333	0.98945	0.1464	0.96748
0.0377	0.98834	0.1613	0.96442
0.0420	0.98725	0.1786	0.96193
0.0461	0.98618	0.2009	0.95788
0.0514	0.98490	0.2169	0.95585
0.0547	0.98406	0.2876	0.94085
0.0585	0.98338	0.3548	0.92916
0.0630	0.98240	0.4247	0.91358
0.0709	0.98123	0.5248	0.88965
0.0740	0.98053	0.5956	0.87756
0.0778	0.97974	0.6886	0.86034
0.0816	0.97901	0.7442	0.85011
0.0857	0.97817	0.8164	0.83722
0.0904	0.97745	0.8977	0.82270
0.0957	0.97632	1.0000	0.80555

liquid mixtures. Such structural absorption in pure liquids is explained in refs. 19 and 20 in terms of presence of voids or openings in the liquid. In ref. 19, the pressure dependence of the structural absorption is examined in terms of volume changes, while in ref. 20 the temperature dependence is examined.

The presence of concentration fluctuations also contributes to the bulk viscosity, and hence to the ultrasonic absorption. This contribution α_{CF}/f^2 is of course not present in the pure liquids. It is also negligible if the concentration fluctuations are very small, or if such concentration fluctuations lead to very small volume fluctuations.

It is assumed here that there are no contributions to α_B/f^2 from the presence of equilibria between any specific intermolecular complexes. If such a contribution exists, then the experimental α_{CF}/f^2 value would be less than that determined here. In aqueous systems, contributions to absorption due to changes involving an enthalpy change can usually be neglected (16) as the temperature changes caused by the adiabatic passage of a sonic wave are small.

In systems such as methanol–octanol, water–dimethylsulfoxide (21), and aniline-ethanol (22) there should be essentially no absorption due to concentration fluctuations. The V^{mix} does not have the anomalous behaviour leading to relatively large values of $(\partial^2 V^{mix}/\partial X^2)$ which vary significantly with composition. It is also unlikely that there is any absorption arising from vibrational relaxation (16) due to the polar nature of the components. Thus the absorption in excess of α_c/f^2 can reasonably safely be assumed to be due to structural absorption. In each case α_S/f^2

Can. J. Chem. Downloaded from www.nrcresearchpress.com by 210.87.254.6 on 09/05/12
For personal use only.

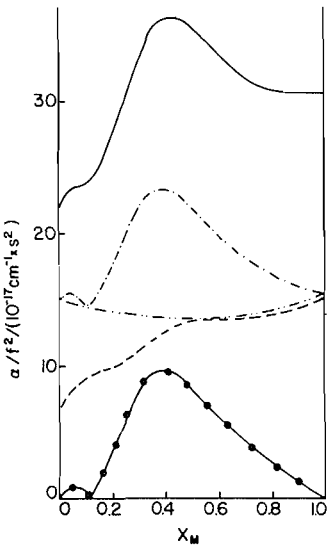

FIG. 5. Experimental, classical, bulk structural, and concentration-fluctuation ultrasonic absorption for methanol–water at 25.0 °C, 31.6 MHz. —, Experimental (α/f^2); - - -, classical (α_c/f^2); -·-·-, excess ($\alpha_B/f^2 = \alpha_s/f^2 + \alpha_{CF}/f^2$); ·····, structural ($\alpha_s/f^2$); ●, concentration-fluctuation (α_{CF}/f^2).

as a function of composition has a dependence which has a slight negative deviation from linearity.

The excess absorption of α_B/f^2 was thus in the case of methanol–water divided into the α_S/f^2 and α_{CF}/f^2 parts by estimating the α_S/f^2 to be of a shape suggested by the results of the above three systems. There were three points to guide the selection of this curve, as α_{CF}/f^2 also disappears at a composition where $(\partial^2 V^{mix}/\partial X_M^2) = 0$. There is nevertheless considerable arbitrariness in drawing in the curve for α_S/f^2 as illustrated in Fig. 5 for the 25 °C data. This arbitrariness can be removed if it were possible to make a measurement of α/f^2 at a high frequency (>1 GHz) where $1/f \ll$ relaxation time of the concentration fluctuations, and where thus $\alpha_{CF}/f^2 \simeq 0$.

Summary of the Romanov–Solovyev Concentration-fluctuation Theory

The theory of Romanov and Solovyev (12, 13) predicts α_{CF}/f^2 to be given by

$$[3] \qquad \frac{\alpha_{CF}}{f^2} = \frac{\rho v k T}{4D}\left(\frac{V''}{G''}\right)^2 I(\omega)$$

where

$$[4] \qquad V'' = \left(\frac{\partial^2 V^{mix}}{\partial X_M^2}\right)$$

$$G'' = \left(\frac{\partial^2 G^{mix}}{\partial X_M^2}\right)$$

$$[5] \quad I(\omega) = k_{max}\left\{1 - \frac{y}{2\sqrt{2}}\left[\tfrac{1}{2}\ln\left(\frac{1 + y\sqrt{2} + y^2}{1 - y\sqrt{2} + y^2}\right) + \arctan\left(\frac{y\sqrt{2}}{(y^2 - 1)}\right)\right]\right\}$$

In [5], y is given through $y^2 = \omega/2Dk_{max}^2$, and k_{max} is the maximum wave number of the Fourier expansion of the concentration fluctuations. It is estimated as the reciprocal of the average distance between the molecules of one solution component, *i.e.* $k_{max} = (N_A/V)^{1/3}$ if $N_A < N_B$ or $k_{max} = (N_B/V)^{1/3}$ if $N_B < N_A$. At frequencies which are relatively low ($y < 1$), the function $I(\omega)$ approaches k_{max}. This is the case here where $\omega \simeq 1.8 \times 10^8$ rad s^{-1}, $D \simeq 1 \times 10^{-5}$ cm^2 s^{-1}, $k_{max} = 2 \times 10^7$ cm^{-1}, $y \simeq 0.15$. Thus the weak dependence of α_{CF}/f^2 on frequency noted is in agreement with the predictions of the theory.

Examination of Volume Data

Volume properties of methanol–water at 0 °C were obtained from the data in Table 6. These data are described by a polynomial:

$$[6] \quad \rho(X_M) = 0.9994 - 0.3327X_M + 1.3601X_M^2 - 5.1096X_M^3 + 8.7608X_M^4 - 6.9951X_M^5 + 2.1226X_M^6$$

This and other polynomials were calculated using a regression program distributed by Hewlett–Packard for use on the HP9830A calculator.

It was found necessary to use a polynomial of at least the sixth degree to describe the density. A fit with fewer parameters smooths out the data excessively with consistently negative deviations in the lower mole fraction region. This behaviour is in agreement with the analysis of evaluating partial molal volumes given in ref. 23. The Gibbs–Duhem volume relationship was not introduced into the density analysis represented by [6]. Since the experimental data is considerably more sparse in the region of large X_M, then [6] does not describe the density data well in that

concentration region, especially as the form of the polynomial is unsuitable for $X \rightarrow 1$.

The data as represented by [6] agree with other density data (10 points) in ref. 24 for this system at 0 °C with an average difference 0.003 g cm^{-3} (0.3%) and a maximum difference 0.0065 g cm^{-3}. The densities as given in ref. 24 are all higher than those represented by [6]. This difference may in part be due to uncertainties in the densitometer constant. The apparatus and experimental method used here are more appropriate for obtaining accurate relative densities, as desired, rather than absolute accuracy.

The apparent molar volume $\overline{V}$ can then be obtained from [6] using

$$[7] \quad \overline{V}(X_M) = \{X_M M_M + (1 - X_M)M_W\}/\rho$$

and the volume of mixing V^{mix} using

$$[8] \quad V^{mix}(X_M) = \overline{V} - (X_M \overline{V}_M^{\cdot} + (1 - X_M)\overline{V}_W^{\cdot})$$

Here $\overline{V}_M^{\cdot}$ and $\overline{V}_W^{\cdot}$ are the partial molar volumes of pure methanol and pure water.

The partial molar volume of methanol in a solution, $\overline{V}_M = (\partial V/\partial n_M)$, can be obtained from

$$[9] \quad \overline{V}_M(X_M) = \overline{V}_M^{\cdot} + V^{mix} + (1 - X_M)(\partial V^{mix}/\partial X_M)$$

There is a minimum in $\overline{V}_M$ at low mole fractions of alcohol for methanol–water as is the case with other alcohol–water systems (25). This minimum results in a zero value for V'' (see [4]) at some value of X_M, and gives the double maximum in the curves in Fig. 6.

As can be seen in [3], the α_{CF}/f^2 is proportional to $(V'')^2$. In terms of densities, V'' is given by:

$$[10] \quad V''(X_M) = 2(M_W - M_M)\cdot(\partial\rho/\partial X_M)/\rho^2 + \{X_M M_M + (1 - X_M)M_W\} \times \{2(\partial\rho/\partial X_M)^2/\rho^3 - (\partial^2\rho/\partial X_M{}^2)/\rho^2\}$$

The V'' data are extrapolated to zero at $X_M \rightarrow 0$ as V^{mix} is linear with X_M in the limit $X_M \rightarrow 0$. However, this region of linearity is only for $X_M < 0.001$ (25) and the limited precision of the density apparatus used prevents the obtaining of meaningful V'' values in this region.

For analysis at 25.0 °C, the density data of Griffiths (26) was used. Because of the smaller number of data points (24 in all, with only 7 at $X_M < 0.15$), an analysis for V'' using polynomial fits is not meaningful. Thus V'' was obtained by a numerical point by point analysis which resulted in considerable scatter.

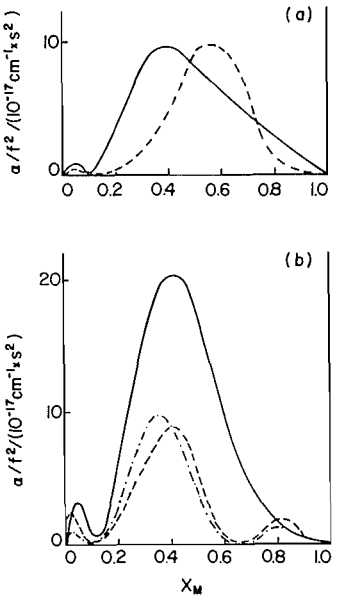

FIG. 6. Ultrasonic absorption due to concentration-fluctuations in methanol–water at 31.6 MHz as obtained from experimental data and theory (*a*) 25.0 °C —, experimental; 25.0 °C - - -, theoretical; (*b*) 0.0 °C —, experimental; - - -, theoretical; -·-·-, theoretical using extrapolated vapour pressure data.

Other density determinations at 25.0 °C for methanol–water have even fewer data points, 10 in ref. 27 and 12 in ref. 28. The data from refs. 26, 27, and 28 show very good agreement. The data from refs. 27 and 28 give (second degree) polynomial fits for V^{mix}, which are within 0.7% of each other while that from ref. 26 gives a V^{mix} about 3% lower in the whole composition range.

Examination of Free Energy Data

The free energy of mixing G^{mix} and G'' (see [4]) were obtained for the system at 0 °C from two different sources: the vapour pressure measurements made at 0.0 °C and data obtained by extrapolating data at 20, 40, 60, 80, and 100 °C as given in ref. 29. As can be seen in Table 5, the experimental data shows a slight negative deviation from Raoult's law at 0.0 °C, while the extrapolated data shows a slight positive deviation.

Separation of the total pressure into contributions from water, p_W, and methanol, p_M, was done by application of the Gibbs–Duhem relationship. An equation with five parameters

Can. J. Chem. Downloaded from www.nrcresearchpress.com by 210.87.254.6 on 09/05/12
For personal use only.

Can. J. Chem. Downloaded from www.nrcresearchpress.com by 210.87.254.6 on 09/05/12
For personal use only.

similar to the three-parameter equation of Christian (30) was used to fit the total pressure data. This method gave ratios p_M/p_W which were consistently about 3% lower than the ratios obtained from extrapolation of the data from ref. 29, where the activities (partial pressures) of methanol and water are given separately.

The quantity G'' (eq. 4) was then calculated by fitting $\ln(p_M/p_W)$ to a polynomial and setting, after ref. 7,

$$[11] \qquad G''(X_M) = \frac{\partial(RT \ln(p_M/p_W)}{\partial X_M}$$

The curve fitting for $\ln(p_M/p_W)$ was done without using the extreme X_M points in order to avoid the appearance of infinities.

For 25.0 °C, the partial pressure data from ref. 31 was used to obtain G''. The data extrapolated to obtain the 0.0 °C data (29) was used to obtain interpolated values of partial pressures at 25.0 °C in order to check the consistency of the data. The values of p_M from ref. 31 are consistently higher than the values interpolated from ref. 29, especially at lower values of X_M, when the difference is as great as 20%.

Examination of Diffusion Data

Free energy (*i.e.* vapour pressure) data must also be used if experimental mutual diffusion coefficients D are unavailable. Values of D can then be obtained from free energy data and values of self-diffusion coefficients D^*. The mutual diffusion coefficients were calculated assuming an expression similar to the Hartley–Crank relation (32, 33).

$$[12] \quad D(X_M) = \frac{d \ln p_M}{d \ln X_M} \cdot \frac{1}{\eta} \times \{(1 - X_M) D_M^{*\cdot} \eta_M^{\cdot} + X_M D_W^{*\cdot} \eta_W^{\cdot}\}$$

The values of the self-diffusion coefficients of pure methanol and pure water ($D_M^{*\cdot}$, $D_W^{*\cdot}$) were taken to be 2.48×10^{-5} (34) and 2.23×10^{-5} $cm^2\ s^{-1}$ (34) at 25 °C and 1.60×10^{-5} (34) and $1.05 \times 10^{-5}\ cm^2\ s^{-1}$ (35) at 0.0 °C respectively for methanol and water. Values of p_M and η were taken from polynomial fits of the previously presented data.

Such relationships often show poor agreement with experimental diffusion coefficients if the systems are not nearly ideal. The methanol–water system is however very close to ideal from the free energy point of view, as shown by the vapour pressure data. A calculation comparing values of D at 25.0 °C evaluated from [12], and from D_M^* and D_W^* values measured in the whole concentration range (36) show agreement to within 5% for $X_M < 0.6$. As $X_M \to 1$ there is more disagreement.

Discussion

The V'', G'', and D values obtained as described above were used to calculate α_{CF}/f^2 through [3]. Figure 6 shows the comparison between such calculated α_{CF}/f^2 curves and those obtained from ultrasonic absorption measurements. Two calculated curves are shown for 0.0 °C, one calculated on the basis of experimental vapour pressures, and the other on the basis of the extrapolated vapour pressures.

The third maximum (at $X_M \simeq 0.8$) in the calculated curves of α_{CF}/f^2 at 0.0 °C is an artifact due to the high degree of polynomial used to fit the density data. As pointed out previously, such a polynomial in powers of X_M is not meaningful for X_M approaching 1. The small difference between the two calculated 0 °C curves shows that much of the difference between the two sets of vapour pressure data in Table 5 (about 20%) does not affect the G'' (eq. 4) and the $d \ln p_M/d \ln X_M$ (eq. 12). Other types of inaccuracies in pressure and density data can, however, be magnified in carrying out the differentiation needed to obtain G'' and V''.

Inaccuracies also appear in the calculated α_{CF}/f^2 due to the assumptions inherent in the Romanov–Solovyev theory; *e.g.* the validity of hydrodynamic equations down to wavelengths as short as tens of Ångstroms, the presence of a Debye distribution of wave numbers for concentration fluctuations, the cut-off of wave numbers at $k_{max} = (N/V)^{1/3}$. Removal of such assumptions seem to involve numerous difficulties. There is also some uncertainty in the separation of α_{CF}/f^2 and α_S/f^2. However, the maximum ($X_M = 0.4$) α_{CF}/f^2 obtained from experiment at 0 °C would change (increase) only by about 20% if the example of previous analyses is followed and α_{CF}/f^2 equated to the α/f^2 in excess of a linear variation with X_M.

The calculations presented here would seem to be the most extensive for testing the concen-

Can. J. Chem. Downloaded from www.nrcresearchpress.com by 210.87.254.6 on 09/05/12
For personal use only.

tration and temperature dependence of this theory. It is unlikely that more accurate measured or calculated α_{CF}/f^2 data can be obtained for this or any system without gathering a great amount of precise density, vapour pressure, diffusion, and ultrasonic data. Thus removal of both experimental and theoretical inaccuracies involve considerable additional work.

Considering the above aspects, the agreement between the calculated and measured absorption can be said to be satisfactory. There is good qualitative and reasonable semiquantitative agreement. The smaller $(\alpha_{CF}/f^2)_{calcd}$ at 0 °C is only about half that of the measured, but the similarity in the shapes of the curves suggests an inaccuracy in the theory or the thermodynamic–dynamic data to be the cause, rather than the existence of another relaxation mechanism. Some of the differences in the two 25 °C curves may be due to the sparseness of the density data used. Thus there seems to be no need to postulate the existence of an additional absorption mechanism, *e.g.* the formations of specific, localized alcohol–water complexes. This does not mean that such complexes do not necessarily form, but only that if they form, then they are likely to contribute little to the ultrasonic absorption.

Light-scattering studies of methanol–water mixtures at 25.0 °C have been carried out (37). A comparison of the actual concentration scattering ratio with that for an ideal mixture shows more fluctuations in concentration in the real mixture than if it were ideal, *i.e.* a positive deviation from Raoult's law in agreement with pressure measurements. Anisotropic Rayleigh ratios indicate only small (if any) deviations from a random distribution of mutual orientations of adjacent molecules at high (=0.8) alcohol mole fractions. Thus there are no indications of specific complexes. The presence of any such complexes should presumably show up in ir studies, but no such studies seem to have been carried out for methanol–water.

The Rayleigh ratio in methanol–water increases monotonically with X_M (37) unlike the light scattering in *n*-propanol–water mixtures (18) which shows a double maximum (Fig. 4). The ultrasonic absorption peak corresponds to neither of the light scattering peaks. Ultrasonic absorption is due to volume differences, and light scattering is due to refractive index (polarization) differences. These two phenomena are thus not directly related, even though a relationship exists between changes in volume and in refractive index (38). The light scattering maxima in *n*-propanol–water suggest that molecular complexes may be formed in that system, but that this formation does not directly affect sound absorption.

Ultrasonic absorption in several water–alcohol systems has now been analysed assuming both the concentration-fluctuation theory and the presence of discrete relaxation times: *tert*-butyl alcohol (7, 4), *n*-propanol (12, 5, 9), ethanol (12, 8). No analysis of the methanol–water data has been attempted assuming discrete relaxations, as the work of Burton (2) suggested that there was no excess absorption. The data presented here do not have a sufficient frequency range to test the applicability of discrete relaxation theories to the frequency dependence. The concentration dependence in methanol–water fits into the trend set by the other alcohol–water systems, *i.e.* the absorption maximum is lower and occurs at a higher alcohol mole fraction as the size of the alcohol decreases. Thus it is most likely that the methanol–water data can be explained assuming discrete relaxations as adequately as the data for other alcohol–water systems.

As suggested by Blandamer (11) the two approaches may actually be describing the same phenomenon. The postulated specific alcohol–water or alcohol–alcohol complexes are themselves quite short-range, with a reciprocal distance beyond the k_{max} assumed for concentration fluctuations. The effect of the presence of such a complex may however stretch to longer distances and manifest itself as longer wavelength concentration fluctuations. The presence of complexes should in any case affect the values of V^{mix} and G^{mix} used in the concentration-fluctuation analysis. If the complexes in such systems are assumed to be very localized, and are treated as such, then any excess ultrasonic absorption due to their equilibria must be in addition to the absorption due to concentration fluctuation. In this case it seems invalid to assume the total excess absorption to be due to the discrete relaxations of these localized complexes.

A clearer picture of the structure and dynamics in alcohol–water (and in particular methanol–water) systems can be achieved by investigating

Can. J. Chem. Downloaded from www.nrcresearchpress.com by 210.87.254.6 on 09/05/12
For personal use only.

the following aspects: (*i*) Development of a theory for calculating the structural absorption α_S/f^2 in liquid mixtures. (*ii*) High frequency, hypersonic investigation of methanol–water to obtain the relaxation of α_{CF}/f^2, and to obtain α_S/f^2 experimentally. With data available in a wider frequency range, a test can be made of the frequency dependence as predicted by the Romanov–Solovyev theory and by theories assuming discrete relaxation times. (*iii*) Extension of high precision density and vapour pressure measurements both at 25 and 0 °C. (*iv*) Mutual diffusion measurements for the system at various temperatures to test self-diffusion – mutual diffusion relationships. Mutual-diffusion coefficients are available for methanol–water only at 15 °C (39). (*v*) Examination of the contributions from the enthalpy of mixing to ultrasonic absorption, although these should be negligible, especially in water-rich systems near 4 °C. (*vi*) Further examination of relationships between ultrasonic absorption, infrared absorption, light scattering intensities, thermodynamic, dynamic, and other data.

Conclusions

The existence of a double maximum in the ultrasonic absorption in alcohol–water systems is noted for the first time. This phenomenon is in agreement with predictions of the concentration-fluctuation theory. A separation of the excess absorption into contributions from "structural" and "concentration-fluctuation" effects has been carried out in a semiquantitative way. Such a separation has not been carried out in previous estimations of α_{CF}/f^2.

Density and vapour pressure data for the system methanol–water at 0.0 °C is presented. In the analysis of this and literature data for application of the concentration-fluctuation theory, an examination is made of the reasonableness of methods for obtaining partial pressures from total vapour pressure, and mutual-diffusion coefficients from self-diffusion data.

The agreement between experimental ultrasonic absorption and that calculated from the Romanov–Solovyev theory is reasonable. This indicates that long range concentration fluctuations most likely account for essentially all the absorption and that any localized intermolecular complexing is not likely to contribute to ultrasonic absorption in methanol–water to any degree.

Acknowledgments

The authors wish to thank Mr. I. D. Babcock and Mr. A. Troicuk for technical assistance; Dr. G. C. Benson for advice and standard density liquids; Dr. W. A. Adams and the Inland Waters Branch, Environment Canada, for use of their densitometer and calculator; and Dr. P. M. Laughton for use of his vapour pressure apparatus. The project was supported financially by the National Research Council of Canada.

1. I. G. MIKHAILOV and S. B. GOUREVITCH. C. R. (Dokl.) Acad. Sci. URSS, **52**, 673 (1946).
2. C. J. BURTON. J. Acoust. Soc. Am. **20**, 186 (1948).
3. J. THAMSEN. Acustica, **16**, 14 (1965).
4. M. J. BLANDAMER, D. E. CLARKE, N. J. HIDDEN, and M. C. R. SYMONS. Trans. Faraday Soc. **64**, 2691 (1968).
5. M. J. BLANDAMER, N. J. HIDDEN, M. C. R. SYMONS, and N. C. TRELOAR. Trans. Faraday Soc. **64**, 3242 (1968).
6. R. J. FANNING and P. KRUUS. Can. J. Chem. **48**, 2052 (1970).
7. P. KRUUS, L. K. KUDRYASHOVA, I. G. MIKHAILOV, and V. P. ROMANOV. Sov. Phys. Acoust. **19**, 82 (1973).
8. S. G. BRUUN, P. GRAAE SØRENSEN, and Aa. HVIDT. Acta Chem. Scand. Ser. A, **28**, 1047 (1974).
9. S. NISHIKAWA, M. MASHIMA, and T. YASUNAGA. Bull. Chem. Soc. Jpn. **48**, 661 (1975).
10. D. SETTE. Nuovo Cimento Ser. X **1**, 800 (1955) as quoted in ref. 10.
11. M. J. BLANDAMER. Water. A comprehensive treatise, Vol. 2. *Edited by* F. Franks. Plenum, New York. 1973.
12. V. P. ROMANOV and V. A. SOLOVYEV. Sov. Phys. Acoust. **11**, 68 (1965).
13. V. P. ROMANOV and V. A. SOLOVYEV. Water in biological systems. Vol. 2. *Edited by* M. F. Vuks and A. I. Sidorova. Consultants Bureau, New York. 1971.
14. J. H. ANDREAE, P. D. EDMONDS, and J. F. MCKELLAR. Acustica, **15**, 74 (1965).
15. W. A. ADAMS, R. YANK, R. O. CHRISTIE, and J. KRUUS. Can. J. Chem. Eng. **52**, 121 (1974).
16. K. F. HERZFELD and T. A. LITOVITZ. Absorption and dispersion of ultrasonic waves. Academic Press, New York. 1959.
17. G. C. BENSON and H. D. PFLUG. J. Chem. Eng. Data, **15**, 382 (1970).
18. M. F. VUKS and L. V. SHURUPOVA. Zh. Struk. Khim. **12**, 712 (1970).
19. I. G. MIKHAILOV and V. M. POLUNIN. Sov. Phys. Acoust. **18**, 236 (1972).
20. K. M. SWAMY, K. LAKSHMINARAYANA, J. S. MURTY, and P. S. SWAMY. Acustica, **27**, 23 (1972).
21. D. R. DICKSON and P. KRUUS. Can. J. Chem. **49**, 3107 (1971).
22. D. SETTE. Acustica, **5**, 195 (1955).

23. C. D. SINCLAIR and C. A. VINCENT. J. Chem. Soc. Faraday Trans. II, **70**, 1926 (1974).
24. V. A. ZHANTALI and M. M. KARAVAEV. Zh. Prikl. Khim. (Leningrad), **47**, 293 (1974).
25. F. FRANKS and G. J. G. IVES. Q. Rev. **20**, 1 (1966).
26. V. S. GRIFFITHS. J. Chem. Soc. I, 860 (1954).
27. G. CLIFFORD and J. A. CAMPBELL. J. Am. Chem. Soc. **73**, 5449 (1951).
28. S. Z. MIKHAIL and W. R. KIMEL. J. Chem. Eng. Data, **6**, 533 (1961).
29. T. KATAYAMA. Kagaku Kogaku, **26**, 490 (1962).
30. S. D. CHRISTIAN. J. Chem. Phys. **64**, 764 (1960).
31. J. A. V. BUTLER, D. W. THOMSON, and W. H. MACLENNAN. J. Chem. Soc. I, 674 (1933).
32. Y. OISHI, Y. KAMEI, and H. SUMIE. J. Chem. Phys. **61**, 2227 (1974).
33. R. K. GHAI and F. A. L. DULLIEN. J. Phys. Chem. **78**, 2283 (1974).
34. D. E. O'REILLY and E. M. PETERSON. J. Chem. Phys. **55**, 2155 (1971).
35. K. T. GILLEN, D. C. DOUGLASS, and M. J. R. HOCH. J. Chem. Phys. **57**, 5117 (1972).
36. E. G. TIBOR, G. INGELT, and P. FODOR-CSANYI. Magy. Kem. Foly. **79**, 20 (1973).
37. G. D. PARFITT and J. A. WOOD. Trans. Faraday Soc. **64**, 2081 (1968).
38. A. IKEGAMI. J. Polym. Sci. Part A, **2**, 907 (1964).
39. P. A. JOHNSON and A. L. BABB. Chem. Rev. **56**, 387 (1956).

Can. J. Chem. Downloaded from www.nrcresearchpress.com by 210.87.254.6 on 09/05/12
For personal use only.

Evidence for a second kind of trapped electron in some deuterated aqueous glasses at low temperatures. A pulse radiolysis study

GEORGE V. BUXTON,[1] HUGH A. GILLIS, AND NORMAN V. KLASSEN
Division of Physics, National Research Council of Canada, Ottawa, Canada K1A 0R6

Received July 21, 1975

GEORGE V. BUXTON, HUGH A. GILLIS, and NORMAN V. KLASSEN. Can. J. Chem. **54**, 367 (1976).

Several deuterated aqueous glasses have been pulse-irradiated at 76 K. In addition to the well known visible absorption band of e_t^-, a second intense infrared absorption band, with $\lambda_{max} > 3200$ nm, has been found in (*a*) 50% by volume ethylene glycol, (*b*) 9.5 *M* LiCl, and (*c*) 2.5 and 4 *M* $MgCl_2$ glasses. Electron scavengers decrease the intensities of both bands, but to different extents. An increase in temperature decreases the intensity of the infrared band, but not that of the visible band. These and other features lead us to conclude that the infrared band is due to shallowly trapped electrons which are distinctly different from trapped electrons which absorb in the visible region.

The decay of the infrared band extends over several orders of magnitude in time and, unlike that of the visible band, is independent of wavelength. In the two chloride glasses the decay of the infrared band is accompanied by emission ($\lambda_{max} \approx 410$ nm) and is probably due to a spur reaction between an electron and hydroxyl radical to form excited hydroxide ion. No emission is found in the ethylene glycol glass, but growth of the visible band matches the decay of the infrared band in this case.

By comparing the amount of Ag^0 produced in an ethylene glycol glass containing Ag^+ with the decrease in intensity of the infrared and visible bands, we obtain $\epsilon_{1400} = (5.7 \pm 0.8) \times 10^3$ M^{-1} cm^{-1}. From the shape of the infrared band, which is Lorentzian on the high energy side, we estimate $\lambda_{max} \approx 3600$ nm and $\epsilon_{max} \approx 4.9 \times 10^4$ M^{-1} cm^{-1}.

GEORGE V. BUXTON, HUGH A. GILLIS et NORMAN V. KLASSEN. Can. J. Chem. **54**, 367 (1976).

On a irradié, par pulsation à 76 K, plusieurs verres aqueux deutériés. En plus de la bande d'absorption visible bien connue de e_t^-, une deuxième bande d'absorption infrarouge intense avec $\lambda_{max} > 3200$ nm, a été trouvée dans des verres à (*a*) 50% par volume d'éthylène glycol, (*b*) 9.5 *M* LiCl et (*c*) $MgCl_2$ à 2.5 et 4 *M*. Des piégeurs d'électron diminuent l'intensité de chacune des bandes mais à des degrés différents. Une augmentation de la température diminue l'intensité de la bande infrarouge mais ne diminue pas celle de la bande visible. Ces caractéristiques ainsi que d'autres nous amènent à conclure que la bande infrarouge est due à des électrons piégés d'une façon superficielle qui sont différents d'une façon distincte des électrons piégés qui absorbent dans la région du visible.

La disparition de la bande infrarouge s'étend sur plusieurs ordres de grandeur dans le temps et contrairement à ce qui est observé pour la bande visible, cette disparition est indépendante de la longueur d'onde. Dans les deux verres de chlorure, la disparition de la bande infrarouge est accompagnée par une émission ($\lambda_{max} \approx 410$ nm) et est probablement due à une réaction dans une branche entre un électron et un radical hydroxyle pour former un ion hydroxyde excité. On ne trouve aucune émission dans le verre d'éthylène glycol mais la croissance de la bande visible correspond à la disparition de la bande infrarouge dans ce cas.

En comparant la quantité de Ag^0 produite dans un verre d'éthylène glycol contenant du Ag^+ avec la diminution d'intensité des bandes infrarouges et visibles, on obtient $\epsilon_{1400} = (5.7 \pm 0.8) \times 10^3$ M^{-1} cm^{-1}. A partir de la forme de la bande infrarouge, qui est du type de Lorentz sur le côté de l'énergie élevée, on estime que le $\lambda_{max} \approx 3600$ nm et $\epsilon_{max} \approx 4.9 \times 10^4$ M^{-1} cm^{-1}.

[Traduit par le journal]

Introduction

Extensive studies have been made in the last ten years of the trapped electron, e_t^-, in several low temperature (usually 77 K) aqueous glasses because, in these systems, e_t^- is stabilized and can

[1]This work was carried out while G.V.B. was a Visiting Research Officer at the National Research Council of Canada, June–September, 1974. Permanent address: University of Leeds, Cookridge Radiation Research Centre, Cookridge Hospital, Leeds LS16 6QB, England.

Can. J. Chem. Downloaded from www.nrcresearchpress.com by 210.87.254.42 on 09/05/12
For personal use only.

Can. J. Chem. Downloaded from www.nrcresearchpress.com by 210.87.254.42 on 09/05/12
For personal use only.

readily be studied using methods such as optical absorption and electron spin resonance spectroscopy (1, 2). In most cases e_t^- is characterized by a single, broad, and intense optical absorption band which is asymmetric because of a high energy tail, and which has λ_{max} in the range 500–600 nm depending on the particular matrix. An exceptional case is ethylene glycol – water glass which, at temperatures <30 K, is reported (3) to show a second band increasing in intensity between 1200 and 2000 nm.

More recently, pulse radiolysis studies of two low temperature aqueous glasses (12 *M* OH^- and 9.5 *M* LiCl) have revealed (4, 5) that the absorption band of e_t^- in the visible region at short times ($<10^{-6}$ s) is considerably broader than the corresponding band at long times. This broadening is due to an increased absorption on the long wavelength side of the band and is accompanied by a red shift in λ_{max} from 575 to 625–650 nm. As time elapses the absorption at $\lambda > 575$ nm decays while the absorption at $\lambda < 575$ nm remains constant, and this accounts for the narrower and blue shifted spectrum observed in γ-irradiation experiments (1). In the pulse radiolysis experiments on aqueous glasses, hitherto, no measurements have been reported at $\lambda >$ 1100 nm.

In the pulse radiolysis experiments reported here we have extended the spectral measurements to include the infrared region out to 3200 nm by using D_2O as the solvent. We have investigated twelve different systems, and in three cases, namely ethylene glycol – water (50:50 by volume), 9.5 *M* LiCl, and 2.5 or 4 *M* $MgCl_2$, we have observed a second absorption band, which increases with wavelength in this region, and which we attribute to a trapped electron. A preliminary report of our findings has been given elsewhere (6)

Experimental

All samples were prepared in D_2O (99.7 atom% D, from Merck, Sharp and Dohme) which was used as received. Solutes were analytical reagent grade and were also used without further purification. The water of crystallisation in $MgCl_2.6H_2O$ and $Mg(CH_3COO_2).4H_2O$ was converted to >98 atom% D by several cycles of addition of D_2O to a 2.5 *M* solution followed by evaporation to the original concentration.

Samples were generally irradiated in high-purity quartz cells of optical path 0.025, 0.2, 0.5, or 1 cm with 40 ns pulses of 35 MeV electrons. The dose per pulse was usually in the range 4–9 krad. Each sample was pulsed many times without noticing any effect due to total accumulated dose. All spectra were corrected for weak absorptions found on irradiating empty cells at 76 K. The cells were supported in a Dewar equipped with optical windows. The Dewar was either filled with liquid N_2, or cold N_2 gas was flowed through it, depending on the temperature required. Temperature was measured with a copper–constantan thermocouple.

The dose per pulse was monitored with a secondary emission monitor which was calibrated for each experiment by using aqueous 5 m*M* KSCN solution saturated with O_2. Differences in electron density between the glass samples and the dosimeter solution were corrected for. The densities of the corresponding solutions were measured at room temperature, and their volume contraction on cooling to liquid N_2 temperature (never more than 7%) was measured with a simple dilatometric device. Absorbance per unit energy absorbed is expressed as $G\epsilon$ where G is the number of e_t^-, etc., produced per 100 eV and ϵ is the decadic molar extinction coefficient in units of M^{-1} cm^{-1}.

The analysing light intensity was simultaneously monitored at two wavelengths, one of which was fixed as the reference, usually at 650 nm, while the other was varied. In the majority of the experiments the following light detectors were used: for $\lambda < 450$ nm a Philips XP-1003 photomultiplier; for 450 nm $\leq \lambda \leq$ 1000 nm an EG&G SHS-100 silicon photodiode; and for $\lambda > 900$ nm a Barnes A-100 room temperature InAs photodiode. The 0–98% response time of the oscilloscope–detector system was <50 ns for the first two detectors, and <80 ns for the last one (7*c*). In a few experiments a Philco-Ford L-4521 germanium photodiode was used for 900 nm $< \lambda <$ 1400 nm. The time response of this detector is complicated (7), with one fast (ns) and one slow (μs) component. The 0–98% response time of the fast component is 10 ns. Kinetic measurements were made only for the first 200 ns with this detector, to keep errors due to this two-component behaviour to a minimum.

Other details of the pulse radiolysis apparatus have been described elsewhere (8).

Results

(1) Spectrum of e_t^- at 76 K

The spectrum of e_t^- was measured at 76 K at the end of a 40 ns pulse in pure ethylene glycol and in the following D_2O glasses: 50% by volume ethylene glycol (EG/D_2O), 9.5 *M* LiCl, 2.5 *M* and 4 *M* $MgCl_2$, 4 *m* $Mg(ClO_4)_2$, 4 *m* $Mg(CH_3CO_2)_2$, 4 *M* $CaCl_2$, 8 *M* $NaClO_4$, 7 *M* HCOONa, 7 *M* NaOD, 10 *M* KOD, 5 *M* K_2CO_3.

In the first three glasses the spectrum consisted of a band in the visible with λ_{max} at about 650 nm, and a band in the infrared which increased in intensity out to the limit of detectability, which was 1900, 2400, and 3200 nm for the EG/D_2O, LiCl, and $MgCl_2$ glasses, respectively. The spectra are shown in Fig. 1. The intensity of the infrared band relative to the absorption at

TABLE 1. Spectral details and yields of e_t^- which absorb in the visible region in D_2O glasses at 76 K[a]

Glass	(λ_{max} ± 20) (nm)	($\lambda_{1/2}$ ± 20) (nm)	$W_{1/2}$ (eV)	$10^{-4}G\epsilon_{max}$
50/50 v/v EG/D_2O	650	470;870	1.2	3.0 ±0.2
Pure EG	550	—;760	—	2.7 ±0.5
9.5 *M* LiCl	640	480;880	1.2	2.8 ±0.1
2.5 *M* $MgCl_2$	650	480;875	1.2	1.2 ±0.1
4 *M* $CaCl_2$	650	460;890	1.3	3.6 ±0.2
4 *m* $Mg(ClO_4)_2$	575	430;710	1.0	3.6 ±0.1
4 *m* $Mg(CH_3CO_2)_2$	600	—;870	—	0.22±0.02
8 *M* $NaClO_4$	575	450;715	1.0	3.9 ±0.3
7 *M* NaO_2CH	575	445;745	1.1	1.10±0.03
7 *M* NaOD	600	455;825	1.2	5.4 ±0.3
10 *M* KOD	630	455;780	1.1	6.5 ±0.4
5 *M* K_2CO_3	575	450;680	1.0	5.6 ±0.2

[a]Measured at the end of a 40 ns pulse and corrected for contribution from the infrared band where necessary.

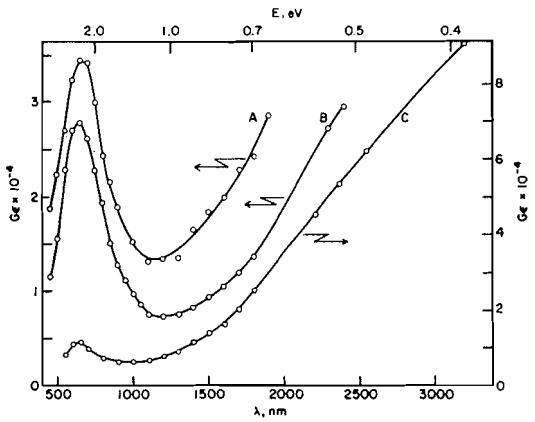

FIG. 1. Absorption spectra observed at 76 K and 100 ns after the start of a 40 ns pulse in 50/50 v/v EG/D_2O glass (*A*), 9.5 *M* LiCl glass (*B*), and 2.5 or 4.0 *M* $MgCl_2$ glass (*C*). Spectrum *A* has been displaced upwards by 0.5 unit.

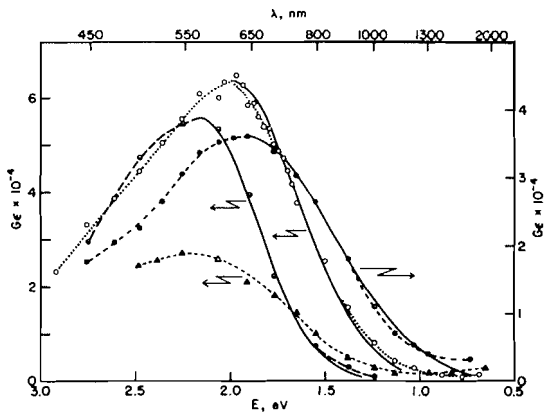

FIG. 2. Absorption spectra observed at 76 K and 100 ns after the start of a 40 ns pulse in 10 *M* KOD glass (○), pure ethylene glycol glass (△), 4 *M* $CaCl_2$ glass (●), and 5 *M* K_2CO_3 glass (◒). The full lines are Gaussian curves fitted to the spectra for $\lambda \geq \lambda_{max}$.

650 nm was independent of the dose per pulse. For example, in the case of 2.5 *M* $MgCl_2$ glass the ratio of the optical densities at 2360 and 650 nm was the same for a 5 krad pulse and a 0.5 krad pulse. In all the glasses other than EG/D_2O, LiCl, and $MgCl_2$, the infrared band was absent or a very minor feature (see examples in Fig. 2). The yields and spectral features of the visible band are summarized in Table 1, and it is clear from these that there are substantial differences in the position, width, and intensity of this band from one glass to another. Most of the variation in bandwidth occurs at $\lambda > \lambda_{max}$. We found no evidence of any fine structure in the visible band of e_t^- in these glasses.

(2) Decay of e_t^- at 76 K

(a) Visible Band

In all cases the absorption at $\lambda > 600$ nm decreased with time, and the fractional decay in a given time increased with λ. This loss of absorption at long wavelengths accounts for the generally narrower and blue shifted spectra observed in γ-radiolysis studies. Figure 3 shows that the decays were approximately proportional to log (time).

In most of the glasses the absorption at $\lambda <$ 550 nm did not change with time over the observation period of 100 μs. Exceptions were (*i*) EG/D_2O where a growth of absorption occurred over about 75 μs, the maximum in-

Can. J. Chem. Downloaded from www.nrcresearchpress.com by 210.87.254.42 on 09/05/12
For personal use only.

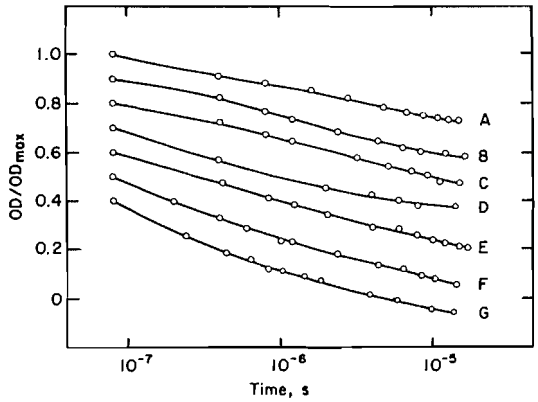

FIG. 3. Decay of absorption at 900 nm at 76 K in the following glasses: 10 *M* KOD (*A*), 2.5 *M* $MgCl_2$ (*B*), 9.5 *M* LiCl (*C*), 7 *M* NaOD (*D*), 4 *M* $CaCl_2$ (*E*), 7 *M* HCO_2Na (*F*), and 5 *M* K_2CO_3 (*G*). The ordinate axis is numbered for curve *A*. Subsequent curves are dropped in steps of 0.1 units for a better display.

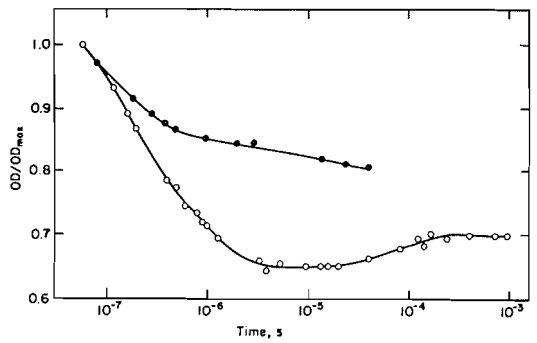

FIG. 4. Decay of absorption at 650 nm in 2.5 *M* $MgCl_2$ glass at 76 K (○); and 107 K (●). The ordinate is the ratio of the optical density at time *t* to the maximum optical density after a 40 ns pulse.

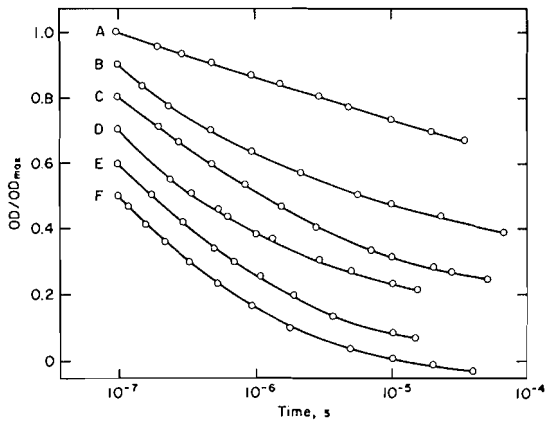

FIG. 5. Effect of CrO_4^{2-} on the decay of the infrared band in glasses at 76 K. 2.5 *M* $MgCl_2$ (*A*), 2.5 *M* $MgCl_2$ containing 4.4 m*M* CrO_4^{2-} (*E*), EG/D_2O (*B*), EG/D_2O containing 5 m*M* CrO_4^{2-} (*D*), 9.5 *M* LiCl (*C*), and 9.5 *M* LiCl containing 5 m*M* CrO_4^{2-} (*F*). The ordinate axis is numbered for curve *A*. Subsequent curves are dropped in steps of 0.1 units for a better display.

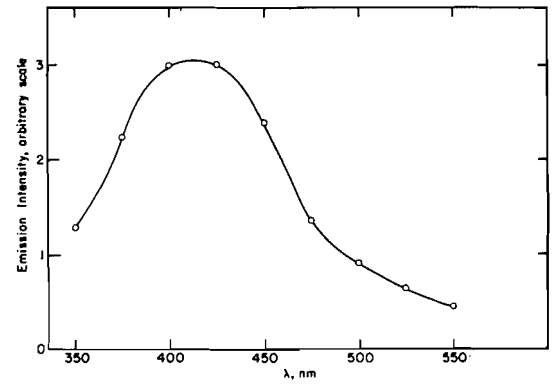

FIG. 6. Spectrum of emission observed at 76 K and 80 ns after the start of a 40 ns pulse in 9.5 *M* LiCl glass. The spectrum has been corrected for the wavelength discrimination of the optical system.

crease (25%) being observed at 550 nm; (*ii*) 8 *M* $NaClO_4$ where a similar, but much smaller, growth was observed, the maximum increase (5%) occurring at 500 nm; (*iii*) pure ethylene glycol where 2.5% growth at the λ_{max} (550 nm) between 80 and 120 ns was followed by decay; and (*iv*) $MgCl_2$, where, at 650 nm, the absorption first decayed by ~35% in 10 μs and then increased by ~10% in the next 100 μs (see Fig. 4).

(b) Infrared Band

In contrast to that of the visible band, the decay of this band was independent of λ for $\lambda > 1400$ nm. The band decayed at different rates in the three glasses where it was observed, and the decay extended over several orders of magnitude in time. Examples of these decays are shown in Fig. 5. In the EG/D_2O glass the rate of decay of the infrared band was similar to the rate of growth of the visible band.

(3) Light Emission

Light emission which persisted after the pulse was observed in LiCl and $MgCl_2$ glasses. Emission spectra were corrected for wavelength variations in the efficiency of the light gathering, analyzing, and detecting systems. The spectrum of this emission was the same for both glasses and is shown in Fig. 6. The reciprocal of the emission intensity was approximately linear in time. In

Can. J. Chem. Downloaded from www.nrcresearchpress.com by 210.87.254.42 on 09/05/12
For personal use only.

TABLE 2. Effect of electron scavengers on the initial yields of trapped electrons (visible and infrared absorbing) in EG/D_2O, LiCl, and $MgCl_2$ glasses at 76 K

[Scavenger]	$\frac{G}{G_0}$ (±10%, 650 nm)[a]	$\frac{G}{G_0}$ (±10%, 1400 or 1800 nm)[a,b]	$\frac{G/G_0 \text{ (infrared)}}{G/G_0 \text{ (650 nm)}}$	r (nm)[c]
		50/50 v/v EG/D_2O		
0.005 *M* CrO_4^{2-}	1.0	0.71[d]	0.71	3.0 (1.8)[e]
0.04 *M* $(CH_3)_2CO$	0.72	0.54[d]	0.75	1.4
0.01 *M* Ag^+	1.06	0.87	0.82	2.0 (0.6)[e]
0.02 *M* Ag^+	0.88	0.82	0.93	1.2
0.03 *M* Ag^+	0.87	0.71	0.82	1.4
		9.5 *M* LiCl		
0.0024 *M* CrO_4^{2-}	0.81	0.51[d]	0.63	4.1 (1.7)[f]
0.0052 *M* CrO_4^{2-}	0.61	0.30[d]	0.49	3.8
0.02 *M* $(CH_3)_2CO$	0.74	0.37[d]	0.50	2.4 (0.6)[f]
0.2 *M* HCl	0.97	1.07[d]	1.10	—(0.7)[f]
0.8 *M* HCl	0.91	0.92[d]	1.01	—
		2.5 *M* $MgCl_2$		
0.002 *M* CrO_4^{2-}	0.97	0.65	0.67	4.3
0.0044 *M* CrO_4^{2-}	0.90	0.46	0.51	3.9
0.0066 *M* CrO_4^{2-}	0.76	0.32	0.42	3.7
0.02 *M* $(CH_3)_2CO$	0.63	0.34	0.54	2.3
0.2 *M* HCl	1.06	1.22	1.15	—

[a]Yields were obtained by extrapolation back to the middle of the 40 ns pulse or the 20 ns pulse (used with Ag^+ only).
[b]Measured at 1400 nm with a Ge photodiode unless otherwise indicated.
[c]r is calculated to be the maximum separation between infrared absorbing trapped electrons and scavenger molecules which form encounter pairs (see Discussion sect. 4*a*). The values of r in parentheses were determined by others for the visible absorbing trapped electrons.
[d]Measured at 1800 nm with an InAs photodiode. The extrapolation to mid-pulse is less accurate than the extrapolation of data measured with a Ge photodiode.
[e]G. V. Buxton and K. G. Kemsley, unpublished results.
[f]Reference 33.

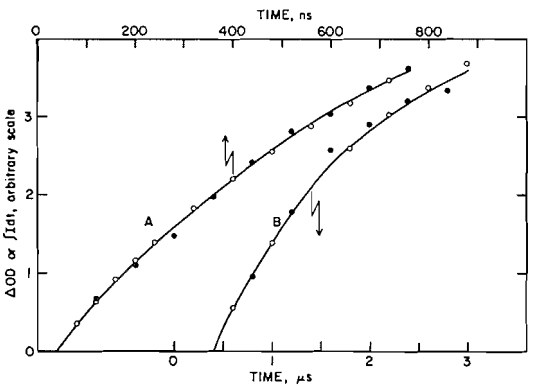

FIG. 7. Comparison of the change with time in: infrared absorption, —ΔOD (●), measured at 2350 nm, and integrated emission intensity, $\int I dt$ (○), measured at 425 nm after a 40 ns pulse in 2.5 *M* $MgCl_2$ glass at 76 K (*A*), and 102 K (*B*).

Fig. 7 the change in optical density in the infrared band over a given period of time is compared to the integrated intensity of emitted light over the same period of time. The change in optical density and $\int I dt$ are seen to correspond closely to each other after normalization of the ordinate scales. This correspondence was found to hold for both LiCl and $MgCl_2$ glasses regardless of temperature. It is to be noted that in Fig. 7 the curve for 76 K refers to an initial part of the decay, and the curve for 102 K refers to a later part. No post-pulse emission was detected at temperatures where the infrared band was absent. No estimates of absolute emission intensities were made because of the variable degree of cracking in the samples which markedly affected the collection efficiency of the optical system.

No post-pulse emission was observed in any of the other glasses. Emission was evident during the pulse but we were unable to distinguish this from normal Cerenkov emission.

The further investigations reported below were confined to the EG/D_2O, LiCl, and $MgCl_2$ glasses.

(4) Effect of Electron Scavengers at 76 K

(a) On the Yields of e_t^-

Addition of acetone or CrO_4^{2-} to each of the glasses decreased the initial intensities of both the visible and infrared bands but the fractional decrease in the latter was always greater. The yields, shown in Table 2, were corrected by ex-

Can. J. Chem. Downloaded from www.nrcresearchpress.com by 210.87.254.42 on 09/05/12
For personal use only.

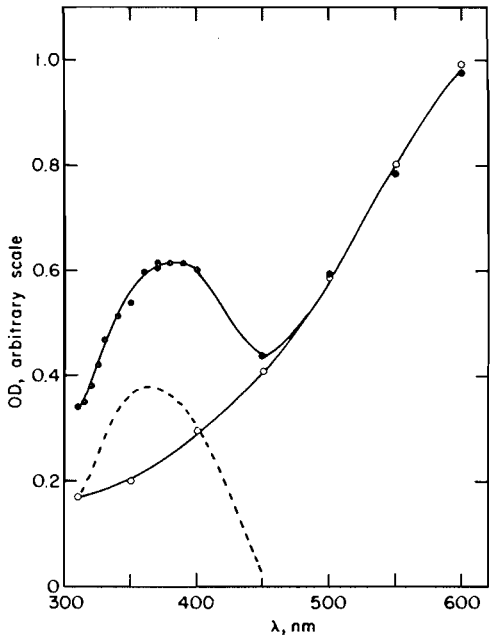

FIG. 8. Spectra observed at 76 K and 100 ns after the start of a 40 ns pulse: in EG/D_2O glass (○), in EG/D_2O glass containing 1.7×10^{-2} *M* Ag^+; (●), and their difference (- - -). The spectra indicated by ○ and ● were normalized to each other in the wavelength range 500–600 nm.

trapolating back to the middle of the pulse. This correction was large when the InAs detector was used, because the earliest measurements were made 100 ns after the start of the pulse. Smaller corrections were necessary when using a Ge photodiode and a 20 ns pulse in which case the first measurements were made 30 ns after the start of the pulse. Table 2 shows that, in contrast to the effect of acetone and CrO_4^{2-}, the addition of HCl to LiCl and $MgCl_2$ glasses scarcely affected the intensities of either the visible or infrared bands.

When Ag^+ was present in an EG/D_2O glass a new absorption band with $\lambda_{max} = 370$ nm (see Fig. 8) was observed, as well as the decrease in intensity of the visible and infrared bands. This new band did not grow after the pulse. We assign it to Ag^0 because of its similarity to the band ($\lambda_{max} = 360$ nm) attributed to Ag^0 formed in aqueous solutions by the reaction (9, 10)

[1] $$Ag^+ + e_{aq}^- \rightarrow Ag^0$$

This reaction provides an opportunity for estimating the extinction coefficient of the infrared-absorbing electron by comparing the decrease in electron absorption to the increase in the 370 nm band. However, we could not find a value for $\epsilon(Ag^0)$ in the literature, and so measured it ourselves in the following manner. The decay of e_{aq}^- and the growth of Ag^0 were followed at 715 and 360 nm, respectively, in an aqueous solution of 10^{-4} *M* $AgClO_4$ and 0.1 *M* *tert*-BuOH at early times following a 20 ns pulse. We found $k_1 = 3.6 \times 10^{10}\ M^{-1}\ s^{-1}$, in agreement with earlier work (9). The growth of Ag^0 was equated to the decay of e_{aq}^- with small corrections made for the loss of Ag^0 via $Ag^0 + Ag^+ \rightarrow Ag_2^+$ (9, 10) the decay of e_{aq}^- by reactions other than [1] and the absorption at 360 nm due to e_{aq}^-. We took $\epsilon_{715}(e_{aq}^-) = 1.8 \times 10^4\ M^{-1}\ cm^{-1}$ and calculated that $\epsilon_{360}(Ag^0) = (1.9 \pm 0.3) \times 10^4\ M^{-1}\ cm^{-1}$ in aqueous solution at room temperature.

For EG/D_2O glasses containing 0, 0.01, 0.02, and 0.03 *M* $AgClO_4$ the absorbance at 360, 650, and 1400 nm was measured following a 20 ns pulse and extrapolated to mid-pulse. The infrared absorbance was monitored at 1400 nm, rather than at longer wavelengths where absorbance was greater, in order to use the Ge photodiode rather than the slower InAs detector. The formation of Ag^0 was equated to the reduction in the yield of trapped electrons compared to their yield in the absence of Ag^+. A value of $2 \times 10^4\ M^{-1}\ cm^{-1}$ was taken for $\epsilon_{650}(e_t^-)$ which is the value obtained by Hase and Kevan (11) for a 10 *M* OH^- glass. For Ag^0 ϵ_{max} ($\lambda_{max} = 370$ nm) was taken to be $(1.9 \pm 0.3) \times 10^4\ M^{-1}\ cm^{-1}$ as determined for aqueous solutions. For the glasses containing 0.01, 0.02, and 0.03 *M* $AgClO_4$ we calculate $\epsilon_{1400} = 5.7 \times 10^3$, 5.5×10^3, and $5.9 \times 10^3\ M^{-1}\ cm^{-1}$ respectively for an average $\epsilon_{1400} = (5.7 \pm 0.8) \times 10^3\ M^{-1}\ cm^{-1}$. There is no evidence that, at the concentrations used, Ag^+ scavenged any electrons which would not otherwise have been trapped by the matrix.

(b) On the Decay of e_t^-

Table 3 shows the fraction of e_t^- which decayed in the time intervals 0.1–1 and 0.1–10 μs after the beginning of a 40 ns pulse in the presence and absence of electron scavengers. In the ethylene glycol – water glass the scavengers eliminate the growth at 650 nm and do not significantly increase the decay rate of the infrared band. In the LiCl glass the scavengers increase the decay rate at 650 nm and again do not significantly affect the decay rate of the infrared

Can. J. Chem. Downloaded from www.nrcresearchpress.com by 210.87.254.42 on 09/05/12
For personal use only.

Can. J. Chem. Downloaded from www.nrcresearchpress.com by 210.87.254.42 on 09/05/12
For personal use only.

TABLE 3. Effect of scavengers on the decay of e_t^- in EG/D_2O, LiCl, and $MgCl_2$ glasses at 76 K

	Fractional decay[a]			
	650 nm		Infrared band	
[Scavenger]	0.1–1 μs	0.1–10 μs	0.1–1 μs	0.1–10 μs
	50/50 v/v EG/D_2O			
None	0.08[b]	0.10[b]	0.41	0.64
0.005 *M* CrO_4^{2-}	0	0	0.47	0.70
0.04 *M* $(CH_3)_2CO$	0	0	0.48	0.68
0.017 *M* Ag^+	0	0	0.38	0.65
0.056 *M* Ag^+	0	0	0.47	0.72
	9.5 *M* LiCl			
None	0	0	0.43	0.73
0.0024 *M* CrO_4^{2-}	0.28	0.41	0.47	0.77
0.0052 *M* CrO_4^{2-}	0.33	0.52	0.52	0.74
0.02 *M* $(CH_3)_2CO$	0.33	0.47	0.57	0.81
0.1 *M* HCl	0.02	0.04	0.41	0.69
0.2 *M* HCl	0.09	0.16	0.41	0.68
0.8 *M* HCl	0.23	0.38	0.46	0.71
	2.5 *M* $MgCl_2$			
None	0.29[c]	0.36	0.20	0.40
0.002 *M* CrO_4^{2-}	0.44	0.63	0.44	0.72
0.0044 *M* CrO_4^{2-}	0.51	0.70	0.50	0.77
0.0066 *M* CrO_4^{2-}	0.59	0.75	0.60	0.84
0.02 *M* $(CH_3)_2CO$	0.42	0.64	0.49	0.73
0.2 *M* HCl	0.23	0.46	0.14	0.37

[a]Time = 0 refers to the beginning of a 40 ns pulse.
[b]Growth observed in this case.
[c]See Fig. 4.

band. In the $MgCl_2$ glass the scavengers increase the decay rate of both the visible and infrared bands. The decay rate of the infrared band in the pure $MgCl_2$ glass is somewhat less than that for the other two glasses without scavengers.

(c) On the Decay of the Post-pulse Emission

In both 9.5 *M* LiCl and 2.5 *M* $MgCl_2$ glasses post-pulse emission was observed in the presence of electron scavengers, and its decay correlated well with that of the infrared band. This is perhaps not surprising in the LiCl case because scavengers scarcely affect the decay of the infrared band, but it is significant in the $MgCl_2$ case where appreciable enhancement of the decay is evident (see Table 3). Furthermore, when 1 *M* acetone was present in the $MgCl_2$ glass the infrared absorption band and the post-pulse emission were both eliminated.

(5) Effect of Temperature in the Absence of Electron Scavengers

The effect of increasing the temperature of the glass up to 133 K on the intensities of the visible and infrared absorption bands is illustrated in Fig. 9. This figure shows that the infrared band steadily decreases in intensity while the visible band remains practically constant up to 120 K and then increases. For the LiCl glass, part of the

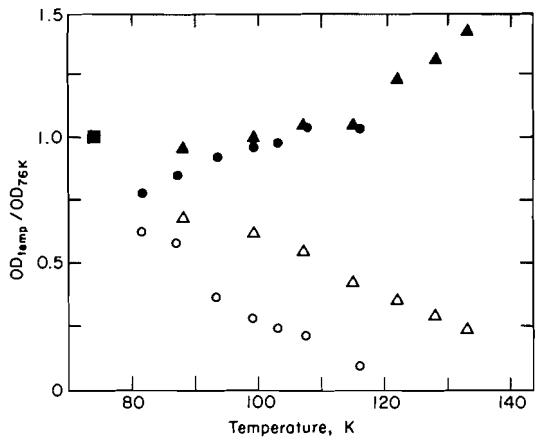

FIG. 9. Effect of temperature on the relative initial intensities of the visible and infrared bands: LiCl, 2360 nm (○); LiCl, 650 nm (●); $MgCl_2$, 2360 nm (△); $MgCl_2$, 650 nm (▲); and one point common to all (■).

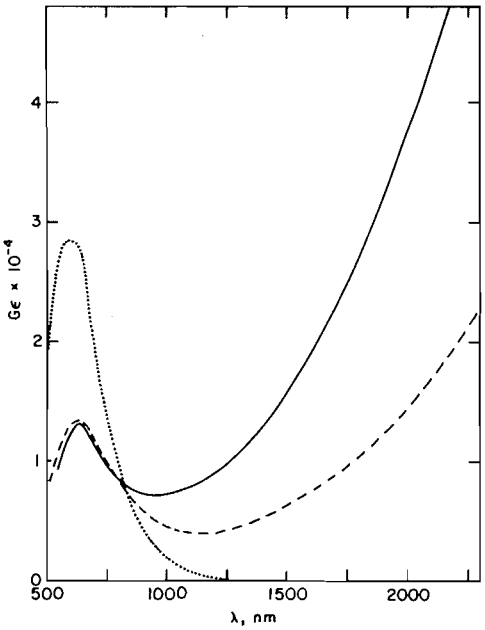

FIG. 10. Absorption spectra observed at 100 ns after the start of a 40 ns pulse in 2.5 *M* $MgCl_2$ glass at 76 K (—); 118 K (- - -); and 167 K (· · ·).

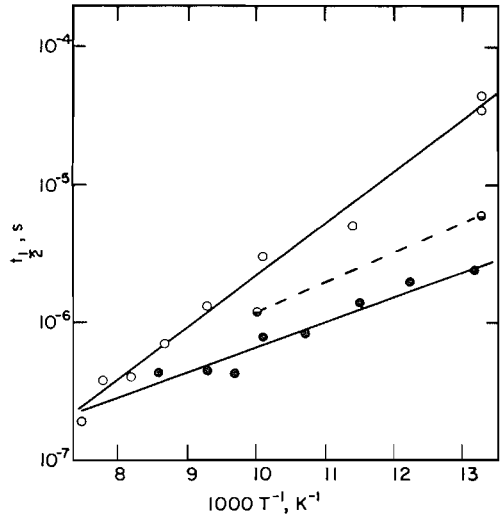

FIG. 11. Effect of temperature on the first observable half life, $t_{1/2}$, of the infrared absorption band in 2.5 *M* $MgCl_2$ glass (○); 50/50 v/v EG/D_2O glass (◒); and 9.5 *M* LiCl glass (●).

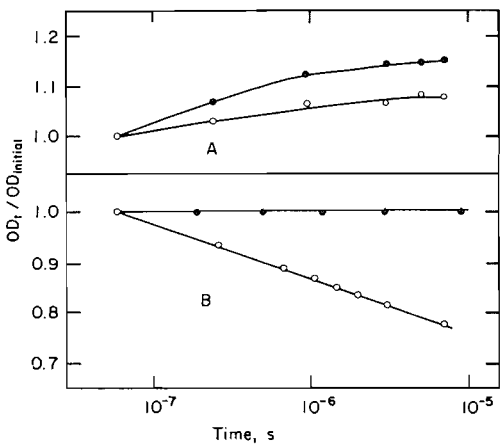

FIG. 12. (*A*) Growth of absorption at 650 nm in 50/50 v/v EG/D_2O glass at 76 K (●) and 100 K (○). (*B*) Decay of absorption at 650 nm in 9.5 *M* LiCl glass at 76 K (●) and 116 K (○).

decrease in intensity in the infrared band is due to the faster decay at higher temperatures (see Fig. 11) which results in more decay before our first observation at ~100 ns. However, in $MgCl_2$ glass this effect was negligible up to 114 K. We found no changes in either the positions or the shapes of the bands up to 133 K, but at higher temperatures where the infrared band was absent, the maximum of the visible band moved to a shorter wavelength and the intensity of the band increased. These changes are exemplified in Fig. 10 for the $MgCl_2$ system, and similar effects have been seen previously in the LiCl system (5).

The rate of decay of the infrared band increased with temperature in all three glasses but the kinetics remained complex. Figure 11 shows that a plot of log (first observable half life) against T^{-1} is linear for the LiCl and $MgCl_2$ glasses, giving apparent activation energies for the decays of 3.6 and 7.5 kJ mol^{-1} K^{-1} respectively. We have not obtained sufficient data to estimate an activation energy for the EG/D_2O glass, but it is probably similar to the LiCl value. We have not investigated in detail the effect of temperature on the visible band, but at 650 nm at higher temperatures the decay rate is increased in the LiCl glass and retarded in the $MgCl_2$ glass, while the growth in the ethylene glycol – water glass is diminished. Exemplary data are shown in Figs. 4 and 12.

(6) Cl_2^- Yields

We found a peak at 350 nm in the LiCl and $MgCl_2$ glasses, and measured $G\epsilon$ as 4×10^4 and 2×10^4, respectively. This is probably due to Cl_2^-; λ_{max} for Cl_2^- in aqueous solution at room temperature is 340 nm (12). However there could be a contribution from $ClOH^-$, which has a λ_{max}

Can. J. Chem. Downloaded from www.nrcresearchpress.com by 210.87.254.42 on 09/05/12
For personal use only.

Can. J. Chem. Downloaded from www.nrcresearchpress.com by 210.87.254.42 on 09/05/12
For personal use only.

at 350 nm in aqueous solution at room temperature (12). We found no decay of the 350 nm peak over our period of observation of 800 μs.

Discussion

(1) Spectrum of e_t^-

The most striking feature of the data is the large infrared band produced in the EG/D_2O, LiCl, and $MgCl_2$ glasses, and the effect of electron scavengers on its intensity (Table 2) and on its rate of decay (Table 3). These data clearly indicate that this band is associated with trapped electrons. A possibility which must be considered is that the band is due to the dielectron, that is, two electrons in the same trap. An analogous species is quite well known in alkali halide crystals as the F′ centre (13). The absorption spectrum of the dielectron has been reported in γ-irradiated 10 *M* NaOH glass at 75 K as being a very broad band in the near infrared with a maximum around 1000 nm (14). We consider that the infrared band observed in the present work is not due to the dielectron for the following reasons: (*a*) the maximum of the band which we observe is at a much longer wavelength than 1000 nm; (*b*) our measurements were made typically with 5 krad pulses, whereas in ref. 14 absorption attributed to the dielectron was observed only for doses greater than 10 Mrad; (*c*) we find that the absorbance per krad at 2360 nm in 2.5 *M* $MgCl_2$ glass is the same for 5 and 0.5 krad pulses; (*d*) we found no growth in the visible band as the infrared band decayed in the LiCl glass. A growth would be expected if the dielectron were decaying to e_t^-.

It is evident from the different effects of electron scavengers (Table 2) and temperature (Figs. 9 and 10), and from the different rates of decay in the visible and in the infrared, that there must be two distinct kinds of trapped electrons giving rise to the visible and infrared bands. The different behaviour of the two bands enables us to resolve them. We subtracted the spectrum at 118 K for the $MgCl_2$ glass from that obtained at 76 K (see Fig. 10) to obtain the resolved infrared band shown in Fig. 13. This procedure should be valid because the visible band seems to be independent of temperature in both shape and magnitude between 76 and 118 K. As far as we can tell, the infrared band has the same position

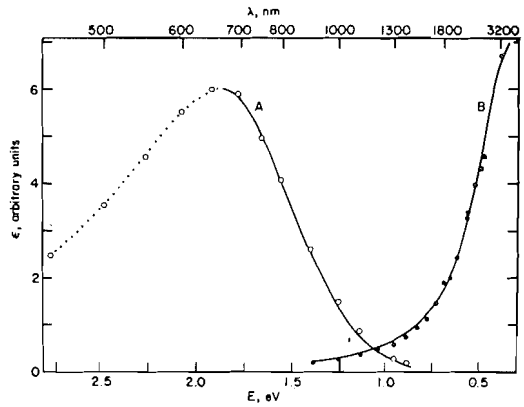

FIG. 13. Resolved visible and infrared absorption bands of the spectra shown in Fig. 1. The data shown are for 50/50 v/v EG/D_2O glass (*A*) and for 2.5 *M* and 4 *M* $MgCl_2$ glasses (*B*). The full lines are Gaussian (*A*) and Lorentzian (*B*) curves fitted to experimental points.

and shape for the EG/D_2O, LiCl, and $MgCl_2$ glasses, and when subtracted from the total spectrum, leaves a visible band with the same λ_{max} and shape for these three glasses. The visible band shown in Fig. 13 is for the EG/D_2O glass, where we have the best data. The visible band maximum is not the same in all aqueous glasses, as Table 1 and Fig. 2 clearly show, but there is no evident dependence of the maximum on the cation or anion of the salt, so it seems likely that the trapping sites are "water-walled", as suggested previously (15).

(2) Band Shapes

(a) Visible Band

The long wavelength edge of the resolved visible band in Fig. 13 has a Gaussian shape, which probably reflects a statistical variation of the environment of the trapped electron. If we assume this is the edge of a symmetrical band with λ_{max} at 650 nm, there is a second component to the visible band which gives rise to a high energy tail. This is shown in Fig. 14 for the EG/D_2O glass. The onset of this tail coincides with the increase in photoconductivity which has been observed in this glass (16), and furthermore, the fractional absorption due to this component correlates quite well with the quantum efficiency for recombination luminescence (16) (see Fig. 14). These observations are consistent with the visible band in EG/D_2O glass comprising a number of bound–bound transitions giving rise to the Gaussian component, and

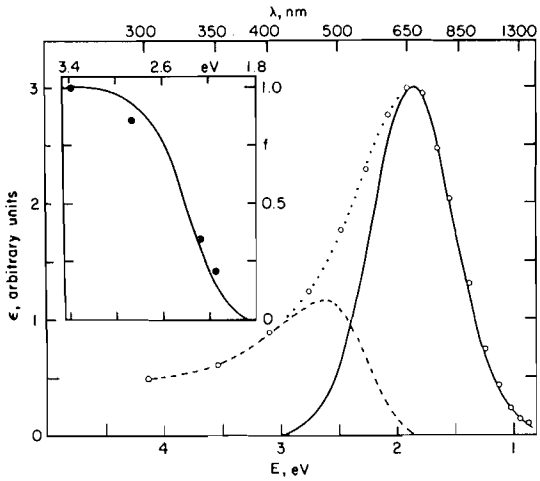

FIG. 14. Resolution of the visible absorption band in 50/50 v/v EG/D_2O glass at 76 K (○) into a low energy Gaussian band (—) and a high energy component (- - -). Inset: Comparison of the fractional contribution f, of the high energy component to the total absorption (—) with the relative quantum efficiency of photostimulated recombination luminescence (●) in the corresponding H_2O water glass containing 2.5 mM tryptophan (data from ref. 16).

bound–free transitions in which the electron is excited to levels in the continuum.

The visible bands in all the other glasses investigated here are also Gaussian in shape for $\lambda > \lambda_{max}$. This might suggest that in all cases the long wavelength edge is due to bound–bound transitions, with a contribution from bound–free transitions giving rise to the high-energy tail. This suggestion is in accord with the conclusion of Shida *et al.* (17), based on a hydrogenic model for absorption spectra of electrons in amorphous solids, that in aqueous solids most of the absorption in the visible band should be due to a bound–bound transition. In contrast to this generalization, in 10 M NaOH glass the efficiency for photocurrent production matches the absorption band, and this has been taken to mean that only bound–free transitions occur in this glass (18). We conclude that our resolution of the visible absorption band in EG/D_2O glass into a Gaussian bound–bound component and a bound–free component at higher energies may not be applicable to all aqueous glasses.

(b) Infrared Band

The resolved infrared band (Fig. 13) closely fits a Lorentzian function on the high energy side, and although we have not been able to make measurements beyond 3200 nm, the parameters of the function predict λ_{max} to be at 3600 nm. From our measured $\epsilon_{1400} = (5.7 \pm 0.8) \times 10^3\ M^{-1}\ cm^{-1}$ and the extrapolation to 3600 nm, we calculate $\epsilon_{max} = (4.9 \pm 0.7) \times 10^4\ M^{-1}\ cm^{-1}$. The shape of the partial band is similar to the band shapes observed by Jou and Dorfman (19) for the solvated electron in several ethers, where λ_{max} occurs in the range 1800 to 2300 nm. These authors find that the band shapes are Lorentzian on the high energy side of λ_{max} and Gaussian on the low energy side. We have no information on the shape of the infrared band (Fig. 13) for $\lambda > 3200$ nm but it seems likely that it will be steeper than Lorentzian since the latter predicts a significant absorption intensity at zero energy. On the assumption that the band is Lorentzian, we calculate an oscillator strength of 0.8. On the other hand, we calculate an oscillator strength ≈ 0.5 for a band with $\lambda_{max} = 3600$ nm and the shape, for wavelengths $> \lambda_{max}$, predicted by Huang and Ellison (20) for photodetachment spectra of trapped electrons. An oscillator strength > 0.5 is in keeping with the large values generally found for trapped electrons.

Generally, infrared spectra of e_t^- are associated with nonpolar media and, in the absence of long range forces, bound–free transitions will make a major contribution to their oscillator strengths (17). The infrared band which we observe in polar glasses (Fig. 13) is probably due, therefore, to electrons trapped in an effectively nonpolar environment. Since we also see an infrared band in crystalline D_2O ice (6) which is very similar to the band in Fig. 13, it seems probable that this nonpolar environment in the glasses is an ice structure. This will be discussed in more detail in a paper on excess electrons in crystalline ice.

(3) Decay of e_t^-

(a) Visible Band

The wavelength dependent decay of this band in the absence of electron scavengers appears to be a general feature of the spectrum of e_t^- in aqueous glasses in this, and other work (4, 5). Similar changes have been seen in hydrocarbon (21) and alcohol glasses (8, 22). Dipole relaxation was invoked to explain these changes in hydrocarbon glasses (21). For the alcohol glasses the changes were again attributed to reorientation of dipoles about the trapped electron (8, 22), or to

Can. J. Chem. Downloaded from www.nrcresearchpress.com by 210.87.254.42 on 09/05/12
For personal use only.

Can. J. Chem. Downloaded from www.nrcresearchpress.com by 210.87.254.42 on 09/05/12
For personal use only.

electron tunnelling from shallow to deep traps (8). In the EG/D_2O glass there is growth at short wavelengths which we believe is due to retrapping of electrons from the infrared band (see below). In the LiCl and $MgCl_2$ glasses no growth was seen at any wavelength for the first 10 μs, so that migration of electrons from shallow to deeper traps and dipole reorientation seem to be unimportant. Apparently some of the trapped electrons causing the visible band are sufficiently close to the geminate holes so that they can recombine with them by a tunnelling mechanism. The rate of such a process is expected to depend on the trap depth (23) so that, if the shape of the long wavelength edge of the band reflects the various trap lengths, we would expect the longer the wavelength, the faster the decay. Figure 3 shows that these decays are approximately logarithmic in time which is a characteristic of tunnelling reactions (24), whereas dipole reorientation is more likely to be a first order process, or a series of first order processes.

The decay of the visible band in the $MgCl_2$ glass at 650 nm (Fig. 4) is odd in two respects: first, because of the rapid partial decay at 76 K, and secondly, because this decay becomes slower as the temperature is increased. A tentative explanation of these phenomena is that radiation generated protons are able to migrate to, and destroy e_t^- to a limited extent. The migration process would require the presence of suitable ice-like microstructures in the glass, and increase in temperature would tend to destroy these specific structures and prevent proton migration. That a significant yield of protons is formed in the $MgCl_2$ glass is suggested by the low yield of Cl_2^- in this system. The reactions forming these species may be envisaged as [2] and [3]:

$$[2] \quad D_2O^+ + Cl^- \rightarrow D_2O\,(\text{or } D + OD) + Cl\,(\xrightarrow{Cl^-} Cl_2^-)$$

$$[3] \quad D_2O^+ + D_2O \rightarrow D_3O^+ + OD$$

and the lower concentration of Cl^- in the $MgCl_2$ glass (2.5 *M*), compared with the LiCl glass (9.5 *M*), would increase the extent of reaction 3 at the expense of reaction 2. Dipole reorientation may also be occurring, as the subsequent small growth at 76 K and 650 nm suggests (see Fig. 4).

When the glasses contain electron scavengers there is good evidence that the trapped electrons (visible band) react with the scavengers by a tunnelling mechanism (5, 23), and that the tunnelling rates differ from one glass to another (5). The different rates have been interpreted (5) in terms of the relative number of trapping sites in each glass and the occurrence of direct and indirect trap-to-solute tunnelling. The data in Table 3 are consistent with this interpretation if the relative number of trapping sites is much greater for the EG/D_2O glass compared with the chloride glasses. Evidence that this is so is provided by the data in Table 2, since the effectiveness of scavengers in reducing $G(e_t^-)$ is expected (5) to be greatest in the glasses having the least number of traps. A similar conclusion was reached by Moan (25).

(b) Infrared Band

The logarithmic time dependence of the decay of this band is again characteristic of a tunnelling process, and seems to rule out dipole relaxation to form deep traps as an important decay mode. However, in contrast to the decay rate of the visible band, the decay rate of the infrared band is independent of wavelength, and increases with temperature (Fig. 11). The wavelength independence may readily be explained if the observed part of the infrared band is due to transitions from only one type of trap, rather than to transitions from traps of various depths. The temperature effect suggests that some molecular motion causes the electrons to be released from their traps. This is not inconsistent with a tunnelling mechanism if this motion merely increases the probability that the energy levels of the donor and acceptor are matched, which is a requirement for tunnelling to take place. In fact the apparent activation energies are only a few kJ mol^{-1} (see above). We do not know the nature of the suggested molecular motion, but it may correspond to the secondary relaxations which have been detected (26) in aliphatic alcohols below their glass transitions temperatures, and which have low Arrhenius activation energies.

The correlation of the decay of the infrared band with the increase of the integrated emission in the LiCl and $MgCl_2$ glasses suggests that electron–hole recombination is at least partly responsible for the decay, and that recombination is the rate determining step in the emission process. The enhancement of the decay rate by electron scavengers (Table 3) indicates, however, that reaction with the scavenger also occurs. That the rates of absorption decay and integrated emission increase remain correlated in the pres-

Can. J. Chem. Downloaded from www.nrcresearchpress.com by 210.87.254.42 on 09/05/12
For personal use only.

ence of scavengers, or when the temperature is raised, implies that the *fraction* of electrons recombining with holes is independent of time in each case.

The lack of effect of HCl on the intensity and decay rate of the infrared band is striking (see Tables 2 and 3), and confirms that neither dry nor shallow trapped electrons react with protons. This lack of effect of acid would seem to eliminate the reaction

[4] $$e_t^- + D_3O^+ \rightarrow D + D_2O^*$$

as the recombination process giving rise to the emission spectrum of Fig. 6. Another reaction to be considered as the source of the emission is

[5] $$e_t^- + Cl_2^- \rightarrow Cl_2^{2-*} \text{ or } Cl^{-*} + Cl^-$$

This reaction has been proposed as the source of the long-lived spontaneous isothermal (25, 27), and photo stimulated (27) emission observed from γ-irradiated glasses at 77 K, which has a spectrum similar to that of Fig. 6. However, the emission of Fig. 6 must originate from a species with a life-time much shorter than that of the infrared absorbing electrons, and hence is likely to be fluorescence and therefore is not obviously related to the long-lived emission of refs. 25 and 27. Reaction 5 does not seem to account for the fast emission we observed because we saw no decay of the 350 nm absorption peak due to Cl_2^- while the infrared absorbing electrons were decaying, and the yield of the latter is appreciable for both the LiCl and $MgCl_2$ glasses (see Table 4).

Another possible decay reaction of the shallowly trapped electrons is a spur reaction with a hydroxyl radical:

[6] $$e_t^- + OD \rightarrow OD^{-*}$$

The electron affinity of the hydroxyl radical has been estimated as $\sim$3.3 eV (28), with all species hydrated, so that on energetic grounds reaction 6 is a feasible source of the 415 nm (3.0 eV) emission of Fig. 6. Both fluorescence (29) and phosphorescence (28, 30) have been observed from systems containing hydroxide ion, and they are thought to originate from the excited hydroxide ion (28, 29) although the excited hydroxyl radical has also been proposed as the emitting source (30). The λ_{max} observed for fluorescence in hydroxide-doped alkali halide crystals is in the range of 294–342 nm (30), but there is probably strong coupling of the electronic states to lattice vibrations, so that a shift of λ_{max} to 415 nm in an aqueous system is not unlikely. We conclude that reaction 6 is the most likely decay reaction of the infrared absorbing electrons which leads to emission.

The behaviour of the EG/D_2O glass is different from that of the LiCl and $MgCl_2$ glasses in that no emission was detected after the pulse, and an appreciable growth of the visible band accompanied the decay of the infrared band. Evidently in this glass tunnelling from shallow traps to deep traps is significant. Similar spectral changes were reported by Hase *et al.* (3) for γ-irradiated EG/H_2O glasses between 4 and 77 K and were attributed to dipole relaxation. The data in Table 3 indicate that electron scavengers do not enhance the rate of decay of the infrared band in this glass as much as in the $MgCl_2$ glass, so that tunnelling to scavenger is not important. This is confirmed by the lack of growth in Ag^0 after the pulse when Ag^+ was present.

Since the growth of the visible band does not account completely for the loss of infrared absorbing electrons (see below) some electron–hole recombination must be occurring which does not result in observable emission. It is unlikely that hydroxyl radicals will persist in the presence of 50% ethylene glycol, so that this result is not inconsistent with our proposal for the emission mechanism in the other cases already discussed. It is interesting to note that emission is observed from irradiated EG/H_2O glass when suitable scavengers of positive ions are present (31).

(4) Electron Yields

(a) Effects of Scavengers and Temperature

If electron scavengers merely intercepted mobile electrons before they became trapped in deep or shallow traps, we would expect the values of G/G_0 for the visible and infrared electrons to be identical. The data in Table 2 show that this is not the case, and we do not believe the discrepancy can be attributed to errors in the extrapolation of yields to mid-pulse. A possible explanation of the greater reduction of infrared electrons is the formation of encounter pairs in which the electrons are trapped within the reaction volume of the scavenger and react before detection (32). Evidence for the formation of such encounter pairs involving deeply trapped electrons has already been reported (5). The probability, P, that an encounter pair is formed is

$$P = 1 - \exp(-2.52[S]r^3)$$

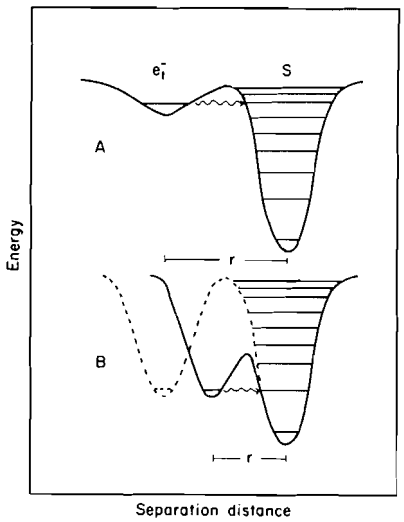

FIG. 15. Schematic representation of an e_t^- – scavenger encounter pair for an electron in a shallow trap (*A*) and a deep trap (*B*), showing the dependence of the encounter pair separation distance *r* on electron trap depth. The scavenger is represented by S and tunnelling is indicated by ⟿.

where [S] is the scavenger concentration and *r* is the reaction radius in nm. At the solute concentrations used in the experiments described in Table 2, we calculate from the values of *r* for the deeply trapped electrons previously determined (33) and listed in Table 2 that the probability of deeply trapped electrons forming encounter pairs is small. Therefore the reduction in visible absorbing e_t^- designated by G/G_0 in Table 2 is due only to the competition for mobile electrons by scavengers and traps. A similar reduction in infrared absorbing e_t^- must also occur, so that only the reduction greater than this can be attributed to the formation of encounter pairs. Therefore we can equate *P* for the shallowly trapped electrons with the ratios of the values of G/G_0 for the infrared and visible bands, and thus calculate the values of *r* for the shallowly trapped electrons shown in Table 2. It is seen that these values of *r* are similar for the Cl^- glasses, and rather smaller for the EG/D_2O glass, and that the *r* values for the shallowly trapped electrons are larger than for the deeply trapped electrons. This is not surprising, first because of the much smaller energy barrier separating the trapped electron from the solute, and secondly because of the higher density of acceptor levels available to the electron. This situation is presented schematically in Fig. 15, which illustrates how *r* must be decreased for deeply trapped electrons to reduce the barrier height and width so that tunnelling becomes as probable as in the case of shallowly trapped electrons.

The decrease in the yield of infrared electrons with increasing temperature seems to be too large to be entirely due to their accelerated decay. Moreover, Moan (25) observed that the luminescence produced from LiCl glass during X-irradiation decreased in intensity with increasing temperature above 77 K, becoming zero at about 120 K. This is precisely the range in which we find the intensity of the infrared band approaching zero (see Fig. 9). Therefore, in view of the correlation of the luminescence with the infrared band noted above, we conclude that the yield of shallowly trapped electrons does diminish in this temperature range. On the other hand no noticeable change occurs in the yield of deeply trapped electrons, indicating that rapid trap deepening does not take place. Thus the effect of increasing temperature appears to result in a decrease in the number, or trapping efficiency, of shallow traps, conceivably because of the same molecular motion which accelerates the decay of the infrared band. It seems unlikely that the ionization yield would be affected by temperature, so that the deficiency in shallowly trapped electrons must be compensated for by recombination of the untrapped electrons with the holes, rather than by deep trapping. This in turn reinforces the implication that the shallowly trapped electrons are largely correlated with the positive holes. Such a correlation is also a property of electrons trapped in nonpolar media, and provides another pointer to the nonpolar nature of the shallow traps in these aqueous glasses.

Steen and Strand (30) have suggested: (*a*) that the X-ray induced luminescence of indoles in EG/H_2O glass comes from the recombination of shallowly trapped electrons and (*b*) that these are much closer to positive ions than are the bulk of stable, deeply trapped electrons. We agree with suggestion (*b*). However, part of the reason for their suggestion was their conclusion that the scavenger concentration needed to halve the yield of ion recombination is roughly one order of magnitude larger than the concentration which reduces the yield of stably trapped electrons to one-half (34). In contrast, as indicated above, we find that scavenger reduces the yield of shallowly

Can. J. Chem. Downloaded from www.nrcresearchpress.com by 210.87.254.42 on 09/05/12
For personal use only.

TABLE 4. Absolute yields of visible and infrared absorbing e_t^- in EG/D_2O, LiCl, and $MgCl_2$ glasses at 76 K

Glass	$G(e_t^-)$ Visible	Infrared	Total	$G(Cl_2^-)$
50/50 v/v EG/D_2O	1.5	2.0	3.5	—
9.5 *M* LiCl	1.4	1.2	2.6	4.6
2.5 *M* $MgCl_2$	0.6	2.1	2.7	2.3

trapped electrons more efficiently than that of deeply trapped electrons. Presumably the difference in conclusions is related to the difference in methods of measuring yields of shallowly trapped electrons, and is probably also due to the fact that we measured yields of deeply trapped electrons at short times (<100 ns), but in ref. 34 these yields were measured some seconds after the beginning of irradiation when appreciable decay of e_t^- would already have occurred.

(b) Absolute Yields of e_t^-

The absolute yields of e_t^- are listed in Table 4. We have assumed that the values of ϵ_{1400} determined for the EG/D_2O glass applies also to the Cl^- glasses, which seems reasonable in view of the similarity in shapes obtained for the resolved infrared bands. Also shown are the values of $G(Cl_2^-)$ obtained by assuming the 350 nm peak is all due to Cl_2^-, and by taking ϵ_{350} for $Cl_2^- = 8.6 \times 10^3\ M^{-1}\,cm^{-1}$ (35).

The values of $G(e_t^-)$ in Table 4 show that EG/D_2O glass is more efficient than the Cl^- glasses at trapping electrons, which is in accord with the smaller effect of scavengers in this glass, and with the transfer of electrons from shallow to deep traps. However, the yields also show that the 25% growth in the visible band in the EG/D_2O glasses at 76 K accounts for only 20% of the decay of the infrared band, so that electron–hole recombination is the major mode of decay of this band.

Acknowledgements

The authors gratefully acknowledge the very capable assistance of Mr. G. G. Teather in the experimental work.

1. B. G. ERSHOV and A. K. PIKAEV. Radiation chemistry I. *Edited by* R. F. Gould. American Chemical Society, Washington, D.C. 1968. p. 1.
2. L. KEVAN. Radiation chemistry of aqueous systems. *Edited by* G. Stein. The Weizmann Science Press of Israel, Jerusalem. 1968. p. 21.
3. H. HASE, M. NODA, and T. HIGASHIMURA. J. Chem. Phys. **54**, 2975 (1971).
4. G. V. BUXTON, F. C. R. CATTELL, and F. S. DAINTON. Trans. Faraday Soc. **67**, 687 (1971).
5. G. V. BUXTON and K. G. KEMSLEY. J. Chem. Soc. Faraday Trans. 1, **71**, 568 (1975).
6. G. V. BUXTON, H. A. GILLIS, and N. V. KLASSEN. Chem. Phys. Lett. **32**, 533 (1975).
7. (*a*) J. H. BAXENDALE, C. BELL, and J. MAYER. Int. J. Radiat. Phys. Chem. **6**, 117 (1974); (*b*) W. A. SEDDON, E. B. SELKIRK, and J. W. FLETCHER. Int. J. Radiat. Phys. Chem. **5**, 323 (1973); (*c*) G. G. TEATHER, N. V. KLASSEN, and H. A. GILLIS. Int. J. Radiat. Phys. Chem. In press.
8. N. V. KLASSEN, H. A. GILLIS, G. G. TEATHER, and L. KEVAN. J. Chem. Phys. **62**, 2474 (1975).
9. J. PUKIES, W. ROEBKE, and A. HENGLEIN. Ber. Bunsenges. Phys. Chem. **72**, 842 (1968).
10. FARHATAZIZ, I. MIHALCEA, L. J. SHARP, and R. R. HENTZ. J. Chem. Phys. **59**, 2309 (1973).
11. H. HASE and L. KEVAN. J. Chem. Phys. **54**, 908 (1971).
12. G. G. JAYSON, B. J. PARSONS, and A. J. SWALLOW. J. Chem. Soc. Faraday Trans 1, **9**, 1597 (1973).
13. J. H. SCHULMAN and W. D. COMPTON. Color centers in solids. The MacMillan Co., New York. 1963. p. 107.
14. L. KEVAN, D. R. RENNEKE, and R. J. FRIAUF. Solid State Commun. **6**, 469 (1968).
15. G. V. BUXTON, F. S. DAINTON, T. E. LANTZ, and F. P. SARGENT. Trans. Faraday Soc. **66**, 2962 (1970).
16. J. MOAN. Chem. Phys. Lett. **17**, 565 (1972).
17. T. SHIDA, S. IWATA, and T. WATANABE. J. Phys. Chem. **76**, 3683 (1972); **76**, 3691 (1972).
18. L. KEVAN. J. Phys. Chem. **76**, 3830 (1972).
19. F. Y. JOU and L. M. DORFMAN. J. Chem. Phys. **58**, 4715 (1973).
20. J. J. HUANG and F. O. ELLISON. Chem. Phys. Lett. **28**, 189 (1974).
21. N. V. KLASSEN, H. A. GILLIS, and G. G. TEATHER. J. Phys. Chem. **76**, 3847 (1972).
22. L. KEVAN. J. Chem. Phys. **56**, 838 (1972).
23. J. R. MILLER. J. Chem. Phys. **56**, 5173 (1972).
24. (*a*) J. R. MILLER. Chem. Phys. Lett. **22**, 180 (1973); (*b*) K. I. ZAMARAEV and R. J. KHAIRUTDINOV. Chem. Phys. **4**, 181 (1974); (*c*) J. KROH and CZ. STRADOWSKI. Int. J. Radiat. Phys. Chem. **7**, 23 (1975).
25. J. MOAN. J. Chem. Phys. **60**, 3859 (1974).
26. G. P. JOHARI and M. GOLDSTEIN. J. Chem. Phys. **55**, 4246 (1971).

Can. J. Chem. Downloaded from www.nrcresearchpress.com by 210.87.254.42 on 09/05/12
For personal use only.

27. S. KHORANA, P. B. MERKEL, and W. H. HAMILL. J. Chem. Phys. **56**, 2807 (1972).
28. P. B. MERKEL and W. H. HAMILL. J. Chem. Phys. **55**, 2174 (1971).
29. H. KOSTLIN. Solid State Commun. **4**, 81 (1965).
30. H. J. MARIA and S. P. MCGLYNN. J. Chem. Phys. **52**, 3402 (1970).
31. H. B. STEEN and O. STRAND. J. Chem. Phys. **60**, 5043 (1974).
32. G. CZAPSKI and E. PELED. J. Phys. Chem. **77**, 893 (1973).
33. G. V. BUXTON, F. C. R. CATTELL, and F. S. DAINTON. J. Chem. Soc. Faraday Trans. 1, **71**, 115 (1975).
34. H. B. STEEN, O. KAALHUS, and M. KONGSHAUG. J. Phys. Chem. **75**, 1941 (1971).
35. G. V. BUXTON. *In* Fast processes in radiation chemistry and biology. *Edited by* G. E. Adams, E. M. Fielden, and B. D. Michael. Wiley, London. 1975. p. 95.

Can. J. Chem. Downloaded from www.nrcresearchpress.com by 210.87.254.42 on 09/05/12
For personal use only.

Metal complexes as antioxidants. II. Reaction of nickel di-*n*-butyldithiocarbamate and nickel diisopropyldithiophosphate with alkylperoxy radicals[1]

J. A. HOWARD[2] AND J. H. B. CHENIER
Division of Chemistry, National Research Council of Canada, Ottawa, Canada K1A 0R9

Received June 13, 1975

J. A. HOWARD and J. H. B. CHENIER. Can. J. Chem. **54**, 382 (1976).

Nickel di-*n*-butyldithiocarbamate and nickel diisopropyldithiophosphate inhibit the α,α'-azo-bis-isobutyronitrile initiated autoxidation of tetralin, styrene, and cyclohexa-1,4-diene by scavenging chain propagating alkylperoxy radicals. The rapid reaction of these complexes with alkylperoxy radicals has been confirmed by low temperature electron spin resonance studies. Kinetic data obtained by these two techniques are reported. Product studies suggest that alkylperoxy radicals (ROO·) are reduced by reaction with the nickel complex to the alcohol (ROH) while the nickel complex is oxidized to a Lewis acid.

J. A. HOWARD et J. H. B. CHENIER. Can. J. Chem. **54**, 382 (1976).

Le di-*n*-butyldithiocarbamate de nickel et le diisopropyldithiophosphate de nickel inhibent l'autooxydation, initiée par l'α,α' azo-bis-isobutyronitrile, de la tétraline, du styrène et du cyclohexadiène-1,4 en piégeant les radicaux alkylpéroxy qui propagent la chaîne. On a confirmé la réaction rapide de ces complexes avec les radicaux alkylperoxy par des études de résonance paramagnétique électronique à basse température. On rapporte les données cinétiques obtenus par ces deux techniques. Une étude des produits suggère que les radicaux alkylperoxy (ROO·) sont réduits par réaction avec le complexe de nickel pour conduire à l'alcool alors que le complexe de nickel est oxydé en acide de Lewis.

[Traduit par le journal]

Introduction

Lubricating oils and many other petroleum products are required to function under conditions that become more severe every year. This has generated a never-ending search for better high temperature antioxidants. It has been discovered empirically that certain heavy metal compounds are very effective antioxidants, but the exact mechanism by which the majority of these compounds inhibit autoxidation has not been elucidated. The most important of the commercial metal-containing antioxidants are the zinc dialkyldithiophosphates and related complexes. The mechanism of inhibition by these compounds has been studied fairly intensively (ref. 1 and references cited therein) but relatively little attention has, so far, been paid to similar compounds of other heavy metals. In this paper, we extend our previous studies (1) to the nickel complexes of diisopropyldithiophosphoric acid, Ni(i-Pr_2dtp)$_2$ and di-*n*-butyldithiocarbamic acid, Ni(n-Bu_2dtc)$_2$.

[1]NRCC No. 15012.

[2]To whom all correspondence should be addressed.

Experimental

Materials

Nickel di-*n*-butyldithiocarbamate was a commercial sample which was recrystallized from chloroform–hexane. Nickel diisopropyldithiophosphate was prepared by reaction of diisopropyldithiophosphoric acid with nickel acetate. The crude product was recrystallized from chloroform–hexane.

Azocumene was prepared by the method described by Nelsen and Bartlett (2). The melting point was 87 °C, lit. (2) 86.9–88.7 °C and the ultraviolet spectrum gave an extinction coefficient of 44 at 367 nm, lit. $\epsilon = 43$ (2).

Tetraphenylbutane was prepared by the method of Müller and Roscheinsen (3). The melting point was 119–123 °C, lit. (4) 122–123 °C. Both the initial rate of oxygen absorption and the total concentration of oxygen absorbed by a standard solution indicated that it was 100% pure.

Dicumyl hyponitrite (5) was synthesized from α-cumyl bromide and silver hyponitrite by a procedure identical to the one described by Kiefer and Traylor (6) for di-*tert*-butyl hyponitrite using pentane as solvent. Cooling the filtrate produced a colourless, crystalline material which melted at 66–70 °C with nitrogen evolution. The yield of nitrogen was close to 1 mol per mol of hyponitrite, indicating that the hyponitrite was ~100% pure.

The oxidizable hydrocarbons, inert solvents, azo-bis-isobutyronitrile, azoisobutane, and di-*tert*-butyl peroxide were commercial samples which were purified as describe previously (1, 7, 8). Great care was taken to exclude

Can. J. Chem. Downloaded from www.nrcresearchpress.com by 210.87.254.5 on 09/05/12
For personal use only.

Can. J. Chem. Downloaded from www.nrcresearchpress.com by 210.87.254.5 on 09/05/12
For personal use only.

adventitious hydroperoxides from the hydrocarbons that were used as substrates.

Procedures

Liquid-phase Autoxidations

Nickel complex inhibited autoxidations of styrene and tetralin at 50 °C and cyclohexa-1,4-diene at 30 °C were studied using the same experimental procedure as was used for the zinc complexes (1). Photochemical initiation was, however, not employed because of the intense color of nickel complex solutions. α,α'-Azo-bis-isobutyronitrile (AIBN) was used as the thermal source of radicals and it was introduced into the reaction mixture after the complex and hydrocarbon had reached thermal equilibrium with an atmosphere of oxygen. Inhibited rates of oxidation were determined from the initial slope of oxygen uptake *vs.* time curves. In some instances measurable rates of autoxidation were obtained before the initiator was added because of a radical generating reaction between the complex and adventitious hydroperoxide (see next paper in this series). These runs were abandoned.

Induction periods (τ) were determined by the method of Boozer *et al.* (9), using cumene as substrate. This method involves measuring the time taken to consume a known concentration of complex at a known rate of chain initiation (R_i). A stoichiometric factor n, *i.e.*, the number of alkylperoxy radicals scavenged by each molecule of inhibitor, can be calculated from $n = R_i\tau/[A]_0$, where $[A]_0$ is the initial concentration of inhibitor.

The concentration of the nickel complex during the induction period was followed by uv spectroscopy (Cary 15). The rate of chain initiation divided by the rate of disappearance of nickel complex $R_i/(-d[A]/dt)$ is an alternative method of determining stoichiometric factors.

Electron Spin Resonance Studies

Reaction of the nickel complexes with *tert*-butylperoxy and 2-ethyl-2-propylperoxy radicals was studied kinetically by electron spin resonance spectroscopy (1, 7, 8). *tert*-Butylperoxy radicals were generated by photolysis of azoisobutane (0.02 *M*) in an oxygen saturated solvent (isopentane, toluene, and fluorotrichloromethane). 2-Ethyl-2-propylperoxy radicals were produced by photolysis of di-*tert*-butyl peroxide (5%) in oxygen saturated isopentane. Radical decays were followed in the presence of a large excess of the complex after the light was shuttered.

Stoichiometric factors were determined by titrating a known concentration of $(CH_3)_3COO\cdot$ with a nickel complex at −90 °C using esr spectroscopy to monitor the peroxy radical concentration (8).

Reaction Products

Products from the decomposition of azocumene and tetraphenylbutane at 50 °C in the absence and presence of nickel di-*n*-butyldithiocarbamate and nickel diisopropyldithiophosphate in an oxygen saturated solvent were determined.

In a typical experiment azocumene (0.033 g, 0.12 mmol) and Ni(*n*-Bu_2dtc)$_2$ (0.058 g, 0.12 mmol) were dissolved in chlorobenzene and shaken in an atmosphere of oxygen for 50 h (*i.e.*, for *ca.* 10 half lives of azocumene). The volatile products and solvent were efficiently pumped into a trap maintained at the temperature of liquid nitrogen. Reaction products were identified by gas–liquid chromatography (F and M model 240 chromatograph equipped with a SE-30 column) in conjunction with mass spectrometry. Yields were determined relative to standard authentic samples and were based on the total concentration of radicals produced. The efficiency of radical production from azocumene is 75% (2) while tetraphenylbutane gives radicals in 100% yield (4).

Yields of the products formed by decomposition of dicumyl hyponitrite in the absence and presence of Ni(*n*-Bu_2dtc)$_2$ in deoxygenated chlorobenzene were also determined by glc.

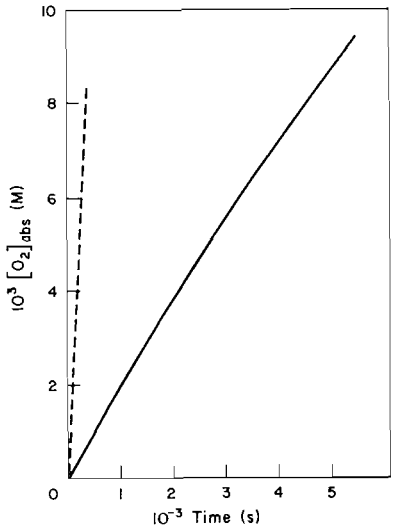

FIG. 1. Oxygen absorption *vs.* time for the AIBN (0.02 *M*) initiated, Ni(*i*-Pr_2dtp)$_2$ (0.016 *M*) inhibited autoxidation of styrene (7 *M*). The broken line represents the uninhibited absorption of oxygen.

Results and Discussion

Inhibited Autoxidations

Rates of α,α'-azo-bis-isobutyronitrile initiated autoxidations of a variety of hydrocarbons (tetralin, styrene, and cyclohexa-1,4-diene) are reduced by millimolar concentrations of nickel di-*n*-butyldithiocarbamate, Ni(*n*-Bu_2dtc)$_2$ and nickel diisopropyldithiophosphate, Ni(*i*-Pr_2dtp)$_2$ (see *e.g.*, Figs. 1 and 2). Initial rates of oxidation were measured at different initiator and inhibitor concentrations and the results are gathered in Tables 1–3. The data presented in these tables indicate that these nickel complexes scavenge alkylperoxy radicals and that the simplest kinetic expression for inhibition by peroxy radical scavenging antioxidants, eq. 1, is very approximately obeyed.

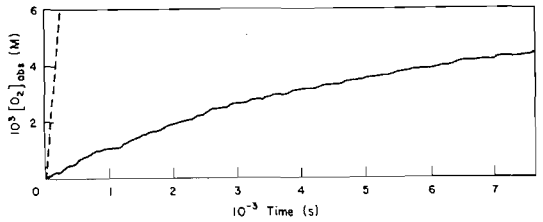

FIG. 2. Oxygen absorption *vs.* time for the AIBN (0.02 *M*) initiated, Ni(*n*-Bu_2dtc)$_2$ (0.02 *M*) inhibited autoxidation of styrene (8.7 *M*). The broken line represents the uninhibited absorption of oxygen.

TABLE 1. Ni(*i*-Pr_2dtp)$_2$ and Ni(*n*-Bu_2dtc)$_2$ inhibited autoxidation of tetralin (5.9 *M*)*

Ligand	$[A]_0 \times 10^3$ (*M*)	$R_i \times 10^8$ ($M\,s^{-1}$)	$(-d[O_2]/dt)_0 \times 10^7$ ($M\,s^{-1}$)	$\frac{nk_{inh}}{k_p}$
—	—	17	120	—
i-Pr_2dtp	0.4	17	50	500
i-Pr_2dtp	1.0	17	21	480
i-Pr_2dtp	2.0	17	14	360
i-Pr_2dtp	3.0	17	6	560
i-Pr_2dtp	1.0	8.4	10	490
i-Pr_2dtp	1.0	4.2	9	270
n-Bu_2dtc	0.4	4.3	6.3	1000

*At 50 °C and 700 Torr.

TABLE 2. Ni(*n*-Bu_2dtc)$_2$ and Ni(*i*-Pr_2dtp)$_2$ inhibited autoxidation of styrene (7.0 *M*)*

Ligand	$[A]_0 \times 10^3$ (*M*)	$R_i \times 10^8$ ($M\,s^{-1}$)	$(-d[O_2]/dt)_0 \times 10^7$ ($M\,s^{-1}$)	$\frac{nk_{inh}}{k_p}$
—	—	4.3†	240	—
n-Bu_2dtc	2	4.3	15	100
n-Bu_2dtc	4	4.3	15	50
n-Bu_2dtc	10	4.3	11	27
n-Bu_2dtc	20	4.3	6.4	23
n-Bu_2dtc	40	18.4‡	15.5	22
i-Pr_2dtp	16	0.43	1.6	10
i-Pr_2dtp	8	4.3	51	7
i-Pr_2dtp	16	4.3	21	9

*At 50 °C and 700 Torr.
†[AIBN] = 0.02 *M*.
‡Tetraphenylbutane (0.002 *M*) was used as initiator for this run.

TABLE 3. Ni(*i*-Pr_2dtp)$_2$ inhibited autoxidation of 1,4-cyclohexadiene (1.1 *M*)*

$[A]_0 \times 10^3$ (*M*)	$R_i \times 10^8$ ($M\,s^{-1}$)	$(-d[O_2]/dt)_0 \times 10^7$ ($M\,s^{-1}$)	$\frac{nk_{inh}}{k_p}$
—	0.8	30	—
0.8	0.8	2.4	46
1.6	0.8	1.0	55
1.6	0.2	0.32	43

*At 30 °C and 700 Torr.

$$[1] \qquad \left(\frac{-d[O_2]}{dt}\right)_0 = \frac{k_p[RH]_0 R_i}{nk_{inh}[A]_0}$$

where $[RH]_0$ is the initial hydrocarbon concentration, $[A]_0$ the initial antioxidant concentration, and n the number of peroxy radicals scavenged by each molecule of A.

Inhibited autoxidations that obey expression 1 can be described by the following elementary reactions:

Initiation:

[2] Production of R· at a rate = R_i

Propagation:

[3] $$R\cdot + O_2 \rightarrow ROO\cdot$$

[4] $$ROO\cdot + RH \xrightarrow{k_p} ROOH + R\cdot \text{ (or } ROORH\cdot)$$

Termination:

[5] $$ROO\cdot + A \xrightarrow{k_{inh}} X$$

[6] $$(n-1)ROO\cdot + X \xrightarrow{\text{fast}} \text{Nonradical products}$$

where k_p and k_{inh} are the rate controlling propagation and termination rate constants.

The values of nk_{inh} calculated from eq. 1 using known values of k_p (ref. 10 and references cited therein) are summarized in Table 4.

These values of nk_{inh} are subject to substantial errors because of the difficulties associated with obtaining precise kinetic data for inhibited autoxidations that are autoretarding and that are extremely sensitive to traces of adventitious hydroperoxide.[3] It would, however, appear that the dithiocarbamate is a more efficient radical scavenger than the dithiophosphate. It would also appear that both complexes are less efficient in styrene than in tetralin. This may be because radicals formed in the rate controlling inhibition step are more efficient propagating species for the autoxidation of styrene than tetralin. This is not unreasonable if these are sulphur centered radicals since it is well known that these radicals add efficiently to olefins but are reluctant to abstract a hydrogen atom (11).

The larger value of nk_{inh} in cyclohexa-1,4-diene may be because hydroperoxyl radicals, which

[3]Addition of the nickel complexes to hydrocarbons containing hydroperoxide produces a pro-oxidant effect which can overshadow the inhibiting effect of these complexes (see next paper in this series).

Can. J. Chem. Downloaded from www.nrcresearchpress.com by 210.87.254.5 on 09/05/12
For personal use only.

TABLE 4. Approximate values of nk_{inh} for inhibition of hydrocarbon autoxidation by nickel complexes

Hydrocarbon	Nickel complex	Temperature (°C)	$\frac{nk_{inh}}{k_p}$	k_p (M^{-1} s^{-1})	$nk_{inh} \times 10^{-3}$ (M^{-1} s^{-1})
Tetralin	*n*-Bu_2dtc	50	1000	13.6	14
Tetralin	*i*-Pr_2dtp	50	440	13.6	6
Styrene	*n*-Bu_2dtc	50	53	98	5
Styrene	*i*-Pr_2dtp	50	9	98	0.9
c-C_6H_8	*i*-Pr_2dtp	30	48	1480	70

are the chain propagating and terminating peroxy species in this substrate (12), are more reactive than alkylperoxy radicals towards the nickel complexes.

We have previously reported values of nk_{inh} for Zn(*i*-Pr_2dtp)$_2$ at 50 °C determined in styrene (1.6×10^4 M^{-1} s^{-1}) and tetralin (8×10^3 M^{-1} s^{-1}). The value in styrene is about an order of magnitude larger than the value reported in this work for the analogous nickel complex while the values of nk_{inh} for Ni(*i*-Pr_2dtp)$_2$ and Zn(*i*-Pr_2dtp)$_2$ determined in tetralin are very similar. These comparisons imply that changing the metal atom from zinc to nickel has no dramatic effect on the peroxy radical scavenging efficiency of metal complexes.

Electron Spin Resonance Studies

Ni(n-Bu$_2$dtc)$_2$

Photolysis of azoisobutane in oxygen saturated CCl_3F and $C_6H_5CH_3$ containing Ni(*n*-Bu_2dtc)$_2$ ($0.2–2 \times 10^{-4}$ M) gave a rather weak singlet absorption centered at $g = 2.015$ which was attributed to $(CH_3)_3COO^{\cdot}$. This radical disappeared very rapidly when the light was shuttered and plots of ln [$(CH_3)_3COO^{\cdot}$] *vs.* time were linear indicating first-order decays. Pseudo-first-order rate constants (k_ψ) were linearly dependent on the complex concentration (Table 5). The second-order rate expression

$$[7] \quad \frac{-d[(CH_3)_3COO^{\cdot}]}{dt} = nk_7[(CH_3)_3COO^{\cdot}][Ni(n\text{-}Bu_2dtc)_2]$$

was, therefore, strictly obeyed.

Values of nk_7 were close to 2×10^4 M^{-1} s^{-1} over the entire temperature range indicating that reaction of $(CH_3)_3COO^{\cdot}$ with Ni(*n*-Bu_2dtc)$_2$ requires little or no activation energy. This rate constant is in reasonable agreement with the rate constants estimated from Ni(*n*-Bu_2dtc)$_2$ inhibited autoxidations of styrene and tetralin at 50 °C (Table 4).

TABLE 5. Rate constants for reaction of $(CH_3)_3COO^{\cdot}$ with Ni(*n*-Bu_2dtc)$_2$ in CCl_3F

Temperature (°C)	$[A]_0 \times 10^6$ (M)	k_ψ (s^{-1})	$nk_7 \times 10^{-4}$ (M^{-1} s^{-1})
−94	2.0	0.056	2.8
−94	10.0	0.32	3.2
−74	2.0	0.05	2.5
−74	10.0	0.3	3.0
−54	10.0	0.25	2.5
−15	10.0	0.15	1.5
−15	20.0	0.24	1.2

When the reaction was carried out in isopentane radicals decays were still exponential but values of k_ψ were much smaller. Slow rates of radical decay could be because 2-ethyl-2-propylperoxy radicals were formed from the solvent during the dark reaction. This would mean that reaction of ROO$^{\cdot}$ with Ni(*n*-Bu_2dtc)$_2$ produces a radical reactive enough to abstract a H-atom from isopentane at low temperatures. Hydrogen atom abstraction from toluene does not appear to complicate rate constants determined in this solvent probably because benzylperoxy radicals would disappear rapidly by reaction with $(CH_3)_3COO^{\cdot}$.

Ni(i-Pr$_2$dtp)$_2$

Pseudo-first-order rate constants for reaction of $(CH_3)_3COO^{\cdot}$ with this complex were about two orders of magnitude smaller than rate constants for reaction of 2-ethyl-2-propylperoxy radicals. Furthermore, values of k_ψ were not linearly dependent on the dithiophosphate concentration, the reactant exponent being closer to zero than one (see *e.g.* Table 6). These kinetic complications could be because of interference from decomposition of *cis*-azoisobutane during the dark reaction (13), self-association of Ni(*i*-Pr_2-

Can. J. Chem. Downloaded from www.nrcresearchpress.com by 210.87.254.5 on 09/05/12
For personal use only.

TABLE 6. Kinetic data for reaction of 2-ethyl-2-propylperoxy radicals with Ni(*i*-Pr_2dtp)$_2$

Temperature (°C)	$[Ni(i\text{-}Pr_2dtp)_2]_0 \times 10^4$ (M)	k_ψ (s^{-1})
−90	0.2	0.62
−90	1.07	1.07
20	0.2	1.72
20	0.37	1.6
20	1.0	2.5
20	1.9	1.8

dtp)$_2$ in organic solvents,[4] and complex formation between peroxy radicals and Ni(*i*-Pr_2dtp)$_2$, the decay of the complex being rate controlling. We could, however, find no experimental evidence to support any of these explanations. We are, therefore, forced to conclude that the kinetic electron spin resonance spectroscopic method cannot be used to give reliable rate constants for reaction of *t*-ROO· with Ni-(R_2dtp)$_2$.[5]

Radical	$[Zn(i\text{-}Pr_2dtp)_2]_0 \times 10^3$	k_ψ (s^{-1})
$(CH_3)_3COO\cdot$	0.0025	0.1
$(CH_3)_3COO\cdot$	0.025	0.055
$(CH_3)_3COO\cdot$	0.25	0.024
$(CH_3)_3COO\cdot$	2.5	0.09
$C_2H_5C(CH_3)_2OO\cdot$	0.0025	0.125
$C_2H_5C(CH_3)_2OO\cdot$	0.025	0.04
$C_2H_5C(CH_3)_2OO\cdot$	0.25	0.04
$C_2H_5C(CH_3)_2OO\cdot$	2.5	0.03

The rate parameters obtained by this technique quoted in ref. 1 are, therefore, almost certainly incorrect.

Stoichiometric Factors

Two *tert*-butylperoxy radicals were destroyed by each molecule of Ni(*n*-Bu_2dtc)$_2$ and Ni(*i*-Pr_2dtp)$_2$ when known concentrations of the nickel complexes were added to known concentrations of the radical in the dark at −90 °C. The stoichiometric factor n is, therefore, equal to 2.0 for both complexes.

Induction periods (τ) obtained for Ni(*n*-Bu_2dtc)$_2$ and Ni(*i*-Pr_2dtp)$_2$ inhibited autoxidations of cumene are given in Table 7 along with the induction period obtained for 2,6-di-*tert*-butyl-4-methoxyphenol. In all cases the overall rate of autoxidation at the end of the induction period was close to the uninhibited rate.[6] Values of $R_i\tau/[A]$ for the dithiocarbamate were >2 while the dithiophosphate gave values <2. The values of n obtained from rates of complex disappearance during the induction period were, however, closer to the values of 2.0 obtained at low temperatures. It would, therefore, appear that each molecule of Ni(*i*-Pr_2dtp)$_2$ and Ni(*n*-Bu_2dtc)$_2$ does scavenge two alkylperoxy radicals and that the Boozer and Hammond method cannot be used for these compounds.

Products of the Reaction of Alkylperoxy Radicals with the Nickel Complexes

Cumylperoxy Radicals

The products and yields obtained from decomposition of azocumene in oxygen saturated chlorobenzene in the absence and presence of Ni(*n*-Bu_2dtc)$_2$ and Ni(*i*-Pr_2dtp)$_2$ are summarized in Table 8.

In the absence of the inhibitor, acetophenone and α-cumyl alcohol were the principal reaction products. These products are consistent with the accepted mechanism for the decomposition of azocumene in the presence of oxygen and the self-reaction of cumylperoxy radicals (10) *i.e.*,

$$[11]\quad RN{=}NR \xrightarrow{k_{11}} [R\cdot\ N_2\ \cdot R]_{cage}$$

$$[12]\quad [R\cdot\ N_2\ \cdot R]_{cage} \begin{cases} \rightarrow \text{Cage products} \\ \rightarrow 2R\cdot + N_2 \end{cases}$$

$$[13]\quad R\cdot + O_2 \rightarrow ROO\cdot$$

$$[14]\quad 2ROO\cdot \rightleftharpoons [ROOOOR]_{cage}$$

$$[15]\quad [ROOOOR]_{cage} \rightarrow [RO\cdot + O_2 + \cdot OR]_{cage}$$

$$[16]\quad [RO\cdot + O_2 + \cdot OR]_{cage} \begin{cases} \rightarrow \text{Cage products} \\ \rightarrow 2RO\cdot + O_2 \end{cases}$$

$$[17]\quad RO\cdot + RH \rightarrow ROH + R\cdot$$

$$[18]\quad RO\cdot \rightarrow C_6H_5COCH_3 + CH_3\cdot$$

where R represents $C_6H_5(CH_3)_2C$.

The yield of acetophenone reported here is

[4]There is ample experimental evidence for association of metal diisopropyldithiophosphates in solution (14).

[5]We have carefully reinvestigated the reaction of *tert*-alkylperoxy radicals with zinc diisopropyldithiophosphate at −100 °C by KESR and find that the rate of this reaction is also virtually independent of the complex concentration.

[6]The unhibited rate was, however, only maintained for a short time before autoinhibition was apparent. Oxygen was then absorbed slowly for a considerable length of time whereupon the rate increased until the uninhibited rate was again reached. The second 'induction period' was about four times longer than the first one.

Can. J. Chem. Downloaded from www.nrcresearchpress.com by 210.87.254.5 on 09/05/12
For personal use only.

TABLE 7. Induction periods and rates of inhibitor disappearance for the Ni(n-Bu_2dtc)$_2$ and Ni(i-Pr_2dtp)$_2$ inhibited autoxidation of cumene (7.2 M) at 50 °C*

Complex	Concentration $\times 10^4$ (M)	Induction period (s)	$\frac{R_i\tau}{[A]}$	$\frac{-d[O_2] \times 10^6}{dt}$ ($M\,s^{-1}$)†	$\frac{-d[A] \times 10^8}{dt}$ ($M\,s^{-1}$)	$\frac{R_i}{-d[A]/dt}$
BMeOP‡	4.0	18 000	2.0	4.4	—	—
Ni(n-Bu_2dtc)$_2$	2.0	18 300	4.0	4.1	—	—
Ni(n-Bu_2dtc)$_2$	4.0	35 000	3.5	3.8	1.6	2.7
Ni(i-Pr_2dtp)$_2$	2.0	2 700	0.5	2.3	—	—
Ni(i-Pr_2dtp)$_2$	4.0	—	—	—	3.0	1.4
Ni(i-Pr_2dtp)$_2$	8.0	14 400	1.5	4.5	—	—

*[AIBN] = 0.02 M; $R_i = 4.3 \times 10^{-8}$ $M\,s^{-1}$.
†Rate of oxidation at the end of the induction period.
‡2,6-Di-*tert*-butyl-4-methoxyphenol.

TABLE 8. Some of the products from reaction of alkylperoxy radicals with nickel complexes*

Alkylperoxy radical	Initiator concentration (M)	Ligand	Initial complex concentration (M)	$[O_2]_{abs}$ (M)	Product-yield† $C_6H_5COCH_3$	Olefin	$C_6H_5C(CH_3)_2OH$
$C_6H_5C(CH_3)_2OO\cdot$	0.026	—	—	0.04	0.5	0	0.27
$C_6H_5C(CH_3)_2OO\cdot$	0.026	n-Bu_2dtc	0.013	0.046	0.15	0.55§	0.04
$C_6H_5C(CH_3)_2OO\cdot$‡	0.04	n-Bu_2dtc	0.02	0.038	0.14	0.30§	0.17
$C_6H_5C(CH_3)_2OO\cdot$	0.026	i-Pr_2dtp	0.035	0.043	0.16	0.41§	0.13
$(C_6H_5)_2CH_3COO\cdot$	0.0045	—	—	0.01	0.18	0	—
$(C_6H_5)_2CH_3COO\cdot$	0.04	n-Bu_2dtc	0.02	0.073	0.38	0.46‖	—
$(C_6H_5)_2CH_3COO\cdot$‡	0.04	n-Bu_2dtc	0.02	0.106	0.32	0.52‖	—

*At 50 °C in chlorobenzene.
†Yields are in mol per mol of peroxy radical generated, the yield of cumylperoxy radicals from azocumene is 150% and the yield of 1,1-diphenylethylperoxy radicals from tetraphenylbutane is 200%.
‡Plus 5% acetic acid.
§α-Methylstyrene.
‖1,1-Diphenylethylene.

similar to that obtained by Blanchard (15) from an analysis of the products formed from the chain termination reaction during autoxidation of cumene. The yield of α-cumyl alcohol seems high but it almost certainly arises by a hydrogen atom abstraction reaction involving cumyloxy radicals. No attempt was made to estimate the yield of dicumyl peroxide (the cage product) or determine the fate of the methyl radicals formed in reaction 18.

When the decomposition of azocumene was carried out in the presence of Ni(n-Bu_2dtc)$_2$ and Ni(i-Pr_2dtp)$_2$ the principal reaction product was α-methylstyrene along with smaller amounts of acetophenone and α-cumyl alcohol. The formation of α-methylstyrene from the decomposition of cumene hydroperoxide by sulphur- and phosphorus-containing antioxidants is well known (16) and has been attributed to the dehydration of α-cumyl alcohol by a Lewis acid formed in the system. These products strongly suggest that cumylperoxy radicals are deoxygenated by the nickel complexes to give cumyloxy radicals which must abstract a hydrogen atom from the ligand to give α-cumyl alcohol. The nickel complex must be oxidized to a Lewis acid which is strong enough to dehydrate α-cumyl alcohol.

1,1-Diphenylethylperoxy Radicals

Decomposition of tetraphenylbutane in oxygen saturated chlorobenzene in the absence and presence of Ni(n-Bu_2dtc)$_2$ gave the products summarized in Table 8.

In the absence of the scavenger 1,1-diphenylethylperoxy radicals interact by a rather more complex mechanism than the one for cumylperoxy radicals (17). Initially the reaction can be described by reactions analogous to reactions 14, 15, and 16 with R = $(C_6H_5)_2CH_3C$. 1,1-Diphenylethoxy radicals, however, undergo a

Can. J. Chem. Downloaded from www.nrcresearchpress.com by 210.87.254.5 on 09/05/12
For personal use only.

Can. J. Chem. Downloaded from www.nrcresearchpress.com by 210.87.254.5 on 09/05/12
For personal use only.

TABLE 9. Some of the products from reaction of cumyloxy radicals* with nickel di-*n*-butyldithiocarbamate†

$[n\text{-}Bu_2dtc]_0$ (M)	$[C_6H_5C(CH_3)_2OH]$ $\times 10^2$ (M)	$[C_6H_5COCH_3]$ $\times 10^2$ (M)	$[C_6H_5C(CH_3){=}CH_2]$ $\times 10^2$ (M)	$[p\text{-}ClC_6H_4CH_3]$ $\times 10^2$ (M)
—	—	2.8	0.11	0.5
0.02	2.2	0.7	0.22	0.11

*Initial cumyl hyponitrite concentration = 0.02 M.
†Solvent, chlorobenzene; reaction temperature, 50 °C.

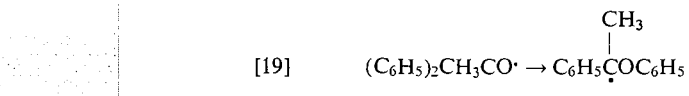

1,2-phenyl shift (reaction 19) rather than β-scission,

$$[19] \qquad (C_6H_5)_2CH_3CO^{\cdot} \rightarrow C_6H_5\overset{\displaystyle CH_3}{\underset{\cdot}{C}}OC_6H_5$$

This new carbon centered radical reacts with oxygen to give a peroxy radical which also undergoes a series of reactions analogous to reactions 14, 15, and 16 to give 1-phenyl-1-phenoxyethoxy radicals which undergo β-scission to give acetophenone:

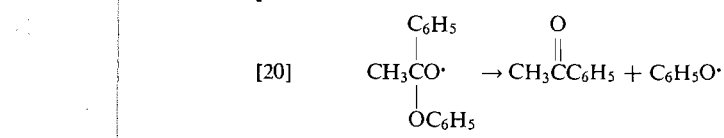

$$[20] \qquad CH_3\overset{\displaystyle C_6H_5}{\underset{\displaystyle OC_6H_5}{C}}O^{\cdot} \rightarrow CH_3\overset{\displaystyle O}{\overset{\|}{C}}C_6H_5 + C_6H_5O^{\cdot}$$

In the absence of a nickel complex 1,1-diphenylethylperoxy radicals interact to give acetophenone (18%) and no 1,1-diphenylethanol. However, in the presence of $Ni(n\text{-}Bu_2dtc)_2$ the acetophenone yield is 30–40% with diphenylethylene (60–70%) making up the balance. By analogy with the cumylperoxy radical – nickel complex system 1,1-diphenylethylene must be formed by dehydration of 1,1-diphenylethanol, the alcohol being produced from 1,1-diphenylethoxy radicals by H-atom transfer. Production of 1,1-diphenylethanol and acetophenone in this system confirms that alkoxy radicals are formed from reaction of alkylperoxy radicals with nickel complexes.

When α-cumyl alcohol was added to the tetraphenylbutane–nickel complex system it was efficiently dehydrated to α-methylstyrene. This indicates unambiguously that a Lewis acid is formed in these systems.

Further evidence for the involvement of alkoxy radicals was obtained from the products formed by decomposition of cumyl hyponitrite (a source of cumyloxy radicals) in the absence and presence of $Ni(n\text{-}Bu_2dtc)_2$ (Table 9). In the absence of the dithiocarbamate the principal reaction product was acetophenone (70%) while in the presence of the dithiocarbamate α-cumyl alcohol (55%), acetophenone (18%), and α-methylstyrene (3%) were formed. The ratio ([α-cumyl alcohol] + [α-methylstyrene])/[acetophenone] in this system = 3.3 and is identical to this ratio obtained in the cumylperoxy–$Ni(n\text{-}Bu_2dtc)_2$ system. There is, however, an interesting difference in the ratio of α-cumyl alcohol to α-methylstyrene produced from the two oxy radicals. In the cumyloxy system only a small amount of dehydration of α-cumyl alcohol occurred. This suggests that alkoxy radicals do not oxidize the nickel complex to a Lewis acid as efficiently as alkylperoxy radicals.

Conclusions

Both nickel di-*n*-butyldithiocarbamate and nickel diisopropyldithiophosphate can inhibit AIBN initiated hydrocarbon autoxidation by scavenging alkylperoxy radicals. Rate constants, calculated from a kinetic analysis of these reactions, fall in the range 0.3–3 $\times 10^4$ M^{-1} s^{-1} at 50 °C with the dithiocarbamate slightly more efficient than the dithiophosphate. The magnitude of k_{inh} does, however, appear to depend on the nature of the substrate indicating that radicals are formed in the rate controlling inhibition reaction which are capable of propagating the chain. Values of k_{inh}, therefore, give a measure of inhibitor efficiency rather than an absolute reactivity to peroxy radicals.

Both $Ni(n\text{-}Bu_2dtc)_2$ and $Ni(i\text{-}Pr_2dtp)_2$ destroyed two alkylperoxy radicals. Induction periods obtained from hydrocarbon autoxidation for the dithiocarbamate were longer than would have been predicted by an n-value of 2, implying that an efficient radical scavenger was formed during the induction period. Conversely induction periods for the dithiophosphate were shorter than would have been predicted, suggesting that additional free radicals were formed during the induction period which consume the inhibitor. In both cases rates of autoxidation

Can. J. Chem. Downloaded from www.nrcresearchpress.com by 210.87.254.5 on 09/05/12
For personal use only.

after the induction period were close to the uninhibited rate but decelerated as oxygen was absorbed, implying that secondary radical scavengers were formed.

Kinetic esr spectroscopy indicated that rate constants for reaction of tertiary alkylperoxy radicals with Ni(*n*-Bu_2dtc)$_2$ in toluene and fluorotrichloromethane are *ca.* 10^4 M^{-1} s^{-1} from -15 to -94 °C. Rate constants were significantly smaller in isopentane which implies that radicals are formed from reaction of peroxy radicals with Ni(*n*-Bu_2dtc)$_2$ which are capable of reacting with the solvent to regenerate *t*-ROO·. Rate constants for reaction of *t*-ROO· with Ni(*i*-Pr_2dtp)$_2$ could not be measured because pseudo-first-order rate constants were virtually independent of the complex concentration.

The radical derived products from reaction of alkylperoxy radicals with Ni(*n*-Bu_2dtc)$_2$ and Ni(*i*-Pr_2dtp)$_2$ suggest that this reaction involves an oxygen atom transfer from the peroxy radical to the nickel(II) complex to give an alkoxy radical and a nickel complex in a higher oxidation state. The production of a reactive alkoxy radical in this reaction is consistent with the kinetic results obtained from inhibited autoxidations and esr studies.

We have previously concluded (1) that reaction of zinc dialkyldithiophosphates and related zinc complexes with alkylperoxy occurs at the metal center by a mechanism that involves either an electron transfer reaction

$$[21] \quad ROO\cdot + ZnX_2 \rightarrow ROO^- + ZnX^+ + X\cdot$$

or an S_H2 process

$$[22] \quad ROO\cdot + ZnX_2 \rightarrow ROOZnX + X\cdot$$

The results presented in this paper certainly favour reaction 22 over a mechanism that comprises formation of alkylperoxide ion. However, reaction 22 as it is written involves substitution of a bidentate chelating ligand with a monodentate ligand, a most unlikely situation. Furthermore, the oxidation state of the metal ion would remain unchanged. It, therefore, seems more likely that the peroxy radical adds to the metal complex to give a zinc or nickel(III) complex ($ROOMX_2$) which is thermally unstable and undergoes O–O homolysis. Only a fraction of the alkoxy radicals produced must escape the solvent cage or these compounds would not inhibit hydrocarbon autoxidation. The exact mechanism for the production of alkoxy radical derived products in these systems is, however, still in doubt although a concerted decomposition of a $ROOMX_2$ species may be involved. We hope that an investigation of the fate of the nickel and zinc complexes after reaction with alkylperoxy radicals will shed more light on the mechanism of reaction 22. Further work along these lines is in progress.

Acknowledgments

The authors wish to thank Dr. K. U. Ingold for his continuing interest and advice throughout the course of this work and the referees for their helpful comments.

1. J. A. Howard, Y. Ohkatsu, J. H. B. Chenier, and K. U. Ingold. Can. J. Chem. **51**, 1543 (1973).
2. S. F. Nelsen and P. D. Bartlett. J. Am. Chem. Soc. **88**, 137 (1966).
3. E. Müller and G. Roscheinsen. Ber. **90**, 543 (1957).
4. L. R. Mahoney. J. Am. Chem. Soc. **88**, 3035 (1966).
5. H. Keifer and T. G. Traylor. Abstract of paper presented to the International Symposium on the Chemistry of Organic Peroxides. Berlin-Adlershof, September 1967.
6. H. Keifer and T. G. Traylor. Tetrahedron Lett. 6163 (1966).
7. J. A. Howard and E. Furimsky. Can. J. Chem. **51**, 3738 (1973).
8. J. H. B. Chenier, E. Furimsky, and J. A. Howard. Can. J. Chem. **52**, 3682 (1974).
9. C. E. Boozer, G. S. Hammond, C. E. Hamilton, and J. N. Sen. J. Am. Chem. Soc. **77**, 3233 (1955).
10. J. A. Howard. Adv. Free Radical Chem. **4**, 49 (1972).
11. J. L. Kice. Free Radicals, **2**, 711 (1973).
12. J. A. Howard and K. U. Ingold. Can. J. Chem. **45**, 785 (1967).
13. J. E. Bennett, J. A. Eyre, C. P. Rimmer, and R. Summers. Chem. Phys. Lett. **26**, 69 (1974).
14. J. R. Wasson, G. M. Woltermann, and H. J. Stoklosa. Fortschr. Chem. Forsch. **35**, 65 (1973).
15. H. S. Blanchard. J. Am. Chem. Soc. **81**, 4548 (1959).
16. K. J. Humphris and G. Scott. J. Chem. Soc. Perkin Trans. II, 831 (1973).
17. J. A. Howard and K. U. Ingold. Can. J. Chem. **47**, 3797 (1969).

Metal complexes as antioxidants. III. Reaction of nickel dialkyldithiocarbamates and nickel dialkyldithiophosphates with alkyl hydroperoxides[1]

J. A. HOWARD[2] AND J. H. B. CHENIER
Division of Chemistry, National Research Council of Canada, Ottawa, Canada K1A 0R9

Received June 13, 1975

J. A. HOWARD and J. H. B. CHENIER. Can. J. Chem. **54**, 390 (1976).

Alkyl hydroperoxides are shown to react with nickel dialkyldithiocarbamates and nickel dialkyldithiophosphates in the liquid-phase at 30 °C to generate free radicals. These radicals are capable of inducing the decomposition of the hydroperoxide and destroying the nickel complex. Rates of radical generation, as determined from hydrocarbon autoxidation, are similar to rates of complex disappearance and are *ca.* 1/5th rates of hydroperoxide disappearance. Rates of disappearance of both reactants are retarded by the addition of hydrogen atom donating antioxidants, the rate of hydroperoxide disappearance is reduced to the rate of radical generation and the rate of complex disappearance is significantly less than the rate of radical generation. These results are consistent with a mechanism for decomposition which involves cycling of the nickel complex. Decomposition of cumene hydroperoxide to α-cumyl alcohol, α-methylstyrene and acetophenone suggests the intermediacy of cumyloxy radicals in this system while the electron spin resonance spectroscopic method indicates that alkylperoxy radicals are also transient intermediates.

J. A. HOWARD et J. H. B. CHENIER. Can. J. Chem. **54**, 390 (1976).

On montre que les hydroperoxydes d'alkyles réagissent avec les dialkyldithiocarbamates et les dialkyldithiophosphates de nickel en phase liquide à 30 °C pour conduire à des radicaux libres. Ces radicaux sont capables d'induire la décomposition de l'hydroperoxyde et de détruire le complexe de nickel. Les taux de formation des radicaux, tels que déterminés par l'autooxydation d'hydrocarbures, sont semblables aux taux de disparition du complexe et sont approximativement 5 fois plus lents que les taux de disparition de l'hydroperoxyde. Les taux de disparition des deux réactifs sont retardés par addition d'antioxydant pouvant donner des atomes d'hydrogène; le taux de disparition de l'hydroperoxyde est réduit au taux de génération des radicaux et la vitesse de disparition du complexe est beaucoup plus faible que la vitesse de génération des radicaux. Ces résultats sont en accord avec un mécanisme pour la décomposition qui implique un recyclage du complexe de nickel. La décomposition de l'hydroperoxyde de cumène en alcool α-cumyle, en α-méthylstyrène et en acétophénone suggère que les radicaux cumyloxy sont des intermédiaires dans ce système alors que des études de spectroscopie de résonance paramagnétique électronique indiquent que les radicaux alkylperoxy sont aussi des intermédiaires de courte durée.

[Traduit par le journal]

Introduction

It is now well established that zinc and nickel complexes of dialkyldithiocarbamic acids and dialkyldithiophosphoric acids can inhibit autoxidation by scavenging chain-propagating alkylperoxy radicals (1, 2). These compounds are also believed to function as preventive antioxidants because of their ability to decompose chain-initiating hydroperoxides to nonradical products (3–9). The initial reaction between some of these complexes and alkyl hydroperoxides has been shown to generate free radicals which are capable of *initiating* autoxidation (4, 5) and it has been suggested that these complexes function as antioxidants because they are oxidized to a catalyst capable of decomposing hydroperoxides heterolytically (3, 4).

As part of our investigation of the inhibition of autoxidation by metal complexes we have studied the reaction of nickel dialkyldithiocarbamates and nickel dialkyldithiophosphates with alkyl hydroperoxides. This work, which is reported here, has produced results which are at variance with those reported in the literature and indicates that these nickel complexes cannot be expected to function as preventive antioxidants at ambient temperature.

[1]NRCC No. 15013.
[2]To whom all correspondence should be addressed.

Can. J. Chem. Downloaded from www.nrcresearchpress.com by 210.87.254.42 on 09/05/12
For personal use only.

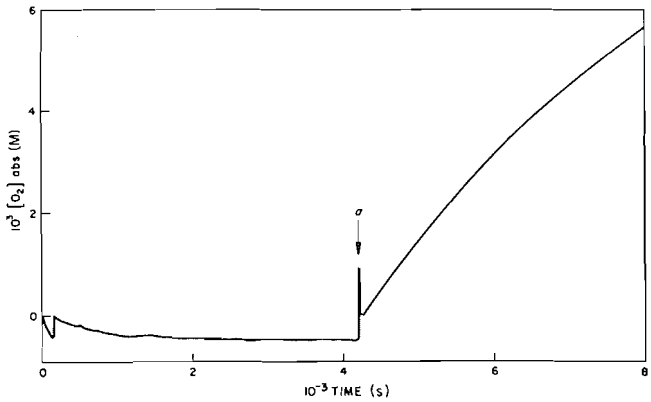

FIG. 1. Oxygen absorption as a function of time for the autoxidation of styrene (1.74 *M*) in chlorobenzene initiated by Ni(*i*-Pr_2dtp)$_2$ (0.016 *M*) and $(CH_3)_3COOH$ (0.01 *M*) at 30 °C. *a* indicates the time that the hydroperoxide was added.

Experimental

Materials

Nickel dialkyldithiocarbamates, Ni(R_2dtc)$_2$, and dialkyldithiophosphates, Ni(R_2dtp)$_2$, were prepared by reaction of the acid or sodium salt with nickel acetate. Cumene hydroperoxide was purified via its sodium salt, *tert*-butyl hydroperoxide by recrystallization from pentane followed by vacuum distillation, while α-tetralin hydroperoxide was prepared by autoxidation of tetralin. The hydroperoxides were better than 99% pure by iodometric titration. The oxidizable hydrocarbons and solvents were purified by standard techniques.

Kinetic Procedure

Autoxidations were followed with the automatic recording apparatus described previously (10). Reactions between the hydroperoxides and nickel complexes were followed by uv spectroscopy (nickel complex disappearances were followed at λ = 320 nm (dtp) and λ = 326 and 394.5 nm (dtc)), infrared spectroscopy (hydroperoxide disappearance at $\nu = 3550\ cm^{-1}$), and iodometric titration. The reactions were performed in the presence and absence of the phenolic inhibitors 2,6-di-*tert*-butyl-4-methoxyphenol (BMeOP) and 2,6-di-*tert*-butyl-4-methylphenol (BMP). All reactions described in this work were carried out at 30 °C.

Products

Volatile reaction products were identified by gas–liquid chromatography in conjunction with mass spectrometry. Yields were determined by comparison with standard authentic samples. The 1-methyl-1-alkylperoxy-3,5-di-*tert*-butylcyclohexadiene-2,5-dione-4's were isolated and identified by standard techniques. Yields of these products were determined by the infrared spectroscopic method. The accumulation of products during reaction was followed by ir spectroscopy.

Electron Spin Resonance Studies

Reactions of alkyl hydroperoxides with the nickel complexes in CCl_4 were performed *in situ* in the cavity of a Varian E-4 spectrometer at 30 °C in the dark with argon bubbling through the sample. Prior to the addition of one of the reactants the spectrometer was set at the magnetic field corresponding to the maximum peak height of the first derivative of the alkylperoxy radical signal with the field sweep switched off. Changes in the signal intensity were monitored continuously with the X–Y recorder provided with the spectrometer as soon as the reactants were thoroughly mixed.

Results

Initiation of Hydrocarbon Autoxidation

It has been reported (4, 5) that zinc complexes of dialkyldithiophosphoric acids and dialkyldithiocarbamic acids exert a pro-oxidant effect on the initial stages of hydrocarbon autoxidation containing hydroperoxide because of a homolytic reaction between the complex and hydroperoxide. We found that zinc dialkyldithiophosphates and dialkyldithiocarbamates reacted with added hydroperoxide during AIBN initiated autoxidation of styrene at 50 °C to give more efficient radical scavengers, a process which overshadowed any enhanced initiation (1). Only zinc isopropylxanthate gave a detectable pro-oxidant effect.

On the other hand the analogous nickel complexes were all found to exert very pronounced catalysis of autoxidations containing hydroperoxide (see *e.g.*, Fig. 1).[3] Initial rates of autoxida-

[3]Nickel complexes of carboxylic acids are also able to initiate hydrocarbon autoxidation in the presence of hydroperoxide. Thus Wallace and Skomoroski (11) have found that nickel cyclohexane butyrate in combination with cumene hydroperoxide is an effective catalyst for the autoxidation of cumene at 104 °C.

Can. J. Chem. Downloaded from www.nrcresearchpress.com by 210.87.254.42 on 09/05/12
For personal use only.

Can. J. Chem. Downloaded from www.nrcresearchpress.com by 210.87.254.42 on 09/05/12
For personal use only.

TABLE 1. Initial rates of autoxidation of styrene (1.74 M)[a] at 30 °C initiated by reaction between a nickel complex and *tert*-butyl hydroperoxide[b]

Ligand	$[A]_0 \times 10^3$ (M)	$[ROOH]_0 \times 10^3$ (M)	$(-d[O_2]/dt)_0 \times 10^7$ ($M\,s^{-1}$)
i-Pr_2dtp	1.6	10	5.0
i-Pr_2dtp	4.0	10	7.2
i-Pr_2dtp	8.0	10	23
i-Pr_2dtp	16	1	1.2
i-Pr_2dtp	16	4	6.8
i-Pr_2dtp	16	10	41
i-Pr_2dtp	1.0	1.0	44.5
Et_2dtc	10	10	170
i-Pr_2dtc	10	10	>1000

[a]Chlorobenzene as diluent.
[b]Cumene hydroperoxide gave almost identical initial rates.

tion of styrene at different initial complex and hydroperoxide concentrations are given in Table 1 and were found to increase as the initial concentration of each reactant was increased.[4] Unfortunately, because of the difficulties associated with measuring accurate initial rates, precise concentration exponents could not be obtained from these experiments. However, it would appear that the order with respect to each reactant is close to 1.0.

We have previously concluded (2) that initial rates of Ni(*i*-Pr_2dtp)$_2$ and Ni(*n*-Bu_2dtc)$_2$ inhibited, α,α'-azobisisobutyronitrile initiated autoxidation of styrene, $(-d[O_2]/dt)_0$, very approximately obey the rate expression

$$[1] \qquad \left(\frac{-d[O_2]}{dt}\right)_0 = \frac{k_p[RH]_0 R_i}{2k_{inh}[A]_0}$$

where $[RH]_0$ is the initial hydrocarbon concentration, $[A]_0$ the initial nickel complex concentration, R_i is the rate of chain initiation, and k_p and k_{inh} are the rate controlling propagation and termination rate constants. It was suggested that these autoxidations can be represented by the following elementary reactions

Initiation:

[2] Production of R· at a rate = R_i

Propagation:

$$[3] \qquad R\cdot + O_2 \xrightarrow{\text{fast}} ROO\cdot$$

$$[4] \qquad ROO\cdot + RH \xrightarrow{k_p} ROORH\cdot$$

Termination:

$$[5] \qquad ROO\cdot + A \xrightarrow{k_{inh}} X$$

$$[6] \qquad ROO\cdot + X \xrightarrow{\text{fast}} \text{Nonradical products}$$

where X is an intermediate which reacts rapidly with ROO· but does not propagate the chain. There was, however, some evidence which suggested that the mechanism may be complicated by a chain transfer reaction between the complex and alkylperoxy radicals.

$$[7] \qquad ROO\cdot + A \rightarrow Y\cdot + \text{other products}$$

where Y· could be an alkoxy radical or a sulphur radical derived from A.

The nickel complex – alkyl hydroperoxide initiated autoxidation of styrene should also be described by the same elementary reactions with the initiation reaction taking the form

$$[2'] \qquad ROOH + A \rightarrow \text{Free radicals}$$

The observation that $(-d[O_2]/dt)_0$ increases as the nickel complex concentration is increased, at a constant hydroperoxide concentration, does, however, imply that the order with respect to [A] in the initiation reaction is higher than it is in the termination reaction.

Autoxidations initiated by reaction 2′ were completely inhibited by the H-atom donating antioxidant, 2,6-di-*tert*-butyl-4-methoxyphenol (see *e.g.*, Fig. 2). Overall rates of chain initiation

[4]A typical feature of these autoxidations was the dramatic decrease in the rate of autoxidation after the absorption of a small amount of oxygen presumably because of complete destruction of the nickel complex in radical scavenging reactions. For instance, addition of $(CH_3)_3COOH$ (0.01 M) to a mixture of nickel diisopropyldithiocarbamate (0.01 M) and styrene (1.74 M) in chlorobenzene gave an initial rate of oxygen absorption $> 10^{-4}$ $M\,s^{-1}$. Absorption of oxygen, however, ceased completely after ~0.0055 M of O_2 had been absorbed.

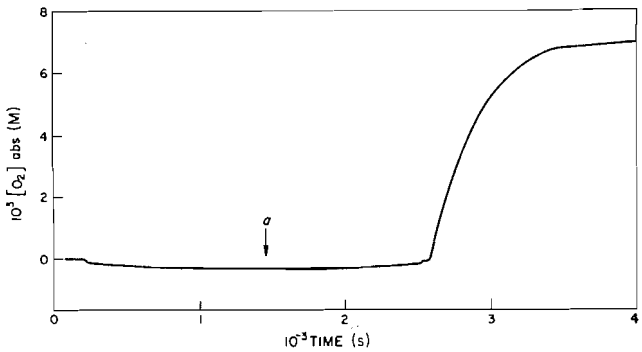

FIG. 2. Oxygen absorption as a function of time for the autoxidation of styrene (1.74 *M*) in chlorobenzene at 30 °C initiated by Ni(*n*-Bu_2dtc)$_2$ (0.0016 *M*) and $(CH_3)_3$-COOH (0.005 *M*) and inhibited by 2,6-di-*tert*-butyl-4-methoxyphenol (0.007 *M*). *a* indicates the time that the hydroperoxide was added.

TABLE 2. Kinetic data for the nickel complex – *tert*-butyl hydroperoxide initiated autoxidation of styrene (1.74 *M*)[a] at 30 °C in the presence of BMeOP

Ligand	$[A]_0 \times 10^3$ (*M*)	$[ROOH]_0 \times 10^3$ (*M*)	$[BMeOP]_0 \times 10^3$ (*M*)	Induction period $\times$ 10^{-4} (s)	$(-d[O_2]/dt)_0 \times 10^7$ ($M\ s^{-1}$)	$R_i \times 10^7$ ($M\ s^{-1}$)
i-Pr_2dtp	1.6	10	0.6	2.8	4.0	0.43
i-Pr_2dtp	4.0	10	0.6	1.2	14	1.0
i-Pr_2dtc	0.8	10	1.4	0.2	194	13.7
i-Pr_2dtc	1.6	5	0.7	0.11	192	12.3
i-Pr_2dtc	0.8	10	1.4	0.2	223	13.3
i-Pr_2dtc	0.8	10	2.8	0.45	112	12.4
i-Pr_2dtc	1.6	10	2.8	0.18	184	31
i-Pr_2dtc	1.6	10	2.8	0.22	182	26

[a]Chlorobenzene as solvent.

were obtained from the time taken to consume a known concentration of BMeOP and were found to increase as the concentration of each reactant was increased (Table 2).

If the rate of chain initiation is given by $R_i = k[A][ROOH]$, where k is a bimolecular rate constant which takes into account the number of radicals generated by reaction 2′ and the efficiency with which radicals are produced, a value of $k = 0.0026\ M^{-1}\ s^{-1}$ can be calculated for the dithiophosphate and $k = 0.16\ M^{-1}\ s^{-1}$ for the dithiocarbamate.

The initial rates of autoxidation of styrene were significantly slower than would be predicted from uninhibited autoxidations, confirming that the nickel complexes retard hydrocarbon autoxidation by scavenging free radicals. If the values of $(-d[O_2]/dt)_0$ obey rate expression 1,[5] the following approximate values of nk_{inh} can be calculated; *ca.* $10^3\ M^{-1}\ s^{-1}$ for the dithiophosphate and *ca.* $6 \times 10^3\ M^{-1}\ s^{-1}$ for the dithiocarbamate; rate constants which are close to the values expected at 30 °C from autoxidations initiated by AIBN in the absence of hydroperoxide at 50 °C (2).

Reaction in the Absence of an Oxidizable Substrate

Reaction of the nickel complexes with alkyl hydroperoxides exhibited no induction period. Rates of disappearance of the complexes in the presence of a large excess of alkyl hydroperoxide were pseudo-first-order since plots of $\ln [A]_0 - \ln [A]_t$ *vs.* time were linear over the entire

[5]This must be an oversimplification because if $R_i \propto$ [ROOH][A] and the rate of termination $\propto$ [ROO·][A] the rate of inhibited autoxidation would be independent of [A]. Precise kinetic orders are extremely difficult to obtain in these systems. Until these orders have been precisely measured we prefer to make the gross assumption that eq. 1 is obeyed.

Can. J. Chem. Downloaded from www.nrcresearchpress.com by 210.87.254.42 on 09/05/12
For personal use only.

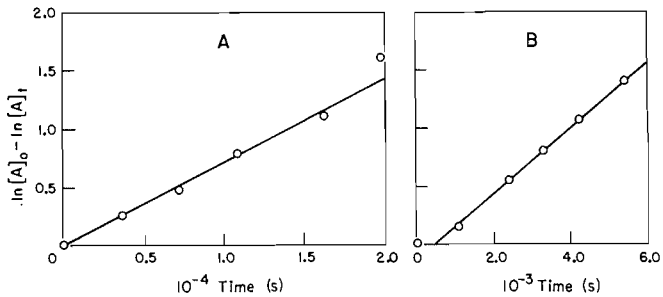

FIG. 3. Plots of $\ln [A]_0 - \ln [A]_t$ against time for reaction between nickel complexes and cumene hydroperoxide. (*A*) $[Ni(i\text{-}Pr_2dtp)_2]_0 = 1.5 \times 10^{-5}$ *M*, $[ROOH]_0 = 10^{-2}$ *M*; (*B*) $[Ni(n\text{-}Bu_2dtc)_2]_0 = 1.5 \times 10^{-5}$ *M*, $[ROOH]_0 = 2 \times 10^{-3}$ *M*.

TABLE 3. Kinetic data for reaction of nickel diisopropyldithiocarbamate with cumene hydroperoxide[a]

$[A]_0 \times 10^4$ (*M*)	$[ROOH]_0 \times 10^2$ (*M*)	$(-d[A]/dt)_0 \times 10^8$ ($M\,s^{-1}$)	$\frac{(-d[A]/dt)_0}{[A]_0[ROOH]_0}$ ($M^{-1}\,s^{-1}$)	$\frac{k_\psi}{[ROOH]_0}$ ($M^{-1}\,s^{-1}$)
1.5	1.0	—	—	0.14
1.1	1.0	14	0.13	—
1.0	1.0	15	0.15	—
1.5	0.1	—	—	0.15
1.4	0.1	4.0	0.29	—
1.3	0.1	1.4	0.11	—
1.07	0.1	1.9	0.18	—
0.3	0.1[b]	—	—	0.13
0.29	0.1	0.8	0.27	—
0.15	0.2	—	—	0.14
0.14	0.2	0.26	0.09	—
0.11	0.2	0.32	0.15	—

[a]Solvent: chlorobenzene.
[b]$(CH_3)_3COOH$ gave $k_\psi/[ROOH]_0 = 0.12\ M^{-1}\,s^{-1}$.

concentration range (see *e.g.* Fig. 3). Pseudo-first-order rate constants (k_ψ) were independent of the initial complex concentration and were linearly dependent on the hydroperoxide concentration. The rate law

$$\frac{-d[A]}{dt} = k'[A][ROOH]$$

where k' is a bimolecular rate constant and $k_\psi = k'[ROOH]$, was, therefore, strictly obeyed. Initial rates of complex disappearance also obeyed this kinetic expression. The kinetic data obtained for reaction of $Ni(i\text{-}Pr_2dtp)_2$ and $Ni(i\text{-}Pr_2dtc)_2$ with cumene hydroperoxide are summarized in Tables 3 and 4. The "best" values of k' were 0.004 and 0.16 $M^{-1}\,s^{-1}$, respectively. Rate constants k' are, therefore, very similar to the bimolecular rate constants k calculated from nickel complex – hydroperoxide initiated autoxidations.

Values of k' were independent of the alkyl moiety in the dithiocarbamate (methyl, ethyl, isopropyl, and *n*-butyl) and the nature of the hydroperoxide (*tert*-butyl, α-cumyl, and α-tetralyl).

At the molar ratios of hydroperoxide to nickel complex shown in Tables 3 and 4 the hydroperoxide concentration remained unchanged. There was, therefore no evidence for significant heterolytic hydroperoxide decomposition. This result is in variance with the reports by Scott and coworkers (4, 9) that traces of nickel dialkyldithiophosphates and dialkyldithiocarbamates decompose cumene hydroperoxide to give phenol and acetone.

Reactant concentration – time profiles are

Can. J. Chem. Downloaded from www.nrcresearchpress.com by 210.87.254.42 on 09/05/12
For personal use only.

TABLE 4. Kinetic data for reaction of nickel diisopropyldithiophosphate with cumene hydroperoxide (0.01 M)[a]

$[A]_0 \times 10^4$ (M)	$(-d[A]/dt)_0 \times 10^8$ ($M\,s^{-1}$)	$\frac{(-d[A]/dt)_0}{[A]_0[ROOH]_0}$ ($M^{-1}\,s^{-1}$)	$\frac{k_\psi}{[ROOH]_0}$ ($M^{-1}\,s^{-1}$)
0.08	0.071	0.009	—
0.10	0.059	0.006	—
0.132	0.098	0.0074	—
0.15[a]	—	—	0.007
0.44	0.072	0.0016	—
0.45	—	—	0.002
1.2	0.36	0.003	—
1.4	0.52	0.004	—
1.5	—	—	0.003
4.3	1.2	0.003	—
4.8	1.3	0.003	—
5.0[a]	—	—	0.003

[a]In chlorobenzene.

shown in Fig. 4 for reaction of nickel diisopropyldithiophosphate and cumene hydroperoxide. It is quite clear from this figure that $-d[ROOH]/dt$ is greater than $-d[A]/dt$ and that the stoichiometric factor is >5.

Rates of hydroperoxide decomposition in the presence of excess nickel complex were measured and found to fit the kinetic expression

$$\frac{-d[ROOH]}{dt} = ak'[A][ROOH]$$

where a is the stoichiometric factor. Values of ak' obtained from $-d[ROOH]/dt$ were about 5 times larger than values of k' determined from $-d[A]/dt$, implying that a is ~ 5.

Stoichiometric factors for this reaction were determined from the concentration of one reactant that disappeared when the other reactant was completely consumed. The results of these studies are summarized in Table 5 and suggest that 5–15 molecules of hydroperoxide are decomposed by each molecule of nickel complex.

The hydroperoxide derived products from reaction of the nickel complexes with cumene hydroperoxide are presented in Table 6. α-Cumyl alcohol is the principal product along with significant quantities of α-methylstyrene and acetophenone. In all cases 100% of the hydroperoxide could be accounted for by these three products. α-Methylstyrene almost certainly arises by dehydration of α-cumyl alcohol during reaction. Reduction of α-cumyl hydroperoxide to α-cumyl alcohol can be achieved either by a free-radical induced reaction or a stoichiometric reaction. However, the concurrent production of acetophenone is indicative of the intermediacy of cumyloxy radicals and hence a homolytic process.

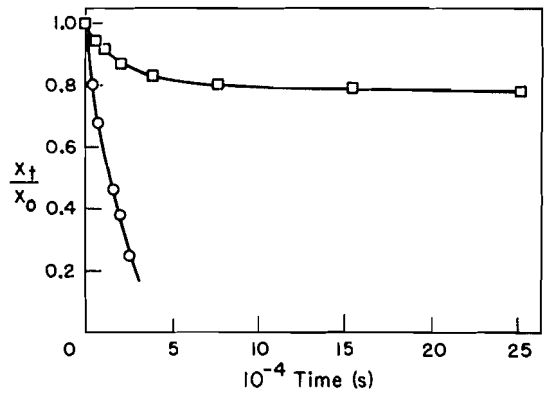

FIG. 4. The concentrations of the reactants (x) as a function of time for reaction of nickel diisopropyldithiophosphate (5×10^{-3} M), □, with cumene hydroperoxide (5×10^{-3} M), ○.

Electron Spin Resonance Studies

When nickel di-*n*-butyldithiocarbamate and *tert*-butyl hydroperoxide were allowed to react in the cavity of an electron spin resonance spectrometer the *tert*-butylperoxy radical (broad singlet at $g = 2.015$) was the only radical species that could be detected. The variation of the concentration of the peroxy radical and the nickel complex during reaction of $Ni(n\text{-}Bu_2dtc)_2$ (10^{-4} M) and $(CH_3)_3COOH$ (1.5×10^{-2} M) in CCl_4 at 30 °C are shown in Fig. 5. The peroxy

Can. J. Chem. Downloaded from www.nrcresearchpress.com by 210.87.254.42 on 09/05/12
For personal use only.

Can. J. Chem. Downloaded from www.nrcresearchpress.com by 210.87.254.42 on 09/05/12
For personal use only.

TABLE 5. Stoichiometric factors for reaction of nickel complexes with alkyl hydroperoxides[a]

Ligand	Initial reactant concentration (M) $[A]_0$	Initial reactant concentration (M) $[(CH_3)_3COOH]_0$	$\frac{[ROOH]_0}{[A]_0}$	$\frac{\Delta[ROOH]}{\Delta[A]}$
n-Bu_2dtc	0.005	0.01	20	14
n-Bu_2dtc	0.001	0.02	20	11
n-Bu_2dtc	0.00002	0.0001	5	15
n-Bu_2dtc	0.0002	0.001	5	7
n-Bu_2dtc	0.0004	0.001	2.5	5
n-Bu_2dtc	0.00002	0.0001	5	8
n-Bu_2dtc	0.0001	0.001	10	7
i-Pr_2dtp	0.00004	0.0001	2.5	17

[a]Almost identical stoichiometric factors were obtained with α-tetralin hydroperoxide.

TABLE 6. Hydroperoxide derived products from reaction of cumene hydroperoxide with some nickel complexes at 30 °C[a]

Ligand	$[A]_0 \times 10^3$ (M)	$[ROOH]_0 \times 10^3$ (M)	Products (mol/mol ROOH) Acetophenone	α-Methylstyrene	α-Cumyl alcohol
i-Pr_2dtp	5	10	0.21	0.22	0.61
i-Pr_2dtp	10	3.3	0.13	0.26	0.67
i-Pr_2dtp	5	5	0.23	0.27	0.58
i-Pr_2dtp	10	10	0.12	0.22	0.6
i-Pr_2dtc	10	10	0.08	0.22	0.64
n-Bu_2dtc	10	0.1	[b]	0.4	0.23

[a]Chlorobenzene used as solvent.
[b]Not detected.

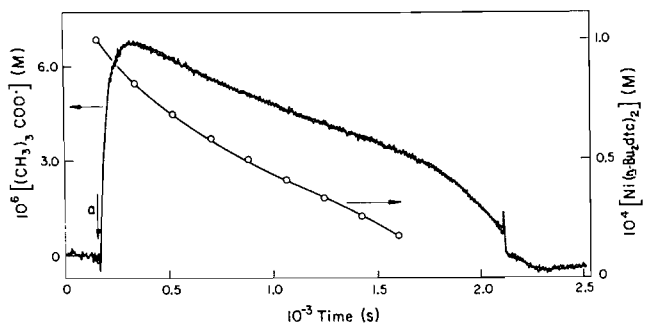

FIG. 5. The change in the *tert*-butylperoxy radical and nickel complex concentration with respect to time for reaction of Ni(n-$Bu_2dtc)_2$ (10^{-4} M) with *tert*-butyl hydroperoxide (1.5×10^{-2} M).

radical concentration increased to a maximum value and then slowly decreased as the nickel complex was consumed. Maximum yields of $(CH_3)_3COO^\cdot$ at different initial reactant concentrations are gathered in Table 7 and demonstrate that the radical concentration increased as the concentration of each reactant was increased.

α-Tetralylperoxy radicals are produced when α-tetralin hydroperoxide was used instead of *tert*-butyl hydroperoxide. The maximum concentration of this radical was about a factor of 4 smaller than the maximum concentration of $(CH_3)_3COO^\cdot$ under identical experimental conditions.

Reaction of Ni(i-$Pr_2dtp)_2$ with *tert*-butyl hydroperoxide also produces *tert*-butylperoxy radicals. The maximum radical yields were, however, about a factor of 10 lower than for the dithio-

Can. J. Chem. Downloaded from www.nrcresearchpress.com by 210.87.254.42 on 09/05/12
For personal use only.

TABLE 7. Maximum yields of *tert*-butylperoxy radicals from reaction of nickel di-*n*-butyldithiocarbamate and *tert*-butyl hydroperoxide[a]

$[A]_0 \times 10^4$ (M)	$[ROOH]_0 \times 10^2$ (M)	$[ROO\cdot]_{max} \times 10^6$[b] ($M$)
0.33	1.0	6.0
1.0	0.33	2.0
3.3	1.0	60
1.0	1.0	7.2
1.0	5.0	20

[a]At 30 °C in CCl_4.
[b]Maximum radical concentration.

carbamate, with radical generation lasting very much longer because the complex was consumed more slowly.

Influence of Phenolic Antioxidants

Rates of disappearance of the nickel complexes in the presence of a large excess of hydroperoxide were considerably slower in the presence of 2,6-di-*tert*-butyl-4-methoxyphenol (BMeOP) and 2,6-di-*tert*-butyl-4-methylphenol (BMP). Plots of $\ln [A]_0 - \ln [A]_t$ against time were linear (see *e.g.* Fig. 6) and the slopes of these plots were proportional to the first power of the hydroperoxide concentration. Values of $(-d[A]/dt)_0$ were proportional to the first power of the concentration of each reactant. The overall rate must, therefore, obey the kinetic expression

$$\frac{-d[A]}{dt} = k''[A][ROOH]$$

where k'' is the bimolecular rate constant. The 'best' values of k'' for Ni(*i*-Pr_2dtp)$_2$ and Ni(*i*-Pr_2dtc)$_2$ were 0.00005 M^{-1} s^{-1} and 0.006 M^{-1} s^{-1}, respectively.

Rates of hydroperoxide decomposition were faster than $-d[A]/dt$ and obeyed the kinetic expression

$$\frac{-d[ROOH]}{dt} = bk''[A][ROOH]$$

where b is the stoichiometric factor.

Stoichiometric factors were determined by the same technique as was employed for reactions in the absence of phenolic antioxidant and the results are summarized in Table 10. Stoichiometric factors are significantly larger in the presence of BMP than they are in the absence of this additive. This is because addition of BMP

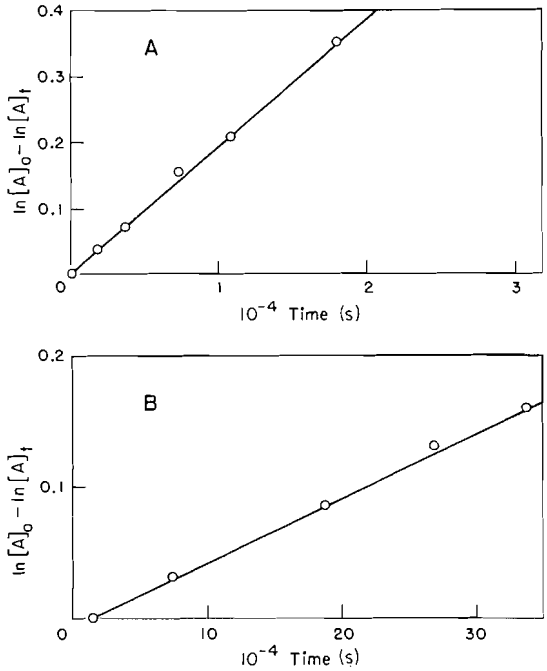

FIG. 6. Plots of $\ln [A]_0 - \ln [A]_t$ against time for reaction between nickel complexes and alkyl hydroperoxides in the presence of phenolic antioxidants. (*A*) Ni(*n*-Bu_2dtc)$_2$ = 10^{-4} M, $(CH_3)_3COOH$ = 10^{-2} M, BMP = 10^{-2} M. (*B*) Ni(*i*-Pr_2dtp)$_2$ = 2×10^{-4} M; $C_6H_5C(CH_3)_2OOH$ = 10^{-2} M, BMeOP = 2×10^{-3} M.

inhibits free radical destruction of the complex enabling it to take part in more hydroperoxide destroying reactions.

The decrease in the concentration of the reactants and the increase in the concentration of the products with respect to time for reaction of Ni(*n*-Bu_2dtc)$_2$ (0.0002 M) and $(CH_3)_3COOH$ (0.02 M) in the presence of BMP (0.01 M) appear in Fig. 7. At these initial reactant concentrations all of the nickel complex was destroyed and the hydroperoxide concentration decreased to 0.003 M, which is consistent with the stoichiometric factors given in Table 10. The hydroperoxide appears to have been converted to *tert*-butyl alcohol (~50%) and *tert*-butylperoxy radicals (~50%), the latter being trapped by 2,6-di-*tert*-butyl-4-methylphenoxy radicals as 1-methyl-1-*tert*-butylperoxy-3,5-di-*tert*-butylcyclohexadiene-2,5-dione-4, **1**.[6] A trace of iso-

[6]The percentage of *tert*-butyl alcohol was based on the yield of this product and the *tert*-butylperoxy radical percentage was based on the yield of **1**.

Can. J. Chem. Downloaded from www.nrcresearchpress.com by 210.87.254.42 on 09/05/12
For personal use only.

TABLE 8. Kinetic data for reaction of $Ni(R_2dtc)_2$ with some tertiary alkyl hydroperoxides in the presence of hindered phenols

$[A]_0 \times 10^4$ (M)	$[ROOH]_0 \times 10^2$ (M)	$(-d[A]/dt)_0 \times 10^8$ (M^{-1} s^{-1})	$\frac{(-d[A]/dt)_0}{[A][ROOH]}$ (M^{-1} s^{-1})	$\frac{k_\psi}{[ROOH]_0}$ (M^{-1} s^{-1})
0.1[a,f]	1.0[d]	0.024	0.0024	0.0023
0.2[a,f]	5.0[d]	0.4	0.004	0.005
0.3[a,f]	0.1[d]	0.006	0.002	0.002
1.0[a,f]	1.0[d]	0.2	0.002	0.002
0.15[b,e]	0.1[c]	0.006	0.004	0.005
0.15[b,e]	0.2[c]	0.016	0.005	0.005
0.3[b,e]	0.1[c]	0.02	0.007	0.005
0.3[b,e]	0.2[c]	0.04	0.007	0.006
1.5[b,e]	0.2[c]	0.2	0.007	0.006

[a] $Ni(n\text{-}Bu_2dtc)_2$.
[b] $Ni(i\text{-}Pr_2dtc)_2$.
[c] α-Cumene hydroperoxide.
[d] *tert*-Butyl hydroperoxide.
[e] 2,6-Di-*tert*-butyl-4-methoxyphenol.
[f] 2,6-Di-*tert*-butyl-4-methylphenol.

TABLE 9. Kinetic data for reaction of nickel diisopropyldithiophosphate with cumene hydroperoxide in the presence of 2,6-di-*tert*-butyl-4-methoxyphenol

$[A]_0 \times 10^4$ (M)	$[ROOH]_0 \times 10^2$ (M)	$(-d[A]/dt)_0 \times 10^8$ (M s^{-1})	$\frac{(-d[A]/dt)_0}{[ROOH]_0[A]_0}$ (M s^{-1})	$\frac{k_\psi}{[ROOH]_0}$ (M^{-1} s^{-1})
2.0	1.0	0.01	0.00005	0.00005
4.0	1.0	0.02	0.00005	0.00005

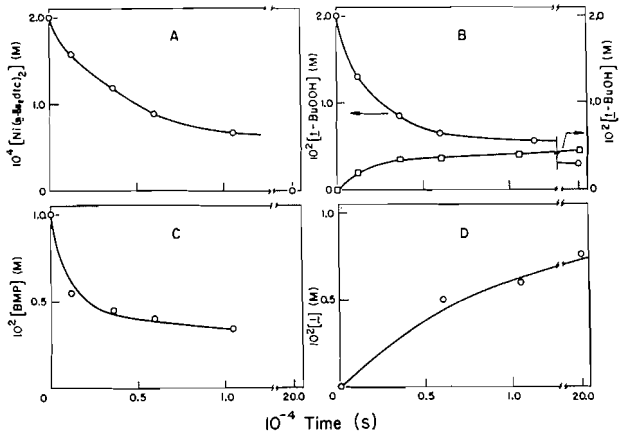

FIG. 7. The concentration of reactants and products as a function of time for reaction between nickel di-*n*-butyl dithiocarbamate (2×10^{-4} M) and *tert*-butyl hydroperoxide (2×10^{-2} M) in the presence of 2,6-di-*tert*-butyl-4-methylphenol. (*A*) $Ni(n\text{-}Bu_2dtc)_2$; (*B*) $(CH_3)_3COOH$ and $(CH_3)_3COH$; (*C*) BMP; (*D*) 1-methyl-1-*tert*-butylperoxy-3,5-di-*tert*-butylcyclohexadiene-2,5-dione.

butylene was formed and the yield of di-*tert*-butyl peroxide was <0.4%.

When cumene hydroperoxide was used instead of *tert*-butyl hydroperoxide the reaction products summarized in Table 11 were obtained. Almost all of the cumene hydroperoxide could be accounted for as α-cumyl alcohol, α-methylstyrene, acetophenone and 1-methyl-1-α-cumylperoxy-3,5-

TABLE 10. Stoichiometries for nickel complex – *tert*-butyl hydroperoxide reaction in the presence of BMP[a]

Ligand	Initial reactant concentration (M) $[A]_0$	Initial reactant concentration (M) $[(CH_3)_3COOH]_0$	$\frac{[ROOH]_0}{[A]_0}$	$\frac{\Delta[ROOH]}{\Delta[A]}$
n-Bu_2dtc	0.0002	0.02	100	60
n-Bu_2dtc	0.0001	0.02	200	44
n-Bu_2dtc	0.0001	0.003	30	40
i-Pr_2dtp	0.0001	0.02	200	40

[a]Almost identical stoichiometric factors were obtained with α-tetralin hydroperoxide.

TABLE 11. Hydroperoxide derived products from reaction of Ni(*n*-Bu_2dtc)$_2$ (6×10^{-4} M) with α-cumene hydroperoxide (2×10^{-2} M) in the presence of 2,6-di-*tert*-4-methylphenol (2×10^{-2} M)

Reaction product	Yield (M)	% yield/mol ROOH
α-Methylstyrene	7.6×10^{-3}	38
Acetophenone	1.2×10^{-3}	6
Cumyl alcohol	5.7×10^{-3}	28
2	1.0×10^{-2}	50

di-*tert*-butylcyclohexadiene-2,5-dione-4, **2**. The yield of cumyloxy derived products (α-cumyl alcohol, α-methylstyrene, and acetophenone) is again approximately equal to the yield of the cumylperoxy radical derived product. A very small concentration of phenol was also formed in this system, implying a minor heterolytic pathway. Production of phenol is probably a consequence of the long reaction times in the presence of BMP giving a heterolytic process time to make a contribution to the reaction products.

Influence of Complexing Agents

Rates of disappearance of the nickel complexes in the absence and presence of BMP were retarded by addition of small concentrations of materials which coordinate metal ions, *e.g.*, Ni(*i*-Pr_2dtc)$_2$ in the presence of pyridine (0.1 M) gave values of $k' = 0.045\ M^{-1}\ s^{-1}$ and $k'' = 0.001\ M^{-1}\ s^{-1}$.

Rates of accumulation of $(CH_3)_3COO\cdot$ as determined by the esr spectroscopic method from reaction of Ni(*n*-Bu_2dtc)$_2$ with $(CH_3)_3COOH$ were also retarded by millimolar concentrations of pyridine.

These results imply that the principal reaction between a nickel complex and an alkyl hydroperoxide involves prior coordination between the hydroperoxide and the nickel complex.

Discussion

There are two mechanisms by which hydroperoxides can be decomposed catalytically, a heterolytic process catalyzed by a Lewis acid and a radical induced decomposition initiated by metal ion – hydroperoxide interactions. The latter mechanism can be represented by

$$[8] \qquad M^n + ROOH \rightarrow M^{n+1} + RO\cdot + OH^-$$

$$[9] \qquad M^{n+1} + ROOH \rightarrow M^n + ROO\cdot + H^+$$

where M is a metal ion and associated ligands (12). These two mechanisms can usually be distinguished by determining the hydroperoxide derived products, *e.g.*, cumene hydroperoxide gives phenol and acetone by a heterolytic decomposition while α-cumyl alcohol, α-methylstyrene, and acetophenone are formed by a radical induced reaction. Furthermore, radical induced decompositions obey a rate law which is first-order in each reactant (13).

Decomposition of cumene hydroperoxide by Ni(R_2dtc)$_2$ and Ni(R_2dtp)$_2$ to α-cumyl alcohol, α-methylstyrene, and acetophenone and a rate expression that is first-order in each reactant suggest that these nickel complexes react by a mechanism analogous to the variable valence transition metal complexes studied by Hiatt *et al.* (13) and that a radical mechanism is prevalent.

Hiatt *et al.* (13) considered that metal ion catalyzed decomposition of tertiary alkyl hydroperoxides can be described by reactions 8 and 9 followed by

$$[10] \qquad RO\cdot + ROOH \rightarrow ROH + ROO\cdot$$

$$[11] \qquad ROO\cdot + ROO\cdot \rightarrow 2RO\cdot + O_2$$

$$[12] \qquad ROO\cdot + ROO\cdot \rightarrow ROOR + O_2$$

The rates of decomposition of the tertiary alkyl hydroperoxides (*tert*-butyl and α-cumyl)

Can. J. Chem. Downloaded from www.nrcresearchpress.com by 210.87.254.42 on 09/05/12
For personal use only.

Can. J. Chem. Downloaded from www.nrcresearchpress.com by 210.87.254.42 on 09/05/12
For personal use only.

and the rates of nickel complex disappearance are consistent with this mechanism if the chain initiation reaction is given by reaction 2′.

Several experimental observations, however, indicate that reactions 11 and 12 are not important for the nickel complexes. First, rates of oxygen evolution were less than 1/100th rates of radical production. Secondly, the maximum concentration of α-tetralylperoxy radicals produced from α-tetralin hydroperoxide, as determined by esr spectroscopy, was only about 1/4 the maximum concentration of $(CH_3)_3COO^\cdot$ produced from $(CH_3)_3COOH$. If termination involved self-reaction of alkylperoxy radicals $[\alpha\text{-}C_{10}H_{11}OO^\cdot]_{max}$ would be $\sim 1/75$th $[(CH_3)_3COO^\cdot]_{max}$ since the termination rate constants for these radicals are 7.4×10^6 and $1.3 \times 10^3\ M^{-1}\ s^{-1}$, respectively (14).

We have previously shown that $Ni(R_2dtc)_2$ and $Ni(R_2dtp)_2$ can inhibit autoxidation at 30 °C by scavenging alkylperoxy radicals (2). It is, therefore, conceivable that this reaction overshadows self-reaction of alkylperoxy radicals in the induced hydroperoxide decomposition.

The observation that $-d[ROOH]/dt > -d[A]/dt$ does, however, demand that radicals capable of reacting with the hydroperoxide are formed from reaction of peroxy radicals with the nickel complex. Our previous kinetic electron spin resonance studies of this reaction (2) indicated that a radical reactive enough to abstract a hydrogen atom from isopentane at −90 °C was formed. Furthermore, the products of this reaction suggest the intermediacy of alkoxy radicals (2).

Overall rates of reaction were slower in the presence of 2,6-di-*tert*-butyl-4-methylphenol, $-d[ROOH]/dt$ being reduced to about R_i while $-d[A]/dt$ was significantly $< R_i$. This latter result implies that the nickel complex is cycled in the initiation process in a manner analogous to reactions 8 and 9.

A reaction scheme that explains all the ramifications of the induced decomposition of alkyl hydroperoxides by $Ni(R_2dtc)_2$ and $Ni(R_2dtp)_2$ is given by the following elementary reactions.

[13] $A + ROOH \rightarrow A^{\cdot+} + RO^\cdot + {}^-OH$

[14] $A^{\cdot+} + ROOH \rightarrow A + ROO^\cdot + H^+$

[10] $RO^\cdot + ROOH \rightarrow ROH + ROO^\cdot$

[15] $ROO^\cdot + A \rightarrow$ Nonradical products

[7] $ROO^\cdot + A \rightarrow Y^\cdot$

where $Y^\cdot$ is most probably an alkoxy radical.

In the presence of a H-atom donating antioxidant such as 2,6-di-*tert*-butyl-4-methylphenol reactions 15 and 7 are overshadowed by reactions 16 and 17

[16] $ROO^\cdot +$ 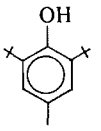 $\rightarrow ROOH +$ 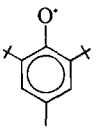

[17] $ROO^\cdot +$ 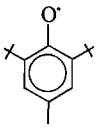 $\rightarrow$ 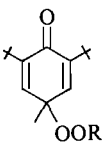

Chien and Boss (15) envisaged that reaction between $Ni(R_2dtc)_2$ and alkyl hydroperoxides initially involved a molecular reaction at a ligand sulphur atom in a manner analogous to reaction of other organosulphur compounds with hydroperoxides (16), *i.e.*,

[18] 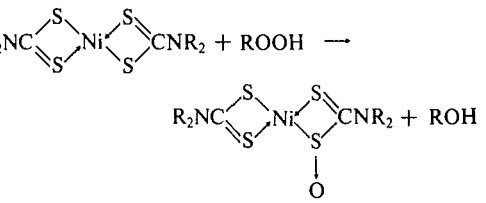

Further reaction with the other sulphur atoms in the ligands results in the reduction of six molecules of hydroperoxide per molecule of complex. This sequence of reactions eventually produces sulphur dioxide which could bring about heterolytic hydroperoxide decomposition. Our results certainly indicate that this is not the major reaction pathway at 30 °C.

Conclusions

Nickel dialkyldithiocarbamates and dialkyldithiophosphates react rapidly with alkyl hydroperoxides by a reaction that is first order in each reactant to generate free radicals. These radicals induce the decomposition of the hydroperoxide and destroy the complex and are capable of initiating hydrocarbon autoxidation. Approximately 10 molecules of hydroperoxide are decomposed by each molecule of nickel complex. Bimolecular rate constants k' determined from rates of complex disappearance are $\sim 0.15\ M^{-1}\ s^{-1}$ for the dithiocarbamates and $\sim 0.004\ M^{-1}\ s^{-1}$

Can. J. Chem. Downloaded from www.nrcresearchpress.com by 210.87.254.42 on 09/05/12
For personal use only.

for the dithiophosphates. Dithiocarbamates are, therefore, more efficient catalysts than dithiophosphates for hydroperoxide initiated autoxidation. The radical generating reaction between a nickel complex and a hydroperoxide must be a fairly efficient process because rates of chain initiation (as determined by hydrocarbon autoxidation) are very similar to rates of nickel complex disappearance (in the absence of a phenolic antioxidant) and rates of hydroperoxide disappearance (in the presence of a phenolic antioxidant).

Reactions of the nickel complexes with the hydroperoxides were much slower in the presence of the phenolic antioxidants, 2,6-di-*tert*-butyl-4-methylphenol and 2,6-di-*tert*-butyl-4-methoxyphenol, because these additives prevent induced decomposition of the hydroperoxide and destruction of the complex. Approximately 45 molecules of hydroperoxide were destroyed by each molecule of nickel complex and the bimolecular rate constants (k'') were $\sim 5 \times 10^{-3}$ M^{-1} s^{-1} for the dithiocarbamates and $\sim 5 \times 10^{-5}$ M^{-1} s^{-1} for the dithiophosphates.

Reaction products are indicative of a mechanism that is principally homolytic with the possibility of very minor contributions from stoichiometric and heterolytic decompositions.

Decomposition of alkyl hydroperoxides by the nickel complexes appears to be kinetically and mechanistically very much simpler than decomposition by the analogous zinc complexes. We could find no evidence for a catalyzed heterolytic decomposition and the ability of the nickel complexes to inhibit autoxidation at ambient temperature is, therefore, only due to their ability to scavenge free radicals. The zinc complexes, on the other hand, appear to be both radical scavengers and preventive antioxidants.

1. J. A. HOWARD, Y. OHKATSU, J. H. B. CHENIER, and K. U. INGOLD. Can. J. Chem. **51**, 1543 (1973) and references cited therein.
2. J. A. HOWARD and J. H. B. CHENIER. Can. J. Chem. This issue.
3. G. W. KENNERLEY and W. L. PATTERSON, JR. Ind. Eng. Chem. **48**, 1917 (1956).
4. J. D. HOLDSWORTH, G. SCOTT, and D. WILLIAMS. J. Chem. Soc. 4692 (1964).
5. D. SHOPOV, S. IVANOV, and V. V. IVANOVA. Rev. Inst. Fr. Petr. **10**, 1520 (1967).
6. A. J. BURN. Adv. Chem. Ser. **75**, 323 (1968).
7. A. J. BURN, R. CECIL, and V. O. YOUNG. J. Inst. Petrol. **57**, 319 (1971).
8. E. ROSSI and L. IMPARATO. Chim. Ind. **53**, 838 (1971).
9. G. SCOTT. Br. Polym. J. **3**, 24 (1971).
10. J. A. HOWARD and K. U. INGOLD. Can. J. Chem. **47**, 3809 (1969).
11. T. J. WALLACE and R. M. SKOMOROSKI. Chem. Ind. 348 (1965).
12. R. HIATT. Organic peroxides. Vol. II, *Edited by* D. Swern, J. Wiley and Sons, Inc., 1971. Chapt. 1.
13. R. HIATT, K. C. IRWIN, and C. W. GOULD. J. Org. Chem. **33**, 1430 (1968).
14. J. A. HOWARD. Adv. Free Radical Chem. **4**, 49 (1972).
15. J. C. W. CHIEN and C. R. BOSS. J. Polym. Sci. Part A-1, **10**, 1579 (1972).
16. J. A. HOWARD. Rubber Chem. Tech. **47**, 976 (1974).

On the hydrodynamics of the polarographic maxima of the first kind

R. N. O'Brien and F. P. Dieken

Department of Chemistry, University of Victoria, Victoria, British Columbia V8W 2Y2

Received July 22, 1975

R. N. O'Brien and F. P. Dieken. Can. J. Chem. **54**, 402 (1976).

The mechanism of polarographic maxima of the first kind, positive and negative, was investigated. Tracks of suspended particles photographed at 16 fps were analysed and found to obey a power law consistent with increasing speeds towards the mercury drop surface pointing to even more rapid movement of the mercury surface. The motions of large particles trapped in specific parts of the flow patterns were photographed and their velocities analysed. Particle motion in the mainly stagnant layer below the drop outlined by interferometry was contrasted with the motion of particles in the streaming region. Finally particles deposited on the drop were used to show the motion of the surface of the bottom hemisphere of the drop. High speed motion picture photography was used to record the change of shape of the drop on sudden polarization and to find the resonant frequency of the drop.

R. N. O'Brien et F. P. Dieken. Can. J. Chem. **54**, 402 (1976).

On a étudié le mécanisme des maxima polarographiques de la première sorte, positif et négatif. On a analysé les tracés de particules suspendues, photographiées à 16 pps, et on a trouvé qu'elles obéissent à une loi de puissance en accord avec des augmentations de vitesse vers la surface de la goutte de mercure indiquant qu'il y a un mouvement encore plus rapide de la surface de mercure. On a aussi photographié les mouvements des grosses particules, captés dans des parties spécifiques de patrons d'écoulement et on a aussi analysé leurs vitesses. Le mouvement des particules dans la fraction principalement stagnante en dessous de la goutte, tel qu'il se profile par interférométrie, était contrasté par le mouvement des particules dans la région qui coule. Enfin, on a utilisé les particules déposées sur la goutte pour montrer le mouvement de la surface dans le bas de l'hémisphère de la goutte. On a utilisé la photographie en mouvement à haute vitesse pour enregistrer les changements de forme de la goutte lors d'une polarisation soudaine et on a trouvé la fréquence de résonance de la goutte.

[Traduit par le journal]

The phenomenon known as the polarographic maximum of the first kind has been extensively studied by polarography (1). Optical studies are limited to those of Antweiler (2) and O'Brien and co-workers (3, 4). Antweiler used a Schlieren-interferometric technique whose results have been recently confirmed and corrected by O'Brien and Dieken (4). In the paper by O'Brien and Dieken, some areas required further definition. These included: the significance of the equator of the drop as the tangent point of flow of the rapid streams of electrolyte, a valid extrapolation of speeds of particles *vs.* distance from the drop, and the relationship of suddenly applied potentials to surface tension. This work is devoted to these ends and to supply further interesting details of phenomena observed above and below the equator. The work adds further reasons for choosing the Levich theory among those still given some consideration.

Experimental

The apparatus used was a Fabry–Perot interferometer, the same one as described in ref. 4. All solutions were made in the same way and from the same materials and in some cases were the same solutions since this work directly followed that published in refs. 3 and 4 and was in fact a continuation of that work. Measuring techniques were used that were evolved in some other polarographic work since published (5) and some motion picture photography without interference fringes was done. The cell was also fitted with uncoated windows when high speed motion picture photography was used.

Four main electrolyte systems were studied. They appear in Table 1. All of these solutions were used with and without suspended activated charcoal particles. The drop time was 5 ± 1 s. A series of experiments was done to record the distortion of the drop when a sudden potential was applied. High speed motion picture photography was used to record the drop distortion. Some frames showing motions of particles in the wake of the drop were rephotographed through a microscope to better present detail observed when the original film was projected at high magnification.

Results and Discussion

As greater amounts of data were obtained it became possible to draw a generalized diagram of the flow patterns around the drop in the

Can. J. Chem. Downloaded from www.nrcresearchpress.com by 210.87.254.5 on 09/05/12
For personal use only.

Can. J. Chem. Downloaded from www.nrcresearchpress.com by 210.87.254.5 on 09/05/12
For personal use only.

TABLE 1. Electrolyte solutions studied

Electroactive species	Supporting electrolyte (0.1 *M*)	Drop times (s)
0.004 *M* Cu^{2+} (sulphate)	$NaClO_4$	5.26
0.005 *M* Cu^{2+} (sulphate)	$NaClO_4$	5.26
0.008 *M* Cu^{2+} (sulphate)	$NaClO_4$	5.26
0.010 *M* Cu^{2+} (sulphate)	$NaClO_4$	5.26
0.010 *M* Cu^{2+} (sulphate)	KCl	5.26
0.010 *M* Co^{2+} (sulphate)	$NaClO_4$	5.28
0.032 *M* Co^{2+} (sulphate)	$NaClO_4$	7.40
0.005 *M* $S_2O_8^{2-}$ (potassium)	$NaClO_4$	5.26
0.0013 *M* O_2 (air saturated)	$NaClO_4$	5.26

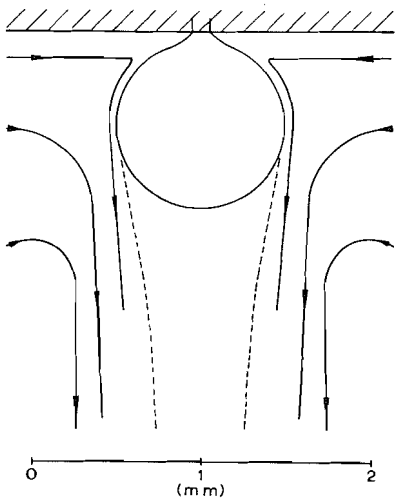

FIG. 1. General flow pattern in the positive maximum.

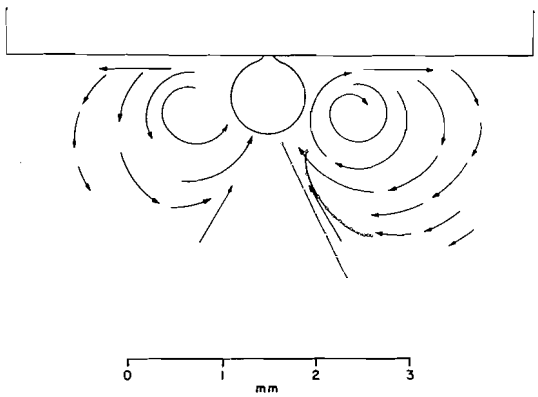

FIG. 2. General flow pattern in the negative maximum. One track shows successive positions of a particle at $\frac{1}{8}$ s intervals.

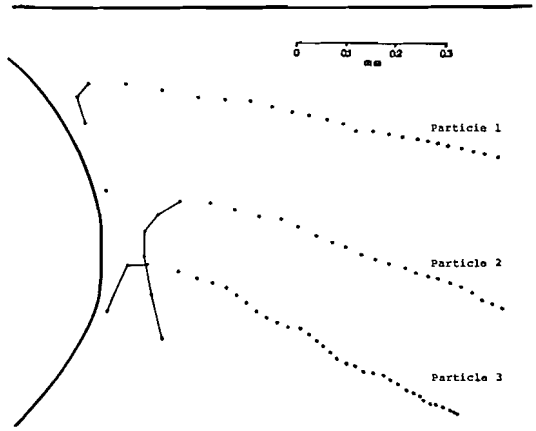

FIG. 3. Plots of three particles approaching the drop during a positive maximum. Individual points are at 0.004 s intervals and connected points are at 0.002 s intervals.

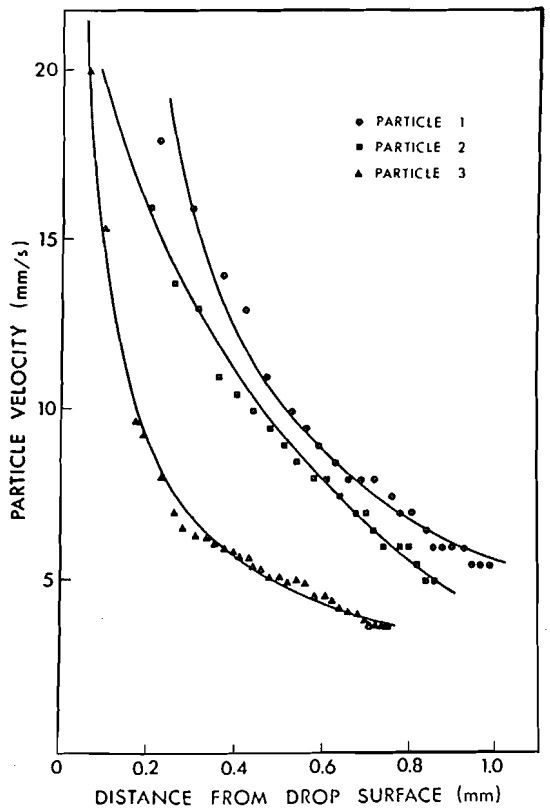

FIG. 4. Particle velocity *vs.* distance from the drop of the three particles in Fig. 3 during a positive maximum.

positive (downward streaming) and negative (upward streaming) maxima. Figure 1 shows the general flow pattern found for the positive maximum and Fig. 2 that for the negative. Figure 3 shows the paths of three particles as they moved towards the drop. Figure 4 shows the velocities

TABLE 2. Particle velocity – distance relationships during the positive maximum

Particle number	Equation	a	b	Correlation coefficient
1	$v = aX^b$	5.60	−0.86	0.987
2	$v = aX^b$	8.15	−0.10	0.379
3	$v = aX^b$	3.06	−0.67	0.988
2	$v = a \exp(bX)$	22.37	−1.74	0.988

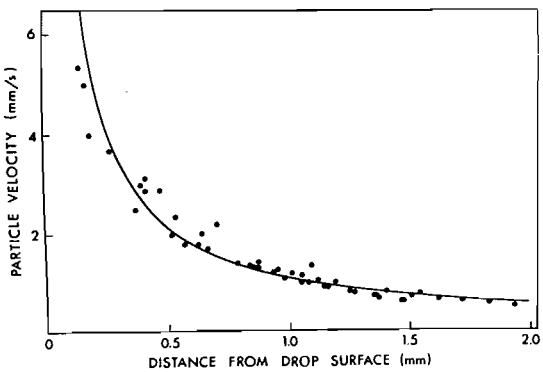

FIG. 5. Particle velocity *vs.* distance from the drop during a negative maximum.

achieved by the three different particles at various distances from the drop. It must be remembered that only the component parallel to the plane of focus of the camera is shown. Since the focal depth is 0.2 mm and there is evidence for precession from coriolus effect, some tracks require rationalization with these effects in mind. They all obviously accelerated as they approached the drop. The solid lines are computer-generated least-squares best fit curves. Table 2 gives the results of using a function of the form $v = ax^b$ and an exponential form $v = a \exp(bx)$ with the values of a and b as given ($a = 5.6$, $b = -0.086$ etc.) and x is the distance from the mercury drop. For laminar flow it is well known that the velocity distribution function for circular pipes is proportional to the square of the distance from the wall. This suggests that the power form should give the best fit which it does for all but particle 2. It also gives the best fit for negative maximum particles. Figure 5 shows that for the negative maximum a large number of particle tracks analysed for velocity at a given distance can be described by one curve of the power form with $a = 1.1$ and $b = -0.95$ with a correlation coefficient of 0.96. Velocities were measured along the best straight line of the trajectories of the particles. This seemed the best procedure to adopt because the system (the positive maximum) is not exactly the reciprocal situation to having a liquid flow around a sphere, which is the system assumed by Levich in his theoretical treatment of the problem (6). Levine and O'Brien (7) have obtained an almost identical solution to that of Levich using the same model, but getting a solution of more general applicability. The attached mercury drop is shielded by the end of the capillary which can be equated to a semi-infinite wall. This undoubtedly is a major contributor to the observed peculiarities of the maximum streaming. Since one expression can reasonably describe the position–velocity data for the negative maximum, a general symmetry of motion is suggested and this is consistent with a torus as found and previously reported. The torus does not, however, correspond to laminar flow past a drop. By analysing the interferograms of the event, before and during streaming, it became obvious that no bulk electrolyte flow of comparable velocity to that in the torus occurred to the bottom area of the drop. A rough estimate of that area would be that intersected by a solid angle of 30° centred on a vertical line through the drop from the capillary bore. The solution within the torus had a concentration which was 3 to 4% below that in the bulk, and the motion of the electrolyte is fast enough to reduce the thickness of the diffusion layer below the limit of detection (about 10^{-3} mm) in this apparatus. Below the drop where the particles were seen to move slowly and more or less randomly upward, there was diminution in concentration before the onset of the maximum (but with at least one-half the limiting current flowing which is usually enough to show a depletion) but there was not after the maximum started. The appearance of the fringes outlining this relatively stagnant volume were reminiscent of those showing the stagnant annular core below the drop during the positive maximum, but of course here they outlined a cone rather than an annulus.

From following the individual particles as they advanced into and receded out of the plane of focus of the camera, it became obvious that the path of the electrolyte in the torus was not circular, but circular with precession around the drop, or a helical motion was indicated. When it is considered that the polarizing electrode was not the mercury pool, but introduced to the side

Can. J. Chem. Downloaded from www.nrcresearchpress.com by 210.87.254.5 on 09/05/12
For personal use only.

Can. J. Chem. Downloaded from www.nrcresearchpress.com by 210.87.254.5 on 09/05/12
For personal use only.

of the drop giving a slightly asymmetric field for the charges of the electrolyte to rotate in, the precession or helical motion would be expected. The effect of this asymmetrical field was also manifested in the slight variation from vertical in the path of the falling drop as outlined by the depleted solution stripped from the falling drop. This may also indicate more rapid streaming on one side.

When a sphere, albeit hanging from a narrow neck, is the electrode of interest and the polarizing electrode is effectively planar and distant, some of the spherical surface will be electrolytically 'shielded'. If the drop is now hung from a capillary whose flat bottom could be considered a semi-infinite wall more shielding will occur, but perhaps not a significant amount more. It has been shown by some authors (8*a*) though others disagree (8*b*) that fine-tipped capillaries produce vigorous maxima stirring. Taylor *et al.* (9) moved a blunt capillary towards a drop on a fine-tipped capillary undergoing a maximum and found that at a certain distance the streaming stopped, then reversed as it was moved closer. Our own experience was that a shaved tip did not affect the positive maximum but caused the torus of the negative maximum to increase in radius (10).

The distribution of velocities inside the approaching stream of electrolyte in the positive maximum clearly shows that the velocity–position plot has another variable, or that a value for the Y direction as well as the X (using the usual cartesion coordinate nomenclature) is necessary. The velocity of approach then clearly depends on the part of the drop the electrolyte is approaching, which could be related to a conventional coordinate system, probably most appropriately, polar coordinates. Figures 1 and 3 also show that tracks of particles converge as they approach the drop, or those well above the equator of the drop have a downward component and those at or near the equator level an upward component until they are close to the drop and adsorbed in the annular flows.

That the power to which x was raised in the velocity–distance function was negative is appropriate, since the velocity decreases away from the surface that is assumed to be moving (the mercury drop surface) according to the theory of Levich. That it is not two is also appropriate since the standard formula for flow in a pipe requires continuous contact with the pipe walls rather than just a momentary contact over less than half of the drop's surface in this case. The power would, therefore, be expected to be less than two.

Directly beneath the drop, a region of depletion has been outlined by interferometric methods. The work of Taneda (11) on wakes behind moving spheres shows wakes similar to those optically outlined for positive maxima. Using Taneda's expression $R = Vd/\eta$ where R is the Reynolds number, V is velocity of the sphere (or solution), d is the diameter of the sphere, and η the kinematic viscosity; $R = 160$ which Taneda finds causes turbulence in the wake. The existence of this region of depletion is incompatible with electrolyte streaming theories which predict that the base of the drop acts as a centre for major downward stirring. Original concepts of stirring in this area of the electrode were based upon particle movement believed to be emanating from the base of the drop; however, particle movement in this area must be carefully scrutinized since particles moving from the bulk electrolyte to the drop either from in front of or behind the drop can exhibit upward or downward motion depending upon their spatial orientation and proximity to the drop. Previous researchers may have observed the downward movement of particles on either side of the drop and extrapolated this type of motion to particles that appeared to be located directly beneath the drop.

In this work, the focal plane of the camera was always the perimeter of the drop. The laser light was effectively plane parallel and the focal depth was about 0.2 mm or less than one-quarter drop diameter at drop fall. Since the proposed dead volume's diameter, as outlined interferometrically, is just less than the drop diameter immediately below the drop (Fig. 1), the quality of being in focus is the principal method of judging whether the particle is or is not really in the region of observed depletion.

Of course, those particles moving towards the drop from in front of or behind the focal plane, and getting reasonably close before altering their trajectories to downward, could merge with the drop image or disappear behind it. The fast moving particles in the bulk or annulus exhibited measured velocities in the approximate range of 1–10 mm s^{-1}. Therefore, if a particle remained

Can. J. Chem. Downloaded from www.nrcresearchpress.com by 210.87.254.5 on 09/05/12
For personal use only.

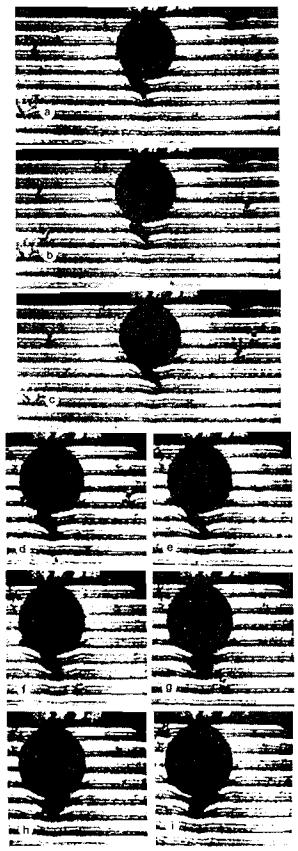

FIG. 6. Large particle movement directly under the base of the drop during a positive maximum; solution 0.10 M Cu_2SO_4 in 0.10 M $NaClO_4$, $\frac{1}{8}$ s interval between frames.

clearly observable for more than $\frac{1}{2}$ s, it must have been out of the fast flowing stream. Also, if the particle had more than one major change in direction it could not have been located in the main stream. A variety of short term, random type particle motions can be observed in what appears to be the region directly below the drop. In this work, considerable effort was devoted to the exact position of the particle(s) relative to the base of the drop.

A very convincing phenomenon was observed several times and photographed once (10). A large charcoal particle whose longest dimension was 0.5 mm became trapped directly beneath the drop during the typical positive maximum observed for Cu^{2+}. This large particle (see Fig. 6) which appears as a platelet of charcoal trapped in the depleted volume rotated continuously counterclockwise until the drop fell. The total observed duration of rotation was about 2.5 s at about 0.8 revolutions per second. The angle of the flat side of the platelet was about 45° to the vertical and it swept out a helix in the depleted solution of about 0.2 mm radius. Allowing for no slippage, the *upward* velocity of the stream would have to be about 0.2 to 0.3 mm s^{-1}; this is clearly too slow a movement for the fast annular stream, but suggests that there may be a velocity gradient near the inside diameter of the annulus and that mild turbulence is probably present. Selected frames ($\frac{1}{8}$ s interval) (Fig. 6) clearly show the large rotating platelet and the black arrow on the right hand side of the drop points to a particle advancing to the drop from the bulk electrolyte. The behaviour of this small particle is typical of particles moving to the drop during the positive maximum.

Figure 7 is a series of frames selected from considerable film footage of the positive maximum for Cu ion taken at 500 fps. This sequence was selected because two particles can be followed and assigned to different streams during the positive maximum. A particle (long arrow particle I) about 0.03 mm on edge is advancing from the bulk solution to the drop. Time intervals between frames (*a*) to (*f*) and (*f*) to (*h*) were 0.016 and 0.008 s respectively. Particle I in the sequence moves upward until frame (*d*) and to the right until frame (*e*). Its upward movement was approximately +0.024 mm and its horizontal motion +0.187 mm in the usual cartesian coordinate sense. After frame (*e*) particle I abruptly changes direction and moves directly downward until at frame (*h*) its vertical motion reached −0.661 mm. The general direction of movement and trajectory of this particle closely resembles that shown schematically in Fig. 1.

The movement of particle I should be contrasted with particle II (white wedge in drop image). A black dot marked R in frame (*a*) is an imperfection in an optical component which remains stationary. Particle II moves slowly upward, moving approximately 0.1 mm during the time that particle II was moving a total of approximately 0.85 mm vertically and approximately 0.15 mm horizontally. Clearly these two particles are moving in different streams during the positive maximum.

Another series of frames showing slow upward, then downward movement of two other

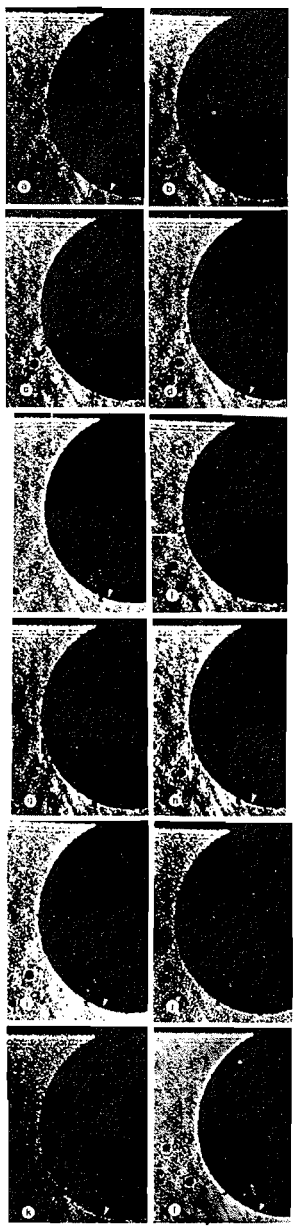

FIG. 7. Upward motion of a particle near but below the bottom of the drop and downward motion of one above the equator of the drop during a positive maximum, 0.010 *M* $CuSO_4$ in 0.10 *M* $NaClO_4$. Time between successive frames was (*a*)–(*e*) 0.016 s, (*f*)–(*i*) 0.008 s and (*j*)–(*l*) 0.022 s.

particles is available (10). Also nearly stationary, discrete particle movement, possibly from in front of to behind the focal plane, was observed. Frame (*e*) of Fig. 7 shows that particle II is not attached to the drop (a distinct gap appears between it and the drop).

In the negative maximum experiments with Co^{2+}, no real change in the flow diagram presented previously (4) is necessary. In one experiment a large platelet of activated charcoal became trapped at the vortex of the torus and rotated for about 3 s until drop detachment (4). The largest dimension of the platelet was about equal to the diameter of the drop (~0.4 mm) when it first became trapped.

The drop including neck was about $1\frac{1}{4}$ times its equator diameter in vertical extent, which is the normally observed dimension. The area swept out by the particle was from a minimum depth of just under one drop radius below the capillary to a maximum depth of just over two drop radii, or almost opposite the bottom of the drop. Laterally its closest approach to the drop was about $\frac{1}{2}$ radius and the farthest it appeared away from the drop was about two drop radii. This gives a roughly circular motion about $1\frac{1}{2}$ drop radii in diameter. The particle, still rotating, quite abruptly precessed counterclockwise to the opposite side of the drop, then either stopped precessing or precessed very slowly till drop detachment. As would be expected, the size of the torus increased in all dimensions with drop growth. The behaviour of this particle, and other particles, large and small, show the centre of the toroidal stirring whorl in the negative maximum to be approximately opposite the equator of the drop, not substantially below the equator as previously believed. As previously mentioned, a shaved capillary did not change the general structure of the stirring flow, only the radius of the toroidal whorl increased, its centre staying approximately opposite the equator of the drop.

When a positive maximum was occurring in the system 0.010 *M* $CuSO_4$, 0.100 *M* $NaClO_4$, islands of solid, said to be copper,[1] were observed on the surface of the mercury. The movements the islands made included moving from near the equator to the drop on one side, across the bottom of the drop to near the equator on the other side. Their movements were uncoordinated with the movement of adjacent suspended carbon particles (3*b*). Movement of the islands is loosely coordinated; that is if a

[1]A. T. Hubbard, private communication.

Can. J. Chem. Downloaded from www.nrcresearchpress.com by 210.87.254.5 on 09/05/12
For personal use only.

Can. J. Chem. Downloaded from www.nrcresearchpress.com by 210.87.254.5 on 09/05/12
For personal use only.

group of islands is moving down on one side of the drop, there will also be counterparts moving upward on the other side of the drop. The total observed motion of the islands indicated that during the positive maximum there was random movement of the surface of the mercury below the equator. In a hanging drop experiment, when the islands completely covered the bottom hemisphere, the maximum abruptly ceased.

The greatest velocities were experienced in positive maxima and when the electroactive species to supporting electrolyte ratio was 1:10, *i.e.* the 0.010 *M* $CuSO_4$, 0.100 *M* $NaClO_4$ solution, as reported by Heyrovsky and Kuta (1). This was also true for the negative (Co^{2+}) maximum studied.

Because the distribution of velocities tended to support Levich's theory which involves a change of surface tension because of unequal potentials in the double layer of the drop when the potential is near the electrocapillary maximum, it was decided to attempt an independent check on how the surface tension of the mercury changed with the sudden application of the potential of the polarographic maximum. Accordingly for a 0.005 *M* $CuSO_4$ in 0.100 *M* $NaClO_4$ solution and 0.005 *M* $K_2S_2O_8$ in 0.100 *M* $NaClO_4$ solution; potentials of −0.45 V *vs.* the s.c.e. were suddenly applied from the rest potential, which is near the electrocapillary maximum potential (near −0.55 *vs.* the s.c.e.). In another experiment a voltage corresponding to a simple limiting current range (1.00 V *vs.* the s.c.e.) was also applied. The results are displayed for the copper solution in Fig. 8 and those for persulfate in Fig. 9.

Rayleigh's equation (12) for the instability of charged conducting drops modified by Langmuir and Yeh (13) is of the form:

$$[1] \qquad \omega^2 = \frac{n(n-1)}{\rho r^3}\left|(n+2)\gamma - \frac{V^2}{4\pi r}\right|$$

where ω is the angular frequency (s^{-1}), n is the order of the spherical surface harmonic mode of oscillation, ρ is the density of the drop (g cm^{-3}), r is the radius of the drop (cm), γ is the surface tension (dyn cm^{-1}), and V is the potential of the sphere (V in esu). The frequency of the drop predicted, $\omega/2\pi$ when γ is 400 (dyn cm^{-1}), r is 0.045 (cm), and n is 2, is 200 s^{-1} analogous to the fundamental frequency of a vibrating string. Table 3 summarizes the results.

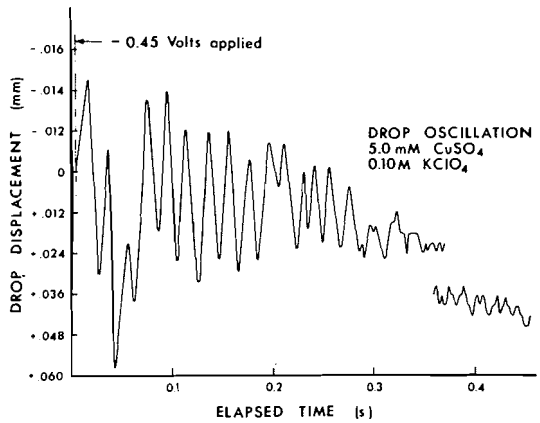

FIG. 8. Drop oscillation on application of −0.45 *V vs.* s.c.e. in 0.10 *M* $NaClO_4$ and 0.005 *M* $CuSO_4$. Detached plot at 0.4 s is open circuit oscillation.

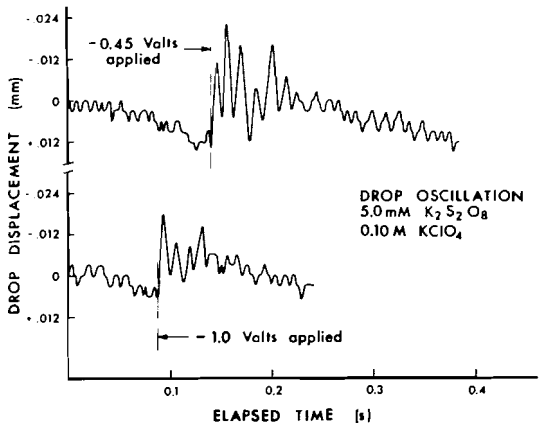

FIG. 9. Drop oscillation on application of −1.0 V *vs.* s.c.e in 0.10 *M* $NaClO_4$ and 0.005 *M* $K_2S_2O_8$.

Open circuit frequencies are about one-half that predicted by the equation. They should be lower since the equation is for use when the drop is suspended in vacuum, not a relatively viscous medium like water (H_2O viscosity is about 1.0 cP, Hg is about 1.55 cP at room temperature).

In both solutions, the bottom of the slightly elongated spherical drop took up a more spherical shape, which is the behaviour expected on a sudden increase in surface tension. This behaviour could be explained on the basis of neutral adsorbed organic molecules (usually present even in very pure solutions) being displaced by ions as the potential of the drop is suddenly changed by a moderate amount (100 mV) from near the PZC. The lower frequencies associated

TABLE 3. Oscillation frequencies of the dropping mercury electrode

Electrolyte solution (5.0 m*M*)	Applied voltage *vs.* s.c.e. (V)	Drop weight* (mg)	Frequency (s^{-1})		
			Open circuit	Region of largest oscillation	Damped oscillations
$CuSO_4$	−0.45	5.90	100	50	85
$K_2S_2O_8$	−0.45	2.65	100	75	90
$K_2S_2O_8$	−1.0	2.23	100	75	90

*Measurements obtained immediately prior to applied voltage.

with the copper maximum could result from the formation of a copper amalgam on the surface, as contrasted with the desorption of the soluble sulphate ion in the persulphate maximum. The persulphate maximum is the most violent giving maximum particle velocities more than twice those for copper. The oxygen maximum which was also studied (10) with and without charcoal particles is the least violent. Runs in which charcoal was used compared favorably in current increases to literature values. The addition of charcoal particles increased the maximum to about the same extent as in the other systems.

Conclusions

All of the evidence here presented supports the theory of Levich. These data may be summarized as follows: (*1*) In the positive maximum the downward flow has the shape of an annulus, following the curvature of the drop and breaking off from the surface near the equator of the drop. (*2*) Inside the annulus and directly below the drop for at least one drop diameter, the flow is slowly and erratically upward, perhaps with a counterclockwise helical motion. The annular flow may also be slightly helical in the counterclockwise sense. (*3*) Movement of the mercury surface below the drop equator is slow and erratic, much slower than the annular stream, but the movement of one side seems to be concerted with the other. (*4*) In the negative maximum, the centre of the toroidal whorl is approximately opposite the equator of the drop. The diameter of the torus appears to increase with increasing drop diameter. (*5*) There is erratic precession of the toroidal ring around the drop.

Since the velocity gradient increases with a power function as the drop is approached, the surface of the drop must be moving faster, and must be the source of the energy to move the electrolyte. Previously presented interferograms showing the onset of a negative maximum show that the motion begins in the region of the drop surface. Sudden fluctuations in concentration at the equator of the drop precede solution movement which appear to start near the equator. The demonstrated patterns of flow are consistent with a difference of potential in the solution adjacent to the mercury surface causing a surface tension gradient on the drop and subsequent rapid movement of surface layers from regions of low to high tension. The free oscillations of the drop on sudden application of a maximum-causing potential have lower frequencies for the Hg soluble product consistent with lower surface tension and less violent maxima.

There is finally the objection of Heyrovsky and Kuta (1) that motion of an atomically smooth, small drop's surface cannot make distant layers of solution move as dramatically as they are observed to do during the maximum. Data of Leja and co-workers (14)[2] showed interferograms wherein monolayers of surfactant moving over the surface of water instantaneously moved a layer of water about 0.1 mm thick with it and simultaneously water at a depth of more than 0.5 mm in the narrow langmuir trough began to flow in the opposite direction. When the film reached the end of the trough, the motion ceased abruptly. The velocities are about equal to those obtained by extrapolation of the equations of Table 2 and agree with von Stackelberg's (15) calculated value of 20–25 cm s^{-1} as reported by Heyrovsky and Kuta (1).

The conclusion must therefore be, that since all flow evidence is supportive, that the mathematical solution of Levich has been verified by a different mathematical approach, that the diffi-

[2]Presented at the Colloid Symposium, Ottawa, Canada, June, 1973.

Can. J. Chem. Downloaded from www.nrcresearchpress.com by 210.87.254.5 on 09/05/12
For personal use only.

culty of moving layers of water of the right thickness by a charged surface has been demonstrated, that therefore the surface tension theory is correct.

Acknowledgements

We are indebted to J. Leja for helpful suggestions, to M. W. Mitchell who performed some supporting experiments and to the National Research Council of Canada for general financial support and a Fellowship awarded to one of us (F.P.D.).

1. J. Heyrovsky and J. Kuta. Principles of polarography. Academic Press, New York. 1966. p. 86; Henry Bauer. J. Electroanal. Chem. In press; Robert N. O'Brien. Rev. Anal. Chem. **2**, 343 (1975).
2. H. J. Antweiler. Z. Electrochem. **43**, 596 (1937). H. J. Antweiler. Z. Electrochem. **44**, 719, 831, 888 (1938).
3. J. Leja and R. N. O'Brien. Nature, **210**, 1217 (1966).
4. R. N. O'Brien and F. P. Dieken. Can. J. Chem. **48**, 2651 (1970).
5. (*a*) R. N. O'Brien and F. P. Dieken. Electroanal. Chem. **42**, 25 (1973); (*b*) R. N. O'Brien and F. P. Dieken. Electroanal. Chem. **42**, 37 (1973).
6. (*a*) A. N. Trumphin and V. G. Levich. J. Phys. Chem. **19**, 573 (1953); (*b*) V. G. Levich. Physiochemical hydrodynamics. Prentice-Hall, Englewood Cliffs, New Jersey. 1962. p. 570.
7. S. Levine and R. N. O'Brien. J. Colloid Interface Sci. **43**, 616 (1973).
8. (*a*) J. Flemming and H. Berg. J. Electroanal. Chem. **8**, 291 (1964); (*b*) H. Triebel and H. Berg. J. Electroanal. Chem. **2**, 467 (1961).
9. D. T. Taylor, R. G. Barradas, and M. J. Dignam. J. Electroanal. Chem. **36**, 475 (1972).
10. F. P. Dieken. Ph.D. Thesis, University of Victoria, Victoria, British Columbia. 1971.
11. Sadatashi Taneda. J. Phys. Soc. Jpn. **11**, 1104 (1966).
12. Lord Rayleigh. Phil. Mag. Ser. 5, **14**, 184 (1882).
13. D. B. Langmuir and G. C. K. Yeh. A simple physical interpretation of Rayleigh's formula for instability of charged droplets. Ramo-Wolldridge Research Laboratories, Canoga Park, California. 1969.
14. R. N. O'Brien, A. I. Feher, and J. Leja. J. Colloid Interface Sci. **51**, 366 (1975).
15. M. von Stackelberg. Advances in polarography. *Edited by* I. S. Langmuir. Pergamon, Oxford. 1960. p. 68.

Can. J. Chem. Downloaded from www.nrcresearchpress.com by 210.87.254.5 on 09/05/12
For personal use only.

The use of ceric ammonium nitrate in pyrrole chemistry

JOHN B. PAINE III[1]
Department of Chemistry, Harvard University, Cambridge, Massachusetts 02138
AND
DAVID DOLPHIN[2]
Department of Chemistry, The University of British Columbia, Vancouver, British Columbia V6T 1W5

Received July 14, 1975

JOHN B. PAINE III and DAVID DOLPHIN. Can. J. Chem. **54**, 411 (1976).

Ceric ammonium nitrate, in aqueous acetic acid buffered with sodium acetate, rapidly oxidizes 2,2′-dipyrromethanes to the corresponding 2,2′-dipyrroketones.

JOHN B. PAINE III et DAVID DOLPHIN. Can. J. Chem. **54**, 411 (1976).

Le nitrate d'ammonium cérique, dans l'acide acétique aqueux tamponné avec de l'acétate de sodium, oxyde rapidement les dipyrro-2,2′ méthanes en dipyrro-2,2′ cétones correspondantes.
[Traduit par le journal]

Can. J. Chem. Downloaded from www.nrcresearchpress.com by 210.87.254.5 on 09/05/12
For personal use only.

While trying to effect the conversion of 2-carbobenzyloxy-3,4,5-trimethylpyrrole (**1**, R = $CH_2\phi$) to 2-carbobenzyloxy-5-formyl-3,4-dimethylpyrrole (**2**, R = $CH_2\phi$) but finding sulfuryl chloride, the usual reagent of choice (1), inadequate to the task, the use of Ce(IV) suggested itself. There had been several reports on the use of ceric ammonium nitrate for the oxidation of toluenes (2, 3) and benzyl alcohols (4, 5) to benzaldehydes in high yields without further oxidation to the benzoic acids.

The commercially available water-soluble cerium(IV) salts are the sulfate, ammonium sulfate, and ammonium nitrate and perchlorate. Of these only the nitrate resists aqueous hydrolysis and at the same time shows reasonable solubility in organic solvents, particularly acetic acid. Since nitric acid is a by-product of the reduction of ceric ammonium nitrate, solutions in aqueous acetic acid were buffered with an excess of sodium acetate.

The reaction of ceric ammonium nitrate, suitably buffered, with several derivatives of 3,4,5-trimethylpyrroles did indeed lead to the 5-formylpyrroles, but the yields were highly variable and depended both upon the rate of addition of oxidant, and the reaction temperature. The best yield obtained was with the 2-carbethoxy derivative (**2**, R = Et), while the benzyl ester (**1**, R = $CH_2\phi$) gave only 42% of the aldehyde (**2**, R = $CH_2\phi$), but in addition gave an 8% yield of what proved to be the symmetrical dipyrroketone (**3**, R = $CH_2\phi$) which was also prepared by the ceric oxidation of the dipyrromethane (**6**, R = $CH_2\phi$). Evidently some of the intermediate hydroxymethylpyrrole had been solvolyzed to the dipyrromethane with the loss of formaldehyde (1), and the dipyrromethane had then been oxidized to the dipyrroketone. In addition the cyano-acrylate ester (**4**) could be oxidized to the aldehyde (**5**) but the yield was poor (15%). Being only a one-electron oxidant, and of a high molecular weight, we concluded that the use of ceric ammonium nitrate for converting pyrrolmethyl to pyrrylaldehyde, was uneconomical, especially as the yields were only fair, and by-products were formed.

However, having found a pyrroketone among the by-products we next investigated the suitability of ceric ammonium nitrate for the oxidation of dipyrromethanes to dipyrroketones. The published procedures for this oxidation specified the use of either lead tetraacetate with lead dioxide (6), or sulfuryl chloride with bromine (7), but these procedures require either long reaction times, or give poor yields.

A model dipyrromethane diester, 5,5-dicarbethoxy-3,3′,4,4′-tetramethyl-2,2′-dipyrromethane (**6**, R = Et) was oxidized with four equiv. of ceric ammonium nitrate in aqueous acetic acid buffered with sodium acetate, with the formation of the expected dipyrroketone (**3**, R = Et) in 57% yield within a very brief reaction time

[1]National Science Foundation Postdoctoral Fellow 1968–1972.

[2]Author to whom correspondence should be addressed.

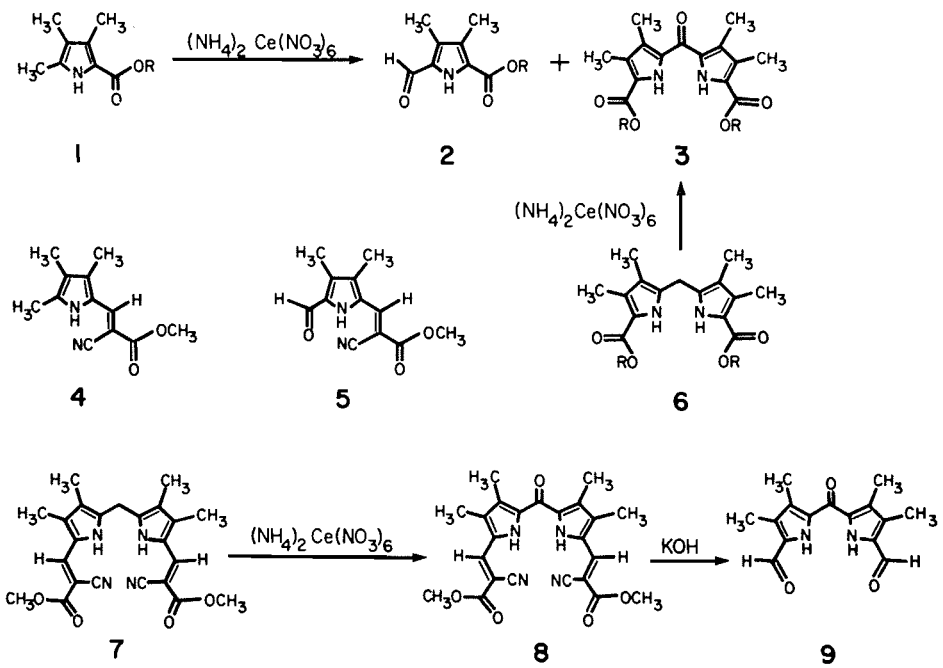

(10–15 min). The product was easily isolated by filtration after diluting the reaction mixture with water.

Similarly the dipyrromethane bis cyanoacrylate ester (**7**) gave the corresponding dipyrroketone (**8**) under similar conditions, but in a lower yield of 38%. In this case sodium acetate may have rendered some of the product water soluble, as was the case during the halogenative decarboxylation of cyanovinyl pyrroles (8). Removal of the cyanovinyl protecting groups with strong base gave the corresponding 5,5′-diformyl-2,2′-dipyrroketone (**9**), and this route provides a convenient alternative to the procedure of Clezy *et al.* (7).

The required bis cyanovinyl dipyrromethanes required for this synthesis of 5,5′-diformyl-2,2′-dipyrroketones may be prepared either by the Friedel-Crafts coupling of two monopyrroles (8) or by the protection, under Knoevenagel conditions, of a diformyl dipyrromethane, prepared by more traditional means (7). Either approach (Scheme 1) can give a symmetrical or an unsymmetrical product. The procedure will be most convenient when only alkali-impervious β-substituents are present. Propionate side-chain esters prove readily re-esterifiable by treatment with diazoalkane. Whether acetic ester side chains survive the deprotection step, or else suffer decarboxylation, has not yet been established.

Experimental

Melting points were determined in a Thomas–Hoover capillary melting point apparatus and are uncorrected. The ir spectra (KBr) were determined in a Perkin-Elmer 137 spectrophotometer. The pmr spectra were obtained on a Varian Associates A-60 spectrometer with tetramethylsilane as internal standard and deuteriochloroform as solvent. Chemical shifts were expressed in the δ-scale. Combustion analyses were carried out by Scandinavian Microanalytical Laboratories, Herlev, Denmark.

2-Carboethoxy-5-formyl-3,4-dimethylpyrrole

2-Carboethoxy-3,4,5-trimethylpyrrole (9.26 g, 0.05 mol), sodium acetate (32.55 g, 0.4 mol), and acetic acid (250 ml) were heated on a steam bath until the sodium acetate had almost dissolved. Ceric ammonium nitrate (110.5 g, 0.20 mol) and water (50 ml) were added and heating was continued for a few minutes after the last of ceric ammonium nitrate had dissolved. The pale yellow solution was diluted with water but no organic product separated. The reaction mixture was then extracted with methylene chloride. The combined organic phases were concentrated on a steam bath. Ice and water were then added to the light orange oil which soon solidified. The water was decanted from the product which was then dissolved in methylene chloride. This solution was dried, taken down to a small volume, and diluted with hexane. The product which separated on cooling was collected by filtration and washed with hexane to give 6.42 g (65.6%) mp 109.5 °C (lit. (7) 108–109 °C).

Can. J. Chem. Downloaded from www.nrcresearchpress.com by 210.87.254.5 on 09/05/12
For personal use only.

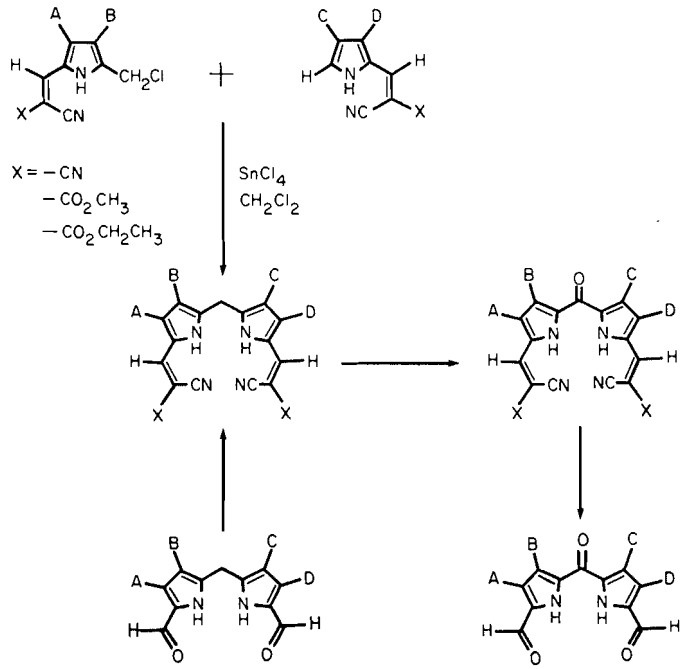

SCHEME 1

2-Carbobenzyloxy-5-formyl-3,4-dimethylpyrrole

2-Carbobenzyloxyl-3,4,5-trimethylpyrrole (12.18 g, 0.05 mol), sodium acetate (36.97 g, 0.46 mol), and acetic acid (250 mol) were heated on a steam bath. A further 150 ml of acetic acid and water (10 ml) were added and the mixture cooled in an ice bath. Ceric ammonium nitrite (121.55 g, 0.22 mol) was dissolved in water (100 ml) and was added to the cold pyrrolic solution in one portion. After standing at 15 °C for 25 min the solution was heated on a steam bath. By 60 °C the mixture had turned red and opaque but still gave a positive starch–iodide color. At 80 °C some gas was evolved but the color did not darken and some granular material had separated. The mixture was maintained at 80 °C for 15 min, then diluted to 800 ml with water, and a white crystalline solid was collected by filtration. The filtrate was then further diluted with water to give an orange crystalline precipitate. The mixture was allowed to stand overnight and the product collected by filtration and washed with water. The product was crystallized from methylene chloride – hexane, and then from acetone to give chunky light tan colored crystals. Total yield from two crops 4.2 g (42%) mp 119–119.5 °C, (lit. (10) 119–120 °C).

The white precipitate collected at the end of the reaction was shown to be 5,5-dicarbobenzyloxy-3,3′,4,4′-tetraethyl-2,2′-dipyrroketone by comparison with an authentic sample (*vide infra*).

5,5′-Dicarbobenzyloxy-3,3′,4,4′-tetramethyl-2,2′-dipyrroketone

5,5′-Dicarbobenzyloxy-3,3′,4,4′-tetramethyl-2,2′-dipyrromethane (1.0 g, 2.13 mmol), sodium acetate (700 mg, 8.35 mmol), and acetic acid (125 ml) were heated in a 250 ml erlenmeyer flask until the mixture was homogeneous. The solution was then cooled, and a solution of ceric ammonium nitrate (4.76 g, 8.53 mmol) in water (5 ml) was added in one portion. Addition of the oxidant caused the mixture to become bright orange, and after a few minutes a negative starch iodide test was obtained. The mixture was stirred for a further 10 min and then poured into cold water (200 ml). The resultant pink-orange solid was collected by filtration, washed with water, and air dried to give 882 mg of a pink solid. Crystallization from methylene chloride – ether gave 469 mg (45%) of off-white needles. An analytical sample was recrystallized from methylene chloride – ether, mp 182–183 °C; ir ν 3200 (NH), 1660, 1640 (C=O); pmr 2.23 (s, 6H), 2.38 (s, 6H), 4.95 (s, 4H), 7.33 (s, 10H), and 11.17 (bs, 2H). *Anal.* Calcd. for $C_{29}H_{28}N_2O_5$: C 71.89, H 5.82, N 5.78; found: C 71.89, H 5.90, N 5.64.

2-(2-Carbomethoxy-2-cyanovinyl)-5-formyl-3,4-dimethylpyrrole

2-(2-Carbomethoxy-2-cyanovinyl)-3,4,5-trimethylpyrrole (2.20 g, 0.01 mol), and sodium acetate (10.03 g, 0.12 mol) were dissolved in warm acetic acid (100 ml) and then water (20 ml) was added. Ceric ammonium nitrate (22.06 g, 0.04 mol) was added in one portion and the mixture heated on the steam bath for 15 min by which time the solution became dark red-brown. The reaction mixture was cooled, diluted with ice water and extracted with methylene chloride. The combined organic layers were taken down to dryness and the residual oil triturated with water to give a dark brown crystalline product. This solid was refluxed with methanol (30 ml) and filtered to remove a small amount of brown amorphous material. The methanol was removed and the residue crystallized from methylene chloride – hexane. The product was collected

Can. J. Chem. Downloaded from www.nrcresearchpress.com by 210.87.254.5 on 09/05/12
For personal use only.

Can. J. Chem. Downloaded from www.nrcresearchpress.com by 210.87.254.5 on 09/05/12
For personal use only.

by filtration and washed with methanol to give 0.34 g (14.7%), mp 190–191 °C (lit. (11) 190–191 °C); pmr 2.20 (s, 3H), 2.32 (s, 3H), 3.91 (s, 3H), 8.05 (s, 1H), 9.80 (s, 1H), and 10.05 (bs, 1H).

5,5'-Dicarbethoxy-3,3',4,4'-tetramethyl-2,2'-dipyrroketone, **7**

5,5'-Dicarbethoxy-3,3',4,4'-tetramethyl-2,2'-dipyrromethane, (9) (3.48 g, 0.01 mol) and anhydrous sodium acetate (8.04 g, ~0.10 mol) were dissolved in acetic acid (200 ml). A solution of ceric ammonium nitrate (22.42 g, ~0.04 mol) in water (25 ml) was added in one portion at room temperature. The pale yellow solution immediately became a deep orange-red and a finely-divided precipitate formed.

The mixture was heated on a steam bath, and the starch–iodide test soon became negative. The solution was then diluted with an equal volume of water, and filtered; this latter operation taking some time due to the small particle size of the product. After washing with water, the filter cake was allowed to dry in air. The yield of light pink solids was 2.07 g. (57.5%). When recrystallized from chloroform–hexane, a reddish color contaminated the product unless a few drops of triethylamine had been added, mp 212–214 °C (lit. (7) 203–205 °C); pmr 1.30 (t, 6H, J = 7.5 Hz), 2.24 (s, 6H), 2.28 (s, 6H), 3.99 (q, 4H, J = 7.5 Hz), 10.9 very weak.

5,5'-Bis-(2-carbomethoxy-2-cyanovinyl)-3,3',4,4'-tetramethyl-2,2'-dipyrroketone

5,5'-Bis-(2-carbomethoxy-2-cyanovinyl)-3,3',4,4'-tetramethyl-2,2'-dipyrromethane, **8** (0.84 g, 2.0 mmol) and anhydrous sodium acetate (4.4 g, 0.05 mol) were heated in acetic acid (50 ml) until they dissolved (at approximately 90 °C). Water (10 ml) was then added, followed by a solution of ceric ammonium nitrate (5.1 g, 0.01 mol = 4.384 g) in water (10 ml) over a 2 min period, at 80–95 °C. The color darkened from yellow to a deep greenish, then lightened as the remaining oxidant was added. After standing a few minutes, the solution was diluted with water (200 ml) to precipitate the product. The solid was filtered off, and washed with water. The filtrates were bright yellow, due to solubilized pyrroles, and not to quadrivalent cerium, as the color was not discharged with hydrogen peroxide. The solid was dissolved in methylene chloride, filtered, and the filtrate taken down to dryness. The residue was crystallized from methanol, collected by filtration and washed with methanol and then hexane to give 0.33 g (38%). An analytical sample was recrystallized from methylene chloride – methanol, mp 273–279 °C; ir ν 3400 (NH), 2210 (C≡N), 1720 (C=O), and 1590 (C=C); cm^{-1}; pmr 2.23 (s, 6H), 2.26 (s, 6H), 3.91 (s, 6H), 8.11 (s, 2H), and 10.12 (bs, 2H); ms, m/e = 434. *Anal.* Calcd. for $C_{23}H_{22}N_4O_5$: C 63.58, H 5.10, N 12.90; found: C 63.19, H 5.27, N 12.65.

5,5'-Diformyl-3,3',4,4'-tetramethyl-2,2'-dipyrroylketone

5,5'-Bis-(2-carbomethoxy-2-cyanovinyl)-3,3',4,4'-tetramethyl-2,2'-dipyrroketone (0.22 g, 0.51 mmol) was dissolved in ethanol (20 ml) and treated with potassium hydroxide (2.5 g) in water (5 ml). The mixture was heated on the steam bath for 3 h under nitrogen and the residue treated with water. The product was collected by filtration and crystallized from methanol to give 0.06 g (49%) of yellow prisms, mp 266–268 °C (lit. (7) 267–269 °C).

Acknowledgments

This work was supported by the United States National Science Foundation and National Institutes of Health and the National Research Council of Canada. The authors wish to thank P. E. Garrett for her help with a portion of the experimental work.

1. H. Fischer and H. Orth. Die chemie des pyrrols. Johnson Reprint Company, New York, New York. 1968.
2. L. Syper. Tetrahedron Lett. 4493 (1966).
3. W. S. Trahanovsky and L. B. Young. J. Org. Chem. **31**, 2033 (1966).
4. W. S. Trahanovsky and L. B. Young. J. Chem. Soc. 5777 (1965).
5. W. B. Trahanovsky, L. B. Young, and G. L. Brown. J. Org. Chem. **32**, 3865 (1967).
6. J. M. Osgerby and S. F. MacDonald. Can. J. Chem. **40**, 1585 (1962).
7. P. S. Clezy, A. J. Liepa, A. W. Nichol, and G. A. Smythe. Aust. J. Chem. **23**, 589 (1970).
8. D. Dolphin, J. B. Paine III, and R. B. Woodward. J. Org. Chem. In press.
9. A. W. Johnson, I. T. Kay, E. Markham, R. Price, and K. B. Shaw. J. Chem. Soc. 3416 (1959).
10. G. M. Badger and A. D. Ward. Aust. J. Chem. **17**, 655 (1964).
11. H. Fischer and H. Höfelmann. Ann. Chem. **533**, 216 (1938).

Butenolides from citraconic anhydride and acetophenone: rearrangement to a 2,3-dihydro-3-furanone related to bullatenone

GEORGE M. STRUNZ AND PAVLE I. KAZINOTI
Canadian Forestry Service, P.O. Box 4000, Fredericton, New Brunswick E3B 5G4

Received July 17, 1975

GEORGE M. STRUNZ and PAVLE I. KAZINOTI. Can. J. Chem. **54**, 415 (1976).

Two related butenolides, one having fungitoxic properties, were obtained from the reaction of acetophenone with citraconic anhydride in the presence of *n*-butyllithium. The butenolides rearranged to a 3(2*H*)-furanone related to bullatenone on acid treatment.

GEORGE M. STRUNZ et PAVLE I. KAZINOTI. Can. J. Chem. **54**, 415 (1976).

Deux buténolides apparentés, dont l'un est doué d'une activité fongitoxique, ont été obtenus par la réaction de l'acétophénone avec l'anhydride citraconique en présence de *n*-butyllithium. Les buténolides, par traitement avec de l'acide, se transforment en 2*H*-furannone-3, voisin de la bullaténone.

The reaction of acetylacetone with citraconic anhydride was reported by Berner (1) in 1952 to give rise to the adduct **1**, evidently by *C*-acylation of the β-diketone, followed by formation of the cyclic enol ether via a Michael addition. A somewhat related sequence of reactions has recently been explored for the synthesis of tetronic acid fungal metabolites (2). It appeared that a similar route could in principle lead to a facile synthesis of structures closely related to the naturally occurring 3(2*H*)-furanone bullatenone, **2** (3). Indeed, a model experiment showed that ethyl acetoacetate and citraconic anhydride yielded on prolonged heating the expected adduct **3** (*cf.* ref. 1), which could be

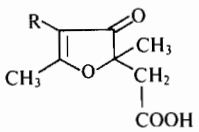

1 R = $COCH_3$
3 R = $COOC_2H_5$
4 R = H

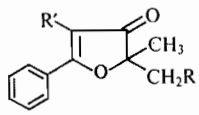

2 R = R′ = H
5 R = COOH
R′ = $COOC_2H_5$
6 R = COOH
R′ = H

hydrolyzed and decarboxylated smoothly to give **4** by heating with an aqueous acetic – hydrochloric acid mixture.[1] Attempts to isolate the analogous adduct **5** from reaction of citraconic anhydride with ethyl benzoyl acetate under the same conditions were not fruitful. The desired product could, however, be obtained in modest yield when sodium acetate was present as catalyst. Because of difficulties encountered in the subsequent hydrolysis and decarboxylation of **5**,[1] the base-catalyzed reaction of acetophenone with citraconic anhydride was investigated as an alternative route to **6**. The results of this study, of enhanced interest because of the fungitoxic properties associated with the intermediate butenolide **8**, are described herein.

The enolate, generated from acetophenone by reaction with *n*-butyllithium in tetrahydrofuran, was treated with one equivalent of citraconic anhydride at ambient temperature for 3–4 h. The reaction mixture, after work-up and preparative layer chromatography, afforded two crystalline products[2] in addition to unreacted starting materials and citraconic acid.

The major product (~36% yield based on unrecovered acetophenone), $C_{13}H_{12}O_4$, was readily identified as **7** on the basis of its spectral charac-

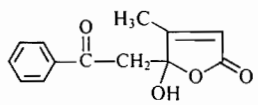

7

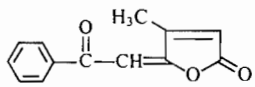

8

teristics. In this respect the nmr spectrum was particularly revealing, displaying clearly the hydroxylic and phenyl proton absorptions, an AB quartet ($J \sim 16$ Hz) corresponding to the methylene protons, and appropriate signals for the allylic methyl group coupled ($J \sim 1.5$ Hz) with the olefinic hydrogen. The chemical shifts of the latter signals establish the position of the

[1]G. M. Strunz and W. Y. Ren, unpublished data.
[2]Yields have not been optimized.

Can. J. Chem. Downloaded from www.nrcresearchpress.com by 210.87.254.105 on 09/05/12
For personal use only.

Can. J. Chem. Downloaded from www.nrcresearchpress.com by 210.87.254.105 on 09/05/12
For personal use only.

methyl group with respect to the conjugated carbonyl system (see Experimental). While nucleophilic attack (by an amine) on *n*-pentylmaleic anhydride has been observed to occur at the carbonyl group remote from the alkyl chain (4), the center affected in the formation of **7** is consistent with the known behavior of citraconic anhydride towards nucleophiles (1).

The less abundant crystalline product (~4% yield based on consumed ketone) was a lemon-yellow substance, $C_{13}H_{10}O_3$, embodying an extended cross-conjugated chromophore. Its spectroscopic properties (see Experimental) and mechanistic considerations identified it as **8**, the anhydro derivative of **7**.[3]

When the reaction was conducted under similar conditions using sodium hydride as base, **8** became the predominant condensation product, but was isolated in only 14% yield (based on consumed ketone), while the yield of **7** dwindled to 5%. An unexpected by-product from this reaction was the pinacol, 2,3-diphenylbutane-2,3-diol, obtained in low yield as a diasteromeric mixture (5), from which the *dl* component could be separated readily by crystallization. Using 1.6 equiv. of sodium hydride from different batches per equivalent acetophenone, the yields of pinacol obtained were around 0.8–1.5% (although one particular batch of hydride gave a 7% yield of pinacol, based on total ketone). (This compound was also produced in the absence of citraconic anhydride and in the dark.) While it is conceivable that the pinacol could be formed via a one-electron transfer from sodium hydride to the ketone, such a reduction has not been observed previously to our knowledge (*cf.* ref. 6). The presence of a small quantity of free metallic sodium in the hydride suspension[4] could perhaps more readily account for the observed results.

Acid treatment of either **7** or **8** resulted in rearrangement to the desired 3(2*H*)-furanone **6**, $C_{13}H_{12}O_4$, whose spectra were in accord with the assigned structure (see Experimental). The nmr spectrum showed a multiplet at δ 7.25–7.92 for the aromatic hydrogens, a singlet at δ 6.05 corresponding to the olefinic proton, a singlet at δ 2.90 attributed to the methylene protons, a singlet at δ 1.55 for the methyl hydrogens, and a broad singlet at δ 10.38 corresponding to the acid proton.

In bioassays using the disc method, the yellow compound **8** showed antifungal activity against selected test organisms, including *Ceratocystis ulmi*.[5] The hydroxy butenolide, **7**, appeared to be devoid of activity against the fungi tested.

Experimental

Melting points were determined on a hot-stage apparatus and are uncorrected. Infrared spectra were recorded on either a Beckman IR-10 or Acculab 2 spectrophotometer. Ultraviolet spectra were obtained using either a Beckman DK-2A or a Perkin-Elmer 402 spectrophotometer. Nuclear magnetic resonance spectra were recorded for solutions in deuteriochloroform with a Varian T-60 instrument, employing tetramethylsilane as internal standard. Mass spectra were obtained with an Hitachi–Perkin-Elmer RMU-6D mass spectrometer. Microanalyses were performed by Spang Microanalytical Laboratory, Ann Arbor, Michigan.

Condensation Reaction, Butyllithium as Base

To acetophenone (1.20 ml, 1.23 g, 10.3 mmol) in dry tetrahydrofuran (~50 ml) was added by syringe under nitrogen, *n*-butyllithium (6.0 ml of 15% heptane solution, 14.1 mmol). The mixture was stirred at ambient temperature in a nitrogen atmosphere for 1 h, and citraconic anhydride (0.90 ml, 1.12 g, 10.0 mmol) was then added by syringe. The mixture was stirred under the same conditions for 3.5 h. The amorphous mixture obtained on work-up was separated on preparative layer plates of silica gel (85% benzene, 15% acetone). In addition to zones yielding unreacted acetophenone (664 mg), citraconic anhydride and acid, two other bands were readily separated.

The less mobile band yielded the hydroxy butenolide **7** (395 mg): colorless crystals from methylene chloride–cyclohexane, mp 119–127 °C; ir (KBr) 1750, 1655, 1450, 1240, 1215, 1075, and 940 cm^{-1}; ir ($CHCl_3$) 3350, 1775 (sh), 1760, and 1670 cm^{-1}; uv λ_{max} (CH_3CN), nm (ε), 243(10 700), 277(infl. 2200), and 338(3000); nmr ($CDCl_3$ 60 MHz) δ 2.13 (3H, d, $J \sim 1.5$ Hz), 3.36 (2H, q, $J \sim 16$ Hz), 5.85 (1H, q, $J \sim 1.5$ Hz), 6.80 (1H, s, exchangeable with D_2O), 7.42–7.67 (3H, m), and 7.78–8.02 (2H, m); mass spectrum, *m/e* 232($M^{+\cdot}$), 214 ($M - H_2O)^{+\cdot}$, 187 ($M - CO{\cdot}OH)^+$, 120($C_8H_8O)^{+\cdot}$, 105($C_7H_5O)^+$. *Anal.* Calcd. for $C_{13}H_{12}O_4$: C 67.23, H 5.21; found: C 67.00, H 5.12.

Material from the less polar yellow band was crystallized from methylene chloride–cyclohexane yielding **8** (39 mg); lemon-yellow crystals, mp 95–110 °C; ir (KBr) 1805, 1795 (sh), 1665, and 1610 cm^{-1}; uv λ_{max} (EtOH) 294 nm (ε 28 000); nmr ($CDCl_3$ 60 MHz) δ 2.29 (3H, d, $J \sim 1.5$ Hz), 6.19 (1H, poorly resolved q, $J \sim 1.5$ Hz),

[3]Hydroxy butenolide **7** was readily converted to **8** (*ca.* 85% yield) on treatment with acetic anhydride at ambient temperature for 15 h.

[4]Sodium hydride from Metal Hydrides, Inc. may contain up to 0.5% free sodium. Personal communication: Ventron Corporation.

[5]M. A. Stillwell, unpublished data.

6.33 (1H, s) 7.19–7.63 (3H, m), and 7.80–7.87 (2H, m); mass spectrum, *m/e* 214 (M^+). *Anal.* Calcd. for $C_{13}H_{10}O_3$: C 72.89, H 4.71; found: C 72.82, H 4.64.

Condensation Reaction, Sodium Hydride as Base

To sodium hydride (672 mg, 60% dispersion in mineral oil, 16.8 mmol) in anhydrous tetrahydrofuran (~50 ml, freshly distilled from lithium aluminum hydride) was added dropwise by syringe under nitrogen 1.18 ml acetophenone (1.21 g, 10.1 mmol). The mixture was stirred at ambient temperature in a nitrogen atmosphere for 45 min, and citraconic anhydride (0.90 ml, 1.12 g, 10.0 mmol) was then added by syringe. The resulting dark red mixture was stirred under the same conditions for 3 h.

The amorphous mixture obtained on work-up was separated on preparative layer plates of silica gel (85% benzene, 15% acetone). In addition to unreacted acetophenone (616 mg), citraconic anhydride and acid, the chromatography yielded, after crystallization, the hydroxy butenolide **7** (62 mg) and the yellow product **8** (150 mg).

Preparative layer chromatography of the mother liquors from crystallization of the yellow butenolide **8**, afforded a colorless product which was recrystallized from methylene chloride–cyclohexane to give the pinacol, (*dl*) 2,3-diphenylbutane-2,3-diol (*cf.* ref. 5): colorless crystals, mp 124–125 °C; ir (KBr) *inter alia*, 3450 (br), 1495, 1445, 1375, 1350, 1205, 1145, 1065, 1030, 935, 920, 765, and 705 cm^{-1}; nmr ($CDCl_3$ 60 MHz) δ 1.50 (6H, s), 2.61 (2H, s, exchangeable with D_2O), and 7.23 (10H, s); mass spectrum, *inter alia*, *m/e* 242 ($M^{+\cdot}$), 224 ($M - H_2O)^{+\cdot}$, 181 $(M - H_2O - CH_3CO)^+$, 121 (base peak) $(M - C_8H_9O)^+$. *Anal.* Calcd. for $C_{16}H_{18}O_2$: C 79.31, H 7.49; found: C 79.54, H 7.43.

The nmr spectrum of the crude mother liquors, specifically additional signals at δ 1.56 (methyl) and 2.36 ppm (hydroxyl), indicated that the *meso* pinacol was also present (5).

Acid-catalyzed Rearrangement of Butenolides

A mixture of **7** (40 mg, 0.17 mmol), aqueous hydrochloric acid (10 ml of 7.4% solution) and acetic acid (1 ml, glacial) was heated under reflux for 2.5 h. The mixture was made alkaline with sodium bicarbonate solution, and washed with ether. The aqueous solution was then reacidified by addition of dilute hydrochloric acid and extracted repeatedly with chloroform. The organic phase was dried over sodium sulfate, and chloroform and acetic acid were removed under vacuum. Crystallization of the residue from methylene chloride–cyclohexane yielded 35 mg (88%) of **6**, colorless crystals, mp 130–140 °C, ir (KBr) 3600–2400, 1730, 1660, 1610, 1590, and 1565 cm^{-1}; uv λ_{max} (EtOH) nm (ε), 242(10 400), 295(21 000), and 304(21 600); nmr ($CDCl_3$ 60 MHz) δ 1.55(3H, s), 2.90(2H, s), 6.05(1H, s), 7.25–7.60(3H, m), 7.65–7.92(2H, m), and 10.38(1H, br s); mass spectrum, *m/e* 232($M^{+\cdot}$), 188$(M - CO_2)^{+\cdot}$, 187$(M - COOH)^+$, 172$(M - C_2H_4O_2)^{+\cdot}$, 130$(C_9H_6O)^{+\cdot}$, 102$(M - C_9H_6O)^{+\cdot}$. *Anal.* Calcd. for $C_{13}H_{12}O_4$: C 67.23, H 5.21; found: C 67.30, H 5.13.

Acid-catalyzed rearrangement of **8** (50 mg, 0.23 mmol) similarly gave 45 mg (83%) of **6**.

Acknowledgments

We thank Mr. M. A. Stillwell, Maritimes Forest Research Centre, for the bioassays, and Mrs. M. Austria, University of New Brunswick for the mass spectra.

1. E. Berner. Acta Chem. Scand. **6**, 646 (1952); E. Berner and P. Kolsaker. Tetrahedron, **24**, 1199 (1968).
2. A. Svendsen and P. M. Boll. Tetrahedron Lett. 2821 (1974).
3. W. Parker, R. A. Raphael, and D. I. Wilkinson. J. Chem. Soc. 3871 (1958).
4. N. H. Anderson, W. D. Ollis, J. E. Thorpe, and A. D. Ward. Chem. Commun. 420 (1974).
5. H. Agahigian, J. F. Moraveck, and H. Gauthier. Can. J. Chem. **41**, 194 (1963); D. J. Cram and K. R. Kopecky. J. Am. Chem. Soc. **81**, 2748 (1959).
6. G. E. Lewis. J. Org. Chem. **30**, 2433 (1965).

Can. J. Chem. Downloaded from www.nrcresearchpress.com by 210.87.254.105 on 09/05/12
For personal use only.

Revised structure for the γ-lactone derived from acid treatment of dihydroisopimaric acid[1,2]

JOHN W. APSIMON AND ANDREW M. HOLMES
Department of Chemistry, Carleton University, Ottawa, Canada K1S 5B6
AND
HELMUT BEIERBECK AND JOHN K. SAUNDERS
Département de Chimie, Université de Sherbrooke, Sherbrooke, Québec J1K 2R1

Received May 15, 1975

JOHN W. APSIMON, ANDREW M. HOLMES, HELMUT BEIERBECK, and JOHN K. SAUNDERS. Can. J. Chem. **54**, 418 (1976).

The γ-lactone obtained from acid treatment of dihydroisopimaric acid was found to have a *cis*-A/B ring fusion. This structure revision was based on ^{13}C nmr chemical shift data and spin–lattice relaxation time (T_1) measurements. Using the same methods, the δ-lactone derived from the same acid was shown to have the previously proposed structure.

JOHN W. APSIMON, ANDREW M. HOLMES, HELMUT BEIERBECK et JOHN K. SAUNDERS. Can. J. Chem. **54**, 418 (1976).

On a trouvé que la jonction des cycles A et B de la γ-lactone obtenue par traitement acide de l'acide dihydroisopimarique possède une géométrie *cis*. Cette structure revisée est basée sur des données de déplacements chimiques en rmn du ^{13}C et sur des mesures de temps de relaxation (T_1) spin–réseau. Utilisant les mêmes méthodes, on a montré que la δ-lactone obtenue à partir du même acide possède la structure proposée antérieurement.

[Traduit par le journal]

Reaction of the diterpenes dihydroabietic acid **1***a* or dihydropimaric acid **1***b* with sulphuric acid leads to backbone rearrangement and lactone formation (1). A γ-lactone **2***a* or **2***b*, respectively, was reported to be the major product isolated when the reaction is carried out at −5 °C for 1 h, whereas more vigorous conditions (25 °C, 5 h) result in the formation of a δ-lactone (**3***a* or **3***b*, respectively) as the major product. The γ-lactone derived from dihydroabietic acid was postulated by Barton (1*a*) to arise from a carbonium ion process in which the angular methyl group migrates from C-10 to C-9. Accordingly, structure **2***a* was assigned to this compound.[3] The *trans*-A/B ring junction was deduced on the basis of energetic arguments; a $\Delta^{5(10)}$ olefinic intermediate was believed to participate in the rearrangement and addition to this double bond would be expected to take place in a *trans* manner to give the more stable *trans* ring fusion. Subluskey and Sanderson (1*b*) also used conformational arguments in order to assign the same stereochemistry at C-5 and C-10 of this compound.

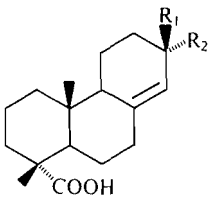

1*a* R_1 = *i*-propyl, R_2 = H
b R_1 = C_2H_5, R_2 = CH_3

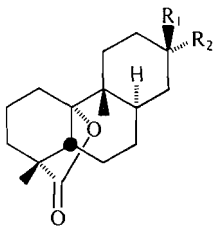

2*a* R_1 = *i*-propyl, R_2 = H
b R_1 = C_2H_5, R_2 = CH_3

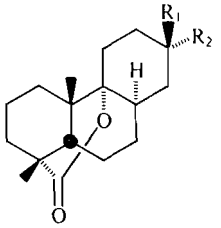

3*a* R_1 = *i*-propyl, R_2 = H
b R = C_2H_5, R_2 = CH_3
c R_1 = CH_3, R_2 = C_2H_5

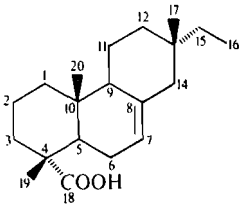

4

[1]Considered as Part V of Diterpene Chemistry. For Part IV see ref. 9.
[2]Part II of Carbon-13 Relaxation Times in Natural Products. For Part I see ref. 5.
[3]No stereochemistry was implied at C-13.

Can. J. Chem. Downloaded from www.nrcresearchpress.com by 210.87.254.42 on 09/05/12
For personal use only.

Can. J. Chem. Downloaded from www.nrcresearchpress.com by 210.87.254.42 on 09/05/12
For personal use only.

During a recent study on the mechanism of acid-catalyzed rearrangements in terpenes, we reexamined the two lactones obtained from dihydroisopimaric acid **4** using ^{13}C nmr spectroscopy. The data obtained confirm the accepted structures for the δ-lactone **3***c*, but show the previously postulated representation of the γ-lactone **5** (*cf.* **2***a*,*b*) to be incorrect.[4]

A number of ^{13}C nmr parameters can be used in structural analysis. The use of the chemical shift is well documented (2) with several methods of predicting chemical shift being available (3, 4). Our method of choice (4) is to use a base chemical shift depending on the type of carbon atom and then to consider the number of β-gauche CH and CC interactions as well as the number of γ and δ steric interactions. In this report, the recorded shifts for *trans*- or *cis*-decalin (3) will be used as the base and the number of gauche and steric interactions at the β and γ carbons respectively, arising from substitution, will be used to predict the carbon shift. For example, the chemical shift of C-12 of **2***b* is calculated as follows (see Fig. 1):[5]

28.0(C-2 of decalin) + 6.3(axial CH_3 group) + 9.4(equatorial CH_2 moiety) − 4.5(γ steric effect of CH_3 of ethyl group) − 4.5(γ effect of C-20 CH_3 group) = 34.7 ppm

The spin-lattice relaxation time T_1 can also be of use, both in assigning an absorption to the type of carbon and, in the case of CH_3 groups, to gaining structural and conformational information (5). The C-13 T_1 value in compounds studied here is given by

$$\frac{1}{T_1} = \frac{N\hbar^2\gamma_H^2\gamma_C^2}{(r_{C-H})^6}\tau_c$$

where N is the number of attached protons. Thus $T_1(CH) = 2T_1(CH_2) \ll T_1(C)$ with $T_1(CH_3)$ ranging in value from $\frac{1}{3}T_1(CH)$ to $3T_1(CH)$ depending on the rate of internal rotation about the C—CH_3 bond. The correlation time τ_i, for internal reorientation can be deduced from (6)

$$\frac{T_1(CH)}{3T_1(CH_3)} = \frac{1}{9}\left[1 + \frac{16}{6+\rho}\ \frac{16}{3+2\rho}\right]$$

where $\rho = \tau_c/\tau_i$.

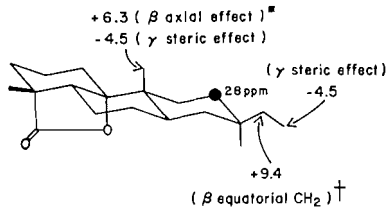

FIG. 1. Calculation of the chemical shift of C-12 in the γ-lactone **2***b*. *One gauche CH (4.7 ppm), 1 gauche CC (1.6 ppm) interaction. †Two gauche CH interactions.

Results and Discussion

The chemical shift data for the γ-lactone **6**, previously considered to be **5**, resulting from treatment of the acid **4** with H_2SO_4 at −5 °C are given in Table 1. The resonances were assigned to C, CH, CH_2, or CH_3 carbons from (180° − τ − 90°) pulse sequences with τ values such that the CH_2 and then the CH carbons were nulled. The remaining assignments were made from the $Pr(fod)_3$ induced shifts given in Table 1 and from the recorded chemical shifts of other terpenoid compounds (7).

This leaves the problem of assigning the configuration of the A/B ring junction. The shifts predicted for the *cis* and *trans* structures are also given in Table 1. As can be seen, reasonable agreement between calculated and observed shifts is obtained for both configurations with the exception of C-1 and C-11 for the *cis*-structure **6** and C-1 and C-7 for the *trans*-structure **5**. The predicted shifts are for carbons in gauche orien-

[4]Our studies with dihydroabietic acid show a parallel behaviour with the isopimaric series, but problems with product purification prevented unambiguous analysis of all the spectroscopic results.

[5]The following reference shifts and increments have been used throughout this work:

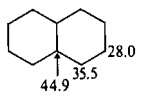

CH_3 = 5.9 ppm

Increments:

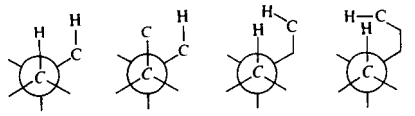

β_{C-H}	β_{C-C}	γ	δ
4.7 ppm	1.6 ppm	−4.5 ppm	−1.1 ppm

The effect of heteroatoms can be deduced in a similar fashion (4*b*).

Can. J. Chem. Downloaded from www.nrcresearchpress.com by 210.87.254.42 on 09/05/12
For personal use only.

TABLE 1. Chemical shifts (δ)* and lanthanide induced shifts ($\Delta\delta$) for the lactones derived from dihydroisopimaric acid

	γ-Lactone				δ-Lactone	
	Observed		δ Predicted			
	δ	$\Delta\delta$	**5**	**6**	δ	$\Delta\delta$
1	27.6	2.2	32.8	32.4	36.6	2.6
2	19.9	2.3	19.0	19.0	21.3	3.6
3	34.9	3.6	36.8	33.5	41.0	6.1
4	49.5	4.1			42.7	7.1
5	48.4	2.6	47.8	46.9	49.2	4.3
6	25.4	2.0	26.0	24.0	21.4	3.0
7	26.4	1.5	31.0	28.2	25.1	3.5
8	32.5	1.3	34.8	34.8	34.6	3.5
9	38.0	1.5	39.2	39.2	89.0	
10	88.0				36.9	3.3
11	27.3	1.2	26.6	31.1	25.6	2.7
12	32.3	0.6	34.8	34.8	31.7	1.8
13	32.4	0.5			32.4	1.3
14	39.9	0.8	41.2	41.2	39.5	2.3
15	28.2	0.4	30.0	30.0	37.7	0.4
16	8.0	0.2	7.6	7.6	7.6	0.4
17	28.9	0.3	29.7	29.7	21.0	0.9
18	178.0					
19	16.9	3.8			22.5	7.1
20	14.4	0.8	12.4	16.2	25.1	1.7

*In ppm from TMS.

tations and do not take into account possible chemical shift changes arising from conformational distortions. Hence, from chemical shift arguments it is difficult to assign the stereochemistry at C-5. However, inspection of the two possibilities shows that in the *trans*-configuration

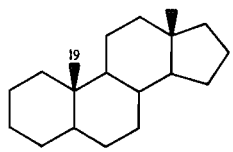

9

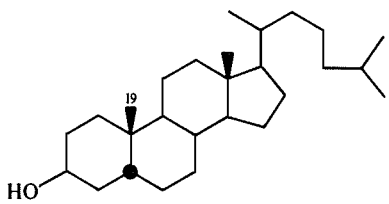

10

5, the C-20 CH_3 group would be in a similar steric environment as C-19 of androstane **9** as it experiences five 1,3-CH_3–H diaxial interactions,

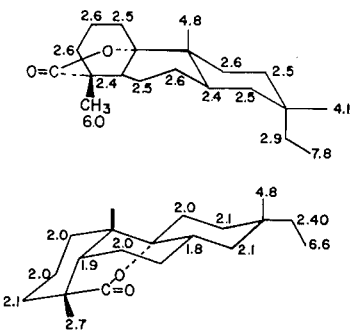

FIG. 2. Relaxation time (T_1) data for the lactones obtained from dihydroisopimaric acid.

whereas for the *cis*-fused configuration **6**, the C-20,C-9 bond is virtually eclipsing the C-1,C-10 bond. We would therefore expect a large difference in the τ_i values for the two compounds with the *trans*-configuration **5** exhibiting a value close to $\tau_i = 0.6 \times 10^{-12}$ s, the recorded value for C-19 of androstane **9** (5). The T_1 data for the γ-lactone are illustrated in Fig. 2, from which τ_i for C-20 is calculated to be 9×10^{-12} s which is 15 times longer than that recorded for C-19 of androstane. This indicates that the γ-lactone must have a *cis* A/B ring junction with the slower rotation rate about the C-20,C-9 bond being a consequence of an increase in the barrier to rotation caused by the relative orientation of C-20 and C-1. The lack of agreement between predicted and observed chemical shift values for C-1 and C-11 is a result of more intense γ interactions than that found in axial methyldecalin, which is used as the model system.

It should be noted that two other γ-lactone structures can be postulated, namely *trans-transoid-cis* **7** and *cis-transoid-cis* **8**. However, both these possibilities can be eliminated using

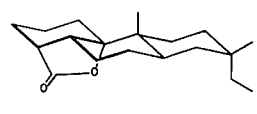

trans - transoid - trans
5

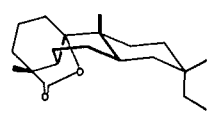

cis - transoid - trans
6

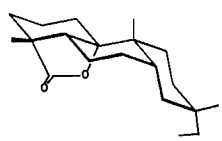

trans - transoid - cis
7

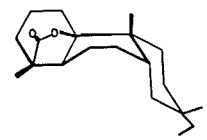

cis - transoid - cis
8

Can. J. Chem. Downloaded from www.nrcresearchpress.com by 210.87.254.42 on 09/05/12
For personal use only.

chemical shift arguments, with particular reference to the CH_3 groups C-20 and C-17. In **7**, we would predict a chemical shift for C-20 at about 25 ppm as it is in a similar environment to C-19 of *cis*-cholestanol **10** whereas this carbon in **8** would appear in the region of 27 ppm as it only has two γ steric interactions, although one (that with C-1) is more severe than normal. In both **7** and **8**, C-17 is axial and would thus absorb in the region of 21.0 ppm as was recorded for the δ-lactone **3***c*. Since the C-20 resonance is at 14.4 ppm and that of C-17 at 28.9 ppm, neither **7** or **8** can be the correct formulation for the γ-lactone.

The chemical shift data for the δ-lactone **3***c* are recorded in Table 1 and the relaxation time data in Fig. 2. The resonances were assigned by use of the $(180° - \tau - 90°)$ sequence followed by the prediction of chemical shifts as outlined earlier. A reasonable correlation between predicted and calculated shifts was obtained. Any other possible structure could be ruled out by considering the chemical shifts of the methyl groups C-17 and C-20. In a *cis-transoid-cis* configuration, C-17 would be equatorial and consequently would appear in the region of 29.0 ppm. No other δ-lactone having the observed number of C, CH, CH_2, and CH_3 carbon atoms can be envisaged. There exists the remote possibility of an ϵ-lactone to C-8 or a γ-lactone with an unusual infrared spectrum, both of these are eliminated by the chemical shift data presented in Table 1. In order to confirm the assignments, a quantitative study of $Pr(fod)_3$ induced shifts (8) was made. Reasonable correlation could be obtained between calculated and observed shifts with the exception of those for C-7 and C-3 with the former having experimental shifts less than calculated whereas the latter showed the reverse behaviour. A much better correlation could be observed by making the C_9—O—C—C_4 bonds planar. This deformation not only increases the overlap between the oxygen orbitals and the C=O of the lactone, but also alleviates the serious nonbonded interaction between the protons of C-1 and C-11. Thus the ^{13}C spectral parameters appear to be in complete agreement with the previously proposed structure (1).

The variation in T_1 values for the CH_3 groups is a consequence of different steric environment. In **3***c*, C-17 is axial and has a 1,3-diaxial interaction with the protons of C-8 and C-11 whereas in **6**, this group is equatorial and its rotation rate is thus significantly slower. In both compounds, NT_1 (C-15) is only marginally longer than that of the ring carbons and this slower rate relative to a CH_3 group is attributable to inclusion of the energy of the barrier to rotation about the C-15,C-16 bond to that about the C-15,C-13 bond. It is of interest to note the difference in τ_i for C-19 in the two compounds. The rotation rate about the C-19,C-4 bond is significantly faster in **6** than in **3***c* with the chemical shift of C-19 in **6** being shielded by 5–6 ppm relative to that observed in **3***c*. This must be interpreted in terms of a larger γ steric effect in **6** resulting in increased shielding and a decrease in the barrier to rotation.

Experimental

Melting points were determined on a Fisher-Johns melting point apparatus and are uncorrected. Infrared (ir) spectra were recorded on a Perkin-Elmer 237 Infracord spectrophotometer. Proton magnetic resonance (pmr) spectra were taken on a Varian Associates Model T-60A spectrometer in deuteriochloroform with tetramethylsilane as internal standard. Methyl singlets are quoted (in ppm). ^{13}C nmr spectra were recorded on a Bruker HX-90 instrument equipped with a Nicolet 1083 computer in the Fourier transform mode. The solvent was $CDCl_3$ with TMS as internal reference. The T_1 data were obtained from $(180° - \tau - 90°)$ sequences as described previously (5). The mass spectra were recorded on an AEI MS12 instrument at Trent University.

9,10-Friedoisopimaran-18:10-olide, **6**

To concentrated sulphuric acid (9.5 ml) at −5 °C was added dihydroisopimaric acid **4** (519 mg). The mixture was stirred for 1 h at this temperature, poured over crushed ice (65 g), and extracted with ether (4 × 30 ml). The combined organic layers were washed with water (5 × 30 ml), dried ($MgSO_4$), and concentrated *in vacuo* to give a pale yellow oil. The oil was adsorbed on silica gel (25 g) and eluted with 30 ml portions of benzene. Fractions 4 to 8 inclusive were combined, yielding a white solid (241 mg, 46%). Recrystallization from methanol–water gave the γ-lactone **6** as white needles (143 mg), mp 105.5–106.5 °C (lit. (1*g*) 105–106 °C); ir (Nujol) 1765 cm^{-1} (five-membered lactone); pmr 0.80, 0.84, 1.08 δ; cmr Table 1; mass spectrum M^+ 304.

5β-Isopimaran-18:9-olide, **3***c*

Dihydroisopimaric acid **2** (537 mg) was stirred in concentrated sulphuric acid (9.5 ml) at room temperature for 4.5 h. Work-up as above gave a yellow oil which was adsorbed on silica gel (30 g). Elution with benzene and then benzene–ether (19:1) gave, in the later fractions, a mixture containing mainly the δ-lactone **3***c*. Further chromatography on silica gel yielded pure **3***c* (78 mg, 15%), which could not be induced to crystallize; ir (neat) 1720 cm^{-1} (six-membered lactone); pmr 0.85, 1.11, 1.23 δ; cmr Table 1; mass spectrum M^+ 304.

1. (*a*) D. H. R. BARTON. Chem. Ind. 638 (1948); (*b*) L. A. SUBLUSKEY and T. F. SANDERSON. J. Am. Chem. Soc. **76**, 3512 (1954); (*c*) L. VELLUZ, G. MULLER, A. PETIT, and J. MATHIEU. Bull. Soc. Chim. Fr. 401 (1954), and references cited therein; (*d*) LE-VAN THOI and J. OURGAUD. Bull. Soc. Chim. Fr. 202 (1956); 205 (1956), and previous papers; (*e*) E. WENKERT and J. W. CHAMBERLIN. J. Am. Chem. Soc. **81**, 688 (1959); (*f*) O. E. EDWARDS and R. HOWE. Chem. Ind. 629 (1958); Can. J. Chem. **37**, 760 (1959); (*g*) W. HERZ and H. J. WAHLBORG. J. Org. Chem. **30**, 1881 (1965).
2. J. B. STOTHERS. Carbon-13 nuclear magnetic resonance spectroscopy. Academic Press, New York. 1972.
3. D. K. DALLING, D. M. GRANT, and E. G. PAUL. J. Am. Chem. Soc. **95**, 3718 (1973); D. K. DALLING and D. M. GRANT. J. Am. Chem. Soc. **96**, 1827 (1974).
4. (*a*) H. BEIERBECK and J. K. SAUNDERS. Can. J. Chem. **53**, 1307 (1975); (*b*) H. BEIERBECK and J. K. SAUNDERS. Can. J. Chem. In press.
5. J. W. APSIMON, H. BEIERBECK, and J. K. SAUNDERS. Can. J. Chem. **53**, 338 (1975); J. K. SAUNDERS. 168th National Meeting of the American Chemical Society, Atlantic City. 1974.
6. A. ALLERHAND, D. DODDRELL, and R. KOMOROSKI. J. Chem. Phys. **55**, 189 (1971).
7. E. WENKERT and B. L. BUCKWALTER. J. Am. Chem. Soc. **94**, 4367 (1972).
8. J. W. APSIMON, H. BEIERBECK, and J. K. SAUNDERS. Can. J. Chem. **51**, 3874 (1973).
9. J. W. APSIMON and H. KREHM. Can. J. Chem. **47**, 2865 (1969).

Can. J. Chem. Downloaded from www.nrcresearchpress.com by 210.87.254.42 on 09/05/12
For personal use only.

Nitration of *p*-cymene. Exchange and rearomatization reactions of *p*-cymene adducts

ALFRED FISCHER AND ROLF RÖDERER
Department of Chemistry, University of Victoria, Victoria, British Columbia V8W 2Y2

Received August 1, 1975

ALFRED FISCHER and ROLF RÖDERER. Can. J. Chem. **54**, 423 (1976).

Nitration of *p*-cymene in acetic anhydride gives a mixture of *cis*- and *trans*-1-isopropyl-4-methyl-4-nitro-1,4-dihydrophenyl acetate as the main product as well as 2- and 3-nitro-*p*-cymene and *p*-nitrotoluene. Acid-catalysed methanolysis of the acetoxynitro adduct gives a mixture of the *cis*- and *trans*-methoxynitro adducts. Under basic conditions the acetate adduct is converted into the corresponding alcohol which is in turn rearomatized to 2-isopropyl-4-methylphenol. The adducts rearomatize to 2-nitro-*p*-cymene in strong acid.

ALFRED FISCHER et ROLF RÖDERER. Can. J. Chem. **54**, 423 (1976).

La nitration du *p*-cymène dans l'anhydride acétique conduit à un mélange d'acétates d'isopropyl-1 méthyl-4 nitro-4 dihydro-1,4 phényle *cis* et *trans* comme produits principaux de même qu'aux nitro-2 et -3 *p*-cymènes et au *p*-nitrotoluène. La méthanolyse, catalysée par les acides, de l'adduit acétoxynitro donne un mélange d'adduits méthoxynitros *cis* et *trans*. Utilisant des conditions basiques, l'adduit acétate est transformé en alcool correspondant qui est à son tour réaromatisé en isopropyl-2 méthyl-4 phénol. Les adduits se réaromatisent en nitro-2 *p*-cymène en milieu fortement acide.

[Traduit par le journal]

Introduction

Appropriately substituted toluenes and related arenes undergo addition of acetyl nitrate (as nitronium acetate) via *ipso* (1) nitration (2–4). The present study deals with the formation and reactions of the adducts of *p*-cymene. In the course of our work on *p*-cymene Hahn and Strack reported the formation of the diastereoisomeric acetyl nitrate adducts and their conversion to *p*-cymene and thymol acetate in acetic acid and to 2-nitro-*p*-cymene in 78% sulfuric acid (3*b*). We have studied the exchange reactions leading to the formation of methoxynitro dienes, the base-catalysed cleavage of the acetoxynitro dienes, the rearomatization and exchange reactions of the new dienes, and the rearomatization reactions of the acetoxynitro dienes under a variety of conditions.

Results and Discussion

Formation of Adducts and their Interconversion (Exchange) Reactions

Nitration of *p*-cymene in acetic anhydride gave 57% of diene adducts, 26% 2-nitro-*p*-cymene, 12% *p*-nitrotoluene and 5% 3-nitro-*p*-cymene. Low temperature chromatography of the product afforded the diastereoisomers[1] of the acetoxynitro dienes **1***a* and **1***b*, the nitro-*p*-cymenes, *p*-nitrotoluene, the hydroxynitro diene **2***a*, and 2-*p*-tolyl-2-propanol. The last product appeared to be formed, presumably from the adducts, during chromatography. The formation of side-chain derivatives, of which 2-*p*-tolyl-2-propanol is an example, is a prevalent reaction in the nitration of *p*-xylene and its derivatives (5–7). The same side-chain derivatives are obtained from acetyl nitrate adducts of these aromatic compounds. It has been established that the methyl group substituted is that *ipso* to the acetate in the adduct and not that *ipso* to the nitro group (8). It is consistent with this that it is the isopropyl group and not the methyl group of the *p*-cymene which is substituted since it is the isopropyl group which is *ipso* to the acetate in the adduct. No evidence of an adduct with nitro *ipso* to isopropyl could be detected. Loss of the isopropyl group as a cation following *ipso* attack by nitronium ion is rapid, even at −40 °C, and *p*-nitrotoluene is the only product obtained. The effect of the addition of the shift reagent tris-(1,1,1,2,2,3,3-

[1]Individual members of a pair of diastereoisomeric adducts are designated as *a* and *b*.

Can. J. Chem. Downloaded from www.nrcresearchpress.com by 210.87.254.105 on 09/05/12
For personal use only.

TABLE 1. Relative gradients (gradient 1-OAc = 1.00) of proton chemical shifts for diene adducts resulting from the addition of Eu([$^2H_9$]fod)$_3$

Compound	2-H	3-H	4-CH_3	8-H	9-H
1*a*	0.74	0.26	0.17	0.83	0.30
1*b*	0.73	0.33	0.20	0.90	0.27

heptafluoro-7,7-[$^2H_6$]dimethyl-4,6-[$^2H_3$]octanedionato)europium(III){Eu([$^2H_9$]fod)$_3$} confirms the structural assignment of acetate *ipso* to isopropyl in the isolated adducts since in both **1***a* and **1***b* the methine proton moved about as rapidly downfield as the acetate methyl protons and faster than the 4-methyl protons (Table 1). Although the 4-methyl protons moved downfield faster in **1***b* than in **1***a*, which would suggest that **1***b* is *trans* and **1***a* is *cis*, the difference in gradients is small and in fact less than that for the 3-H. Thus the assignment of stereochemistry is not conclusive. Similar difficulties have been met with other tertiary acetate adducts (8).

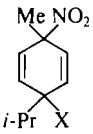

1[1] X = OAc
2 X = OH
3 X = OMe

Reaction of the acetoxynitro diene **1***a* with methanolic sodium methoxide resulted in cleavage of the acetate group and the formation of the hydroxynitro diene **2***a*, presumably by the $B_{AC}2$ mechanism (9). The hydroxynitro diene **2***a* was in turn converted into 2-isopropyl-4-methylphenol (see below). Under the same conditions the acetoxynitro diene **1***b* was also converted into 2-isopropyl-4-methylphenol, presumably via the hydroxynitro diene **2***b* although in this case the intermediate formation of **2***b* could not be demonstrated, possibly because it is converted into the phenol as fast as it is formed. The acid-catalysed methanolysis of **1***a* gave both diastereoisomers of the methoxynitro diene **3***a* and **3***b*. Similarly, the hydroxy diene **2***a* gave both methoxy dienes **3***a* and **3***b* on acid-catalysed methanolysis. These acid-catalysed exchange reactions presumably involve the intermediate formation of the *ipso*-cyclohexadienyl cation **4** ($A_{AL}1$ mechanism; Scheme 1) and parallel the

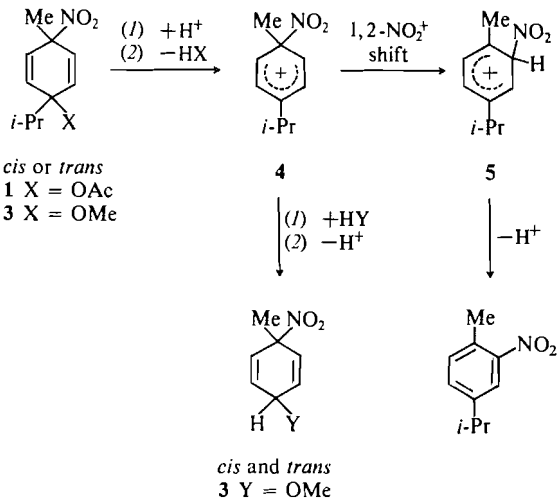

SCHEME 1

exchange reactions of the pseudocumene and *p*-xylene adducts (8). The hydroxy diene **2***a* did not exchange the hydroxyl group for the less nucleophilic acetate in acidified acetic acid and rearomatization occurred (see below).

Rearomatization Reactions

In the rearomatization of the acetyl nitrate adducts of *p*-xylene three types of reaction were observed: (*i*) migration of the nitro group to give 2-nitro-*p*-xylene; (*ii*) formation of side-chain derivatives, and (*iii*) 1,2-shift of the acetate group to form 2,5-xylyl acetate (8*b*).

Reaction of any of the *p*-cymene adducts **1**, **2**, or **3** with strong acid (trifluoroacetic acid, sulfuric acid, or boron trifluoride etherate) resulted in the formation of 2-nitro-*p*-cymene. As in the case of the acetyl nitrate adducts of *p*-xylene these reactions presumably follow the mechanism suggested by Myhre (4) for the formation of 3-nitro-*o*-xylene from the acetyl nitrate adduct of *o*-xylene: acid-catalysed loss of acetate, hydroxyl, or methoxyl, to generate the *ipso*-cyclohexadienyl cation **4** which undergoes migration of the nitro group to form the cyclohexadienyl cation **5**, followed by deprotonation to the 2-nitro-*p*-cymene (Scheme 1). As mentioned above attempts to observe the exchange of hydroxyl by acetate were unsuccessful, rearomatization via both nitro migration and loss of the nitro group occurring instead. Acetic acid is less nucleophilic than methanol and apparently sufficiently so that it cannot capture the *ipso*-

Can. J. Chem. Downloaded from www.nrcresearchpress.com by 210.87.254.105 on 09/05/12
For personal use only.

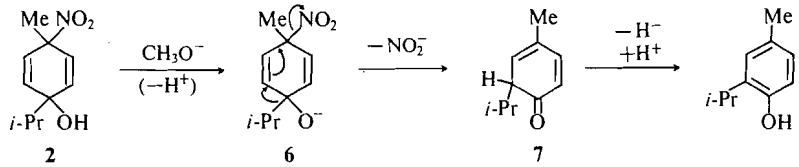

2 6 7

SCHEME 2

cyclohexadienyl cation **4** at a rate competitive with the nitro migration or loss. The reaction with acidified acetic acid gives rise to a complex mixture of products including *p*-methylacetophenone (59%), *p*-nitrotoluene (7%), 3-nitro-*p*-cymene (2%), as well as the 2-nitro-*p*-cymene (33%). It seems clear that the *p*-methylacetophenone and *p*-nitrotoluene must arise from *p*-cymene (itself formed by loss of nitronium ion from **4**) by attack of (possibly incipient) acetylium ion and nitronium ion, respectively, *ipso* to the isopropyl group followed by loss of the isopropyl cation.

Reaction of acetoxydiene **1***a* in neat acetic acid or in acetic acid containing acetic anhydride, at ambient temperature, gave thymol acetate in a slow reaction ($t_{1/2} \sim 100$ h). Diene **1***a* was not epimerized to **1***b* in the course of the reaction and thus under these weakly acid conditions cation **4** can only be formed very slowly indeed. When the reaction was repeated in 33% aqueous [$^2H_4$]-acetic acid, thymol acetate was again obtained and the reaction was complete in 1 h. Clearly the acetate group, which is not exchanged with the solvent, undergoes an intramolecular 1,2-shift. These results provide further support for the proposed mechanism involving the concerted loss of the elements of nitrous acid and the simultaneous cyclic migration of the acetate group (8*b*).

A striking feature of the rearomatization reactions is the apparent absence of significant amounts of side-chain products. The benzylic hydrogens in the *p*-xylene, pseudocumene, and other polymethylbenzene[2] side-chain derivatives (7, 8) appear in a region of the nmr spectrum uncomplicated by absorptions from other constituents of the mixture. It is more difficult to detect the formation of side-chain products from *p*-cymene, in which the only saturated hydrogens are those of the methyl groups, than from *p*-xylene and the polymethylbenzenes. Nevertheless it is clear that side-chain derivatives cannot be present to any large extent in the rearomatization products from the *p*-cymene adducts. As mentioned, a small amount of 2-*p*-tolyl-2-propanol was isolated from the nitration of *p*-cymene. It is likely that the alcohol is not the primary side-chain product but is derived from such a product, such as the acetate ester, nitrate ester or nitro derivative, during work-up (8*b*). In the glc – mass spectrum of the products from reaction of hydroxy diene **2** with acetic acid containing sulfuric acid a minor glc peak of mass 150 was probably that of the side-chain alcohol and a peak underlying the peak for 2-nitro-*p*-cymene and which gave rise to an apparent mass spectra parent peak of mass 133 was probably a side-chain ester whose molecular ion cleaved before detection to form the *p*-tolyldimethyl carbinyl cation ($m/e = 133$).

Reaction of adduct **2** with methanolic sodium methoxide resulted in the formation of 2-isopropyl-4-methylphenol. The proposed mechanism is depicted in Scheme 2. In the anion **6**, the conjugate base of the hydroxy diene **2**, the isopropyl group undergoes a 1,2-shift with concurrent loss of nitrite anion to give the 2,4-hexadienone **7** which is the keto form of the product phenol. Presumably the driving force of the reaction is the resonance stabilization of the dienone together with the greater anionic stability of nitrite compared with the alkoxide **6**. Anion **6** appears to be an essential intermediate since the methoxynitro diene **3** was recovered unchanged on treatment with strong base.

Experimental

Microanalyses were by Dr. D. McGillivray. Nitric acid and solvents were purified as previously described (2*b*). *p*-Cymene, 2-isopropyl-4-methylphenol, and 2-isopropyl-5-methylphenol (thymol) were from Aldrich. 2-Isopropyl-5-methylphenyl acetate (thymol acetate) was prepared by reaction of thymol with acetic anhydride containing sulfuric acid, nmr ($CDCl_3$) τ 1.88 (nq,[3] 1, $J = 8.5$ Hz,

[2]In unpublished work with D.R.A. Leonard it has been shown that large amounts of side-chain derivatives are obtained in the rearomatization reactions of the tetramethylbenzene adducts.

[3]One-half of an AB quartet (10).

Can. J. Chem. Downloaded from www.nrcresearchpress.com by 210.87.254.105 on 09/05/12
For personal use only.

Can. J. Chem. Downloaded from www.nrcresearchpress.com by 210.87.254.105 on 09/05/12
For personal use only.

3-*H*), 2.08 (nq, 1, J = 8.5 Hz, 4-*H*), 2.25 (s, 1, 6-*H*), 7.05 (septet, J = 7 Hz, C*H*$(CH_3)_2$), and 8.84 (d, 6, J = 7 Hz, CH(C*H*$_3)_2$).

Nitration of p-Cymene in Acetic Anhydride

A cold solution of nitric acid (9.5 cm^3, 0.23 mol) in acetic anhydride (35 cm^3) was added slowly with stirring to a solution of *p*-cymene (20 g, 0.15 mol) in acetic anhydride (40 cm^3) at −45 °C. The mixture was allowed to warm to −15 °C and maintained at that temperature for 12 h.[4] The mixture was worked up in the usual manner to yield an oil (27 g) consisting of (by nmr) 51% diene adducts, 28% nitro-*p*-cymenes, 11% *p*-nitrotoluene, and 10% *p*-cymene.

Chromatography on 400 g of alumina at −45 °C and elution with pentane and ether–pentane mixtures gave a mixture (6.1 g) of *p*-cymene, *p*-nitrotoluene, and 2- and 3-nitro-*p*-cymene (ratio 5:1 by glc) in the 10% ether fraction, a mixture (7.2 g) of one diastereoisomer of 1-isopropyl-4-methyl-4-nitro-1,4-dihydrophenyl acetate, **1***a*, and nitro compounds (40%) in the 20% ether fraction, pure **1***a* (4.1 g) in the 25% ether fraction, a mixture (1.8 g) of **1***a* and its diastereoisomer **1***b* in the 30% ether fraction and **1***b* (2.0 g) in the 50–70% ether fractions. The 80–100% ether fractions contained a mixture of 1-isopropyl-4-methyl-4-nitro-1,4-dihydrophenol, **2**, and 2-*p*-tolyl-2-propanol.

The *p*-nitrotoluene was separated from the nitrocymenes by dry column chromatography and the nitrocymenes separated by preparative glc. The nitro compounds had characteristic nmr ($CDCl_3$): *p*-nitrotoluene τ 1.90 (nq, 2, J = 8.5 Hz, 3-*H* and 5-*H*), 2.66 (nq, 2, J = 8.5 Hz, 2-*H* and 6-*H*), and 7.56 (s, 3, C*H*$_3$); 2-nitro-*p*-cymene τ 2.15 (d, 1, J = 2 Hz, 3-*H*), 2.60 (d of d, 1, J = 2 and 8 Hz, 5-*H*), 2.72 (nq, 1, J = 8 Hz, 6-*H*), 7.08 (septet, J = 7 Hz, C*H*$(CH_3)_2$), 7.52 (s, 3, 1-C*H*$_3$), and 8.77 (d, 6, J = 7 Hz, CH(C*H*$_3)_2$); 3-nitro-*p*-cymene τ 2.52 (s, 1, 2-*H*), 2.58 (s, 2, 5-*H* and 6-*H*), 6.65 (septet, 1, J = 7 Hz, C*H*$(CH_3)_2$), 7.66 (s, 3, 1-C*H*$_3$), and 8.76 (d, 6, J = 7 Hz, CH(C*H*$_3)_2$). The alcohol was separated from the hydroxynitro diene by distillation under reduced pressure.

After recrystallization from acetone-pentane the first diastereoisomer of 1-isopropyl-4-methyl-4-nitro-1,4-dihydrophenyl acetate, **1***a*, had mp 33 °C; uv (CH_3OH) 197 nm (ϵ 1220 m^2mol^{-1}); ir (Nujol) 1760 and 1240 ($OCOCH_3$), 1560 (NO_2), 1015 and 815 cm^{-1}; nmr ($CDCl_3$) τ 3.78 (nq, 2, J = 10.5 Hz, 3-*H* and 5-*H*), 4.04 (nq, 2, J = 10.5 Hz, 2-*H* and 6-*H*), 8.00 (s, 3, OCOC*H*$_3$), 7.95 (septet, 1, J = 6.6 Hz, C*H*$(CH_3)_2$), 8.21 (s, 3, 4-C*H*$_3$), and 9.12 (d, 6, J = 6.6 Hz, CH(C*H*$_3)_2$).

The second diastereoisomeric acetoxynitro adduct **1***b* was recrystallized from chloroform–pentane, mp 36–37 °C; uv (CH_3OH) 196 nm (ϵ 1270 m^2mol^{-1}); ir (Nujol) 1755 and 1245 ($OCOCH_3$), 1560 (NO_2), 1020 and 810 cm^{-1}; nmr ($CDCl_3$) 3.67 (nq, 2, J = 10.6 Hz, 3-*H* and 5-*H*), 3.95 (nq, 2, J = 10.6 Hz, 2-*H* and 6-*H*), 8.03 (s, 3, OCOC*H*$_3$), 7.79 (septet, 1, J = 6.7 Hz, C*H*$(CH_3)_2$), 8.29 (s, 3, 4-C*H*$_3$), and 9.11 (d, 6, J = 6.7 Hz, CH(C*H*$_3)_2$). *Anal.* Calcd. for $C_{12}H_{17}NO_{21}$ (M_r 239): C 60.24, H 7.16, N 5.85; found (244): C 60.43, H 7.18, N 5.65.

The single diastereoisomer of 1-isopropyl-4-methyl-4-nitro-1,4-dihydrophenol, **2***a*, crystallized from ether–pentane as faintly yellow needles, mp 56–57 °C; uv (CH_3OH) 192 nm (ϵ 2030 m^2mol^{-1} ; ir (film) 3390 (OH), 1550 and 1345 (NO_2), 1030 and 820 cm^{-1}; nmr ($CDCl_3$) τ 3.89 (nq, 2, J = 10.5 Hz, 3-*H* and 5-*H*), 3.98 (nq, 2, J = 10.5 Hz, 2-*H* and 6-*H*), 8.15 (s, 1, O*H*), 8.2 (m, 1, C*H*$(CH_3)_2$), 8.26 (s, 3, 4-C*H*$_3$), and 9.13 (d, 6, J = 7 Hz, CH(C*H*$_3)_2$). *Anal.* Calcd. for $C_{10}H_{15}NO_3$: C 60.90, H 7.67, N 7.10; found: C 60.87, H 7.68, N 6.94.

2-*p*-Tolyl-2-propanol had bp 111–112 °C; ir (film) 3390 (OH); nmr ($CDCl_3$) τ 2.66 (nq, 2, J = 8.3 Hz, 2-*H* and 6-*H*), 2.88 (nq, 2, J = 8.3 Hz, 3-*H* and 5-*H*), 7.6 (1, O*H*), 7.70 (s, 3, 4-C*H*$_3$), and 8.45 (s, 6, C(C*H*$_3)_2$); mass spectrum (70 eV) *m/e* (relative intensity) 150 (14, M), 135 (44, M − CH_3), 132 (4), 91 (15), 77 (7), 43 (100, C_3H_7).

Reaction of Adduct 1 with Acidified Methanol: 1-Isopropyl-4-methyl-4-nitro-1,4-dihydrophenyl Methyl Ether, 3

The acetoxynitro adduct **1** (8.1 g, 34 mmol) was dissolved in methanol (150 cm^3) and sulfuric acid (200 mm^3) was added with stirring. The mixture was stirred at room temperature for 2 h.[5] Sodium bicarbonate (2 g) was added and the methanol evaporated at 14 °C. After addition of water (5 cm^3) extraction with ether and work-up, the oil obtained (7.5 g) was shown by nmr to consist of 60% diene adducts and 40% of aromatic product. Chromatography on alumina at −40 °C and elution with pentane and ether–pentane mixtures gave a mixture (2.2 g, 15 mmol) of isopropyl-methoxy-methylbenzenes in the 0–5% ether fractions and a mixture (2.6 g, 11 mmol) of the diastereoisomeric methoxynitro adducts, **3**; ir (film) 2830 (OCH_3), 1550 and 1345 (NO_2), 1070 (C—O—C), and 815 cm^{-1}; mass spectrum (70 eV) *m/e* (relative intensity) 196 (7, M − CH_3), 136 (31), 125 (72), 124 (74), 121 (100) in the 15–40% ether fractions. Rechromatography of the mixture of adducts at −45 °C using an alumina:substrate ratio of 100:1 effected only partial separation of the individual diastereoisomers.

The diastereoisomers of 1-isopropyl-4-methyl-4-nitro-1,4-dihydrophenyl methyl ether, **3**, had nmr ($CDCl_3$) τ 3.71 (nq, J = 10.5 Hz, 3-*H* and 5-*H*), 4.17 (nq, J = 10.5 Hz, 2-*H* and 6-*H*), 6.98 (s, OC*H*$_3$), 8.26 (s, 4-C*H*$_3$), 9.15 (d, J = 7 Hz, CH(C*H*$_3)_2$) and 3.73 (nq, J = 10.5 Hz, 3-*H* and 5-*H*), 4.19 (nq, J = 10.5 Hz, 2-*H* and 6-*H*), 6.93 (s, OC*H*$_3$), 8.31 (s, 4-C*H*$_3$), and 9.15 (d, J = 7 Hz, CH-(C*H*$_3)_2$), respectively.

Reaction of the Acetoxynitro Adduct, 1, with Sodium Methoxide: 1-Isopropyl-4-methyl-4-nitro-1,4-dihydrophenol, 2

Adduct **1***a* (90 mg, 0.38 mmol) was reacted with an equimolar amount of sodium [$^2H_3$]methoxide in [$^2H_4$]-methanol (0.5 cm^3) in an nmr tube. The hydroxynitro adduct **2***a* formed rapidly and slowly decomposed (70% in 24 h) to form 2-isopropyl-4-methylphenol. Neutralization and work-up gave 2-isopropyl-4-methylphenol with identical nmr and glc retention time to that of an authentic

[4]Preliminary studies by nmr indicated that the yield of adducts was close to the maximum at −15 °C and no rearomatization of the adducts occurred at this temperature.

[5]Subsequent experiments showed that the exchange was complete in 15 min and that shorter reaction times reduced the amount of rearomatization products.

Can. J. Chem. Downloaded from www.nrcresearchpress.com by 210.87.254.105 on 09/05/12
For personal use only.

sample and which exhibited the expected molecular ion peak at *m/e* 150.

On a preparative scale the mixture of acetoxynitro adduct **1** and nitro compounds obtained from nitration of *p*-cymene was treated with a two-fold excess of sodium methoxide in methanol. The reaction was complete after 10 min. The mixture was diluted with water and extracted with ether. The etheral solution was washed and dried and the ether evaporated to give an oil containing 37% of the hydroxynitro adduct, by nmr. The dark red residual oil was dissolved in pentane and on standing at 5 °C the hydroxynitro adduct **2***a* (2.75 g, 14 mmol) crystallized and was filtered off.

When the nmr tube experiment was repeated using **1***b* as the substrate no intermediate formation of a hydroxynitro adduct could be detected and the phenol was formed rapidly (50% in 25 min.).

*Reaction of Adduct **1** in Acetic Acid*

The acetoxynitro adduct **1***a* (70 mg) was added to acetic acid (0.5 cm^3) and the reaction followed by nmr. Thymol acetate was formed ($t_{1/2}$ = 90 h) and epimerization of **1***a* was not observed. The same result was obtained when acetic acid made anhydrous by heating under reflux with acetic anhydride was used, except that the reaction was slightly slower ($t_{1/2}$ = 109 h). When the reaction was repeated using 33% aqueous [$^2H_4$]acetic acid thymol acetate was again obtained and the reaction was complete in 1 h.

*Reaction of Adduct **1** with Trifluoroacetic Acid and with Boron Trifluoride*

Adduct **1***a* (80 mg) was dissolved in a solution of trifluoroacetic acid (0.1 cm^3) in deuteriochloroform (0.4 cm^3). A vigorous decomposition to 2-nitro-*p*-cymene (88%), 3-nitro-*p*-cymene (9%), and *p*-cymene (3%) ensued. The presence of the minor constituents was detected by glc. When the decomposition was carried out in the presence of mesitylene, 2-nitro-*p*-cymene was obtained and no biaryl was formed.

The reaction was repeated using boron trifluoride etherate (10 mm^3) in deuteriochloroform (0.5 cm^3) as the reagent. The same products were obtained. Addition of mesitylene (150 mg) to the reaction solution did not divert the reaction from the formation of the nitrocymene and no biaryl was formed.

*Reaction of Adduct **2a** with Acidified Methanol*

The hydroxynitro adduct **2***a* (80 mg) was reacted with [$^2H_4$]methanol (0.5 cm^3) containing a catalytic amount of sulfuric acid and the reaction was followed by nmr. The characteristic pattern of the diene protons of **2***a* smoothly disappeared and was replaced by the pattern for the diastereoisomeric mixture of the methoxynitro adducts **3** in a reaction with a half-life of 16 min.

*Reaction of Adduct **2a** with Acetic Acid Containing Sulfuric Acid*

A preliminary nmr experiment showed that the hydroxynitro adduct **2***a* reacted rapidly (~25 min) with a solution of sulfuric acid (10 mm^3) in [$^2H_4$]acetic acid (0.5 cm^3) and gave rise to a complex mixture of aromatic products. The adduct (0.5 g) was reacted with a solution of sulfuric acid (20 mm^3) in acetic acid (1 cm^3). Gas–liquid chromatography of the product after work-up showed two major and two minor constituents. Chromatography on silica gel and elution with 5% ether–pentane separated the major products shown to be 2-nitro-*p*-cymene (39% from the glc of the reaction product) and *p*-methyl acetophenone; 49%, ir 1700 (C=O), 1625, 1375, 1280, and 825 cm^{-1}; nmr ($CDCl_3$) τ 2.23 (nq, J = 8 Hz, 2-*H* and 6-*H*), 2.83 (nq, J = 8 Hz, 3-*H* and 5-*H*), 7.54 (s, CH_3CO), 7.69 (s, $ArCH_3$); mass spectrum 134 (M); glc retention time, identical with an authentic sample. The minor constituents were present in the nitro-cymene fraction and were shown to be *p*-nitrotoluene (12%) and 3-nitro-*p*-cymene (5%) by glc and glc – mass spectrometry. Also present under the glc peak of 2-nitro-*p*-cymene was a component which gave a mass spectrum with a highest mass peak of mass 133. In the glc of the *p*-methylacetophenone fraction minor peaks having masses of 148 and 150 respectively (chemical ionization mass spectrometry) were present.

*Reaction of Adduct **2a** with Strong Acids*

Adduct **2***a* (75 mg) was reacted with a catalytic amount of sulfuric acid in mesitylene. 2-Nitro-*p*-cymene was formed (nmr, tlc). The same result was obtained for the sulfuric acid-catalysed decomposition in deuteriochloroform containing in one instance phenol and in another anisole and no biaryl was obtained in either case.

Adduct **2***a* (90 mg) was reacted with boron trifluoride etherate (10 mm^3) in deuteriochloroform (0.4 cm^3). 2-Nitro-*p*-cymene was formed (nmr, tlc). When the reaction was repeated in the presence of an equivalent amount of anisole or mesitylene the 2-nitro-*p*-cymene was still formed and no coupling product was detected.

*Reaction of Adduct **3** with Strong Acids*

The methoxynitro adduct **3** (100 mg) in deuteriochloroform (0.5 cm^3) was treated with boron trifluoride etherate (10 mm^3). 2-Nitro-*p*-cymene was formed together with a lesser amount of a product tentatively identified as an aryl methyl ether.

When the experiment was repeated adding trifluoroacetic acid (0.1 cm^3) or sulfuric acid (0.1 cm^3) instead of the boron trifluoride etherate a vigorous reaction to give 2-nitro-*p*-cymene together with small amounts of 3-nitro-*p*-cymene and *p*-cymene occurred.

*Attempted Reaction of Adduct **3** with Strong Base*

The methoxynitro adduct **3** was recovered unchanged after treatment with butyllithium in ether and with sodium methoxide in methanol.

1. C. L. PERRIN and G. A. SKINNER. J. Am. Chem. Soc. **93**, 3389 (1971).
2. (*a*) D. J. BLACKSTOCK, A. FISCHER, K. E. RICHARDS, J. VAUGHAN, and G. J. WRIGHT. Chem. Commun. 641 (1970); (*b*) A. FISCHER, C. C. GREIG, and R. RÖDERER. Can. J. Chem. **53**, 1570 (1975).
3. (*a*) R. C. HAHN and M. B. GROEN. J. Am. Chem. Soc. **95**, 6128 (1973); (*b*) R. C. HAHN and D. L. STRACK. J. Am. Chem. Soc. **96**, 4335 (1974); (*c*) M. W. GALLEY and R. C. HAHN. J. Am. Chem. Soc. **96**, 4337 (1974).
4. P. C. MYHRE. J. Am. Chem. Soc. **94**, 7921 (1972).
5. (*a*) R. ROBINSON and H. W. THOMPSON. J. Chem. Soc. 2015 (1932); (*b*) R. ROBINSON. J. Chem. Soc. 1289 (1970).

6. H. SUZUKI, K. NAKAMURA, and K. MARUYAMA. Bull. Chem. Soc. Jpn. **41**, 1487 (1968); (*b*) H. SUZUKI and T. HANAFUSA. Bull. Chem. Soc. Jpn. **47**, 2625 (1974).
7. D. J. BLACKSTOCK, A. FISCHER, K. E. RICHARDS, and G. J. WRIGHT. Aust. J. Chem. **26**, 775 (1973).
8. (*a*) A. FISCHER and J. N. RAMSAY. J. Am. Chem. Soc. **96**, 1614 (1974); (*b*) A. FISCHER and J. N. RAMSAY. Can. J. Chem. **52**, 3960 (1974).
9. C. K. INGOLD. Structure and mechanism in organic chemistry. 2nd ed. Cornell University Press, Ithaca, New York. 1969. Chapt. 15.
10. F. A. BOVEY. Nuclear magnetic resonance spectroscopy. Academic Press, New York, New York. 1961. p. 249.

Can. J. Chem. Downloaded from www.nrcresearchpress.com by 210.87.254.105 on 09/05/12
For personal use only.

Ring C substituted 14-hydroxymorphinans and isomorphinans as narcotic antagonists

MARCEL MENARD, PIERRE RIVEST, BERNARD BELLEAU, JEAN-PAUL DARIS, AND YVON G. PERRON
Bristol Laboratories of Canada, Candiac, Quebec J5R 1J1

Received July 25, 1975

MARCEL MENARD, PIERRE RIVEST, BERNARD BELLEAU, JEAN-PAUL DARIS, and YVON G. PERRON. Can. J. Chem. **54**, 429 (1976).

The synthesis of morphinans incorporating a hydroxyl group at position 14 as well as an appropriate alkyl substitution in ring C is described. It is shown that the spatial area around ring C plays an important role at the analgesic receptor level. A novel morphine structure with ring C frozen in a boat conformation is also described.

MARCEL MENARD, PIERRE RIVEST, BERNARD BELLEAU, JEAN-PAUL DARIS et YVON G. PERRON. Can. J. Chem. **54**, 429 (1976).

La synthèse de morphinanes, comprenant à la fois un groupe hydroxyle en position 14 et un groupement alkyle approprié sur le noyau C, est décrite. L'activité analgésique de ces composés démontre l'influence remarquable de la région de l'anneau C sur les contacts substrats-récepteurs. Dans un des morphinanes décrits, le cycle C est rigide et de conformation bateau.

Can. J. Chem. Downloaded from www.nrcresearchpress.com by 210.87.254.5 on 09/05/12
For personal use only.

Previous publications (1) from this laboratory have demonstrated the importance of a 14-β-hydroxyl group for high, side effect free, agonistic–antagonistic activity in the morphinan class of analgesics. Oxilorphan and butorphanol were found to be potent and pharmacologically 'clean' antagonists, the latter possessing high non-narcotic analgesic properties in man. Recently, the drug diprenorphine, which lacks the 14-hydroxyl group of oxilorphan and butorphanol but incorporates the bulky ring C substituents of Bentley-type compounds, was reported to be a pure antagonist, more potent than naloxone and somewhat longer acting.

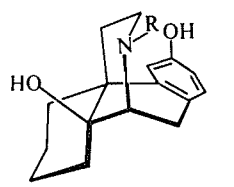

Butorphanol, R =
Oxilorphan, R =

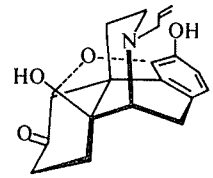

Naloxone

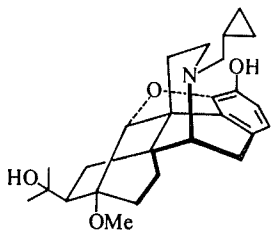

Diprenorphine

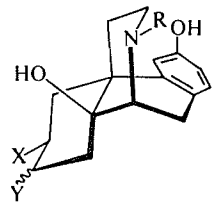

1

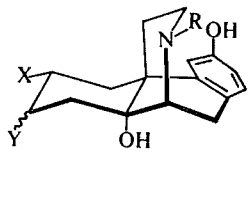

2

New insights into the role of ring C substitution at the receptor level appeared essential if any progress in developing better analgesics was to be made. To this end, we prepared a series of hybrid compounds incorporating a hydroxyl group at position 14 as well as an appropriate substitution in ring C of the morphinan molecule. This new series, represented by general formulae **1** and **2** includes not only the morphinan skeleton **1**, but also the isomorphinan stereochemistry **2**, where the ring C part of the Bentley-type compounds is approximated better than in structures of type **1**.

These compounds were synthesized by the general method previously developed in our laboratories. We shall restrict our discussion of this approach to questions of stereochemistry since the general methodology is now well documented (1). Scheme 1 illustrates the preparation of the key intermediate **13**, which provides an entry, as shown in Scheme 2, into the morphinan

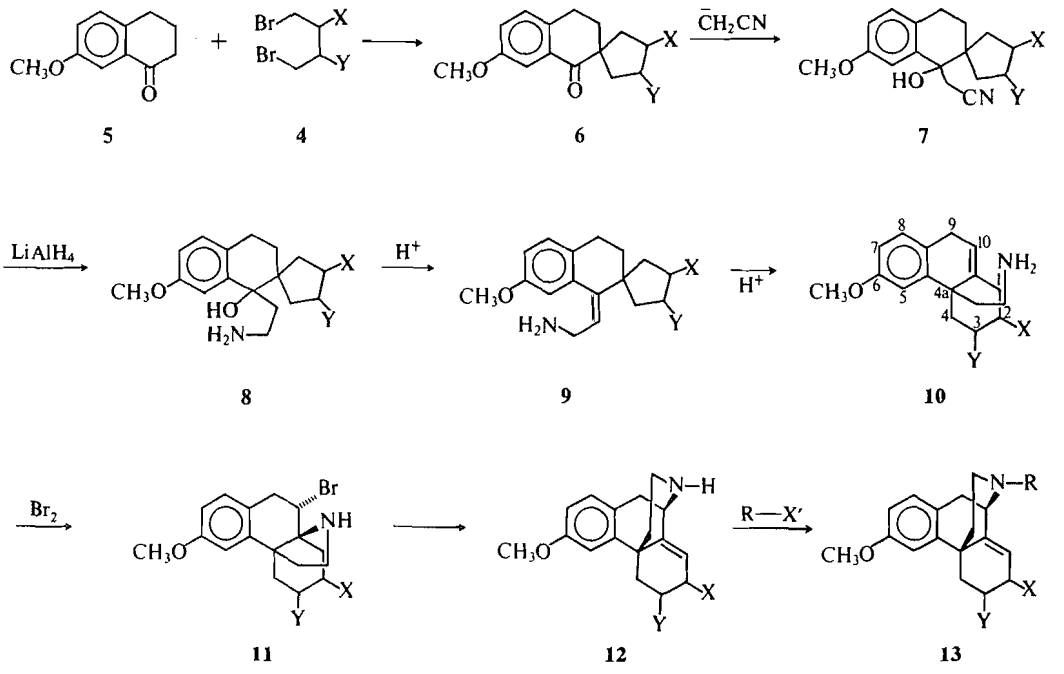

SCHEME 1

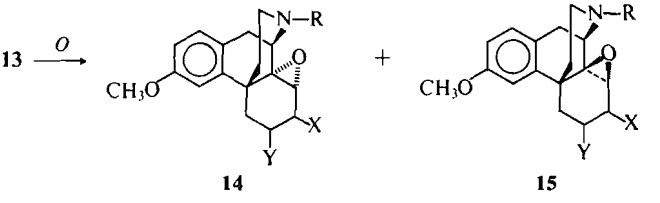

SCHEME 2

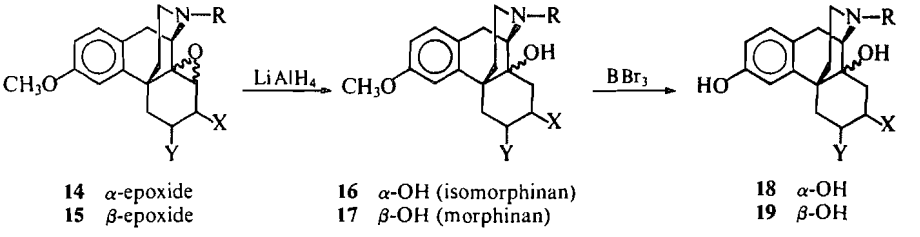

14 α-epoxide
15 β-epoxide
16 α-OH (isomorphinan)
17 β-OH (morphinan)
18 α-OH
19 β-OH

SCHEME 3

or isomorphinan systems. Transformation of these intermediates to the desired α- and β-14-hydroxyisomorphinans and morphinans is illustrated in Scheme 3.

Scheme 4 illustrates a chemical proof that structures of the type of **14** possess the isomorphinan stereochemistry as based on the stereochemical requirements (*1b*) of the epoxide cyclization **21** → **22**. It is clear that this sequence can only lead to the isomorphinan system.

Whereas the tertiary alcohol **8** (X = Y = H) (*1*) gave exclusively the expected unsaturated rearranged amine **10** when treated with aqueous acid at 35–40 °C, the substituted alcohols **8***a*–**8***e*

Can. J. Chem. Downloaded from www.nrcresearchpress.com by 210.87.254.5 on 09/05/12
For personal use only.

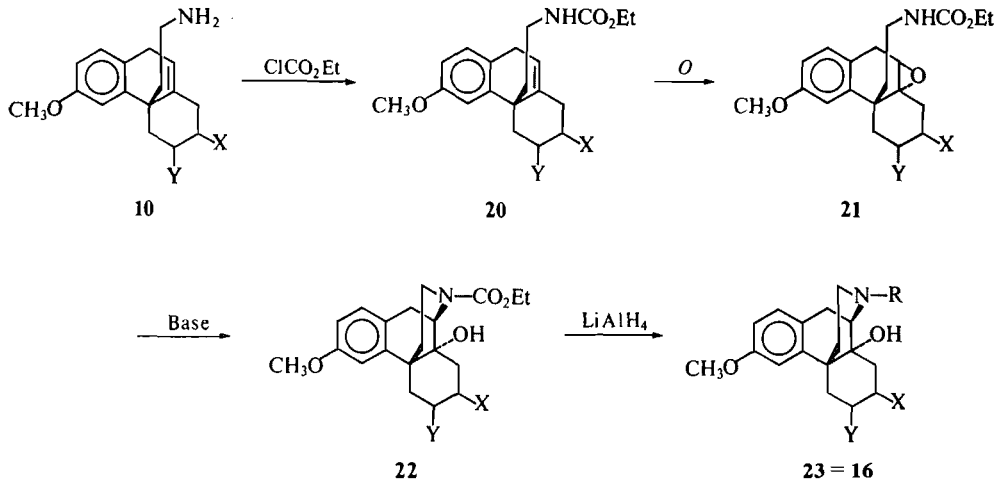

SCHEME 4

TABLE 1. Identification of the substitution X and Y. Throughout this paper the letters *a*, *b*, *c*, *d*, and *e* following a compound number have the meaning described. Capital letters *A* to *E* represent the proposed correct space structures for *a* to *e*.

Code	X	Y	Configuration
a	—$(CH_2)_4$—		*trans*
b	—$(CH_2)_4$—		*cis*
c			*trans*
d	CH_3—	CH_3—	*trans*
e	CH_3—	CH_3—	*cis*

afforded mainly the dehydration products **9** under the same conditions. This may not be surprising in view of the fact that rearrangement of **8***a*–**8***e* to the corresponding unsaturated amines **10** appears to be opposed by nonbonded interactions between the ring C substituents. The activation energy required for the desired 1,2-shift may be expected to be higher for the substituted **8**. However, this barrier was readily overcome by using a higher reaction temperature (80–100 °C) which caused the alcohols **8** or the unrearranged unsaturated amines **9** to yield the hexahydrophenanthrene amines **10** as the only products.

Strong indications were obtained (tlc, nmr) that the unsaturated amines **10** are produced as simple racemic rather than diastereomeric mixtures. In fact, nmr evidence was obtained that single isomers of the unsaturated compounds **12** are generated upon rearrangement of the precursors (epimerisation at center **4***b* when going from **10** to **12** is impossible).[1] Since the amino alcohols **8** must exist as a pair of diastereoisomers, it follows that the Wagner–Meerwein rearrangement of these alcohols may not proceed by a concerted mechanism.[2] The structures of each final product in this synthetic approach can best be explained on the basis that the compound resulting from this rearrangement is the thermodynamically more stable of the two expected diastereoisomers. This could mean that the 1,2-shift is reversible so as to allow equilibration to the more stable isomer or else the transition state resembles the preferred geometry of the end product sufficiently so as to favor a selective migration of only one of the spiro C—C bonds in order to produce the more stable isomer.

Of the two possible diastereoisomers for **10***a* that having structure **10***A* and possessing a *trans-syn*-quasi *trans* arrangement about the hexahydroanthracene part, will be preferred over **10***F* (*trans-anti*-quasi *trans*) (3). Compounds **10***c* and **10***d* are expected to possess similar structures. In the *cis* series *b* and *e*, structures with a *cis-anti*-quasi *trans* conformation will be pre-

[1]H-8 (morphinan nomenclature) is a sharp singlet at 5.35 δ for **12***a*, at 5.9 δ for **12***c* (not as sharp) and at 5.32 for **12***d*; 90° coupling with H-7. H-8 is a sharp doublet centered at 5.42 δ for **12***b* and **12***e*, J_{7-8} = 5.5 Hz ≃ 30° coupling.

[2]Also, optically active **8** (X = Y = H) is rearranged to enantiomeric **10** (I. Monković, unpublished results). The unrearranged amines **9** give **10** which is identical to **10** arising from **8**.

Can. J. Chem. Downloaded from www.nrcresearchpress.com by 210.87.254.5 on 09/05/12
For personal use only.

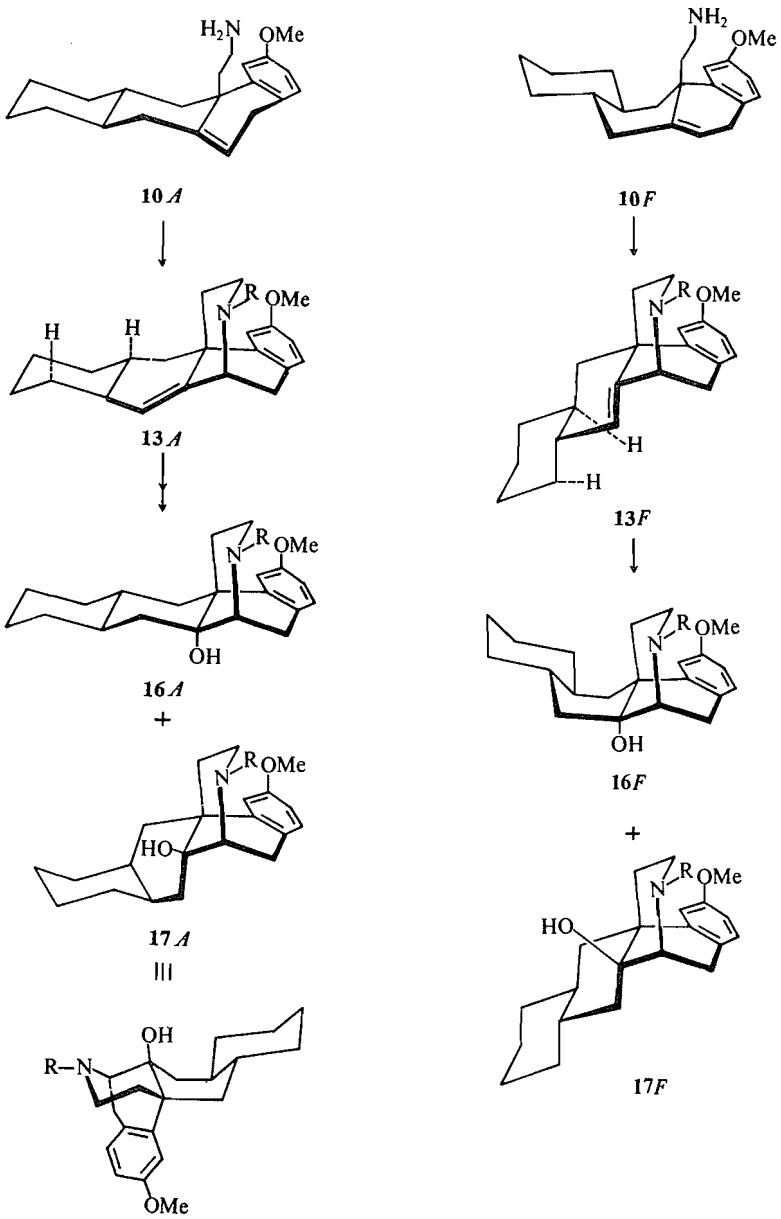

SCHEME 5. *trans*-Series. Stereochemistry of the steps **10** → **16** indicating the structures of the morphinans and isomorphinans resulting from the two possible isomers from the Wagner–Meerwein rearrangement of **8**.

ferred on conformational grounds (3).

Bromination and cyclization to **12** cannot alter the basic stereochemistry of these structures and the resulting **13** will have structures depicted in **13***A* and not **13***F* since the latter would arise from a less stable conformer of **10**.

Taking into account that the epoxidation of the unsubstituted compounds **13** (X = Y = H) takes place predominantly on the β-face of the molecule (1) (80% β, 20% α) a structure like **13***F* would be expected to afford almost exclusively the β-epoxide since the steric hindrance of the two axial hydrogen atoms in **13***F* would orient the epoxidation reaction in the same direction as the nitrogen participation. On the other hand, the same two protons in **13***A* would oppose the

Can. J. Chem. Downloaded from www.nrcresearchpress.com by 210.87.254.5 on 09/05/12
For personal use only.

Can. J. Chem. Downloaded from www.nrcresearchpress.com by 210.87.254.5 on 09/05/12
For personal use only.

TABLE 2. Yields (isolated) of the epoxidation reaction **13** → **14** + **15**.

13	R	14 (α) (%)	15 (β) (%)
a	▷—CO	50	10
a	CF_3CO	35.5	—
a	◇—CO	36	30
b	◇—CO	71	
c	▷—CO	56	17
d	◇—CO	47	31
e	◇—CO	90	—
e	▷—CO	55	

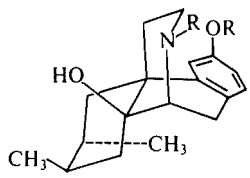

19*D*

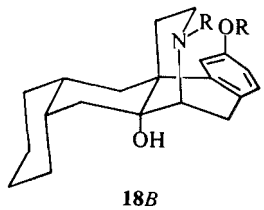

18*B*

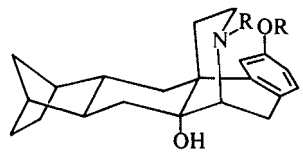

18*C*

β-attack and would be likely to increase the proportion of α-epoxidation. In actual fact, **13***a* (Table 2) yields predominantly the α-epoxides **14** which demonstrates the correctness of the structural assignment **13***A*. This conclusion is also valid for the *cis* series.

Reduction of the epoxides **14** and **15** to the alcohols **16** and **17** proceeded as expected. In the case of the epoxides **14***a* and **14***d* reduction afforded amino alcohols **16***a* and **16***d* which were found to be identical to the amino alcohols **23***a* and **23***d* obtained through Scheme 4. This demonstrates that **14***a* and **14***d* are indeed α-epoxides and also establishes the intermediacy of the unsaturated amides of structure **13***A* (and not **13***F* since **13***A*, like **21**, gives ultimately an all chair isomorphinan **16***A* and BDE-*chair* C-*boat* morphinan **17***F*). Compound **13***F* would give a stereochemical arrangement about the C ring of **16** which is impossible to obtain from **21**.

In the *trans*-dimethyl series, because of the flexibility of ring C, the same reasoning implies that the methyl groups at 6 and 7 possess a diaxial conformation in the morphinans **17***d* and **19***d* and a diequatorial conformation in the isomorphinans **16***d* and **18***d*. The correct spatial structures for other compounds are as indicated in Table 3. Structures **17***a*, **18***a*, **16***c*, **17***d*, and **16***e* were confirmed by ^{13}C nmr spectroscopy.[3]

The pharmacological data for compounds **18–19** are presented in Table 3. Compound **18***a* (R = ▷—CH_2), a 14-β-hydroxymorphinan with the *trans*-tetramethylene substitution and a boat conformation for ring C, is an *analgesic antagonist more potent* than the parent compound BC-2605. It is almost free of any analgesic agonistic activity and appears to be a purer antagonist than naloxone. A unique feature of this structure consists in that a change from *N*-cyclopropylmethyl to *N*-cyclobutylmethyl did not cause any agonistic activity to appear. Because ring C exists in a boat conformation, the spatial arrangement in **19***a* is rather similar to that of the corresponding isomorphinan of structure **18***a*. In fact, both share similar pharmacological properties. Since in these two compounds the 14-hydroxyl group points in opposite directions, it may be that the spatial area around ring C is more decisive in the agonist–antagonist interactions at the receptor level than the area surrounding position 14. This is also substantiated by the fact that the *N*-methyl substituted **18***a* does not show the expected level of agonistic activity and also possesses a slight but definite antagonistic component.

In the *trans*-dimethyl series **18–19***d*, the two equatorial ring C methyl groups in the isomorphinan **18***d* (14α-hydroxyl) (R = ◇—CH_2) eliminated the expected agonistic properties but with the two methyl groups in the axial arrangement (14-β-hydroxy morphinan **19***d*) this did not happen because the agonistic–antagonistic properties of **19***d* closely resembled those of the parent compound BC-2627.

Limited data for the bulkier *c* series indicate that the same pattern already noted in the *a* series appears to apply.

In conclusion, it can be said that the spatial area around the remote end of ring C in the morphinan and isomorphinan series of analgesics plays an important role at the receptor level in

[3]We are grateful to Dr. John Saunders, Université de Sherbrooke, for the determination and interpretation of these ^{13}C nmr spectra. Dr. Saunders will publish his results in a separate communication.

TABLE 3. Pharmacological data. Agonist–antagonist analgesic activity

Compound	C–E[a]	OH[b]	Structure[k]	R	Agonist[c]	Antagonist OSTM[d]	Antagonist RTF[e]
19*a*	*trans*	β	**17***A*	▷—CH_2	~40	0.04	0.03
				◇—CH_2	>40	5	ND
19*d*	*trans*	β	**19***D*	◇—CH_2	0.15	2.5	ND
BC-2605[f]		β		▷—CH_2	8.7	0.3	0.03
BC-2627[g]				◇—CH_2	0.06	3.2	0.38
18*a*[h]	*trans*	α	**16***A*	▷—CH_2	80	0.48	0.04
				◇—CH_2	~80	3	0.3
				CH_3	8.8	30	ND
				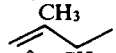	>40	~3	ND
18*b*	*cis*	α	**18***B*	◇—CH_2	23	11	ND
18*c*	*trans*	α	**18***C*	▷—CH_2	>40	0.7	~0.5
18*d*	*trans*	α	(**16***A*)	▷—CH_2	~60	0.3	0.04
				◇—CH_2	>40	2	ND
18*e*	*cis*	α	(**18***B*)	▷—CH_2	9	0.16	ND
				◇—CH_2	0.32	3.5	ND
iso-2605[i]		α		▷—CH_2	10	0.6	ND
iso-2627[j]		α		◇—CH_2	7	9	ND
Naloxone		β		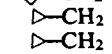	80	0.03	

[a]Stereochemistry of the C–E ring junction or the 6,7-substitution.
[b]Configuration of the 14-hydroxyl group.
[c]ED_{50} for the inhibition of phenylquinone-induced writhing in the mouse, mg/kg, s.c.
[d]ED_{50} for the antagonism of oxymorphone-induced Straub tail in the mouse, mg/kg, s.c.
[e]ED_{50} for the antagonism of morphine analgesic (rat tail flick), mg/kg, s.c.
[f]*dl*-Mixture corresponding to oxilorphan.
[g]*dl*-Mixture corresponding to butorphanol.
[h]The reactivity resides in the *levo*-isomer.
[i]*dl*-Isomorphinan analog of oxilorphan.
[j]*dl*-Isomorphinan analog of butorphanol.
[k]Correct stereostructure for the substitution at C_6 and C_7 (axial–equatorial).

that it can serve to control the agonistic–antagonistic relationships. This role is as important or even more important than the substitution patterns at positions 14 and 17.

Experimental

Melting points (Fisher Mel-Temp) are not corrected. All compounds possessed ir (Unicam SP-200G) and nmr (Varian A-60A) spectra consistent with their structure. Combustion analyses were performed by Microtech Laboratories.

The starting bisbromomethyl compounds were known with the exception of **4***c*: **4***a* (4); **4***b* (5); **4***d* and **4***e* (6). Compounds **4***a*, **4***b* and **4***c* were prepared by a modification reported by Blomquist and Verdol (7) for 1,2-bis(bromoethyl)cyclobutane. The alcohol used to prepare **4***c* was described by Birch *et al.* (8).

Detailed experimental procedures are given for the *trans*-cyclohexane series only. Procedures were identical for the other series unless cited otherwise. Physical constants for the compounds **6**–**19** are given in Tables 4 and 5.

Preparation of the Spiro[7'-methoxy-cis- or trans-substituted Cyclopentane-1,2'-tetra-1'-one], 6

A solution of 7-methoxy-1-tetralone (121.0 g, 0.69 mol) and *trans*-1,2-bis(bromomethyl)cyclohexane (188.0 g, 0.695 mol) in anhydrous benzene (1500 ml) was added, in a fast stream from an addition funnel, to a refluxing mixture of potassium *tert*-butoxide (155.0 g, 1.38 mol) in anhydrous benzene (1500 ml). The mixture was stirred and refluxed for 24 h. The above operations were carried out under an atmosphere of nitrogen. After cooling, the mixture was washed with 10% hydrochloric acid and with water. Drying and concentration of the organic phase left an oil which was crystallized in methanol to give **6***a* as a white solid; 140 g, 69.5%, mp 103–104 °C.

6*c* required a 6 day reflux period in toluene; **6***d* and **6***e* a 3 day reflux in benzene.

Preparation of the Spiro[1'-β-aminoethyl-1'-hydroxy-7'-methoxy-cis- or trans-substituted Cyclopentane-1,2'-tetralins], 8

A solution of acetonitrile (23 g, 0.56 mol) in dry THF (500 ml) was added, under nitrogen, over a period of 10 min, to a solution of *n*-butyllithium (0.564 mol of the commercial 1.6 *M* solution in hexane) in dry THF (338 ml) cooled at −78 °C. After a 1 h stirring period at −78 °C, a solution of the spiroketone **6***a* (160 g, 0.56 mol) in THF (600 ml) was added as rapidly as possible from an addition funnel. The cooling bath was removed and the solution was stirred for 15 min. Solid lithium aluminum hydride (34 g, 0.90 mol) was added in one portion and the resulting mixture was stirred for 3 h at room temperature. After cooling to 0 °C, the excess of hydride was decomposed by the dropwise addition of water (34 ml), aqueous sodium hydroxide (25.5 ml of a 20% solution) and again water (119 ml). The precipitated hydroxides were re-

Can. J. Chem. Downloaded from www.nrcresearchpress.com by 210.87.254.5 on 09/05/12
For personal use only.

Can. J. Chem. Downloaded from www.nrcresearchpress.com by 210.87.254.5 on 09/05/12
For personal use only.

TABLE 4. Physical constants of compounds **6–12**[a]

Compound	Melting point (°C)	Solvent	Yield (%)	Formula	Analysis % Calculated C	Calculated H	Calculated N	Found C	Found H	Found N
6*a*	104–105	MeOH	70	$C_{19}H_{24}O_2$	80.24	8.51		80.53	8.46	
6*b*	74–77	Petroleum ether	25	$C_{19}H_{24}O_2$	80.24	8.51		80.32	8.32	
6*c*	174–175	EtOAc	25	$C_{20}H_{24}O_2$	81.04	8.16		80.96	8.21	
7*b*	117–118	CCl_4	46	$C_{21}H_{27}NO_2$	77.50	8.36	4.30	77.45	8.45	4.28
8*b*·$C_2H_2O_4$	204–205	MeOH–Et_2O	90	$C_{23}H_{33}NO_6 \cdot \frac{1}{2}H_2O$	64.46	8.00	3.27	64.92	7.97	3.40
8*c*	135–137	Petroleum ether	70	$C_{22}H_{31}NO_2$	77.38	9.15	4.10	77.29	9.29	4.01
9*b*·$C_2H_2O_4$	203	MeOH	55	$C_{23}H_{31}NO_5 \cdot \frac{1}{2}H_2O$	67.29	7.86	3.41	67.36	7.81	3.70
10*a*·HCl	155–160	EtOH·Et_2O	76	$C_{21}H_{30}ClNO \cdot C_2H_5OH$	70.14	9.21	3.55	70.51	8.76	3.74
10*b*·HCl	170–175	PrOH·Et_2O	75	$C_{21}H_{30}ClNO$	72.49	8.69	4.03	72.32	8.41	4.27
10*c*·HCl	145–160	PrOH·Et_2O	68	$C_{22}H_{30}ClNO$	69.91	8.53	3.70	70.43	8.11	3.67
10*d*·$C_2H_2O_4$	195–197 (dec.)	EtOH·Et_2O	75	$C_{21}H_{29}NO_5 \cdot H_2O$	64.10	7.94	3.55	64.70	7.79	3.58
10*e*·$C_2H_2O_4$	204–207	EtOH·Et_2O	55	$C_{21}H_{29}NO_5$	67.17	7.85	3.73	67.00	7.90	3.71
11*a*·HBr	228–231	CH_3COCH_3	65	$C_{21}H_{29}Br_2NO$	53.52	6.20	2.97	53.21	6.17	3.06
11*c*·HBr	235 (dec.)	CH_3COCH_3	70	$C_{22}H_{29}Br_2NO$	54.67	6.05	2.90	54.77	6.07	2.85
11*d*·HBr	182–185 (dec.)	EtOH·Et_2O	50	$C_{19}H_{27}Br_2NO \cdot H_2O$	49.26	6.31	3.02	49.40	6.34	2.86
12·$C_2H_2O_4$	186–187	MeOH·Et_2O	95	$C_{23}H_{29}NO_5$	69.15	7.32	3.51	68.87	7.53	3.46

[a]The following compounds were difficult to purify and were not analysed. The crude product was used for the next step: **6***d* (bp 144–148 °C/0.1 Torr), **6***e* (bp 148–154 °C/0.05 Torr), **7***a*,**7***c*, **7***d*, **7***e*, **8***a* (·HCl, mp 196–200 °C), **8***d*, **8***e*, **11***b* (·HBr, mp 197–200 °C), **11***e*, **12***b*, **12***c*, **12***d*, and **12***e*.

Can. J. Chem. Downloaded from www.nrcresearchpress.com by 210.87.254.5 on 09/05/12
For personal use only.

TABLE 5. Physical constants of compounds **13–19**[a]

Compound	R	Melting point (°C)	Solvent	Yield (%)	Formula	Analysis (%) Calculated C	H	N	Found C	H	N
13*a*	▷—CO	187–189	EtOAc	80	$C_{25}H_{31}NO_2$	79.54	8.28	3.71	79.33	8.25	3.58
13*a*	◇—CO	155–157	EtOAc–petroleum	85	$C_{26}H_{33}NO_2$	79.75	8.49	3.57	80.04	8.44	3.48
14*a*	▷—CO	162–164	CH_2Cl_2–Et_2O^{ether}	48	$C_{25}H_{31}NO_3$	76.30	7.94	3.56	76.59	8.01	3.48
14*a*	◇—CO	198–200	$C_6H_6 \cdot Et_2O$	35	$C_{26}H_{33}NO_3$	77.47	8.74	3.15	77.58	8.35	2.98
14*a*	CF_3CO	132–134	MeOH	35	$C_{23}H_{26}F_3NO_3$	65.55	6.22	3.32	65.90	6.18	3.30
15*a*	◇—CO	135–138	$C_6H_6 \cdot Et_2O$	30	$C_{26}H_{33}NO_3 \cdot \frac{1}{2}C_6H_6$	77.47	8.74	3.15	77.50	8.12	3.02
16*a*	▷—CH_2	255–260[b]	EtOH·Et_2O	90	$C_{25}H_{36}ClNO_2$	71.83	8.68	3.35	71.84	8.70	3.27
16*a*	◇—CH_2	255–265	MeOH·Et_2O	50	$C_{26}H_{38}ClNO_2$	72.28	8.87	3.24	72.28	8.88	3.16
16*a*	CH_3	251–257 (dec.)[b]	EtOH·Et_2O	80	$C_{22}H_{32}ClNO_2 \cdot H_2O$	66.73	8.66	3.54	67.03	8.73	3.58
16*a*	H	282–285[b]	EtOH·Et_2O	50	$C_{21}H_{30}ClNO_2 \cdot \frac{1}{2}H_2O$	67.63	8.38	3.76	66.67	8.50	3.70
16*a*	CH_2=$CHCH_2$	192–194[b]	EtOH·Et_2O		$C_{25}H_{34}ClNO_2 \cdot H_2O$	68.30	8.59	3.32	68.58	8.50	3.35
16*d*	H	290 (dec.)[b]	EtOH	35	$C_{19}H_{28}ClNO_2$	67.54	8.35	4.15	67.60	8.50	4.00
17*a*	◇—CH_2	92–94	EtOH	75	$C_{26}H_{37}NO_2$	78.94	9.43	3.54	78.67	9.54	3.43
18*a*	▷—CH_2	272–273[b]	MeOH·Et_2O	50	$C_{24}H_{34}ClNO_2$	71.35	8.48	3.47	71.28	8.53	3.27
18*a*	▷—CH_2	200–205[c]	MeOH		$C_{26}H_{36}NO_5 \cdot \frac{1}{2}CH_3OH$	69.40	8.35	3.05	69.50	8.12	3.28
18*a*	▷—CH_2	195–200[d]	MeOH		$C_{26}H_{36}NO_3 \cdot \frac{1}{2}CH_3OH$	69.40	8.35	3.05	69.32	8.06	3.37
18*a*	◇—CH_2	276–277[b]	MeOH·Et_2O	65	$C_{25}H_{36}ClNO_2$	71.83	8.68	3.35	71.37	8.74	3.12
18*a*	CH_2=$CHCH_2$	275–280[b]	EtOH·Et_2O	72	$C_{23}H_{32}ClNO_2 \cdot \frac{1}{2}H_2O$	69.24	8.34	3.51	69.40	8.25	3.53
18*a*	CH_3	190–193	MeOH	60	$C_{21}H_{29}NO_2$	77.02	8.93	4.28	76.91	9.26	4.36
18*b*	◇—CH_2	312–315 (dec.)[b]	MeOH·Et_2O	67	$C_{25}H_{36}ClNO_2 \cdot \frac{1}{4}CH_3OH$	71.19	8.75	3.28	71.13	8.67	3.16
18*c*	▷—CH_2	218–223 (dec.)[b]	PrOH·Et_2O	32	$C_{25}H_{34}ClNO_2 \cdot 2H_2O$	66.43	8.47	3.09	66.42	7.67	2.77
18*d*	▷—CH_2	190–193	Petroleum ether	52	$C_{22}H_{31}NO_2$	77.37	9.15	4.10	77.47	9.35	4.08
18*d*	◇—CH_2	173–174	Petroleum ether	37	$C_{23}H_{33}NO_2$	77.70	9.35	3.94	77.72	9.52	3.85
18*e*	▷—CH_2	227–230	EtOH·H_2O	67	$C_{22}H_{31}NO_2$	77.37	9.15	4.10	77.17	9.23	3.92
18*e*	◇—CH_2	187–189	EtOH·H_2O	82	$C_{23}H_{33}NO_2$	77.70	9.35	3.94	77.43	9.68	3.80
19*a*	▷—CH_2	271–274[b]	EtOH·Et_2O	42	$C_{24}H_{34}ClNO_2$	71.35	8.48	3.47	71.06	8.59	3.40
19*a*	◇—CH_2	267–274[b]	EtOH·Et_2O	67	$C_{25}H_{36}ClNO_2$	71.83	8.68	3.35	71.90	8.72	3.23
19*d*	◇—CH_2	283–285[b]	EtOH·Et_2O	56	$C_{23}H_{34}ClNO_2$	70.47	8.74	3.57	70.05	8.86	3.41

[a]The following compounds were difficult to crystallize. They were cleaned by column chromatography and the residue from the proper fractions were employed in the next step: **13***a* (CF_3CO) oil; **13***b* (◇—CO) mp 98–100 °C; **13***c* (▷—CO) oil; **13***d* (◇—CO); **13***e* (◇—CO) oil; **13***e* (▷—CO); **14***a* (H) oil; **14***b* (◇—CO) mp 110–115 °C; **14***c* (▷—CO); **14***d* (◇—CO); **14***e* (◇—CO); **14***e* (▷—CO) mp 158–162 °C; **15***d* (◇—CO); **16***b* (◇—CH_2) mp 270–280 °C (dec.); **16***c*[b] (▷—CH_2), **16***d*[b] (▷—CH_2) mp 250–255 °C (dec.); **16***d*[b] (◇—CH_2) mp 246; **17***d* (◇—CH_2).

[b]Hydrochloric acid salt.

[c]*d*-Tartaric acid salt of the levo-isomer, $[\alpha]_D^{20} \times (MeOH) = -93.75$.

[d]*l*-Tartaric acid salt of the dextro-isomer, $[\alpha]_D^{25}(MeOH) = +96.73$.

Can. J. Chem. Downloaded from www.nrcresearchpress.com by 210.87.254.5 on 09/05/12
For personal use only.

moved by filtration over Celite and washed with ether (300 ml). The combined filtrates were treated with hydrochloric acid (500 ml of a 10% solution) which brought about the separation of an oil (the hydrochloride of **8***a* is insoluble in water) which crystallized upon cooling. After filtration, the solid was triturated with acetonitrile and dried to give the crude hydrochloride of **8***a* as a white powder; mp 196–200 °C, 140 g, 68%. This crude material was used as such in the next step.

Preparation of the Spiro[1'-cyanomethyl-1'-hydroxy-7'-methoxy-cis- or trans-substituted Cyclopentane-1,2'-tetralins], **7**

To a stirred solution of *n*-butyllithium (27.6 ml of the commercial 1.6 *M* solution in hexane) in dry THF (26 ml) cooled at −78 °C was added, under nitrogen and over a period of 10 min, a solution of acetonitrile (2.1 ml, 0.069 mol) in dry THF (40 ml). After stirring at −78 °C for 1 h, a solution of the spiroketone **6***b* (11.36 g, 0.04 mol) in THF (40 ml) was added as rapidly as possible from an addition funnel. The cooling bath was removed and the solution was stirred 15 min at room temperature. The above operations were carried out under an atmosphere of nitrogen. The solution was poured into ice-cold dilute (*ca.* 2%) hydrochloric acid (50 ml) and extracted with benzene (3 × 50 ml). The combined organic phases were washed with water, dried (Na_2SO_4), and concentrated to leave a reddish oil. The oil was crystallized in ethyl acetate – petroleum ether and recrystallized from carbon tetrachloride to give colorless crystals of **7***b*; 6.0 g, 46%.

Reduction of the Nitriles, **7**

To a slurry of lithium aluminum hydride (0.114 g, 0.03 mol) in dry THF (2 ml) was added dropwise a solution of the spironitrile **7***b* (0.67 g, 0.002 mol) in dry THF (5 ml). After stirring at room temperature for 3 h, the excess of hydride was decomposed at 0 °C by the dropwise addition of water (0.11 ml), aqueous sodium hydroxide (0.082 ml of a 20% solution), and water (0.385 ml). The precipitated hydroxides were removed by filtration over Celite and washed with ether (20 ml). The combined filtrates were extracted with hydrochloric acid (2 × 10 ml of a 10% solution). The combined acidic layers were made basic with concentrated ammonium hydroxide and extracted with ether (3 × 20 ml). After drying (Na_2SO_4) and concentration of the ether phases, an oil was obtained. It was redissolved in anhydrous ether and treated with an excess of ethereal oxalic acid. The yellow solid formed was recrystallized from methanol–ether to give the oxalate salt of **8***b* as a white hygroscopic powder, mp 204.5–205 °C, 90%.

*Elimination of the Alcohols **8** without Rearrangement*; *Preparation of **9***

A mixture of the hydrochloride **8***b* (5.36 g, 0.0153 mol), concentrated hydrochloric acid (5 ml), and ether (20 ml) was stirred and refluxed under an atmosphere of nitrogen for 5 h. Removal of the ether phase by decantation, neutralization with ammonium hydroxide, extraction with ether, drying, and concentration left **9***b* as an oil. Preparation of an oxalate salt in ether gave a white solid which was purified by recrystallization from methanol; 3.0 g, mp 203–203.5 °C.

Preparation of the 4a-β-Aminoethyl-1,2,3,4,4a,9-hexahydro-6-methoxy Phenanthrenes, **10**

A mixture of the hydrochloride of **8***a* (95 g, 0.26 mol) (or the equivalent amount of the unsaturated amine **9**), concentrated hydrochloric acid (200 ml), and benzene (400 ml) was stirred and refluxed for 3 h under a nitrogen atmosphere. The hot solution was transferred to a separatory funnel and the phases decanted. The aqueous phase was extracted with benzene (200 ml) and the combined benzene layers were diluted with ether (600 ml). Upon cooling the hydrochloric acid salt of **10***a* separated as colorless crystals. A further crop of solid was obtained by concentration of the filtrates and dilution with ether. Recrystallization from ethanol–ether gave the pure hydrochloride **10***a* as crystals; mp 155–160 °C, 76%.

Preparation of the 9-α-Bromo-3-methoxy-6,7-substituted Hasubanan Hydrobromides, **11**

A solution of the amine **10***a* (101.6 g, 0.32 mol, free base prepared from the hydrochloride) in reagent grade chloroform (200 ml) was added in one portion to a vigorously stirred solution of bromine (52.8 g, 0.32 mol) in chloroform (7000 ml). After stirring for 5 min, the reaction mixture was concentrated on a rotary evaporator at 35–40 °C under water-aspirator vacuum. The resulting solid residue was recrystallized from acetone; 102.0 g 65%, mp 225–228 °C (dec.).

Preparation of the 3-Methoxy-6,7-substituted-Δ^8-morphinans, **12**

A mixture of the amine hydrobromide **11***a* (97.34 g, 0.206 mol), anhydrous sodium bicarbonate (17.3 g, 0.207 mol), and dry DMF (700 ml) was heated in an oil bath at 110–115 °C for 1.5 h with vigorous stirring. After cooling, the mixture was poured into a saturated sodium bicarbonate solution (1000 ml) and extracted with benzene (3 × 200 ml). The combined benzene layers were washed with water (5 × 100 ml) dried (Na_2SO_4), and concentrated to leave an oil (63.7 g), (100%). This oil can be used as such for the next step. The oil was dissolved in ether and treated with an excess of oxalic acid in ether to give a semisolid mass. This was dissolved in a minimum amount of methanol and diluted with a large volume of ether to give the oxalic acid salt of **12***a* as a white solid; mp 186–187 °C, 95%.

Preparation of the 17-Acylated-3-methoxy-6,7-substituted-Δ^8-morphinans, **13**

(*a*) Cyclopropylcarbonyl chloride (4.5 g, 0.043 mol) (or the equivalent amount of cyclobutylcarbonyl chloride) was added dropwise to a stirred and cooled (0 °C) solution of the amine **12***a* (11.62 g, 0.037 mol) and pyridine (3.75 g, 0.047 mol) in methylene chloride (45 ml). After the end of the addition, the mixture was stirred for 10 min at 0 °C and poured into ice-cold hydrochloric acid (25 ml of a 10% solution). The aqueous phase was decanted and the organic phase was washed with water (25 ml), dried (Na_2SO_4), and concentrated. The residue was recrystallized from ether; 11 g, 80%, mp 186–188 °C.

(*b*) Trifluoroacetic anhydride (80 ml, 0.56 mol) was added as rapidly as possible, keeping the temperature at 0–5 °C, to an ice-cooled vigorously stirred mixture of the amine **12***a* (20.25 g, 0.095 mol) and anhydrous Na_2CO_3

Can. J. Chem. Downloaded from www.nrcresearchpress.com by 210.87.254.5 on 09/05/12
For personal use only.

(60 g, 0.7 mol) in anhydrous ether (160 ml). The mixture was stirred vigorously at room temperature for 1 h, ice was added to hydrolyse the excess of anhydride and the mixture was decanted, the ether phase washed with water, dried and concentrated to leave 37 g of an oily residue. Chromatography of this oil on silica gel (900 g) gave 29.49 g (77%) (ether – petroleum ether, 1:4) of pure oil which was used as such for the next step.

*Preparation of the 17-Acylated-8,14-α- and β-epoxy-3-methoxy-6,7-substituted Isomorphinans and Morphinans, **14** and **15***

m-Chloroperbenzoic acid (6.15 g of the commercial 85% compound) was added portionwise to a stirred and cooled (0 °C) solution of the unsaturated amide **13***a* (R = ▷—CO—) (10.0 g, 0.0255 mol) in methylene chloride (300 ml). After stirring at room temperature for 18 h, the mixture was washed with a 10% solution of sodium bisulfite (50 ml), with a 10% solution of sodium carbonate (3 × 50 ml), and with a saturated salt solution (2 × 50 ml). After drying and concentration of the organic phase, the oily residue was crystallized in ether to yield 48% of the α-epoxide **14***a*. The ether filtrates were concentrated and chromatographed over silica gel (500 g) eluting with 30% ether in petroleum ether. The order of elution was as follows **13***a*, **14***a*, and the desired β-epoxide **15***a* (20% yield).

In most cases, the separation of the two isomeric-epoxides was achieved by chromatography only.

*Preparation of 17-Alkyl-14-α and β-hydroxy-3-methoxy-6,7-substituted Isomorphinans and Morphinans, **16** and **17***

(*a*) R = alkyl: the amido epoxide **14***a* (R = cyclopropylcarbonyl), or an equivalent amount of the morphinan epoxides **15**, (11.57 g, 0.0295 mol) was added in small portions to a slurry of lithium aluminum hydride (6.0 g, 0.16 mol) in dry THF (100 ml). The mixture was heated under reflux for 1 h, cooled to 0 °C, and decomposed by the dropwise addition of water (6.0 ml), aqueous sodium hydroxide (4.5 ml of a 20% solution) and water (21.0 ml). The precipitated hydroxides were removed by filtration over Celite and washed with ether (200 ml). The combined filtrates were extracted with hydrochloric acid (3 × 50 ml of a 10% solution), the combined acidic layers were made alkaline with concentrated ammonium hydroxide and extracted with methylene chloride (3 × 100 ml). Drying (Na_2SO_4) and concentration left an oil which was dissolved in ether and petroleum ether (200 ml, 1:1). After drying with Na_2SO_4, it was filtered over Celite and the Celite washed with 200 ml of the ether – petroleum ether mixture. Dry HCl was bubbled through the solution and the solid hydrochloride was collected by filtration and washed with ether – petroleum ether; 11.26 g, 90%, mp 255–260 °C.

(*b*) R = allyl: a mixture of the amino alcohol **16***a* (R = H) (from 2.20 g, 0.0065 mol of the HCl salt, Na_2CO_3 and CH_2Cl_2), triethylamine (2.7 g, 0.027 mol) and allyl bromide (1.1 g, 0.01 mol) in absolute ethanol (25 ml) was heated under reflux for 18 h. After cooling, the mixture was poured into Na_2CO_3 (100 ml of a 10% solution) and extracted with methylene chloride (3 × 15 ml). Drying and concentration of the combined methylene chloride extract left an oil which was dissolved in ether and filtered over Celite. An excess of a saturated solution of hydrogen chloride in ether was added to the filtrates. The solid hydrochloride salt of **16***a* (R = allyl) was collected by filtration and recrystallized from methanol–ether; mp 192–194 °C.

*Preparation of 17-Alkyl-3,14-dihydroxy-6,7-substituted Isomorphinans and Morphinans, **18** and **19***

(*a*) R = alkyl: a solution of the amine **16***a* (R = cyclopropylmethyl) (from 1.75 g of the hydrochloride neutralized with ammonium hydroxide and extracted with methylene chloride) in methylene chloride (40 ml) was added over a period of 1 h to a stirred and cooled (0 °C) solution of boron tribromide (1.25 ml, 0.019 mol) in methylene chloride (15 ml). After the end of the addition, the mixture was stirred 3 h at room temperature, cooled to 0 °C, and decomposed with water (15 ml) and concentrated ammonium hydroxide (20 ml). After decantation, the aqueous phase was again extracted with methylene chloride (40 ml) and the combined organic layers were washed with a saturated salt solution (15 ml). After drying (Na_2SO_4) and concentration, the residue was dissolved in ether (100 ml) and treated with hydrochloric acid (20 ml of a 10% solution). The solid hydrochloride of **14***a* was collected by filtration and recrystallized from methanol–ether; 50%, mp 272–273 °C.

(*b*) R = allyl: a solution of sodium ethanethiolate was prepared, under nitrogen, from sodium hydride (1.59 g of the 57% suspension in mineral oil, 0.037 mol) and ethanethiol (2.8 ml, 2.32 g, 0.0374 mol) in DMF (10 ml) at 0 °C. A solution of the methoxy compound **16***a* (R = $CH_2CH{=}CH_2$) (from 1.5 g of the HCl salt, NH_4OH and CH_2Cl_2) in DMF (20 ml) was added to the above solution and the mixture was stirred and refluxed for 2 h, cooled, poured into ice water (50 ml), acidified to p*H* 6 with hydrochloric acid, and made basic with ammonium hydroxide. It was extracted with benzene (4 × 50 ml), dried over Na_2SO_4, and concentrated. The residual oil was dissolved in ether and treated with an excess of a solution of hydrogen chloride in ether. The solid hydrochloride salt was collected by filtration and recrystallized from ethanol–ether; mp 275–280 °C.

*Resolution of **18***a* (R = ▷—CH_2—)*

A boiling solution of *d*-tartaric acid (1.52 g, 0.0102 mol) in methanol (5 ml) was added to a boiling solution of **18***a* (R = ▷—CH_2—) (3.73 g, 0.0102 mol) in methanol (25 ml). After standing at room temperature for 24 h, the crystals were collected by filtration: 3.0 g, no optical rotation. Repeated recrystallization at high dilution from methanol gave the pure *d*-tartaric acid salt of *l*-**18***a*, mp 200–205 °C, $[\alpha]_D^{20} = -93.75$.

The *d*-isomer was prepared like the *l*-isomer, starting with *l*-tartaric acid and the free base obtained from the filtrates of crystallization of the *l*-isomer. Isolated as the half salt of *l*-tartaric acid; $[\alpha]_D^{20} = 96.73$ (methanol), mp 195–200 °C (dec.).

*Preparation of the 8,14-α-Epoxy-3-methoxy-6,7-substituted Isomorphinans, **14a** and **14d** (R = H)*

A mixture of **14***a* (R = CF_3CO—) (5.5 g, 0.013 mol) and sodium borohydride (0.495 g, 0.013 mol) in absolute ethanol (30 ml) was heated under reflux for 10 min. After cooling, the mixture was poured into dilute hydrochloric

acid (25 ml of a 10% solution) and the solution washed with ether. The aqueous layer was made basic with concentrated ammonium hydroxide and extracted with ether (3 × 20 ml). The combined ether layers were dried over Na_2SO_4 and concentrated to give 5.2 g of **14***a* (R = H) as an oil which was used as such for the next step.

Preparation of the 14-α-Hydroxy-3-methoxy-6,7-substituted Isomorphinans, ***16a*** *and* ***16d*** *(R = H)*

(*a*) The amino epoxide **14***a* (R = H) (5.2 g, 0.016 mol) in THF (50 ml) was added dropwise to a stirred suspension of $LiAlH_4$ (3.0 g, 0.079 mol) in THF (25 ml). The mixture was heated under reflux for 1 h, cooled, and decomposed with water (3 ml), sodium hydroxide (2.25 ml of a 20% aqueous solution), and water (10.5 ml). Filtration over Celite and concentration left a colorless oil which was dissolved in ether (100 ml) and treated with an excess of a saturated hydrogen chloride solution in ether. The solid was collected by filtration and recrystallized from ethanol–ether; 2.90 g, 50%, mp 282–285 °C.

(*b*) The amine **10***a* (9.60 g, 0.03 mol) and pyridine (3.0 g, 0.035 mol) in chloroform (150 ml) was treated, dropwise and at 0 °C, with ethylchloroformate (3.8 g, 0.035 mol) in chloroform (50 ml). After stirring for 10 min, the reaction was worked up in the usual manner to leave 13.0 g of an oily reaction residue, **20***a*.

The above oil, epoxidized with metachloroperbenzoic acid as described for **14**, gave 13.3 g of crude epoxide **21***a*.

The above crude epoxide was cyclized in the following manner: to a solution of sodium isoamylate, prepared from sodium hydride (0.04 mol) and isoamyl alcohol (3.1 g, 0.035 mol) in benzene (100 ml), was added dropwise a solution of the crude epoxide in benzene (250 ml). After a 24 h reflux period, the mixture was cooled and washed with water, dried with Na_2SO_4, and concentrated to give 6.42 g of **22***a* as a reddish oil.

The above oil (3.0 g) was refluxed for 45 min with a solution of KOH (2.8 g) in octanol (25 ml), cooled, and poured into ice water. The usual acid–base extraction afforded crude **23***a* which was purified through its hydrochloric acid salt; 1.0 g, mp 282–285 °C, identical (ir, nmr, tlc, mixture mp) with a sample of **16***a* (R = H) prepared by method *a*.

Acknowledgments

We wish to thank Dr. A. W. Pircio of Bristol Laboratories, Syracuse, New York, for the pharmacological data.

1. (*a*) I. MONKOVIĆ, T. T. CONWAY, H. WONG, Y. G. PERRON, I. J. PACHTER, and B. BELLEAU. J. Am. Chem. Soc. **95**, 7910 (1973); (*b*) B. BELLEAU, H. WONG, I. MONKOVIĆ, and Y. G. PERRON. J. Chem. Soc. Chem. Commun. 603 (1974); (*c*) M. SAUCIER and I. MONKOVIC. Can. J. Chem. **52**, 2736 (1974); (*d*) B. BELLEAU, T. T. CONWAY, T. W. DOYLE, L. MORRIS, and W. VERBESTEL. Can. J. Chem. **53**, 237 (1975).
2. (*a*) J. W. LEWIS. Abstr. 1st International Conference on Narcotic Antagonists, Warrenton, Va. 1972. pp. 4–26; (*b*) L. S. HARRIS. Abstr. 13th National Med. Chem. Symposium, Am. Chem. Soc. Div. Med. Chem., Iowa City, Iowa. 1972. pp. 21–24; (*c*) J. W. LEWIS and M. J. READHEAD. J. Chem. Soc. Perkin. Trans. 1, 881 (1972); (*d*) J. W. LEWIS, M. J. READHEAD, and A. C. B. SMITH. J. Med. Chem. **16**, 9 (1973).
3. E. L. ELIEL, N. L. ALLINGER, S. J. ANGYAL, and G. A. MORRISON. Conformational analysis. Interscience Publishers, New York. 1965. p. 235.
4. G. A. HAGGIS and L. N. OWEN. J. Chem. Soc. 389 (1953).
5. E. L. SCHUMANN, M. G. VAN HAMPEN, JR., and C. H. TILFORD. J. Org. Chem. **23**, 763 (1958).
6. G. E. MCCASLAND and S. PROSKOW. J. Am. Chem. Soc. **76**, 3486 (1954).
7. A. T. BLOMQUIST and J. A. VERDOL. J. Am. Chem. Soc. **77**, 1806 (1955).
8. S. F. BIRCH, N. J. HUNTER, and D. T. MCALLAN. J. Org. Chem. **21**, 970 (1956).

Can. J. Chem. Downloaded from www.nrcresearchpress.com by 210.87.254.5 on 09/05/12
For personal use only.

Aqueous trifluoroacetic acid as a medium for organic reactions. I. Acidity functions and the identity of the manganese(VII) species found in powerfully acidic media[1]

UDO A. SPITZER, TREVOR W. TOONE, AND ROSS STEWART
Department of Chemistry, University of British Columbia, Vancouver, British Columbia V6T 1W5

Received June 3, 1975

UDO A. SPITZER, TREVOR W. TOONE, and ROSS STEWART. Can. J. Chem. **54**, 440 (1976).

The H_R acidity function has been determined for the trifluoroacetic acid – water system, and extended beyond 100% acid by the addition of trifluoroacetic anhydride, to 99.5 wt.% anhydride. The existing H_0 acidity function is corrected and extended to 100% trifluoroacetic acid, confirming Eaborn's observation that H_0 attains a minimum value at approximately 97% acid. Comparison of the acidity functions shows that although trifluoroacetic acid is only weakly protonating, it is a strongly protonating-dehydrating medium. Changes in the uv–visible spectrum of potassium permanganate produced by changing acid concentration are used to calculate the degree of further ionization of the permanganate ion; the correlation of this with the H_R acidity function further suggests the presence of the permanganyl cation, MnO_3^+, or its trifluoroacetate complex or ester, $MnO_3 \cdot O_2CCF_3$, in these solutions. A cryoscopic investigation into the mode of ionization of permanganate in trifluoroacetic acid reveals that extensive ion-pair formation occurs in this solvent. Although this effect prevents an unequivocal determination of the number of solute particles being made the results are consistent with the presence of a permanganyl species in solution.

UDO A. SPITZER, TREVOR W. TOONE et ROSS STEWART. Can. J. Chem. **54**, 440 (1976).

On a déterminé la fonction d'acidité H_R du système acide trifluoroacétique – eau, et on l'a étendue au delà de 100% d'acide par addition d'anhydride trifluoroacétique jusqu'à 99.5% en poids d'anhydride. On a corrigé la fonction d'acidité H_0 existante et on l'à étendue à l'acide trifluoroacétique 100% confirmant l'observation d'Eaborn que H_0 atteint une valeur minimale à environ 97% d'acide. Une comparaison des fonctions d'acidité montre que quoique l'acide trifluoroacétique n'est que faiblement protonant, c'est un milieu fortement protonant et déshydratant. Des modifications dans le spectre uv–visible du permanganate de potassium, produites par des changements de concentration d'acide, ont été utilisées pour calculer le degré d'ionisation subséquente de l'ion permanganate; la corrélation de ceci avec la fonction d'acidité H_R suggère de plus la présence dans ces solutions du cation permanganyle, MnO_3^+, ou de son complexe trifluoro acétate ou ester, $MnO_3 \cdot O_2CCF_3$. Une étude cryoscopique du mode d'ionisation du permanganate dans l'acide trifluoroacétique révèle qu'il y a une formation importante de paires d'ions dans ce solvant. Quoique cet effet empêche une détermination non-équivoque du nombre de particules de soluté, les résultats sont en accord avec la présence d'espèces permanganyles en solution.

[Traduit par le journal]

Recent interest has been shown in trifluoroacetic acid solutions as media for a variety of reactions, including electrophilic aromatic substitutions (1), displacement reactions (2), conductivity processes (3), and oxidations (4, 5); in addition H_0 and H_- acidity functions have been determined for this medium (6). A major reason for the interest shown in this solvent system is its ability to dissolve both ionic salts and organic compounds.

We have found that aqueous trifluoroacetic acid can be used for the homogeneous oxidation of hydrocarbons by potassium permanganate. The oxidation rate increases with increasing acidity of the medium but the increase is much greater than can be accounted for by the increase in acidity as measured by the H_0 or H_- acidity functions (5). Accordingly, we undertook an examination of the chemical equilibria involving permanganate and trifluoroacetic acid making use of three approaches; firstly, a determination of the H_R acidity function, which might be expected to correlate the activation more satisfactorily than either the H_0 or H_- functions; secondly, an examination of the change in

[1]Taken in part from the Ph.D. Thesis of U. A. Spitzer, University of British Columbia, 1972.

Can. J. Chem. Downloaded from www.nrcresearchpress.com by 210.87.254.6 on 09/05/12
For personal use only.

Can. J. Chem. Downloaded from www.nrcresearchpress.com by 210.87.254.6 on 09/05/12
For personal use only.

position of the equilibrium between permanganate ion and the green species observed in strong acids (see below) as the acid concentration changes, monitored by following changes in the ultra-violet and visible spectra; and thirdly, a cryoscopic investigation of the behaviour of potassium permanganate in pure trifluoroacetic acid.

It has long been known that when potassium permanganate is dissolved in concentrated acids such as sulfuric (7) or perchloric (8) a green solution results, in contrast to the familiar purple colour observed in more aqueous media. Solutions of permanganate containing more than 90% trifluoroacetic acid are also green, and we hoped the present study would aid in identifying the species responsible. Three species have been proposed to account for the green colour; permanganyl cation (MnO_3^+) (a proposal based on cryoscopic and conductiometric measurements in sulfuric acid) (9), its complex with an acid anion A^- ($AMnO_3$) (based on conductiometric measurements in sulfuric acid) (10), and permanganic acid ($HMnO_4$) (8, 11). The latter possibility now appears unlikely since solid permanganic acid has recently been prepared and found to be a deep violet colour (12).

Acidity Functions in Trifluoroacetic Acid

(a) H_R Acidity Function

This function was determined by standard techniques (13, 14) using a series of triarylcarbinols, whose behaviour in acid solution is known to be governed by the following equation:

$$R^+ + H_2O \overset{K_{R^+}}{\rightleftharpoons} ROH + H^+$$

The H_R function is defined as follows:

$$H_R = pK_{R^+} + \log \frac{[ROH]}{[R^+]} = -\log \frac{a_{H^+} f_{ROH}}{a_{H_2O} f_{R^+}}$$

where

$$K_{R^+} = \frac{a_{ROH} a_{H^+}}{a_{R^+} a_{H_2O}} = \frac{[ROH]\, a_{H^+}}{[R^+] a_{H_2O}} \cdot \frac{f_{ROH}}{f_{R^+}}$$

Highly parallel ionization plots were obtained over the entire range of acid concentration, suggesting that high reliance may be placed on the derived H_R and pK_{R^+} values.

H_R was extended beyond 100% trifluoroacetic acid by measuring the ionization of 4,4′-dinitrotriphenylmethanol in mixtures of trifluoroacetic acid and trifluoroacetic anhydride. Solutions of indicator in acid–anhydride mixtures were the expected yellow colour, but the colour was lost on transferring samples, and slowly restored (taking 10–15 min for full restoration, the longer times being recorded for those solutions containing a higher proportion of anhydride). Since the colour was fully restored (with a small loss due to the slow decomposition of the indicator in this medium), oxidation of the indicator was ruled out as a cause of this phenomenon. It was found that bubbling air through the solutions temporarily removed the colour, but this did not occur if the air was carefully dried by passing it twice through concentrated sulfuric acid. Thus water causes the equilibrium to shift away from the carbonium ion, and the equilibrium is only restored slowly. The disappearance of the carbonium ion may reflect a shift in the position of the equilibrium as the binary system (acid–anhydride) becomes a tertiary system (acid–anhydride–water), the original equilibrium being restored as the small quantity of water reacts with anhydride to give trifluoroacetic acid. Alternatively the carbinol formed may react quickly with anhydride to give the trifluoroacetate ester, which ionizes slowly to restore the equilibrium. (If the latter alternative is true, then as the equilibrium is between an ester and a carbonium ion, it is not, strictly speaking, the H_R acidity function being measured in these solutions.)

Since the indicator is not fully ionized in mixtures of trifluoroacetic acid and anhydride, the extinction coefficient of the carbonium ion was measured in sulfuric acid (as was that for 3,3′,3″-trichlorotriphenylmethanol). Comparison of the extinction coefficients of the carbonium ions generated from more basic carbinols in sulfuric and trifluoroacetic acids showed this to be a reasonable approximation, since values in the two acids are generally similar, neither acid giving consistently higher values. However, this approximation, and the fact that the carbonium ion decomposes slowly in this medium (necessitating using the maximum optical density value recorded as colour is restored as the 'true' optical density of the solution), coupled with the difficulties of working with trifluoroacetic anhydride (bp 39.5–40.1 °C) at 25 °C, means that the values of H_R above 100% trifluoroacetic acid should be regarded as approximate.

The ionization of 4,4′-dinitrotriphenylmeth-

TABLE 1. pK_{R^+} values for triarylcarbinols

Substituent	pK_{R^+}	$pK_{R^+}(H_2SO_4)$*	λ_{max}†	log ε†
(1) 4,4′,4″-Trimethoxy	0.92	0.82	480	5.04
(2) 4,4′-Dimethoxy-4″-methyl	−0.28	—	487	4.93
(3) 4,4′-Dimethoxy	−0.97	−1.24	495	4.88
(4) 4,4′,4″-Trimethyl	−2.81	−3.56	446	4.97
(5) 4-Methoxy	−3.18	−3.40	469	4.82
(6) 4,4′-Dimethyl	−3.78	—	451	4.81
(7) 4-Methyl	−4.81	−5.24	450	4.70
(8) Unsubstituted	−6.44	−6.63	425	4.60
(9) 4,4′,4″-Trichloro	−8.13	−7.74	460	5.02
(10) 4-Nitro	−9.77	−9.15	436	4.51
(11) 3,3′,3″-Trichloro	−10.50	−11.03	412	—‡
(12) 4,4′-Dinitro	−12.83	−12.90	447	—‡

*Reference 13.
†The values of λ_{max} and log ε for the carbonium ion generated in trifluoroacetic acid used in the evaluation of ionization ratios.
‡The value of log ε not measureable in trifluoroacetic acid.

anol reaches a maximum at about 66% anhydride in trifluoroacetic acid, and correspondingly H_R attains a minimum value at this point.

Values of pK_{R^+} and H_R are given in Tables 1 and 2. Satisfactory agreement exists between the pK_{R^+} values determined in this work and those determined in sulfuric acid, although it is worthy of note that 4-methoxy- and 4,4′,4″-trimethyltriphenylmethanol fall in the order predicted by their $\sum\sigma^+$ values, whereas this order is reversed in sulfuric acid.

D_R was also examined and found to be essentially the same as H_R. Although solutions of CF_3CO_2D–D_2O of the same molarity as the protium system were more ionizing the differences between pK_{R^+} (H_2O) and pK_{R^+} (D_2O) were the same as between pH and pD, *i.e.* pD = pH + 0.40 (15), and $\log([R^+]/[ROH])_{D_2O} = \log([R^+]/[ROH])_{H_2O} + 0.40$, with the result that $D_R = H_R$ as was observed for H_2SO_4–H_2O and D_2SO_4–D_2O (16).

(b) H_0 Acidity Function

The H_0 acidity function in aqueous trifluoroacetic acid has been measured to approximately 90% acid by Randles and Tedder (6), and the accuracy of this work confirmed by Satchell (17). Eaborn *et al.* (18) have measured the ionization of 2,4-dichloro-6-nitroaniline in concentrated trifluoroacetic acid at 20 °C, and showed that a minimum value of H_0 is attained in the region of 97% acid. Unfortunately the overlap with the least basic indicator used by Randles and Tedder is not extensive, and no H_0 function for the entire range of acid concentration has been established. In order to establish such a scale the ionization of 2-chloro-6-nitroaniline was measured, and the overlap method used to extend the scale of Randles and Tedder to 100% acid. The H_0 scale is given in Table 2. (The original H_0 scale was anchored using 4-nitroaniline, assuming a pK_a value of 1.11. This has been corrected to a 'best' value of 0.99 (14).)

The data confirm Eaborn's observation that a minimum value of H_0 is obtained before 100% acid is reached, and the protonating ability of the medium decreases beyond this point. Unfortunately the indicator colour fades rapidly in solutions of trifluoroacetic anhydride in acid, presumably owing to trifluoroacetylation, but by extrapolating the drop in optical density with time to the time of mixing, it was possible to confirm that the protonating ability of the medium continues to decrease above 100% acid. (A solution containing 1.7% anhydride in acid has an H_0 value of −2.70.)

Overlap with 2,4-dichloro-6-nitroaniline (as measured by Eaborn) is good, particularly above 95% acid, despite the 5 °C difference in the temperature of measurement. (The pK_a of 2,4-dichloro-6-nitroaniline, as calculated by the overlap method, is −3.20.) This suggests that the H_0 function is independent of the particular indicator used in its evaluation over the entire range of trifluoroacetic acid – water concentrations, despite the observation that H_0 values are often a function of the particular indicator used in solutions of low dielectric constant (19).

(c) $H_{R'}$ Acidity Function

It has been shown that the $H_{R'}$ acidity function (= H_R − log (activity of water)) can be used to

Can. J. Chem. Downloaded from www.nrcresearchpress.com by 210.87.254.6 on 09/05/12
For personal use only.

Can. J. Chem. Downloaded from www.nrcresearchpress.com by 210.87.254.6 on 09/05/12
For personal use only.

TABLE 2. Acidity function values in trifluoroacetic acid

Acid normality*	Wt.% acid	$-H_R$	$-H_0$	$-H_{R'}$
0.1	0.7	−1.18	−1.16	−1.18
0.2	1.6	−0.81	−0.78	−0.81
0.3	2.5	−0.56	−0.59	−0.57
0.4	3.7	−0.35	−0.43	−0.36
0.6	6.0	−0.11	−0.29	−0.12
0.8	8.2	0.12	−0.14	0.10
1.0	10.4	0.30	−0.05	0.28
1.5	15.2	0.69	0.08	0.65
2.0	20.2	1.11	0.17	1.06
2.5	24.8	1.52	0.23	1.45
3.0	29.3	1.89	0.28	1.81
3.5	34.0	2.52	0.34	2.42
4.0	38.2	3.01	0.39	2.89
4.5	42.3	3.29	0.46	3.13
5.0	46.2	3.71	0.52	3.55
5.5	50.1	4.11	0.59	3.93
6.0	53.8	4.51	0.58	4.31
6.5	57.2	4.84	0.64	4.62
7.0	60.8	5.20	0.71	4.95
7.5	64.2	5.58	0.77	5.30
8.0	67.4	5.97	0.84	5.65
8.5	70.6	6.36	0.93	6.00
9.0	73.9	6.89	1.04	6.47
9.5	77.0	7.27	1.21	6.80
10.0	79.9	7.61	1.39	7.07
10.5	82.8	8.26	1.65	7.65
11.0	86.0	8.99	1.95	8.26
11.5	89.4	9.49	2.28	8.56
12.0	92.9	10.03	2.59	8.74
12.2	94.4	10.30	2.70	8.85
12.4	95.9	10.61	2.78	8.84
12.5	96.6	10.77	2.79	8.81
12.6	97.3	10.91	2.80	8.77
12.7	98.0	11.04	2.80	8.72
12.8	98.8	11.15	2.78	8.51
12.9	99.4	11.24	2.75	
12.97	100.0	11.30	2.71	
	Wt.% anhydride			
13.0	2.4	11.32		
13.2	20.0	11.74		
13.4	37.5	12.21		
13.6	53.4	12.50		
13.8	68.9	12.70		
14.0	83.7	12.62		
14.2	98.0	12.18		
14.25	99.5	11.84		

*Normality is used in preference to molarity in order to provide a continuous measure of acid concentration from water to 100% anhydride, through 100% acid.

describe the protonation of diarylalkenes in sulfuric acid (20). The $H_{R'}$ acidity function for aqueous trifluoroacetic acid was calculated by subtracting the logarithm of the activity of water (21) (converted to molarity units) from the measured H_R values. Values are given in Table 2. It may be seen that the $H_{R'}$ function also attains a minimum value before 100% trifluoroacetic acid is reached, at about the same concentration as that for H_0. Thus trifluoroacetic acid – water mixtures attain a maximum protonating power at about 96% acid; the continuing decrease in H_R beyond this point may be attributed to the strongly dehydrating nature of the medium.

(d) Checks on the H_R Acidity Function

It has been shown that the ionizations of 9-aryl-9-fluorenols accurately follow the H_R acidity function in sulfuric acid (22). It was therefore decided to measure the ionization of a suitable 9-aryl-9-fluorenol as a stringent test of the general applicability of the H_R function.

Optical densities of solutions of 9-(*m*-methoxyphenyl)-9-fluorenol ($pK_{R^+} = -11.11$ (22)) were measured over a range of trifluoroacetic acid – water and trifluoroacetic acid – anhydride compositions. The optical density rose with increasing acid concentration to 100% acid, and continued to rise as the anhydride content was increased, to 32% anhydride. Beyond this maximum a slow decrease in optical density to 40% anhydride occurred, followed by a more rapid decrease. Since the optical density in 32% anhydride exceeded that in sulfuric acid, this was taken as the fully ionized value, and ionization ratios calculated thereon. Results are given in Table 3. (Slow ionizations were observed for the fluorenol, as for the triarylcarbinols, in solutions containing anhydride, and the maximum optical density attained was used. Since the fluorenol was found to decompose slowly in pure trifluoroacetic acid, a stock solution was made up in methanol, and acid concentrations corrected for this. Decomposition was fast in solutions containing more than 90% anhydride, and values in this region are approximate.)

The relative constancy of the calculated $pK_{R^+}(H_R + \log(\text{ionization ratio}))$ value up to, and just above, 100% acid, suggests that the H_R values have considerable validity in this region. In solutions containing a larger proportion of anhydride, however, pK_{R^+} values vary markedly, suggesting that the values in this region are a function of the particular indicator used in their evaluation.

As a further check on the generality of the H_R function, the ionization of 4,4′-diethoxydiphenylcarbinol was measured. A plot of log (ionization

Can. J. Chem. Downloaded from www.nrcresearchpress.com by 210.87.254.6 on 09/05/12
For personal use only.

TABLE 3. The ionization of 9-(*m*-methoxyphenyl)-9-fluorenol

Acid normality*	Wt.% acid	$-H_R$	log I	pK_{R^+}
11.74	91.17	9.86	−0.949	−10.81
11.88	92.13	9.96	−0.743	−10.70
11.97	92.80	10.01	−0.542	−10.55
12.10	93.73	10.18	−0.358	−10.54
12.21	94.50	10.35	−0.208	−10.56
12.35	95.55	10.56	−0.009	−10.57
12.51	96.66	10.79	0.215	−10.57
12.67	97.82	11.00	0.441	−10.56
12.69	97.98	11.03	0.371	−10.66
12.80	98.73	11.15	0.599	−10.55
12.94	99.70	11.28	0.959	−10.17
12.94	99.70	11.28	1.107	−10.32
	Wt.% anhydride			
12.98	8.97	11.31	1.091	−10.22
12.99	9.58	11.32	0.981	−10.34
13.64	55.52	12.58	0.842	−11.74
13.71	64.87	12.65	0.706	−11.94
13.89	76.87	12.70	0.446	−12.25
13.99	81.59	12.64	0.312	−12.33
14.22	100.0	12.10	−0.469	−12.57

*See footnote to Table 2.

ratio) *vs.* H_R was linear (correlation coefficient 0.998) with a slope of 0.84 (H_R (half-ionization) = −5.98). This compares with a slope of 0.83 found for the ionization of diphenylcarbinol versus H_R in sulfuric acid (22).

(e) Relationships between the Acidity Functions

It has been shown that in strong acids different acidity functions are frequently linearly related (23). A plot of H_R versus H_0 in trifluoroacetic acid below $H_0 = 0$ shows such linearity, but in two distinct parts. Up to approximately 70% acid the plot is linear with a slope of 7.4; at 70% the plot shows sharp curvature, and becomes linear with a slope of 2.0 up to 93% acid, where the plot curves as H_0 nears a minimum value. This behaviour is unexpected since the water activity begins to decrease sharply in the region of 80% acid, and H_R might be expected to decrease even more rapidly, rather than less rapidly, when compared with H_0 in this region. Similar, though less marked, behaviour occurs in formic acid, in which a plot of H_R versus H_0 (values of ref. 24) shows a slope of 3.4 below 60% acid and curves sharply down to 2.1 between 60 and 96% acid.

Visible Spectroscopy

The green species found in solutions of trifluoroacetic acid has absorption maxima at 283 (ε 3600), 456 (ε 512) and 630 (ε 100) nm. These values are very near those found in perchloric and sulfuric acids (7, 8, 9). It has been suggested (10) that this spectrum, which is similar to the spectra of ions of the type $ROCrO_3^-$ (25) and CrO_3F^- (26), indicates that the species in sulfuric acid solution is $O_3Mn{\cdot}OSO_3H$. Royer (9) has argued that if this were the case, then the low energy absorption should be an allowed transition, and show greater intensity, and has shown that the spectrum can be reasonably explained in terms of the molecular orbitals of MnO_3^+.

The equilibria that govern the formation of permanganyl cation, MnO_3^+, and its trifluoroacetate complex or ester, $MnO_3{\cdot}O_2CCF_3$, can be shown as follows

[1] $$MnO_4^- + 2\,CF_3CO_2H \rightarrow MnO_3^+ + H_2O + 2\,CF_3CO_2^-$$

[2] $$MnO_4^- + 2\,CF_3CO_2H \rightarrow MnO_3{\cdot}O_2CCF_3 + H_2O + CF_3CO_2^-$$

Neither of these reactions correspond to any of the conventional acidity functions, although what might be called the protonation-dehydration aspects of each reaction might lead one to expect a much closer correlation to H_R than to H_0 or H_-, particularly for production of MnO_3^+. The conversion of permanganate ion to the green species (referred to herein as 'ionization') was measured by following the change in optical density at 546 nm (λ_{max} for permanganate ion) as the acidity was changed, and values of the logarithm of the ratio [green species]/[MnO_4^-] calculated (Table 4). (It should be noted that literature values for the pK_a of permanganic acid (8, 11) are based on observations of this equilibrium, and are therefore in error.)

Plots of log I, where I = [green species]/[MnO_4^-], versus H_0 are linear over part of the measurable range, but curve upwards at higher acidities as the extent of ionization increases, despite the protonating-power of the medium (as measured by H_0) reaching a maximum. Half-ionization is reached at $H_0 = -2.3$. Plots of log I *vs.* H_R, on the other hand, are linear over the entire measurable range (Fig. 1). The best straight line, fitted by the method of least squares, gives a correlation coefficient of 0.997, with a slope of −0.76 and H_R (half-ionization) value of

Can. J. Chem. Downloaded from www.nrcresearchpress.com by 210.87.254.6 on 09/05/12
For personal use only.

TABLE 4. The ionization of permanganate ion

Acid normality*	Wt.% acid	log I†
10.16	80.7	−1.198
10.30	81.6	−0.993
10.59	83.4	−0.863
10.81	84.8	−0.679
11.00	86.0	−0.536
11.29	88.0	−0.329
11.42	88.9	−0.148
11.68	90.7	0.093
11.95	92.6	0.319
12.08	93.5	0.517
12.28	95.0	0.800
12.47	96.4	0.970
12.61	97.4	1.114

*See footnote to Table 2.
†I = [green species]/[MnO_4^-]. It is assumed that [green species] = [MnO_4^-]stoichiometric − [MnO_4^-]experimental.

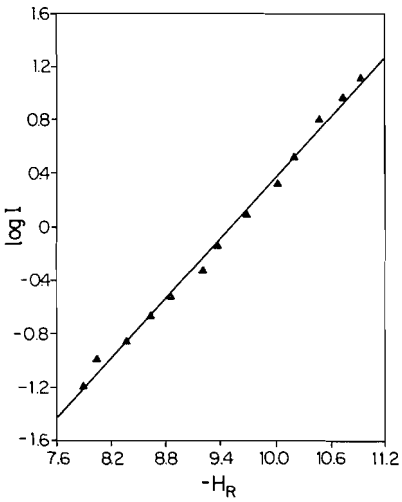

FIG. 1. Plot of log I ([green species]/[MnO_4^-]) versus H_R.

−9.51. Half-ionization in sulfuric acid occurs at approximately 60% acid (11), corresponding to $H_0 = -4.4$ and $H_R = -9.5$ (although slopes of log I versus H_0 and H_R seem to be lower in sulfuric acid). The correspondence of the H_R (half-ionization) values further suggests that the equilibrium is closely related to the protonation-dehydration equilibrium used to define H_R.

Another example of a protonation-dehydration equilibrium is the generation of nitronium ion from nitric acid in strong acids, and this also is believed to be governed by the H_R acidity function, or, more exactly, the function (H_R + log (activity of water)), since nitric acid exists as a monohydrate in these solutions (27). Rates of aromatic nitration correlate with this function (28), just as rates of oxidation in solutions of potassium permanganate in trifluoroacetic acid correlate well with the H_R acidity function (5).

Cryoscopy

Trifluoroacetic acid would seem to be a good medium in which to carry out cryoscopic measurements. It melts at −15.25 °C and has the advantage of being monoprotic, reducing the number of particulation schemes possible. Unfortunately, it has a low dielectric constant ($\epsilon = 8.22$ (29)) which causes extensive ion-pairing, and, as will be seen, this effect prevents its being used to determine unequivocally the number of solute particles present in the green solution formed when potassium permanganate is dissolved.

A non-electrolyte, benzene, was examined at several concentrations, and a plot of ΔT, the freezing-point depression, *vs.* molality was found to be linear and pass through the origin. The freezing-point depression produced by another solute, ΔT_{solute}, at a given molality, may be divided by the depression caused by the same concentration of benzene, $\Delta T_{benzene}$, to give the number of particles, n, produced by the solute in solution, *i.e.* $n = \Delta T_{solute}/\Delta T_{benzene}$. This approach was verified using toluene ($n = 1$) and sodium acetate ($n = 3$) as solutes, although the latter showed positive deviations at very low concentrations, indicating that benzene was not an ideal model for electrolytes.

This method was used to evaluate the number of particles produced by several electrolytes (such as potassium trifluoroacetate, potassium bicarbonate, triphenylcarbinol, and sodium nitrate) in solution. Nearly all electrolytes showed evidence of extensive ion-pair formation at high concentrations, although most tended to approach the theoretical value of 'n' at low concentrations. Values of 'n' for potassium permanganate varied from 3.0 at high concentration (0.05 molal) to 5.2 at low concentration (0.004 molal). Interestingly water appeared to behave like an electrolyte at low concentration ($n = 1.8$ at 0.012 molal), although conductivity studies have shown that it is not an electrolyte (3, 30). Similar anomalous behaviour has been observed for water in nitric acid (31).

Since the comparisons with benzene were in-

Can. J. Chem. Downloaded from www.nrcresearchpress.com by 210.87.254.6 on 09/05/12
For personal use only.

conclusive, an alternative approach was used. Instead of using benzene, for which $n = 1$, as a standard to provide a ΔT *vs.* molality plot, potassium trifluoroacetate, for which 'n' theoretically equals 2, was used instead, the plot for this compound being a smooth curve. The number of particles produced by a given solute then equals twice the depression of freezing-point produced by the solute divided by the depression produced by the same concentration of potassium trifluoroacetate, and the effects of ion-pairing are nullified, but only if this does not vary from cation to cation. Unfortunately, the values obtained for potassium permanganate by this treatment were not constant but varied from 6.1 at 0.05 molal to 5.7 at 0.004 molal, passing through a minimum value of 5.1 at 0.015 molal. Using data on potassium bicarbonate or sodium nitrate instead of potassium trifluoroacetate gave similarly inconclusive results. Thus the degree of ion-pairing must vary with the identity of the cation, and this effect, together with the anomalous behaviour of water, prevents any conclusive data being obtained on the ionization of permanganate ion by cryoscopy in trifluoroacetic acid. Nevertheless, the high values of 'n' obtained for potassium permanganate are consistent with the existence of either permanganyl cation or its ester or complex being present in solution.

Conclusions

In concentrated trifluoroacetic acid the spectrum of potassium permanganate is identical to that in sulfuric acid. Royer has provided cryoscopic evidence that at low concentrations manganese(VII) exists as the permanganyl ion in sulfuric acid (9). Further evidence is afforded by the identification of π-complexes between MnO_3^+ and various aromatics in sulfuric acid (32). The equilibrium between permanganate ion and the green species correlates well with the H_R acidity function, suggesting that the equilibrium is a protonation-dehydration process. It is possible, however, that the permanganyl cation exists in equilibrium with the complex or ester $MnO_3 \cdot O_2CCF_3$. Evidence for the ester being present in solutions containing high concentrations of permanganate in acid is provided by the distillation of a green impurity with trifluoroacetic acid when the acid is distilled from solutions containing high concentrations of potassium permanganate. The halides of the permanganyl cation are also green, *e.g.* MnO_3F (33) and MnO_3Cl (34).

Even if the ester or complex exists in equilibrium with permanganyl ion at kinetic concentrations, the ion is almost certainly the more reactive electrophile and oxidant, and will be largely responsible for oxidative processes in these solutions.

Experimental

Reagents

All inorganic salts were of AnalaR grade except potassium trifluoroacetate and potassium bicarbonate. Potassium trifluoroacetate was prepared by mixing equimolar quantities of AnalaR potassium hydroxide and distilled trifluoroacetic acid; the solution was evaporated to dryness and the white salt crystallized twice from methanol. Reagent grade potassium bicarbonate was crystallized twice from water; titration against standard acid showed the sample to be at least 99.7% pure.

Organic compounds were recrystallized or distilled prior to use. Trifluoroacetic acid was distilled from a small amount (0.1 g per k) of potassium permanganate using a Vigreaûx column, bp 71.0–71.5 °C. (Distillation from large quantities of permanganate produces a distillate containing a green-coloured impurity.)

Cryoscopy

The experimental technique used was essentially the same as that used by Royer (9) in his investigation of the mode of ionization of potassium permanganate in sulfuric acid. In a typical experiment a 20.0 ml sample of pure trifluoroacetic acid was super-cooled to 10 °C below its freezing point by means of a Dry Ice – acetone bath. Crystallization was induced by touching the wall of the vessel with a small piece of Dry Ice. The solution was completely frozen to degas it and then remelted. Next it was cooled to 1 °C below the freezing-point and crystallization was again induced with a piece of Dry Ice. The resulting warming curve was measured using a Beckmann thermometer and recorded until the temperature reached the equilibrium plateau indicative of the liquid–solid equilibrium temperature. When the solution was supercooled by no more than 2 °C this plateau extended over a time interval of 2–4 min, allowing precise determination of the freezing-point. Once the freezing-point had been verified for the pure compound the sample of interest was added and completely dissolved. Then using the same supercooling technique the new freezing-point was determined and verified at least twice. No correction was made for supercooling, but since the temperature obtained after crystallization was initiated changed very little over a period of several minutes, extrapolation of the plateau to the cooling-curve (35) would make little difference. The freezing-points so obtained are therefore not of the highest precision, and probably exaggerate slightly the freezing-point depression and 'n', the number of particles. Sometimes when larger amounts of compound were added the solutions tended to supercool too much, giving no warming plateau. Whenever this occurred the acetone bath temperature was slowly lowered until crystallization

Can. J. Chem. Downloaded from www.nrcresearchpress.com by 210.87.254.6 on 09/05/12
For personal use only.

could be maintained. In this manner freezing-points could be determined to ±0.01 °C. For pure trifluoroacetic acid the reproducibility was ±0.005 °C. Fresh acid was used for each sample investigated and all determinations were performed under a nitrogen atmosphere.

Determination of Acidity Functions

Stock solutions of the indicators were made up in neat trifluoroacetic acid of such concentration that when conveniently measurable small quantities were made up to 5.0 or 10.0 ml the fully ionized (or in the case of 2-chloro-6-nitroaniline, the unionized) absorbance value would be near 0.8. Stock solutions remained stable for several weeks. Absorbances of a series of solutions were measured on a Cary 16 spectrophotometer at 25 °C, the uncertainty of the absorbance measurement being ±0.1%. The acidity of each solution was then determined by titration with 2.00 *N* sodium hydroxide. It was found that titration of solutions containing trifluoroacetic acid and anhydride failed to give consistent results, and so these solutions were made up in volumetric flasks by weight, and theoretical normalities calculated. (N = (g CF_3CO_2H per litre/114.022) + (2 × (g $(CF_3CO)_2O$ per litre/210.03))).

Indicators 1 and 2 (Table 1) were used to tie the H_R function into the standard pH function. Both were appreciably ionized in solutions which had measurable pH values. A Radiometer model no. 26 pH meter was used and standardized at pH = 2.00.

To test the validity of Beer's Law in 100% trifluoroacetic acid solutions containing various concentrations of 9-(*m*-methoxyphenyl)-9-fluorenol and 2-chloro-6-nitroaniline were examined. It was found that neither indicator obeyed Beer's Law exactly; in both cases increasing concentration of indicator causes a decrease in the percentage ionization, as might be expected in a medium of low dielectric constant. However, the departure from Beer's Law is fairly small, and since ionization measurements were carried out at constant indicator concentrations the effect on acidity function values will be small.

Acknowledgments

The financial support of the National Research Council of Canada is gratefully acknowledged.

1. (*a*) H. C. Brown and R. A. Wirkkala. J. Am. Chem. Soc. **88**, 1447 (1966); (*b*) S. L. Cotter, L. J. Andrews, and R. M. Keefer. J. Am. Chem. Soc. **84**, 793 (1962); (*c*) C. Eaborn, P. M. Jackson, and R. Taylor. J. Chem. Soc. B, 613 (1966); (*d*) L. M. Stock and M. R. Wasielewski. J. Org. Chem. **36**, 1002 (1971); (*e*) U. A. Spitzer and R. Stewart. J. Org. Chem. **39**, 3936 (1974).
2. J. E. Norlander and W. G. Deadman. J. Am. Chem. Soc. **90**, 1590 (1968).
3. M. G. Harriss and J. B. Milne. Can. J. Chem. **49**, 1888 (1971); **50**, 3789 (1972).
4. D. G. Lee and D. T. Johnson. Can. J. Chem. **43**, 1952 (1965).
5. U. A. Spitzer and R. Stewart. To be published.
6. J. E. B. Randles and J. M. Tedder. J. Chem. Soc. 1218 (1955).
7. M. H. Aschoff. J. Prakt. Chem. **81**, 29 (1860).
8. N Bailey, A. Carrington, K. A. K. Lott, and M. C. R. Symons. J. Chem. Soc. 290 (1960).
9. D. J. Royer. J. Inorg. Nucl. Chem. **17**, 159 (1961).
10. H. C. Mishra and M. C. R. Symons. J. Chem. Soc. 4411 (1962).
11. R. Stewart and M. M. Mocek. Can. J. Chem. **41**, 1160 (1963).
12. N. A. Frigerio. J. Am. Chem. Soc. **91**, 6200 (1969).
13. N. C. Deno, J. J. Jaruzelski, and A. Schriesheim. J. Am. Chem. Soc. **77**, 3044 (1955).
14. C. H. Rochester. Acidity functions. Academic Press, London. 1970.
15. P. K. Glascoe and F. A. Long. J. Phys. Chem. **64**, 188 (1960).
16. E. DeFabrizio. Ric. Sci. **36**, 1321 (1966); cited by C. H. Rochester, ref. 13, pp 73–74.
17. D. P. N. Satchell. J. Chem. Soc. 3904 (1958).
18. C. Eaborn, P. M. Jackson, and R. Taylor. J. Chem. Soc. B, 613 (1966).
19. J. C. James and J. G. Knox. Trans. Faraday Soc. **46**, 254 (1950).
20. N. C. Deno, P. T. Groves, and G. Saines. J. Am. Chem. Soc. **81**, 5790 (1959).
21. N. G. Zarakhani and N. P. Vorob'eva. Zh. Fiz. Khim. **46**, 2426 (1972).
22. (*a*) T. W. Toone, E. Lee-Ruff, and A. C. Hopkinson. Can. J. Chem. **53**, 1635 (1975); (*b*) T. W. Toone, E. Lee-Ruff, P. G. Khazanie, and A. C. Hopkinson. J. Chem. Soc. Perkin Trans. 2, 607 (1975).
23. K. Yates and R. A. McClelland. J. Am. Chem. Soc. **89**, 2686 (1967).
24. R. Stewart and T. Matthews. Can. J. Chem. **38**, 602 (1960).
25. U. Kläning and M. C. R. Symons. J. Chem. Soc. 3204 (1962).
26. L. Helmholtz, H. Brennen, and M. Wolfsberg. J. Chem. Phys. **23**, 853 (1955).
27. R. B. Moodie, K. Schofield, and M. J. Williamson. Tetrahedron, **20**, (1964). Suppl. **1**, 89.
28. (*a*) R. B. Moodie, J. R. Penton, and K. Schofield. J. Chem. Soc. B, 578 (1969); (*b*) P. J. Brignell, A. R. Katritzky, and H. O. Tarhan. J. Chem. Soc. B, 1477 (1968).
29. G. P. Nilles and R. D. Schuetz. J. Chem. Educ. **50**, 267 (1973).
30. J. H. Simons and K. E. Lorentzen. J. Am. Chem. Soc. **74**, 4746 (1952).
31. R. J. Gillespie, E. D. Hughes, and C. K. Ingold. J. Chem. Soc. 2552 (1950).
32. D. Dimitrov, A. Stefanova, F. Fratev, S. Voinova, and M. Korova. God. Vissh. Khimikotekhnol Inst. Sofia, **14**, 209 (1971).
33. A. Englebrecht and A. V. Grosse. J. Am. Chem. Soc. **76**, 2042 (1954).
34. O. Michel and A. Doiwa. Naturwissenschaften, **53**, 129 (1966).
35. B. J. Mair, A. R. Glasgow, and F. D. Rossini. J. Res. Nat. Bur. Stand. **26**, 591 (1941).

Thermolysis of the sodium salt of tricarbonyl(acetophenone)chromium *p*-tosylhydrazone

MUHAMMAD ASHRAF[1]
Institute of Chemistry, University of the Punjab, Lahore, Pakistan

Received May 6, 1975

MUHAMMAD ASHRAF. Can. J. Chem. **54**, 448 (1976).

Thermolysis of the sodium salt of tricarbonyl(acetophenone)chromium *p*-tosylhydrazone was carried out at 116–118 °C in pyridine, both in the presence and absence of 1,1-diphenylethylene and cyclohexene. The products, separated by column chromatography, were shown by analyses to be acetophenone azine, symmetrical and unsymmetrical tricarbonyl(acetophenone azine)chromium complexes, and a diastereomeric mixture of hexacarbonyl(2,3-diphenylbutane)dichromium and 1-tricarbonyl(phenyl)chromium-1-methyl-2,2-diphenylcyclopropane. The formation of these compounds has been rationalised by the combination of a diazo intermediate and tricarbonyl(methylphenylcarbene)chromium. Their stereochemistry has been discussed in the light of various spectroscopic results.

MUHAMMAD ASHRAF. Can. J. Chem. **54**, 448 (1976).

On a effectué la thermolyse du sel de sodium de la *p*-tosylhydrazone du tricarbonyle acétophénone chrome; cette réaction a été effectuée à 116–118 °C dans la pyridine en présence et en l'absence de diphényl-1,1 éthylène et de cyclohexène. On a montré que les produits, séparés par chromatographie sur colonne, sont l'azine de l'acétophénone, les complexes symétriques et non-symétriques du tricarbonyle(acétophénone azine)chrome et un mélange diastéréoisomère d'hexacarbonyl(diphényl-2,3 butane)dichrome et du tricarbonyl(phényl)chrome-1 méthyl-1 diphényl-2,2 cyclopropane. On a rationnalisé la formation de ces composés par une combinaison des intermédiaires diazo avec le tricarbonyl(méthylphénylcarbène)chrome. On a discuté de leur stéréochimie à la lumière des divers résultats spectroscopiques.

[Traduit par le journal]

Introduction

Pyrolysis (2) and photolysis (3) of hydrazone salts are well known methods for the generation of carbenes. But it appears that a carbene bearing a tricarbonylchromium moiety in the aromatic portion has not been studied so far. It was, therefore, decided to investigate the pyrolytic decomposition of the sodium salt of tricarbonyl(acetophenone)chromium *p*-tosylhydrazone, **1**, in order to generate tricarbonyl(methylphenylcarbene)chromium, to study the effect of the tricarbonylchromium group on the spin state of this carbene and the stereochemistry of various products obtained. This was accomplished by the thermal decomposition of **1** in pyridine at 116–118 °C both in the presence and absence of external unsaturated system, *e.g.*, 1,1-diphenylethylene (**2**) and cyclohexene.

Results and Discussion

Thermolysis in the Absence of an Olefin

Chromatography afforded an orange-yellow compound (**5**) which exhibited two carbonyl active stretching modes at *ca.* 1875 and 1990 cm^{-1} along with $\nu_{C=N}$ at 1608 cm^{-1} (*cf.* ref. 7). The mass spectrum showed peaks at *m/e* 372 (molecular ion), 344, 316, and 288 for the stepwise loss of CO molecules followed by peaks associated with the fragmentation of acetophenone azine (8, 9). These observations indicated this to be tricarbonyl(acetophenone azine)chromium. Its nmr spectrum showed two methyl signals at τ 7.82 and 7.68 (in CCl_4). This azine complex was decomposed to the free ligand only after bubbling air through its ethereal solution for several days. The solvent was removed and the nmr spectrum again showed two separate signals for methyl groups at τ 7.44 and 7.56 (in $CDCl_3$) suggesting that this azine was the unsymmetrical isomer **9** (*cf.* ref. 10). This eliminated the possibility of the other two symmetrical isomers **10** and **11**. If one assumes that the azine stereochemistry did not change during decomposition the tricarbonylchromium complex has either structure **5***a* or **5***b*. However, it is not possible to distinguish between these isomers.

Chromatography also gave a light-yellow com-

[1]Present address: Department of Chemistry, Makerere University, P.O. Box 7062, Kampala, Uganda.

Can. J. Chem. Downloaded from www.nrcresearchpress.com by 210.87.254.5 on 09/05/12
For personal use only.

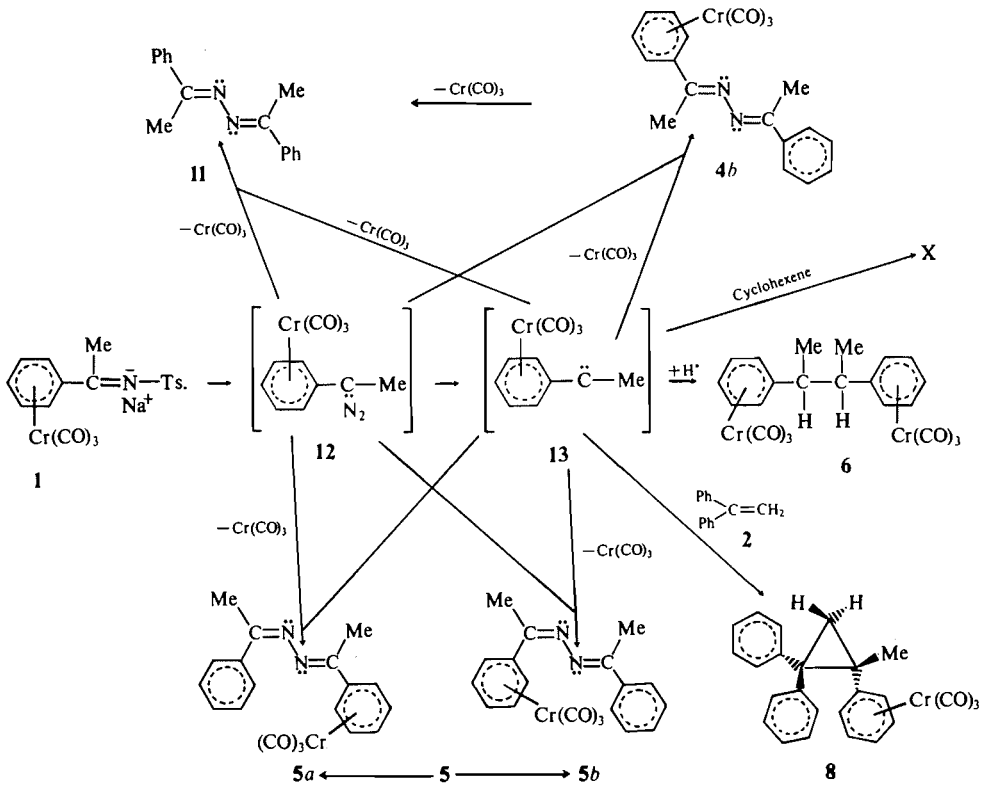

SCHEME 1. Pyrolytic decomposition of the sodium salt of tricarbonyl(acetophenone)chromium *p*-tosylhydrazone.

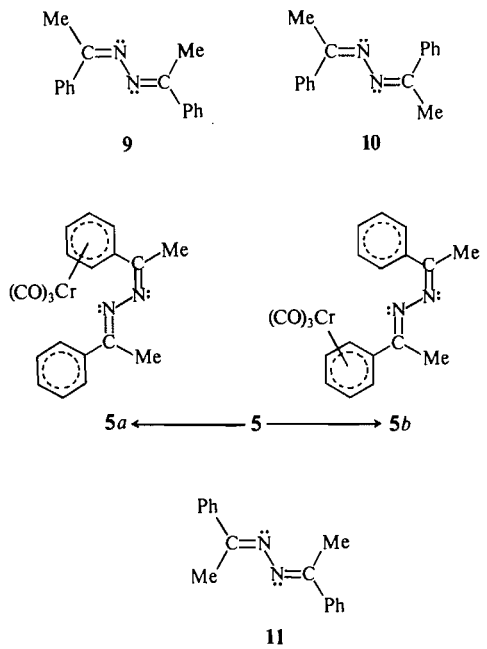

pound, **4**, which had a similar but not identical infrared spectrum to the tricarbonyl(acetophenone azine)chromium, **5**, suggesting that it was a stereoisomer of **5**. The material correctly analysed for C, H, and N. The mass spectrum did not show any molecular ion peak at *m/e* 372 but fragment ions were obtained which agreed with a published mass spectrum of an acetophenone azine (8, 9) together with peaks associated with *m/e* 344, 288 and chromium. The nmr spectrum of this azine complex, **4**, showed only one signal at τ 7.68 for the methyl groups. In the stereoisomer **5** the tricarbonylchromium group had little effect on the value of the methyl groups. Thus, the two methyl groups absorbed at τ 7.56, 7.44 ($\Delta\tau$ 0.12) in the free ligand and at τ 7.82, 7.68 ($\Delta\tau$ 0.14) in the tricarbonylchromium complex. If a similar assumption is made for **4** then this chromium complex is considered to be derived from one of the symmetrical azine isomers **10** or **11** and thus must have the structure **4***a* or **4***b*.

Can. J. Chem. Downloaded from www.nrcresearchpress.com by 210.87.254.5 on 09/05/12
For personal use only.

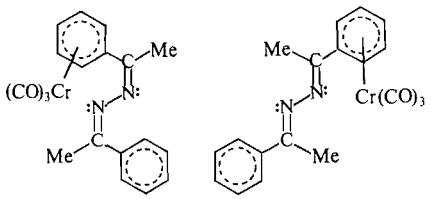

4*a* ⟵ 4 ⟶ 4*b*

A very small amount of a yellowish white compound, **3**, mp 119–121 °C, was obtained whose infrared spectrum ($\nu_{C=N}$ 1610 cm^{-1}) strongly resembled that of the acetophenone azine complex **4** but did not show any metal carbonyl absorptions. This suggested that this azine might have been obtained by losing $Cr(CO)_3$ from **4** during the reaction or during work-up. The mass spectrum indicated a molecular ion peak at *m/e* 236 corresponding to acetophenone azine and the fragmentation pattern was again in agreement with a published spectrum (8, 9). These results indicated that the acetophenone azine **3** most probably corresponded to either **10** or **11**. This suggestion is supported by the fact that the acetophenone azine, mp 123–124 °C, has been reported by French workers (11) to have an *anti–anti* configuration (*i.e.* either **10** or **11**) as evidenced by one methyl signal in their nmr spectrum.

Elution with light petroleum – ether (5:1) (*i.e.* petroleum ether (30–60 °C) – diethyl ether, throughout) gave **6** whose infrared spectrum and elemental analysis were consistent with a mixture of two isomers **6***a* and **6***b* of hexacarbonyl(2,3-diphenylbutane)dichromium. The mass spectrum showed a molecular ion peak at *m/e* 482 and gave the expected fragmentations. Each diastereomer showed separate signals of nearly equal intensity at τ 8.80 and 8.73 (for their methyl groups) and well spaced multiplets at τ 8.50 and 7.32 due to the benzylic protons of each isomer. This suggested that it was a mixture

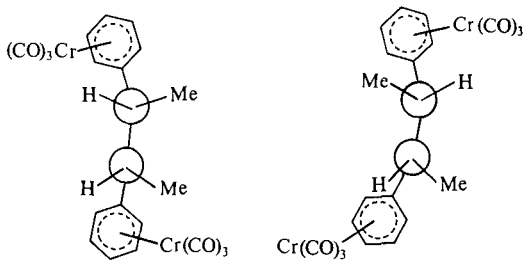

6*a* ⟵ 6 ⟶ 6*b*

containing almost equal proportions of the *meso* **6***a* and the racemic **6***b* isomers.

Pyrolysis in the Presence of 1,1-Diphenylethylene

The sodium salt **1** was pyrolysed in pyridine in the presence of 1,1-diphenylethylene to detect any product formed from interaction of an intermediate carbene with the olefin **2**. In this connection light petroleum – ether (19:1) eluted the tricarbonylchromium complex **8**. Accurate mass analysis showed its molecular weight to be 420.9629 (calcd. 420.4324). The ir spectrum clearly showed two carbonyl absorptions at 1965 and 1875 cm^{-1}. Its nmr spectrum was consistent with 1-tricarbonyl(phenyl)chromium-1-methyl-2,2-diphenylcyclopropane, **8**, formed by the interaction of tricarbonyl(methylphenylcarbene)chromium and 1,1-diphenylethylene, **2**. The hydrogen atoms in the cyclopropane ring appeared as unresolved multiplets centred on τ 8.46 and 7.70. This observation appears to be in contrast with ring protons of unsubstituted cyclopropane which absorb at higher τ values. However, the methylene protons in this compound may be nonequivalent in agreement with various cyclic systems (13).

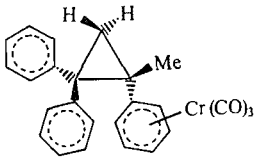

8

Pyrolysis in the Presence of Cyclohexene

When the sodium salt **1** was pyrolysed in the presence of cyclohexene, **3**, **4**, **5**, and **6** were obtained but no addition product with this olefin could be detected. A repeat experiment on an identical scale also failed to afford any addition compound with cyclohexene.

Formation of Products

Formation of tricarbonyl(acetophenone azine)-chromium and other products (Scheme 1) can easily be explained by the combination of the diazo compound **12** and tricarbonyl(methylphenylcarbene)chromium, **13**. The formation of azines, as the major products, is in agreement with a reported work on diaryldiazomethanes (14). A small amount of pentacarbonyl(pyridine)-chromium obtained might be the result of reversible removal of the chromiumcarbonyl groups by pyridine from the reaction mixture.

Can. J. Chem. Downloaded from www.nrcresearchpress.com by 210.87.254.5 on 09/05/12
For personal use only.

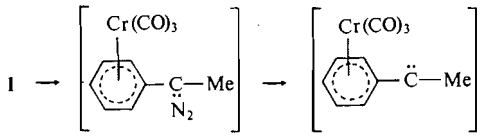

12 13

The carbene **13** may be considered to rearrange to the corresponding styrene complex in analogy with various alkyl- and dialkylcarbenes. But intramolecular stabilization leading to the expected olefin complex by hydride shift of primary hydrogen appears to be unfavourable as compared with secondary and tertiary hydrogens (15, 16). Moreover, dimerization of carbenes is a statistically unlikely process, especially in solution, since they are much shorter lived species, where their concentration will always be low (17). Consequently, the formation of **6** is rationalised by the abstraction of a hydrogen atom by the carbene **13** from the solvent to give an intermediate radical. The radical appears to be sufficiently stable to give the dimer in conformity with most of the diarylcarbenes (18). It may therefore be inferred that the reactions of carbene **13** are similar to those of arylcarbenes. A similar intermediate has also been proposed to explain the formation of benzoylferrocene azine in the thermolysis of benzoylferrocene tosylhydrazone sodium salt (19).

Spin State of Carbene

The most incisive information concerning the chemical characteristics of singlet and triplet carbenes comes from the study of addition reactions involving the carbon–carbon double bond. In this connection, relative reactivities of various olefinic substrates towards carbenes serve as useful criteria regarding their singlet and triplet states (20). Thus, the formation of **6** in the presence of cyclohexene indicates that the carbene involved is a triplet. The fact that this carbene adds to 1,1-diphenylethylene also suggests its triplet nature, since this particular olefin is known to be an effective triplet carbene trap (21). If a singlet carbene like dichloromethylene were present, it should be expected to add equally well to cyclohexene (22), which it does not.

The role of the $Cr(CO)_3$ group on the singlet/triplet state of the carbene (**13**) must be viewed through very complex evidence which suggests that it is strongly electron withdrawing, perhaps comparable to the *p*-nitro group (23, 24). Moreover, coordination of the phenyl ring with the $Cr(CO)_3$ group is known to considerably influence the effective positive charge on the aromatic ring carbon σ-orbitals, thereby increasing their electronegativity (25). Therefore, $Cr(CO)_3$ may be regarded as a strongly electron-attracting moiety, irrespective of the mode of its electron withdrawal. Thus, it is likely to destabilize the carbene (**13**) which appears to be stabilized by the donor solvent. Hence, in analogy with aryl/diaryl carbenes (1), it is reasonable to suggest that tricarbonyl(methylphenylcarbene)-chromium has apparently reacted in its triplet state. Nevertheless, in view of the peculiar nature of the $Cr(CO)_3$ group, it is difficult to generalize about its effect upon the characteristic reactivity of singlet and triplet carbenes, which warrants additional studies before a comprehensive generalization may be made.

Experimental

General

Melting points were determined on a Kofler microscope hot-stage and are uncorrected. Hexacarbonylchromium (Stem Chemical Inc.) was sublimed on a boiling water bath at 0.3 Torr and crystallised from chloroform. Deactivated alumina was obtained by shaking overnight alumina (2.5 kg) (Spence grade H) with water (100 ml) containing glacial acetic acid (10 ml).

Spectra

Infrared absorption spectra were recorded on a Perkin-Elmer 'Infracord' (137) spectrometer (NaCl optics). Ultraviolet and visible spectra were recorded on a Perkin-Elmer double beam spectrometer (402). Mass spectra were determined with an AE1 MS9, using the heated inlet system and operating at 70 eV. The nmr spectra were recorded for CCl_4, $CDCl_3$, and CD_3COCD_3 solutions (as specified) containing TMS, except where otherwise mentioned, as internal standard using a Varian HA 100 spectrometer.

Acetophenone Tosylhydrazone

The tosylhydrazone of acetophenone was prepared by the method of Caglioti and Magi (4). Acetophenone (2.4 g; 0.02 mol) was added to a solution of *p*-toluenesulphonylhydrazine (4.65 g; 0.025 mol) in methanol (120 ml). The mixture was boiled under reflux for 4 h which on cooling gave acetophenone-*p*-toluenesulphonylhydrazone (3.9 g; 68%), mp 145–147 °C, improved to 148–149 °C upon crystallization from methanol. Anal. found: C 62.7, H 5.6, N 9.9, S 11.2; $C_{15}H_{16}N_2O_2S$ requires: C 62.5, H 5.6, N 9.7, S 11.1.

Tricarbonyl(acetophenone)chromium

Acetophenone (7 ml) and hexacarbonylchromium (2.2 g) were refluxed in diglyme (12 ml) for 1.5 h to give the complex (1.42 g; 55%), mp 83–86 °C (lit. (5) 91–92.5 °C).

Can. J. Chem. Downloaded from www.nrcresearchpress.com by 210.87.254.5 on 09/05/12
For personal use only.

Can. J. Chem. Downloaded from www.nrcresearchpress.com by 210.87.254.5 on 09/09/12
For personal use only.

TABLE 1. Reaction parameters of thermolysis of the sodium salt of tricarbonyl(acetophenone)chromium *p*-tosylhydrazone (**1**) and results of chromatographic separation on deactivated alumina

						Compound eluted with light petroleum – ether							
						1:0			19:1		17:3	5:1	1:1
Sodium salt of **1** (g)	Pyridine (ml)	N_2 flushing time (h)	Olefin added (ml)	Reaction time (h)	Sodium *p*-toluene-sulphinate precipitated (g(%))	Olefin recovered (%)	PCPC (mg)	**3**[c] (mg)	**4**[d] (mg)	**8**[g] (mg)	**5**[e] (mg)	**6**[f] (mg)	**7** unidentified (mg)
2.0	130	0.5	—	1.5	0.696(87)	—	10.5	2.0	9.5	—	85	29	3(mp 180–185 °C dec.)
0.5	70	—	1.3[a]	2.0	0.150(75)	90[a]	—	—	Decomposed		10.5	Small amount	
2.0	225	0.5	3.0[a]	1.0	0.498(62)	83[a]	4.0	—	5	115	65	25	6.0
2.0	100	0.5	10[b]	1.5	0.657(82)	99[b]	12.0	3.5	6.9	—	68	23	2.5
2.0	100	0.5	10[b]	1.5	0.660(82)	98.5[b]	10.0	4.0	7.3	—	75	20	4.0

[a]1,1-Diphenylethylene.
[b]Cyclohexene; PCPC = pentacarbonyl(pyridine)chromium, mp 96–97 °C (lit. (6,12) 95.5–96.5 °C).
[c]Acetophenone azine, mp 119–121 °C (lit. (11) 123–124 °C).
[d]Light-yellow tricarbonyl(acetophenone azine)chromium, mp 121–122 °C.
[e]Orange-yellow tricarbonyl(acetophenone azine)chromium, mp 131–132 °C.
[f]Diastereomers of hexacarbonyl(2,3-diphenylbutane)dichromium, mp 165–170 °C (dec.).
[g]1-Tricarbonyl(phenyl)chromium-1-methyl-2,2-diphenylcyclopropane.

Can. J. Chem. Downloaded from www.nrcresearchpress.com by 210.87.254.5 on 09/05/12
For personal use only.

Tricarbonyl(acetophenone)chromium p-Tosylhydrazone

p-Toluenesulphonylhydrazine (5.58 g; 0.03 mol) and tricarbonyl(acetophenone)chromium (6.91 g; 0.027 mol) were refluxed in methanol (300 ml) for 6 h to give crystalline needles of the complex (8.4 g; 73%), mp 180–181 °C (dec.). Anal. found: C 51.0, H 3.7, N 6.6; $C_{18}H_{16}CrN_2O_5S$ requires: C 50.9, H 3.8, N 6.6; Nuclear magnetic resonance (acetone-d_6) signals, τ 7.86 (singlet, 3H), 7.59 (singlet, 3H), 4.11 (triplet, 3H, J = 7 Hz), 3.95 (doublet, 1H, $J \simeq$ 2 Hz), 3.92 (doublet, 1H, $J \simeq$ 2 Hz), 2.61 (doublet, 2H, J = 8.5 Hz), 2.16 (doublet, 2H, J = 8.5 Hz), and 0.36 (broad singlet, NH).

Sodium Salt of Tricarbonyl(acetophenone)chromium p-Tosylhydrazone (cf. Ref. 2)

A 50% suspension of sodium hydride (0.72 g; 0.015 mol) in dry tetrahydrofuran (100 ml) was rapidly stirred and cooled. The hydrazone (6.36 g; 0.015 mol) was added to this solution over 5 min with vigorous stirring. Precipitation of the sodium salt commenced after 10 min and the mixture was stirred with cooling for a further period of 1 h. Excess of sodium hydride was then decomposed with 2–3 drops of ethanol. The sodium salt (6.0 g; 90%) was obtained by filtration, washed with ether, and dried. The formation of the sodium salt was confirmed by the loss of —NH absorption in the infrared spectrum and disappearance of the —NH signal in the nmr spectrum (recorded in deuterated dimethylsulphoxide).

Thermolysis of the Sodium Salt of Tricarbonyl-(acetophenone)chromium p-Tosylhydrazone in Pyridine in the Absence and Presence of Added Olefin

The sodium salt **1** and the olefin 1,1-diphenylethylene or cyclohexene, where necessary, were dissolved in dry pyridine and flushed with N_2 gas. The nitrogen atmosphere was maintained and the reaction mixture heated at 116–118 °C. The precipitated sodium-*p*-toluenesulphinate was removed and washed with ether. Most of the solvent was removed from the filtrate under reduced pressure. The residue was cooled in an ice bath, acidified, and extracted with ether (8 × 100 ml). The ethereal extract was washed with water (2 × 100 ml), sodium hydroxide (20%; 2 × 100 ml), and water respectively. The neutral ethereal portion was dried ($MgSO_4$) and the solvent removed on a rotary evaporator. The orange yellow viscous residue was chromatographed on deactivated alumina. The results are recorded on Table 1. The spectroscopic data of various compounds is given below.

Compound **3**: the yellowish white acetophenone azine had mp 119–121 °C; ir (KBr disc) ν *ca.* 3400, 2900, 2850 (shoulder), 1610, 1550(w), 1525 (shoulder), 1475(w), 1425, 1350, 1300, 1275, 1170, 1063, 1024, 918, 760, and 690; ms peaks at *m/e* 235(76), 220(100), 208(5),193(8), 179(12), 159(21), 143(6), 133(9), 132(12), 118(26), 104(29), 103(32), 91(9), 77(88), and a metastable peak at M^* 205.95.

Compound **4**: the light-yellow tricarbonyl(acetophenone azine)chromium complex had mp 121–122 °C; ir (KBr disc) ν *ca.* 3400, 2900, 2850 (shoulder), 1975, 1895, 1610, 1550(w), 1525 (shoulder), 1475(w), 1425, 1350, 1300(w), 1275, 1170, 1063, 1024, 918(w), 760, and 690; ms peaks at *m/e* 372(0), 344(2), 288(10), 236(90), 221(100), 208(5), 194(6), 179(12), 159(18), 143(5), 133(10), 132(12), 118(32), 104(10), 103(23), 102(33), 91(13), 77(95), 52(10), and 51(33); nmr signals at τ 7.68 (singlet, 6H), 4.92 (triplet, 3H, J = 7 Hz), 4.80 (doublet. 1H, $J \simeq$ 2 Hz), 4.74 (doublet, 1H, $J \simeq$ 2 Hz), 2.59 (triplet, 3H, $J \simeq$ 3 Hz), 2.05 (doublet, 1H), and 2.12 (doublet, 1H). Anal. found: C 61.2, H 4.3, N 7.6; calcd. for $C_{19}H_{16}CrN_2O_3$: C 61.3, H 4.3, N 7.5.

Compound **5**: the orange-yellow tricarbonyl(acetophenone azine)chromium had mp 131–132 °C; ir (KBr disc) ν *ca.* 1990, 1875, 1608, 875, 820, 760, 740, 690, and 685; the ultraviolet and visible spectrum in methanol showed absorption maxima at λ_{max} 410 (ϵ 3456), 323 (ϵ 12 288), 295 (shoulder, ϵ 14 848), 260 (ϵ 25 805), and 217 nm (ϵ 33 203); ms peaks at *m/e* 372(9), 344(3), 316(4), 288(83), 236(10), 221(12), 206(40), 170(18), 169(13), 155(15), 143(14), 129(42), 118(6), 104(9), 103(8), 93(72), 91(4), 77(30), and 52(100); nmr signals at τ 7.82 (singlet, 3H), 7.68 (singlet, 3H), 4.65 (triplet, 3H, J = 7 Hz), 4.04 (doublet, 1H, J = 2 Hz), 3.97 (doublet, 1H, J = 2 Hz), 2.66 (triplet, 3H), 2.18 (doublet, 1H), and 2.12 (doublet, 1H). Anal found: C 61.1, H 4.3, N 7.7; $C_{19}H_{16}CrN_2O_3$ requires: C 61.3, H 4.3, N 7.5.

Compound **6**: the mixture of diastereomers of hexacarbonyl(2,3-diphenylbutane)dichromium complex (**6**) had mp 165–170 °C (dec.); ir (KBr disc) ν *ca.* 3025, 2850, 1975, 1900, 1600, 830, 815, 786, and 700; nmr signals at τ 8.80 (singlet, CH_3), 8.73 (singlet, CH_3), 8.50 (multiplet, 2H), 7.32 (multiplet, 2H), 5.03 (triplet, 6H, J = 7 Hz), and 4.73 (doublet, 4H, J = 2.5 Hz); ms peaks at *m/e* 482(16), 398(10), 346(2.5), 370(10), 314(25), 262(70), 210(1), 158(14), 156(13), 129(14), 105(14), 104(2), 91(3), 77(2), and 52(53). Anal. found: C 55.2, H 3.6; $C_{22}H_{18}Cr_2O_6$ requires: C 54.8, H 3.3.

Compound **8**: the viscous oil **8** which failed to crystallize had ir (KBr film) ν *ca.* 1965, 1875, 1660, 1600, 800, 755, 690, and 655; accurate mass analysis showed mol. wt. 420.9629 (calcd. 420.4324). Anal. found: C 71.9, H 5.2; $C_{25}H_{20}CrO_3$ requires: C 71.4, H 4.8. Nuclear magnetic resonance signals at τ 8.75 (multiplet, 3H), 8.46 (multiplet, 1H), 7.7 (multiplet, 1H), 4.84 (multiplet, 5H), and 2.8 (multiplet, aromatic protons) which agrees with 1-tricarbonyl(phenyl)chromium-1-methyl-2,2-diphenylcyclopropane.

Acknowledgement

The author is grateful to Professor W. R. Jackson of Monash University, Victoria, Australia, for his interest, useful criticism, and discussion on the entire manuscript.

1. (*a*) R. W. Brandson, G. L. Closs, and C. A. Hutchison. J. Chem. Phys. **37**, 1878 (1962); (*b*) R. W. Murray, A. M. Trozzolo, E. Wasserman, and W. A. Yager. J. Am. Chem. Soc. **84**, 3213 (1962); (*c*) A. M. Trozzolo, R. W. Murray, and E. Wasserman. J. Am. Chem. Soc. **84**, 4990 (1962).
2. R. M. McDonald and R. A. Krueger. J. Org. Chem. **31**, 488 (1966).
3. W. M. Jones and L. Ennis. J. Am. Chem. Soc. **89**, 3069 (1967).
4. L. Caglioti and M. Magi. Tetrahedron, **19**, 1127 (1963).

5. B. NICHOLLS and M. C. WHITING. J. Chem. Soc. 551 (1959).
6. H. BEHRENS and W. KLEK. Z. Anorg. Chem. **292**, 151 (1957).
7. R. MATHIS-NÖEL, L. LAFAILLE, and A. LATTES. C. R. Acad. Sci. Paris, Ser. B, **265**, 306 (1967).
8. R. G. COOKS and S. W. TAM. Org. Mass Spectrom. **1**, 583 (1968).
9. S. E. SCHEPPLE, R. D. GRIGSBY, E. D. MITCHELL, D. W. WILLER, and G. R. WALLER. J. Am. Chem. Soc. **90**, 3521 (1968).
10. I. FLEMING and J. HARLEY-MASON. J. Chem. Soc. 5560 (1961).
11. J. ELGUERO, R. JACQUIER, and C. MARZIN. Bull. Soc. Chim. Fr. No. 2, 713 (1968).
12. C. S. KRAIHANZEL and F. A. COTTON. Inorg. Chem. **2**, 533 (1963).
13. K. W. BENTLEY. *In* Technique of organic chemistry. Vol. XI. *Edited by* A. Weissberger. Elucidation of structures by physical and chemical methods. Part 1. Interscience Publishers, New York. 1963, p. 199.
14. (*a*) H. STAUDINGER and O. KUPFER. Ber. Deut. Chem. Ges. **44**, 2197 (1911); (*b*) H. STAUDINGER and J. GOLDSTEIN. Ber. Deut. Chem. Ges. **49**, 1923 (1916).
15. L. FRIEDMAN and H. SHECHTER. J. Am. Chem. Soc. **81**, 5512 (1959).
16. G. L. CLOSS. J. Am. Chem. Soc. **84**, 809 (1962).
17. T. L. GILCHRIST and C. W. REES. Carbenes, nitrenes and arynes. The Pitman Press, Bath, Great Britain. 1969. pp. 82, 96.
18. W. KIRMSE, L. HORNER, and H. HOFFMANN. Ann. **614**, 19 (1958).
19. A. SONODA, I. MORITANI, T. SARAIE, and T. WADA. Tetrahedron Lett. 2943 (1969).
20. P. S. SKELL and A. Y. GARNER. J. Am. Chem. Soc. **78**, 5430 (1956).
21. R. M. ETTER, H. S. SKOVRONEK, and P. S. SKELL. J. Am. Chem. Soc. **81**, 1008 (1959).
22. A. SONODA, I. MORITANI, and Y. YASUDA. Unpublished work.
23. J. L. FLETCHER and M. J. MCGLINCHEY. Can. J. Chem. **53**, 1525 (1975).
24. M. ASHRAF and W. R. JACKSON. J. Chem. Soc. Perkin Trans. 2, 103 (1972).
25. S. P. GUBIN and V. S. KHANDKAROVA. J. Organomet. Chem. **22**, 449 (1970).

Can. J. Chem. Downloaded from www.nrcresearchpress.com by 210.87.254.5 on 09/05/12
For personal use only.

Photochemical rearrangements of substituted thiochromanone sulfoxides[1]

I. W. J. STILL,[2] P. C. ARORA, M. S. CHAUHAN, M.-H. KWAN, AND M. T. THOMAS[3]
Department of Chemistry and Erindale College, University of Toronto, Toronto, Ontario M5S 1A1

Received August 21, 1975

I. W. J. STILL, P. C. ARORA, M. S. CHAUHAN, M.-H. KWAN, and M. T. THOMAS. Can. J. Chem. **54**, 455 (1976).

The photochemical behavior of a number of substituted derivatives of thiochroman-4-one 1-oxide has been examined. In contrast to the analogous sulfones these sulfoxides undergo a variety of photochemical rearrangements. At least three distinct pathways have been recognized; β-hydrogen abstraction or rearrangement to cyclic sulfenates, which then undergo further reaction by homolysis of the S—O bond, appearing to be particularly favorable processes. In a small number of examples, photochemical deoxygenation is observed as a competing reaction. Mechanisms which attempt to account for the influence of structural variations on the particular pathway followed have been proposed.

I. W. J. STILL, P. C. ARORA, M. S. CHAUHAN, M.-H. KWAN et M. T. THOMAS. Can. J. Chem. **54**, 455 (1976).

On a examiné le comportement photochimique d'un certain nombre de dérivés de la thiochromanone-4 oxyde-1 substituée. Par opposition avec les sulfones correspondantes, ces sulfoxydes subissent une variété de réarrangements photochimiques. On a reconnu, au moins trois chemins distincts; les processus qui semblent particulièrement favorables sont l'enlèvement d'un hydrogène-β ou le réarrangement en sulfénates cycliques qui subissent une réaction ultérieure par homolyse du lien S—O. Dans un petit nombre d'exemples on observe une désoxygénation photochimique comme réaction compétitive. On propose des mécanismes qui tentent d'expliquer l'influence des variations structurales sur les chemins particuliers suivis au cours des réactions.

[Traduit par le journal]

Introduction

Interest in the photochemistry of cyclic sulfoxides has increased dramatically since the work of Archer and Kitchell (1) on the rearrangement of 2,2-dimethylthiochroman 1-oxide appeared in 1966. Schultz and Schlessinger (2, 3), Lawesson and co-workers (4), and Ganter and Moser (5) have been among the workers active in this area, while the topic has been reviewed by Block (6). We wish now to report our own results, obtained upon irradiation of a series of thiochromanone sulfoxides, which have been the subject of earlier communications (7, 8). Evidence will be presented in support of three distinct types of rearrangement pathway, in each of which the sulfoxide group appears to undergo a formal α-cleavage reaction. The dependence of the particular pathway followed upon the (alkyl) substitution pattern and the possible reasons for this dependence will also be presented.

Results and Discussion

After some initial difficulties had been overcome a satisfactory general procedure for synthesizing sulfoxides in the thiochroman-4-one, **1**, and isothiochromanone, **2**, series was discovered. We have examined the effects of ultraviolet irradiation on close to 20 such compounds, most of which have not been reported previously.

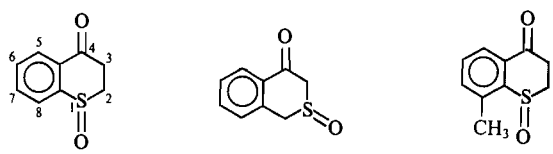

1 **2** **3**

One very notable feature of the photochemistry of thiochromanone sulfoxides is that it differs dramatically from that of the analogous sulfides,

[1]Presented in part at the 56th Annual Conference of the Chemical Institute of Canada, Montreal, Quebec, June, 1973, and at the Vth International Symposium on Organic Sulfur Chemistry, Lund, Sweden, June, 1972.

[2]Author to whom correspondence should be addressed.

[3]Taken in part from the Ph.D. thesis of M. T. Thomas, University of Toronto, 1970.

Can. J. Chem. Downloaded from www.nrcresearchpress.com by 210.87.254.6 on 09/05/12
For personal use only.

Can. J. Chem. Downloaded from www.nrcresearchpress.com by 210.87.254.6 on 09/05/12
For personal use only.

reported a few years ago by Berchtold and co-workers (9, 10), in which rearrangements via thiacyclobutanone intermediates and photofragmentation processes are common, and that of the analogous sulfones (11) for which simple photoreduction to pinacols predominates. Apart from a relatively small number of instances in which the sulfoxides were decomposed too rapidly to allow isolation of the photoproducts, it appears that we can sub-divide the photoreactions of these sulfoxides into three categories:

(*A*) those in which electron-releasing substituents (such as CH_3, OCH_3) are present at positions 6 or 8 of the thiochromanone system;

(*B*) those in which at least one substituent (CH_3) is present at the C-3 position, although another substituent (CH_3 or C_6H_5) may also be present at C-2;

(*C*) those in which at least one substituent (CH_3 or C_6H_5) is present at C-2, but C-3 is completely unsubstituted.

The first example of a reaction of type *A* was encountered on photolysis in benzene of 8-methylthiochroman-4-one 1-oxide, **3** (8). The only characterizable product, isolated in 10% yield from this reaction, showed a molecular ion at *m/e* 390, indicative of a dehydrodimer type structure. The possibilities of a disulfide or a peroxide type structure presented themselves, but the latter was rejected when the usual organic peroxide tests proved negative. (Intuitively, the formation of a peroxide which was not only stable at its mp (133–134 °C), but showed a molecular ion with intensity 13% of the base peak, had seemed highly improbable.) The spectral evidence, particularly the low frequency for the carbonyl group in the ir, pointed towards the disulfide structure **4**. This was confirmed by a relatively straightforward synthesis from *o*-cresol (Scheme 1). The Fries rearrangement conditions could be controlled to obtain predominantly *ortho*-migration of the 3-chloropropanoyl group in the ester **5**. No attempt to optimize the yield in the conversion of **6** into **4** has been made. The sample of **4** obtained by this route was identical in all respects with the photoproduct described above. A considerable amount (40%) of the starting sulfoxide was recovered from the irradiation of the 8-methyl sulfoxide.

Similarly, photolysis of 6-methyl- and 6-methoxythiochroman-4-one 1-oxide (**7***a*, **7***b*) gave the analogous disulfide products (**8***a*, **8***b*) in yields of

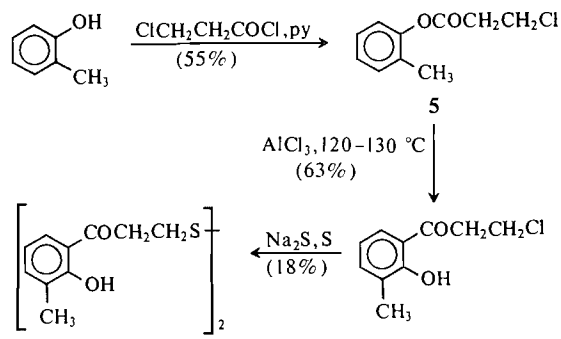

SCHEME 1

6 and 7.5%, respectively. On the other hand, no such product could be isolated from the irradiation of 8-carbomethoxythiochroman-4-one 1-oxide, **9**. These facts suggested an electronic rather than a steric effect of the substituent in the aromatic ring and we thus propose the mechanism shown in Scheme 2 in which an electron-

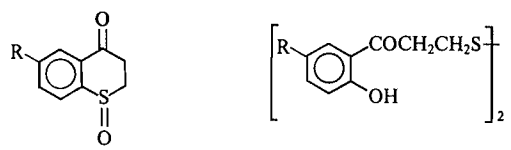

7*a* R = CH_3 **8***a* R = CH_3
7*b* R = OCH_3 **8***b* R = OCH_3

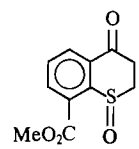

9

releasing group at position 8 (or 6) would be expected to stabilize the initially produced cyclohexadienyl radical **10** (or, possibly, a simple phenyl radical produced by α-cleavage of the sulfoxide). Collapse of **10** to the cyclic sulfenate **11**,[4] followed by a second photolytic step would lead to the biradical **12**. Coupling of the thiyl radicals, and hydrogen abstraction (from solvent or other substrate molecules) by the phenyloxy radicals would lead to **4**. It is a necessary consequence of this proposal that the sulfoxide oxygen becomes the phenolic OH group in the product.

[4]As discussed later for the 3-methyl substituted case, we cannot at present rule out the possibility of a concerted rearrangement of **3** to **11**.

Can. J. Chem. Downloaded from www.nrcresearchpress.com by 210.87.254.6 on 09/05/12
For personal use only.

We have confirmed that this is the case by repeating the irradiation, under otherwise identical conditions, on the ^{18}O-labelled sulfoxide, prepared by the procedure of Montanari and coworkers (12). The mass spectral fragmentation pattern (see Experimental) strongly supports the exclusive location of the ^{18}O-label on the phenolic hydroxyl group.

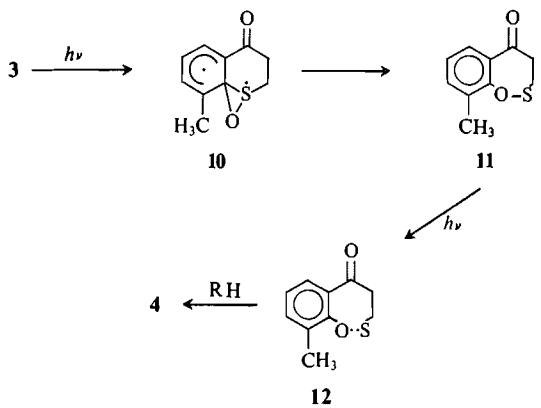

SCHEME 2

Photolysis of the 3-methylthiochroman-4-one 1-oxide, **13***a*, is typical of a number of 3-substituted sulfoxides which, like the sulfoxides already discussed, give products derived by opening of the hetero-ring, but from which in addition the sulfur atom has been subsequently lost (type *B* reaction). Irradiation of 3-methylthiochroman-4-one 1-oxide in benzene (7) was found to give three identifiable products, along with recovered starting material (15%). The least polar product eluted on chromatography was a mobile liquid with a single carbonyl band

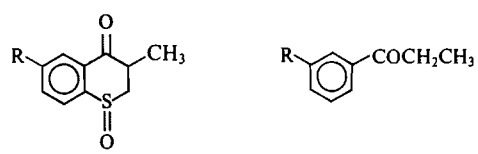

13*a* R = H
13*b* R = CH_3

14*a* R = H
14*b* R = CH_3

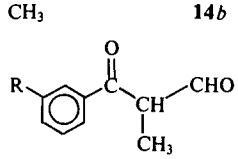

15*a* R = H
15*b* R = CH_3

(1685 cm^{-1}) and the characteristic pattern of an ethyl group in the nmr. Direct comparison with an authentic sample showed unmistakably that this compound was propiophenone, **14***a*, and this was further confirmed by comparison of the semicarbazone derivatives of the two samples.

A second product isolated from the chromatography was a solid, with bands in the ir at 1724 and 1680 cm^{-1}, indicative of two carbonyl groups. That one of these was an aldehyde functionality was indicated by the characteristic singlet at δ 9.86 ppm in the nmr. The presence of a monosubstituted benzene ring and the molecular formula $C_{10}H_{10}O_2$ indicated that this product was probably 2-benzoylpropanal, **15***a*. This was confirmed by synthesizing the latter compound by base-catalyzed condensation of propiophenone and ethyl formate and direct spectral comparison of the two samples.

The third product, also a solid, was comparatively easily identified as benzoic acid, **16**, by virtue of its mp, molecular formula ($C_7H_6O_2$), and characteristic reaction with aqueous sodium bicarbonate.

Our mechanistic proposal (Scheme 3) assumes that the initial photoproduct is 2-benzoylpropanal, **15***a*. Support for this suggestion was obtained by subjecting **15***a* independently to photolysis. Irradiation of **15***a* in dry benzene gave virtually no change after 30 h, but if the irradiation was conducted in benzene previously shaken with water, benzoic acid (67%) and propiophenone (13%) were isolated after 12 h. Some benzoic acid was also obtained when a sample of **15***a* was allowed to stand at 25 °C in the dark for 2 weeks. We are presently unable to advance a reason for the dramatic effect of added water on the photolysis of **15***a*, other than the obvious comment that it appears to require attack of water on an excited state of the keto-aldehyde.

The nature of the products obtained from the 3-methyl sulfoxide, and particularly the absence of sulfur, raised the possibility that these products might have arisen by complete photochemical cleavage of the hetero-ring, followed by attack of the fragments so produced on solvent benzene. This possibility could be eliminated following the photolysis of 3,6-dimethylthiochroman-4-one 1-oxide, **13***b*, which was found to produce only the expected propiophenone analogue, 1-*m*-tolyl-1-propanone, **14***b* (9%), and no

Can. J. Chem. Downloaded from www.nrcresearchpress.com by 210.87.254.6 on 09/05/12
For personal use only.

isomeric tolyl ethyl ketones, thus showing that the aromatic ring in the keto-aldehyde is that originally present in the sulfoxide. Photolysis of **13***b* also produced the expected keto-aldehyde **15***b* (7%) (although no *m*-toluic acid was found) and some recovered sulfoxide (13%).

Irradiation of 3,3-dimethylthiochroman-4-one 1-oxide, **17**, in benzene proceeded in an analogous manner. Chromatography again led to the isolation of three products, identified as isobutyrophenone, **18** (15%), 2-methyl-2-benzoylpropanal, **19** (15%), and benzoic acid (25%). The isobutyrophenone was identified by spectral comparison with an authentic sample and also by mp and mixture mp of the semicarbazone derivative. The keto-aldehyde structure **19** was initially assigned by analogy with the similar products obtained earlier, and finally confirmed by direct comparison with an authentic sample of 2-methyl-2-benzoylpropanal, synthesized by benzoylation of the morpholine enamine of isobutyraldehyde (13). The mp of the (mono) 2,4-dinitrophenylhydrazones of the two samples remained undepressed on admixture. A small amount of starting sulfoxide (8%) was also recovered in the later stages of the chromatography of the photolysate.

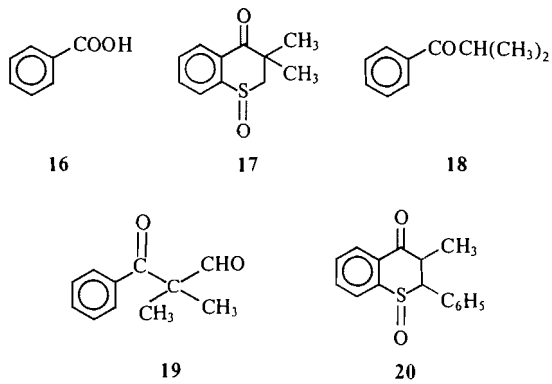

Once again, we attempted to establish the formation of 2-methyl-2-benzoylpropanal, **19**, as the primary photochemical process by independent irradiation of this compound in benzene. After only 1 h, decomposition was essentially complete and afforded isobutyrophenone (71%), accompanied by benzoic acid (14%). The possibility that some reaction is occurring by a ground state (acid- or base-catalyzed) pathway cannot be completely eliminated, in view of the well known susceptibility of non-enolizable β-keto aldehydes to hydrolytic cleavage (13). However, the results of deuterium-labelling experiments, to be discussed below, make it unlikely that this is anything more than a minor decomposition pathway. The high yield of isobutyrophenone obtained in the irradiation of **19** is surprising, in that it appears to be at variance both with the results of the original irradiation of **17** and also with the results of irradiation of the β-keto aldehyde **15***a*, where benzoic acid was the principal product. We can advance no really satisfactory explanation for the first anomaly but it is possible that the presence of a large amount of the hydroxymethylene tautomer of 2-benzoylpropanal makes attack of water at the ketone carbonyl (whether in the ground state or the excited state) greatly preferred in the latter case, accounting for the large amount of benzoic acid formed.

Irradiation of 3-methyl-2-phenylthiochroman-4-one 1-oxide, **20**, under similar conditions

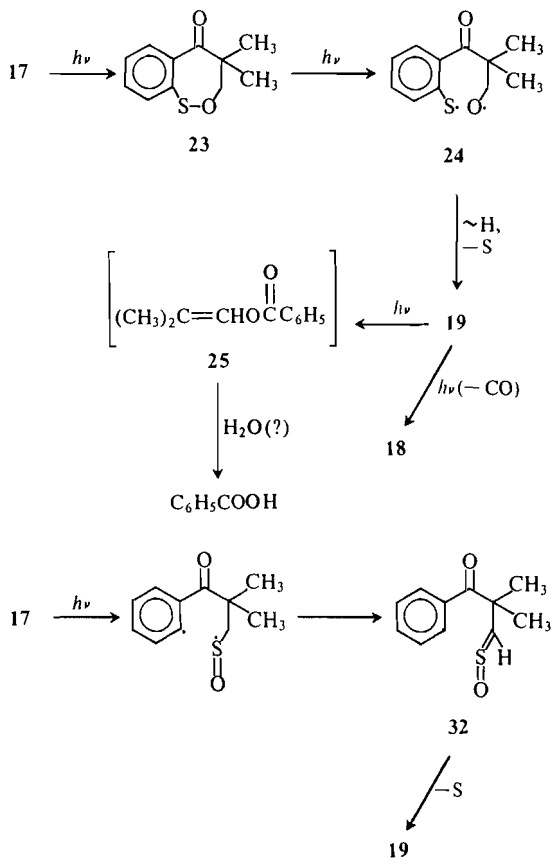

SCHEME 3

Can. J. Chem. Downloaded from www.nrcresearchpress.com by 210.87.254.6 on 09/05/12
For personal use only.

produced a crystalline product (39%) for which elemental analysis indicated the formula $C_{16}H_{14}O_2$. Analogy with the previous results and the spectral properties of this compound indicated that it was the expected 1,1-dibenzoylethane, **21**. This was readily confirmed by direct comparison with an authentic sample of the latter prepared by (mono) methylation of dibenzoylmethane with methyl iodide – silver oxide (14). Unlike the keto-aldehydes which were the

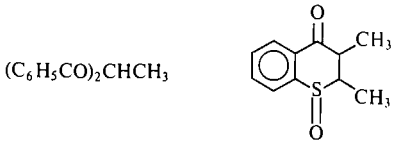

21 **22**

primary photoproducts in the earlier type *B* reactions, this β-diketone is not particularly susceptible to further photolysis, which accounts for both its relatively high yield and the almost complete absence (<0.5%) of benzoic acid in this photolysis. The only other product definitely identified in this reaction was recovered starting sulfoxide (12%).

Somewhat inadequate (spectral) evidence for the formation of the analogous 1-acetyl-1-benzoylethane was encountered in a small scale photolysis of 2,3-dimethylthiochroman-4-one 1-oxide, **22**. As the starting sulfoxide was difficult to synthesize and purify, no attempt has been made to confirm this result.

The results obtained from the photolyses of the 3-substituted thiochromanone sulfoxides lead us to postulate the alternative mechanisms shown in Scheme 3 for the type *B* photoreaction. Ring expansion of the 3,3-dimethyl sulfoxide **17**, for example, to the cyclic sulfenate **23** has ample analogy in mass spectrometry (15) and might proceed in either a concerted or a stepwise fashion. Further photolysis of the sulfenate leading to the biradical **24**, followed by desulfurization[5] and (intramolecular) hydrogen transfer from C-2 to the phenyl ring position vacated by sulfur, would lead to the initially formed keto-aldehyde **19**. Results of a deuterium-labelling experiment (to be discussed in detail below) further suggest that the secondary photochemical decarbonylation of **19** is either concerted (via a singlet excited state) or proceeds by a stepwise, cage-recombination process, since the formyl hydrogen (deuterium) is retained in the product **18**. The production of benzoic acid may be explained by α-cleavage of the benzoyl group, and recombination at oxygen rather than carbon, leading to the enol benzoate **25**. This possibility is supported by the report of the isolation of 2-butenyl acetate, albeit in low yield, from the photolysis of the β-diketone, 3-methyl-2,4-pentanedione (16). Finnegan and Hagan (17*a*) have reported the isolation of benzoylacetaldehyde, acetophenone, and benzoic acid from the photolysis of vinyl benzoate itself, the yields of the three products varying with the solvent used in the photolysis. Finnegan and Hagen have proposed a general category of photochemical rearrangement (of which the photo-Fries reaction is another example) of the type X—A—B=C → [A=B=C]· + X· → A=B—C—X, which may be reversible in certain instances.

An alternative proposal (Scheme 3) for the formation of **19** involves initial α-cleavage of the aryl C—S bond. Although this is the stronger of the two C—S bonds, the difference in bond energies is only about 7 kcal/mol and examples of aryl C—S bond cleavage in sulfides, sulfoxides, and sulfones have been reported by Kharasch and Khodair (17*b*). Hydrogen abstraction from C-2 by the reactive phenyl radical could then lead to an intermediate sulfine **32** (or the isomeric oxathiiran) which, from the work of Schultz and Schlessinger, would be expected to lose sulfur readily to give **19**.

Partial support for one of the above mechanisms was obtained by the photolysis of 2,2-di-

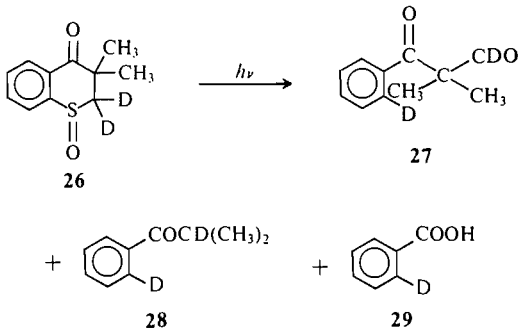

26 **27**

28 **29**

[5]As one of the referees has pointed out, this step appears significantly endothermic, and is perhaps, therefore, the major weakness in this suggested mechanism. However, we have not ascertained the fate of the extruded sulfur atom and Pryor and Walling have earlier shown the existence of the reaction RS· + A → R· + SA (*cf.* J. Am. Chem. Soc. **95**, 945 (1973)).

Can. J. Chem. Downloaded from www.nrcresearchpress.com by 210.87.254.6 on 09/05/12
For personal use only.

deuterio-3,3-dimethylthiochroman-4-one 1-oxide, **26**, synthesized by the procedure of Mock (18). This led to the deuterated keto-aldehyde **27** and the isobutyrophenone **28**, in each case with retention of the two deuterium atoms, and to the monodeuterated benzoic acid **29**, in yields comparable to those originally obtained for the unlabelled sulfoxide. Furthermore, attempts to incorporate external deuterium by conducting the photolysis of the unlabelled sulfoxide in benzene-d_6 or toluene-d_8 were without success. Thus the transfer of hydrogen from C-2 to the aryl ring, whatever the detailed mechanism of this step, must be *intra*molecular. Likewise, as postulated previously, the decarbonylation step must proceed without external incorporation of hydrogen (deuterium), and is thus presumably photochemical, not hydrolytic, in nature.

Other mechanistic studies conducted on the type *B* photolysis include an attempt to trap an

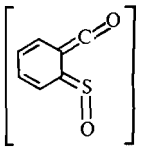

30

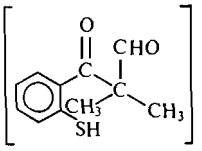

31

intermediate such as **30**, which might be formed by a photochemical fragmentation reaction analogous to that observed by Berchtold (10) for the keto-sulfides of similar structure or the mass spectrometric (*retro*-Diels–Alder) fragmentation observed earlier by us (19) for related sulfoxides. Trapping attempts (with methanol) were unsuccessful, as were attempts to isolate isobutylene from the effluent gas stream, indicating that **17** at least does not undergo significant photochemical reaction by this pathway. Preliminary attempts to carry out the irradiation of 3,3-dimethylthiochroman-4-one 1-oxide at lower temperatures (−10 °C) were not encouraging. Some evidence was obtained, however, in one experiment for a labile precursor to the keto-aldehyde **19**. Among the possible structures for this intermediate are the cyclic sulfenate **23**, the thiol **31**, or the sulfine **32**. A synthetic programme is currently in progress to attempt to identify sulfenates as real intermediates in these reactions.

The third well-defined category of photochemical behavior of thiochromanone sulfoxides

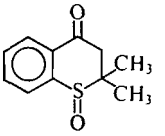

33

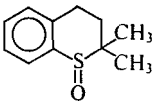

34

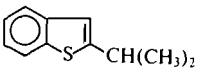

35

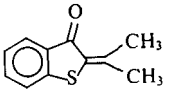

36

was first observed in the photolysis of 2,2-dimethylthiochroman-4-one 1-oxide **33**. As mentioned previously, Archer and Kitchell (1) had reported the photochemical ring contraction of 2,2-dimethylthiochroman 1-oxide, **34**, to 2-isopropylbenzothiophene, **35**, and also the conversion of **33** into 2-isopropylidene-3-thiaindanone, **36**, by heating with acetic anhydride (Pummerer reaction). We were interested to discover whether the presence of the carbonyl group in **33** would inhibit β-hydrogen abstraction by the excited sulfoxide chromophore at C-3, leading eventually, by the mechanism proposed by Archer and Kitchell, to **36**, or whether other photochemical processes would predominate. It may be noted that if β-hydrogen abstraction does occur it could also involve one of the C-2 methyl groups, leading to products other than **36**. We will return to this possibility later.

One other point concerning the synthesis of the 2,2-dimethylthiochroman-4-one 1-oxide (see Experimental) is worthy of brief comment. Cyclization of 3-methyl-3-phenylthiobutanoic acid to 2,2-dimethylthiochroman-4-one, **37**, the precursor of the desired sulfoxide **33**, failed completely if the reagent normally employed for such cyclizations, concentrated sulfuric acid, was used. Similarly poor results were obtained using polyphosphoric acid or phosphorus oxychloride which also have been successfully used for other thiochromanones and thioflavanones. A successful cyclization was achieved, however, with

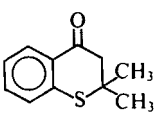

37

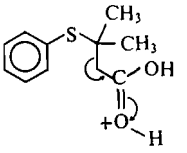

38

Can. J. Chem. Downloaded from www.nrcresearchpress.com by 210.87.254.6 on 09/05/12
For personal use only.

very dry phosphorus pentoxide in boiling benzene. We attribute the failure of the earlier attempts to fragmentation of the protonated butanoic acid derivative **38**, leading to the formation of a particularly stable (sulfur-stabilized) tertiary carbonium ion centre, and hence eventually to water-soluble products only.

Irradiation of 2,2-dimethylthiochroman-4-one 1-oxide in benzene showed considerable destruction of the sulfoxide band (ir) in 4 h. Chromatographic isolation of the products led to the isolation (in very low yield, 3%) of a crystalline ketone $C_{11}H_{10}OS$, shown by direct comparison with an authentic sample, to be identical with 2-isopropylidene-3-thiaindanone, **36**.

A crystalline product (8%), of similar polarity, was later shown to be identical with 2,2-dimethylthiochroman-4-one, **37**. This represents a product of formal deoxygenation of the starting sulfoxide. (The possibility that **37** was already present as an impurity in the starting sulfoxide has been eliminated.) Gurria and Posner (20) recently reported the photochemical deoxygenation of a number of diaryl sufoxides, and the mixed aryl alkyl sulfoxide **39**, in excellent yield. It may well be the case, based on the results of these authors and our own findings, that photochemical deoxygenation becomes an important pathway when other alternatives, such as β-hydrogen abstraction and α-cleavage processes, are impossible or disfavored in energy terms. Gurria and Posner (20) adduced evidence that the triplet excited state of their sulfoxides was responsible for the deoxygenation reaction and

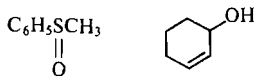

39 **40**

were also able to obtain evidence for the formation (direct or indirect) of singlet oxygen by a trapping experiment with cyclohexene. From the fact that they were able to isolate 2-cyclohexen-1-ol, **40**, in 41% yield by sodium iodide reduction of the photolysate, they concluded that formation of the corresponding hydroperoxide precursor indicated that the deoxygenation of the sulfoxides led to $^1O_2$, and not to atomic oxygen, which would be expected to react with cyclohexene to give the epoxide or cyclohexanone. We have attempted to carry out similar oxygen trapping experiments in the photolysis of **33**, without success. Since we have earlier shown (11), however, that thiochromanone sulfones are photolyzed only in the presence of a good hydrogen donor and are photochemically inert in benzene, we are quite confident in asserting that we have observed in the formation of **37** another genuine deoxygenation reaction, and not simply a disproportionation of the sulfoxide to equimolar amounts of sulfide and sulfone.

Some unreacted sulfoxide (46%) was recovered from the later stages of the chromatographic separation, and was the only other identifiable material present on photolysis of **33** in benzene.

Schultz and Schlessinger (21) have recently reported a similar photochemical ring contraction of a cyclic sulfoxide **41**. On the strength of a successful trapping experiment with methanol they propose a mechanism (Scheme 4) like that of Archer and Kitchell (1), involving β-hydrogen abstraction, ring closure to a highly strained tetracovalent sulfur species **42** and (acid-catalyzed?) rearrangement via the carbonium ion species **43** to the thiophene **44** (in benzene) or the dihydrothiophene **45** (in methanol). For this

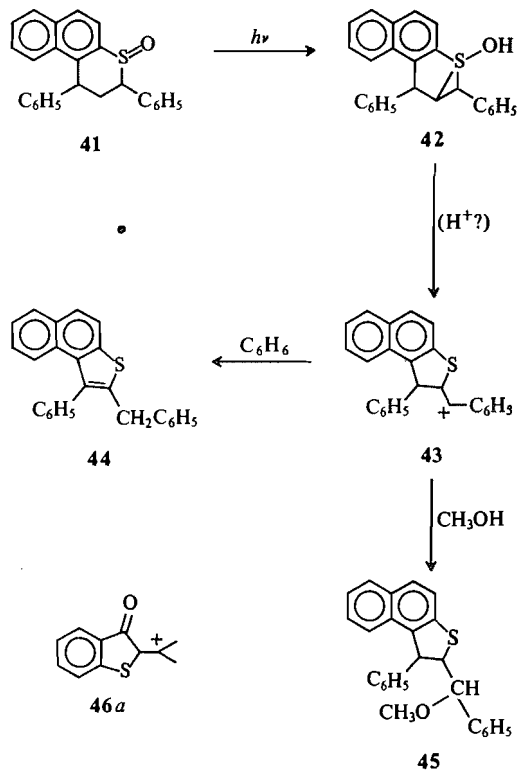

41 **42** **43** **44** **45** **46a**

SCHEME 4

Can. J. Chem. Downloaded from www.nrcresearchpress.com by 210.87.254.6 on 09/05/12
For personal use only.

reason, we have conducted the photolysis of 2,2-dimethylthiochroman-4-one 1-oxide, **33**, in methanol to see if products corresponding to the reaction of the (presumed) intermediate carbonium ion **46***a* could be obtained. We have so far been quite unsuccessful in this endeavour, thus suggesting that an entirely different mechanism is responsible for the formation of the ring-contraction product **36** or, possibly, that the intermediate involved in our case is not **46***a*, but a radical species of similar structure **46***b* (see Scheme 5).

From the irradiation of **33** in methanol (and also in various mixtures of methanol and benzene) we have isolated, however, a new product $C_{11}H_{12}OS$ in 6–11% yield, accompanied only by recovered starting sulfoxide (36%) and without formation of any of the deoxygenation product **37** or the ring-contraction product **36**. The presence of a weak band in the ir at 2450 cm^{-1} and of a singlet (1H) in the nmr at δ 1.58 ppm, completely removed by shaking with D_2O, led us to identify the new product as a thiol. The presence of an allylic CH_3 group (3H, s) at δ 1.58 and of the broadened doublet pattern characteristic of the $C{=}CH_2$ unit at δ 4.91 ppm, along with the mass spectral and analytical data, lead us to postulate the structure **47** for this compound. Since this product corresponds to a formal photoreduction process we repeated the irradiation of **33** in 50:50 isopropyl alcohol–benzene. Rather surprisingly, none of the thiol **47** appears to be formed under these conditions, although a small amount (4%) of the deoxygenation product **37** and recovered sulfoxide (30%) were isolated.

The foregoing results appear to point to a rather inefficient photochemical decomposition of **33**, characterized by the formation of free radical, rather than ionic, intermediates. The mechanistic scheme (Scheme 5) which we propose must be regarded as somewhat tentative but is more in accord with our findings than that proposed by Archer and Kitchell (1). Initial β-hydrogen abstraction from the two possible sites, followed by electronic reorganization, leads to two isomeric sulfenic acids **48***a* and **48***b*. This process, incidentally, is formally analogous to the formation of unsaturated aldehydes, following α-cleavage of cyclic ketones, and we certainly cannot rule out the possibility that α-cleavage precedes hydrogen abstraction. Homolytic decomposition of these unstable species by fission of the S—O bond would be expected to lead to the corresponding thiyl radicals. Cyclization of the thiyl radical **49***a* could lead to **46***b* and hence to **36**, and cyclization of **49***b* could eventually lead to the product of formal deoxygenation **37**. On the other hand, in the presence of a superior hydrogen donor (methanol) **49***b* is converted exclusively to the thiol **47**. We cannot at present answer the question as to why methanol does not appear to reduce the other thiyl radical **49***a* (or **46***b* for that matter) in a similar fashion. Nevertheless, although we cannot exclude other free-radical processes at this stage (including the involvement of a cyclic sulfenate), the mechanistic scheme which we propose satisfactorily accounts for the formation of all the products

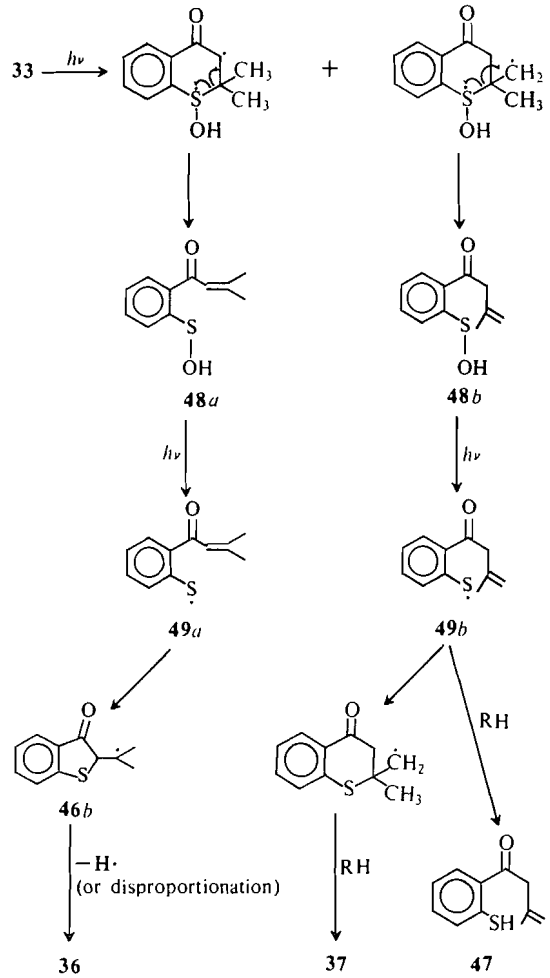

SCHEME 5

Can. J. Chem. Downloaded from www.nrcresearchpress.com by 210.87.254.6 on 09/05/12
For personal use only.

isolated and enables one to rationalize the rather surprising formation of the unconjugated thiol **47** and the absence of products arising from methanol addition more satisfactorily than a polar or ionic mechanism.

Similar irradiation of 2-methylthiochroman-4-one 1-oxide in benzene led, disappointingly, to a very rapid decomposition to a very viscous product from which no identifiable products could be obtained. A similar result was obtained with thiochroman-4-one 1-oxide, **1**, itself, which in this instance does resemble its sulfide analogue, earlier examined by Berchtold (10). Irradiation of 6-methyl-2-phenylthiochroman-4-one 1-oxide, **50**, however, in benzene afforded as the only identifiable product (14%) the ring-contracted analogue of **36**, 5-methyl-2-benzylidene-3-thiaindanone **51**, identified by comparison with an authentic sample prepared by aldol condensation of 5-methyl-3-thiaindanone with benzaldehyde. The stereochemistry of this compound has not been established; the vinylic proton signal is overlapped by the aromatic proton signals in the nmr, making an unambiguous assignment of the stereochemistry very difficult. The starting sulfoxide (44%) was also recovered in this irradiation.

Irradiation of isothiochromanone 2-oxide, **2**, and its 3,3-dimethyl derivative produced no isolable product, even when irradiation of the latter was conducted at −20 °C. We had also

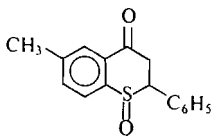

50

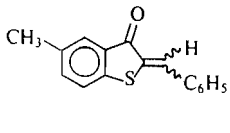

51

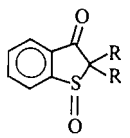

52
(R = H,CH_3)

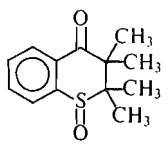

53

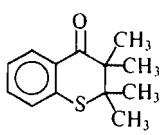

54

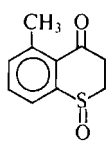

55

intended to examine the photochemical behavior of some thiaindanone sulfoxides **52**, but the unexpected difficulties encountered in their synthesis and the labile nature of the sulfide precursors induced us to abandon this attempt.

The irradiation of 2,2,3,3-tetramethylthiochroman-4-one 1-oxide, **53**, provides an example of a situation where both the 2- and 3-positions are completely substituted. In this case, of course, neither ring-contraction by β-hydrogen abstraction from C-3, nor the usual formation of β-dicarbonyl products from C-3 substituted analogues is possible. β-Hydrogen abstraction (from a C-2 methyl group) or γ-hydrogen abstraction (from a C-3 methyl group) remain formal possibilities but although we obtained liquid products showing spectral (nmr) evidence for vinylic protons, we were unable to isolate and separate any pure compounds from the photolysis mixture by any chromatographic technique, including glc.

Interestingly, the only product actually isolated, apart from small amounts of starting sulfoxide, was the product of deoxygenation, 2,2,3,3-tetramethylthiochroman-4-one, **54**, obtained in 33% yield. This yield was not significantly increased by changing the solvent to acetone. The isolation of the deoxygenation product, however, lends support to our suggestion that deoxygenation of the sulfoxide group is only likely when other photochemical pathways are impossible or disfavored.

The ultraviolet spectra of thiochromanone sulfoxides (Table 1) show a marked similarity to those of the analogous sulfones reported by us previously (11). However, in contrast to the sulfones, which are photochemically inert in solvents which are poor hydrogen-donors and give only moderate yields of pinacolic reduction products in alcoholic solvents, the foregoing discussion clearly reveals a very complex photochemistry for the keto-sulfoxides studied in this paper. In view of the fact that these photolyses proceed in essentially the same manner, albeit more slowly, in Pyrex as well as with Vycor filtration, and since the major emission bands of the (medium-pressure) mercury lamps being used are at 313 and 366 nm, it seems likely that absorption of light at approximately 290–295 nm (band B) is responsible for the photochemistry observed. The exact nature of this absorption is not known with certainty except that it appears

TABLE 1. Ultraviolet spectra of thiochromanone sulfoxides[a]

Sulfoxide	Band A nm (ε)	Band B nm (ε)	Band C nm (ε)
Thiochroman-4-one 1-oxide	243(10 300)	288(1920)	333sh(50)[b]
2,2-Dimethylthiochroman-4-one 1-oxide	243(10 500)[b]	296(1700)[b]	333sh(~100)[b]
3-Methylthiochroman-4-one 1-oxide	244(9040)	288(1910) 295sh(1790)	340(175)
6-Methylthiochroman-4-one 1-oxide	250(7950)	298(1780)	345(560)
8-Carbomethoxythiochroman-4-one 1-oxide	250sh(8600)	289(950) 298sh(830)	342(430)
2,2,3,3-Tetramethylthiochroman-4-one 1-oxide	242(—)[c]	301(—)[c]	[c]
Isothiochromanone 2-oxide	253(9880)	294(1580)	[c]

[a]In methanol or 95% ethyl alcohol.
[b]Reference 22.
[c]Not recorded.

likely to be some sort of combination band involving both the C=O and the S=O chromophores (22). The interesting possibility that essentially all of the light is absorbed by the carbonyl chromophore is suggested by our experience on irradiation of 5-methylthiochroman-4-one 1-oxide, **55**. In sharp contrast to the behavior of the other thiochromanone and isothiochromanone sulfoxides, even those which do not lead to identifiable products, **55** could be recovered in 90% yield after 24 h irradiation. This is believed due to the readiness with which *o*-methyl substituted aryl ketones undergo 'unproductive' photoenolization and suggests that the carbonyl group is playing an essential role, perhaps as an intramolecular sensitizer, in the photochemistry of the sulfoxide group which is ultimately observed.

The photochemical behavior of the S=O chromophore is frequently compared with that of the much better known carbonyl chromophore. Our results, and those of previous workers, suggest that the photochemical behavior of sulfoxides may indeed be as complex as that of ketones, but that there are important differences. The potential for the sulfoxide group to rearrange initially to bivalent sulfenate (or sulfenic acid) derivatives is formally analogous to the relatively rare formation of oxacarbenes, but the tendency for further homolysis of the much weaker S—O bond accounts for much of the unique photochemistry observed for sulfoxides. Recent evidence suggests that β-hydrogen abstraction processes may also be involved in the photochemistry of sulfoxides in certain cases, in contrast to that of the carbonyl group, in which γ-hydrogen abstraction is virtually the rule. Examination of Dreiding models of sulfoxides appears to confirm the likelihood of such processes occurring. Instances of γ-hydrogen abstraction involving the sulfoxide group, leading to fragmentation products akin to those in Norrish type II processes, however, have also been reported (6).

Experimental

General

The ir spectra (cm^{-1}) were recorded on a Perkin-Elmer 337 grating spectrophotometer and the low resolution mass spectra were obtained on a Bell and Howell 21-490 spectrometer. Accurate mass measurements were obtained on the A.E.I. MS-902 instrument. Nuclear magnetic resonance spectra (δ) were recorded on Varian T-60 and EM-360 spectrometers, with TMS as internal standard. Elemental analyses were performed by the Scandinavian Microanalytical Laboratory, Box 25, DK 2730, Herlev, Denmark. A water-cooled Hanovia 115 W medium-pressure mercury arc lamp was normally employed as the light source in irradiation experiments, with the filter (Vycor or Pyrex) indicated. All melting points and boiling points are uncorrected.

Thiochromanones

Thiochroman-4-one is now available commercially and the syntheses of its 2-,3-,5-, and 8-methyl and 8-carbomethoxy analogues, and of isothiochromanone (11) as well as the 2,2- and 3,3-dimethylthiochromanones have been described previously (23,24). The synthesis of 3,3-dimethylisothiochromanone has also been described earlier (25). Two representative procedures (Methods *A*, *B*) are described below.

Sulfoxides

These were synthesized by oxidation of the appropriate thiochromanone by the same general procedure which we have already described (19,24) (see Table 2).

Method A

6-Methylthiochroman-4-one 1-Oxide

p-Toluenethiol (12.5 g) was added to a 20% aqueous

Can. J. Chem. Downloaded from www.nrcresearchpress.com by 210.87.254.6 on 09/05/12
For personal use only.

Can. J. Chem. Downloaded from www.nrcresearchpress.com by 210.87.254.6 on 09/05/12
For personal use only.

sodium hydroxide solution (20 ml), and β-propiolactone (7.2 g) added to the mixture at 0–5 °C, with stirring. After 3 h, the reaction mixture was acidified (HCl) and the product, 3-*p*-tolylthiopropanoic acid (11.0 g, 57%) collected by filtration as a white solid, mp 64–65 °C.

The thio acid (5.0 g) was then cyclized in concentrated sulfuric acid (75 ml) at 25 °C for 26 h. The dark red mixture was poured over crushed ice and extracted with ether. Washing the ethereal extracts with water, drying ($MgSO_4$), and evaporation gave a solid product which on recrystallization from petroleum ether (bp 60–70 °C) gave 6-methylthiochroman-4-one (3.3 g, 73%), mp 61–62 °C.

The sulfoxide was prepared by the usual procedure as a white solid (76%), which was recrystallized from benzene–petroleum ether, mp 110–111 °C; lit. mp (26) 110 °C.

Method B

3-Methyl-2-phenylthiochroman-4-one 1-Oxide

α-Methylcinnamic acid was prepared by the Perkin reaction by heating benzaldehyde (21.0 g), propionic anhydride (32.0 g) and freshly fused sodium propionate (20.0 g) at 130–135 °C for 30 h. The reaction mixture was poured into water and the solution neutralized with solid sodium carbonate. Removal of excess benzaldehyde by steam distillation and acidification gave the cinnamic acid (21.0 g, 64%).

α-Methylcinnamic acid (32.0 g), benzenethiol (30.0 g), and piperidine (4 ml) were refluxed in absolute alcohol (100 ml) for 72 h. Upon cooling, the p*H* was adjusted to 4–5 and excess thiol removed by steam distillation. The insoluble oily residue remaining in the distilling flask rapidly solidified and was recrystallized from benzene–petroleum ether. The 2-methyl-3-phenyl-3-phenylthiopropanoic acid so obtained (42.0 g, 76%) was a white solid, mp 119–120 °C.

The thio acid (7.0 g) was cyclized by heating with phosphorus oxychloride (30.0 g) at 100 °C for 1 h. After cooling and pouring the reaction mixture over crushed ice the crude product was extracted with ether. Washing the combined ethereal extracts (aqueous NaOH, H_2O), drying ($MgSO_4$), and evaporation gave the 2-phenyl-3-methylthiochroman-4-one (6.0 g, 89%).

Oxidation of the above product by the usual procedure gave a rather impure product in virtually quantitative yield. Purification by chromatography on silica gel and elution with 2–5% acetone in methylene chloride gave what appeared to be a diastereoisomeric mixture of the expected sulfoxide. The expected strong bands (1690, 1026 cm^{-1}) in the infrared were present and the expected molecular ion at *m/e* 270 was observed, but the nmr spectrum was more complex than expected for a single diastereomer: δ ($CDCl_3$) 1.2 (3H, dd), 3.2 (1H, q), 4.2 (1H, m), 7.3–8.2 (9H, m) ppm. No further purification was attempted and irradiation was carried out on the mixture (*q.v.*).

2,3-Dimethylthiochroman-4-one 1-Oxide

Oxidation of the sulfide (*cis/trans* mixture) obtained by the method already described (23) gave, after chromatography on silica gel, what was believed to be a mixture of diastereoisomeric sulfoxides (53%). The liquid mixture did not crystallize on prolonged cooling at −10 °C and was used directly for the irradiation (*q.v.*)

3,3-Dimethylisothiochromanone 2-Oxide

Oxidation of 3,3-dimethylisothiochromanone by the procedure used for isothiochromanone (*q.v.*) gave a liquid sulfoxide (86%) which decomposed on attempted distillation, but could be readily purified by chromatography on silica gel and elution with methylene chloride–acetone mixtures; ir (neat) 1681, 1047 cm^{-1}; nmr ($CDCl_3$) δ 1.50 (3H, s), 1.57 (3H, s), 4.26 (2H, AB quartet, J_{AB} = 10 Hz), 7.2–7.7 (3H, m), 8.08 (1H, dd, J = 2.0, 7.0 Hz) ppm.

Irradiation of 8-Methylthiochroman-4-one 1-Oxide

The sulfoxide (1.5 g) was irradiated (Vycor) under N_2 in dry, degassed benzene for 24 h, by which time the sulfoxide band in the ir at 1020 cm^{-1} had almost disappeared. After evaporation of the solvent the disulfide product (0.145 g, 10%) was obtained by chromatography on silica gel by elution with 1–2% acetone in methylene chloride. Apart from some brown polymeric material the only other compound isolated was the starting sulfoxide (40%), eluted with acetone.

Trituration of the crude disulfide with petroleum ether gave a white solid, which was recrystallized from petroleum ether (bp 60–70 °C), mp 133–134 °C; ir (Nujol) 1634, 1610 cm^{-1}; nmr ($CDCl_3$) δ 2.23 (6H, s), 3.07 (4H, t, J = 6 Hz), 3.43 (4H, t, J = 6 Hz), 6.85 (2H, t, J = 7.5 Hz), 7.38 (2H, d, J = 7.5 Hz), 7.66 (2H, d, J = 7.5 Hz), 12.46 (2H, s) ppm; λ_{max} (MeOH) 259(14 000), 330(5700) nm; *m/e* 390(M^+) (13), 163(63), 162(30), 161(13), 145(12), 135(100), 105(10), 79(17), 78(50), 77(36). *Anal.* calcd. for $C_{20}H_{22}O_4S_2$: C 61.22, H 5.61, S 16.32; found: C 61.47, H 5.80, S 16.47.

Attempts to form the semicarbazone, 2,4-dinitrophenylhydrazone, or oxime of the photoproduct were unsuccessful, and the compound showed no positive reaction with $FeCl_3$. Attempts to degrade the disulfide by employing various oxidizing agents, Raney nickel or acid-catalyzed hydrolysis were likewise unsuccessful. Essentially the same results were obtained when the irradiation was conducted in acetonitrile or acetone, and if the Vycor filter was replaced by Pyrex.

*o-Tolyl 3-Chloropropanoate, **5***

A mixture of *o*-cresol (10.8 g), 3-chloropropanoyl chloride (28.0 g) and pyridine (1 ml) were refluxed for 10 h in benzene (50 ml). After evaporation the residue was extracted with ether and the ethereal extracts washed thoroughly with water and dried ($MgSO_4$). After evaporation of solvent the ester (11.0 g, 55%) was collected at 90–92 °C/2 Torr; ir (neat) 1755 (C=O) cm^{-1}; nmr ($CDCl_3$) δ 2.16 (3H, s), 2.90 (2H, t, J = 6.5 Hz), 3.75 (2H, t, J = 6.5 Hz), 7.0–7.3 (4H, m) ppm. *Anal.* calcd. for $C_{10}H_{11}ClO_2$: C 60.45, H 5.54, Cl 17.88; found: C 60.52, H 5.60, Cl 17.84.

*1-(2-Hydroxy-3-methylphenyl)-3-chloro-1-propanone, **6***

The *o*-cresyl ester (2.0 g) was subjected to the Fries rearrangement by heating with anhydrous aluminum chloride (4.0 g) at 120–130 °C for 30 min. After cooling and cautious addition of water, the aqueous solution was extracted with ether. Washing (H_2O), drying ($MgSO_4$), and evaporation of the ethereal extracts gave the desired propiophenone derivative (1.3 g, 63%) as a white solid, mp 82–83 °C (95% EtOH); ir (Nujol) 1635 (C=O) cm^{-1};

Can. J. Chem. Downloaded from www.nrcresearchpress.com by 210.87.254.6 on 09/05/12
For personal use only.

TABLE 2. Analytical data

Sulfoxide	% Yield (from sulfide)	mp (deg)	Calculated			Found		
			C	H	S	C	H	S
Thiochroman-4-one 1-oxide	79	49–50	60.00	4.48	17.77	59.65	4.63	17.63
Isothiochromanone 2-oxide	62[a]	170–171[b]	60.00	4.48	17.77	60.15	4.64	17.63
2-Methylthiochroman-4-one 1-oxide	75	109–110[b]	61.86	5.15	16.49	61.61	5.08	16.52
3-Methylthiochroman-4-one 1-oxide (27)	73	116–117[c]	61.86	5.15	16.49	61.64	5.17	16.62
5-Methylthiochroman-4-one 1-oxide	60	112–113[c]	61.86	5.15	16.49	61.63	5.23	16.54
8-Methylthiochroman-4-one 1-oxide	90	83–84[c]	61.86	5.15	16.49	61.98	5.25	16.55
6-Methoxythiochroman-4-one 1-oxide	90[d]	98–99[c]	57.14	4.76	15.24	57.35	4.97	15.07
2,2-Dimethylthiochroman-4-one 1-oxide	49[e]	91–92[c]	63.46	5.77	15.38	63.45	5.81	15.37
3,3-Dimethylthiochroman-4-one 1-oxide	90	(bp) 140–142/0.5 Torr	63.46	5.77	15.38	63.85	6.02	14.97
3,6-Dimethylthiochroman-4-one 1-oxide	88	106–107[c]	63.46	5.77	15.38	63.15	5.62	15.40
6-Methyl-2-phenylthiochroman-4-one 1-oxide	33	140–141[e,f]	71.10	5.22	11.84	71.28	5.14	11.93
2,2,3,3-Tetramethylthiochroman-4-one 1-oxide	81	73–74[g]	66.08	6.83	13.55	66.20	6.68	13.59

[a]A much shorter time (2–4 h) is required for the oxidation in this case.
[b]Recrystallized from benzene.
[c]Recrystallized from benzene–petroleum ether (bp 60–70 °C).
[d]In the preceding cyclization step considerable demethylation occurred, leading to 6-hydroxythiochroman-4-one, mp 141–142 °C.
[e]The synthesis of 2,2-dimethylthiochroman-4-one has been reported (23) but the mp of this compound should read 60–61 °C and not as reported previously. The intermediate 3-methyl-3-phenylthiobutanoic acid has mp 68–69 °C and may be isolated in 58% yield by the method described (23).
[f]Arndt (27) reports mp 177–178 °C, but admits that his sulfoxide is likely contaminated with the sulfone, mp 191–192 °C.
[g]Recrystallized from *n*-hexane.

Can. J. Chem. Downloaded from www.nrcresearchpress.com by 210.87.254.6 on 09/05/12
For personal use only.

nmr ($CDCl_3$) δ 2.25 (3H, s), 3.35–4.05 (4H, A_2B_2 system), 6.77 (1H, t, J = 7.5 Hz), 7.32 (1H, dd, J = 1.5, 7.5 Hz), 7.53 (1H, dd, J = 2.0, 8.0 Hz), 12.23 (1H, s) ppm. *Anal.* calcd. for $C_{10}H_{11}ClO_2$: C 60.45, H 5.54, Cl 17.88; found: C 60.36, H 5.49, Cl 18.26.

Conversion of **6** *into the Disulfide,* **4**

Sodium disulfide was prepared by refluxing a mixture of sodium sulfide (90 mg) and sulfur (12 mg) in 95% ethyl alcohol (25 ml) until the sulfur had dissolved. The hot solution was then added slowly to a refluxing solution of **6** (85 mg) in 95% ethyl alcohol (12 ml). After a further 2.5 h refluxing the reaction mixture was cooled and filtered, and the filtrate made slightly acidic with dilute hydrochloric acid. After evaporation of the solvent the residue was sublimed to remove excess sulfur and the remaining solid was recrystallized from methanol to afford **4** (15 mg, 18%). The solid so obtained was identical (mp, mixture mp, ir, nmr) with the photoproduct obtained as described earlier.

8-Methylthiochroman-4-one 1-[^{18}O]-oxide

This compound was made by essentially the general method of Montanari and co-workers (12). A solution of iodobenzene dichloride (1.4 g) in anhydrous pyridine (3.0 ml) was added dropwise to a stirred solution of 8-methylthiochroman-4-one (0.9 g) in aqueous pyridine containing 0.8 ml $H_2{}^{18}O$ (20% enrichment) and 3.2 ml pyridine. After stirring for 30 min at 20 °C the mixture was diluted with chloroform (30 ml), washed with 10% sulfuric acid and water, and dried (Na_2SO_4). Evaporation and repeated recrystallization of the residue from benzene–hexane gave the labelled sulfoxide (0.7 g, 71%), mp 81–82 °C. The mass spectrum of the sulfoxide showed the expected enhancement in the intensity of the (M + 2) peak at m/e 196.

Irradiation of the labelled sulfoxide under the same conditions as described for the unlabelled 8-methylthiochroman-4-one 1-oxide gave the same crystalline disulfide, mp 133–134 °C. The relevant mass spectral data are reported below:

		Mass	
m/e	Formula	Calculated	Experimental
394(M+4)	$C_{20}H_{22}{}^{18}O_2{}^{16}O_2S_2$	394.1044	394.1048
392(M+2)	$C_{20}H_{22}{}^{18}O^{16}O_3S_2$	392.1001	392.0994
390(M)	$C_{20}H_{22}O_4S_2$	390.0959	390.0961
$165\left(\frac{M}{2}-S+2\right)$	$C_{10}H_{11}{}^{18}O^{16}O$	165.0801	165.0801
$163\left(\frac{M}{2}-S\right)$	$C_{10}H_{11}O_2$	163.0758	163.0756
$137\left(\frac{M}{2}-S,-C_2H_4,+2\right)$	$C_8H_7{}^{18}O^{16}O$	137.0488	137.0487
$135\left(\frac{M}{2}-S,-C_2H_4\right)$	$C_8H_7O_2$	135.0446	135.0443
$121\left(\frac{M}{2}-S,-C_2H_4,-O,+2\right)$	$C_8H_7{}^{18}O$	(Intensity too low for mass measurement)	
$119\left(\frac{M}{2}-S,-C_2H_4,-O\right)$	C_8H_7O	119.0497	119.0497
$91\left(\frac{M}{2}-S,-C_2H_4,-O,-CO\right)$	C_7H_7	91.0548	91.0548

Irradiation of 6-Methylthiochroman-4-one 1-Oxide

The sulfoxide (500 mg) was irradiated in dry, degassed benzene (80 ml) for 22 h under essentially the same conditions as those described for the 8-methyl analogue. Chromatography on silica gel afforded the starting material (75 mg, 15%) and the disulfide product **8***a* (30 mg, 6%). The disulfide had mp 128–129 °C; ir (Nujol) 1635, 1610 cm^{-1}; nmr ($CDCl_3$) δ 2.38 (6H, s), 3.33 (8H, A_2B_2 system), 6.9–7.6 (6H, m), 11.91 (2H, s) ppm. *Mol Wt.* calcd. for $C_{22}H_{22}O_4S_2$: 390.0959; found: 390.0959.

Irradiation of 6-Methoxythiochroman-4-one 1-Oxide

The sulfoxide (400 mg) was irradiated in dry, degassed benzene (150 ml) for 23 h. Chromatography on preparative tlc plates of silica gel afforded starting material (220 mg, 55%) and the disulfide product **8***b* (30 mg, 7.5%), mp 125–126 °C; ir (Nujol) 1640, 1610 cm^{-1}; nmr ($CDCl_3$) δ 3.09 (4H, t, J = 8 Hz), 3.44 (4H, t, J = 8 Hz), 3.82 (6H, s), 6.9–7.3 (6H, m), 11.79 (2H, s) ppm. *Mol. Wt.* calcd. for $C_{20}H_{22}O_6S_2$: 422.0856; found: 422.0857.

Irradiation of 3-Methylthiochroman-4-one 1-Oxide

The sulfoxide (2.0 g) was irradiated in degassed benzene (250 ml) under nitrogen in quartz for 35 h, by which time almost all of the sulfoxide band in the ir had disappeared. After evaporation of solvent, the residue was dissolved

Can. J. Chem. Downloaded from www.nrcresearchpress.com by 210.87.254.6 on 09/05/12
For personal use only.

in a mixture of methylene chloride – carbon tetrachloride (75:25) and chromatographed on silica gel.

A yellow liquid (136 mg, 10%) was eluted in 90% CH_2Cl_2–CCl_4; ir (neat) 1685 cm^{-1}; nmr ($CDCl_3$) δ 1.21 (3H, t, J = 7.5 Hz), 2.92 (2H, q, J = 7.5 Hz), 7.2–7.5 (3H, m), 7.8–8.0 (2H, m) ppm. Spectral comparison with propiophenone and a mp (174 °C) and mixture mp comparison of the semicarbazones showed this product to be identical with authentic propiophenone.

A second solid fraction (278 mg) was obtained on elution with 2% acetone in methylene chloride. This material proved to be rather impure and was rechromatographed on silica, affording a white solid (140 mg, 8%), mp 119–120 °C (cold crystallization from $CHCl_3$); ir ($CHCl_3$) 1724, 1680 cm^{-1}. *Anal.* calcd. for $C_{10}H_{10}O_2$: C 74.07, H 6.17; found: C 73.40, H 5.88.

Comparison of the ir and nmr spectra of an authentic sample of 2-benzoylpropanal, prepared by the base-catalyzed condensation of propiophenone with ethyl formate (29), with those of the photoproduct confirmed the identity of the photoproduct.

The third product isolated (110 mg, 9%) by elution with 2–5% acetone in methylene chloride was also a white solid, mp 121–122 °C, shown to be identical with benzoic acid by mp, mixture mp, and ir and nmr spectral comparisons.

Apart from considerable quantities of brown gummy, uncharacterizable material the only other compound recovered was the starting sulfoxide (294 mg, 15%), by elution with 30% acetone in methylene chloride.

Irradiation of 2-Benzoylpropanal

A solution of the keto-aldehyde (0.2 g) in degassed benzene (150 ml) was irradiated for 48 h in a quartz vessel, under nitrogen. Chromatography on silica gel led to the isolation of small quantities of benzoic acid, but no propiophenone. Starting material was also recovered. On repeating the irradiation in moist benzene after 12 h benzoic acid (67%) and propiophenone (13%) were recovered.

Irradiation of 3,6-Dimethylthiochroman-4-one 1-Oxide

The sulfoxide (0.9 g) was irradiated in degassed benzene (200 ml) with Vycor filtration for 24 h, under nitrogen. Chromatography of the crude product on silica gel gave, on elution with methylene chloride, a yellow oil (58 mg, 9%); ir (neat) 1685 cm^{-1}; nmr ($CDCl_3$) δ 1.20 (3H, t, J = 7 Hz), 2.38 (3H, s), 2.96 (2H, q, J = 7 Hz), 7.2–7.4 (2H, m), 7.65–7.8 (2H, m) ppm. The general similarity of the ir and nmr spectra to those of propiophenone led us to assign the 1-*m*-tolyl-1-propanone structure to this product.

A semisolid fraction obtained on elution with 2% acetone in methylene chloride was rechromatographed and afforded a white crystalline solid (50 mg, 7%) on elution with 2% acetone. After cold crystallization from chloroform a sample of this compound was further purified by recrystallization from cyclohexane; mp 122–123 °C; ir 1725, 1685 cm^{-1}; nmr (acetone-d_6) δ 1.35 (3H, m), 1.83 (3H, s), 3.05 (1H, m), 7.3–7.7 (3H, m), 8.09 (1H, dd, J = 2.0, 7.5 Hz), 9.86 (1H, s) ppm. *Anal.* calcd. for $C_{11}H_{12}O_2$: C 75.00, H 6.82; found: C 74.42, H 6.65.

Apart from considerable amounts of brown gummy material, some starting sulfoxide (121 mg, 13%) was recovered by elution with 50% acetone–methylene chloride.

Irradiation of 3,3-Dimethylthiochroman-4-one 1-Oxide

The sulfoxide (1.0 g) dissolved in 200 ml degassed benzene was irradiated under nitrogen in a quartz vessel with Vycor filtration for 10 h. The residue obtained on evaporation was chromatographed on silica gel.

A liquid product (106 mg, 15%) obtained on elution with 90% methylene chloride – carbon tetrachloride showed ir 1685 cm^{-1}; nmr ($CDCl_3$) δ 1.21 (6H, d, J = 7 Hz), 3.55 (1H, septet, J = 7 Hz), 7.3–7.6 (3H, m), 7.8–8.05 (2H, m) ppm. These spectra were identical with those of an authentic sample of isobutyrophenone and the semicarbazone of the photoproduct (mp 180–181 °C) was undepressed on admixture with that of isobutyrophenone.

Elution with 2% acetone in methylene chloride gave a semicrystalline product (314 mg, 37%) which showed two carbonyl peaks (1720, 1675 cm^{-1}) in the ir. The material was rechromatographed on silica gel affording a colorless oil (131 mg, 15%), bp 85–90 °C/1 Torr; nmr ($CDCl_3$) δ 1.47 (6H, s), 7.4–7.9 (5H, m), 9.73 (1H, s) ppm. This product was identical (ir, nmr) with an authentic sample of 2-methyl-2-benzoylpropanal prepared by benzoylation of isobutyraldehyde (morpholine) enamine by the method of Inukai and Yoshizawa (13). The (mono) 2,4-dinitrophenylhydrazone, mp 149–50 °C (ethanol) showed no depression of mp on admixture with a sample prepared from the known compound.

Elution with 5% acetone in methylene chloride afforded a crystalline product (151 mg, 25%) shown to be identical (mp, mixture mp) with benzoic acid.

The final fraction (81 mg, 8%), eluted with 50% acetone in methylene chloride, was shown to consist of the starting sulfoxide.

Irradiation of 2-Benzoyl-2-methylpropanal

A solution of the keto-aldehyde (0.3 g) in degassed benzene was irradiated under nitrogen in a quartz vessel, with a Vycor filter. After 1 h, the solution was evaporated and the product chromatographed on silica. Isobutyrophenone (180 mg, 71%) and benzoic acid (30 mg, 14%) were isolated as described in the original photolysis.

2,2-Dideuterio-3,3-dimethylthiochroman-4-one 1-Oxide

3,3-Dimethylthiochroman-4-one 1-oxide (0.33 g) in dioxan (10 ml) containing deuterium oxide (2 ml) and potassium *tert*-butoxide (0.25 g) was refluxed with stirring for 4 h. After acidification (20% deuterium chloride) the solution was evaporated under vacuum to remove most of the dioxan and a further 5–10 ml of deuterium oxide was added. Extraction with methylene chloride, washing (D_2O), and drying ($MgSO_4$) gave, on evaporation and distillation, (140 °C/0.5 Torr) a viscous liquid (0.23 g, 69%). Unlike the protonated precursor, this sulfoxide showed complete absence of the AB quartet at δ 3.45 ppm, indicating that exchange at the 2-position was complete.

Irradiation of 2,2-Dideuterio-3,3-dimethylthiochroman-4-one 1-Oxide

Irradiation in benzene and the subsequent column chromatography and isolation of the products were conducted exactly as described for the undeuterated 3,3-dimethylthiochroman-4-one 1-oxide. The isobutyrophe-

Can. J. Chem. Downloaded from www.nrcresearchpress.com by 210.87.254.6 on 09/05/12
For personal use only.

none thus isolated showed a molecular ion at *m/e* 150 showing that it retained two deuterium atoms. In the nmr of this product the methyl groups appeared as a *singlet* at δ 1.43 while the septet at δ 3.49 due to the methine proton had completely disappeared. Furthermore, the integrated intensities of the two groups of aromatic protons were now in the ratio 3:1 instead of 3:2, indicating that the other deuterium atom had replaced a hydrogen *ortho-* to the carbonyl group.

The keto-aldehyde (2-benzoyl-2-methylpropanal) also showed a molecular ion two units higher than the undeuterated analogue, at *m/e* 178, confirming that it was also doubly labelled. In the nmr the characteristic aldehyde proton signal at δ 9.70 ppm had disappeared and the integrated intensities of the two groups of aromatic protons had again become 3:1, instead of 3:2, thus confirming the presence of a deuterium atom in the formyl group and *ortho-* to the aromatic carbonyl group.

The benzoic acid isolated showed a molecular ion at *m/e* 123, indicating a singly-labelled compound. The 3:1 ratio for the aromatic protons and the presence of the characteristic acidic proton as a broad singlet at δ 12.6 ppm confirmed the C-2 position as the location of the deuterium atom.

Irradiation of 3-Methyl-2-phenylthiochroman-4-one 1-Oxide

A solution of the sulfoxide (1.0 g) in degassed benzene was irradiated under the usual conditions for 48 h. Chromatography on silica gel produced a rather impure product, which, after being rechromatographed and eluted with 1% acetone in methylene chloride, afforded white crystals (347 mg, 39%), mp 83–84 °C (cyclohexane); ir (Nujol) 1695, 1678 cm^{-1}; nmr ($CDCl_3$) δ 1.60 (3H, d, J = 7.5 Hz), 5.30 (1H, q, J = 7.5 Hz), 7.3–7.6 (6H, m), 7.8–8.1 (4H, m) ppm. *Anal.* calcd. for $C_{16}H_{14}O_2$: C 80.67, H 5.88; found: C 80.85, H 5.79.

The results suggest that this compound is 1,1-dibenzoylethane and this was confirmed by comparison (mp, mixture mp, ir, nmr) with an authentic sample prepared by methylation of dibenzoylmethane with methyl iodide and silver oxide (14).

Further fractions from the original chromatography produced only traces (<0.5%) of benzoic acid and some starting sulfoxide (117 mg, 12%).

Irradiation of 2,2-Dimethylthiochroman-4-one 1-Oxide

Method A

A solution of the sulfoxide (0.5 g) in degassed benzene (200 ml) was irradiated under nitrogen, with a Vycor filter, for 4 h. The residue was chromatographed on silica.

Elution with 1% acetone in methylene chloride gave a product (14 mg, 3%) which crystallized on standing; ir (Nujol) 1675 cm^{-1}; nmr ($CDCl_3$) δ 2.15 (3H, s), 2.52 (3H, s), 7.1–7.6 (3H, m), 7.87 (1H, dd, J = 1.5, 7.5 Hz) ppm. The spectral data and the mp (102–103 °C) for this compound are in accord with those reported for 2-isopropylidene-3-thiaindanone, mp 103–105 °C (30). Comparison with an authentic sample synthesized by the procedure of Morin *et al.* confirmed this conclusion.

A further solid product (38 mg, 8%) was obtained with the same eluent. This compound was shown by mp, mixture mp and spectral comparison to be identical with 2,2-dimethylthiochroman-4-one.

The starting sulfoxide (230 mg, 46%) was also recovered by elution with 50% acetone-methylene chloride.

Method B

Irradiation of the sulfoxide (0.5 g) in methanol (200 ml) with a Vycor filter, for 2 h and chromatography on silica gel led to the recovery of a new product (27 mg, 6%) by elution with benzene and 2% ether in benzene. This product was obtained as a white crystalline solid, mp 110–111 °C (benzene–petroleum ether); ir ($CHCl_3$) 2450 (w) and 1685(s) cm^{-1}; nmr ($CDCl_3$) δ 1.58 (1H, s, exchanges with D_2O), 1.85 (3H, s), 3.71 (2H, s), 4.91 (2H, br d, J_{gem} = 8 Hz), 7.1–7.35 (2H, m), 7.7–7.95 (2H, m) ppm; *m/e* 192 (M^+), 190, 177, 158, 145, 136 (100). *Anal.* calcd. for $C_{11}H_{12}OS$: C 68.75, H 6.25, S 16.66; found: C 68.84, H 5.84, S 16.88. This evidence is in accord with the thiol structure **47**. Starting material (180 mg, 36%) was also recovered on elution with ether.

Irradiation of the sulfoxide in mixtures of benzene and methanol containing 10–50% methanol gave essentially the same results. Use of a low-pressure (2 W Hanovia) mercury lamp gave a slightly improved conversion to thiol product (11%) after 4 h, but much less starting material was recovered in this experiment.

Method C

Irradiation of the sulfoxide (0.5 g) in a degassed mixture of benzene (100 ml) and isopropyl alcohol (100 ml) after 4 h, followed by the usual isolation procedure, indicated that no thiol was formed. The only identifiable compounds isolated from this experiment were 2,2-dimethylthiochroman-4-one (20 mg, 4%) and starting sulfoxide (150 mg, 30%).

Irradiation of 6-Methyl-2-phenylthiochroman-4-one 1-Oxide

A solution of the sulfoxide (1.0 g) in degassed benzene (200 ml) was irradiated under nitrogen for 24 h. Chromatography on silica gel gave among the early fractions an impure crystalline material which was rechromatographed and eluted with 1% ether in benzene as orange needles (125 mg, 14%) ir (Nujol) 1672 cm^{-1}; nmr ($CDCl_3$) δ 2.35 (3H, s), 7.3–7.9 (9H, m) ppm. The mp (144–145 °C; ethanol) of the photoproduct and the spectral data indicated the structure 5-methyl-2-benzylidene-3-thiaindanone (lit. (31) mp 145.5 °C). A sample of this compound was prepared by the alkaline condensation of benzaldehyde and 5-methylthiaindanone, synthesized by the method of Auwers and Arndt (31). The ir and nmr spectra of the samples were identical and the mp of the photoproduct remained undepressed on admixture with the authentic sample.

Further confirmation of the identity of the photoproduct was established by direct comparison of its dibromide, mp 111–113 °C, prepared on addition of bromine in chloroform, with the corresponding dibromide of 5-methyl-2-benzylidene-3-thiaindanone, lit (31) mp 116 °C.

The only other identifiable compound obtained on chromatography was the starting sulfoxide (441 mg, 44%) on elution with 30% acetone in methylene chloride.

Irradiation of 2,2,3,3-Tetramethylthiochroman-4-one 1-Oxide

Method A

Irradiation of the sulfoxide (200 mg) in dry benzene

(200 ml) in Pyrex for 6 h under nitrogen afforded on evaporation a yellow oil. Chromatography on silica gel and elution with 70–90% methylene chloride – carbon tetrachloride afforded an essentially colorless oil (62 mg, 33%), shown by ir and nmr spectral comparison to be identical with 2,2,3,3-tetramethylthiochroman-4-one. Starting sulfoxide (19 mg, 10%), eluted with 15% acetone in methylene chloride, and dark viscous oils were the only other materials obtained.

Method B

Irradiation of the sulfoxide (200 mg) in degassed acetone (150 ml) in Pyrex for 6 h under nitrogen, followed by a similar chromatographic separation afforded 2,2,3,3-tetramethylthiochroman-4-one (70 mg, 38%) and the starting sulfoxide (24 mg, 12%) as the sole identifiable products.

Acknowledgement

We thank the National Research Council of Canada for partial support of this work.

1. R. A. Archer and B. S. Kitchell. J. Am. Chem. Soc. **88**, 3463 (1966).
2. A. G. Schultz and R. H. Schlessinger. Tetrahedron Lett. 3605 (1973); 4787 (1973).
3. A. G. Schultz and R. H. Schlessinger. Chem. Commun. 1051 (1970); 1294 (1970).
4. B. S. Larsen, J. Kolc, and S.-O. Lawesson. Tetrahedron, **27**, 5163 (1971).
5. C. Ganter and J.-F. Moser. Helv. Chim. Acta, **54**, 2228 (1971).
6. E. Block. Q. Rep. Sulfur Chem. **4**, 317 (1969).
7. I. W. J. Still and M. T. Thomas. Tetrahedron Lett. 4225 (1970).
8. I. W. J. Still, M. S. Chauhan, and M. T. Thomas. Tetrahedron Lett. 1311 (1973).
9. W. C. Lumma and G. A. Berchtold. J. Org. Chem. **34**, 1566 (1969).
10. P. Y. Johnson and G. A. Berchtold. J. Org. Chem. **35**, 584 (1970).
11. I. W. J. Still and M. T. Thomas. J. Org. Chem. **33**, 2730 (1968).
12. G. Barbieri, M. Cinquini, S. Colonna, and F. Montanari. J. Chem. Soc. C, 659 (1968).
13. T. Inukai and R. Yoshizawa. J. Org. Chem. **32**, 404 (1967).
14. R. D. Abell. J. Chem. Soc. **101**, 989 (1912).
15. J. H. Bowie, D. H. Williams, S.-O. Lawesson, J. Ø. Madsen, C. Nolde, and G. Schroll. Tetrahedron, **22**, 3515 (1966).
16. C. K. Johnson, B. Dominy, and W. Reusch. J. Am. Chem. Soc. **85**, 3894 (1963).
17. (*a*) R. A. Finnegan and A. W. Hagen. Tetrahedron Lett. 365 (1963); (*b*) N. Kharasch and A. I. A. Khodair. Chem. Commun. 98 (1967).
18. W. L. Mock. J. Am. Chem. Soc. **92**, 6918 (1970).
19. A. G. Harrison, M. T. Thomas, and I. W. J. Still. Org. Mass Spectrom. **3**, 899 (1970).
20. G. M. Gurria and G. H. Posner. J. Org. Chem. **38**, 2419 (1973).
21. A. G. Schultz and R. H. Schlessinger. Tetrahedron Lett. 4787 (1973).
22. G. Kresze and W. Amman. Spectrochim. Acta A, **26**, 647 (1970).
23. M. S. Chauhan and I. W. J. Still. Can. J. Chem. **53**, 2880 (1975).
24. I. W. J. Still, M. S. Chauhan, and M. T. Thomas. Can. J. Chem. **51**, 839 (1973).
25. I. W. J. Still, M. T. Thomas, and A. M. Clish. Can. J. Chem. **53**, 276 (1975).
26. F. Krollpfeiffer, H. Schultze, E. Schlumbohm, and E. Sommermeyer. Chem. Ber. **58**, 1654 (1925).
27. F. Arndt. Chem. Ber. **58**, 1612 (1925).
28. R. Wolffenstein and J. Rolle. Chem. Ber. **41**, 733 (1908).
29. S. Takagi and H. Yasuda. Yakugaku Zasshi, **79**, 467 (1959).
30. R. B. Morin, D. O. Spry, and R. A. Mueller. Tetrahedron Lett. 849 (1969).
31. K. Auwers and F. Arndt. Chem. Ber. **42**, 541 (1909).

Can. J. Chem. Downloaded from www.nrcresearchpress.com by 210.87.254.6 on 09/05/12
For personal use only.

Fumaramine and bicucullinine: two minor alkaloids of *Corydalis ochroleuca* Koch

R. G. A. RODRIGO AND R. H. F. MANSKE
Department of Chemistry, University of Waterloo, Waterloo, Ontario N2L 3G1
AND
H. L. HOLLAND AND D. B. MACLEAN
Department of Chemistry, McMaster University, Hamilton, Ontario L8S 4M1

Received August 28, 1975

R. G. A. RODRIGO, R. H. F. MANSKE, H. L. HOLLAND, and D. B. MACLEAN. Can. J. Chem. **54**, 471 (1976).

The structures of two minor alkaloids of *Corydalis ochroleuca* have been resolved. Alkaloid F-46 is identical with fumaramine (**1**). Alkaloid F-45, bicucullinine, is a benzil, apparently derived from bicuculline, and possesses structure **3**.

R. G. A. RODRIGO, R. H. F. MANSKE, H. L. HOLLAND et D. B. MACLEAN. Can. J. Chem. **54**, 471 (1976).

On a élucidé la structure de deux alcaloides mineurs du *Corydalis ochroleuca*. L'alcaloide F-46 est identique à la fumaramine (**1**). L'alcaloide F-45, la bicucullinine, est un benzile qui semble être dérivé de la bicuculline et qui possède la structure **3**.

[Traduit par le journal]

The recent assignment (1) of structure **1** to the alkaloid fumaramine, isolated from *Fumaria paviflora* and *F. vaillanti* (2) and of structure **2** to an alkaloid of *F. offincinalis* (3), prompted this report of our concurrent investigation of two minor alkaloids of *Corydalis ochroleuca* designated F-45 and F-46 upon isolation (4).

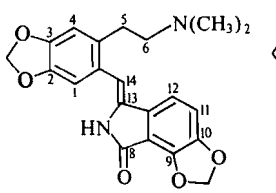

1

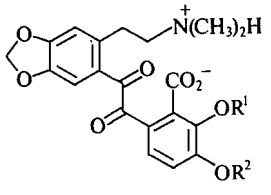

2 $R^1 = R^2 = CH_3$
3 $R^1 + R^2 = CH_2$

Alkaloid F-46, mp 227 °C, $C_{21}H_{20}N_2O_5$[1] exhibited spectral properties (pmr and ir) virtually identical with those reported (1, 2) for fumaramine (mp (2) 220–221 °C). Mass spectral data clearly indicated the presence of two nitrogen atoms, and determination of fragment ion compositions by high resolution mass spectrometry indicated a fragmentation pattern entirely consistent with structure **1**. Characteristic ions appeared at *m/e* 335(3) $C_{19}H_{13}NO_5$ ($M - C_2H_7N$), 293(2) $C_{17}H_{11}NO_4$ ($M - C_4H_9NO$), 204(12) $C_{12}H_{14}NO_2$, and 58(100) C_3H_8N. We therefore conclude that alkaloid F-46 is identical with fumaramine, and is correctly represented by structure **1**.

A second minor alkaloid of *C. ochroleuca*, F-45, mp 268 °C, for which we now propose the trivial name bicucullinine was originally suspected to be phenolic because of its solubility characteristics (4). Investigation of this alkaloid was hampered by extreme insolubility in organic solvents, and such spectral data as were readily available could not be consistently assigned to any known group of isoquinoline alkaloids. The proton magnetic resonance spectrum at 220 MHz (basic D_2O) showed absorption at δ 2.08 (6H, s), 2.34 (2H, m), 2.87 (2H, m), 5.90 (2H, s), 6.02 (2H, s), 6.75 (2H, broad s), and 7.32 (2H, broad s). Repetitive scanning at 220 MHz of a saturated solution of F-45 in CD_2Cl_2, with C.A.T. analysis, clearly showed two distinct signals at δ 6.70 and 7.82, assignable to single aromatic protons, and an AB quartet at δ 6.91 and 7.20 (J = 8 Hz) assignable to adjacent aromatic protons. The presence of a dimethylaminoethyl substituent and two methylenedioxy groups and the absence of other saturated proton absorptions was also apparent, and this, together with other spectral

[1]The molecular formula was determined by high resolution mass spectrometry and confirmed by elemental analysis.

Can. J. Chem. Downloaded from www.nrcresearchpress.com by 210.87.254.42 on 09/05/12
For personal use only.

Can. J. Chem. Downloaded from www.nrcresearchpress.com by 210.87.254.42 on 09/05/12
For personal use only.

and solubility data, led to the proposal of structure **3** for bicucullinine. This structure accords with other spectral data; ^{13}C nmr (basic D_2O) showed signals at 190.0 and 190.4 ppm downfield from TMS, attributable to carbonyl carbons, and a signal at δ 168.0 assignable to the carbon of a carboxylate anion. Structure **3** has been proposed for a minor alkaloid of *F. officinalis*, mp 275 °C (3), but no physical data were presented. Comparison of the spectral data available for **2** (3), however, with that of F-45, establishes the identity of the skeletal structure of the two alkaloids. Cryptopleurospermine, **4**, an alkaloid of *C. pleurosperma* (5), is a further

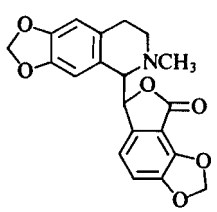

5

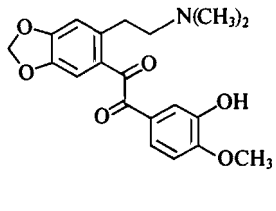

4

example of a naturally occurring benzil, and comparison of the spectral data of bicucullinine with that reported for **4** (5), strengthens the assignment of structure **3** to bicucullinine. It may be of significance that both F-45 and F-46 occur in a plant which contains bicuculline, **5**, as a major alkaloid component; the possibility that imides such as **1** are produced from phthalideisoquinolines during extraction has been noted (1, 6). The occurrence of bicucullinine in *C. ochroleuca* does, however, suggest that oxidative processes involving phthalideisoquinolines may occur *in vivo*.

Experimental

Melting points are uncorrected. Infrared spectra were obtained with a Beckman IR-5 spectrophotometer and proton magnetic resonance spectra at 100 MHz on a Varian HA 100 and at 220 MHz on the Varian HR 220 instrument of the Ontario Research Foundation, Sheridan Park, Ontario. Carbon magnetic resonance spectra were obtained at 22.62 MHz on a Brucker WH-90 instrument. Mass spectra were recorded on a CEC 21-110B spectrometer. High resolution mass measurements were performed by the reported method (7).

Isolation of the Alkaloids

The isolation and purification of fumaramine (F-46) and bicucullinine (F-45) has been previously described (4).

Fumaramine

Infrared (KBr), ν_{max} 1040, 1250, 1705, and 2700–3200 cm^{-1}; pmr (δ), 2.24 (6H, s, 2 × N—Me), 2.2–2.9 (4H, m, C-5 and C-6 H's), 5.95 (2H, s, —O—CH_2—O—), 6.18 (2H, s, —O—CH_2—O—), 6.41 (1H, s, C-14H), 6.77 (1H, s, aromatic H), 6.83 (1H, s, aromatic H), 7 03 and 7.27 (2H, ABq, C-11 and C-12 H's), and 8.10 (1H, broad s, N—H).

Bicucullinine

Infrared (KBr), ν_{max} 1040, 1595, 1625, and 1675 cm^{-1}; pmr, see text; cmr (δ), 28.0 (C-5), 40.5 (N—CH_3), 56.2 (C-6), 99.3, 99.7 (O—CH_2—O), 104.9, 108.8, 109.4, 118.9, 121.4, 122.4, 125.1, 137.8, 142.0, 142.5, 148.9, 149.8 (aromatic carbons), 168.0 (C-8), 190.0, and 190.4 (C-13, C-14); ms *m/e* (%)[2] 413(1), 395(52) $C_{21}H_{17}NO_7$, 377(56) $C_{21}H_{15}NO_6$, 365(14) $C_{20}H_{15}NO_6$, 352(34) $C_{19}H_{12}O_7$, 334(78) $C_{19}H_{10}O_6$, 322(100) $C_{18}H_{10}O_6$, 220(24) $C_{12}H_{14}NO_3$, 218(22) $C_{12}H_{12}NO_3$, 205(12) $C_{11}H_{11}NO_3$, 203(38) $C_{11}H_9NO_3$, 192(10) $C_9H_4O_5$, 50 (80) C_3H_8N. *Anal.* calcd. for $C_{21}H_{19}NO_8$:C 61.01, H 4.60, N 3.39; found: C 60.61, H 4.76, N 3.30.

Acknowledgment

We thank the National Research Council of Canada for financial support.

1. M. Shamma and J. L. Moniot. Chem. Commun. 89 (1975).
2. I. A. Ismailov, M. S. Yunusov, and S. Yu. Yunusov. Khim. Prir. Soedin. **6**, 588 (1970); Chem. Abstr. **74**, 42528m (1971); Chem. Nat. Comp. (USSR), **6**, 603 (1973).
3. P. Forgacs, J. Provost, R. Tiberghien, J.-F. Desconclois, G. Buffard, and M. Pesson. C. R. Acad. Sci. Paris, **276**, 105 (1973).
4. R. H. F. Manske. Can. J. Res. **17***B*, 95 (1939).
5. S. R. Johns, J. A. Lamberton, A. A. Sioumis, and R. I. Willing. Aust. J. Chem. **23**, 353 (1970).
6. J. Hodková, Z. Veselý, Z. Koblicová, J. Holubek, and J. Trojánek. Lloydia, **35**, 61 (1972).
7. C. K. Yu and D. B. MacLean. Can. J. Chem. **49**, 3025 (1971).

[2]The relative abundance of ions showed a marked dependence upon temperature. The quoted spectrum was recorded at 270 °C.

A total synthesis of myrrhine, (±)-hippodamine, and (±)-convergine

WILLIAM A. AYER, ROBIN DAWE, REINHOLD A. EISNER, AND KIMIAKI FURUICHI
Department of Chemistry, University of Alberta, Edmonton, Alberta T6G 2G2

Received September 8, 1975

WILLIAM A. AYER, ROBIN DAWE, REINHOLD A. EISNER, and KIMIAKI FURUICHI. Can. J. Chem. **54**, 473 (1976).

A seven-step, stereoselective, total synthesis of the ladybug defensive substance myrrhine (**5**) from 2,4,6-collidine is presented. Successive alkylation and acylation of 2,4,6-collidine followed by ketalization provides 2-(3-[2-(1,3-dioxolanyl)]propyl)-6-(2-methyl-2-[1,3-dioxolanyl]methyl)-4-methylpyridine (**14**). Sodium–alcohol reduction gives the corresponding all-*cis* piperidine **17**. Hydrolysis of **17** followed by acid-catalyzed cyclization provides ketone **26**. Reduction of the carbonyl group in **26** gives myrrhine (**5**). Cyclization using pyrrolidine – acetic acid gives a mixture of ketones (**26** and **31**). Reduction of **31** gives (±)-hippodamine (**4**). Oxidation of (±)-hippodamine with peracid gives (±)-convergine (**3**).

WILLIAM A. AYER, ROBIN DAWE, REINHOLD A. EISNER et KIMIAKI FURUICHI. Can. J. Chem. **54**, 473 (1976).

On présente une synthèse totale stéréosélective en sept étapes à partir de la collidine-2,4,6 pour la myrrhine (**5**), la substance défensive du moustique femelle. Une alkylation et une acylation de la collidine-2,4,6 suivies par une acétalisation fournit la ([(dioxolanyl-1,3)-2]-3 propyl)-2 (méthyl-2[dioxolanyl-1,3]-2 méthyl)-6 méthyl-4 pyridine (**14**). La réduction par le sodium dans l'éthanol conduit à la pipéridine toute *cis* correspondante (**17**). L'hydrolyse de **17**, suivie par une cyclisation acido catalysée, fournit la cétone **26**. La réduction du groupement carbonyle dans **26** donne la myrrhine (**5**). La cyclisation sous l'influence de la pyrrolidine et de l'acide acétique donne un mélange de cétones (**26** et **31**). La réduction de **31** donne la (±)-hippodamine (**4**). L'oxydation de la (±)-hippodamine par un peracide fournit la (±)-convergine (**3**).

[Traduit par le journal]

Can. J. Chem. Downloaded from www.nrcresearchpress.com by 210.87.254.5 on 09/05/12
For personal use only.

Coccinellidae (ladybugs or ladybirds) are colorful insects of importance in the natural control of aphids, mealy bugs, and scale insects (1). When molested these insects release droplets of orange liquid at their joints, known as *reflex bleeding*, and this has been shown to provide efficient protection against certain predators (2, 3). In recent years, Tursch and co-workers have isolated and determined the structures of the defensive substances present in several species of Coccinellidae[1] and have shown that most of these are stereoisomers of 2-methylperhydro-9b-azaphenalene and the corresponding *N*-oxides. These include coccinelline **1**, and the corresponding free base precoccinelline **2** (5, 6), convergine **3**, and its free base hippodamine **4** (7), and myrrhine **5** (4). We wish at this time to report the total synthesis of myrrhine **5**, and racemic convergine **3**, and hippodamine **4**.

Some years ago we reported (8) the synthesis of (±)-dihydrodeoxyepiallocernuine, **6**, a degradation product of the *Lycopodium* alkaloid cernuine (enantiomer of **7**). The striking similarity between the BCD ring system of **6** and myrrhine prompted us to investigate a similar approach to the synthesis of the ladybug defen-

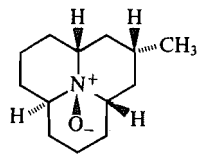

1
2 (free base of **1**)

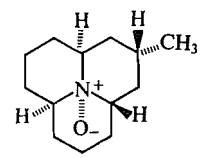

3
4 (free base of **3**)

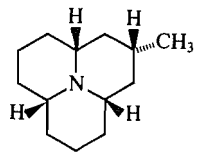

5

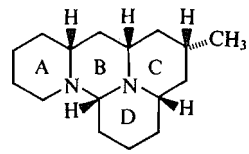

6

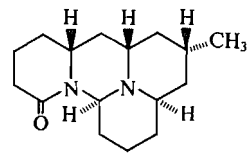

7

[1]For summarizing articles see refs. 3 and 4.

Can. J. Chem. Downloaded from www.nrcresearchpress.com by 210.87.254.5 on 09/05/12
For personal use only.

sive substances. In particular, our initial objective was the all-*cis* keto aldehyde **8**, designed to serve as a precursor of the immonium ion **9**, which we hoped could be induced to cyclize to the perhydro-9b-azaphenaline system of precoccinelline, **2**, and/or myrrhine, **5**.

Alkylation of the monolithium derivative, **10**, of 2,4,6-collidine, generated by treatment of the latter with either *n*-butyllithium or phenyllithium in ether, with β-bromopropionaldehyde dimethyl acetal (9) gave the acetal **11** in 41% yield. Alternatively, **11** could be prepared in 40% overall yield by alkylation of collidyllithium, **10**, with β-chloropropionaldehyde diethyl acetal followed by acid-catalyzed acetal exchange.

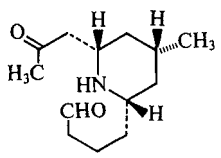

8

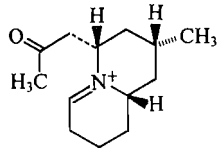

9

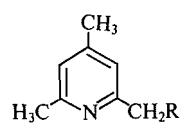

10 R = Li
11 R = $-CH_2CH_2CH(OCH_3)_2$
15 R = $-COCH_3$
16 R = 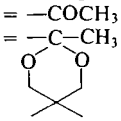

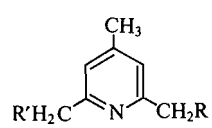

12 R = $-CH_2CH_2CH(OCH_3)_2$
R′ = $-COCH_3$
14 R = $-CH_2CH_2CH$
R′ = 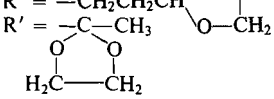

The introduction of an acetyl group into the 6-methyl group of **11** proved somewhat troublesome. The acylation of the methyl group of α-picoline has been studied in some detail by Wibaut and co-workers (10), who found acetonitrile to be the most convenient acetylating agent. Treatment of **11** with phenyllithium in ether, followed by very slow addition of one equivalent of acetonitrile in ether provides, after workup, the ketone **12** in 35–45% yield along with considerable amounts of unreacted starting material. Use of excess acetonitrile led to diminished yields, presumably due to the competition between addition and proton abstraction. Use of acetyl chloride as the acylating agent gave mainly **13**, the product of double addition. Treatment of the lithio derivative of **11** with *N*,*N*-dimethylacetamide in ether at −30 °C (11) provided ketone **12** in only 15% yield.

Separation of keto acetal **12** from starting material **11** either by distillation or chromatography proved difficult. Since the next step in the projected synthesis involved protection of the carbonyl function in **12**, it was found more efficient to treat a toluene solution of the crude product obtained from the acylation reaction with an excess of ethylene glycol and an acid catalyst. During this treatment the dimethyl acetal was exchanged for the ethylene acetal (in both **11** and **12**) and the keto group in **12** was transformed to the ethylene acetal to give **14**. The mixture of acetals could be separated by careful chromatography over alumina. In this way **11** may be transformed into **14** in 40–45% yield using acetonitrile as the acylating agent. In addition approximately 40% of **11** is recovered (as the ethylene acetal).

8-Acetoxyquinoline has been used successfully as an acylating agent for Grignard reagents (12). Treatment of an ether solution of the lithio derivative of **11** with 8-acetoxyquinoline at 0 °C followed by transformation of the crude products into the ethylene acetals and chromatography provided **14** in 37% yield, along with starting material **11** (as the ethylene acetal, 14%), and **13** (as the ethylene acetal, 9%). Although this method provides **14** almost as efficiently as the acetonitrile method, the latter is preferred since the reagent is much less expensive. Proof that acetylation has occurred at the 6-methyl group rather than the 4-methyl of **11** is provided by the proton magnetic resonance (pmr) spectra of **12** and **14** which clearly show the presence of a pyridine γ-methyl group (δ 2.38 in each) (8, 13).

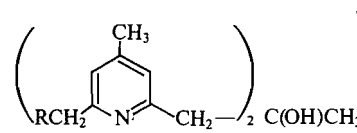

13 R = $CH_2CH_2CH(OCH_3)_2$

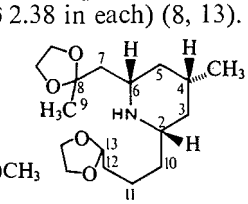

17

Can. J. Chem. Downloaded from www.nrcresearchpress.com by 210.87.254.5 on 09/05/12
For personal use only.

The alternative route to **14** involving first addition of the keto side chain then addition of the aldehyde side chain was investigated briefly. Treatment of collidyllithium, **10**, with acetonitrile gave the ketone **15** in 34% yield. Treatment of the ethylene acetal of **15** with phenyllithium in ether followed by allyl bromide led to a product mixture which did not contain an ethylene acetal signal in the nmr. Since ethylene acetals are known to be unstable towards strong bases (14), **15** was transformed to the neopentyl acetal **16**. Treatment of **16** with one equivalent of phenyllithium followed by deuterium oxide gave a monodeuterated **16** in which the signal for the methylene group adjacent to both the protecting group and the pyridine ring (δ 3.18) integrated for only one proton, indicating the formation of the lithio derivative at this position rather than at the desired 6-methyl position. This approach was not pursued further.

Reduction of the diacetal **14** with sodium in isoamyl alcohol provided a mixture of stereoisomers of which the major component was the desired all-*cis* piperidine **17**. Separation of **17** (in about 60% yield) from the remaining stereoisomers was achieved by chromatography over silica gel. Compound **17** has a higher R_f value than the remaining isomers and is eluted first on chromatography. The more polar isomers (tlc indicated at least two) were not separated from one another by this method. Structure **17** was assigned to the major component of the reduction on the following basis. The mass spectrum showed a weak molecular ion at *m/e* 313, a base peak at *m/e* 198 corresponding to ion **18**, and a peak at *m/e* 212 corresponding to **19**. The pmr spectrum is consistent with the assigned constitution (see Experimental). Dissolving metal reduction of **14** is expected to give the thermodynamically more stable all-*cis* isomer **17** as the major product (8). Confirmation of this assignment is obtained by consideration of the ^{13}C nuclear magnetic resonance (cmr) spectrum (Table 1) of **17**. By application of chemical shift theory and standard decoupling techniques (15, 16) it is possible to assign all the carbon shifts for compound **17**. The proton decoupled cmr spectrum displays 16 signals, one signal corresponding to two carbons, and the off-resonance decoupled spectrum reveals the substitution (methyl, methylene, etc.) of these carbons as shown in Table 1. The shifts of the side-chain carbons were assigned by direct analogy with the reported values for **20** (17). The models chosen for calculating the shifts of the carbons of the piperidine ring and the 4-methyl group were piperidine, 2-methylpiperidine, 2-propylpiperidine (16), 4-methylpiperidine (15), and the isomeric 1,3,5-trimethylcyclohexanes (15*a*). For example, the methine carbon of 4-methylpiperidine resonates at δ 31.3. In **17** the C-4 methine signal appears at δ 31.5. If either the C-2 or C-6 side chain were axial, a γ-gauche effect would shift the C-4 resonance upfield by 5–6 ppm (15). The methyl group in 4-methylpiperidine (equatorial) resonates at δ 22.5, in **17** the C-4 methyl signal is at δ 22.3. In the 1,3,5-trimethylcyclohexanes, an axial methyl resonates about 4 ppm to higher field than equatorial methyl and a similar shift would be expected in the 2,4,6-substituted piperidines if the methyl were axially orientated. Similar considerations lead to the remaining assignments in Table 1. The cmr data, combined with proof of the *cis*-relationship of the side chains at C-2 and C-6 discussed below, provide firm evidence that the major product of the reduction is the desired all *cis* isomer **17**.

TABLE 1. ^{13}C chemical shifts for **17**[a]

Chemical shift (δ TMS)	Substitution	Assignment[b]
20.6	$>CH_2$	C-11
22.3	$-CH_3$	C-4 methyl
24.3	$-CH_3$	C-9
31.5	$>CH$	C-4
34.0	$>CH_2$	C-10
36.9	$>CH_2$	C-12
41.1	$>CH_2$	C-5[c]
42.3	$>CH_2$	C-3[c]
45.3	$>CH_2$	C-7
53.2	$>CH$	C-6
56.4	$>CH$	C-2
64.4	$>CH_2$	ethylene acetals
64.7	$>CH_2$	ethylene acetals
64.8[d]	$>CH_2$	ethylene acetals
104.6	$>CH$	C-13
110.2	$-\overset{\vert}{\underset{\vert}{C}}-$	C-8

[a]Spectrum determined in $CDCl_3$.
[b]See **17** for numbering system.
[c]C-5 and C-3 may be reversed.
[d]Two carbons.

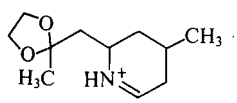

18

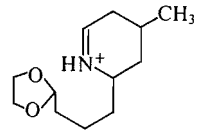

19

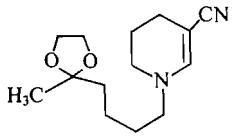

20

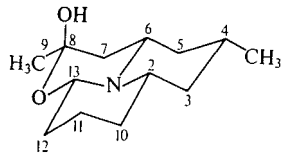

21

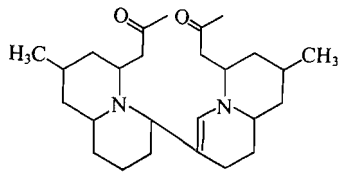

22

Removal of the protecting groups from **17** was accomplished by hydrolysis with 5% aqueous hydrochloric acid. The crystalline product has the molecular composition $C_{13}H_{23}NO_2$ expected for the keto aldehyde **8**, but does not show carbonyl absorption in the infrared (ir). The ir spectrum does however show hydroxyl absorption, as well as intense Bohlmann bands (18) in the region 2600–2870 cm^{-1}. The pmr spectrum shows a methyl doublet at δ 0.90, a methyl singlet at δ 1.43, and a one proton multiplet at δ 4.02. The product is thus the hemiketal **21** of the carbinolamine form of keto aldehyde **8**. The appearance of intense Bohlmann bands in the infrared spectrum of **21** indicates that at least two of the hydrogens on carbons α to nitrogen *and* the nitrogen lone pair are antiperiplanar (18). *Assuming that all the six-membered rings are in the chair conformation, the only configuration which meets this condition is the all cis (referring to H's at ring junctions) configuration shown for* ***21***. This provides additional evidence that the side chains at C-2 and C-6 in **17** are *cis*-related. The methyl group at C-4 in **21** resonates at δ 22.0 in the cmr spectrum, indicating its equatorial nature (see above). The methyl at C-8 appears at δ 30.2 and is also assigned the equatorial configuration, using 5-*tert*-butyl-2,2-dimethyl-1,3-dioxane (equatorial methyl δ 27.98, axial methyl δ 20.28 (19)) as a model compound.

When the hemiketal **17**, which crystallizes in hydrated form, is heated to 60–70 °C *in vacuo*, it is transformed into a compound showing strong carbonyl absorption (1715 cm^{-1}) and olefinic absorption (1655 cm^{-1}) in the ir. The mass spectrum of this material shows an apparent molecular ion at *m/e* 414 and an intense fragment peak at *m/e* 357. It is known that *N*-substituted 2-piperideines dimerize readily (20) and structure **22** is suggested for this substance, the peak at *m/e* 357 in the mass spectrum resulting from loss of an acetonyl side chain.

Our attention now turned to methods for generating the immonium salt **9** and its enol **23** (Y = OH) or enamine **23** (Y = NR_2) forms which should be capable of cyclization as illustrated in **23**. 'Top-side' addition of the enol or enamine to the immonium double bond (arrow *a*) would lead to the ketone **24** possessing the stereochemistry of precoccinelline (**2** = **25**), while 'bottom-side' attack (arrow *b*) would lead to the ketone **26**, possessing the myrrhine (**5** = **27**) configuration. *A priori*, the preferred direction of cyclization could not be predicted with con-

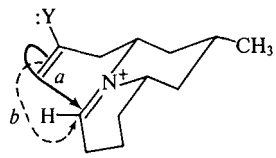

23

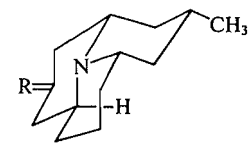

24 R = O
25 R = H,H

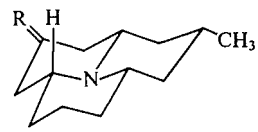

26 R = O
27 R = H,H

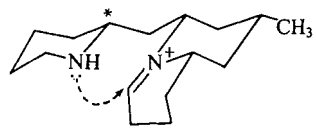

28

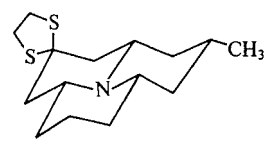

29

Can. J. Chem. Downloaded from www.nrcresearchpress.com by 210.87.254.5 on 09/05/12
For personal use only.

Can. J. Chem. Downloaded from www.nrcresearchpress.com by 210.87.254.5 on 09/05/12
For personal use only.

fidence. In the case of the immonium ion **28**, an intermediate in the synthesis of dihydrodeoxyepiallocernuine (8), addition of the amine to the immonium double bond occurs exclusively from the 'bottom-side'. However, in the case of the compound epimeric with **28** at the carbon bearing the asterisk, both modes of cyclization are observed (8).

Attempts to cyclize the hemiketal **21** by heating with aqueous acid or base were unsuccessful. However, when a toluene solution of **21** was heated in the presence of two equivalents of *p*-toluenesulfonic acid the ketone **26** was obtained in high yield. The ir spectrum of the ketone shows carbonyl absorption at 1728 cm^{-1} and strong Bohlmann bands, this latter feature serving to distinguish **26** from the other possible isomer, **24**. Ketone **26** proved to be rather unstable, rapidly discoloring when exposed to air, and in most cases the crude product resulting from the cyclization was converted directly into the thioketal **29**. After chromatography, the crystalline thioketal **29** was obtained in 60% overall yield from hemiketal **21**. The thioketal also shows very pronounced Bohlmann bands in the ir confirming the stereochemical assignment.

The thioketal **29** was desulfurized using W-2 Raney nickel in refluxing ethanol. Distillation of the crude product, which showed only one spot on tlc, gave myrrhine[2] (**5** = **27**) in 64% yield. Oxidation of the synthetic myrrhine with *m*-chloroperbenzoic acid provided crystalline myrrhine *N*-oxide, **30**, identical in all respects[3] with that prepared from myrrhine. In connection with the cmr assignments discussed above, it is worthwhile noting that the signal for the methyl carbon in **30** appears at δ 21.4, approximately the same shift as in **17** and **21**.

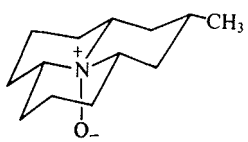

30

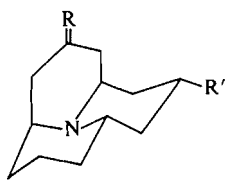

31 R = H,H, R′ = CH_3
32 R = O, R′ = CH_3
33 R = O, R′ = H

The acid-catalyzed cyclization of **21**, presumably through the intermediate enol immonium ion **23** (Y = OH), appears to proceed completely via 'bottom-side' attack (arrow *b* in **23**), although this may be the result of a thermodynamic rather than a kinetic process. In an effort to obtain the coccinelline geometry, other methods of cyclization were investigated. When the hemiketal **21** was heated with pyrrolidine and acetic acid in tetrahydrofuran, the resulting product (ir 1725 cm^{-1}) consisted of two components (by tlc), one having the same R_f as ketone **26**, the other being more polar. The mixture was treated with ethanedithiol–BF_3, and the resulting mixture of thioketals (two spots on tlc) desulfurized in the usual manner. The crude product from the desulfurization also showed two spots on tlc, one having an R_f value identical with that of myrrhine, the other similar to that of precoccinelline (**2** = **25**). The two components were separated by preparative tlc and the component of higher R_f was identified as myrrhine (**5** = **27**). The other component, isomeric with myrrhine (mass spectrum) and lacking Bohlmann bands in the ir, was expected to be precoccinelline. However, the ir spectrum was clearly different from that of precoccinelline. This isomeric base was transformed to the *N*-oxide. Comparison of the spectra of this *N*-oxide and its hydrochloride with those of coccinelline, **1**, and coccinelline hydrochloride again revealed differences. *However, comparison of the spectra of our synthetic base and its N-oxide with those of hippodamine, **4**, and convergine, **3**, respectively, showed that they were identical.*[4] The overall yields of myrrhine and racemic hippodamine from hemiketal **21** were 33% and 23%, respectively.

The formation of hippodamine (**4** = **31**) requires epimerization of the side chain at C-6 prior to cyclization. In the presence of both acid and base this may involve a reversible shift of the immonium double bond as illustrated in Scheme 1. Although ion **c** is expected to be a minor component in the equilibrium mixture, the axial side chain is ideally situated for ring closure (to **32**) and the rate of cyclization of **c** may well exceed that of **a**.

We have been unable to define reaction condi-

[2]The ir spectrum of synthetic myrrhine was identical with that of natural myrrhine. We wish to thank Prof. B. Tursch for the ir spectrum of myrrhine.

[3]We wish to thank Prof. B. Tursch for making this comparison.

[4]We wish to thank Prof. B. Tursch for providing comparison samples and spectra of coccinelline, precoccinelline, hippodamine, and convergine.

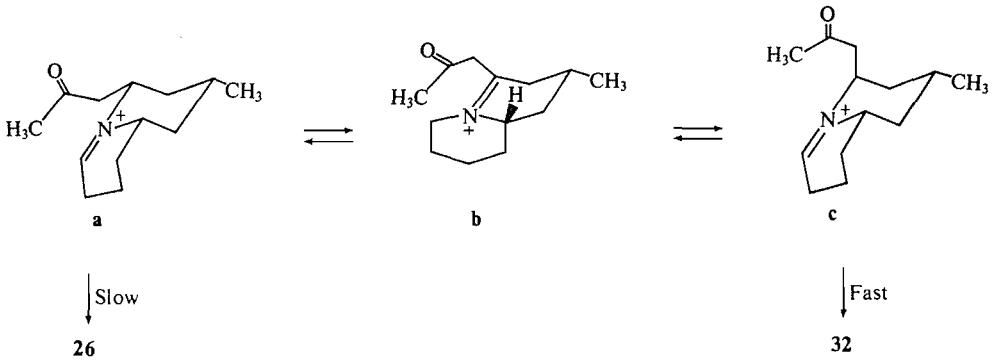

SCHEME 1

ions which lead to cyclization of **21** to give ketone **24**, and thus coccinelline. However, it is noted that ketone **33**, *potentially* available by this route starting from 2,6-lutidine instead of 2,4,6-collidine, is a possible precursor of precoccinelline, **2**. Replacement of the carbonyl group in **33** with an equatorial methyl group gives **2**. This route is being investigated.

Experimental

Solutions were dried over anhydrous magnesium sulfate unless otherwise specified. Skellysolve B refers to Skelly Oil Company light petroleum, bp 62–70 °C. Melting points were determined on a Fisher-Johns or Leitz–Wetzlar hot-stage melting point apparatus and are uncorrected. Microanalyses were performed by the Microanalytical Laboratory of this department.

Infrared spectra were recorded on a Perkin-Elmer Model 337 grating ir spectrophotometer, a Unicam SP 1000 grating ir spectrophotometer, or a Perkin-Elmer Model 421 dual grating ir spectrophotometer.

Proton magnetic resonance spectra were measured using a Varian Associates Model A-60 spectrometer or a Varian Model HR-100 spectrometer with tetramethylsilane as internal standard. Spectra were determined in $CDCl_3$ unless otherwise noted. Only significant signals are quoted.

^{13}C nuclear magnetic resonance spectra were obtained on natural abundance samples in $CDCl_3$ at 22.63 MHz (Bruker HFX-90 interfaced to a Nicolet 1085 computer) in the pulse Fourier mode. Shifts are quoted relative to internal tetramethylsilane (δ_{TMS}).

Mass spectra including high resolution measurements (hrms) were recorded on a A.E.I. model MS-9 mass spectrometer and are reported as *m/e* (relative intensity). Unless diagnostically significant only peaks over *m/e* 50 and at least 20% as intense as the base peak are recorded.

3-Bromo-1,1-dimethoxypropane, ***9***

A stirred solution of anhydrous methanol (23.1 g) and freshly distilled acrolein (40.3 g) was cooled to −15 °C and hydrogen bromide bubbled in until 123.4 g had absorbed. The resulting mixture was poured into a cold separatory funnel and the layers allowed to separate. The bottom layer was drawn off, dried over $CaCl_2$, and then distilled rapidly (60–80 °C/16 Torr) to prevent polymerization. The resultant mixture of 1,3-dibromo-1-methoxypropane and 3-bromo-1,1-dimethoxypropane (80 g) was added slowly to anhydrous methanol (300 ml) cooled in an ice bath. The resulting solution was kept at room temperature for 20 h. The methanol was then removed under reduced pressure on a rotary evaporator to leave a clear brown oil (59.2 g) which by nmr (δ 2.23 (2,H q, J = 6.5 Hz), 3.37 (3H, s), 3.43 (2H, t, J = 6.5 Hz), 4.55 (1H, t, J = 6.5 Hz)) appears to be essentially pure 3-bromo-1,1-dimethoxypropane. Distillation of the product gives a clear distillate which by pmr appears to be a mixture of the desired compound and 1,1,3-trimethoxypropane. Undistilled material was used directly in the next step.

2-(4,4-Dimethoxybutyl)-4,6-dimethylpyridine, ***11***

Using 3-Bromo-1,1-dimethoxypropane

2,4,6-Collidine (26.0 g, 0.215 mol, freshly distilled Eastman–Kodak or BDH reagent grade; Matheson, Coleman and Bell technical grade proved unsatisfactory since it contains considerable amounts of 2,3,6-trimethylpyridine which are not readily removed by distillation) in ether (200 ml) was added dropwise over 30 min to a solution of phenyllithium (18 g, 0.215 mol, prepared from bromobenzene and lithium metal) in ether (200 ml) under nitrogen. The resultant blood-red solution was stirred at room temperature for 1 h, then a solution of 3-bromo-1,1-dimethoxypropane (39.2 g, 0.214 mol) in ether (70 ml) was added dropwise over 1 h. The solution was stirred overnight and then water (80 ml) added dropwise. The layers were separated, the aqueous layer washed with ether (2 × 50 ml), and the combined ether solutions washed with water and saturated brine. Removal of the ether left a reddish brown oil (43.4 g) which was distilled under reduced pressure. After a forerun consisting mainly of 2,4,6-collidine and the bromoacetal (10.2 g, bp 25–73 °C/5 Torr), compound **11** (19.3 g, 41%), bp 107–112 °C/1 Torr, n_D^{22} 1.4904, was obtained as a colorless liquid. *Anal.* calcd. for $C_{13}H_{21}NO_2$: C 69.96, H 9.42, N 6.28; found: C 70.16, H 9.54, N 6.26.

Infrared spectrum: ν_{max} (neat) 1610, 1570, 1120, and 1065 cm^{-1}. Proton magnetic resonance spectrum: δ 2.28 (3H, s, C-2 methyl), 2.51 (3H, s, C-4 methyl), 3.35 (6H, s,

Can. J. Chem. Downloaded from www.nrcresearchpress.com by 210.87.254.5 on 09/05/12
For personal use only.

Can. J. Chem. Downloaded from www.nrcresearchpress.com by 210.87.254.5 on 09/05/12
For personal use only.

methoxyls), 4.43 (1H, t, J = 5 Hz, acetal H), and 6.87 (2H, s, aromatic protons). Mass spectrum: 223 (1, M^+), 192(92), 191(28), 176(35), 148(49), 121(100), 75(84). *Mol. Wt.* calcd. for $C_{13}H_{21}NO_2$ (molecular ion): 223.1572; found: 223.1566.

Using 3-Chloro-1,1-diethoxypropane Followed by Ketal Exchange

To a solution of phenyllithium (6.72 g, 0.08 mol) in ether (250 ml) under nitrogen was added dropwise a solution of 2,4,6-collidine (9.7 g, 0.08 mol) in ether (30 ml). The mixture was stirred for 2 h at room temperature and then to the blood-red solution was added dropwise a solution of 3-chloro-1,1-diethoxypropane (Aldrich Chemicals, 13.3 g, 0.08 mol) in ether (30 ml). The mixture was stirred overnight and worked up as above. Distillation afforded 2-(4,4-diethoxybutyl)-4,6-dimethylpyridine (9.1 g, 45%), bp 120–124 °C/1.2 Torr, n_D^{23} 1.4844. Infrared spectrum: ν_{max} (neat) 1610, 1570, 1125, and 1060 cm^{-1}. *Anal.* calcd. for $C_{15}H_{25}NO_2$: C 71.71, H 9.96, N 5.58; found: C 71.59, H 9.99, N 5.56. *Mol. Wt.* calcd. for $C_{15}H_{25}NO_2$: 251; found (ms): 251.

The diethyl acetal (10.3 g) was dissolved in dry methanol (250 ml) and *d*-10-camphorsulfonic acid (10.2 g) added. The solution was distilled slowly during which time methanol was added dropwise to maintain the volume. After 100 ml of methanol was collected, the solution was cooled and sodium carbonate (10 g) added. The mixture was stirred vigorously, filtered, and evaporated. The residue was partitioned between ether and water. The ether solution was dried and distilled to give 2-(4,4-dimethoxybutyl)-4,6-dimethylpyridine (**11**, 8.3 g), identical with that described above.

2-(3-[2-(1,3-Dioxolanyl)]propyl-6-(2-methyl-2-[1,3-dioxolanyl]methyl)-4-methylpyridine, ***14***

Acetonitrile Method

A solution of 2-(4,4-dimethoxybutyl)-4,6-dimethylpyridine (**11**, 12.0 g, 0.054 mol) in anhydrous ether (20 ml) was added dropwise, under nitrogen, to a stirred solution of phenyllithium (4.54 g, 0.054 mol) in ether (40 ml) at room temperature. After 30 min, freshly distilled acetonitrile (2.1 g, 0.051 mol) in ether (100 ml) was added dropwise over a period of 4 h. The solution was stirred for an additional hour, then 2.4 *N* HCl in dry methanol (100 ml) was added dropwise. The solution turned yellow (from blood-red) and a precipitate separated. This mixture was stirred overnight, then triethylamine (25 g, 0.25 mol) was added dropwise, and the solution poured into saturated sodium bicarbonate (100 ml). The layers were separated, the aqueous layer washed with ether (2 × 50 ml), and the combined ether layers washed with saturated sodium bicarbonate, then saturated brine. Removal of the ether gave a dark brown oil (13.7 g, ν_{max} (neat) 1720 cm^{-1}, crude **12**) which was dissolved in toluene (20 ml) and added to a solution of ethylene glycol (15.0 g, 0.24 mol) and *p*-toluenesulfonic acid monohydrate (13.1 g, 0.07 mol) in toluene (350 ml). The mixture was heated under reflux (Dean–Stark water separator) for 18 h, then cooled and triethylamine (7.1 g, 0.07 mol) added. The solution was washed with 5% sodium bicarbonate, water, and brine. Removal of the toluene under reduced pressure gave a dark oil which was chromatographed over alumina (300 g, Alcoa F-20, activity I-II), Elution with toluene (6 l) provided the ethylene acetal of **11** (4.8 g), elution with toluene–ether (1 l of 4:1) gave a mixture of **11** (ethylene acetal) and **14**, and elution with toluene–ether (4 l of 1:1) gave the title compound **14** (5.7 g, 41%), bp 146–149 °C/0.08 Torr, n_D^{23} 1.5132. *Anal.* calcd. for $C_{17}H_{25}NO_4$: C 66.45, H 8.14, N 4.56; found: C 66.58, H 8.27, N 4.53. *Mol. Wt.* calcd. for $C_{17}H_{25}NO_4$: 307.1784; found (hrms): 307.1769.

Infrared spectrum: ν_{max} 1610, 1570, 1130, and 1045 cm^{-1}. Proton magnetic resonance spectrum: δ 1.36 (3H, s), 1.82 (4H, m), 2.28 (3H, s), 2.77 (2H, m), 3.05 (2H, s), 3.90 (8H, m), 4.87 (1H, t, J = 4.5 Hz), 6.85 (1H, s), and 6.95 (1H, s). Mass spectrum: 307(1, M^+), 221(55), 207(16), 187(100).

8-Acetoxyquinoline Method

A solution of compound **11** (2.23 g, 8.9 mmol) in anhydrous ether (20 ml) was added dropwise to a solution of phenyllithium (0.87 g, 10.4 mmol) in ether (8 ml) at room temperature. The solution was stirred for 2 h, then cooled to 0 °C, and a solution of 8-acetoxyquinoline (1.87 g, 10 mmol) in ether (20 ml) was rapidly added. The temperature rose to 15 °C and the solution was stirred at this temperature for 15 min, then water (20 ml) added. The yellow precipitate which separated was removed by filtration, the filtrate diluted with chloroform (150 ml), washed with saturated sodium bicarbonate, and evaporated to leave a brown oil (2.95 g). This oil was then ketalized as described under 'acetonitrile method'. The resulting product (2.57 g) was chromatographed over alumina (100 g). Elution with benzene (500 ml) gave starting material (0.30 g, as ethylene acetal). Elution with benzene–ether (500 ml of 4:1) gave the title compound **14** (1.15 g, 37%), identical with that described above. Elution with ether (300 ml) gave the ethylene acetal of the double addition product **13** (0.39 g, 9%), ν_{max} 3300 (br), 1612, and 1570 cm^{-1}. The structure of this product is apparent from the molecular weight (M^+ = 484) and the pmr spectrum: δ 1.14 (3H, s, HO—C(—CH_3)—), 1.6–2.0 (8H, m), 2.27 (6H, s, pyridine γ-methyls), 2.74 (4H, t, J = 6.5 Hz), 2.88 (4H, s), 3.75–3.95 (8H, m), 4.87 (2H, t, J = 4.5 Hz), 6.82 (2H, s), and 6.86 (2H, s).

2-(3-[2-(1,3-Dioxolanyl)]propyl)-cis-4-methyl-cis-6-(2-methyl-2[1,3-dioxolanyl]methyl)-piperidine, ***17***

Sodium (5.2 g) was added to a refluxing solution of compound **14** (2.63 g) in freshly distilled isoamyl alcohol (70 ml) in a nitrogen atmosphere. Heating was continued until all the sodium had reacted (*ca.* 1.5 h), then water (70 ml) was added and the layers separated. The aqueous layer was extracted with chloroform (3 × 50 ml) and the combined organic layers washed with water and brine. Removal of the solvents under reduced pressure left a viscous oil (3.1 g) which was chromatographed over silica gel (60 g) using chloroform–methanol–dimethylamine (100:10:1) as the eluant at a flow rate of 3 ml/h. Three ml fractions were collected. Fractions 51 to 68 gave the title compound **17** (1.65 g, 62%) as a colorless oil. Fractions 71 to 100 gave material (0.66 g) isomeric (by ms) with **17**.

An analytical sample of **17** was prepared by molecular distillation (120–130 °C/0.05 Torr), n_D^{20} 1.4784. *Anal.* calcd. for $C_{17}H_{31}NO_4$: C 65.18, H 9.90, N 4.47; found:

Can. J. Chem. Downloaded from www.nrcresearchpress.com by 210.87.254.5 on 09/05/12
For personal use only.

C 65.39, H 10.08, N 4.64. *Mol. Wt.* calcd. for $C_{17}H_{31}NO_4$: 313.2253; found (hrms): 313.2246.

Infrared spectrum: ν_{max} 3320, 1120, and 1030 cm^{-1}. Proton magnetic resonance spectrum: δ 0.90 (3H, d, J = 5.5 Hz), 1.35 (3H, s), 3.95 (8H, m), and 4.87 (1H, t, J = 4 Hz). ^{13}C magnetic resonance spectrum: see Table 1. Mass spectrum: 313(1, M^+), 212(12), 198(100), 87(20).

Hemiketal 21

A solution of compound **17** (1.25 g) in 5% aqueous hydrochloric acid (25 ml) was stirred at room temperature for 18 h. The solution was made basic by the addition of 5% aqueous sodium bicarbonate and extracted with methylene chloride. Evaporation left a solid residue (1.10 g) which was recrystallized from ether–hexane to give **21** (0.76 g), mp 58–60 °C (dec.). Hemiacetal **21** crystallizes in hydrated form and it has not been possible to obtain consistent combustion analyses. The infrared spectrum of crystalline **21** dissolved in chloroform shows, besides hydroxyl absorption at 3595, bands due to water (21) at 3680 and 1605 cm^{-1}. After azeotropic removal of the water and redissolving in chloroform, the bands at 3680 and 1605 cm^{-1} are no longer present. Attempts to remove water by heating *in vacuo* lead to 'dimerization' to **22**. *Mol. Wt.* calcd. for $C_{13}H_{23}NO_2$: 225.1729; found (hrms): 225.1724.

Infrared spectrum: ν_{max} (KBr) 3500, 3200 (broad), 2820, 2780, 2740, 2630, and 2610 cm^{-1} (Bohlmann bands). Proton magnetic resonance spectrum: δ 0.88 (3H, d, J = 6 Hz), 1.42 (3H, s), and 4.00 (1H, m). ^{13}C magnetic resonance spectrum: δ 94.6(C-8), 84.8(C-13), 59.3(C-6), 55.3(C-2), 41.9(CH_2), 41.6(CH_2), 41.2(CH_2), 32.7(CH_2), 31.8(CH_2), 30.2(C-4), 30.2(C-9), 22.3(CH_2), and 22.0(CH_3 at C-4). Mass spectrum: 225(8, M^+), 224(17), 210(11), 207(20), 150(100).

Thioketal 29

The hemiketal **21** (296 mg) was dissolved in toluene (50 ml) and *p*-toluenesulfonic acid monohydrate (499 mg) added. The vigorously stirred mixture was heated under reflux (Dean–Stark water separator) in a nitrogen atmosphere for 3 h, then cooled and triethylamine (1 ml) added. The solution was poured into saturated sodium bicarbonate and the layers separated. The aqueous layer was washed twice with methylene chloride and the organic layers combined and concentrated under reduced pressure to give crude ketone **26** as a pale yellow oil (294 mg). Infrared spectrum: ν_{max} (neat) 2795, 2755, 2715, 2610 (Bohlmann bands), and 1725 (C=O) cm^{-1}. Proton magnetic resonance spectrum: δ 0.92 (3H, d, J = 5.5 Hz). Mass spectrum: 207(62, M^+), 206(48), 192(27), 165(21), 164(100), 150(43). The crude ketone **26** (294 mg) was dissolved in ethanedithiol (2 ml) and boron trifluoride–etherate (0.4 ml) added. After 18 h at room temperature the solution was diluted with methylene chloride (50 ml) and washed with 4 *N* aqueous sodium hydroxide (4 × 20 ml), water and brine. Removal of solvent left a pale yellow oil (356 mg) which was chromatographed over silica gel. The eluant was chloroform–methanol–aqueous ammonia (95:5:0.5); 3 ml fractions were collected. Fractions 12 and 13 provided thioketal **29** (218 mg), mp 51–52 °C (from ether–Skellysolve B). *Anal.* calcd. for $C_{15}H_{25}NS_2$: C 63.55, H 8.89, N 4.94; found: C 63.33, H 8.78, N 4.87. *Mol. Wt.* calcd. for $C_{15}H_{25}NS_2$: 283.1429 (^{32}S); found (hrms): 283.1410.

Infrared spectrum: ν_{max} 2800, 2755, 2735, 2680, 2610 (Bohlmann bands), and 1125 cm^{-1}. Proton magnetic resonance spectrum: δ 0.88 (3H, d, J = 5.5 Hz) and 3.27 (4H, bs). Mass spectrum: 283(41, M^+), 282(26), 222(30), 190(51), 151(100).

Myrrhine (5 = 27)

To a solution of thioketal **29** (0.38 g) in ethanol (20 ml) was added a slurry of W-2 Raney nickel (*ca.* 4 g) in ethanol (25 ml). The mixture was heated under reflux with vigorous stirring for 2 h, then filtered and concentrated HCl (1 ml) added. The solvent was removed under reduced pressure. The residue was dissolved in methylene chloride and anhydrous potassium carbonate added with stirring. Filtration and evaporation of solvent gave a pale-yellow oil (0.21 g) which was distilled at 90 °C (bath temperature) (0.1 Torr) to give myrrhine (**5** = **27**, 166 mg) as a colorless oil. The infrared spectrum was identical with that of authentic myrrhine. Infrared spectrum: ν_{max} (film) 2790, 2760, 2725, 2610 (Bohlmann bands), 1445, 1385, 1325, 1255, 1220, 1130, 1120, 1042, 1020, and 730 cm^{-1}. Proton magnetic resonance spectrum: δ 0.88 (3H, d, J = 5.5 Hz). Mass spectrum: identical with the published (4) spectrum.

Myrrhine N-oxide, 30

Myrrhine (11 mg) in chloroform (2 ml) was treated with *m*-chloroperbenzoic acid (15 mg) in chloroform (1 ml). After 4 h the reaction mixture was poured onto a column of alumina (1 g) and eluted with chloroform (25 ml). Evaporation left a colorless solid (11 mg) which was crystallized from methylene chloride – ether. The colorless needles slowly decomposed when heated above 150 °C. The synthetic material was identical (ir, nmr, ms) with authentic myrrhine *N*-oxide.

^{13}C magnetic resonance spectrum: δ 73.6(CH), 73.3(2 × CH), 35.8(2 × CH_2), 35.6(2 × CH_2), 30.1(CH), 27.4(2 × CH_2), 23.4(2 × CH_2), and 21.4(CH_3).

(±)-Hippodamine (4 = 31)

Pyrrolidine (0.042 ml) and acetic acid (0.058 ml) were added to a solution of hemiketal **21** (113 mg) in dry tetrahydrofuran (10 ml) and the resulting solution was heated under reflux in a nitrogen atmosphere for 24 h. After addition of saturated aqueous sodium bicarbonate (10 ml) most of the tetrahydrofuran was removed under reduced pressure. The aqueous solution was extracted with methylene chloride to give a pale yellow oil (103 mg) which showed carbonyl absorption at 1725 cm^{-1} and two spots on tlc (silica gel). A portion (84 mg) of the oil was dissolved in ethanedithiol (2 ml), boron trifluoride–etherate (0.2 ml) added, and the solution left overnight. Work-up as above gave a pale yellow oil (115 mg) which showed two spots on tlc differing in R_f values from the ketones above. The crude thioketals were desulfurized in the same manner as for **29**. The product (65 mg) showed two spots, R_f values 0.8 and 0.2, on tlc (alumina, developed with ethyl acetate). The components were separated by preparative tlc (alumina, ethyl acetate). The component of higher R_f value (27 mg) was identical with myrrhine. The component of lower R_f value (19 mg) was purified by molecular distillation (90 °C/0.1 Torr). The ir, pmr, and ms were identical with those of authentic hippodamine (**4** = **31**).

(±)-*Convergine*, *3*

(±)-Hippodamine (10 mg) was transformed to the *N*-oxide in the same manner as described for myrrhine. The hygroscopic solid obtained showed spectral properties (ir, ms, pmr) identical with those of authentic convergine. The synthetic material was transformed into the hydrochloride which was recrystallized from methylene chloride – ether, mp 225–230 °C (dec.). The infrared spectrum was identical with that of authentic convergine hydrochloride.

Acknowledgements

We thank the National Research Council of Canada for financial support, and Prof. B. Tursch, Université Libre de Bruxelles, for his help in establishing the identity of the synthetic materials.

1. K. S. HAGEN. Natl. Geographic, **137**, 543 (1970).
2. G. M. HAPP and T. EISNER. Science, **134**, 329 (1961).
3. J. M. PASTEELS, C. DEROE, B. TURSCH, J. C. BRAEKMAN, D. DALOZE, and C. HOOTELE. J. Insect Physiol. **19**, 1771 (1973).
4. B. TURSCH, D. DALOZE, C. HOOTELE, J. C. BRAEKMAN, and J. M. PASTEELS. Tetrahedron, **31**, 1541 (1975).
5. B. TURSCH, D. DALOZE, M. DUPONT, C. HOOTELE, M. KAISIN, J. M. PASTEELS, and D. ZIMMERMAN. Chimia, **25**, 307 (1971).
6. R. KARLSSON and D. LOSMAN. Chem. Commun. 626 (1972).
7. B. TURSCH, D. DALOZE, J. C. BRAEKMAN, C. HOOTELE, A. CRAVADOR, D. LOSMAN, and R. KARLSSON. Tetrahedron Lett. 409 (1974).
8. W. A. AYER and K. PIERS. Can. J. Chem. **45**, 451 (1967).
9. A. KIRRMANN, M. GOUDARD, and M. CHAHIDZADEH. Bull. Soc. Chim. Fr. **2**, 2148 (1935).
10. J. P. WIBAUT and J. I. DEJONG. Recl. Trav. Chem. **68**, 485 (1949), and references therein.
11. P. T. IZZO and S. R. SAFIR. J. Org. Chem. **24**, 701 (1959).
12. T. SAKAN and Y. MORI. Chem. Lett. 793 (1972).
13. L. M. JACKMAN and S. STERNHELL. Applications of nuclear magnetic resonance spectroscopy in organic chemistry. 2nd ed. Pergamon Press, Oxford. 1969. p. 174.
14. C. H. HEATHCOCK, J. E. ELLIS, and R. A. BADGER. J. Heterocycl. Chem. **6**, 139 (1969).
15. (*a*) J. B. STOTHERS. Carbon-13 NMR spectroscopy. Academic Press, New York, New York. 1972; (*b*) G. C. LEVY and G. L. NELSON. Carbon-13 nuclear magnetic resonance for organic chemists. Wiley-Interscience, New York, New York. 1972.
16. E. WENKERT, J. S. BINDRA, C.-J. CHANG, D. W. COCHRAN, and F. M. SCHELL. Acc. Chem. Res. **7**, 46 (1974).
17. E. WENKERT, B. CHAUNCY, K. G. DAVE, A. R. JEFFCOAT, F. M. SCHELL, and H. P. SCHENK. J. Am. Chem. Soc. **95**, 8427 (1973).
18. F. BOHLMANN. Chem. Ber. **91**, 2157 (1958).
19. A. J. JONES, E. L. ELIEL, D. M. GRANT, M. C. KNOEBER, and W. F. BAILEY. J. Am. Chem. Soc. **93**, 4772 (1971).
20. N. J. LEONARD and F. P. HAUCK. J. Am. Chem. Soc. **79**, 5279 (1957).
21. C. N. R. RAO. Chemical applications of infrared spectroscopy. Academic Press, New York. 1963. pp. 355–356.

Can. J. Chem. Downloaded from www.nrcresearchpress.com by 210.87.254.5 on 09/05/12
For personal use only.

Studies of the pyrolysis of diethylzinc by the toluene carrier method and of the reaction of ethyl radicals with toluene

AHTI A. KOSKI, S. JAMES W. PRICE,[1] AND BARRY C. TRUDELL
Chemistry Department, University of Windsor, Windsor, Ontario N9B 3P4

Received July 25, 1975

AHTI A. KOSKI, S. JAMES W. PRICE, and BARRY C. TRUDELL. Can. J. Chem. **54**, 482 (1976).

The thermal decomposition of diethylzinc in a toluene carrier system has been studied over the temperature range of 669 to 762 K, and percent decomposition of 3.8 to 97.2%. The decomposition occurs by a two step mechanism, the second step rapidly following the first,

[1] $$Zn(C_2H_5)_2 \rightarrow ZnC_2H_5 + C_2H_5\cdot$$

[2] $$ZnC_2H_5 \rightarrow Zn + C_2H_5\cdot$$

The overall progress of the reaction was followed by determination of the residual diethylzinc by hydrolysis followed by analysis for zinc by atomic absorption. In selected runs two additional methods were used: (*i*) measurement and analysis of the gas evolved during the hydrolysis and (*ii*) full analysis of all pyrolysis products involving the C_2H_5 group.

In the absence of zinc oxide the decomposition is essentially homogeneous and

$$\log k_1\,(s^{-1}) = 14.3 \pm 0.6 - \frac{49\,000 \pm 2\,000}{4.58T}$$

or $-205\,000/19.15T$ if the activation energy is expressed in joules rather than calories. The presence of zinc oxide causes marked catalysis of the overall decomposition but does not appear to affect reaction 3 or reaction 6.

[3] $$C_2H_5 + C_6H_5CH_3 \rightarrow C_2H_6 + C_6H_5CH_2$$

[6] $$C_2H_5 \rightarrow C_2H_4 + H$$

$$\log k_3\,(cc\ mol^{-1}\ s^{-1}) = 11.12 \pm 0.15 - \frac{9\,800 \pm 500}{4.58T}$$

$$\log k_6\,(s^{-1}) = 11.0 - \frac{30\,300}{4.58T}\ (\text{at 15 mm pressure})$$

Reaction 6 is in a strongly pressure dependent region and is based on very limited data.

AHTI A. KOSKI, S. JAMES W. PRICE et BARRY C. TRUDELL. Can. J. Chem. **54**, 482 (1976).

On a étudié la décomposition thermique du diéthylzinc dans un système contenant du toluène comme diluant; ces études ont été réalisées entre 669 et 762 K et amenées des pourcentages de décomposition de 3.8 à 97.2%. La décomposition se produit par un mécanisme en deux étapes; la deuxième étape suit rapidement la première

[1] $$Zn(C_2H_5)_2 \rightarrow ZnC_2H_5 + C_2H_5\cdot$$

[2] $$ZnC_2H_5 \rightarrow Zn + C_2H_5\cdot$$

On a suivi le progrès globale de la réaction en déterminant le diéthylzinc résiduel par une hydrolyse suivie par une analyse du zinc par absorption atomique. Dans un certain nombre de cas spécifiques, on a utilisé deux méthodes supplémentaires: (*i*) la mesure et l'analyse du gas qui s'échappe au moment de l'hydrolyse et (*ii*) l'analyse complète de tous les produits de pyrolyse impliquant le groupe C_2H_5.

En l'absence d'oxyde de zinc, la décomposition est essentiellement homogène et

$$\log k_1\,(s^{-1}) = 14.3 \pm 0.6 - \frac{49\,000 \pm 2\,000}{4.58T}$$

ou $-205\,000/19.15T$ si l'énergie d'activation est exprimé en joules plutôt qu'en calories. La présence d'oxyde de zinc produit une catalyse importante pour la décomposition globale mais ne semble pas affecter les réactions 3 ou 6.

---

[1]To whom correspondence should be addressed.

Can. J. Chem. Downloaded from www.nrcresearchpress.com by 210.87.254.42 on 09/05/12
For personal use only.

[3] $$C_2H_5 + C_6H_5CH_3 \rightarrow C_2H_6 + C_6H_5CH_2$$

[6] $$C_2H_5 \rightarrow C_2H_4 + H$$

$$\log k_3 \text{ (cc mol}^{-1}\text{ s}^{-1}) = 11.12 \pm 0.15 - \frac{9\,800 \pm 500}{4.58T}$$

$$\log k_6 \text{ (s}^{-1}) = 11.0 - \frac{30\,300}{4.58T} \text{ (à 15 mm de pression)}$$

La réaction 6 dépend grandement de la pression et est basée sur très peu de données expérimentales.

[Traduit par le journal]

Introduction

Although the pyrolysis of a number of compounds of the type $M(C_2H_5)_n$, $n = 2, 3, 4$, has been studied only very limited data are available on $D((C_2H_5)_{n-1}M—C_2H_5)$ bond dissociation energies or on the energetics of the subsequent reaction of the ethyl radicals released (1, 2). The present study is the second in a series from this laboratory on such alkyls and is closely related to previous work on methyl metallic alkyls.

Experimental

Materials

Toluene

The toluene employed was toluene from sulfonic acid, number X325 as supplied by Eastman Organic Chemicals. It was dried by refluxing under vacuum at least 24 h over freshly pressed sodium ribbon and then degassed by bulb-to-bulb distillation.

Diethylzinc

The diethylzinc was obtained from Alfa Inorganics, stock number 85101. It was used as supplied, except for a vigorous degassing. Analysis of residue remaining after decomposition by water yielded 99+% $ZnEt_2$, measured as Zn^{2+} using atomic absorption. Analysis of the decomposition gases showed up to 4% of a methyl-containing impurity, probably dimethylzinc. This impurity was reduced to less than 0.5% by a few degassings. The small quantity remaining would presumably remain inert during passage through the furnace and be subsequently collected in the condensable liquids trap (3).

Apparatus and Procedure

The experiments were carried out in a system similar to that used in previous work (4). The reaction vessel had a volume of 156 cc. To test for surface effects a vessel was packed with small quartz tubes. This vessel had a volume of 101 cc and a surface-to-volume ratio 20 times that of the unpacked vessel. Both vessels were treated with hot concentrated nitric acid before use. The residual acid was baked out under vacuum after the vessels were installed in the reaction system. Zinc oxide surfaces were prepared by decomposition of the alkyl followed by passage of oxygen over the fresh zinc surface.

The gaseous products were analyzed using a Perkin–Elmer model 154 gas chromatograph equipped with a $\frac{1}{4}$ in. × 6 ft silica gel column. The column was maintained at 80 °C, and a helium flow rate of 20 cm^3 per min was used.

The liquid products from selected runs were analyzed on a Perkin–Elmer model 800 gas chromatograph equipped with a flame ionization detector. A 0.02 in. id 150 ft open tubular column coated with poly(propylene glycol) (Perkin–Elmer Column R) was used. The column and injection port temperatures were set at 75 and 135 °C respectively. Nitrogen was used as the carrier gas.

To check for dissolved butane in the condensable products, a butane standard was prepared following procedures simulating conditions in a run. The resulting standard solution of butane in toluene was warmed to −12 °C and analyzed immediately on the Perkin–Elmer 800. A precooled syringe was used for all injections. Both the standard and run samples were also run at room temperature using benzene as an internal standard. As an added precaution, the toluene was checked after each run for traces of accumulated contaminants, mainly benzene and ethylbenzene, and the appropriate corrections made. Corrections were necessary only in several runs where the first and last fractions of a particular batch of toluene were used.

Diethylzinc was recovered as a dilute solution in toluene and hydrolysed over a period of 5–10 min. The zinc hydroxide formed was dissolved by the addition of a small quantity of nitric acid and the resulting solution was quantitatively diluted to bring the Zn^{2+} concentration into the 0–6 ppm range required for optimum analysis on a Pye Unicam SP 90 Atomic Absorption – Flame Emission Spectrometer equipped with a hollow zinc cathode lamp.

In a number of runs the gas evolved during the hydrolysis of the residual diethylzinc was collected and analyzed using the same procedures employed for analysis of the gaseous pyrolysis products.

Results and Discussion

Typical experimental conditions and results are shown in Table 1[2] while selected analytical data are given in Table 2. These results may be discussed in terms of the following mechanism:

[2]A complete table of the pyrolysis data is available, at a nominal charge, from the Depository of Unpublished Data, CISTI, National Research Council of Canada, Ottawa, Canada K1A 0S2.

Can. J. Chem. Downloaded from www.nrcresearchpress.com by 210.87.254.42 on 09/05/12
For personal use only.

TABLE 1. Pyrolysis data for diethylzinc

T (K)	Total Pressure (mm)	Contact time (s)	Initial alkyl concentration (mol $cc^{-1} \times 10^8$)	Length of run (min)	% decomposition (based on zinc analysis)[a]	k_{Zn} (s^{-1})	k_d (s^{-1})
756	15.1	1.37	0.59	65	74.6	1.01	0.97
739	15.4	1.20	0.69	20	52.5	0.623	0.630
733	15.7	1.22	0.89	20	38.2	0.395	0.440
726	14.3	1.22	1.18	20	33.9	0.341	0.310
713	14.7	1.20	0.70	20	20.9	0.195	0.170
713	14.7	1.06	0.68	20	18.2	0.190	0.180

[a](moles $Zn(C_2H_5)_2$ used − moles zinc recovered in traps)/(moles $Zn(C_2H_5)_2$) × 100.

TABLE 2. Experimental parameters and product analysis

T (K)	Pressure (mm)	Toluene/Alkyl (molar ratio)	Products from pyrolysis of $Zn(C_2H_5)_2$ (mol × 10^4)						Hydrolysis products (mol × 10^4)[a]			
			H_2	CH_4	C_2H_4	C_2H_6	C_4H_{10}	*n*-Propyl benzene	H_2	CH_4	C_2H_4	C_2H_6
756	15	84	1.95	0.080	4.82	2.06	2.90	—	0.05	0.40	0.08	3.88
739	15	73	1.54	0.064	3.94	1.79	1.92	0.185	0.12	0.68	0.19	9.18
733	16	59	1.18	0.081	3.10	1.52	1.97	0.182	0.11	1.10	0.27	14.6
713	15	73	0.36	0.040	0.57	0.97	1.51	0.137	0.33	0.11	0.33	17.2
713	15	73	0.54	0.026	1.73	1.09	0.69	0.089	0.24	0.12	0.24	19.2
700	15	74	0.38	0.040	1.10	0.66	0.42	0.162	0.19	0.19	0.55	16.3

[a]From slow decomposition of $Zn(C_2H_5)_2$ when the toluene solution recovered after the run is mixed with water in the absence of oxygen.

[1] $Zn(C_2H_5)_2 \rightarrow Zn(C_2H_5) + C_2H_5\cdot$

[2] $Zn(C_2H_5) \rightarrow Zn + C_2H_5\cdot$

The ethyl radicals produced in the decomposition will then abstract hydrogen atoms from either the ring or the side chain of toluene to yield ethane, recombine to produce butane, disproportionate to give ethylene and ethane, or decompose:

[3] $C_2H_5\cdot + C_6H_5CH_3 \rightarrow C_2H_6 + (C_6H_5CH_2 \text{ or } C_6H_4CH_3)$

[4] $C_2H_5\cdot + C_2H_5\cdot \rightarrow C_4H_{10}$

[5] $\rightarrow C_2H_4 + C_2H_6$

[6] $C_2H_5\cdot \rightarrow C_2H_4 + H\cdot$

A combination reaction between benzyl radicals formed in reaction 3 and ethyl radicals was also found to occur as evidenced by the production of significant amounts of propylbenzene:

[7] $C_2H_5\cdot + C_6H_5CH_2\cdot \rightarrow C_6H_5C_3H_7$

Numerous reactions involving methyl and hydrogen radicals also occur:

[8] $H\cdot + C_6H_5CH_3 \rightarrow CH_3\cdot + C_6H_6$

[9] $\rightarrow H_2 + C_6H_5CH_2\cdot$

[10] $CH_3\cdot + C_6H_5CH_3 \rightarrow CH_4 + C_6H_5CH_2\cdot$

[11] $CH_3\cdot + C_2H_5\cdot \rightarrow C_3H_8$

[12] $CH_3\cdot + C_2H_5ZnC_2H_5 \rightarrow CH_3ZnC_2H_5 + C_2H_5\cdot$

[13] $H\cdot + C_2H_5ZnC_2H_5 \rightarrow HZnC_2H_5 + C_2H_5\cdot$

Reaction 11 seems negligible in that only minute traces of propane were found. A displacement reaction similar to reaction 12 has been observed to occur between CH_3 and $B(C_2H_5)_3$ (5, 6).

Reactions represented by [12] and [13] are proposed on the basis of evidence that significant amounts of methane and hydrogen were produced when residual alkyl was decomposed with water at the end of the run. A portion of the CH_4 is due to the small $Zn(CH_3)_2$ impurity but this cannot account for all the CH_4 found. The decomposition of small amounts of diethylzinc by water has been the subject of several investigations (7, 8), and the only volatile product reported formed was ethane. An earlier study (9), utilizing considerably more drastic conditions for the decomposition, in which relatively large samples of the alkyl were decomposed with water or acid, did yield hydrogen and ethylene in small quantities. To test the possibility that the same situation might obtain in the present study,

Can. J. Chem. Downloaded from www.nrcresearchpress.com by 210.87.254.42 on 09/05/12
For personal use only.

Can. J. Chem. Downloaded from www.nrcresearchpress.com by 210.87.254.42 on 09/05/12
For personal use only.

a sample of diethylzinc obtained directly from the storage vessel was decomposed under the same conditions as the residual alkyl normally would have been. No traces of ethylene or hydrogen were detected in the decomposition gases.

First order rate constants were calculated from the usual expression

$$k = \frac{2.303}{t_c} \log \frac{100}{100 - x}$$

where x denotes the percent decomposition and t_c is the contact time or the average time that a molecule spends in the reaction zone in the furnace. This was calculated from the expression

$$t_c = \frac{V}{22416} \cdot \frac{P}{760} \cdot \frac{273}{T} \cdot \frac{1}{F}$$

where V is the reaction zone volume in cc, P is the average total pressure in mm mercury, T is the absolute temperature in the reaction zone, and F is the flow rate through the furnace in mol s^{-1}.

The percent decomposition, x, was evaluated by three separate methods, (*i*) by analysis of zinc residue using atomic absorption techniques, (*ii*) by decomposition gas analysis via gas chromatography, and (*iii*) product analysis. For runs in which two or more methods were used the agreement is generally favourable. The first two methods are compared in Table 1. Values of k_1 obtained by the third method are plotted in Fig. 1 along with the values obtained by method *i*.

The agreement between the methods shows that, unlike the case of dimethylzinc (3), reaction 2 follows rapidly after reaction 1. This is not unexpected. The slow decomposition of $ZnCH_3$ was governed by the fact that this simple fragment was decomposing under conditions of temperature and pressure that placed the decomposition reaction close to or in its second order region. This is not true for ZnC_2H_5 which should have twice the effective number of oscillators.

The runs in the unpacked reaction vessel actually represent runs in three different vessels subjected to a variety of conditioning processes. In addition to the standard HNO_3 rinsing and baking procedure, rinsing with HF and coating with deposits from the decomposition of other alkyls ($Sb(CH_3)_3$, $Sn(C_2H_5)_4$) were tried. All of these treatments produced the same lower limit for k_1 at any given temperature. On this basis it

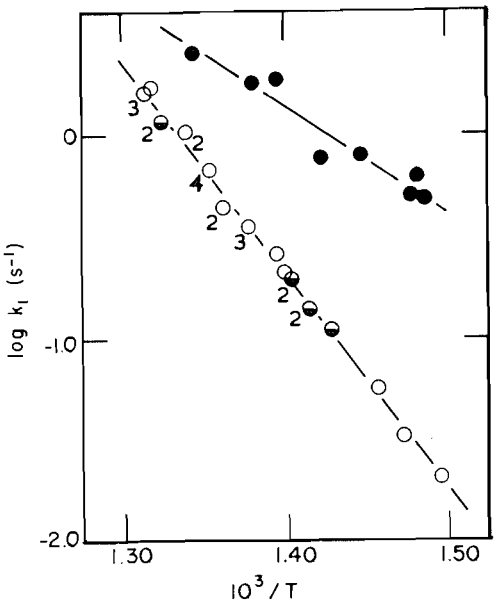

FIG. 1. Arrhenius plot for the pyrolysis of diethylzinc. ○, based on residual zinc analysis; ◒, based on product analysis; ●, runs catalysed by zinc oxide.

seems probable that major surface effects are not present in runs done in the clean and conditioned vessels. However, in the first runs in the packed vessel (surface-to-volume ratio 20 times that of the unpacked vessel) oxide was present and subsequent cleaning, although removing all visible oxide, still led to values of k_1 that indicate the possibility of up to 15% heterogeneous reaction in the unpacked vessel. The packed vessel was made with the quartz packing sealed in so that the small quartz tubes had to be cleaned *in situ* and the cleaning process may not have been entirely satisfactory.

The marked affect of zinc oxide on the decomposition of diethylzinc may be seen by comparing the two Arrhenius plots in Fig. 1. The upper curve (zinc oxide on surface) may be represented by

$$\log k_1 (s^{-1}) = 7.6 \pm 1.6 - \frac{24\,000 \pm 5\,000}{4.58T}$$

while the predominately homogeneous reaction (lower curve) is given by

$$\log k_1 (s^{-1}) = 14.3 \pm 0.6 - \frac{49\,000 \pm 2\,000}{4.58T}$$

A similar rate enhancement was previously encountered in a study on the related compound

Can. J. Chem. Downloaded from www.nrcresearchpress.com by 210.87.254.42 on 09/05/12
For personal use only.

dimethylzinc (10). If the activation energy for reaction 1 is accepted as a reasonable measure of the bond dissociation energy D_0^0, then D_{298}^0 is approximately 47.5 kcal mol^{-1}.

Assuming ΔH_{f298}^0 ($C_2H_5\cdot$, g) = 25.3 kcal mol^{-1} (11), ΔH_{f298}^0 (Zn, g) = 31.19 kcal mol^{-1} (12), and ΔH_{f298}^0 ($Zn(C_2H_5)_2$, g) = 12.1 kcal mol^{-1} (11) and that the recombination process (the reverse of reactions 1 and 2 have zero activation energies

$$D_1(C_2H_5Zn—C_2H_5) + D_2(Zn—C_2H_5) = 31.2 + (2 \times 25.3) - 12.1 = 69.7 \text{ kcal mol}^{-1}$$

Then at 298 K, since $D_1 = 47.5$ kcal mol^{-1}, $D_2 = 22.7$ kcal mol^{-1}. Since previous studies have shown that the decomposition of $ZnCH_3$ yields Zn atoms in their ground state (1, 3) this is likely to also be the case for ZnC_2H_5. Thus the A factor for reaction 2 will probably be limited to a maximum value of 10^9 to 10^{10} s^{-1}. However even with this restriction on A_2, k_2 will be at least 200 times greater than the corresponding k_1 value. This is consistent with the observation that to satisfy the analytical data k_2 must be much greater than k_1.

Hydrogen Abstraction by Ethyl Radicals

The rate expressions for reactions 3 and 4 may be written as

$$\frac{d[C_2H_6—C_2H_4^*]}{dt} = k_a[C_2H_5\cdot][C_6H_5CH_3]$$

and

$$\frac{d[C_4H_{10}]}{dt} = k_r[C_2H_5\cdot]^2$$

respectively. (Note: $C_2H_4^* = C_2H_4$ from disproportionation only.) Thus

$$\frac{k_a}{k_r^{1/2}} = \frac{d[C_2H_6—C_2H_4^*]/dt}{(d[C_4H_{10}]/dt)^{1/2}[C_6H_5CH_3]}$$

The disproportionation/combination ratio for ethyl radicals was approximated as 0.11 on the basis of previous studies (13) so that

$$\text{moles } C_2H_4^* = 0.11 \text{ (moles } C_4H_{10})$$

The values of k_3 used to construct Fig. 2 were obtained from these expressions and log k_4 (cc mol^{-1} s^{-1}) = 12.6 (14). With the combined data from the two sources of ethyl radicals

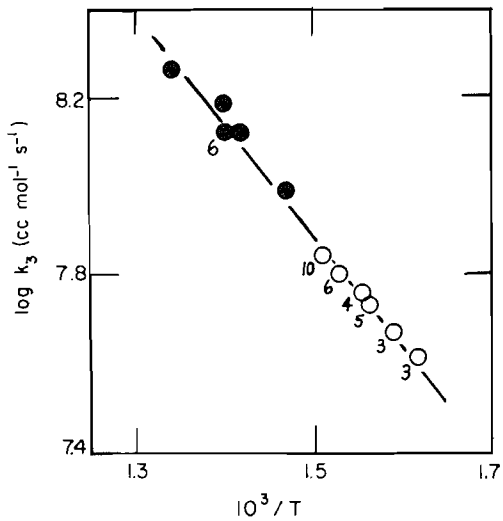

FIG. 2. Arrhenius Plot for the abstraction of hydrogen from toluene by ethyl radicals. ●, radical source $Zn(C_2H_5)_2$ (present work); ○, radical source $Hg(C_2H_5)_2$ (ref. 2).

$$\log k_3 \text{ (cc mol}^{-1}\text{ s}^{-1}) = 11.12 \pm 0.15 - \frac{9\,800 \pm 500}{4.58T}$$

The slightly steeper overall slope compared to the individual sets of data is the result of increasing nonuniformity of $[C_2H_5]$ with increasing temperature. Three of the nine points from the present work are from zinc oxide catalysed runs. As expected the presence of the oxide on the surface of the reaction vessel has no effect on the value of k_3.

Decomposition of the Ethyl Radical

The rate expression for reaction 6 may be written as

$$\frac{d[C_2H_4^t—C_2H_4^*]}{dt} = k_6[C_2H_5\cdot]$$

where t = total, $C_2H_4^* = C_2H_4$ from disproportionation. The determination of $C_2H_4^*$ and $[C_2H_5\cdot]$ has been discussed in the previous section. The limited data (seven points) may be represented by the very approximate Arrhenius equation

$$\log k_6(5) = 11.0 - \frac{30\,300}{4.58T} \quad \text{(at 15 mm pressure)}$$

The major significance of this equation is that it adequately represents points from both runs in a

clean vessel and runs in an oxide coated vessel. This is a good indication that even though the main decomposition process is essentially a heterogeneous reaction when the surface is coated with zinc oxide, the ethyl radical decomposition is not surface catalysed.

Acknowledgments

This work has been supported by a grant from the National Research Council of Canada.

1. S. J. W. PRICE. Comprehensive chemical kinetics. Vol. 4. Elsevier, Amsterdam. 1972. pp. 208–257.
2. A. C. LALONDE and S. J. W. PRICE. Can. J. Chem. **49**, 3367 (1971).
3. A. N. DUNLOP and S. J. W. PRICE. Can. J. Chem. **48**, 3205 (1970).
4. M. KRECH and S. J. W. PRICE. Can. J. Chem. **41**, 224 (1963).
5. M. V. ENCINA and E. A. LISSI. J. Organomet. Chem. **29**, 21 (1971).
6. J. GROTEWOLD, E. A. LISSI, and J. C. SCIANO. J. Chem. Soc. B, 1189 (1971).
7. I. M. ISHIMORI, O. NAKASUGI, N. TAKEDA, and T. TSURATA. Makromol. Chem. **115**, 103 (1968).
8. R. J. HEROLD, S. L. AGGARWAL, and V. NEFF. Can. J. Chem. **41**, 1368 (1963).
9. A. S. CARSON, K. HARTLEY, and H. A. SKINNER. Trans. Faraday Soc. **45**, 1159 (1949).
10. I. LAMBERT. J. Chim. Phys. **62**, 516 (1965).
11. Technical Note 3, suppl. for Kinetic Data of Gas Phase Unimolecular Reactions, NSRDS-NBS21, Washington. 1972.
12. Handbook of Chemistry and Physics, 54th ed. The Chemical Rubber Co., Cleveland, Ohio. 1973–1974.
13. Tables of Bimolecular Gas Reactions, NSRDS-NBS 9, Washington. 1967. p. 111.
14. J. A. KERR and E. RATAJCZAK. Second supplementary tables of bimolecular gas reactions. Chemistry Department, University of Birmingham, Birmingham, England. 1973.

Can. J. Chem. Downloaded from www.nrcresearchpress.com by 210.87.254.42 on 09/05/12
For personal use only.

Etude sur les carbéthoxy-3 pyrazolinones-5: contribution à l'étude des formes tautomériques et préparation de sels d'hydrazinium et de guanidinium[1]

J. ZAUHAR ET B. F. LADOUCEUR
Collège militaire royal de Saint-Jean, Saint-Jean, Québec J0J 1R0

Reçu le 11 juillet 1975

J. ZAUHAR et B. F. LADOUCEUR. Can. J. Chem. **54**, 488 (1976).

Les carbéthoxy-3 pyrazolinones-5 adoptent de préférence la forme tautomérique NH à l'état solide et en solution; le solvant ne cause pas de changement radical de forme parce que les molécules, passablement polaires, semblent stabilisées par un système fortement conjugué et, possiblement aussi, par une chélation due à la formation d'une liaison hydrogène entre le groupement carbonyle, du groupement carbéthoxy en position 3, avec l'atome d'hydrogène attaché à l'atome d'azote en position 2.

Ces carbéthoxy-3 pyrazolinones-5 forment des sels d'hydrazinium et de guanidinium, par transfert d'un proton, en présence d'hydrazine et de guanidine en solution éthanolique.

J. ZAUHAR and B. F. LADOUCEUR. Can. J. Chem. **54**, 488 (1976).

The tautomeric NH-form is preferentially adopted by 3-carbethoxy-5-pyrazolinones in the solid state and in solution; the solvent does not cause a radical change in form because these molecules are quite polar and appear to be stabilized by a rather extended conjugated system and possibly also by chelation of the carbonyl group of the carbethoxy group in position 3 with the hydrogen atom attached to the nitrogen atom in position 2.

These 3-carbethoxy-5-pyrazolinones form hydrazinium and guanidinium salts in the presence of hydrazine and guanidine in ethanolic solution by means of a proton transfer.

Introduction

La condensation de quelques carbéthoxy-3 pyrazolinones-5, **1**, avec l'hydrate d'hydrazine bouillant a permis à certains auteurs (1–4) d'isoler les hydrazides correspondantes, **2**.

[1] 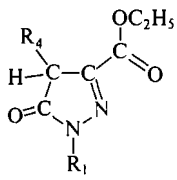 $+ NH_2NH_2 \cdot H_2O \rightarrow$

1

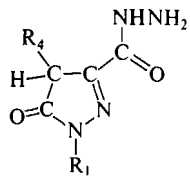 $+ C_2H_5OH + H_2O$

2

De même, quelques esters simples ont conduit à une réaction semblable avec la guanidine (5), selon [2].

[2] 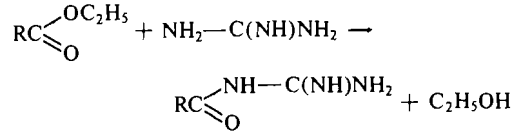

Toutefois, lorsque les carbéthoxy-3 pyrazolinones-5 réagissent avec l'hydrazine ou la guanidine dans des conditions moins sévères (solution éthanolique à la température de reflux), on obtient des dérivés solides dans lesquels le groupement carbéthoxy est resté intact. Ces solides sont des sels d'hydrazinium ou de guanidinium des carbéthoxy-3 pyrazolinones-5, **3**.

Nous avons pensé que, dans ces conditions,

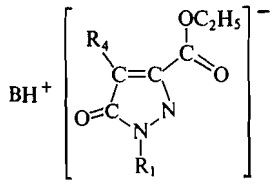

3

[1]La recherche pour cette publication a été subventionnée en partie par le Conseil de recherches pour la défense, numéro d'octroi 9530-25.

Can. J. Chem. Downloaded from www.nrcresearchpress.com by 210.87.254.40 on 09/05/12
For personal use only.

Can. J. Chem. Downloaded from www.nrcresearchpress.com by 210.87.254.40 on 09/05/12
For personal use only.

les carbéthoxy-3 pyrazolinones-5 adopteraient possiblement une forme tautomérique dans laquelle un proton est plus facilement arraché par le réactif basique que ne l'est le groupement éthoxy. Une étude des formes tautomériques de ces composés a alors été entreprise.

Résultats et discussion

Contribution à l'étude des formes tautomériques des carbéthoxy-3 pyrazolinones-5

Plusieurs auteurs (1–4, 6–12, 14) ont apporté par leurs travaux des informations sur les formes tautomériques des pyrazolinones-5. En 1964, Katritzky et Maine (8) ont dressé un inventaire des travaux déjà faits et ont par la suite contribué largement à éclairer le sujet (9, 12). Les formes tautomériques (**4** *a–c*) varient selon que le composé est à l'état solide ou dissous dans un solvant, et selon la nature et le nombre de substituants qu'il porte.

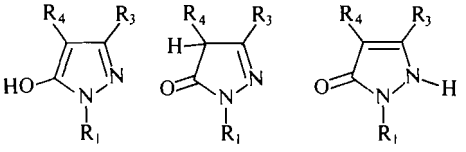

4*a* (forme OH) **4***b* (forme CH) **4***c* (forme NH)

Selon Katritzky (8), les pyrazolinones-5 portant des substituants méthyles ou phényles en positions 1 et 3 existent essentiellement sous la forme CH, **4***b*, en solution dans le chloroforme ou le tétrachlorure de carbone. Toutefois, l'addition d'un substituant en position 4 modifie la forme; par exemple, des solutions fraîchement préparées de la diméthyle-3,4 phényle-1 pyrazolinone-5 dans ces mêmes solvants donnent des spectres qui démontrent l'existence de fortes proportions de la forme NH, **4***c*, proportions qui diminuent par vieillissement de la solution. Puis, en solution aqueuse, c'est la forme NH qui prédomine et qui est en équilibre avec environ 10% de la forme OH, **4***a*. Enfin, à l'état solide, selon ce même auteur, ces composés adoptent une forme NH fortement associée par liaison hydrogène dans laquelle un transfert d'un proton conduisant à la forme OH peut très bien se produire:

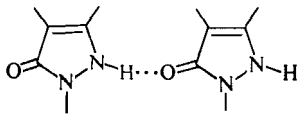

ou

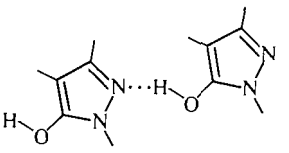

Nous avons étudié les carbéthoxy-3 pyrazolinones-5 suivantes:

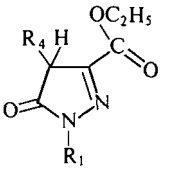

5 R_1 = H, R_4 = H
6 R_1 = Me, R_4 = H
7 R_1 = Ph, R_4 = H
8 R_1 = H, R_4 = Me
9 R_1 = Ph, R_4 = Ph
10 R_1 = Ph, R_4 = Me

Les tentatives faites pour préparer les trois dérivés phényle-4, diméthyle-1,4 et méthyle-1 phényle-4 ont toutes été vaines; nous avons toujours plutôt obtenu une dihydrazide de l'acide oxalique, soit un produit de dégradation de formule $(RNHNHCO)_2$ dans laquelle R = H ou Me.

Nous avons basé notre étude des formes tautomériques des carbéthoxy-3 pyrazolinones-5 sur leurs spectres ir, rmn et uv.

Spectres infrarouges

Les spectres ir pris à l'état solide dans KBr (tableau 1) montrent que les carbéthoxy-3 pyrazolinones-5 absorbent beaucoup dans la région au-délà de 2000 cm^{-1}. D'abord, pour les composés non substitués en 1 (**5**, **8**), on trouve une bande assez forte et un peu élargie vers 3440–3330 cm^{-1} due au groupement NH libre; puis, dans la région 3400–3100 cm^{-1}, où l'absorption est toujours appréciable, il ressort dans tous les cas étudiés une petite bande vers 3180–3070 cm^{-1}, même lorsque la position 1 est substituée, ce qui semble indiquer un groupement NH associé. De plus, dans tous les spectres examinés, une bande d'absorption très large et d'intensité assez forte entre 2800 et 2200 cm^{-1}, qui persiste lorsque le spectre est pris dans le chloroforme et qui garde alors une intensité constante, fait conclure à une association intramoléculaire ou à une chélation assez forte. La bande large entre 2000 et 1800 cm^{-1}, attribuable à une association intermoléculaire NH—OH dans les pyrazolinones non carbéthoxylées (8), n'apparaît pas dans les spectres des carbéthoxy-3 pyrazolinones-5 étudiées.

On retrouve également dans tous les cas deux bandes d'absorption ν C=O, l'une d'intensité

Can. J. Chem. Downloaded from www.nrcresearchpress.com by 210.87.254.40 on 09/05/12
For personal use only.

TABLEAU 1. Données spectrales ir des carbéthoxy-3 pyrazolinones-5 (cm^{-1})[a]

Composé	Phase	ν OH libre ν OH associé	ν NH libre	ν NH associé	Chélation	ν C=O ester	ν C=O cycle	Ph	ν C=C cycle	ν C—O—C asym.	ν C—O—C sym.?
5	KBr		3368f	3300–3050m (3162m)	2800–2500m	1737m	1722f 1715f	—	1572m	1286f	1195f
	$CHCl_3$[b]	3680fa 3590fa	3360m	3250–3050m (3170m,3100m)	2800–2500m	1720m	1705f	—	1580f	1268f	1180m
6	KBr		3441fa	3300–3050fa (3178m)	2800–2100m	1737m	1727f	—	1578d,f	1224f	1186f
	$CHCl_3$	3670fa[c] 3580fa–m[c]		3400–3050m (3155m)	2800–2100m	1738f	1725f 1715f	—	1575f	1288f	1165f
7	KBr		3436fa	3300–3050fa (3157fa,3080m)	2900–2100m	1737m	1724f	1597f	1564f 1559f	1264f	1171f
	$CHCl_3$[b]	3680fa 3580fa		3300–3050fa	2800–2400fa	1740m	1725f	1598m	1565fa	(1311m)	—
8	KBr		3330f	3150–3050f (3090m–f)	2800–2200f	1737m	1715mu,f	—	1595m 1564m	1270mu,f	1196f
	$CHCl_3$[b]	3690fa[c] 3580fa[c]	3460m 3380f	3250–3050m (3155m)	2850–2400m	1725m	1700mu,f	—	1592m	1260l,m	1180l,m
9	KBr		3440fa	3300–3050fa (3072fa)	2800–2200m	1737m	1725d,f	1610m 1596m	1580m	1275mu,m	1185m 1150f
	$CHCl_3$	3660fa[c] 3540m[c]	3330fa	3300–3050m	2800–2300fa	1740m	1720l,f	1610fa 1596f	1575f	1300mu,f	1165l,f 1125f
10	KBr	3425fa		3350–3050m	2800–2200m	1736m	1715d,f	1597m	1575m	1265l,f	1168f

[a]Abbréviations: d = double, f = forte, fa = faible, l = large, m = médium, mu = multiple.
[b]Solvant non satisfaisant, absorption faible.
[c]Intensité augmente avec dilution.

Can. J. Chem. Downloaded from www.nrcresearchpress.com by 210.87.254.40 on 09/05/12
For personal use only.

très forte et quelquefois multiple à environ 1725 cm^{-1} et l'autre de moindre intensité à 1737 cm^{-1}, visible comme une épaule bien définie; ces bandes sont aussi présentes dans les spectres pris dans le chloroforme, à une fréquence un peu plus basse, soit vers 1725–1700 cm^{-1} et vers 1740–1720 cm^{-1}. La première bande est attribuable au groupement C=O du cycle; selon Katritzky (8), cette bande très intense apparaît vers 1700 cm^{-1} dans les spectres des pyrazolinones non carbéthoxylées, uniquement lorsqu'ils sont pris dans le chloroforme ou le tétrachlorure de carbone (formes CH ou NH), et elle est absente dans les spectres de ces mêmes composés pris à l'état solide (forme OH ou NH—OH associée). De ceci, on peut conclure que les carbéthoxy-3 pyrazolinones-5 existent de façon prédominante sous la forme NH, à l'état solide ou en solution. La seconde bande ν C=O est due au groupement carbéthoxy de la position 3, et sa plus faible intensité pourrait s'expliquer par une chélation de ce groupement CO avec l'atome d'hydrogène localisé sur l'atome d'azote de la position 2 de la forme NH, **11**; Leonard *et al.* (13) ont observé un tel affaiblissement d'absorption du groupement CO dans certains α-cétoesters cycliques énolisables et l'ont attribué à une chélation de ce genre. Cette attribution de ces deux bandes d'absorption à des vibrations C=O est en parfait accord avec celle de Maquestiau *et al.* (14) qui ont observé ces deux bandes à 1732 cm^{-1}, intensité medium, et à 1682 cm^{-1}, intensité très forte, dans le spectre ir de la molécule modèle de type NH, soit la carbéthoxy-4 méthyle-2 phényle-1 pyrazolinone-5, pris dans le chloroforme.

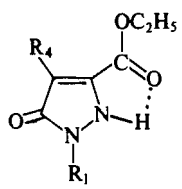

11

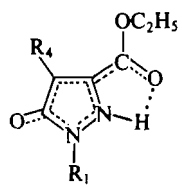

11*a*

Comme l'absorption entre 1700 et 1600 cm^{-1} est nulle, on peut conclure à l'absence d'une liaison C=N et par conséquent exclure les formes CH et OH. Cependant, la présence d'une bande d'intensité assez forte vers 1592–1575 cm^{-1} pourrait provenir d'une conjugaison assez forte et d'une chélation. Le spectre de la molécule modèle de type NH de Maquestiau *et al.* (14) donne aussi une bande à 1569 cm^{-1}, d'intensité forte, attribuée à une vibration C=C. D'une façon analogue, on pourrait attribuer cette bande aux vibrations du cycle fortement conjugué et chélaté représenté par la formule **11***a*.

Les carbéthoxy-3 pyrazolinones-5 sont très peu solubles dans le tétrachlorure de carbone de sorte que leurs spectres pris dans ce solvant n'ont pas de valeur. Cependant, leur solubilité est meilleure dans le chloroforme et les spectres obtenus dans ce solvant, en particulier pour les composés **6** et **9**, sont valables; ils sont comparables à ceux qui ont été pris à l'état solide, mais ils sont moins bien définis. Néanmoins, on doit noter dans ces spectres l'apparition de deux bandes vers 3670 et 3550 cm^{-1} dont l'intensité augmente avec la dilution, particulièrement dans le cas de la deuxième bande. Ceci indiquerait une association d'un groupement OH avec le solvant: une certaine proportion de la forme OH existerait donc en solution dans le chloroforme.

De cette étude spectroscopique ir, il est donc logique de conclure que les carbéthoxy-3 pyrazolinones-5 adoptent préférablement la forme NH. Cette forme semble stabilisée par une forte conjugaison et par une chélation pour devenir passablement polaire (12), ce qui expliquerait en partie la solubilité assez limitée de ces composés dans les solvants peu ou non polaires.

Spectres de résonance magnétique nucléaire

L'étude des spectres rmn (tableau 2) de ces carbéthoxy-3 pyrazolinones-5 confirme les informations obtenues des spectres ir. La présence d'une bande très large à champ faible, aux environs de 11–13 ppm, serait due à un groupement NH dont le proton est très déblindé par liaison intramoléculaire avec le groupement CO ester (7). Plus le solvant utilisé dans la préparation des spectres est polaire, plus la forme NH semble stable, en accord avec Katritzky (8).

Pour les composés non substitués en position 1, les spectres pris dans le DMSO deutéré montrent deux bandes NH séparées, chacune d'intensité 1H, vers 13 et 10 ppm, et dans les spectres pris dans le $CDCl_3$, une seule bande NH d'intensité 2H qui apparaît à champ un peu plus élevé, vers 8–9 ppm. Lorsque la position 1 porte une substitution, une seule bande NH d'intensité 1H est observée vers 11 ppm dans le DMSO et un peu plus haut dans le $CDCl_3$. (Il y a une

TABLEAU 2. Données spectrales rmn des carbéthoxy-3 pyrazolinones-5 (δ en ppm, TMS)[a]

Composé	Solvant	Position 1	Position 2	Position 3	Position 4
5	DMSO-d_6	10.4b(1H)	12.5b(1H)	1.29t(3H) 4.26q(2H)	5.92s(1H)
	$CDCl_3$	8.1b(2H)		1.42t(3H) 4.48q(2H)	6.22s(1H)
6	DMSO	3.61s(3H)	11.4b(1H)	1.24t(3H) 4.19q(2H)	5.76s(1H)
	$CDCl_3$	3.70s(3H)	11.1b(1H)	1.28t(3H) 4.28q(2H)	5.93s(1H)
7	DMSO	7.6m(5H)	11.9b(1H)	1.29t(3H) 4.26q(2H)	5.97s(1H)
	$CDCl_3$	7.5m(5H)	3.75s(1H)[b]	1.38t(3H) 4.40q(2H)	6.10s(1H)
8	DMSO	9.5b(1H)	13.0b(1H)	1.30t(3H) 4.26q(2H)	2.05s(3H)
	$CDCl_3$	8.7b(2H)		1.44t(3H) 4.43q(2H)	2.20s(3H)
9	DMSO	7.5m(5H)	11.4b(1H)	1.18t(3H) 4.20q(2H)	7.50m(5H)
	$CDCl_3$	7.3m(5H)	7.8b(1H)	1.14t(3H) 4.15q(2H)	7.30m(5H)
10	DMSO	7.6m(5H)	11.0b(1H)	1.30t(3H) 4.30q(2H)	2.15s(3H)
	$CDCl_3$	7.3m(5H)	9.4b(1H)	1.31t(3H) 4.30q(2H)	2.05s(3H)

[a]Abbréviations: b = bande, m = multiplet, q = quadruplet, s = singulet, t = triplet.
[b]Exception.

exception pour le composé 7 pour lequel cette bande ressort beaucoup plus bas à 3.75 ppm dans le $CDCl_3$. Nous n'avons pas pu expliquer cette anomalie.) Toutes ces bandes disparaissent par addition de D_2O.

De plus, le signal donné par le ou les protons de la position 4 est toujours un singulet, sauf pour les protons aromatiques, et son intensité est toujours équivalente à 1, 3 ou 5 protons selon que cette position est non substituée, méthylée ou phénylée. Ce fait exclut la forme CH. La présence du groupement carbéthoxy en position 3 doit stabiliser la forme NH, par allongement du système conjugué et possiblement par chélation.

Spectres ultraviolets

L'examen des spectres d'absorption uv (fig. 1) semble aussi confirmer ces avancés. Dans le cyclohexane, la solubilité des carbéthoxy-3 pyrazolinones-5 est très faible et le calcul du coefficient d'extinction molaire n'est pas possible en pratique. Cependant, ce calcul a été possible en utilisant l'éthanol absolu comme solvant. On observe deux bandes d'absorbtion, l'une d'intensité forte vers 225 nm et l'autre d'intensité plus faible vers 270 nm: ceci amène à conclure à la

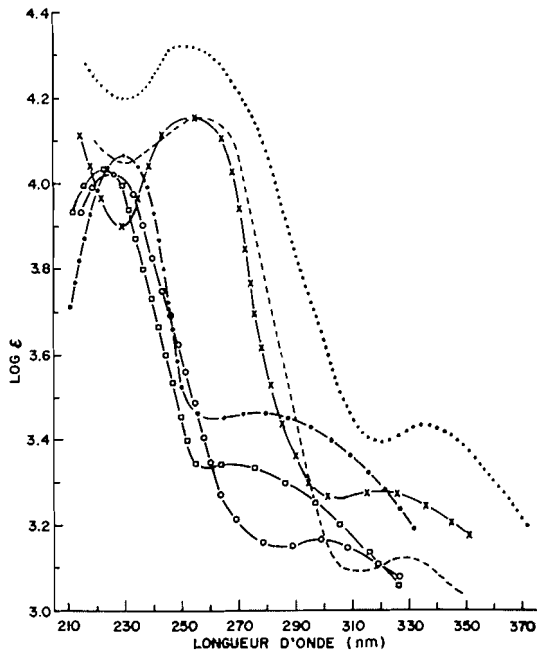

FIG. 1. Spectres uv des carbéthoxy-3 pyrazolinones-5 (ethanol): non-substituée □—□—□—□, méthyle-1 ○—○—○—○, phényle-1 ×—×—×—×—×, méthyle 4 ·—·—·—·, diphényle-1,4 ·····, méthyle-4 phényle-1 — — — —.

Can. J. Chem. Downloaded from www.nrcresearchpress.com by 210.87.254.40 on 09/05/12
For personal use only.

TABLEAU 3. Sels d'hydrazinium des carbéthoxy-3 pyrazolinones-5

Composé	Point de fusion (°C)	Solvant de cristallisation	Rendement brut (%)	Formule	Trouvé C	Trouvé H	Trouvé N	Calculé C	Calculé H	Calculé N
12*a*	125–26	EtOH abs.	>80	$C_7H_{14}N_4O_3$	41.40	6.96	27.42	41.58	6.93	27.72
12*b*	135–37	EtOH, 95%	>90	$C_{12}H_{16}N_4O_3$	54.94	6.12	21.05	54.53	6.10	21.58
12*c*[a]	≃115–16(dec.)	EtOH abs.	>90	$C_7H_{14}N_4O_3$	—	—	—	—	—	—
12*d*	197–98	EtOH, 95%	>90	$C_{18}H_{20}N_4O_3$	63.56	5.93	16.71	63.53	5.88	16.47
12*e*	162–64	EtOH abs.	>90	$C_{13}H_{18}N_4O_3$	55.86	6.73	20.19	56.10	6.52	20.13

[a]**12***c* se décompose durant la recristallisation; il n'a pu être suffisamment purifié pour analyse.

TABLEAU 4. Sels de guanidinium des carbéthoxy-3 pyrazolinones-5

Composé	Point de fusion (°C)	Solvant de cristallisation	Rendement brut (%)	Formule	Trouvé C	Trouvé H	Trouvé N	Calculé C	Calculé H	Calculé N
13*a*	129–31	EtOH, 95%	55	$C_7H_{13}N_5O_3\cdot H_2O$	36.26	6.34	29.95	36.05	6.48	30.03
13*b*	182–84	EtOH–EtOAc	>90	$C_8H_{15}N_5O_3\cdot H_2O$	38.76	7.06	27.88	38.86	6.88	28.33
13*c*	182–83	H_2O	>90	$C_{13}H_{17}N_5O_3\cdot\frac{1}{2}H_2O$	52.37	5.96	23.23	52.00	6.00	23.33
13*d*	192–93	H_2O	>90	$C_8H_{15}N_5O_3\cdot H_2O$	39.16	6.96	28.54	38.86	6.88	28.33
13*e*	240–42	EtOH abs.	>90	$C_{19}H_{21}N_5O_3\cdot C_2H_5OH$	61.16	6.38	16.84	61.02	6.53	16.95
13*f*	182–86(dec.)	EtOH–$CHCl_3$	>80	$C_{14}H_{19}N_5O_3\cdot\frac{1}{2}H_2O$	53.47	6.35	22.05	53.61	6.41	22.28

présence d'un système conjugué dont un groupement C=O, tel que trouvé dans les esters α, β insaturés. La présence d'un substituant phényle en position 1 cause un déplacement bathochromique des deux bandes d'absorption vers 255 et 330 nm et augmente l'intensité de la première bande, indiquant possiblement un allongement de la conjugaison.

Sels d'hydrazinium et de guanidinium des carbéthoxy-3 pyrazolinones-5

Les travaux concernant la réaction des carbéthoxy-3 pyrazolinones-5, **1**, avec l'hydrate d'hydrazine qui sont décrits dans la littérature (1–4) mentionnent uniquement la formation de produits de condensation avec le groupement carbéthoxy, soit l'obtention d'hydrazides **2** servant d'intermédiaires dans la préparation des azides correspondants. Ces hydrazides (éq. 1, R_1 = Ph, PhCO; R_4 = Me, Et, Ph, Bz) sont obtenues en faisant réagir l'hydrate d'hydrazine bouillant avec les carbéthoxy-3 pyrazolinones-5 correspondantes.

D'autre part, aucune réaction semblable avec la guanidine n'est rapportée dans la littérature.

Lorsque les carbéthoxy-3 pyrazolinones-5 substituées (**6**–**10**) réagissent avec l'hydrazine ou la guanidine en solution éthanolique, à une température ne dépassant pas 80 °C, la réaction ne se fait pas (ou très peu) avec le groupement carbéthoxy; il se produit plutôt un transfert d'un proton vers la base et il en résulte des ions hydrazinium ou guanidinium, de sorte que les sels d'hydrazinium ou de guanidinium correspondants des pyrazolinones (**12** et **13**) sont formés.

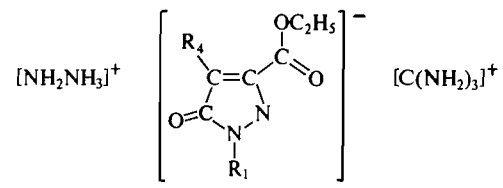

12

a R_1 = Me, R_4 = H
b R_1 = Ph, R_4 = H
c R_1 = H, R_4 = Me
d R_1 = Ph, R_4 = Ph
e R_1 = Ph, R_4 = Me

13

a R_1 = H, R_4 = H
b R_1 = Me, R_4 = H
c R_1 = Ph, R_4 = H
d R_1 = H, R_4 = Me
e R_1 = Ph, R_4 = Ph
f R_1 = Ph, R_4 = Me

On obtient ces différents sels par évaporation à sec de la solution car ils sont en général très solubles dans le milieu réactionnel. Les rendements des produits purifiés n'ont pas été calculés parce qu'une perte élevée de substance est subie lors de la recristallisation de ces solides, passablement solubles dans les solvants polaires (eau et alcool) et très peu solubles dans les solvants non polaires. Les rendements bruts sont cependant élevés, dépassant 80%.

Le sel d'hydrazinium **12***c* n'a pu être isolé à

Can. J. Chem. Downloaded from www.nrcresearchpress.com by 210.87.254.40 on 09/05/12
For personal use only.

Can. J. Chem. Downloaded from www.nrcresearchpress.com by 210.87.254.40 on 09/05/12
For personal use only.

TABLEAU 5. Données spectrales ir des sels d'hydrazinium, cm^{-1} (fenêtre KBr)[a]

Composé	ν NH libre	ν NH associé		ν NH_3^+		ν C=O ester	ν C=O cycle	Ph	ν C=C cycle	?	ν C—O—C asym.	ν C—O—C sym.?
12*a*	3358fa	3300–3265m	3160–3140m	2900–2500m	2150–2100fa	1736fa 1720m 1703f	1689f		1582f	1475mu,f	1245f	1136f 1075f
12*b*	3343m	3290fa 3222fa	3140m 3068–3050m	2900–2300m	2180–2060fa	1736fa 1720m 1703f	1698f 1693f	1602m	1588m 1565m	1470mu,f	1265f	1155m 1128m
12*c*[b]	3350f	3290–3100f		2900–2300f	2220–2040fa	1737fa 1720m 1704f	1685m 1640m		1570f	1500f 1479f	1250f	1125f 1090f
12*d*	3364m	3300fa	3065m	2900–2500m	2160–2080fa	1740fa 1722m 1707m	1689f	1603f	1577m 1540f	1517f 1496m 1444f	1247f	1168m 1112m
12*e*	3357m	3293fa	3063m	2900–2400m	2200–2100fa	1737fa 1721m 1703f	1699f	1598m	1562m 1556m	1505m 1480m 1432f	1249f	1170m 1118m

[a]Abbréviations: f = forte; fa = faible; m = médium; mu = multiple.
[b]Produit brut, non recristallisé.

Can. J. Chem. Downloaded from www.nrcresearchpress.com by 210.87.254.40 on 09/05/12
For personal use only.

TABLEAU 6. Données spectrales ir des sels de guanidinium, cm^{-1} (fenêtre KBr)[a]

Composé	H_2O	ν NH libre		ν NH de $(NH_2)_3C^+$		ν C=O ester	ν C=O cycle	δNH de $(NH_2)_3C^+$	Ph	ν C=C cycle	?	ν C—O—C asym.	ν C—O—C sym.?
13*a*	3540b,m	3400f	3353f	3250–3100f	2900–2400m–fa	1738fa 1722fa 1704m	1690f	1660mu,f	—	1579f 1575f 1558m	1498m 1433f	1283f	1148f 1111m
13*b*	3540b,m	3440f	3350f	3300–3100f	2900–2400m–fa	1737fa 1720m 1713f	1685m	1660mu,f	—	1562f 1555f 1537m	1490m 1430f	1271f	1183f 1110m
13*c*	3520b,m	3420f	3380f	3300–3100m 3075m	2900–2400m–fa	1737fa 1720m 1708f	1685m	1660mu,f	1599f	1560m 1550f 1537m	1495m 1484m 1429f	1246f 1209m	1149m 1109f
13*d*	3520–3470b,m	3460–3370b,f	3315f	3200–3100f	2900–2400m–fa	1736fa 1720m 1702f	1697f	1665mu,f	—	1571f 1567f 1555m	1422f	1253f	1085f
13*e*	—	3438f 3415f	3350m	3250b,m 3200–3060m	2850–2400m–fa	1737fa 1720fa 1703f	1698f 1695f	1665mu,f	1599f	1545m 1535m 1528m	1492m 1442f 1420f	1217f	1153f 1052m
13*f*	3550m	3475m	3360b,m	3155b,m	2900–2500m–fa	1737fa 1720fa 1704m	1680f 1675f	1665mu,f	1598m	1564m 1557m	1514m 1500m 1440f	1249f	1160m 1089m

[a]Abbréviations: b = bande, f = forte, fa = faible, m = médium, mu = multiple.

TABLEAU 7. Données spectrales rmn des sels d'hydrazinium des carbéthoxy-3 pyrazolinones-5, pris dans le DMSO-d_6 (glissements chimiques en δ ppm, TMS)[a]

Composé	$(NH_2NH_3)^+$	N—CH_3	C=C—H	C=C—CH_3	C_6H_5	CH_2CH_3 (ester)
12*a*	6.95s(5H)	3.44s(3H)	5.22s(1H)			1.22t(3H) 4.14q(2H)
12*b*	6.8s(5H)		5.37s(1H)		7.8mu(5H)	1.29t(3H) 4.24q(2H)
12*d*	4.95s(7H)[b]				7.5mu(10H)	1.24t(3H) 4.26q(2H)
12*e*	6.75s(5H)			2.00s(3H)	7.5mu(5H)	1.30t(3H) 4.22q(2H)

[a]Abbréviations: b = bande, mu = multiplet, q = quadruplet, s = singulet, t = triplet.
[b]Intensité 5H de $NH_2NH_3^+$ et 2H de H_2O résiduelle de DMSO.

l'état pur car sa recristallisation redonnait toujours la pyrazolinone de départ **8**; néanmoins, on a réussi à l'identifier à l'état brut par analyse spectrale ir. Il faut noter aussi que les sels de guanidinium ont cristallisé sous forme d'hydrates (**13** *a–d*, **13***f*) ou sous forme d'éthanolate **13***e*.

Parmi les carbéthoxy-3 pyrazolinones-5 étudiées, nous avons remarqué que celle qui est non substituée **5** est moins réactive. Le rendement brut de son sel de guanidinium **13***a* n'a pas dépassé 50% et son sel d'hydrazinium (**12**, R_1 et R_4 = H) n'a pas été obtenu, le produit alors isolé avec un rendement de 30% étant plutôt l'hydrazide correspondante, déjà rapportée dans la littérature (15).

Les tableaux 3 et 4 donnent le point de fusion et l'analyse de ces différents sels.

Les analyses spectrales confirment la nature de ces sels. Les spectres ir (tableaux 5 et 6) révèlent plusieurs bandes d'absorption caractéristiques des ions hydrazinium et guanidinium (vers 3400–3050 cm^{-1} et 2900–2700 cm^{-1}) et font voir que la fréquence de la bande d'absorption du groupement C=O du cycle a baissé à 1700–1685 cm^{-1}, soit un déplacement d'environ 20 à 30 cm^{-1}, possiblement causé par un accroissement d'intensité du système conjugué. On retrouve encore cette bande d'intensité assez forte vers 1570 cm^{-1} attribuable au groupement C=C selon Maquestiau *et al.* (14).

La forme CH n'est plus possible dans le cas de ces sels des carbéthoxy-3 pyrazolinones-5, et les formes OH et NH deviennent équivalentes et conduisent, par perte d'un proton, au même système conjugué stabilisé **14**.

L'analyse spectrale rmn (tableaux 7 et 8) révèle aussi des glissements chimiques caractéristiques des ions hydrazinium et guanidinium, massifs assez étroits dans le cas des sels d'hydrazinium, mais plus élargis pour les sels de guanidinium, peut-être à cause de la présence d'eau d'hydratation dans ces derniers; leur déplacement chimique est en général voisin de 7 ppm. Les autres protons, ceux de l'anion cyclique, subissent les glissements chimiques attendus et n'apportent pas d'autre information vu que cet anion ne peut adopter qu'une seule forme, celle donnée ci-haut.

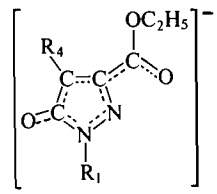

14

Partie expérimentale

Les points de fusion ont été déterminés dans des tubes capillaires et ne sont pas corrigés. Les analyses spectrales ont été faites avec les appareils suivants: ir, Perkin-Elmer, modèle 647; rmn, Varian, modèle T-60, avec TMS comme standard interne; uv, Bausch and Lomb, modèle spectronic 600.

Les analyses élémentaires ont été réalisées par Micro-Tech Laboratories, Inc., Skokie, Illinois.

Carbéthoxy-3 pyrazolinones-5 (5–10)

Toutes les carbéthoxy-3 pyrazolinones-5 ont été préparées par la méthode de Wislicenus et Arnold (16) en condensant les oxosuccinates d'éthyle correspondants avec l'hydrate d'hydrazine et ses dérivés. Parmi elles, seules les méthyle-4 et éthyle-4 ne sont pas rapportées dans la littérature: (*i*) méthyle-4: pf: 190–92 °C (eau); *Anal.* calc. pour $C_7H_{10}N_2O_3$: C 49.42, H 6.01, N 16.39, trouvé: C 49.40, H 5.92, N 16.47; (*ii*) éthyle-4: pf:

Can. J. Chem. Downloaded from www.nrcresearchpress.com by 210.87.254.40 on 09/05/12
For personal use only.

TABLEAU 8. Données spectrales rmn des sels de guanidinium des carbéthoxy-3 pyrazolinones-5, pris dans le DMSO-d_6 (glissements chimiques en δ ppm, TMS)[a]

Composé	$(NH_2)_3C^+$	N—H	N—CH_3	C=C—H	C=C—CH_3	C_6H_5	CH_2CH_3 (ester)
13*a*	6.92b(9H)[b]	(6.92)[b]	—	5.11s(1H)	—	—	1.29t(3H) 4.20q(2H)
13*b*	6.3b(8H)[c]		3.33s(3H)	5.03s(1H)			1.22t(3H) 4.12q(2H)
13*c*	7.2b(7H)[d]			5.09s(1H)		7.8mu(5H)	1.25t(3H) 4.18q(2H)
13*d*	6.8b(9H)[b]	(6.8)[b]			1.91s(3H)		1.27t(3H) 4.18q(2H)
13*e*	3.7b(6H)[e]					7.8mu(10H)	1.28t(3H) 4.26q(2H)
13*f*	7.2b(7H)[d]				1.91s(3H)	7.6mu(5H)	1.26t(3H) 4.20q(2H)

[a]Abbréviations: b = bande, mu = multiplet, q = quadruplet, s = singulet, t = triplet.
[b]Massif de 6H de $(NH_2)_3C^+$ avec 2H de H_2O et 1H de NH (position 1).
[c]Massif de 6H de $(NH_2)_3C^+$ avec 2H de H_2O.
[d]Massif de 6H de $(NH_2)_3C^+$ avec 1H de H_2O.
[e]Massif de 6H de $(NH_2)_3C^+$ caché sous le triplet de CH_2 (δ 3.5) provenant de CH_3CH_2OH de cristallisation. Le quadruplet de CH_3 provenant de CH_3CH_2OH apparaît à 1.15 ppm.

192–193 °C (alcool); *Anal.* calc. pour $C_8H_{12}N_2O_3$: C 51.22, H 6.64, N 15.27; trouvé: C 51.72, H 6.56, N 15.21.

Sels d'hydrazinium (12a–e)

Les carbéthoxy-3 pyrazolinones-5 (0.01 à 0.10 mol) sont agitées mécaniquement dans de l'alcool éthylique absolu (50–100 ml). Le mélange est alors porté à la température de reflux et un léger excès (10%) d'hydrate d'hydrazine est ajouté lentement. L'agitation et le reflux sont maintenus durant une période variant de 4 à 8 h. Le sel cristallise en partie par refroidissement de la solution et est séparé par filtration; en vaporisant entièrement le solvant dans un évaporateur, on obtient le reste du solide, souvent coloré, que l'on recristallise avec la première portion, soit dans l'eau ou l'alcool. Les analyses élémentaires et spectrales ir et rmn sont données dans les tableaux 3, 5 et 7.

Sels de guanidinium (13a–f)

Les carbéthoxy-3 pyrazolinones-5 (0.01 à 0.05 mol) sont agitées dans de l'éthanol absolu (50–100 ml) et le mélange est chauffé avec agitation à une température voisine de 65 °C; puis une solution alcoolique de guanidine est ajoutée lentement, en léger excès (10%). Le mélange est maintenu à cette même température, avec agitation, pour une période variant de 7 à 24 h. Les sels sont isolés par évaporation complète du solvant et sont recristallisés soit dans l'eau, soit dans l'éthanol. Les résultats des analyses élémentaires et spectrales uv et rmn apparaissent dans les tableaux 4, 6 et 8.

Remerciements

Nous tenons à remercier sincèrement les Drs J.-C. Richer et M. St-Jacques de l'Université de Montréal pour l'aide apportée à l'analyse spectrale rmn, et M. André Fouquet du C.M.R. pour son assistance technique.

1. P. E. GAGNON, J. L. BOIVIN, P. A. BOIVIN et R. N. JONES. Can. J. Chem. **29**, 182 (1951).
2. P. E. GAGNON, J. L. BOIVIN, P. A. BOIVIN et H. M. CRAIG. Can. J. Chem. **30**, 52 (1952).
3. P. E. GAGNON, J. L. BOIVIN et A. CHISHOLM. Can. J. Chem. **30**, 904 (1952).
4. P. E. GAGNON, J. L. BOIVIN et M. TREMBLAY. Can. J. Chem. **31**, 673 (1953).
5. W. TRAUBE. Chem. Ber. **26**, 2553 (1893).
6. F. SNAVELY, W. S. STRAHANOVSKY et F. H. SUYDAM. J. Org. Chem. **27**, 994 (1962).
7. R. JONES, A. J. RYAN, S. STERNHELL et S. E. WRIGHT. Tetrahedron, **19**, 1497 (1963).
8. A. R. KATRITZKY et F. W. MAINE. Tetrahedron, **20**, 299 (1964).
9. A. R. KATRITZKY, F. W. MAINE et S. GOLDING. Tetrahedron, **21**, 1693 (1965).
10. H. YASUDA et H. MIDORIDAWA. J. Org. Chem. **31**, 1722 (1966).
11. G. J. LESTINA et T. H. REGAN. J. Org. Chem. **34**, 1685 (1969).
12. A. R. KATRITZKY. Chimia, **24**, 134 (1970).
13. N. J. LEONARD, H. S. GUTOWSKY, W. J. MIDDLETON et E. M. PETERSEN. J. Am. Chem. Soc. **74**, 4070 (1952).
14. A. MAQUESTIAU, Y. VAN HAVERBEKE et R. JACQUERYE. Bull. Soc. Chim. Belg. **82**, 233 (1973).
15. R. VON ROTHENBURG. J. Prakt. Chem. **51**, 56 (1894).
16. W. WISLICENUS et E. ARNOLD. Ann. Chem. **246**, 329 (1888).

Can. J. Chem. Downloaded from www.nrcresearchpress.com by 210.87.254.40 on 09/05/12
For personal use only.

A facile synthesis of sulfonyl chlorides

RICHARD F. LANGLER[1]

Chemistry Department, Scarborough College, University of Toronto, West Hill, Ontario M1C 1A4

Received July 15, 1975

RICHARD F. LANGLER. Can. J. Chem. **54**, 498 (1976).

Benzylic sulfides have been shown to furnish sulfonyl chlorides in excellent yields, upon reaction with molecular chlorine in aqueous acetic acid. The reaction most likely proceeds through the intermediacy of the corresponding sulfenyl chloride.

RICHARD F. LANGLER. Can. J. Chem. **54**, 498 (1976).

On a montré que les sulfures benzyliques fournissent des chlorures de sulfonyle avec d'excellents rendements par réaction avec du chlore moléculaire en solution acide acétique aqueux. Il est plus que probable que la réaction possède par l'intermédiaire des chlorures de sulfényle correspondants.

[Traduit par le journal]

A great deal of work has been done on the chlorination of sulfides and sulfoxides under a variety of reaction conditions with a wide range of chlorinating agents (1–9).

In a preliminary report (10) we have indicated that the chlorination of sulfides and sulfoxides, in aqueous media, may be a useful method for the synthesis of sulfonyl chlorides, although this reaction requires the intermediacy of α-poly chlorosulfoxides which restricts starting materials to α-chloro or symmetrical sulfides.

In a recently reported study (2) we have realized a good yield of methanesulfonyl chloride from the chlorination of benzyl methyl sulfide in aqueous acetic acid. At that time we proposed that methanesulfenyl chloride was the principal intermediate in the reaction.

In an attempt to support the intermediacy of the sulfenyl chlorides in these reactions, we prepared and chlorinated benzyl methyl sulfoxide under the same conditions which we had previously utilized for benzyl methyl sulfide (2). Our hope was that the sulfoxide might undergo hydrolysis, persuant to oxochlorosulfonium chloride formation, furnishing some benzyl methyl sulfone which was not observed as a product from the experiment on the sulfide. In this way the intermediacy of the sulfoxide could be dismissed from consideration.[2] Unfortunately, the results from the chlorination of benzyl methyl sulfoxide were identical to those from the chlorination of the sulfide, which fails to establish the intermediacy of the sulfenyl chlorides in the aqueous chlorination of benzylic sulfides. However, this result is consistent with our observation in a similar comparison of a β-sulfonyl benzylic sulfide and a β-sulfonyl benzylic sulfoxide under the same reaction conditions (2).

TABLE 1. Yields of sulfonyl chlorides from the corresponding benzylic sulfides

Sulfide	Sulfonyl chloride	Yield (%)
$PhCH_2SCH_3$(2)	CH_3SO_2Cl	75
$PhCH_2SCH_2CH_3$	$CH_3CH_2SO_2Cl$	99
$PhCH_2S(CH_2)_2CH_3$	$CH_3(CH_2)_2SO_2Cl$	98
$PhCH_2S(CH_2)_3CH_3$	$CH_3(CH_2)_3SO_2Cl$	96
$PhCH_2S(CH_2)_4CH_3$	$CH_3(CH_2)_4SO_2Cl$	95
$PhCH_2SCH_2Ph$*	$PhCH_2SO_2Cl$	74

*J. S. Grossert and R. F. Langler, unpublished results.

In order to establish the utility of benzylic sulfides as precursors for the synthesis of sulfonyl chlorides, we have prepared and chlorinated a representative selection of precursors. The results are depicted in Table 1. In each case benzyl acetate and benzyl chloride were also formed as shown below.

$$PhCH_2\cdot S\cdot R + Cl_2/H_2O \xrightarrow{HOAc} PhCH_2OAc + PhCH_2Cl + R\cdot SO_2\cdot Cl$$
$$\sim 15\% \qquad \sim 80\% \qquad \sim 95\%$$

The synthetic utility of benzylic sulfides as intermediates in the synthesis of sulfonyl chlor-

[1]Enquiries should be addressed to: Dr. R. F. Langler, Chemistry Department, Dalhousie University, Halifax, Nova Scotia B3H 4J3.

[2]This approach was not unreasonable in view of the fact that both Durst and Tin (11) and Cinquini *et al.* (12) have observed sulfone formation via nucleophilic attack on oxochlorosulfonium cations.

Can. J. Chem. Downloaded from www.nrcresearchpress.com by 210.87.254.105 on 09/05/12
For personal use only.

Can. J. Chem. Downloaded from www.nrcresearchpress.com by 210.87.254.105 on 09/05/12
For personal use only.

ides is clearly superior to that of symmetrical sulfides, since a benzylic group is selectively cleaved rather than a potentially complex R-group. Furthermore, the chlorination of dialkyl sulfides consumes a great deal more chlorine since α-polychlorosulfoxides intervene which react sluggishly resulting in the bulk of the chlorine passing through the reaction mixture unused.

Experimental

General

The ir spectra were recorded on a Beckman IR-10 grating spectrophotometer and the nmr spectra were obtained on a Varian T-60 instrument using TMS as the internal standard.

Preparation of Benzylic Sulfides

The preparation of the benzylic sulfides was essentially the method of Buchi *et al.* (13) as illustrated by the details provided below for the preparation of benzyl ethyl sulfide.

Sodium metal (2.047 g) was dissolved in absolute ethanol (100 ml) followed by benzyl thiol (10 ml). A solution of ethyl bromide (13.126 g) in 10 ml of absolute ethanol was added dropwise over a period of *ca.* 15 min and the reaction stirred at ambient temperature for 54 h. Water (100 ml) was added and the solution washed with chloroform (three 100-ml aliquots). The chloroform layers were combined, dried ($MgSO_4$), filtered, and the chloroform rotary evaporated. The residue was rectified at reduced pressure furnishing benzyl ethyl sulfide (9.893 g bp 119–120 °C/31 Torr).

Preparation of Sulfonyl Chlorides

In each case the appropriate alkyl benzyl sulfide (5–6 g) was added to a solution of distilled water (3.3 ml) in glacial acetic acid (25 ml). Molecular chlorine was bubbled through the solution at *ca.* 200 ml/min. During the chlorination the reaction temperature was maintained below 30 °C with an ice-water bath. Chlorination was continued until the reaction was no longer exothermic (~10–20 min). Upon completion of the chlorination, water (35 ml) was added and the solution washed with chloroform (three 50-ml aliquots). The combined chloroform layers were washed with 2.5% w/v NaOH (two 50-ml aliquots). The chloroform was then dried ($MgSO_4$), filtered, and rotary evaporated.

Yields were calculated from the molar ratios of the products as obtained from an nmr spectrum of the crude. Sulfonyl chlorides could be detected in crude mixtures on tlc using sodium iodide–acetone spray (14).

Identification of the components in each case was achieved by resolving a small sample of crude mixture on preparative thin layer chromatography plates. Five preparative plates were spotted with concentrate from the chlorination reaction (100 mg/plate). The plates were eluted with chloroform giving rise to three bands, R_F 0.49 (uv light), R_F 0.60–0.70 (variable, detected on analytical plates with NaI–acetone spray), and R_F 0.88 (uv light). The upper bands (R_F 0.88) were scraped and combined, covered with chloroform (150 ml), and stirred for 1 h. After filtration and concentration benzyl chloride was obtained, which was identical with authentic material by tlc, ir, and nmr. The whole area between the upper and lower band (R_F 0.60–0.70) was subjected to the same procedures as described for the upper bands. Upon concentration the appropriate sulfonyl chloride was obtained which was identical to authentic material by nmr, ir, and bp. Isolation of the lower band material always furnished a compound identical to authentic benzyl acetate by tlc, nmr, and ir.

Acknowledgements

It is a pleasure to acknowledge the kindness of Dr. T. T. Tidwell during the course of this work. Ms. J. R. Jardine and Mr. D. Hitchmough provided technical assistance which is gratefully acknowledged. The University of Toronto provided some financial assistance.

1. K. Fries and W. Vogt. Ann. **381**, 337 (1911).
2. W. R. Hardstaff, R. F. Langler, J. Leahy, and M. J. Newman. Can. J. Chem. **53**, 2664 (1975), and references therein.
3. I. B. Douglass. J. Org. Chem. **39**, 563 (1974).
4. M. Cinquini, S. Colonna, and F. Montanari. J. Chem. Soc. Perkin Trans. 1, 1719 (1974).
5. M. Cinquini, S. Colonna, and F. Montanari. J. Chem. Soc. Perkin Trans. 1, 1723 (1974).
6. H. Stollar and J. Klein. J. Chem. Soc. Perkin Trans. 1, 1763 (1974).
7. S. Iriuchijima, M. Ishibashi, and G. Tsuchihashi. Bull. Chem. Soc. Jpn. **46**, 921 (1973).
8. S. Bory, R. Lett, B. Moreau, and A. Marquet. C. R. Acad. Sci. Ser. C, 1323 (1973).
9. I. Granoth. J. Chem. Soc. Perkin Trans. 1, 2166 (1974).
10. J. S. Grossert, W. R. Hardstaff, and R. F. Langler. Chem. Commun. 50 (1973).
11. T. Durst and K. C. Tin. Can. J. Chem. **49**, 2374 (1971).
12. M. Cinquini, R. Annunziata, and S. Colonna. J. Chem. Soc. Perkin Trans. 1, 2057 (1972).
13. I. J. Buchi, M. Prost, H. Eichenberger, and R. Lieberherr. Helv. Chim. Acta, **35**, 1527 (1952).
14. J. R. Jardine and R. F. Langler. J. Chromatogr. In press.

Studies of *p*-nitrobenzoic acid and the *p*-nitrobenzoate ion in the electrical double layer of oriented cationic and anionic nematic phases

YUNKO LEE AND LEONARD W. REEVES
Department of Chemistry, University of Waterloo, Waterloo, Ontario N2L 3G1

Received July 14, 1975

YUNKO LEE and LEONARD W. REEVES. Can. J. Chem. **54**, 500 (1976).

The *p*-nitrobenzoate ion and its conjugate acid have been oriented in both cationic and anionic detergent based lyomesophases. In the cationic phase there is no marked change in the order of the C_2 axis as the hydrogen ion concentration of the water region of the phase is varied. The degree of order along the C_2 axis is decreased considerably in passing to the anionic detergent based phase and in this phase the degree of order of the ion does increase in the expected manner on protonation. The orientation of the larger organic counter ion and its acid is probably complicated by insertion into the hydrophobic region and use of the $-NO_2$, $-CO_2^-$, or —COOH moieties as head groups.

YUNKO LEE et LEONARD W. REEVES. Can. J. Chem. **54**, 500 (1976).

On a orienté l'ion *p*-nitrobenzoate et son acide conjugué dans des lyomésophases basées sur des détergents cationiques et anioniques. Dans la phase cationique, il n'y a pas de changement important dans l'ordre de l'axe C_2 à mesure que la concentration en ion hydrogène de la région aqueuse de la phase varie. Le degré d'ordre le long de l'axe C_2 diminue considérablement lorsque l'on passe à la phase basée sur le détergent anionique; dans cette phase, le degré d'ordre de l'ion augmente de la façon attendue lorsqu'il y a protonation. L'orientation de l'ion organique plus gros et de son acide est probablement compliquée par l'insertion dans la région hydrophobique et l'utilisation des fonctions $-NO_2$, $-CO_2^-$ ou —COOH comme groupes de tête.
[Traduit par le journal]

Introduction

Lyotropic liquid crystals provide important model research problems, which have impact in widely differing areas of chemistry and biology (1). The superstructure arrangements of the amphiphilic molecules or ions are determined by the hydrophobic effect and divide these mesophases into three separate regions: (*a*) aqueous, (*b*) electrical double layer (edl) or polar layer, and (*c*) lipophillic hydrocarbon chains (2). These three divisions are essential aspects of the operations of the lipid bilayer model of biological membranes (3).

Magnetic fields used in the nuclear magnetic resonance (nmr) studies of these systems provide a mechanism for spontaneous orientation of the nematic mesophases (4). Two distinctly different nematic lyomesophases can be distinguished according to the direction of alignment of the nematic axis in a magnetic field. A type I nematic phase orients parallel to the magnetic field and a type II nematic phase perpendicular to the magnetic field (4, 5). The type II phase can be shown to have a cylindrical superstructure reported earlier in similar systems by Luzzati *et al.* (2).

One very important model aspect of lyomesophases is the edl or polar interface regions and the high concentration of interface per unit volume which make them particularly convenient to study by nmr methods. The orientation of small counter ions with respect to the perpendicular direction to the interface becomes accessible to experimental study in these systems. It is clear also that the distribution of ions as a function of distance from the interface can be investigated at least indirectly in terms of the local degree of orientation with respect to the interface.

The chemistry of the edl can be varied almost at will in these mesophases as we have recently shown (6–11). The sign of the charge on the detergent ion can be positive or negative and successful nematic phases have been recently synthesized with mixtures of detergent cations and anions. The interface charge density can be varied by additions of neutral amphiphiles such as decanol or cholesterol (5) and the aqueous part of the electrical double half layer can be varied by the addition of balanced electrolytes or small polar molecules such as methanol, ethylene carbonate, aromatic nitrogen

Can. J. Chem. Downloaded from www.nrcresearchpress.com by 210.87.254.40 on 09/05/12
For personal use only.

Can. J. Chem. Downloaded from www.nrcresearchpress.com by 210.87.254.40 on 09/05/12
For personal use only.

TABLE 1. Compositions of the lyotropic nematic phases prepared in this study

Sample	Wt.% DACl	D_2O	NH_4Cl	CsNB*
1	30.0	63.2†	1.6	5.3
2	32.6	60.7	1.7	5.0
3	32.3	63.3‡	1.5	2.9

Sample	Wt.% CsDS	D_2O	*n*-Decanol	CsNB*
4	36.9	52.5†	4.1	6.5
5	37.8	52.4	3.5	6.3
6	38.7	54.4§	3.8	3.1

*CsNB = cesium *p*-nitrobenzoate.
†D_2O (0.01 *N* NaOH).
‡D_2O (0.2 *N* HCl).
§D_2O (0.2 *N* H_2SO_4).

bases, etc. (1*b*, 5, 11). The ability to sustain nematic properties with these chemical variables enables the experimenter to bring to bear, probably for the first time, all the anisotropic nmr parameters on the edl problem.

Recently Lee and Reeves (11) have shown a 60- to 90-fold increase in the magnitude of the degree of order of C_∞ axis of the cation, $[CH_3TlCH_3]^+$, present in the form of added electrolyte, when the nematic phase is changed from one prepared using a cationic detergent to that using an anionic detergent.

In this present study, the hydrogen ion concentration of the aqueous component is controlled in order to study the orientation of *p*-nitrobenzoic acid and its conjugate base in both cationic and anionic detergent nematic phases.

Experimental

The proton nmr spectra of the oriented *p*-nitrobenzoate ion and its conjugate acid in the lyotropic nematic phases were recorded on a Varian HA-100 spectrometer, with sample spinning at a probe temperature of 30.7 ± 0.2 °C. The spectrometer was operated in a locked mode. The calibration of the position of the individual peaks was achieved by the difference frequency from the lock signal. *p*-Nitrobenzoate (or protonated *p*-nitrobenzoate) ion was oriented in both cationic and anionic nematic phases. The cationic nematic phases were made from decylammonium chloride (DACl), ammonium chloride, and deuterium oxide. The anionic nematic phases were composed of cesium decylsulfate (CsDS), *n*-decanol, and deuterium oxide. The compositions of the nematic phases made in the present study are listed in Table 1. Samples 1, 2, and 3 are basic, neutral, and acidic cationic nematic phases, while samples 4, 5, and 6 are basic, neutral, and acidic anionic phases respectively. Cesium *p*-nitrobenzoate was prepared by neutralizing *p*-nitrobenzoic acid with cesium carbonate. The product was recrystallized in a water–ethanol solvent mixture. Cesium decylsulfate was prepared by neutralizing cesium carbonate with decylsulfuric acid, which was formed by passing sodium decylsulfate through an acidified chromatographic column containing Dowex 50-H^+ ion exchange resin. Decylammonium chloride was prepared from the reaction of decylamine and hydrochloric acid.

TABLE 2. The analysis of the proton spectrum of the cesium *p*-nitrobenzoate in the isotropic solution

Parameter	Value (Hz)
J_{12}	2.48 ± 0.03
J_{34}	1.92 ± 0.03
$J_{13} = J_{24}$	0.34 ± 0.02
$J_{14} = J_{23}$	8.45 ± 0.02
$\Delta\delta$	20.4 ± 0.03
rms error	0.06

Results and Discussion

The proton magnetic resonance spectrum of cesium *p*-nitrobenzoate was recorded from isotropic aqueous solutions of the salt at 100 MHz. The concentration of the salt was maintained close to that of the mesophases which contained the oriented ion. The spectrum was also obtained from unoriented micellar solutions prepared as closely as possible to the mesophase compositions. The $AA'BB'$ spectrum was analyzed with the UEA computer program (12) which gave the parameters listed in Table 2 for several averaged spectra. No significant variation of these parameters occurred on protonation of the ion or when the isotropic medium was varied. The root-mean-square error of ±0.06 Hz from the computed 12 line spectrum was deemed satisfactory. The enumeration of the scalar couplings J_{ij} are denoted in Fig. 1

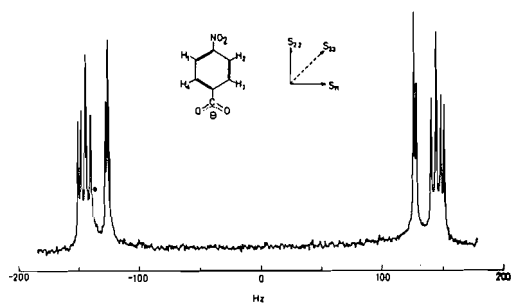

FIG. 1. Proton magnetic resonance spectrum of the *p*-nitrobenzoate ion oriented in a lyotropic nematic phase of cesium decylsulfate, decanol, and deuterium oxide.

TABLE 3. The direct couplings, the ratios of the various interproton distances, and the orientation parameters in cesium *p*-nitrobenzoate with D_{2h} symmetry

Parameter	Value					
	Sample 1	Sample 2	Sample 3	Sample 4	Sample 5	Sample 6
D_{12} (Hz)	−1.03	−1.62	−10.8	−15.8	−23.9	−13.5
D_{13} (Hz)	36.5	42.1	33.3	−1.43	−2.11	15.9
D_{14} (Hz)	1103.6	1277.8	1139.7	188.3	286.3	665.9
r_{14}/r_{12}	0.5892	0.5885	0.5895	0.5854	0.5847	0.5882
r_{13}/r_{12}	1.1607	1.1603	1.1608	1.1590	1.1584	1.1601
S_{11}	3.14×10^{-4}	5.03×10^{-4}	3.32×10^{-3}	4.96×10^{-3}	7.52×10^{-3}	4.18×10^{-3}
S_{22}	-6.94×10^{-2}	-8.04×10^{-2}	-7.15×10^{-2}	-1.19×10^{-2}	-1.80×10^{-2}	-4.19×10^{-2}
S_{33}	6.90×10^{-2}	7.99×10^{-2}	6.82×10^{-2}	0.69×10^{-2}	1.05×10^{-2}	3.77×10^{-2}

which gives the protons numbered positions on the ring. These scalar couplings and the chemical shifts were assumed to be invariant in the change from isotropic to mesophase solution and were used to reduce the number of parameters needed for iteration to fit the spectra from anisotropic media. The *p*-nitrobenzoate ion and its conjugate acid were oriented in the phases described in Table 1 and a 12 line proton magnetic resonance spectrum typical of an $AA'BB'$ nuclear spin system was recorded. An example of the spectrum is shown as Fig. 1 for the basic phase cesium decylsulfate, decanol, water, and cesium *p*-nitrobenzoate. The spectral analyses of the oriented acid and ion in both cationic and anionic lyomesophases are presented in Table 3.

In the cationic decylammonium chloride based phase, the direct dipolar coupling constants between *meta* protons D_{12} are smaller than those between *para* protons D_{13}, although quite a good fit to the experimental spectrum can be obtained by interchanging the *meta* and *para* values. The small dipolar coupling constant between *meta* protons leads to physically meaningful orientation parameters and internuclear distance ratios. The opposite is true in the anionic detergent phases based on the decylsulfate system. Assuming an internal chemical shift $\delta_1 = \delta_2 \neq \delta_3 = \delta_4$, and $D_{12} = D_{34}$, the best fit between the experimental and computed spectrum using the UEA program gives a root-mean-square error of 0.2 Hz or less for the difference between frequencies for all computed and experimental lines. This is in agreement with the random error analysis of the experimental peak positions. Since the two *para*-substituents on the benzene ring are different, one would expect the four protons of the *p*-nitrobenzoate ion to be on a plane with C_{2v} symmetry rather than a D_{2h} symmetry. However the C_{2v} symmetry was not detected in the present study. The dipolar coupling constants depend on the interproton distances. A very small difference between the interproton distances of the two pairs of *meta*-protons would probably make the C_{2v} symmetry indistinguishable within experimental error from a D_{2h} symmetry. The cases of *p*-chlorofluorobenzene and *p*-bromofluorobenzene are similar, but in these molecules the symmetry of C_{2v} has not been detected (13).

The relations between the ratios of the various interproton distances and the direct dipolar coupling constants for an $AA'BB'$ spin system with D_{2h} symmetry are given by the following equations (14):

$$[1] \quad D_{14}(r_{14}/r_{12})^5 - D_{13}[1 + (r_{14}/r_{12})^2]^{5/2} = -D_{12}$$

$$[2] \quad (r_{13}/r_{12})^2 = 1 + (r_{14}/r_{12})^2$$

Equations 1 and 2 indicate that the ratios (r_{14}/r_{12}) and (r_{13}/r_{12}) in the *p*-nitrobenzoate ion can be determined unambiguously, independent of orientation. The interproton distance ratios obtained in this study are listed in Table 3. The present results show that there are no significant changes in the geometry of the *p*-nitrobenzoate *ion* or protonated *p*-nitrobenzoate ion in both the cationic and anionic lyotropic nematic phases. The ratio of the *meta* to *ortho* proton distances found for the *p*-nitrobenzoate ion is comparable to those found for a *p*-dihalobenzene (15).

The orientation parameters S_{11} and S_{22} are related to the interproton distances and to the various dipolar coupling constants by [3] and [4] respectively:

Can. J. Chem. Downloaded from www.nrcresearchpress.com by 210.87.254.40 on 09/05/12
For personal use only.

Can. J. Chem. Downloaded from www.nrcresearchpress.com by 210.87.254.40 on 09/05/12
For personal use only.

[3] $$S_{11} = -(2\pi^2/h\gamma^2)D_{12}r_{12}^3$$

[4] $$S_{22} = -(2\pi^2/h\gamma^2)D_{14}r_{14}^3$$

It is obvious that the values of S_{11} and S_{22} can be determined only if one of the interproton distances is known. The distance between the *ortho* protons chosen for the present calculations is 2.47 Å, which is typical for *para*-disubstituted benzene molecules. Values of the orientation parameters calculated are also included in Table 3.

It has been proposed in our previous work that electrostatic interactions play quite a significant role on the orientation of an ion in a lyotropic nematic phase (11). The parameter S_{22} defined here is related to the orientation of the C_2-symmetry axis. A comparison of the S_{22} values of the *p*-nitrobenzoate ion in the decylammonium chloride phase with those in the decylsulfate phase shows that the C_2-symmetry axis of the ion is more highly ordered in the cationic detergent phase than in the anionic detergent phase. This reflects a stronger electrostatic interaction between the *p*-nitrobenzoate ion and its conjugate acid and the positively charged electrical double half layer of decylammonium ions. There is no large change in degree of order in any direction as the acidity of the aqueous region changes. This shows no strong preferential orienting forces at the positive interface as the ion changes to conjugate acid. In this case therefore the charge on the species has little effect in providing an orienting electrostatic force. There is a large change in degree of order of the *p*-nitrobenzoate ion and its conjugate acid in passing to the anionic nematic phase which decreases the order parameter S_{22} by a factor about 2 to 4 times. This factor is however much smaller than that observed for the dimethylthallium ion in passing from cationic to anionic phase (11). There is a notable increase in degree of order S_{22} in the anionic phase as the *p*-nitrobenzoate ion is protonated (Table 3). The approximately twofold increase in S_{22} can be associated with removal of the negative charge on the ion, decreasing the repulsive forces with the anionic detergent head groups. The ionic detergent head groups in these lyotropic nematic phases are known to be the most highly ordered regions of the phase (7–10) and an increase in degree of order in a counter ion principal axis is associated with a more intimate contact at the edl.

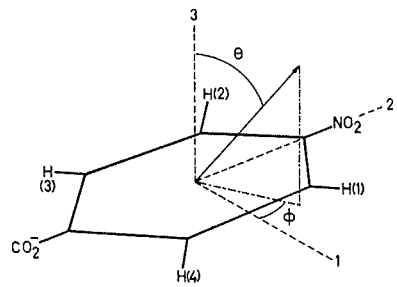

FIG. 2. The coordinate system and numbering of protons for *p*-nitrobenzoate ion.

The anisotropic motion of the counter ion can be described with a probability function $P(\theta,\phi)$, which is the probability per unit solid angle that the applied magnetic field direction is θ and ϕ in spherical polar coordinates relative to the molecule-fixed Cartesian coordinate system (8). With the spherical polar coordinates as defined in Fig. 2, and assuming that the lyotropic nematic phases are oriented perpendicular to the applied magnetic field (4, 5), the probability function $P(\theta,\phi)$ of the oriented *p*-nitrobenzoate ion can be expressed as (16)

[5] $$P(\theta,\phi) = \left(\frac{1}{4\pi}\right) + \left(\frac{5}{16\pi}\right)S_{33} - \left(\frac{15}{16\pi}\right)S_{33}\cos^2\theta - \left(\frac{5}{16\pi}\right)(S_{11} - S_{22})\sin^2\theta\cos 2\phi$$

The probability functions $P(\theta,\phi)$ were evaluated for the *p*-nitrobenzoate ion (or protonated *p*-nitrobenzoate ion) in all the samples studied,

$$P(\theta,\phi) = 0.0864 - 0.0206\cos^2\theta - 0.0069\sin^2\theta\cos 2\phi \quad \text{(Sample 1)}$$

$$P(\theta,\phi) = 0.0875 - 0.0238\cos^2\theta - 0.0080\sin^2\theta\cos 2\phi \quad \text{(Sample 2)}$$

$$P(\theta,\phi) = 0.0864 - 0.0204\cos^2\theta - 0.0074\sin^2\theta\cos 2\phi \quad \text{(Sample 3)}$$

$$P(\theta,\phi) = 0.0803 - 0.0021\cos^2\theta - 0.0017\sin^2\theta\cos 2\phi \quad \text{(Sample 4)}$$

$$P(\theta,\phi) = 0.0806 - 0.0031\cos^2\theta - 0.0025\sin^2\theta\cos 2\phi \quad \text{(Sample 5)}$$

$$P(\theta,\phi) = 0.0833 - 0.0113\cos^2\theta - 0.0046\sin^2\theta\cos 2\phi \quad \text{(Sample 6)}$$

$P(\theta,\phi)$ has a maximum at $\theta = 90°$ and $\phi = 90°$, which suggests that the most probable orientation of the *p*-nitrobenzoate ion is with its C_2-axis in the direction of the applied magnetic field. However, the results reported here suggest that more complex factors than charge alone could also influence the orientation of the organic ions and their conjugate acids at the edl interface. These complicating factors in the case of the organic ion and its acid could be the distribution between aqueous and hydrophobic environments and the ability of the $-CO_2^-$, $-NO_2$, and —COOH moieties to act as head groups with the organic part of the ion or molecule in the hydrophobic medium. This suggests more extensive surveys of different ionic and molecular types in similar investigations. The only clear effect of protonation is indicated in the increased order of S_{22} in the anionic phases.

Acknowledgments

This work was supported by the National Research Council of Canada and the Defense Research Board of Canada in operating grants to L.W.R.

1. (*a*) G. H. Brown, J. W. Doane, and V. D. Neff. A review of the structure and physical properties of liquid crystals. C.R.C. Press, Cleveland, Ohio. 1971; (*b*) L. W. Reeves. Chemical physics, series of monographs on physical chemistry. *Edited by* C. A. McDowell. MTP Press, London. 1975.
2. V. Luzzati, H. Mustacchi, A. Skoulios, and F. Husson. Acta Crystallogr. **13**, 660 (1960).
3. (*a*) S. J. Singer and G. L. Nicolson. Science, **175**, 720 (1972); (*b*) M. S. Bretscher. Science, **181**, 622 (1973); (*c*) L. L. M. Van Deenen. The molecular basis of membrane function. *Edited by* D. C. Tostesen. Prentice-Hall, New Jersey. 1969.
4. (*a*) K. Radley, L. W. Reeves, and A. S. Tracey. J. Phys. Chem. In press; (*b*) K. Radley and L. W. Reeves. Can. J. Chem. **53**, 2998 (1975).
5. F. Fujiwara and L. W. Reeves. J. Am. Chem. Soc. In press.
6. L. W. Reeves, J. Sanches de Cara, M. Suzuki, and A. S. Tracey. Mol. Phys. **25**, 1481 (1973).
7. L. W. Reeves, A. S. Tracey, and M. M. Tracey. J. Am. Chem. Soc. **95**, 3799 (1973).
8. L. W. Reeves, J. M. Riveros, R. A. Spragg, and J. R. Vanin. Mol. Phys. **25**, 9 (1973).
9. L. W. Reeves and A. S. Tracey. J. Am. Chem. Soc. **96**, 1198 (1974).
10. D. Bailey, A. D. Buckingham, F. Fujiwara, and L. W. Reeves. J. Magn. Reson. **18**, 344 (1975).
11. Y. Lee and L. W. Reeves. Can. J. Chem. **53**, 161 (1975).
12. J. A. Ferretti and R. K. Harris. J. Magn. Reson. **3**, 84 (1970).
13. P. Diehl, C. L. Khetrapal, and U. Lienhard. Org. Magn. Reson. **1**, 93 (1969).
14. P. Diehl and C. L. Khetrapal. NMR basic principles and progress. Vol. 1. Springer-Verlag, New York, Heidelberg, Berlin. 1969.
15. J. Bulthuis, J. Gerritsen, C. W. Hilbers, and C. MacLean. Recl. Trav. Chim. Pays-Bas, **87**, 417 (1968).
16. P. Diehl, C. L. Khetrapal, H. P. Kellerhals, U. Lienhard, and W. Niederberger. J. Magn. Reson. **1**, 527 (1969).

Can. J. Chem. Downloaded from www.nrcresearchpress.com by 210.87.254.40 on 09/05/12
For personal use only.

Can. J. Chem. Downloaded from www.nrcresearchpress.com by 210.87.254.105 on 09/05/12
For personal use only.

Canadian Journal of Chemistry

Published by
THE NATIONAL RESEARCH COUNCIL OF CANADA

Journal canadien de chimie

Publié par
LE CONSEIL NATIONAL DE RECHERCHES DU CANADA

Volume 54 Number 4 February 15, 1976 Volume 54 numéro 4 15 février 1976

The radiation chemistry of aqueous solutions of sodium 9,10-anthraquinone-2-sulfonate

CHARLES EUGENE BURCHILL, DOUGLAS MICHAEL SMITH, AND JAMES LESLIE CHARLTON
Department of Chemistry, University of Manitoba, Winnipeg, Manitoba R3T 2N2

Received February 21, 1975[1]

CHARLES EUGENE BURCHILL, DOUGLAS MICHAEL SMITH, and JAMES LESLIE CHARLTON. Can. J. Chem. **54**, 505 (1976).

The ^{60}Co γ-radiolysis of aqueous solutions of sodium 9,10-anthraquinone-2-sulfonate has been studied in acidic, unbuffered, and alkaline conditions and with addition of N_2O and 2-propanol. Mechanisms are proposed to account for the yields of H_2O_2 and hydroxylated anthraquinone sulfonates. In neutral solution, in the absence of O_2, the $OH^\cdot$ and e^- adducts undergo preferential cross termination. Reduction of the $OH^\cdot$ adduct leads to dehydration and regeneration of the quinone.

CHARLES EUGENE BURCHILL, DOUGLAS MICHAEL SMITH et JAMES LESLIE CHARLTON. Can. J. Chem. **54** 505 (1976).

On a étudié la radiolyse-γ par du ^{60}Co de solutions aqueuses d'anthraquinone-9,10 sulfonate-2 de sodium; ces études ont été effectuées en milieu acide, basique et non-tamponné et avec addition de N_2O et de propanol-2. On propose des mécanismes pour tenir compte des rendements en H_2O_2 et en sulfonates d'anthraquinones hydroxylés. En milieu neutre, en l'absence de O_2, les adduits de $OH^\cdot$ et e^- subissent de préférence une terminaison croisée. La réduction de l'adduit $OH^\cdot$ conduit à une déshydratation et à la régénération de la quinone.

[Traduit par le journal]

Introduction

There is a considerable body of literature on the photochemistry of anthraquinones and related species in alcoholic and aqueous solutions. Recent papers by Clark and Stonehill (1, 2) have suggested mechanisms for the photohydroxylation of the 9,10-anthraquinone-2-sulfonate anion (AQS) in aqueous solution. In these mechanisms a number of free-radical intermediates are proposed, including the $OH^\cdot$ radical and species equivalent to the adducts with AQS of the $OH^\cdot$ radical, e^-_{aq}, or $H^\cdot$. Gamma irradiation of aqueous solutions of AQS, alone and in the presence of specific radical scavengers, should permit the generation of these species selectively and in controlled amounts. Although accounts of pulse radiolysis of AQS solutions have been published (3, 4) and there have been references (1–4) to the results of γ-irradiation of aqueous solutions there has been no detailed report of the products of conventional γ-radiolysis.

It was our hope that such a study would elucidate the free-radical chemistry of AQS and thus reduce the mechanistic possibilities for its photochemistry.

Experimental

Sodium 9,10-anthraquinone-2-sulfonate (Aldrich) was recrystallized twice from aqueous solution and stored in the dark.

Water for solution preparation was redistilled once from alkaline permanganate solution and once from acid dichromate.

[1]Revision received October 6, 1975.

TABLE 1. Radiation chemical yields[a] for the ^{60}Co γ-radiolysis of aqueous solutions of 9,10-anthraquinone-2-sulfonate (maximum dose $\approx 10^{21}$ eV l^{-1}, [AQS] = 6×10^{-4} M)

Conditions	pH 2 (0.005 M H_2SO_4)		Neutral (unbuffered)		pH 12 (0.01 M KOH)	
	G(AQSOH)	$G(H_2O_2)$	G(AQSOH)	$G(H_2O_2)$	G(AQSOH)	$G(H_2O_2)$
Air-saturated	2.24[b]	2.64	2.47[b]	2.64	2.18[c]	2.63
Air-saturated + 10^{-2} M IPA	0	3.13	0	2.82	0	3.07
Degassed	0.17[d]	1.11	0.22[d]	0.99	1.07[c]	1.73
Degassed + 10^{-2} M IPA	0	2.65	0	2.54	0	2.76
N_2O-saturated	—	—	2.32[b]	0.76	2.64[c]	0.96

[a]Yields measured after opening samples to air.
[b]Isomeric ratio estimated $[\alpha]/[\beta] = 0.62/0.38$.
[c]Only β isomer.
[d]After irradiation to $\sim 6 \times 10^{21}$ eV l^{-1}.

All other materials were of reagent grade and used without further treatment.

All manipulations of prepared solutions were carried out in a darkened room to minimize photochemical processes induced by ambient light.

Irradiations were done in a Gammacell 220 ^{60}Co source (AECL) with dose rates estimated by ferrous sulfate dosimetry (5). All G values reported are based on apparently linear yield–dose curves having a minimum of four (and usually six) points

Concentrations of hydroxylated anthraquinone sulfonates were estimated spectrophotometrically by adjusting the pH of the irradiated solutions to 13 and measuring their absorbance at 476 and at 491 nm. The extinction coefficients and position of the apparent absorption maximum given by Clark and Stonehill (2) were used to calculate concentrations and isomeric ratios.

H_2O_2 was measured by a modification of the tri-iodide spectrophotometric method (6). Because AQS and its hydroxylated derivatives absorb at 350 nm, the blank for each measurement was an aliquot of the irradiated solution buffered, like the sample, to pH 4 with biphthallate and diluted to the same volume. Control experiments established that the reaction of H_2O_2 with I^- and the absorbance of I_3^- were unaffected by the presence of AQS.

Absorption spectra of products unstable to air were recorded on a Cary 14 spectrophotometer using samples which had been irradiated in sealed quartz ampoules.

Electron spin resonance spectra were recorded using a Varian E-3 X-band spectrometer with a flat silica aqueous solution cell. Samples were irradiated in the cell.

Results and Discussion

Only H_2O_2 and mono-hydroxylated anthraquinone sulfonates were identified as permanent products after irradiation and subsequent exposure to air (or when irradiated without initial deaeration). (Long irradiations of solutions with low initial concentrations of AOS led to the formation of polyhydroxy products as the starting material was depleted but the results reported here refer only to initial yields at low conversions.) Two spectrophotometrically distinguishable hydroxylated products were obtained. These have been characterized by Clark and Stonehill (2) as α and β isomers and are equivalent to the 1-hydroxy-6-sulfonate and the 2-hydroxy-6-sulfonate, respectively. The ratio $[\alpha]/[\beta]$ for irradiated acid or neutral solutions was 0.62/0.38. In alkaline solution only the β isomer was obtained as a product. This is essentially the same as observed for photohydroxylation (2). The principal results are given in Table 1.

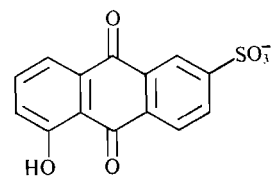

α

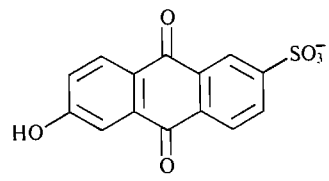

β

For comparisons between the stoichiometric predictions based on proposed mechanisms and the measured yields, the following primary

Can. J. Chem. Downloaded from www.nrcresearchpress.com by 210.87.254.105 on 09/05/12
For personal use only.

Can. J. Chem. Downloaded from www.nrcresearchpress.com by 210.87.254.105 on 09/05/12
For personal use only.

yields for irradiated aqueous solutions were assumed (7): $G_{e^-_{aq}} = 2.65$, $G_H = 0.55$, $G_{OH} = 2.70$, $G_{H_2} = 0.45$, $G_{H_2O_2} = 0.70$.

In neutral air-saturated solutions the yield of hydroxylated products was independent of AQS concentration (between 3×10^{-4} and 3×10^{-3} M) and nearly equivalent to G_{OH}. In acid and alkaline solutions the yield of hydroxylated products increased slightly with increasing AQS concentration (to ~2.5 at [AQS] = 3×10^{-3} M). We suggest that, in neutral solutions, all primary OH radicals are scavenged by AQS to give hydroxyl radical adducts which are subsequently oxidized by O_2 to give the observed products and H_2O_2. (The product of the reaction of OH with AQS has been concluded to be the adduct since the kinetic salt effect on its bimolecular disappearance is consistent with a unit negative charge (4).)

[1] $2AQSOH^{\cdot} + O_2 \rightarrow 2AQSOH + H_2O_2$

The lower yield of hydroxylated products and their concentration dependence in acid and alkaline solutions may be a consequence of competitive scavenging of $OH^{\cdot}$ by an impurity in the base or by the acid itself (H_2SO_4) in the acid solutions.

If the other primary radicals (e^-_{aq},$H^{\cdot}$) react directly with O_2, or indirectly via addition to AQS and subsequent oxidation by O_2, leading ultimately to H_2O_2, the yield of H_2O_2 expected would be

$$G(H_2O_2) = \tfrac{1}{2}(G_{e^-_{aq}} + G_{OH} + G_H) + G_{H_2O_2} = 3.65$$

The observed yield was, in all cases, substantially less than this. This may, in part, be attributed to peroxide-destroying secondary reactions. At the doses used, H_2O_2 accumulates to a concentration sufficient to become a competitive scavenger for primary free radicals (particularly e^-_{aq}) and perhaps for intermediate radical species. While the yield–dose curves were all apparently linear this is not a particularly sensitive test for back reactions (8) and a few experiments with smaller total doses gave somewhat higher values for $G(H_2O_2)$.

Addition of 10^{-2} M 2-propanol reduced hydroxylation to below the level of detection in air-saturated solutions, while the peroxide yield increased slightly. Using lower concentrations of the alcohol, G(hydroxylation) was measured as a function of alcohol concentration. If reactions 2 and 3 represent the competing reactions of OH, and if the alcohol-derived radicals are oxidized by O_2, the yield of hydroxylation should be given by eq. 4.

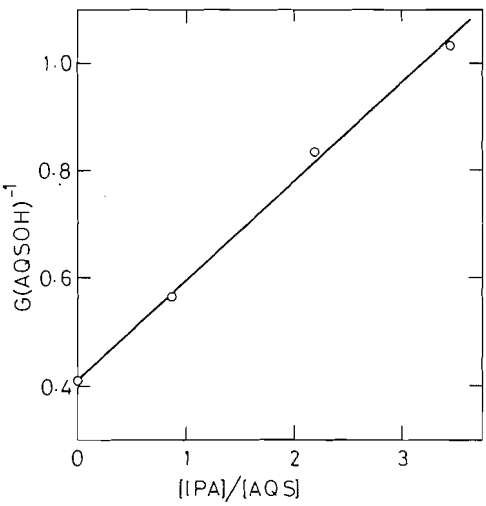

FIG. 1. Competition plot for reaction of 2-propanol and AQS with OH radicals (see eq. 4).

[2] $OH^{\cdot} + (CH_3)_2CHOH \rightarrow H_2O + (CH_3)_2\dot{C}OH + \dot{C}H_2(CH_3)CHOH$ (85%) (15%)

[3] $OH^{\cdot} + AQS \rightarrow AQSOH^{\cdot}$

$$[4] \quad \frac{1}{G(\text{hydroxylation})} = \frac{1}{G_{OH}}\left(1 + \frac{k_2[IPA]}{k_3[AQS]}\right)$$

A plot of eq. 4 for results using [AQS] = 6×10^{-4} M is shown in Fig. 1. From the slope and intercept a value of $k_2/k_3 = 0.45$ may be calculated. This is in reasonable agreement with a value of 0.35 for this ratio from independent measurements of these rate constants by pulse radiolysis (4, 9). Thus the effect of 2-propanol on hydroxylation yields in air-saturated solutions can be accounted for solely by the competitive scavenging of OH by the alcohol. Similar results have been reported by Clark and Stonehill (15), using 2-propanol and other $OH^{\cdot}$ scavengers.

The observed increase in $G(H_2O_2)$ in the presence of the alcohol is less readily accounted for. If all radicals are oxidized by O_2 to give

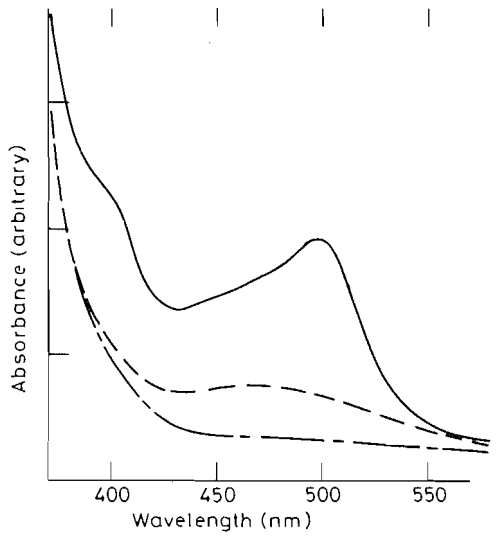

FIG. 2. Absorption spectra of alkaline aqueous solutions of AQS: ------ deaerated, unirradiated; —after irradiation; - - - after admission of air.

$\frac{1}{2}H_2O_2$ the yield should be unaffected by the addition of alcohol except as it reflects an increase in the effective primary yields induced by the increased scavenging power of the solution. In acid and alkaline solutions, particularly, the increases seem too large to be attributed to such an effect. The measured yield is still, however, less than the expected stoichiometry, based on primary yields. If this shortfall is a consequence of peroxide-destroying back-reactions, a change in the nature of the substrate radicals responsible when alcohol is present might explain the results.

In deaerated acid and neutral solutions the absorption spectrum of a sample irradiated to $\sim 10^{21}$ eV l^{-1} was not noticeably different from that of an unirradiated solution nor was there an apparent change when air was admitted. At these doses, the presence of hydroxylated products was undetectable in the irradiated solution. After this paper was initially submitted for publication, Clark and Stonehill (15) reported a G(hydroxylation) of 0.7 for anaerobic neutral and acid solutions. We have repeated the experiments for doses up to 6×10^{21} eV l^{-1} and find G(hydroxylation) to be 0.22 ± 0.05 and 0.17 ± 0.05 for neutral and acid solutions respectively.

In deaerated alkaline solution the absorption spectrum of an irradiated sample corresponds to that of the semiquinone radical anion ($AQS^{\cdot -}$, the electron adduct of AQS) (2, 4) plus that of the β-hydroxy-anthraquinone-2-sulfonate (2). The esr spectrum of $AQS^{\cdot -}$ (characterized by twenty-one approximately equally spaced lines of ~ 0.25 separation) (10) may be observed in the irradiated solution. On admission of air the esr and absorption spectra of $AQS^{\cdot -}$ disappear and the absorption spectrum of β-AQSOH remains (see Fig. 2).

The mutual disproportionation of the semiquinone radical is known to be a pH dependent equilibrium giving the quinone and dihydroquinone in neutral solution but the radical being the predominant form in base. The hydroxyl radical adduct of AQS has been reported to decay bimolecularly giving a half yield of monohydroxyAQS (4). We suggest that in neutral solution, when the semiquinone radical anion and the hydroxyl radical adduct are formed in roughly equivalent yields, their cross-termination is the most important decay mode. (A similar possibility has recently been suggested for the electron and hydroxyl radical adducts of benzene in aqueous solution (11).) Moreover, the low yield of characterizable products from AQS suggests that the reduction of the hydroxyl radical adduct leads to dehydration and regeneration of the quinone (reaction 5).[2]

[5] 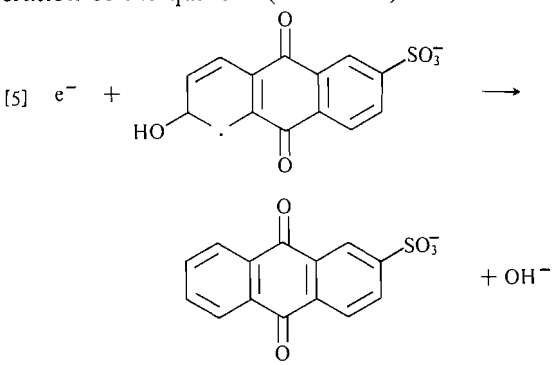

We suggest that, in neutral solution, the three radical termination reactions (reactions 6–8) occur.

[6] $2AQSOH^{\cdot} \rightarrow AQS + AQSOH + H_2O$

[7] $AQS^{\cdot -} + AQSOH^{\cdot} \rightarrow 2AQS + OH^-$

[8] $2AQS^- + 2H_2O \rightarrow AQS + AQSH_2 + 2OH^-$

[2]If this were also the case for the hydroxyl radical adduct of benzene it would account for the low net yields of product formation from deaerated aqueous benzene solutions.

Can. J. Chem. Downloaded from www.nrcresearchpress.com by 210.87.254.105 on 09/05/12
For personal use only.

Can. J. Chem. Downloaded from www.nrcresearchpress.com by 210.87.254.105 on 09/05/12
For personal use only.

If $2k_6 = k_7 = 2k_8$ (*i.e.* statistically equivalent rate constants), under steady-state conditions, the hydroxylation yield would be given by

$$G(\mathrm{AQSOH}) = \frac{(G_{\mathrm{OH}})^2}{2(G_{e^-_{aq}} + G_{\mathrm{H}} + G_{\mathrm{OH}})} = 0.62$$

However, Hulme *et al.* (4) have reported that the bimolecular decay of $AQS^{\cdot -}$ is "much slower" than that of $AQSOH^{\cdot}$. If this is the case the cross reaction (reaction 7) would be the most important if $k_7 \approx 2k_8$. Redox balance would require

$$G(\mathrm{AQSH_2}) = \tfrac{1}{2}(G_{e^-_{aq}} + G_{\mathrm{H}} - G_{\mathrm{OH}}) + G(\mathrm{AQSOH})$$

and, on opening to air,

$$G(\mathrm{H_2O_2}) = G_{\mathrm{H_2O_2}} + \tfrac{1}{2}(G_{e^-_{aq}} + G_{\mathrm{H}} - G_{\mathrm{OH}} + G(\mathrm{AQSOH}) = 1.17$$

The observed $G(H_2O_2)$ after opening to air was not far short of this value.

In acid solution the low yield of hydroxylated products again suggests that cross reaction (equivalent to reaction 7) is the most important radical decay mode. Below p*H* 3.25 the reduced species will be the semiquinone radical $AQSH^{\cdot}$ (4) and the bimolecular decay constant for the semiquinone has been reported to be essentially equivalent to that for $AQSOH^{\cdot}$. In order for the cross reaction to dominate, its rate constant would have to be significantly greater than $2k_6$. While this may seem improbable with $2k_6 = 3.2 \times 10^9$ (4) the stoichiometry of H_2O_2 found is consistent with this interpretation.

To account for the observed yields and absorption spectra for alkaline deaerated solutions we assume that not only is the disproportionation of the semiquinone radical anion stopped by base but also its reaction with the hydroxyl radical adduct. If the hydroxyl radical adduct undergoes only mutual termination by disproportionation (reaction 6), the expected yield of hydroxylation would be $\frac{1}{2}G_{\mathrm{OH}}$. The observed yield was almost precisely one-half that obtained from an aerated alkaline solution. If all reducing radicals lead to $AQS^{\cdot -}$ which is subsequently oxidized on admission of air, the expected yield of H_2O_2 would be

$$G(\mathrm{H_2O_2}) = G_{\mathrm{H_2O_2}} + \tfrac{1}{2}(G_{e^-_{aq}} + G_{\mathrm{H}}) = 2.30$$

As in most other instances the observed yield was less than this value but it was also significantly greater than that in deaerated neutral solutions.

The suggestions as to the probably reactions of the radical adducts of AQS are supported by the results of the remaining experiments.

In degassed acid and neutral solutions with 10^{-2} *M* 2-propanol added, all OH radicals will react with the alcohol to give ~85% ketyl radicals (12) which are expected to reduce the quinone to semiquinone (4). (The remaining radicals from 2-propanol are non-reducing substituted alkyl radicals (13) which will probably simply couple.) Disproportionation of the semiquinone species would give the dihydroquinone. A strong absorption spectrum corresponding to the dihydroquinone (14) was observed which disappeared on admission of air. The stoichiometry of H_2O_2 production on the basis of these assumptions would be

$$G(\mathrm{H_2O_2}) = \tfrac{1}{2}(0.85G_{\mathrm{OH}} + G_{e^-_{aq}} + G_{\mathrm{H}}) + G_{\mathrm{H_2O_2}} = 3.45$$

In degassed alkaline solutions with 10^{-2} *M* 2-propanol added the only absorption spectrum observed was that of the semiquinone radical anion, which disappeared on admission of air. The anticipated yield of H_2O_2 would be the same as for neutral solutions. In all of acid, neutral, and alkaline solutions the yield of H_2O_2 was less than the expected value but the increase over that without alcohol was consistent with the proposed reactions.

In neutral solutions saturated with N_2O the yield of H_2O_2 was essentially the primary yield. N_2O reacts with e^-_{aq}, generating an $OH^{\cdot}$ radical, but $H^{\cdot}$ reacts much more slowly and would probably be scavenged by the quinone to give a semiquinone. Cross termination of these few semiquinone radicals with the hydroxyl radical adduct and mutual termination of the remaining $OH^{\cdot}$ adducts to give a half yield of hydroxylated products would require

$$G(\text{hydroxylation}) = \tfrac{1}{2}(G_{\mathrm{OH}} + G_{e^-_{aq}} - G_{\mathrm{H}}) = 2.40$$

and

$$G(\mathrm{H_2O_2}) = G_{\mathrm{H_2O_2}} = 0.70$$

which were almost precisely the observed results. In one experiment in which a small, but un-

Can. J. Chem. Downloaded from www.nrcresearchpress.com by 210.87.254.105 on 09/05/12
For personal use only.

known, concentration of O_2 was present in addition to N_2O the yield of hydroxylated products was 4.3. Although this result could not be analyzed quantitatively it is consistent with the majority of e^-_{aq} reacting with N_2O but the resulting $OH^\cdot$ adducts of AQS being largely oxidized by O_2, rather than disproportionating.

In N_2O-saturated solutions at pH 12, the majority of primary H atoms will be scavenged by the quinone to give the radical anion which, at this pH, has been observed to be stable but, on admission of air, reacts to give H_2O_2. Thus we expect

$$G(H_2O_2) = G_{H_2O_2} + \tfrac{1}{2}G_H = 1.02$$

With increasing concentrations of AQS, $G(H_2O_2)$ increased (to 1.33 at [AQS] = 3×10^{-3} M), presumably as the quinone became a competitive scavenger for e^-_{aq}. The expected yield of hydroxylated product would be

$$G(\text{hydroxylation}) = \tfrac{1}{2}(G_{OH} + G_{e^-_{aq}}) = 2.68$$

if there were no scavenging of e^-_{aq} by the quinone. With increased concentration of AQS the yield of hydroxylation did not show the expected decrease but remained essentially constant. The possibility that $AQS^{\cdot -}$ might reduce N_2O was considered but was discounted when an alkaline solution containing both N_2O and 2-propanol was irradiated. Strong absorption and esr spectra of the radical anion were obtained.

The principal conclusions drawn from this study are: (*1*) In neutral and acidic aqueous solutions the cross termination between the semiquinone radical of anthraquinone-2-sulfonate and the hydroxyl radical adduct is more important than that of either mutual termination. (*2*) In alkaline solution the radical anion does not reduce the hydroxyl radical adduct. The hydroxyl radical adduct may, however, react by disproportionation. (*3*) Reduction of the hydroxyl radical adduct, whether by another species or as one-half of its disproportionation, leads to dehydration and regeneration of the quinone.

Although the magnitudes of the observed yields (particularly those for H_2O_2) do not, in all cases, correspond to the assumed stoichiometry, the pattern of the results is consistent with the mechanisms proposed.

The apparent inability of the semiquinone radical anion to reduce the hydroxyl radical adduct in alkaline solution is somewhat puzzling, as is the change in the isomeric ratio of hydroxylated products over the same pH range. The most obvious explanation for these phenomena would be a base-induced change in the nature of the radical species involved. Clark and Stonehill (1, 15) have proposed that the hydroxyl radical adducts undergo acid dissociation of the hydroxyl group and isomerization in the pH range 9–11. However, Hulme *et al.* reported there was no change in the absorption spectrum of the hydroxyl radical adduct in the pH range 3–12. Moreover, in a recent study the pK_a's of a series of β-hydroxyalkyl radicals were estimated to be in the range of 14–15 (16). These observations do not rule out ionization of the hydroxyl group but they do suggest some caution in assuming it.

The disproportionation of the semiquinone radical anion is known to be a pH-dependent equilibrium. If all three radical–radical reactions (reactions 6–8) were naively written as equilibria (reactions 6*a* to 8*a*) the mutual termination of the hydroxyl radical adduct would be the least affected by increasing pH.

$$[6a] \qquad 2AQSOH^\cdot \rightleftarrows AQS + AQSOH + H_2O$$

$$[7a] \quad AQS^{\cdot -} + AQSOH^\cdot \rightleftarrows 2AQS + OH^-$$

$$[8a] \quad 2AQS^{\cdot -} + 2H_2O \rightleftarrows AQS + AQSH_2 + 2OH^-$$

However the implication of this is that there should be some mildly alkaline pH at which a deaerated aqueous solution of anthraquinone-2-sulfonate would undergo a spontaneous dark reaction leading to hydroxylated products and semiquinone radical anions. To our knowledge this has never been observed.

Acknowledgments

Financial support from the National Research Council of Canada and the Department of Chemistry of the University of Manitoba (Departmental Assistantship to D.M.S.) is gratefully acknowledged. We thank Dr. H. I. Stonehill for making available to us results in advance of their publication.

1. K. P. Clark and H. I. Stonehill. J. Chem. Soc. Faraday Trans. I, **68**, 577 (1972).
2. K. P. Clark and H. I. Stonehill. J. Chem. Soc. Faraday Trans. I, **68**, 1676 (1972).
3. B. E. Hulme, E. J. Land, and G. O. Phillips. Chem. Commun. 518 (1969).
4. B. E. Hulme, E. J. Land, and G. O. Phillips. J. Chem. Soc. Faraday Trans. I, **68**, 1992 (1972).

5. H. A. J. BATTAERD and G. N. TREGEAR. Rev. Pure Appl. Chem. **16**, 83 (1966).
6. A. O. ALLEN, C. J. HOCHANADEL, J. A. GHORMLEY, and T. N. DAVIS. J. Phys. Chem. **56**, 575 (1952).
7. I. G. DRAGANIĆ and Z. D. DRAGANIĆ. The radiation chemistry of water. Academic Press, New York. 1971. p. 140.
8. G. CZAPSKI. *In* Radiation chemistry I. *Edited by* R. F. Gould. Am. Chem. Soc. Adv. Chem. **81**, 107 (1968).
9. M. ANBAR and P. NETA. Int. J. Appl. Radiat. Isotop. **18**, 493 (1967).
10. P. J. BAUGH, G. O. PHILLIPS, and J. C. ARTHUR. J. Phys. Chem. **70**, 3061 (1966).
11. D. G. MARKETOS, A. MARKETOU-MANTAKA, and G. STEIN. J. Phys. Chem. **78**, 1987 (1974).
12. C. E. BURCHILL and G. F. THOMPSON. Can. J. Chem, **49**, 1305 (1971).
13. C. WALLING and S. KATO. J. Am. Chem. Soc. **93**. 4275 (1971).
14. G. O. PHILLIPS, N. W. WORTHINGTON, J. F MCKELLAR, and R. R. SHARPE. J. Chem. Soc. A, 767 (1969).
15. K. P. CLARK and H. I. STONEHILL. Private communication to J.L.C.
16. Y. KIRINO. J. Phys. Chem. **79**, 1296 (1975).

Can. J. Chem. Downloaded from www.nrcresearchpress.com by 210.87.254.105 on 09/05/12
For personal use only.

The aqueous photochemistry of sodium 9,10-anthraquinone-2-sulfonate

JAMES LESLIE CHARLTON, RHONDA GAIL SMERCHANSKI, AND CHARLES EUGENE BURCHILL
Department of Chemistry, University of Manitoba, Winnipeg, Manitoba R3T 2N2

Received February 21, 1975[1]

JAMES LESLIE CHARLTON, RHONDA GAIL SMERCHANSKI, and CHARLES EUGENE BURCHILL. Can. J. Chem. **54**, 512 (1976).

The aqueous photochemistry of sodium 9,10-anthraquinone-2-sulfonate is described and a new mechanism for the photohydroxylation is proposed. The participation of kinetically free hydroxyl radicals is ruled out.

JAMES LESLIE CHARLTON, RHONDA GAIL SMERCHANSKI et CHARLES EUGENE BURCHILL. Can. J. Chem. **54**, 512 (1976).

On décrit la photochimie en phase aqueuse de l'anthraquinone-9,10 sulfonate-2 de sodium et on propose un nouveau mécanisme pour la photohydroxylation. On exclut la possibilité de la participation de radicaux hydroxyles cinétiquement libres.

[Traduit par le journal]

Introduction

Prior to 1970 several investigators had studied the aqueous photochemistry of sodium anthraquinone-2-sulfonate (AQS). Wells had first noted the formation of coloured products in 1961 (1) and these were later identified as isomeric monohydroxy derivatives by Mooney and Stonehill (2), and by Broadbent (3). Due to the nature of the products, Broadbent suggested the intermediacy of an OH radical produced by electron abstraction from water by the excited state quinone. A similar phenomenon had been invoked previously to explain the photochemistry of xanthene dyes (4) and more recently for *p*-benzoquinone (5). The fact that hydroxy benzoic acids were produced from irradiating solutions of benzoic acid and AQS also seemed to provide evidence for participation of the hydroxyl radical (3).

In 1972 Clark and Stonehill provided considerable kinetic data for photohydroxylation in both neutral and basic solutions (6). For neutral solutions they make two significant observations: (*a*) the rate of photohydroxylation increases with quinone concentration, and (*b*) the yields of hydroxylated quinone are matched by an equal yield of hydrogen peroxide. They proposed two schemes that would account for their kinetic data and these are outlined briefly below.

Scheme I

$$AQS \xrightarrow{h\nu} AQS^*$$
$$AQS^* + H_2O \rightarrow AQSOH^- + H^+$$
$$AQSOH^- \rightarrow AQS + OH^-$$
$$AQSOH^- + AQS \rightarrow AQSOH\cdot + AQS^{-\cdot}$$
$$AQSOH\cdot + O_2 \rightarrow AQSOH + HO_2\cdot$$
$$2HO_2\cdot \rightarrow O_2 + H_2O_2$$

Scheme II

$$AQS \xrightarrow{h\nu} AQS^*$$
$$AQS^* + AQS \rightarrow AQS^{\cdot -} + AQS^{\cdot +}$$
$$AQS^{\cdot +} + H_2O \rightarrow AQS + OH\cdot + H^+$$
$$OH\cdot + AQS \rightarrow AQSOH\cdot$$
$$AQSOH\cdot + O_2 \rightarrow AQSOH + HO_2\cdot$$
$$2HO_2\cdot \rightarrow O_2 + H_2O_2$$

Derivatives such as $AQSOH^-$, $AQSOH\cdot$, and AQSOH denote a mixture of α (1, 4, 5, or 8 hydroxy) and β (3, 6, or 7 hydroxy) compounds.

Both mechanisms are capable of explaining the dependence of the yield on AQS concentration and the equal yield of H_2O_2 and hydroxy anthraquinone-2-sulfonate (AQSOH). Each mechanism has a rather dubious step however. In Scheme I it seems surprising that the oxidation of the hydroxide adduct $AQSOH^-$ by AQS can compete effectively with return to starting material. It is also difficult to see how AQS could photocatalyse the hydroxylation of benzoic acid if water adds to the excited state of the quinone.

[1]Revision received October 6, 1975.

Can. J. Chem. Downloaded from www.nrcresearchpress.com by 210.87.254.42 on 09/05/12
For personal use only.

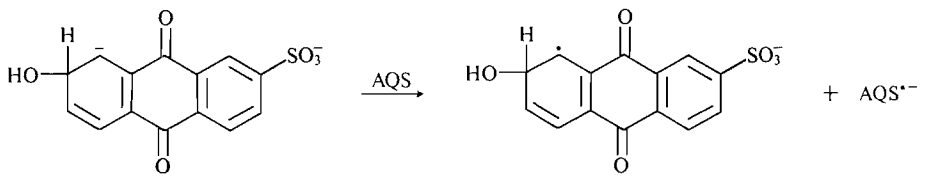

In Scheme II one wonders why oxidation of water by $AQS^{\bullet+}$ can compete with addition of water to the cation radical. This possibility was not considered by the authors despite the fact that it leads directly to the hydroxyl radical adduct AQSOH•.

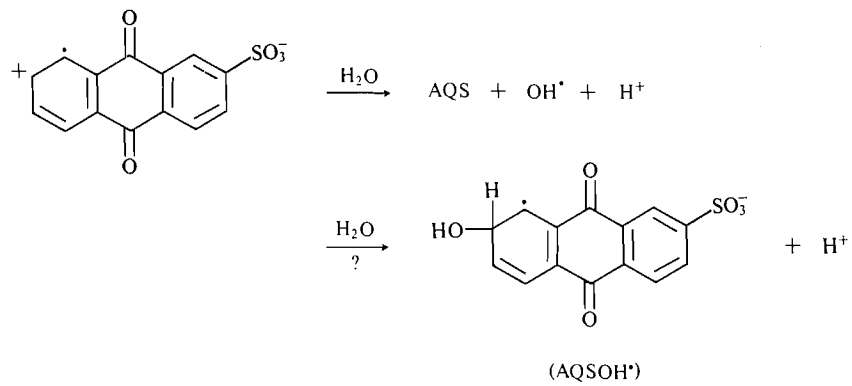

Broadbent and Newton have also studied the action of Fenton's reagent on AQS (7). They note a similarity in product composition to photohydroxylation and use this as support for OH radical intermediacy in the photolysis case.

We have attempted to trap the intermediate OH radical with isopropyl alcohol and have compared the results to those obtained by γ-radiolysis. Experiments in vigorously degassed solutions also tend to shed some doubt on the validity of the mechanisms proposed by Stonehill and Clark (6).

Experimental

Quantum Yields

The light source used for quantum yield studies was a 200 W HBO Osram mercury lamp and 1/4 meter Jarrell Ash monochrometer set at 366 nm. Light intensities were measured by ferrioxalate actinometry according to the method of Parker and co-worker (8). Hydrogen peroxide was determined by treatment with iodide and titrating the I_3^- with sodium thiosulfate. Hydroxylation was determined according to the method of Clark and Stonehill (6). For neutral solution, 0.17 ml of 3.02 *N* potassium hydroxide was added to a 5 ml sample and the absorption measured at 476 and 491 nm. The extinction coefficients for α and β hydroxy anthraquinone-2-sulphonates were assumed to be

$$\epsilon_{\beta(476)} = 3.6 \times 10^3 \text{ l mol}^{-1} \text{ cm}^{-1}$$
$$\epsilon_{\beta(491)} = 3.4 \times 10^3 \text{ l mol}^{-1} \text{ cm}^{-1}$$
$$\epsilon_{\alpha(476)} = 5.09 \times 10^3 \text{ l mol}^{-1} \text{ cm}^{-1}$$
$$\epsilon_{\alpha(491)} = 5.65 \times 10^3 \text{ l mol}^{-1} \text{ cm}^{-1}$$

as given in part by Clark and Stonehill (6). It was assumed in neutral solution the ratio of α-AQSOH to β-AQSOH was always 3 to 2 (6).

Hydroxylation of Sodium Anthraquinone-2-sulfonate in the Presence of Isopropyl Alcohol and Oxygen

Oxygenated samples of AQS (5.0 ml, 3.89×10^{-3} *M*) in water, containing various concentrations of isopropyl alcohol, were irradiated and subsequently analysed for hydroxylated products and hydrogen peroxide. The results are tabulated in Table 1.

Photohydroxylation in Basic Solutions

Aerated samples of AQS (5.0 ml, 3.89×10^{-3} *M*) in 0.02 *N* potassium hydroxide were irradiated and analysed for hydroxylated products. The quantum yield for hydroxylation was 0.095. A similar sample was degassed by freezing in liquid nitrogen and evacuating to 10^{-3} Torr and repeating several times. The quantum yield of photohydroxylation was thus reduced to 0.048. Adding 1% isopropyl alcohol to the samples gave quantum yields of 0.062 (aerated) and 0.011 (degassed).

Can. J. Chem. Downloaded from www.nrcresearchpress.com by 210.87.254.42 on 09/05/12
For personal use only.

Can. J. Chem. Downloaded from www.nrcresearchpress.com by 210.87.254.42 on 09/05/12
For personal use only.

TABLE 1. Effect of isopropyl alcohol on photolysis of AQS

%IPA[a]	Φ_{AQSOH}
0	0.038
0.1	0.040
1.0	0.027
3.0	0.016
5.0	0.012
10.0	0.007[b]

[a]% by volume.
[b]$\Phi_{H_2O_2}$ for this sample was 0.595.

Photohydroxylation in Degassed Neutral Solutions

Samples of AQS (5.0 ml, 3.89×10^{-3} *M*) were degassed as described above and irradiated. The quantum yield of hydroxylation was measured to be 0.003. No hydrogen peroxide could be detected.

Results and Discussion

The γ-radiation induced hydroxylation of AQS has been found (9) to give a product distribution identical to that of photohydroxylation implying the intermediacy of the hydroxyl radical adduct AQSOH$^{\cdot}$ and the electron adduct AQS$^{\cdot -}$ in both reactions.

In rigorously degassed neutral solutions the yield of hydroxylated products was less than 10% of that in aerated solution ($\phi = 0.003$ *vs.* 0.038). This is in qualitative agreement with the statement by Clark and Stonehill (6) that photohydroxylation in anaerobic solutions is "much slower" than in aerobic solutions. On the other hand it is in marked disagreement with a recent report (10) that deoxygenation has no effect on the rate of photohydroxylation. This result is also similar to the effect of deoxygenation in the γ-radiolysis of neutral solutions. We suggest that, as in the case of radiolysis, the reduced yield in deoxygenated solution is a consequence of the preferential cross-reaction between AQSOH$^{\cdot}$ and AQS$^{\cdot -}$ to give back the starting material (*i.e.* AQSOH$^{\cdot}$ + AQS$^{\cdot -} \rightarrow$ 2AQS + OH$^-$). Now this is simply the reverse of the reaction proposed by Clark and Stonehill in their Scheme I to generate AQSOH$^{\cdot}$ and AQS$^{\cdot -}$. If, as we suggest, the bimolecular reaction of the radicals is essentially diffusion controlled, the reverse reaction is a rather improbable radical source.

It has been found that 1 volume% of isopropyl alcohol will quench the hydroxylation of AQS (6×10^{-4} *M*) when the solution is γ-irradiated (9). If OH radicals are involved in the photohydroxylation of AQS a similar quenching effect would be expected. The quantum yields of photohydroxylation at various isopropyl alcohol concentrations are tabulated in Table 1.

Even at 10 volume% significant hydroxylation occurs eliminating the possibility that this reaction involves OH radicals.[2]

The decrease in quantum yield can be accounted for by a direct interception of the excited state quinone with isopropyl alcohol, a reaction that leads only to hydrogen peroxide and acetone in oxygenated solution.

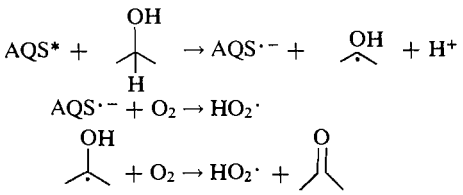

We would like to propose a modified mechanism for the photohydroxylation and it is outlined below.

$$AQS \xrightarrow{h\nu} AQS^*$$
$$AQS^* + AQS \rightarrow AQS^{\cdot -} + AQS^{\cdot +}$$
$$AQS^{\cdot -} + AQS^{\cdot +} \rightarrow 2AQS$$
$$AQS^{\cdot +} + H_2O \rightarrow AQSOH^{\cdot} + H^+$$
$$AQS^{\cdot -} + O_2 \rightarrow AQS + O_2^{\cdot -}$$
$$AQSOH^{\cdot} + O_2 \rightarrow AQSOH + HO_2^{\cdot}$$
$$AQSOH^{\cdot} + AQS^{\cdot -} \rightarrow 2AQS + OH^-$$
$$2AQSOH^{\cdot} \rightarrow AQS + AQSOH + H_2O$$

This mechanism can explain the dependence of hydroxylation on quinone concentration and an equal yield of hydroxylation and peroxide production. In the absence of oxygen AQS$^{\cdot -}$ is no longer scavenged by O_2 and the reactions with AQS$^{\cdot +}$ and AQSOH$^{\cdot}$ will become more important leading to a lowered yield of AQSOH. It could also explain the AQS catalysed hydroxylation of benzoic acid, as presumably the excited quinone could oxidize the benzoic acid to its radical cation as well.

We have carried out no experiments to determine the nature of the excited states involved; however, it seems likely that the triplet state is involved.

[2]The same conclusion has also been reached by Clark and Stonehill, private communication to J.L.C.

Can. J. Chem. Downloaded from www.nrcresearchpress.com by 210.87.254.42 on 09/05/12
For personal use only.

There is the possibility that a similar mechanism might be involved in cases where one electron oxidation of water by excited state molecules has been proposed. In particular, recent papers by Harbour and Tollins (5) describe the one-electron oxidation of water and ethanol by excited state *p*-benzoquinone. They use esr detection of the solvent radical as evidence. We suggest that these esr data might also be explained by solvent addition to a radical cation of *p*-benzoquinone. Experiments are now in progress to isolate possible products of such a reaction.

Finally, we have examined the photolysis of AQS in basic solution. We find that the product is solely β-hydroxy AQS (3, 6, or 7 mono hydroxy) as previous authors have reported.

The quantum yield in oxygenated solution is 0.095 and in deoxygenated solution 0.042. A similar halving of yield for deoxygenated solutions is found on γ-radiolysis (9). This implies, that in basic deoxygenated solution, the cross reaction of $AQSOH^{\cdot}$ and $AQS^{\cdot -}$ does not occur, and that mutual reaction of $AQSOH^{\cdot}$ is the only path leading to AQSOH. Why this occurs and why only β AQSOH is found still remains unexplained. The suggestion that $AQSOH^{\cdot}$ ionizes at the hydroxylic position, and stops cross reaction, seems rather unlikely, since this OH group is comparable to an allylic alcohol, although this mechanism has been postulated by Stonehill and Clark (6). In oxygenated alkaline solutions the increase in photohydroxylation over that in neutral solution may be a consequence of the more efficient scavenging of $AQS^{\cdot +}$ by OH^- compared to that by H_2O.

Acknowledgment

We would like to acknowledge the financial assistance of the National Research Council of Canada.

1. C. F. Wells. Trans. Faraday Soc. **57**, 1703 (1961); **57**, 1719 (1961).
2. B. Mooney and H. I. Stonehill. Chem. Ind. 1309 (1961).
3. A. D. Broadbent. Chem. Commun. 382 (1967).
4. T. Ohno, Y. Usui, and M. Korzumi. Bull. Chem. Soc. Jpn. **38**, 1023 (1965).
5. J. R. Harbour and G. Tollin. Photochem. Photobiol. **19**, 147 (1974).
6. K. P. Clark and H. I. Stonehill. J. Chem. Soc. Faraday Trans. I, **68**, 577, 1676 (1972).
7. A. D. Broadbent and R. P. Newton. Can. J. Chem. **50**, 381 (1972).
8. C. A. Parker. Proc. R. Soc. **A220**, 104 (1953); C.G. Hatchard and C. A. Parker. Proc. R. Soc. **A235**, 518 (1956).
9. C. E. Burchill, D. M. Smith, and J. L. Charlton. Can. J. Chem. This issue.
10. A. D. Broadbent, H. B. Matheson, and R. P. Newton. Can. J. Chem. **53**, 826 (1975).

Comments on "The aqueous photochemistry . . . ", and "The radiation chemistry of aqueous solutions of sodium 9,10-anthraquinone-2-sulfonate"

H. I. STONEHILL AND K. P. CLARK

Department of Chemistry and Metallurgy, Royal Military College of Science, Shrivenham, Swindon, Wilts., England

Received April 23, 1975

H. I. STONEHILL and K. P. CLARK. Can. J. Chem. **54**, 516 (1976).

Some of the mechanistic conclusions of the title articles are criticized because they are inconsistent with other results available to the present authors. Further, the mechanisms of the title articles would not operate in aerobic systems for which alone the present authors' mechanisms were designed.

H. I. STONEHILL et K. P. CLARK. Can. J. Chem. **54**, 516 (1976).

Quelques conclusions mécanistiques des articles mentionnés dans le titre sont critiquées parce qu'elles ne sont pas en accord avec d'autres résultats obtenus par les présents auteurs. De plus,les mécanismes des articles mentionnés dans le titre ne seraient pas opérationnels dans des systèmes aérobiques pour lesquels les mécanismes proposés par les présents auteurs avaient été uniquement désignés.

[Traduit par le journal]

In the preceding two papers (1, 2) the authors present over-simplified versions of two alternative schemes which we proposed (3) to account for the observed photohydroxylation kinetics of the title compound AQS; they omit important branchings without which the kinetic effects of AQS and OH^- are inexplicable. While this does not affect their main conclusions, it would have been advisable to indicate the significance of these omissions, which are also relevant to their alternative proposed scheme.

Burchill *et al.* reject the intermediacy of kinetically free $OH^\bullet$ in the photolysis on the basis of the much greater hydroxylation-quenching effect of *i*-PrOH in γ-radiolysis (where $OH^\bullet$ certainly is an intermediate) than in photolysis. In a recently completed investigation (4) we have reached the same conclusion but on the basis of wider evidence involving comparison of the effects of several $OH^\bullet$-scavengers and of high $[OH^-]$ on hydroxylation yields in γ-radiolysis and photolysis. In γ-radiolysis, initial (0–10 min) G(hydroxylation) is 2.54 (oxygen present) and 0.8 (deaerated), independent of dose rate between 100 and 3300 krad h^{-1} and pH in the range 2–12, decreasing at pH > 12 to reach 0.87 (aerobic) and 0.18 (anaerobic) at pH 14. This decrease, which is independent of [AQS], we attribute to ionisation of $OH^\bullet$ to $O^{\bullet-}$, which unlike $OH^\bullet$ does not give a stoichiometric hydroxylation yield with AQS (4). By contrast, in photolysis Φ(hydroxylation) increases with $[OH^-]$ up to pH 14 and shows no sign of decrease at higher alkalinity. As to radical scavenger effects, we have previously mentioned (3) that these differ qualitatively in photolysis and γ-radiolysis. In photolysis, scavengers such as HCOONa, NaN_3, KCNS, MeOH, EtOH, and *i*-PrOH are much less effective in alkaline (pH 13) than in neutral or slightly acidic media, no such pH effect being observed in radiolysis, while at any pH their effectiveness is always less in photolysis than in radiolysis (4). We have consequently (3) modified our AQS*/AQS scheme (Scheme 2 in ref. 1) by omitting the $OH^\bullet$ intermediate, thereby (4) obtaining a scheme of which the alternative proposed scheme in ref. 1 is an over-simplified version. We emphasize that this modification does not alter the kinetic predictions of the scheme, so we still have two rival schemes, both leading to the kinetics observed in aerated solutions (3).

The near-zero photolytic and low (G originally zero, later altered to ~0.2) radiolytic hydroxylation yield in acid or neutral (but not alkaline) deaerated solutions reported by Burchill *et al.* (1, 2) contrasts with our higher yields which reflect several consistent results and not one or two isolated determinations. The implicit suggestion that the discrepancy might be due to the greater efficiency of freeze–thaw deaeration compared with our inert gas bubbling technique is

Can. J. Chem. Downloaded from www.nrcresearchpress.com by 210.87.254.40 on 09/05/12
For personal use only.

Can. J. Chem. Downloaded from www.nrcresearchpress.com by 210.87.254.40 on 09/05/12
For personal use only.

difficult to uphold, since any residual trace of O_2 after gas-bubbling would be removed by semiquinone produced in the first few seconds of irradiation, after which deaeration is complete, and, according to Burchill *et al.*, no hydroxylation should occur. We actually observed a steady linear-with-time build-up of hydroxy-product over considerable periods both in photolysis (3) and in radiolysis (4). Similarly, other solutes added to neutral deaerated AQS are also photohydroxylated (5).

To explain their low hydroxylation yield Burchill *et al.* suggest that in acid or neutral solution the semiquinone radical ion $AQS^{\cdot -}$ and the OH·-adduct AQSOH· undergo mutual destruction

[1] $$AQS^{\cdot -} + AQSOH^{\cdot} \rightarrow 2AQS + H_2O$$

Since AQSH· has an acid–base pK_a of 3.25 (6), the radical ion $AQS^{\cdot -}$ is the only semiquinone species observable at $pH > 4$, as *e.g.* in pulse-radiolysed Ar-saturated solutions of AQS (7). It undergoes a rapid disproportionation reaction 3 in neutral solution, but not in alkaline solution ($pH > 10$), where the semiquinone formation equilibrium constant is much greater (8). Reaction 1 would therefore be expected to be more important in alkaline solutions (higher steady-state $[AQS^{\cdot -}]$) than in neutral solution, in complete contrast to the findings of Burchill *et al.* who are unable to explain why alkali suppresses reaction 1. We believe that reaction 1 occurs, but with a rate constant which is low enough to preclude it from being a predominant mode of AQSOH· removal except at high $[AQS^{\cdot -}]$. We pulse-radiolysed Ar-saturated AQS solutions at pH 4, and observed a second order decay velocity constant $(1.45 \pm 0.23) \times 10^9\ M^{-1}\ s^{-1}$ independent of monitoring λ over the range 280–491 nm. This is a composite of three possible decays, *viz.* reaction 1 above and

[2] $$2AQS \rightarrow AQS + H_2O + ROH \text{ (hydroxy-product)}$$

[3] $$2AQS^{\cdot -} \text{ (or } AQS^{\cdot -} + AQSH^{\cdot}\text{, or } 2AQSH^{\cdot}) \rightarrow AQS + AQS^{2-} \text{ (or } AQSH^{-}\text{, or } AQSH_2)$$

In reaction 3, rapid ionisation interconversion of the semiquinone species occurs, and reaction 1 is second order because both reactants are produced in equimolar amounts. Separate measurements in N_2O-saturated solutions (4) give the velocity-constant of reaction 2 as $(1.41 \pm 0.17) \times 10^9\ M^{-1}\ s^{-1}$, while for reaction 3 the constant at pH 4 is (4) $(1.33 \pm 0.18) \times 10^9\ M^{-1}\ s^{-1}$ (*cf.* Hulme's value (7) $1.6 \times 10^9\ M^{-1}\ s^{-1}$ at pH 1.7). Since all these constants are roughly equal to *ca.* $1.5 \times 10^9\ M^{-1}\ s^{-1}$, the constant for reaction 1 must be of the same order. Thus reaction 1 cannot be overwhelmingly faster than reaction 2, which argues against Burchill's explanation of low hydroxylation yield. We have actually suggested earlier (3*b*) that reaction 1 is important in *alkaline* solution when $[AQS^{\cdot -}]$ builds up, so that photoreduction–hydroxylation in deaerated solution stops at *ca.* 25–30% of reduction, *not* at *zero* conversion. In a γ-radiolysis of AQS at pH 13, previously electroreduced to *ca.* 25% conversion to $AQS^{\cdot -}$, we obtained G(hydroxylation) = 0.12, compared with 2.54 for aerated and 0.8 for deaerated (but not electroreduced) solution. This again supports the analogue of reaction 1 but for *alkaline* solution, and again shows that reaction 1 is not overwhelmingly faster than reaction 2 in such media.

No explanation is offered by Burchill *et al.* for the change in α:β isomer ratio of the hydroxy-products, both photolytic and radiolytic, in going from neutral to alkaline conditions. Our previously proposed mechanism (3) for this, based on mobile equilibration of α and β isomers of adduct AQSOH·, conditioned by their ionisation, provides a quantitative explanation of observed isomer ratios. The mobility of the OH· group in adducts thereof, facilitating α–β isomerisation, has been reported for other systems (9), and the values 11.2 and 9.4 required by our mechanism for the acid-base pK_a's of the α and β adducts are not inconsistent with low values (5.5–12.2) reported for α-hydroxyalkyl radicals ·CRR′OH in which pK_a decreases as electron affinity of substituents R,R′ increases (10).

Burchill *et al.* state (1) that back-reaction 1 is "simply the reverse of" our reaction in Scheme 1 to generate AQSOH· and $AQS^{\cdot -}$. They go on to suggest that reaction 1 is "essentially diffusion-controlled, [so that] the reverse reaction is a rather improbable radical source". Now reaction 1 is *not* the reverse of our radical-generating reaction which involves one triplet state and one ground-state AQS molecule, not two ground-state molecules. Thus the subsequent conclusion about improbability as a radical source is false.

Finally we must point out that both of our proposed photolysis schemes (3, 4), which

account quantitatively for observed Φ values, were designated for aerated solutions where back-reaction between $AQSOH^{\bullet}$ and $AQS^{\bullet-}$ is irrelevant since O_2 rapidly scavenges $AQS^{\bullet-}$, and not for deaerated solutions, where, as previously stated, we believe some $AQSOH^{\bullet}$, but not the major part, is removed by the back-reaction.

1. J. L. CHARLTON, R. G. SMERCHANSKI, and C. E. BURCHILL. Can. J. Chem. This issue.
2. C. E. BURCHILL, D. M. SMITH, and J. L. CHARLTON. Can. J. Chem. This issue.
3. K. P. CLARK and H. I. STONEHILL. J. Chem. Soc. Faraday I, (*a*) **68**, 577 (1972); (*b*) **68**, 1676 (1972).
4. K. P. CLARK and H. I. STONEHILL. J. Chem. Soc. Faraday I. To be published.
5. J. BOLTON. Private communication.
6. B. E. HULME and G. O. PHILLIPS. Chem. Commun. 518 (1969).
7. B. E. HULME, E. J. LAND, and G. O. PHILLIPS. J. Chem. Soc. Faraday I, **68**, 1992 (1972).
8. R. GILL and H. I. STONEHILL. J. Chem. Soc. 1845. (1952).
9. O. VOLKERT and D. SCHULTE-FROHLINDE. Tetrahedron Lett. 2151 (1968).
10. M. SIMIC, P. NETA, and E. HAYON. J. Phys. Chem. **73**, 4214 (1969). P. S. RAO and E. HAYON. J. Am. Chem. Soc. **96**, 1287 (1974). J. EIBEN and R. W. FESSENDEN, J. Phys. Chem. **75**, 1186 (1971). K. D. ASMUS, A. HENGLEIN, A. WIGGER, and G. BECK. Ber. Bunsenges. Phys. Chem. **70**, 756 (1966).

Can. J. Chem. Downloaded from www.nrcresearchpress.com by 210.87.254.40 on 09/05/12
For personal use only.

The photochemistry of some bisethylenediamine and cyclam complexes of rhodium(III)

JAMES SELLAN AND ROBERT RUMFELDT
Department of Chemistry, University of Windsor, Windsor, Ontario N9B 3P4

Received July 3, 1975

JAMES SELLAN and ROBERT RUMFELDT. Can. J. Chem. **54**, 519 (1976).

The visible and uv photolysis of *trans*-$[Rh(A_4)X_2]^+$ and *cis*-$[Rh(A_4)Y_2]^+$ have been studied where A_4 is the macromolecule 1,4,8,11-tetraazacyclotetradecane (cyclam) or two ethylenediamine (en) molecules, X is Cl, Br, or I, and Y is Cl. With the exception of *cis*-$[Rh(en)_2Cl_2]^+$, all photoreactions proceeded via halide aquation with complete isomeric retention for both ligand field and charge transfer excitation. In the case of *cis*-$[Rh(en)_2Cl_2]^+$, amine aquation is the principal reaction with some isomerization occurring through a secondary reaction. The quantum yield of halide increased in the order Cl < Br < I for *trans*-$[Rh(A_4)X_2]^+$, but was found to be almost equally sensitive to the degree of chelation of the amine system so that the photoactivity of *trans*-$[Rh(NH_3)_4Cl_2]^+$ and *trans*-$[Rh(cyclam)I_2]^+$ were nearly equal ($\phi(Cl^-)$ = 0.13 and $\phi(I^-)$ = 0.14). These systems were also found to be more sensitive to charge transfer excitation than ligand field excitation with *cis*-$[Rh(cyclam)Cl_2]^+$ being the most sensitive complex ($\phi(Cl^-)$ = 0.47 at 254 nm).

The photochemistry of the systems studied has been interpreted in terms of a dominant influence of electronic factors in determining the type of photoreaction with the quantitative aspects being significantly influenced by mechanistic factors.

JAMES SELLAN et ROBERT RUMFELDT. Can. J. Chem. **54**, 519 (1976).

On a étudié la photolyse dans le visible et l'uv des $[Rh(A_4)X_2]^+$-*trans* et $[Rh(A_4)Y_2]^+$-*cis* dans lesquels A_4 est la macromolécule tétraaza-1,4,8,11 cyclotétradécane (cyclam) ou deux molécules d'éthylènediamine (en), X = Cl, Br ou I et Y = Cl. A l'exception du $[Rh(en)_2Cl_2]^+$-*cis*, toutes les photoréactions se produisent par l'intermédiaire d'une aquation de l'halogénure avec une rétention complète de l'isomérie pour les excitations de champ de ligand et de transfert de charge. Dans le cas du $[Rh(en)_2Cl_2]^+$-*cis*, l'aquation de l'amine est la réaction principale avec un peu d'isomérisation se produisant par l'intermédiaire d'une réaction secondaire. Le rendement quantique de l'halogène augmente dans l'ordre Cl < Br < I pour $[Rh(A_4)X_2]^+$-*trans*; on a toutefois trouvé que ce rendement est aussi sensible au degré de chélation du système de l'amine d'une façon telle que les photoactivités des $[Rh(NH_3)_4Cl_2]^+$-*trans* et $[Rh(cyclam)I_2]^+$-*trans* sont pratiquement égales ($\phi(Cl^-)$ = 0.13 et $\phi(I^-)$ = 0.14). On a aussi trouvé que ces systèmes sont plus sensibles à des excitations de transfert de charge qu'à des excitations de champ de ligand; le $[Rh(cyclam)Cl_2]^+$-*cis* est le complexe le plus sensible ($\phi(Cl^-)$ = 0.47 à 254 nm).

On a interprété la photochimie des systèmes étudiés en termes d'une influence prédominante de facteurs électroniques dans la détermination du type de photoréaction avec des aspects quantitatifs qui sont influencés d'une façon importante par des facteurs mécanistiques.

[Traduit par le journal]

The photochemistry of transition metal complexes has in the main been concentrated on complexes of Cr(III) and Co(III); however, a number of interesting studies of Rh(III) have been reported recently (1, 2), which indicate significant variations in photochemical behaviour from both Cr(III) and Co(III). Thus, the adherence of mixed ligand systems of Cr(III) to "Adamson's Emperical Rules" (3) is not entirely paralleled by Rh(III) complexes. For example, whereas ammonia release would be predicted from halopentaammine complexes and this was found to be the case for $[Rh(NH_3)_5I]^+$, with $[Rh(NH_3)_5Cl]^+$ chloride aquation is apparently the exclusive process. Whilst this pattern was operative for irradiation of both *d–d* and charge transfer to metal (cttm) bands, the curious effect was observed that photoaquation was more efficient for *d–d* than cttm excitation (1).

At least a partial explanation for these photochemical observations of the rhodium(III)–haloammines is provided by the photochemical model developed by Zink (4, 5). The model, which is based on fundamental crystal field and molecular orbital theories, analyses the antibonding properties of the excited states. Whereas

Can. J. Chem. Downloaded from www.nrcresearchpress.com by 210.87.254.6 on 09/05/12
For personal use only.

Can. J. Chem. Downloaded from www.nrcresearchpress.com by 210.87.254.6 on 09/05/12
For personal use only.

such an analysis was sufficient for successfully predicting the photoreactions of a wide variety of Cr(III) complexes, it has recently been demonstrated that steric factors in Rh(III) complexes can have a significant influence on the overall reaction (2). Thus, while Zink's model correctly predicts chloride aquation for the three electronically similar complexes $[Rh(NH_3)_4Cl_2]^+$, $[Rh(en)_2Cl_2]^+$, and $[Rh(cyclam)Cl_2]^+$ (where the ethylene diamine = en complex and 1,4,8,11-tetraazocyclotetradecane = cyclam complexes exhibit virtually identical electronic spectra) the yields progressively decrease with the increasing chelation.

The purpose of this investigation is to further explore the relative effects of both structural and electronic effects on the photochemistry of a series of Rh(III) complexes.

Experimental

The preparation of complexes used in this study was by methods described in the literature (6, 7), except that these compounds were separated as the perchlorate salts. The absorption spectra were in close agreement with reported values (6). All solutions were freshly prepared using triple distilled H_2O and reagent grade CH_3CN.

The perchlorate salt of each complex was chosen since using the corresponding halide would involve (*a*) a large blank correction in the yield analyses, (*b*) anion photolysis in the case of the 2537 Å irradiation of the iodide complexes, (*c*) a possible homogeneous anation reaction, and (*d*) a possible undetectable heterogeneous anation reaction if any of the various complexes employed were susceptible to ion-pairing. The insolubility of $[Rh(cyclam)X_2]^+(ClO_4)^-$ (where X = Cl^-, Br^-, or I^-) in H_2O required 10% CH_3CN in H_2O as the solvent. Acidification caused the complexes to precipitate, thus all solutions were irradiated at 'natural p*H*'. The $[Rh(en)_2X_2]^+(ClO_4)^-$ complexes were water soluble, thus avoiding CH_3CN; however, these solutions were also used at natural p*H* since precipitation occurred upon acidification.

An Oriel model C-13-62 low pressure Hg lamp operated with a stabilized power supply in conjunction with a 22 mm H_2O filter was used as the source for 2537 Å irradiations. A 1 cm spectrophotometer cell served as a reaction cell and irradiations were at ambient temperature (24 ±2 °C). Intensities were measured using the differential technique with the ferrioxalate actinometer (8).

An Oriel model 6111 system employing a 150 W high pressure xenon lamp in conjunction with an Oriel model 7155 filter monochromator was employed as the source for irradiations in the 400 and 500 nm region. A water cooled (24 ± 0.2 °C) 11.5 cm pathlength cell with quartz windows was used for irradiations with this system. Light intensities were determined using the Reineckate ion as the actinometer (9) with the concentrations being used so as to achieve a computed optical density of 2 (for the total pathlength of the cell) for the various wavelengths employed. Similarly, the concentrations of all sample solutions were adjusted to provide the same optical density as that of the actinometer. Actinometry was repeated both before and after each run to ensure constant light intensity.

Halide ion analyses were performed using appropriate Orion selective ion electrodes with a double junction reference electrode and Orion model 801 meter. This meter was also used for p*H* measurements. The use of reagent blanks in preparing halide calibration curves was especially important with the CH_3CN–H_2O solvent as a considerable displacement relative to H_2O occurred; however, the sensitivity was not affected.

Spectra were recorded using a Beckman DK-1A Far UV recording spectrophotometer. For some single wavelength analyses a Hitachi–Perkin-Elmer model 139 spectrophotometer was used. Spectrophotometric and ion analyses of thermal blanks prepared with each series of photochemical runs revealed (with the exception of *cis*-$[Rh(en)_2Cl_2]^+$) negligible effects due to dark reactions.

Results

For the low energy irradiations the wavelengths were selected to correspond to first spin allowed ligand field band for each complex. When the 254 nm line was used absorption would be by the first band of the dichloro complexes, a combination of the first and second bands of the dibromo complexes, and the second and third bands of the diiodo complexes.[1] In any event, regardless of the wavelength selected, the principal reaction was aquation via halide elimination for the photolysis of *trans*-$[Rh(A_4)X_2]^+$ (where A_4 = $(en)_2$ or cyclam, and X = Cl, Br, or I) and *cis*-$[Rh(cyclam)Cl_2]^+$.

The quantum yields listed in Table 1 were computed from the initial linear portion of yield *vs.* reaction time plots. Although curvature was observed in several plots, the onset appeared only after 25–30% decomposition and thus did not influence the accuracy in determining the initial slopes. The yields for the *trans* complexes irradiated in the ligand field region are in reasonably good agreement with values previously reported for *trans*-$[Rh(cyclam)Cl_2]^+$ and *trans*-$[Rh(en)X_2]^+$. On the other hand, Muir and Huang (10) have reported values for the 254 nm irradiation of *trans*-$[Rh(en)_2X_2]^+$ which are significantly lower than those given in Table 1. Since the higher values reported here establish the pattern that ct excitation produces larger yields than *d–d* excitation, whereas the results of

[1]The band reported (6) at 226 nm (ϵ = 22 800) was due mainly to free I^-. This band is removed in the ClO_4^- salt with a new peak appearing at 238 nm (ϵ = 3800).

TABLE 1. The photolysis of some *trans*-dihalorhodium(III) amines

Complex	Quantum yield of halide	
	2537 Å	First ligand field band
trans-$Rh(NH_3)_4Cl_2^+$	—	0.13 ± 0.02[a]
trans-$Rh(en)_2Cl_2^+$	0.12 ± 0.02	0.08 ± 0.01
trans-$Rh(cyclam)Cl_2^+$	0.035 ± 0.002	0.008 ± 0.001
trans-$Rh(NH_3)_4Br_2^+$	—	—
trans-$Rh(en)_2Br_2^+$	0.12 ± 0.02	0.07 ± 0.01
trans-$Rh(cyclam)Br_2^+$	0.10 ± 0.01	0.03 ± 0.003
trans-$Rh(NH_3)_4I_2^+$	(0.20)[b]	0.48[b]
trans-$Rh(en)_2I_2^+$	0.27 ± 0.02	0.20 ± 0.02
trans-$Rh(cyclam)I_2^+$	0.18 ± 0.01	0.14 ± 0.01

[a]Reference 2.
[b]Reference 1.

TABLE 2. The photolysis of *cis*-$[Rh(A_4)Cl_2]^+$

Complex	Quantum yield of halide	
	2537 Å	First ligand field band
cis-$[Rh(cyclam)Cl_2]^+$	0.47 ± 0.02	0.37 ± 0.02
cis-$[Rh(en)_2Cl_2]^+$	0.1[a]	—

[a]Reference 10. ϕ ($-H^+$) $\simeq$ 0.4).

Muir and Huang indicate the opposite trend, the discrepancy is seen to be serious.

The origin of the discrepancy is not immediately clear. The main analytic techniques employed appear identical in both instances with comparable yields being obtained at long wavelengths and the yields appear to be independent of the counterion employed (X^-, NO_3^-, or ClO_4^-) and p*H*. In order to ensure the reliability of our apparatus and techniques, several experiments were performed using N_2O saturated solutions of aqueous I^- and $Fe(CN)_6^{4-}$ and no difficulty was experienced in reproducing literature values (11, 12). Thus, while we cannot identify the source of the difference with the results of Muir and Huang, we are confident in the accuracy of our own results.

Spectrophotometric examination of the photolysed solutions indicated a total retention of configuration not only for the *trans* complexes but also for the photohydrolysis of *cis*-$[Rh(cyclam)Cl_2]^+$, for which the results are given in Table 2.

In addition to the complexes listed in Table 1, the photolysis of *cis*-$[Rh(en)_2Cl_2]^+$ was also investigated. Unfortunately in this case the chloride could not be determined accurately due to a large correction required by a relatively rapid dark reaction due presumably to base hydrolysis. Using a spectrophotometric analysis a quantum yield of $\sim$0.5 for 254 nm excitation was estimated for the disappearance of *cis*-$[Rh(en)_2Cl_2]^+$. Based on either the approximate chloride yields obtained or previously reported data (10), only a fraction of this yield can be associated with chloride aquation. Significantly, the p*H* was observed to increase upon photolysis and corresponded to an initial value of $\phi(-H^+) \sim 0.5$. This is in marked contrast to a very slight decrease observed for photolysis of *trans*-$[Rh(en)_2X_2]^+$ (*i.e.* for X = Cl, the p*H* decreased from 3.53 to 3.52 and for X = Br from 3.72 to 3.69).

Figure 1 illustrates the efficient bleaching of the 348 nm band of the *cis*-$[Rh(en)_2Cl_2]^+$. The isosbestic point observed was not developed initially, thus indicating an origin by a secondary photolysis. An examination of a more complete spectrum of curve *E* revealed besides the very intense bands at and beyond 205 nm new bands in the form of weak shoulders at 410, 315, and 276 nm and a more intense shoulder at 243 nm. These features are strongly characteristic of the presence of *trans*-$[Rh(en)_2Cl_2]^+$ and also suggest the formation of *trans*-$[Rh(en)_2OHCl]^+$. The failure to develop an isosbestic point initially is

Can. J. Chem. Downloaded from www.nrcresearchpress.com by 210.87.254.6 on 09/05/12
For personal use only.

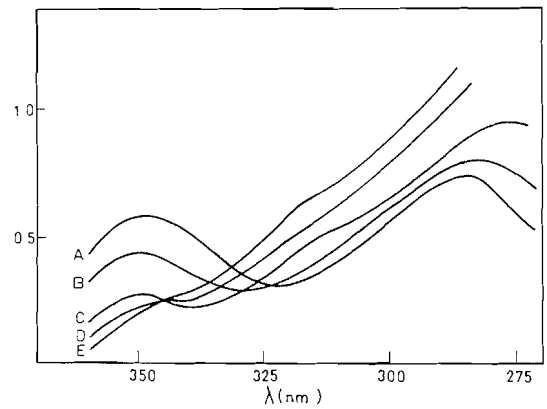

FIG. 1. The solution spectra of *cis*-$[Rh(en)Cl_2]^+$ and its 254 nm photolysis products. Curve *A* is the unirradiated solution with curves *B*, *C*, *D*, and *E* being the spectra of solutions irradiated for successively longer periods.

indicative of the formation of more than one absorbing species. This reflects the presence of an unstable product or the formation of multiple primary products. At low per cent conversion the initial product spectrum was too diffuse to be of analytical value and the attempt to generate sufficient product to facilitate product identification was frustrated by the onset of the secondary photoreaction.

Discussion

Using a matrix isolation technique and ligand field excitation, Thomas and Crosby (13) characterized the emission from Rh(III) amine complexes as phosphorescence from the lowest triplet state. Their results suggest that intersystem crossing in these complexes occurs with near unit efficiency. If the same primary processes are operative in the ligand field excitation of aqueous *trans*-$[Rh(A_4)X_2]^+$, then the initially excited first ligand field band ($^1E_g \leftarrow {}^1A_{1g}$) should lead to formation of the ^3E_g state as the lowest electronic state within the *d–d* manifold. The photoactivity of these complexes would thus be related to the properties of this state.

Since the formation of either the singlet or triplet E_g state represents the transfer of an electron from the nonbonding or weakly π^*-antibonding e_g (d_{xz}, d_{yz}) orbital to a σ^*-antibonding orbital, photosubstitution via a dissociative mechanism can be regarded as a natural consequence. In D_{4h} symmetry there are two nonequivalent σ^*-antibonding levels represented by the metal centered a_{1g} and b_{1g} orbitals which correspond to the d_{z^2} and $d_{x^2-y^2}$ orbitals respectively. Although both the $(d_{xz}, d_{yz})^3(d_{z^2})^1$ and $(d_{xz}, d_{yz})^3(d_{x^2-y^2})^1$ configurations transform as E_g, neither is an eigenfunction of the low-lying ^3E_g state; however, a wavefunction can be constructed using the linear combinations

$$[1a]\quad \psi(^3E_g) = \sqrt{3}/2[(xy)^2(yz)^2(xz)^1(z^2)^1] + (1/2)[(xy)^2(yz)^2(xz)^1(x^2-y^2)^1]$$

$$[1b]\quad = -\sqrt{3}/2[(xy)^2(yz)^1(xz)^2(z^2)^1] + (1/2)[(xy)^2(yz)^1(xz)^2(x^2-y^2)^1]$$

The numerous additional ^3E_g states of higher energy which are possible for a d^6 ion in a D_{4h} field, can lead to perturbations of this function via configuration interaction. The magnitude of such mixing will only be significant for those states whose unperturbed energy levels are not too widely separated; thus, for simplicity only the interaction between the two lowest ^3E_g states has been computed and leads to the revised wavefunction for the lowest excited level of

$$[2]\quad \psi(^3E_g) = 0.5\,(1+a^2)^{-\frac{1}{2}}\{(\sqrt{3}-a)[(xy)^2(xz)^2(yz)^1(z^2)^1] + (1+\sqrt{3}a)[(xy)^2(xz)^2(yz)^1(x^2-y^2)^1]\}$$

where a is the mixing coefficient and has the value of

$$a = -(1.73D_s + 2.16D_t)/(8B + 2D_s + 10D_t)$$

and D_s and D_t are the distortion parameters defined by Ballhausen (14).

Unfortunately, the paucity of spectral data prohibits an accurate evaluation of the critical parameters B, D_s, and D_t. A crude estimate can be made of the mixing coefficient if it is assumed that the magnitude of D_t for the Rh(III) complexes will be at least as great as that calculated for their Co(III) analogues (15) and that the ratio D_t/D_s found for *trans*-$[Cr(en)_2X_2]^+$ (16) may also be applied to the Rh(III) complexes. The value thus calculated suggests at least a 90% contribution by the d_{z^2} orbital which is comparable to the computed value for similar Cr(III) complexes (17). Following the model proposed by Zink (4, 5), these calculations identify the weak field or dihalo axis as the dominant axis of labilization, a qualitative feature which is immediately confirmed by reference to the data in Table 1.

Can. J. Chem. Downloaded from www.nrcresearchpress.com by 210.87.254.6 on 09/05/12
For personal use only.

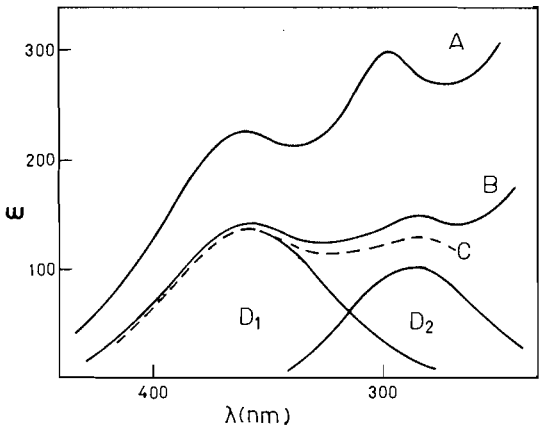

FIG. 2. The spectra of *cis*-$[Rh(A_4)Cl_2]^+$. Curve *A* is the observed spectrum of *cis*-$[Rh(cyclam)Cl_2]^+$ and curve *B* the observed spectrum of *cis*-$[Rh(en)Cl_2]^+$. Curve *C* represents the sum of the theoretical bands *D* (1) and *D* (2).

Treating the *cis* complexes in an analogous fashion identifies the weak field as lying along the N—Rh—Cl axis which then becomes the axis of labilization. As shown by Zink (4), the repulsive energy will be localized in the bond containing the strongest ligand; therefore, the N would be predicted to be the labilized ligand. Thus, the photoactivity of *cis*-$[Rh(en)_2Cl_2]^+$, which is similar to that reported for *cis*-$[Cr(en)_2Cl_2]^+$ (18), involves the antithermal, primary dissociation of a Rh—N bond and is accurately predicted by Zink's model. Although Cl^- was also obtained, it cannot be immediately identified as a primary product since the failure to establish an isosbestic point indicated product instability. Therefore, the relatively low yield of Cl^- as well as the isomerized products may only reflect the occurrence of secondary reactions. The importance of secondary reactions in multiple product formation has recently been demonstrated by Wong and Kirk (19).

In contrast to *cis*-$[Rh(en)_2Cl_2]^+$, a large Cl^- yield is obtained with *cis*-$[Rh(cyclam)Cl_2]^+$ without evidence of any other product or isomerization. From the experience with *cis*-$[Rh(en)_2Cl_2]^+$ and Zink's model, the anticipated reaction would have been dissociation of a Rh—N bond. Since the N is essentially locked into its coordination site by the stereo-rigid structure of the cyclam ring, geminate recombination would be prevalent and no net photoreaction would be predicted. The results clearly contradict this prediction.

It should be recalled that the implied premise in deriving the *weak field – strong ligand* prediction is that the ligands of the *cis* complex are arranged along three orthogonal axes. Although formally the complex will belong to C_{2v} symmetry, the effective group will be tetragonal. In the case where the tetragonal distortion is not too severe, the Rh can be considered to be in an approximately octahedral environment. In order to test this hypothesis the synthetic spectrum depicted by curve *C* in Fig. 2 was constructed using matrix elements based on O_h symmetry for the $^1T_{1g} \leftarrow {}^1A_{1g}$ and $^1T_{2g} \leftarrow {}^1A_{1g}$ transitions with weighted average values for the parameters D_q, *B*, and *C* as calculated from spectra of $[RhCl_6]^{3-}$ and $[Rh(en)_3]^{3+}$ (20). The bands represented by curve *D* in Fig. 2 were calculated using these computed energies and assuming a Gaussian function with averaged half-band widths. The intensities were chosen to correspond to that of an octahedral amine complex, in this case $[Rh(NH_3)_6]^{3+}$ (20) and the two curves (*D*) summed to give the synthetic spectrum *C*.

The coincidence between the observed spectrum of *cis*-$[Rh(en)_2Cl_2]^+$ and the theoretical spectrum is supportive of the assumption that this complex is essentially tetragonal and the *weak field – strong ligand* prediction should be valid. The spectrum of *cis*-$[Rh(cyclam)Cl_2]^+$ is distinguished by its marked increase in intensity which is characteristic of a significant distortion from O_h symmetry. Thus, a weak field axis can no longer be identified with one or other of a set of bond axes. It becomes necessary to describe new sets of wavefunctions in which the linear combinations will span contributions from all six ligands. If the coefficients could be evaluated then an estimate might be made of the change in bonding and antibonding properties between the ground state and the lowest excited state and the ligand or set of ligands experiencing the maximum destabilization might be identified. Such a treatment is in fact just an extension of Zink's model to a mixed ligand system lacking tetragonal symmetry. Rather than constituting an exception to the rule, *cis*-$[Rh(cyclam)Cl_2]^+$ demonstrates the potential inadequacy of any predictive model in the absence of good wavefunctions, a circumstance which may easily prevail whenever the effective symmetry must be assumed.

The relative quantum yields from the *trans*

Can. J. Chem. Downloaded from www.nrcresearchpress.com by 210.87.254.6 on 09/05/12
For personal use only.

Can. J. Chem. Downloaded from www.nrcresearchpress.com by 210.87.254.6 on 09/05/12
For personal use only.

complexes appear to follow a trend which is suggested by [2]. Thus, as D_t increases, the d_{z^2} orbital becomes increasingly dominant in [2]. Since D_t should ordinarily increase in the order $Cl < Br < I$ and the yields follow the same order with $\phi(Cl^-) < \phi(Br^-) < \phi(I^-)$, this would seem to be the predicted order on the basis of Zink's model. The difficulty with this interpretation is that it implies a competition between axial and equatorial labilization; however, if this was the case, then the decrease in halide yield observed with the *trans* dichloro complexes as compared to the *trans* diiodo complexes should be complimented by a yield of amine. In fact all the evidence supports the presence of a single hydrolysed product formed by substitution of a halide ligand.

It is noteworthy that the increased photoactivity which accompanies the increasing tetragonal distortion is very nearly matched in magnitude by a chelation effect (*e.g.* *trans*-$[Rh(cyclam)I_2]^+$, $\phi(I^-) = 0.14$ and *trans*-$[Rh(NH_3)_4Cl_2]^+$, $\phi(Cl^-) = 0.13$). Since the electronic spectra exhibit little dependence on the amine system, it is unlikely that the chelation effect is electronic in origin. On the other hand, increasing chelation would be expected to exhibit a definite effect if the photoefficiency of these systems was dependent upon the structure of the five coordinate intermediate. A trigonal bipyramidal intermediate, while satisfying the demand for stereomobility, seems improbable due to the complete isomeric retention in the hydrolysed product. A square pyramidal intermediate would account for the isomeric retention but would not explain the chelation effect. A tetragonal pyramidal intermediate, however, would not only satisfy both criteria but would also account for the very large difference in the yield between *trans*-$[Rh(cyclam)Cl_2]^+$ and *cis*-$[Rh(cyclam)Cl_2]^+$. In the latter case it is easily seen that only a minor rearrangement is required to achieve such a structure in the five coordinate intermediate.

Contrary to the decreased photoactivity with decreasing wavelength previously reported for some Rh(III) systems (1, 10), all of the systems studied here were more sensitive to ct excitation than to ligand field excitation. Consequently, internal conversion between the two manifolds of states must be negligible and the ct excitation produces its own unique photoactive state. Nevertheless, the same qualitative and quantitative trends are produced by both exciting luminations, suggesting that common controlling factors are operative in both cases.

For the *trans* complexes the lowest energy ct state correlates with the configuration $(e_u)^3(b_{2g})^2(e_g)^4(a_{1g})^1$ where the e_u orbitals are essentially chlorine centered nonbonding π orbitals. Destabilization will occur through population of σ^* antibonding a_{1g} and since this correlates with the metal d_{z^2} orbital, labilization is naturally directed along the weak field axis and the same ligand specificity is observed for both ct and ligand field excitation.

Since the reaction precursor is a ct state, a possible redox mechanism was considered. However, in forming the ct state the ligand electron deficiency is in a nonbonding orbital so that the major repulsive effect is defined by the highest filled orbital (*e.g.* the metal d_{z^2} orbital). In prospect, it seems that the more facile reaction coordinate would involve a halide ion rather than a halogen atom as the leaving group since the former would not only be more sensitive to metal–ligand repulsion but would experience the advantage of solvent stabilization. Thus, the ct and ligand field mechanism should be virtually the same. The higher charge density localized on the metal in the ct case would effect a greater metal–ligand repulsion thus providing a reason for the larger yields.

For both ligand field and ct excitation Zink's model has proven to be an effective basis for developing a qualitative interpretation of the photoreactions of the Rh(III) complexes included in this investigation. The model tends to accurately predict the principal reaction products; however, the situation becomes ambiguous with respect to secondary products. Thus for example, [2] correctly predicts the predominant axial labilization and could be employed to explain the increasing yield as D_t increases. Therefore, the logical inference is that some equatorial activation should also occur as a complimentary process to compensate for the otherwise low absolute yield in the *trans*-Cl_2 complexes. Since this is not the case then it is unlikely that purely electronic factors are controlling the quantitative aspects of the yields. On the other hand, both the pronounced chelation effect and the marked structural effect exhibited by the photosensitivity of the *cis* complexes are strongly suggestive of mechanistic influences as a

major factor in determining the magnitude of the yields. In summarizing his model, Zink (4) acknowledges the potential importance of mechanism to the overall photoefficiency of the system and the results presented here reinforce this concern.

Acknowledgment

The authors wish to acknowledge the National Research Council of Canada for financial assistance and for the award of a scholarship to James Sellan.

1. T. L. KELLY and J. F. ENDICOTT. J. Am. Chem. Soc. **92**, 5733 (1970); **94**, 1797 (1972); J. Phys. Chem. **76**, 1937 (1972).
2. C. KUTAL and A. W. ADAMSON. Inorg. Chem. **12**, 1454 (1973).
3. A. W. ADAMSON. J. Phys. Chem. **71**, 798 (1967).
4. (*a*) J. I. ZINK. J. Am. Chem. Soc. **94**, 8039 (1972); (*b*) J. I. ZINK. Mol. Photochem. **5**, 151 (1973).
5. J. I. ZINK. Inorg. Chem. **12**, 1018 (1973).
6. E. J. BOUNSALL and S. R. KOPRICH. Can. J. Chem. **48**, 1481 (1970).
7. (*a*) E. J. BOUNSALL. Ph.D. Thesis, Imperial College, University of London, London, England. 1964; (*b*) S. A. JOHNSON and F. BASOLO. Inorg. Chem. **1**, 925 (1962).
8. C. HATCHARD and C. PARKER. Proc. R. Soc. London, Ser. A, **235**, 518 (1956).
9. E. E. WEGER and A. W. ADAMSON. J. Am. Chem. Soc. **88**, 394 (1966).
10. M. MUIR and W. HUANG. Inorg. Chem. **12**, 1831 (1973).
11. F. S. DAINTON and S. LOGAN. Proc. R. Soc. London, Ser. A, **287**, 281 (1965).
12. W. L. WALTZ and A. W. ADAMSON. J. Phys. Chem. **73**, 4250 (1969).
13. T. R. THOMAS and G. A. CROSBY. J. Mol. Spectrosc. **38**, 118 (1971).
14. C. J. BALLHAUSEN. Introduction to ligand field theory. McGraw-Hill, New York. 1962.
15. A. B. P. LEVER. Inorganic electronic spectroscopy. Elsevier, Amsterdam. 1968.
16. M. KEETON, B. FA-CHUN CHOU, and A. B. P. LEVER. Can. J. Chem. **49**, 192 (1971).
17. J. I. ZINK. Inorg. Chem. **12**, 1957 (1973).
18. A. D. KIRK, K. C. MOSS, and J. G. VALENTINE. Can. J. Chem. **49**, 1524 (1971).
19. C. F. C. WONG and A. D. KIRK. Can. J. Chem. **52**, 3384 (1974).
20. C. K. JORGENSON. Acta Chem. Scand. **10**, 500 (1956).

Can. J. Chem. Downloaded from www.nrcresearchpress.com by 210.87.254.6 on 09/05/12
For personal use only.

An inequality formulation of conformational energy differences

JOHANNES PIETER COLPA, H. BERNHARD SCHLEGEL,[1] AND SAUL WOLFE
Department of Chemistry, Queen's University, Kingston, Ontario K7L 3N6

Received July 25, 1975

JOHANNES PIETER COLPA, H. BERNHARD SCHLEGEL, and SAUL WOLFE. Can. J. Chem. **54**, 526 (1976).

A theoretical analysis has been performed of the effects of geometry optimization upon computed barriers to rotation and pyramidal inversion. It is shown that, where ΔE is the true energy difference between the energy minimum and the transition state for a particular conformational process, (barrier using the optimized geometry of the lower state) $> \Delta E >$ (barrier using the optimized geometry of the higher state). Some numerical tests of this inequality are discussed. These reveal certain limitations upon the assumption that an optimized geometry is transferable from one basis set to another.

JOHANNES PIETER COLPA, H. BERNHARD SCHLEGEL et SAUL WOLFE. Can. J. Chem. **54**, 526 (1976).

On a effectué l'analyse théorique des effets de l'optimisation de la géométrie sur les barrières calculées pour la rotation et pour l'inversion pyramidale. On a montré que, lorsque ΔE est la vraie différence d'énergie entre l'énergie minimum et l'état de transition pour un processus conformationel déterminé, (la barrière utilisant la géométrie optimisée de l'état le plus bas) $> \Delta E >$ (la barrière utilisant la géométrie optimisée de l'état le plus élevé). On discute de quelques essais numériques de cette inéquation. Ceux-ci rélèvent certaines limitations concernant l'hypothèse qu'une géométrie optimisée est transférable d'une base à une autre.
[Traduit par le journal]

Introduction

A number of workers have suggested recently (1) that the conventional explanation of the first and second of Hund's rules[2] may be incorrect, because this explanation overemphasizes effects of electron–electron repulsion upon energy differences within a multiplet (2). While there is no doubt that electron repulsion is largest in the state having the lower energy, for neutral systems nuclear–electron *attraction* is also largest (most negative) in the state having the lower energy, and this attractive term is always the dominant component in a Hund multiplet.

To rationalize this result, Colpa (3) proposed a reformulation of the theory of Hund's rules in which certain unnecessary assumptions concerning the role of electron repulsion were deleted. In the Restricted Hartree Fock (RHF) scheme, this reformulation has the mathematical form of a series of inequalities. In the case of the singlet–triplet energy difference of an open shell $\pi\pi^*$ excited configuration, the appropriate inequality is

$$[1] \qquad 2K^{S}_{\pi\pi^*} \leq \Delta E_{RHF} \leq 2K^{T}_{\pi\pi^*}$$

in which ΔE_{RHF} is the energy difference between the exact RHF energy levels, and $K^{S}_{\pi\pi^*}$ and $K^{T}_{\pi\pi^*}$ are the exchange integrals for the exact RHF π and π^* orbitals of the singlet and triplet states, respectively.

As has been shown elsewhere (4), $2K^{S}_{\pi\pi^*}$ and $2K^{T}_{\pi\pi^*}$ are the energy differences which result when both states are described by singlet or by triplet RHF orbitals, respectively. These energy differences correspond to the use of a "frozen" orbital model which maintains the identity of orbitals in different states. According to the inequality of eq. 1, the true energy difference in the RHF approximation lies between the values of the two differences obtained with the frozen orbital approximation.

The significance of such work is that it provides insight into why an energy difference computed within a particular frozen orbital approximation may either underestimate or overestimate the true energy difference, according

[1]Holder of a National Research Council of Canada 1967 Science Scholarship.

[2]Hund's first rule states that, for a given configuration in an atom, the state of lowest energy is the state with the highest multiplicity. The second rule states that, within the manifold of states with the same multiplicity, the state with the largest angular momentum quantum number has the lowest energy.

Can. J. Chem. Downloaded from www.nrcresearchpress.com by 210.87.254.42 on 09/05/12
For personal use only.

Can. J. Chem. Downloaded from www.nrcresearchpress.com by 210.87.254.42 on 09/05/12
For personal use only.

to the particular frozen orbital model which is selected. This situation has a parallel in the computation of conformational energy differences. Much work, especially by Veillard (5), has shown that full geometry optimization along the reaction coordinate is necessary to reproduce barriers to torsion about bonds or pyramidal inversion at a tricoordinate centre. The purpose of the present work is to demonstrate, by means of an inequality formulation of the problem, the relationship between barriers computed within a particular rigid rotor model and the true value of the barrier.

Theory

For the analysis of rotation in ethane, we employ a two-symbol descriptor to represent the state of the molecule. The first symbol describes the conformation, *i.e.*, staggered or eclipsed. The second (bracketed) symbol refers to the particular optimized geometry employed to describe this conformation.[3] Thus St(St) describes a staggered conformation with CC and CH bond lengths and HCH angles optimized for this conformation; this is the true equilibrium situation for the staggered conformation. In the same way, Ecl(St) describes an eclipsed conformation which has the CC and CH bond lengths and HCH angles of the staggered conformation. The energies of the various states are given by $E_{\mathrm{St(St)}}$, etc.; and $\Delta E = E_{\mathrm{Ecl(Ecl)}} - E_{\mathrm{St(St)}}$ is the energy difference between the true equilibrium conformations Ecl(Ecl) and St(St).

The transformation from St(St) to Ecl(Ecl) can be supposed to proceed in two stages. In the first, rotation takes place within a rigid rotor model, *i.e.*, St(St) → Ecl(St). The energy difference associated with this process is designated B(St). In the second step, the state Ecl(St) relaxes to its true equilibrium geometry Ecl(Ecl).

Since

$$E_{\mathrm{Ecl(St)}} \geq E_{\mathrm{Ecl(Ecl)}}$$

it follows that

$$E_{\mathrm{Ecl(St)}} - E_{\mathrm{St(St)}} \geq E_{\mathrm{Ecl(Ecl)}} - E_{\mathrm{St(St)}}$$

i.e.

$$[2] \qquad B(\mathrm{St}) \geq \Delta E$$

[3] It is known (5) that the CC and CH bond lengths as well as the HCH angles of the staggered and eclipsed conformations of ethane are not the same.

Proceeding analogously for the transformation from Ecl(Ecl) to St(St), with B(Ecl) the energy difference for the step Ecl(Ecl) → St(Ecl), and noting that

$$E_{\mathrm{St(Ecl)}} \geq E_{\mathrm{St(St)}},$$

leads to

$$E_{\mathrm{Ecl(Ecl)}} - E_{\mathrm{St(Ecl)}} \leq E_{\mathrm{Ecl(Ecl)}} - E_{\mathrm{St(St)}}$$

i.e.

$$[3] \qquad B(\mathrm{Ecl}) \leq \Delta E$$

Combining [2] and [3] gives

$$[4] \qquad B(\mathrm{St}) \geq \Delta E \geq B(\mathrm{Ecl})$$

One can easily generalize the proof of this inequality to

[5] Barrier for lower state rigid rotor $\geq \Delta E \geq$ Barrier for higher state rigid rotor

Equations similar to [4] and [5] are also derived readily for an inversion barrier.

It is evident that these inequalities are formally similar to the inequality of [1]. However, there are important differences: eq. 1 is rigorously correct within the RHF scheme; but eqs. 4 and 5 will apply to exact wavefunctions, to Hartree Fock (HF) wavefunctions, or even to approximate HF wavefunctions, so long as the equilibrium geometry is computed exactly within the particular approximation selected. These geometries will, of course, be somewhat different within the various approximations. Some numerical tests of [5] follow in the next section.

Numerical Tests of the Theory

Table 1 summarizes the results of computations on ethane employing a minimal (STO-3G) and an extended (4-31G) basis set (6) with Gaussian 70 (7). The energy differences computed with the extended basis set are B(St) = 2.90 kcal/mol, ΔE = 2.77 kcal/mol, and B(Ecl) = 2.64 kcal/mol, in agreement with [4].[4]

The calculations just described are relatively expensive in terms of costs of computer time, because of the need to optimize the geometry of both states. It has, therefore, become customary (8) to compute the optimized geometry with the STO-3G basis set and then calculate energy differences with the 4-31G basis set, the assump-

[4] Veillard (5) has reported ΔE = 3.07 kcal/mol.

TABLE 1. Total energies and rotational barriers in ethane

Conformation	Energy[a] Staggered optimized parameters (St)	Eclipsed optimized parameters (Ecl)
Minimal basis set (optimization with the minimal basis set)		
Staggered	−78.306138[b]	−78.305778[c]
Eclipsed	−78.301493[b]	−78.301525[c]
Difference	B(St) = 2.92 > ΔE = 2.90 > B(Ecl) = 2.67[d]	
Extended basis set (optimization with the minimal basis set)		
Staggered	−79.115732[b]	−79.115466[c]
Eclipsed	−79.111189[b]	−79.111297[c]
Difference	B(St) = 2.85 > ΔE = 2.78 > B(Ecl) = 2.62[d]	
Extended basis set (optimization with the extended basis set)		
Staggered	−79.115927[e]	−79.115726[f]
Eclipsed	−79.111302[e]	−79.111514[f]
Difference	B(St) = 2.90 > ΔE = 2.77 > B(Ecl) = 2.64[d]	

[a]Total energies in hartrees; 1 hartree = 627.71 kcal/mol.
[b]r_{CC} = 1.5452 Å; r_{CH} = 1.0858 Å; ∠CCH = 110.66°
[c]r_{CC} = 1.5587 Å; r_{CH} = 1.0849 Å; ∠CCH = 111.02°
[d]Energy differences in kcal/mol.
[e]r_{CC} = 1.5300 Å; r_{CH} = 1.0834 Å; ∠CCH = 110.07°
[f]r_{CC} = 1.5412 Å; r_{CH} = 1.0828 Å; ∠CCH = 111.64°

tion being made that the optimized geometry does not change appreciably as the basis set is changed. Equation 4 can be employed to assess the validity of this procedure and the assumption of transferability of geometry from one basis set to another. In this connection, it is useful to note that, for a problem such as the rotational barrier of ethane, one should expect that

$$[6] \quad E_{\mathrm{Ecl(St)}} - E_{\mathrm{Ecl(Ecl)}} \simeq E_{\mathrm{St(Ecl)}} - E_{\mathrm{St(St)}}$$

because both sides of this approximate equality refer to relaxation to an equilibrium geometry; and the same bonds and valence angles are involved.

When eq. 6 is a strict equality, we have

$$[7] \quad \Delta E = \tfrac{1}{2}(B_{\mathrm{St}} + B_{\mathrm{Ecl}})$$

The computations on ethane with the 4-31G basis set obey eq. 7 very closely; the average of B(St) and B(Ecl) is 0.004416 hartree, as compared to ΔE = 0.004413 hartree.

In contrast to these results, a computation on ethane with the STO-3G basis set and a single optimization cycle led to the energy differences B(St) = 2.92 kcal/mol, ΔE = 2.90 kcal/mol, and B(Ecl) = 2.67 kcal/mol. Although these data still obey [4], it is clear that [7] is not obeyed. A further analysis showed that [6] was not obeyed and that $E_{\mathrm{Ecl(St)}} \sim E_{\mathrm{Ecl(Ecl)}}$. This analysis of rotation in ethane thus shows that a single optimization cycle at the STO-3G level is insufficient. Using the geometries computed by one STO-3G optimization cycle, the energy differences computed at the 4-31G level are B(St) = 2.85 kcal/mol, ΔE = 2.78 kcal/mol, and B(Ecl) = 2.62 kcal/mol. Equation 4 is again obeyed; however, ΔE is not the average of B(St) and B(Ecl), although the deviation is less marked than for the STO-3G results.

Table 2 summarizes computations on pyramidal inversion in ammonia. These show that the geometry computed with an STO-3G basis set cannot be used to calculate 4-31G energy differences. In this case, the inequality of [5] should be

$$[8] \quad B(\text{optimization at pyramidal geometry}) \geq \Delta E \geq B(\text{optimization at planar geometry})$$

The energy differences computed with STO-3G optimized geometries and the STO-3G basis set are B(pyr) = 12.50 kcal/mol, ΔE = 11.13 kcal/mol, and B(plan) = 9.78 kcal/mol, in agreement with [8]. However, when these geometries are

Can. J. Chem. Downloaded from www.nrcresearchpress.com by 210.87.254.42 on 09/05/12
For personal use only.

TABLE 2. Total energy and inversion barriers in ammonia

Conformation	Energy[a] Pyramidal optimized parameters (Py)	Energy[a] Planar optimized parameters (Pl)
Minimal basis set (optimization with the minimal basis set)		
Pyramidal	−55.455390[b]	−55.453250[c]
Planar	−55.435481[b]	−55.437665[c]
Difference	$B(\mathrm{Py}) = 12.50 > \Delta E = 11.13 > B(\mathrm{Pl}) = 9.78$[a]	
Extended basis set (optimization with the minimal basis set)		
Pyramidal	−56.099081[b]	−56.100586[c]
Planar	−56.100260[b]	−56.104912[c]
Difference	$B(\mathrm{Py}) = -0.74 > \Delta E = -3.66 \not> B(\mathrm{Pl}) = -2.71$[a]	
Extended basis set (optimization with the extended basis set)		
Pyramidal	−56.106692[d]	−56.106613[e]
Planar	−56.105948[d]	−56.105997[e]
Difference	$B(\mathrm{Py}) = 0.49 > \Delta E = 0.44 > B(\mathrm{Pl}) = 0.39$[a]	

[a]See Table 1.
[b]r_{NH} = 1.0318 Å; ∠HNH = 104.77° for pyramidal structure.
[c]r_{NH} = 1.0052 Å; ∠HNH = 120.00° for planar structure.
[d]r_{NH} = 0.991 Å; ∠HNH = 115.8° for pyramidal structure.
[e]r_{NH} = 0.986 Å; ∠HNH = 120.00° for planar structure.

used to calculate the energy differences with the 4-31G basis set, negative barriers are observed, *i.e.*, $B(\mathrm{Pyr}) = -0.74$ kcal/mol, $\Delta E = -3.66$ kcal/mol, and $B(\mathrm{plan}) = -2.71$ kcal/mol. In addition, these negative barriers do not satisfy [8].

The barriers computed with the 4-31G basis set and 4-31G optimized geometry do satisfy [8]. However, ΔE is lower than the experimental value (5.9 kcal/mol) (9). The experimental ΔE for ammonia has been reproduced with a very extended basis set which included *d*-type polarization functions on nitrogen and *p*-type functions on hydrogen (10).

Our results are thus entirely in accord with the view (10, 11) that barriers to pyramidal inversion are extraordinarily sensitive to the nature and quality of the basis set as well as the nature of the geometry optimization scheme employed. At the same time, the inequality formulation of the problem suggests that the qualitative comparison of barriers to pyramidal inversion of a series of closely related molecules should be valid, provided that geometry optimization of both the pyramidal and planar conformations is performed, and the same basis set is employed for the geometry optimization and the computation of energy differences.

It is, perhaps, useful to recognize that inequalities of the type discussed in this paper will exist regardless of the nature of the optimization that is performed, so long as both the upper and lower states are optimized in the same way. The present example of geometry optimization can, therefore, be regarded as a subset of a more complete optimization scheme in which basis set optimization would be included. However, basis set optimization is usually not practical for polyatomic molecules, and our numerical examples were restricted to geometry optimization using the standard STO-3G and 4-31G basis sets.

Acknowledgement

We thank the National Research Council of Canada for financial support of this research.

1. E. R. DAVIDSON. J. Chem. Phys. **42**, 4199 (1965); R. P. MESSMER and F. W. BIRSS. J. Phys. Chem. **73**, 2085 (1969); J. KATRIEL. Theor. Chim. Acta, **23**, 309 (1972).
2. J. P. COLPA and M. F. J. ISLIP. Mol. Phys. **25**, 701 (1973); J. P. COLPA and R. E. BROWN. Mol. Phys. 26, 1455 (1973).
3. J. P. COLPA. Mol. Phys. **28**, 501 (1974).
4. J. P. COLPA, A. J. THAKKAR, V. H. SMITH, and P. RANDLE. Mol. Phys. **26**, 1861 (1975).

Can. J. Chem. Downloaded from www.nrcresearchpress.com by 210.87.254.42 on 09/05/12
For personal use only.

5. A. VEILLARD. Theor. Chim. Acta, **18**, 21 (1970).
6. W. J. HEHRE, R. F. STEWART, and J. A. POPLE. J. Chem. Phys. **51**, 2657 (1969); R. DITCHFIELD, W. J. HEHRE, and J. A. POPLE. J. Chem. Phys. **54**, 724 (1971).
7. W. J. HEHRE, W. A. LATHAN, R. DITCHFIELD, M. D. NEWTON, and J. A. POPLE. GAUSSIAN 70. Quantum Chemistry Program Exchange. Indiana University, Bloomington, Ind. No. 236.
8. W. A. LATHAN, L. A. CURTISS, W. J. HEHRE, J. B, LISLE, and J. A. POPLE. Progr. Phys. Org. Chem. **11**. 175 (1974).
9. J. D. SWALEN and J. A. IBERS. J. Chem. Phys. **36**, 1914 (1962).
10. A. RAUK, L. C. ALLEN, and E. CLEMENTI. J. Chem. Phys. **52**, 4133 (1970).
11. R. E. KARI and I. G. CSIZMADIA. J. Chem. Phys. **50**, 1443 (1969).

Can. J. Chem. Downloaded from www.nrcresearchpress.com by 210.87.254.42 on 09/05/12
For personal use only.

The pulse radiolysis of 1-propanol at 147 to 300 K

L. GILLES AND A. W. BOYD[1]

Section de Recherches et Interaction du Rayonnement avec la Matiere C.E.N. Saclay, B.P. No. 2, 91190 Gif-sur-Yvette, France

Received August 20, 1975

L. GILLES and A. W. BOYD. Can. J. Chem. **54**, 531 (1976).

Using ~20 ns electron pulses the spectra and kinetics of the electron and an absorption in the uv in 1-propanol have been determined at temperatures from 147 to 300 K. The uv absorption is attributed to the hydroxy propyl radical, $CH_3CH_2\dot{C}HOH$; it is formed within ~20 ns over this temperature range and disappears by second order kinetics. The results for the formation of the solvated electron are in agreement with those of Baxendale and Wardman. The temperature dependence of both the radical–radical reaction and the reaction of the solvated electron with N_2O is very nearly the same as that of T/η.

L. GILLES et A. W. BOYD. Can. J. Chem. **54**, 531 (1976).

Le spectre d'absorption de l'electron ainsi qu'une absorption dans l'uv ont été observés entre 147 et 300 K dans la radiolyse pulsé du propanol normal. Dans la gamme de températures considérées le spectre uv est formé dans l'impulsion (~20 ns) et il disparait selon une cinetique du second ordre. On l'attribue aux radicaux hydroxypropyliques $CH_3CH_2\dot{C}HOH$. Les resultats relatifs a l'évolution du spectre de l'électron avec le temps sont en bon accord avec ceux de Baxendale et Wardman. La réaction de disparition des radicaux et celle de l'électron avec N_2O varient en fonction de la température comme T/η.

Introduction

Three distinct absorptions have been observed in the pulse radiolysis of the simple liquid aliphatic alcohols. The first of these to be reported is characterized by a broad apparently structureless spectrum with peaks depending on alcohol and temperature, in the range of 500 to 900 nm (1–4). This species, which has a lifetime of a few microseconds in the pure alcohol at room temperature (5), reacts with electron scavengers with rates similar to those of the hydrated electron in water. It has thus been identified as the solvated electron and has been shown to be formed within picoseconds after an electron pulse at room temperature (6).

For ethyl, butyl, and 1-propyl alcohols, at temperatures near their melting points, the spectrum of the absorption of the solvated electron appears only after several nanoseconds (7). The spectrum that appears immediately after the pulse (the second of the three absorptions) shows an absorption which extends from 400 to 1400 nm. Its disappearance is coincident with the appearance of the solvated electron spectrum and it is believed to be a precursor of the solvated electron. It is presumably formed in conjunction with the positive ion in the primary process, reaction 1.

[1] $$RCH_2OH \rightsquigarrow RCH_2OH^+ + e^-$$

and is solvated as in reaction 2.

[2] $$e^- + 1\text{-}RCH_2OH \rightarrow e_{solv}^-$$

Measurements (8) have been made of the rate of reaction 2 at temperatures between those of Baxendale and Wardman (7) and room temperature. These give rate constants of the order $1\text{–}4 \times 10^{10}\ s^{-1}$ and activation energies of the order of 5 kcal mol^{-1}. Further measurements of the decay rate at room temperature of the absorption at 1050 nm (9) give a direct determination of the solvation processes; the values obtained are in the same order of magnitude as the values previously calculated (10) or extrapolated (8).

The third type of spectrum is in the uv with increasing absorption at lower wavelength. This absorption is found in the radiolysis of aqueous solutions of alcohols as well as in the pure alcohols (11–12). It is formed within nanoseconds at room temperature and its decay follows second order kinetics with a rate constant

[1]On leave of absence 1974–1975 from Physical Chemistry Branch, Atomic Energy of Canada Limited, Chalk River, Ontario.

Can. J. Chem. Downloaded from www.nrcresearchpress.com by 210.87.254.105 on 09/05/12
For personal use only.

of the order of $10^9\ M^{-1}\ s^{-1}$ (11–13). In methanol and ethanol, the species responsible for this uv spectrum have been identified as CH_2OH and $CH_3\dot{C}HOH$: it is believed that these are formed by reaction 3 or reactions 4 and 5:

[3] $RCH_2OH^+ + RCH_2OH \rightarrow RCH_2OH_2^+ + R\dot{C}HOH$

[4] $RCH_2OH^+ + RCH_2OH \rightarrow RCH_2OH_2^+ + RCH_2O^\bullet$

[5] $RCH_2O^\bullet + RCH_2OH \rightarrow RCH_2OH + R\dot{C}HOH$

and reactions 6*a* or 6*b* and 7

[6*a*] $e_{solv}^- + RCH_2OH_2^+ \rightarrow H + RCH_2OH$

[6*b*] $e_{solv}^- + RCH_2OH \rightarrow H + RCH_2O^-$

[7] $H + RCH_2OH \rightarrow H_2 + R\dot{C}HOH$

This uv absorption has also been observed in glassy alcohols (77 K) and attributed to the hydroxy radicals (14–15) whose decay follows second order kinetics. Nevertheless, no observations of this uv absorption at low temperature in liquid alcohols have been reported. It is thus of interest to determine the rates of formation and decay of the radical species in these conditions. As a first approach, we chose to study 1-propanol as did Baxendale and Wardman (7), because of its low melting point. We have also measured the rate constant for the reaction of the solvated electron in 1-propanol with N_2O at several temperatures between 140 and 200 K to confirm that the reaction is diffusion controlled (7, 16).

Experimental

The irradiation source was a modified Febetron 707. The electron pulse from the Febetron tube window was dispersed by an electromagnet (17) and only electrons in the range 1.7 to 1.8 MeV were selected. The total pulse length was thus reduced to about 20 ns with a width at half height of 10 ns. The absorbed dose can be varied from 10 to ~300 krads.

The irradiation cell was constructed of 1 mm thick suprasil. The optical path length was 2.5 cm and the depth of the solution in the electron beam was 2.5 mm. To reduce the concentration gradient of the optically observed species the width of the analyzing light was limited to 0.05 cm. This is small compared to the range of Febetron electrons in propanol.

To obtain the low temperatures, the cell was mounted on a copper block inside a vacuum chamber. A commercial temperature control system (Air Liquide) was used to regulate the temperature of the copper block and a calibration curve, determined prior to the irradiations with two calibrated thermocouples, gave the temperature inside the cell as a function of the temperature of the copper block.

It was found that the dose per pulse varied but the relative dose could be monitored by insulating the cell holder and measuring the total charge with a charge integrating circuit. The induced voltage was linearly proportional to the absorbed dose (as measured with $10^{-2}\ M$ potassium ferricyanide) within ±5% from 10 to 300 krads. In these experiments the spectra were determined by normalization of the optical densities to an arbitrary value of 1 V on our capacitive system (~100 krads).

The optical system included a Zeiss M4 Q III prism monochromator and a 450 W Xe arc lamp. The intensity of the latter could be increased by a factor of up to 200 for ~200 μs by means of a condenser bank discharge (18). The wavelength range of the photomultiplier (Hamamatsu R446) is 185–850 nm. Further details may be found in previous publications (19, 20).

It was found that when commercially available 1-propanol (Merck fur Chromatographie, Merck zur Analyse, Prolabo) was irradiated after degassing by bubbling with argon there was fluorescence in the region 230–280 nm and the lifetime of the solvated electron was less than 100 ns. With alcohol purified by distillation the fluorescence disappeared and the lifetime of the electron increased to several hundred nanoseconds. The distillation was carried out using a packed 1.5 m Dewar jacketed column. The extent of refluxing was controlled to give a throughput of 5 ml per hour and the first and last quarters of the distillate were discarded. No further changes in the transient absorption spectra or in the electron life-time were observed with redistilled alcohol.

The nitrous oxide was Air Liquide N40 (>99.99% N_2O) and the argon Air Liquide N55 (>99.9995% Ar). The irradiation cell was filled with alcohol previously deaerated with argon (or saturated with N_2O) at room temperature, and then cooled down to the desired temperature.

Results and Discussion

Room Temperature (25 °C)

Spectra were measured 30 ns after the beginning of the pulse over the range 220 to 700 nm. In Ar purged solutions the spectrum above 400 nm is similar to that obtained previously (3) for the solvated electron. The kinetics of its decay are intermediate between first and second order. For a dose of ~20 krads the half life is approximately 350 ns. This is shorter than that found at lower doses (3) but this decrease in lifetime is to be expected (5).

The uv spectrum of 1-propanol has not been previously reported; it is obtained with alcohol saturated with N_2O ($[N_2O] \approx 1.34 \times 10^{-1}$) in order to suppress any contribution of the solvated electron. The shape is similar to that observed in the uv for other alcohols (12). The decay (usually measured at 230 nm) follows second order kinetics. If the radical yield expressed as the number of radicals produced per 100 eV absorbed is assumed to be 5 (21) then the rate constant is about $1 \times 10^9\ M^{-1}\ s^{-1}$, which is similar to the values obtained for the

Can. J. Chem. Downloaded from www.nrcresearchpress.com by 210.87.254.105 on 09/05/12
For personal use only.

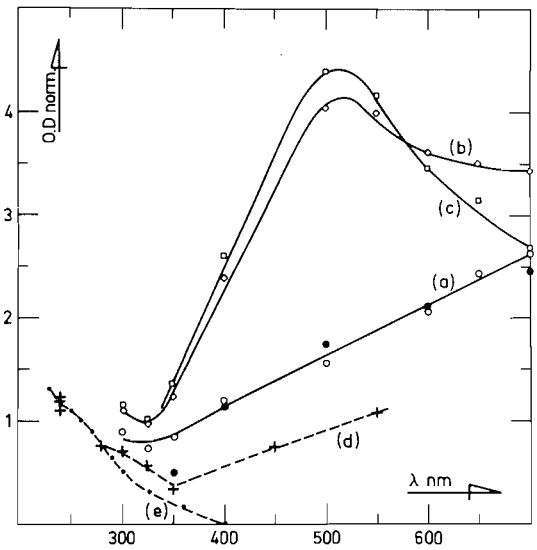

FIG. 1. Spectra observed in pulsed Ar purged in 1-propanol at 147 K. Optical/densities normalized to 1 V on charge integrator. (*a*) ○, Experimental points immediately after the 20 ns pulse; ●, from Baxendale and Wardman (7). (*b*) ◊, 2.5 μs after the pulse. (*c*) □, 5 μs after the pulse, N_2O saturated 1-propanol. (*d*) +, 147 K, immediately after the 20 ns pulse. (*e*) ●, 152 K, 15 μs after the pulse.

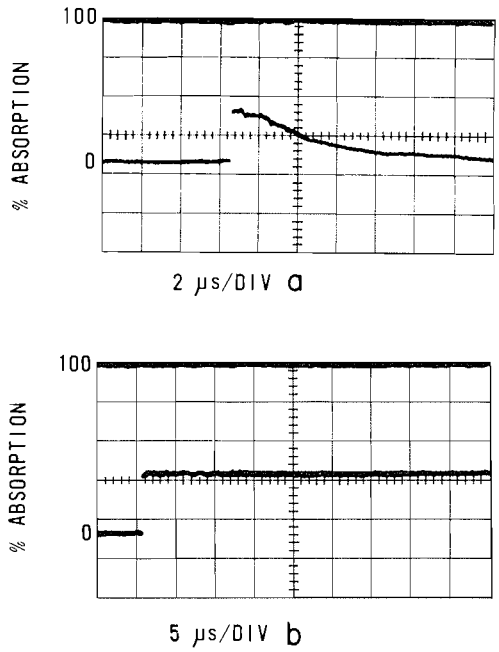

FIG. 2. N_2O saturated 1-propanol at 152 K. (*a*) λ = 550 nm, horizontal sweep, 2 μs/div; (*b*) λ = 230 nm, horizontal sweep, 5 μs/div.

disappearance of $CH_3\dot{C}HOH$ in ethanol (13). Since the decay is second order and since the principal products of radical–radical reactions in 1-propanol are hexane-3,4-diol, and propionaldehyde (21) this species is most probably $CH_3CH_2\dot{C}HOH$; the radical $CH_3CH_2CH_2O\cdot$ would not give the dimeric alcohol and its decay would follow pseudo first order kinetics as in reaction 5.

Low Temperatures

The spectra in Ar purged solutions at 147 K at various times after the pulse are shown in Fig. 1 along with values obtained by Baxendale and Wardman (7). From 400–700 nm the agreement between the two spectra is very good though there is a small difference in the lifetime of solvation. We obtained a half life for the solvation (at λ = 550 nm) of 614 ns, Baxendale and Wardman obtained this value at 137 K.

In N_2O saturated solutions at 147 K, the yield of the precursor of the solvated electron is reduced by about 60% and the apparent solvation time is reduced to ~200 ns. Since the N_2O reacts with the precursor as well as the solvated electron it is not possible to derive an accurate rate constant for reaction 2 in the presence of N_2O. In these solutions the spectrum below 350 nm (Fig. 1) is similar to that obtained at room temperature, but the contribution of the precursor of the solvated electron only becomes negligible (as seen with the change in absorption due to the solvation process) below 280 nm. The difference at 350 nm between our results and those of Baxendale and Wardman (7) is probably due to the photodiode that they used which has a cut-off near 360 nm. At 230 nm, the absorption appears immediately after the pulse and does not change up to several microseconds (Fig. 2*b*). Even in N_2O solutions the decay of e^- (Fig. 2*a*) prevents the precise determination of the uv spectrum at short times. The spectrum after electron decay (15 μs) is shown in Fig. 1.

The decay of the uv spectrum (measured principally at 230 nm) follows second order kinetics and it would appear that this absorption, as at room temperature, is due to the radical $CH_3CH_2\dot{C}HOH$ (again, if it were the radical $CH_3CH_2CH_2O\cdot$, its decay should be pseudo first order as in reaction 5). If, as seem most likely, reaction 3 occurs (22), then it has a rate constant greater than $2 \times 10^7\ M^{-1}\ s^{-1}$ (assuming $t_{1/2} \approx$ 20 ns) even at 147 K; this value is in good agreement with the values determined by Fowles (22). If reaction 4 also occurs, there are at least two possibilities:

Can. J. Chem. Downloaded from www.nrcresearchpress.com by 210.87.254.105 on 09/05/12
For personal use only.

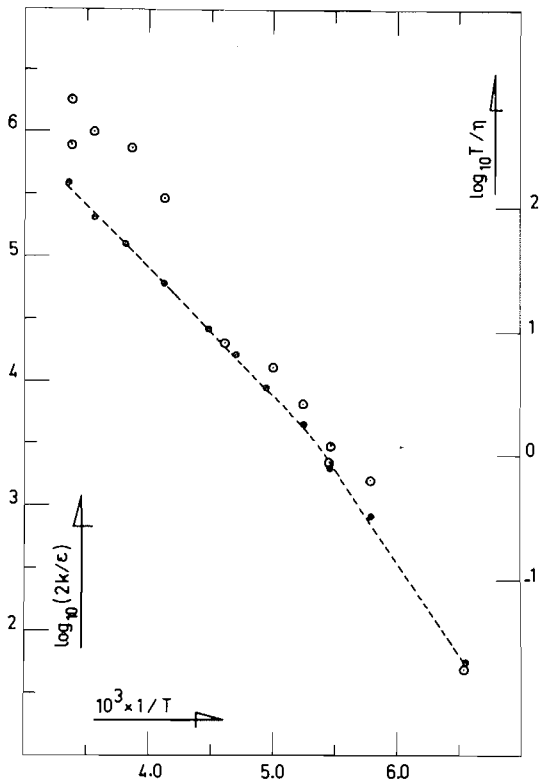

FIG. 3. Arrhenius plot for radical decay: ○, experimental relative rate constants ($2k/\epsilon$) estimated error ±15%; - -●- -, calculated relative rate constants ($k = AT/\eta$).

(*1*) As has been previously assumed for $CH_3O\cdot$ and CH_2OH in the radiolysis of methanol (23), $CH_3CH_2CH_2O\cdot$ has the same spectrum and the same extinction coefficient as $CH_3CH_2\dot{C}HOH$ in the region studied. The quite different structures of these two kinds of radicals make this hypothesis less probable.

(*2*) The oxy radicals absorb below 230 nm and are converted in less than 20 ns into hydroxyradicals (reaction 5) even at 147 K or more plausibly recombine to give the aldehyde. The results of γ radiolysis of pure ethanol and aqueous solutions of ethanol (24) suggest this kind of reaction as a possible source of molecular acetaldehyde.

Sargent *et al.* (25) using a spin trapping method in the radiolysis of liquid methanol concluded that $CH_3O\cdot$ and $\dot{C}H_2OH$ are both present but a direct esr detection of radicals in various alcohols (26) has only shown hydroxyradicals even at −50 °C. It appears that direct optical spectroscopic studies cannot differentiate between the two kinds of radicals in the radiolysis of alcohols.

The decay of the absorption at 230 nm was determined at several temperatures in the range 150 to 300 K. Figure 3 is an Arrhenius plot of the relative experimental second order rate constants ($2k/\epsilon$) (27) and of the relative rate constants given by the expression $k = AT/\eta$. The values of the viscosity, η, are from ref. 28. It can be seen that the temperature dependence of the two sets of values is very nearly the same which leads us to assume that reaction 8 is essentially diffusion controlled.

[8] $$2CH_3CH_2\dot{C}HOH \rightarrow P$$

As stated at 152 K, the solvated electron has completely disappeared by reaction with N_2O. This reaction is generally assumed to be

[9] $$e_{solv}^- + N_2O \xrightarrow{CH_3CH_2CH_2OH} \cdot OH + N_2$$

OH radicals are known to react with alcohols by hydrogen abstraction. At room temperature the rate constant for this process is $\sim 2.5 \times 10^9\ M^{-1}\ s^{-1}$ and 66% of these radicals react at the α carbon atom (29).

[10] $$\dot{O}H + CH_3CH_2CH_2OH \rightarrow CH_3CH_2\dot{C}HOH + H_2O$$

If we assume as is suggested by the above results, that the solvated electron does not absorb at 230 nm, then the effect of reactions 9 and 10 should be an increase of the absorption at this wavelength due to either the OH or the hydroxypropyl radicals formed. But as can be seen in Fig. 2, there is no change in absorption at 230 nm coincident with the disappearance of the solvated electron. Sargent and Gardy (26) reported that when methanol was saturated with N_2O, there was no change in the intensity of the $\dot{C}H_2OH$ spectrum compared with the deaerated solution. To explain this they proposed that H abstraction by hydrogen atoms, [6*a*], [6*b*], and [7], was replaced by the abstraction of OH radicals, [9] and [10]. This explanation is not consistent on our time scale (*i.e.*, with no increase in the 230 nm absorption coincident with e_{solv}^- disappearance). The two remaining possibilities are: (*1*) oxy and hydroxy radicals OH and e_{solv}^- all have the same absorption below 280 nm, (*2*) OH is not produced concurrently with the disappearance of e_{solv}^- by reaction with N_2O. The latter of these would seem to be more likely (30). It is difficult to derive more

Can. J. Chem. Downloaded from www.nrcresearchpress.com by 210.87.254.105 on 09/05/12
For personal use only.

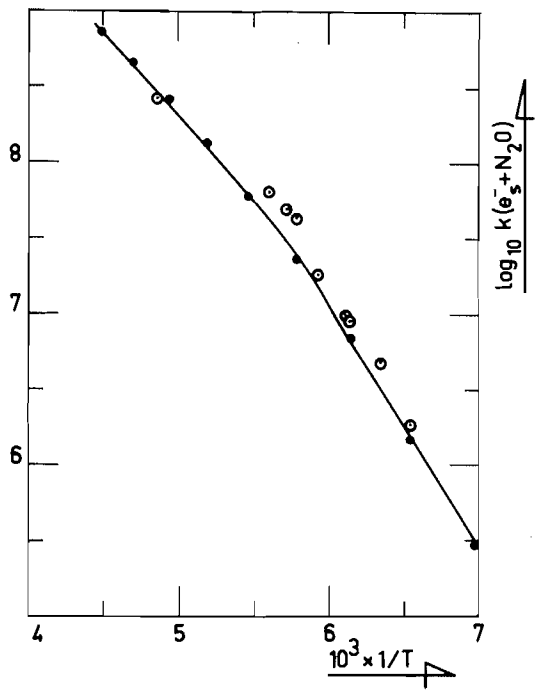

FIG. 4. Arrhenius plot for the reaction of the solvated electron with N_2O: ○, experimental rate constants (using $|N_2O| = 1.34 \times 10^{-1}$ M) estimated error ±15%; —●—, calculated rate constants ($k = 8\pi RT/3\eta$).

information by measurements at longer times after the pulse, because of the second order decay of the radical of 1-propanol.

Figure 4 is an Arrhenius plot of the rate constant for the reaction of the solvated electron with N_2O at temperatures from 140 to 200 K. The Arrhenius plot of the rate constants from Smoluchowski–Einstein–Stokes approximation, $k = 8\pi RT/3\eta$, is also given in this figure. The activation energies derived from the experimental and calculated values in the range 170–200 K are 4.2 kcal mol^{-1} in good agreement with the previous assumption (16) for this diffusion controlled reaction.

Conclusions

An absorption in the uv which is produced in the pulse radiolysis of 1-propanol is most probably due to the formation of the hydroxy radical $CH_3CH_2\dot{C}HOH$. This radical is believed to result from the proton transfer reaction 3 of the positive ion. As the uv absorption appears within 20 ns from 147 to 300 K, we conclude that this reaction, unlike the electron solvation reaction 2 is very fast even at low temperatures.

No increase in the uv absorption is observed at 152 K on the addition of N_2O concurrent with the decrease over ~10 μs in the absorption due to the solvated electron. This implies that the species N_2O^- does not immediately react at this temperature to produce hydroxyl radicals.

As the decay of the uv absorption is second order, the hydroxyradicals presumably disappear by recombination. Both this recombination and the reaction of the solvated electron with N_2O have rate constants whose temperature dependence is directly proportional to T/η. Thus both reactions are diffusion controlled.

1. I. A. TAUB, M. C. SAUER, and L. M. DORFMAN. Discuss. Faraday Soc. **36**, 206 (1963).
2. I. A. TAUB, D. C. HARTER, M. C. SAUER, and L. M. DORFMAN. J. Chem. Phys. **41**, 979 (1964).
3. M. C. SAUER, S. ARAI, and L. M. DORFMAN. J. Chem. Phys. **42**, 708 (1965).
4. G. E. ADAMS, J. H. BAXENDALE, and J. W. BOAG. Proc. R. Soc. London, Ser. A, **277**, 549 (1966).
5. J. W. FLETCHER, P. J. RICHARDS, and W. A. SEDDON. Can. J. Chem. **48**, 1645 (1970).
6. M. J. BRONSKILL, R. K. WOLFF, and J. W. HUNT. J. Chem. Phys. **53**, 4201 (1970).
7. J. H. BAXENDALE and P. WARDMAN. J. Chem. Soc. Faraday Trans. I, **69**, 584 (1973).
8. L. GILLES, J. E. ALDRICH, and J. W. HUNT. Nature (London), Phys. Sci. **243**, 70 (1973).
9. K. Y. LAM and J. W. HUNT. Int. J. Radiat. Phys. Chem. **7**, 317 (1975).
10. G. BECK and J. K. THOMAS. J. Phys. Chem. **76**, 3856 (1972).
11. I. A. TAUB and L. M. DORFMAN. J. Am. Chem. Soc. **84**, 4053 (1962).
12. M. SIMIC, P. NETA, and E. HAYON. J. Phys. Chem. **73**, 3794 (1969).
13. J. W. FLETCHER, P. J. RICHARDS, and W. A. SEDDON. Can. J. Chem. **48**, 3765 (1970).
14. A. HABERSBERGEROVA, LJ. JOSIMOVIC, and J. TEPLY. (*a*) Trans. Faraday Soc. **66**, 656 (1970); (*b*) Trans. Faraday Soc. **66**, 669 (1970).
15. S. FUJII and J. E. WILLARD. J. Phys. Chem. **74**, 4313 (1970).
16. K. N. JHA and G. R. FREEMAN. J. Chem. Phys. **51**, 2839 (1969).
17. B. LESIGNE and R. SAUNEUF. Rev. Sci. Instrum. To be published.
18. L. GILLES, C. LEMOINE, B. LESIGNE, P. NACASS, and G. SUTTER. Rapport CEA R 4645. 1975.
19. B. LESIGNE, L. GILLES, and R. J. WOODS. Can. J. Chem. **52**, 1135 (1974).
20. R. J. WOODS, B. LESIGNE, L. GILLES, C. FERRADINI, and J. PUCHEAULT. J. Phys. Chem. In press.
21. R. A. BASSON and H. J. VAN DER LINDE. J. Chem. Soc. A, 1182 (1967).

Can. J. Chem. Downloaded from www.nrcresearchpress.com by 210.87.254.105 on 09/05/12
For personal use only.

22. P. FOWLES. Trans. Faraday Soc. **67**, 428 (1971).
23. D. H. ELLISON, G. A. SALMON, and F. WILKINSON. Proc. R. Soc. London Ser. A, **323**, 23 (1972).
24. J. C. ROUX. Thesis, Universite de Bordeaux I, 1974.
25. F. P. SARGENT, E. M. GARDY, and H. R. FALLE. Chem. Phys. Lett. **24**, 120 (1974).
26. F. P. SARGENT and E. M. GARDY. J. Phys. Chem. **78**, 1977 (1974).
27. M. S. MATHESON and L. M. DORFMAN. *In* Pulse radiolysis. MIT, Press Cambridge. 1969, Chapt. 5.
28. V. G. KOMARENKO, V. G. MANZHELII, and A. V. RADTSIG. Ukr. Fiz. Zh. **12**, 47 (1967).
29. L. M. DORFMAN and G. E. ADAMS. NSRDS-NBS46 (1973).
30. F. S. DAINTON, P. O'NEILL and G. A. SALMON. J. Chem. Soc. Chem. Commun. 1001 (1972).

Can. J. Chem. Downloaded from www.nrcresearchpress.com by 210.87.254.105 on 09/05/12
For personal use only.

The flash thermolysis of allyl sulphides[1]

H. Gwynne Giles, Robert A. Marty, and Paul de Mayo
Department of Chemistry, University of Western Ontario, London, Ontario N6A 5B7

Received August 15, 1975

H. Gwynne Giles, Robert A. Marty, and Paul de Mayo. Can. J. Chem. **54**, 537 (1976).

The flash thermolysis of allyl sulphides has been shown to generate thiocarbonyl compounds. The reaction provides a route to very reactive substances such as thioacrolein, thiobenzaldehyde, and monothiobiacetyl; these have been characterized spectroscopically.

H. Gwynne Giles, Robert A. Marty et Paul de Mayo. Can. J. Chem. **54**, 537 (1976).

On a montré que la thermolyse éclair de sulfures d'allyle conduit à des composés thiocarbonylés. La réaction permet d'obtenir des substances très réactives comme la thioacroléine, le thiobenzaldéhyde et le monothiobiacétyl; on a caractérisé ces composés par spectroscopie.
[Traduit par le journal]

Can. J. Chem. Downloaded from www.nrcresearchpress.com by 210.87.254.105 on 09/05/12
For personal use only.

In contrast to their oxygen analogues, thiocarbonyl compounds have been comparatively little studied.[2] One important reason for this lies in their impressive tendency to oligo- or polymerize, a property which results in several chemically intelligent potential routes to thiones leading to intractable or undesirable products. Although many difficulties have been overcome (simple aliphatic thiones have, for instance, recently been isolated free from enethiol (4)), paths to the more reactive thiones and to thials in monomeric form, are lacking. The present report describes a route to very reactive thiocarbonyl compounds which then may be trapped at low temperature.[3]

The thermolysis of allyl ethers has been shown to lead to the formation of carbonyl compounds together with an olefin (6–8). It seemed probable that a similar reaction should be available to allyl sulphides, but thermolysis in a static system would suffer from the same restrictions as other techniques with regard to subsequent polymerisation of the product; the technique of flash thermolysis was, therefore, used. The apparatus has been described elsewhere (9, 10).

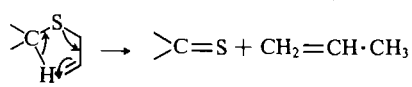

The simple approach was tested on two compounds, allyl *exo*-2-bornyl sulphide (**1**) and allyl cyclohexyl sulphide (**2**), since the expected products of reaction, thiocamphor and cyclohexanethione, were known substances of widely differing stability; thiocamphor is stable for prolonged periods, whereas **5** rapidly undergoes chemical reaction at room temperature (11, 12).

The conditions of the thermolyses are indicated in Table 1; the calculated contact times (13) were of the order of 1 ms. The thiocarbonyl compounds obtained in both cases were those expected and were identified by comparison with authentic specimens. The initial reactions appeared to proceed with high efficiency as judged by the high yields of propene. Hexa-1,5-diene (derived from the combination of allyl radicals) was not detected in major amount, indicating the incursion of free radical processes was probably of minor importance (14). The products to be expected from elimination processes, born-2-ene (**3**) and cyclohexene, were not important constituents of the thermolysates (<1 and 6% respectively), but this observation should be interpreted with caution since these hydrocarbons are labile under some thermolytic conditions (15, 16).

The quantitative estimation of **4** and **5** is difficult because of the occurrence of secondary thermolysis and/or the inefficiency of the analytical reactions employed. Camphor itself has been shown to give over 20 products on flash thermolysis (17). Similarly, we have shown that thiocamphor is labile under the conditions used for its generation. The products were not identified, but it seems probable that the fission between the quaternary centres C_1 and C_7 is the primary

[1]Flash Thermolysis. Part 11.
[2]For reviews see refs. 1–3.
[3]Part of the material has been reported in preliminary form (5).

TABLE 1. Conditions of thermolysis

Starting material	Precise mass Calcd.	Precise mass Exptl.	Thermolysis temperature (°C ± 5)	Propene (%)	Thiocarbonyl (%)	Starting material (%)
1	210.144	210.144	650	99	28	0
2	156.097	156.097	615	54	31[b]	17
10	—	—	650	91	[c]	0
11	164.065	164.066	615	75	75[d]	14
12	144.059	144.061	660	90	91	0
13	[a]	[a]	800	170	—	0

[a]No parent peak. *Anal.* calcd. for $C_9H_{16}S_2$: C 57.45, H 8.51, S 34.04; found: C 57.27, H 8.43, S 33.82.
[b]Estimated as trimer.
[c]Polymer adhered too strongly to be weighed.
[d]Crude polymer converted in 80% yield to β-trithiobenzaldehyde.

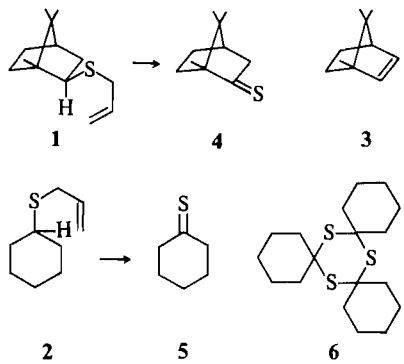

process. For convenience **5** was estimated as the cyclic trimer **6**, but the nonquantitative conversion of monomer to trimer has been noted previously (18, 19); the yields of **4** and **5** reported in Table 1 are thus minimal.

The temperature used for the thermolysis was not necessarily optimal and a knowledge of the reaction temperature profile seemed desirable. This could be obtained by the coupling of a quadrupole mass spectrometer to the exit of the furnace and monitoring the peaks with *m/e* values corresponding to the molecular weights of the molecules of interest. It was, unfortunately, not possible to use the preparative furnace for this purpose (that used was of the type employed for making spectroscopic measurements on the cryostat) and so the profile obtained is not directly transferable. In addition there were, of necessity, pressure differences. Low energy electrons were employed to minimise molecular fragmentation, and the plots are corrected for contributions from the starting material. The profile of the process **1** → **4** (Fig. 1) shows, indeed, that **4** is further transformed since the optimum yield is obtained over a fairly narrow

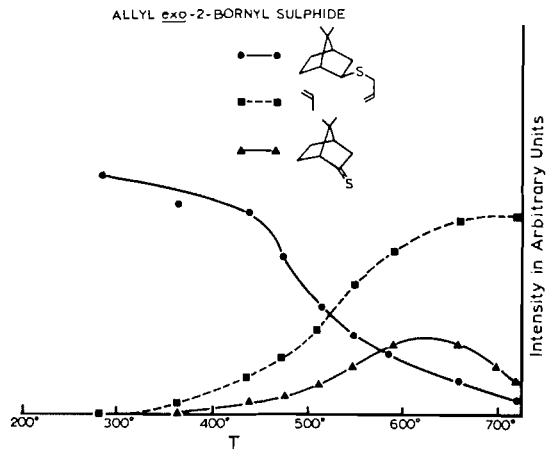

FIG. 1. Temperature profile for allyl bornyl sulphide.

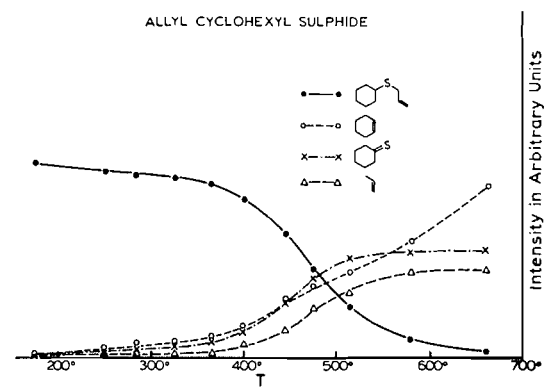

FIG. 2. Temperature profile for allyl cyclohexyl sulphide.

temperature range. Cyclohexanethione **5**, on the other hand, appears to be, thermally, comparatively stable (Fig. 2).

The aposynthetic technique has been applied

Can. J. Chem. Downloaded from www.nrcresearchpress.com by 210.87.254.105 on 09/05/12
For personal use only.

Can. J. Chem. Downloaded from www.nrcresearchpress.com by 210.87.254.105 on 09/05/12
For personal use only.

to the preparation of three highly reactive compounds, *viz.* thioacrolein **7**, thiobenzaldehyde **8**, and monothiobiacetyl **9**. The starting materials were diallyl sulphide **10**, and allyl benzyl sulphide **11**, and 3-allylthio-2-butanone **12**, respectively.

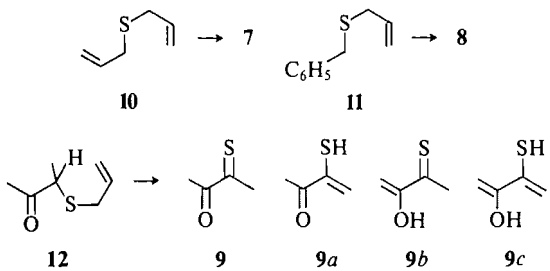

In all cases the initial reaction appeared to proceed well as judged, again, by the propene yields. A direct measurement of the yields of these thiocarbonyl substances was not possible because of their extremely ready polymerization far below ambient temperatures. The polymers of thiobenzaldehyde and of **9** were soluble in chloroform; that of thioacrolein was not and adhered strongly to glass. The polymeric thiobenzaldehyde could be converted in high yield to β-trithiobenzaldehyde.

Temperature profiles again showed the production of a substance of the same molecular weight as the desired thiocarbonyl compound and of propene. The curves resembled Fig. 2 rather than Fig. 1.

The characterization of these reactive species was of interest because few saturated aldehydes (20) and no simple, conjugated aldehydes[4] have been spectroscopically detected, and but a few complex heterocyclic thioaldehydes isolated (ref. 22 and references cited therein). In addition, no aliphatic α-ketothione has yet been reported though monothiobenzil has been recently described (23, 24). The electronic spectra of **7** and **8** have been calculated (25).

The low temperature (*ca.* 77 K) spectra of **7**, **8**, and **9** were obtained by deposition on a sodium chloride plate in a cryostat (26). For these determinations the flash thermolysis conditions were arranged such that there was essentially no starting material in the thermolysates. In the electronic spectrum **7** showed maxima at 276 and 580 nm (Fig. 3); **8** at ~228,

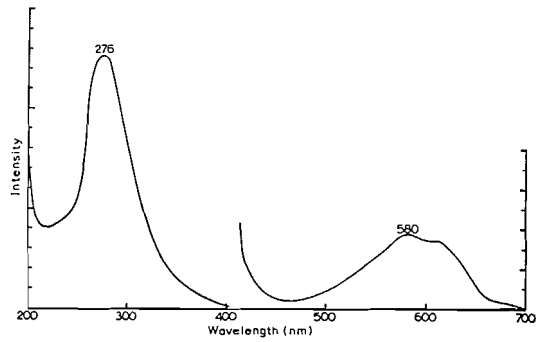

FIG. 3. Absorption spectrum (77 K) of acrolein.

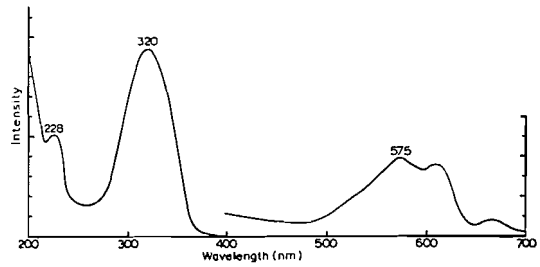

FIG. 4. Absorption spectrum (77 K) of thiobenzaldehyde.

320, and 575 nm (Fig. 4); and **9** at ~240, 380, and 625 nm. The calculated (25) spectrum of **7** includes maxima at 265 and 570 nm[5] and that of **8** at 226, 231, 296, 302, and 567 nm. The agreement is, therefore, good.

In view of the ready thioenolization of thiocarbonyl compounds the exact tautomeric form in which **9** might be found is uncertain. Aside from **9** itself, other possibilities were **9***a*, **9***b*, and **9***c*. *If* the material of which the spectrum was recorded consisted of a single tautomer then of these **9***a* and **9***c* may be immediately excluded; the band at 625 nm is certainly the $\pi^* \leftarrow$ n transition of some conjugated form of thiocarbonyl group. The nature of the 380 nm band is perplexing. It is of low intensity. It could be attributed to the carbonyl of **9**, but this is seemingly excluded by the absence of an appropriate carbonyl stretching frequency in the infrared spectrum. It does not appear likely that it could be a $\pi^* \leftarrow$ n of a conjugated carbonyl, again because the carbonyl stretch is not intense enough. We are presently unable to make an assignment.

The infrared spectra of thermolysates con-

[4]An inorganic complex of thioacrolein has been isolated recently (21).

[5]The CNEBI approach yields similar results.

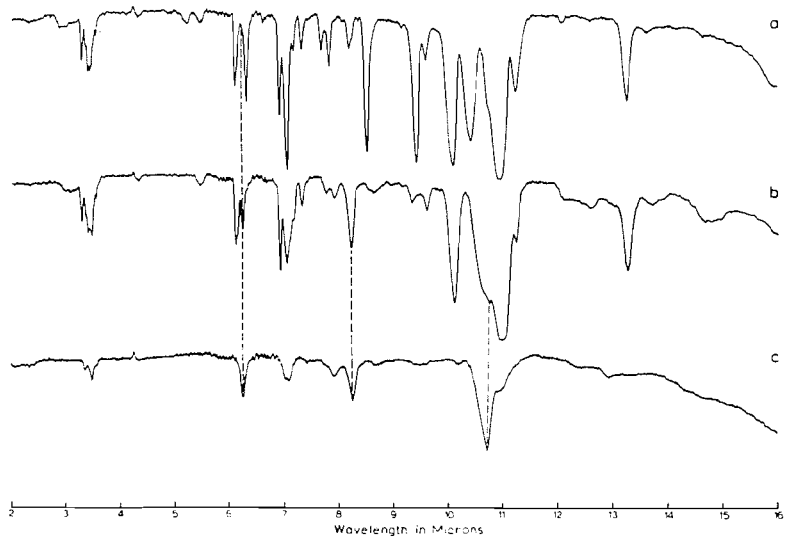

FIG. 5. Infrared spectrum (77 K) of the thermolysate of **7** (*a*) on depositing, (*b*) after warming to *ca.* 100 K, and (*c*) at room temperature after pumping.

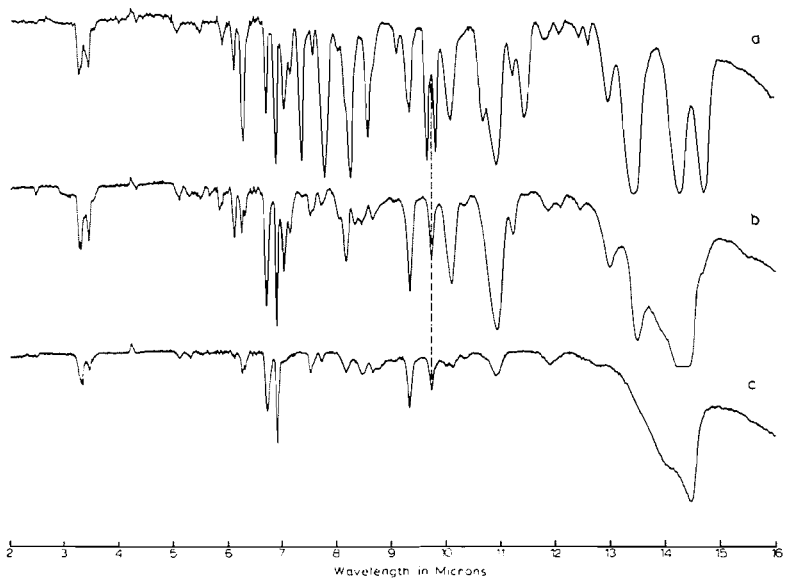

FIG. 6. Infrared spectrum (77 K) of the thermolysate of **8** (*a*) on deposition, (*b*) after warming to *ca.* 100 K, and (*c*) at room temperature after pumping.

taining **7**, **8**, and **9** are shown in Figs. 5, 6, and 7 respectively. The monitoring of these spectra has shown that **7** reacts slowly at 77 K (under these conditions), **8** is unreactive up to 110 K, and **9** is unreactive up to 100 K. In each of Figs. 5–7 (*a*) is the infrared spectrum of these deposits, (*b*) is the spectrum after reaction, and (*c*) the residue at ambient temperatures after removal of volatile substances, propene in particular, by pumping.

It was of interest to determine if the reaction could be induced twice in the same molecule, and if so whether simultaneously or consecutively. The substance chosen was the bis-sulphide **13**.

Can. J. Chem. Downloaded from www.nrcresearchpress.com by 210.87.254.105 on 09/05/12
For personal use only.

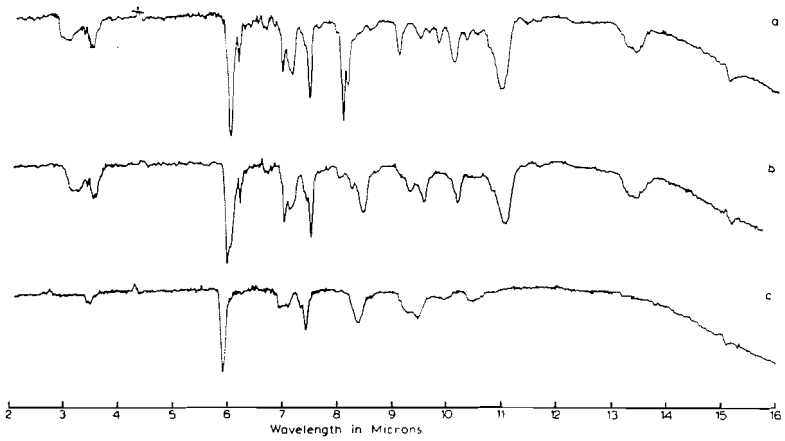

FIG. 7. Infrared spectrum (77 K) of the thermolysate of **9** (*a*) on deposition, (*b*) after warming to *ca.* 100 K, and (*c*) at room temperature after pumping.

Preparative thermolyses indicated that **15** was formed since 1.7 mol of propene were obtained, but, as expected, the product polymerised rapidly. Determination of the thermal profile showed that at no temperature was the reaction clean, but it appeared that the maximum amount of **15** was formed at the expense of **14**; that is, the reaction is at least, in part, stepwise.

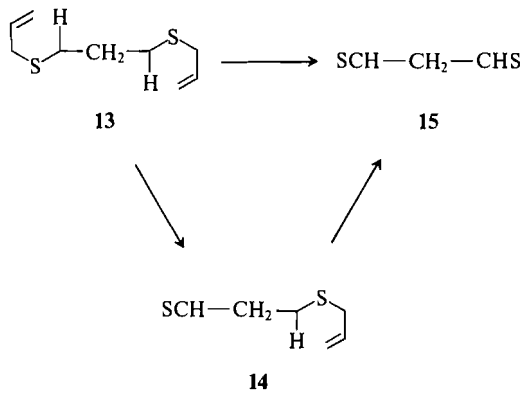

Experimental

Melting points were determined on a Reichert hot stage apparatus, infrared spectra on a Beckman-IR5 or IR5A spectrometer. Electronic spectra were determined point-by-point with an Hitachi–Perkin-Elmer 139 spectrometer. Proton magnetic resonance spectra were determined at 60 MHz with TMS as internal standard. Low resolution mass spectra were obtained on an EAI/QUAD 1100A spectrometer. Precise mass determinations were obtained from calibrated spectra from a Varian M-66 mass spectrometer. The apparatus employed for the thermolyses and low temperature spectra have been described previously (9, 10, 26).

Allyl Sulphides

Diallyl sulphide was obtained from Eastman Kodak and was distilled *in vacuo* prior to use. Allyl benzyl sulphide has been prepared previously (27). The remaining compounds were prepared by the condensation of the alkyl mercaptan with allyl bromide, or the alkyl bromide with allyl mercaptan (28). Purity was determined in all cases by thin layer chromatography and pmr spectra. The pmr spectra of these compounds showed very characteristic complex multiplets in the region δ (CCl_4) 4.9–6.5 (see for example, ref. 29). In addition, methyl signals were observed for **1** at δ (CCl_4) 0.81, 0.88, and 0.96,[6] and for **12** at δ (CCl_4) 1.38 (J = 7 Hz). In all cases the allylic methylene protons appeared as a quasi doublet near δ 3.1.

Allyl Butan-3-onyl Sulphide ***12***

To a mixture of 3-bromo-butan-2-one (Eastman Kodak) 4.0 g, 0.0265 mol) and allyl mercaptan (Aldrich, 70%+, 3.15 g, 0.0425 mol) in ethanol (50 ml) was added sodium hydroxide (1.8 g, 0.045 mol in 10 ml 1:1 H_2O–EtOH) with stirring over 15 min. After 15 min further stirring the mixture was diluted with water and the product isolated with ether. Preparative tlc (1:1 petroleum ether (60–80 °C – $CHCl_3$) gave the sulphide (1.9 g, 50%).

Analysis

Only **4** is sufficiently unreactive to allow quantitative determination. A sample prepared by the action of hydrogen sulphide on camphor (11) was found to be identical (tlc, vpc, pmr, and mass spectrum) with the product of thermolysis of **1**. The yield of **4** was determined gravimetrically after tlc purification. The product from **2** was treated with hydrogen chloride and yielded a white solid. Crystallization from methanol gave trithiocyclohexanone **6**, mp 100.5–101 °C (lit. (19, 20) 101–102 °C). The mp of a mixture with an authentic specimen was not depressed. The polymer from thiobenzaldehyde

[6]The stereochemical configuration of **1** was assigned by analogy with the pmr spectra of *exo* and *endo* bicyclic alcohols (30).

Can. J. Chem. Downloaded from www.nrcresearchpress.com by 210.87.254.105 on 09/05/12
For personal use only.

was converted in methylene dichloride solution by the action of hydrogen chloride into β-trithiobenzaldehyde identical (mp, mixed mp, tlc, mass spectrum) with an authentic specimen (31).

Thermolyses

In a typical experiment the sulphide (*ca.* 100 mg) was allowed to distil through the furnace over a period of 2 h. The thermolysate was trapped on the cold finger at 77 K. On warming the colour of the thermolysate was discharged, the volatile products being distilled into a vacuum line. The residue was subsequently extracted with solvent. The distillate was separated into liquids (traces) and gases using a methylenechloride – carbon dioxide slurry.

1. R. MAYER. Angew. Chem. Int. Ed. Engl. **3**, 277 (1964).
2. D. PAQUER. Int. J. Sulfur Chem. Part B, **7**, 269 (1972); **8**, 173 (1973).
3. E. CAMPAIGNE. *In* The chemistry of the carbonyl group. *Edited by* S. Patai. Interscience Publishers, New York. 1966. pp. 917–959.
4. D. PAQUER and J. VIALLE. Bull. Soc. Chim. Fr. 4407 (1971).
5. H. G. GILES, R. A. MARTY, and P. DE MAYO. J. Chem. Soc. Chem. Commun. 409 (1974).
6. M. J. MOLERA and E. ARIZA. An. R. Soc. Esp. Fis. Quim. Ser. B, **56**, 851 (1960).
7. R. C. COOKSON and S. R. WALLIS. J. Chem. Soc. B, 1245 (1966).
8. H. KWART, S. F. SARNER, and J. SLUTSKY. J. Am. Chem. Soc. **95**, 5234 (1973).
9. P. DE MAYO. Endeavour, **31**, 135 (1972).
10. J. F. KING, P. DE MAYO, C. L. MCINTOSH, K. PIERS, and D. J. H. SMITH. Can. J. Chem. **48**, 3704 (1970).
11. D. C. SEN. J. Indian Chem. Soc. **12**, 647 (1935).
12. D. C. SEN. J. Indian Chem. Soc. **13**, 268 (1936).
13. M. TAKAHASI. Bull. Chem. Soc. Jpn. **33**, 801 (1960).
14. E. HEDAYA and D. MCNEIL. J. Am. Chem. Soc. **89**, 4213 (1967).
15. W. C. HERNDON and J. M. MANION. J. Org. Chem. **33**, 4504 (1968).
16. F. O. RICE, P. M. RUOFF, and E. L. RODOWSKAS. J. Am. Chem. Soc. **60**, 955 (1938).
17. T. SATO. Tetrahedron, **21**, 2947 (1965).
18. J. MORGENSTERN and R. MAYER. J. Prakt. Chem. **34**, 116 (1966).
19. E. FROMM. Ber. **60**, 2090 (1927).
20. K. J. ROSENGREN. Acta Chem. Scand. **16**, 2284 (1962).
21. K. TAKAHASHI, M. IWANAMI, A. TSAI, P. L. CHANG, R. L. HARLOW, L. E. HARRIS, J. E. MCCASKIE, C. E. PFLUGER, and D. C. DITTMER. J. Am. Chem. Soc. **95**, 6113 (1973).
22. S. MCKENZIE and D. H. REID. J. Chem. Soc. C, 145 (1970).
23. D. C. DITTMER and G. E. KUHLMANN. J. Org. Chem. **35**, 4224 (1970).
24. B. SAVILLE and M. STEER. Chem. Commun. 616 (1972).
25. J. FABIAN. Z. Phys. Chem. (Leipzig), **250**, 377 (1972).
26. R. BLOCH, R. A. MARTY, and P. DE MAYO. Bull. Soc. Chim. Fr. 2031 (1972).
27. J. BÜCHI, M. PROST, H. EICHENBERGER, and R. LIEBERHERR. Helv. Chim. Acta, **35**, 1527 (1952).
28. E. E. REID. Organic chemistry of bivalent sulfur. Vol. II. Chemical Publishing Co., New York. 1960. p. 25.
29. N. S. BHACCA, L. F. JOHNSON, and J. N. SHOOLERY. N.M.R. spectra catalog. Varian Associates, 1962.
30. T. J. FLAUTT and W. F. ERMAN. J. Am. Chem. Soc. **85**, 3212 (1963).
31. E. CAMPAIGNE, N. F. CHAMBERLAIN, and B. E. EDWARDS. J. Org. Chem. **27**, 135 (1962).

Can. J. Chem. Downloaded from www.nrcresearchpress.com by 210.87.254.105 on 09/05/12
For personal use only.

Branched-chain sugars. Reaction of 1,2:5,6-di-*O*-isopropylidene-α-D-*ribo*-hexofuranos-3-ulose with sodium cyanide and methyl nitroacetate

ALEX ROSENTHAL AND B. L. CLIFF

Department of Chemistry, The University of British Columbia, Vancouver, British Columbia V6T 1W5

Received July 14, 1975

ALEX ROSENTHAL and B. L. CLIFF. Can. J. Chem. **54**, 543 (1976).

Treatment of 1,2:5,6-di-*O*-isopropylidene-α-D-*ribo*-hexofuranos-3-ulose (**1**) with sodium cyanide in anhydrous ethanol followed by addition of an equimolar amount of methyl nitroacetate gave 3-*C*-cyano-1,2:5,6-di-*O*-isopropylidene-α-D-glucofuranose (**2**) in 57% yield. When methyl nitroacetate was first added to sodium cyanide in alcohol followed by the addition of ketose **1** then the *allo*-cyanohydrin epimer **4** was produced in 85% yield. 3-*C*-(Carbomethoxy-*R*,*S*-nitromethyl)-1,2:5,6-di-*O*-isopropylidene-α-D-allofuranose (**6**) was produced in low yield in the latter reaction and was isolated and characterized as its 3-*O*-acetate derivative **7**. Selective acetolysis of the 5,6-*O*-isopropylidene group of the branched-chain sugars was achieved using acetic anhydride and *p*-toluenesulfonic acid monohydrate. The proof of structure of the cyanohydrins is described.

ALEX ROSENTHAL et B. L. CLIFF. Can. J. Chem. **54**, 543 (1976).

Le traitement du di-*O*-isopropylidène-1,2:5,6 α-D-*ribo*-hexofuranne ulose-3 (**1**) avec le cyanure de sodium dans l'éthanol anhydre, suivi par l'addition d'une quantité équimoléculaire de nitroacétate de méthyle, conduit au cyano-3-*C* di-*O*-isopropylidène-1,2:5,6 α-D-glucofurannose (**2**) avec un rendement de 57%. Lorsque l'on additionne en premier lieu le nitroacétate de méthyle au cyanure de sodium dans l'alcool puis le cétose **1**, il y a alors formation de l'*allo*-cyanohydrine épimère, **4**, avec un rendement de 85%. On obtient le (carbométhoxy-*R*,*S*-nitrométhyl)-3-*C* di-*O*-isopropylidène-1,2:5,6 α-D-allofurannose (**6**) avec un faible rendement dans cette dernière réaction; on l'a isolé et caractérisé sous forme de son dérivé 3-*O*-acétate **7**. On a effectué une acétolyse sélective du groupe *O*-isopropylidène-5,6 des s cres à chaîne ramifiée en utilisant l'anhydride acétique et le monohydrate de l'acide *p*-toluènesulfonique. On décrit la preuve de structure des cyanohydrines.

[Traduit par le journal]

Although the Kiliani and Fischer cyanohydrin synthesis (1) has been widely applied to aldoses the procedure has been very little used to prepare branched-chain sugars from ketoses. Bourgeois (2) has recently reported in a preliminary communication application of the cyanohydrin synthesis to 1,2:5,6-di-*O*-isopropylidene-α-D-*ribo*-hexofuranos-3-ulose, **1**, (3) to yield an epimeric mixture of cyanohydrins. The structures of the cyanohydrins were not proven but were assumed on mechanistic grounds.

During the past decade our laboratory has been involved in a study of glycosyl α-amino acids (4–7) related to the polyoxins (8). Because our first reported routes (4–7) involved many steps we have investigated the application of the cyanohydrin and methyl nitroacetate addition synthesis to ketoses as novel facile routes for the synthesis of branched-chain glycosyl α-amino acids. In this communication we wish to present proof of structure of the cyanohydrins from ketose **1**, the effect of p*H* on controlling proportions of products, and in addition, present some of the preliminary work dealing with the branched-chain methyl nitroacetate adduct of the same ketose.

As depicted in Table 1, treatment of ketose **1** with one molar equivalent of sodium cyanide in anhydrous ethanol, followed by chromatographic purification of the cyanohydrin on silica using 1:1 benzene – ethyl acetate as developer, afforded crystalline 3-*C*-cyano-1,2:5,6-di-*O*-isopropylidene-α-D-glucofuranose, **2**, in 35% yield. The yield of **2** was increased to 57% by adding, after the addition of sodium cyanide to the ketose, one molar equivalent of methyl nitroacetate. Less than a 5% yield of *allo*-cyanohydrin **4** accompanied the *gluco*-epimer. After column chromatography there was no evidence (in the pmr spectrum) of any methyl nitroacetate-ketose addition compound **6**.

Very surprisingly, when the order of addition of methyl nitroacetate to the ketose was changed then the *allo*-cyanohydrin **4** was formed pre-

Can. J. Chem. Downloaded from www.nrcresearchpress.com by 210.87.254.6 on 09/05/12
For personal use only.

TABLE 1. Application of the cyanohydrin synthesis to ketose **1** in the presence of methyl nitroacetate (MNA)

Procedure	Ketose (g)	NaCN (g)	MNA (g)	Solvent (ml)	Reaction time (h)	T (°C)	Cyanohydrin *gluco*(**2**) (%)	Cyanohydrin *allo*(**4**) (%)	MNA(**6**) (%)[a]
A	1.06	0.195	None	EtOH(2)	18	20	35	3	
A	1.43	0.290	0.706	EtOH(2)	18	20	57	4	
B	1.14	0.219	0.525	EtOH(5)	18	22	6	85	7
B	1.10	0.21	None	EtOH(5) AcOH(0.25)	18	22	5	71	

[a]Per cent yield of **6** calculated from an analysis of the pmr spectrum of the product mixture.

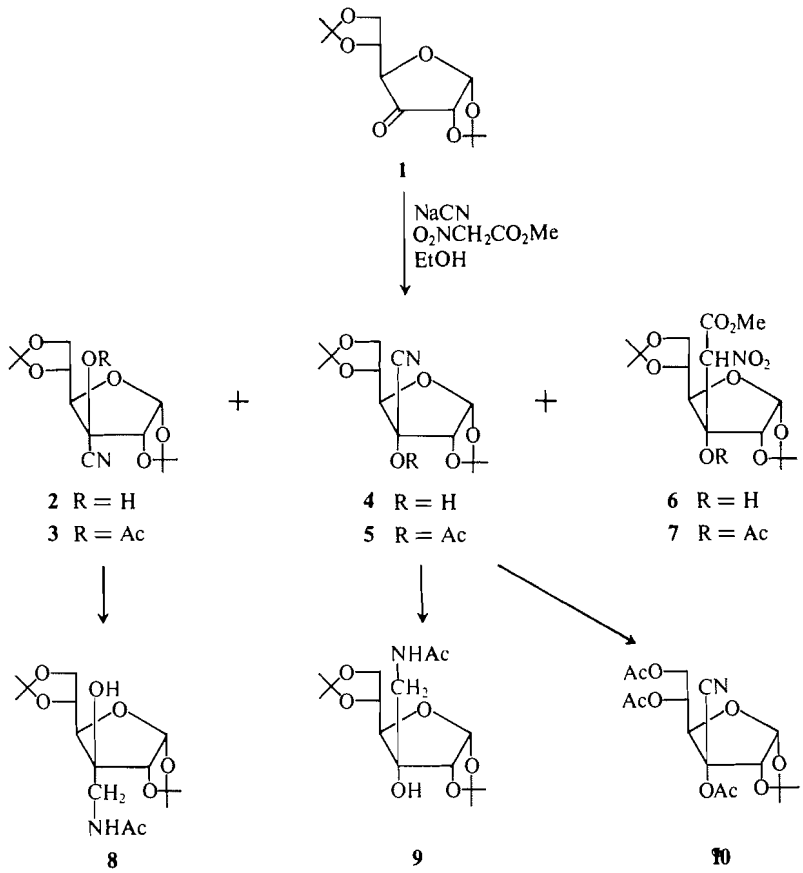

ponderantly. Thus, addition of the ketose **1** to a previously formed equimolar mixture of sodium cyanide and methyl nitroacetate in ethanol gave, after chromatographic separation on silica gel using 4:6 benzene – ethyl acetate as developer, the *allo*-epimer **4** in 85% yield. This product also could be directly crystallized out of the product mixture. The mp of **4** was substantially higher than that reported by Bourgeois (2). An analysis of the pmr spectrum of the residue obtained from the mother liquor, after removal of the *allo*-epimer, showed the presence of about 6% of *gluco*-cyanohydrin **2**, and a low yield (approximately 7%) of the methyl nitroacetate-ketose addition compound **6**. Attempts to obtain pure **6** by repeated chromatography were unsuccessful because **6** was quite unstable. Approximately the same ratio of *allo*:*gluco*-epimers was obtained when glacial acetic acid was used instead of methyl nitroacetate.

Can. J. Chem. Downloaded from www.nrcresearchpress.com by 210.87.254.6 on 09/05/12
For personal use only.

Can. J. Chem. Downloaded from www.nrcresearchpress.com by 210.87.254.6 on 09/05/12
For personal use only.

The proof of structure of the epimeric cyanohydrins **2** and **4** was provided in the following way. Lithium aluminum hydride reduction of the *gluco*-cyanohydrin **2** followed by acetylation afforded the corresponding 3-*C*-acetaminomethyl *gluco*-derivative **8**, which had a pmr spectrum identical to that of a substance which was obtained (9) by application of the nitromethane synthesis (10, 11) to ketose **1** followed by reduction and acetylation. Unequivocal proof of structure of a substance identical with compound **8** has been provided (9). Similar treatment of the epimeric *allo*-cyanohydrin **4** afforded the known 3-*C*-acetamidomethyl-1,2:5,6-di-*O*-isopropylidene-α-D-allofuranose **9** (9).

When a molar equivalent of ketose **1** was added to a mixture of one equivalent of sodium cyanide and one equivalent of methyl nitroacetate in ethanol, and the resulting mixture allowed to react for 18 h at room temperature followed by an immediate acetylation of the partially purified product mixture with acetic anhydride in the presence of *p*-toluenesulfonic acid monohydrate as catalyst, four products were obtained. The mixture of products was chromatographed on silica using 9:1 benzene – ethyl acetate as developer to afford the *O*-acetyl derivatives of each product, namely, the *gluco*-cyanohydrin **3**, the *allo*-cyanohydrin **5**, the methyl nitroacetate adduct **7**, and the tri-*O*-acetyl *allo*-cyanohydrin **10** in the ratio of 1:23:4:72, respectively. Proof of the structure of compound **10** was provided by the fact that selective hydrolysis of the 5,6-*O*-isopropylidene group of the *allo*-cyanohydrin **5** followed by acetylation afforded a substance identical (mp and pmr) with compound **10**. This selective acetolysis of the 5,6-*O*-isopropylidene group of di-*O*-isopropylidene sugar derivatives using *p*-toluenesulfonic acid monohydrate is a catalyst is noteworthy as it can provide a means of markedly reducing the number of steps required in some nucleoside syntheses.

Experimental

Nuclear magnetic resonance spectra were determined in deuteriochloroform solution with TMS as the internal standard using a Varian HA-100 spectrometer. Optical rotations were measured at room temperature with a Perkin-Elmer automatic polarimeter Model 141. Chemical analyses were performed by Mr. P. Borda of the Microanalytical Laboratory, University of British Columbia.

*Treatment of 1,2:5,6-di-O-Isopropylidene-α-D-ribo-hexofuranos-3-ulose, **1**, with Sodium Cyanide and Methyl Nitroacetate*

*Procedure A to Yield gluco-Cyanohydrin **2***

To a solution of ketose **1** (1.43 g) in a hydrous ethanol (2 ml) was added sodium cyanide (0.290 g). A solution of methyl nitroacetate (0.706 g) in anhydrous ethanol (2 ml) was added dropwise and the reaction mixture stirred for 18 h at room temperature. The ethanol was removed by evaporation under reduced pressure. After the addition of 10 ml of chloroform, a precipitate of non-carbohydrate material was removed by filtration. Water (10 ml) was added and the mixture extracted with chloroform (5 × 20 ml). The combined chloroform extracts were dried over magnesium sulfate, filtered, and evaporated to yield a syrup (1.13 g). This syrup was chromatographed on silica (50 g, 24 × 2.8 cm) using 1:1 benzene – ethyl acetate as developer to yield ketose **1** (0.44 g) and 0.739 g (61%) of a syrup which crystallized on standing.

3-*C*-Cyano-1,2:5,6-di-*O*-isopropylidene-α-D-glucofuranose, **2**, was recrystallized from benzene–hexane, mp 99–100 °C; $[\alpha]_D^{24}$ +51.6° (*c* 1.4, chloroform); τ ($CDCl_3$), 4.08 (d, 1H, H-1, $J_{1,2}$ = 4), 5.45 (d, 1H, H-2), 5.6–6.0 (m, 5H, one proton exchanges in D_2O), 8.45, 8.49, 8.64, and 8.66 (12H, CH_3). *Anal.* calcd. for $C_{13}H_{19}NO_6$: C 54.73, H 6.71, N 4.91; found: C 54.87, H 6.77, N 4.92. The ratio of *gluco*- to *allo*-epimers was 13:1.

*Procedure B to Yield allo-Cyanohydrin **4***

To a mixture of sodium cyanide (0.219 g) in anhydrous ethanol (2 ml) was added methyl nitroacetate (0.525 g), followed immediately by a solution of ketose **1** (1.14 g) in 5 ml ethanol. After the reaction mixture was stirred overnight, the precipitate of non-carbohydrate material was removed by filtration. Evaporation of the filtrate afforded a syrup which was triturated with 20 ml of water and extracted with chloroform (5 × 20 ml). The combined chloroform extracts were dried ($MgSO_4$), filtered, and evaporated to yield a clear syrup. This syrup was chromatographed on a column of silica (130 g, 5 × 16 cm) using 4:6 benzene – ethyl acetate as developer to yield ketose **1** (0.247 g) and a syrup (0.986 g). The syrup was crystallized from benzene–hexane to afford 3-*C*-cyano-1,2:5,6-di-*O*-isopropylidene-α-D-allofuranose, **4**, (0.75 g, 85% on reacted ketose), mp 61–64 °C; $[\alpha]_D^{24}$ +8.6° (*c* 1.4, chloroform); τ ($CDCl_3$), 4.18 (d, 1H, H-1, $J_{1,2}$ = 4), 5.31 (d, 1H, H-2, $J_{2,1}$ = 4), 5.40–6.29 (overlapping signals, 4H), 6.35 (s, 1H, OH, exchanges in D_2O), 8.51, 8.64, and 8.72 (s, 4 methyl groups). *Anal.* calcd. for $C_{13}H_{19}NO_6$: C 54.73, H 6.71, N 4.91; found: C 54.89, H 6.81, N 4.98.

The nmr spectrum of the syrup obtained from the mother liquors after crystallization of **4** showed the presence of **4**, the *gluco*-cyanohydrin **2**, and the methyl nitroacetate addition compound **6**. The ratio of products **4**, **2**, and **6** was 87:6:7, respectively. Attempts to obtain pure **6** by repeated slow chromatography led to the decomposition of compound **6**.

Procedure C

The reaction was carried out in the same way as

Can. J. Chem. Downloaded from www.nrcresearchpress.com by 210.87.254.6 on 09/05/12
For personal use only.

described in Procedure B up to the chromatographic separation. The product mixture (1.266 g) was acetylated with acetic anhydride (10 ml) and *p*-toluenesulfonic acid monohydrate (0.17 g) for 4 h at 80–85 °C. The volatile components of the mixture were co-distilled with toluene under reduced pressure to yield a dark syrup which was dissolved in chloroform (100 ml) and then washed with water (3 × 15 ml). After the chloroform solution was dried over sodium sulfate, evaporation of the filtrate afforded a syrup which was chromatographed on silica (110 g, 3 × 40 cm) using 9:1 benzene – ethyl acetate as developer to afford the acetates of the *gluco*-cyanohydrin **3** (0.009 g, 0.8%), the *allo*-cyanohydrin **5** (0.188 g, 15.6%), the methyl nitroacetate addition compound **7** (0.040 g, 2.6%), and the tri-*O*-acetyl *allo*-cyanohydrin **10** (0.651 g, 47.6%). The ratio of yields of compounds **3**, **5**, **7**, and **10** was 23:1:4:72, respectively.

3-*O*-Acetyl-3-*C*-(carbomethoxy-*R* or *S*-nitromethyl)-1,2:5,6-di-*O*-isopropylidene-α-D-allofuranose, **7**, was crystallized from ether–hexane, mp 136–137 °C; $[\alpha]_D^{24}$ +71° (*c* 5.3, chloroform); τ ($CDCl_3$), 4.07 (d, 1H, H-1, $J_{1,2}$ = 3.5), 4.10 (s, 1H, H-1′), 5.10 (d, 1H, H-2), 5.13 (s, 1H), 5.66 (s, 3H), 6.20 (s, 3H, OCH_3), 7.92 (s, 3H, OAc), 8.50, 8.57, 8.63, and 8.67 (4S, 12H, CH_3); ν_{max} ($CHCl_3$), 1740 cm^{-1} (C=O), 1360, and 1570 (NO_2). The nmr and mp of **7** suggest that only one diastereoisomer was isolated. Both diastereoisomers were likely formed. *Anal.* calcd. for $C_{17}H_{25}NO_{11}$: C 48.69, H 6.01, N 3.34; found: C 48.86, H 6.08, N 3.10.

3-O-Acetyl-3-C-cyano-1,2:5,6-di-O-isopropylidene-α-D-glucofuranose, ***3***

The *gluco*-cyanohydrin **2** (0.40 g) was acetylated with acetic anhydride (4 ml) and *p*-toluenesulfonic acid monohydrate (0.02 g) for 0.5 h at 80 °C. The product was worked-up in the usual way to afford 0.49 g of syrup which was chromatographed on silica using 8:2 benzene – ethyl acetate as developer. The *gluco*-acetate **3** (83% yield) was crystallized from hexane, mp 79–80 °C; $[\alpha]_D^{23}$ +45° (*c* 1.3, chloroform); τ ($CDCl_3$), 4.00 (d, 1H, H-1, $J_{1,2}$ = 4), 5.43 (d, 1H, H-2), 5.52–6.00 (overlapping signals, 4H, H-4, H-5, H-6), 7.87 (s, 3H, OAc), 8.37, 8.43, 8.57, and 8.62 (12H, CH_3). *Anal.* calcd. for $C_{15}H_{21}NO_7$: C 55.04, H 6.47, N 4.28; found: C 55.22, H 6.56, N 4.29.

3-O-Acetyl-3-C-cyano-1,2:5,6-di-O-isopropylidene-α-D-allofuranose, ***5***

The *allo*-cyanohydrin **4** was acetylated and purified using the same procedure utilized for the preparation for compound **3**. Compound **5**, mp 115–115.5 °C; $[\alpha]_D^{21}$ +38° (*c* 1.1, chloroform); τ ($CDCl_3$), 4.05 (d, 1H, H-1, $J_{1,2}$ = 4), 4.79 (d, 1H, H-2), 5.48–5 68 (o, 1H), 5.75–6.00 (overlapping m, 3H), 7.86 (s, 3H, OAc), 8.50, 8.55, 8.64, and 8.68 (12H, CH_3). *Anal.* calcd. for $C_{15}H_{21}NO_7$: C 55.04, H 6.47, N 4.28; found: C 55.13, H 6.45, N 4.40.

3,5,6-Tri-O-acetyl-3-C-cyano-1,2-O-isopropylidene-α-D-allofuranose, ***10***

The *allo*-cyano acetate **7** (0.20 g) was treated with 66% acetic acid for 24 h at room temperature. The acetic acid was then removed by co-distillation with toluene under reduced pressure. The residual syrup was then acetylated in the usual way using acetic anhydride and pyridine to afford the tri-*O*-acetate **10** which was purified by chromatography on silica using 8:2 benzene – ethyl acetate as developer. Compound **10** was crystallized from benzene–hexane, mp 131.5–132.5 °C; $[\alpha]_D^{26}$ +73° (*c* 1, chloroform); τ ($CDCl_3$), 4.01 (d, 1H, H-1, $J_{1,2}$ = 4), 4.56 (o, 1H, H-5, $J_{4,5}$ = 7.5, $J_{5,6b}$ = 5, $J_{5,6a}$ = 2.8), 4.74 (d, 1H, H-2), 5.38 (q, 1H, H-6a, $J_{6a,6b}$ = 12.5), 5.64 (d, 1H, H-4), 5.77 (q, 1H, H-6b), 7.82, 7.90, and 7.92 (3s, 9H, OAc), 8.45 and 8.64 (2s, 6H, CH_3). *Anal.* calcd. for $C_{16}H_{21}NO_9$: C 51.75, H 5.70, N 3.77; found: C 51.61, H 5.60, N 3.55.

3-C-Acetamidomethyl-1,2:5,6-di-O-isopropylidene-α-D-glucofuranose, ***8***, *and the Allofuranose Epimer* ***9***

The *gluco*-cyanohydrin **2** (100 mg) was dissolved in tetrahydrofuran (THF) (1 ml) and added dropwise to a mixture of lithium aluminum hydride (LAH) (50 mg) in THF (4 ml). After stirring for 1½ h, the excess LAH was decomposed by the addition of 3 ml ethyl acetate. The solution was then filtered, evaporated, and dissolved in chloroform (20 ml). The chloroform was washed with water (2 × 5 ml), dried over sodium sulphate, and evaporated to give a crystalline white solid in quantitative yield, mp 112–113.5 °C.

This solid (100 mg), without further purification, was then dissolved in anhydrous methanol (5 ml) and acetic anhydride (1 ml). After 24 h, the reaction was dumped into ice water (30 ml) and the solution was extracted with chloroform (5 × 20 ml). The combined extracts were dried over sodium sulphate and evaporated to yield 90 mg (79%) of a clean colourless syrup. Initial crystallization from benzene–ether followed by a second recrystallization gave 76 mg (66%) of white crystalline needles; mp 126–127 °C (lit. mp (9) 120–121 °C), $[\alpha]_D^{24}$ +67.3° (*c* 1.46, ethanol) (lit. value (9) $[\alpha]_D^{23}$ +63.8° (*c* 1.44, ethanol)); τ ($CDCl_3$), 3.44 (broad triplet, 1H, NHAc), 4.19 (d, 1H, H-1, $J_{1,2}$ = 4.5), 5.10 (s, 1, exchanges in D_2O,OH), 5.67 (sex, H-5, $J_{4,5}$ = 8.0, $J_{5,6a}$ = 6.0, $J_{5,6b}$ = 5.5), 5.68 (d, H-2), 5.91 (q, H-6a, $J_{6a,6b}$ = 8.5), 6.05 (q, H-6b), 6.25 (d, H-4), 6.26 (q, H-3a, $J_{3'a,3'b}$ = 14.5, $J_{3'a,NH}$ = 5.0), 6.54 (q, H-3′b, $J_{3'b,NH}$ = 7), 8.00 (s, 3H, Ac), 8.53, 8.61, 8.67, and 8.72 (4 C—CH_3).

Compound **4** (100 mg) was treated identically to yield compound **9** (86 mg, 74%) which after recrystallization from benzene–ether–hexane gave white crystalline needles, mp 158–158.5 °C (lit. mp (9) 156–156.5 °C), $[\alpha]_D^{24}$ +64.3° (*c* 1.43, ethanol) (lit. value (9) $[\alpha]_D^{23}$ +56.3° (*c* 1.0, ethanol)), τ ($CDCl_3$), 3.73 (broad d, 1, exchange in D_2O, N*H*Ac), 4.23 (d, 1H, H-1, $J_{1,2}$ = 4.0), 5.77 (d, 1H, H-a), 5.83–6.31 (overlapping signals, 4H, H-4, 5, 6) 6.32 (d, 1, H-3a, $J_{3'a,b}$ = 14), 6.71 (q, 1H, H-3′b, $J_{3'b,NHAc}$ = 3.5), 6.91 (s, 1, exchanges in D_2O, OH), 7.99 (s, 3H, Ac), 8.44, 8.57, and 8.67 (3s, 12H, CH_3).

Acknowledgment

The support of the National Research Council of Canada is gratefully acknowledged.

1. C. S. HUDSON. Adv. Carbohydr. Chem. **1**, 1 (1945).
2. J. M. BOURGEOIS. Helv. Chim. Acta, **56**, 2879 (1973).
3. (*a*) P. J. BEYNON, P. M. COLLINS, and W. G. OVEREND. Proc. Chem. Soc. London, 342 (1964); (*b*) K. ONODERA, S. HIRANO, and N. KASHIMURA. J. Am. Chem. Soc. **87**, 4651 (1965); (*c*) K. ONODERA, S. HIRANO, and N. KASHIMURA. Carbohydr. Res. **6**, 276 (1968).

4. A. ROSENTHAL and K. SHUDO. J. Org. Chem. **37**, 4391 (1972).
5. A. ROSENTHAL, C. M. RICHARDS, and K. SHUDO. Carbohydr. Res. **27**, 353 (1973).
6. A. ROSENTHAL and C. M. RICHARDS. Carbohydr. Res. **27**, 412 (1973).
7. A. ROSENTHAL and C. M. RICHARDS. Carbohydr. Res. **31**, 331 (1973).
8. K. ISONO, K. ASAHI, and S. SUZUKI. J. Am. Chem. Soc. **91**, 7490 (1969).
9. J. YOSHIMURA, K. KOBAYASHI, K. SATO, and M. FUNABASHI. Bull. Chem. Soc. Jpn. **45**, 1806 (1972).
10. A. ROSENTHAL, K. S. ONG, and D. BAKER. Carbohydr. Res. **13**, 113 (1970).
11. H. P. ALBRECHT and J. G. MOFFATT, Tetrahedron Lett. 3733 (1969).

Can. J. Chem. Downloaded from www.nrcresearchpress.com by 210.87.254.6 on 09/05/12
For personal use only.

Carbon catalyzed organic reactions: racemization of 1,1′-binaphthyl by carbon surfaces

RICHARD E. PINCOCK, WYNONA M. JOHNSON, AND JOHN HAYWOOD-FARMER[1]

Department of Chemistry, University of British Columbia, Vancouver, British Columbia V6T 1W5

Received July 15, 1975

RICHARD E. PINCOCK, WYNONA M. JOHNSON, and JOHN HAYWOOD-FARMER. Can. J. Chem. **54**, 548 (1976).

Rotation around the bond joining the two naphthalene rings (*i.e.*, racemization) in 1,1′-binaphthyl is very effectively catalyzed by carbon blacks and decolorizing carbons. In acetone at 20 °C where a small fraction of binaphthyl is reversibly absorbed, the activity of various carbons increases with surface area (relative catalytic rates are in the order Acetylene Black < Spheron 6 < Norit < Carbolac 1). The racemization is inhibited by structurally analogous compounds (naphthalene, anthracene) and poisoned by small concentrations (*ca.* 10^{-5} *M*) of larger polynuclear aromatics (pyrene, perylene). The barrier to inversion is lowered to $\Delta H^{\ddagger}$ = 16 kcal/mol in acetone by Spheron 6 as catalyst ($\Delta H^{\ddagger}$ = 22 kcal/mol for the uncatalyzed reaction). Although reaction via a relatively small number of specific active sites on the catalyst has not been eliminated, the kinetic data and inhibition effects also correlate with catalysis by more general adsorption of binaphthyl on the planar surfaces of the graphite-like lattice of active carbons.

RICHARD E. PINCOCK, WYNONA M. JOHNSON et JOHN HAYWOOD-FARMER. Can. J. Chem. **54**, 548 (1976).

La rotation autour du lien reliant les deux cycles naphtaléniques (*i.e.* recémisation) de binaphtyles-1,1′ est catalysée d'une façon très efficace par du noir animal et des charbons à décolorer. Dans l'acétone, à 20 °C alors qu'une petite fraction de binaphtyle est adsorbée d'une façon réversible, l'activité des divers charbons augmente avec la surface et les taux relatifs des catalyses sont dans l'ordre noir d'acétylène < Sphéron 6 < Norit < Carbolac 1. La racémisation est empêchée par des composés qui ont des structures analogues (naphtalène et l'anthracène) et empoisonnée par des faibles concentrations (*ca.* 10^{-5} *M*) de produits aromatiques de poids moléculaires plus élevés (pyrène et le périylène). Lorsque le Sphéron 6 est utilisé comme catalyseur dans l'acétone, il y a un abaissement de la barrière à l'inversion jusqu'à $\Delta H^{\ddagger}$ = 16 kcal/mol; le $\Delta H^{\ddagger}$ pour la réaction sans catalyseur est de 22 kcal/mol. Quoique l'on ne puisse pas éliminer la possibilité d'une réaction par l'intermédiaire d'un nombre relativement faible de sites actifs spécifiques sur le catalyseur, les données cinétiques et les effets inhibiteurs sont en accord avec une catalyse par l'adsorption plus générale du binaphtyle sur les surfaces planaires des espaces ressemblant au graphite des charbons activés.

[Traduit par le journal]

Introduction

The commercial use of carbon (as carbon blacks or decolorizing carbons) is of great technological importance and carbon is the subject of an immense number of studies of its structural and physical properties (1, 2). Nevertheless, the detailed chemical reactivity of activated carbon in organic reactions is not at all well established. Leaving aside the great number of uses of carbon as a support for metal catalysts, there are a variety of reactions in which carbon itself is a specific catalyst (3–5). Most of these are 'simple' inorganic reactions (*e.g.*, hydrogen–deuterium exchange (6), production of sulphuryl chloride from SO_2 and Cl_2, decomposition of H_2O_2 and H_2NNH_2 (7), isomerization of metal ligands (8)). When an organic material is involved, an oxidation–reduction reaction may be promoted by carbon (*e.g.*, oxidation of amino acids and of oxalic acid) (4). In these cases it is often unclear whether or not metallic ions present as impurities and oxygen present on the carbon surface are directly involved. In any case the mechanisms of such reactions are unknown.

There are a few but often brief reports of carbon acting distinctly as a catalyst for organic reactions such as double bond migrations (9), *cis–trans* isomerizations (10), transesterifications (11), and ester hydrolysis (12). These are sufficient

[1]Visiting Professor from Bishop's University, Lennoxville, Quebec.

Can. J. Chem. Downloaded from www.nrcresearchpress.com by 210.87.254.6 on 09/05/12
For personal use only.

to point out the potential of carbon as a catalyst for a variety of reactions and it may be that the activity of catalytic carbon can be better defined and made useful. The work reported here concerns the catalysis by carbon of one of the simplest of reactions, *i.e.*, the bond rotation that interconverts the two enantiomers of 1,1′-binaphthyl.

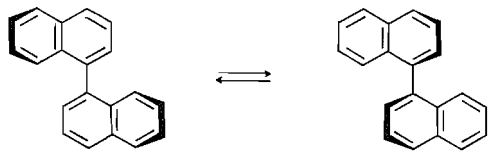

R-(−)-1,1′-Binaphthyl *S*-(+)-1,1′-Binaphthyl

Solutions of optically active binaphthyl are completely racemized within minutes at room temperature by small amounts (*ca.* 1 mg/ml) of active carbons (13), whereas the uncatalyzed racemization has a half-life of *ca.* 12 h (14). The kinetic results reported here may be a useful basis for exploring catalytic effects of various active carbons in a wider variety of organic reactions.

Results

The uncatalyzed racemization of binaphthyl in solution is sufficiently slow at room temperature to allow quenching of the carbon catalyzed reaction simply by filtering out the carbon. Rates could then be followed by polarimetric analysis of individual samples taken from a kinetic run. Although the catalyzed reaction is heterogeneous it did not depend on the rate of mixing of the suspended carbon; with slow or fast rates of stirring, or with different types of stirring apparatus, the same rate of racemization was obtained. However, the use of well purified binaphthyl was necessary for reproducibility. Multiple recrystallizations and pretreatments with decolorizing carbons (Norit) before optical resolution were necessary to obtain reproducible rates with various binaphthyl preparations. Rates were otherwise slow, no doubt due to inhibition by impurities (see below). In some runs a short and irreproducible loss of optical activity was observed before settling down to a reproducible rate. Use of highly purified binaphthyl essentially eliminated this curious effect as well.

Although an individual carbon from the same lot gave consistent results, the activity of at least Spheron 6 varied between two different commercial batches. The variable and sensitive nature of carbon surfaces is also pointed out by the observation that simply degassing of Spheron 6 in vacuum for 16 h at 100 °C resulted in a halving of the observed rate of catalyzed racemization. However, the observed rate was not affected by water (in acetone or ethanol with or without 2% water), and the catalyzed reaction proceeded at comparable rates in cyclohexane as well as in acetone and ethanol.

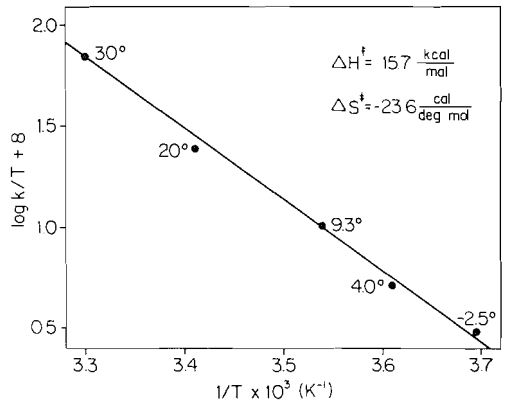

FIG. 1. Plot of log (k_{obs}/T) against $1/T$ for racemization of binaphthyl (0.015 *M*) with 1.55 g/ml of Spheron 6 in acetone.

Kinetic plots of log (observed rotation) against time were generally straight lines (see the figure of ref. 13), but with Spheron 6 a small decrease in the observed rate constant was noticeable after about one half-life. Deactivation of catalysis by traces of strongly absorbed products (possibly formed by oxidation of binaphthyl by surface oxides) was suspected but this possibility was eliminated by stirring Spheron 6 with acetone (up to 48 h), or with racemic binaphthyl in acetone (17 h) followed by addition of optically active binaphthyl. These solutions gave the same rate of reaction as a freshly prepared solution of the same concentration. The cause of the apparent slight deactivation of catalysis during a run remains unknown.

Initial first-order rate constants could be obtained from the plots of log α *vs.* time. Measurements over a temperature of 30 to −2 °C with a standard concentration of binaphthyl and of Spheron 6 in acetone (see Fig. 1) allowed the calculation of the apparent activation

Can. J. Chem. Downloaded from www.nrcresearchpress.com by 210.87.254.6 on 09/05/12
For personal use only.

Can. J. Chem. Downloaded from www.nrcresearchpress.com by 210.87.254.6 on 09/05/12
For personal use only.

parameters $\Delta H^{\ddagger} = 15.7$ kcal/mol and $\Delta S^{\ddagger} = -23.6$ cal/deg mol. This may be contrasted with the values obtained for a wide range of solvents (13), $\Delta H^{\ddagger} = 22$ kcal/mol and $\Delta S^{\ddagger} = -6$ cal/deg mol. The measured activation enthalpy of the catalyzed reaction is not directly related to the actual activation enthalpy of the surface catalyzed racemization; it contains as well the heat of adsorption on the catalysis surface (15). However, the transition state for the catalyzed reaction is at least 6 kcal/mol lower in energy than the transition state for the uncatalyzed reaction. Since adsorption leads to a decrease in entropy the more negative entropy term is consistent with the restrictions involved in an adsorption mechanism.

The extent of adsorption of binaphthyl on active carbon from acetone or cyclohexane solutions was investigated by gas–liquid chromatography and by ultraviolet spectrophotometry. At the concentrations of binaphthyl (0.015 *M*) and of carbon (1.0 mg/ml) commonly used in the kinetics runs no loss of binaphthyl from solution was detected after treatment and then removal of the carbon (Spheron 6 or Norit) by filtering. A 2–5% loss would have been detected.

Activity of Various Carbons

The observed first-order rate constants were, as shown in Fig. 2 for Spheron 6 in acetone, proportional to the amount of suspended catalyst (in g/ml). The catalytic activity of various carbons is presented in Table 1 where observed rate constants (corrected for the contribution of uncatalyzed racemization) per mg of carbon (see column four) may be compared to the known (16) surface areas and p*H*'s of aqueous suspensions of the carbons. Catalytic activity varies from nil for low surface carbons (graphite, Sterling FT) to a high activity comparable to that of enzymatic catalysis (13) for a high surface carbon (Carbolac 1, Norit). The pattern of activity shows no relationship to the p*H* characteristic of the carbons (which is a measure of the total acidic and basic character of the myriad of various functional groups present on carbon surfaces (1,7,17). In this regard cellulose powder, alumina, and platinum metal do not racemize binaphthyl.

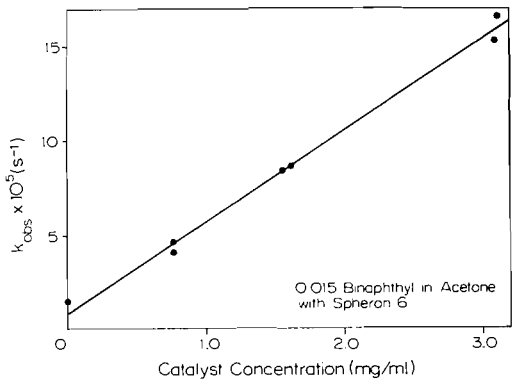

FIG. 2. Relationship of observed rate constant at 20 °C to concentration of Spheron 6 in acetone.

The possibility of a stereospecific carbon catalyst which would distinguish between the two enantiomers of binaphthyl was investigated. Spheron 6 with either *R* or *S* binaphthyl showed the same catalytic rate and Norit on cellulose

TABLE 1. Catalytic activity of various carbons[a]

Catalyst	Concentration (mg/ml)	k_{obs} ($s^{-1} \times 10^5$)	Relative activity[b] (s^{-1} g^{-1} ml $\times 10^5$)	Area[c] (m^2/g)	p*H*[d]
None	—	1.64	—	—	—
Graphite	1.50	1.52	0.0	Small	7
Sterling FT	1.64	1.32	0.0	16	9
Acetylene Black	1.62	3.42	1.10	64	4.8
Spheron 6	1.58	8.65	4.44	110	4–5
Norit SG1	0.16	23.6	137	750	7.8–8.3
Carbolac 1	0.163	47.6	281	950	2.6–3.0
Cellulose powder	3.86	1.57	0.0	—	—
Norit on cellulose[e]	0.16	14.4 with (+)-binaphthyl			
Norit on cellulose[e]	0.16	15.7 with (−)-binaphthyl			

[a]In acetone at 20 °C with 0.015 *M* binaphthyl.
[b]Relative activity = $(k_{obs} - k_{obs,unc})$/(mg of carbon/ml).
[c]Area in m^2/g as determined by nitrogen adsorption. See refs. 16 and 19.
[d]See ref. 16.
[e]Weight ratio of 1 to 25.

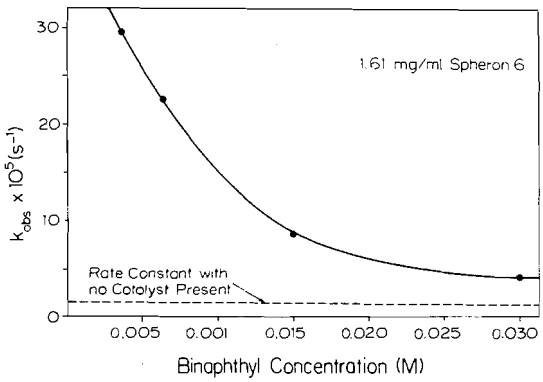

FIG. 3. Relationship of observed rate constant to binaphthyl concentration with 1.61 mg/ml of Spheron 6 in acetone.

(1 to 25 by weight) as a chiral support showed a 40% decrease in activity which, however, was the same for either enantiomer of binaphthyl. The possibility still remains that certain chiral compounds which adsorb on carbon may promote enantiomeric stereoselectivity, but this was not explored further.

Inhibition Effects

With a standard amount of carbon catalyst the observed first-order rate constants varied with the total binaphthyl concentration as shown in Fig. 3. At the lowest concentration allowed by the method of analysis (3.7×10^{-3} *M*) the rate constant was seven fold greater than with 30×10^{-3} *M* binaphthyl. At higher concentrations the binaphthyl inhibited its own catalyzed reaction and the rate constant decreased towards that for the uncatalyzed reaction.

Compounds structurally analogous to binaphthyl also inhibit or poison the catalytic effect of carbon. For example, the catalyzed racemization with any type of carbon is completely stopped by use of benzene as solvent. However, compared to a series of higher molecular weight aromatics, benzene is not an effective inhibitor. As shown in Table 2, the inhibition properties of unsubstituted aromatic compounds increase with the size of aromatic (benzene $\ll$ naphthalene $<$ anthracene $<$ pyrene $<$ perylene). Both 2-naphthol and 1-nitronaphthalene are about as effective in inhibition as naphthalene itself, while the sterically hindered 2,6-di-*tert*-butylnaphthalene is not a good inhibitor.

TABLE 2. Effect of various compounds on observed rate constants for binaphthyl racemization[a]

Added compound	Concentration (mol/l $\times 10^4$)	k_{obs} ($s^{-1} \times 10^5$)
None	—	7.68[b]
Benzene	7.08	7.73
Naphthalene	0.936	5.54
Naphthalene	0.92	5.91
Naphthalene	1.37	5.72
Naphthalene	1.87	5.31
Naphthalane	3.78	4.63
Naphthalene	7.57	3.39
2-Naphthol	3.90	3.17
1-Nitronaphthalene	4.16	3.16
2,6-*tert*-Butylnaphthalene	127	3.83
Anthracene	7.79	1.93
Anthracene	0.785	2.52
Pyrene	0.168	2.22
Perylene	6.2	1.31
Perylene	0.12	2.26

[a]Temperature 20 °C; binaphthyl at 0.015 *M* in acetone; carbon catalyst (Spheron 6) at 1.57 mg/ml.
[b]Note that $k_{obs,unc} = 1.6 \times 10^{-5}\ s^{-1}$ = rate constant for uncatalyzed reaction with no carbon present.

Discussion

Kinetic Equations

The pattern of kinetic effects described above fits the simplest possible reaction scheme involving adsorption on the carbon surface. With the addition of the uncatalyzed spontaneous racemization (*i.e.*, k_{unc}), which is usually negligible under catalyzed conditions, the complete reaction scheme is as follows.

$$R \underset{}{\overset{k_{unc}}{\rightleftharpoons}} S$$

$$R + C^* \underset{k_{-1}}{\overset{k_1}{\rightleftharpoons}} C^*B \underset{k_{-2}}{\overset{k_2}{\rightleftharpoons}} S + C^*$$

$$C^* + I \underset{k_{-I}}{\overset{k_I}{\rightleftharpoons}} C^*I$$

R and *S* denote the two enantiomeric forms of binaphthyl, C* the active sites on carbon, C*B is the intermediate complex formed at the active sites, and I and C*I are the inhibitor and the inhibitor complex, respectively.

Since the catalyst shows no preference for either *R* or *S* binaphthyl the scheme may be further simplified by equating the rate constants $k_1 = k_{-2}$ and $k_2 = k_{-1}$. Assuming a steady state concentration of C*B and C*I, the observed

Can. J. Chem. Downloaded from www.nrcresearchpress.com by 210.87.254.6 on 09/05/12
For personal use only.

first-order rate constants for racemization are then given by

$$k_{obs} = k_{obs,\,unc} + \frac{2k_1k_2[C_{total}]}{k_1[\text{binaphthyl}] + 2k_2 + 2k_2k_I[I]/k_{-I}}$$

This equation summarizes all of the observed kinetic results; the observed rate constants are proportional to the total carbon suspended in solution (see Fig. 2), inversely proportional to total binaphthyl concentration (Fig. 3), and inversely proportional to the concentration of any inhibitor present. Since no more than 5% of binaphthyl is adsorbed from solution by carbon at 1 mg/ml, the equilibrium constant for adsorption, $K = k_1/k_2$ must be small. With the assumption that $k_1 \ll k_2$, together with the slope of the line in Fig. 2 for a binaphthyl concentration of 0.015 *M*, the rate constant for reaction of binaphthyl with active sites on Spheron 6 may be calculated, *i.e.*, $k_1 = ca.\ 5 \times 10^{-5}\ s^{-1}\,mg^{-1}\,ml$. Even at as low a 'concentration' of suspended carbon as 1 mg/ml the rate of catalyzed reaction is several times the rate for spontaneous rotation of binaphthyl (*ca.* $1 \times 10^{-5}\ s^{-1}$).

The above kinetic equation fits only qualitatively with the observed inhibition by binaphthyl itself (Fig. 3). At higher concentrations of binaphthyl, and with a practical amount of carbon present, the predominate mode of racemization becomes the uncatalyzed racemization. Under these conditions a large amount of both *R* and *S* binaphthyl competes for relatively few active sites. At the other extreme, the observed rate constant increases with lower concentrations of binaphthyl but rate measurements at a very low concentration of binaphthyl ($<10^{-3}$ *M*) were limited by the method of analysis. These factors prevented the determination of the catalyzed rate constant over a wide variety of concentrations of binaphthyl. According to the kinetic scheme above, the rate constant for desorption (k_2) could otherwise have been determined from the slope of a plot of reciprocal observed rate constant minus the uncatalyzed rate constant against binaphthyl concentration.

The competitive inhibition incorporated into the kinetic scheme predicts a linear relationship of the reciprocal of ($k_{obs} - k_{obs,unc}$) against inhibitor concentration. This was shown with variation of naphthalene concentration as presented in Fig. 4, which also shows the relative effects of benzene and anthracene. The slopes of the lines are proportional to the equilibrium constant for adsorption of inhibitor at the active sites, *i.e.* $K_I = k_I/k_{-I}$. On this scale the relative inhibition properties of aromatics increase with size in the order benzene, nil; naphthalene, 0.05; anthracene, 1.3; pyrene, 10; and perylene, 13. Neither electron donating nor withdrawing substituents on naphthalene fail to modify inhibition activity greatly (2-naphthol and 1-nitronaphthalene are at 0.13 and 0.12, respectively on this scale), but the sterically hindered compound 2,6-di-*tert*-butylnaphthalene (relative inhibition 0.002) does not compete well with binaphthyl for adsorption sites.

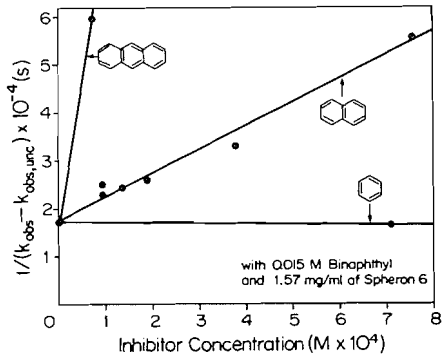

FIG. 4. Reciprocal of observed rate constant minus uncatalyzed rate constant against inhibitor concentration in acetone at 20 °C.

Nature of the Active Sites

The transition state for rotation of biaryls is generally assumed to be planar (18). On this basis the adsorption of binaphthyl on the planar graphite-like surfaces of active carbons is an attractive possibility for the transition state for catalyzed racemization. Spheron 6, for example, contains crystallites with planes of average diameter 23 Å (19) with 'incompletely saturated (residual) valencies' (20) which are usually considered to be responsible for adsorption properties. These could accommodate binaphthyl in a *trans*-planar arrangement and lead directly to racemization. The increase in catalytic activity with the total surface area of various carbons, the inhibition by larger planar aromatic compounds, and to some degree, the absence of discrimination between *R* and *S* binaphthyl are consistent with this simple model for catalyzed

Can. J. Chem. Downloaded from www.nrcresearchpress.com by 210.87.254.6 on 09/05/12
For personal use only.

Can. J. Chem. Downloaded from www.nrcresearchpress.com by 210.87.254.6 on 09/05/12
For personal use only.

racemization. Since binaphthyl racemization is known to be accelerated by complexing with planar aromatic acceptors (21), the greater catalytic properties of the larger, more active surfaces of carbon can be expected.

On the other hand, the specific case of uncatalyzed rotation of the two naphthalene units of binaphthyl is believed to proceed by a nonlinear (*meso*) transition state in which the 1,1′ bond and the 8 and the 8′ bonds to hydrogen are bent out of planarity with each of the naphthalene rings and the two naphthalene rings are themselves not in the same plane (22). This type of mechanism for rotation may also apply to the surface catalyzed reaction if bending of these bonds is somehow aided by adsorption of at least one naphthalene ring. There is the further possibility of catalysis by a more specific arrangement of some functional groups which are situated on the edges of the planar carbon surfaces. This could involve electrophilic groups which could add to an adsorbed molecule and aid rotation of the naphthalene units. A mechanism for racemization of diaryls by electrophilic addition of protons to the atoms of the interannular bond has been suggested (23). This seems unlikely with binaphthyl itself since the racemization reaction shows little or no rate differences between hydroxylic and nonhydroxylic solvents and the catalyzed rate is not related to the acidic or basic character of the carbons (see Table 1).

Finally, since carbon blacks can act as reducing (as well as oxidizing) agents, the racemization might be promoted by a reversible electron transfer to binaphthyl which can result in greater resonance stabilization and less hindrance between the naphthalene rings (24). A final distinction between these various mechanisms would require knowledge of the activity of carbons in catalyzing racemization of binaphthyls substituted with electron withdrawing or donating groups. Kinetic studies of carbon as a catalyst for other types of organic reactions would also be useful.

Experimental

Binaphthyl was purified by chromatography on alumina (20 g to 500 g) with elution by a 9:1 mixture of petroleum ether (30–60 °C) – benzene. After recrystallization from acetone this material was divided into *ca.* 2.5 g batches, treated with 'seeds' of resolved binaphthyl and resolved by the thermal solid state resolution method (25). These samples gave rotations of $[\alpha]_D$ +222, +232, +239, +224, +226, +195, and +235°. The combined material was recrystallized two times from acetone between room temperature and −70 °C. The final rotation was $[\alpha]_D^{25}$ +235° at 0.025 *M* in benzene. In the earliest runs similar samples of binaphthyl but with lower optical activity were used; some of these had been treated with Norit to remove impurities.

Acetone for kinetic runs was freshly distilled from permanganate. In the usual kinetic run 20 ml of a binaphthyl solution, equilibrated at the temperature of a run, was pipetted onto a weighted amount of carbon in a V-shaped flask. Stirring was by an overhead Corning Vibrastir or by a magnetic stirbar; variation of speed had no effect on the rate. At various times a *ca.* 1 ml sample of the suspension was removed, the syringe fitted with a Swinny syringe filter and, if no dilution was required, rapidly transferred through the filter to the optical cell. A Bendix type 143A automatic polarimeter was used at 5890 Å with a 1 cm cell. Plots of log (observed rotation) against time were generally straight lines (see text).

The carbon blacks and activated carbons were commercial materials used as supplied by Cabot Corporation, Billerica, Massachusetts (Spheron 6, Carbolac 1, and Sterling FT), by Gulf Oil Company, Shawinigan, Quebec (Acetylene Black), and American Norit Company, Jacksonville, Florida (Norit SG). Another sample of Spheron 6 and one of graphite (grade SP-1) were supplied by Professor Gilbert Hooley, University of British Columbia. Inhibitors were recrystallized before use (except 2,6-di-*tert*-butylnaphthalene which was used as supplied).

Acknowledgments

The support of the National Research Council of Canada is gratefully acknowledged. We also wish to thank Professor Gilbert Hooley for samples of various carbons and for helpful suggestions, and Dr. Keith Wilson for pointing out the phenomenon of catalyzed binaphthyl racemization.

1. J. S. Mattson and H. B. Mark, Jr. Activated carbon. Marcel Dekker, New York. 1971.
2. M. Smišek and S. Černy. Active carbon. Elsevier, Amsterdam. 1970.
3. V. R. Dietz. Bibliography of solid adsorbents. Natl. Bur. Stand. Washington. 1944; and Supplement (Circ. No. 566). 1956.
4. V. A. Garten and D. E. Weiss. Rev. Pure Appl. Chem. **7**, 69 (1957).
5. R. W. Coughlin. Proc. 4th Int. Congr. Catal. 2, 322 (1971).
6. B. M. W. Trapnell. *In* Catalysis. Vol. III. *Edited by* P. H. Emmett. Reinhold, New York. 1955. p. 1.
7. G. Brinkman. Angew. Chem. **61**, 378 (1949).
8. R. J. Mureinik and M. Spiro. J. Chem. Soc. Dalton Trans. 2493 (1974).
9. J. A. Meier and L. W. Hill. J. Catal. **32**, 80 (1974).
10. T. W. J. Taylor and E. M. W. Lavington. J. Chem. Soc. 980 (1934).
11. J. B. Adams. Biochim. Biophys. Acta, **62**, 17 (1962).

12. V. A. LIFEROVA, Z. D. SKRIPNIK, and G. F. YANKOVSKAYA. Adsorbtsiya Adsorbenty, **2**, 43 (1974); Chem. Abstr. **81**, 104246 (1974).
13. R. E. PINCOCK, W. M. JOHNSON, K. R. WILSON, and J. HAYWOOD-FARMER. J. Am. Chem. Soc. **95**, 6477 (1973).
14. A. K. COLTER and L. M. CLEMENS. J. Phys. Chem. **68**, 651 (1964).
15. J. C. JUNGERS and J. C. BALACEANU. *In* Technique of organic chemistry. Vol. VIII, Part A. *Edited by* A. Weissberger. Interscience, New York. 1961. p. 664.
16. C. L. MANTELL. Carbon and graphite handbook. Interscience, New York. 1968. p. 98.
17. J. B. DONNET. Carbon, **6**, 161 (1968). S. S. BARTON, D. GILLESPIE, and B. H. HARRISON. Carbon, **11**, 649 (1973).
18. F. H. WESTHEIMER. *In* Steric effects in organic chemistry. *Edited by* M. S. Newman. Wiley, New York. 1956. p. 523.
19. Technical information from G. L. Cabot, Inc., Cambridge, Mass.
20. D. E. WEISS. Proc. 5th Conf. Carbon. Vol. 1. Pergamon, New York. 1962. p. 65.
21. A. K. COLTER and L. M. CLEMENS. J. Am. Chem. Soc. **87**, 847 (1965).
22. A. S. COOKE and M. M. HARRIS. J. Chem. Soc. 2365 (1963).
23. M. CRAWFORD and I. F. B. SMYTH. J. Chem. Soc. 3464 (1954).
24. G. J. HOIJTINK. Recl. Trav. Chim. **74**, 1525 (1955).
25. K. R. WILSON and R. E. PINCOCK. J. Am. Chem. Soc. **95**, 1474 (1975).

Can. J. Chem. Downloaded from www.nrcresearchpress.com by 210.87.254.6 on 09/05/12
For personal use only.

Réactions ion–molécule dans les méthylbutènes: radiolyse du méthane

GUY J. COLLIN

Département des Sciences Pures, Université du Québec à Chicoutimi, Chicoutimi, Québec G7H 2B1

Reçu le 29 juillet 1975

GUY J. COLLIN. Can. J. Chem. **54**, 555 (1976).

La radiolyse du méthane en présence de l'un des trois méthylbutènes provoque une isomérisation importante de l'additif. Les observations rapportées sont compatibles avec un mécanisme ionique initié par les ions CH_5^+ et $C_2H_5^+$ formés dans la radiolyse directe du méthane. L'isomérisation progresse dans un mécanisme en chaîne courte où le porteur de chaîne pourrait être l'ion *tert*-$C_5H_{11}^+$. Dans le cas du méthyl-3-butène-1, l'ion $(CH_3)_2CHCHCH_3^+$ initialement formé s'isomérise en *tert*-$C_5H_{11}^+$ avant d'amorcer l'isomérisation observée.

GUY J. COLLIN. Can. J. Chem. **54**, 555 (1976).

The radiolysis of gaseous methane has been studied in the presence of one of the three methylbutenes. We have observed an important isomerization of the added olefin. An ionic mechanism initiated by the CH_5^+ and $C_2H_5^+$ ions seems to be compatible with the observations reported. Isomerization proceeds through a chain mechanism where the chain carrier may be the *tert*-$C_5H_{11}^+$ ion. In the presence of 3-methyl-1-butene, the initially formed $(CH_3)_2CHCHCH_3^+$ ion isomerizes to the tertiary structure before producing the observed isomerization.

Introduction

Récemment, nous avons montré que l'irradiation gamma du néopentane gazeux en présence de dérivés insaturés comme les méthylbutènes provoque le déplacement de la double liaison le long de la chaîne carbone–carbone. Le mécanisme suggéré propose un mécanisme ionique initié par l'ion *tert*-$C_4H_9^+$ formé dans la radiolyse directe du néopentane. L'ion *tert*-$C_5H_{11}^+$ sert de porteur de chaîne. Ainsi dans le cas du méthyl-2-butène-1 (M2B1) le mécanisme serait le suivant:

[1] néo-$C_5H_{12} \rightsquigarrow$ *tert*-$C_4H_9^+ + CH_3 + e^-$

[2] *tert*-$C_4H_9^+ + M2B1 \rightarrow$ iso-$C_4H_8 +$ *tert*-$C_5H_{11}^+$
$\Delta H = -3.3$ kcal mol^{-1}

[3] *tert*-$C_5H_{11}^+ + M2B1 \rightarrow CH_3CH{=}C(CH_3)_2$
$+$ *tert*-$C_5H_{11}^+ \quad \Delta H = -1.5$ kcal mol$^-$

Ce type d'isomérisation est aussi observé avec le méthyl-2-butène-2 (M2B2) avec les mêmes caractéristiques. Cependant celle-ci n'est pas observée avec le méthyl-3-butène-1 (M3B1) (1) contrairement à ce qui est observé dans la photoionisation du cyclohexane (2).

Nous avons repris cette étude en utilisant le méthane comme source d'ions positifs. La radiolyse de ce composé est bien connue. Celle-ci produit des ions CH_5^+ et $C_2H_5^+$ en quantités importantes et de plus ces ions ne réagissent pas avec le méthane. Comme les réactions de transfert de proton de ces deux ions vers chacun des trois méthylbutènes sont exothermiques, nous avons utilisé ce système pour tester le mécanisme proposé.

Méthode expérimentale

Produits chimiques

Tous les hydrocarbures (produits API) sauf le méthane sont utilisés sans autre purification (pureté minimum: 99.9%) après dégasage sous vide (10^{-6} Torr) à la température de l'azote liquide. Le méthane, Matheson of Canada Research grade, contient 0.0034% d'éthane et est employé tel que reçu. Le méthane-d_4, pureté isotopique $CD_3H/CD_4 \leq 0.03$, et le méthylcyclohexane-d_{14}, pureté isotopique $C_7D_{13}H/C_7D_{14} = 12.2 \pm 0.3\%$, sont des produits Merck, Sharp and Dohme of Canada et sont aussi utilisés tels que reçus. Le méthane-d_4 contient de l'éthane (0.0060%) et de l'éthylène (0.0069%). L'oxygène et l'ammoniac (99.99%) sont des produits Matheson de même que les gaz rares (99.99%).

Echantillons et irradiations

La préparation et les techniques d'irradiation ont déjà été décrites (1). Tous les échantillons contiennent de l'oxygène. Afin de limiter l'absorption d'énergie par les additifs, et en particulier par les hydrocarbures, on a limité autant que possible le rapport hydrocarbure/méthane à 0.02. Les temps d'irradiations sont de 1200 min sauf cas indiqués. La vitesse de dose mesurée par la mesure du courant de saturation (3) est de 2.45×10^{16} eV/(mol s) ce qui se compare bien avec la vitesse de dose mesurée dans le néopentane gazeux (1).

Analyses

Les analyses sont faites par chromatographie en phase gazeuse (double ionisation de flamme) sur une colonne d'alumine programmée entre 30 et 150 °C ou sur une colonne de squalane à la température de la chambre.

Can. J. Chem. Downloaded from www.nrcresearchpress.com by 210.87.254.42 on 09/05/12
For personal use only.

TABLEAU 1. Radiolyse du méthane en présence d'additifs

Mélanges irradiés (pression: Torr)				Rendements G				
CH_4	M2B1	O_2	Additif	C_2H_6	C_2H_4	M3B1	M2B2	iso-C_5H_{12}
200	1.6	4.1	—	0.45	1.09	n.m.[a]	4.7	0.22
200	1.6	4.0	NH_3:1.4	0.25	1.22	0.025	0.38	0.00
250	2.8	5.0	MCH[b]:2.9	1.32[c]	0.99	0.02	3.75[d]	0.36

[a]Non mesuré.
[b]Méthylcyclohexane-d_{14}.
[c]$G(C_2H_5D) \simeq 0.66$ et $G(C_2H_6) \simeq 0.6$.
[d]$C_5H_9D/C_5H_{10} \leq 0.03$

TABLEAU 2. Radiolyse du méthane en présence d'additifs

Mélanges irradiés (pression: Torr)				Rendements G				
CH_4	M2B2	O_2	Additif	C_2H_6	C_2H_4	M3B1	M2B1	iso-C_5H_{12}
114	1.0	4.2	—	0.40	1.09	0.03	0.82	0.12
230	2.0	8.6	—	0.33	0.97	0.06	0.82	0.12
115	1.0	4.8	NH_3:1.6	0.12	1.00	0.004	0.36	<0.01
226	2.0	8.1	NH_3:2.1	0.06	0.94	<0.01	0.52	<0.01
124	1.0	4.3	MCP[a]:2.0	1.07	0.95	<0.01	0.50	0.45[c]
230	2.1	8.6	MCP:4.3	1.15	0.75	n.m.[b]	0.51	0.40[c]
100	1.3	12.2	He:100	0.30	1.24	n.m.	0.52	0.13

[a]Méthylcyclopentane.
[b]Non mesuré.
[c]25% de cette quantité d'isopentane est formée dans la radiolyse du mélange indiqué mais ne contenant pas de méthane.

Les analyses par spectrométrie de masse ont été faites sur des échantillons séparés par chromatographie (détecteur thermique) et introduits dans un appareil CEC-21-104.

Résultats

Les rendements sont exprimés en valeurs $G(X)$ qui représentent le nombre de molécules X formées pour une absorption d'énergie de 100 eV par le méthane. L'incertitude relative sur chaque mesure est de l'ordre de 10%.

L'addition de l'un des trois méthylbutènes au mélange CH_4–O_2 (100:4) produit les deux autres méthylbutènes au cours de l'irradiation. En présence de M2B1 (tableau 1), l'addition d'ammoniac perturbe le rendement en éthylène, supprime la formation d'isopentane et diminue fortement le rendement en C_5H_{10}. L'addition de méthylcycloalcane augmente de façon importante le rendement en éthane et en isopentane, ne diminue que faiblement le rendement en éthylène et en C_5H_{10}. On retrouve ces mêmes caractéristiques dans la radiolyse en présence de M2B2 (tableau 2). Dans ce cas cependant on note des valeurs $G(C_5H_{10})$ inférieures à celles observées en présence de M2B1. Il ne semble pas y avoir d'effet de pression dans le domaine étudié tout au moins sur les rendements des produits en C_5. L'addition d'hélium ne modifie pas non plus de façon importante les rendements obtenus. On retrouve ces mêmes caractéristiques dans les irradiations faites en présence de M3B1 (tableau 3). Il faut cependant relever ici un effet de pression: les rendements $G(C_5H_{10})$ diminuent fortement lorsque la pression passe de 100 Torr à 350 Torr.

En plus de ces résultats et des analyses isotopiques indiquées au bas des tableaux il faut aussi ajouter que les analyses des isopentanes formés en présence de CD_4 ou de méthylcyclohexane-d_{14} contiennent un mélange d'iso-C_5H_{12}, iso-$C_5H_{11}D$ et iso-$C_5H_{10}D_2$ qu'il était difficile d'analyser étant donné la présence de CO_2 qui interferre aux masses 44 et 45 dans le spectre de masse.

Discussion

Radiolyse du méthane

Etant donnée l'importance relative du méthane dans les mélanges irradiés, on peut admettre en première approximation que l'éner-

Can. J. Chem. Downloaded from www.nrcresearchpress.com by 210.87.254.42 on 09/05/12
For personal use only.

TABLEAU 3. Radiolyse du méthane en présence d'additifs

Mélanges irradiés (pression: Torr)				Rendements G				
CH_4	M3B1	O_2	Additif	C_2H_6	C_2H_4	M2B2	M2B1	iso-C_5H_{12}
115	1.6	2.2	—	n.m.[b]	n.m.	0.51	0.09	0.22
115	3.4	2.8	—	n.m.	n.m.	0.53	n.m.	0.20
254(d_4)[a]	2.5	6.1	—	n.m.	n.m.	0.25	0.03	0.21
100	1.1	12.0	He:100	0.13	1.56	0.52	0.07	0.30
100	1.1	10.0	A:280[i]	1.8 (0.34)[c]	2.2 (0.41)[c]	1.76 (0.33_5)[c]	0.24 (0.04_5)[c]	0.96 (0.18_4)[c]
117(d_4)	1.2	4.5	MCP[d]:1.1	n.m.	n.m.	0.26	0.05	0.36
374(d_4)	2.2	8.1	MCP:2.1	1.21	0.72	0.17	0.02	0.32
100	1.0	2.0	MCH[e]:1.1	0.93	1.01	0.34[f]	0.03_2	0.25
351	2.0	10.2	MCH[e]:2.1	0.90	0.72	0.20[f]	0.02	0.20
117(d_4)	1.1	4.6	NH_3:1.6	n.m.	n.m.	0.36[g]	0.48[h]	0.00
310	2.5	4.7	NH_3:2.5	0.82	1.01	0.39	0.61	0.00

[a]Méthane-d_4.
[b]Non mesuré.
[c]G' calculé par rapport à l'énergie absorbée par le méthane et l'argon.
[d]Méthylcyclopentane.
[e]Méthylcyclohexane-d_{14}.
[f]$C_5H_9D/C_5H_{10} < 0.15$.
[g]$C_5H_9D/C_5H_{10} = 80/20$.
[h]$C_5H_9D/C_5H_{10} = 86/14$.
[i]Temps d'irradiation: 600 min.

gie absorbée par le méthane est responsable des phénomènes observés. La radiolyse du méthane forme des atomes chauds ou non, des radicaux excités ou non, des ions, etc. Etant donnée l'importance quantitative du méthane les radicaux excités doivent avoir disparu avant de rencontrer les additifs. La majorité des radicaux thermiques et des atomes d'hydrogène sont interceptés par l'oxygène puisque le rapport oxygène/C_5H_{10} est le plus souvent supérieur ou égal à 2.0. Ceux des atomes d'hydrogène qui sont interceptés par le méthylbutène forment le radical pentyl correspondant lui aussi intercepté par l'oxygène. Quant aux ions formés directement dans la radiolyse du méthane, ils consistent essentiellement en ions CH_4^+ et CH_3^+ (4 et les références qui y sont citées). Ces deux ions réagissent très vite avec le méthane (presqu'à chaque collision):

[4] $CH_4^+ + CH_4 \rightarrow CH_5^+ + CH_3$
$k = 1.20 \times 10^{-9}$ cm^3 molécule^{-1} s^{-1}

(réfs. 5, 6 et les références qui y sont citées);

[5] $CH_3^+ + CH_4 \rightarrow C_2H_5^+ + H_2$
$k = 1.15 \times 10^{-9}$ cm^3 molécule^{-1} s^{-1}

(réf. 6 et les références qui y sont citées). Les rendements de ces deux ions sont importants: $G(C_2H_5^+) = G(CH_5^+) = 1.35 \pm 0.10$ aux pressions utilisées ici et comptent pour près de 75% du total des ions primaires (4). Ils ne réagissent pas ou très lentement avec le méthane (7 et les références qui y sont citées) ou l'oxygène (8, 9). Les autres ions CH_n^+ ($n = 0$, 1 ou 2) réagissent aussi très rapidement avec le méthane ($k = 1.6 \times 10^{-9}$ cm^3 molécule^{-1} s^{-1}) en formant en particulier des ions $C_2H_4^+$, $C_2H_3^+$ et $C_2H_2^+$ (6). Les ions $C_2H_4^+$ ne réagissent pas ou lentement avec le méthane et les ions $C_2H_3^+$ et $C_2H_2^+$ réagissent pour former des ions $C_3H_5^+$ qui à leur tour ne semblent pas réagir avec le méthane (6). Quant aux espèces radicalaires excitées (en particulier CH_2) elles réagissent avec le méthane sauf probablement les atomes d'hydrogène chauds. L'addition d'hélium ne modifie pas les rendements obtenus de façon importante (tableaux 2 et 3). L'énergie directement absorbée par l'hélium dans les mélanges rapportés ne doit pas dépasser 20% de celle absorbée par le méthane. Par transfert de charge des ions He^+ vers le méthane on ne peut donc prévoir qu'une augmentation mineure des rendements mesurés. Par contre, on peut exclure la participation des atomes d'hydrogène excités à l'isomérisation observée.

Radiolyse en présence des méthylbutènes

L'ensemble des observations rapportées s'accomodent bien du mécanisme ionique déjà proposé (1). L'absence d'effet important de l'hélium, mais surtout l'effet de l'ammoniac, des méthyl-

Can. J. Chem. Downloaded from www.nrcresearchpress.com by 210.87.254.42 on 09/05/12
For personal use only.

cycloalcanes et les analyses isotopiques peuvent se satisfaire d'un tel mécanisme. L'initiation de l'isomérisation est probablement le fait des ions CH_5^+ et $C_2H_5^+$ (cas du M2B1):

[6] $C_nH_5^+ + M2B1 \rightarrow C_nH_4 + tert\text{-}C_5H_{11}^+$
$\Delta H = -77$ kcal mol^{-1} ($n = 1$);
$\Delta H = -36.5$ kcal mol^{-1} ($n = 2$)

(les valeurs $\Delta H_f^0(X)$ sont tirées de Franklin *et al.* (10*a*), sauf la valeur $\Delta H_f^0(tert\text{-}C_5H_{11}^+)$ qui provient de Solomon et Field (10*b*)). Cette réaction est suivie de la réaction 3. Ces deux réactions sont en compétition avec les réactions de condensation et la réaction 3 l'est avec la réaction de transfert de proton en résonnance (11). En présence de M2B2 le mécanisme est similaire: la réaction 3 étant remplacée par la suivante:

[7] $tert\text{-}C_5H_{11}^+ + M2B2 \rightarrow M2B1 + tert\text{-}C_5H_{11}^+$
$\Delta H = 1.5$ kcal mol^{-1}

L'endothermicité de cette réaction est compensée par l'exothermicité de la réaction correspondante à la réaction 6 bien que la majorité de l'énergie emmagasinée par l'ion $tert\text{-}C_5H_{11}^+$ au cours de la réaction 6 soit dissipée par collision avant la réalisation de la réaction 7. Cela explique aussi les rendements moins élevés dans ce système par rapport au précédent. Remarquons aussi qu'un autre ion méthylbutyl peut être formé dans les réactions initiales et qu'il peut aussi former le M2B2 et le M3B1:

[8] $C_nH_5^+ + M2B2 \rightarrow C_nH_4 + (CH_3)_2CHCHCH_3^+$
$\Delta H = -68$ kcal mol^{-1} ($n = 1$);
$\Delta H = -27.5$ kcal mol^{-1} ($n = 2$)

[9] $(CH_3)_2CHCHCH_3^+ + M2B2 \rightarrow M3B1 + tert\text{-}C_5H_{11}^+$
$\Delta H = 0.0$ kcal mol^{-1}

[10] $(CH_3)_2CHCHCH_3^+ + M2B2 \rightarrow M2B2 + tert\text{-}C_5H_{11}^+$
$\Delta H = -4$ kcal mol^{-1}

Ces réactions sont toujours en compétition avec les réactions de transfert de proton en résonnance et les réactions de condensation. En présence de M3B1, le rendement relativement élevé en M2B1 surtout en présence d'ammoniac ne peut s'expliquer que sur la base de l'isomérisation de l'ion méthylbutyl formé (12):

[11] $C_nH_5^+ + M3B1 \rightarrow C_nH_4 + (CH_3)_2CHCHCH_3^+$
$\Delta H = -72$ kcal mol^{-1} ($n = 1$);
$\Delta H = -31.5$ kcal mol^{-1} ($n = 2$)

[12] $(CH_3)_2CHCHCH_3^+ \rightarrow tert\text{-}C_5H_{11}^+$
$\Delta H = 4$ kcal mol^{-1}

[13*a*] $tert\text{-}C_5H_{11}^+ + M3B1 \rightarrow M2B2 + (CH_3)_2CHCHCH_3^+$
$\Delta H = 0.0$ kcal mol^{-1}

[13*b*] $\rightarrow M2B1 + (CH_3)_2CHCHCH_3^+$
$\Delta H = 2.0$ kcal mol^{-1}

[14*a*] $tert\text{-}C_5H_{11}^+ + NH_3 \rightarrow M2B2 + NH_4^+$
$\Delta H = -13$ kcal mol^{-1}

[14*b*] $\rightarrow M2B1 + NH_4^+$
$\Delta H = -11$ kcal mol^{-1}

L'exothermicité des réactions 11 est probablement suffisante pour contrebalancer l'énergie d'activation de la réaction 12. L'effet de pression observé dans ce système sur les rendements en C_5H_{10} est peut-être dû à une réaction de désactivation par collision de l'ion $C_5H_{11}^+$ formé dans les réactions 11. En admettant que tous les ions $(CH_3)_2CHCHCH_3^+$ formés dans la réaction 11 s'isomérisent (processus 12), les rapports k_{13a}/k_{13b} et k_{14a}/k_{14b} sont égaux à 8 ± 2 et à 0.7 ± 0.1 respectivement. On peut cependant penser que tel n'est pas le cas et que les ions $(CH_3)_2CHCHCH_3^+$ qui ne s'isomérisent pas forment uniquement le M2B2 en réagissant avec le M3B1 ou l'ammoniac. C'est le cas en particulier des ions $C_4H_{11}^+$ formés dans le réaction 13. L'importance relative du rendement en M2B1 en présence d'ammoniac indique que plus de la moitié des ions $(CH_3)_2CHCHCH_3^+$ sont isomérisés (réaction 12). A 125 Torr, au moins 60% des ions $C_5H_{11}^+$ ont la structure tertiaire puisque le rapport M2B1-d_1/C_5H_9D est égal à 0.60. Il faut noter que les réactions 6, 8 et 11 ont des constantes de vitesse du même ordre de grandeur que les réactions mettant en jeu les ions CH_5^+ et $C_2H_5^+$ avec l'ammoniac (9), puisque cet additif ne modifie pas de façon brutale les rendements en isomérisation, sauf dans le cas du M2B1, où la chaîne cinétique semble plus longue.

[15] $C_nH_5^+ + NH_3 \rightarrow$ Produit

Cela est également apparent à la lecture des rendements en éthylène, confirmant ainsi que les trois réactions de transfert de proton de l'ion $C_2H_5^+$ vers chacun des trois méthylbutènes sont toujours efficaces. Il est néanmoins difficile, étant donnée l'incertitude relative sur chaque mesure et les réactions possibles, de chiffrer l'importance relative de chacun de ces transferts. En présence de méthylcycloalcane on observe la

Can. J. Chem. Downloaded from www.nrcresearchpress.com by 210.87.254.42 on 09/05/12
For personal use only.

formation de l'éthane à travers le transfert d'ion hydrure (voir note *c*, tableau 1), réaction aussi observée avec le M2B1 (13):

[16] $C_2H_5^+ + RD \rightarrow C_2H_5D + R^+$

Quant à l'isopentane, une part importante de celui-ci est formé via les réactions suivantes:

[17] $RH_2^+ + C_5H_{10} \rightarrow R^+ + \text{iso-}C_5H_{12}$

[18] $RH_2 + C_5H_{10}^+ \rightarrow R^+ + \text{iso-}C_5H_{12}$

C'est le cas en particulier lors des irradiations faites en présence de méthylcycloalcane (1) (voir résultats). Il ne semble pas que les réactions du type *tert*-$C_5H_{11}^+ + C_5H_{10}$ ou *tert*-$C_5H_{11}^+ + CH_3$-cy-C_5H_9 conduisent à ce produit (1) ni les réactions du type $C_5H_{10}^+ + C_5H_{10}$ (14–16).

Remerciements

Nous voulons remercier J. A. Herman et P. Gagnon de L'Université Laval pour l'aide qu'ils nous ont apportée à la réalisation des irradiations dans la bombe au cobalt du département de Chimie de L'Université Laval. Nous remercions aussi le Centre de Recherches de Valcartier et particulièrement, M. R. Voyzelle, qui nous ont gracieusement offert les analyses par spectrométrie de masse.

1. G. J. Collin. J. Phys. Chem. Sous presse.
2. G. J. Collin et P. Ausloos. Can. J. Chem. **53**, 680 (1975).
3. R. M. Leblanc et J. A. Herman. J. Chim. Phys. 1055 (1966).
4. P. Ausloos et S. G. Lias. Actions Chim. Biol. Radiat. 11ème Ser. (1967).
5. A. S. Blair et A. G. Harrisson. Can. J. Chem. **51**, 1645 (1973).
6. A. A. Herod et A. G. Harrisson. Int. J. Mass. Spectrom. Ion Phys. **4**, 415 (1970).
7. F. H. Field. Acc. Chem. Res. **1**, 42 (1968).
8. P. Ausloos, S. G. Lias et R. Gorden, Jr. J. Chem. Phys. **39**, 3341 (1963).
9. M. S. B. Munson et F. H. Field. J. Am. Chem. Soc. **87**, 4242 (1965).
10. (*a*) J. L. Franklin, J. G. Dillard, H. M. Rosenstock, J. T. Herron, K. Draxl et F. H. Field. Natl. Stand. Ref. Data Ser. Natl. Bur. Stand. No. 26 (1969). (*b*) J. J. Solomon et F. H. Field. J. Am. Chem. Soc. **95**, 4483 (1973).
11. G. J. Collin. Can. J. Chem. **52**, 2341 (1974).
12. J. Long et B. Munson. J. Am. Chem. Soc. **94**, 3339 (1972).
13. S. G. Lias et P. Ausloos. J. Chem. Phys. **37**, 877 (1962).
14. H. Gagnon, G. J. Collin et C. Bertrand. J. Phys. Chem. **78**, 98 (1974).
15. G. J. Collin et C. Bertrand. J. Photochem. **3**, 123 (1974).
16. G. J. Collin et C. M. Gaucher. Can. J. Chem. **52**, 34 (1974).

Can. J. Chem. Downloaded from www.nrcresearchpress.com by 210.87.254.42 on 09/05/12
For personal use only.

Substituent effects of phosphorus and arsenic containing groups in aromatic substitution. VI. Orientation in nitration of some anilides and phenyl esters

TOMASZ A. MODRO[1]
Department of Chemistry, University of Toronto, Toronto, Ontario M5S 1A1
AND
JERZY PIOCH
Institute of Chemistry, University of Gdansk, Gdansk, Poland

Received September 15, 1975

TOMASZ A. MODRO and JERZY PIOCH. Can. J. Chem. **54**, 560 (1976).

The orientation in nitration of *N*-acyl derivatives of aniline and *O*-acyl derivatives of phenol in aqueous H_2SO_4 and in acetic anhydride has been studied. Acetyl and methanesulfonyl derivatives are exclusively *ortho/para* directing, whereas the *N*- and *O*-phosphorylated compounds yield in both media considerable amounts of the *meta* isomer. The observed differences in orientation are discussed in terms of different protonation sites and strong π_p–π_d interactions of the oxygen or nitrogen and the P(IV) atom.

TOMASZ A. MODRO et JERZY PIOCH. Can. J. Chem. **54**, 560 (1976).

On a étudié l'orientation de la nitration des dérivés *N*-acyl de l'aniline et *O*-acyl du phénol dans le H_2SO_4 aqueux et dans l'anhydride acétique. Les dérivés acétylés et méthanesulfonylés dirigent exclusivement en *ortho/para* alors que les composés *N*- et *O*-phosphorylés conduisent dans les deux milieux à des quantités considérables d'isomère *méta*. Les différences observées dans l'orientation sont discutées en termes de différents sites de protonation et d'interactions fortes π_p–π_d de l'oxygène ou de l'azote et de l'atome P(IV).

[Traduit par le journal]

It has long been known that the isomer proportions obtained in the nitration of such substrates as anilides or aromatic ethers vary significantly as the reaction conditions are changed (1). Different explanations have been proposed to account for this behavior (2), and a recent paper of Hartshorn *et al.* (3) presents a comprehensive study of the mechanism of nitration of some *N*-acylated derivatives of aniline, both in aqueous H_2SO_4 and in acetic anhydride.

In our studies on the substituent effects of various groups containing the P(IV) atom (4), we have found that the presence of the phosphoryl function results in an abnormally high proportion of *ortho* substitution (together with a negligible substitution at the *para* position), most likely as a consequence of initial attack of an electrophile at the oxygen atom of the phosphoryl group, followed by rearrangement into the benzene ring. A similar mechanism was postulated (3) for the nitration of anilides with sufficiently nucleophilic oxygens in acetic anhydride. In order to obtain a better understanding of the structure–reactivity relationship in systems containing tetravalent phosphorus in different structural environments, we have investigated the orientation pattern in the nitration of *N*-phosphorylated aniline and *O*-phosphorylated phenol in strongly acidic and in aprotic media. The results have been compared with those obtained in this work and by other authors for analogous compounds derived from organic acids of different types. It was expected that the direct comparison of the substituent effects in the systems Ph—NH—Y and Ph—O—Y (Y = COR, $P(O)(OR)_2$, SO_2R) would provide useful information concerning such problems as the protonation site of the substituent, and the relative involvement of the nitrogen or oxygen nonbonding electrons in conjugative interactions with the benzene ring and with the acid residue Y.

Experimental

Solvents were purified by conventional methods. Melting points and boiling points are uncorrected. Solutions of sulfuric acid were obtained by diluting AnalaR sulfuric acid (*d* 1.83) with distilled water and standardizing with aqueous NaOH. AnalaR nitric acid (*d* 1.42) was distilled

[1]Author to whom correspondence should be addressed.

Can. J. Chem. Downloaded from www.nrcresearchpress.com by 210.87.254.5 on 09/05/12
For personal use only.

Can. J. Chem. Downloaded from www.nrcresearchpress.com by 210.87.254.5 on 09/05/12
For personal use only.

from an equal volume of concentrated H_2SO_4 immediately before use. Ultraviolet spectra were determined with a Perkin-Elmer 402 or a Carl Zeiss-Jena VSU-2 spectrophotometer. Nuclear magnetic resonance spectra were obtained with a Tesla BS-487 (80 MHz) spectrometer with TMS as internal standard.

Substrates

Acetanilide and phenyl acetate were commercial products. Substrates **2**, **5**, and **6** were prepared from the corresponding acyl chlorides and aniline or phenol: diethylphosphoric anilide **2**, mp 93–94 °C (lit. (5) mp 96 °C); diethylphenyl phosphate **5**, bp 120–123 °C/1.4–1.5 Torr (lit. (ref. 5, p. 330) bp 131 °C/2 Torr); phenyl methanesulfonate **6**, mp 61–62 °C (lit. (7) mp 62 °C). All substrates were purified by crystallization or distillation until chromatographically pure (tlc).

Nitration in Sulfuric Acid

A solution of the aromatic substrate in sulfuric acid (or in a mixture of sulfuric acid and a small amount of acetic acid) was added dropwise at 0 °C with stirring to a solution of a stoichiometric amount of nitric acid in sulfuric acid. At the end of the reaction, which was followed by tlc (usually less than 1 h), the reaction mixture was poured on ice and refluxed for 12–24 h, until tlc showed that the hydrolysis was complete.[2] The aqueous solution was then extracted with ether (for aniline derivatives after neutralization, with Na_2CO_3), dried ($MgSO_4$), and the composition of the organic layer was determined as described before (8).

Nitration in Acetic Anhydride

The solution of acetyl nitrate in acetic anhydride was prepared from nitric acid and an excess of Ac_2O at 0 °C, and added slowly to a solution of the substrate in acetic anhydride at 20 °C. The reaction mixture was kept at 20 °C for 24–48 h, then poured on ice, and worked-up as described above.

In some cases the pmr spectra of the reaction products after hydrolysis were recorded and the relative proportions of isomers were determined from the relative intensities of the corresponding signals. Good agreement with the results of the tlc–uv analysis was always obtained.

Results and Discussion

Substrates **1**, **2**, **4**, **5**, and **6** were nitrated with nitric acid in aqueous H_2SO_4 at 0 °C and in Ac_2O at 20 °C. In H_2SO_4 the reaction is very fast and the products of nitration were formed in practically quantitative yields. In Ac_2O the reaction is much slower and the products were analyzed after the reaction reached 40–60% completion. Thin layer chromatography showed that the remaining material was unreacted substrate, and that the isomer proportions were insensitive to the extent of reaction. The reaction product was hydrolyzed to a mixture of isomeric nitroanilines or nitrophenols and the product composition was then determined by the quantitative tlc–spectrophotometric method described previously (8). The results are shown in Tables 1 and 2, together with some data taken from the literature.

In aqueous H_2SO_4 of concentrations above 70%, acetanilide **1** reacts entirely as a conjugate acid and the increase in the *o/p* ratio with decreasing acidity was attributed to changes in solvation of the cationic substituent (3). The conjugate acid is, in this case, in accordance with the general view on the protonation of carboxylic amides (10), certainly the *O*-protonated species Ph—NH—C(OH)CH_3^+. The observed almost exclusive *p/o* substitution indicates that the nitrogen lone pair is not significantly involved in conjugative interactions with the protonated carbonyl group, and thus selectively activates these positions. Methanesulfonic anilide **3** is nitrated as a free base (3), in aqueous H_2SO_4, and being more reactive than **1** shows lower selectivity between *ortho* and *para* positions; the amount of *meta* isomer is again negligible because of the strong +M effect of the nitrogen nonbonding electrons.

Diethylphosphoric anilide **2** gives rise to an apparently different substitution pattern. The most striking feature is that for H_2SO_4 concentrations of 97–70% a large proportion of the *meta* isomer is formed; such orientation has never been observed for any anilide so far studied. Secondly, a 1/2 *o:p* ratio greater than unity is found and is virtually insensitive to changes in the acidity of the medium. Although the basicity of the phosphoroamidate system is not available, it has been suggested (11) that it should be similar to that of carboxylic amides. Diethylphosphoric anilide **2** reacts therefore at the given acidity range almost certainly also as a conjugate acid, exhibiting, however, a different net substituent effect from that of protonated acetanilide. The most plausible explanation for the observed difference in orientation between the conjugate acids of **1** and **2** is to invoke *N*-protonation for the *N*-phosphorylated derivative:

[2]Separate experiments showed that when no nitric acid was added, all substrates studied could be quantitatively recovered from sulfuric acid solutions under the conditions of the nitration reaction. This proves that there is no nitroaniline or nitrophenol in the reaction product formed via nitration of the primarily hydrolyzed substrate.

TABLE 1. Isomer proportions for nitration in strong acids*

Substrate	Conditions	Isomers (%) *ortho*	*meta*	*para*	1/2 *o:p*	1/2 *m:p*	Reference
Ph—NH—$COCH_3$ **1**	HNO_3–98% H_2SO_4, 25 °C	5	<2	95	0.026	—	3
	HNO_3–80.9% H_2SO_4	17	<2	83	0.10	—	
	HNO_3–77.4% H_2SO_4	23	<2	77	0.15	—	
	HNO_3–69.9% H_2SO_4	40	<2	60	0.33	—	
	HNO_3–conc. H_2SO_4, 20 °C	19.4	≤2.1	78.5	0.125	—	2, p. 97
	90% HNO_3, −20 °C	23.5	—	76.5	0.15	—	
	HNO_3–98% H_2SO_4, 0 °C				0.025	—	9
	HNO_3–97% H_2SO_4, 0 °C	23	≤1	76	0.15	—	This work
Ph—NH—$P(O)(OEt)_2$ **2**	HNO_3–97% H_2SO_4, 0 °C	42	38	20	1.05	0.95	This work
	HNO_3–90% H_2SO_4	47	33	20	1.17	0.82	
	HNO_3–85% H_2SO_4	46	37	17	1.35	1.09	
	HNO_3–80% H_2SO_4	47	35	18	1.25	0.95	
	HNO_3–75% H_2SO_4	48	34	18	1.33	0.95	
	HNO_3–70% H_2SO_4	48	29	23	1.04	0.63	
Ph—NH—SO_2Me **3**	HNO_3–98% H_2SO_4, 25 °C	30	<1	70	0.21	—	3
Ph—O—$COCH_3$ **4**	HNO_3–97% H_2SO_4, 0 °C	25	≤1	74	0.17	—	This work
Ph—O—$P(O)(OEt)_2$ **5**	HNO_3–97% H_2SO_4, 0 °C	21	33	46	0.23	0.36	This work
	HNO_3–85% H_2SO_4	23	29	48	0.24	0.30	
	HNO_3–75% H_2SO_4	25	23	52	0.24	0.22	
	HNO_3–65% H_2SO_4	28	18	54	0.26	0.17	
Ph—O—SO_2Me **6**	HNO_3–97% H_2SO_4, 0 °C	13	≤1	86	0.07	—	This work

*The results obtained in this work are the average of at least five independent determinations and are accurate to better than ±10%.

TABLE 2. Isomer proportions for nitration in acetic anhydride*

Substrate	Conditions	Isomers (%) *ortho*	*meta*	*para*	1/2 *o:p*	1/2 *m:p*	Reference
1	HNO_3–Ac_2O, 20 °C	67.8	≤2.5	29.7	1.15	—	2, p. 97
	HNO_3–Ac_2O, 25 °C	77	—	23	1.67	—	3
	HNO_3–Ac_2O, 0 °C	72			2.1	—	9
	HNO_3–Ac_2O, 20 °C	76	<1	24	1.58	—	This work
2	HNO_3–Ac_2O, 20 °C	60	19	21	1.43	0.45	This work
3	HNO_3–Ac_2O, 25 °C	60	—	40	0.75	—	3
4	HNO_3–Ac_2O, 20 °C	27	≤1	72	0.19	—	This work
5	HNO_3–Ac_2O, 20 °C	42	17	41	0.51	0.21	This work
6	HNO_3–Ac_2O, 20 °C	53	—	47	0.56	—	This work

*The results obtained in this work are the average of at least five independent determinations and are accurate to better than ±10%.

[1] $$2 \rightleftharpoons^{H^+} Ph—\overset{+}{N}H_2—P(O)(OEt)_2$$

The positive pole adjacent to the benzene ring would then account for the large amount of *meta* substitution. *N*-Protonation of phosphinanilides has been also postulated in studies on acid-catalyzed hydrolysis of these compounds (12). We hope that more unambiguous conclusions can be reached by nmr studies on the protonation of phosphoroamidate system; such work is in progress in these laboratories.

The high value of the *ortho/para* ratio (*ca.* 10

Can. J. Chem. Downloaded from www.nrcresearchpress.com by 210.87.254.5 on 09/05/12
For personal use only.

times higher than that for protonated **1**) indicates that the special '*ortho*' mechanism operates in this case, outweighing the deactivation of *ortho* positions by the inductive effect of the positive pole. This can be visualized in terms of an initial attack of the electrophile at the phosphoryl oxygen still available as a nucleophilic centre, followed by selective transfer to the *ortho* position of the ring:

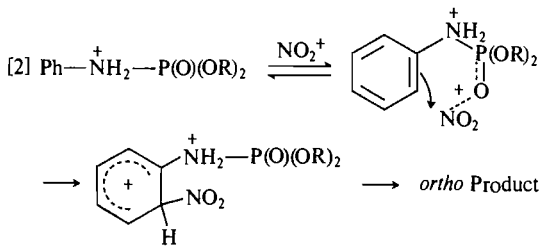

The above sequence of substituent effects in the nitration of anilides **1**–**3** in aqueous H_2SO_4 is to some extent repeated in a series of the corresponding phenyl esters **4**–**6**. Phenyl acetate and methanesulfonate give an orientation almost identical with that found for acetanilide and methanesulfonic anilide. The *O*-phosphorylated compound **5** shows again the characteristic feature of yielding a considerable amount of *meta* substitution product. In our opinion, this result does not necessarily provide evidence for the protonation of the oxygen of the Ar—O—P linkage in **5**. The phosphoryl oxygen is probably the most basic centre in this compound; the low value of the *ortho/para* ratio supports this conclusion, since no special '*ortho*' mechanism would be expected if the phosphoryl group were involved in protonation equilibrium. It is, however, well known (13) that in quasiphosphonium systems strong π_p–π_d interactions between oxygen and phosphorus take place, and a large fraction of the positive charge can be still present at the phenolic oxygen (resonance structure **5***b*), being responsible for the observed *meta* orientation:[3]

[3] **5** $\overset{H^+}{\rightleftharpoons}$ Ph—O—P(OR)$_2$ ↔ Ph—O=P(OR)$_2$
OH OH
5*a* **5***b*
↔ Other canonical structures

The proportion of *meta* isomer decreases with the decrease of acidity, attaining at 65% H_2SO_4 the value obtained for nitration in acetic anhydride (Table 2). This is almost certainly the result of an increasing contribution of nitration of the free base, since ester **5** should be considerably less basic than the anilide **2**.

Isomer proportions obtained for nitration in acetic anhydride are shown in Table 2. When a reaction through the conjugate acid of a substrate is not possible, all aromatic systems containing neutral groups having unshared electrons adjacent to the ring are considered as almost exclusively *ortho/para* directing in electrophilic substitution (15). Acetylated and sulfonylated aniline and phenol (compounds **1**, **3**, **4**, and **6**) give results in full accord with this; the phosphorylated derivatives **2** and **5**, on the other hand, show again an intramolecular selectivity pattern which justifies their classification as a separate group. For both compounds significant amounts of the *meta*-nitro product are found; this is in fact not much less than that formed in H_2SO_4 solutions, where the protonation of the substituent has been taken into account. It seems to us that the striking contrast between the behavior of these two substrates and the remaining anilides and esters can be best explained in terms of the high tendency of the N and O nonbonding electrons to get involved in donor π_p–π_d interactions with the adjacent P(IV) atom, even when the substituent is formally neutral. Some evidence exists that the charge on the quasiphosphonium P atom has little effect on the degree of π_p–π_d conjugation; the ^{31}P shielding in the $(MeO)_3PO/(MeO)_4P^+$ and $(Me_2N)_3PO/(Me_2N)_3POMe^+$ pairs has been found to be very similar (16). It has been also reported (17) that phenyl groups do not compete effectively with the P(IV) atom in conjugation with nitrogen or oxygen nonbonding electrons, since no essential difference in π_p–π_d bonding was observed for Z_3PO when Z = NMe_2 was changed to Z = NPh_2, or Z = OMe to Z = OPh.

If the phosphate moiety decreases the +M effect of a Y–P(O)$(OR)_2$ substituent (Y = N, O)

[3]Nesmeyanov *et al.* (14) observed only *para* substitution in nitration of the triphenyloxonium ion. It might suggest that in the case of compound **5** it is not so much a positive charge, but the vacant *d* orbitals of the adjacent phosphorus which constitute an electron sink, effectively diminishing the availability of the oxygen unshared pairs for the mesomeric activation of the *ortho* and *para* positions.

Can. J. Chem. Downloaded from www.nrcresearchpress.com by 210.87.254.5 on 09/05/12
For personal use only.

Can. J. Chem. Downloaded from www.nrcresearchpress.com by 210.87.254.5 on 09/05/12
For personal use only.

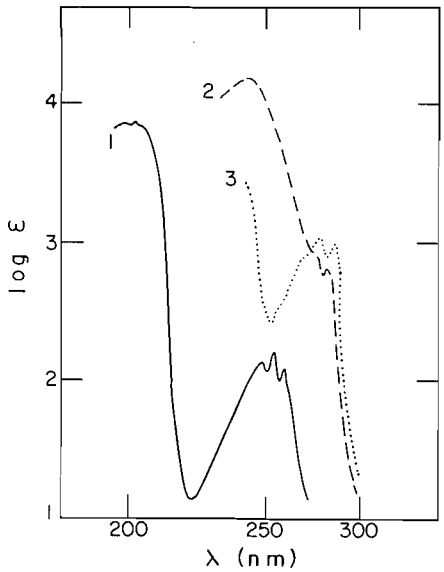

FIG. 1. Ultraviolet absorption spectra of: **1**, anilinium ion; **2**, acetanilide; **3**, diethylphosphoric anilide. Spectra of **1** and **2** are taken from ref. 18.

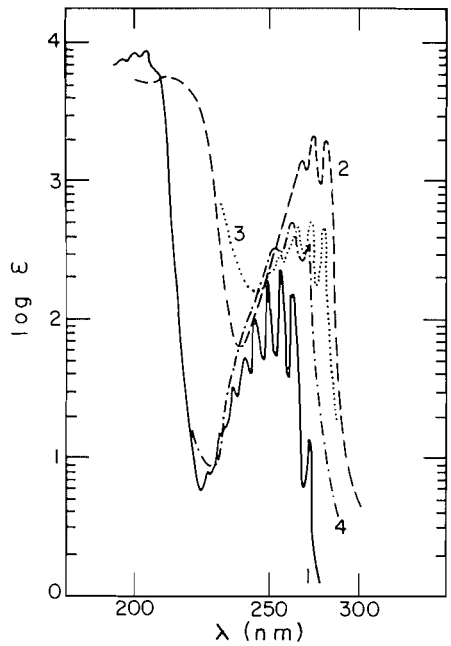

FIG. 2. Ultraviolet absorption spectra of: **1**, benzene; **2**, phenol; **3**, phenyl acetate; **4**, diethylphenyl phosphate. Spectra of **1** and **2** are taken from ref. 18.

relative to the corresponding carboxylic derivatives, this effect should be also detected in the electronic spectra of these compounds. In Fig. 1 the uv absorption spectra of anilides **1** and **2** are shown together with that of anilinium ion, where the nitrogen lone pair is fully involved in covalent bonding. The absorption curve of the diethylphosphoric anilide, although considerably shifted towards longer wavelengths and increased intensity, resembles the spectrum of the $Ph—NH_3^+$ ion much more than does the acetanilide, for which the 'benzenoid' structure of the spectrum had almost disappeared, a result that has usually been attributed to strong interactions of the unshared *p* electrons with the aromatic system (19). A similar, but even stronger trend can be seen in the uv spectra of phenyl esters of diethylphosphoric, **5**, and acetic, **4**, acid (Fig. 2), where they are compared with the spectra of phenol and benzene.

The reason for large scatter in the values of the *o/p* ratio in acetic anhydride (Table 2) is not quite clear. According to Schofield *et al.* (3) the special '*ortho*' mechanism operates in this medium for acetanilide ($1/2$ *o:p* > 1), but not for methanesulfonic anilide, because of the low nucleophilicity of the SO_2 group. We believe that this mechanism takes place also for diethylphosphoric anilide ($1/2$ *o:p* $= 1.43$) and probably for phenyldiethyl phosphate **5** and phenyl methanesulfonate **6**, since for these two substrates the *o/p* ratio is considerably higher in acetic anhydride than in sulfuric acid. Phenyl acetate gives predominantly *para* orientation in both media. However, it has to be remembered that some of the compounds studied may react in acetic anhydride at or near to the encounter rate, *i.e.* under conditions where the intramolecular selectivity does not always reflect the properties of substituents, observed when the attack of the electrophile is the rate-determining step (6).

1. R. O. C. NORMAN and R. TAYLOR. Electrophilic substitution in benzenoid compounds. Elsevier, Amsterdam. 1965. Chapt. 3.1.f.
2. J. C. HOGGETT, R. B. MOODIE, J. R. PENTON, and K. SCHOFIELD. Nitration and aromatic reactivity. Cambridge University Press, London. 1971. Chapt. 5.3.4.
3. S. R. HARTSHORN, R. B. MOODIE, and K. SCHOFIELD. J. Chem. Soc. B, 2454 (1971).
4. E. MALINSKI, A. PIEKOS, and T. A. MODRO. Phosphorus, In press; and preceding papers of this series.
5. K. SASSE. Methoden der organischen chemie, Vol. XII/2. Georg Thieme Verlag, Stuttgart. 1964. p. 422.
6. S. R. HARTSHORN and K. SCHOFIELD. Progress in organic chemistry. Vol. 8. Butterworths, London. 1973.

7. T. KAMETANI, O. UMEZAWA, K. SEKINE, T. ODA, M. ISHIGURA, and D. MIZUNO. Yakugaku Zasshi, **84**, 237 (1964); Chem. Abstr. **61**, 600 (1964).
8. T. A. MODRO and J. PIOCH. Rocz. Chem. **48**, 161 (1974).
9. B. M. LYNCH, C. M. CHEN, and Y. Y. WIGFIELD. Can. J. Chem. **46**, 1141 (1968).
10. M. LILER. Reaction mechanisms in sulphuric acid. Academic Press, London. 1971. Chapt. 3.3.2.5.
11. T. KOIZUMI and P. HAAKE. J. Am. Chem. Soc. **95**, 8073 (1973).
12. D. A. TYSSEE, L. P. BAUSHER, and P. HAAKE. J. Am. Chem. Soc. **95**, 8066 (1973).
13. T. A. MODRO and A. PIEKOS. Tetrahedron, **28**, 3867 (1972).
14. A. N. NESMEYANOV, T. P. TOLSTAYA, L. S. ISAEVA, and A. V. GRIB. Dokl. Akad. Nauk. SSSR, **133**, 602 (1960).
15. C. K. INGOLD. Structure and mechanism in organic chemistry. *Edited by* G. Bell, London. 1969. Chapt. VI.20(d).
16. A. SCHMIDPETER and C. WEINGAND. Z. Naturforsch. **246**, 177 (1969).
17. J. R. VAN WAZER and J. H. LETCHER. Topics in phosphorus chemistry. Vol. 5. Interscience, New York. 1967. p. 190.
18. UV atlas of organic compounds. Vol. I (1966); Vol. III (1967); Vol. IV (1968). Verlag Chemie, Weinheim.
19. C. N. R. RAO. Ultra-violet and visible spectroscopy. Butterworths, London. 1967. Chapt. 5.

Can. J. Chem. Downloaded from www.nrcresearchpress.com by 210.87.254.5 on 09/05/12
For personal use only.

Intermolecular hydrogen bonds and molecular conformations. A 220 MHz nuclear magnetic resonance study of the piperazine ring in 1-thiobenzoyl-3,5-dimethylpiperazine[1,2]

ADRIAN O. FULEA[3] AND PETER J. KRUEGER[4]
Department of Chemistry, University of Calgary, Calgary, Alberta T2N 1N4

Received August 5, 1975

ADRIAN O. FULEA and PETER J. KRUEGER. Can. J. Chem. **54**, 566 (1976).

In the 220 MHz ^{1}H nmr spectrum of the acetone-d_6 complex of the title compound some distortion of the piperazine ring is observed, and separate $NH_e\cdots O$ (dominant) and $NH_a\cdots O$ (secondary) proton signals are seen over a 90 °C temperature interval because of a reduction in the N inversion rate due to hydrogen bonding. The chemical shift of the former is strongly temperature dependent, while that of the latter is not, leading to a signal cross-over near 30 °C. A single NH signal is found for the title compound in $CDCl_3$ solution, with a maximum near 30 °C in the chemical shift *vs.* temperature plot. This is explained by rapid $NH_e\cdots Cl_3CD \rightleftharpoons Cl_3CD\cdots NH_a$ exchange, with the same type of temperature dependence for NH_a and NH_e in these complexes as found in acetone-d_6. Infrared evidence for these energetically competitive complexes is presented. The NH group is shown to be a good spectroscopic probe for conformational studies in hydrogen bonded complexes.

ADRIAN O. FULEA et PETER J. KRUEGER. Can. J. Chem. **54**, 566 (1976).

Dans le spectre rmn du proton à 220 MHz du complexe de l'acétone-d_6 avec le composé du titre, on observe quelques distorsions du noyau pipérazine et on voit des signaux séparés pour les protons $NH_e\cdots O$ (prédominant) et $NH_a\cdots O$ (secondaire) sur un intervale de température de 90 °C à cause de la réduction de la vitesse d'inversion de l'azote dû à un pont hydrogène. Le déplacement chimique du premier est fortement dépendant sur la température alors qu'il ne l'est pas pour le dernier; ceci conduit à un recoupement des signaux près de 30 °C. On trouve un signal NH unique pour le composé du titre en solution dans le $CDCl_3$ avec un maximum près de 30 °C dans la courbe du déplacement chimique en fonction de la température. On explique ce résultat par un échange $NH_e\cdots Cl_3CD \rightleftharpoons Cl_3CD\cdots NH_a$ avec le même type de dépendance sur la température pour NH_a et NH_e dans ces complexes que dans ceux trouvés pour l'acétone-d_6. On présente des preuves infrarouges pour les complexes énergétiquement compétitifs. On montre que le groupe NH est une bonne sonde spectroscopique pour des études conformationnelles de complexes comportant des ponts hydrogène.

[Traduit par le journal]

Introduction

Recently the spectroscopic and structural properties of 1-(2′-hydroxythiobenzoyl)piperidines and -morpholines have been investigated in this laboratory (1). In general they are characterized by a strong intramolecular $OH\cdots S$ hydrogen bond and by non-planarity of the phenyl ring with the thioamide group, leading to the existence of two molecular conformations in which the aromatic $H_{6'}$ atom interferes sterically with either one or with both of the *anti* NCH_2 protons of the hetero-ring (2). These conformers interchange rapidly by ring inversion (except if the hetero-ring is biased by methyl groups) and by rotation about the Ph—C(S) and C—N bonds, although the last two processes are slow at low temperatures. In acetone-d_6, the intramolecular $OH\cdots S$ hydrogen bond is slowly replaced by an intramolecular $O\cdots HS$ bond, and two distinctly different $SH\cdots O$ peaks separated by 6–8 Hz are seen over an 80 °C temperature range in 300 MHz nmr spectra, in spite of a large temperature dependence of the chemical shift of this doublet (3).

This paper summarizes an investigation of the conformational implications of 220 MHz ^{1}H nmr spectra of 1-thiobenzoyl-3,5-dimethylpiperazine, **1**, in several solvents. In view of the established sensitivity of intramolecularly hydrogen bonded OH and SH groups as conforma-

[1]Presented in part at the 12th European Congress on Molecular Spectroscopy, Strasbourg, France, July, 1975.
[2]From the Ph.D. Thesis of A. O. Fulea.
[3]Isaac Walton Killam Scholar; on leave of absence from the University of Bucharest.
[4]Author to whom correspondence should be addressed.

Can. J. Chem. Downloaded from www.nrcresearchpress.com by 210.87.254.42 on 09/05/12
For personal use only.

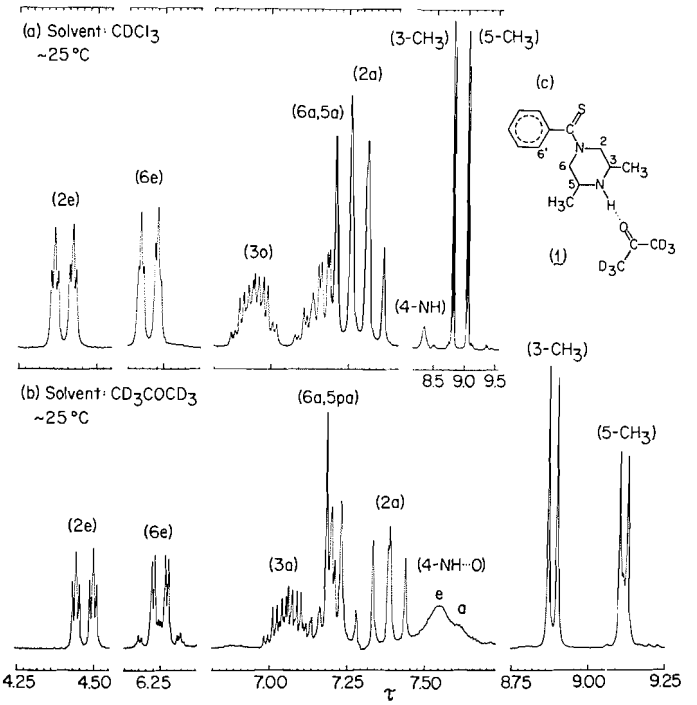

FIG. 1. 220 MHz ^{1}H nmr spectra of piperazine ring and methyl protons of **1** relative to internal TMS reference in (*a*) $CDCl_3$, (*b*) CD_3COCD_3. Assignments according to numbering in (*c*), which shows hydrogen bonded complex of **1** in CD_3COCD_3. For stereochemical considerations see text.

tional probes, it was of particular interest to see if an NH group which was hydrogen bonded to solvent molecules exhibited similar behaviour.

Experimental

Compound **1** was prepared from benzaldehyde, sulfur, and 2,6-dimethylpiperazine in pyridine by the Willgerodt–Kindler reaction (4), and was purified by recrystallization from petroleum ether (bp 65–100 °C) to give yellow crystals in 79% yield, mp 123–125 °C.[5] Infrared spectra were obtained with a Perkin-Elmer Model 621 spectrophotometer. The 220 MHz nmr spectra were obtained at the Canadian 220 MHz NMR Centre, Sheridan Park, Ontario, under the direction of Dr. A. E. Grey.

Results and Discussion

The nmr spectra of **1** in chloroform-*d* and acetone-d_6 solution at ambient temperature are shown in Fig. 1 *a* and *b*, respectively. The hetero-ring chair–chair inversion is frozen on the nmr time scale by the methyl substituents. These are equatorial, since the *syn* NCH_a proton signal is a triplet, implying that in addition to geminal coupling, J_{aa} also exists, and therefore H_3 is axial. The chemical shift of H_5 is very similar to that of H_3, and it is therefore also axial. No *trans* isomer of 2,6-dimethylpiperazine was detected in the starting material for the synthesis of **1**.

The *syn* NCH_e proton signal is a doublet of triplets in both solvents ($J_{gem} = 12$ Hz, $J_{ea} \approx J^4_{ee} \approx$ 2.3 Hz), whereas the *anti* NCH_e proton signal is a doublet of triplets in chloroform-*d*, but a clear doublet of doublets in acetone-d_6 ($J_{gem} =$ 10 Hz, $J^4_{ee} \approx 2.3$ Hz). The long range coupling (5) $J^4_{2e,6e}$ between the NCH_e protons is approximately equal to J_{ae}.[6] The fact that the *anti* NCH_e peak is a doublet of doublets in acetone-d_6 solution implies that H_{5a} (see numbering in Fig. 1*c*) is no longer axial, but *pseudoaxial* (6), with the 5-methyl group being pseudoequatorial and the piperazine ring somewhat more

[5]We thank Mrs. C. Fulea for the preparation of this compound during her stay at the University of Calgary as a Guest Worker.

[6]This long range coupling does not exist in piperazine itself, proving that here the 2 and 6 equatorial hydrogen atoms are in a plane in the well-known 'W'-conformation.

Can. J. Chem. Downloaded from www.nrcresearchpress.com by 210.87.254.42 on 09/05/12
For personal use only.

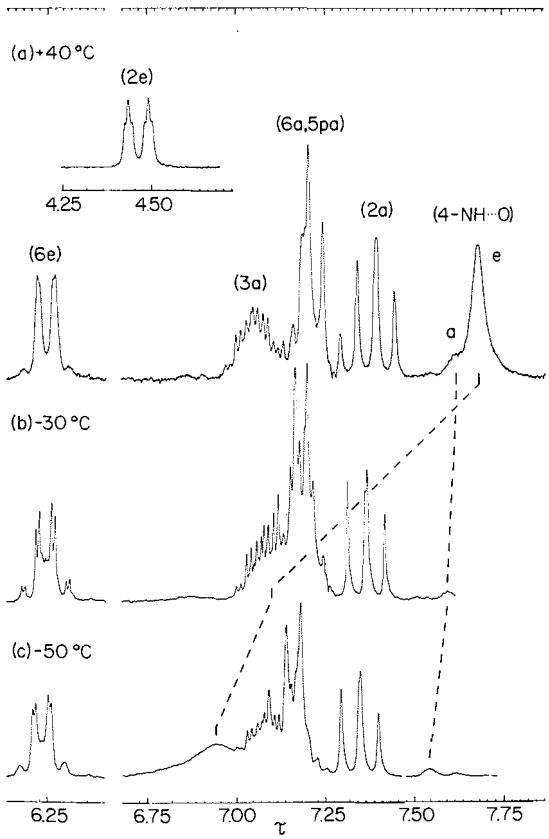

FIG. 2. 220 MHz ^{1}H nmr spectra of piperazine ring and methyl protons of **1** at +40, −30, and −50 °C in CD_3COCD_3. The spectrum at +40 °C in particular should be compared with that at ~25 °C in Fig.1*b* with respect to the NH_a/NH_e signal cross-over.

puckered than normally on the side *anti* to the thiocarbonyl group. This can be established from the fact that the spectra show $J_{ae} = 0$ for the H_5 atom. From the known dependence of the vicinal coupling constant on $\cos^2$ of the dihedral angle between the C—H bonds involved, it follows that $\angle H_{6e}C—CH_{5a}$ must be close to 90° in **1** instead of 60° as in the normal chair conformation found for **1** in $CDCl_3$ solution.

At 40 °C the NH proton signal of **1** in chloroform-*d* is 400 Hz downfield from TMS, while in acetone-d_6 a pair of signals is observed, the dominant peak being at 510 Hz, with a weak secondary peak at ~520 Hz. The temperature dependence of these signals (Fig. 2) shows unequivocally that the dominant 4-NH signal in acetone-d_6 is very strongly hydrogen bonded to solvent molecules, as in Fig. 1*c*. Its chemical

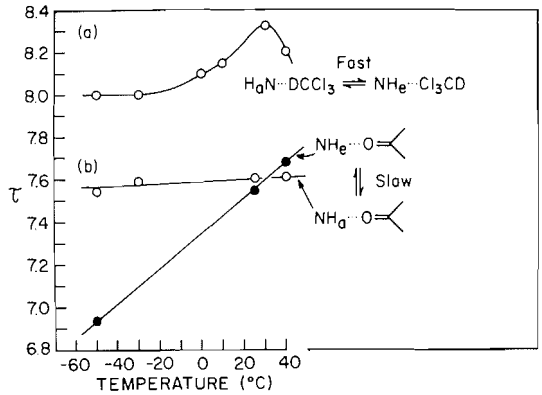

FIG. 3. Temperature dependence of NH signals of **1** in (*a*) $CDCl_3$, (*b*) CD_3COCD_3.

shift displacement over the range 40 to −50 °C in acetone-d_6 is 160 Hz, and is linearly related to temperature (Fig. 3). The secondary NH signal shifts very little with temperature, with a resulting signal cross-over near 30 °C. Since the axial NH is expected to be more sterically hindered and the equatorial NH more acidic (7), a preference for the latter which exceeds that in piperazine itself (8) is expected in the acetone-d_6 complex of **1** (9). Presumably steric factors severely limit the $NH_a···O=C$ configurations relative to those allowed for $NH_e···O=C$, and also may impose a greater $NH_a···O$ distance leading to a more weakly bonded complex. Contraction of the average $NH_e···O$ distance and a progressive shift to the configuration with the strongest hydrogen bond as the temperature is lowered can account for the pronounced temperature dependence of the $NH_e···O=C$ proton signal, and the dominance of this conformation because of the greater strength of this hydrogen bond accounts for the linearity of the temperature dependence. The appearance of separate NH_e and NH_a signals implies that inversion at N is drastically slowed down by the hydrogen bond to the solvent, and this phenomenon has been well documented (10).

In contrast, much weaker NH···Cl and $CCl_3CD···N$ hydrogen bonds are expected in chloroform-*d* solution, which may be envisaged schematically in Scheme 1. Nitrogen inversion barriers in chloroform-*d* are only ~0.5 kcal/mol higher than in hydrocarbon solvents (10). Infrared spectroscopic studies of amines in both chloroform and chloroform-*d* demonstrate that both NH···Cl and CD···N interactions are

Can. J. Chem. Downloaded from www.nrcresearchpress.com by 210.87.254.42 on 09/05/12
For personal use only.

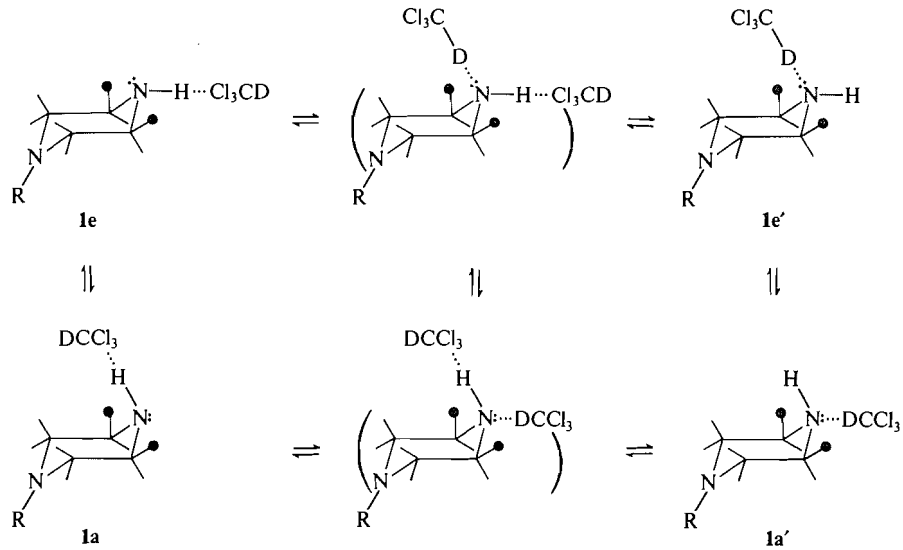

SCHEME 1

important (P. J. Krueger, unpublished results).

While the 1:2 complexes shown in Scheme 1 would have a much lower probability than the 1:1 complexes, they may facilitate the transition between **1e** and **1e′**, and between **1a** and **1a′** energetically. However, only one NH proton signal is observed, signifying rapid exchange on the nmr time scale over the temperature range investigated. A maximum in the chemical shift *vs.* temperature plot (Fig. 3*a*) can be understood in terms of the equilibria in Scheme 1, provided that the temperature dependence of the chemical shift of two of the major species involved is different and leads to a cross-over (as in acetone-d_6). The principal difference between the chloroform-*d* and acetone-d_6 complexes of **1** is therefore the $NH_a \rightleftharpoons NH_e$ exchange rate. It may be noted that the temperature of the maximum in the chemical shift plot for the chloroform-*d* complex (Fig. 3*a*) corresponds to the cross-over point in the analogous plot for the acetone-d_6 complex (Fig. 3*b*). In chloroform-*d* solution the conformational NH acidity differences in **1** are likely to favour **1e** and N basicity differences likely to favour **1a′** (7), while NH···Cl and CD···N interactions in the 1:2 complexes would be synergetic (steric factors permitting).

The specific interaction of the hydrogen bonded acetone molecule with the C_5 portion of the hetero-ring is further demonstrated by the band shape differences for the 3- and 5-methyl groups (Fig. 1). In chloroform-*d* (Fig. 1*a*) the signals are virtually identical for these two groups; in acetone-d_6 the 5-methyl signal is significantly broadened (Fig. 1*b*), even at 40 °C, and this broadening increases at lower temperature. Similar distortion (*i.e. anti* NCH_e a doublet of doublets) occurs for **1** in the proton-accepting solvents pyridine and dimethylsulfoxide-d_6, demonstrating that the size and geometry of the acceptor is not a determining factor in the distortion of the piperazine ring, but that the presence of an intermolecular NH···X hydrogen bond is the important factor.[7] Since typical NH···O hydrogen bond distances of 3.04 Å have been observed in crystals (11), it is hard to envisage direct steric interaction between the methyl groups of the acetone molecule and the

[7]There is a slight suggestion of distortion of the *anti* NCH_e doublet of triplets of **1** in $CDCl_3$ solution, but the triplet remains well-defined. Furthermore, a slight broadening of the 5-methyl group signal is observed at low temperature. These observations indicate a small amount of piperazine ring distortion is also present in $CDCl_3$ solution, and this correlates with the weaker but still significant NH···Cl hydrogen bond.

Can. J. Chem. Downloaded from www.nrcresearchpress.com by 210.87.254.42 on 09/05/12
For personal use only.

Can. J. Chem. Downloaded from www.nrcresearchpress.com by 210.87.254.42 on 09/05/12
For personal use only.

methyl substituents on the piperazine ring, particularly an interaction with only the *anti* side of the ring. The primary cause of this distortion must therefore be sought within the molecule, such as the steric $H_{6'}\cdots H_6$ interactions which may generate a torque whose effect appears to be localized at C_5 in the presence of a strong $NH\cdots X$ hydrogen bond. It may be of significance that the N lone pair is axial and antiperiplanar to H_{6a} and H_{3a} in the dominant $NH_e\cdots O$ complex, geometrical conditions under which a partial participation of the N lone pair in an antibonding σ^* C—H orbital has been proposed by Hamlow *et al.* (12). Strong $NH_e\cdots O$ hydrogen bonding would favour this, and the preferential involvement of H_{6a} as opposed to H_{3a} may provide for easier ring deformation as the N_4—C_5 bond is weakened. No similar distortion of the morpholine ring is found in 4-(4′-nitrothiobenzoyl)-2,6-dimethylmorpholine in acetone-d_6.

Infrared spectra of very dilute CCl_4 solutions of piperidine and piperazine show a fundamental NH stretching doublet, with the dominant high frequency component characteristic of NH_e and the minor low frequency component characteristic of NH_a (7). While both probably interact weakly with the solvent ($NH\cdots Cl$), the greater acidity and less hindered orientation of the NH_e group, as opposed to the lower acidity and more hindered orientation of the NH_a group are consistent with these spectra, and indeed the solvent effect of CCl_4 must be small as the relative proportions of the two conformers do not change significantly from the vapour phase value (9). These measurements are compared in Scheme 2 with those for **1** in three solvents, with the vertical bars giving an approximate indication of relative intensity within each doublet. In CCl_4 the NH doublet of **1** resembles that in piperazine, except for a shift to lower frequency by some 15 cm^{-1} due to the *N*-thiobenzoyl group and the sp^2 N atom in the ring. In $CDCl_3$ this

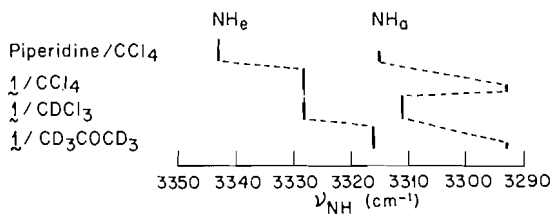

SCHEME 2

doublet shows a dramatic reversal in relative intensity, with no frequency shift for the NH_e band ($NH_e\cdots Cl$ as in CCl_4 solution) while the NH_a peak moves to *higher* frequency by some 18 cm^{-1}, *i.e.* it becomes more 'free', suggesting that $NH_a\cdots Cl$ interaction is unfavourable (on steric grounds and due to the lower NH_a acidity) as a stronger $CD\cdots N$ bond forms to the equatorial lone pair electrons of N. The higher basicity of the NH_a nitrogen atom appears to favour this complex, and the infrared data strongly suggest that of the complexes shown in Scheme 1, the **1e** $\rightleftharpoons$ **1a**′ equilibrium is the most important. The corresponding NH peaks are more nearly equal in intensity here than in the other solvents, indicating that the complexes involved are energetically quite competitive. The apparent lack of an $NH_a\cdots Cl$ bond provides a logical basis for the difference in the temperature dependence of the chemical shift for NH_a and NH_e proposed earlier in this paper to explain the maximum in Fig. 3*a*.

In acetone-d_6 the $NH_e\cdots O$ peak again becomes dominant, with a further downward displacement in frequency by 12 cm^{-1} due to the stronger hydrogen bond. The minor $NH_a\cdots O$ peak reverts to the frequency found in $CDCl_3$, indicative of much weaker hydrogen bonding to acetone than in $NH_e\cdots O$. This explains the much smaller temperature dependence actually observed for the NH_a signal in Fig. 3*b*.

While the NH group in **1** is too far removed from the thioamide group to feel any differences due to the conformational interchange described in the Introduction, it is a good spectroscopic probe for the study of N inversion and molecular conformations in hydrogen bonded complexes.

Acknowledgments

The financial support of the National Research Council of Canada is gratefully acknowledged. The infrared spectral measurements were made by Mrs. Marelle Bertram.

1. P. J. KRUEGER, A. O. FULEA, C. FULEA, and F. CORNEA. Spectrosc. Lett. **8**, 141 (1975).
2. P. J. KRUEGER and A. O. FULEA. Tetrahedron, **31**, 1813 (1975).
3. P. J. KRUEGER and A. O. FULEA. Proc. 12th European congress on molecular spectroscopy. Elsevier, Amsterdam. In press.

4. W. WALTER and J. VOSS. *In* The chemistry of amides. *Edited by* J. Zabicky. Interscience, London. 1970. pp. 426–429, and references cited therein.
5. M. BARFIELD and B. CHAKRABARTE. Chem. Rev. **69**, 757 (1969), and references cited therein.
6. H. S. ISBELL and R. S. TIPSON. J. Res. Natl. Bur. Stand. **64**A, 171 (1960).
7. P. J. KRUEGER and J. JAN. Can. J. Chem. **48**, 3236 (1970).
8. M. J. COOK, R. A. Y. JONES, A. R. KATRITZKY, M. M. MANAS, A. C. RICHARDS, A. J. SPARROW, and D. L. TREPANIER. J. Chem. Soc. Perkin Trans. 2, 325 (1973).
9. R. A. Y. JONES, A. R. KATRITZKY, A. C. RICHARDS, R. J. WYATT, R. J. BISHOP, and L. E. SUTTON. J. Chem. Soc. B, 127 (1970).
10. J. B. LEHN. Fortschr. Chem. Forsch. **15**, 311 (1970); J. B. LAMBERT. *In* Topics in stereochemistry. Vol. 6. *Edited by* N. L. Allinger and E. L. Eliel. Wiley-Interscience, New York. 1971. pp. 45–47, and references cited in these two review articles.
11. G. C. PIMENTEL and A. L. MCCLELLAN. The hydrogen bond. W. H. Freeman, San Francisco. 1960. p. 289.
12. H. P. HAMLOW, S. OKUDA, and N. NAKAGAWA. Tetrahedron Lett. 2553 (1964).

Can. J. Chem. Downloaded from www.nrcresearchpress.com by 210.87.254.42 on 09/05/12
For personal use only.

Esters chromiques dérivés du tertiobutanol

JEAN-MARIE HACHEY, HÉLÈNE GHALI ET JEAN-BAPTISTE SAVARD
Département des sciences pures, Université du Québec à Chicoutimi, Chicoutimi, Québec G7H 2B1

Reçu le 12 septembre 1975

JEAN-MARIE HACHEY, HÉLÈNE GHALI et JEAN-BAPTISTE SAVARD. Can. J. Chem. **54**, 572 (1976).

La composition du mélange d'esters chromiques issus de la réaction entre le tertiobutanol et des quantités croissantes de trioxyde de chrome a été calculée à partir du spectre rmn du proton et confirmée par la détermination de la teneur en chrome des mélanges d'esters chromiques. Les esters chromiques pouvant se former sont le chromate, le dichromate et le trichromate de ditertiobutyle.

JEAN-MARIE HACHEY, HÉLÈNE GHALI, and JEAN BAPTISTE SAVARD. Can. J. Chem. **54**, 572 (1976).

The composition of the mixture of chromate esters obtained from the reaction between *tert*-butyl alcohol and increasing amounts of chromium trioxide has been calculated from the pmr spectrum and confirmed through the determination of the chromium content of these mixtures. The chromate esters formed are the ditertiarybutyl mono-, di-, and trichromate.

Introduction

Dans un récent article, Behr et Fuchs (1) signalent la formation des esters mono, di et trichromique dérivés du tertiobutanol.[1] Ces auteurs appuient la formation de ces esters sur la teneur en CrO_3 ainsi que l'étude du spectre infrarouge.

Il est intéressant de souligner ici le comportement singulier du *tert*-BuOH en présence de CrO_3. En effet, les nombreux esters chromiques dérivés d'alcools tertiaires décrits dans la littérature (pour une revue, voir les réfs. 2 et 3) sont des diesters monochromiques de formule générale $ROCrO_2OR$. Il faut ajouter que ces esters sont souvent obtenus (3–5) en faisant réagir un grand excès de CrO_3 (jusqu'à deux fois la quantité stoïchiométrique) avec l'alcool tertiaire.

Ce travail a pour objet d'étudier l'influence de l'excès de trioxyde de chrome sur la nature et la répartition des esters chromiques pouvant se former lors de la réaction entre le *tert*-BuOH et le CrO_3 dans le CCl_4. La détermination de la composition du mélange d'esters par rmn du proton s'est avérée une méthode rapide et efficace. L'analyse par rmn est confirmée par la détermination de la teneur en chrome.

[1]Dans cet article ester monochromique ou chromate ou monochromate de ditertiobutyle se réfère au composé $ROCrO_2OR$ (**1**), ester dichromique ou dichromate de ditertiobutyle désigne le composé $RO(CrO_2O)_2R$ (**2**) et ester trichromique ou trichromate de ditertiobutyle se rapporte au composé $RO(CrO_2O)_3R$ (**3**), (R = *tert*-Bu).

Resultats et discussion

Les résultats de la réaction entre le *tert*-BuOH et des quantités croissantes de CrO_3 sont rassemblés au tableau 1. La figure 1 permet de mieux apprécier l'influence de la concentration des réactifs sur la composition du mélange d'esters chromiques.

Les produits de la réaction tert-BuOH + CrO_3 dans le CCl_4 (T = 25 °C)

Les résultats expérimentaux illustrés à la figure 1 permettent de constater qu'il est possible d'obtenir le produit **1** pur en faisant un choix judicieux des concentrations initiales. Des méthodes de synthèse de **1** sont d'ailleurs décrites dans la littérature (3,4). Cependant, ce mode de

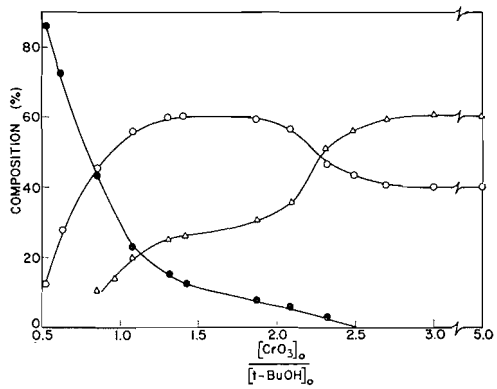

FIG. 1. Variation de la composition du mélange d'esters chromiques en fonction des rapports molaires initiaux des réactifs: esters **1** (●), **2** (○) et **3** (△).

Can. J. Chem. Downloaded from www.nrcresearchpress.com by 210.87.254.42 on 09/05/12
For personal use only.

Can. J. Chem. Downloaded from www.nrcresearchpress.com by 210.87.254.42 on 09/05/12
For personal use only.

TABLEAU 1. Caractéristiques de la réaction entre le *tert*-BuOH et le CrO_3 dans le CCl_4 à 25 °C

$[CrO_3]_0/[tert\text{-BuOH}]_0$*	Composition (%)†			
	tert-BuOH	**1**	**2**	**3**
0.52	18	71(87)	11(13)	—
0.56	11	73(82)	16(18)	—
0.59	10	70(78)	20(22)	—
0.63	9	66(73)	25(27)	—
0.74	3	60(61)	37(39)	—
0.86	1	43(44)	45(45)	11
0.97	Trace	34	52	14
1.01	—	32	52	16
1.08	—	23	57	20
1.20	—	17	61	22
1.30	—	15	60	25
1.42	—	13	60	27
1.87	—	8	60	32
2.09	—	7	57	36
2.32	—	3	46	51
2.50	—	—	44	56
2.70	—	—	41	59
3.0	—	—	40	60
5.0	—	—	40	60

*Rapport molaire initial.
†Déterminée par rmn; écart ±0.5 (au moins 3 déterminations dans chaque cas).

synthèse ne permet pas d'obtenir un mélange réactionnel contenant plus de ~63% de l'ester **2**, cet ester est obtenu en présence de **1** (~12%) et de **3** (~25%). La figure 1 indique également que le rendement en **3** augmente sensiblement avec augmentation de l'excès de CrO_3; toutefois, au-delà du rapport des concentrations molaires initiales $[CrO_3]_0/[tert\text{-BuOH}]_0 \simeq 2.3$, le mélange réactionnel laisse voir une augmentation du rendement en **3** et une diminution en **2**. Dans les deux cas, le rendement semble se stabiliser autour de 60% pour **3** et 40% pour **2** même si un grand excès de CrO_3 est utilisé. En effet, la composition du mélange reste pratiquement constante dès que le rapport $[CrO_3]_0/[tert\text{-BuOH}]_0$ atteint 3. La détermination de la teneur en chrome (6) s'accorde très bien avec cette composition du mélange calculée à partir du spectre rmn. De plus, il est possible de constater que le rendement en **1** décroît de façon continue avec l'augmentation de la concentration en CrO_3. Par ailleurs, l'ester **2** atteint un rendement maximum de l'ordre de 60% pour des valeurs $[CrO_3]_0/[tert\text{-BuOH}]_0$ comprises entre ~1.3 et ~1.9; au-delà de ~2, le rendement en ester **2** décroît puis se stabilise à ~40% du moins jusqu'aux valeurs limites étudiées. Pour ce qui est de l'ester **3** son rendement croît jusqu'à $[CrO_3]_0/[tert\text{-BuOH}]_0 \sim 3$ puis tend à se stabiliser vers 60%.

Les résultats du tableau 1 indiquent que le mélange réactionnel contient du *tert*-BuOH jusqu'à ce que l'on fasse réagir des quantités équimoléculaires de *tert*-BuOH et de CrO_3; mais à ce moment le mélange contient déjà beaucoup (~52%) de **2** et un peu de **3** (~16%).

Les demiesters chromiques

La formation des demiesters chromiques *tert*-$BuO(CrO_2O)_nH$, $n = 1,2,3$ n'a pu être mise en évidence. D'ailleurs, il n'a pas encore été possible de mettre en évidence ces demiesters bien qu'ils aient été suggérés comme intermédiaires lors de la formation de diesters monochromiques $ROCrO_2OR$ (4). En fait, un balayage en rmn jusqu'à 20 ppm ne donne aucun signal supplémentaire. Le spectre infrarouge confirme également l'abscence de bandes OH. Ces résultats attestent donc de la grande réactivité des demiesters chromiques d'où la difficulté de les observer.

Comportement du tert-BuOH en présence de CrO_3

Le fait que le *tert*-BuOH conduise à la formation des esters **2** et **3** dans des conditions où les autres alcools tertiaires étudiés jusqu'à présent ne donnent lieu qu'à la formation de diesters monochromiques $ROCrO_2OR$ nous amène à faire les remarques suivantes.

(*i*) Le CrO_3 est un polymère (7*a*) qui peut être dépolymérisé par dissolution dans l'eau, le *tert*-BuOH, la pyridine et l'anhydride acétique (7*b*).

(*ii*) La solubilité du *tert*-BuOH, du CrO_3 et des demiesters dans l'eau, tout en facilitant le contact de ces réactifs, favoriserait d'autant la formation des esters **2** et **3**.

(*iii*) L'hydrolyse du chromate **1** est facile (8). En effet, dans le cas de l'ester **1**, le caractère hydrophobe serait réduit comparativement aux autres esters chromiques dérivés d'alcools tertiaires aliphatiques hydrocarbonés qui renferment des chaînes hydrocarbonées plus longues.

(*iv*) L'encombrement stérique réduit du *tert*-BuOH par rapport aux autres alcools tertiaires utilisés jusqu'à présent pourrait également expliquer son comportement avec le CrO_3.

Après la réaction, un examen par rmn de la phase aqueuse contenant le CrO_3 en vue d'y déceler la présence d'esters polychromiques n'a révélé aucun nouveau signal. Cette observation confirme donc la composition du mélange d'esters chromiques calculée à partir du spectre

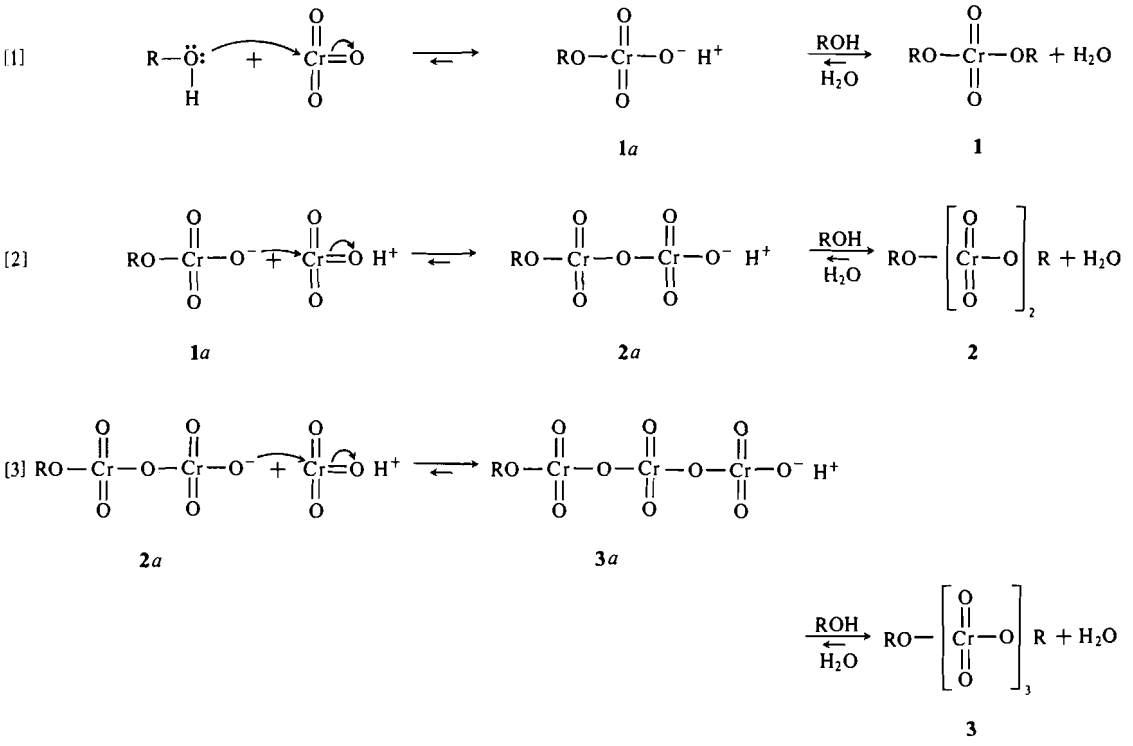

rmn ainsi que la teneur en chrome de ce mélange d'esters solubles dans le CCl_4. Par ailleurs, il est intéressant de constater que la quantité relative des esters **2** et **3** à l'équilibre (40 et 60% respectivement) est la même que la quantité relative de groupements chromates requis pour chacun de ces esters: la composition du mélange des esters chromiques à l'équilibre se trouverait ainsi à refléter l'équilibre et la contribution à la stabilisation par résonance des intermédiaires **2***a* et **3***a*. Des études complémentaires pourraient être entreprises pour étudier l'influence de la nature du solvant, de la concentration et de la température.

Le mécanisme suivant est suggéré pour la réaction entre le *tert*-BuOH et le CrO_3 dans le CCl_4 à 25 °C.

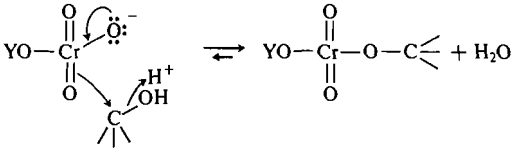

Y = *tert*-Bu(**1***a*); Y = *tert*-$BuOCrO_2$(**2***a*);
Y = *tert*-$BuOCrO_2OCrO_2$(**3***a*)

Le passage du demiester à l'ester correspondant se ferait selon le mécanisme suivant inspiré de celui proposé par Zeiss et Matthews (4) pour la formation d'esters monochromiques.

Caractérisation des esters 2 et 3 dérivés du tert-BuOH

Après des essais de chromatographie sur colonnes d'alumine et de silice, Behr et Fuchs (1) font part du fait qu'il leur a été impossible de séparer et de purifier les esters **2** et **3**. Dans ce travail, nous n'avons pas tenté de nouvelles méthodes de séparation et purification de ces esters chromiques; cependant, nous avons utilisé une méthode, la rmn du proton, qui nous permet de déterminer la composition du mélange d'esters. En effet, les esters **1**, **2** et **3** apparaissent sous forme de singulet à 1.47, 1.59 et 1.65 ppm respectivement; le déblindage des protons est donc sensiblement accrû par l'augmentation du nombre de groupements chromates. La composition du mélange d'esters chromiques calculée à partir du spectre rmn du proton est confirmée par la détermination de la teneur en chrome. Il convient également de signaler que le déplacement chimique de **1** rapporté dans cette étude est identique à celui déterminé antérieurement (3).

Can. J. Chem. Downloaded from www.nrcresearchpress.com by 210.87.254.42 on 09/05/12
For personal use only.

Can. J. Chem. Downloaded from www.nrcresearchpress.com by 210.87.254.42 on 09/05/12
For personal use only.

Conclusion

La réaction entre le *tert*-BuOH et le CrO_3 présente un cas particulier en ce que le *tert*-BuOH est le seul alcool tertiaire connu jusqu'à présent pouvant conduire à la formation de mono, di et trichromate de ditertiobutyle dans des conditions où les autres alcools tertiaires ne donnent que des diesters monochromiques $ROCrO_2OR$, R: alkyle tertiaire.

Suite à des études récentes (9,10), il serait intéressant d'examiner le comportement du di et du trichromate de ditertiobutyle comme inhibiteurs de corrosion et également comme agents oxydants de composés organiques.

Partie expérimentale

Les spectres ir ont été pris sur un appareil Unicam, modèle SP-1000; solvant, CCl_4. Les spectres rmn ont été mesurés à l'aide d'un appareil Hitachi–Perkin-Elmer, modèle R-24 à 60 MHz; solvant: CCl_4, concentration ~50% (P/V) dans CCl_4; standard interne TMS.

Le CrO_3 *Reagent* fut conservé au dessicateur. Le *tert*-BuOH et le CCl_4 étaient de qualité *Spectro* et ont été distillés avant usage.

Réaction entre le tert-BuOH et le CrO_3

Le *tert*-BuOH est dissous dans 20 ml de CCl_4 anhydre contenu dans un ballon de 50 ml; la réaction se fait à 25 ± 1 °C. Tout en maintenant l'agitation, une quantité appropriée de CrO_3 anhydre est ajoutée. Il y a coloration immédiate de la solution et apparition de gouttelettes d'eau au fond du ballon. L'agitation est poursuivie durant 3 min à la température ambiante. Le mélange réactionnel est ensuite décanté, transféré dans une fiole conique puis séché sur Na_2SO_4 anhydre. Après décantation du desséchant, les spectres rmn et infrarouge sont déterminés sans évaporation du solvant. La quantité utilisée de *tert*-BuOH, 1.1 g; CrO_3, entre 0.77 et 7.4 g, La réaction est faite à l'abri de la lumière.

Analyse du chrome

Après avoir fait réagir les quantités appropriées de *tert*-BuOH et de CrO_3 durant ~3 min dans le CCl_4 (à l'abri de la lumière), la solution est séchée sur Na_2SO_4 anhydre et le solvant est évaporé sous pression réduite. Un spectre infrarouge est alors pris sur le mélange d'esters et le spectre rmn est ensuite déterminé. Le mélange est alors pesé et on procède enfin à l'analyse du chrome selon la méthode décrite antérieurement (3, 6).

Remerciements

Les auteurs remercient vivement le Ministère de l'Education du Québec pour son aide financière.

1. W. J. Behr et J. Fuchs. Z. Naturforsch. **28**b, 597 (1973).
2. W. Treibs. Chemiker-Ztg/Chem. Apparatur, **24**, 953 (1967).
3. J. C. Richer et J. M. Hachey. Can. J. Chem. **53**, 3087 (1975).
4. H. H. Zeiss et C. N. Matthews. J. Am. Chem. Soc. **78**, 1694 (1956).
5. L. F. Fieser et G. Ourisson. Bull. Soc. Chim. Fr. **20**, 1152 (1953).
6. A. I. Vogel. A text book of quantitative inorganic analysis. 3ième ed. Longmans, London. 1961. p. 311.
7. (*a*) J. S. Stephens et D. W. J. Cruickshank. Acta Crystallogr. B**26**, 222 (1970); (*b*) H. O. House. Modern synthetic reactions. 2ième ed. Benjamin, California. 1972. p. 257; R. Stewart. Oxidation in organic chemistry, Part A, *Edited by* K. B. Wiberg. Academic Press, New York. 1965. pp. 69–184.
8. A. Leo et F. H. Westheimer. J. Am. Chem. Soc. **74**, 4383 (1952).
9. E. L. Ghali, B. Girard et J. M. Hachey. Can. J. Chem. Sous presse.
10. J. C. Richer et J. M. Hachey. Can. J. Chem. **52**, 2475 (1974).

Synthesis of some long-chain spiropyranindolines[1]

ILONA GRUDA AND ROGER M. LEBLANC
Département de Chimie-Biologie, Université du Québec à Trois-Rivières, Trois-Rivières, Québec G9A 5H7

Received August 1, 1975

ILONA GRUDA and ROGER M. LEBLANC. Can. J. Chem. **54**, 576 (1976).

Nine new spiropyranindolines containing an *n*-hexadecyl substituent at the 1′ or 3′ position have been synthesized. Their spectral properties (nmr, uv, visible) are described.

The equilibrium constant between the colored and colorless species of some of the compounds have been measured. The results show that the presence of a long aliphatic chain promotes the colored form.

ILONA GRUDA et ROGER M. LEBLANC. Can. J. Chem. **54**, 576 (1976).

Nous avons synthétisé neuf spiropyranindolines possédant un substituant *n*-hexadécyle à la position 1′ ou 3′. Les propriétés spectrales de ces composés ont été examinées, en particulier celles de rmn, uv, visible.

La constante d'équilibre entre les formes colorées et incolores a été mesuree. Ces données montrent que l'introduction d'une longue chaîne aliphatique favorise la forme colorée.

Solid photochromic films have a number of useful applications, such as recording media for information storage and retrieval systems, and protection against sunlight, intense flashes of light, or lasers (1). As an example, spiropyrans dissolved in a plastic matrix have been used as photochromic sunglasses to protect man's eyes (2).

The photochromic pigments in the chloroplast and in the photoreceptor cell of the vision system have a monolayer organization (3,4). It is known that the monolayer assemblies favour the energetic transformations. To our knowledge no synthetic photochromic compounds have been studied in monolayers. In order to perform this study, we needed a long-chain photochromic compound.

As preliminary work we present in this paper the synthesis and spectral properties of some spiropyranindolines containing an aliphatic long-chain substituent.

Results and Discussion

The most general method of synthesis of a spiropyranindoline consists of the condensation of a 2-alkylideneindoline **1** with an *ortho*-hydroxyaldehyde **2**. The long-chain substituent could be introduced as R_1, R_2 or R_3.

In order to prepare compound **1** with a long-chain substituent we attempted to perform the reaction of alkylation using 3-hexadecyl-2-methylindole, 1,2-dimethyl-3-hexadecylindole, 1-hexadecyl-2-methylindole, and 2,3-dimethyl-1-hexadecylindole as starting materials and alkyl iodides (5) or esters of aromatic sulfonic acids (6) as alkylation agents. All these attempts were unsuccessful.

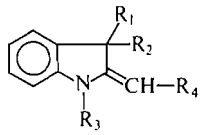

1

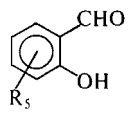

2

Another possible reaction pathway was to start with indolenines which are stronger bases and react more readily with quaternizing agents. The 2,3,3-trimethylindolenine **3** was commercially available, 2,3-dimethyl-3-hexadecylindolenine **4** was prepared by the Grignard method using 3-hexadecyl-2-methylindole and methyl iodide. Compound **3** was alkylated by hexadecyl iodide giving the quaternary iodide which was decomposed by sodium hydroxide to give 1-hexadecyl-3,3-dimethyl-2-methyleneindoline **5**. Compound **4** alkylated by dimethyl sulfate, gave 1,3-dimethyl-3-hexadecyl-2-methyleneindoline **6** after decomposition of the quaternary methyl sulfate. All these compounds (indoles, indolenines, and indolines) were characterised by nmr spectra, and their purity checked by glc.

The condensation of compounds **5** and **6** with salicylaldehyde, 3-methoxysalicylaldehyde, 5-nitrosalicylaldehyde, 3-nitrosalicylaldehyde, 2-hydroxynaphtaldehyde, and 6-nitro-2-hydroxy-

[1]Part I of Photochromic Studies in Monolayers.

Can. J. Chem. Downloaded from www.nrcresearchpress.com by 210.87.254.105 on 09/05/12
For personal use only.

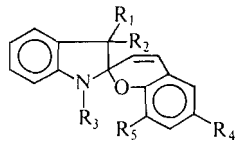

7

a $R_1 = R_2 = CH_3$, $R_3 = C_{16}H_{33}$, $R_4 = R_5 = H$

b $R_1 = R_2 = CH_3$, $R_3 = C_{16}H_{33}$, $R_4 = H$, $R_5 = OCH_3$

c $R_1 = R_2 = CH_3$, $R_3 = C_{16}H_{33}$, $R_4 = NO_2$, $R_5 = H$

d $R_1 = R_2 = CH_3$, $R_3 = C_{16}H_{33}$, $R_4 = H$, $R_5 = NO_2$

e $R_1 = R_3 = CH_3$, $R_2 = C_{16}H_{33}$, $R_4 = H$, $R_5 = OCH_3$

f $R_1 = R_3 = CH_3$, $R_2 = C_{16}H_{33}$, $R_4 = NO_2$, $R_5 = H$

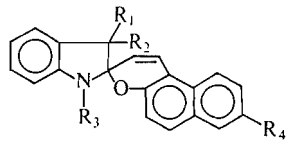

8

a $R_1 = R_2 = CH_3$, $R_3 = C_{16}H_{33}$, $R_4 = H$

b $R_1 = R_2 = CH_3$, $R_3 = C_{16}H_{33}$, $R_4 = NO_2$

c $R_1 = R_3 = CH_3$, $R_2 = C_{16}H_{33}$, $R_4 = NO_2$

naphtaldehyde gave the long-chain spiropyranindolines **7** and **8**.

In the case of spiropyranindolines containing two asymetric centers (*7e*, *7f*, and **8***c*) some interesting observations were made. As an example the nmr spectrum of a freshly prepared solution of the compound *7e* in CCl_4 had one signal at τ 7.30, corresponding to the *N*-methyl protons. This peak decreased with time and simultaneously another appeared at τ 7.38. An equilibrium was reached after 2 h with a ratio of the integrated area under the peaks (τ 7.30/τ 7.38) of 1.7. The spectrum had also two peaks for the methoxy protons (τ 6.36 and τ 6.40). The double signals for some protons on the nmr spectra of these compounds are attributed to the existence of two isomers: *cis* and *trans* characterised respectively by the long-chain on the side of the double bond **9**, and of the oxygen of the 2*H*-pyran ring **10**:

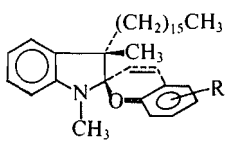

9

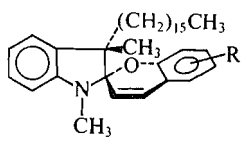

10

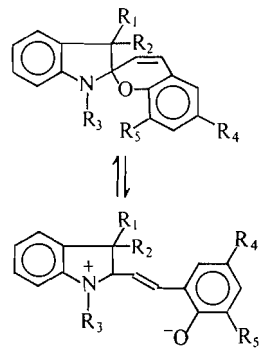

[1]

The equilibrium [1] between the colored and the colorless species of some spiropyranindolines in solution was measured by the method of Flannery (7), and compared with his results for a spiropyranindoline without a long-chain.

From the values given in Table 1 it seems that the long aliphatic chain promotes the colored (opened) form of a spiropyranindoline. Table 2 gives the absorption bands in the uv and visible for the synthesized spiropyranindolines in 95% ethanol.

Figure 1 represents the uv and visible spectra of 3′,3′-dimethyl-1′-hexadecyl-6-nitrospiro-(2*H*-1-benzopyran-2,2′-indoline), *7c*, and 3,3-dimethyl-1 hexadecyl-8′-nitrospiro[indoline-2,3′-(3*H*)-naphto(2,1-*b*)pyran], **8**b. Preliminary results of these compounds as monolayers at the air–water interface show a solid isotherm in the interval 10 to 40 dyn cm^{-1}.

Experimental

Melting points are uncorrected. Microanalyses were performed by Schwarzkopf Microanal. Lab., New York,

TABLE 1. The equilibrium between colored and colorless species of some spiropyranindolines. K_e = [colored form]/[colorless form]

Compound	Solvent	$K_e \times 10^5$*
7a	Ethanol	38.3 ± 1.9
7b	Ethanol	560 ± 33
7c	Benzene	9.68 ± 0.26
	Acetone	396 ± 23
	Isopropanol	1229 ± 73
	Ethanol	2369 ± 19
7e	Ethanol	1215 ± 65
1′,3′,3′-trimethyl-6-nitro-	Benzene	4.10†
spiro[2*H*-1-benzopyran-	Acetone	134†
2,2′-indoline]	Ethanol	843†

*The value 3.5×10^4 l mol^{-1} cm^{-1} for the molar extinction coefficient (ϵ) was used for polar solvents and 5.2×10^4 l mol^{-1} cm^{-1} for benzene (7, 8). The relative error that we give for the K_e is an experimental error and does not reflect the uncertainty in ϵ.

†Values from ref. 7.

Can. J. Chem. Downloaded from www.nrcresearchpress.com by 210.87.254.105 on 09/05/12
For personal use only.

TABLE 2. Spectral characteristics (uv and visible) of spiropyranindolines in 95% ethanol

	Absorption maxima* (λ ± 0.5 nm)											
7*a*	208.0	220.0^S		248.5	270.5^S	299.0				≈420		571.5
7*b*	206.5	225.5		247.5	269.0^S	296.5	323.0^S			≈420		592.0
7*c*	203.5	224.0	230.5^S	244.5	265.0	300.5		335.5			590.0	
7*d*	210.5			246.5		288.0		347.5			562.0	
7*e*	203.5	225.0		246.5^S	263.5	275.0^S	294.0	327.5		≈419		590.0
7*f*	204.5	224.0^S	230.0^S	243.0	266.0^S	297.0		337.5			540.5	
8*a*	203.5	217.5^S	233.5^S	244.0	262.5	299.5	311.4	345.5	359.0	406.5	540.0^S	572.0
8*b*	206.0		229.5	250.0^S	269.5	300.0		349.0^S	364.0	385.0^S	539.5^S	574.0
8*c*	203.5		230.5	248.0^S	270.0^S	298.0		347.5^S	363.5	382.5^S	536.0^S	572.0

*S = shoulder. For absorption in the visible, we used concentrations higher than 10^{-3} mol l^{-1}, except for the compounds **7***d*, **8***b*, and **8***c* where the concentration was ≈10^{-4} mol l^{-1}.

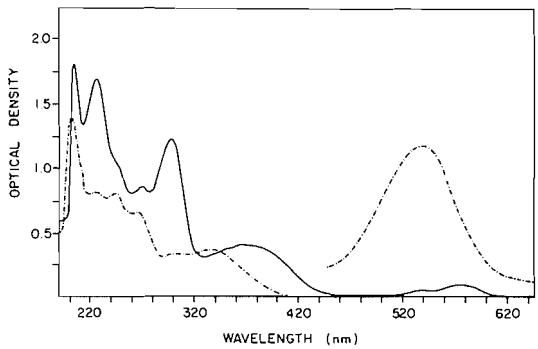

FIG. 1. Absorption spectra of 3′,3′-dimethyl-1′-hexadecyl-6-nitrospiro-(2*H*-1-benzopyran-2,2′-indoline), **7***c*, concentration: 5.0×10^{-5} mol l^{-1} in the uv and 1.0×10^{-3} mol l^{-1} in the visible (— · — · —); and 3,3-dimethyl-1-hexadecyl-8′-nitrospiro[indoline-2,3′-(3*H*)-naphto(2,1-*b*)-pyran], **8***b*, concentration: 2.93×10^{-5} mol l^{-1} (—). Spectra taken in 95% ethanol at 300 K, path length 1.0 cm.

N.Y. The absorption spectra were measured with a Perkin-Elmer 124 or a Unicam SP 1800. The nuclear magnetic resonance spectra were recorded at 60 MHz using a Perkin-Elmer R-12 spectrometer with TMS as standard.

3-Hexadecyl-2-methylindole was prepared by the Fisher synthesis (9), mp 46–48 °C. 2-Hydroxy-6-nitronaphtaldehyde was prepared by the method described in ref. 10, mp 235 °C.

2,3-Dimethyl-3-hexadecylindolenine

A concentrated solution of 3-hexadecyl-2-methylindole (0.06 mol) in anhydrous ether was added dropwise with stirring to a Grignard reagent of methyl iodide (0.06 mol) in 15 ml of anhydrous ether. The resulting solution was refluxed for 3 h. An equimolar amount of methyl iodide was added and the reflux was continued for 24 h. After hydrolysis the organic layer was separated, dried (KOH), and the solvent evaporated. The nmr spectrum and glc analysis of the oily residue showed that the product contained about 67% of 2,3-dimethyl-3-hexadecylindolenine and 33% of unreacted 3-hexadecyl-2-methylindole. The next reaction was performed without further purification of the product.

1,3-Dimethyl-3-hexadecyl-2-methyleneindoline

Crude 2,3-dimethyl-3-hexadecylindolenine (0.033 mol of pure compound) was dissolved in chloroform (30 ml), warmed to the boiling point, and dimethyl sulfate (0.066 mol) added dropwise with stirring. The solution was stirred at room temperature for 1 h and evaporated. To the residue, water and benzene were added and the two layers were separated. The aqueous layer was washed twice with benzene and made basic with a concentrated solution of sodium hydroxide. The solution was extracted several times with ether, the organic layer was dried (KOH), and the solvent evaporated. The residual oil crystallized on cooling to give 8 g (63%) of 1,3-dimethyl-3-hexadecyl-2-methyleneindoline, mp 49–50 °C. Recrystallization in ethanol gave reddish crystals, mp 55–56 °C. The nmr spectrum (CCl_4) had multiplets at τ 2.90–3.65 (four aromatic protons), a doublet centered at τ 6.25 (two olefinic protons), a singlet at τ 6.98 (*N*-methyl protons), a multiplet centered at τ 8.70 (30 methylene protons and three methyl protons), and a triplet centered at τ 9.10 (methyl group of the long-chain).

1-Hexadecyl-2,3,3-trimethylindoleninium Iodide

A solution of 2,3,3-trimethylindolenine (0.125 mol) and hexadecyl iodide (0.187 mol) in chloroform (40 ml) was boiled at reflux temperatures for 20 h. The solvent was evaporated and the residue washed with ether. A reddish solid was separated and dried to give 42.5 g (83.2%) of 1-hexadecyl-2,3,3-trimethylindoleninium iodide, mp 100 °C.

The nmr spectrum ($CDCl_3$) had a broad singlet at τ 2.10 (four aromatic protons), a triplet centered at τ 5.25 (*N*-methylene group), a singlet at τ 6.8 (three 2-methyl protons), a singlet at τ 8.25 (six 3,3-dimethyl protons), a multiplet centered at τ 8.65 (28 methylene protons), and a triplet centered at τ 9.05 (methyl group of the long-chain).

3,3-Dimethyl-1-hexadecyl-2-methyleneindoline

1-Hexadecyl-2,3,3-trimethylindoleninium iodide (0.039 mol) was suspended in water and a concentrated solution of sodium hydroxide was added. The mixture was extracted with ether and the organic layer was dried (KOH) and evaporated to leave 10.3 g (70%) of red liquid 3,3-dimethyl-1-hexadecyl-2-methyleneindoline.

The nmr spectrum (CCl_4) had multiplets at τ 2.90–3.70 (four aromatic protons), a singlet at τ 6.25 (two olefinic

Can. J. Chem. Downloaded from www.nrcresearchpress.com by 210.87.254.105 on 09/05/12
For personal use only.

Can. J. Chem. Downloaded from www.nrcresearchpress.com by 210.87.254.105 on 09/05/12
For personal use only.

protons), a triplet centered at τ 6.80 (*N*-methylene protons), a multiplet centered at τ 8.70 (28 methylene protons and six 3,3-dimethyl protons), and a triplet centered at τ 9.10 (three methyl protons of the long chain).

Condensation of 2-Methyleneindolines with ortho-Hydroxyaldehydes

To a warm solution of an *ortho*-hydroxyaldehyde (0.006 mol) in ethanol (10 ml) was added slowly a solution of a 2-methyleneindoline (0.005 mol) in ethanol. The mixture was refluxed for an additional 6 h. After cooling, a solid was separated and recrystallized several times in ethanol and cyclohexane. The following compounds were obtained:

(*i*) 3′,3′-Dimethyl-1′-hexadecylspiro-(2*H*-1-benzopyran-2,2′-indoline), mp 25 °C. *Anal.* calcd. for $C_{34}H_{49}NO$: C 83.78, H 10.16, N 2.89; found: C 84.21, H 10.21, N 3.16. The nmr spectrum (CCl_4) had multiplets at τ 2.90–3.70 (eight aromatic and one olefinic proton), a doublet centered at τ 4.30 (one olefinic proton), a triplet centered at τ 6.85 (*N*-methylene protons), a multiplet centered at τ 8.70 (28 methylene protons), a singlet at τ 8.80 (six 3′,3′-dimethyl protons), and a triplet centered at τ 9.05 (long-chain methyl protons).

(*ii*) 3′,3′-Dimethyl-1′-hexadecyl-6-nitrospiro-(2*H*-1-benzopyran-2,2′-indoline), mp 84–85 °C. *Anal.* calcd. for $C_{34}H_{48}N_2O_3$: C 76.69, H 9.02, N 5.26; found: C 76.71, H 9.01, N 5.14. The nmr spectrum (CCl_4) had multiplets at τ 1.90–2.10 (two aromatic protons), and τ 2.90–3.70 (five aromatic and one olefinic proton), a doublet centered at τ 4.15 (one olefinic proton), a triplet centered at τ 6.85 (*N*-methylene protons), a multiplet centered at τ 8.70 (28 methylene protons and three 3′-methyl protons), a singlet at τ 8.80 (three 3′-methyl protons), and a triplet at τ 9.05 (long-chain methyl protons).

(*iii*) 3′,3′-Dimethyl-1′-hexadecyl-8-methoxyspiro-(2*H*-1-benzopyran-2,2′-indoline), mp 43–44 °C. *Anal.* calcd. for $C_{35}H_{51}NO_2$: C 81.24, H 9.86, N 2.71; found: C 80.79, H 9.55, N 2.55. The nmr spectrum (CCl_4) had multiplets at τ 2.90–3.65 (one olefinic and seven aromatic protons), a doublet centered at τ 4.32 (one olefinic proton), a triplet centered at τ 6.85 (*N*-methylene protons), a singlet at τ 6.40 (methoxy group), a multiplet at τ 8.75 (28 methylene protons and a methyl groups at 3′), and a triplet at τ 9.10 (methyl protons of the long chain).

(*iv*) 1′,3′-Dimethyl-3′-hexadecyl-6-nitrospiro-(2*H*-1-benzopyran-2,2′-indoline), mp 81–82 °C. *Anal.* calcd. for $C_{34}H_{48}N_2O_3$: C 76.69, H 9.02, N 5.26; found: C 76.58, H 9.06, N 5.18. The nmr spectrum (CCl_4) had a multiplet at τ 1.90–2.10 (two aromatic protons), a multiplet at τ 2.90–3.60 (one olefinic and five aromatic protons), a doublet centered at τ 4.17 (one olefinic proton), two singlets at τ 7.30 and τ 7.40 (*N*-methyl group of two isomers), a multiplet centered at τ 8.75 (30 methylene protons and methyl group at 3′), and a triplet centered at τ 9.10 (methyl group of the long chain).

(*v*) 3,3-Dimethyl-1-hexadecylspiro[indoline-2,3′-(3*H*-naphto(2,1-*b*)pyran], mp 63 °C. *Anal.* calcd. for $C_{38}H_{51}NO$: C 84.92, H 9.50, N 2.61; found: C 84.69, H 9.55, N 2.79. The nmr spectrum (CCl_4) had multiplets at τ 2.00–3.65 (one olefinic and ten aromatic protons), a doublet centered at τ 4.25 (one olefinic proton), a triplet centered at τ 6.80 (*N*-methylene group, a multiplet at τ 8.70 (28 methylene protons and three 3′-methyl protons), a singlet at τ 8.80 (three 3′-methyl protons), and a triplet at τ 9.05 (long-chain methyl protons).

(*vi*) 3′,3′-Dimethyl-1′-hexadecyl-8-nitrospiro-(2*H*-1-benzopyran-2,2′-indoline), mp 62 °C. *Anal.* calcd. for $C_{34}H_{48}N_2O_3$: C 76.69, H 9.02, N 5.26; found: C 76.08, H 9.48, N 5.30. The nmr spectrum (CCl_4) had multiplets at τ 2.24–3.65 (one olefinic and seven aromatic protons), a doublet centered at τ 4.25 (one olefinic proton), a triplet centered at τ 6.85 (*N*-methylene protons), a multiplet at τ 8.75 (28 methylene protons and six 3′-methyl protons), and a triplet at τ 9.05 (long-chain methyl group).

(*vii*) 1′,3′-Dimethyl-3′-hexadecyl-8-methoxyspiro-(2*H*-1-benzopyran-2,2′-indoline), mp 68–69 °C. *Anal.* calcd. for $C_{35}H_{51}NO_2$: C 81.24, H 9.86, N 2.71; found: C 80.94, H 9.88, N 3.01. The nmr spectrum (CCl_4) had multiplets at τ 2.90–3.70 (one olefinic and seven aromatic protons), a doublet centered at τ 4.36 (one olefinic proton), two singlets at τ 7.30 and τ 7.38 (*N*-methyl group of two isomers), two singlets at τ 6.36 and τ 6.40 (methoxy, group of two isomers), a multiplet at τ 8.70 (30 methylene and six 3′-methyl protons), and a triplet centered at τ 9.05 (methyl group of the long-chain).

(*viii*) 3,3-Dimethyl-1-hexadecyl-8′-nitrospiro[indoline-2,3′-(3*H*)-naphto(2,1-*b*)pyran], mp 72.5 °C. *Anal.* calcd. for $C_{38}H_{50}N_2O_3$: C 78.35, H 8.59, N 4.81; found: C 78.13, H 9.08, N 5.11. The nmr spectrum (CCl_4) had multiplets at τ 1.35–3.55 (one olefinic and nine aromatic protons), a doublet centered at τ 4.10 (one olefinic proton), a triplet centered at τ 6.80 (*N*-methylene group), a multiplet at τ 8.70 (28 methylene protons and six 3-methyl protons), and a triplet centered at τ 9.05 (methyl group of the long chain).

(*ix*) 1,3-Dimethyl-3-hexadecyl-8′-nitrospiro[indoline-2,3′-(3*H*)-naphto(2,1-*b*)pyran], mp 139 °C. *Anal.* calcd. for $C_{38}H_{50}N_2O_3$: C 78.35, H 8.59, N 4.81; found: C 77.87, H 9.11, N 5.09. The nmr spectrum (CCl_4) had multiplets at τ 1.50–3.70 (one olefinic and nine aromatic protons) a, doublet centered at τ 4.15 (one olefinic proton), two singlets at τ 7.30 and τ 7.40 (*N*-methyl group of two isomers), a multiplet at τ 8.75 (30 methylene protons), and a superposed singlet and triplet at τ 8.90–9.10 (methyl groups).

Acknowledgments

We wish to thank Mr. Y. Thibeault for his help in this study. This research was supported by grants from the Ministère de l'éducation du Québec (FCAC) and the National Research Council of Canada.

1. G. H. Brown (*Editor*). Photochromism in techniques of chemistry. Vol. III. Wiley-Interscience, New York, New York. 1971.
2. R. C. Bertelson, K. D. Glanz, D. B. McQuain, and F. D. Thomson. Final report on contract AF41 (609), AD645730 (1966).
3. E. Rabinowitch. Proceedings of the 5th International Congress of Biochemistry. Vol. VI. 15 (1963).
4. E. A. Dratz, J. E. Gaw, S. Schwartz, and Wei-Mei Ching. Nature, **237**, 99 (1972).

5. S. N. NAGARAJA and S. V. SUNTHANKAR. J. Sci. Ind. Res. (India) Sect. B, **17**, 457 (1958).
6. I. I. LEVKOEV and A. YA. BASHKIROVA. Zh. Prikl. Khim. **35**, 688 (1962).
7. J. B. FLANNERY, JR. J. Am. Chem. Soc. **90**, 5660 (1968).
8. J. G. CALVERT and J. N. PITTS, JR. Photochemistry. John Wiley and Sons Inc., New York, New York. 1966.
9. NGUYEN P. BUU-HOÏ and P. JACQUIGNON. C. R. Acad. Sci. **251**, 1297 (1960).
10. P. RUGGLI and E. BURCKHARDT. Helv. Chim. Acta, **23**, 445 (1940).

Can. J. Chem. Downloaded from www.nrcresearchpress.com by 210.87.254.105 on 09/05/12
For personal use only.

Di-*tert*-butyl peroxide decomposition behind shock waves

DAVID K. LEWIS
Department of Chemistry, Colgate University, Hamilton, New York 13346

Received August 20, 1973[1]

DAVID K. LEWIS. Can. J. Chem. **54**, 581 (1976).

The homogeneous, gas phase thermal decomposition of di-*tert*-butyl peroxide has been studied in a single pulse shock tube. Samples containing 0.05% to 0.5% reactant in argon were heated to 528–677 K at total pressures of about 1 atm. Acetone and ethane were the only significant products. The reaction obeyed first order kinetics. The Arrhenius parameters, log A (s^{-1}) = 15.33 ± 0.50, E_{act} (kJ/mol) = 152.3 ± 5.8, are in agreement with the bulk of the earlier reported results of lower temperature work, and with a recently reported result obtained via the very low pressure pyrolysis technique. Indications from some of the earlier work that the A factor may decline at high temperatures are not supported by the present study.

DAVID K. LEWIS. Can. J. Chem. **54**, 581 (1976).

On a étudié, dans un tube à choc pulsé simple, la décomposition thermique en phase gaseuse et homogène du peroxyde du di-*tert*-butyle. On a chauffé des échantillons contenant de 0.05 à 0.5% réactif dans l'argon à des températures de 528 à 677 K et à des pressions totales d'environ 1 atm. L'acétone et l'éthane sont les deux seuls produits formés en quantité notable. La cinétique de la réaction est du premier ordre. Les paramètres d'Arrhénius sont log A (s^{-1}) = 15.33 ± 0.50, E_{act} (kJ/mol) = 152.3 ± 5.8, qui sont en accord avec l'ensemble des données rapporté antérieurement pour des travaux à plus basse température et avec un résultat rapporté récemment obtenu par l'intermédiaire de la technique de pyrolyse à basse pression. Les résultats obtenus au cours de la présente étude n'offrent aucun support aux indications provenant de travaux antérieurs à l'effet que la valeur de A peut diminuer à haute température.

[Traduit par le journal]

The gas phase thermal decomposition of di-*tert*-butyl peroxide (DTBP) has been studied in conventional static and flow reactors over the temperature range 363–623 K by numerous workers. In the most recent report, Shaw and Pritchard (1) provided, along with their results, a comprehensive and critical review and reanalysis of all previously reported studies. They concluded that the homogeneous reaction can be completely accounted for by a direct unimolecular process

$$DTBP \rightarrow 2CH_3COCH_3 + 2CH_3$$

and recommended the Arrhenius parameters log A (s^{-1}) = 15.80 ± 0.03 and E_{act} (kJ/mol) = 158.07 ± 0.25 over the range 363–623 K. However, there was some indication that this very high pre-exponential factor was beginning to decrease at the high end of this temperature range, and the need for data at higher temperatures was indicated.

A shock tube study of the decomposition kinetics of a series of *tert*-butyl alkyl ethers has been in progress in this laboratory for some time now (2). In elucidating the mechanisms of these reactions, it became necessary to produce *tert*-butoxy radicals and monitor their subsequent decomposition at 1000–1200 K; DTBP was the obvious choice as the source of these radicals, because the fragmentation is complete and essentially instantaneous on the ~1 ms experimental time scale at these temperatures. That study provided an opportunity to make experimental runs at lower temperatures, 528 to 677 K, in which range the DTBP decomposition goes 0.10%–97.9% to completion during the ~1.2 ms reaction time. The results of these lower temperature experiments are the subject of this paper.

While this manuscript was in preparation, there appeared a report of a study of DTBP decomposition kinetics at 507–660 K via the very low pressure pyrolysis technique (3). Because of the low pressures involved, measured rate constants required correction for falloff effects; k_∞ values were determined via RRKM calculations. Resulting Arrhenius parameters reported were E_{act} = 154.0 kJ/mol (from acetone yield) and E_{act} = 156.3 kJ/mol (from DTBP loss). The A factors for both sets of data are $10^{15.6}$ s^{-1};

[1]Revision received August 25, 1975.

Can. J. Chem. Downloaded from www.nrcresearchpress.com by 210.87.254.40 on 09/05/12
For personal use only.

TABLE 1. Summary of experimental conditions (reaction times $\approx$ 1200 μs; total pressures behind reflected shocks $\approx$ 1 atm)

Set	Symbols (Fig. 1)	% DTBP	Initial pressure range (Torr)	Reaction temperature range (K)
A	○, ●	0.05	90–160	546–677
B	△, ▲	0.10	95–160	553–640
C	□	0.50	116–160	528–593

however, in the RRKM calculations, the transition state model was chosen to give this value, so it cannot be considered an independent result.

Experimental Section

Materials

DTBP was obtained from K and K Laboratories. It was subjected to a purification process involving three successive freeze–pump–thaw–distill cycles in a vacuum line. At each distillation only the middle portion was kept. After purification there was no detectable impurity upon gas chromatographic analysis; the estimated maximum undetectable impurity concentration was 0.01%. Matheson "Ultra-High Purity" argon (99.999%) was used as the diluent gas for preparation of 0.05 to 0.5% DTBP samples.

Apparatus

A 10 cm i.d. stainless steel single-pulse shock tube was used in the study. This apparatus and details of its operation have been described previously (4).

Analyses

Reactant and product samples were analyzed on a Varian Aerograph 1440 chromatograph equipped with a hydrogen flame detector. The column was a 10 ft $\times$ $\frac{1}{8}$ in. column of 20% polypropylene glycol saturated with silver nitrate on 80/100 mesh chromosorb W at 40 °C. The instrument was calibrated with 0.25% samples of ethane, acetone, and DTBP before and after each day's experiments to be certain that the calibration factors had not changed during that time. Peak areas were evaluated by the "cut and weigh" method. The products of each shock were analyzed two or three times.

Conditions

Series of single-pulse shock tube experiments were run on mixtures of 0.050%, 0.10%, and 0.50% DTBP in argon. Experimental conditions are summarized in Table 1.

Calculations

Temperatures for all shocks were computed from measured incident shock velocities on the basis of ideal one-dimensional shock theory. Vibrational assignments and structural data for DTBP reported by McKean *et al.* (5), supplemented by our estimates for unassigned torsional vibrations, were used originally in computing thermodynamic data for DTBP/argon mixtures. A recent recalculation using the torsional frequency values chosen by Perona and Golden (3) on the basis of entropy considerations resulted in negligibly small changes.

The initial step in the reaction, the scission of DTBP to form two *tert*-butoxy radicals, has a $\Delta H_{298}^0 = +156.9$ kJ/mol (6); but the net reaction which forms two acetone molecules and one ethane molecule from each DTBP (see Results) is quite exothermic: $\Delta H_{298}^0 = -180.3$ kJ/mol (6). The combination of methyl radicals to form ethane is sufficiently rapid under these experimental conditions (7) to yield most of the heat from this process during the reaction time, rather than during the subsequent cooling period. The net effect is that the temperature of the reacting gas mixture will rise if large amounts of DTBP are allowed to fragment. In these experiments, extents of conversion did not exceed 46% in the 0.10% mixture or 6.5% in the 0.50% mixture. Changes in gas temperatures from exothermicity should not have exceeded 6 K, and were not corrected for in the analysis.

Although the gas sample is heated almost instantaneously ($t \approx 10^{-11}$ s) as the shock wave passes through it, the cooling process is much slower ($\lesssim 6 \times 10^4$ K/s) and significant amounts of product ($\lesssim 25\%$ of the total) are formed during the cooling process. For each experiment we have integrated over the reflected shock dwell time and cooling period, determined from oscillosope records of pressure histories, and have substracted out the amounts of products attributable to the cooling process before calculating rate constants.[2] For these corrections, we assumed that the reaction is first order and assumed that the Arrhenius parameters reported by Shaw and Pritchard (1) are applicable under the conditions of these experiments. Both of these assumptions are justified by the experimental results.

Rate constants for consumption of DTBP were calculated for each experiment using the integrated rate expression for an irreversible first order reaction.

Results

The DTBP decomposition was observed to proceed cleanly over the range of experimental conditions. Only acetone and ethane and trace amounts of methane were produced. The rate data are displayed in Fig. 1. The amounts of acetone and ethane were stoichiometric (2:1) within the $\pm 5\%$ experimental error of the

[2]Experimental data and discussion of data reduction procedures may be obtained, at a nominal charge, from the Depository of Unpublished Data, CISTI, National Research Council of Canada, Ottawa, Canada K1A 0S2.

Can. J. Chem. Downloaded from www.nrcresearchpress.com by 210.87.254.40 on 09/05/12
For personal use only.

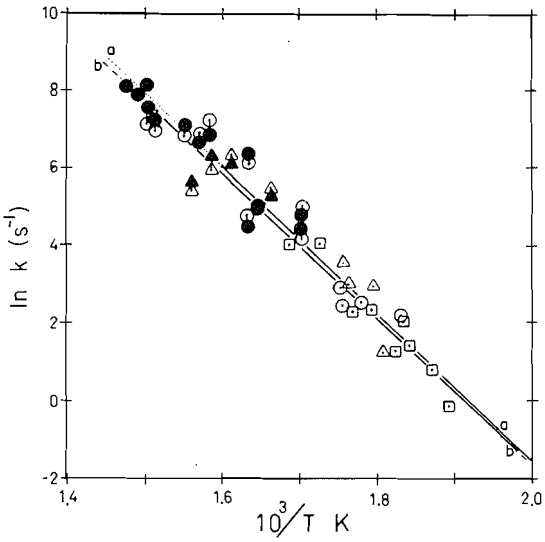

FIG. 1 Arrhenius plot of rate data for DTBP decomposition, as determined from ethane and acetone production (open symbols) and DTBP depletion (closed symbols). The short vertical lines connect data points from the same experiment. ○, ●, 0.05% DTBP; △, ▲, 0.10% DTBP; □, 0.50% DTBP. Lines represent earlier published parameters: (*a*) recommended by Shaw and Pritchard (1); (*b*) results of Perona and Golden (3).

analysis, with no discernable trends to indicate higher relative concentrations of either product. Their concentrations as determined from multiple vpc analyses were averaged before rate constants were calculated. Values for rate constants determined from acetone and ethane product concentrations are included in Fig. 1 only for experiments in which less than 90% decomposition of DTBP occurred. Above that limit the analytical imprecision can introduce an error of more than a factor of two in calculated k values. Figure 1 also displays rate constants determined from extents of DTBP loss. In this case, values of k for experiments in which less than 10% decomposition occurred are subject to large errors and were omitted. For experiments in the range 10% to 90% decomposition, rate constants calculated from reactant loss and from product formation were usually in good agreement. However, four experiments in which the calculated k values differed by more than a factor of two were discarded. Four other shocks were also discarded because the velocity gauge signals could not be unambiguously distinguished from background noise on the oscilloscope traces and/or because of poorly formed pressure traces.

A comparison of the data from the three reaction mixtures in Fig. 1 indicates that the reaction shows first order behavior throughout the range of experimental conditions. The Arrhenius parameters deduced from the data are log A (s^{-1}) = 15.33 ± 0.50, E_{act} = 152.3 ± 5.8 kJ/mol. These values are identical, within the uncertainty specified (one standard deviation in the least squares analysis), to the values recommended by Shaw and Pritchard (1) over the range 363–623 K, and to the values deduced by Perona and Golden (3) over the range 506–660 K. If the five experiments at temperatures above 645 K, corresponding to >80% decomposition, are removed from the least squares reduction, the values log A = 15.84 ± 0.67, E_{act} = 157.9 ± 7.5 kJ/mol are obtained. As a matter of record, inclusion of the eight points that were thrown out for what were deemed justifiable reasons would result in a considerable increase in scatter in Fig. 1 and therefore higher standard deviation; but the change in E_{act} would be an increase of 4 kJ/mol. In the least squares reduction that yielded the above results, $1/T$ was taken as the independent variable, log k the dependent variable.

Discussion

In performing kinetics studies in shock tubes, it is often the case that uncertainties associated with measurements of the reaction temperature are much larger on a relative basis than uncertainties in logarithms of rate constants calculated from measured extents of reaction. When temperatures are determined from calculations based on incident or reflected shock velocity, scatter on an Arrhenius plot amounting to ±25 to ±50 K is common. This lack of precision can be overcome by making use of the relative rate technique, in which another noninterfering first order reaction, with similar, well known Arrhenius parameters is run simultaneously as a standard, or by performing a large number of experiments and using statistical methods of data reduction to obtain the desired information. In this study no standard reaction could be found which met all the requirements, so the latter approach was taken. The scatter in Fig. 1 indicates a maximum random error of ±30 K, and most points lie within ±15 K of the least squares line. This latter value is the estimated maximum uncertainty associated with the

Can. J. Chem. Downloaded from www.nrcresearchpress.com by 210.87.254.40 on 09/05/12
For personal use only.

Can. J. Chem. Downloaded from www.nrcresearchpress.com by 210.87.254.40 on 09/05/12
For personal use only.

reading of shock arrival times at velocity gauges from the oscilloscope records.

Systematic errors in calculated temperatures are usually more difficult to assess; the effects of shock attenuation, boundary layer growth, heating or cooling of the gas by the reaction taking place and other non-ideal processes may be considerable. The shock tube used in this study has been found to yield shock speed temperature values that agree with temperatures calculated from extents of reaction of cyclohexene decyclization (4), cyclopentene dehydrogenation (8), and other reactions (2) in the range 900–1100 K. In some of the present experiments, four shock arrival times were recorded, allowing three velocity measurements. The final gauge (also used for monitoring the gas pressure history) was close to the downstream end of the tube. There was no consistent trend to indicate that speed-up or attenuation of the incident shock was occurring. The location of the gauges prevented the need for extrapolating measurements at one location to a reacting gas at another location along the tube.

A final argument against significant systematic temperature error (more than a few degrees K) is the excellent agreement between rate constants from the shock tube data and the earlier reported results, particularly in the 525–550 K range where the latter are believed to be quite reliable.

The measurement of reaction times can introduce systematic errors into calculated rate constants, if performed improperly. In the present study, because of the large tube diameter (10 cm i.d.) and small sample withdrawn for analysis ($\sim$50 cm^3), the sample should have occupied only a short length of the tube during reaction. Thus, there is no need for reaction time averaging. Also, the pressure transducer and sampling port are located such that the samples withdrawn for analysis should have been located at the transducer under reflected shock conditions, so no correction from the reaction time indicated on the pressure history was necessary. A necessary condition for the foregoing arguments to be correct is that there was no significant mixing of the gas after the initial shock heating/cooling cycle, by subsequent unattenuated waves. With our apparatus and experimental procedure it is impossible to detect small amounts of post-experiment mixing, and it would be naive to assume that absolutely no perturbations propagated through the gas after cooling. However, if such perturbations did occur, they were not of sufficient intensity to introduce driver gas into the samples extracted for analysis. A series of five shocks was run on pure argon at $T \approx 600$–700 K, using as the driver gas helium to which substantial amounts of *n*-butane were added. Products withdrawn immediately after the shocks contained no traces of organic material.

Another source of error in rate constants is the boundary layer of cool gas that forms along the shock tube walls. Inclusion of some of this gas in the analyzed sample will cause apparent rate constants to be too low. Samples containing 1–5% unheated gas will result in log k values that are subject to negligible error if the reaction temperatures are low, but the errors become important at higher temperatures at which large extents of reaction are expected. In these experiments the large tube diameter and short reaction time should have resulted in relatively low percentages of boundary layer gas in the analyzed samples. However, it will be noted in Fig. 1 that the five experiments above 645 K give rate constants which group slightly below the least squares line and which lower the calculated activation energy by 4.6 kJ/mol. Thus the experiments in which extents of conversion exceeded 80% may have been affected significantly by this source of error.

Conclusions

This single-pulse shock tube study of the thermal decomposition kinetics of di-*tert*-butyl peroxide has yielded Arrhenius parameters that are in excellent agreement with results from earlier studies in static and flow reactors as reviewed by Shaw and Pritchard, and with the very low pressure pyrolysis study by Perona and Golden. This adds support to the validity of the VLPP technique and supports the adequacy of the RRKM calculations as applied to this system. The possible downward curvature of the Arrhenius Plot noted at high temperatures by Shaw and Pritchard in their compilation of earlier published data is not reproduced in this study. Thus the A factor appears to remain very high and constant from 363–677 K, over which range the rate constant varies by ten orders of magnitude. Even at the highest temperatures,

with very high extents of decomposition, the pyrolysis is essentially free of side reactions under the homogeneous shock tube conditions.

Acknowledgments

The author wishes to thank the Colgate University Research Council for support of this work, and Mr. Michael Sarr for performing a preliminary study of DTBP decomposition in this laboratory.

1. D. H. SHAW and H. O. PRITCHARD. Can. J. Chem. **46**, 2721 (1968).
2. D. K. LEWIS, S. RAPPARD, L. ROCCA, and M. SARR. Decomposition of *tert*-butyl alkyl ethers in shock waves. Presented at 6th Northeast Regional Meeting of the American Chemical Society, Burlington, Vt., August, 1974. Manuscript in preparation.
3. M. J. PERONA and D. M. GOLDEN. Int. J. Chem. Kinetics, *V*, 55 (1973).
4. D. LEWIS, M. KEIL, and M. SARR. J. Am. Chem. Soc. **96**, 4398 (1974).
5. D. C. MCKEAN, J. L. DUNCAN, and R. K. M. HAY. Spectrochim. Acta, **23A**, 605 (1967).
6. S. W. BENSON and H. E. O'NEAL. Kinetic data on gas phase unimolecular reactions. NSRDS-NBS 21, U.S. Govt. Printing Office. 1970. pp. 430, 597.
7. A. SHEPP. J. Chem. Phys. **24**, 939 (1956).
8. D. LEWIS, M. SARR, and M. KEIL. J. Phys. Chem. **78**, 436 (1974).

Can. J. Chem. Downloaded from www.nrcresearchpress.com by 210.87.254.40 on 09/05/12
For personal use only.

Raman spectra of pyridine adsorbed on a series of ion-exchanged forms of zeolite Y

T. A. EGERTON,[1] A. H. HARDIN,[2] AND N. SHEPPARD
School of Chemical Sciences, The University of East Anglia, Norwich, United Kingdom

Received June 11, 1975

T. A. EGERTON, A. H. HARDIN, and N. SHEPPARD. Can. J. Chem. **54**, 586 (1976).

As with other silicas and aluminas, it is shown that a broad general fluorescence from Y zeolite samples excited by irradiation with the 6328 Å line of a He/Ne laser can be greatly reduced by heating the zeolite in oxygen at 500 °C. This general fluorescence is attributed to the presence of traces of unsaturated hydrocarbon impurities which can be burned off by the oxygen treatment. A narrower residual fluorescence in the region of 14 000 – 14 500 cm^{-1} is attributed to the presence of Fe^{3+} impurities.

Successful Raman spectra using He–Ne laser excitation have been obtained from pyridine adsorbed on oxygen-treated NaY zeolite, and on samples of this zeolite in which the majority of sodium ions have been replaced by Li^+, K^+, Co^{2+}, Cu^{2+}, Ce^{3+} or H^+ (decationated Y zeolite). The position of the ν_1 Raman band from the ring-breathing mode of pyridine is found to give a linear correlation with q/r for the metal ions (where q is the charge and r the radius of an ion) strongly suggesting that the main adsorption is at cation sites. During adsorption of pyridine on CeY the spectrum changes as a function of time. Adsorption on Ce^{3+} appears to be the final situation and intermediate Raman spectra suggest that pyridine adsorbs and forms hydrogen bonds with surface OH groups; quite different Raman spectra are obtained from these two surface species. The Raman spectra of pyridine on HY zeolite is consistent with the coexistence of pyridinium ions and hydrogen-bonded pyridine molecules.

T. A. EGERTON, A. H. HARDIN et N. SHEPPARD. Can. J. Chem. **54**, 586 (1976).

Comme avec d'autres silices et alumines, on montre qu'une fluorescence générale large provenant d'échantillons de zéolithe-Y excitée par une irradiation avec la ligne 6328 Å de laser He/Ne peut être grandement réduite par chauffage de la zéolithe dans l'oxygène à 500 °C. On attribue cette fluorescence générale à la présence de traces d'impuretés d'hydrocarbures insaturés qui peuvent être brûlés par le traitement avec de l'oxygène. On attribue une fluorescence résiduelle plus étroite dans la région de 14 000 à 14 500 cm^{-1} à la présence d'impuretés de Fe^{3+}.

On a pu obtenir des spectres Raman, utilisant l'excitation laser He/Ne, pour de la pyridine adsorbée sur une zéolithe NaY traitée à l'oxygène et sur des échantillons de cette zéolithe dans lesquels la majorité des ions sodium ont été remplacés par des ions Li^+, K^+, Co^{2+}, Cu^{2+}, Ce^{3+} ou H^+ (zéolithe-Y décationnée). On a trouvé que la position de la bande Raman ν_1 pour le mode de pulsation du cycle de la pyridine donne une corrélation linéaire avec q/r pour les ions métalliques (q est la charge et r est le rayon de l'ion), ce résultat suggère fortement que l'adsorption principale est au niveau des sites cationiques. Durant l'adsorption de la pyridine sur le CeY, le spectre change en fonction du temps. L'adsorption sur Ce^{3+} semble être la situation finale; les spectres Raman intermédiaires suggèrent que la pyridine s'adsorbe et forme des ponts hydrogènes avec les groupes OH de la surface. On obtient des spectres Raman très différents à partir de ces deux espèces de surface. Le spectre Raman de la pyridine sur la zéolithe HY est en accord avec la co-existence d'ions pyridinium et de molécules de pyridine liées par des ponts hydrogènes.

[Traduit par le journal]

Introduction

Infrared spectroscopy has been widely used in studies of zeolite surface chemistry (1). Early studies focussed attention on the hydroxyl groups that remained in the zeolite after dehydration (2). Later papers reported the spectra of adsorbed species and showed that the infrared spectra of adsorbed molecules were, in suitable cases, sensitive to the nature of the charge-balancing cations (3, 4). By using such probe molecules, information about the electrical fields at the zeolite surface was obtained (3).

Ward has shown that pyridine is a most useful

[1]Present address: Tioxide International Ltd., Billingham, Teesside, England.

[2]Present address: Energy Research Laboratory, Department of Energy, Mines and Resources, 555 Booth Street, Ottawa, Canada K1A 0G1.

Can. J. Chem. Downloaded from www.nrcresearchpress.com by 210.87.254.6 on 09/05/12
For personal use only.

Can. J. Chem. Downloaded from www.nrcresearchpress.com by 210.87.254.6 on 09/05/12
For personal use only.

probe molecule for studies of zeolite surfaces (5, 6). The pyridine can adsorb on zeolites in at least four different ways, (*a*) by physical adsorption, (*b*) by hydrogen-bonding to surface OH groups, (*c*) by proton-transfer from a surface OH group to form a pyridinium ion, and (*d*) by the formation of a coordinate bond, either to a charge-balancing cation or to three-coordinate Al^{3+} ions of the aluminosilicate framework. The latter Al^{3+} sites may be generated during the thermal decomposition of the hydrogen form of the zeolite. Each of these main types of interaction gives rise to characteristic bands in the infrared spectrum (5), but the infrared spectra are not readily distinguishable for the two possibilities of forming coordinate linkages with the surface.

In this paper we describe some features of the Raman spectra of pyridine adsorbed on ion-exchanged forms of zeolite Y, and considerably extend our earlier brief report of the spectrum of pyridine on NaY (7*b*). The spectrum of pyridine on the ammonium-exchanged form of mordenite has been reported by Hendra *et al.* (8). At monolayer coverage a single Raman line at 1004 cm^{-1} was observed and assigned to pyridine hydrogen-bonded to the surface. Buechler and Turkevich (9), as part of a survey laser-Raman study of a number of surfaces, reported the Raman and fluorescence spectra of the Eu(III) Y zeolite itself. Angell (10) has recently recorded Raman spectra of 16 natural and synthetic zeolites and also obtained Raman spectra of acetonitrile, propylene, acrolein, and carbon dioxide adsorbed on the sodium forms of A, X, and Y zeolites. The spectra of the adsorbed molecules were in these cases very similar to the liquid-state spectra, indicating that only weak adsorption had occurred.

The application of laser-Raman spectroscopy to surface chemistry studies has recently been reviewed (11*a*, 11*b*). It is not yet a routine matter. A major problem has been the minimization of a broad background emission which is associated with the adsorbent itself (7–12, footnote 3), although it may become enhanced in the presence of certain types of adsorbate (7*b*, 9, footnote 3). If this emission is not reduced it gives rise to a strong background signal upon which the Raman spectrum of the adsorbed species is superimposed. Since in a photon-counting situation the noise is proportional to the square root of the *total* signal, the much weaker Raman spectrum of the surface species can easily become lost in the overall noise level.

Egerton *et al.* (7*a*, 7*b*) on the one hand, Buechler and Turkevich (9) and more recently Cooney *et al.* (11*a*), have independently shown that with oxide-based catalysts this emission can be much reduced, and for some silicas eliminated, by heating the sample in oxygen for a number of hours (at 500 °C is suggested in refs. 7*a*, 7*b*; at 600–650 °C is suggested in ref. 9). These groups attribute the success of these procedures to the 'burning-off' of small amounts of fluorescent hydrocarbon impurities from the oxide surfaces. Increases in emission when such samples are initially heated to intermediate temperatures in air or in vacuum (7, 8, 10, 12, footnote 3) may, in this picture, be attributed to the conversion of saturated hydrocarbon impurities to unsaturated and conjugated ones which generate fluorescence but can only be 'burnt-off' at higher temperatures in oxygen. Others (12) have attributed the 'fluorescence' to the presence of tightly hydrogen-bonded water molecules close to Lewis sites.

It has been found (7*b*) that the oxygen treatment of a number of aluminas, silica-aluminas and zeolites, leaves behind a residual weaker but still broad fluorescence of different characteristic frequency (*ca.* 14 100 cm^{-1}, of half-width *ca.* 1000 cm^{-1}). This has been provisionally attributed to the presence of small amounts of fluorescent Fe^{3+} ions which have replaced a proportion of Al^{3+} ions in tetrahedral environments.

Work by Buechler and Turkevich (9) and in this laboratory[4] has shown that, unlike the sharper Raman features whose wavenumbers move precisely with that of the exciting line, the broad background emissions remain essentially fixed in position although the intensities vary as the exciting line approaches. These experiments show that these broad emissions may be correctly termed fluorescence (or phosphorescence) backgrounds.

In this paper we report the main features of the fluorescent background spectra obtained from seven cation-exchanged forms of zeolite Y, and the Raman spectra of pyridine adsorbed on

[3]A. H. Hardin and N. Sheppard, unpublished results.

[4]D. Flint and N. Sheppard, unpublished results.

Can. J. Chem. Downloaded from www.nrcresearchpress.com by 210.87.254.6 on 09/05/12
For personal use only.

these samples after heating with oxygen had reduced the fluorescence to a minimum.

In Angell's earlier work (10) successful Raman spectra from adsorbed molecules were only obtained on Na-zeolites. He reported that the purest zeolite samples gave the weakest backgrounds but that, where such a background was present, heating in oxygen, air, or vacuum at 500 °C did not eliminate but increased it. Our finding is that, as before (7), heating our zeolite samples in oxygen greatly *reduced* the initial fluorescence but did not eliminate it, there being a residual fluorescence of different profile as described above for alumina-containing samples. The initial fluorescence grew back slowly with time on heating in vacuum. It should be borne in mind that Angell's measurements were made using the 4880 Å Ar line. Also Buechler and Turkevich (9) found that only Raman lines from EuY were excited by the 6371 Å line of an Ar/Kr laser whereas the 4880 Å line excited both a Raman and a fluorescence spectrum. The differences in excitation may hence account for the differences in comparative strengths of the fluorescence backgrounds.

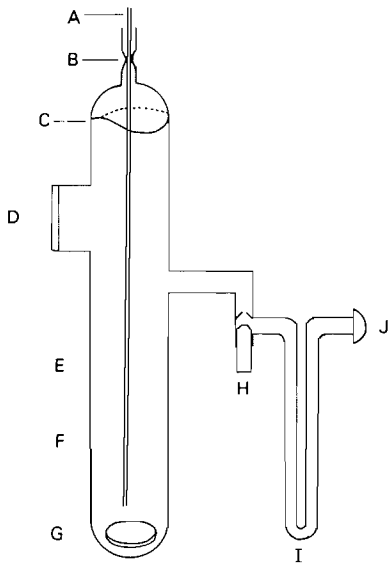

FIG. 1. A sealed cell for obtaining Raman spectra of zeolite adsorbents and adsorbates under grease-free conditions. A, oxygen entry; B, seal-off point; C, disc entry; D, optical window; E, quartz-to-glass seal; F, quartz tube; G, sample disc; H, Rotaflo Teflon tap; I, low-temperature trap; J, ball-joint.

Experimental

The ion-exchanged zeolites used in these experiments were prepared from two different batches of Linde NaY zeolite. (SK-40 Lot Nos. 51-31 and 12996-46). Both batches had a silica–alumina ratio in agreement with the formula $Na_{56}(AlO_2)_{56}(SiO_2)_{136}\cdot 264H_2O$. The latter batch was used for studies of pure NaY and for preparation of highly exchanged (>70%) LiY and KY. Lot No. 51-31 was used for the preparation of CuY-50,[5] CoY-80, CeY-71, and NH_4Y-64. The exchange procedures have been described previously (13). The NH_4Y-64 was converted to HY-64 by heating to 500 °C for 12 h in air.

For spectroscopic studies 1 g portions of the hydrated zeolite were pressed into self-supporting 25 mm discs at 10 tons psi. The cells were designed in the light of our earlier experience, which showed that stopcock-grease vapours can contribute strongly to the background fluorescence (*7b*). The design is illustrated in Fig. 1. The Rotaflo Teflon taps gave adequate vacua when properly set and cleaned. As an added precaution the cells were protected by liquid-nitrogen traps from any source of condensable vapours in the vacuum line. Typically, the cell was precleaned by heating it empty for 4 h at 500 °C. Sample discs were introduced at C, (Fig. 1), and the cell was sealed. With the Teflon tap H removed, a slow stream of oxygen was passed in through A and out at H, while the zeolites were heated at 80, 130, 330 °C for successive 1 h periods and then above 500 °C. When heating was complete the tube A was withdrawn and the cell was sealed by drawing off the inlet at B, and then immediately evacuated for 1 h, usually at 330 °C, but in some cases at a lower temperature in order to keep the background low. Details of zeolite pretreatment are given in Table 1. Background spectra of the zeolites in the untreated, oxygen-treated, and final evacuated state were recorded from $\Delta\nu = -1500\ cm^{-1}$ to $\Delta\nu = +3500\ cm^{-1}$ with respect to the red exciting line at 15 802 cm^{-1} (6328 Å).

The discs were allowed to cool to 20 °C before being exposed to pyridine vapour. The pyridine adsorbate (redistilled BDH Analar Grade) was degassed by four freeze–pump–thaw cycles before use. Adsorption of the vapour was initially from doses of fixed size and finally from the vapour in equilibrium with the liquid adsorbate. Generally the spectrum was observed after the addition of several 0.2 mmol aliquots. Spectra were not always observable at low coverage, but in all cases at least one Raman feature was observed after the disc had been exposed to the equilibrium vapour pressure of pyridine. In the cases of CoY-80 and CuY-50 the blue or mauve discs absorbed a considerable fraction of the red excitation line and gave weak Raman spectra.

Raman spectra were recorded with a Spex Industries laser Raman spectrometer using a Spectra-Physics Model 125 He–Ne laser, 90° illumination–collection optics, and a Model 1401 double monochromator. The principal neon lasing line at 15 802 cm^{-1} was employed. It yielded 40–60 mW with r.f. stabilization. Sample discs were held at an angle of 30° (from grazing) to the exciting radiation. The

[5]Through this paper the nomenclature MY-X will be used to describe an NaY zeolite in which X% of the sodium has been replaced by cations of M.

TABLE 1. Details of the pretreatment of the zeolite samples

Zeolite	Oxygen pretreatment Temperature (°C)	Oxygen pretreatment Time (h)	Vacuum pretreatment Temperature (°C)	Vacuum pretreatment Time (h)	Fluorescence recovery at 430 cm^{-1}
NaY-100	500	16	330	1	2.5×
LiY->70	570	72	250	1	1.5×
KY->70	610	24	330	1	6×
HY-64	500	45	100	1	2×
CoY-80	510	21	330	1	2×
CuY-50	520	18	330	1	4×
CeY-71	520	40	330	1	2×

beam was focussed to a point behind the front face of the sample disc to avoid localized heating (when localized heating occurred it sometimes led to an increase of the background fluorescence when adsorbate was present). Other details of sample alignment, cell holders, and spectrometer conditions have been reported elsewhere (*7b*).

Spectra were usually recorded at 8.0 cm^{-1} resolution in order to give higher energy at the detector, but even then scan speeds as low as 5 or 10 cm^{-1}/min had to be used. In a few special cases the 1000 cm^{-1} region was scanned at 2.5 or 4.0 cm^{-1} resolution. Survey spectra were also run at 8 cm^{-1} resolution but at 100 cm^{-1}/min and with a time constant of 0.25 s. Consequently these spectra were noisy and weak features were difficult to locate to within ± 10 cm^{-1}. We did not investigate in detail the weak spectra of the zeolites themselves. Frequencies within the spectra of each pyridine–zeolite system were calibrated with respect to the non-lasing lines.

All spectra were measured with the samples at 20 °C neglecting any heating of the zeolite disc by the laser beam. The latter could have been of importance when making measurements with the highly coloured Cu^{2+} and Co^{2+} samples. A conventional glass vacuum system, capable of maintaining a vacuum of 10^{-6} Torr, was used for disc pretreatment and for dosing the adsorbate.

Results

Fluorescent background spectra were normally very broad and strong for zeolite samples that had not been heated in oxygen at 500 °C or above and it was not feasible to obtain Raman spectra of adsorbed molecules (or of the zeolite itself) from these. Fluorescence maxima occurred between 15 000 and 15 500 cm^{-1}; ($\Delta\nu \sim$ 800–300 cm^{-1}).

After initial heating of the zeolite samples in oxygen, as specified in Table 1, Raman spectra from the adsorbents were obtainable superimposed on the much weaker scattering backgrounds. Figure 2*a* shows such a spectrum from a zeolite HY sample. The residual fluorescence, centred in different samples between $\bar{\nu} \sim$ 14 000 – 14 500 cm^{-1} ($\Delta\bar{\nu} \sim$ 1800–1300 cm^{-1}), is similar in form to that found previously with alumina-containing oxides (*7b*) and attributed to the presence of Fe^{3+} impurities. Table 2*a* lists the frequencies of the fluorescence maxima and approximate half-widths of the bands. Additional fluorescence reappeared when the zeolites were subsequently evacuated at elevated temperatures (Table 1) and the same information is given for these fluorescence spectra in Table 2*b*. The maxima at this stage normally fell in the original higher frequency region of 15 000 – 15 500 cm^{-1} and a spectrum from zeolite HY is shown in

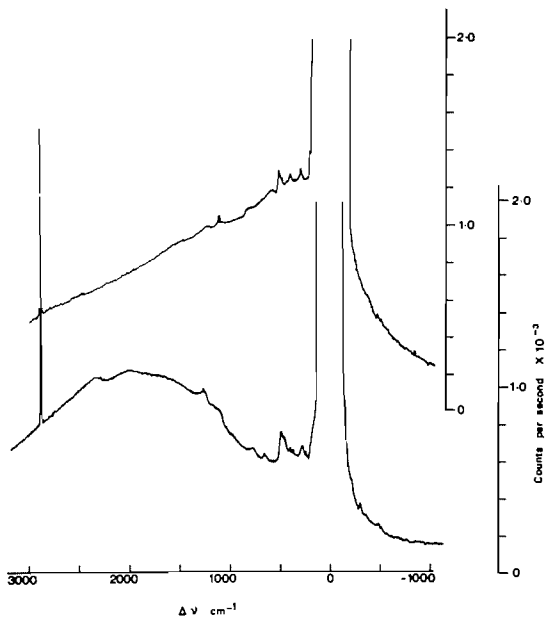

FIG. 2. Raman and fluorescence spectra of an HY zeolite sample after heating the zeolite in oxygen at 500 °C (lower spectrum) and after subsequently retaining the sample *in vacuo* for 1 h at 100 °C (upper spectrum).

Can. J. Chem. Downloaded from www.nrcresearchpress.com by 210.87.254.6 on 09/05/12
For personal use only.

Can. J. Chem. Downloaded from www.nrcresearchpress.com by 210.87.254.6 on 09/05/12
For personal use only.

TABLE 2. Positions (cm^{-1}) of maxima in the residual fluorescence of samples that had been preheated in oxygen near 500 °C, and in spectra showing increased fluorescence after subsequent heating in vacuum as specified in Table 1

(*a*) Frequencies at the maxima of residual fluorescence features, and their half-widths, after heating above 500 °C in oxygen (Table 1)

Zeolite	Frequencies (cm^{-1})			
LiY-70	14 330	—	—	—
KY-70	14 210	—	—	—
NaY-100	14 390	—	—	—
HY-64	~14 000(~2000)	—	13 780	13 450
CoY-80	14 200	—	—	—
CuY-50	14 490	14 020	—	—
CeY-71	14 400	14 200	13 730	—
ZnY-62	14 380	—	—	—

(*b*) Frequencies of main fluorescence background features after subsequent evacuation as specified in Table 1

Zeolite	Frequencies (cm^{-1})		
LiY-70	15 440	14 370	—
KY-70	15 180	—	—
NaY-100	15 050	14 350	—
HY-64	15 200	14 310	—
CoY-80	—	—	13 890
CuY-50	15 110	14 390	—
CeY-71	15 120	—	—
ZnY-62	15 420	—	—

Fig. 2*b*. A renewed cycle of heating in oxygen led reproducibly to the same residual fluorescence spectrum.

It was possible to observe Raman lines superimposed on these weaker fluorescent backgrounds without difficulty, particularly those obtained after heating in oxygen. With our experimental arrangement some of these sharp features arise from the quartz window of the cell and others from the zeolite samples themselves. Because it is difficult to make clear-cut distinctions between weak sub-maxima on the fluorescent backgrounds and the Raman lines, except in the region below $\Delta\nu = 550\ cm^{-1}$ where the stronger Raman lines of the zeolites are expected, Table 3 lists only the sharp features observed in the readily accessible region of $\Delta\nu \sim 550$ to $250\ cm^{-1}$ for the samples heated in oxygen. Our experiments using the relatively weak He–Ne laser were not designed so as to obtain strong spectra from the zeolites. Much stronger Raman spectra of quartz and Y-zeolite have been observed by Angell (10) using the 4880 Å line from an argon–krypton laser; his frequencies are also recorded in Table 3. The less significant features in our spectra that can be assigned to Raman scattering from the quartz window are indicated by italics.

Raman scattering from pyridine adsorbed on the oxygen-pretreated zeolites were recorded over the accessible range of fundamental frequencies *i.e.* 350–3200 cm^{-1}. The positions, half-height widths, and relative peak heights of all the bands observed in the spectra of pyridine adsorbed on HY-64, LiY->70, NaY-100, and KY->70 are shown in Table 4 and compared with the values for pyridine liquid run at the same resolution. In the cases of pyridine adsorbed on CoY-80 and CuY-50 only single weak bands were observed, at 1018 cm^{-1} in both experiments. Since the bands in this region of the spectrum of pyridine are normally much stronger than any others, the other frequency regions were not scanned for pyridine on these

TABLE 3. Raman frequencies ($\pm 10\ cm^{-1}$) observed from zeolites after heating in O_2 above 500 °C

Zeolite	Frequencies (cm^{-1})*				
LiY-70		320(m)		410(s)	485(s)	
NaY-100						505(s)‡
KY-70		300(w)			*470*(s)	500(s)
HY-64		297(m)	*350*(w)	*405*(w)	*465*(s)	510(s)
Quartz†	*268*(w)		*355*(m)	*403*(w)	*466*(vs)	
NaY-100†		~290(m)	350(w)			505(vs)
CoY-80		275(w)			440(m)	
CuY-50		300(m)	375(w)	420(s)	*450*(s)	
CeY-71		275(s)	370(w)		*455*(s)	515(w)

*s = strong, m = medium, w = weak, v = very. None are very strong on an absolute scale.
†From ref. 10.
‡The only Raman line observed.

Can. J. Chem. Downloaded from www.nrcresearchpress.com by 210.87.254.6 on 09/05/12
For personal use only.

TABLE 4. Principal bands in the Raman spectra of pyridine adsorbed on ion-exchanged zeolites

Symmetry	Mode	Position $\Delta\nu$ (cm^{-1})					Half-height width $\delta\nu_{1/2}$ (cm^{-1})					Relative peak height (rph)				
		Liquid*	HY	LiY	NaY	KY	Liquid*	HY	LiY	NaY	KY	Liquid*	HY	LiY	NaY	KY
(B_1)	ν_{20b}	3089	3066	3063	3070	3064	sh	33	30	25	18	—	11	11	11	11
(A_1)	$\nu_{2,13}$	3054					23					14				
(A_1)	ν_{8a}	1583	1592	1594†	1596†	1589†	16	16	14	10	11	8	7	12	8	7
(B_1)	ν_{8b}	1572	1574	—	1574	1572†	14	14	—	12	13	7	7	—	6	5
(B_1,A_1)	ν_3,ν_{9a}	1218	1222	1223	1218	1222	18	16	20	16	20	7	12	11	15	12
(A_1)	ν_{12}	1030	1035	1036	1036	1034	8	9	13	10	9	78	46	25	61	59
(A_1)	ν_1	—	1014‡	—	—	—	—	sh	—	—	—	—	24	—	—	—
(A_1)	ν_1	991	999	1002	1002	996	7	12	14	12	10	100	100	100	100	100
(B_1)	ν_{6b}	652	651	651	654	652	15	10	13	14	10	15	25	14	20	23
(A_1)	ν_{6a}	605	—	—	613	612	18	—	—	12	12	6	—	—	7	9

*Spectra recorded at 8 cm^{-1}, as for the adsorbed state.

†Ward (6) gives the following values for infrared bands that can probably be assigned to ν_{8a} and ν_{8b} respectively: Li, 1594(s), 1573(m); Na, 1588(s), 1570(w); K, 1590(s), 1575(m); in the Raman spectrum of NaY and KY we observed additional weak lines at 1615 (Na); 1607 (K). These are close to infrared frequencies assigned to combination bands in Fermi resonance with the nearby fundamentals.

‡Initial stages of adsorption.

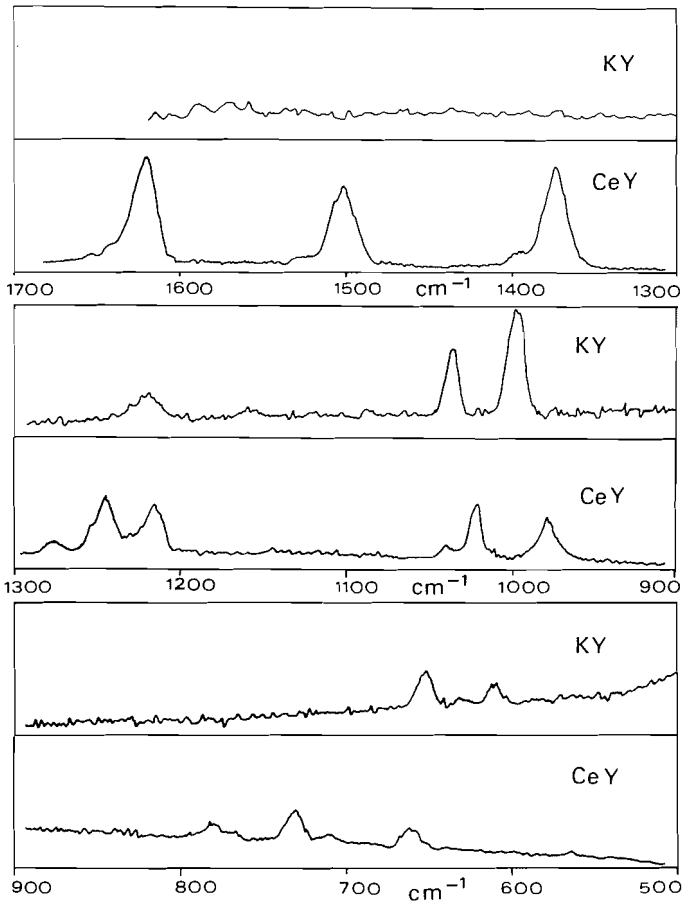

FIG. 3. A comparison of complete Raman spectra of pyridine adsorbed on KY and on CeY zeolites. The spectrum on CeY was the final one to be obtained (see Fig. 6).

zeolites. CuY and CoY are very probably poor Raman scatterers because of their colours. The dehydrated CuY turned from pale green to purple after exposure to pyridine vapour and the CoY was a dark blue throughout the experiment. Attempts to increase the intensity of the Raman radiation scattered from CuY were not successful. Focussing the laser beam upon the face of the zeolite disc only caused the background to rise sharply but this stopped when the beam was defocussed. This effect is probably caused by localized heating. Hendra (14), has estimated that this can amount to as much as 300 °C above ambient for black or blue samples.

The Raman spectrum observed for CeY-71 which had been exposed to pyridine for an extended period was markedly different from other spectra of pyridine that we have observed on zeolites, aluminas or silicas. The frequencies observed in the pyridine on CeY-71 spectrum are as follows: 1654(w), 1638(w), *1619*(s), 1534(vw), *1503*(s), 1397(w), *1374*(s), 1278(w), *1246*(m), *1215*(m), 1042(w), *1020*(m), 998(w), *979*(m), 781(w), 729(m), 664(w), 436(w). The Raman spectra of pyridine on KY-70 and on CeY-71 are contrasted in Fig. 3.

In all previous work with adsorbed pyridine the strong Raman lines in the 1000 cm^{-1} region arising from the fundamentals ν_1 and ν_{12} proved to be most sensitive to environment and to adsorption processes (7, 8). The positions, halfband-widths, and relative intensities of the observed pyridine Raman lines between 975 and 1040 cm^{-1} are summarized in Table 5. Since

Can. J. Chem. Downloaded from www.nrcresearchpress.com by 210.87.254.6 on 09/05/12
For personal use only.

TABLE 5. Raman spectra in the 1000 cm^{-1} region of pyridine adsorbed on ion-exchanged zeolites at different pressures of pyridine vapour

	P_c (Torr)	Position $\Delta\nu$ (cm^{-1})			$\delta\nu_{1/2}$ (cm^{-1})			Relative peak height		
		ν_{12}	ν_1	ν_{17a}	ν_{12}	ν_1	ν_{17a}	ν_{12}	ν_1	ν_{17a}
Liquid (ir)		1028	990							
(Raman)		1030	991	980	8	7		78	100	
HY-64	small		1014			sh				
	4	1035	999		9	12		46	100	
	(17)		(1001)							
LiY->70	1	1036	1002		13	14		25	100	
	(15)		(1004)							
NaY-100	16*	1036	1002		10	12		61	100	
KY->70	1	1034	996		9	10		59	100	
	(16)		(997)							
CoY-80	10.5		1018†			11			100	
CuY-50	16.5		1018†			11			100	
CeY-71	16‡		1020	979		12	17		100	63
			998			sh			sh	
	16§	1028	998		15	~10		90	100	

*Spectrum little changed by pumping for 12 h at 20 °C.
†Weak spectra.
‡Intermediate spectrum, see text.
§Final spectrum, see text.

the band positions depend somewhat on coverage the $\Delta\nu$ values observed both at equilibrium (16–17 Torr) and at lower pressures of pyridine are listed in some cases. For CuY, CoY, and CeY, ν_1 is close to 1020 cm^{-1} and for these samples no bands were observed of measurable intensity near 1035 cm^{-1}. However, as noted earlier, the CuY and CoY spectra are very weak because of the strong sample colouration.

Figure 4 shows the 1000 cm^{-1} region of the spectrum for pyridine adsorbed on KY-70 as a function of pyridine dosage. The first seven doses of pyridine were of approximately equal size (~200 μmol) but for doses eight to eleven the sample disc was exposed to pyridine vapour in equilibrium with the liquid for different periods. In Fig. 5 the intensities of the ν_1 and ν_{12} Raman bands for KY-70 are plotted as a function of the number of pyridine doses to which the sample had been exposed. The bands initially increased approximately linearly with dosage but reached a maximum intensity soon after six or seven doses of pyridine had been adsorbed. By contrast similar plots for the adsorption *vs.* dosage on HY-64 were also smooth but had no initial linear sections.

Small changes were observed in the intensities, widths, and frequencies of some of the Raman bands on standing or on pumping. Rescanning

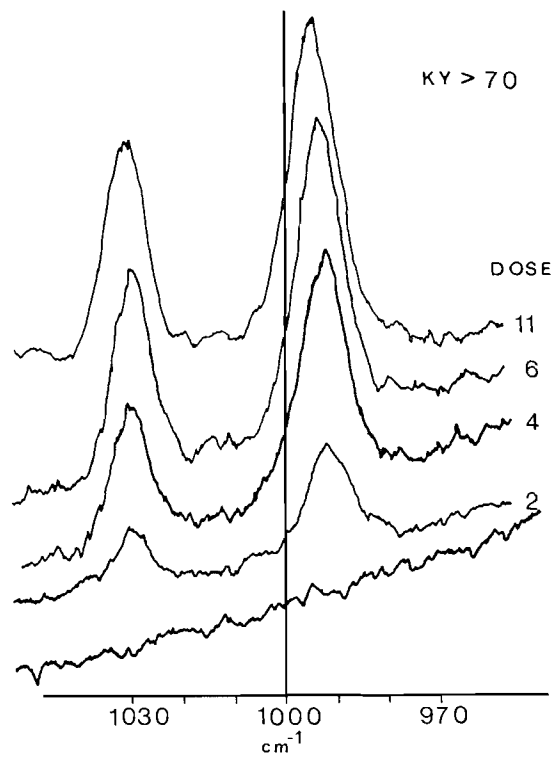

FIG. 4. The growth of the ν_1 and ν_{12} Raman lines of pyridine on KY zeolite as a function of dosage by the adsorbate.

Can. J. Chem. Downloaded from www.nrcresearchpress.com by 210.87.254.6 on 09/05/12
For personal use only.

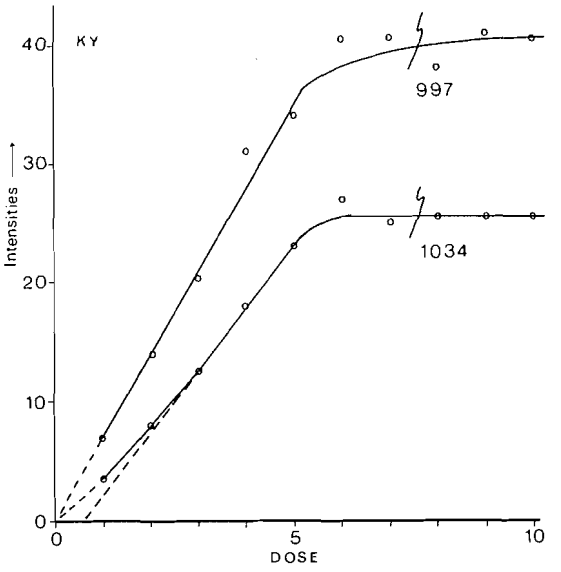

FIG. 5. The intensities of the ν_1 and ν_{12} Raman lines of pyridine on KY zeolite as a function of dosage.

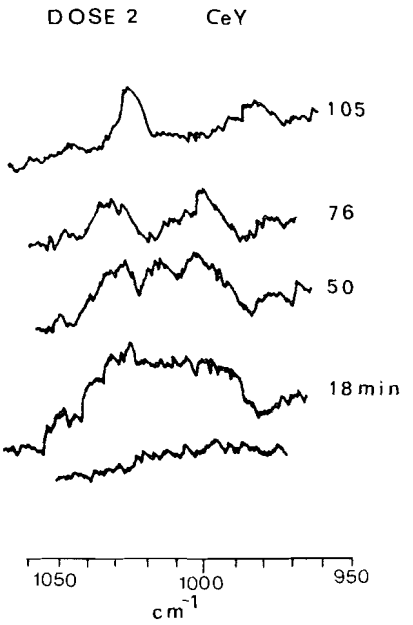

FIG. 6. The Raman spectra in the 1000 cm^{-1} region from pyridine adsorbed on a CeY zeolite developing as a function of time under the saturated vapour pressure of pyridine.

a sample with a dose of adsorbed pyridine after several hours sometimes gave bands with reduced half-widths. In addition to expected losses in intensity, pumping at room or higher temperatures frequently gave rise to residual bands of somewhat greater width. These changes were sometimes accompanied by frequency changes slightly in excess of the normal uncertainties of ± 2 cm^{-1}.

No spectrum was observed when the first dose of pyridine was adsorbed on CeY-71. The CeY was subsequently exposed to the saturated vapour pressure of pyridine for 80 min, and during this time the ν_1–ν_{12} region was scanned continuously. Initially a very broad ill-defined band appeared, as shown in Fig. 6. After 76 min the broad band resolved itself into two components at *ca.* 998 and 1028 cm^{-1}. Four minutes later the tap to the adsorption cell was closed and after another 12 min the spectrum showed that the bands had shifted to considerably lower frequencies, 979 and 1020 cm^{-1}. The 1020 cm^{-1} band is stronger but a weak shoulder could still be seen at 998 cm^{-1} in subsequent spectra. The cell, sample, and alignment were not altered during these spectral measurements. There were no further significant changes in band positions, although the intensities increased slightly.

Desorption of pyridine from the CeY-71 sample by pumping for 7 h at 20 °C and 20.5 h at 65 °C decreased the 1020 and 979 cm^{-1} band heights by 40% but the widths and positions remained constant.

Discussion

The high fluorescence background obtained from many oxide adsorbents has limited the Raman data that can be obtained from adsorbed molecules. In our previous work (*7a*, *7b*) and that of Buechler and Turkevich (9) it has been shown that for the silicas this fluorescence can be virtually eliminated by heating the sample in oxygen above 500 or 600 °C and that, with this type of adsorbent, the fluorescence does not rapidly return on standing *in vacuo* at temperatures between 500 °C and ambient. Both groups of workers attribute this oxygen-removable fluorescence to the presence of hydrocarbon impurities that can be burned off in oxygen.

With alumina-containing adsorbents (as with the zeolite samples studied here) heating in oxygen above 500 °C again greatly reduces fluorescence, but this is more liable to grow back again under heated vacuum conditions (*7b*). In the silica case the evidence that hydrocarbon impurities cause this oxygen-removable

Can. J. Chem. Downloaded from www.nrcresearchpress.com by 210.87.254.6 on 09/05/12
For personal use only.

Can. J. Chem. Downloaded from www.nrcresearchpress.com by 210.87.254.6 on 09/05/12
For personal use only.

fluorescence is indirect but nevertheless strong. Thus the fluorescence is greatest with oxide samples that are known to be contaminated with hydrocarbons or near warm grease vacuum-taps, and it becomes stronger in the presence of added hydrocarbons such as *n*-heptane or benzene or other organic molecules such as furan (9, footnote 3). The re-growth of fluorescence with a similar frequency profile when alumina-containing absorbents and zeolites remain for periods *in vacuo* at elevated temperatures may plausibly be attributed to recontamination with traces of hydrocarbons despite experimental precautions to minimize this. The combination of vacuum conditions and higher temperature is most conductive to the diffusion of impurities in the gas phase. The resulting intensity of the band depended sensitively on the temperature and time of evacuation. For example the intensity of background scattering near 500 cm^{-1} in HY-64 zeolite grew by more than two orders of magnitude over the value for the oxygen-treated sample when heated 1 h at 330 °C in a cell vacuum of 5×10^{-5} Torr. By contrast evacuation at 100 °C for 1 h led to an increase of only a factor of 2 near $\Delta\nu = 600\ cm^{-1}$ (Fig. 2*b*). The other zeolites could be evacuated at temperatures up to 330 °C without too serious a regrowth in fluorescence. The finding that a similar regrowth of fluorescence is much less pronounced with silica adsorbents may be accounted for by postulating that the acidic alumina surfaces more readily decompose saturated hydrocarbon impurities into unsaturated and fluorescent products. If this is true the absence of fluorescence is not necessarily an indication of the absence of traces of impurities in the form of saturated hydrocarbons.

Unlike ourselves and Cooney *et al.* (11*a*), Angell (10) has not found heating in oxygen at 500 °C to be efficacious at greatly reducing fluorescence from his zeolite samples. However the finding, that 'activating' zeolite samples (10) or aluminas (Careri *et al.* (12)) at higher temperatures leads to increased fluorescence, is also explicable in terms of conversion of hydrocarbon contaminants into fluorescent forms. Careri *et al.* (12), and more recently Hendra and Turner,[6] have shown that heating such samples *in vacuo* at very high temperatures (> 800 °C) removes the fluorescence once again, perhaps by volatilization of the residual hydrocarbons.

We have previously shown that with alumina-containing adsorbents there remains a weaker fluorescence background with a different profile (broad maxima centre in the $\bar{\nu} = 14\,000\ cm^{-1}$ region). By analogy with work by Pott and McNicol (15*a*, 15*b*) on transition metal impurities in alumina-containing oxides and zeolites, we have attributed this weaker residual fluorescence to Fe^{3+} ions replacing Al^{3+} in tetrahedral environments. They found an Fe^{3+} emission band between 15 000 and 13 700 cm^{-1} depending on the state of zeolite hydration (15) and, as described in the experimental section, all our residual fluorescence peaks from different zeolites fall within the centre part of this frequency range. However neither Fe^{3+} in tetrahedral or octahedral environments can be postulated as the source of the original or the regenerated fluorescence in the 15 000 – 15 500 cm^{-1} region and the assignment of this to hydrocarbon impurities seems the most satisfactory one.

We do not propose to discuss in detail the Raman bands listed in Table 3 which arise from vibrations in the bulk of the crystalline zeolite framework. However we note that changes in cation led to changes in the detailed frequencies of lines which might be worth further investigation. This should preferably be carried out using higher-power laser excitation (such as the 4880 Å argon line used by Angell (10)) and an experimental arrangement that minimises contributions to the spectra from the quartz window.

Fairly complete Raman spectra from adsorbed pyridine were obtained for HY, LiY, NaY, and KY and the main features of these are listed in Table 4. The very different final spectra obtained on CeY is listed in the text of the results section. More complete results for the 1000 cm^{-1} region of the Raman spectra, which contains the adsorption-sensitive ring-breathing modes of vibration ν_1 and ν_{12} of pyridine, are given in Table 5 for these zeolites and for CuY and CoY which gave weak single-line spectra.

Infrared studies show that the surface concentrations of OH groups is very small for the alkali-metal Y-zeolites after heating above 450 °C (5, 6, 16, 17). With CuY and CoY two zeolite surface OH groups have been detected at 450 °C but they are weak in comparison with those

[6]P. J. Hendra and I. D. M. Turner, private communication.

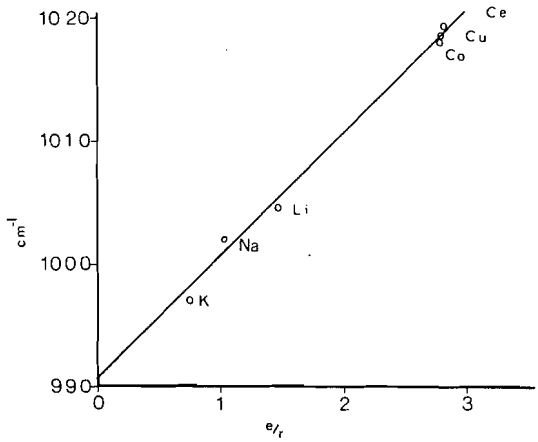

FIG. 7. The position of the ν_1 Raman lines of pyridine adsorbed on different cation-containing zeolites as a function of q/r where q is the ionic charge and r the ionic radius.

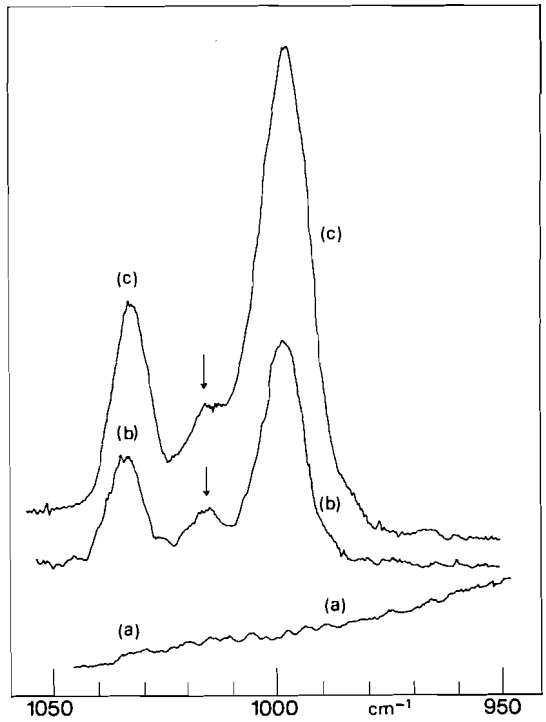

FIG. 8. Raman spectra of pyridine adsorbed on HY zeolite as a function of dosage. (*a*) background, (*b*) dose 2, (*c*) dose 4.

observed with HY (18). Nonacidic hydroxyl groups are also present and are assigned to MOH^+ species. It will be recalled that all our samples have been heated for several hours at 500 °C in oxygen. It seems unlikely that in these cases the pyridine molecules interact mainly by hydrogen bonding, or by proton transfer, with surface OH groups. By analogy with the results of Barrer *et al.* (19) for benzene adsorption on NaX, we would expect a limiting adsorption of approximately five pyridine molecules in each supercage of NaY. Up to four charge-balancing cations could occupy the site II positions surrounding any given supercage. Therefore few pyridine molecules will be unaffected by the presence of the charge-balancing cations. The charge-balancing cations therefore seem the most likely sites of specific adsorption and it is very satisfactory to find that the frequency ν_1 of the main band correlates in a linear fashion (Fig. 7) with q/r, where q is the cation charge and r its radius as taken from the *Handbook of Chemistry and Physics* (20). In the cases of CuY, CoY, and CeY it is assumed that ν_1 is to be identified with the strongest line (or the only line observed) in this region of the Raman spectrum. The straight-line plot in Fig. 7 extrapolates very satisfactorily to 991 cm^{-1} *i.e.* very close to the value of ν_1 for liquid pyridine. These results are in good general agreement with infrared measurements involving the *ca.* 1440 cm^{-1} frequencies of the pyridine molecule which also indicate interaction with the cations of the alkali metals (5, 6). In Fig. 7 it has been assumed that we are still dealing with Ce(III). It should perhaps be mentioned that some oxidation to Ce(IV) might have resulted from the oxygen treatment at elevated temperatures.

For the same series of zeolites there are also indications (Table 4) that increasing q/r leads to weaker ν_{12} bands compared with ν_1, and the former band is missing in the spectra of CuY, CoY, and CeY. ν_{6a} and ν_{6b} show increasing intensities along the alkali metal series Li to K.

In the case of decationated HY, the initial 'balancing cation' is a proton which immediately forms OH groups attached to the aluminosilicate framework. Infrared studies show that there are two main types of OH groups with frequencies near 3650 and 3545 cm^{-1}, of which the former is more acidic and forms pyridinium ions (17, 21, 22), while the latter hydrogen-bonds to adsorbed pyridine. The observed Raman spectra from pyridine on HY (Fig. 8) seem to be consistent with the infrared findings. Thus the

Can. J. Chem. Downloaded from www.nrcresearchpress.com by 210.87.254.6 on 09/05/12
For personal use only.

Can. J. Chem. Downloaded from www.nrcresearchpress.com by 210.87.254.6 on 09/05/12
For personal use only.

pair of bands at 1035 and 999 cm^{-1} are consistent with values of ν_{12} and ν_1 expected for hydrogen-bonding to OH groups; they may also in part be caused by interaction with the residual Na^+ ions in HY-64. Another Raman line at about 1014 cm^{-1} (possibly with two components) is observed at lower coverages and persists at higher coverages. It is as expected for a pyridinium ion (7*b*, 8) such as has previously been identified by infrared spectroscopy (23). Hendra *et al.* (24) have recently discussed the difficulty of characterising pyridinium ions on surfaces in the presence of hydrogen-bonded species. However the zeolite HY, with its multiple acidic OH's, possibly constitutes a favourable case. These alternative sites possibly account for a nonlinear increase of intensity of ν_1 and ν_{12} from hydrogen-bonded species with dosage.

CeY is an intermediate case in that infrared studies show that the same type of OH groups are present as on decationated HY (17) but that adsorption to Ce^{3+}, rather than the formation of pyridinium ions, occurs at room temperature. Infrared work also suggests that pyridinium ions are only formed after heating to 70 °C (17) or after co-adsorption of water at room temperature.

It was pointed out in the results section (see also Fig. 6) that the Raman spectra show particularly complex changes as a function of time when pyridine is adsorbed on CeY-71. However the frequency of the strongest band in the final spectrum in the 1000 cm^{-1} region occurs at 1020 cm^{-1}. This frequency fits in very well on the plot of ν_1 *vs.* q_1/r_1 as shown in Fig. 7 and suggests ultimate interaction with the cations. The broad and ill-defined spectra in this region observed during the earlier phrases of adsorption (Fig. 6) implies the presence of a variety of surface species. The changes of spectra with time may be associated with activated diffusion of pyridine from initial sites to more stable ones (17), *e.g.* in supercages, or possibly with the movement of Ce^{3+} ions from inaccessible to accessible sites in the presence of pyridine as has been observed for Cu^{2+} and Ni^{2+} ions (25).

As emphasized in Fig. 3, the final strong spectrum obtained from pyridine on CeY-71 is very substantially different from that observed with liquid pyridine or with pyridine adsorbed on KY. Thus in parallel to the movement of ν_1 to 1020 cm^{-1}, which implies a strong Lewis-type interaction with the triply charged cation, Ce^{3+}, there are remarkable increases in intensity of the bands at 1619, 1503, 1374, and 1246 cm^{-1} compared with the normal pyridine spectrum. The bands at 1028 and 998 cm^{-1} observed in the penultimate spectrum (Fig. 6) suggest the earlier presence of pyridine hydrogen-bonded to OH groups which is later replaced by pyridine bonded to the Ce^{3+} Lewis sites. Earlier poorly defined spectra imply extra bands near 1015 cm^{-1} which might originate from pyridinium ions.

Acknowledgments

We thank the Science Research Council (Grants B/SR/1065 and B/SR/6085) and the Hydrocarbon Research Group of the Institute of Petroleum for support of this research programme. One of us (T.A.E.) is grateful for an I.C.I. Fellowship during the tenure of which this work was carried out.

1. D. J. C. Yates. Catal. Rev. **2**, 113 (1968).
2. J. L. Carter, P. J. Lucchesi, and D. J. C. Yates. J. Phys. Chem. **68**, 1385 (1964).
3. (*a*) C. L. Angell and P. Schaffer. J. Phys. Chem. **70**, 1413 (1966); (*b*) J. A. Rabo, C. L. Angell, P. H. Kasai, and V. Schomaker. Discuss. Faraday Soc. **41**, 328 (1966).
4. C. L. Angell. J. Phys. Chem. **70**, 2420 (1966).
5. J. W. Ward. J. Catal. **10**, 34 (1968).
6. J. W. Ward. J. Colloid. Sci. **28**, 269 (1968).
7. T. A. Egerton, A. H. Hardin, Y. Kozirovski, and N. Sheppard. (*a*) Chem. Commun. 887 (1971); (*b*) J. Catal. **32**, 343 (1974).
8. P. J. Hendra, J. R. Horder, and E. J. Loader. J. Chem. Soc. A, 1766 (1971).
9. E. Buechler and J. Turkevich. J. Phys. Chem. **76**, 2325 (1972).
10. C. L. Angell. J. Phys. Chem. **77**, 222 (1973).
11. (*a*) R. P. Cooney, G. Curthoys, and Nguyen The Tam. Advan. Catal. **24**, 293 (1975); (*b*) T. A. Egerton and A. H. Hardin. Catal. Rev. **11**, 71 (1975).
12. G. Careri, V. Mazzacurati, N. Sampoli, and G. Signorelli. J. Catal. **26**, 494 (1972).
13. T. A. Egerton and F. S. Stone. Trans. Faraday Soc. **66**, 2364 (1970).
14. P. J. Hendra. Symposium on Chemisorption and Catalysis. Institute of Petroleum, London. 1970.
15. (*a*) B. D. McNicol and G. T. Pott. J. Catal. **25** 223 (1972); (*b*) G. T. Pott and B. D. McNicol. Discuss. Faraday Soc. **52**, 121 (1971).
16. C. L. Angell and P. C. Schaffer. J. Phys. Chem. **69**, 3463 (1965).
17. L. C. Christner, B. V. Liengme, and W. K. Hall. Trans. Faraday Soc. **64**, 1679 (1968).
18. J. W. Ward. Trans. Faraday Soc. **67**, 1489 (1971).
19. R. M. Barrer, J. W. Bultitude, and F. W. Sutherland. Trans. Faraday Soc. **53**, 1111 (1957).

20. Handbook of Chemistry and Physics. 49th ed. C.R.C. Press, Cleveland, Ohio. 1968–1969.
21. J. W. WARD. J. Phys. Chem. **71**, 3106 (1967).
22. T. R. HUGHES and H. M. WHITE. J. Phys. Chem. **71**, 2192 (1967).
23. B. V. LIENGME and W. K. HALL. Trans. Faraday Soc. **62**, 3229 (1966).
24. P. J. HENDRA, I. D. M. TURNER, E. J. LOADER, and M. STACEY. J. Phys. Chem. **78**, 300 (1974).
25. P. GALLEZOT, Y. BEN TAARIT, and B. IMELIK. (*a*) C.R. Acad. Sci. Ser. C, **272**, 261 (1971); (*b*) J. Catal. **26**, 295 (1972); (*c*) J. Catal. **26**, 481 (1972).

Can. J. Chem. Downloaded from www.nrcresearchpress.com by 210.87.254.6 on 09/05/12
For personal use only.

Mass spectra of some deuterium-labelled methylsilanes and the analysis of mixtures

DAVID I. BRADSHAW, RICHARD B. MOYES, AND PETER B. WELLS
Department of Chemistry, The University, Hull, HU6 7RX, England

Received May 21, 1975

DAVID I. BRADSHAW, RICHARD B. MOYES, and PETER B. WELLS. Can. J. Chem. **54**, 599 (1976).

Positive ion mass spectra of CH_3SiH_3 and of CH_3SiD_3 (*m/e* 28–49) at 18 eV are reported and the appearance potentials of the most abundant ions measured. Modifications to published mechanisms of ion fragmentation are proposed.

Methylsilane gives no parent ion and fragmentation is extensive. Accurate analysis of mixtures containing CH_3SiX_3 (X = H or D) can be achieved for any sample containing two or three of these isotopically distinguishable methylsilanes, or of all four if the composition possesses a certain symmetry. The deuterium content can be determined for a sample of any composition.

DAVID I. BRADSHAW, RICHARD B. MOYES et PETER B. WELLS. Can. J. Chem. **54**, 599 (1976).

On rapporte l'observation des ions positifs du spectre de masse de CH_3SiH_3 et de CH_3SiD_3 (*m/e* 28–49) à 18 eV et on a mesuré les potentiels d'apparition des ions les plus abondants. On propose des modifications aux mécanismes publiés pour la fragmentation des ions.

Le méthylsilane ne donne pas d'ion moléculaire et la fragmentation est importante. Des analyses précises de mélanges contenant CH_3SiX_3 (X = H ou D) peuvent être effectuées pour n'importe quel échantillon contenant deux ou trois de ces méthylsilanes qui peuvent être distingués d'une façon isotopique, ou pour les quatre si la composition possède une certaine symétrie. Le contenu en deutérium peut être déterminé pour un échantillon de n'importe quelle composition.

[Traduit par le journal]

Introduction

Mass spectrometric analysis of hydrocarbons in which some hydrogen atoms are exchanged for deuterium is widely practised, and isotope tracer studies have greatly advanced our understanding of hydrocarbon reactivity. By comparison, isotope exchange in silicon hydrides has been almost completely neglected, largely because of analytical difficulties associated with low or zero parent ion yields in the mass spectra.

The objects of the present work have been to examine the mass spectrum of CH_3SiD_3 which has not been reported before, and to validate a method of analysis for mixtures of deuterium-labelled methylsilanes. This analysis represents a difficult case, since the parent ion concentrations are zero and ion fragmentation considerable.

Experimental

Materials

CH_3SiH_3 was pure as supplied. CH_3SiD_3 was prepared by the reduction of methyltrichlorosilane with lithium aluminium deuteride in dibutyl ether solution at 273 K. Isotopic purity was >99%. The product contained less than 1% dimethylsilane as the only chemical impurity.

Apparatus and Methods

Mass spectra and appearance potentials were obtained using a Vacuum Generators Micromass 6 mass spectrometer. Source pressures were such (10^{-5}–10^{-6} Torr) that pressure-dependent reactions of ions were not observed. Appearance potentials were determined by the vanishing current method (1). Ionisation energy was varied in steps of 0.2 eV, and ion current intensities were measurable to ±1 pA. The ionisation energy scale was calibrated by measurement of the ionisation potentials of helium, argon, and xenon. Mass spectra have been corrected for the natural abundance of ^{29}Si, ^{30}Si, and of ^{13}C.

Results

Positive ion mass spectra of CH_3SiH_3 and of CH_3SiD_3 were recorded for electron beam energies in the range 12–70 eV.[1] The spectrum of CH_3SiH_3 at 70 eV agreed with a literature report (2). For the purpose of analysis, it was necessary to use an electron beam energy lower than 20 eV in order to restrict fragmentation, but higher than 16 eV in order to maintain a sufficient total ion current. Spectra of both CH_3SiH_3 and CH_3SiD_3 at 18.0 eV, together with

[1]Full details can be obtained from ref. 5 or by correspondence with the authors.

Can. J. Chem. Downloaded from www.nrcresearchpress.com by 210.87.254.105 on 09/05/12
For personal use only.

Can. J. Chem. Downloaded from www.nrcresearchpress.com by 210.87.254.105 on 09/05/12
For personal use only.

TABLE 1. Mass spectra of CH_3SiH_3 and of CH_3SiD_3 at 18.0 eV

	CH_3SiH_3		CH_3SiD_3	
m/e	Ion current (%)	Major contributing ions[a]	Ion current (%)	Major contributing ions[a]
48[b]			0.3	$CSiH_2D_3^+$
47			23.0	$CSiH_3D_2^+$
46	0.0	$CSiH_6^+$	4.7	$CSiH_2D_2^+$
45	28.4	$CSiH_5^+$	39.5	$CSiH_3D^+$
44	44.1	$CSiH_4^+$	5.2	$CSiH_2D^+$
43	9.2	$CSiH_3^+$	3.0	$CSiH_3^+$
42	0.3	$CSiH_2^+$	0.6	$CSiH_2^+$
41	0.0	$CSiH^+$	0.2	$CSiH^+$
34			3.7	SiD_3^+
33			0.1	$SiHD_2^+$
32			9.4	SiD_2^+
31	3.1	SiH_3^+	1.0	$SiHD^+$
30	8.9	SiH_2^+	0.5	SiD^+
29	1.0	SiH^+	1.9	SiH^+
28	6.2	Si^+	7.3	Si^+

[a]See Discussion.
[b]Ion current at *m/e* 49 ($CSiH_3D_3^+$) was zero.

the designation of the major contributing ions (see Discussion) are presented in Table 1.

Appearance potentials are recorded in Table 2. Breaks in the curves of ion current against electron energy reported by earlier workers (3) were not observed.

The mass spectrum of CH_3SiD_3 contained four peaks (m^* = 41.2, 39.3, 24.5, and 17.4), corresponding to the decomposition of metastable ions. These m^*-values confirm the original assignment of the three metastable ions derived from CH_3SiH_3 (2).

Discussion

Mechanisms of Fragmentation

The ions formed in greatest abundance from CH_3SiH_3 have been assigned the structures $CH_3SiH_2^+$, CH_3SiH^+, and CH_3Si^+ largely on the grounds that the dissociation energies of Si—H are generally lower than those of corresponding C—H bond, and that the ionisation potentials of silyl radicals are normally lower than those of the corresponding alkyl radicals. Potzinger and Lampe (3) assign the ion at *m/e* 45 in the spectrum of CH_3SiH_3 as $CH_3SiH_2^+$ in the neighbourhood of the appearance potential, with a contribution from $CH_2SiH_3^+$ above 12.9 eV where these authors report a break in the ionisation efficiency curve. The spectrum of CH_3SiD_3 (Table 1) confirms that the formation of $CH_3SiD_2^+$ is a favoured process. However, loss of protium from carbon to give the ion $CH_2SiD_3^+$ at *m/e* 48 was negligible under all conditions, and no break was evident in our ionisation efficiency curves. Thus, by analogy, the ion at *m/e* 45 in the spectrum of CH_3SiH_3 is almost entirely $CH_3SiH_2^+$ under all conditions.

TABLE 2. Appearance potentials

	CH_3SiH_3	CH_3SiD_3	
m/e	Appearance potential (eV)	*m/e*	Appearance potential (eV)
45	11.8 (11.80)[a]	47	11.8
44	11.3 (11.45)	46	11.4
43	12.8 (14.05)	45	11.5
31	12.5 (12.8)	44	11.4
30	11.7 (11.50, 11.62)	43	12.1
29	14.8	34	12.4
28	12.1	32	11.6
		28	11.8

[a]Literature values (3, 4) in parentheses.

Fragmentation of CH_3SiH_3 by loss of two atomic mass units (2 amu) to give CH_3SiH^+ in the neighbourhood of the appearance potential, with primary formation of $CH_2SiH_2^+$ above 12.4 eV has been proposed (3). Secondary formation of $CH_2SiH_2^+$ may occur by intramolecular rearrangement of CH_3SiH^+, since resonance stabilisation would tend to render the process energetically favourable. These primary and secondary routes to $CX_2SiX_2^+$ (X = H or D) become distinguishable in the fragmentation of CH_3SiD_3 (reactions 1 and 2).

$$[1] \qquad CH_3SiD_3 \xrightarrow{-H_C,\ -D_{Si}} CH_2SiD_2^+$$

$$[2] \qquad CH_3SiD_3 \xrightarrow{-2D_{Si}} CH_3SiD^+ \rightarrow CH_2SiHD^+$$

Table 1 shows that the loss of four atomic mass units is more important by an order of magnitude than the loss of three. However, the ions at *m/e* 45 and 46 in the spectrum of CH_3SiD_3 have virtually identical appearance potentials (Table 2) and rupture of the C—Si bond provides $SiHD^+$ at *m/e* 31. Thus, a small but significant proportion of ions at *m/e* 45 has the structure CH_2SiHD^+. Analogously, therefore, a small proportion of ions at *m/e* 44 in the spectrum of CH_3SiH_3 has the structure of $CH_2SiH_2^+$.

The same workers attribute ions of mass 43 formed from CH_3SiH_3 to the structure CH_3Si^+

Can. J. Chem. Downloaded from www.nrcresearchpress.com by 210.87.254.105 on 09/05/12
For personal use only.

(on admittedly slender grounds) with a contribution from CH_2SiH^+ above 15.5 eV. In the spectrum of CH_3SiD_3 the ion current at *m/e* 44 ($CSiH_2D^+$) exceeds that at *m/e* 43 ($CSiH_3^+$). Thus protium loss from carbon appears to have been important, although the situation is confused by the possibility that a proportion of these ions may have been formed in the ion source by secondary processes involving the decomposition of the potentially metastable ion $CH_3SiD_2^+$.

The formation of SiD_3^+ from CH_3SiD_3 shows that simple carbon–silicon bond cleavage occurs as a minor fragmentation reaction.

The metastable ions observed reveal that Si^+ originates in decompositions of CH_3SiX^+ and of SiX_2^+ (X = H or D). Such decompositions in the ion source are responsible for ions at *m/e* 28.

Analysis of Mixtures

The analysis of mixtures of deuterium-containing methylsilanes by positive ion mass spectrometry presents special difficulties because of the absence of parent ions and the complexity of fragmentation. In the method described below, the reported spectra of CH_3SiH_3 and of CH_3SiD_3 are used to obtain the fragmentation spectrum of CH_3SiH_2D and of CH_3SiHD_2. A set of equations is derived which describes the composition of each ion current over the *m/e* range 43–47 for the situation in which all four methylsilanes having protium or deuterium bonded to silicon are present together. Accurate information concerning mixture compositions can be obtained in certain cases, and the deuterium content of samples can be obtained in all cases.

Fragmentation factors are defined as follows. The loss of one H atom bonded to silicon (H_{Si}) from CH_3SiH_3 is accorded the fragmentation factor *X*. (For example, $X = 28.4$ at 18.0 eV (Table 1)). Similarly, *M* represents the fragmentation of CH_3SiD_3 by loss of one deuterium atom.

Fragmentation of CH_3SiD_3 by loss of 2X (X = H or D) gives products distinguishable as to mass (reaction 3), whereas the analogous fragmentation of CH_3SiH_3 does not (reaction 4). $[CH_3SiH^+]/[CH_2SiH_2^+]$ is assumed equal to P/N.

[3] $CH_3SiD_3 \xrightarrow{-2D_{Si}} CH_3SiD^+$ fragmentation factor = *P*

$CH_3SiD_3 \xrightarrow{-H_C,\ -D_{Si}} CH_2SiD_2^+$ fragmentation factor = *N*

[4] $CH_3SiH_3 \xrightarrow{-2H_{Si}} CH_3SiH^+$ fragmentation factor = *Y*

$CH_3SiH_3 \xrightarrow{-H_C,\ -H_{Si}} CH_2SiH_2^+$

Similarly, for fragmentation by overall loss of 3X (X = H or D) the factors are as described in reactions 5 and 6 and it is assumed that $[CH_3Si^+]/[CH_2SiH^+] = R/Q$.

[5] $CH_3SiD_3 \xrightarrow{-3D_{Si}} CH_3Si^+$ fragmentation factor = *R*

$CH_3SiD_3 \xrightarrow{-2D_{Si},\ -H_C} CH_2SiD^+$ fragmentation factor = *Q*

[6]

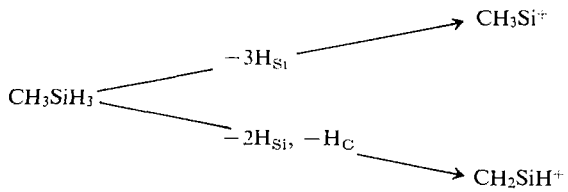

fragmentation factor = Z

The fragmentation spectra of CH_3SiH_2D and of CH_3SiHD_2 have been derived on the assumption that when H-atom loss occurs the relevant factor is that observed for the analogous process in CH_3SiH_3, and *mutatis mutandis* for D-atom loss. For example, the spectrum of CH_3SiH_2D is given by equations 7.

[7]
$$i_{46} = 2X/3$$
$$i_{45} = M/3 + 2NY/3(N + P) + PY/3(N + P)$$
$$i_{44} = N/3 + PY/3(N + P) + P/3 + QZ/3(Q + R)$$
$$i_{43} = QZ/3(Q + R) + Q/3 + R/3$$

Thus, the introduction into the mass spectrometer of a mixture containing CH_3SiH_3, CH_3SiH_2D, CH_3SiHD_2, and CH_3SiD_3 will result in ion currents the compositions of which are:

[8*a*] $$i_{47} = a_{1,1}[CH_3SiH_3] + a_{1,2}[CH_3SiH_2D] + a_{1,3}[CH_3SiHD_2] + a_{1,4}[CH_3SiD_3]$$

. . . . .

. . . . .

. . . . .

[8*e*] $$i_{43} = a_{5,1}[CH_3SiH_3] + a_{5,2}[CH_3SiH_2D] + a_{5,3}[CH_3SiHD_2] + a_{5,4}[CH_3SiD_3]$$

where $a_{x,y}$ are arithmetical expressions involving M, N, P, Q, R, X, Y, and Z. Coefficients, $a_{x,y}$, derived from the mass spectra of CH_3SiH_3 and CH_3SiD_3 at 18 eV (Table 1) are given in Table 3.

Although the matrix [8] provides five equations containing four unknowns, equations for i_{43} and i_{44} can be generated from the remainder, and hence solutions in the general case are not obtainable. Nevertheless, solutions can be obtained, and hence useful analyses can be achieved, in the following special cases.

Case 1. Equations 8*a*, 8*b*, and 8*c* allow the composition of a mixture of any two or any three of the components CH_3SiX_3 (X = H or D) to be determined. For example, mass spectrometric analysis of a standard mixture containing 65.8 ± 1.0% CH_3SiH_3 and 34.2 ± 1.0% CH_3SiD_3 gave by use of eqs. 8 the composition 63.1% CH_3SiH_3 and 36.9% CH_3SiD_3. This is satisfactory agreement in view of the assumptions involved. Similarly, mixtures of CH_3SiH_3 with CH_3SiH_2D and CH_3SiHD_2 obtained by the stepwise exchange of CH_3SiH_3 with molecular deuterium catalysed by metals have been analysed in this way (5).

TABLE 3. Coefficients $a_{x,y}$ for equations 8*a*–8*e* (ionisation energy = 18.0 eV)

	$a_{x,1}$	$a_{x,2}$	$a_{x,3}$	$a_{x,4}$
$a_{1,y}$	0.000	0.000	0.118	0.310
$a_{2,y}$	0.000	0.236	0.226	0.062
$a_{3,y}$	0.354	0.301	0.371	0.511
$a_{4,y}$	0.536	0.372	0.215	0.067
$a_{5,y}$	0.110	0.090	0.070	0.049

Case 2. Samples of deuterium-labelled methylsilane may arise by exchange reactions involving CH_3SiH_3 and CH_3SiD_3 as reactants. When the initial ratio of reactants is unity, the rate of formation of CH_3SiH_2D and of CH_3SiHD_2 will be equal, as will the rate of removal of each reactant. The number of unknowns is then reduced to two, eq. 8*a* can be solved simultaneously with 8*b* or 8*c*, and the remaining equation used as a check of the values obtained. Proportions (per cent) determined experimentally for a mixture initially containing 48.0% CH_3SiH_3 and 52.0% CH_3SiD_3 equilibrated over a molybdenum film at 195 K, with equilibrium proportions expected on a statistical basis shown in parentheses, are CH_3SiH_3, 11.9, (11.0); CH_3SiH_2D, 35.1, (35.9); CH_3SiHD_2, 38.2, (39.0); CH_3SiD_3, 14.8, (14.1).

Can. J. Chem. Downloaded from www.nrcresearchpress.com by 210.87.254.105 on 09/05/12
For personal use only.

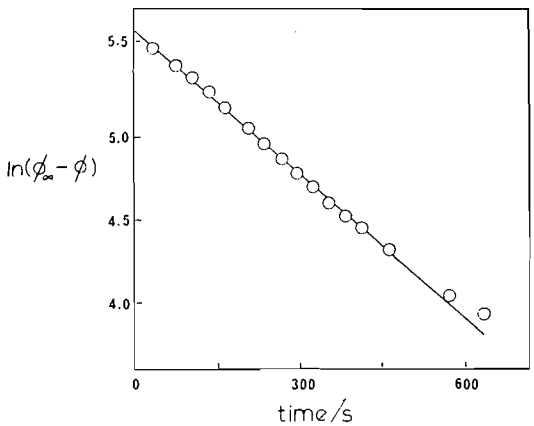

FIG. 1. First order exchange of protium for deuterium in the silyl group of CH_3SiH_3 catalyzed by an evaporated molybdenum film at 195 K. Film weight = 19 mg. Initial pressures of methylsilane = 1 Torr and of deuterium = 10 Torr. ϕ is defined in the text; ϕ_∞ is the value of ϕ at equilibrium.

Finally, a most important feature of this analysis is that the deuterium content, ϕ, of *any* sample containing CH_3SiX_3 (X = H or D) can be determined using eq. 9:

$$[9] \quad \phi = i_{46}/a_{2,2} + i_{47}(2.000 - a_{2,3}/a_{2,2})$$

where, following custom (6) $\phi = (\%\ CH_3SiH_2D) + 2(\%\ CH_3SiHD_2) + 3(\%\ CH_3SiD_3)$. For example, Fig. 1 shows the standard function plot (6) for the determination of the first order rate coefficient for the appearance of deuterium in methylsilane during exchange between CH_3SiH_3 and D_2 catalysed by an evaporated molybdenum film at 195 K. The figure shows linear behaviour to 85% conversion, whereas analysis under special case 1 was possible only as far as 20% conversion. Thus it is possible to undertake kinetic investigations of deuterium incorporation into methylsilane under conditions where neither special case illustrated above applies.

Acknowledgments

We thank the Science Research Council for the award of grants for the purchase of the mass spectrometer and of a maintenance grant (to D.I.B.).

1. F. H. FIELD and J. F. FRANKLIN. Electron impact phenomena. Academic Press, New York. 1957. p. 28.
2. G. P. VAN DER KELEN, O. VOLDERS, H. VAN ONCKELEN, and Z. EECKHAUT. Z. Anorg. Allg. Chem. **338**, 106 (1965).
3. P. POTZINGER and F. W. LAMPE. J. Phys. Chem. **74**, 587 (1970); **74**, 719 (1970).
4. W. C. STEELE, L. D. NICHOLS, and F. G. A. STONE. J. Am. Chem. Soc. **84**, 4441 (1962).
5. D. I. BRADSHAW. Ph.D. Thesis. University of Hull, Hull, England. 1975.
6. C. KEMBALL. Adv. Catal. **11**, 223 (1959).

Can. J. Chem. Downloaded from www.nrcresearchpress.com by 210.87.254.105 on 09/05/12
For personal use only.

The reaction of *cis*- and *trans*-1,2-dianisyl-2-phenylvinyl-2-^{13}C bromides with acetic acid and silver acetate

CHOI CHUCK LEE AND MITSUO OKA

Department of Chemistry and Chemical Engineering, University of Saskatchewan, Saskatoon, Saskatchewan S7N 0W0

Received July 11, 1975

CHOI CHUCK LEE and MITSUO OKA. Can. J. Chem. **54**, 604 (1976).

The reaction of *cis*- or *trans*-1,2-dianisyl-2-phenylvinyl-2-^{13}C bromide with HOAc–AgOAc gave a 1:1 mixture of *cis*- and *trans*-1,2-dianisyl-2-phenylvinyl-2-^{13}C acetates with no isotopic scrambling according to pmr and cmr analyses. The lack of degenerate 1,2-phenyl shift in this system is in contrast with the finding of about 7% scrambling in the analogous reaction with triphenylvinyl-2-^{13}C bromide and mechanistic implications of this difference are discussed.

CHOI CHUCK LEE et MITSUO OKA. Can. J. Chem. **54**, 604 (1976).

La réaction des bromures de dianisyl-1,2 phényl-2 vinyl-2 ^{13}C *cis* ou *trans* avec un mélange d'acide acétique et d'acétate d'argent conduit à un mélange d'acétates de dianisyl-1,2 phényl-2 vinyl-2 ^{13}C *cis* et *trans* dans lequel il n'y a pas eu de répartition des isotopes; ces analyses ont été effectuées par rmp et rmc. L'absence de déplacement dégénéré de phényle des positions 1 à 2 dans ce système est en opposition avec les résultats obtenus antérieurement alors que l'on avait observé 7% de répartition des isotopes dans la réaction analogue du bromure de triphényl-vinyl-2 ^{13}C; on discute des implications mécanistiques de cette différence.

[Traduit par le journal]

There is considerable interest in vinyl cations and a number of reviews on the subject are available (1–4). Recently in this laboratory, ^{13}C-labeling coupled with cmr analysis was used to measure the extents of degenerate rearrangements arising from 1,2-aryl shifts in triarylvinyl cations (5, 6). It was found, for example, that the reaction of triphenylvinyl-2-^{13}C bromide (**1**-Br-2-^{13}C) and of trianisylvinyl-2-^{13}C bromide (**2**-Br-2-^{13}C) with HOAc–AgOAc resulted, respectively, in about 7 and 20% scrambling of the label from C-2 to C-1. In the present work, the same technique is utilized in a study with *cis*- and *trans*-1,2-di-*p*-methoxyphenyl-2-phenylvinyl-2-^{13}C (1,2-dianisyl-2-phenylvinyl-2-^{13}C) bromides (*cis*- and *trans*-**3**-Br-2-^{13}C) in an attempt to gain further information regarding the mechanistic aspects of degenerate rearrangements in triarylvinyl cationic systems.

Rappoport and Apeloig (7) have prepared and determined the stereochemistry of *cis*- and *trans*-**3**-Br. Various solvolytic experiments were carried out including the AgOAc catalyzed acetolysis which gave a 1:1 mixture of *cis*- and *trans*-**3**-OAc from either *cis*- or *trans*-**3**-Br. Very recently, these same workers (8, 9) reported further on their extensive work on *cis*- and *trans*-**3**-Br as well as the *cis*-chloride and the *cis*- and *trans*-mesylates under a variety of solvolytic conditions, implicating the involvement of ion pairs and dissociated ions and their return processes. An equilibrium *cis–trans* distribution in HOAc for the bromides, chlorides, and acetates was found to be 54:46 (8), which was a slight modification of the previously reported ratio of 1:1 (7).

For the present study on possible degenerate 1,2-phenyl shifts, *cis*- and *trans*-**3**-Br-2-^{13}C were prepared by the reactions outlined in Scheme 1.

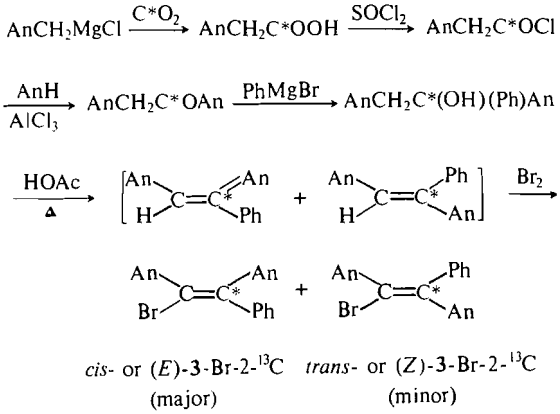

SCHEME 1

Acetolysis of *cis*- or *trans*-**3**-Br-2-^{13}C in the presence of AgOAc gave an essentially 1:1 mixture (no attempt was made to differentiate between 1:1 and 54:46) of *cis*- and *trans*-**3**-O-Ac

Can. J. Chem. Downloaded from www.nrcresearchpress.com by 210.87.254.42 on 09/05/12
For personal use only.

Can. J. Chem. Downloaded from www.nrcresearchpress.com by 210.87.254.42 on 09/05/12
For personal use only.

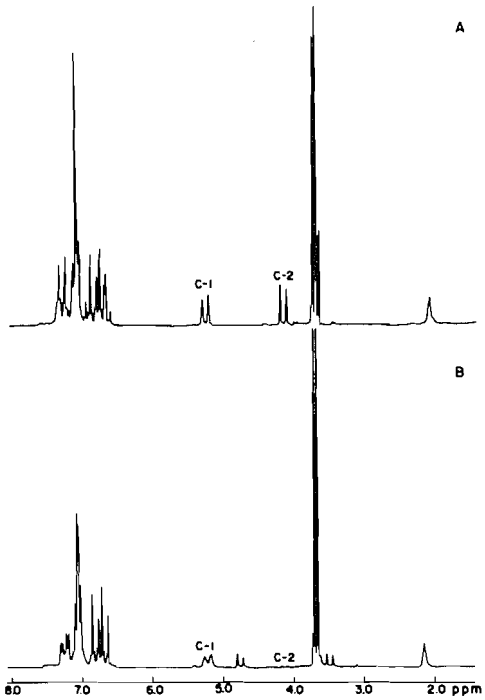

FIG. 1. The pmr spectra of 1,2-dianisyl-2-phenylethanol, **4**. (*A*) unlabeled diastereomeric mixture; (*B*) purified major diastereomer (**4***a*-2-^{13}C) derived from reaction with 90% enriched *cis*-1,2-dianisyl-2-phenylvinyl-2-^{13}C bromide (*cis*-**3**-Br-2-^{13}C).

x-^{13}C. For pmr and cmr analyses, this mixture of acetates was converted to 1,2-dianisyl-2-phenylethanol-*x*-^{13}C (**4**-*x*-^{13}C) (5, 6), which was of advantage since the C-1 and C-2 ^{13}C signals would be clearly separated from the aromatic region and their absorptions would be enhanced by the nuclear Overhauser effect.

Formation of **4** should give a mixture of the *erythro* and *threo* diastereomers. Figure 1*A* shows the pmr spectrum of ordinary **4** prepared from unlabeled *cis*- and *trans*-**3**-OAc. From the intensities of the CH_3O absorptions, the ratio of the two diastereomers, to be designated **4***a* and **4***b*, was found to be about 70:30. Figure 1*B* shows the pmr spectrum of the purified major isomer, **4***a*-*x*-^{13}C, derived from the *cis*- and *trans*-**3**-OAc-*x*-^{13}C product obtained from the reaction of 90% enriched *cis*-**3**-Br-2-^{13}C with HOAc–AgOAc. The chemical shifts for this isomer, in both the pmr and cmr spectra, are summarized in Table 1. From Fig. 1*B*, the ^{13}C satellites for the C-2 proton can be clearly seen (J = 127 Hz), while there are no measurable

TABLE 1. Proton and carbon-13 magnetic resonance of 1,2-dianisyl-2-phenylethanol (one isomer, *erythro* or *threo*, **4***a*-2-^{13}C)

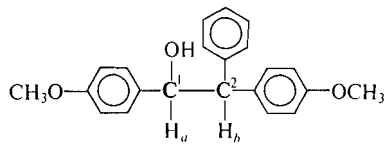

(*a*) Proton magnetic resonance

Proton		δ($CDCl_3$), ppm from TMS
OH	1H broad singlet	2.15
OCH_3	6H 2 singlets	3.68, 3.72
H_b	1H doublet $J_{H_aH_b}$ = 9 Hz $J_{^{13}CH_b}$ = 127 Hz	4.12
H_a	1H doublet	5.22
Aromatic	12H multiplets	6.64–7.32

(*b*) Carbon-13 magnetic resonance

Carbon	δ(acetone-d^6), ppm from TMS
C-1	76.4
C-2 $J_{^{13}C_1{}^{13}C_2}$ = 38 Hz	59.9
CH_3O	55.2 (55.12, 55.20)*
Aromatic carbons	113.6, 114.0, 126.3, 128.5, 128.7, 129.3, 130.7
Aromatic quaternary carbons	135.3, 137.0, 144.2, 158.7, 159.1

*Numbers in the parentheses show the two methoxyl absorptions when the spectral width was expanded from 5000 Hz to 1000 Hz.

satellites for the C-1 proton, suggesting no scrambling of the ^{13}C-label from C-2 to C-1. The same conclusion was drawn from the pmr spectrum of a 20:80 mixture of **4***a*-*x*-^{13}C and **4***b*-*x*-^{13}C, a fraction of the diastereomeric mixture which contained a greater proportion of the minor isomer, **4***b*-*x*-^{13}C. These results, indicating no isotopic scrambling, are in agreement with the observations from the cmr studies described below, and thus **4***a*-*x*-^{13}C and **4***b*-*x*-^{13}C are actually **4***a*-2-^{13}C and **4***b*-2-^{13}C.

In the cmr studies, the ^{13}C contents at C-1 and C-2 can be obtained, as described previously (6), by measuring the relative intensities in the cmr spectrum using the CH_3O absorption containing ^{13}C in its natural abundance as an internal standard. Reactions with HOAc–AgOAc were carried out with 45 and 90% enriched *cis*-**3**-Br-

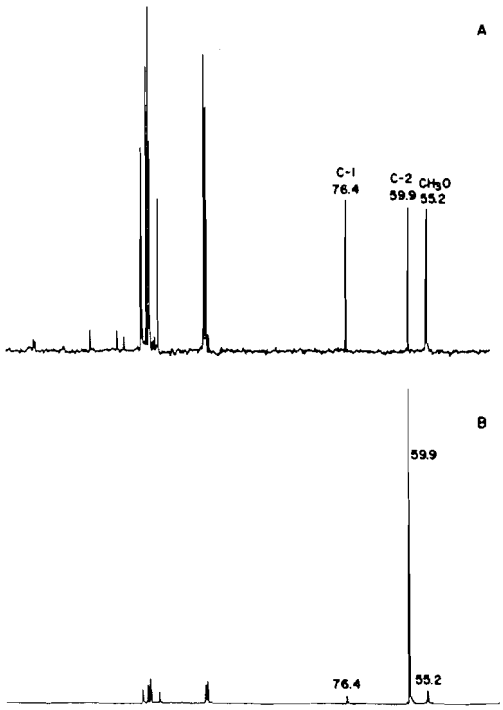

FIG. 2. ^{1}H-decoupled cmr spectra of 1,2-dianisyl-2-phenylethanol, **4**. (*A*) unlabeled diastereomer **4***a*; (*B*) **4***a*-2-^{13}C derived from reaction with 30% enriched *trans*-1,2-dianisyl-2-phenylvinyl-2-^{13}C bromide (*trans*-**3**-Br-2-^{13}C).

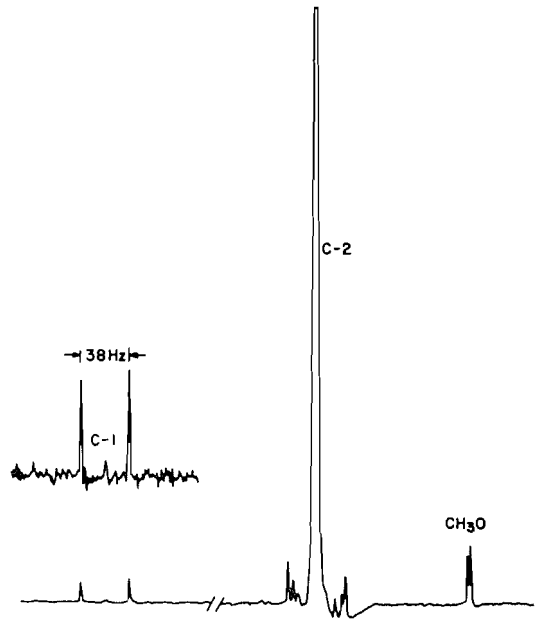

FIG. 3. Expanded cmr spectrum showing the C-1, C-2, and CH_3O absorptions of **4***a*-2-^{13}C derived from reaction with 90% enriched *cis*-**3**-Br-2-^{13}C.

2-^{13}C and with 30% enriched *trans*-**3**-Br-2-^{13}C. Figure 2, *A* and *B*, respectively, show the ^{1}H-decoupled cmr spectra of unlabeled **4***a* and **4***a*-2-^{13}C derived from one of the acetolysis experiments, in this case, the reaction with 30% enriched *trans*-**3**-Br-2-^{13}C. As stated earlier, the chemical shifts are summarized in Table 1. The intensity ratios from the cmr spectra and related data are given in Table 2. Since I_1/I_s for the unenriched **4***a* with its natural ^{13}C abundance of 1.1% and for the **4***a*-*x*-^{13}C derived from the reaction with 30% enriched *trans*-**3**-Br-2-^{13}C are, respectively, 1.08 and 0.66, the ^{13}C content at C-1 in the **4***a*-*x*-^{13}C from this reaction would be $(0.66/1.08) \times 1.1 = 0.7\%$. This ^{13}C intensity for C-1 is less than natural abundance because of the decrease in absorption due to $^{13}C_1$–$^{13}C_2$ coupling. An illustration of this decrease in intensity for the C-1 absorption is given by Fig. 3, which is an expanded and amplified spectral region showing the C-1, C-2, and CH_3O absorptions for the **4***a*-2-^{13}C derived from the reaction with 90% enriched *cis*-**3**-Br-2-^{13}C. In the reaction

TABLE 2. Data from the cmr spectra of 1,2-dianisyl-2-phenylethanol (purified diastereomer **4***a* or **4***a*-2-^{13}C) derived from reaction of *cis*- or *trans*-1,2-dianisyl-2-phenylvinyl-2-^{13}C bromide (*cis*- or *trans*-**3**-Br-2-^{13}C) with HOAc–AgOAc

Reactant	^{13}C enrichment (%)*	Intensity ratio†		^{13}C content at C-1 (%)‡	
		I_1/I_s	I_2/I_s	From cmr	Calculated for no scrambling
	Unenriched	1.08	1.01		
cis-**3**-Br-2-^{13}C	90	0.06	—	0.1	0.1
cis-**3**-Br-2-^{13}C	45	0.38	—	0.4	0.6
trans-**3**-Br-2-^{13}C	30	0.66	—	0.7	0.8

*Based on the commercial designation of 90% enrichment without dilution or diluted with carrier by factors of 2 and 3.

†I_1, I_2, and I_s are, respectively, the integrated intensities for C-1, C-2, and the CH_3O internal standard, I_2/I_s for the labeled compounds being too large for measurement.

‡^{13}C at C-1 less decrease due to $^{13}C_1$–$^{13}C_2$ coupling.

Can. J. Chem. Downloaded from www.nrcresearchpress.com by 210.87.254.42 on 09/05/12
For personal use only.

Can. J. Chem. Downloaded from www.nrcresearchpress.com by 210.87.254.42 on 09/05/12
For personal use only.

with 30% enriched *trans*-**3**-Br-2-^{13}C, if there were no ^{13}C scrambling from C-2 to C-1, correcting for the $^{13}C_1$–$^{13}C_2$ coupling, the calculated ^{13}C content at C-1 would be $(1.0 - 0.3) \times 1.1 = 0.8\%$, which is in agreement with the value obtained from the cmr intensity ratios. Similar agreements were observed for the reaction with 90 or 45% enriched *cis*-**3**-Br-2-^{13}C (Table 2), indicating that there was no *detectable* isotopic scrambling resulting from degenerate 1,2-phenyl shifts in the reaction of *cis*- or *trans*-**3**-Br-2-^{13}C with HOAc–AgOAc.[1]

The absence of degenerate rearrangement and the formation of a nearly equal mixture of *cis*- and *trans*-**3**-OAc from the reaction of *cis*- or *trans*-**3**-Br with HOAc–AgOAc indicated that, in agreement with previous conclusions (7–9), the reaction took place via classical vinyl cations without anchimeric assistance. However, it is of interest to note that for the analogous reaction of triphenylvinyl-2-^{13}C bromide (**1**-Br-2-^{13}C) with HOAc–AgOAc, about 7% scrambling of the label from C-2 to C-1 was observed (5). In discussing the relative migratory aptitudes of the anisyl and phenyl groups in vinyl cationic systems, such as in solvolyses of *cis*- and *trans*-2-anisyl-1,2-diphenylvinyl bromide (*cis*- and *trans*-**5**-Br), Rappoport and Houminer (10) have pointed out that a number of factors have to be considered. If the bridged ions **6** and **7** were taken as models for the transition states in the Ph and

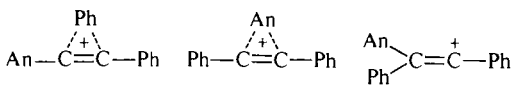

6 **7** **8**

An migrations, their relative stabilities compared with ion **8** would depend on such factors as the stabilization achieved by charge delocalization on the bridging group, the deconjugation of the migrating group and the enhanced conjugation of the nonmigrating group with the vinylic double bond, and the possibility of partial positive charge formation at the β-carbon. The effect of ground state conjugation between the α-aryl group and the vinylic double bond in accounting for the lower solvolytic reactivity of arylvinyl relative to saturated systems has been demonstrated by Yates and Périé (11). Extending the treatment to the β-aryl substituents, it has been suggested (ref. 10, and private communication with Z. Rappoport) that the loss of conjugation between the migrating group and the double bond in going from ion **8** to **6** or **7** may be more important for the anisyl than the phenyl group, thus favoring **6** over **7** and accounting for the observation that the ratio of anisyl to phenyl migration in vinylic systems is apparently lesser than in saturated systems.

In considering the possible degenerate 1,2-phenyl shift in the present 1,2-dianisyl-2-phenylvinyl system in relation to that in the triphenylvinyl system, if bridged ions **9** and **10** were taken as models of the transition states for the phenyl migration, since the migrating group in both cases is the same, the effects of stabilization by

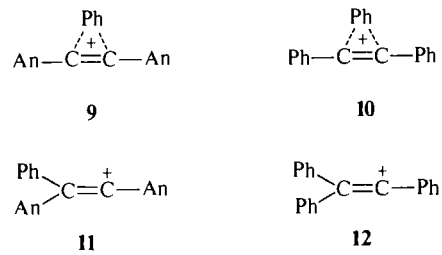

9 **10**

11 **12**

charge delocalization on the bridging group and of the loss of conjugation of the migrating group with the vinylic double bond should be similar. On the other hand, enhanced conjugation of the nonmigrating group and possible partial positive charge formation at the β-carbon should favor **9** over **10**, and increase the possibility of Ph migration in the 1,2-dianisyl-2-phenylvinyl system. The observed results are contrary to this expectation. The lack of scrambling in the reaction of *cis*- or *trans*-**3**-Br-2-^{13}C with HOAc–AgOAc noted in the present study may, therefore, be attributed to the greater stability of the α-anisyl substituted ion **11** over that of the α-phenyl substituted ion **12**, so that the conversion of **11** to **9** would require a higher activation energy than the conversion of **12** to **10**. It may also be pointed out that Bonner and Putkey (12) have found that there was less

[1]Since experimental errors in the nmr intensity measurements may be relatively large, small extents of scrambling may not be detectable by this method. The present results do indicate that the scrambling is very low, probably $0 \pm 2\%$. Professor Z. Rappoport (private communication) has informed us that under different conditions, such as the reaction of *cis*- and *trans*-**3**-Br with 2,2,2-trifluoroethanol in the presence of lutidine, some degenerate 1,2-phenyl shift was observed.

Can. J. Chem. Downloaded from www.nrcresearchpress.com by 210.87.254.42 on 09/05/12
For personal use only.

1,2-anisyl migration in the deamination of 1,2,2-trianisylethylamine-1-^{14}C than 1,2-phenyl migration in a similar deamination of 1,2,2-triphenylethylamine-1-^{14}C. The delocalization of the cationic charge at the migration terminus has been suggested as playing an important role (12, 13). From this point of view, the greater charge delocalization in **11** over **12**, thus giving a less electrophilic migration terminus and lesser tendency for migration for **11**, would also fit the present results.

It is of interest to note that Stang and Dueber (14, 15) have found that solvolyses of *trans*-1,2-dimethyl-2-phenylvinyl triflate involved the phenyl bridged ion with anchimeric assistance, while reaction of the *cis*-isomer proceeded via the classical vinyl cation. It is also well known that an increase in the stability of a carbocation generally decreases the probability of anchimeric assistance (16, 17). In triarylvinyl cationic systems, when the α-aryl group is anisyl, the stability of the classical cation is high and there is no anchimeric assistance in reactions involving α-anisylvinyl cations. In the case of the triphenylvinyl cation, however, its stability being intermediate between the 1,2-dianisyl-2-phenylvinyl and 1,2-dimethyl-2-phenylvinyl cations, the possibility cannot be excluded that phenyl participation with anchimeric assistance may be an explanation of the scramblings observed in the reaction of triphenylvinyl-2-^{13}C bromide with HOAc–AgOAc (5) or in the solvolyses of triphenylvinyl-2-^{14}C triflate (18). A comparison of the triarylvinyl and the 1,2,2-triarylethyl systems is also of interest. Bonner's work (12) indicated that the anisyl shift in the 1,2,2-trianisylethyl cation is less than the phenyl shift in the 1,2,2-triphenylethyl cation, and this is in contrast with the observation of more anisyl shift in the trianisylvinyl cation than phenyl shift in the triphenylvinyl cation (5, 6). If phenyl participation were to play a role in the triphenylvinyl system, and if only classical ions were involved in the trianisylvinyl system, than a direct comparison should not be made with the saturated triarylethyl systems since both the 1,2,2-triphenylethyl and the 1,2,2-trianisylethyl cases apparently involved classical ions. Further work is currently underway in this laboratory in an effort to ascertain whether phenyl participation occurs in reactions with triphenylvinyl systems.

Experimental

Desoxyanisoin-carbonyl-^{13}C (13)

p-Anisylacetic acid-carboxyl-^{13}C was prepared from reaction of $AnCH_2MgCl$ with $^{13}CO_2$ (90% enriched as $Ba^{13}CO_3$, Merck, Sharp and Dohme Canada Ltd.) as previously described for the analogous preparation of the ^{14}C-labeled acid (19). The labeled acid (3.25 g, 19.5 mmol) was converted to the acid chloride by refluxing for 1 h with 5.0 g (42 mmol) of $SOCl_2$. Cyclohexane (10 ml) was added and the excess of $SOCl_2$ was removed with the cyclohexane under reduced pressure. The residual labeled acid chloride was used directly for the Friedel–Crafts acylation.

To a solution of the labeled acid chloride and 4.30 g (40 mmol) of anisole in 40 ml of CS_2 was added gradually 4.0 g (30 mmol) of $AlCl_3$. The deep red reaction mixture was stirred at room temperature for 15 min. The excess CS_2 was distilled off and the residue was poured into cold 2 *N* HCl. The white precipitate was collected and redissolved in 200 ml of tetrahydrofuran (THF). The solution was washed with 10% NaOH and then with a saturated solution of NaCl. After removal of the solvent, the product was recrystallized from ethanol, giving 3.70 g (74% based on the *p*-anisylacetic acid-carboxyl-^{13}C) of **13**, mp 110–111 °C (an unlabeled, commercial sample (Aldrich) melted at 110–112 °C), pmr ($CDCl_3$) for the unlabeled compound, δ 3.73, 3.80 (two CH_3O, two singlets), 4.15 (CH_2, s), and 6.77–8.07 (aromatic, m). For the labeled compound, the methylene protons showed long range coupling with the carbonyl-^{13}C, $J_{^{13}CCH_2} = 6$ Hz. *Anal.* calcd. for $C_{16}H_{16}O_3$ (90% ^{13}C enriched at the carbonyl carbon): C 75.10, H 6.27; found: C 75.08, H 6.24.

1,2-Dianisyl-1-phenylethanol-1-^{13}C (14)

A solution of 3.70 g (14.5 mmol) of **13** (90% enriched) in 80 ml of THF was added over a period of 1 h to a Grignard solution prepared from PhBr (6.0 g, 38 mmol), Mg (1.5 g, 62 mmol), and THF (60 ml). The resulting mixture was refluxed for 2 h and then poured into 200 ml of H_2O containing NH_4Cl (20 g) and NH_4OH (4 ml). The crude product was collected, washed with CCl_4, and recrystallized from ethanol, giving 3.80 g (79%) of **14**, mp 111–112 °C. The pmr spectrum of the unlabeled compound, prepared in the same way, showed δ 2.30 (OH, broad s), 3.53 (CH_2, s), 3.68, 3.72 (two CH_3O, two singlets), and 6.60–7.43 (aromatic, m). The labeled compound also showed long range coupling of the CH_2 protons with the ^{13}C at C-1 ($J_{^{13}CCH_2} = 4$ Hz). *Anal.* calcd. for $C_{22}H_{22}O_3$ (90% ^{13}C enriched at C-1): C 79.06, H 6.62; found: C 79.02, H 6.63.

The mp of unlabeled **14**, previously prepared by the same reaction but with benzene as solvent, was reported as 84–85 °C (7), considerably lower than the presently observed 111–112 °C. In the mass spectrum, the base peak for unlabeled **14** has $m/e = 213$ ($M - AnCH_2$), while m/e of the base peak for desoxyanisoin is 135 ($AnCO^+$). The previous workers (7) reported that the base peak for unlabeled **14** was 135, suggesting that possibly their sample might be contaminated by desoxyanisoin. Moreover, the reported analytical data also suggested con-

Can. J. Chem. Downloaded from www.nrcresearchpress.com by 210.87.254.42 on 09/05/12
For personal use only.

tamination since the H content was found to be 6.32% in comparison with the calculated value of 6.63%.

cis- and trans-1,2-Dianisyl-2-phenylvinyl-2-^{13}C Bromides (cis- and trans-3-Br-2-^{13}C)

A solution of 3.80 g (11.3 mmol) of **14** in 200 ml of HOAc was heated in an oil bath at 85 °C for 3 h. The resulting solution was cooled in an ice bath, 1.0 ml of Br_2 in 8.0 ml of HOAc was added gradually, and the mixture was stirred for 10 min before being poured into H_2O which contained 1.0 g of $Na_2S_2O_3$ to destroy the excess Br_2. The resulting mixture was left standing overnight before the precipitated product was collected. Analysis by pmr (7) indicated that the crude product consisted of a mixture of *cis*- and *trans*-3-Br-2-^{13}C in a ratio of about 9:1. Fractional crystallization was effected with CH_3OH as solvent, with the minor *trans*-isomer being recovered from the concentrated mother liquor after long standing (1–2 days). Several crops of the major or minor product were combined and recrystallized from CH_3OH to give 2.0 g (45%) of *cis*-3-Br-2-^{13}C, mp 116–117 °C (lit. (7) mp 117 °C), and 0.25 g (5%) of *trans*-3-Br-2-^{13}C, mp 122–123 °C (lit. (7, 11) mp 135–136 °C, 131 °C). *Anal.* calcd. for $C_{22}H_{19}BrO_2$ (90% ^{13}C enriched at C-2): C 66.92, H 4.83; found: (*cis*-isomer), C 66.94, H 4.98, (*trans*-isomer), C 66.94, H 5.16. The pmr spectra of the unlabeled *cis*- and *trans*-3-Br, prepared in the same way as described above, were in agreement with previously reported data (7), pmr ($CDCl_3$) *cis*-isomer, δ 3.68, 3.75 (two CH_3O, two singlets), and 6.50–7.37 (aromatic, m); *trans*-isomer, δ 3.73; 3.80 (two CH_3O, two singlets), and 6.63–7.45 (aromatic, m).

Reaction of cis- or trans-3-Br-2-^{13}C with HOAc–AgOAc

The procedure for the acetolysis of *cis*- or *trans*-3-Br-2-^{13}C in the presence of AgOAc was similar to that described by Rappoport and Apeloig (7). A mixture of 1.5 g (3.8 mmol) *cis*-3-Br-2-^{13}C (90% enriched), 0.70 g (4.2 mmol) AgOAc, 35 ml HOAc, and 2.5 ml Ac_2O was heated under reflux for 1.5 h. The hot reaction mixture was filtered and the solvent was evaporated off. The residue was redissolved in CCl_4, washed with H_2O and $NaHCO_3$ solution, dried, and the solvent removed to give a product mixture (1.2 g, 85%) whose pmr was consistent with that reported for unlabeled *cis*- and *trans*-1,2-dianisyl-2-phenylvinyl acetates, pmr ($CDCl_3$) δ 1.95, 2.00 (two AcO, two singlets, 1:1 ratio), 3.77, 3.83 (two CH_3O, two singlets), and 6.65–7.33 (aromatic, m). This product was utilized without further purification for conversion to 1,2-dianisyl-2-phenylethanol-*x*-^{13}C for cmr analysis.

For the acetolysis of *trans*-3-Br-2-^{13}C, the labeled bromide (0.20 g, 90% enriched) was diluted with 0.40 g of unlabeled material and the resulting 30% enriched *trans*-3-Br-2-^{13}C was treated with HOAc–AgOAc in the same way as in the reaction with the *cis*-isomer. A 1:1 mixture of *cis*- and *trans*-3-OAc-*x*-^{13}C (0.45 g, 90%) was obtained, pmr ($CDCl_3$) δ 1.97, 2.00 (two AcO, two singlets, 1:1 ratio), 3.78, 3.83 (two CH_3O, two singlets), 6.67–7.32 (aromatic, m).

1,2-Dianisyl-2-phenylethanol-x-^{13}C (4-x-^{13}C)

The 1:1 mixture of *cis*- and *trans*-3-OAc-*x*-^{13}C obtained from the reaction of *cis*- or *trans*-3-Br-2-^{13}C with HOAc–AgOAc was converted to 4-*x*-^{13}C (*erythro* and *threo*) for cmr examination using the XL-100-15 spectrometer by the same procedures as previously described for 1,2,2-trianisylethanol-*x*-^{13}C (6). In a typical experiment, the mixture of *cis*- and *trans*-3-OAc-*x*-^{13}C from the reaction of 90% enriched *cis*-3-Br-2-^{13}C was reduced twice with $LiAlH_4$ in THF (6). The resulting oil was crystallized from ethanol, the pmr spectrum of which indicated that it consisted of a mixture of diastereomers, formed in a ratio of about 70:30 based on the CH_3O absorptions. In an analogous run with unlabeled materials, a similar 70:30 mixture of diastereomers was obtained, pmr ($CDCl_3$) δ 2.06 (OH, broad s), 3.62, 3.68, 3.72 (CH_3O, three singlets, major isomer, 3.68, 3.72, minor isomers, 3.62, 3.68), 4.12 (C-2 H, d, J = 9 Hz), 5.22 (C-1 H, d), and 6.56–7.35 (aromatic, m).

After the labeled 70:30 mixture of diastereomers was recrystallized three times from ethanol, the major diastereomer, 4*a*-*x*-^{13}C (0.25 g) was obtained, mp 123–124 °C. Its pmr and cmr data, as given in Tables 1 and 2, indicate no scrambling and that 4*a*-*x*-^{13}C is in fact 4*a*-2-^{13}C. *Anal.* calcd. for $C_{22}H_{22}O_3$ (90% ^{13}C enriched at C-2): C 79.06, H 6.61; found: C 79.16, H 6.35.

Acknowledgments

The financial support given by the National Research Council of Canada and valuable comments and information supplied by Professor Z. Rappoport are sincerely acknowledged.

1. M. Hanack. Acc. Chem. Res. **3**, 209 (1970).
2. G. Modena and U. Tonellato. Adv. Phys. Org. Chem. **9**, 185 (1971).
3. P. J. Stang. Prog. Phys. Org. Chem. **10**, 205 (1973).
4. L. R. Subramanian and M. Hanack. J. Chem. Educ. **52**, 80 (1975).
5. F. H. A. Rummens, R. D. Green, A. J. Cessna, M. Oka, and C. C. Lee. Can. J. Chem. **53**, 314 (1975).
6. M. Oka and C. C. Lee. Can. J. Chem. **53**, 320 (1975).
7. Z. Rappoport and Y. Apeloig. J. Am. Chem. Soc. **91**, 6734 (1969).
8. Z. Rappoport and Y. Apeloig. J. Am. Chem. Soc. **97**, 821 (1975).
9. Z. Rappoport and Y. Apeloig. J. Am. Chem. Soc. **97**, 836 (1975).
10. Z. Rappoport and Y. Houminer. J. Chem. Soc. Perkin Trans. 2, 1506 (1973).
11. K. Yates and J. J. Périé. J. Org. Chem. **39**, 1902 (1974).
12. W. A. Bonner and T. A. Putkey. J. Org. Chem. **27**, 2348 (1962).
13. M. J. McCall, J. M. Townsend, and W. A. Bonner. J. Am. Chem. Soc. **97**, 2743 (1975).
14. P. J. Stang and T. E. Dueber. J. Am. Chem. Soc. **95**, 2683 (1973).
15. P. J. Stang and T. E. Dueber. J. Am. Chem. Soc. **95**, 2686 (1973).
16. A. Streitwieser, Jr. Solvolytic displacement reactions. McGraw-Hill, New York. 1962. p. 104.
17. D. Bethell and V. Gold. Carbonium ions, an introduction. Academic Press, New York. 1967. p. 278.
18. C. C. Lee, A. J. Cessna, B. A. Davis, and M. Oka. Can. J. Chem. **52**, 2679 (1974).
19. C. C. Lee, D. Newman, and D. P. Thornhill. Can. J. Chem. **41**, 520 (1963).

Dipolar and calorimetric study of the complexes between *N,N*-dimethyl-*N'*-phenylformamidines and phenols

ALFRED F. FOUBERT AND PIERRE L. HUYSKENS
University of Leuven, Celestijnenlaan 200-F, B-3030 Heverlee, Belgium

Received July 8, 1975

ALFRED F. FOUBERT and PIERRE L. HUYSKENS. Can. J. Chem. **54**, 610 (1976).

The dipole moments μ_b of *N,N*-dimethyl-*N'*-phenylformamidine and its 4-methylphenyl and 4-chorophenyl derivatives and the dipole moments μ_{ab} of some 20 complexes of these bases with phenols were determined in cyclohexane at 298 K. Assuming the additivity of the bond moments, the angles α_b between μ_b and the axis C_1C_4 of the phenyl group were computed for the three bases. Dipole increments $\Delta\vec{\mu} = \vec{\mu}_{ab} - \vec{\mu}_a - \vec{\mu}_b$ were then computed assuming the hydrogen bond involved the electron pair of the sp_2 hybridized imino nitrogen atom. The variation of the $\Delta\mu$ computed in this way with the complexation enthalpy ΔH_{ab} is described by the same curve as that for the systems phenols–anilines and phenols–pyridines. This is not the case when other structures are chosen for computing $\Delta\mu$ and this provides evidence for the 'imino' structure of the complexes. For a given amidine, the dipole increment increases when the proton donor becomes more acidic. The derivative $d\Delta\mu/dpK_a$ here is of the order of -0.5 D per pK_a unit whereas this value is only -0.2 for the pyridines. The absolute values of $\Delta\mu$ are also greater for the amidines. This can be ascribed in part to a higher proportion of H-bonds of the ion pair type $O^-\cdots H^+N$, when the amidine is complexed by the same phenol as the pyridines.

ALFRED F. FOUBERT et PIERRE L. HUYSKENS. Can. J. Chem. **54**, 610 (1976).

Les moments dipolaires μ_b de la *N,N*-diméthyl *N'*-phénylamidine et de ses dérivés 4-méthylphényl et 4-chlorophényl ainsi que les moments dipolaires d'une vingtaine de complexes de ces bases avec divers phénols d'acidité croissante ont été déterminés dans le cyclohexane à 298 K. Les angles α_b entre la direction de μ_b et celle de l'axe C_1C_4 du groupe phényle ont été calculés pour les trois bases en supposant l'additivité des moments de liaison. Les incréments dipolaires $\Delta\vec{\mu} = \vec{\mu}_{ab} - \vec{\mu}_a - \vec{\mu}_b$ ont été calculés dans l'hypothèse où le pont d'hydrogène se forme dans la direction de la paire électronique de l'atome d'azote imino avec une hybridation sp_2. Les valeurs de $\Delta\mu$ ainsi déterminées varient avec l'enthalpie de complexation ΔH_{ab} suivant une fonction qui est la même que celle des systèmes phénols–pyridines et phénols–anilines. Ceci n'est pas le cas lorsque l'on calcule $\Delta\mu$ sur la base d'une structure différente. Ces résultats constituent donc un argument en faveur de la structure 'imino' de ces complexes. Pour une amidine donnée, l'incrément dipolaire augmente avec l'acidité du donneur de proton. La dérivée $d\Delta\mu/dpK_a$ est ici de l'ordre de -0.5 D par unité pK_a alors qu'elle n'atteint que -0.2 dans le cas des pyridines. La valeur absolue de $\Delta\mu$ est aussi plus élevée pour les amidines. Ceci peut être attribué, en partie, à une proportion plus élevée de ponts d'hydrogène du type ionique $O^-\cdots H^+N$ lorsque l'amidine est complexée par le même phénol que les pyridines.

Introduction

Amidines can be represented by the general formula

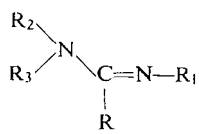

As a rule these molecules have two basic sites, namely, the two lone pairs of electrons of both nitrogen atoms. As shown by Smith and Taylor (1), it appears that the first pK_a of these substances in a 50:50 water–ethanol mixture is highly sensitive to the nature of the group R_1, while, according to the earlier results of Lorz and Baltzly (2), modifying R_2 or R_3 only weakly affects the pK_a. Grivas and Taurin (3), studying the infrared spectrum of the *N,N*-dimethyl- and *N,N*-diethylamidinium ions, found intensive bands due to the absorption by the $=N=H_2^+$ group while absorption bands of the $\equiv N-H^+$ group did not appear. The nmr spectra of the cations of a series of *N,N*-dimethylamidines were investigated by Rens (4) who found a peak of two protons in the vicinity of $\delta = 10$ ppm, which could be assigned to the $=N=H_2^+$ group. It is therefore generally assumed that the most basic site of the amidines is the 'imino' nitrogen atom.

When amidines form hydrogen bonds with proton donors the imino electron pair will thus be preferentially involved.

Can. J. Chem. Downloaded from www.nrcresearchpress.com by 210.87.254.6 on 09/05/12
For personal use only.

Can. J. Chem. Downloaded from www.nrcresearchpress.com by 210.87.254.6 on 09/05/12
For personal use only.

The stability of the hydrogen bonds depends on the acidic strength of the proton donor and on the basic strength of the proton acceptor (5) and thus will be influenced by the substitution in both molecules.

In a recent work Zeegers-Huyskens and coworkers (6) determined the complexation constants of *N*,*N*-dimethyl-*N'*-phenylformamidine derivatives with several phenols in cyclohexane at 298 K. The complexation constants K_{ab} depend on the Hammett parameter σ_b of the substituent of the phenyl group of the amidine and σ_a of the substituent of the phenol according to a relation of the type

$$[1] \quad \log K_{ab} = 1.90 + 1.18\sum\sigma_a - 0.66\sum\sigma_b - 0.6(\sum\sigma_a)(\sum\sigma_b)$$

The formation of a hydrogen bond brings about displacements of the electrons and of the nuclei which result in a difference between the dipole moment of the complex and the vector sum of the individual moments of the components.

$$[2] \quad \Delta\vec{\mu} = \vec{\mu}_{ab} - \vec{\mu}_a - \vec{\mu}_b$$

This dipole increment can be considered as a quantitative indication of the 'polarity' of the hydrogen bond. As shown by Ratajczak and Sobczyk (7) and by ourselves (8, 9), in a given family of complexes with O—H···N bonds the dipole increment also increases with both the strength of the acid and the strength of the base. The value of $\Delta\mu$ computed from the dipole moments of the complex and of the separate components depends on the chosen values of the angles between these vectors.

In this work the values for $\Delta\mu$ for several amidine–phenol complexes are computed, assuming that the hydrogen bond involves the imino electron pair and that all the rotamers around the H-bond are equally represented. Under these circumstances the values of $\Delta\mu$ show relations with respect to the complexation enthalpy ΔH_{ab} which fully agree with the relations observed for other O—H···N bonds, thus corroborating the predominance of this structure for the ab complexes.

Dipole Moments of the Amidines and of the Complexes

Principle of the Determinations

Starting from the theory of Fröhlich (10), it can be shown that the dipole moments μ_j of the various *dissolved* entities obey the following equation

$$[3] \quad \sum\mu_j^2 C_j = \frac{9kT}{4\pi N_A}\left[\frac{(\epsilon - n^2)(2\epsilon + n^2)}{\epsilon(n^2+2)^2} - F_s\bar{V}_s^0\frac{(\epsilon_s - n^2)(2\epsilon_s + n_s^2)}{\epsilon_s(n_s^2+2)^2}\right]$$

where C_j is the real concentration of the dissolved entity j, F_s the formal concentration of the solvent in the solution, and $\bar{V}_s^0$ the molar volume of the pure solvent. The other subscripts refer to the pure solvent (s). ϵ corresponds to the dielectric constant and n to the refractive index.

Let us now consider ternary solutions of the acid and of the base in the solvent, where the formal concentration F_b of the base is much higher than that of the acid F_a.

The following quantity Ω can be determined from the dielectric constants, the refractive indices (no correction for atomic polarization is made here), and the densities of the solutions and of the pure solvent:

$$[4] \quad \Omega \equiv \frac{9kT}{4\pi N_A}\frac{1}{F_b}\left\{\frac{(\epsilon - n^2)(2\epsilon + n^2)}{\epsilon(n^2+2)^2} - F_s\bar{V}_s^0\frac{(\epsilon_s - n_s^2)(2\epsilon_s + n_s^2)}{\epsilon_s(n_s^2+2)^2}\right\}$$

When F_b is sufficiently large such that the complexation is practically complete, and when no complexes of higher stoichiometry are formed, the quantity Ω must vary linearly with the ratio F_a/F_b, following the relation (11):

$$[5] \quad \Omega = \mu_b^2 + (\mu_{ab}^2 - \mu_b^2)\frac{F_a}{F_b}$$

When Ω is plotted against the ratio F_a/F_b, it is thus possible to determine μ_b from the ordinate at the origin and $(\mu_{ab}^2 - \mu_b^2)$ from the slope. (A correction can be made if the complexation is not complete but, owing to the large values of the complexation constant in the present case (6), this was not necessary here.)

The determinations were made with formalities F_b of the order of magnitude of 0.5 mol l^{-1} in cyclohexane at 298 K. Some 10 solutions with ratios F_a/F_b going from 0 to 0.1 were used. In Fig. 1 we give as an example the evolution of

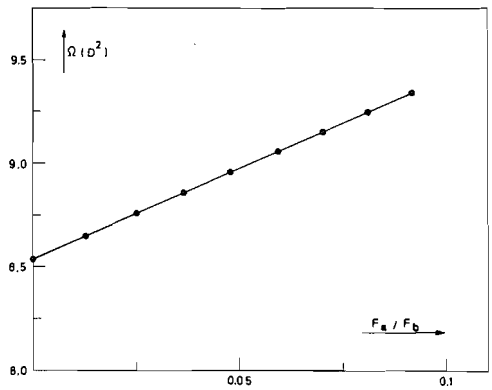

FIG. 1. A plot of Ω *vs.* F_a/F_b for the system phenol–*N*,*N*-dimethyl-*N*′-phenylformamidine.

Ω *vs.* F_a/F_b for the system phenol–*N*,*N*-dimethyl-*N*′-phenylformamidine.

Experimental Results

In Table 1 we give the intercept (which corresponds to μ_b^2) and the slope of the function with its mean deviation. The values of μ_b^2 are very similar for all the systems with the same base. The mean value of μ_b^2 was used to compute μ_{ab}^2 from the slope of the lines. Also tabulated in Table 1 are the values of μ_{ab} and the value of the dipole moment of the phenol taken from the literature.

The formation of a_2b complexes with two molecules of acid would cause the appearance of an higher term in [5] and thus perturb the linearity of the function. From the observed linearity one can thus deduce that in the present conditions the formation of a_2b complexes is negligible. This can be expected from the order of magnitude of the addition constants (6) and from the very low concentration of free acid in these experiments (lower than 0.002 mol l^{-1}). Owing to the absence of a second proton donor site on the acid, hydrogen bonded ab_2 complexes cannot be formed. On the other hand, the formation of aggregates between an ab complex and a base molecule by dipole–dipole interactions does not appear to be important in this concentration range. In order to check this, additional

TABLE 1. Ordinate at the origin and slope of the functions Ω against F_a/F_b. Dipole moments of the amidine and of the complexes. Dipole moments of the phenols taken from the literature

Base	Substituent of phenol	Intercept (D^2)	Slope (D^2)	μ_{ab} (D)	μ_a (D)
N,*N*-Dimethyl-	4-CH_3	7.45	8.56±0.24	4.00	1.40*
N′–4-methylphenylformamidine	4-*tert*-butyl	7.46	8.74±0.26	4.02	1.47*
	3,5-$(CH_3)_2$	7.45	8.17±0.20	3.95	1.40*
	—	7.42	9.82±0.17	4.15	1.39*
	4-F	7.42	16.60±0.21	4.90	2.02*
	4-Cl	7.36	18.96±0.18	5.14	2.05†
	3,5-Cl_2	7.27	22.16±0.60	5.44	2.05‡
	3,4,5-Cl_3	7.43	30.71±0.73	6.18	2.81*
		Mean 7.41	μ_b = 2.72 D		
N,*N*-Dimethyl-	4-CH_3	8.56	7.29±0.09	3.98	1.40*
N′-phenylformamidine	4-*tert*-butyl	8.54	7.74±0.14	4.03	1.47*
	3,5-$(CH_3)_2$	8.53	7.65±0.05	4.02	1.40*
	—	8.52	8.98±0.08	4.19	1.39*
	4-F	8.58	15.98±0.38	4.95	2.02*
	4-Cl	8.47	17.32±0.18	5.08	2.05†
	3,5-Cl_2	8.60	18.50±0.20	5.20	2.05‡
	3,4,5-Cl_3	8.53	28.00±0.17	6.04	2.81*
		Mean 8.54	μ_b = 2.92 D		
N,*N*-Dimethyl-	—	18.04	4.08±0.39	4.73	1.39*
N′-4-chlorophenylformamidine	4-F	18.53	9.81±0.23	5.29	2.02*
	4-Cl	17.98	10.79±0.16	5.39	2.05†
	3,5-Cl_2	18.47	14.30±0.16	5.71	2.05‡
		Mean 18.25	μ_b = 4.27 D		

*Reference 14.
†Reference 9.
‡Value as for 4-chlorophenol.

Can. J. Chem. Downloaded from www.nrcresearchpress.com by 210.87.254.6 on 09/05/12
For personal use only.

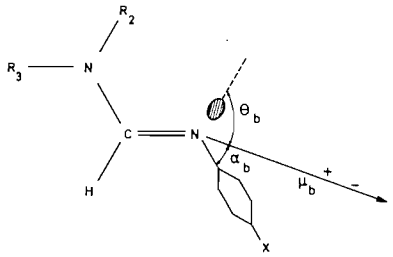

FIG. 2. μ_b of amidines.

experiments were carried out for the system 4-methylphenol–*N*,*N*-dimethyl-*N'*-phenylformamidine using a formality of F_b of 0.25 mol l^{-1} instead of 0.5 mol l^{-1}. The deviation of μ_{ab} is smaller than the experimental errors. We can therefore conclude that the values of Table 1 refer to 1:1 complexes within the margin of experimental error.

Orientation in the Dipole Moments of the Amidines

The dipole moments of the amidines studied here are fairly large. As a first approximation one can neglect the component which is perpendicular to the plane of the amidine group. In this plane, $\vec{\mu}_b$ can be resolved into a component parallel to the N···X axis (Fig. 2) and into another component in the perpendicular direction. As a first approximation it will be assumed that this last component remains the same for the three amidines which are studied.

Hence

$$[6] \qquad \frac{\sin \alpha_b}{\sin \alpha_{b'}} = \frac{\mu_b}{\mu_b}$$

The difference between the parallel components of the 4-chlorophenyl derivative and of the unsubstituted phenyl derivative can be taken equal to the dipole moment of chlorobenzene, assuming the additivity of the bond moments. In the same solvent, using a similar equation, Debecker (12) found a value of 1.564 D for C_6H_5Cl. This leads to the equation

$$[7] \qquad \mu_H \cos \alpha_H + 1.564 = \mu_{Cl} \cos \alpha_{Cl}$$

where the subscripts H and Cl refer respectively to phenylformamidine and to the 4-chlorophenyl derivative. Combining [6] and [7] it is possible to compute the angle α_b between μ_b and the N···X axis. Assuming an sp_2 hybridization of this nitrogen atom, this axis forms an angle of 120° with the lone pair of electrons. If θ_b is the angle between μ_b and the direction of the lone pair of electrons

$$[8] \qquad \theta_b = 120 - \alpha_b$$

In Table 2 the values of α_b and θ_b are tabulated.

TABLE 2. Angle α_b between the dipole moment of the amidines and the N···X axis. Angle θ_b between the dipole moment of the amidines and the lone pair of electrons of the imino nitrogen atom. pK_a of the amidine in water–ethanol (50:50 mixture) at 298 K

Compound	α_b (deg)	θ_b (deg)	pK_a
N,*N*-Dimethyl-*N'*-4-methylphenylformamidine	41	79	8.45
N,*N*-Dimethyl-*N'*-phenylformamidine	37.5	82.5	8.35
N,*N*-Dimethyl-*N'*-4-chlorophenylformamidine	24.5	95.5	7.54

Dipole Increment Resulting from the Formation of the H-Bond

If it is assumed that the dipole increment has the direction of the O—H bond, that the hydrogen bond has the direction of the lone pair of electrons of the imino nitrogen atom, and that all rotamers around the hydrogen bond are equally represented, then the dipole increment $\Delta\mu$ is given by the following equation:

$$[9] \qquad \Delta\mu = \sqrt{\mu_{ab}^2 - \mu_a^2 \sin^2 \theta_a - \mu_b^2 \sin^2 \theta_b} - \mu_a \cos \theta_a - \mu_b \cos \theta_b$$

Here θ_a is the angle between the direction of μ_a and the O—H axis of the phenol. These angles were computed previously (13). The results are given in Table 3.

Enthalpy of the H-Bond Formation

The complexation enthalpy ΔH_{ab} was determined by adiabatic calorimetry, dissolving a given amount of amidine in a solution of the phenol in cyclohexane. The concentration of the amidine after dilution was of the order of 0.08 mol l^{-1}. Several phenol solutions were used where F_a varied from 0 to 0.04 mol l^{-1}. The concentration C_{ab} of the complex was computed using the values of K_{ab} obtained by infrared spectrometry (6). ΔH_{ab} is computed from the temperature variations ΔT and ΔT^0 respectively

Can. J. Chem. Downloaded from www.nrcresearchpress.com by 210.87.254.6 on 09/05/12
For personal use only.

Can. J. Chem. Downloaded from www.nrcresearchpress.com by 210.87.254.6 on 09/05/12
For personal use only.

TABLE 3. Experimental values of the dipole increment $\Delta\mu$ of the complexes. Calculated value from [11]: complexation enthalpy; log K_{ab} (ref. 6): ΔpK_a; pK_a of the phenol and angle θ_a between the dipole moment of the phenol and the O—H axis

Base	Substituent of phenol	$\Delta\mu$ (D) Exptl.	$\Delta\mu$ (D) Calcd. [11]	ΔH_{ab} (kJ mol^{-1})	log K_{ab}	ΔpK_a	pK_a	θ_a (deg)
N,*N*-Dimethyl-	4-CH_3	1.23	1.31	−38.5	1.86	−1.81	10.26	35
N'-4-methylphenylformamidine	4-*tert*-butyl	1.31	1.29	—	—	−1.83	10.28	46
	3,5-$(CH_3)_2$	1.16	1.35	−38.0	—	−1.73	10.18	35
	—	1.38	1.50	−37.5	1.99	−1.54	9.99	25
	4-F	1.66	1.57	—	—	−1.36	9.81	−19
	4-Cl	1.91	1.75	−41.5	2.36	−0.93	9.38	−20
	3,5-Cl_2	2.27	2.33	−43.0	2.91	+0.27	8.18	−20
	3,4,5-Cl_3	2.51	2.57	—	—	+0.70	7.75	−33
N,*N*-Dimethyl-	4-CH_3	1.08	1.19	−37.5	1.76	−1.91	10.26	35
N'-phenylformamidine	4-*tert*-butyl	1.21	1.17	—	—	−1.93	10.28	46
	3,5-$(CH_3)_2$	1.15	1.23	−35.0	—	−1.73	10.18	35
	—	1.33	1.38	−38.0	1.89	−1.64	9.99	25
	4-F	1.67	1.45	—	—	−1.46	9.81	−19
	4-Cl	1.81	1.63	−40.0	2.30	−1.03	9.38	−20
	3,5-Cl_2	1.95	2.21	−42.0	2.77	+0.17	8.18	−20
	3,4,5-Cl_3	2.34	2.45	—	—	+0.00	7.75	−33
N,*N*-Dimethyl-	—	1.23	1.11	−38.0	1.75	−2.45	9.99	25
N'-4-chlorophenylformamidine	4-F	1.60	1.28	—	—	−2.27	9.81	−19
	4-Cl	1.72	1.46	−38.5	1.97	−1.84	9.38	−20
	3,5-Cl_2	2.22	2.04	—	2.52	−0.64	8.18	−20

in the presence and in the absence of phenol, by means of the equation

$$[10] \qquad \Delta H_{ab} = \frac{-C_p(\Delta T - \Delta T^0)}{C_{ab}V}$$

where C_p is the heat capacity of the calorimeter (of the order of 450 J K^{-1}) and V the volume of the solution (of the order of 250 cm^3). For a given system the values of ΔH_{ab} are constant within 3%. The mean values are tabulated in Table 3.

pK_a of the Amidines

The pK_a of the amidines was deduced from the pH at half-neutralization in a water–ethanol mixture (50:50 in volume). The base was titrated by 0.01 N HCl using a potentiometric method. The results are given in Table 2.

Discussion

Influence of the Strength of the Acid and of the Base on the Polarity of the Amidine–Phenol Complexes

From the data of Table 3 it clearly appears that, for a given amidine, the dipole increment systematically increases when the proton donor becomes more acidic. The overall value of the derivative $d\Delta\mu/dpK_a$, computed from the extreme points, reaches −0.5 D per pK_a unit for the three amidines studied here.

The effect of changing the pK_a of the acid on the polarity of the hydrogen bonds is thus fairly strong for these bases. As a matter of fact, according to the data of our previous work (9), the value of $d\Delta\mu/dpK_a$ in the same range of pK_a of the acids is only −0.2 D per pK_a unit for the pyridines. The absolute values of $\Delta\mu$ are also greater for the amidines. This can be ascribed to the higher basic strength of the amidines studied here. When for a given nitrogen base $\Delta\mu$ is plotted against the pK_a of an extended family of proton donors, the curve generally shows a sigmoidal shape (7–9), the inflection of which can be ascribed to the appearance of important amounts of hydrogen bonds of the ion pair type (14). The higher absolute value of $d\Delta\mu/dpK_a$ observed for the amidines indicates that the corresponding part of the $\Delta\mu$–pK_a curve lies nearer to the inflection of the sigmoid. In this connection it can be pointed out that it was not possible to determine the dipole moment of the complexes of the amidines with still stronger acids because of the lack of solubility of these complexes. This low solubility also suggests a high polarity of the corresponding complexes.

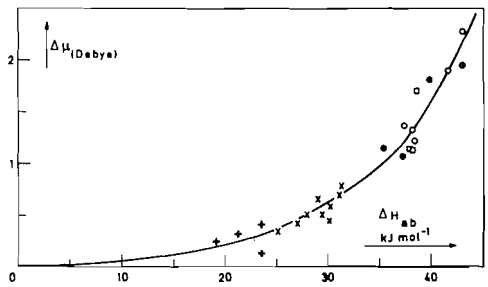

FIG. 3. Plot of $\Delta\mu$ *vs.* ΔH_{ab}: +, anilines, × pyridines, ●, ○, □ amidines.

From the data of Table 3 it also appears that for a given acid there is a general tendency to increase $\Delta\mu$ when the amidine becomes more basic. These effects of the substitution in both partners on the polarity of the hydrogen bond can be roughly expressed in terms of a Hammett relation:

$$[11] \qquad \Delta\mu = 1.33 + 1.1\sum\sigma_a - 0.7\sum\sigma_b$$

Dipole Increment and Complexation Enthalpy

A priori one can expect that the energy of a hydrogen bond is related to the extent of displacement of charges which accompanies its formation. Of course, if the two partners do not exert specific forces on each other and the complexation enthalpy is zero, there will not be any displacement of charges and the dipole increment will also vanish.

In Fig. 3, $\Delta\mu$ is plotted against ΔH_{ab} for the complexes studied here and also for other O—H···N bonds, for which the data was taken from the literature, namely complexes between phenol and anilines (8, 15) and complexes between pyridines and phenols (9, 16, 17). It clearly appears that within experimental error all the experimental points *lie on the same curve.*

It must be emphasized here that this could no longer be the case if, for instance, a uniform value of $\theta_b = 90°$ was used for the three amidines (which corresponds to the formation of a hydrogen bond involving the 'amino' nitrogen atom). Indeed, in this case the computed values of $\Delta\mu$ would be much higher for the two first amidines.

One can thus conclude *that the structure which*

Can. J. Chem. Downloaded from www.nrcresearchpress.com by 210.87.254.6 on 09/05/12
For personal use only.

Can. J. Chem. Downloaded from www.nrcresearchpress.com by 210.87.254.6 on 09/05/12
For personal use only.

was assumed for the computation of $\Delta\mu$ leads to coherent results, compared with other systems where no doubt exists about the orientation.

This provides supplementary evidence for the assumption that the imino nitrogen atom is the most basic site of the amidine molecule. On the other hand, the plot of $\Delta\mu$ *vs.* ΔH_{ab} is not linear but shows an upward curvature. The strong enhancement of $\Delta\mu$ when $-\Delta H_{ab}$ surpasses 35 kJ mol^{-1} can be ascribed, in part, to the formation of a large proportion of ion pairs, which involves a fairly large displacement of the proton

$$-\mathrm{O}-\mathrm{H} + \mathrm{N}\begin{matrix}\diagup\\ -\\ \diagdown\end{matrix} \rightarrow \mathrm{O}^{-}\cdots\mathrm{H}^{+}\mathrm{N}\begin{matrix}\diagup\\ -\\ \diagdown\end{matrix}$$

As shown in a previous work (18), this formation becomes important in O—H···N bonds when $-\Delta H_{ab}$ exceeds 37 kJ mol^{-1}.

Experimental Section

Apparatus

Dielectric constants within 0.0001 were determined by a W.T.W. DMO1 Dipolmeter (2 MHz). Refractive indices were measured by a Pulfrich refractometer of Bellingham and Stanley. Density measurements were performed by means of a hydrostatic balance. The volume of the adiabatic calorimeter was of the order of 250 cm^3. The heat capacity C_p was determined by means of an electrical device calibrated by the TRIS method.

Products

Fluka cyclohexane 'für uv spektroskopie' was dried on molecular sieve 4A. The origin and the purification of the phenols was the same as in a previous work (13).

The amidines were synthesized according to the method described by Bredereck (19). The amidine is extracted by benzene and dried on potassium carbonate. It is further purified by vacuum distillation. Its purity was controlled by nmr spectra and by gas chromatography.

Acknowledgments

The authors wish to thank the Fonds voor Kollektief Fundamenteel Onderzoek, the Katholieke Universiteit te Leuven for their support, and Professor L. Ghosez for fruitful discussions.

1. J. A. Smith and H. J. Taylor. J. Chem. Soc. B, 66 (1969).
2. E. Lorz and R. Baltzly. J. Am. Chem. Soc. **71**, 3992 (1949).
3. J. C. Grivas and A. Taurin. Can. J. Chem. **37**, 1260 (1959).
4. M. Rens. Thèse de doctorat, Louvain-la-Neuve, Belgium. 1974.
5. (*a*) J. Rubin, B. Z. Senkowski, and G. S. Panson. J. Phys. Chem. **68**, 1601 (1964); (*b*) A. M. Dierckx, P. Huyskens, and Th. Zeegers-Huyskens. J. Chim. Phys. **62**, 336 (1965); (*c*) K. R. Bashar and S. Singh. Spectrochim. Acta, Part A, **23**, 1155 (1967); (*d*) M. L. Lin and R. M. Scott. J. Phys. Chem. **76**, 587 (1972).
6. J. Vaes, A. Foubert, and Th. Zeegers-Huyskens. Can. J. Chem. **53**, 604 (1975).
7. H. Ratajczak and L. Sobczyk. J. Chem. Phys. **50**, 556 (1969); Bull. Acad. Pol. Sci. Ser. Chim. **18**, 93 (1970); J. Jadzyn and J. Malecki. Acta Phys. Pol. A, **41**, 599 (1972).
8. G. Debecker and P. Huyskens. J. Chim. Phys. **68**, 295 (1971).
9. R. Nouwen and P. Huyskens. J. Mol. Struct. **16**, 459 (1973).
10. H. Fröhlich. Trans. Faraday Soc. **44**, 328 (1948); Theory of dielectrics. Oxford University Press, London. 1949.
11. P. Huyskens and C. Hernandez. Ind. Chim. Belge, **38**, 1237 (1973).
12. G. Debecker. Ann. Soc. Sci. Bruxelles, Ser. 1, **84**, 117 (1970).
13. H. Pauwels and P. Huyskens. Bull. Soc. Chim. Belg. **83**, 427 (1974).
14. P. Huyskens and Th. Zeegers-Huyskens. J. Chim. Phys. **61**, 81 (1964).
15. D. Neerinck. Thesis. Leuven. 1968.
16. D. Neerinck and L. Lamberts. Bull. Soc. Chim. Belg. **75**, 473 (1968); **75**, 484 (1968).
17. S. S. Barton, J. P. Kraft, T. R. Owens, and L. K. Rinner. J. Chem. Soc. Perkin Trans. 2, 339 (1972).
18. P. Huyskens. Ind. Chim. Belge, **37**, 15 (1972).
19. H. Bredereck. Berichte, 92 (1959).

The influence of manganese(II) and copper(II) on ^{13}C nuclear relaxation rates in imidazole

RODERICK E. WASYLISHEN AND MOIRA R. GRAHAM
Department of Chemistry, University of Winnipeg, Winnipeg, Manitoba R3B 2E9

Received August 13, 1975

RODERICK E. WASYLISHEN and MOIRA R. GRAHAM. Can. J. Chem. **54**, 617 (1976).

^{13}C nuclear relaxation rates have been measured for aqueous solutions of imidazole at 31 °C for several values of p*H*. The influence of Mn(II) and Cu(II) on these relaxation rates has been examined. The results indicate that ^{13}C transverse relaxation rates of imidazole in the presence of these metals are completely dominated by the scalar mechanism. Because of the important influence of this mechanism it is not possible to obtain the geometry of complexes between imidazole-like ligands and Mn(II) or Cu(II) from ^{13}C line-width measurements.

RODERICK E. WASYLISHEN et MOIRA R. GRAHAM. Can. J. Chem. **54**, 617 (1976).

On a mesuré les taux de relaxation nucléaire du ^{13}C pour des solutions aqueuses d'imidazole, à 31 °C et à plusieurs valeurs de p*H*. On a examiné l'influence du Mn(II) et du Cu(II) sur les taux de relaxation. Les résultats indiquent que les taux de relaxation transversale du ^{13}C pour l'imidazole en présence de ces métaux sont complètement dominés par un mécanisme scalaire. A cause de l'influence importante de ce mécanisme, il n'est pas possible d'obtenir la géométrie des complexes entre des ligands du type imidazole et le Mn(II) ou le Cu(II) à partir de mesures de largeur de raies du ^{13}C.

[Traduit par le journal]

Introduction

The imidazole ring of the histidine moiety frequently serves as a ligand for transition metal ions in many biologically important systems (1–6). Proton nuclear magnetic resonance (^1H nmr) line-width experiments, which allow calculation of the influence of paramagnetic metal ions on transverse relaxation times ($T_{2,p}$) have been used extensively to study the nature of transition metal complexes. For example, Ihnat (7) and Ihnat and Bersohn (8) have used this technique to estimate relative Cu(II) – histidyl ring proton separations in Cu(II) – ribonuclease A and Cu(II)–carnosine complexes. Similar measurements have recently been carried out to estimate the relative separations between protons and metal ions in Mn(II)–benzylpenicillin and Cu(II)–benzylpenicillin complexes (9).

Although there are two possible mechanisms, the dipolar and scalar interactions (10–12), which can be responsible for transverse relaxation of ligand nuclei by unpaired electron(s) of a cation, it has been customary to assume that the effect of the scalar mechanism is negligible. In principle this allows calculation of r, the metal–ligand nuclei separation, since the dipolar interaction depends on r^{-6}. The scalar interaction is independent of distance but depends on the formation of a metal–ligand bond which may be very transient in nature.

Recent technical innovations, notably the introduction of the Fourier transform technique in nmr (13), have made spin–lattice relaxation time, T_1, measurements almost routine. The contribution a paramagnetic metal makes to this relaxation rate, $T_{1,p}^{-1}$, for a given ligand nucleus is generally dependent only on the dipolar interaction (14, 15). Thus recent proton T_1 and T_2 relaxation measurements of ligand nuclei in the presence and absence of paramagnetic metal ions have demonstrated that one can generally not assume that the scalar mechanism makes a negligible contribution to proton transverse relaxation rates (16–18). Here we report the influence of Mn(II) and Cu(II) on spin–lattice and transverse nmr relaxation rates of ^{13}C nuclei in imidazole, and discuss the relative importance of the dipolar and scalar interactions. It will be shown that the latter interaction completely dominates ^{13}C transverse relaxation in imidazole making it impossible to determine the geometry of Mn(II) or Cu(II) imidazole-like ligands from nmr line-width measurements. Our results also show that it is not valid to calculate the geometry of such metal complexes using the dipolar parts of the Solomon–

Can. J. Chem. Downloaded from www.nrcresearchpress.com by 210.87.254.105 on 09/05/12
For personal use only.

Can. J. Chem. Downloaded from www.nrcresearchpress.com by 210.87.254.105 on 09/05/12
For personal use only.

Bloembergen equations (10–12) which are based on the point-dipole approximation.

The expected influence of Mn(II) and/or Cu(II), which may be present as impurities in peptides, on the ^{13}C line widths of histidyl residues is also briefly discussed in this paper. The effect of paramagnetic impurities in ^{1}H and ^{13}C nmr relaxation rates has recently been of considerable interest (16, 19–21).

Experimental

Imidazole was obtained from Sigma Chemical Company and used without further purification. All nmr relaxation studies were carried out on aqueous imidazole (3 *M*) solutions which contained 1 *M* NaCl (99.0% Baker Analyzed). p*H* was adjusted using HCl and NaOH and p*H* meter readings were taken on a Corning Digital 109 p*H* meter.

Stock solutions of $MnCl_2 \cdot 4H_2O$ (certified ACS, Fisher Scientific Company and 99% Research Organic/Inorganic) and $CuCl_2 \cdot 2H_2O$ (99.9% Fisher Scientific Company) were prepared and when required, aliquots were added to the imidazole solutions using a Gilson micropipet.

Proton-decoupled ^{13}C nmr spectra were obtained on a Varian CFT-20 spectrometer (10 mm probe) using a sweep width of 500 Hz and a data acquisition time of 4.095 s. A co-axial tube containing D_2O provided the necessary deuterium lock for the CFT-20. All spectra were obtained at 31 ± 2 °C unless otherwise stated. The nOe factors, η, were measured using the gated proton decoupler on the CFT-20. Variable temperature spectra were obtained on the CFT-20 using an 8 mm variable temperature probe. Spin–lattice relaxation rates were measured using the inversion–recovery pulse sequence ($d - 180° - \tau - 90°$). The 90° pulse width was 19 μs, and d, the pulse delay, was always greater than $5T_1$. The 90° pulse was measured for a 3 *M* imidazole sample. The nmr spectra were generally obtained for 10 different τ values, and T_1 was calculated from the slope of a plot of $\ln (A_\infty - A_\tau)$ *vs.* τ. Sensitivity enhancement factors of 1.5 and 0.1 were used in all T_2 and T_1 measurements respectively. The exponential weighting factor of 1.5 makes a very small contribution (<0.25 Hz) to the observed line widths.

Theory

Before presenting and discussing our experimental results it will be helpful to briefly present the theory of nmr relaxation rates pertinent to this study.

1. ^{13}C Nuclear Relaxation Rates in the Absence of Paramagnetic Ions

In the absence of paramagnetic impurities the spin–lattice relaxation rates of ^{13}C nuclei with directly bonded protons are usually dominated by the carbon–proton dipole–dipole mechanism. For small molecules such as imidazole in aqueous solution at 31 °C,

$$[1] \qquad \frac{1}{T_{1,\mathrm{d-d}}} = \frac{n\gamma_C^2\gamma_H^2\hbar^2}{r_{C-H}^6}\tau_{\mathrm{eff}}$$

where n is the number of directly attached protons, γ_C and γ_H are the carbon and proton gyromagnetic ratios, $\hbar$ is Planck's constant divided by 2π, r_{C-H} is the C—H bond length, and τ_{eff} is the effective correlation time (22). The importance of the carbon–proton dipole–dipole mechanism can be calculated from the measured nOe factor (23, 24).

$$[2] \qquad \%\mathrm{DD} = \frac{\eta}{1.988} \times 100$$

Although ^{13}C spin–spin relaxation values in small molecules are often significantly shorter than the corresponding T_1 values (25, 26) the observed ^{13}C nmr line widths in FT-nmr are generally not determined by T_2 but by one or more of the following factors: magnetic field inhomogeneity, the efficiency of the proton decoupler, the acquisition time, or the number of data points.

2. Nuclear Relaxation in the Presence of Paramagnetic Metal Ions (14, 15, 27, 28)

The increase in nuclear relaxation rates of ligand nuclei due to the presence of paramagnetic metal ions can be calculated using the following equations:

$$[3] \qquad \frac{1}{T_{1,\mathrm{p}}} = \frac{1}{T_{1,\mathrm{obs}}} - \frac{1}{T_{1,\mathrm{o}}}$$

and

$$[4] \qquad \frac{1}{T_{2,\mathrm{p}}} = \frac{1}{T_{2,\mathrm{obs}}} - \frac{1}{T_{2,\mathrm{o}}} = \pi(\nu_{1/2,\mathrm{obs}} - \nu_{1/2,\mathrm{o}})$$

where $1/T_{1,\mathrm{obs}}$ and $1/T_{2,\mathrm{obs}}$ are the observed relaxation rates in the presence of the paramagnetic metal ions and $1/T_{1,\mathrm{o}}$ and $1/T_{2,\mathrm{o}}$ are the rates of relaxation for the same ligand nuclei in the absence of paramagnetic metal ions. $\nu_{1/2,\mathrm{obs}}$ and $\nu_{1/2,\mathrm{o}}$ are, respectively, the observed line widths at half height in the presence and in the absence of paramagnetic metal ions.

The influence of paramagnetic metal ions on the relaxation rates of ligand nuclei depends upon the molar ratio of metal ions to ligand molecules, p, and on the number of ligands, q, bound to the

Can. J. Chem. Downloaded from www.nrcresearchpress.com by 210.87.254.105 on 09/05/12
For personal use only.

metal in an identical way. Of course, $T_{1,p}^{-1}$ and $T_{2,p}^{-1}$ also depend upon the efficiency of the metal in relaxing ligand nuclei at the bound site, T_{1M}^{-1} and T_{2M}^{-1}. In certain situations, the lifetime of the ligand in the metal coordination sphere, τ_M, and the difference in chemical shift between ligand nuclei bound and free, ω_M, are also important.

For Mn(II) and Cu(II) one can assume that $T_{2M}^{-2} \gg \Delta\omega_M^2$ (29); for this case, Swift and Connick (30), Luz and Meiboom (31), and Granot and Fiat (32) have shown that

$$[5] \qquad T_{1,p}^{-1} = pq/(T_{1M} + \tau_M)$$

and

$$[6] \qquad T_{2,p}^{-1} = pq/(T_{2M} + \tau_M)$$

For the case of fast exchange, $T_{1M} \gg \tau_M$, and $T_{1,p}^{-1}$ and $T_{2,p}^{-1}$ are directly proportional to T_{1M}^{-1} and T_{2M}^{-1}, respectively. T_{1M}^{-1} and T_{2M}^{-1} are given by the Solomon–Bloembergen equations (10–12):

$$[7] \qquad \frac{1}{T_{1M}} = \frac{2}{15}\frac{\gamma_I^2 g^2 \beta^2 S(S+1)}{r^6}\left(3\tau_c + \frac{7\tau_c}{1+\omega_s^2\tau_c^2}\right)$$

$$[8] \qquad \frac{1}{T_{2M}} = \frac{1}{15}\frac{\gamma_I^2 g^2 \beta^2 S(S+1)}{r^6} \times \left(7\tau_c + \frac{13\tau_c}{1+\omega_s^2\tau_c^2}\right) + \frac{1}{3}S(S+1)\frac{A^2}{\hbar^2}\tau_e$$

where γ_I is the nuclear magnetogyric ratio (equal to γ_c for carbon; see eq. 1), g is the electronic 'g' factor, β is the Bohr magneton, S is the total electron spin, and r is the distance between the unpaired electron(s) and the ligand. $A/\hbar$ is the isotropic scalar coupling constant in rad/s between the unpaired electron(s) and the ligand nucleus. τ_c and τ_e are correlation times which modulate the dipolar and scalar interactions, respectively; they are related to other time-dependent processes:

$$[9] \qquad \frac{1}{\tau_c} = \frac{1}{\tau_r} + \frac{1}{\tau_s} + \frac{1}{\tau_M}$$

$$[10] \qquad \frac{1}{\tau_e} = \frac{1}{\tau_s} + \frac{1}{\tau_M}$$

where τ_r is the correlation time for rotation of the complex and τ_s is the electron longitudinal relaxation time. In writing the Solomon–Bloembergen equations as given in eqs. 7 and 8 we have assumed that $\omega_I\tau_c \ll 1$ and $\omega_s\tau_e \gg 1$. For the results discussed below, ω_I and ω_s represent the Larmor precession frequencies of the ^{13}C nuclei and unpaired metal electrons, respectively; at 18.7 kG $\omega_I = 1.26 \times 10^8$ rad/s and $\omega_s = 3.2 \times 10^{11}$ rad/s. For imidazole–metal complexes, τ_c will be slightly longer than τ_{eff}. Using eq. 1 (see discussion below) we calculate $\tau_{eff} \simeq 5.5 \times 10^{-12}$ s. τ_e will probably be determined by τ_s since τ_s is generally much less than τ_M; for both Mn(II) and Cu(II), $\tau_s > 10^{-10}$ s (15, 33–35).

In the discussion which follows it will be of interest to consider the ratio of $T_{1,p}$ to $T_{2,p}$. If the scalar interaction makes a negligible contribution to T_{2M}^{-1}, as is often assumed, and if one is in the region of fast exchange, $\tau_M \ll T_{1M}$, T_{2M}, then by substituting eqs. 7 and 8 into eqs. 5 and 6, respectively, $T_{1,p}/T_{2,p} = 1$ for $\omega_s^2\tau_c^2 \ll 1$. In the case where $\omega_s^2\tau_c^2 \gg 1$ but $\omega_I^2\tau_c^2 \ll 1$, then $T_{1,p}/T_{2,p} = 7/6$.

Summarizing then, in the region of fast exchange $1 \leq T_{1,p}/T_{2,p} \leq 7/6$ if the scalar mechanism makes a negligible contribution to $T_{2,p}$. If, however, the scalar mechanism is important, $T_{1,p}/T_{2,p} > 7/6$.

Finally, it should be mentioned that the dipolar terms in eqs. 7 and 8 are based on the point dipole approximation which takes the two interacting spins, I and S as point dipoles (10). Although this is probably not a good approximation it does not influence the conclusions reached in this study.

Results and Discussion

In aqueous solution imidazole (**1**) exists in one of two equivalent forms between which there is rapid exchange, thus the C_4 and C_5 ^{13}C nuclei show chemical shift equivalence (36–39). The C_2 carbon nucleus resonates at lowest field, 136.2 ppm, while the $^{13}C_4$ and $^{13}C_5$ nuclei resonate at 122.3 ppm from TMS. The pK_a of imidazole is approximately 7.1 so that at pH values below 6.1

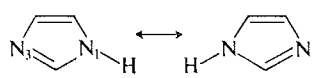

1

TABLE 1. T_1 values, in seconds, and nOe factors (given in parentheses) for C_2 and $C_{4,5}$ carbon nuclei in 3 M imidazole solutions at 31 °C ± 2 °C*

pH	C_2	$C_{4,5}$
2.6	7.4(1.5)	8.0(1.8)
8.0	7.1(1.5)	7.3(1.7)
11.0	8.3(2.0)	7.9(2.0)

*Errors in T_1 values are less than 10% while errors in nOe factors are less than ±0.2.

imidazole exists almost exclusively as a cation in which both nitrogens are protonated. ^{13}C chemical shifts of imidazole as a function of pH have previously been discussed (37). Stability constants and geometries of metal–imidazole complexes have been reviewed (1, 40).

1. ^{13}C Nuclear Magnetic Resonance Relaxation Rates of Imidazole in the Absence of Metals

^{13}C spin–lattice relaxation times and nOe factors, η, of imidazole at three different pH values are given in Table 1. The T_1 values for C_2 and $C_{4,5}$ are similar and essentially independent of pH. The nOe factors indicate that the intramolecular dipole–dipole relaxation mechanism completely dominates ($\geq 75\%$). The spin–rotation mechanism (13, 22) may be of some importance ($\leq 25\%$) and probably accounts for the nOe factors less than 2.0.

Taking $T_{1,d-d} = 8$ s and a C—H bond length of 1.08 Å one calculates $\tau_{eff} = 5.5 \times 10^{-12}$ s. Previously we measured a proton T_1 of 42 s for $H_{4,5}$ of 0.073 M imidazole in D_2O at 20 °C (16). This value represents a lower limit in the dipole–dipole relaxation time due to the H_4–H_5 interaction. Assuming that the H_4–H_5 separation is 2.75 Å (41) we calculate $\tau_{eff} \leq 11 \times 10^{-12}$ s, which is in fair agreement with the more reliable value calculated from our ^{13}C nmr data in Table 1. The τ_{eff} calculated from the ^1H T_1 value is a correlation time describing reorientation of the H_4–H_5 vector. From ^{14}N line-width measurements at 18 °C, Richards and Thomas (42) have calculated $\tau_q = 18.9 \times 10^{-12}$ s for 0.2 M solutions of imidazole. Here, τ_q is the correlation time representing reorientations which affect the electric field gradient at the nitrogen.

Scalar relaxation of the second kind is important in relaxing (T_2) the C_2 and $C_{4,5}$ nuclei of the imidazolium cation. Here the mechanism results from scalar coupling between two rapidly relaxing quadrupolar nuclei (^{14}N, $I=1$) and the

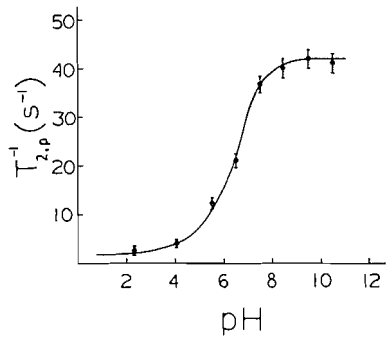

FIG. 1. pH dependence of $T_{2,p}^{-1}$ for $^{13}C_{4,5}$ in 3 M imidazole in the presence of 2×10^{-4} M Mn(II).

^{13}C nuclei. This mechanism is more important for the cation than the neutral species since the spin–spin coupling constant, $J(^{14}N, ^{13}C)$ is probably much greater in the cation. For example, in pyridine, $^1J(^{14}N, ^{13}C)$ is 0.3 Hz while in pyridinium hydrochloride this coupling constant increases to 8.5 Hz (43). For the imidazolium cation $\nu_{1/2,o}(C_2) \simeq 10$ Hz while $\nu_{1/2,o}(C_{4,5}) \simeq 3.5$ Hz and for the neutral species $\nu_{1/2,o}$ is less than 1.5 Hz for both $^{13}C_2$ and $^{13}C_{4,5}$. The scalar mechanism is more effective for the C_2 carbon nucleus since it is directly bonded to two ^{14}N nuclei, while C_4 or C_5 are only directly bonded to one nitrogen. Finally, it is easy to show that the scalar mechanism discussed above makes a negligible contribution to the ^{13}C spin–lattice relaxation rates (13, 22).

Because of the importance of the scalar interaction between the ^{14}N and $^{13}C_2$ nuclei at p$H \leq 7.5$ we have concentrated our ^{13}C relaxation studies in the presence of metals on the $C_{4,5}$ nuclei of imidazole.

2. Influence of Mn(II) on ^{13}C Nuclear Magnetic Resonance Relaxation Rates of $^{13}C_{4,5}$ in Imidazole

The pH dependence of $T_{2,p}^{-1}$ values for the $C_{4,5}$ carbon-13 nuclei of imidazole in the presence of 2×10^{-4} M Mn(II) is shown in Fig. 1. $T_{2,p}^{-1}$ values measured as a function of pH in the presence of 8×10^{-5} M Mn(II) displayed the same behavior as those in Fig. 1 but were smaller by a factor of 2.5. Below p$H \simeq 5$ the Mn(II) is not very effective in altering $T_{2,p}^{-1}$ and above p$H \simeq 12$ $T_{2,p}^{-1}$ also decreases. The presence of a precipitate, probably manganese hydroxide, was observed in the strongly alkaline solutions. Increasing the temperature of the

Can. J. Chem. Downloaded from www.nrcresearchpress.com by 210.87.254.105 on 09/05/12
For personal use only.

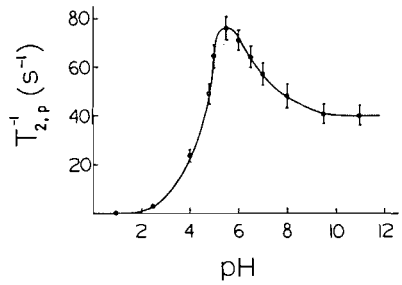

FIG. 2. pH dependence of $T_{2,p}^{-1}$ for $^{13}C_{4,5}$ in 3 M imidazole in the presence of 2×10^{-4} M Cu(II).

TABLE 2. Influence of 8×10^{-5} M Mn(II) on the ^{13}C nmr relaxation rates of the C_4 and C_5 carbon nuclei in 3 M imidazole solutions at 31 °C ± 2 °C

pH	$T_{2,p}^{-1}$ (s^{-1})	$T_{1,p}^{-1}$ (s^{-1})	$T_{1,p}/T_{2,p}$
2.6	0.3	0.009	—
8.0	14.8	0.259	57 ± 20
11.0	16.5	0.309	53 ± 20

Mn(II)–imidazole solutions resulted in linewidth narrowing indicating that one is in the region of fast exchange. For example, for the pH 9.5 solution, $\nu_{1/2,obs}$ varied from 15 Hz at 28 °C to 10 Hz at 59 °C.

Observed $T_{1,p}^{-1}$ and $T_{2,p}^{-1}$ values for Mn(II)–imidazole complexes are given in Table 2. The large ratio of $T_{1,p}$ to $T_{2,p}$ indicates that the first term in eq. 8, due to the dipolar interaction, is negligible compared to the scalar interaction term. Lam *et al.* (44) have recently made similar observations for the adenine base ^{13}C nuclei of the Mn(II)–ATP complexes; however in this case $T_{1,p}/T_{2,p}$ did not exceed 20 for any given ^{13}C nucleus. Finally, for the carboxyl ^{13}C of Mn(II)–pyruvate, Fung *et al.* (45) found $T_{1,p}/T_{2,p} \simeq 80$, indicating that the scalar term is also important when metal-binding takes place through carboxylate oxygen atoms.

3. *Influence of Cu(II) on ^{13}C Nuclear Magnetic Resonance Relaxation Rates of $^{13}C_{4,5}$ in Imidazole*

Observed $T_{2,p}^{-1}$ values for the $C_{4,5}$ ^{13}C nuclei of 3 M imidazole solutions in the presence of 2×10^{-4} M Cu(II) as a function of pH are shown in Fig. 2. At very low pH Cu(II) does not appear to be effective in competing with the protons for binding sites on imidazole; however above pH 3, Cu(II) increases $T_{2,p}^{-1}$ until it reaches a maximum at p$H \backsim 5.5$. At p$H > 7$, $T_{2,p}^{-1}$ decreases, probably because of the formation of copper hydroxide complexes. Variable temperature studies at p$H \simeq 8$ indicate that $\tau_M < T_{2M}$ for the Cu(II)–imidazole complexes, thus the conditions of fast exchange are satisfied.

For 3 M imidazole at pH 7.2 and in the presence of 10^{-4} M Cu(II), $T_{1,p}^{-1}$ and $T_{2,p}^{-1}$ are approximately 0.086 s^{-1} and 30 s^{-1}, respectively, therefore $T_{1,p}/T_{2,p} = 350 \pm 150$. An nOe factor, η, of 1.2 was also observed for the above solution indicating that although $T_{2,p} \simeq 30\ s^{-1}$ the dominant mechanism for spin–lattice relaxation is the proton–carbon dipole–dipole mechanism. At pH 11.0 $T_{1,p}/T_{2,p} = 344 \pm 150$; however, at p$H$ 2.6 the presence of 2×10^{-4} M Cu(II) did not influence the observed T_1 of $^{13}C_{4,5}$.

Kotowycz (46) has also found the scalar relaxation mechanism to be important in 5′-CMP-Cu(II) complexes. For the cytosine base (**2**) ^{13}C nuclei, $T_{1,p}/T_{2,p}$ values for C_2, C_4, and C_5

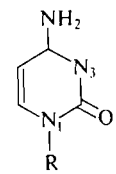

2

were 3.3, 2.0, and 45.2, respectively. It is interesting to note that although binding probably takes place at N_3, line-broadening is greatest for the $^{13}C_5$ nucleus. Doddrell *et al.* (47) have observed similar long-range scalar coupling between Cu(II) in copper acetylacetonate and ^{13}C nuclei in a variety of aliphatic amines.

Finally, it is of interest to mention that proton nmr studies also indicate large hyperfine interactions and hence large unpaired spin densities at carbon atoms in imidazole-like ligands. For pH 7 solutions of 7.3×10^{-2} M imidazole in the presence of 3×10^{-5} M Cu(II) at 20 °C we find $T_{1,p}/T_{2,p} = 40.7$ for $H_{4,5}$ and 18.2 for H_2. These data were obtained at 220 MHz (16) and are in good agreement with the values recently reported by Espersen *et al.* (17) which were obtained at 100 MHz.

For bis(1,2,4-triazolato)copper(II), Inoue and Kubo (48) have estimated unpaired spin densities as large as 0.1 at carbon atoms in this heterocyclic ring system. The esr spectra of tetrakisimidazole copper(II) iodide (49) show hyperfine splitting due to the nitrogen atoms, providing

Can. J. Chem. Downloaded from www.nrcresearchpress.com by 210.87.254.105 on 09/05/12
For personal use only.

Can. J. Chem. Downloaded from www.nrcresearchpress.com by 210.87.254.105 on 09/05/12
For personal use only.

further evidence for appreciable delocalization of the unpaired electron on the imidazole rings.

Unpaired spin densities in the imidazole ring of this magnitude can be expected to make significant contributions to T_{1M}^{-1}. Therefore in the case of imidazole or for other ligands where $T_{1M}/T_{2M} \gg 7/6$, values of r calculated using eq. 7 are expected to be too short since all unpaired spin density is not localized on the metal atom.

4. Effect of Mn(II) or Cu(II) as Impurities on the ^{13}C Nuclear Magnetic Resonance Spectra of Histidyl Residues in Peptides

Transition metals are often present as impurities in water, amino acids, and peptides as well as in nucleic acid components. In some cases, the concentration of these metals has been high enough to lead to the misinterpretation of nmr data (19, 50, 51). The large values of $T_{1,p}/T_{2,p}$ for the imidazole ring nuclei indicate that trace amounts of Mn(II) or Cu(II), [metal]/[imidazole] $> 10^{-4}$, may be effective in broadening ^{13}C resonances of the histidyl residue so that they may be difficult to detect. However, it is unlikely that trace amounts of Cu(II) will influence ^{13}C T_1 values of this moiety. Also, the data in Figs. 1 and 2 indicate that metal ions are less likely to be a problem at low pH values. We have also found this to be the case for the peptide antibiotic, bacitracin (R. Wasylishen and M. Graham, unpublished results).

Conclusion

For Cu(II)–imidazole and Mn(II)–imidazole complexes, the scalar interaction between unpaired electron(s) and the $^{13}C_{4,5}$ nuclei provides a very efficient relaxation (transverse) mechanism for these nuclei. Our results together with the data of others (44–47) indicate that it is not valid to neglect the scalar contribution to $T_{2,M}^{-1}$ and therefore one should not use ^{13}C nmr line-width data to calculate Mn(II) and Cu(II) metal–ligand ^{13}C nuclei separations.

Acknowledgments

The support of the National Research Council of Canada is gratefully acknowledged. We wish to thank Valerie Wasylishen and Charles Pilger for technical assistance, and Dr. Jack S. Cohen for his assistance in obtaining the ^1H nmr spectra at 220 MHz and for valuable discussions. We would also like to thank Professor R. B. Martin and Dr. W. G. Espersen for communicating their results prior to publication.

1. R. J. Sundberg and R. B. Martin. Chem. Rev. **74**, 471 (1974).
2. R. Österberg. Coord. Chem. Rev. **12**, 309 (1974).
3. H. C. Freeman. *In* Inorganic biochemistry. Vol. 1. *Edited by* G. L. Eichhorn. Elsevier Scientific Publishing Company, New York. 1973. p. 121.
4. E. Breslow. *In* Inorganic biochemistry. Vol. 1. *Edited by* G. L. Eichhorn. Elsevier Scientific Publishing Company, New York. 1973. p. 227.
5. A. S. Mildvan. *In* The enzymes. Vol. 2, 3rd ed *Edited by* P. D. Boyer. Academic Press, New York. 1970. p. 445.
6. H. Sigel. *In* Metal ions in biological systems. Vol. 2. *Edited by* H. Sigel. Marcel Dekker, Inc., New York. 1973. p. 63.
7. M. Ihnat. Biochemistry, **11**, 3483 (1972).
8. M. Ihnat and R. Bersohn. Biochemistry, **9**, 4555 (1970).
9. G. V. Fazakerley and G. E. Jackson. J. Chem. Soc. Perkin Trans. 2, 567 (1975).
10. I. Solomon. Phys. Rev. **99**, 559 (1955).
11. N. Bloembergen. J. Chem. Phys. **27**, 572 (1957).
12. N. Bloembergen and L. O. Morgan. J. Chem. Phys. **34**, 842 (1961).
13. T. C. Farrar and E. D. Becker. Pulse and fourier transform nmr. Academic Press, New York. 1971.
14. R. A. Dwek. Nuclear magnetic resonance in biochemistry. Clarendon Press, Oxford. 1973. Chapts. 9 and 10.
15. A. S. Mildvan and J. I. Engle. *In* Methods in enzymology. Vol. 26, Part C. *Edited by* C. H. W. Hirs and S. N. Timasheff. Academic Press, New York. 1972. p. 654.
16. R. E. Wasylishen and J. S. Cohen. Nature, **249**, 847 (1974).
17. W. G. Espersen, W. C. Hutton, S. T. Chow, and R. B. Martin. J. Am. Chem. Soc. **96**, 8111 (1974).
18. K. B. Dillon and F. J. C. Rossotti. J. Chem. Soc. Dalton Trans. 1005 (1973).
19. H. Pearson, D. Gust, I. M. Armitage, H. Huber, J. D. Roberts, R. E. Stark, R. R. Vold, and R. L. Vold. Proc. Natl. Acad. Sci. U.S.A. **72**, 1599 (1975).
20. J. S. Cohen, R. B. Bradley, and T. R. Clem. J. Am. Chem. Soc. **97**, 908 (1975).
21. I. C. P. Smith, R. Deslauries, H. Saitô, R. Walter, C. Garrigou-Lagrange, H. McGregor, and D. Sarantakis. Ann. N.Y. Acad. Sci. **222**, 597 (1973).
22. J. R. Lyerla, Jr. and G. C. Levy. *In* Topics in carbon-13 nmr spectroscopy. Vol. 1. *Edited by* G. C. Levy. Wiley–Interscience, New York. 1974, p. 79.
23. K. F. Kuhlmann and D. M. Grant. J. Am. Chem. Soc. **90**, 7355 (1968).
24. K. F. Kuhlmann, D. M. Grant, and R. K. Harris. J. Chem. Phys. **52**, 3439 (1970).
25. R. R. Shoup and D. L. VanderHart. J. Am. Chem. Soc. **93**, 2053 (1971).

26. R. FREEMAN and H. D. W. HILL. *In* Molecular spectroscopy 1971. Institute of Petroleum, London. 1971. p. 105.
27. R. A. DWEK, R. J. P. WILLIAMS, and A. V. XAVIER. *In* Metal ions in biological systems. Vol. 4. *Edited by* H. Sigel. Marcell Dekker, New York. 1974. p. 61.
28. T. J. SWIFT. *In* NMR of paramagnetic molecules. *Edited by* G. N. La Mar and W. D. Horrocks, Jr. Academic Press, New York. 1973. p. 53.
29. R. A. DWEK. Nuclear magnetic resonance in biochemistry. Clarendon Press, Oxford. 1973. Section 9.8.1, pp. 202–207, and p. 657.
30. T. J. SWIFT and R. E. CONNICK. J. Chem. Phys. **37**, 307 (1962).
31. Z. LUZ and S. MEIBOOM. J. Chem. Phys. **40**, 2686 (1964).
32. J. GRANOT and D. FIAT. J. Magn. Reson. **15**, 540 (1974).
33. D. C. MCCAIN and R. J. MYERS. Mol. Phys. **28**, 1109 (1974).
34. S. H. KOENIG, R. D. BROWN, III, and F. BREWER. Proc. Natl. Acad. Sci. U.S.A. **70**, 475 (1973).
35. B. P. GABER, R. D. BROWN, S. H. KOWNIG, and J. A. FEE. Biochim. Biophys. Acta, **271**, 1 (1972).
36. F. J. WEIGERT and J. D. ROBERTS. J. Am. Chem. Soc. **90**, 3543 (1968).
37. R. J. PUGMIRE and D. M. GRANT. J. Am. Chem. Soc. **90**, 4232 (1968).
38. M. C. THORPE and W. C. COBURN, JR. J. Magn. Reson. **12**, 225 (1973).
39. R. E. WASYLISHEN and G. TOMLINSON. Biochem. J. **147**, 605 (1975).
40. H. SIGEL and D. B. MCCORMICK. Acc. Chem. Res. **3**, 201 (1970).
41. G. WILL. Z. Kristallogr. Kristallgeom. Kristallphys. Kristallchem. **129**, 211 (1969).
42. R. E. RICHARDS and N. A. THOMAS. J. Chem. Soc. Perkin Trans. 2, 368 (1974).
43. R. L. LICHTER and J. D. ROBERTS. J. Am. Chem. Soc. **93**, 5218 (1971).
44. Y. LAM, G. P. P. KUNTZ, and G. KOTOWYCZ. J. Am. Chem. Soc. **96**, 1834 (1974).
45. C. H. FUNG, A. S. MILDVAN, A. ALLERHAND, R. KOMOROSKI, and M. C. SCRUTTON. Biochemistry, **12**, 620 (1973).
46. G. KOTOWYCZ. Can. J. Chem. **52**, 924 (1974).
47. D. DODDRELL, I. BURFITT, and N. V. RIGGS. Aust. J. Chem. **28**, 369 (1975).
48. M. INOUE and M. KUBO. Inorg. Chem. **5**, 70 (1966).
49. F. AKHTAR, D. M. L. GOODGAME, M. GOODGAME, G. W. RAYNER-CANHAM, and A. C. SKAPSKI. Chem. Commun. 1389 (1968).
50. I. M. ARMITAGE, H. HUBER, H. PEARSON, and J. D. ROBERTS. Proc. Natl. Acad. Sci. U.S.A. **71**, 2096 (1974).
51. Y. P. WONG. J. Am. Chem. Soc. **95**, 3511 (1973).

Can. J. Chem. Downloaded from www.nrcresearchpress.com by 210.87.254.105 on 09/05/12
For personal use only.

Thermodynamic properties of aqueous organic solutes in relation to their structure. Part III. Apparent molal volumes and heat capacities of low molecular weight alcohols and polyols at 25 °C

CARMEL JOLICOEUR AND GHYSLAIN LACROIX
Department of Chemistry, Université de Sherbrooke, Sherbrooke, Québec J1K 2R1

Received June 30, 1975

CARMEL JOLICOEUR and GHYSLAIN LACROIX. Can. J. Chem. **54**, 624 (1976).

The density and specific heat of dilute aqueous solutions of various alcohols and polyols have been measured at 25 °C. Such measurements have been carried out for the following solutes: methanol, ethanol, *n*-propanol, *n*-butanol, isobutanol, *s*-butanol, *tert*-butyl alcohol, *n*-pentanol, 3-pentanol, *neo*-pentanol, ethyleneglycol, 1,4-butanediol, 1,6-hexanediol, dimethyl-2,2-propanediol, 1,1,1-tris(hydroxymethyl)ethane, and pentaerythritol.

The limiting apparent molal volume ϕ_v^0 and heat capacities ϕ_c^0 derived from these data exhibit some variations among the properties of isomers (*e.g.* branched *vs.* normal alkyl groups), but these variations cannot be conclusively attributed to specific effects in the hydration of the alkyl groups. On the other hand, the data allows one to derive group contributions to ϕ_v^0 and ϕ_c^0, namely $\Delta\phi^0(CH_2)$ for the methylene group, $\Delta\phi^0(OH)$ for the OH functional group and $\Delta\phi^0(H)$ for the C—H of a terminal methyl group.

The concentration dependence of ϕ_v and ϕ_c brings out some interesting new features. With most of the alcohols, ϕ_v decreases with concentration, in a way related to the degree of hydrophobicity of the alcohol. Solute–solute interactions contribute to reduce ϕ_c of the hydrophilic solutes, but the opposite effect is observed with the most hydrophobic alcohols.

CARMEL JOLICOEUR and GHYSLAIN LACROIX. Can. J. Chem. **54**, 624 (1976).

La densité et la chaleur spécifique de solutions aqueuses diluées d'une variété d'alcools mono- et polyfonctionnels de faible poids moléculaire ont été mesurées à 25 °C. La série d'alcools ainsi étudiée comprend les composés suivants: méthanol, éthanol, *n*-propanol, *n*-butanol, isobutanol, *s*-butanol, *t*-butanol, *n*-pentanol, pentanol-3, *néo*-pentanol, ethylèneglycol, butanediol-1,4, hexanediol-1,6, diméthyl-2,2-propanediol, tris(hydroxyméthyle)-1,1,1 éthane et pentaérythritol.

Les volumes ϕ_v^0 et capacités calorifiques ϕ_c^0 apparents molaires (dilution infinie) obtenus de ces données permettent une analyse détaillée des contributions dues aux différentes portions de la molécule en solution, soit: $\Delta\phi^0(CH_2)$, la contribution du groupement méthylène, $\Delta\phi^0(OH)$, celle du groupe hydroxy et $\Delta\phi^0(H)$, la contribution due à un groupe C—H sur un méthyle en bout de chaîne. On observe également des variations dans les valeurs limites ϕ_v^0 et ϕ_c^0 parmi les différents isomères du butanol, ou ceux du pentanol, mais elles ne peuvent être attribuées uniquement à la solvatation du résidu alcoyle du soluté.

Par ailleurs, la variation de ϕ_v et de ϕ_c selon la concentration démontre que les interactions soluté–soluté tendent à réduire ϕ_v et à augmenter ϕ_c d'une façon apparentée au caractère hydrophobe de l'alcool.

Introduction

In previous investigations (1, 2) we have studied some thermodynamic properties of aqueous solutes containing various hydrocarbon residues. The aim of these studies was mainly to establish whether the thermodynamic properties of these solutes depend on the shape of their hydrocarbon groups. If as inferred from the earlier results, such a relationship can be demonstrated, it should prove useful for understanding the solvent structural influences which are believed to play an important role in the solvation of hydrocarbons (3–6). Since these hydration effects also add significant contribution to solute–solute pair potentials (7), the understanding of excess thermodynamic functions provide further incentive for such studies.

As continuation of earlier work, we have determined the apparent molal volumes and heat capacities of a variety of alcohols in aqueous solution. The alcohols were chosen so as to emphasize the effects of (*1*) increasing the length of the hydrocarbon residue, (*2*) branching of this alkyl residue, and (*3*) addition of other hydroxy groups in several typical molecules. The study of polyols presents obvious interest in

Can. J. Chem. Downloaded from www.nrcresearchpress.com by 210.87.254.6 on 09/05/12
For personal use only.

Can. J. Chem. Downloaded from www.nrcresearchpress.com by 210.87.254.6 on 09/05/12
For personal use only.

relation to the solution behavior of sugars. The choice of heat capacity measurements follows from the high sensitivity of this property towards changes in weak molecular interactions (4).

From previous data on the isomeric butanols, significant differences had been observed in the limiting solution properties of the isomers (*e.g.* apparent molal volumes (8, 9), solvation enthalpies and entropies (10, 11), and also in their excess thermodynamic functions (*e.g.* excess free energies (12) and enthalpies (13)). It is difficult, however, to determine how much of the differences found can be attributed to solvation effects at the hydrocarbon group, against those occurring at the polar OH group. It has been shown recently (14) that the 'acidity' of the OH group, and presumably its interaction with the solvent water, depends on the size and degree of branching of the alkyl substituent. Thus the 'solute geometrical effect' we seek here can, at best, be evidenced from studies involving different series of isomers.

In spite of these fundamental limitations, the alcohols still offer interesting features as compared, for example, to tetraalkylammonium halides which have been widely studied as typical hydrophobic solutes. As will be seen below, some of the effects observed with alkylsubstituted ammonium salts are reproduced with the alcohols. However, the absence of coulombic interactions (ion–ion and ion–dipole) in solutions of the latter, allows a clearer description of the role of the hydrocarbon residue in solute–solute interactions. The solution properties of several polyols also enable new information to be derived.

Experimental

All solutions were prepared by weight, using water doubly distilled over alkaline permanganate and equilibrated with atmospheric CO_2. The alcohols used were obtained from the following suppliers: methanol, ethanol, and *n*-propanol (Fisher Certified); *n*-butanol (Anachemia); isobutanol and *s*-butanol (Baker Reagent); *tert*-butyl alcohol (Fisher Certified); *n*-pentanol, 3-pentanol, and *neo*-pentanol (Aldrich 99%); ethyleneglycol (Fisher Certified); 1,4-butanediol (Aldrich 99%); 1,6-hexanediol (Aldrich); dimethyl-2,2-propanediol (Eastman); 1,1,1-tris(hydroxymethyl)ethane (Fluka); pentaerythritol (Aldrich).

Materials having a specified purity $\geq$99% were used as such after verifying that they gave a single peak gc chromatogram on a Carbowax 20-M column using a Hewlett Packard (Model HP-5750) chromatograph. Liquid alcohols of unspecified purity were distilled and only a small middle fraction ($\sim$10%) was retained for the present measurements; as estimated by gc, the purity of these fractions was at least 98%. Solid materials were recrystallized twice from appropriate solvents.

The solution densities (d) and volumetric specific heats (σ) were measured using a flow densimeter (15) and a flow microcalorimeter (16) described earlier; the detection limits attainable, in differential measurements, were respectively $\pm 2 \times 10^{-6}$ g cm^{-3} and $\pm 1 \times 10^{-5}$ J K^{-1} cm^{-3}. In this study, the same closed-loop thermostat was used to regulate the temperature of both the densimeter and the microcalorimeter. Under the flowrates (1.0 cm^3 min^{-1}) and heating power (21 mW) used, the temperature increment during the specific heat measurements was $\sim$0.3 °C. Thus, the heat capacity data were recorded at a mean temperature of $\sim$25.15 °C.

Results

The apparent molal volume ϕ_v and heat capacity ϕ_c of the various alcohols were calculated from the data using the following equations (2, 17):

$$[1] \qquad \phi_v = \frac{M_2}{d} - \frac{1000\,(d - d_0)}{mdd_0}$$

$$[2] \qquad \phi_c = \phi_v\sigma_0 + \frac{1000\,(\sigma - \sigma_0)}{c}$$

d_0 is the density of water taken as 0.997047 g cm^{-3} (18) and σ_0 is the volumetric specific heat in J K^{-1} cm^{-3}. The latter was obtained from the weight specific heat taken as 4.1793 J K^{-1} g^{-1} (19). The results were fitted by least-squares methods to equations of the form

$$[3] \qquad \phi = \phi^0 + Bc$$

in which c represents the molar concentration of the solute.

The resulting coefficients are collected in Table 1 which includes the limiting values of ϕ_v^0 and ϕ_c^0 for the 16 alcohols and the corresponding slopes B_v and B_c. Standard deviations on these quantities are also reported as obtained from six to nine duplicate measurements in the concentration range quoted. The complete set of experimental data is available elsewhere upon request.[1]

For more than half of the compounds studied

[1]Values of d, c_p, ϕ_c, ϕ_v for the various compounds are available, at a nominal charge, from the Depository of Unpublished Data, CISTI, National Research Council of Canada, Ottawa, Canada K1A 0S2.

here, a comparison of the ϕ_v^0 data with earlier literature values is possible and shows satisfactory agreement in most cases (Table 1). In some instances, the discrepancy with previous data is larger than our standard deviation on ϕ_v^0. This may result from either impurities in the alcohols or minor systematic errors in one of the studies. As will become evident below, such discrepancies

TABLE 1. Apparent molal volumes and heat capacities of various alcohols at 25 °C*

Alcohol		ϕ_v^0 (cm^3 mol^{-1})	B_v	ϕ_c^0 (J K^{-1} mol^{-1})	B_c	Concentration range
Methanol	—OH	38.25 (0.01)	−0.17 (0.01)	158.2 (0.1)	−4.10 (0.09)	0.44 -2.2
Ethanol		55.12 (0.01)	−0.57 (0.01)	260.3 (0.1)	−0.6 (0.2)	0.13 -0.97
Propanol		70.63 (0.02)	−0.82 (0.03)	352.9 (0.2)	3.8 (0.3)	0.16 -1.0
n-Butanol	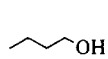	86.48 (0.02)	−0.98 (0.03)	437.0 (0.5)	15.6 (0.8)	0.20 -0.92
2-Butanol		86.53 (0.03)	−1.44 (0.04)	449.1 (0.3)	9.7 (0.5)	0.14 -0.98
Isobutanol		86.75 (0.02)	−1.35 (0.04)	432.5 (0.4)	11.6 (0.7)	0.29 -0.94
tert-Butyl alcohol		87.73 (0.02)	−1.61 (0.02)	464.0 (0.6)	11.7 (0.9)	0.27 -0.94
n-Pentanol		102.88 (0.04)	−4.55 (0.40)	523.8 (0.3)	28.7 (2.9)	0.027-0.19
neo-Pentanol		101.87 (0.06)	(0.05) (0.78)	503.5 (0.7)	(−18.6) (9.8)	0.020-0.12
3-Pentanol		101.14 (0.02)	−2.09 (0.09)	539.8 (0.4)	10.8 (1.6)	0.052-0.39
Ethyleneglycol		54.63 (0.01)	−0.08 (0.01)	191.9 (0.1)	−5.5 (0.1)	0.18 -1.4
1,4-Butanediol	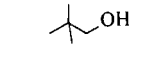	88.23 (0.02)	−0.61 (0.03)	346.8 (0.3)	−13.6 (0.6)	0.088-1.0
1,6-Hexanediol	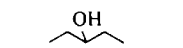	120.49 (0.01)	−1.24 (0.04)	521.6 (0.2)	−28.9 (0.7)	0.047-0.54
Dimethyl-2,3-propanediol		102.34 (0.01)	−1.00 (0.02)	432.3 (0.3)	−8.8 (0.6)	0.19 -0.79
1,1,1-Tris(hydroxymethyl)ethane	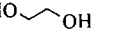	102.30 (0.01)	−0.52 (0.02)	373.3 (0.2)	−10.8 (0.6)	0.048-0.50
Pentaerythritol	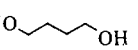	101.81 (0.01)	0.23 (0.04)	328.8 (0.2)	−9.1 (0.6)	0.070-0.57

*The standard deviation is given in parentheses below each result; data shown in parentheses are considered unreliable due to limited concentration range accessible. Literature values of ϕ_v^0 data for aqueous alcohols are MeOH, 38.17 (22); EtOH, 55.08 (22); PrOH, 70.74 (22); *n*-BuOH, 86.63 (22), 85.90 (8), 85.72 (9); isoBuOH, 86.15 (8), 86.07 (9); *s*-BuOH, 86.33 (8), 86.02 (9), 86.66 (20); *tert*-butyl alcohol, 87.95 (8); *n*-PenOH, 102.55 (22); 3-PenOH, 101.28 (20); ethylene glycol, 54.65 (22); 1,4-butanediol, 88.36 (22), 88.2 (21); 1,6-hexanediol, 120.39 (22).

Can. J. Chem. Downloaded from www.nrcresearchpress.com by 210.87.254.6 on 09/05/12
For personal use only.

Can. J. Chem. Downloaded from www.nrcresearchpress.com by 210.87.254.6 on 09/05/12
For personal use only.

are of little consequence on the information extracted from the data.

Discussion

The following discussion of the results is presented in three sections. The first part merely summarizes some qualitative observations on the data, which relate directly to the purpose of our study. The second part reports a more quantitative analysis of the results carried out to evaluate the contribution to ϕ_v^0 and ϕ_c^0 of the different portions of the alcohol solute molecule. Finally, the third part describes the consequence of solute–solute interactions on ϕ_v and ϕ_c of aqueous alcohols.

(1) Limiting Apparent Molal Quantities ϕ_v^0 and ϕ_c^0

A comparison of the ϕ_v^0 and ϕ_c^0 data among the isomers of BuOH and PenOH shows that there are marked, but inconsistent, variations in these properties associated with the isomerization of the alkyl residue. Similar inconsistencies are evident also in the ϕ_v^0 data for the isomers of $BuNH_3Cl$ and those of BuCOONa (23). As pointed out in the introductory remarks, this difficulty arises presumably because of changes in the hydration at the polar groups as the geometry of the alkyl substituent is varied. Within the series of data available thus far, this effect apparently obscures the consequence of alkyl group branching on either ϕ_v^0 or ϕ_c^0 (24).

The changes in ϕ_v^0 and ϕ_c^0 resulting from the addition of one or more OH groups on the hydrocarbon chain of an aliphatic alcohol are quite striking. While the apparent molal volume of the alcohol is hardly affected by the replacement of a hydrogen atom (C—H) by an OH group, the apparent molal heat capacity is sharply reduced. This is in agreement with the results of earlier studies on ϕ_v^0 and ΔC_p^0 (pure liquid → dilute solution) of propanol, propanediols, and glycerol (25, 26). With the polyols derived by successive OH substitution on *neo*-PenOH, the sequential changes in ϕ_v^0 or ϕ_c^0 exhibit trends which can be understood from interference in the hydration of CH_3 and CH_2OH groups on the quaternary carbon.

(2) Group Contributions to ϕ_v^0 and ϕ_c^0

For predictive purposes, as well as for understanding the hydration of the various functional groups on a given molecule, it is of interest to evaluate the contribution of each group to the measured quantity (20, 25–28). From the present data, combined with several others from the literature, a group contribution assignment has been carried out based on operations which are best visualized from the following definitions (referring to either ϕ_v^0 or ϕ_c^0):

(*a*) $\Delta\phi^0(CH_2)$: methylene group contribution derived from the homologous series of *n*-alcohols.

(*b*) $\Delta\phi^0(H\cdots OH)$: Combined contributions from the OH group, $\Delta\phi^0(OH)$, and from a hydrogen atom on the terminal methyl group, $\Delta\phi^0(H)$. This quantity is obtained as the extrapolation to zero chain length of a plot of the data for *n*-ROH against number of carbon atoms, and is assumed to represent

$$[\Delta\phi^0(H) + \Delta\phi^0(OH)]$$

(*c*) $\Delta\phi^0(H \rightarrow OH)$: change in ϕ^0 found for the substitution of an H atom by an OH group, which we identify to

$$[\Delta\phi^0(OH) - \Delta\phi^0(H)]$$

While these definitions imply nonthermodynamic group additivity assumptions, they yield by simple arithmetic on the data in Table 1, values for $\Delta\phi^0(H)$ and $\Delta\phi^0(OH)$ which will be shown quite consistent.

In Table 2, we summarize the estimated group contributions $\Delta\phi^0(CH_2)$, $\Delta\phi^0(OH)$, and $\Delta\phi^0(H)$. $\Delta\phi^0(CH_2)$ values were obtained from the slopes of the plots of ϕ^0 against number of carbon atoms (N) as shown in Figs. 1 and 2, and are in good agreement with previous results (27–30). The extrapolation of these plots to $N = 0$ yields $\Delta\phi_v^0(H\cdots OH)$ as 23 cm^3 mol^{-1} and $\Delta\phi_c^0(H\cdots OH) = 90$ J K^{-1} mol^{-1}. The OH group contribution was taken as one-half of the value obtained when extrapolating the data for α,ω-diols to $N = 0$, giving $\Delta\phi_v^0(OH) = 11$ cm^3 mol^{-1} and $\Delta\phi_c^0(OH) = 10$ J K^{-1} mol^{-1}. These independent results yield, from the additivity assumed above, the following $\Delta\phi^0(H)$ values: $\Delta\phi_v^0(H) = 12$ cm^3 mol^{-1} and $\Delta\phi_c^0(H) = 80$ J K^{-1} mol^{-1}.

The consistency of these estimated group contributions can be tested by first verifying that they adequately predict the effect of the H → OH substitution on ϕ_v^0 and ϕ_c^0. From the data for various pairs of solutes which differ only by their

TABLE 2. Estimates of various group contributions to ϕ_v^0 and ϕ_c^0

Group	$\Delta\phi_v^0$ ($cm^3\ mol^{-1}$)	$\Delta\phi_c^0$ ($J\ K^{-1}\ mol^{-1}$)
1 —CH_2—	15.9*	88*
2 —OH	11	10
3 —C—H (terminal)	12	80
4 H → OH	−1 [−0.5 to 1.8]†	−70 [−45 to −71]†
5 (H···H)	24 [12 to 23]†	160 [100 to 250]†

*The average values exclude the data for methanol. The methylene group contributions to ϕ_v^0 and ϕ_c^0 have been reported by Desnoyers and co-workers as 15.9 $cm^3\ mol^{-1}$ (30) and 88 ± 3 $J\ K^{-1}\ mol^{-1}$ (29).

†*4* and *5* are given as predicted from *2* and *3*. The ranges quoted in brackets were obtained as described in text. For *5*, the range in ϕ_v^0 and ϕ_c^0 include model estimates reported earlier as well as other literature data (see text).

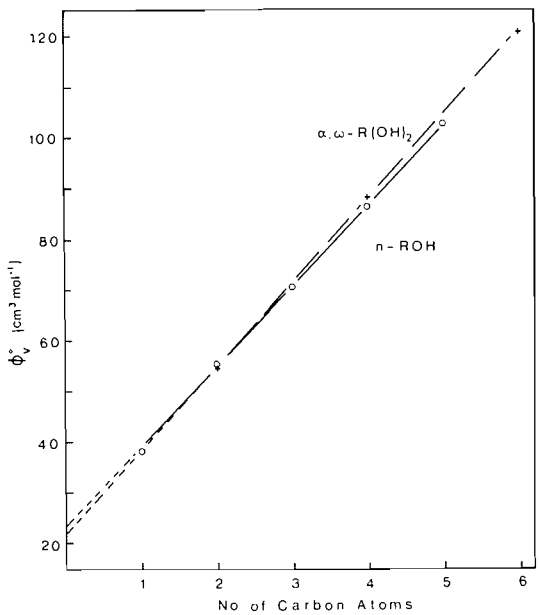

FIG. 1. Limiting apparent molal volumes ϕ_v^0 of *n*-alcohols and α,ω-diols in water at 25 °C.

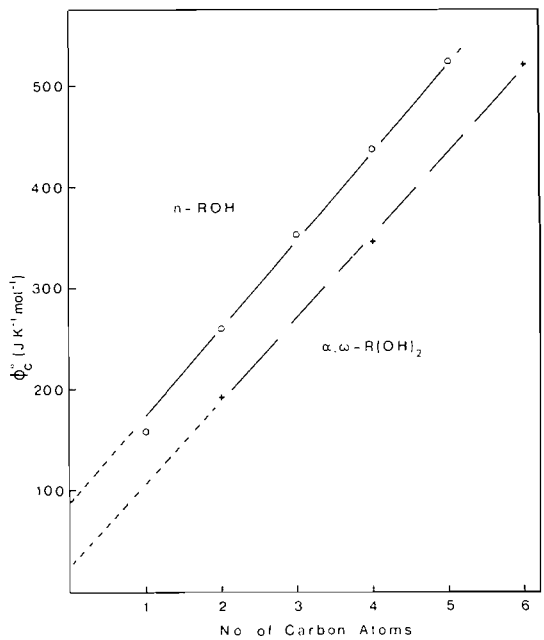

FIG. 2. Limiting apparent molal heat capacities ϕ_c^0 of *n*-alcohols and α,ω-diols in water at 25 °C.

number of OH groups (Table 1), we calculated $\Delta\phi_v^0(H \rightarrow OH)$ and $\Delta\phi_c^0(H \rightarrow OH)$; the values obtained lie within the ranges given in Table 2 (brackets).

Further indication that $\Delta\phi_v^0(H)$ and $\Delta\phi_c^0(H)$ are meaningful quantities is given by data on model compounds which can illustrate the effect of removing two terminal C—H protons from hydrocarbon residues. Examples of such model systems would be those representing: dimerization (*e.g.* 2EtOH → 1,4-butanediol) and cyclisation (*e.g.* 3-pentanol → *c*-pentanol).[2] The contribution of two terminal C—H protons $\Delta\phi_v^0(H\cdots H)$ and $\Delta\phi_c^0(H\cdots H)$ have been calculated from data on the following model systems: 'chemical dimer models': alcohols (present data), alkylammonium and diazonium ions (31), alkanes (32); 'cyclisation models':

[2]$\Delta\phi^0(H\cdots H)$ values obtained from these model processes include, of course, changes in the intrinsic properties of the solutes, as well as those originating in hydration effects. Although there are usually no accurate means of sorting out these various contributions, we know that in many cases the changes in the intrinsic properties are not the most important (2, 31). (In ref. 31, the difference between ϕ_c^0 values of *n*- and *c*-$HexNH_3Br$ should read −110 rather than −60 $J\ K^{-1}\ mol^{-1}$ as quoted in footnote 4.)

Can. J. Chem. Downloaded from www.nrcresearchpress.com by 210.87.254.6 on 09/05/12
For personal use only.

Can. J. Chem. Downloaded from www.nrcresearchpress.com by 210.87.254.6 on 09/05/12
For personal use only.

alcohols and alkylamines (20) and alkylammonium ions (2, 29, 30). The extreme values of $\Delta\phi^0(H\cdots H)$ obtained from the different data sets are given in Table 2 in brackets.

The rather broad range of $\Delta\phi^0(H\cdots H)$ values found is not too surprising in view of the vastly different types of model systems examined. However, the derived group contributions point, with insistence, to the fact that the removal of a terminal H atom on a hydrocarbon chain produces an unexpectedly large reduction in the apparent molal volume and heat capacity of the solute molecules. These observations imply that there exist important differences in the hydration effects associated with methyl and methylene groups.

A rationalization of the magnitudes of the various group contributions obtained above will presumably be feasible only as other regularities are found in ϕ_v^0 and ϕ_c^0 data on hydrocarbon-like solutes in aqueous and nonaqueous media. At present, some aspects seem qualitatively explainable as, for example, the relative magnitude of $\Delta\phi_c^0(H)$ and $\Delta\phi_c^0(OH)$. The latter might be understood as the replacement of several weak $C—H\cdots H_2O$ interactions (and possibly $H_2O\cdots HOH$ interactions in the solvent structural effect) by one or a few (three at most) stronger $R—OH\cdots H_2O$ interactions.[3] However, other results such as the close similarity of $\Delta\phi_v^0(CH_2)$ and $\Delta V_1^0(CH_2)$, *i.e.* in the pure liquid hydrocarbon (2, 34), raises questions which do not readily find an answer within the current concepts of the hydration of alkyl groups!

(3) Concentration Dependence of ϕ_v and ϕ_c

The B_v and B_c coefficients of [3] are plotted in Figs. 3 and 4 against the limiting apparent molal volume of the alcohols. From the volume data, the general trend is that B_v is negative and decreases with increasing size of the hydrocarbon group, as reported by several other workers (8, 20, 30). This is apparently true for diols as well as for monohydric alcohols, though diols

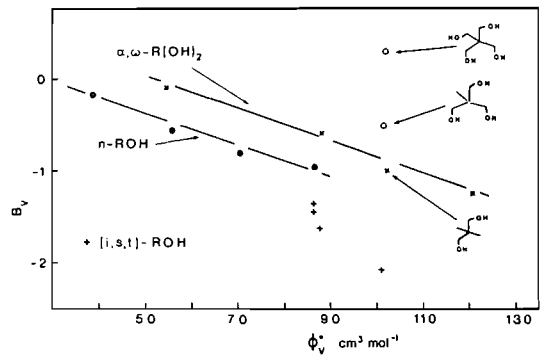

FIG. 3. Molar concentration dependence of ϕ_v for various alcohols and polyols in water at 25 °C.

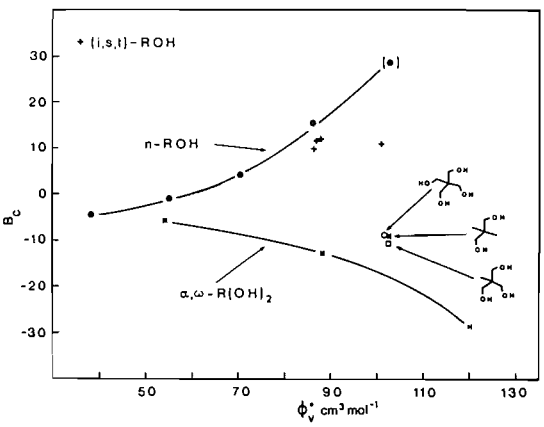

FIG. 4. Molar concentration dependence of ϕ_c for various alcohols and polyols in water at 25 °C.

and polyols exhibit less negative B_v values. The present data show in addition that branching of the hydrocarbon residue leads, in all cases, to slightly more negative B_v values (8). This would be more readily interpreted if, similarly, branching of the hydrocarbon group always increased ϕ_v^0 of the alcohols.

The consequence of solute–solute interactions on the apparent molal heat capacity of alcohols reveals unambiguous features. The B_c coefficients increase from ~ -5 to ~ 30 in going from MeOH to *n*-PenOH. Since B_c values for diols are negative and decrease with increasing number of carbon atoms, the positive slopes are readily attributed to interactions which involve the hydrophobic ends of the alkyl chains. Thus, near room temperature, 'hydrophobic interactions' among *n*-alcohol molecules in water lead to an *increase* in the apparent heat capacity

[3]A group contribution analysis to the enthalpies of hydration ΔH_s^0(gas → dilute solution) from data on the heat of solution of *n*-alcohols (11) and *n*-alkanes (32) leads to the inference that $\Delta H_s^0(H)$ and $\Delta H_s^0(CH_2)$ are both exothermic and of similar low magnitude (33). $\Delta H_s^0(OH)$, on the other hand, is large, exothermic, and not greatly different in water as compared to other solvents.

of the solute (29, 31, 35). This is consistent with the variations in the magnitude of the B_e coefficients of some large organic ions as reported earlier (31).

The data in Fig. 4 also indicate that the effect of branching in the alkyl residue would be to reduce B_e. On the other hand, addition of a third and fourth hydroxy group to a diol does not appear to change B_e values any further.

Conclusion

The limiting partial molal volumes and heat capacities of various low molecular weight alcohols exhibit a chain length dependence which is consistent with the effects observed in other series of homologous compounds. On the other hand, the data show no regular change in ϕ_v^0 or ϕ_e^0 with the degree of branching (shape) of the hydrocarbon chain of the alcohols.

Assuming group contribution additivity to ϕ_v^0 and ϕ_e^0, the contribution of —CH_2—, C—OH and terminal C—H groups have been derived from the data on *n*-alcohols and α,ω-diols. The estimated group contributions point to an important difference in the hydration effects of methylene groups and terminal methyl groups. This conclusion finds support in the comparison of the properties of model solutes such as 2(Ethanol) *vs.* 1,4-butanediol or 3-PenOH *vs.* *c*-PenOH. Through such comparisons, we had previously sought a basis for understanding the influence of geometrical factors in the hydration of alkyl residues (2, 31). It now appears that the loss of terminal C—H protons may be responsible for a significant change in ϕ_v^0 and ϕ_e^0 of aqueous organic solutes, an effect we plan to further verify through measurements on various unsaturated alcohols.

The concentration dependence of ϕ_v and ϕ_e for the various alcohols and polyols exhibit regular trends as function of chain length, degree of branching and extent of —OH substitution. A remarkable feature of these excess functions is the finding that solute–solute interactions enhance the apparent molal heat capacity of *n*-alcohols bearing an alkyl residue larger than C_2H_5.

Acknowledgments

The authors gratefully acknowledge the financial support of the Ministère de l'Education du Québec and of the National Research Council of Canada, and the assistance of Mr. P.-A. Leduc in processing the data.

1. C. Jolicoeur and G. Lacroix. Can. J. Chem. **51**, 3051 (1973).
2. C. Jolicoeur, J. Boileau, S. Bazinet, and P. Picker. Can. J. Chem. **53**, 716 (1975).
3. H. S. Frank and M. W. Evans. J. Phys. Chem. **13** 507 (1945).
4. H. S. Frank and W. Y. Wen. Discuss. Faraday Soc. **24**, 133 (1957).
5. A. Ben-Naim. *In* Water and aqueous solutions. *Edited by* R. A. Horne. Wiley Interscience, New York. 1972. p. 425.
6. F. Franks. *In* Water a comprehensive treatise. Vol. 2. *Edited by* F. Franks. Plenum Press, New York. 1973. p. 1.
7. P. S. Ramanathan, C. V. Krishnan, and H. L. Friedman. J. Solution Chem. **1**, 237 (1972).
8. F. Franks and H. T. Smith. J. Chem. Eng. Data, **13**, 538 (1968).
9. M. E. Friedman and H. A. Scheraga. J. Phys. Chem. **69**, 3795 (1965).
10. J. A. V. Butler. Trans. Faraday Soc. **33**, 229 (1937).
11. C. V. Krishnan and H. L. Friedman. J. Phys. Chem. **73**, 1572 (1969).
12. J. J. Kozak, W. S. Knight, and W. Kauzmann. J. Chem. Phys. **48**, 675 (1968).
13. C. V. Krishnan and H. L. Friedman. J. Solution Chem. **2**, 119 (1973).
14. E. M. Arnett, L. E. Small, R. T. McIver, and J. Scott Miller. J. Am. Chem. Soc. **96**, 5638 (1974).
15. P. Picker, E. Tremblay, and C. Jolicoeur. J. Solution Chem. **3**, 377 (1974).
16. P. Picker, P. A. Leduc, P. R. Philip, and J. E. Desnoyers. J. Chem. Thermodyn. **3**, 631 (1971).
17. J. L. Fortier, P. A. Leduc, and J. E. Desnoyers. J. Solution Chem. **3**, 323 (1974).
18. G. S. Kell. J. Chem. Eng. Data, **12**, 66 (1967).
19. A. Eucken and M. Eigen. Z. Elektrochem. Dtsch. **55**, 343 (1951).
20. S. Cabani, G. Conti, and L. Lepori. J. Phys. Chem. **78**, 1030 (1974).
21. K. Nakanishi, N. Kato, and M. Maruyama. J. Phys. Chem. **71**, 814 (1967).
22. T. Nakajima, T. Komatsu, and T. Nakagawa. Bull. Chem. Soc. Jpn. **48**, 783 (1975).
23. M. Sakurai. Bull. Chem. Soc. Jpn. **46**, 1596 (1973); M. Sakurai, T. Komatsu, and T. Nakagawa. J. Solution Chem. **4**, 511 (1975).
24. E. M. Arnett, W. B. Kover, and J. V. Carter. J. Am. Chem. Soc. **91**, 4028 (1969).
25. F. Franks, M. A. J. Quickenden, D. S. Reid, and B. Watson. Trans. Faraday Soc. **66**, 582 (1970).
26. F. Franks, D. S. Reid, and A. Suggett. J. Solution Chem. **2**, 99 (1973).
27. K. Kusano, J. Suurkuusk, and I. Wadsö. J. Chem. Thermodyn. **5**, 757 (1973).
28. S. Cabani, G. Conti, A. Martinelli, and E. Matteoli. J. Chem. Soc. Faraday Trans. I, **69**, 2112 (1973).

Can. J. Chem. Downloaded from www.nrcresearchpress.com by 210.87.254.6 on 09/05/12
For personal use only.

29. P. A. LEDUC, J. L. FORTIER, and J. E. DESNOYERS. J. Phys. Chem. **78**, 1217 (1974).
30. J. E. DESNOYERS and M. AREL. Can. J. Chem. **47**, 547 (1969).
31. C. JOLICOEUR and J. BOILEAU. J. Solution Chem. **3**, 889 (1974).
32. R. D. WAUCHOPE and R. HAQUE. Can. J. Chem. **50**, 133 (1972).
33. C. V. KRISHNAN and H. L. FRIEDMAN. J. Solution Chem. **2**, 37 (1973).
34. Physical Properties of Chemical Compounds, Advances in Chemistry Series. Vols. 15 (1955) and 22 (1959). American Chemical Society, Washington, D.C.
35. W. H. STRENG and W. Y. WEN. J. Solution Chem. **3**, 865 (1974).

Can. J. Chem. Downloaded from www.nrcresearchpress.com by 210.87.254.6 on 09/05/12
For personal use only.

The shielding effect of heterosubstituents in ^{13}C nuclear magnetic resonance

H. BEIERBECK AND J. K. SAUNDERS
Département de Chimie, Université de Sherbrooke, Sherbrooke, Québec J1K 2R1

Received June 9, 1975

H. BEIERBECK and J. K. SAUNDERS. Can. J. Chem. **54**, 632 (1976).

The effect of a heterosubstituent X on ^{13}C chemical shifts, in conformations characterized by dihedral angles of 60°, is analyzed in terms of α-shifts, heteroatom–carbon (XC), hydrogen–heteroatom (HX) and carbon–heteroatom (CX) *gauche* interactions, and nonbonded γ(X) and δ(X) interactions. The more general parameters HX $\times$ cos ϕ and CX $\times$ cos ϕ describe the β-heteroatom shifts in conformations in which the dihedral angles ϕ differ from 60°. The shielding effects of chlorine, exocyclic oxygen, and endocyclic nitrogen are analyzed.

H. BEIERBECK et J. K. SAUNDERS. Can. J. Chem. **54**, 632 (1976).

On analyse l'effet d'un hétérosubstituant X sur les déplacements chimiques du ^{13}C dans des conformations caractérisées par des angles dièdres de 60°; cette analyse est faite en termes de déplacements α et d'interactions hétéroatome–carbone (XC), hydrogène–hétéroatome (HX) et carbone–hétéroatome (CX) et d'interactions nonliées γ(X) et δ(X). Les paramètres plus généraux HX $\times$ cos ϕ et CX $\times$ cos ϕ décrivent les déplacements des hétéroatomes β dans des conformations dans lesquelles les angles dièdres ϕ sont différents de 60°. On analyse les effets de blindages du chlore, de l'oxygène exocyclique et de l'azote endocyclique.

[Traduit par le journal]

Introduction

The ^{13}C chemical shift is a sensitive function of the chemical environment of a carbon nucleus, particularly its structural relation to the β- and γ-substituents. The substituent effects of the β- and γ-groups are approximately additive, and several sets of shielding parameters for the derivation of ^{13}C chemical shifts in saturated hydrocarbons have been reported (1–7).

We have recently proposed the use of *gauche* interactions as a basis for β-carbon shielding parameters since they represent the simplest description of the steric relation between a carbon nucleus and its β-carbons (7). *Gauche* parameters not only provide the most convenient representation for the β-substituent effects of any general group X, in substrates of staggered conformation, but they are also readily adapted to cases where dihedral angles differ from 60°. This is demonstrated here with the derivation of ^{13}C chemical shifts for a series of hydroxides, amines, and chlorinated hydrocarbons.

Results and Discussion

The ^{13}C chemical shifts for saturated hydrocarbons which exist in staggered conformations (dihedral angles of 60°) may be derived in the following manner (7). The resonances for the primary carbons of ethane, the secondary carbon in propane, the tertiary carbon in isobutane, and the quaternary carbon in neopentane serve as reference shifts for primary, secondary, tertiary, and quaternary carbons, respectively. To these reference values shift increments are added which are associated with hydrogen–carbon (HC) and exocyclic carbon–carbon (CC) *gauche* interactions, and with nonbonded γ- and *syn*-axial δ-interactions, γ(C) and δ(C).

By analogy, the derivation of the chemical shifts of heterosubstituted carbons may be based on the resonances in the substrates CH_3X, CH_3CH_2X, $(CH_3)_2CHX$, and $(CH_3)_3CX$, respectively. The shielding parameters of the group X are again based on those configurations which are not already present in the reference substrates, namely XC, HX, and CX *gauche* interactions, and nonbonded γ(X) and δ(X) interactions (Table 1). Since endo- and exocyclic CC parameters were found to be nonequivalent (7), endo- and exocyclic XC and CX configurations are also treated separately.

With these parameters the chemical shifts for X-substituted carbons may be derived from the resonances in the appropriate reference substrates CH_3X etc., by adding the sum of the

Can. J. Chem. Downloaded from www.nrcresearchpress.com by 210.87.254.105 on 09/05/12
For personal use only.

TABLE 1. Structural parameters for the derivation of heterosubstituent effects on ^{13}C chemical shifts

Parameters		Derivation of chemical shifts: From structural units	From parent hydrocarbon resonances	
Reference		C—X	Hydrocarbon	Hydrocarbon
α-shift		—	>C—X–>C—H	>C—X–>C—CH_3
α		XC	XC–HC	XC–CC
β		HX	HX	HX–HC
β		CX	CX	CX–CC
γ		γ(X)	γ(X)	γ(X)–γ(C)
δ		δ(X)	δ(X)–γ(C)	δ(X)–δ(C)

shielding contributions from HC, CC, γ(C), δ(C), and XC interactions. The resonances for the remaining carbons are given by the shifts in the corresponding references CH_3CH_3 etc., plus the sum of the shift increments associated with HC, CC, γ(C), δ(C), HX, CX, γ(X), and δ(X) configurations.

Alternatively, chemical shifts may be derived from the corresponding resonances in the parent hydrocarbons. In this case two modifications are necessary. Since exocyclic X replaces hydrogen, whereas endocyclic X replaces carbon, these modifications differ slightly for exo- and endocyclic substituents. First, an α-shift has to be added to the hydrocarbon resonance, if the carbon in question is heterosubstituted. In the exocyclic case the α-shift corresponds to the difference (>C—X) – (>C—H), and in the endocyclic case to (>C—X) – (>C—CH_3). These α-shifts may be derived from resonances in reference substrates, or in compounds related to the molecules under investigation. For instance, the α-hydroxyl shift for the prediction of the chemical shifts in decalols (*v.i.*) may be taken to be the difference in chemical shifts in isopropanol and propane, or in equatorial cyclohexanol and cyclohexane. Secondly, X not only introduces, but also replaces, structural features and may therefore eliminate shift increments which contributed to the resonance in the parent hydrocarbon. Thus, an exocyclic β-heteroatom, replacing a hydrogen in an HC *gauche* configuration, causes the β-substituent shift (XC–HC). For example, introduction of an axial hydroxyl group into the cyclohexane ring replaces two HC by OC *gauche* interactions, and therefore gives rise to an α-shift plus two (OC–HC) shift increments.

TABLE 2. Chemical reference shifts and carbon shielding parameters, in ppm, for the derivation of ^{13}C resonances in hydrocarbons, hydroxides, and amines[a]

Carbon reference shifts and shielding factors (ppm)		
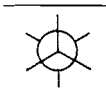 5·9	49·3	28·3
16·1	57·3	36·9
25·2	63·7	43·0
27·9	68·7	47·2
4·73	1·74	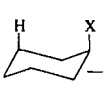 −4·50

[a]The chemical shifts for the hydrocarbons were taken from refs. 2 and 8 (ethane), for the hydroxides from ref. 9, for the amines from ref. 10, and the values for the parameters HC, CC, and γ(C) from ref. 7.

Can. J. Chem. Downloaded from www.nrcresearchpress.com by 210.87.254.105 on 09/05/12
For personal use only.

TABLE 3. Structural parameters, observed, and differences between calculated and observed ^{13}C chemical shifts for a series of decalols

Carbon	Substituent	Parameters[a]	Δ chemical shift (calcd. − exptl.)[b] Structural	Resonance	Chemical shift (exptl.)[c]
1	1β-OH	3 0 0 1 1 0 0 0 0 0	3.3	0.6	74.6
1	1α-OH	1 0 0 1 3 0 0 0 0 0	−2.0	0.2	70.4
2	2α-OH	2 0 0 1 0 0 0 0 0 0	3.0	−0.1	70.2
2	2β-OH	0 0 0 1 2 0 0 0 0 0	−2.9	−1.1	66.6
1	1β-OH,10-Me	3 1 0 1 2 0 0 0 0 0	0.0	1.1	79.6
1	1α-OH,10-Me	2 1 0 1 3 0 0 0 0 0	−0.3	3.2	75.2
2	2α-OH,10-Me	2 0 1 1 0 0 0 0 0 0	1.8	−1.6	66.9
2	2β-OH,10-Me	0 0 0 1 2 1 0 0 0 0	−3.9	−2.4	67.6
3	3β-OH,10-Me	2 0 0 1 0 0 0 0 0 0	2.2	−0.6	71.0
3	3α-OH,10-Me	0 0 0 1 2 0 0 0 0 0	−2.9	−0.8	66.6
4	4α-OH,10-Me	3 0 1 1 1 0 0 0 0 0	3.4	0.2	70.0
4	4β-OH,10-Me	1 0 0 1 3 1 0 0 0 0	−3.4	−1.7	71.8
2	1β-OH	2 0 0 0 0 0 2 0 0 0	−0.6	−0.1	35.8
9	1β-OH	4 0 0 0 0 0 0 0 1 0	−0.8	−1.2	29.1
10	1β-OH	4 0 0 0 0 0 1 1 0 0	0.5	0.0	50.4
2	1α-OH	2 0 0 0 0 0 1 1 0 0	−1.9	−0.7	34.3
3	1α-OH	2 0 0 0 0 0 0 0 1 0	−1.2	0.5	20.0
5	1α-OH	4 0 0 0 0 0 0 0 1 0	1.8	1.7	35.6
9	1α-OH	4 0 0 0 0 0 0 0 1 0	−1.3	−1.7	29.6
10	1α-OH	4 0 0 0 0 0 0 2 0 0	0.7	0.8	47.4
1	2α-OH	4 0 0 0 0 0 2 0 0 0	1.7	0.1	43.0
3	2α-OH	2 0 0 0 0 0 2 0 0 0	−0.4	0.1	35.6
1	2β-OH	4 0 0 0 0 1 1 0 0 0	1.4	0.6	40.4
3	2β-OH	2 0 0 0 0 1 1 0 0 0	−1.5	−0.3	33.9
4	2β-OH	4 0 0 0 0 0 0 1 0 0	0.7	0.3	27.6
10	2β-OH	4 0 0 0 0 0 0 1 0 0	1.0	0.9	36.4
10	1β-OH,10-Me	0 4 0 0 0 0 0 2 0 0	−0.4	−0.8	39.2
11	1β-OH,10-Me	6 0 4 0 0 0 0 0 1 0	−0.2	−0.5	9.8
10	1α-OH,10-Me	0 4 0 0 0 0 0 2 0 0	0.5	0.1	38.3
11	2β-OH,10-Me	6 0 3 0 0 0 0 0 0 1	0.6	0.6	17.9
11	4β-OH,10-Me	6 0 3 0 0 0 0 0 0 1	−0.6	−0.6	19.1

[a]The geometric parameters are given in the order: HC, exocyclic CC, γ(C); α-shift, exocyclic OC, eliminated γ(C), HO, exocyclic CO, γ(O), and δ(O). For every δ(O) interaction a γ(C) interaction is removed at the carbinyl carbon.
[b]Differences between calculated and observed chemical shifts. The chemical shifts are calculated from simple structural units (left column), as well as from the resonances in the corresponding hydrocarbons (right column).
[c]The chemical shifts for the decalols and the corresponding decalins are taken from ref. 11.

An equatorial hydroxyl group, on the other hand, neither introduces OC nor removes HC interactions, and its substituent effect at C(1) therefore constitutes the α-hydroxyl shift. While exocyclic XC replaces an HC *gauche* interaction, endocyclic XC replaces a CC *gauche* configuration. The combinations of introduced and replaced structural features are included in Table 1.

An analysis of the shielding effects of exocyclic oxygen and endocyclic nitrogen may serve as illustration. The required reference shifts are given in Table 2. Tables 3 and 4 show the ^{13}C chemical shifts for some *trans*-decalols and quinolizidines, which were used to derive the oxygen and nitrogen shielding parameters. The structural variables are also included in Tables 3 and 4. Multiple linear regression analyses between the structural variables and observed chemical shifts gave the shielding parameters in Table 5. The hydroxyl parameters in Table 5 were then used to predict substituent shifts in oxygenated steroids (Table 6).

The shielding parameters in Table 5 require a few comments. Two sets of parameters were derived, basing the prediction of the chemical shifts (*a*) on the reference values in Table 2 and (*b*) on the corresponding hydrocarbon resonances. Since exocyclic NC, CN, and γ(N) *gauche* configurations occur only in axial methylquinolizidines, and since the chemical shifts for the cor-

Can. J. Chem. Downloaded from www.nrcresearchpress.com by 210.87.254.105 on 09/05/12
For personal use only.

TABLE 4. Structural parameters, observed, and differences between calculated and observed ^{13}C chemical shifts for some quinolizidines

Carbon	Substituent	Parameters[a]	Δ chemical shift (calcd. − exptl.)[b]		Chemical shift (exptl.)[c]
			Structural	Resonance	
1	nil	3 0 0 0 1 0 0	0.2	−0.5	33.6
3	nil	1 0 0 0 1 0 0	−1.7	−0.3	26.0
4	nil	4 0 0 0 0 0 0	−1.1	−1.8	56.9
10	nil	4 0 0 0 0 0 0	−1.3	−1.7	63.2
1	1β-methyl	2 1 0 0 1 0 0	3.3	0.6	36.6
3	1β-methyl	1 0 0 0 1 0 0	−1.6	0.4	25.9
9	1β-methyl	3 0 1 0 1 0 0	−0.6	−0.1	29.9
10	1β-methyl	5 1 0 0 0 0 0	−1.1	−1.1	69.5
1	1α-methyl	1 2 0 0 0 1 0	−1.0	—[d]	37.0
3	1α-methyl	1 0 1 0 1 0 0	−1.1	—	20.9
9	1α-methyl	3 0 1 0 1 0 0	−1.0	—	30.3
10	1α-methyl	4 1 0 1 0 0 0	−0.3	—	65.9
11	1α-methyl	4 0 2 0 0 0 1	0.0	—	13.8
1	2β-methyl	4 1 0 0 1 0 0	0.9	—	39.3
3	2β-methyl	2 1 0 0 1 0 0	−0.6	—	31.4
4	2β-methyl	4 0 1 0 0 0 0	0.6	—	50.7
10	2β-methyl	4 0 1 0 0 0 0	0.4	—	57.0
1	2α-methyl	5 0 0 0 1 0 0	0.9	−0.2	42.3
3	2α-methyl	3 0 0 0 1 0 0	−0.6	0.1	34.4
4	2α-methyl	4 0 0 0 0 0 0	−0.8	−1.5	56.6
3	3β-methyl	1 0 0 0 1 0 0	2.1	0.6	31.3
4	3β-methyl	6 0 0 0 0 0 0	−1.4	−2.6	66.7
1	3α-methyl	3 0 1 0 1 0 0	0.8	—	28.5
3	3α-methyl	0 1 0 0 0 1 0	1.0	—	28.6
4	3α-methyl	5 0 0 1 0 0 0	0.3	—	62.1
11	3α-methyl	4 0 1 0 0 0 1	0.0	—	18.3
3	4α-methyl	3 0 0 0 1 0 0	−1.7	0.4	35.5
4	4α-methyl	3 1 0 0 0 0 0	−0.3	0.0	59.2
6	4α-methyl	4 0 1 0 0 0 0	−0.6	−0.1	51.9
11	4α-methyl	2 0 1 0 2 0 0	−3.0	−3.6	20.8
1	10-methyl	4 1 0 0 1 0 0	−0.3	0.4	40.5
4	10-methyl	4 0 1 0 0 0 0	1.3	0.1	50.0
10	10-methyl	0 4 0 0 0 0 0	1.0	0.0	53.2
11	10-methyl	4 0 4 0 2 0 0	3.7	3.1	10.1

[a]The geometric parameters are given in the order: HC, exocyclic CC, γ(C); exocyclic NC, HN, exocyclic CN, and γ(N).
[b]Differences between calculated and observed chemical shifts. The chemical shifts are calculated from structural units (left column), as well as from the parent hydrocarbon resonances (right column).
[c]The chemical shifts for the quinolizidines are taken from ref. 12, those for the corresponding decalins from ref. 5.
[d]The chemical shifts for the corresponding methyldecalins were not available.

responding axial methyldecalins were not available, the shift increments NC, CN, and γ(N) could not be rederived by method *b*.

The α-heterosubstituent effects are predicted using a combination of α-shift increments and XC *gauche* parameters. Endocyclic XC configurations occurred only in the quinolizidine series, where the NC parameter value was found to be insignificant. The values for the exocyclic XC parameters depend on the choice of α-shift increments. For instance, the use of the $(CH_3)_2$-$CHOH$–$(CH_3)_2CH_2$ shift difference of 47.6 ppm gave a small OC value (set equal to zero in Table 5). If, however, the *trans*-4-*tert*-butylcyclohexanol–*tert*-butylcyclohexane shift difference of 43.2 ppm (9) was chosen, an OC shift contribution of 2.44 ppm was derived. The second choice gives somewhat better results (Table 3), presumably because conformational effects on the carbinyl carbon resonances are similar in the cyclohexanol and decalol systems.

The β-substituent parameters HO, CO and HN, CN correspond to the β-carbon parameters HC, CC (7). Endocyclic CX interactions occurred only in the quinolizidine series and, like the endocyclic CC parameter, the shift increment

Can. J. Chem. Downloaded from www.nrcresearchpress.com by 210.87.254.105 on 09/05/12
For personal use only.

TABLE 5. Heterosubstituent parameters, in ppm, derived with the structural variables and ^{13}C chemical shifts in Tables 3 and 4

Hydroxides			Amines		
	I[a]	II[b]		I[a]	II[b]
OC	0.00[c]	2.44[d]	NC	1.90	—
HO	4.84	4.42	HN	3.7	3.49
CO	1.97	2.27	CN	2.63	—
γ(O)	−6.72	−6.40	γ(N)	−2.02	—
δ(O)	−2.28	−1.70			

[a]The chemical shift calculations are based on the reference values in Table 2.
[b]The chemical shift computations are based on the resonances in the parent decalins.
[c]The OC parameter was found to be insignificant and was set equal to zero.
[d]The *trans*-4-*tert*-butylcyclohexanol–*tert*-butylcyclohexane shift difference of 43.2 ppm (9) was used as α-hydroxyl shift.

associated with the endocyclic CN configuration was found to be insignificant.

The *gauche* γ(O) parameter is directly observable and does not require any explanation. This parameter is rather sensitive to variations in the structural environment. An antiperiplanar heterosubstituent may also cause noticeable upfield shifts (13). However, because of the unknown nature of conformational effects on carbon resonances no anti γ(X) parameter was included in the present analysis.

A δ-substituent needs to be considered only if it is *syn*-axial to the carbon in question. Such an arrangement occurs in the decalol series. The present interpretation of δ(O) differs from that given previously (11). Introduction of a *syn*-axial hydroxyl group shifts the δ-carbon resonance downfield. However, it also removes a γ(C) interaction. The observed displacement is therefore a δ(O)–γ(C) effect and the δ(O) parameter itself is an upfield shift, rather than a downfield shift.

Other additivity schemes for the prediction of oxygen (9, 14) and nitrogen (10, 12) substituent effects are available. However, these methods generally consist of correlating chemical shifts in heterosubstituted molecules with resonances in the corresponding hydrocarbons, rather than with structural features.

To illustrate the use of the parameters, the calculations of the chemical shifts for C(1) and C(2) of 1β-hydroxydecalin and for C(9) and C(10) of 1β-methylquinolizidine are described in detail (see also Table 7). Consider first the derivation from the resonances in the structural units in Table 2. The fragments C(2)—*C*(1)—OH—C(10) and C(3)—*C*(2)—C(1) correspond to isopropanol and propane, leading to reference shifts of 63.7 and 16.1 ppm, respectively. The only additional contribution to the C(1) resonance, 3×4.73 ppm, comes from the three HC *gauche* interactions between the axial hydrogen on C(1) and C(3), C(5) and C(9). The shift contribution from the OC *gauche* interaction is taken to be zero. Two HC *gauche* interactions between the axial hydrogen on C(2) with C(4) and C(10), and two HO *gauche* interactions between the hydrogens on C(2) and the hydroxyl group contribute 2×4.73 ppm and 2×4.84 ppm to the resonance value of C(2). The fragments C(8)—*C*(9)—C(10) and C(9)—*C*(10)—N—C(1) correspond to propane and isopropylamine, leading to reference shifts of 16.1 ppm and 43.0 ppm, respectively. Three HC *gauche* interactions between the axial hydrogen on C(9) and C(1) and C(7), and the equatorial hydrogen on C(9) with C(1), the γ(C) interaction between the equatorial hydrogen on C(9) and the methyl group, and the HN *gauche* interaction between the axial hydrogen on C(9) and nitrogen contribute 3×4.73, 1×-4.50, and 1×3.47 ppm to the resonance of C(9). Five HC *gauche* interactions between the hydrogen on C(10) and C(2), C(4), C(6), C(8), and C(11), and the exocyclic CC *gauche* interaction C(9)—C(10)—C(1)—C(11) add 5×4.73 and 1×1.74 ppm to the chemical shift of C(10).

If the chemical shifts are to be derived from the resonances in the parent hydrocarbons, the chemical shifts of C(1) and C(2) in decalin, 34.3 and 26.9 ppm, become the reference shifts for C(1) and C(2) of 1β-hydroxydecalin. The α-hydroxyl shift is taken to be 43.2 ppm. The (OC–HC) *gauche* interaction contributes (2.44–4.73) ppm to the resonance of C(1). The HC *gauche* interactions are already present in decalin and are now ignored. Two HO *gauche* interactions between the axial and equatorial hydrogens of C(2) with the hydroxyl group add 2×4.42 ppm to the chemical shift of C(2). The resonances for the corresponding carbons in 1β-methyldecalin, 31.0 and 50.6 ppm, become the

Can. J. Chem. Downloaded from www.nrcresearchpress.com by 210.87.254.105 on 09/05/12
For personal use only.

TABLE 6. Structural parameters, observed, and differences between calculated and observed ^{13}C chemical shifts for some hydroxylated steroids and terpenes[a]

Substrate	Reference	Carbon	Parameters	Chemical shift HR	Chemical shift HOR	Δ (res.)
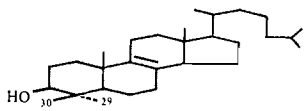	16/17[b]	2	0 0 0 2 0 0 0	19.1	27.9	0.0
		3	1 2 0 0 0 0 0	42.4	79.0	2.0
		4	0 0 0 0 2 0 0	33.5	39.0	−1.0
		29	0 0 0 0 0 0 1 0	33.5	28.1	−1.0
		30	0 0 0 0 0 0 1 0	22.0	15.4	0.2
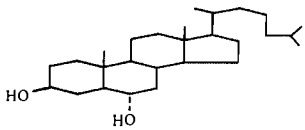	11/18	4	0 0 0 0 0 1 0	38.3	32.3	−0.4
		5	0 0 0 1 1 0 0	45.0	51.6	0.1
		6	1 1 0 0 0 0 0	28.9	69.3	0.5
		7	0 0 0 2 0 0 0	32.6	41.7	−0.3
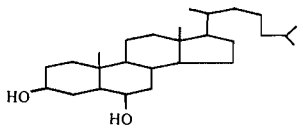	11/18	4	0 0 0 0 0 1 0	38.3	35.4	−3.5
		5	0 0 0 0 2 0 0	45.0	47.3	2.2
		6	1 3 1 0 0 0 0	28.9	71.9	−2.2
		7	0 0 0 1 1 0 0	32.6	36.9	2.4
		8	0 0 0 0 0 1 0	36.0	30.4	−0.8
		19	0 0 0 0 0 0 1	12.5	15.8	−0.5
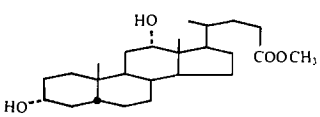	19/19	9	0 0 0 0 0 1 0	40.9	34.1	0.4
		11	0 0 0 1 1 0 0	21.3	29.2	−1.2
		12	1 3 0 0 0 0 0	40.7	73.5	3.5
		13	0 0 0 0 2 0 0	43.2	47.0	0.7
		14	0 0 0 0 0 1 0	57.0	48.6	2.0
		17	0 0 0 0 0 1 0	56.5	47.6	2.5
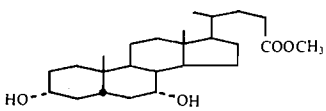	19/19	4	0 0 0 0 0 0 1	37.0	40.1	−0.3
		6	0 0 0 1 1 0 0	27.7	35.7	−1.3
		7	1 3 1 0 0 0 0	26.9	68.8	−1.1
		9	0 0 0 0 0 1 0	40.9	33.5	1.0
		14	0 0 0 0 0 1 0	57.0	51.1	−0.5
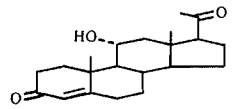	20/20	1	0 0 0 0 0 0 1	35.1	36.9[c]	1.0
		9	0 0 0 1 1 0 0	53.1	58.1	0.7
		11	1 1 1 0 0 0 0	20.5	67.1	−1.2
		12	0 0 0 2 0 0 0	37.9	49.4	−2.7
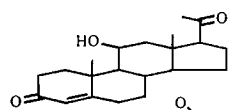	20/20	8	0 0 0 0 0 1 0	34.9	31.0	−2.5
		9	0 0 0 0 2 0 0	53.1	55.6	2.0
		11	1 3 2 0 0 0 0	20.5	66.2	0.4
		12	0 0 0 1 1 0 0	37.9	46.8	−2.2
		18	0 0 0 0 0 0 1	12.9	15.3	0.4
		19	0 0 0 0 0 0 1	16.8	20.3	−0.7
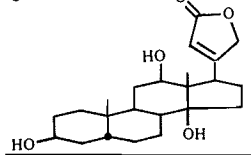	21/21	11	0 0 0 2 0 0 0	21.7	30.0	0.5
		12	1 2 0 0 0 0 0	40.4	74.8	4.2
		13	0 0 0 0 2 0 0	50.3	56.4	−1.6
		18	0 0 0 0 0 1 0	16.1	9.4	0.3

[a]Explanation of column headings: (*i*) ref. *x*/*y*: *x* = reference for oxygenated substrate, *y* = reference for corresponding hydrocarbon; (*ii*) parameters: they are given in the sequence α-shift, exocyclic OC, removed γ(C), HO, exocyclic CO, γ(O), and δ(O); for every δ(O) interaction a γ(C) interaction is removed at the carbinyl carbon; (*iii*) HR: chemical shift in the hydrocarbon; (*iv*) HOR: chemical shift in the hydroxyl derivative; (*v*) res.: difference between calculated and experimental chemical shifts; the parameters in column II of Table 5 were used for the calculations.

[b]The HR resonances are those for a $\Delta^{8(9)}$-pimaradiene (17), rather than the corresponding triterpene.

[c]The assignments of the C(1) and C(2) resonances of 11α-hydroxyprogesterone (20) have been reversed.

reference shifts for C(9) and C(10) of 1β-methylquinolizidine. The shift difference of (43.0–25.2) ppm for C(2) in isopropylamine and isobutane is taken to be the α-nitrogen shift. The replacement of the HC interaction of the axial hydrogen in C(9) with C(5) by an HN interaction contributes the shift increment (3.49–4.73) ppm to the resonance of C(9).

Can. J. Chem. Downloaded from www.nrcresearchpress.com by 210.87.254.105 on 09/05/12
For personal use only.

Can. J. Chem. Downloaded from www.nrcresearchpress.com by 210.87.254.105 on 09/05/12
For personal use only.

TABLE 7. Sample calculations of ^{13}C chemical shifts[a]

From structural units						From parent hydrocarbon[b]					
Parameter	C(1)	C(2)	Parameter	C(9)	C(10)	Parameter	C(1)	C(2)	Parameter	C(9)	C(10)
Ref.	63.7	16.1	Ref.	16.1	43.0	Ref.	34.3	26.9	Ref.	31.0	50.6
α	—	—	α	—	—	α	43.9	—	α	—	17.8
HC	3×4.73	2×4.73	HC	3×4.73	5×4.73	HC	—	—	HC	—	—
CC	0×1.74	0×1.74	CC	0×1.74	1×1.74	CC	—	—	CC	—	—
γ(C)	0×−4.50	0×−4.50	γ(C)	1×−4.50	0×−4.50	γ(C)	—	—	γ(C)	—	—
OC	1×0.00	0×0.00	NC	0×1.90	0×1.90	OC–HC	1×−2.58	0×−2.58	NC–CC	—	—
HO	0×4.84	2×4.84	HN	1×3.47	0×3.47	HO	0×4.42	2×4.42	HN–HC	1×−1.24	0×−1.24
CO	0×1.97	0×1.97	CN	0×2.63	0×2.63	CO	0×2.27	0×2.27	CN–CC	—	—
γ(O)	0×−6.72	0×−6.72	γ(N)	0×−2.02	0×−2.02	γ(O)	0×−6.40	0×−6.40	γ(N)–γ(C)	—	—
δ(O)	0×−2.28	0×−2.28				δ(O)–γ(C)	0×2.80	0×2.80			
Pred.	77.9	35.2	Pred.	29.3	68.4	Pred.	75.6	35.7	Pred.	29.8	68.4
Obs.	74.6	35.8	Obs.	29.9	69.5	Obs.	74.6	35.8	Obs.	29.9	69.5
Δ	3.3	−0.6	Δ	−0.6	−1.1	Δ	1.0	−0.1	Δ	−0.1	−1.1

[a]Examples: C(1) and C(2) of 1β-hydroxydecalin and C(9) and C(10) of 1β-methylquinolizidine.
[b]Chemical shifts for decalins are taken from ref. 5 (comparison with quinolizidines) and from ref. 11 (comparison with decalols).

Can. J. Chem. Downloaded from www.nrcresearchpress.com by 210.87.254.105 on 09/05/12
For personal use only.

TABLE 8. General β-carbon and β-hydroxyl shielding parameters HC/CC and HO/CO, in ppm, derived with ^{13}C chemical shifts in substrates, in which the dihedral angles differ from 60°[a]

Parameter	cos ϕ		cos^2 ϕ	
	[b]	[c]	[b]	[c]
HC	8.69	9.46	10.35	18.92
CC	2.86	3.48	4.40	6.96
RMS	1.62	1.74	1.66	5.11
HO	10.54	9.68	11.67	19.44
CO	4.84	3.94	6.31	8.12
RMS	1.55	1.75	2.01	5.59

[a]Two expressions are considered:
'cos ϕ' $\delta(\beta) = R_1X \times \cos\phi_1 + R_2X \times \cos\phi_2$
'cos^2 ϕ' $\delta(\beta) = R_1X \times \cos^2\phi_1 + R_2X \times \cos^2\phi_2$.
[b]The values for HC/CC and HO/CO are optimized.
[c]Previously derived values for HC/CC and HO/CO are used (see Table 5):
'cos ϕ' HC = 2 × 4.73, CC = 2 × 1.74, HO = 2 × 4.84, CO = 2 × 1.97
'cos^2 ϕ' HC = 4 × 4.73, CC = 4 × 1.74, HO = 4 × 4.84, CO = 4 × 1.97.

The interpretation of ^{13}C chemical shift contributions of β-groups in terms of *gauche* parameters implies a general dependence of β-substituent effects on the dihedral angles. An angular dependence of β-carbon shifts has already been suggested to rationalize qualitatively the observed shielding trends in D-rings of steroids (15). An angular dependence is most simply introduced by multiplying the *gauche* parameters by a trigonometric function of the dihedral angle ϕ. The fact that β-substituent shifts in ecclipsed fragments (Tables 9 and 10) are about twice as large as the β-parameters derived from staggered structural units suggests a cos ϕ dependence, since cos 0° = 2 × cos 60°.

$$[1] \quad \delta(\beta) = R_1X \times \cos\phi_1 + R_2X \times \cos_2 \qquad 0° \leq \phi \leq 90°$$

(R_1, R_2 = H or C; X = C, O, or Cl)

As Tables 9–11 show, a cos ϕ dependence gives indeed an adequate description of the angular variation of methyl, hydroxyl, and chlorine β-shifts. The function cos^2 ϕ could also be used to predict the β-substituent shifts in Tables 9 and 10, but the corresponding parameters (Table 8) do not show the necessary relation to the HC, CC and HO, CO shift increments, given by cos^2 0° = 4 × cos^2 60°. It was assumed throughout that interactions at angles greater than 90° do not contribute to the chemical shifts. Their inclusion

TABLE 9. *Gauche* interactions, dihedral angles, observed and predicted β-methyl substituent effects in norbornane derivatives

Carbon	Compound	Parameters				Chemical shifts Calcd.[a]		Chemical shifts Exptl.[b]
1	2-*endo*-Methylnorbornane	45	CC	85	HC	2.8	3.3	5.4
3	2-*endo*-Methylnorbornane	0	HC	>90	—	8.7	9.5	10.6
1	2-*exo*-Methylnorbornane	35	HC	85	CC	7.4	8.1	6.7
3	2- *xo*-Methylnorbornane	0	HC	>90	—	8.7	9.5	10.2
1	2,3-*endo*-Dimethylnorbornane	45	CC	85	HC	2.8	3.3	5.4
2	2,3-*endo*-Dimethylnorbornane	0	CC	>90	—	2.9	3.5	0.8
1	2-*endo*,3-*exo*-Dimethylnorbornane	45	CC	85	HC	2.8	3.3	5.5
2	2-*endo*,3-*exo*-Dimethylnorbornane	0	HC	>90	—	8.7	9.5	10.0
3	2-*endo*,3-*exo*-Dimethylnorbornane	0	HC	>90	—	8.7	9.5	8.8
4	2-*endo*,3-*exo*-Dimethylnorbornane	35	HC	85	CC	7.4	8.1	6.7
1	2,3-*exo*-Dimethylnorbornane	35	HC	85	CC	7.4	8.1	7.6
2	2,3-*exo*-Dimethylnorbornane	0	CC	>90	—	2.9	3.5	3.5
2	1-Methylnorbornane	45	HC	85	HC	6.9	7.5	6.8
7	1-Methylnorbornane	60	HC	60	HC	8.7	9.5	6.7
1	7-Methyl orbornane	60	HC	60	CC	5.8	6.5	3.8
1	1,2-*exo*-Dimethylnorbornane	45	CC	85	CC	2.3	2.8	1.5
2	1,2-*exo*-Dimethylnorbornane	45	CC	85	HC	2.8	3.3	4.0
1	1,2-*endo*-Dimethylnorbornane	45	CC	85	CC	2.3	2.8	2.4
2	1,2-*endo*-Dimethylnorbornane	45	HC	85	CC	6.4	7.0	5.4
1	1,7-Dimethylnorbornane	60	CC	60	CC	2.9	3.5	0.5
7	1,7-Dimethylnorbornane	60	HC	60	CC	5.8	6.5	3.8

[a]The chemical shifts are calculated with equation 1. The parameters were 8.69/2.86 (left column) and 9.46/3.48 (right column).
[b]The experimental data from 2-*endo*-methylnorbornane to 2,3-*exo*-dimethylnorbornane are taken from ref. 22, the rest from ref. 23.

TABLE 10. *Gauche* interactions, dihedral angles, observed and predicted β-hydroxyl substituent effects in molecules where the dihedral angles differ from 60°

Carbon	Compound	Parameters				Chemical shifts Calcd.[a]		Chemical shifts Exptl.[b]
1	2-*endo*-Norbornanol	45	CO	85	HO	4.3	3.6	5.9
3	2-*endo*-Norbornanol	0	HO	>90	—	10.5	9.7	7.5
1	2-*exo*-Norbornanol	35	HO	85	CO	9.1	8.3	7.3
3	2-*exo*-Norbornanol	0	HO	>90	—	10.5	9.7	11.9
1	Borneol	45	CO	85	CO	3.8	3.1	3.2
3	Borneol	0	HO	>90	—	10.5	9.7	10.4
1	Isoborneol	35	CO	85	CO	4.4	3.6	2.5
3	Isoborneol	0	HO	>90	—	10.5	9.7	11.9
1	2-*endo*-Hydroxy,3-*endo*-methylnorbornane	45	CO	85	HO	4.3	3.6	6.0
3	2-*endo*-Hydroxy,3-*endo*-methylnorbornane	0	CO	>90	—	4.8	3.9	2.8
1	2-*endo*-Hydroxy,3-*exo*-methylnorbornane	45	CO	85	HO	4.3	3.6	6.5
3	2-*endo*-Hydroxy,3-*exo*-methylnorbornane	0	HO	>90	—	10.5	9.7	9.2
1	2-*exo*-Hydroxy,3-*endo*-methylnorbornane	35	HO	85	CO	9.1	8.3	7.7
3	2-*exo*-Hydroxy,3-*endo*-methylnorbornane	0	HO	>90	—	10.5	9.7	12.1
1	2-*exo*-Hydroxy,3-*exo*-methylnorbornane	35	HO	85	CO	9.1	8.3	8.1
3	2-*exo*-Hydroxy,3-*exo*-methylnorbornane	0	CO	>90	—	4.8	3.9	7.0
2	1-Twistanol[c]	35	HO	85	HO	9.6	8.8	9.1
6	1-Twistanol	35	HO	85	CO	9.1	8.3	9.0
10	1-Twistanol	45	HO	75	HO	10.2	9.4	8.6
3	4-*endo*-Twistanol	45	CO	75	HO	6.2	5.3	6.6
5	4-*endo*-Twistanol	30	HO	90	CO	9.1	8.4	11.7
3	4-*exo*-Twistanol	45	HO	75	CO	8.7	7.9	9.0
5	4-*exo*-Twistanol	30	HO	90	HO	9.1	8.4	10.7
13	17α-Hydroxyandrostane	35	CO	85	CO	4.4	3.6	4.5
16	17α-Hydroxyandrostane	10	HO	>90	—	10.4	9.5	11.9
13	17β-Hydroxyandrostane	30	CO	90	CO	4.2	3.4	2.1
16	17β-Hydroxyandrostane	10	HO	>90	—	10.4	9.5	10.1

[a]The chemical shifts are calculated with equation 1. The parameter values are 10.54/4.84 (left column) and 9.68/3.94 (right column).
[b]The chemical shifts for the borneols, norbornanols and their parent hydrocarbons are taken from ref. 23, and for the methylnorbornanols and parent hydrocarbons from ref. 24 and 23 respectively; the chemical shifts for twistane and the twistanols are unpublished results from this laboratory, and the steroid shifts are taken from ref. 18.
[c]Twistane numbering system:

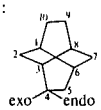

TABLE 11. *Gauche* interactions, dihedral angles, observed and predicted β-chloro substituent shifts

Carbon	Compound	Parameters				Calcd.[a]	Exptl.[b]
2	*eq*-Chlorocyclohexane	60	HX	60	HX	11.6	10.6
2	*ax*-Chlorocyclohexane	60	HX	60	CX	7.6	6.9
2	1-Chloroadamantane	60	HX	60	HX	11.6	10.0
1	2-Chloroadamantane	60	HX	60	CX	7.6	7.1
1	2-*endo*-Chlorobornane	45	CX	85	CX	2.8	3.7
3	2-*endo*-Chlorobornane	0	HX	>90	—	11.6	10.8
1	2-*exo*-Chlorobornane	35	CX	85	CX	3.2	2.9
3	2-*exo*-Chlorobornane	0	HX	>90	—	11.6	13.4
2	1-Chlorotwistane	35	HX	85	HX	10.5	11.9
6	1-Chlorotwistane	35	HX	85	CX	9.8	11.3
10	1-Chlorotwistane	45	HX	75	HX	11.2	10.8

[a]The chemical shifts are calculated with equation 1. The parameter values are: HX = 11.59, CX = 3.53.
[b]The substituent shifts for the cyclohexanes are taken from ref. 25, for the bornanes from ref. 23, and the twistane shifts are unpublished results from this laboratory.

Can. J. Chem. Downloaded from www.nrcresearchpress.com by 210.87.254.105 on 09/05/12
For personal use only.

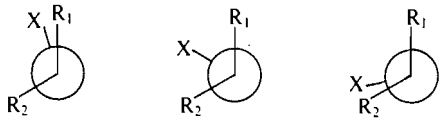

$2R_1X$ $R_1X + R_2X$ $2R_2X$

had little effect on parameters or calculated resonance values. Equation 1 indicates that a pronounced variation of β-substituent shifts with torsional angles is to be expected only if X interacts with two different groups $R_1 \neq R_2$. The sum $(\phi_1 + \phi_2)$ is always close to 120° and the sum $(\cos\phi_1 + \cos\phi_2)$ is nearly invariant over the range $0° \leq \phi \leq 90°$ (angles greater than 90° are ignored). If $R_1 = R_2$, the substituent effect is virtually independent of ϕ, and eclipsed and staggered conformations have similar β-substituent shifts.

Acknowledgment

We thank the National Research Council of Canada for their generous financial support.

1. G. B. Savitsky and K. Namikawa. J. Phys. Chem. **68**, 1956 (1964).
2. D. M. Grant and E. G. Paul. J. Am. Chem. Soc. **86**, 2984 (1964).
3. L. P. Lindeman and J. Q. Adams. Anal. Chem. **43**, 1245 (1971).
4. J. Mason. J. Chem. Soc. A, 1038 (1971).
5. D. K. Dalling, D. M. Grant, and E. G. Paul. J. Am. Chem. Soc. **95**, 3718 (1973).
6. D. K. Dalling and D. M. Grant. J. Am. Chem. Soc. **96**, 1827 (1974).
7. H. Beierbeck and J. K. Saunders. Can. J. Chem. **53**, 1307 (1975).
8. H. Spiesecke and W. G. Schneider. J. Chem. Phys. **35**, 722 (1961).
9. J. D. Roberts, F. J. Weigert, J. I. Kroschwitz, and H. J. Reich. J. Am. Chem. Soc. **92**, 1338 (1970).
10. H. Eggert and C. Djerassi. J. Am. Chem. Soc. **95**, 3710 (1973).
11. S. H. Grover and J. B. Stothers. Can. J. Chem. **52**, 870 (1974).
12. R. T. LaLonde and T. N. Donvito. Can. J. Chem. **52**, 3778 (1974).
13. E. L. Eliel, W. F. Bailey, L. D. Kopp, R. L. Willer, D. M. Grant, R. Bertrand, K. A. Christensen, D. K. Dalling, M. W. Duch, E. Wenkert, F. M. Schell, and D. W. Cochran. J. Am. Chem. Soc. **97**, 322 (1975).
14. G. Engelhardt, E. Lippmaa, and T. Pehk. J. Prakt. Chem. **312**, 935 (1970).
15. T. Yamagishi, K. Hayashi, H. Mitsuhari, M. Imanari, and K. Matsushita. Tetrahedron Lett. 3531 (1973).
16. S. A. Knight. Org. Magn. Res. **6**, 603 (1974).
17. E. Wenkert and B. L. Buckwalter. J. Am. Chem. Soc. **94**, 4367 (1972).
18. J. W. ApSimon, H. Beierbeck, and J. K. Saunders. Can. J. Chem. **51**, 3874 (1973).
19. D. Leibfritz and J. D. Roberts. J. Am. Chem. Soc. **95**, 4996 (1973).
20. N. S. Bhacca, D. D. Giannini, W. S. Jankowski, and M. E. Wolff. J. Am. Chem. Soc. **95**, 8421 (1973).
21. K. Tori, H. Ishii, Z. W. Wolkowski, C. Chachaty, M. Sangaré, F. Piriou, and G. Lucacs. Tetrahedron Lett. 1077 (1973).
22. J. B. Stothers, C. T. Tan, and K. C. Teo. Can. J. Chem. **51**, 2893 (1973).
23. E. Lippmaa, T. Pehk, J. Paasivirta, N. Belikova, and A. Platé. Org. Magn. Res. **2**, 581 (1970).
24. J. B. Grutzner, M. Jautelat, J. B. Dence, R. A. Smith, and J. D. Roberts. J. Am. Chem. Soc. **92**, 7107 (1970).
25. O. A. Subbotin and N. M. Sergeyev. J. Am. Chem. Soc. **97**, 1080 (1975).

Can. J. Chem. Downloaded from www.nrcresearchpress.com by 210.87.254.105 on 09/05/12
For personal use only.

Photoelectron studies on intramolecularly hydrogen-bonded systems. I. The photoelectron spectra of *cis*- and *trans*-2-aminocyclopentanol, and *cis*- and *trans*-2-(*N,N*-dimethylamino)cyclopentanol

R. S. BROWN

Department of Chemistry, University of Alberta, Edmonton, Alberta T6G 2G2

Received August 1, 1975

R. S. BROWN. Can. J. Chem. **54**, 642 (1976).

The photoelectron spectra of *cis*- and *trans*-2-aminocyclopentanol and *cis*- and *trans*-2-(*N,N*,-dimethylamino)cyclopentanol have been recorded and interpreted. The *cis* isomers exhibit N lone pair ionizations at higher ionization energy, and O lone pair ionizations at lower ionization energy than their *trans* isomers.

The results are most consistent with the existence and observation of intramolecular hydrogen-bonding in the *cis* isomers. Infrared data on these systems also show that the *cis* isomers exist in the intramolecularly hydrogen-bonded state.

R. S. BROWN. Can. J. Chem. **54**, 642 (1976).

On a enregistré et interprété les spectres photoélectroniques des amino-2 cyclopentanols *cis* et *trans* et des (*N,N*-diméthylamino)-2 cyclopentanols *cis* et *trans*. Pour les isomères *cis*, l'ionisation des paires d'électrons libres de l'azote s'effectue à des énergies d'ionisation plus élevées alors que celle des paires d'électrons des oxygènes requière des énergies d'ionisation plus basses que celles des isomères *trans*.

Les résultats sont en accord avec l'existence et l'observation de ponts hydrogènes intramoléculaires dans les isomères *cis*. Les données infrarouges sur ces systèmes montrent qu'il existe des ponts hydrogènes intramoléculaires dans les isomères *cis*.

[Traduit par le journal]

The phenomenon known as hydrogen-bonding has been the subject of intense interest as evidenced by the appearance of at least 5000 pertinent publications over the last 35 years (for an excellent compendium of leading works see ref. 1). Infrared spectroscopy (ir) has proved to be a most convenient technique for determining the existence of both inter- and intramolecular hydrogen bonds. While such measurements provide definite evidence for hydrogen bonds they do so by indirect methods since it is the change in the stretching frequency of the bond *adjacent* to the hydrogen bond that is measured. Direct observation of the electron pair involved in a hydrogen bond would perhaps offer insight into the subtle electronic changes occurring during this most interesting process.

Photoelectron spectroscopy (pes) has recently proved to be an invaluable aid to the elucidation of the electronic structures of molecules (2). Particularly accessible to pe study are lone pairs of electrons isolated on various atoms,[1] since these pairs are usually well removed in terms of energy from the more bonding electrons. Of the myriad of papers available concerning hydrogen-bonding, to our knowledge only two involved the use of pe spectroscopy (3, 4). These investigated the temperature induced changes of the pe spectra of flexible amino alcohols (3) and carboxylic acid dimers (4). However, neither of these studies were conclusive in that such spectral changes could have arisen from complicating effects such as conformational heterogeneity and anomalous temperature effects. The following study was therefore undertaken in the hopes of clarifying the situation by determining what electronic changes occurred during intramolecular hydrogen-bonding of well defined systems.

Since pe spectroscopy is at present limited to the study of single molecular species, the molecules to be investigated must contain both the hydrogen donor and acceptor in a well-

[1]The term 'nonbonding' electrons is misleading since it implies little or no association of the lone pair with adjacent orbitals. Recent pe investigations of amines indicate the lone pair ionization has considerable breadth, indicative of a change in the molecular geometry between the ground and ion states. Such can be taken to imply that the orbital giving rise to that ionization has some bonding (or antibonding) character (2).

Can. J. Chem. Downloaded from www.nrcresearchpress.com by 210.87.254.105 on 09/05/12
For personal use only.

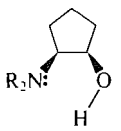
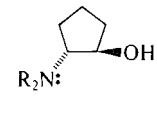

1*a* R = H
b R = CH_3

2*a* R = H
b R = CH_3

defined stereochemical relationship. The compounds chosen for study were *cis*- and *trans*-2-aminocyclopentanol (**1***a* and **2***a*), and *cis*- and *trans*-2-(*N*,*N*-dimethylamino)cyclopentanol (**1***b* and **2***b*).

It was felt that these molecules offered the best opportunity of observing spectral changes which might be attributable to hydrogen-bonding. Firstly the amine lone pair ought to be clearly distinguishable from other bands since it should appear at low ionization potential ($(CH_3)_2\ddot{C}H\ddot{N}H_2$, IP_a = 8.86 eV (5)). Increasing substitution on the amine should separate it further from other ionizations ($(CH_3)_3\ddot{N}$, IP_a = 8.12 eV (5)). Additionally, since adiabatic IP's have been correlated with gas phase basicity (6), it was hoped that the greater basicity of the N lone pair over the O lone pair (6*f*) should facilitate the formation of a single hydrogen bonded species **3***a* rather than a mixture of **3***a* with appreciable quantities of **3***b*. The ir results of Krueger and

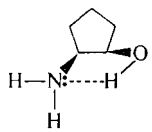
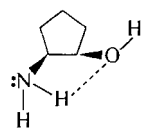

3*a* **3***b*

Mettee on some ethanolamines (7) suggest that the O—H - - -:N form is 1–2 kcal/mol more stable than the O: - - - HN form. Lastly, the *cis* and *trans* isomers should provide well-defined spacial orientations of the interacting groups. The *cis* isomers (**1***a* and **1***b*) should hold the amino and hydroxyl groups in positions permitting the maximum interaction allowable in these systems, while the *trans* compounds (**2***a* and **2***b*) rigidly hold the two groups far enough apart to preclude appreciable hydrogen-bond formation. Being isomers however, it is felt that each *cis* and *trans* pair should experience similar inductive and substituent effects.

Experimental

trans-2-Aminocyclopentanol (**2***a*) was prepared by opening of cyclopentene oxide with ammonia as described by Bannard *et al.* (8). It could be easily converted to *cis*-2-aminocyclopentanol (**1***a*) by the oxazoline inversion method (8). *trans*-2-(*N*,*N*-Dimethylamino)cyclopentanol was prepared by the opening of cyclopentene oxide with dimethylamine according to the procedure of Friess and Baldridge (9), while the corresponding *cis* compound (**1***b*) was prepared by an Eschweiller–Clarke methylation of **1***a* (10).

Photoelectron spectra were run using a MacPherson Model 36 ESCA machine equipped with a He(I) ionization source, and were calibrated using argon as an internal standard. The resolution of the Ar $2P_{3/2}$–$2P_{1/2}$ doublet was found to be 30–40 meV during actual spectral recording.

Infrared spectra were monitored using a Perkin-Elmer 421 grating spectrophotometer and tetrachloroethylene as a solvent. Temperature studies of **1***a* and **1***b* were performed in 1.0 cm matched fused-quartz cells transparent to 2500 cm^{-1}. These cells were inserted in a thermostated cell holder connected to a temperature regulated Haake FE water circulating pump. Temperatures were measured by a thermocouple inserted through the Teflon stopper of a cell in the thermostated block and connected to a Biddle-Gray TC Potentiometer. Temperatures are generally believed accurate to ±0.3 °C.

Results and Discussion

The pe spectra for compounds **1***a*, **2***a*, and **1***b*, **2***b* are presented in Figs. 1 and 2 while the corresponding data and assignments for the first two bands of each spectrum are presented in Table 1.

It can be clearly seen from Figs. 1 and 2 that in each case, the *cis* isomer displays the N lone pair at higher ionization or binding potential. Thus the difference in the first vertical[2] IP for **1***a* and **2***a* is 0.45 eV while that for the *cis*- and *trans*-(*N*,*N*-dimethylamino) derivatives **1***b* and **2***b* is 0.39 eV. Correspondingly, there is a somewhat smaller *decrease* of 0.13 eV in the oxygen lone pair ionizations of the *cis* compounds over the *trans* compounds. Intuitively, one expects that in

[2]The IP really applicable to this study is the adiabatic IP, since the vertical IP represents not the $0' \leftarrow 0$ transition, but the $X' \leftarrow 0$ transition where X' represents some upper vibrational level of the ion state. While one might argue that the changes attributed to hydrogen bonding in these spectra are simply due to shifts in the Franck–Condon envelope, if one takes the onset potential as being representative of the adiabatic IP, it can be seen that the onset potentials parallel the trends shown in the vertical IP's. Additionally, the half-widths of the N ionizations for **1***b* and **2***b* are constant at 0.76 ± 0.02 eV, showing no broadening of the Franck–Condon envelope. Because of ease of measurement, we shall use the vertical IP's throughout the article since it is believed that the vertical and adiabatic IP's show the same trends.

Can. J. Chem. Downloaded from www.nrcresearchpress.com by 210.87.254.105 on 09/05/12
For personal use only.

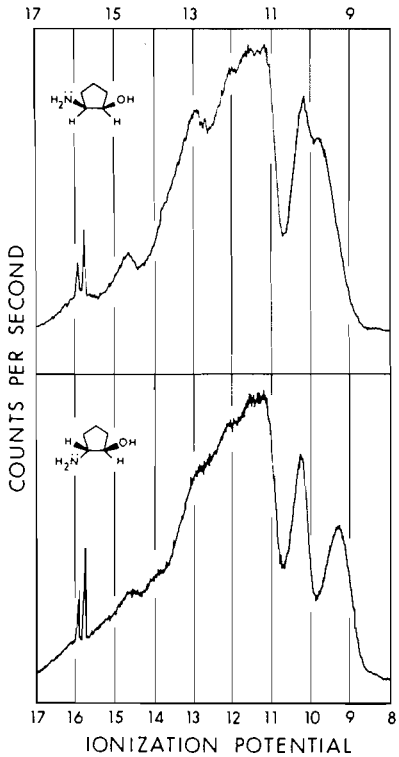

FIG. 1. Photoelectron spectra of *cis*- and *trans*-2-aminocyclopentanol (**1***a* and **2***a* respectively) using argon as an internal calibrating gas.

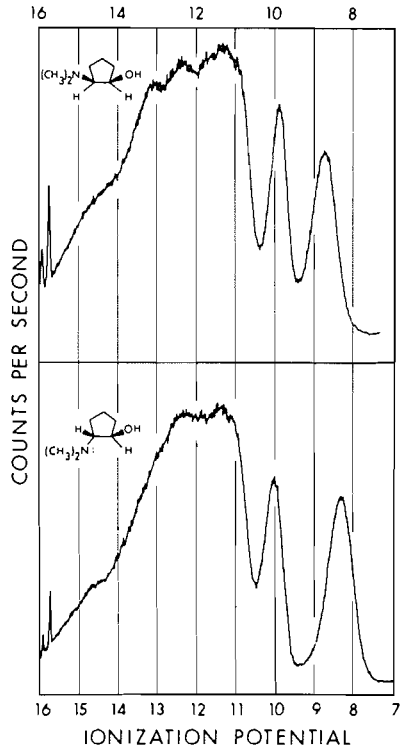

FIG. 2. Photoelectron spectra of *cis*- and *trans*-2-(*N*,*N*-dimethylamino)cyclopentanol (**1***b* and **2***b* respectively) using argon as an internal calibration.

hydrogen-bonded systems the amine lone pair ought to become more bonding and move to higher IP. Concomitantly as the hydrogen of the OH moiety associates with the N lone pair, the oxygen ought to experience an increase in electron density which should facilitate removal of an electron from the O lone pair. Recent theoretical calculations (11) concerning the Mulliken populations of hydrogen-bonded dimers are in agreement with these ideas and observations.

That the *cis*-amino alcohols in fact exist in an intramolecularly hydrogen-bonded state is amply illustrated by ir spectroscopy. Pertinent data are listed in tabular form in Table 2. Dilution studies on the *trans* compounds (**2**) show a diminution of the intermolecularly bonded OH absorption with increasing dilution, while the *cis* compounds (**1**) show no change in the ratios of the bonded to unbonded absorptions with diminishing concentration. Such studies provide strong evidence for the existence of intramolecular hydrogen-

TABLE 1. Ionization potentials of *cis*- and *trans*-2-aminocyclopentanol (**1***a* and **2***a*) and of *cis*- and *trans*-2-(*N*,*N*-dimethylamino)cyclopentanol (**1***b* and **2***b*)

Compound	Nitrogen IP (eV)		Oxygen IP (eV)	
	Vertical	Adiabatic*	Vertical	Adiabatic*
cis-2-Aminocyclopentanol	9.70	8.61	10.11	†
trans-2-Aminocyclopentanol	9.25	8.30	10.24	†
cis-2-(*N*,*N*-Dimethylamino)cyclopentanol	8.69	7.80	9.89	9.25
trans-2(*N*,*N*-Dimethylamino)cyclopentanol	8.30	7.45	10.02	9.36

*Adiabatic IP's are taken to be the onset potential for the band.
†The adiabatic IP was not observable due to strong band overlap.

Can. J. Chem. Downloaded from www.nrcresearchpress.com by 210.87.254.105 on 09/05/12
For personal use only.

TABLE 2. Infrared O—H stretching frequencies of aminocyclopentanols **1** and **2** determined in $Cl_2C{=}CCl_2$ solution at room temperature

Compound	ν_{OH} (cm^{-1}) 'Free'	'Bonded'
cis-2-Aminocyclopentanol (**1***a*)	3630	3445*
trans-2-Aminocyclopentanol (**2***a*)	3625	3350†‡
cis-2(*N*,*N*-Dimethylamino)cyclopentanol (**1***b*)	‖	3455*
trans-2(*N*,*N*-Dimethylamino)cyclopentanol (**2***b*)	3620	3400†§

*Exhibits no change in the relative spectral intensities with increasing dilution.
†Exhibits diminution of bonded intensity and increase in free intensity with increasing dilution.
‡Exhibits a broad second maximum at 3275 cm^{-1} which also diminishes with increasing dilution.
§Exhibits broad second maximum at 3160 cm^{-1} which also diminishes with increasing dilution.
‖Free OH band is not observable in this spectrum, but is assumed to be roughly the same as in the *trans* compound (**2***b*).

bonding in the latter. Unfortunately low volatility of compounds (**1**) prevented gas phase ir studies, but it is expected in the gas phase (where pe measurements were made) that the *cis*-amino alcohols (**1**) will also exist in their intramolecularly hydrogen-bonded states.

Several points should be made regarding the ir data. Within each series, the *trans* isomer shows $\Delta\nu$ ('free' OH − 'bonded' OH) to be larger than the *cis* isomer. It has been observed that 1,2- and 1,3-amino alcohols (12) and diols (13) show larger $\Delta\nu$ values for intermolecular than intramolecular hydrogen-bonding presumably due to geometric restraints in the latter which prevent optimum interaction. Certainly the data of Table 2 do not contradict these observations. On the other hand, one might expect that increasing the basicity of the nitrogen by substitution (6) should increase the hydrogen bond strength (12). If it is assumed that the controversial Badger–Bauer rule (14) holds, which states that $\Delta\nu$ is indicative of the enthalpy of the hydrogen-bond, then we would expect the ir data for **1***a* and **1***b* might reflect the different hydrogen-bond strengths. A comparison of the $\Delta\nu$ values for **1***a* (185 cm^{-1}) and **1***b* ($\sim$ 180 cm^{-1}) shows no difference in $\Delta\nu$ even though the basicity of **1***b* is undoubtedly larger than that of **1***a* (6). Either the Badger–Bauer rule does not apply in these systems, or the ΔH values for the bonded *vs.* free forms of **1***a* and **1***b* are equal. The Badger–Bauer rule has been shown not to be applicable to several systems such as the α–ω diol monomethyl ethers (15) and equilibria in which alkyl halides act as hydrogen acceptors (16).

From an ir temperature relationship similar to that used by Krueger and Mettee (7) one can calculate the $-\Delta H$ value for *cis*-2-aminocyclopentanol (**1***a*) to be 1.92 kcal/mol (correlation coefficient 0.96). Unfortunately one cannot apply the same treatment to 2-(*N*,*N*-dimethylamino)-cyclopentanol (**1***b*) because the free OH group is not observable even at 90 °C. One can, however, predict a lower limit for the $-\Delta G$ value for the hydrogen-bonded to free state of **1***b* of 3.34 kcal/mol if we assume that at 90 °C we could see greater than 1% of the free OH form. Since one can observe a free OH absorption for **1***a* it is clear that $-\Delta G$ for the hydrogen-bonded to free form of **1***a* is smaller than for **1***b*. However, in the absence of entropy values, no prediction can be made concerning the relative values of enthalpies for the hydrogen-bonded forms of **1***a* and **1***b*.

It is tempting in the light of the spectra presented in Figs. 1 and 2 to ascribe to hydrogen-bonding those differences in the pe spectra of the *cis*- and *trans*-aminocyclopentanols. While pe spectroscopy has been used before to test the presence of hydrogen-bonding in open chain amino alcohols (3), previous studies relied on increasing temperature to break hydrogen bonds in flexible systems. While one could argue that such small observed differences (in many cases barely outside experimental error) were simply due to conformational heterogeneities of the ill-defined rotomers, such is not the case here. By use of the relatively rigid isomeric aminocyclopentanols, one has frozen out all extraneous rotations about the C—C bonds and ensured well-defined geometries. That lone pair–lone pair interactions are not responsible for the observed spectral shifts is illustrated in **4**. Direct through-space interactions (17) which should be maximized in the *cis* isomers are expected to increase

Can. J. Chem. Downloaded from www.nrcresearchpress.com by 210.87.254.105 on 09/05/12
For personal use only.

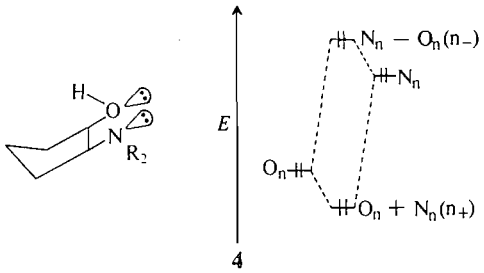

4

the N–O separations rather than decrease them as observed, while a through-bond mechanism (17) can possibly operate in both *trans* and *cis* forms and would also be expected to lower the N orbital IP.

While the observed spectral shifts are most consistent with intramolecular hydrogen-bonding, it is not clear at this time whether pe spectroscopy might offer a quantitative evaluation of the intramolecular hydrogen-bond strength. Although the readily visible bands in the pe spectra do shift markedly, there are subtle shifts in the shape of the σ-envelope that defy analysis. One expects that in addition to the observed changes in the oxygen and nitrogen lone pair ionizations, there ought to be significant changes in the O—H σ-bond and N—H and N—C bonds as well. Unfortunately the bands arising from electrons within these orbitals are obscured by the large σ-envelope. It does not appear that one can assume such changes in the σ-ionizations will exactly compensate one another, and thus simply regard the oxygen and nitrogen lone pairs as being the only orbitals significantly altered by the presence of the hydrogen bond.

In conclusion, the above study illustrates that pe spectroscopy can be used to detect intramolecular hydrogen-bonding in well-defined rigid systems. Such observations directly probe the electron pair actually involved in the hydrogen bond, and may in future provide new insight into the phenomenon of hydrogen bonding.

Acknowledgments

The author gratefully acknowledges the financial assistance of the University of Alberta and of the National Research Council of Canada.

1. (*a*) M. D. JOESTEN and L. J. SCHAAD. Hydrogen bonding. Marcel Dekker Inc., New York. 1974; (*b*) G. C. PIMENTEL and A. L. MCCLELLAND. The hydrogen bond. W. H. Freeman and Company, San Francisco. 1960.
2. D. W. TURNER, C. BAKER, A. D. BAKER, and C. R. BRUNDLE. Molecular photoelectron spectroscopy. Wiley Interscience, London. 1970.
3. S. LEAVELL, J. STEICHEN, and J. L. FRANKLIN. J. Chem. Phys. **59**, 4343 (1973).
4. R. K. THOMAS. Proc. R. Soc. London, Ser. A, **331**, 249 (1972).
5. M. I. AL-JOBOURY and D. W. TURNER. J. Chem. Soc. 4434 (1964).
6. (*a*) R. H. STALEY and J. L. BEAUCHAMP. J. Am. Chem. Soc. **96**, 1604 (1974); (*b*) J. L. BEAUCHAMP. Annu. Rev. Phys. Chem. **22**, 527 (1971); (*c*) D. H. AUE, H. M. WEBB, and M. T. BOWERS. J. Am. Chem. Soc. **94**, 4726 (1972); (*d*) J. I. BRAUMAN, J. M. RIVEROS, and L. K. BLAIR. J. Am. Chem. Soc. **93**, 3914 (1971); (*e*) K. YOSHIKAWA, M. HASHIMOTO, and I. MORISHIMA. J. Am. Chem. Soc. **96**, 288 (1974); (*f*) R. W. TAFT. *In* Proton transfer reactions. *Edited by* E. F. Caldin and V. Gold. Chapman and Hall Ltd., London. 1975.
7. P. J. KRUEGER and H. D. METTEE. Can. J. Chem. **43**, 2970 (1965).
8. R. A. B. BANNARD, N. C. C. GIBSON, and J. H. PARKKARI. Can. J. Chem. **49**, 2064 (1971).
9. S. L. FRIESS and H. D. BALDRIDGE. J. Am. Chem. Soc. **78**, 2482 (1956).
10. H. T. CLARKE, H. B. GILLESPIE, and S. Z. WEISSHAUSE. J. Am. Chem. Soc. **55**, 4571 (1933).
11. J. E. DELBENE. J. Am. Chem. Soc. **95**, 5460 (1973).
12. L. P. KUHN, R. A. WIRES, W. RUOFF, and H. KWART. J. Am. Chem. Soc. **91**, 4790 (1969).
13. L. P. KUHN. J. Am. Chem. Soc. **74**, 2492 (1952).
14. R. BADGER and S. BAUER. J. Chem. Phys. **5**, 839 (1937).
15. L. P. KUHN and R. A. WIRES. J. Am. Chem. Soc. **86**, 2161 (1964).
16. R. WEST, D. POWELL, L. WHATLEY, M. LEE, and P. VON R. SCHLEYER. J. Am. Chem. Soc. **84**, 3221 (1962).
17. R. HOFFMAN. Acc. Chem. Res. **4**, 1 (1971).

Can. J. Chem. Downloaded from www.nrcresearchpress.com by 210.87.254.105 on 09/05/12
For personal use only.

Pyrolysis of benzophenone oxime carbonates: a potential route to aryl imino ethers (aryl imidates)

P. E. TITUS, P. A. FORTE, AND J. M. PROKIPCAK[1]

Department of Chemistry, University of Guelph, Guelph, Ontario N1G 2W1

Received August 14, 1975

P. E. TITUS, P. A. FORTE, and J. M. PROKIPCAK. Can. J. Chem. **54**, 647 (1976).

Aryl ketoxime carbonates have been found to undergo decompositions at temperatures ranging from 180–200 °C to give carbon dioxide and aryl imino ethers (imidates). This pyrolysis could prove to be a general method for preparing aryl imino ethers. Formation of different imidates from the two geometric isomers (*E*- and *Z*-forms) of the ketoxime carbonates supports a mechanism involving the migration of the aryl group *trans* to the carbonate grouping. This is similar to that observed in the Beckmann rearrangement of ketoximes.

P. E. TITUS, P. A. FORTE et J. M. PROKIPCAK. Can. J. Chem. **54**, 647 (1976).

On a trouvé que les carbonates d'aryle cétoximes subissent des décompositions à des températures allant de 180–200 °C pour conduire à du dioxyde de carbone et des éthers aryl-iminos (imidates). Cette pyrolyse pourrait s'avérer être une méthode générale pour préparer les éthers aryl-iminos. La formation de différents imidates à partir des deux isomères géométriques (formes *E et Z*) des carbonates de cétoxime est en accord avec un mécanisme impliquant la migration du groupe aryle *trans* par rapport au groupement carbonate. Ceci est semblable à ce qui est observé dans le réarrangement de Beckmann des cétoximes.

[Traduit par le journal]

Introduction

There are several generally accepted methods of preparing imino ethers or imidates (1). In most cases these imidates are starting compounds for the Chapman reaction (2) which converts the imidates to diphenyl amides and eventually diphenyl amines. The most frequently encountered method for preparing the imidates involves basically three steps; the benzanilide formation, conversion to the imidoyl chloride, and then conversion to the imidate. We wish to report a new method of preparing aryl imidates via the pyrolysis of benzophenone oxime carbonates. It was found that the nature of the final imidate can be altered by using differently substituted ketoxime carbonates and also by using different geometric isomers *i.e.* the *E*- and *Z*-forms of the

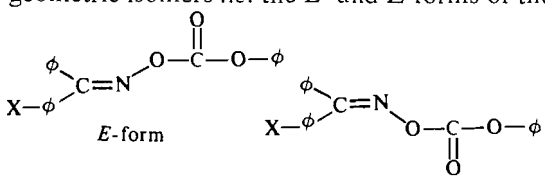

ketoxime carbonates. Some speculation on the mode of decomposition is made on the basis of the products formed.

[1]Author to whom correspondence should be sent.

Various aromatic ketoximes **1** including differently substituted as well as geometric isomers were prepared from the corresponding benzophenones. These were then treated with phenyl chloroformate to yield the desired ketoxime carbonates **2** which upon heating to 180–200 °C decomposed to give carbon dioxide and aryl imidates **3**. The overall sequence is outlined in eq. 1.

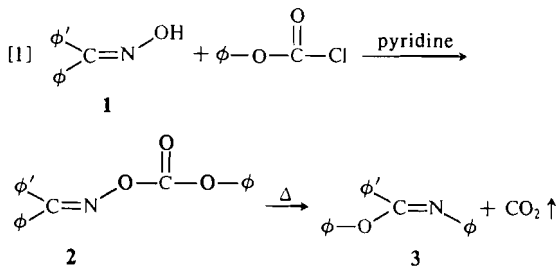

Experimental

In carrying out the studies, use was made of benzophenones which were readily available commercially. These were used without further purification and included the *p*-methoxy-, *p*-methyl-, *p*-chloro-, and *p*-nitrobenzophenones.

Preparation of Oximes and Separation of the Geometric Isomers

The benzophenone oximes were prepared by the well established reaction of ketones with hydroxylamine. The

Can. J. Chem. Downloaded from www.nrcresearchpress.com by 210.87.254.42 on 09/05/12
For personal use only.

Can. J. Chem. Downloaded from www.nrcresearchpress.com by 210.87.254.42 on 09/05/12
For personal use only.

geometric isomers (*E*- and *Z*-forms) were separated using previously reported methods; *p*-methoxybenzophenone oximes (3), *p*-methylbenzophenone oximes (4), *p*-chlorobenzophenone oximes (4), and *p*-nitrobenzophenone oximes (5). The only variation in the above methods occurred in the separation of the *p*-methylbenzophenone oximes. It was found that fractional crystallization from an ethanol–water mixture gave a better separation of the isomers than the originally reported acetic acid – water mixture. The *E*-isomer crystallized readily from the mixture while the filtrate contained the *Z*-isomer. All the oximes were finally crystallized from a chloroform – petroleum ether (bp 30–60 °C) mixture.

Preparation of Ketoxime Carbonates

The same general procedure was used for the preparation of the ketoxime carbonates, their pyrolysis and subsequent product identification. This procedure will be outlined for *E*-*p*-methoxybenzophenone oxime.

In a 500 ml round-bottomed flask were placed 150 ml of anhydrous diethyl ether, 2.3 ml pyridine and 4.8 g (0.023 mol) *E*-*p*-methoxybenzophenone oxime. While cooling this solution in an ice bath, 3.9 g (0.025 mol) phenyl chloroformate dissolved in 25 ml anhydrous ether were added slowly with stirring over a period of 1 h. The reaction mixture was stirred for an additional 2 h at 0 °C and then allowed to stand overnight. The reaction mixture was poured onto ice and the ether layer separated. This ethereal layer was washed twice with water, dried over anhydrous magnesium sulfate, and the solvent was removed *in vacuo* whereupon a solid formed (6.5 g, 86% yield). Recrystallization from chloroform – petroleum ether (bp 30–60 °C) gave pure *E*-*p*-methylbenzophenone oxime carbonate, mp 152–153 °C which had the following spectral data: ir ($CHCl_3$) 1780 cm^{-1} (C=O stretch), 1600 cm^{-1} (C=N stretch), and 1190–1250 cm^{-1} (ester C—O stretch); nmr ($CDCl_3$) δ (ppm) 2.34 (3H singlet, methyl) and 7.0–7.67 (14H multiplet, aromatic). *Anal.* calcd. for $C_{21}H_{17}NO_3$: C 76.37, H 5.17, N 4.23; found: C 76.26, H 5.02, N 4.22.

Pyrolysis of Ketoxime Carbonates

The pure *E*-*p*-methylbenzophenone oxime carbonate (5.0 g, 0.015 mol) was placed in a flask along with 10 ml diphenyl ether and the solution was heated until a steady stream of CO_2 evolved (190–200 °C). The flask contents were kept at this temperature for 8 h. The diphenyl ether was then removed by vacuum distillation leaving an oil which yielded 7.63 g (77%) of the crude solid imidate. Recrystallization of this solid from chloroform – petroleum ether (bp 30–60 °C) yielded pure phenyl *N*-*p*-tolylbenzimidate, mp 118–120 °C (reported (6) 117–119 °C) which had the following spectral data: ir ($CHCl_3$) 1660 cm^{-1} (C=N stretch); nmr ($CDCl_3$) δ (ppm), 2.23 (3H singlet, methyl) and 6.8–8.0 (14H multiplet, aromatic. *Anal.* calcd. for $C_{20}H_{17}NO$: C 83.58, H 5.97, N 4.87; found: C 83.67, H 6.02, N 4.85. The structure of the imidate was further checked by hydrolyzing it with aqueous H_2SO_4 whereupon *N*-tolyl benzamide, mp 158 °C was obtained. The benzamide was verified via mixed melting point with an authentic sample of benzamide prepared by an alternate, well-established method.

Results and Discussion

The results of the preparation and decomposition of the ketoxime carbonates along with the elemental analysis of the carbonates and imidates are shown in Table 1. The configuration of each of the oxime phenyl carbonates was assumed to be identical to that of the parent oxime since the synthesis of the carbonates did not involve cleavage of the N—O bond. Furthermore, work done by Curtin *et al.* (7) and Philips (8) would indicate that isomerization between the *E*- and *Z*-forms around the imino double bond is very unlikely to occur under the reactions conditions.

It can be seen from Table 1 that the yields of the imino ethers depend to a certain extent on the nature of the phenyl group *trans* to that of the carbonate grouping. The yields appear to be best in the cases of the ketoxime carbonates which have an electron-donating group on the phenyl ring *trans* to the departing carbonate function. Since this group eventually becomes attached to the nitrogen atom, this means that the Chapman rearrangement of the imino ether would also be enhanced (9). Thus it would seem that for electron-donating substituents, this modification would be useful for the Chapman synthesis; when electron-withdrawing substituents are present, this route would not be as satisfactory. Diphenyl ether was initially chosen as the solvent for the decompositions and presented no work-up problems. When triglyme and hexamethylphosphoramide were used in place of diphenyl ether, no improvement in yields was observed whereas actual product isolation was made more difficult. Thus diphenyl ether was used for all the decompositions carried out in this study. However, other solvents are still being considered to see if improved yields could be obtained.

Since the present work encompasses only the identification of the major products of the pyrolysis reaction, namely, the imino ether and CO_2, no conclusions can be made on the mechanism for the decomposition. However, some speculation is possible since product identification and yields have been obtained for a series of substituted benzophenone oxime carbonates. On the basis of the imino ethers formed from the various oxime carbonates, it is felt that this reaction belongs to a Beckmann class of reactions. Just as in the case of the Beckmann

Can. J. Chem. Downloaded from www.nrcresearchpress.com by 210.87.254.42 on 09/05/12
For personal use only.

TABLE 1. Synthesis and pyrolysis of benzophenone oxime carbonates

		Oxime phenyl carbonate*								Imino ether*							
		Melting point	Yield	Calcd. (%)			Found (%)			Melting point	Yield	Calcd. (%)			Found (%)		
R	R′	(°C)	(%)	C	H	N	C	H	N	(°C)	(%)	C	H	N	C	H	N
H	Meo	114.5–116	60	72.59	4.94	4.03	72.77	4.94	4.08	84–86	64	79.16	5.65	4.61	79.00	5.96	4.82
Meo	H	121–123	55	72.59	4.94	4.03	72.15	5.35	4.00	97.5–99	96	79.16	5.65	4.61	79.20	5.82	4.61
H	Me	112–113	94	76.37	5.17	4.23	76.18	5.16	3.97	70–72	63.5	83.58	5.97	4.87	83.26	6.40	4.76
Me	H	152–153	86	76.37	5.17	4.23	76.26	5.02	4.22	118.5–120.5	77	83.58	5.97	4.87	83.67	6.02	4.85
H	H	173–175	84.5	75.70	4.76	4.41	75.53	4.63	4.28	103–105	62	83.49	5.53	5.12	83.38	5.49	5.09
H	Cl	98–101	80	68.29	4.01	3.98	67.80	3.89	3.71	59–62	52	74.14	4.59	4.55	74.09	4.95	4.49
Cl	H	128.5–130.5	51	68.29	4.01	3.98	68.05	3.88	3.88	108–110	46	74.14	4.59	4.55	74.20	4.95	4.49
H	NO_2	97–99	58	66.30	3.89	7.73	67.54	4.42	6.39	‡							
NO_2	H	128–130	40	66.30	3.89	7.73	66.14	4.05	7.72	‡							

*General Structures: Oxime Carbonate 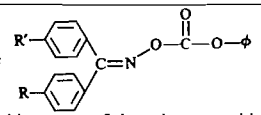 Imidate 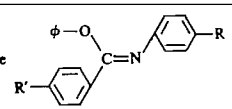

†Analysis not within limits due to unstable nature of the substance which appeared to be breaking down to ketone under isolation procedure.
‡These compounds yielded ketone as the major product.

Can. J. Chem. Downloaded from www.nrcresearchpress.com by 210.87.254.42 on 09/05/12
For personal use only.

reaction where there is an *anti*-migration (10) of the group relative to the hydroxyl group, the products obtained in this study appear to support a similar *trans*-migration of the aryl ring which is *trans* to the departing carbonate function. Furthermore, imidate yields and reactions times seem to indicate that electron-donating substituents on the *trans* aryl group enhance the reaction. Similar observations were recorded by Chapman and Fidler (4) in the thermal Beckmann rearrangement of ketoxime picryl ethers.

It was found that the *p*-nitrobenzophenone oxime carbonates yielded no imino ethers whatsoever. The major product in the case of both the *E*- and *Z*-isomers was *p*-nitrobenzophenone. The strong electron-withdrawing nitro group makes the carbonates unstable quite possibly by making the imino double bond highly prone to hydrolysis by trace amounts of water.

With the compounds that did yield imino ethers, the electronic effects support a mechanism where the migrating group is a negative species and any electron-donating groups on the migrating ring enhance the migrating tendencies of the group. From the reported results, conclusions cannot be made on whether the reaction is concerted, whether it is intramolecular with the formation of a close ion-pair, or whether a planar intermediate is formed. However, the products isolated do indicate that the imino ethers formed are very dependent on the nature of the group *trans* to the carbonate grouping. Furthermore it appears that one isomer is the major product,

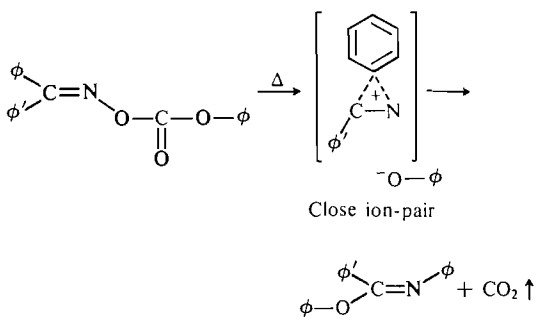

that being the imino ether formed with the migration of the *trans* aryl group. On the basis of these results a possible mechanism is outlined below involving a three-membered transition state very similar to that involved in the Beckmann rearrangement of oximes.

Conclusions

The work presented appears to offer an alternate route to the preparation of aryl imino ethers and a more extensive list of aryl ketones is being investigated to get an idea of the full implications of the preparative value of this reaction. A great deal of work on the kinetics and solvent effects is planned to help determine the decomposition mechanism. Even though the completed work does favour a concerted type of *trans*-migration, no concrete conclusions can be made regarding the mechanism.

Acknowledgments

The authors wish to thank the National Research Council of Canada for financial assistance in the form of NRC Scholarships to Patricia E. Titus and Peter A. Forte.

1. R. Roger and D. G. Neilson. Chem. Rev. **61**, 179 (1961).
2. A. W. Chapman. J. Chem. Soc. 1992 (1925); 2296 (1926); 1749 (1927).
3. R. W. Johnson and J. Stieglitz. J. Am. Chem. Soc. **56**, 1905 (1924).
4. A. W. Chapman and E. A. Fidler. J. Chem. Soc. 448 (1936).
5. L. E. Sutton and T. W. J. Taylor. J. Chem. Soc. 2190 (1931); 63 (1933).
6. D. H. Hey and T. M. Moyneham. J. Chem. Soc. 1563 (1959).
7. D. Y. Curtin, E. J. Grubbs, and C. G. McCarty. J. Am. Chem. Soc. **88**, 2275 (1966).
8. W. D. Philips. Ann. N.Y. Acad. Sci. **70**, 817 (1958).
9. A. W. Chapman. J. Chem. Soc. 1743 (1927).
10. P. A. S. Smith. Molecular rearrangements. Vol. 1. *Edited by* P. DeMayo. Interscience, New York. 1963. pp. 528–567.

A re-examination of the adiabatic correction term for the hydrogen molecule

HUW O. PRITCHARD AND LUTOSŁAW WOLNIEWICZ[1]

Centre for Research in Experimental Space Science, York University, Downsview, Ontario M3J 1P3

Received September 8, 1975

HUW O. PRITCHARD and LUTOSŁAW WOLNIEWICZ. Can. J. Chem. **54**, 651 (1976).

The adiabatic coupling correction term $\langle \Delta_R \rangle$ has been evaluated by two methods, the one used by Kołos and Wolniewicz in 1964 and the one suggested by Kari, Chan, Hunter, and Pritchard in 1973. The difference between the two procedures for H_2 amounts to 0.04 cm^{-1} and is almost independent of internuclear separation in the range R = 1.0–1.8 a.u. Thus, the method of computing the Δ_R-term does not affect the vibrational energy level spacings.

HUW O. PRITCHARD et LUTOSŁAW WOLNIEWICZ. Can. J. Chem. **54**, 651 (1976).

On a évalué, par deux méthodes, le terme de correction de couplage adiabatique $\langle \Delta_R \rangle$; les deux méthodes utilisées sont celle de Kołos et de Wolniewicz en 1964 et celle suggérée par Kari, Chan, Hunter et Pritchard en 1973. Pour H_2, la différence entre les deux méthodes équivaut à 0.04 cm^{-1} et est pratiquement indépendente de la séparation internucléaire dans l'écart de R = 1.0–1.8 u.a. Donc la méthode de calcul du terme Δ_R n'affecte pas l'espacement des niveaux d'énergie vibrationnelle.

[Traduit par le journal]

Introduction

This paper sets out to compare two alternative methods of computing the adiabatic coupling correction term for the hydrogen molecule, and at the same time to examine the nature of any approximations involved. Over a decade ago, Kołos and Wolniewicz (1) made an extensive study of the adiabatic corrections to the potential energy curve for the ground state of the hydrogen molecule, and the accuracy of their calculations was confirmed when repeated in double-length arithmetic a few years later (2). To simplify the computations, they assumed that the wave equation was satisfied exactly and that the derivative of the nonlinear parameter in the wave function could be neglected. Tests at the equilibrium internuclear separation established the validity of neglecting these derivatives, which again is equivalent to saying that the wave equation was satisfied. With modern computers, however, it is relatively easy to avoid these simplifying assumptions. More recently, it was pointed out (3) that another simplifying assumption, that of treating the mass-polarisation term as a perturbation rather than including it in the electronic Hamiltonian, could be avoided also. This would improve the variational characteristics of the result, but is clearly a second-order effect. With the continuing interest in the comparison of theoretical and experimental energies for hydrogen, it is logical to examine the nature and magnitude of the corrections arising when these refinements are included in the computational scheme.

Theory

For the symmetric hydrogen molecule, after separating off the centre of mass motion and measuring the electronic coordinates from the geometric centre of the molecule, one gets the Hamiltonian in the form

$$H = H_{\text{cl.n}} - \frac{1}{2\mu}\Delta_R - \frac{1}{8\mu}(\nabla_1 + \nabla_2)^2 \qquad [1]$$

where $H_{\text{cl.n}}$ is the clamped nuclei Hamiltonian, μ is the reduced mass of the nuclei, and R is the internuclear distance. The adiabatic internuclear potential is given as an integral over the electronic coordinates

$$U_{\text{ad}}(R) = \int \Psi H \Psi \, d\tau \qquad [2]$$

[1]Visiting Fellow. Permanent address: Institute of Physics, Nicholas Copernicus University, Grudziadzka 5, 87-100 Torun, Poland.

Can. J. Chem. Downloaded from www.nrcresearchpress.com by 210.87.254.5 on 09/05/12
For personal use only.

with Ψ being the electronic wave function of the molecule satisfying the Schrödinger equation

[3] $$H_0\Psi = E(R)\Psi$$

where H_0 is the electronic Hamiltonian. As was mentioned in the Introduction, the total Hamiltonian, H, can be split into

$$H = H_0 + H'$$

in more than one way: thus, we can write

[4] $$H_0 = H_{\text{cl.n}}$$
$$H' = -\frac{1}{2\mu}\Delta_R - \frac{1}{8\mu}(\nabla_1 + \nabla_2)^2$$

as was done originally by Kołos and Wolniewicz (1) or

[5] $$H_0 = H_{\text{cl.n}} - \frac{1}{8\mu}(\nabla_1 + \nabla_2)^2$$
$$H' = -\frac{1}{2\mu}\Delta_R$$

as was suggested by Kari *et al.* (3); [4] and [5] are equivalent to [5*a*] and [5*c*] of ref. 3.

The electronic wave function employed in the present investigation was the same as that used previously (1, 3), *i.e.* the expansion

[6] $$\Psi = \sum_i c_i g_i$$
$$g_i = e^{-\alpha(\xi_1+\xi_2)}\rho^{\mu_1}\{\xi_1^{r_i}\eta_1^{s_i}\xi_2^{\bar{r}_i}\eta_2^{\bar{s}_i} + \xi_1^{\bar{r}_i}\eta_1^{\bar{s}_i}\xi_2^{r_i}\eta_2^{s_i}\}$$

where ξ_j, η_j are the elliptic coordinates and $\rho = 2r_{12}/R$. The linear parameters c_i were determined from the equations

[7] $$\sum_k (H_{ik}^0 - E^0 S_{ik})c_k = 0$$

independently for the two electronic Hamiltonians [4] and [5], using the values of α as given in ref. 1, and the wave functions thus obtained were used to compute the appropriate expectation value of H'. The most costly part of the electronic computations is that of selecting suitable terms in the wave function and optimizing the nonlinear parameter α. However, it was found that the same value of α led to a minimum in the appropriate variational energy by either procedure, and thus, with α and the functions g_i given, one can use either of the electronic Hamiltonians [4] and [5] equally easily. Therefore we will not go into any details of the electronic computations and concentrate on the evaluation of the adiabatic correction arising from $-(1/2\mu)\Delta_R$.

As was shown previously (1), one can simplify the computations considerably if one uses the fact that $R\rho = 2r_{12}$ commutes with Δ_R, and we recall briefly the relevant formulas. The expectation value of Δ_R is expressed in the form

[8] $$\langle\Delta_R\rangle = \int \Psi\Delta_R\Psi d\tau = \int \Psi\frac{\partial^2}{\partial R^2}\Psi d\tau + \int \Psi\sum_i \left(\frac{\mu_i(\mu_i+1)}{R^2} - \frac{2\mu_i}{R}\frac{\partial}{\partial R}\right)c_i g_i d\tau$$
$$- \int \Psi\sum_i \frac{\mu_i}{R} c_i\rho^{\mu_i} D_1\bar{g}_i d\tau + \int \Psi\sum_i \rho^{\mu_i} D_1\frac{\partial}{\partial R} c_i\bar{g}_i d\tau + \int \Psi\sum_i c_i\rho^{\mu_i} D_2\bar{g}_i d\tau$$

In the right hand side of [8], D_1 and D_2 are operators acting on the elliptic coordinates of the electrons, $\bar{g}_i = \rho^{-\mu_i} g_i$, and in the differentiation R and the elliptic coordinates are treated as independent variables. The operators D_j are defined by eq. 20 of ref. 1 and we will not rewrite them here.

Can. J. Chem. Downloaded from www.nrcresearchpress.com by 210.87.254.5 on 09/05/12
For personal use only.

By making use of the identity

$$[9] \qquad \int \Psi \frac{\partial^2}{\partial R^2} \Psi d\tau = \frac{2I}{R^2} - \int \left(\frac{\partial \Psi^2}{\partial R} \right) d\tau$$

one gets $\langle \Delta_R \rangle$ expressed in terms of integrals containing Ψ and its first derivative with respect to R,

$$[10] \qquad \frac{\partial \Psi}{\partial R} = \sum_i \left[\frac{dc_i}{dR} g_i - \frac{d\alpha}{dR} (\xi_1 + \xi_2) c_i g_i \right]$$

The derivatives dc_i/dR are given by the equations

$$[11] \qquad \sum_k (H_{ik}^0 - E^0 S_{ik}) \frac{dc_k}{dR} = \sum_k \left(\frac{2H_{ik}^0 - V_{ik}}{R} - \frac{dE^0}{dR} S_{ik} \right) c_k + \frac{d\alpha}{dR} \sum_k \{ \xi_1 + \xi_2, H^0 - E^0 \}_{ik} c_k$$

$$\sum_{ik} c_k S_{ki} \frac{dc_i}{dR} = -\frac{3}{R} + \frac{d\alpha}{dR} \sum_{ik} c_i (\xi_1 + \xi_2)_{ik} c_k$$

The braces denote anticommutators and double subscripts denote matrix elements, *e.g.*

$$\int g_i (\xi_1 + \xi_2) g_k \, d\tau \equiv (\xi_1 + \xi_2)_{ik} \qquad \text{etc.}$$

Clearly, E depends on both the internuclear distance R and α, and thus

$$[12] \qquad \frac{dE}{dR} = \frac{\partial E}{\partial R} + \frac{\partial E}{\partial \alpha} \frac{d\alpha}{dR}$$

$$\frac{\partial E}{\partial R} = -\frac{2E^0 - \langle V \rangle}{R}$$

$$\frac{\partial E}{\partial \alpha} = -\langle \{ \xi_1 + \xi_2, H^0 - E^0 \} \rangle$$

where $\langle \ \rangle$ stands for an expectation value. Previously (1), the energy was minimized with respect to α and so $\partial E/\partial \alpha$ did not appear in the equations for dc_i/dR. Here, in order to study the influence of different choices of $d\alpha/dR$ on the final result and also in order to determine the extent to which α was optimized, $\partial E/\partial \alpha$ will not be omitted.

Similarly, as [12] holds for the energy, we have for the coefficients c_i:

$$[13] \qquad \frac{dc_i}{dR} = \frac{\partial c_i}{\partial R} + \frac{d\alpha}{dR} \frac{\partial c_i}{\partial \alpha} \equiv b_i' + \frac{d\alpha}{dR} d_i'$$

and b_i', d_i' satisfy the sets of equations

$$[14] \qquad \sum_k (H_{ik}^0 - E^0 S_{ik}) b_i' = \sum_k \left(\frac{2H_{ik} - V_{ik}}{R} - \frac{E^0 - \langle V \rangle}{R} S_{ik} \right) c_k$$

$$\sum_{ik} S_{ik} c_i b_k' = -\frac{3}{R}$$

$$[15] \qquad \sum_k (H_{ik}^0 - E^0 S_{ik}) d_k' = \sum_k \left(\{ \xi_1 + \xi_2, H^0 - E^0 \}_{ik} + \frac{\partial E}{\partial \alpha} S_{ik} \right) c_k$$

$$\sum_{ik} S_{ik} c_i d_k' = \langle (\xi_1 + \xi_2) \rangle$$

with $\partial E/\partial \alpha$ given by [12]. Now in view of [8], [9], and [13] it is obvious that $\langle \Delta_R \rangle$ is a second

Can. J. Chem. Downloaded from www.nrcresearchpress.com by 210.87.254.5 on 09/05/12
For personal use only.

order polynomial in $d\alpha/dR$:

$$[16] \qquad \langle \Delta_R \rangle = \langle \Delta_R \rangle_0 + \langle \Delta_R \rangle_1 \frac{d\alpha}{dR} + \langle \Delta_R \rangle_2 \left(\frac{d\alpha}{dR}\right)^2$$

where $\langle \Delta_R \rangle_0$ is the expectation value of Δ_R computed with $d\alpha/dR = 0$. The remaining coefficients read:[2]

$$[17] \qquad \langle \Delta_R \rangle_1 = -2\sum S_{ik} b_i' d_k' + 2\sum (\xi_1 + \xi_2)_{ik} b_i' c_k - 2\sum S_{ik} c_i \frac{\mu_k}{R} d_k' + 2\sum (\xi_1 + \xi_2)_{ik} c_i \frac{\mu_k}{R} c_k + \sum (D_1)_{ik} c_i d_k' - \sum [D_1(\xi_1 + \xi_2)]_{ik} c_i c_k$$

$$[18] \qquad \langle \Delta_R \rangle_2 = -\sum S_{ik} d_i' d_k' + 2\sum (\xi_1 + \xi_2)_{ik} c_i d_k' - \sum [(\xi_1 + \xi_2)^2]_{ik} c_i c_k$$

From the above formulas one can infer that for accurate variational functions the linear and quadratic terms in $d\alpha/dR$ are very small. Indeed, if an infinite expansion of the form [6] was used the choice of α would be immaterial and one would get from [7] a function satisfying

$$[19] \qquad \frac{\partial \Psi}{\partial \alpha} = 0$$

or

$$[20] \qquad \sum_i \frac{\partial c_i}{\partial \alpha} g_i = \sum_i c_i (\xi_1 + \xi_2) g_i$$

Thus we could write for an operator $\boldsymbol{O}$

$$[21] \qquad \sum_i O_{ki} d_i' = \sum_i [\boldsymbol{O}(\xi_1 + \xi_2)]_{ki} c_i$$

Clearly, for a finite expansion [6], [21] does not hold. Nonetheless if the expansion is reasonably long [21] can be expected to hold approximately. Therefore the consecutive terms in the right hand side of [17] should cancel pairwise and each of the two negative terms in [18] should be approximately equal to one-half of the positive contribution to $\langle \Delta_R \rangle_2$. We can conclude therefore that $\langle \Delta_R \rangle_1$ and $\langle \Delta_R \rangle_2$ should decrease with increasing accuracy of the wave function and this explains why the results obtained by Kołos and Wolniewicz in 1964 (1) were practically insensitive to the choice of $d\alpha/dR$.

It is worth noting that what was said above can be generalized in a straightforward manner to the case of two or more nonlinear parameters. This has some practical consequences: should the adiabatic corrections for higher excited states of H_2 be computed, the R dependence of the nonlinear parameters could be ignored in computing the expectation value of Δ_R and this would simplify the computations significantly.

Numerical Results

Calculations were performed with a series of wave functions up to and including $N = 54$ terms in the electronic expansion [6], as used previously by Kołos and Wolniewicz (1), for values of $R = 1.0$, 1.4, and 1.8 a.u.; this range covers the important region for the determination of the low-lying vibrational energy levels.

First we examined the effect of neglecting terms in $d\alpha/dR$ and $(d\alpha/dR)^2$ in [16]. It was found, as expected, that $\langle \Delta_R \rangle_1$ and $\langle \Delta_R \rangle_2$ are small, and that the pairwise cancellation of terms in [17] and [18] did in fact occur: for example, for $R = 1.4$ a.u., $\alpha = 1.0$, and $N = 20$, [17] becomes

$$\langle \Delta_R \rangle_1 = 20.5926 - 20.5998 + 18.3855 - 18.3956 + (2.0300 + \delta) - (2.0065 + \delta)$$
$$\approx 5.3 \times 10^{-3} \text{ a.u.}$$

[2]It is understood that in matrix elements containing D_1, ρ^μ stands to the *left* of the operator.

Can. J. Chem. Downloaded from www.nrcresearchpress.com by 210.87.254.5 on 09/05/12
For personal use only.

TABLE 1. The convergence of $\langle \Delta_R \rangle$ and $\partial E/\partial \alpha$ with increasing expansion length N for three trial wave functions (all quantities are given in atomic units)

Wave function parameters	N	$\langle \Delta_R \rangle_0$	$\langle \Delta_R \rangle_1$	$\langle \Delta_R \rangle_2$	$\partial E/\partial \alpha$
$R = 1.0; \alpha = 0.8025$	20	−0.322	1.1×10^{-2}	-2.9×10^{-3}	4.1×10^{-4}
	30	−0.321	7.1×10^{-3}	-2.0×10^{-3}	7.7×10^{-5}
	40	−0.318	1.4×10^{-3}	-2.4×10^{-4}	-1.3×10^{-5}
	50	−0.318	9.8×10^{-4}	-1.4×10^{-4}	4.8×10^{-6}
$R = 1.4; \alpha = 1.027$	20	−0.322	7.6×10^{-3}	-1.7×10^{-3}	3.4×10^{-4}
	30	−0.322	3.3×10^{-3}	-7.6×10^{-4}	5.2×10^{-5}
	40	−0.321	1.0×10^{-3}	-1.6×10^{-4}	2.4×10^{-6}
	50	−0.321	6.6×10^{-4}	-9.0×10^{-5}	1.4×10^{-6}
$R = 1.8; \alpha = 1.249$	20	−0.332	9.0×10^{-3}	-1.9×10^{-3}	4.4×10^{-4}
	30	−0.332	3.0×10^{-3}	-5.3×10^{-4}	1.4×10^{-4}
	40	−0.332	1.5×10^{-3}	-2.0×10^{-4}	3.9×10^{-5}
	50	−0.332	7.3×10^{-4}	-1.1×10^{-4}	2.3×10^{-6}

TABLE 2. Specimen results for 54-term wave functions, as used by Kołos and Wolniewicz (1), for the hydrogen molecule

Approximation	Method	$R = 1.0$ a.u. $\alpha = 0.8025$	$R = 1.4$ a.u. $\alpha = 1.027$	$R = 1.8$ a.u. $\alpha = 1.249$
Clamped nucleus energy	[4]	−1.124533158 a.u.	−1.174470001 a.u.	−1.155061581 a.u.
Energy including mass-polarisation	[4]	−1.124107499 a.u.	−1.174122559 a.u.	−1.154761767 a.u.
	[5]	−1.124107608 a.u.	−1.174122647 a.u.	−1.154761845 a.u.
Difference		-0.024 cm^{-1}	-0.019 cm^{-1}	-0.017 cm^{-1}
Adiabatic energy	[4]	−1.123934323 a.u.	−1.173947711 a.u.	−1.154581022 a.u.
	[5]	−1.123934521 a.u.	−1.173947888 a.u.	−1.154581195 a.u.
Difference		-0.043 cm^{-1}	-0.039 cm^{-1}	-0.038 cm^{-1}

where δ stands for $2R^{-1}\langle \xi_1 + \xi_2 \rangle$ which cancels identically and was therefore not evaluated; likewise, [18] becomes

$$\langle \Delta_R \rangle_2 = -21.2881 + 42.5918 - 21.3050 \approx -1.3 \times 10^{-3} \text{ a.u.}$$

The first term in the expansion $\langle \Delta_R \rangle_0$ is about 3.2×10^{-1} a.u.

Results were then computed for three specific cases: $R = 1.0$ a.u., $\alpha = 0.8025$; $R = 1.4$ a.u., $\alpha = 1.027$; and $R = 1.8$ a.u., $\alpha = 1.249$, these values of α being the optimum values found previously (1) for the 54-term wave function. Table 1 shows that as the expansion length N is increased from 20 to 54, the value of $\langle \Delta_R \rangle_0$ remains roughly constant near 3.2×10^{-1} a.u. in all three cases, but the cancellation illustrated above for $\langle \Delta_R \rangle_1$ and $\langle \Delta_R \rangle_2$ improves. As N increases from 20 to 54, $\langle \Delta_R \rangle_1$ falls by an order of magnitude, $\langle \Delta_R \rangle_2$ by a little more, and $\partial E/\partial \alpha$ by about two orders of magnitude. Since $d\alpha/dR$ is of the order of 0.7 a.u. and $\langle \Delta_R \rangle$ has to be multiplied by $(2M)^{-1}$ in the final expression for the total energy, neglect of these terms at $N = 54$ amounts only to a few hundredths of a wave number. Thus, the neglect of the terms in $d\alpha/dR$ and $(d\alpha/dR)^2$ is justified for any calculation where the expansion length N is large enough to achieve spectroscopic accuracy and α is optimised in the normal way; these conclusions hold for both methods of performing the calculation, *i.e.* using [4] or [5] to partition the Hamiltonian.

Thus, ignoring the $d\alpha/dR$ terms, the total energy was calculated for all orders from $N = 20$ to $N = 54$ using both the methods of [4] and [5] for these three choices of R and α. In each case,

Can. J. Chem. Downloaded from www.nrcresearchpress.com by 210.87.254.5 on 09/05/12
For personal use only.

as expected, the electronic energy including mass-polarisation came out *very* slightly lower using [5], the improvement being of the order of 0.02 cm^{-1}, independent of the expansion length N in the range $20 \leqslant N \leqslant 54$. Then $\langle \Delta_R \rangle_0$ was calculated for each wave function, and again the correction was slightly more negative for [5] than for [4], by about 0.02 cm^{-1} at each value of R, and again, virtually independent of N in the range $20 \leqslant N \leqslant 54$. Specimen results are shown in Table 2.

We conclude that the calculation based on [5] is slightly better than that based on [4], although the improvement in energy is an order of magnitude less than the expected non-adiabatic corrections. This small improvement does little towards the resolution of the remaining discrepancies between theory and experiment for hydrogen (3) and deuterium (4) (especially since the improvement for D_2 is only one-fourth as big as it is for H_2). Our results, however, strongly support the conclusion that $\langle \Delta_R \rangle_1$ and $\langle \Delta_R \rangle_2$ can be neglected, and it seems quite likely that this should also be true for other electronic states.

Acknowledgment

This work was supported by the National Research Council of Canada.

1. W. Kołos and L. Wolniewicz. J. Chem. Phys. **41**, 3663 (1964).
2. W. Kołos and L. Wolniewicz. J. Chem. Phys. **49**, 404 (1968).
3. R. E. Kari, A. C. H. Chan, G. Hunter, and H. O. Pritchard. Can. J. Chem. **51**, 2055 (1973).
4. R. J. LeRoy and M. G. Barwell. Ground state D_2 dissociation energy from the near-dissociation behaviour of rotational level spacings. University of Waterloo Chemical Physics Research Report CP-39, March, 1975.

Can. J. Chem. Downloaded from www.nrcresearchpress.com by 210.87.254.5 on 09/05/12
For personal use only.

Nematic phase nuclear magnetic resonance studies of the molecular structures of cyclobutanone and methylenecyclobutane[1]

K. C. COLE AND D. F. R. GILSON

Chemistry Department, McGill University, P.O. Box 6070, Station A, Montreal, Quebec H3C 3G1

Received August 5, 1975

K. C. COLE and D. F. R. GILSON. Can. J. Chem. **54**, 657 (1976).

The nematic phase proton magnetic resonance spectra of cyclobutanone and methylenecyclobutane have been analyzed and the direct dipole coupling constants corrected for the averaging effects of the ring puckering vibrations. The nmr data have been used in conjunction with microwave spectroscopic results to derive the molecular structures.

K. C. COLE et D. F. R. GILSON. Can. J. Chem. **54**, 657 (1976).

On a analysé les spectres rmn en phase nématique de la cyclobutanone et du méthylène cyclobutane et on a corrigé les constantes de couplage dipolaires directes pour le fait que les vibrations de plissement du cycle conduisent à des valeurs moyennes. On a aussi utilisé les données de rmn, de concert avec des résultats de spectroscopie de micro-ondes, pour en déduire les structures moléculaires.

[Traduit par le journal]

Can. J. Chem. Downloaded from www.nrcresearchpress.com by 210.87.254.40 on 09/05/12
For personal use only.

Introduction

Four-membered ring molecules possess an out-of-plane vibrational mode with a potential function that depends upon the opposing forces of ring strain, tending to maintain planarity, and torsional effects which relieve interactions between eclipsed protons and favour non-planarity. The potential functions are of the general form

$$[1] \quad V(z) = k_2 z^2 + k_4 z^4 + k_a \exp(-k_b z^2)$$

where z is a ring puckering coordinate and the k's are constants. A negative value of k_2 or the presence of the exponential term produces a barrier at the planar conformation such that, if the barrier is sufficiently high, the molecule will be puckered in the ground state. In some cases the barrier is small and the ground state lies above the maximum. Even-numbered vibrational levels are strongly perturbed by the barrier since these have finite probabilities at the planar conformation; the odd levels are less perturbed since these have a node at this position.

A wide variety of experimental techniques have been used to study molecules of this type as the values of bond lengths and angles in highly strained rings are of considerable interest. Most molecular structure determinations emphasize the heavy atom coordinates at the expense of the hydrogen positions since protons exert only weak influences on electron diffraction or microwave measurements. The data obtainable from the analyses of nmr spectra of molecules partially oriented in a nematic liquid crystal solvent are particularly useful for determining relative proton distances and thus this method provides a complementary technique for structural determination. We have reported earlier on the structures of cyclobutane (1) and trimethylene oxide and trimethylene sulphide (2). The present work extends these studies to two compounds which possess exocyclic substituents: cyclobutanone and methylenecyclobutane.

Scharpen and Laurie have studied the microwave spectra of both cyclobutanone (3) and methylenecyclobutane (4). For cyclobutanone a puckering potential was derived which fits both the microwave and far-infrared data (5):

$$[2] \quad V(\mathrm{cm}^{-1}) = 13.21Q^2 + 11.51Q^4 + 47.70 \exp(-0.8854Q^2)$$

where Q is a mass weighted coordinate.[2] The

[1]This paper is dedicated to Professor C. A. Winkler of McGill University on the occasion of his sixty-fifth birthday by one of his colleagues (D.F.R.G.).

[2]The potential function can be expressed in different forms. Some confusion has arisen when the appropriate transformations are not applied. See ref. 6.

potential function has a small barrier of 8 cm^{-1} at the planar position and the ground state lies 9 cm^{-1} above the barrier.

The far-infrared spectrum of methylenecyclobutane shows a generalized absorption from 50 to 100 cm^{-1} from which it is not possible to obtain a puckering potential (7). However, Durig *et al.* (7) have examined the Raman spectrum and derived a potential function which also explained the microwave data (4) and infrared combination bands (8).

$$[3] \qquad V(cm^{-1}) = -91.07Q^2 + 14.75Q^4$$

This potential function has a barrier of 141 cm^{-1} and the ground state and first two excited vibrational levels lie below the barrier. An exponential term was not required in this function. Cyclobutanone and methylenecyclobutane thus differ in that the ground state is nonplanar in the latter case but planar in cyclobutanone.

The model commonly used to describe the puckering motions in four-membered rings was derived by Chan *et al.* (9) for trimethylene oxide. The ring is assumed to bend about the C_α–C_α and C_β–O diagonals without any stretching of bonds. This motion is conveniently described by a parameter ω which has a value of zero for symmetrical bending, -1 for bending across the C_α–C_α diagonal with no change in the $C_\alpha C_\beta C_\alpha$ and $C_\alpha O C_\alpha$ angles, and a value of $+1$ for bending across the C_β–O diagonal with no change in the $C_\beta C_\alpha O$ angles. The protons of the methylene groups are assumed to move with a curvilinear motion such that there is no stretching of the C—H bonds or deformation of the methylene angles.

In analysing the results obtained from microwave investigations it is possible to derive the rotational constants for each vibrational level and express the rotational constants as power series in the puckering coordinate. The results can be extrapolated to a (hypothetical) planar state and a structure derived. For methods such as nematic phase nmr, or electron diffraction, it is not possible to study the individual vibrational states and results appropriate to an average over all occupied vibrational levels are obtained and must be treated accordingly. For cyclobutane (1) and trimethylene oxide and trimethylene sulphide (2) this averaging over the vibrational motion was incorporated in the nematic phase nmr analysis by deriving correction terms to the direct dipole coupling constants, D_{ij}. The correction terms were calculated as the expectation values of the even powers of the puckering coordinate from the solution of the Schrödinger equation with the known puckering potential and simple harmonic oscillator basis functions.

TABLE 1. Spectral parameters for cyclobutanone

Parameter	Value
$\nu_1 - \nu_5$*	185.26±0.20
$J_{12} - J_{56}$	−6.91±0.53 (Hz)
J_{13}	−3.49±0.46
J_{14}	+4.77±0.59
J_{15}	+10.01±0.17
J_{16}	+6.49±0.16
D_{12}	+3567.17±0.19
D_{13}	−40.80±0.22
D_{14}	−229.26±0.24
D_{15}	−659.05±0.13
D_{16}	+10.63±0.16
D_{56}	+3558.73±0.30

*Chemical shift difference in Hz at 220 MHz.

The nematic phase nmr spectrum of cyclobutanone has been reported by d'Annibale *et al.* (10) and by Swinton (11) who analysed the structure as a rigid planar molecule without averaging over the vibrational motions.

Experimental

Cyclobutanone and methylenecyclobutane were obtained from commercial sources and used without further purification. Solutions were prepared in the nematic liquid crystal *p*-ethoxybenzylidene-*p*-*n*-butylaniline (EBBA); cyclobutanone 24 mol%, and methylenecyclobutane 18 mol%, and spectra obtained at 220 MHz at the Canadian 220 MHz NMR Centre, Sheridan Park, Ontario. The sample temperature was 18 °C in each case. Analysis of the spectra and calculations followed the procedures described earlier (2), except for the spectrum of the eight-spin methylenecyclobutane system which was analysed with the computer program SPECSYM, written in this laboratory.

Results

The spectrum of cyclobutanone resembles those of trimethylene oxide and trimethylene sulphide reported earlier (2). Seventy-eight lines were used in the analysis and fitted with an rms deviation in line position of 0.96 Hz. The spectral parameters are listed in Table 1.

Can. J. Chem. Downloaded from www.nrcresearchpress.com by 210.87.254.40 on 09/05/12
For personal use only.

Can. J. Chem. Downloaded from www.nrcresearchpress.com by 210.87.254.40 on 09/05/12
For personal use only.

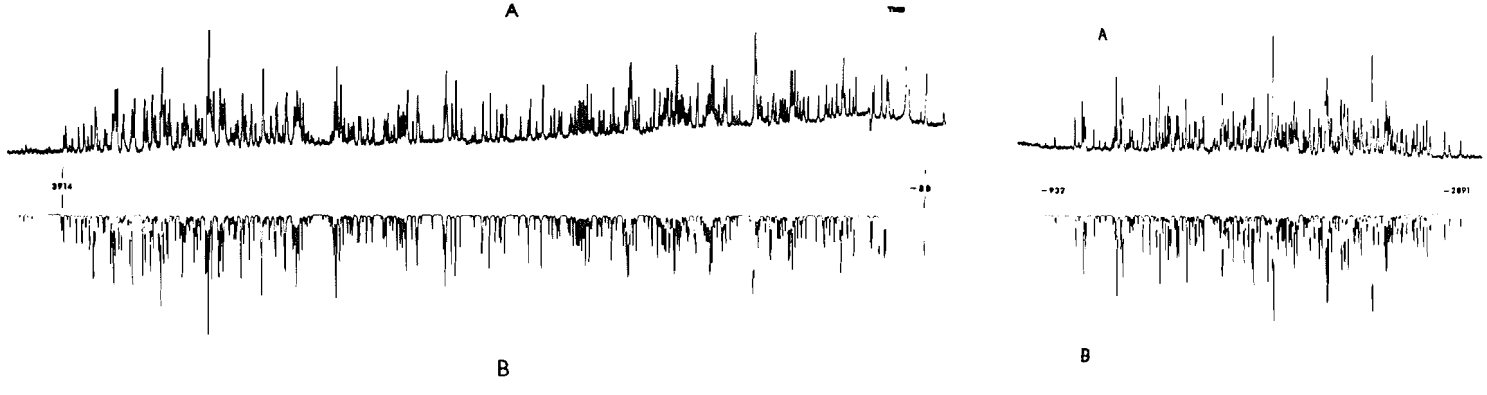

FIG. 1. Proton nmr spectrum of partially oriented methylene cyclobutane: (*A*) experimental spectrum, (*B*) computed spectrum.

TABLE 2. Spectral parameters for methylenecyclobutane

Parameter	Value†	Parameter	Value
ν_1*	592.27±0.04		
ν_5	404.03±0.05		
ν_7	996.61±0.05		
J_{12}	−14.72±2.27 (Hz)	D_{12}	+3414.31±0.45 (Hz)
J_{13}	−3.05±0.08	D_{13}	+38.75±0.08
J_{14}	+0.84±0.07	D_{14}	−75.60±0.08
J_{15}	+9.61±0.06	D_{15}	−569.63±0.06
J_{16}	+6.45±0.06	D_{16}	+15.92±0.05
J_{17}	(−2.3 ±0.5)	D_{17}	−458.44±0.75
J_{18}	(−2.8 ±0.5)	D_{18}	−142.36±0.60
J_{56}	−9.98±2.28	D_{56}	+3054.19±0.11
J_{57}	(0.0)	D_{57}	−158.66±0.10
J_{78}	0.49±0.09	D_{78}	−398.33±0.08

*Chemical shifts in Hz from TMS at 220 MHz.
†Assumed parameters in parentheses.

The direct coupling constants cannot be compared with those of d'Annibale *et al.* (10) since a different nematic solvent was used. The same solvent was used by Swinton (11), but a different solute concentration and possibly a different sample temperature resulted in a different degree of orientation of the solute molecule.

The spectrum of methylenecyclobutane was extremely complex, Fig. 1. Of the 2930 symmetry allowed transitions some 770 lines were of observable intensity and 350 of those used in the analysis. The rms deviation between experimental and calculated frequencies was 0.59 Hz. The relatively large chemical shifts between the olefinic and ring protons leads to some first order character so that the off-diagonal terms $(2J_{ij} - D_{ij})$ are less well determined than the corresponding diagonal terms $(J_{ij} + D_{ij})$ and it was not possible to obtain, with accuracy, the indirect coupling constants J_{17} and J_{18} from the partially oriented spectrum. Values were assumed for these couplings based on those reported for similar compounds. The final spectral parameters for methylenecyclobutane are given in Table 2.

Discussion

Cyclobutanone

The proton geometry of a rigid planar cyclobutanone molecule can be described by four independent distances, Fig. 2, but only a relative geometry can be derived due to the interdependence of the distance functions and motional constants in the direct dipole moment

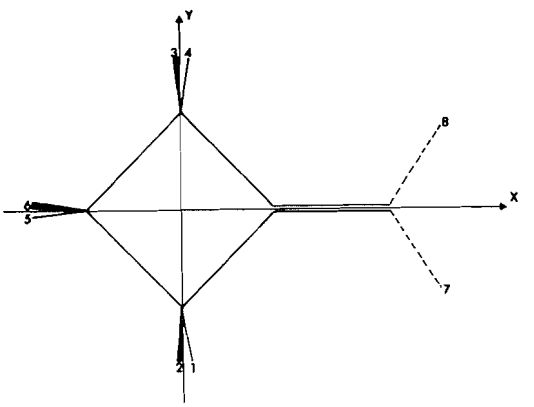

FIG. 2. Proton numbering scheme and distances in cyclobutanone and methylenecyclobutane; $d_1 = x_2 - x_6$, $d_2 = y_3$, $d_3 = z_2$, $d_4 = z_6$, $d_5 = x_7 - x_2$, $d_6 = y_8$.

expressions (12). One distance can therefore be assumed in order to scale the geometry and with the two motional constants required to describe the degree of orientation there remains five parameters with which to fit the six experimental direct dipole coupling constants. The best fit for a rigid planar geometry was obtained with the distances given in column I of Table 3 with an rms deviation between the experimental and calculated D_{ij} values of 3.4 Hz.

In order to include the effects of ring puckering it was necessary to determine the parameter ω, described earlier, which was not reported by Scharpen and Laurie for cyclobutanone (3). A comparison of calculated and experimental variations in rotational constants with vibrational quantum numbers gave good agreement

Can. J. Chem. Downloaded from www.nrcresearchpress.com by 210.87.254.40 on 09/05/12
For personal use only.

TABLE 3. Structural results for cyclobutanone

Parameter	Value I Rigid planar	II $\eta = 0$	III η varied
d_1* (Å)	(1.7446)	(1.7446)	(1.7446)
d_2	1.8960	1.7401	1.7660±0.0018
d_3	0.9221	0.9170	0.9100±0.0005
d_4	0.9228	0.9035	0.9074±0.0004
$C_{3z^2-r^2}$	−0.2083	−0.2150	−0.2065±0.0004
$C_{x^2-y^2}$	+0.0159	+0.0259	+0.0216±0.0002
η	—	0	−0.2907±0.0051
ΔD_{ij} rms (Hz)	3.37	3.95	0

*Assumed parameter.

for $\omega = -0.4$. The negative value of ω indicates that bending occurs principally about the C_α–C_α diagonal which is to be expected since bending about the other diagonal would involve the more highly strained carbonyl bond angle. With this model the thermally averaged functions at 291 K were calculated to be $\langle z^2\rangle_T = 8.563 \times 10^{-3}$ Å^2 and $\langle z^4\rangle_T = 1.595 \times 10^{-4}$ Å^4. The nonplanar four membered ring no longer retains C_{2v} symmetry and, therefore, the orientation in the liquid crystal cannot be described by only two motional constants. It is convenient to introduce the third required motional constant C_{xz} via the expression $C_{xz} = \eta z$, *i.e.* proportional to the puckering amplitude. The term η can be used as an additional variable parameter but this leads to an equal number of 'knowns and unknowns' and an exact fit can be made to the direct dipole coupling constants and there is no redundant parameter. With the inclusion of the thermally averaged puckering correction terms and the η term the D_{ij} expressions are:

$$D_{12} = D_{12}^{\,p} + 861.16C_{3z^2-r^2} + 330.88C_{x^2-y^2} - 202.40\eta$$

$$D_{13} = D_{13}^{\,p} + 91.96C_{3z^2-r^2} + 159.28C_{x^2-y^2}$$

$$D_{14} = D_{14}^{\,p} + 17.83C_{3z^2-r^2} + 34.65C_{x^2-y^2} - 4.70\eta$$

$$D_{15} = D_{15}^{\,p} - 521.13C_{3z^2-r^2} + 131.02C_{x^2-y^2} + 147.30\eta$$

$$D_{16} = D_{16}^{\,p} + 23.45C_{3z^2-r^2} + 13.86C_{x^2-y^2} + 7.44\eta$$

$$D_{56} = D_{56}^{\,p} + 1548.60C_{3z^2-r^2} - 894.09C_{x^2-y^2} - 643.59\eta$$

where the superscript p refers to the planar geometry. Calculations were performed with η set equal to zero and with η as a variable parameter. In the first case the fit is worse than for the rigid planar case. The preferred distance values are given in column III of Table 3 where the error limits are calculated probable errors based upon the errors in the measured direct dipole coupling constants (13). The nmr data can be combined with the microwave results to give a more complete structure. The ring atom bond lengths and angles were taken from the r_s structure of Scharpen and Laurie (3). The C—H bond length was assumed to be 1.097 Å, the value found for trimethylene oxide (2), and the proton geometry scaled to fit the structure. The parameters which remain to be determined are the bond angles at the methylene groups and the carbon–oxygen bond length. This bond length was not quoted by Scharpen and Laurie (3) but can be obtained from the rotational constants once the proton coordinates are known. The proposed structure is given in Table 5. The proton distances in this structure differ slightly from the values given in Table 3 due to the scaling procedure. The bisector of the methylene group is displaced 2.6° toward the carbonyl group and away from the bisector of the interior ring angle. A similar effect was reported by d'Annibale *et al.* (10) who based their proposed structure on a rigid planar molecule and concluded that ring puckering effects were negligible. The angle in this treatment was found to be 11.5°.

Methylenecyclobutane

The procedures used for methylenecyclobutane were the same as those used for cyclobutanone. For a rigid planar molecule (C_{2v}

Can. J. Chem. Downloaded from www.nrcresearchpress.com by 210.87.254.40 on 09/05/12
For personal use only.

TABLE 4. Structural results for methylenecyclobutane

Parameter	Value I Rigid planar	II $\eta = 0$	III η varied
d_1	1.6521	1.7777	1.7651±0.0013
d_2*	(1.7369)	(1.7369)	(1.7369)
d_3	0.8446	0.9325	0.9190±0.0007
d_4	0.8766	0.9183	0.9159±0.0002
d_5	2.5561	3.0555	2.9426±0.0054
d_6	0.8829	0.9872	0.9707±0.0004
$C_{3z^2-r^2}$	−0.1532	−0.2251	−0.2113±0.0006
$C_{x^2-y^2}$	+0.0648	+0.0971	+0.0907±0.0004
η	—	0	−0.1311±0.0048
ΔD_{ij} (Hz)	10.43	4.46	2.92

*Assumed parameter.

symmetry) there are six distances required to specify the proton geometry and two motional constants to describe the orientation and thus seven parameters are to be determined from ten D_{ij} values. The best least squares fit gave a large rms deviation of 10.4 Hz for a rigid planar molecule and this is obviously not an acceptable structure. The value of ω was not given in the microwave study (4) and an attempt to determine this parameter was unsuccessful. No value of ω would adequately reproduce the dependence of all three rotational constants upon the vibrational level and, therefore, the value found for cyclobutanone, −0.4, was adopted. It was also assumed that the olefin group was rigid, *i.e.* no rocking or bending occurred. The following results were obtained:

$$\langle z^2\rangle_T = 1.562 \times 10^{-2}\ \text{Å}^2$$

$$\langle z^4\rangle_T = 4.112 \times 10^{-4}\ \text{Å}^4$$

$$D_{12} = D_{12}^{P} + 1643.39C_{3z^2-r^2} + 590.71C_{x^2-y^2} - 401.57\eta$$

$$D_{13} = D_{13}^{P} + 34.67C_{3z^2-r^2} + 64.19C_{x^2-y^2} - 9.41\eta$$

$$D_{14} = D_{14}^{P} + 171.55C_{3z^2-r^2} + 297.14C_{x^2-y^2}$$

$$D_{15} = D_{15}^{P} - 941.59C_{3z^2-r^2} + 245.53C_{x^2-y^2} + 253.42\eta$$

$$D_{16} = D_{16}^{P} + 28.68C_{3z^2-r^2} + 30.06C_{x^2-y^2} + 17.75\eta$$

$$D_{17} = D_{17}^{P} - 14.26C_{3z^2-r^2} + 71.83C_{x^2-y^2} - 67.00\eta$$

$$D_{18} = D_{18}^{P} - 29.87C_{3z^2-r^2} + 2.16C_{x^2-y^2} - 29.01\eta$$

$$D_{56} = D_{56}^{P} + 3018.26C_{3z^2-r^2} - 1742.59C_{x^2-y^2} - 1193.56\eta$$

$$D_{57} = D_{57}^{P} + 30.96C_{3z^2-r^2} - 55.81C_{x^2-y^2} + 17.26\eta$$

$$D_{78} = D_{78}^{P}$$

Inclusion of the correction terms for the puckering motion but neglect of the third motional constant reduced the rms deviation between experimental and calculated direct dipole coupling constants to 4.5 Hz, Table 4. The inclusion of η as an eighth variable parameter reduced the deviation to 2.9 Hz and although this is probably an acceptable fit for eight variables to the ten D_{ij} values, certain coupling constants showed large deviations. Attempts to obtain a better fit by using alternative values of ω or by including methylene group rocking motions did not lead to any substantial improvement.

A combination of nmr and microwave data can also be used for methylenecyclobutane. It is necessary to assume four parameters to give a complete structure. In this case the C—H bond length for both methylene groups was taken as 1.097 Å and the C_α—C_β bond length as 1.550 Å, which seems to be an appropriate value for cyclobutane (1) and trimethylene oxide (2) and is close to the value obtained for cyclobutanone. The olefinic bond length was assumed to be 1.340 Å (14). The proposed structure is given in Table 5. The ring structure is very similar to that of cyclobutanone. The olefinic proton bond lengths appear to be slightly longer than normal but this may not be significant. The bending of the α-methylene protons toward the substituent group is observed again; in this case the angle between the

Can. J. Chem. Downloaded from www.nrcresearchpress.com by 210.87.254.40 on 09/05/12
For personal use only.

TABLE 5. Molecular structures of cyclobutanone and methylenecyclobutane

Parameter	Value	
	Cyclobutanone	Methylenecyclobutane
$r(C_\alpha—C_\beta)$	1.556 (Å)	(1.550) (Å)
$r(C—C_1)$	1.527	1.534
$r(C—H)$	(1.097)	(1.097)
$r(C=O)$	1.216	—
$r(C=C)$	—	(1.340)
$r(C—H)$olef.	—	1.109
$\angle C_\alpha C_\beta C_\alpha$	90.9°	91.1°
$\angle C_\beta C_\alpha C_1$	88.0°	88.3°
$\angle C_\alpha C_1 C_\alpha$	93.1°	92.4°
$\angle HC_\alpha H$	110.8°	112.0°
$\angle HC_\beta H$	110.3°	111.4°
$\angle$HCH,olef	—	120.1°
ϕ*	2.6°	3.8°

*Angle between the bisector of the methylene group angle and the bisector of the interior ring angle.

TABLE 6. Comparison of cyclic molecules and their open chain analogues

Molecule	$r(C_\alpha—X)$ (Å)	$\angle C_\alpha X C_\alpha$ (deg)	Reference
Cyclobutane	1.548	90	1
Propane	1.526	112.4	21
Trimethylene oxide	1.449	91.9	2
Dimethyl ether	1.410	111.7	22
Trimethylene sulphide	1.845	78.4	2
Dimethyl sulphide	1.802	98.9	23
Cyclobutanone	1.527	93.1	This work
Acetone	1.517	116.0	24
Methylenecyclobutane	1.534	92.4	This work
Isobutene	1.508	115.6	25

methylene bisector and the ring angle bisector is 3.8°.

The bond lengths and bond angles for these ring compounds can be compared with the open chain analogues, Table 6. The bond lengths are significantly longer in the cyclic molecules and bond angles are consistently some 20° less. The bond lengthening in cyclobutane has been attributed to repulsive forces between diagonally opposite atoms (15, 16) and in this series of molecules the C—X bond length increases O < C < S, *i.e.* proportional to the size of the substituent atom and also inversely proportional to the magnitude of the bond stretching force constant. The methylene group bond angles, within the assumption of a C—H bond length of 1.097 Å, all lie in the range 110 to 112°, *i.e.* between the values for ethane 107.4 ± 0.3° (17) and cyclopropane 115.2 ± 0.1° (18). In all four compounds a bending of the α-methylene protons towards the substituent atom or group occurs. The angles are small but consistent and this deformation appears to be an additional mechanism whereby the forces between eclipsed methylene protons can be relieved.

Bevan *et al.* have derived a complete r_s structure for trimethylene sulphoxide and reported details of the specific configuration of the methylene groups (19). There is a tilting of the β-methylene group and for the α-methylene groups, which do not lie on a symmetry element, bending and twisting occurs in addition to tilting. The bending angle in trimethylene sulphoxide is 5° 3′.

The calculated values of the thermally averaged square of the puckering coordinate $\langle z^2 \rangle_T$ can be used to derive the puckering angle θ_{rms}, the averaged angle between the $C_\alpha—C_\beta—C_\alpha$ and $C_\alpha—X—C_\alpha$ planes. A similar puckering

Can. J. Chem. Downloaded from www.nrcresearchpress.com by 210.87.254.40 on 09/05/12
For personal use only.

angle exists for the C_β—C_α—X planes if the motion is not symmetrical but this angle will not differ too much from θ_{rms}. The values obtained were: cyclobutane, 29.0°; trimethylene oxide, 18.1°; trimethylene sulphide, 26.5°; cyclobutanone, 19.8°; and methylenecyclobutane, 26.7°. The molecules which have ground state vibrational levels below the hump in the potential barrier have puckering angles greater than 26° whereas trimethylene oxide and cyclobutanone, which have ground state levels above the hump, have puckering angles of about 19°. Thus the description 'effectively planar' is not appropriate in the latter cases, since it is based upon the perturbed ground state conformation, and to give a more appropriate description of the structure of molecules which undergo ring puckering motions the actual distribution over the occupied states should be included. Calculated distribution functions for different temperatures have been reported for only one species, trimethylene sulphide, by Gwinn and Luntz (20), and calculations are presently underway on other molecules in the series.

It is possible that the structure of a molecule can be perturbed by the anisotropic environment in the nematic liquid crystal. The agreement between our previously reported results for trimethylene oxide and sulphide (2) and the microwave and electron diffraction structures (26, 27) of those compounds is very good; this encourages the belief that no serious perturbation of the structure is occurring.

1. K. C. Cole and D. F. R. Gilson. J. Chem. Phys. **60**, 1191 (1974).
2. K. C. Cole and D. F. R. Gilson. Mol. Phys. **29**, 1749 (1975).
3. L. H. Scharpen and V. W. Laurie. J. Chem. Phys. **49**, 221 (1968).
4. L. H. Scharpen and V. W. Laurie. J. Chem. Phys. **49**, 3041 (1968).
5. T. R. Borgers and H. L. Strauss. J. Chem. Phys. **45**, 947 (1966).
6. J. S. Gibson and D. O. Harris. J. Chem. Phys. **57**, 2318 (1972).
7. J. R. Durig, A. C. Shing, L. A. Carreira, and Y. S. Li. J. Chem. Phys. **57**, 4397 (1972).
8. T. B. Malloy, Jr., F. Fisher, and R. M. Hedges. J. Chem. Phys. **52**, 5325 (1970).
9. S. I. Chan, J. Zinn, and W. D. Gwinn. J. Chem. Phys. **34**, 1319 (1961).
10. A. d'Annibale, L. Lunazzi, G. Fronza, R. Mondelli, and S. Bradamante. J. Chem. Soc. Perkin Trans. II, 1908 (1973).
11. P. F. Swinton. J. Magn. Reson. **13**, 304 (1974).
12. L. C. Snyder. J. Chem. Phys. **43**, 4041 (1965).
13. K. C. Cole and D. F. R. Gilson. Can. J. Chem. **52**, 281 (1974).
14. Tables of Interatomic Distances. Chemical Society Special Publ., Chem Soc., London. 1958.
15. E. Goldish. J. Chem. Educ. **36**, 408 (1959).
16. J. D. Dunitz and V. Schomaker. J. Chem. Phys. **20**, 1703 (1952).
17. K. Kuchitsu. J. Chem. Phys. **49**, 4456 (1968).
18. N. J. D. Lucas. Mol. Phys. **22**, 233 (1971).
19. J. W. Bevan, A. C. Legon, and D. J. Millen. J. Chem. Soc. Chem. Commun. 659 (1974).
20. W. D. Gwinn and A. Luntz. Trans. Am. Crystallogr. Assoc. **2**, 90 (1966).
21. D. R. Lide. J. Chem. Phys. **33**, 1514 (1960).
22. U. Blukis, P. H. Kasai, and R. J. Myers. J. Chem. Phys. **38**, 2753 (1963).
23. L. Pierce and M. Hayashi. J. Chem. Phys. **35**, 479 (1961).
24. T. Iijima. Bull. Chem. Soc. Jpn. **45**, 3526 (1972).
25. I. Tokue, T. Fukuyama, and K. Kuchitsu. J. Mol. Struct. **17**, 207 (1973).
26. R. A. Creswell. Mol. Phys. **30**, 217 (1975).
27. K. Karakida and K. Kuchitsu. Bull. Chem. Soc. Jpn. **48**, 1691 (1975).

Can. J. Chem. Downloaded from www.nrcresearchpress.com by 210.87.254.40 on 09/05/12
For personal use only.

Behaviour of vanadia-catalyzed SO_2 oxidation in the presence of inert, diluent gases

KRISHNA KUMAR RUNGTA[1], ROBERT ROSS HUDGINS, AND PETER LEWIS SILVESTON

Department of Chemical Engineering, University of Waterloo, Waterloo, Ontario N2L 3G1

Received August 5, 1975

KRISHNA KUMAR RUNGTA, ROBERT ROSS HUDGINS, and PETER LEWIS SILVESTON. Can. J. Chem. **54**, 665 (1976).

Observations on the effect of diluent gas on the rate of oxidation of SO_2 over a commercial vanadia catalyst reported by Yeramian *et al.* in a 1970 paper in this journal have been extended in this study.

A pronounced increase in rate is observed when inert diluents krypton and C_4F_8 are substituted for helium. The influence of other diluents was less marked. The increase in rate has been found to depend upon the partial pressure of the diluent and to be extremely sensitive to the ratios of the reactants.

KRISHNA KUMAR RUNGTA, ROBERT ROSS HUDGINS et PETER LEWIS SILVESTON. Can. J. Chem. **54**, 665 (1976).

Dans cette étude, on élargit les observations rapportées par Yeramian et coll. dans une publication parue dans ce journal en 1970 et ayant trait à l'effet d'un gaz diluant sur la vitesse d'oxydation du SO_2 sur un catalyseur commercial au vanadium.

On observe une augmentation prononcée de la vitesse quand on remplace l'hélium par du krypton et du C_4F_8. L'influence d'autres diluants est moins marquée. On a trouvé que l'augmentation de la vitesse dépend de la pression partielle du diluant et qu'elle est extrêmement sensible aux rapports de réactifs.

[Traduit par le journal]

Introduction

Baron, Manning, and Johnstone (1) first established the existence of the influence of a diluent gas on the rate of the heterogeneous oxidation of SO_2 over a V_2O_5 catalyst. This result was later confirmed by Yeramian *et al.* (2) and published in this journal. The purpose of this paper is to communicate additional observations on this system. The diluent gas effect is so unusual in terms of conventional understanding of catalysis, that this paper will be devoted mainly to providing additional data and observations rather than attempting extensive interpretation of them. In a recent review article, a number of explanations for the diluent gas effect (DGE) in heterogeneous catalysis were examined by Hudgins and Silveston (3) and will not be repeated here.

Experimental Details

The reactor apparatus for this study has been described by Yeramian *et al.* (2). The main modification made to the previous apparatus was the small reactor tube which was used to eliminate thermal and mass transfer limitations in the differential reactor bed. The reaction section itself consisted of a 316-stainless steel union plugged at both ends with 120-mesh stainless steel screen. As in the previous study, the reactor was immersed in the fluidized sand bath, whose temperature was controlled by a proportional temperature controller.

The catalyst was of the type previously used by Yeramian *et al.* (2), namely, Cyanamid Aero SA vanadium oxide catalyst. For use in the reactor, a few pellets were crushed and sieved and the 40/50 US mesh particles (average diameter 0.358 mm) used for catalytic tests. These particles were mixed with quartz particles of the same mesh size. The function of the quartz was twofold: to reduce error because of any catalyst carry-over and to reduce temperature differences over the length of the catalyst bed because of the exothermicity of reaction. The activity of each sample of the catalyst was checked by measuring the steady-state rate at a standard condition with 60% argon at 405 °C, and found to be reproducible.

To prevent condensation of SO_3, all valves and lines from the sand bath to the sampling section were heated by asbestos-covered nichrome resistance wire. A Nupro fine-metering valve in the exit line was used to control total pressure. Total pressure and pressure drop across the packed bed were measured by means of a mercury manometer.

The method of sampling and analyzing the reaction products was similar to that described by Yeramian *et al.* (2), standard deviation of replicated SO_3 conversion runs was found to be 5.6%. The standard deviation of the actual analytical method was determined to be about 2%.

In the experiments a total flow rate of 0.3 mol/h was used. This flow was sufficient to keep the reactor differential (conversion did not exceed 1.2%), as well as to eliminate

[1]Present address: Ontario Hydro, Bruce Heavy Water Plant, Tiverton, Ontario.

Can. J. Chem. Downloaded from www.nrcresearchpress.com by 210.87.254.40 on 09/05/12
For personal use only.

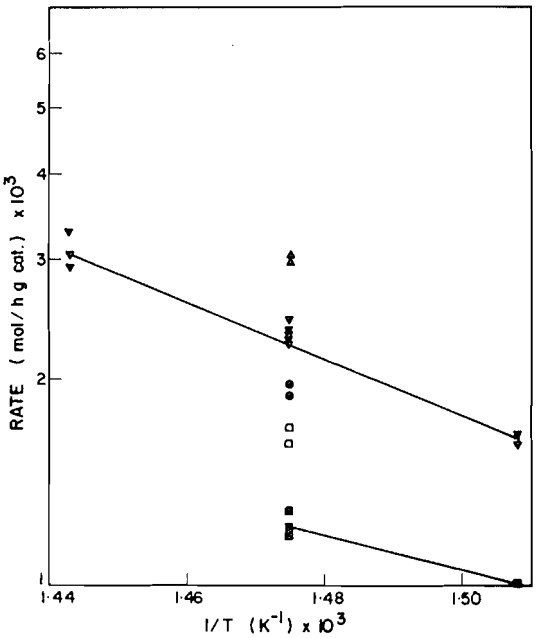

FIG. 1. Arrhenius plots of catalytic SO_2 oxidation using monatomic diluents. Mole percentage in feed: SO_2:O_2:diluent = 15:25:60. Diluents: ▲, Kr; ▼, Ar; ●, Ne; □, no diluent; ■, He.

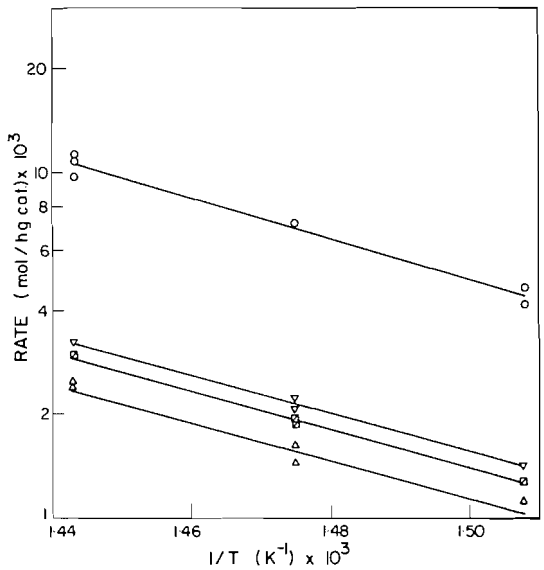

FIG. 2. Arrhenius plots of catalytic SO_2 oxidation using polyatomic diluents. Mole percentages in feed as in Fig. 1. Diluents: △, CF_4; ▨, C_2F_6; ▽, SF_6; ○, C_4F_8.

film transport effects around the catalyst particles. A constant pressure of 1.20 atm (122 kPa) was used. All runs within a set of experiments were done in random order.

When not in use, the reactor was maintained by flushing continuously with argon. The temperature was allowed to drop only a few degrees below the usual reaction temperature of 405 °C.

Prior to the start of the experiments, some blank runs were made without catalyst in the reactor. Some conversion was caused by the walls and the preheater of the reactor at the outset, but within three or four days this activity had dropped to zero. When quartz was used in place of the catalyst no conversion was found (4).

Results and Discussion

Four main sets of results are presented in this paper: (*1*) evidence of the effect of different diluent gases on the catalytic oxidation rates of SO_2; (*2*) the influence of diluent gases on the initial rate of approach to steady state; (*3*) the influence of different diluent gas concentrations on the rates; and (*4*) the influence of the reactant ratio SO_2/O_2 on the presence of the diluent gas effect.

The Arrhenius plots of Figs. 1 and 2 show the influence of various diluent gases on the steady state rates of SO_2 oxidation over vanadia catalyst. These results have been divided into two groups representing essentially homologous series of diluents. This was done because molecular properties within a homologous series will change more uniformly than within a non-homologous series. Figure 1 shows two points labelled 'no diluent'. Measurements for these points were made at higher partial pressures of the reactants and extrapolated to conditions comparable to those used for the remaining rate measurements by an empirical formula. Justification for the extrapolation is given in the Appendix.

The similarity of the slopes on these lines is striking. Table 1 further shows that the apparent energies of activation overlap considerably with

TABLE 1. Apparent activation energies

Diluent gas	Experimental value of E showing 95% confidence interval* (kcal/mol)
He	12 ± 17
Ar	19 ± 3
SF_6	25 ± 10
C_2F_6	26 ± 10
CF_4	24 ± 7
C_4F_8	27 ± 4

*Using a pooled estimate of the standard error of the apparent activation energy from all runs.

Can. J. Chem. Downloaded from www.nrcresearchpress.com by 210.87.254.40 on 09/05/12
For personal use only.

Can. J. Chem. Downloaded from www.nrcresearchpress.com by 210.87.254.40 on 09/05/12
For personal use only.

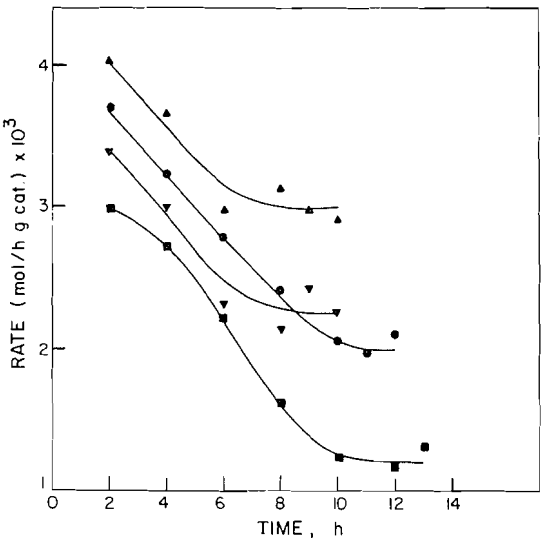

FIG. 3. Reaction rate *vs.* time at 405 °C. Mole percentages as in Fig. 1. Diluents: ▲, Kr; ▼, Ar; ●, Ne; ■, He.

the exception of Ar and C_4F_8 diluent series. The values of the apparent activation energies are approximately a factor of ten higher than those expected in the case of reaction controlled by diffusion of reactant to the periphery of the catalyst particles. In addition, calculations made using available criteria from the literature, indicate the absence of intraparticle mass and heat transfer limitations, as well as the absence of mass and heat transfer limitations in the gaseous film around catalyst particles (5–8).

The apparent activation energies for helium and argon diluents in Table 1 are substantially less than those observed by Yeramian *et al.* (2) (for helium 35.7 ± 2.4 kcal/mol and for argon 28.5 ± 2.0 kcal/mol). Although the two studies were performed at slight differences of the partial pressures, it is unlikely that these differences are sufficient to reconcile the differences in activation energies. Instead, it must be noted that the present study is confined to a temperature range between 390 and 420 °C, whereas the previous range was between 370 and 462 °C. In that paper (2), the possibility of a break in the Arrhenius plots was noted near 420 °C, but sufficient data were not taken to establish a slope change. In the present study, the more restricted temperature range does indeed give rise to a lower apparent activation energy with helium and argon.

The approach to the steady state indicates some unusual behaviour that appears to be related to the diluent gas effect. Figure 3 shows that a considerable period of time is required to obtain the steady state. It was assumed that the steady state was attained when, after 6 h of running time, three successive reaction rates sampled an hour apart showed a standard deviation within 10% of their mean value. A comparison below of the times required to reach steady state with the steady state rate indicates that the two measurements appear to be related.

Diluent	Approximate time to attain steady state (h)	Reaction rate at steady rate (mol/h g-catalyst × 10^3)
He	6	1.2
Ne	6	1.9
Ar	10	2.3
Kr	10	3.0

Figure 3 also shows an often observed but still unexplained phenomenon. After a change in conditions, the rate of reaction always decays to a steady state and apparently never rises. The starting condition of the catalyst is not reproducible, as may be seen by the initial rates in Figure 3. Exploitation of this phenomenon by oscillating the feed composition to the catalyst shows that the total yield from the reactor can be augmented as much as 25% over the steady state (9). It is, in fact, because perturbations to

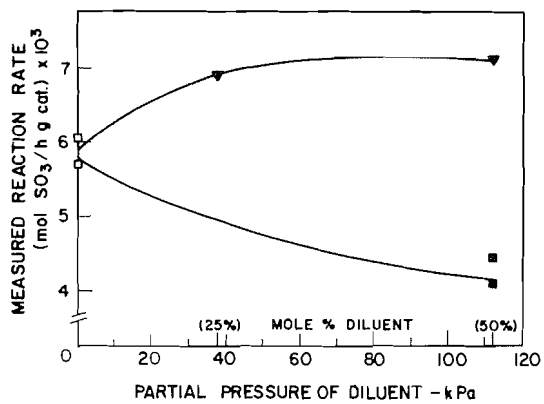

FIG. 4. Dependence of reaction rate (405 °C) on diluent gas added. Diluent: □, none; ■, He; ▼, Ar. p_{SO_2} = 42.0 kPa; p_{O_2} = 70.0 kPa; flow of SO_2 plus O_2 = 0.75 mol/h.

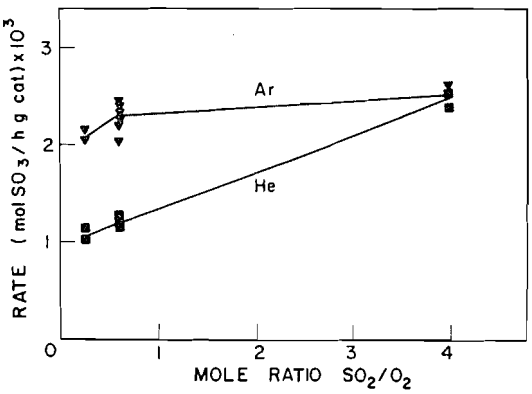

FIG. 5. Dependence of reaction rate (405 °C) on SO_2/O_2 ratio. Total pressure = 121.3 kPa; total flow = 0.3 mol/h; 60% diluent.

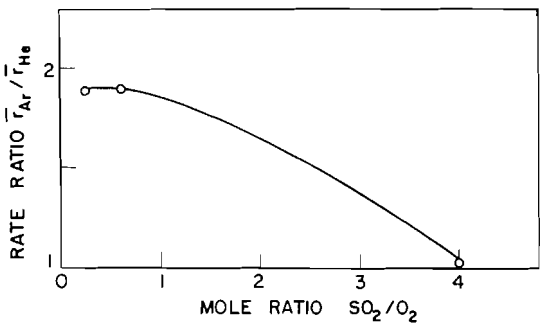

FIG. 6. Ratio of mean reaction rates from Fig. 5 *vs.* SO_2/O_2 ratio. $\bar{r}_{Ar}$ = mean reaction rate with Ar diluent. $\bar{r}_{He}$ = mean reaction rate with He diluent.

the feed can cause this increase in activity of the catalyst plus the long stabilization times required that steady-state rate data are so difficult to collect for this system.

Figure 4 gives the result of a few measurements with varying quantities of Ar diluent. These results show that the addition of helium inhibits the rate of reaction found in the absence of diluents, but that the addition of argon has an opposite effect. The results also suggest that the promoting effect of argon to the 'undiluted' reaction rate is not proportional to the quantity of argon present in the gas and suggest that some type of saturation limit occurs with respect to the diluent.

Figure 5 shows the influence of the SO_2/O_2 ratio at constant diluent gas partial pressures on the rates of oxidation with helium and with argon diluents. It is clear that the effect on the rate of reaction of increasing the ratio from 0.25 to 4 is much more pronounced with helium diluent than with argon. Figure 6 shows the relative change in rates as a function of the SO_2/O_2 ratio, indicating that there is essentially no difference in the rates with different diluents at SO_2/O_2 molar ratios of 4. A similar conclusion was inferred from the factorially designed experiments of Rhodey *et al.* (10) in this system. These observations are not consistent with the momentum exchange or thermal accommodation models for the DGE, detailed in a recent review article (3), since they do not permit the rate of reaction to vary substantially with the change in ratio of reactants of a gas in which the diluent predominates. These observations could probably be accounted for in a theory invoking a condensed phase on the catalyst surface sensitive to the partial pressures of the reactants in the reacting gas mixture.

Table 2 demonstrates the tolerably good correlation that exists between the rate of reaction and the molecular weight of the gas. These

TABLE 2. Steady-state reaction rates at 405 °C

Diluent	Mean molar mass of feed gas (g/mol)	Mean reaction rate (mol/h g-catalyst) $\times 10^3$	No. in sample
Noble gases			
He	20.0	1.22	3
Ne	29.7	1.94	2
Ar	41.6	2.32	9
Kr	67.8	3.00	2
Fluorocarbons			
CF_4	70.4	1.54	2
C_2F_6	100.4	1.89	2
C_4F_8	137.6	7.14	1

Can. J. Chem. Downloaded from www.nrcresearchpress.com by 210.87.254.40 on 09/05/12
For personal use only.

Can. J. Chem. Downloaded from www.nrcresearchpress.com by 210.87.254.40 on 09/05/12
For personal use only.

results have been separated into two homologous series of diluents: the noble gases and the fluorocarbons. Each series indicates an increase in the rates of SO_2 oxidation as the molecular weight of the diluent increases. Since other properties of gases are related to the molecular weight, it is not surprising that other correlations are possible, *e.g.* rate *vs.* normal boiling point of the diluent gas, rate *vs.* thermal conductivity of the diluent gas. Such correlations, however, are unable to establish any causal relationship.

Conclusions

The study of SO_2 oxidation over vanadium oxide catalyst originally carried out by Yeramian *et al.* has been extended to a wide range of diluent gases, and shows several additional unexpected phenomena, especially the dependence of the diluent gas effect on the molar ratio of the reactants. The results appear consistent with a thermodynamic rather than a thermal accommodation explanation of the diluent gas observations.

Acknowledgments

The authors wish to acknowledge financial support of the National Research Council of Canada in the form of a research grant, and to the Petroleum Research Fund (5452-AC7) for partial support of this project.

Catalyst was provided by Cyanamid of Canada, Limited.

1. T. Baron, W. R. Manning, and H. F. Johnstone. Chem. Eng. Prog. **48**, 125 (1952).
2. A. A. Yeramian, P. L. Silveston, and R. R. Hudgins. Can. J. Chem. **48**, 1175 (1970).
3. R. R. Hudgins and P. L. Silveston. Catal. Rev. Sci. Eng. **11**, 167 (1975).
4. K. K. Rungta. Ph.D. Thesis, University of Waterloo, Waterloo, Ontario, 1974.
5. P. B. Weisz and J. S. Hicks. Chem. Eng. Sci. **17**, 265 (1962).
6. R. R. Hudgins. Can. J. Chem. Eng. **50**, 427 (1972).
7. R. R. Hudgins. Chem. Eng. Sci. **23**, 94 (1968).
8. D. E. Mears. J. Catal. **20**, 127 (1971).
9. M. P. Unni, R. R. Hudgins, and P. L. Silveston. Can. J. Chem. Eng. **51**, 623 (1973).
10. W. G. Rhodey, P. M. Reilly, P. L. Silveston, and R. R. Hudgins. J. Catal. In press.
11. P. L. Calderbank. J. Appl. Chem. London, **2**, 482 (1952).

Appendix

Table A1 shows the influence the concentration of diluent has on the rate of SO_2 oxidation. In obtaining these results, the measured rates have been converted to a common base of the partial pressure of SO_2 and O_2 through the use of the empirical formula $r = kp_{SO_2}p_{O_2}^{1/2}$ used, among others, by Calderbank (11).

The justification of this approach can be seen in Table A1. While this comparison cannot be made between runs done at exactly the same percentage of diluent gas, a semi-quantitative comparison is still possible. For He diluent, the rates appear to be similar and the same is true for Ar diluent. Thus, the use of the empirical rate model for purposes of extrapolating appears to be reasonable. This being so, the rate measurements in the absence of any diluent gas is assumed to be reasonable also, and has been plotted in Fig. 1. (The original data measured in the absence of diluent are given in Fig. 4.)

Table A1. Comparison of measured and calculated rates at 405 °C, p_{SO_2} = 18.2 kPa, and p_{O_2} = 30.3 kPa

Diluent	Mean reaction rate (mol/h g-catalyst) $\times 10^3$	No. in sample
He (60%)	1.22	3
He (50%)	1.19*	2
Ar (60%)	2.32	9
Ar (50%)	2.01*	1

*Extrapolated from data of Fig. 4, using formula $r = kp_{SO_2}p_{O_2}^{1/2}$.

COMMUNICATIONS

Arylsulfonyltetrazoles as highly efficient condensing reagents for polynucleotide synthesis[1]

J. STAWINSKI, T. HOZUMI, AND S. A. NARANG
Division of Biological Sciences, National Research Council of Canada, Ottawa, Canada K1A 0R6

Received October 1, 1975

J. STAWINSKI, T. HOZUMI, and S. A. NARANG. Can. J. Chem. **54**, 670 (1976).

Various arylsulfonyltetrazoles have been investigated to build the phosphotriester bond between appropriately protected oligonucleotides. These reagents have been found to be highly effective with respect to the time of reaction and yields.

J. STAWINSKI, T. HOZUMI et S. A. NARANG. Can. J. Chem. **54**, 670 (1976).

On a étudié comment divers arylsulfonyltétrazoles peuvent être utilisés pour former le lien phosphotriester entre des oligonucléotides protogés d'une façon appropriée. On a trouvé que ces réactifs sont extrêmement efficaces tant par rapport aux temps de réaction qu'aux rendements.

[Traduit par le journal]

Previously, we reported arylsulfonyltriazoles (1) as useful new condensing reagents for oligonucleotide synthesis and for the first time demonstrated that the modified triester method (2, 3) is capable of producing large amounts of defined sequences of deoxyoligonucleotides with demonstrated biological activity (4, 5). However, despite their effectiveness, especially with guanosine containing units, the triazoles are rather slow in completing the condensation (4). Our continued efforts to improve the triester methodology led us to attempt the use of arylsulfonyltetrazole derivatives but these compounds could not be prepared in satisfactory yield according to the published procedure (1). Recently we have accomplished their syntheses by a modified method and in this communication we wish to report their syntheses and also applications in building the longer chains of deoxyoligonucleotides by the modified triester approach.

To arylsulfonyl chloride (10 m*M*) and tetrazole (10 m*M*) in dioxane (20 ml) was added triethylamine (10 m*M* in 10 ml of dioxane) with stirring at 5 °C. After 1.5 h, the precipitate was filtered off and the dioxane solution was evaporated to dryness under vacuum. The crystalline residue was dissolved in chloroform (50 ml), washed

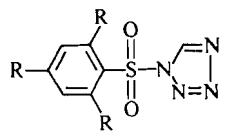

1 R = H
2 R = CH_3
3 R = $HC(CH_3)_2$

with water (2 × 20 ml), and after drying over Na_2SO_4 the residue was recrystallized from benzene. Triisopropylbenzenesulfonyl (TPS-tetr) mp 95–97 °C and mesitylenesulfonyltetrazole (MS-tetr) mp 108–110 °C were obtained in 80% yield. In the case of benzenesulfonyltetrazole (BS-tetr), because of its instability towards heat, the recrystallization with benzene was difficult. Finally analytically pure sample was obtained by dissolving the crude sample in benzene, shaking it with silica gel, and after removing silica gel the solution was evaporated under vacuum to dryness. Benzenesulfonyltetrazole, mp 88–90 °C was obtained in 60–70% yield.[2] All arylsulfonyltetrazoles were found to decompose during storage in a dessicator and the most unstable was benzenesulfonyltetrazole which de-

[1]NRCC No. 15121.

[2]These compounds are characterized satisfactorily by elemental and spectral analyses.

Can. J. Chem. Downloaded from www.nrcresearchpress.com by 210.87.254.105 on 09/05/12
For personal use only.

TABLE 1. Comparison of the time periods for the completion of condensation reactions using different arylsulfonyltetrazoles*

5′-Protected oligonucleotide (size)	5′-Hydroxyl oligonucleotide (size)	BS-tetr		MS-tetr		TPS-tetr		Product
		Time (min)	Yield (%)	Time (h)	Yield (%)	Time (h)	Yield (%)	
Monomer	Monomer	30	74	0.75	82	1	85	Dimer
Dimer	Monomer	30	77	0.75	85	1	85	Trimer
Trimer	Trimer	45	74	4	78	6	80	Hexamer
Hexamer	Hexamer	120	67	12	62	15	60	Dodecomer

*The data in the table represents the yields and time period for the synthesis of thymidine oligonomers. Similar results were also obtained in the case of dA, dG, and dC.

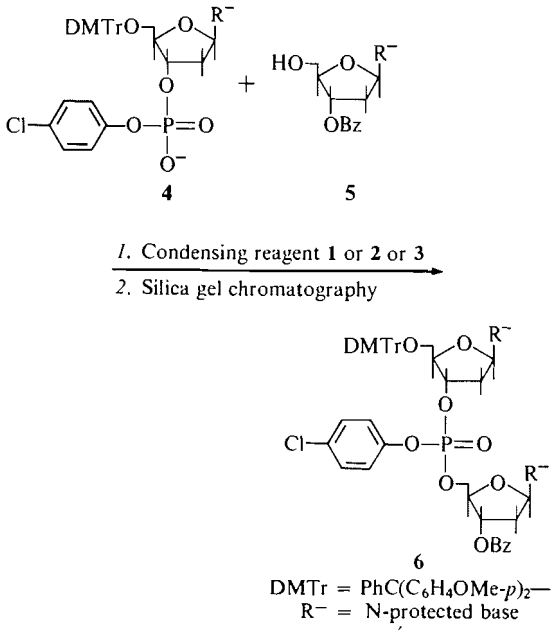

SCHEME 1

composed completely after 10 days. Therefore it is advisable to use these reagents as quickly as possible.

The coupling efficiency of these reagents was studied by carrying out a condensation between suitably protected nucleotides as outlined in Scheme 1. A typical condensation reaction was carried out by treating an anhydrous pyridine solution of 5′-dimethoxytrityldeoxynucleoside 3′-(*p*-chlorophenyl)phosphate **4** and 3′-benzoyl N-protected nucleoside **5** (equimolar with respect to **4**) and arylsulfonyl tetrazole(2–3 molar equiv.) for 30 min to 15 h (depending upon the chain length) at room temperature. The reaction mixture was then decomposed with aqueous pyridine, followed by extraction with chloroform, and the organic layer was backwashed with 0.1 *M* triethylammonium bicarbonate p*H* 7.5. The chloroform solution was then co-evaporated with toluene to a gum and the desired product was isolated by silica gel column chromatography. The reaction conditions and isolated yields are given in Table 1.

Although the rate of condensation was dependent upon the substitution in the benzene ring such that the phenyl > 2,4,6-trimethylphenyl > 2,4,6-triisopropyl phenyl groups, all these analogs reacted faster than the triazole reagents (4), even triisopropylbenzenesulfonyl chloride (3, 6). The most commonly used condensing reagents such as dicyclohexylcarbodiimide (DDC) could not be used in the triester approach due to its failure to activate the diester phosphate, and mesitylenesulfonyl chloride (MS) caused extensive sulfonation at the 5′-hydroxyl group of one of the coupling units. It is noteworthy to mention that no sulfonated side product was observed in the case of arylsulfonyltetrazoles during the condensation reaction.

In conclusion, the use of arylsulfonyltetrazoles, especially benzenesulfonyltetrazole, in the synthesis of oligonucleotides by the improved triester approach gives a much reduced time period of reaction with much higher yields which is of immense practical significance for the synthesis of longer biologically important polynucleotides.

1. N. KATAGIRI, K. ITAKURA, and S. A. NARANG. Chem. Commun. 325 (1974); J. Am. Chem. Soc. **97**, 7332 (1975).
2. K. ITAKURA, C. P. BAHL, N. KATAGIRI, J. J. MICHNIEWICZ, R. H. WIGHTMAN, and S. A. NARANG. Can. J. Chem. **51**, 3649 (1973).

Can. J. Chem. Downloaded from www.nrcresearchpress.com by 210.87.254.105 on 09/05/12
For personal use only.

3. J. C. CATLIN and F. CRAMER. J. Org. Chem. **38**, 275 (1973).
4. K. ITAKURA, N. KATAGIRI, S. A. NARANG, C. P. BAHL, K. J. MARIANS, and R. WU. J. Biol. Chem. **250**, 4590 (1975).
5. C. P. BAHL, K. J. MARIANS, R. WU, K. ITAKURA, N. KATAGIRI, and S. A. NARANG. Fed. Proc. (Abstract) **34**, 608 (1975).
6. N. J. CUSACK, C. B. REESE, and J. H. VAN BROOM. Tetrahedron Lett. 2209 (1973).

Can. J. Chem. Downloaded from www.nrcresearchpress.com by 210.87.254.105 on 09/05/12
For personal use only.

Can. J. Chem. Downloaded from www.nrcresearchpress.com by 210.87.254.42 on 09/05/12
For personal use only.

Canadian Journal of Chemistry

Published by
THE NATIONAL RESEARCH COUNCIL OF CANADA

Journal canadien de chimie

Publié par
LE CONSEIL NATIONAL DE RECHERCHES DU CANADA

Volume 54 Number 5 March 1, 1976

Volume 54 numéro 5 1 mars 1976

The acidolysis of *p*-nitrophenyl sulfate. A kinetic spectrophotometric method for evaluation of pK_a

ERWIN BUNCEL AND CLAUDIO CHUAQUI
Department of Chemistry, Queen's University, Kingston, Ontario K7L 3N6

Received July 8, 1975

ERWIN BUNCEL and CLAUDIO CHUAQUI. Can. J. Chem. **54**, 673 (1976).

A kinetic spectrophotometric method for evaluation of pK_a has been developed. In the present study this has been utilized towards the pK_a determination, in methanol, of the conjugate acids of 4-picoline, aniline, hydroxylamine, methoxyamine, and hydrazinium ion. For the first two cases the pK_a values determined by the present method could be compared with the potentiometrically measured values, in a methanol solvent, with satisfactory agreement. Our proposed method involves essentially the spectrophotometric determination of the rate of the acid catalyzed conversion of *p*-nitrophenyl sulfate to *p*-nitrophenol in methanol in the presence of the acidic species whose pK_a in this medium is required.

ERWIN BUNCEL et CLAUDIO CHUAQUI. Can. J. Chem. **54**, 673 (1976).

On a développé une méthode spectrophotométrique cinétique pour déterminer les pK_a. Dans l'étude présente, on a utilisé cette méthode pour déterminer le pK_a, dans le méthanol, d'acides conjugés de la picoline-4, de l'aniline, de l'hydroxylamine, de la méthoxyamine et de l'ion hydrazinium. Pour les deux premier cas, les valeurs de pK_a déterminées par la méthode actuelle peuvent être comparées avec les valeurs mesurées d'une façon potentiométrique dans le méthanol comme solvant et ceci avec une bonne corrélation. La méthode proposée implique essentiellement la détermination spectrophotométrique de la vitesse de conversion acido-catalysée du sulfate de *p*-nitrophényle en *p*-nitrophénol dans le méthanol en présence de l'espèces acide pour laquelle on veut déterminer le pK_a dans ce milieu.

[Traduit par le journal]

We reported recently on the kinetic study of methyl *p*-nitrophenyl sulfate with some nucleophilic reagents in methanol (1–3). It was found that a reagent HNu causes two reaction stages to occur, of which the first stage (A → B) yielding *p*-nitrophenyl sulfate is nucleophile catalyzed while the second (B → C) yielding *p*-nitrophenol is acid catalyzed [1]. A convenient method for dissection of the rate constants, k_A and k_B, from the spectrophotometrically measured reaction rates was given (4) for the case that k_A and k_B are comparable in magnitude.

An interesting situation arose when the reaction was performed with the $H_2NNH_3^+$/$^+H_3NNH_3^+$ combination, or with $^+H_3NNH_3^+$ alone in methanol solvent (3). In such systems the methanolysis reaction (HNu = CH_3OH)

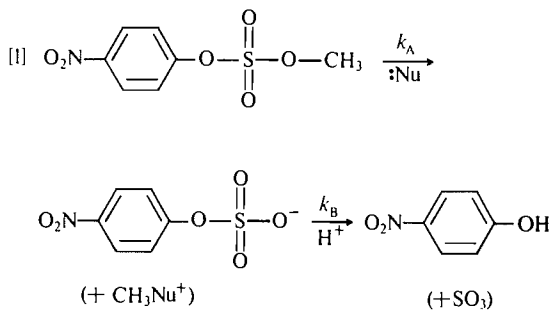

Can. J. Chem. Downloaded from www.nrcresearchpress.com by 210.87.254.42 on 09/05/12
For personal use only.

competes effectively with the hydrazinolysis ($HNu = H_2NNH_3^+$), giving rise in each case to *p*-nitrophenyl hydrogen sulfate as the product of the first reaction stage. The hydrogen ion thus generated augments the hydrogen ion concentration derived from dissociation of $^+H_3NNH_3^+$; together the two sources of H^+ (solvated) induce the second stage of reaction, the conversion of *p*-nitrophenyl sulfate ion to *p*-nitrophenol. Appropriate treatment of k_B then yielded an estimated pK_a value for $^+H_3NNH_3^+$ in methanol as 3.85 (3). This value appeared reasonable though it could not be compared with a literature value as such has not been reported (in water $^+H_3NNH_3^+$ has pK_a −0.67 (5)).

In the present study we have placed this kinetic method for pK_a evaluation on a firmer footing and have also simplified the procedure to make it more readily applicable. The kinetic technique has been simplified by isolating the $B \rightarrow C$ reaction independently of the $A \rightarrow B$ reaction. This can be done by using B as the reactant rather than A. By causing reaction to occur in the presence of the acidic species of interest, the measured rate constant (k_ψ) is used to calculate the pK_a of the catalyzing acid. The specific rate constant (k_{H^+}) for the conversion of *p*-nitrophenyl sulfate to *p*-nitrophenol in methanol is determined in prior experiments using mineral acid.

Results and Discussion

We have performed the reaction between potassium *p*-nitrophenyl sulfate and 4-picolinium chloride, as well as anilinium chloride, in methanol at 25 °C. The pK_a values derived from the reaction rates could be compared with literature data measured potentiometrically. The method, thus validated, has been used to obtain the pK_a values in methanol for the conjugate acids of hydroxylamine and methoxyamine, as well as to improve upon the hydrazinium pK_a. In addition we have made exploratory measurements in an ethanol medium in order to evaluate the general applicability of the kinetic spectrophotometric method for determination of pK_a.

Reaction of 4-picolinium chloride with potassium *p*-nitrophenyl sulfate in methanol at 25 °C was followed spectrophotometrically, making use of the characteristic absorptions of reactant and product in the ultraviolet region. The spectral observations in a typical experiment, using a substrate concentration of 5×10^{-5} *M* and reagent concentration of 34.21×10^{-3} *M*, consisted of a decrease in the absorption at 283 nm and a gradual growth of a peak at 311 nm as the reaction proceeded, with a tight isosbestic point at 294 nm maintained throughout the course of reaction. The final spectrum corresponds to quantitative formation of *p*-nitrophenol. A plot of $\log (A_\infty - A_t)$ *vs.* *t* for the absorbance changes at 311 nm exhibited a linear plot which yielded a pseudo first-order rate constant $k_\psi = 2.64 \times 10^{-4}\ s^{-1}$.

The mechanism of the acid induced conversion of *p*-nitrophenyl sulfate ion to *p*-nitrophenol has been established (6, 7) as proceeding according to eqs. 2 and 3 (Ar = *p*-nitrophenyl). The SO_3

[2] $$Ar{-}O{-}SO_3^- + H^+ \overset{\text{fast}}{\rightleftharpoons} Ar{-}\overset{+}{O}(H){-}SO_3^-$$

[3] $$Ar{-}\overset{+}{O}(H){-}SO_3^- \xrightarrow{\text{slow}} ArOH + SO_3$$

produced will be rapidly solvolyzed yielding methyl hydrogen sulfate, thus regenerating H^+. The overall reaction can be described as A-1, namely a unimolecular specific-hydrogen ion catalyzed process.

It is evident from eqs. 2 and 3 that the rate of transformation of *p*-nitrophenyl sulfate ion to *p*-nitrophenol, as induced by 4-picolinium ion, gives a direct measure of the hydrogen ion concentration in the reaction medium. Thus $k_\psi = k_{H^+}[H^+]$ and $k_{H^+} = 1.855\ M^{-1}\ s^{-1}$, from independent measurement of the reaction rate in HCl containing methanolic medium at 25 °C (3). Hence one obtains for the 4-picolinium ion reacting system $[H^+] = 2.64 \times 10^{-4}/1.855\ (M) = 1.428 \times 10^{-4}\ M$. The acidity constant for 4-picolinium ion can be obtained from the relationship $K_a = [H^+][C_6H_7N]/[C_6H_7NH^+]\ (M) = (1.428 \times 10^{-4})^2/34.07 \times 10^{-3}\ (M) = 5.98 \times 10^{-7}\ M$; *i.e.* $pK_a = 6.22$. The reported value (8*a*) for the pK_a of 4-picolinium ion in methanol, as measured potentiometrically, is 6.09.

A more accurate pK_a value is obtained from the present results by taking into account the fact that hydrogen chloride is incompletely dissociated in methanol ($pK_a = 1.23$ (8)) and therefore a correction is needed for a common

TABLE 1. Rate and equilibrium data in acidolysis of *p*-nitrophenyl sulfate effected by amine conjugate acids

$R_3N^+HCl^-$	$[R_3NH^+Cl^-]_0$[a] $\times 10^3$ *M*	k_ψ[b] $\times 10^4$ s^{-1}	$[H^+]$[c] $\times 10^5$ *M*	$[HCl]$[d] $\times 10^5$ *M*	$[R_3NH^+]$[e] $\times 10^3$ *M*	K_a[f]	pK_a[g]	Literature value
4-Picolinium	34.21	2.64	14.28	8.27	33.98	9.48×10^{-7}	6.02 ± 0.05	6.09(8*a*)
	68.42	3.60	19.40	22.40	65.99	1.19×10^{-6}	5.93 ± 0.05	
$C_6H_5NH_3^+$	50.67	3.18	17.10	14.65	50.35	1.08×10^{-6}	5.97 ± 0.05	5.80(8*b*)
	50.67	3.12	16.80	14.40	50.36	1.04×10^{-6}	5.98 ± 0.05	
$HONH_3^+$	14.20	1.42	7.65	1.85	14.11	5.15×10^{-7}	6.29 ± 0.05	
	14.20	1.46	7.86	1.89	14.10	5.44×10^{-7}	6.26 ± 0.05	
$CH_3ONH_3^+$	2.46	2.39	12.90	0.54	2.33	7.44×10^{-6}	5.13 ± 0.05	
	2.46	2.38	12.80	0.53	2.33	7.34×10^{-6}	5.13 ± 0.05	
$^+H_3NNH_3^+$[h]	2.46	12.97	69.90	5.71	1.70	2.94×10^{-4}	3.53 ± 0.05	
	2.46	12.61	67.88	5.61	1.73	2.74×10^{-4}	3.56 ± 0.05	

[a]Stoichiometric concentrations.
[b]Pseudo first-order rate constants at 25 °C.
[c]Calculated from $k_\psi = k_{H^+}[H^+]$ where $k_{H^+} = 1.855$ M^{-1} s^{-1}.
[d]Calculated from $[HCl] = \dfrac{[H^+]\,[R_3NH^+Cl^-]_0}{K_{HCl} + [H^+]}$.
[e]Calculated from $[R_3NH^+] = [R_3NH^+Cl^-]_0 - [H^+] - [HCl]$.
[f]Calculated from eq. 7.
[g]Error limit is based on $\pm5\%$ overall error in k_ψ and k_{H^+} (see text).
[h]For this diprotic acid the calculations are appropriately modified where necessary.

ion effect due to the amine hydrochloride introduced. Thus for the dissociation process given by eq. 4, one has at equilibrium the following

$$[4]\quad R_3NH^+ + Cl^- \overset{K_a}{\rightleftharpoons} R_3N + H^+ + Cl^- \overset{1/K_{HCl}}{\rightleftharpoons} R_3N + HCl$$

mass balance relationships,

$$[5]\quad [R_3N] = [H^+] + [HCl]$$

$$[6]\quad [R_3N] + [R_3NH^+] = [R_3NH^+Cl^-]_0 = [Cl^-] + [HCl]$$

and it follows that K_a is given by

$$[7]\quad K_a = [H^+]\left\{\frac{[R_3NH^+Cl^-]_0 + (K_{HCl} + [H^+])}{[R_3NH^+Cl^-]_0 K_{HCl}/[H^+] - (K_{HCl} + [H^+])}\right\}$$

For the 4-picolinium ion reaction with $[C_6H_7NH^+Cl^-]_0 = 34.21 \times 10^{-3}$ *M* and $[H^+] = 1.428 \times 10^{-4}$ *M* (from $k_\psi = k_{H^+}[H^+]$), one obtains $K_a = 9.48 \times 10^{-7}$ *M* and $pK_a = 6.02$. Other equilibrium quantities of interest in this system which can readily be calculated are $[HCl] = 8.27 \times 10^{-5}$ *M*, $[C_6H_7N] = 2.25 \times 10^{-4}$ *M* and $[C_6H_7NH^+] = 3.40 \times 10^{-2}$ *M* (Table 1). The uncertainty in the pK_a value can be estimated as follows. If the measured k_ψ has an associated error of $\pm3\%$, and if k_{H^+} has an error of $\pm2\%$, then $[H^+] = k_\psi/k_{H^+}$ will have an error of $\pm5\%$. Performing the calculation according to eq. 7 with these error limits leads to pK_a values of 5.98 and 6.07 respectively. Hence a given calculated pK_a has an associated error of ±0.05 units. We have found that replicate experiments yield an upper error limit of ±0.10 units in the pK_a value (Table 1).

The validity of the treatment for suppression of HCl dissociation due to added $R_3NH^+Cl^-$ could be confirmed independently. Thus reaction of *p*-nitrophenyl sulfate ion to *p*-nitrophenol, as induced by HCl in methanol, has been performed in the absence and in the presence of added tetraethylammonium chloride and k_ψ values have been determined. From the known pK_a of HCl (1.23) and the initial concentrations of Et_4NCl and HCl one can readily calculate the effective H^+ concentration and hence, using k_ψ, the specific rate coefficient k_{H^+}. The results, given in Table 2, show that k_{H^+} is constant within experimental error, *i.e.*, $k_{H^+} = 1.90 \pm 0.03$ M^{-1} s^{-1}. The good agreement with the previously determined value (3) for k_{H^+} (1.855 M^{-1} s^{-1}) shows that the treatment is self consistent and that no unusual salt effect is operating. These results give added confidence to the pK_a method described herein.

We have used the kinetic procedure outlined above for the pK_a determination of the amine conjugate acids given in Table 1, which also

Can. J. Chem. Downloaded from www.nrcresearchpress.com by 210.87.254.42 on 09/05/12
For personal use only.

TABLE 2. Rate data for acidolysis of *p*-nitrophenyl sulfate in the presence of tetraethylammonium chloride to demonstrate the common ion effect

$[HCl]_0$[a] $\times 10^3$ *M*	$[Et_4NCl]_0$[a] $\times 10^3$ *M*	k_ψ[b] $\times 10^4$ s^{-1}	$[H^+]$[c] $\times 10^4$ *M*	k_{H^+}[d] M^{-1} s^{-1}
1.000	—	18.7	9.84	1.90
1.000	33.3	11.9	6.41	1.86
1.000	67.0	9.05	4.69	1.93

[a]Initial concentrations.
[b]Measured pseudo first-order rate constants at 25 °C.
[c]Calculated from $[H^+] = \frac{1}{2}\{-K_{HCl} + [Et_4NCl]_0 + \sqrt{[(K_{HCl} + [Et_4NCl]_0)^2 + 4K_{HCl}[HCl]_0]}\}$.
[d]Calculated from $k_{H^+} = k_\psi/[H^+]$.

records the measured rate data and some calculated equilibrium quantities for these systems. The anilinium ion case was chosen as an additional acid of known pK_a in methanol (8*b*). The value for hydrazinium ion was determined as a confirmation of the value obtained by the earlier, more elaborate, method (3).[1] Hydroxylamine and methoxyamine are commonly used nucleophiles in a variety of investigations (9) and hence their pK_a in a non-aqueous medium was deemed to be of interest. The range of pK_a values covered in Table 1 is 3.5–6.3. However, it can readily be shown that the effectively accessible pK_a range for the *p*-nitrophenyl sulfate ion acidolysis reaction in methanol is actually *ca.* 2–8, by choosing initial concentrations of $R_3NH^+Cl^-$ between 10^{-3} *M* and 10^{-1} *M* while k_ψ at 25 °C is allowed to cover a range of conveniently measurable values, from 6×10^{-5} s^{-1} ($T_{1/2} \sim 3$ h) to 2×10^{-3} s^{-1} ($T_{1/2} \sim 6$ min). The pK_a range can be extended somewhat by performing the rate measurements at temperatures other than 25 °C.[2]

The method for pK_a determination which we have described should be capable of application to media other than methanol.[3] Preliminary experiments in ethanol have been performed. We have found that *p*-nitrophenyl sulfate reacts in ethanol containing HCl to yield *p*-nitrophenol with a second-order coefficient $k_{H^+}(EtOH) = 1.17 \times 10^{-2}$ M^{-1} s^{-1}. This appreciably smaller rate constant than for methanol (1.86 M^{-1} s^{-1}) means in effect that the ethanol medium is suitable for measuring pK_a's of stronger acids compared to methanol medium.

A variety of methods for the determination of acidity constants are known and these have been critically reviewed (10–12). It is clear that for highly precise pK_a values the established methods based, for example, on measurement of conductivity or electromotive force, are to be strongly preferred. However, in many cases data of such high precision have not been needed and then a variety of other methods have been used with their particular advantages and disadvantages. A kinetic method applicable to moderately concentrated acid media has been developed by Bunnett and Olsen (13). The rate of hydrolysis of ethylene acetal (14), which is known to be subject to specific hydrogen ion catalysis (15), was used to determine the pK_a of cacodylic acid by a principle analogous to the present. However, the experimental method used (14), namely following the reaction rate by dilatometry, has disadvantages compared with the spectrophotometric method employed in our work. Moreover, with compounds which do not have a characteristic absorption in the ultraviolet or visible region of the spectrum, so that standard spectrophotometric methods (11, 16) for pK_a determination (based on indicator ratio measurement) are not applicable, the presently described method should be of particular advantage. A noteworthy aspect of the present method, which is in contrast with many of the others (10–12), is that the extent of dissociation of the acid the pK_a of which is measured can be quite small (*e.g.* for the

[1]In the previous work (3) the common ion effect of added hydrazinium chloride was not taken into account. Recalculation of the earlier results (3) according to the present method yields for $^+H_3NNH_3^+$ $pK_a = 3.60$.

[2]Care must be exercised with relatively strong acids ($pK \leq 2$). In using eq. 7, (as when using the familiar eq. $K_{HA} = [H^+]^2/(C_0 - [H^+])$), an error in $[H^+]$ (obtained kinetically) of *ca.* ±5%, will be exaggerated when $[H^+]$ approaches $[R_3NH^+Cl^-]_0$ (*i.e.* for strong acids). The situation becomes considerably improved of course if the error in rate measurements can be reduced to, say, ±1%.

[3]In media of low dielectric constant, ion association can become a complicating factor, and a cautionary note is needed in this regard.

Can. J. Chem. Downloaded from www.nrcresearchpress.com by 210.87.254.42 on 09/05/12
For personal use only.

Can. J. Chem. Downloaded from www.nrcresearchpress.com by 210.87.254.42 on 09/05/12
For personal use only.

4-picolinium ion case *ca.* 1%, Table 1) owing to the sensitivity of the rate of the reaction followed to acid catalyst.

Experimental

Materials and Methods

The hydrochloride salts of picoline and of aniline were prepared as crystalline compounds by the action of HCl on ethereal solutions of the amines; the others were commercially procured. Methanol and ethanol solvents were dried and distilled. Potassium *p*-nitrophenyl sulfate was purchased from Sigma Chemicals. The purity of this compound can be ascertained by examining the spectrum in alkaline solution for the presence of *p*-nitrophenoxide ion and by the quantitativeness of the conversion to *p*-nitrophenol in acidic medium. In most of the present work it was found convenient to prepare a solution of potassium *p*-nitrophenyl sulfate *in situ* by the alkaline methanolysis of methyl *p*-nitrophenyl sulfate (17) and this method will be described in detail.

A stock solution of potassium *p*-nitrophenyl sulfate was prepared in a 10 ml volumetric flask by addition of 1 ml 0.275 *M* CH_3OK/CH_3OH to 1 ml of 1.50×10^{-2} *M* methyl *p*-nitrophenyl sulfate – ether solution and making up to mark with methanol. The resulting solution (90% methanol – 10% ether) was 1.50×10^{-3} *M* in *p*-nitrophenyl sulfate and 2.60×10^{-2} *M* in base due to quantitative reaction of the methyl aryl sulfate (1). This alkaline stock solution is stable for long periods of time. A second stock solution of 2.60×10^{-2} *M* HCl in methanol was prepared by appropriate dilution. Reaction mixtures were prepared by addition to a 1 cm cuvette of 0.100 ml of the two stock solutions, an appropriate volume of methanolic amine hydrochloride, and sufficient methanol to make up to 3.00 ml (the *p*-nitrophenyl sulfate solution was added last to the thermostatted cell to initiate the reaction). A Bausch and Lomb SP 505 spectrophotometer with a thermostatted cell block was used, scanning over the region 220 to 370 nm.

Tests for Buffer Catalysis and for Common Ion Effects

Tests for buffer catalysis were made in the case of the hydrazinium ion system. Reaction was performed using a buffer solution with $[H_2NNH_3^+] = [^+H_3NNH_3^+] = 2.5 \times 10^{-3}$ *M* and k_ψ determined as 5.07×10^{-4} s^{-1}. Another (duplicate) experiment was performed with $[H_2NNH_3^+] = [^+H_3NNH_3^+] = 5.0 \times 10^{-3}$ *M* which gave $k_\psi = 5.11 \times 10^{-4}$ s^{-1}, showing that no detectable buffer catalysis obtains.

Experiments with added tetraethylammonium chloride were performed to demonstrate the common ion effect on HCl association. The technique employed was analogous to that with the amine hydrochlorides but using instead HCl as the catalyst and determining the rate of conversion of *p*-nitrophenyl sulfate ion to *p*-nitrophenol in the usual way. The results are given in Table 2.

Acknowledgment

Continued financial support of this research by the National Research Council of Canada is acknowledged with thanks.

1. E. BUNCEL, A. RAOULT, and J. F. WILTSHIRE. J. Am. Chem. Soc. **95**, 799 (1973).
2. E. BUNCEL, C. CHUAQUI, P. FORSYTHE, S. MAHONEY, A. RAOULT, and J. F. WILTSHIRE. J. Chem. Soc. Perkin Trans. 2, 478 (1975).
3. E. BUNCEL and C. CHUAQUI. Can. J. Chem. **53**, 1275 (1975).
4. E. BUNCEL, A. RAOULT, and J. F. WILTSHIRE. J. Chem. Educ. **51**, 814 (1974).
5. J. J. CHRISTENSEN, R. M. IZATT, D. P. WRATHALL, and L. D. HANSEN. J. Chem. Soc. A, 1212 (1969).
6. J. L. KICE and J. M. ANDERSON. J. Am. Chem. Soc. **88**, 5242 (1966).
7. E. J. FENDLER and J. H. FENDLER. Chem. Commun. 1261 (1967).
8. (*a*) C. D. RITCHIE. *In* Solute–solvent interactions. *Edited by* C. D. Ritchie and J. F. Coetzee. Dekker, New York. 1969; (*b*) A. L. BACARELLA, E. GRUNWALD, H. P. MARSHALL, and E. L. PURLEE. J. Org. Chem. **20**, 747 (1955).
9. W. P. JENCKS. Catalysis in chemistry and enzymology. McGraw-Hill, New York. 1969.
10. E. J. KING. Acid–base equilibria. Pergamon Press, Oxford. 1965.
11. A. ALBERT and E. P. SERJEANT. The determination of ionization constants. 2nd ed. Chapman and Hall, London. 1971.
12. R. F. COOKSON. Chem. Rev. **74**, 5 (1974).
13. J. F. BUNNETT and F. P. OLSEN. Can. J. Chem. **44**, 1916 (1966).
14. M. L. KILPATRICK. J. Am. Chem. Soc. **71**, 2607 (1949).
15. J. N. BRONSTED and C. GROVE. J. Am. Chem. Soc. **52**, 1394 (1930).
16. A. DOLENKO, K. MAHENDRAN, and E. BUNCEL. Can. J. Chem. **48**, 1736 (1970); R. A. Cox and E. BUNCEL. Can. J. Chem. **51**, 3143 (1973).
17. E. BUNCEL and A. RAOULT. Can. J. Chem. **50**, 1907 (1972).

The log k_{exo} *vs.* log k_{endo} correlation as a mechanistic criterion; on the mechanisms of solvolysis of norbornyl derivatives and base-catalyzed isotope exchange of norbornanones

SUJIT BANERJEE AND NICK HENRY WERSTIUK[1]
Department of Chemistry, McMaster University, Hamilton, Ontario L8S 4M1

Received August 1, 1975

SUJIT BANERJEE and NICK HENRY WERSTIUK. Can. J. Chem. **54**, 678 (1976).

Rate data for the acetolysis of *exo*-norbornyl-sulfonates have been correlated with those for the corresponding *endo* isomers. It is shown that the slopes of the log k_{exo} *vs.* log k_{endo} plots reflect the difference in delocalization between the transition states derived from the *exo* and *endo* isomers, respectively. The log k_{exo} *vs.* log k_{endo} plot, which is comprised of the parent norbornyl sufonate and its derivatives substituted at the 5, 6, and 7 positions, has a slope of 1.11 ± 0.08, which establishes that σ bridging is absent in the transition state obtained from the *exo* isomer. A similar analysis of base-catalyzed hydrogen–deuterium exchange rates of norbornanones reveals that *exo* proton exchange is more sensitive to substituent effects than the corresponding *endo* process.

SUJIT BANERJEE et NICK HENRY WERSTIUK. Can. J. Chem. **54**, 678 (1976).

On a fait une corrélation entre les données de vitesse d'acétolyse des sulfonates d'*exo*-norbornyle avec celles des isomères *endo* correspondants. On a montré que les pentes des courbes du log k_{exo} *vs.* log k_{endo} réflètent la différence de délocalisation entre les états de transition dérivés respectivement des isomères *exo* et *endo*. La courbe de log k_{exo} *vs.* k_{endo} qui est formée par le sulfonate de norbornyle non substitué et ses dérivés substitués aux positions 5, 6 et 7 a une pente de 1.11 ± 0.08 qui établie que le pontage σ est absent dans l'état de transition obtenu à partir de l'isomère *exo*. Une analyse similaire des taux d'échange hydrogène–deutérium, catalysés par les bases, de la norbornanone révèle que l'échange des protons *exo* est plus sensible aux effets de substituants que le processus pour les hydrogènes *endo* correspondants.

[Traduit par le journal]

Introduction

Recent work by Brown and co-workers (1) and others (2) has provided evidence of the absence of σ-bridged cations in the solvolysis of norbornyl derivatives. According to Brown's thesis, the large *exo/endo* rate ratios observed in solvolysis are derived from differences in steric environment rather than from participation of the C_1—C_6 bond during solvolysis of the *exo* stereoisomer. Other workers, however, have attributed the difference in stereochemical reactivity to σ bridging in the *exo* transition state (3, 4).

Quantitative definition of substituent effects has been attempted by standard linear free energy methods. For example, solvolytic rate data for benzonorbornen-2-yl-brosylates and benzonorbornen-9-yl-brosylates bearing substituents on the aromatic ring correlate well with σ or σ^+ (5–7). However, the origin of the variation of *exo/endo* rate ratios in these and other processes remains to be established.

Our interest in the area stems from our studies on stereoselective base-catalyzed exchange in norbornanones (8, 9, 12), where variation of the *exo/endo* rate ratio with structure is well known (8–12). In this paper we interpret acetolysis rate data by means of log k_{exo} *vs.* log k_{endo} plots, and show that the available data argue against σ participation in simple norbornyl derivatives.

Discussion

Solvolysis of Norbornyl Derivatives

From a study of the solvolysis of a number of 2-substituted norbornyl derivatives, Brown and co-workers have concluded that σ bridging is unimportant in the reaction of the *exo* isomers (13–15). These views have been based on the insensitivity of the *exo/endo* rate ratio to electron demand, and on the similarity of σ^+ values for the solvolysis of *exo*-norbornyl-, *endo*-norbornyl-,

[1]Author to whom enquiries should be addressed.

Can. J. Chem. Downloaded from www.nrcresearchpress.com by 210.87.254.5 on 09/05/12
For personal use only.

Can. J. Chem. Downloaded from www.nrcresearchpress.com by 210.87.254.5 on 09/05/12
For personal use only.

TABLE 1. Acetolysis rates of *exo*-2, *endo*-2, *syn*-9, and *anti*-9-benzonorbornenyl brosylates at 77.6 °C*

		log $k_{exo(anti)}$	log $k_{endo(syn)}$
2-Benzonorbornenyl brosylate	**1**	−2.427	−6.089
6-Methoxy-**1**	**2**	−0.174	−5.662
7-Methoxy-**1**	**3**	−2.572	−6.019
7-Methoxy-6-nitro-**1**	**4**	−5.388	−6.889
7-Nitro-**1**	**5**	−5.439	−7.087
6,7-Dinitro-**1**	**6**	−7.452	−8.024
9-Benzonorbornenyl brosylate	**7**	−4.827	−7.893
6-Chloro-**7**	**8**	−6.178	−8.410
6-Nitro-**7**	**9**	−8.684	−9.325
6-Methyl-**7**	**10**	−4.074	−7.690
6-Methoxy-7	**11**	−3.093	−7.684

*Taken from refs. 5–7.

and cyclopentyl esters (13). Linear free energy correlations of this type are, however, limited to systems bearing aromatic moieties, and are not generally applicable with any precision to simple substrates with a variety of substituents at different sites. On the other hand, a plot of log k_{exo} *vs.* log k_{endo} circumvents the need for external parameters such as σ or σ^+. The slope of this plot should therefore reflect differential delocalization between the transition states derived from the *exo* and *endo* isomers, respectively.

Tanida and co-workers have correlated the acetolysis rates of a series of benzonorbornen-2-yl-brosylates (**1–6** *exo* and *endo*) and benzonorbornen-9-yl-brosylates (**7–11** *syn* and *anti*) with σ and σ^+ (5–7). For the former series they have obtained ρ values of −3.26 and −1.31 for the *exo* and *endo* isomers respectively. The kinetic data are summarized in Table 1, and the log $k_{exo(anti)}$ *vs.* log $k_{endo(syn)}$ plot for these derivatives is illustrated in Fig. 1. The slopes of these lines (2.9 ± 0.3, corr. coeff. = 0.97 for the 2-brosylates and 3.1 ± 0.4, corr. coeff. = 0.98 for the 9-brosylates)[2] establish that the solvolytic rates of the *exo* and *anti* isomers are more sensitive to substituents than are the rates of the corresponding *endo* and *syn* isomers.[3] Accordingly,

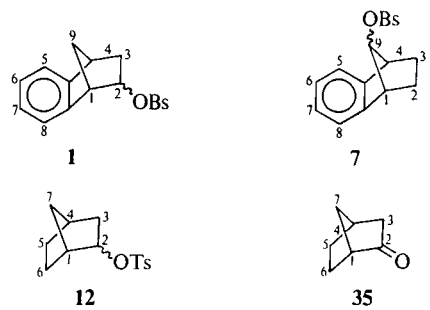

1 **7** **12** **35**

in keeping with Tanida's conclusions, participation of the aryl ring is more important in stabilizing the developing positive charge for the solvolysis of the *exo* and *anti* isomers than it is for that of the *endo* and *syn* isomers. Thus, we establish that plots of the type shown in Fig. 1

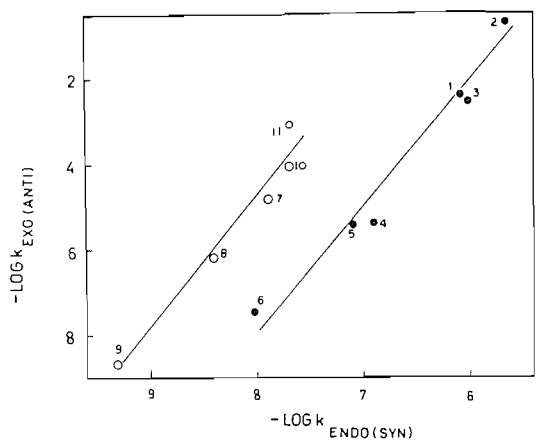

FIG. 1. Plot of log k_{exo} *vs.* log k_{endo} for benzonorbornen-2-yl brosylates (●) and log k_{anti} *vs.* log k_{syn} for benzonorbornen-9-yl brosylates (○).

[2]The 6-OMe substituent in both the 2-(**1–6**) and the 9-(**7–11**) substituted norbornenyl systems deviates from the line which correlates non-lone pair containing substituents. This deviation signals the incursion of an additional stabilizing mechanism involving the 6-OMe group. When the 6-OMe group is omitted from both correlations, the slopes are 2.6 and 2.8, respectively.

[3]The similar slopes obtained from the 2- and 9-substituted norbornyl substrates perhaps identifies comparable π participation in the transition states.

TABLE 2. Acetolysis rates of 2-norbornyl tosylates at 25 °C

		log k_{exo}	log k_{endo}	Reference
2-Norbornyl tosylate	**12**	−4.619	−7.089	17
5-Methoxy-**12**	**13**	−6.485	−8.451	17
6-Methoxy-**12**	**14**	−5.481	−7.487	17
7-*anti*-Methoxy-**12**	**15**	−5.710	−7.511	17
6,6-Dimethyl-**12**	**16**	−6.036	−8.350	18
5,5-Dimethyl-**12**	**17***	−5.060	−7.222	19
7-*syn*-Chloro-**12**	**18**	−7.179	−9.570	20
7-*anti*-Chloro-**12**	**19**	−7.367	−9.269	20
7-*syn*-Phenyl-**12**	**20**	−5.219	−7.524	23
7-*anti*-Phenyl-**12**	**21**	−5.246	−7.631	23
5-Keto-**12**	**22***	−8.548	−10.176	21
7-Keto-**12**	**23**	−7.842	−7.062	22
7,7-Dimethyl-**12**	**24***	−3.591	−7.203	19
3,3-Dimethyl-**12**	**25***	−4.960	−8.052	19
3-*exo*-Phenyl-**12**	**26**	−7.217	−9.973	23
3-*endo*-Phenyl-**12**	**27**	−5.636	−7.196	23

*Rates for the brosylates have been converted by division by a factor of 3.

are sufficiently sensitive to detect a difference in transition state stabilization where it unquestionably occurs in a pair of stereoisomers.[4]

We now turn our attention to the question of σ bridging in simple norbornyl substrates. If the *exo* transition state is indeed bridged, then in the absence of steric, torsional, and strain effects, the influence of substituents through an inductive effect would manifest itself by affecting the solvolysis rate of the *exo* derivative more than that of the corresponding *endo* isomer. That is, since the electron density at the site of electron donation, namely the C_1—C_6 bond, should be depleted or increased through the effects of substituents at C_4, C_5, C_6, and C_7, the rate ratio should be altered.[5] Consequently, the slope of the log k_{exo} *vs.* log k_{endo} plot would exceed unity if σ participation was of significance in the solvolysis of the *exo* isomer.

Rate data for the solvolysis of norbornyl tosylates substituted at the 3, 5, 6, and 7 positions are listed in Table 2, and a plot of log k_{exo} *vs.* log k_{endo} is illustrated in Fig. 2. The slope of the line is 1.11 ± 0.08, (corr. coeff. = 0.98)[6] which indicates that the transition states derived from the *exo* and *endo* isomers respectively are equally affected by inductive variations, and does not support the concept of σ-bridging

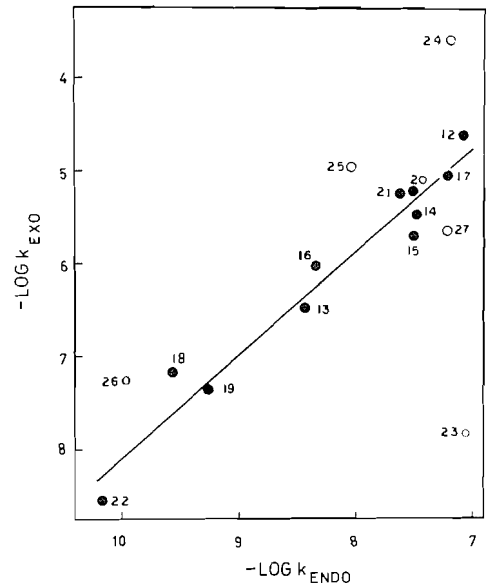

FIG. 2. Plot of log k_{exo} *vs.* log k_{endo} for substituted norbornyl sulfonates.

[4]A referee has pointed out that the linear regression analysis used here is inapplicable to the equation described. While recognizing the validity of this criticism we note that (*a*) the data analyzed in this paper were obtained in various laboratories, presumably with varying uncertainties, and (*b*) some of the data were obtained through extrapolations in temperature or corrections for the nature of the leaving group. Hence, since the errors in the individual data points are unknown, and vary considerably, little is to be gained by the application of more rigorous regression analysis.

[5]That substituents alter the effectiveness of σ-type participation, as well as that of the π type, has been established in studies of the cyclopropyl carbinyl system (16).

[6]Substrates **23**–**27** have been omitted from the least-squares analysis.

Can. J. Chem. Downloaded from www.nrcresearchpress.com by 210.87.254.5 on 09/05/12
For personal use only.

TABLE 3. Acetolysis rates of 1-substituted norbornyl tosylates at 25 °C*

		log k_{exo}	log k_{endo}
1-Phenyl-**12**†	**28**	−4.020	−7.247
1-*p*-Nitrophenyl-**12**	**29**	−5.108	−8.379
1-*p*-Chlorophenyl-**12**	**30**	−4.175	−7.724
1-*m*-Methoxyphenyl-**12**	**31**	−4.015	−7.311
1-*p*-Toluyl-**12**	**32**	−3.801	−7.268
1-*p*-Methoxyphenyl-**12**	**33**	−3.726	−7.206
1-*o*-Methoxyphenyl-**12**	**34**	−3.318	−6.119

*Taken from ref. 25.
† Taken from ref. 23.

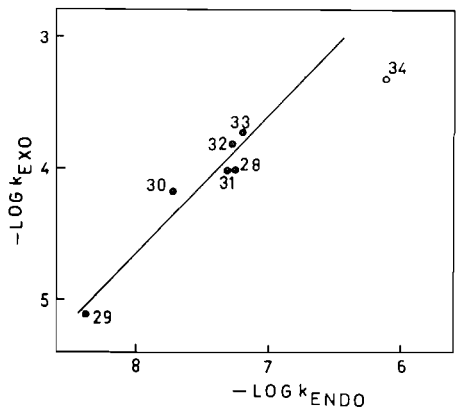

FIG. 3. Plot of log k_{exo} *vs.* log k_{endo} for substituted-1-aryl norbornyl tosylates.

in the transition state for solvolysis of the *exo* isomer.

Deviations from the least-squares line in Fig. 2 establish the involvement of other rate influencing factors. The deviation of the 7-keto derivative **23** from the line is in keeping with the enhanced reactivity of the *endo* isomer, which is 320 times more reactive than expected (22), and probably arises from participation of the carbonyl oxygen or its solvated moiety in the transition state. Steric acceleration in the reaction of the 7,7-dimethyl derivative **24** could account for the deviation of this compound. The deviations present in the 3-substituted compounds are less serious, but are also less easily rationalized. The marked difference in reactivity between the *exo*-3-phenyl-**12** (**26**) and the *endo*-3-phenyl-**12** (**27**) derivatives are of particular significance. While this might, to a certain extent, be attributed to differences in ground state energy, an alternate explanation involving steric inhibition to solvation is perhaps more important (23).

The solvolysis of 1-aryl-2-norbornyl tosylates is also of interest. Kinetic data are summarized in Table 3, and the *exo–endo* relationship is outlined in Fig. 3. Although the range of reactivity is more limited in this case, the slope (1.1 ± 0.1, corr. coeff. = 0.977[7] suggests that σ bridging does not occur in the transition state obtained from the *exo* isomer.[8] Interestingly, although the lines in Figs. 2 and 3 are nearly parallel, the latter is located at approximately 1.5 log units above the former. This difference originates in all likelihood from the steric acceleration to ionization of the 1-aryl-*exo*-2-derivatives. If such is the case, then the difference in intercept, a factor of 30, between the lines in Figs. 2 and 3 is a measure of this acceleration.

The validity of the relationships summarized in Figs. 1–3 is dependent upon the constancy of the ground stage energy difference between the *exo* and *endo* epimers as well as upon the constancy of internal return processes and solvation effects. However, the difference in energy between *exo* and *endo* isomers with remote substituents is expected to be small as compared to the activation energy, and minor variations in the equilibrium constant are not likely to cause any serious error. Although the effect of sub-

[7]Substrate **34** has been omitted from the least-squares analysis. The special effect of the OMe substituent is indicated by a change in $\Delta S^{\ddagger}$ for the reaction. The solvolysis of *exo*-**34** has $\Delta S^{\ddagger} = -4.2$ compared to $\Delta S^{\ddagger} = -0.3$ to -2.6 for the other *exo* members of the series. Similarly $\Delta S^{\ddagger}$ for *endo*-**34** is -1.6, whereas *endo*-**28** to **33** are associated with $\Delta S^{\ddagger}$ values of -5.2 to -7.9 (23, 24).

[8]For this particular series, the log k_{exo} *vs.* log k_{endo} slope equals ρ_{exo}/ρ_{endo}. Reported values of ρ_{exo} and ρ_{endo} are -1.36 and -1.06 respectively (25). However, for the compounds considered we find $\rho_{exo} = -1.32$ and $\rho_{endo} = -1.19$, from which $\rho_{exo}/\rho_{endo} = 1.1$, in agreement with our value for the slope.

Can. J. Chem. Downloaded from www.nrcresearchpress.com by 210.87.254.5 on 09/05/12
For personal use only.

TABLE 4. Rates of base-catalyzed hydrogen–deuterium exchange in norbornanones in 60% dioxane – 40% D_2O at 25 °C

		log k_{exo}	log k_{endo}	Reference
2-Norbornanone	**35**	−1.415	−4.229	8
5-Methylene-**35**	**36**	−0.466	−3.907	12
6,6-Dimethyl-**35**	**37**	−1.785	−4.587	12
4,6,6-Trimethyl-**35**	**38**	−2.005	−4.597	12
5-Methylene-6,6-dimethyl-**35**	**39**	−0.883	−4.126*	12
4,6,6-Trimethyl-5-methylene-**35**	**40**	−1.167	−4.138	8
3-Chloro-**35**	**41**	2.424	−1.973†	
Norbornenone	**42**	−3.270	−5.218*	31
Benzonorbornenone	**43**	−1.705	−4.480*	31
1,7,7-Trimethyl-**35**	**44**	−3.155	−4.484	31
6-Methylene-**35**	**45**	−1.157	−4.879	12

*These rates were obtained in 2:1 dioxane–D_2O. They were converted to the above solvent system by multiplication by 0.736 (the ratio of the exchange rates of **35** in the two solvent systems).

†These rates have been corrected for the ground state energy difference between the two stereoisomers as well as for a small temperature difference. The observed *exo*/*endo* rate ratio is 11 500.

stituents on the extent of internal return has yet to be assessed, no major changes are expected in the case of C_5, C_6, and *anti*-C_7 substituted systems because of the remoteness of substituents from the reaction site. That this is the case is supported by the quality of the data in Fig. 2 for non-sterically perturbed substrates.

Base-catalyzed Exchange of Norbornanones

The high *exo–endo* rate ratios observed in base-catalyzed hydrogen–deuterium exchange in norbornanones has been interpreted as indicative of steric hindrance to *endo* proton abstraction (26). From a study on the isomerization of exocyclic olefins, Bank *et al.* have presented evidence for a twisted allylic ion intermediate (27). Since rates of ketone enolization correlate[9] well with those of olefin isomerization (27–29), it is likely that the enols or enolates involved are twisted to some extent. Consequently, the transition state arising from one of the epimers will possess greater enolic character than the other, and the *exo*/*endo* exchange ratio observed might in part derive from the preferential overlap in one of the two transition states. We have been able to correlate *exo* and *endo* exchange rates for the series of bicyclic ketones listed in Table 4. The plot in Fig. 4 has a slope of 1.72 ± 0.08 (corr. coeff. = 0.993) implying that the *exo* process is the more sensitive to substituent effects.[10,11] Hence, more charge is developed on C_2 during *exo* proton abstraction than it is for the corresponding *endo* process. The value of the slope can be accounted for if the intermediate enol or enolate is twisted towards the *endo*

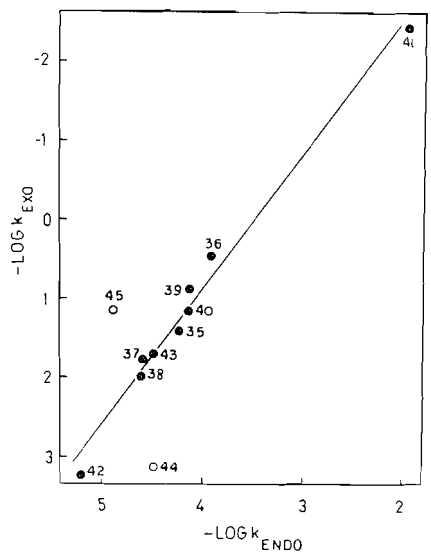

FIG. 4. Plot of log k_{exo} *vs.* log k_{endo} for H–D exchange for substituted 2-norbornanones.

[9]N. H. Werstiuk and S. Banerjee, unpublished results.

[10]We have previously observed that exchange of the *endo* protons in norbornanones proceeds through two competing processes (9). However, the observed *exo*/*endo* rate ratios are only about 10–20% less than the true stereoselectivities. Consequently, the errors will appear in the intercept of the line in Fig. 4 rather than in the slope.

[11]Substrates **44** and **45** have been omitted from the least-squares analysis.

Can. J. Chem. Downloaded from www.nrcresearchpress.com by 210.87.254.5 on 09/05/12
For personal use only.

direction, that is, the anion derived from *endo* proton abstraction overlaps better with the carbonyl π system in the transition state than does the anion obtained from *exo* proton abstraction. Some support for this rationale is available from a comparison of the solvolysis rates of the **12**-*exo*- and **12**-*endo*-tosylates with the *exo*- and *endo*-3-methylene-2-norbornyl-tosylates (30). The

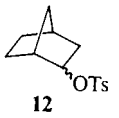

12

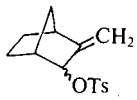

	k_{solv}	k_{solv}
exo	2.36×10^{-5} s^{-1}	1.02×10^{-4} s^{-1}
endo	8.28×10^{-8} s^{-1}	2.62×10^{-5} s^{-1}

reasons for this twisted geometry are not yet clear. However, models show that a developing lone pair (or *p* orbital in the cation) with *endo* stereochemistry is more easily brought into coplanarity with the carbonyl π orbital (or double bond) through an *endo* twist that opens up the C-1, C-2, C-3 bond angle to better accommodate the developing sp^2 center. The *exo* twist is not favoured because such a twist would close the C-1, C-2, C-3 bond angle and thus decrease the ease of introduction of an sp^2 center at C-2. Also, the *exo* twist increases the non-bonded interaction between the *syn* hydrogen at C-7 and the reacting *exo* site at C-2. However, in the absence of further evidence, this view must be regarded as tentative.

As in the case of solvolysis of norbornyl systems, only those substrates which possess special features such as steric and homoconjugative influences would be expected to deviate from the least-squares line in Fig. 4.

Comparison of the solvolytic and exchange data reveal several features of interest. The magnitude of the deviation of the 7,7-dimethyl derivative **44** in Fig. 4 is similar and opposite in sign to that of **24** in Fig. 2, and probably owes its origin to similar steric factors. Thus if steric acceleration is responsible for the deviation of the 7,7-dimethyl-ester **24** in Fig. 2, then steric hindrance to approach of base quite reasonably accounts for the deviation of **44**, in Fig. 4.

Tidwell has argued that bis-homo-*anti*-aromatic delocalization in the enol or enolate obtained from norbornenone, **42**, results in its decreased reactivity with respect to norcamphor, **35** (31). However, the presence of unsaturation should affect the *exo* rate but leave the *endo* rate relatively unaltered, so that π interaction of the proposed type would lead to significant deviation in Fig. 4. This is evidently not the case. Consequently, we believe that partial ground state interaction of the double bond with the carbonyl group (for which there is spectroscopic evidence (32)) reduces the electron-withdrawing nature of the carbonyl group. These same arguments apply to the benzonorbornene derivative **43**.

The deviation of **45** from the lines is surprising, and points to some hitherto unsuspected special effects inherent in the molecule.

Conclusions

In summary, we have established that log k_{exo} *vs.* log k_{endo} or related relationships are useful on two accounts: they correlate changes in stereoselectivity with variations in substrate structure and they provide a means of estimating the importance of special features associated with compounds which deviate from the norm.

Insofar as norbornyl ester solvolysis is concerned, our interpretation demonstrates the absence of significant charge delocalization in the transition state for *exo* solvolysis relative to that for the *endo* reaction. This conclusion considered in conjunction with other results and viewpoints (1, 2) makes the σ bridged norbornyl cation an unnecessary and improbable species in solvolytic processes.

Acknowledgment

We thank the National Research Council of Canada for financial support.

1. E. N. Peters and H. C. Brown. J. Am. Chem. Soc. **97**, 2892 (1975), and references cited therein.
2. F. K. Fong. J. Am. Chem. Soc. **96**, 7638 (1974).
3. P. D. Bartlett. Nonclassical ions. W. A. Benjamin, New York, N.Y. 1965.
4. C. F. Wilcox, Jr., L. M. Loew, R. G. Jesaitis, S. Belin, and J. N. C. Hsu. J. Am. Chem. Soc. **96**, 4061 (1974).
5. H. Tanida, Y. Hata, S. Ikegami, and H. Ishitobi. J. Am. Chem. Soc. **89**, 2928 (1967).
6. H. Tanida, H. Ishitobi, T. Irie, and T. Tsushima. J. Am. Chem. Soc. **91**, 4512 (1969).
7. H. Tanida, T. Irie, and T. Tsushima. J. Am. Chem. Soc. **92**, 3404 (1970).
8. N. H. Werstiuk and R. Taillefer. Can. J. Chem. **48**, 3966 (1970).
9. S. Banerjee and N. H. Werstiuk. Can. J. Chem. **53**, 1099 (1975).

Can. J. Chem. Downloaded from www.nrcresearchpress.com by 210.87.254.5 on 09/05/12
For personal use only.

10. G. A. ABAD, S. P. JINDAL, and T. T. TIDWELL. J. Am. Chem. Soc. **95**, 6326 (1973).
11. W. O. CRAIN. Ph.D. Thesis, Indiana University, Bloomington, Indiana. 1969.
12. R. TAILLEFER. Ph.D. Thesis, McMaster University, Hamilton, Ontario. 1973.
13. H. C. BROWN and M. RAVINDRANATHAN. J. Am. Chem. Soc. **97**, 2895 (1975).
14. H. C. BROWN, M. RAVINDRANATHAN, K. TAKEUCHI, and E. N. PETERS. J. Am. Chem. Soc. **97**, 2899 (1975).
15. H. C. BROWN, E. N. PETERS, and M. RAVINDRANATHAN. J. Am. Chem. Soc. **97**, 2900 (1975).
16. H. G. RICHEY. Cyclopropyl carbonium ions. Vol. 3 of Carbonium ions. *Edited by* G. A. Olah and P. v. R. Schleyer. Wiley, New York. 1972.
17. P. v. R. SCHLEYER, P. J. STANG, and D. J. RABER. J. Am. Chem. Soc. **92**, 4725 (1970).
18. P. v. R. SCHLEYER, M. M. DONALDSON, and W. E. WALTS. J. Am. Chem. Soc. **87**, 375 (1965).
19. A. COLTER, E. C. FRIEDRICH, N. J. HOLNESS, and S. WINSTEIN. J. Am. Chem. Soc. **87**, 378 (1965).
20. P. G. GASSMAN and J. M. HORNBACK. J. Am. Chem. Soc. **91**, 4280 (1969).
21. J. C. GREEVER and D. E. GWYNN. Tetrahedron Lett. 813 (1969).
22. P. G. GASSMAN and J. L. MARSHALL. J. Am. Chem. Soc. **88**, 2822 (1966).
23. D. C. KLEINFELTER, E. S. TRENT, J. E. MALLORY, T. E. DYE, and J. H. LONG, JR. J. Org. Chem. **38**, 4127 (1973).
24. J. A. BERSON. Molecular rearrangement. Part One. *Edited by* P. de Mayo. Interscience, New York. 1963.
25. P. v. R. SCHLEYER and D. C. KLEINFELTER. 138th Meeting, Am. Chem. Soc., New York. September, 1960. Abstracts, p. 43P.
26. G. D. SARGENT. Carbonium ions. *Edited by* G. A. Olah and P. v. R. Schleyer. Wiley, New York. 1972.
27. S. BANK, C. A. ROWE, JR., A. SCHRIESCHEIM, and L. A. NASLUND. J. Am. Chem. Soc. **89**, 6897 (1967).
28. A. SCHRIESCHEIM, R. J. MULLER, and C. A. ROWE, JR. J. Am. Chem. Soc. **84**, 3164 (1962).
29. A. SCHRIESCHEIM, C. A. ROWE, JR., and L. NASLUND. J. Am. Chem. Soc. **85**, 2111 (1963).
30. C. F. WILCOX, JR. and R. G. JESAITIS. Chem. Commun. 1046 (1967).
31. T. T. TIDWELL. J. Am. Chem. Soc. **92**, 1448 (1970).
32. N. H. WERSTIUK, R. TAILLEFER, R. A. BELL, and B. SAYER. Can. J. Chem. **51**, 3010 (1973).

Can. J. Chem. Downloaded from www.nrcresearchpress.com by 210.87.254.5 on 09/05/12
For personal use only.

The reduction of acetals with cobalt carbonyl catalysts[1]

BRUCE I. FLEMING AND HENRY I. BOLKER

Pulp and Paper Research Institute of Canada, and Department of Chemistry, McGill University, Montreal, Quebec H3C 3G1

Received August 25, 1975

BRUCE I. FLEMING and HENRY I. BOLKER. Can. J. Chem. **54**, 685 (1976).

When heated with a dicobalt octacarbonyl ($Co_2(CO)_8$) catalyst under synthesis gas, acetals of aromatic aldehydes (in contrast to aliphatic acetals) gave good yields of the products of reductive cleavage, but no products of hydroformylation. A mechanism is proposed to explain the products of cyclic acetals of benzaldehyde which yielded not only the expected hydroxy-ethers, but also considerable amounts of dibenzyl ethers. The room temperature reductive cleavage of aromatic acetals by pure $HCo(CO)_4$ in organic solvents indicates that $HCo(CO)_4$ might be the active species in the catalytic reductions. Since acetals of benzaldehyde *para*-substituted with electron-releasing groups cleaved faster than those substituted with electron-withdrawing groups, the mechanism probably involves a carbonium ion intermediate.

The previously observed formation of dibenzyl ether during benzaldehyde reduction with cobalt carbonyl catalysts can now be explained via the reductive cleavage of hemiacetal or acetal intermediates.

BRUCE I. FLEMING et HENRY I. BOLKER. Can. J. Chem. **54**, 685 (1976).

Lorsque l'on chauffe des acétals d'aldéhydes aromatiques (par opposition aux acétals aliphatiques) en présence d'un catalyseur octacarbonyl de dicobalt ($Co_2(CO)_8$) dans une atmosphère de gaz de synthèse, on obtient de bons rendements de produits de rupture réductrice; il n'y a toutefois pas de formation de produits d'hydroformylation. On propose un mécanisme pour expliquer la nature des produits formés à partir d'acétals cycliques du benzaldéhyde; dans ce cas il y a formation, en plus des hydroxy-éthers attendus, de quantités considérables d'éthers dibenzyliques. La coupure réductrice d'acétals aromatiques par $HCo(CO)_4$ dans des solvants aromatique à température de la piéce, indique que le $HCo(CO)_4$ peut être l'entité réactive dans les réductions catalytiques. Puisque les acétals de benzaldéhydes substitués en *para* par des groupes électro-donneurs se coupent plus rapidement que ceux substitués par des groupes électroaffinitaires, le mécanisme implique probablement une carbocation comme intermédiaire.

Il avait été observé antérieurement qu'il y a formation d'un éther dibenzylique lors de la réduction du benzaldéhyde par des catalyseurs de carbonyles de cobalt; on peut maintenant expliquer ce résultat grâce à une rupture réductrice d'intermédiaires hémiacétals ou acétals.

[Traduit par le journal]

Of eight reports (1–8) of reactions between cobalt carbonyl catalysts, synthesis gas, and acetals, five (1–5) concern acetals of formaldehyde. The literature contains few references to reactions of higher aliphatic acetals, presumably because the product mixtures are very complex.[2] As an example, Fig. 1*a* shows a gas chromatogram of the product mixture obtained by heating propionaldehyde diethylacetal with dicobalt octacarbonyl ($Co_2(CO)_8$) under synthesis gas. In contrast, the product from formaldehyde dimethylacetal, treated similarly, yielded only seven peaks in the gas chromatogram.[3] The multitude of products from higher aliphatic acetals may arise from an intermediate α,β-unsaturated ether formed in the presence of an acidic catalyst such as hydrocobalt tetracarbonyl ($HCo(CO)_4$).[4] Once formed, the α,β-unsaturated ether may (*i*) react to yield reduction or hydroformylation products with $HCo(CO)_4$, or (*ii*) form new acetals by condensing with starting material (acetal) (16*a*). Because formals cannot give α,β-unsaturated ethers, they yield simpler reaction products.

We have found that heating aromatic acetals with cobalt carbonyl catalysts in the presence of

[1]Taken from the Ph.D. Thesis of B. I. Fleming, McGill University, Montreal 1974.

[2]See ref. 59 for a discussion of the literature.

[3]Three of these corresponded to CH_3OH, CH_3OCH_3, and $CH_3OCH_2CH_2OH$.

[4]$HCo(CO)_4$, a strong acid (9–13), is known to form when cobalt carbonyls are heated under synthesis gas (14, 15). One of the preparative routes to α,β-unsaturated ethers is the treatment of an acetal with a strong acid (16*b*).

Can. J. Chem. Downloaded from www.nrcresearchpress.com by 210.87.254.105 on 09/05/12
For personal use only.

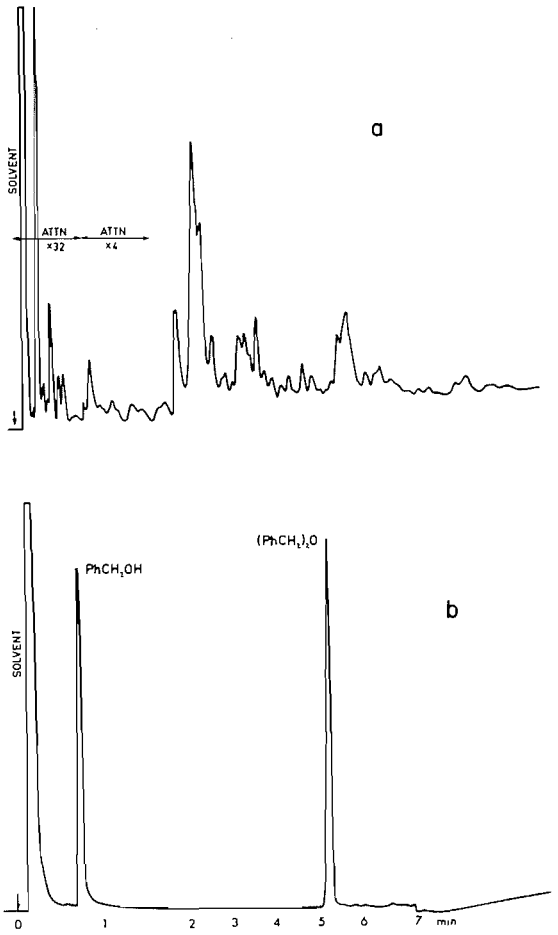

FIG. 1. Gas liquid chromatograms of the products obtained by heating (*a*) propionaldehyde diethylacetal (*b*) benzaldehyde dibenzylacetal with $Co_2(CO)_8$ under synthesis gas.

synthesis gas yields even simpler product mixtures than those obtained from the formals. Thus, Fig. 1*b* shows the gas chromatogram of the reduction products of benzaldehyde dibenzylacetal. In general, simple acetals of benzaldehyde give good yields of the products of reductive cleavage, a benzyl ether and an alcohol (Table 1, experiments 1 and 2). Acetophenone diethylketal (Table 1, experiment 3) also gives a good yield of the corresponding ether. The accompanying ethylbenzene probably results from slight further cleavage of the benzyl ether product (likewise the toluene detected in experiments 4 and 5), in agreement with the findings of Li (8). The high yield of reduction product from acetophenone diethylketal is surprising, as this compound, and also phenacetaldehyde dimethylacetal (experiment 6), can form α,β-unsaturated ethers by elimination.[5] A possible explanation is that in these examples the double bond formed by elimination is conjugated with the aromatic ring, and such double bonds are reduced, not hydroformylated, by the catalyst mixture (25, and ref. 26, p. 171). This effect is greater when there are other substituents on the double bond. Thus, styrene itself gave only 25% ethylbenzene and the remainder was hydroformylated, but α-methyl styrene gave 69% isopropylbenzene and only 9% hydroformylated material (15). Therefore, any α,β-unsaturated ether formed in experiments 3 and 6 will mostly be reduced to the same ether product which would have resulted from a reductive cleavage of the acetal.

Reductions of cyclic acetals of benzaldehyde with cobalt carbonyl exhibit two differences from those of acyclic acetals: (*i*) unreacted starting material remains after treatment under fairly forcing conditions; (*ii*) a dibenzyl ether product is obtained.

The Formation of Diethers

We propose the following mechanism (Scheme 1) for diether formation during the reduction of cyclic aromatic acetals (**1**): as the reductive cleavage proceeds and product alcohol (**2**) begins to accumulate, transacetalation with unreacted starting material (**1**) may occur to yield the new acyclic acetal **3**. Provided that the latter cleaves at a rate comparable to that of the cyclic starting material and that transacetalation is fast, a large amount of the alcohol **2** will be converted into the diether **4**. Experiment 7 (Table 2) provides some support for this hypothesis. When benzaldehyde and an excess of dry methanol were heated with the catalyst for a short time at 85 °C, the product contained benzaldehyde dimethylacetal in 70% yield as measured by glc, and 55% by actual isolation. This experiment demonstrated the ability of the cobalt carbonyl – synthesis gas combination to catalyse the formation of acetals of benzaldehyde. Although acetals were previously known to form in the presence of this catalyst (18–23), and transacetalations are also

[5]As an example phenacetaldehyde dimethylacetal yields the α,β-unsaturated ether when passed over a catalyst at a high temperature, exactly as do aliphatic acetals (27).

Can. J. Chem. Downloaded from www.nrcresearchpress.com by 210.87.254.105 on 09/05/12
For personal use only.

TABLE 1. Reduction of some aromatic acetals with $Co_2(CO)_8$ catalyst[a]

Experiment	Acetal	Product	Yield[b] (%)	Unreacted starting material (%)	Initial conditions (2400 psig H_2:CO 2:1)
1	$\phi CH(OMe)_2$	ϕCH_2OMe	96(83)[c]	0	160 °C,2 h
2	$\phi CH(OCH_2\phi)_2$	$\phi CH_2OCH_2\phi$ ϕCH_2OH	95 92	0	128 °C,1 h
3	$\phi C(OEt)_2Me$	$\phi CH(OEt)Me$ ϕCH_2Me EtOH	93(81)[c] 4 106	0	170 °C,3 h
4	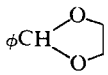	$\phi CH_2OCH_2CH_2OH$ $\phi CH_2OCH_2CH_2OCH_2\phi$ ϕCH_3	37(28)[d] 50(41)[d,e] 9	3	210 °C,6 h
5	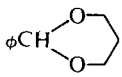	$\phi CH_2O(CH_2)_3OH$ $\phi CH_2O(CH_2)_3OCH_2\phi$ ϕCH_3	26(18)[d] 40(37)[d,e] 2	30(28)[d]	164 °C,4 h
6	$\phi CH_2CH(OMe)_2$	ϕCH_2CH_2OMe + 8 minor products	65(53)[c]	0	180 °C,2 h

[a]In a benzene solvent, [acetal] = 3 *M*, $[Co(CO)_8]$ = 0.15 *M*.
[b]Analysis by glc using 'bracketing' standards of authentic samples. Figures in parentheses are yields (mol%) of isolated material.
[c]By distillation.
[d]By SiO_2 chromatography.
[e]The yields of the diethers are based on 2 mol acetal ⟶ 1 mol diether.

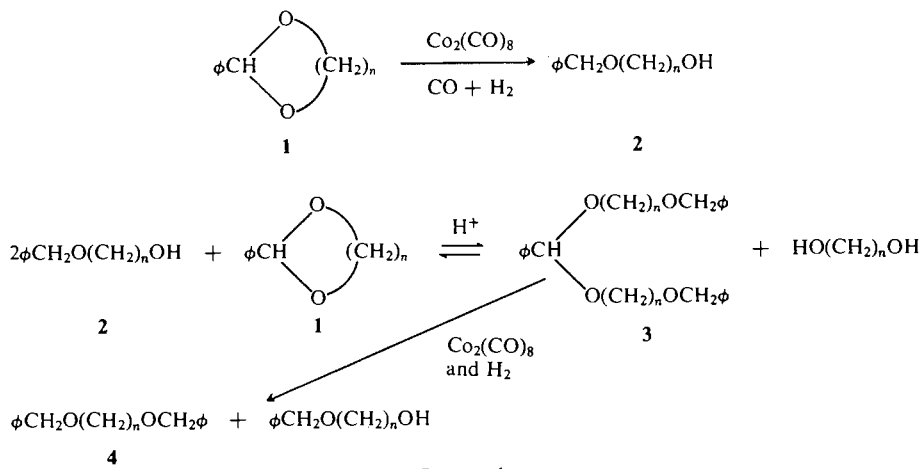

SCHEME 1

known (24), the documentation of such reactions remains rather meager.

When benzaldehyde, methanol, and catalyst were heated for longer times and at higher temperatures (experiment 8), the composition of the product mixture closely resembled that obtained from pure benzaldehyde dimethylacetal (experiment 1, Table 1). Evidently the cobalt carbonyl catalyst mixture possesses the unusual ability to catalyse both the formation and the reductive cleavage of aromatic acetals.

The Reductive Cleavage of Acetals by $HCo(CO)_4$ Solutions

Under conditions close to ambient, solutions of pure $HCo(CO)_4$ in organic solvents (28) were found to bring about the reductive cleavage of aromatic acetals [1]. This observation supports

Can. J. Chem. Downloaded from www.nrcresearchpress.com by 210.87.254.105 on 09/05/12
For personal use only.

TABLE 2. Reductions of benzaldehyde–alcohol mixtures with $Co_2(CO)_8$ catalyst[a]

Experiment	Substrate[b]	Molar ratio, (benzaldehyde: alcohol)	Reaction time (h)	Reaction temperature (°C)	Product yield by glc (mol%)		Product isolated (mol%)[c]
7	Benzaldehyde + methanol	1:10	0.2	85 ± 5	Benzaldehyde dimethylacetal	70	55[d]
					Benzaldehyde	23	
					Benzyl methyl ether	7	
8	Benzaldehyde + methanol	1:4	1.4	161 ± 2	Benzyl methyl ether	90	79[d]
					Benzyl alcohol	1	1[e]
					Dibenzyl ether	1	1[e]
9	Benzaldehyde + benzyl alcohol	1:2	1.8	158 ± 2	Dibenzyl ether	87	92
					Benzyl alcohol	45	32[f]
10	Benzaldehyde + *p*-chlorobenzyl alcohol	1:2	2.0	162 ± 3	*p*-Chlorobenzyl benzyl ether	75	70
					Benzyl alcohol	10	7
					Dibenzyl ether	5	1
					p-Chlorobenzyl alcohol	51	41[f]
11	Benzaldehyde + benzyl alcohol	1:3	0.25	85 ± 5	Benzaldehyde	80	
					Benzaldehyde dibenzylacetal	15	14[d]
					Dibenzyl ether	2	
					Benzyl alcohol	[g]	
12	Benzaldehyde dibenzylacetal	—	1.0	128	Dibenzyl ether	95	
					Benzyl alcohol	92	

[a]In benzene solvent, [φCHO] = 4 *M*, [$Co_2(CO)_8$] = 0.15 *M*. Synthesis gas ($2H_2$:1CO) pressure = 2500 psig.
[b]Added to catalyst only after reaction temperature attained.
[c]By SiO_2 chromatography except where noted. Ether yields based on (1 mol aldehyde → 1 mol ether).
[d]This compound was isolated by distillation.
[e]Isolated by SiO_2 chromatography of the distillation residue.
[f]Recovery of starting alcohol.
[g]Detected but not quantified.

TABLE 3. The reaction of benzaldehyde dibenzylacetal with $HCo(CO)_4$ under stoichiometric conditions at 22 °C

Experiment	Acetal (mmol)	$HCo(CO)_4$ (mmol)	Solvent and volume (ml)	Approximate reaction time (h)[a]	Ether produced (mol%)[b]
13	1.0	2.5	C_6H_{14}(26)	212–260	43[c]
14	0.5	1.2	C_6H_{14}(3)+C_6H_6(10)	94–117	60
15	1.0	2.3	C_6H_{14}(5)+THF(10)	1–2	53
16	1.0	1.3	C_6H_{14}(5)+THF(10)	1–2	76
17	1.0	2.4	C_6H_6(5.3)	25–92	47
18	1.0	1.9	C_6H_6(6)+C_6H_5Cl(10)	44–104	55

[a]Until $HCo(CO)_4$ no longer detectable (by smell, or by precipitation of $Co(CO)_4^-$ as nickel tri-*o*-phenanthroline complex).
[b]Estimated by gas chromatography, yield calculation is based on eq. 1. Besides unreacted starting material, benzyl alcohol was also detected, but as it is formed by hydrolysis as well as by reduction it was not quantified.
[c]$Co_2(CO)_8$ isolated as orange crystals, mp 50–52 °C, by cooling the hexane solution to −78 °C. Calcination yielded 108 mg Co_3O_4, equivalent to 1.35 mmol $Co(CO)_4$.

the concept that $HCo(CO)_4$ is the active species in the catalytic reduction of acetals with $Co_2(CO)_8$ and hydrogen. Table 3 shows the results

[1] $PhCH(OR)_2 + 2HCo(CO)_4 = PhCH_2OR + ROH + Co_2(CO)_8$

obtained in the reduction of the dibenzyl acetal of benzaldehyde by $HCo(CO)_4$ solutions. Experiments 13, 14, and 15 show that increasing solvent polarity greatly increases the rate of the reaction of benzaldehyde dibenzylacetal with $HCo(CO)_4$ (see also Fig. 2). The *yield* of ether produced is not greatly affected by the solvent. Experiment 16 does show a higher yield, but it differs from

Can. J. Chem. Downloaded from www.nrcresearchpress.com by 210.87.254.105 on 09/05/12
For personal use only.

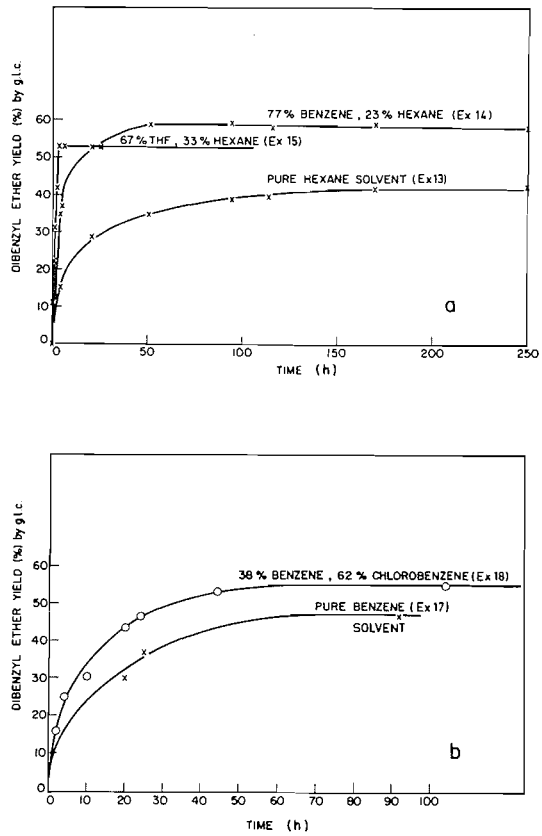

FIG. 2. The reduction of benzaldehyde dibenzylacetal by $HCo(CO)_4$ solutions in various solvents at 22 °C (see Table 3). The upper curve in Fig. 2*b* was obtained by adding chlorobenzene to a benzene solution of $HCo(CO)_4$ and the acetal. The dilute solution so formed reacted faster than a benzene solution of over three times the concentration (lower curve).

experiment 15 by having about half the amount of $HCo(CO)_4$. Consequently, acetal is present in excess, and the yield is based on $HCo(CO)_4$. The improvement of yield may be a result of reduced loss of $HCo(CO)_4$ according to eq. 2.

$$[2] \qquad 2HCo(CO)_4 \rightarrow Co_2(CO)_8 + H_2$$

Experiments 17 and 18 illustrate the effect of adding chlorobenzene to the reaction mixtures. After chlorobenzene addition, the reaction mixture in experiment 18 was three times more dilute than that in experiment 17, but still reacted slightly faster (Fig. 2*b*). The increase in reaction rate produced by polar solvents is considered evidence for a polar intermediate in acetal cleavage.

The recovery of cobalt as $Co_2(CO)_8$ from the completed reductions was only 55% of the theoretical yield. The clear yellow colour of the filtrate confirmed the removal of $Co_2(CO)_8$, which, when present, gives almost black solutions. Some cobalt therefore remains in solution, perhaps as a complex with the product alcohol. Incomplete cobalt recovery as $Co_2(CO)_8$ has previously been noted in the stoichiometric reduction of aldehydes to alcohols with $HCo(CO)_4$ (29).

The Mechanism of Acetal Cleavage with $HCo(CO)_4$

It is reasonable to anticipate a carbonium ion mechanism for the reduction of acetals with $HCo(CO)_4$. We know that acetal formation is catalysed by $HCo(CO)_4$, and that, in general, acetal formation is a reversible reaction proceeding via carbonium ions derived from protonated hemiacetals (ref. 16, p. 316). Therefore we can also expect the facile formation of carbonium ions from acetals in the presence of $HCo(CO)_4$. The most straightforward description of acetal formation and cleavage is illustrated in Scheme 2.

Reduction of similarly generated carbonium ions is the generally accepted mechanism for the reaction of *p*-methoxybenzyl alcohol with $HCo(CO)_4$ (25, 30). Such carbonium ions also play a role when this catalyst reduces benzhydrols (25, 31) and when hydroformylation products are generated from formaldehyde dimethylacetal (5).

The reduction step in Scheme 2 must be relatively slow, or isolation of the acetal from aldehyde, alcohol, and $HCo(CO)_4$ mixtures (experiment 7, Table 2) would not be possible. Evidence for the role of a carbonium ion in the reductive cleavage of acetals was obtained (Table 4) by comparing the rates of cleavage of the benzyl acetals of *para*-substituted benzaldehydes in competitive reactions. Low temperatures were necessary in these reactions to avoid cleavage of all the acetal before the hydrogenator could be cooled, since the apparatus provided no means of direct liquid sampling. The yields shown in Table 4 do not provide an exact quantitative measure of the reactivity of the acetals, but, just as Wender and co-workers (31) have found for benzhydrols, clearly indicate that an electron-releasing group in the *para* position enhances the reduction rate and an electron-withdrawing substituent diminishes it.

Ether Formation During Benzaldehyde Reduction

The literature contains references to the forma-

Can. J. Chem. Downloaded from www.nrcresearchpress.com by 210.87.254.105 on 09/05/12
For personal use only.

TABLE 4. Competitive reductions of pairs of acetals of the type p-X-$C_6H_4CH(OCH_2Ph)_2$[a]

X	Reaction temperature (°C)	Unreacted starting material (%)[b]	Product ether formed (%)[b]
MeO + H	75	12	59
		74	7
H + Cl	80	41	42
		65	16

[a]Procedure as described in Experimental but with 1 mmol of each acetal + 5 ml hexane in the ampoule. Catalyst equilibrium established by heating at 90–100 °C for 25 min before mixing the contents at the reaction temperature and allowing the autoclave to cool to ambient (~2 h).
[b]Analysed by glc.

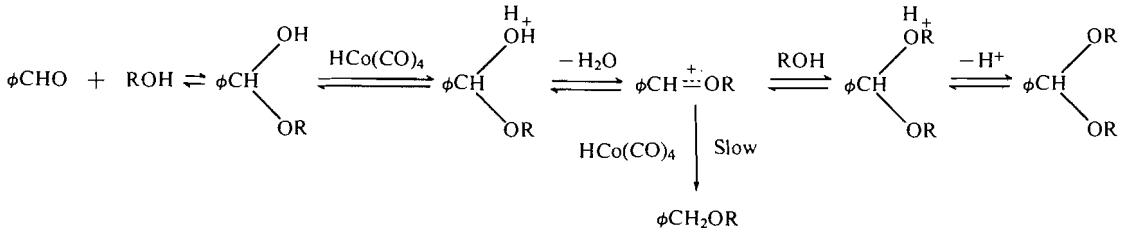

SCHEME 2

tion of ethers during the reduction of benzaldehyde with synthesis gas and cobalt carbonyl catalysts:

Yields of over 50%[6] of dibenzyl ether were obtained when benzaldehyde and catalyst were heated under synthesis gas for 2 h or less at 180–200 °C (58, 60). The ratio of benzyl alcohol to benzyl ether in the product strongly depends on the initial concentration of the aldehyde (58). Wender *et al.* (60) at first thought the ether was formed by dehydration of benzyl alcohol, but in subsequent work (61) found that under the same conditions, though for a somewhat longer time, benzyl alcohol yielded only toluene and phenethyl alcohol. The same two products were the only ones isolated by Ziesecke (62) in numerous experiments with benzyl alcohol, cobalt catalysts, and synthesis gas under varied conditions. Dawydoff (58) heated benzyl alcohol and catalytically generated $HCo(CO)_4$ for up to 5 h at 200 °C with and without benzene solvent but obtained only a 2% yield of dibenzyl ether.

Thus, the formation of large amounts of dibenzyl ether during benzaldehyde reductions has so far remained unexplained, but is readily accounted for by Scheme 2 (R = ϕCH_2—); benzyl alcohol, initially formed by reduction of benzaldehyde (63–65), can readily react with unchanged starting material to yield hemiacetal or acetal, and finally dibenzyl ether.[7] The formation of benzyl alcohol is first order in benzaldehyde (65), but hemiacetal formation requires a second molecule of benzaldehyde. Thus Scheme 2 explains qualitatively the experimental finding that in dilute solution the dibenzyl ether yield is low, but that it increases rapidly at the expense of benzyl alcohol as the concentration of the starting aldehyde is raised (58).

Support for Scheme 2 is provided by experiment 9 (Table 2) wherein benzaldehyde was treated with 2 equiv. of benzyl alcohol and gave, under milder conditions than Wender *et al.* employed, a nearly quantitative yield of dibenzyl ether, while almost half of the benzyl alcohol was recovered.

Experiment 10 resembled the preceding experiment except that p-chlorobenzyl alcohol was used. The chief product was p-chlorobenzyl benzyl ether [3], but some reduction of benzaldehyde to benzyl alcohol did occur, with subsequent formation of a little dibenzyl ether. No bis-(p-chloro-

[6]Based on 2 mol aldehyde yielding 1 mol of ether.

[7]A similar scheme for silane reductions appears in ref. 66.

Can. J. Chem. Downloaded from www.nrcresearchpress.com by 210.87.254.105 on 09/05/12
For personal use only.

Can. J. Chem. Downloaded from www.nrcresearchpress.com by 210.87.254.105 on 09/05/12
For personal use only.

[3] 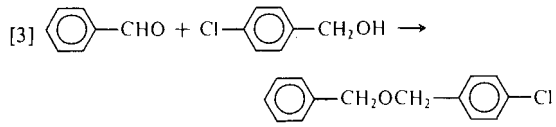

benzyl)ether was detected. The result of experiment 10 indicates that the ether formed during benzaldehyde reductions is derived from 1 molecule of aldehyde and 1 molecule of alcohol.

The isolation, in 14% yield, of benzaldehyde dibenzylacetal, **5**, from the benzaldehyde – benzyl alcohol – catalyst mixture treated under mild conditions (experiment 11), and the subsequent cleavage of **5** to dibenzyl ether and benzyl alcohol under more drastic conditions (experiment 12) both offer strong support for Scheme 2.

Reduction vs. Hydroformylation

Both steric and electronic effects determine whether the fate of alkyl and aryl cobalt carbonyls will be reduction, or CO-insertion yielding hydroformylated products. Bulky groups (*e.g.* secondary and tertiary alkyl, phenyl groups) decrease the amount of CO-insertion relative to a primary alkyl cobalt carbonyl (32). Insertion of carbon monoxide is also inhibited if electron-withdrawing groups are substituted into the alkyl moiety (33, 34).

If the reduction step in aromatic acetal cleavage proceeds via an intermediate such as **6**, one expects, for both the above reasons, to

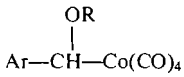

6

obtain little hydroformylation product. The expectation is borne out by the present experiments: no hydroformylation products have been detected from the reductive cleavage of α-aryl acetals, and the reduction products (ethers) have been obtained in yields approaching 100%. This observation is entirely consistent with the distribution of hydroformylated and reduced products obtained from related compounds by other workers.[8]

Experimental

Reduction of Acetals at Elevated Temperatures under Synthesis Gas

The reductive cleavage of 2-phenyl-1,3-dioxane (Table 1, experiment 5) is representative of the general procedure. A stainless steel hydrogenator,[9] having a removable glass liner and internal volume (with the liner in place) of 255 ml, was employed. A quantity of the acetal (4.33 g) was supported in a small, open ampoule above the catalyst mixture (0.44 g $Co_2(CO)_8$ in 3.8 ml benzene) inside the liner. After purging with carbon monoxide, the hydrogenator was pressurized to 2400 psig with a 2:1 H_2–CO mixture and the temperature was raised to 160 °C in 45 min. Then the apparatus was tilted to mix the acetal and the catalyst, and heating was continued at 165 ± 5 °C. After 4 h, the hydrogenator was cooled to room temperature and vented, and its contents were made up to 50 ml in benzene. A glc analysis of this solution revealed the following components: unchanged starting material, 28%, 3-benzyloxy-1-propanol, 26%, 1,3-dibenzyloxypropane, 40%,[10] as major constituents; toluene, 1.8%, and a trace of benzaldehyde, <1%, were also evident.

A 40 ml portion of the benzene solution was now evaporated under reduced pressure (30 °C, ~15 torr) and the residue was allowed to stand open to the atmosphere for 24 h to permit the catalyst to oxidise. (A repeat glc analysis after this procedure showed that catalyst oxidation did not affect the organic materials). A little benzene was next added to the product and the resulting mixture, consisting of dissolved organic material and suspended oxidised catalyst, was applied to a silica gel column. The fractions thus obtained in order of elution[11] were as follows.

(*i*) 1,3-Dibenzyloxypropane, 0.99 g (37%); $n_D^{22.3}$ 1.5361; authentic sample, $n_D^{22.2}$ 1.5386; glc retention time and pmr spectrum were identical to those of a synthesized sample;

(*ii*) 2-Phenyl-1,3-dioxane, starting material, 1.04 g (30%); mp 46–47 °C, mixture mp with starting material 46–47.5 °C;

(*iii*) 3-Benzyloxy-1-propanol, 0.59 g (18%); n_D^{20} 1.5168 (lit. (35) n_D^{20} 1.5152), glc retention time and pmr spectrum were identical to those of a synthesized sample.

When this experiment was repeated with the catalyst omitted, 2-phenyl-1,3-dioxane was found to be perfectly stable, and, being unable to form an α,β-unsaturated ether by elimination, was also stable under the same conditions in the presence of *p*-toluenesulphonic acid (0.05 g). This behaviour contrasts with that of acetone *n*-butyl ketal which decomposed completely under the acidic conditions.

Because of a report (17) that benzaldehyde diethylacetal undergoes disproportionation at 200 °C in the presence of thorium oxide (eq. 4), it was also thought necessary to perform a blank experiment with benzaldehyde dimethylacetal, **7**, under the reaction conditions. In the absence of catalyst, **7** was unchanged after 3½ h at 160 °C.

[4] $$\phi CH(OEt)_2 \xrightarrow[ThO_2]{200\ ^\circ C} \phi CH_2OEt + MeCHO$$

[8]A summary of the related literature appears in ref. 59, p. 76.

[9]American Instrument Co. model 406-01M.

[10]The quantitative analysis of this compound was actually made from a second, later glc analysis, after the compound had been isolated and identified.

[11]Benzene eluent for the first two fractions, benzene + ether (15% by volume) for fraction *iii*.

Can. J. Chem. Downloaded from www.nrcresearchpress.com by 210.87.254.105 on 09/05/12
For personal use only.

Stoichiometric Reductions of Acetals with $HCo(CO)_4$ Solutions

Solutions of $HCo(CO)_4$ in hydrocarbon solvents were prepared according to Kirch and Orchin (28). Even after stirring for 1 h with anhydrous sodium sulphate (36), the solutions contained too much moisture for acetal reductions. Further drying was achieved by transferring the solution by syringe to a serum capped, carbon monoxide filled, erlenmeyer flask containing 5 g of molecular sieve (Linde 5A). In agreement with the published spectra (28), hexane solutions thus prepared showed the following carbonyl stretching frequencies (cm^{-1}): 2115 (w), 2070 (m), 2053 (s), 2030 (s), and 1992 (w).

From this point on, experiment 9 (Table 3) will be described as typical of the general procedure. The pale yellow solution of $HCo(CO)_4$ was analysed gasometrically (37) as follows: a 1 ml sample of solution was injected into excess aqueous potassium iodide – iodine solution in a flask connected to a carbon monoxide filled gas burette.[12] A 51.5 ml volume of carbon monoxide (saturated with water and hexane at 23 °C) was produced. This gas (36.6 ml, dry at NTP) is equivalent to 0.41 mmol of $HCo(CO)_4$.

Six ml of the $HCo(CO)_4$ solution (2.46 mmol $HCo(CO)_4$) was added by syringe to an erlenmeyer flask containing 1 mmol of benzaldehyde dibenzylacetal in 20 ml of hexane under a CO atmosphere. Standing at room temperature, the mixture darkened very slowly. The progress of the reaction was followed by removing samples (2 μl) by syringe for gas chromatography. For up to 212 h after mixing, $HCo(CO)_4$ was detectable in these aliquots by its odour. After 260 h, the mixture composition, as determined by glc, remained constant at 43% dibenzyl ether, 25% starting material, 29% benzaldehyde (formed by hydrolysis), and an unquantified amount of benzyl alcohol.[13]

The almost black solution was next cooled in a dry ice – acetone mixture, whereupon small orange crystals of dicobalt octacarbonyl separated, mp 50–52 °C (lit. (38) 51–52 °C). The crystals were filtered and roasted at 750 °C in a weighed porcelain crucible. Yield of Co_3O_4 = 108 mg, equivalent to 1.35 mmol of cobalt (55% recovery).

Isolation of benzaldehyde dibenzylacetal (**5**) from the product mixture of experiment 11 was achieved as follows: the product mixture (in benzene solution) was stirred with 1 *N* sodium hydroxide solution and extracted with ether. The extract was dried (K_2CO_3), the ether was evaporated, and the benzene, benzaldehyde, and benzyl alcohol were distilled off at 100 °C under reduced pressure. The high boiling residue was distilled to yield 4.25 g of **5** (14%, based on 10.6 g φCHO starting material), bp 190 °C/0.85 torr; n_D^{25} 1.5735; pmr (py-d_5) δ 7.8–7.1 (m, 15H), 5.8 (s, 1H), 4.7 (s, 2H), 4.6 (s, 2H), identical to the spectrum of synthesized material (lit. (44) bp 170 °C/0.2 torr; n_D^{20} 1.5776).

Sources of Starting Materials

Propionaldehyde diethylacetal was prepared in 46% yield according to ref. 39. Boiling point 124–125 °C/757 torr; n_D^{22} 1.3890 (lit. (39) bp 123 °C/740 torr; $n_D^{25.5}$ 1.3872).

Formaldehyde dimethylacetal (methylal) was obtained from Baker Chemical Co.

Benzaldehyde dimethyl acetal was prepared in 35% yield according to Fischer and Giebe (40). Boiling point 97.5 °C/30 torr (lit. (40) bp 198–199 °C/762 torr).

Acetophenone diethyl ketal was prepared according to Fuson and Burness (41). Boiling point 103 °C/16 torr; n_D^{20} 1.4781 (lit. (41) bp 101.5 °C/15 torr; n_D^{20} 1.4773).

Benzaldehyde dibenzylacetal and the following two compounds were prepared by Salmi's method (42), yield 65%. Boiling point 163–166 °C/0.04–0.05 torr; n_D^{24} 1.5765 (lit. (43) bp 'about 168 °C'/0.1 torr, (44) 170 °C/0.2 torr; n_D^{20} 1.5776).

2-Phenyl-1,3-dioxolane, yield 66%, bp 123–124 °C/26 torr; n_D^{22} 1.5264 (lit. (45) bp 116 °C/20 torr, (46) bp 129 °C/25 torr; n_D^{18} 1.5285).

2-Phenyl-1,3-dioxane, yield 85%, bp 126–127 °C/15 torr; mp 46–48 °C (lit. (47) bp 125 °C/14 torr; mp 49–51 °C).

Phenylacetaldehyde dimethylacetal was prepared in 53% yield according to ref. 48. Boiling point 84–84.5 °C/6 torr; n_D^{24} 1.4930 (lit. (48) bp 219–221 °C/754 torr).

p-Methoxybenzaldehyde dibenzylacetal was prepared by the method of Gualtieri *et al.* (49), but some decomposition of this reactive acetal was found (pmr) to occur during distillation. Boiling point 192–198 °C/0.2–0.25 torr (lit. (49), bp 195 °C/0.25 torr). Moreover, decomposition in the heated injection port of the glc caused difficulty in estimating the purity of the product by this technique. However, since all contaminants are relatively volatile, a pure product was obtained without distillation of the acetal. After the reaction, the mixture was stirred with a large excess of aqueous potassium carbonate. The upper layer was separated, washed twice with water, and its volatile materials were removed under reduced pressure. After 2 h in an oil bath at 120 °C under 0.08 torr pressure, the residual pale yellow oil was completely pure *p*-methoxybenzaldehyde dibenzylacetal as far as could be detected by pmr, yield 85%, n_D^{20} 1.5756. This product is pure enough for most purposes, but if necessary, the yellow colour may be removed by silica gel chromatography.

p-Chlorobenzaldehyde dibenzylacetal does not appear to have been previously reported. It was prepared from *p*-chlorobenzaldehyde (Eastman, practical, 40 g, 0.28 mol) and benzyl alcohol (130 g, 1.2 mol) with *p*-toluenesulphonic acid (0.1 g) as catalyst. The water produced was removed as a benzene–water azeotrope, using 300 ml of benzene and a Dean–Stark separator. After 3 h of refluxing, no further water was obtained, and the reaction mixture was stirred with excess saturated aqueous sodium carbonate solution. The upper layer was separated, washed with water, and distilled under reduced pressure. The final fraction of distillate, bp 196–198 °C/0.1 torr was the pure acetal; yield, 76 g (80%); n_D^{20} 1.5816; pmr; δ 4.40 (4H, s, benzyl methylenes), 5.51 (1H, s, methine), 7.2 (14H, m, aromatic). *Anal.* calcd. for $C_{21}H_{19}ClO_2$: C 74.4, H 5.65, Cl 10.5; found: C 74.4, H 5.63, Cl 10.7.

Sources of Authentic Samples of the Reduction Products

Benzyl methyl ether, *2-(benzyloxy)ethanol* and *ethylbenzene* were obtained from Eastman Kodak Co.

[12]The flask also contained some hexane to maintain saturation of the gas in the burette.

[13]In another experiment conducted in benzene solution, dibenzyl ether was isolated in 43% yield (59).

Can. J. Chem. Downloaded from www.nrcresearchpress.com by 210.87.254.105 on 09/05/12
For personal use only.

Dibenzyl ether was obtained from the Aldrich Chemical Co.

α-Methylbenzyl ethyl ether was prepared according to Mislow (50).

Phenethyl methyl ether was synthesized from phenethyl alcohol, methyl iodide, and silver oxide, according to ref. 51. The sweet-smelling product was purified by chromatography on silica gel. Yield 60%, $n_D^{23.5}$ 1.4962 (lit. (52) n_D^{21} 1.5001).

3-Benzyloxy-1-propanol was made according to ref. 54. Boiling point 130 °C/10 torr; n_D^{26} 1.5110 (lit. (54) bp 114 °C/0.9 torr; n_D^{20} 1.5184, (55) bp 155 °C/23 torr).

1,2-Dibenzyloxyethane was prepared by a Williamson synthesis in which 2-(benzyloxy)ethanol (Eastman, 10 g, 0.066 mol) was stirred with excess (2 g) sodium and xylene (25 ml) for 24 h. The excess sodium was removed, benzyl chloride (5.3 g, 0.041 mol) was added, and the mixture was boiled under reflux for 4 h. The precipitated sodium chloride was filtered off, and the filtrate was distilled under vacuum. Yield 5.3 g (53%), bp 123–125 °C/0.05–0.07 torr; n_D^{26} 1.5436 (lit.(53) bp 139 °C/0.1 torr).

1,3-Dibenzyloxypropane was made from 3-benzyloxy-1-propanol by a Williamson synthesis as described above. Yield, 65%; bp 145–146 °C/0.03 torr; $n_D^{22.2}$ 1.5386; pmr; δ 7.19 (10H, m, aromatic), 4.35 (4H, s, Ph—CH_2—O—), 3.46 (4H, t, —O—CH_2—C), 1.81 (2H, quintet, C—CH_2—C). *Anal.* calcd. for $C_{17}H_{20}O_2$; C 79.7, H 7.87; found: C 79.7, H 7.96.

p-Chlorobenzyl benzyl ether was prepared by a Williamson synthesis as described in ref. 56. Yield 70%, bp 113 °C/0.1 torr; n_D^{20} 1.5692 (lit. (56) bp 114 °C/0.1 torr; n_D^{20} 1.5698).

p-Methoxybenzyl benzyl ether was made similarly (56). Yield 51%, bp 125 °C/0.1 torr; n_D^{20} 1.5636 (lit. (56) bp 146–147 °C/0.4 torr; n_D^{22} 1.5625).

Acknowledgments

This work was supported by grants from the National Research Council of Canada, and B.I.F. was the grateful recipient of an NRCC Scholarship (1973–1974).

1. K. Pieroh. German Patent No. 875,802 (1953).
2. M. Müller-Cunradi, K. Pieroh, and L. Lorenz. German Patent No. 890,945 (1953).
3. W. F. Gresham and R. E. Brooks. U.S. Patent No. 2,449,470 (1948).
4. W. F. Gresham and R. E. Brooks. U.S. Patent No. 2,525,793 (1950).
5. K. Hamada, K. Baba, and N. Hagihara. Osaka University Inst. Sci. and Ind. Res. Mem. **14**, 207 (1957).
6. J. D. C. Wilson. U.S. Patent No. 2,555,950 (1951).
7. A. Rosenthal. Advan. Carbohydr. Chem. **23**, 59 (1968).
8. C. M. Li. M.Sc. Thesis, McGill University, Montreal, Quebec. 1972.
9. W. Hieber and W. Hübel. Z. Naturforsch. Teil B, **7**, 322 (1952).
10. W. Hieber. Angew. Chem. **64**, 400 (1952).
11. W. Reppe. Ann. **582**, 116 (1953).
12. H. W. Sternberg, I. Wender, R. A. Friedel, and M. Orchin. J. Am. Chem. Soc. **75**, 2717 (1953).
13. W. Hieber and W. Hübel. Z. Elektrochem. **57**, 235 (1957).
14. I. Wender, H. W. Sternberg, and M. Orchin. J. Am. Chem. Soc. **75**, 3041 (1953).
15. M. Orchin, L. Kirch, and I. Goldfarb. J. Am. Chem. Soc. **78**, 5450 (1956).
16. S. Patai (*Editor*). The ether link. Interscience, New York. 1967. (*a*) p. 322, (*b*) p. 337.
17. H. Meerwein and R. Schmidt. Ann. **444**, 224 (1925).
18. L. Roos, R. W. Goetz, and M. Orchin. J. Org. Chem. **30**, 3023 (1965).
19. J. Falbe, N. Huppes, and F. Korte. Brennst. Chem. **47**, 207 (1966).
20. J. Falbe. Brennst. Chem. **48**, 183 (1967).
21. P. L. Barrick and A. A. Pavlic. U.S. Patent No. 2,506,571 (1950); Chem. Abstr. **44**, 7344*e* (1950).
22. C. H. McKeever and G. H. Agnew. U.S. Patent No. 2,533,276 (1950); Chem. Abstr. **45**, 3415d (1951).
23. H. Adkins and G. Krsek. J. Am. Chem. Soc. **71**, 3051 (1949).
24. P. Pino. Gazz. Chim. Ital. **81**, 625 (1951).
25. M. Orchin. Adv. Catal. **5**, 385 (1953).
26. B. R. James. Homogeneous hydrogenation. Wiley, New York. 1973. p. 171.
27. O. Bayer. Methoden der organischen chemie. Vol. 7/1. Houben-Weyl. 1954. p. 437.
28. L. Kirch and M. Orchin. J. Am. Chem. Soc. **81**, 3597 (1959).
29. R. W. Goetz and M. Orchin. J. Org. Chem. **27**, 3698 (1962).
30. H. W. Sternberg and I. Wender. Chem. Soc. Spec. Publ. (London) **13**, 35 (1959).
31. Y. C. Fu, H. Greenfield, S. J. Metlin, and I. Wender. J. Org. Chem. **32**, 2837 (1967).
32. L. Marko. Chem. Ind. 260 (1962).
33. R. B. King. Adv. Organomet. Chem. **2**, 157 (1964); see p. 240.
34. R. F. Heck and D. S. Breslow. J. Am. Chem. Soc. **84**, 2499 (1962).
35. E. L. Eliel, V. G. Badding, and M. N. Rerick. J. Am. Chem. Soc. **84**, 2371 (1962).
36. R. W. Goetz and M. Orchin. J. Am. Chem. Soc. **85**, 2782 (1963).
37. H. W. Sternberg, I. Wender, and M. Orchin. Anal. Chem. **24**, 174 (1952).
38. I. Wender and P. Pino. Organic syntheses via metal carbonyls. Vol. 1. Interscience, New York. 1968. p. 39.
39. H. W. Post. J. Org. Chem. **5**, 244 (1940).
40. E. Fischer and G. Giebe. Ber. **31**, 545 (1898).
41. R. C. Fuson and D. M. Burness. J. Am. Chem. Soc. **68**, 1270 (1946).
42. E. J. Salmi. Ber. B, **71**, 1803 (1938).
43. Z. Foldi. Acta. Chim. Acad. Sci. Hung. **6**, 191 (1955); Chem. Abstr. **50**, 9324g.
44. S O. Lawesson and C. Berglund. Ark. Kemi, **16**, 287 (1961).
45. B. E. Leggetter and R. K. Brown. Can. J. Chem. **42**, 990 (1964).
46. P. Mastagli, Z. Zafiriadis, and G. Lagrange. Compt. Rend. **237**, 187 (1953).
47. E. Fischer. Ber. **27**, 1537 (1894).

48. E. FISCHER and E. HOFFA. Ber. **31**, 1991 (1898).
49. F. GUALTIERI, H. JOHNSON, H. MAIBACH, D. SKIDMORE, and W. SKINNER. J. Pharm. Sci. **61**, 577 (1972).
50. K. MISLOW. J. Am. Chem. Soc. **73**, 4043 (1951).
51. S. S. DESHAPANDE. J. Indian Chem. Soc. **15**, 509 (1938).
52. L. SUMMERS and M. L. LARSON. J. Am. Chem. Soc. **74**, 4498 (1952).
53. H. NORMANT and T. CUVIGNY. Bull. Soc. Chim. Fr. 1866 (1965).
54. J. D. GENZER, C. P. HUTTRER, and G. C. VAN WESSEM. J. Am. Chem. Soc. **73**, 3159 (1951).
55. G. BENNETT and A. L. HOCK. J. Chem. Soc. 472 (1927).
56. R. L. HUANG and S. S. SI-HOE. J. Chem. Soc. 3988 (1957).
57. I. WENDER, H. GREENFIELD, and M. ORCHIN. J. Am. Chem. Soc. **73**, 2656 (1951).
58. W. DAWYDOFF. Chem. Tech. (Berlin), **11**, 431 (1959).
59. B. I. FLEMING. Ph.D. Thesis, McGill University, Montreal, Quebec. 1974.
60. I. WENDER, R. LEVINE, and M. ORCHIN. J. Am. Chem. Soc. **72**, 4375 (1950).
61. I. WENDER, H. GREENFIELD, and M. ORCHIN. J. Am. Chem. Soc. **73**, 2656 (1951).
62. K.-H. ZIESECKE. Brennst. Chem. **33**, 385 (1952).
63. R. W. GOETZ and M. ORCHIN. J. Org. Chem. **27**, 3698 (1962).
64. L. MARKO. Proc. Chem. Soc. 67 (1962).
65. C. L. ALDRIDGE and H. B. JONASSEN. J. Am. Chem. Soc. **85**, 886 (1963).
66. M. P. DOYLE, D. J. DEBRUYN, and D. A. KOOISTRA. J. Am. Chem. Soc. **94**, 3659 (1972).

Can. J. Chem. Downloaded from www.nrcresearchpress.com by 210.87.254.105 on 09/05/12
For personal use only.

The addition of 2,4-dinitrobenzenesulfenyl chloride to a series of phenyl substituted *cis*- and *trans*-1-phenylpropenes[1]

GEORGE H. SCHMID AND VINCENT J. NOWLAN
Department of Chemistry, University of Toronto, Toronto, Ontario M5S 1A1

Received July 29, 1975

GEORGE H. SCHMID and VINCENT J. NOWLAN. Can. J. Chem. **54**, 695 (1976).

The rate of addition of 2,4-dinitrobenzenesulfenyl chloride to *cis* and *trans* 3-NO_2, 4-Cl, 4-CH_3, 4-OCH_3, 4-OC_6H_5, 4-$OCH(CH_3)_2$ substituted-1-phenylpropenes has been measured in 1,1,2,2-tetrachloroethane at 25 °C and the product stereochemistry has also been determined. While a plot of log k_2 *vs.* either σ or σ^+ is linear a better correlation is obtained with σ. Such a linear relationship is obtained even though the product stereochemistry changes from stereospecific and nonregiospecific for electron-withdrawing substituents (3-NO_2, 4-Cl) to regiospecific and nonstereospecific for electron-donating substituents (4-OCH_3, 4-OC_6H_5, and 4-$OCH(CH_3)_2$). These results suggest that the rate determining step for all the additions is bridged and that any open ion is formed after this step.

GEORGE H. SCHMID et VINCENT J. NOWLAN. Can. J. Chem. **54**, 695 (1976).

Travaillant dans le tétrachloro-1,1,2,2 éthane à 25 °C, on a mesuré la vitesse d'addition du chlorure de dinitro-2,4 benzènesulfényle à des phényl-1 propènes *cis* et *trans* substitués sur le noyau aromatique par des nitro-3, chloro-4, méthyl-4, méthoxy-4, phénoxy-4 et isopropoxy-4; on a aussi déterminé la stéréochimie des produits. Alors que l'on obtient une relation linéaire entre log k_2 *vs.* soit σ ou σ^+ on obtient une meilleure corrélation avec σ. On obtient une telle relation linéaire même si la stéréochimie des produits change de stéréospécifique et non-régiospécifique pour les substituants électro-attracteurs (nitro-3 et chloro-4) à régiospécifique et non stéréospécifique pour les substituants électro-donneurs (méthoxy-4, phénoxy-4 et isopropoxy-4). Les résultats suggèrent que l'étape déterminante, pour toutes ces additions, est un ion ponté et que tous les ions ouverts se forment après cette étape.

[Traduit par le journal]

The recent report of the addition of 2,4-dinitrobenzenesulfenyl chloride to *cis*- and *trans*-anethole is the first example of a nonstereospecific addition of an arenesulfenyl chloride to an alkene (2). In this reaction an open carbonium ion is clearly involved as an intermediate prior to the product determining step. However it is not clear if the first formed intermediate is also an open carbonium ion. In an attempt to obtain more information about the mechanism of this reaction we have examined the rate of addition of 2,4-dinitrobenzenesulfenyl chloride to a series of phenyl substituted *cis*- and *trans*-1-phenylpropenes (**1***a–g* and **2***a–g*).

The purpose of this study is to determine if there is a break in the Hammett $\sigma\rho$ plot at the point where the addition becomes nonstereospecific. In this way, we should be able to determine if there is a change in the structure of the rate determining transition state as the product stereochemistry changes.

[1]Reactions of Sulfenyl Chlorides and their Derivatives. XII. For Part XI see ref. 1.

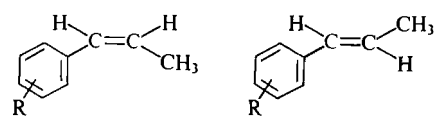

1 **2**

R		R	
a	3-NO_2	*e*	4-OC_6H_5
b	4-Cl	*f*	4-OCH_3
c	H	*g*	4-$OCH(CH_3)_2$
d	4-CH_3		

Results

The rates of addition of 2,4-dinitrobenzenesulfenyl chloride to a series of phenyl substituted *cis*-(**1***a–g*)- and *trans*-(**2***a–g*)-1-phenylpropenes were measured at 25 °C in 1,1,2,2-tetrachloroethane (TCE) by two methods: a titrimetric method and a dilatometry method using an Anton Paar precision density meter. The additions were found to exhibit normal second-order kinetics, first-order in alkene and first-order in sulfenyl chloride to 80% completion of the reaction. The rate data are presented in Table 1.

The *trans* alkenes were obtained by standard

TABLE 1. The specific rate constants for addition of 2,4-dinitrobenzenesulfenyl chloride to a series of phenyl substituted 1-phenylpropenes in 1,1,2,2-tetrachloroethane at 25.00 °C

Substituent	σ	σ^+	k_2 (M^{-1} s^{-1}) *cis*	k_2 (M^{-1} s^{-1}) *trans*
3-NO_2	0.71[a]	0.67[c]	$3.1 \pm 0.1 \times 10^{-6}$	$1.23 \pm 0.06 \times 10^{-6}$
4-Cl	0.23[a]	0.114[b]	$7.0 \pm 0.1 \times 10^{-5}$	$5.60 \pm 0.80 \times 10^{-5}$
H	0[a]	0[b]	$1.58 \pm 0.08 \times 10^{-4}$	$5.1 \pm 0.2 \times 10^{-4}$
4-CH_3	−0.17[a]	−0.31[b]	$7.33 \pm 0.05 \times 10^{-4}$	$2.73 \pm 0.03 \times 10^{-3}$
4-OC_6H_5	−0.32[a]	−0.90[d]	$9.1 \pm 0.4 \times 10^{-4}$	$4.85 \pm 0.07 \times 10^{-3}$
4-OCH_3	−0.27[a]	−0.78[b]	$2.3 \pm 0.2 \times 10^{-3}$	$1.15 \pm 0.08 \times 10^{-2}$
4-$OCH(CH_3)_2$	−0.45[a]	−0.99[d]	$4.92 \pm 0.08 \times 10^{-3}$	$1.33 \pm 0.05 \times 10^{-2}$

[a]Reference 25.
[b]Reference 26.
[c]Reference 7.
[d]Reference 27.

synthetic methods. The *cis* alkenes were obtained by catalytic hydrogenation of the substituted 1-phenylpropynes. In a few cases the *cis* alkene was obtained by the photochemical isomerization of the more readily available *trans* isomer followed by separation of the *cis–trans* mixture by preparative glc. The identity of the isomers can be established on the basis of their nmr spectra. The methyl group of the *trans* isomer gives rise to a sharp doublet at δ 1.85 while the methyl signal of the *cis* isomer appears as a doublet of doublets centered at δ 1.90. The extra splitting in the case of the *cis* isomer is caused by long range coupling to the vinyl proton α to the ring with a coupling constant $J \approx 1.5$ Hz.

The addition of an arenesulfenyl chloride to 1-phenylpropene can result in the formation of the four products illustrated in Fig. 1. Previous work has established that there are two main effects which determine the relative positions of the protons of these four isomeric adducts in the nmr. First it has been shown that the *erythro*

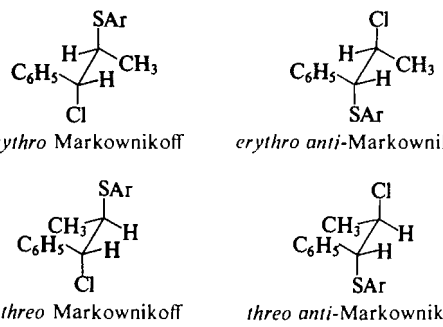

FIG. 1. The four possible isomeric adducts formed by addition of an arenesulfenyl chloride to 1-phenylpropene.

and *threo* configurations of 1,2-disubstituted-1-arylpropanes may be assigned on the basis of the chemical shift of the methyl protons provided the values of both isomers are available (3). Thus the methyl protons of the *threo* isomer are found at higher field than those of the *erythro* isomer. Secondly it is known that protons next to chlorine are deshielded relative to protons next to sulfur (4, 5). These spectral correlations were found applicable to the products of addition of 2,4-dinitrobenzenesulfenyl chloride to *cis*- and *trans*-anethole (2) and 1-phenylpropene (6) reported previously. We have used this nmr method to establish the regiospecificity and stereochemistry of the products obtained in this study. The relevant nmr parameters are given in Table 2 along with the initially formed adduct mixture.

Discussion

Considerable work has been done on the addition of arenesulfenyl chlorides to alkenes and a general two step mechanism has been postulated (6). In the rate determining first step the alkene is attacked by the electrophile to form a cationic intermediate which is subject to nucleophilic attack in the subsequent product forming step. In the majority of additions, the products are formed stereospecifically by *anti* addition which indicates that both the product and rate determining transition states are bridged.

From the results reported in Table 2, it is clear that the stereochemistry and the regiospecificity of the products can change as the electron-donating ability of the substituents on the alkene

TABLE 2. The nmr parameters and product composition of the adducts formed by the addition of 2,4-dinitrobenzenesulfenyl chloride to a series of phenyl substituted *cis*- and *trans*-1-phenylpropenes at 25 °C in 1,1,2,2-tetrachloroethane

(*a*) Adducts from the *cis* alkenes

Substituent	Chemical shifts[a] H_a	H_b	H_c	Assignment[a]	%
3-NO_2	5.22	4.10	1.46	*threo* M	30
	4.84	4.50	1.65	*threo* aM	70
4-Cl	5.04	4.00	1.40	*threo* M	70
	4.65	4.40	1.53	*threo* aM	30
H	5.12	4.10	1.44	*threo* M	60
	4.73	4.46	1.56	*threo* aM	40
4-CH_3	5.07	4.03	1.43	*threo* M	>95
	[b]	[b]	~1.65		Trace
4-OCH_3	5.07	3.96	1.43	*threo* M	70
	4.92	3.96	1.65	*erythro* M	30
4-OC_6H_5	5.09	4.07	1.48	*threo M*	75
	4.96	~4.00[c]	1.64	*erythro* M	25
4-$OCH(CH_3)_2$	5.07	~4.00[c]	1.41	*threo* M	52
	4.92	~4.00[c]	1.62	*erythro* M	48

(*b*) Adducts from the *trans* alkenes

Substituent	Chemical shifts[a] H_a	H_b	H_c	Assignment[a]	%
3-NO_2	5.16	4.03	1.64	*erythro* M	100
4-Cl	4.93	3.88	1.54	*erythro* M	100
H	5.05	4.00	1.63	*erythro* M	100
4-CH_3	4.95	3.93	1.65	*erythro* M	100
4-OCH_3	4.92	3.96	1.65	*erythro* M	>95[d]
4-OC_6H_5	4.95	3.90	1.63	*erythro* M	>95[d]
4-$OCH(CH_3)_2$	4.92	3.95	1.62	*erythro* M	>95[d]

[a]The structure of the adducts is 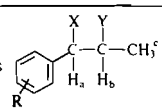

When X = Cl and Y = $SC_6H_3(NO_2)_2$ the adduct is defined as Markownikoff (M). When reversed the adduct is defined as *anti*-Markownikoff (aM). The *erythro* adduct is defined as *anti* addition to the *trans* alkene.

[b]Not detectable.

[c]Obscured by another peak.

[d]In these cases a small amount of the *threo* Markownikoff adducts are also observed.

change. Thus in the *cis* series the addition changes from stereospecifically *anti* and non-regiospecific for the three alkenes **1***a–c* to regio-specific and nonstereospecific for the four alkenes **1***d–g*. In the *trans* series the change is not as dramatic. The addition is regiospecific for all the alkenes, stereospecifically *anti* for alkenes **2***a–d* and stereoselectively *anti* for alkenes **2***e–g*.

In order to learn if the change in the overall stereochemistry of the reaction is due to a change in the structure of the rate determining transition state we have correlated the rate data against both σ and σ^+ using the substituent constants listed in Table 1. The results are tabulated in Table 3 and illustrated in Fig. 2. For the addition of 2,4-dinitrobenzenesulfenyl chloride the correlation *vs.* σ is superior to that *vs.* σ^+ for both series. The important point illustrated by Fig. 2 is that a linear relationship is obtained for all the compounds in both series.

TABLE 3. Correlations of the rate of 2,4-dinitrobenzenesulfenyl chloride to a series of phenyl substituted *cis*- and *trans*-1-phenylpropenes at 25 °C in 1,1,2,2-tetrachlorethane *vs.* σ and σ^+

Alkene series	Substituent constant	ρ	r^a	s^b
cis	σ	-2.7 ± 0.2	0.986	0.2
trans	σ	-3.7 ± 0.2	0.990	0.2
cis	σ^+	-1.7 ± 0.2	0.956	0.2
trans	σ^+	-2.3 ± 0.3	0.948	0.4

[a]Correlation coefficient.
[b]Standard deviation of the fit.

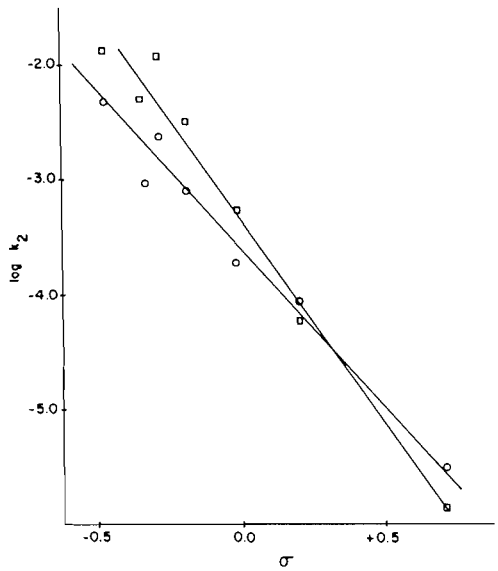

FIG. 2. Plot of log k_2 *vs.* σ for the addition of 2,4-dinitrobenzenesulfenyl chloride to ring substituted *cis*- and *trans*-1-phenylpropenes: □ *trans* compounds, $\rho = -3.7$; ○ *cis* compounds, $\rho = -2.7$.

This indicates that the polar factors must be similar in the rate determining transition state for all the alkenes in both series. Since we know that the rate determining transition states for the addition to alkenes **1***a–c* and **2***a–c* are bridged, this implies that a bridged rate determining transition state must also be involved in the addition to the other alkenes where products resulting from nonstereospecific additions are observed. This conclusion permits us to rule out any mechanism involving the rate determining formation of an open ion.

The defining reaction for the σ^+ substituent constants (7) is one in which direct conjugative interaction between the substituent and a carbonium ion α to the ring is possible. A poorer correlation of the rates with σ^+ indicates that little of the stabilization supplied by the phenyl ring is due to a resonance interaction. This is confirmed by the small values of R obtained in the Yukawa–Tsuno relationship (8). The following equations are obtained for the *cis* and *trans* series respectively using only five substituents (3-NO_2, 4-Cl, 4-H, 4-CH_3, 4-CH_3O).

$$\log k_X/k_H = -2.5[\sigma + 0.34(\sigma^+ - \sigma)]$$

$$\log k_X/k_H = -3.8[\sigma + 0.20(\sigma^+ - \sigma)]$$

In contrast to these results, the additions of bromine (9) and chlorine (10) to styrene systems have been shown to correlate with σ^+ rather than σ. However the magnitude of ρ^+ does not indicate the relative bridging ability of bromine and chlorine in their respective rate determining transition states since ρ^+ is -4.55 for bromination (9) and only -3.2 for chlorination (10). This lower value for chlorination was explained by invoking an earlier rate determining transition state (10). A similar argument can be proposed to account for the more positive value of ρ for the *cis* series. An alternate explanation is that the rate determining transition state for the *cis* is more bridged than the *trans* series. In other words there is more charge on the benzylic carbon in the rate determining transition for addition to the *trans* alkenes. While we favor the latter explanation, the available data are too sparse to arrive at a definite conclusion.

The value of ρ for the *trans* series is more negative than the value obtained for the same reaction series in acetic acid by Fueno and coworkers (11) and by Orr and Kharasch (12) for the addition of 2,4-dinitrobenzenesulfenyl chloride to styrene in acetic acid. This is due to the fact that both values of the rate of the 4-methoxyl derivative in acetic acid lie well above the line.

In addition some variation of ρ with solvent might be expected.

It should be noted that the k_c/k_t ratios show a small but regular variation with the electron-donating ability of the substituent. When the substituent is electron donating $k_c/k_t < 1$ while with electron-withdrawing substituents $k_c/k_t > 1$. The former ratio is usually found for phenyl substituted ethylenes (13) while the latter ratio is normally found for alkyl substituted ethylenes (14). This variation is also evident in the different ρ values obtained for the two series. This effect can be assigned to the greater tendency of the phenyl ring to adopt a planar conformation as its electron-releasing ability increases. For addition to the *cis* relative to the *trans* series, this will cause a larger steric interaction in the thiiranium ion-like rate determining transition state for the 4-methoxy than for the 3-nitro substituent. As a result the inversion in the k_c/k_t ratio occurs with increasing electron-donating ability of the substituents.

The product data in Table 2 clearly indicate that there is a difference in the product determining transition states not only between the two series but also within the *cis* alkene series. The stereospecific formation of Markownikoff and *anti*-Markownikoff adducts in the addition to *cis*-1-phenylpropene and the *cis* alkenes containing electron-withdrawing substituents is clearly in accord with a bridged product determining transition state. The formation of both *erythro* and *threo* Markownikoff adducts in the addition to *cis* alkenes containing electron-donating substituents indicates that the product determining transition state has an open-ion like structure. As indicated by the linearity of the Hammett correlation, the intermediate formed in the rate determining step of the addition in the *cis* series is structurally similar for all substituents. Therefore it follows that in the presence of electron-donating substituents, the first formed intermediate rearranges to a significant degree before the product determining transition state.

In the *trans* series the exclusive formation of Markownikoff adducts indicates a higher charge on the benzylic carbon in the rate determining transition state than for the *cis* series. Also the structure of the intermediate formed in the addition to the *trans*-1-phenylpropenes does not change appreciably between the rate and product determining transition states.

If we regard the reaction of arenesulfenyl chlorides with alkenes as a nucleophilic substitution reaction at sulfur rather than the usual electrophilic addition reaction, we are led to the conclusion that the two step mechanism usually proposed is not unique. Two mechanisms which have been proposed for nucleophilic displacements at sulfur are shown in Fig. 3. Path *a*, which is the sulfur analog of the S_N2 mechanism, leads to a single intermediate and is identical to the usual two step mechanism. Path *b* involves formation of a tetravalent sulfur intermediate, **3**, which may ionize to the thiiranium ion or may proceed directly to the products. Evidence for

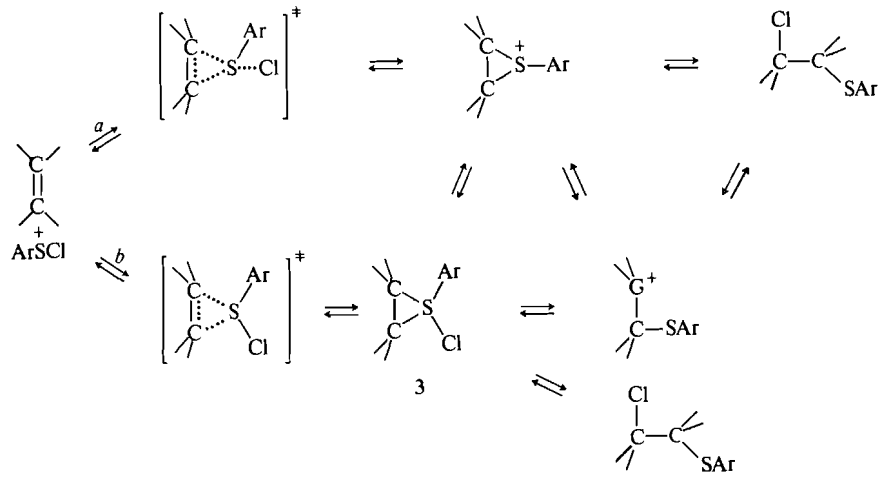

FIG. 3. Possible S_N2-like and addition–elimination mechanisms.

both the S_N2-like transition state (15) and the tetravalent intermediate (16) in nucleophilic displacement reactions at sulfur has been presented while isolation of the selenium analog of **3** has been reported (17). A thiiranium ion-like rate determining transition state seems to be the most consistent with the sign and magnitude of ρ. Whether this transition state is formed via a direct S_N2-like step or by rate limiting ionization of the tetravalent sulfur intermediate is still not clear.

Experimental

All melting and boiling points are uncorrected. Nuclear magnetic resonance spectra were recorded on Varian T-60 or HA-100 spectrometers using tetramethylsilane as internal standard. Microanalyses were carried out by A.B. Gygli Microanalysis Laboratories, Toronto.

trans-Anethole was obtained commercially from Eastman Organic Chemicals and purified by distillation, bp 76.5–77 °C/1.5 torr.

cis-Anethole was obtained by photochemical isomerization and purified by preparative glc on a 25-ft UCON column.

2,4-Dinitrobenzenesulfenyl chloride was prepared by the method of Lawson and Kharasch (18) mp 96–97 °C (lit. (18) mp 97–98 °C).

1,1,2,2-Tetrachloroethane was purified as previously described (6).

4-Phenoxypropiophenone was prepared in 82% yield by reacting diphenyl ether and propionic anhydride under Friedel–Crafts conditions according to the method of Ingersoll *et al.* (19), bp 135–140 °C/0.06 torr; nmr δ 1.2 (t, 3H), 2.8 (q, 2H), 6.8–9.0 (m, 9H).

1-(4-Phenoxyphenyl)propyne was prepared by heating to 120 °C the selenadiazole prepared from 4-phenoxypropiophenone according to the method of Yalpani and coworkers (20), bp 108–109 °C/0.07 torr; nmr δ 2.00 (s, 3H), 6.8–8.0 (m, 9H).

cis-1-(4-Phenoxyphenyl)propene was prepared by hydrogenating 2.2 g (0.011 mol) of 1-(4-phenoxy)propyne in a Parr hydrogenation vessel using 0.05 g of freshly prepared Raney nickel in 25 ml of 95% ethanol. The reaction was stopped after the consumption of 1 equiv. of hydrogen. The reaction product consisted of 80% *cis* olefin with some dihydrogenated product and some unreduced acetylene. The *cis* olefin was isolated by glc on a 20 ft × $\frac{3}{8}$ in. 30% SE-30 column at 215 °C with a flow rate of 50 ml per min. The retention time was 22.5 min, nmr δ 1.90 (dd, 3H), 5.71 (m, 1 H), 6.41 (br d, 1H), 6.8–7.5 (9H). *Anal.* calcd. for $C_{15}H_{14}O$: C 85.68, H 6.71; found: C 85.87, H 6.52.

trans-1-(4-Phenoxyphenyl)propene was prepared by the reduction of 8.2 g (0.036 mol) of 4-phenoxypropiophenone with a slight excess of $LiAlH_4$ in diethyl ether. The crude alcohol obtained was added to a solution of 0.5 g of 4-toluenesulfonic acid in 100 ml refluxing benzene. The reaction solution was refluxed using a Dean and Stark trap to remove water. After 2 h the amount of water remained constant. The reaction mixture was cooled to room temperature, extracted with water to remove the sulfonic acid, then dried over $MgSO_4$. The benzene was removed on a rotary evaporator leaving a pale yellow liquid which was distilled under reduced pressure. After a 0.5 ml fore-run, a constant boiling fraction was collected, 4.6 g (61% from the ketone) of *trans*-1-(4-phenoxyphenyl)propene, bp 119 °C/0.1 torr; nmr δ 1.85 (d, 3H), 6.17 (m, 1H), 6.36 (d, 1H), 6.8–7.5 (9H). *Anal.* calcd. for $C_{15}H_{14}O$: C 85.68, H 6.71; found: C 85.49, H 6.69.

trans-1-(4-Chlorophenyl)propene was prepared in 26% yield from commercially available 4-chloropropiophenone by the same method used for *trans*-1-(4-phenoxyphenyl)-propene, bp 75–76 °C/6 torr; nmr δ 1.86, (d, 3H), 6.15 (m, 1H), 6.23 (d, 1H), 7.18 (s, 4H). *Anal.* calcd. for C_9H_9Cl: C 70.82, H 5.94, Cl 23.24; found: C 71.09, H 6.11, Cl 23.20.

cis-1-(4-Chlorophenyl)propene was obtained by way of the selenadiazole using the same procedure as in the case of the 4-phenoxy derivative. In this manner 10.5 g of 4-chlorophenylpropyne was prepared in 15% yield from the ketone. Pyrolysis of the selenadiazole again occurred at 120 °C; the acetylene was collected by cooling the receiver in an ice water bath, bp 25 °C/0.07 torr; nmr δ 2.02 (s, 3H), 7.23 (s, 4H).

Hydrogenation of the acetylene in 95% ethanol over Raney nickel resulted in the isolation of 6.4 g (61%) of *cis*-1-(4-chlorophenyl)propene, nmr δ 1.85 (dd, 3H), 5.80 (m, 1H), 6.30 (br d, 1H), 7.21 (s, 4H). *Anal.* calcd. for C_9H_9Cl: C 70.82, H 5.94, Cl 23.24; found: C 70.90, H 6.11, Cl 23.17.

trans-1-(4-Tolyl)propene was obtained in 65% yield by dehydration of 1-(4-tolyl)propanol prepared by the reaction of ethyl magnesium bromide with 4-tolualdehyde, bp 36–38 °C/0.1 torr; nmr δ 1.88 (d, 3H), 2.33 (s, 3H), 6.20 (m, 1H), 6.35 (d, 1H), 6.9–7.3 (m, 4H). *Anal.* calcd. for $C_{10}H_{10}$: C 90.85, H 9.15; found: C 91.02, H 9.17.

cis-1-(4-Tolyl)propene was obtained by way of the selenadiazole. In this manner 1-(4-tolyl)propyne was prepared, bp 58–59 °C/10 torr; nmr δ 2.02 (s, 3H), 2.30 (s, 3H), 7.10 (q, 3H).

Hydrogenation over Raney nickel in 95% ethanol gave *cis*-1-(4-tolyl)propene which was isolated by preparative glc. Retention time on a 20 ft × $\frac{3}{8}$ in. 30% SE-30 column at 140 °C, with a flow rate of 45 ml per min is 27 min; nmr δ 1.89 (dd, 3H), 2.35 (s, 3H), 5.81 (m, 1H), 6.16 (br d, 1H), 6.9–7.3 (4H). *Anal.* calcd. for $C_{10}H_{10}$: C 90.85, H 9.15; found: C 90.76, H 9.15.

4-Isopropoxypropiophenone was prepared by the Friedel–Crafts acylation of phenyl isopropyl ether according to the procedure of Ingersoll *et al.* (19). The phenyl isopropyl ether was made according to the procedure of Olsen *et al.* (21).

trans-1-(4-Isopropoxyl)propene was prepared by reduction of 4-isopropoxypropiophenone with excess $LiAlH_4$ to produce the alcohol which was dehydrated with *p*-toluenesulphonic acid in benzene. Distillation of the product under reduced pressure gave 4.8 g (50% from the ketone) of *trans*-1-(4-isopropoxyphenyl)propene, bp 62 °C /0.4 torr; nmr δ 1.28 (d, 6H), 1.82 (d, 3H), 4.40 (m, 1H), 6.0 (m, 1H), 6.25 (d, 1H), 6.6–7.2 (4H). *Anal.* calcd. for $C_{12}H_{16}O$: C 81.77, H 9.15; found: C 81.68, H 8.98.

cis-1-(4-Isopropoxyphenyl)propene. Using the method of Vogel (22), 4-iodophenol was obtained from 4-iodoaniline;

TABLE 4. Microanalysis data for the adducts of 2,4-dinitrobenzenesulfenyl chloride and substituted 1-phenylpropenes

Substituent	Configuration	Calculated (%)				Found (%)			
		C	H	N	S	C	H	N	S
3-NO_2	*trans*	45.33	3.04	10.57	8.07	45.32	2.84	10.44	7.87
	cis	45.33	3.04	10.57	8.07	45.33	3.19	10.56	8.11
4-Cl	*trans*	46.56	3.13	7.24	8.29	46.33	3.08	7.15	8.30
	cis	46.56	3.13	7.24	8.29	46.22	3.50	7.12	8.18
4-CH_3	*trans*	52.44	4.12	7.65	8.75	52.36	4.41	7.75	8.73
	cis	52.44	4.12	7.65	8.75	52.41	3.99	7.78	8.64
4-OC_6H_5	*trans*	56.69	3.85	6.30	7.21	56.49	3.86	6.18	7.29
4-$OCH(CH_3)_2$	*trans*	52.24	4.66	6.82	7.80	52.44	4.80	6.67	7.69

8.4 g of this phenol was converted to 4-iodophenyl isopropyl ether by the method of Olsen *et al.* (21). The method of Castro *et al.* (23) was used to prepare 4-isopropoxyphenylpropyne by the reaction of propynyl copper and 4-iodophenyl isopropyl ether in 72% yield, bp 54–55 °C/0.3 torr; nmr δ 1.30 (d, 6H), 2.01 (s, 3H), 4.52 (m, 1H), 6.95 (q, 4H).

Hydrogenation of this acetylene over Raney nickel in 95% ethanol resulted in a mixture of the *cis* and *trans* olefins as well as some dihydrogenated product. The *cis*-1-(4-isopropoxyphenyl)propene was collected by preparative glc. Retention time on a 20 ft × $\frac{3}{8}$ in. 30% SE-30 column, at 185 °C, with a flow rate of 100 ml per min, is 20.0 min; nmr δ 1.30 (d, 6H), 1.88 (dd, 3H), 4.50 (m, 1H), 5.78 (m, 1H), 6.30 (br d, 1H), 7.0 (q, 4H). *Anal.* calcd. for $C_{12}H_{16}O$: C 81.77, H 9.15; found: C 81.71, H 9.18.

1-(3-Nitrophenyl)propanone was prepared by the method of Zenitz and Hartung (24) from propiophenone and fuming nitric acid. The *meta* isomer was separated from the *ortho* isomer by fractional crystallization from 95% ethanol, mp 98–99.5 °C (lit. (19) mp 97–100 °C).

cis- and trans-1-(3-Nitrophenyl)propene were prepared in 91% yield by the polyphosphoric acid catalyzed dehydration of 1-(3-nitrophenyl)propanol, obtained by reduction of the ketone with sodium borohydride. After removal of the benzene solvent, the irradiation of the alkene mixture (95:5 *trans:cis*) in cyclohexane was carried out through Pyrex and a 10% aqueous $CuSO_4$ solution. An equilibrium mixture (7:3; *trans:cis*) was obtained after about 50 h irradiation. The alkene mixture was purified by distillation bp 88 °C/0.02 torr and the isomers were separated by glc on a 20 ft × $\frac{3}{8}$ in. 30% SE-30 column at 170 °C with a flow rate of 60 ml per min. Retention time of the *cis* isomer is 44 min, that of the *trans* 55 min. Nuclear magnetic resonance of the *cis* isomer, δ 1.90 (dd, 3H), 5.98 (m, 1H), 6.42 (br d, 1H), 7.3–8.2 (4H); nmr of the *trans* isomer, δ 1.90 (d, 3H), 5.95–6.5 (m, 2H), 7.2–8.2 (4H). *Anal.* calcd. for $C_9H_9NO_2$:C 66.24, H 5.56, N 8.58; found (for the *cis* isomer): C 66.21, H 5.47, N 8.56; found (for the *trans* isomer): C 66.38, H 5.54, N 8.63.

Nuclear Magnetic Resonance Analysis of Products

Reacting solutions in tetrachloroethane were subjected to nmr analysis as follows. From a solution of the olefin (0.1–0.2 *M*) and 2,4-dinitrobenzenesulfenyl chloride reacting at 25 °C a sample for nmr purposes was withdrawn. The methyl region of the nmr spectrum of this sample was examined periodically during the reaction. In cases where more than one adduct was formed, adduct ratios were determined from the integrals of the nmr signals corresponding to the methyl groups of the adducts. The chemical shifts reported for the adducts are those obtained from solutions in deuteriochloroform using tetramethylsilane as internal standard.

Kinetic Measurements

Titrimetric

The method of obtaining rate constants by a titrimetric method has been previously described (2).

Densitometric

Solutions of 2,4-dinitrobenzenesulfenyl chloride and olefin were made up to give a final concentration of the limiting reagent of approximately 0.05 *M*. The solutions were equilibrated at 25 °C, then mixed rapidly. A sample of this solution was then inserted into the oscillator tube of the densitometer. Approximately 5 min were required for complete temperature equilibration before readings of the period of oscillation could be obtained. Measurements of this period were then recorded throughout the reaction.

Analytical samples were prepared as previously described (13). Analyses for adducts which have not been previously reported are given in Table 4.

Acknowledgments

We thank the National Research Council of Canada for continued financial assistance. The technical assistance of Dennis G. Garratt in the preparation of 1-(3-nitrophenyl)propene is greatly appreciated. Financial assistance to VJN in the form of Province of Ontario Graduate Fellowships and a National Research Council of Canada Bursary is also gratefully acknowledged.

1. C. L. DEAN, D. G. GARRATT, T. T. TIDWELL, and G. H. SCHMID. J. Am. Chem. Soc. **96**, 4958 (1974).
2. G. H. SCHMID and V. J. NOWLAN. J. Org. Chem. **37**, 3086 (1972).

3. G. H. SCHMID. Can. J. Chem. **46**, 3415 (1968).
4. J. R. CAVANAUGH and B. P. DAILEY. J. Chem. Phys. **34**, 1093 (1961).
5. B. P. DAILEY and J. N. SCHOOLERY. J. Am. Chem. Soc. **77**, 3977 (1955).
6. G. H. SCHMID, V. M. CSIZMADIA, V. J. NOWLAN, and D. G. GARRATT. Can. J. Chem. **50**, 2457 (1972).
7. Y. OKAMOTO, T. INUKUI, and H. C. BROWN. J. Am. Chem. Soc. **80**, 4969 (1958).
8. Y. YUKAWA and Y. TSUNO. Bull. Chem. Soc. Jpn. **32**, 971 (1959).
9. K. YATES and R. S. MCDONALD. J. Org. Chem. **38**, 2460 (1973).
10. H.-W. LEUNG. Ph.D. Thesis, University of Toronto, Toronto, Ontario. 1970.
11. K. IZAWA, T. OKUYAMA, and T. FUENO. Bull. Chem. Soc. Jpn. **47**, 1480 (1974).
12. W. L. ORR and N. KHARASCH. J. Am. Chem. Soc. **78**, 1201 (1956).
13. G. H. SCHMID and D. G. GARRATT. Can. J. Chem. **52**, 1807 (1974).
14. G. H. SCHMID, D. G. GARRATT, and C. L. DEAN. Can. J. Chem. In press.
15. J. L. KICE. *In* Sulfur in organic and inorganic chemistry. Vol. 1. *Edited by* A. Senning. Marcel Dekker, New York. 1971. Chapt. 6. p. 176.
16. D. C. OWSLEY, G. K. HELMKAMP, and M. F. RETTIG. J. Am. Chem. Soc. **91**, 5239 (1969).
17. D. G. GARRATT and G. H. SCHMID. Can. J. Chem. **52**, 1027 (1974).
18. D. D. LAWSON and N. KHARASCH. J. Org. Chem. **24**, 858 (1959).
19. A. W. INGERSOLL, J. H. BROWN, C. K. KIM, W. D. BEAUCHAMP, and G. JENNINGS. J. Am. Chem. Soc. **58**, 1808 (1936).
20. I. LALEZARI, A. SHAFIEE, and M. YALPANI. J. Org. Chem. **36**, 2836 (1971).
21. W. T. OLSEN, H. F. HIPSCHER, C. M. BUESS, I. A. GOODMAN, I. HART, J. H. LAMNECK, JR., and L. C. GIBBONS. J. Am. Chem. Soc. **69**, 2451 (1947).
22. A. I. VOGEL. A textbook of practical organic chemistry. 3rd ed. Longmans, London. 1957. p. 651.
23. C. E. CASTRO, E. J. GAUGHAN, and D. C. OWSLEY. J. Org. Chem. **31**, 4071 (1966).
24. B. L. ZENITZ and W. H. HARTUNG. J. Org. Chem. **11**, 444 (1946).
25. D. H. MCDANIEL and H. C. BROWN. J. Org. Chem. **23**, 420 (1958).
26. H. C. BROWN and Y. OKAMOTO. J. Am. Chem. Soc. **80**, 4979 (1958).
27. C. G. SWAIN and E. C. LUPTON, JR. J. Am. Chem. Soc. **90**, 4028 (1968).

The ionic free energy and enthalpy of In^{3+} ion, and some other properties of indium trichloride

ALAN N. CAMPBELL
Chemistry Department, University of Manitoba, Winnipeg, Manitoba R3T 2N2

Received August 25, 1975

ALAN N. CAMPBELL. Can. J. Chem. **54**, 703 (1976).

The following properties have been investigated: the standard ionic free energy and ionic enthalpy of formation of In^{3+} ion, in water at 25 °C. They are: $\Delta G^0 = -22.9 \pm 0.2$ kcal mol^{-1}, $\Delta H^0 = -57.8 \pm 0.2$ kcal mol^{-1}. The entropy of formation of $InCl_3$(aq) has also been determined.

In addition, the partially miscible systems indium trichloride – ethyl ether – water, and indium trichloride – *n*-butyl alcohol – water have been investigated.

A solution of indium trichloride causes the inversion of cane sugar. On the assumption that this is due to hydrolysis, the hydrolysis constant has been calculated.

ALAN N. CAMPBELL. Can. J. Chem. **54**, 703 (1976).

On a étudié les propriétés suivantes: l'énergie libre ionique standard et l'enthalpie de formation ionique de l'ion In^{3+} dans l'eau à 25 °C. Les valeurs sont $\Delta G^0 = -22.9 \pm 0.2$ kcal mol^{-1} et $\Delta H^0 = -57.8 \pm 0.2$ kcal mol^{-1}. On a aussi déterminé l'entropie de formation du $InCl_3$(aq).

De plus, on a étudié les systèmes partiellement miscibles: $InCl_3$–Et_2O–H_2O et $InCl_3$–*n*BuOH–H_2O.

Une solution de $InCl_3$ provoque une inversion du sucre de canne. En faisant l'hypothèse que ce résultat provient d'une hydrolyse, on a calculé la constante d'hydrolyse.

[Traduit par le journal]

Introduction

Three recent papers (1–3) have dealt with various properties, chiefly thermodynamic, of indium trichloride and the In^{3+} ion. As a conclusion to this work on indium chloride the ionic free energy and enthalpy of the In^{3+} ion have been determined, as well as the distribution of indium trichloride between water and ethyl ether and between water and *n*-butyl alcohol. The inversion of cane sugar by indium chloride has also been studied.

Apparatus and Materials

These have been described in previous publications, refs. 1 to 3.

Ionic Free Energy

The cell

$$In_{(s)}/In_2(SO_4)_{3(N=1)}//CuSO_{4(N=1)}/Cu_{(s)} \qquad (1)$$

corresponding to the reaction

$$2In + 3CuSO_4 \rightarrow In_2(SO_4)_3 + 3Cu$$

or

$$2In + 3Cu^{2+} \rightarrow 2In^{3+} + 3Cu$$

was set up and the emf measured; it was found to be 0.694 V at 25 °C.

From this, the decrease in Gibbs free energy for the above reaction in stoichiometric quantities ($\nu = 6$) results as -9.614×10^4 cal. Using the figure of 1.591×10^4 cal for Cu^{2+}, ΔG^0(ionic) for In^{3+} results as -24.21 kcal mol^{-1}.

In accordance with the above equation, metallic indium does actually, and readily, displace copper from solution. Aluminum, the nearest congener of indium, does not do this, despite its negative electrode potential. The reason is well known to be the existence of a protective skin of oxide which forms on the surface of aluminum.

Taking ΔH^0 for $InCl_3$(aq) as -177.5 kcal mol^{-1} (2), we have

$$In^{3+} + 3Cl^- \rightarrow InCl_{3(aq)}$$

$$\Delta H^0_{In^{3+}} = -177.5 - 3(-39.9)$$

whence

$$\Delta H^0_{In^{3+}} = -57.8 \text{ kcal mol}^{-1}$$

The above experiment was repeated, using $N/10$ strength for both solutions, and again with

Can. J. Chem. Downloaded from www.nrcresearchpress.com by 210.87.254.5 on 09/05/12
For personal use only.

TABLE 1. Electromotive force of cells (I) and (II) at various concentrations

Concentration (N)	Electromotive force (V)	
	(I)	(II)
1	0.6943	0.7060
0.1	0.6815	0.6762
0.01	0.6750	0.6513

$N/100$ solutions. The cell

$$In_{(s)}/InCl_{3(aq)}//CuCl_{2(aq)}/Cu_{(s)} \qquad (II)$$

was then set up, corresponding to the reaction

$$2In + 3Cu^{2+} \rightarrow 2In^{3+} + 3Cu$$

The emf's of cells (I) and (II) at different concentrations are given in Table 1.

If the figures of Table 1 are plotted in the form V *vs.* N, it appears as if the value of V for $N = 0.01$, for cell II, were too low. If, however, V is plotted against $-\log N$, a pretty close approximation to linearity results, and this has been done in Fig. 1. This procedure does not permit of extrapolation to zero concentration, so the value of V for $N = 0.01$ has been taken as representing infinite dilution. Using the figure for the most dilute solutions (0.6513) ΔG^0 for the reaction becomes -90.19 kcal mol^{-1} and ΔG for In^{3+} -21.23 kcal mol^{-1} in reasonably good agreement with the previous result.

Finally, two cells, *viz.*

$$In_{(s)}/InCl_{3(sat'd)}//HCl_{a=1}/Pt(Cl_{2(g)}) \qquad (III)$$

and

$$Hg_{(l)}/Hg_2Cl_{2(s)},KCl_{(sat'd)}//InCl_{3(sat'd)}/In_{(s)} \qquad (IV)$$

were established. The first cell corresponds to

$$In + \tfrac{3}{2}Cl_2 \rightarrow InCl_3$$

and had an emf of 1.6875 V. The second cell had an emf of 0.5825 V. From the known emf of the saturated calomel electrode, the single electrode potential, $In/InCl_3$ saturated, results as -0.3410 V. From the known potential of the chlorine electrode as $+1.358$ V, the calculated emf of the first cell results as 1.699 V, as against the experimental 1.6875 V. From the experimental figure (1.6875 V), ΔG^0 for the reaction

$$In + \tfrac{3}{2}Cl_2 \rightarrow InCl_3$$

results as -116.8 kcal mol^{-1}. ΔH^0 for the reaction, from the known molar enthalpy, is -154.25 kcal mol^{-1} whence $\Delta S^0 = -125.7$ eu.

The figures for In^{3+} ($\Delta G^0 = -22.87$ kcal mol^{-1} and $\Delta H^0 = -57.8$ kcal mol^{-1}) should be compared with the corresponding figures for Al^{3+}, *viz.* $\Delta G^0 = -115.5$, $\Delta H^0 = -126.3$.

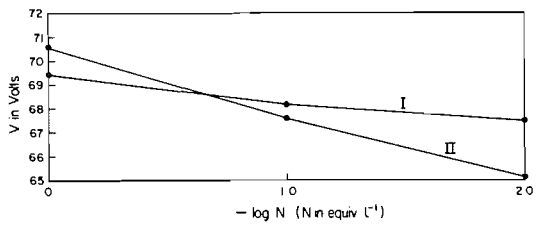

FIG. 1. Plot of V *vs.* $-\log N$ for cells I and II.

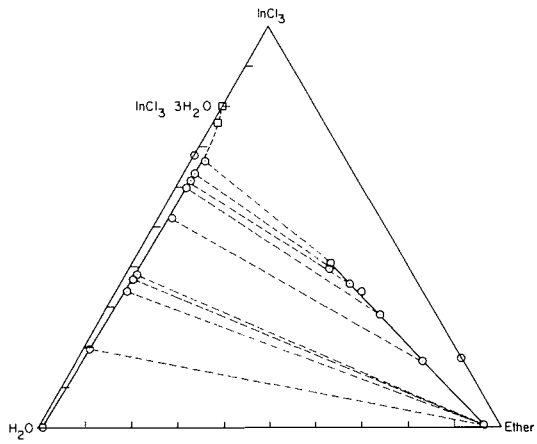

FIG. 2. System $InCl_3$ – ethyl ether – water at 25 °C.

The System $InCl_3$ – Ethyl Ether – Water

The homogeneous phases of this system were analyzed by chloride determination and density. The data are to be found in the Depository of Unpublished Data, and the results are expressed graphically in Fig. 2.[1] The miscibility gap is cut off by the occurrence of a solid phase ($InCl_3.3H_2O$) so that a critical solution cannot be formed. Two isothermal invariant points exist: (*1*) $InCl_3.3H_2O_{(s)}$, saturated aqueous layer, saturated ethereal layer. (*2*) $InCl_3.3H_2O_{(s)}$, $InCl_{3(s)}$, saturated ethereal layer.

The first invariant is readily realisable experimentally, as Fig. 2 shows, but the latter cannot be. Crystals of $InCl_3.3H_2O$ dissolve completely in excess ether, without formation of a second

[1]Complete set of tables is available, at a nominal charge, from the Depository of Unpublished Data, CISTI, National Research Council of Canada, Ottawa, Canada K1A 0S2.

Can. J. Chem. Downloaded from www.nrcresearchpress.com by 210.87.254.5 on 09/05/12
For personal use only.

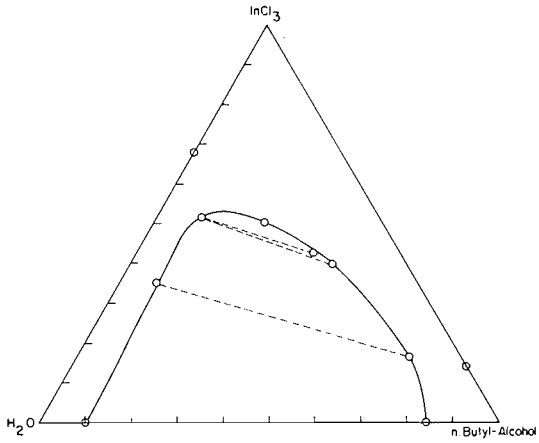

FIG. 3. System – *n*-butyl alcohol – water at 25 °C.

(aqueous) layer. It is obvious that the second invariant contains very little water.

There are two invariant triangles, the equilibrium phases of which are, respectively: (*1*) $InCl_3.3H_2O_{(s)}$, saturated aqueous solution, saturated ethereal solution; and (*2*) $InCl_3$.anhydrous$_{(s)}$, $InCl_3.3H_2O_{(s)}$, and saturated ethereal solution.

The System $InCl_3$ – n-Butyl Alcohol – Water

The data are to be found in Depository.[1] Figure 3 expresses the results graphically. Here the curve of congruent solutions is complete: it is not cut by the occurrence of a solid phase. The critical composition is: 50.1% $InCl_3$, 24.0% *n*-butyl alcohol, 25.9% water.

Inversion of Cane Sugar and Hydrolysis Constant

A solution of indium trichloride brings about the inversion of cane sugar, presumably as a consequence of the presence of hydrogen ion due to hydrolysis. Equal volumes of cane sugar solution (10 g/100 cc) and of 0.45 *M* $InCl_3$ were mixed and the inversion followed polarimetrically, at 25 °C. The value of the rate constant was found to be $k = 6.2 \times 10^{-4}$ min^{-1}. Repeating the experiment with 0.1 *N* HCl instead of the $InCl_3$ solution, gave $k = 5.63 \times 10^{-3}$. Assuming a hydrogen ion concentration of 0.05 mol l^{-1} in the second experiment and that hydrogen ion concentration is proportional to k, the hydrogen ion concentration in the indium trichloride solution results as 0.0055 *N*, or $pH \simeq 2.3$. If the hydrolysis is correctly represented by

$$In^{3+} + 3H_2O \rightleftharpoons In(OH)_3 + 3H^+$$

(it probably is not) then

$$K_h = [H^+]^3/[In^{3+}] = 6.8 \times 10^{-7}$$

Discussion

Discussion is not called for in this purely experimental paper. It is the author's intention to proceed to an investigation of the properties of indium tribromide.

1. A. N. CAMPBELL. Can. J. Chem. **51**, 3006 (1973).
2. A. N. CAMPBELL, E. M. KARTZMARK, and O. N. BHATNAGAR. Can. J. Chem. **52**, 1954 (1974).
3. A. N. CAMPBELL. Can. J. Chem. **53**, 1761 (1975).

Can. J. Chem. Downloaded from www.nrcresearchpress.com by 210.87.254.5 on 09/05/12
For personal use only.

A kinetic study of nickel(II)–murexide complex formation in dimethylsulfoxide/nitromethane mixed solvents[1]

JAMES P. K. TONG AND COOPER H. LANGFORD[2]
Department of Chemistry, Carleton University, Ottawa, Canada K1S 5B6

Received November 7, 1975

JAMES P. K. TONG and COOPER H. LANGFORD. Can. J. Chem. **54**, 706 (1976).

The rates of nickel(II)–murexide complex formation were studied in dimethylsulfoxide/nitromethane mixed solvents at 25 °C with the latter being an "inert" solvent, to elucidate the mechanism of the reaction. Results do not fit in detail with a D mechanism and the five-coordinated intermediate interpretation. I_d mechanisms are able to explain the observations with and without invoking a nitromethane-containing intermediate, $Ni(DMSO)_5NM^{2+}$. Both mechanisms were tested with the aid of nmr data on solvation (second coordinate sphere nitromethane population). Ligand solvation unavoidably plays a major role in the determination of the encounter as well as the complex formation equilibrium. The simplest mechanism assumes an I_d process in which the probability of encounter between $Ni(DMSO)_6^{2+}$ and murexide ion is quite sensitive to solvent composition.

JAMES P. K. TONG et COOPER H. LANGFORD. Can. J. Chem. **54**, 706 (1976).

On a étudié les vitesses de formation du complexe nickel(II)–muréxure afin de déterminer le mécanisme de la réaction; ces études ont été effectuées, à 25 °C, dans des solvants mixtes de diméthylsulfoxyde/nitrométhane alors que ce dernier était considéré comme un solvant "inerte". Les résultats ne corroborent pas entièrement un mécanisme D et l'interprétation faisant appel à un intermédiaire pentacoordonné. Des mécanisme I_d peuvent expliquer tous les résultats en faisant et en ne faisant pas appel à un intermédiaire contenant du nitrométhane, $Ni(DMSO)_5NM^{2+}$. On a évalué les deux mécanismes à l'aide de données rmn sur la solvatation (population du nitrométhane dans la deuxième sphère de coordination). La solvatation du ligand joue d'une façon non équivoque un rôle important dans la détermination de la rencontre aussi bien que dans l'équilibre conduisant à la formation du complexe. Le mécanisme le plus simple implique un processus I_d dans lequel la probabilité de rencontre entre $Ni(DMSO)_6^{2+}$ et l'ion muréxure est sensible à la composition du solvant.

[Traduit par le journal]

Introduction

Solvent exchange rate studies are important in the determination of complex formation mechanisms with transition metal ions in solutions. Complex formation kinetics of nickel(II) in non-aqueous solvents or solvent mixtures have drawn considerable attention; nevertheless, detailed mechanisms remain ambiguous. Frankel (1) studied dimethylsulfoxide (DMSO) exchange at nickel(II) in DMSO and its mixed solvents with nitromethane (NM) and dichloromethane (DCM). The results indicate constant DMSO exchange rates in both the neat solvent and the solvent mixtures. Low temperature nmr signal analysis also indicates that the added solvents, NM and DCM, do not, to any noticeable extent, enter the coordination sphere of nickel(II); *i.e.* they are "inert" solvents and the only equilibrium species detectable in the solution is $Ni(DMSO)_6^{2+}$ without, say, $Ni(DMSO)_5NM^{2+}$. These observations led Frankel to conclude that nickel(II) complex formation in DMSO goes by a dissociative (D) mechanism involving a five-coordinated intermediate. Langford and Tsiang (2) tested the mechanism by studying the complex formation rates of nickel(II) with thiocyanate (SCN^-) in DMSO/NM mixed solvents. Experimental difficulties forced the use of excess SCN^-, which invited the complications of erroneous observations due to higher complex formation.

We here report the results of a similar, but more convenient, experiment with nickel(II) and murexide anion. The overall reaction may be presented as:

[1] $Ni(DMSO)_6^{2+} + L^- \rightarrow Ni(DMSO)_5L^+ + DMSO$

L = murexide anion 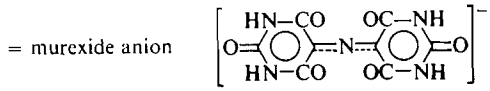

[1]We thank the National Research Council for grants and a scholarship to J.P.K.T.

[2]To whom correspondence should be addressed.

Can. J. Chem. Downloaded from www.nrcresearchpress.com by 210.87.254.105 on 09/05/12
For personal use only.

Can. J. Chem. Downloaded from www.nrcresearchpress.com by 210.87.254.105 on 09/05/12
For personal use only.

Although the murexide ion structure may function as a bidentate ligand, complex formation kinetics will be straightforward if ring closure is fast. It seems to be so in pure DMSO (2).

Experimental

$Ni(DMSO)_6(NO_3)_2$ was prepared according to the scheme suggested by Cotton and Francis (3), and was recrystallized from DMSO. DMSO and NM were obtained as spectral grade reagents from Fisher Scientific Company and dried over 4A molecular sieve. Murexide was obtained as ammonium murexide from Fisher. Complex formation kinetics were followed using a Durrum-Gibson stopped-flow spectrophotometer thermostatted to 25.0 °C at wavelengths 540 nm and 450 nm, corresponding to maxima for murexide consumption and for complex formation respectively. In all cases, the nickel(II) concentrations were kept at least 10 times higher than the murexide concentration, which was in the order of 10^{-5} *M*, to ensure pseudo-first order kinetics and 1:1 complexation. The nickel(II) concentrations were extended up to 4×10^{-3} *M*, unless the pseudo-first order rates reached the detection limit of the spectrophotometer, *i.e.* a pseudo-first order rate constant of about 350 s^{-1}. Judging from the results of repetitive runs, we claim less than a 5% standard deviation in each data point. Simple spectral determinations and recording of spectra were accomplished with a Gilford spectrophotometer. Nuclear magnetic resonance measurements were made on a Varian T-60 NMR spectrometer.

Results

The electronic spectra of murexide and the nickel murexide complex in DMSO are presented in arbitrary units in Fig. 1. The molar extinction coefficient of murexide at 540 nm is approximately 2×10^4. There is little noticeable change in the murexide and the complex electronic spectra as a function of solvent composition.

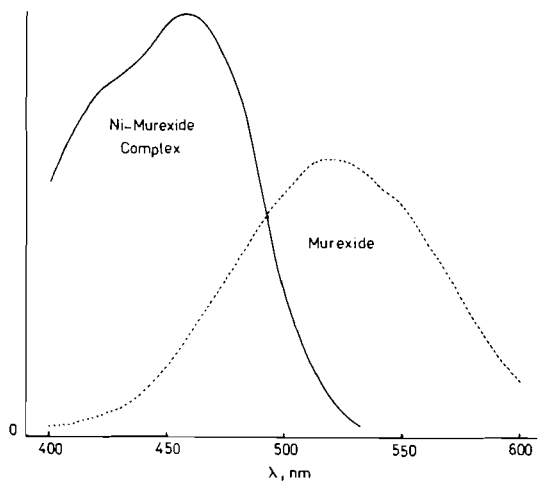

FIG. 1. Electronic spectra of murexide and nickel murexide complex in DMSO at room temperature.

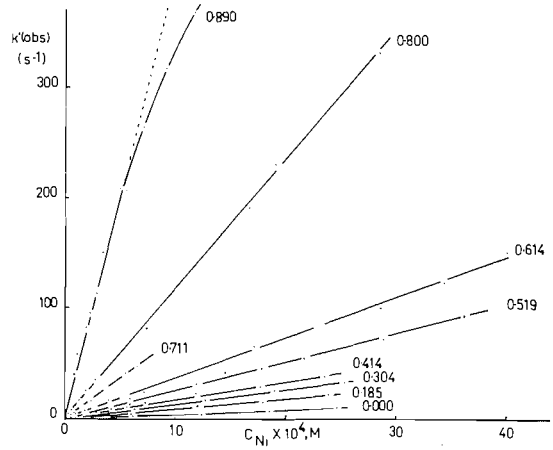

FIG. 2. Metal ion concentration dependence of pseudo-first order rate constants of nickel murexide complex formation in DMSO/NM mixed solvent at 25 °C. Solvent compositions are indicated by mole fraction NM.

The psuedo-first order rate constants, k'(obs), of complex formation at 25.0 °C are plotted as a function of nickel(II) concentrations in Fig. 2. The results obtained by following at both wavelengths agreed within experimental uncertainties. The ionic strengths of the reacting systems are controlled by the $Ni(DMSO)_6(NO_3)_2$ concentrations. In each case, the pseudo-first order rate constants are linear with respect to nickel(II) concentration, and pass through the origin. The indication of comparatively slow dissociation is supported by an equilibrium study. The complex formation equilibrium quotients, K_f, of the nickel murexide complex in DMSO and DMSO/NM mixed solvents were estimated by measuring the absorbance of murexide at 540 nm as a function of nickel(II) added at constant murexide concentrations. The estimated K_f's are listed in Table 1. The magnitudes of K_f's indicate that, if

TABLE 1. Estimated formation constants, K_f, of nickel murexide complex in DMSO/NM mixed solvents at room temperature

x_{NM}	K_f (M^{-1})
0.00	5.5×10^5
0.30	1.1×10^6
0.57	1.6×10^6
0.89	$\geq 10^7$

TABLE 2. Second order rate constants of nickel murexide complex formation in DMSO/NM mixed solvents at 25 °C

x_{DMSO}	x_{NM}	$[DMSO]^{-1}$ (M^{-1})	$(x_{DMSO})^{-1}$	$k(obs) \times 10^{-3}$ (M^{-1} s^{-1})	log k(obs)
1.00	0.00	0.0714	1.000	3.80	3.580
0.815	0.185	0.0837	1.23	9.20	3.964
0.696	0.304	0.0952	1.44	13.8	4.140
0.586	0.414	0.111	1.71	17.0	4.230
0.481	0.519	0.131	2.08	25.8	4.412
0.386	0.614	0.159	2.59	36.7	4.565
0.289	0.711	0.206	3.46	73.1	4.864
0.200	0.800	0.286	5.00	119	5.076
0.110	0.890	0.500	9.09	400	5.602

a ratio of rate constants describes K_f

$$[2] \qquad K_f = \frac{k(\text{formation})}{k(\text{dissociation})}$$

then k(dissociation) is small. The plots in Fig. 2 should pass essentially through the origin. The second order rate constants of complex formation, k(obs), derived from the slopes are tabulated in Table 2, and are plotted logarithmically as a function of solvent composition in Fig. 3. It is noteworthy that the K_f values support the limited ionic strength independence seen in complex formation rates.

The nmr linewidths (at half height) of the NM protons in DMSO/NM mixed solvents with 0.1 M $Ni(DMSO)_6^{2+}$ varied little throughout the whole solvent composition range, fluctuating between 2.0 and 2.4 Hz. The linewidth is about 1.0 Hz in the absence of $Ni(DMSO)_6^{2+}$. Since the linebroadening effect arises solely from outer sphere interactions with the nickel solvatocomplex, there is little or no preferential solvation of $Ni(DMSO)_6^{2+}$ in the mixed solvents. This implies that the composition of the solvation shell around $Ni(DMSO)_6^{2+}$ parallels the bulk composition. This interpretation is explained in ref. 4 and several papers cited therein.

Considering the D mechanism for complex formation with a five-coordinate intermediate, the reaction steps are as follows:

$$[3] \qquad Ni(DMSO)_6 \underset{k_{-1}}{\overset{k_1}{\rightleftharpoons}} Ni(DMSO)_5 + DMSO$$

$$Ni(DMSO)_5 + L \xrightarrow{k_2} Ni(DMSO)_5L$$

The rate expression where k's are the rate constants for the appropriate steps, takes the following form:

$$[4] \qquad k(\text{obs}) = \frac{k_1 k_2}{k_{-1}[DMSO] + k_2[L]}$$

Since the pseudo-first order rate plots were all accurately linear, it would imply that $k_2[L] \ll$

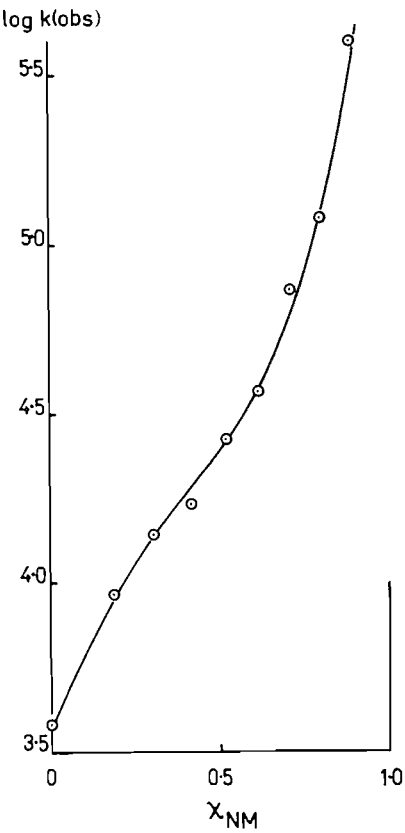

FIG. 3. Rate constants of nickel murexide formation in DMSO/NM mixed solvents at 25 °C.

Can. J. Chem. Downloaded from www.nrcresearchpress.com by 210.87.254.105 on 09/05/12
For personal use only.

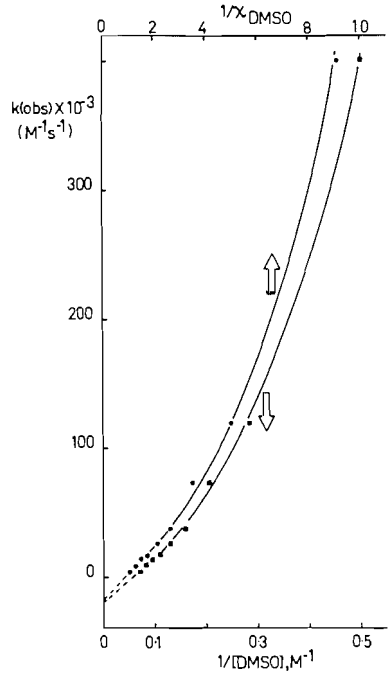

FIG. 4. Plots of rate constants *vs.* reciprocal DMSO contents of the mixed solvents.

k_{-1}[DMSO]. Then eq. 4 may be simplified as:

[5] $$k(\text{obs}) = k_1k_2/k_{-1}[\text{DMSO}]$$

Equation 5 suggests that a plot of k(obs) *vs.* $[\text{DMSO}]^{-1}$ should be linear as long as preferential solvation is not substantial, and will be independent of the nature of the added "inert" solvent. Moreover, the algebra demands that the plot passes through the origin. The results as presented in Fig. 4 do not suggest such relationship. Unless k_{-1} and/or k_2 change substantially with solvent composition, this mechanism may be ruled out.

An alternate possible mechanism may be a coupled I_d mechanism involving an NM substituted intermediate. If the D mechanism is ruled out, this must be the explanation of Frankel's results (1). The reaction scheme may be represented as follows for complex formation with ligand L.

[6] $$\text{Ni(DMSO)}_6 + \text{L} \overset{(K_E)}{\rightleftharpoons} \text{Ni(DMSO)}_6\text{.L}$$

$$\text{Ni(DMSO)}_6\text{.L} \xrightarrow{k_L} \text{Ni(DMSO)}_5\text{L} + \text{DMSO}$$

$$\text{Ni(DMSO)}_6 + \text{NM} \overset{K}{\rightleftharpoons} \text{Ni(DMSO)}_5\text{NM} + \text{DMSO}$$

$$K = \frac{[\text{Ni(DMSO)}_5\text{NM}][\text{DMSO}]}{[\text{Ni(DMSO)}_6][\text{NM}]}$$

$$\text{Ni(DMSO)}_5\text{NM} + \text{L} \overset{(K_E')}{\rightleftharpoons} \text{Ni(DMSO)}_5\text{NM.L} \xrightarrow{k_L'} \text{Ni(DMSO)}_5\text{L} + \text{NM}$$

where K_E is an encounter equilibrium constant and k_L a first order rate constant. The prime designates a process involving the NM containing species. The derived rate expression at reasonably low nickel concentrations is given as

[7] $$k(\text{obs}) = K_Ek_L + KK_E'k_L'([\text{NM}]/[\text{DMSO}]) = K_Ek_L + KK_E'k_L'(1/\chi_{\text{DMSO}} - 1)$$

where χ_{DMSO} is the mole fraction of DMSO in the solvent mixture. In eq. 7, k_L and k_L' may be compared to the solvent exchange rates, k_{ex} and k_{ex}', of DMSO and NM at nickel(II) respectively. Again, eq. 7 suggests a linear dependence of k(obs) on $(\chi_{\text{DMSO}})^{-1}$ with an intercept at $(K_Ek_L - KK_E'k_L')$ if K_E, K_E', and K are reasonably solvent composition insensitive. Indeed, in Fig. 4, extrapolation from the closest set of data points gives an intercept at approximately -16×10^3 M^{-1} s^{-1}. This agrees with the fact that k_L', and hence rate of NM exchange at nickel(II), is much larger than k_L or rate of DMSO exchange. Deviations from linearity of the plot in mixed solvents of high NM content may simply be a reflection of solvent dependences of K_E or K_E', which is plausible. Although the simple Fuoss–Eigen formulation of ion-pairing (5) suggests little variation of K_E and K_E' resulting from changing the medium dielectric constant from 49 of DMSO to 39 of NM (6), the incorporation of consideration of solvation of the murexide anion may render the medium dielectric only a secondary parameter. A very obvious set of examples that demonstrate the importance of solvation rather than the medium dielectric upon ion pairing is provided by D'Aprano *et al.* (7). Hinz and Margerum (8, 9) have shown that ligand solvation can be a dominating factor in determining complex formation equilibria. Our preliminary studies on the formation constants, K_f, of the nickel murexide complex in DMSO/NM mixed solvents indicated substantial increase in K_f at high NM contents, suggesting poorer solvation of murexide by NM (since nmr data implied little preference for DMSO or NM for the outer sphere of Ni(DMSO)_6). If this is a

Can. J. Chem. Downloaded from www.nrcresearchpress.com by 210.87.254.105 on 09/05/12
For personal use only.

correct interpretation, it would arise from solvent effects on the encounter equilibrium constants K_E and/or K_E'. Such an interpretation of the observations is adequate, allowing for the substantial variation of encounter equilibrium constants with solvent compositions.

Given these arguments, another arises which is simpler and just as good. The simple I_d interpretation which is represented as follows is equally plausible (*i.e.* only the first part of mechanism (6) is important).

$$[8]\quad Ni(DMSO)_6 + L \overset{K_E}{\rightleftharpoons} Ni(DMSO)_6.L \xrightarrow{k_L} Ni(DMSO)_5L + DMSO$$

The general expression for observed rate constants is derived as

$$[9]\quad k(\text{obs}) = K_E k_L/(1 + K_E[Ni(DMSO)_6])$$

When $K_E[Ni(DMSO)_6]$ is considerably smaller than unity, eq. 9 reduces to

$$[10]\quad k(\text{obs}) = K_E k_L$$

Frankel's experiments suggested that k_{ex}, and hence k_L, are essentially independent of solvent composition. Our results then imply a large solvent effect (changes in murexide solvation) on K_E, as discussed earlier. Indeed, the pseudo-first order rate constant plot in Fig. 2 does show some curvature for the highest NM content solvent mixture studied. Such curvature implies a large encounter equilibrium constant as required by this mechanism. Since the curvature occurs fairly close to the equipment sensitivity limit, we shall not attempt to extract further parameters. Unfortunately, there is no direct method to study the solvation behaviour of murexide ion in this mixed solvent system; nor is there a good solvating solvent for murexide which is "inert" to $Ni(DMSO)_6^{2+}$ to elucidate this problem further. We cannot distinguish eq. 10 with variable K_E from eq. 7.

1. L. S. FRANKEL. Inorg. Chem. **10**, 814 (1971),
2. C. H. LANGFORD and H. G. TSIANG. Inorg. Chem. **9**, 2346 (1970).
3. F. A. COTTON and R. FRANCIS. J. Am. Chem. Soc. **82**, 2986 (1960).
4. C. H. LANGFORD and T. R. STENGLE. *In* NMR of paramagnetic molecules. *Edited by* G. N. LaMar, R. Holm, and W. D. Horrocks. Academic Press. New York. 1974. Chapt. 10.
5. S. PETRUCCI. *In* Ionic interactions. Vol. 1. *Edited by* S. Petrucci. Academic Press, New York. 1971. Chapt. 3.
6. A. J. GORDON and R. A. FORD. The chemists' companion. Wiley–Interscience, New York. 1972.
7. A. D'APRANO, M. GOFFREDI, and R. TRIOLO. Faraday Trans. (I), **71**, 1188 (1975).
8. F. P. HINZ and D. W. MARGERUM. J. Am. Chem. Soc. **96**, 4993 (1974).
9. F. P. HINZ and D. W. MARGERUM. Inorg. Chem. **13**, 2941 (1974).

Can. J. Chem. Downloaded from www.nrcresearchpress.com by 210.87.254.105 on 09/05/12
For personal use only.

Preparation, Mössbauer and vibrational spectra of diorganotin chromates and carbonates

R. G. GOEL AND H. S. PRASAD
Department of Chemistry, University of Guelph, Guelph, Ontario N1G 2W1
AND
G. M. BANCROFT AND T. K. SHAM
Department of Chemistry, University of Western Ontario, London, Ontario N6A 3K7

Received September 5, 1975

R. G. GOEL, H. S. PRASAD, G. M. BANCROFT, and T. K. SHAM. Can. J. Chem. **54**, 711 (1976).

Dimethyltin chromate and basic dimethyltin and diphenyltin carbonates have been isolated for the first time. Structural features of these compounds, as well as of the previously known basic dimethyltin chromate, have been investigated by examining their infrared, Raman, and Mössbauer spectra. Infrared, Raman, and Mössbauer spectra of $[Me_2Sn(NCS)]_2O$ have also been examined, and by comparing its spectroscopic data with those for $(Me_2Sn)_2OCrO_4$, $(Me_2Sn)_2OCO_3$, and $(Ph_2Sn)_2O(CO_3)$, possible structures have been suggested for the latter compounds. From the combined infrared and Mössbauer data, a structure is also proposed for Me_2SnCrO_4. All compounds are indicated to have polymeric structures with bridging CrO_4^{2-} or CO_3^{2-}.

R. G. GOEL, H. S. PRASAD, G. M. BANCROFT et T. K. SHAM. Can. J. Chem. **54**, 711 (1976).

On a isolé pour la première fois le chromate de diméthylétain et les carbonates basique de diméthylétain et de diphénylétain. On a étudié les caractéristiques structurales des composés de même que celles du chromate basique de diméthylétain qui était déjà connu; ces études ont été réalisées par un examen des spectres ir, Raman et Mössbauer de ces composés. On a aussi examiné les spectres ir, Raman et Mössbauer du $[Me_2Sn(NCS)]_2O$, et en comparant ces propriétés spectroscopiques avec celles du $(Me_2Sn)OCrO_4$, du $(Me_2Sn)OCO_3$ et du $(Ph_2Sn)_2O(CO_3)$, on a pu suggérer des structures possibles pour ces derniers composés. A partir des données ir et Mössbauer, on peut aussi proposer une structure pour le Me_2SnCrO_4. Il existe, pour chacun de ces composés, des indications à l'effet que des ponts CrO_4^{2-} ou CO_3^{2-} provoquent la formation de structures polymériques.

[Traduit par le journal]

Introduction

Recent structural studies on dimethyltin derivatives of the type Me_2SnX_2, where X = an anionic group, show the prevalence of polymeric structures involving six-coordinate tin and bridging X groups. In dimethyltin difluoride (1) each tin atom is surrounded by four symmetrically bridging fluorine atoms in a plane, with methyls above and below the plane. Recently, dimethyltin bis(fluorosulfate) (2) has been shown to have a similar structure in which each tin atom is coordinated to four oxygens and two methyls in the *trans*-positions. A tetrahedral structure had been established for dimethyltin dichloride by an electron diffraction study (3) in the vapour phase. A similar structure had been postulated in the solid state on the basis of infrared spectroscopy (4). However, the crystal structure of Me_2SnCl_2 (5) indicates that Me_2SnCl_2 consists of chains of distorted tetrahedral molecules linked by weak interactions between neighbouring Sn and Cl atoms. In this manner, the Sn atoms acquire a distorted octahedral environment. Association has also been detected by X-ray crystallography in $Me_2Sn(NCS)_2$ (6, 7).

Mössbauer spectroscopy has also been useful for inferring association in such compounds. First, the quadrupole splitting for an unassociated Me_2SnX_2 compound is considerably smaller than for an associated Me_2SnX_2 compound (8, 9). Second, an associated compound normally gives a larger room temperature absorption than an unassociated compound (10, 11).

Apart from some recent spectroscopic work, little structural information is, however, available on dimethyltin derivatives of dibasic acids. On the basis of infrared and Mössbauer spectroscopic data (12), a polymeric structure involv-

Can. J. Chem. Downloaded from www.nrcresearchpress.com by 210.87.254.40 on 09/05/12
For personal use only.

TABLE 1. Mössbauer spectral parameters at 110 and 295 K*

Compound	At 110 K			At 295 K			
	C.S.†	Q.S.	Γ	C.S.†	Q.S.	Γ	R‡
Me_2SnCrO_4	1.37	3.92	1.26	1.40	3.85	1.13	0.34
$(Me_2Sn)_2O(CrO_4)$	1.26	3.15	1.24	1.12	3.16	1.08	0.17
$(Me_2Sn)_2O(CO_3)$	1.13	3.18	1.19	1.10	3.24	1.15	0.12
$(Ph_2Sn)_2O(CO_3)$	1.04	2.23	0.98	0.97	2.29	0.98	0.17
	1.09	3.96	0.98	1.16	3.93	0.98	
$[(Me_2SnNCS)_2O]_2$	1.25	3.38	1.04	1.20	3.36	0.95	0.10

*The errors in C.S. and Q.S. are ±0.02 mm s^{-1}; the error in Γ = ±0.05 mm s^{-1}.
†All C.S. values are quoted relative to the centroid of a $BaSnO_3$–$BaSnO_3$ room temperature spectrum.
‡R is the ratio of the normalized intensities of the room temperature to liquid nitrogen spectra, A_{295}/A_{110}.

ing bridging SO_4 or SeO_4 groups and *trans*-octahedral coordination around the tin atoms has been indicated for dimethyltin sulfate and selenate. Mössbauer data (13, 14) for Me_2SnMoO_4 have also been interpreted in terms of a polymeric *trans*-octahedral structure. Mössbauer data (15) for Me_2SnWO_4, $Me_2SnC_2O_4.H_2O$, and $(Me_2Sn)_2O(CrO_4)$ have also been reported although no interpretation of the data has been provided. The formation of Me_2SnCrO_4 and Me_2SnCO_3 has also been inferred (16) from infrared measurements but neither compound has hitherto been isolated in the pure form.

In the present work Me_2SnCrO_4 has been isolated and characterized, but the infrared spectrum attributed to Me_2SnCO_3, in the previous work (16), has been shown to be that of previously unknown $(Me_2Sn)_2O(CO_3)$. Basic diphenyltin carbonate has also been prepared. Using Mössbauer infrared and Raman spectroscopy, combined with the recent crystal structure of the stannoxane $[Me_2Sn(NCS)]_2O$ (17), we are able to propose possible structures for the basic chromate and carbonates. On the basis of the combined infrared and Mössbauer data a new structure is also proposed for dimethyltin chromate.

Results and Discussion

Dimethyltin Chromate

The metathetical reaction of aqueous dimethyltin dichloride with silver chromate afforded a water-soluble yellow crystalline product for which the analytical data correspond to the formula Me_2SnCrO_4. Its infrared spectrum was identical to that reported (16) for the product obtained by stirring dimethyltin dichloride and silver chromate in anhydrous acetone or acetonitrile. Thus, there can be little doubt that the previously reported (16) infrared spectrum was indeed due to Me_2SnCrO_4.

The infrared spectrum of Me_2SnCrO_4 has been interpreted previously in terms of a polymeric structure containing tetrahedrally coordinated tin atoms and bidentate chromate groups (16). Confirmation of the proposed structure was sought in the present work by Raman and Mössbauer spectroscopic measurements. Attempts to measure the Raman spectrum failed due to the decomposition of the compound by the laser beam. However, the Mössbauer parameters (Table 1) suggest that Me_2SnCrO_4 has a polymeric structure containing octahedrally coordinated tin with axial methyl groups (8). The large R value is indicative of a polymeric structure, while the large Q.S. is consistent with a six-coordinate structure with axial methyl groups and a Me—Sn—Me angle of less than 180° (18). Suggestions for a four-coordinate structure were based mainly on the assumption that dimethyltin(IV) compounds containing nonlinear Me—Sn—Me linkages, such as Me_2SnCl_2, contained tetrahedrally coordinated tin. From the recently reported crystal structure determination of $Me_2Sn(NCS)_2$ (6, 7) and other tin(IV) compounds (for a summary, see ref. 18), it is now apparent that dimethyltin(IV) derivatives often adopt six-coordinate structures containing nonlinear Me—Sn—Me groups. In view of these results, the infrared spectrum of Me_2SnCrO_4 can be interpreted in terms of a six-coordinate structure containing nonlinear Me—Sn—Me groups, in which each chromate oxygen is coordinated to a tin atom in such a manner that the two Cr—O bonds are lengthened in comparison with the other two Cr—O bonds. An example of such bonding between tin and chromate oxygens is provided by the recently reported (19) crystal structure of polymeric tris(trimethyltin) chromate

Can. J. Chem. Downloaded from www.nrcresearchpress.com by 210.87.254.40 on 09/05/12
For personal use only.

Can. J. Chem. Downloaded from www.nrcresearchpress.com by 210.87.254.40 on 09/05/12
For personal use only.

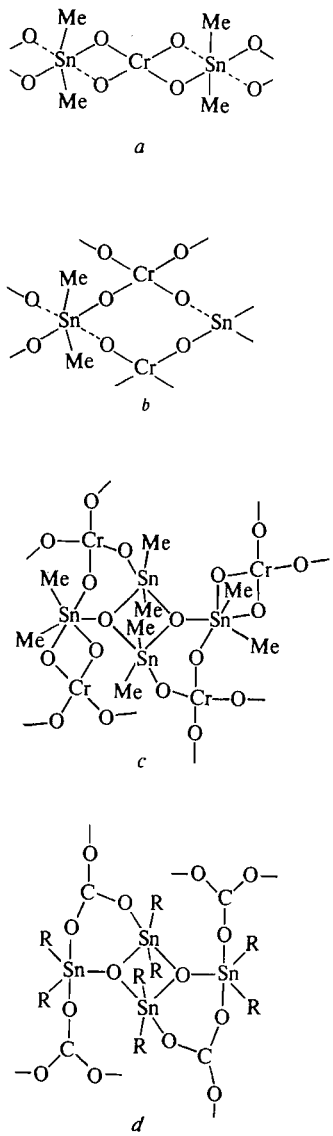

FIG. 1. Proposed schematic structures for *a* and *b*, Me_2SnCrO_4; *c*, $(Me_2Sn)_2O(CrO_4)$; *d*, $(Me_2Sn)_2O(CO_3)$ and $(Ph_2Sn)_2O(CO_3)$.

hydroxide, $(Me_3Sn)_3CrO_4(OH)$. In this compound each chromate oxygen is bonded to penta-coordinate tin atoms and the two Cr—O bonds are shortened and the other two Cr—O bonds are lengthened as compared with the mean Cr—O distances observed for $(NH_4)_2CrO_4$. Thus, the infrared and Mössbauer spectra of Me_2SnCrO_4 are consistent with structures as shown in Fig. 1 (*a*) or (*b*).

The magnitude of the quadrupole splitting is of use in discussing the structure of analogous dimethyltin compounds. Me_2SnCrO_4 has a substantially smaller Q.S. than that of Me_2SnSO_4 or Me_2SnSeO_4 (5.00 mm s^{-1} and 4.82 mm s^{-1} respectively) (12), but a splitting in between that of Me_2SnMoO_4 and Me_2SnWO_4 (4.10 mm s^{-1} and 3.53 mm s^{-1} respectively) (15). The quadrupole splitting increases with an increase in degree of association (8, 9) and an increase in Me—Sn—Me angle (18). Thus, the quadrupole splittings indicate that the degree of association and the Me—Sn—Me angle increase in the order $WO_4 < CrO_4 < MoO_4 < SeO_4 < SO_4$.

Basic Dimethyltin Chromate

As reported by Rochow and co-workers (20), basic dimethyltin chromate, $(Me_2Sn)_2O(CrO_4)$ was precipitated upon mixing aqueous solutions of dimethyltin dichloride and sodium or potassium chromate. The observed infrared bands for the solid $(Me_2Sn)_2O(CrO_4)$ together with their suggested assignments are recorded in Table 2. Attempts to measure the Raman spectrum of this compound also failed due to its decomposition by the laser beam. The assignments for the infrared bands in the 3000–2900 (C—H stretch), 1400–1200 (C—H deformation), 800 (Sn—CH_3 rock) and 520 (Sn—C symmetric stretch) cm^{-1} regions follow from those for dimethyltin dichloride (4, 20). The bands at 963, 935, 866, 750, 420, 388, 372, and 325 cm^{-1} are similar to those observed for dimethyltin chromate and can be attributed to the vibrations of the coordinated chromate group of C_{2v} or C_s symmetry. The bands at 600, 555, and 265 cm^{-1} are similar to those observed for $[Me_2Sn(NCS)]_2O$ and their assignments are discussed below.

As shown by an X-ray crystallographic study (17), $[Me_2Sn(NCS)]_2O$ has a polymeric structure containing a dimeric unit which has a dioxo-bridged four membered

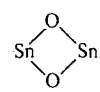

ring. The tin atoms of the ring have a distorted trigonal bipyramidal configuration and each oxygen atom of the ring is also bonded to another tin atom which is formally six-coordinate. The observed infrared frequencies in the 4000 to 250 cm^{-1} region, and the Raman frequencies in the region below 900 cm^{-1}, for $[Me_2Sn(NCS)]_2O$, together with their suggested assignments are listed in Table 2. Apart from the frequencies

TABLE 2. Infrared and Raman spectral frequencies* for $(Me_2Sn)_2O(CrO_4)$, $(Me_2Sn)_2O(CO_3)$, and $[Me_2Sn(NCS)]_2O$

Infrared $(Me_2Sn)_2O(CrO_4)$	$(Me_2Sn)_2O(CO_3)$		$[Me_2Sn(NCS)]_2O$		Assignments
	Infrared	Raman	Infrared	Raman	
3000vw 2910vw	3000vw 2905vw				C—H stretch
			2080vs 2015vs		ν(CN)
	1510vs				ν_3, (CO_3)
1405w	1410sh		1405w		C—H deformation
	1385vs				ν_3, (CO_3)
1200mw	1200m		1210mw		C—H deformation
	1105m				ν_3, (CO_3)
963s 935s 866s					ν_3, (CrO_4)
	832m				ν_2, (CO_3)
				885w 820w	ν(CS)
795s	795s 780s		800s		Sn—CH_3 rock
750s					ν_1, (CrO_4)
	700m	697w			ν_4, (CO_3)
600s	655s		635s		$\nu(Sn_2O_2)$
	580m 570m	581w 571w	580m	578m	Antisymmetric Sn—CH_3 stretch
555s		550w	545s		$\nu(Sn_2O_2)$
520m	525m	531s 524s	525sh	535s 521s	Symmetric Sn—CH_3 stretch
	500s	495w		510w	$\nu(Sn_2O_2)$
			480mw 420mw 400mw	485w	o(NCS)
420m 388m 372m					ν_4, (CrO_4)
	345m				$\nu(Sn_2O_2)$
325m					ν_2, (CrO_4)
265m	275m		280m		ν(SnO)
		215m		226m	Sn—CH_3 bend
		130m		156m 141m	

*In cm^{-1} in the solid state. Abbreviations: m, medium; s, strong; sh, shoulder; v, very; w, weak.

due to the internal vibrations of the CH_3 and NCS groups and a strong band due to the Sn—CH_3 rocking mode, the infrared frequencies for this compound include strong bands at 635 and 545 cm^{-1}, a medium–strong band at 280 cm^{-1} and medium to weak bands at 580, 525, 480, 420, and 400 cm^{-1}. The Raman frequencies in this region include two strong bands at 535 and 521 cm^{-1}, and three medium to weak bands at 578, 510, and 485 cm^{-1}, and a medium band at

Can. J. Chem. Downloaded from www.nrcresearchpress.com by 210.87.254.40 on 09/05/12
For personal use only.

Can. J. Chem. Downloaded from www.nrcresearchpress.com by 210.87.254.40 on 09/05/12
For personal use only.

226 cm^{-1}. The bands at *ca.* 535 and 521 cm^{-1} are undoubtedly due to the symmetric Sn—CH_3 stretching frequencies (4, 21) of the two inequivalent $Sn(CH_3)_2$ groups and the 580–578 cm^{-1} band is due to the antisymmetric Sn—CH_3 stretching frequency (4, 21) which is apparently similar for the four $Sn(CH_3)_2$ groups. The bands in the 485 to 400 cm^{-1} region are due to the NCS bending frequencies (22) of the two inequivalent NCS groups, and the 226 cm^{-1} band can be assigned to a Sn—CH_3 bending mode. Thus the strong infrared bands at 635 and 545 cm^{-1} and the weak Raman band at 510 cm^{-1} are associated with the bridge vibrations of the Sn_2O_2 ring. As shown by Wing and Callahan (23), a dioxobridged M_2O_2 ring of D_{2h} symmetry gives rise to four stretching frequencies of which two are infrared active and the other two are Raman active. Thus, the assignments for the 635 and 545 cm^{-1} infrared bands and the 510 cm^{-1} Raman band are consistent with the crystal structure data. The medium-strong infrared band at 280 cm^{-1} can be assigned to the stretching mode of the Sn—O bonds between the bridging oxygens and hexacoordinated tin atoms.

Although it is difficult to ascertain the structure of $(Me_2Sn)_2O(CrO_4)$ from the infrared spectroscopic data, close similarities of the 600, 555, and 262 cm^{-1} bands with the 635, 545, and 280 cm^{-1} bands of $[Me_2Sn(NCS)]_2O$ indicate that both compounds contain a similar network of Sn_2O_2 and Sn—O bonds. In addition, the Mössbauer parameters for $(Me_2Sn)_2O(CrO_4)$ are very similar to those for $[Me_2Sn(NCS)]_2O$. By analogy with the structure for the latter compound, a structure as shown in Fig. 1(*c*) is proposed for the basic chromate. Both structures contain five-coordinate and six-coordinate Sn atoms which give coincidentally overlapping Sn resonances. This overlap is not surprising if the two MeSnMe bond angles are similar (18) (as they are in $[Me_2Sn(NCS)]_2O$).

Basic Carbonates

The reaction of dimethyltin dichloride with alkali metal or silver carbonate, in water or methanol, gave dimethyltin oxide as the only tin-containing species. However, the reaction of aqueous potassium carbonate with an acetone solution of dimethyltin dichloride which had been saturated with carbon dioxide afforded basic dimethyltin carbonate $(Me_2Sn)_2O(CO_3)$. Its infrared spectrum was found to be identical to that attributed previously (16) to Me_2SnCO_3, except that the doublets observed in the present work at *ca.* 795–780 and 580–570 cm^{-1} were not resolved in the previous work. Thus the product formulated in the previous study (16) as Me_2SnCO_3 was in fact $(Me_2Sn)_2O(CO_3)$. Basic diphenyltin carbonate $(Ph_2Sn)_2O(CO_3)$ was also obtained from a similar reaction of diphenyltin dichloride with cesium carbonate.

The revised assignments for the infrared spectrum of $(Me_2Sn)_2O(CO_3)$ along with its Raman spectral data in the region below 900 cm^{-1} are presented in Table 2. The infrared bands due to the C—H stretching and deformation modes, and the Sn—CH_3 rocking mode are similar to those for $(Me_2Sn)_2O(CrO_4)$. The carbonate infrared bands for the basic carbonate compare very well with those reported (24) for rare earth dioxymonocarbonates. The observed splittings of the degenerate modes and the appearance of the infrared inactive symmetric CO stretching mode are indicative of a C_{2v} or C_s symmetry for the carbonate groups. However, the observed carbonate frequencies do not give any indication of the presence of nonequivalent carbonate groups.

The strong Raman bands at 531 and 524 cm^{-1} and a medium infrared band at 525 cm^{-1} observed for the basic carbonate can be assigned to the symmetric Sn—CH_3 stretching frequencies. Similarly, weak Raman bands at 581 and 571 cm^{-1} and medium infrared bands at 580 and 570 cm^{-1} can be assigned to the antisymmetric Sn—CH_3 stretching frequencies. Therefore, this compound is also indicated to contain two inequivalent dimethyltin groups. The strong infrared bands at 655 and 500 cm^{-1} are similar to the 635 and 545 cm^{-1} bands observed for $[Me_2Sn(NCS)]_2O$ and can be assigned to the stretching vibrations of the Sn_2O_2 ring. The infrared band at 345 cm^{-1} can also be assigned to a stretching frequency of the dioxobridged Sn_2O_2 ring, and the 275 cm^{-1} infrared band can be assigned to a Sn—O stretching frequency.

Due to the presence of numerous phenyl bands, it is difficult to make clear-cut assignments for the skeletal frequencies in the case of basic diphenyltin carbonate. However, by comparison of its infrared spectrum with that of diphenyltin dichloride, it is possible to ascertain

TABLE 3. Analytical data

Compound	Calcd. (%)			Found (%)		
	C	H	Sn	C	H	Sn
Me_2SnCrO_4*	9.07	2.28	44.8	9.04	2.11	44.15
$(Me_2Sn)_2O(CrO_4)$	11.18	2.81		11.13	2.88	
$(Me_2Sn)_2O(CO_3)$	16.07	3.23	63.55	16.52	3.28	63.36
$(Ph_2Sn)_2O(CO_3)$	48.34	3.24	38.21	48.68	3.81	37.54
$[Me_2Sn(NCS)]_2O$†	16.77	2.82		16.82	3.23	

*Percent Cr: calcd., 19.64; found, 19.54.
†Percent N: calcd., 6.52; found, 6.43.

that the bands at 1510, 1383, 1095, and 820 cm^{-1}, observed for the basic carbonate are due to the carbonate group. Infrared spectrum of the basic carbonate also showed bands at 660, 650, 583, 425, 325, and 310 cm^{-1} which were not observed in the spectrum of the dichloride. The 660 cm^{-1} band appeared very strongly in the Raman spectrum which also showed weak bands at 590 and 320 cm^{-1}. Since a band at *ca.* 660 cm^{-1} is also reported (25, 26) to appear in the infrared and Raman spectra of Ph_3SnCl and $PhSnCl_3$, it is most likely that the 660 and 650 cm^{-1} bands are due to the vibrations of the phenyl rings. Thus, by comparison with the spectra of the methyl compound the infrared or Raman bands at 583, 425, and 325 cm^{-1} can be attributed to the stretching vibrations of the Sn_2O_2 ring and the 310 cm^{-1} band can be assigned to the Sn—O stretching frequency.

In summary, the infrared and Raman data for both $(Me_2Sn)_2O(CO_3)$ and $(Ph_2Sn)_2O(CO_3)$ are in accord with a polymeric structure containing bridging carbonates and four-membered Sn_2O_2 rings. Again by analogy with the structure of $[Me_2Sn(NCS)]_2O$, a structure as shown in Fig. 1(*d*) is proposed for these compounds.

As shown in Table 1, the Mössbauer data indicates that there are substantial differences between MeSnMe angles and PhSnPh angles in the two basic carbonates. The $(Me_2Sn)_2O(CO_3)$ spectrum shows a relatively narrow doublet indicating that the two Sn resonances coincidentally overlap, as in $[\{Me_2SnNCS\}_2O]_2$ (and in $(Me_2Sn)_2O(CrO_4)$) due to similar MeSnMe angles. In contrast, the two distinct doublets for $(Ph_2Sn)_2O(CO_3)$ indicate that one PhSnPh angle approaches 90° while the other approaches 180° (18).

Experimental

Diphenyltin dichloride and dimethyltin dichloride were obtained from M&T Chemicals Inc. Dimethyltin dichloride was recrystallized from a mixture of acetone and petroleum ether (b.p. 35–60 °C). Diphenyltin dichloride was used without further purification. Methanol was refluxed over magnesium and subsequently distilled. Other solvents and chemicals were reagent grade. Elemental analyses were performed by Schwarzkopf Microanalytical Laboratory, Wood Side, New York. Analytical data are recorded in Table 3.

Dimethyltin Chromate

Dimethyltin dichloride (2.196 g, 0.01 mol) and silver chromate (3.3166 g, 0.01 mol) were stirred in 25 ml of water for 3–4 h, at room temperature. The mixture was then filtered and the filtrate was concentrated *in vacuo* until bright yellow crystals appeared which were filtered and washed several times with acetonitrile. The product was finally washed with diethyl ether and dried *in vacuo*. Yield 20%.

Basic Dimethyltin Chromate

This compound was prepared according to the method of Rochow and co-workers (20).

Basic Dimethyltin Carbonate

An acetone solution of dimethyltin dichloride (1.098 g, 0.005 mol) saturated with carbon dioxide was mixed slowly with an aqueous solution of potassium carbonate (0.6910 g, 0.005 mol). The white solid which precipitated immediately was filtered, washed several times with carbonated water, then dried at room temperature. Yield 50%.

Basic Diphenyltin Carbonate

A solution of diphenyltin dichloride (1.146 g, 0.0033 mol) in methanol was mixed slowly with a methanol solution of cesium carbonate (1.086 g, 0.0033 mol), in a nitrogen-filled dry box. The precipitated solid was filtered, washed with methanol, and dried *in vacuo*. Yield 60%.

Tetramethyl-1,3-diisothiocyanatodistannoxane

This compound was prepared by the published methods of Okawara and co-workers (27).

Spectroscopic Measurements

Infrared spectra were obtained on a Beckman IR-12 double beam spectrophotometer using KRS-5 and polyethylene windows. Samples were prepared as mulls in Nujol and halocarbon oil and the spectra were recorded in the 4000 to 250 cm^{-1} region. Raman spectra of solid

Can. J. Chem. Downloaded from www.nrcresearchpress.com by 210.87.254.40 on 09/05/12
For personal use only.

samples were obtained from 100 to 1000 cm^{-1} using a spex model 1400 spectrophotometer and the Ar^+ 5145 Å line. The carbonates gave good spectra but the yellow chromates decomposed in the laser beam even when the samples were mounted in a spinning sample holder on top of a Hg_2Cl_2 layer. Mössbauer spectra were obtained at ~110 K using a 5 mCi $BaSnO_3$ source at room temperature and an Austin Science Associates spectrometer. Calibration was performed with a 99.99% Fe foil. Centre shifts are quoted relative to the centroid of a $BaSnO_3$–$BaSnO_3$ room temperature spectrum (28). All spectra were fitted to Lorentzian line shapes using the program written by Stone. Except for the room temperature spectrum of $(Ph_2Sn)_2O(CO_3)$, all χ^2 values were 500 ± 50 for 512 channel mirror image spectra.

Acknowledgment

Financial assistance from the National Research Council of Canada is gratefully acknowledged.

1. E. O. Schlemper and W. C. Hamilton. Inorg. Chem. **5**, 995 (1966).
2. F. H. Allen, J. A. Lerbscher, and J. Trotter. J. Chem. Soc. (A), 2507 (1971).
3. H. A. Skinner and L. E. Sutton. Trans. Faraday Soc. **40**, 164 (1944).
4. P. Taimsalu and J. L. Wood. Spectrochim Acta, **20**, 1043 (1964).
5. A. G. Davies, H. J. Milledge, D. C. Puxley, and P. J. Smith. J. Chem. Soc. (A), 2862 (1970).
6. R. A. Forder and G. M. Sheldrick. J. Organometal. Chem. **22**, 611 (1970).
7. Y. M. Chow. Inorg. Chem. **9**, 794 (1970).
8. G. M. Bancroft and R. H. Platt. Adv. Inorg. Radiochem. **15**, 59 (1972) and references cited therein.
9. A. G. Maddock and R. H. Platt. J. Chem. Soc. (A), 1181 (1971).
10. H. A. Stockler, H. Sano, and R. H. Herber. J. Chem. Phys. **47**, 1567 (1967); H. A. Stockler and H. Sano. Phys. Rev. **165**, 406 (1968); Phys. Lett. **25**, A, 550 (1967).
11. G. M. Bancroft, K. D. Butler, and T. K. Sham. J. Chem. Soc. (Dalton), 1483 (1975).
12. B. F. E. Ford, J. R. Sams, R. G. Goel, and D. R. Ridley. J. Inorg. Nucl. Chem. **33**, 23 (1971).
13. B. A. Goodman and N. N. Greenwood. Chem. Commun. 1105 (1969).
14. N. E. Erickson. Chem. Commun. 1349 (1970).
15. M. Vuvelic. Croat, Chem. Acta, **40**, 255 (1968).
16. H. C. Clark and R. G. Goel. Inorg. Chem. **4**, 1428 (1965); J. Organomet. Chem. **7**, 263 (1967).
17. Y. M. Chow. Inorg. Chem. **10**, 673 (1971).
18. T. K. Sham and G. M. Bancroft. Inorg. Chem. **14**, 2281 (1975).
19. A. M. Domingos and G. M. Sheldrick. J. Chem. Soc. Dalton, 477 (1974).
20. E. G. Rochow, D. Seyferth, and A. C. Smith, Jr. J. Am. Chem. Soc. **75**, 3099 (1953).
21. T. Tanaka. Organometal. Chem. Rev. (A), **5**, 1 (1970), and references cited therein.
22. R. A. Bailey, S. L. Kozak, T. W. Michelsen, and W. N. Mills. Coord. Chem. Rev. **6**, 407 (1971), and references cited therein.
23. R. M. Wing and K. P. Callahan. Inorg. Chem. **8**, 871 (1969).
24. R. P. Turcotte, J. O. Sawyer, and L. Eyring. Inorg. Chem. **8**, 238 (1969).
25. J. R. Durig, C. W. Sink, and S. F. Bush. J. Chem. Phys. **45**, 66 (1966).
26. J. Kriegsmann and H. Beissler. Z. Anorg. Chem. **323**, 170 (1963).
27. M. Wada, M. Nixhika, and R. Okawara. J. Organomet. Chem. **3**, 70 (1965).
28. G. M. Bancroft. Mössbauer spectroscopy: an introduction for inorganic chemists and geochemists. McGraw-Hill, London, England, 1973 and Wiley, New York, 1974.

Can. J. Chem. Downloaded from www.nrcresearchpress.com by 210.87.254.40 on 09/05/12
For personal use only.

A ^{13}C nuclear magnetic resonance study of aliphatic ketone protonation in sulfuric acid solutions

ROBERT A. MCCLELLAND AND WILLIAM F. REYNOLDS
Department of Chemistry, University of Toronto, Toronto, Ontario M5S 1A1

Received September 12, 1975

ROBERT A. MCCLELLAND and WILLIAM F. REYNOLDS. Can. J. Chem. **54**, 718 (1976).

A ^{13}C nmr investigation of the protonation in sulfuric acid of the aliphatic ketones MeCOR (R = Me, Et, *i*-Pr, *tert*-Bu), 3-pentanone, and the cyclic ketones from cyclobutanone through cyclooctanone is reported. With the exception of cyclobutanone which is considerably less basic, these ketones are all very similar in their basicity, with half-protonation in the region 73–78% H_2SO_4. The acidity dependence of the protonation is discussed; there appears to be a small dependence on molecular size. ^{13}C nmr is shown to be a suitable alternative to ^1H nmr in the study of the protonation of weak organic bases in strongly acidic solutions.

ROBERT A. MCCLELLAND et WILLIAM F. REYNOLDS. Can. J. Chem. **54**, 718 (1976).

On rapporte les résultats d'une étude par rmn du ^{13}C, de la protonation dans l'acide sulfurique des cétones aliphatiques CH_3COR (R = Me, Et, *i*-Pr et *tert*-Bu), de la pentanone-3 et des cétones cycliques allant de la cyclobutanone à la cyclooctanone. A l'exception de la cyclobutanone qui est de beaucoup moins basique que les autres, ces cétones ont toutes des basicités semblables et leur demi-protonation se situe dans la région de H_2SO_4 à 73–78%. On discute de la dépendance de la protonation sur l'acidité; il semble qu'il existe une légère dépendance sur la grosseur moléculaire. On montre que la rmn du ^{13}C s'avère être une bonne alternative à la rmn du ^1H pour l'étude de la protonation des bases organiques faibles dans des solutions acides fortes.

[Traduit par le journal]

The protonation of weak organic bases in non-dilute acid solutions has been one of the most intensively investigated topics of physical organic chemistry (1, 2). A major problem in such studies has involved finding a suitable experimental method for the measurement of the concentrations of protonated and unprotonated species. This is particularly the case with non-aromatic species, where often the uv technique cannot be applied. In recent years, extensive use has been made of ^1H nmr spectroscopy in which the chemical shift variation can be taken as a measure of the extent of protonation (see, for example, refs. 3–5). A logical extension is ^{13}C nmr spectroscopy, a technique which has been used quite successfully in studying acid–base behaviour in the p*H* region (*e.g.*, ref. 6). Its applicability to more strongly acid solutions is suggested by a partial titration curve published for the carbonyl carbon chemical shift of acetone (7).

In addition to the benefits obtained with ^1H nmr when compared to other techniques (8, 9), ^{13}C nmr offers further advantages. Both because of the inherently larger variations observed with structural changes (10), and because a nucleus closer to the site of protonation can be probed, larger chemical shift changes on protonation should be obtained. This should result in more accurate measurements; precision is one of the major problems with ^1H nmr studies (8, 9). Additionally, with proton decoupling very simple ^{13}C nmr spectra can be produced even for complex molecules. The major drawback of the technique is that using natural abundance samples, relatively long measuring times (0.5–6 h) are required to produce suitable spectra, so that acid sensitive systems are not amenable to study. It should be pointed out however that as with ^1H nmr studies (3) completely stable solutions are not absolutely required since the chemical shifts are still accurately measurable even in the presence of quite substantial amounts of decomposed material. Proton-decoupled ^{13}C nmr is superior to ^1H nmr in this respect since, due to the greater chemical shift range and the fact that there is one sharp peak for each carbon, there is a much lower probability of spectral interference by decomposition products.

For our investigation of the applicability of

Can. J. Chem. Downloaded from www.nrcresearchpress.com by 210.87.254.40 on 09/05/12
For personal use only.

Can. J. Chem. Downloaded from www.nrcresearchpress.com by 210.87.254.40 on 09/05/12
For personal use only.

this technique we have chosen a series of 10 simple aliphatic ketones, both acyclic and cyclic. This system was chosen for several reasons. Such species are relatively stable to even very concentrated acid solutions, so that the previously mentioned problem should not be too serious. Additionally the protonation of an extensive series of simple ketones has not been satisfactorily studied. Numerous reports, using various techniques, are available concerning acetone protonation (4, 11, 12), and are not in particularly good agreement (13). A ^1H nmr study on three simple acyclic ketones has also appeared (8). The ultraviolet spectra (in the $n-\pi^*$ region) of essentially the same compounds of this study have been measured in H_2SO_4 solutions (12), but these are subject to very pronounced medium effects so that little more than the qualitative protonation behaviour can be reliably obtained.

On the other hand there are now a number of reports concerning the protonation of conjugated ketone systems (1, 2, 4, 14). It is well recognized that, with a few exceptions, ketones do not behave as Hammett bases, *i.e.* that slopes of plots of log $[XH^+]/[X]$ *vs.* $-H_0$ are different from unity (4). However, unlike other functional classes which seem at least to generate a characteristic acidity function of their own (2), the ketones do not (4), the acidity function behaviour of the individual members apparently being dependent on the conjugative ability of the groups attached to the carbonyl (4). Thus a further goal of this study is an evaluation of the acidity dependence for the protonation of aliphatic ketones, which differ only in the size and nature of alkyl groups attached to the carbonyl.

Results and Discussion

Ketone ^{13}C Nuclear Magnetic Resonance in Acid Solutions

The ketones employed in this study were MeCOR (R = Me, Et, *i*-Pr, *tert*-Bu), 3-pentanone, and the simple cyclic ketones from cyclobutanone through cyclooctanone. ^{13}C chemical shifts as a function of sulfuric acid concentration (in general from water to 30% SO_3–H_2SO_4), were obtained, relative to the external standard dioxane (20% in D_2O). Assignments of the peaks were made essentially by comparison with known spectra (15); in a few cases relative intensities were also taken into account. Some ambiguity exists with respect to C_3 and C_4 of both cycloheptanone and cyclooctanone. In no case was there a problem in assigning the carbonyl carbon or the α-carbons.

Although solutions in the more concentrated acids were faintly yellow, no extraneous peaks appeared in the spectra, and the ketones could be recovered after the recording, indicative that decomposition is not a problem (with two exceptions). Interestingly the time required to obtain satisfactory Fourier transform spectra is strongly acid dependent, ranging from a minimum of 6 h in dilute acids to periods of 20–30 min in acids above 90% H_2SO_4. (This is due to much shorter ^{13}C spin-lattice relaxation times in the highly viscous H_2SO_4 solutions). In consequence the measuring time in these latter acids is not a great deal longer than that of, for example, ^1H nmr or uv spectroscopy and the decomposition problem is not as severe as might be anticipated. The two exceptions were cyclobutanone and 3,3-dimethylbutanone where solutions in 30% SO_3–H_2SO_4 went immediately bright red and no peaks at all appeared in the ^{13}C spectrum. These two, however, were sufficiently stable in 100% H_2SO_4 to obtain spectra without difficulty.

In Figs. 1 and 2 the chemical shift variations for the carbons of 2-butanone and cyclohexanone are shown. These figures are typical of those for the entire series of ketones, with the exception of cyclobutanone (see later). For the carbonyl carbons sigmoidal titration curves typical of weak bases undergoing protonation are obtained, with quite substantial downfield chemical shifts associated with the protonation (Table 1). This latter behaviour is not surprising (as discussed previously), particularly here where the carbonyl carbon should be very sensitive to protonation. Interestingly this downfield shift is quite similar throughout the series, with the exception of cyclobutanone. Protonation of the conjugated ketones, acetophenone, and cyclopropyl methyl ketone, results in significantly smaller downfield shifts for the carbonyl carbons (Table 1).

For the other carbons of the aliphatic ketones, the chemical shift changes on protonation are considerably smaller, and examples of both downfield and upfield shifts can be found (Table 1). Significantly, for the conjugated ketones,

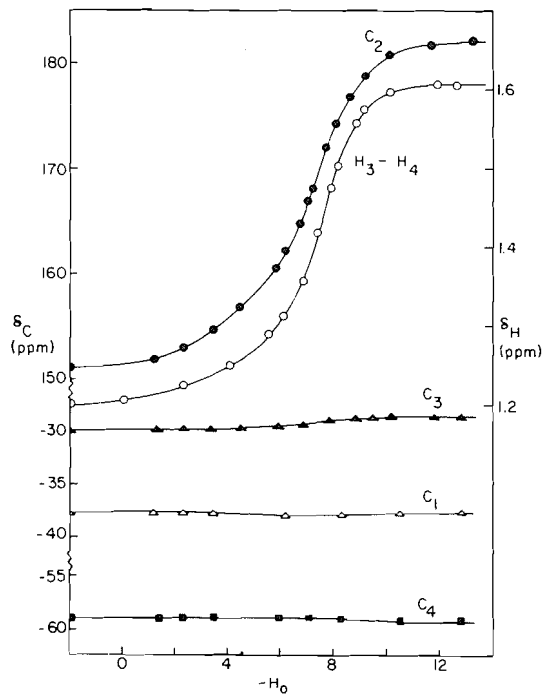

FIG. 1. Chemical shift variation as a function of acidity for 2-butanone. ^{13}C nmr data are relative to an external dioxane standard.

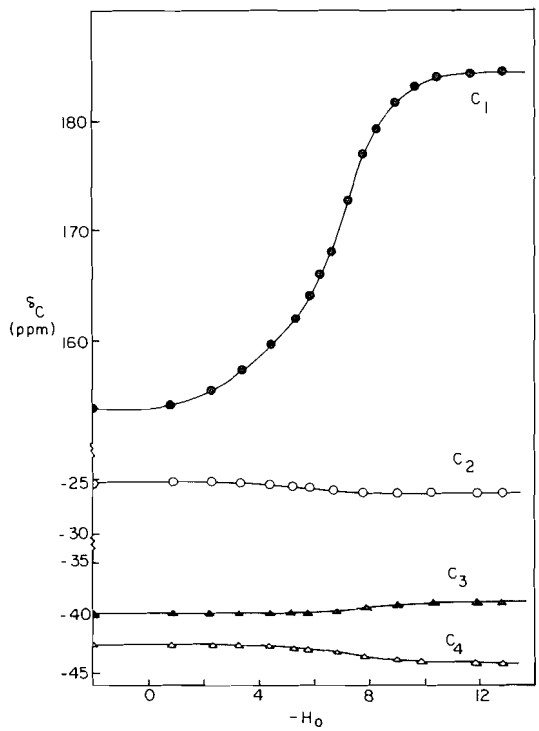

FIG. 2. Chemical shift variation as a function of acidity for cyclohexanone. Data are relative to an external dioxane standard.

protonation produces large changes with some of the other carbons as well.[1]

Finally, it is noted that the even-number cyclic ketones appear to show an alternation of signs of chemical shift changes on protonation (*e.g.* see Fig. 2), possibly indicative of the alternating inductive effect proposed by Pople *et al.* (18).

Dilute Acids Medium Effect on Protonation

Thus the ^{13}C chemical shifts of the carbonyl carbons would appear to be a sensitive indicator of protonation behaviour. Very similar sigmoidal curves are in fact found in ^{1}H nmr studies, as for example that in Fig. 1 for 2-butanone. The one disturbing aspect common to both types of studies concerns the behaviour in the dilute acids. Although there are very definite plateaus at the concentrated acid end, this is not true in the dilute acids. There are two explanations.[2] This can be attributed to a medium effect on the unprotonated ketone, as for example a hydrogen bonding interaction between the carbonyl and an acidic species (20), or it can be taken as an indication of the onset of protonation. At present these two alternatives are difficult to distinguish. However, it is equally as difficult to introduce a medium effect correction term into the analysis of these titration curves without making unwarranted assumptions. In consequence, in the following discussion we will assume that there is no medium effect, and that the chemical shift behaviour is due to protonation only.

This interpretation will mean that the ketones of this study are undergoing protonation over virtually the entire range of sulfuric acid solutions. This may seem unlikely but the behaviour of these ketones is very far removed from that of typical Hammett bases which protonate over

[1]The ^{13}C nmr of various conjugated ketones and their conjugate acids have been discussed (17).

[2]A third possibility is that hydrate formation complicates the situation in dilute acids. This however can be ruled out since the extent of such hydration is very small. Acetone, for example, exists only 0.2% in the hydrated form, and with the bulkier ketones this number will be even smaller (19).

Can. J. Chem. Downloaded from www.nrcresearchpress.com by 210.87.254.40 on 09/05/12
For personal use only.

TABLE 1. Ketone ^{13}C chemical shift variation between water and 100.8% H_2SO_4

	$\delta(H_2SO_4) - \delta(H_2O)$[a] (ppm)					
	C_1	C_2	C_2	C_4	C_5	C_6
Acetone	+0.10	+30.12				
2-Butanone	−0.09	+30.28	+1.26	−0.79		
2-Methyl-2-butanone	+0.17	+30.42	+1.57	−0.13		
3,3-Dimethyl-2-butanone	+1.48	+30.40	+2.54	−0.19		
3-Pentanone	−0.61	+1.20	+30.46			
Cyclobutanone[b]	+34.01	−1.61	+1.44			
Cyclopentanone	+30.00	+2.59	−0.10			
Cyclohexanone	+30.24	−1.25	+0.58	−2.10		
Cycloheptanone	+29.91	+0.12	−0.28[c]	−1.15[c]		
Cyclooctanone	+30.27	+0.32	+2.78[c]	−0.47[c]	+1.21	
Acetophenone[d]	−11.09	+6.62	+1.65	+11.00	+15.51	+2.09
Cyclopropyl methyl ketone[e]	+6.51	+21.91	−2.65	+17.40		

[a]Corrected for bulk susceptibility (16).
[b]Not completely protonated in 100.8% H_2SO_4.
[c]Assignments uncertain.
[d]C_1–C_4 refer to aromatic carbons, C_5 to C=O, C_6 to CH_3.
[e]C_1, CH_3; C_2, C=O; C_3, C_α (ring); C_4, C_β (ring).

much narrower acidity ranges. Similar shallow acidity dependencies are found in fact for aliphatic ethers (21) and alcohols (22), and as will be seen later the behaviour of the aliphatic ketones is not inconsistent. Additional support comes from the remarkable similarity of the results obtained from the two different types of nmr (Fig. 1, see also Table 3). In terms of a medium effect explanation this would have to mean that the effect on both techniques is identical, which would be surprising. It is true that the carbonyl carbon of acetone undergoes lowfield shifts in protic solvents which have been attributed to strong hydrogen bonding (23). However, this is based on the unproven assumption that no protonation occurs in these media.

Finally, it should be noted that the changes in dilute acid are quite small when compared to the overall chemical shift variation, so that regardless of the assumption regarding this region, the protonation can still be defined with reasonable accuracy.

Ketone Concentration Effects

Most measurements of protonation of weak bases by strong acids have been carried out by uv spectroscopy and utilize base concentrations in the range 10^{-3}–10^{-4} *M*. This includes measurements of base protonation used in defining acidity scales. However, nmr spectroscopic measurements (particularly ^{13}C nmr) require much higher concentrations. To check whether this affected the accuracy of our results, acetone uniformly labelled with *ca.* 45 mol% ^{13}C was used, allowing the preparation of much more dilute solutions (0.001 g/ml, as compared to 0.04 g/ml for the natural abundance samples). As shown in Table 2, this 40-fold dilution has minimal effect on chemical shifts. The greatest difference is found in the intermediate acidity region and is consistent with the expected acidity decrease as acetone concentration increases. However, the differences are small and lead to only small errors in the basicity measurements.

Ketone Ionization Ratios

The ionization ratios I ($[XH^+]/[X]$) for the various ketones have been calculated from the

TABLE 2. Dependence of chemical shift on acetone concentration

	$\delta(C{=}O) - \delta(CH_3)$ (ppm)	
H_2SO_4 (%)	0.001 g/ml[a]	0.04 g/ml[a]
Water	185.3	185.1
31.0	186.3	186.1
54.5	189.3	189.1
70.7	195.1	194.4
80.2	203.1	202.4
92.7	212.8	212.5
99.7	215.5	214.9
30% SO_3	216.5	216.2

[a]Concentration of acetone in acid solutions.

Can. J. Chem. Downloaded from www.nrcresearchpress.com by 210.87.254.40 on 09/05/12
For personal use only.

TABLE 3. Ionization ratios for 2-butanone

	log I				
$-H_0$	C_2–C_1	C_2–C_3	C_2–C_4	H_3–H_4[b,c]	H_1–H_4[c]
4.5	−0.67	−0.70	−0.70	−0.73	−0.73
5.0	−0.56	−0.58	−0.59	−0.65	−0.65
5.5	−0.46	−0.46	−0.47	−0.55	−0.55
6.0	−0.34	−0.36	−0.35	−0.46	−0.45
6.5	−0.18	−0.20	−0.20	−0.35	−0.29
7.0	0.00	−0.02	−0.01	−0.17	−0.09
7.5	0.21	0.18	0.18	0.10	0.17
8.0	0.41	0.37	0.36	0.36	0.45
8.5	0.61	0.58	0.56	0.64	0.75
9.0	0.81	0.80	0.77	0.85	0.97
m[a]	0.35	0.34	0.34	0.36	0.38
$(H_0)_{1/2}$	−6.70	−6.80	−6.78	−6.91	−6.76
ϕ	0.58	0.70	0.69	0.68	0.65
pK_{SH^+}	−2.82	−2.82	−2.83	−2.97	−3.06

[a]See Table 4 for meaning of symbols.
[b]Reference 8.
[c]This work.

standard equation

$$[XH^+]/[X] = \Delta\Delta - \Delta\Delta_B/\Delta\Delta_{BH^+} - \Delta\Delta$$

The quantities used here are the differences in chemical shift between two of the nuclei (*i.e.* the carbonyl carbon and one of the others). Rather than using the individual chemical shifts this approach is recommended since it avoids bulk susceptibility corrections (for an external standard), and also may work to minimize medium effects. In our calculations the term $\Delta\Delta_B$ is taken to be that in water, $\Delta\Delta_{BH^+}$ as the value in 30% $SO_3 \cdot H_2SO_4$. (For 3,3-dimethylbutanone $\Delta\Delta_{BH^+}$ is the value for 100.0% H_2SO_4.)

This assumes that the chemical shifts in 30% $SO_3 \cdot H_2SO_4$ represent the chemical shifts of the completely protonated ketone rather than, for example, the chemical shifts of a Lewis acid adduct of the ketone. In support of this view we note that the chemical shifts for all carbons show smooth titration curves with only small chemical shift changes from 100% H_2SO_4 to 30% SO_3–H_2SO_4 and no discontinuities which could be associated with adduct formation. ^1H chemical shift titration curves for ketones in SO_3–H_2SO_4 also show normal titration curves (9). Finally, ^1H nmr spectra of ketones in even stronger Lewis acid media (HSO_3F–SbF_5, HF–SbF_5, HSO_3F–SbF_5–SO_2, etc.) actually show peaks due to the OH protons of protonated ketones (24), confirming protonation in strong Lewis acid media.

In Table 3 ionization ratios determined for 2-butanone using various combinations in both the ^{13}C and ^1H nmr spectra are compared. Excellent agreement is seen amongst the various sets of data, both in the individual log I values as well as in the derived basicity parameters. This table further emphasizes the agreement between the two different nmr techniques. This is also true with other published ketone ^1H nmr data (4, 8) when compared with our ^{13}C nmr results.

Ketone Basicity Constants

Ideally, to determine a thermodynamic basicity constant from log I – acidity data, it is necessary to have or determine an acidity function appropriate to the substrate undergoing protonation. This is not possible in the present case, both because of the fact that none of the ketones are sufficiently protonated in very dilute acid to anchor such a scale, and also because it is doubtful if such a common scale exists for ketones (ref. 4, and later discussion). Two empirical approaches have arisen to estimate pK_{SH^+} values in such a case. That of Yates (25) recognizes that acidity functions are in general linear in each other, and utilizes the equation

$$\log I = mH_0 + pK_{SH^+}$$

where m and pK_{SH^+} are respectively the slope and intercept of a plot of log I *vs.* $-H_0$. Alternatively, the Bunnett–Olsen treatment (26) uses

Can. J. Chem. Downloaded from www.nrcresearchpress.com by 210.87.254.40 on 09/05/12
For personal use only.

TABLE 4. Basicity constants for ketone protonation based on ^{13}C nmr

	Chemical shift	log I vs. $-H_0$			Bunnett–Olsen	
		m[a]	pK_{SH^+}[a]	$(H_0)_{1/2}$[b]	ϕ[c]	pK_{SH^+}[c]
Acetone	C_2–C_1	0.32	−2.16	−6.74	0.71	−2.72
2-Butanone	C_2–C_1	0.35	−2.35	−6.70	0.69	−2.82
2-Methyl-2-butanone	C_2–C_1	0.34	−2.32	−6.83	0.70	−2.81
3,3-Dimethyl-2-butanone	C_2–C_1	0.39	−2.68	−6.87	0.65	−3.12
3-Pentanone	C_3–C_2	0.37	−2.52	−6.88	0.67	−2.97
Cyclobutanone[d]				> −9		
Cyclopentanone	C_1–C_2	0.31	−2.06	−6.63	0.73	−2.59
Cyclohexanone	C_1–C_2	0.35	−2.27	−6.48	0.69	−2.76
Cycloheptanone	C_1–C_2	0.37	−2.37	−6.40	0.67	−2.85
Cyclooctanone	C_1–C_2	0.39	−2.49	−6.39	0.64	−2.98

[a]Least-squares slope, m, and intercept, pK_{SH^+}, of plot of log I vs. $-H_0$. Correlation coefficients greater than 0.98. Deviation in m is 0.01–0.02. Deviation in pK_{SH^+} is 0.1–0.2.
[b]pK_{SH^+}/m.
[c]Least-squares slope, ϕ, and intercept, pK_{SH^+}, of plot of log $I + H_0$ vs. log $[H^+] + H_0$. Correlation coefficients greater than 0.99. Deviation in ϕ is 0.01–0.02. Deviation in pK_{SH^+} is 0.1–0.2.
[d]Not completely protonated in most concentrated acid of this study.

the equation

$$\log I + H_0 = \phi(H_0 + \log [H^+]) + pK_{SH^+}$$

where ϕ and pK_{SH^+} are obtained as the slope and intercept of a plot of log $I + H_0$ vs. $H_0 +$ log $[H^+]$.

Results of the application of both approaches to the ketone protonation data are given in Table 4. Also quoted are the values of $(H_0)_{1/2}$, the H_0 value for half-ionization (log $I = 0$) as determined from the log I vs. $-H_0$ plot. The agreement between the pK_{SH^+} values is quite poor, those of the Yates plot being consistently 0.5 units less negative. This is probably due to the large extrapolation (and assumption of continuing linearity) in the Yates treatment (27).

Nevertheless, the basic conclusion must be that, with one exception, these aliphatic ketones are very similar in their base strengths, with half-protonation occurring in the region 73–78% H_2SO_4. The one exception is cyclobutanone, which is considerably less basic, so much so that we are unable to obtain a reliable pK_{SH^+} value. The weaker basicity of the ketone has been noted before (9, 12) and probably arises out of the different hybridization of this molecule (28).

Acidity Dependence

Recently considerable effort has been devoted to an understanding of 'acidity function failure', the fact that different types of weak bases respond differently to increasing acidity (4, 29, 30). These variations arise out of different solvation requirements of the conjugate acid–base pair (differing acidity dependencies of the activity coefficient ratio f_{BH^+}/f_B) and appear as the slope parameters 'm' and 'ϕ' in the two treatments used here. In Table 5 these values are compared for a series of oxygen bases, and it can be seen that the behaviour of the alkyl ketones is consistent. This series of results can be explained in terms of the ability of the protonated species to disperse the positive charge (4, 30); the same effect is also in operation when considering ketones of differing degrees of conjugation (4).

TABLE 5. Values of 'm' and 'ϕ' for oxygen bases in sulfuric acid

Base	'm'	'ϕ'	Reference
Alcohols	0.25	0.85	22
Alkyl ethers	0.25–0.30	0.72–0.85	21
Alkyl ketones	0.31–0.39	0.64–0.71	This work
Alkyl esters	0.5–0.6	0.5–0.6	32
Amides	0.55–0.7	0.42–0.55	33

Additionally, however, examination of Table 4 reveals that there is a very definite trend within the series of aliphatic ketones themselves. Although the effect is small,[3] the larger ketones have associated with the protonation larger 'm' values and smaller 'ϕ' values (the two parameters are inversely related). This dependency on

[3]The standard deviations in m and ϕ are of the order of 0.01 to 0.02. Thus the overall variation is just outside the limit of experimental error. We feel additionally that the regularity of the trend adds further weight to its validity.

Can. J. Chem. Downloaded from www.nrcresearchpress.com by 210.87.254.40 on 09/05/12
For personal use only.

TABLE 6. Typical recording times for ketone ^{13}C nmr spectra

H_2SO_4 (%)	Time (h)
0	6[a]
30	6[a]
60	5
75	2
90	0.5
100	0.5
30% SO_3	0.5

[a]For the larger ketones where solubility dictated the use of more dilute solutions, considerably longer times (up to 24 h) were required.

molecular size has seen little recognition in studies of this type. A recent review however suggested that size does play an important role, and discussed the factors responsible (30). This study then further underlines this dependency, although one must conclude on the basis of the much larger effect of varying conjugation (4), that size may be a secondary consideration. In any event the final conclusion is that even this series of structurally similar ketones fails to follow a common acidity function behaviour.

Experimental

Materials

All ketones were commercially available and were used without further purification. A sample of acetone *ca.* 45% ^{13}C enriched in each carbon was obtained by mixing acetone-90% $^{13}C_1$ and acetone-90% $^{13}C_2$ (Merck, Sharpe & Dohme Canada Ltd.). Sulfuric acid solutions were prepared and standardized as previously described (31), except that solutions above 96% H_2SO_4 were standardized by titration. Solutions of the ketones in the acids were near 0.04 g/ml; in cases where solubility was limited, saturated solutions were used. With the enriched acetone, concentrations near 0.001 g/ml were employed.

Nuclear Magnetic Resonance

^{13}C spectra at 20 MHz and probe temperature (40 °C) were recorded on a Varian CFT-20 nmr spectrometer in pulsed Fourier transform – proton noise decoupled mode. A capillary tube containing 20% dioxane in D_2O was used to provide the deuterium lock signal and the external (dioxane) ^{13}C reference signal. ^1H spectra of 2-butanone were recorded on a Varian spectrometer. The observed chemical shift differences for the protons of C_3 and C_4 agreed with those previously reported (8).

Stability of Solutions

Typical times required to generate suitable spectra are shown in Table 6. All ketones were stable throughout the entire range of acidity, with the exception of cyclobutanone and 3,3-dimethyl-2-butanone which decomposed in solutions above 100% H_2SO_4. This stability was shown by the absence of extraneous peaks, and the reproducibility of the spectra on dilution. In addition with each ketone the 100% H_2SO_4 solutions upon recording were diluted to *ca.* 30% H_2SO_4, and extracted with methylene chloride. Gas chromatographic analysis of this solution showed only the presence of the original ketone.

Acknowledgment

The authors thank the National Research Council of Canada for their financial support.

1. E. M. ARNETT. Prog. Phys. Org. Chem. **1**, 223 (1963).
2. C. H. ROCHESTER. *In* Acidity functions. Academic Press, London. 1970; M. LILER. *In* Reaction mechanisms in sulfuric acid. Academic Press, London. 1971.
3. D. G. LEE and M. H. SADAR. J. Am. Chem. Soc. **96**, 2862 (1974).
4. A. LEVI, G. MODENA, and G. SCORRANO. J. Am. Chem. Soc. **96**, 6585 (1974).
5. A. KOEBERG-TELDER and H. CERFONTAIN. J. Chem. Soc. Perkin Trans. II, 226 (1975).
6. A. R. QUIRT, J. R. LYERLA, JR., I. R. PEAT, J. S. COHEN, W. F. REYNOLDS, and M. H. FREEDMAN. J. Am. Chem. Soc. **96**, 570 (1974).
7. W. H. DE JEU. J. Phys. Chem. **74**, 822 (1970).
8. D. G. LEE. Can. J. Chem. **48**, 1919 (1970).
9. G. C. LEVY, J. D. CARGIOLI, and W. RACELA. J. Am. Chem. Soc. **92**, 6238 (1970).
10. J. B. STOTHERS. *In* Carbon-13 nmr spectroscopy. Academic Press, New York. 1972; G. C. LEVY. *In* Carbon-13 nmr for organic chemists. Wiley-Interscience, New York. 1972.
11. H. LEMAIRE and H. J. LUCAS. J. Am. Chem. Soc. **72**, 5198 (1951); S. NAGAKURI, A. MINEGESHI, and K. STANFIELD. J. Am. Chem. Soc. **79**, 1033 (1957); U. L. HALDNA and V. A. PALM. Dokl. Akad. Nauk SSSR, **135**, 667 (1960); N. C. DENO and M. J. WISOTSKY. J. Am. Chem. Soc. **85**, 1735 (1963); U. L. HALDNA and R. K. PÜSS. Russ. J. Phys. Chem. **38**, 1529 (1964); U. L. HALDNA and K. E. LAANESTE. Org. React. USSR, **3**, 61 (1966); C. F. WELLS. Trans. Faraday Soc. **62**, 2815 (1966).
12. H. J. CAMPBELL and J. T. EDWARD. Can. J. Chem. **38**, 2109 (1960).
13. E. M. ARNETT, R. P. QUIRK, and J. J. BURKE. J. Am. Chem. Soc. **92**, 1260 (1970).
14. R. STEWART and K. YATES. J. Am. Chem. Soc. **80**, 6355 (1958); A. FISCHER, B. A. GRIGAR, J. PACKER, and J. VAUGHAN. J. Am. Chem. Soc. **83**, 4208 (1961); R. STEWART, M. R. GRANGER, R. B. MOODIE, and J. M. MUENSTER. Can. J. Chem. **41**, 1065 (1963); T. G. BONNER and J. PHILLIPS. J. Chem. Soc. B, 650 (1966); R. I. ZALEWSKI and G. E. DUNN. Can. J. Chem. **46**, 2469 (1968).
15. L. M. JACKMAN and D. P. KELLY. J. Chem. Soc. B, 102 (1970); F. J. WEIGERT and J. D. ROBERTS. J. Am. Chem. Soc. **92**, 1347 (1970).
16. E. D. BECKER. *In* High resolution NMR. Academic Press, London. 1969. pp. 63–64.

Can. J. Chem. Downloaded from www.nrcresearchpress.com by 210.87.254.40 on 09/05/12
For personal use only.

17. G. L. NELSON, C. G. LEVY, and J. D. CARGIOLI. J. Am. Chem. Soc. **94**, 3089 (1972); G. A. OLAH, Y. HALPERN, Y. K. MO, and G. LIANGA. J. Am. Chem. Soc. **94**, 3554 (1972).
18. J. A. POPLE and D. L. BEVERIDGE. *In* Approximate molecular orbital theory. McGraw-Hill, New York. 1970. Chapt. 4.
19. R. P. BELL. Adv. Phy. Org. Chem. **4**, 1 (1966).
20. P. E. PETERSON. J. Org. Chem. **31**, 439 (1966).
21. D. G. LEE and R. CAMERON. Can. J. Chem. **50**, 445 (1972).
22. D. G. LEE and R. CAMERON. J. Am. Chem. Soc. **93**, 4724 (1971).
23. G. E. MACIEL and J. J. NATTERSTAD. J. Chem. Phys. **42**, 2752 (1965).
24. G. A. OLAH, A. M. WHITE, and D. H. O'BRIEN. Chem. Rev. **70**, 561 (1970).
25. K. YATES and R. A. MCCLELLAND. J. Am. Chem. Soc. **89**, 2686 (1967); K. YATES. Acc. Chem. Res. **4**, 136 (1971).
26. J. F. BUNNETT and F. P. OLSEN. Can. J. Chem. **44**, 1899 (1966).
27. C. J. GIFFNEY and C. J. O'CONNOR. J. Chem. Soc. Perkin Trans. II, 706 (1975).
28. D. H. AUE, H. M. WEBB, and M. T. BOWERS. J. Am. Chem. Soc. **97**, 4137 (1975).
29. H. WAI, K. YATES, G. WELCH, and R. A. MCCLELLAND. J. Am. Chem. Soc. **95**, 418 (1973).
30. K. YATES and R. A. MCCLELLAND. Prog. Phys. Org. Chem. **11**, 323 (1974).
31. K. YATES and R. A. MCCLELLAND. Can. J. Chem. **52**, 1098 (1974).
32. D. G. LEE and M. H. SADAR. J. Am. Chem. Soc. **94**, 2862 (1974).
33. K. YATES, J. B. STEVENS, and A. R. KATRITZKY. Can. J. Chem. **42**, 1957 (1964).

Can. J. Chem. Downloaded from www.nrcresearchpress.com by 210.87.254.40 on 09/05/12
For personal use only.

X-ray analysis of the structure and correlation with the spectra of haplophytine

P.-T. CHENG, S. C. NYBURG, F. N. MACLACHLAN, AND PETER YATES
Lash Miller Chemical Laboratories, University of Toronto, Toronto, Ontario M5S 1A1

Received July 17, 1975

P.-T. CHENG, S. C. NYBURG, F. N. MACLACHLAN, and PETER YATES. Can. J. Chem. **54**, 726 (1976).

Haplophytine crystallizes as the methanolate in the orthorhombic space group $P2_12_12_1$ with $a = 13.874(4)$, $b = 10.628(4)$, $c = 22.890(9)$ Å, $Z = 4$. X-Ray structure analysis confirms that the previously assigned structure **3** is correct and that haplophytine undergoes reversible rearrangement on conversion to its dihydrobromide **1**. The dimensions of **3** provide evidence supporting previous interpretations of unusual features of the infrared and proton magnetic resonance spectra of haplophytine.

P.-T. CHENG, S. C. NYBURG, F. N. MACLACHLAN et PETER YATES. Can. J. Chem. **54**, 726 (1976).

L'haplophytine sous forme de méthanolate cristallise dans le système orthorhombique avec un groupe d'espace $P2_12_12_1$ et $a = 13.874(4)$, $b = 10.628(4)$, $c = 22.890(9)$ Å, $Z = 4$. Une analyse de la structure par rayons-X confirme que la structure **3** attribuée antérieurement est correcte et que l'haplophytine subit un réarrangement réversible lors de sa conversion en dibromohydrate **1**. Les dimensions de **3** fournissent des données en accord avec l'interprétation faite antérieurement des caractéristiques non usuelles trouvées dans les spectres infrarouges et rmn de l'haplophytine.

[Traduit par le journal]

Introduction

Haplophytine is the principal alkaloid of *Haplophyton cimicidum (Apocyanaceae)* (1). In 1967 a crystal structure analysis was carried out on the dihydrobromide **1** (2, 3) and structure **2** was assigned to haplophytine itself (2). Subsequently it became apparent that conversion to the dihydrobromide must have been accompanied by rearrangement of the parent alkaloid, whose structure was then reassigned as **3** on spectroscopic and degradative evidence (4). This rearrangement can be reversed on treatment of **1** with aqueous sodium bicarbonate. Because of this unusual circumstance and the novelty of structure **3**, we have undertaken an X-ray crystal structure analysis of haplophytine, which, it was hoped, would also throw light on some unusual spectroscopic features of this and related alkaloids (2, 4, 5). This analysis confirms that the reassigned structure **3** is correct.

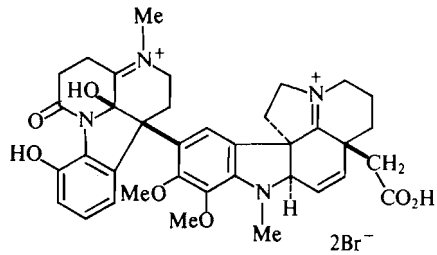

1

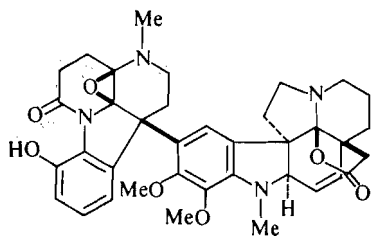

2

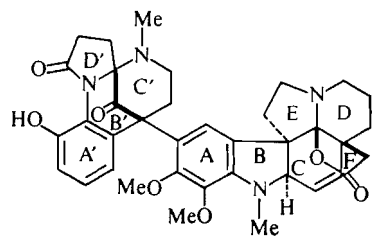

3

Can. J. Chem. Downloaded from www.nrcresearchpress.com by 210.87.254.42 on 09/05/12
For personal use only.

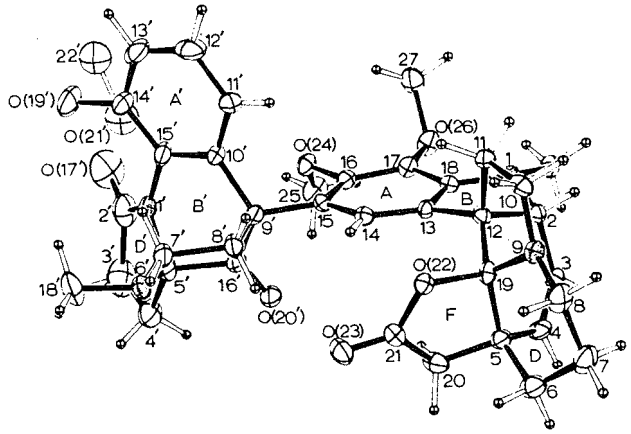

FIG. 1. ORTEP plot of molecule showing 20% probability thermal ellipsoids, except for hydrogen atoms which are represented by arbitrary isotropic spheres.

Experimental

Crystals obtained from methanol by slow evaporation were well formed and colorless.

Crystal Data

$C_{37}H_{40}N_4O_7.CH_3OH$ fw = 684.3

Orthorhombic, $a = 13.874(4)$, $b = 10.628(4)$, $c = 22.890(9)$ Å, $V = 3375.1(9)$ Å^3, $\rho_o = 1.33(1)$, $Z = 4$, $\rho_c = 1.35$ (CuKα, $\lambda = 1.542$ Å).

The crystal used for data collection was a prism of dimensions *ca.* $0.1 \times 0.1 \times 0.5$ mm mounted about the *y*-axis, parallel to the longest dimension. Cell parameters and their standard deviations were obtained from diffractometer angular settings of 12 well-centered high 2θ reflections using CuKα radiation. Intensities were collected on a computer-controlled Picker four-circle diffractometer equipped with pulse height analyzer using Ni-filtered CuKα radiation. Scanning was in the θ–2θ mode at 1 ° min^{-1}, $\sin\theta \leq 0.90$, with take-off angle 3.0°. Backgrounds were determined for 1 min at each end of the scan range of 2° adjusted for α-splitting. During the course of data collection there was a random variation of $\leq 7\%$ from the mean in the standard intensity, recorded every 30 reflections. Counting statistics and an Abrahams factor (6) of 0.02 were used to estimate $\sigma(I)$. Of the 3139 independent reflections measured, 2834 were considered significant on the criterion $|F_o| > \sigma(F_o)$. Absorption corrections were not applied.

The crystal structure was determined by direct methods from the 488 reflections having $|E| > 1.32$ using the MULTAN program of Germain *et al.* (7). Twelve out of forty-eight nonhydrogen atoms of the alkaloid were clearly identified on the first electron density map and the remainder from three successive Fourier maps. Refinement was by full matrix anisotropic least squares using programs XFLS-3 of Oak Ridge National Laboratories, the function minimized being $\sum w\Delta^2$ where $\Delta = |F_o| - |F_c|$ and $w = \sigma^{-2}(F_o)$. The atomic scattering factors used were those of Cromer and Mann (8) for C, N, O and of Stewart *et al.* (9) for H. All hydrogen atoms except that on O(19′) (see Fig. 1) were located on the final difference map as were the carbon and oxygen atoms (but not hydrogen atoms) of one molecule of methanol. The 39 locatable hydrogen atoms were given theoretical positions (C—H = 1.0 Å) and included in the refinement with isotropic thermal factors. The carbon and oxygen atoms of methanol were included in the refinement with variable occupancy, reaching finally 0.8 (in keeping with the smaller ρ_o value). The final residual for all observed reflections, $R = \sum|\Delta|/\sum|F_o| = 0.082$ with esd for unit observation equal to 1.18.[1] Final positional and thermal parameters are listed in Table 1 *a* and *b*.

Description and Discussion of Structure

The molecular structure, confirming the assignment **3**, is shown in Fig. 1. Bond lengths and angles are given in Fig. 2 *a* and *b*.

The overall conformation is as expected from Dreiding models. In the tetrahydrocarbazole system (rings A, B, C), ring A is slightly puckered (maximum deviation 0.04 Å) as is the same ring in **1**, but the deviations do not match well. (Best least squares planes are given in Table 2 *a* and *b*.)

The two methoxyl groups are bent in opposite directions away from the mean plane of ring A. Ring B has an envelope conformation with C(2) as the flap. In ring C the double bond at C(3)—C(4) keeps C(2), C(3), C(4), C(5) coplanar, atoms C(12) and C(19) being twisted out of this plane in opposite senses. The indolizidine system (rings D, E) is, as expected, different from that in the

[1]Table containing F_o, F_c data is available, at a nominal charge, from the Depository of Unpublished Data, CISTI, National Research Council of Canada, Ottawa, Canada K1A 0S2.

Can. J. Chem. Downloaded from www.nrcresearchpress.com by 210.87.254.42 on 09/05/12
For personal use only.

TABLE 1

(*a*) Atomic fractional coordinates ($\times 10^4$) and anisotropic temperature factors ($\times 10^4$) of form $\exp -(h^2\beta_{11} + k^2\beta_{22} + l^2\beta_{33} + 2hk\beta_{12} + 2hl\beta_{13} + 2kl\beta_{23})$

Atom	*x*	*y*	*z*	β_{11}	β_{22}	β_{33}	β_{12}	β_{13}	β_{23}
N(1)	4603(3)	1645(5)	1473(2)	41(3)	72(5)	21(1)	−12(3)	3(1)	−1(2)
C(2)	5002(4)	357(6)	1324(2)	38(3)	91(7)	16(1)	−11(4)	−1(2)	1(2)
C(3)	5251(4)	289(6)	678(2)	52(4)	96(8)	15(1)	−11(5)	6(2)	4(3)
C(4)	4990(5)	−579(7)	327(3)	71(4)	131(8)	14(1)	−10(5)	11(2)	3(3)
C(5)	4385(4)	−1734(6)	483(3)	57(4)	97(8)	18(1)	−14(5)	8(2)	−7(3)
C(6)	4851(6)	−2981(8)	265(3)	90(6)	135(10)	24(2)	−26(7)	14(3)	−13(4)
C(7)	5649(6)	−3457(8)	621(4)	71(6)	126(9)	40(3)	20(6)	10(3)	−14(4)
C(8)	5293(6)	−3620(7)	1253(4)	76(6)	92(8)	40(2)	22(6)	2(3)	−7(4)
N(9)	4941(4)	−2402(5)	1464(2)	46(3)	113(7)	23(1)	11(4)	0(2)	−7(3)
C(10)	4775(5)	−2225(7)	2074(3)	66(4)	121(8)	17(1)	−2(5)	−9(2)	2(3)
C(11)	4235(4)	−994(7)	2119(2)	50(4)	110(7)	14(1)	4(5)	0(2)	0(3)
C(12)	4151(4)	−539(6)	1484(2)	43(3)	96(7)	14(1)	−4(4)	−4(2)	4(2)
C(13)	3272(4)	320(5)	1404(2)	37(3)	77(6)	15(1)	12(4)	2(2)	0(2)
C(14)	2314(4)	76(6)	1396(2)	47(4)	79(6)	17(1)	0(4)	−1(2)	−2(3)
C(15)	1621(4)	1071(6)	1356(2)	37(3)	101(7)	14(1)	9(4)	−4(2)	−1(3)
C(16)	1957(4)	2298(6)	1362(2)	48(3)	98(7)	15(1)	16(4)	1(2)	3(2)
C(17)	2947(4)	2607(6)	1418(3)	51(4)	75(7)	22(1)	0(4)	4(2)	0(3)
C(18)	3618(4)	1584(6)	1414(2)	45(3)	90(7)	14(1)	1(4)	−1(2)	−3(3)
C(19)	4224(4)	−1743(6)	1146(2)	39(3)	69(6)	20(1)	0(4)	4(2)	8(2)
C(20)	3370(5)	−1657(7)	253(3)	85(5)	126(9)	17(1)	−22(6)	−3(2)	−4(3)
C(21)	2786(5)	−2404(7)	689(3)	52(4)	121(9)	21(1)	−5(5)	−3(2)	−6(3)
O(22)	3268(3)	−2452(4)	1195(2)	48(2)	100(5)	18(1)	−8(3)	4(1)	−2(2)
O(23)	1989(4)	−2871(5)	639(2)	64(3)	146(7)	29(1)	−29(4)	−8(2)	−1(3)
O(24)	1283(3)	3238(4)	1361(2)	50(3)	98(5)	21(1)	22(3)	3(1)	7(2)
C(25)	1344(6)	4182(8)	918(4)	86(6)	140(11)	30(2)	34(7)	6(3)	19(4)
O(26)	3257(4)	3809(4)	1447(2)	68(3)	80(5)	32(1)	3(3)	8(2)	2(2)
C(27)	3022(6)	4467(8)	1987(4)	71(5)	114(9)	44(3)	2(6)	−6(3)	−29(4)
C(28)	5230(5)	2723(7)	1363(3)	54(4)	113(8)	24(2)	−11(5)	5(2)	−3(3)
N(1′)	−1253(4)	2129(7)	1155(3)	35(3)	150(8)	30(2)	20(4)	−1(2)	−8(3)
C(2′)	−1733(7)	3122(10)	957(6)	76(6)	133(12)	59(4)	13(8)	−2(4)	−8(6)
C(3′)	−1868(9)	2988(15)	268(6)	110(9)	300(24)	54(4)	16(14)	−5(5)	45(9)
C(4′)	−1324(6)	1795(12)	117(4)	68(5)	254(21)	28(2)	32(10)	−7(3)	17(6)
C(5′)	−929(5)	1247(9)	689(3)	42(4)	191(13)	23(2)	14(6)	−5(2)	0(4)
N(6′)	−1240(4)	−14(7)	753(3)	42(3)	152(9)	28(2)	9(5)	−6(2)	−15(3)
C(7′)	−786(4)	−783(8)	1219(3)	45(4)	127(9)	31(2)	−15(5)	7(2)	−20(4)
C(8′)	307(4)	−619(7)	1260(3)	38(4)	119(8)	29(2)	3(5)	−3(2)	−11(3)
C(9′)	562(4)	817(7)	1301(3)	37(3)	144(9)	15(1)	5(5)	3(2)	0(3)
C(10′)	−29(4)	1338(7)	1817(3)	41(4)	121(8)	20(1)	−2(5)	7(2)	−9(3)
C(11′)	279(5)	1044(9)	2383(3)	71(5)	195(12)	16(1)	−19(7)	4(2)	−1(3)
C(12′)	−302(8)	1338(11)	2865(3)	130(8)	234(16)	18(2)	−65(10)	10(3)	−2(4)
C(13′)	−1189(7)	1876(11)	2772(4)	90(7)	198(15)	34(3)	−54(9)	31(4)	−27(5)
C(14′)	−1514(5)	2195(10)	2210(4)	60(5)	213(15)	34(2)	−8(7)	15(3)	−41(5)
C(15′)	−924(4)	1927(8)	1737(3)	42(4)	138(10)	33(2)	−11(5)	14(2)	−19(4)
C(16′)	181(4)	1295(8)	724(3)	48(4)	163(10)	14(1)	10(5)	2(2)	1(3)
O(17′)	−2056(8)	3977(10)	1238(5)	149(8)	197(11)	78(4)	54(9)	−14(5)	−6(6)
C(18′)	−2305(6)	−160(9)	786(5)	58(5)	137(12)	70(4)	10(7)	−18(4)	−38(6)
O(19′)	−2409(5)	2681(9)	2164(4)	76(4)	289(15)	59(3)	12(7)	29(3)	−53(5)
O(20′)	671(3)	1573(6)	310(1)	58(3)	200(8)	16(1)	4(4)	1(1)	3(2)

dihydrobromide **1** because the π-bond at the nitrogen atom in the latter causes its bonds to be coplanar whereas in the parent alkaloid this atom is pyramidal. Ring D is in a chair form and ring E an envelope with C(19) as flap. In the lactone ring F, it is only C(5) that is significantly out of plane.

In the other part of the molecule the atoms of ring A′ are more closely coplanar than in ring A (maximum deviation <0.02 Å). The atoms

Can. J. Chem. Downloaded from www.nrcresearchpress.com by 210.87.254.42 on 09/05/12
For personal use only.

TABLE 1 (*Concluded*)
(*b*) Atomic fractional coordinates ($\times 10^4$) and isotropic, *B*, temperature factors, for methanol C(22′) and O(21′) atoms and hydrogen atoms (*B* factors for latter rounded to 0.5)

Atom	*x*	*y*	*z*	*B*
O(21′)	−1996(10)	6516(13)	1343(6)	11.98(59)
C(22′)	−2406(13)	6952(18)	1919(7)	11.49(69)
H(2)	5594	159	1563	3.50
H(3)	5644	922	454	6.00
H(4)	5248	−391	−75	6.50
H(6*A*)	5088	−2832	−144	5.00
H(6*B*)	4327	−3639	256	5.00
H(7*A*)	5885	−4275	464	7.00
H(7*B*)	6195	−2823	618	7.00
H(8*A*)	4750	−4256	1264	6.00
H(8*B*)	5830	−3927	1512	6.00
H(10*A*)	4376	−2936	2237	6.50
H(10*B*)	5404	−2181	2295	6.50
H(11*A*)	3579	−1119	2293	5.50
H(11*B*)	4606	−367	2361	5.50
H(14)	2121	−835	1410	5.00
H(20*A*)	3318	−2049	−147	6.50
H(20*B*)	3132	−768	236	6.50
H(25*A*)	2004	4598	911	10.00
H(25*B*)	1268	3768	524	10.00
H(25*C*)	838	4839	952	10.00
H(27*A*)	3617	4441	2231	9.00
H(27*B*)	2449	4086	2173	9.00
H(27*C*)	2901	5376	1861	9.00
H(28*A*)	5821	2673	1608	8.00
H(28*B*)	4853	3511	1455	8.00
H(28*C*)	5400	2727	934	8.00
H(3′*A*)	−1596	3737	71	10.00
H(3′*B*)	−2577	2908	179	10.00
H(4′*A*)	−784	1994	−153	8.50
H(4′*B*)	−1776	1172	−70	8.50
H(7′*A*)	−926	−1693	1141	6.00
H(7′*B*)	−1074	−533	1606	6.00
H(8′*A*)	614	−979	899	7.00
H(8′*B*)	553	−1063	1614	7.00
H(11′)	914	609	2445	5.50
H(12′)	−70	1133	3274	7.50
H(13′)	−1604	2031	3121	8.00
H(18′*A*)	−2423	−1090	757	8.50
H(18′*B*)	−2617	313	445	8.50
H(18′*C*)	−2501	167	1170	8.50

directly attached to this ring, O(19′), N(1′), and C(9′), are out of plane in the same direction by 0.08, 0.10, and 0.24 Å, respectively. Ring B′ is quite buckled. Its atoms can be considered to lie on three planes with the 'folds' at N(1′) . . . C(9′) and C(5′) . . . C(9′). Ring C′ has a chair conformation with, as expected, pyramidal rather than planar N(6′) found in the dihydrobromide. Ring D′ and O(17′) are coplanar. In ring D′ C(2′)—C(3′) is extremely long, 1.60(2) Å. Furthermore, a comparison of the equivalent ring in L-pyroglutamyl-L-histidine (10) shows interesting bond angle differences. In this latter structure the internal angles at C(4′) and at C(3′) are 104.0 and 105.9°, respectively. In haplophytine, ring D′, the order is reversed, 107.6 and 104.0°. This may well be due to conflict between H(4′B) and H(18′B) which are only 1.89 Å apart. This short contact seems to be related to the differences in angle at N(6′): C(18′)—N(6′)—C(5′) (114.1°) and C(18′)—N(6′)—C(7′) (109.1°).

The lengths of bonds C(19)—O(22) and

Can. J. Chem. Downloaded from www.nrcresearchpress.com by 210.87.254.42 on 09/05/12
For personal use only.

Can. J. Chem. Downloaded from www.nrcresearchpress.com by 210.87.254.42 on 09/05/12
For personal use only.

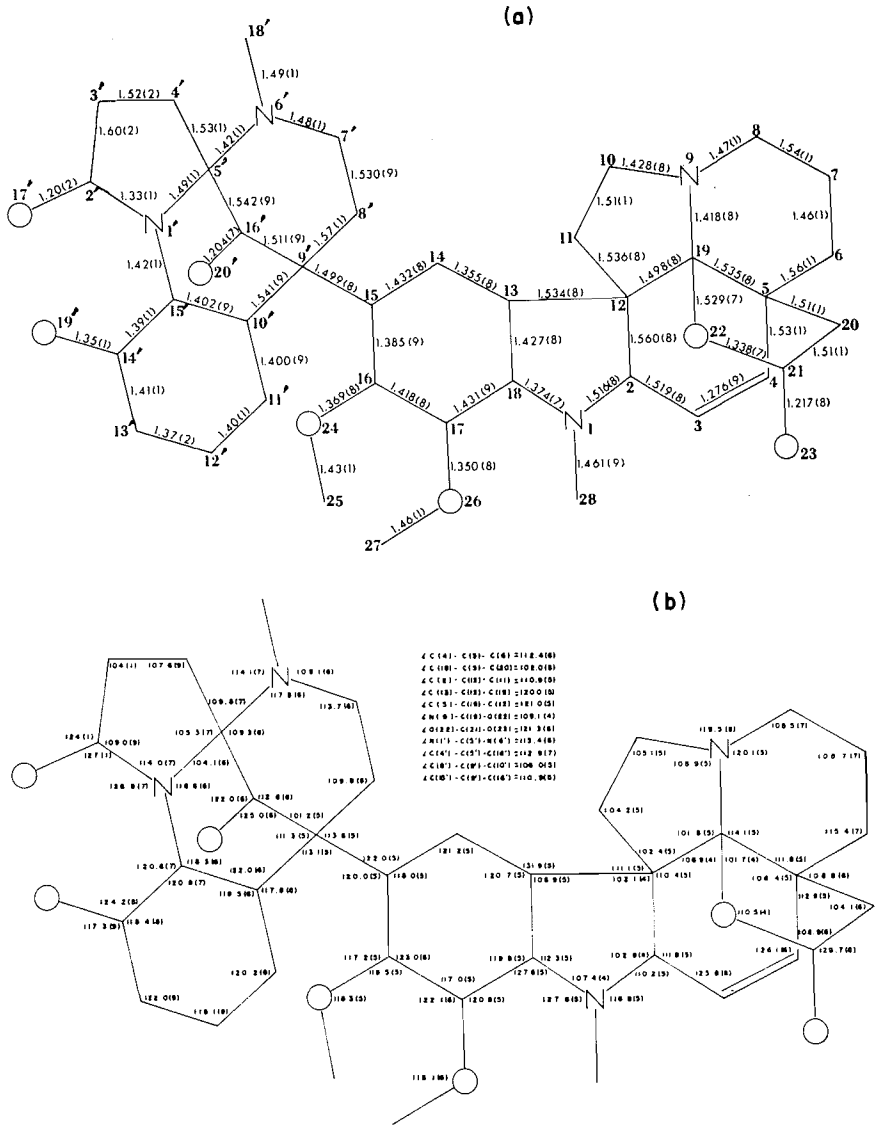

FIG. 2. (*a*) Bond lengths. (*b*) Bond angles.

TABLE 2. Coefficients of best least squares planes $AX + BY + CZ = D$ where X, Y, Z are real orthogonal coordinates (in Å) with X along x and Z along z^*

Plane	Ring	*A*	*B*	*C*	*D*
1	A	0.049(2)	0.001(2)	−0.999(7)	−3.003(2)
2	B	−0.023(3)	0.018(3)	−1.000(8)	−3.376(2)
3	C	−0.822(9)	0.484(5)	−0.302(6)	−6.293(2)
4	D	0.762(43)	0.646(37)	−0.052(20)	3.263(3)
5	E	0.862(25)	0.494(15)	−0.115(13)	4.080(3)
6	F	0.341(6)	−0.916(16)	−0.213(9)	3.298(3)
7	A′	−0.430(22)	−0.899(45)	−0.078(8)	−1.590(4)
8	B′	0.426(17)	0.901(35)	−0.088(17)	0.933(3)
9	C′	0.405(4)	−0.439(4)	−0.802(8)	−2.141(3)
10	D′	0.847(32)	0.519(20)	−0.116(9)	−0.595(4)

Can. J. Chem. Downloaded from www.nrcresearchpress.com by 210.87.254.42 on 09/05/12
For personal use only.

TABLE 3. Deviations from best least squares planes (10^{-3} Å). Asterisked atoms were not included in calculating plane

Plane	Atom	Deviation	Atom	Deviation	Atom	Deviation
1	C(13)	16(5)	C(14)	−31(6)	C(15)	12(5)
	C(16)	22(6)	C(17)	−39(6)	C(18)	15(5)
	N(1)*	−52(5)	C(12)*	−108(6)	C(9′)*	66(6)
	O(24)*	−19(4)	O(26)*	−82(6)		
2	N(1)	−111(5)	C(2)	193(6)	C(12)	−163(6)
	C(13)	65(5)	C(18)	53(5)	C(28)*	141(7)
3	C(2)	−138(6)	C(3)	−11(6)	C(4)	82(7)
	C(5)	70(6)	C(12)	261(6)	C(19)	−209(6)
4	C(5)	126(7)	C(6)	−212(9)	C(7)	263(9)
	C(8)	−300(8)	N(9)	139(5)	C(19)	−130(6)
5	N(9)	181(5)	C(10)	−86(7)	C(11)	−97(6)
	C(12)	208(6)	C(19)	−247(5)		
6	C(5)	227(7)	C(19)	−163(6)	C(20)	−216(8)
	C(21)	23(8)	O(22)	51(4)	O(23)*	125(6)
7	C(10′)	5(7)	C(11′)	2(9)	C(12′)	−18(12)
	C(13′)	14(11)	C(14′)	2(11)	C(15′)	−9(8)
	N(1′)*	98(7)	C(9′)*	242(7)	O(19′)*	81(9)
8	N(1′)	131(7)	C(5′)	−427(9)	C(9′)	−82(7)
	C(10′)	−37(7)	C(15′)	15(8)	C(16′)	267(8)
	O(20′)*	906(6)				
9	C(5′)	−227(8)	N(6′)	70(6)	C(7′)	−172(8)
	C(8′)	290(7)	C(9′)	−314(6)	C(16′)	308(6)
	C(18′)*	−521(11)	O(20′)*	1214(4)		
10	N(1′)	−9(6)	C(2′)	28(10)	C(3′)	−22(14)
	C(4′)	−1(10)	C(5′)	9(8)	O(17′)*	46(10)

C(19)—N(9) are particularly noteworthy. The former (1.53 Å) is significantly longer than the corresponding bonds (1.45—1.47 Å) in several γ-lactones that have recently been measured (11), while the latter bond (1.42 Å) is unusually short for a C(sp^3)—N bond.[2] These observations lend considerable support to the previous interpretation of the unusually long wavelength of the C=O stretching band in the infrared spectrum of **3** and related compounds (5) in terms of a contribution of a dipolar canonical structure **5** to the carbinolamine lactone function **4**.[3]

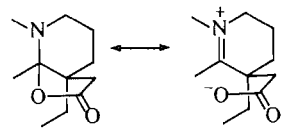

4 **5**

Two short intramolecular distances are found from O(17′): to O(19′), 2.58 Å, and to O(21′) of the methanol molecule, 2.71 Å. There are thus clearly hydrogen bonds here but the hydrogen atoms involved could not be located unambiguously and were omitted from F_c.

There is only one short intermolecular distance O(19′) . . . H(11*A*) (at $-x, \frac{1}{2}+y, \frac{1}{2}-z$), 2.41 Å.

It was previously suggested (2) that the fact that one of the methoxyl proton signals in the pmr spectrum of **3** occurs at unusually high field (δ 3.00) is attributable to shielding of the C(25) methyl group by ring A′. A corresponding effect was considered to account for the high-field position (δ 6.27) of one of the aromatic proton

[2]Thus the lengths of the C(sp^3)—N bonds in **3** and in several other alkaloids that have recently been measured (12) fall in the range 1.42–1.52 Å; the average length of the thirty such bonds is 1.47 Å. It must be noted, however, that the C(19)—N(9) bond is not significantly shorter than the C(10)—N(9) bond.

[3]A related interpretation can be postulated for the unusual position of the δ-lactone C=O stretching band in swietenine (13) and is supported by bond length measurements (14).

signals; this was assigned to the proton at C(11′) which it was suggested, is shielded by ring A. With the assumption that the conformation of **3** in solution resembles that in the crystalline state (*vide supra*), qualitative support for these spectroscopic interpretations can be adduced from the X-ray crystallographic data in that estimations (15) based on the geometrical relationships revealed by these data predict significant shielding of the C(25) and C(11′) protons by rings A′ and A, respectively.

Acknowledgment

We thank the National Research Council of Canada for support of this work.

1. E. F. ROGERS, H. R. SNYDER, and R. F. FISCHER. J. Am. Chem. Soc. **74**, 1987 (1952); H. R. SNYDER, R. F. FISCHER, J. F. WALKER, H. E. ELS, and G. A. NUSSBERGER. J. Am. Chem. Soc. **76**, 2819 (1954); **76**, 4601 (1954); H. R. SNYDER, H. F. STROHMAYER, and R. A. MOONEY. J. Am. Chem. Soc. **80**, 3708 (1958).
2. I. D. RAE, M. ROSENBERGER, A. G. SZABO, C. R. WILLIS, P. YATES, D. E. ZACHARIAS, G. A. JEFFREY, B. DOUGLAS, J. L. KIRKPATRICK, and J. A. WEISBACH. J. Am. Chem. Soc. **89**, 3061 (1967).
3. D. E. ZACHARIAS. Acta Crystallogr. Sect. B, **26**, 1455 (1970).
4. P. YATES, F. N. MACLACHLAN, I. D. RAE, M. ROSENBERGER, A. G. SZABO, C. R. WILLIS, M. P. CAVA, M. BEHFOROUZ, M. V. LAKSHMIKANTHAM, and W. ZEIGER. J. Am. Chem. Soc. **95**, 7842 (1973).
5. M. P. CAVA, M. V. LAKSHMIKANTHAM, S. K. TALAPATRA, P. YATES, I. D. RAE, M. ROSENBERGER, A. G. SZABO, B. DOUGLAS, and J. A. WEISBACH. Can. J. Chem. **51**, 3102 (1973).
6. S. C. ABRAHAMS and J. L. BERNSTEIN. Acta Crystallogr. **18**, 926 (1965).
7. G. GERMAIN, P. MAIN, and M. M. WOOLFSON. Acta Crystallogr. Sect. A, **27**, 368 (1971).
8. D. T. CROMER and J. B. MANN. Acta Crystallogr. Sect. A, **24**, 321 (1968).
9. R. F. STEWART, E. R. DAVIDSON, and W. T. SIMPSON. J. Chem. Phys. **42**, 3175 (1965).
10. M. COTRAIT and M. ALLARD. C. R. Acad. Sci. Ser. C, **276**, 1671 (1973).
11. B. SHELDRICK. Acta Crystallogr. Sect. B, **29**, 2631 (1973); J. L. FLIPPEN. Acta Crystallogr. Sect. B, **28**, 2046 (1972); H. M. BERMAN, R. D. ROSENSTEIN, and J. SOUTHWICK. Acta Crystallogr. Sect. B, **27**, 7 (1971); G. D. ANDREETTI, A. MANGIA, M. NARDELLI, and G. PELIZZI. Gazz. Chim. Ital. **103**, 257 (1973); A. FURUSAKI and T. WATANABE. Bull. Chem. Soc. Jpn. **45**, 2288 (1972).
12. C. RICHE. Acta Crystallogr. Sect. B, **30**, 1386 (1974); **29**, 2147 (1973); K. SASAKI and Y. HIRADA. Acta Crystallogr. Sect. B, **29**, 547 (1973); M. CESARIO and C. PASCARD-BILLY. Acta Crystallogr. Sect. B, **29**, 529 (1973); H. IRIE, K. OHNO, K. OSAKI, T. TAGA, and S. UYEO. Chem. Pharm. Bull. **21**, 451 (1973); P. A. LUHAN and A. T. MCPHAIL. J. Chem. Soc. Perkin Trans. II, 2006 (1972); D. N. J. WHITE, A. T. MCPHAIL, and G. A. SIM. J. Chem. Soc. Perkin Trans. II, 1280 (1972).
13. J. CHAKRAVARTY and A. CHATTERJEE. J. Indian Chem. Soc. **32**, 179 (1955).
14. A. T. MCPHAIL and G. A. SIM. J. Chem. Soc. B, 318 (1966).
15. F. A. BOVEY. Nuclear magnetic resonance spectroscopy. Academic Press, New York. 1969. pp. 64–65, 264–274.

Can. J. Chem. Downloaded from www.nrcresearchpress.com by 210.87.254.42 on 09/05/12
For personal use only.

Succinimidyl esters of fatty acids for amino acid acylations[1]

ALENKA PAQUET
Food Research Institute, Research Branch, Canada Agriculture, Ottawa, Canada K1A 0C6

Received June 25, 1975

ALENKA PAQUET. Can. J. Chem. **54**, 733 (1976).

Fatty acid *N*-hydroxysuccinimide esters have been prepared from the thallium(I) salt of *N*-hydroxysuccinimide and the corresponding acyl chlorides in essentially quantitative yields. These active esters were used for acylation of amino acid esters in organic solvents, or of free amino acids in aqueous medium. The title compounds were found to be selective towards the side chain amino group of lysine. An efficient preparation of ε-*N*-benzyloxycarbonyl-L-lysine using benzyl succinimidyl carbonate is described.

ALENKA PAQUET. Can. J. Chem. **54**, 733 (1976).

On a préparé les esters *N*-hydroxysuccinimides d'acide gras à partir du sel de thallium(I) de la *N*-hydroxysuccinimide et des chlorures d'acyles correspondants. Les rendements de ces esters sont pratiquement quantitatifs. On a utilisé ces esters actifs pour l'acylation d'esters d'acides aminés dans des solvants organiques ou d'acides aminés libres dans les milieux aqueux. On a trouvé que les composés mentionnés dans le titre sont sélectifs vis-à-vis le groupe aminé de la chaîne latérale de la lysine. On décrit une préparation efficace de ε-N-benzyloxycarbonyl-L-lysine utilisant le carbonate de la benzylsuccinimidyle.

[Traduit par le journal]

Long chain acylamino acids possessing appropriate lipophilic–hydrophilic balance are generally emulsifiers and surfactants and are suggested to possess bactericidal activity. The physicochemical characteristics which relate to their potential usefulness as surfactants, such as critical micelle concentration, foaming, and emulsifying properties, have been studied by Fieser *et al.* (1), Heitmann (2), and recently by Takehara *et al.* (5) and Smith and Barden (6). The surface and interfacial behaviour of these compounds are of interest as they may be of use in various industrial applications relying upon foaming and emulsifying properties.

The objective of this work was to develop a method, adaptable to the preparation of long chain acylamino acids, for use in physicochemical and biological studies. Fatty acyl ε-*N*-lysine derivatives having the $RCH_2NH_3^+COO^-$ zwitterion are expected to possess different physicochemical properties than fatty acyl monoamino acids. Therefore it was also an objective to devise a convenient method for the preparation of long chain ε-*N*-acyl derivatives of unprotected lysine.

Many syntheses of fatty acyl monoamino acids have been reported using the Schotten–Baumann or mixed anhydride method (1–4). However these procedures are not expected to acylate selectively the ε-amino group of lysine in view of the work of Leclerc and Benoiton (7). These authors demonstrated that, in contrast to anhydrides and acyl chlorides, active esters react exclusively with the ε-amino group of lysine at $pH > 11$. This was established using *p*-nitrophenyl esters (7). Therefore attention was focussed on the active ester method.

Succinimidyl esters (OHSu esters) of N-protected amino acids have been widely used in peptide syntheses giving good yields of N-protected peptides (8–10). OHSu esters are of particular interest for the syntheses of fatty acyl derivatives because *N*-hydroxysuccinimide is a water soluble by-product in the step of acylamino acid formation. Therefore the use of OHSu esters of fatty acids for acylations of monoamino acids and for selectivity experiments was investigated.

The dicyclohexylcarbodiimide method (8, 9, 11) or mixed anhydride method (12) has been used for the preparation of OHSu esters of acylamino acids. A decision was made to explore the use of the thallium(I) salt of *N*-hydroxysuccinimide (TlOSu). The expected smooth reaction with acyl chlorides would be convenient for our purposes particularly for experiments with unsaturated fatty acids. Taylor and Kienzle (13) reported the preparation of the thallium(I) salt

[1]Contribution No. 262 from the Food Research Institute, Agriculture Canada, Ottawa, Canada.

Can. J. Chem. Downloaded from www.nrcresearchpress.com by 210.87.254.105 on 09/05/12
For personal use only.

Can. J. Chem. Downloaded from www.nrcresearchpress.com by 210.87.254.105 on 09/05/12
For personal use only.

of 1-hydroxy-2(1*H*)-pyridone by the reaction of the thallous ethoxide with 1-hydroxy-2(1*H*)-pyridone. The authors showed that the reaction of the thallium(I) salt of 1-hydroxy-2(1*H*)-pyridone with chlorides of N-protected amino acids gave very reactive esters in high yields. Paquette (14) who prepared the above mentioned esters from 2-ethoxypyridine-1-oxide and the appropriate acyl chloride also reported their extreme sensitivity to hydrolysis and aminolysis. It is unlikely that these esters could be used for selective acylations.

Thus the reaction of thallous ethoxide (15) with *N*-hydroxysuccinimide in chloroform at room temperature gave a quantitative yield of the thallous salt $C_4H_4NO_2Tl$, **1**, which was water soluble and stable, except for slight light sensitivity.

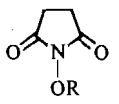

1 R = Tl
2 R = $OCOCH_2$–C$_6$H$_5$
3 R = $COCH_3$
4 R = $COC_{15}H_{31}$
5 R = $COC_{19}H_{39}$
6 R = $COC_{21}H_{43}$
7 R = $COC_{17}H_{31}$

The TlOSu was converted to OHSu esters in chloroform at room temperature by reaction with the appropriate acyl chloride. The following esters were synthesized: acetate **3** (11), palmitate **4**, arachidate **5**, behenate **6**, and linoleate **7**. These compounds were stable (except the unsaturated ester **7**) and their smooth reactivity with amino acid esters was demonstrated by the reaction of **4** with glycine ethyl ester, and lysine ethyl and methyl esters in organic solvent giving the corresponding acylamino acids in high yield. α-*N*,ϵ-*N*-Dipalmitoyl-L-lysine ethyl ester was saponified with 3% methanolic potassium hydroxide to α-*N*,ϵ-*N*-dipalmitoyllysine. The infrared spectrum was found to be identical with the spectrum of the compound obtained by acylation of L-lysine by palmitoyl chloride. Similarly α-*N*,ϵ-*N*-dilinoleoyl-L-lysine methyl ester was prepared using **7**.

Reactions of OHSu esters with free amino acids were performed in water–acetone or water–ethanol medium in the presence of 2 equiv. of triethylamine. No reaction occurred when only 1 equiv. of triethylamine was added. Glycine, L-alanine, β-alanine, and L-aspartic acid were used, giving good yields of acylamino acids.

Under these conditions OHSu esters acylate exclusively the side chain amino group of lysine. This was proven as follows. ϵ-*N*-Palmitoyl-L-lysine $C_{22}H_{44}N_2O_3$, was obtained by the reaction of an equivalent amount of **4** with unprotected L-lysine in 87% yield. The same yield of ϵ-*N*-palmitoyl-L-lysine was obtained when **4** was used in excess (2 equiv.). Infrared spectra and melting points of both products were identical. ϵ-*N*-Palmitoyl-L-lysine was allowed to stir with 2 equiv. of **4** under the above described conditions for several hours: unchanged ϵ-*N*-palmitoyl-L-lysine was isolated from the reaction mixture in quantitative yield. ϵ-*N*-Acetyl-L-lysine was submitted to the same reaction with 2 equiv. of **4**. No difference in ninhydrin colour was observed when compared to a control sample to which no **4** had been added.

The evidence for the structure of ϵ-*N*-palmitoyl-L-lysine is as follows. (*i*) The infrared spectrum (which is similar to the spectrum of ϵ-*N*-acetyl-L-lysine) in Nujol shows absorption for an ionized carboxyl group (1590 cm^{-1}) and both amide bands (1650 and 1540 cm^{-1}); absorption at 1710–1720 cm^{-1}, which would indicate unionized carboxyl due to α-*N*-substitution, was not observed. (*ii*) Reaction of ϵ-*N*-palmitoyl-L-lysine with benzyl chlorocarbonate in the presence of base in a water–acetone suspension gave α-*N*-benzyloxycarbonyl-ϵ-*N*-palmitoyl-L-lysine, $C_{30}H_{50}N_2O_5$, with yields of 91% of the crude, and 78% of the recrystallized products, mp 96–98 °C. This compound was identical with the product obtained by the reaction of authentic α-*N*-benzyloxycarbonyl-L-lysine with an equivalent amount of **4** in acetone–water medium containing 2 equiv. of triethylamine. A yield of 92% of the crude and 77% of the recrystallized product was obtained, mp 98 °C. There was no doubt as to the identity of these compounds on the basis of their identical ir spectra in chloroform (1710–1745, 1640, 1520–1550 cm^{-1}) and their mixture melting point.

In experiments designed to explore the further use of the TlOSu, benzyl succinimidyl carbonate (Z-OSu) **2** was prepared in essentially quantitative yield by the reaction of an equivalent amount of benzyl chlorocarbonate with TlOSu in organic solvent at room temperature. (The preparation of some other derivatives using TlOSu will be published later.)

Z-OSu can be conveniently used for the preparation of benzyloxycarbonyl amino acids as

TABLE 1. Succinimidyl esters*

Ester group	Melting point (°C)	Composition	N analysis (%) Calcd.	Found
Benzyl carbonate	75 (lit. (16) 78–80)	$C_{12}H_{11}NO_5$	5.61	5.69
Acetate	128 (lit. (11) 131–134)	$C_6H_7NO_4$	8.91	8.74
Palmitate	84	$C_{20}H_{35}NO_4$	3.90	4.00
Arachidate	98	$C_{24}H_{43}NO_4$	3.41	3.59
Behenate	88–90	$C_{26}H_{47}NO_4$	3.20	3.32
Linoleate	Oily	$C_{22}H_{35}NO_4$	Purification caused decomposition of the compound	

*All products exhibited typical infrared spectra and nmr spectra in accordance with their structures.

shown by Frankel *et al.* (16) and Gross and Bilk (17) but has been rarely used for this purpose since the previously reported syntheses of Z-OSu were cumbersome. No yield was reported by Frankel *et al.* who synthesized **2** from *N*-hydroxysuccinimide and benzyl chlorocarbonate. Gross and Bilk obtained **2** by the reaction of succinimidyl chlorocarbonate (obtained from the reaction of the potassium salt of *N*-hydroxysuccinimide with phosgene) with benzyl alcohol in an overall yield of 53%.

In the light of this work the selectivity of **2** could be expected. It would lead to the facile preparation of ε-*N*-benzyloxycarbonyllysine without first having protected the α-amino group. Thus ε-*N*-benzyloxycarbonyl-L-lysine was obtained in 85% yield by reaction of equimolar amounts of Z-OSu and L-lysine monohydrochloride in water–methanol medium in the presence of 3 equiv. of potassium hydroxide. Infrared spectra of this compound and the authentic compound were identical.

Selectivity experiments using **3** under the conditions described for acylation of lysine by OHSu esters gave results which were in agreement with those obtained by Leclerc and Benoiton (7). The ε-amino group was acylated exclusively when 1 or 2 equiv. of **3** were used. However in less concentrated solutions the use of even 2 equiv. of **3** left some residual amino acid. The reaction mixtures were analyzed on an amino acid analyzer by comparison with standards.

Experimental

Melting points were determined on a Koffler Block and are uncorrected. Nuclear magnetic resonance spectra were recorded on a Varian T-60 spectrometer in deuteriochloroform. Infrared spectra were measured on a Beckman IR-20 spectrometer in chloroform unless stated otherwise. Optical rotations were determined using a Perkin-Elmer 141 polarimeter. Amino acid analyses were performed on a Beckman 121M amino acid analyzer. Colorimetric determination of amino acids was performed on a Coleman spectrophotometer 20 (Bausch and Lomb) at 570 μm. Thin layer chromatography was carried out on silica gel plates (Type 60, Brickmann Instruments, Canada) and column chromatography on silica gel Bio-Sil-HA (minus 325 mesh, Bio-Rad laboratories, California, USA). Fatty acid chlorides were obtained from NU CHEK PREP. INC., Minnesota, U.S.A. and thallous ethoxide from Fisher Scientific Co., Ottawa, Canada.

N-Hydroxysuccinimide Thallium(I) Salt (TlOSu), 1

To a solution of *N*-hydroxysuccinimide (11.5 g, 0.1 mol, previously dried by evaporation with ethanol and drying under reduced pressure for about 1 h) in absolute ethanol (20 ml), thallous ethoxide (24.9 g, 0.1 mol) was added dropwise under vigorous stirring at room temperature. Stirring was continued for 1 h and the reaction mixture was allowed to stand at 0 °C overnight. Within this period the yellow precipitate changed to a white semicrystalline mass which was collected by filtration and washed with cold ethanol yielding 31.8 g (quantitative yield) of **1**. A small amount was recrystallized from water–ethanol in order to obtain an analytical sample; mp 208–210 °C. *Anal.* calcd. for $C_4H_4NO_2Tl$: C 15.08, H 1.26, N 4.39; found: C 15.23, H 1.40, N 4.36.

N-Hydroxysuccinimide Derivatives 2–7

The derivatives were prepared as follows. To a stirred suspension of **1** (10 mmol) in chloroform acyl chloride (10 mmol) in the same solvent was slowly added at room temperature. After stirring for 1 h, the suspension of thallium chloride was filtered off, resuspended in chloroform, filtered, and thoroughly washed with the same solvent. The combined filtrate was washed with a small amount of water, dried over sodium sulfate, and evaporated under reduced pressure giving essentially quantitative yields of the products. The results are shown in Table 1.

Acylamino Acid Esters

The acylamino acid ethyl or methyl esters were prepared under the following conditions. To a solution of 5 mmol of amino acid ester hydrochloride (a suspension in the case of lysine esters) in chloroform, equivalent

Can. J. Chem. Downloaded from www.nrcresearchpress.com by 210.87.254.105 on 09/05/12
For personal use only.

Can. J. Chem. Downloaded from www.nrcresearchpress.com by 210.87.254.105 on 09/05/12
For personal use only.

amounts of active ester and triethylamine were added with stirring at room temperature. Stirring was continued for at least 2 h, and in some cases overnight.

N-Palmitoylglycine Ethyl Ester

The reaction mixture was stirred overnight, washed with water, dried over sodium sulfate, and evaporated, yielding 86% of recrystallized product (ethanol); mp 80–81 °C (lit. (18) 80–82 °C). Infrared ν_{max} 1700–1740 (ester), 1670, 1510 cm^{-1} (amide).

N-Palmitoyl-L-alanine Ethyl Ester

A slight excess of triethylamine was used in this case and the reaction mixture was kept for 2 h at room temperature. The solvents and the excess of triethylamine were evaporated under reduced pressure and the residue was dissolved in ethanol. Water was slowly added until crystallization ensued and was completed by standing at 0 °C overnight. The product, isolated in quantitative yield, was recrystallized from ethanol giving a 95% yield of the product; mp 62 °C; $[\alpha]_D^{20}$ +7 (*c* 0.55, chloroform). Infrared 1740 ν_{max} (ester), 1680, 1515 cm^{-1} (amide). *Anal.* calcd. for $C_{21}H_{41}NO_3$: N 3.83; found: N 3.90.

α-N,ε-N-Dipalmitoyl-L-lysine Ethyl Ester

The reaction mixture was stirred for 3 h and after removal of the solvent under reduced pressure the product was crystallized from ethanol–water yielding 85% of the diamide; mp 96 °C; $[\alpha]_D^{20}$ +4.4 (*c* 0.90, chloroform). Infrared ν_{max} 1740 (ester), 1660, 1510 cm^{-1} (amide). *Anal.* calcd. for $C_{40}H_{78}N_2O_4$: C 73.79, H 12.07, N 4.30; found: C 73.72, H 11.86, N 4.33.

α-N,ε-N-Dipalmitoyl-L-lysine Methyl Ester

The reaction mixture was kept overnight, the solvent evaporated under reduced pressure, the residue dissolved in methanol, and water was slowly added until crystallization started. The product was recrystallized from methanol giving 88% of the ester; mp 98 °C; $[\alpha]_D^{20}$ +3.6 (*c* 0.74, chloroform). Infrared ν_{max} 1735 (ester), 1650–1510 cm^{-1} (amide). *Anal.* calcd. for $C_{39}H_{76}N_2O_4$: N 3.96; found: N 4.08.

α-N,ε-N-Dipalmitoyllysine

The ethyl ester (1.58 g) was heated to gentle reflux with 3% methanolic sodium hydroxide for 2 h, and left at room temperature overnight. The soapy material was acidified to p*H* 2 with cold 1 *N* HCl and the white solid was collected and recrystallized from acetone–water giving 88% (1.31 g) of the free acid; mp 104–106 °C. Infrared (Nujol) ν_{max} 1715 (carboxyl), 1640, 1560 cm^{-1} (amide). *Anal.* calcd. for $C_{38}H_{74}N_2O_4 \cdot \frac{1}{2}H_2O$: C 72.21, H 11.96, N 4.43; found: C 72.32, H 11.64, N 4.41.

α-N,ε-N-Dilinoleoyl-L-lysine Methyl Ester

The reaction mixture was stirred for 3 h, washed with water, dried over sodium sulfate, and evaporated under reduced pressure yielding 90% of an oily product which was chromatographed on a column containing 10 times its weight of silica gel. Chloroform–hexane (2:3) eluates gave a 55% yield. $[\alpha]_D^{20}$ +2.6 (*c* 0.38, chloroform). Infrared ν_{max} 1730–1750 (ester), 1660, 1520 cm^{-1} (amide). Further purification of the product resulted in partial decomposition precluding valid elemental analysis.

Free Acylamino Acids

These were prepared under the following general conditions. To an aqueous solution of amino acid equivalent amounts of active ester in acetone or ethanol suspension and 2 equiv. of triethylamine were added. The reaction mixture was stirred at room temperature for at least 2 h and in some cases overnight. The products were isolated as described for each separate acylamino acid.

N-Palmitoylglycine

Glycine (1 mmol, in 1.5 ml of water) and **4** (1 mmol, in 2 ml of acetone) were allowed to react overnight. Triethylamine was thoroughly evaporated by repeated evaporation with ethanol under reduced pressure. The residue was suspended in water and the product was extracted into chloroform. The combined extract was washed with water, dried over sodium sulfate, and evaporated under reduced pressure giving a 92% yield of crude material which, upon crystallization from 96% ethanol, gave an 85% yield of the pure product; mp 96 °C (95% ethanol), 120–122 °C (petroleum ether) (lit. (3) 121–122 °C (petroleum ether)). *Anal.* calcd. for $C_{18}H_{35}NO_3$: C 68.99, H 11.26, N 4.46; found: C 69.01, H 11.14, N 4.37.

N-Palmitoyl-L-alanine

L-Alanine (1.5 mmol in 2 ml of water) and **4** (1.5 mmol in 2 ml of ethanol) were condensed at room temperature overnight. Reaction mixture was acidified to p*H* 2 with 1 *N* HCl and kept at 0 °C overnight. The precipitated title compound was collected, washed with cold water, giving an 80% yield of crystalline solid; mp 89 °C. $[\alpha]_D^{20}$ −13.1 (*c* 0.13, 96% ethanol). *Anal.* calcd. for $C_{19}H_{37}NO_3$: C 69.68, H 11.38, N 4.27; found: C 69.42, H 11.39, N 4.38.

N-Palmitoyl-β-alanine

The title compound was prepared essentially as above except that the product was extracted into chloroform – isopropropyl alcohol (3:2) after the acidification of the reaction mixture. The combined extract was washed with water, dried over sodium sulfate, and evaporated to an oily residue which crystallized from chloroform–hexane in 88% yield; mp 105–107 °C. *Anal.* calcd. for $C_{19}H_{37}NO_3$: C 69.68, H 11.38, N 4.27; found: C 69.71, H 11.77, N 4.33.

N-Arachidoyl-L-alanine

L-Alanine (0.5 mmol in 2 ml of water) and **5** (0.5 mmol in 2 ml of acetone) were stirred at room temperature overnight. The reaction mixture was acidified to p*H* 2 with 1 *N* HCl and left at 0 °C overnight. The precipitated title compound was collected, washed with cold water, and dried giving an 88% yield of the crude compound desired which was recrystallized from methylene chloride; mp 107 °C; $[\alpha]_D^{20}$ −2.6 (*c* 0.23, 96% ethanol). *Anal.* calcd. for $C_{23}H_{45}NO_3$: N 3.64; found: N 3.80.

ε-N-Palmitoyl-L-lysine

To the solution of L-lysine (1 mmol) in water (2 ml) and triethylamine (0.27 ml, 2 mmol) 1 mmol of **4** (suspended in 2 ml of acetone) was added at room temperature under stirring. Stirring of the reaction mixture was continued for 4 h. Triethylamine was removed under reduced pressure, the precipitate was collected by filtra-

Can. J. Chem. Downloaded from www.nrcresearchpress.com by 210.87.254.105 on 09/05/12
For personal use only.

tion, washed with water, and dried giving an 87% yield of the title compound; mp 210–220 °C; $[\alpha]_D$ +3.3 (*c* 0.15, 0.5 *N* methanolic KOH). Infrared (Nujol) ν_{max} 1635 (amide), 1590 (carboxyl), 1510–1530 cm^{-1} (amide). *Anal.* calcd. for $C_{22}H_{44}N_2O_3$: N 7.28; found: N 6.98.

From the experiment carried out with 2 mmol of **4** under the same conditions the title compound was isolated in essentially the same yield. Infrared spectra of both compounds were identical.

N-Palmitoyl-L-aspartic Acid

L-Aspartic acid (1 mmol in 0.5 ml of water) and **4** (1 mmol in 1.5 ml of acetone) were allowed to react for 4 h. Acetone was removed under reduced pressure and the reaction mixture was acidified to p*H* 2 with 1 *N* HCl. The crystalline product was separated, washed with a small amount of ice water, and dried; yield 88%; mp 117 °C. Recrystallization from ethanol–water gave mp 119 °C; $[\alpha]_D^{20}$ +13.3 (*c* 0.30, 96% ethanol). *Anal.* calcd. for $C_{20}H_{37}NO_5$: C 64.65, H 10.03, N 3.77; found: C 64.89, H 10.80, N 3.93.

N-Linoleoyl-L-aspartic Acid

The title compound was prepared from L-aspartic acid and **7** using the procedure described for *N*-palmitoyl-L-aspartic acid. The oily product exhibited $[\alpha]_D^{20}$ +1.4 (96% ethanol). Infrared ν_{max} 1710–1745 (carboxyl), 1640–1670, 1510–1550 cm^{-1} (amide). *Anal.* calcd. for $C_{22}H_{37}NO_5$; N 3.75; found: N 3.94.

A slightly modified Schotten–Baumann method gave the title compound in 90% yield. Infrared spectra of both products were identical.

ε-N-Benzyloxycarbonyl-L-lysine

To the solution of 27.3 mg (0.15 mmol) of L-lysine monohydrochloride in 0.5 ml of water and 0.9 ml of 0.5 *N* methanolic potassium hydroxide (0.45 mmol) 37.3 mg (0.15 mmol) of Z-OSu was added under stirring at room temperature. After 15 min the reaction mixture was carefully neutralized with 1 *N* HCl. The methanol was evaporated and the precipitated title product was collected by filtration, washed with water, and recrystallized from hot water giving an 85% yield; mp 252 °C. The infrared spectrum in Nujol was identical with the spectrum of the authentic ε-*N*-benzyloxycarbonyl-L-lysine.

α-N-Benzyloxycarbonyl-ε-N-palmitoyllysine

From α-N-Benzyloxycarbonyl-L-lysine

α-*N*-Benzyloxycarbonyl-L-lysine (0.5 mmol) and **4** (0.5 mmol) in 1.4 ml of water and 1.4 ml of acetone were stirred in the presence of 0.14 ml of triethylamine (1 mmol) for 2 h. Water (2 ml) was added and the reaction mixture acidified to p*H* 2 with 1 *N* HCl and the crystalline solid was separated by filtration, washed with water, and dried; 92% of the crude and 77% of the recrystallized product (methylene chloride) was obtained; mp 96–98 °C $[\alpha]_D^{20}$ +14.3 (*c* 0.28, chloroform). *Anal.* calcd. for $C_{30}H_{50}N_2O_5$: C 69.46, H 9.73, N 5.39; found: C 69.68, H 9.40, N 5.61.

From ε-N-Palmitoyl-L-lysine

To the suspension of 187 mg (0.47 mmol) of ε-*N*-palmitoyl-L-lysine in 3 ml of water and 2 ml of dioxane 0.12 ml of 4 *N* NaOH (0.47 mmol) was added under stirring and cooling. Then 93 mg (0.5 mmol) of benzyl chlorocarbonate and 0.13 ml (0.51 mmol) of 4 *N* NaOH were added under the same conditions. Another 2 ml of water and 1 ml of dioxane were added and the reaction mixture was kept at 0 °C overnight. After acidification to p*H* 2 by 1 *N* HCl the product was separated, washed with water, dried, and recrystallized from methylene chloride (77%). Yields of crude and recrystallized products, and their melting points were comparable to those obtained from above described reaction. Infrared spectra in chloroform were identical as discussed earlier in this paper.

Acknowledgements

The author wishes to acknowledge Mr. G. Morris for elemental analyses, (Analytical Services, CBRI, Agriculture Canada). The author is grateful to Dr. L. Benoiton for his help in discussing and preparing this manuscript and acknowledges the samples of ε-*N*-acetyl-L-lysine and α-*N*-benzyloxycarbonyl-L-lysine obtained from him. The author is indebted to the director of this Institute, Dr. J. Holme, for valuable suggestions when this work was planned.

1. M. Fieser, L. F. Fieser, E. Toromanoff, Y. Hirata, H. Heymann, M. Tefft, and S. Bhattacharya. J. Am. Chem. Soc. **78**, 2825 (1956).
2. P. Heitmann. Eur. J. Biochem. **3**, 346 (1968).
3. E. Jungermann, J. F. Gerecht, and I. J. Krems. J. Am. Chem. Soc. **78**, 172 (1956).
4. M. Takehara, I. Yoshimura, and K. Takizawa. J. Am. Oil Chem. Soc. **49**, 157 (1972).
5. M. Takehara, H. Mariyuki, and I. Yoshimura. J. Am. Oil Chem. Soc. **49**, 143 (1972).
6. G. D. Smith and R. E. Barden. Chem. Phys. Lipids, **14**, 1 (1975).
7. J. Leclerc and L. Benoiton. Can. J. Chem. **46**, 1047 (1968).
8. G. W. Anderson, J. E. Zimmerman, and F. M. Callahan. J. Am. Chem. Soc. **85**, 3039 (1963).
9. G. W. Anderson, J. E. Zimmerman, and F. M. Callahan. J. Am. Chem. Soc. **86**, 1839 (1964).
10. J. P. Greenstein and M. Winitz. *In* Chemistry of the amino acids. Vol. 2. Wiley, New York. 1961. p. 1027.
11. D. G. Lindsay and S. Shall. Biochem. J. **121**, 737 (1971).
12. G. W. Anderson, F. M. Callahan, and J. E. Zimmerman. J. Am. Chem. Soc. **89**, 178 (1967).
13. E. C. Taylor and F. Kienzle. J. Org. Chem. **35**, 1672 (1970).
14. L. A. Paquette. J. Am. Chem. Soc. **87**, 5186 (1965).
15. M. Fieser and L. F. Fieser. *In* Reagents for organic chemistry. Vol. 2. Wiley, New York. 1969. p. 407.
16. M. Frankel, D. Ladkany, C. Gilon, and Y. Wolman. Tetrahedron Lett. **39**, 4765 (1966).
17. H. Gross and L. Bilk. Ann. Chem. **725**, 212 (1969).
18. A. Koebner. J. Chem. Soc. 564 (1941).

The crystal and molecular structure of 1,1-bis(diphenylphosphino)-2,2-dimethylhydrazine

J. BRIAN FAUGHT

Department of Chemistry, Dalhousie University, Halifax, Nova Scotia, B3H 4J3

Received September 26, 1975

J. BRIAN FAUGHT. Can. J. Chem. **54**, 738 (1976).

The structure of 1,1-bis(diphenylphosphino)-2,2-dimethylhydrazine, $[(C_6H_5)_2P]_2NN(CH_3)_2$ has been determined crystallographically. The compound crystallizes from *n*-heptane in the space group $P2_1/c$ with $a = 8.910(1)$, $b = 9.686(1)$, $c = 27.489(4)$ Å, and $\beta = 102.94(2)°$ with four molecules per unit cell. The structure was solved from 2669 independent reflections with $I > 3\sigma(I)$ and refined by block diagonal least squares methods to $R = 0.032$ and $R_\omega = 0.048$. Each diphenylphosphino group is bonded to the same hydrazine nitrogen and the geometry about this nitrogen is nearly planar. The average dimensions of the structure are P—C = 1.828 ± 0.005, P—N = 1.715 ± 0.014, N—N = 1.451, and N—C = 1.457 ± 0.003 Å, ∠C—P—C = 101.6 ± 0.6, ∠C—P—N = 104.5 ± 0.8, ∠P—N—P = 126.31, ∠P—N—N = 116.8 ± 0.6, and ∠N—N—C = 111.5 ± 1.3°.

J. BRIAN FAUGHT. Can. J. Chem. **54**, 738 (1976).

On a déterminé la structure de la bis(diphénylphosphino-1,1) diméthyl-2,2 hydrazine, $[(C_6H_5)_2P]_2NN(CH_3)_2$, par la diffraction des rayons X. Le composé recristallise du *n*-heptane dans le groupe spatial $P2_1/c$ avec quatre molécules par maille, $a = 8.910(1)$, $b = 9.686(1)$, $c = 27.489(4)$ Å, $\beta = 102.94(2)°$. La structure cristalline, qui a été résolue à partir de 2669 réflexions indépendantes avec $I > 3\sigma(I)$, est affinée par moindres carrés (blocs diagonaux) jusqu'à une valeur de $R = 0.032$ ($R_\omega = 0.048$), en utilisant l'approximation diagonale. Les deux groupes diphénylphosphino sont liés avec le même azote de l'hydrazine; l'entourage de cet azote est presque planaire. Les dimensions moléculaires moyennes sont P—C = 1.828 ± 0.005, P—N = 1.715 ± 0.014, N—N = 1.451, N—C = 1.457 ± 0.003 Å, ∠C—P—C = 101.6 ± 0.6, ∠C—P—N = 104.5 ± 0.8, ∠P—N—P = 126.31, ∠P—N—N = 116.8 ± 0.6, et ∠N—N—C = 111.5 ± 1.3°.

[Traduit par le journal]

Introduction

Phosphinohydrazines present us with the possibility of studying the P—N—N system, which may be looked upon as a homolog of triazane and higher nitrogen chain compounds. We wish to report the structure of 1,1-bis-(diphenylphosphino)-2,2-dimethylhydrazine, the first phosphinohydrazine structure to be reported.

Experimental

1,1-Bis(diphenylphosphino)-2,2-dimethylhydrazine was prepared according to the method of Nielsen and Sisler (1). Crystals of this compound suitable for diffraction purposes were grown from *n*-heptane at room temperature, mp 143–144 °C, literature value 129.5–132.5 °C (1). Proton magnetic resonance, infrared and mass spectra were consistent with 1,1-bis(diphenylphosphino)-2,2-dimethylhydrazine.

Crystal Structure Analysis

Crystal data are as follows:

$[(C_6H_5)_2P]_2NN(CH_3)_2$ f.w. = 428.5

Monoclinic, $a = 8.910(1)$, $b = 9.686(1)$, $c = 27.489(4)$ Å, $\beta = 102.94(2)°$, $V = 2312.1$ Å^3, $\rho_{obs} = 1.23$ g cm^{-3}, $Z = 4$, $\rho_{calc} = 1.231$ g cm^{-3}, (23 °C, CuK$_{\alpha 1}$, $\lambda = 1.54051$ Å).

Preliminary photographic data showed the crystals to be monoclinic with the following systematic absences: $h0l$, $l = 2n + 1$; $0k0$, $k = 2n + 1$. These absences indicate the space group is $P2_1/c$. The unit cell dimensions and their standard deviations were obtained from a least-square refinement of 12 independent reflections.[1]

A crystal (0.23 × 0.27 × 0.27 mm) was mounted with the *b* axis nearly parallel to the ϕ axis of the diffractometer, a Picker FACS-1 automated diffractometer with a graphite monochromator. Data were collected by the θ–2θ scan technique using a scan range of 1.75° and a rate of 1° min^{-1}. Stationary background counts were taken for 20 s at either side of the scan range. Intensities were measured with a scintillation counter. Since the instrument has no attenuators, the reflections below $2\theta = 30°$ were measured with the X-ray tube operating at reduced amperage. The take-off angle of the X-ray tube was 3.0°.

Two complete octants of data were measured, hkl and

[1]Crystal orientation, centering of reflections, least-squares refinement of cell parameters and orientation parameters, and the θ–2θ scan were all performed using the programs written originally by Busing and Levy (2) and adapted by the Picker Corporation to the PDP8/E computer which forms part of the FACS-1 system.

Can. J. Chem. Downloaded from www.nrcresearchpress.com by 210.87.254.105 on 09/05/12
For personal use only.

Can. J. Chem. Downloaded from www.nrcresearchpress.com by 210.87.254.105 on 09/05/12
For personal use only.

$\bar{h}\bar{k}l$ in the 2θ range from 5–120°. Three reflections, 2 1 15, 2 $\bar{6}$ 3, and $\bar{1}$ $\bar{5}$ 12, were monitored every 30 reflections. There was a decrease in intensity of 2 1 15 by 20%, 2 $\bar{6}$ 3 by 19%, and $\bar{1}$ $\bar{5}$ 12 by 18%. The decrease appeared to be linear and corrections were applied as such. The linear absorption coefficient for CuK_α radiation $\mu = 17.92$ cm^{-1}. An absorption correction was applied to the data using a $4 \times 4 \times 4$ grid[2] and the transmission factors ranged from 0.618 to 0.703. Lorentz and polarization corrections were applied using the expression $(L_p)^{-1} = (\sin 2\theta)(1+\cos^2 2\theta_m)/(\cos^2 2\theta_m + \cos^2 2\theta)$ where $2\theta_m$ is the monochromator setting angle.

Of the 3442 independent reflections collected, 2669 reflections for which $I > 3\sigma(I)$ were considered observed.

$$\sigma(I) = \left[\text{total} + 0.25\left(\frac{t_s}{t_b}\right)^2 (B_1 + B_2) + (0.03I)^2\right]^{1/2}$$

where total is the total count of the scan, B_1 and B_2 are background counts, I is net count, t_s is total scan time and t_b = single background time.

The structure was determined by the application of symbolic addition procedures (4). The phosphorus, nitrogen, and methyl carbon atoms as well as two of the four phenyl rings were found in the E-map. A structure factor calculation based on these atoms led to a conventional R factor of 0.435 where $R = \sum||F_o| - |F_c||/\sum F_o$. Temperature and scale factors were taken from the Wilson plot. A three-dimensional electron density map calculated at this point indicated the positions of the remaining carbon atoms. Block diagonal least-squares refinement with isotropic thermal parameters and unit weights converged at $R = 0.096$. The function minimized was $\sum\omega(|F_o| - |F_c|)^2$. A difference electron density map indicated clearly the positions of all 26 hydrogen atoms. Each hydrogen atom had an electron density of between 0.3 and 0.5 e Å^{-3}.

The refinement was continued with anisotropic thermal parameters for all non-hydrogen atoms and isotropic thermal parameters for the six methyl hydrogen atoms. The phenyl hydrogen atoms were not refined, but assigned to calculated positions with a C—H bond length of 0.95 Å and $B = 5.0$ Å^2. The weighting scheme used was

$$\omega = \frac{1}{(\sigma_F)^2}$$

where

$$\sigma_F = \frac{k}{2(L_p \times I)^{1/2}}\,\sigma(I)$$

where k is a scale factor. Continued block diagonal refinement on observed reflections only converged (shifts $< 0.3\sigma$) with $R = 0.032$ and $R_\omega = 0.048$ where

$$R_\omega = \left[\frac{\sum\omega(|F_o| - |F_c|)^2}{\sum\omega(F_o)^2}\right]^{1/2}$$

The final "goodness of fit", defined as $[\sum\omega(|F_o| - |F_c|)^2/(m-n)]^{1/2}$ was 1.87 where m = number of observations and n = number of refined parameters.

[2]The programs used in the data reduction, solution and refinement are local modifications of the programs of Ahmed *et al.* (3). All computations were performed on the CDC 6400 computer at Dalhousie University.

A final difference electron density map was featureless with the highest residual electron density of 0.2 e Å^{-3} in the vicinity of the phosphorus atoms. There were no trends in the quantity $\sum\omega(|F_o| - |F_c|)^2$ as a function of $|F_o|$, sin 2θ or $|h|$.

The scattering curves for neutral P, N, C, and H atoms were taken from the compilation of Hanson *et al.* (5). No corrections for $\Delta f'$ and $\Delta f''$ were made.

Results and Discussion

A drawing of the molecule of 1,1-bis(diphenylphosphino)-2,2-dimethylhydrazine projected on to the plane containing the phosphorus and nitrogen atoms is shown in Fig. 1. The atom notation is indicated in this figure. Table 1 contains the list of final fractional co-ordinates and thermal parameters for all atoms except the phenyl hydrogen atoms. The final observed and calculated structure factors with weights based on these positional and thermal parameters are available from the Depository of Unpublished Data.[3] Table 2 is a list of calculated bond lengths and angles with standard deviations.

The molecule consists of two diphenylphosphino groups attached to one of the hydrazine nitrogen atoms and the two methyl groups to the other. The $\begin{matrix}P(2)\\P(1)\end{matrix}\!\!>$N(1)—N(2) framework may be described as nearly planar with N(1) only 0.026(2) Å out of the plane described by P(1), P(2), and N(2). The equation of the plane is

$$0.1347X - 0.9335Y - 0.3324Z + 3.7990 = 0$$

where X, Y, and Z are an orthogonal set of axes, X along a, Y in the ab plane, and Z along c^*. The average P—N bond length 1.715 ± 0.014 Å is significantly shorter than the accepted P—N single bond length of 1.77 Å in $NaPO_3NH_3$ (6). Delocalization of the lone-pair electrons of N(1) into empty phosphorus d-orbitals would account for the shorter bond. The decrease in bond length is not as dramatic as in other examples of P—N bonds with the atoms in the same valence state, *e.g.* F_2P—$N(CH_3)_2$ (7) where P—N is 1.628 Å. In our case, the delocalization takes place over 2 P—N bonds. The near planarity of the P and N atoms is consistent with the delocalization of the nitrogen lone-pair electrons. The P—N—P angle is 126.31(5)° and is substantially larger than

[3]Tabular data are available, at a nominal charge, from the Depository of Unpublished Data, CISTI, National Research Council of Canada, Ottawa, Canada K1A 0S6.

Can. J. Chem. Downloaded from www.nrcresearchpress.com by 210.87.254.105 on 09/05/12
For personal use only.

TABLE 1. Positional and thermal parameters* for $[(C_6H_5)_2P]_2NN(CH_3)_2$

(*a*) Non-hydrogen atoms

Atom	*x*	*y*	*z*	U_{11}†	U_{22}	U_{33}	U_{12}	U_{13}	U_{23}
P(1)	0.40127(7)	0.30093(7)	0.16022(2)	361(3)	451(4)	409(4)	8(3)	62(3)	28(3)
P(2)	0.46912(7)	0.41411(7)	0.06346(2)	417(4)	442(4)	421(4)	−12(3)	112(3)	16(3)
N(1)	0.3478(2)	0.3560(2)	0.09989(6)	366(10)	496(11)	425(11)	3(9)	63(9)	43(9)
N(2)	0.1841(2)	0.3611(2)	0.07757(7)	384(11)	599(13)	498(11)	31(10)	48(9)	11(10)
C(1)	0.1412(3)	0.2711(3)	0.03430(10)	594(17)	749(20)	559(15)	−109(15)	27(14)	−43(15)
C(2)	0.1349(3)	0.5031(3)	0.06554(10)	641(16)	693(19)	708(19)	240(16)	74(15)	68(16)
C(3)	0.2805(3)	0.3998(2)	0.19347(8)	463(14)	449(14)	410(15)	−31(12)	101(11)	29(11)
C(4)	0.3554(3)	0.4825(3)	0.23277(9)	569(16)	599(17)	501(15)	−99(14)	117(13)	−25(13)
C(5)	0.2740(3)	0.5657(3)	0.25867(10)	810(20)	714(20)	586(19)	−142(16)	234(16)	−176(16)
C(6)	0.1159(3)	0.5677(3)	0.24556(10)	837(20)	621(19)	681(19)	20(16)	368(16)	−65(16)
C(7)	0.0386(3)	0.4852(3)	0.20713(9)	569(16)	705(19)	570(15)	51(14)	213(14)	22(15)
C(8)	0.1194(3)	0.4013(3)	0.18161(9)	493(15)	604(17)	482(15)	−26(13)	111(12)	−28(13)
C(9)	0.3159(3)	0.1284(2)	0.15805(8)	425(14)	461(14)	482(15)	55(12)	79(12)	53(11)
C(10)	0.2449(3)	0.0789(3)	0.19460(9)	556(16)	534(16)	589(15)	6(13)	172(13)	40(13)
C(11)	0.1985(3)	−0.0575(3)	0.19468(10)	679(18)	552(17)	807(19)	−28(15)	278(16)	80(16)
C(12)	0.2208(3)	−0.1468(3)	0.15823(11)	809(20)	475(16)	880(23)	−38(15)	238(17)	30(16)
C(13)	0.2916(4)	−0.1000(3)	0.12201(11)	1186(26)	475(18)	743(19)	39(17)	337(19)	−32(15)
C(14)	0.3409(3)	0.0358(3)	0.12234(10)	872(20)	503(17)	632(19)	82(15)	288(16)	40(14)
C(15)	0.6083(3)	0.2747(2)	0.06494(9)	460(14)	450(15)	563(15)	−52(12)	182(12)	−32(12)
C(16)	0.7270(3)	0.2420(3)	0.10572(10)	559(16)	560(17)	700(19)	34(14)	127(14)	−39(14)
C(17)	0.8264(3)	0.1337(3)	0.10320(12)	649(19)	596(18)	953(23)	119(16)	148(17)	69(17)
C(18)	0.8095(4)	0.0580(3)	0.06017(12)	915(23)	547(18)	113(27)	156(17)	408(20)	−22(18)
C(19)	0.6946(4)	0.0892(3)	0.01998(12)	1257(29)	712(22)	884(23)	190(20)	323(21)	−256(19)
C(20)	0.5945(3)	0.1974(3)	0.02205(10)	844(21)	683(19)	639(19)	79(17)	155(16)	−148(16)
C(21)	0.5885(3)	0.5448(2)	0.10124(8)	466(14)	389(13)	509(15)	−5(11)	102(12)	40(11)
C(22)	0.5455(3)	0.6163(3)	0.13943(10)	711(18)	511(17)	716(19)	−66(14)	280(16)	−59(14)
C(23)	0.6341(4)	0.7247(3)	0.16345(11)	955(23)	542(18)	773(19)	−73(17)	259(17)	−161(16)
C(24)	0.7662(3)	0.7632(3)	0.14901(11)	783(21)	494(17)	899(23)	−123(15)	45(17)	−94(16)
C(25)	0.8096(3)	0.6944(3)	0.11078(11)	602(18)	607(18)	987(23)	−138(15)	187(17)	−16(17)
C(26)	0.7223(3)	0.5864(3)	0.08723(10)	577(16)	533(17)	689(19)	−51(14)	185(14)	−18(14)

(*b*) Hydrogen atoms

Atom	*x*	*y*	*z*	*U*‡
H(1A)	0.191(3)	0.299(3)	0.0067(9)	40(8)
H(1B)	0.024(3)	0.278(2)	0.0222(9)	35(7)
H(1C)	0.169(3)	0.169(2)	0.0427(9)	43(8)
H(2A)	0.014(3)	0.503(3)	0.0544(10)	60(9)
H(2B)	0.183(3)	0.545(3)	0.0375(9)	42(8)
H(2C)	0.161(3)	0.562(3)	0.0961(9)	36(7)

*The form of the anisotropic vibration is $\exp[-2\pi^2(a^{*2}h^2U_{11} + \ldots + 2a^*b^*hkU_{12} + \ldots)]$.
†$U_{ij} \times 10^4$.
‡$U \times 10^3$ Å^2.

TABLE 2. Interatomic distances and angles (esd's in parentheses)

Atoms	Distance (Å)	Atoms	Angle (deg)
P(1)—N(1)	1.705(2)	N(1)—P(1)—C(3)	104.8(1)
P(2)—N(1)	1.724(2)	N(1)—P(1)—C(9)	103.3(1)
N(1)—N(2)	1.451(3)	C(3)—P(1)—C(9)	101.9(1)
N(2)—C(1)	1.455(3)	N(1)—P(2)—C(15)	104.9(1)
N(2)—C(2)	1.459(4)	N(1)—P(2)—C(21)	104.9(1)
P(1)—C(3)	1.831(2)	C(15)—P(2)—C(21)	101.2(1)
P(1)—C(9)	1.831(2)	P(1)—N(1)—P(2)	126.31(5)
P(2)—C(15)	1.828(2)	P(1)—N(1)—N(2)	117.2(1)
P(2)—C(21)	1.821(2)	P(2)—N(1)—N(2)	116.4(1)
C(3)—C(4)	1.390(3)	N(1)—N(2)—C(1)	112.4(1)
C(4)—C(5)	1.384(4)	N(1)—N(2)—C(2)	110.5(2)
C(5)—C(6)	1.374(4)	C(1)—N(2)—C(2)	111.6(2)
C(6)—C(7)	1.379(4)	P(1)—C(3)—C(4)	117.1(2)
C(7)—C(8)	1.378(4)	P(1)—C(3)—C(8)	125.2(1)
C(8)—C(3)	1.399(3)	P(1)—C(9)—C(10)	123.0(2)
C(9)—C(10)	1.387(3)	P(1)—C(9)—C(14)	118.9(1)
C(10)—C(11)	1.385(4)	P(2)—C(15)—C(16)	125.1(1)
C(11)—C(12)	1.371(4)	P(2)—C(15)—C(20)	116.9(2)
C(12)—C(13)	1.370(4)	P(2)—C(21)—C(22)	123.8(2)
C(13)—C(14)	1.386(4)	P(2)—C(21)—C(26)	118.1(1)
C(14)—C(9)	1.385(4)	C(8)—C(3)—C(4)	117.7(2)
C(15)—C(16)	1.395(4)	C(3)—C(4)—C(5)	121.3(2)
C(16)—C(17)	1.384(4)	C(4)—C(5)—C(6)	119.8(2)
C(17)—C(18)	1.371(5)	C(5)—C(6)—C(7)	120.0(2)
C(18)—C(19)	1.362(5)	C(6)—C(7)—C(8)	120.2(2)
C(19)—C(20)	1.385(5)	C(7)—C(8)—C(3)	120.9(2)
C(20)—C(15)	1.379(4)	C(14)—C(9)—C(10)	117.5(2)
C(21)—C(22)	1.382(4)	C(9)—C(10)—C(11)	121.0(2)
C(22)—C(23)	1.388(4)	C(10)—C(11)—C(12)	120.6(2)
C(23)—C(24)	1.375(4)	C(11)—C(12)—C(13)	119.2(2)
C(24)—C(25)	1.371(4)	C(12)—C(13)—C(14)	120.4(2)
C(25)—C(26)	1.376(4)	C(13)—C(14)—C(9)	121.2(2)
C(26)—C(21)	1.392(3)	C(20)—C(15)—C(16)	118.1(2)
C(1)—H(1A)	1.00(2)	C(15)—C(16)—C(17)	120.7(2)
C(1)—H(1B)	1.02(3)	C(16)—C(17)—C(18)	120.0(2)
C(1)—H(1C)	1.03(3)	C(17)—C(18)—C(19)	119.9(2)
C(2)—H(2A)	1.05(3)	C(19)—C(20)—C(15)	120.7(2)
C(2)—H(2B)	1.04(2)	C(26)—C(21)—C(22)	117.7(2)
C(2)—H(2C)	1.00(3)	C(21)—C(22)—C(23)	121.0(2)
		C(22)—C(23)—C(24)	120.0(2)
		C(23)—C(24)—C(25)	119.8(2)
		C(24)—C(25)—C(26)	120.2(2)
		C(25)—C(26)—C(21)	121.3(2)
		N(2)—C(1)—H(1A)	112(1)
		N(2)—C(1)—H(1B)	107(1)
		N(2)—C(1)—H(1C)	113(1)
		N(2)—C(2)—H(2A)	107(1)
		N(2)—C(2)—H(2B)	112(1)
		N(2)—C(2)—H(2C)	110(1)
		H(1A)—C(1)—H(1B)	109(2)
		H(1A)—C(1)—H(1C)	107(2)
		H(1B)—C(1)—H(1C)	108(2)
		H(2A)—C(2)—H(2B)	110(2)
		H(2A)—C(2)—H(2C)	106(2)
		H(2B)—C(2)—H(2C)	110(2)

the ideal trigonal planar angle. Figure 1 shows quite clearly that the large P—N—P angle is not due to steric factors. A large angle at nitrogen has been reported in the structure of tetraphenylhydrazine $(C_6H_5)_2NN(C_6H_5)_2$ (8, 9). In this case, the delocalization of the nitrogen lone-pair elec-

Can. J. Chem. Downloaded from www.nrcresearchpress.com by 210.87.254.105 on 09/05/12
For personal use only.

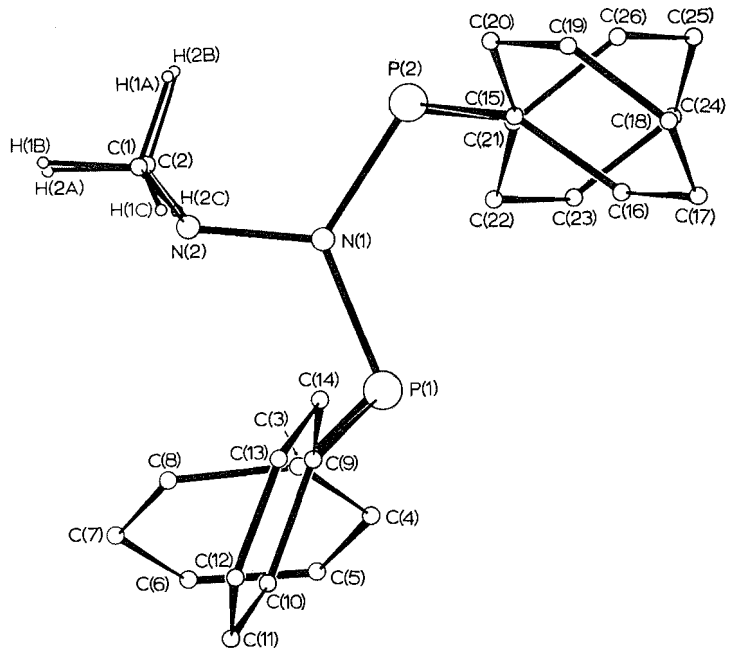

FIG. 1. A view of the molecule $[(C_6H_5)_2P]_2NN(CH_3)_2$ projected onto the P(1)—P(2)—N(2) plane.

trons makes the C—N and N—N bond lengths shorter than normal single bond lengths and an almost planar molecule. Here, the bulky phenyl groups contribute to the large C—N—C angle. In $[(C_6H_5)P_2]_2NN(CH_3)_2$, the large P—N—P angle can be rationalized from VSEPR theory (10). The electronegativity of N(2) is greater than that of the P atoms and bond angles increase with decreasing ligand electronegativity.

The N—N bond, 1.451(3), is the same within standard deviations as that found for H_2NNH_2 by electron-diffraction, 1.449(4) (11) (Table 2). The average N—methyl bond is 1.457 ± 0.003 Å and the N—N—C angle is 111.5 ± 1.3°. This indicates a slightly distorted tetrahedral arrangement of atoms about N(2).

The 24 independent C—C distances in the phenyl rings range from 1.362 to 1.399 Å averaging 1.381 ± 0.008 Å, as compared to the accepted C—C (aromatic) value of 1.394 ± 0.005 (12). The C—C—C angles range from 117.5° to 121.3° average 120.0 ± 1.3°. The internal angles at the P-bonded carbon atoms are consistently less than 120°, averaging 117.8 ± 0.2°. This deviation from D_{6h} symmetry has been noted in other phenylphosphorus compounds (13, 14). The average P—C bond is 1.828 ± 0.005 Å.

TABLE 3. Shortest intermolecular distances

From atom in x,y,z	To atom	In position	Distance (Å)
H(C17)	H(C8)	1+x,y,z	2.64
H(C26)	H(2A)	1+x,y,z	2.40
H(1C)	H(C19)	1−x,−y,−z	2.64
H(C19)	H(C14)	1−x,−y,−z	2.54
H(1A)	H(C26)	1−x,1−y,−z	2.55
H(C12)	H(2C)	x,−1+y,z	2.56
H(C6)	H(C17)	1−x,½+y,½−z	2.87
H(C10)	H(C6)	−x,−½+y,½−z	2.73
H(C11)	H(C7)	−x,−½+y,½−z	2.58

Each phenyl ring is planar, rms deviation from planarity being 0.007 Å for C(3)—C(8), 0.008 Å for C(9)—C(14), 0.002 Å for C(15)—C(20), and 0.003 Å for C(21)—C(26). P(2) is essentially coplanar with phenyl ring C(15)—C(20) (deviation is 0.007 Å), but is displaced from the C(21)—C(26) plane by 0.18 Å. P(1) is displaced from the C(3)—C(8) and C(9)—C(14) planes by 0.09 and 0.19 Å respectively.

The dihedral angles of the phenyl rings attached to P(1) and P(2) are 65.2 and 69.8° respectively.

Figure 2 is a projection of the structure on to the *ac* plane. There is no evidence for any C—H

Can. J. Chem. Downloaded from www.nrcresearchpress.com by 210.87.254.105 on 09/05/12
For personal use only.

Can. J. Chem. Downloaded from www.nrcresearchpress.com by 210.87.254.105 on 09/05/12
For personal use only.

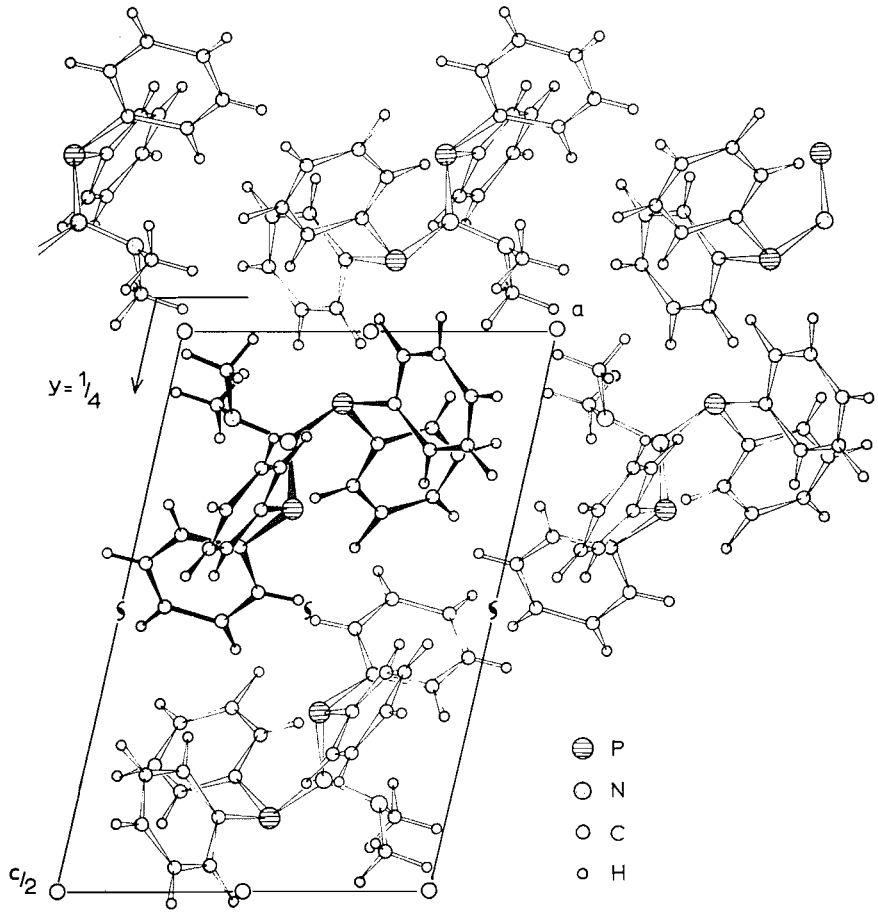

FIG. 2. Packing diagram of $[(C_6H_5)_2P]_2NN(CH_3)_2$, projected onto the *ac* plane. The atoms in the molecule with the filled in bonds correspond to those listed in Table 2.

. . . N hydrogen bonds. Table 3 lists the shortest intermolecular distances.

1. R. P. NIELSEN and H. H. SISLER. Inorg. Chem. **2**, 753 (1962).
2. W. R. BUSING and H. A. LEVY. Acta Crystallogr. **22**, 457 (1967).
3. F. R. AHMED, S. R. HALL, M. E. PIPPY, and C. P. HUBER. NRC-Crystallographic programs for the IBM/360 System. National Research Council of Canada, 1970.
4. J. KARLE and I. L. KARLE. Acta Crystallogr. **21**, 849 (1966).
5. H. P. HANSON, F. HERMAN, J. D. LEA, and S. SKILMAN. Acta Crystallogr. **17**, 1040 (1964).
6. D. W. J. CRUICKSHANK. Acta Crystallogr. **17**, 671 (1964).
7. E. D. MORRIS, JR. and C. E. NORDMAN. Inorg. Chem. **8**, 1673 (1969).
8. A. HOEKSTRA, A. VOS, P. B. BRAUN, and J. HORNSTRA. Acta Crystallogr. B**31**, 1708 (1975).
9. A. HOEKSTRA and A. VOS. Acta Crystallogr. B**31**, 1722 (1975).
10. R. J. GILLESPIE. Molecular geometry. VAN NOSTRAND-REINHOLD, London. 1972.
11. Y. MORINO, T. IIJIMA, and Y. MURATA. Bull. Chem. Soc. Jpn. **33**, 46 (1960).
12. L. E. SUTTON. *In* Tables of interatomic distances and configuration in molecules and ions. Chem. Soc. Spec. Publ. No. **18**, S16S (1975).
13. M. R. CHURCHILL and S. W.-Y. CHANG. Inorg. Chem. **14**, 98 (1975).
14. A. DOMENICANO, A. VACIAGO, and C. A. COULSON. Acta Crystallogr. B**31**, 1630 (1975).

Molecular structure effects on electron ranges and mobilities in liquid hydrocarbons: chain branching and olefin conjugation: mobility model[1]

J.-P. DODELET, K. SHINSAKA, AND G. R. FREEMAN
Chemistry Department, University of Alberta, Edmonton, Alberta T6G 2G2

Received June 20, 1975

J.-P. DODELET, K. SHINSAKA, and G. R. FREEMAN. Can. J. Chem. **54**, 744 (1976).

The effect of molecular structure on electron behavior in liquids was studied by measuring secondary electron penetration ranges b_{GP} and thermal electron mobilities u_e in substituted methanes and ethylenes. The penetration ranges are smaller (energy transfer cross sections are larger) when the alkane molecules are less rigid. It was confirmed that the epithermal electron energy transfer interaction radius in a liquid phase alkane molecule is limited to two C—C bonds in series. This modifies the earlier noted correlation between b_{GP} and the degree of sphericity of the molecules. For example, the density normalized range $b_{GP}d$ in the relatively sphere-like tetraethylmethane (54×10^{-8} g/cm^2) is more similar to that in the distinctly non-spherical diethylmethane (*n*-pentane, 43×10^{-8} g/cm^2) than to that in the sphere-like tetramethylmethane (126×10^{-8} g/cm^2). Tetraethylmethane is too large for the entire molecule to interact with an electron in the liquid phase, and the possibility of rotations about the C—C bonds in the ethyl groups makes the molecule less rigid. Electrons sense these relatively sphere-like molecules to be similar to those of a *n*-alkane. Connecting *tert*-butyl groups to olefinic or acetylenic carbons creates sphere-like quasi neopentyl groups which greatly enhance electron ranges in the unsaturated compounds. In conjugated olefins *cis–trans* effects are largely overshadowed by the general efficiency of these compounds as electron energy sinks. The earlier noted correlation between b_{GP} and u_e contains fine structure. For a given value of b_{GP}, u_e increases in the order *n*-alkane < cyclo or branched alkane < olefin. Electron mobilities are interpreted in terms of a model that contains a Gaussian distribution of solvated electron state energies, a conduction band, and thermally activated transitions between them. The model is a combination of our treatment of electrons in ethers and Schiller's treatment of electrons in hydrocarbons. The percolation model does not provide a sufficiently complete interpretation of electron migration in hydrocarbons.

J.-P. DODELET, K. SHINSAKA et G. R. FREEMAN. Can. J. Chem. **54**, 744 (1976).

L'effet de la structure moléculaire sur le comportement des électrons en excès dans les liquides a été étudié en mesurant, pour différentes substitutions du méthane et de l'éthylène, le parcours des électrons secondaires, b_{GP}, et les mobilités des électrons thermalisés, u_e. Lorsque les molécules d'alcanes perdent leur rigidité, les parcours électroniques sont plus courts. La probabilité de transfert d'énergie par l'électron épithermique est donc plus importante. Le rayon d'interaction de ce dernier avec les molécules d'alcanes a été confirmé à deux liens C—C en série. Ceci modifie la corrélation précédente entre b_{GP} et le degré de sphéricité des molécules. Par exemple, le parcours, normalisé pour la densité, ($b_{GP}d = 54 \times 10^{-8}$ g/cm^2) dans le tetraéthylméthane ressemble plus au parcours électronique dans le *n*-pentane (43×10^{-8} g/cm^2) qu'à celui dans le tetraméthylméthane (126×10^{-8} g/cm^2). L'électron voit le tetraéthylméthane, une molécule quasi sphérique, comme il voit un alcane normal. Ceci est dû à la grandeur de la molécule qui ne permet pas une interaction globale, ainsi qu'à la possibilité de rotation autour des liens C—C des groupements éthyles, qui rendent cette molécule moins rigide. Lorsqu'un groupement tertiobutyle est attaché à un carbone oléfinique ou acétylénique, la molécule resultante contient un groupement quasi néopentyle ce qui accroît considerablement le parcours de l'électron dans ces liquides non saturés. L'effet *cis–trans* observé pour les oléfins conjuguées est pratiquement masqué par l'efficacité de ces molécules en tant que récepteurs d'énergie. La corrélation entre b_{GP} et u_e, mentionnée précédemment, contient une structure fine. Pour une valeur de b_{GP} donnée, u_e augmente dans l'ordre suivant: *n*-alcane < alcane cyclique ou ramifié < oléfine. Les mobilités électroniques sont interprétées en fonction d'un modèle qui comporte une répartition gaussienne des états d'énergie pour l'électron solvaté, une bande de conduction et des transitions, fonctions de la température, entre ces deux états. Ce modèle est une combinaison de notre traitement des électrons dans les éthers et du traitement de Schiller pour les électrons dans les hydrocarbures. Le modèle de percolation n'apporte pas une interprétation complète de la migration électronique dans les hydrocarbures.

[1]Assisted financially by the National Research Council of Canada.

Can. J. Chem. Downloaded from www.nrcresearchpress.com by 210.87.254.5 on 09/05/12
For personal use only.

Can. J. Chem. Downloaded from www.nrcresearchpress.com by 210.87.254.5 on 09/05/12
For personal use only.

Introduction

The ease of penetration of low energy electrons into liquids depends on the nature of the compound (1–9). Penetration ranges are shorter when the electrons are more quickly de-energized, and vice versa. However, the properties that govern these processes are not clearly known. In small alkanes the range increases with increasing degree of sphericity of the molecule (7, 9), but the basic reason for it remains to be discovered. The properties that govern penetration in unsaturated hydrocarbons are obscure (5).

In the present article, ranges are reported and compared for several different geometries of open chain saturated and unsaturated hydrocarbons. For example, the range is large in the globular compound tetramethylmethane (2,2-dimethylpropane) (1, 2, 7). How much smaller is it in the somewhat less globular tetraethylmethane (3,3-diethylpentane)? One suspects that it is much smaller in the latter, because the relatively short energy transfer interaction distance of electrons in liquids (7) should prevent the electron from sensing the entire tetraethylmethane molecule. The range in tetraethylmethane might therefore be closer to that in diethylmethane (*n*-pentane) than to that in tetramethylmethane.

Furthermore, electron penetration into liquid olefins and acetylenes is affected by whether or not the unsaturated group is terminal and by the overall shape of the molecule (5). To get more information about the behavior of electrons in unsaturated liquids, two series of experiments were done. The first was to try to partially shield the multiple bond with the large *tert*-butyl group. The second was to associate double bonds with each other in different geometries of polyolefins.

The mobilities of thermal electrons were also measured where possible. The results are interpreted in terms of a model for electron migration in liquid hydrocarbons.

Experimental

Materials

The purities of the hydrocarbons obtained from the suppliers were ≥99%, unless otherwise mentioned.

The 2-methylpropane, *n*-pentane, and 2,2-dimethylbutane were Phillips Research Grade. The 2-methylpentane (≥98%), 3-methylpentane (≥98%), 2,3-dimethylbutane (97%), and 1,3,5-hexatriene were from Aldrich Chemicals. The 3-ethylpentane, 3,3-dimethylpentane, 3,3-diethylpentane, 2,2,5,5-tetramethyl-3-hexyne, *cis,cis*-2,4-hexadiene (98%), and *trans,trans*-2,4-hexadiene were from Chemical Samples. Chemical Procurement Labs supplied 3,3-dimethyl-1-butene, 2-methyl-2-butene, 4,4-dimethyl-*cis*-2-pentene, 4,4-dimethyl-*trans*-2-pentene, and 2,2,5,5-tetramethyl-*trans*-3-hexene, all Research Grade.

Each saturated hydrocarbon except 2-methylpropane was shaken at room temperature (~22 °C) overnight with concentrated sulfuric acid. The separated hydrocarbon was then shaken with solid barium carbonate to remove traces of acid, then decanted onto lithium aluminum hydride in a bulb attached to a vacuum rack. The bulb was closed by inserting a Teflon plug (with O rings of Viton A) into the glass barrel of the large stopcock on the filling tube. The liquid was pumped on to partially remove air and carbon dioxide by boiling. The bulb was then cooled in liquid nitrogen, evacuated to $<10^{-3}$ Torr, then closed from the vacuum and warmed. The contents were magnetically stirred for several hours. The hydrocarbon was then distilled onto sodium–potassium alloy and stirred for ≥10 h.

2-Methylpropane was stirred in a closed bulb on the vacuum system with concentrated sulfuric acid for 18 h at ~15 °C, then distilled successively onto potassium hydroxide pellets, lithium aluminum hydride powder, and sodium–potassium liquid alloy, and stirred with each for 2–3 h at ~5 °C.

The mono-olefins were stirred successively with the hydroxide, hydride, and alloy, all in bulbs on the vacuum line.

Alkynes and conjugated olefins react with sodium–potassium alloy, so after treatment with lithium aluminum hydride they were distilled into an electrolysis cell and electrolyzed at 1.1 kV/cm for ≥10 h.

The liquids were thoroughly degassed during rapid distillations in the vacuum system, while continually pumping the collection traps. Each compound was finally condensed into the conductance cell which was sealed off after the pressure at 77 K had been reduced to less than 5×10^{-6} Torr. The final criterion of purity for liquids that do not react with electrons was to have an electron conductance transient with a decay half life of ~1 μs. In some cases it was much longer than that.

Apparatus and Techniques

The conductance cells and methods of measuring radiolysis free ion yields and electron mobilities were the same as those described in refs. 5, 10, and 11. Briefly, a 1 μs (or 0.1 μs) pulse of 1.7 MeV X-rays delivered $\sim 5 \times 10^{19}$ (or 1×10^{19}) eV/g to the sample. Free ion yields $G_{fi}{}^{E}$ were measured at electric field strengths E between 2 and 20 kV/cm, using the charge clearing technique. The penetration ranges of the secondary electrons were estimated by fitting a theoretical model (5, 12–14) to the experimental results. Thermal electron mobilities u were usually determined at field strengths between 2 and 20 kV/cm, using the magnitude of the electron conductance transient as a measure of $G_{fi}{}^{E}u$ and taking the ratio $(G_{fi}{}^{E}u/G_{fi}{}^{E}) = u$. The positive ion mobilities were assumed to be negligible compared to those of the electrons.

In some instances electron mobilities were measured by the "ramp method". At the higher field strengths the

TABLE 1. G_{fl}^0 and most probable electron range b_{GP} in hydrocarbon liquids

Liquid	T (K)	d[a] (g/cm³)	ϵ	G_{fl}^0	b_{GP}[b] (Å)	$b_{GP}d$ (10^{-8} g/cm²)	$(b_{GP}d)_{av}$ (10^{-8} g/cm²)
			Alkanes				
2-Methylpropane	169	0.710	2.004[d]	0.12	98	70	65
	188	0.680	1.968	0.15	97	67	
	210	0.660	1.921	0.19	98	65	
	235	0.629	1.869	0.24	100	63	
	252	0.608	1.833	0.29	104	63	
	273	0.581	1.785	0.35	108	63	
	296	0.553	1.727	0.44	117	65	
2,2-Dimethylbutane	186	0.750	2.124[e]	0.26	112	84	80
	214	0.725	2.073	0.32	110	80	
	257	0.683	1.990	0.43	111	76	
	293	0.649	1.926	0.58	120	78	
	324	0.620	1.872	0.71	127	79	
	340	0.604	1.843	0.81	135	82	
2,3-Dimethylbutane	293	0.661	1.95[e]	0.22	74	49	49
n-Pentane	163	0.744	2.045[c]	0.029	57	42	43
	182	0.728	2.015	0.038	57	42	
	204	0.709	1.980	0.056	61	43	
	228	0.688	1.944	0.076	62	43	
	254	0.664	1.904	0.11	68	45	
	293	0.626	1.844	0.17	70	44	
2-Methylpentane	293	0.653	1.88[e]	0.19	71	47	47
3-Methylpentane	293	0.664	1.90[e]	0.18	67	45	45
3-Ethylpentane	179	0.792	2.12[e]	0.038	56	44	46
	214	0.764	2.06	0.064	59	45	
	253	0.731	2.00	0.10	61	44	
	293	0.698	1.94	0.18	67	47	
	332	0.655	1.87	0.26	73	48	
	355	0.647	1.85	0.32	74	48	
3,3-Dimethylpentane	197	0.774	2.08[e]	0.15	85	66	64
	226	0.749	2.04	0.19	86	64	
	254	0.726	1.99	0.25	88	64	
	293	0.693	1.90	0.35	93	64	
	324	0.666	1.89	0.41	93	62	
	357	0.639	1.84	0.53	100	64	
3,3-Diethylpentane	293	0.753	2.02[e]	0.23	73	55	54
	324	0.729	1.97	0.28	74	54	
	354	0.706	1.93	0.34	75	53	
	380	0.686	1.90	0.40	78	54	
			Alkenes				
3,3-Dimethyl-1-butene	237	0.709	2.145[d]	0.12	64	45	48
	253	0.693	2.101	0.16	70	49	
	293	0.653	1.992	0.23	73	48	
	327	0.618	1.899	0.31	80	49	
2-Methyl-2-butene	229	0.730	2.129[d]	0.11	65	48	47
	246	0.712	2.094	0.13	66	47	
	258	0.699	2.064	0.15	68	47	
	277	0.679	2.022	0.19	70	47	
	295	0.660	1.980	0.22	72	48	

Can. J. Chem. Downloaded from www.nrcresearchpress.com by 210.87.254.5 on 09/05/12
For personal use only.

TABLE 1 (*Concluded*)

Liquid	T (K)	d^a (g/cm³)	ϵ	G_{fl}^0	b_{GP}^b (Å)	$b_{GP}d$ (10^{-8} g/cm²)	$(b_{GP}d)_{av}$ (10^{-8} g/cm²)
4,4-Dimethyl-*cis*-2-pentene	168	0.811	2.320[d]	0.072	70	56	56
	215	0.769	2.215	0.13	70	54	
	259	0.731	2.119	0.19	72	53	
	293	0.699	2.044	0.28	78	55	
	322	0.675	1.979	0.35	82	55	
	342	0.657	1.935	0.41	87	57	
	368	0.634	1.877	0.51	93	59	
4,4-Dimethyl-*trans*-2-pentene	293	0.690	1.982[d]	0.21	71	49	51
	314	0.670	1.949	0.26	74	50	
	339	0.648	1.909	0.33	79	51	
	364	0.626	1.869	0.42	85	53	
2,2,5,5-Tetramethyl-	293	0.715[d]	1.97[c]	0.43	102	73	75
trans-3-hexene	329	0.683	1.91	0.56	109	74	
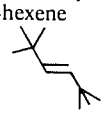	359	0.658	1.87	0.71	109	78	
			Alkyne				
2,2,5,5-Tetramethyl-3-hexyne	293	0.712	1.98[c]	0.47	107	76	78
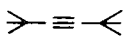	331	0.674	1.91	0.61	114	77	
	359	0.646	1.86	0.72	121	78	
	376	0.628	1.83	0.83	129	81	
			Conjugated olefins				
1,3-Butadiene[f]	269	0.650	2.05	0.038	39	26	27
cis,cis-2,4-Hexadiene	239	0.774	2.281[d]	0.045	41	32	30
	269	0.744	2.220	0.057	41	31	
	292	0.721	2.173	0.070	42	30	
	322	0.691	2.110	0.085	43	29	
	354	0.659	2.042	0.11	44	29	
trans,trans-2,4-Hexadiene	234	0.779	2.250[d]	0.033	38	30	28
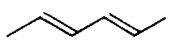	266	0.747	2.186	0.044	38	28	
	293	0.720	2.131	0.056	39	28	
	313	0.700	2.091	0.066	40	28	
	334	0.679	2.049	0.078	41	28	
	353	0.660	2.010	0.096	43	28	
1,3,5-Hexatriene	272	0.753[d]	2.338[d]	0.035	32	24	24
cis and *trans* mixture	293	0.734	2.285	0.043	33	24	
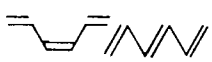	313	0.719	2.243	0.050	33	24	
	333	0.707	2.203	0.057	34	24	
	353	0.699	2.163	0.068	35	24	
1,3-Cyclohexadiene[g]	292	0.842	2.35	0.075	40	34	34
Benzene[h]	292	0.880	2.29	0.081	42	37	38

[a] References 15 and 16.
[b] Based upon the gas phase value $G_{tot} = 4.3$.
[c] Reference 17.
[d] This work.
[e] $\epsilon \simeq n_D^2$. The value of the refractive index n_D at one temperature was obtained from ref. 15 or 18 and the Lorenz–Lorentz equation was used to calculate the values at other temperatures.
[f] Reference 5, using $G_{tot} = 4.0$ for this compound (21).
[g] Reference 27.
[h] Reference 11.

Can. J. Chem. Downloaded from www.nrcresearchpress.com by 210.87.254.5 on 09/05/12
For personal use only.

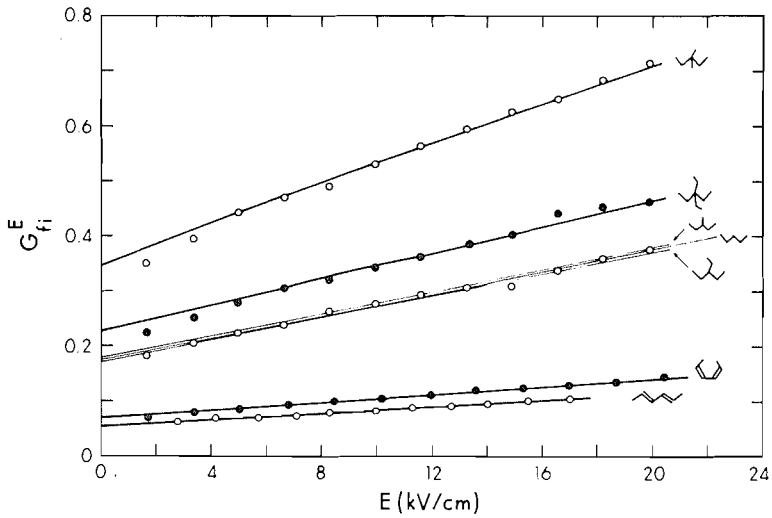

FIG. 1. Free ion yields $G_{fi}{}^E$ as a function of applied electric field strength E at 293 K. Structural representations of the compounds are shown in the figure. The points in the central cluster of curves are for 3-ethylpentane. All curves were calculated from the model, using the parameter values in Table 1.

electron conductance transient signal decayed linearly with time. When the decay is linear the mobility can be obtained from eq. 1.

$$[1] \qquad u = l^2/Vt_d$$

where l is the distance between the electrodes, V is the applied voltage, and t_d is the signal decay time, corresponding to the time required for an electron to drift the distance l.

At field strengths where mobilities could be estimated by both methods the values agreed within 10%.

Physical Properties of the Liquids

The densities d (15, 16) and dielectric constants ϵ (17, 18) were obtained from data in the references quoted or were measured during the present work. Details of the measurements will be published elsewhere, together with extensive tables (19). Relevant values are listed in Table 1.

Total ionization yields in the liquids are not known. For lack of better information they were taken equal to the average gas phase value $G_{tot} = 4.3$ for a number of similar hydrocarbons (20–22).

Results

Free Ion Yields

The yields increase with field strength and temperature in the manner illustrated in Figs. 1 and 2, respectively. The curves were extrapolated to zero field strength to obtain $G_{fi}{}^0$, using eq. 2 (5).

$$[2] \qquad G_{fi}{}^E = G_{tot}\int_0^\infty F(y)\phi(y,E)\mathrm{d}y$$

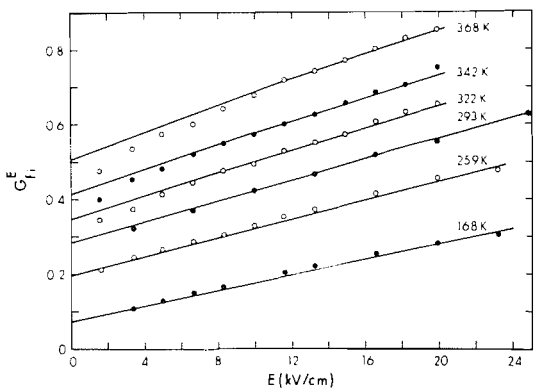

FIG. 2. Free ion yields $G_{fi}{}^E$ as a function of field strength E in 4,4-dimethyl-*cis*-2-pentene at different temperatures. The curves were calculated from the model, using the parameter values in Table 1.

where G_{tot} is the total number of ion–electron pairs generated per 100 eV absorbed by the liquid, $F(y)\mathrm{d}y$ is the fraction of thermalized electron–ion pairs that have initial intrapair separation distances between y and $y + \mathrm{d}y$, and $\phi(y,E)$ is the probability that a pair with a given separation distance y will escape geminate neutralization (become free ions) in the presence of an applied field E.

$$[3] \quad \phi(y,E) = \mathrm{e}^{-r/y} \times\left(1 + \mathrm{e}^{-\beta y}\sum_{n=1}^{\infty}\frac{(\beta y)^n}{(n+1)!}\sum_{j=0}^{n-1}(n-j)\frac{(r/y)^{j+1}}{(j+1)!}\right)$$

Can. J. Chem. Downloaded from www.nrcresearchpress.com by 210.87.254.5 on 09/05/12
For personal use only.

TABLE 2. Thermal electron mobilities (u_e) and activation energies (E_u) in liquid hydrocarbons

Liquid	T (K)	u_e (cm^2 V^{-1} s^{-1})	E_u (kcal/mol)
	Alkanes		
2-Methylpropane	296	7.3	1.8
2,2-Dimethylbutane	295	12.4	1.4
2,3-Dimethylbutane	293	1.1	—
n-Pentane	293	0.15	4.2
2-Methylpentane	293	0.29	—
3-Methylpentane	293	0.18	—
3-Ethylpentane	293	0.10	4.6
3,3-Dimethylpentane	293	2.3	—
3,3-Diethylpentane	293	0.76	—
	Alkenes		
3,3-Dimethyl-1-butene	293	1.9	~3[a]
2-Methyl-2-butene	295	2.8	2.5[b]
2,3-Dimethyl-2-butene[c]	293	5.8	1.2
4,4-Dimethyl-*cis*-2-pentene	293	3.4	2.1
4,4-Dimethyl-*trans*-2-pentene	294	1.7	3.1

[a]Value at $T > 280$ K. E_u increases at lower temperatures.
[b]Value at $T > 240$ K. E_u increases at lower temperatures.
[c]Reference 10, curve redrawn in the present Fig. 3. $E_u > 1.2$ kcal/mol at $T < 270$ K.

where $r = \xi^2/\epsilon kT$, $\xi = 4.803 \times 10^{-10}$ esu, ϵ is the dielectric constant of the liquid, k is Boltzmann's constant, T is the absolute temperature, and $\beta = (\xi E/300kT)$.

The distribution function $F(y)$ was taken to have the form [4], which has been designated YGP (5).

$$[4]\quad \begin{cases} F(y) = 0.96\mathrm{YG} & y < 2.4b_{GP} \\ F(y) = 0.96[\mathrm{YG} + 0.5b_{GP}^2/y^3] & y > 2.4b_{GP} \end{cases}$$

where 0.96 is a normalization factor, YG is the three dimensional Gaussian function $(4y^2/\pi^{1/2}b_{GP}^3)\exp(-y^2/b_{GP}^2)$, while b_{GP} is the dispersion parameter and is also the most probable value of y.

Calculated and experimental yields were compared by calculating the average % error:

$$[5]\quad \text{Average \% error} = 100\sum|G^E_{fi,calc} - G^E_{fi,exp}|/\sum G^E_{fi,exp}$$

Calculations were done with a series of b_{GP} values to find the one that gave the minimum average % error. This value of b_{GP} was then used to calculate G_{fi}^0.

$$[6]\quad G_{fi}^0 = G_{tot}\int_0^\infty F(y)e^{-r/y}dy$$

The calculated curves and experimental points in Figs. 1 and 2 display the extent of agreement obtained under different conditions. The curve parameter values are given in Table 1. The curves pass through the experimental points at the lower temperatures, but the theoretical slope is somewhat smaller than the experimental slope at the highest temperatures (Fig. 2).

The yields at zero field strength and the most probable electron ranges are listed in Table 1 for all the liquids studied.

Yields at 296 K had been reported earlier for *n*-pentane, 2,2- and 2,3-dimethylbutane, 2- and 3-methylpentane (6). The values were lower than the present ones by a factor 1.2 ± 0.1 except in 2,2-dimethylbutane where the factor is 1.9. The reason for the discrepancy is unknown.

Electron Mobilities

Mobilities were measured in the alkanes and mono-olefins, with one exception, and the results are given in Fig. 3 and Table 2. In 2,2,5,5-tetramethyl-*trans*-3-hexene the electrons reacted (probably with impurities) with a half life somewhat smaller than the response time of the measuring circuit, ~50 ns, so an accurate value of the mobility could not be obtained in that liquid.

Electrons react with conjugated polyolefins and with alkynes (or impurities in alkynes). Electron signals were therefore not obtained in these liquids.

Can. J. Chem. Downloaded from www.nrcresearchpress.com by 210.87.254.5 on 09/05/12
For personal use only.

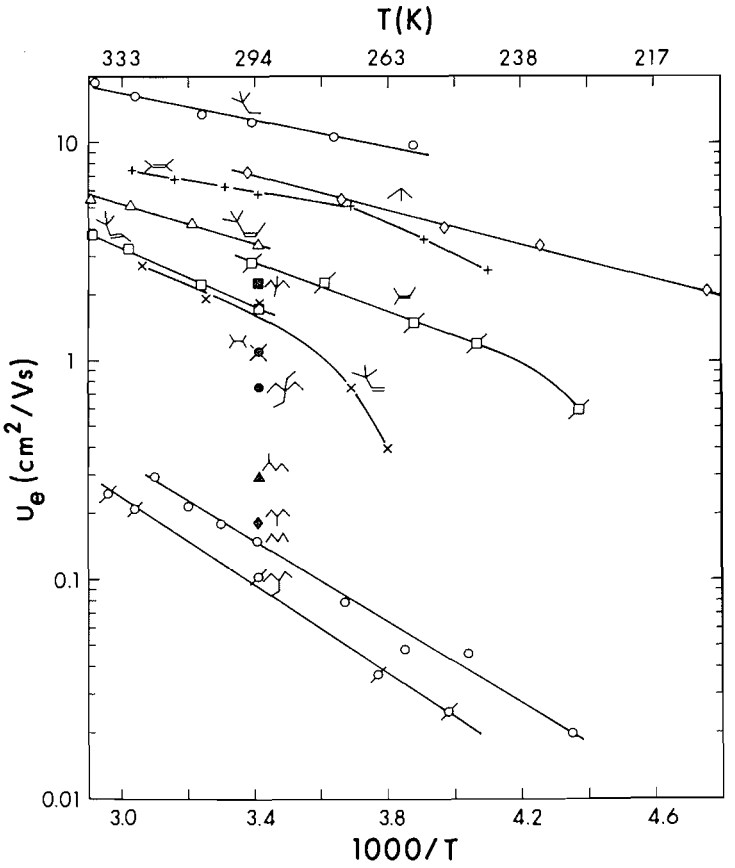

FIG. 3. Electron mobilities in liquid hydrocarbons as functions of the inverse temperature. The compounds are identified on the graph by their carbon skeletal structures. The points for 2,3-dimethyl-2-butene were taken from ref. 10 and the curve was redrawn to display the deviation from linearity at low temperatures and to recalculate the activation energy E_a at high temperatures (Table 2).

The measured mobilities were independent of field strength over the range 2 to 20 kV/cm.

Discussion

Free Ion Yields and Penetration Ranges of Secondary Electrons

To compare the ranges in different liquids, the values of b_{GP} were normalized by multiplying them by the liquid density. The density-normalized range $b_{GP}d$ in a given liquid is essentially independent of temperature (Table 1).

Alkanes

Large free ion yields (and electron ranges) in liquid hydrocarbons have been associated with a high degree of sphericity of the molecules (1, 7), or with the presence of tertiary and, especially, quaternary carbon atoms in the molecules (2, 6). However, the relative effects of methyl and ethyl substitution have not been delineated.

Density-normalized ranges in methyl- and ethyl-substituted methanes are compared in Table 3. Addition of either a methyl or an ethyl group to methane destroys its tetrahedral symmetry and sphere-like shape, and causes the electron range to decrease drastically. Ethyl substitution reduces the range slightly more than does methyl substitution (Table 3). Addition of two methyl or ethyl groups reduces the range somewhat more. Further substitution causes the range to increase again, but the amount of increase is much smaller for ethyl than for methyl (Table 3). The range in tetraethylmethane is approximately equal to those in monoethyl- and monomethylmethane, whereas that in tetramethylmethane is double those values. The

Can. J. Chem. Downloaded from www.nrcresearchpress.com by 210.87.254.5 on 09/05/12
For personal use only.

Can. J. Chem. Downloaded from www.nrcresearchpress.com by 210.87.254.5 on 09/05/12
For personal use only.

TABLE 3. Density normalized ranges in methyl- and ethyl-substituted methanes and ethylenes

Compound	$b_{GP}d$ (10^{-8} g/cm^2) Methyl	Ethyl
Methanes		
Unsubstituted[a]	235	235
Mono-[a]	58	52
Di-	52[a]	43
Tri-	65	46
Tetra-	126[b]	54
Ethylenes		
Unsubstituted[a]	23	23
Mono-	29[a]	33[c]
1,1-Di-[c]	41	—
1,2-Di-*cis*-[c]	46	38
1,2-Di-*trans*-[c]	32	36
Tri-	47(52[d])	—
Tetra-[c]	72	—

[a]Reference 9.
[b]Reference 7.
[c]Reference 5.
[d]Reference 5 corrected for the dielectric constant measured in the present work.

quaternary carbon atom in itself seems to be relatively unimportant in these considerations. The ranges are an inverse function of the electron energy loss cross sections of the liquid molecules acting in concert. The cross section is larger for tetraethylmethane than for tetramethylmethane. This does not result from the relative sizes of the molecules (7), but seems to be related to the lower degree of sphericity and smaller rigidity of the former molecules. The ethyl groups can take different rotational orientations on the molecule, which renders the sphericity less than that of neopentane. In fact, the electron seems to see tetraethylmethane (3,3-diethylpentane) much more like *n*-pentane (diethylmethane) than like neopentane (tetramethylmethane), judging from the relative values of $b_{GP}d$ in Table 3. This is consistent with an earlier conclusion about the myopic character of electrons in liquids (7). The effective interaction distance of an electron with an alkane molecule in the liquid phase encompasses only two C—C bonds in series.

The small influence of tertiary carbon atoms is evidenced by the similarity of $b_{GP}d$ in 2,3-dimethylbutane (49×10^{-8} g/cm^2) and *n*-butane (47×10^{-8} g/cm^2) (9), or in 3-methyl-, 2-methyl-, and *n*-pentane (Table 1).

The fact that $b_{GP}d$ in 3,3-dimethylpentane is greater than that in 3,3-diethylpentane (Table 1) is attributed to the more globular and rigid nature of the former as sensed by the myopic electron.

Alkenes and Alkynes

In liquid ethylene the range is smaller than that in an alkane (9), which indicates that electron energy loss is more efficient in the former than in the latter. Substitution of the ethylenic hydrogens by methyl groups increases the electron range in the liquid olefin, but also gives rise to unexplained structure effects such as that in *cis*- and *trans*-2-butene (Table 3). Replacement of the ethylenic hydrogens by ethyl groups, on the other hand, leads to only a small *cis–trans* effect (Table 3). Rotations in the ethyl groups tend to obscure structural differences between the *cis* and *trans* isomers.

Substitution of the ethylenic hydrogens by *tert*-butyl groups creates quasi neopentyl groups in the molecule and greatly enhances the electron ranges. For example, $b_{GP}d = 47 \times 10^{-8}$ g/cm^2 in *tert*-butylethylene, whereas it is only 29×10^{-8} g/cm^2 in methylethylene (Table 4). The quasi neopentyl group in the former compound is evidently a poor energy sink for the secondary electrons, as is the neopentyl group (7).

Replacement of one of the methyls by a *tert*-butyl group in *cis*- and *trans*-2-butene increases $b_{GP}d$ in the *trans* more than that in the *cis* isomer (Table 4). The *cis–trans* effect is thereby diminished.

Substitution of methyl groups for both hydrogens on acetylene causes $b_{GP}d$ to triple, and substitution of *tert*-butyl groups nearly quadruples it (Table 4). Hydrogenation of the disubstituted acetylenes to *trans*-olefins reduces the normalized range in the dimethyl compound by 50%, but has only a slight effect on that in the di-*tert*-butyl compounds (Table 4). Hydrogenation of the *trans* olefins to alkanes increases the ranges in both liquids by a factor of 1.4 ± 0.1. *cis*-Di-*tert*-butylethylene is unstable due to steric hindrance of the *tert*-butyl groups and could not be studied. However, it is curious that ranges in the *tert*-butyl compounds are greater than those in the dimethyl compounds by nearly the same factor (2.2 ± 0.1) for the *trans* olefins and the alkanes. One might have expected the *tert*-butyl groups to shield the double bond and that the ratio of $b_{GP}d$ values (di-*tert*-butyl/dimethyl) would be much greater in the *trans* olefins than in the alkanes.

The behavior does not fit a simple pattern.

TABLE 4. Effects of methyl and *tert*-butyl substitution and of subsequent hydrogenation on $b_{GP}d$ in unsaturated compounds[a]

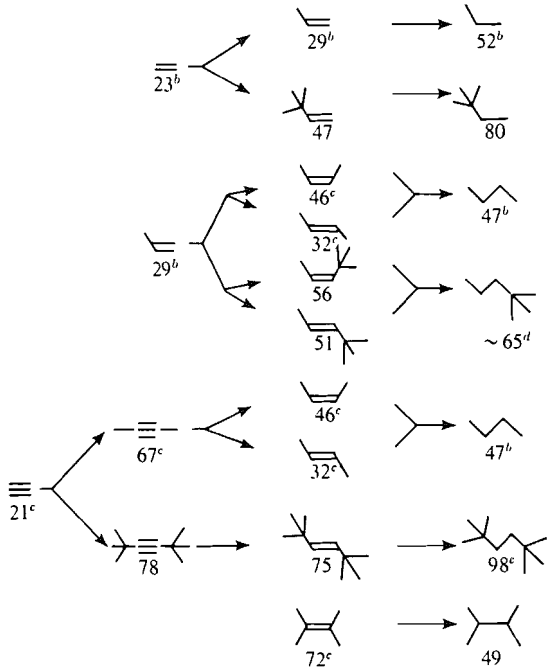

[a]The numbers below the structural diagrams are $b_{GP}d$ in units of 10^{-8} g/cm².
[b]Reference 9. The value of b_{GP} in *n*-butane at 293 K recorded in Table 1 of ref. 9 should read 83 Å (not 93 Å) and $b_{GP}d = 48 \times 10^{-8}$ g/cm² (not 54×10^{-8}).
[c]Reference 5.
[d]Assumed, by comparison with values for other alkanes.
[e]Reference 7.

Another puzzling result is that for the dimethyl compounds the normalized range is greater in the acetylene than in the alkane, whereas the reverse is true in the di-*tert*-butyl compounds (Table 4). Still another is that $b_{GP}d$ in tetramethylethylene is considerably greater than that in the corresponding alkane, whereas the reverse order is normally observed between olefins and alkanes (Table 4 and ref. 5).

Conjugated Olefins

Conjugated olefins have a positive electron affinity (23) and therefore a tendency to form negative ions. Electron spin resonance spectra of anion radicals of conjugated olefins in 2-methyltetrahydrofuran glass at 77 K have been reported (24, 25), and the compounds are efficient electron scavengers in liquid alkanes (26). The interactions of low energy electrons with conjugated olefins are therefore strong and the penetration ranges are short (5).

The *cis–trans* effect is noticeable in 2,4-hexadiene (Table 1), but it is largely overshadowed by the general efficiency of conjugated olefins as electron energy sinks. Electron energy transfer to the *cis,cis* isomer would also be enhanced by the favored extended configuration (as opposed to the possible cyclic configuration) and by the lack of rigidity of the molecule (hindered rotation about the central bond). These influences would diminish the difference between the electron interactions with the *cis* and *trans* isomers. In support of this suggestion, $b_{GP}d = 34 \times 10^{-8}$ g/cm² in 1,3-cyclohexadiene (27) is larger than that in *cis,cis*-2,4-hexadiene (30×10^{-8} g/cm²), and $b_{GP}d = 38 \times 10^{-8}$ g/cm² in benzene (11) is much larger than that in 1,3,5-hexatriene (24×10^{-8} g/cm², Table 1).

The ranges in the nonconjugated olefins propadiene (26×10^{-8} g/cm² (5)) and ethene (23×10^{-8} g/cm² (9)) are shorter than one might expect in the present context. Additional series of compounds must be studied to aid the disentanglement of influences of molecular shape and other properties on electron penetration into liquids.

Electron Mobilities

Arrhenius plots of the mobilities are given in Fig. 3 and the activation energies E_u derived from them are listed in Table 2. The activation energy tends to be smaller in liquids in which the mobilities are larger, as noted previously (7, 10, 28).

In olefins for which $u_e > 1$ cm² V^{-1} s^{-1} at ~300 K the value of E_u increases at low temperatures (see curves for 2,2-dimethyl-1-butene, 2-methyl-2-butene, and 2,3-dimethyl-2-butene in Fig. 3). In an earlier study of olefins (10) the data for 2,3-dimethyl-2-butene had been erroneously approximated by a straight line to calculate E_u, so they are replotted in Fig. 3; at $T > 270$ K $E_u = 1.2$ kcal/mol. At lower temperatures the larger activation energy of electron migration is probably due to the formation of deeper traps for the solvated electron. Similar behavior has been observed in other olefins (27).

Mobility Model

A model for electron migration in ethers (29) can be generalized to apply to other liquids. In ethers two mechanisms contribute to electron transport, their relative importance depending

Can. J. Chem. Downloaded from www.nrcresearchpress.com by 210.87.254.5 on 09/05/12
For personal use only.

Can. J. Chem. Downloaded from www.nrcresearchpress.com by 210.87.254.5 on 09/05/12
For personal use only.

on the ether and the temperature. An ion-like mechanism in which $u_e \approx 2u_{anion}$ dominates at low temperatures, while at higher temperatures a conduction band or hopping mechanism becomes important. The ion-like process does not contribute appreciably to electron migration in alkanes under conditions studied thus far (29), so only the second mechanism is treated here.

The electrons are considered to be distributed among localized and conduction band states. In an ether the distribution of occupied energy states was empirically related to the optical absorption spectrum of the solvated electrons (29). The low energy side of the spectrum has an approximately Gaussian shape, and in diethyl ether at ~297 K the value of the dispersion parameter is $\sigma \approx 0.18$ eV (29, 30). This parameter is also approximately equal to the thermal energy fluctuation parameter in the liquid, 0.16 eV/molecule, calculated by the method of Schiller *et al.* (31) to be discussed later. The near coincidence of these two parameter values suggested the following modification of the earlier model (29).

The energy states of electrons in liquids are affected by thermal fluctuations (31). It appears that the dispersion of the energies of electron states in ethers is similar to that of the thermal fluctuations, and the same is assumed to be true for electrons in alkanes.[2] The states are therefore taken to have a Gaussian distribution $N(V)$ about a mean energy $\bar{V}$ with a dispersion parameter σ.

$$[7] \quad N(V) = \pi^{-1/2}\sigma^{-1} \exp\left[-\left(\frac{V-\bar{V}}{\sigma}\right)^2\right]$$

where $\pi^{-1/2}\sigma^{-1}$ is a normalization factor.

The bottom of the lowest conduction band in the liquid is at energy V_0. The fraction F_{cb} of electrons in the conduction band is given approximately by [8].

$$[8] \quad F_{cb} = \int_{-\infty}^{\infty} N(V) f(V_0 - V) dV$$

where, assuming the entropy change is small when an electron is excited from a trap into the conduction band,

$$[9] \quad f(V_0 - V) = \{1 + \exp[(V_0 - V)/kT]\}^{-1}$$

The observed mobility u_e of electrons is

$$[10] \quad u_e = u_{cb}F_{cb}$$

where u_{cb} is the mobility of electrons in the conduction band.

Equation 10 represents thermal excitation of electrons from a lower distribution of states $N(V)$ into a level at V_0. There is also a distribution of upper levels, but it is assumed for simplicity that the total distribution of excitation energies involved can be represented by the Gaussian eq. 7, with a somewhat larger value of σ than that pertaining to the lower states alone.

To calculate u_e one must have values for u_{cb}, V_0, $\bar{V}$, and σ. The value of u_{cb} is approximately 100 $cm^2 V^{-1} s^{-1}$ in alkanes (7, 28). A self-consistent set of experimental values of V_0 relative to the potential energy of an electron in a vacuum (32) has recently been published for a number of liquid hydrocarbons (33). No direct information about $\bar{V}$ is available, so it is used as an adjustable parameter.

The dispersion parameter σ of the energy states of the localized electrons is not necessarily equal to that of the thermal energy fluctuations of the molecules, but the two seem to be related (29, 31). The energy of the electron states is affected by fluctuations of molecular orientation and fluid density in the immediate vicinity of the electron. The thermal fluctuation parameter can be estimated from the heat capacity of the liquid (31). However, the canonical ensemble model (fluctuating energy, constant number of molecules per cell and cell volume) chosen by Schiller *et al.* seems too restrictive. In this model the value of σ is estimated from the constant volume heat capacity C_v and it would be too small. The grand canonical ensemble model may be more realistic, with fluctuations in both the amount of energy and the number of molecules in the constant volume cell. Under these circumstances the dispersion parameter for the energy fluctuations can be estimated from [11].[3]

$$[11] \quad \sigma^2 = 2kT^2[C_p - \alpha(H + TS) + (\kappa HS/\underline{V})]$$

where the factor 2 converts the "normal distribution" dispersion parameter (31) to that of the simple Gaussian eq. 7, C_p is the heat capac-

[2]In the hydrogen bonded liquids ammonia, water, and alcohols the energy distributions of solvated electron states, judging from the optical spectra, are three to four times broader than the thermal fluctuations per molecule.

[3]B. L. Clarke, private communication.

Can. J. Chem. Downloaded from www.nrcresearchpress.com by 210.87.254.5 on 09/05/12
For personal use only.

ity of the system at constant pressure, $\alpha = \underline{V}^{-1}(\partial \underline{V}/\partial T)_{P'}$ $\kappa = -\underline{V}^{-1}(\partial \underline{V}/\partial P)_{T'}$ $\underline{V}$ is the volume of the system, and H and S are the average amounts of enthalpy and entropy in excess of those in the crystalline state at 0 K. The system in the present instance can be considered to be the number of molecules with which an electron interacts relatively strongly at a given time, and is probably of the order of ten. The bulk liquid acts as a reservoir. In estimating the over-all energy fluctuations the values of C_p, $\underline{V}$, H, and S refer to the system, $\sim$10 molecules, and are approximately proportional to the molar quantities for the solvent since the solution is extremely dilute. The magnitude of the fluctuations in the potential energies of the electron states is probably only a fraction of the over-all energy fluctuations. The size of the fraction is sought by trial and error.

Calculations with *n*-pentane at 293 K show that the last two terms on the right side of [11] nearly cancel each other.[4] One may therefore take[5]

$$[12] \qquad \sigma^2 \approx 2kT^2C_p$$

Sets of values of u_e (7, 28, 36–38), V_0 (33), and C_p (16, 35) are available for only a few liquids. These quantities were used in [10] and [12], with $u_{cb} = 100\ cm^2\ V^{-1}\ s^{-1}$, to estimate $\bar{V}$ in a number of *n*-alkanes and tetramethylsilane at 293 K. Calculations were done using several magnitudes of σ^2, ranging from values corresponding to 11% of the thermal value for one molecule to the full thermal value for nine molecules. Results appear to be not unreasonable when σ^2 is in the range corresponding to one to four molecules,[6] *i.e.* equivalent to $\sim$10–40% of the total energy fluctuation of an $\sim$10 molecule "system". The data for these two limiting cases are listed in Table 5.

Several comments are worthwhile:

(*a*) σ_1 and σ_4 represent values of σ estimated by using C_p equivalent to one and four molecules of solvent, respectively. Although the values of σ in earlier models were not elaborated in this manner, Schiller *et al.* (31) used σ_1 and Kestner and Jortner (39) used σ_4. In both earlier models it was assumed that $\bar{V}$ had the same value in all alkanes and in tetramethylsilane, the value being picked to give the best over-all results in the mobility calculations (31, 39). The present model gives $\bar{V}$ nearly constant when σ_1 is used, but for larger values of σ such as σ_4, the deduced value of $\bar{V}$ decreases with increasing V_0. When one considers possible mechanisms of electron localization in alkanes, for example with nonspherical molecules oriented in a nonrandom way about the electron center, one might expect V to decrease and V_0 to increase with decreasing degree of sphericity of the molecules. Reality might therefore fall somewhere between σ_1 and σ_4.

(*b*) The value of u_{cb} seems to be approximately the same in all the liquids from tetramethylsilane to *n*-decane. The reason for this is not obvious. However, the estimated value of $\bar{V}$ varies only slowly with the assumed value of u_{cb}, so differences in the latter give rise to relatively little error in the former: $(V_0 - \bar{V})_{estimated} \lesssim (\log u_{cb})_{assumed}$ for $u_e/u_{cb} < 0.1$.

The adjustable parameter actually used in the calculations was $(V_0 - \bar{V})$. The values of this quantity at several temperatures were estimated from the corresponding electron mobilities, using [10] and [12] with $u_{cb} = 100\ cm^2\ V^{-1}\ s^{-1}$. The quantity varied approximately linearly with temperature and values of $d(V_0 - \bar{V})/dT$ are recorded in Table 6. Conventional ideas about electron solvation lead one to expect that the derivative would be slightly negative. Negative values were only obtained for liquids in which u_e is high (Table 6). The positive values obtained for the *n*-alkanes might be an artifact that would result if the true value of σ varied less with T

[4]For liquid *n*-pentane at 293 K

$C_p = 1.77 \times 10^{-3}$ eV deg^{-1} molecule^{-1} (16)
$\underline{V} = 1.91 \times 10^{-22}$ cm^3 molecule^{-1}
$\alpha = 1.66 \times 10^{-3}$ deg^{-1} (34)
$\kappa = 3.37 \times 10^{-22}$ cm^3 eV^{-1} (34)
$H = \int_0^{T_m} C_p dT + \Delta H_m + \int_{T_m}^{293} C_p dT$
$= 0.395$ eV molecule^{-1}
T_m = melting point = 143 K
$S = \int_0^{T_m} C_p d \ln T + \Delta S_m + \int_{T_m}^{293} C_p d \ln T$
$= 2.72 \times 10^{-3}$ eV deg^{-1} molecule^{-1} (35)
$C_p - \alpha(H + TS) + (\kappa HS/\underline{V})$
$= (1.77 - 1.98 + 1.90) \times 10^{-3}$
$= 1.69 \times 10^{-3}$ eV deg^{-1} molecule^{-1}

[5]Contrary to what may have been assumed earlier (31), the difference between C_p and C_v is greater in liquids than in gases. In low pressure gases $(C_p - C_v) = R = 2$ cal deg^{-1} mol^{-1}, whereas in liquid *n*-pentane at 293 K, $(C_p - C_v) = T\underline{V}\alpha^2/\kappa = 11$ cal deg^{-1} mol^{-1} $= 0.35C_v$.

[6]σ^2 is proportional to the number of molecules, through C_p.

Can. J. Chem. Downloaded from www.nrcresearchpress.com by 210.87.254.5 on 09/05/12
For personal use only.

TABLE 5. Estimated values of $\bar{V}$ in open chain hydrocarbons and tetramethylsilane at 293 K

Liquid	u_e[a] ($cm^2\ V^{-1}\ s^{-1}$)	C_p[b] (10^{-3} eV deg^{-1} $molecule^{-1}$)	V_0[c] (eV)	σ_1[d] (eV)	$\bar{V}$[e] (eV)	σ_4[d] (eV)	$\bar{V}$[e] (eV)
Tetramethylsilane	90	2.10	−0.57	0.177	−0.40	0.354	−0.25
2,2-Dimethylpropane	50	~1.7	−0.37	0.16	−0.37	0.32	−0.37
	(70)[f]				(−0.31)		(−0.25)
2,2,4,4-Tetramethylpentane	24	~2.7	−0.33	0.20	−0.43	0.40	−0.53
2,2-Dimethylbutane	12	~1.94	−0.27	0.17	−0.42	0.34	−0.56
2,2,4-Trimethylpentane	7	2.33	−0.17	0.186	−0.37	0.372	−0.56
2-Methylpentane	0.29	1.98	0.02	0.172	−0.34	0.344	−0.66
3-Methylpentane	0.18	~1.98	0.01	0.17	−0.37	0.34	−0.70
n-Pentane	0.15	1.77	0.03	0.163	−0.34	0.326	−0.67
n-Hexane	0.08	2.02	0.07	0.173	−0.35	0.346	−0.72
n-Octane	0.039	2.60	0.13	0.196	−0.37	0.392	−0.82
n-Decane	0.025	~3.2	0.18	0.217	−0.38	0.434	−0.91

[a]References 7, 28, 36, 37.
[b]References 16, 35. The values marked ~ were obtained by interpolation or extrapolation from those for similar compounds.
[c]Average of the values in ref. 33 *a* and *b*.
[d]σ_1 and σ_4 were estimated using C_p equivalent to one and four molecules of solvent, respectively.
[e]Estimated relative to V_0, using [10] and [12] with u_{eb} = 100 $cm^2\ V^{-1}\ s^{-1}$.
[f]References 28, 38.

TABLE 6. Temperature dependences of V_0, σ, and $(V_0 - \bar{V})$

Liquid	T range (K)	u_e range ($cm^2\ V^{-1}\ s^{-1}$)	dV_0/dT[a] (10^{-3} eV/deg)	$d\sigma/dT$[b] (10^{-3} eV/deg)		$d(V_0 - \bar{V})/dT$[c] (10^{-3} eV/deg)	
				σ_1	σ_4	Using σ_1	Using σ_4
Tetramethylsilane	260 to 293	90 to 90	−2.7	0.8	1.6	−0.6	−1.1
2,2-Dimethylpropane	260 to 333	50 to 54	—	0.8	1.6	−0.1	−0.4
2,2,4,4-Tetramethylpentane	293 to 333	24 to 33	—	0.8	1.6	−0.5	−1.5
2,2-Dimethylbutane	260 to 333	10 to 17	−3.3	0.8	1.6	0.0	−0.3
n-Pentane	260 to 333	0.058 to 0.35	−2.6	0.8	1.5	0.7	1.4
n-Hexane	260 to 333	0.026 to 0.23	−2.5	0.7	1.5	0.5	1.0
n-Octane	293 to 400	0.039 to 0.31	—	0.9	1.8	0.8	1.8
n-Decane	293 to 400	0.025 to 0.14	—	1.0	2.0	1.3	2.8

[a]From data in ref. 33.
[b]Estimated from [12] and C_p data in refs. 16 and 36 (see Table 5).
[c]Estimated from u_e at different temperatures, using [10] and [12] with u_{eb} = 100 $cm^2\ V^{-1}\ s^{-1}$.

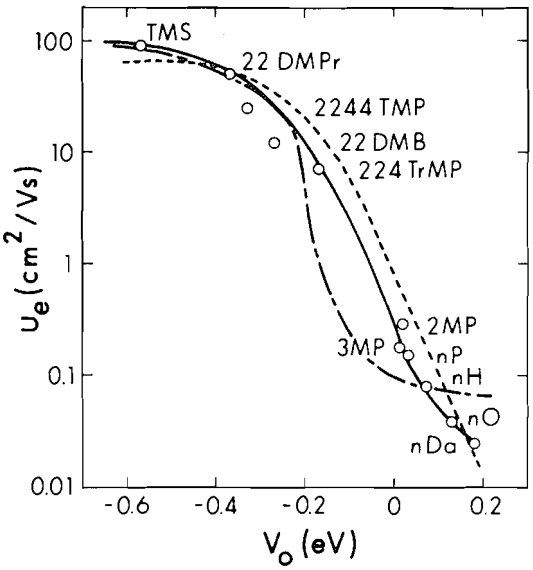

FIG. 4. Correlation of electron mobilities with V_0. ○, experimental values from Table 5; —, curve calculated from eq. 10 using $u_{cb} = 100$ cm^2 V^{-1} s^{-1}, σ_1 from Table 5 and $\bar{V} = -0.36$ eV; - - -, curve from ref. 31; – – –, curve from ref. 39.

than indicated by [12].[7] Reducing the temperature dependence of σ_1 to 40% of the value in Table 6 would make all values of $d(V_0 - \bar{V})/dT$ slightly negative or zero.

The steep decrease of u_e in olefins at low temperatures (Fig. 3 and ref. 27) can be attributed to a relatively large negative value of $d(V_0 - \bar{V})/dT$. The energy V_0 of the conduction band presumably behaves normally, but the energy $\bar{V}$ of the localized state might decrease due to increasing involvement of a negative ion state as the temperature is lowered (27).

At this point a comment should be offered about the percolation model (39). Although percolation might make a contribution to restraining electron migration at the top end of the mobility range, it does not provide an interpretation of the lower mobilities (37). The present treatment interprets the entire mobility range and does not require a contribution from percolation (Fig. 4). However, many problems remain. The detailed significance of the parameters u_{cb}, V_0, and σ are not known. For example, it is surprising that the empirical value of u_{cb} can be taken to be independent of temperature and to have approximately the same value for the series of liquids. This parameter might contain several factors, the details of which depend on the model adopted. The experimental magnitude of V_0 might not be simply the energy of an electron in the bottom of the conduction band relative to that in a vacuum, but it might also be influenced by the scattering properties of the liquid. And the use of [12] for the dispersion of electron transition energies is an oversimplification.

Correlation between u_e and b_{GP}

The general correlation that exists between thermal electron mobilities and secondary electron ranges in liquids (7, 10) contains fine structure. The structure is displayed in a semilog plot of u_e against b_{GP} (Fig. 5). The trend is for u_e to increase with b_{GP}, but the points on the left side of the graph fall into layers. The bottom layer includes the *n*-alkanes, di-*n*-alkyl ethers, and *p*-dioxan. The next layer contains branched and cyclic alkanes, terminal olefins, *trans*-2-butene, substituted cyclohexenes, and cyclic monoethers. The uppermost layer contains the benzenes, unsubstituted cycloolefins, *cis*-2-butene, the more highly substituted olefins, and globular alkanes. 1,4-Cyclohexadiene lies above the top layer.

The layering reflects differences between the relative interactions of thermal and those of epithermal electrons with different kinds of liquids. Choosing the middle layer as a reference, the lower mobilities in the *n*-alkanes and ethers reflect the formation of more stable solvated states of electrons (larger $(V_0 - \bar{V})$) in these liquids. By contrast, the upper layer may be attributed mainly to displacement of the points to lower ranges, due to larger energy transfer cross sections of aromatic and simple cycloolefinic liquids. The highest mobilities and ranges occur in the more globular compounds (Fig. 5); these liquids have small energy transfer cross sections for low energy electrons.

The basic reasons for the above behavior are not known.

It has been noted that the liquid density d influences the depth of the solvated electron states, as reflected in the optical absorption spectra (40, 41). The optical absorption energy (trap depth) tends to increase with increasing liquid density. One might therefore expect u_e to

[7] C_p increases with T, so [12] predicts $\sigma \propto T^x$ with $x > 1.0$. Recent work with ethers by F.-Y. Jou in this laboratory indicates $x < 1.0$.

Can. J. Chem. Downloaded from www.nrcresearchpress.com by 210.87.254.5 on 09/05/12
For personal use only.

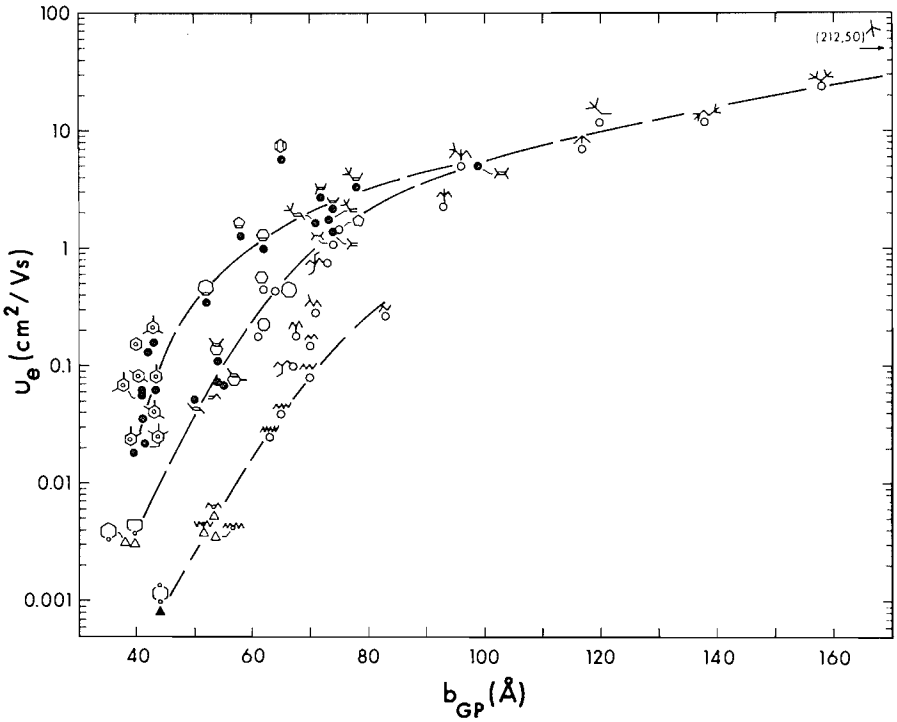

FIG. 5. Correlations between thermal electron mobilities u_e and secondary electron ranges b_{GP} in organic liquids at 294 ± 2 K. The data were taken from Tables 1 and 2 and refs. 5, 7, 10, 11, 27, 29, and 37: ●, unsaturated hydrocarbon; ○, saturated hydrocarbon; △, ether.

decrease with increasing d. The penetration range in a given type of liquid is also density dependent: $b_{GP} \propto d^{-1}$ (5–7). The electron mobilities at 294 ± 2 K were plotted against d^{-1} in Fig. 6 to compare with the mobility–range plot in Fig. 5. As in Fig. 5, the points in Fig. 6 may be grouped in layers and several interesting points emerge.

(*a*) u_e tends to increase with increasing d^{-1} as expected.

(*b*) The lowest stratum of mobilities in the d^{-1} plot is comprised of the *n*-alkyl ethers and two simple olefins, 1-butene and *trans*-2-butene. The strongly polar nature of the ethers (dipole moments 1.2 D (42)) allows one to rationalize the relatively deep traps and low mobilities in those liquids. However, *trans*-2-butene is nonpolar and the dipole moment of 1-butene is only 0.34 D (42), smaller than that of isobutene (0.50 D) in which the mobility is much larger. An effect other than polarity must explain the low mobilities in the two olefins. One possibility is the participation of transient negative ions (27).

$$e^- + C_4H_8 \rightleftharpoons C_4H_8^-$$

(*c*) The second lowest layer includes the cyclic ethers and *n*-alkanes. It is arbitrarily chosen as reference. The mobilities in the high density cyclic ethers are near the ion-like limit, towards which all strata except the top one converge.

(*d*) The next higher layer contains the benzenes, cycloalkanes, and most of the olefins. The conclusion that mobilities in most olefins are relatively high emerges from both the range and the density plots. This is contrary to common expectation and has not been explained. An empirical factor that seems to favor the high electron mobilities is the relative rigidity of the molecules (27).

(*e*) The more globular alkanes and 1,4-cyclohexadiene form the top layer, similar to the behavior in Fig. 5.

There are certain differences between the groupings of compounds in the strata of Figs. 5 and 6. The *n*-alkanes have exchanged layers with butene-1 and *trans*-2-butene. This indicates that the latter liquids are especially effective

Can. J. Chem. Downloaded from www.nrcresearchpress.com by 210.87.254.5 on 09/05/12
For personal use only.

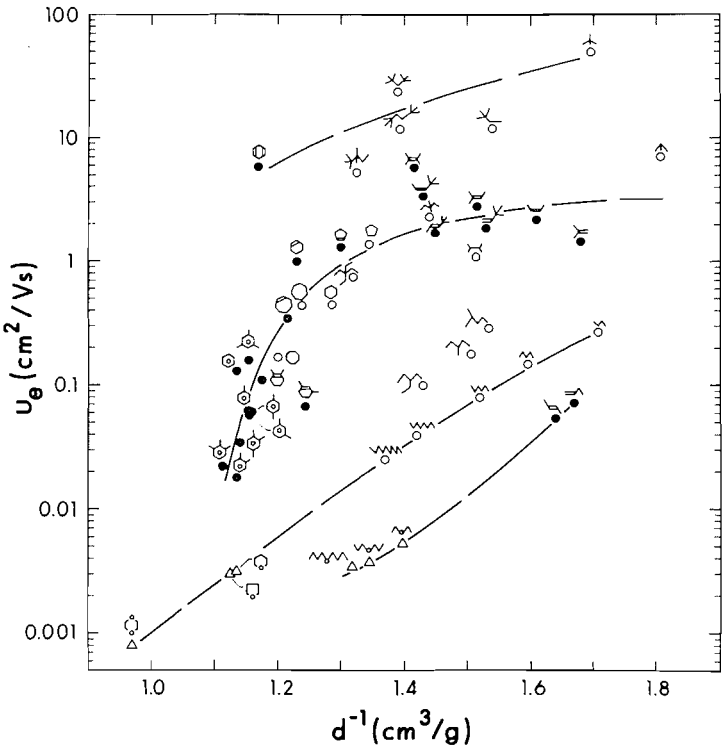

FIG. 6. Plot of electron mobility at 294 ± 2 K against the inverse of the liquid density. The points correspond to those in Fig. 4 and the data were taken from the same references.

energy sinks for electron thermalization, which causes b_{GP} to be relatively small for liquids of that density. Furthermore, the globular alkanes lie directly above the olefins on the d^{-1} plot, but are much off to the right in the b_{GP} plot. The globular alkanes are relatively poor energy sinks for electron thermalization.

Plotting the mobilities against the product $b_{GP}d$ tends to compress and merge the layers but does not yield additional information.

Acknowledgments

We wish to thank the staff of the Radiation Research Center for help with the electronics.

1. P. H. TEWARI and G. R. FREEMAN. J. Chem. Phys. **49**, 4394 (1968).
2. W. F. SCHMIDT and A. O. ALLEN. J. Phys. Chem. **72**, 3730 (1968).
3. K. N. JHA and G. R. FREEMAN. J. Am. Chem. Soc. **95**, 5891 (1973).
4. M. G. ROBINSON and G. R. FREEMAN. Can. J. Chem. **51**, 1010 (1973).
5. J.-P. DODELET, K. SHINSAKA, U. KORTSCH, and G. R. FREEMAN. J. Chem. Phys. **59**, 2376 (1973).
6. W. F. SCHMIDT and A. O. ALLEN. J. Chem. Phys. **52**, 2345 (1970).
7. J.-P. DODELET and G. R. FREEMAN. Can. J. Chem. **50**, 2667 (1972).
8. M. G. ROBINSON and G. R. FREEMAN. Can. J. Chem. **51**, 641 (1973).
9. M. G. ROBINSON and G. R. FREEMAN. Can. J. Chem. **52**, 440 (1974).
10. J.-P. DODELET, K. SHINSAKA, and G. R. FREEMAN. J. Chem. Phys. **59**, 1293 (1973).
11. K. SHINSAKA and G. R. FREEMAN. Can. J. Chem. **52**, 3495 (1974).
12. L. ONSAGER. Phys. Rev. **54**, 554 (1938).
13. G. R. FREEMAN. J. Chem. Phys. **39**, 1580 (1963).
14. J. TERLECKI and J. FIUTAK. Int. J. Radiat. Phys. Chem. **4**, 469 (1972).
15. R. R. DREISBACH. Adv. Chem. Soc. **22** (1959).
16. R. W. GALLANT. Physical properties of hydrocarbons. Vol. 1. Gulf Publishing Co., Houston, Texas. 1968.
17. A. A. MARYOTT and E. R. SMITH. Tables of dielectric constants of pure liquids. NBS Circular 514, U.S. Dept. Commerce, Washington 25, D.C. 1951.
18. R. C. WEAST (*Editor*). Handbook of chemistry and physics. 50th ed. Chemical Rubber Co., Cleveland, Ohio. 1969.
19. J.-P. DODELET, K. SHINSAKA, and G. R. FREEMAN. To be published.
20. P. ALDER and H. K. BOTHE. Z. Naturforsch. **20***a*, 1700 (1965).

Can. J. Chem. Downloaded from www.nrcresearchpress.com by 210.87.254.5 on 09/05/12
For personal use only.

21. R. M. LEBLANC and J. A. HERMAN. J. Chim. Phys. **63**, 1055 (1966).
22. T. A. STONEHAM, D. R. ETHRIDGE, and G. G. MEISELS. J. Chem. Phys. **54**, 4054 (1971).
23. G. R. FREEMAN. Radiat. Res. Rev. **1**, 1 (1968).
24. T. SHIDA and W. H. HAMILL. J. Am. Chem. Soc. **88**, 5371 (1966).
25. T. SHIGA and A. LUND. Ber. Bunsenges. Phys. Chem. **78**, 259 (1974).
26. E. D. STOVER and G. R. FREEMAN. Can. J. Chem. **46**, 2109 (1968).
27. K. SHINSAKA, J.-P. DODELET, and G. R. FREEMAN. Can. J. Chem. **53**, 2714 (1975).
28. R. M. MINDAY, L. D. SCHMIDT, and H. T. DAVIS. J. Phys. Chem. **76**, 442 (1972).
29. J.-P. DODELET and G. R. FREEMAN. Can. J. Chem. **53**, 1263 (1975).
30. F.-Y. JOU and L. M. DORFMAN. J. Chem. Phys. **58**, 4715 (1973).
31. R. SCHILLER, SZ. VASS, and J. MANDICS. Int. J. Radiat. Phys. Chem. **5**, 491 (1973).
32. R. A. HOLROYD. J. Chem. Phys. **57**, 3007 (1972).
33. (*a*) R. A. HOLROYD, B. K. DIETRICH, and H. A. SCHWARZ. J. Phys. Chem. **76**, 3794 (1972); (*b*) R. A. HOLROYD and R. L. RUSSELL. J. Phys. Chem. **78**, 2128 (1974).
34. R. C. REID and T. K. SHERWOOD. The properties of gases and liquids. 2nd ed. McGraw-Hill, Toronto. 1966. Chapt. 6.
35. J. TIMMERMANS. Physico-chemical constants of pure organic compounds. Vol. 1. Elsevier, Amsterdam. 1950.
36. W. F. SCHMIDT and A. O. ALLEN. J. Chem. Phys. **52**, 4788 (1970).
37. J.-P. DODELET, K. SHINSAKA, and G. R. FREEMAN. J. Chem. Phys. **63**, 2765 (1975).
38. K. SHINSAKA and G. R. FREEMAN. Can. J. Chem. **52**, 3556 (1974).
39. N. R. KESTNER and J. JORTNER. J. Chem. Phys. **59**, 26 (1973).
40. K. N. JHA, G. L. BOLTON, and G. R. FREEMAN. J. Phys. Chem. **76**, 3876 (1972).
41. G. R. FREEMAN. J. Phys. Chem. **77**, 7 (1973).
42. R. D. NELSON, JR., D. R. LIDE, JR., and A. A. MARYOTT. Selected values of electric dipole moments for molecules in the gas phase. NSRDS-NBS 10. Superintendent of Documents, Washington, D.C. 1967.

Can. J. Chem. Downloaded from www.nrcresearchpress.com by 210.87.254.5 on 09/05/12
For personal use only.

An exciplex mechanism for the quenching of singlet excited states of aliphatic ketones by carbon tetrachloride

RAFIK O. LOUTFY AND ALLAN C. SOMERSALL

Xerox Research Centre of Canada Limited, 2480 Dunwin Drive, Mississauga, Ontario L5L 1J9

Received September 22, 1975

RAFIK O. LOUTFY and ALLAN C. SOMERSALL. Can. J. Chem. **54**, 760 (1976).

Non-classical energy transfer from the excited singlet states of aliphatic ketones to carbon tetrachloride leads to sensitized decomposition products and fluorescence quenching. The correlation of the ionization potentials for a wide variety of such ketones with the corresponding quenching constants from fluorescence data has been rationalized by an exciplex mechanism. The correlation implies that charge transfer from the excited ketone to the carbon tetrachloride is a major contribution to the exciplex state for which two possible structures are tentatively proposed.

RAFIK O. LOUTFY et ALLAN C. SOMERSALL. Can. J. Chem. **54**, 760 (1976).

Le transfert d'énergie non-classique des états excités singulets de cétones aliphatiques au tétrachlorure de carbone conduit à des produits de décomposition sensibilisée et à l'extinction de la fluorescence. On a rationalisé la corrélation qui existe entre le potentiel d'ionisation d'une grande quantité de telles cétones et les constantes correspondantes d'extinction obtenues à partir de données de fluorescence à l'aide d'un mécanisme d'exciplexe. La corrélation implique que le transfert de charge de la cétone excitée au tétrachlorure de carbone contribue d'une façon prépondérante à l'état exciplexe pour lequel on propose d'une façon non définitive deux structures possibles.

[Traduit par le journal]

The quenching of fluorescence by molecules which cannot function by classical electronic energy transfer has been the focus of many investigations in recent years. A considerable body of evidence has given direct support for formation of excited-state complexes in many such systems (1).

Halogenated alkanes (2), dienes (3), and amines (4) have typically been investigated as quenchers of the fluorescence of aromatic hydrocarbons and their derivatives. The observation of fluorescence quenching in such cases where there is negligible overlap of donor emission and acceptor absorption spectra (required for classical transfer) was rationalized by Hammond and co-workers (3) in terms of an exciplex intermediate.[1] Klein *et al.* (2*a*) later developed a model in which the formation rate of this exciplex was considered as the rate-determining step in the excitation quenching process. The model predicts that the quenching rate constants (k_q) for a series of donors by an acceptor are related by the following expression:

$$[1] \quad \ln k_q \propto -(IP_D - EA_A - C - P - E_s)/kT$$

where IP_D is the ionization potential of the donor, EA_A is the electron affinity of the acceptor, C is the coulomb energy, and P is the polarization energy of the separated charges. E_s represents the energy of the first excited state. Generally, for a common fluorescent donor and a series of different electron-deficient quenchers, the bimolecular rate constants can be correlated with the corresponding EA values of the quenchers. Other correlations have sometimes been made for different fluophores and a single quencher but both IP and E_s values change simultaneously in the series of aromatics which have been reported so that k_q had to be correlated with $(IP - E_s)$.

We wish to report some linear free energy correlations for the fluorescence quenching of a wide variety of aliphatic ketones by carbon tetrachloride which affords some insight into the exciplex intermediate in this system (5). The quenching of the singlet excitation of aliphatic ketones by a common quencher affords a rather unique system where E_s proves to be practically constant while IP varies significantly.

The photochemistry of ketones in carbon tetrachloride has been reported earlier (5). The

[1]This is consistent with the definition proposed formally by J. B. Birks: "An exciplex is an electronically excited atomic or molecular complex of definite stoichiometry, which is dissociated in its electronic ground state" in ref. 20.

Can. J. Chem. Downloaded from www.nrcresearchpress.com by 210.87.254.105 on 09/05/12
For personal use only.

TABLE 1. Fluorescence quenching rate constants of n,π^* singlet aliphatic ketones by carbon tetrachloride, plus the ionization potentials and Taft polar substituent constants for the ketones

Experiment	Ketone R—CO—R′		$k_q{}^1\tau$ (M^{-1})	$^1\tau^b$ (ns)	$k_q \times 10^7$ (M^{-1} s^{-1})	IP[c] (eV)	$-\sigma^{*d}$
	R	R′					
1	CH_3	CH_3	0.076	1.85	4.20	9.70	0.00
2	CH_3	C_2H_5	0.232	2.50	9.28	9.53	0.10
3	CH_3	C_3H_7	0.112	1.8	6.22	9.39	0.12
4	CH_3	i-C_3H_7	0.31	2.7[a]	11.5	9.32	0.19
5	CH_3	C_5H_{11}	0.092	0.9[a]	10.2	9.33	0.15
6	CH_3	C_6H_{13}	0.08	0.8[a]	10.0	9.38	0.16
7	CH_3	$tert$-C_4H_9	0.86	4.2	20.5	9.17	0.30
8	i-C_3H_7	i-C_3H_7	0.65	4.2[a]	15.5	8.94	0.38
9	C_2H_5	C_2H_5	0.38	2.8[a]	14.0	9.32	0.20
10	C_3H_7	C_3H_7	0.20	1.3	15.4	9.23	0.24
11	C_4H_9	C_4H_9	0.12	0.6[a]	20.0	9.16	0.26
12	C_5H_{11}	C_5H_{11}	0.12	0.5[a]	24.0	9.10	0.30
13	C_7H_{15}	C_7H_{15}	0.12	0.5[a]	24.0	9.08	0.31
14	$C_{11}H_{23}$	$C_{11}H_{23}$	0.13	0.5[a]	26.0	9.11	0.32
15	Cyclopentanone		0.58	1.9	29.0	9.25	0.22
16	Cyclohexanone		0.95	2.6	38.0	9.14	0.28
17	2-Methylcyclohexanone		1.50	3.0	50.0	9.10	0.30
18	Cycloheptanone		0.174	2.67[a]	6.50	9.49	0.24
19	Cyclooctanone		0.117	1.56[a]	7.50	9.45	0.25

[a]Reference 14, calculated value.
[b]References 15–17, measured by single photon counting technique, estimated error ± 10%.
[c]References 11 and 18.
[d]Reference 19.

chemical products observed were formed by radiationless energy transfer from the excited $^1(n,\pi^*)$ ketone to the carbon tetrachloride. We have now extended the fluorescence quenching measurements to include symmetric, asymmetric, and cyclic aliphatic ketones. The data has been treated by typical Stern–Volmer kinetics as illustrated in Fig. 1. The Stern–Volmer equation is given as

$$[2] \qquad \frac{I_f^0}{I_f} = \frac{\phi_f^0}{\phi_f} = 1 + k_q{}^1\tau\,[CCl_4]$$

where I_f^0, I_f represent the intensities of fluorescence of the ketone in the absence and the presence of quencher respectively, and ϕ_f^0, ϕ_f are the corresponding quantum yields. The slopes of the straight line plots give values for $k_q{}^1\tau = K_{sv}$ from which the k_q values have been derived. Values of the singlet lifetime ($^1\tau$) of ketones in cyclohexane were obtained from ϕ_f measurements and integrated absorption spectra or from the reported literature values. The data is summarized in Table 1.

Carbon tetrachloride quenches the fluorescence of the lowest excited singlet state of aliphatic ketones at a rate of about three orders of magnitude slower than that characteristic of a room temperature diffusion-controlled process

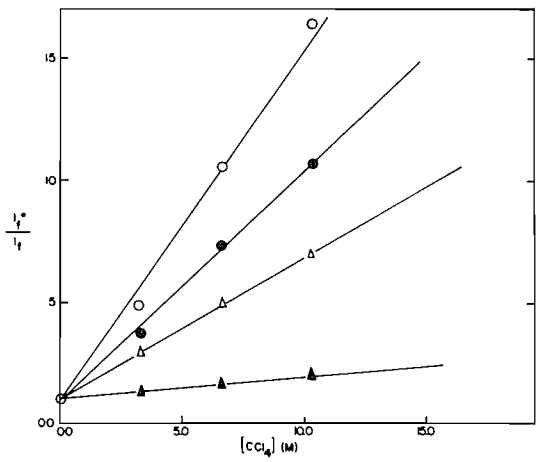

FIG. 1. Stern–Volmer plots for quenching of n,π^* singlet excited aliphatic ketones: (○) 2-methylcyclohexanone, (●) cyclohexanone. (△) cyclopentanone, and (▲) 2-hexanone in cyclohexane excited at 313 nm (with carbon tetrachloride).

Can. J. Chem. Downloaded from www.nrcresearchpress.com by 210.87.254.105 on 09/05/12
For personal use only.

Can. J. Chem. Downloaded from www.nrcresearchpress.com by 210.87.254.105 on 09/05/12
For personal use only.

(5×10^{10} M^{-1} s^{-1}). In addition, the rate of fluorescence quenching is considerably faster than can be accounted for by chemical quenching.[2] Thus, the quenching is believed to proceed via an intermediate donor–acceptor (DA) exciplex formed between the excited ketone and carbon tetrachloride. According to this model, the rate of formation of the exciplex depends on the energy difference $E_{DA} - E_s$. From the similarity of absorption and fluorescence spectra, E_s for the series of aliphatic ketones studied is presumed to be constant, thus the relative rate of exciplex formation will depend on its energy E_{DA}.

In order to check the validity of eq. 1 with respect to the model above, we measured the fluorescence quenching rate constant for a series of aliphatic ketones (RCOR′) where the substituents R and R′ were varied, systematically increasing their inductive effect. The inductive effect of the alkyl substituent leads to a predictable decrease in the adiabatic ionization potential of the ketones, even though the alkyl groups are not directly bound to the carbonyl oxygen atom. This is due to the fact that the carbonyl π system, being readily polarizable, transmits the polar effects of the alkyl group with very little reduction in their magnitude (6). It was found that the rate of quenching (k_q) increases as IP decreases.

A plot of log k_q *vs.* IP is given in Fig. 2. The linear correlation suggests that E_s, C, and P values are practically constant and that there is significant charge transfer in the excited state intermediate complex. However, the slope (1.4 eV^{-1}) is much less than $1/2.30RT$ ($\simeq$17 eV^{-1}) which is to be expected from eq. 1. We therefore believe that, though the direction of the rate constants indicates significant charge-transfer character in the complex, such transfer is probably not a complete one-electron transfer at the transition state or in the complex. It is worth noting that the effect of ketone structure on the rate of fluorescence quenching with CCl_4 in energy units ($\Delta E = 2.303RT\,\Delta \log k_q$) is about a tenth of the effect on its ionization potential. Similar observations were reported by Kochevar and Wagner (7) and Caldwell *et al.* (8) for the effect of olefin structure on its rate constant for quenching of aromatic ketone triplets.

[2]For example, the rate of reaction of alkyl radicals with carbon tetrachloride does not exceed 10^4–10^5 M^{-1} s^{-1} (see ref. 21).

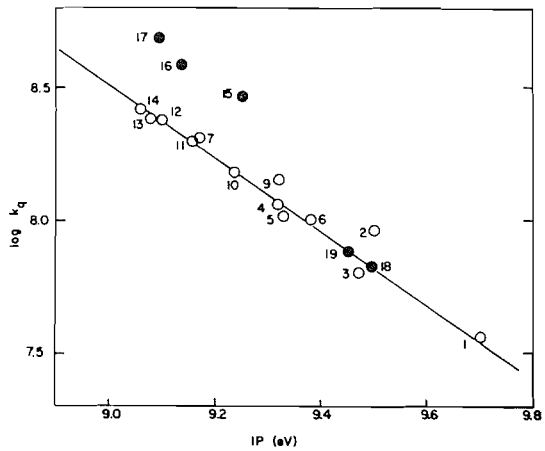

FIG. 2. The relation between the measured fluorescence quenching rate constant and the ionization potential of (○) acyclic and (●) cyclic ketones.

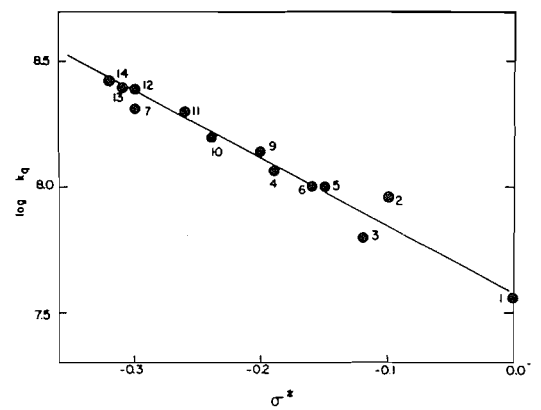

FIG. 3. Plot of log k_q *vs.* Taft σ^* polar substituent constants.

A similar correlation of log k_q with Taft σ^* polar substituent constants is again linear, as shown in Fig. 3. The ρ value (slope) of -2.7 indicates moderate charge development in the transition state with net positive charge on the ketone. Similar correlations for quenching of substituted naphthalenes with a diazo-compound or trimethylamine (9) quencher afford ρ values of $+2.24$ and $+2.5$ respectively, indicating in these cases that a negative charge develops on the aromatic fluophore in the intermediate complexes in such cases.

The rate of quenching of acetone fluorescence using a series of chloromethanes is given in Table 2. In Fig. 4, log k_q is plotted against the

Can. J. Chem. Downloaded from www.nrcresearchpress.com by 210.87.254.105 on 09/05/12
For personal use only.

TABLE 2. Fluorescence quenching rate constant of singlet acetone by chloromethanes and the electron affinities of the quenchers

Experiment	Quencher	EA[a] (eV)	$k_q \times 10^6$ (M^{-1} s^{-1})
1	Carbon tetrachloride	2.12	42.0±0.5
2	Chloroform	1.75	5.2±0.3
3	Methylene chloride	1.36	1.4±0.3

[a]Reference 2*c*.

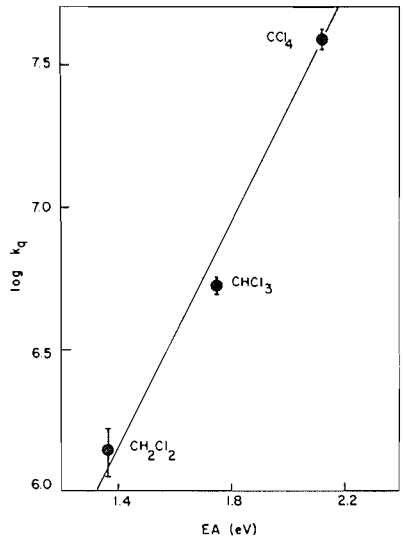

FIG. 4. The dependence of quenching rate constant of acetone fluorescence on the electron affinity of the chloromethane quenchers.

electron affinity (EA) of the quenchers. Although there are only three points, these data satisfy a linear relationship verifying eq. 1 and indicating that the chloromethane quenchers act as an acceptor.

The marked substituent effects on the rate constants for ketone fluorescence quenching would also suggest that the carbonyl carbon atom is intimately involved in the intermediate exciplex interaction. Turro *et al.* (10) found that the vacant n-orbital on oxygen is involved in the quenching of ketones by electron-rich olefins. On the other hand, they provided strong evidence that fluorescence quenching of the excited ketone singlet by electron-deficient olefins involves attack on the nucleophilic carbonyl π^*_{CO} orbital (11). In our case, the quencher has an affinity for electrons, so it is likely that the electron promoted to the π^* orbital of the ketone

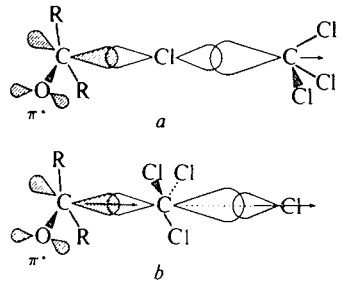

FIG. 5. Proposed exciplex structures.

interacts with a chlorine atom of the CCl_4 leading to dissociation of the CCl_4. This is similar to chain transfer reactions to CCl_4 solvent molecules in free radical polymerizations. It is not unreasonable to propose that CCl_4 may also be polarized in a non-equilibrium conformation, so that the central carbon atom attached to the four electronegative chlorines is somewhat electron-deficient and interacts with the π^*_{CO} orbital in the vicinity of the carbonyl carbon of the ketone. These tentative rationalizations are illustrated in Fig. 5 *a* and *b* respectively.

The low values of k_q which are 2–3 orders of magnitude less than the diffusion limit, the failure to observe expected curvature in the Stern–Volmer plots due to instantaneous quenching at high quencher concentration (up to 10 *M*), and the absence of thermal acceleration up to 60 °C, would all imply that such an energy transfer process via the exciplex is limited by steric and/or entropic barriers rather than by a thermal energy barrier.

Comparisons of the k_q values for cyclopentanone (15), cyclohexanone (16), and 2-methylcyclohexanone (17) with those of acyclic alkanones having the same ionization potentials (*e.g.* di-*n*-propyl ketone (10), di-*n*-butyl ketone (11), and di-*n*-pentyl ketone (12), respectively) reveal a substantial increase in k_q, by a factor of two going from acyclic to cyclic ketones. Approach of CCl_4 to the nucleophilic π^*_{CO} orbital of the n,π^* excited state of the acyclic ketone is probably more sterically hindered than its approach to that of cyclic ketones.

Recently Dalton and Snyder (12) observed similar steric effects in fluorescence quenching of alkanones by amines. Comparison of the quenching rate by carbon tetrachloride of ^{1}n,π^* of ketones and $^1\pi,\pi^*$ of methyl benzenes (2*c*) shows that log k_q correlates linearly with

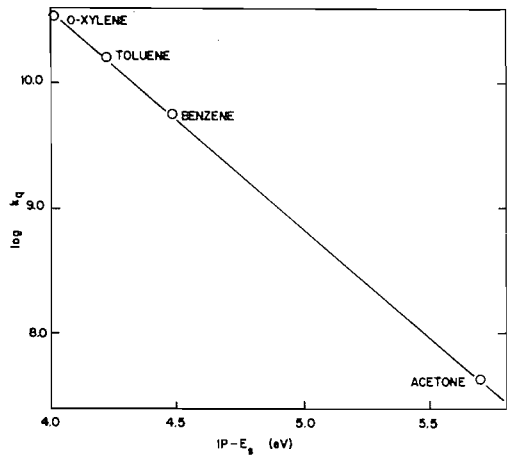

FIG. 6. The relation between the quenching rate constant of methylbenzenes and aliphatic ketones fluorescence and the term (IP $-$ E_s).

(IP $-$ E_s) for both series (Fig. 6). The nature of the excited state has no apparent effect on the quenching rate. This is not surprising since in both cases the carbon π^* orbital of the ketone or benzene is the one which is involved in the interaction.

Finally, we note that Ware and Lewis (2*b*) have demonstrated that non-classical fluorescence quenching can be observed when non-fluorescent *ground-state* complexes between the fluophore and quencher compete for excitation. Nemzek (13) has recently measured the excited state lifetime of acetone by single photon counting in neat cyclohexane and carbon tetrachloride and obtained values of 1.85 and 1.00 ns respectively. From these values the estimated value of k_q in this case is 4.6×10^7 compared to 4.3×10^7 M^{-1} s^{-1} derived from our fluorescence quenching data. This is totally consistant with the exciplex mechanism above and the absence of a discernible difference for acetone absorption spectra in carbon tetrachloride implies that such a ground-state complex is not important in this case.

1. BRIAN STEVENS. Adv. Photochem. **8**, 161 (1971).
2. (*a*) J. KLEIN, V. P. PLAZANET, and G. LAUSTRIAT. J. Chim. Phys. Physicochim. Biol. **67**, 302 (1970); (*b*) W. R. WARE and C. LEWIS. J. Chem. Phys. **57**, 3546 (1972). (*c*) D. SAPERSTEIN and E. LEVIN. J. Chem. Phys. **62**, 3560 (1975).
3. D. A. LABIANCA, G. N. TAYLOR, and G. S. HAMMOND. J. Am. Chem. Soc. **94**, 3679 (1972), and references therein.
4. (*a*) D. REHM and A. WELLER. Isr. J. Chem. **8**, 259 (1970); (*b*) A. WELLER and H. BEENS. *In* Organic molecular photophysics. Vol. 2. *Edited by* J. B. Birks, Wiley, New York. 1975. p. 158.
5. J. O. PAVLIK, P. I. PLOOARD, A. C. SOMERSALL, and J. E. GUILLET. Can. J. Chem. **51**, 1435 (1973).
6. B. J. COCKSEY, J. H. D. ELAND, and C. J. DANBY. J. Chem. Soc. (B), **5**, 790 (1971).
7. I. KOCHEVAR and P. WAGNER. J. Am. Chem. Soc. **92**, 5742 (1970); **94**, 3859 (1972).
8. R. A. CALDWELL, G. W. SOVOCOOL, and R. P. GAJEWSKI. J. Am. Chem. Soc. **95**, 2549 (1973).
9. R. H. YOUNG and R. L. MARTIN. J. Am. Chem. Soc. **94**, 5183 (1972).
10. N. J. TURRO, J. C. DALTON, G. FARRINGTON, M. NIEMCZYK, and D. M. POND. J. Am. Chem. Soc. **92**, 6978 (1970).
11. N. J. TURRO, M. NIEMCZYK, and D. M. POND. Mol. Photochem. **2**, 345 (1970), and references therein.
12. J. C. DALTON and J. J. SNYDER. J. Am. Chem. Soc. **97**, 5192 (1975).
13. T. NEMZEK. Private communication.
14. A. C. SOMERSALL and J. GUILLET. Macromolecules, **5**, 410 (1972).
15. J. C. DALTON and N. J. TURRO. J. Am. Chem. Soc. **93**, 3569 (1971).
16. O. L. CHAPMAN and D. S. WEISS. Org. Photochem. **3**, 239 (1972), and references therein.
17. J. C. DALTON and R. J. STERNFELS. Mol. Photochem. **6**, 307 (1974).
18. K. WATANOBE, T. NAKAYAMA, and J. MOTTL. J. Quant. Spectrosc. Rad. Transfer, **2**, 369 (1962).
19. P. ZUMAN. Substituent effects in organic polarography. Plenum Press, New York. 1967. p. 170.
20. J. B. BIRKS. *In* Molecular luminescence. *Edited by* E. C. Lim. W. A. Benjamin Inc., New York. 1969. p. 906.
21. F. W. BILLMEYER. Textbook of polymer science. Wiley, New York. 1971. pp. 293–301.

Can. J. Chem. Downloaded from www.nrcresearchpress.com by 210.87.254.105 on 09/05/12
For personal use only.

Polymorphism in *n*-alkylammonium chlorides: X-ray powder diffraction studies

D. F. R. GILSON,[1] A. S. KERTES,[2] R. ST. J. MANLEY, AND J. TSAU[3]

Department of Chemistry, McGill University, P.O. Box 6070, Station A, Montreal, Quebec H3C 3G1

AND

G. DONNAY

Department of Geological Sciences, McGill University, P.O. Box 6070, Station A, Montreal, Quebec H3C 3G1

Received September 29, 1975

D. F. R. GILSON, A. S. KERTES, R. ST. J. MANLEY, J. TSAU, and G. DONNAY. Can. J. Chem. **54**, 765 (1976).

The *n*-alkylammonium halides which have thermal transitions above room temperature adopt either a monoclinic or an orthorhombic form when recrystallized at temperatures below the lowest transition. On heating a transition to a tetragonal structure occurs but on subsequent cooling the crystals do not return to their original form but to a different monoclinic structure.

D. F. R. GILSON, A. S. KERTES, R. ST. J. MANLEY, J. TSAU et G. DONNAY. Can. J. Chem. **54**, 765 (1976).

Les halogénures de *n*-alkylammonium qui ont des transitions thermiques au-dessus de la témperature de la pièce adoptent soit une forme monoclinique ou une forme orthorhombique lorsqu'on les recristallise à des températures en dessous de leur transition la plus basse. Lorsqu'on les chauffe, une transition vers une structure tétragonale se produit; toutefois lorsqu'on les refroidit, les cristaux ne retournent pas à leurs formes originales mais à une structure monoclinique différente.

[Traduit par le journal]

Introduction

Crystal structure data for homologous series of *n*-alkyl compounds have been reported for carboxylic acids (1), their salts (2), and for *n*-alcohols (3). Although a partial structure determination of the room temperature monoclinic phase of *n*-dodecylammonium chloride was reported by Gordon, Stenhagen, and Vand (4) in 1953, there is no recent structural information available on the *n*-alkylammonium halide series. Much earlier studies indicated that the chloride salts of the lower members of the series are tetragonal at room temperature, except for the ethylammonium salts which are monoclinic. The longer chain compounds are either monoclinic, C_{12}, C_{14}, C_{16}, or orthorhombic, C_{13} and C_{18}. Gordon *et al.* (4) observed that *n*-dodecyclammonium chloride undergoes a transition at 59 °C on heating to another monoclinic or triclinic form but on cooling returns to a structure with a slightly different long spacing. The long spacings reported by these authors for *n*-dodecylammonium chloride and bromide were 17.86 and 35.8 Å, respectively. Kertes, Gutman, and Mayer (5), however, reported values of 35.3 and 17.7 Å respectively.

A differential scanning calorimetric (dsc) study of the chlorides and bromides from methyl to hexadecyl showed that a complex sequence of transitions occurs (6) and the longer chain compounds exhibit a nonreversible behaviour in that the first time the samples were heated a single dsc transition was observed but on both cooling and subsequent re-heating cycles three or more transitions occurred at temperatures different from the initial heating scan. Wide line nuclear magnetic resonance studies confirmed this nonreversible behaviour (7, 8). The second moment values showed abrupt decreases from values which indicate the presence of a torsional motion of the chain to values much lower than those calculated for chain rotation alone. A more extensive motion must therefore be present. For samples which had been previously heated through this transition region, the second moment behaviour as a function of temperature resembled that of the shorter members of the series, for which a plateau region is observed where chain rotation alone occurs, and the more extensive motion follows at higher temperatures.

A simple qualitative explanation is that these

[1]To whom correspondence should be addressed.

[2]Permanent address: Hebrew University of Jerusalem, Jerusalem, Israel.

3NRCC Studentship 1966–1969.

Can. J. Chem. Downloaded from www.nrcresearchpress.com by 210.87.254.6 on 09/05/12
For personal use only.

TABLE 1. Crystallographic parameters for *n*-alkylammonium chlorides

n	*a* (Å)	*b* (Å)	*c* (Å)	*β* (deg)	Z	Reference
10	5.83	6.62	16.05	91.18	2	12
11	5.71	6.98	16.37	90.50	2	This work
12	5.68	7.16	17.86	91.26	2	4
13	7.57	7.61	56.49	—	8	10
13	5.35	5.28	28.15	—		This work
14	5.67	7.20	20.13	95.87	2	10
15	5.75	7.14	21.47	92.08	2	13
16	5.71	7.24	22.56	98.35	2	10
17	—	—	34.46	—		This work
18	5.45	5.40	69.40	—	4	11
18	—	—	35.84	—		This work
19	—	—	36.88	—		This work

transitions involve a change from a "low" temperature monoclinic or orthorhombic structure to a "high" temperature tetragonal form. The occurrence of chain rotation in the high temperature phase is consistent with the observed tetragonal unit cell in which the site symmetry is incompatible with the molecular symmetry unless disordering occurs. The dependence of transition temperature upon chain length shows that for the chloride salts the transitions occur below room temperature for chain lengths of nine carbon atoms or less and above room temperature for longer chains. The nonreversible behaviour of the transition for the longer chains and the inconsistency in the reported long spacings for the dodecylammonium compounds suggest that the thermal history of the sample may influence the crystal structure. We have therefore undertaken a study of the long spacings of the *n*-alkylammonium chlorides under controlled experimental conditions in order to examine the thermal effects.

Experimental

The amines or their hydrochlorides were obtained from commercial sources, and, in the cases of the free amines, the salts prepared by addition of dilute hydrochloric acid to a solution of the amine in chloroform, and recrystallized from chloroform. The alkylammonium chlorides were re-dissolved in chloroform and cooled. The first crystals to form were discarded and after further cooling the required crystals were obtained. All such recrystallizations were performed at temperatures *below the lowest transition temperature observed in the dsc studies* (6). The materials crystallize exceedingly thin soft laths which, in addition, are usually twinned. Intensity data of sufficient quality for structural studies are very difficult to obtain.

Powder diffraction photographs were obtained using nickel filtered CuK_α radiation $\lambda = 1.5418$ Å with a modified Rigaku–Denki low angle camera. Samples were mounted in glass capillaries placed in an oven constructed from an insulated aluminium block with a thermocouple placed next to the sample. Diffraction patterns were taken for each sample first at room temperature, then at 130 °C, then again at room temperature.

The 130 °C value was chosen since it is approximately mid-way between the highest observed dsc transition temperature and the melting point and provided a common temperature for all samples.

Some additional data were obtained from Debye–Scherrer photographs at other temperatures (9), and also by the Gandolfi single crystal method.

Results and Discussion

Tables 1 and 2 contain both experimental results obtained in the present study and a survey of the literature data. The long spacings, *d*(001), observed in the present study for *n*-tridecyl- and *n*-octadecylammonium chlorides are half the values reported previously (10, 11). For *n*-tridecylammonium chloride this is due to a different choice of unit cell. The phases which have not been heated above their transition temperatures are either monoclinic or orthorhombic and these will be referred to as "primary" phases. When these samples are heated to 130 °C the long spacings increase and for the primary monoclinic phase the long spacing is approximately doubled in the high temperature (tetragonal) phase. This latter phase is, of course, the stable room temperature phase for the shorter members of the series. On cooling to room temperature the samples do not return to the original primary phase and adopt instead a secondary phase which is monoclinic with a long spacing slightly larger than that of the tetragonal phase, *i.e.* a negative coefficient of expansion in this direction. The

Can. J. Chem. Downloaded from www.nrcresearchpress.com by 210.87.254.6 on 09/05/12
For personal use only.

TABLE 2. Long spacings (Å) for *n*-alkylammonium chloride*

n	Primary phase	Reference	Secondary monoclinic phase	Reference	Tetragonal phase	Temperature (K)	Reference
1					5.06		16
2	6.95	14			—		
3			7.27 (143K)	15	7.38		15
4					14.88		17
5					16.72		18
6					19.59		18
7					21.13		18
8			25.40	This work	24.20	333	18
9			28.50	This work	26.20	343	This work
10			31.11	This work	28.00	383	This work
11	16.37	This work	32.72	This work	29.90	383	This work
12	17.71	10	35.30	5	32.80	403	This work
	17.86	4	35.62	This work			
13	27.15	This work	37.12	This work	34.60	403	This work
14	20.03	10	38.74	This work	36.30	403	This work
	19.99	This work					
15	21.04	This work	41.67	This work	39.09	403	This work
	21.43	13					
16	22.32	10	43.28	This work	40.51	403	This work
	22.64	This work					
17	34.46	This work	46.05	This work	42.20	403	This work
18	35.84	This work	48.90	This work	45.40	403	This work
19	36.88	This work	49.77	This work	46.35	403	This work

*At room temperature unless otherwise stated.

long spacings are plotted as a function of the number of carbon atoms in the chain, Fig. 1. The four straight lines in Fig. 1 correspond to four different crystal forms which exist under the specific conditions employed in the present experiments: (*i*) a common high temperature tetragonal phase existing above the highest transition temperature. The space group is $P4/nmm$, two molecules per unit cell; (*ii*) a secondary monoclinic phase obtained by cooling from the tetragonal phase and which is presumably common to all members, and (*iii*) and (*iv*) the primary monoclinic and orthorhombic structures for crystals which have not received thermal treatment. This change from the primary monoclinic or orthorhombic to the secondary monoclinic structure explains the nonreversible behaviour observed in the dsc and nmr studies and the inconsistencies in earlier X-ray studies.

If a similar behaviour occurs for the *n*-alkylammonium bromide series, then it may be concluded that Gordon *et al.* (4) must have examined the primary monoclinic structure of *n*-dodecylammonium chloride and the secondary monoclinic phase of the bromide, whereas Kertes *et al.* (5) reported data for the secondary monoclinic

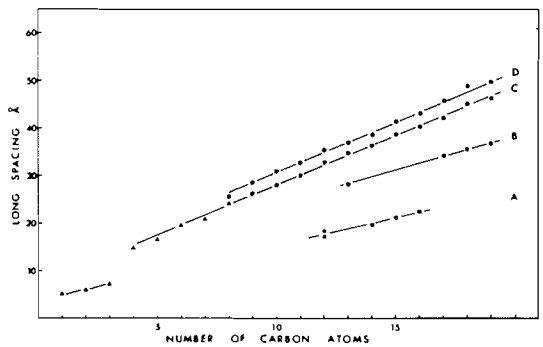

FIG. 1. Long spacings of *n*-alkylammonium chlorides. Lines A and B, primary monoclinic and orthorhombic phases. Line C, tetragonal phase. Line D, secondary monoclinic phase. Triangles are literature values, circles are from the present study.

chloride and primary monoclinic bromide.

Irreversible transitions such as these are better known for inorganic systems (12) and generally involve small differences in internal energy between the two forms but a large activation energy exists for conversion from one form to the other. The enthalpy change observed for the nonreversible transition to the tetragonal phase is 2.5 kcal mol^{-1} for *n*-tridecylammonium chloride

Can. J. Chem. Downloaded from www.nrcresearchpress.com by 210.87.254.6 on 09/05/12
For personal use only.

but greater than 6 kcal mol^{-1} for the *n*-tetradecyl-, *n*-pentadecyl-, and *n*-hexadecyl-compounds. There was no evidence of diffuse X-ray scattering on diffraction photographs of either the primary monoclinic or the primary orthorhombic phases and these must be the only ordered phases with the monoclinic more stable than the orthorhombic. The observation of three or more transitions in the dsc study (6) implies that other intermediate phases must exist. The present investigation is concerned with the low and high temperature limiting cases only.

Acknowledgements

The financial support of the National Research Council of Canada is acknowledged. The authors are indebted to Mr. L. Marcotte and Mr. T. Campbell for technical assistance.

1. E. VON SYDOW. Arkiv Kemi, **9**, 231 (1956).
2. A. E. SKOULIOS and V. LUZZATI. Acta Cryst. **14**, 278 (1961).
3. K. TANAKA, T. SETO, A. WATANABE, and T. HAYASHIDA. Bull. Inst. Chem. Res. Kyoto University, **37**, 281 (1959).
4. M. GORDON, E. STENHAGEN, and V. VAND. Acta. Cryst. **6**, 739 (1953).
5. A. S. KERTES, H. GUTMAN, and I. MAYER. J. Appl. Cryst. **4**, 93 (1971).
6. J. TSAU and D. F. R. GILSON. J. Phys. Chem. **72**, 4082 (1968).
7. J. TSAU and D. F. R. GILSON. Can. J. Chem. **51**, 1990 (1973).
8. J. TSAU and D. F. R. GILSON. Can. J. Chem. **52**, 2421 (1974).
9. J. TSAU. Ph.D. Thesis, McGill University, Montreal, Quebec. 1970.
10. G. L. CLARK and C. R. HUDGENS. Science, **112**, 309 (1950).
11. J. D. BERNAL. Z. Kristallogr. **83**, 153 (1932).
12. C. N. R. RAO and K. J. RAO. Progr. Solid State Chem. **4**, 131 (1967).
13. G. DONNAY and T. CAMPBELL. Unpublished results.
14. F. JELLINEK. Acta Cryst. **11**, 626 (1958).
15. M. V. KING and W. N. LIPSCOMB. Acta Cryst. **3**, 222 (1950).
16. E. W. HUGHES and W. N. LIPSCOMB. J. Am. Chem. Soc. **68**, 1970 (1946).
17. S. B. HENDRICKS. Z. Kristallogr. **67**, 119 (1928).
18. S. B. HENDRICKS. Z. Kristallogr. **68**, 189 (1928); **74**, 29 (1930).

Can. J. Chem. Downloaded from www.nrcresearchpress.com by 210.87.254.6 on 09/05/12
For personal use only.

Potential energy calculations of the rotational barriers of molecular solids. II. The dynamic structures of adamantane and hexamethylenetetramine in the solid state and the nature of the phase transition in adamantane[1]

C. A. FYFE[2] AND D. HAROLD-SMITH[3]

Guelph-Waterloo Centre for Graduate Work in Chemistry, Guelph Campus, Chemistry Department, University of Guelph, Guelph, Ontario N1G 2W1

Received January 17, 1975[4]

C. A. FYFE and D. HAROLD-SMITH. Can. J. Chem. **54**, 769 (1976).

Nonbonded atom–atom potential functions have been used in conjunction with literature crystal structure data from diffraction measurements to calculate the sublimation energies and also the energy barriers for rotation around the molecular axes for both α and β phases of adamantane and also for hexamethylenetetramine. These results are compared with experimental values and the nature of the dynamic structures deduced.

In addition, a detailed consideration of individual intermolecular interactions in the case of adamantane is presented which explains in detail the observed high temperature disordered structure and the nature of the associated order–disorder transition.

C. A. FYFE et D. HAROLD-SMITH. Can. J. Chem. **54**, 769 (1976).

On a utilisé des fonctions de potentiel atome–atome nonliés de concert avec des données de la littérature concernant des structures cristallines dérivées de mesures de diffraction pour calculer les énergies de sublimation et aussi les barrières d'énergie à la rotation autour des axes moléculaires des phases α et β de l'adamantane et de l'hexaméthylènetétramine. On compare ces résultats avec les valeurs expérimentales et on en déduit la nature des structures dynamiques.

De plus on présente dans le cas de l'adamantane une considération détaillée des interactions intermoléculaires individuelles qui explique en détail la structure désordonnée observée à haute température et la nature de la transition ordre–désordre qui l'accompagne.

[Traduit par le journal]

Introduction

In recent years, empirical potential functions describing the interaction between nonbonded atoms have been used with varying degrees of success to describe the conformational structures of simple organic molecules, polymers, and biopolymers. For the solid state, these functions have been used to describe and predict the lattice structures, small-angle vibrational motions, and the sublimation energies of the crystals.

In addition to these small-amplitude vibrations in crystals it is known that, in certain cases, molecular motions of much greater amplitude can occur, involving the complete reorientation of groups or whole molecules (1). For example, in the case of crystalline benzene the individual molecules can move in their molecular planes by a jumping motion around the hexad axis.

The energy barriers associated with these jumping motions in the solid state may be deduced from the variation of the nmr linewidth with temperature or from the Waugh estimate of $T = 27E_a$, where T is the temperature of transition in degrees K and E_a is the energy barrier in kcal/mol. Both these techniques are empirical, however, and a better estimate is obtained from measurements of the spin–lattice relaxation time, T_1, or $T_1\rho$, the spin–lattice relaxation time in the rotating frame of the magnetic nuclei. These parameters are very temperature dependent if motion is present, as the movement of the molecules provides a relaxation mechanism for the nuclei, and the temperature dependence can be treated exactly, yielding reliable values for the barrier height (1).

In the preceding paper in this series (2), a model was developed and used to calculate the

[1]Presented at the Canadian Chemical Conference of the Chemical Institute of Canada, Regina, Saskatchewan, June 1974.

[2]To whom correspondence should be addressed.

[3]Present address: Department of Chemistry, Northwestern University, Evanston, Illinois.

[4]Revision received November 17, 1975.

Can. J. Chem. Downloaded from www.nrcresearchpress.com by 210.87.254.5 on 09/05/12
For personal use only.

Can. J. Chem. Downloaded from www.nrcresearchpress.com by 210.87.254.5 on 09/05/12
For personal use only.

reorientational energies for a series of planar polycyclic aromatics, which gave good agreement with the experimentally observed values. An important simplification in the calculations for those particular compounds was the absence of *intra*molecular rotation, the molecules being treated as rigid. The present work is an attempt to apply the method of calculation to more complex systems, while still keeping this particular simplification. These requirements are satisfied in the case of rigid cage-like aliphatic molecules. The two most studied molecules of this type are adamantane (**1**) and its nitrogen substituted analogue hexamethylenetetramine (**2**).

Adamantane, or tricyclo[3,3,1,$1^{3,7}$] decane (**1**), is the simplest cage-like hydrocarbon having its carbon atoms arranged in the tetrahedral structure characteristic of the diamond lattice. Substitution of nitrogen for all four methyne carbons yields the compound hexamethylenetetramine (**2**). Carbon skeletons of adamantane (**1**) and carbon, nitrogen skeleton of hexamethylenetetramine (**2**) are as follows:

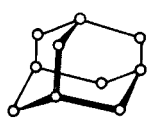

1

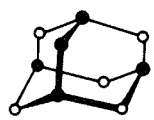

2

Below 208.62 K adamantane crystallizes in an ordered structure. A tetragonal structure, space group $P\bar{4}2_1C$, $a = 6.60$, $c = 8.81$ Å, $Z = 2$, has been reported for this phase (3), and the structure has been further refined by other workers (4). At 208.62 K adamantane undergoes a phase transition (5) to a face centered cubic disordered structure, space group $Fln3m$, with $a = 9.45$ Å and $Z = 4$ (3). The structure indicates a random distribution of the molecules between two positions which are related to each other by a 90° rotation about a molecular twofold axis passing through two methylene groups.

Hexamethylenetetramine (**2**) has been the subject of several X-ray diffraction studies, aimed at measuring both the static and the dynamic features of its structure. It crystallizes in the body-centered cubic space group $I\bar{4}3m$ with $a = 7.02$ Å at 298 K (6).

The high temperature, or α phase of adamantane is plastic crystalline; hexamethylenetetramine and the β phase of adamantane are not. Much of the interest in these three phases has been focused on measuring the structural differences among them in order to determine what properties produce plastic crystallinity. Nuclear magnetic resonance studies have shown that both rotational and translational diffusion are much more rapid in α-adamantane than they are in either β-adamantane or hexamethylenetetramine (7–9). A variety of symmetry axes are available for both molecules, and the purpose of the present work was to try to calculate the complete dynamic structures of both and to relate these results to those from X-ray, neutron diffraction, and nmr measurements. A subsequent paper will describe the predictions made from similar calculations for the dynamic structures of other molecules of this class where fewer experimental data are available (10).

In the present paper, while continuing the type of calculation done in Part I, we also seek to extend the capabilities of these calculations in three ways:

For planar molecules, in plane rotations are much more probable than those about other axes. For 'three-dimensional' molecules, however, the axis (or axes) of rotation may be more difficult to identify. Furthermore, rotations about more than one axis may be significant in the same temperature range and this may be difficult to detect by nmr or other experiments. Hence determining the axis or axes of rotation is a definite objective in extending these calculations to nonplanar molecules. Secondly, for some compounds, a metastable orientation of the molecule may exist which lies at an energy minimum not much greater than that of the equilibrium orientation indicated by X-ray diffraction measurements. In these cases a 'second-order' calculation may be performed in which the effect of populating this metastable orientation is investigated. In this paper we perform such 'second-order' computations on adamantane.

While it is apparent that in an order–disorder transition the energy required for a molecule to rotate to an orientation of disorder must depend on the orientations of its neighboring molecules, very little quantitative information is extant about specific potentials for large-angle molecular motions and how these potentials are changed by the corresponding orientation of nearby molecules. Discussions of such transitions often

Can. J. Chem. Downloaded from www.nrcresearchpress.com by 210.87.254.5 on 09/05/12
For personal use only.

employ 'order parameters' which detail the amount of disordering introduced during the transition but which give no information as to the molecular mechanism involved. Second order calculations of the type described above provide a possible method for the investigation of order–disorder transitions, and we have used them in an attempt to determine how the dynamic structure of the ordered β phase leads to the disordered high temperature α phase.

Experimental

All calculations were performed on an I.B.M. 360-75 computer using Fortran IV programs written by the authors. Copies of these programs and additional information are available on request.

Results and Discussion

Calculations of the rotational barriers around all the axes of molecular symmetry of adamantane in both of its phases and of hexamethylenetetramine have been made, as well as a detailed breakdown of the interactions which produce the phase-transition of adamantane. For clarity of presentation, the different parts of these calculations will be described in separate sections:

Adamantane: Model and Choice of Potential Functions

It is assumed that the potential energy of interaction between any two molecules in a crystal is given by a sum over atom–atom pair interactions. The latter are assumed to be a function only of the distance between the two atoms, to be independent of the nature of the rest of the molecule of which the given atom forms a part, and to be unaffected by the presence of nonbonded atoms on a third molecule with which the two atoms under consideration may be simultaneously interacting. The particular functional form used for such pairwise additive atom–atom potentials is the exponential-6 function:

$$[1] \qquad V_{ij} = -Ar^{-6} + B\exp(-Cr)$$

The potential energy of interaction between two nonbonded atoms, V_{ij}, is thus a simple function of the distance r between them; the empirically determined parameters A, B, and C are different for chemically differing pairs of atoms. The experimental information used to obtain these parameters are the observed crystal structures for a series of molecular crystals, and the enthalpies of sublimation. Williams (11) has determined that for hydrocarbons the atom-centered functions (eq. 1) are superior to bond-centered models. A convenient review of much of the work on potential functions has been done by Mason (12).

If the equilibrium crystal structure is known, all interatomic distances can be computed and the equilibrium lattice-sum for potential energy found:

$$[2] \qquad U = \frac{1}{2}\sum_{i=1}^{n}\sum_{j}^{\infty} V_{ij}(r_{ij})$$

where n is the number of atoms in the molecule and the sum to infinity over j implies that the interaction energy of atom i with all atoms of all other molecules in the crystal must be accounted for. Each term V_{ij} is given by the appropriate form of [1]; since V_{ij} is zero where r_{ij} is infinite, U is measured relative to the energy of the molecules at infinite separation from one another, *i.e.* relative to the ideal gas. Thus, the sublimation enthalpy at absolute zero (taken as positive) is given by:

$$[3] \qquad (\Delta H_{sub}{}^{0})_{T=0} = -U - E_0$$

where E_0 is the zero-point energy (taken as positive) associated with the lattice modes. In the present work, the summation over j, in [2], was not carried out to infinity, but was restricted to $r_{ij} < 8$ Å or < 10 Å. All V_{ij} terms become extremely small outside this range, and since the object of the present work was to compute energy *differences*, the small errors introduced by cutting off the summation will very nearly cancel.

In the initial calculations, the mechanical model for the motion was the simplest possible one in which one molecule (M) was considered to move while all the other molecules were kept static in the lattice at the positions of minimum potential as indicated by the X-ray diffraction structure. Intramolecular motions and any concerted motions between the molecules were neglected. The only justification for such a simple model is its success in explaining the experimental data in both the previous work (2, 10) and also the present investigations. This is not to say that molecular distortions or concerted motions may not occur; but if they do, they do not exert a large influence on the physical properties presently being calculated.

TABLE 1
(*a*) Calculated and measured heats of sublimation

Phase	ΔH_{sub} (measured)	ΔU (calcd)	Cell dimensions
β-Adamantane	13.5[a]	14.4[d]	$a_0 = 6.60$ $c_0 = 8.81$
α-Adamantane	12.7[b]	12.9[e]	$a_0 = 9.426$
		13.1[d]	$a_0 = 9.426$
		13.0[d]	$a_0 = 9.45$
Hexamethylenetetramine	18.1[c]	15.5[f]	$a_0 = 6.910$ (34 K)
		16.5[f]	$a_0 = 6.931$ (100 K)
		16.9[f]	$a_0 = 7.021$ (298 K)
Adamantane (HMT lattice)	—	8.5[f]	$a_0 = 7.37$
Hexamethylenetetramine (α-adamantane lattice)	—	14.3[f]	$a_0 = 9.30$
Hexamethylenetetramine (β-adamantane lattice)	—	16.4[f]	$a_0 = 6.60$ $b_0 = 8.81$

[a]Reference 14.
[b]Reference 13.
[c]Reference 25.
[d]Reference 11*c*, Table 1B.
[e]Reference 11*c*, Table 1C.
[f]Reference 11*b*.

(*b*) Parameters used in the evaluation of V_{ij} (eq. 1)

Atom pair	A (kcal mol^{-1} Å^6)	B (kcal mol^{-1})	C (Å^{-1})	Reference
C–C	565.01	75 523	3.60	11*c*, Table 1B
C–H	108.15	10 352	3.67	
H–H	20.7	1 729	3.74	
C–C	512.57	71 782	3.60	11*c*, Table 1*C*
C–H	111.84	8 503	3.67	
H–H	24.4	2 171	3.74	
C–C	5.68	83 620	3.60	11*b*
C–H	1.25	8 766	3.67	
H–H	27.3	2 654	3.74	

The mechanics of the calculations have been outlined previously and will be only briefly reviewed here.

In the application of this model, the molecule of interest (M) was placed in the correct position as indicated by X-ray diffraction measurements in a unit cell which itself was placed at the center of a group of 26 or more unit cells. The potential energy from the nonbonded interactions of the atoms in this molecule with the atoms of the other molecules in its own unit cell and those of all the molecules in the surrounding unit cells was evaluated as a sum of the appropriate pair potentials.

When the molecule (M) is thus located in the position given by the X-ray structure, the intermolecular potential evaluated corresponds to the experimentally measurable sublimation energy ΔH_{sub}.

The molecule (M) was then rotated by an angle θ around a chosen axis to a new set of coordinates, with all the other molecules in the surrounding unit cells kept static in their original positions, and the intermolecular potential between (M) and all the rest was evaluated as a function of the angle of reorientation. For comparison with experimental data the difference in energy between the zero rotation and the computed maximum in this curve was equated to the activation energy for motion about this axis.

β Phase Adamantane

The angular dependence of the potential energy for rotation of the adamantane molecule in the β phase about both its twofold and threefold axes was calculated using the model outlined above, using hydrogen coordinates generated from the carbon coordinates with a C—H bond length of 1.08 Å as in previous calculations, and using Williams' most recent parameters for aliphatic compounds only (11). These results are tabulated in Table 1 and presented diagramatically in Fig. 1 *A* and *B*.

Can. J. Chem. Downloaded from www.nrcresearchpress.com by 210.87.254.5 on 09/05/12
For personal use only.

Can. J. Chem. Downloaded from www.nrcresearchpress.com by 210.87.254.5 on 09/05/12
For personal use only.

In the case of rotation of the molecule about its threefold axis in the β phase (Fig. 1*A*), the potential repeats every 120° as required by the symmetry of the axis, 120° movements bringing the molecule back to a position of minimum potential where the positions of all atoms are identical to those in the original 0° rotation.

Less obvious from the crystal structure is the symmetry of each 120° phase about its midpoint; and the subminimum at each of these midpoints was totally unpredictable. The calculated barrier to rotation was 4.4 kcal/mol, in acceptable agreement with the experimental values of 5.8 and 6.5 kcal/mol from T_1 measurements reported for E_R of β-adamantane. Examination of the molecular packing in the β phase shows that the potential for rotation about the twofold axis is expected to be asymmetric, and this asymmetry is reflected in the calculated potential. According to the calculations, the twofold axis rotational barrier is 5.6 or just 1.2 kcal/mol larger than the threefold axis barrier. Measurements of E_R by pulse nmr undoubtedly reflect a weighted average or rotations about several axes.[5]

Thus at very low temperatures, adamantane will be completely rigid in its lattice. Wide line nmr measurements indicate that motion on this timescale is occurring in the β phase at temperatures >125 K (8). The above results indicate that orientation will occur initially by movement around the threefold axis and then with a gradual admixture of motion around the twofold axis. Because the two barriers are similar in energy, a single second moment transition is expected, as is observed experimentally, and the barrier heights from T_1 measurements will be a weighted average. It is also thought that at these temperatures a small proportion ($<6\%$) of the molecules will occupy the positions indicated by the subminima in Fig. 1 *A* and *B*.

The calculated sublimation energy of 14.4 kcal/mol (Table 1) is in reasonable agreement with the experimental value of 13.5 kcal/mol.

[5]For rotation about an arbitrarily chosen axis orthogonal to the twofold axis, we calculated a potential barrier of 4.7 kcal/mol. Because of the nearly spherical symmetry of the molecule, the maximum repulsions produced by rotations about various axes are nearly equal. Combinations of rotations about other axes equivalent to a 60 or 120° jump about the threefold axis or a 70, 110, or 180° jump about the twofold axis are required for the molecule to return to one of the positions of minimum potential shown in Figs. 1 *A* and *B* at the end of its rotational jump.

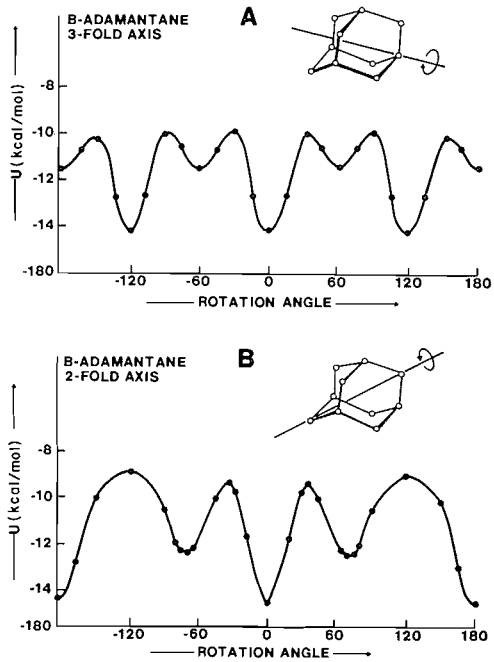

FIG. 1. (*A*) Potential for rotation of the test molecule M about the threefold axis in β-adamantane. (*B*) Potential for rotation of M about the twofold axis in β-adamantane.

α Phase Adamantane

Since the crystal structure of α-adamantane indicates that the molecules are randomly distributed between two disordered positions (Fig. 4*A*), the potential energy for each rotation angle of the test molecule was calculated twice: once with all the other lattice molecules in one of the disordered orientations, and a second time with the lattice molecules in the other orientation. The measured energy is approximated in the present case by the average of these two calculations. In fact, for any given molecule, there will be a unique potential function which will be a weighted average of the two potential functions depending on the particular distribution of the surrounding molecules over the two sites available to each molecule.

Figure 2*A* shows the potential for rotation of the test molecule about the twofold axis when all of the molecule's neighbors have been artificially given the same orientation. Figure 2*B* is the average of Fig. 2*A* and the potential generated by rotation of the test molecule about the twofold axis with all of the surrounding molecules in the *other* of the two disordered orientations. The latter potential is not illustrated since, except for

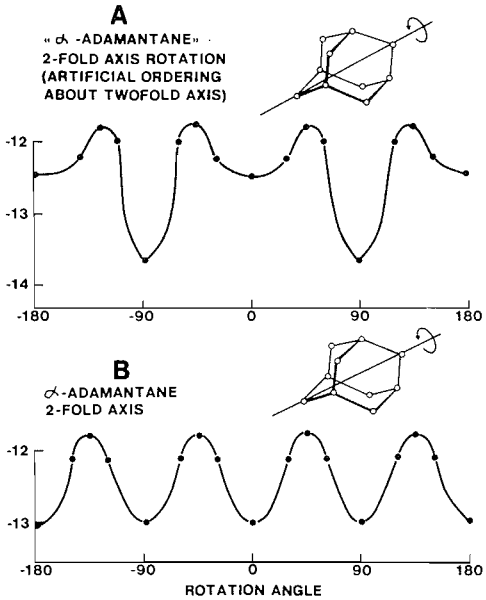

FIG. 2. (*A*) Potential for rotation of M about the twofold axis in an artificially ordered 'α-adamantane' lattice. All of the lattice molecules are in the same one of the two disorder orientations. (*B*) Potential for rotation of M about the twofold axis in the true, disordered α-adamantane lattice, assuming an equal distribution of the surrounding molecules over the two possible orientations for each.

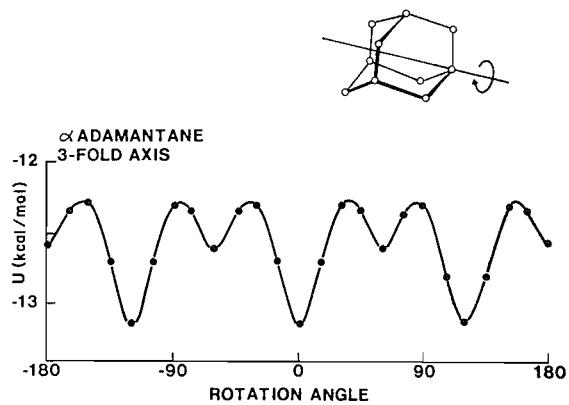

FIG. 3. Potential for rotation of M about the threefold axis in α-adamantane, assuming an equal distribution of the surrounding molecules over the two sites available for each.

being 90° out of phase, it is identical to Fig. 2*A*. The potentials for rotation of adamantane about its threefold axis as calculated in this manner are shown in Fig. 3. The results are tabulated in Table 1. Again the potential shown is only an approximate representation of the energy barrier involved. Any particular molecule will have a specific potential function for reorientation which will depend on the distribution of the surrounding molecules over the two sites available to each.

The calculated lattice energy for α-adamantane is 13.2 kcal/mol compared to the experimental lattice enthalpy of 12.8 kcal/mol (13). The calculated value for the difference between the lattice energies of the α and β forms is thus 1.2 kcal/mol, which is in excellent agreement with the measured value of 0.8 kcal/mol (5). It is also in agreement with the value of 1.3 kcal/mol quoted by Wu *et al.* (13), who used potential functions of the type described here to explain the observed ir frequencies of solid adamantane and used these to investigate the phase transition in solid adamantane. Although complete details are not given, they also made preliminary calculations of the transition energy and the barriers to rotation about the twofold axis.

The Mechanism of the Order–Disorder Transition of Adamantane

The cell dimension of (cubic) α-adamantane is $a_\alpha = 9.4$ Å, and for β-adamantane (tetragonal) the dimensions are $a_\beta = 6.6$, $c_\beta = 8.8$ Å. Nordman and Schmitkons (3) observed that when α-adamantane was cooled into the low temperature form, the directions of the tetragonal c axis always coincided with the direction of one or more of the three cubic a axes. Thus, as can be seen from Fig. 4, the order–disorder transition in adamantane takes place through a reorientation of the molecules about their twofold axes. According to the X-ray diffraction measurements, the reorientation angle is either 9 or 81°, depending on which of the two disorder positions the individual adamantane molecule assumes in the disordered phase.

Because it seems probable that the subminima in the calculated potentials for the β phase be responsible for the transition to the high temperature phase, a second-order recalculation of the potentials in Fig. 1 has been performed to try to elucidate the mechanism of the transition. In this calculation the molecules surrounding the test molecule have been reoriented to the positions which were metastable in the first-order calculation. This was done not only to improve the accuracy of the first-order calculation, but because it was hoped that the second-order calculation might give at least some qualitative

Can. J. Chem. Downloaded from www.nrcresearchpress.com by 210.87.254.5 on 09/05/12
For personal use only.

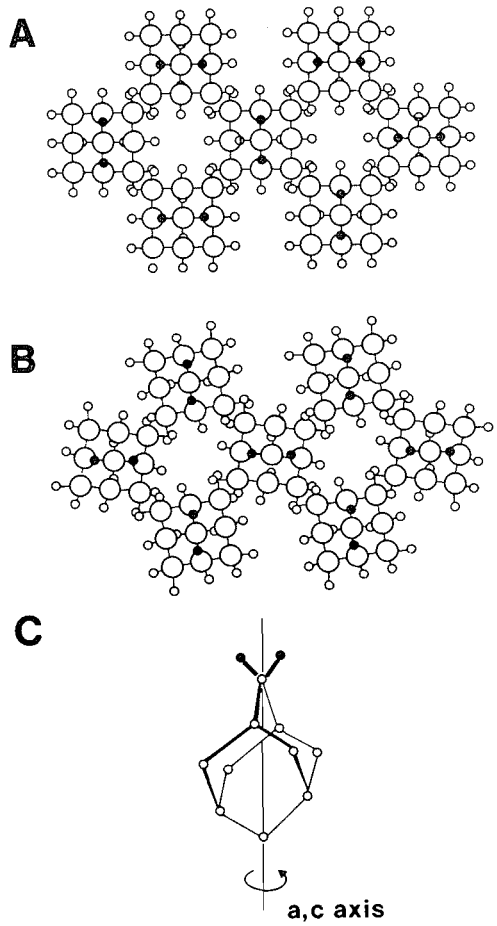

FIG. 4. Illustration of the rotation about the molecular twofold axis which produces the order–disorder transition in adamantane. The projections in (*A*) and (*B*) are down the axis of rotation. (*A*) The high-temperature, α phase. The random distribution of the molecules between two orientations, which are interchangeable by a 90° rotation about the projection axis is illustrated by the upper methylene hydrogens (dark circles). The cubic *a* axis is diagonal. (*B*) The low-temperature, β phase. Ordered phase produced by molecular rotations of 9 and 81°. The projection axis coincides with the tetragonal *c* axis, and the *a* axis is vertical. (*C*) Illustration of the adamantane molecules projected in (*A*) and (*B*). All of the hydrogen atoms have been omitted, except the upper pair of methylene hydrogens (dark circles). The plane of the other methylene group (lowermost carbon) is orthogonal to the plane of the methylene group shown.

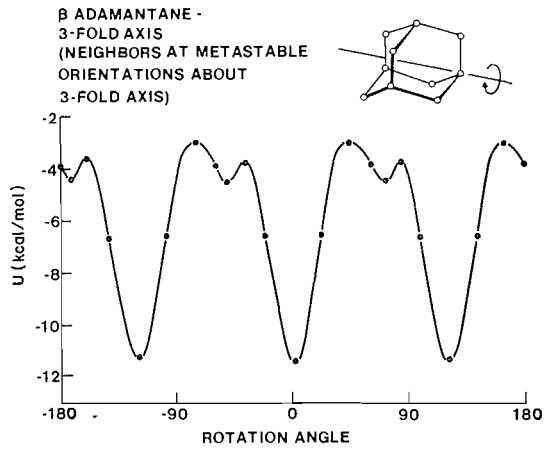

FIG. 5. Potential for rotation of M about the threefold axis when all the neighboring molecules have been rotated about their threefold axes to metastable orientations.

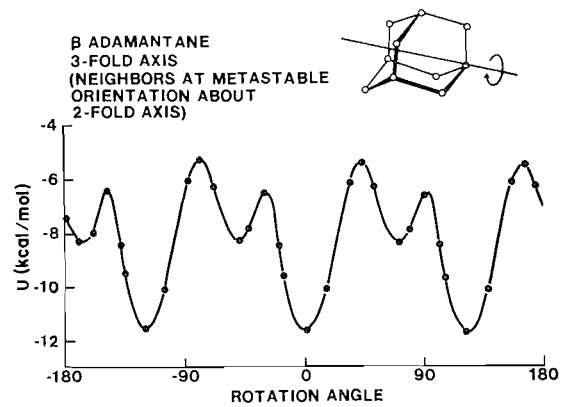

FIG. 6. Potential for rotation of M about the threefold axis when all the neighboring molecules have been rotated about their twofold axes to metastable orientations.

information about the mechanism of the phase transition. In particular, it was hoped that rotation of some molecules to nonequilibrium positions would lower the metastable potential for rotation of the test molecule about its twofold axis and shift the position of the subminimum from 70° closer to 90°. It was also hoped that a molecule-by-molecule consideration of the potentials between the test molecule and its neighbors would make possible a quantitative treatment of the 'coupling' which produces the phase transition and indicate clearly why this ends in statistical disorder about the twofold axis in the α phase.

Figures 5 to 8 show the effects on the two- and threefold axes potentials of rotating *all* the molecules in the lattice to a given orientation of subminimum energy. For example (Fig. 5), when all the surrounding molecules are rotated 60° about the threefold axis, the potential energy of the test molecule at its equilibrium position is raised from -14.4 to -11.5 kcal/mol and the

Can. J. Chem. Downloaded from www.nrcresearchpress.com by 210.87.254.5 on 09/05/12
For personal use only.

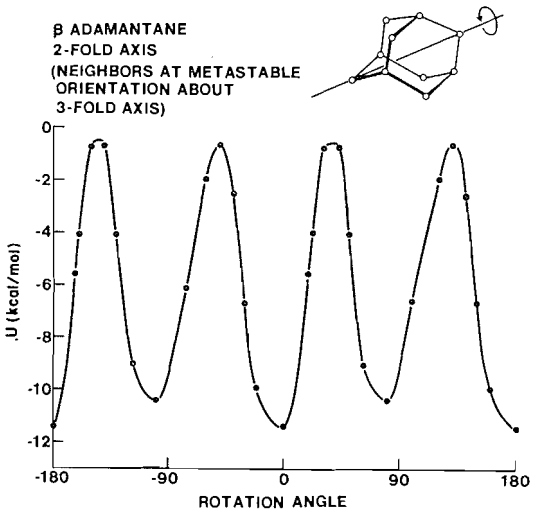

FIG. 7. Potential for rotation of M about the twofold axis when all the neighboring molecules have been rotated about their threefold axes to metastable orientations.

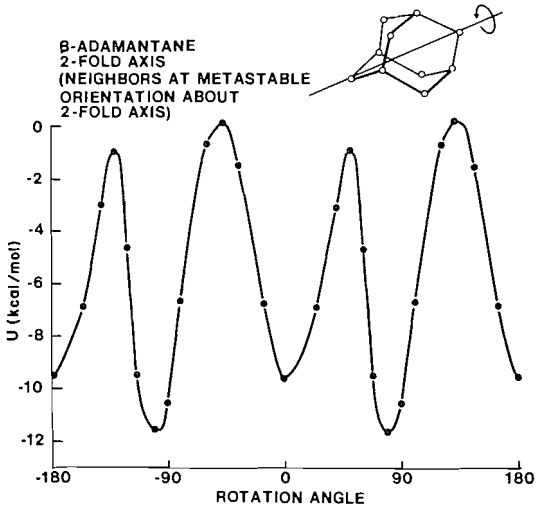

FIG. 8. Potential for rotation of M about the twofold axis when all the neighboring molecules have been rotated about their twofold axes to metastable orientations.

barrier to rotation about its threefold axis increases from 4.5 to 8.4 kcal/mol. Furthermore, the energy difference between the metastable and the equilibrium orientations increase from 2.9 to 6.9 kcal/mol. (The position of the metastable orientation also shifts from 60° to about 65°.) If a random distribution of reoriented molecules is assumed, this type of motion therefore tends to be self-quenching, although this may not be true of specific molecular pairs.

Figure 6 shows the effect on the threefold axis rotation when the surrounding molecules are reoriented about their twofold axes. Again, motion about the threefold axis tends to be quenched, although the effects are weaker. The sublimation energy of the test molecule is reduced in this case also, from 14.4 to 11.7 kcal/mol.

Figures 7 and 8 show the results of analogous second-order calculations for rotation of the test molecule about its twofold axis. It is this type of reorientation which, according to the X-ray diffraction studies, produces the disordered phase. In both calculations, the sublimation energy has been reduced to about 11.6 kcal/mol.

As shown in Fig. 7, the effect of orienting the surrounding molecules at their metastable orientation about their threefold axes is to increase the barrier to rotation of the test molecule about its twofold axis and to lower the difference in energies between the equilibrium and metastable positions.

Figure 8 shows the effects of orienting the surrounding molecules at their metastable orientation about their twofold axes on the rotation of the test molecule about its twofold axis. In this case, the potential of the 'metastable' orientation is now *lower* than the potentials of the 'equilibrium' orientation. Qualitatively, then, the potential in Fig. 8 has exactly those properties necessary to produce the observed phase transition; (*1*) the position of the minimum has shifted from 70 to 85° (observed, 90°), (*2*) the position of the barrier to rotation is shifted from 35 to 45°, (*3*) the 'metastable' energy is now lower than the 'equilibrium' energy. This last feature is crucial, since it means that the more molecules jump to the metastable orientation, the easier it becomes for other molecules to make this same jump and the more difficult it is for the molecules in the metastable position to jump back. Eventually, at equilibrium (when the phase transition is complete) the potential energies for both orientations of the test molecule must be the same and the rates of 'forward' and 'backward' jumps must be equal. Thus, the situation described in Fig. 8 is one which will not be reached in practice. It does, however, contain all the information about the effect of orienting any one of the surrounding molecules at its metastable orientation.

Table 2 summarizes the (molecular) pair-wise interactions which produce the phase transition.

Can. J. Chem. Downloaded from www.nrcresearchpress.com by 210.87.254.5 on 09/05/12
For personal use only.

TABLE 2. Calculated and measured activation enthalpies for rotation (kcal mol^{-1}) of adamantane and hexamethylenetetramine in their molecular crystals

Phase	Molecular axis	E_R Calculated	E_R Measured Reference 7	E_R Measured Reference 25
β-Adamantane	Twofold	4.4	6.50	4.1
	Threefold	5.6		
α-Adamantane	Twofold	1.5	3.08	
	Threefold	1.0		
Hexamethylenetetramine	Twofold	18.0	19.3	17.9, 18.7
	Threefold	20.3		

TABLE 3

(*a*) Roles of neighboring molecules in the order–disorder transition of adamantane in the solid state

Axis of rotation	Cell	D	ΔE_θ[a] $\theta = 70°$	$\theta = 0°$	$\theta = 35°$	E_{Rf}	E_{Rb}
Twofold	1,6,8,10	6.42	−0.37	+0.21	0.00	5.0	3.5
Twofold	3,5,7,9	6.42	−0.23	+0.20	+0.06	5.1	3.3
Twofold	2,3,4,5	6.60	+0.15	+0.25	+1.09	6.0	4.1
Threefold	2	6.60	+0.10	+0.23	+0.44	5.4	3.4
Threefold	3	6.60	+0.18	+0.59	+1.39	6.0	4.3
—	—	0	0	0	0	5.2	3.1

[a] ΔE_θ is the change in potential of the test molecule (at a rotation angle of θ degrees) when *one* of the molecules named by column 2 has been reoriented from its equilibrium orientation about the axis listed in column 1 to the subminimum orientation for that axis of rotation. Energies are in kcal/mol. D is the distance in Angströms between the center of mass of the molecule and the center of mass of the test molecule. E_{Rf} is the difference between the maximum potential encountered during rotation and the equilibrium potential. E_{Rb} is the difference between the maximum potential and the potential of the metastable orientation.

(*b*) Locations of unit cells referred to in (*a*)

Cell	X	Y	Z
1	0	0	0
2	1	0	0
3	−1	0	0
4	0	1	0
5	0	−1	0
6	−1	0	−1
7	0	0	−1
8	0	−1	−1
9	−1	−1	−1
10	−1	−1	0

Columns 1, 2, and 3 list the neighboring molecule, its cell, and the axis about which it has been rotated respectively. The rotations were 70 and 60° about the two- and threefold axes, respectively, these being the metastable orientations in the first order calculation (see Fig. 1), ΔE_θ is the difference between the potentials of the test molecule (rotated θ degrees from equilibrium) when the neighboring molecule has undergone the indicated reorientation, and when it is at its equilibrium position. E_{Rf} and E_{Rb} are the activation energies for rotation from the equilibrium to the metastable orientations and *vice versa*. θ = 0, 80, and 35° are, respectively, the equilibrium, metastable, and potential submaximum orientations. Several conclusions may be quickly noted: (*1*) Except for next nearest neighbors in cells 2 and 3, rotation of neighboring

Can. J. Chem. Downloaded from www.nrcresearchpress.com by 210.87.254.5 on 09/05/12
For personal use only.

molecules about their threefold axes does not promote the transition. (*2*) Rotations of these molecules aid the transition only because they raise the energy of the test molecule at its equilibrium orientation more than they increase the potential of its metastable orientation. (*3*) Only eight molecules promote the transition by both lowering the energy of the metastable orientation of the test molecule and raising the energy of its equilibrium orientation. These eight are the nearest neighbors and may be divided into two groups of four equivalent molecules. Both types increase the equilibrium potential of the test molecule by about 0.2 kcal/mol; but the one type decreases the potential of the metastable orientation of the test molecule by 0.23 kcal/mol while the other produces a greater effect by decreasing its metastable potential by 0.37 kcal/mol. (See Table 3.)

Hexamethylenetetramine: Model and Choice of Potential Functions

The same model of the reorientation processes was used in which a single molecule was rotated, the rest of the lattice being held rigid at the positions indicated by the X-ray structure. An additional problem exists for hexamethylenetetramine (HMT), however, in that the addition of the nitrogen atoms requires three new interatomic potential functions: N–N, N–H, and N–C. Some of the parameters used by various workers have been briefly reviewed by Venkatachalam and Ramachandran (14) and later by Scheraga (15).

Three sets of published parameters for nitrogen were tried in calculations on hexamethylenetetramine. These included two sets based on Kitaigorodskii's approach (16) (KI and KII in refs. 14 and 15) and the set used by Scheraga (15). None of the three yielded calculated values of the sublimation energy and rotation barrier which were even close to correct. For example, the latter set, which gave the best values among the three, is illustrated in Fig. 10*B*. The total N–N, N–C, N–H potential for rotation of hexamethylenetetramine about its twofold axis varied by less than 0.5 kcal/mol, although it was known from a calculation on the hydrocarbon portion of the molecule that the contribution from the nitrogen interactions was at least 10 kcal/mol. Therefore, an alternative approach was chosen.

While recognizing that bond-centered potentials may be theoretically preferable to atom-centered potentials, it is thought that the published empirical coefficients for the latter model give more accurate results than those available for the bond-centered model. In the present model, the electron lone-pair and nucleus of nitrogen are considered to be similar to a hydrogen bonded to a carbon. Thus a nitrogen atom and its lone pair are treated exactly as a hydrogen bonded to a carbon except that the 'C—H' bond distance is shorter for nitrogen. This allows us to treat the three additional pair interactions created by insertion of nitrogen into a hydrocarbon with just one parameter, rather than the nine additional parameters which would otherwise be required. Its chief justification, however, lies in the agreement it gives between calculated quantities and their measured values.

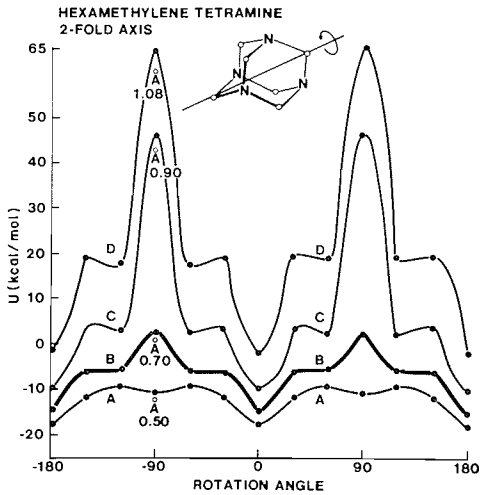

FIG. 9. Dependence of the potential for rotation of the test molecule M about the twofold axis of hexamethylenetetramine on the length of the hypothetical nitrogen–hydrogen bond.

Figure 9 shows how the total potential calculated for rotation of hexamethylenetetramine about its twofold axis varies as the hypothetical N—H bond distance is changed. Since the measured activation energy for rotation of hexamethylenetetramine is 19.3 kcal/mol (7), and 'N—H' distance of 0.7 Å gives the best agreement between calculation and measurement. There is support for this value in the work of Allinger and Thai (17) who calculated the potentials for approach of a helium atom toward an ammonia molecule along both the electron lone pair and the H—N bond axis. The two

Can. J. Chem. Downloaded from www.nrcresearchpress.com by 210.87.254.5 on 09/05/12
For personal use only.

Can. J. Chem. Downloaded from www.nrcresearchpress.com by 210.87.254.5 on 09/05/12
For personal use only.

potential curves have nearly identical shapes and were separated by a distance of 0.69 Å. This distance is almost identical to the difference between the N—H bond length and the distance of the centroid of the lone pair from the nitrogen nucleus (18). Furthermore, this method of treating the effect of elements with lone pairs of electrons is analogous to models for predicting the geometries of small molecules which have been so successful, in which the effect of lone pairs of electrons is considered similar to that of bonds (19, 20). The present work merely extends this approach to intermolecular interactions involving these orbitals, and puts it on a quantitative basis.

Reorientation in Hexamethylenetetramine

The crystal structure of hexamethylenetetramine has been carefully studied by both X-ray and neutron diffraction (21–24). The most recent and accurate study is by Becka and Cruickshank, who obtained anisotropic atomic-vibration amplitudes at 298, 100, and 34 K (24). The compound is ideally suited for this kind of study because of its cubic molecular and crystal symmetries. Information about both translational and small-angle rotational vibrations was obtained in that study.

Large-jump rotation, translation, and impurity diffusion have been studied by nmr. Smith (25) obtained values for the rotational activation energy of 17.9 and 18.7 kcal/mol from second moment studies and T_1 measurements; Resing (7) obtained a value of 19.3 kcal/mol. Correlation times for translational self-diffusion were too long to be measured even by $T_{1\rho}$ (7).

Thermodynamic studies of HMT include low temperature calorimetric work by Westrum (5) and measurements of the vapor pressure by Stranski *et al.* (26).

Probably the major motivation for most of the work which has been done to date on HMT has been to establish why HMT is not plastic-crystalline in spite of its close structural similarity to adamantane. From the nmr studies, it seems certain that the lack of plastic crystallinity in HMT as compared to adamantane is connected with its lack of rotational and translational mobility, but it is unclear just how the substitution of four nitrogen atoms for four C—H groups produces the drastic reduction in mobility. Smith has offered a discussion of this

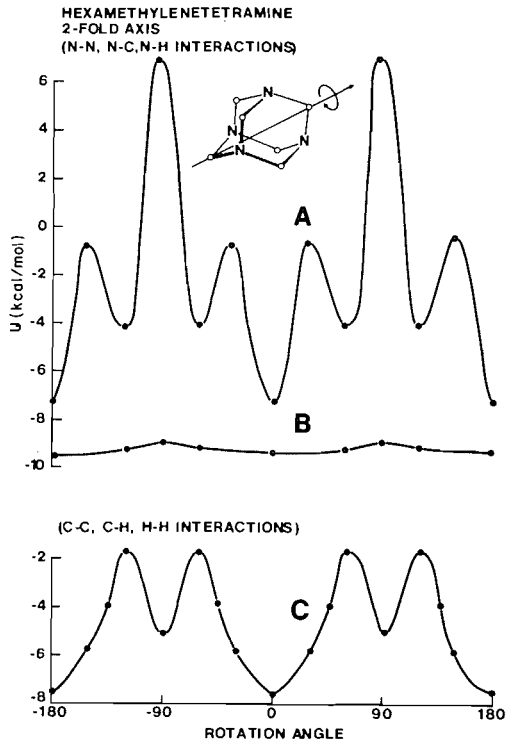

FIG. 10. Potential for rotation of M about the twofold axis broken down into the sum of the interactions involving nitrogen and the sum of the interactions not involving nitrogen. (*A*) Sum of the interactions involving nitrogen computed with hypothetical nitrogen–hydrogen bonds on each nitrogen (bond length 0.7 Å). (*B*) 'Best' sum of the interactions involving nitrogen computed without hypothetical nitrogen–hydrogen bonds (Scheraga's parameters for nitrogen). (*C*) Sum of the C—C, C—H, and H—H potentials for rotation of hexamethylenetetramine about the twofold axis. Most of the barrier to rotation of hexamethylenetetramine about the twofold axis comes from interactions involving the nitrogen lone pairs.

problem in terms of specific atomic interactions (25), but the treatment was largely qualitative and hence inconclusive. He divided the barrier to rotation for HMT into two parts: (*1*) hydrogen bonding between molecules and (*2*) 'steric' interactions. The 'steric' interactions in HMT were assumed to be equal to those in adamantane, and the difference between E_R (HMT) and E_R (adamantane) was then supposed to be entirely due to the hydrogen bonding in the former. This left a value of 0.7 kcal/mol for each hydrogen bond. He also concluded that the threefold axes were probably the axes of rotation. However, the ordered cubic structure of HMT and the disordered cubic structure of adamantane do not

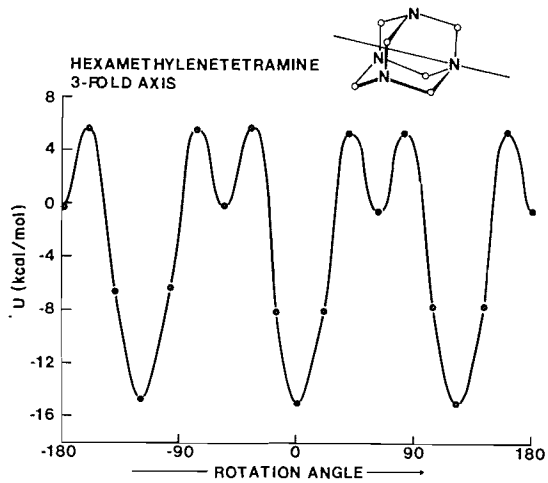

FIG. 11. Potential for rotation of M about the threefold axis in hexamethylenetetramine.

belong to the same space group; and there is no reason to suppose these 'steric' interactions be equal.

Figure 10 shows the variation of the potential energy of HMT as it is rotated about its twofold axis. The computed value of E_R is 17.0 kcal/mol, in satisfactory agreement with the measured value of about 19 kcal/mol. Figure 10 also shows the total potential broken down into two potentials, one which includes all the nitrogen interactions, and one which includes only interactions involving carbon and hydrogen. The latter potential, with its subminimum between two maxima in a period of 180° is qualitatively similar to the analogous potentials of adamantane in both its α and β phases. In HMT, however, no metastable orientation is available to the molecule due to the strongly repulsive nitrogen interactions at and near the position of 90° rotation.

The potential for rotation of HMT about its threefold axis is illustrated in Fig. 11. Like the potential for rotation of adamantane about its threefold axis, the HMT potential contains a subminimum at the center of each 120° period. For HMT, however, the energy of this position is so high that the population of this orientation is negligible. The computed value of E_R for rotation about the threefold axis is 20.3 kcal/mol. This suggests that the measured values of E_R include a weighted average for rotations about both the two- and threefold axes. Energetically, rotation about the twofold axis is favored roughly 3:1 over rotation about the threefold axis; but the relative entropies of activation may be of greater importance in determining the relative jump frequencies.

Finally, it is useful to compare the computed sublimation energy with the measured enthalpy of sublimation for HMT. Along with the measured value of E_R, this provides two observational equations which must be fit by the one empirical parameter, the 'N—H' bond distance. Our computed sublimation energy is 15.1 kcal/mol at 34 K, 16.1 kcal/mol at 100 K, and 16.6 kcal/mol at 298 K. From the data of Stranski *et al.* (26), Smith (25) has obtained a sublimation enthalpy of 18.1 kcal/mol from literature data. Thus, the computed sublimation energy appears to be 1 to 2 kcal/mol too small. The sum of the carbon–carbon, carbon–hydrogen, and hydrogen–hydrogen contributions to the net lattice energy is about 7.5 kcal/mol.

An attempt may also be made within the format of these calculations to understand why, despite their similar molecular structures, adamantane and hexamethylenetetramine crystallize in different lattices. This may be done by comparing the computed sublimation energies for the actual structure with those calculated for HMT in the adamantane structure and for adamantane in the HMT structure. The lattice energy of adamantane crystallized with the HMT lattice has been calculated as a function of the unit cell dimension and is found to reach a maximum value of 8.8 kcal/mol at $\alpha_0 = 7.35$ Å. By comparison, the sublimation energy of the disordered, cubic form of adamantane (calculated) is 13.1 kcal/mol; and the sublimation energy of the low temperature form is 14.4 kcal/mol. The lattice energy of HMT crystallized in the β form of adamantane is 16.4 kcal/mol. For the α form an illustrative calculation was performed in which all the HMT molecules occupied one of the two possible positions of the disordered forms; this yielded a lattice energy of 14.3 kcal/mol.

These calculations show unequivocally that the HMT structure is not available to adamantane. But the energies calculated for HMT in the two structures of adamantane are equal, within experimental error, to the calculated lattice energy of HMT in its observed crystal structure. This may be due to the use of 'incorrect' values

Can. J. Chem. Downloaded from www.nrcresearchpress.com by 210.87.254.5 on 09/05/12
For personal use only.

Can. J. Chem. Downloaded from www.nrcresearchpress.com by 210.87.254.5 on 09/05/12
For personal use only.

for the empirical parameters in the N–N, C–N, and N–H potential functions. Or it may be that the forms of the potential functions are inadequate and that the octupole moment of HMT is the force which causes it to crystallize in a lattice different from those of adamantane. The work of Kihara (27) supports the latter interpretation.

Recently, Dolling *et al.* (28) have suggested that the systematic difference between the measured librational frequencies of HMT and the values which they calculated might be due to the octupole moment of the HMT molecule. In their calculation, they used the pair-potential parameters of Kitaigorodskii (29) for the C–C, C–H, and H–H interactions and used the carbon parameter for nitrogen. Since this method ignores the lone electron pair of nitrogen (and since we find that Kitaigorodskii's parameters do not give good results for the rotational activation energies), it seems probable that the error in the dispersion and repulsion terms of their calculation be larger than the octupole contribution.

The HMT octupole moment arises from the sum of the dipole moment associated with each nitrogen. The nitrogen dipole moment is caused by the difference in the electron distributions of the lone pair and the three N—C bonds. Since the distance between intramolecular nitrogens is comparable to the intermolecular distance between nearest-neighbor molecules, it is more accurate to treat the dipoles individually than it is to approximate their molecular sum as a point octupole. In fact, we have chosen to reduce the approximation by replacing the point dipoles with point charges at the nitrogen nucleus and bonds.

The coordinate differences between the bond midpoints and the electron 'centers of gravity' may be taken from the difference between the coordinates derived from neutron and X-ray diffraction measurements, respectively. These measurements show that the center of seven electrons is shifted 0.018 Å along the direction of the lone pair from the nitrogen protons (28).

Inclusion of the octupole term increases the sublimation energy of HMT by 0.4 kcal/mol and increases the calculated rotational activation energy by 1.0 kcal/mol. Since the values computed without the octupole term for these two quantities were each about 2 kcal/mol smaller than the measured values, inclusion of the octupole term does improve the agreement between measurement and calculation. Calculations on hexamethylenetetramine crystallized with the lattice structure of β-adamantane show that in this case the contribution of the octupole term to the lattice energy is negligible.

In order to form some idea of the dependence of ΔE_{sub} and E_R on the nitrogen dipole moment in HMT, the calculation has been repeated assuming a charge separation of 0.036 Å. (This is double the experimental value and equivalent to the diffraction coordinates each being in error by 0.009 Å. This is not unreasonable, since the estimated standard deviations alone are about 0.004 Å and molecular rotation etc. introduces systematic errors of this magnitude (24).) This increased the sublimation energy by 1.0 kcal/mol and the rotational activation energy by 1.3 kcal/mol. We therefore conclude that the inclusion of the four dipoles of hexamethylenetetramine constitute only a small correction to our calculations.

NOTE ADDED IN PROOF:

The subminima for rotation about the two- and three-fold axes in adamantane shown in Fig. 1 have been found to be true subminima on a three dimensional energy surface and not 'saddle points' (30).

1. (*a*) J. G. POWLES. Arch. Sci. (Geneva), **12**, 87 (1959); (*b*) E. R. ANDREW. J. Phys. Chem. Solids, **18**, 9 (1961); (*c*) E. R. ANDREW and P. S. ALLEN. J. Chem. Phys. **63**, 85 (1966); (*d*) C. A. FYFE. *In* Molecular complexes. Vol. 1. *Edited by* R. Foster. Paul Elek (Scientific Books) Ltd., London. 1973. Chapt. 2.
2. R. K. BOYD, C. A. FYFE, and D. A. WRIGHT. J. Phys. Chem. Solids, **35**, 1355 (1974).
3. C. E. NORDMAN and D. L. SCHMITKONS. Acta Crystallogr. **18**, 764 (1965).
4. J. DONOHUE and I. H. GOODMAN. Acta Crystallogr. **22**, 352 (1967).
5. S. S. CHANG and E. F. WESTRUM, JR. J. Phys. Chem. **64**, 1547 (1960).
6. L. N. BECKA and D. W. J. CRUICKSHANK. Proc. R. Soc. London, Ser. A, **273**, 435 (1963).
7. H. A. RESING. Mol. Cryst. Liq. Cryst. **9**, 101 (1969).
8. D. W. MCCALL and D. C. DOUGLAS. J. Chem. Phys. **33**, 777 (1960); G. W. SMITH. J. Chem. Phys. **35**, 1134 (1961).
9. N. I. LIU and J. JONAS. Chem. Phys. Lett. **14**, 555 (1972).
10. C. A. FYFE and D. HAROLD-SMITH. J. Chem. Soc. Faraday Trans. II, 967 (1975).
11. D. E. WILLIAMS. (*a*) J. Chem. Phys. **45**, 3770 (1966); (*b*) J. Chem. Phys. **47**, 4680 (1967); (*c*) Trans. Am. Crystallogr. Assoc. **6**, 21 (1966).

12. R. MASON. Mol. Cryst. Liq. Cryst. **9**, 3 (1969).
13. P.-J. WU, L. HSU, and D. A. DOWS. J. Chem. Phys. **54**, 2714 (1971).
14. C. M. VENKATACHALAM and G. N. RAMACHANDRAN. *In* Conformation of biopolymers. *Edited by* G. N. Ramachandran. Academic Press, London. 1967.
15. H. A. SCHERAGA. Adv. Phys. Org. Chem. **6**, 103 (1968).
16. A. I. KITAIGORODSKII. Tetrahedron, **14**, 230 (1961).
17. N. L. ALLINGER and J. C. THAI. J. Am. Chem. Soc. **87**, 1227 (1965).
18. R. MASON. Proc. R. Soc. London, Ser. A, **304**, 501 (1968).
19. N. V. SIDGWICK and H. M. POWELL. Proc. R. Soc. London, Ser. A, **176**, 153 (1940).
20. R. J. GILLESPIE. J. Am. Chem. Soc. **82**, 5978 (1963).
21. A. F. ANDERSON. Acta Crystallogr. **10**, 107 (1957).
22. B. BRILL, H. G. GRIMM, C. HERMANN, and A. PERERS. Ann Phys. Leipzig, **34**, 393 (1939).
23. P. A. SHAFFER, JR. J. Am. Chem. Soc. **69**, 435 (1947).
24. L. N. BECKA and D. W. J. CRUICKSHANK. Proc. R. Soc. London, Ser. A, **273**, 435 (1963).
25. G. W. SMITH. J. Chem. Phys. **36**, 3081 (1962).
26. J. N. STRANSKI, G. KLIPPING, A. F. BOGENSCHUETZ, H. J. HEINRICH, and H. MAENNIG. Adv. Catal. **9**, 406 (1957).
27. T. KIHARA. Adv. Chem. Phys. **20**, 1 (1971).
28. G. DOLLING, G. S. PAWLEY, and B. M. POWELL. Proc. R. Soc. London, Ser. A, **333**, 363 (1973).
29. A. I. KITAIGORODSKII. J. Chem. Phys. **63**, 8 (1966).
30. T. KOEHLER. Private communication.

Can. J. Chem. Downloaded from www.nrcresearchpress.com by 210.87.254.5 on 09/05/12
For personal use only.

Potential energy calculations of the mechanisms of self-diffusion in molecular crystals: adamantane

C. A. FYFE[1] AND D. HAROLD-SMITH[2]

Guelph-Waterloo Centre for Graduate Work in Chemistry, Guelph Campus, Chemistry Department, University of Guelph, Guelph, Ontario N1G 2W1

Received January 17, 1975[3]

C. A. FYFE and D. HAROLD-SMITH. Can. J. Chem. **54**, 783 (1976).

A simple but physically well-defined model for self-diffusion in molecular solids is described. This is combined with semi-empirical atom–atom pair potentials for nonbonded atoms to test various possible diffusion mechanisms in the two phases of adamantane. For adamantane it is found that (*1*) diffusion occurs by jumps to single-vacancy holes at nearest-neighbor lattice sites, (*2*) the four molecules closest to the midpoint of the jumps are cooperatively distributed among their equilibrium orientations, and (*3*) the jump trajectory is curved. The computed enthalpy of activation is in good agreement with the experimental value obtained from $T_1\rho$ and vapor pressure measurements. The rate of self-diffusion in β-adamantane has not been reported, but the enthalpy of activation has been calculated for various mechanisms and indicates the critical role of lattice disorder in the self-diffusion of plastic crystals.

C. A. FYFE et D. HAROLD-SMITH. Can. J. Chem. **54**, 783 (1976).

On décrit un modèle simple mais bien défini pour l'auto-diffusion dans les solides moléculaires. On combine ce modèle avec des potentiels semi-empiriques de paires atome–atome pour des atomes non-liés afin de vérifier divers mécanismes possibles de diffusion dans les deux phases de l'adamantane. Pour l'adamantane, on a trouvé que: (*1*) la diffusion se produit par sauts vers des trous d'une unité des sites du réseau voisin le plus près; (*2*) les quatre molécules les plus près de la demi-hauteur des sauts se redistribuent d'une façon coopérative entre leurs orientations d'équilibre et (*3*) les trajectoires des sauts sont courbées. La valeur calculée pour l'enthalpie d'activation est en bon accord avec la valeur expérimentale obtenue à partir de mesures de $T_1\rho$ et de pression de vapeur. On ne rapporte pas le taux d'auto-diffusion du β-adamantane mais on a calculé l'enthalpie d'activation pour divers mécanismes et ces calculs indiquent que le désordre dans le réseau joue un rôle critique dans l'auto-diffusion des cristaux plastiques.

[Traduit par le journal]

Introduction

The study of self-diffusion was first made possible by the discovery of isotopes, particularly those which are radioactive (1). The radiotracer technique makes it possible to measure the net self-diffusion which takes place in a macroscopic object over a period of several hours or days. But because the number of individual atomic or molecular jumps in this length of time is astronomical, it is extremely difficult to deduce the mechanisms of translational diffusion from such measurements.

In recent years a wide variety of nuclear magnetic resonance techniques have been developed to measure self-diffusion including second-moment, T_1 and $T_1\rho$ measurements, as well as measurements of the transverse relaxation time in a magnetic field gradient (2). T_1 and $T_1\rho$ measurements detect diffusion on time scales characteristic of the individual translational jumps of the molecules and provide a direct measurement of the jump time τ. If it is assumed that the molecules undergo random jumps of mean-squared distance $\langle r^2 \rangle$, τ can be related to the macroscopic self-diffusion coefficient D through the equation (3)

$$[1] \qquad \tau = \langle r^2 \rangle / 6D$$

Some information about diffusion mechanisms is potentially available by comparison of nmr and macroscopic diffusion measurements through [1]. Folland *et al.* (4) have discussed five plastic crystalline compounds for which both $T_1\rho$ and radiotracer measurements have been made. The two types of data are in good agreement for two of the compounds. But for the others there are

[1]To whom correspondence should be addressed.

[2]Present address: Department of Chemistry, Northwestern University, Evanston, Illinois.

[3]Revision received November 17, 1975.

Can. J. Chem. Downloaded from www.nrcresearchpress.com by 210.87.254.42 on 09/05/12
For personal use only.

Can. J. Chem. Downloaded from www.nrcresearchpress.com by 210.87.254.42 on 09/05/12
For personal use only.

substantial differences between the diffusion coefficients, the activation enthalpies for diffusion, or both, and there are not yet sufficient data nor theoretical understanding to determine if the differences stem from the purities of the samples, the measurements, or diffusion mechanisms for which [1] is not valid.

In the absence of a theoretical understanding of the mechanisms of self-diffusion in plastic crystals, various attempts have been made to correlate activation enthalpies of self-diffusion with thermodynamic parameters, even though thermodynamic data measure equilibrium properties and self-diffusion is a part of the dynamic structure of the crystal lattice. It has been suggested that for plastic crystals with entropies of fusion greater than $1.9R$, the activation enthalpies of self-diffusion seem to be approximately twice the respective heats of sublimation ($\Delta H_{act} \simeq 2\Delta H_{sub}$). This has been taken to indicate that self-diffusion occurs by a single vacancy mechanism in these lattices. (The heat of sublimation is just the enthalpy required to form a single vacancy by removal of a molecule in the lattice to infinity.) The trends for plastic crystals with entropies of fusion less than $1.9R$ were less clear, but it seemed that for many $\Delta H_{act} \simeq \Delta H_{sub}$, and it was suggested that this indicates diffusion by a more complicated defect mechanism (5). In a more recent study of five plastic crystals, Folland *et al.* (4) concluded that their compounds could not be neatly divided into these two categories, but did report the general trend ΔH_{act} decreased as the entropy of diffusion decreased.

Recently semi-empirical potential functions which describe the interactions between nonbonded atoms have been used to interpret and predict the lattice structure and sublimation energies (6), small-angle vibrational motions (7), and modes of rotational diffusion in molecular crystals (8–10). The success of these treatments of nontranslational motion suggested that it might be possible to calculate the molecular potentials for self-diffusion in the organic solid-state. Successful calculations of these potentials would determine the mechanism(s) of diffusion and to what extent there exists a basis for the empirical correlation of the parameters of self-diffusion with thermodynamic parameters. Since the measured values of the correlation time for self-diffusion depend on the assumed model of diffusion (3, 11–13), such calculations might also lead to the more accurate interpretation of experimental data.

Adamantane was chosen for study because it has a high temperature phase (α–adamantane) which is plastic crystalline and a low temperature structure (the β phase) which is not. Several nmr studies of the dynamic behavior of this compound have been made (14–17). Furthermore, calculations of the potentials for molecular rotation have produced a detailed understanding of the mechanisms of rotational diffusion in the two phases and of the order–disorder transition between them (9).

Diffusion

Model and Choice of Potential Functions

The functional form chosen for the pairwise-additive atom–atom potentials is the exponential-6 function:

$$[2] \qquad V_{ij} = -A_{ij}r^{-6} + B_{ij}\exp(-C_{ij}r)$$

The values of A, B, and C were chosen from the published values of Williams (18) and were the same as those used in the previous calculations on adamantane (9).

In the calculations the atomic coordinates from crystallographic data were used to generate the diffusing molecule, M. This molecule was then surrounded by its neighboring molecules at their equilibrium positions, and a single-vacancy hole was created by removal of a molecule at a designated lattice site. The molecule M was then translated along the designated path to the vacancy, and the molecular potential was calculated from [3] for a series of positions of M along the path.

$$[3] \qquad U = \tfrac{1}{2}\sum_{i=1}^{n}\sum_{j}^{\infty} V_{ij}(r_{ij})$$

where n is the number of atoms in the molecules and the sum to infinity over j implies that the interaction energy of atom i with all other atoms on all other molecules in the crystal must be taken.

In the initial calculations, the model for the motion was the simplest one possible: All other molecules were kept fixed in the lattice at the positions of minimum potential as indicated by the X-ray diffraction structure. Intramolecular motions and rotations of either M or of other molecules in the lattice were ignored. The

Can. J. Chem. Downloaded from www.nrcresearchpress.com by 210.87.254.42 on 09/05/12
For personal use only.

assumptions are similar to those made in previous studies of rotational diffusion (8–10). In subsequent calculations, the translating molecule and/or its neighbors were allowed to rotate about the axes of molecular symmetry. Thus, in the trial models, diffusion occurs by jumps to single-vacancy holes and jumps are between neighboring lattice sites. A jump without molecular rotation corresponds to the simplest possible diffusion mechanism; the other trial mechanisms were adopted to test the role of correlation effects between molecular rotation and translation.

The initial potential of the diffusing molecule M is (ignoring the zero-point energy difference and corrections from absolute zero to the temperature of the crystallographic structure data) the enthalpy of sublimation minus the molecular pair potential which would exist between M and a molecule at the vacancy site. Both quantities had previously been calculated. The potentials of M before and after the jump are identical, and the enthalpy of activation for self-diffusion is equated with the difference between this potential and the maximum potential encountered by M between its initial and final lattice sites.[4] Thus the simplest model implicitly assumes a perfect crystal, except for the random distribution of isolated vacancies whose number is constant.

Self-Diffusion in α-Adamantane

Each molecule in the cubic lattice of the disordered phase of adamantane has twelve nearest neighbors, and the distance between the center of mass of nearest neighbors is 6.60 Å.

Simple Diffusion

Figure 1 shows the potential barrier encountered by an adamantane molecule diffusing without rotation to a nearest-neighbor vacancy in an artificially ordered lattice. The diffusion path is along $x = 0$, $y = z$, with the hole initially at the lattice site with its center at the orthogonal coordinates (0, 4.71, 4.71) and the diffusing molecule at (0, 0, 0). The potential is symmetrical about the midpoint of the path, and the barrier height is ~110 kcal/mol. This

[4]A negative activation enthalpy would correspond to a stable interstitial defect. The energy and enthalpy of activation are identical in this model since there is no change of volume.

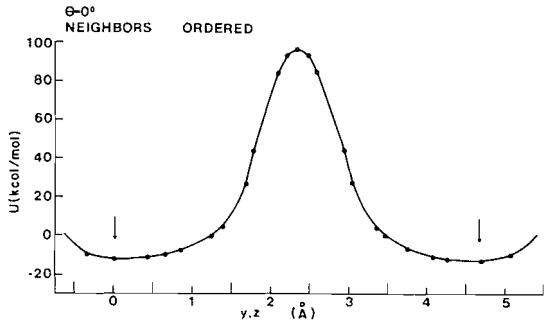

FIG. 1. Potential for the translation of an adamantane molecule to a single-vacancy hole at a nearest-neighbor position in an artificially ordered α-adamantane lattice. The jump trajectory is along $x = 0$, $y = z$; and no other motion occurs. Arrows mark the lattice sites.

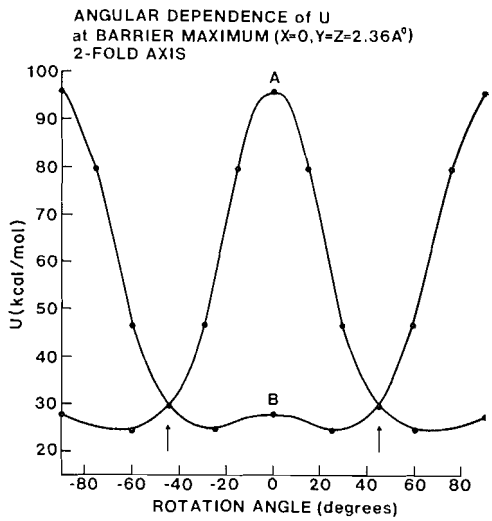

FIG. 2. Potentials generated by rotation about the twofold axis of an adamantane molecule at the midpoint of a translational jump. The two curves are for artificially ordered lattices with the molecules at 0° orientation (*A*) and at 90° orientation (*B*).

is about four times the measured enthalpy of activation for self-diffusion in α-adamantane.

Diffusion by Combined Rotation–Translation

In Fig. 2 the possibility that the adamantane molecule might reduce the potential at the maximum by a rotation about the molecular twofold axis parallel to the z axis of the lattice is investigated. For one of the curves all of the molecules surrounding M are at one of the two disorder orientations; the other curve was generated by placing all of the surrounding molecules at the other disorder orientation. The two curves are

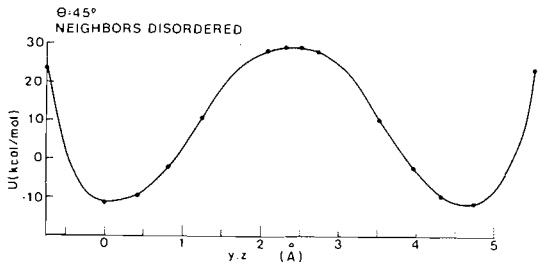

FIG. 3. Potential for the translation of a molecule rotated 45° about the twofold axis.

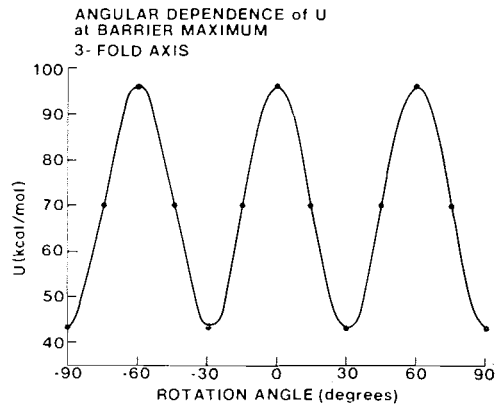

FIG. 4. Potential generated by rotation about the threefold axis of an adamantane molecule at the midpoint of a translational jump. The combined rotation–translation lowers the barrier to self-diffusion but is not an important mechanism.

identical except for being 90° out of phase, since the two orientations of disorder are related to each other by a 90° rotation. If half of the surrounding molecules are at one orientation and half at the other, the potential in the lattice is represented by the average of these two curves. This is, of course, a special situation corresponding to one of many possible distributions but is instructive in finding the approximate energies involved for different pathways and will be replaced by a consideration of the optimum local ordering (see later).

Examination of Fig. 2 reveals that the average of the two potentials is smallest for an angle of $\pm 45°$ (or $\pm 135°$) of the diffusing molecule. The equilibrium orientations of the molecule at the lattice site are 0, ± 90, 180°. Hence the molecule can reduce the translational barrier to 41.5 kcal/mol (Fig. 3) by combining a rotation to an orientation midway between the equilibrium angles with the translational jump. This barrier is still larger than the experimental value of the activation enthalpy (23.9 kcal/mol) (15, 22), and the combined rotation–translation mechanism contributes much less than 0.01% of the total diffusion in α-adamantane.

The potential generated by a threefold axis rotation of M at the midpoint of the translational jump is shown in Fig. 4. Although a 30° rotation of M about this axis greatly reduces the barrier, the potential is still 13.5 kcal/mol greater than the minimum barrier attained by a rotation about the twofold axis. Hence diffusion with rotation about the threefold axis is not a significant mechanism.

Diffusion with Local Ordering

Examination of the individual molecule–molecule pair potentials between the diffusing molecule M and each of its neighbors reveals that large repulsions occur only between M and the four neighbors nearest to the midpoint of the jump path. The lattice sites of these molecules are (± 4.71, 0, 4.71) and (± 4.71, 4.71, 0), while the center of M at the jump midpoint is at (0, 2.36, 2.36). Each of these molecules may have two possible orientations. If M starts with the same orientation as one of these molecules and does not rotate during the jump, the molecular pair-potential is +25 kcal/mol. If all four neighbors are in the same orientation as M, this produces a huge net repulsive potential. However, by being in the 'correct' orientation as defined by M, each of these neighbors can reduce its pair-potential with M to either 1.9 or 13.7 kcal/mol, without changing its net potential with the rest of the lattice by more than 1 kcal/mol.[5] The way in which this occurs shows how the introduction of disorder into the crystal, combined with the molecular and lattice symmetries, can greatly reduce the activation enthalpy of self-diffusion.

If the four neighbors jump 90° to the other disorder orientation from that of M, each molecular pair potential between M and the two neighbors in the $X = +C/2$ plane is 13.7 kcal/mol, while the corresponding potentials with the two neighbors in the $X = -C/2$ plane are only 1.9 kcal/mol each. If all five molecules then rotate 90° to their other equiva-

[5]See Fig. 2*A*, ref. 9.

Can. J. Chem. Downloaded from www.nrcresearchpress.com by 210.87.254.42 on 09/05/12
For personal use only.

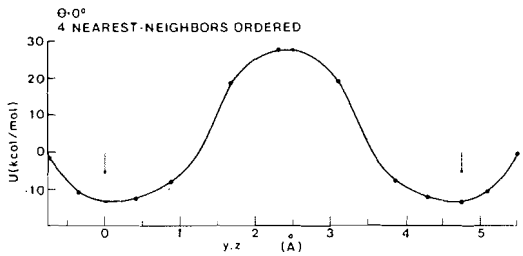

FIG. 5. Potential for the translation of a molecule with 0° orientation angle along $x = 0$, $y = z$ when the four molecules closest to the midpoint of the jump are in the other orientation. An identical potential is generated if M and the four neighbors exchange their disorder orientations relative to each other.

lent orientation, the geometry is inverted, the large and small pair-potentials are exchanged, and the net potential is unchanged. Hence the minimum barrier to self-diffusion is established whenever all four special molecules have the same orientation and M has the other orientation.

The net potential is shown in Fig. 5. The barrier is the difference between the maximum potential (27.5 kcal/mol) encountered during the jump and the initial potential (−12.1 kcal/mol) of the diffusing molecule. For a 0° orientation of M this potential may be deduced from Fig. 2 as the average of $2A$ and $2B$ at 0° rotation angle, but with $2A$ shifted 90° to coincide with $2B$. From this same figure it may also be seen that the barrier maximum varies only a few kcal/mol between $\sim \pm 40°$ for the orientation angle of M and reaches a minimum value of 36.6 kcal/mol at $\pm 30°$.

Each molecule spends one-half of its time in each of the two orientations; hence there is a $2 \times (\frac{1}{2})^4 = \frac{1}{8}$ probability at any instant that the four molecules have the 'correct' distribution of orientations. As shown by experiment (15) and previous calculations (9) the barrier to molecular rotation between equilibrium orientations is $\lesssim 3$ kcal/mol, so that the reorientation frequency for an individual molecule is $\gtrsim 10^8$ Hz (15). Hence, even if it is assumed that all four molecules adjacent to M and the hole must have the 'correct' orientation *before* M can translate, this occurs with a frequency $\gtrsim 10^7$ times per second.

Diffusion with Curved Jump Paths

The potential in Fig. 5 is generated by the shortest possible jump from the initial lattice site of M to the nearest-neighbor hole. At the midpoint of the jump the net repulsion between M and the two molecules at (4.71, 0, 4.71) and (4.71, 4.71, 0) is 23.6 kcal/mol greater (or less) than the net potential between M and the two molecules at (−4.71, 0, 4.71) and (−4.71, 4.71, 0).

Therefore, the barrier to diffusion is lower if M follows a curved path which takes it closer to one of these pairs of molecules than to the other pair. The calculations show that the minimum barrier occurs when the jump midpoint is 0.4 Å from the $X = 0$ plane and the orientation angle of M is 0 or 90°. The potential of M at this point is 12.1 kcal/mol, and the calculated enthalpy of activation for the self-diffusion is 24.2 kcal/mol.

The rate of diffusion in a crystal is proportional to both the rate of hole motion and the number of holes, or $D \propto \exp(-\Delta H_{act}/KT) \exp(-\Delta H_{sub}/KT)$. Hence, the nmr experiment measures an apparent enthalpy of activation, $\Delta H_{app} = \Delta H_{act} + \Delta H_{sub}$. The reported values of ΔH_{app} and the enthalpy of sublimation are 36.7 kcal/mol (15) and 12.8 kcal/mol (22), respectively. Hence, the experimental value for ΔH_{act} is 23.9 kcal/mol. As the barrier maximum the distances between nonbonded atoms are short, the repulsive forces are very steep functions of the distances, and small uncertainties in the atomic coordinates produce relatively large uncertainties in the net potential. Furthermore, the uncertainty in the experimental value of ΔH_{act} is the sum of the errors in two experiments. Hence the agreement between the calculated and measured values of ΔH_{act} is reasonable.

Temperature Dependence of ΔH_{act}

Another effect which produces an uncertainty in the experimental value of ΔH_{act} is the fact that presumably it is temperature dependent due to the thermal expansion of the lattice. Unfortunately, there is no experimental way to estimate this effect. In the model presented here the temperature variation of ΔH_{act} can be calculated by varying the lattice dimensions while holding all else constant. A 1.2% increase in the edge of the cubic unit cell produced a calculated decrease of 4 kcal/mol in ΔH_{act}. From the thermal expansivity of α-adamantane (23, 24) this corresponds to approximately 0.5×10^{-2} kcal mol^{-1} K^{-1} for the temperature dependence

Can. J. Chem. Downloaded from www.nrcresearchpress.com by 210.87.254.42 on 09/05/12
For personal use only.

Can. J. Chem. Downloaded from www.nrcresearchpress.com by 210.87.254.42 on 09/05/12
For personal use only.

of the enthalpy of activation. This indicates that the temperature dependence of ΔH_{act} can probably be neglected in experimental determinations without introducing significant errors.

Self-diffusion in β-Adamantane

Each molecule in β-adamantane has eight nearest neighbors. In an orthonormal coordinate system whose origin is at the center of mass of the chosen molecule M, the nearest neighbors of M are centered at $x = \pm 3.30$, $y = \pm 3.30$, $z = \pm 4.40$ Å. M also has four next-nearest neighbors at $x = \pm 6.60$, $y = z = 0.0$ and $y = \pm 6.60$, $x = z = 0.0$ Å; and two third-nearest neighbors at $x = y = 0.0$, $z = \pm 8.80$. The distances between the molecular centers of mass of M and these neighbors are 6.42, 6.60, and 8.80 Å, respectively. The diffusion of M into vacancies at each of these lattice sites will be considered. In each case M diffuses through a lattice which is perfect, except for the absence of a single molecule at the lattice site to which it jumps.

Diffusion to a Third-nearest Neighbor Vacancy

The first diffusional motion considered was a simple 8.8 Å jump of M along the *c* axis to a third-nearest neighbor vacancy, without any other motion in the lattice or of M. A translational jump of this distance appeared *a priori* to be extremely unlikely, and this was confirmed by the calculations. At one-quarter of the way along the jump path the repulsive potential reaches 250 kcal/mol, and at the jump midpoint many of the distances between the atoms of the surrounding molecules are less than the normal lengths between bonded atoms. Because of these extremely short distances between nonbonded atoms, no combination of rotations of M and motions by the surrounding molecules can reduce the potential to a reasonable value.

Diffusion to a Next-nearest Neighbor Vacancy

The barrier to diffusion to a next-nearest neighbor hole in the lattice is 71.2 kcal/mol if the diffusing molecule does not rotate. The barrier is reduced to 65 kcal/mol by a rotation of 60° by the molecule about one of its threefold axes, and to 62.4 kcal/mol by a rotation of 60° about the molecular twofold axis which is parallel to the *c* axis of the crystal and orthogonal to the translational path. By contrast, any rotation about one of the other twofold axes increases the potential sharply. Since the initial potential of the diffusing molecule is −14.2 kcal/mol, the minimum activation energy for diffusion to a next-nearest neighbor vacancy is about 77 kcal/mol.

Diffusion to a Nearest-neighbor Vacancy

The barrier to diffusion without molecular rotation for a 6.4 Å jump to a nearest-neighbor hole is the same as for the 6.60 Å jump to a next-nearest-neighbor vacancy, 71 kcal/mol. However, molecular rotation is somewhat more effective in reducing the potential maximum for the shorter jump path. A 20° rotation about a threefold axis results in an activation energy of 62 kcal/mol, and a 60° rotation about the special twofold axis parallel to the lattice *c* axis reduces the activation energy to 56 kcal/mol.

Unfortunately the enthalpy of activation for self-diffusion in β-adamantane has not yet been measured. Nuclear magnetic resonance measurements on α- and β-adamantane show that the rate of self-diffusion becomes too slow to detect by $T_1 p$ measurements about 100 °C above the phase transition. Hence self-diffusion in the ordered phase must be studied by radiotracer measurements. Since the β phase is not cubic, this should preferably be done with a single crystal.

The eight nearest-neighbors to a molecule in the β-adamantane lattice form a body-centered cube, and the site asymmetry between the 'special' *c* axis and the *a* and *b* axes begins only with the four next-nearest neighbors. Nearest-neighbor jumps are expected to be about 2 exp (77 − 56) as frequent as jumps to next-nearest neighbor vacancies. The former motion moves the molecule ±4.4 Å along the *c* axis and ±3.3 Å along the *a* or *b* axis, while the latter motion produces a translation of ±6.6 Å along the *a* or *b* axis. Since the rate of diffusion is equal to the jump frequency times the square of the jump distance (eq. 1) and the fraction of self-diffusion occurring by next-nearest neighbor jumps is insignificant, the diffusion is predicted to be nearly twice as fast along the *c* axis as in the other two directions. The predicted activation enthalpy is ≤70 kcal/mol, which is nearly 45 kcal/mol greater than the barrier to self-diffusion in α-adamantane. The effect of cooperative motions of the surrounding molecules

mechanism might not have been considered and might reduce the diffusional barrier, and 70 kcal/mol can only be considered an upper limit on the enthalpy of activation.

Conclusion

Several possible mechanisms of self-diffusion have been considered for each phase of adamantane.

In β-adamantane the crystal is ordered and each molecule has only one equilibrium orientation. Thus, there is no other distribution of the molecules among equivalent orientations which could lower the activation barrier. By combining rotation with translation, the diffusing molecule can somewhat reduce the barrier to self-diffusion.

The two phases illustrate why it can be expected in general that phases with low entropies of fusion will have relatively low activation enthalpies of self-diffusion. A low entropy of fusion is symptomatic of orientational disorder in the crystal, so that each molecule assumes a number of orientations which (in the absence of defects) have equal energies and equal probabilities. Thus each molecule along the transitional jump can 'choose' the orientation which produces the smallest potential with the diffusion molecule and the lowest activation barrier. However, there is no direct connection between the enthalpy of sublimation and the enthalpy of activation for diffusion (25).

In α-adamantane the most favorable mechanism involves the cooperative orientation of the four molecules closest to the midpoint of the jump path, and the diffusing molecule moves along a curved trajectory. The closeness of the calculated barrier for diffusion to the experimental value gives credence to the diffusion model and also to the atomic-pair potentials which were used.

Because of the disorder in the lattice and the cooperative orientation of nearby molecules, the diffusing molecules need not rotate during the translational jumps.

These calculations indicate that from crystal structures and a quantitative treatment of the interactions between nonbonded atoms it may be possible to determine in some detail the molecular mechanisms of self-diffusion in crystals.

1. G. Hevesy and F. Paneth. Z. Anorg. Chem. **82**, 323 (1913).
2. E. O. Stejskal and J. E. Tanner. J. Chem. Phys. **42**, 288 (1965).
3. H. C. Torrey. Phys. Rev. **92**, 962 (1953).
4. R. Folland, R. R. Jackson, J. H. Strange, and A. V. Chadwick. J. Phys. Chem. Solids, **34**, 1713 (1973).
5. P. Bladon, N. C. Lockhart, and J. N. Sherwood. Mol. Phys. **20**, 577 (1971).
6. D. E. Williams. Acta Crystallogr. Sect. A, **28**, 629 (1972).
7. G. S. Pawley. Phys. Status Solidi, **20**, 347 (1967).
8. R. K. Boyd, C. A. Fyfe, and D. A. Wright. J. Phys. Chem. Solids, **35**, 1355 (1974).
9. C. A. Fyfe and D. Harold-Smith. Can. J. Chem. This issue.
10. C. A. Fyfe and D. Harold-Smith. J. Chem. Soc. Faraday Trans. II, 967 (1975).
11. H. A. Resing and H. C. Torrey. Phys. Rev. **131**, 1102 (1963).
12. M. Eisenstadt and A. G. Redfield. Phys. Rev. **132**, 635 (1963).
13. D. Z. Wolf. Z. Naturforsch, **26a**, 1816 (1971).
14. G. W. Smith. J. Chem. Phys. **35**, 1134 (1961).
15. H. A. Resing. Mol. Cryst. Liq. Cryst. **9**, 101 (1969).
16. D. W. McCall and D. C. Douglas. J. Chem. Phys. **33**, 777 (1960).
17. N. I. Liu and J. Jonas. Chem. Phys. Lett. **14**, 555 (1972).
18. D. E. Williams. J. Chem. Phys. **47**, 4680 (1967).
19. C. E. Nordman and D. L. Schmitkons. Acta Crystallogr. **18**, 764 (1965).
20. J. Donohue and I. H. Goodman. Acta Crystallogr. **22**, 352 (1967).
21. S. S. Chang and E. F. Westrum, Jr. J. Phys. Chem. **64**, 1547 (1960).
22. P.-J. Wu, L. Hsu, and D. A. Dows. J. Chem. Phys. **54**, 2714 (1971).
23. S. M. Breitling, A. D. Jones, and R. H. Boyd. J. Chem. Phys. **54**, 3959 (1971).
24. C. W. F. T. Pistorius and H. A. Resing. Mol. Cryst. Liq. Cryst. **5**, 353 (1969).
25. A. V. Chadwick and J. N. Sherwood. *In* Diffusion processes. *Edited by* J. N. Sherwood *et al.* Gordon and Breach, New York. 1971.

Can. J. Chem. Downloaded from www.nrcresearchpress.com by 210.87.254.42 on 09/05/12
For personal use only.

A study of ^{13}C-^{15}N couplings and revised ^{13}C shieldings in ^{15}N-enriched *E*-acetophenone oximes

GERALD W. BUCHANAN AND BRIAN A. DAWSON
Department of Chemistry, Carleton University, Ottawa, Canada K1S 5B6

Received October 2, 1975

GERALD W. BUCHANAN and BRIAN A. DAWSON. Can. J. Chem. **54**, 790 (1976).

^{13}C nmr chemical shifts and ^{13}C–^{15}N couplings through one, two, and three bonds are reported for *E*-acetophenone oxime and five *para*-substituted derivatives. It is shown that earlier assignments for three of these compounds, based on lanthanide induced shifts and CNDO calculations, are erroneous. With the exception of the methoxyl group, couplings are relatively insensitive to the nature of the *para*-function. For geminal ^{13}C–^{15}N interactions, the proximity of the nitrogen lone pair to the carbon terminus greatly enhances the absolute value of the coupling constant.

GERALD W. BUCHANAN et BRIAN A. DAWSON. Can. J. Chem. **54**, 790 (1976).

On rapporte les déplacements chimiques des ^{13}C en rmn et les couplages ^{13}C–^{15}N à travers un, deux et trois liens pour l'oxime (*E*) de l'acétophénone et pour cinq de ses dérivés substitués en position *para*. On montre que les attributions faites antérieurement pour trois de ces composés et basées sur des déplacements chimiques induits par les lanthanides et par des calculs CNDO sont en erreur. A l'exception du groupe méthoxyle, les couplages sont relativement insensibles à la nature de la fonction en *para*. Pour les interactions ^{13}C–^{15}N géminales, la présence du carbone au voisinage de la paire d'électron libre de l'azote augmente considérablement la valeur absolue de la constante de couplage.

[Traduit par le journal]

Introduction

There has been recent interest in the application of ^{13}C–^{15}N coupling constants to configurational and conformational analysis. Lichter *et al.* (1) have found that the absolute values of 1- and 2-bond ^{13}C–^{15}N couplings in *E*-acetaldehyde oxime are considerably larger than those for the *Z*-isomer. Results for *E*-benzaldoxime (1) and *E*-mesitaldoxime (2) below, indicate that direct C–N couplings are attenuated when the aromatic ring is twisted out of coplanarity with the C=N bond, as in the mesityl system.

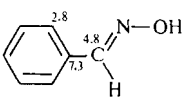

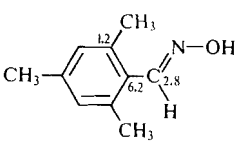

The fact that the vicinal ^{13}C–^{15}N coupling in the planar (3) benzaldoxime is 1.6 Hz larger than for the mesityl compound suggests the existence of a dihedral dependence for these couplings, however a detailed analysis of the geometrical requirements has not yet been carried out. Recently, the importance of the orientation of the nitrogen lone pair in determining the magnitudes of ^{13}C–^{15}N couplings has been suggested by Berger and Roberts (4).

At the outset of this study, no ^{13}C–^{15}N couplings had been reported for acetophenone oximes. Also, we have chosen to examine *para*-substituent effects on these parameters since electronic effects are known to influence the magnitude of couplings of ^{13}C to other magnetic nuclei (5).

Results and Discussion

(a) Chemical Shifts

The only ^{13}C chemical shift data for acetophenone oximes have been reported by Sterk Steininger (6) for *E*-acetophenone oxime and its 4-methyl and 4-chloro derivatives. These workers have attempted to calculate ^{13}C shifts of oximes using a Molecular Orbital approach and the diamagnetic and paramagnetic contributions to the shielding expression. Spectral assignments were based solely on $Pr(fod)_3$-d_{27} induced shifts and their results are included in Table 1.

In order to verify the previous assignments we initially examined the ^1H spectrum of *E*-acetophenone oxime and found, for the aromatic

TABLE 1. ^{13}C chemical shifts for *E*-acetophenone oximes (δ_c from TMS ± 0.1)

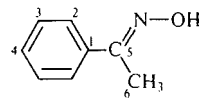

Compound	Substituent	C-1	C-2	C-3	C-4	C-5	C-6	OCH_3	4-CH_3
1[a]	4-H	136.2	127.0	125.8	128.1	155.7			
1[b]	4-H	136.5	126.0	128.5	129.1	155.9	12.4		
1[c]	4-H	138.2	129.0	129.4	126.6	154.5	11.6		
2[a]	4-CH_3	139.0	128.9	125.6	133.5	155.5			
2[b]	4-CH_3	133.8	126.0	129.2	139.2	155.8	12.3		21.1
3[a]	4-Cl	135.1	128.9	126.9	134.5	154.9			
3[b]	4-Cl	135.4	127.4	128.8	135.0	155.2	12.3		
4[b]	4-Br	135.5	127.6	131.7	123.6	155.2	12.0		
5[b]	4-OCH_3	129.1	127.3	113.8	160.5	155.4	12.1	55.2	
6[c]	4-NO_2	144.0	127.4	124.1	148.8	153.9	11.4		

[a]Reference 6; unspecified concentration in $CDCl_3$.
[b]Present work; 0.5 *M* in $CDCl_3$.
[c]Present work; 0.5 *M* in acetone-d_6.

TABLE 2. Predicted and observed (in parentheses) aryl carbon shieldings relative to benzene for *para*-substituted *E*-acetophenone oximes

Compound	Substituent	C-1	C-2	C-3	C-4
1[a]	4-H	(+7.8)	(−2.7)	(−0.2)	(+0.4)
1[b]	4-H	(+9.5)	(+0.3)	(+0.7)	(−2.1)
2[a]	4-CH_3	+4.7(+5.1)	−2.9(−2.7)	+0.4(+0.5)	+9.5(+10.5)
3[a]	4-Cl	+5.5(+6.7)	−1.7(−1.3)	−0.3(+0.1)	+6.0(+6.3)
4[a]	4-Br	+6.8(+6.8)	−0.5(−1.1)	+3.1(+3.0)	−5.0(−5.1)
5[a]	4-OCH_3	−1.1(+0.4)	−2.7(−1.4)	−15.7(−14.9)	+30.6(+31.8)
6[b]	4-NO_2	+15.5(+15.3)	+1.1(−1.3)	−4.6(−4.6)	+17.5(+20.1)

[a]0.5 *M* solutions in $CDCl_3$.
[b]0.5 *M* solution in acetone-d_6.

protons, a 3-proton multiplet centered at δ 7.32 and a 2-proton multiplet at δ 7.61 (0.5 *M* solution in $CDCl_3$). Although the anisotropic properties of the C=N bond are not well known, it is likely that the *ortho*-aromatic protons experience an anisotropic deshielding influence from the C=N group in the planar conformation, using the C=O group as an analogy (7). Selective irradiation at δ 7.61 sharpened the carbon resonance at δ 126.0 rather than that at 128.5 which is inconsistent with the results from Sterk and Steininger (6). Further support for the reversal of the earlier assignments comes from the spectrum of the ^{15}N enriched *E*-acetophenone oxime. The resonance at δ 126.0 exhibits a substantial coupling to ^{15}N (2.9 Hz), which is nearly identical to the 3-bond coupling found in *E*-benzaldoxime (1). By contrast, the resonance at δ 128.5 shows no resolvable coupling (<0.6 Hz) to ^{15}N, indicating a more distant (4-bond) relationship between ^{15}N and this carbon. Other spectral assignments were made from off-resonance decoupling experiments, intensity ratios (for protonated carbons), and earlier ^{13}C work on aliphatic oximes (8). In addition, it is known (5) that *para*-substituent effects on aromatic ^{13}C resonances are usually additive within ± 1 ppm, and thus assignments for **2**–**6** can be checked since the additivy parameters for the CH_3, Cl, Br, OCH_3, and NO_2 functions employed here are well documented (5).

Table 2 contains the predicted (relative to benzene δ 128.7) shifts for the aromatic carbons of **2**–**6**, with the observed values in parentheses. Except for C-4 of **6**, the agreement between calculated and experimental findings is near ± 1 ppm. For the 4-CH_3 derivative, **2**, it is important to note that in addition to the reversal of C-2 and C-3 assignments, our results

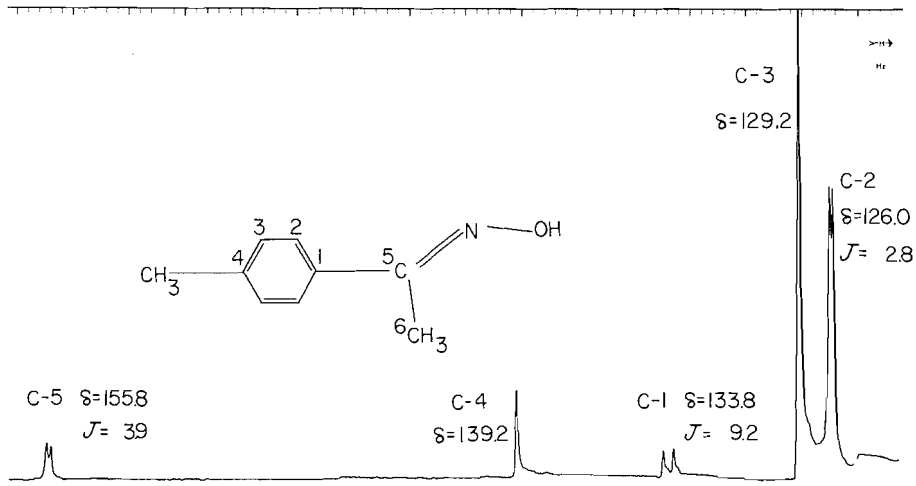

FIG. 1. ^{13}C nmr spectrum (aromatic and oxime carbons) of 97% ^{15}N-enriched *p*-CH_3-*E*-acetophenone oxime.

TABLE 3. $^{13}C-^{15}N$ couplings (Hz) (absolute values)

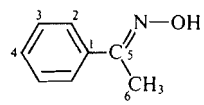

Compound	Substituent	^1J (C–N)	^2J (C_1–C–N)	^2J (C_6–C–N)	^3J (C_2–C–C–N)
1[a]	4-H	3.9	9.3	1.0	2.9
1[b]	4-H	2.4	9.7	1.5	2.7
2[a]	4-CH_3	3.9	9.2	0.7	2.8
3[a]	4-Cl	4.0	9.5	0.8	2.9
4[a]	4-Br	3.8	9.5	0.6	2.7
5[a]	4-OCH_3	3.9	9.3	4.4	2.4
6[b]	4-NO_2	2.7	10.1	<0.6	3.4

[a]0.5 *M* solution in $CDCl_3$.
[b]0.5 *M* in acetone-d_6.

indicate that the previous (6) assignments for C-1 and C-4 are also in error. Using the shifts reported by the German workers (6) the deviations from additivy for C-1 and C-4 of **2** are near 5 ppm. Our findings are confirmed by the large 2-bond $^{13}C-^{15}N$ coupling (9.2 Hz) exhibited by the resonance at δ 138.8, whereas C-4 which is five bonds removed from the ^{15}N shows no resolvable coupling (Fig. 1).

For the 4-Cl derivative **3**, again the early assignments (6) for C-2 and C-3 must be reversed from consideration of additivity and $^{13}C-^{15}N$ couplings. Results for **6** are reported for an acetone-d_6 solution only, due to the low solubility of **6** in $CDCl_3$. Considerable solvent effects (up to 3 ppm) are noted for **1** in $CDCl_3$ *vs.* acetone-d_6. A series of dilution experiments involving **1** in $CDCl_3$ were carried out, but only minor ($\pm$0.1 ppm) changes as a function of concentration in the range 0.1 $\rightarrow$ 2.0 *M* were noted.

To summarize, the fact that the earlier (6) chemical shift assignments are almost totally in error emphasizes the need for extreme caution in the use of CNDO methods for predicting small differences in ^{13}C shifts. Also, care is required in the interpretation of lanthanide induced shifts in molecules such as oximes, where the complexing site is not unambiguous.

(b) Coupling Constants

Table 3 contains the absolute values of $^{13}C-^{15}N$ couplings for **1**–**6**. For the 1-bond interactions, there is little effect of substituent

and the magnitudes are similar to that of 4.8 Hz reported for *E*-benzaldoxime (1). The smaller coupling for **6** appears to be primarily the result of an acetone-d_6 induced solvent effect. On the assumption that the Fermi contact mechanism dominates the direct $^{13}C-^{15}N$ interaction, Binsch *et al.* (9) proposed a simple dependence of J on the S characters of the coupled nuclei [1].

$$[1] \qquad \%S_N \times \%S_C = 80J_{NC}$$

Using 33% S character for C and N the expected 1-bond couplings in **1–6** are *ca.* 12 Hz *i.e.* a factor of three greater than the observed. It has been pointed out, however, that the lack of experimental agreement with eq. 1 does not necessarily preclude the dominance of the Fermi contact term, and INDO MO calculations on this basis do reproduce several observed trends in C–N J's for related molecules (1).

In discussing the geminal couplings *i.e.* C_1-C-N and C_6-C-N in **1–6** it is useful to note the results for *E* and *Z* 2-cyclohexenone oximes (1). The enhancement of the 2-bond coupling in the *E* isomer is suggested to be associated with the proximity of the nitrogen lone pair. Findings for 2-butenone oximes (1) and quinoline (10) can be similarly rationalized.

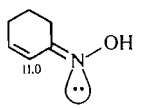

E

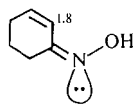

Z

Differences in dihedral angle are not deemed to be the dominant factor (1) in determining these couplings. For **1–6** it is clear that the trends are analogous to those for the butenones and cyclohexenones. The minor importance of hybridization changes is also implied since the couplings of ^{15}N to the CH_3 of **1**, **2**, **3**, **4**, and **6** are only slightly smaller (*ca.* 1 Hz) than to the α-olefinic carbon of the *Z*-enone oximes.

The only remarkable substituent effect is for **5** in which an increase in ^2J (C_6-C-N) to a value of 4.4 Hz is observed. This result may be a consequence of conjugative electron release by the methoxyl group such that resonance form **5***b*, is a substantial contributor. In **5***b* one of the lone pairs on nitrogen will be spatially much closer to the C-6 CH_3 group than will the single nitrogen lone pair in **5***a*, and this would be

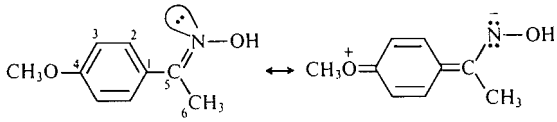

5a *5b*

expected to increase the absolute value of the observed coupling.

Vicinal couplings in **1–6** are not particularly sensitive to substituent and are close to the value of 2.9 Hz observed for *E*-benzaldoxime (1). Due to free rotation about the $^1C-^5C$ bond and assuming planar conformations for **1–6** (3), the observed coupling reflects an average of 0° and 180° dihedral angles. As mentioned previously, the three bond coupling in mesitaldoxime (1) is notably smaller (1.2 Hz) which suggests a dihedral dependence for vicinal $^{13}C-^{15}N$ J's. Further work in these laboratories is being directed toward the synthesis of *ortho*-alkylated acetophenone oximes in order to explore this relationship more fully.

Experimental

Spectra

^{13}C spectra were obtained using the pulsed Fourier transform method at 25.16 MHz on a Varian XL-100-12 nmr spectrometer. The free induction decays were stored in a Nicolet BNC-12 computer (20 K memory) and were transformed after a sufficient number had been accumulated. Normally 8192 data points were used in the interferogram accumulation.

For chemical shift determinations spectral widths were routinely 5000 Hz and the solutions contained 4% TMS as an internal standard. 0.5 *M* solutions in $CDCl_3$ or acetone-d_6 were contained in 8 mm o.d. tubes. For coupling constant determinations, spectral widths of 500 and 1000 Hz were employed with 8192 data points. Decoupler settings were optimized to give the sharpest possible ^{13}C resonances in order to resolve the small (< 1 Hz) couplings. Normally spectra were recorded with complete proton noise decoupling. For the selective decoupling experiments irradiation was performed at low decoupler power in the absence of noise modulation.

Materials

The oximes were prepared using known procedures from the corresponding acetophenone and hydroxylamine hydrochloride. ^{15}N enriched (97%) hydroxylamine HCl was obtained from Merck Sharp and Dohme Canada Ltd.

For **1–5**, the following experimental procedure was employed: The ketone (0.001 mol), the hydroxylamine hydrochloride (100 mg), and potassium hydroxide (200 mg) were added to a 10 ml round-bottomed flask. Ethanol (3 ml of 95%) was added and refluxed on an oil bath for 3 h. During the refluxing, some solid usually remained on the bottom of the flask. After refluxing, the solution and solid were washed from the flask with cold water (10 ml). This solution was then made slightly acidic by

adding HCl (1 *N*). The solution was cooled and the crystals collected and air dried. Yields ranged from 40–92%. Compound **1**, mp 57.5–58 °C (lit. (11) 60 °C); **2**, mp 82.5–83 °C (lit. (12) 85–87 °C); **3**, mp 92.5–93 °C (lit. (13) 97.5–98 °C); **4**, mp 124–125 °C (lit. (13) 127–129 °C); **5**, mp 83–84 °C (lit. (13) 87–88 °C).

For **6**, the following procedure was used: *p*-nitroactephenone (0.001 mol), hydroxylamine hydrochloride (100 mg), water (3 ml) and 10% sodium hydroxide (1 ml) were heated on a steam bath. Enough ethanol (95%) was added to the hot solution to make it clear. The solution was then warmed for an additional 15 min. The solution was then cooled in an ice bath and the crystals collected and air dried. Yield 88%, mp 169.5–170 °C (lit. (14) 171–172 °C).

Acknowledgments

We thank the National Research Council of Canada for generous financial aid.

1. R. L. Lichter, D. E. Dorman, and R. Wasylishen. J. Am. Chem. Soc. **96**, 930 (1974).
2. M. Chistl, J. P. Warren, B. L. Hawkins, and J. D. Roberts. J. Am. Chem. Soc. **95**, 4392 (1973).
3. S. Basu and C. W. N. Cumper. J.Chem. Soc. Perkin Trans. II, 325 (1974).
4. S. Berger and J. D. Roberts. J. Am. Chem. Soc. **96**, 6757 (1974).
5. J. B. Stothers. Carbon-13 NMR spectroscopy. Academic Press, New York, N.Y. 1972. Chap. 10.
6. H. Sterk and H. Steininger. Z. Naturforsch. **29***a*, 1685 (1974).
7. J. W. ApSimon, P. V. Demarco, D. W. Mathieson, W. G. Craig, A. Karin, L. Saunders, and W. B. Whalley. Tetrahedron, **26**, 119 (1970).
8. G. C. Levy and G. L. Nelson. J. Am. Chem. Soc. **94**, 4897 (1972).
9. G. Binsch, J. B. Lambert, B. W. Roberts, and J. D. Roberts. J. Am. Chem. Soc. **86**, 5564 (1964).
10. P. S. Pregosin, E. W. Randall, and A. I. White. J. Chem. Soc. Perkin Trans. II, 1 (1972).
11. R. C. Weast. (*Editor*). Handbook of chemistry and physics. 53rd ed. Chemical Rubber Co., Cleveland. 1972.
12. K. N. Campbell and J. F. McKenna. J. Org. Chem. **4**, 198 (1939).
13. A. B. Sen and D. D. Mukeji. J. Ind. Chem. Soc. **28**, 161 (1951).
14. K. Eichenberger, E. Ganz, and J. Drury. Helv. Chim. Acta, **38**, 284 (1955).

On the rigidity of planar tricoordinate carbon

SAUL WOLFE, H. BERNHARD SCHLEGEL, AND MYUNG-HWAN WHANGBO
Department of Chemistry, Queen's University, Kingston, Ontario K7L 3N6

Received July 10, 1975

SAUL WOLFE, H. BERNHARD SCHLEGEL, and MYUNG-HWAN WHANGBO. Can. J. Chem. **54**, 795 (1976).

A linear relationship has been found between the computed out-of-plane bending force constants of the methylene group and the total charge transfer from X to CH_2 for the series XCH_2^+ (X = H, CH_3, NH_2, OH, F) and $CH_2{=}X$ (X = O, NH, CH_2, S). As the electron-withdrawing power of X increases, out-of-plane bending becomes more difficult in all cases. Two complementary interpretations of this result are proposed.

SAUL WOLFE, H. BERNHARD SCHLEGEL et MYUNG-HWAN WHANGBO. Can. J. Chem. **54**, 795 (1976).

On a trouvé une relation linéaire entre la vibration de déformation angulaire hors plan du groupe méthylène et la charge de transfert totale de X à CH_2 pour une série de XCH_2^+ (X = H, CH_3, NH_2, OH, F) et de $CH_2{=}X$ (X = O, NH, CH_2, S). A mesure que le pouvoir électroaffinitaire de X augmente, la vibration de déformation angulaire hors plan devient plus difficile et ce dans tous les cas. On propose deux interprétations complémentaires pour expliquer ce résultat.
[Traduit par le journal]

Introduction

In general, carbonium ions[1] and carbanions are characterized, respectively, by trigonal planar (2) and pyramidal (3) configurations at carbon. Therefore, substitution at a carbanionic centre can be expected to affect both its stability and its stereochemical capabilities (*e.g.*, the barrier to pyramidal inversion), but in the case of a carbonium ion, only the first of these effects would appear to be susceptible to ready experimental observation. Thus, although many physical and spectroscopic properties of carbonium ions have been described (1, 4), to our knowledge there has been no systematic determination of the rigidity or 'degree of planarity' (*i.e.*, ease of out-of-plane bending) of any series of carbonium ions.

It is reasonable to assume that the degree of planarity of a planar species should be subject to recognizable substituent effects because, from a theoretical standpoint, the single well potential associated with the distortion from planarity of a carbonium ion is just a special case of the double well potential characteristic of carbanions (3). In the case of carbanions, it is well established that relative stabilization of a planar conformation occurs as the substituents are made larger (*i.e.*, steric effects), electron-delocalizing (*i.e.*, conjugative effects), and electron-releasing (*i.e.*, inductive effects). The inductive effect associated with an electron-withdrawing substituent causes relative stabilization of a nonplanar conformation. If these same effects were operative upon the degree of planarity of carbonium ions then, depending on the balance between an electron-withdrawing inductive effect on the one hand, and a combination of steric, conjugative, and electron-releasing inductive effects on the other hand, bending of the carbonium ion might become facilitated.

The present work was undertaken to assess the balance of effects just mentioned, by a theoretical study of the out-of-plane bending force constants of the series of cations XCH_2^+ (X = H, CH_3, OH, NH_2, F). In the case of $HOCH_2^+$, the force constants were calculated for both the all planar energy minimum **1** (5) and the conformation **2**, in which the π-conjugative effect is substantially reduced. The results of the computations were rather unexpected, and the work was, therefore, extended to the neutral molecules $CH_2{=}O$, $CH_2{=}NH$, $CH_2{=}CH_2$, and $CH_2{=}S$.

1 **2**

Calculations

Force constants were computed by the force method (6). The forces, *i.e.*, the negative of the

[1]This terminology refers to trivalent ('classical') carbenium ions. See ref. 1.

Can. J. Chem. Downloaded from www.nrcresearchpress.com by 210.87.254.6 on 09/05/12
For personal use only.

TABLE 1. Charge transfer [a] and out-of-plane bending force constants[b] of the carbonium ions $X-CH_2^+$ [c]

X	π ($X \rightarrow CH_2^+$)	σ ($X \rightarrow CH_2^+$)	Total ($X \rightarrow CH_2^+$)	k
H		0.344	0.344	0.418(0.431)
CH_3	0.135	0.143	0.278	0.441(0.440)
NH_2	0.517	−0.291	0.226	0.438
OH[d]	0.379	−0.354	0.025	0.481(0.465)
	0.263	−0.300	−0.037	0.567
F	0.222	−0.420	−0.198	0.508

[a]In units of electrons.
[b]In units of mdyn Å.
[c]The following geometrical parameters were employed:
CH_3^+: r_{CH} = 1.077 Å, ∠HCH = 120°
$CH_3CH_2^+$: $r_{CH}(CH_3)$ = 1.1 Å, $r_{CH}(CH_2^+)$ = 1.077 Å, r_{CC} = 1.44 Å, ∠HC⁺C = 121°, ∠HCC⁺ = 109.5°
$NH_2CH_2^+$: r_{CH} = 1.103 Å, r_{NH} = 1.038 Å, r_{CN} = 1.292 Å, ∠NCH = ∠CNH = 120°
$HOCH_2^+$: r_{CH} = 1.114 Å, r_{OH} = 1.003 Å, r_{CO} = 1.252 Å, ∠COH = 114.7°, ∠HCO(HC *syn* to OH) = 123°, ∠HCO(HC *anti* to OH) = 116.4°
FCH_2^+: r_{CH} = 1.127 Å, r_{CF} = 1.265 Å, ∠FCH = 120°.
[d]The first row refers to computations on conformation 1, and the second row to computations on conformation 2.

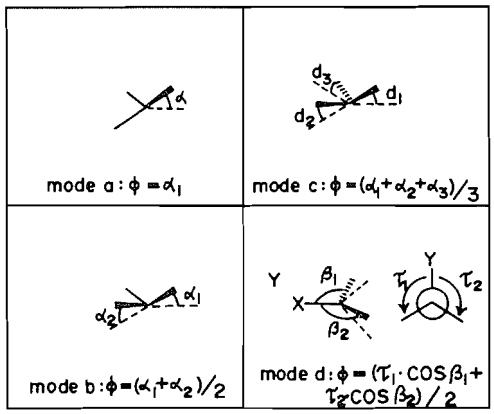

FIG. 1. Possible choices for the out-of-plane bending coordinate (ϕ) for a tricoordinate species.

first derivatives of the energy with respect to the nuclear coordinates, are computed analytically. These are then differentiated numerically to obtain the force constants. The SCF computations were performed using the Gaussian 70 programme system (7) and the standard 4-31G basis set (8). The forces and force constants were calculated using a series of programmes written in this laboratory (9). Various test systems have shown that the 4-31G basis set gives force constants that agree well with experimental and other theoretical work (10).

There are a number of choices for the out-of-plane bending coordinate ϕ. These are illustrated in Fig. 1, as follows: (*a*) mode a, in which one atom moves out of the plane; (*b*) mode b, in which two atoms move out of the plane; (*c*) mode c, in which three atoms move out of the plane; (*d*) mode d, in which the out-of-plane motion is specified in terms of the dihedral angles. With the indicated normalization of the out-of-plane bending coordinate, each of these modes leads to the same harmonic force constant.[2] For convenience, mode d was chosen.

The bending force constants of CH_3^+, $CH_3CH_2^+$, and $HOCH_2^+$ were also calculated, using mode b, by fitting computed energies to a quadratic equation of the internal coordinate. The energies were obtained, using the IBMOL 4 programme system (11), and a double zeta basis set of contracted gaussian functions $(13^s7^p/4^s2^p$ for C and O (12), and $4^s/2^s$ for H (13)).

Results and Discussion

Table 1 summarizes the results obtained for the cations XCH_2^+. The last column shows the computed out-of-plane bending force constants obtained by the force method; the numbers in parentheses are the values obtained by fitting a quadratic equation to the IBMOL 4 computed energies, and it is seen that the same trends are predicted by both methods.

The rigidities of these cations are found to be:

[1] $FCH_2^+ > HOCH_2^+ > CH_3CH_2^+ \gtrsim NH_2CH_2^+ > CH_3^+$

[2]However, the quartic force constants will depend upon the choice of coordinate.

Can. J. Chem. Downloaded from www.nrcresearchpress.com by 210.87.254.6 on 09/05/12
For personal use only.

Can. J. Chem. Downloaded from www.nrcresearchpress.com by 210.87.254.6 on 09/05/12
For personal use only.

This finding is just the opposite of that expected by the assumption that increasing the ligand electronegativity should have led to a decrease in the rigidity of the carbonium ion centre, except for the relative positions of $CH_3CH_2^+$ and CH_3^+.[3]

It follows that inductive effects are not a dominant factor in determining the ease of out-of-plane bending of these carbonium ions. Although none of the substituents shown in eq. 1 is particularly bulky, consideration of *A* values (15) as a measure of their steric effects suggests that these should increase in the order

[2] $$F < OH < NH_2 < CH_3$$

Clearly, the trend seen in eq. 1 is also not compatible with an assumption that steric effects are important in determining the flexibility of these carbonium ions. Therefore, it seemed to follow that the π-conjugative effect of X must be the dominant factor which decides the orderings of eq. 1. According to the classical view, p_π–p_π conjugation is associated with increasing stability of planar configurations at the interacting centres. This leads to the unreasonable conclusion that in the present system the extent of such conjugation increases in the direction

[3] $$CH_3,NH_2 < OH < F$$

To take this point further, the out-of-plane bending force constant was calculated for conformation **2** of $HOCH_2^+$. Since the degree of π-conjugation in **2** must be less than in **1**, the bending force constant of **2** should have been smaller than that of **1**. However, as seen in Table 1, this is not the case. The bending force constants of **1** and **2** are 0.481 and 0.567 mdyn Å, respectively.

Thus none of the classical effects which are commonly considered to influence molecular structure can be responsible for our findings. To gain additional insight into the problem, the amount of charge transfer from X (X = H, CH_3, NH_2, OH, F) to the CH_2^+ moiety was computed, based upon the Mulliken population analysis (see columns 1–3 of Table 1).[4] This quantity can be partitioned into the π and σ contributions (5). The former is the gross charge of the *p*-orbital, and will be zero when there is no π-type charge delocalization between X and CH_2^+. The total charge transfer in XCH_2^+ is the sum of the gross atomic charges on the CH_2^+ group minus seven.

The magnitude of the π-charge transfer may be considered as a measure of the extent of π-conjugation. As was already deduced from the computations on **1** and **2**, it is evident that the amount of π-conjugation does not correlate with the rigidity of the carbonium ion centre. On the other hand, the σ-charge transfer and, even more strikingly, the total charge transfer correlate well with the out-of-plane bending force constants. This means that, as the electron-withdrawing power of the substituent increases, the out-of-plane bending of the carbonium ion becomes more difficult.[5]

This result demonstrates that it is not valid to assume that substituent effects that operate upon barriers to pyramidal inversion of carbanions and on the rigidity of carbonium ions are the same. An electron-withdrawing substituent causes relative stabilization of the geometry of the energy minimum, regardless of whether its conformation is pyramidal or planar.

Our results can be rationalized in two ways. In terms of the Walsh–Mulliken model (18), the pyramidality of CH_3^- can be regarded as the result of electron occupation of the vacant *p*-orbital of CH_3^+, which is planar. This model predicts that π-electron transfer from X to CH_2^+ in XCH_2^+ will facilitate the bending of the carbonium ion centre or, conversely, that the carbonium ion will become more rigid as π-bonding becomes less effective. This is the

[3] This presumes that methyl is to be regarded as an electron-releasing substituent (however, *vide infra*). It should be noted that the force constant computed for ethylcarbonium ion in the present work refers to out-of-plane bending of a trigonally planar carbonium ion centre. Although the CH_2^+ group is slightly non-planar in the fully optimized geometry of the classical structure of ethylcarbonium ion (14), the average structure of the CH_2^+ group is planar because of the very low barrier to internal rotation.

[4] The discussion which follows is subject to the usual caveats concerning the basis set dependence of the Mulliken population analysis (16). However, our argument is based upon trends rather than absolute magnitudes and, in any event, all computations were performed with the same basis set.

[5] It will be noted that, relative to hydrogen, methyl is not electron-releasing but electron-withdrawing because of the combination of its σ and π effects. The polarizable nature of this group (17) allows it to stabilize both cationic and anionic centres.

Can. J. Chem. Downloaded from www.nrcresearchpress.com by 210.87.254.6 on 09/05/12
For personal use only.

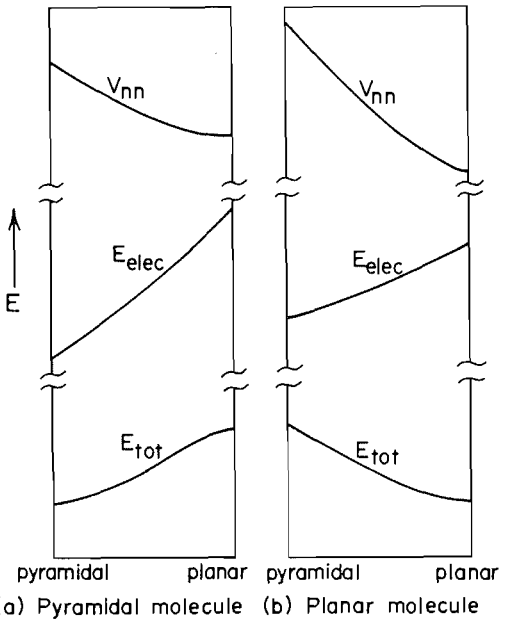

FIG. 2. Schematic diagrams showing the total energy and its nuclear and electronic components for pyramidal (*a*) and planar (*b*) species.

observation in the series FCH_2^+, $HOCH_2^+$ (**1**), and $H_2NCH_2^+$, and it accounts for the difference between the two conformations of $HOCH_2^+$. The same reasoning may be applied to the behaviour of carbanions. In XCH_2^-, conjugation results in π-electron transfer from $^-CH_2$ to X, and it leads to a decrease in the pyramidality of the carbanionic centre (19). What is significant about this model is that the effects of π-electron transfer upon the geometries of adjacent carbonium ions and carbanions are predicted correctly, in contrast to the classical view which predicts incorrectly that both systems become more planar with increasing π-electron transfer.[6]

On the other hand, we have found that our results are better correlated with the total charge transfer than either the σ- or π-effects alone. It is appropriate, therefore, to search for a rationalization of the results which focusses upon the whole system and not just one of the interactions present in this system. Such a rationalization can be provided by making use

[6]The argument just presented is based upon comments communicated to us independently by Professors W. J. Hehre (personal communication), F. Bernardi and N. D. Epiotis (to be published) and L. C. Allen (20). We thank these workers for drawing our attention to the predictive utility of the Walsh–Mulliken model.

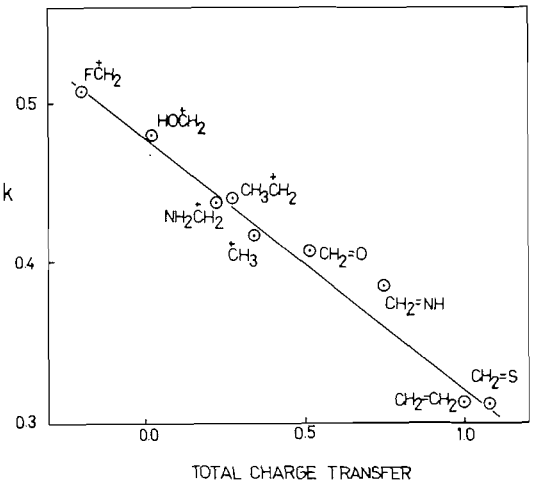

FIG. 3. A plot of total charge transfer versus out-of-plane bending force constant for the cations XCH_2^+ and the molecules CH_2X.

of energy component analysis (21). Figure 2*a* shows the behaviour of the electronic and nuclear components of the total energy for a pyramidal molecule. In this case, the total energy is dominated by the electronic component, so that electron pair repulsion considerations (22) (which are part of the electronic component) correctly simulate the behaviour of the total energy. However, as seen in Fig. 2*b*, for a planar molecule it is the nuclear component which dominates. In terms of such an analysis, it is easy to understand why the removal of electronic charge from a carbonium ion centre will make this centre more rigid, because this increases further the dominance of the nuclear term.

The above arguments should be applicable not only to carbonium ions but to all systems which have trigonal planar geometry about a central atom, *e.g.*, planar neutral molecules. The available experimental data support this view. Thus, the out-of-plane bending frequencies of $CH_2{=}CH_2$, $CH_2{=}NH$, and $CH_2{=}O$ are found at 949 cm^{-1} (23), 1120 or 1057 cm^{-1} (24), and 1167 cm^{-1} (25), respectively. Table 2 summarizes the computed charge transfer[7] and bending force constants of the neutral molecules $CH_2{=}X$ (X=O, NH, CH_2, S). This table again shows the correlation between out-of-plane bending force constants and the total charge transfer.

[7]The charge transfer was calculated by treating $CH_2{=}X$ as $^+CH_2{-}X^-$.

TABLE 2. Charge transfer[a] and out-of-plane bending force constants[b] of the neutral molecules $CH_2{=}X$[c]

X	π ($X \rightarrow CH_2^+$)	σ ($X \rightarrow CH_2^+$)	Total	k
O	0.734	−0.220	0.514	0.408
NH	0.885	−0.136	0.749	0.384
CH_2	1.0	0.0	1.0	0.314
S	0.831	0.244	1.08	0.313

[a]In units of electrons. The charge transfer was calculated by assuming that these species consist of carbonium ions bearing negatively charged substituents, *i.e.*, $^+CH_2{-}O^-$, $^+CH_2{-}NH^-$, $^+CH_2{-}CH_2^-$, $^+CH_2{-}S^-$.

[b]In units of mdyn Å.

[c]The following geometrical parameters were employed:
CH_2O: $r_{CH} = 1.09$ Å, $r_{CO} = 1.21$ Å, $\angle OCH = 120°$
C_2H_4: $r_{CH} = 1.086$ Å, $r_{CC} = 1.337$ Å, $\angle CCH = 121.35°$
CH_2S: $r_{CH} = 1.09$ Å, $r_{CS} = 1.6375$ Å, $\angle SCH = 120°$
CH_2NH: r_{CH}(CH *syn* to NH) = 1.091 Å, r_{CH}(CH *anti* to NH) = 1.089 Å, $r_{NH} = 1.048$ Å, $r_{CN} = 1.273$ Å, $\angle CNH = 109.1°$, $\angle HCN$(CH *syn* to NH) = 125.4°, $\angle HCN$(CH *anti* to NH) = 119.1°.

Figure 3 plots the computed bending force constants *vs.* the total charge transfer for all of the systems studied in the present work. The linear relationship observed in this figure may be taken as evidence that effects of substituents upon the rigidities of carbonium ions and planar neutral molecules are the same.

Acknowledgments

We thank the National Research Council of Canada and the donors of the Petroleum Research Fund, administered by the American Chemical Society, for financial support of this research. One of us (H.B.S.) also thanks the National Research Council for the award of a 1967 Science Scholarship. A number of helpful discussions with Professor I. G. Csizmadia are also gratefully acknowledged.

1. G. A. OLAH. Carbocations and electrophilic reactions. John Wiley and Sons, New York. 1974.
2. J. E. WILLIAMS, JR., R. SUSTMANN, L. C. ALLEN, and P. v. R. SCHLEYER. J. Am. Chem. Soc. **91**, 1037 (1969).
3. J. M. LEHN. Top. Curr. Chem. **15**, 311 (1970); A. RAUK, L. C. ALLEN, and K. MISLOW. Angew. Chem. Int. Ed. Engl. **9**, 400 (1970).
4. G. A. OLAH and P. v. R. SCHLEYER (*Editors*). Carbonium ions. Vol. 1. 1968; (*b*) G. A. OLAH, G. D. MATEESCU, L. A. WILSON, and M. H. GROSS. J. Am. Chem. Soc. **92**, 7231 (1970); (*c*) G. A. OLAH and A. M. WHITE. J. Am. Chem. Soc. **91**, 5801 (1969); (*d*) T. KOENIG, T. BALLE, and W. SNELL. J. Am. Chem. Soc. **97**, 662 (1975).
5. F. BERNARDI, I. G. CSIZMADIA, H. B. SCHLEGEL, and S. WOLFE. Can. J. Chem. **53**, 1144 (1975).
6. P. PULAY. Mol. Phys. **17**, 197 (1969).
7. W. J. HEHRE, W. A. LATHAN, R. DITCHFIELD, M. D. NEWTON, and J. A. POPLE. Quantum Chemistry Program Exchange, Indiana University, Bloomington, Indiana.
8. R. DITCHFIELD, W. J. HEHRE, and J. A. POPLE. J. Chem. Phys. **54**, 724 (1971).
9. H. B. SCHLEGEL. PhD Thesis. Queen's University, Kingston, Ontario. 1975.
10. H. B. SCHLEGEL, S. WOLFE, and K. MISLOW. J. Chem. Soc. Chem. Comm. 246 (1975); H. B. SCHLEGEL, S. WOLFE, and F. BERNARDI. J. Chem. Phys. **63**, 3632 (1975).
11. A. VEILLARD. IBMOL: Computation of wavefunctions for molecules of general geometry, Version 4. IBM Research Laboratory, San Jose, California.
12. S. HUZINAGA and S. SAKAI. J. Chem. Phys. **50**, 1371 (1969).
13. H. BASCH, M. B. ROBIN, and N. A. KUEBLER. J. Chem. Phys. **47**, 1201 (1967).
14. P. C. HARIHARAN, W. A. LATHAN, and J. A. POPLE. Chem. Phys. Lett. **14**, 385 (1972).
15. J. A. HIRSCH. Top. Stereochem. **1**, 199 (1967).
16. R. S. MULLIKEN. J. Chem. Phys. **36**, 3428 (1962); P. POLITZER and R. S. MULLIKEN. J. Chem. Phys. **55**, 5135 (1971); S. FLISZAR, A. GOURSOT, and H. DUGAS. J. Am. Chem. Soc. **96**, 4358 (1974).
17. W. J. HEHRE and J. A. POPLE. Tetrahedron Lett. 2959 (1970); J. A. POPLE and M. S. GORDON. J. Am. Chem. Soc. **89**, 4253 (1967).
18. R. J. BUENKER and S. D. PEYERIMHOFF. Chem. Rev. **74**, 127 (1974).
19. S. WOLFE, H. B. SCHLEGEL, I. G. CSIZMADIA, and F. BERNARDI. Can. J. Chem. **53**, 3365 (1965).
20. E. D. JEMMIS, V. BUSS, P. v. R. SCHLEYER, and L. C. ALLEN. J. Am. Chem. Soc. Submitted for publication.
21. V. BUSS, P. v. R. SCHLEYER, and L. C. ALLEN. Top. Stereochem. **7**, 262 (1972).
22. R. J. GILLESPIE and R. S. NYHOLM. Q. Rev. Chem. Soc. **11**, 339 (1957); R. J. GILLESPIE. J. Chem. Educ. **40**, 295 (1963).
23. W. H. FLETCHER and W. T. THOMPSON. J. Mol. Spectrosc. **25**, 240 (1968).
24. D. E. MILLIGAN. J. Chem. Phys. **35**, 1491 (1961); C. B. MOORE, G. C. PIMENTEL, and T. D. GOLDFARB. J. Chem. Phys. **43**, 63 (1965).
25. J. L. DUNCAN and P. D. MALLINSON. Chem. Phys. Lett. **23**, 597 (1973).

Can. J. Chem. Downloaded from www.nrcresearchpress.com by 210.87.254.6 on 09/05/12
For personal use only.

The sign of the 'through-space' spin–spin coupling between methyl protons and the fluorine nucleus in 2,6-dimethylbenzoyl fluoride

TED SCHAEFER, KALVIN CHUM, AND KIRK MARAT

Department of Chemistry, University of Manitoba, Winnipeg, Manitoba R3T2N2

AND

RODERICK E. WASYLISHEN

Department of Chemistry, University of Winnipeg, Winnipeg, Manitoba R3B 2E9

Received September 22, 1975

TED SCHAEFER, KALVIN CHUM, KIRK MARAT, and RODERICK E. WASYLISHEN. Can. J. Chem. **54**, 800 (1976).

The spin–spin coupling constant over five formal bonds between ^{19}F and methyl protons, $^{5}J_{o}^{F,CH_3}$, in 2,6-dimethylbenzoyl fluoride is -3.1 Hz. Observation of a nonzero $^{6}J_{p}^{H,COF}$ indicates an out-of-plane conformation for the carbonyl fluoride group and implies substantial non-bonded repulsions between the methyl and carbonyl fluoride groups. It is argued that $^{5}J_{o}^{F,CH_3}$ is as small as -7 Hz when the C—F bond lies *cis* to a methyl group and that its magnitude is a consequence of the so-called 'through-space' coupling mechanisms. On the basis of INDO–MO–FPT computations, it is suggested that such observed couplings are a composite of large contributions of either sign and, therefore, that observed through-space $^{1}H,^{19}F$ couplings may be of either sign if conformational averaging occurs.

TED SCHAEFER, KALVIN CHUM, KIRK MARAT et RODERICK E. WASYLISHEN. Can. J. Chem. **54**, 800 (1976).

La constante de couplage spin–spin à travers cinq liens formels entre le ^{19}F et les protons du méthyle, $^{5}J_{o}^{F,CH_3}$, dans le fluorure de diméthyl-2,6 benzoyle est de -3.1 Hz. L'observation d'une constante $^{6}J_{p}^{H,COF}$ qui n'est pas égale à zéro indique que le groupement fluorocarbonyle existe dans une conformation hors plan et implique des répulsions non liées substantielles entre les groupes méthyle et fluorocarbonyle. On suggère que $^{5}J_{o}^{F,CH_3}$ est aussi petit que -7 Hz quand le lien C—F et le groupe méthyle sont *cis* l'un par rapport à l'autre et que l'amplitude de ce couplage est une conséquence des mécanismes de couplage communément appelé 'à travers l'espace'. En se basant sur des calculs INDO–MO–FPT, on suggère que de tels couplages observés sont dus à une superposition de contributions larges de signes divers et qu'en conséquences les couplages $^{1}H,^{19}F$ observés à travers l'espace peuvent être de n'importe quel signe si une moyenne des conformations se produit.

[Traduit par le journal]

Introduction

The size of so-called 'through-space' spin–spin coupling constants between nuclear pairs like $^{19}F,^{19}F$ and $^{1}H,^{19}F$, among others, apparently is steeply dependent on the internuclear distance and becomes relatively small when this distance exceeds the sum of the van der Waals radii of the corresponding atoms (1–15). The sign of the $^{19}F,^{19}F$ coupling constants, $^{n}J^{F,F}$, is positive in a variety of bonding situations and when the number, n, of formal intervening bonds is four or five (5, 7–9, 15–17). One semiempirical theory relates the magnitude of $^{n}J^{F,F}$ to the overlap between the valence orbitals centered on the nuclei and predicts a positive sign (18), while another (19) finds a negative sign for relatively large internuclear distances when n is four but a positive sign when n is five. A molecular orbital model (20) rationalizes a positive sign for $^{n}J^{F,F}$.

For $^{1}H,^{19}F$ through-space couplings a negative sign is calculated by a sum-over-states perturbation method based on INDO molecular orbitals (19). Indeed, in derivatives **1** and **2**, of *o*-fluorophenol and of *o*-hydroxybenzotrifluoride, $^{4}J_{o}^{OH,F}$ and $^{5}J_{m}^{OH,CF_3}$ are negative for the indicated, proximate bond orientations (21,22). INDO–MO–FPT (23) calculations

1

2

Can. J. Chem. Downloaded from www.nrcresearchpress.com by 210.87.254.6 on 09/05/12
For personal use only.

Can. J. Chem. Downloaded from www.nrcresearchpress.com by 210.87.254.6 on 09/05/12
For personal use only.

agree as to the signs and suggest a sensitivity of the magnitudes of these couplings to the H,F distance (21) in **1** and **2**. These calculations, in common with the other theoretical treatments, invoke the Fermi contact interaction as the underlying coupling mechanism.

On the other hand, it may be argued that **1** and **2** represent a weak hydrogen bonding situation and that the mechanism of transfer of spin state information depends on the properties of the hydrogen bond wave function.[1] Consequently, the sign of $J^{H,F}$ may change when the proximity of ^1H and ^{19}F nuclei arises for steric reasons, *viz.*, when strong nonbonded repulsions occur between the relevant molecular fragments.

Recently (26), exploratory INDO–MO–FPT computations of $J^{H,F}$ for a variety of bonding situations demonstrate a complexity of the through-space coupling phenomenon. Large negative or positive values are found, depending on the relative orientation of the proximate bonds containing the nuclei. Conformational mobility could then lead to small, averaged, observed couplings; presumably of either sign.

In this paper the sign of $^5J_o^{F,CH_3}$ in 2,6-dimethylbenzoyl fluoride is determined. In this molecule the nonbonded interactions are apparently large enough to twist the carbonyl fluoride group out of the benzene plane, thereby ensuring substantial nonbonded interactions between H and F atoms.

Experimental

Fluorination of 2,6-dimethylbenzoic acid with sulfur tetrafluoride yielded the benzoyl fluoride (27). SF_4 (13.6 mmol) was condensed from a metal vacuum system into a 75 ml stainless steel cylinder containing 2 g (13 mmol) of the acid and 10 ml of CH_2Cl_2. After 10 min at room temperature, gaseous products were vented and the remaining liquid was fractionated to yield 1.1 g (56%) of the benzoyl fluoride, bp 66 °C/1 torr. Product identity was confirmed by mass, ^1H, and ^{19}F nmr spectra.

A 25 mol% solution of 2,6-dimethylbenzoyl fluoride in CS_2 contained small amounts of internal tetramethylsilane and CF_3CCl_3 and was degassed by the freeze–pump–thaw technique. The pmr spectrum was repeatedly calibrated on an HA-100 spectrometer, using the frequency-sweep mode and sweep rates of 0.01 and 0.02 Hz s^{-1}. The ^{19}F nmr spectrum was recorded at 56.4 MHz on an HA60 spectrometer, also in the frequency-sweep mode. Partial decoupling (28) and weak irradiation experiments (29) of the usual kind established the relative signs of the $^1H,^{19}F$ spin–spin coupling constants.

INDO–MO–FPT (23) calculations were performed on an IBM 370/158 system and convergence to 0.01 Hz in the coupling constants was demanded. A regular geometry (30) was assumed for the benzene and methyl group moieties. The geometry of the carbonyl fluoride group was based on microwave data for acetyl fluoride (31) and had C—F 1.348, C=O 1.181, and C—C 1.46 Å; ∠CCF 110.3° and ∠CCO 128.3°.

Results and Discussion

1. Spectral Analysis

The pmr spectrum of 2,6-dimethylbenzoyl fluoride corresponds to the $ABB'X_3X_3'$ part of an $ABB'X_3X_3'R$ spin system. However, $^6J_p^{H,CH_3}$ and $^4J_o^{H,CH_3}$ in toluene differ by only 0.1 Hz (32) and are unlikely to differ by more than this in the benzoyl fluoride derivative. Consequently, the spectrum is insensitive to $^4J_m^{H,H} \equiv J_{BB'}$ and to $^5J_m^{CH_3,CH_3}$ and can be adequately analyzed as an AB_2X_6R spectrum; yielding $(^4J_o^{H,CH_3} + {}^6J_p^{H,CH_3})/2$. In any event, the coupling of real interest in this paper is $^6J_o^{F,CH_3}$, the error in which is certainly less than 0.05 Hz. An iterative fit to the observed spectrum was performed with the computer program LAME (33, 34) and the final parameters are given in Table 1.

Double irradiation experiments demonstrated that $^6J_p^{H,COF}/{}^5J_o^{F,CH_3} > 0$ and that $^5J_m^{H,COF}/{}^5J_o^{F,CH_3} < 0$. A fit of the ^{19}F spectrum could not be achieved if $^5J_m^{H,COF}$ and $^6J_p^{H,COF}$ had the same sign but the spectrum was insensitive to the sign of $^5J_o^{F,CH_3}$. In 2-fluoro-6-chlorobenzoyl fluoride we have shown that $^5J_m^{H,COF}/{}^3J_o^{H,F} > 0$ and as $^3J_o^{H,F}$ is positive (35, 36), the signs in Table 1 are firmly established.

2. Out-of-plane Twisting of the Carbonyl Fluoride Group

Steric hindrance from the methyl groups in **3** may destroy coplanarity of the carbonyl fluoride group and the benzene ring. The most direct evidence for a substantial deviation from coplanarity of these moieties is the observed value of -0.37 Hz for $^6J_p^{H,COF}$. This coupling

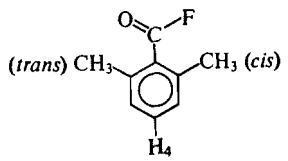

3

[1]When a stronger bond holds ^1H and ^{19}F together, *i.e.* as in the HF molecule, $J^{H,F}$ is +530 Hz (24), in disagreement with calculations based on the approximations inherent to all the above theories, but in fair agreement with a sum-over-states calculation of +836 Hz (25).

TABLE 1. Chemical shifts* and coupling constants† in 2,6-dimethylbenzoyl fluoride

Parameter	Value	Parameter	Value
ν_{CH_3}	234.067(1)‡	$^5J_m^{H,COF}$	1.087(3)
$\nu_{3,5}$	696.365(1)	$^6J_p^{H,COF}$	−0.370(3)
ν_4	716.425(1)	$^5J_o^{CH_3,COF}$	−3.091(2)
ν_5§	7629.2	Error (rms)†	0.0127
$^3J_o^{H,H}$	7.689(1)	Largest error†	0.043
$(^4J_o^{H,CH_3} + {}^6J_p^{H,CH_3})/2$	−0.644(1)	Transitions assigned	404
$^5J_m^{H,CH_3}$	0.343(1)	Transitions calculated‖	466

*In Hz at 100 MHz to low field of internal TMS of a 25 mol% solution in carbon disulfide.
†In Hz.
‡The numbers in brackets give the standard deviation in the last place.
§In Hz to low field of internal CF_3CCl_3 at 56.443 MHz.
‖Intensities greater than 0.01, *i.e.*, observable at reasonable gain settings.

is not observed in benzoyl fluoride (36), presumably because it is transmitted via a $\sigma-\pi$ mechanism which is inoperative when the C—F bond lies in the benzene plane. Analogous behaviour is found in benzaldehyde and 2,6-dichlorobenzaldehyde, $^6J_p^{H,CHO}$ being unobserved in the former but amounting to —0.15 Hz in the latter compound (38). Because the COF and CH_3 groups likely suffer at least as great a mutual steric hindrance as do the CHO and Cl entities, an average out-of-plane conformation of the COF group in **3** may be safely assumed. The barriers to internal rotation in benzaldehyde and benzoyl fluoride are equal (39, 40).

A rough estimate of the angle of twist about the C—C bond in **3** is made below. Of greater interest here is the fact that a twisted conformation implies a substantial nonbonded interaction of the fluoride (and oxygen) atom(s) with the hydrogen atoms of the methyl groups. Consequently, a through-space coupling interaction, $^5J_o^{F,CH_3}$, likely occurs.

3. The Negative Signs of $^5J_o^{F,CH_3}$

$^5J_o^{F,CH_3}$ is −3.09 Hz in **3** and represents a simple average of the *cis* and *trans* couplings, $^5J_c^{F,CH_3}$ and $^5J_t^{F,CH_3}$, schematically marked in **3**. On the assumption that the nonproximate, five-bond coupling, $^5J_t^{F,CH_3}$, has a magnitude of 1 Hz it follows that $^5J_c^{F,CH_3}$ is -6.2 ± 1 Hz; implying a considerable magnitude for a coupling mechanism dependent on the proximity of the C—F and C—H bonds.

Further insight into the manner in which nuclear spin state information is transmitted via the electrons when proximate bond orientations exist is provided by the INDO–MO–FPT calculations of $^5J_o^{F,CH_3}$, tabulated in Table 2. Consider an essentially coplanar arrangement (angle of twist, $\theta = 1°$) of the carbonyl fluoride and benzene fragments, as in **4**. In **4** the methyl

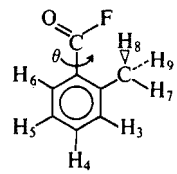

4

group is staggered about the C—F bond so that the C—H_7 bond eclipses the C—C bond of the benzene ring.[2] One striking computational prediction is the large positive coupling of 25.8 Hz to H_7 in a C—H bond which is coplanar with, but pointing away from, fluorine. Such an interaction has been discussed previously (26) for similar bond orientations in other molecules and is an example of a direct (41) mechanism involving the orbitals on the carbon atom of the C—H_7 bond. Another striking prediction is the great sensitivity of $^5J_o^{F,CH_3}$ to the distance between ^{19}F and H_8 and H_9 in **4**. With the geometry given under Experimental, the H_9,F distance is 2.01 Å and the H_8,F distance is 2.03 Å. The corresponding couplings are −1.59 Hz and −0.46 Hz, respectively, when $\theta = 1°$, *i.e.*, when F in **4** lies slightly below the plane of the paper. The average value of $^5J_c^{F,CH_3}$ for **4** is +7.9 Hz.

However, it was argued above that considerable out-of-plane twisting of the COF group occurs. The calculated values in Table 2 for

[2]Only one methyl group is used in the calculations in order to reduce the computational expense; convergence was not achieved for $\theta = 0°$.

Can. J. Chem. Downloaded from www.nrcresearchpress.com by 210.87.254.6 on 09/05/12
For personal use only.

TABLE 2. INDO–MO–FPT values* for $^1H,^{19}F$ spin–spin coupling constants in 2-methylbenzoyl fluoride (Hz)

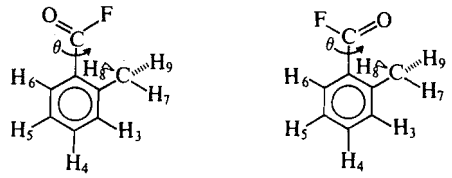

	θ(deg.)†						
	cis				*trans*		
Coupling	1‡	10	20	30	1	10	20
$^4J_o^{F,H}$	1.22	1.21	1.16	1.06	−1.05	−0.77	−0.11
$^5J_m^{F,H_3}$	−0.41	−0.39	−0.27	−0.03	4.48	4.47	4.46
$^5J_m^{F,H_5}$	5.59	5.53	5.38	5.19	−0.26	−0.21	−0.05
$^6J_p^{F,H_4}$	0.65	0.60	0.44	0.15	0.52	0.46	0.26
$^5J_o^{F,H_7}$	25.79	23.11	16.66	9.88	0.65	0.59	0.49
$^5J_o^{F,H_8}$	−0.46	2.18	2.06	1.51	−0.58	−0.83	−0.77
$^5J_o^{F,H_9}$	−1.59	−8.55	−15.96	−17.50	−0.49	0.01	0.68

*Geometries are specified under Experimental.
†The angle of twist, θ, represents a clockwise rotation about the C—C(OF) bond, *e.g.*, θ = 1° represents a conformation in which the F atom lies just below the plane of the paper.
‡Convergence was not achieved when θ was 0°.

θ = 10, 20, and 30° demonstrate a strong dependence on θ and, therefore, on the H,F distance. The average value of $^5J_c^{F,CH_3}$ becomes −2.0 Hz at θ = 30°. Of course, torsional oscillations of the methyl and carbonyl fluoride groups occur in the molecule and, in a situation where the coupling is so exceedingly sensitive to the H,F distance, will certainly help to determine[3] the actual value of $^5J_c^{F,CH_3}$.

Nevertheless, it may be concluded that the signs of observed through-space $^1H,^{19}F$ coupling constants will vary, depending as they apparently do on the relative magnitudes of positive and negative contributions. These magnitudes, in turn, depend on a delicate balance of the nonbonded interactions which determine the precise electron and nuclear arrangement in the relevant molecular fragments. In 2,6-dimethylbenzoylfluoride the negative contributions to $^5J_c^{F,CH_3}$ outweigh the positive ones. The calculated values of $^5J_t^{F,CH_3}$ suggest that its magnitude is below 0.2 Hz and therefore, perhaps, that $^5J_c^{F,CH_3}$ is indeed as small as −7 Hz.

[3]A conformation in which a C—H bond of the methyl group eclipses the C—F bond (within one degree) yields a calculated *J* of −324 Hz, corresponding to an internuclear distance of 1.33 Å. Naturally, such a conformation is energetically very unfavourable.

4. The Other Couplings to ^{19}F

The measured $^6J_p^{H,COF}$ of −0.37 Hz in **3** has been partly discussed above. The calculated values in Table 2 are too large, indicating a positive number at θ = 0°. However, they apparently follow a $\sin^2\theta$ law, at least for the *cis* form between θ = 1° and 30°. In fact, the calculated changes in $^6J_p^{H,CFO}$, as θ changes, suggest $^6J_p^{H,COF}$ as −2.1 ± 0.1 Hz at θ = 90°; assuming that $^6J_p^{H,COF}$ vanishes at θ = 0°, as in benzoyl fluoride itself (37). It follows that θ ~ 25° in 2,6-dimethylbenzoyl fluoride. This estimate of θ is very rough. A comparison between calculated and observed values of $^5J_o^{F,CH_3}$ in Tables 1 and 2 implies a value of nearer 40° for θ. Both estimates are to be considered as tentative.

$^5J_m^{H,COF}$ is 1.09 Hz in **3** but is 1.33 Hz in benzoyl fluoride, indicating a nonzero angle of twist, θ, in **3** if it is assumed that the largest magnitude occurs for the planar 'zig-zag' or 'all-*trans*' arrangement of the intervening bonds and that the methyl groups do not exert an intrinsic substituent effect on $^5J_m^{H,COF}$. Substituents in the *para* position do not alter $^5J_m^{H,COF}$ appreciably (42). The calculated numbers in Table 2 imply an intrinsic substituent effect on $^5J_m^{H,COF}$ and also overestimate the

Can. J. Chem. Downloaded from www.nrcresearchpress.com by 210.87.254.6 on 09/05/12
For personal use only.

magnitude of the coupling. In these calculations the C—C bond length in the C—COF fragment is taken as 1.46 Å and a change in this parameter may well alter the calculated magnitudes (42).

Acknowledgment

We are grateful to the National Research Council of Canada for financial assistance.

1. P. C. MYHRE, J. W. EDMONDS, and J. D. KRUGER. J. Am. Chem. Soc. **88**, 2459 (1966).
2. K. L. SERVIS and F. R. JEROME. J. Am. Chem. Soc. **93**, 1535 (1971).
3. G. W. GRIBBLE and J. R. DOUGLAS, JR. J. Am. Chem. Soc. **92**, 5764 (1970).
4. F. R. JEROME and K. L. SERVIS. J. Am. Chem. Soc. **94**, 5896 (1972).
5. R. D. CHAMBERS, L. H. SUTCLIFFE, and G. J. T. TIDDY. Trans. Faraday Soc. **66**, 1025 (1970).
6. R. J. ABRAHAM, D. F. WILEMAN, G. R. BEDFORD, and D. GREATBANKS. Org. Magn. Reson. **4**, 343 (1972).
7. C. SCHUMANN and F. CAVAGNA. J. Magn. Reson. **18**, 172 (1975).
8. C. W. HAIGH, J. HILTON, L. H. SUTCLIFFE, and G. J. T. TIDDY. J. Magn. Reson. **18**, 241 (1975).
9. R. A. FLETTON, R. D. LAPPER, and L. F. THOMAS. Chem. Commun. 1049 (1969).
10. F. B. MALLORY, C. W. MALLORY, and M.-C. FEDARKO, J. Am. Chem. Soc. **96**, 3536 (1974).
11. G. R. MILLER, A. W. YANKOWSKY, and S. O. GRIM. J. Chem. Phys. **51**, 3185 (1969).
12. R. E. RICHARDS and T. SCHAEFER. Trans. Faraday Soc. **54**, 1447 (1958).
13. L. PETRAKIS and C. H. SEDERKOLM. J. Chem. Phys. **35**, 1243 (1961).
14. J. JONAS, L. BOROWSKI, and H. S. GUTOWSKY. J. Chem. Phys. **47**, 2441 (1967).
15. T. SCHAEFER, W. NIEMCZURA, and K. MARAT. J. Chem. Soc. Faraday Trans. II, 1526 (1975).
16. S. L. MANATT, M. A. COOPER, C. W. MALLORY, and F. B. MALLORY. J. Am. Chem. Soc. **95**, 975 (1973).
17. D. F. EVANS, S. L. MANATT, and D. D. ELLEMAN. J. Am. Chem. Soc. **85**, 238 (1963).
18. A. D. BUCKINGHAM and J. E. CORDLE. J. Chem. Soc. Faraday Trans. II, **70**, 994 (1974).
19. K. HIRAO, H. NAKATSUJI, and H. KATO. J. Am. Chem. Soc. **95**, 31 (1973).
20. F. B. MALLORY. J. Am. Chem. Soc. **95**, 7747 (1973).
21. T. SCHAEFER and J. B. ROWBOTHAM. Chem. Phys. Lett. **29**, 633 (1974).
22. J. B. ROWBOTHAM, M. SMITH, and T. SCHAEFER. Can. J. Chem. **53**, 986 (1975).
23. J. A. POPLE, J. W. MCIVER, JR., and N. S. OSTLUND. J. Chem. Phys. **49**, 2960 (1968); **49**, 2965 (1968).
24. J. S. MUENTER and W. KLEMPERER. J. Chem. Phys. **52**, 6033 (1970).
25. J. N. MURRELL, M. A. TURPIN, and R. DITCHFIELD. Mol. Phys. **18**, 271 (1970).
26. R. E. WASYLISHEN and M. BARFIELD. J. Am. Chem. Soc. **97**, 4545 (1975).
27. W. C. SMITH. Angew. Chem. Int. Ed. Engl. **1**, 467 (1962).
28. J. P. MAHER and D. F. EVANS. Proc. Chem. Soc. 208 (1961).
29. R. FREEMAN and W. A. ANDERSON. J. Chem. Phys. **37**, 2053 (1962).
30. J. A. POPLE and M. GORDON. J. Am. Chem. Soc. **89**, 4253 (1967).
31. L. PIERCE and L. C. KRISHER. J. Chem. Phys. **31**, 875 (1959).
32. M. P. WILLIAMSON, R. KOSTELNIK, and S. M. CASTELLANO. J. Chem. Phys. **49**, 2218 (1968).
33. S. CASTELLANO and A. A. BOTHNER-BY. Mellon Institute Publications, Pittsburgh, Pennsylvania. 1967.
34. C. W. HAIGH and J. M. WILLIAMS. J. Mol. Spectrosc. **32**, 398 (1969).
35. P. DIEHL and I. GRÄNACHER. J. Chem. Phys. **34**, 1846 (1961).
36. A. SAUPE. Z. Naturforsch, **19***a*, 161 (1964); **20**, 572 (1965).
37. R. J. KOSTELNIK, M. P. WILLIAMSON, D. E. WISNOSKY, and S. M. CASTELLANO. Can. J. Chem. **47**, 3313 (1969).
38. C. L. BELL, S. S. DANYLUK, and T. SCHAEFER. Can. J. Chem. **47**, 3529 (1969).
39. W. G. FATELEY, R. K. HARRIS, F. A. MILLER, and R. E. WITKOWSKI. Spectrochim. Acta, **21**, 231 (1965).
40. R. K. KAKAR. J. Chem. Phys. **56**, 1189 (1972).
41. M. BARFIELD and M. KARPLUS. J. Am. Chem. Soc. **91**, 1 (1969).
42. H. BILDSOE and K. SCHAUMBURG. J. Magn. Reson. **14**, 223 (1974).

Can. J. Chem. Downloaded from www.nrcresearchpress.com by 210.87.254.6 on 09/05/12
For personal use only.

The influence of remote substituents upon ionization potential. Part I. The effect of two allylic oxygens upon the ionization of the π-bond

R. S. BROWN

Department of Chemistry, University of Alberta, Edmonton, Alberta T6G 2E1

Received August 6, 1975

R. S. BROWN. Can. J. Chem. **54**, 805 (1976).

The photoelectron (pe) spectrum of ascaridole (**1**) shows an unusually high binding potential for the π-bond. Several possible explanations both conjugative and inductive in nature can be envisioned to account for these observations. To probe which of these mechanisms was prominent, several symmetrical bisallylic oxygen compounds as well as their saturated analogues were synthesised and their pe spectra recorded. Substitution at the allylic centres was chosen to be nearly constant in each case, but the orientation of the symmetrically placed oxygens varied about the π-bond from 0° in ascaridole (**1**) to 90° in 1,4-dimethoxybicyclo[2.2.2]oct-2-ene (**6**). In each unsaturated case the position of the ionization attributable to the π-bond is the same. Conjugative interactions of the oxygens with the π-bond cannot account for the pe results since these are expected to show marked dependence upon geometrical constraints. It is postulated that in these systems, the greater electronegativity of oxygen relative to carbon is responsible for the observed result.

R. S. BROWN. Can. J. Chem. **54**, 805 (1976).

Le spectre de l'ascaridole photoelectronique (pe) (**1**) indique la présence d'un potentiel particulièrement élevé pour le lien-π. On peut envisagé plusieurs explications possibles, de nature conjugative et inductive, pour expliquer ces résultats. Afin de pouvoir évaluer l'importance de chacun de ces mécanismes, on a synthétisé plusieurs composés oxygénés bisallyliques symétriques ainsi que leurs analogues saturés et on a enregistré leurs spectres pe. On a choisi des substitutions aux centres allyliques qui étaient pratiquement constantes dans chaque cas mais l'orientation des oxygènes, placés d'une façon symétrique autour du lien-π, variait de 0° dans l'ascaridole (**1**) jusqu'à 90° dans le diméthoxy-1,4 bicyclo[2.2.2]octène-2 (**6**). Dans chaque composé insaturé, la position de l'ionisation attribuable au lien-π est la même. Des interactions de conjugaison des oxygènes avec les liens-π ne peuvent expliquer les résultats pe puisque de telles interactions devraient varier d'une façon importante avec les contraintes géométriques. On postule que dans ces systèmes, la plus grande électronégativité de l'oxygène, par rapport au carbone, est responsable des résultats observés.

[Traduit par le journal]

Some time ago during a study designed to investigate certain organic peroxides by photoelectron (pe) spectroscopy (1), we observed that the double bond of ascaridole (**1**) appeared at an unusually high binding energy. The vertical ionization potential (VIP) for the π-bond in **1** is 9.70 eV while that in the carbocyclic analogues **3***a*, **3***b*, and **3***c* appear at 8.97 eV (2*a*), 9.05 eV (2*a*), and 9.00 eV (2*b*) respectively.

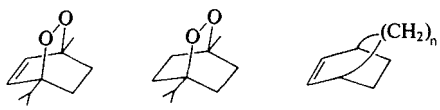

1 **2** **3** *a*; $n=1$ *b*; $n=2$ *c*; $n=3$

Although ascaridole (**1**) is substituted at the bridgehead positions by alkyl groups while **3***a–c* are not, such substitution is expected to lower the IP of the π-bond in contrast to what is actually observed (3). Hence simple substitution effects cannot account for the 0.65 eV (~15 kcal) stabilization of the π-bond of **1** as compared to **3***b*.

Recognizing that the double-bond position was undoubtedly influenced by the presence of the two oxygens at the allylic positions, we set out to determine the cause of the stabilization. *A priori*, one might list several types of possible interactions: (*a*) interactions of the π-bond with the peroxide linkage (homoconjugation), (*b*) a through-bond interaction of the π-bond with the perpendicularly-oriented C—O σ-bonds (hyperconjugation), or (*c*) a removal of electron density from the π-system by the more electronegative oxygens (inductive).

In order to test which of these effects were operative a series of similarly substituted un-

Can. J. Chem. Downloaded from www.nrcresearchpress.com by 210.87.254.6 on 09/05/12
For personal use only.

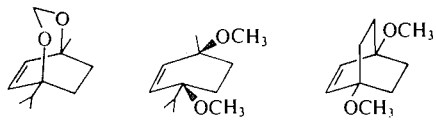

4 5 6

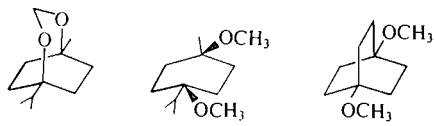

7 8 9

saturated compounds (**4**–**6**) and their saturated analogues (**7**–**9**) were synthesized and their pe spectra studied. The following represents the findings of this study.

Experimental

Photoelectron spectra were recorded on a MacPherson Model 36 Esca spectrometer equipped with an He(I) ionization source. While under optimum conditions the resolution of the argon $2P_{3/2}$–$2P_{1/2}$ doublet was 17 meV and 10^5 counts/s, a resolution of between 25 and 35 meV was noticed during actual spectral recording. Continued monitoring of all spectra over a several hour period showed no spectral changes.

All melting points and boiling points are uncorrected. Nuclear magnetic resonance (pmr) spectra were recorded using a Varian A56-60 or Perkin-Elmer 90 mHz spectrometer. Infrared spectra were determined in $CHCl_3$ solution using a Perkin-Elmer 421 grating infrared spectrometer.

Ascaridole (**1**) *(1,4-Epidioxy-p-menth-2-ene)*

This was obtained from the Fluka A.G. Chemische Fabrik (Switzerland) and was purified by low temperature recrystalization from isopentane at −78 °C to a constant melting point of 3 °C (lit. (4) 3.3 °C).

Dihydroascaridole (**2**) *(1,4-Epidioxy-p-menthane)*

This was prepared by catalytic hydrogenation of an ethanol solution of ascaridole over Adam's Catalyst according to the procedure of Paget (5); pmr ($CDCl_3$) δ 2.17–1.45 (m, 9H), 1.12 (s, 3H), 0.88 (d, 6H, J = 6.5 Hz); ir ($CHCl_3$) 3025, 3000, 2970, 2930, 2892, 2888, 2800, 1472, 1465, 1450, 1387, 1376, 1370, 1440, 1260, 1225 (br), 1140, 1118, 1107, 1077, 1035, 1000 cm^{-1}; Raman (neat), O–O stretch 724 cm^{-1}; mp 19 °C (lit. (5) 19.5 °C).

cis-p-Menth-2-ene-1,4-diol was prepared by the procedure of Schenck *et al.* (6).

Δ^6-1-Methyl-5-isopropyl-2,4-dioxabicyclo[3.2.2]nonene (**4**)

This could not be prepared by an acid catalysed formylation of *cis-p*-menth-2-ene-1,4-diol since this procedure produced only *p*-cymene (**10**) (TsOH catalysed) or Δ^4-1-methyl-4-isopropyl-6,8-dioxabicyclo[4.3.0]nonene (**11**) (BF_3—$O(C_2H_5)_2$). An alternative anionic route to produce **4** was used successfully.

To a 1 litre 3-necked flask equipped with an addition funnel, reflux condensor, magnetic stirrer, and N_2-inlet tube was added 400 cc dimethoxyethane (distilled from $LiAlH_4$) and 50 cc of dry DMSO followed by 3.4 g (2×10^{-2} mol) of *cis-p*-menth-2-ene-1,4-diol prepared as above. To the stirring solution held at room temperature was added 1.68 g (4×10^{-2} mol of 57% NaH in oil) NaH suspension over a period of 15 min. The suspension was stirred an additional $\frac{1}{2}$ h and refluxed for a total of 3 h more to ensure maximum conversion to the alkoxide. After cooling the mixture to room temperature, 2.6 g (2×10^{-2} mol) redistilled bromochloromethane was added to it at once and the mixture gently brought to reflux overnight. After cooling and filtering excess DME was removed under reduced pressure, and the remaining dark liquid distilled at 20–30 torr to yield a distillate containing roughly 90% DMSO to 10% product. This distillate was diluted with 20 ml 5% aqueous K_2CO_3 and extracted with several small portions of pentane which were ultimately combined and dried over Na_2SO_4. Filtration and removal of solvent and finally bulb to bulb distillation at 1 torr pressure yielded 600 mg of desired **4**; pmr ($CDCl_3$) δ 6.02 (AB quartet, 2H, J = 9 Hz), 4.73 (s, 2H), 2.30–1.42 (m, 5H), 1.34 (s, 3H), 0.93 (d, 6H, J = 7 Hz); ir (neat) 3055, 2980, 2945, 2895, 1475, 1455, 1384, 1374, 1267, 1210, 1197, 1142, 1095, 1078, 1040, 1030, 1018, 940 cm^{-1}. *Exact Mass* calcd. for $C_{11}H_{18}O_2$: 182.1307; found: 182.1310.

1-Methyl-5-isopropyl-2,4-dioxabicyclo[3.2.2]nonane (**7**)

This was produced by the acid-catalysed condensation of *cis-p*-menthane-1,4-diol (synthesised by Al(Hg) reduction of dihydroascaridole as described by Schenck *et al.* (6)) with formaldehyde.

To 15 g (0.09 mol) of crude *cis-p*-menthane-1,4-diol in 100 ml benzene was added 10 g of paraformaldehyde and 100 mg *p*-toluene sulfonic acid. The mixture was refluxed and the theoretical amount of H_2O removed by azeotropic distillation. Work-up consisted of rapid filtration while hot, and extraction with 2 × 100 ml portions of 5% aqueous K_2CO_3. After drying the organic phase over Na_2SO_4 and removal of benzene the residue was distilled at reduced pressure to yield 12.1 g (80%) of **7**, bp 75 °C/2 torr; pmr ($CDCl_3$) δ 4.92 (s, 2H), 2.15–1.38 (m, 9H), 1.20 (s, 3H), 0.88 (d, 6H, J = 6.5 Hz); ir ($CHCl_3$) 3000, 2970, 2935, 2880, 2775, 1495, 1470, 1460, 1451, 1400, 1384, 1377, 1367, 1345, 1270, 1243 (br), 1178, 1151, 1131, 1090, 1038, and 1010 cm^{-1}. *Exact Mass* calcd. for $C_{11}H_{20}O_2$: 184.1463; found: 184.1460. *Anal.* calcd. for $C_{11}H_{20}O_2$: C 71.74, H 10.87; found: C 71.48, H 10.78.

cis-1,4-Dimethoxy-p-menth-2-ene (**5**)

This was produced by an alkylation procedure described by Diner *et al.* (7). From 3.4 g of *cis-p*-menth-2-ene-1,4-diol (2×10^{-2} mol prepared as above) dissolved in 100 ml anhydrous DME (distilled from $LiAlH_4$ prior to use) containing 6 g (8.4×10^{-2} mol) CH_3I and 2 g 57% NaH suspension (2×10^{-2} mol) was produced 3.4 g (86%) **5**, bp 68.5 °C/2 torr; pmr ($CDCl_3$) δ 5.76 (AB quartet, 2H, J = 10 Hz), 3.25 (s, 3H), 3.22 (s, 3H), 2.47–1.32 (m, 5H), 1.20 (s, 3H), 0.87 (d of d, 6H, J = 6.5 Hz); ir (neat) 3070, 2970, 2880, 2830, 1465 (br), 1385, 1368, 1195, 1125, 1107, 1079 (br), 1035, 1010, 940, 907 cm^{-1}. *Anal.* calcd. for $C_{12}H_{22}O_2$: C 72.73, H 11.11; found: C 72.78; H 11.08.

cis-1,4-Dimethoxy-p-menthane (**8**)

This was prepared by an alkylation (7) of *cis-p*-men-

Can. J. Chem. Downloaded from www.nrcresearchpress.com by 210.87.254.6 on 09/05/12
For personal use only.

Can. J. Chem. Downloaded from www.nrcresearchpress.com by 210.87.254.6 on 09/05/12
For personal use only.

thane-1,4-diol in 70% yield, bp 78–80 °C/2.5 torr; pmr ($CDCl_3$) δ 3.23 (s, 3H), 3.12 (s, 3H), 2.30–1.23 (m, 9H), 1.16 (s, 3H), 0.87 (d, 6H, J = 6.5 Hz); ir ($CHCl_3$) 3005, 2965, 2845, 1475, 1445 (sh), 1395, 1385, 1375, 1267, 1132, 1115, 1075, 1007, 984 cm^{-1}. *Exact Mass* calcd. for $C_9H_{17}O_2$ ($M^+ - C_3H_7$): 157.1229; found: 157.1232.

1,4-Dimethoxybicyclo[2.2.2]oct-2-ene

This was prepared via the following sequence.

Birch reduction (8) of *p*-dimethoxybenzene in contrast to yielding the expected 1,4-dimethoxy-1,4-cyclohexadiene as reported (8), in our hands yielded a bright yellow liquid in 60% yield, bp 81–82 °C/10 torr which proved to be the isomerized material 1,4-dimethoxy-1,3-cyclohexadiene; pmr ($CDCl_3$) δ 4.83 (s, 2H), 3.50 (s, 6H), 2.33 (s, 4H); ir ($CHCl_3$) 3075, 3000, 2950, 2900, 2835, 1655, 1619, 1505, 1465, 1450, 1438, 1423, 1379, 1291, 1215 (br), 1155, 1137, 1125 cm^{-1}. Additionally 10% of the further reduced 1,4-dimethoxy-1-cyclohexene was isolated.

1,4-Dimethoxybicyclo[2.2.2]oct-5-ene-2,3-dicarboxylic Acid Anhydride

To 1.40 g (0.01 mol) of 1,4-dimethoxy-1,3-cyclohexadiene (prepared as above) in 10 ml ethyl acetate was added 0.98 (0.01 mol) maleic anhydride (recrystallized from $CHCl_3$). Immediately the solution turned a brilliant orange–red. The solution was stirred and refluxed overnight at which time it appeared yellow; further refluxing did not alter this final color. Work-up consisted of removal of the solvent, and trituration of the residue with 10 ml of 1:1 ether:chloroform to yield a white powder. Recrystallization from 1:1 ether:chloroform gave 1.75 g solid (70%) mp 123–125 °C; pmr ($CDCl_3$) δ 6.23 (s, 2H), 3.53 (s, 2H), 3.48 (s, 6H), 2.28–1.48 (m, 4H); ir ($CHCl_3$) 3020 (br), 2940 (br), 2875, 2835, 1871, 1835, 1785 (br), 1460, 1443, 1372, 1200 (br), 1158, 1133, 1073, 1031 cm^{-1}.

1,4-Dimethoxybicyclo[2.2.2]octane-2,3-dicarboxylic Acid Anhydride

To 1.2 g (0.005 mol) 1,4-dimethoxybicyclo[2.2.2]oct-5-ene-2,3-dicarboxylic acid anhydride in 20 ml THF was added 0.1 g Pt_2O, and the mixture hydrogenated at atmospheric pressure until 1 equiv. of H_2 was consumed. The mixture was then filtered and stripped of solvent and the residue recrystallized from 3:1 acetone:ether to give quantitatively the desired bicyclo octane mp 100–103 °C; pmr ($CDCl_3$) δ 3.55 (s, 2H), 3.33 (s, 6H), 1.97–1.58 (m, 4H); ir ($CHCl_3$) 3100 br, 2968 (d), 2885, 2840, 1950 (br), 1789 (br), 1485, 1412, 1350, 1325, 1281, 1220 (br), 1167, 1120, 1075, 1030 cm^{-1}.

1,4-Dimethoxybicyclo[2.2.2]octane-2,3-dicarboxylic Acid

To 1.20 g (0.005 mol) of the bicyclooctane anhydride was added 20 ml of 20% aqueous $KHCO_3$ and the mixture stirred and refluxed until all solids dissolved and then an additional 30 min. The solution was cooled and acidified to p*H* 3 by the addition of concentrated HCl, and then set in the freezer overnight to crystalize. Filtration yielded 850 mg (60%) of the diacid, mp 160–165.5 °C (—CO_2); pmr (DMSO-d_6) δ 11.18 (br s, 2H, exchanges with D_2O), 3.17 (s, 2H), 3.08 (s, 6H), 2.26–2.46 (m, 2H), 1.75 (br s, 4H), 1.43–1.67 (m, 2H); ir (Nujol) 3500 (sh), 3380 (br), 1750, 1695, 1460, 1380, 1315, 1300, 1275, 1237, 1214, 1190, 1120, 1090, 1072, 1020 (d) cm^{-1}.

1,4-Dimethoxybicyclo[2.2.2]oct-2-ene (**6**)

This was prepared from the bicyclooctane diacid via the procedure of Grob *et al.* (9). From 19.3 g starting diacid, 5.1 g (40%) of **6** was produced, bp 91 °C/10 torr; pmr ($CDCl_3$) δ 6.25 (s, 2H), 3.33 (s, 6H), 1.63 (AB quartet, 4H, J = 8 Hz); ir ($CHCl_3$) 3025, 3000, 2950, 2910, 2875, 2830, 1608 (w), 1465, 1453, 1375, 1367, 1330, 1220 (br), 1160, 1140, 1110 (br), 1038, 1015 cm^{-1}. *Anal.* calcd. for $C_{10}H_{16}O_2$: C 71.43, H 9.52; found: C 71.04, H 9.58.

1,4-Dimethoxybicyclo[2.2.2]octane (**9**)

This was prepared by catalytic hydrogenation of 1 g (**6**) in 10 ml THF over Pt_2O. The mixture was filtered, solvent removed and distilled to yield 80% **9**, bp 77 °C/4 torr; pmr ($CDCl_3$) δ 3.17 (s, 6H), 1.77 (s, 12H); ir ($CHCl_3$) 3020, 2960, 2875, 2815, *2400*, 1520 (br), 1458, 1425, 1355, 1215 (vs), 1170, 1100, 1035 cm^{-1}. *Anal.* calcd. for $C_{10}H_{18}O_2$: C 70.59, 10.59; found: C 70.37, H 10.58.

Results and Discussion

The synthesis of **4** proved rather interesting and a few points should be made concerning it. Initial attempts to synthesise **4** involved an acid-catalysed condensation of *cis-p*-menth-2-ene-1,4-diol and formaldehyde as shown in Scheme 1. While this procedure was successful when applied to the saturated *cis-p*-menthane-1,4-diol, the presence of the double bond presents additional complications. Acid catalysis produced only the aromatic derivative by dehydration, while BF_3–etherate complex catalysis produced *p*-cymene and **11**. Presumably **11** was produced by a mechanism proposed in Scheme 2.

Since all cationic approaches produced undesirable products, an anionic approach was used. This consisted of prior formation of the dianion of *cis-p*-menth-2-ene-1,4-diol in an inert solvent which was then treated with bromochloromethane as outlined in Scheme 3. This latter scheme produced the desired **4**, albeit in low yields.

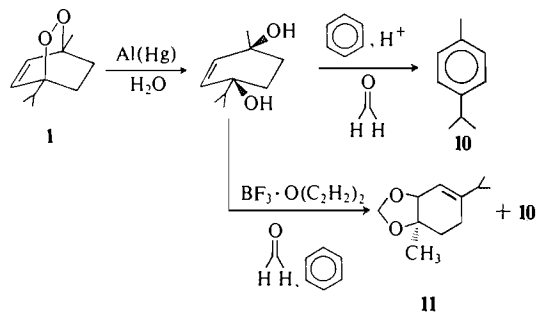

SCHEME 1

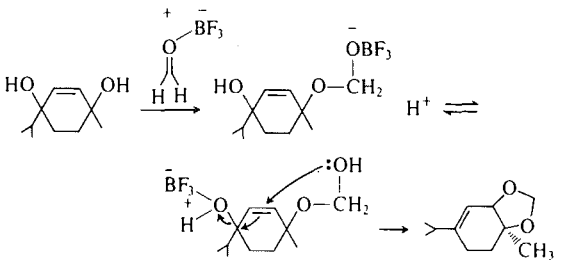

11

SCHEME 2

In investigating the effects of remote substituents on the IP of the double bond in these systems, it is expected that conjugative orbital interactions ought to be separable from inductive effects since the former should show marked geometrical dependence.

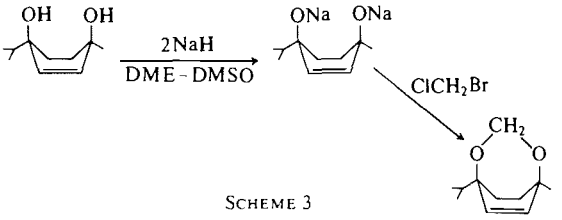

4

SCHEME 3

Hence, whereas ascaridole (**1**) may possibly possess a homoconjugative interaction of the double bond with the peroxide moiety reminiscent of that present in norbornadiene or bicyclooctadiene (10) such cannot be the case for 1,4-dimethoxybicyclo[2.2.2]oct-2-ene (**6**). Since direct homoconjugative interaction of the methoxyl groups and double bond in **6** is minimal or nonexistent, to a first approximation only the inductive influence of the oxygens will be experienced by the double bond.

Figure 1 illustrates the pe spectrum of ascaridole (**1**) and dihydroascaridole (**2**) while Figs. 2, 3, and 4 illustrate the pe spectra of compound pairs **4**, **7**; **5**, **8**; and **6**, **9** respectively. The corresponding data and assignments for these compounds are presented in Table 1.

From the data presented in Table 1, one can see that in each unsaturated molecule the ionization ascribed to the π-bond appears at 9.68 $\pm$ 0.02 eV. Perhaps this might seem surprising in view of the following discussion.

Homoconjugative Interactions

Ascaridole (**1**), the first molecule investigated exhibited an unusually stabilized (in terms of

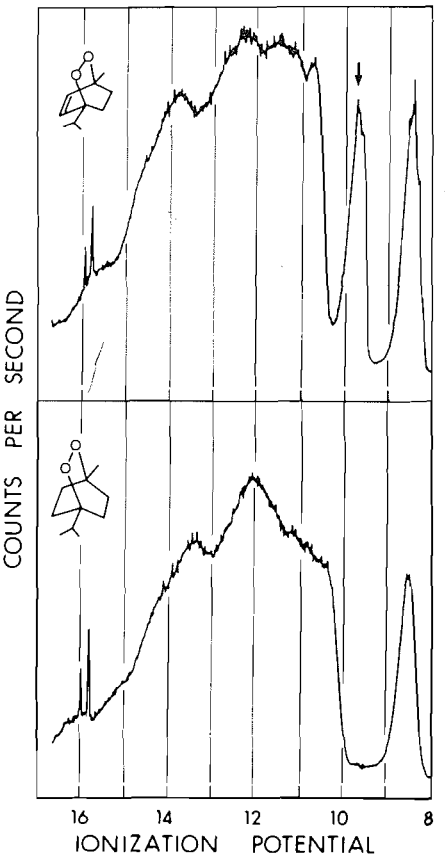

FIG. 1. Photoelectron spectra of ascaridole (**1**) and dihydroascaridole (**2**) using argon as an internal calibrating gas.

increased binding potential) π-bond. There is undoubtedly significant orbital overlap between the peroxide lone pairs and the π-system analogous to that evident in bicyclooctadiene (10*b*). It is evident from symmetry arguments that the only combination of the oxygen lone pairs which is allowed to interact with the π-bond is n_+ as shown in **12**. That the n_- combination does not mix appreciably with π, is illustrated by observing that n_- in dihydro-

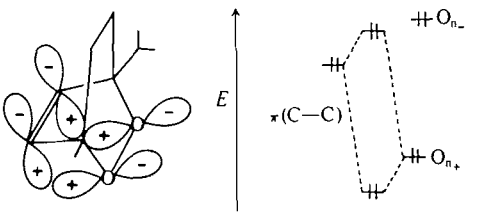

12

Can. J. Chem. Downloaded from www.nrcresearchpress.com by 210.87.254.6 on 09/05/12
For personal use only.

Can. J. Chem. Downloaded from www.nrcresearchpress.com by 210.87.254.6 on 09/05/12
For personal use only.

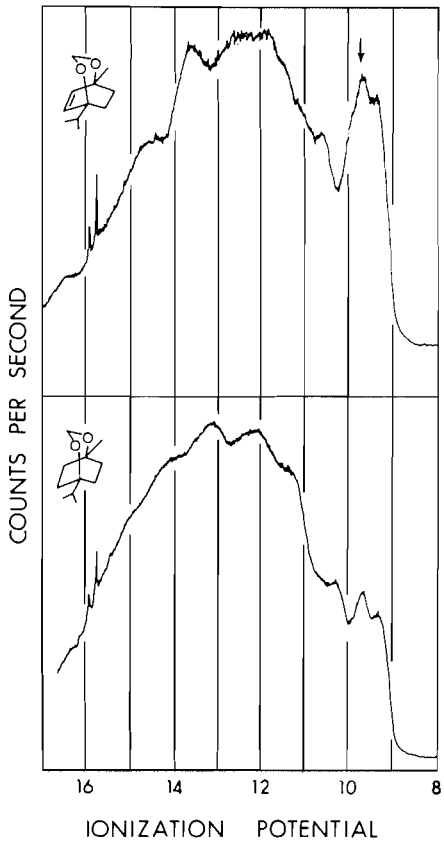

FIG. 2. Photoelectron spectra of Δ^6-1-methyl-5-isopropyl-2,4-dioxabicyclo[3.2.2]nonene (**4**) and 1-methyl-5-isopropyl-2,4-dioxabicyclo[3.2.2]nonane (**7**) using argon as an internal calibrating gas.

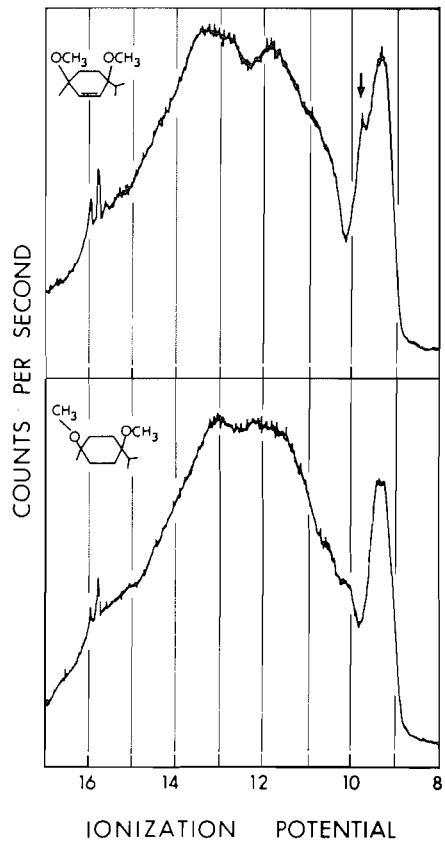

FIG. 3. Photoelectron spectra of *cis*-1,4-dimethoxy-*p*-menth-2-ene (**5**) and *cis*-1,4-dimethoxy-*p*-menthane (**8**) using argon as an internal calibrating gas.

TABLE 1. Vertical ionization potentials of compounds **1**, **2**, **4**–**9** in eV

Compound	$IP_v(n^-)$	$IP_v(\pi)$	$IP_v(n_+)$	Others[b]
1 Ascaridole	8.42[a]	9.70		10.71(σ_-(C—O))
2 Dihydroascaridole	8.50			10.36(σ_-(C—O))
4 Δ^6-1-Methyl-5-isopropyl-2,4-dioxabicyclo[3.2.2]nonene	9.31	9.66	9.91	10.59
7 1-Methyl-5-isopropyl-2,4-dioxabicyclo-[3.2.2]nonane	9.29		9.63	10.29
5 *cis*-1,4-Dimethoxy-*p*-menth-2-ene	9.21	9.69	(9.21)[c]	10.46
8 *cis*-1,4-Dimethoxy-*p*-menthane	9.26		(9.26)[c]	10.1
6 1,4-Dimethoxybicyclo[2.2.2]oct-2-ene	9.24	9.70	9.41	10.44
9 1,4-Dimethoxybicyclo[2.2.2]octane	9.14		9.35	10.06

[a]Exhibits vibrational spacings of 1008 ± 50 cm^{-1}.
[b]Represents the vip of the first σ-orbital.
[c]From the peak intensity and shape, it is speculated that n_+ and n_- are nearly degenerate.

Can. J. Chem. Downloaded from www.nrcresearchpress.com by 210.87.254.6 on 09/05/12
For personal use only.

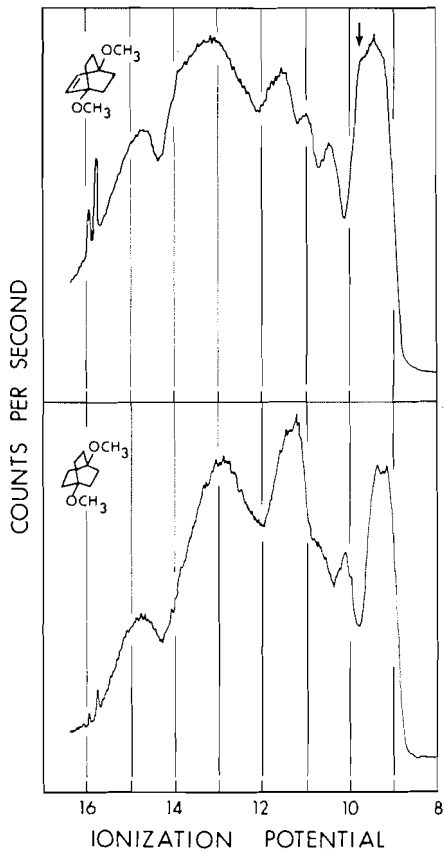

FIG. 4. Photoelectron spectra of 1,4-dimethoxybicyclo[2.2.2]oct-2-ene (**6**) and 1,4-dimethoxybicyclo[2.2.2]-octane (**9**) using argon as an internal calibrating gas.

ascaridole (**2**) appears at virtually the same IP as in ascaridole (**1**).

However, such interaction as in **12** (if significant) would be expected to *decrease* the π-IP since the π-orbital will become destabilized. Evidently such interaction is small if any. The apparent anomaly can be resolved by arguments similar to that of Heilbronner and co-workers (10*d*) concerning homoconjugation. Perturbation theory (11) indicates that the interaction of π_1 with n_+ will give rise to second order shifts (ΔE) in the energies of both the π_1 and n_+ orbitals as given by eq. 1.

$$[1] \qquad |\Delta E| = \frac{(\pi_1|H|n_+ d\tau)^2}{|E_{\pi_1} - E_{n_+}|} = \frac{(m\beta)^2}{|E_{\pi_1} - E_{n_+}|}$$

where $\beta = 2.5$ eV (10*d*) and $m = 0.12$ (derived for bicyclooctadiene).

The pe spectrum of **1** does not give an accurate value for n_+, since this ionization is buried under the σ-envelope. However molecular orbital calculations[1] on ascaridole place the n_-, n_+ separation at roughly 9.5 eV. With this value as a guide, it can be seen that the ΔE value expected for the π_1 bond and n_+ is exceedingly small ($\Delta E \simeq 0.01$ eV). Hence, because π_1 and n_+ are well separated in terms of energy, interaction between them will be minimal.

While it is apparent from the above that one can safely neglect the n_+, π interactions in the peroxides, such is not the case in the analogous hydrazine compounds as shown by Nelsen and Buschek (13). In such compounds, the interaction appears significant because $E_{\pi_1}-E_{n_-}$ separation is small.

Hyperconjugative Interactions

Also of correct symmetry to interact with the π-bond of **1** are certain linear combinations of the C—O σ-framework. One expects that symmetry allowed $\sigma-\pi$ interaction of the C—O σ-bonds will drive the π-level up in energy as illustrated in **13**. However such is not the case with the appropriate symmetry antibonding C—O σ-bonds. Calculated orbitals for *cis* H_2O_2 (14) indicate that the LUMO is a symmetric combination of antibonding σ-orbitals (σ_+*). If we are allowed to extrapolate these calculations to ascaridole (also a *cis* peroxide) an interaction such as that evident in **14** could be

[1]CNDO/2 calculations were performed on appropriate models for compounds **1**, **4**, and **6**. The model for ascaridole (**1**) and formal **4** simply replaced the bridgehead isopropyl with a methyl group, while that chosen for **6** was bicyclo-[2.2.2]oct-2-ene-1,4-diol. Molecular coordinates were obtained by measurements of Dreiding models of these compounds and are recognized as imperfect. Complementary results were obtained using the calculation method of Caulton and Fenske (12). (A modification of this program was kindly supplied by A. Sarapu.)

Assignments of the uppermost orbitals were based upon calculation and comparison of the saturated and unsaturated analogues. Since the π-ionization is readily visible, such spectral comparison is relatively straightforward for compound pairs **1**, **2**; **5**, **8**; and **6**, **9**. However, simple spectral comparison is not without ambiguity for compounds **4** and **7**. In this case, the reliance upon calculated orbitals is quite large, and the computed ordering of the three highest occupied molecular orbitals in **4** is $n_- > \pi > n_+$. One should accept these assignments with caution however, since it is expected that such ordering may be heavily dependent upon the molecular geometry used as input data.

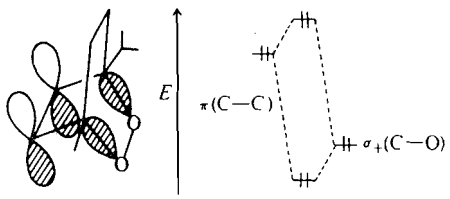

13

envisioned. This interaction might possibly *stabilize* the π-bond as observed. However unlikely this may appear (particularly in view of the large energy difference between π(C—C) and σ_+*(C—O)), we can test for this possibility in two ways. Firstly, breaking the peroxide linkage but still maintaining the C—O σ-bonds parallel to the π-system ought to alter the position of the σ_+* combination significantly thereby altering any interaction with the π-bond. That the π-bond appears at the same position in the pe spectrum of both **1** and **4** indicates interactions similar to those in **14** are either insignificant, or that certain opposite effects are compensating each other.

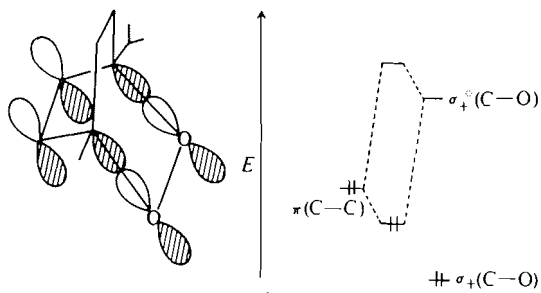

14

In formal **4**, the pe spectrum (Fig. 2) illustrates that the n_+, n_- separation is roughly 0.6 eV which corresponds nicely to the 0.55 eV splitting noticed in 1,3-dioxolane (15). In such systems, the n_+, n_- splitting has been said to be of either a through-bond nature (1,3-dioxolane) or a through-space nature (1,3-dioxane) (15). While our results give no direct indication of the nature of such splitting in **4** or **7**, both through-space and through-bond mechanisms can be envisioned (15). Molecular models indicate that direct overlap between n_+ and π is not likely to be as large as in ascaridole. Hence, a reduction in the numerator of eq. 1 also causes significant reduction of the ΔE induced in π_1 and n_+ even though their energy levels are more closely matched. That the ionization assigned to the π-bond (π_1) in formal **4** appears at the same place as that in ascaridole (**1**) gives credence to the idea that the π_1, n_+ interaction is small or nonexistent probably due to poor overlap between them.

Further rotation of the C—O σ-bonds out of planarity with the π-system will decrease even further any possible homoconjugative (n, π) or hyperconjugative (σ–π) interactions. Molecular models of *cis*-1,4-dimethoxy-*p*-menth-2-ene (**5**) in the half-chair conformation indicate that the C—O σ-bonds are displaced 30° from planarity with the π-system. Again the ionization assigned to removal of a π-electron appears at 9.69 eV as a shoulder on the bands assigned to removal of electrons from the n_+ and n_- orbitals. Further rotation so that the C—O σ-bonds are 90° to the π-system is finally accomplished in 1,4-dimethoxybicyclo[2.2.2]oct-2-ene (**6**). Once again the π-system ionization appears at 9.70 eV, identical to that of **1**, **4**, and **5**.

Invariance of the ionization potential of the π-bond in these systems, to rotation of the allylic C—O bonds indicates that conjugative stabilization of the π-bond by the allylic oxygens is not important whether homo- or hyperconjugative in nature. Such rotational variations have been used before to test for conjugative interactions (16) in other systems. On the other hand barring slight changes in bond lengths such rotation does not alter the distance from each oxygen to its allylic carbons. Hence inductively[2] the effect of the oxygens is the same in **1**, **4**, **5**, and **6**. It is proposed then, that as a consequence of the greater electronegativity of oxygen relative to carbon, significant electron density is removed from the more polarizable π-system making its ionization more difficult. Such changes are noticed in other systems as well as illustrated by stabilization of the π-system of 2-propene-1-ol as compared to

[2]Whether such substituent effects originate from a through-bond mechanism or field mechanism is still an open question (for pertinent references see ref. 17). For the purposes of the above discussion we will make no distinction between them. Hence we use inductive to mean those effects caused by differences in electronegativity between interacting groups. It is also expected that minor variations in the substitution of each oxygen will not significantly alter its ability to pull electron density towards itself. Hence, while not strictly correct, it is assumed that the inductive effect of the oxygens in ascaridole will be to a first approximation equivalent to that of the oxygens in both **5** and **6**.

Can. J. Chem. Downloaded from www.nrcresearchpress.com by 210.87.254.6 on 09/05/12
For personal use only.

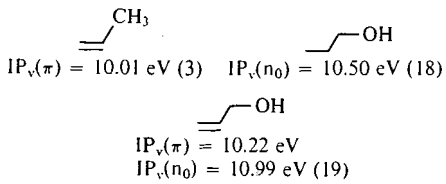

1-propene, (also caused by the presence of the electronegative oxygen).

Conclusions

It has been demonstrated that in systems designed to exhibit similar substitution, that pe spectroscopy can be used to determine the effects of remote substituents upon π-bonds. Inductive effects can be distinguished from conjugative interactions by observing that the latter effects ought to show marked geometrical dependence. That the ionization of the π-bond in the above systems is invariant to the orientation of the two allylic oxygens illustrates that the predominant stabilizing influence exerted on the π-system by the remote oxygens is that due to the greater electronegativity of oxygen relative to carbon.

Acknowledgments

The author gratefully acknowledges the financial assistance of the University of Alberta and the National Research Council of Canada.

1. R. S. BROWN. Can. J. Chem. **53**, 3439 (1975).
2. (*a*) P. BISCHOF, J. A. HASHMALL, E. HEILBRONNER, and V. HORNUNG. Helv. Chim. Acta, **54**, 783 (1971); (*b*) E. HEILBRONNER. Isr. J. Chem. **10**, 143 (1972).
3. P. MASCLET, D. GROSJEAN, G. MOUVIER, and J. DUBOIS. J. Electron Spectrosc. Relat. Phenom. **2**, 225 (1973).
4. R. C. WEAST (*Editor*). Handbook of chemistry and physics. 50th ed. Chemical Rubber Co. Press, Cleveland, Ohio. 1969–1970.
5. H. PAGET. J. Chem. Soc. 829 (1938).
6. G. O. SCHENCK, K. GOLLNICK, G. BUCHWALD, S. SCHROETER, and G. OHLOFF. Ann. **674**, 93 (1964).
7. U. E. DINER, F. SWEET, and R. K. BROWN. Can. J. Chem. **44**, 1591 (1966).
8. A. J. BIRCH. J. Chem. Soc. 102 (1947).
9. G. A. GROB, M. OHTA, E. RENK, and A. WEISS. Helv. Chim. Acta, **41**, 1191 (1958).
10. (*a*) R. HOFFMANN. Acc. Chem. Res. **4**, 1 (1971); (*b*) P. BISCHOF, J. A. HASHMALL, E. HEILBRONNER, and V. HORNUNG. Helv. Chim. Acta, **52**, 1745 (1969); (*c*) R. HOFFMANN, E. HEILBRONNER, and R. GLEITER. J. Am. Chem. Soc. **92**, 706 (1970); (*d*) P. BISCHOF, R. GLEITER, and E. HEILBRONNER. Helv. Chim. Acta, **53**, 1425 (1970).
11. W. T. BORDEN. Modern molecular orbital theory for organic chemists. Prentice-Hall Inc., Englewood Cliffs, N.J. 1974.
12. K. G. CAULTON and R. F. FENSKE. Inorg. Chem. **7**, 1273 (1968).
13. S. F. NELSEN and J. M. BUSCHEK. J. Am. Chem. Soc. **96**, 6987 (1972).
14. U. KALDOR and I. SHAVITT. J. Chem. Phys. **44**, 1823 (1966).
15. D. A. SWEIGART and D. W. TURNER. J. Am. Chem. Soc. **94**, 5599 (1972).
16. (*a*) W. HANSTEIN, H. J. BERWIN, and T. G. TRAYLOR. J. Am. Chem. Soc. **92**, 7476 (1970); (*b*) A. L. GOODMAN and R. H. EASTMAN. J. Am. Chem. Soc. **86**, 908 (1964); (*c*) W. G. DAUBIN and G. H. BEREZIN. J. Am. Chem. Soc. **89**, 3449 (1967); (*d*) J. C. MARTIN and B. R. REE. J. Am. Chem. Soc. **91**, 5882 (1969).
17. T. W. COLE, C. J. MAYERS, and L. M. STOCK. J. Am. Chem. Soc. **96**, 4555 (1974).
18. M. B. ROBIN and N. A. KUEBLER. J. Electron Spectrosc. Relat. Phenom. **1**, 13 (1972).
19. G. W. MINES and H. W. THOMPSON. Spectrochim. Acta, **29**, 1377 (1973).

Can. J. Chem. Downloaded from www.nrcresearchpress.com by 210.87.254.6 on 09/05/12
For personal use only.

A stereodynamic investigation of antivitamins K in the dicoumarol series. II. Differentiation between the two hydroxyl groups by the nuclear Overhauser effect

CLAUDE LARUELLE AND JEAN-JACQUES GODFROID

Laboratoire de Pharmacochimie Moléculaire, Université de Paris VII, 2, Place Jussieu, 75221, Paris Cedex 05, France

Received July 14, 1975

CLAUDE LARUELLE and JEAN-JACQUES GODFROID. Can. J. Chem. **54**, 813 (1976).

Dicoumarol derivatives, substituted at the bridgehead, show a double restricted rotation. This hindered rotation is manifest through the appearance of two signals, the hydroxyl protons being diastereotopic at low temperatures.

In this work we assign the two respective signals by the nuclear Overhauser effect. The high-field signal corresponds to a hydroxyl site close to the bridgehead tertiary proton, while the other corresponds to a site in proximity to the substituent R. The case of structurally analogous dimethones has been investigated by the same technique with identical conclusions. This disproves the interpretation made previously on the basis of steric and anisotropic effects.

The interatomic distances concerned have been calculated, and these have yielded an estimate of deformations induced by the bridgehead substituents.

Evidence is supplied for the different behavior of the two sites and this study gives evidence for a very facile intermolecular chemical exchange of the hydroxyl site close to the tertiary bridgehead proton in the presence of traces of protonated compounds.

The overall behavior is the result of the asymmetry of the molecules of this series in their chelated form.

CLAUDE LARUELLE ET JEAN-JACQUES GODFROID. Can. J. Chem. **54**, 813 (1976).

Les dérivés du dicoumarol, substitués au niveau du pont présentent une double rotation restreinte qui se manifeste par l'apparition de deux signaux, les protons hydroxyles étant diastéréotropiques à basse température.

La présente publication permet d'attribuer, par effet Overhauser nucléaire, les deux signaux aux groupes hydroxyles incriminés. Le signal à haut champ correspond au site hydroxyle proche du proton tertiaire du pont, alors que l'autre correspond au site proche du substituant R. D'autre part, le cas des dimethones, analogues structuraux, a été étudié par la même technique et les conclusions sont identiques, ce qui annule l'interprétation inverse qui a été faite antérieurement à partir d'interprétations stériques et anisotropiques.

Les distances interatomiques concernées ont été calculées et les déformations induites par les substituants du pont estimées.

Le comportement différencié des deux sites est mis en évidence et l'étude conclut à un échange chimique intermoléculaire très facile du site hydroxyle proche du proton tertiaire du pont avec des traces de composés protonés.

L'ensemble des propriétés mises en évidence est la conséquence de l'asymétrie des molécules de cette série dans leur forme chélatée.

Introduction

An nmr investigation at variable temperatures has been carried out on dicoumarol (R = H) and bridgehead substituted analogs (Fig. 1) with antivitamin K activity. We have found evidence for a double restricted rotation of both 4-hydroxy coumarin moities around the two bonds at the bridge (1) through hydrogen bonding. We have determined that both hydroxyl protons are diastereotopic and give distinct nmr signals (1). In this report we (*a*) identify the two signals by nOe at low temperature, (*b*) assign the two hydroxyl groups, (*c*) determine the interatomic distances and estimate the deformation caused by the bridgehead substituents, and (*d*) compare the exchange characteristics of both hydroxyl protons.

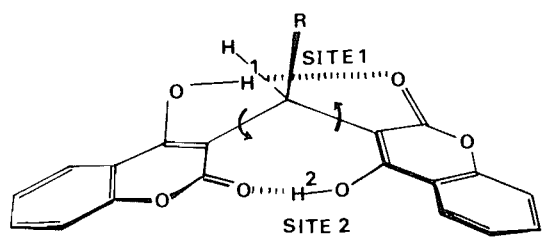

FIG. 1. Dicoumarols R = H **1**, R = CH_3 **2**, R = C_2H_5 **3**, R = *n*-propyl **4**, R = *i*-propyl **5**.

Can. J. Chem. Downloaded from www.nrcresearchpress.com by 210.87.254.6 on 09/05/12
For personal use only.

TABLE 1. Assignment of hydroxyl peaks (OH^1 and OH^2) by nOe, at -55 °C in $CDCl_3$ dicoumarol ($R = CH_3$) **2**, and dimethone ($R = CH_3$) **6**

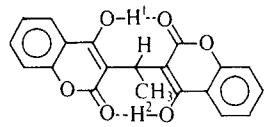

Methyldicoumarol **2**

ω irrad. (ppm)	nOe observed OH^2	nOe observed OH^1
1.87 (methyl)	+25%	−8%
4.72 (tertiary H)	+14%	+49%
3.00 (reference)	0%	0%

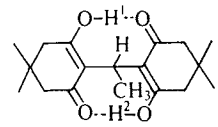

Methyldimethone **6**

ω irrad. (ppm)	nOe observed OH^2	nOe observed OH^1
1.52 (methyl)	+26%	−6%
4.16 (tertiary H)	−10%	0%
3.00 (reference)	0%	0%

Results and Discussion

Most nOe experiments are made on compact molecules with a rigid structure. Although it has been accepted that measurements on protons involved in exchanging sites are non-conclusive if their lifetimes were of the same order as their relaxation times (2), Basselier and co-workers (3) have established the relationship between the enhancements and the general Bloch equations modified by Solomon for a quantitative interpretation of nOe. In particular, they proved that if the lifetime of a nuclear spin in a given state is long in comparison with the relaxation time in this site, thermal equilibrium is attained for each site, and therefore the exchange has no effect on the Overhauser enhancements.

The intramolecular nOe is based on dipolar relaxation mechanisms of nuclear spins. This method allows for the estimate of spatial proximity of atomic groups within the distance interval of 2.3–3.2 Å (4–8). In general, in order to observe a nOe between two protons, their mutual relaxation is a sufficient condition. The phenomenon is enhanced if the protons are in close spatial proximity, but drops off if they are involved in conformational exchange, or if they are in chemical (intra- and intermolecular) exchange. All three situations were found to be present in the dicoumarols.

Identification and Assignment of OH Signals

Forsen *et al.* have assigned the high-field signal to the OH proton close to R for dimethones (9). In fact, the assignment should be reversed: the low-field signal is *syn* in relation to R, and the interpretation is unambiguous as indicated in Table 1. Irradiation of the methyl protons of the methyldimethone **6**, at 55 °C, increases the area of the low-field signal of the OH proton by 26%. Saturation of the tertiary proton has no effect on the signal of the more shielded proton, but the rare negative nOe (−10%) that is observed on the other proton contributes further evidence to these assignments (11).

Similar effects are obtained for methyldicoumarol **2**. Irradiation of the bridgehead proton produces a 49% nOe enhancement (maximum obtainable is 50%), when the more shielded OH proton is observed. Irradiation of the methyl yields a 25% nOe enhancement while observing the other proton.

Deformations Induced by Bridgehead R Substituents

The nOe observed follows a linear correlation with Taft's steric factor E_s (10) for four aliphatic R substituents (R = Me, Et, propyl, isopropyl). Beyond that point there is a decrease with steric hindrance (Tables 2 and 3), following a linear relationship of high significance ($F_{1,2} = 710.14$; $F_{1.2;\alpha 0.005} = 198.50$). % nOe $= 48.4 + 70.6E_s$, where $n = 4$, $r = 0.99$, and $s = 1.03$. The low exchange criterion of the measured nOe corresponds to the following inter-proton distances (8): H–(H^1—O) = 2.31 Å; (CH_3)–(H^2—O) =

Can. J. Chem. Downloaded from www.nrcresearchpress.com by 210.87.254.6 on 09/05/12
For personal use only.

TABLE 2. The nOe observed for dicoumarols with R ≠ H

R		Temperature	ω irrad. (ppm) (tertiary H	nOe observed OH[2]	nOe observed OH[1]
$CH_2—CH_3$	**3**	−30 °C	4.31	+3%	+43%
$CH_2—CH_2—CH_3$	**4**	−30 °C	4.43	−5%	+22%
$CH(CH_3)_2$	**5**	−30 °C	3.92	0	+16%
$CH(CH_3)_2$	**5**	+30 °C	3.94	0	+16%

NOTE: (*a*) the previous assignment is confirmed; (*b*) the intensity of the nOe enhancement varies with the size of R; (*c*) maximum nOe enhancement is obtained already at room temperature for R = $CH(CH_3)_2$ since the conformational exchange is sufficient at that temperature.

TABLE 3. Relationship between nOe enhancement and Taft's steric parameter (E_s) for aliphatic R in the series of bridge substituted dicoumarols

R		E_s	% nOe*
CH_3	**2**	0	+49
$CH_2—CH_3$	**3**	−0.07	+43
$CH_2—CH_2—CH_3$	**4**	−0.36	+22
$CH(CH_3)_2$	**5**	−0.47	+16

*The nOe observed on the signal corresponding to the more shielded OH.

2.73 Å. For dicoumarol **1** itself (R = H), (C=O)-(H—O) = 2.6 Å (12).

These results allow for a precise description of deformations induced by a bridgehead substituent R, which are enhanced when passing from R = CH_3 to R = isopropyl. We observe (*a*) a torsion of the CHR bridge in the direction of OH^1, (*b*) a decrease in the $C\overset{H}{\underset{R}{\updownarrow}}$ angle, (*c*) an increase in the $OH^1\cdots O{=}C$ distance, and (*d*) a decrease in the $OH^2\cdots O{=}C$ distance.

Comparison of the Exchange Properties of the Two Hydroxyl Protons

When the nmr spectra are recorded without special precautions, both OH signals have a different half-width. The high field signal (I) is wider than the low-field one (II). Furthermore, the integrated value for II is greater than that of I. Several hypotheses may be put forward to explain this phenomenon.

By recreating and amplifying the phenomenon, we have established that it is an intermolecular chemical exchange with exchangeable, non-identical protons present in solution (alcohol of recrystallization, acid impurity, residual water, etc.), and therefore an artefact. For example, at normal temperature (37 °C), the addition of a drop of methyl alcohol brings about the total exchange of the high-field proton, while the low-field proton exchanges only partially. At −60 °C, the phenomenon is similar. However since the rate of exchange is slowed down at site 1, the total exchange of OH^2 with the alcoholic OH (Fig. 2) was not obtained. These differences in exchange properties may be related to the two pK_a values for the dicoumarols. In general, a first facile dissociation corresponds to pK_a between 1 and 5, while a

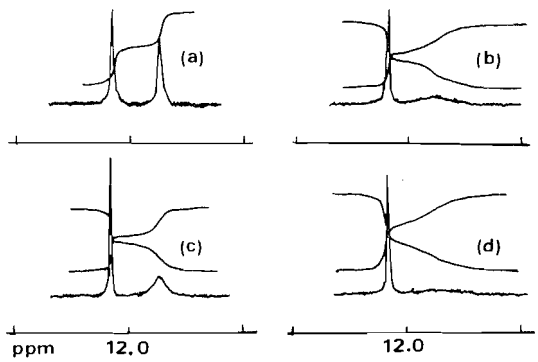

FIG. 2. The nmr spectra of dicoumarol **4** (R = *n*-propyl) in the hydroxyl proton region (between 10 and 14 ppm): (*a*) $CDCl_3$ solvent at −60 °C, (*b*) after the addition of 3 drops CH_3OH at −60 °C, (*c*) in the same solvent dried over molecular sieves (4 Å) after addition of 1 drop of CH_3OH at −60 °C, and (*d*) as in *c* after the addition of 3 drops of CH_3OH at −60 °C.

Can. J. Chem. Downloaded from www.nrcresearchpress.com by 210.87.254.6 on 09/05/12
For personal use only.

second more difficult dissociation requires a pK_a between 7 and 10. Although this has not been established, we may suggest that, by analogy with differential exchange properties, the first dissociation takes place at the proton *syn* to the tertiary bridge proton. Furthermore, the application of the nOe provides access to a dynamic exchange phenomenon and completes the evidence, since if a drop of water is added to the solution observed by nmr, the irradiation of the water signal at 4.7 ppm decreases the intensity of both OH signals, the OH^1 intensity being less than that of OH^2. In general, irradiation of one of the three signals present (OH^1, OH^2 or H_2O) brings about the disappearance or decrease of the other two, depending on the rate of exchange.

Asymmetry of the Dicoumarols

Both properties, namely (*a*) magnetic nonequivalence and (*b*) difference exchange characteristics of the hydroxyl protons, are the consequence of the asymmetry of molecules derived from dicoumarol in their chelated form. This asymmetry has been confirmed for 1-isopropyldicoumarol containing two diastereotopic methyl groups (13). These data provide evidence for a chiral center in bridge-substituted dicoumarins. The coalescences of the hydroxyl and methyl signals through temperature elevation suggest that they originate with the same phenomenon, which is in fact a conformational racemization. In a forthcoming paper we intend to detail the pharmacological implications of the chirality concept in bridge substituted dicoumarols (14).

Experimental

Nuclear Overhauser Effect (nOe)

Measurements were made on 5% solutions in deuteriochloroform. The solutions should be filtered and degassed with care in order to eliminate the dissolved paramagnetic oxygen which contributes markedly to the relaxation of the protons. The samples were degassed by bubbling nitrogen through the solution or, better, by multiple freeze–thaw cycles under vacuum (0.1 torr) before sealing the nmr sample tubes. The results mentioned and utilized in our quantitative analysis are the mean of five integrations obtained on a Varian HA-100 spectrometer. The second radio frequency field was supplied by a low frequency generator. For other details we refer the reader to the experimental procedure of Bell and Saunders (8) which was followed in detail.

Correlation

Abbreviations used: n = number of data points, r = correlation coefficients, s = standard deviation, F = F test.

Acknowledgments

We wish to express thanks for various nOe measurements to Mrs. L. Lacombe of the 'Laboratoire de Chimie Organique, Collège de France', and Dr. U. Sheidegger, Varian A.G., Zug (Switzerland). We acknowledge the contribution of Dr. M. L. Martin and Dr. Filleux-Blanchard of the 'Laboratoire de Chimie Organique Physique, Université de Nantes'.

1. C. Laruelle, J. J. Godfroid, and C. Courteix. Bull. Soc. Chim. Fr. 2111 (1974).
2. J. K. Saunders and R. A. Bell. Can. J. Chem. **48**, 512 (1970).
3. S. Combrisson, B. Roques, P. Rigny, and J. J. Basselier. Can. J. Chem. **49**, 904 (1971).
4. J. Noggle and R. E. Shirmer. The nuclear Overhauser effect, chemical application. Academic Press, London and New York. 1971.
5. G. Moreau. Bull. Soc. Chim. Fr. 1770 (1969).
6. G. E. Bachers and T. Shaefer. Chem. Rev. **6**, 617 (1971).
7. P. D. Kennewell. J. Chem. Educ. 278 (1970).
8. R. A. Bell and J. K. Saunders. Can. J. Chem. **48**, 114 (1970).
9. S. Forsen, W. E. Frankle, P. Laszlo, and J. Lubochinsky. J. Magn. Reson. **1**, 327 (1969).
10. R. W. Taft. Steric effects in organic chemistry. *Edited by* M. S. Newmann. John Wiley, N.Y. 1956. p. 556.
11. R. A. Bell and J. K. Saunders. Can. J. Chem. **46**, 3421 (1968).
12. G. Bravic, J. Gaultier, and C. Haun. C.R. Acad. Sc. **267**, 1790 (1968).
13. C. Courteix. Thèse de 3ème cycle. Université de Paris VI. 1973.
14. C. Laruelle and J. J. Godfroid. Eur. J. Med. Chem. In preparation.

Can. J. Chem. Downloaded from www.nrcresearchpress.com by 210.87.254.6 on 09/05/12
For personal use only.

The vibrational spectrum and normal coordinate analysis of tellurium chloride pentafluoride

W. V. F. BROOKS, M. ESHAQUE, CLEMENT LAU, AND JACK PASSMORE

Chemistry Department, University of New Brunswick, Fredericton, New Brunswick E3B 5A3

Received August 5, 1975

W. V. F. BROOKS, M. ESHAQUE, CLEMENT LAU, and JACK PASSMORE. Can. J. Chem. **54**, 817 (1976).

The infrared and Raman spectra of $TeClF_5$ have been recorded. Assignments have been made on the basis of C_{4v} symmetry. A normal coordinate analysis was carried out on $SClF_5$, $SeClF_5$, $TeClF_5$, SF_6, SeF_6, and TeF_6 and the derived force constants compared.

W. V. F. BROOKS, M. ESHAQUE, CLEMENT LAU et JACK PASSMORE. Can. J. Chem. **54**, 817 (1976).

On a enregistré les spectres Raman et infrarouge du $TeClF_5$. On a fait les attributions des bandes en se basant sur une symétrie C_{4v}. On a effectué une analyse normale des coordonnées des $SClF_5$, $SeClF_5$, $TeClF_5$, SF_6, SeF_6 et TeF_6 et on a comparé les constantes de force qui en dérivent.

[Traduit par le journal]

Introduction

We recently reported a convenient preparative route to tellurium chloride pentafluoride (1), first prepared in low yield by Fraser *et al.* (2). The microwave spectrum has been investigated by Legon (3) who proposed a structure of C_{4v} symmetry. The vibrational and normal coordinate analysis of tellurium chloride pentafluoride was undertaken in order to assign the spectrum and compare it and the derived force constants with those obtained for selenium chloride pentafluoride (4), sulphur chloride pentafluoride (5–7), and the group VI hexafluorides.

Experimental

The preparation and purification of $TeClF_5$ has been described (1). The infrared spectrum was recorded on a Perkin-Elmer 457 spectrometer in the range 4000–250 cm^{-1}, and a Beckman IR 12 spectrometer in the range of 450–200 cm^{-1}. A stainless steel cell of path length 10 cm fitted with AgCl windows and a 10 cm glass cell fitted with polyethylene windows were used as the sample containers. The Raman spectra of liquid $TeClF_5$ were recorded on a Spex Ramalab spectrometer using a 2 W Ar/Kr ion laser with emitting line either 6471 or 5145 Å. Polarization measurements were carried out by means of an Ednalite polarization rotator. Samples were condensed into a glass capillary and vacuum sealed. It was found that the best Raman spectra were obtained when traces of chlorine were present in the sample.

Vibrational Spectra and Assignments

Figure 1 shows the infrared spectrum of gaseous $TeClF_5$ in the region 1600–250 cm^{-1}, and Fig. 2 shows the spectrum in the 450–200 cm^{-1} region on an expanded scale. Figure 3 shows the Raman spectrum of liquid $TeClF_5$. Spectra were calibrated against known frequencies and have an accuracy of $\pm 2\ cm^{-1}$. Table 1 lists the observed frequencies.

Tellurium chloride pentafluoride should have C_{4v} symmetry, and on this basis have 11 fundamental vibrational modes: $4a_1$(R,p; ir) + $2b_1$ (R,dp) + b_2 (R,dp) + $4e$ (R,dp; ir).

The four a_1 modes should be polarized in the Raman spectrum and also be present in the infrared. There are five clearly polarized bands in the Raman at 708, 659, 413, 407, and 312 cm^{-1}. The bands 413 and 407 cm^{-1} on the basis of intensity and separation (Table 5) must be the $Te^{35}Cl$ and $Te^{37}Cl$ stretching vibrations. The infrared spectrum shows a shoulder at 711 cm^{-1}, a weak peak at 662, and fairly strong bands at 410.5, 404, and 317 cm^{-1}. It is not possible to ascertain whether or not the 711 band has PQR structure, but this is a feature of the other a_1 bands; the P–R separations are close to the predicted value of 12 cm^{-1} (8). By analogy with related molecules, (*e.g.* $SeClF_5$ (4), $HOTeF_5$ derivatives (9), IOF_5 (10), and TeF_5^- (11)), the frequencies at 708 and 659 cm^{-1} can be assigned to the TeF (axial) and symmetrical TeF_4 (equatorial) stretching vibrations, respectively. Since the vibrations at 413 and 407 cm^{-1} are assigned to the TeCl stretching

Can. J. Chem. Downloaded from www.nrcresearchpress.com by 210.87.254.105 on 09/05/12
For personal use only.

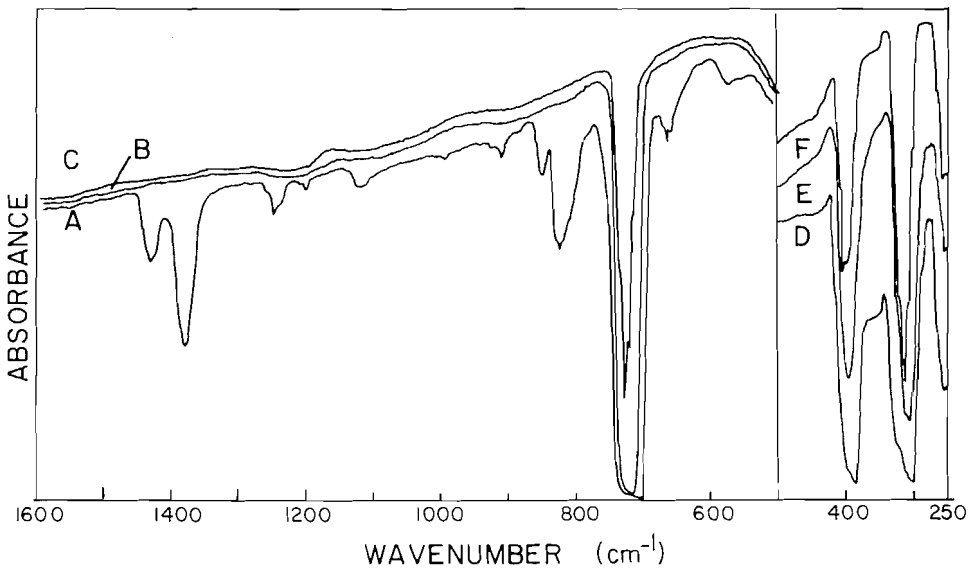

FIG. 1. Infrared spectrum of gaseous $TeClF_5$ at (*A*) 400, (*B*) 50, and (*C*) ~2 Torr pressure in a 10-cm cell with AgCl windows; (*D*) 180, (*E*) 15, and (*F*) ~5 Torr pressure in a 10-cm cell with polyethylene windows.

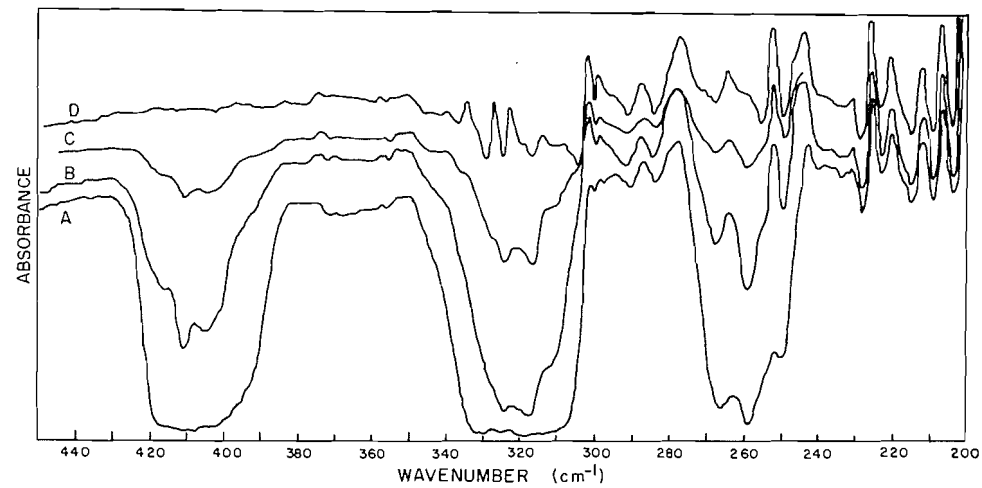

FIG. 2. Infrared spectrum of gaseous $TeClF_5$ on expanded scale at (*A*) 50, (*B*) 10, (*C*) ~1, and (*D*) 0 Torr pressure in 10-cm cell with polyethylene windows.

mode, the 312 cm^{-1} band is assigned as a TeF_4 umbrella deformation.

The depolarized Raman bands at 726, 327, and 259 cm^{-1} also appear in the infrared and are therefore identified as belonging to symmetry class *e*. Infrared spectra below 200 cm^{-1} were not obtained, but the Raman band at 167 cm^{-1} is tentatively assigned as an *e* mode by analogy with $SeClF_5$ (4) and $SClF_5$ (5, 6). The two other depolarized bands in the Raman spectrum at 651 (see Fig. 3) and 302 cm^{-1}, are assigned as b_1 and b_2 vibrations. A complete listing of observations and assignments is given in Table 1.

One mode, ν_6 (the b_1 out-of-plane deformation), is not accounted for. The same problem has occurred with $SClF_5$ and $SeClF_5$ spectra (4–6); we assume, following Christe *et al.* (4), that the ν_6 mode has low intensity and is not observed.

Can. J. Chem. Downloaded from www.nrcresearchpress.com by 210.87.254.105 on 09/05/12
For personal use only.

TABLE 1. Vibrational spectrum of $TeClF_5$

Infrared (gas) (cm^{-1})	Raman (liquid) (cm^{-1})[b]	Assignment
1429[a] w		$2\nu_1$
1380[a] mw		$\nu_5+\nu_8$ or $\nu_1+\nu_2$
1245[a] vw		?
1195 vvw		imp or $3\nu_4$?
1120 vw		$\nu_1+\nu_4$?
980 vvw		$\nu_5+\nu_9$ or $\nu_2+\nu_3$ or imp?
909 vw		$\nu_5+\nu_{10}$
856 vw		imp?
849 vw		?
820[a] w		$2\nu_4$
726[a] vvs	726 (6) dp	ν_8
711 sh,m	708 (31) p	ν_1
662 vw	659 (100) p	ν_2
	651 (8) dp	ν_5
570 vvw		$\nu_3+\nu_{10}$
410.5[a] ms	413 (77) p	ν_4 (^{35}Cl)
404[a] m	407 (23) p	ν_4 (^{37}Cl)
324.5[a] ms	327 (9) dp	ν_9
317[a] s	312 (8) p	ν_3
	302 (5) dp	ν_7
259[a] m	259 (17) dp	ν_{10}
	167 (18) dp	ν_{11}

[a]PQR branches observed. The frequency reported is for the Q branch.
[b]Relative intensities are given in parentheses.

Structure

The structural parameters used in the vibrational analysis are given in Table 2. The $SClF_5$ and $TeClF_5$ structures were derived from microwave data (3, 12) by a least-squares method modified to deal with linear dependence (13).

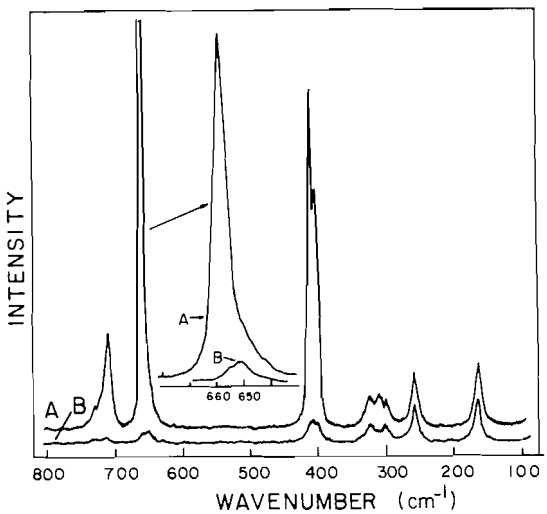

FIG. 3. Raman spectrum of liquid $TeClF_5$, slit width 2 cm^{-1}, exciting line 5145 Å: (*A*) obtained with incident polarization perpendicular; (*B*) incident polarization parallel.

Using generalized coordinates orthogonal to that combination of axial–equatorial fluorine distances which leads to a singularity, it is possible to find a well-defined best value of the axial–equatorial angle. Of the two fluorine bond distances, it is only possible to say that they probably differ by less than 0.02 Å in each case but with no indication from the microwave data as to which is the longer. Therefore, equality is assumed. Legon (3) proposed structures derived from a different analysis of the data which differ slightly from ours. For $SeClF_5$, we assume an angle intermediate between those found for $SClF_5$ and $TeClF_5$, and use the bond distances estimated by Christe *et al.* (4).

Force Constants

Our vibrational analysis uses the Wilson **F** and **G** matrix method (14) and a least-squares fitting program to determine the best values of the force constants. The force field is a general valency-force field (gvff) with certain assumptions that reduce the number of constants to be determined.

We first found a set of force constants for the group VI hexafluorides. In most respects our

Can. J. Chem. Downloaded from www.nrcresearchpress.com by 210.87.254.105 on 09/05/12
For personal use only.

TABLE 2. Structural parameters for $XClF_5$ and XF_6 molecules (distances in Angströms, 1 Å = 0.1 nm)

Molecule	X—F_{eq}	X—F_{ax}	X—Cl	$\angle F_{ax}$—X—F_{eq} (deg)
SF_6[a]	1.564			90
$SClF_5$[b]	1.576±0.010[c]	1.576∓0.020[c]	2.030±0.001	88.36±0.01
SeF_6[a]	1.688			90
$SeClF_5$[d]	1.68	1.68	2.14	88.30
TeF_6[e]	1.824			90
$TeClF_5$[f]	1.830±0.005[c]	1.830∓0.010[c]	2.2504±0.0004	88.26±0.01

[a]Reference 32.
[b]Calculated from data of ref. 12.
[c]Error limits are for correlated (not independent) variation.
[d]Assumed angles, distances from ref. 4.
[e]Reference 33.
[f]Calculated from data of ref. 3.

TABLE 3. Force constants[a] of group VI hexafluorides and chloride pentafluorides[b]

Parameter	Value					
	SF_6	$SClF_5$	SeF_6	$SeClF_5$	TeF_6	$TeClF_5$
f_r	4.845	4.593	4.946	4.514	5.081	4.760
f_R		4.623		4.836		4.929
f_D		2.749		2.737		2.864
f_α[c]	2.227	2.076	1.470	1.319	1.039	0.962
f_β		1.859		1.202		0.923
f_δ		2.248		1.534		1.125
f_{rr}	0.347	0.261	0.122	0.081	0.067	0.045
$f_{Rr} = f_{Dr}$		(0.3)		(0.11)		(0.06)
$f_{rr'}$[d]	0.463	0.348	0.162	0.108	0.089	0.060
f_{DR}		(0.4)		(0.14)		(0.078)
$f_{r\alpha}$[e]	0.535	(0.48)	0.290	(0.26)	0.183	(0.18)
$f_{\alpha\alpha}$ (coplanar)[f]	0.170	(0.15)	0.087	(0.08)	0.060	(0.054)
$f_{\alpha\alpha'}$ (perpendicular)[g]	0.290	(0.26)	0.185	(0.16)	0.158	(0.14)
$f_{\alpha\delta}$ (perpendicular)		0.149		0.100		0.094

[a]Force constants in mdyn/Å, 1 mdyn/Å = 10^2 N/m.
[b]Values in parentheses are XF_6 constants multiplied by 0.9.
[c]Bending coordinates are all of the form $\rho\Delta\alpha$, ρ = 1 Å = 0.1 nm.
[d]$f_{rr'} = \frac{4}{3} \times f_{rr}$, $f_{DR} = \frac{4}{3} \times f_{Dr}$.
[e]Plus $f_{r\beta}$, $f_{r\delta}$, $f_{R\beta}$, $f_{D\delta}$ interactions of $XClF_5$.
[f]Plus $f_{\beta\delta}$, $f_{\beta\beta}$, $f_{\delta\delta}$ interactions of $XClF_5$.
[g]Plus $f_{\alpha\beta}$, $f_{\beta\beta'}$, $f_{\delta\delta'}$ interactions of $XClF_5$.

approach and results are identical to the work of Labonville *et al.* (15). We assume that (*a*) for stretch–stretch interactions $f_{rr'}$ (opposite) = $\frac{4}{3} f_{rr}$ (adjacent) (16) and (*b*) all stretch–bend and bend–bend interactions are zero if the two coordinates do not have a common bond. We differ from Labonville *et al.* in using a total of six constants in order to fit closely all six fundamentals. The constants are given in Table 3 and the observed and calculated frequencies in Table 4.

We note that the stretching force constants of the hexafluorides increase on descending the group. This trend is inconsistent with the relative values of the average bond dissociation energies (SF_6, 330; SeF_6, 305; TeF_6, 343 kJ/bond (ref. 17 and references cited therein)). It is usual to expect the force constant to increase with bond dissociation energy (18); however, these are two separate quantities which are simply related only if the potential energy surfaces for the molecules are of exactly the same form. There are various other examples where this relationship does not hold (*e.g.* CF_4 and SiF_4 (19)), including the case of diatomic fluorine and chlorine (20). Indeed, on the basis

Can. J. Chem. Downloaded from www.nrcresearchpress.com by 210.87.254.105 on 09/05/12
For personal use only.

TABLE 4. Observed[a] and calculated frequencies of SF_6, SeF_6, and TeF_6

	Frequency					
	SF_6		SeF_6		TeF_6	
Class	Obsvd.	Calcd.	Obsvd.	Calcd.	Obsvd.	Calcd.
a_{1g}	773.5	773.5	706.9	707.0	697.1	697.1
e_g	641.7	642.0	658.7	659.2	670.3	670.8
t_{1u}	939	939.1	780	779.8	752	751.7
	614	613.9	437	437.0	325	325.0
t_{2g}	525	525.0	405	405.0	314	314.1
t_{2u}	347	346.9	264	264.0	197	197.0

[a]Reference 34.

of the higher force constant for fluorine relative to chlorine, a proposal was made (21) that the value of the bond dissociation energy of fluorine should be higher than that reported.

The force constants of $SClF_5$ (22, 7) and $SeClF_5$ (4) have been determined previously, assuming 90° angles throughout. Our purpose in redoing these molecules is to treat $SClF_5$, $SeClF_5$, and $TeClF_5$ using better angular data and a consistent treatment so that comparisons will be useful even though the force constants may not be uniquely determined. We follow Christe *et al.* (4) in the designation of bond coordinates and force constants.

For the force constant analysis, the gaseous (infrared) frequencies are to be preferred where there is a choice, but for the ν_1 and ν_3 vibrations the Raman data are better. The ν_1 band appears as a shoulder in the infrared so the Raman measurement is used. For ν_3 in the infrared the resolution is only fair, and neighboring bands cause some difficulty; further, the infrared frequency is above the Raman, but for $SClF_5$ and $SeClF_5$ the Raman frequency of ν_3 is higher than the infrared. Therefore, the 312 Raman line, which is relatively isolated and clearly an a_1 mode, is used for the datum. The ν_{11} vibration is infrared active but out of the range of our instrument.

The general quadratic force constant matrix of $XClF_5$ (C_{4v}) contains 38 independent force constants. We reduce this number by relating adjacent and opposite stretch–stretch interactions as was done for the hexafluorides, and by transferring most of the off-diagonal constants from the corresponding hexafluorides.

We have tried other strategies and all give similar results for the diagonal constants.

The variable quantities are the diagonal constants: f_r = equatorial stretch, f_R = axial fluorine stretch, f_D = chlorine stretch, f_α = equatorial bend (F_{eq}—X—$F_{eq'}$), f_β = (F_{ax}—X—F_{eq}), f_δ = (Cl—X—F_{eq}); and the off-diagonals: f_{rr} = adjacent equatorial stretch–stretch term, $f_{rr'} = \frac{4}{3} f_{rr}$, and $f_{\alpha\delta}$. The remaining off-diagonals are simply transferred from the hexafluoride and multiplied by 0.9. The factor 0.9 is used because previous studies and preliminary trials of ours indicate a general weakening of force constants in $XClF_5$ compared to XF_6. We treated all $XClF_5$ bonds the same in this transfer, *i.e.* no correction for the change from F to Cl or for the angle changes. This may be justified because the final fitting is not very sensitive to small changes (20% or less) in individual off-diagonal constants. Thus we use 10 (or 11 when the ^{37}Cl stretching is assigned) frequencies to determine 8 independent force constants. The final force constants are given in Table 3 and the observed and calculated frequencies in Table 5. The observed–calculated fit is satisfactory and the consistency of the force field for the three molecules confirms that the assignments are consistent.

The quantities of greatest interest in the force constant solutions are the stretching constants since these are a measure of bond strength. Different assignments, different assumptions, or even different initial values for the solution of the equations can lead to different force constant values; but the stretching assignments are relatively well-determined, and their values are not very sensitive to changes in the assignments of ν_6 and ν_{11} nor to different assumptions about the off-diagonal constants. In a number of trials using different approaches, the $f_R > f_r$

Can. J. Chem. Downloaded from www.nrcresearchpress.com by 210.87.254.105 on 09/05/12
For personal use only.

TABLE 5. Observed and calculated vibrational frequencies of group VI chloride pentafluorides

		Frequencies					
		$SClF_5$		$SeClF_5$		$TeClF_5$	
Mode	Vibration	Obsvd.[a]	Calcd.	Obsvd.[b]	Calcd.	Obsvd.[c]	Calcd.
a_1	ν_1	855	856.0	729	728.9	708	709.0
	ν_2	707	706.7	654	654.7	662	662.1
	ν_3	602	599.5	440	446.6	312	311.1
	ν_4	402	403.1	384	376.0	410.5	411.4
	$\nu_4(^{37}Cl)$	396	394.7	—	369.6	404	403.1
b_1	ν_5	625	628.3	636	631.2	651	650.1
	ν_6	—	332.1	—	256.2	—	199.1
b_2	ν_7	505	505.4	380	380.8	302	301.7
e	ν_8	909	907.0	745	748.3	726	727.6
	ν_9	579	578.7	421	420.0	324.5	324.9
	ν_{10}	441	442.1	334	332.6	259	259.4
	ν_{11}	287	287.2	213	211.9	167	167.4

[a]Frequencies from ref. 5, assignments ref. 4.
[b]Reference 4.
[c]This work ν_1, ν_3, ν_5, ν_7, and ν_{11} are Raman frequencies, others ir.

pattern persisted; and the f_r and f_D values for $SeClF_5$ were consistently lower than the corresponding values for $SClF_5$ and $TeClF_5$. We feel that the relative values rounded to the nearest 0.1 are valid for purposes of comparison.

The previous force constant calculations on $SClF_5$ (4, 22, 7) and $SeClF_5$ (4) have all been isolated treatments; thus the constants collected by Christe *et al.* (4) for comparison are not clearly derived from equivalent calculations using comparable approximations. The force constants of Venkateswarlu and Sathianandan for $SClF_5$ (7) differ significantly from ours, but they determine 13 constants from 11 frequencies and their *e*-type symmetry coordinates do not factor properly (a correct set of symmetry coordinates is given by Smith and Begun (10)). However, all these find $f_R > f_r$ with the exception of Yeranos (22) who assumed that the two stretching constants were the same.

Replacement of a fluorine in hexafluoride by chlorine, as expected, leads to a general drop in the force constants of the remaining bonds.

The differences between axial and equatorial stretching constants are noteworthy. These results are similar to those reported for ClF_5, BrF_5, IF_5 (23), SF_5^-, SeF_5^-, TeF_5^- (11), IOF_5 (10), and $WClF_5$ (24). For BrF_5 (25), TeF_5^- (26), and IF_5 (25, 27) accurate axial and equatorial bond distances are reported; for these the axial distances are shorter. Thus the usual force constant – bond distance relationship and the results from similar molecules suggest that the axial distances for the three molecules studied here are probably slightly shorter than the equatorial distances. These results are consistent with the valence shell electron pair repulsion model (28) and a molecular orbital study of tellurium hexafluoride derivatives (29). The former theory accounts for the angle $F_{ax}—X—F_{eq}$ (X = S, Te) being slightly less than 90°. (See Table 2.)

Replacement of fluorine in SeF_6 and TeF_6 by O^- giving $SeOF_5^-$ and $TeOF_5^-$ leads to a substantial drop in Se—F and Te—F stretching force constants (30). Unlike the cases cited above the axial force constants are smaller than the equatorial force constants, in contrast to the related molecule IOF_5 (10). We also note that an electron diffraction study of SF_5NF_2 (31), indicated that the axial S—F bond was longer than the corresponding equatorial bonds.

Acknowledgments

We wish to thank the National Research Council of Canada and the Defence Research Board (Grant No. 9530-128) for financial assistance.

1. C. LAU and J. PASSMORE. Inorg. Chem. **13**, 2278 (1974).
2. G. W. FRASER, R. D. PEACOCK, and P. M. WATKINS. Chem. Commun. 1257 (1968).

Can. J. Chem. Downloaded from www.nrcresearchpress.com by 210.87.254.105 on 09/05/12
For personal use only.

3. A. C. LEGON. J. Chem. Soc. Faraday Trans. II, **69**, 29 (1973).
4. K. O. CHRISTE, C. J. SCHACK, and E. C. CURTIS. Inorg. Chem. **11**, 583 (1972).
5. J. E. GRIFFITHS. Spectrochim. Acta, Part A, **23**, 2145 (1967).
6. L. H. CROSS, H. L. ROBERTS, P. GOGGIN, and L. A. WOODWARD. Trans. Faraday Soc. **56**, 945 (1960).
7. K. VENKATESWARLU and K. SATHIANANDAN. Opt. Spectrosc. **11**, 24 (1961).
8. S. L. GERHARD and D. M. DENNISON. Phys. Rev. **43**, 197 (1933).
9. H. BURGER. Z. Anorg. Allg. Chem. **360**, 97 (1968).
10. D. F. SMITH and G. M. BEGUN. J. Chem. Phys. **43**, 2001 (1965).
11. K. O. CHRISTE, E. C. CURTIS, C. J. SCHACK, and D. PILIPOVICH. Inorg. Chem. **11**, 1679 (1972).
12. R. KEWLEY, K. S. R. MURTY, and T. M. SUGDEN. Trans. Faraday Soc. **56**, 1732 (1960).
13. R. M. LEES. J. Mol. Spectrosc. **33**, 124 (1970).
14. E. B. WILSON, J. C. DECIUS, and P. C. CROSS. Molecular vibrations. McGraw-Hill, New York. 1955.
15. P. LABONVILLE, J. R. FERRARO, M. C. WALL, and L. J. BASILE. Coord. Chem. Rev. **7**, 257 (1972).
16. W. VAN BRONSWYK, R. J. H. CLARK, and L. MARESCA. Inorg. Chem. **8**, 1395 (1969).
17. D. A. JOHNSON. *In* Sulphur in organic and inorganic chemistry. Vol. 2, *Edited by* A. Senning. Marcel Dekker Inc., New York. 1972. pp. 37–69.
18. F. A. COTTON and G. WILKINSON. Advanced inorganic chemistry. 3rd ed. Interscience, New York. 1972. p. 123.
19. A. RUOFF. Spectrochim. Acta, Part A, **23**, 2421 (1967).
20. R. A. DURIE and A. G. GAYDON. J. Phys. Chem. **56**, 316 (1952).
21. M. G. BROWN. Trans. Faraday Soc. **55**, 9 (1959).
22. W. A. YERANOS. Mol. Phys. **9**, 455 (1965).
23. G. M. BEGUN, W. H. FLETCHER, and D. F. SMITH. J. Chem. Phys. **42**, 2236 (1965).
24. A. J. KALE and K. SATHIANANDAN. Spectrochim. Acta, Sect. A, **26**, 1337 (1970).
25. A. G. ROBIETTE, R. H. BRADLEY, and P. N. BRIER. Chem. Commun. 1567 (1971).
26. A. J. EDWARDS and M. A. MOUTY. J. Chem. Soc. A, 703 (1969).
27. R. D. BURBANK and G. R. JONES. Inorg. Chem. **13**, 1071 (1974).
28. R. J. GILLESPIE. J. Chem. Educ. **47**, 18 (1970).
29. D. R. ARMSTRONG, G. W. FRASER, and G. D. MEIKLE. Inorg. Chim. Acta, **15**, 39 (1975).
30. E. MAYER and F. SLADKY. Inorg. Chem. **14**, 589 (1975).
31. J. HAASE, H. OBERHAMMER, W. ZEIL, O. GLEMSER, and R. HEWS. Z. Naturforsch. Teil A, **26**, 1333 (1971).
32. V. C. EWING and E. L. SUTTON. Trans. Faraday Soc. **59**, 1241 (1963).
33. H. M. SEIP and R. STOLEVIK. Acta Chem. Scand. **20**, 1535 (1966).
34. H. H. CLASSEN, G. L. GOODMAN, J. H. HOLLOWAY, and H. SELIG. J. Chem. Phys. **53**, 341 (1970).

Can. J. Chem. Downloaded from www.nrcresearchpress.com by 210.87.254.105 on 09/05/12
For personal use only.

Partial molar volumes of aqueous 1:1 and 2:1 electrolytes and a structure model

LOWELL W. BAHE AND KATHRYN A. JUNG[1]

Department of Chemistry, University of Wisconsin-Milwaukee, Milwaukee, Wisconsin 53201

Received June 3, 1975

LOWELL W. BAHE and KATHRYN A. JUNG. Can. J. Chem. **54**, 824 (1976).

An expression for partial molar volumes is derived from the free energy equation based on field-dielectric-gradient forces, as well as coulombic forces, between ions in structured solution. Qualitative agreement between the model and experimental partial molar volume data is very good. Excellent quantitative agreement is obtained by adopting for a universal parameter of the theory a value that implies $(\partial \ln k/\partial P) = 76 \times 10^{-6}$ bar^{-1} for water at 25 °C and 1 atm. The latter value is compatible with data obtained from direct measurements.

LOWELL W. BAHE et KATHRYN A. JUNG. Can. J. Chem. **54**, 824 (1976).

On a dérivé une expression pour les volumes molaires partiels à partir de l'équation d'énergie libre basée sur des gradients de forces de champs diélectriques ainsi que sur les forces coulombiques entre ions dans une solution structurée. La corrélation qualitative entre les données expérimentales de volumes molaires partiels et celles calculées à partir du modèle est très bonne; on obtient une corrélation quantitative excellente si on adopte pour un paramètre universel de la théorie une valeur qui implique que $(\partial \ln k/\partial P) = 76 \times 10^{-6}$ bar^{-1} pour l'eau à 25 °C et à 1 atm. Cette valeur est compatible avec des données obtenues par des mesures directes.

[Traduit par le journal]

Introduction

The properties of strong, binary 1:1 and 2:1 electrolytes in aqueous solution have been interpreted on the basis of a model of a loose lattice structure that results from the field-dielectric-gradient interaction, in addition to the coulombic interaction, between all ion pairs (1–3). The fundamental equation which results from this analysis is (1, 3)

$$[1] \qquad \log f_{\pm} = -Ac^{1/3} + Bc$$

where $f_{\pm}$ is the mean mole fraction ionic activity coefficient, c is the concentration in mol l^{-1}, and

$$[2] \qquad A = \frac{A''z_+z_-N}{(\ln 10)vRTk} a_{A''} \left(\frac{N}{1000}\right)^{1/3}$$

where A'' is the Madelung constant, z_+ and z_- are the charges on the cation and anion, respectively, N is Avogadro's number, $v = v_+ + v_-$ for the salt $C_{v_+}A_{v_-}$, R is the gas constant, T is the temperature, k is the dielectric constant of the solvent, $a_{A''}$ is the factor for converting a particular structure into the distance of ionic separation (3), and B is a constant which depends upon the interaction between an ion and the surrounding dielectric medium (1, 3).

Equation 1 agrees well with experimental data for activity coefficients (free energies) for 1:1 (1) and 2:1 (3) electrolytes at 25 °C. The temperature derivative of eq. 1 predicts heats of dilution of 1:1 electrolytes which show excellent agreement with experimental observations (2). This paper will show that the pressure derivative of eq. 1 leads to excellent agreement with partial molar volume data for 1:1 and 2:1 electrolytes and gives a new value for the pressure derivative of the dielectric constant of water at 1 atm.

Equation for Partial Molar Volumes

The partial molar Gibbs free energy for an electrolyte in solution is given by

$$[3] \qquad \bar{G}_2 = \bar{G}_2^{\,0} + RT \ln f_{\pm}^{\,v} X_{\pm}^{\,v}$$

where $X_{\pm}$ is the mean ionic mole fraction of electrolyte in solution. Since $(\partial \bar{G}/\partial P)_{T,n's} = \bar{V}$, the

[1]Present address: Department of Oceanography, Dalhousie University, Halifax, Nova Scotia.

Can. J. Chem. Downloaded from www.nrcresearchpress.com by 210.87.254.40 on 09/05/12
For personal use only.

pressure derivative of eq. 3 at constant temperature and constant composition gives

$$[4] \qquad \bar{V}_2 = \bar{V}_2^0 + vRT\left(\frac{\partial \ln f_\pm}{\partial P}\right)_{T,n's}$$

The pressure derivative of eq. 1 gives

$$[5] \qquad \frac{1}{\ln 10}\left(\frac{\partial \ln f_\pm}{\partial P}\right)_{T,n's} = -A\left(\frac{\partial c^{1/3}}{\partial P}\right)_{T,n's} - c^{1/3}\left(\frac{\partial A}{\partial P}\right)_{T,n's} + B\left(\frac{\partial c}{\partial P}\right)_{T,n's} + c\left(\frac{\partial B}{\partial P}\right)_{T,n's}$$

Since k is the only pressure sensitive variable in eq. 2, we obtain

$$[6] \qquad \left(\frac{\partial A}{\partial P}\right)_{T,n's} = -A\left(\frac{\partial \ln k}{\partial P}\right)_{T,n's}$$

while the pressure derivative of the concentration, c, gives

$$[7] \qquad \left(\frac{\partial c}{\partial P}\right)_{T,n's} = \beta c$$

where β ($= -(1/V)(\partial V/\partial P)_{T,n's}$) is the isothermal compressibility. Combining eqs. 4, 5, 6, and 7, we obtain

$$[8] \qquad \bar{V}_2 = \bar{V}_2^0 + vRT\,(\ln 10)A\left[\left(\frac{\partial \ln k}{\partial P}\right)_{T,n's} - \frac{\beta}{3}\right]c^{1/3} + vRT\,(\ln 10)\left[\beta B + \left(\frac{\partial B}{\partial P}\right)_{T,n's}\right]c$$

$$[9] \qquad = \bar{V}_2^0 + A_p c^{1/3} + B_p c$$

where

$$[10] \qquad A_p = vRT(\ln 10)A\left[\left(\frac{\partial \ln k}{\partial P}\right)_{T,n's} - \frac{\beta}{3}\right]$$

and

$$[11] \qquad B_p = vRT\,(\ln 10)\left[\beta B + \left(\frac{\partial B}{\partial P}\right)_{T,n's}\right]$$

We can now compare the predictions of eq. 9 with actual experimental determinations of partial molar volumes.

Coefficient of $c^{1/3}$

A_p in eqs. 9 and 10 should be determinable since β has been measured repeatedly, and $(\partial \ln k/\partial P)_{T,n's}$ has been reported from direct measurements on pure water (4–7). However, it has also been suggested that $(\partial \ln k/\partial P)_{T,n's}$ be found from partial molar volume data rather than direct measurement since the value of $(\partial \ln k/\partial P)_{T,n's}$ from direct measurement is difficult to obtain and much variation has existed among reported values (8). On the other hand, it has also been noted that a thorough and careful analysis on the basis of a complete theory, such as that of Debye and Hückel, is necessary to account for the variation of $\bar{V}$ or ϕ_v with c to avoid mistaken conclusions (9). And lastly, it is now claimed that both procedures give the same results, at least for the interpretation on the basis of the Debye–Hückel theory (10).

The direct measurement of $(\partial \ln k/\partial P)_T$ at 1 atm is difficult. One reported value for $(\partial \ln k/\partial P)_{25\,C,P=1}$ is 47.10×10^{-6} bar^{-1}, which gives a value for $(\partial k/\partial P)_{25°C,P=1}$ of about 3.7×10^{-3} bar^{-1} (4). To find measurable changes in k, the accuracy of which is no better than ± 0.01, the increments in P must be fairly large; the increments reported range around 75–100 bars, and k changes by a few tenths with this pressure change (5). A common procedure involves measuring k at 1, 100, 200 bars, etc. and then curve fitting the results so that a function of k equals a function of P; the

Can. J. Chem. Downloaded from www.nrcresearchpress.com by 210.87.254.40 on 09/05/12
For personal use only.

derivative is then found from this functional relationship. In our case we need the value of $(\partial \ln k/\partial P)_T$ at $P = 1$. Finding the slope of a fitted curve at the very end of the curve with data whose measured increments are very large makes one apprehensive. One could feel less apprehensive if the data could be collected at increments of perhaps 1 atm or less, but inaccuracies of method will not allow such measurements at the present time.

In view of this difficulty we have chosen to follow a procedure similar to that of Redlich and Meyer (8), namely, to find A_p from $\bar{V}_2$ data rather than use the values reported for the direct measurement of $(\partial \ln k/\partial P)_{T,P=1}$. The important criterion that must be met is that a single value for $[(\partial \ln k/\partial P)_T - \beta/3]$ (eq. 8) must be found that will apply to all strong, binary salts for which partial molar volume data are available.

Experimental Partial Molar Volumes

Commonly results are reported in terms of ϕ_v, apparent molar volumes, rather than in terms of $\bar{V}$, since ϕ_v is obtained easily from density data while $\bar{V}$ is more involved. The relationships are

$$[12] \qquad \phi_v = \frac{V - n_1 \bar{V}_1^0}{n_2}$$

where V is the volume of the solution, n_1 is the number of moles of solvent, $\bar{V}_1^0$ is the molar volume of pure solvent, and n_2 is the number of moles of solute. From eq. 12 it follows that

$$[13] \qquad \left(\frac{\partial V}{\partial n_2}\right)_{T,P,n_1} = \bar{V}_2 = \left(\frac{\partial(m\phi_v)}{\partial m}\right)_{T,P,n_1} = \phi_v + m\left(\frac{\partial \phi_v}{\partial m}\right)_{T,P,n_1}$$

where m is the molality of the salt. At very low concentrations the last term on the right of eq. 9 can be disregarded and c can be replaced by $\rho_0 m$, where ρ_0 is the density of pure water, so that eqs. 9 and 13 can be combined to give

$$[14] \qquad \frac{\partial(m\phi_v)}{\partial m} = \bar{V}_2^0 \ (\equiv \phi_v^0) + A_p \rho_0^{1/3} m^{1/3}$$

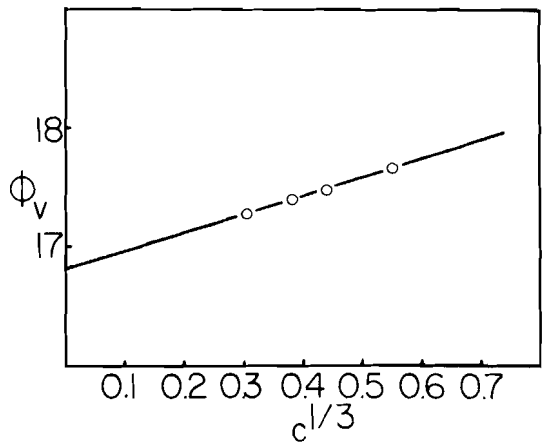

FIG. 1. Apparent molar volume, ϕ_v, plotted against $c^{1/3}$ for LiCl (12).

which can be integrated to yield

$$[15] \qquad \phi_v = \phi_v^0 + \frac{3}{4} A_p c^{1/3}$$

Equation 15 predicts that, at low concentrations, a plot of ϕ_v *vs.* $c^{1/3}$ should give a straight line. Data for LiCl with four points from $c = 0.02$ to $c = 0.16$ (11) are shown in Fig. 1 and a straight line with slope 1.50 is obtained. The value for the slope was obtained by linear regression analysis.

As was the case with heats of dilution, data of very high accuracy at very low concentrations are needed for a plot such as that in Fig. 1. Even then, the linear term in c, as will be seen below, cannot be disregarded for many salts. Fortunately, LiCl has a small B_p (see below) so that the analysis of Fig. 1 is quite good.

Two approaches are available for testing the data over a greater concentration range. Since ϕ_v is the experimental quantity and $\bar{V}$ is the quantity most directly related to the theory one can either convert the ϕ_v data to $\bar{V}$ quantities or one can rearrange eq. 9 into the ϕ_v form. The latter, as can be seen from eqs. 9 and 13, requires that

$$[16] \quad \phi_v = \bar{V}_2^0 + A_p\left[\frac{1}{m}\int_0^m c^{1/3} dm\right] + B_p\left[\frac{1}{m}\int_0^m c\, dm\right]$$

In principle, the integrations of eq. 16 can be carried out either graphically or numerically after which $\bar{V}_2^0$ and the two coefficients, A_p

Can. J. Chem. Downloaded from www.nrcresearchpress.com by 210.87.254.40 on 09/05/12
For personal use only.

TABLE 1. Parameters of eq. 17 determined by multiple linear regression analysis

Salt	Concentration range	v'	a'	b'	Reference
CsBr	0.12–0.30	47.422	2.58823	4.65514	14
$BaCl_2$	0.18–0.8	22.999	5.6629	1.6009	15
$CaCl_2$	0.18–0.8	17.402	5.22203	1.17759	15
RbF	0.12–0.48	11.461	1.60900	1.03098	14
KF	0.1 –0.6	7.509	1.79849	0.79410	14
RbBr	0.07–0.34	37.948	0.69720	1.21394	14
RbCl	0.1 –1.0	31.689	1.74024	0.50880	11
KCl	0.1 –1.0	26.682	1.59892	0.54125	11
CsCl	0.1 –1.0	38.875	1.82712	0.39930	11
NaCl	0.1 –1.0	16.419	1.58046	0.46495	11
NaBr	0.1 –1.0	23.402	1.44425	0.36911	12
KI	0.19–0.90	45.072	1.504	0.26296	13
NaI	0.1 –1.0	35.034	1.00365	0.38896	12
LiCl	0.1 –1.0	16.851	1.40160	0.22329	11
KBr	0.1 –1.0	33.037	2.76130	−0.21908	13
LiBr	0.1 –1.0	23.692	1.26303	0.13412	12
LiI	0.1 –1.0	35.232	1.28987	−0.12159	12

and B_p, can be found by suitable analysis. In practice, this procedure worked poorly; the values obtained for the three constants, $\bar{V}_2^0$, A_p, and B_p, were inconsistent and not reproducible even when multiple regression analysis was used.

The alternative method requires that ϕ_v be converted into $\bar{V}_2$. The raw data can be fitted to the empirical relation

$$[17] \qquad \phi_v = v' + a'm^{1/3} + b'm$$

by multiple regression analysis. The form of eq. 17 was chosen since, as eq. 16 indicates, this form would result if $c = m$. The values obtained for v', a', and b' were not intended to be significant other than as curve fitting results. The derivative of eq. 17 gives

$$[18] \qquad \frac{\partial \phi_v}{\partial m} = \frac{1}{3}a'm^{-2/3} + b'$$

and eqs. 17 and 18 can be combined according to eq. 13 to give

$$[19] \qquad \bar{V}_2 = v' + \frac{4}{3}a'm^{1/3} + 2b'm$$

Equation 19 allows the evaluation of $\bar{V}_2$ at various m and should be most valid between the highest and lowest values of m. Thus v' is an empirical constant not necessarily the same as $\bar{V}^0$. Also, the a' and b' are to be considered empirical. Because the experimental error increases very rapidly as c becomes small (9), values below about 0.1 m were not included in finding the empirical constants in eq. 17. In addition, since previous results have indicated that deviations occur at fairly high concentrations (1–3) and because the equating of m to c becomes worse at high concentrations, experimental results above about 1 M were not used. The values of v', a', and b' obtained for several salts are shown in Table 1.

Values of $\bar{V}_2$ obtained from a set of data should be independent of the method used to evaluate $\bar{V}_2$. In the ORNL report (16) covering his NaCl data, Vaslow determined values for $\bar{V}_2$ using an equation based on $\partial\phi_v/\partial\sqrt{c}$ as suggested by the Debye-Hückel theory. Values of $\bar{V}_2$ determined from eq. 19 were either identical to or slightly lower (never more than 0.02 ml mol^{-1} or 0.1%) than the NaCl values recorded by Vaslow up to concentrations of 1 M.

Before proceeding with the calculations, an analysis of the possible errors which may be encountered should be considered. Equation 9 indicates that the error in A_p can be estimated from

$$[20] \qquad \delta A_p = \frac{\delta\bar{V}_2 + \delta\bar{V}_2^0 + \delta(B_p c) + A_p\delta c^{1/3}}{c^{1/3}}$$

The values of $\bar{V}_2$ will be found from ϕ_v and $(\partial\phi_v/\partial m)$ (eq. 10). Even though the experimental values of ϕ_v may be accurate to perhaps ± 0.002 (depending on the method and the

Can. J. Chem. Downloaded from www.nrcresearchpress.com by 210.87.254.40 on 09/05/12
For personal use only.

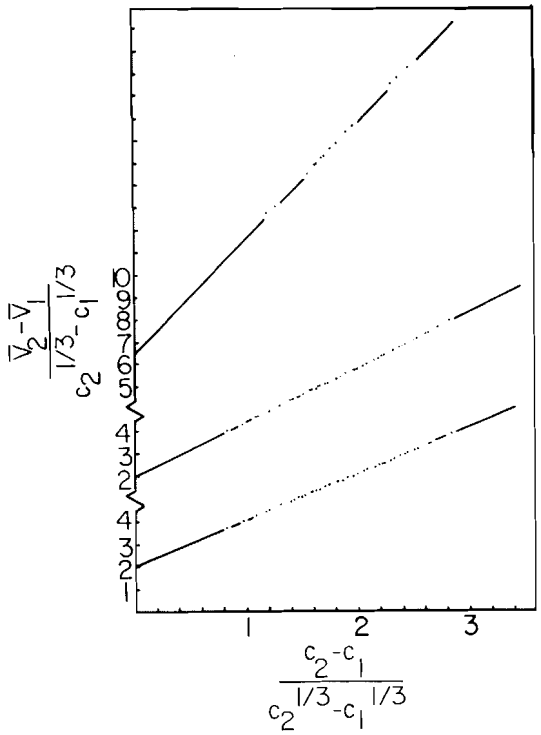

FIG. 2. The left-hand-side of eq. 21 plotted against $(c_2 - c_1)/(c_2^{1/3} - c_1^{1/3})$. Top curve, $CaCl_2$; middle curve, KCl; bottom curve, NaCl. The data were taken from Vaslow (12) and Dunn (15).

concentration range where measured), the numerical evaluation of a derivative increases the error appreciably (17). Not only this, but $\bar{V}_2^0$ is obtained by extrapolation outside the range of experimental values which will introduce additional error. Contributions of several hundredths to as much as 0.1 to the error in A_p might be anticipated from $\bar{V}_2$ and $\bar{V}_2^0$. Since the error in the concentration should normally be limited to something near $\pm 10^{-4}$, the error contributions of the last two terms in the numerator of eq. 20 should be small. The $c^{1/3}$ term in the denominator of eq. 20 could increase the error by as much as a factor of 4 or 5 when c is as low as 0.01 ($0.01^{1/3} \simeq 0.22$).

Equation 9 can be recast as

$$[21] \quad \frac{(\bar{V}_2)_2 - (\bar{V}_2)_1}{c_2^{1/3} - c_1^{1/3}} = A_p + B_p \frac{c_2 - c_1}{c_2^{1/3} - c_1^{1/3}}$$

to eliminate the $\bar{V}_2^0$ obtained by extrapolation, and a similar error analysis would lead to an error estimate of several hundredths to one-tenth in the value of A_p. Even to achieve this accuracy, very accurate data on ϕ_v over a considerable concentration range must be available. By eliminating one of the constants, eq. 21 proved useful for testing experimental data and for evaluating A_p and B_p.

TABLE 2. Slopes, B_p, and intercepts, A_p, of eq. 21 for the electrolytes shown in Fig. 2

Salt	B_p	A_p
NaCl	1.0309	2.0105
KCl	1.2108	2.0096
$CaCl_2$	2.6085	6.7402

The left-hand-side of eq. 21 is plotted against $(c_2 - c_1)/(c_2^{1/3} - c_1^{1/3})$ in Fig. 2 for the salts NaCl, KCl, and $CaCl_2$. Very nice straight lines are obtained. The values for the slopes and intercepts, determined by linear regression analysis, are given in Table 2. A statistical error treatment (18) of the data in Fig. 2 indicated that the error in the slope and intercept might be as small as 0.02. However, from our discussion of the errors in A_p, above, we doubt that the accuracy is as good as the statistical analysis indicates. The curve fitting has apparently made a particular set of data internally more satisfactory than is truly allowable. Analysis of data for other salts, though also internally consistent, confirmed that the error in A_p is probably larger than 0.02.

It was pointed out above that the value for $([(\partial \ln k)/(\partial P)]_{T,n's} - \beta/3)$ must be the same for all strong binary salts. Table 2 shows that NaCl and KCl have identical A_p within the experimental error. In addition, eq. 10 indicates that the ratio of A_p for 1:1 and 2:1 salts must be given by (1, 3)

$$[22] \quad \frac{(A_p)_{11}}{(A_p)_{21}} = \frac{(\nu_{11})(A_{11})}{(\nu_{21})(A_{21})} = \frac{(2)(0.28894)}{(3)(0.64100)} = 0.3005$$

and the ratio from Table 2 is 2.01/6.74 = 0.298. In addition to these numbers, we should also remember, as indicated by eq. 15, that the slope of ϕ_v *vs.* $c^{1/3}$ at very low concentrations should be 3/4 of A_p; the results in Fig. 1 for LiCl indicated a slope of 1.50 which gives $A_p = 2.00$

Can. J. Chem. Downloaded from www.nrcresearchpress.com by 210.87.254.40 on 09/05/12
For personal use only.

Can. J. Chem. Downloaded from www.nrcresearchpress.com by 210.87.254.40 on 09/05/12
For personal use only.

TABLE 3. Slopes, B_p, and intercepts, $\bar{V}_2^0$, for the 1:1 and 2:1 electrolytes shown in Fig. 3.

Salt	B_p	$\bar{V}_2^0$
CsBr	4.08	45.32
$BaCl_2$	3.88	23.37
$CaCl_2$	2.62	17.50
RbF	2.18	11.52
KF	1.89	7.67
RbBr	1.37	37.54
RbCl	1.26	31.82
KCl	1.20	26.73
CsCl	1.11	39.06
NaCl	1.01	16.46
NaBr	0.72	23.35
KI	0.58	45.05
NaI	0.44	34.70
LiCl	0.38	16.77
KBr	0.50	33.86
LiBr	0.10	23.53
LiI	−0.41	35.09

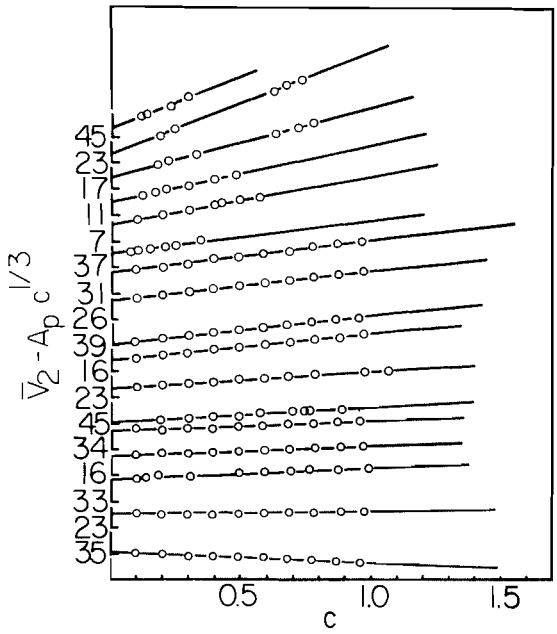

FIG. 3. The left-hand-side of eq. 24 plotted against c. The curves are arranged in the same order, from top to bottom, as the salts in Table 3 with CsBr on top and LiI on the bottom. Each increment on the ordinate represents 1 ml mol^{-1}. The number to the left of each right angle represents the value of that intersection in ml mol^{-1}.

to compare with the 2.01 obtained from NaCl and KCl. We therefore have three 1:1 salts and one 2:1 salt which give the same value for $([(\partial \ln k)/(\partial P)]_{T,n's} - \beta/3)$. We adopt a value of 2.0 ± 0.1 and 6.7 ± 0.3 as the value for A_p in eq. 9 for 1:1 and 2:1 salts, respectively. More will be said below about the resulting value of $(\partial \ln k/\partial P)_{25°C,P=1}$ for water. Many other salts have been examined according to the procedure just outlined for eq. 21 but not all behave as consistently as the three cited. Extremely accurate experimental results are necessary to use eq. 21.

Vaslow's data have been used preferentially because of their great accuracy and because the concentration range is large. Data on NaCl from other investigators have been examined, and, though none were apparently as accurate as those of Vaslow, the results confirmed the values obtained from Vaslow's data. Smith (19) measured ϕ_v for NaCl at 25 °C over the concentration range of $0.002m$ to $0.09m$. At these small concentrations where $c = \rho^0 m$, eq. 16 can be cast in the integrated form as

$$[23] \qquad \phi_v - \frac{B_p}{2}c = \phi_v^0 + \frac{3}{4}A_p c^{1/3}$$

Using B_p determined above from Vaslow's results this equation gave a value of 1.97 for A_p by linear regression analysis, using Smith's data from $0.01m$ to $0.09m$. Millero (20) also reported ϕ_v as a function of m for NaCl at 25 °C. Again using eq. 16 in the integrated form, which is valid at low concentrations, where $c = \rho^0 m$, we evaluated $\phi_v^0 = \phi_v - 1.50c^{1/3} - 0.51c$ for Millero's seven values between $0.01m$ and $0.20m$ and found an average of 16.48 with a standard deviation of 0.05 with no discernable trend in the values.

The universality of the A_p's can be demonstrated for many salts. Equation 9 can be rearranged to give

$$[24] \qquad \bar{V}_2 - A_p c^{1/3} = \bar{V}_2^0 + B_p c$$

so that the left-hand-side of eq. 24 plotted against c should give a straight line. The results of doing this using the universal values found above for A_p are shown in Fig. 3. Very nice straight lines are obtained for fifteen 1:1 and two 2:1 salts. The intercepts, $\bar{V}_2^0$, and slopes, B_p, are shown in Table 3.

A further check on the consistency of the results may be obtained by testing the additivity of the $\bar{V}_2^0$'s. A partial list of the possible comparisons is shown in Table 4. Only results from

TABLE 4. Comparison of $\Delta\bar{V}_2^0$ for several 1:1 electrolytes

Salts	$\Delta\bar{V}_2^0$
NaCl–NaI	−18.24
LiCl–LiI	−18.32
NaCl–LiCl	−0.31
NaBr–LiBr	−0.28
NaI–LiI	−0.39
LiBr–LiCl	6.76
NaBr–NaCl	6.89
NaI–NaBr	11.35
LiI–LiBr	11.56

the data of Vaslow (11, 12) have been included since our previous work indicated that his data were very good. Comparisons of values which include data from other investigators give somewhat larger, but adequate, differences of differences. Allowing an error of about 0.1–0.2 ml mol^{-1} in $\bar{V}_2^0$ indicates that the $\bar{V}_2^0$ are additive.

Discussion

The partial molar volume data agree well with the model of structured ions in solution for a number of 1:1 and 2:1 electrolytes. These results are further evidence supporting this model, and they show additional evidence for the validity of the field-dielectric-gradient force operating between ions in solution. All strong 1:1 electrolytes apparently assume a loose face-centered-cubic structure in solution while strong 2:1 electrolytes assume a loose fluorite structure in solution.

The value 2.0 for A_p for 1:1 electrolytes allows the determination of the value for the pressure derivative of the dielectric constant of water. From eq. 10 we see that

$$[25]\quad \left(\frac{\partial \ln k}{\partial P}\right)_{25°C,n's,P=1} - \frac{\beta}{3} = \frac{A_p}{\nu RT\,(\ln 10)A} = 61 \times 10^{-6}\ \text{atm}^{-1}$$

and if we use the value $\beta = 45.24 \times 10^{-6}$ bar^{-1} (21), we obtain

$$[26]\quad \left(\frac{\partial \ln k}{\partial P}\right)_{25°C,n's,P=1} = 76 \times 10^{-6}\ \text{bar}^{-1}$$

for water at 1 bar. This value is considerably larger than the recent value of 47.10×10^{-6} bar^{-1} (4) found by directly measuring k as a function of P. The discussion above pointed out some of the difficulties inherent in the direct measurement of k at various P to determine the value of this derivative. We have drawn in Fig. 4 a plot of the three data points reported by Harris *et al.* (5) at 25.6 °C along with the value from Owen *et al.* (4) at 100 bar corrected by the ratio of dielectric constants at 1 atm to put it on the same temperature scale. We have drawn an arbitrary line through the experimental k's with the slope our results indicate at 1 atm pressure. Until better data have been collected, or until a theory for the expected behavior of the dielectric constant as a function of pressure has been developed, we conclude that the slope generated by our $\bar{V}_2$ treatment is not impossible and may even be preferable to that obtained by direct measurement.

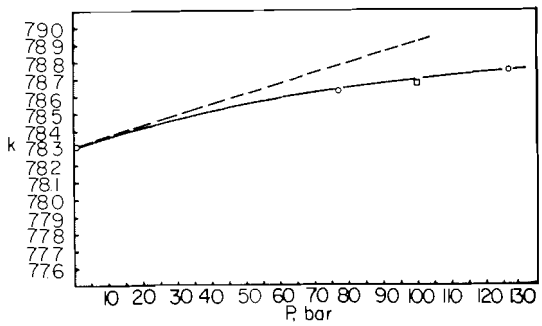

FIG. 4. The dielectric constant of water as a function of pressure. ○, ref. 6: □, ref. 5. The Owen *et al.* value at 100 bars was multiplied by the ratio of dielectric constants at $P = 1$ to put it on the same scale. The solid line is an arbitrary line drawn through the data points with the slope at $P = 1$ predicted from the $\bar{V}_2$ treatment. The dashed line is the slope drawn through k at 1 atm.

The results obtained here also give a value for B_p in eq. 9. The values for this coefficient, as expected, are specific to each salt, and have both positive and negative values as shown in Table 3. Since B can be determined from activity coefficient data and β for water is available, the pressure derivative of B, $(\partial B/\partial P)_{T,n's}$, can also be evaluated for each salt, as shown by eq. 11. The values for $(\partial B/\partial P)_{T,n's}$, shown in Table 5 for those salts for which B is available (1, 3), display both positive and negative values. Though the correlation is not perfect, in general for the same cation the value increases as the ionic weight of the anion decreases, and for the same anion the value

Can. J. Chem. Downloaded from www.nrcresearchpress.com by 210.87.254.40 on 09/05/12
For personal use only.

Can. J. Chem. Downloaded from www.nrcresearchpress.com by 210.87.254.40 on 09/05/12
For personal use only.

TABLE 5. Values for the pressure derivative of B

Salt	B^* (l mol^{-1})	$\frac{\partial B}{\partial P} \times 10^3$ (ml mol^{-1} atm^{-1})
KCl	0.0680	7.58
NaCl	0.0970	4.58
KBr	0.0785	0.89
NaBr	0.1230	0.83
KI	0.0967	0.77
NaI	0.1540	−3.06
LiBr	0.0955	−3.43
LiCl	0.1713	−4.38
$CaCl_2$	0.3982	−2.50
$BaCl_2$	0.2896	9.87

*References 1 and 3.

increases as the ionic weight of the cation increases.

One of the referees has pointed out that eq. 23 of ref. 3 implies that the B's of eq. 1 should be additive, *i.e.*, that $B_{NaCl} - B_{KCl}$ leads to $B_{Na+} - B_{K+}$, and a similar additive result should therefore be expected for $(\partial B/\partial P)_i$. The values of B and of $\partial B/\partial P$ are not additive as can be seen by examining the various tables. The non-additivity of the B's apparently resides in the inability to determine individual-ion activity coefficients. Writing

$$[27] \qquad f_{\pm}^{\nu} = f_{+}^{\nu_+} f_{-}^{\nu_-}$$

is a mathematical convenience without physical significance; only the mean ionic activity coefficients can be measured (22). Let us cast the function

$$[28] \quad \log \frac{f_{\pm}^{\nu}(NaCl) f_{\pm}^{\nu}(KBr)}{f_{\pm}^{\nu}(KCl) f_{\pm}^{\nu}(NaBr)} = \nu(B_{NaCl} + B_{KBr} - B_{KCl} - B_{NaBr})C$$

If eq. 27 were physically valid then the left-hand-side of eq. 28 should be zero (all activity coefficients referring to the same concentration). The left-hand-side of eq. 28 is a thermodynamic relationship; the values are independent of any theory of behavior in solution. Experimental values of activity coefficients substituted into the left-hand-side of eq. 28 do not give a value of zero which confirms the physical invalidity of eq. 28. Correspondingly eq. 23 of ref. 3 substituted into the right-hand-side of eq. 28 implies that $\Delta B = 0$, but the measured values of B do not give a value of zero. Thus the non-additivity of the B's apparently resides in the impossibility of determining individual-ion activity coefficients. Guggenheim (23) has considered the limitations on relationships between single-ion activity coefficients. His "specific salt" effects come into play in the B's and B_p's and therefore two salts which differ in one or both ions, even at the same concentration, are not in the same "media" as Guggenheim has defined "media." Comparison of the additivity of the $\bar{V}_2^0$'s, however, as was done in Table 4, is legitimate since at zero concentration the effects of electrical interactions and specific salt effects has been removed.

Finding $\bar{V}_2^0$'s as was done above does not require that the model and the resulting equations be valid at all concentrations down to zero concentration. $\bar{V}_2^0$ has the properties of an integration constant which can be evaluated over the domain of the function. Operationally $\bar{V}_2^0$ can be evaluated by an extrapolation to zero concentration, but it can also be evaluated without such an extrapolation. The properties of the function (eq. 9) are such that $\bar{V}_2^0$ measures the partial molar volume of a salt when the contributions of the coulombic and field-dielectric-gradient electrical interactions to the volume have been removed from the structured model. Values of $\bar{V}_2^0$ evaluated over the domains of other functions, such as that of Debye and Hückel, may also be obtained and compared. The values of $\bar{V}_2^0$ obtained from different functions will probably not be the same, yet each set can have a physical interpretation that can be valid and significant. The values of $\bar{V}_2^0$ obtained from the structured model are very close to those obtained from a square-root, linear function, the values in Table 3 often being smaller by a few hundredths of a ml mol^{-1} (24).

Acknowledgment

It is a pleasure to acknowlege the support of the University of Wisconsin-Milwaukee Graduate School for one of us (L.W.B.), and the National Science Foundation through its Undergraduate Research Participation Program for the support for the other (K.A.J.).

1. L. W. BAHE. J. Phys. Chem. **76**, 1062 (1972).
2. L. W. BAHE. J. Phys. Chem. **76**, 1608 (1972).
3. L. W. BAHE and D. PARKER. J. Am. Chem. Soc. **97**, 5664 (1975).
4. B. B. OWEN, R. C. MILLER, C. E. MILNER, and H. L. COGAN. J. Phys. Chem. **65**, 2065 (1961).

5. F. E. HARRIS, E. W. HAYCOCK, and B. J. ALDER. J. Phys. Chem. **57**, 978 (1953).
6. G. FALKENBERG. Ann. Phys. **61**, 145 (1920).
7. S. KYROPOULOS. Z. Phys. **40**, 507 (1926).
8. O. REDLICH and D. MEYER. Chem. Rev. **64**, 221 (1964).
9. B. B. OWEN and S. R. BRINKLEY, Jr. Ann. N. Y. Acad. Sci. **51**, 753 (1949).
10. O. REDLICH. J. Phys. Chem. **67**, 496 (1963).
11. F. VASLOW. J. Phys. Chem. **70**, 2286 (1966).
12. F. VASLOW. J. Phys. Chem. **73**, 3745 (1969).
13. L. A. DUNN. Trans. Faraday Soc. **64**, 1898 (1968).
14. A. F. SCOTT. J. Phys. Chem. **35**, 2315 (1931).
15. L. A. DUNN. Trans. Faraday Soc. **63**, 2348 (1967).
16. F. VASLOW. Oak Ridge National Laboratory Report ORNL-TM-1438, April 1966.
17. K. S. KUNZ. Numerical analysis. McGraw-Hill, New York. 1957. p. 126.
18. Y. BEERS. Introduction to the theory of error. 2nd ed. Addison-Wesley, Reading, Mass. 1957.
19. H. T. SMITH. Ph.D. Thesis. University of Bradford, Yorkshire, England. 1967.
20. F. J. MILLERO. J. Phys. Chem. **74**, 356 (1970).
21. R. C. WEAST (*Editor*). Handbook of chemistry and physics. 49th ed. Chemical Rubber Co., Cleveland, Ohio. 1968. p. F-5.
22. R. FOWLER and E. A. GUGGENHEIM. Statistical thermodynamics. Cambridge University Press, London. 1949. p. 400.
23. E. A. GUGGENHEIM. J. Phys. Chem. **33**, 842 (1929).
24. J. E. DESNOYERS, M. AREL, G. PERRON, and C. JOLICOEUR. J. Phys. Chem. **73**, 3346 (1969).

Can. J. Chem. Downloaded from www.nrcresearchpress.com by 210.87.254.40 on 09/05/12
For personal use only.

^{15}N-^{13}C spin-spin coupling constants in some aniline derivatives

RODERICK E. WASYLISHEN

Department of Chemistry, University of Winnipeg, Winnipeg, Manitoba R3B 2E9

Received September 29, 1975

RODERICK E. WASYLISHEN. Can. J. Chem. **54**, 833 (1976).

Nitrogen–carbon spin–spin coupling constants in aniline-^{15}N and some of its derivatives have been measured using ^{13}C Fourier transform nmr spectroscopy. Observed values of $^1J(^{15}N,^{13}C)$ in these aniline derivatives are dependent on the nature of the substituent as well as the solvent. Observed values of $^1J(^{15}N,^{13}C)$ in the amino fragment of a number of amine derivatives are linearly related to the corresponding $^1J(^{15}N,H)$ values in these compounds. The $^1J(^{15}N,^{13}C)$ values in these compounds also appear to be related to the N(*s*)—C(*s*) bond order. Comparison of observed $^1J(^{15}N,^{13}C)$ values in a number of compounds with those calculated using INDO–MO theory indicate that $^1J(^{15}N,^{13}C)$ in aniline and its derivatives is negative, that is, $^1K(N,C)$ is positive. Observed and calculated ^{15}N–^{13}C spin–spin coupling constants over two and three bonds are also presented.

RODERICK E. WASYLISHEN. Can. J. Chem. **54**, 833 (1976).

On a mesuré les constantes de couplage spin–spin entre l'azote et le carbone dans l'aniline-^{15}N et quelques-uns de ses dérivés; pour ce faire, on a utilisé la spectroscopie rmn du ^{13}C par transformation de Fourier. Les valeurs observées pour $^1J(^{15}N,^{13}C)$ dans ces dérivés de l'aniline dépendent de la nature des substituants et du solvant. Les valeurs observées pour $^1J(^{15}N,^{13}C)$, dans la portion aminée d'un certain nombre de dérivés d'amines, sont reliés d'une façon linéaire avec les valeurs $^1J(^{15}N,H)$ correspondantes dans ces composés. Les valeurs de $^1J(^{15}N,^{13}C)$ dans ces composés semblent être aussi reliés à l'ordre de la liaison N(*s*)—C(*s*). Une comparaison des valeurs $^1J(^{15}N,^{13}C)$ observées dans un certain nombre de composés avec celles calculées en faisant appel à la théorie INDO–MO indique que la constante $^1J(^{15}N,^{13}C)$ de l'aniline et de ses dérivés est négative ce qui indique que $^1K(N,C)$ est positif. On présente aussi les constantes de couplage observées et calculées pour des couplages spin–spin ^{15}N–^{13}C s'effectuant sur deux et trois liens.

[Traduit par le journal]

Introduction

A number of studies (1–9) of the one bond ^{15}N–H coupling constant in aniline derivatives have established that the magnitude of this coupling constant is at least qualitatively related to the nature of the hybridization of the nitrogen atom. Comparing an sp^3-hybridized nitrogen (*e.g.*, anilinium) to one approaching sp^2 hibridization (*e.g.*, 2,4-dinitroaniline), $^1J(^{15}N,H)$ varies from −76.0 to −92.6 Hz (4, 9). As well as being sensitive to ring substituents $^1J(^{15}N,H)$ values in aniline and its derivatives also depend upon the solvent. For example, in aniline $^1J(^{15}N,H)$ decreases from −78.0 Hz in chloroform to −82.3 Hz in dimethyl sulfoxide (10).

Several years ago the following relationship between $^1J(N,C)$ and hybridization was proposed (1):

$$[1] \qquad 80\,^1J(^{15}N,^{13}C) = s_N s_C$$

Here s_N and s_C represent the percent 2*s* character of the nitrogen and the carbon hybrid orbitals which overlap to form the N—C bond. Although several studies have shown that this equation is not of general applicability (11, 12) it is of interest to determine whether there is a qualitative relationship between $^1J(^{15}N,^{13}C)$ and hybridization in certain nitrogen compounds. This problem is best studied by examining $^1J(^{15}N,^{13}C)$ values in a series of closely related compounds of known hybridization. Aniline derivatives serve as a good model since their hybridization states are quite well understood (3, 9, 13–15). Thus in this study, $^1J(^{15}N,^{13}C)$ has been measured for aniline-^{15}N and some of its derivatives. For aniline-^{15}N solvent effects on $^1J(^{15}N,^{13}C)$ are also examined.

Semi-empirical MO calculations of $^1J(^{15}N,^{13}C)$ at the INDO level of approximation (16–18) have also been carried out for aniline, the anilinium ion, acetanilide, and several other nitrogen compounds. Calculated values are compared with those observed in this study and those reported by other workers.

Can. J. Chem. Downloaded from www.nrcresearchpress.com by 210.87.254.105 on 09/05/12
For personal use only.

TABLE 1. Observed values of $^1J(^{15}N,^{13}C)$ and $^1J(^{15}N,H)$ in some amines containing the —NHR fragment*

^{15}N compound	Solvent	$\lvert^1J(^{15}N,^{13}C)\rvert$	$^1J(^{15}N,H)$	Reference
Aniline	Neat	10.9±0.3		
	CCl_4	11.1±0.3	−78.0	10
	$CDCl_3$	10.9±0.3	−78.0	10
	Acetone-d_6	11.6±0.3	−82.1	10
	DMSO-d_6	12.1±0.3	−82.3	10
	TFA-*d*	8.9±0.3	—	
	DCl	8.9±0.3	−76.0	4
4-Methylaniline	$CDCl_3$	10.5±0.3	−76.5	9
2-Methylaniline	$CDCl_3$	10.5±0.3	—	
4-Nitroaniline	Acetone-d_6	14.9±0.3	−88.9	19, 20
	DMSO	15.0±0.3	−89.4	9
	DCl	9.2±0.3	−76.0	4
2-Aminobenzoic acid	NaOD (p*D* 12)	10.7±0.5	—	
Acetanilide	$CDCl_3$	C_1 14.3±0.5	—	
		*C*O		
	Acetone-d_6	C_1 14.7±0.5	−91.3†	15
		*C*O		
Formamide	H_2O	14.8	−89.1‡	21
Methylamine	Neat	4.5±0.5	−65.0	22
Pyrrole	—	12.98	−96.5	24§

*$J(^{15}N,^{13}C)$ values in this study were determined for ~20% solutions.
†Determined in DMSO-d_6.
‡Average value.
§H. Jakobsen, private communication.

Experimental

All ^{13}C nmr spectra were obtained at 29 °C on a Varian CFT-20 nmr spectrometer. Acquisition times of 5.0 s or longer were used to obtain the data reported here. In some cases the free induction decay was multiplied by an exponential weighting factor (SE > −5 s). Line widths at half height were typically less than or equal to 0.5 Hz.

Aniline-^{15}N, *ortho*- and *para*-toluidine-^{15}N, and anthranilic acid-^{15}N were obtained from Prochem, Maplewood, New Jersey. Deuterated solvents and *p*-nitroaniline-^{15}N were supplied by Merck Sharp and Dohme Canada Limited. The acetanilidine-^{15}N was obtained from Dr. T. Schaefer, University of Manitoba.

Results and Discussion

1. One-bond ^{15}N–^{13}C Coupling Constants

Observed values of $^1J(^{15}N,^{13}C)$ and $^1J(^{15}N,H)$ for several amine derivatives are given in Table 1. All $^1J(^{15}N,^{13}C)$ values for aniline and its derivatives were determined in this study. The signs of the $^1J(^{15}N,H)$ values are assumed negative on the basis of the accepted sign for $^1J(^{15}N,H)$ in ammonium ions (25, 26) and the observed negative sign in methylamine (22). Only the magnitude of the $^1J(^{15}N,^{13}C)$ values are given in Table 1, however, double resonance experiments have shown that the sign of this coupling constant is negative in methylamine (22) and pyrrole-^{15}N.[1] Below it is argued that $^1J(^{15}N,^{13}C)$ is negative in sign for all of the compounds in Table 1.

The magnitude of $^1J(^{15}N,^{13}C)$ found for aniline-^{15}N, 47% w/w, in acetone is in good agreement with the precise value of 11.47 ± 0.03 Hz previously reported by Hansen and Jakobsen (27). The values of $^1J(^{15}N,^{13}C)$ in aniline are solvent dependent varying from 10.9 ± 0.3 Hz in $CDCl_3$ to 12.1 ± 0.3 Hz in DMSO-d_6. Similar results have been reported for $^1J(^{15}N,H)$ in aniline where the magnitude of this coupling constant parallels the hydrogen-bonding capability of the solvents (10). Hinton *et al.* (28) recently found $^1J(^{15}N,^{13}C)$ values for aqueous solutions of formamide-^{15}N to be concentration dependent, varying from 13.9 Hz in the neat liquid to 14.8 Hz for a dilute solution in water. It was suggested that this increase results from an increase in the double bond character of the carbon–nitrogen bond. A similar argument may be invoked to explain the increase in $^1J(^{15}N,^{13}C)$ observed for aniline in polar solvents where resonance structure **1***b* is of greater importance than in the case of non-polar solvents. Solvent

[1] H. Jakobsen, private communication.

Can. J. Chem. Downloaded from www.nrcresearchpress.com by 210.87.254.105 on 09/05/12
For personal use only.

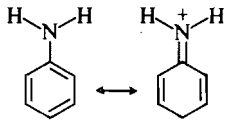

1a **1b**

dependent ^{13}C chemical shifts of aniline also indicate that resonance structure **1***b* is important in polar solvents. An upfield shift of 2.8 ppm is observed for C_4 on going from CCl_4 to DMSO solutions (29). This upfield shift strongly suggests an increase in electron density at C_4 in the more polar solvent.

Further evidence that $^1J(^{15}N,^{13}C)$ is related to the N—C bond order comes from noting the influence of the 4-nitro group on $^1J(^{15}N,^{13}C)$ in aniline. $^1J(^{15}N,^{13}C)$ is approximately 25% larger in magnitude in 4-nitroaniline-^{15}N, **2**, than in aniline-^{15}N. It is of interest to point out that in 4-nitrotoluene, $^1J(^{13}CH_3,^{13}C) = 43.45$ Hz while in toluene, $^1J(^{13}CH_3,^{13}C) = 44.19$ Hz (30). That is, $^1J(^{13}CH_3,^{13}C)$ decreases by only 1.7%. A resonance structure analogous to **2***b* is certainly not important for 4-nitrotoluene, therefore it is reasonable to attribute the large substituent effect on $^1J(^{15}N,^{13}C)$ observed in the 4-nitroaniline to an increase in double bond character (**2***b*).

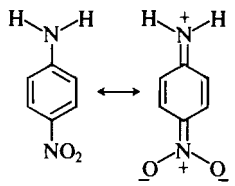

2a **2b**

The substituent effects on $^1J(^{15}N,^{13}C)$ in amine derivatives also parallel those observed for $^1J(^{15}N,H)$, however changes in $^1J(^{15}N,^{13}C)$ are about one-third those observed for $^1J(^{15}N,H)$. In Fig. 1 observed values of $^1J(^{15}N,H)$ are plotted against the corresponding $^1J(^{15}N,^{13}C)$ values observed for the same compound in the same solvent. All values were taken from Table 1. Since the $^1J(^{15}N,H)$ values in these compounds have been qualitatively related to the hybridization at the nitrogen (1–9) the relatively good correlation observed in Fig. 1 suggests a similar relationship between $^1J(^{15}N,^{13}C)$ values and hybridization in these amine derivatives. From Fig. 1, one finds

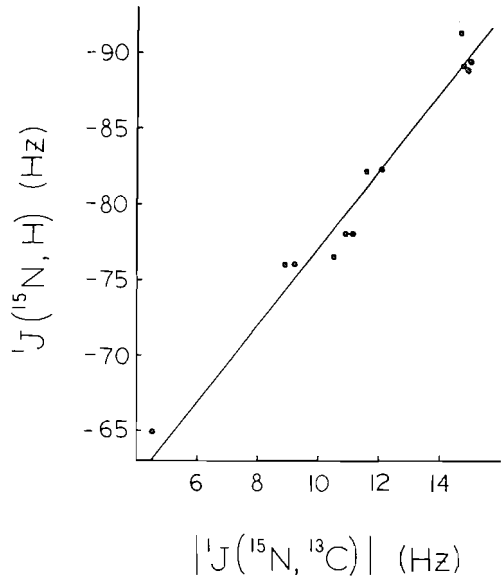

FIG. 1. Plot of observed $|^1J(^{15}N,^{13}C)|$ values *vs.* $^1J(^{15}N,H)$ values for some of the amine derivatives given in Table 1.

$$[2]\quad |^1J(^{15}N,^{13}C)| \simeq 0.392|^1J(^{15}N,H)| - 20.2$$

Substituting an expression derived by Binsch *et al.* (1) which relates % 2*s* character at the nitrogen to $^1J(^{15}N,H)$, into eq. 2, one calculates

$$[3]\quad |^1J(^{15}N,^{13}C)| = 0.912\,\%\,2s(N) - 14.7$$

Thus for sp^3 and sp^2 hybridization at the nitrogen the magnitude of $J(^{15}N,^{13}C)$ is calculated to be 8.1 and 15.7 Hz, respectively. It must be stressed that this relationship is probably roughly valid *only* for compounds containing the $^{13}C—^{15}N\langle^{H}_{R}$ fragment. Also, eq. 3 does not take into account changes in hybridization at the carbon in a direct manner. A more accurate and theoretically satisfying expression would probably relate $^1J(^{15}N,^{13}C)$ and $P^2_{s(N)s(C)}$ where $P_{s(N)s(C)}$ is the bond order between the valence-shell *s* orbitals of nitrogen and carbon.

Finally it is of interest to point out that the magnitudes of $^1J(C,C)$ and $^1J(N,N)$ also generally increase with the intervening bond order (30, 31).

2. *Sign of* $^1J(^{15}N,^{13}C)$ *for the Compounds in Table 1*

Although all known $^1J(C,C)$ values are positive (26, 30, 32) and all $^1J(^{19}F,^{13}C)$ values are

Can. J. Chem. Downloaded from www.nrcresearchpress.com by 210.87.254.105 on 09/05/12
For personal use only.

Can. J. Chem. Downloaded from www.nrcresearchpress.com by 210.87.254.105 on 09/05/12
For personal use only.

TABLE 2. Some calculated $^1J(^{15}N,^{13}C)$ and $^1J(^{15}N,H)$ values in Hz*

Compound	$^1J(^{15}N,^{13}C)$ (Hz)	$^1J(^{15}N,H)$ (Hz)	Geometry reference†
Aziridine	7.60	−7.56	41
Oxaziridine	1.53	8.88	41
Methylamine	−3.74	−34.78	41
Methylammonium cation	−10.07	−75.38	41
Aniline (pyramidal N)	−16.33	−59.74	41
(planar N)	−29.43	−92.91	41
Anilinium ion	−4.39	−72.36	41
4-Nitroaniline (pyramidal N)	−16.40	−62.20	18, 41‡
(planar N)	−29.34	−93.58	18, 41‡
4-Methylaniline (pyramidal N)	−16.33	−59.48	18, 41‡
Acetanilide N-C_1	−25.11	−73.48	41
N-CO	−23.59	—	
Formamide	−26.43	H_c −80.89	41
		H_t −86.09	41
Pyrrole	−29.96	−79.15	41
Pyridinium ion	−27.49	−100.71	41
Benzonitrile-*N*-oxide	−73.52	—	48

*The $^1J(^{15}N,H)$ results here are similar to those recently reported by Ley *et al.* (47).
†See ref. 41 for original references.
‡The geometry of the aniline moiety was as in ref. 41 and standard geometries (18) were used for the nitro and methyl groups.

negative (32, 33), both positive and negative $^1J(^{15}N,^{13}C)$ values are known (22, 34–37).[1]

The reasonably good correlation observed in Fig. 1 together with experimental evidence that $^1J(^{15}N,^{13}C)$ is negative in methylamine (22) and pyrrole[1] strongly suggest that $^1J(^{15}N,^{13}C)$ is negative for all of the compounds in Table 1. A negative sign for $^1J(^{15}N,^{13}C)$ requires that the reduced coupling constant, $^1K(N,C)$ is positive since the gyromagnetic ratio of the ^{15}N nucleus is negative.[2] One would not expect the magnitude of $^1K(N,C)$ to be directly related to C—N bond order unless $^1K(N,C)$ is in fact positive (11). Also, a negative sign for $^1J(^{15}N,^{13}C)$ for the compounds in Table 1 appears to be confirmed by the calculations discussed below.

3. *INDO–MO Calculations of* $^1J(^{15}N,^{13}C)$

It has been shown that semi-empirical INDO–MO calculations of $^1J(^{15}N,^{13}C)$ are successful in qualitatively reproducing some experimental trends (38, 39). In this and previous studies (11, 38, 39) only the Fermi contact contribution to $^1J(^{15}N,^{13}C)$ has been calculated. The Fermi contact mechanism has been shown to completely dominate $^1J(C,C)$ (33), also it is generally the most important mechanism for one bond $^{19}F-^{13}C$ coupling constants (33, 40). The orbital and spin-dipolar mechanisms are most important when the two coupled nuclei are joined by multiple bonds. Thus in the $^{13}C—^{15}N\langle^{H}_{R}$ fragment it is expected that the orbital and dipolar contributions to $^1J(^{15}N,^{13}C)$ will be much smaller than the Fermi contact contribution.

Calculated values of $^1J(^{15}N,^{13}C)$ and $^1J(^{15}N,H)$ for a number of nitrogen compounds are given in Table 2. These calculations were carried out as previously described (41); references to the geometry used in the calculations are also included in Table 2.

The calculations predict a positive value for $^1J(^{15}N,^{13}C)$, that is, a negative sign for $^1K(N,C)$, in the three-membered ring systems considered. The only known positive value of $^1J(^{15}N,^{13}C)$ has in fact been measured for an oxaziridine derivative (36). The smallest known values of $^1K(C,C)$ or $^1J(C,C)$ also occur in strained ring systems. For example, in cyclopropane-carboxylic acid $^1J(C_1,C_2)$ = 10.05 Hz (30*d*) compared to a value of 34.6 Hz (42) in ethane.

For methylamine the calculations predict that $^1J(^{15}N,^{13}C)$ = −3.75 Hz, in good agreement with the observed value of −4.5 Hz. On

[2]The reduced coupling constant, $K(i,j) = \frac{4\pi^2}{h\gamma_i\gamma_j} J(i,j)$. The units of $K(i,j)$ are cm^{-3}.

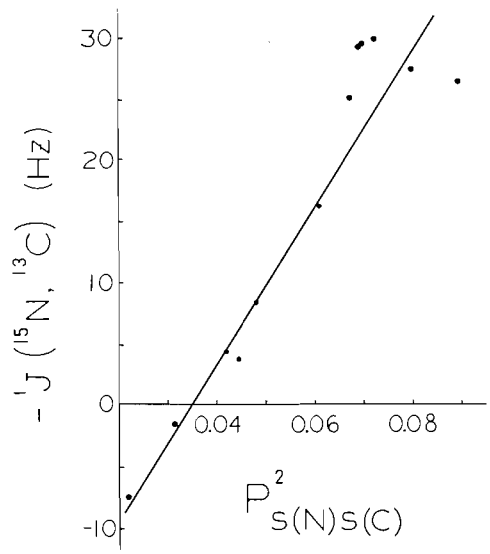

FIG. 2. Plot of calculated $^1J(^{15}N,^{13}C)$ values *vs.* $P^2_{s(N)s(C)}$ values for some of the amine derivatives given in Table 2. Three points fall at $^1J(^{15}N,^{13}C) \simeq -16.3$ Hz and $P^2_{s(N)s(C)} \simeq 0.061$.

protonation of methylamine, $^1J(^{15}N,^{13}C)$ is predicted to become more negative. This coupling constant has been observed to increase in magnitude upon the protonation of aliphatic amines. For example, upon protonation of 1-propylamine and quinuclidine, $^1J(^{15}N,^{13}C)$ increases in magnitude from 3.9 and 2.1 Hz respectively, to 4.4 and 4.8 Hz (39). Similarly, in glycine and alanine, $^1J(^{15}N,^{13}C)$ increases in magnitude when the nitrogen becomes protonated (43). However, in aniline, $^1J(^{15}N,^{13}C)$ is predicted to *decrease* in magnitude upon nitrogen protonation. This is confirmed by experiment since in both aniline and 4-nitroaniline, $^1J(^{15}N,^{13}C)$ decreases in magnitude upon protonation of the nitrogen. The calculated value of $^1J(^{15}N,^{13}C)$ in aniline, assuming a pyramidal nitrogen, is in fair agreement with experiment; however, the magnitude of the value calculated assuming a planar amino group is much too large. A pyramidal structure for aniline is known from microwave spectroscopy (44).

The INDO calculations predict the 4-nitro and 4-methyl substituent to have little or no influence on the $^1J(^{15}N,^{13}C)$ value in aniline provided the geometry of the amino fragment is fixed. Thus, the large observed value of $|^1J(^{15}N,^{13}C)|$ in 4-nitroaniline indicates an increase in the planarity of the amino group in **2** compared with that in **1**. There is also evidence from X-ray diffraction data that the amino group in 4-nitroaniline is approximately planar in the solid state (45).

The influence of nitrogen planarity on calculated values of $^1J(^{15}N,^{13}C)$ for both methylamine and formamide has been examined. As one goes from a pyramidal nitrogen to a planar amino group, calculated values of $P^2_{s(N)s(C)}$ and $|^1J(^{15}N,^{13}C)|$ increase in an approximately linear fashion.

For the compounds in Table 2, calculated values of $^1J(^{15}N,^{13}C)$ are also related to $P^2_{s(N)s(C)}$, however for some compounds there are significant deviations from linearity. See Fig. 2. Compounds containing triple bonds, *e.g.* $CH_3C{\equiv}N$, $CH_3N{\equiv}C$, and several other compounds including pyridine show considerable deviation from the curve shown in Fig. 2.

Calculated values of $^1J(^{15}N,^{13}C)$ for pyrrole and the pyridinium ion are too large in magnitude.

The calculations are successful in correctly predicting the magnitude of $^1J(^{15}N,^{13}C)$ in a derivative of benzonitrile-*N*-oxide where $^1J(^{15}N,^{13}C)_{obs} = 77.5 \pm 0.5$ Hz (12) while the calculated value in benzonitrile-*N*-oxide itself is -73.52 Hz.

Qualitatively, for compounds containing the $^{13}C{-}^{15}N{<}^{R}_{H}$ fragment, the calculations predict that as the nitrogen becomes more planar (sp^2-like in character), $^1J(^{15}N,H)$ and $^1J(^{15}N,^{13}C)$ both become more negative. Although exact agreement between observed and calculated $^1J(^{15}N,^{13}C)$ values (Tables 1 and 2, respectively) is not realized, the observed trends are qualitatively accounted for by the calculations. No attempt has been made to correct the calculations for variations in effective nuclear charge (11); the values of $s^2(N)_0$ and $s^2(C)_0$ are the same as those used by Pople and co-workers (11, 16–18).

Despite the qualitative agreement between theory and experiment observed in this study, the calculations are not capable of accounting for the negative sign observed for $^1J(^{15}N,^{13}C)$ in acetonitrile (11). In this case it is possible that the spin-dipolar and orbital mechanisms are important.

Can. J. Chem. Downloaded from www.nrcresearchpress.com by 210.87.254.105 on 09/05/12
For personal use only.

Can. J. Chem. Downloaded from www.nrcresearchpress.com by 210.87.254.105 on 09/05/12
For personal use only.

4. $^nJ(^{15}N,^{13}C)$ values where n = 2 or 3

For aniline-^{15}N in $CDCl_3$, $^2J(^{15}N,^{13}C) = -2.8 \pm 0.3$ Hz and $^3J(^{15}N,^{13}C) = -1.2 \pm 0.3$ Hz, in good agreement with the values previously determined (27). For the anilinium ion in deuterated trifluoroacetic acid we find $|^2J(^{15}N,^{13}C)| = 1.5 \pm 0.3$ Hz and $|^3J(^{15}N,^{13}C)| = 2.1 \pm 0.3$ Hz, respectively. The assignment of the ^{13}C nmr spectrum was made on the basis of the results given for the anilinium ion in methanesulfonic acid (29). The ^{15}N–^{13}C coupling constants do not appear to change sign upon protonation of the nitrogen.

The INDO–MO calculations predict $^2J(^{15}N,^{13}C)$ to increase from -0.5 to $+2.7$ Hz upon nitrogen protonation. $^2J(^{15}N,^{13}C)$ does in fact become more positive. $^3J(^{15}N,^{13}C)$ is predicted to decrease from -0.8 Hz in aniline to -3.3 Hz in the anilinium ion. The observed value of $^3J(^{15}N,^{13}C)$ actually does decrease, though only by about 0.9 Hz.

Again the calculations predict the observed experimental trends, however the magnitude of the changes predicted is too large.

It is of interest to point out that in *o*-anthranilic acid ($pD \geqslant 12$), $^3J(^{15}N,^{13}CO_2) \leqslant 0.5$ Hz. This represents another example of a very small $^3J(^{15}N,^{13}C)$ value (23, 46).

For acetanilide, $^2J(^{15}N,^{13}CH_3) = 9.0 \pm 0.3$ Hz, similar to the value observed in acrylamide (46). This large ^{15}N–^{13}C coupling constant, which is almost certainly negative, has been compared with the large observed values of: $^2J(^{13}C,^{13}C)$ in acetone, $^2J(^{13}C,H)$ in aldehydes, and $^2J(H,H)$ in formaldehyde (46).

A detailed discussion of solvent and substituent effects on $^nJ(^{15}N,^{13}C)$ values (where $n \geqslant 2$) will require more precise measurements than currently possible in our laboratory.

Conclusion

We have found some evidence that $^1J(^{15}N,^{13}C)$ values are linearly related to the corresponding $^1J(^{15}N,H)$ values for a number of amine derivatives. Further work will be necessary to establish the reliability and utility of the relationships proposed here.

Although initial INDO calculations considering only the Fermi contact mechanism showed poor agreement with experiment (11) the results presented here indicate that such calculations may be useful in qualitatively predicting observed trends in $^1J(^{15}N,^{13}C)$ for compounds containing the ^{13}C—$^{15}N\lessgtr^{H}_{R}$ fragment.

Acknowledgments

I would like to thank Dr. T. Schaefer for several interesting discussions, for allowing me to carry out some of the calculations in his laboratory and for the acetanilide-^{15}N sample. Also, I would like to thank Dr. H. Jakobsen for sending his experimental data on pyrrole. The assistance of Valerie Wasylishen in preparing the figures is also acknowledged. I am grateful to the National Research Council of Canada for financial support.

1. G. Binsch, J. B. Lambert, B. W. Roberts, and J. D. Roberts. J. Am. Chem. Soc. **86**, 5564 (1964).
2. A. J. R. Bourn and E. W. Randall. Mol. Phys. **8**, 567 (1964).
3. R. E. Wasylishen and T. Schaefer. Can. J. Chem. **51**, 3087 (1973).
4. T. Axenrod, M. J. Wieder, G. Berti, and P. L. Barili. J. Am. Chem. Soc. **92**, 6066 (1970).
5. T. Axenrod. *In* Nuclear magnetic resonance spectroscopy of nuclei other than protons. *Edited by* T. Axenrod and G. A. Webb. Wiley-Interscience, New York. 1974. p. 81.
6. T. Axenrod. *In* Nitrogen nmr. *Edited by* G. A. Webb and M. Witanowski. Plenum Publishing Co., New York. 1973. p. 261.
7. R. L. Lichter. *In* Determination of organic structures by physical methods. Vol. 4. *Edited by* F. C. Nachod and J. J. Zuckerman. Academic Press, New York. 1971. p. 195.
8. E. W. Randall and D. G. Gillies. *In* Progress in nuclear magnetic resonance spectroscopy. Vol. 6. *Edited by* J. W. Emsley, J. Feeney, and L. H. Sutcliffe. Pergamon Press, Oxford. 1971. p. 119.
9. T. Axenrod, P. S. Pregosin. M. J. Wieder, E. D. Becker, R. B. Bradley, and G. W. A. Milne. J. Am. Chem. Soc. **93**, 6536 (1971).
10. L. Paolillo and E. D. Becker. J. Magn. Reson. **2**, 168 (1970).
11. G. E. Maciel, J. W. McIver, Jr., N. S. Ostlund, and J. A. Pople. J. Am. Chem. Soc. **92**, 11 (1970).
12. M. Christl, J. P. Warren, B. L. Hawkins, and J. D. Roberts. J. Am. Chem. Soc. **95**, 4392 (1973).
13. (*a*) P. J. Krueger. Can. J. Chem. **40**, 2300 (1962); (*b*) L. Krause and M. A. Whitehead. J. Chem. Soc. B, 2433 (1971); (*c*) G. Cazzoli, D. Damiani, and D. G. Lister. J. Chem. Soc. Faraday Trans. II, **69**, 119 (1973); (*d*) A. Hastie, D. G. Lister, R. L. McNeil, and J. K. Tyler. J. Chem. Soc. Chem. Commun. 108 (1970); (*e*) D. Christen, D. Norbury, D. G. Lister, and P. Palmieri. J. Chem. Soc. Faraday Trans. II, **71**, 438 (1975); (*f*) F. J. Lovas, F. O. Clark, and E. Tiemann. J. Chem. Phys. **62**, 1925 (1975).

14. T. YONEMOTO, W. F. REYNOLDS, H. M. HUTTON, and T. SCHAEFER. Can. J. Chem. **43**, 2668 (1965).
15. R. E. WASYLISHEN, J. B. ROWBOTHAM, L. ERNST, and T. SCHAEFER. Can. J. Chem. **50**, 2575 (1972).
16. J. A. POPLE, J. W. MCIVER, Jr., and N. S. OSTLUND. Chem. Phys. Lett. **1**, 465 (1967).
17. J. A. POPLE, J. W. MCIVER, Jr., and N. S. OSTLUND. J. Chem. Phys. **49**, 2960 (1968); **49**, 2965 (1968).
18. J. A. POPLE and D. L. BEVERIDGE. Approximate molecular orbital theory. McGraw-Hill Book Co., New York. 1970.
19. M. R. BRAMWELL and E. W. RANDALL. J. Chem. Soc. Chem. Commun. 250 (1969).
20. E. W. RANDALL and J. J. ZUCKERMAN. J. Am. Chem. Soc. **90**, 3167 (1968).
21. R. J. CHUCK, D. G. GILLIES, and E. W. RANDALL. Mol. Phys. **16**, 121 (1969).
22. L. PAOLILLO and E. D. BECKER. J. Magn. Reson. **3**, 200 (1970).
23. R. DIBLASI and K. D. KOPPLE. J. Chem. Soc. Chem. Commun. 33 (1975).
24. J. M. BRIGGS, E. RAHKAMAA, and E. W. RANDALL. J. Magn. Reson. **12**, 40 (1973).
25. R. B. JOHANNESEN. J. Chem. Phys. **48**, 1414 (1968).
26. C. J. JAMESON and H. S. GUTOWSKY. J. Chem. Phys. **51**, 2790 (1969).
27. M. HANSEN and H. J. JAKOBSEN. Acta Chem. Scand. **26**, 2151 (1972).
28. J. F. HINTON, K. H. LADNER, and W. E. STEWART. J. Magn. Reson. **12**, 90 (1973).
29. G. L. NELSON, G. C. LEVY, and J. D. CARGIOLI. J. Am. Chem. Soc. **94**, 3089 (1972).
30. (*a*) J. L. MARSHALL and A. M. IHRIG. Org. Magn. Reson. **5**, 235 (1973); (*b*) G. E. MACIEL. *In* Nuclear magnetic resonance spectroscopy of nuclei other than protons. *Edited by* T. Axenrod and G. A. Webb. Wiley-Interscience, New York. 1974. p. 187; (*c*) J. L. MARSHALL, A. M. IHRIG, and D. E. MILLER. J. Mol. Spectrosc. **43**, 323 (1972); (*d*) F. J. WEIGERT and J. D. ROBERTS. J. Am. Chem. Soc. **94**, 6021 (1972).
31. S. BULUSU, J. R. AUTERA, and T. AXENROD. J. Chem. Soc. Chem. Commun. 602 (1973).
32. W. MCFARLANE. Q. Rev. Chem. Soc. **23**, 187 (1969).
33. A. C. Blizzard and D. P. SANTRY. J. Chem. Phys. **55**, 950 (1971).
34. W. MCFARLANE. Mol. Phys. **10**, 603 (1966).
35. W. MCFARLANE. J. Chem. Soc. A, 1660 (1967).
36. W. B. JENNINGS, D. R. BOYD, C. G. WATSON, E. D. BECKER, R. B. BRADLEY, and D. M. JERINA. J. Am. Chem. Soc. **94**, 8501 (1972).
37. H. J. C. YEH, H. ZIFFER, D. M. JERINA, and D. R. BOYD. J. Am. Chem. Soc. **95**, 2741 (1973).
38. R. L. LICHTER, D. E. DORMAN, and R. E. WASYLISHEN. J. Am. Chem. Soc. **96**, 930 (1974).
39. S. BERGER and J. D. ROBERTS. J. Am. Chem. Soc. **96**, 6757 (1974).
40. R. L. LICHTER and R. E. WASYLISHEN. J. Am. Chem. Soc. **97**, 1808 (1975).
41. R. E. WASYLISHEN and T. SCHAEFER. Can. J. Chem. **50**, 2989 (1972).
42. D. M. GRAHAM and C. E. HOLLOWAY. Can. J. Chem. **41**, 2114 (1963).
43. R. L. LICHTER and J. D. ROBERTS. J. Am. Chem. Soc. **93**, 5218 (1971).
44. (*a*) D. G. LISTER and J. K. TYLER. J. Chem. Soc. Chem. Commun. 152 (1966); (*b*) A. HATTA, M. SUZUKI, and K. KOZIMA. Bull. Chem. Soc. Jpn. **46**, 2321 (1973).
45. (*a*) K. N. TRUEBLOOD, E. GOLDISH, and J. DONOHUE. Acta Crystallogr. **14**, 1009 (1961); (*b*) D. L. HUGHES and J. TROTTER. J. Chem. Soc. A, 2181 (1971).
46. R. L. LICHTER, C. G. FEHDER, P. H. PATTON, J. COMBES, and D. E. DORMAN. J. Chem. Soc. Chem. Commun. 114 (1974).
47. B. E. LEY, A. E. FOTI, and S. M. ROTHSTEIN. J. Am. Chem. Soc. **97**, 2030 (1975).
48. M. SHIRO, M. YAMAKAWA, T. KUBOTA, and H. KOYAMA. J. Chem. Soc. Chem. Commun. 1409 (1968).

Can. J. Chem. Downloaded from www.nrcresearchpress.com by 210.87.254.105 on 09/05/12
For personal use only.

ERRATUM

Erratum: Esters chromiques dérivés d'alcools tertiaires

JEAN-CLAUDE RICHER ET JEAN-MARIE HACHEY
Département de chimie, Université de Montréal, Montréal, Québec H3C 3V1

Reçu le 10 décembre 1975

(Ref.: Can. J. Chem. **53**, 3087 (1975))

(*i*) La formule du chromate de di(méthyl-3 hexyl-3) illustrée dans le tableau 1 devrait se lire comme suit:

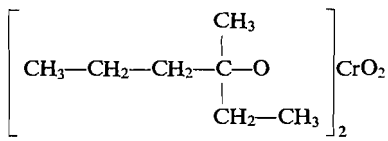

(*ii*) Le nom (chromate de di(diméthyl-2,3 hexyl-2)) devrait figurer immédiatement sous la formule de ce produit illustrée dans le tableau 1 à la page 3088.

Can. J. Chem. Downloaded from www.nrcresearchpress.com by 210.87.254.6 on 09/05/12
For personal use only.

Can. J. Chem. Downloaded from www.nrcresearchpress.com by 210.87.254.5 on 09/05/12
For personal use only.

Canadian Journal of Chemistry

Published by
THE NATIONAL RESEARCH COUNCIL OF CANADA

Journal canadien de chimie

Publié par
LE CONSEIL NATIONAL DE RECHERCHES DU CANADA

Volume 54 Number 6 March 15, 1976

Volume 54 numéro 6 15 mars 1976

The crystal structures of $Cu_{1.8}Se$, Cu_3Se_2, α- and γCuSe, $CuSe_2$, and $CuSe_2$II

ROBERT DONALD HEYDING AND RITCHIE MACLAREN MURRAY
Department of Chemistry, Queen's University, Kingston, Ontario K7L 3N6

Received October 20, 1975

ROBERT DONALD HEYDING and RITCHIE MACLAREN MURRAY. Can. J. Chem. **54**, 841 (1976).

The crystal structures of a number of copper selenides have been re-examined using X-ray powder diffraction intensity data. $|F_o|$ values for $Cu_{1.8}Se$ at room temperature (a = 5.765 Å) are satisfied by a model based on space group *Fm3m* with 4 Se atoms per unit cell on the *fcc* sites, 5.2 Cu atoms on the tetrahedral sites, and 2.0 Cu atoms on the trigonal sites in the Se sublattice. Cu_3Se_2 is tetragonal, $P\bar{4}2_1m$, a = 6.402, c = 4.279 Å, with Cu(1) in 2(*a*), Cu(2) in 4(*e*) with $x = 0.147 \pm 5$, $z = 0.781 \pm 9$, and Se in 4(*e*) with $x = 0.272 \pm 3$, $z = 0.264 \pm 7$. $CuSe_2$ has the orthorhombic *C*18 *marcasite* structure, *Pnnm*, a = 5.005, b = 6.182, c = 3.740 Å, with Cu in 2(*a*), and Se in 4(*g*) with $x = 0.184 \pm 1$, $y = 0.385 \pm 1$. $CuSe_2$II has the cubic *C*2 *pyrite* structure, *Pa*3, a = 6.116 Å, with Cu in 4(*a*), and Se in 8(*c*) with $x = 0.3891 \pm 5$.

Neither αCuSe nor γCuSe have the CuS *covellite* structure.

These results are discussed in some detail.

ROBERT DONALD HEYDING et RITCHIE MACLAREN MURRAY. Can. J. Chem. **54**, 841 (1976).

On a réexaminé les structures cristallines d'un certain nombre de séléniure de cuivre utilisant des données d'intensité de diffraction de rayons-X de poudre. Les valeurs de $|F_o|$ pour le $Cu_{1.8}Se$ à température de la pièce (a = 5.765 Å) sont satisfaites par un modèle basé sur un groupe d'espace *Fm3m* avec 4 atomes de sélénium par la maille unitaire situés sur les sites *fcc*, 5.2 atomes de cuivre sur les sites tétraédriques et de 2.0 atomes de cuivre sur les sites trigonaux dans le sous réseau du sélénium. Le Cu_3Se_2 est tétragonal $P\bar{4}2_1m$, a = 6.402, c = 4.279 Å avec Cu(1) dans la position 2(*a*), Cu(2) dans la position 4(*e*) avec $x = 0.147 \pm 5$, $z = 0.781 \pm 9$ et le sélénium dans la position 4(*e*) avec $x = 0.272 \pm 3$, $z = 0.264 \pm 7$. Le $CuSe_2$ a la structure orthorhombique de la *marcasite* *C*18, *Pnnm*, a = 5.005, b = 6.182, c = 3.740 Å avec le cuivre dans la position 2(*a*) et le sélénium dans la position 4(*g*) avec $x = 0.184 \pm 1$, $y = 0.385 \pm 1$. Le $CuSe_2$II a la structure cubique de la *pyrite* *C*2, *Pa*3, a = 6.116 Å avec le cuivre dans la position 4(*a*) et le sélénium dans la position 8(*c*); $x = 0.3891 \pm 5$.

Ni l'αCuSe ni le γCuSe n'ont la structure *covellite* du CuS.

On discute de ces résultats en détail.

[Traduit par le journal]

Introduction

Compounds in the copper/selenium system exhibit a variety of phenomena which have been of some interest in recent years. Three of the eight solid phases exist as minerals (*berzelianite*, $Cu_{2-x}Se$; *umangite*, Cu_3Se_2; *klockmannite*, αCuSe). Earlier confusion regarding the composition of berzelianite has been resolved, but the structure of klockmannite defies analysis. This compound exhibits a first order transformation just above room temperature followed immediately by a second order transformation which terminates when the original structure is regained. The selenium-rich phase $CuSe_2$ exhibits a classical *marcasite* → *pyrite* transformation under pressure. The copper-rich phase

Can. J. Chem. Downloaded from www.nrcresearchpress.com by 210.87.254.5 on 09/05/12
For personal use only.

$Cu_{2-x}Se$ appears to belong to a class of M_3Y_2 defect structures in which both trigonal and tetrahedral sites are occupied at random by metal ions in an *fcc* chalcogen sublattice. The electrical properties of this phase have been the subject of numerous studies and are undoubtedly related to the structure and the remarkably high mobility of copper ions in the lattice.

We reported recently on a study of the phase relationships in this system (1). Using specimens chosen from those prepared for the phase studies, we have examined the crystal structures of $Cu_{2-x}Se$, αCuSe, γCuSe, $CuSe_2$, and $CuSe_2$II using X-ray powder diffraction data and the least squares refinement program developed by Finger (2). A specimen of *umangite* was used to redetermine the atom positions in Cu_3Se_2. The results of these calculations are given in this paper.

Experimental

Intensity data were obtained from integrating Debye-Scherrer or Guinier – de Wolff powder diffraction cameras using monochromated CuK_α radiation (λ = 1.5418 Å) (3). Non-integrated high temperature Guinier–Lenne patterns were used to estimate intensities for γCuSe. Relative line intensities were estimated using film density wedges and a recording microphotometer. Corrections were applied for polarization of the incident radiation and for film envelope absorption. The Guinier – de Wolff specimen windows were very lightly dusted with −400 mesh powder, and sample absorption corrections were not applied (see further comments in the discussion on $CuSe_2$II below).

All observed reflections ($I/I_m \geq 1$) were given unit weight provided they could be indexed unambiguously; overlapping and unobserved reflections were given zero weight in the initial refinement. Anomalous dispersion and extinction corrections were not applied. The Hartree–Fock atomic scattering factor equations of Cromer and Mann (4) were used. Thermal vibrations were assumed to be isotropic. The agreement indices recorded here are unweighted ($R = \sum|F_o| - |F_c|/\sum|F_o|$) and the standard deviations are those derived by the program from the diagonal elements of the inverse matrix. The structural models were refined by the Burroughs B6700 computer in the Computing Centre at Queen's University.

Results and Discussion

$Cu_{2-x}Se$

The $Cu_{2-x}Se$ phase is related to the *B*4 (ZnO) and C1 (CaF_2) structures. Four selenium atoms form a simple face centred cubic sublattice with six to eight copper atoms (depending on the composition) occupying the octahedral, tetrahedral, and trigonal sites, more or less at random, in the selenium sublattice. Structure factor calculations by Rahlfs (5) and Borchert (6), and more recently by Stevels and Jellinek (7, 8), indicate that one set of tetrahedral sites, as in the *B*4 structure, are completely occupied. Stevels' model of the high temperature form of $Cu_{1.80}Se$ places 0.6 of the remaining 3.2 copper atoms on octahedral sites, and the balance in pseudo-trigonal sites which are displaced slightly from the face of the tetrahedron towards an unoccupied tetrahedral site.

The Finger program permits refinement of site occupancies as well as positional and temperature parameters, and is therefore an excellent vehicle for re-examining defect structures of this kind. Observed structure factors for 12 independent reflections were obtained for $Cu_{1.80}Se$ from integrated Debye–Scherrer patterns at 298 K (a = 5.765 Å). Some of the models refined by the computer program allowed for variation in occupancies at four sites, in one positional parameter, and in two temperature parameters. In view of the small number of observed structure factors, the results must be regarded with some skepticism, although, in the event, some models containing only two or three variables refined well.

The first series of models was based on space group $F\bar{4}3m$ (Borchert (6)) with atoms in the following positions:

Atom	Site	Position	
Cu(4)	16(*e*)	$x,x,x;x,\bar{x},\bar{x}$	(trigonal sites)
Cu(3)	4(*d*)	3/4,3/4,3/4	(tetrahedral sites)
Cu(2)	4(*c*)	1/4,1/4,1/4	(tetrahedral sites)
Cu(1)	4(*b*)	1/2,1/2,1/2	(octahedral sites)
Se	4(*a*)	0,0,0	

Some of the models are described in Table 1, with the results of the computer refinement for each.

Models in which the copper atoms were confined to octahedral and tetrahedral sites (Trials 1 and 2, Table 1) did not refine well, giving unreasonably large temperature factors for Cu and relatively large agreement indices (R). Refinements based on models suggested in the literature with 4 atoms in one set of tetrahedral sites and the remaining 3.2 atoms distributed over the remaining lattice sites (Trials 3 and 4) indicated that the occupancy of the octahedral

TABLE 1. Summary of results of structure factor refinement on selected models for $Cu_{1.80}Se$*

(*a*) Series 1, space group $F\bar{4}3m$; 4 Se atoms in 4(*a*)

Trial	Copper site occupancy, atoms/unit cell 4(*b*)	4(*c*)	4(*d*)	16(*e*)	*x* (in 16(*e*))	B_{Se} (Å^2)	B_{Cu} (Å^2)	*R*
1	2.32	*4.00*	0.88			1.3±5	5.9±1.9	0.114
2	1.90	*3.20*	2.10			1.5±7	9.2±2.9	0.158
3	0.13	*4.00*	1.56	1.51	0.67±1	2.3±2		0.047
4	0.08	*4.00*	1.68	1.44	0.67±1	2.2±6	2.4±9	0.048
5	0.04	2.71	2.61	1.82	0.67±1	1.9±4	2.6±5	0.030
6		*4.00*	1.63	1.57	*0.667*	2.2±6	2.3±9	0.050
7		*3.20*	2.08	1.91	*0.667*	2.0±3	2.5±5	0.036

(*b*) Series 2, space group $Fm3m$; 4 Se atoms in 4(*a*)

Trial	Copper site occupancy, atoms/unit cell 8(*c*)	32(*f*)	*x* (in 32(*f*))	B_{Se} (Å^2)	B_{Cu} (Å^2)	*R*
8	5.05	2.15	*0.333*	*2.0*	*2.3*	0.034
9	5.18	2.02	*0.333*	2.0±3	2.5±4	0.031
10	4.98	2.22	0.327±7	1.9±3	2.4±5	0.035

*Numbers in italics fixed during trial refinement, $R = \Sigma||F_o| - |F_c||/\Sigma|F_o|$.

sites is small, and that the copper atoms in positions 16(*e*) are almost exactly in the trigonal holes of the selenium sublattice ($x = 2/3$). These results were confirmed in the refinement of the completely general model in which all parameters were allowed to vary, constrained only by the total number of copper atoms in the unit cell (Trial 5). Although this trial produced the smallest agreement index of all of the models examined, the refinement gives a sum of occupancies in 4(*d*) and 16(*e*) greater than four, implying that adjacent trigonal and tetrahedral sites, or two adjacent trigonal sites, may be occupied simultaneously. Neither of these conditions is possible.

In subsequent models the positional parameter of the atoms in 16(*e*) was fixed at 2/3, and to ensure that no tetrahedron need be occupied by more than one copper atom, the occupancies of the 4(*c*) sites were fixed at values between 4.0 and 3.2. Results for the limiting models are given in Trials 6 and 7. The values of *R* varied monotonically with 4(*c*) occupancy for models not recorded in Table 1.

The model described in Trial 7 satisfies the diffraction intensities of overlapping and unobserved reflections as well as those used in the structure analyses.[1] With 3.2 copper atoms per unit cell in the tetrahedral sites at 1/4,1/4,1/4, the remaining 4 atoms are divided essentially equally between the tetrahedral and trigonal sites of the tetrahedra centred on 3/4,3/4,3/4.

Assuming the refinement process is credible, there seems to be no chemical rational for the non-equivalence of tetrahedral sites. Accordingly a second series of models was examined in which these sites are equivalent. These are based on space group $Fm3m$ (No. 225) with atoms in the following positions:

Atom	Site	Position
Cu(2)	32(*f*)	±(*x*,*x*,*x*; *x*,$\bar{x}$,$\bar{x}$ ↻) (trigonal sites)
Cu(1)	8(*c*)	1/4,1/4,1/4; 3/4,3/4,3/4 (tetrahedral sites)
Se	4(*a*)	0,0,0

The results of the refinements are summarized in Table 1, Trials 8–10. The model described in Trial 9 satisfies the diffraction intensities of overlapping and unobserved reflections as well as those used in the structure analysis.[1] The

[1]Tables of $|F_o|$ and $|F_c|$ values are available, at nominal charge, from Depository of Unpublished Data, CISTI, National Research Council of Canada, Ottawa, Canada, K1A 0S2.

Can. J. Chem. Downloaded from www.nrcresearchpress.com by 210.87.254.5 on 09/05/12
For personal use only.

Can. J. Chem. Downloaded from www.nrcresearchpress.com by 210.87.254.5 on 09/05/12
For personal use only.

small shift in Cu(2) positions from the 'ideal' trigonal site on refinement (Trial 10) is not significant. With 5.2 Cu on tetrahedral sites and the balance on trigonal sites the model is as reasonable as any based on $F\bar{4}3m$. We favor this structure over those represented by Trials 5 and 7 because the tetrahedral sites are equivalent.

The conclusion to be drawn from the refinement is that the best agreement between $|F_o|$ and $|F_c|$ is obtained when the electron density at the tetrahedral sites is equivalent to 0.65 copper atoms, and to 0.063 copper atoms at trigonal sites. If this is interpreted as a random distribution of 5.2 and 2.0 Cu atoms per unit cell on tetrahedral and trigonal sites respectively, the following applies:

Atom pair	Distance*
Cu(1)—Cu(1)	3.6 nn at 2.88 Å
Cu(1)—Cu(2)	1.7 nn at 2.50 Å
Cu(2)—Cu(2)	1 nn at 2.35 or 2.50 Å

*nn = nearest neighbour.

When 5 tetrahedral sites are occupied by Cu(1) in the unit cell, 20 of the 36 trigonal sites, those in the faces of the 5 tetrahedra, cannot also be occupied. When a trigonal site in one of the 'vacant' tetrahedra is occupied, five more tetrahedral sites cannot be occupied; three are in the same tetrahedron at 1.35 Å and two in adjacent tetrahedra at 1.93 Å. The six remaining sites available to the second Cu(2) atom are at 2.35 and 2.50 Å.

The Cu(1)—Se distance is 2.50 Å, and the Cu(2)—Se distance 2.35 Å.

This model applies to $Cu_{1.80}Se$ at room temperature. A number of authors refer to low and high temperature modifications of $Cu_{2-x}Se$, manifest in part by abnormal lattice thermal expansion coefficients below *ca.* 523 K (6, 7), anomalous behaviour in magnetic susceptibility, and variation in diffraction intensities (7). This transition has not been evident in our samples (1). In the most recent of a comprehensive series of papers by Ogorelec and co-workers (9), reference is made to the disappearance of the (200) reflection and the appearance of the (422) reflection with increasing temperature. In our patterns the (200) reflection is very weak ($I/I_m = 2.7$) at all temperatures, while the intensity of the (422) reflection is relatively strong ($I/I_m = 22.1$) and temperature independent at least to 570 K. Borchert assigns a relative intensity of 30 to this reflection at 293 K. This contradictory evidence indicates that the structure of $Cu_{2-x}Se$ may be history or trace impurity dependent, or both.

The electrical conductivity of $Cu_{2-x}Se$ increases with decreasing copper concentration and the temperature dependence is metallic. This behaviour is generally attributed to a 'self doping' effect. The copper vacancies are assumed to create low-lying acceptor levels in the band gap, all of which are occupied at temperatures at which the phase is stable, creating a number of holes in the valence band equal to the number of vacancies. Presumably these vacancies must now refer to tetrahedra which contain no copper atom either in the tetrahedral site or in one of the trigonal sites. Since no tetrahedron may contain more than one copper atom, the stoichiometric composition is Cu_2Se (*i.e.*, $x = 0$). At this composition the compound should be non-metallic. This does not appear to be so (10–12). However if the acceptor levels are associated with the copper atoms in trigonal sites rather than vacancies (or as well as vacancies), the conductivity need not approach zero at the stoichiometric composition, since there is no reason to believe that only tetrahedral sites in Cu_2Se are occupied.

Cu_3Se_2

Structure factor data for Cu_3Se_2 were obtained from integrated Guinier – de Wolff patterns of *umangite* rather than synthetic Cu_3Se_2 because of better definition of higher order reflections from the mineral. Samples were selected from a Beaverlodge specimen containing *malachite* and *albite* as well as the selenide. The tetragonal unit cell dimensions were $a = 6.4024 \pm 5$ and $c = 4.2786 \pm 4$ Å, somewhat larger than those of synthetic specimens (1). Electron probe analysis on polished specimens indicated 0.5–1.0% Si (probably carry-over from the silicate phase during polishing) and trace amounts ($\leq 0.1\%$) of Fe, Ag, S, and Cl.

Morimoto and Koto (13) have shown by single crystal studies that Cu_3Se_2 belongs to space group $P\bar{4}2_1m$, with atoms in the following positions:

Atom	Site	Position
Se	4(*e*)	$\left.\begin{matrix}x,1/2+x,z;\ \bar{x},1/2-x,z\\ 1/2+x,\bar{x},\bar{z};\ 1/2-x,x,\bar{z}\end{matrix}\right\}$ $x=0.275$ $z=0.250$
Cu(2)	4(*e*)	
Cu(1)	2(*a*)	0,0,0; 1/2,1/2,0

Can. J. Chem. Downloaded from www.nrcresearchpress.com by 210.87.254.5 on 09/05/12
For personal use only.

These atom positions were used as initial values in the Finger refinement using intensity data for 26 reflections. The final values, giving an agreement index $R = 0.061$, were:

Atom	Position
Se	$x=0.272\pm3$, $z=0.264\pm7$; $B=1.9\pm6$ Å^2
Cu(2)	$x=0.147\pm5$, $z=0.781\pm9$; $B=2.3\pm5$ Å^2

Four observed reflections were not included in the refinement because of overlap or unusually large variation in intensities from specimen to specimen. Agreement between $|F_o|$ and $|F_c|$ for these reflections was satisfactory.[1] Calculated structure factors for twelve reflections which were not observed indicated that three should have been observable with $1 \leq I/I_m \leq 3$, although two of these would very nearly overlap with relatively strong reflections.

The results confirm the structure proposed by Morimoto and Koto, with only minor differences in interatomic distances. Each Cu(1) is surrounded by four Cu(2) at 2.62 Å and four Se at 2.54 Å; each Cu(2) by four Se at 2.36, 2.46, 2.46, and 2.48 Å; two Cu(1) at 2.62 Å and one Cu(2) at 2.66 Å. Okamoto *et al.* (14) have described the structure in terms of the distribution of copper atoms in a distorted *fcc* sublattice of Se atoms. Stevels' description (7) is based on a distorted *bcc* Se sublattice with Cu atoms in the distorted tetrahedral sites. These descriptions may be misleading in two senses. The first is that the number of 'holes' in the Se sublattices is greater than the number of Cu atoms present, and the ordering of the occupancies is not readily apparent. The second is that, as Morimoto and Koto observed, the structure is determined primarily by interactions between copper atoms.

The following is an alternative description. Each Cu(1) atom is surrounded by four Cu(2) atoms at the corners of a distorted tetrahedron. Each Cu(2) atom is shared by two tetrahedra, and has one other Cu(2) atom as a neighbor. Sheets of Cu tetrahedra are formed which are parallel to (001). In each unit cell the copper atoms form eight distorted semi triakis tetrahedral vacancies defined by four Cu(2) atoms and two Cu(1) atoms as shown in Fig. 1. Half of these sites are occupied by Se in opposite 'octants' of the unit cell.

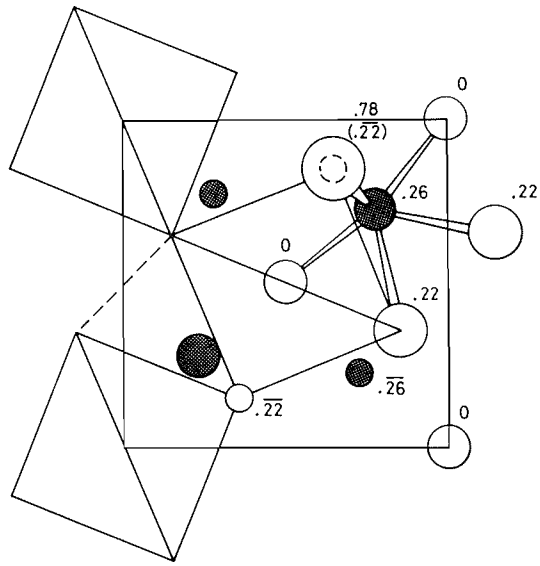

FIG. 1. Projection of atom positions in Cu_3Se_2 on (001) showing the tetrahedral network of copper atoms and the coordination of six copper atoms to a selenium atom. Copper and selenium are represented by open and shaded circles respectively.

α- and γCuSe

αCuSe (*klockmannite*) is generally regarded as isostructural with CuS (*covellite*), which Berry (15) has shown belongs to space group $P6_3/mmc$, with atoms on the following positions:

Atom	Site	Position
Cu(2)	4(*f*)	1/3,2/3,*z*
S(2)	4(*e*)	0,0,*z*
Cu(1)	2(*d*)	1/3,2/3,3/4
S(1)	2(*c*)	1/3,2/3,1/4

Berry's assignment of CuSe to the same structure was made with considerable reservation. Early (16) observed very weak reflections in single crystal patterns indicating a twelve-fold multiplicity in the *a* axis. The problem of the structure of the ordered modification of αCuSe has been discussed by Taylor and Underwood (17), by Lipmann (18), and by Elliott *et al.* (19). We did not observe reflections from newly prepared specimens which could not be indexed on a simple hexagonal cell with $a = 3.934$, $c = 17.217$ Å, although extra reflections appeared in aged specimens (1). This slow ordering process, also

Can. J. Chem. Downloaded from www.nrcresearchpress.com by 210.87.254.5 on 09/05/12
For personal use only.

observed by Berry and by Stevels (7), suggested that αCuSe might have the *covellite* structure when first formed, that is, on cooling from temperatures above the α–β transition point.

In this study, intensities for 26 unambiguous reflections were obtained from integrated Guinier – de Wolff patterns in which no superlattice reflections could be observed. Berry's values of z_{Se} and z_{Cu} were used to begin the calculations.

These data did not refine well. The minimum agreement index R obtained for observed reflections was 0.24. Calculated structure factors for reflections from three of four (*hk*0) planes, which are independent of the values of z for Cu(2) and Se(2) in the model, were much smaller than those observed. In addition, the refinements showed that some of the unobserved reflections, particularly the (002), (004), and (203), should be clearly visible.

Trial refinements using Early's intensity data resulted in an R value of 0.41, with the same discrepancies.

We are satisfied that αCuSe is not isostructural with *covellite*. A number of alternate models based on simple modifications of the *covellite* structure were examined and found to have little merit. Structure factors calculated for the model suggested by Arunsingh *et al.* for films of CuSe produced by pulse annealing (20) did not agree with our observed values.

It is unlikely that the correct structure can be determined from powder diffraction data.

γCuSe, which is stable above 393 K, is also hexagonal with similar unit cell dimensions (a = 3.984, c = 17.288 Å at 430 K) and a diffraction pattern very similar to that of αCuSe. To see if this modification might be isostructural with *covellite*, intensities of the nine observable reflections at 430 K were estimated from Guinier – Lenne patterns. While the R index for the refinement based on these reflections was promising (0.14), large $|F_c|$ values for several unobserved reflections indicated that the model was not correct.

$CuSe_2$

The low pressure modification of $CuSe_2$ has the orthorhombic *marcasite* structure (*C*18, *Pnnm*, a = 5.005, b = 6.182, c = 3.740 Å) with atoms on the following positions:

Atom	Site	Position
Se	4(*g*)	±(x,y,0); ±(1/2+x,1/2−y,1/2); x=0.176, y=0.387
Cu	2(*a*)	0,0,0; 1/2,1/2,1/2

The atom positions were determined by Gattow (21, 22).

Intensity data for 26 unambiguous reflections were obtained from integrated Guinier – de Wolff patterns. Refinement led to the following values of the several variables, with an agreement index R = 0.041:

Atom	Position
Se	x=0.184±1, y=0.385±1; B=1.6±3 Å^2
Cu	B=3.1±4 Å^2

Calculated structure factors for ten overlapping or weak reflections were in good agreement with observed values with one exception ((410), (331) overlap, I/I_m observed ≈1, calculated 7). $|F_c|$ values for seven reflections which were not observed indicated that all should be below minimum observable intensity.[1]

The values of the fractional coordinates for Se are in excellent agreement with those determined recently by Kjekshus *et al.* via powder neutron diffraction (23).

In this structure each copper atom is surrounded by six selenium atoms at 2.55 Å in a distorted octahedral arrangement. Each selenium is in a distorted tetrahedral configuration with three copper neighbors and with one selenium neighbor at 2.33 Å. The minimum Cu—Cu distance is 3.74 Å.

$CuSe_2II$

The high pressure modification of $CuSe_2$ has the pyrite *C*2 structure (*Pa*3) (24) with atoms in the following positions:

Atom	Site	Position
Se	8(*c*)	±(x,x,x); ±(1/2+x,1/2−x,$\bar{x}$); ±($\bar{x}$,1/2+x,1/2−x); ±(1/2−x,$\bar{x}$,1/2+x)
Cu	4(*a*)	0,0,0; 1/2,1/2,0

Integrated Guinier – de Wolff intensities for 15 unambiguous reflections were used in the initial

TABLE 2. Summary of interatomic distances (Å) and coordination numbers in parentheses

Phase	Atom	Interatomic distance Cu—Cu	Cu—Se	Se—Se
$Cu_{1.8}Se$	Cu(1)	2.50 (1.7 Cu(2)) 2.88 (3.6 Cu(1))	2.50 (4)	4.08
	Cu(2)	2.35 or (1.0 Cu(2)) 2.50	2.35 (3)	
Cu_3Se_2	Cu(1)	2.62 (4 Cu(2))	2.54 (4)	3.79
	Cu(2)	2.62 (2 Cu(1)) 2.66 (1 Cu(2))	2.36 to 2.48 (4)	
$CuSe_2$		3.74 (2) 4.39 (8)	2.55 (6)	2.33 (1)
$CuSe_2II$		4.32 (12)	2.57 (6)	2.35 (1)

refinement (a = 6.116 Å). From this refinement $|F_c|$ values for four sets of overlapping pairs of reflections were then used to divide the total intensities of each pair so that further refinement could be made on 23 $|F_o|$ values. The final values of the parameters giving an agreement index R = 0.032 were[1]

Atom	Position
Se	$x = 0.3891 \pm 5$; $B = 1.6 \pm 3$ Å^2
Cu	$B = 2.4 \pm 3$ Å^2

Refinement in which the temperature coefficients were made equal led to values of x and B of 0.389 ± 7 and 1.9 ± 3 Å^2. Refinement on $|F_o|$ values corrected for sample absorption (estimated by a laborious process of measuring particle size distributions on each specimen window and applying spherical particle absorption corrections (3)) led to the same value of x and slightly larger temperature coefficients.

In this modification each Cu atom has six Se neighbors at 2.57 Å in a distorted octahedral configuration. Each Se atom has three Cu and one Se (at 2.35 Å) at the corners of a distorted tetrahedron.

General Discussion

The nearest-neighbor interatomic distances in these compounds are summarized in Table 2. Copper–copper interactions are important components of the two copper-rich selenides, and apparently dominate in Cu_3Se_2. It is remarkable that of the four compounds only Cu_3Se_2 exhibits Curie–Weiss type paramagnetism consistent with the presence of d^9 ions; the others are either diamagnetic or show weak temperature independent paramagnetism (14, 24). The majority of the Cu—Se distances in all four compounds lie between 2.46 and 2.57 Å, the shorter ranges predominating in the copper-rich structures. Both $Cu_{1.8}Se$ and Cu_3Se_2 contain very short Cu—Se distances of 2.35 Å, although there is only one such distance per Se atom in Cu_3Se_2 while in $Cu_{1.8}Se$ each trigonal copper site which is occupied involves three such interactions.

The *marcasite/pyrite* pressure dependent transformation has been observed for FeS_2, $FeSe_2$, $FeTe_2$, $CoSe_2$, $CoTe_2$, and $NiAs_2$ as well as $CuSe_2$ (25). These *marcasites* are all 'normal' *marcasites*, *i.e.*, Class B in Kjekshus' notation (23). (In all probability $NiSb_2$ will undergo the same transformation.) In each of these compounds the same electronic configuration for the metal ion is to be expected in both modifications. The dominant feature in both structures is the presence of pairs of chalcogen atoms at distances comparable to the interatomic distances in the elements themselves. For $CuSe_2$ the Se—Se distances are essentially equal to the intrachain distance of 2.32 Å in hexagonal selenium. The distortion of the octahedral configuration of Se about Cu is dictated by the existence of these pairs and the requirement for tetrahedral configuration about each Se atom. The degree of distortion of the polyhedra are indicated by the

Can. J. Chem. Downloaded from www.nrcresearchpress.com by 210.87.254.5 on 09/05/12
For personal use only.

TABLE 3. Summary of bond angles in the *marcasite* and *pyrite* modifications of $CuSe_2$

Configuration	Bond	Angle	
		Marcasite	*Pyrite*
Octahedral	Se—Cu—Se	88.0°, 92.0°, 180°	86.0°, 94.0°, 180°
Tetrahedral	Cu—Se—Cu	119.0° (2), 94.2°	114.9°
Tetrahedral	Cu—Se—Se	108.8° (2), 106.5°	103.3°

interatomic distances in Table 2 and the bond angles in Table 3. The distortion of the octahedra is greater in the *pyrite* modification (4°) than in the *marcasite* (2°), while the reverse is true for the tetrahedra (6° and 15° max., respectively). The energy associated with the further distortion of the octahedra during the *marcasite* → *pyrite* transformation is balanced in part by the improvement in the tetrahedral configuration, and by the decrease in molar volume from 34.86 to 34.45 $cm^3\ mol^{-1}$.

Acknowledgements

We are indebted to Dr. Douglas Scott for instruction and assistance in the use of the Finger program. Most of the technical operations were performed by Mr. Brian Forbes. The microprobe analyses of *umangite* were done for us by Mr. David Kempson. This work was supported by an operating grant from the National Research Council of Canada.

1. R. M. MURRAY and R. D. HEYDING. Can. J. Chem. **53**, 878 (1975).
2. L. W. FINGER. Carnegie Inst. Wash. Yearbook. **67**, 216 (1967).
3. R. D. HEYDING and R. J. C. BROWN. Rev. Sci. Instr. **43**, 1602 (1972).
4. D. T. CROMER and J. B. MANN. Acta Crystallogr. A**24**, 321 (1968).
5. P. RAHLFS. Z. Phys. Chem. B**31**, 157 (1936).
6. W. BORCHERT. Z. Kristallogr. **106**, 5 (1945).
7. A. L. N. STEVELS. Philips Res. Rep. Suppl. No. 9, 124 pp. (1969).
8. A. L. N. STEVELS and F. JELLINEK. Recl. Trav. Chim. **90**, 273 (1971).
9. A. TONJEC, Z. OGORELEC, and B. MESTNIK. J. Appl. Crystallogr. **8**, 375 (1975).
10. G. A. EFENDIEV, M. YA. BAKIROV, and E. S. ZARDOVA. Izv. Akad. Nauk SSSR, Neorg. Mater. **5**, 1460 (1969).
11. R. ROUTIE, M. SUDRES, and J. MAHENC. J. Chim. Phys. Physicochem. Biol. **67**, 1013 (1970).
12. Z. OGORELEC, B. MESTNIK, and J. TURKOVIC. Solid State Commun. **12**, 857 (1973).
13. N. MORIMOTO and K. KOTO. Science, **152**, 345 (1966).
14. K. OKAMOTO, S. KAWAI, and R. KIRIYAMA. Jpn. J. Appl. Phys. **8**, 718 (1969).
15. L. G. BERRY. Am. Mineral. **39**, 504 (1954).
16. J. W. EARLY. Am. Mineral. **34**, 435 (1949).
17. C. A. TAYLOR and F. A. UNDERWOOD. Acta Crystallogr. **13**, 361 (1960).
18. F. LIPMANN. Neues Jahrb. Mineral. Monatsh. 99 (1962).
19. J. A. ELLIOTT, J. A. BICKNELL, and R. G. COLLENGE. Acta Crystallogr. B**25**, 2420 (1969).
20. ARUNSINGH, O. N. SRIVASTAVA, and B. DAYAL. Acta Crystallogr. B**28**, 635 (1972).
21. G. GATTOW. Naturwissen. **52**, 258 (1965).
22. G. GATTOW. Z. Anorg. Allg. Chem. **340**, 312 (1965).
23. A. KJEKSHUS, T. RAKKI, and A. F. ANDRESEN. Acta Chem. Scand. A**28**, 996 (1974).
24. T. A. BITHER, R. J. BOUCHARD, W. H. CLOUD, P. C. DONOHUE, and J. W. SIEMONS. Inorg. Chem. **7**, 2208 (1968).
25. F. HULLIGER. *In* Structure and bonding. Vol. 4. *Edited by* C. K. Jorgensen *et al.* Springer-Verlag. 1968. p. 83.

Can. J. Chem. Downloaded from www.nrcresearchpress.com by 210.87.254.5 on 09/05/12
For personal use only.

C-Nucleosides and related compounds. VI. Carbocyclic analogues of *C*-nucleosides: synthesis and derivatives of some useful intermediates

GEORGE JUST, GRANT READER,[1] AND BERNADETTE CHALARD-FAURE
Department of Chemistry, McGill University, Montreal, Quebec H3C 3G1

Received July 7, 1975

GEORGE JUST, GRANT READER, and BERNADETTE CHALARD-FAURE. Can. J. Chem. **54**, 849 (1976).

The Diels–Alder adduct of cyclopentadiene and β-bromo acrylic acid **1** was converted to D,L-*exo*-6,7-(dihydroxy-di-*O*-isopropylidene)-2-hydroxy-3-oxabicyclo[3.2.1]octane (**9**) in an eight-step sequence and a 24% yield based on **1**. Alternatively, the hemiacetal **9** was obtained in five steps and 22% yield from norbornadiene through the intermediate lactone **11**. The thiosemicarbazone and semicarbazone of **9** were prepared. The synthesis of the free aldehyde **13** as well as that of the Wittig reaction products **12** and **19** are described.

GEORGE JUST, GRANT READER et BERNADETTE CHALARD-FAURE. Can. J. Chem. **54**, 849 (1976).

La réaction de l'acide β-bromo acrylique **1** sur le cyclopentadiène conduit au produit d'addition de Diels–Alder correspondant; ce dernier peut être transformé en huit étapes avec un rendement global de 24% basé sur **1** en D,L-*exo*-(dihydroxy-di-*O*-isopropylidène-6,7 hydroxy-2-oxa-3 bicyclo[3.2.1]octane **9**. L'hémiacétal **9** a également été obtenu en cinq étapes avec un rendement de 22% à partir du norbornadiène et en passant par la lactone **11**. On décrit la préparation de la thiosemicarbazone et de la semicarbazone de **9** ainsi que la synthèse de l'aldéhyde **13** et des produits **12** et **19** provenant de réactions de Wittig.

In a preliminary communication (1), we reported the synthesis of lactol **9** and lactone **11**. In this paper, we are giving a full account of this work and the description of a second pathway leading to **9** and **11**. The syntheses of related derivatives and of the free aldehyde **13** are also described. These compounds are potential intermediates for the preparation of carbocyclic analogues of *C*-nucleosides.

Condensation of β-bromoacrylic acid **1** with cyclopentadiene in benzene (2) gave the Diels–Alder adduct **2** in 75% yield. This compound was almost exclusively the *endo* carboxylate isomer (3). Treatment of the acid **2** with diazomethane gave, in essentially quantitative yield, the ester **2***a* which was oxidized to the diol **3** with hydrogen peroxide and a catalytic (4) amount of osmium tetroxide. The diol **3**, mp 145 °C, was obtained in 50% yield. The stereochemistry of the hydroxy groups in **3** was assigned on the basis of previous work (4, 5) which had shown the preferential *exo*-hydroxylation of bicyclic[2.2.1] systems of type **2**.

Attempts to hydroxylate the acid **2** directly were unsuccessful. Crude diol **3** was converted to its isopropylidene derivative **3***a* in 60% yield based on adduct **2**. Elimination of hydrogen bromide by treatment of **3***a* with 1,5-diazabicyclo[5.4.0]undec-5-ene afforded the olefinic ester **4**. Upon treatment of diol **3** with acetic anhydride – pyridine, the olefinic diacetate **4***a* was obtained. Similarly, the olefinic carbonate derivative **4***b* was the major product from the reaction of diol **3** with phosgene in pyridine. It was not possible to obtain a pure sample of **3***a* for elemental analysis, although the compound was otherwise well characterized. Attempts at purification by column chromatography, on either silica gel or alumina (activity I or III) always gave some elimination product **4**. The α,β-unsaturated ester **4** could in fact be prepared by passing **3***a* through an alumina (activity I) column.

Ozonolysis of **4** in methylene chloride at low temperature gave a stable ozonide which was assigned structure **6**. Its nmr spectrum is consistent with this formulation. The carbomethoxy substituent does not influence the chemical shift of protons H_5 and H_6, which appear as a singlet at δ 4.92. Proton H_3 gives a sharp doublet at δ 6.0 (J = 7 Hz). Models indicate that protons H_3 and H_4 are eclipsed in structure **6** while a dihedral angle of 35° is found in the correspond-

[1]Holder of a National Research Council of Canada Scholarship, 1971–1973.

Can. J. Chem. Downloaded from www.nrcresearchpress.com by 210.87.254.42 on 09/05/12
For personal use only.

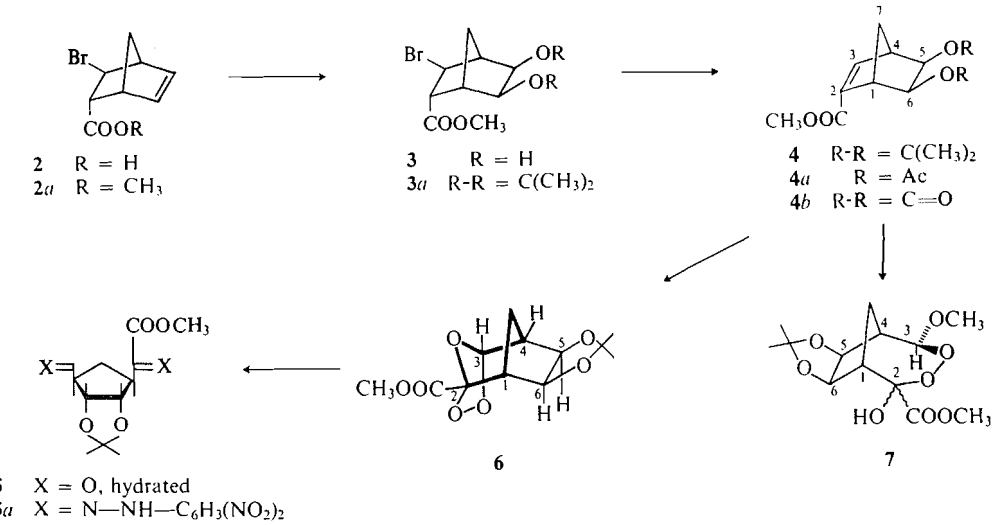

SCHEME 1

ing isomeric ozonide. Comparison with sugar derivatives having a similar degree of substitution (6–9) suggests that a dihedral angle of 0° is more appropriate for a coupling constant of 7 Hz.

Ozonolysis of the unsaturated ester **4** in methanol gave a white crystalline product, mp 123–124 °C. The compound was assigned the structure **7** on the basis of the following evidence. The compound liberated iodine from acidified potassium iodide (10, 11), but failed to react with lead tetraacetate in both benzene and acetic acid (11). This indicated the presence of a dialkyl peroxide, and not a hydroperoxide. Hydroperoxides react with lead tetraacetate releasing oxygen (11). Also in the nmr spectrum the exchangeable proton absorbed at δ 4.53 whereas the proton of a hydroperoxide absorbs around δ 9–9.5 (10). There are two sharp three-proton singlets at δ 3.47 and 3.84 assigned to the —OMe acetal and —OMe ester groups respectively. The C_5 and C_6 protons give an AX system at δ 4.40 and 5.25, J = 6 Hz, with the implication that one is very much deshielded with respect to the other. This is consistent with an '*exo*' attack of methanol on the intermediate zwitterion —$\overset{+}{C}$—O—$\bar{O}$ (12) giving a product with the stereochemistry at C_3 indicated in **7**. The methoxy group is far removed from the proton at C_5. We consider the formation of the zwitterion at C_3 to be more likely than at C_2, which is α to a carbomethoxy group. The proton at C_3 appears as a singlet in the nmr spectrum, but this would be expected with either of the possible stereochemistries at C_3. The cyclic peroxide structure is similar to that found for the product of ozonolysis in methanol of phenanthrene (11). If ozonide **6** is treated with methanol at −60 °C a mixture of products is formed and not the product of ozonolysis using methanol as solvent.

The ozonide **6** was smoothly reduced with dimethyl sulfide (13) to give the aldehydo-keto-ester **5**. The nmr spectrum of **5** in deuterated chloroform or acetone-d_6, showed a complex system of peaks in the isopropylidene regions and in the region of absorption of the methyl ester. The low field spectrum indicated that the free aldehyde was present to the extent of only 30%. In solution, the free aldehyde **5** is in equilibrium with its bridged hydrated form (14, 15). Treatment of **5** in dimethyl formamide with 2 molar equiv. of 2,4-dinitrophenylhydrazine and anhydrous hydrogen chloride gave a crystalline bis-2,4-dinitrophenylhydrazone, **5***a*.

Reduction of **5**, either with lithium aluminum hydride, or more conveniently with sodium borohydride, gave the triol **8** which was characterized as its oily triacetate **8***a*. Treatment of **8** in aqueous solution with 1 mol equiv. of sodium periodate (16) gave the hydroxy-aldehyde **9** which exists entirely in its hemiacetal form, as a mixture of isomers. Acetylation gave the monoacetate **9***a*, again as a mixture of isomers (from the nmr spectrum). Oxidation of **9** with Collins' (17, 18) or Fetizon's (19) reagents gave the lactone **11**. Oxidation with ruthenium tetroxide proved to be unsatisfactory in this instance.

Can. J. Chem. Downloaded from www.nrcresearchpress.com by 210.87.254.42 on 09/05/12
For personal use only.

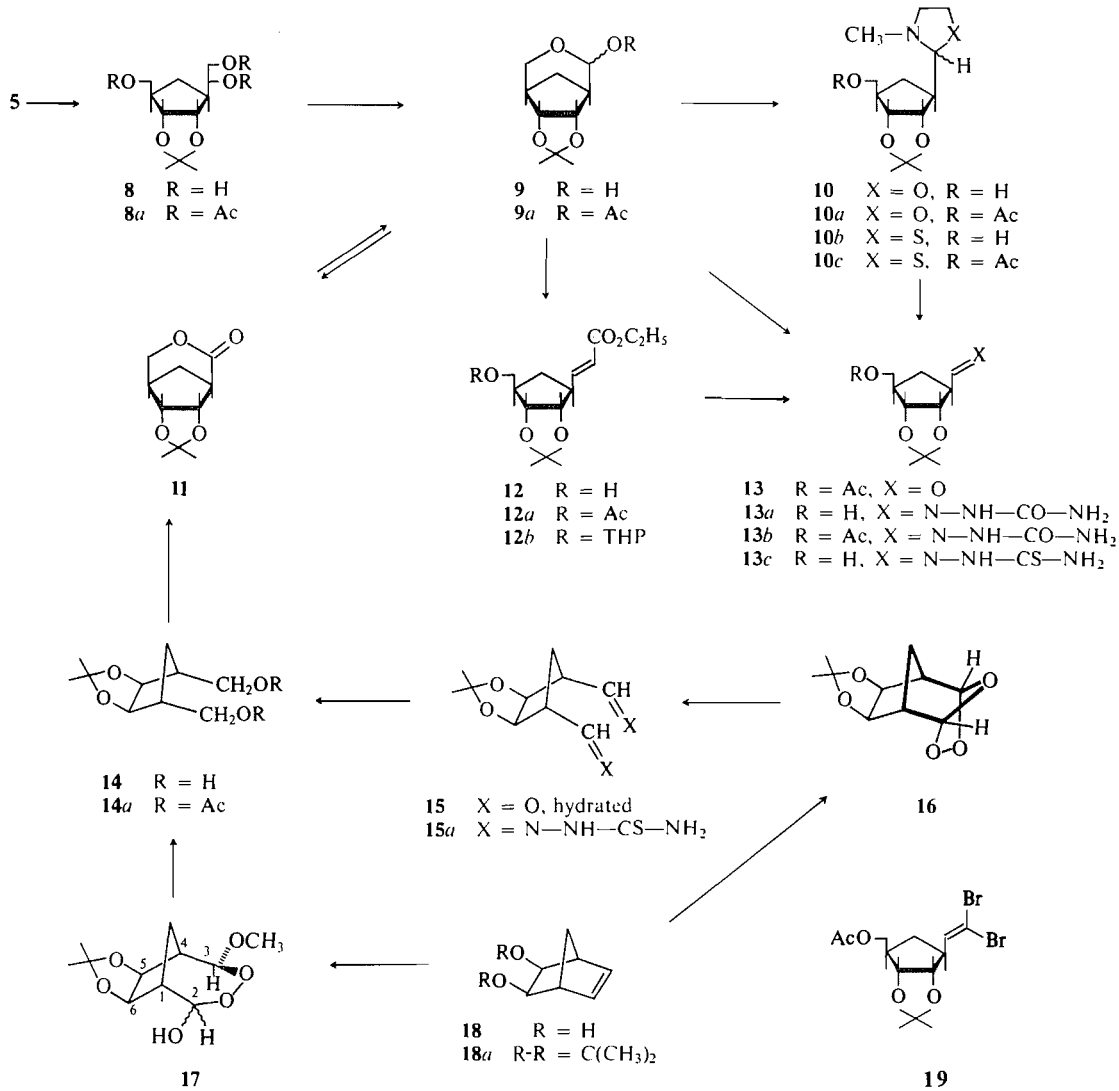

SCHEME 2

Alternatively, permanganate oxidation of norbornadiene according to the procedure of Shealy and Clayton (20) afforded the diol **18** in 28% yield. We attempted to improve the yield of this reaction using catalytic osmylation (4) with osmium tetroxide and hydrogen peroxide but the yield did not exceed 30%.

Treatment of the diol **18** with acetone, 2,2-dimethoxypropane, and a trace of *p*-toluenesulfonic acid afforded the isopropylidene derivative **18***a* in quantitative yield. Upon ozonolysis in methylene chloride at low temperature, olefin **18***a* gave ozonide **16** which could be isolated by prompt evaporation of the solvent. The structure of **16** was assigned by analogy with that of **6** but this compound was not stable and was directly reduced at low temperature with dimethyl sulfide according to the procedure of Pappas *et al.* (13). The resulting dialdehyde **15** existed mainly in its bridged hydrated form (14, 15) as a mixture of several isomers and was characterized by its bis-thiosemicarbazone **15***a*, mp 168 °C (dec.). Attempts to reduce selectively one of the aldehyde functions failed.

Reduction of the dialdehyde **15** with sodium borohydride or lithium aluminium hydride gave

Can. J. Chem. Downloaded from www.nrcresearchpress.com by 210.87.254.42 on 09/05/12
For personal use only.

Can. J. Chem. Downloaded from www.nrcresearchpress.com by 210.87.254.42 on 09/05/12
For personal use only.

the corresponding diol **14**. However, good yields of **14** with minimum handling were obtained when the olefin **18***a* was ozonolyzed in methanol at low temperature followed by a direct reduction with an excess of sodium borohydride at room temperature (21). During the ozonolysis, a white crystalline material, mp 124–125 °C, precipitated out of solution and was isolated by concentration of the solvent. The structure of this compound **17** was assigned in an analogous manner to that of peroxide **7** and had a similar stereochemistry at C_3. Direct reduction of peroxide **17** with sodium borohydride in methanol afforded diol **14**, mp 51 °C, in 65–70% yield. Acetylation gave the oily diacetate **14***a* in quantitative yield.

Oxidation of **14** with Fetizon's reagent (19) in refluxing benzene provided the lactone **11**, mp 128–129 °C, in 98% yield.

Reduction of **11** with diisobutylaluminium hydride (22) at low temperature afforded the lactol **9**, mp 119.5–121 °C, in quantitative yield. The compound existed entirely in its hemiacetal form which appeared to be a (1:1) mixture of isomers at C_2 as shown by nmr spectroscopy. Two multiplets were found at δ 4.80 and 5.10 for the anomeric proton H_2.

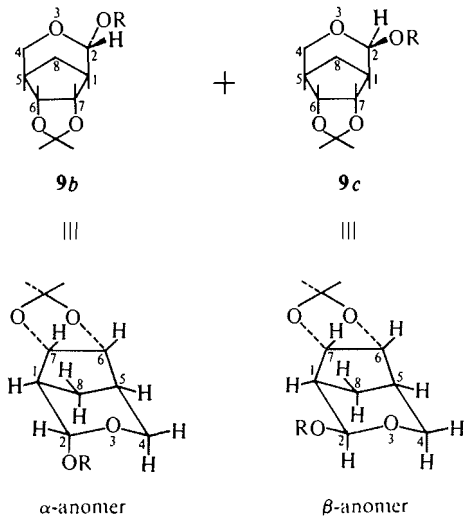

The doublet at δ 5.10 was tentatively assigned to the anomeric proton of the *endo* or α-anomer **9***b*. This conclusion was based on analogy with carbohydrates, in which the equatorial anomeric proton gives a signal at lower field (by about 0.4 ppm) than the epimeric axial one (23).

Similarly, the nmr spectrum of the acetate **9***a* suggested a 3:2 mixture of isomers at the 2 position. Although they had very close R_f values, it was possible to separate the two compounds by thin layer chromatography on silica gel using hexane – ethyl ether (5:4) as eluant. The two anomers **9***b* and **9***c* had virtually identical infrared and mass spectra but different nmr spectra on which were based their structural identification.

The major and less polar isomer (on silica gel), mp 98–99 °C, was assigned structure **9***b* or the α conformation. In its nmr spectrum, the C_6 and C_7 protons had the same chemical shift, giving an apparent singlet at δ 4.57.[1] The fact that neither of them was influenced by the acetate substituent at the 2 position suggested that the latter was attached as depicted in **9***b*. Also, as in carbohydrates (23), the anomeric equatorial proton, H_2, appeared at lower field than the similar but axial hydrogen of the isomer **9***c*, giving a doublet at δ 5.90. The C_4 protons were nonequivalent, giving an AB quartet with the axial proton, H_4, being more deshielded by 1,3 diaxial interaction with the acetoxy group.

The minor and more polar isomer, mp 94–96 °C, was assigned the alternate structure **9***c*. In this case, the equatorial acetoxy group possibly had a deshielding effect on the C_7 proton which was no longer equivalent to C_6 and both protons appeared as an AB quartet (J_{vic} = 6 Hz). As expected from models, the anomeric proton gave a singlet at δ 5.60. Also the AB quartet of the C_4 protons collapsed due to the upfield shift of the axial H_4 doublet in the absence of 1,3-diaxial interaction with the acetoxy substituent.

Treatment of hemiacetal **9** with semicarbazide gave the semicarbazone **13***a* which was converted to its crystalline acetate **13***b*, mp 158–159 °C. The crystalline thiosemicarbazone **13***c* was similarly prepared from **9**. In both cases, only one geometric isomer was obtained as shown by a clear low field doublet (—C*H*=N—).

The lactol **9** failed to react with unstabilized Wittig reagents. However, condensation of **9** with carboethoxymethylenetriphenylphosphorane in dimethylformamide at 90 °C (24) provided the α,β-unsaturated ester **12** as the pure *trans* isomer. The ester **12** was further converted to its acetate **12***a* and tetrahydropyranyl **12***b* derivatives. When the Wittig reaction mixture was evaporated and acetylated *in situ*, the acetate **12***a* was obtained in up to 85% yield.

Because of the lack of reactivity of lactol **9**

Can. J. Chem. Downloaded from www.nrcresearchpress.com by 210.87.254.42 on 09/05/12
For personal use only.

towards unstabilized Wittig reagents, the free aldehyde **13** was prepared in the following manner.

Hemiacetal **9** reacted slowly with *N*-methylethanolamine in boiling benzene with continuous removal of water. The resulting oxazolidine **10** was too unstable for purification (25) and was directly converted to its acetate derivative **10***a*. Attempts to purify the latter by chromatography led to a mixture of compounds. Accordingly, the crude acetate **10***a* was hydrolyzed with aqueous acetic acid to the aldehyde **13**, the nmr spectrum of which showed a low field singlet for the aldehydic proton at δ 9.78 ppm. The compound appeared to decompose upon standing at room temperature in chloroform (25). For analytical purposes, it could be purified from minor impurities by rapid chromatography through a short column of alumina (neutral, grade IV) using ethyl ether as eluent.[2] The crude aldehyde **13** was characterized as its crystalline semicarbazone **13***b*, mp 158–159 °C, obtained in 48% yield based on the lactol **9** and identical in all respects to the derivative obtained from the lactol **9** via the sequence **9** → **13***a* → **13***b*.

N-Methylthioethanolamine (27) was similarly condensed with the hemiacetal **9**. The stable *N*-methylthiazolidine **10***b* obtained in 60% yield was further converted to its acetate **10***c*. Regeneration of the free aldehyde **13** from such derivatives can be performed with mercuric chloride in tetrahydrofuran–water (28). However, since the reagent itself was difficult to prepare as well as being very hygroscopic, this procedure was discarded.

The most practical route to the free aldehyde **13** which allowed the use of acid sensitive protecting groups for the primary hydroxy function involved, as starting material, the unsaturated ester **12***a*. Treatment of a methylene chloride solution of the ester **12***a* with ozone at −60 °C followed by reduction with dimethyl sulfide (13) afforded an oily product homogeneous on tlc. The material gave a positive test for aldehydes using acidic dinitrophenyl hydrazine as a spray on tlc plates. It was found to be identical to the product previously obtained from the oxazolidine **10***b* and gave the same semicarbazone derivative **13***b*. Ethyl glyoxalate, formed during the reaction, was easily removed under high vacuum, and dimethylsulfoxide, the other by-product, was washed away with water. Conversion of the ester **12***a* to the pure aldehyde **13** was nearly quantitative.

The free aldehyde **13** reacted with unstabilized Wittig reagents in the expected manner. For example, **13** reacted with triphenylphosphine and carbon tetrabromide in the presence of zinc dust (29) to give the dibromo olefin **19** in 60% yield. In the nmr spectrum of **19** the olefinic proton appeared as a low field doublet at δ 6.40 and the mass spectrum showed the characteristic pattern of a dibromo product (30) with base peaks at m/e = 385 ($M^+ - CH_3$, Br^{81}), 383 ($M^+ - CH_3$, $Br^{79,81}$), and 381 ($M^+ - CH_3$, Br^{79}).

The use of hemiacetal **9**, lactone **11**, and olefins **12***a* and **19** as precursors of carbocyclic analogues of *C*-nucleosides will be discussed in following papers.

Experimental

Melting points were determined on a Gallenkamp block and are uncorrected. Mass spectra were obtained on an AEI-MS-902 mass spectrometer at 70 eV using a direct insertion probe. Nuclear magnetic resonance spectra were recorded on Varian T-60 and HA-100 spectrophotometers using tetramethylsilane as an internal standard. Infrared spectra were determined on Unicam SP-1000 and Perkin-Elmer PE-257 infrared spectrophotometers. Analytical thin layer chromatography (tlc) was performed on silica gel coated plastic plates (Eastman Kodak) and on a preparative scale on silica gel (E.M. $HF_{254+366}$) coated glass plates (20 cm × 20 cm × 1 mm). Woelm alumina (neutral) and silica gel were used for column chromatography. Microanalyses were carried out by Dr. C. Daessle, Montreal.

2-Bromonorborn-5-ene 3-Carboxylic Acid, **2**

The compound was prepared in a manner similar to the method described by Alder *et al.* (2). Freshly distilled cyclopentadiene (37 ml) was added to *trans*-β-bromoacrylic acid, **1** (5 g) dissolved in 37 ml of benzene. The solution was refluxed for 1.5 h and then stripped of solvent and excess cyclopentadiene. Petroleum ether (20 ml) was added to the residue and evaporated under reduced pressure. This was repeated. The residue was filtered and washed with small portions of petroleum ether. The product was recrystallized from ethyl acetate –

[2]Aldehydes of types **13** are subject to epimerization (26). In our case, we have no evidence of such an epimerization as there appeared to be only one spot on tlc for the aldehyde, and the nmr spectrum showed only one low field aldehyde proton signal. However, as noted by Moffatt (25), chromatography of such molecules should not be used as a preparative procedure. For example, an attempt to recover from a reaction some unreacted aldehyde **13** led to the isolation of a mixture which had been partially converted to its more stable *trans* isomer as shown by two aldehyde peaks in the nmr spectrum (δ 9.74 and 9.82).

Can. J. Chem. Downloaded from www.nrcresearchpress.com by 210.87.254.42 on 09/05/12
For personal use only.

petroleum ether: yield 75%, mp 130–136 °C (lit. (2) mp 134 °C). If the solution was refluxed for longer than 1.5 h, it became difficult to separate the desired product from the dicyclopentadiene formed as a by-product of the reaction. The product is a mixture of both isomers with the *endo* acid as the major product. Infrared (KBr) 1720 (acid C=O), 3450 cm^{-1} (acid OH); nmr ($CDCl_3$) δ 1.77 (1H), 2.12 (1H, AB, J = 10 Hz), 3.22 (m, 1H), 3.55 (d, 2H), 4.04 (m, 1H), 6.25 (br s, 2H).

2-Bromo-3-carbomethoxynorborn-5-ene, ***2a***

Diazomethane in ether (approximately 0.4 *M* solution) was added dropwise to a stirred solution of 2-bromonorborn-5-ene 3-carboxylic acid, **2**, (2 g) in 50 ml of ether, until a faint yellow colour persisted. The solution was evaporated to dryness, leaving a pale yellow liquid. Filtration of a chloroform solution of the product through a short silica gel column (30 g, activity I) gave the product, after evaporation of the solvent under reduced pressure. The yield was quantitative. Infrared (film) 1745 cm^{-1} (C=O); nmr (neat, external TMS) δ 2.02, 2.36 (2H, AB, J = 9 Hz), 3.52 (m, 3H), 3.95 (s, 3H), 4.36 (m, 1H), 6.50 (br s, 2H). *Anal.* calcd. for $C_9H_{11}O_2Br$: C 46.8, H 4.8, Br 34.6; found: C 46.6, H 4.7, Br 34.4.

2-Bromo-3-carbomethoxy-exo-5,6-dihydroxynorbornane, ***3***

Ester **2***a* (5 g, 18.9 mmol) and osmium tetroxide (15 mg in 3 ml of *tert*-butyl alcohol) were dissolved in 100 ml of ethyl ether. Hydrogen peroxide (30%, 2.7 ml, 2.7 mmol) was added in five lots over 8 h. Evaporation under reduced pressure followed by addition of ether gave, on cooling, a white crystalline product. The crystals were separated by filtration, and a further crop of crystals was obtained from the filtrate. The diol was recrystallized from ether or carbon tetrachloride: mp 144–145 °C, yield 50%. Infrared (KBr) 1733 (C=O), 3290, 3430 cm^{-1} (OH); nmr (acetone-d_6, internal TMS) δ 1.87 (m, 2H), 2.46 (m, 3H), 3.28 (m, 1H), 4.33 (m, 2H), 3.75 (s, 3H), 3.60 (br, 2H). *Anal.* calcd. for $C_9H_{13}O_4Br$: C 40.8, H 4.9, Br 30.1; found: C 40.9, H 5.0, Br 30.3.

2-Bromo-3-carbomethoxy-5,6-(dihydroxy-di-O-isopropylidene)norbornane, ***3a***

The diol obtained above, **3**, (5 g, 16.4 mmol) was added to approximately 80 ml of reagent acetone containing 10 ml of 2,2-dimethoxypropane. *p*-Toluenesulfonic acid monohydrate (10 mg) was added and the solution was stirred at room temperature for 40 min. Evaporation to near dryness was followed by addition of 40 ml of methylene chloride. The organic solution was washed twice with 10 ml of 1 *M* sodium carbonate and once with brine. The methylene chloride solution was dried over magnesium sulphate, and evaporated to give a heavy oil which failed to crystallize. Repeated attempts to purify a sample by chromatography on alumina and silica gel resulted in at least partial elimination of hydrogen bromide. Infrared (film) 1738 (C=O), 1380 cm^{-1} (acetonide); nmr ($CDCl_3$) δ 1.23 (s, 3H), 1.41 (s, 3H), 1.86 (m, 2H), 2.65 (m, 2H), 3.16 (m, 1H), 3.74 (s, 3H), 4.09 (m, 3H). The product was used without purification to prepare the norbornene derivative **4**.

2-Carbomethoxy-exo-5,6-(dihydroxy-di-O-isopropylidene)norborn-2-ene, ***4***

The crude product **3***a* from the above reaction was dissolved in anhydrous ether (100 ml) and 1,5-diazabicyclo-[5.4.0]undec-5-ene (DBU) (5 ml, 30 mmol), was added dropwise with cooling and vigorous stirring of the ether solution. After all the DBU had been added the solution was stirred for 30 min, the white precipitate (presumably DBU:HBr) was filtered off and washed several times with anhydrous ether. The ether solutions were combined and washed three times with 0.5 *M* hydrochloric acid and once with brine. Drying over magnesium sulphate and evaporation gave a colourless or pale yellow oil which crystallized on standing. The yield based on **3** was essentially quantitative. The product was best purified by dry column chromatography on Woelm 211 dry column alumina (activity III), eluting with chloroform; mp 60–62 °C. Infrared (KBr) 1719 (C=O), 1600 (C=C), 1390 cm^{-1} (acetonide); nmr ($CDCl_3$) δ 1.35 (s, 3H), 1.52 (s, 3H), 1.82, 2.12 (2H, AB, J = 9 Hz), 3.00 (m, 1H), 3.19 (br s, 1H), 3.76 (s, 3H), 4.29 (br s, 2H), 6.97 (d, 1H, J = 4 Hz); uv (methanol) λ_{max} 233 nm (ϵ 6700). *Anal.* calcd. for $C_{12}H_{16}O_4$: C 64.3, H 7.2; found: C 64.3, H 7.4.

2-Carbomethoxy-exo-5,6-diacetoxynorborn-2-ene, ***4a***

The diol obtained from 2 g of **2** was dissolved in 30 ml of pyridine and to the solution was added 5 ml of acetic anhydride. The solution was allowed to stir overnight at room temperature and was then worked up in the usual way. The product was chromatographed on a dry alumina column (Woelm, activity III), eluting with chloroform. This gave on evaporation a colourless oil, which failed to crystallize, in 90% yield. Infrared (film) 1728, 1752 cm^{-1} (C=O); nmr ($CDCl_3$) δ 2.04 (s, 3H), 2.10 (s, 3H), 2.10 (center of AB, J = 10 Hz), 3.03 (m, 1H), 3.23 (br s, 1H), 3.78 (s, 3H), 4.81 (d, 2H), 7.03 (d, 1H, J = 4 Hz); uv (methanol) λ_{max} 228 nm, (ϵ 9000). *Anal.* calcd. for $C_{13}H_{16}O_6$: C 58.2, H 6.0; found: C 58.1, H 6.2.

2-Carbomethoxy-5,6-dihydroxynorborn-2-ene-di-O-carbonate, ***4b***

Diol **3** (1.2 g, 4.3 mmol) was dissolved in 35 ml of dry pyridine. The solution was cooled in ice water and 3.6 ml of a 12% solution of phosgene (12 mmol) in methylene chloride was added. The solution was slowly allowed to come to room temperature, and stirring was continued for 6 h. Crushed ice was then slowly added to the reaction mixture, and after the excess phosgene had been destroyed the reaction mixture was extracted with chloroform (3 × 30 ml). The solution was evaporated to near dryness. The oily residue was taken up in 40 ml of chloroform and the resulting solution was washed with 0.5 *M* hydrochloric acid (3 × 15 ml). The chloroform layer was dried over sodium sulphate, and evaporated to give 550 mg of a light brown oil, which crystallized on standing. The product was recrystallized from hexane – methylene chloride; yield: 60%; mp 118–119 °C. Infrared (KBr) 1720 (ester C=O), 1800 cm^{-1} (carbonate C=O); nmr ($CDCl_3$) δ 1.97 (m, 2H), 3.20 (m, 1H), 3.54 (br s, 1H), 4.82 (s, 3H), 4.73 (s, 2H), 6.99 (d, 1H, J = 4 Hz); uv (methanol) λ_{max} 223 nm, (ϵ 8400). *Anal.* calcd. for $C_{10}H_{10}O_5$: C 57.1, H 4.8; found: C 56.9, H 5.1.

2-Carbomethoxy-5,6-(dihydroxy-di-O-isopropylidene)-norborn-2-ene Ozonide, ***6***

The unsaturated ester **4** (2 g) was dissolved in dry methylene chloride (50 ml), cooled to −60 °C, and treated

Can. J. Chem. Downloaded from www.nrcresearchpress.com by 210.87.254.42 on 09/05/12
For personal use only.

with ozone in oxygen at the rate of 7 mmol of ozone per h. The reaction was continued until the blue colour characteristic of ozone persisted. The temperature of the solution was allowed to rise to room temperature and the solvent was evaporated under reduced pressure with the temperature of the water bath at 35 °C. The ozonide was obtained as a colourless oil in quantitative yield. Infrared (film) 1762 cm^{-1} (ester C=O); nmr ($CDCl_3$) δ 1.35 (s, 3H), 1.24 (s, 3H), 1.67 (br s, 2H), 2.65 (d of d, 1H, J_{34} = 7 Hz, J_{14} = 3 Hz), 2.94 (d, 1H, J = 3 Hz), 3.88 (s, 3H), 4.92 (s, 2H), 6.00 (d, 1H, J_{34} = 7 Hz). The ozonide was not further characterized.

Methyl-2-(2α,3α-dihydroxy-di-O-isopropylidene-4β-aldehydocyclopent-1β-yl)glyoxylate, **5**

The methylene chloride solution of the ozonide **6** prepared from 3 g of **4** was cooled to −60 °C in a dry ice – acetone bath under nitrogen and dimethyl sulfide (4 ml) was added. The solution was stirred, and allowed to come slowly to room temperature. Stirring was continued for a total of 4 h. The methylene chloride solution was washed with saturated sodium chloride solution (5 × 15 ml). Drying over magnesium sulphate, and evaporation gave the oily aldehydo-ketoester. This compound was characterized as its bis-2,4-dinitrophenylhydrazone. Mass spectrum of **5**, 257 (M^+ − OH), 241 (M^+ − H_2O − CH_3, base peak).

2,4-Dinitrophenylhydrazone of **5**, **5a**

2,4-Dinitrophenylhydrazine (400 mg, 2 mmol) was dissolved in a minimum volume of dimethylformamide and **5** (260 mg, 1 mmol) was added. Anhydrous hydrogen chloride gas was bubbled through the solution for a few seconds and the solution was then left to stand. After a few minutes an orange material precipitated. The product was filtered and washed several times with small portions of cold methanol. The nmr spectrum of the product, which is soluble in chloroform, indicated the presence of 1 mol of dimethylformamide of crystallization. The product was dissolved in methylene chloride and then reprecipitated with dropwise addition of methanol and slow evaporation of methylene chloride. This procedure was repeated.

The product **5a** was obtained in 60% yield, decomposition >175 °C. Infrared (KBr) 3380 (NH), 1675 (C=O), 1630 (C=N), 1600 (phenyl), 1520, 1345 cm^{-1} (—NO_2); nmr ($CDCl_3$) δ 1.38 (s, 3H), 1.53 (s, 3H), 2.13 (m, 2H), 2.95 (m, 2H), 3.97 (s, 3H), 4.94 (m, 2H), 6.02 (m, 1H), 7.87 (m, 6H), 9.00 (m, 2H). *Anal.* calcd. for $C_{24}H_{24}N_8O_{12}$: C 46.8, H 3.8, N 18.2; found: C 47.0, H 3.9, N 18.2.

2-Carbomethoxy-7,8-(dihydroxy-di-O-isopropylidene)-2-hydroxy-5-methoxy-3,4-dioxabicyclo[4.2.1]nonane, **7**

A solution of **4** (2.5 g in 40 ml methanol) at −60 °C was treated with ozone in oxygen at the rate of 7 mmol of ozone per h. After 1 equiv. of ozone had been added the solution was allowed to rise to room temperature and concentrated to approximately one third of its volume. The white, analytically pure, crystalline precipitate was filtered off and washed twice with small portions of cold methanol, yield 85%, mp 123–124 °C. Infrared (KBr) 3470 (O—H), 1740 (ester, C=O), 1380 cm^{-1} (acetonide); nmr ($CDCl_3$) δ 1.28 (s, 3H), 1.42 (s, 2H), 1.82–2.65 (m, 4H), 3.47 (s, 3H), 3.84 (s, 3H), 4.40 (d, 1H, J_{67} = 6 Hz, C_6), 4.53 (s, 1H, exchangeable), 4.56 (br s, 1H), 5.21 (d, 2H, C_7). *Anal.* calcd. for $C_{13}H_{20}O_8$: C 51.3, H 6.6; found: C 51.5, H 6.6.

(2α,3α-Dihydroxy-di-O-isopropylidene-4β-hydroxymethyl-cyclopent-1β-yl)ethyleneglycol, **8**

The compound **5** (0.5 g) obtained from dimethyl sulfide work up of the ozonide **6** was dissolved in 40 ml of methanol, and sodium borohydride (600 mg) was added. The addition was strongly exothermic. The solution was allowed to stir for 3 h, then 0.5 *M* hydrochloric acid was added carefully over 10–15 min until the p*H* was approximately 4. The solution was evaporated to dryness and the residue, A, was extracted three times with hot chloroform. The chloroform was evaporated to leave 450 mg of the crude product as a colourless oil. Nuclear magnetic resonance (D_2O, external TMS) δ 1.40 (s, 3H), 1.56 (s, 3H), 2.16 (m, 4H), 3.72 (m, 4H), 4.57 ppm (m, 3H).

No attempts were made to further purify the triol, and the product was characterized as the triacetate.

1-(4β-Acetoxymethyl-2α,3α-dihydroxy-di-O-isopropylidenecyclopent-1β-yl)ethyleneglycol Triacetate, **8a**

The triol **8** obtained above was dissolved in 15 ml of pyridine and 5 ml of acetic anhydride. The solution was stirred at room temperature overnight and worked up in the usual way. The oily product was chromatographed on 20 × 20 cm × 1 mm silica gel plates, eluting with chloroform – ethyl acetate (3:2). The product was a colourless oil which failed to crystallize; yield, 60%, based on **5**. Infrared (film) 1750, 1762 (acetate), 1380 cm^{-1} (acetonide); nmr ($CDCl_3$) δ 1.28 (s, 3H), 1.48 (s, 3H), 2.07 (s, 6H), 2.10 (s, 3H), 2.24 (m, 4H), 4.27 (m, 6H), 5.18 (m, 1H). *Anal.* calcd. for $C_{17}H_{26}O_8$: C 57.0, H 7.3; found: C 57.0, H 7.3.

A higher yield (75%) of the triacetate is obtained if residue A is acetylated directly without extraction with chloroform.

exo-6,7-(Dihydroxy-di-O-isopropylidene)-2-hydroxy-3-oxabicyclo[3.2.1]octane, **9**

A. From Triol **8**

Powdered sodium periodate (500 mg), was added to a stirred solution of the crude triol **8** (500 mg) in 40 ml of water. The solution was warmed slightly and was stirred for 15 min. The aqueous solution was then extracted with chloroform (4 × 15 ml), the organic solutions were combined, dried (magnesium sulfate), and evaporated to leave a colourless oil which crystallized on standing. Yield based on **5** as starting material, was 50%.

The yield of hemiacetal **9** could be improved to 70%, based on **5**, if the periodate cleavage was carried out *in situ*, without isolation of the triol, as described in the following paragraph.

The aldehydo-ketoester **5** (1 g) was treated with 300 mg of sodium borohydride in 50 ml of isopropyl alcohol. After the mixture was stirred for 3 h, dilute hydrochloric acid was carefully added to bring the p*H* of the solution to 5. The mixture was stirred for 20 min, filtered, and the filtrate evaporated to dryness. The residue was dissolved in water (100 ml) and treated with 1 g of powdered sodium periodate. After work up as above, a 70% yield of the hemiacetal **9** was obtained. The product reduced Fehling's solution and gave a positive test with purpald.

Can. J. Chem. Downloaded from www.nrcresearchpress.com by 210.87.254.42 on 09/05/12
For personal use only.

B. From Lactone **11**

A fresh solution of diisobutylaluminium hydride in toluene (0.181 *M*, 5.5 ml, 1 mmol) was added dropwise over a period of 20 min to a solution of lactone **11** (198 mg, 1 mmol) in dry toluene (20 ml) at −25 °C under nitrogen. The reaction mixture was then stirred at this temperature for another 20 min after which tlc showed the disappearance of the starting material. The aluminium complex was precipitated by addition, at −20 °C, of 2 ml of 2 *M* isopropanol in toluene and the aluminium complex was destroyed at 0 °C by shaking with 0.2 ml of water and then 1 ml of ethyl acetate. Kieselghur (200 mg) and sodium sulfate were added and the mixture was filtered through a bed of Kieselghur. The solid mass was washed several times with toluene – ethyl acetate (4:1) and the combined filtrates were evaporated to give the white crystalline hemiacetal **9** as a mixture of anomers (1:1). An analytical sample was recrystallized from benzene–hexane. Yield 195 mg (98%); mp 119.5–121 °C. Infrared (KBr) 3370 (O—H), 2970 (C—H aliphatic), 1390 cm^{-1} (acetonide); nmr ($CDCl_3$) δ 1.38 and 1.49 (2s, 6H, $C(CH_3)_2$), 2.18 (m, 4H, H_1, H_5, C—CH_2—C), 3.66 (br s, 1H exch. O*H*), 4.08 (m, 2H, —CH_2O), 4.78 (m, 2H, H_6, H_7), 4.80 (m, 0.5H, H_2), 5.10 ppm (m, 0.5H, H_2). No detectable absorption in the aldehyde region. Mass spectrum m/e = 185 ($M^+ - CH_3$), 119, 100, 81. *Anal.* calcd. for $C_{10}H_{16}O_4$: C 59.98, H 8.05; found: C 60.17, H 8.09.

endo,exo-2-Acetoxy-exo-6,7-(dihydroxy-di-O-isopropylidene)-3-oxabicyclo[3.2.1]octane, ***9a***

The hemiacetal **9** (150 mg, 0.75 mmol) was acetylated with acetic anhydride (3 ml) in pyridine (5 ml) overnight. Work up as usual afforded the crude acetate which was purified by preparative tlc silica gel plates using ether–hexane (6:5) as eluant. Extraction of the large band (R_f 0.6–0.45) gave the white crystalline acetate **9** as a mixture of C_2-anomers (3:2).

A sample was recrystallized from ether–hexane. Yield 135 mg (90%); mp 73–74 °C. Infrared (KBr) 1750 (C=O), 1380 (acetonide), 1040 cm^{-1} (C—O). Mass spectrum m/e = 242(M^+), 227($M^+ - CH_3$), 183($M^+ - OCOCH_3$), 167, 143, 125, 79. *Anal.* calcd. for $C_{12}H_{18}O_5$: C 59.49, H 7.49; found: C 59.71, H 7.80.

The two anomers were separated by preparative tlc on silica gel plates using ethyl ether – hexane (6:5) as eluant.

(exo-2-Acetoxy) Isomer (or α-Anomer), ***9b***

Extraction of the top of the large band (R_f 0.6) after the chromatography plate provided the pure α-anomer **9***b* mp 98–99 °C. Nuclear magnetic resonance ($CDCl_3$) δ 1.37 and 1.50 (2s, 6H, $C(CH_3)_2$), 1.60–2.33 (m, 4H, C—CH_2—C, H_1, H_5), 2.08 (s, 3H, $OCOCH_3$), 3.80 (ABq, 2H, J = 11 Hz, —CH_2O—), 4.57 (s, 2H, H_6, H_7), 5.90 (d, 1H, J = 3 Hz, H_2).

(endo-2-Acetoxy) Isomer (or β-Anomer), ***9c***

The lower part of the band (R_f 0.45–0.5) afforded the β-anomer mp 94.5–96 °C. Nuclear magnetic resonance ($CDCl_3$) δ 1.37 and 1.50 (2s, 6H, $C(CH_3)_2$), 1.93–2.23 (m, 4H, C—CH_2—C, H_1, H_5), 2.09 (s, 3H, $OCOCH_3$), 3.73 (m, 2H, —CH_2O—), 4.63 (ABq, 2H, J = 6 Hz, H_6, H_7), 5.60 (s, 1H, H_2).

exo-6,7-Dihydroxy-di-O-isopropylidene-2-oxo-3-oxabicyclo[3.2.1]octane, ***11***

A. From Hemiacetal ***9***

With Collins' Reagent—Collins' reagent, $CrO_3 \cdot 2py$, (2.3 g, 9 mmol), was added in a nitrogen atmosphere, to a stirred solution of **9** (300 mg, 1.5 mmol) in 50 ml of dry methylene chloride. The solution became deep red and a dark red-brown precipitate quickly formed. Stirring was continued for 20 min, the mixture was then filtered, and the precipitate washed thoroughly with methylene chloride. The combined organic layers were washed with 1 *M* sodium bicarbonate (3 × 15 ml), once with 15 ml of 0.5 *M* hydrochloric acid, and once with brine. The organic layer was dried (magnesium sulfate), and evaporated to give the crystalline product, crude yield 80%. A chloroform solution of the lactone was filtered through a short silica gel (activity III) column. The lactone was recrystallized from hexane – methylene chloride, yield 70%, mp 128–129 °C.

With Fetizon's Reagent (Silver Carbonate–Celite)—Fetizon's reagent (19) (3 g) was added to a solution of the hemiacetal **9** (100 mg, 0.5 mmol) in 70 ml of dry benzene. The solution was refluxed vigorously for 24 h. After this time tlc indicated the presence of starting material, so a further 2 g of Fetizon's reagent was added and refluxing was continued for a further 14 h. The solution was then filtered through Celite, and evaporated to leave 70 mg of the crude product, yield 70%. The lactone was purified as above.

B. From Diol ***14***

Fetizon's reagent (3 g) was added to a solution of the diol **14** (150 mg, 0.75 mmol) in 60 ml of dry benzene. The solution was stirred vigorously and refluxed overnight using a Dean–Stark condenser. At that time, tlc showed the absence of starting material and the solution was filtered through a bed of Celite. The solid material was washed several times with hot benzene and the combined filtrates evaporated under vacuum. The lactone **11** was obtained as white crystals.

An analytical sample was recrystallized from hexane–dichloromethane. Yield 148 mg (98%); mp 128–129 °C. Infrared (KBr) 2970 (C—H aliphatic), 1750 (C=O), 1390 (acetonide) 1030 cm^{-1} (C—O); nmr ($CDCl_3$) δ 1.33 and 1.48 (2s, 6H, $C(CH_3)_2$), 2.01 (m, 2H, H_8), 2.43 (m, 1H, H_5), 2.97 (m, 1H, H_1), 4.23 (m, 2H, —CH_2O), 4.60 (br s, 2H, H_6, H_7). Mass spectrum m/e = 183 ($M^+ - CH_3$), 141, 101, 99. *Anal.* calcd. for $C_{10}H_{14}O_4$: C 60.60, H 7.07; found: C 60.47, H 7.12.

cis-exo-5,6-Dihydroxy-di-O-isopropylidenenorborn-2-ene, ***18a***

Diol **18** (1.2 g, 10 mmol) (20) was dissolved in 25 ml of dry acetone containing 10 ml of 2,2-dimethoxypropane and a crystal of *p*-toluenesulfonic acid. The solution was then stirred at room temperature for 3 h. After concentration under vacuum (35 °C) to about 2 ml, chloroform was added and the organic layer was washed twice with brine, once with 10 ml of water, and then dried over magnesium sulfate. Evaporation gave a yellow brown liquid which was passed through a short column of alumina (neutral Grade 3) using hexane–chloroform (8:2) as eluant. The

Can. J. Chem. Downloaded from www.nrcresearchpress.com by 210.87.254.42 on 09/05/12
For personal use only.

product **18***a* was obtained as a colourless liquid in quantitative yield.

A sample for analysis was distilled, mp 19 °C; bp 75.5 °C/16 torr. Infrared (film) 2990, 2970 (C—H aliphatic), 1387, 1377 cm^{-1} (acetonide); nmr ($CDCl_3$) δ 1.32 and 1.42 (2s, 6H, $C(CH_3)_2$), 1.63 (m, 1H, H_{7b}, 1.92 (m, 1H, H_{7a}), 2.72 (m, 2H, H_1, H_4), 4.20 (m, 2H, H_2, H_3), 6.70 (m, 2H, H_5, H_6). Mass spectrum m/e = 151 ($M^+ - CH_3$), 108, 100, 79, 66. *Anal.* calcd. for $C_{10}H_{14}O_2$: C 72.28, H 8.43; found: C 71.93, H 8.37.

cis-exo-5,6-Dihydroxy-di-O-isopropylidenenorborn-2-ene Ozonide, ***16***

The olefin **18***a* (250 mg, 1.5 mmol) was dissolved in dry methylene chloride (40 ml), cooled to −60 °C and treated with ozone in oxygen at a rate of 7 mmol of ozone per h. The reaction was continued until the blue colour characteristic of ozone persisted. The excess of ozone was removed by bubbling nitrogen through the solution. Evaporation of the solvent under reduced pressure (temperature of the bath below 35 °C) gave the ozonide **16** as a white foam in quantitative yield. Infrared ($CHCl_3$) 1390, 1380 cm^{-1} (acetonide); nmr ($CDCl_3$) δ 1.32 and 1.41 (2s, 6H, $C(CH_3)_2$), 1.48 (m, 2H, $—CH_2—$), 1.93–2.73 (m, 2H, H_1, H_4), 4.93 (s, 2H, H_5, H_6), 5.93 (d, 2H, J = 6 Hz, H_2, H_3). The ozonide was not further characterized.

2,4-Dihydroxy-exo-6,7-(dihydroxy-di-O-isopropylidene)-3-oxabicyclo[3.2.1]octane, ***15***

A methylene chloride solution of the ozonide **16** prepared from 400 mg (2.4 mmol) of the olefin **18***a* was cooled to −60 °C under nitrogen and dimethyl sulfide (1 ml) was added. The solution was allowed to warm up slowly to room temperature and stirred for a total of 4 h. The solution was then washed with brine (5 × 10 ml), dried over magnesium sulfate, and evaporated to give the dialdehyde **15** as a white foam. Yield 456 mg (99% based on olefin **18***a*). Infrared ($CHCl_3$) 3400 (O—H), 2970 (aliphatic C—H), 2700 (aldehydic C—H), 1730 (weak, C=O aldehyde), 1390 cm^{-1} (acetonide); nmr ($CDCl_3$) δ 1.35 and 1.48 (2s, 6H, $C(CH_3)_2$), 1.83–3.23 (m, 4H, $—CH_2—$, H_1, H_5), 4.40–5.30 (m, 6H, H_2, H_4, H_7, 2 exch. O—H), 9.67 (s, 0.2H, aldehyde). Mass spectrum m/e = 216 (M^+), 215 ($M^+ - H$), 200 ($M^+ - CH_3—H$), 199 ($M^+ - OH$), 183 ($M^+ - CH_3 - H_2O$), 171, 111. The compound was characterized as its dithiosemicarbazone **15***a*.

Dithiosemicarbazone of ***15***, ***15a***

Hemiacetal **15** (107 mg, 0.5 mmol) was dissolved in 15 ml of methanol containing 100.5 mg (2 equiv.) of thiosemicarbazide. The mixture was warmed up to 40–50 °C to dissolve the reactants and then allowed to stand at room temperature for 2 h. The white precipitate formed was collected by filtration and washed with small portions of methanol. An analytical sample was recrystallized from methanol–ether. Yield 85 mg (50%); mp 168 °C (dec.). Infrared (Nujol) 3440, 3380, 3310 (NH, NH_2), 1610 (C=N), 1540 (C=S), 1075, 1050 cm^{-1}; nmr (DMSO-d_6) δ 1.28 and 1.43 (2s, 6H, $C(CH_3)_2$), 1.73–2.23 (m, 2H, $—CH_2—$), 2.66–2.90 (m, 2H, H_1, H_4), 4.73 (m, 2H, H_2, H_3), 7.43 (d, 2H, J = 5 Hz, $—CH=N$), 7.97 (br, s, 4H exch., NH_2), 11.10 (2H exch., NH). Mass spectrum m/e = 344 (M^+), 329 ($M^+ - CH_3$), 268 ($M^+ - CH_3 - CSNH_2 - H$), 254 ($M^+ - CH_3 - NHCSNH_2$), 194 ($M^+ - 2$ ($NHCSNH_2$)), 179 ($M^+ - CH_3 - 2$ ($NHCSNH_2$)), 133, 131, 116, 101 ($CH=NHCSNH_2$), 91. *Anal.* calcd. for $C_{12}H_{20}N_6O_2S_2$: C 41.86, H 5.85, N 24.40, S 18.68; found: C 42.09, H 5.66, N 24.20, S 18.91.

2-Hydroxy-5-methoxy-7α,8α-(dihydroxy-di-O-isopropylidene)-3,4-dioxabicyclo[4.2.1]nonane, ***17***

A solution of the olefin **18***a* (200 mg, 1.2 mmol) in 40 ml of methanol was treated at −60 °C with ozone in oxygen at the rate of 7 mmol of ozone per h. After 1 equiv. of ozone had been added, the solution was allowed to warm to room temperature and concentrated to 5 ml. The white crystalline precipitate was filtered off and washed twice with small portions of cold methanol. Yield 90%; mp 125–126 °C. Infrared (KBr) 3430 (O—H), 1390 cm^{-1} (acetonide); nmr ($CDCl_3$) δ 1.23 and 1.37 (2s, 6H, $C(CH_3)_2$), 1.93 (m, 2H, $—CH_2—$), 2.37 (m, 2H, H_1, H_6), 3.43 (s, 3H, OCH_3), 3.50 (s, 1H exch., OH), 4.34 (d, 1H, J_{67} = 6 Hz, H_7), 4.56 (br s, 1H, H_5), 5.18 (d, 1H, J_{81} = 6 Hz, H_8), 5.26 (m, 1H, H_2). Mass spectrum: m/e = 232 ($M^+ - CH_3 - H$), 214, 186, 142, 125, 111. *Anal.* calcd. for $C_{11}H_{18}O_6$: C 53.65, H 7.31; found: C 53.71, H 7.23.

1β,4β-Dihydroxymethyl-2α,3α-(dihydroxy-di-O-isopropylidene)cyclopentane, ***14***

A solution of the olefin **18***a* (2g, 12 mmol) in 60 ml of dry methanol was cooled to −50 °C and treated with ozone in oxygen at the rate of 7 mmol of ozone per h. After 1 equiv. of ozone had been added, nitrogen was bubbled through the solution to remove the excess of ozone. The solution was allowed to warm up to room temperature and sodium borohydride (1 g, 4 equiv.) was added slowly such that the temperature did not exceed 40 °C. After stirring overnight at room temperature, the excess of reagent was destroyed by slow addition of dilute hydrochloric acid until neutralization. The methanol was evaporated under vacuum and the aqueous layer, saturated with potassium carbonate, was extracted with ethyl acetate (3 × 40 ml). The extracts were combined, dried over sodium sulfate and evaporated to give the diol **14** as a colourless oil. The product crystallized from petroleum ether – dichloromethane. Yield 1.70 g (70%); mp 51–51.5 °C. Infrared ($CHCl_3$) 3400 (OH), 2970 (C—H), 1390 cm^{-1} (acetonide); nmr ($CDCl_3$) δ 1.32 and 1.52 (2s, 6H, $C(CH_3)_2$), 1.87–2.23 (m, 4H, $—CH_2—$, H_1, H_4), 3.12 (s, 2H exch., OH), 3.12 (d, 4H, J = 6 Hz, $—CH_2OH$), 4.42 (m, 2H, H_2, H_3). Mass spectrum m/e = 187 ($M^+ - CH_3$), 169 ($M^+ - CH_3 - H_2O$), 145, 127 ($M^+ - CH_3 - 2CH_2O$), 109, 81. *Anal.* calcd. for $C_{10}H_{18}O_4$: C 59.40, H 8.97; found: C 59.83, H 9.09.

1β,4β-Diacetoxymethyl-2α,3α-(dihydroxy-di-O-isopropylidene)cyclopentane ***14a***

Acetic anhydride (3 ml) was added to a solution of the diol **14** (100 mg, 0.5 mmol) in 5 ml of dry pyridine. The solution was stirred overnight and then poured in ice water (10 ml). The solution was extracted with chloroform and the organic layer was washed with dilute hydrochloric acid and then water. After evaporation of the solvent, the crude diacetate was obtained. Purification by passage through a short column of silica gel (grade 3) using ethyl

Can. J. Chem. Downloaded from www.nrcresearchpress.com by 210.87.254.42 on 09/05/12
For personal use only.

ether as eluant gave **14***a* as a colourless oil. Yield 140 mg (98%). Infrared ($CHCl_3$) 2970 (C—H), 1745 (C=O ester), 1390 (acetonide), 1030 cm^{-1} (C—O); nmr ($CDCl_3$) δ 1.33 and 1.51 (2s, 6H, $C(CH_3)_2$), 1.90–2.66 (m, 4H —CH_2—, H_1, H_4), 2.10 (s, 6H, $OCOCH_3$), 4.18 (d, 4H, J = 5 Hz, —CH_2OAc), 2.73 (m, 2H, H_2, H_3). Mass spectrum m/e = 271 ($M^+ - CH_3$), 228 ($M^+ - CH_3 - COCH_3$), 169, 151, 127, 109, 91. *Anal.* calcd. for $C_{14}H_{22}O_6$: C 58.73, H 7.75; found: C 58.63, H 7.57.

1β-Formyl-2α,3α-(dihydroxy-di-O-isopropylidene)-4β-hydroxymethylcyclopentane Thiosemicarbazone, ***13c***

Thiosemicarbazide (75 mg, 0.8 mmol) was added to a solution of the hemiacetal **9** (150 mg, 0.75 mmol) in 20 ml of methanol. The solution was refluxed with a Dean–Stark trap containing molecular sieves (type 3A) for 20 h. Evaporation and purification of the residue by preparative tlc using ethyl acetate – ether (9:1) as the solvent system afforded 175 mg of white foam. The product crystallized from chloroform–ether. Yield 85%; mp 127–128 °C. Infrared ($CHCl_3$) 3520, 3380 (NH_2), 3350, 3180 (multiple bands, O—H, NH), 1590 (C=N), 1525 (C=S), 1385 cm^{-1} (acetonide); nmr ($CDCl_3$) δ 1.33 and 1.53 (2s, 6H, $C(CH_3)_2$), 1.92–2.50 (m, 3H,—CH_2—, H_4), 2.73–3.10 (m 1H, H_1), 3.23 (br s, 1H exch., O*H*), 3.67 (d, 2H, J = 6 Hz, —CH_2OH), 4.40–4.77 (m, 2H, H_2, H_3), 7.13 (m, 2H exch., NH_2), 7.56 (d, 1H, J = 5 Hz, —C*H*=N), 10.33 (br s, 1H exch., N*H*). Mass spectrum m/e = 273 (M^+), 258 ($M^+ - CH_3$), 241 ($M^+ - CH_3 - NH_2$), 199 ($M^+ - CH_3 - CSNH$), 198 ($M^+ - NH_2 - CSNH$), 184 ($M^+ - NH_2CSNHN$), 102 ($CH - N - NH - CSNH_2$). Anal. calcd. for $C_{11}H_{19}N_3O_3S$: C 48.34, H 7.01, N 15.38, S 11.71; found: C 47.93, H 7.16, N 15.79, S 11.59.

1β-Formyl-2α,3α-(dihydroxy-di-O-isopropylidene)-4β-hydroxymethylcyclopentane Semicarbazone, ***13a***

The hemiacetal **9** (150 mg, 0.75 mmol) in 20 ml of methanol was added to a solution of semicarbazide hydrochloride (92 mg, 0.75 mmol) and sodium acetate (67.5 mg, 1 equiv.). The resulting mixture was stirred overnight at room temperature. After evaporation of the solvent, the residue was purified by chromatography on a column of alumina (neutral Grade 4) using ethyl acetate – methanol (7:3) as eluant. The semicarbazone **13***a* was recovered as a white foam which failed to crystallize.

Alternatively, the semicarbazone **13***a* was prepared by refluxing a mixture of lactol **9** and semicarbazide (1 equiv.) for 1 h. Semicarbazide was obtained by treatment of its hydrochloride salt with Dowex (OH^-) resin. Yield 70%. Infrared (film) 3500 to 3350 (multiple bands, NH_2, NH, OH), 1690 (C=O amide), 1385 cm^{-1} (*gem*-dimethyl); nmr (acetone-d_6) δ 1.27 and 1.43 (2s, 6H, $C(CH_3)_2$, 1.77–2.43 (m, 4H, —CH_2—, H_4, O*H*), 2.67–3.00 (m, 1H, H_1), 3.53 (d, 2H, J = 6 Hz, —CH_2OH), 4.37–4.80 (m, 2H, H_2, H_3), 6.38 (br s, 2H exch., NH_2), 7.26 (d, 1H, J = 5 Hz, —C*H*=N), 9.93 (br s, 1H exch., N*H*). Mass spectrum m/e = 257 (M^+), 242 ($M^+ - CH_3$), 199 ($M^+ - CH_3 - CONH$), 183 ($M^+ - CH_3 - NH_2CONH$), 168 ($M^+ - CH_3 - CONH_2 - CH_2O$), 156 ($M^+ - CH_3 - CH{=}N{-}NH - CONH_2$), 131, 103.

1β-Formyl-4β-acetoxymethyl-2α,3α-(dihydroxy-di-O-isopropylidene)cyclopentane Semicarbazone, ***13b***

The semicarbazone **13***a* (60 mg, 0.54 mmol) was dissolved in 3 ml of pyridine, and 2 ml of acetic anhydride were added. The solution was stirred at room temperature overnight. After evaporation of the solvent, the residue was purified by preparative tlc. Elution with ethyl acetate–methanol (7:3) afforded 170 mg of oily product (R_f 0.8). The compound crystallized from ether – petroleum ether. Yield 95%; mp 158–159 °C. Infrared ($CHCl_3$) 3540, 3420 (NH_2), 1745 (C=O ester), 1700 (C=O amide), 1640 (C=N), 1390 cm^{-1} (*gem*-dimethyl); nmr ($CDCl_3$) δ 1.33 and 1.50 (2s, 6H, $C(CH_3)_2$), 2.10 (s, 3H, $OCOCH_3$), 1.87–2.60 (m, 3H), 2.88 (m, 1H, H_1), 4.12 (d, 2H, J = 6 Hz, —CH_2OAc), 4.50 (m, 2H, H_2, H_3), 5.83 (br s, 2H exch., NH_2), 7.26 (d, 1H, J = 5 Hz, —C*H*=N), 9.83 (br s, 1H exch., N*H*). Mass spectrum m/e = 299 (M^+), 284 ($M^+ - CH_3$), 255 ($M^+ - CONH_2$), 241 ($M^+ - CH_3 - COCH_3$), 215, 199, 169, 151, 95; uv (EtOH) λ_{max} 269 nm. *Anal.* calcd. for $C_{13}H_{21}O_5N_3$: C 52.16, H 7.07, N 14.04; found: C 52.37, H 7.08, N 14.30.

trans-Ethyl-3-(2′α,3′α-dihydroxy-di-O-isopropylidene-4′β-hydroxymethylcyclopent-1′β-yl)acrylate, ***12***

Carboethoxymethylenetriphenylphosphorane (550 mg, 2.75 mmol) was added to the hemiacetal **9** (300 mg, 1.5 mmol) in 15 ml of dimethylformamide. The solution was heated at 95 °C for 6 h, cooled, and stripped of solvent by evaporation under high vacuum using toluene as a chaser. The residue was purified by chromatography on a silica gel column (activity 3) eluting with ethyl acetate – methanol (7:3). The unsaturated ester was recovered as a yellow oil. Yield 75%; Infrared (film) 3400 (O—H), 1725 (C=O ester), 1665 (C=C), 1380 cm^{-1} (*gem*-dimethyl); nmr ($CDCl_3$) δ 1.26 (t, 3H, J = 7 Hz, —CH_2—CH_3), 1.28 and 1.50 (2s, 6H, $C(CH_3)_2$), 1.73–3.00 (m, 4H, C—CH_2—C, $H_{1'}$, $H_{4'}$), 3.60 (d, 2H, J = 5 Hz, —CH_2OH), 4.10 (q, 2H, J = 7 Hz, —CH_2—CH_3), 4.35 (m, 2H, $H_{2'}$, $H_{3'}$), 5.79 (d of d, 1H, J = 16 Hz, J = 2 Hz, H_2), 6.83 (d of d, 1H, J = 16 Hz, J = 7 Hz, H_3). *Anal.* calcd. for $C_{14}H_{22}O_5$: C 62.38, H 8.20; found: C 62.40, H 7.95.

trans-Ethyl-3-(4′β-acetoxymethyl-2′α,3′α-dihydroxy-di-O-isopropylidenecyclopent-1′β-yl)acrylate, ***12a***

The crude unsaturated ester **12** (400 mg) was acetylated with acetic anhydride – pyridine in the usual way. After evaporation of the solution to dryness, the residue was purified by chromatography on a silica gel column (activity III) eluting with ethyl acetate. The acetate was obtained as a slightly yellow oil. Yield 395 mg (85%, based on the hemiacetal **9**). Infrared (film) 1750 (C=O acetate), 1725 (C=O ethyl ester), 1660 (C=C), 1380 cm^{-1} (*gem*-dimethyl); nmr ($CDCl_3$) δ 1.27 (t, 3H, J = 7 Hz, —CH_2—CH_3), 1.29 and 1.50 (2s, 6H, $C(CH_3)_2$), 2.06 (s, 3H, $OCOCH_3$), 1.92–3.03 (m, 4H, C—CH_2—C, $H_{1'}$, $H_{4'}$), 4.10 (d, J = 5 Hz, —CH_2OAc), 4.13 (q, 2H, J = 7 Hz, —CH_2—CH_3), 4.40 (m, 2H, $H_{2'}$, $H_{3'}$), 5.75 (d of d, 1H, J = 16 Hz, J = 2 Hz, H_2), 6.97 (d of d, 1H, J = 16 Hz, J = 7 Hz, H_3); uv (EtOH) λ_{max} 220 nm (ϵ = 13 000). Mass spectrum m/e = 297 ($M^+ - CH_3$), 271, 267 ($M^+ - OC_2H_5$), 254 ($M^+ - CH_3 - COCH_3$), 252 ($M^+ - CH_3 - OC_2H_5$), 209 ($M^+ - CH_3 - COCH_3 - OC_2H_5$), 194, 177, 149, 98, 91. *Anal.* calcd. for $C_{16}H_{24}O_6$: C 61.5, H 7.8; found: C 61.9, H 7.47.

trans-Ethyl-3-(2′α,3′α-dihydroxy-di-O-isopropylidene-4′β-tetrahydropyranylcyclopent-1′β-yl)acrylate, ***12b***

To a solution of unsaturated ester **12** (238 mg, 0.76 mmol) in anhydrous ether (25 ml) was added dihydro-

Can. J. Chem. Downloaded from www.nrcresearchpress.com by 210.87.254.42 on 09/05/12
For personal use only.

pyran (64 mg, 10 equivl.) and a crystal of *p*-toluenesulfonic acid. The reaction mixture was stirred overnight at room temperature. After evaporation of the solvent, the residue was passed through an alumina column (neutral, Grade IV), eluting with hexane – ethyl acetate (4:1). The tetrahydropyranyl ether was recovered as a slightly yellow oil. Yield 255 mg (95%). Infrared (film) 1730 (C=O ester), 1665 (C=C), 1390, 1380 cm^{-1} (*gem*-dimethyl); nmr ($CDCl_3$) δ 1.27 (t, 3H, J = 7 Hz, $-CH_2-CH_3$), 1.30 and 1.52 (2s, 6H, $C(CH_3)_2$), 1.67 (m, 6H, $-CH_2-(CH_2)_3-CH$), 2.00–3.03 (m, 4H, $-CH-CH_2-CH$, $H_{1'}$, $H_{4'}$), 3.34–3.87 (m, $-CH_2O-CH-$), 3.70 (d, 2H, J = 5 Hz, $-CH_2OTHP$), 4.18 (q, 2H, J = 7 Hz, OCH_2-CH_3), 4.43–4.58 (m, 3H), 5.88 (d of d, 1H, J = 16 Hz, J = 2 Hz, H_2), 6.97 (d of d, 1H J = 16 Hz, J = 7 Hz, H_3). Mass spectrum m/e = 354 (M^+), 339 ($M^+ - CH_3$), 309 ($M^+ - OC_2H_5$), 255 ($M^+ - CH{=}CH{-}CO_2C_2H_5$), 212, 183, 177, 149, 91, 85. *Anal.* calcd. for $C_{19}H_{30}O_6$: C 64.38, H 8.53; found: C 63.83, H 8.56.

N-Methyl-2-(2'α,3'α-dihydroxy-di-O-isopropylidene-4'β-hydroxymethylcyclopent-1'β-yl)oxazolidine, ***10***

Hemiacetal **9** (100 mg, 0.5 mmol) was dissolved in 15 ml of dry benzene containing *N*-methylethanolamine (76 mg, 1 mmol) and the resulting mixture was refluxed with a Dean–Stark trap filled with molecular sieves (type 3A) for 48 h. After evaporation of the solvent, under vacuum, the oxazolidine **10** was obtained as a crude oil (145 mg). Attempts to purify the product by chromatography led to its decomposition. Infrared (film) 3420 (O—H), 2820 (N—CH_3), 1470, 1390 cm^{-1} (*gem*-dimethyl); nmr ($CDCl_3$) δ 1.30 and 1.48 (2s, 6H, $C(CH_3)_2$), 1.73–2.33 (m, 3H), 2.27 (s, 3H, N—CH_3), 2.43–2.77 (m, 2H), 3.67 (d, 2H, J = 6 Hz, $-CH_2OH$), 3.67–4.00 (m, 5H, $-CH_2-O$, H_2), 4.37–4.67 ppm (m, 2H, $H_{2'}$, H_3). Mass spectrum (70 eV) m/e = 257 (M^+), 242 ($M^+ - CH_3$), 226 ($M^+ - CH_2OH$), 187, 86.

N-Methyl-2-(2'α,3'α-dihydroxy-di-O-isopropylidene-4'β-hydroxymethylcyclopent-1'β-yl)thiazolidine, ***10b***

A mixture of the hemiacetal **9** (100 mg, 0.5 mmol) and *N*-methylthioethanolamine (48 mg, 1.1 equiv.) was refluxed in benzene with a Dean–Stark trap filled with molecular sieves (type 3A) for 48 h. Evaporation of the solvent afforded 150 mg of oily product which was purified by preparative tlc (ethyl ether as solvent system). The thiazolidine **9** was recovered as a colourless oil (R_f 0.3). Yield 85 mg (60%). Infrared ($CHCl_3$) 3360 (O—H), 2900 (N—CH_3), 1380 (*gem*-dimethyl) 1100 cm^{-1}; nmr ($CDCl_3$) δ 1.33 and 1.50 (2s, 6H, $C(CH_3)_2$), 1.97–2.33 (m, 4H, $H_{1'}$, $H_{4'}$, $H_{5'}$), 2.17 (s, 1H exch., O*H*), 2.38 (s, 3H, N—CH_3), 2.83–3.23 (AA'BB', 4H, $-S-CH_2-CH_2$), 3.67 (d, 2H, J = 6 Hz, $-CH_2OH$), 4.00–4.23 (m, 1H, H_2), 4.37–4.51 (m, 2H, $H_{2'}$, $H_{3'}$). Mass spectrum m/e = 273 (M^+), 258 ($M^+ - CH_3$), 226 ($M^+ - CH_3 - S$), 198, 185, 168, 102. The analysis was carried on the acetate derivative **10***c*.

N-Methyl-2-(4'β-acetoxymethyl-2'α,3'α-dihydroxy-di-O-isopropylidenecyclopent-1'β-yl)thiazolidine, ***10c***

The thiazolidine **10***b* (75 mg, 0.28 mmol) was acetylated with pyridine acetic anhydride in the usual way. The crude acetate was purified on an alumina column (activity III) eluting with ethyl ether. The product was obtained as a colourless oil. Yield 98%. Infrared ($CHCl_3$) 2800 (N—CH_3), 1745 (C=O acetate), 1390 cm^{-1} (*gem*-dimethyl); nmr ($CDCl_3$) δ 1.37 and 1.57 (2s, 6H, $C(CH_3)_2$), 2.10 (s, 3H, $COCH_3$), 2.11–2.65 (m, 4H, $H_{1'}$, $H_{4'}$, $H_{5'}$), 2.30 (s, 3H, —N—CH_3), 3.10 (AA'BB', 4H, $-S-CH_2-CH_2$), 4.17 (d, 2H, J = 6 Hz, $-CH_2OAc$), 4.20–4.67 (m, 3H, $H_{2'}$, $H_{3'}$, H_2). Mass spectrum m/e = 315 (M^+), 300 ($M^+ - CH_3$), 268 ($M^+ - CH_3 - S$), 257 ($M^+ - CH_3 - COCH_3$), 240, 227, 183, 125, 102. *Anal.* calcd. for $C_{15}H_{25}NO_4S$: C 57.13, H 7.99, N 4.44, S 10.15; found: C 56.86, H 7.66, N 4.23, S 10.03. The compound was directly acetylated.

1β-Formyl-4β-acetoxymethyl-2α,3α-(dihydroxy-di-O-isopropylidene)cyclopentane, ***13***

A. From Oxazolidine ***10***

The crude oxazolidine **10** (145 mg) was treated with acetic anhydride (3 ml) in pyridine (5 ml) at room temperature overnight. After evaporation of the solution to dryness, the crude acetate **10***a* was treated with aqueous acetic acid (50%, 10 ml) for ½ h. The aqueous solution was extracted with dichloromethane (3 × 15 ml). The combined extracts were washed with cold water, dried over sodium sulfate, and evaporated to dryness giving 95 mg of crude aldehyde **13**.

The aldehyde **13** was characterized as its semicarbazone which crystallized from the reaction mixture after several days. This compound was identical in all respects to **13***b* as obtained from **9**. Yield 75 mg (48%, based on the hemiacetal **9**), mp 156–157 °C.

B. From Ester ***12a***

A solution of the acrylate **12***a* (196 mg, 0.63 mmol) in dry methylene chloride (30 ml) was treated at −60 °C with ozone in oxygen at a rate of 7 mmol of ozone per h. The reaction was continued until the blue colour characteristic of ozone persisted. Excess of ozone was removed by bubbling nitrogen through the solution and dimethyl sulfide (1 ml) was added at −40 °C. The solution was stirred and allowed to rise slowly to room temperature. The methylene chloride solution was then washed with saturated sodium chloride (3 × 15 ml) and dried over sodium sulfate. Evaporation under high vacuum afforded the aldehyde **13** as a colourless oil. Yield 98%. Infrared ($CHCl_3$) 2990 (C—H aliphatic), 2730 (C—H aldehydic), 1730, 1735 (C=O ester, aldehyde), 1390 cm^{-1} (*gem*-dimethyl); nmr ($CDCl_3$) δ 1.33 and 1.50 (2s, 6H, $C(CH_3)_2$), 1.80–2.73 (m, 3H, H_5, H_4), 2.05 (s, 3H, $OCOCH_3$), 3.99 (d, 2H, J = 6 Hz, $-CH_2OAc$), 4.17 (m, 1H, H_1), 4.42 (m, 1H, H_2), 4.93 (m, 1H, H_3), 9.74 (s, 1H, C*H*O). Mass spectrum m/e = 242 (M^+), 227 ($M^+ - CH_3$), 184 ($M^+ - CH_3 - COCH_3$), 142, 124, 95, 79. *Anal.* calcd. for $C_{12}H_{16}O_5$: C 59.49, H 7.49; found: C 59.27, H 7.34.

This aldehyde was characterized as its crystalline semicarbazone, mp 158–160 °C. This compound was identical in all respects to that prepared from **10***a*.

4β-Acetoxymethyl-1β-(2',2'-dibromoethylene)-2α,3α-(dihydroxy-di-O-isopropylidene)cyclopentane, ***19***

A solution of the aldehyde **13** (194 mg, 0.8 mmol) in methylene chloride was added dropwise, under nitrogen, to a reagent prepared from interaction of zinc dust (2 equiv.), triphenylphosphine (2 equiv.), and carbon tetrabromide (2 equiv.) in dry methylene chloride at room

temperature for 24–30 h. The cloudy purple solution turned clear and the reaction mixture was stirred at room temperature for 20 h. When tlc showed complete disappearance of the starting material, the solution was concentrated to a small volume and filtered through a column of silica gel (activity 3) eluting with ether–hexane (1:1). The resulting dibromo olefin was obtained as a colourless oil. Yield 55–65%. Infrared ($CHCl_3$) 1745 (C=O ester), 1390, 1380 (*gem*-dimethyl), 870 cm^{-1} (C—Br_2); nmr ($CDCl_3$) δ 1.33 and 1.57 (2s, 6H, $C(CH_3)_2$), 1.83–2.50 (m, 3H, H_5, H_5, H_4), 2.17 (s, 3H, $OCOCH_3$), 2.83–3.13 (m, 1H, H_1), 4.17(d, 2H, J = 6 Hz, —CH_2OAc), 4.40–4.48 (m, 2H, H_2, H_3), 6.40 (d, 1H, J = 9 Hz, CH=CBr_2). Mass spectrum m/e = 400 (M^+, Br^{81}), 398 (M^+, $Br^{79,81}$), 396 (M^+, Br^{79}), 385 ($M^+ - CH_3$,Br^{81}), 383 ($M^+ - CH_3$,$Br^{79,81}$), 381 ($M^+ - CH_3$,Br^{79}), 342 (385 − $COCH_3$), 340 (383 − $COCH_3$), 338 (342 − $COCH_3$), 304 ($M^+ - CH_3 - Br$,Br^{81}), 302 ($M^+ - CH_3 - Br$,Br^{79}), 280, 263, 214, 212 (CH=CH—CH=CBr_2), 210. *Anal.* calcd. for $C_{13}H_{18}O_4Br_2$: C 37.4, H 4.77, Br 40.2; found: C 37.15, H 4.55, Br 40.14.

Acknowledgment

We wish to thank the National Research Council of Canada for financial support.

1. G. Just and G. Reader. Tetrahedron Lett. 1521 (1973); G. Just and G. Reader. Tetrahedron Lett. 1525 (1973).
2. K. Alder, F. Brockhagen, C. Kaiser, and W. Roth. Ann. **593**. 1 (1955).
3. H. Brouwer and J. B. Stothers. Can. J. Chem. **49**, 2152 (1971).
4. R. Daniels and J. L. Fischer. J. Org. Chem. **28**, 320 (1963).
5. K. C. Murdock and R. B. Angier. J. Am. Chem. Soc. **84**, 3758 (1962).
6. D. H. Williams and N. S. Bhacca. J. Am. Chem. Soc. **86**, 2742 (1964).
7. L. D. Hall. Adv. Carbohydr. Chem. **19**, 51 (1964).
8. H. Booth. Tetrahedron Lett. 411 (1965).
9. P. Laszlo and P. von R. Schleyer. J. Am. Chem. Soc. **85**, 2709 (1963).
10. C. S. Foote, M. T. Wuesthoff, S. Wexler, J. G. Burstain, R. Denny, G. O. Schenck, and K. H. Schulte-Elte. Tetrahedron, **23**, 2583 (1967).
11. P. S. Bailey. J. Am. Chem. Soc. **78**, 3811 (1956); J. P. Wibault and T. J. DeBoer. Recl. Trav. Chim. **78**, 183 (1959).
12. R. L. Augustine (*Editor*). Oxidation. Vol. 1. Marcel Decker Inc., New York. 1969.
13. J. J. Pappas, W. P. Keaveney, E. Gancher, and M. Berger. Tetrahedron Lett. 4273 (1966).
14. R. D. Guthrie and J. Honeyman. J. Chem. Soc. 2441 (1959).
15. J. N. Baxter and A. S. Perlin. Can. J. Chem. **38**, 2217 (1960).
16. E. J. Reist and P. H. Christie. J. Org. Chem. **35**, 3521 (1970).
17. J. C. Collins, W. W. Hess, and F. J. Frank. Tetrahedron Lett. 3363 (1968).
18. W. G. Dauben, M. Lorber, and D. S. Fullerton. J. Org. Chem. **34**, 3587 (1969).
19. M. Fetizon, M. Golfier, and J. M. Louis. Chem. Commun. 1118 (1969).
20. Y. F. Shealy and J. D. Clayton. J. Am. Chem. Soc. **91**, 3075 (1969).
21. H. Grob. Helv. Chim. Acta, **53**, 2156 (1970).
22. J. Schmidlin and A. Wettsein. Helv. Chim. Acta, **46**, 2799 (1963).
23. E. L. Eliel, N. L. Allinger, S. J. Angyal, and G. A. Morrison. Conformational analysis. Wiley–Interscience, New York. 1967. p. 399.
24. N. K. Kochetkov and B. A. Dimitriev. Tetrahedron, **21**, 803 (1965).
25. H. P. Albrecht, D. B. Repke, and J. G. Moffatt. J. Org. Chem. **38**, 1836 (1973).
26. J. A. Montgomery, K. Hewson, and A. G. Laseter. Carbohydr. Res. **27**, 303 (1973); also G. H. Jones and J. G. Moffatt, Abstracts, 158th National Meeting of the American Chemical Society, New York, 1969, CARB. 15.
27. D. S. Tarbell and D. P. Cameron. J. Am. Chem. Soc. **78**, 2731 (1956).
28. L. J. Altman and S. L. Richeimer. Tetrahedron Lett. 4709 (1971).
29. E. J. Corey and P. L. Fucks. Tetrahedron Lett. 3769 (1972).
30. H. Budzikiewicz, C. Djerassi, and D. H. Williams. Mass spectrometry of organic compounds. Holden-Day Inc. San Francisco. 1967.

Can. J. Chem. Downloaded from www.nrcresearchpress.com by 210.87.254.42 on 09/05/12
For personal use only.

C-Nucleosides and related compounds. VII. Synthesis of carbocyclic analogues of *C*-nucleosides

GEORGE JUST AND BERNADETTE CHALARD-FAURE
Department of Chemistry, McGill University, Montreal, Quebec H3C 3G1

Received July 7, 1975

GEORGE JUST and BERNADETTE CHALARD-FAURE. Can J. Chem. **54**, 861 (1976).

Condensation of lactone **1** and aminoguanadine provides the amino-triazole carbocyclic analogue of *C*-nucleoside **2***a*. Lead tetraacetate oxidation of the semicarbazone derivative **4** leads to the amino-oxadiazole derivative **5**. Isoxazolines **11** and **12** are obtained by 1,3-dipolar addition of mesitonitrile oxide with the α,β-unsaturated ester **13**. Addition of diazomethane onto ester **13** gives the pyrazoline **16** which can be oxidized with bromine to the corresponding carboethoxy-pyrazole **17**. The latter is converted to the carboxamido-pyrazole **18** by treatment with ammonia.

GEORGE JUST et BERNADETTE CHALARD-FAURE. Can. J. Chem. **54**, 861 (1976).

L'amino-triazole **2***a*, analogue carbocyclique de *C*-nucléoside, est obtenu par condensation de la lactone **1** avec l'aminoguanidine. L'oxidation de la semicarbazone **4** par le tétraacétate de plomb conduit au dérivé amino-oxadiazolique **5**. L'addition dipolaire-1,3 de l'oxide de mésitonitrile **10** sur l'ester α,β-insaturé **13** donne les isoxazolines **11** et **12**. L'addition du diazométhane sur ce même ester **13** conduit à la pyrazoline **16** qui peut être oxidée en carboéthoxy-pyrazole correspondant par le brome. L'ammoniac réagit avec ce dernier pour donner le carboxamido-pyrazole **18**.

In the preceding (1) paper, we described the synthesis of potential precursors to carbocyclic analogues of *C*-nucleosides. The synthetic utility of some of these compounds is illustrated here.

Condensation of the lactone **1** with aminoguanidine bicarbonate in pyridine, according to the procedure of Ried and Valentin (2) gave the amino-triazole **2**, mp 206–207 °C, in 85% yield after purification by chromatography. Treatment of **2** with dilute trifluoroacetic acid in water cleaved the isopropylidene group, leading to the oily carbocyclic *C*-nucleoside **2***a*.

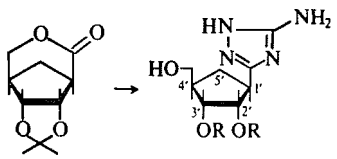

1 **2** R = $C(CH_3)_2$
2*a* R = H

SCHEME 1

Analogue **2***a* exhibited no virus inhibition when tested against nine different viruses in the agar diffusion assay and against vaccinia and herpes virus in plaque-reduction assays. The same results were observed with its ribofuranosyl analogue (15).

Lead tetraacetate oxidation (4) of the semicarbazone derivative **4** at low temperature under nitrogen, provided crystalline amino-oxadiazole **5**.

Elemental analysis and mass spectrometry indicated that the product had either structure **5** or that of the isomeric hydroxytriazole **7** or its triazolinone tautomer **8**. It has been shown (5) that, under the conditions used, cyclization to oxygen is favoured. The structure assignment was confirmed by the nmr spectrum, which showed the absence of an enolic O—H peak, and by the ir spectrum, which indicated the presence of a primary amino group and the absence of amide-type absorption. The acetal **6** was obtained as a minor side-product of the oxidation (5) of **4** and possibly arose from further oxidation of an initially formed azo-acetate **9** (6). Compound **6** was unstable and decomposed at room temperature to give the aldehyde **3**.

Treatment of the oxadiazole **5** with a catalytic amount of sodium in methanol afforded the crude alcohol **5***a*, the nmr spectrum of which showed no acetate peak. However, attempts to remove the isopropylidene group with trifluoroacetic acid in water led to a mixture of products due to the instability of amino-1,3,4-oxadiazoles towards acidic conditions (7). Consequently, **5***b* could not be characterized and submitted for biological testings.

Can. J. Chem. Downloaded from www.nrcresearchpress.com by 210.87.254.6 on 09/05/12
For personal use only.

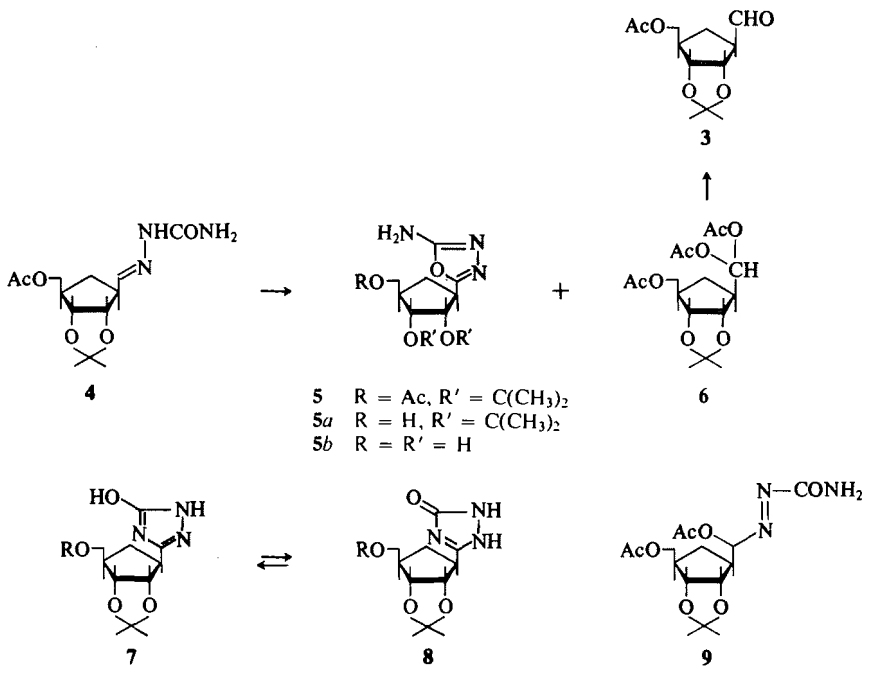

Unsaturated ester **13** proved to be a suitable precursor for the elaboration of five-membered heterocyclic systems via 1,3-dipolar additions. Cycloaddition of **13** with mesitonitrile oxide **10** (8) in refluxing benzene gave a mixture of two isomeric 2-isoxazolines **11** and **12** in approximately equal amounts. This was shown by two sets of triplets for the methyl of the carboethoxy group in the nmr spectrum. Previous work (9, 10) on the cycloaddition of mesitonitrile oxide onto olefinic and acetylenic esters (11) indicated that the addition was sterically controlled, leading to the isoxazolines with the ester group β to the oxygen atom. Models showed that the addition giving **11** and **12** was in fact favored, and that approach of the dipole from both sides of the double bond of **13** was equally feasible. It is also known that 1,3-dipolar additions are stereospecific, giving *cis* additions (12). On the basis of the preceding data, we assumed that the reaction product of **10** and **13** consisted mainly of an equimolecular mixture of the two diastereoisomeric 4-carboethoxy-2-isoxazolines **11** and **12**. The nmr spectrum of the reaction product corroborated our assumption. The C_5 proton gave a multiplet at δ 5.15 consistent with the chemical shift observed for this proton in similar 5-glycosyl-2-isoxazolines (10). Had the addition of **10** to **13** occurred in the reverse manner, H_4 should have been found at markedly higher field.

It is known that 4-carbethoxy-2-isoxazolines decarboxylate easily (13) upon hydrolysis. Hydrolysis of the crude cycloaddition product with ethanolic potassium hydroxide resulted in loss of both the acetate and the carbethoxy group and the formation of **15**, confirming the structures of **11** and **12**. Attempts to oxidize the isoxazolines **11** and **12** to the corresponding isoxazole **14** failed (14, 15).

The ester **13** underwent a facile addition with an excess of diazomethane at room temperature. In this case, the addition was electronically controlled, and attack occurred in a Michael fashion, leading to the pyrazoline **16** with the nitrogen β to the activating group (10, 11, 16), presumably via a 1-pyrazoline which rapidly isomerized. Its nmr spectrum showed multiple signals for the ethyl ester substituent suggesting a mixture of epimers at C_4. Accordingly, dehydrogenation to the corresponding pyrazole was carried out on the crude product **16**. The pyrazoline **16** was stirred at 0 °C with $1\frac{1}{2}$ molar equiv. of bromine in chloroform (16, 17). Evaporation of the solvent left a crude oil, the nmr spectrum of which showed that the isopropylidene group had been partially hydrolyzed.

Can. J. Chem. Downloaded from www.nrcresearchpress.com by 210.87.254.6 on 09/05/12
For personal use only.

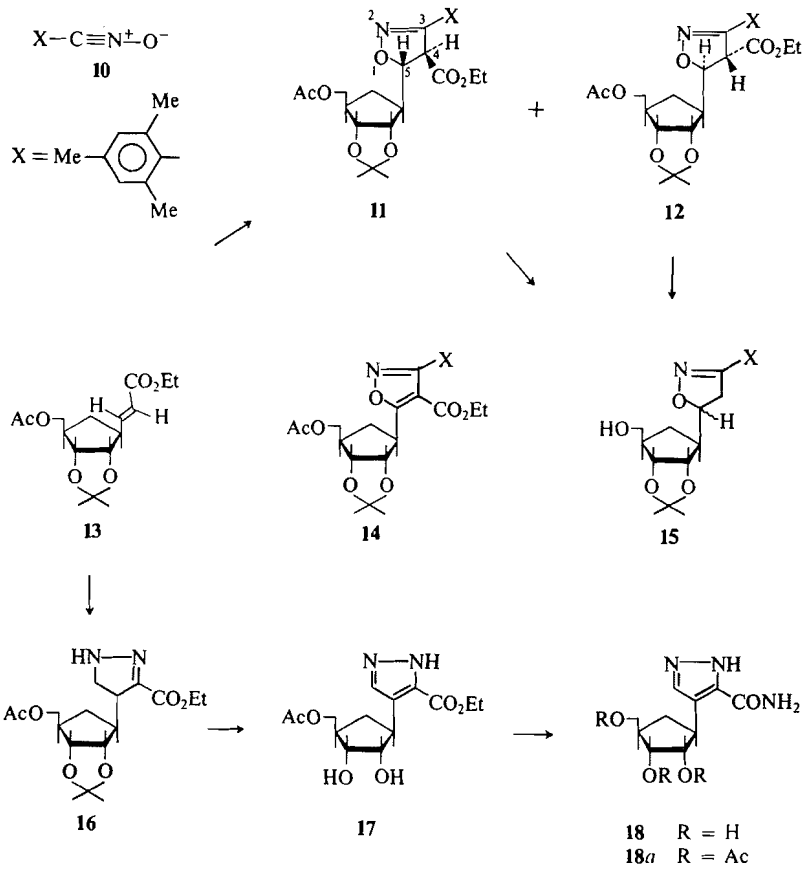

Stirring with a solution of sodium sulfite to complete the hydrolysis and destroy excess bromine gave, after chromatography, the oily pyrazole **17** in an overall yield of 65% based on the unsaturated ester **13**.

It should be noted that use of bromine as a dehydrogenating agent led to somewhat irreproducible results. Since the isopropylidene group was partially removed during the process, it is possible that the hydroxy functions were subsequently oxidized by bromine.

Treatment of the carboethoxy-pyrazole **17** with saturated methanolic ammonia at room temperature for five days afforded the carboxamidopyrazole **18**, mp 180–181 °C, in 65% yield (3).

The compound **18** was characterized by its triacetate derivative **18***a*. Although the tetraacetate was most likely formed in a first step, the *N*-acetyl group in pyrazole is known to be very labile (17) and its elimination probably occurred during purification on silica gel plates.

Although **18** has not been submitted for testing yet it should be mentioned that its ribofuranosyl analogue (15) showed no activity in the assay in which **2***a* has been tested.

Experimental

Melting points were determined on a Gallenkamp block and are uncorrected. Mass spectra were obtained on an AEI-MS-902 mass spectrometer at 70 eV using a direct insertion probe. Nuclear magnetic resonance spectra were recorded on Varian T-60 and HA-100 spectrophotometers using tetramethylsilane as an internal standard. Infrared spectra were determined on Unicam SP-1000 and Perkin-Elmer PE-257 infrared spectrophotometers. Analytical thin layer chromatography was performed on silica gel coated plastic plates (Eastman Kodak) and on a preparative scale on 20 cm × 20 cm × 1 mm silica gel (E.M. $HF_{254+366}$) coated glass plates. Woelm alumina (neutral) and silica gel were used for column chromatography. Microanalyses were carried out by Dr. C. Daessle, Montreal.

3-Amino-5-(2′α,3′α-dihydroxy-di-O-isopropylidene-4′β-hydroxymethylcyclopent-1′β-yl)-1,2,4-triazole, **2**

Aminoguanidine bicarbonate (205 mg, 1.5 mmol) was added to the lactone **1** (1) (300 mg, 1.5 mmol) in 8 ml of

Can. J. Chem. Downloaded from www.nrcresearchpress.com by 210.87.254.6 on 09/05/12
For personal use only.

Can. J. Chem. Downloaded from www.nrcresearchpress.com by 210.87.254.6 on 09/05/12
For personal use only.

pyridine and the reacton mixture was refluxed for 10 h. Filtration through Celite and evaporation of the solvent under high vacuum (using toluene as a chaser) afforded a semi-crystalline residue which was purified by chromatography on 20 × 20 cm silica gel plates. A mixture of ethyl acetate – methanol (7:3) was used as eluant and the band having a R_f = 0.6 under these conditions gave **2** as white crystals. Yield 325 mg (85%); mp 206–207 °C. Infrared (KBr) 3410 (O—H), 3220 (N—H), 1650 (C=N), 1380 cm^{-1} (acetonide); nmr (pyridine-d_5) δ 1.33 and 1.60 (2s, 6H, $C(CH_3)_2$), 2.57 (m, 3H, $—CH_2—$, $H_{4'}$), 3.63 (m, 1H, $H_{1'}$), 3.90 (d, 2H, J = 5 Hz, $—CH_2OH$), 4.86 (m, 1H, $H_{3'}$), 5.31 (m, 1H, $H_{2'}$), 6.66 (br s, 2H exch., NH_2), 7.85 (br s, 1H exch., NH); uv (MeOH) λ_{max} 217 nm (ϵ 2500). Mass spectrum m/e = 254 (M^+), 239 ($M^+ - CH_3$), 224 ($M^+ - CH_2O$), 209 ($M^+ - CH_3 - CH_2O$), 196, 179, 165, 149, 126, 111 (B* + 28), 110 (B + 27) (B = heterocyclic base). *Anal.* calcd. for $C_{11}H_{18}N_4O_3$: C 51.95, H 7.14, N 22.03; found: C 51.64, H 7.12, N 22.03.

3-Amino-5-(2′α,3′α-dihydroxy-4′β-hydroxymethyl-cyclopent-1′β-yl)-1,2,4-triazole, 2a

The acetonide **2** (100 mg, 0.4 mmol) was dissolved in 5 ml of trifluoroacetic acid – water (9:1) and the solution was stirred at room temperature for 10 min. After dilution with 10 ml of water, the reaction mixture was extracted with chloroform (3 × 10 ml). Evaporation of the aqueous layer under high vacuum (using methanol as chaser) afforded a glassy product which failed to crystallize. Yield 85 mg. Infrared (film) 3240 (O—H), 3220 (N—H), 1640 cm^{-1} (C=N); nmr (D_2O, external TMS) δ 1.23–1.60 (m, 1H, $H_{5'}$), 2.03–2.43 (m, 2H, $H_{5'}$, $H_{4'}$), 3.00–3.20 (m, 1H, $H_{1'}$), 3.57 (d, 2H, J = 6 Hz, $—CH_2OH$), 3.83–4.33 (m, 2H, $H_{2'}$, $H_{3'}$); uv (MeOH) λ_{max} 214 nm (ϵ 2500). Mass spectrum m/e = 214 (M^+), 197 ($M^+ - NH_3$), 167 ($M^+ - NH_3 - CH_2O$), 155, 138, 127, 111 (B + 28), 110 (B + 27). *Anal.* calcd. for $C_8H_{14}N_4O_3 \cdot H_2O$: C 41.4, H 6.9, N 24.1; found: C 41.1, H 6.8, N 24.1.

2-Amino-5-(4′β-acetoxymethyl-2′α,3′α-dihydroxy-di-O-isopropylidenecyclopent-1′β-yl)-1,3,4-oxadiazole, 5

A methylene chloride solution of the semicarbazone acetate **4** (1) (120 mg, 0.4 mmol in 6 ml of CH_2Cl_2) was added dropwise, at 0 °C under nitrogen, to a suspension of lead tetraacetate (266 mg, 1.5 equiv.) in the same solvent. The reaction mixture was vigorously stirred at 0 °C for 1 h and then hydrolyzed with ice cold water (10 ml). After filtration through a bed of Celite, the organic layer was separated, washed with cold water followed by cold sodium bicarbonate solution and dried over sodium sulfate. Evaporation gave a yellowish oil which was purified by preparative tlc (elution with ethyl acetate). The main band (R_f 0.5) afforded 65 mg of oily oxadiazole **5** which crystallized from ether–chloroform. Yield 65%; mp 158–160 °C. Infrared ($CHCl_3$) 3500, 3420 (NH_2), 1740 (C=O acetate), 1660 (C=N), 1385 cm^{-1} (*gem*-dimethyl); nmr ($CDCl_3$) δ 1.33 and 1.52 (2s, 6H, $C(CH_3)_2$), 1.83–2.73 (m, 3H, $—CH_2—$, $H_{4'}$), 2.07 (s, 3H, $OCOCH_3$), 3.27–3.60 (m, 1H, $H_{1'}$), 4.07 (d, 2H, J = 6 Hz, $—CH_2OAc$), 4.37–4.57 (m, 1H, $H_{3'}$), 4.73–4.90 (m, 1H, $H_{2'}$), 5.73 (br s, 2H exch., NH_2); uv (EtOH) λ_{max} 222 ϵ 9500). Mass spectrum m/e = 297 (M^+), 282 ($M^+ - CH_3$), 240 ($M^+ - CH_3 - CONH_2$), 239 ($M^+ - CH_3 - COCH_3$), 210 (240 − N), 180, 169, 162, 150, 126, 112 (B + 28), 111 (B + 27), 94 (B = base). *Anal.* calcd. for $C_{13}H_{19}N_3O_5$: C 52.52, H 6.40, N 14.14; found C 52.46, H 6.07, N 14.34.

4β-Acetoxymethyl-1β-di-O-acetoxymethyl-2α,3α-(dihydroxy-di-O-isopropylidene)cyclopentane, 6

This compound was obtained as a side product of the oxidation of **4** to the oxadiazole **5**.

The crude product of lead tetraacetate oxidation of **4** was purified by chromatography on silica gel plates (ethyl acetate as solvent system). The top band (R_f 0.85) afforded the acetal **6** as a yellowish oil. Yield 10–30%. Infrared ($CHCl_3$) 1750–1745 (C=O esters), 1390 cm^{-1} (*gem*-dimethyl); nmr ($CDCl_3$) δ 1.33 and 1.53 (2s, 6H, $C(CH_3)_2$), 2.10 (s, 9H, $OCOCH_3$) 2.00–2.60 (m, 3H, H_4, 2 × H_5), 3.20 (m, 1H, H_1), 4.05 (d, 2H, J = 6 Hz, $—CH_2$-OAc), 4.38–4.62 (m, 2H, H_2, H_3), 6.83 (d, 1H, J = 5 Hz, $—CH(OAc)_2$). Mass spectrum m/e = 329 ($M^+ - CH_3$), 301 ($M^+ - COCH_3$), 285 ($M^+ - OCOCH_3$), 271, 243 ($M^+ - 2COCH_3$), 227, 224, 199, 185, 167, 139.

Upon standing at room temperature, this acetal decomposed to give the corresponding aldehyde **3** (1). Partial decomposition most likely occurred during the isolation process on silica gel.

4-Carboethoxy-5-(4′β-acetoxymethyl-2′α,3′α-dihydroxy-di-O-isopropylidenecyclopent-1′β-yl)-3-(2,4,6-trimethylphenyl)-2-isoxazolines, 11 + 12

Mesitonitrile oxide **10** (80 mg, 0.48 mmol) was added to a solution of the unsaturated acetoxy ester **13** (1) (150 mg, 0.48 mmol) in 7 ml of benzene and the resulting mixture was refluxed for 14 h. The solution was cooled and evaporated to dryness under vacuum. The crude residue was purified by preparative tlc eluting with ethyl acetate – hexane (1:1). The product (R_f 0.7) was recovered as a colourless oil. Yield 220 mg (95%). Infrared (film) 3030 (C—H, aromatic), 2970 (C—H, aliphatic), 1745, 1735 (C=O, acetate, ester), 1620 (C=N, aryl isoxazoline), 1380, 1390 cm^{-1} (*gem*-dimethyl); nmr ($CDCl_3$) δ 0.93 and 0.97 (2t, 3H, J = 7 Hz, $CO_2CH_2CH_3$), 1.30 and 1.51 (2s, 6H, C (CH_3)$_2$), 2.08 (s, 3H, $OCOCH_3$), 2.27 (s, 9H, $—C_6H_2(CH_3)_3$), 2.00–2.60 (m, 3H, $H_{5'}$, $H_{5'}$, H_4'), 3.03 (m, 1H, $H_{1'}$), 3.87–4.56 (m, 7H, $—OCH_2CH_3$ $—CH_2OAc$, $H_{2'}$, $H_{3'}$, $H_{4'}$), 4.97–5.50 (m, 1H, H_5), 6.90 (br s, 2H, $—C_6H_2$); uv (EtOH) λ_{max} 217 nm (ϵ 12 000). Mass spectrum m/e = 473 (M^+), 458 ($M^+ - CH_3$), 415 ($M^+ - CH_3 - COCH_3$), 370 ($M^+ - CH_3 - COCH_3 - OC_2H_5$), 260 (B), 231, 185, 95 (B = heterocyclic base). *Anal.* calcd. for $C_{26}H_{35}NO_7$: C 65.94, H 7.45, N 2.96; found: C 65.63, H 7.57, N 2.78.

5-(2′α,3′α-Dihydroxy-di-O-isopropylidene-4′β-hydroxymethylcyclopent-1′β-yl)-3-(2,4,6-trimethylphenyl)-2-isoxazoline, 15

The crude mixture of isoxazolines **11** + **12** (100 mg) was treated with methanolic potassium hydroxide at room temperature for 18 h. After evaporation of the solvent and addition of water (10 ml), the solution was neutralized with dilute hydrochloric acid (10%) to pH 5. The aqueous solution was extracted with ethyl acetate (3 × 10 ml) and the combined extracts were dried over sodium sulfate. Evaporation of the solvent afforded 35 mg of oily product which was purified by preparative tlc using ethyl acetate as eluant. The compound was

Can. J. Chem. Downloaded from www.nrcresearchpress.com by 210.87.254.6 on 09/05/12
For personal use only.

recovered as a white solid. Yield 33%, based on ester **13**. Infrared ($CHCl_3$) 3400 (O—H), 3030 (C—H aromatic), 2980 (C—H aliphatic), 1620 (C=N), 1390 cm^{-1} (*gem*-dimethyl); nmr ($CDCl_3$) δ 1.32 and 1.52 (2s, 6H, $C(CH_3)_2$), 2.30 (s, 9H, $—C_6H_2(CH_3)_3$), 2.02–2.60 (m, 3H, $H_{5'}$, $H_{5''}$, $H_{4'}$), 3.02 (m, 1H), 3.62 (m, 2H), 3.87 (m, 7H), 5.20 (m, 1H), 6.93 (m, 2H, $—C_6H_2—$); uv (EtOH) λ_{max} 212 nm (ϵ 10 000). Mass spectrum m/e = 359 (M^+), 344 ($M^+ - CH_3$), 216 (B + 27), 214, 188, 159, 145, 119, 91 (B = heterocyclic base).

3-Carboethoxy-4-(4'β-acetoxymethyl-2'α,3'α-dihydroxy-di-O-isopropylidenecyclopent-1'β-yl)-2-pyrazoline, ***16***

The unsaturated ester **13** (1) (100 mg, 0.32 mmol) was dissolved in 5 ml of an etheral solution of diazomethane (1.5% by weight). The solution was stirred at room temperature for 6 h and then evaporated to dryness under vacuum. The pyrazoline was obtained as a yellow oil in quantitative yield and was not further purified. Infrared ($CHCl_3$) 3380 (N—H), 1745 (C=O ester, acetate), 1635 (C=N), 1380 cm^{-1} (*gem*-dimethyl); nmr ($CDCl_3$) δ 1.27 (t, 3H, $—OCH_2CH_3$), 1.29 and 1.47 (2s, 6H, $C(CH_3)_2$), 2.06 (2, 3H, $OCOCH_3$), 1.85–2.66 (m, 4H), 3.40–3.90 (m, 3H), 4.07–4.50 (m, 6H, $—CH_2OAc$, $—OCH_2CH_3$, $H_{2'}$, $H_{3'}$), 6.04 (br s, 1H exch., N*H*); uv (EtOH) λ_{max} 285 nm (ϵ 3900). Mass spectrum m/e = 355 ($M^+ + 1$), 354 (M^+), 340 (355 − CH_3), 339 ($M^+ - CH_3$), 311 ($M^+ - COCH_3$), 297 (340 − $COCH_3$), 251 ($M^+ - CH_3 - COCH_3 - OC_2H_5$), 236, 195, 141, 121, 95.

5(3)-Carboethoxy-4-(4'β-acetoxymethyl-2'α,3'α-dihydroxycyclopent-1'β-yl)pyrazole, ***17***

To a solution of pyrazoline **16** (344 mg, 0.94 mmol) in chloroform at 0 °C, was added dropwise a solution of bromine in chloroform (1.5 mmol). The reaction was stirred at 0 °C for 1 h after which tlc showed complete disappearance of the starting material. A solution of sodium sulfite (10%, 10 ml) was added and the solution was stirred for another 15 min. After evaporation to dryness, the residue was extracted with ethyl acetate (3 × 15 ml). Evaporation of the combined extracts gave the crude oily pyrazole which was purified by preparative tlc using ethyl acetate – methanol (7:3) as solvent system. Extraction of the lower band (R_f 0.6) afforded the oily pyrazole **17**. Yield 190 mg (65%). Infrared ($CHCl_3$) 3450 (N—H), 3300 (O—H), 1735, 1720 (C=O acetate, ester), 1475 cm^{-1} (C=N); nmr (pyridine-d_5), δ 1.30 (t, 3H, $CO_2CH_2CH_3$), 1.20–1.4 (m, 1H, $H_{5'}$), 2.03 (s, 3H, $OCOCH_3$), 2.21 (m, 2H, $H_{5'}$, $H_{4'}$), 3.5 (m, 1H, $H_{1'}$), 3.72–4.43 (m, 6H, $—CH_2OAc$, $H_{2'}$, H_3', $—CO_2CH_2CH_3$), 6.23 (br s, 3H exch., O*H*, N*H*), 7.60 (s, 1H, H_5); uv (EtOH) λ_{max} 222 nm (ϵ 7000).

3(5)-Carboxamido-4-(2'α,3'α-dihydroxy-4'β-hydroxymethylcyclopent-1'β-yl)pyrazole, ***18***

A solution of the pyrazole **17** (90 mg, 0.28 mmol) in methanol (8 ml) was saturated with ammonia at −60 °C and left at room temperature for one week. After evaporation to dryness, the residue was partitioned between chloroform and water. The aqueous layer was washed twice with chloroform and evaporated to dryness leaving 60 mg of crude pyrazole **18** which crystallized from methanol. Yield 65%; mp 180–181 °C. Infrared (film) 3450, 3300 (N—H, O—H), 1670 (C=O amide), 1600 cm^{-1} (C=N); nmr (D_2O, external TMS) δ 1.15–1.50 (m, 1H, $H_{5'}$), 1.83–2.50 (m, 2H, $H_{4'}$, $H_{5'}$), 3.00–3.40 (m, 1H, $H_{1'}$), 3.60 (d, 2H, J = 5 Hz, $—CH_2OH$), 3.87 (m, 2H, $H_{2'}$, $H_{3'}$), 8.20 (s, 1H, H_5); uv (EtOH) λ_{max} 220 nm (ϵ 7000). Mass spectrum 241 (M^+ − H), 221 (241 − H_2O), 205, 192, 138, 121 (B + 27 − NH). *Anal.* calcd. for $C_{10}H_{15}O_4N_3$: C 49.78, H 6.27, N 17.42; found: C 49.58, H 6.57, N 17.25.

3(5)-Carboxamido-4-(4'β-acetoxymethyl-2'α,3'α-diacetoxycyclopent-1'β-yl)pyrazole, ***18a***

The pyrazole **18** (50 mg) was treated with acetic anhydride (3 ml) in pyridine (5 ml) overnight. After evaporation to dryness, the residue was purified by preparative tlc silica gel plates eluting with ethyl acetate. The band (R_f 0.75) afforded the triacetate **18a**. Yield 65%. Infrared ($CHCl_3$) 3520–3460 (NH_2, NH), 1740 (C=O esters), 1685 (C=O amide), 1590 cm^{-1} (C=N); nmr ($CDCl_3$) δ 1.20 (m, 2H, 2 × $H_{5'}$), 2.07 (s, 3H, CH_2OCOCH_3), 2.10 (s, 6H, 2 × $OCOCH_3$), 2.5 (m, 2H, $H_{1'}$, $H_{4'}$), 4.15 (d, 2H, J = 5 Hz, CH_2OAc), 5.00–5.50 (m, 2H, $H_{2'}$, $H_{3'}$), 7.45 (s, 1H, H_5). Mass spectrum m/e = 368 ($M^+ + 1$), 265 ($M^+ - 2COCH_3 - NH_2$) 247, 223, 205, 187, 138 (B + 28), 137 (B + 27), 121 (137 − NH_2).

Acknowledgements

We wish to thank the National Research Council of Canada for financial support. Thanks are due to Drs. D. C. DeLong, R. Nagarajan, G. E. Gutowski and K. Gerzon, Lilly Research Laboratories, Indianapolis, Ind. for biological tests.

1. G. JUST, G. READER, and B. CHALARD-FAURE. Can. J. Chem. This issue.
2. W. RIED and J. VALENTIN. Chem. Ber. **101**, 2117 (1968).
3. H. P. ALBRECHT, D. B. REPKE, and J. G. MOFFAT. J. Org. Chem. **39**, 2176 (1974).
4. A. M. CAMERON, P. R. WEST, and J. WARKENTIN. J. Org. Chem. **34**, 3230 (1969).
5. P. WEST and J. WARKENTIN. J. Org. Chem. **33**, 2089 (1968).
6. W. A. F. GLADSTONE, J. B. AYLWARD, and R. O. C. NORMAN. J. Chem. Soc. C, 2587 (1969).
7. L. G. BEHR. *In* Five and six-membered compounds with nitrogen and oxygen. Vol. 17 of the Chemistry of heterocyclic compounds. *Edited by* R. H. Wiley. Wiley–Interscience, New York and London. 1962. p. 271.
8. C. GRUNDMANN and J. M. DEAN. J. Org. Chem. **30**, 2809 (1965).
9. C. GRUNDMANN and P. GRUNANGER. The nitrile oxides. Springer-Verlag, New York, Heidelberg, Berlin. 1971 p. 107.
10. J. M. J. TRONCHET, S. JACCARD-THORNDAHL, L. FAIVRE, and P. MASSARD. Helv. Chim. Acta, **56**, 1303 (1973); J. BASTIDE and O. HENRI-ROUSSEAU.
11. J. BASTIDE, J. HAMELIN, F. TEXIER, and Y. V. QUANG. Bull. Soc. Chim. Fr. 2555 (1973); 2871 (1973).
12. R. HUISGEN. Angew Chem. Int. Ed. Engl. **21**, 565 (1963); **21**, 635 (1963).

13. A. R. KATRITZKY (*Editor*). Advances in heterocyclic chemistry. Vol. 2. Academic Press, New York and London. 1963. p. 410.
14. P. K. MARTIN. J. Org. Chem. **33**, 3758 (1968).
15. M. RAMJEESINGH. Ph.D. Thesis, McGill University, Montreal. 1975.
16. R. FUSCO. *In* The chemistry of heterocyclic compounds. Vol. 22. *Edited by* A. Weissberger. Interscience, New York. 1967. p. 1.
17. A. R. KATRITZKY and A. J. BOULTON (*Editors*). Advances in heterocyclic chemistry. Vol. 6. Academic Press, New York and London. 1966. p. 385.

Can. J. Chem. Downloaded from www.nrcresearchpress.com by 210.87.254.6 on 09/05/12
For personal use only.

2,3-Oxazabicyclo[2.2.1]heptane

GEORGE JUST AND LUIGI CUTRONE
Department of Chemistry, McGill University, Montreal, Quebec H3C 3G1

Received September 19, 1975

GEORGE JUST and LUIGI CUTRONE. Can. J. Chem. **54**, 867 (1976).

The title compound **5** was synthesized by adding nitroso derivative **2***e* to cyclopentadiene. The resulting adduct was reduced with diborane followed by acetic acid, and the dinitrobenzoyl group then removed with potassium hydroxide or ammonia.

GEORGE JUST et LUIGI CUTRONE. Can. J. Chem. **54**, 867 (1976).

Le composé **5** a été synthétisé par l'addition du dérivé nitrosé **2***e* au cyclopentadiène. Le produit obtenu fut réduit avec le diborane, suivit par de l'acide acétique, et le groupement protecteur enlevé avec de l'hydroxyde de potassium ou de l'ammoniaque.

The primary prostaglandins PGG and PGH have a 2,3-dioxabicyclo[2.2.1]heptane skeleton (**5**, NH=O). In view of their biological importance, we were interested in synthesizing analogs in which one of the oxygens of the *endo*-peroxide bridge is replaced by nitrogen. Only one member of this class of compounds, *N*-phenyl-2,3-oxazabicyclo[2.2.1]hept-5-ene (**3**, R = Ph), has been described (1). It is reported to decompose slowly at 0 °C.

The Diels–Alder route leading to compounds **3**, **4**, and **5** seemed more attractive than others, and we therefore sought to develop a dienophile bearing a nitroso group which would form a stable adduct of type **3**, and in which, after saturation of the double bond, the group R could be removed without destruction of the molecule.

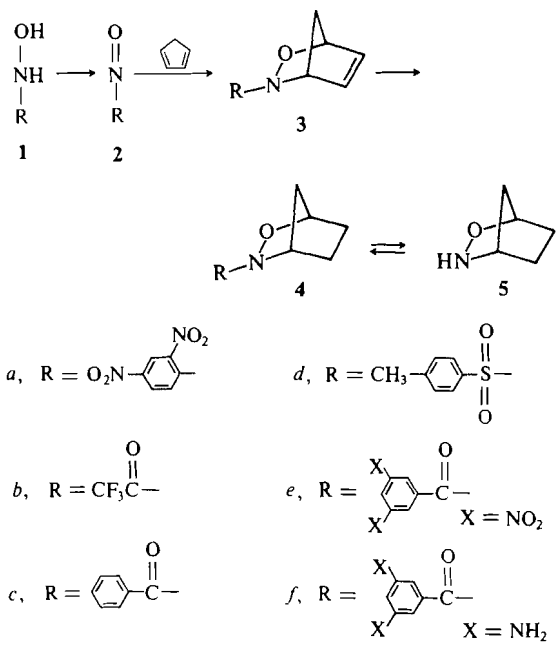

Preliminary experiments using 1-chloro-1-nitrosocyclohexane as dienophile indicated that low temperature reaction with cyclopentadiene gave a product which decomposed at −30 °C with formation of a black tar.

It has been reported that nitrosobenzene bearing an electron-withdrawing group at the *para*-position underwent the Diels–Alder reaction in much higher yield than nitrosobenzene bearing an electron-donating group (2). We therefore studied the reactions of various nitroso derivatives **2** in which R is an electron-withdrawing group.

Reaction of 2,4-dinitronitrosobenzene **2***a* (3) with cyclopentadiene gave the expected bicyclic adduct **3***a*, mp 101–102.5 °C in 82% yield. The adduct could be recovered unchanged even after boiling in carbon tetrachloride for 24 h. Attempts to reduce the double bond catalytically failed and resulted in decomposition of the product, presumably because of reduction of the nitro groups, which are necessary for the stabilization of the bicycloheptene system **3***a*. Reduction of **3***a* with diimine (4) gave **4***a*, mp 122–125 °C. Attempts to remove the dinitrophenyl group using Amberlite OH resin (5) proceeded poorly, and the use of mercaptoethanol, which is reported (6) to liberate amines from *N*-substituted 2,4-dinitroanilines, resulted in cleavage of the O—N bond and the formation of **6**.

Since electron-withdrawing groups such as dinitrophenyl accelerate the Diels–Alder reaction and stabilize the Diels–Alder adduct formed, we focussed our attention on nitroso compounds

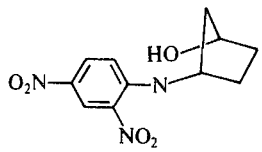

6

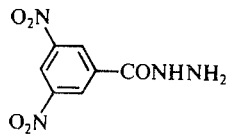

7

bearing acyl groups, in which the acyl group could be removed readily after Diels–Alder reaction and saturation of the double bond. Because of the ease of hydrolysis of trifluoroacetamides, we first studied the condensation of cyclopentadiene with CF_3CONO. Trifluoroacetohydroxamic acid **1***b* was added at −70 °C to cyclopentadiene and benzyltrimethylammonium periodate (7). The resulting product had the spectral characteristics (ir, nmr, ms) required for **3***b* but turned brown after standing at 40 °C in solution for a few minutes. Catalytic reduction gave the oily saturated bicyclic system **4***b*. Treatment of **4***b* with sodium borohydride (8) gave the oily oxazabicycloheptane **5**, which was characterized as its 2,4-dinitrophenyl derivative **4***a*.

We next investigated the nitroso compound **2***c* derived from benzhydroxamic acid (**1***c*). Its reaction with cyclopentadiene gave in low yield a product having the nmr spectrum appropriate for the expected adduct **3***c*. However, it decomposed at 40 °C and was therefore not further characterized.

Reaction of the nitroso compound **2***d* derived from *p*-toluenesulfinic acid (9) with cyclopentadiene gave in 30% yield the crystalline, stable, adduct **3***d* which gave a good mass spectrum. However, extreme insolubility made this product unattractive as an intermediate.

The nitroso derivative **2***c* derived from 3,5-dinitrobenzhydroxamic acid **1***e* (10) turned out to be most appropriate for the construction of **5**.

Addition of **1***e* to cyclopentadiene and benzyltrimethylammonium periodate at −20 °C gave a good yield of a crystalline adduct **3***e*, which when refluxed for 24 h in carbon tetrachloride was recovered unchanged. Catalytic reduction of **3***e*, under conditions which would reduce only the nitro groups, gave **3***f* as an oil. It decomposed upon standing at room temperature. We attempted a selective reduction of the double bond with diimine (4) generated by oxidation of hydrazine. The reaction, however, resulted in the cleavage of the amide bond and formation of 3,5-dinitrobenzhydrazide **7**, and no oxazobicycloheptane **5** was isolated. Treatment of **3***e* with diborane (11), followed by hot acetic acid, gave the saturated bicyclic system **4***e*, which was converted with either methanolic ammonia or potassium hydroxide to **5**, which was characterized as its dinitrophenyl derivative **4***a*.

In conclusion, it appears that an electron-withdrawing group is essential for the stabilization of bicyclic olefins of type **3**.

Experimental

General

All melting points were determined in open capillaries on a Gallenkamp melting point apparatus and are uncorrected. The ir spectra were recorded on a Unicam SP-1000. The nmr spectra were recorded on a Varian T-60 spectrometer operating at 60 MHz. Merck silica gel HF was used for tlc. Mass spectra were obtained on an AEI-MS-902 mass spectrometer at 70 eV using direct insertion probe.

N-2,4-Dinitrophenyl-2,3-oxazabicyclo[2.2.1]hept-5-ene, 3a

Freshly distilled cyclopentadiene 3.30 g (0.05 mol) was slowly added to a solution of 1.97 g (0.01 mol) of 2,4-dinitronitrosobenzene in 50 ml of acetone at −20 °C. After 2 h, the excess cyclopentadiene and acetone were removed under vacuum and the solid residue was recrystallized from ethanol to afford 2.15 g (82%) of light yellow crystals: mp 96–100 °C, one further recrystallization from ethanol raised the melting point to 101–102.5 °C; nmr ($CDCl_3$) δ 1.9 (2H, q), 5.4 (2H, d), 6.2 (1H, m), 6.7 (1H, m), 7.5 (1H, d), 8.3 (1H, q), 8.6 (1H, d) ppm; ir (KBr) 1620, 1610, 1590, 1530, 1520 cm^{-1}; *m/e* 263 (M^+); *Anal.* calcd. for $C_{11}H_9N_3O_5$: C 50.19, H 3.45, N 15.97; found: C 49.89, H 3.35, N 16.11.

N-2,4-Dinitrophenyl-2,3-oxazabicyclo[2.2.1]heptane, 4a

A solution of 1.10 g (4.18 mmol) of the olefin in 15 ml of 95% ethanol was cooled to 0 °C in an ice bath and to it was added 1.5 ml of 95% hydrazine and 0.25 ml of 1% solution of cupric sulfate pentahydrate with vigorous stirring. When a precipitate started to appear 0.75 ml of 30% hydrogen peroxide was slowly added (15 to 20 min). After 30 min the product was filtered off and was recrystallized from ethanol to afford 500 mg (45%) of light orange crystals: mp 123–125 °C; nmr ($CDCl_3$) δ 2.0 (6H, m), 4.3 (1H, m), 4.7 (1H, m), 7.3 (1H, d), 8.3 (1H, q), 9.5 (1H, d) ppm; ir (KBr) 1610, 1590, 1530, 1520 cm^{-1}; *m/e* 265 (M^+). *Anal.* calcd. for $C_{11}H_{11}N_3O_5$: C 49.81, H 4.18, N 15.84; found: C 49.83, H 4.30, N 15.73.

N-(2,4-Dinitrophenyl)-3-hydroxycyclopentylamine, 6

To a solution of 100 mg (0.38 mmol) of the 2,4-DNP derivative in 10 ml of methanol and 10 ml of water was added 43 mg (0.55 mmol) of 2-mercaptoethanol and the p*H* was adjusted to 8. After 1 h the mixture was acidified with acetic acid. Evaporation of the solvents and extraction with chloroform afforded 65 mg (65%) of orange crystals; mp 78–80 °C, after recrystallization from ethanol; nmr ($CDCl_3$) δ 2.0 (6H, m), 3.3 (1H, s), 4.2

(1H, m), 4.5 (1H, m), 6.9 (1H, d), 8.1 (1H, q), 8.8 (1H, d), 9.0 (1H, d) ppm; ir (KBr) 3580, 2980 1650, 1600, 1520, 1440, 1360 cm^{-1}; *m/e* 267 (M^+).

N-Trifluoroacetyl-2,3-oxazabicyclo[2.2.1]hept-5-ene, 3b

A solution of 1.29 g (0.01 mol) of trifluoroacetohydroxamic acid in methylene chloride was slowly added to a solution of 3.41 g (0.01 mol) of benzyltrimethylammonium periodate and 3.30 g (0.05 mol) of freshly distilled cyclopentadiene in 50 ml of methylene chloride at −70 °C. After completion of the addition, the temperature was allowed to rise to −20 °C and was kept there for 1 h. Once the addition was completed the mixture was allowed to warm up to room temperature and was filtered. The filtrate was washed twice with a 10% solution of sodium thiosulfate, once with water, and dried over sodium sulfate. Evaporation of the solvent afforded 1.25 g (78%) of a yellow oil. The product was purified by passing it through a column of silica gel (silica gel Woelm, Act I), using chloroform as the eluent; nmr δ 1.9 (2H, d), 5.3 (2H, d), 6.5 (2H, m) ppm; ir (neat) 1720, 1690, 1580, 1240, 1210 cm^{-1}; *m/e* 193 (M^+).

N-Trifluoroacetyl-2,3-oxazabicyclo[2.2.1]heptane, 4b

A solution of 1.0 g (5 mmol) of the olefin in 25 ml of ethanol was hydrogenated over 50 mg of platinum oxide at room temperature and 3 atm pressure. After 1 h the mixture was filtered through Celite and evaporation of the solvent afforded 0.93 g (92%) of the reduced product as an oil; nmr ($CDCl_3$) δ 1.7 (6H m) 4.9 (2H, d); ir (neat) 2980, 1710, 1690, 1230, 1170 cm^{-1}; *m/e* 195(M^+).

2,3-Oxazabicyclo[2.2.1]heptane, 5

To a solution of 129 mg (1 mmol) of the trifluoroacetyl derivative in 5 ml of ethanol was added 152 mg (4 mmol) of sodium borohydride. After 1 h the excess reducing agent was destroyed by the addition of 5 ml of acetone. Evaporation of the solvent afforded 65 mg (67%) of the oxazabicycloheptane as an oil. The product was characterized as the 2,4-DNP derivative **4***a*, mp 123–125 °C.

N-Benzo-2,3-oxazabicyclo[2.2.1]hept-5-ene, 3c

To a solution of 1.1 g (0.016 mol) of cyclopentadiene and 1.98 g (0.005 mol) of benzyltrimethylammonium periodate in 50 ml of nitromethane at −70 °C was slowly added a solution of 1.05 g (0.008 mol) of benzohydroxamic acid in 25 ml of nitromethane. After a few minutes the solution turned to a dark color. After 1 h the reaction mixture was filtered and the solvent was removed under vacuum. The residue was passed through a column of silica gel using methylene chloride as the eluent affording a light yellow oil: 80 mg (15%); nmr ($CDCl_3$) δ 1.9 (2H, q), 5.4 (2H, s), 6.4 (2H, m), 7.6 (4H, d). The compound decomposes spontaneously at 40 °C.

N-Toluenesulfonyl-2,3-oxazabicyclo[2.2.1]hept-5-ene, 3d

A solution of 170 mg (0.001 mol) of *p*-toluenesulfinic acid in 15 ml of ether was added to a solution of 117 mg (0.001 mol) of amyl nitrite acid 132 mg (0.002 mol) of cyclopentadiene. Upon addition of the sulfinic acid the solution turned green, which subsequently disappeared. After 1 h the solvent was removed under vacuum; the residue was taken up in dioxane and upon addition of water a white precipitate was obtained. Yield 75 mg (30%); ir (KBr) 2980, 1600, 1390, 1330, 1310 cm^{-1}; *m/e* 251 (M^+); mp 108–110 °C.

3,5-Dinitrobenzo-2,3-oxazabicyclo[2.2.1]hept-5-ene, 3e

A solution of 2.27 g (0.010 mol) of 3,5-dinitrobenzohydroxamic acid in 10 ml of ether was slowly added to a solution of 3.90 g (0.011 mol) of benzyltrimethylammonium periodate and 3.30 g (0.05 mol) of freshly distilled cyclopentadiene in 50 ml of methylene chloride at −20 °C. After 1 h the mixture was filtered and the filtrate was washed twice with 10% solution of sodium thiosulfate and once with water. Evaporation of the solvents gave an oil which solidified upon standing. The product was purified by passing it through a column of silica gel, using methylene chloride as the eluent. Yield 2.4 g (82%); mp 105–106.5 °C; nmr ($CDCl_3$) δ 2.2 (2H, m), 5.5 (2H, m), 6.4 (1H, m), 6.7 (1H, m), 9.2 (3H, m) ppm; ir (KBr) 3020, 1650, 1630, 1550, 1530, 1350, 1320 cm^{-1}; *m/e* 291 (M^+).

3,5-Dinitrobenzo-2,3-oxazabicyclo[2.2.1]heptane, 4e

A solution of 582 mg (2 mmol) of the olefin in 10 ml of tetrahydrofuran was treated with a solution of BH_3 in tetrahydrofuran (4 ml, 4 mmol) at 0 °C under nitrogen. After 2 h, 2 ml of acetic acid was added to hydrolize the borane complex. After 1 h of refluxing the solvent was removed under vacuum and the residue was extracted with methylene chloride, washed with 5% sodium bicarbonate and water, and dried over magnesium sulfate. Evaporation of the solvent afforded 380 mg (65%) of light yellow oil: nmr ($CDCl_3$) δ 2.0 (6H, m), 4.7 (1H, m), 5.3 (1H, m), 9.2 (3H, m) ppm; ir (neat) 2920, 1640, 1560, 1550, 1360 cm^{-1}; *m/e* 293 (M^+).

2,3-Oxazabicyclo[2.2.1]heptane, 5

A solution of 100 mg (0.34 mmol) of the 3,5-dinitrobenzo derivative in 5 ml of methanol was added to a 25 ml of methanol saturated with ammonia. After 12 h the methanol was removed under vacuum and the residue was dissolved in chloroform and extracted with 0.5 *N* hydrochloric acid. The aqueous layer was neutralized with sodium carbonate and extracted with ether. Evaporation of the solvent afforded 22 mg (68%) of a colorless oil: ir ($CHCl_3$) 3420, 2970, 1610, 1270, 1110 cm^{-1}; *m/e* 97 (M^+).

Reduction of 3e

A solution of 50 mg of **3***e* in 15 ml of ethyl acetate was hydrogenated over 5 mg of platinum oxide at room temperature and 3 atm pressure. After 20 min the reduction was stopped, the mixture was filtered through Celite, and evaporation of the solvent afforded 43 mg of the reduced product as an oil. The nmr spectrum showed the presence of the olefinic protons at 6.7 ppm and the NH protons at 7.1 ppm. No further characterization was done because the compounds decomposed upon standing at room temperature.

Acknowledgments

We wish to thank the National Research Council of Canada, and Abbott Laboratories, Montreal, for financial support.

1. G. KRESZE and G. SCHULTZ. Tetrahedron, **12**, 7 (1961).

2. S. ITO, S. NARITA, and K. ENDO. Bull. Chem. Soc. Jpn. **46**, 3517 (1973).
3. W. BORSCHE. Ber. Dtsch. Chem. Ges. **56**, 1494 (1923).
4. E. J. COREY, W. L. MOCK, and D. J. PASTO. Tetrahedron Lett. 347 (1961).
5. P. F. LLOYD and M. STACEY. Tetrahedron, **9**, 116 (1960).
6. F. CHILEMI and R. B. MERRIFIELD. Biochemistry, **8**, 4344 (1969).
7. G. W. KIRBY and J. G. SWEENY. Chem. Commun. 704 (1973).
8. F. WEYGAND and E. FRAUENDORFER. Chem. Ber. **103**, 2437 (1970).
9. G. KRESZE and W. KORT. Chem. Ber. **94**, 2624 (1961).
10. M. A. STOLBERG, W. A. MOSHER, and T. WAGNER-JAUREGG. J. Am. Chem. Soc. **79**, 2615 (1957).
11. H. C. BROWN and K. MURRAY. J. Am. Chem. Soc. **81**, 4108 (1959).

Reactions of $NaBH_2S_3$ with some typical organic nitrogen compounds

JEAN-ROCK BRINDLE, JEAN-LOUIS LIARD, AND NORMAND BÉRUBÉ
Département des Sciences Pures, Université du Québec, Rimouski, Québec G5L 3A1

Received March 17, 1975[1]

JEAN-ROCK BRINDLE, JEAN-LOUIS LIARD, and NORMAND BÉRUBÉ. Can. J. Chem. **54**, 871 (1976).

The following substrates react with sulfurated sodium borohydride, $NaBH_2S_3$, to give the corresponding products as shown by the formulas in parentheses: azobenzene (p-$H_2N\phi$—ϕNH_2), azoxybenzene (p-$H_2N\phi$—ϕNH_2, $C_6H_5NNC_6H_5$), phenyl isocyanate ($C_6H_5NH_2$, $C_6H_5NHCH_3$), *N*-nitrosodiphenylamine ($(C_6H_5)_2NH$, $(C_6H_5)_2NNH_2$), diphenylcarbamyl chloride ($(C_6H_5)_2NH$), phenyl isothiocyanate ($C_6H_5NH_2$), benzyl carbamate ($C_6H_5CH_2OH$), benzyl *N*-phenylcarbamate ($C_6H_5CH_2OH$, $C_6H_5NH_2$, $C_6H_5CH_2SH$), benzyl nitrite ($C_6H_5CH_2OH$), benzyl nitrate ($C_6H_5CH_2OH$), benzyl thiocyanate ($C_6H_5CH_2S_2CH_2C_6H_5$), and pyridine-1-oxide (C_5H_5N). Benzotriazole, pyridine, phthalimide, and *N*,*N*′-diphenylurea were found to be stable towards $NaBH_2S_3$.

The advantage of sulfurated sodium borohydride, $NaBH_2S_3$, over sodium borohydride, $NaBH_4$, as a reducing agent was also proven when it was found that most of the above substrates were inert toward $NaBH_4$ except for the following organic nitrogen compounds which reacted with $NaBH_4$ to give the products indicated in parentheses: *N*-nitrosodiphenylamine ($(C_6H_5)_2NH$), diphenylcarbamyl chloride ($(C_6H_5)_2NCH_3$), phenyl isothiocyanate ($C_6H_5NHCH_3$), benzyl *N*-phenylcarbamate ($C_6H_5CH_2OH$, $C_6H_5NHCH_3$), and benzyl thiocyanate ($C_6H_5CH_2S_2CH_2C_6H_5$).

JEAN-ROCK BRINDLE, JEAN-LOUIS LIARD et NORMAND BÉRUBÉ. Can. J. Chem. **54**, 871 (1976).

Les substances suivantes réagissent avec le borohydrure de sodium sulfuré, $NaBH_2S_3$, et donnent les produits tel qu'indiqué par les formules entre parenthèses: azobenzène (p-$H_2N\phi$—ϕNH_2), azoxybenzène (p-$H_2N\phi$—ϕNH_2, $C_6H_5NNC_6H_5$), isocyanate de phényle ($C_6H_5NH_2$, $C_6H_5NHCH_3$), *N*-nitroso diphénylamine ($(C_6H_5)_2NH$, $(C_6H_5)_2NNH_2$), chlorure de diphénylcarbamate ($(C_6H_5)_2NH$), isothiocyanate de phényle ($C_6H_5NH_2$), carbamate de benzyle ($C_6H_5CH_2OH$), *N*-phényl carbamate de benzyle ($C_6H_5CH_2OH$, $C_6H_5NH_2$, $C_6H_5CH_2SH$), nitrite de benzyle ($C_6H_5CH_2OH$), nitrate de benzyle ($C_6H_5CH_2OH$), thiocyanate de benzyle ($C_6H_5CH_2S_2CH_2C_6H_5$) et l'oxyde-1-pyridine (C_5H_5N). Le benzotriazole, la pyridine, la phtalimide et la *N*,*N*′-diphénylurée ne réagissent pas avec $NaBH_2S_3$.

L'avantage du borohydrure de sodium sulfuré, $NaBH_2S_3$, par rapport au borohydrure de sodium, $NaBH_4$, en tant qu'agent de réduction fut aussi démontré lorsque des tentatives de réduction à l'aide de $NaBH_4$ s'avérèrent négatives avec la plupart des substances azotées mentionnées plus haut, à l'exception des substances suivantes, lesquelles conduisent aux produits indiqués entre parenthèses: *N*-nitrosodiphenylamine ($(C_6H_5)_2NH$), chlorure de diphénylcarbamate ($(C_6H_5)_2NCH_3$), isothiocyanate de phényle ($C_6H_5NHCH_3$), *N*-phénylcarbamate de benzyle ($C_6H_5CH_2OH$, $C_6H_5NHCH_3$) et le thiocyanate de benzyle ($C_6H_5CH_2S_2CH_2C_6H_5$).

In previous papers we have reported the use of sulfurated sodium borohydride (1) for the reduction of some nitrogen compounds (2–4). It was found that $NaBH_2S_3$ is a mild reducing agent which often shows an intermediate reducing potential between lithium aluminum hydride ($LiAlH_4$) and sodium borohydride ($NaBH_4$), and often gives sulfurated products of great interest. Moreover, the reducing potential of $NaBH_2S_3$ was found to be occasionally even more selective than that of $LiAlH_4$ allowing, for example, the reduction of the nitro group in the presence of esters (3).

It was decided to extend the scope of these reactions to more nitrogen compounds as listed below. Azobenzene ($C_6H_5NNC_6H_5$), azoxybenzene ($C_6H_5N(O)NC_6H_5$), phenyl isocyanate (C_6H_5NCO), *N*-nitrosodiphenylamine ($(C_6H_5)_2NNO$), diphenylcarbamyl chloride ($(C_6H_5)_2NCOCl$), phenyl isothiocyanate (C_6H_5NCS), benzyl carbamate ($C_6H_5CH_2OCONH_2$), benzyl *N*-phenylcarbamate ($C_6H_5CH_2OCONHC_6H_5$), benzyl nitrite ($C_6H_5CH_2ONO$), benzyl nitrate ($C_6H_5CH_2ONO_2$), benzyl thiocyanate ($C_6H_5CH_2SCN$), pyridine-1-oxide ($C_5H_5N(O)$, pyridine (C_5H_5N), benzotriazole

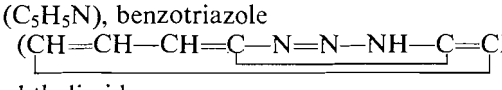

phthalimide,

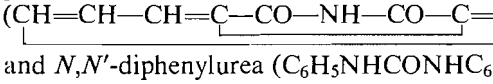

and *N*,*N*′-diphenylurea ($C_6H_5NHCONHC_6H_5$).

[1]Revision received December 1, 1975.

Can. J. Chem. Downloaded from www.nrcresearchpress.com by 210.87.254.5 on 09/05/12
For personal use only.

TABLE 1. Reactions of some nitrogen compounds with $NaBH_2S_3$

Substrate	Molar ratio $NaBH_2S_3$: substrate	Reflux time in THF (h)	Substrate used (%)	Product yield (%)*					
				$H_2N\phi—\phi NH_2$	$\phi NN\phi$	ϕNH_2	$\phi NHCH_3$	ϕ_2NH	ϕ_2NNH_2
$\phi NN\phi$	4:1	3	80	80					
	2:1	3	80	80					
	1:1	3	80	80					
	1:2	3	40	40					
$\phi N(O)N\phi$	4:1	18	90	85	5				
	2:1	18	75	60	15				
	1:1	18	70	40	30				
	1:2	18	40	35	5				
ϕNCO	4:1	18	92			62	30		
	2:1	18	97			60	37		
	1:1	18	50			25	25		
ϕ_2NNO	4:1	18	97					93	4
	2:1	18	98					90	8
	1:1	18	90					90	Traces
	1:2	18	65					65	Traces
ϕ_2NCOCl	4:1	18	100					100	
ϕNCS	4:1	18	50			50			

*ϕ = C_6H_5— or p-C_6H_4— in the case of $H_2N\phi—\phi NH_2$.

We have compared our results with the reductions obtained with other common reducing agents. Tables 1 and 2 give the best reaction conditions leading to an optimum yield of products for a given substrate, whereas Table 3 compares, for certain substrates, the results obtained with different reducing agents such as, borane (B_2H_6), lithium aluminum hydride ($LiAlH_4$), sodium borohydride ($NaBH_4$), aluminum hydride (AlH_3), and sulfurated sodium borohydride ($NaBH_2S_3$).

Azobenzene

Results indicate that the stoichiometry of this reaction requires a molar ratio of 1:1; an 80% yield of benzidine is obtained. This reaction is of a special interest since, apart from catalysed hydrazine reductions (5) and anodic reductions (6), there is no other efficient way to reduce azobenzene to hydrazobenzene or to 4,4′-diaminobiphenyl. For example, a mixture of $NaBH_4$ and AlH_3 is known to reduce azobenzene to aniline (12).

Azoxybenzene

A molar ratio of 4:1 in favor of sulfurated sodium borohydride gives a very high yield of benzidine while a molar ratio of 1:1 gives a 70% yield of almost equal quantities of benzidine and azobenzene.

Phenyl Isocyanate

The reduction of isocyanates generally leads to the formation of amines. With $NaBH_2S_3$, an excess of reducing agent gives an almost quantitative yield of a mixture of *N*-methylaniline and aniline, the predominance of the latter making this reaction important for the production of $C_6H_5NH_2$ from phenyl isocyanate since the action of other reducing agents generally favors the production of *N*-methylaniline.

N-Nitrosodiphenylamine

We have already reported the synthesis of aniline from nitrozobenzene in the presence of $NaBH_2S_3$ (3), and it is known that $LiAlH_4$ in the presence of C_6H_5NO gives azobenzene instead of aniline (15). It seems that $LiAlH_4$ reacts with *N*-nitroso compounds such as *N*-nitrosodiphenylamine to give a moderate yield of diphenylamine (16) while the same secondary amine is produced almost quantitatively when *N*-nitrosodiphenylamine reacts with $NaBH_2S_3$.

Diphenylcarbamyl Chloride

Sulfurated sodium borohydride seems to react with $(C_6H_5)_2NCOCl$ the same way as it does with C_6H_5NCO, yielding amines; a quantitative yield of diphenylamine is indeed obtained from the reduction of $(C_6H_5)_2NCOCl$ with an excess of $NaBH_2S_3$, whereas $NaBH_4$ reduces $(C_6H_5)_2$-

Can. J. Chem. Downloaded from www.nrcresearchpress.com by 210.87.254.5 on 09/05/12
For personal use only.

Can. J. Chem. Downloaded from www.nrcresearchpress.com by 210.87.254.5 on 09/05/12
For personal use only.

NCOCl to the tertiary amine $(C_6H_5)_2NCH_3$ under the same experimental conditions.

Phenyl Isothiocyanate

It has been mentioned already that the reaction of an excess of $NaBH_2S_3$ with C_6H_5NCO leads to an almost quantitative yield of *N*-methylaniline and aniline. By comparison, it was found that an excess of $NaBH_2S_3$ reacts more slowly with C_6H_5NCS but gives a 50% yield of aniline as the only product of the reaction. Once more, the specific potential of other reducing agents leads to the production of *N*-methylaniline, whereas the action of $NaBH_2S_3$ on C_6H_5NCS leads to the production of $C_6H_5NH_2$.

Benzyl Carbamate

It was found that $C_6H_5CH_2OCONH_2$ reacts quantitatively with an excess of $NaBH_2S_3$ to yield $C_6H_5CH_2OH$. The formation of $C_6H_5CH_2OH$ resulting from the action of $LiAlH_4$ on $C_6H_5CH_2OCONH_2$ (17) is also known, but no mention is made of the yield of the reduction.

Benzyl N-Phenylcarbamate

It seems that a 94% consumption of benzyl *N*-phenylcarbamate requires a 2:1 molar ratio in favor of the reducing agent, resulting in the formation of a mixture of compounds where aniline accounts for 47% of the total consumption, followed by benzyl alcohol, α-toluenethiol, and benzyl disulfide. Once again the specific potentials of $NaBH_4$ and $NaBH_2S_3$ cause the former to react quantitatively with $C_6H_5CH_2OCONHC_6H_5$ yielding equal proportions of $C_6H_5CH_2OH$ and $C_6H_5NHCH_3$. Under similar experimental conditions, $NaBH_2S_3$ will also react quantitatively with the substrate to give a 100% yield of $C_6H_5NH_2$, the complementary products being equal proportions of $C_6H_5CH_2OH$ and $C_6H_5CH_2SH$.

Benzyl Nitrite and Benzyl Nitrate

It has been reported that most nitrates and nitrites are reduced to the corresponding alcohols when $LiAlH_4$ (18) is used, suggesting the possibility of producing benzyl alcohol from benzyl nitrate and benzyl nitrite. Our work proved that $NaBH_2S_3$ can give a quantitative yield of $C_6H_5CH_2OH$ when acting with $C_6H_5CH_2ONO$ or $C_6H_5CH_2ONO_2$, even though there is evidence that $C_6H_5CH_2ONO$ is very slowly hydrolysed to the corresponding alcohol in dilute acidic solutions.

Benzyl Thiocyanate

As reported by Strating and Backer it seems that $LiAlH_4$ reacts with thiocyanates to yield the corresponding thiols (19). On the other hand, we have found that sodium borohydrides act on $C_6H_5CH_2SCN$ to give high yields of $C_6H_5CH_2S_2CH_2C_6H_5$ and that further conversion of $C_6H_5CH_2S_2CH_2C_6H_5$ to $C_6H_5CH_2SH$ is possible for $LiAlH_4$ (19) and $NaBH_2S_3$, but impossible for $NaBH_4$.[2] Total inertness of $C_6H_5CH_2SCH_2C_6H_5$ towards $LiAlH_4$ is reported (19) and was also checked for $NaBH_4$ and $NaBH_2S_3$.

Pyridine-1-oxide

In spite of its low solubility in THF, pyridine-1-oxide is completely reduced to pyridine when reacting with $NaBH_2S_3$. Although no yield is reported, it seems that the action of $LiAlH_4$ on pyridine-1-oxide also leads to the formation of pyridine, whereas $NaBH_4$[2] was found inert towards pyridine-1-oxide.

Pyridine, Benzotriazole, Phthalimide, and N,N'-Diphenylurea

A large excess of $NaBH_2S_3$ refluxed in THF (tetrahydrofuran) for 24 h with these substrates showed total stability of these groups toward sulfurated sodium borohydride.

Discussion

From a study of Tables 1 and 2, it appears that $NaBH_2S_3$ generally gives very high yields of reduced products from the following substrates: azobenzene, azoxybenzene, phenyl isocyanate, *N*-nitrosodiphenylamine, diphenylcarbamyl chloride, phenyl isothiocyanate, benzyl carbamate, benzyl *N*-phenylcarbamate, benzyl nitrite, benzyl nitrate, benzyl thiocyanate, and pyridine-1-oxide.

It was also shown that pyridine, benzotriazole, and phthalimide are totally inert with $NaBH_2S_3$, indicating that cyclic nitrogen atoms are much less accessible to $NaBH_2S_3$ than open chain nitrogen atoms. *N,N'*-Diphenylurea was also found inert with $NaBH_2S_3$ probably because of its low solubility in THF in our experimental conditions.

Although it was suggested in earlier papers on the reactions of oxime, nitrile, amide, and nitroso groups with sulfurated sodium borohydride (2–4) that this borohydride would normally be classified as a medium reducing agent

[2] $NaBH_2S_3$ and $NaBH_4$ were made in our laboratory.

TABLE 2. Reactions of some nitrogen compounds with $NaBH_2S_3$

Substrate	Molar ratio $NaBH_2S_3$: substrate	Reflux time in THF(h)	Substrate used (%)	Product yield (%)*				
				ϕCH_2OH	ϕNH_2	ϕCH_2SH	$\phi CH_2S_2CH_2\phi$	C_5H_5N
ϕCH_2OCONH_2	4:1	30	100	100				
$\phi CH_2OCONH\phi$	4:1	18	100	56	100	44		
	2:1	18	94	54	94	20	20	
	1:1	18	50	50	50			
ϕCH_2ONO	2:1	18	100	100				
	1:2	18	100	100				
ϕCH_2ONO_2	2:1	18	100	100				
ϕCH_2SCN	4:1	18	100				68	
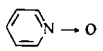	1:1	18	100					100

*$\phi = C_6H_5-$

because it usually has an intermediate reduction potential as compared to $LiAlH_4$ and $NaBH_4$, we can see from Table 3 that, for a given substrate such as azobenzene, $NaBH_2S_3$ sometimes reacts even more strongly than $LiAlH_4$ in order to lead easily to the formation of benzidine. Under similar reaction conditions, $LiAlH_4$ is reported to reduce azobenzene to hydrazobenzene after a reaction time of 3 days (20).

Furthermore, as was proven earlier for the reduction of aromatic nitro groups to amines with $NaBH_2S_3$ (3), Table 3 gives more examples where $NaBH_2S_3$ is found to yield totally different products compared with other reducing agents. Such is the case for azobenzene, azoxybenzene, phenyl isocyanate, diphenylcarbamyl chloride, phenyl isothiocyanate, and benzyl *N*-phenylcarbamate. Table 3 also illustrates the versatility of $NaBH_2S_3$. It was found, indeed, that azobenzene, azoxybenzene, phenyl isocyanate, benzyl nitrate, and pyridine-1-oxide are inert to $NaBH_4$ but easily reduced by $NaBH_2S_3$. Another interesting fact is that *N*-nitrosodiphenylamine, benzyl carbamate, and pyridine-1-oxide will react with $NaBH_2S_3$ to give equal or even higher yields of reduced compounds when compared with the action of $LiAlH_4$ and $NaBH_4$ on the same substrates.

In conclusion, it is recognized that sulfurated sodium borohydride is an interesting reducing agent towards organic nitrogen compounds giving a reducing pattern different from other known reducing agents currently used in organic chemistry.

Experimental

The nmr measurements were made with a Perkin-Elmer R-12A apparatus. The ir measurements were made with a Pye Unicam SP200G spectrophotometer. The vpc measurements were made with a Pye 104 chromatograph using an 8 ft 10% Carbowax column.

Each experiment described in this text was performed in an inert atmosphere of nitrogen.

Azobenzene

To a suspension of 0.05 mol (6.60 g) of $NaBH_2S_3$ in 100 ml of tetrahydrofuran (THF) prepared as described by Lalancette *et al.* (1), 0.05 mol (9.10 g) of azobenzene in 100 ml of THF was added dropwise. The reaction mixture was stirred and refluxed for 3 h, and was then evaporated to dryness under reduced pressure at room temperature. The residual solid was covered with 200 ml of ethyl ether and hydrolysed with a 10% hydrochloric acid solution until the p*H* of the reaction mixture was 1.0. The precipitated sulfur was filtered off and the filtrate washed repeatedly with ethyl ether. The 'organic fraction' was dried over $MgSO_4$ and evaporation of ether gave 1.80 g (20%) of unreacted azobenzene. The 'aqueous fraction' was then covered with 200 ml of ethyl ether and neutralized with a 20% solution of NaOH until the p*H* of the reaction mixture was 11.0. After separation of the two layers and successive washings of the aqueous layer with ethyl ether, the ethereal extracts were dried over $MgSO_4$ and evaporated, yielding 7.30 g (80%) of 4,4′-diaminobiphenyl. The positive identification of the unreacted azobenzene and of the amine was made by comparison of mp, ir, and nmr measurements obtained with the authentic products.

The terms 'organic fraction' and 'aqueous fraction' that will be used in the following discussions refer to exactly the same steps already described for azobenzene.

Azoxybenzene

A mixture of 0.20 mol (26.40 g) of $NaBH_2S_3$ and 0.05 mol (9.90 g) of azoxybenzene was refluxed in THF for 18 h. The nmr analysis of the 'organic fraction' gave a 10% yield of unreacted $C_6H_5N(O)NC_6H_5$ (τ (CCl_4)

Can. J. Chem. Downloaded from www.nrcresearchpress.com by 210.87.254.5 on 09/05/12
For personal use only.

Can. J. Chem. Downloaded from www.nrcresearchpress.com by 210.87.254.5 on 09/05/12
For personal use only.

TABLE 3. Selective reductions of different reducing agents (similar reaction conditions)

Substrate	B_2H_6 Product	Yield(%)	Ref.	$LiAlH_4$ Product	Yield(%)	Ref.	$NaBH_4$* Product	Yield(%)	AlH_3 Product	Yield(%)	Ref.	$NaBH_2S_3$* Product	Yield(%)
ϕ—N=N—ϕ §	ϕNH_2	†	7–9	NR‡		11	NR		NR		10	$H_2N\phi$—ϕNH_2	80
ϕ—N=N—ϕ ↓ O	NR		9	ϕ—N=N—ϕ	90	11	NR		NR		10	$H_2N\phi$—ϕNH_2	85
ϕ—N=C=O	$\phi NHCH_3$	†	9	$\phi NHCH_3$	80	13,14	NR		—			ϕNH_2 $\phi NHCH_3$	62 30
ϕ_2N—N=O	—			ϕ_2NH	70	16	ϕ_2NH	45	—			ϕ_2NH	90
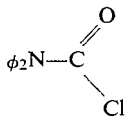	—			—			ϕ_2NCH_3	95	—			ϕ_2NH	100
ϕ—N=C=S	—			$\phi NHCH_3$	78	14	$\phi NHCH_3$	85	—			ϕNH_2	50
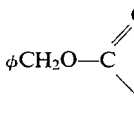	—			ϕCH_2OH	†	17	—		—			ϕCH_2OH	100
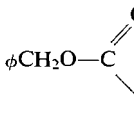	—			—			ϕCH_2OH $\phi NHCH_3$	100 100	—			ϕCH_2OH ϕNH_2 ϕCH_2SH	56 100 44
ϕCH_2O—N=O	—			—			—		—			ϕCH_2OH	100
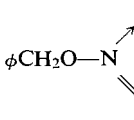	—			—			NR		—			ϕCH_2OH	100
ϕCH_2S—C≡N	—			—			$\phi CH_2S_2CH_2\phi$	97	—			$\phi CH_2S_2CH_2\phi$ Polysulfides	68 32
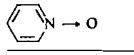	C_5H_5N	†	9	—			NR		—			C_5H_5N	100

*$NaBH_4$ and $NaBH_2S_3$ made in our laboratory.
†Not reported.
‡NR, no reaction.
§ϕ = C_6H_5— or p-C_6H_4— in the case of $H_2N\phi$—ϕNH_2.

Can. J. Chem. Downloaded from www.nrcresearchpress.com by 210.87.254.5 on 09/05/12
For personal use only.

complex at 2.25) and a 5% yield of $C_6H_5NNC_6H_5$ (τ (CCl_4), complex at 2.35). Final analysis of the 'aqueous fraction' gave 7.70 g (85%) of 4,4′-diaminobiphenyl (mp 128–129 °C), which was also readily identified by comparison of ir and nmr measurements with the authentic product (τ (deuterated acetone) complex of 8 protons at 3.05, broad singlet of 4 protons at 5.90).

Phenyl Isocyanate

A mixture of 0.20 mol (26.40 g) of $NaBH_2S_3$ and 0.05 mol (5.95 g) of C_6H_5NCO was refluxed in THF for 18 h. Investigation of the 'organic fraction' showed 8% of unreacted C_6H_5NCO which analysed as symmetrical diphenylurea, whereas 4.50 g of products obtained from the 'aqueous fraction' were identified by nmr and gas chromatography measurements as a mixture of 62% (2.90 g) $C_6H_5NH_2$ and 30% (1.60 g) $C_6H_5NHCH_3$.

N-Nitroso Diphenylamine

A mixture of 0.10 mol (13.20 g) of $NaBH_2S_3$ and 0.05 mol (9.90 g) of $(C_6H_5)_2NNO$ was refluxed in THF for 18 h. Investigation of the 'organic fraction' (7.80 g) by nmr analysis showed mainly $(C_6H_5)_2NH$ (τ (CCl_4) complex of 10 protons at 3.00, broad singlet of 1 proton at 4.60) (90%) and traces of unreacted $(C_6H_5)_2NNO$ (τ (CCl_4) complex at 2.80) which was found previously to be stable in the presence of a 10% HCl solution. A comparative ir analysis with the authentic products confirmed the presence of $(C_6H_5)_2NNO$ and $(C_6H_5)_2NH$. The nmr and ir study of the 'aqueous fraction' (0.73 g) showed the presence of $(C_6H_5)_2NNH_2$ (8%) (τ (CCl_4) complex of 10 protons at 3.00, broad singlet of 2 protons at 6.25); mp 49–50 °C.

Diphenylcarbamyl Chloride

A mixture of 0.10 mol (13.20 g) of $NaBH_2S_3$ and 0.025 mol (5.80 g) of $(C_6H_5)_2NCOCl$ was refluxed in THF for 18 h. Comparative ir and nmr analysis of the 'organic fraction' (4.20 g) showed the presence of $(C_6H_5)_2NH$ (100%); this quantitative yield of amine being confirmed by the absence of products in the 'aqueous fraction'.

Phenyl Isothiocyanate

To a suspension of 0.10 mol (13.20 g) of $NaBH_2S_3$ in boiling THF, 0.025 mol (3.38 g) of C_6H_5NCS was added dropwise and the mixture was refluxed for 18 h. Following normal procedures as described above for azobenzene, investigation of the 'organic fraction' showed 50% (1.60 g) of unreacted C_6H_5NCS analysed as 1,3-diphenyl-2-thiourea, whereas comparative ir and nmr analysis of the 'aqueous fraction' (1.15 g) confirmed the presence of $C_6H_5NH_2$ (50%).

Benzyl Carbamate

A mixture of 0.20 mol (26.40 g) of $NaBH_2S_3$ and 0.05 mol (7.56 g) of $C_6H_5CH_2OCONH_2$ was refluxed in THF for 30 h. Comparative ir, nmr, and silica gel thin-layer chromatography studies of the 'organic fraction' (5.50 g) revealed the presence of $C_6H_5CH_2OH$ (100%).

Benzyl N-Phenylcarbamate

A mixture of 0.10 mol (13.20 g) of $NaBH_2S_3$ and 0.025 mol (5.69 g) of $C_6H_5CH_2OCONHC_6H_5$ was refluxed in THF for 18 h. Investigation of the 'organic fraction' by nmr analysis showed the presence of $C_6H_5CH_2SH$ (22%) (τ (CCl_4) singlet of 5 protons at 2.80, doublet of 2 protons at 6.30, triplet of 1 proton at 8.45) and of $C_6H_5CH_2OH$ (28%) (τ (CCl_4) singlet of 5 protons at 2.80, singlet of 2 protons at 5.40, broad singlet of 1 proton variable between 5.00 and 7.70). Treatment of the 'aqueous fraction' showed the presence of 2.30 g of $C_6H_5NH_2$ proving that the substrate has been entirely used up. Comparative ir, nmr, and silica gel thin-layer chromatography studies confirmed the composition of these two fractions.

Benzyl Nitrite

A mixture of 0.025 mol (3.30 g) of $NaBH_2S_3$ and 0.05 mol (6.85 g) of $C_6H_5CH_2ONO$ was refluxed in THF for 18 h. The reaction mixture was evaporated to dryness under reduced pressure at room temperature and the residual solid was washed repeatedly with many portions of ethyl ether. This ethereal fraction was dried over $MgSO_4$ and evaporation of the solvent left no product to be analysed, indicating total consumption of $C_6H_5CH_2ONO$ by $NaBH_2S_3$ to form an insoluble intermediate. Following, at this point, the procedures described earlier for azobenzene, ir and nmr analysis of the 'organic fraction' showed the presence of C_6H_5OH. A continuous liquid–liquid extraction (24 h) on the 'aqueous fraction' using ethyl ether gave a small quantity of $C_6H_5CH_2OH$. The two portions of alcohol (5.80 g) confirmed the 100% yield.

Benzyl Nitrate

A mixture of 0.08 mol (10.56 g) of $NaBH_2S_3$ and 0.04 mol (6.12 g) of $C_6H_5CH_2ONO_2$ was refluxed in THF for 18 h. Investigation of the 'organic and aqueous fractions' as mentioned above for benzyl nitrite, showed the presence of 4.30 g of $C_6H_5CH_2OH$ (100%) which was positively identified by a comparative ir and nmr study with the authentic alcohol.

Benzyl Thiocyanate

A mixture of 0.10 mol (13.20 g) of $NaBH_2S_3$ and 0.025 mol (3.73 g) of $C_6H_5CH_2SCN$ was refluxed in THF for 18 h. A column chromatography analysis of the 'organic fraction', using a silica gel column and carbon tetrachloride (CCl_4) as eluant, revealed a 68% yield of $C_6H_5CH_2SSCH_2C_6H_5$ (2.10 g, mp 70–71 °C) and a 32% yield of a complex mixture of polysulfides. The absence of benzyl thiocyanate in the organic and aqueous fractions indicated total reaction of the initial substrate with $NaBH_2S_3$. Positive identification of benzyl disulfide was made by ir and nmr comparative studies with authentic $C_6H_5CH_2S_2CH_2C_6H_5$ (τ (CCl_4) singlet of 5 protons at 2.76, singlet of 2 protons at 6.48).

Pyridine-1-oxide

A mixture of 0.05 mol (6.60 g) of $NaBH_2S_3$ and 0.05 mol (4.75 g) of pyridine-1-oxide was refluxed in THF for 18 h. Analysis of the 'organic fraction' showed the absence of products while investigation of the 'aqueous fraction', after being submitted to a continuous liquid–liquid extraction (24 h) with ethyl ether, revealed the presence of 3.80 g of pyridine which was positively identified by ir and nmr measurements.

When relevant, the same procedures as those mentioned above were used for the action of $NaBH_4$ on a given substrate, as indicated in Table 3.

Acknowledgments

The authors thank the National Research Council of Canada (grant A6830) for financial assistance.

1. J. M. LALANCETTE, R. MONTEUX, and A. FRÊCHE. Can. J. Chem. **46**, 2754 (1968).
2. J. M. LALANCETTE and J. R. BRINDLE. Can. J. Chem. **48**, 735 (1970).
3. J. M. LALANCETTE and J. R. BRINDLE. Can. J. Chem. **49**, 2990 (1971).
4. J. M. LALANCETTE, A. FRÊCHE, J. R. BRINDLE, and M. LALIBERTÉ. Synthesis, **10**, 526 (1972).
5. A. FURST and R. E. MOORE. J. Am. Chem. Soc. **79**, 5492 (1957).
6. T. T. TSAI, W. E. MCEWEN, and J. KLEINBERG. J. Org. Chem. **25**, 1186 (1960).
7. H. C. BROWN and B. C. SUBBA RAO. J. Org. Chem. **22**, 1135 (1957).
8. H. C. BROWN and B. C. SUBBA RAO. J. Am. Chem. Soc. **82**, 681 (1960).
9. H. C. BROWN. J. Am. Chem. Soc. **92**, 1637 (1970).
10. H. C. BROWN and NUNG MIN YOON. J. Am. Chem. Soc. **88**, 1464 (1966).
11. R. F. NYSTROM and W. G. BROWN. J. Am. Chem. Soc. **70**, 3738 (1948).
12. H. C. BROWN and B. C. SUBBA RAO. J. Am. Chem. Soc. **78**, 2582 (1956).
13. R. WESSELY and W. SWOBODA. Monatsh. Chem. **82**, 621 (1951).
14. W. RIED and F. MÜLLER. Chem. Ber. **85**, 470 (1952).
15. W. C. BROWN. Org. React. **6**, 471 (1951).
16. F. W. SCHUELER and C. HANNA. J. Am. Chem. Soc. **73**, 4996 (1951).
17. N. G. GAYLORD. Reduction with complex metal hydribes. Interscience Publishers Inc., New York. 1956. p. 636.
18. L. M. SOFFER, E. W. PARROTTA, and J. DI DOMENICO. J. Am. Chem. Soc. **74**, 5301 (1952).
19. J. STRATING and H. J. BACKER. Rec. Trav. Chim. **69**, 638 (1950); **69**, 909 (1950).
20. F. BOHLMANN. Chem. Ber. **85**, 390 (1952).

Can. J. Chem. Downloaded from www.nrcresearchpress.com by 210.87.254.5 on 09/05/12
For personal use only.

Etude de Mn(II) en solution aqueuse perchlorique par résonance paramagnétique électronique

OUASSINI BENALI-BAITICH

Université d'Alger, Faculté des Sciences, Département de Chimie, 2, Rue Didouche Mourad, Alger, Algérie

ET

EDGAR WENDLING[1]

Université de Metz, Faculté des Sciences, Laboratoire de Chimie Minérale Physique, Ile du Saulcy, 57000-Metz, France

Reçu le 10 février 1975[2]

OUASSINI BENALI-BAITICH et EDGAR WENDLING. Can. J. Chem. **54**, 878 (1976).

Le comportement du perchlorate de manganèse(II) en solution aqueuse perchlorique ($0 < C_{HClO_4} < 11.85$) est étudié par rpe à 25 et 55 °C.

L'élargissement de la raie lors de l'addition d'$HClO_4$ dépasse nettement celui provoqué normalement par l'augmentation de la viscosité. Ce résultat est interprété en envisageant la formation d'un complexe monoperchlorato-interne en équilibre avec le complexe externe.

La diminution de l'intensité relative du signal lors de l'addition d'$HClO_4$ confirme la présence d'un complexe monoperchlorato-interne et permet d'évaluer sa constante de stabilité $(8.0 \pm 1.5) \times 10^{-2}$. La stabilité relative du monoperchlorato de Mn(II) comparée à celle de Co(II) et Ni(II) s'explique par la considération de l'énergie de stabilisation du champ des coordinats.

OUASSINI BENALI-BAITICH and EDGAR WENDLING. Can. J. Chem. **54**, 878 (1976).

The behaviour of manganese(II) perchlorate in aqueous perchloric acid solution ($0 < C_{HClO_4} < 11.85$) was studied by epr at 25 and 55 °C. The broadening of the band following addition of $HClO_4$ considerably exceeds that normally caused by the increase in the viscosity. This result is interpreted in terms of the formation of an internal monoperchlorato complex in equilibrium with the external complex. The decrease in the relative intensity of the signal following addition of $HClO_4$ confirms the presence of an internal monoperchlorato complex and permits the evaluation of its stability constant, $(8.0 \pm 1.5) \times 10^{-2}$. The relative stability of the Mn(II) monoperchlorato complex compared to those of Co(II) and Ni(II) is explained by a consideration of the ligand field stabilization energy.

[Journal translation]

Introduction

Dans un article précédent (1) consacré à l'étude du comportement des perchlorates de Co(II), Ni(II) et Cu(II) en milieu aqueux perchlorique, nous avons mis en évidence la formation de perchlorato-complexes dont la structure et la stabilité ont pu être déterminés par spectrophotométrie d'absorption.

Malheureusement, cette étude n'a pu être étendue à l'ion Mn(II) dont le spectre d'absorption visible est formé de bandes d'intensités très faibles et qui pour être détectées exigeraient soit des largeurs de cuves démesurées soit des concentrations en $Mn(ClO_4)_2$ incompatibles avec la solubilité de ce sel dans $HClO_4$ aqueux.

Par contre, l'ion Mn(II) présente en solution un spectre rpe facilement observable même à de très faibles concentrations et dont la largeur et l'intensité des raies évoluent lors de l'addition d'anions du fait de la formation de complexes aussi bien en milieu aqueux (2, 3) qu'en milieu non aqueux (4–6). Plus récemment Burlamacchi et ses collaborateurs ont analysé les phénomènes déterminant la forme de la raie rpe de l'ion Mn(II) dans les solvants mixtes (7).

Le but de ce travail est l'étude de l'effet de $HClO_4$ aqueux sur le spectre rpe de l'ion $Mn(H_2O)_6^{2+}$ en relation avec la coordination de l'anion ClO_4^- laquelle n'a été mise en évidence jusqu'à présent que par spectroscopie Raman (8) et rmn de ^{35}Cl (9) sans que ni la nature ni la stabilité du complexe formé n'aient encore été précisées.

Nous avons donc suivi la variation de la largeur et de l'intensité de la quatrième raie hyperfine (à partir des champs faibles) des spectres rpe des solutions de $Mn(ClO_4)_2$ dans

[1]Toute correspondance est à adresser à E. Wendling, Université de Metz, Faculté des Sciences, Laboratoire de Chimie Minérale Physique, Ile du Saulcy, 57000-Metz, France.

[2]Revision reçue le 10 décembre 1975.

Can. J. Chem. Downloaded from www.nrcresearchpress.com by 210.87.254.105 on 09/05/12
For personal use only.

TABLEAU 1. Largeur de raie ΔH (en gauss) en fonction de C_{HClO_4} (M/l) à 25 et 55 °C (concentration en Mn(II) 3×10^{-2} M/l)

	C_{HClO_4}											
	0.18	4.40	6.55	7.60	8.15	8.65	9.20	9.70	10.25	10.75	11.20	11.85
$\Delta H_{25°C}$	21	21	23	26	29	32	34	38	42	44	47	51
$\Delta H_{55°C}$	13	16	21	27	30	34	37	42	44	45	48	50
$\left(\frac{\eta}{\rho.T}\right)10^3$ (25 °C)	3.12	3.05	3.78	4.41	4.82	5.24	5.73	6.16	6.70	7.28	7.87	8.58
$\left(\frac{\eta}{\rho.T}\right)10^3$ (55 °C)	1.54	1.73	2.15	2.52	2.68	2.90	3.13	3.37	3.66	3.93	4.20	4.56

$HClO_4$ aqueux en fonction de C_{HClO_4} (M/l) à 25 et 55 °C. Le choix de cette raie correspondant à $M_I = \frac{1}{2}$ se justifie car elle se prête le mieux à l'étude des phénomènes de relaxation (2).

Partie expérimentale

Les spectres de résonance paramagnétique électronique des solutions de perchlorate de manganèse (3×10^{-2} M/l) dans $HClO_4$ aqueux ($0 < C_{HClO_4} < 11.85$ M/l) sont enregistrés suivant la dérivée première de l'absorption à l'aide d'un spectromètre bande X de type Varian V 4502 doté d'une double cavité pour les mesures de l'intensité du signal. La température (55 °C) est maintenue constante à ±2 °C à l'aide d'un courant d'air chaud envoyé dans la cavité. Le champ magnétique statique est mesuré à l'aide d'un gaussmètre de précision muni d'une sonde à effet Hall. La largeur de raie ΔH est mesurée "pic à pic" avec une incertitude inférieure à ±1 gauss.

Les solutions de perchlorate de Mn(II) dans $HClO_4$ aqueux sont préparées de la même façon que dans la réf. 1. Pour chaque solution un test au $AgNO_3$ et au $BaCl_2$ est effectué pour vérifier l'absence des ions étrangers en particulier Cl^- et SO_4^{2-}.

Les mesures de l'intensité du signal sont effectuées par référence au DPPH. Il faut noter que pour les solutions de concentration $C_{HClO_4} \geq 10.75$ M/l, les six raies hyperfines commencent à se recouvrir ce qui augmente l'imprécision dans la détermination des paramètres de la raie; c'est pourquoi l'étude a été limitée à $C_{HClO_4} \leq 11.85$ M/l, concentration maximum pour laquelle les six raies hyperfines sont encore résolues. Compte tenu de l'importance de l'incertitude commise sur les mesures d'intensité (de l'ordre de 10%), nous avons adopté la relation approximative $\Delta H^2.h$ (h étant la hauteur de la raie) pour la détermination de l'intensité relative du signal dans tout le domaine de concentration. Enfin, puisque l'intensité du signal diminue pour des solutions de même concentration en Mn(II) lorsque C_{HClO_4} augmente, il est plus intéressant de rapporter cette intensité à celle de la solution aqueuse normalisée à 100. De cette façon, l'intensité relative du signal (I/I_0) s'exprimera en % et sera comprise entre 0 et 100.

Résultats et discussions

Largeur de raie

Il faut d'abord noter qu'il n'y a aucune variation du facteur g (2.004 ± 0.002) dans les spectres des solutions étudiées ce qui est caractéristique des complexes de Mn(II) (5).

Le tableau 1 donne les largeurs de raie à 25 et 55 °C pour chaque solution ainsi que la valeur correspondante du rapport $\eta/\rho.T$ (η, ρ, T représentent respectivement les viscosité, densité et température) calculé à partir des données de la réf. 10.

On constate que la largeur de raie augmente fortement lorsque C_{HClO_4} augmente; cependant à 25 °C cette augmentation n'est effective qu'à partir de $C_{HClO_4} \geq 6.55$ M/l. Le spectre de la solution la plus diluée correspond donc logiquement à celui de l'ion $Mn(H_2O)_6^{2+}$ non influencé par ClO_4^- (2). L'accroissement de la largeur de raie lorsque C_{HClO_4} augmente ne permet pas de conclure immédiatement à la formation de complexes car la viscosité des solutions augmente notablement avec C_{HClO_4} (10) et contribue à elle seule à un élargissement de la raie.

En effet le mécanisme de relaxation le plus important pour l'ion $Mn(H_2O)_6^{2+}$ est du à la modulation du "zero-fiel-splitting" introduit lors de la distorsion de l'ion par les fluctuations du solvant avec un temps de corrélation τ_c (11, 12). Dans le cas limite $\omega\tau_c \ll 1$ (ω fréquence de Larmor des électrons), la largeur de raie est proportionnelle à τ_c, lui même proportionnel à $\eta/\rho.T$. Ainsi, si l'ion $Mn(H_2O)_6^{2+}$ était la seule espèce présente en solution, on devrait observer une variation linéaire de ΔH par rapport à $\eta/\rho.T$; ce qui en portant ΔH en fonction de

Can. J. Chem. Downloaded from www.nrcresearchpress.com by 210.87.254.105 on 09/05/12
For personal use only.

Can. J. Chem. Downloaded from www.nrcresearchpress.com by 210.87.254.105 on 09/05/12
For personal use only.

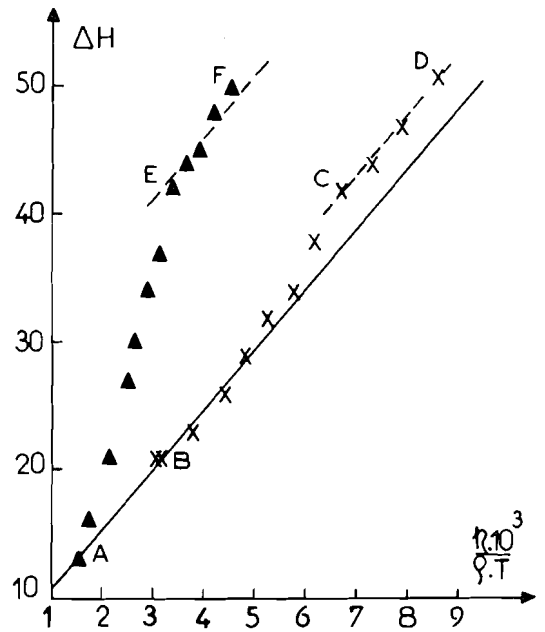

FIG. 1. Variation de la largeur de raie ΔH (gauss) en fonction de $\eta/\rho.T$ (centipoise/K). Concentration en Mn(II) 3×10^{-2} M/l. ×: $T = 25$ °C, ▲: $T = 55$ °C. La droite AB représente la variation correspondant à l'ion $Mn(H_2O)_6^{2+}$ seul.

$\eta/\rho.T$ devrait donner une droite sur laquelle se placeraient tous les points quelque soit la température, comme c'est le cas pour les solutions de $Mn(ClO_4)_2$ dans l'eau (12). A l'aide des données de la réf. 12, nous avons tracé la droite représentant la variation correspondant à l'ion $Mn(H_2O)_6^{2+}$ seul (voir fig. 1). Cette droite passe d'ailleurs par les 2 points A et B relatifs à la solution aqueuse (55 et 25 °C).

D'après la fig. 1, non seulement les points ne s'alignent pas sur cette droite mais s'en écartent de plus en plus lorsque C_{HClO_4} augmente (surtout à 55 °C, segment AE). On constate d'ailleurs que l'évolution de la largeur de raie lors de l'addition d'$HClO_4$ est différente à 25 et 55 °C. Si à 25 °C la largeur de raie observée ne dépasse celle estimée pour $Mn(H_2O)_6^{2+}$ seul qu'à partir de $C_{HClO_4} > 9.70$ M/l, à 55 °C l'accroissement de la largeur de raie est déjà plus important.

Puisque l'élargissement de la raie dépasse nettement celui provoqué par l'augmentation de la viscosité, il est donc certain que l'ion ClO_4^- se coordine à Mn(II).

Nos résultats ne sont d'ailleurs pas sans rappeler ceux obtenus par Hayes et Myers (2) pour l'effet de l'ion Cl^- dans les solutions aqueuses de perchlorate de Mn(II). Les perchlorato-complexes étant beaucoup moins stables que les chloro-complexes, on s'explique qu'à 25 °C l'excès de la largeur de raie par rapport à celle estimée pour l'ion libre ne commence à être effectif (portion CD fig. 1) que pour de fortes concentrations en $HClO_4$. Ces auteurs attribuent le très petit élargissement de la raie observé aux faibles températures à la formation du complexe externe et celui très important observé aux fortes températures à la formation du complexe interne et relient cet élargissement aux cinétiques de formation.

Par analogie avec leur description, il nous faut envisager les deux équilibres suivants:

$$[1]\quad Mn(H_2O)_6^{2+} + ClO_4^- \underset{k_{ba}}{\overset{k_{ab}}{\rightleftharpoons}} Mn(H_2O)_6^{2+}, ClO_4^-$$

$$[2]\quad Mn(H_2O)_6^{2+}, ClO_4^- \underset{k_{cb}}{\overset{k_{bc}}{\rightleftharpoons}} Mn(H_2O)_5ClO_4^+ + H_2O$$

et définir les constantes de stabilité dans le cadre de l'approximation faite dans la réf. 1:

$$[3]\quad K'_{ab} = \frac{[Mn(H_2O)_6^{2+}, ClO_4^-]}{[Mn(H_2O)_6^{2+}].a_{ClO_4^-}} = \frac{k_{ab}}{k_{ba}}$$

$$[4]\quad K'_{bc} = \frac{[Mn(H_2O)_5ClO_4^+].a_{H_2O}}{[Mn(H_2O)_6^{2+}, ClO_4^-]} = \frac{k_{bc}}{k_{cb}}$$

ainsi que les temps de demi-réaction:

$$[5]\quad \tau_{ab} = (k_{ab}a_{ClO_4^-})^{-1} \qquad \tau_{ba} = 1/k_{ba}$$
$$\tau_{bc} = 1/k_{bc} \qquad \tau_{cb} = (k_{cb}a_{H_2O})^{-1}$$

Si l'on appelle t_{2A}, t_{2B} et t_{2C} les temps de relaxation respectifs de l'ion libre, du complexe externe et du complexe interne, il est évident que $t_{2A} > t_{2B} > t_{2C}$ puisque l'asymétrie du complexe se prononce lorsque l'on passe de l'aquoion au complexe interne. Lorsque C_{HClO_4} augmente, τ_{ab} diminue fortement (car $a_{ClO_4^-}$ augmente) tandis que τ_{cb} augmente (car a_{H_2O} diminue).

Par comparaison avec le système $Mn(ClO_4)_2 - H_2O - Cl^-$ (2), on est sûr que pour les solutions les plus concentrées en $HClO_4$, les conditions $\tau_{ab} \ll t_{2A}$ et $\tau_{cb} \gg t_{2C}$ sont satisfaites et ce, d'autant mieux à 55 qu'à 25 °C; ce qui signifie que pour l'équilibre 1, il y a échange rapide et pour l'équilibre 2, échange lent. Dans ces conditions, le complexe interne ne contribue pas

Can. J. Chem. Downloaded from www.nrcresearchpress.com by 210.87.254.105 on 09/05/12
For personal use only.

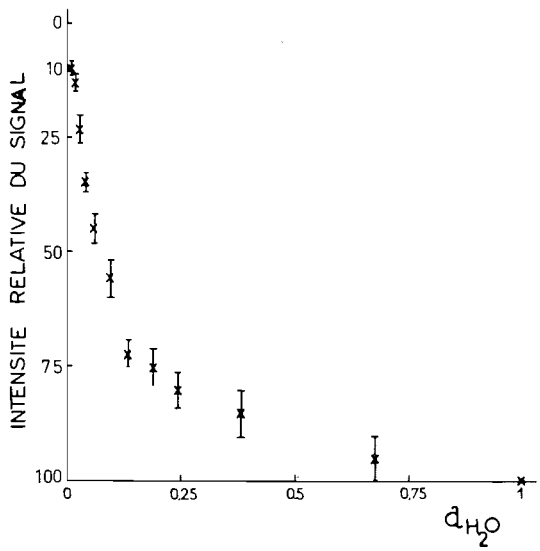

FIG. 2. Variation de l'intensité relative du signal pour les solutions de $Mn(ClO_4)_2$ 3×10^{-2} M/l en fonction de l'activité de l'eau à 25 °C. Les concentrations des solutions d'$HClO_4$ en M/l correspondantes sont celles du tableau 1. Les traits verticaux indiquent l'incertitude estimée sur la mesure de l'intensité relative du signal pour chaque solution.

directement à l'élargissement de la raie (par l'intermédiaire de t_{2C}): c'est sa vitesse de formation $1/\tau_{bc}$ qui est déterminante.

Comme $1/\tau_{bc}$ augmente avec la température, on comprend que l'élargissement soit plus important à 55 qu'à 25 °C. On doit s'attendre à ce que l'excès de la largeur de raie par rapport à celle de l'ion libre tende vers une limite dès que la formation du complexe externe est complète. Ceci semble être le cas d'après la fig. 1 pour $C_{HClO_4} \geq 9.70$ M/l à 55 °C (segment EF) et pour $C_{HClO_4} \geq 10.25$ M/l à 25 °C (segment CD). Compte tenu du nombre d'inconnues (constantes de vitesse et t_{2B}), il n'est pas possible de déterminer les constantes de stabilité à partir de l'élargissement de la raie; néanmoins, il est à prévoir que celles-ci sont plus fortes à 55 qu'à 25 °C.

Intensité du signal

La fig. 2 montre qu'à 25 °C l'intensité relative du signal par rapport à celui de la solution aqueuse décroît lorsque l'activité de l'eau diminue, jusqu'à atteindre la valeur de 10% pour la solution concentrée. (Pour la détermination de a_{H_2O} *cf.* réf. 1).

La décroissance de l'intensité du signal, très rapide à partir de $C_{HClO_4} > 8.15$ M/l, doit être attribuée à la formation du complexe interne. En effet le temps de relaxation t_{2C} de celui-ci, voisin de 10^{-11} s (3), est très court, ce qui donne lieu à une raie trop large pour être détectée. La présence du complexe interne se manifeste donc par une diminution de l'intensité du signal due à une diminution de la concentration globale des espèces contribuant au signal (ion libre et complexe externe).

Ceci nous permet d'évaluer la constante de stabilité K'_{bc} si l'on admet avec Burlamacchi et Tiezzi (3) que la concentration du complexe interne est proportionnelle à la diminution de l'intensité relative du signal. Pour C_{HClO_4} suffisamment élevée, l'équilibre 1 est déplacé vers la droite et la relation 4 s'écrit alors:

$$[6] \qquad K'_{bc} = \frac{(I_0 - I)}{I} \cdot a_{H_2O}$$

Le traitement des résultats de la fig. 2 par la méthode des moindres carrés nous permet d'estimer cette constante à $(8.0 \pm 1.5) \times 10^{-2}$ à 25 °C, tandisque les mesures à 55 °C nous donnent $(9.5 \pm 1.5) \times 10^{-2}$.

Ces résultats paraissent raisonnables devant ceux trouvés pour le monoperchlorato-interne de Mn(II) par rpe mais en milieu non aqueux (6). L'ordre de stabilité CH_3OH > DMF ~ DMSO > H_2O est conforme à l'augmentation de la constante diélectrique du solvant. Par ailleurs, la stabilité relative du monoperchlorato de Mn(II) comparée à celle de Co(II) et Ni(II) (constantes respectivement égales à 3.1×10^{-2} et 1.3×10^{-2}) (1) s'explique si l'on considère l'énergie de stabilisation du champ de coordinat.

D'après Jørgensen (13), l'énergie de stabilisation contribuant à la formation d'un complexe à partir d'un aquo-ion lors de la substitution d'une molécule d'eau, est approximativement égale à

$$[7] \qquad \Delta E = -\rho(10Dq_{complexe} - 10Dq_{aquo})/5$$

pour des complexes octaédriques non sujets à l'effet Jahn-Teller où le paramètre $\rho = 2a - 3b$ avec a nombre d'électrons t_{2g} et b nombre d'électrons e_g.

Pour un perchlorato-complexe, $10Dq_{complexe} < 10Dq_{aquo}$; d'après l'équation 7, il y a donc déstabilisation ce qui explique déjà l'instabilité des perchlorato-complexes. De plus cette dé-

stabilisation croît lorsque l'on passe de Mn(II) à Co(II) et Ni(II), puisque les valeurs respectives de ρ sont 0, 4, 6 d'où l'ordre $\Delta E_{Mn(II)} < \Delta E_{Co(II)} < \Delta E_{Ni(II)}$ qui entraîne par conséquent pour les constantes de stabilité l'ordre suivant $K_{Mn(II)} > K_{Co(II)} > K_{Ni(II)}$.

Cet ordre est le même que celui observé pour les chloro- et sulfato-complexes mais il est contraire à celui de la série d'Irving et Williams établie, il est vrai, par la considération des complexes aminés.

1. O. Benali-Baitich et E. Wendling. J. Inorg. Nucl. Chem. **37**, 1217 (1975).
2. R. G. Hayes et R. J. Myers. J. Chem. Phys. **40**, 877 (1964).
3. L. Burlamacchi et E. Tiezzi. J. Mol. Struct. **2**, 261 (1968).
4. S. I. Chan, B. M. Fung et H. Lutje. J. Chem. Phys. **47**, 2121 (1967).
5. H. Levanon et Z. Luz. J. Chem. Phys. **49**, 2031 (1968).
6. L. Burlamacchi, G. Martini et E. Tiezzi. J. Phys. Chem. **74**, 3980 (1970).
7. L. Burlamacchi, G. Martini et M. Romanelli. J. Chem. Phys. **59**, 3008 (1973)
8. M. M. Jones, E. A. Jones, D. F. Harmon et R. T. Semmes. J. Am. Chem. Soc. **83**, 2038 (1961).
9. F. Klanberg, J. P. Hunt et H. W. Dodgen. Inorg. Chem. **2**, 139 (1963).
10. A. A. Zinovev et V. P. Babaeva. Zh. Neorg. Khim. **2**, 2188 (1957).
11. N. Bloembergen et L. O. Morgan. J. Chem. Phys. **34**, 842 (1961).
12. B. B. Garrett et L. O. Morgan. J. Chem. Phys. **44**, 890 (1966).
13. C. K. Jørgensen. Modern aspects of ligand field theory. North-Holland. 1971. p. 384.

Can. J. Chem. Downloaded from www.nrcresearchpress.com by 210.87.254.105 on 09/05/12
For personal use only.

Synthetic morphinans and hasubanans. VI.[1] Total synthesis of 3-hydroxyisomorphinans, 3-hydroxyhasubanans, and 3,9-dihydroxyhasubanans

IVO MONKOVIĆ AND HENRY WONG
Bristol Laboratories of Canada, 100 Industrial Blvd., Candiac, Quebec J5R 1J1

Received August 20, 1975

IVO MONKOVIĆ and HENRY WONG. Can. J. Chem. **54**, 883 (1976).

A new total synthesis of racemic 3-hydroxyisomorphinans (**3**), 3-hydroxyhasubanans (**9**), 3,9α-dihydroxyhasubanans (**5**), and 3,9β-dihydroxyhasubanans (**7**), via 4a-(2-aminoethyl)-1,2,3,4,4a,9-hexahydro-6-methoxyphenanthrene (**1***a*) is described.

IVO MONKOVIĆ et HENRY WONG. Can. J. Chem. **54**, 883 (1976).

On décrit une nouvelle synthèse totale des hydroxy-3 isomorphinanes (**3**), hydroxy-3 hasubananes (**9**), dihydroxy-3,9α hasubananes (**5**) et dihydroxy-3,9β hasubananes (**7**) par l'intermédiaire du (amino-2 éthyle)-4a hexahydro-1,2,3,4,4a,9 méthoxy-6 phénanthrène (**1***a*).
[Traduit par le journal]

Introduction

In the previous papers in this series, we have reported on the total synthesis of a number of 3,14-dihydroxymorphinans I (Chart 1), via 3-methoxy-$\Delta^{8,14}$-morphinan II, some of which have been found to possess valuable pharmacological properties as analgesics and narcotic antagonists (1, 2). We also reported on the total synthesis of various 3,14-dihydroxyisomorphinans III (3, 4) and several hasubanan alkaloids IV (4, 5). The common intermediate in all of the above syntheses is 4a-(2-aminoethyl)-1,2,3,4,4a,9-hexahydro-6-methoxyphenanthrene **1***a* (Chart 2).

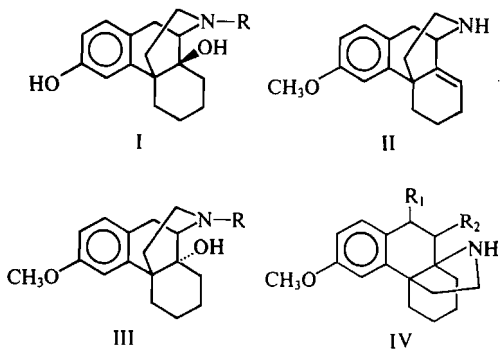

R = H, CH_3, and various C_3H_5–C_5H_9 substituents.
R_1 = H, β-SH R_2 = H, α-OH, α-Br.

CHART 1

We now report on its utilization in the synthesis of isomorphinans **3** and various hasubanan alkaloids **5**–**9**.

Results and Discussion

Several routes developed by Gates and coworkers led to the synthesis of the isomorphinan skeleton **3** (6, 7), the most practical being a modified Grewe approach (8). In view of potent analgesic and narcotic antagonist activity of some of these compounds, and a successful application of amine **1***a* in the synthesis of various related structures (1–5), we decided to attempt a total synthesis of the 3-hydroxyisomorphinan system **3** via the same intermediate. This was carried out in the following manner. Treatment of unsaturated amides (**1***b* and **1***c*) (4) with diborane in THF, followed by hydrogen peroxide and sodium hydroxide led to the stereo- and regioselective formation of B/C *trans*-fused α-hydroxyphenanthrenes **2***a* and **2***d* respectively, accompanied by some tertiary bases **2***b* and **2***e*. This stereochemical assignment is consistent with the reaction sequence described below. Treatment of **2***a* and **2***d* with methanesulfonyl chloride and pyridine afforded esters **2***c* and **2***f* which were cyclized to isomorphinans **3***a* and **3***c* respectively, by treatment with sodium hydride in DMF. Alkaline hydrolysis of **3***a* afforded 3-methoxyisomorphinan **3***b*, a versatile intermediate for the synthesis of various nitrogen substituted 3-hydroxyisomorphinans. Thus by a series of standard reactions, we prepared 17-

[1]For part V, see ref. 1.

Can. J. Chem. Downloaded from www.nrcresearchpress.com by 210.87.254.105 on 09/05/12
For personal use only.

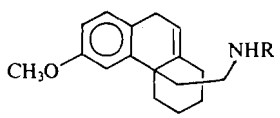

1

a R = H
b R = $COCF_3$
c R = CO—◁
d R = CO_2Et

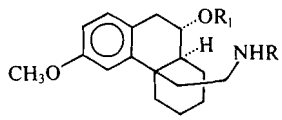

2

a R = $COCF_3$, R_1 = H
b R = CH_2CF_3, R_1 = H
c R = $COCF_3$, R_1 = SO_2CH_3
d R = CO—◁, R_1 = H
e R = CH_2—◁, R_1 = H
f R = CO—◁, R_1 = SO_2CH_3

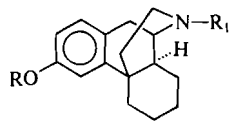

3

	R	R_1
a	CH_3	$COCF_3$
b	CH_3	H
c	CH_3	CO—◁
d	CH_3	CH_2—◁
e	H	CH_2—◁
f	CH_3	CO—◇
g	CH_3	CH_2—◇
h	H	CH_2—◇
i	CH_3	CO_2Et
j	H	CO_2Et
k	H	CH_3

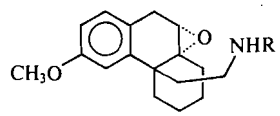

4

a R = CO_2Et
b R = CO—◁
c R = CH_3

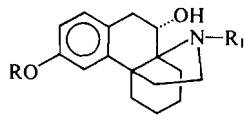

5

	R	R_1
a	CH_3	CO_2Et
b	H	CO_2Et
c	H	CH_3
d	CH_3	CO—◁
e	H	CO—◁
f	H	CH_2—◁
g	CH_3	CH_3

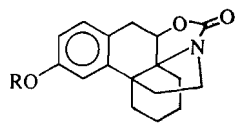

6

a R = CH_3
b R = H

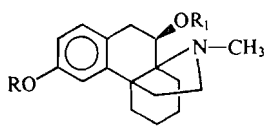

7

	R	R_1
a	CH_3	H
b	H	H
c	CH_3	SO_2CH_3

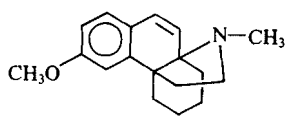

8

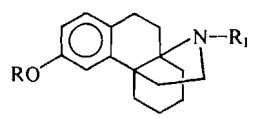

9

	R	R_1
a	CH_3	CO_2Et
b	CH_3	CH_3
c	CH_3	H
d	CH_3	$COCF_3$
e	CH_3	CO—◁
f	H	CO—◁
g	H	CH_2—◁

CHART 2

cyclobutylmethyl-3-hydroxyisomorphinan **3***h* and 3-hydroxy-17-methylisomorphinan **3***k*, which was identical in every respect to an authentic specimen. Similarly, **3***c* was reduced to **3***d* and demethylated to **3***e*.

Our earlier experience with the acid-catalysed cyclizations of certain δ,ε-unsaturated systems (5, 9) led us to explore the reactivity of various epoxides, **4**, (4) and amides, **1**, under acidic conditions. These efforts gave rise to two new

Can. J. Chem. Downloaded from www.nrcresearchpress.com by 210.87.254.105 on 09/05/12
For personal use only.

Can. J. Chem. Downloaded from www.nrcresearchpress.com by 210.87.254.105 on 09/05/12
For personal use only.

synthetic approaches to the hasubanan skeleton. Thus, treatment of epoxy amides **4***a* and **4***b* with dilute perchloric acid in THF afforded 9α-hydroxy-3-methoxyhasubanans **5***a* and **5***b* respectively in good yields. Further transformations of these to the dihydroxyhasubanans **5***c* and **5***f* were easily accomplished by standard procedures, except that the usual reaction sequence, *i.e.* reduction of amide function followed by demethylation, was reversed. The reversed reaction sequence was applied after an unsuccessful demethylation attempt on the previously reported 9α-hydroxy-3-methoxy-17-methylhasubanan **5***g* (4).

The epimeric 3,9β-dihydroxyhasubanan **7***b* was prepared from **5***a* in three reaction steps as follows. (*i*) Treatment of **5***a* with phosphorus oxychloride in pyridine afforded oxazolidone **6***a* in an intramolecular displacement–inversion reaction.[2] (*ii*) Demethylation of **6***a* by treatment with boron tribromide to give **6***b*, followed by reduction with lithium aluminum hydride afforded 3,9β-dihydroxy-17-methylhasubanan **7***b*. (*iii*) Reduction of **6***a* (lithium aluminum hydride) to **7***a*, followed by treatment with methanesulfonyl chloride afforded an ester **7***c*, which was subjected to a reaction with sodium hydride in DMF, whereupon 3-methoxy-17-methyl-$\Delta^{9,10}$-hasubanan **8** was obtained.

Our initial attempts to effect a one step synthesis of the hasubanan skeleton via acid-catalysed (sulfuric acid) cyclization of urethane **1***d* led to intractable mixtures. However, treatment of **1***b*, **1***c* and **1***d* with trifluoroacetic acid at reflux temperature afforded the corresponding hasubanans **9***a*, **9***b*, and **9***c* in good yields. Alkaline hydrolysis of **9***a* yielded 3-methoxyhasubanan **9***c* which could be easily transformed to the various N-substituted 3-hydroxyhasubanans. Alternatively, demethylation of **9***e* followed by reduction directly afforded 17-cyclopropylmethyl-3-hydroxyhasubanan **9***g*.

A summary of the various synthetic applications of the unsaturated amine **1***a* toward morphinan and hasubanan ring systems with structural correlations is shown in Scheme 1. We shall attempt to rationalize the high order of stereo- and regioselectivity of most of these reactions as follows. The stereospecific α-epoxidation and hydroboration of various acyl derivatives of **1***a* can be rationalized in terms of the steric effect of the amidoethano function. The bromocyclization of **1***a* to 9α-bromohasubanan IV rather than the respective 14-bromoisomorphinan is in accordance with the known preferential formation of five- to that of six-membered rings in the bromocyclization reactions (10, 11). Such preference in the case of **1***a* should be further enhanced by the fact that the probable intermediate bromonium ion should be asymmetric with higher charge distribution on the tertiary carbon (C_{14}) over that of the secondary one (C_9).

The regioselectivity of the epoxide ring opening reaction is influenced by several factors of steric and electronic nature, and it is usually difficult to assess the relative importance of each of these factors (12). However, due to the intramolecular nature of all the reactions studied, a number of important factors such as substitution of the epoxide ring, electrophilicity of the neighbouring group, and the size of the new ring to be formed, are easily recognized and the results can be rationalized as follows. The acid-catalysed reaction is expected to proceed by protonation of the epoxide oxygen atom and opening of the epoxide ring via neighbouring group participation of the acyl amine function. In such reactions, the tertiary carbocation intermediate as well as the size of the newly formed ring are expected to be dominant factors favoring 5-membered rings (hasubanans) over six-membered ones as pointed out in the course of the discussion of the bromocyclization reaction.

On the other hand, factors influencing the reactivity of aminoepoxide **4***c* (under non-catalyzed conditions) seem to be in a delicate balance resulting in equal amounts of the two possible products 9α-hydroxyhasubanan **5***g* and 14-hydroxyisomorphinan III (R = CH_3) (4). To put it another way, the preference (kinetic, or both kinetic and thermodynamic?) for formation of five- over six-membered rings successfully competes with the expected preferential opening of the epoxide with an amine at the less substituted carbon atom. However, this preference is insufficient when the nucleophilicity of the neighbouring group is enhanced such as in the case of base-catalysed cyclizations of various epoxides **4**, which result in exclusive formation

[2]Similar cyclizations in the cyclouridine series (18) using partially hydrolized phosphorus oxychloride, and in the series of β-hydroxyurethanes (19) using thionyl chloride and phosphorus pentoxide have been reported.

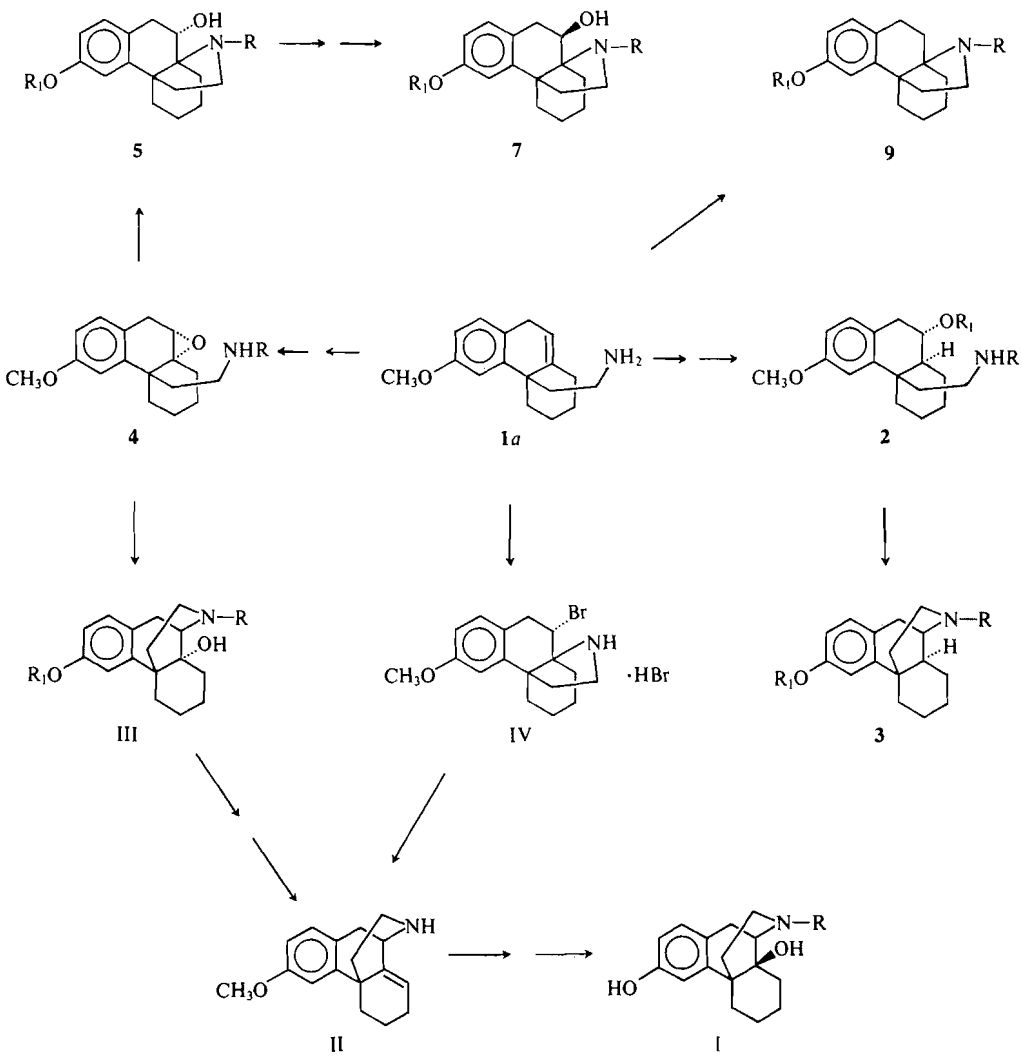

SCHEME 1

of 14-hydroxyisomorphinans III (4).

The preferred acid-catalysed cyclization of **1***b*, **1***c*, and **1***d* to hasubanan rather than morphinan ring systems is predictable on the basis of both ring size and a tertiary carbocation intermediate. This cyclization at the time of execution appeared to be a novel synthetic approach to a wide variety of heterocyclic compounds, particularly pyrrolidines and piperidines. Subsequently, we found two recorded examples in the literature describing the synthesis of spirolactams VI (Scheme 2) (13) and VIII (14, 15), from the respective cyclohexenyl derivatives V and VII.

It is interesting to note that some closely related systems such as IX under similar reaction conditions have been reported to give products of oxygen participation X. Similarly, various *N*-allylamides and related compounds give products of oxygen (sulfur) rather than nitrogen participation (5, 16, 17).

Pharmacological Results

A number of new compounds (in particular *N*-alkyl-3-hydroxy derivatives) have been screened for analgesic and narcotic antagonist activities

Can. J. Chem. Downloaded from www.nrcresearchpress.com by 210.87.254.105 on 09/05/12
For personal use only.

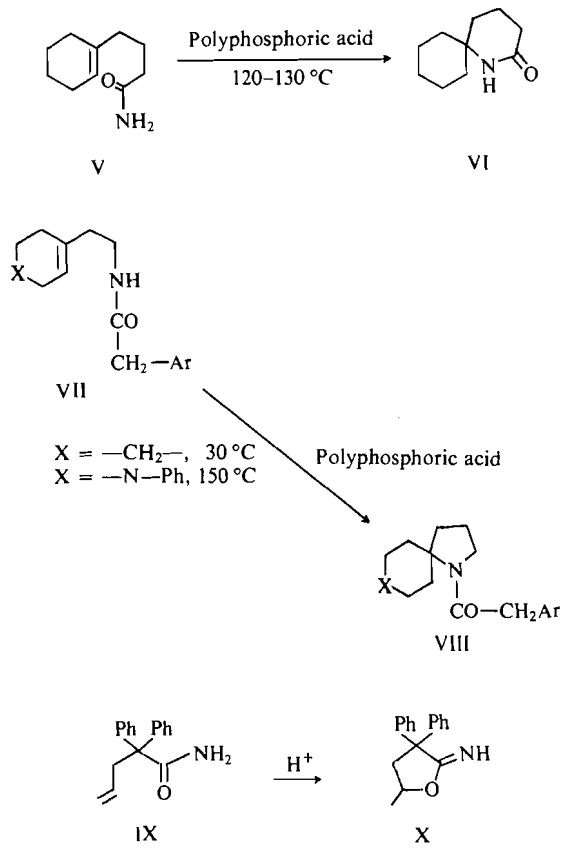

SCHEME 2

in mice by Dr. A. W. Pircio of the Bristol Laboratories, Syracuse, N.Y., according to the previously reported procedures (1). Some of the compounds have been found to possess moderate levels of activities as shown in Table 1, however, none was considered to be of therapeutic value.

Experimental

The melting points were determined on a Gallenkamp apparatus, and are uncorrected. The infrared (ir) spectra were recorded on a Unicam SP-200G grating ir spectrometer. The nmr spectra were recorded on a Varian A-60A spectrometer using deuteriochloroform. The chemical shifts are expressed in δ values using tetramethylsilane as internal reference. Microanalyses were performed by Micro-Tech Laboratories Inc., Skokie, Illinois.

Trifluoroacetamido Alcohol, 2a, and Trifluoroethylamino Alcohol, 2b

To a cooled (ice), stirred solution of **1***b* (4) (10.5 g) in dry THF (80 ml) was added dropwise 1 *M* solution of diborane in THF (75 ml). The mixture was allowed to stand for 18 h at 5 °C, followed by 4 h at room temperature. It was then treated successively with water (3 ml), 5 *N* sodium hydroxide (16 ml), and 30% hydrogen peroxide (4.4 ml), and the resulting mixture was heated to an internal temperature of 45–50 °C for 30 min. After cooling, it was diluted with ice cold water (100 ml), acidified with concentrated hydrochloric acid, and extracted with benzene. The acid layer was set aside and the benzene extract was dried and evaporated *in vacuo* to yield 11.7 g of crude **2***a* as an oil. The analytical sample was purified by chromatography on a silica gel column (eluent, benzene–ether 3:2); ir (neat), 3340, 3100, 1720 cm^{-1}; nmr δ 6.8–7.2 (3H, m), 3.82 (3H, s), 1.1–3.9 (16H, m). *Anal.* calcd. for $C_{19}H_{24}F_3NO_3$: C 61.44, H 6.51, N 3.77; found: C 61.60, H 6.74, N 3.63.

TABLE 1. Analgesic and narcotic antagonist activities (in mice) of some of the compounds studied

Compound	ED_{50} (mg/kg s.c.) Antagonist activity (oxymorphone-induced Straub tail)	ED_{50} (mg/kg s.c.) Analgesic activity (mouse writhing)
3*h*	7	0.3
5*c*	>40	20
5*f*	15	24
7*b*	>40	9
9*g*	>40	13

The aqueous acidic solution was made basic with ammonium hydroxide and extracted with dichloromethane. Drying and evaporation of solvent gave 450 mg of amino alcohol **2***b* as an oil; ir (neat) 3380 cm^{-1}; nmr ($CDCl_3$) δ 6.5–7.0 (3H, m), 3.9 (1H, m), 3.72 (3H, s), 1.1–3.5 (17H, m). The oxalate salt of **2***b* was recrystallized from methanol–ether; mp 170–172 °C. *Anal.* calcd. for $C_{19}H_{26}F_3NO_2 \cdot C_2H_2O_4$: C 56.37, H 6.31, N 3.13; found: C 56.41, H 6.61, N 3.17.

Methanesulfonyl Ester 2c

To a cooled and stirred mixture of crude amido alcohol **2***a* (11.2 g) and triethylamine (4.5 g) in benzene (50 ml) was added dropwise a solution of methanesulfonyl chloride (5.16 g) in benzene (10 ml). The reaction mixture was stirred for 3 h at room temperature and then partitioned between water and dichloromethane. The organic layer was dried and evaporated *in vacuo*. The residual oil was dissolved in a small amount of benzene and to this solution was added a large amount of ether. The solid deposited was collected by filtration to give 5.54 g of **2***c*. Recrystallization from 2-propanol gave an analytical sample; mp 118–120 °C; ir (Nujol) 3360, 1720 cm^{-1}; nmr δ 6.6–7.1 (3H, m), 4.6–5.1 (1H, m), 3.77 (3H, s), 3.03 (3H, s), 1.1–3.7 (15H, m). *Anal.* calcd. for $C_{20}H_{26}F_3NO_5S$: C 53.44, H 5.83, N 3.12; found: C 53.26, H 6.00, N 3.04.

Amido Alcohol 2d and Amino Alcohol 2e

To a solution of unsaturated amide **1***c* (9.75 g) in dry THF was added 1 *M* solution of diborane in THF (63 ml) and the mixture left at 5 °C for 18 h, at the end of which period, it was treated consecutively with water (1.5 ml), 5 *N* sodium hydroxide (13.5 ml), and 30% hydrogen

Can. J. Chem. Downloaded from www.nrcresearchpress.com by 210.87.254.105 on 09/05/12
For personal use only.

Can. J. Chem. Downloaded from www.nrcresearchpress.com by 210.87.254.105 on 09/05/12
For personal use only.

peroxide (4.4 ml). The mixture was heated under reflux for 30 min, cooled, diluted with water, and acidified with concentrated hydrochloric acid. The acidic solution was extracted with benzene and left aside. The benzene extract was dried and evaporated *in vacuo* to give an oil, which crystallized from ether. A yield of 65% (6.9 g) of **2***d* was obtained; mp 130–131 °C from dichloromethane–ether; ir (Nujol) 3480, 3280, 1630 cm^{-1}; nmr δ 6.6–7.2 (3H, m), 3.8 (3H, s), 3.7–4.1 (1H, m), 0.4–3.5 (20H, m). *Anal.* calcd. for $C_{21}H_{29}NO_3$: C 73.44, H 8.51, N 4.08; found: C 73.40, H 8.59, N 4.07.

The aqueous solution was made alkaline with ammonium hydroxide and extracted with dichloromethane to yield, after drying and evaporation, 1.4 g of amino alcohol **2***e* as an oil; ir (neat) 3380 cm^{-1}; nmr δ 6.6–7.2 (3H, m), 3.8 (3H, s), 3.8–4.2 (1H, m), 0.0–3.7 (22H, m).

A sample for analysis was purified as the oxalate salt by recrystallization from acetone; mp 193–195 °C. *Anal.* calcd. for $C_{21}H_{31}NO_2 \cdot C_2H_2O_4$: C 65.85, H 7.93, N 3.34; found: C 65.50, H 7.94, N 3.31.

Methanesulfonyl Ester 2f

The ester **2***f* was obtained in 93% yield from alcohol **2***d* by the procedure given for the preparation of **2***c*; mp 123–124 °C from dichloromethane–ether; ir (Nujol) 3280, 1640 cm^{-1}; nmr δ 6.6–7.1 (3H, m), 4.7–5.2 (1H, m), 3.8 (3H, s), 2.98 (3H, s), 0.4–3.6 (20H, m). *Anal.* calcd. for $C_{22}H_{31}NO_5S$: C 62.68, H 7.41, N 3.32; found: C 62.32, H 7.39, N 3.18.

3-Methoxy-17-trifluoroacetylisomorphinan 3a and 3-Methoxyisomorphinan 3b

To a cooled and stirred suspension of sodium hydride (580 mg of 55%, washed with hexane) in DMF (5 ml) was added dropwise a solution of methanesulfonyl ester **2***c* (4.05 g) in DMF (20 ml) and the mixture stirred at room temperature for 6 h. It was then cooled and partitioned between ice-cold water and a benzene–ether mixture. The organic layer was washed several times with cold water and extracted with dilute hydrochloric acid. The acidic extract was set aside, and the organic layer was washed with water, dried, and evaporated to dryness to give 1.25 g of isomorphinan **3***a* as an oil; bp 140–145 °C/0.02 torr; ir (neat) 1720 cm^{-1}; nmr δ 6.6–7.3 (3H, m), 4.1–4.6 (1H, m), 3.85 (3H, s), 0.8–3.6 (15H, m). *Anal.* calcd. for $C_{19}H_{22}F_3NO_2$: C 64.58, H 6.28, N 3.96; found: C 64.40, H 6.34, N 3.97.

The acidic extract was made basic with ammonium hydroxide and extracted with ether. The ethereal extract was dried, filtered with charcoal, and concentrated *in vacuo* to give 1.35 g of isomorphinan **3***b* as an oil; ir (neat) 3300 cm^{-1}; nmr δ 6.6–7.3 (3H, m), 3.83 (3H, s), 1.1–3.6 (15H, m), 0.85 (1H, d, $J \simeq 10$ Hz). The hydrochloride salt (1.42 g) was recrystallized from methanol–acetone; mp 293–295 °C. *Anal.* calcd. for $C_{17}H_{23}NO \cdot HCl$: C 69.49, H 8.23, N 4.77; found: C 69.48, H 8.38, N 4.62.

By varying the solvent composition and work-up temperature, the ratio of **3***a* and **3***b* can be adjusted. In another experiment, the starting material **2***c* (9.09 g) was dissolved in THF (25 ml) and added to a suspension of sodium hydride (1.6 g of 55%) in DMF (10 ml) under the same conditions as above. During work-up, the reaction mixture was cooled with an ice–salt bath. This procedure afforded 5.7 g of **3***a* and 1.1 g of **3***b*.

The hydrolysis of **3***a* to **3***b* is effected by treatment with sodium hydroxide in aqueous ethanol. A mixture of **3***a* (5.4 g) and 1 *N* sodium hydroxide in 80% aqueous ethanol (20 ml) was heated under reflux for 15 min. The usual work-up gave 4.0 g of **3***b*. This procedure can be applied to the crude mixture of **3***a* and **3***b* to obtain exclusively **3***b*.

17-Cyclopropylcarbonyl-3-methoxyisomorphinan 3c

The isomorphinan **3***c* (an oil) was similarly obtained in quantitative yield from **2***d*. The reaction time was 18 h. A sample for analysis was distilled at 165–170 °C/0.2 torr; ir (neat) 1630 cm^{-1}; nmr δ 6.6–7.2 (3H, m), 3.82 (3H, s), 3.8–5.0 (2H, m), 4.5–3.6 (19H, m). *Anal.* calcd. for $C_{21}H_{27}NO_2$: C 77.50, H 8.36, N 4.30; found: C 77.56, H 8.44, N 4.15.

17-Cyclopropylmethyl-3-methoxyisomorphinan 3d

To a solution of lithium aluminum hydride (0.23 g) in dry ether (10 ml) was added dropwise under nitrogen a solution of amide **3***c* (1.46 g) in ether (15 ml) and the mixture heated under reflux for 2 h. After cooling and the usual work-up, 1.17 g of **3***d* was obtained as an oil; nmr δ 6.6–7.1 (3H, m), 3.82 (3H, s), 0.0–3.3 (23H, m). A sample was purified as its hydrochloride salt by recrystallization from methanol–acetone; mp 237–239 °C. *Anal.* calcd. for $C_{21}H_{29}NO_2 \cdot HCl$: C 72.49, H 8.69, N 4.03; found: C 72.37, H 8.83, N 3.97.

3-Hydroxy-17-cyclopropylmethylisomorphinan 3e

A solution of 3-methoxyisomorphinan **3***d* (3.0 g) in hydrobromic acid (30 ml, 48%) was heated under reflux under nitrogen for 5 min. After cooling, the mixture was poured onto ice and ammonium hydroxide and extracted with dichloromethane. The extract was dried and evaporated *in vacuo*. The residual oil was dissolved in acetone and filtered over a celite–charcoal mixture. The filtrate was treated with a solution of hydrogen chloride in ether to give 2.05 g of the solid hydrochloride salt of **3***e*. Recrystallization from ethanol gave an analytical sample; mp 266–268 °C; ir (free base, neat) 3250 cm^{-1}; nmr δ 6.25–6.9 (3H, m), 0.0–3.2 (23H, m). *Anal.* calcd. for $C_{20}H_{27}NO \cdot HCl$: C 61.94, H 8.45, N 4.20; found: C 71.71, H 8.33, N 4.09.

17-Cyclobutylcarbonyl-3-methoxyisomorphinan 3f

To a cooled and stirred solution of **3***a* (5.0 g) and triethylamine (2.12 g) in dichloromethane (50 ml) was added dropwise a solution of cyclobutylcarbonyl chloride (2.49 g) in dichloromethane (10 ml). The mixture was then washed with water, dried, and evaporated *in vacuo* to give 5.98 g of **3***f* as an oil. A sample was distilled at 165–170 °C/0.2 torr; ir (neat) 1630 cm^{-1}; nmr δ 6.7–7.3 (3H, m), 4.0–5.3 (2H, m), 3.82 (3H, s), 1.2–3.7 (20H, m), 0.75–1.15 (1H, m). *Anal.* calcd. for $C_{22}H_{29}NO_2$: C 77.84, H 8.61, N 4.13; found: C 77.55, H 8.72, N 4.01.

17-Cyclobutylmethyl-3-methoxyisomorphinan 3g

A solution of amide **3***f* (5.67 g) in dry THF (40 ml) was added dropwise to a solution of lithium aluminum hydride (1.0 g) in THF (10 ml) and the mixture heated under reflux for 4.5 h. After cooling and the usual work-up, 4.55 g of **3***g* was obtained as an oil. A sample was distilled at 160–165 °C/0.01 torr; nmr δ 6.6–7.2 (3H, m), 3.8 (3H, s), 1.1–3.3 (24H, m), 0.86 (1H, d, m, poor

Can. J. Chem. Downloaded from www.nrcresearchpress.com by 210.87.254.105 on 09/05/12
For personal use only.

resolution, $J = 10$ Hz). *Anal.* calcd. for $C_{22}H_{31}NO$: C 81.18, H 9.60, N 4.30; found: C 81.30, H 9.67, N 4.18.

17-Cyclobutylmethyl-3-hydroxyisomorphinan 3h

A solution of methoxyisomorphinan **3g** (4.25 g) in dichloromethane (130 ml) was added dropwise over a period of 30 min to a cooled (ice–salt) and stirred solution of boron tribromide (6.77 g) in dichloromethane (10 ml). The mixture was stirred for another 30 min and then treated with cold water, followed by ammonium hydroxide, and the layers were separated. The organic layer was dried and evaporated to dryness. The residual oil was purified as its hydrochloride salt by two recrystallizations from 90% ethanol to give 2.1 g of **3h** hydrochloride; mp 263–265 °C; ir (neat) 3260 cm^{-1}; nmr δ 6.6–7.2 (3H, m), 1.1–3.3 (24H, m), 0.85 (1H, d, $J = 10$ Hz). *Anal.* calcd. for $C_{21}H_{29}NO \cdot HCl$: C 72.49, H 8.69, N 4.03; found: C 72.27, H 8.79, N 4.08.

17-Methoxycarbonyl-3-methoxyisomorphinan 3i

To a cooled (ice) stirred solution of 3-methoxyisomorphinan **3b** (1.80 g) and triethylamine (1.02 g) in dichloromethane (20 ml) was added dropwise a solution of methylchloroformate (0.66 g) in dichloromethane (5 ml). The mixture was then washed with water followed by dilute hydrochloric acid, dried, and evaporated *in vacuo* to give 1.84 g of **3i** as an oil; ir (neat) 1680 cm^{-1}; nmr δ 6.5–7.1 (3H, m), 4.1–4.5 (1H, m), 3.72 (3H, s), 3.65 (3H, s), 1.1–3.5 (14H, m), 0.9 (1H, d, $J = 10$ Hz). *Mol. Wt.* calcd. for $C_{19}H_{25}NO_3$; found (mass spectrum) 315.

3-Hydroxy-17-methoxycarbonylisomorphinan 3j

To a cooled (ice–salt) solution of boron tribromide (1.5 g) in dichloromethane (10 ml) a solution of methoxyisomorphinan **3i** (0.90 g) in dichloromethane (10 ml) was introduced dropwise under nitrogen. The mixture was stirred at room temperature for 4 h, and then worked up as usual to give 0.70 g of **3j** as an oil; ir (neat) 3340, 1675 cm^{-1}; nmr δ 6.4–7.0 (3H, m), 4.1–4.5 (1H, m), 3.63 (3H, s), 1.1–3.5 (14H, m), 0.85 (1H, d, $J = 10$ Hz). A sample solidified after distillation at 190 °C/0.05 torr; mp 102–105 °C. *Anal.* calcd. for $C_{18}H_{23}NO_3$: C 71.73, H 7.69, N 4.64; found: C 71.62, H 7.61, N 4.61.

3-Hydroxy-17-methylisomorphinan 3k

The hydroxyisomorphinan **3k** was obtained in quantitative yield by essentially the same procedure as given for the preparation of **3h**. At first an oil, it crystallized on standing. Recrystallization from ethyl acetate gave an analytical sample; mp 216–218 °C, reported mp 217–218.5 °C (6); ir (Nujol) 3100 cm^{-1}; nmr δ 6.5–7.0 (3H, m), 3.6–4.0 (1H, m), 2.32 (3H, s), 1.1–3.5 (14H, m), 0.98 (1H, d, $J = 10$ Hz). *Anal.* calcd. for $C_{17}H_{23}NO$: C 79.33, H 9.01, N 5.44; found: C 79.10, H 9.08, N 5.52.

17-Ethoxycarbonyl-9α-hydroxy-3-methoxyhasubanan 5a

To a cooled (ice), stirred solution of epoxy urethane **4a** (4) (4.5 g) in THF (40 ml) was added dropwise 30% perchloric acid (4 ml), and the mixture allowed to stand at room temperature for 2 h. It was then partitioned between aqueous ammonium hydroxide and benzene. The benzene layer was washed with water, dried, and evaporated to dryness. The residual oil crystallized from ether to yield 2.8 g of **5a**; mp 109–110 °C. Recrystallization from 2-propanol gave an analytical sample; mp 113–114 °C; ir (Nujol) 3340, 1665 cm^{-1}; nmr δ 6.6–7.1 (3H, m), 4.2 (1H, unresolved), 4.15 (2H, q, $J = 7$ Hz), 3.72 (3H, s), 2.6–3.8 (4H, m), 1.3 (3H, t, $J = 7$ Hz), 0.9–2.2 (10H, m). *Anal.* calcd. for $C_{20}H_{27}NO_4$: C 69.54, H 7.88, N 4.06; found: C 69.45, H 8.06, N 4.06.

3,9α-Dihydroxy-17-ethoxycarbonylhasubanan 5b

To a cooled (ice) stirred solution of **5a** (1.78 g) in dichloromethane (20 ml) was added in a few portions a solution of boron tribromide (2.75 g) in dichloromethane (10 ml). The mixture was allowed to stand at room temperature for 2 h and then it was treated with ice cold ammonium hydroxide and methanol. When all of solid was dissolved, the mixture was partitioned between water and dichloromethane. The organic layer was dried and evaporated *in vacuo* to give 950 mg of solid **5b**; mp 180–182 °C. Recrystallization from benzene afforded an analytical sample; mp 185–187 °C; ir (Nujol) 3220, 1645 cm^{-1}; nmr δ 6.5–7.0 (3H, m), 4.15 (2H, q, $J = 7$ Hz), 4.0–4.3 (1H, unresolved), 2.7–3.9 (4H, m), 0.9–2.2 (10H, m), 1.27 (3H, t, $J = 7$ Hz). *Anal.* calcd. for $C_{19}H_{25}NO_4$: C 68.86, H 7.60, N 4.23; found: C 68.60, H 7.63, N 4.14.

3,9α-Dihydroxy-17-methylhasubanan 5c

To a solution of lithium aluminum hydride (250 mg) in THF (20 ml) was added dropwise a solution of dihydroxyhasubanan **5b** (500 mg; containing 1 mol of benzene of crystallization) in THF (10 ml) and the mixture heated under reflux for 3 h. After cooling and the standard work-up procedure, the product was dissolved in a benzene–ether mixture and extracted with 1 *N* hydrochloric acid. The acidic extract was made basic with ammonium hydroxide and extracted with a benzene–ether mixture to give, after drying and evaporation of solvent, 360 mg of **5c** as a white solid; mp 183–186 °C. Recrystallization from acetone–benzene gave an analytical sample; mp 190–192 °C; ir (Nujol) 3270, 3440 cm^{-1}; nmr δ 6.4–6.9 (3H, m), 4.05 (1H, dd, $J_1 = 10$ Hz, $J_2 = 6$ Hz), 2.4–3.0 (4H, m), 2.4 (3H, s), 0.9–2.0 (10H, m). *Anal.* calcd. for $C_{17}H_{23}NO_2$: C 74.69, H 8.48, N 5.12; found: C 74.52, H 8.69, N 5.13.

17-Cyclopropylcarbonyl-9α-hydroxy-3-methoxyhasubanan 5d

The epoxide **4b** (4) was treated with perchloric acid as described above to give **5d** as an oil in 55% yield, which crystallized from ether; mp 99–101 °C. Another crop of 21% yield was obtained from mother liquors by column chromatography (silica gel, ether) for a total of 82%; ir (Nujol) 3200, 1610 cm^{-1}; nmr δ 6.6–7.1 (3H, m), 4.14 (1H, dd, $J_1 = 10$ Hz, $J_2 = 6$ Hz), 3.75 (3H, s), 3.6–4.0 (2H, m), 2.82 (3H, s, and d, $J = 3$ Hz), 0.6–2.3 (10H, m). *Anal.* calcd. for $C_{21}H_{27}NO_3$: C 73.87, H 7.97, N 4.10; found: C 73.66, H 8.09, N 4.01.

3,9α-Dihydroxy-17-cyclopropylcarbonylhasubanan 5e

The dihydroxyhasubanan **5e** was obtained in 76% yield, as a white solid containing 1 mol of benzene of crystallization, by treatment of methoxyhasubanan **5d** with boron tribromide as described for the preparation of **5b**. Recrystallization from acetone gave an analytical sample containing $\frac{1}{2}H_2O$ of crystallization; mp 193–194 °C; ir (Nujol) 3180, 1605 cm^{-1}; nmr δ 6.5–7.0

Can. J. Chem. Downloaded from www.nrcresearchpress.com by 210.87.254.105 on 09/05/12
For personal use only.

(3H, m), 3.6–4.4 (3H, m), 2.7–3.1 (3H, m), 0.6–2.4 (10H, m). *Anal.* calcd. for $C_{20}H_{25}NO_3 \cdot \frac{1}{2}H_2O$: C 71.40, H 7.79, N 4.16; found: C 71.19, H 7.63, N 4.28.

3,9α-Dihydroxy-17-cyclopropylmethylhasubanan 5f

The dihydroxyhasubanan **5f** was obtained in 83% yield, as a white solid, mp 82–92 °C from **5e** by a procedure given for the preparation of **5c**. Recrystallization from methanol gave an analytical sample containing $\frac{1}{2}CH_3OH$ of crystallization; mp 106–108 °C; ir (Nujol) 3420, 3295 cm^{-1}; nmr δ 6.4–7.0 (3H, m), 3.9 (1H, dd, J_1 = 10 Hz, J_2 = 6 Hz), 2.4–3.3 (6H, m), 0.0–2.1 (15H, m). *Anal.* calcd. for $C_{20}H_{27}NO_2 \cdot \frac{1}{2}CH_3OH$: C 75.19, H 8.71, N 4.18; found: C 75.19, H 8.89, N 4.22.

Oxazolidone 6a

To a cold (ice) solution of hydroxyurethane **5a** (1.56 g) in pyridine (10 ml) was added dropwise phosphorus oxychloride (3 ml) under nitrogen and the mixture allowed to stand at room temperature for 4 h. It was then poured carefully onto ice water and extracted with ether. The ether extract was washed with cold dilute hydrochloric acid followed by water, dried, and evaporated to dryness. The residual oil (1.30 g) was chromatographed over alumina (150 g, dry column eluent chloroform) to give 850 mg of **6a** as a heavy oil; ir (neat) 1752 cm^{-1}; nmr δ 6.5–7.1 (3H, m), 4.7 (1H, t, J = 3 Hz), 3.73 (3H, s), 1.1–3.3 (14H, m). A sample for analysis was distilled at 155 °C/0.05 torr to give an amorphous solid. *Anal.* calcd. for $C_{18}H_{21}NO_3$: C 72.22, H 7.07, N 4.68; found: C 72.34, H 7.16, N 4.57.

Oxazolidone 6b

To a cold (ice-salt) solution of boron tribromide (1.0 g) in dichloromethane (10 ml) was added dropwise a solution of oxazolidone **6a** (550 mg) in dichloromethane (10 ml) under nitrogen and the mixture was stirred at room temperature for 1.5 h. It was then poured onto ice – ammonium hydroxide and the layers separated. The organic layer was washed with water, dried (Na_2SO_4), and evaporated *in vacuo* to give 430 mg of solid **6b**. Recrystallization from ether gave an analytical sample; mp 234–236 °C; ir (Nujol) 3260, 1740 cm^{-1}; nmr δ 6.4–7.0 (3H, m), 4.78 (1H, t, J = 3 Hz), 1.1–3.3 (14H, m). *Anal.* calcd. for $C_{17}H_{19}NO_3$: C 71.56, H 6.71, N 4.91; found: C 71.29, H 6.60, N 4.76.

9β-Hydroxy-3-methoxy-17-methylhasubanan 7a

To a solution of lithium aluminum hydride (0.50 g) in THF (10 ml) was added dropwise a solution of oxazolidone **6a** (1.0 g) in THF (20 ml) and the mixture was heated under reflux for 18 h. Work-up as usual gave 900 mg of solid **7a**. It was purified as its hydrochloride salt by recrystallization from methanol–ether; mp 273–275 °C; ir (Nujol) 3200 cm^{-1}; nmr (free base) δ 6.5–7.1 (3H, m), 3.03 (1H, dd, J_1 = 8 Hz, J_2 = 5 Hz), 7.78 (3H, s), 2.44 (3H, s), 1.1–3.3 (14H, m). *Anal.* calcd. for $C_{18}H_{25}NO_2 \cdot HCl$: C 66.76, H 8.09, N 4.33; found: C 66.29, H 8.18, N 4.07.

3,9β-Dihydroxy-17-methylhasubanan 7b

This compound was prepared in 65% yield by the method described for the preparation of **6b**; an oil; nmr δ 6.4–7.0 (3H, m), 4.03 (1H, dd, poor resolution), 2.4 (3H, s), 1.1–3.2 (14H, m). A sample purified as its hydrochloride salt by recrystallization from methanol–ether contained 1 mol of water of crystallization; mp 273–275 °C; ir (Nujol) 3310, 3220 cm^{-1}. *Anal.* calcd. for $C_{17}H_{23}NO_2 \cdot HCl \cdot H_2O$: C 62.28, H 7.99, N 4.27; found: C 62.08, H 7.49, N 4.10.

3-Methoxy-17-methyl-$\Delta^{9,10}$-hasubanan 8

9β-Hydroxyhasubanan **7a** (350 mg) in benzene (5 ml) was treated with methanesulfonyl chloride (170 mg) and triethylamine (150 mg) for 4 h to give after the usual work-up, 440 g of 9β-methanesulfonate **7c** as an oil; nmr δ 6.5–7.1 (3H, m), 4.3 (1H, dd, J_1 = 11 Hz, J_2 = 6 Hz), 3.73 (3H, s), 3.03 (3H, s), 2.36 (3H, s), 1.1–3.8 (14H, m). This was treated with sodium hydride (100 mg) in DMF (10 ml) under reflux for 15 min to yield after work-up 260 mg of **8**, an oil, identical to an authentic sample prepared by another route.[3]

17-Ethoxycarbonyl-3-methoxyhasubanan 9a

A solution of urethane **1d** (1.2 g) in trifluoroacetic acid (12 ml) was heated under reflux under nitrogen for 10 min. The mixture was evaporated *in vacuo* and the residual oil was dissolved in ether and triturated with petroleum ether. This solution was filtered with charcoal and the filtrate concentrated *in vacuo* to give 1.08 g of **9a** as an oil, which solidified upon standing; mp 78–80 °C; ir (Nujol) 1695 cm^{-1}; nmr δ 6.6–7.1 (3H, m), 4.10 (2H, q, J = 7 Hz), 3.78 (3H, s), 1.3–3.6 (16H, m), 1.2 (3H, t, J = 7 Hz). *Anal.* calcd. for $C_{20}H_{27}NO_3$: C 72.90, H 8.26, N 4.25; found: C 73.00, H 8.21, N 4.15.

3-Methoxy-17-methylhasubanan 9b

Urethane **9a** was reduced to the *N*-methyl derivative **9b** by treatment with lithium aluminum hydride by the standard procedure. The product so obtained contained some of the 3-methoxyhasubanan **9c**. Formaldehyde was added to the mixture which was then hydrogenated with Raney Nickel as catalyst, to give a 72% yield of **9b**, isolated as its hydrochloride salt; mp 258–262 °C, identical by mixture mp determination with a sample of **9b** as previously reported (5).

3-Methoxyhasubanan 9c

To a solution of **9a** (3.29 g) in 1-octanol (20 ml) was added potassium hydroxide pellets (2.8 g) and the mixture was heated under reflux for 1 h. After cooling, ether (100 ml) was added and this solution was extracted several times with 1 *N* hydrochloric acid, followed by water (5 × 20 ml). The combined extracts were made basic with ammonium hydroxide and extracted with ether. The ether extract was dried and evaporated *in vacuo* and the residual oil **9c** was purified as its hydrochloride salt by recrystallization from methanol–ether to afford 1.5 g, mp 263 °C, identical to that previously reported (5).

3-Methoxy-17-trifluoroacetylhasubanan 9d

A solution of amide **1b** (2 g) in trifluoroacetic acid (20 ml) was heated under reflux under nitrogen for 30 min. The acid was then removed by evaporation *in vacuo* and the residual oil was treated with 5 *N* sodium hydroxide (10 ml) and ethanol (40 ml) at reflux temperature for 10 min. Then the mixture was cooled, diluted

[3]Unpublished work from these laboratories.

with water, acidified with hydrochloric acid, and extracted with ether to give, after drying and evaporation of ether, an oil which crystallized from ether – petroleum ether. Compound **9***d* (1.0 g) was obtained as a white solid; mp 102–104 °C (from ether); ir (Nujol) 1710 cm^{-1}; nmr δ 6.6–7.2 (3H, m), 3.78 (3H, s), 3.0–4.0 (3H, m), 1.2–3.0 (13H, m). *Anal.* calcd. for $C_{19}H_{22}F_3NO_2$: C 64.58, H 6.27, N 3.96; found: C 64.41, H 6.41, N 3.91.

17-Cyclopropylcarbonyl-3-methoxyhasubanan **9***e*

A solution of **1***c* (4.0 g) in trifluoroacetic acid (40 ml) was heated under reflux under nitrogen for 30 min. Then the mixture was concentrated to small volume, and the residue was partitioned between aqueous ammonium hydroxide and ether. The organic layer was dried, filtered over celite–charcoal, and evaporated *in vacuo* to give 3.9 g of solid **9***e*; mp 109–111 °C (from ether – petroleum ether); ir (Nujol) 1630 cm^{-1}; nmr δ 6.6–7.2 (3H, m), 3.85 (3H, s), 0.5–3.85 (21H, m). *Anal.* calcd. for $C_{21}H_{27}NO_2$: C 77.50, H 8.36, N 4.30; found: C 77.46, H 8.45, N 4.26.

17-Cyclopropylcarbonyl-3-hydroxyhasubanan **9***f*

The hydroxyamide **9***f* was obtained in quantitative yield, as a white solid from **9***e* by a procedure given for the preparation of **6***b*; mp 216–218 (from methanol); ir (neat) 3125, 1610 cm^{-1}; nmr δ 6.6–7.1 (3H, m), 0.4–3.8 (21H, m). *Anal.* calcd. for $C_{20}H_{25}NO_2$: C 77.14, H 8.09, N 4.50; found: C 77.13, H 8.21, N 4.39.

17-Cyclopropylmethyl-3-hydroxyhasubanan **9***g*

The hydroxyhasubanan **9***g* was obtained in 74% yield isolated as its hydrochloride salt, by reduction of **9***f* with lithium aluminum hydride as described above; mp 254–256 °C, from 2-propanol; ir (free base, neat) 3320 cm^{-1}; nmr δ 6.6–7.2 (3H, m), 0.0–3.6 (24H, m). *Anal.* calcd. for $C_{20}H_{27}NO \cdot HCl$: C 71.94, H 8.45, N 4.20; found: C 71.92, H 8.60, N 4.03.

Acknowledgments

The financial support of the National Research Council of Canada through its Industrial Research Assistance Program is gratefully acknowledged. We also thank Professor B. Belleau and Drs. I. J. Pachter and Y. G. Perron for encouragement.

1. I. Monković, H. Wong, A. W. Pircio, Y. G. Perron, I. J. Pachter, and B. Belleau. Can. J. Chem. **53**, 3094 (1975).
2. I. Monković, T. T. Conway, H. Wong, Y. G. Perron, I. J. Pachter, and B. Belleau. J. Am. Chem. Soc. **95**, 7910 (1973).
3. B. Belleau, H. Wong, I. Monković, and Y. G. Perron. J. Chem. Soc. Chem. Commun. 603 (1974).
4. I. Monković, H. Wong, B. Belleau, I. J. Pachter, and Y. G. Perron. Can. J. Chem. **53**, 2515 (1975).
5. M. Saucier and I. Monković. Can. J. Chem. **52**, 2736 (1974).
6. M. Gates and W. G. Webb. J. Am. Chem. Soc. **80**, 1186 (1958).
7. M. Gates and T. Montzka. J. Med. Chem. **7**, 127 (1968).
8. M. Gates. *In* Narcotic antagonists; advances in biochemical psychopharmacology. Vol. **8**. *Edited by* M. C. Braude *et al.* Raven Press, New York, 1973. p. 51.
9. I. Monković. Can. J. Chem. **53**, 1189 (1975).
10. D. L. H. Williams, E. Bienvenue Goetz, and J. E. Dubois. J. Chem. Soc. B, 517 (1969).
11. V. I. Staninets and E. A. Shilov. Russ. Chem. Rev. **36**, 272 (1971).
12. J. G. Buchanan and H. Z. Sable. *In* Selective organic transformations. Vol. 2. *Edited by* B. S. Thyagarajan. Wiley-Interscience, New York. 1972. p. 2.
13. R. K. Hill. J. Org. Chem. **22**, 830 (1957).
14. R. R. Wittekind, C. Weissman, S. Farber, and R. I. Meltzer. J. Heterocycl. Chem. **9**, 143 (1967).
15. R. R. Wittekind and C. Weissman. J. Heterocycl. Chem. **9**, 111 (1972).
16. S. P. McManus, J. T. Carroll, and C. H. Pittman. Jr. J. Org. Chem. **35**, 3768 (1970).
17. C. U. Pittman, Jr., S. P. McManus, and J. W. Larsen. Chem. Rev. **72**, 357 (1972).
18. Y. Furukawa and M. Honjo. Chem. Pharm. Bull. Jpn. **16**, 2286 (1968).
19. A. L. P. Coll. Spanish Patent No. 288,893 (1964).

Can. J. Chem. Downloaded from www.nrcresearchpress.com by 210.87.254.105 on 09/05/12
For personal use only.

Infrared spectra of the ammonium ion in crystals. III. The ammonium ion in crystal sites of symmetry S_4[1,2]

IAN A. OXTON AND OSVALD KNOP
Department of Chemistry, Dalhousie University, Halifax, Nova Scotia B3H 4J3
AND
MICHAEL FALK
Atlantic Regional Laboratory, National Research Council of Canada, Halifax, Nova Scotia B3H 3Z1

Received August 8, 1975

IAN A. OXTON, OSVALD KNOP, and MICHAEL FALK. Can. J. Chem. **54**, 892 (1976).

The infrared spectra of the isotopically isolated NH_3D^+ ion in polycrystalline ammonium perrhenate, NH_4ReO_4, and ammonium tetrachlorocuprate(II) dihydrate, $(NH_4)_2CuCl_4.2H_2O$, have been recorded at room and liquid-nitrogen temperatures. In the crystals of both compounds the ammonium ions are located at sites of S_4 symmetry. The N—D stretching mode of NH_3D^+ in NH_4ReO_4 is a singlet, as expected for this site symmetry. In $(NH_4)_2CuCl_4.2H_2O$, however, a doublet is observed which reveals the occurrence of two non-equivalent orientations of the ammonium ion. The spectra of the undeuterated compounds contain bands due to combination modes involving the librations of the ammonium ion. This shows that the ions are non-rotating.

IAN A. OXTON, OSVALD KNOP et MICHAEL FALK. Can. J. Chem. **54**, 892 (1976).

On a enregistré, à la température ambiante et à celle de l'azote liquide, les spectres infrarouge de l'ion NH_3D^+ isotopiquement dilué dans le perrhénate d'ammonium, NH_4ReO_4, et dans $(NH_4)_2CuCl_4.2H_2O$ polycristallins. Dans les cristaux des deux composés, les ions ammonium sont situés à des sites de symétrie S_4. Conformément à cette symétrie, un seul mode de vibration de valence N—D est observé dans le spectre du perrhénate. Par contre, dans le $(NH_4)_2CuCl_4.2H_2O$, on observe un doublet, ce qui indique la présence de deux orientations non-équivalentes de l'ion ammonium. Les spectres des composés non-deutérés contiennent des bandes dues à des modes de combinaison. La présence de ces modes, qui impliquent des librations de l'ion ammonium, met en évidence que les ions NH_4^+ ne sont pas en rotation.

In the first two papers of this series we described the ir spectra of the NH_3D^+ ion at crystal sites of tetrahedral (1) and trigonal (2) symmetry. It was shown that the N—D stretching (ν_1) and N—D bending (ν_{4bc}) modes of isotopically dilute NH_3D^+ ions accurately reflect the environments of the ammonium ions in the compounds studied. We also discussed the evidence for hydrogen bonding in some ammonium salts on the basis of rotating, or non-rotating, ammonium ions (2).

The present paper is concerned with the ammonium ion at sites of symmetry S_4-$\bar{4}$ as exemplified by NH_4ReO_4 and $(NH_4)_2CuCl_4.2H_2O$. The simultaneous presence of NH_4^+ and water of crystallization in the second compound introduces a situation which has not previously been encountered in our study of the ion. It merits special attention, for the absorption due to ν_{OD} in the N—D stretching region of the ir spectrum could interfere with $\nu_1(NH_3D^+)$: ν_{OD}(HDO) has been found to occur in the range of 2650–2400 cm^{-1} (3) whilst previously tabulated $\nu_1(NH_3D^+)$ frequencies have been in the 2425–2250 cm^{-1} region (1, 2, 4).

The spectra of the two compounds were also examined for absorptions due to combination modes involving the librational mode ν_6. The appearance of bands due to such modes in the ir spectra of ammonium salts has been used to establish that ammonium ions are not rotating in many cases (5, 6). We again adopt the definition of hydrogen bonding that was used in ref. 2.

Spectroscopic Expectations from Crystallographic Data

The crystallographic data for the two tetragonal compounds are summarized in Table 1. In both compounds all ammonium ions occupy equivalent sites and each ion is surrounded by two sets of nearest-neighbour atoms that are

[1]For Part II, see ref. 2.
[2]NRCC No. 15081.

Can. J. Chem. Downloaded from www.nrcresearchpress.com by 210.87.254.40 on 09/05/12
For personal use only.

TABLE 1. Crystallographic data for NH_4ReO_4 and $(NH_4)_2CuCl_4.2H_2O$

Atom	Equipoint	Site symmetry	x	y	z
		NH_4ReO_4 (scheelite-type), $I4_1/a$ (No. 88)*			
N	4(*b*)	$\bar{4}$-S_4	0	0	$\frac{1}{2}$
Re	4(*a*)	$\bar{4}$-S_4	0	0	0
O	16(*f*)	1-C_1	0.209	0.131	0.085
		$(NH_4)_2CuCl_4.2H_2O$, $P4_2/mnm$ (No. 136)†			
N	4(*d*)	$\bar{4}$-S_4	0	$\frac{1}{2}$	$\frac{1}{4}$
Cu	2(*a*)	*mmm*-D_{2h}	0	0	0
Cl(1)	4(*f*)	*mm*-C_{2v}	0.2161	0.2161	0
Cl(2)	4(*g*)	*mm*-C_{2v}	0.7262	0.2738	$\frac{1}{2}$
O	4(*e*)	*mm*-C_{2v}	0	0	0.2484

*a = 5.883 Å, c = 12.979 Å at 25 °C (7); Z = 4. The positional parameters are for $KReO_4$ (8); origin as in ref. 13.
†a = 7.598(2) Å, c = 7.966(2) Å (converted to accepted wavelengths) (9); a = 7.594(1) Å, c = 7.967(1) Å at 25 °C (10); Z = 2. The positional parameters are for $K_2CuCl_4.2H_2O$ (11).

potential hydrogen-bond acceptors. Each set contains four atoms related by S_4 through the N atom. Although only one crystallographically distinct type of oxygen atom exists in the structure of NH_4ReO_4, four of the nearest-neighbour oxygens are at a distance d(N . . . O) from the N atom and the other four, at a different distance d(N . . . O′) (Fig. 1). In the absence of an accurate crystal-structure determination the numerical values of these distances can only be estimated. The best estimate that can be obtained at present is based on the lattice parameters of NH_4ReO_4 (7) combined with the positional parameters[3] as determined for $KReO_4$ (8); it gives d(N . . . O) = 2.85 Å and d(N . . . O′) = 2.98 Å, with an uncertainty of at least 0.05 Å. The two angles, ∠ONO = 104° and ∠O′NO′ = 117°, are fairly close to the tetrahedral angle.

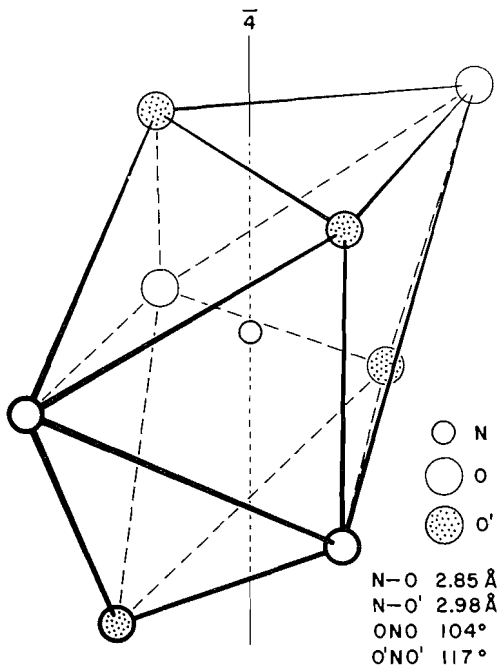

FIG. 1. Environment of an ammonium ion in NH_4ReO_4 based on crystallographic data of Table 1. The two sets of oxygen atoms at different distances from the N atom are distinguished by O and O′.

In $(NH_4)_2CuCl_4.2H_2O$ each set of four chlorine neighbours of an N atom is crystallographically distinct, one set consisting of Cl(1) and the other, of Cl(2) (Fig. 2); each Cl(2) is hydrogen-bonded to a water molecule. Here, too, the N . . . Cl(1) and N . . . Cl(2) distances can only be estimated by combining the lattice parameters of the ammonium compound with the positional parameters of the chlorines as determined for $K_2CuCl_4.2H_2O$ by neutron diffraction (11): d[N . . . Cl(1)] = 3.36 Å, d[N . . . Cl-(2)] = 3.35 Å.

The predicted ir spectrum of the NH_3D^+ ion at a site of symmetry S_4 is based on the 'effective' molecular symmetry of the ion, which is given by the intersection of the point-group C_{3v} of the 'free' ion with the site point group S_4 (*i.e.* $C_{3v} \cap S_4$) and is C_1. However, under the site symmetry S_4 all four N . . . X distances for either acceptor set are equal. Hence, instead of the multiplicity of vibrational modes which would normally be expected from a NH_3D^+ ion in four distinct

[3]The positional parameters of the oxygen in NH_4ReO_4 quoted by Wyckoff (13) (x = 0.25, y = 0.11, z = 0.07) are due to Beintema (12) and are at best *typical* values for the alkali perrhenates and periodates as a group.

Can. J. Chem. Downloaded from www.nrcresearchpress.com by 210.87.254.40 on 09/05/12
For personal use only.

Can. J. Chem. Downloaded from www.nrcresearchpress.com by 210.87.254.40 on 09/05/12
For personal use only.

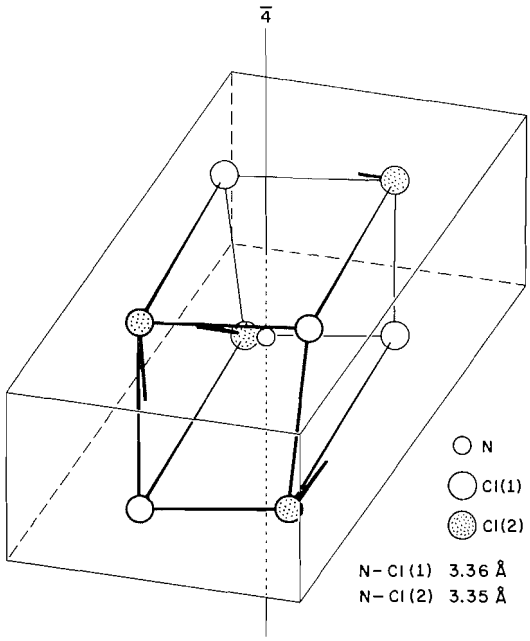

FIG. 2. Environment of an ammonium ion in $(NH_4)_2CuCl_4.2H_2O$ based on crystallographic data of Table 1. The thin solid line outlines the lower half of a tetragonal unit cell. The chlorine atoms are in the basal planes of this half-cell. Line segments on Cl(2) atoms indicate the directions of Cl(2)...OH_2 vectors (see Fig. 1 of ref. 17 for a more complete drawing of the structure).

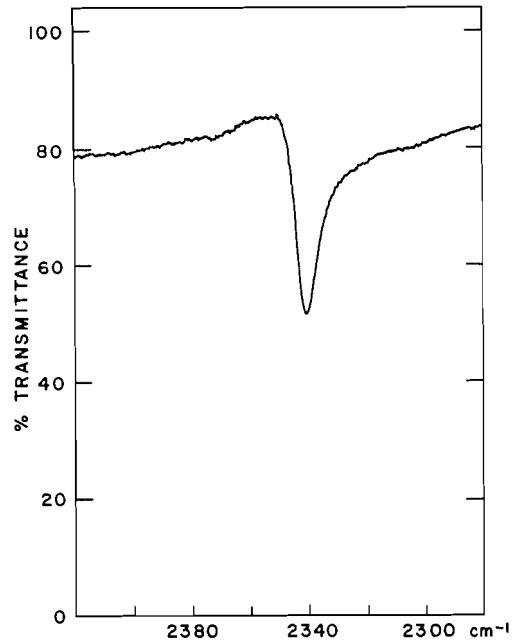

FIG. 3. The N—D stretching region of the ir spectrum of NH_4ReO_4 (1% D) at liquid-nitrogen temperature.

orientations of C_1 symmetry, we predict that the spectrum will be consistent with that given by a direct correlation as in Table 2. Thus ν_1 and ν_{4bc}, which have been found to be the most readily observed NH_3D^+ modes (2), should give rise to one and two bands respectively.

TABLE 2. Correlation of vibrational modes of 'free' (C_{3v}) NH_3D^+ ion with those in C_1 symmetry

C_{3v}	C_1
$\nu_1(a)$	$\nu_1(a)$
$\nu_2(e)$	$\nu_{2a}(a) + \nu_{2b}(a)$
$\nu_{3a}(a_1)$	$\nu_{3a}(a)$
$\nu_{3bc}(e)$	$\nu_{3b}(a) + \nu_{3c}(a)$
$\nu_{4a}(a_1)$	$\nu_{4a}(a)$
$\nu_{4bc}(e)$	$\nu_{4b}(a) + \nu_{4c}(a)$

Experimental

Ammonium perrhenate, NH_4ReO_4, was obtained commercially (Alfa Chemicals) and was recrystallized from water. Its ir spectrum agreed with that reported by Müller (14). The sample of low D concentration was obtained by recrystallization from a mixture of H_2O and D_2O of the appropriate composition.

Ammonium tetrachlorocuprate(II) dihydrate, $(NH_4)_2CuCl_4.2H_2O$, was prepared by slow evaporation of an aqueous solution containing the stoichiometric amounts of NH_4Cl and $CuCl_2$. Its ir spectrum was in agreement with that shown in Nyqvist and Kagel's compilation (15). The partially deuterated sample was obtained in an analogous manner using an appropriate mixture of H_2O and D_2O.

Spectra of Nujol mulls were recorded, at room and liquid-nitrogen temperatures, on a Perkin-Elmer model 180 spectrophotometer. The mulls were supported on KBr windows. The reported frequencies are believed to be correct to ± 0.5 cm^{-1}.

Results

The spectroscopic data described below are summarized in Table 3.

NH_4ReO_4

The N—D stretching region of the ir spectrum of NH_4ReO_4 (1% D) at liquid-nitrogen temperature is shown in Fig. 3. The absorption in this region consists of a *single* sharp band at 2341 cm^{-1} and may be assigned unambiguously to $\nu_1(NH_3D^+)$. The region 1300–1200 cm^{-1} (Fig. 4) contains two strong sharp bands, at 1272.1 and 1259.0 cm^{-1}, which are assigned to ν_{4b} and ν_{4c}

Can. J. Chem. Downloaded from www.nrcresearchpress.com by 210.87.254.40 on 09/05/12
For personal use only.

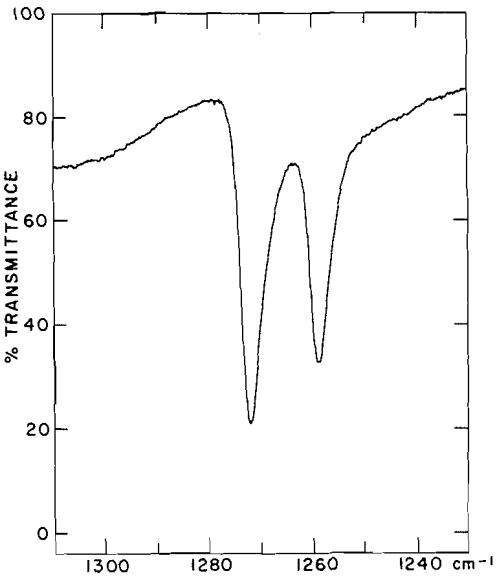

FIG. 4. The N—D bending region of the ir spectrum of NH_4ReO_4 (1% D) at liquid-nitrogen temperature.

of NH_3D^+. A doublet at 1611.4 and 1606.3 cm^{-1}, is assigned to the components of $\nu_2(NH_3D^+)$.

The spectrum of undeuterated NH_4ReO_4 is rich in absorptions at liquid-nitrogen temperature. A strong band at 1670 cm^{-1} (with shoulder at 1661 cm^{-1}) could be assigned to either ν_2 or $\nu_4 + \nu_6$ of NH_4^+. In view of previous assignments made for these modes (5, 6) the former seems more likely.

The region 2000–1750 cm^{-1} contains many bands of a variety of intensities. These absorptions arise from the combination modes $\nu_4 + \nu_6$ and $\nu_2 + \nu_6$ of the ammonium ion, with possibly a small contribution from $2\nu_3(ReO_4^-)$. Two fairly sharp bands are found on the high-frequency

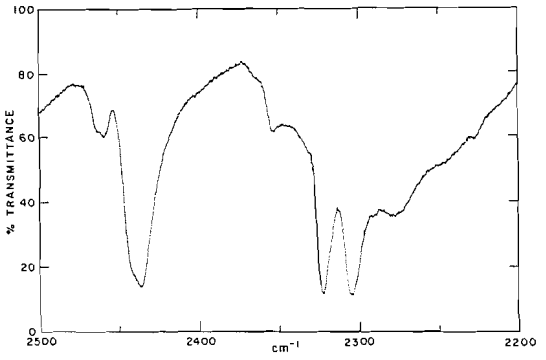

FIG. 5. The N—D stretching region of the ir spectrum of $(NH_4)_2CuCl_4.2H_2O$ (1% D) at liquid-nitrogen temperature.

wing of the N—H stretching absorptions, at 3478 and 3392 cm^{-1}, and probably arise from such combination modes as $\nu_1 + \nu_5$ and $\nu_3 + \nu_5$, ν_5 being a translatory mode. The antisymmetric bending fundamental ν_4 occurs as an intense absorption at about 1410 cm^{-1}.

$(NH_4)_2CuCl_4.2H_2O$

The N—D stretching region of $(NH_4)_2CuCl_4.2H_2O$ (1% D) is shown in Fig. 5. The absorption arising from the isotopically dilute NH_3D^+, in this region, consists of a *doublet* with maxima at 2322 and 2304 cm^{-1}.[4] The ratio of the integrated intensities of the components of this doublet is 1 ± 0.05. The band at 2441 cm^{-1} may be assigned to the O—D stretch of isotopically dilute HDO (16, 17) and is close to the absorption due to the overtones of the N—D bending modes of NH_3D^+. That band is broader than the corresponding band in the spectrum of $Rb_2CuCl_4.2H_2O$, and exhibits marked asymmetry. This will be discussed elsewhere (16). The absorption due to ν_{4b} and ν_{4c} of NH_3D^+ consists of a single, slightly asymmetric band at 1263 cm^{-1}. This band is broad compared with the corresponding bands in NH_4ReO_4 (see above) and that found for $(NH_4)_2PtCl_6$ (1).

A higher deuteration reveals a doubling of certain vibrational modes. An example is the doublet which is assigned to $\nu_{2a}(NH_2D_2^+)$ (1). This non-degenerate mode gives rise to two bands, of approximately equal intensity, at 1561 and 1557 cm^{-1}.

The ir spectrum of undeuterated $(NH_4)_2CuCl_4.2H_2O$ at liquid-nitrogen temperature contains a large number of bands similar in appearance to those found for NH_4ReO_4 and assigned to combination and overtone modes of NH_4^+. A doublet assigned to ν_2 is found at 1674 (shoulder) and 1671 cm^{-1}. Bands arising from $\nu_2 + \nu_6$ appear at 1997 and 1967 cm^{-1}, whilst those due to $\nu_4 + \nu_6$ are observed around 1750 cm^{-1}. A more detailed description of the $(NH_4)_2CuCl_4.2H_2O$ spectrum will be made elsewhere (16).

Discussion

Hydrogen Bonding

The ir spectra of undeuterated NH_4ReO_4 and

[4]The broad absorption on which these two sharp bands are superimposed is due to the combination modes $\nu_2 + \nu_L$ of H_2O, as is evident from a comparison with the spectrum of undeuterated $(NH_4)_2CuCl_4.2H_2O$.

Can. J. Chem. Downloaded from www.nrcresearchpress.com by 210.87.254.40 on 09/05/12
For personal use only.

TABLE 3. Frequencies ν and half-widths $\Delta\nu_{1/2}$ (in cm^{-1}) of absorptions due to the vibrational modes of NH_3D^+ in partially deuterated NH_4ReO_4 and $(NH_4)_2CuCl_4.2H_2O$ at liquid-nitrogen temperature

	NH_4ReO_4		$(NH_4)_2CuCl_4.2H_2O$	
Mode	ν	$\Delta\nu_{1/2}$	ν	$\Delta\nu_{1/2}$
$2\nu_{4b}$, $2\nu_{4c}$	2535, 2508		2513	
ν_1	2341	8	2322, 2304	8, 9
ν_{2a}, ν_{2b}	1611.4, 1606.3	—	1612	10
ν_{4b}, ν_{4c}	1272.1, 1259.0	4, 5	1263	10

$(NH_4)_2CuCl_4.2H_2O$ both contain medium-strong absorptions in the regions 2000–1900 and 1800–1700 cm^{-1} (Table 4) which are assigned to components of the combination modes $\nu_2 + \nu_6$ and $\nu_4 + \nu_6$, respectively. This observation is consistent with the absence of rotation of the ammonium ion in each crystal (5, 6). Using the definition of ref. 2, we conclude that in each case the ammonium ion is hydrogen-bonded.

It has been found previously (1, 2) that the room-temperature spectra of the NH_3D^+ ion in crystals of low D concentration are not informative owing to the breadth of the absorption bands. In the case of NH_4ReO_4, however, bands due to the N—D stretching and bending modes appear even at room temperature and are sufficiently well-defined to yield reasonably accurate frequencies. The band due to $\nu_1(NH_3D^+)$ is shifted to lower frequency by 17 cm^{-1} on cooling to liquid-nitrogen temperature, whilst its half-width decreases from *ca.* 30 to 8 cm^{-1}. The broad band in the room-temperature spectrum due to ν_{4b} and ν_{4c} of NH_3D^+, with a half-width of *ca.* 20 cm^{-1}, is split on cooling into two sharp bands at somewhat higher frequency, of half-widths 4 and 5 cm^{-1} respectively. Both frequency shifts are indicative of increased hydrogen bonding at the lower temperature, but it is difficult at present to assess the significance of the shifts. It is quite possible that the increased hydrogen bonding, on cooling, arises from an overall contraction of the crystal structure, but no crystallographic data are available to clarify this point.

TABLE 4. Combination modes involving ν_6 observed in undeuterated NH_4ReO_4 and $(NH_4)_2CuCl_4.2H_2O$ at liquid-nitrogen temperature*

	Frequency	
Mode	NH_4ReO_4	$(NH_4)_2CuCl_4.2H_2O$
$\nu_2 + \nu_6$	1950 sh, 1909	1997, 1967
$\nu_4 + \nu_6$	~1800	1747, 1728, 1718

*Frequencies in cm^{-1}; sh = shoulder.

The absorption arising in $(NH_4)_2CuCl_4.2H_2O$ from $\nu_1(NH_3D^+)$, at room temperature, consists of a single band, $\Delta\nu_{1/2} \approx 55\ cm^{-1}$, centred on 2324 cm^{-1}. It thus appears that no significant frequency change, and hence change in the strength of hydrogen bonding, occurs on cooling to liquid-nitrogen temperature.

The conclusion that ammonium ions in NH_4ReO_4 and $(NH_4)_2CuCl_4.2H_2O$ are hydrogen-bonded is further supported by the anomalously small c/a ratios of the ammonium compounds compared with the corresponding isostructural alkali and silver compounds.[5] In a plot of c/a against the cube root $(V/4)^{1/3}$ of the normalized unit-cell volume of $MReO_4$ (Fig. 6*A*; room-temperature values), the points for the alkali and silver compounds lie on a straight line but the NH_4ReO_4 point is significantly below.[6] The contraction of the unit cell of NH_4ReO_4 along the c-axis relative to the alkali compounds reflects an adjustment of the immediate neighbourhood of the NH_4^+ ion to optimize the hydrogen bonding between the ion and the oxygen acceptors; indeed, the estimated ONO angles are closer to the tetrahedral angle than the observed (8) OKO angles in $KReO_4$. A similar situation is seen to exist for MIO_4 and $MTcO_4$ even though the lines for these two series

[5]The anomalously low c/a values of NH_4ReO_4 and NH_4IO_4 were pointed out by Beintema (12) but were not ascribed to hydrogen bonding.

[6]Figures 6 and 7 are based on unit-cell dimensions derived from the following sources: $MReO_4$ (scheelite): Na, Rb (12); Ag (22), K (8, 22), NH_4 (7). MIO_4 (scheelite): Na (21, 25, 26), Ag (7), K (21, 27), Rb (23), NH_4 (12). $MTcO_4$ (scheelite): Na, Ag (19, 24); K, NH_4 (20, 24); Rb (24). $CsMO_4$ (*Pnma*): Re, I (12); Tc (20, 24). $M_2CuCl_4.2H_2O$: K, Rb, NH_4 (10); Cs (18).

Can. J. Chem. Downloaded from www.nrcresearchpress.com by 210.87.254.40 on 09/05/12
For personal use only.

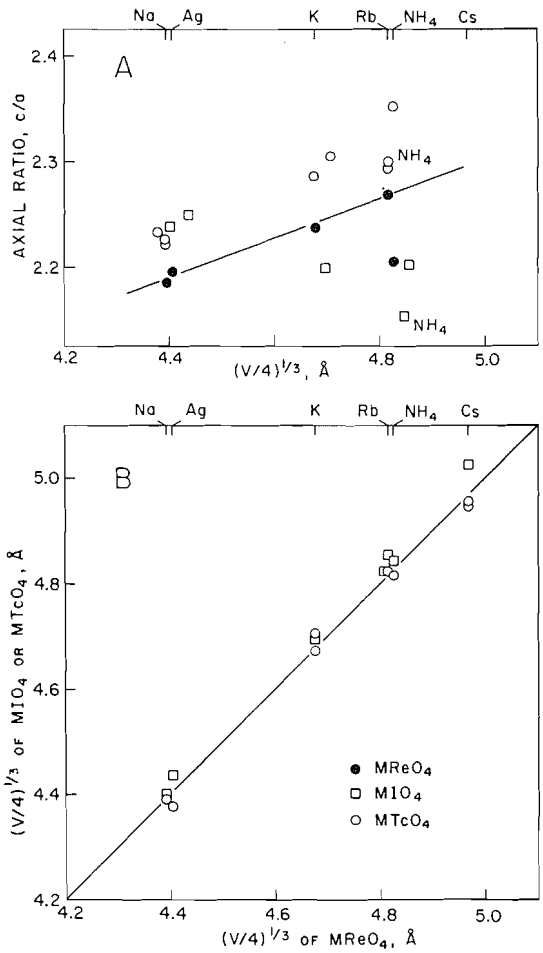

FIG. 6. (*A*) Plot of the *c/a* axial ratio against the cube root $(V/4)^{1/3}$ of the normalized unit-cell volume for the isostructural series $MReO_4$, MIO_4, and $MTcO_4$ (room temperature). The best straight line is for $MReO_4$. (*B*) Plot of $(V/4)^{1/3}$ of MIO_4 and $MTcO_4$ against $(V/4)^{1/3}$ of $MReO_4$. A 45° line is drawn for reference. The Cs compounds are of a different structure type but isostructural among themselves. Data from two independent sources are shown where available.

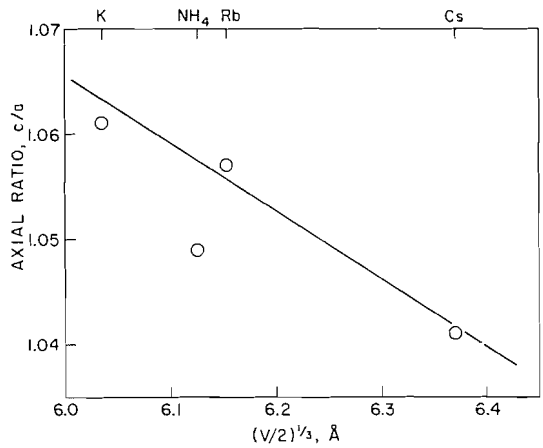

FIG. 7. Plot of the *c/a* axial ratio against $(V/2)^{1/3}$ of $M_2CuCl_4.2H_2O$ (room temperature).

are much less well-defined (the scatter is not evident in the $(V/4)^{1/3}$ values, Fig. 6*B*). An analogous contraction along the *c*-axis is observed for $(NH_4)_2CuCl_4.2H_2O$ (Fig. 7).

Spectrum of the NH_3D^+ Ion in NH_4ReO_4

The ir spectra of the isotopically isolated NH_3D^+ ion show that only one N—D . . . X distance occurs in the crystal at liquid-nitrogen temperature. Consequently all the ammonium ions are equivalent, consistent with the crystallographic evidence (Table 1), and each ion forms four hydrogen bonds of equal length, so that all the ions have the same orientation relative to their oxygen environment. Consideration of the geometry of the environment of the ammonium ion (Fig. 1) shows that three orientations are compatible with the existence of a unique $\nu_1(NH_3D^+)$ and the formation of four hydrogen bonds equivalent under S_4: that involving normal hydrogen bonds at N . . . O distances of about 2.85 Å, that involving normal bonds at N . . . O distances of *ca.* 2.98 Å, and that involving bifurcated bonds. The first situation appears to offer the most favourable possibilities for the formation of four equivalent, fairly straight N—H . . . O bonds.

The frequency of $\nu_1(NH_3D^+)$ may be qualitatively compared with that found for the straight N—D . . . O bond in $(NH_4)_2Pb(SO_4)_2$ (2). In the latter case the N . . . O distance was estimated to be *ca.* 2.74 Å and the appropriate $\nu_1(NH_3D^+)$ frequency was 2311.5 cm^{-1}. Since the hydrogen bonds in NH_4ReO_4 are longer than 2.74 Å and are also bent, we would expect $\nu_1(NH_3D^+)$ at a somewhat higher frequency than 2311.5 cm^{-1}; this mode is actually observed at 2341.0 cm^{-1}.

Spectrum of the NH_3D^+ Ion in $(NH_4)_2CuCl_4.2H_2O$

The absorptions observed in the N—D stretching region of the ir spectrum of $(NH_4)_2CuCl_4.2H_2O$ (1% D) (Fig. 5) are clearly not as expected from the Introduction and Table 2. The presence of *two* bands arising from $\nu_1(NH_3D^+)$ requires

Can. J. Chem. Downloaded from www.nrcresearchpress.com by 210.87.254.40 on 09/05/12
For personal use only.

detailed consideration. The duplication cannot be due to factor-group splitting, as the bands arise from isotopically dilute NH_3D^+ ions. Nor are the two bands of comparable intensity produced by Fermi resonance between $\nu_1(NH_3D^+)$ and an overtone or combination mode. The lowest-frequency mode, $\nu_{4b,c}$, is observed at 1263 cm^{-1} while the overtones arising from these modes would be expected at frequencies almost 200 cm^{-1} higher than $\nu_1(NH_3D^+)$, making the chance of such a strong resonance remote. The existence of *two different orientations* of the NH_4^+ ion in the structure thus appears to be the most likely explanation of the band doubling.

Each ammonium ion in $(NH_4)_2CuCl_4.2H_2O$ is surrounded by four Cl(1) and four Cl(2) atoms at N . . . Cl distances estimated to be 3.35 and 3.36 Å respectively, and both acceptor angles Cl(1)—N—Cl(1) and Cl(2)—N—Cl(2) are close to the tetrahedral angle. An ammonium ion would thus be expected to show little preference for either possible orientation N . . . 4Cl(1) and N . . . 4Cl(2).[7] As the doubling of $\nu_1(NH_3D^+)$ indicates, *both* orientations occur in the crystal.

The intensity of $\nu_1(NH_3D^+)$ can be expected to increase with the strength of hydrogen bonding, *i.e.* with decreasing frequency. The frequency difference between the N—D . . . Cl(1) and N—D . . . Cl(2) stretches, however, is 18 cm^{-1} and little difference in ir absorptivity is to be expected between these oscillators. We thus conclude, from the 1:1 intensity ratio of the two $\nu_1(NH_3D^+)$ bands, that approximately equal numbers of NH_4^+ ions adopt each orientation. This is a result that demonstrates the usefulness of our spectroscopic isotopic dilution method, in that it could not have been predicted *with any certainty* from the available, inadequate crystallographic information.

Summary

The ir spectrum of the isotopically dilute NH_3D^+ ion in NH_4ReO_4 was found to be consistent with the site symmetry for the ammonium ion in this compound. In contrast, the observed spectrum of the isotopically dilute NH_3D^+ ion in $(NH_4)_2CuCl_4.2H_2O$ revealed a duplication of certain vibrational modes, including a splitting of 18 cm^{-1} in $\nu_1(NH_3D^+)$. This unexpected observation is explained as arising from two distinct orientations, relative to the immediate neighbourhood, of the ammonium ions in the crystal. The 1:1 intensity ratio of the two $\nu_1(NH_3D^+)$ bands points to an approximately equal distribution of the ammonium ions between the two orientations.

The isotopic dilution method appears to be readily applicable to the study of hydrates of ammonium salts. The concomitant appearance of ν_{OD}(HDO) near the N—D stretching region in the ir spectrum of $(NH_4)_2CuCl_4.2H_2O$ caused no difficulties in assignment of NH_3D^+ absorptions. The only difficulty which may arise in such cases could be the encroachment of components of $\nu_2 + \nu_L$ of H_2O into the N—D stretching region.

The spectra of undeuterated NH_4ReO_4 and $(NH_4)_2CuCl_4.2H_2O$ are consistent with the absence of rotation of the ammonium ions. This has been considered, on the criterion adopted in ref. 2, as an indication that the ammonium ions are hydrogen-bonded.

[7]The effect of the hydrogen bond between H_2O and Cl(2) (Fig. 2) on the acceptor strength of Cl(2) cannot be assessed at present.

Acknowledgment

The grant-in-aid of research from the National Research Council of Canada to one of us (O.K.) is acknowledged.

1. I. A. Oxton, O. Knop, and M. Falk. Can. J. Chem. **53**, 2675 (1975).
2. I. A. Oxton, O. Knop, and M. Falk. Can. J. Chem. **53**, 3394 (1975).
3. M. Falk and O. Knop. *In* Water: a comprehensive treatise. Vol. 2. *Edited by* F. Franks. Plenum Press, New York. 1973. Chap. 2.
4. L. L. Oden and J. C. Decius. Spectrochim. Acta, **20**, 667 (1964).
5. T. C. Waddington. J. Chem. Soc. 4340 (1958).
6. J. T. R. Dunsmuir and A. P. Lane. Spectrochim. Acta, **28A**, 45 (1972).
7. H. E. Swanson, M. I. Cook, T. Isaacs, and E. H. Evans. U.S. Natl. Bur. Stand. Circ. 539, **9**, 7, 49 (1960).
8. J. C. Morrow. Acta Crystallogr. **13**, 443 (1960).
9. A. L. Greenberg and G. H. Walden, Jr. J. Chem. Phys. **8**, 645 (1940).
10. H. E. Swanson, H. F. McMurdie, M. C. Morris, E. H. Evans, B. Paretzkin, J. H. De Groot, and S. J. Carmel. U.S. Natl. Bur. Stand. Monogr. 25, **9**, 8, 34 (1971).
11. R. Chidambaram, Q. O. Navarro, A. Garcia, K. Linggoatmodjo, S.-C. Lin, I.-H. Suh, A. Sequeira, and S. Srikanta. Acta Crystallogr. B, **26**, 827 (1970).
12. J. Beintema. Z. Kristallogr. **97A**, 300 (1937); F. M.

JAEGER and J. BEINTEMA. Proc. Acad. Sci. Amsterdam, **36**, 523 (1960).
13. R. W. G. WYCKOFF. Crystal structures. Vol. 3. 2nd ed. Interscience, New York. 1965.
14. A. MÜLLER. Z. Naturforsch. **20a**, 745 (1965).
15. R. A. NYQVIST and R. O. KAGEL. Infrared spectra of inorganic compounds. Academic Press, New York. 1971.
16. D. A. OTHEN, O. KNOP, and M. FALK. To be published.
17. G. H. THOMAS, M. FALK, and O. KNOP. Can. J. Chem. **52**, 1029 (1974).
18. R. PERRET. Bull. Soc. Chim. Fr. 769 (1966).
19. K. SCHWOCHAU. Z. Naturforsch. **17a**, 630 (1962).
20. B. J. MCDONALD and G. J. TYSON. Acta Crystallogr. **15**, 87 (1962).
21. H. E. SWANSON, N. T. GILFRICH, and M. I. COOK. U.S. Natl. Bur. Stand. Circ. 539, **7**, 41, 48 (1957).
22. H. E. SWANSON, N. T. GILFRICH, M. I. COOK, R. STINCHFIELD, and P. C. PARKS. U.S. Natl. Bur. Stand. Circ. 539, **8**, 41, 53 (1959).
23. H. E. SWANSON, M. C. MORRIS, R. P. STINCHFIELD, and E. H. EVANS. U.S. Natl. Bur. Stand. Monogr. 25, **2**, 31 (1963).
24. C. KELLER and B. KANELLAKOPULOS. Radiochim. Acta, **1**, 107 (1963).
25. V. T. DESHPANDE, S. V. SURYANARAYANA, and R. R. PAWAR. Acta Crystallogr. **A24**, 398 (1968).
26. A. KÁLMÁN and D. W. J. CRUICKSHANK. Acta Crystallogr. **B26**, 1782 (1970).
27. V. T. DESHPANDE, R. R. PAWAR, and S. V. SURYANARAYANA. Curr. Sci. **36**, 513 (1967).

Can. J. Chem. Downloaded from www.nrcresearchpress.com by 210.87.254.40 on 09/05/12
For personal use only.

A comparison of methods for pK_a determination in strongly basic systems applied to the deprotonation of some heterocyclic methiodide salts

ROBIN A. COX AND ROSS STEWART
University of British Columbia, Vancouver, British Columbia V6T 1W5
AND
MICHAEL J. COOK, ALAN R. KATRITZKY, AND ROBERT D. TACK
School of Chemical Sciences, University of East Anglia, Norwich, England NOR 88C

Received September 12, 1975

ROBIN A. COX, ROSS STEWART, MICHAEL J. COOK, ALAN R. KATRITZKY, and ROBERT D. TACK. Can. J. Chem. **54**, 900 (1976).

Ionization values for the deprotonation of the methiodide salts **1–8**, which occurs in strongly basic DMSO/water mixtures containing 0.047 *M* base, are used to determine pK_a values by the Bunnett–Olsen and Marziano–Cimino–Passerini techniques, which involve extrapolation to the purely aqueous state. The resulting values are compared with those obtained using the H_0^q acidity function; agreement is good in most cases.

ROBIN A. COX, ROSS STEWART, MICHAEL J. COOK, ALAN R. KATRITZKY et ROBERT D. TACK. Can. J. Chem. **54**, 900 (1976).

Les valeurs d'ionisation pour la déprotonation des sels de méthiodures **1–8**, qui se produit dans des milieux fortement basiques de DMSO dans l'eau contenant 0.047 *M* de base, ont été utilisées pour déterminer les valeurs de pK_a par les techniques de Bunnett–Olsen et Marziano–Cimino–Passerini qui impliquent des extrapolations jusqu'à des états aqueux purs. Les valeurs résultantes sont comparées avec celles obtenues en utilisant des fonctions d'acidité H_0^q; la corrélation est bonne dans la plupart des cas.

[Traduit par le journal]

Introduction

Two methods have recently been developed for determining acidity constants of very weak acids (1) based on the work of Bunnett and Olsen (2), and of Marziano *et al.* (3). Both make use of measurements of degree of ionization in mixtures of water and dimethyl sulfoxide (DMSO) containing dilute base, and central to each is an assumption regarding the behaviour of the activity coefficient term, log ($f_{R^-}/f_{RH}f_{OH^-}$). As with the better known acidity function (AF) method (4) both refer to the standard state of pure water, but more directly, by extrapolation, rather than through an acidity function, whose construction requires a series of well-behaved overlapping indicators and whose use requires the compound under investigation to be similarly well-behaved.

An acidity function of some sort is necessary for the use of the Bunnett–Olsen (BO) method (2), and an overlapping series of ionization ratios in the media under investigation is necessary for the use of the Marziano–Cimino–Passerini (MCP) method (3) although the acidity function, as such, is not needed in this case (1). The BO and MCP approaches to acidity constant measurements have the advantage that pK values for compounds that are poorly behaved Hammett indicators (those whose ionization plots are not parallel to those of their neighbours) can be estimated with some degree of confidence by these means.

We now apply these methods to the deprotonation of some methyl quaternary salts to give neutral heterocyclic bases, which occurs in strongly basic solutions, in order to compare the resulting pK_a values with those previously obtained using an acidity function (5). The reaction in this case is positive ion $\rightleftharpoons$ neutral species (*i.e.* described by an H_0 function) (4), rather than the neutral species $\rightleftharpoons$ negative ion reaction (H_- function) considered up to now, and thus should provide an interesting test of the methods.

Results and Discussion

The reaction under consideration is the deprotonation of CH_3, CH_2Ph, $CHPh_2$, or NH_2, in

Can. J. Chem. Downloaded from www.nrcresearchpress.com by 210.87.254.40 on 09/05/12
For personal use only.

Can. J. Chem. Downloaded from www.nrcresearchpress.com by 210.87.254.40 on 09/05/12
For personal use only.

the iodide salts of **1–8** by hydroxide ion in DMSO/water mixtures.

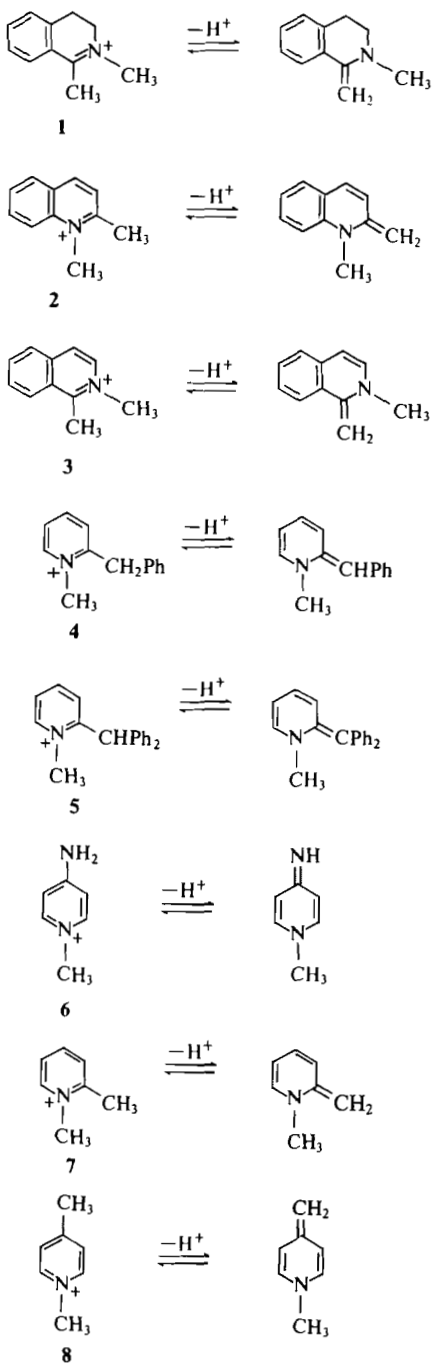

The above processes can be generalized as in eq. 1. From the equilibrium constant, eq. 2,

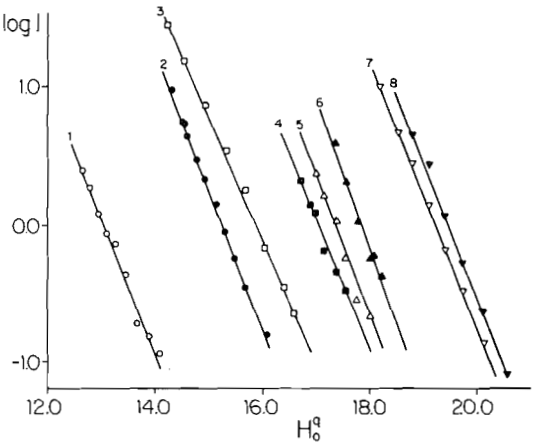

FIG. 1. Plot of log I values for **1–8** as a function of H_0^q. See Table 1.

[1] $$RH^+ + OH^- \overset{K_b}{\rightleftharpoons} R + H_2O$$

[2] $$K_b = K_a/K_w = a_R a_{H_2O}/a_{RH^+}a_{OH^-}$$

where the symbols have their usual meanings (1, 4), eq. 3 can be obtained, where log I = log (C_{RH^+}/C_R).

[3] $$pK_a - \log I = pK_w + \log C_{OH^-} - \log a_{H_2O} - \log (f_R/f_{RH^+}f_{OH^-})$$

[4] $$\log (f_{R_1}/f_{R_1H^+}f_{OH^-}) = \log (f_{R_2}/f_{R_2H^+}f_{OH^-})$$

[5] $$pK_{a_2} - pK_{a_1} = \log I_2 - \log I_1 = \Delta \log I$$

Making the assumption that for adjacent indicators 1 and 2, eq. 4, which is the Hammett cancellation assumption (6), holds, eq. 3 applied to the two indicators leads to eq. 5. Equation 5 implies that the pK_a difference between two adjacent indicators is given by Δ log I. The validity of the cancellation assumption is shown by the degree of parallelism found when log I values for different compounds are plotted as a function of medium composition (1).

Applying this treatment to the data obtained for compounds **1–8** given in Table 1 leads to the previously obtained (5) AF pK_a values given in Table 2, and these lead directly to values of the appropriate acidity function, H_0^q, via eq. 6 (see Table 1); the scale is anchored on the pK_a

[6] $$H_0^q = pK_a - \log I$$

of **1**, 13.06, measured in water (5). A plot of log I *vs.* H_0^q for **1–8** is shown in Fig. 1; the high degree of parallelism illustrates that the H_0^q function is a quite satisfactory one.

Can. J. Chem. Downloaded from www.nrcresearchpress.com by 210.87.254.40 on 09/05/12
For personal use only.

TABLE 1. Ionization ratio data and derived H_0^q values[a]

Mol% DMSO	log I	H_0^q	Mol% DMSO	log I	H_0^q
	Compound **1**			Compound **5**	
0.00	0.39	12.67	24.8	0.369	16.96
0.90	0.27	12.79	26.2	0.212	17.12
1.83	0.08	12.98	27.5	0.020	17.31
2.79	−0.07	13.13	29.0	−0.253	17.58
3.86	−0.15	13.21	30.4	−0.557	17.89
5.00	−0.36	13.42	32.0	−0.669	18.00
6.08	−0.73	13.79			
7.34	−0.81	13.87		Compound **6**	
8.57	−0.90	14.01	27.6	0.59	17.28
			29.1	0.30	17.57
	Compound **2**		30.4	0.02	17.85
9.35	1.15	14.08	31.9	−0.25	18.12
9.94	0.98	14.25	32.6	−0.25	18.12
10.8	0.75	14.48	33.4	−0.38	18.25
11.1	0.73	14.50			
11.2	0.64	14.59		Compound **7**	
11.9	0.47	14.76	33.4	0.997	18.25
12.7	0.33	14.90	35.4	0.658	18.59
13.55	0.15	15.08	37.2	0.439	18.81
14.2	−0.06	15.29	39.1	0.128	19.12
15.2	−0.24	15.47	41.0	−0.201	19.45
16.2	−0.47	15.70	43.2	−0.503	19.75
18.2	−0.81	16.04	45.5	−0.870	20.12
	Compound **3**			Compound **8**	
9.7	1.45	14.44	37.2	0.649	18.82
11.1	1.19	14.70	39.1	0.433	19.12
12.7	0.87	15.02	41.0	0.050	19.41
14.4	0.54	15.35	43.2	−0.289	19.75
16.2	0.25	15.64	45.5	−0.646	20.10
18.05	−0.17	16.06	47.9	−1.122	20.58
20.2	−0.46	16.35	50.4	−1.514	20.97
21.2	−0.65	16.54			
	Compound **4**				
22.4	0.315	16.70			
23.6	0.135	16.86			
24.8	0.008	17.00			
26.2	−0.198	17.21			
27.5	−0.354	17.36			
29.0	−0.490	17.50			

[a]The method used for obtaining the log I data is reported elsewhere (5).

However, the assumption of eq. 4 does not have to be made; as previously discussed (1) we can make the alternative and less drastic assumption that eqs. 7 and 8 hold. Here the activity coefficient terms are assumed to be linear functions of one another, rather than to cancel out. A Bunnett–Olsen equation (2) can be derived

$$[7]\quad \log (f_R/f_{RH^+}f_{OH^-}) = (\phi + 1)[\log (f_{A^-}/f_{AH}f_{OH^-})]$$

$$[8]\quad = m^*[\log (f_{A_*^-}/f_{A_*H}f_{OH^-})]$$

from eq. 7 as before (1), expressed here in terms of the H_- acidity function and the aniline and diphenylamine acids, AH, used to set it up, given as eq. 9; a Marziano–Cimino–Passerini equation [4] can be derived from eq. 8 (1). In the latter case the activity coefficient ratio for one

$$[9]\quad H_- + \log I = \phi(H_- - pK_w - \log C_{OH^-} + \log a_{H_2O}) + pK_a$$

TABLE 2. pK_a values for **1–8** given by the three methods

Compound	No. of points	pK_a[a] (AF)	pK_b[b] (BO)	Slope[b] ϕ	r[b,c]	pK_a[d] (MCP)	Slope[d] m^*	r[c,d]
1	9	13.06	13.06	0.71	0.936	13.07	1.54	0.987
2	12	15.23	15.52	1.10	0.980	15.76	2.18	0.996
3	8	15.89	15.52	0.61	0.979	15.95	1.86	0.999
4	6	17.01	15.80	0.16	0.804	15.80	1.20	0.997
5	6	17.33	17.03	0.52	0.928	17.11	1.61	0.990
6	6	17.87	17.99	0.67	0.925	18.19	1.81	0.987
7	7	19.25	19.27	0.62	0.994	19.19	1.66	0.998
8	7	19.46	20.24	0.82	0.992	20.27	1.90	0.997

[a]Acidity function method.
[b]Bunnett–Olsen method.
[c]Correlation coefficient.
[d]Marziano–Cimino–Passerini method.

$$[10]\quad pK_w + \log C_{OH^-} - \log a_{H_2O} + \log I = m^*[\log (f_{A*}^-/f_{H*A}f_{OH^-})] + pK_a$$

compound A_*H (in our case 2,4,4′-trinitrodiphenylamine) (1), which can be calculated at any medium composition from a series of overlapping log I measurements (1, 3), is used instead of an acidity function. This is eq. 10.

The results of applying eqs. 9 and 10, using the H_-, log a_{H_2O}, etc. data previously tabulated (1), to compounds **1–8** are tabulated in Table 2 and are illustrated in Figs. 2 and 3. The pK_a values obtained in the three possible ways are plotted against one another, and compared to ideal lines of unit slope in Fig. 4. The standard deviations between pK_a's measured in the different ways are: BO/AF, ±0.55; MCP/AF, ±0.57; BO/MCP, ±0.19. The MCP slopes (m^*) for the eight compounds average out to 1.72 ± 0.27.

It would appear that the assumption of eqs. 7 and 8 is justified, despite the difference in charge type between compounds **1–8** and the H_- indicators used in the BO and MCP methods. The only evidence of curvature in Figs. 2 and 3 appears to be in the BO plots for **2** and **3**. Thus the H_- function may not be the best one to use in the BO method for these two compounds, and one might predict somewhat higher pK_a values than the linearly extrapolated ones in these two cases. The MCP plots for **2** and **3**, however,

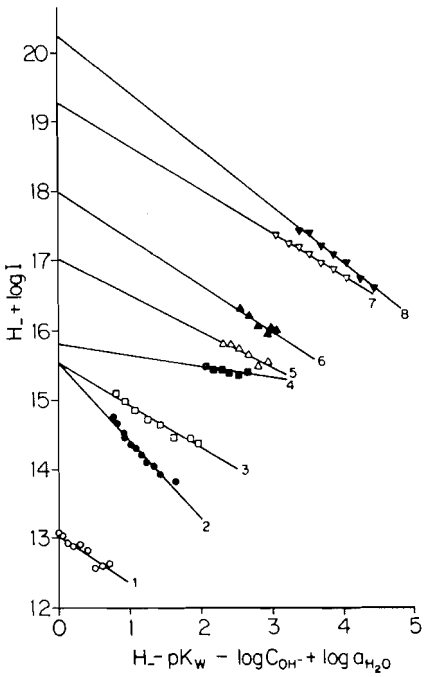

FIG. 2. Bunnett–Olsen plots for **1–8**. $H_- + \log I$ plotted vertically against the 'excess basicity' $H_- - pK_w - \log C_{OH^-} + \log a_{H_2O}$ (1); pK_a values are y-axis intercepts.

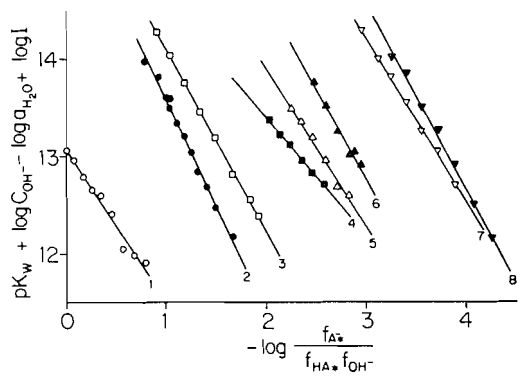

FIG. 3. Marziano–Cimino–Passerini plots for **1–8**, using eq. 10.

Can. J. Chem. Downloaded from www.nrcresearchpress.com by 210.87.254.40 on 09/05/12
For personal use only.

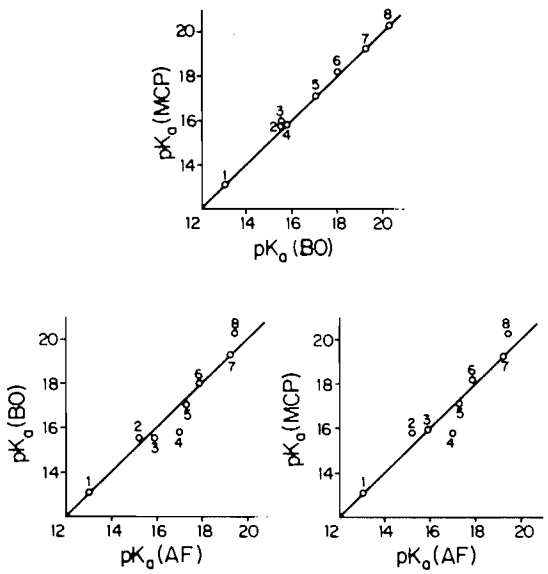

Fig. 4. Comparison of pK_a values of **1–8** measured in different ways. Both axes are pK_a values; the line has the theoretical unit slope. Top: MCP values (y-axis) compared with BO values. Left: BO compared with AF. Right: MCP compared with AF.

show excellent linearity, and do indeed extrapolate to rather higher pK_a values than the BO ones. In all other cases the linearity is very good, and the agreement between BO and MCP pK_a values is excellent.

Agreement between the AF pK_a's and the others is also very good for compounds **1**, **3**, **5**, **6**, and **7**. For **2** and **8**, the AF pK_a's seem too low, and for **4** the AF pK_a appears to be more than one unit too high. From Fig. 2, especially, it appears that the good parallelism and overlap of Fig. 1 may be somewhat illusory. Since H_- and log I differ, in the sense that one increases while the other decreases, experimental error, curvature, and poor overlap become much easier to see in the BO method, where log $I + H_-$ is plotted, rather than log I itself. Nevertheless, it is also apparent that the AF technique has a self-correcting property, *i.e.* high pK_a values are not unduly affected by poor overlap between compounds at lower pK_a values. The AF pK_a values of **5**, **6**, and **7** appear to be unaffected by the large deviation in that for **4**.

The conjugate bases of **1–8** were used earlier (5) as fixed models in tautomeric equilibrium studies and their AF pK_a values, and those of the corresponding mobile systems, afforded K_T data by the basicity method (7). The present study indicates that K_T values for the following require amending (figures in parentheses are those reported previously): 2-methylquinoline, pK_T = 9.9 (9.40); 2-benzylpyridine, pK_T = 10.7 (11.9); 4-methylpyridine, pK_T = 14.2 (13.44).

1. R. A. Cox and R. Stewart. J. Am. Chem. Soc. **98**, 488 (1976); R. A. Cox and R. Stewart, presented at the 58th Canadian Chemical Conference, Toronto, May 1975. Paper No. 228.
2. J. F. Bunnett and F. P. Olsen. Can. J. Chem. **44**, 1899 (1966).
3. N. C. Marziano, G. M. Cimino, and R. C. Passerini. J. Chem. Soc. Perkin Trans. II, 1915 (1973).
4. C. H. Rochester. Acidity functions. Academic Press, New York. 1970; M. A. Paul and F. A. Long. Chem. Rev. **57**, 1 (1957).
5. M. J. Cook, A. R. Katritzky, P. Linda, and R. D. Tack. J. Chem. Soc. Perkin Trans. II, 1080 (1973); Swee-Ong Chua, M. J. Cook, and A. R. Katritzky. J. Chem. Soc. Perkin Trans. II, 2111 (1973).
6. L. P. Hammett and A. J. Deyrup. J. Am. Chem. Soc. **54**, 2721 (1932); L. P. Hammett, Physical organic chemistry, 2nd ed. McGraw-Hill, New York. 1970. Chap. 9.
7. A. R. Katritzky and M. J. Lagowski. Adv. Heterocycl. Chem. **1**, 311 (1963).

Can. J. Chem. Downloaded from www.nrcresearchpress.com by 210.87.254.40 on 09/05/12
For personal use only.

Réactions de substitution homolytique. V. Stéréosélectivité de différents radicaux cyclohexyles

MICHEL GRUSELLE, JACQUES FOSSEY ET DANIEL LEFORT
G.R. n° 12, C.N.R.S., 2 Rue H. Dunant, 94320, Thiais, France
ET
CLAUDE LAMARRE ET JEAN-CLAUDE RICHER
Département de Chimie, Université de Montréal, B.P. 6210 Succursale A, Montréal, Québec H3C 3V1

Reçu le 9 octobre 1975

MICHEL GRUSELLE, JACQUES FOSSEY, DANIEL LEFORT, CLAUDE LAMARRE et JEAN-CLAUDE RICHER. Can. J. Chem. **54**, 905 (1976).

En utilisant la décarboxylation thermique de peracides de structure "adequate", les auteurs étudient l'influence de l'environnement d'un centre radicalaire sur la stéréosélectivité de la réaction de substitution homolytique de radicaux cyclohexyles diversement substitués sur l'oxygène peroxydique d'un peracide. Cette réaction conduit à des alcools stéréoisomères

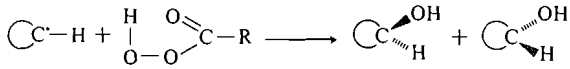

Le radical se comporte comme s'il était plan et en général l'entrée du réactif par la face axiale est nettement favorisée sauf quand on augmente l'encombrement stérique de celle-ci.

La stéréosélectivité est expliquée en termes d'importance relative des effets stériques (pour l'entrée axiale) et d'effets d'interactions de liaison (pour l'entrée équatoriale); elle dépend également de la "flexibilité" du cycle.

MICHEL GRUSELLE, JACQUES FOSSEY, DANIEL LEFORT, CLAUDE LAMARRE, and JEAN-CLAUDE RICHER. Can. J. Chem. **54**, 905 (1976).

The influence of the environment near the radical site on the stereoselectivity of the homolytic substitution reaction of variously substituted cyclohexyl radicals on the peroxidic oxygen of a peroxy acid has been studied using the thermal decarboxylation of peroxy acids. This reaction leads to stereoisomeric alcohols

The radical behaves as if it were planar and, in general, an axial approach of the reagent is strongly favoured except when substituents increase the steric hindrance of the radical.

The stereoselectivity is explained in terms of the relative importance of steric effects (for the axial approach) and of bond interactions (for the equatorial approach). It also depends on the flexibility of the ring.

[Journal translation]

Introduction

Les réactions de substitution homolytique constituent une part importante des processus radicalaires et la stéréosélectivité concernant les radicaux dont les deux faces sont inéquivalentes, a fait l'objet de plusieurs études. Mais en général les auteurs ont considéré la réaction d'un radical, par exemple le radical cyclohexyle, sur divers substrats (1, 2). Pour notre part, nous nous sommes intéressés à l'influence de l'environnement du centre radicalaire sur la stéréosélectivité de la réaction du radical considéré sur un même substrat. Pour mener à bien cette étude nous avons utilisé la décomposition thermique des peracides dont l'un d'entre nous a démontré (3) qu'il s'agit d'un mécanisme radicalaire en chaîne

[1] 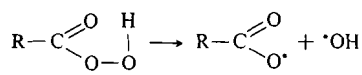

[2] 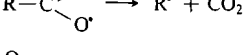

[3] 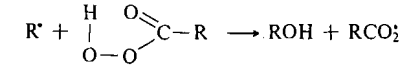

[4] 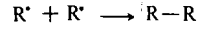

Can. J. Chem. Downloaded from www.nrcresearchpress.com by 210.87.254.5 on 09/05/12
For personal use only.

Can. J. Chem. Downloaded from www.nrcresearchpress.com by 210.87.254.5 on 09/05/12
For personal use only.

Ce système a les avantages suivants.

(*i*) Le peracide est à la fois l'amorçeur de la réaction, la source de radicaux et le substrat. Le mélange réactionnel s'en trouve simplifié. La seule réaction radicalaire secondaire qui peut avoir une certaine importance est celle de transfert sur le solvant

$$R^{\cdot} + HS \rightarrow RH + S^{\cdot}$$

et ce radical issu du solvant peut alors réagir sur le peracide

$$S^{\cdot} + RCO_3H \rightarrow SOH + RCO_2^{\cdot}$$

Toutes les expériences étant effectuées dans le cyclohexane, la séparation des deux alcools ROH et cyclohexanol ne pose aucun problème, d'autant plus que, dans les cas étudiés au cours de ce travail, les quantités de cyclohexanol sont faibles.

(*ii*) La réaction est très exothermique (5) (environ 45 kcal/mol); l'état de transition ressemblera donc probablement aux produits de départ, en particulier au radical libre.

(*iii*) L'alcool ROH est formé avec un bon rendement (80%).

L'étape 3, dont l'existence a été justifiée précédemment (3–5), a donc été utilisée pour étudier la stéréosélectivité de la réaction de substitution de radicaux cyclohexyles diversement substitués sur les peracides correspondants. Les groupements substituants ont été choisis dans le but de déterminer l'influence relative des effets stériques, des interactions de liaisons et de conformation de cycle. Nous avons donc préparé les peracides indiqués dans le tableau ci-dessous et déterminé le rapport des alcools stéréoisomères formés selon le schéma réactionnel écrit précédemment.

Resultats

Les peracides sont décomposés en solution dans le cyclohexane à ébullition, à une concentration de 0.1 mol/l. En fin de réaction le rapport des alcools stéréoisomères est déterminé par chromatographie en phase gazeuse.

Les résultats rassemblés dans le tableau 1 montrent que (*i*) lorsque le cyclohexyle n'a pas de substituant en position 3 *axiale* par rapport au centre radicalaire, l'arrivée du réactif par la face *axiale* est toujours très nettement préférentielle (radicaux *A*, *B*, *C*, *D* et *F* comparés aux radicaux *E* et *G*); (*ii*) qu'un CH_3 en position 2 *axiale* favorise l'entrée *axiale* (*B*); et (*iii*) que l'entrée *axiale* est légèrement favorisée quand le centre radicalaire appartient à un cyclohexane plutôt qu'à un motif décalinique (radicaux *A* et *F* par rapport aux radicaux *E* et *G*).

Discussion

Au cours d'une précédente étude (5) et en comparant les résultats stéréochimiques obtenus pour des radicaux cyclohexyles à ceux déjà publiés pour des réactions de type ionique, nous étions arrivés à la conclusion qu'un radical cyclohexyle est plan, ou se conduit comme tel au cours de la réaction de substitution homolytique; cette conclusion est d'ailleurs en accord avec les observations faites par divers auteurs en rpe (6).

Quelle que soit la configuration du peracide de départ (par exemple **1***a* ou **1***b*) on obtient toujours le même rapport des alcools stéréoisomères; en reprenant les arguments déjà exposés (5), la stéréosélectivité de la réaction 3 qui conduit à la formation de l'alcool, dépend de l'importance relative des effets stériques lorsque le peracide arrive sur le radical par la face axiale et des interactions de liaison lorsque l'arrivée se fait par la face équatoriale.

Pour interpréter les résultats consignés dans le tableau, nous distinguerons deux catégories d'effets: celle relative à la présence de CH_3 en position 2 ou 3 par rapport au centre radicalaire et celle ayant pour origine la conformation du cycle.

Influence des méthyles en position 2 ou 3

(*i*) La présence d'un CH_3 en 3 (radicaux *E* et *G*) diminue relativement l'entrée *axiale* du fait de l'augmentation des effets stériques. Celle d'un CH_3 en 2 *axial* (*B*) augmente les interactions de torsion, du sens de Cherest et Felkin (7), pour l'entrée *équatoriale* et favorise ainsi l'entrée *axiale*.

(*ii*) Un CH_3 en position 2 *équatorial* (*C*) diminue l'entrée *axiale* par suite d'une nouvelle interaction butane gauche dans l'état de transition.

Dans le cas du radical *D* nous avons les effets conjugués des deux situations précédentes et nous constatons que l'effet de torsion dû au CH_3 en *axial* l'emporte sur celui du CH_3 en *équatorial*; cette conclusion est conforme aux observations faites pour les radicaux *B* et *C* puisqu'un CH_3 en axial apporte un $\Delta(\Delta G)$ de 500 cal pour 200 seulement dans le cas de

TABLEAU 1. Alcools stéréoisomères formés par décarboxylation thermique des peracides en solution 0.1 *M* dans le cyclohexane. Température de la réaction, 80 °C

Peracides*			Radical intermediaire	Rapport des alcools formés ax./éq.	$\delta(\Delta G)^{\neq}$ (cal/mol) éq. − ax.
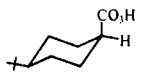	ou	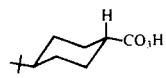		80/20	980
1*a*		**1***b*	*A*		
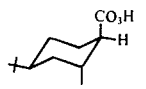	ou	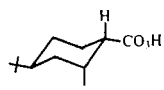	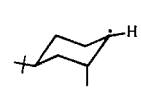	90/10	1500
2*a*		**2***b*	*B*		
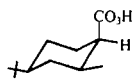	ou	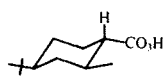		75/25	780
3*a*		**3***b*	*C*		
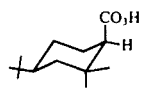	ou	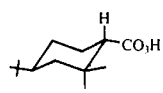		83/17	1120
4*a*		**4***b*	*D*		
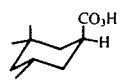	ou	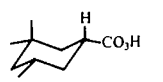	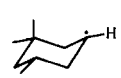	37/63	−375
5*a*		**5***b*	*E*		
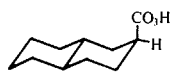	ou	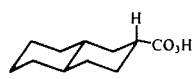	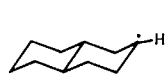	71/29	640
6*a*		**6***b*	*F*		
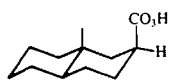	ou	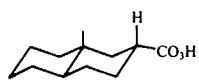	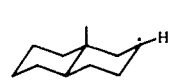	25/75	−775
7*a*		**7***b*	*G*		

*Les résultats concernant les peracides **1**, **2**, **3** et **7** ont déjà fait l'objet d'une précédente publication (5).

CH_3 en *équatorial*. On peut visualiser ces interactions par le schéma 1.

Dans le cas d'une attaque equatoriale, l'angle α_2 entre la liaison qui se forme et C_2R_2 est de 20° environ[1] alors que α_1, dans le cas de l'attaque axiale, est de 80°. Ceci explique l'influence plus importante d'un CH_3 en *axial*.

[1]Calculs faits pour un radical *tert*-butyl-4 cyclohexyle (donc non substitué) par Mme Fournier et M. B. Waegell (Université de Marseille) que nous remercions vivement.

Influence de la conformation du cycle

Si on compare les stéréosélectivités observées pour les radicaux ayant même encombrement de la face axiale c'est à dire *E* et *G* d'une part et *A* et *F* d'autre part on s'aperçoit que l'entrée axiale du réactif est un peu plus favorisée dans le cas des radicaux cyclohexyles "bloqués" par un *tert*-butyle en 4 (*A*) ou par des méthyles (*E*), que dans celui où le cyclohexyle fait partie d'un motif décalinique; on peut expliquer cette différence

Can. J. Chem. Downloaded from www.nrcresearchpress.com by 210.87.254.5 on 09/05/12
For personal use only.

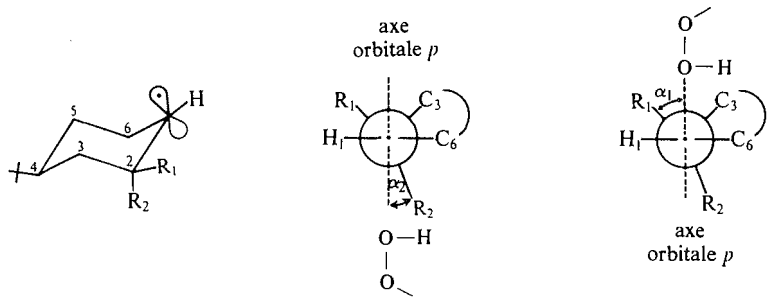

$E_T^{\neq}$ attaque éq. $E_T^{\neq}$ attaque ax.

SCHÉMA I

par une plus grande rigidité du cycle dans le cas du modèle décalinique qui accroît légèrement l'effet de l'encombrement stérique de H ou CH_3 en position 9. On retrouve d'ailleurs des différences analogues dans le cas d'époxydation de doubles liaisons juxtacycliques (8) ou de réduction de cétones cycliques (*tert*-butyl-4 cyclohexanone et *trans*-décalone-2) (9).[2]

Conclusion

Les résultats présentés au cours de ce travail permettent d'aboutir à plusieurs conclusions sur la stéréosélectivité de la réaction de substitution homolytique étudiée, réaction pour laquelle l'état de transition est certainement très proche des produits de départ.

(*i*) La stéréosélectivité, comme dans le cas des réactions ioniques, est le résultat de l'importance relative des effets stériques pour l'entrée du réactif par la face axiale, et des effets d'interactions de liaison qui se forme et de liaisons déjà existantes pour l'entrée équatoriale. Le radical cyclohexyle se conduit comme s'il était plan.

(*ii*) La stéréosélectivité est faiblement fonction de la "flexibilité" du cycle, selon que celui-ci a une conformation bloquée par des substituants alkyles (CH_3 ou *tert*-Bu) ou par jonction *trans* dans un motif décalinique.

Partie expérimentale

Produits de départ

Le cyclohexane utilisé comme solvant est un produit commercial purifié par lavage avec H_2SO_4 et distillation avant emploi. Les acides correspondants aux peracides **4** et **5** ont été obtenus selon réf. 10. L'acide *trans* décaline carboxylique est un produit commercial. Les spectres ir ont été exécutés avec un appareil Hitachi EPI G2, les chromatogrammes en phase gazeuse avec des appareils Girdel ou Aerograph 1200 et les spectres rmn au moyen d'un appareil Varian A 60.

Préparation des peracides

Les peracides sont préparés selon la méthode de Swern et ses collaborateurs (11) que nous avons déjà utilisée précédemment (5). Les peracides **4**, **5** et **6** sont obtenus respectivement avec un rendement de 70, 95 et 80% (pureté déterminée par iodométrie). Pour chaque peracide: ir (CCl_4) ν_{OH} 3250 cm^{-1}, $\nu_{C=O}$ 1730 cm^{-1}.

Décomposition des peracides

Chacun des peracides est décomposé en solution dans le cyclohexane à ébullition (80 °C), à une concentration d'environ 0.1 mol/l, selon un mode opératoire déjà décrit (5). Après $\frac{1}{2}$ h le peracide est complètement décomposé (indice de peroxyde nul).

Analyse du mélange réactionnel

Le rapport des alcools stéréoisomères formés est déterminé en cpg par comparaison avec des échantillons authentiques. Les conditions analytiques sont rassemblées dans le tableau 2.

Lorsque la totalité du peracide a disparu, la solution cyclohexanique est traitée de façon à éliminer les traces d'acide formé par des réactions secondaires; sur le mélange des alcools stéréoisomères ainsi obtenu on effectue un spectre rmn (dans CCl_4). Pour le mélange $a + b$ on observe pour les protons en α de OH, un multiplet à 192 Hz (H éq.) et un massif non résolu à 186 Hz (largeur 20 Hz, H ax.). En ce qui concerne le mélange $c + d$ on a deux multiplets à 226 Hz (H éq.) et 212 Hz (H ax.). Dans ce dernier cas l'intégration de ces deux signaux donne un rapport c/d = 40/60 (trouvé en cpg 37/63).

Remerciements

Les auteurs remercient vivement le Conseil National de Recherches du Canada et les autorités chargées d'administrer les accords scientifiques franco-québécois pour l'aide financière apportée sous forme de subventions et de

[2]Dans ce travail, les auteurs ont étudié la stéréosélectivité de la réduction des cyclohexanones et des décalones-2 dans les mêmes conditions réactionnelles; la comparaison des résultats est donc significative.

Can. J. Chem. Downloaded from www.nrcresearchpress.com by 210.87.254.5 on 09/05/12
For personal use only.

TABLEAU 2. Les conditions analytiques pour les déterminations des rapports des alcools stéréoisomères

Alcools		Colonne* phase stat./ % impregn.	Temperature (°C)		Temps retention† (sec)
			Injecteur	Colonne	
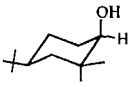	*a*	Carbowax 20 M	180	140	1000
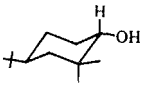	*b*				1152
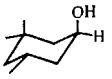	*c*	EGSSX 15%	130	100	160
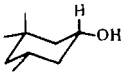	*d*				224
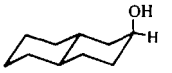	*e*	EGSSX 15%	160	120	500
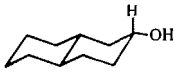	*f*				595

*Longeur 2 m; diametre interne 2 mm.
†Mesurés à partir du pic solvant.

frais de mission. Les auteurs sont aussi reconnaissants à Mlles E. de Lamirande et M. Masquelier pour leur aide technique.

1. J. KOCHI. Free radicals. J. Wiley, New York. 1973.
2. F. JENSEN, L. GALE et J. RODGERS. J. Am. Chem. Soc. **90**, 5793 (1968).
3. D. LEFORT, J. SORBA et D. ROUILLARD. Bull. Soc. Chim. 2219 (1961).
4. M. GRUSELLE. Tetrahedron, À paraître.
5. M. GRUSELLE, M. TICHY et D. LEFORT. Tetrahedron, **28**, 3885 (1972).
6. R. FESSENDEN. J. Phys. Chem. **71**, 74 (1967).
7. M. CHEREST et H. FELKIN. Tetrahedron Lett. 2205 (1968).
8. R. CARLSON et N. BEHN. J. Org. Chem. **32**, 1363 (1967).
9. P. TACHEAU. Thèse, Université de Paris-Sud, Centre d'Orsay, Orsay. 1975.
10. J. C. RICHER et C. LAMARRE. Can. J. Chem. **53**, 2033 (1975).
11. L. SILBERT, E. SIEGEL et D. SWERN. J. Org. Chem. **27**, 1336 (1962).

Can. J. Chem. Downloaded from www.nrcresearchpress.com by 210.87.254.5 on 09/05/12
For personal use only.

Can. J. Chem. Downloaded from www.nrcresearchpress.com by 210.87.254.6 on 09/05/12
For personal use only.

Metabolites of bird's nest fungi. Part 4.[1] The isolation and structure determination of cybullol, a metabolite of *Cyathus bulleri* Brodie

WILLIAM A. AYER AND MICHAEL G. PAICE
Department of Chemistry, University of Alberta, Edmonton, Alberta T6G 2G2

Received November 26, 1975

WILLIAM A. AYER and MICHAEL G. PAICE. Can. J. Chem. **54**, 910 (1976).

Cybullol, a metabolite of *Cyathus bulleri* Brodie, has been shown to be (2*S*,5*S*,6*S*,10*S*)-*cis*-6, *trans*-10-dimethyl-*r*-2-*cis*-5-decalindiol (**1**) by a combination of chemical and physical methods. The mass spectra and the ^1H and ^{13}C magnetic resonance spectra of cybullol and derivatives are discussed. The absolute configuration of cybullol was deduced from the circular dichroism spectrum of the ketol **3**. Cybullol has been transformed into the fungal metabolite (−)-geosmin (**11**). This correlation establishes the absolute configuration of (−)-geosmin.

WILLIAM A. AYER et MICHAEL G. PAICE. Can. J. Chem. **54**, 910 (1976).

On a montré que le cybullol, un métabolite du *Cyathus bulleri* Brodie, est le (2*S*,5*S*,6*S*,10*S*)-diméthyl-6 *cis* 10 *trans* décalindiol-2*r* 5 *cis* (**1**). On est arrivé à ces conclusions par une combinaison de méthodes chimiques et physiques. On discute des spectres de masse et des spectres de résonance magnétique nucléaire du proton et du ^{13}C du cybullol et de ses dérivés. On a déduit la configuration absolue du cybullol à partir du spectre de dichroïsme circulaire du cétol **3**. On a transformé le cybullol en métabolite fongeux (−)-géosmine (**11**). Cette corrélation a permis d'établir la configuration absolue de la (−)-géosmine.

[Traduit par le journal]

The small gasteromycetous fungi known as the Nidulariaceae or bird's nest fungi are widely distributed in nature (4). We have previously reported (2, 3) on the diterpenoid metabolites of one species, *Cyathus helenae* Brodie, indigenous to the Rocky Mountains of Alberta (5). We now wish to report the structure of a metabolite obtained when *Cyathus bulleri* Brodie, first discovered in the West Indies (6) and subsequently in Hawaii (7), is grown in 'still surface' culture on a liquid medium. The original culture of *C. bulleri* used in this work was obtained from the collection of H. J. Brodie and was grown on a liquid medium developed by Brodie (8). After a 30 day growth period, the culture broth was extracted with ethyl acetate to provide the crude metabolite used in this work.

Preliminary investigation of the crude metabolite by thin layer chromatography (tlc) revealed the presence of at least six components. By a combination of column chromatography and preparative tlc (ptlc) the major component (as evidenced by gas chromatography (gc)) has been isolated in pure form. This substance, for which we propose the name cybullol, has been shown to possess structure **1** on the basis of the evidence discussed below.

[1]References 1, 2, and 3 are considered as Parts 1, 2, and 3 respectively.

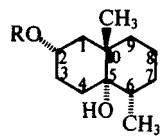

1 R = H
2 R = Ac

Cybullol, **1**, $C_{12}H_{22}O_2$, is an optically active colorless crystalline compound, mp 125–126 °C, $[\alpha]_D^{25}$ −16°. The ir spectrum of cybullol shows strong OH absorption but does not show carbonyl absorption. Acetylation of cybullol provides a monoacetate, **2**, which shows extremely weak hydroxyl absorption in the ir. However, cybullol exchanges two hydrogens when dissolved in CH_3OD (determined by mass spectrometry) confirming that both oxygens are present as hydroxyl groups.

The proton magnetic resonance (pmr) spectrum of cybullol contains signals at δ 0.81 (3H, d, J = 6 Hz, CH—CH_3), 1.03 (3H, s, —C—CH_3), and 3.9 (1H, m, C*H*OH). Since only one proton is geminal to hydroxyl, cybullol contains a tertiary and a secondary hydroxyl group. As mentioned, acetylation provides a monoacetate. The signal for the hydrogen geminal to oxygen in the acetate appears as a multiplet at δ 5.0. In both the alcohol and the acetate this signal appears as an apparent symmetrical heptet (splitting ~5 Hz)

Can. J. Chem. Downloaded from www.nrcresearchpress.com by 210.87.254.6 on 09/05/12
For personal use only.

which approximates a triplet of triplets, of J's 5 and 10 Hz. The width at half height ($W_{1/2}$), 25 Hz, indicates that the proton geminal to the oxygen function is axial (9) and the coupling pattern indicates it is flanked on both sides by methylene groups. Since cybullol shows no olefinic absorption in its ir, pmr, or ^{13}C nuclear magnetic resonance (cmr) spectra it must be a bicyclic diol.

A small sample of cybullol was dehydrogenated over palladium–charcoal. Gas chromatography indicated the formation of four products. These were separated by gc and shown by high resolution mass spectrometry to have apparent molecular formulas $C_{11}H_{10}$ (*A*), $C_{12}H_{12}$ (*B*), $C_{11}H_{10}O$ (*C*), and $C_{12}H_{12}O$ (*D*). Compound *A* was shown to be 1-methylnaphthalene by its uv spectrum, mass spectrum, and gc retention time (on a column which resolves 1-methyl- and 2-methylnaphthalene). The uv and mass spectra indicate that *B* is a dimethylnaphthalene, *C* is a methylnaphthol, and *D* is a dimethylnaphthol. This result suggested the presence of the decalin system[2] in cybullol. The presence of 1-methylnaphthalene coupled with the absence of 2-methylnaphthalene in the dehydrogenation product indicated that the secondary methyl group is located at a carbon adjacent to the ring junction. Since the tertiary methyl and the tertiary hydroxyl cannot be geminal (high field methyl signal in pmr) these groups must be located at the ring junction of the decalin system. This latter consideration also rules out the possibility that cybullol contains a spiro[5.4]decane system.

Oxidation of cybullol with Jones' reagent furnishes a ketol, **3**, absorbing at 1710 cm^{-1} in the ir, indicating that the secondary hydroxyl is located in a six-membered ring, and mitigating against the presence of a perhydroazulene system. Reduction of ketol **3** with sodium borohydride provides cybullol, **1**, and epicybullol, **4**, in a ratio of 1:4. The pmr spectrum of **4** shows a 3-proton doublet at δ 0.79 for the methyl at C-6, a 3-proton singlet at δ 1.29 for the methyl at C-10 and a 1-proton multiplet ($W_{1/2}$ = 8 Hz) for the equatorial proton (9) at C-2. The large downfield shift of the tertiary methyl in **4** relative to **1** (Δ = 0.26 ppm) indicates that the C-10 methyl and the newly formed hydroxyl group are in a 1,3-diaxial relationship (10). Ketol **3** was recovered unchanged after treatment with hot alcoholic KOH and thus did not appear to be a β-hydroxy ketone. At this point partial structure **5** was compatible with the evidence obtained, with the secondary hydroxyl located at either C-2 or C-8.

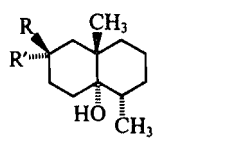

3 R = R′ = Carbonyl
4 R = OH, R′ = H

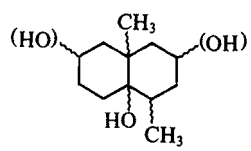

5

Consideration of the mass spectra of cybullol, **1**, and the ethylene acetal, **6**, derived from ketol **3**,

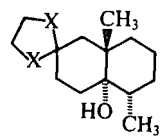

6 X = O
12 X = S

favored the location of the hydroxyl group at C-2. The mass spectrum of cybullol (Fig. 1) shows intense fragments at *m/e* 128 ($C_7H_{12}O_2$)[3] and 126 ($C_8H_{14}O$). Fragmentation as indicated in Scheme 1, similar to that observed with 5-

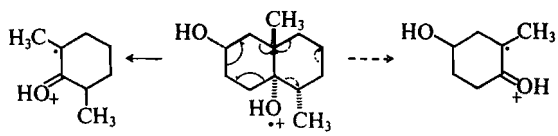

m/e 126 *m/e* 128

SCHEME 1

hydroxysteroids (11), accounts for these fragments provided the secondary hydroxyl and secondary methyl are not in the same ring. In agreement with this hypothesis is the observation that fragmentation of ketol **3** does not produce an *m/e* 128 ion but only an *m/e* 126 ion which under high resolution is a doublet arising from a $C_8H_{14}O^+$ fragment (75%) and a $C_7H_{10}O_2^+$ fragment (25%).

The fragmentation patterns of ethylene acetals have been extensively studied (12). By analogy with the previous work (12), the acetal **6** is predicted to give rise to fragments *m/e* 99, 126, and

[2]Spiro[5.4]decanes and perhydroazulenes can also, by simple Wagner–Meerwein rearrangement, lead to naphthalene precursors.

[3]The formulas of all fragment ions shown in Schemes 1, 2, and 3 were determined by high resolution mass spectrometry (hrms).

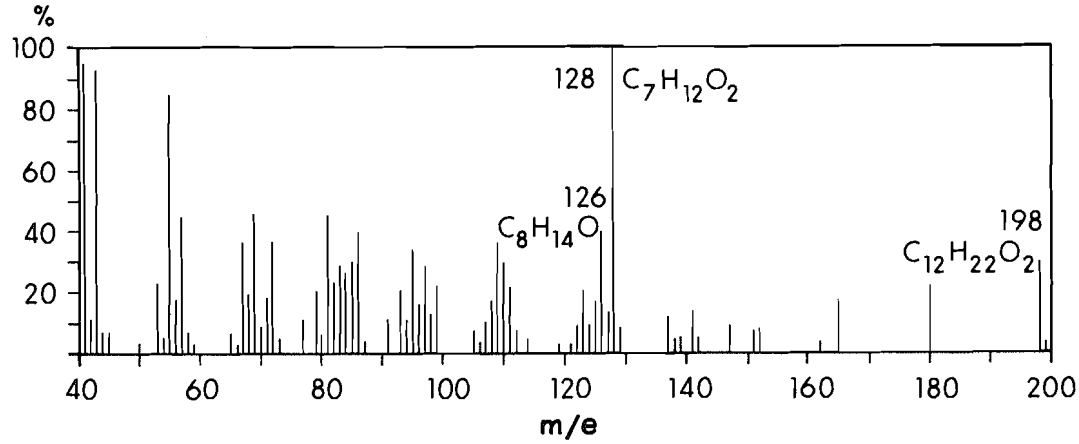

FIG. 1. Mass spectrum of cybullol, **1**.

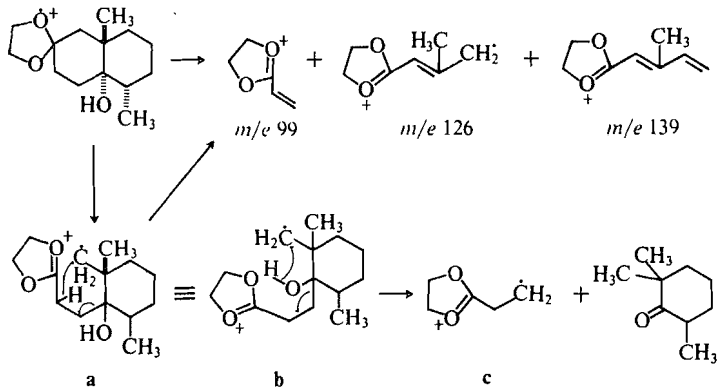

SCHEME 2

139 (Scheme 2). All of these peaks are observed in the mass spectrum of acetal **6**. In addition to these peaks, intense peaks are observed at *m/e* 100 (base peak) and *m/e* 113 (40% of base peak). The intense peak at *m/e* 99 is believed (12) to arise by hydrogen transfer and cleavage as illustrated in ion **a** (Scheme 2). Alternatively, hydrogen transfer from the hydroxyl group and cleavage as illustrated in ion **b** would lead to a stable neutral molecule (trimethylcyclohexanone) and the ion radical **c** of *m/e* 100. The ion of *m/e* 113 is believed to arise as illustrated in Scheme 3, by analogy with a well documented process (ref. 12, p. 37).

Cybullol was first assigned the relative stereochemistry shown in **1** on the following basis. It has been shown (13) that in compounds containing vicinal methyl and hydroxyl groups, substantial downfield shifts of the methyl protons are noted in pyridine solution (relative to chloroform) when the methyl group and the

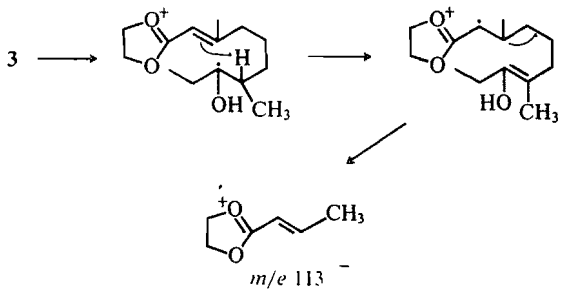

SCHEME 3

hydroxyl group are synclinal ($\delta_{CDCl_3} - \delta_{py} = \Delta_{py} -0.20$ to -0.27 ppm), whereas relatively little shift is observed when the groups are antiperiplanar ($\Delta_{py} -0.03$ ppm) (13).

In order to confirm that this method may be

Can. J. Chem. Downloaded from www.nrcresearchpress.com by 210.87.254.6 on 09/05/12
For personal use only.

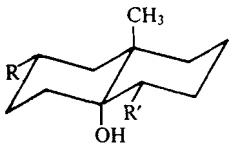

7 R = R′ = H
10 R = OH, R′ = CH_3
11 R = H, R′ = CH_3

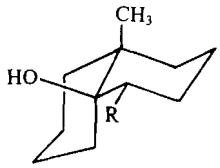

8 R = H
9 R = CH_3

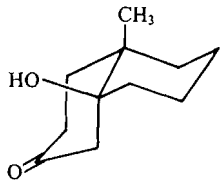

13

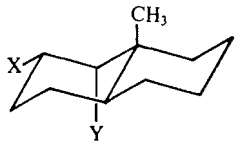

14 X = OH, Y = H
15 X = H, Y = OH
16 X = Y = H

applied to 10-methyl-5-decalols the pyridine induced shifts of the tertiary methyl groups in *trans*-10-methyl-5-decalol, **7**,[4] *cis*-10-methyl-5-decalol, **8**,[4] and *trans*-4,10-dimethyl-*cis*-5-decalol, **9**,[5] were measured and found to be −0.01, −0.14, and −0.18 ppm, respectively. In cybullol, Δ_{py} is −0.03 ppm for the tertiary methyl, and −0.14 ppm for the secondary methyl. Since the equatorial secondary hydroxyl at C-2 should not influence these induced shifts (13), this datum suggests that the tertiary hydroxyl is antiperiplanar to the tertiary methyl and synclinal to the secondary methyl, *i.e.*, cybullol has the relative stereochemistry shown in **10** = **1**.

Confirmation of the relative stereochemistry at C-5, C-6, and C-10 in cybullol was obtained by transformation of cybullol into geosmin, **11**, the fungal metabolite responsible for the 'earthy' odor of freshly plowed soil (14) and the 'muddy' taste of certain surface waters (15) and trout (16). The constitution of geosmin was first suggested by Gerber (17) and the structure and relative stereochemistry, **11**, proven by Marshall's stereoselective synthesis (18) of the racemic form. Transformation of the ketol **3** to the thioacetal **12** and subsequent desulfurization with Raney nickel provided (−)-geosmin, **11**, identified by comparison of ir, pmr, and mass spectra, and by its characteristic and penetrating odor!

The circular dichroism spectrum of the ketol **3** from cybullol shows a positive Cotton effect at 286 nm ($\Delta\epsilon$ +1.73). Application of the octant rule (19, 20) indicates that structure **3** represents the absolute stereochemistry of **3** and thus **1** represents the absolute stereochemistry of cybullol. The absolute stereochemistry of (−)-geosmin, not previously determined, is therefore as shown in **11**.

The cmr spectrum of cybullol (see Experimental) is worthy of comment.[6] The position of the tertiary methyl signal (δ 21.1) in cybullol, when compared with the corresponding signals in **8** (δ 22.4),[4] **9** (δ 22.3),[5] **13** (δ 21.5),[7] **14** (δ 16.6) (21), **15** (δ 16.1) (21), and **16** (δ 15.7) (22) seemed in better agreement with a *cis*-decalin system for cybullol. However, in *trans*-10-methyl-5-decalol (**7**)[4] the methyl signal also appears at low field (δ 20.4). The origin of this unusual (21, 23) deshielding by antiperiplanar hydroxyl is under investigation.[7]

Biogenetically cybullol, **1**, like geosmin, **11**, (17) appears to be a degraded eudesmane-type sesquiterpene. We have isolated from cultures of *C. bulleri* very small amounts of a compound $C_{15}H_{28}O_3$ which appears to be a bicyclic triol of the eudesmane type (see Experimental). We are currently endeavoring to obtain sufficient amounts of this C_{15} compound to allow its structure determination.

Experimental

Mass spectra were recorded on an A.E.I. model MS-2, MS-9, or MS-12 mass spectrometer and are reported as *m/e* (relative intensity). Unless diagnostically significant only peaks at least 20% as intense as the base peak are reported. Infrared spectra were recorded on a Unicam SP1000 or Perkin-Elmer model 421 dual grating spectrophotometer, uv spectra on a Cary model 14M spectrophotometer, cd spectra on a Jasco model SS-20-2 spectropolarimeter, and optical rotations on a Perkin-Elmer Model 141 automatic polarimeter. Proton magnetic resonance spectra were measured using a Varian HA-100 spectrometer with tetramethylsilane as internal standard. Melting points were recorded on a Fisher-Johns melting point apparatus and are uncorrected.

Silica gel tlc plates were 0.5 mm silica gel G (E. Merck, Darmstadt) containing 1% electronic phosphor (General Electric, Cleveland); materials were detected by spraying with 30% sulfuric acid and charring. Unless otherwise specified the solvent system used for development was methylene chloride–methanol (10:1). All solvents were reagent grade and were distilled prior to use.

[4]Kindly furnished by Dr. L. M. Browne of these laboratories.

[5]We wish to thank Prof. J. A. Marshall for a sample of **9**.

[6]We wish to thank Prof. J. B. Stothers for determination of the spectra and for valuable discussion.

[7]J. B. Stothers, private communication.

Can. J. Chem. Downloaded from www.nrcresearchpress.com by 210.87.254.6 on 09/05/12
For personal use only.

Can. J. Chem. Downloaded from www.nrcresearchpress.com by 210.87.254.6 on 09/05/12
For personal use only.

Gas chromatographic analyses were carried out with a Hewlett Packard Model 5700A gas chromatograph fitted with a flame ionization detector, a 10 ft × ¼ in. glass column packed with 3% OV-225 on 100/120 Gas Chrom Q (Applied Sciences), and using N_2 as carrier gas.

Growth of C. bulleri on Liquid Medium and Isolation of the Crude Metabolites

The aqueous medium used for culture growth (Brodie liquid medium) has the following composition (per litre): maltose, 5.0 g; dextrose, 2.0 g; yeast extract (Difco), 2.0 g; KH_2PO_4, 0.5 g; $Ca(NO_3)_2 \cdot 4H_2O$, 0.5 g; $MgSO_4$, 0.24 g; peptone, 0.2 g; asparagine, 0.2 g; $Fe_2(SO_4)_3$, trace; glycerol, 6 ml. The medium was autoclaved at 120 °C for 20 min before use.

Agar slant tube cultures of *C. bulleri* were obtained from Prof. H. J. Brodie and were used to inoculate 500 ml erlenmeyer flasks containing 200 ml of the above medium. These were allowed to mature at 25 °C for at least 30 days. To initiate large scale growths the contents of one 500 ml erlenmeyer were blended (Waring blender) and 10 ml portions of the resulting suspension were transferred under sterile conditions to 4 l Fernbach flasks containing 1 l of the above liquid medium. After 30 days growth at 25 °C the mycelium was removed by filtration through cheesecloth and the clear culture broth extracted with an equal volume of ethyl acetate. Concentration of the yellowish ethyl acetate extract provided the crude metabolites as a yellowish-brown semisolid (~50 mg/l of culture broth).

Isolation of Cybullol

The crude metabolites were chromatographed over silica gel (Woelm, <0.063 mm particle size) using ethyl acetate as eluant and a substrate to adsorbent ratio of 1:100. In a typical separation using 1.0 g of crude extract and collecting 10 ml fractions (flow rate ~10 ml/h), cybullol (detected by tlc on silica gel, R_f 0.42 and by gc) eluted in fractions 10–13. These fractions were usually further purified either by column chromatography over silica gel using methylene chloride – methanol (20:1) as the eluant, or by ptlc over silica gel G (0.5 mm layer, eluant methylene chloride – methanol (10:1)). In this fashion chromatographically pure cybullol could be isolated in about 2.5% overall yield from crude metabolite. Cybullol crystallizes from methylene chloride – Skellysolve B as colorless plates, mp 125–126 °C, $[\alpha]_D^{25}$ −16° (*c* 0.4, methanol). Infrared spectrum (KBr disc): 3500–3380, 1040, 945 cm^{-1}; pmr spectrum ($CDCl_3$): δ 0.81 (3H, d, J = 6 Hz), 1.03 (3H, s), 3.90 (1H, apparent septet, splitting 5 Hz); cmr spectrum ($CDCl_3$): δ_{TMS} 15.3 (CH_3 on C-6), 20.3 (C-8), 21.1 (CH_3 on C-10), 29.8, 30.3, 31.2 (C-7, C-3, C-4, assignments tentative), 33.9 (C-6), 34.7 (C-9), 38.8 (C-10), 45.0 (C-1), 66.8 (C-2), 73.6 (C-5). Mass spectrum: see Fig. 1. *Anal.* calcd. for $C_{12}H_{22}O_2$: C 72.68, H 11.18; found: C 72.61, H 11.15. *Mol. Wt.* calcd. for $C_{12}H_{22}O_2$: 198.1620; found (hrms): 198.1614.

Acetylation of Cybullol

Cybullol (8 mg) was dissolved in acetic anhydride (1 ml) and pyridine (4 drops) added. After 4 h at room temperature the solvent was removed *in vacuo* to yield a colorless oil (8.6 mg) which was purified by tlc on silica gel (R_f 0.53). This same product was obtained when the reaction mixture was heated under reflux for 1 h. Infrared spectrum (CCl_4): 3620 (w), 1740, 1250 cm^{-1}; pmr spectrum ($CDCl_3$): δ 0.80 (3H, d, J = 6 Hz), 1.07 (3H, s), 2.01 (3H, s), 5.00 (1H, apparent septet, splitting 5 Hz). Mass spectrum: 240 (14, M^+, calcd. for $C_{14}H_{24}O_3$, 240.1726 amu, found 240.1718 amu), 180 (100), 165 (34), 162 (29), 126 (42), 111 (38), 110 (38), 95 (29), 81 (30), 55 (32).

Oxidation of Cybullol

Jones' reagent (8 *N* in CrO_3) was added dropwise to a solution of cybullol (8 mg) in acetone (2 ml) until the solution remained orange. After 20 min isopropyl alcohol was added to discharge the orange color and the solution diluted with brine. Extraction with ether provided the ketol **3** (6 mg) as a colorless oil which showed a single spot on tlc (R_f 0.60). Infrared spectrum (CCl_4): 3600, 1705 cm^{-1}; pmr spectrum ($CDCl_3$): δ 0.90 (3H, d, J = 6.5 Hz), 0.97 (3H, s). Mass spectrum: 196 (50, M^+, calcd. for $C_{12}H_{20}O_2$, 196.2144 amu, found 196.2136 amu), 126 (98), 125 (52), 111 (30), 109 (31), 107 (80), 69 (48), 55 (90). Optical rotatory dispersion spectrum (methanol, *c* 0.5): $[\Phi]_{315}$ +3,400°, $[\Phi]_{275}$ −3,000°; cd spectrum (methanol, *c* 0.5): $\Delta\epsilon_{296}$ +1.73.

Attempted Dehydration of Ketol 3

The ketol **3** (1 mg) was heated under reflux in 2% ethanolic KOH (5 ml) of 4 h. The cooled solution was diluted with saturated brine (10 ml) and extracted with ether. The dried ether solution was evaporated to yield ketol **3** (1 mg), identified by ms, tlc, and gc.

Reduction of Ketol 3

Ketol **3** (7.7 mg) in ethanol (2 ml) was treated with $NaBH_4$ (5 mg) at room temperature for 15 min. Dilution with water and extraction with ether yielded a mixture of cybullol, **1**, and epicybullol, **4**, in a ratio of ~1:4 (by gc). Separation was achieved by ptlc (R_f's, cybullol 0.42, epicybullol 0.50). Epicybullol, **4**: pmr spectrum ($CDCl_3$): δ 0.79 (3H, d, J = 6 Hz), 1.26 (3H, s), 4.1 (1H, m, $W_{1/2}$ = 8 Hz); mass spectrum: 198 (20, M^+), 128 (100), 126 (19), 110 (28), 109 (22), 95 (20), 86 (30), 81 (27), 69 (22), 57 (24), 55 (36).

Dehydrogenation of Cybullol

Cybullol (8.5 mg) was mixed with 5% palladium-on-charcoal (80 mg) and the mixture heated to 250 °C in a sealed tube for 4 h. The reaction mixture was triturated first with methylene chloride then with methylene chloride – methanol (10:1). Evaporation of the methylene chloride gave an oil (1.8 mg) which consisted mainly of two components which were separated by gc (temperature programmed 80–240 °C at 8 °C/min, fractions collected in 10 cm capillary tubes packed with Amberlite XAD-2 resin (24)). Component *A*, retention time 8.40 min, mol. wt. 142.0783 amu (hrms) (calcd. for $C_{11}H_{10}$, mol. wt. 142.0779 amu) was identical in retention time, mass spectrum, and uv spectrum with 1-methylnaphthalene. Under these gc conditions, 2-methylnaphthalene has retention time 8.12 min. Component *B*, retention time 10.36 min, showed mol. wt. 156.0947 amu (calcd. for $C_{12}H_{12}$, 156.0939 amu). Evaporation of the methylene chloride – methanol extract yielded an oil (1.3 mg); (uv spectrum (MeOH) λ_{max} 227 nm shifted to 232 and 244 nm on addition of base) which consisted chiefly of two components which were separated by gc. Component *C*, retention time 17.5 min, possessed mol. wt. 158.0740 amu

Can. J. Chem. Downloaded from www.nrcresearchpress.com by 210.87.254.6 on 09/05/12
For personal use only.

(calcd. for $C_{11}H_{10}O$, 158.0732 amu). Component *D*, retention time 19.6 min, had mol. wt. 172.0881 amu (calcd. for $C_{12}H_{12}O$, 172.0888 amu).

Preparation of Acetal **6**

A solution of ketol **3** (5 mg) in benzene (2 ml) containing ethylene glycol (0.50 ml) and a trace of *p*-toluenesulfonic acid was heated under reflux for 15 h during which time water was continuously removed by passing the refluxing benzene over 4A molecular sieves. The cooled solution was washed with dilute aqueous $NaHCO_3$ (5 ml), water (2 × 5 ml), and dried ($MgSO_4$). Removal of the solvent left the acetal **6** (5 mg) as a colorless oil, R_f 0.60 (tlc, silica gel). Infrared spectrum (CCl_4): 3600, 1090 cm^{-1}; pmr spectrum ($CDCl_3$): δ 0.79 (3H, d, J = 6 Hz), 1.13 (3H, s), 3.90 (4H, m). Mass spectrum: 240 (2, M^+, calcd. for $C_{14}H_{24}O_3$, 240.1726 amu, found, 240.1718 amu), 139 (6, calcd. for $C_8H_{11}O_2$, 139.0759 amu, found 139.0763 amu), 126 (13, calcd. for $C_7H_{10}O_2$, 126.0681 amu, found, 126.0678 amu), 113 (40, calcd. for $C_6H_9O_2$, 113.0603 amu, found, 113.0608 amu), 100 (100, calcd. for $C_5H_8O_2$, 100.0524 amu, found, 100.0525 amu), 99 (48, calcd. for $C_5H_7O_2$, 99.0446 amu, found, 99.0448 amu), 55 (33).

Preparation of Thioacetal **12**

To a solution of ketol **3** (13 mg) in acetic acid (1 ml) was added ethanedithiol (40 μl) and BF_3–etherate (10 μl). After 3.5 h the solution was diluted with saturated brine (10 ml) and extracted with ether (3 × 10 ml). The ether extract was washed with 10% aqueous sodium hydroxide (3 × 10 ml), saturated brine (10 ml) and dried ($MgSO_4$). Evaporation of solvent gave a mixture (5.2 mg) of starting ketol **3** and thioacetal **12** in a ratio of about 1:3 (by gc). The mixture was separated by ptlc over silica gel (CH_2Cl_2–MeOH, 49:1). The product of higher R_f (~4 mg) was characterized as the thioacetal **12** by mass spectrometry and used directly in the next experiment. Mass spectrum: 274 (11, $M + 2$), 272 (100, M^+), 254 (23), 239 (11), 179 (52), 161 (35), 149 (36), 132 (44), 131 (40), 99 (40), 55 (81).

Desulfurization of **12**

The crude thioacetal **12** (8 mg) in ethanol (2 ml) was heated under reflux with W-2 Raney nickel (excess) for 4 h. The solution was filtered and evaporated under reduced pressure at room temperature. The residue was taken up in ether (3 ml), washed with saturated brine, and dried ($MgSO_4$). The ether solution was concentrated to small volume and geosmin isolated by gas chromatography (5 ft × ¼ in. glass column, 3% OV-225 on Gas Chrom Q, 140 °C, N_2 carrier gas (100 ml/min), fractions collected in 10 cm capillary tubes packed with Amberlite XAD-2 resin (24) and eluted from the resin with CCl_4 (for ir spectrum) and $CDCl_3$ (for pmr spectrum)). The major component, retention time 8.56 min, was identical in ir spectrum (15), pmr spectrum (15), and mass spectrum (15) with geosmin **11**. The specific rotation, determined on two separate samples (~1 mg each) of the geosmin prepared from cybullol, in methanol (2 ml) was $[\alpha]_D^{25}$ ~ −140° (reported (14), $[\alpha]_D^{25}$ −16.5° (*c* 0.005, $CHCl_3$)). Since only small quantities of this volatile substance were available, the rotation data is not considered to be accurate. However, the rotation was distinctly levorotatory. The rotation measured in carbon tetrachloride (~2 mg geosmin in 2 ml CCl_4) was also levorotatory (~ −100°).

Characterization of Compound $C_{15}H_{28}O_3$ from C. bulleri

The compound $C_{15}H_{28}O_3$ was present in fractions 13–16 of the ethyl acetate column chromatogram of crude metabolites (see isolation of cybullol) and was further purified by ptlc over silica gel (R_f 0.35). After crystallization from methylene chloride it melted at 152–153 °C, $[\alpha]_D^{25}$ −18.5° (*c* 0.07, methanol). Infrared spectrum (Nujol): 3400 cm^{-1}; pmr spectrum ($CDCl_3$): δ 1.04 (3H, d, J = 7 Hz, $>CHCH_3$), 1.05 (3H, s, $\geqslant C—CH_3$), 1.30 (6H, s, $HO>C(CH_3)_2$), 3.5 (1H, m, $CHOH$). Mass spectrum: 256 (4, apparent M^+, calcd. for $C_{15}H_{28}O_3$, 256.2039 amu, found, 256.2046 amu), 238 (12), 223 (4), 220 (5), 180 (22), 170 (81, calcd. for $C_{10}H_{18}O_2$, 170.1307 amu, found, 170.1301), 162 (30), 152 (45), 123 (43), 109 (46), 85 (45), 81 (64), 59 (93, calcd. for C_3H_7O, 59.0497 amu, found, 59.0499 amu), 55 (71), 43 (100).

Acetylation of this compound with acetic anhydride – pyridine provided a monoacetyl derivative. Treatment of the C_{15} compound with trichloroacetyl isocyanate in a nmr tube followed by recording of the spectrum of the resulting derivative revealed (25) the presence of three hydroxyl groups in the C_{15} compound.

Acknowledgements

We wish to thank the National Research Council of Canada for financial support, Dr. H. J. Brodie for cultures of *C. bulleri* and for his interest, and Dr. D. R. Taylor for helpful discussion.

1. A. D. Allbutt, W. A. Ayer, H. J. Brodie, B. N. Johri, and H. Taube. Can. J. Microbiol. **17**, 1401 (1971).
2. W. A. Ayer and H. Taube. Can. J. Chem. **51**, 3842 (1973).
3. W. A. Ayer and L. L. Carstens. Can. J. Chem. **51**, 3157 (1973).
4. H. J. Brodie. Can. Field Nat. **82**, 2 (1968).
5. H. J. Brodie. Can. J. Bot. **44**, 1235 (1966).
6. H. J. Brodie. Bull. Torrey Bot. Club, **94**, 68 (1967).
7. H. J. Brodie. Can. J. Bot. **50**, 643 (1972).
8. H. J. Brodie. Sven. Bot. Tidskr. **62**, 201 (1968).
9. A. Hassner and C. Heathcock. J. Org. Chem. **29**, 1350 (1964).
10. Y. Kawazoe, Y. Sato, M. Natsume, H. Hasegawa, T. Okamoto, and K. Tsuda. Chem. Pharm. Bull. **10**, 338 (1962).
11. A. Rotman, A. Mandalbaum, and Y. Mazur. Tetrahedron, **29**, 1303 (1973).
12. H. Budzikiewicz, C. Djerassi, and D. H. Williams. Structure elucidation of natural products by mass spectrometry. Vol. 2. Holden-Day, San Francisco. 1964. pp. 24–49.
13. P. V. Demarco, E. Farkas, D. Doddrell, B. L. Mylari, and E. Wenkert. J. Am. Chem. Soc. **90**, 5480 (1968).
14. N. N. Gerber and H. A. Lechevalier. Appl. Microbiol. **13**, 935 (1965).

15. L. L. MEDSKER, D. JENKINS, and J. F. THOMAS. Environ. Sci. Technol. **2**, 461 (1968).
16. M. YURKOWSKI and J.-A. L. TABACHEK. J. Fish. Res. Board Can. **31**, 1851 (1974).
17. N. N. GERBER. Tetrahedron Lett. 2971 (1968).
18. J. A. MARSHALL and A. R. HOCHSTETLER. J. Org. Chem. **33**, 2593 (1968).
19. W. MOFFITT, R. B. WOODWARD, A. MOSCOWITZ, W. KLYNE, and C. DJERASSI. J. Am. Chem. Soc. **83**, 4013 (1961).
20. D. N. KIRK and W. KLYNE. J. Chem. Soc. Perkin Trans. I, 1076 (1974).
21. S. H. GROVER and J. B. STOTHERS. Can. J. Chem. **52**, 870 (1974).
22. D. K. DALLING, D. M. GRANT, and E. G. PAUL. J. Am. Chem. Soc. **95**, 3718 (1973).
23. E. L. ELIEL, W. F. BAILEY, L. D. KOPP, R. L. WILLER, D. M. GRANT, R. BERTRAND, K. A. CHRISTENSEN, D. K. DALLING, M. W. DUCH, E. WENKERT, F. M. SCHELL, and D. W. COCHRAN. J. Am. Chem. Soc. **97**, 322 (1975).
24. J. S. FRITZ. J. Org. Chem. **38**, 3006 (1973).
25. I. R. TREHAN, C. MONDER, and A. K. BOSE. Tetrahedron Lett. **67** (1968).

Can. J. Chem. Downloaded from www.nrcresearchpress.com by 210.87.254.6 on 09/05/12
For personal use only.

^{13}C nuclear magnetic resonance studies. 58.[1] ^{13}C spectra of a variety of bicyclo[2.2.2]octane derivatives. Further definition of the deshielding δ effect

J. B. STOTHERS AND C. T. TAN

Department of Chemistry, University of Western Ontario, London, Ontario N6A 5B7

Received November 21, 1975

J. B. STOTHERS and C. T. TAN. Can. J. Chem. **54**, 917 (1976).

The ^{13}C nmr spectra of 35 bicyclo[2.2.2]octane and -octene derivatives have been determined to extend our examinations of the effects of stereochemistry on the shieldings of closely neighboring carbons. This series includes a variety of methyl substituted bicyclooctanols and -octenols as well as the corresponding hydrocarbons and some bicyclooctanones. With the bicyclo[2.2.2]-octane skeleton it is possible to examine an array of systems having substituents separated by three and four bonds in a variety of orientations. The interactions, termed γ and δ effects, respectively, produce distinctive shielding variations which are useful for stereochemical elucidations. Particularly interesting are the pronounced shifts observed for the carbons *bearing* closely neighboring substituents. Characteristically, for vicinal substituents, these carbons are shielded while for *syn*-axial δ interactions, these carbons are deshielded by as much as 8.6 ppm. The results are compared with the trends found in other sterically crowded systems.

J. B. STOTHERS et C. T. TAN. Can. J. Chem. **54**, 917 (1976).

Afin d'étendre nos études sur les effets de la stéréochimie sur le blindage des carbones à proximité, on a déterminé les spectres rmn du ^{13}C de 35 dérivés des bicyclo[2.2.2]octane et -octène. Cette série comprend un certain nombre de bicyclooctanols et -octénols substitués par des groupes méthyles de même que les hydrocarbures correspondants et quelques bicyclo-octanones. Avec le squelette du bicyclo[2.2.2]octane, il est possible d'examiner un grand nombre de systèmes ayant des substituants séparés par trois et quatre liens dans une grande variété d'orientation. Les interactions, dénommées effet γ et δ, produisent respectivement des variations de blindages caractéristiques qui sont utiles pour des élucidations stéréochimiques. Il est particulièrement intéressant de noter les effets importants provoqués sur les carbones portant des substituants très rapprochés. D'une façon caractéristique, on trouve que pour des substituants vicinaux, ces carbones sont blindés alors que, pour des interactions *syn*-axiales δ, ces carbones sont déblindés par des valeurs allant jusqu'à 8.6 ppm. On compare ces résultats avec les tendances trouvées dans d'autres systèmes stériquement encombrés.

[Traduit par le journal]

Introduction

As an extension of our examination of the effects of molecular geometry on ^{13}C shieldings, we have obtained the spectra of a series of bicyclo[2.2.2]octane derivatives for comparison with the results for other bicyclic systems (1). The principal virtue of such systems for an investigation of stereochemical effects is their relatively rigid skeleton which permits one to study the shielding variations as a function of fairly well-defined substituent orientations. The shifts produced by substituents separated by three and four bonds are of particular interest because of their potential application as probes for conformational analysis in mobile systems and as a tool for stereochemical elucidations. The trends associated with interactions between vicinal substituents are the most generally recognized and have been applied in a wide variety of systems (2), since it is found that a carbon involved in a vicinal *gauche* or eclipsed interaction is more strongly shielded than its counterpart in an *anti* arrangement. Furthermore, in a number of cases, a carbon in the latter situation is shielded relative to one having a dihedral angle, ϕ, near 120° with respect to a vicinal carbon or heteroatom (3). For substituents separated by four bonds, so-called δ interactions, a *syn*-axial arrangement tends to deshield the terminal carbon(s) as has been demonstrated for several methyl–methyl and methyl–hydroxyl interactions (4). More recently, it has been found that the carbons bearing these substituents suffer much more pronounced downfield shifts, by comparison with the shieldings expected on the basis of simple additivity (1*c*, 5). The consistency

[1]For Part 57 see ref. 19.

Can. J. Chem. Downloaded from www.nrcresearchpress.com by 210.87.254.105 on 09/05/12
For personal use only.

Can. J. Chem. Downloaded from www.nrcresearchpress.com by 210.87.254.105 on 09/05/12
For personal use only.

of substituent effects within families of compounds has led to the general application of simple additivity for estimating ^{13}C shieldings in a host of systems and has proved to be extremely useful, provided the substituents are not close neighbors (for a general discussion see ref. 6). Deviations from additivity for the latter situations appear to reflect, at least qualitatively, stereochemical perturbations exerted through space, although theoretical interpretations of the observed shifts are lacking.

In earlier parts of this series, we have examined in some detail the shielding variations produced by γ and δ interactions between two substituents in several bicyclo[2.2.1]heptanes (1*b*, *c*). In these systems, however, it is conceivable that ring strain may contribute to the observed shifts. Since the bicyclo[2.2.2]octane skeleton is less strained, by 4–6 kcal/mol according to molecular mechanics (7), a comparison of the corresponding interactions could reveal differences ascribable to strain effects. The bicyclo[2.2.2]octane skeleton permits the examination of three different vicinal interactions having dihedral angles of 0°, 60°, and 120°, assuming D_{3h} symmetry. Substituted bicyclooctanes, of course, may assume D_3 symmetry to reduce vicinal interactions but it is difficult to estimate the maximum degree of twist. For the parent hydrocarbon, molecular mechanics and spectroscopic data point to the higher symmetry (8), while an electron diffraction study indicated that the twisting motion has a large amplitude with a turning point of 13° in terms of the twist angle (9). It was concluded that the potential probably has a low hump at the D_{3h} position so the molecule was described as 'quasi-D_{3h}'. Possibly, in substituted cases, skeletal twist can exceed that for disubstituted norbornanes, which may be as large as 14° (10), but it seems reasonable to assume that vicinal substituents at C-2 and C-3 would have similar mutual orientations in each of these bicyclic systems. Thus we have prepared several 2,3-disubstituted examples for comparison. Also, a number of systems having *syn*-axial arrangements of 2,6-substituents were synthesized. These compounds provide several examples of methyl–methyl and methyl–hydroxyl interactions for substituents separated by three and four bonds. In an earlier report, examples with vicinal substituents having $\phi \sim 60°$ were included (11). The data for all of these com-

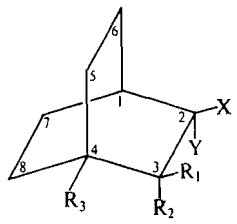

	X	Y	R_1	R_2	R_3
1	Me	H	H	H	H
2	Me	Me	H	H	H
3	Me	H	H	Me	H
4	Me	H	Me	H	H
14	=O		Me	H	H
15	=O		Me	Me	H
5	OH	H	H	H	H
6	OH	H	H	H	Me
17	OH	H	H	Me	H
18	OH	H	Me	H	H
19	OH	H	Me	Me	H

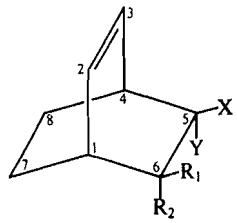

	X	Y	R_1	R_2
7	H	Me	H	H
8	Me	H	H	H
9	Me	H	H	Me
10	Me	H	Me	H
11	Me	Me	H	H
12	H	OH	H	H
13	OH	H	H	H
28	H	OH	Me	Me
31	OH	H	Me	Me

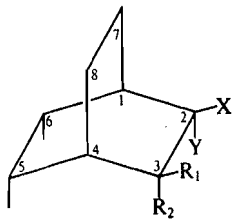

	X	Y	R_1	R_2
16	=O		H	H
21	OH	H	H	H
22	H	OH	H	H
23	H	OH	Me	H
24	H	OH	Me	Me
25	=O		Me	H
26	=O		H	Me
27	=O		Me	Me

Can. J. Chem. Downloaded from www.nrcresearchpress.com by 210.87.254.105 on 09/05/12
For personal use only.

pounds, therefore, allow detailed comparisons for an array of substitution patterns in the bicyclo[2.2.2]octane and norbornane systems, which we wish to present in this paper.

Experimental

Materials

The parent hydrocarbons, bicyclo[2.2.2]octanone, **14** and **15** were available from an earlier study (11), which also provided the ketonic precursors for **5**, **6**, **19**, **20**, and **29**, prepared by reduction with lithium aluminum hydride in ether. In each case a single crystalline alcohol was obtained and each exhibited the expected infrared and proton spectra. Alcohol **5** had mp 205–206 °C (lit. (12) mp 210–212 °C); the physical constants and analytical data for the four new alcohols are listed in Table 1. Mixtures of the following isomeric pairs: **12,13**; **28,31**, and **30,32** were also obtained by $LiAlH_4$ reduction of the appropriate ketones, available from our earlier study (11). Column chromatography on alumina served to separate **28** from **31** and a pure sample of **32** crystallized from the mixture of **30** and **32**; analytical data for the new, pure alcohols are given in Table 1. Reduction of 6-methylbicyclo[2.2.2]oct-2-en-5-one (11) with $LiAlH_4$ followed by hydrogenation in ether using a PtO_2 catalyst furnished a 2:3 mixture of **17** and **18**. Wolff–Kishner reduction of 6,6-dimethylbicyclo[2.2.2]oct-2-en-5-one gave **11** which was hydrogenated over PtO_2 in ether to **2** (13).

Following the procedure described by Russell *et al.* (14) from 1,3-cyclohexadiene and maleic anhydride, olefin **10**, alcohol **21**, and ketone **16** were generated. Reduction of **16** with $LiAlH_4$ furnished a sample of **22**, the physical and

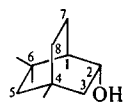

20

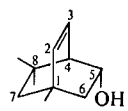

29

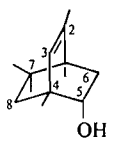

30

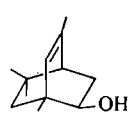

32

analytical data for which are listed in Table 1. The initial adduct was also converted to the *cis*-diethyl ester with $EtOH–HC(OEt)_3$ and isomerized to the *trans*-diethyl ester by refluxing with NaOEt–EtOH. Then with the same sequence used to generate olefin **10**, the *trans*-ester was converted to **9** and subsequently hydrogenated to **3**; hydrogenation of **10** gave **4**. Hydrocarbons **3**, **4**, **9**, and **10** had physical properties closely agreeing with those reported by Petit *et al.* (13) and, as a further check on their identities, precise mass determinations were obtained (Table 1). An analogous approach was employed to prepare **1**, **7**, and **8**. The Diels–Alder reaction of 1,3-cyclohexadiene with acryloyl chloride gave a mixture from which bicyclo[2.2.2]oct-2-ene-*endo*-5-carboxylic acid was isolated (15) after hydrolysis. This acid was reduced to the hydroxymethyl derivative, converted to the tosylate, and then to olefin **8** using the sequence described by Russell *et al.* (14). Hydrogenation over PtO_2 gave **1**. Esterification of the *endo*-acid followed by base-catalyzed equilibration to a mixture of *exo* and *endo* ethyl esters which was taken through the same sequence: $—COOEt \rightarrow —CH_2OH \rightarrow —CH_2OTs \rightarrow —CH_3$ furnished a mixture of **7** and **8**. These three hydrocarbons, **1**, **7**, and **8**, have been reported by Kazanskii and Svirskaya (16).

Ketone **16** was methylated using methyl iodide–sodium amide in ether as described by Corey *et al.* (17) to give a mixture containing 47% of **25**, 3% of **26**, and 37% of **27**. These ketones were separated from unreacted **16** (13%) by gc on a 20% SE 30 column and characterized by precise mass determinations (Table 1). Treatment of **25** and **27** with $LiAlH_4$ in ether gave **23** and **24**, respectively, as the sole products, each as a crystalline solid; their physical and analytical data are listed in Table 1.

All of the compounds **1–32** exhibited the expected infrared and proton spectra. The physical data for those previously reported were in good agreement with the literature values while the data for the new compounds are collected in Table 1.

Nuclear Magnetic Resonance Spectra

Proton and ^{13}C spectra were obtained with Varian T-60, HA-100, and XL-100-15 instruments. The latter was used in the Fourier transform mode with proton noise decoupling for ^{13}C spectra. Off-resonance decoupled ^{13}C spectra were recorded to distinguish carbon types. All compounds were examined in $CDCl_3$ solutions (10–15%) with TMS as an internal reference.

Results and Discussion

The observed shieldings for the hydrocarbons, parent alcohols, and ketones included in this series as model compounds are listed in Table 2, while the data for the more highly substituted compounds are given in Table 3. The results for bicyclo[2.2.2]octane, -octene, -octanone, and the 3-methyl and 3,3-dimethyl derivatives of the latter (**14** and **15**, respectively) were reported previously (11) but the earlier methylene shielding for bicyclooctane was printed incorrectly. The assignments shown in Table 2 were aided by off-resonance decoupled spectra which permitted the distinction of primary, secondary, tertiary, and quaternary carbon signals. Carbonyl, olefinic, and carbinyl carbon absorptions were readily assigned from their characteristic positions and a general knowledge of the relative magnitudes of the effects of methyl groups on the shieldings of neighboring carbons, as established for other closely related systems (1), led to the listed assignments for the remaining nuclei. The overall fit of the data with similar shifts for the corresponding carbons in different compounds offers

Can. J. Chem. Downloaded from www.nrcresearchpress.com by 210.87.254.105 on 09/05/12
For personal use only.

TABLE 1. Physical and analytical data for several bicyclo[2.2.2]octanes

Compound	mp (°C)	Molecular formula	Analysis* Calculated C	Calculated H	Observed C	Observed H	Compound	mp (°C)	Molecular formula	Precise mass determination‡ Calculated	Observed
6	85.5–86.5	$C_9H_{16}O$	77.09	11.50	76.97	11.71	**19**	141–142	$C_{10}H_{18}O$	154.1355	154.1353
20	59–60	$C_{11}H_{20}O$	78.51	11.98	78.85	12.19	**23**	65.0–65.5	$C_{11}H_{20}O$	168.1513	168.1522
22	103–104	$C_{10}H_{18}O$	77.87	11.76	78.17	11.77	**24**	59.0–59.5	$C_{12}H_{22}O$	182.1670	182.1672
25	171–172†	$C_{11}H_{18}O$	79.46	10.91	79.24	11.00	**26**		$C_{11}H_{18}O$	166.1357	166.1363
29	52–53	$C_{11}H_{18}O$	79.46	10.91	79.26	10.93	**27**		$C_{12}H_{20}O$	180.1513	180.1511
30	59–61	$C_{12}H_{20}O$	79.94	11.18	79.39	11.21	**28**		$C_{10}H_{16}O$	152.1201	152.1198
							3		$C_{10}H_{18}$	138.1408	138.1409
							4		$C_{10}H_{18}$	138.1408	138.1404
							9		$C_{10}H_{16}$	136.1251	136.1245
							10		$C_{10}H_{16}$	136.1251	136.1253

*Elemental analyses were performed by Chemalytics, Inc., Tempe, Arizona.
†Melting point of the 3,5-dinitrophenylhydrazone.
‡High resolution mass spectra obtained with a Varian M66 instrument, averaging ten separate measurements of m/e for the molecular ion.

Can. J. Chem. Downloaded from www.nrcresearchpress.com by 210.87.254.105 on 09/05/12
For personal use only.

TABLE 2. ^{13}C shieldings* of several bicyclo[2.2.2]octane derivatives

Compound	Substitution	C-1	C-2	C-3	C-4	C-5†	C-6†	C-7	C-8	Methyl	
Bicyclooctane		24.0	26.1	26.1	24.0	26.1	26.1	26.1	26.1		
1	2-Me	30.4	30.4	35.8	25.2	26.2	20.4	27.5	25.2		21.2
		(6.4)	(4.3)	(9.7)	(1.2)	(0.1)	(−5.7)	(1.4)	(−0.9)		
2	2,2-Me_2	35.1	30.6	42.7	26.5	25.1	23.4	23.4	25.1		30.9
		(11.1)	(4.5)	(16.6)	(2.5)	(−1.0)	(−2.7)	(−2.7)	(−1.0)		
3	*trans*-2,3-Me_2	31.5	40.1	40.1	31.5	27.5	20.2	27.5	20.2		19.2
		(7.5)	(14.0)	(14.0)	(7.5)	(1.4)	(−5.9)	(1.4)	(−5.9)		(−2.0)
4	*cis*-2,3-Me_2	31.8	33.3	33.3	31.8	20.3	20.3	27.4	27.4		15.2
		(7.8)	(7.2)	(7.2)	(7.8)	(−5.8)	(−5.8)	(1.3)	(1.3)		(−6.0)
5	2-OH	31.7	69.5	37.5	24.8	25.6	18.6	23.8	24.5		
		(7.7)	(43.4)	(11.4)	(0.8)	(−0.5)	(−7.5)	(−2.3)	(−1.6)		
6	4-Me-2-OH	31.7	69.8	44.5	28.6	32.8	19.4	24.2	32.0		28.0
		(0.0)‡	(0.3)‡	(7.0)‡	(3.8)‡	(7.2)‡	(0.8)‡	(0.4)‡	(7.5)‡		
Bicyclooctene		29.5	134.1	134.1	29.5	25.8	25.8	25.8	25.8		
7	*exo*-5-Me	30.8	132.9	136.4	36.0	30.4	34.9	26.4	18.9		20.5
		(1.3)	(−1.2)	(2.3)	(6.5)	(4.6)	(9.1)	(0.6)	(−6.9)		
8	*endo*-5-Me	30.5	134.1	132.0	36.8	32.2	36.0	24.3	26.6		23.0
		(1.0)	(0.0)	(−2.1)	(7.3)	(6.4)	(10.2)	(−1.5)	(0.8)		
9	*endo*-5-*exo*-6-Me_2	36.6	136.3	131.5	37.4	41.5	40.8	17.7	27.0	18.6 (*exo*)	22.2 (*endo*)
		(7.1)	(2.2)	(−2.6)	(7.9)	(15.7)	(15.0)	(−8.1)	(1.2)	(−1.9)	(−0.8)
10	*endo*-5-*endo*-6-Me_2	38.5	132.9	132.9	38.5	36.6	36.6	26.0	26.0		17.1
		(9.0)	(−1.2)	(−1.2)	(9.0)	(10.8)	(10.8)	(0.2)	(0.2)		(−5.9)
11	5,5-Me_2	31.5	131.9	136.0	41.7	33.3	42.8	23.7	21.8		30.1 (*exo*)
		(2.0)	(−2.2)	(1.9)	(12.2)	(7.5)	(17.0)	(−2.1)	(−4.0)		32.1 (*endo*)
12	*exo*-5-OH	30.1	135.2	132.0	37.6	68.8	35.4	26.1	17.3		
		(0.6)	(1.1)	(−2.1)	(8.1)	(43.0)	(9.6)	(0.3)	(−8.5)		
13	*endo*-5-OH	30.1	135.9	129.9	37.6	70.2	38.9	24.1	22.1		
		(0.6)	(1.8)	(−4.2)	(8.1)	(44.4)	(13.1)	(−1.7)	(−3.7)		
Bicyclooctanone		42.3	216.7	44.6	27.9	24.8	23.4	23.4	24.8		
14	3-Me	42.3	220.1	47.2	33.9	20.2	24.2	22.7	26.1		13.5
		(0.0)	(3.4)	(2.6)	(6.0)	(−4.6)	(0.8)	(−0.7)	(1.3)		
15	3,3-Me_2	42.7	221.9	45.9	38.5	22.4	23.5	23.5	22.4		23.7
		(0.4)	(5.2)	(1.3)	(10.6)	(−2.4)	(0.1)	(0.1)	(−2.4)		
16	*endo*-5-*endo*-6-Me_2	50.7	216.8	39.8	35.5	32.7	34.6	23.5	26.3		14.9 (5-Me)
		(8.4)	(0.1)	(−4.8)	(7.6)	(7.9)	(11.2)	(0.1)	(1.5)		16.4 (6-Me)

*In ppm from internal TMS for $CDCl_3$ solutions; values in parentheses are the substituent effects $\Delta\delta = \delta_c(RX) - \delta_c(RH)$ where RH is the appropriate parent compound.
†These are *syn* with respect to the 2-substituent in the bicyclooctanes and to the 3-substituent in the bicyclooctanones.
‡Substituent effect of the 4-methyl group, *i.e.* $\delta_c(6) - \delta_c(5)$.

Can. J. Chem. Downloaded from www.nrcresearchpress.com by 210.87.254.105 on 09/05/12
For personal use only.

TABLE 3. ^{13}C shieldings* of some polysubstituted bicyclo[2.2.2]octane derivatives

Parent	Compound	Substitution	C-1	C-2	C-3	C-4	C-5	C-6	C-7	C-8	Methyl		
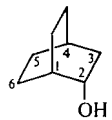	**17**	*trans*-3-Me	32.9 (0.0)	78.1 (−1.1)	41.8 (0.0)	31.3 (0.1)	27.1 (0.1)	18.4 (0.7)	24.1 (0.2)	19.7 (0.9)		18.6 (−2.6)	
	18	*cis*-3-Me	31.8 (−1.1)	70.9 (−8.3)	35.8 (−6.0)	31.3 (0.1)	20.2 (0.3)	18.6 (−0.1)	23.7 (0.8)	26.5 (0.6)		12.8 (−8.4)	
	19	3,3-Me_2	33.7 (−0.5)	77.9 (−8.2)	35.9 (−6.1)	36.5 (0.6)	22.7 (0.1)	17.7 (−0.2)	24.4 (1.6)	22.5 (0.7)	22.4 (*cis*) (−8.5)	29.9 (*trans*) (−1.0)	
	20	4,6,6-Me_3	43.0 (0.2)	72.8 (5.7)	43.4 (−0.1)	31.0 (−0.1)	50.1 (0.4)	30.7 (6.2)	22.5 (0.6)	30.6 (−0.1)	27.9 (4-Me) (−0.1)	32.3 (1.4)	32.5 (1.6)
	21	*anti,cis*-5,6-Me_2	40.1 (0.6)	65.0 (1.3)	32.3 (0.6)	32.7 (0.1)	33.1 (1.4)	32.9 (1.9)	19.9 (0.0)	27.1 (0.2)	15.4 (5-Me) (0.2)	14.6 (6-Me) (−0.6)	
	22	*syn,cis*-5,6-Me_2	39.1 (−0.4)	71.4 (7.7)	31.6 (−0.1)	32.7 (0.1)	33.1 (0.3)	33.3 (7.5)	25.8 (0.7)	26.4 (0.6)	14.8 (5-Me) (−0.4)	17.7 (6-Me) (2.5)	
	23	*trans*-3-*syn,cis*-5,6-Me_3	40.2 (−0.5)	79.6 (6.2)	34.9 (−1.1)	39.7 (0.7)	34.0 (−0.2)	33.5 (8.6)	26.8 (1.6)	21.0 (0.9)	14.6 (5-Me) (−0.6)	17.6 (6-Me) (2.4)	18.3 (3-Me) (−2.9)
	24	3,3-*syn,cis*-5,6-Me_4	40.6 (−1.4)	80.2 (−0.1)	37.1 (0.1)	43.9 (0.2)	36.2 (6.1)	32.8 (8.0)	26.8 (2.7)	25.8 (2.7)	18.6 (5-Me) (3.4)	17.5 (6-Me) (2.3)	25.0 (*cis*-3-Me) (−5.9) 32.8 (*trans*-3-Me) (1.9)
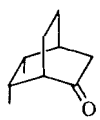	**25**	*anti*-3-*endo,cis*-5,6-Me_3	51.0 (0.3)	219.6 (−0.6)	42.0 (−0.4)	41.2 (−0.3)	33.5 (−0.5)	34.1 (0.2)	24.6 (0.3)	21.8 (0.1)	14.9 (5-Me) (0.0)	16.8 (6-Me) (0.4)	13.1 (3-Me) (−0.4)
	26	*syn*-3-*endo,cis*-5,6-Me_3	50.2 (−0.5)	220.3 (0.1)	47.6 (5.2)	41.7 (0.2)	34.5 (6.4)	36.3 (0.9)	22.6 (−0.2)	29.2 (1.6)	16.3 (5-Me) (1.4)	16.9 (6-Me) (0.5)	15.4 (3-Me) (1.9)
	27	3,3-*endo,cis*-5,6-Me_4	51.1 (0.0)	221.3 (0.7)	46.1 (5.0)	46.1 (0.0)	36.1 (5.8)	35.5 (0.8)	23.0 (−0.6)	26.0 (2.1)	13.2 (5-Me) (3.3)	16.8 (6-Me) (0.4)	25.6 (*exo*-3-Me) (1.9) 27.3 (*endo*-3-Me) (3.6)
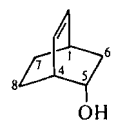	**28**	6,6-Me_2	42.6 (0.3)	136.4 (−0.7)	130.1 (0.3)	39.2 (−0.4)	76.7 (−9.1)	35.1 (−7.8)	21.9 (−0.2)	14.9 (−0.3)	22.7 (*exo*) (−7.4)	32.5 (*endo*) (0.4)	
	29	1,8,8-Me_3	35.4	136.8	133.4	49.9	72.9	40.5	51.5	34.7	25.0 (1-Me)	31.8 (*exo*) (1.7)	33.3 (*endo*) (1.2)
	30	2,4,7,7-Me_4	48.2	145.3	127.6	40.3	73.3	32.2	34.5	41.2	21.8 (4-Me) (−3.2) 21.9 (2-Me)	28.3 (*exo*) (−1.8)	31.5 (*endo*) (−0.6)
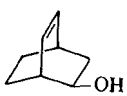	**31**	6,6-Me_2	43.3 (1.0)	138.7 (0.9)	127.9 (0.2)	39.9 (0.3)	79.9 (−7.3)	40.1 (−6.3)	21.7 (1.6)	20.9 (0.9)	29.7 (*exo*) (−0.4)	24.5 (*endo*) (−7.6)	
	32	2,4,7,7-Me_4	48.3	145.6	124.6	41.0	74.6	35.7	34.3	47.9	21.6 (4-Me) (−3.4) 21.9 (2-Me)	29.3 (*exo*) (−0.8)	30.9 (*endo*) (−1.2)

*In ppm from internal TMS for $CDCl_3$ solutions. For the skeletal carbons the values in parentheses are the deviations ($\delta_c^{obsd} - \delta_c^{calc}$) where δ_c^{calc} was obtained assuming additivity of substituent effects from Table 1. For the methyl carbons the parenthetic values are substituent effects $\Delta\delta = \delta_c(R(Me)X) - \delta_c(R(Me)H)$.

Can. J. Chem. Downloaded from www.nrcresearchpress.com by 210.87.254.105 on 09/05/12
For personal use only.

strong support for these assignments. Unequivocal assignments for the skeletal carbons of **16** were obtained from the characteristic effects of deuterium (*1b*) in the spectrum of **16**-3,3-d_2.

The shielding data in Table 2 permit one to generate a set of shielding effects for this array of substituents; these values are given in parentheses in Table 2. The trends are quite normal with carbons one and two bonds from the substituent deshielded (the α and β effects) and vicinal carbons shielded if *gauche* with respect to the substituent. For the latter the effects are more pronounced for sp^3 carbons than for sp^2 carbons. For example, the *endo*-methyl in **8** shields the nearer olefinic carbon (C-3) by -2.1 ppm, while the *exo*-methyl (**7**) shields the *gauche* methylene carbon (C-8) by -6.9 ppm. The through-space interactions in these two cases differ significantly in that the former involves the methyl group and the π cloud of the double bond, while in the latter the methyl group and the *endo*-proton are close neighbors. A similar difference is apparent for alcohols **12** and **13**, in **13** the *endo*-hydroxyl shields the *gauche* olefinic carbon by -4.2 ppm while in **12** the *exo*-hydroxyl shields the *gauche* methylene carbon by -8.5 ppm. It may be noted that the *anti* periplanar vicinal carbon in each of these cases is also shielded relative to its value for bicyclooctene; in **13**, C-8 is shielded by -3.7 ppm while in **12** C-3 is shifted -2.1 ppm. Similar shifts have been noted and discussed for a variety of substituents (3). The effects of methyl–methyl interactions are also included in Table 2 for a few derivatives. For **3** and **9** vicinal methyl groups subtending a dihedral angle of $\sim 120°$ are shielded by -2 ppm from the positions found for the monomethyl compounds, while for **4** and **10**, eclipsed methyl carbons are more strongly shielded (-6 ppm). These shifts are comparable to the values found for the corresponding bicyclo[2.2.1]heptane systems (*1b*) indicating that 'ring strain' has little effect on these shieldings. In fact, the methyl substituent effects in these two bicyclic systems are closely similar, comparing the observed shifts for the carbons in the 6-membered ring in the bicycloheptanes with those for the bicyclooctanes. It is interesting, however, that γ *gauche* effects of a 2-methyl and a 2-hydroxyl group at C-6 are somewhat more shielding by ~ -2 ppm in the bicycloheptane cases. Also these substituents tend to deshield the more remote olefinic carbon in the bicycloheptenes more strongly than in the bicyclooctenes. For example, the 2-hydroxyl group deshields this olefinic centre by ~ 5 ppm in the norbornenols while the corresponding shifts for the bicyclooctenols are < 2 ppm. In these derivatives the carbinyl carbon is significantly less shielded (~ 4 ppm) in the norbornenols. Otherwise, the methyl and hydroxyl substituent effects are comparable for both bicyclic systems with shifts generally within < 1 ppm for the corresponding carbons. Included in Table 2 are values obtained for bridgehead methyl substitution by comparing the shieldings of **5** and **6**. These shifts clearly emphasize the presence of minor perturbations contributing to the shielding of a given carbon atom since similarly disposed carbons are not equally affected by the bridgehead methyl. The three β carbons (C-3, -5, and -8) in **6** exhibit shifts of 7.0, 7.5, and 7.2 ppm, respectively, while the three γ carbons are shifted by 0.3 (C-2), 0.4 (C-6), and 0.8 ppm (C-7). Although these variations are not readily explained but are presumably due to minor alterations in the effects of the hydroxyl group, these data indicate the 'precision' one may expect for a comparison of observed shieldings with those predicted by simple additivity of substituent effects. The α-effect of the bridgehead methyl in the bicyclooctane skeleton is 3.5 ppm smaller than that for the bicycloheptane system (*1c*). The γ and δ effects are also attenuated by ~ 1 ppm in the former case while the β effects are similar for both systems. Interestingly, methyl substitution in isobutane $\rightarrow$ neopentane causes shifts comparable to those for the bicyclooctane system, namely, α and β effects of 2.7 and 7.2 ppm, respectively (18). Hence, it appears that ring strain in the bicyclo[2.2.1]heptane skeleton may accentuate the α effect of bridgehead substitution.

One may compare the shieldings for **3**, **4**, **9**, and **10** with values predicted by assuming additivity of the effects of the individual methyl groups as given by the data for **1**, **7**, and **8**. For **3** and **9** whose vicinal methyl groups subtend a dihedral angle near 120°, the deviations between the observed and predicted shieldings tend to be small, < 0.7 ppm, with the exception of C-3 in **9** for which the difference is 1.1 ppm. Thus, it is apparent that additivity works well. For **4** and **10**, similar agreement is found for the skeletal carbons, except for those bearing the eclipsed methyl groups which absorb 6.8 and 5.8 ppm.

Can. J. Chem. Downloaded from www.nrcresearchpress.com by 210.87.254.105 on 09/05/12
For personal use only.

respectively, upfield from the predicted positions. This behavior is typical for carbons in a fragment having an eclipsed γ interaction of the terminal groups. These deviations are comparable to those found for the corresponding bicyclo[2.2.1]heptanes and -heptenes (1*b*). Additional examples are included in Table 3 in which the γ interactions occur between methyl and hydroxyl groups. The deviations between observed and predicted shieldings, $\delta_c^{obsd} - \delta_c^{calc}$, are given in parentheses and a negative value indicates that a carbon is more highly shielded than additivity predicts. Eclipsed γ interactions occur in **18**, **19**, **28**, and **31** and inspection of the skeletal carbon data reveals that negative deviations in the range 6–9 ppm are found for the carbons bearing the hydroxyl and methyl groups while the remaining carbons absorb close to the predicted positions. It may also be noted that the eclipsed methyl carbons exhibit upfield shifts of 7–8 ppm. In contrast, the deviations are small for **17** in which the dihedral angle between the hydroxyl and methyl groups is ~120°, but the methyl group is slightly shielded, exhibiting a shift comparable to those for **3** and **9**. Clearly these trends are entirely analogous, both qualitatively and quantitatively, to those found for a variety of corresponding norbornane derivatives (1).

Most of the remaining examples in Table 3 were selected to examine δ effects produced by interactions between substituents separated by four bonds. To identify these effects in **21**–**24** we have employed the shifts caused by vicinal methyl substitution as listed in Table 2 for **4**; in this way, the contributions arising from the vicinal interactions are taken into account and the deviations between observed and predicted shieldings may be ascribed to δ interactions. For ketones **25**–**27**, **16** was taken as the parent compound for the same reason. The data for a variety of norbornanols (1*c*) showed that interactions between δ substituents in *syn*-axial orientations, or the equivalent, led to pronounced deshielding of the carbons bearing the substituents which themselves were somewhat deshielded. For other orientations of δ substituents the observed shieldings were predicted satisfactorily by simple additivity. On this basis, of the examples in Table 3, **21** and **25** would be expected to show reasonable agreement between the observed and predicted values while **20**, **22**, **23**, **26**, and **27**, which have one *syn*-axial interaction should show marked deviations similar to those found for the bicyclo[2.2.1]heptane system. This is indeed the case. The deviations for **25** are <0.6 ppm and, although the deviations are somewhat larger for the substituted carbons in **21** none exceeds 2 ppm. It seems reasonable to suggest that the 1.3–1.9 ppm differences for the substituted carbons may arise from a conformational change with skeletal twisting different from that in **4** and **5**, the compounds from which the individual substituent effects were derived. In any event, much more distinctive deviations are apparent for the second group of compounds. Ketones **26** and **27** exhibit differences of 5.0–6.4 ppm for C-3 and C-5, the carbons bearing the *syn*-axial methyl groups, and these methyl carbons are also deshielded. It is interesting that the more highly substituted **27** has the more deshielded methyl carbon. Also, both geminal methyl carbons are deshielded. This behavior is entirely analogous to that found in the norbornane series (1*c*). Similar trends are apparent for alcohols **20**, **22**, and **23** for which C-2 and C-6, bearing the *syn*-axial hydroxyl and methyl groups, are deshielded by 5.7–8.6 ppm from the values predicted by simple additivity. Their 6-methyl carbons also show downfield shifts. For each of these five compounds, the remaining deviations are generally small.

The deviations found for C-5 and C-6 in **24** are large, 6.1 and 8.0 ppm, while those for C-2 and C-3 are very small, ± 0.1 ppm, but each of these carbons bears a substituent involved in a *syn*-axial interaction. For C-2 and C-3, however, their substituents are mutually eclipsed and the resulting γ effect will essentially cancel the downfield shift produced by the *syn*-axial interaction with the 5- and 6-methyl groups. If, instead, the shieldings for **24** are compared with those obtained from the substituent effects of the vicinal 5,6-methyls (from **4**) combined with the data for **19**, deviations of 8.1, 7.0, 6.3, and 7.9 ppm are obtained for C-2, -3, -5, and -6, respectively. Viewed in this manner, the effects of the vicinal interactions are taken into account without masking the δ effects, as was done above for the previous examples. The deviations for C-7 and C-8 become 2.0 and 1.1 ppm, respectively, somewhat less than those from the first analysis (Table 3); these may have a conformational origin arising from a different skeletal twist in the more highly substituted **24**. Although we lack the

Can. J. Chem. Downloaded from www.nrcresearchpress.com by 210.87.254.105 on 09/05/12
For personal use only.

substituent effects of bridgehead methyl substitution in bicyclo[2.2.2]octene, it may be assumed that the γ and δ carbons are not appreciably affected, by analogy with the effects in bicyclooctane noted above. Combining the substituent effects from **11** with the data for **12**, we find deviations of 8.1 and 9.9 ppm for C-5 and C-8, respectively, in **29** and the methyl carbons are slightly deshielded relative to those in **11**.

Finally, a comparison of the shieldings of **30** and **32** shows that the differences are entirely analogous to those between **12** and **13** indicating that 5- and 7-substituents on the same side of the ring system introduce no appreciable perturbations on the individual effects of these substituents. It may be noted, however, that the geminal methyl carbons are slightly shielded. This pattern is identical to that found for the corresponding norbornanols such as *endo*-5-methyl-*endo*-2-norbornanol. The upfield shift exhibited by the bridgehead methyl, relative to the corresponding centre in **29**, is a result of the vicinal interaction with the hydroxyl group, since these have a nominal dihedral angle of 60°.

In summary, the marked deshielding effects apparently arising from steric interactions of closely neighboring substituents in *syn*-axial orientations are similar in the bicyclo[2.2.1]heptane and bicyclo[2.2.2]octane systems, although for the latter the effects are slightly smaller. The most striking differences are found for the carbons bearing the δ substituents while significant, but much smaller, downfield shifts are found for the terminal carbons in a *syn*-axial δ fragment. These trends contrast directly with those found for closely neighboring vicinal substituents for which each carbon in the γ fragment is appreciably shielded, but again the shifts are comparable in both ring systems, indicating that ring strain has little effect on these shieldings. The distinctive shifts exhibited by *syn*-axial arrangements should be helpful in the interpretation of spectra of more complex systems, since the trends appear to be general.

Acknowledgements

We are grateful to the National Research Council of Canada for financial support. We wish to thank Dr. A. K. Cheng for a sample of **11**, K. R. Stephens for samples of **6**, **20–22**, **29**, and **30**, Robert Lazier for mass spectrometric determinations and Ms. J. L. Gough, C. Ferriera, and Inara Grikis for technical assistance.

1. (*a*) S. H. Grover, D. H. Marr, J. B. Stothers, and C. T. Tan. Can. J. Chem. **53**, 1351 (1975); (*b*) J. B. Stothers, C. T. Tan, and K. C. Teo. Can. J. Chem. **51**, 2893 (1973); (*c*) Can. J. Chem. In press.
2. N. K. Wilson and J. B. Stothers. *In* Topics in stereochemistry. Vol. 8. *Edited by* E. L. Eliel and N. L. Allinger. Wiley-Interscience, New York. 1974. Chap. 1.
3. E. L. Eliel, W. F. Bailey, L. D. Kopp, R. L. Willer, D. M. Grant, R. Bertrand, K. A. Christensen, D. K. Dalling, M. W. Duch, E. Wenkert, F. M. Schell, and D. W. Cochran. J. Am. Chem. Soc. **97**, 322 (1975).
4. S. H. Grover, J. P. Guthrie, J. B. Stothers, and C. T. Tan. J. Magn. Reson. **10**, 227 (1973).
5. J. B. Stothers, C. T. Tan, and K. C. Teo. J. Magn. Reson. **20**, 570 (1975).
6. G. C. Levy and G. L. Nelson. ^{13}C nuclear magnetic resonance for organic chemists. Wiley-Interscience, New York. 1972; J. B. Stothers. ^{13}C N.M.R. spectroscopy. Academic Press, New York. 1972; E. Breitmaier and W. Voelter. ^{13}C N.M.R. spectroscopy. Verlag Chemie, Weinheim. 1974.
7. E. M. Engler, J. D. Andose, and P. Von R. Schleyer. J. Am. Chem. Soc. **95**, 8005 (1973); R. H. Boyd, S. N. Sanwal, S. Shary-Tehrany, and D. McNally. J. Phys. Chem. **75**, 1264 (1971).
8. G. J. Gleicher and P. Von R. Schleyer. J. Am. Chem. Soc. **89**, 582 (1967), and references cited therein.
9. A. Yokozeki, K. Kuchitsu, and Y. Morino. Bull Chem. Soc. Jpn. **43**, 2017 (1970).
10. C. Altona and M. Sundaralingam. J. Am. Chem. Soc. **92**, 1995 (1970).
11. K. R. Stephens, J. B. Stothers, and C. T. Tan. *In* Mass spectrometry and N.M.R. spectroscopy in pesticide chemistry. *Edited by* R. Haque and J. F. Biros. Plenum Press, New York. 1974. pp. 179–196.
12. H. M. Walborsky and D. F. Loncrine. J. Am. Chem. Soc. **76**, 5396 (1954).
13. F. Petit, M. Pecque, and M. Blanchard. Bull. Soc. Chim. Fr. 747 (1972).
14. G. A. Russell, G. W. Holland, and C.-Y. Chang. J. Am. Chem. Soc. **89**, 6629 (1967).
15. W. R. Boehme, E. Schipper, W. G. Scharpf, and J. Nichols. J. Am. Chem. Soc. **80**, 5488 (1958).
16. B. A. Kazanskii and P. I. Svirskaya. Zh. Obsch. Khim. **29**, 2584 (1959).
17. E. J. Corey, R. Hartmann, and R. A. Vataken-cherry. J. Am. Chem. Soc. **84**, 2611 (1962).
18. D. M. Grant and E. G. Paul. J. Am. Chem. Soc. **86**, 2984 (1964).
19. D. H. Hunter, R. E. Klinck, R. P. Steiner, and J. B. Stothers. Can. J. Chem. In press.

Use of polymers as protecting groups in organic synthesis. III. Selective functionalization of polyhydroxy alcohols[1,2]

JEAN M. J. FRÉCHET AND LUCY J. NUYENS
Department of Chemistry, University of Ottawa, Ottawa, Canada K1N 6N5

Received August 22, 1975

JEAN M. J. FRÉCHET and LUCY J. NUYENS. Can. J. Chem. **54**, 926 (1976).

Insoluble polymers containing trityl chloride residues were used to block one primary alcohol functional group of several polyhydroxy alcohols. After protecting the remaining hydroxyl groups by benzoylation, the ether linkage between the polymer and the protected alcohol was cleaved in acidic medium. Depending on the reaction conditions and the nature of the starting alcohol, several alcohols or bromides in which only one of the two primary hydroxyls had been esterified, were obtained. In some cases benzoyl migrations were observed. The trityl chloride polymers could be regenerated in one step without degradation or appreciable loss of activity.

JEAN M. J. FRÉCHET et LUCY J. NUYENS. Can. J. Chem. **54**, 926 (1976).

Des polymères insolubles contenant des unités fonctionnelles de chlorure de trityle ont été utilisés pour bloquer un des groupements alcool primaire de plusieurs polyols. Après avoir protégé les groupements hydroxyles restants par benzoylation, la liaison éther entre le polymère et l'alcool protégé a été coupée en milieu acide. Selon les conditions de la réaction et la nature du polyol initial, plusieurs alcools ou les bromures correspondants dans lesquels une seule des fonctions hydroxyles primaires était estérifiée, ont été obtenus. Dans certains cas on a observé des migrations de groupements benzoyles. Les groupements fonctionnels de chlorure de trityle des polymères peuvent être régénérés en une étape sans dégradation ou perte sensible d'activité.

Functionalized insoluble polymers for use as protecting groups or reagents in organic synthesis have been receiving considerable attention since Merrifield (1) first reported the synthesis of a polypeptide using a polymer support. Thus, various cross-linked polystyrene resins were used in the synthesis of selectively monosubstituted derivatives of symmetrical molecules (2, 3) or to prepare selectively substituted derivatives of D-glucose (4–6). The advantages and the uses of polymeric reagents and protecting groups have been recently summarized by Leznoff (7). We now wish to report on the use of a polymer containing trityl chloride pendant groups, **1**, for the synthesis of selectively substituted derivatives of several polyhydroxy alcohols. The polymeric trityl chloride reagent should have most of the advantages of its monomeric counterpart (8), namely its reactivity and selectivity for primary *vs.* secondary or tertiary hydroxyl groups, and the ease of cleavage of the corresponding trityl ethers in acidic medium. In addition the polymeric reagent should behave as a dilute reagent and react with only one end of a molecule containing several primary hydroxyl groups. The insolubility of the reagent will also facilitate the separation of all products and intermediates while the reagent itself should be easily regenerable in one step after use. In some instances the steric bulk of the polymer may also be expected to be the source of some selectivity.

Results and Discussion

In a typical synthetic procedure (Scheme 1) a polyhydroxy alcohol (**2**–**8**) is allowed to react with resin **1** to give a resin (**2***a*–**8***a*) in which one of the primary alcohol functional groups of the starting alcohol is attached to the polymeric support through an ether linkage. Without further purification, the remaining hydroxyl groups are protected by esterification with benzoyl chloride. Cleavage of the ether linkage of the resin (**2***b*–**8***b*) in acidic medium yields a product (**2** *c*–*e*, **8** *c*–*e*) in which selective functionalization has been achieved, and also a resin **1***a* from which the polymeric reagent **1** can be regenerated in one step.

The Polymeric Reagent

The synthesis of the polymeric trityl chloride reagent **1** was achieved by chemical modification

[1]Presented in part before the 170th National Meeting of the American Chemical Society, Chicago, Illinois, August 1975.

[2]For part II see ref. 6.

Can. J. Chem. Downloaded from www.nrcresearchpress.com by 210.87.254.42 on 09/05/12
For personal use only.

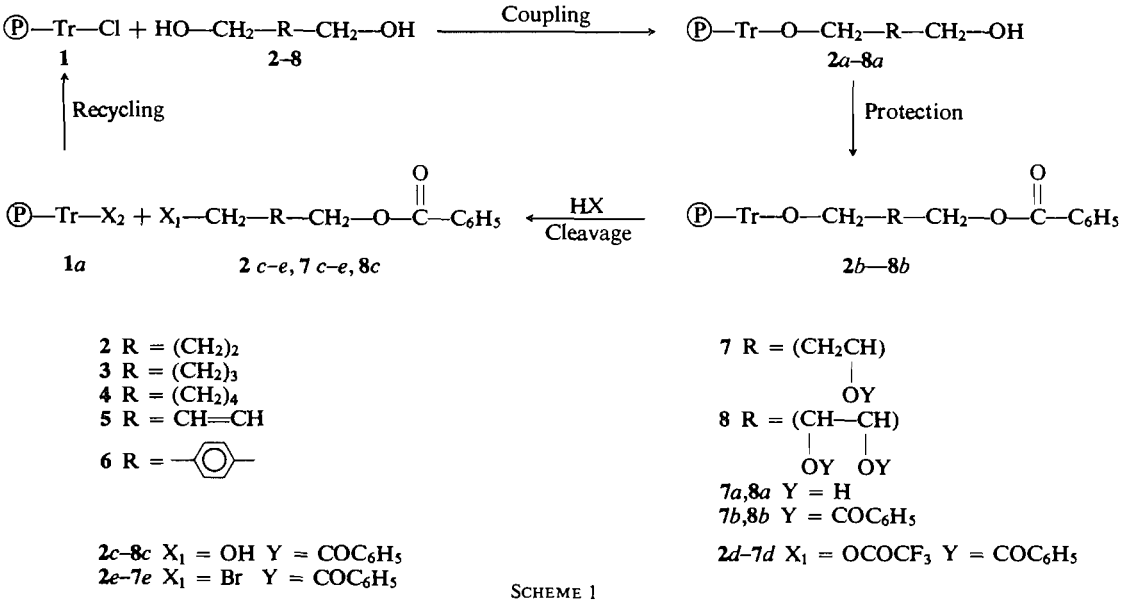

SCHEME 1

(6) of commercially available styrene–divinylbenzene copolymers. Two types of copolymers were tested in this research; one was a rigid macroreticular resin of well defined pore size which does not swell in organic solvents and which can be used in almost any type of solvent, while the second was a copolymer containing 1% divinylbenzene which can only be used at peak efficiency in solvents with good swelling properties such as aromatic solvents, chlorinated hydrocarbons, dioxane, tetrahydrofuran, etc.

In both cases **1** was prepared by benzoylation of the starting resin followed by reaction with an excess of phenylmagnesium bromide and by treatment of the resulting carbinol with acetyl chloride. As had been observed earlier (9), the macroreticular resins were found to be less reactive than their swellable counterparts and their functionalization invariably led to reagents of relatively low capacities (expressed in milliequivalents of functional group per gram). The macroreticular resins do, however, possess some advantages, mainly in their ease of filtration and lack of dependence on swelling prior to reaction, which makes them particularly useful for applications involving packed columns.

The capacities of the trityl chloride resins were estimated by chlorine analyses and found to be of the order of 0.9–2.3 mequiv. of functional group per gram for the swellable resin and of the order of 0.61–0.92 mequiv. of functional group per gram for the macroreticular resin.

Coupling of the Alcohol to the Polymer

The coupling step was carried out in dry pyridine at room temperature using a 50–100% excess of the alcohol.[3] In most cases the intermediate polymer-bound alcohols **2***a*–**8***a* were not isolated since the next step, protection of the remaining hydroxyl groups, could conveniently be carried out in pyridine. In some instances, however, the polymer-bound alcohols were isolated to estimate the yield of the coupling reaction and test the recovery procedure for the excess polyhydroxy alcohol since such recovery could be important in reactions involving rare or expensive materials.

The coupling yields, estimated from the gain in weight of the resin, were generally of the order of 75–90% based on the resin.[4] The excess unreacted alcohol could be recovered by a simple filtration and recycled. The ir spectra of the polymer-bound alcohols included strong OH and C—O absorptions in the 3400–3600 and 1000–1050 cm^{-1} regions. The remaining hydroxyl

[3]The usual reaction scale, 5 g of polymer, was sufficient to produce 1 g or more of the desired product after cleavage.

[4]Lower yields were obtained when the starting alcohols were not thoroughly dried before use.

Can. J. Chem. Downloaded from www.nrcresearchpress.com by 210.87.254.42 on 09/05/12
For personal use only.

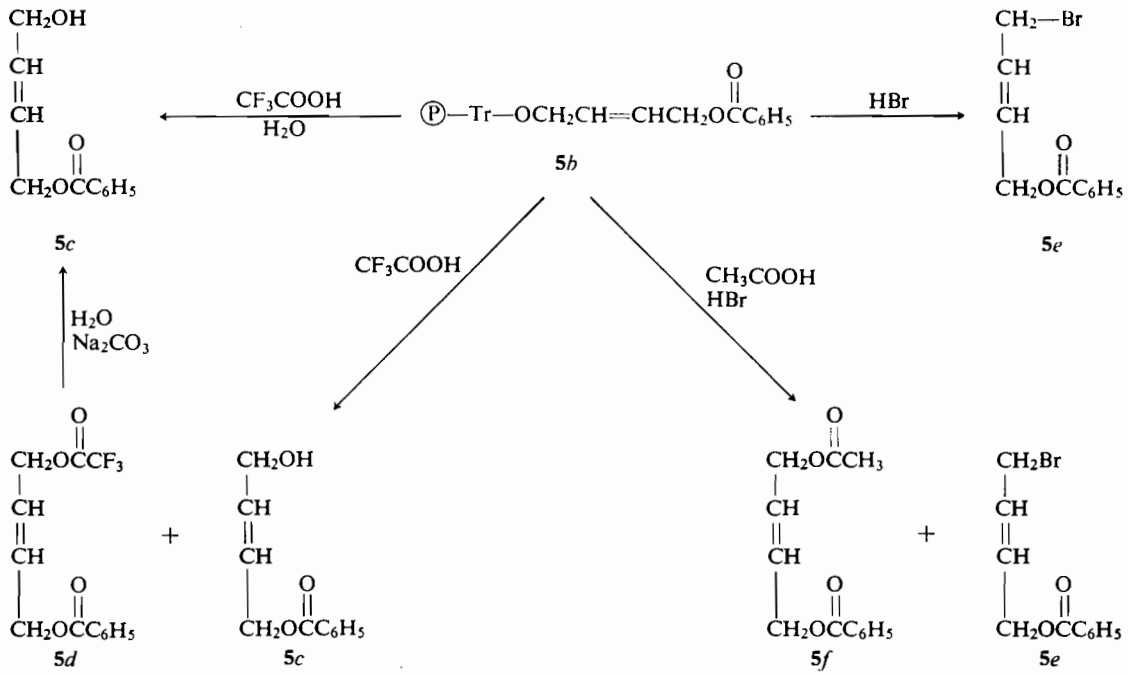

SCHEME 2

groups of **2***a*–**8***a* were protected by reaction with a large excess of benzoyl chloride in pyridine. The reaction proceeded to completion as evidenced by the lack of hydroxyl absorption in the ir spectrum while new carbonyl absorptions appeared near 1720 cm^{-1}.

Cleavage of the Protected Alcohol from its Support

Cleavage of the protected diols **2***b* and **4***b* was effected by passing a current of dry hydrogen bromide through a suspension of the resin in carbon tetrachloride. While the cleavage of normal trityl ethers requires only a very brief contact time, the polymeric trityl ethers were slightly more difficult to cleave and contact times of 10–30 min were used. Excellent yields of **2***c* and **4***c* were obtained by this procedure. For reasons which will become apparent later in this text, the cleavage of the polymeric trityl ethers with anhydrous trifluoroacetic acid was also investigated with resins **2***b*–**5***b*. In every case a mixture of alcohols **2***c*–**5***c* and of trifluoroacetate **2***d*–**5***d* (in approximately equal proportions) was obtained. The trifluoroacetyl groups, however, were quite labile and could be easily hydrolyzed. Thus, the alcohols **2***c*–**5***c* were the only products isolated when the solutions obtained after cleavage and filtration of the resin were shaken with an aqueous sodium bicarbonate solution.

While the free alcohols **2***c*–**4***c* are the products expected from such cleavage, the trifluoroacetates are not, and are probably formed from the corresponding alcohols, perhaps by transesterification with the polymeric trityl trifluoroacetate by-product of the reaction.

In contrast to the results obtained with **2***c* and **4***c*, the cleavage of ethers **5***b*–**8***b* with anhydrous hydrogen bromide did not yield the expected alcohols **5***c*–**8***c*. As can be seen in Scheme 2, the bromide **5***e* was the only product obtained in the cleavage of **5***b* with hydrogen bromide and a mixture of **5***e* and **5***f* was obtained when hydrogen bromide in acetic acid was used. Here again the free allylic alcohol **5***c* is probably produced first; it then reacts further with hydrogen bromide or hydrogen bromide – acetic acid to yield the isolated products. This reaction is interesting since **5***e* which contains three different functionalities should prove useful in a number of applications.

The benzylic ether **6***b* was found to be too

Can. J. Chem. Downloaded from www.nrcresearchpress.com by 210.87.254.42 on 09/05/12
For personal use only.

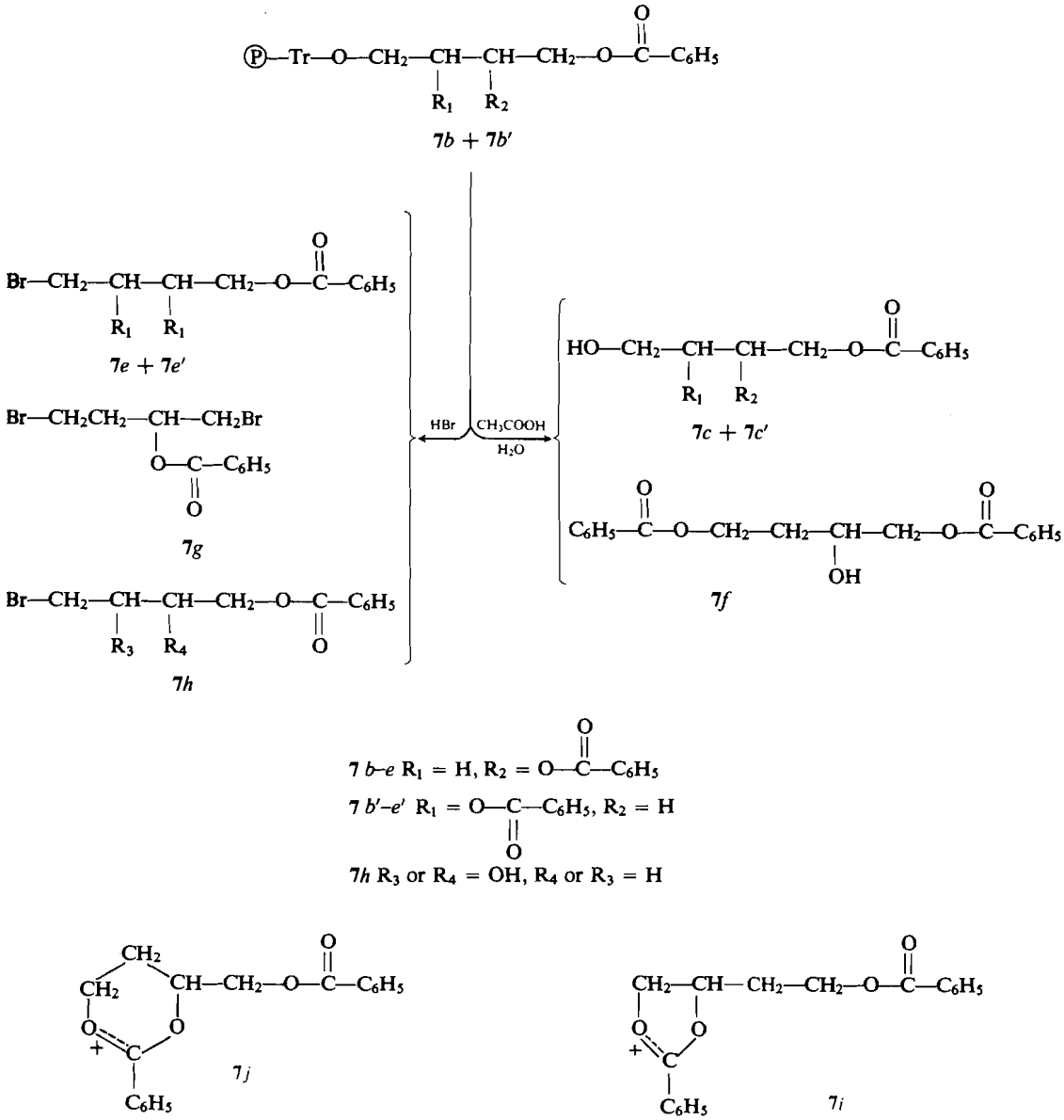

SCHEME 3

sensitive to cleavage under acidic conditions to be useful. Thus, cleavage of **6***b* with hydrogen bromide afforded only 1,4-dichloromethyl benzene and cleavage with trifluoroacetic acid gave a complex mixture of products which was not fully characterized. Better results could perhaps have been obtained by using a weaker acid such as chloroacetic acid for the cleavage.

The cleavage of 7*b* (7*b* + 7*b*′ in Scheme 3) with hydrogen bromide or trifluoroacetic acid also afforded some complex mixtures of products. This was to be expected since **7** is not a symmetrical molecule and attachment to OH-1 or to OH-4 of 1,2,4-butanetriol will lead to different products. It was hoped that due to the different steric requirements of these two primary hydroxyl groups, some selectivity would be obtained. However, difficulties in the separation of isomeric products, protecting group migrations, and other reactions subsequent to the cleavage from the

Can. J. Chem. Downloaded from www.nrcresearchpress.com by 210.87.254.42 on 09/05/12
For personal use only.

Can. J. Chem. Downloaded from www.nrcresearchpress.com by 210.87.254.42 on 09/05/12
For personal use only.

resin prevented the exact measurement of the selectivity.[5]

As indicated in Scheme 3, cleavage with trifluoroacetic acid followed by treatment with aqueous sodium bicarbonate led to a mixture of *7c*, *7c'*, and *7f*. While compounds *7c* and *7c'* (80% of the total product) are the products expected from normal coupling, the presence of *7f* in the reaction mixture could be attributed to the coupling of the polymeric reagent to the secondary hydroxyl group of **7**, which is unlikely, or to the migration of a benzoyl group from the secondary to a primary hydroxyl group. Such an intramolecular transesterification reaction could easily occur through a 5- or 6-membered ring intermediate such as *7i* or *7j*. Confirmation of this benzoyl migration is obtained from the observation that pure *7f* or the mixture *7c* + *7c'* equilibrate at room temperature in chloroform containing trifluoroacetic acid to yield a mixture of *7c*, *7c'*, and *7f*. Similarly, cleavage with anhydrous hydrogen bromide gave a mixture of products from which *7e* + *7e'* (30%), *7g* (30%), and *7h* (15%) were obtained. The formation of *7e* and *7e'* can be rationalized as follows: normal cleavage of the polymeric trityl ether yields the alcohol in a first step, as was the case in the cleavage of *2b*. Since *2b* and *7b* + *7b'* differ only in the presence of a benzoyl group α or β to the ether linkage, the formation of a bromide from *7b* + *7b'* may be due to participation of the neighboring benzoyl group which helps to displace water from the protonated alcohol to yield a cyclic intermediate such as *7i* or *7j*. Attack of bromide on this intermediate would yield the bromide *7e* + *7e'*. Similar cyclic intermediates could be involved in the formation of the dibromide *7g*. Alternately, *7g* could be envisioned as resulting from a process in which the starting diol reacted with the polymeric reagent through both primary alcohol functional groups. This is however unlikely since no such coupling was observed for any of the other alcohols studied.[6]

Finally, the cleavage of *8b* with anhydrous hydrogen bromide or trifluoroacetic acid was studied. The reaction with hydrogen bromide was accompanied by extensive rearrangements which gave rise to numerous products and therefore make this reaction impractical. Cleavage with trifluoroacetic acid resulted in a mixture of two products of very different mobility on tlc. The slowest moving component (75% of the mixture) was identified as *8c* while the fastest moving component *8d* which was unaffected by treatment with aqueous sodium bicarbonate and contained no trifluoroacetyl group could not be positively identified. It was however established that *8d* was formed from *8c* by reaction with trifluoroacetic acid while the reverse transformation did not occur. It is interesting at this juncture to compare the behaviour of *7b* with that of the corresponding polymeric 6-*O*-trityl ether of methyl 2,3,4-tri-*O*-benzoyl-α-D-glucopyranoside, **9** (6). Although both compounds have similar structural features in the vicinity of the ether linkage, their cleavage gives very different results. Thus *7b* reacts with HBr to yield bromides and rearranged products while **9** gives rise almost exclusively to the alcohol methyl 2,3,4-tri-*O*-benzoyl-α-D-glucopyranoside with little or no rearrangement (6).

Regeneration of the Resin

The resins which maintained their mechanical and physical properties throughout the synthetic sequence could be regenerated easily in one step after cleavage of the products and washing of the resin on filter. The polymeric trityl chloride reagent recycled five times is nearly as effective as the original material.

The polymeric trityl chloride reagent therefore seems to be most useful in the selective functionalization of one extremity of a symmetrical diol. Their use can be extended to other alcohols containing more than two hydroxyl groups although mixtures of products may be obtained with unsymmetrical molecules containing more than one primary hydroxyl. Furthermore, acyl migrations may be observed if the alcohol contains hydroxyls α or β to one another. The polymeric trityl chloride reagent has a number of advantages over the acid chloride resin described previously (2). Thus it has a much higher capacity, well adapted to larger laboratory scale syntheses, the ether linkage is easier to cleave than the ester linkage of the acid chloride resin, and finally no degradation of the polymer is observed

[5]The nmr spectrum of the mixture of isomers *7c* + *7c'* indicated a ratio of 7:3 and that of *7e* + *7e'* a ratio of 5:4.

[6]Coupling through both primary hydroxyl groups would have been most likely to occur with a diol such as 1,6-hexanediol which has relatively distant hydroxyls, however, no diol was found in the organic or aqueous phases after cleavage of *4b*.

Can. J. Chem. Downloaded from www.nrcresearchpress.com by 210.87.254.42 on 09/05/12
For personal use only.

and its regeneration is easy and not accompanied by a loss of activity. It should be noted, however, that the two resins complement each other since the link between the resins is acid stable in the case of the acid chloride resin, and base stable in the case of the trityl chloride resin. The possible selectivity of the trityl polymers with unsymmetrical polyhydroxy alcohols such as **7**, using non-migrating protecting groups, is under investigation.

Experimental

Styrene–divinylbenzene copolymers were purchased from Bio-Rad Laboratories (Bio-beads SM-2 for the macroreticular resin and Bio-beads SX-1 for the swellable resins). Both types of resin contained water and were dried under vacuum at 70 °C. Infrared spectra were recorded on a Beckmann IR 20A spectrophotometer using potassium bromide pellets. Nuclear magnetic resonance spectra were measured on a Varian T-60 or Varian HA-100 instrument using tetramethylsilane as the internal standard (δ = 0 ppm; $CDCl_3$ solvent). Mass spectra were recorded on a Hitachi-Perkin-Elmer RMU-6D or an AEI MS 902S mass spectrometer. Dichloromethane, carbon tetrachloride, benzene, toluene, and pyridine were dried over calcium hydride, tetrahydrofuran was dried over lithium aluminum hydride and distilled immediately before use. In the text below, Ⓟ—Tr—Cl refers to the polymeric trityl chloride reagent (chlorodiphenylpolystyrylmethane) and Ⓟ—Tr—OH to the corresponding trityl carbinol resin (diphenylpolystyryl carbinol).

Preparation of the Diphenylpolystyrylcarbinol Resin Ⓟ—Tr—OH

Bio-beads SX-1 (32 g) were stirred into 320 ml of dry CS_2 until the resin was fully swollen. The clear suspension was then refluxed for 30 min and 40 g powdered anhydrous $AlCl_3$ were added to the stirred mixture. After 40 min of stirring, 34 ml of benzoyl chloride were added slowly. The resulting deep red mixture was left stirring under reflux for 3½ h. After cooling, the reaction mixture was poured into 800 ml of a 5:1:1 mixture of dioxane–HCl–H_2O. The slurry was stirred for 30 min then filtered, and the polymer rinsed with dioxane–water 5:1, methyl ethyl ketone, hot water, methyl ethyl ketone, and methanol. The ir spectrum of the polymeric ketone included a large carbonyl absorption centered at 1650 cm^{-1}. To a solution of phenylmagnesium bromide, freshly prepared from 18 g of Mg and 70 ml of bromobenzene in 450 ml of dry tetrahydrofuran, was added 47 g of the polymeric ketone. The mixture was stirred at 65–70 °C for 48 h, then at room temperature for another 48 h. It was then poured in a cold mixture of dioxane–water–HCl 5:1:1. After stirring for 1–2 h, the polymer was collected on a filter and rinsed with dioxane–water–HCl 5:2:1, methyl ethyl ketone, water, methanol, methyl ethyl ketone, and ether. The carbinol polymer Ⓟ—Tr—OH had an ir spectrum with large hydroxyl absorptions centered at 3430 and 3580 cm^{-1}.

*Preparation of the Chlorodiphenylpolystyrylmethane Resin Ⓟ—Tr—Cl, **1***

A slurry of 50 g of Ⓟ—Tr—OH in 800 ml of benzene was stirred and heated until approximately 200 ml of benzene had distilled. The mixture was then cooled to 70 °C and stirred, while 80 ml of acetyl chloride were added slowly. After 4 h of stirring at 70 °C, the mixture was cooled to room temperature and stirred overnight. The polymer was collected on a filter with exclusion of humidity and washed repeatedly with dry benzene, dichloromethane, and finally with petroleum ether. The capacity of the resin **1**, calculated from the chlorine analysis, was found to be ~1.3 mequiv./g. Resins prepared under more drastic reaction conditions contained up to 2.3 mequiv. of functional group per gram.

The macroreticular resins were prepared by a similar procedure. However, since the resin beads were found to be quite fragile, the reaction mixtures were stirred only intermittently while the reactions were carried out at reflux temperatures. The macroreticular resins were easier to wash and filter than their swellable counterparts, but had a lower capacity in the range of 0.61 to 0.92 mequiv. of functional group per gram.

*Preparation of **2c** from 1,4-Butanediol*

A mixture of 3.921 g (5.09 mequiv.) of resin **1** and 1.3 ml of 1,4-butanediol in 40 ml dry pyridine was stirred for 2 days at room temperature. After addition of 10 ml benzoyl chloride, the stirring was continued for another 24 h. The resin was then filtered and rinsed repeatedly with dioxane–water 3:1, dioxane, methyl ethyl ketone, water, methyl ethyl ketone, and methanol. After drying, the resin weighed 4.554 g, which corresponds to about 0.815 g of 1,4-butanediol monobenzoate fixed on the polymer (83% yield based on polymer **1**). The ir spectrum of **2b** included a C=O absorption at 1720 cm^{-1}.

After stirring a suspension of 4.2 g of **2b** in 40 ml of carbon tetrachloride for 2 h, a current of HBr was bubbled through it for 45 min. The mixture was then filtered and the polymer washed with portions of toluene. After washing the filtrate with aqueous $NaHCO_3$, then with water, and drying it with $MgSO_4$, the solvent was evaporated to yield a slightly colored oil (0.707 g or 78% yield based on resin **1**) homogeneous on tlc (ethyl acetate – carbon tetrachloride 1:1) which had an nmr spectrum corresponding to that expected for **2c** (see Table 1).

In a similar experiment carried out on 6.04 g (10.8 mequiv.) of a recycled resin **1**, 1.6 ml of 1,4-butanediol and 12 ml of benzoyl chloride, the cleavage of resin **2b** swollen in chloroform was effected by adding 2 ml of trifluoroacetic acid and stirring for 15 min at room temperature. After filtration and extraction of the polymer with chloroform, the filtrate was evaporated to an oil. The oil, which contained two components of very different mobility on tlc (silica gel, benzene–ether 10:1), was fractionated on a column packed with 100 g of silica gel. Elution with benzene afforded 0.695 g of **2d** (22% yield based on resin **1**, see Table 1). Elution with benzene–methanol 95:5 afforded 0.91 g of **2c** (44% yield based on resin **1**). The yield of **2c** could be increased by shaking a solution of **2d** in chloroform or tetrahydrofuran with an excess of sodium bicarbonate or sodium carbonate in water until the hydrolysis was complete (reaction followed

TABLE 1. Nuclear magnetic resonance data

Compound	Structure*	Nuclear magnetic resonance data†
2*c*	$HOCH_2—CH_2—CH_2—CH_2OR$	3.72(HOCH_2, t); 1.6–2.0(—CH_2—CH_2, m) 4.37(CH_2OR, t); 2.49(OH, s, exch.)
2*d*	$R'OCH_2—CH_2—CH_2—CH_2OR$	4.36(R'OCH_2 and CH_2OR, m); 1.65–2.05(CH_2—CH_2, m)
3*c*	$HOCH_2—(CH_2)_3—CH_2OR$	3.66(HOCH_2, t); 1.5–1.9((CH_2)$_3$, m) 4.33(CH_2OR, t); 1.96(OH, s, exch.)
3*d*	$R'OCH_2—(CH_2)_3—CH_2OR$	4.36(R'OCH_2 and CH_2OR, m); 1.6–2.0((CH_2)$_3$, m)
4*c*	$HOCH_2—(CH_2)_4—CH_2OR$	3.66(HOCH_2, t); 1.4–1.9((CH_2)$_4$, m) 4.35(CH_2OR, t); 1.97(OH, s, exch.)
4*d*	$R'OCH_2—(CH_2)_4—CH_2OR$	4.36(R'OCH_2 and CH_2OR, m); 1.4–2.0((CH_2)$_4$, m)
5*c*	$HOCH_2—CH=CH—CH_2OR$	4.22(HOCH_2, d, 6 Hz); 5.48–5.91(CH=CH, m) 4.81(CH_2OR, d, 6 Hz); 2.24(OH, s, exch.)
5*e*	$BrCH_2—CH=CH—CH_2OR$	4.11(BrCH_2, d, 8 Hz); 5.70-6.14(CH=CH, m) 4.97(CH_2OR, d, 6 Hz)
5*f*	$CH_3COOCH_2—CH=CH—CH_2OR$	2.08(CH_3, s); 4.75 and 4.93(CH_2, 2d, 5.5 Hz) 5.65–6.03(CH=CH, m)

*R = —C—C_6H_5; R' = —C—CF_3.
O O

†Benzoyl resonances not included; s = singlet, d = doublet, t = triplet, m = multiplet, exch. = proton exchangeable with D_2O.

by tlc). In every case, monitoring of the aqueous phases after cleavage showed the absence of 1,4-butanediol.

Preparation of 3c from 1,5-Pentanediol

This reaction was carried out as above using 10 g of resin **1** (macroreticular resin, 0.65 mequiv./g), 1 ml of 1,5-pentanediol, and 10 ml of benzoyl chloride. Cleavage of the resin with 2 ml of trifluoroacetic acid followed by treatment of the product with aqueous sodium bicarbonate afforded 0.361 g of pure **3***c* (27% yield based on macroreticular **1**).

Preparation of 4c from 1,6-Hexanediol

The reaction was carried out as above for **2***c* using 4.7 g (8.5 mequiv.) of resin **1**, 1.6 ml of 1,6-hexanediol, and 10 ml of benzoyl chloride. Cleavage of the product with trifluoroacetic acid followed by treatment with aqueous sodium bicarbonate afforded 1.05 g of pure **4***c*. A second cleavage with trifluoroacetic acid afforded an additional 0.32 g of **4***c* for a total yield of 73% based on resin **1**.

Preparation of 5c from 1,4-Butenediol

The reaction was carried out as above for **2***c* using 5.08 g of resin **1** (1.3 mequiv./g), 1.2 ml of 1,4-butenediol, and 11 ml of benzoyl chloride. Cleavage of the product with trifluoroacetic acid followed by treatment with aqueous sodium bicarbonate gave rise to 0.65 g of **5***c* (52% yield with respect to **1**).

Preparation of 5e and 5f from 1,4-Butenediol

The coupling reaction was carried out as above for **2***c* using 5.01 g (9 mequiv.) of resin **1**, 2 ml of 1,4-butenediol, and 10.5 ml of benzoyl chloride. The cleavage reaction was effected in a carbon tetrachloride suspension using 3.5 g of 30% HBr in acetic acid with a contact time of 10 min. The product which showed two spots on tlc was separated on a column of silica gel (65 g) using petroleum ether (80–100 °C) for elution. The first fraction isolated (0.69 g, 30% with respect to **1**) contained the bromide **5***e*, a second fraction (0.47 g, 21% with respect to **1**) contained a mixture of **5***e* and **5***f*, while the third fraction (0.45 g, 21% with respect to **1**) contained **5***f*. Thus the total yield of the reaction was ~72% with respect to **1**. Nuclear magnetic resonance data for **5***e* and **5***f* are provided in Table 1. *Anal.* calcd. for **5***e* ($C_{11}H_{11}BrO_2$): C 51.78, H 4.35, Br 31.33; found: C 51.51, H 4.40, Br 31.17. *Anal.* calcd. for **5***f* ($C_{13}H_{14}O_4$): C 66.65, H 6.02; found: C 66.55, H 5.96.

In a separate experiment 4.94 g of resin **1** (1.3 mequiv./g) was used to prepare 1.24 g of **5***e* (76% yield with respect to **1**). In this reaction, cleavage of the trityl ether was carried out in carbon tetrachloride saturated with anhydrous hydrogen bromide with a contact time of 30 min.

Attempted Synthesis of 6c from 1,4-Benzene Dimethanol

The reaction of **6** (1.9 g) with resin **1** (5.08 g or 9.1 mequiv.) proceeded as expected to yield **6***a* which was benzolated with 10 ml of benzoyl chloride. Cleavage of the ether linkage in carbon tetrachloride saturated with anhydrous hydrogen bromide with 10 min contact time gave 1.4 g (58% yield with respect to **1**) of a product which was characterized by its nmr spectrum (δ 4.48 and 7.37, singlets, ratio 1:1) and its mass spectrum (M^+ 262 and 266) as being 1,4-dibromo methylbenzene.

Preparation of 7c, 7c', and 7f from 1,2,4-Butanetriol

The coupling reaction was performed as described above with 5.13 g (9.23 mequiv.) of resin **1** and 2 g of 1,2,4-butanetriol. The remaining hydroxyls were protected by reaction with 20 ml of benzoyl chloride and, after the usual processing, the trityl ether was cleaved by the action of 3 ml trifluoroacetic acid. After filtration and treatment of the filtrate with excess sodium carbonate

Can. J. Chem. Downloaded from www.nrcresearchpress.com by 210.87.254.42 on 09/05/12
For personal use only.

TABLE 2. Nuclear magnetic resonance data of compounds 7

Compound	Structure*	Nuclear magnetic resonance data† (δ ppm)
7*c*	$HOCH_2—CH_2—CH(OR)—CH_2OR$	3.78(HO*CH*$_2$, m); 2.02(*CH*$_2$, m); 5.68(*CH*, q); 4.6(*CH*$_2$OR, d)
7*c'*	$HOCH_2—CH(OR)—CH_2—CH_2OR$	3.9(HO*CH*$_2$, d); 5.4(CH, q); 2.28(*CH*$_2$, m); 4.44(CH$_2$OR, m); exch.
7*f*	$ROCH_2—CH_2—CH(OH)—CH_2OR$	4.1–4.75(RO*CH*$_2$, *CH*OH, *CH*$_2$OR, m); 2.85(*OH*, s, exch.); 2.05(CH$_2$, m); exch.
7*e*	$BrCH_2—CH_2—CH(OR)—CH_2OR$	3.52(Br*CH*$_2$, t); 2.4(*CH*$_2$, m); 5.64(*CH*, m); 4.5(*CH*$_2$OR, m)
7*e'*	$BrCH_2—CH(OR)—CH_2—CH_2OR$	3.72(Br*CH*$_2$, d); 5.52(*CH*, m); 2.4(*CH*$_2$, m); 4.5(*CH*$_2$OR, m)
7*g*	$BrCH_2—CH_2—CH(OR)—CH_2Br$	3.5–3.68(Br*CH*$_2$ and *CH*$_2$Br, m); 2.44(*CH*$_2$, m); 5.44(*CH*, s)
7*h*	$BrCH_2—CH(R_1)—CH(R_2)—CH_2OR$	3.53(Br*CH*$_2$, m); 4.0(*CH*OH, m); 2.02(CH$_2$, m); 4.5(*CH*$_2$OR, m) 2.78(OH, exch.)

*R = —C(=O)—C$_6$H$_5$; R$_1$ or R$_2$ = OH; R$_2$ or R$_1$ = H.

†Benzoyl resonances not included; d = doublet, t = triplet, q = quintet, s = sextet, m = multiplet, exch. = proton exchangeable with D$_2$O.

solution, the product which exhibited two spots on tlc was fractionated by passing it through a column packed with 120 g of silica gel. Elution with benzene–ether 100:0.5 afforded first 0.29 g of compound 7*f* which crystallized spontaneously in benzene. After recrystallization from ether – petroleum ether 7*f* had mp 69.5–70 °C. Yield with respect to **1**, 10%. *Anal.* calcd. for $C_{18}H_{18}O_5$: C 68.78, H 5.77; found: C 68.72, H 5.61.

After elution of a fraction containing a mixture of 7*c*, 7*c'*, and 7*f* (0.21 g or 7% with respect to **1**), a fraction containing 7*c* and 7*c'* was obtained (1.24 g or 43% with respect to **1**).

The nmr spectrum of the mixture 7*c* + 7*c'* indicated that 7*c* was preponderant and that the ratio 7*c*:7*c'* was 7:3. *Anal.* calcd. for $C_{18}H_{18}O_5$: C 68.78, H 5.77; found: C 69.00, H 5.87. The nmr data for 7*c*, 7*c'*, and 7*f* is presented in Table 2.

Preparation of 7e, 7e', 7g, and 7h from 1,2,4-Butanetriol

The reaction was carried out as above for **2***c* with 6.47 g (11.6 mequiv.) of resin **1**, 2.3 g of 1,2,4-butanetriol and 20 ml of benzoyl chloride. Cleavage of the trityl ether was accomplished by bubbling anhydrous hydrogen bromide through the polymer suspension for 15 min. After the usual processing, the product which exhibited several spots on tlc, was fractionated by passing it through a column packed with 110 g of silica gel, and eluted with benzene to afford 7*g* (0.674 g or 17% yield with respect to **1**) which was identified by its nmr spectrum (Table 2) and mass spectrum (M^+, 334 and 338).

The second compound eluted was 7*c* + 7*c'* (0.660 g, 15% yield with respect to **1**). The mixture of 7*c* + 7*c'* was also identified by its nmr spectrum (Table 2) and mass spectrum (M^+, 376 and 378). A third compound eluted with benzene–ether 99:1 was identified by its nmr spectrum as being 7*h* (0.307 g or 10% yield with respect to **1**). *Anal.* calcd. for $C_{11}H_{13}O_3Br$: C 48.37, H 4.80, Br 29.26; found: C 48.67, H 4.89, Br 29.54.

Several other fractions totaling 0.579 g were also isolated but were not identified. The total yield of the reaction is approximately 60% with respect to resin **1**.

Preparation of 8c from meso-Erythritol

The coupling reaction was performed using 5.6 g of **1** (2.13 mequiv./g or 12.35 mequiv.) and 2.2 g of dry *meso*-erythritol in 50 ml of dry pyridine. After 2 days at room temperature, 40 ml of dry pyridine and 25 ml of benzoyl chloride were added and the mixture was stirred at room temperature overnight, then at 90 °C for 1 h. After the usual work up, the resin was swollen in 100 ml chloroform and 3 ml of trifluoroacetic acid in 9 ml of chloroform were added. The mixture was stirred for 3 h, then an excess of saturated sodium bicarbonate solution was added, and the mixture was shaken for 2 h. After separating the chloroform phase, washing it with water, and drying over magnesium sulfate, the solvent was evaporated to yield 4.73 g of a product which showed 2 distinct spots on tlc. A 2.02 g portion of the crude reaction product was fractionated on a column packed with 100 g of silica gel. Elution with benzene afforded 0.517 g of an unidentified compound. Elution with

Can. J. Chem. Downloaded from www.nrcresearchpress.com by 210.87.254.42 on 09/05/12
For personal use only.

benzene–ether 97:3 gave **8***c* (1.426 g which corresponds to a 62% yield with respect to resin **1**). Compound **8***c* was crystallized from benzene and recrystallized from ether – petroleum ether (30–60 °C); it had mp 106–108 °C. Its nmr spectrum included signals centered at δ 8.01 and 7.44 (m, benzoyl); δ 5.58 (m, central —*CH*—*CH*—); δ 4.81 (d, *CH*$_2$—O—CO—); δ 4.45 (m, *CH*$_2$—OH); δ 3.35 (d, *OH* exch.). *Anal.* calcd. for $C_{25}H_{22}O_7$: C 69.11, H 5.10; found: C 69.10, H 4.88.

Behaviour of 7c + 7c′ and 5c in Solution Containing Hydrogen Bromide

A solution of **7***c* + **7***c*′ in dichloromethane was saturated with anhydrous hydrogen bromide and the reaction was followed by tlc (silica gel, benzene–ether 10:1). Within a few minutes **7***c* + **7***c*′ (one spot on tlc at R_f = 0.09) disappeared completely and a new compound which had the same R_f as **7***e* + **7***e*′ (R_f = 0.66) had appeared, thus confirming the transformation **7***c* → **7***e*. Similarly **5***c* is rapidly transformed into **5***e* when treated with anhydrous hydrogen bromide in dichloromethane solution while the transformation **2***c* → **2***e* does not occur.

Interconversion of 7c + 7c′ and 7f in Trifluoroacetic Acid Medium

When the mixture of **7***c* + **7***c*′ (R_f = 0.3, silica gel, benzene–ether 2:1) is treated with trifluoroacetic acid in chloroform, a mixture of **7***c* + **7***c*′ + **7***f* is formed. Similarly, when **7***f* (R_f = 0.4) is treated with trifluoroacetic acid in chloroform, the same mixture is formed, indicating that benzoyl migration has occurred.

Regeneration of the Polymeric Reagent

After each cleavage reaction, the product was extracted from the polymer with a suitable solvent. The spent reagent was then soaked in dioxane – HCl 2 *N* (10:2) for 2 h then washed with water, methyl ethyl ketone, benzene–methanol (10:1), and finally dried at 70 °C under reduced pressure. The ir spectrum of the washed polymer was identical to that of the original Ⓟ—Tr—OH. The regeneration was carried out in one step by reaction with acetyl chloride in benzene, as described in the preparation of **1**. A polymer containing 2.13 mequiv. of functional groups per gram was regenerated after being used in the synthesis of a sample of **2***b*; the capacity of the regenerated polymer was 1.85 mequiv./g. After a second coupling–protection–cleavage cycle, the polymer was regenerated again to yield a resin having a capacity of 2.05 mequiv./g, and after five such cycles the polymer had a capacity of 1.97 mequiv./g.

Acknowledgments

The authors thank Dr. Tony Durst for a stimulating discussion, Mr. Philippe Fromage for technical assistance, and the National Research Council of Canada for a grant in aid of this research.

1. R. B. Merrifield. J. Am. Chem. Soc. **85**, 2149 (1963).
2. J. Y. Wong and C. C. Leznoff. Can. J. Chem. **51**, 2452 (1973).
3. C. C. Leznoff and J. Y. Wong. Can. J. Chem. **51**, 3756 (1973).
4. J. M. J. Fréchet and G. Pelle. J. Chem. Soc. Chem. Comm. 225 (1975).
5. S. Hannessian, T. Ogawa, Y. Guindon, J. Kamennof, and R. Roy. Carbohydr. Res. **38**, C15 (1974).
6. J. M. J. Fréchet and K. E. Haque.Tetrahedron Lett. 3055 (1975).
7. C. C. Leznoff. Chem. Soc. Rev. **3**, 65 (1974).
8. B. Helferich, L. Moog, and A. Junger. Chem. Ber. **58**, 872 (1925).
9. J. M. J. Fréchet and K. E. Haque. Macromolecules, **8**, 130 (1975).

Can. J. Chem. Downloaded from www.nrcresearchpress.com by 210.87.254.42 on 09/05/12
For personal use only.

The use of polymer supports in organic synthesis. V.[1] The preparation of monoacetates of symmetrical diols[2]

THOMAS M. FYLES[3] AND CLIFFORD C. LEZNOFF
Department of Chemistry, York University, Downsview, Ontario M3J 1P3

Received December 11, 1975

THOMAS M. FYLES and CLIFFORD C. LEZNOFF. Can. J. Chem. **54**, 935 (1976).

A 2% cross-linked divinylbenzene–styrene copolymer was directly lithiated with *n*-butyllithium in the presence of *N,N,N′,N′*-tetramethylethylenediamine. The lithiated polymer on reaction with a benzophenone gave an insoluble polymer-bound trityl alcohol. Further reaction with acetyl chloride gave a polymer-bound trityl chloride which, on treatment with the primary symmetrical diols 1,10-decanediol, 1,7-heptanediol, and 1,4-butanediol, gave mostly symmetrical diols monoblocked by insoluble polymer-bound trityl groups. Acetylation followed by acid cleavage from the polymer gave the monoacetates of 1,10-decanediol, 1,7-heptanediol, and 1,4-butanediol and some recovered diols. The recovered polymer can be efficiently recycled. The quantity of recovered diol was related to the problem of 'double-binding' of the symmetrical diols to the polymer-bound trityl groups. The extent of 'double-binding' could be greatly reduced by the use of polymer-bound trityl chloride prepared via the lithiated polymer and methyl benzoate or phosgene.

THOMAS M. FYLES et CLIFFORD C. LEZNOFF. Can. J. Chem. **54**, 935 (1976).

On a lithié directement, avec du *n*-butyllithium en présence de la *N,N,N′,N′*-tétraméthyléthylènediamine, un copolymère divinylbenzène–styrène réticulé à 2%. Par réaction du polymère lithié avec une benzophénone, on obtient un alcool tritylique insoluble lié à un polymère. Une réaction subséquente avec du chlorure d'acétyle fournit un chlorure de trityle lié à un polymère qui par traitement avec les diols symétriques primaires décanediol-1,10, heptanediol-1,7 et butanediol-1,4 conduit principalement à des diols symétriques bloqués en un seul endroit par des groupes trityles insoluble liés à un polymère. L'acétylation suivit d'une coupure acide enlève les produits du polymère et conduit aux monoacétates des décanediol-1,10, heptanediol-1,7 et de butanediol-1,4 et à un peu de diols récupérés. On peut recycler d'une façon efficace le polymère récupéré. Les quantités de diols récupérés sont reliées au problème de la "double fixation" des diols symétriques aux groupes trityles reliés au polymère. Les quantités de "double fixation" peuvent être réduites d'une façon considérable par l'utilisation d'un chlorure de trityle lié au polymère préparé par l'intermédiaire d'un polymère lithié et de benzoate de méthyle ou de phosgène.

[Traduit par le journal]

The concept of using insoluble solid phases in multi-step, nonrepetitive, general organic synthesis has been recently demonstrated (1) and reviewed (2, 3). Completely symmetrical difunctional compounds have been monoprotected using insoluble polymer supports, showing how inexpensive symmetrical starting materials such as terephthalaldehyde (2, 4), isophthalaldehyde (2, 4), and symmetrical diols (5, 6) can be used in organic synthesis.

Although we had previously prepared monotrityl (5, 6) and tetrahydropyranyl ethers (6) of symmetrical diols via formation of their polymer-bound monoesters, we were interested in synthesizing insect pheromones (7) directly on polymer supports, and monoprotection of the symmetrical diols through a base stable ether linkage would be a more appropriate approach. In this paper we explore the use of polymer-bound trityl chloride as a monoblocking group of symmetrical primary diols and the subsequent formation of a series of monoacetates of these diols.

Polymer-bound trityl alcohols have been previously prepared by lithiation of a halogenated phenyl group of the polymer, followed by treatment with benzophenone (8) or by a Friedel–Crafts reaction of divinylbenzene (DVB) cross-linked polystyrene with benzoylchloride followed by a phenyl Grignard reagent (9). The former

[1]For part IV see ref. 1.

[2]Presented in part at the 9th Great Lakes Regional Meeting of the American Chemical Society, St. Paul, Minn. June, 1975.

[3]Holder of a National Research Council of Canada Scholarship 1974–1976.

Can. J. Chem. Downloaded from www.nrcresearchpress.com by 210.87.254.105 on 09/05/12
For personal use only.

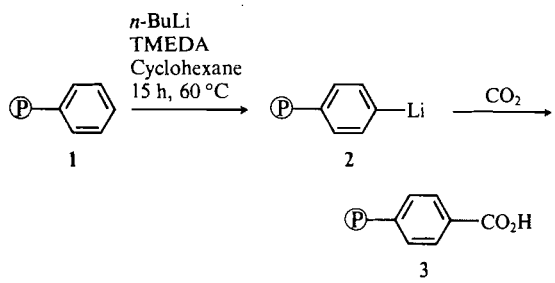

1 2 3

SCHEME 1

preparation is a three stage procedure and the latter is a two step reaction. *Soluble* polystyrene has been *directly* metalated using the 1:1 complex of *n*-butyllithium and *N,N,N',N'*-tetramethylethylenediamine (TMEDA) (10–12). We find that this direct lithiation procedure can be applied to *insoluble* cross-linked polystyrene polymers and that the synthesis of the polymer-bound trityl alcohols is accomplished in a single reaction vessel.

Reaction of a 2% cross-linked DVB-styrene copolymer, **1**, with *n*-butyllithium and TMEDA in purified cyclohexane gave a dark red-brown polymer, **2**, presumed by analogy to lithiated soluble polystyrene to be a polymer lithiated on the phenyl rings (10, 12). This polymer **2** could be quenched with water liberating 3–4 mmol base/g resin. Alternatively, **2** could be quenched with carbon dioxide as shown in Scheme 1 to give a benzoic acid polymer, **3**, showing typical infrared absorbances for the —CO_2H group (see Experimental) and exhibiting by acid–base titration, values of 0.5–1.5 mmol acid/g resin.

As shown in Scheme 2 reaction of **2** with 4,4'-dimethoxybenzophenone, **4**, or benzophenone, **5**, gave polymer-bound 4,4'-dimethoxytrityl alcohol, **6**, or a polymer-bound trityl alcohol, **7**. Treatment of **6** and **7** with acetyl chloride in benzene (9) gave polymer-bound 4,4'-dimethoxytrityl chloride, **8**, and polymer-bound trityl chloride, **9**, respectively. Reaction of **8** and **9** with excess 1,10-decanediol, **10**, and only **9** with 1,7-heptanediol, **11**, and 1,4-butanediol, **12**, gave the polymer-bound monoblocked symmetrical diols **13–16** respectively. The infrared spectra of **13–16** did not exhibit an assignable OH absorbance. However, acetylation of **13–16** with acetic anhydride in pyridine gave the polymer-bound monoblocked symmetrical diol monoacetates **17–20** respectively, all of which showed CO_2R absorbances in their infrared spectra at 1725 cm^{-1}. Acid cleavage of **17–20** liberated free 1,10-decanediol monoacetate, **21**, from **17** and **18**, 1,7-heptanediol monoacetate, **22**, from **19**, and 1,4-butanediol monoacetate, **23**, (13) from **20**, respectively. Polymer **6** was liberated from **17** and polymer **7** from **18–20**. Some diol **10** was recovered from acid cleavage

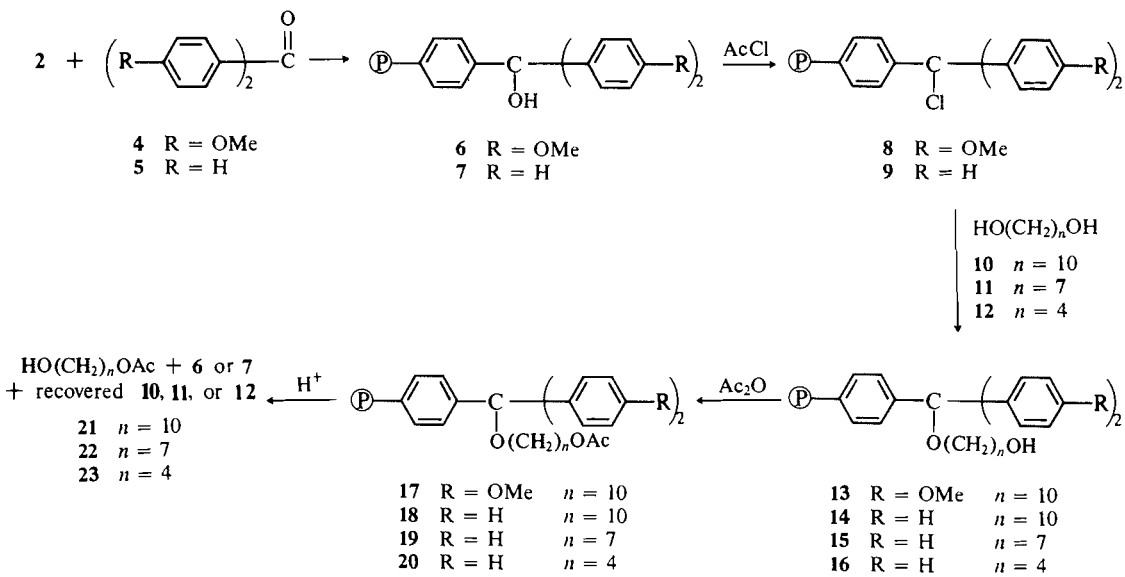

4 R = OMe
5 R = H

6 R = OMe
7 R = H

8 R = OMe
9 R = H

10 n = 10
11 n = 7
12 n = 4

21 n = 10
22 n = 7
23 n = 4

17 R = OMe n = 10
18 R = H n = 10
19 R = H n = 7
20 R = H n = 4

13 R = OMe n = 10
14 R = H n = 10
15 R = H n = 7
16 R = H n = 4

SCHEME 2

Can. J. Chem. Downloaded from www.nrcresearchpress.com by 210.87.254.105 on 09/05/12
For personal use only.

Can. J. Chem. Downloaded from www.nrcresearchpress.com by 210.87.254.105 on 09/05/12
For personal use only.

of **17** and **18** and similarly diols **11** and **12** were recovered from **19** and **20**, respectively. The yields of diol monoacetates and related information are listed in Table 1.

Cleavage of the Diol Monoacetates from the Trityl Polymers

Since reactions on insoluble polymer supports are generally slower than their solution analogs (14), we initially prepared the 4,4′-dimethoxytrityl polymer **4** so that the final cleavage step of the polymer-bound diol monoacetate **17** would be rapid due to the effect of the 4-methoxy substituents on the trityl group in accelerating acid cleavage of trityl ethers (15). Cleavage of polymer **13**, for example, with 80% acetic acid at room temperature overnight (9) yielded as the major component 1,10-decanediol, minor amounts of the desired 1,10-decanediol monoacetate, **21**, and some 1,10-decanediol diacetate. The presence of the latter compound showed that acetylation of the alcohols had occurred under the cleavage conditions. Indeed, control experiments under a variety of conditions showed that 1,10-decanediol itself can be acetylated by acetic acid – water mixtures giving equilibrium amounts of diol, mono- and diacetates.

After extensive investigation, a reagent suitable for the desired cleavage was found to be 0.3 *N* anhydrous HCl in dioxane.[4] Treatment of **13** with this reagent at room temperature for 48 h yielded pure 1,10-decanediol (0.3–0.5 mmol diol/g resin). Under these conditions acetate groups are not affected although free alcohol groups are chlorinated to a small extent (< 1%), especially for acid concentrations greater than 0.5 *N*. More dilute acid only partially cleaved the polymer-bound diol.

Since the 4,4′-dimethoxytrityl containing polymer **13** required more forcing conditions for cleavage than anticipated and resulted in the formation of a diacetate, the preparation of monoacetates of symmetrical diols using polymer-bound trityl alcohols, derived from benzophenone, *i.e.* polymer **5**, was repeated and all the results recorded in Table 1 were obtained using the 0.3 *N* anhydrous HCl cleavage conditions.

In all experiments some diol was recovered from the final cleavage step. Control experiments[5] showed that 1,10-decanediol monoacetate, **21**, was not hydrolyzed under the cleavage conditions. The recovered diols could conceivably have arisen from two sources. Either the acetylation reaction was incomplete or the diols on initial attachment to the polymer-bound trityl chloride, **5**, became attached at both ends, a process which we shall call 'double-binding' (16, 17).[6]

Experiments Designed to Explore the Amount of Double-binding of Diols to the Polymer

Since a large variety of acetylations and other reactions including halogenations, tosylations, and mesylations (18) were attempted on the free alcohol end of polymer-bound diols and in all cases approximately 30–50% of the starting diols were recovered, we strongly suspected that the source of recovered diols was due to double-binding of the initial diols to the polymer.

The extent of double-binding should be a function of the proportion of polymer in which the trityl chloride functional groups are sufficiently close in proximity so that these groups can be bridged by the symmetrical diols. The functional groups may be close due to functionalization of adjacent phenyl groups along the polymer backbone or may be due to conformational mobility of the polymer bringing remote groups close to each other. Despite the fact that a large excess of symmetrical diols was used to react with **9**, it is highly possible that the free alcohol group of a singly bound diol is often closer to a trityl chloride, *within the local environment of the polymer backbone*, than any amount of excess diol in the bulk of the reaction mixture.

The Use of a 20% Cross-linked Macroporous Resin

To reduce the conformational mobility of the polymer, the preparation of 1,10-decanediol monoacetate, **10**, was repeated according to Scheme 2 but using a 20% cross-linked DVB–styrene macroporous copolymer. The direct lithiation of the 20% cross-linked polymer was sluggish, requiring 2 days reaction time. Although subsequent formation of a 20% cross-linked polymer-bound 4,4′-dimethoxytrityl chloride polymer was readily achieved, followed by

[4]The mode of this cleavage is somewhat different than those described in refs. 8 and 9.

[5]Pure **21** or **21** admixed with **1** or **7**, in 0.3 *M* HCl in dioxane was not hydrolyzed.

[6]This is another example of an intraresin reaction, several of which have been previously recorded (16, 17).

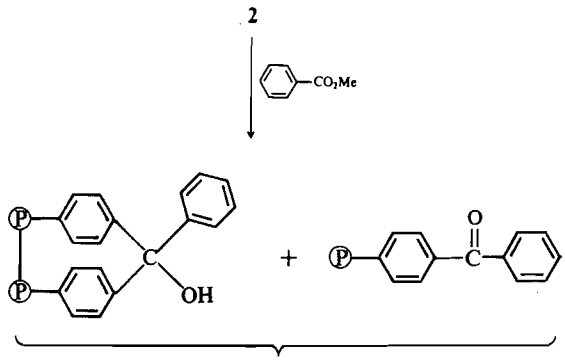

24

SCHEME 3

formation of polymer-bound monoprotected 1,10-decanediol and preparation of the polymer-bound 1,10-decanediol monoacetate, subsequent cleavage from the polymer was very slow requiring forcing acid conditions leading to a low recovery of 1,10-decanediol monoacetate. The large beads of the 20% cross-linked polymer would disintegrate if one used magnetic stirring instead of overhead stirring (19). Drying the polymer under high vacuum divides the large beads giving 'split peas'. Thus further synthesis on 20% cross-linked polymers were abandoned and all the data reported in Table 1 refer to 2% cross-linked polymers.

The Use of Methyl Benzoate and Phosgene in Quenching the Lithiated Polymer

One possibility for eliminating proximal functional sites on the polymer would be to have the lithiated polymer reacting twice with a single substrate. To this end the 2% cross-linked lithiated polymer **2** was treated with methylbenzoate to give a new polymer **24** in which two phenyllithium groups from the polymer can react with one methylbenzoate giving essentially a more highly cross-linked polymer-bound mixture, **24**, of trityl alcohol and benzophenone (Scheme 3) in which proximal phenyllithium groups have been quenched, thereby reducing the likelihood of polymer-bound trityl alcohol groups being close to each other.

Similarly, lithiated polymer **2**, possibly containing *three* reactive polymer-bound phenyllithium groups in close proximity can react with one phosgene giving a highly cross-linked polymer-bound mixture, **25**, of trityl alcohol, benzophenone, and methyl benzoate (from washing the reaction mixture with methanol) as shown in Scheme 4.

Polymer **24**, isolated from the reaction of **2** with methyl benzoate showed absorption in the infrared spectrum at 1670 cm^{-1} typical of the carboxyl absorption of benzophenone. Similarly, polymer **25**, isolated from the reaction of **2** with phosgene, showed absorptions at 1670 cm^{-1} and 1720 cm^{-1} typical of the benzophenone and methyl benzoate moieties. Treatment of **24** and **25** with acetyl chloride gave trityl chloride polymers **26** and **27** containing 0.9 mmol and 0.4 mmol halide/g resin respectively. Polymers **26** and **27**, on treatment with 1,10-decanediol gave polymer-bound monotrityl-1,10-decanediols **28** and **29** respectively. The amount of diol attached to these polymers was determined by acid cleavage to be 0.07 mmol and 0.03 mmol/g resin respectively.[7] Acetylation of **28** and **29** gave polymer-bound monotrityl-1,10-decanediol monoacetates **30** and **31** which on acid cleavage gave 72% and over 90% of 1,10-decanediol monoacetates from **30** and **31** respectively. Repetition of the synthesis of **21** via **24** using

[7]The low loading capacity was probably due to insufficient drying of this particular sample of **10**.

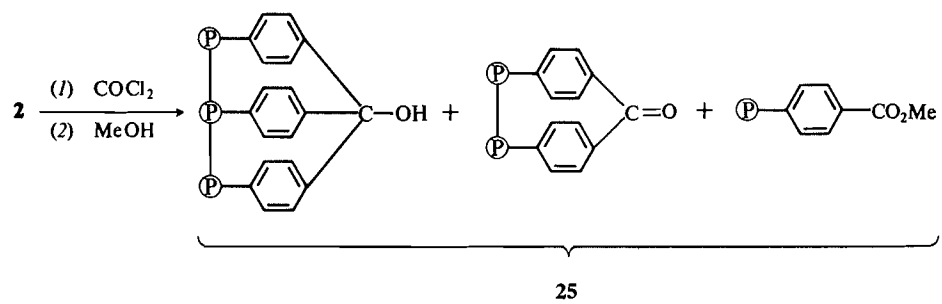

25

SCHEME 4

Can. J. Chem. Downloaded from www.nrcresearchpress.com by 210.87.254.105 on 09/05/12
For personal use only.

TABLE 1. Comparison of the yields of symmetrical diol monoacetates from symmetrical diols bound to different polymers according to Scheme 2

Polymer-bound diol	Halide content[a] (mmol/g)	Bound diol[b] (mmol/g (mg/g))	Diol monoacetate[c] (mmol/g (mg/g))	Recovered diol[d] (mmol/g (mg/g))	Relative yield of monoacetate[e] (%)	Overall yield[f] (%)	Conversion[g] (%)
14	1.42	0.58(101)	0.36(62)	0.16(29)	70	60	86
28	0.90	0.07(12)	0.05(19)	0.03(5)	67	67	100
28[h]	1.32	0.33(58)	0.21(46)	0.08(15)	71	64	84
29	0.40	0.03(5)	—	—	90[i]	—	—
28[j]	1.00	0.27(46)	0.24(52)	0	100	90	100
15	1.25	0.94(124)	0.39(80)	0.46(52)	46	42	82
16	1.25	0.98(88)	0.59(77)	0.29(26)	67	60	86
14[k]	0.80	0.33(58)	0.19(42)	0.14(25)	56	56	100
14[l]	1.00	0.71(123)	0.43(94)	0.23(40)	67	60	89

[a]This number refers to the halide content of the polymer-bound trityl chloride precursor to the polymer-bound diol.
[b]Refers to the quantity of diol attached to the polymer-bound diol.
[c]Refers to the amount of diol monoacetate synthesized via the polymer-bound diol according to Scheme 2.
[d]Yield of diol recovered from the reaction mixture after cleavage of polymer-bound diol monoacetates.
[e]Relative yield of diol monoacetate compared to recovered diol.
[f]Yield of diol monoacetate compared to diol initially bound to polymer.
[g]Yield of diol monoacetate from initially bound diol if the recovered diol is recycled.
[h]Polymer **28**, prepared from scrupulously dry **10**.
[i]Determined by integration of the nmr spectrum of crude **21** and **10** derived from **29**.
[j]Polymer **28**, made via **24**, prepared from a very dilute solution of methyl benzoate in THF.
[k]Polymer **14**, prepared from the trityl alcohol, made via the two step bromination and lithiation procedure (19).
[l]Polymer **14**, prepared from once used trityl alcohol, recovered from the cleavage of **18**.

scrupulously dry **10** showed similar yields but better loading (Table 1). Polymer **24**, prepared when **2** was quenched with a very dilute solution of methyl benzoate and subjected to the normal reaction sequence of Scheme 2, yielded 1,10-decanediol monoacetate with no liberation of starting 1,10-decanediol (see Table 1).

Thus the trapping of the lithiated polymer with methyl benzoate and phosgene yielded polymers in which two or three of the phenyl groups of the trityl moiety were attached to the polymer backbone. In this way the conformational mobility of the polymer was reduced and proximal lithiated sites reacted in such a way as to produce only one trityl moiety, reducing the possibility of having proximal trityl groups. The fact that polymers **24** and **25** gave relatively high yields of 1,10-decanediol monoacetate with little or no starting 1,10-decanediol strongly suggests that the starting diols recovered from cleavage of **18**, **19**, and **20** were derived from double-binding and not incomplete acetylation. A comparison of the yields of the 1,10-decanediol monoacetates from different polymers are given in Table 1.

Other Experiments

The used polymer-bound trityl alcohol **7**, recovered from the cleavage of **18** was recycled to prepare more 1,10-decanediol monoacetate in high yield (Table 1), showing that the polymer is completely regenerable.

Although we have depicted the direct lithiation of **1** giving the *para* lithiated **2**, experiments by Evans *et al.* (12) on lithiation of soluble polystyrene showed that both *meta* and *para* lithiation occurred, with a *meta–para* ratio of 2:1. Thus it is likely that a considerable amount of **2** is actually lithiated in the *meta* position. We were somewhat concerned that our lithiation procedure might thus give more *meta* lithiated polymer than the prior two step procedure of bromination and lithiation and that this difference might give different results in a synthetic scheme. Because of this we made **2** by the two step procedure of Camps *et al.* (19, 20) and prepared 1,10-decanediol monoacetate on this polymer according to Scheme 2. The results were very comparable as shown in Table 1.

Evaluation of Results

Although it is possible to prepare polymers, *e.g.* **24** and **25** which lead to symmetrical diols bound to the polymer at one end only, the capacities of these polymers are lower than optimum (see Table 1). Furthermore, the amount of double-binding observed in polymers **14**, **15**, and **16**, does not seriously affect the synthetic

Can. J. Chem. Downloaded from www.nrcresearchpress.com by 210.87.254.105 on 09/05/12
For personal use only.

Can. J. Chem. Downloaded from www.nrcresearchpress.com by 210.87.254.105 on 09/05/12
For personal use only.

elaboration of the free alcohol end to either monoacetates as shown in this paper or to insect pheromones in continuing work in this laboratory. Double-binding simply removes a small portion of the symmetrical diols from the reaction pathway through inert bis-ether formation and the diols can be recovered and recycled upon final cleavage of the products from the polymer. Our 70–100% yield of decanediol monoacetate, **21**, via polymer supports can be contrasted to our preparation of **21** in a classical acetylation in which two chromatographic separations were required to isolate pure **21** in only 34% yield (see Experimental). The report on the previously prepared **23** does not record a yield (13). We feel that polymer bound trityl chloride will be exceedingly useful for monoprotecting symmetrical diols for use in general organic synthesis.

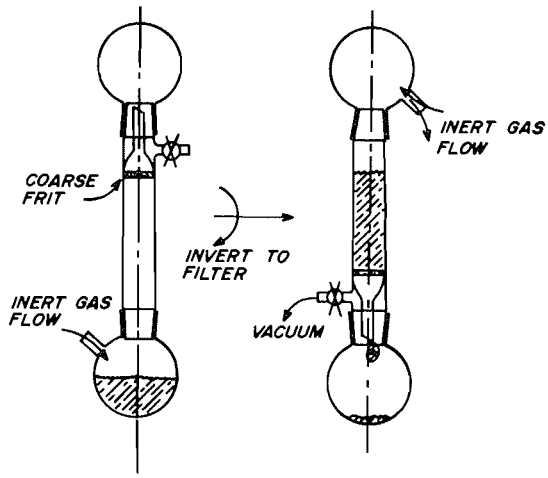

FIG. 1. Apparatus for reaction and vacuum filtration of moisture and oxygen sensitive insoluble polymers.

Experimental

A Bausch and Lomb Abbé 3L refractometer was used to record the refractive index data. Infrared spectra were recorded on a Unicam SP1000 ir spectrophotometer as KBr discs unless otherwise specified. Nuclear magnetic resonance spectra were recorded on a Varian EM360 spectrometer using deuteriochloroform as solvent and tetramethylsilane as internal standard. Mass spectra were recorded on a Perkin-Elmer–Hitachi RMU6E mass spectrometer. The number in brackets after the parent ion shows the percentage of the base peak represented by the parent ion. Silica gel was used for all thin and preparative layer chromatography. Filtration was done under vacuum through sintered glass Buchner funnels. Inert atmosphere filtration was done in a modified fritted Schlenck tube (Fig. 1). Stirring of 2% cross-linked polystyrene polymers was done magnetically, while 20% cross-linked polystyrene polymers were stirred with mechanical overhead stirrers. Microanalyses were performed by G. Gygli of Toronto.

Preparation of Polymer-bound Phenyllithium, 2

In a typical preparation 5 g of cross-linked polystyrene (2% DVB–styrene copolymer BioRad BioBeads SX-2 or 20% DVB–styrene copolymer Rohm and Haas XE-305) was suspended in 50 ml of purified cyclohexane under argon, in a flask fitted with a modified Schlenk tube (Fig. 1). To this mixture 25 ml of *n*-butyllithium (25 mmol, 2 *N* in hexane) followed by 10 ml of *N,N,N′,N′*-tetramethylethylenediamine (TMEDA) (60 mmol) were added by a syringe. The slurry was heated to 60 °C and stirring continued overnight (2% cross-linked polymer) or 48 h (20% cross-linked polymer). The lithiated polymer, **2**, was filtered under dry argon (Fig. 1) washed with 50 ml of cyclohexane (four times) and dried at high vacuum. Hydrolysis of a standard sample of **2** released 3–4 mmol base/g resin.

Preparation of Polymer-bound Benzoic Acid, 3

A 1 g sample of **2** was suspended in 20 ml dry tetrahydrofuran (THF) under dry argon. Carbon dioxide was bubbled into the mixture until the dark colour of the polymer faded (5 min) and continued a further 5 min. The polymer was filtered, washed with 10 ml THF, 10 ml water (four times), 10 ml ethanol, and suspended in 40 ml 20% HCl in dioxane. The mixture was stirred for ½ h. The polymer was filtered, washed with 10 ml dioxane–water (1:1), 10 ml water (five times), 10 ml ethanol (four times), 10 ml ether (four times), and air dried. The ir spectrum of polymer-bound benzoic acid, **3**, exhibited ν_{max} 1690 (shoulder at 1730) cm^{-1} (C=O) and 2500–3600 cm^{-1} (CO_2H). Treatment of **3** suspended in 1:1 dioxane–water with excess standard sodium hydroxide and back titration with standard HCl solution showed **3** to contain 0.6–0.9 mmol acid/g of 2% resin or 1.1–1.5 mmol acid/g of 20% resin.

Preparation of Polymer-bound Trityl Alcohols, 6 and 7

To a suspension of 5 g of 2% cross-linked **2** (containing 3.6 mequiv. base/g) in 80 ml of dry THF under argon was added a total of 20 g of 4,4′-dimethoxybenzophenone, **4**, or benzophenone, **5**, in 80 ml of dry THF in portions during 1 h. The mixture was stirred an additional hour. The mixture was treated with 25 ml THF–water 1:1, filtered, washed with 20 ml water (ten times), 10 ml ethanol (four times), 10 ml dioxane (four times), 10 ml ether (four times), and air dried to **6** and **7** respectively. The ir spectra of **6** and **7** were uninformative.

Preparation of Polymer-bound Trityl Chlorides, 8 and 9

A mixture of 5 g of **6** or **7** in 120 ml of 20% acetyl chloride in benzene (9) was stirred overnight at reflux under argon. The polymer **8** or **9** was rapidly filtered in air, washed with dry benzene, and dried under high vacuum. Analysis for chloride ion was determined by the method of Volhardt as applied to chloromethylated polymers (21) and showed 1.1–1.5 mmol Cl/g of **8** or **9**. The ir spectra of **8** and **9** were uninformative.

Preparation of Polymer-bound 1,10-Decanediol, 14

A typical preparation of the polymer-bound diols **13–16** is given for the preparation of **13** from **9**. A mixture

Can. J. Chem. Downloaded from www.nrcresearchpress.com by 210.87.254.105 on 09/05/12
For personal use only.

of 5 g of **9** (containing 1.42 mmol Cl/g) and 4.3 g (25 mmol) of dry 1,10-decanediol, **10**, in 60 ml of dry pyridine was stirred at room temperature for 48 h. The polymer **14** was filtered rapidly in air, washed with 25 ml dry pyridine (four times), 25 ml dry ether (four times), washed in a Soxhlet extractor for 8 h with ether, and dried under high vacuum. Analysis for chloride showed only trace amounts. The ir spectra of **13–16** were uninformative.

*Isolation of 1,10-Decanediol, **10**, from **14**, **11** from **15**, and **12** from **16***

In a typical cleavage reaction of the diol from polymer, necessary to determine the extent of loading of diol to the polymer, 1 g of **14** was suspended in 40 ml of 0.3 *N* anhydrous HCl in dry dioxane and the mixture was stirred at room temperature for 48 h. The polymer was filtered, washed with 10 ml ethanol, 10 ml water (ten times), 10 ml ethanol (twice), 10 ml ether (four times), and air dried. The filtrate was extracted with ether, washed with water, dried over magnesium sulfate, and evaporated to yield 80–150 mg of crystalline 1,10-decanediol, exhibiting a loading capacity of 0.5–0.9 mmol **10**/g of resin.

The filtrate from **15** and **16** was neutralized with ammonium hydroxide and evaporated to dryness to yield a mixture of salts and oils. The mixture was extracted with three portions of ether, dried over magnesium sulfate, and evaporated giving the pure diols **11** and **12**. This latter procedure is necessary for the lower molecular weight, **11** and **12**, as they are soluble in water.

*Preparation of Polymer-bound 1,10-Decanediol Monoacetate, **18***

A suspension of 1.25 g of **14** (0.55 mmol diol/g) in 60 ml dry pyridine containing 6 ml (60 mmol) acetic anhydride was stirred at 60–80 °C for 48 h. The polymer-bound monoacetate **18** was filtered, washed with 10 ml pyridine (twice), 10 ml ethanol, 10 ml water (ten times), 10 ml ethanol (four times), 20 ml chloroform (twice), 10 ml ether (four times), and air dried. The ir spectrum of **18** exhibited a strong absorbance at ν_{max} 1725 cm^{-1}, (C=O).

*Isolation of 1,10-Decanediol Monoacetate, **21**, from **18***

The isolation of **21** from **18** was identical to that described above for the isolation of **10** from **14**. From 1.0 g of **18**, 106 mg of a light brown oil was obtained. Purification by preparative tlc (eluant 40% ether – 60% benzene) yielded 40 mg of **10** (R_f 0.2) and 65 mg of 1,10-decanediol monoacetate, **21** (R_f 0.6), as an oil. The yield of **21** was 54% based on the amount of **10** attached to **18**. Infrared spectrum, ν_{max} (neat) 1250 (OAc), 1725 (C=O), 3500 cm^{-1} (OH); mass spectrum *m/e* 216 (0.1) (M$^+$); nmr spectrum, 4.00 (t, 2H, CH_2OAc protons, J = 8 Hz), 3.70 (t, 2H, CH_2OH protons, J = 8 Hz), 3.70 (br, 1H, OH proton), 2.00 (s, 3H, Ac), 1.5–1.0 ppm (16H, methylene protons). *Anal.* calcd. for $C_{12}H_{24}O_3$: C 66.63, H 11.18; found: C 66.74, H 11.17.

*1,7-Heptanediol Monoacetate, **22**, and 1,4-Butanediol Monoacetate, **23***

The isolation of **22** from **19** was identical to that described above for the isolation of **11** from **15**. The yield of **22** was 46% based on the amount of **11** attached to **19**. Infrared spectrum, ν_{max} (neat) 1240 (OAc), 1735 (C=O), 3400 cm^{-1} (OH); mass spectrum, *m/e* 174 (0.4) (M$^+$); nmr spectrum, 4.05 (t, 2H, CH_2OAc, J = 8 Hz), 3.60 (t, 2H, CH_2OH, J = 8 Hz), 3.65 (br s, 1H, OH), 1.6–1.2 ppm (br envelope, 10H, methylene protons). *Anal.* calcd. for $C_9H_{18}O_3$: C 62.04, H 10.41; found: C 62.10, H 10.43.

Similarly, the yield of **23** from **20** was 67% based on the amount of **12** attached to **20**. Infrared spectrum, ν_{max} (neat) 1240 (OAc), 1735 (C=O), 3400 cm^{-1} (OH); mass spectrum, *m/e* 132 (1) (M$^+$); nmr spectrum, 4.00 (t, 2H, CH_2OAc, J = 8 Hz), 3.55 (t, 2H, CH_2OH, J = 8 Hz), 3.58 (br s, 1H, OH), 2.00 (s, 3H, Ac), 1.7–1.6 ppm (complex m, 4H, methylene); n_D^{20} 1.4309 (lit. (13) 1.4296).

*Preparation of Doubly-attached Polymer-bound Trityl Alcohol, **24***

To a suspension of 8 g of 2% cross-linked **2** (containing 3.9 mequiv. base/g) in 80 ml dry THF under argon was added 2.5 ml (50 mmol) of methyl benzoate in 80 ml dry THF in portions during 2 h. The work-up was identical to that described for the preparation of **5**. Analytical data of polymers derived from **24** are given in Table 1. The ir spectrum of **24** showed ν_{max} 1670 cm^{-1} (C=O).

*Preparation of Triply-attached Polymer-bound Trityl Alcohol, **25***

Into a mixture of 8 g of 2% cross-linked **2** (containing 3.9 mequiv. base/g) in 60 ml dry THF under argon, phosgene was bubbled for 20 min. The polymer **25** was filtered under argon, washed with 25 ml THF (five times), and dried at high vacuum. The ir spectrum of **25** showed ν_{max} 1670 (C=O) and 1800 cm^{-1} (COCl). This dried polymer was suspended in 40 ml anhydrous methanol, filtered, washed with 20 ml methanol (twice), 20 ml water (four times), 20 ml methanol (four times), 20 ml dioxane (twice), 20 ml ether (four times), and air dried. The ir spectrum of methanol washed **25** shows ν_{max} 1670 (C=O) and 1720 cm^{-1} (CO_2Me).

*Bromination of **1***

Cross-linked polystyrene **1** was brominated as previously described (19) to give a polymer containing 26.79% Br by elemental analysis which corresponds to 3.32 mmol Br/g of polymer.

This polymer was used to make **2**, for comparison of the synthesis of **21** according to Scheme 2, with **2** made by direct lithiation (see Table 1).

*Preparation of **21** Without the Use of Polymer Supports*

To a solution of 1.7 g (20 mequiv.) of 1,10-decanediol, **10**, in 8 ml of pyridine was added 0.6 ml (6 mequiv.) acetic anhydride and the mixture was stirred at reflux for 30 min. The cooled solution was poured into ice water, neutralized (H_2SO_4), and extracted with ether. The ethereal solution was washed with water, dilute $NaHCO_3$, dilute H_2SO_4, dried over magnesium sulfate, and evaporated to yield 2.1 g of oily crystals. This mixture was shown by tlc (eluant 40% ether – 60% benzene) to contain **10**, **21**, and 1,10 decanediol diacetate. Column chromatography (on silica gel, elution gradient benzene – 20% ether + 80% benzene) yielded 0.5 g of a mixture containing predominantly **21** with traces of the diacetate. Preparative tlc (eluant 20% ether – 80% benzene) yielded 0.45 g pure **21** in 34% yield.

Acknowledgments

The authors wish to thank the National Research Council of Canada for a grant in aid of

this research, and Rohm and Haas Co. for a gift of Polymer XE-305.

1. J. Y. WONG, C. MANNING, and C. C. LEZNOFF. Angew. Chem. Int. Ed. Engl. **13**, 666 (1974).
2. C. C. LEZNOFF. Chem. Soc. Rev. **3**, 65 (1974).
3. G. G. OVERBERGER and K. N. SANNES. Angew Chem. Int. Ed. Engl. **13**, 99 (1974).
4. C. C. LEZNOFF and J. Y. WONG. Can. J. Chem. **51**, 3756 (1973).
5. C. C. LEZNOFF and J. Y. WONG. Can. J. Chem. **50**, 2892 (1972).
6. J. Y. WONG and C. C. LEZNOFF. Can. J. Chem. **51**, 2452 (1973).
7. D. A. EVANS and C. L. GREEN. Chem. Soc. Rev. **2**, 75 (1973).
8. L. R. MELBY and D. R. STROBACH. J. Am. Chem. Soc. **89**, 450 (1967); J. M. J. FRÉCHET and K. E. HAQUE. Tetrahedron Lett. 3055 (1975).
9. F. CRAMER and H. KOSTER. Angew. Chem. Int. Ed. Engl. **7**, 473 (1968).
10. A. J. CHALK. J. Polym. Sci. Part B, **6**, 649 (1968); A. J. CHALK and T. J. HOOGEBOOM. J. Organometal. Chem. **11**, 615 (1968).
11. D. C. EVANS, M. H. GEORGE, and J. A. BARRIE. J. Polym. Sci. Polym. Chem. Ed. **12**, 247 (1974).
12. D. C. EVANS, L. PHILLIPS, J. A. BARRIE, and M. H. GEORGE. J. Polym. Sci. Polym. Lett. Ed. **12**, 199 (1974).
13. S. MAMEDOV and Y. U. PAKOVNA. Zh. Obsch. Khim. Engl. Ed. **33**, 3099 (1963).
14. R. L. LETSINGER, M. J. KORNET, V. MAHADEVAN, and D. M. JERINA. J. Am. Chem. Soc. **86**, 5163 (1964); G. R. MARSHALL and R. B. MERRIFIELD. *In* Biochemical aspects of reactions on solid supports. *Edited by* G. R. Stark. Academic Press, New York. 1971, p. 111.
15. H. SCHALLER, G. WEIMANN, G. LEURCH, and H. G. KHORANA. J. Am. Chem. Soc. **85**, 3821 (1963).
16. J. I. CROWLEY, T. B. HARVEY III, and H. RAPOPORT. J. Macromol. Sci. Chem. **7**, 1117 (1973).
17. M. A. KRAUS and A. PATCHORNIK. J. Am. Chem. Soc. **93**, 7325 (1971).
18. T. M. FYLES and C. C. LEZNOFF. Unpublished results.
19. N. M. WEINSHENKER, G. A. CROSBY, and J. Y. WONG. J. Org. Chem. **40**, 1966 (1975).
20. F. CAMPS, J. CASTELS, M. J. FERRANDO, and J. FONT. Tetrahedron Lett. 1713 (1971).
21. J. M. STEWART and J. D. YOUNG. Solid phase peptide synthesis. W. H. Freeman Ltd., San Francisco. 1969. p. 58.

Can. J. Chem. Downloaded from www.nrcresearchpress.com by 210.87.254.105 on 09/05/12
For personal use only.

Intramolecular vibrational energy relaxation. Decomposition of chemically activated alkylcyclobutanes[1,2]

FA-MEI WANG[3] AND B. S. RABINOVITCH

Department of Chemistry, University of Washington, Seattle, Washington 98195

Received September 15, 1975

FA-MEI WANG and B. S. RABINOVITCH. Can. J. Chem. **54**, 943 (1976).

This paper describes an approach to the study of intramolecular energy relaxation of highly vibrationally excited complex molecules. The features of the decomposition of a series of chemically activated alkylcyclobutanes are outlined, including variable selectivity of the initial, non-randomized state of excitation. It is shown how this can afford both a qualitative test of the postulate of internal energy randomization employed in the Rice–Ramsperger–Kassel–Marcus treatment of unimolecular reactions, as well as a quantitative measure of the rate of relaxation. The study of the first members of this series, ethyl and dimethyl cyclobutane, is described. As expected, the first members can provide a lower limit to the relaxation rate, namely, $\lambda > 10^{12}$ s^{-1}.

FA-MEI WANG et B. S. RABINOVITCH. Can. J. Chem. **54**, 943 (1976).

Cette publication décrit une approche pour l'étude de l'énergie de relaxation intramoléculaire de molécules complexes hautement excitées au niveau vibrationnel. On décrit les caractéristiques de la décomposition d'une série d'alkylcyclobutanes activés chimiquement; ceci inclut une sélectivité variable de l'état d'excitation initial qui n'est pas au hasard. On montre comment ceci peut fournir à la fois un test qualitatif du postulat de distribution au hasard d'énergie interne employé dans le traitement des réactions unimoléculaires de Rice–Ramsperger–Kassel–Marcus ainsi qu'une mesure quantitative du taux de relaxation. On décrit l'étude des premiers membres de la série soit l'éthyl et le diméthylcyclobutane. Tel qu'entendu, les premiers membres peuvent fournir une limite inférieure du taux de relaxation soit $\lambda > 10^{12}$ s^{-1}.

[Traduit par le journal]

Introduction

The Rice–Ramsperger–Kassel–Marcus (R.R.-K.M.) theory of unimolecular reaction is well established as a practical working theory (1, 2). As is appropriate, various aspects or limitations of the theory continue to be tested. In recent years, a number of approaches have been proposed or adopted to test the basic assumption of random lifetimes (3–9) used in the theory, and which presupposes that the internal energy of the excited molecule is statistically distributed among all active degrees of freedom of the molecule prior to the reaction event. Many experiments have supported the validity of this postulate *under conventional experimental conditions* (2, 5, 10–14) while only a few unsupported results have suggested otherwise (15, 16). It is apparent, nonetheless, that since the rate of internal relaxation of energy is finite, even though rapid, that the randomization postulate must reach the limit of its utility at some point. The matter at hand, then, is to explore the validity of the assumption of equal probability of all accessible complexions of the system corresponding to a particular energy specification, and to learn the domain of the constraints on effective intramolecular energy relaxation. All of the present experimental techniques are confronted by complications, and much effort, by many groups and by several methods, has been focused on this problem.

One technique, which has been used in this laboratory, takes advantage of the selective state of energization of a molecule obtained by use of chemical activation. A limitation of the random lifetime assumption has been demonstrated in studies of the decomposition of chemically activated fluorobicyclopropyl (7*a*, 17) and fluoroalkylcyclopropane (7*b*, 18) systems. The findings have supported the general experimental feature of a randomized internal energy distribution, perturbed by non-random initial conditions; a large (above 100 kcal mol^{-1}) input of energy, initially localized in a subset of the vibration modes of the excited molecule,[4] relaxes into the

[1]This paper is dedicated to Professor C. A. Winkler of McGill University on the occasion of his sixty-fifth birthday by one of his former students (B.S.R.).

[2]Work supported by the National Science Foundation, U.S.A.

[3]Present address: Department of Chemistry, University of California, Irvine, California.

Can. J. Chem. Downloaded from www.nrcresearchpress.com by 210.87.254.105 on 09/05/12
For personal use only.

Can. J. Chem. Downloaded from www.nrcresearchpress.com by 210.87.254.105 on 09/05/12
For personal use only.

full set to produce a quasi-equilibrium condition. During the transient period, the process of intramolecular energy relaxation suffers competition from the non-random decomposition of the molecule induced by the states initially populated near the critical hypersurface for reaction. The value of the intramolecular relaxation rate was found to be $\sim 10^{12}$ s^{-1} and presently affords the only experimental measurement in such systems.

Depending upon the initial conditions, the reaction rate of non-randomly excited systems may increase, decrease, or remain unchanged as the collision rate increases in the suprahigh pressure region, as governed by the position of the initial states relative to the critical bounding hypersurface for reaction. In the previous studies (7, 17), the systems were preferentially activated on a nascent ring, the locus of decomposition. The states populated initially were those in proximity to the reaction configuration for rupture of the nascent ring; therefore, the apparent decomposition rates (defined as $k_a = \omega D/S$, where ω is the specific collision rate, and D and S are the respective observed amounts of decomposition and stabilization of the excited species) rise with pressure, when the collision rates become high enough to significantly quench the contribution to decomposition by randomized species but are still too low to inhibit the decomposition of nascent non-randomized species.

The present study of alkylcyclobutanes is an effort to enhance the understanding of the nature of intramolecular energy transfer. This may be accomplished in twofold fashion: (*a*) by changing the nature of the substrate from a fluorocarbon to a hydrocarbon, thus drastically altering the spectrum of vibrational behavior that characterizes the molecule; (*b*) by devising a reaction system which effectively permits the selection of the initial states at different locations in the energy-coordinate hyperphase space of the substrate, relative to the critical reaction hyperplane.

In an alkylcyclobutane system, the energy may be deposited at sites which are on, near, or remote from the reaction locus (*i.e.*, the ring), as illustrated for the two extreme cases:

[1*a*] $\square\!\!-(CH_2)_nCH_3 + {}^1CH_2 \rightarrow \square\!\!-(CH_2)_nCH_2CH_3^*$

[1*b*] $\rightarrow CH_3^*\square\!\!-(CH_2)_nCH_3$

[4]Which is loosely represented as energy deposition in the modes of the ring formed in the activation process.

Hence, the randomization 'flows' in the opposite directions in reactions 1*a* and 1*b* with respect to the reaction channels. Any deviation from R.R.K.M. behavior due to initial state selection should be manifested by direct comparison of the two reaction rates. The effect should be even more distinguishable as the side appendage becomes larger so that one of the activated sites (corresponding to a different initial subset of vibrationally excited modes) is moved further away from the reaction site. The present study deals with the smallest system in which observable effects might arise, namely, methylcyclobutane substrate ($n = 0$) which forms ethyl (ECB) and dimethyl cyclobutane (DMCB) products of interest.[5] It is not a favorable case, but its investigation was worthwhile to provide a limit on the magnitude of the intramolecular energy relaxation rate in this hydrocarbon system and for the purposes of completeness of investigation of the series.

Experimental

Ketene was prepared by the pyrolysis of acetic anhydride and was purified by trap-to-trap distillation with slush baths at −110 °C and −160 °C and stored at −196 °C. Prior to each run, it was degassed and then warmed to −78 °C and a ketene sample distilled off. Methylcyclobutane (MCB) (99%) was obtained from Chemical Samples Co., was purified by distillation and gas chromatography, and was stored at −196 °C. The purity was no less than 99.99%. In preparing a mixture of inert bath gases, carbon monoxide (Matheson, CP grade) and oxygen (Airco, 99%) were passed through silica gel trap at 25 °C and then through a copper wool-packed trap at −196 °C. The middle fraction of the condensed liquids were used.

The radiation of a PEK AH6 high pressure mercury lamp was filtered through a $NiSO_4/CoSO_4$ solution (27.6/8.4%, by weight), and was centered around 3100 Å with a band width of ~200 Å.

A standard vacuum system fitted with Teflon O-ring stopcocks was employed for gas handling. The sizes of the quartz reaction vessels ranged from 1.14 ml to 1 l, depending on the total pressure, which varied from 1.69 Torr to 15 atm. Most runs were of 1–4 h duration to give enough decomposition product for analysis. Typical compositions of reaction mixtures were MCB:ketone: O_2:CO = 10:1:1:40 at low pressures, and 10:2:4:60–200 at high pressures. Extra oxygen was added at higher pressures to ensure adequate scavenging of triplet methylene radicals.

At the end of photolysis, after pumping off non-

[5]Cyclobutane substrate, the type molecule, is assumed to lead to a system in which the distinction between a non-randomized moiety and the whole molecule, methylcyclobutane, is minimal or effectively non-existent.

Can. J. Chem. Downloaded from www.nrcresearchpress.com by 210.87.254.105 on 09/05/12
For personal use only.

condensables at −196 °C, the reaction products were passed through a magnesium perchlorate column to remove unreacted ketene. Products were analyzed by gas chromatography with use of a flame ionization detector. Details have been described elsewhere (*7a*). A combination series of 3/16 in. columns of 30 ft 30% $AgNO_3$ glycol and 15 ft 30% dibutylphthalate was employed for analysis. The temperature of the $AgNO_3$ column started at 0 °C for detection of decomposition products, and was then warmed to 25 °C, while the phthalate column was heated to 45 °C for stabilization products, after transit of decomposition products. It was usually necessary to perform preliminary separations for high pressure runs to obtain proper resolution. Calibrations were made from time to time with authentic materials.

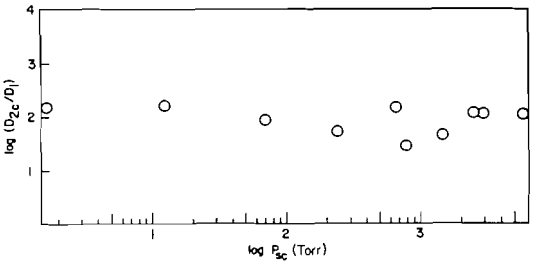

FIG. 1. Plot of ratio, D_l/D_{2c}, *vs.* log P_{sc}, where $P_{sc} = 0.48P_{tot}$ and $\omega_{sc} = 8 \times 10^{10}$ s^{-1} at the highest total pressure (15 atm) used.

Results and Discussion

In cyclobutane systems, only methylene insertion into C—H bonds occurs. The important reaction paths for MCB are:

[2] $^1CH_2 + MCB \rightarrow$ 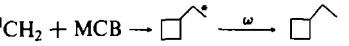 (S_l)

$\xrightarrow{k_a(2)} C_2H_4 + \text{butene-1}$ (D_l)

[3] $^1CH_2 + MCB \rightarrow$

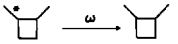 (*cis* and *trans*) (S_{2c}, S_{2t})

$\xrightarrow{k_a(3A)} C_2H_4 + \textit{cis}\text{- and } \textit{trans}\text{-butene-2}$ (D_{2c}, D_{2t})

$\xrightarrow{k_a(3B)} 2C_3H_6$

[4] $^1CH_2 + MCB \rightarrow$ 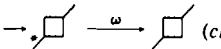 (*cis* and *trans*) (S_3)

$\xrightarrow{k_a(4)} 2C_3H_6$

[5] $^1CH_2 + MCB \rightarrow$ 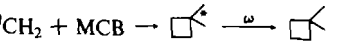 (S_i)

$\xrightarrow{k_a(i)} C_2H_4 + \text{isobutane}$ (D_i)

In reaction 2, the energy is initially deposited mainly in the nascent side chain of ECB and then relaxes among the full set of vibrational modes of the molecule. As the collision rate increases, the inter-collisional time becomes shorter so that the non-randomized species may not relax fully before collisional stabilization occurs. If the non-random component of activation is significant, the rate of unimolecular decomposition, $k_a(2)$, should decrease with increasing collisional rate since the initial rate of non-random decomposition for ECB is small or zero if the ring modes are significantly excluded from the initial subset of excited vibration modes.[6] On the other hand, in reactions 3 and 4, the ring is part of the initial nascent DMCB moiety: the subset of vibrational modes originally excited includes a large number of ring modes, and is taken here to include all of them.[6] An increase in the collision rate can result in an *increase* in the measured decomposition rate, due to a relatively constant contribution to decomposition from the faster reacting, non-randomized ring moiety. The decomposition rate by path [5] represents an intermediate, more equivocal, case and is not as useful.

The differential nature of intramolecular vibrational energy relaxation in this system should, in principle, be perceptible by monitoring the relative amounts of butenes produced via reaction paths [2], [3], and [4], as a function of pressure.

Early in the work, it became apparent that the chromatogram of D_{2t} tended to be less reproducible than that of D_{2c} due to interference by a cyclobutane impurity and by methylcyclopropane which arose by the addition of methylene to propylene. The propylene arose as a decomposition product in reaction 3 and from the photolysis of ketene; in view of its dual origin it, also, was not a useful monitor of reaction path [3] or reaction path [4]. The ratio of (D_l/D_{2c}) is plotted in Fig. 1 as a function of pressure. The pressure given here has been corrected to a strong collider basis by assigning the relative deactivation collision efficiency of CO and O_2 to be 0.46 (see below). Due to analytical difficulties, no run was carried out above a total pressure of 15 atm. The present system enters the conventional chemical activation high pressure limiting region (2, 19) at a pressure below 100 Torr, since the S/D value is ~50 at 100 Torr. Corrections were made for butenes arising from the iso-

[6]More quantitative statements would not be well founded at the present time.

Can. J. Chem. Downloaded from www.nrcresearchpress.com by 210.87.254.105 on 09/05/12
For personal use only.

merization of methylcyclopropane which was 4% at the lowest pressure studied and became negligible in the high pressure region, in agreement with ref. 10.

The constancy of the curve in Fig. 1 indicates that, in the pressure range studied, the internal energy is essentially randomized prior to decomposition.

R.R.K.M. calculations were carried out for the decomposition rates of randomized ethyl cyclobutane (ECB), randomized dimethyl cyclobutane (DMCB), and its corresponding initial MCB moiety.[7] Calculation for the MCB nascent moiety was based on Simons' model II for MCB (20), with minor changes as appropriate. Vibrational frequencies of energized molecules ECB and DMCB were deduced from those of MCB, with necessary extensions and modifications. The frequency assignment for the activated complexes was chosen so as to fit the high pressure Arrhenius parameters of thermal studies (Appendix I). A biradical model of activated complexes was employed, resulting from considerations of orbital symmetry, rather than a concerted mechanism (21); however, such differences are not crucial for our purposes. The decomposition rate of ECB is reported (22) as $k_\infty = 10^{15.6}e^{-62\,000/RT}$, at 713 K, and this corresponds to a critical threshold E_0 of 59.4 kcal mol^{-1}. There are two sets of Arrhenius parameters (23) available for the thermal rate of decomposition of *cis*- and *trans*-DMCB to give *cis*- and *trans*-butenes. No attempt was made here to distinguish between reactions of DMCB isomers. A simple average was adopted since the two sets of values do not differ greatly; $k_\infty = 10^{15.4}e^{-63.0/RT}$ at 680 K. The corresponding critical threshold is then E_0 = 60.6 kcal mol^{-1}.

The total internal energy E^* available for activation of ECB was estimated from the thermochemistry of the reaction

$$^1CH_2 + \square \rightarrow \square^{\wedge}$$

The heat of formation of triplet methylene has been assigned as 95 ± 2 kcal mol^{-1} (24), and the splitting between $CH_2(^1A_1)$ and $CH_2(^3B_1)$ has been established to be ~9 kcal mol^{-1} (25, 26); thus, $\Delta H_{f0}{}^0(^1CH_2) \approx 104$ kcal mol^{-1}. The exothermicity of the process is given by

$$\begin{aligned}\Delta H_{298}{}^0 &= \Delta H_{f298}{}^0(\text{ECB})\,(23b) \\ &\quad - \Delta H_{f298}{}^0(\text{MCB})\,(23b) \\ &\quad - \Delta H_{f298}{}^0(^1CH_2) \\ &\leq -5.2 + 0.6 - 104 \\ &= -109 \text{ kcal mol}^{-1}\end{aligned}$$

On adding thermal energy of 3.0 kcal mol^{-1} for ECB, a lower limit of E^* = 112 kcal mol^{-1} is obtained. The upper limit is provided by the excess photolysis and vibrational energies carried by methylene (20, 25). Based on experimental results for MCB (20), a value of E^* = 115.6 kcal mol^{-1} was used.

Similarly, the E^* for DMCB was estimated to be 117.3 kcal mol^{-1}, with $\Delta H_{f298}{}^0$(DMCB)-(23*b*) = −7.2 kcal mol^{-1} and $E_{th}{}^{298}$(DMCB) = 2.7 kcal mol^{-1}.

The measured and calculated rates of decomposition for two randomized molecules of this system and for the reactive one of the initial 'moiety' are listed in Table 1. The biradical mechanism implicates several reaction channels, with one probably favored over the others due to energy considerations. For simplicity, a reaction path degeneracy d^+ of four was employed; these details have no significance for this study.

A weak-collider stochastic calculation was made, to account for the inefficient collisions induced by CO, based on a step-ladder model with CO represented by a 1600 cm^{-1} down-step size and by 4000 cm^{-1} for the substrates; the

TABLE 1. Calculated and experimental values of decomposition rate constants

	Value		
		DMCB	
Parameter	ECB	Molecule	Moiety
E_0 (kcal mol^{-1})	59.4	60.6	60.6
E_a (kcal mol^{-1})	62.0	63.0	62.1
E^* (kcal mol^{-1})[a]	115.6	117.3	116.4
E^{rem} (kcal mol^{-1})[b]			89.9
$k_{ND}(0)$ (s^{-1})			5.11E8
$k_{RD}(\infty)$ (calc)[c] (s^{-1})	2.80E7	1.59E7	
$k_{RD}(\infty)$ (expt)[d] (s^{-1})	4.3E7	2.8E7	
A (calc) (s^{-1})	3.98E15	2.51E15	4.47E15

[a]Including thermal energy at 298 K (~3 kcal mol^{-1}).
[b]Corresponding to the temperature of molecule at which E^* is as listed (2037 K).
[c]Calculated with $d^+ = 4$, $I^+/I \simeq 1$, $F_w = 1$.
[d]Collision rates calculated from collision diameters, s, based on Lennard-Jones σ constants as follows: $\sigma(\square^{\wedge})$ = 6.0 Å, $\sigma(\square)$ = 5.7 Å, and σ(CO) = 3.8 Å (27).

[7]The initial rate of the decomposition of the nascent ECB moiety is set equal to and, of course, remains zero.

Can. J. Chem. Downloaded from www.nrcresearchpress.com by 210.87.254.105 on 09/05/12
For personal use only.

following relation holds, $\omega_{sc} = 0.48\omega_{tot}$, where subscript sc stands for strong collider and ω_{tot} is the total specific collision rate of excited species with all of the components of the reaction mixture.

The relaxation constant for intramolecular energy transfer process was found in the earlier work on fluorocarbons to be $\lambda \approx 10^{12}\ s^{-1}$. Owing to their characteristically higher frequency of vibration, hydrocarbons might be expected to redistribute their energy faster, *i.e.*, $\lambda > 10^{12}\ s^{-1}$. On the other hand, enhanced anharmonicity in fluorocarbons could invert the inequality. Thus, a value of $\lambda \approx 10^{12}\ s^{-1}$ also appears to be a plausible estimate for the present alkyl cyclobutanes.

Using the rough rule given earlier (*7b*), the collision rate ω_t at which *turn-up* in the decomposition rate has its onset is

$$\omega_t = \frac{x}{0.2}\frac{k_{RD}(\infty)\lambda}{k_{ND}(0)}$$

here $k_{RD}(\infty)$ is the rate of decomposition of the randomized molecule, and $k_{ND}(0)$ is the initial rate of decomposition of the non-randomized molecule (moiety); x stands for the minimum experimentally detectible fractional change 0.1–0.2 of k_a, and the factor 0.2 is a crude mean adjustment parameter to account for the decay of $k_{ND}(0)$ to zero (*7b*). A rise in the apparent value of $k_a(3A)$ for the decomposition of DMCB is predicted to occur around $\omega_t \approx 5 \times 10^{10}\ s^{-1}$. By contrast, since the decomposition in ECB arises solely from randomization, a *decrease* in the apparent rate of $k_a(2)$ should occur when the collision rate is high enough to intercept the relaxation process. The calculated variation of k_a *vs.* ω for the two reaction paths is displayed in Fig. 2; $k_a(3A)$ was calculated on the basis of the non-randomized energy decay model described earlier,[7] and $k_a(2)$ was estimated by employing a simple model,[7] namely, $k_{RD}(t) = k_{RD}(\infty) + [k_{ND}(0) - k_{RD}(\infty)]e^{-\lambda t}$. On this basis, the observable ratio of (D_1/D_{2c}) should begin to drop by a factor of two around $\omega_{sc} = 8 \times 10^{10}\ s^{-1}$, corresponding to 15 atm, the highest pressure attained.

The interpretation of the results is quite straightforward. The fact that the experimental ratios of Fig. 1 do not show any obvious tendency to decline up to $\omega_{sc} \approx 8 \times 10^{10}\ s^{-1}$ suggests that the intramolecular relaxation rate for this system has a higher value, *i.e.*, $\lambda > 10^{12}\ s^{-1}$. Indeed, as is evident from Fig. 2, for an assumed value $\lambda = 5 \times 10^{12}\ s^{-1}$ a non-random contribution to D_{2c} would be experimentally unmeasurable at total pressures below 15 atm.

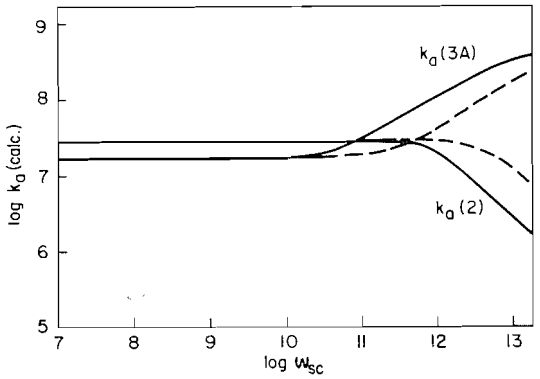

FIG. 2. Plots of calculated values of log $k_a(3A)$ and log $k_a(2)$ *vs.* log ω_{sc} for $\lambda = 10^{12}\ s^{-1}$, —, and for $\lambda = 5 \times 10^{12}$, - - - -.

A non-random phenomenon would become more easily detectible for members of the cyclobutane series which have longer side chains. An extension of two more carbons on the side chain could reduce the critical collision rate ω_t below $10^{10}\ s^{-1}$ and make it more readily accessible.

1. G. M. WIEDER and R. A. MARCUS. J. Chem. Phys. **37**, 1835 (1962).
2. B. S. RABINOVITCH, R. F. KUBIN, and R. E. HARRINGTON. J. Chem. Phys. **38**, 405 (1963).
3. D. L. BUNKER. J. Chem. Phys. **40**, 1946 (1964).
4. R. C. BAETZOLD and D. J. WILSON. J. Phys. Chem. **68**, 3141 (1964).
5. D. W. PLACZEK, B. S. RABINOVITCH, and F. H. DORER. J. Chem. Phys. **44**, 279 (1966).
6. J. L. FRANKLIN and M. A. HANEY. J. Phys. Chem. **73**, 2857 (1969).
7. (*a*) J. D. RYNBRANDT and B. S. RABINOVITCH. J. Phys. Chem. **75**, 2164 (1971). (*b*) J. F. MEAGHER, K. J. CHAO, J. R. BARKER, and B. S. RABINOVITCH. J. Phys. Chem. **78**, 2535 (1974).
8. Y. N. TANG and Y. Y. SU. J. Chem. Phys. **57**, 4048 (1972).
9. (*a*) J. M. PARSON and Y. T. LEE. J. Chem. Phys. **56**, 4658 (1972); (*b*) S. A. SAFRON, N. D. WEINSTEIN, D. R. HERSCHBACH, and J. C. TULLY. Chem. Phys. Lett. **12**, 564 (1972).
10. J. N. BUTLER and G. B. KISTIAKOWSKY. J. Am. Chem. Soc. **82**, 759 (1960).
11. I. OREF, D. SCHUETZLE, and B. S. RABINOVITCH. J. Chem. Phys. **54**, 575 (1971).
12. Y. Y. SU and Y. N. TANG. J. Phys. Chem. **76**, 2187 (1972).
13. L. D. SPICER and B. S. RABINOVITCH. Ann. Rev. Phys. Chem. **21**, 349 (1970).

14. J. ASPDEN, N. KAWAJA, J. REARDON, and D. WILSON. J. Am. Chem. Soc. **91**, 7580 (1969).
15. G. B. SKINNER and B. S. RABINOVITCH. Bull. Soc. Chim. Belg. **82**, 305 (1973).
16. (*a*) J. F. BOTT. J. Chem. Phys. **54**, 181 (1971); (*b*) M. L. DUTTON, D. L. BUNKER, and H. H. HARRIS. J. Phys. Chem. **76**, 2614 (1972).
17. J. D. RYNBRANDT and B. S. RABINOVITCH. J. Chem. Phys. **54** 2275 (1971).
18. B. S. RABINOVITCH, J. F. MEAGHER, K. J. CHAO, and J. R. BARKER. J. Chem. Phys. **60**, 2932 (1974).
19. G. H. KOHLMAIER and B. S. RABINOVITCH. J. Chem. Phys. **38**, 1692 (1963).
20. J. W. SIMONS, W. L. HASE, R. J. PHILLIPS, E. J. PORTER, and F. B. GROWCOCK. Int. J. Chem. Kinet. **7**, 879 (1975).
21. H. M. FREY, G. R. JACKSON, M. THOMPSON, and R. WALSH. J. Chem. Soc. Faraday I, 2054 (1973).
22. R. E. WELLMAN and W. D. WALTERS. J. Am. Chem. Soc. **79**, 1542 (1957).
23. (*a*) H. R. GERBERICH and W. D. WALTERS. J. Am. Chem. Soc. **83**, 3935 (1961); **83**, 4884 (1961); (*b*) S. W. BENSON and H. E. O'NEAL. Kinetic data on gas phase unimolecular reactions. U. S. Department of Commerce, National Bureau of Standards, Washington, D.C., NSRDS-NBS 21, 1970.
24. (*a*) W. A. CHUPKA, J. BERKOWITZ, and K. M. A. REFAEY. J. Chem. Phys. **50**, 1938 (1969); (*b*) V. H. DIBELER, M. KRAUSS, R. M. REESE, and F. N. HARLEE. J. Chem. Phys. **42**, 3791 (1965).
25. (*a*) W. L. HASE, R. J. PHILLIPS, and J. W. SIMONS. Chem. Phys. Lett. **12**, 161 (1971); (*b*) J. W. SIMON. Private communication.
26. (*a*) P. J. HAY, W. J. HUNT, and W. A. GODDARD. Chem. Phys. Lett. **13**, 30 (1972); (*b*) C. F. BENDER, J. F. SCHAEFER, D. R. FRANCESCHETTI, and L. C. ALLEN. J. Am. Chem. Soc. **94**, 6888 (1972).
27. L. D. SPICER and B. S. RABINOVITCH. J. Phys. Chem. **74**, 2445 (1970).

Appendix

Frequency assignment (cm^{-1}) for ECB and DMCB*

(*a*) Molecules

Assignment	Frequency ECB	Frequency DMCB
C—H stretch	2946(11),2854	2946(11),2854
CH_3 and CH_2 def.	1438(7)	1438(8)
C—H bend	1310	1310(2)
CH_2 twist and wag	1243(8)	1243(4)
CH_3 rock, C—CH_3 str. and ring def.	965(8)	965(11)
C—H bend, CH_2 rock and C—C str.	735(5)	735(4)
C—C bend	324(3),150	324(4)
Ring pucker	200	200
C—C torsion	190, 90	190(2)

*Based on ref. 20.

(*b*) Activated complex (only altered frequencies listed)

Assignment	Frequency ECB	Frequency DMCB
CH_2 twist and wag	1247(7)	1247(4)
CH_3 rock, C—CH_3 str, and C—H bend	974(7)	974(9)
CH_2 rock, C—CH_2 str.	724(3)	724(2)
Skel. def., C—C bend	366(4),150	366(4),259(2)
Skel. bend and C—C bend	163(3)	163(2)

(*c*) MCB moiety, C_5H_{10}

Assignment	Frequency Molecule	Frequency Activated complex
C—H str.	2946(9)	2946(9)
CH_3 and CH_2 def.	1438(6)	1438(6)
CH_2 twist and wag, C—H bend	1243(5)	1247(4)
CH_3 rock, ring def., C—CH_3 str.	965(9)	974(8)
C—H bend, CH_2 rock	735(4)	724(2)
C—C bend	324(2)	299(4)
Ring pucker	200	—
C—C torsion	190	190
Skel. bend, C—C bend		163(2)

Can. J. Chem. Downloaded from www.nrcresearchpress.com by 210.87.254.105 on 09/05/12
For personal use only.

Molecular orbitals from group orbitals. I. A perturbational molecular orbital treatment of the electronic structures, shapes and conformations of AH_mBH_n systems

MYUNG-HWAN WHANGBO[1] AND SAUL WOLFE

Department of Chemistry, Queen's University, Kingston, Ontario K7L 3N6

Received May 29, 1975

MYUNG-HWAN WHANGBO and SAUL WOLFE. Can. J. Chem. **54**, 949 (1976).

A procedure is proposed which allows the group orbitals of a fragment AH_m— to be obtained from the molecular orbitals of the molecule AH_m—H. Orbital interaction diagrams constructed from these group orbitals have been found useful in the description of the electronic structures and conformations of a variety of molecular systems of the type AH_mBH_n. The molecules that have been treated by this procedure include ethane, hydrazine, diphosphine, aminophosphine, aminoborane, and sulfonium and phosphonium ylids.

MYUNG-HWAN WHANGBO et SAUL WOLFE. Can. J. Chem. **54**, 949 (1976).

On propose une procédure qui permet d'obtenir les orbitales de groupe d'un fragment AH_m— à partir des orbitales moléculaires de la molécule AH_m—H. On a trouvé que les diagrammes d'interactions orbitalaires, construits à partir de ces orbitales de groupe, sont utiles pour décrire les structures électroniques et les conformations d'un grand nombre de systèmes moléculaires du type AH_mBH_n. On a traité les molécules suivantes d'après cette procédure: éthane, hydrazine, diphosphine, aminophosphine, aminoborane et les ylures de sulfonium et de phosphonium.

[Traduit par le journal]

Introduction

During the last decade, much information of chemical interest has been obtained from the use of qualitative molecular orbital models. Considerations of orbital symmetry conservation (1), in conjunction with applications of perturbational molecular orbital (PMO) theory (2), have become extremely powerful methods for gaining insight into the mechanisms of concerted chemical reactions. Molecular orbital theory also gives rise to qualitative models for the explanation of molecular shapes (3–9). In particular, the Mulliken–Walsh model (3) attempts to correlate changes in orbital energies with changes in molecular geometry, and reasons for the success of this model have been sought from applications of both rigorous molecular orbital theory (7, 9) and the Hellman–Feynman theorem (8).

More recently, PMO models have been applied to the problem of rationalizing stable conformations of molecules (10–18). These applications proceed in two stages. In the first, the molecule under consideration is dissected into two parts or groups of atoms; then the interactions between the orbitals of these groups are examined as a function of their conformational relationship. The obvious rationale of such an approach is the observation that molecular orbitals can often be expressed qualitatively as a linear combination of a small number of typical 'group orbitals' which recur from molecule to molecule (18).

The present work constitutes an attempt to apply this procedure to a number of stereochemical problems of current interest. The nature of group orbitals is considered first. Then an empirical scheme is presented for the construction of molecular orbitals from group orbitals. Finally, a qualitative model is proposed for the rationalization of molecular shapes and conformations of AH_mBH_n systems in terms of group orbital correlation diagrams.

Group Orbitals

An orbital is generally characterized by its nodal property and by its 'orbital energy'. In the Mulliken–Walsh and PMO models, the orbital energy is treated as an orbital eigenvalue of an effective one-electron Hamiltonian[2] so that a change in orbital energies can be related directly to a change in the total energy.

[1]Holder of National Research Council of Canada Scholarship, 1972–1974.

[2]Examples are the Hamiltonians in the Hückel and Extended-Hückel methods (19).

Can. J. Chem. Downloaded from www.nrcresearchpress.com by 210.87.254.6 on 09/05/12
For personal use only.

Can. J. Chem. Downloaded from www.nrcresearchpress.com by 210.87.254.6 on 09/05/12
For personal use only.

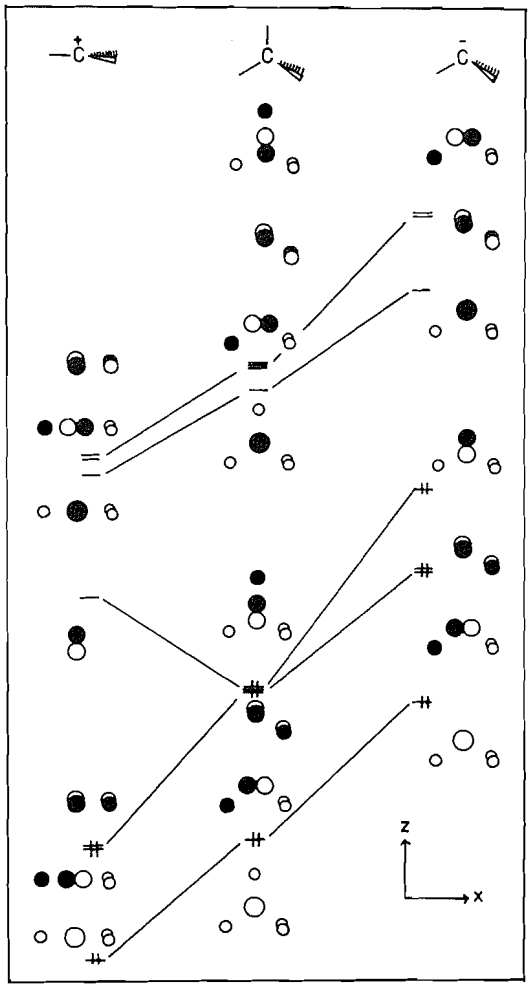

FIG. 1. Schematic representation of the molecular orbitals of CH_3^+, CH_4, and CH_3^-.

Many proposals have been made which attempt to correlate this orbital energy with other theoretical quantities (7, 9, 20).

For a simple molecular system, the relative sequence of orbital eigenvalues seems to be the same regardless of the quality of the particular computation (4, 9, 21). Since this is what is most important in a PMO model, orbital eigenvalues obtained from SCF–MO calculations may therefore be employed as orbital energies in a PMO model.[3] In the present analysis, *ab initio* SCF–MO orbital eigenvalues are used as orbital energies.

[3]The HOMO and LUMO orbital energies estimated, where possible, from experimental data have also been used as the basis of perturbational molecular orbital models (22).

To describe the molecular orbitals of an A_2H_{2m} system, it has been customary to take as the group orbitals of the AH_m fragments the molecular orbitals of AH_m type molecules (4, 21*b*). However, this conventional definition of group orbitals is incomplete when molecules of the type AH_mBH_n are considered, because the relative orderings of the AH_m group orbitals *with respect to* those of the BH_n group orbitals are not determined. For example, CH_3 group orbitals might, in principle, be represented by the molecular orbitals of NH_3, CH_3^-, or CH_3^+ in their pyramidal configurations; and the NH_2 group orbitals might be represented by those of H_2O and BeH_2 in their bent configurations. However, there is an ambiguity as to which combinations of these fragments are appropriate for the construction of the correlation diagram of CH_3NH_2. Therefore, there is a need for an alternative definition of group orbitals which can remove this ambiguity and, at the same time, remain as practical and useful as the conventional definition.

Figure 1 shows the molecular orbitals and the orbital energies of CH_3^+, CH_4, and CH_3^-.[4] It is seen that the nodal properties and relative orderings of the molecular orbitals are the same in CH_3^+ and CH_3^-, as expected from the Mulliken–Walsh model (4, 9). If the hydrogen atom located on the *z*-axis (see Fig. 1) is removed from CH_4, the orbitals of the resulting truncated fragment are found not only to have nodal properties similar to those of the CH_3^+ and CH_3^- molecular orbitals, but also relative orderings which are the same as those of the CH_3^+ or CH_3^- molecular orbitals, if it is considered that those orbitals from which the hydrogen lobe is removed by the truncation show a slight increase in their orbital eigenvalues.[5]

On the basis of these observations, a procedure for obtaining group orbitals will be formulated as follows:

(*a*) the nodal properties of the group orbitals

[4]Unless stated otherwise, the *ab initio* SCF molecular orbitals were generated from wavefunctions computed with double ζ quality basis sets using contracted gaussian type functions: $(13^s7^p/4^s2^p)$ basis set for C, N, O, and F atoms (23*a*), and a $(4^s/2^s)$ basis set for H atom (23*b*).

[5]A slight elongation of the CH bond on the *z*-axis (Fig. 1) reduces the point symmetry from T_d to C_{3v}, and causes a splitting of the three degenerate molecular orbitals. See also ref. 24.

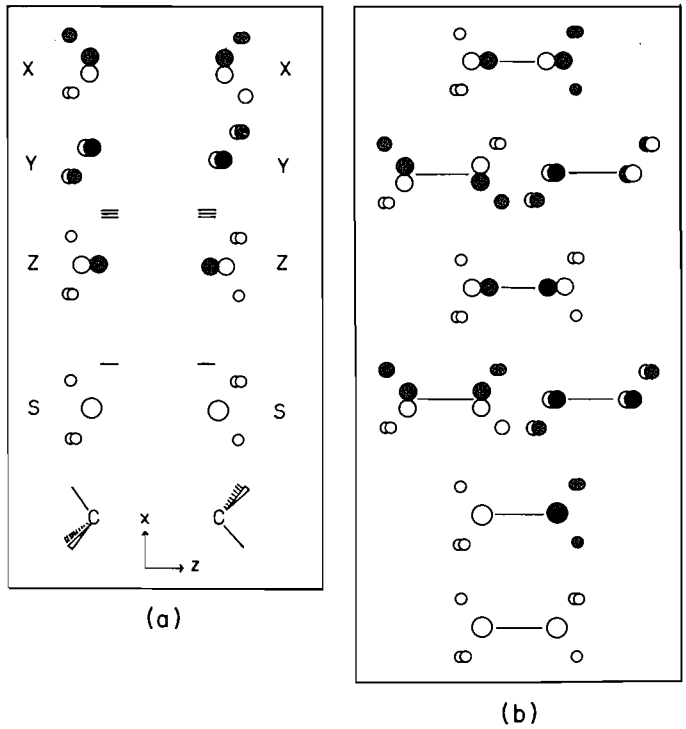

FIG. 2. (*a*) Construction of the molecular orbitals of ethane in terms of the group orbitals of two methyl groups. (*b*) Schematic representation of the molecular orbitals of ethane.

of a fragment are generated from the molecular orbitals of the molecule that would be formed from this fragment by the addition of a hydrogen atom. This scheme is also applied in the case of charged fragments, so that the group orbitals of, for example, $—CH_2^+$ and $—CH_2^-$ are obtained from the molecular orbitals of CH_3^+ and CH_3^-, respectively;

(*b*) the orbital eigenvalues are assumed to be affected in the same way, whether a hydrogen is removed from AH_{m+1} to generate $—AH_m$ or from BH_{n+1} to generate $—BH_n$. The relative positions of the orbital energies of the $—AH_m$ and $—BH_n$ fragments are then obtained from those of AH_{m+1} and BH_{n+1}. The splitting of degenerate molecular orbitals, where this is possible, as a result of symmetry reduction by the removal of a hydrogen atom, will be neglected.

The procedure just described contains a number of assumptions. In the discussion which follows, our objective is to determine whether these group orbitals, coupled with the qualitative orbital interaction model, have predictive utility or permit the rationalization of various experimental observations. It must be emphasized that the present definition of group orbitals is not unique, and that other definitions may exist which allow the ambiguity in the conventional definition to be resolved.

Molecular Orbitals as a Linear Combination of Group Orbitals

Attempts to construct molecular orbitals from group orbitals began with the work of Mulliken in the 1930s (24). For the most part, correlation diagrams between molecular orbitals and group orbitals have tended to emphasize A_2H_{2m} systems (4, 21*b*). In this section, the nodal properties and orderings of the molecular orbitals of AH_mBH_n are examined in terms of those of the $—AH_m$ and $—BH_n$ group orbitals, determined by the procedure described above.

To begin the discussion, the well-known correlation between atomic and molecular orbitals of diatomics (25) is considered first. For homonuclear and heteronuclear diatomic molecules, the nodal properties and orderings of the

Can. J. Chem. Downloaded from www.nrcresearchpress.com by 210.87.254.6 on 09/05/12
For personal use only.

Can. J. Chem. Downloaded from www.nrcresearchpress.com by 210.87.254.6 on 09/05/12
For personal use only.

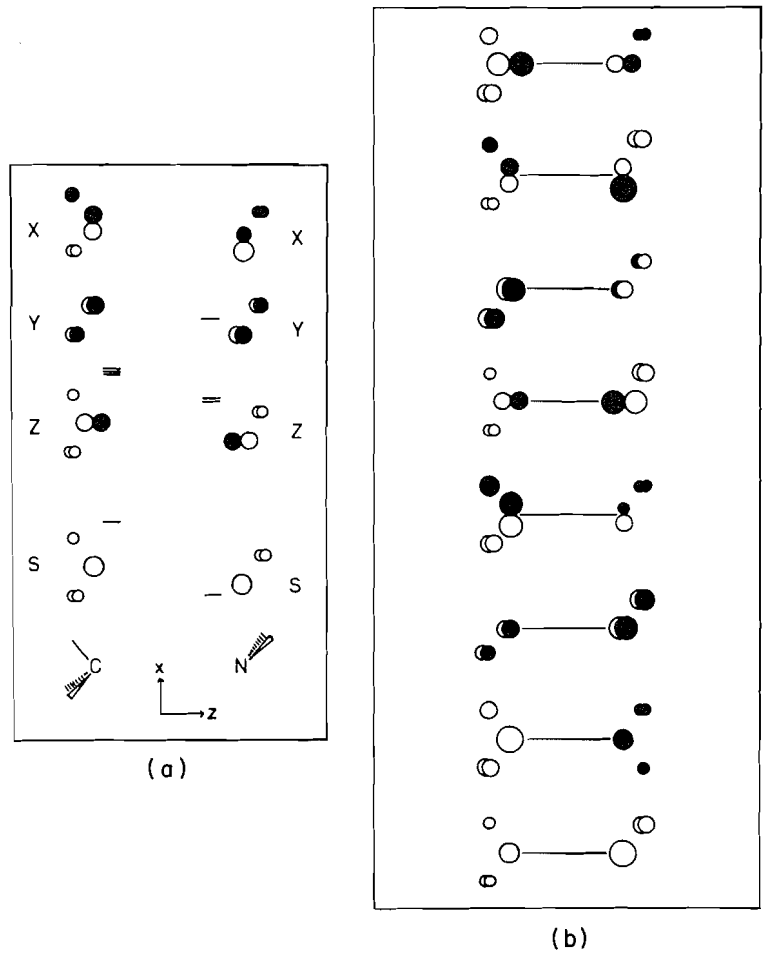

FIG. 3. (*a*) The group orbitals of $-CH_3$ and $-NH_2$ employed in the construction of the molecular orbitals of CH_3NH_2. (*b*) Schematic representation of the molecular orbitals of CH_3NH_2.

molecular orbitals can be represented qualitatively by [1]

$$[1] \quad \sigma_s^+ < \sigma_s^- < \pi_x^+ = \pi_y^+ < \sigma_z^+ < \pi_x^- = \pi_y^- < \sigma_z^-$$

with the internuclear axis chosen as the z-axis. The symbols + and − represent, respectively, the in-phase (bonding) and out-of-phase (antibonding) combinations of the two atomic orbitals, and the subscripts s, x, y, and z refer to the ns, np_x, np_y, and np_z atomic orbitals, respectively, where n is the principal quantum number of the valence atomic orbitals. Core electrons are not included in [1], for which several different notations have been employed (25).

The orderings shown in [1] are usually found to be correct for the resulting molecule, but there are instances in which the relative position of the σ_z^+ molecular orbital changes with respect to the π_x^+ and π_y^+ (or π_x^- and π_y^-) molecular orbitals (25). For homonuclear diatomics, the relative weights of the two atomic orbitals in a molecular orbital are, of course, the same. For heteronuclear diatomics, a larger weight is given to the lower-lying atomic orbital in an in-phase combination, and to the higher-lying atomic orbital in an out-of-phase combination (2*a*, 18, 25*b*).

Several polyatomic molecules will now be examined to determine whether empirical 'rules' can be found, such as [1] for diatomics, which allow the nodal properties and orderings of the molecular orbitals of the whole molecule to be correlated with those of the group orbitals.

Can. J. Chem. Downloaded from www.nrcresearchpress.com by 210.87.254.6 on 09/05/12
For personal use only.

Figure 2 shows the group orbitals of two CH_3 fragments and the molecular orbitals of C_2H_6. Here a convention is adopted in which the group orbitals are arranged so that the bond formed upon combination of the two fragments (in this case, the CC bond) lies on the z-axis. To simplify the notation, the symbols S, X, Y, and Z are employed to identify each individual group orbital (see Fig. 2*a*), and these are assigned by reference to the carbon $2s$, $2p_x$, $2p_y$, and $2p_z$ orbitals which are present in the group orbitals under the given coordinate system. In general AH_mBH_n systems, these orbitals are assigned by reference to the valence atomic orbitals ns, np_x, np_y, and np_z of A and B.[6]

It is now observed that the nodal properties and orderings of the C_2H_6 molecular orbitals are related to those of the CH_3 group orbitals in the following way:

$$[2]\quad (S_a + S_b) < (S_a - S_b) < (X_a + X_b) = (Y_a + Y_b) < (Z_a + Z_b) < (X_a - X_b) = (Y_a - Y_b) < (Z_a - Z_b)$$

in which the symbols + and − again represent the in-phase and out-of-phase combinations, respectively. The subscripts a and b refer to the methyl groups at each end of the CC bond.

A second example is presented in Fig. 3, which shows the correlation between the CH_3NH_2 molecular orbitals and the $-CH_3$ and $-NH_2$ group orbitals. The nodal properties and orderings of the CH_3NH_2 molecular orbitals are seen to be related to those of the $-CH_3$ and $-NH_2$ group orbitals as follows:

$$[3]\quad (\delta S_a + S_b) < (S_a - \delta S_b) < (\delta Y_a + Y_b) < (X_a + \delta X_b) < (\delta Z_a + Z_b) < (Y_a - \delta Y_b) < (\delta X_a - X_b) < (Z_a - \delta Z_b)$$

In this notation, $0 < \delta < 1$, and a and b refer to the $-CH_3$ and $-NH_2$ fragments, respectively.

These examples suggest that the nodal properties of the molecular orbitals of molecules AH_mBH_n can be approximated by pairwise combinations of $-AH_m$ and $-BH_n$ group orbitals that have the same symmetry (*i.e.*, S, X, Y, and Z). By analogy with diatomic systems, [2] and [3] can be simplified to [4] and [5], respectively.

$$[4]\quad \sigma_S^+ < \sigma_S^- < \pi_X^+ = \pi_Y^+ < \sigma_Z^+ < \pi_X^- = \pi_Y^- < \sigma_Z^-$$

$$[5]\quad \sigma_S^+ < \sigma_S^- < \pi_Y^+ < \pi_X^+ < \sigma_Z^+ < \pi_Y^- < \pi_X^- < \sigma_Z^-$$

There is a striking similarity between [1] and [4]. The common feature of [4] and [5] is

$$[6]\quad \sigma_S^+ < \sigma_S^- < \pi^+\text{'s} < \sigma_Z^+ < \pi^-\text{'s} < \sigma_Z^-$$

which is now generalized as *Rule I*.

For each pairwise combination, the relative weights of the two group orbitals can be assigned by application of the usual first and second order orbital interaction diagrams (2*a*, 18, 25*b*) to the two group orbitals under consideration, as in the case of diatomics. The relative orderings of the two pairs of nondegenerate π molecular orbitals (*i.e.*, π_X^+ and π_Y^+ or π_X^- and π_Y^-) in [5] are then explained as follows:

(*a*) the major contributor to π_X^- is the higher-lying of the two X group orbitals, and the major contributor to π_Y^- is the higher-lying of the two Y group orbitals. The higher-lying of the two π^- molecular orbitals is then decided by whichever major contributor (X or Y) is higher-lying

(*b*) the major contributors to π_X^+ and π_Y^+ are the lower-lying of the two X and Y group orbitals, respectively, and the lower-lying group orbital of these two major contributors decides the lower-lying π^+ molecular orbital. These are designated *Rule II*.

Rules I and II permit the nodal properties and orderings of the AH_mBH_n molecular orbitals to be derived qualitatively in terms of the $-AH_m$ and $-BH_n$ group orbitals. Their utility will be demonstrated in the next section by a consideration of various specific examples. From the electronic structures of various

[6]According to this convention, two of the np atomic orbital axes of the atom A of a pyramidal AH_2— group (*e.g.*, NH_2—) will not be aligned exactly along the given coordinate axes. Since this np atomic orbital can be decomposed into np_x, np_y, and np_z components, the axis of the largest contributor can be chosen to label the group orbital type (*i.e.*, X, Y, Z). For convenience, the AH_2— group can be arranged so that the np atomic orbital axis of the AH_3 HOMO is perpendicular to the z-axis (*e.g.*, the arrangement of the NH_2— group in Fig. 3*a*).

AH_mBH_n systems, the AB bond type may be classified as follows:[7]
a single bond has the structure

[7] $$(\sigma_S^+)^2(\sigma_S^-)^2(\pi^+)^4(\sigma_Z^+)^2(\pi^-)^4$$

a double bond has the structure

[8] $$(\sigma_S^+)^2(\sigma_S^-)^2(\pi^+)^4(\sigma_Z^+)^2(\pi^-)^2$$

a triple bond has the structure

[9] $$(\sigma_S^+)^2(\sigma_S^-)^2(\pi^+)^4(\sigma_Z^+)^2$$

Applications of Group Orbital Interaction Diagrams

In the ground state of a closed shell AH_mBH_n system, the σ_Z^+ orbital (commonly denoted σ_{AB}) is doubly occupied, and the σ_Z^- orbital (σ_{AB}^*) is unoccupied. Therefore, if the occupancy of each of the Z type AH_m— and BH_n— group orbitals is assumed to be one, the occupancies of the S, X, and Y type group orbitals can be taken to be the same as those of the molecular orbitals from which they are derived.

There are a number of systems in which it appears that molecular shapes and conformations are dictated by the nature of the highest occupied molecular orbital (4*c*, 8*b*, 8*c*, 26). In particular, molecules of the type AH_mBH_n of a given electronic state tend to adopt that conformation which leads to the lowest possible energy level for the highest occupied molecular orbital. Since, in most AH_mBH_n systems, the σ_Z^+ orbital is not the HOMO, this finding can be rephrased as follows for the PMO treatment: a molecule adopts that conformation which has a maximum two-electron stabilization between the frontier group orbitals of X and Y symmetries and/or a minimum destabilization between the group orbitals which contribute to the HOMO, when the HOMO is of π^- type. Both of these have the effect of lowering the energy of the HOMO. This accounts for the success of conformational analysis based on a consideration of the π-type group orbital interactions across the broken bond.

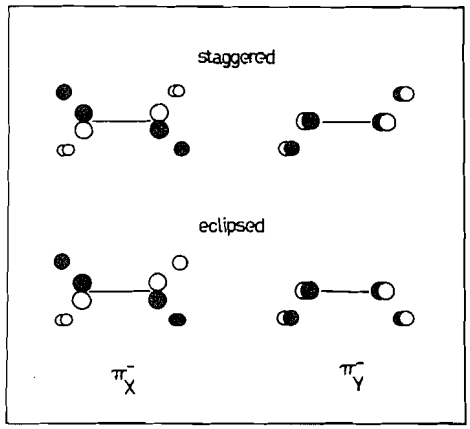

FIG. 4. Schematic representation of the HOMOs of ethane.

The electronic structures and conformations of various molecular systems may now be discussed. As usual, the argument is qualitative in the sense that a first order interaction is larger than a second order interaction, and a large overlap or a small energy gap between the two group orbitals leads to a large second order interaction (2*a*). The examples which follow include two typical and much-studied A_2H_{2m} systems, ethane and hydrazine. They are included for two reasons: (*i*) to establish an argument which will be employed later on to explain the change in the shape of a group when the system is changed from A_2H_{2m} to AH_mBH_n; (*ii*) and to show that the present group orbitals lead to the same predictions as those obtained with the conventional group orbitals. Some repetition of other work is, therefore, necessary.

(A) C_2H_6

A molecular orbital interpretation of the barrier to internal rotation in ethane has been given by Lowe (4*c*, 4*d*), by consideration of the end-to-end hydrogen interactions in the ethane HOMO (4*c*). Essentially the same argument results upon consideration of the group orbital interactions in the ethane HOMOs. The HOMOs of the eclipsed and staggered conformations shown in Fig. 4 correspond to π_X^- and π_Y^-. In both cases the interaction between the group orbitals is destabilizing, but the destabilization

[7]As in the case of [1] for diatomics, the orderings predicted by rules I and II are not always correct. However, it is always possible to use this qualitative molecular orbital construction scheme to interpret the results of MO calculations. The usual exceptions are as follows: for triple bonded systems, the σ_Z^+ MO comes right after the σ_S^- MO; for double bonded systems, the σ_Z^+ MO follows immediately after the lower-lying π^- MO and in some cases, it is the higher-lying π^+ MO and not the π^- MO which becomes the HOMO.

Can. J. Chem. Downloaded from www.nrcresearchpress.com by 210.87.254.6 on 09/05/12
For personal use only.

Can. J. Chem. Downloaded from www.nrcresearchpress.com by 210.87.254.6 on 09/05/12
For personal use only.

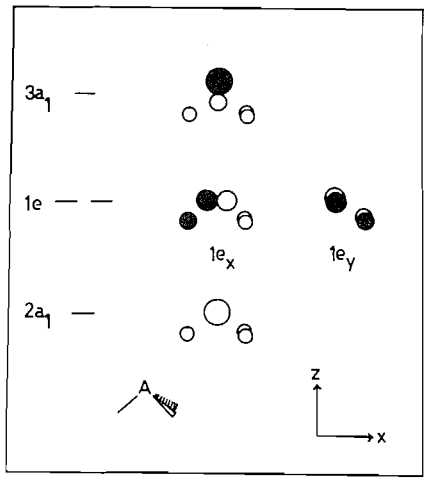

FIG. 5. Schematic representation of the molecular orbitals of molecules AH_3.

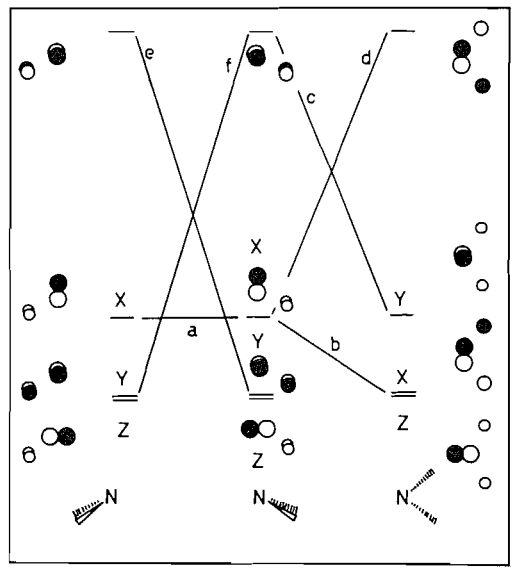

FIG. 6. Group orbital interaction diagram for NH_2NH_2. The combination I*a* and II leads to the *syn* and *anti* conformations, and that of I*b* and II to the *gauche* conformation.

is greater in the eclipsed conformation, because the magnitude of the overlap, for example, between the Y group orbitals which form π_Y^-, is greater in this conformation.

As to the shapes of the two methyl groups, it will be noted that the X and Y group orbitals that form the degenerate HOMOs have the same nodal property as the $1e_x$ and $1e_y$ molecular orbitals of the general molecule AH_3 (see Fig. 5); when these constitute the HOMO of AH_3, the molecule is planar (8). Therefore, if this nodal property were to have a dominant effect upon the shapes of the methyl groups in ethane, a flattening of these groups might be expected. However, the antibonding nature of the interaction between the group orbitals which make up the HOMOs cannot be ignored. Since this antibonding character is larger in the eclipsed conformation, it can be predicted that the HCH valence angle will be smaller in this conformation. This prediction parallels the result obtained in the geometry optimization study of Veillard (27).

(B) NH_2NH_2

The group orbital interaction diagrams required for the construction of the NH_2NH_2 molecular orbitals are shown in Fig. 6. The molecular orbital construction scheme (rules I and II) leads to [10]

$$[10] \quad \pi_Y^+ < \pi_X^+ < \sigma_Z^+ < \pi_Y^- < \pi_X^-$$

for the *syn* and *anti* conformations, and to [11]

$$[11] \quad \pi_Y^+ = \pi_X^+ < \sigma_Z^+ < \pi_Y^- = \pi_X^-$$

for the *gauche* conformation.[8]

The *gauche* conformation of N_2H_4 has C_2 symmetry, and, thus, has no degenerate representation. Therefore, the degeneracies observed in [11] (*i.e.*, $\pi_Y^+ = \pi_X^+$ and $\pi_Y^- = \pi_X^-$) are an accidental result of the simple molecular orbital construction scheme. However, it should be noted that *ab initio* calculations on N_2H_4 reveal these levels to be nearly degenerate (21*a*, 28). Otherwise, the orderings derived in [11] are in agreement with the results of the *ab initio* calculations, but there are some discrepancies in the orderings predicted by [10]. According to the work of Fink *et al.* (28*a*), the molecular orbital levels of the *syn* and *anti* conformations of N_2H_4 should be represented as in [12], and are the same as in ethylene (4, 21*b*).[7]

$$[12] \quad \pi_Y^+ < \sigma_Z^+ < \pi_Y^- < \pi_X^+ < \pi_X^-$$

The interaction which leads to the HOMO of the *syn* and *anti* conformations is first order (interaction *a*), and in the *gauche* conformation,

[8]Here the term '*gauche*' refers to a conformation in which one $—NH_2$ group is rotated by 90° from the *syn* (or *anti*) conformation.

Can. J. Chem. Downloaded from www.nrcresearchpress.com by 210.87.254.6 on 09/05/12
For personal use only.

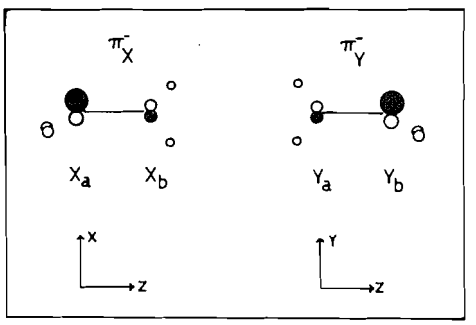

FIG. 7. Schematic representation of the HOMOs of NH_2NH_2.

it is second order (interaction *b*). Since this interaction is destabilizing, the *gauche* conformation of N_2H_4 should be more stable than the *syn* and *anti* conformations. The same conclusion is reached when the two-electron stabilizing interactions between the frontier group orbitals are considered (interactions *c*, *d*, *e*, and *f*). It follows that the *gauche* conformation is predicted to be more stable than either the *syn* or *anti* conformations because there is both minimization of the destabilizing interaction and maximization of the stabilizing interactions, and both of these effects lower the orbital energy of the HOMO.[9]

The orbital interaction diagrams shown in Fig. 6 apply to all singly bonded A_2H_4 systems. We may therefore proceed to a consideration of the nodal property of the $-AH_2$ group orbitals in the A_2H_4 HOMOs. These are shown schematically in Fig. 7 which is the result of the second order orbital interaction leading to the HOMO (see Fig. 6).[10] The major components of the two HOMOs are X_a and Y_b, and their nodal properties are the same as that of the $3a_1$ molecular orbital of the general molecule AH_3 except for the deletion of one hydrogen lobe. This nodal property will thus cause the $-AH_2$ groups of A_2H_4 to be pyramidal. The group orbitals X_b and Y_a are minor components of the HOMOs; their nodal characters are the same as that of the $1e$ molecular orbital of AH_3 and tend to make the $-AH_2$ groups planar. Since the latter effect is less because of the lower weight, it is expected that the $-AH_2$ groups of A_2H_4 will be pyramidal, but less so than in AH_3. This prediction is compatible with the available experimental and theoretical data (28*c*, 29).

In general, the relative heights of barriers to linear or pyramidal inversion are related in a simple way to the degree of angle deformation associated with the conformational change (30). On this basis, the decreased pyramidality of $-AH_2$ in A_2H_4 as compared to AH_3 seems to require that pyramidal inversion of the group $-AH_2$ in A_2H_4 should have a lower barrier than that of AH_3. This is not observed (28*b*, 29). The reason for the failure of this simple argument can be seen upon consideration of the antibonding nature of the interaction between the two $-AH_2$ group orbitals of the A_2H_4 HOMO *both* in the ground state *and* in the transition state of the pyramidal inversion process. However, since the HOMO of AH_3 in the transition state is a pure p_z-orbital of the atom A (see Fig. 6), it has no antibonding character and is stabilized with respect to the HOMO of AH_2 in A_2H_4 in its planar transition state. Therefore, to understand the increased barrier to pyramidal inversion of the $-AH_2$ group in A_2H_4, it is necessary to consider both the destabilization of its transition state resulting from the antibonding nature of the transition state HOMO, as well as the angle deformation.

(C) PH_2NH_2

Ab initio calculations on aminophosphine reveal the most stable conformation to be **1**, in which the nitrogen atom has trigonal planar geometry (31). A recent CNDO/2 calculation by Berthelat *et al.* (32), in which the HNH and HNP and also the HPH and HPN valence angles were optimized separately, has found the NH_2 moiety to be slightly nonplanar. These

1 **2** **3** **4**

[9]In the literature (16, 28*b*, 28*c*), there is a tendency to equate stabilizing and destabilizing orbital interactions with repulsive and attractive interactions (or "repulsion" and "attraction"), respectively. These qualitative ideas should, however, not be confused with the more rigorously derived V_{ee} (electron–electron repulsion) and V_{ne} (electron–nuclear attraction).

[10]In the present qualitative treatment, π_X^- and π_Y^- are degenerate. Consequently, the HOMOs may also be represented by their linear combinations, $(\pi_X^- + \pi_Y^-)$ and $(\pi_X^- - \pi_Y^-)$, which are the nodal properties observed in the SCF–MO computation (21*a*, 28*b*, 28*c*). The following discussion is not affected by the use of these MOs.

Can. J. Chem. Downloaded from www.nrcresearchpress.com by 210.87.254.6 on 09/05/12
For personal use only.

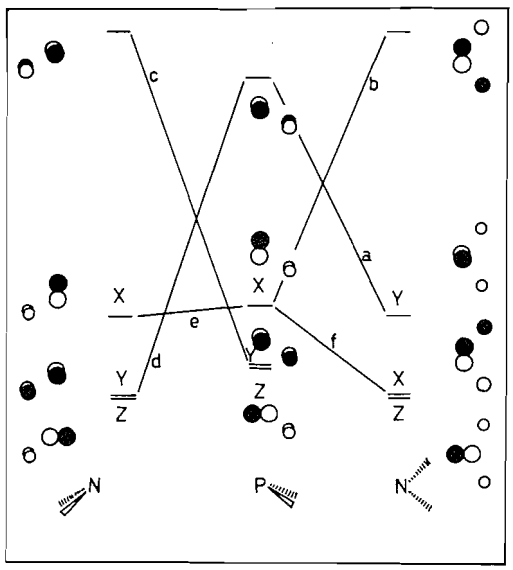

FIG. 8. Group orbital interaction diagram for PH_2NH_2. The combination *Ia* and II leads to conformations **3** and **4**, and that of *Ib* and II to conformation **2**.

workers have therefore suggested that the planarity of nitrogen found by Csizmadia *et al.* (31) may be due to the restriction that $\angle$ HNH = $\angle$ HNP in the optimization procedure. We have performed *ab initio* computations on PH_2NH_2 at the STO-3G level, using the same restriction employed by Csizmadia *et al.* (31), which reveals that the $-NH_2$ group is nonplanar ($\angle$ HNH = 105° in NH_3 and 114° in the NH_2 group of the stable conformation of PH_2NH_2). The point of interest from all of these computations is that the NH_2 moiety of PH_2NH_2 is significantly more planar than NH_3.

The group orbital interaction diagrams are shown in Fig. 8.[11] Consideration of the two-electron stabilizing interactions (*a*, *b*, *c*, and *d*) shows that the *gauche* conformation **2** is the most stable. Information concerning the geometries at nitrogen and phosphorous can be obtained from the molecular orbital construction scheme, which leads to [13]

$$[13] \quad \pi_X^+ < \pi_Y^+ < \sigma_Z^+ < \pi_Y^- < \pi_X^-$$

for the PH_2NH_2 molecular orbitals in the *gauche* conformation. The *ab initio* calculation on conformation **1** shows that these orderings are

[11]The MOs of PH_3 were computed with the 4-31G basis set of the GAUSSIAN 70 program system (33).

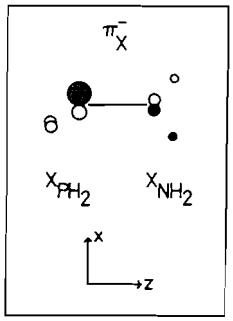

FIG. 9. Schematic representation of the HOMO of PH_2NH_2.

correct except for an interchange between π_Y^+ and σ_Z^+ in [13] (31).

Consideration of the destabilizing interactions which form the HOMOs also leads to the prediction that the *gauche* conformation is more stable than the *syn* (**3**) and *anti* (**4**) conformations (interactions *e* and *f*). A schematic representation of the nodal property of the PH_2NH_2 HOMO in the *gauche* conformation is seen in Fig. 9. The group orbital of the $-PH_2$ moiety has the same nodal property as the $3a_1$ molecular orbital of AH_3, so that the $-PH_2$ group should remain pyramidal. However, the group orbital of the $-NH_2$ moiety in this HOMO has the nodal property of the 1*e* molecular orbital of AH_3. This will tend to make the $-NH_2$ group planar. An alternative rationalization may be offered, in terms of the electron transfer associated with interactions *a* and *b*. On the basis of the energy differences associated with *a* and *b*, more electron transfer is expected in the case of *a*. This will cause greater loss of pyramidal character or, equivalently, greater tendency toward planarity in the $-NH_2$ group.

Csizmadia *et al.* (31) have rationalized their findings on PH_2NH_2 in terms of inductive electron release from P to N. It seems well established (34) that electron withdrawal from a tricoordinate atom causes relative stabilization of the pyramidal structure, while electron release to a tricoordinate atom causes relative stabilization of the planar structure. In aminophosphine, a Mulliken population analysis shows that the $-PH_2$ group has a net decrease in charge, and is an electron releasing ligand when attached to $-NH_2$. An argument based upon inductive effects is based on the electro-

Can. J. Chem. Downloaded from www.nrcresearchpress.com by 210.87.254.6 on 09/05/12
For personal use only.

negativity difference between the directly bonded tricoordinate atoms. On the other hand, the present analysis depends upon the relative energy levels of the group orbitals associated with these atoms. For the specific cases of PH_3 and NH_3, the molecular orbitals associated with the less electronegative atom (*i.e.*, the electron donor) have a relatively higher energy level (see Fig. 8), so that a common basis can be found for seemingly different interpretations.

If the same analysis is applied to the HOMOs of the *syn* and *anti* conformations of PH_2NH_2, the $-PH_2$ and $-NH_2$ group orbitals in the PH_2NH_2 HOMOs are both found to have the same nodal property as the $3a_1$ molecular orbital of AH_3 (see Fig. 8). Therefore, in the *syn* and *anti* conformations of PH_2NH_2, *both* the $-PH_2$ *and* the $-NH_2$ groups are predicted to be pyramidal. This prediction has been checked by *ab initio* computations and has been found to be correct (31*b*).

The major contributor of the π_Y^- molecular orbital of *gauche* PH_2NH_2 is the *Y* group orbital of $-NH_2$, whose nodal property is the same as that of the $3a_1$ molecular orbital of AH_3. In a qualitative sense, the π_X^- and π_Y^- molecular orbitals of *gauche* PH_2NH_2 may, therefore, be equated with the phosphorus and nitrogen lone pairs, respectively; and the phosphorus lone pair is higher in energy than the nitrogen lone pair. However, the photoelectron spectra (35) of substituted aminophosphines, in which the substituents of P are electron withdrawing and those of N are electron releasing, have been interpreted to mean that the nitrogen lone pair is higher in energy than the phosphorus lone pair. This point will be reconsidered later in this paper.

(D) NH_2BH_2

Aminoborane exemplifies a compound in which one of the two π^- molecular orbitals is not occupied. *Ab initio* calculations (36) have shown the planar structure **5** to be the energy minimum. However, geometry optimization of the orthogonal conformation (**6**) indicates (37) that the $-NH_2$ group has become pyramidal.

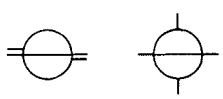

5 **6**

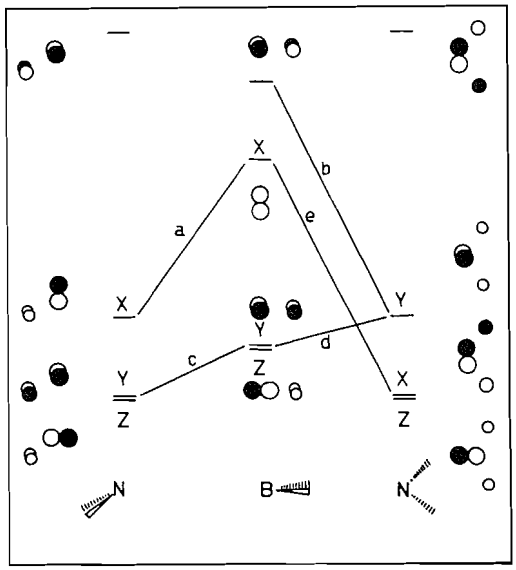

FIG. 10. Group orbital interaction diagram for NH_2BH_2. The combination of I*a* and II leads to conformation **7**, and that of I*b* and II to conformation **8**.

The group orbital interaction diagram for NH_2BH_2 is shown in Fig. 10, making use of the molecular orbitals of pyramidal NH_3 and planar BH_3.[12] Comparison of the group orbital interactions *a* and *b* indicates that conformation **7** will be more stable than conformation **8**.

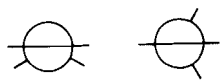

7 **8**

For the application of the molecular orbital construction scheme, the nodal properties and orderings of the NH_2BH_2 molecular orbitals in **7** and **8** are derived first as shown in [14] and [15],

$$[14] \quad \pi_Y^+ < \sigma_Z^+ < \pi_X^+ < \pi_Y^- < \pi_X^-$$

$$[15] \quad \pi_X^+ < \sigma_Z^+ < \pi_Y^+ < \pi_Y^- < \pi_X^-$$

respectively.[13] These orderings are found to be the same as those of the *ab initio* computations of Armstrong *et al.* (36) with a planar $-NH_2$. In their calculations, the orderings of the π_X^+ and π_Y^- levels in the planar structure are the

[12]The MOs of BH_3 have been taken from ref. 21*a*.

[13]In [14] and [15], the ordering of the σ_Z^+ MO and the higher-lying π^+ MO is not the same as that predicted by rules I and II. See footnote 7.

Can. J. Chem. Downloaded from www.nrcresearchpress.com by 210.87.254.6 on 09/05/12
For personal use only.

reverse of those predicted by [14] when small basis sets are used,[14] but the orderings of these two levels are the same as those predicted by [14] when a large basis set is employed. The interactions which lead to the HOMOs of conformations **7** and **8** are shown as *c* and *d* in Fig. 10.

Our analysis can be carried further. In NH_2BH_2, π_X^+, π_Y^+, and π_Y^- are occupied, but π_X^- is not. Therefore, any stabilization of π_Y^+ is offset by the destabilization of π_Y^-, so that the stability of the system is decided by the stabilization of π_X^+.[15] For example, consideration of interactions *a* and *e* again leads to the prediction that conformation **7** is more stable than conformation **8**.

Turning to the shape of the $-NH_2$ moiety, it can be seen that the group orbital of the $-NH_2$ moiety in the HOMO of conformation **7** has the same nodal property as the 1*e* molecular orbital of AH_3. Such nodal property will tend to make the $-NH_2$ group planar in this conformation.[16] On the other hand, the group orbital of the $-NH_2$ moiety in the HOMO of conformation **8** has the nodal property of the $3a_1$ molecular orbital of AH_3. This would tend to make the $-NH_2$ group pyramidal in conformation **8**. Therefore, the change in the geometry of the $-NH_2$ group which takes place during rotation in aminoborane is rationalized in terms of the same model that accounted for the *planarity* of the $-NH_2$ moiety in aminophosphine.

(E) The Model Ylids $\dot{S}H_2\bar{C}H_2$ and $\dot{P}H_3\bar{C}H_2$

The electronic structures of ylids are usually written (38) as resonance hybrids of ylids and ylene forms, *e.g.*,

$$\geqslant\overset{+}{P}-\overset{-}{C}< \longleftrightarrow \geqslant P=C<$$

Although several kinds of experimental observations point to the ylene structure (39), the most recent experimental (40) and theoretical (41) results tend to favor the ylid structure.

The group orbital interaction diagram for

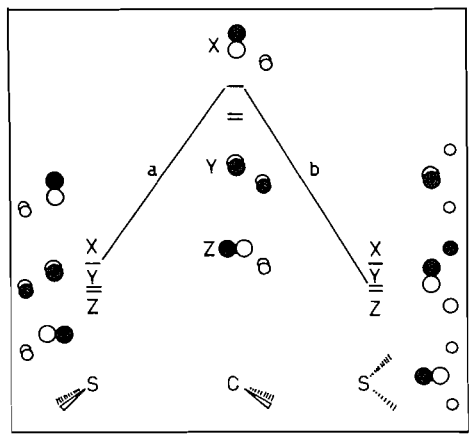

FIG. 11. Group orbital interaction diagram for $\dot{S}H_2\bar{C}H_2$. The combination of I*a* and II leads to the *syn* and *anti* conformations, and that of I*b* and II to the *gauche* conformation.

$\dot{S}H_2\bar{C}H_2$ is shown in Fig. 11. In the construction of this diagram, the group orbitals were obtained from the molecular orbitals of SH_3^+ and CH_3^-.[17] The $\dot{S}H_2\bar{C}H_2$ molecular orbitals of the *gauche* and *syn* (*anti*) conformations are characterized in terms of the molecular orbital construction scheme as shown in [16] and [17], respectively.

[16] $\pi_X^+ < \pi_Y^+ < \sigma_Z^+ < \pi_Y^- < \pi_X^-$

[17] $\pi_Y^+ < \pi_X^+ < \sigma_Z^+ < \pi_Y^- < \pi_X^-$

These orderings agree with the results of the *ab initio* computations.[18] From the interactions *a* and *b*, which lead to the HOMOs, it is predicted that the *gauche* conformation is more stable. This prediction is confirmed by the above calculation.

The shapes of the $-CH_2^-$ and $-SH_2^+$ groups are now considered. In the HOMO of *gauche* $\dot{S}H_2\bar{C}H_2$, the major contributor is the *X* group orbital of the $-CH_2^-$ fragment, which has the same nodal property as that of the $3a_1$ molecular orbital of AH_3. The *X* group orbital of the

[14]That is, these basis sets cause aminoborane to have the same electronic structure as ethylene.

[15]This argument can be employed for systems whose electronic structure is represented by [8].

[16]The conventional explanation would emphasize the conjugation in the B—N bond, *i.e.*, the maximum stabilization of the π_X^+ molecular orbital.

[17]Calculated with the STO-3G basis sets of the GAUSSIAN 70 program system (33). The group orbitals derived from the unoccupied molecular orbitals are not shown in Fig. 11, because the LUMO of SH_3^+ lies lower than the HOMO of CH_3^-. In such a case, the simple orbital interaction picture breaks down as far as the two-electron stabilizing interactions are concerned. This is also the case for the group orbital interaction diagram shown in Fig. 12.

[18]Using an STO-3G basis set.

Can. J. Chem. Downloaded from www.nrcresearchpress.com by 210.87.254.6 on 09/05/12
For personal use only.

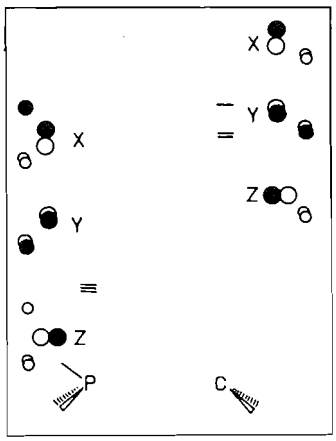

FIG. 12. Group orbital interaction diagram for $\dot{P}H_3\bar{C}H_2$.

$-SH_2^+$ fragment in this HOMO has the nodal property of the $1e$ molecular orbital of AH_3. Thus, the $-SH_2^-$ moiety will tend to be planar, while the $-CH_2^-$ group will remain pyramidal. In agreement with this prediction, the optimized HSH valence angle of *gauche* $\dot{S}H_2\bar{C}H_2$ is 101°, which shows a considerable increase from that of SH_3^+ (95.4°). On the other hand the optimized HCH valence angle of *gauche* $\dot{S}H_2\bar{C}H_2$ is 102°, which is only slightly different from that of CH_3^- (101°).

Inspection of the group orbital interaction diagram (Fig. 11) shows that, in *gauche* $\dot{S}H_2\bar{C}H_2$, the π_X^- molecular orbital can be characterized as the carbon lone pair orbital. The π_Y^- molecular orbital, which according to the molecular orbital construction scheme should have a larger weight on the Y group orbital of $-CH_2^-$ than on that of $-SH_2^+$, actually has a larger weight on $-SH_2^+$ in the SCF–MO calculation.[18,19] This orbital is characterized as the sulfur lone pair orbital. That is, the carbon lone pair lies higher in energy than the sulfur lone pair in $\dot{S}H_2\bar{C}H_2$. This result would not have been predicted if the orbital energy levels of the highest occupied $-SH_2^+$ and $-CH_2^-$ group orbitals had been taken from the sulfur and carbon atomic orbitals, respectively (42). From the molecular orbital energy levels of CH_3^+, CH_4, and CH_3^- (see Fig. 1), it is evident that the presence of a formal positive charge on a group causes a lowering of all its orbital energies, and the presence of a formal negative charge causes a raising of all its orbital energies.[20] Electron-withdrawing and electron-releasing substituents may be considered to operate by producing fractional positive and negative charges on the attached central atoms, respectively. This permits an explanation of the photoelectron spectra of substituted aminophosphines, discussed earlier. Electron-withdrawing substituents on P would lower the group orbital energy levels of the P moiety in comparison to those of $-PH_2$ and electron-releasing substituents on N would raise the group orbital energy levels of the N moiety in comparison to those of $-NH_2$. The available photoelectron spectral data support this view (47).

In previous theoretical investigations of phosphonium ylids $\dot{P}R_3\bar{C}H_2$, $\dot{P}H_3\bar{C}H_2$ has been employed as a model compound (38, 41). However, these calculations have been performed with a planar geometry at carbon.

Figure 12 shows the group orbital interaction diagram of $\dot{P}H_3\bar{C}H_2$. The group orbitals were obtained from the molecular orbitals of PH_4^+ and CH_3^-.[18] The qualitative molecular orbital

9

construction scheme reveals that the molecular orbitals of $\dot{P}H_3\bar{C}H_2$ in conformation **9** can be characterized as shown in [18].

[18] $\quad \pi_Y^+ < \pi_X^+ < \sigma_Z^+ < \pi_Y^- < \pi_X^-$

[19]This finding, together with the comments made in footnote 17, indicate that group orbital energies obtained by the procedure presented herein are less satisfactory when used in group orbital interaction diagrams for molecules of the type $\dot{A}H_m\bar{B}H_n$ than for those of the type AH_mBH_n, $AH_m\dot{B}H_n$, or $AH_m\bar{B}H_n$. However, the qualitative conclusions that follow are not affected by this.

[20]A group that contains an atom bearing a formal positive (negative) charge is considered to be strongly electronegative (electropositive) (43). It follows that an electronegative (electropositive) group will be characterized by low-lying (high-lying) group orbitals. Since an absolute value of an orbital energy can be measured by the ionization potential (44), the above statement in a sense parallels the Mulliken definition of electronegativity (45); *i.e.*, the electronegativity of an atom is given as the average of its ionization potential and electron affinity, with the ionization potential the dominant term (46).

Can. J. Chem. Downloaded from www.nrcresearchpress.com by 210.87.254.6 on 09/05/12
For personal use only.

The major contributor of the $\dot{P}H_3\bar{C}H_2$ HOMO is the X group orbital of the $-CH_2^-$ fragment, which has the nodal property of the $3a_1$ molecular orbital of AH_3. This leads to the prediction that the $-CH_2^-$ moiety in $\dot{P}H_3\bar{C}H_2$ will be pyramidal. This is in agreement with the results of an *ab initio* geometry optimization of $\dot{P}H_3\bar{C}H_2$.[18] The orderings given in [18] are also confirmed. It may therefore be asked whether the experimentally observed planarity (39) of the $-CH_2^-$ group in $\dot{P}R_3\bar{C}H_2$ is a genuine property of the phosphonium ylid. Of course, one has to consider the limitations of the basis set employed in the present calculation.[18] Further, in the present study of $\dot{P}H_3\bar{C}H_2$ and $\dot{S}H_2\bar{C}H_2$, the two-electron stabilizing interactions between the lone pair orbital of $-\bar{C}H_2$ and vacant group orbitals of $-\dot{P}H_3$ and $-\dot{S}H_2$ have been neglected. A more detailed and systematic investigation of the model ylides, $\dot{P}H_3\bar{C}H_2$, $\dot{N}H_3\bar{C}H_2$, $\dot{S}H_2\bar{C}H_2$, and $\dot{O}H_2\bar{C}H_2$ will be reported elsewhere.

Conclusions

The range of examples that has been treated suggests that the definition of group orbitals presented herein may have some utility for an understanding of the shapes, conformations, and electronic structures of AH_mBH_n type molecules. When using the present definition of group orbitals, it is necessary to employ molecular orbitals calculated to the same degree of approximation, since the orbital eigenvalues of a molecular system depend upon the quality of the basis set.

Acknowledgments

We thank the National Research Council of Canada and the donors of the Petroleum Research Fund, administered by the American Chemical Society, for financial support of this research. We are also grateful to a referee for his helpful and critical comments, and to Professor N. D. Epiotis for stimulating discussions which initiated our interest in the type of analysis presented herein.

1. (*a*) R. Hoffmann and R. B. Woodward. Acc. Chem. Res. **1**, 17 (1968); (*b*) R. B. Woodward and R. Hoffmann. The conservation of orbital symmetry. Academic Press, New York. 1970.
2. (*a*) L. Salem. J. Am. Chem. Soc. **90**, 543 (1968); (*b*) K. Fukui. Acc. Chem. Res. **4**, 57 (1971); (*c*) R. G. Pearson. Acc. Chem. Res. **4**, 152 (1971); (*d*) N. D. Epiotis. J. Am. Chem. Soc. **94**, 1294 (1972) and subsequent papers in this series; (*e*) N. D. Epiotis. Angew. Chem. Int. Ed. Engl. **13**, 751 (1974).
3. (*a*) R. S. Mulliken. Rev. Mod. Phys. **14**, 204 (1942); (*b*) A. D. Walsh. J. Chem. Soc. 2260 (1953) and subsequent papers by this author.
4. (*a*) B. M. Gimarc. Acc. Chem. Res. **7**, 384 (1974); (*b*) R. M. Gavin. J. Chem. Educ. **46**, 413 (1969); (*c*) J. P. Lowe. J. Am. Chem. Soc. **92**, 3799 (1970); (*d*) J. P. Lowe. J. Am. Chem. Soc. **96**, 3759 (1974).
5. H. Nakatsuji. J. Am. Chem. Soc. **95**, 345 (1973); **95**, 354 (1973); **95**, 2084 (1973).
6. R. G. Pearson. J. Am. Chem. Soc. **90**, 1252 (1969); **90**, 4947 (1969); J. Chem. Phys. **52**, 2167 (1970); Chem. Phys. Lett. **10**, 31 (1971).
7. L. C. Allen. Theor. Chim. Acta, **24**, 117 (1973).
8. (*a*) C. A. Coulson and B. M. Deb. Int. J. Quantum Chem. **5**, 411 (1971); (*b*) B. M. Deb. J. Am. Chem. Soc. **96**, 2030 (1974); (*c*) B. M. Deb, P. N. Sen, and S. K. Bose. J. Am. Chem. Soc. **96**, 2044 (1974).
9. R. J. Buenker and S. D. Peyerimhoff. Chem. Rev. **74**, 127 (1974).
10. R. Hoffmann, L. Radom, J. A. Pople, P. v. R. Schleyer, W. J. Hehre, and L. Salem. J. Am. Chem. Soc. **94**, 6221 (1972).
11. W. J. Hehre and L. Salem. J. Chem. Soc. Chem. Commun. 754 (1973).
12. N. D. Epiotis, D. Bjorkquist, L. Bjorkquist, and S. Sarkanen. J. Am. Chem. Soc. **95**, 7558 (1973).
13. C. C. Levin, R. Hoffmann, W. J. Hehre, and J. Hudec. J. Chem. Soc. Perkin Trans. II, 201 (1973).
14. S. David, O. Eisenstein, W. J. Hehre, L. Salem, and R. Hoffman. J. Am. Chem. Soc. **95**, 3806 (1973).
15. R. Hoffmann. Acc. Chem. Res. **4**, 1 (1971).
16. N. D. Epiotis. J. Am. Chem. Soc. **95**, 3087 (1973).
17. O. Eisenstein, N. T. Anh, Y. Jean, A. Devaquet, J. Cantacuzène, and L. Salem. Tetrahedron, **30**, 1717 (1974).
18. W. L. Jorgensen and L. Salem. The organic chemist's book of orbitals. Academic Press, New York. 1973.
19. R. Hoffmann. J. Chem. Phys. **39**, 1397 (1963).
20. (*a*) C. A. Coulson and A. H. Neilson. Discuss. Faraday Soc. **35**, 71 (1963); **35**, 217 (1963); (*b*) D. Peters. Trans. Faraday Soc. **62**, 1353 (1966).
21. (*a*) L. C. Snyder and H. Basch. Molecular wave functions and properties. Wiley-Interscience, New York. 1972; (*b*) G. Herzberg. Molecular spectra and structure. III. Electronic spectra and electronic structure of polyatomic molecules. Van Nostrand, Princeton, N.J. 1950.
22. K. N. Houk. J. Am. Chem. Soc. **95**, 4092 (1973); K. N. Houk, J. Sims, R. E. Duke, Jr., R. W. Strozier, and J. K. George. J. Am. Chem. Soc. **95**, 7301 (1973); K. N. Houk, J. Sims, C. R. Watts, and L. J. Luskus. J. Am. Chem. Soc. **95**, 7287 (1973).
23. (*a*) S. Huzinaga and Y. Sakai. J. Chem. Phys. **50**, 1371 (1969); (*b*) H. Basch, M. B. Robin, and N. A. Kuebler. J. Chem. Phys. **47**, 1201 (1967).
24. R. S. Mulliken. J. Chem. Phys. **3**, 517 (1935); J. Chem. Phys. **3**, 506 (1935); Phys. Rev. **47**, 413 (1935).

25. (*a*) R. S. MULLIKEN. Rev. Mod. Phys. **4**, 1 (1932); (*b*) C. A. COULSON. Valence. Oxford University Press, London. 1965; (*c*) J. N. MURRELL, S. F. A. KETTLE, and J. M. TEDDER. Valence theory. John Wiley and Sons, New York. 1965; (*d*) H. B. GRAY. Electrons and chemical bonding. Benjamin, New York. 1964; (*e*) G. HERZBERG. Molecular spectra and molecular structure. I. Spectra of diatomic molecules. Van Nostrand, New York. 1950.
26. R. J. BUENKER, S. D. PEYERIMHOFF, and K. HSU. J. Am. Chem. Soc. **93**, 5005 (1971).
27. A. VEILLARD. Theor. Chim. Acta, **18**, 21 (1970).
28. (*a*) W. H. FINK and L. C. ALLEN. J. Chem. Phys. **46**, 2261 (1967); **46**, 2267 (1967); (*b*) R. HOFFMANN, C. C. LEVIN, and R. A. MOSS. J. Am. Chem. Soc. **95**, 639 (1973); (*c*) J. O. JARVIE and A. RAUK. Can. J. Chem. **52**, 2785 (1974).
29. (*a*) S. WOLFE, L. M. TEL, J. H. LIANG, and I. G. CSIZMADIA. J. Am. Chem. Soc. **94**, 1361 (1972); (*b*) D. R. LIDE. J. Chem. Phys. **22**, 1613 (1954) and references cited therein.
30. (*a*) J. B. LAMBERT. Top. Stereochem. **6**, 19 (1971); (*b*) A. RAUK, L. C. ALLEN, and K. MISLOW. Angew. Chem. Int. Ed. Engl. **9**, 400 (1970); (*c*) J. M. LEHN and B. MUNSCH. Mol. Phys. **23**, 21 (1972); (*d*) A. RAUK, L. C. ALLEN, and E. CLEMENTI. J. Chem. Phys. **52**, 4133 (1970).
31. (*a*) I. G. CSIZMADIA, A. H. COWLEY, M. W. TAYLOR, L. M. TEL, and S. WOLFE. J. Chem. Soc. Chem. Commun. 1147 (1972); (*b*) I. G. CSIZMADIA, A. H. COWLEY, M. W. TAYLOR, M.-H. WHANGBO, and S. WOLFE. To be published.
32. M. BERTHELAT, R. MATHIS, J.-F. LABARRE, and M. MATHIS. C.R. Ser. C, 645 (1975).
33. W. J. HEHRE, W. A. LATHAN, R. DITCHFIELD, M. D. NEWTON, and J. A. POPLE. Quantum Chemistry Program Exchange. Indiana University, Bloomington, Ind. No. 236.
34. (*a*) J. M. LEHN. Fortschr. Chem. Forsch. **15**, 311 (1970); (*b*) K. MISLOW. Trans. N.Y. Acad. Sci. Ser. II, **35**, 227 (1973).
35. A. H. COWLEY, M. J. S. DEWAR, J. W. GILJE, D. W. GOODMAN, and J. R. SCHWEIGER. J. Chem. Soc. Chem. Commun. 340 (1974).
36. D. R. ARMSTRONG, B. J. DUKE, and P. G. PERKINS. J. Chem. Soc. A, 2566 (1969).
37. O. GROPEN and H. M. SEIP. Chem. Phys. Lett. **25**, 206 (1974).
38. (*a*) R. HOFFMANN, D. B. BOYD, and S. Z. GOLDBERG. J. Am. Chem. Soc. **92**, 3929 (1970); (*b*) A. W. JOHNSON. Ylid chemistry. Academic Press, New York. 1966.
39. (*a*) H. SCHMIDBAUR. Adv. Organomet. Chem. **9**, 259 (1970) and references cited therein; (*b*) W. LÜTTKE and K. WILHELM. Angew. Chem. **77**, 867 (1965); (*c*) W. S. SAWDONY. Z. Anorg. Allg. Chem. **368**, 284 (1964); (*d*) J. C. J. BART. Angew. Chem. **80**, 697 (1968); J. Chem. Soc. B, 530 (1969).
40. (*a*) H. SCHMIDBAUR and W. TRÖNICH. Chem. Ber. **101**, 604 (1968); **100**, 1032 (1967); **101**, 595 (1968); (*b*) E. A. C. LUCKEN and C. J. MAZELINE. J. Chem. Soc. A, 1074 (1966); J. Chem. Soc. A, 439 (1967).
41. I. ABSAR and J. R. VAN WAZER. J. Am. Chem. Soc. **94**, 2382 (1972).
42. C. FROESE-FISCHER. At. Data, **4**, 301 (1972).
43. V. RAUTENSTRAUCH. Helv. Chim. Acta, **55**, 2233 (1972).
44. C. C. J. ROOTHAAN. Rev. Mod. Phys. **23**, 69 (1951).
45. P. R. WELLS. Prog. Phys. Org. Chem. **6**, 111 (1968).
46. H. O. PRITCHARD and H. A. SKINNER. Chem. Rev. **55**, 745 (1955).
47. A. H. COWLEY, M. J. S. DEWAR, D. W. GOODMAN, and M. C. PADOLINA. J. Am. Chem. Soc. **96**, 2648 (1974).

Can. J. Chem. Downloaded from www.nrcresearchpress.com by 210.87.254.6 on 09/05/12
For personal use only.

Molecular orbitals from group orbitals. II. Conformational analysis of systems with three heavy atoms. The XCH_2CH_2 system and the anomeric effect

MYUNG-HWAN WHANGBO[1] AND SAUL WOLFE
Department of Chemistry, Queen's University, Kingston, Ontario K7L 3N6

Received June 11, 1975[2]

MYUNG-HWAN WHANGBO and SAUL WOLFE. Can. J. Chem. **54**, 963 (1976).

A procedure for the conformational analysis of systems of the type $AH_mBH_nDH_k$ is proposed, in terms of interactions between AH_mBH_n— and —DH_k fragments. The nodal properties and relative level orderings of the group orbitals of these fragments are obtained from the molecular orbitals of the molecules AH_mBH_{n+1} and DH_{k+1}. Attention is focussed upon two-orbital two-electron stabilizing and two-orbital four-electron destabilizing interactions between these fragments. A consistent interpretation of the conformational behaviour of *n*-propyl and 2-fluoroethyl carbonium ions and carbanions is attempted within the framework of this group molecular orbital procedure. The conformational behaviour of FCH_2OH, a model for the anomeric effect, has also been examined. It is shown that the group molecular orbital approach accommodates two earlier interpretations of the anomeric effect, one of which focusses upon bond–bond interactions; the second focusses upon effects of the oxygen lone pairs. Some limitations of the model are noted, in particular the problem associated with explicit calculation of the magnitudes of different stabilizing and destabilizing interactions.

MYUNG-HWAN WHANGBO et SAUL WOLFE. Can. J. Chem. **54**, 963 (1976).

On propose une procédure pour l'analyse conformationnelle de systèmes du type $AH_mBH_nDH_k$; cette procédure est établie en termes d'interactions entre les fragments AH_mBH_n— et —DH_k. On obtient les propriétés nodales et les arrangements relatifs des niveaux des orbitales de groupe de ces fragments à partir des orbitales moléculaires des molécules AH_mBH_{n+1} et DH_{k+1}. On attire l'attention sur les interactions stabilisantes de deux électrons à deux orbitales et déstabilisantes de quatre électrons à deux orbitales entre ces fragments. On propose une interprétation cohérente du comportement conformationnel des ions carbonium et des carbanions *n*-propyle et fluoro-2 éthyle à l'intérieur du système de cette méthode d'orbitales moléculaires de groupe. On a aussi examiné le comportement conformationnel du FCH_2OH, un modèle pour l'effet anomérique. On a montré que l'approche des orbitales moléculaires de groupe est en accord avec deux interprétations antérieures de l'effet anomérique; une d'elle fait intervenir d'une manière principale les interactions entre liens alors que la deuxième fait appel principalement aux effets des paires d'électrons libres de l'oxygène. On note quelques limitations du modèle, en particulier dans le problème associé avec le calcul explicite des grandeurs de différentes interactions stabilisantes et déstabilisantes.

[Traduit par le journal]

Introduction

In Part I of this series (1), a perturbational molecular orbital (PMO) analysis of the electronic structures and conformations of AH_mBH_n systems was developed, in terms of the interactions between the AH_m— and BH_n— groups. The novel feature of the analysis was the use of *ab initio* wavefunctions of AH_{m+1} and BH_{n+1} to obtain the relative level orderings and nodal properties of the AH_m— and BH_n— group orbitals.

The purpose of the present paper is to extend this approach to some systems of the type $AH_mBH_nDH_k$, which contain three heavy atoms. The procedure adopted is to dissect the whole system into two molecular fragments, *e.g.*, AH_mBH_n— and DH_k—, and to derive the nodal properties and orderings of the group orbitals of these fragments from the molecular orbitals of AH_mBH_{n+1} and DH_{k+1}, respectively.

Results and Discussion

The molecule is placed in the coordinate system shown in Fig. 1, with the B—D bond on the *z*-axis. Since the p_x and p_z components of the

[1]Holder of a National Research Council of Canada Scholarship 1972–1974.

[2]Revision received November 17, 1975.

Can. J. Chem. Downloaded from www.nrcresearchpress.com by 210.87.254.5 on 09/05/12
For personal use only.

Can. J. Chem. Downloaded from www.nrcresearchpress.com by 210.87.254.5 on 09/05/12
For personal use only.

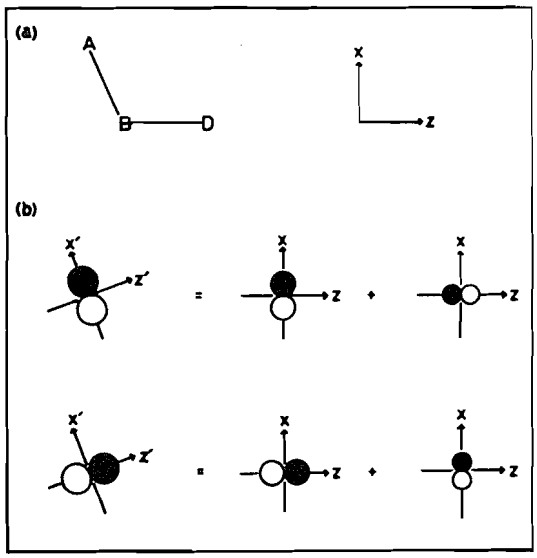

FIG. 1. (*a*) Coordinate system of $AH_mBH_nDH_k$. The ABD valence angle is assumed to be tetrahedral. (*b*) Decomposition of the $p_{x'}$ and $p_{z'}$ orbitals of the atom B into p_x and p_z contributions; the x'- and z'-axes are parallel and perpendicular to the AB bond axis.

$p_{x'}$ and $p_{z'}$ orbitals of the AH_mBH_n— fragment can be seen to exhibit mainly π- and σ-type interactions, respectively, across the z-axis, it is convenient to place the A—B bond on the x-axis. For the same reason, a DH or DH_2 fragment is oriented with the rotational axes of DH_2 and DH_3 orthogonal to the z-axis. Group orbitals which make σ-type interactions across the B—D bond are not included in Fig. 1.

The XCH_2CH_2 System

The conformational behaviour of $FCH_2CH_2^-$ and $FCH_2CH_2^+$ has been discussed by Hoffmann *et al.* (2), and that of $CH_3CH_2CH_2^+$ has been treated by Jorgensen and Salem (3). Two structures are of interest in each of these XCH_2CH_2 species: these are termed (3) eclipsed ($E_\pm$) and bisected ($B_\pm$). To complete the comparative study of this system, we have performed *ab initio* computations on $CH_3CH_2CH_2^-$ (4), which reveal that B_- is more stable than E_-. The results of these various studies may therefore be summarized as follows: in the case of the anions, B_- is more stable than E_- for both X = F and X = CH_3; for the cations E_+ is more stable when X = F, but B_+ is more stable when X = CH_3, *i.e.*, when X = CH_3, B is more stable than E in both the anion and the cation.

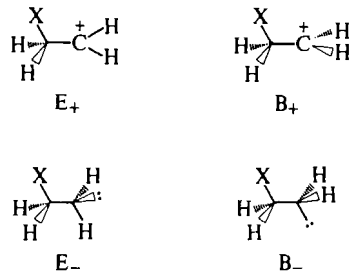

In the earlier PMO analyses of these effects (2, 3), the X substituent (F or CH_3) has been treated as a perturbation upon the orbitals of a methyl group ($CH_3 \rightarrow XCH_2$). This reduces the three heavy atom problem to a two heavy atom problem. However, different criteria were employed in the two studies to position the perturbed methyl group orbitals. In one (2), the orbital raising or orbital lowering effect of X was based on electronegativity considerations; in the other (3), bond energy effects were taken into account.

If we attempt to extend these ideas to the conformational analysis of *n*-propylcarbanion, it is necessary to begin with a definition of perturbed methyl group orbitals appropriate to CH_3CH_2—. Since the electronegativity of CH_3 is greater than that of H (5), we might expect CH_3CH_2— to behave in the same way as FCH_2— (2). This leads to the prediction that the conformational behaviour of $CH_3CH_2CH_2^-$ will resemble that of $FCH_2CH_2^-$, *i.e.*, that B_- will be more stable than E_-. This is the correct prediction.

In the same way, it seems reasonable to expect that $CH_3CH_2CH_2^+$ will resemble $FCH_2CH_2^+$, *i.e.*, that E_+ will be more stable than B_+. This is not correct. The failure of the prediction in this case can be rationalized if it is supposed that CH_3 is electron-withdrawing in the anion and electron-releasing in the cation (6). However, the problem is that, since the treatment of XCH_2 as a perturbed methyl group is a qualitative procedure, it may, as has been seen, lead to uncertainties concerning the positioning of the orbitals of this group. A PMO procedure which avoids this ambiguity would, therefore, be useful.

Figure 2 shows an orbital interaction diagram for $C^3H_3C^2H_2C^1H_2^-$, using CH_3CH_2— and —CH_2^- group orbitals derived from *ab initio* computations on ethane and methylcarbanion, respectively. The C_2—C_3 bond has been placed

Can. J. Chem. Downloaded from www.nrcresearchpress.com by 210.87.254.5 on 09/05/12
For personal use only.

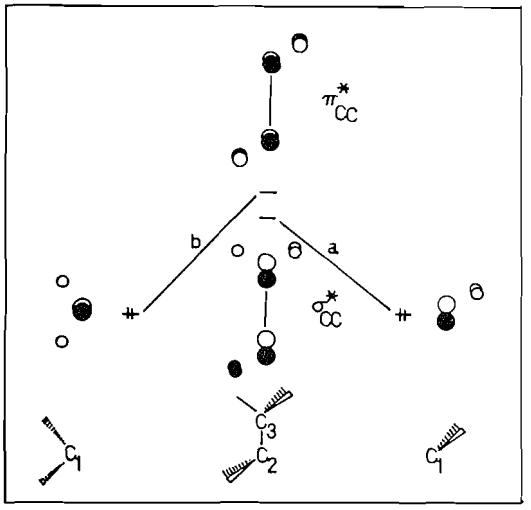

FIG. 2. The interaction diagram of $CH_3CH_2CH_2^-$; the CH_2^- orbital is essentially the carbon lone pair.

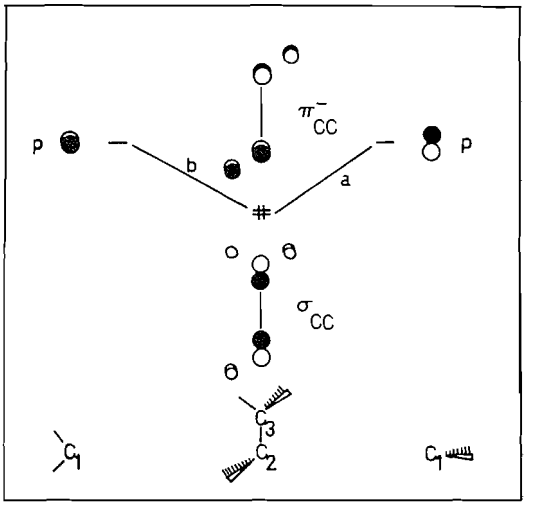

FIG. 3. The interaction diagram of $CH_3CH_2CH_2^+$; the CH_2^+ orbital is an empty p orbital.

on the x-axis, and the interaction between the two groups takes place on the z-axis. The right hand portion of Fig. 2 corresponds to the interactions leading to B_-; the left hand portion of Fig. 2 corresponds to a 90° rotation of the $-CH_2^-$ moiety, and it simulates E_-. The two-orbital two-electron stabilizing interactions to be considered in this diagram involve the highest occupied group orbital of CH_2^- and the lowest lying unoccupied group orbitals of CH_3CH_2-. The two lowest lying unoccupied orbitals of CH_3CH_2- are classified σ_{CC}^* and π_{CC}^*. The relevant interaction in B_- is a and, in E_- it is b. Since a leads to greater stabilization, B_- should be more stable than E_-, in agreement with the *ab initio* calculation on *n*-propylcarbanion.

Figure 3 applies the same procedure to $CH_3CH_2CH_2^+$. The operative two-orbital two-electron stabilizing interaction now involves occupied CH_3CH_2- and unoccupied $-CH_2^+$ orbitals. The two highest occupied orbitals of CH_3CH_2- correspond to σ_{CC} and π_{CC}^-. Inspection of Figs. 2 and 3 reveals immediately that a prediction based upon orbital energy differences in the two conformations will be less certain in the case of the carbonium ion, because the orbital energies of σ_{CC} and π_{CC}^- are nearly the same, whereas those of σ_{CC}^* and π_{CC}^* differ significantly. However, note that interaction b leads to π-bonding in the C_1–C_2 region, and π-antibonding in the C_1–C_3 region, whereas a leads to bonding in both regions. This observation indicates that a, which leads to B_+, will have a greater stabilizing effect than b. The group orbital analysis of the *n*-propyl system has thus rationalized why B is more stable than E in both the anion and the cation.

Figure 4 shows the group orbitals of FCH_2-

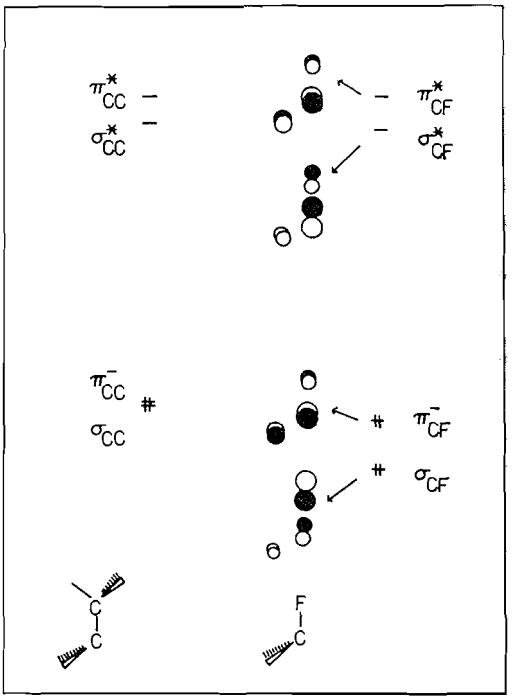

FIG. 4. Comparison of the FCH_2- and CH_3CH_2- group orbitals.

Can. J. Chem. Downloaded from www.nrcresearchpress.com by 210.87.254.5 on 09/05/12
For personal use only.

and CH_3CH_2— which are appropriate for interaction with adjacent $—CH_2^-$ and $—CH_2^+$ moieties. As already discussed, the antibonding orbitals of CH_3CH_2— which interact with an adjacent anionic centre are σ_{CC}^* and π_{CC}^*; the corresponding FCH_2— orbitals are σ_{CF}^* and π_{CF}^*. In both cases, the energies of these two orbitals are seen to differ significantly; the analysis of $FCH_2CH_2^-$ will be the same as that of $CH_3CH_2CH_2^-$, *i.e.*, B_- is more stable than E_-. However, σ_{CF} and π_{CF}^- have quite different orbital energies in contrast to σ_{CC} and π_{CC}^-. Thus for $FCH_2CH_2^+$, the two-orbital two-electron stabilization of the adjacent cationic centre will be greater in E_+. We see from the group orbital analysis of the XCH_2CH_2 system that the principal difference between CH_3 and F is the position of σ_{CX}, which is stabilized by the more electronegative substituent.

The Anomeric Effect (7)

The anomeric effect (the Edward–Lemieux effect (8)) refers to an increased preference for the axial conformation of an electronegative ligand when it is in the α position of a six-membered heterocyclic ring containing oxygen or sulfur (*e.g.*, **1**). Computations on FCH_2OH, which has been employed as a model compound for the theoretical investigation of the anomeric effect (8–10), reveal that the *gauche* conformation **2** is the energy minimum, and that the *anti* conformation **3** is the energy maximum associated with torsion about the C—O bond.

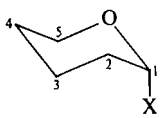

1

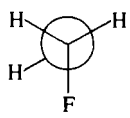

2

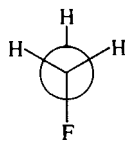

3

In an earlier discussion of the anomeric effect (8, 10), energy component analysis (11) was employed to obtain a physical interpretation of the computed result. This led to the conclusions that the preference for the *gauche* conformation **2** was the result of interactions between the C—F and O—H bonds (in agreement with Chü's finding (12) that the anomeric effect originates in an interaction between the C_5—O and C_1—X bonds), and that the oxygen lone pairs behave as though they are quasi-spherical (non-directional) ligands, when the repulsion between lone pairs and bond pairs is considered. This interpretation of the anomeric effect corresponds to a localized molecular orbital description of the problem (10). It is rigorous within the framework of energy component analysis (16) and localization of canonical molecular orbitals (13).

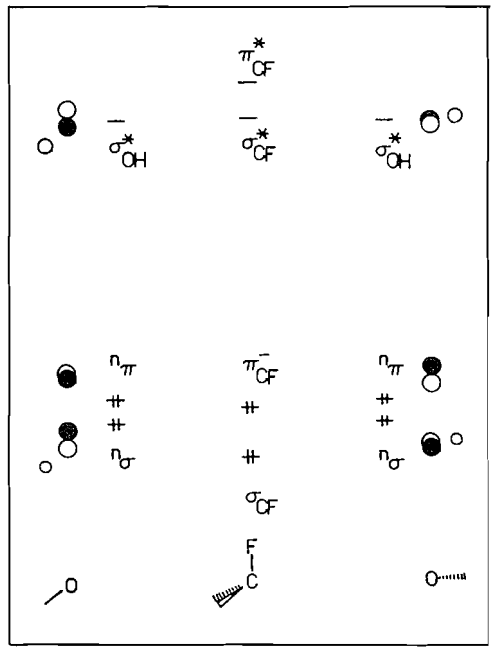

FIG. 5. FCH_2— and —OH group orbitals considered for the construction of the FCH_2OH interaction diagram; n_π and n_σ are the higher and lower lying oxygen lone pairs, respectively.

In a different approach to the problem, David *et al.* (14) and Eisenstein *et al.* (15) employed the PMO method to analyze the anomeric effect. In this analysis, the oxygen lone pairs are treated as canonical molecular orbitals. When the different nodal properties (*i.e.*, directionalities) and orbital energies of the two oxygen lone pairs are taken into consideration explicitly, the anomeric effect can be rationalized. Like the localized molecular orbital description discussed above, this is a rigorous interpretation, within the framework of PMO theory.

We thus have two theoretical interpretations of the anomeric effect. One emphasizes interactions associated with the oxygen lone pairs. The other effectively ignores the lone pairs. It seems reasonable to ask whether these apparently contradictory interpretations can be reconciled.

Figure 5 shows the $—CH_2F$ and —OH group

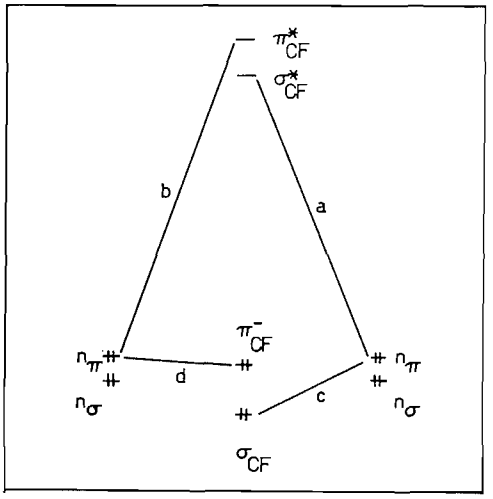

FIG. 6. Interaction between n_π and $-CH_2F$ group orbitals.

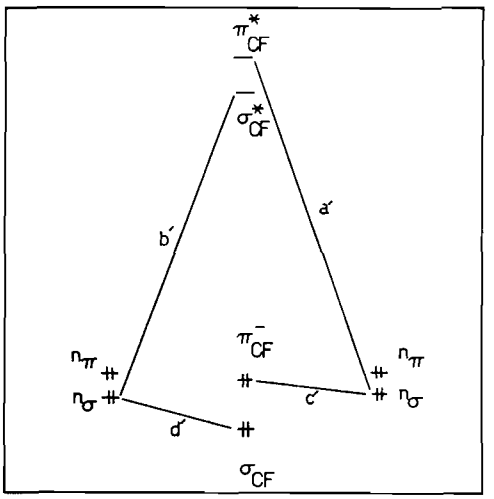

FIG. 7. Interaction between n_σ and $-CH_2F$ group orbitals.

orbitals which are appropriate for the construction of the FCH_2OH interaction diagram. The interaction of $-CH_2F$ with —OH to form *syn* (or *anti*) FCH_2OH is shown on the left; a 90° rotation of the —OH group simulates *gauche* FCH_2OH, and is shown on the right. The two highest occupied —OH orbitals are essentially lone pair orbitals and the lowest unoccupied —OH orbital can be characterized as σ_{OH}*.

Figure 6 shows the interactions between the n_π and $-CH_2F$ group orbitals. Interaction *a* is more stabilizing than interaction *b*, and interaction *c* is less destabilizing than interaction *d*. This means that the *gauche* conformation is favoured by both the two-electron stabilization and the four-electron destabilization interactions associated with n_π.

Figure 7 shows the interactions between the n_σ and $-CH_2F$ group orbitals. This diagram reveals that both the two-electron stabilization and the four-electron destabilization associated with n_σ favour the *syn* (or *anti*) conformation. Thus, the interactions of n_π and n_σ have opposite conformational consequences. To determine the net result of these opposing effects, it would be necessary to estimate the relative magnitudes of the various interactions, at least qualitatively. David *et al.* (14) have attempted to do this in their analysis. Since the present approach does not lend itself readily to quantitative estimation of the various interactions, we present an indirect argument. In the *ab initio* SCF-MO's of FCH_2OH, the nodal properties of the HOMO's of *gauche* and *syn* (or *anti*) FCH_2OH correspond mainly to the out-of-phase combinations of the $-CH_2F$ and —OH group orbitals associated with interactions *c* and *d*. In addition, the rotational dependence of the FCH_2OH HOMO level parallels that of the total energy of FCH_2OH (16)[3]. This result suggests that the behaviour of the whole molecule can be rationalized by consideration of only those interactions which simulate the behaviour of the HOMO. Figure 6 clearly shows that the HOMO level should be lower in the *gauche* than in the *syn* (or *anti*) conformation; and we may, therefore, neglect the effect of interactions associated with n_σ because these do not lead to the HOMO.

Turning to Fig. 8, we now focus on the two-orbital two-electron interactions between occupied $-CH_2F$ and σ_{OH}* orbitals. Since interaction *e* is more stabilizing than interaction *f*, the *gauche* conformation is predicted to be more stable. It is important to note that *e* and *f* refer to interactions between the CF and OH bonds, and their consideration amounts to a rationalization of the *gauche* preference of FCH_2OH

[3]The HOMO eigenvalues are −0.4703, −0.4759, −0.4905, −0.5803, −0.4894, −0.4766, and −0.4721 a.u. for dihedral angles of 0°, 30°, 60°, 90°, 120°, 150°, and 180°, respectively, with a dihedral angle of 0° corresponding to the *syn* conformation. Interestingly, the torsional dependence of the second highest occupied molecular orbital of FCH_2OH has opposite phase and, thus, does not parallel the behaviour of the total energy.

Can. J. Chem. Downloaded from www.nrcresearchpress.com by 210.87.254.5 on 09/05/12
For personal use only.

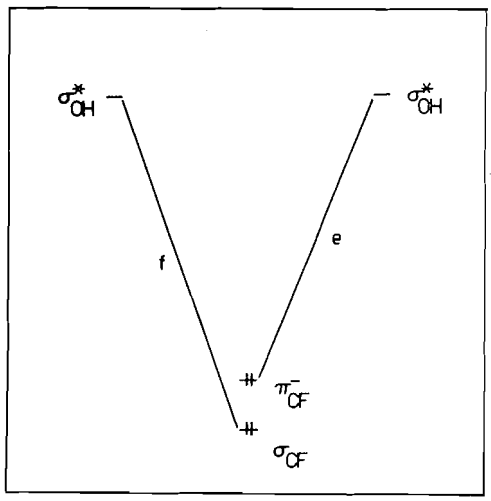

FIG. 8. Interaction between σ_{OH}* and —CH_2F group orbitals.

which does not consider oxygen lone pair effects. In this sense, the argument derived from Fig. 8 may be regarded as the group molecular orbital equivalent of the quasi-spherical lone pair interpretation (8, 10).

The above considerations reveal that both of the earlier interpretations of the anomeric effect can be accommodated within the framework of a group molecular orbital model. The relative importance of interactions *a* and *e* cannot be assessed without a more quantitative treatment of the orbital interactions. We believe, therefore, that further progress in the understanding of these and related (17) conformational effects will require the development of reliable methods to compute explicitly the relative magnitudes of the various two-electron and four-electron interactions that have been discussed (*cf.* ref. 18)). Such an investigation is presently in progress.

Acknowledgment

We thank the donors of the Petroleum Research Fund, administered by the American Chemical Society, for financial support of this research.

1. M. H. WHANGBO and S. WOLFE. Can. J. Chem. This issue.
2. R. HOFFMANN, L. RADOM, J. A. POPLE, P. v. R. SCHLEYER, W. J. HEHRE, and L. SALEM. J. Am. Chem. Soc. **94**, 6221 (1972).
3. W. L. JORGENSEN and L. SALEM. The organic chemist's book of orbitals. Academic Press, New York. 1973.
4. M. H. WHANGBO and S. WOLFE. Unpublished results.
5. P. R. WELLS. Prog. Phys. Org. Chem. **6**, 111 (1968).
6. (*a*) W. J. HEHRE and J. A. POPLE. Tetrahedron, 2959 (1970); (*b*) N. C. BAIRD and M. A. WHITEHEAD. Theor. Chim. Acta, **6**, 167 (1966); Can. J. Chem. **44**, 1033 (1966).
7. (*a*) J. T. EDWARD. Chem. Ind. 1102 (1955); (*b*) R. U. LEMIEUX. Pure Appl. Chem. **25**, 527 (1971); (*c*) E. L. ELIEL. Acc. Chem. Res. **3**, 1 (1970).
8. S. WOLFE, A. RAUK, L. M. TEL, and I. G. CSIZMADIA. J. Chem. Soc. B, 136 (1971).
9. L. RADOM, W. J. HEHRE, and J. A. POPLE. J. Am. Chem. Soc. **93**, 289 (1971); G. A. JEFFREY, J. A. POPLE, and L. RADOM. Carbohydr. Res. **25**, 117 (1972).
10. S. WOLFE, L. M. TEL, W. J. HAINES, M. A. ROBB, and I. G. CSIZMADIA. J. Am. Chem. Soc. **95**, 4863 (1973).
11. (*a*) L. C. ALLEN. Chem. Phys. Lett. **2**, 597 (1968); (*b*) W. H. FINK and L. C. ALLEN. J. Chem. Phys. **46**, 2261 (1967); **46**, 2267 (1971).
12. N. J. CHÜ. Ph.D. Thesis. University of Ottawa, Ottawa, Canada. 1959. p. 97.
13. C. EDMISTON and K. RUEDENBERG. J. Chem. Phys. **43**, S97 (1963); Rev. Mod. Phys. **35**, 457 (1963).
14. S. DAVID, O. EISENSTEIN, W. J. HEHRE, L. SALEM, and R. HOFFMANN. J. Am. Chem. Soc. **95**, 3806 (1973).
15. O. EISENSTEIN, N. T. ANH, Y. JEAN, A. DEVAQUET, J. CANTACUZÈNE, and L. SALEM. Tetrahedron Lett. **30**, 1717 (1974).
16. H. B. SCHLEGEL. Unpublished results.
17. (*a*) J. M. LEHN and G. WIPFF. J. Am. Chem. Soc. **96**, 4048 (1974); (*b*) P. DESLONGCHAMPS, P. ATLANI, D. FRÉHEL, and A. MALAVAL. Can. J. Chem. **50**, 3405 (1972); P. DESLONGCHAMPS, C. LEBREUX, and T. TAILLEFER. Can. J. Chem. **51**, 1665 (1973); P. DESLONGCHAMPS, C. MOREAU, D. FRÉHEL, and R. CHÊNEVERT. Can. J. Chem. **53**, 1204 (1975); P. DESLONGCHAMPS, S. DUBÉ, C. LEBREUX, D. R. PATTERSON, and R. J. TAILLEFER. Can. J. Chem. **53**, 2791 (1975).
18. N. D. EPIOTIS and R. L. YATES. J. Am. Chem. Soc. **98**, 461 (1976).

Can. J. Chem. Downloaded from www.nrcresearchpress.com by 210.87.254.5 on 09/05/12
For personal use only.

Sphere tensiometry: an evaluation and critique

C. HUH AND S. G. MASON

Pulp and Paper Research Institute of Canada and
Department of Chemistry, McGill University, Montreal, Quebec H3C 3G1

Received September 26, 1975

C. HUH and S. G. MASON. Can. J. Chem. **54**, 969 (1976).

An absolute gravimetric method of measuring surface and interfacial tensions of liquids by pulling a sphere through the interface is examined. The method also permits simultaneous measurement of the contact angle of the liquid on the sphere surface; this enables corrections to be made for incomplete wetting of the solid by liquids in measuring the interfacial tension, a feature which the conventional ring and plate methods lack. Simultaneous measurements of the interfacial tension and the difference in phase densities across the interface are in principle also possible. Preliminary experimental results are presented, and the advantages and disadvantages of the method are critically discussed.

C. HUH et S. G. MASON. Can. J. Chem. **54**, 969 (1976).

On examine une méthode gravimétrique absolue pour mesurer les tensions interfaciales et de surface de liquides; cette méthode est basée sur le principe que l'on tire une sphère à travers l'interface. Cette méthode permet aussi de mesurer simultanément l'angle de contact du liquide avec la surface de la sphère; ceci permet de faire des corrections pour un mouillage incomplet du solide par des liquides lorsqu'on mesure les tensions interfaciales, une caractéristique qui manque aux méthodes conventionnelles de disque ou de plaque. Il est en principe aussi possible de mesurer simultanément la tension interfaciale et la différence dans les densités de phase à travers l'interface. On présente des résultats expérimentaux préliminaires et on discute d'une façon critique des avantages et des désavantages de la méthode.

[Traduit par le journal]

Introduction

Surface and interfacial tensions of liquids can be conveniently measured by gravimetric methods in which small solid bodies are weighed as they are pulled under quasi-static conditions through a horizontal fluid/liquid interface. If the shape of the meniscus around the solid is known, the capillary component of the balancing force and thus the tension, can be calculated. The commonly used bodies are the (duNouy) ring and the (Wilhelmy) plate; a much simpler geometry which has scarcely received attention for this purpose is the sphere. Whereas the ring and plate both form menisci with complicated shapes, a sphere does not, thus making it possible to calculate the equilibrium interfacial force rigorously and in a relatively straightforward manner (1). The use of another simple geometry, a circular cylinder vertically protruding through the interface, and of a cylindrical tip with a sharp edge to which the meniscus attaches has also been proposed (2). Because of difficulties of vertical alignment, axisymmetry (required by the theory) may not be exactly realized with cylinders; a sphere presents no such problem. In this paper, we examine the feasibility of using spheres, present some preliminary experimental data, and indicate the advantages and disadvantages of the method.

An immediate advantage is that it is capable of measuring the interfacial tension γ_{23} of a fluid/liquid interface which, for various reasons, may not be visible (γ_{23} is the interfacial tension between phases 2 and 3 (Fig. 1)). For such systems, obviously we cannot use the drop shape methods, or the ring and plate methods because we cannot be certain of the completeness of wetting of the solid with one of the liquids, which is an essential prerequisite. As will be seen, however, the sphere permits simultaneous measurement of γ_{23} and the contact angle θ_0 (measured through the lower liquid phase) which the interface makes with the sphere (Fig. 1). Although the ring method can, in principle, also be modified to determine θ_0, the calculations involved are much more complex than those made here for the sphere. The measurement of θ_0 may not actually be wanted, because to produce a precision solid sphere which is sufficiently smooth to render θ_0 thermodynamically meaningful is a difficult task (3), but it permits corrections if wetting is

Can. J. Chem. Downloaded from www.nrcresearchpress.com by 210.87.254.40 on 09/05/12
For personal use only.

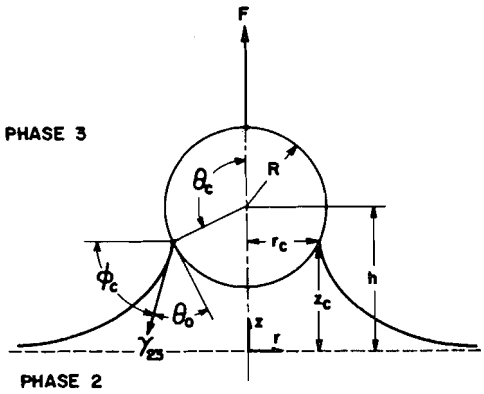

FIG. 1. A solid sphere (phase 1) at a horizontal interface between phases 2 (below) and 3 (above). The sphere is slowly pulled upwards from phase 2 and the force F on the thread is measured as a function of the sphere height h.

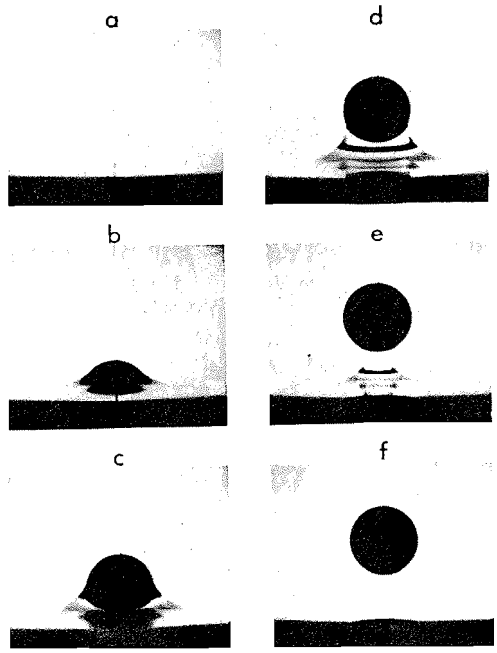

FIG. 2. Photograph of a Teflon sphere (R = 6.35 mm) pulled through the Silicone fluid/water interface. Dow Corning 200 (50 cs) Silicone fluid is the upper phase, and the contact angle $\theta_0 \simeq 0°$. Frame (e) shows the non-equilibrium rupture of the meniscus, completed in (f).

incomplete (*i.e.* $\theta_0 > 0$) in determining γ_{23}. There are other possibilities, one of which is to determine *in situ* the difference of the fluid phase densities ρ_2 and ρ_3 across the interface as well as γ_{23} (ρ_i is density of phase i). When $(\rho_2 - \rho_3)$ is small, separate determination of

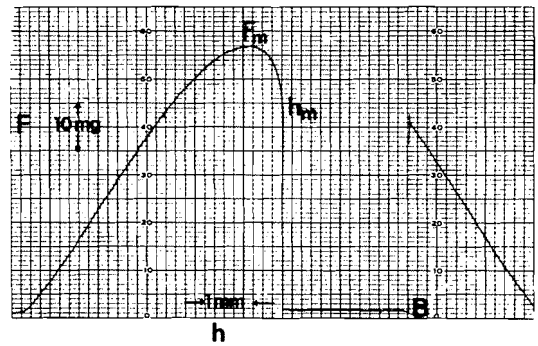

FIG. 3. A typical experimental F–h curve, for a nylon sphere (R = 2.03 mm) at Dow Corning 200 (100 cs) Silicone fluid/water interface. The sphere, pulled upwards, detached from the interface slightly before the maximum equilibrium height h_m; on lowering, the sphere contacted the interface at B, suddenly forming a meniscus around it with an accompanying jump in F.

ρ_2 and ρ_3 can lead to substantial errors in calculating γ_{23}. By the sphere method we can, in principle, simultaneously measure γ_{23}, θ_0, and $(\rho_2 - \rho_3)$.

When a solid sphere (phase 1) of radius R is slowly pulled through a horizontal fluid/liquid interface from the liquid phase 2 to the fluid phase 3 above 2 as shown schematically in Fig. 1, the force F on a thread attached to the sphere increases with height h of the sphere center above the flat level of the interface (Figs. 2 and 3). With further increase of h, F attains a maximum at F_m, decreases until the maximum equilibrium height h_m is reached, whereupon the sphere detaches from the interface. Knowing θ_0 and $(\rho_2 - \rho_3)$, we need only know the maximum F to determine γ_{23}. However, the equlibrium relation between F and h which we measure experimentally as a continuous curve (Fig. 3) provides much more information than the maximum F; utilizing other characteristic features of the F–h curve, we should be able to obtain quantities other than γ_{23}, notably θ_0 or $(\rho_2 - \rho_3)$ as noted above.

A scheme of measuring interfacial tensions by the sphere method similar to ours has recently been reported by Scheludko and Nikolov (4). Their method relies on the photographic measurement of the contact line location on the sphere at the maximum force, which from our experience cannot be accurately measured, especially when the phase 2 liquid in the region of the contact line is very thin which

Can. J. Chem. Downloaded from www.nrcresearchpress.com by 210.87.254.40 on 09/05/12
For personal use only.

Can. J. Chem. Downloaded from www.nrcresearchpress.com by 210.87.254.40 on 09/05/12
For personal use only.

is the case for small values of θ_0. We believe that they have exaggerated accuracy (1 in 10^5) for the surface tension measurements. Our proposed method avoids their difficulties but at the same time recognizes some important sources of error overlooked in ref. 4.

To treat the problem in the simplest mathematical form, we employ the following dimensionless variables

$$[1] \qquad \bar{R} \equiv R\sqrt{C_{23}}$$
$$\bar{h} \equiv h\sqrt{C_{23}}$$
$$D \equiv F\Big/\frac{4}{3}\pi(\rho_2 - \rho_3)gR^3$$

where $C_{23} \equiv (\rho_2 - \rho_3)g/\gamma_{23}$, and g is gravity. Without loss of rigour we set $F \equiv 0$ when the sphere is entirely in phase 2, so that the sphere density ρ_1 is immaterial to the measurement. We have numerically calculated the equilibrium relation between D and $\bar{h}$ for different values of $\bar{R}$ and θ_0. Several parameters identifying the D–$\bar{h}$ curve for various values of $\bar{R}$ and θ_0 have been defined and made available as a numerical tabulation.

When the sphere is lowered (by pushing if necessary) from the upper phase 3 to the lower phase 2, the theoretical treatment of the problem is identical to the case of raising the sphere, provided D, θ_0 and $\bar{h}$ are replaced by $(1 - D)$, $(180° - \theta_0)$, and $-\bar{h}$. This arises due to the mirror symmetry of the system in the horizontal plane $z = 0$.

On the basis of the theoretical and preliminary experimental results, presented below, we discuss the feasibility of sphere tensiometry for absolute measurements of surface and interfacial tensions. As we will see, the method holds considerable promise, but several difficulties must first be surmounted.

Basic Theory

The mechanical equilibrium of the sphere at the interface (Fig. 1) can be expressed as (5)

$$[2] \qquad 2D = 1 + \frac{3}{2}\sin^2\theta_c(\bar{h}/\bar{R}) - \cos^3\theta_c + \frac{3}{\bar{R}^2}\sin\theta_c\sin(\theta_c - \theta_0)$$

where θ_c is the angle between the upward vertical and the normal to the sphere at the contact line. In addition, we have the following geometric relations at the contact line:

$$[3] \qquad \bar{r}_c = \bar{R}\sin\theta_c$$

$$[4] \qquad \bar{z}_c = \bar{h} + \bar{R}\cos\theta_c$$

$$[5] \qquad \phi_c = \theta_c - \theta_0$$

where $r_c \equiv \bar{r}_c/\sqrt{C_{23}}$ and $z_c \equiv \bar{z}_c/\sqrt{C_{23}}$ are the radial and vertical coordinates of the contact line circle and ϕ_c is the slope angle of the liquid meniscus at the contact line. The values of $\bar{r}_c$, $\bar{z}_c$, and ϕ_c are obtained from the equilibrium shape calculations of the meniscus formed around the sphere (1, 6).

For given $\bar{R}$ and θ_0, therefore, [2] to [5] provide equilibrium relations between D and $\bar{h}$. To obtain the D–$\bar{h}$ curve, we have solved numerically the Young–Laplace equation for the equilibrium meniscus shape, employing the integration method of Huh and Scriven (6) and with the same accuracy as that of the earlier calculations (1). When the coordinates and slope angle $(\bar{r}, \bar{z}, \phi)$ of the meniscus were obtained by numerical integration during the computing process, we set them to apply at the contact line $(\bar{r}_c, \bar{z}_c, \phi_c)$ and calculated θ_c from [5] for a given θ_0, and $\bar{R}$, $\bar{h}$, and D from [3], [4], and [2], successively. Interpolation of $\bar{h}$ and D in regular intervals of $\bar{R}$ was made, employing the six-point Aitken–Lagrange interpolation scheme with an upper error bound of 10^{-8}. For given θ_0 and $\bar{R}$, at least 240 sets of $\bar{h}$ and D values were thus collected, from which we constructed a D–$\bar{h}$ curve.

Figure 4 shows the D–$\bar{h}$ curves for $\bar{R} = 0.5$ and different values of θ_0. When $\theta_0 = 0°$, the sphere touches the interface at $\bar{h} = -\bar{R}$ $(= -0.5)$ and D starts to increase from 0 to the maximum value of D_m; and then D decreases until the maximum $\bar{h} = \bar{h}_m$ is attained, whereon the sphere detaches from the interface. In actual experiments, we found that because the slope of the curve rapidly decreased near $\bar{h}_m$, the sphere often detached somewhat before the slope reached $-\infty$ at $\bar{h}_m$. The equilibrium of the sphere between $\bar{h}_m$ and B is believed to be unstable and has not been achieved experimentally. At point B, the sphere is completely in phase 3. When $\theta_0 > 0°$, the contact between the sphere and the interface at $\bar{h} = -\bar{R}$ causes a sudden withdrawal of phase 2 from the

Can. J. Chem. Downloaded from www.nrcresearchpress.com by 210.87.254.40 on 09/05/12
For personal use only.

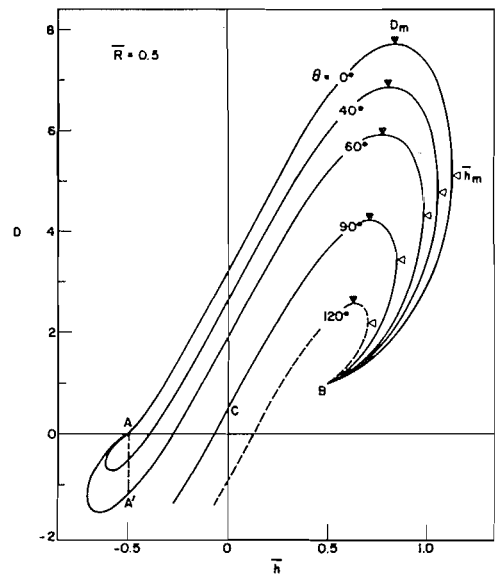

FIG. 4. Equilibrium relation between D and $\bar{h}$ for $\bar{R} = 0.5$ and various θ_0. Note the similarity to the experimental curve in Fig. 3. For further explanation, see text.

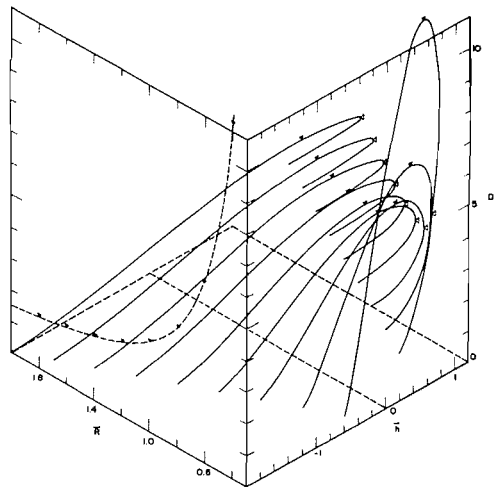

FIG. 5. Perspective view of the equilibrium relation between D and $\bar{h}$ for $\theta_0 = 0°$ and various $\bar{R}$. The points ▼ indicate the maxima $D = D_m$ and △ the maxima $\bar{h} = \bar{h}_m$; D_m's are projected on the D–$\bar{R}$ plane, and show the D_m–$\bar{R}$ relation.

neighborhood of the contacting point and the formation of a meniscus around the sphere (from A to A′ in Fig. 4 when $\theta_0 = 60°$). Accordingly, D suddenly changes from 0 (completely in phase 2) to the negative value at A′. The subsequent behavior as $\bar{h}$ is increased will be substantially identical to that for $\theta_0 = 0°$. We note that the curves for θ_0 and $180° - \theta_0$ are symmetric with respect to the point C ($D = 0.5$ and $\bar{h} = 0$); thus, the curve for $\theta_0 = 120°$ (dotted line) can be easily constructed from that for $\theta_0 = 60°$. This symmetry arises due to the fact that the Young–Laplace equation for the meniscus shape is symmetric with respect to the plane $\bar{z} = 0$ (5).

Two prominent parameters characterizing the curves are (*i*) the maximum D_m which corresponds to the equilibrium force necessary to detach a freely-moving sphere from the interface, and (*ii*) the maximum $\bar{h}_m$ which corresponds to the largest equilibrium height which a sphere may attain at the interface before the rupture of the meniscus. Figure 5 shows, for the particular case of interest of $\theta_0 = 0°$, the D–$\bar{h}$ curves for $\bar{R} = 0.4$ to 2.0. The maximum D_m's are projected on the D–$\bar{R}$ plane, from which the D_m–$\bar{R}$ curve shown can be constructed; the maximum $\bar{h}_m$'s are also projected on the $\bar{h}$–$\bar{R}$ plane, from which the $\bar{h}_m$–$\bar{R}$ curve (not shown) can be constructed. We have prepared a tabulation[1] of D_m and $\bar{h}_m$ for $\bar{R} = 0.21(0.01)0.60(0.02)1.80$ and $\theta_0 = 0°(1°)90°$, where the intervals between the end values are indicated in parentheses. For $\theta_0 = 0°$, Table 1 gives values of D_m, and $\bar{h}$, ϕ_c, $\bar{r}_c$, and $\bar{z}_c$ for the maximum force state, and Table 2 shows $\bar{h}_m$, and ϕ_c, $\bar{r}_c$, and $\bar{z}_c$ for the maximum height state.

When the equilibrium F–h curve is produced experimentally, we cannot convert it to the dimensionless D–h curve since γ_{23} is unknown; however, the equilibrium relations can be expressed in terms of the normalized quantities D/D_m and $\bar{h}/\bar{R}$, which are measurable. The following additional parameters which characterize the D–$\bar{h}$ curve may then be defined in terms of the above normalized quantities and may be utilized to calculate γ_{23} and θ_0:

$$S \equiv \frac{\bar{R}}{D_m}\left(\frac{dD}{d\bar{h}}\right)_m = \frac{R}{F_m}\left(\frac{dF}{dh}\right)_m$$

[6] $$E_1 \equiv \frac{1}{D_m\bar{R}}\int_{D=0}^{D=D_m} D\,d\bar{h} = \frac{1}{F_m R}\int_{F=0}^{F=F_m} F\,dh$$

$$E_2 \equiv \frac{1}{D_m\bar{R}}\int_{D=0}^{\bar{h}=\bar{h}_m} D\,d\bar{h} = \frac{1}{F_m R}\int_{F=0}^{h=h_m} F\,dh$$

[1]These tabulations are available, at a nominal charge, from the Depository of Unpublished Data, CISTI, National Research Council of Canada, Ottawa, Canada K1A 0S2.

Can. J. Chem. Downloaded from www.nrcresearchpress.com by 210.87.254.40 on 09/05/12
For personal use only.

TABLE 1. Conditions at maximum force when $\theta_0 = 0°$*

$\bar{R}$	D_m	$\bar{h}$	ϕ_c (deg)	$\bar{r}_c$	$\bar{z}_c$
0.20	39.83	0.4914	91.02	0.2000	0.4878
0.25	26.173	0.5635	91.52	0.2499	0.5569
0.30	18.714	0.6285	92.09	0.2998	0.6175
0.35	14.189	0.6882	92.71	0.3496	0.6716
0.40	11.233	0.7439	93.37	0.3993	0.7204
0.45	9.1916	0.7967	94.06	0.4489	0.7648
0.50	7.7206	0.8472	94.78	0.4983	0.8055
0.6	5.7831	0.9434	96.26	0.5964	0.8780
0.7	4.5957	1.0354	97.76	0.6936	0.9409
0.8	3.8124	1.1252	99.27	0.7896	0.9963
0.9	3.2666	1.2137	100.77	0.8442	1.0456
1.0	2.8699	1.3017	102.23	0.9773	1.0899
1.1	2.5718	1.3896	103.66	1.0689	1.1299
1.2	2.3417	1.4777	105.04	1.1589	1.1664
1.3	2.1600	1.5662	106.38	1.2473	1.1997
1.4	2.0138	1.6551	107.67	1.3340	1.2303
1.5	1.8943	1.7445	108.91	1.4191	1.2585
1.6	1.7953	1.8345	110.11	1.5025	1.2845
1.7	1.7123	1.9250	111.26	1.5844	1.3087
1.8	1.6419	2.0160	112.36	1.6647	1.3312
1.9	1.5817	2.1075	113.42	1.7434	1.3522
2.0	1.5297	2.1994	114.45	1.8207	1.3717

*D_m values extracted from deposited numerical tabulations. See footnote in text.

TABLE 2. Conditions at maximum height when $\theta_0 = 0°$*

$\bar{R}$	$\bar{h}_m$	ϕ_c (deg)	$\bar{r}_c$	$\bar{z}_c$
0.20	0.5868	117.98	0.1766	0.4929
0.25	0.6894	120.30	0.2159	0.5633
0.30	0.7855	122.38	0.2534	0.6249
0.35	0.8765	124.27	0.2893	0.6795
0.40	0.9634	126.00	0.3236	0.7283
0.45	1.0469	127.60	0.3565	0.7723
0.50	1.1275	129.08	0.3881	0.8123
0.6	1.2816	131.76	0.4475	0.8820
0.7	1.4284	134.13	0.5025	0.9410
0.8	1.5694	136.23	0.5534	0.9917
0.9	1.7057	138.11	0.6009	1.0357
1.0	1.8383	139.82	0.6453	1.0743
1.1	1.9677	141.36	0.6869	1.1085
1.2	2.0945	142.77	0.7260	1.1390
1.3	2.2189	144.07	0.7629	1.1663
1.4	2.3416	145.26	0.7978	1.1912
1.5	2.4624	146.36	0.8309	1.2136
1.6	2.5820	147.38	0.8625	1.2342
1.7	2.7000	148.33	0.8925	1.2531
1.8	2.8167	149.22	0.9211	1.2704
1.9	2.9329	150.05	0.9486	1.2865
2.0	3.0478	150.83	0.9749	1.3014

*$\bar{h}_m$ values from detailed numerical tabulations.

TABLE 3. Characteristic parameters for the D–$\bar{h}$ curve when $\theta_0 = 0°$*

$\bar{R}$	S	E_1	E_2
0.20	0.3689	1.940	2.3968
0.25	0.3956	1.826	2.3069
0.30	0.4190	1.736	2.2334
0.35	0.4399	1.662	2.1708
0.40	0.4586	1.600	2.1164
0.45	0.4755	1.546	2.0682
0.50	0.4909	1.501	2.0252
0.6	0.5179	1.425	1.9504
0.7	0.5407	1.367	1.8878
0.8	0.5603	1.319	1.8341
0.9	0.5773	1.281	1.7872
1.0	0.5921	1.249	1.7464
1.1	0.6051	1.222	1.7099
1.2	0.6166	1.199	1.6772
1.3	0.6268	1.180	1.6476
1.4	0.6360	1.167	1.6207
1.5	0.6442	1.160	1.5962

*Values of D_m are given in Table 1.

The first term derives from the maximum $dD/d\bar{h} \equiv (dD/d\bar{h})_m$ corresponding to the inflexion point in the D–$\bar{h}$ curve; the second and third terms derive, respectively, from the work required to pull (or push) the sphere through the interface, and the work done during the process.

From the analysis of the D–$\bar{h}$ curves for different $\bar{R}$ and θ_0, we have calculated $\bar{R}$, S, E_1, and E_2 as functions of D_m and θ_0. The deposited tabulations include values of $\bar{R}$, S, E_1, and E_2 as functions of $D_m = 2.2(0.1)4.0(0.2)10.0(0.5)20.0$ and $\theta_0 = 0°(5°)90°$. For $\theta_0 = 0°$, Table 3 shows R, S, E_1, and E_2 as functions of D_m. Figures 6 *a* and *b* and 7 *a* and *b* show $\bar{R}$, S, E_1, and E_2, respectively, as functions of D_m and θ_0. We note that for a given D_m, the variations in S, E_1, and E_2 with respect to θ_0 are all small near $\theta_0 = 0°$, but rapidly increase as θ_0 increases.

When we obtain an experimental F–h curve, we calculate D_m from the maximum F and the fluid densities; any conveniently measurable quantities among S, E_1, and E_2 are also obtained; from the above tabulation using these two parameters (D_m and *e.g.*, S) we locate θ_0 and $\bar{R}$; the surface tension can be calculated from

$$[7] \qquad \gamma_{23} = (\rho_2 - \rho_3)g(R/\bar{R})^2$$

which is a component of [1].

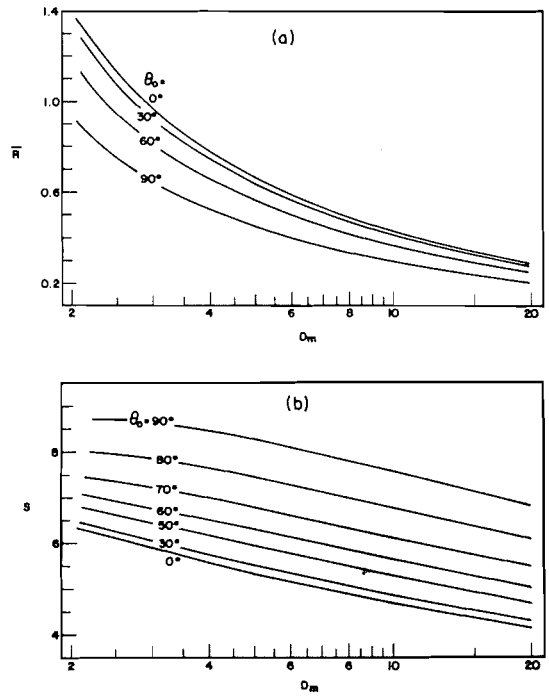

FIG. 6. (*a*) $\bar{R}$, and (*b*) S as functions of D_m and θ_0.

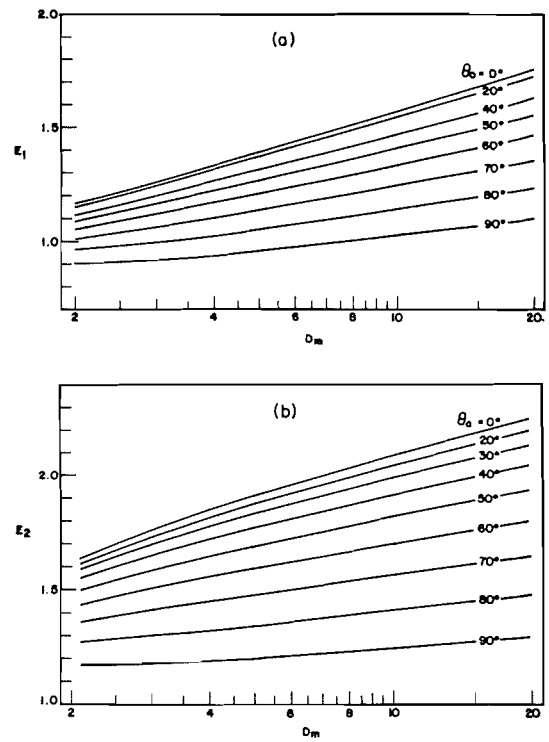

FIG. 7. (*a*) E_1, and (*b*) E_2 as functions of D_m and θ_0.

Can. J. Chem. Downloaded from www.nrcresearchpress.com by 210.87.254.40 on 09/05/12
For personal use only.

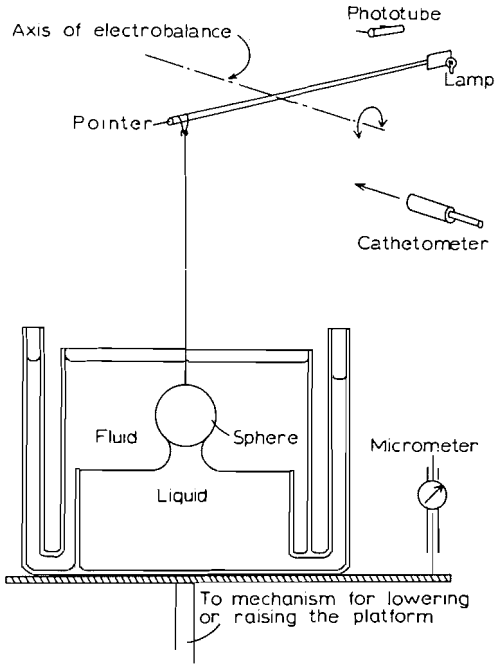

FIG. 8. Schematic of the experimental set-up.

Experimental Part

Apparatus

Figure 8 shows the schematic of the prototype experimental setup, consisting of a weighing device, a specimen cell, and the means of varying the height h. The weighing device consisted of (*i*) a Cahn RG recording electric microelectrobalance, set for 0–1.0 g total range and 0–100 mg recorder range, which measured continuously the force F on a thread attached to a sphere; and (*ii*) a 1 mV span recorder to record the balance output. The balance–recorder arrangement provided about 0.1 mg resolution.

The liquid specimen cell was contained in a cubic enclosure with 20 cm inner sides to protect the specimen liquids from air currents and permit temperature control to ± 0.1 °C. The weighing unit of the balance was located over the enclosure, which had a hole through which a thin wire attached to the top of the sphere passed to the weighing arm of the balance. Two opposite vertical walls of the enclosure were transparent to permit visual observation during experiments. The specimen cell consisted of two vertical cylindrical cups open at the top, one placed inside the other; the inner cup had its rim ground flat with sharp edges to hold the liquid interface, and both cups had branching connections for easy addition and removal of liquids.

A vertical piston on top of which was firmly attached a horizontal platform was used to vary h. The platform which held the specimen cell was made horizontal to $\pm 0.3°$. The piston protruded through the bottom of the enclosure, and could be moved vertically in both directions at constant speeds via geared connections driven by a variable-speed DC motor. The displacement of the piston was also recorded to confirm the displacement shown on the Varian recorder. The piston, gears, and motor were all mounted on the same base as the enclosure.

Nylon spheres were used, which were machine-made (Industrial Tectonics Inc.). A nichrome wire (0.1 mm diameter) was attached to the sphere by drilling a tiny hole on its top. The wire gives rise to an extra force as it emerges from phase 3 into the air, and the corrections for it on F were made. The spheres were soaked in distilled water for several days; this was done to prevent the absorption of water during the measurement period and to form a homogeneous solid surface fully wetted by water. The sphere radius, ranging from $R = 0.163$ to 0.325 cm, was measured with a micrometer; minute swelling of the nylon occurred during soaking, and the corrections for R made. Deviation from sphericity was less than 0.1%.

Materials

The water used for surface tension measurements was purified by passing it through the organics-removal and the standard deionization columns (Barnstead), and followed by distillation. The Dow Corning (Type 200, 100 cs) Silicone fluid was used as received from the manufacturer. In some experiments sodium dodecyl sulfate was added to the water.

Procedure

Before an experiment the cell was repeatedly washed with detergent and flowing tap water; immersed for 3 min twice in an aqueous mixture of 2% hydrofluoric and 50% nitric acids; and rinsed thoroughly 15 to 20 times with the distilled water. The spheres, which were kept soaked in distilled water, were transferred to the distilled water in the cell; the wire of the sphere was attached to the weighing arm, the sphere being positioned at the center of the cell. The lighter liquid phase was added and the liquid/liquid system was equilibrated for one day or more in the cell.

The platform was then lowered at constant speed (~ 0.5 mm/min), with the weighing and recording units operating, until the force exerted on the balance went through a maximum and started decreasing. Before the sphere detached from the interface, the movement of the platform was reversed until the force again went through a maximum and started decreasing to zero. In several cases, the platform was lowered until the sphere detached from the interface.

From the F–h curve obtained, F_m was measured; D_m was calculated from $(\rho_2 - \rho_3)$ which was independently measured by the displacement method. From the curve, S or E_1 was also measured. Because the F–h relation was available as an electrical output, S (or E_1 or E_2) could be obtained directly employing an electrical differentiater (or integrator).

Preliminary Results and Discussion

We attempted to make the correction for finite θ_0 on measurements of γ_{23}. Table 4 shows the experimental results for the Silicone fluid/water interface with and without the addition of sodium dodecyl sulfate. The density difference $(\rho_2 - \rho_3)$ was independently measured by the displacement method, and the interfacial ten-

Can. J. Chem. Downloaded from www.nrcresearchpress.com by 210.87.254.40 on 09/05/12
For personal use only.

Can. J. Chem. Downloaded from www.nrcresearchpress.com by 210.87.254.40 on 09/05/12
For personal use only.

Table 4. Interfacial tensions with corrections for finite θ_0

System	R (cm)	F_m (dyn)	D_m	γ_{23} assuming $\theta_0 = 0°$ (dyn/cm)	S	θ_0 by S	γ_{23} by S (dyn/cm)	E_1	θ_0 by E_1	γ_{23} by E_1 (dyn/cm)
Silicone fluid*/water	0.2853	80.5	13.33	38.5	0.453	20°	39.8			
(γ_{23} = 39.5 dyn/cm)†	0.3315	92.63	10.40	39.0	0.476	24°	41.0			
Silicone fluid*/water	0.2853	42.44	7.034	18.0	0.523	34°	19.9	1.472	9°	18.1
+0.5% sodium dodecyl sulfate	0.2034	26.61	12.17	17.6	0.458	19°	18.1	1.620	4°	17.6
(γ_{23} = 19.6 dyn/cm)†	0.1633	20.09	17.75	17.3	0.438	28°	18.6	1.710	13°	17.6
	0.3248	50.94	5.721	17.9	0.522	14°	18.3	1.405	19°	18.6

*Dow Corning 200 (10 cs) Silicone fluid.
†Independent measurements by the pendant drop shape method. $(\rho_2 - \rho_3) = 0.0633$ g/cm^3 for both systems.

Can. J. Chem. Downloaded from www.nrcresearchpress.com by 210.87.254.40 on 09/05/12
For personal use only.

sion was measured independently by the pendant drop shape method, to compare with the present results.

For the system without sodium dodecyl sulfate, we employed the S parameter, as defined by [6], and a contact angle value of about 22° was calculated for the results. The resultant correction for the interfacial tension values amounted to about +4.2% over the values assuming $\theta_0 = 0°$. For the system with sodium dodecyl sulfate, the contact angle values obtained showed a wide scatter. Thus, when we employed the S parameter, the correction for interfacial tension values ranged from +2.2% to +10.6% over those assuming $\theta_0 = 0°$. When the E_1 parameter was employed, the correction for interfacial tension values ranged from 0% to +3.9%, and was not sufficient to bring the values to agree with that by the pendant drop shape method.

Possible reasons for the large discrepancies are discussed below. Despite these difficulties, we believe that the present sphere method holds definite advantages over the ring and plate methods, as discussed in the Introduction, and the alternative sphere method of Scheludko and Nikolov (4). While the Scheludko–Nikolov method depends on the optical measurement of θ_c at F_m, a measurement which from our experience is extremely difficult, our experimental data are available directly as an electrical output which can be easily processed.

The procedure in using the sphere method to determine simultaneously γ_{23} and $(\rho_2 - \rho_3)$ when θ_0 is known (in particular $\theta_0 = 0°$) is: (*i*) S is determined from the experimental F–h curve; (*ii*) D_m and $\bar{R}$ are read from Tables 1 and 3 for S; and (*iii*) γ_{23} and $(\rho_2 - \rho_3)$ are determined utilizing R and F_m and the definitions of $\bar{R}$ and D_m in [1].

In making the sphere method convenient for simultaneously measuring γ_{23} and θ_0, several practical difficulties must be overcome. The first difficulty arises from the geometry of sphere in that relative to its volume it has a short contact line, compared to the ring or plate. Thus, a small error in the measurement of R causes a substantial loss of accuracy in D_m (see the definition of D in [1]), and accordingly in S, E_1, and E_2 (see [6]). Preparation of precision spheres thus becomes absolutely necessary, although the availability of precision ball bearings makes this surmountable. The second difficulty is that the measurement of the h-variation is susceptible to error. To measure a varying weight continuously, the available electrobalances feed back the information on the weighing arm displacement to reposition the weighing arm at its original setting. The continuous displacement and readjustment of the weighing arm, although minute, cause an error in h when we measure h and F simultaneously. Errors in h cause further loss in accuracy of S, E_1, and E_2. Correction for the weighing arm displacement can be satisfactorily made from the knowledge of F and the direct cathetometric measurement of h but the details will not be discussed here. An alternative is a new design of electrobalance with zero (or negligible) displacement as F varies.

The third difficulty is that θ_0 may vary as h increases. This variation of θ_0 (which in itself would be an average of variations along a given line of contact) may result from roughness and heterogeneity of the surface of the sphere (3, 7, 8), or as a dynamic effect (9). With the use of a precision sphere with a molecularly smooth surface (8), and with a sufficiently slow variation of h in time, *e.g.* less than 1 mm/min as in our experiments, this difficulty may be overcome. From the upward and downward displacements of the sphere (see Fig. 3), we examined the reversibility of the F–h curves, and when they were reversible, *i.e.*, had mirror symmetry, we assumed that θ_0 was constant.

The last, but probably the most serious difficulty is the effect of the finite size of the container which contains the test liquids. The theoretical calculations assume that the horizontal 23 interface extends to infinity. In many practical situations, however, the radius ratio of the sphere to container must be large due to the limited amount of the test liquid available. When $\bar{R} \ll 1$, the meniscus deformation extends to a large distance from the sphere and the container wall effect becomes more severe (10). Either a wide container is employed, or a theoretical correction must be made for the effect of the container wall. How the container wall affects the interfacial tension measurements is qualitatively shown by Fig. 9. Interfacial tensions were measured for the Silicone fluid/water interface which was fixed (11) at the sharp-edged rim of the container. The radius ratio of

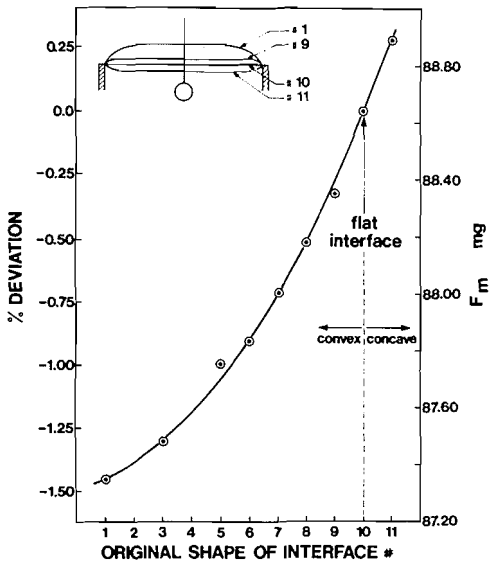

FIG. 9. Effect of the small size of the liquid container on the measurements of γ_{23}. The Dow Corning 200 (10cs) Silicone fluid/water interface, which was remained pinned at the sharp-edged rim of the container, was initially bulged upward; equal volume increments of water were successively removed from the container. The approximate surface contours determined photographically at the various numbered data stations (shown as abscissa) are shown in the inset.

the container to sphere was 9.2, as shown by the inset of Fig. 9. Initially (station 1, Fig. 9), the interface bulged upward, and the measured value of the interfacial tension was smaller than the true one; as the equal volume increments of the water were removed from the container, F_m and the apparent γ_{23} gradually increased, revealing a sizeable effect of the container wall.

Further attempts are being made to overcome these difficulties and to make available the sphere method as a convenient way of measuring surface and interfacial tensions.

Acknowledgment

This investigation was conducted over the period 1969–1975, with the assistance of Mr. Arie Mar to whom we are indebted for many contributions and especially for the experimental work.

1. C. HUH and S. G. MASON. J. Colloid Interface Sci. **47**, 271 (1974).
2. J. F. PADDAY, A. R. PITT, and R. M. PASHLEY. J. Chem. Soc. Faraday Trans. I, **71**, 1919 (1975).
3. J. F. OLIVER, C. HUH, and S. G. MASON. Wetting and spreading: III. Influence of surface roughness (experimental). To be published.
4. A. D. SCHELUDKO and A. D. NIKOLOV. Colloid Polymer Sci. **253**, 396 (1975).
5. H. M. PRINCEN. *In* Surface and colloid science. Vol. 2. *Edited by* E. Matijevic. Wiley (Interscience), New York. 1969. p. 1.
6. C. HUH and L. E. SCRIVEN. J. Colloid Interface Sci. **30**, 323 (1969).
7. R. E. JOHNSON, Jr. and R. DETTRE. *In* Surface and colloid science. Vol. 2. *Edited by* E. Matijevic. Wiley (Interscience), New York, 1969. p. 85.
8. C. HUH and S. G. MASON. Wetting and spreading: I. Influence of surface roughness (theoretical). To be published.
9. G. E. P. ELLIOT and A. C. RIDDIFORD. J. Colloid Interface Sci. **23**, 389 (1967).
10. C. HUH and S. G. MASON. A rigorous theory of ring tensiometry: addendum on the wall effect. Colloid Polymer Sci. In press.
11. J. F. OLIVER, C. HUH, and S. G. MASON. Wetting and spreading: II. Resistance to spreading by a sharp edge. To be published.

Can. J. Chem. Downloaded from www.nrcresearchpress.com by 210.87.254.40 on 09/05/12
For personal use only.

Chemically induced dynamic nuclear and electron polarization. Part IX. The photolysis of tetrafluoro-*p*-benzoquinone in dioxane

HARISH M. VYAS AND JEFFREY K. S. WAN

Department of Chemistry, Queen's University, Kingston, Ontario K7L 3N6

Received September 15, 1975

HARISH M. VYAS and JEFFREY K. S. WAN. Can. J. Chem. **54**, 979 (1976).

The photoreduction of *p*-fluoranil in dioxane was studied by combined CIDNP and CIDEP techniques. It was established that the photoreactive species is the excited triplet of the quinone and the phototriplet mechanism is mainly responsible for the CIDEP observation. The CIDNP observations revealed the cage recombination of the primary radical-pair resulting in the formation of the cross-combination product from the semiquinone and the dioxane radicals. The cage recombination cannot be monitored by the conventional kinetic esr technique. The field dependent CIDNP intensity of the *p*-fluoranil in the photoreduction by fluorohydroquinone was also studied and a calculation based on Lawler's scheme showed that the results can be adequately explained by the radical-pair theory including both the scavenged and cage combination processes.

HARISH M. VYAS et JEFFREY K. S. WAN. Can. J. Chem. **54**, 979 (1976).

On a étudié, par une combinaison des techniques CIDNP et CIDEP, la photoréduction, dans le dioxanne, du *p*-fluoroanil. On a établi que l'éspèce photoréactive est un triplet excité de la quinone et que le mécanisme de phototriplet est le principal responsable pour l'observation CIDEP. Les observations CIDNP révèlent la recombinaison en cage de la paire de radical primaire qui amène la formation d'un produit croisé de combinaison provenant des radicaux de la semiquinone et du dioxanne. La recombinaison en cage ne peut pas être suivie par la technique conventionnelle de cinétique rpe. On a aussi étudié l'intensité CIDNP dépendant du champ du *p*-fluoroanil lors de la photoréduction de la fluorohydroquinone et un calcul basé sur le schéma de Lawler montre que les résultats peuvent être expliqués correctement par la théorie des paires de radicaux incluant les deux processus de piégage et de combinaison en cage.

[Traduit par le journal]

Introduction

In a previous esr study (1) of the photolysis of *p*-fluoranil (tetrafluoro-*p*-benzoquinone) in dioxane solution, we observed the transient *p*-tetrafluorosemiquinone radical and its decay kinetics. These radicals decay by self-disproportionation with a second-order rate constant at room temperature of $3.2 \times 10^9\ M^{-1}\ s^{-1}$. Similar decay kinetics have been reported (2) for other semiquinone radicals in dioxane or isopropanol solution.

The conventional esr spectrometer is not able to detect free radicals with lifetimes shorter than 100 μs and thus only gives a partial resolution to the 'transient' radical intermediates involved in various stages of a chemical reaction. On the other hand, detailed CIDNP studies may yield more insight into the whole chemical reaction system, but the identity of the transient radical intermediates is only inferred from the products. However, when combined with the transient esr technique in which the radicals and their magnetic parameters can be readily obtained, CIDNP study can yield unprecedented detailed information on the nature of the radical intermediates, their various reaction pathways leading to the formation of products. For example, in the previous study (1) of the photoreduction of *p*-fluoranil in dioxane, the conventional ^{19}F nmr analysis revealed only the self-disproportionated products which are the major reactions of the semiquinone radicals, according to the kinetic esr observations. The minor reaction pathways such as the cross-combination with the counter dioxane radicals were not observed. The extremely high sensitivity of CIDNP technique in the present study afforded the direct investigation of these minor reactions and the identification of the products.

In our first correlated CIDNP and CIDEP study of the benzoquinone in isopropanol (3), the CIDNP results also suggest that the semiquinone radicals decay by a minor pathway in a 'cage disproportionation' with the ketyl radicals,

Can. J. Chem. Downloaded from www.nrcresearchpress.com by 210.87.254.5 on 09/05/12
For personal use only.

Can. J. Chem. Downloaded from www.nrcresearchpress.com by 210.87.254.5 on 09/05/12
For personal use only.

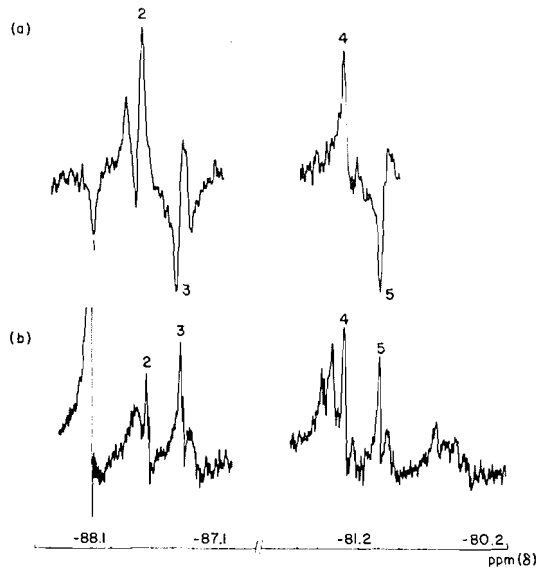

FIG. 1. (*a*) ^{19}F CIDNP spectrum during the photolysis of *p*-fluoranil in dioxane; (*b*) ^{19}F spectrum of the product after prolonged irradiation. Line 1 is the hydroquinone peak, lines 2, 3, 4, 5 are due to the product **1**.

in addition to the major decay path via self-disproportionation. Recently, we have established (4, 5) that in the photochemical carbonyl systems involving primary photochemical reactions from excited triplets, both the radical-pair and the phototriplet mechanisms contribute simultaneously to the electron polarization as well as the nuclear polarization. In quinone systems in which the proton coupling constants of the semiquinone radicals are relatively small, the phototriplet mechanism was found to be dominant in electron polarization of the primary radical-pair. Subsequent secondary reactions of the radical-pair leading to product formations and CIDNP observations can be accounted for mostly by the radical-pair mechanism. Furthermore, it has been clearly demonstrated that the radical-pair mechanism also plays a minor role in the electron polarization of the semiquinone radicals. Because of the relatively unfavorable magnetic parameters of the protons in the semiquinone radicals, simultaneous contribution to CIDNP from the phototriplet mechanism is more difficult to demonstrate. However, by using *p*-fluoranil in which the protons are replaced by fluorines which have larger coupling constants, we are able to establish the contribution of the phototriplet mechanism to the CIDNP of the fluoranil system (6). Here the initial electron polarization of the semiquinone radical derived from the phototriplet mechanism is being transferred to the ^{19}F nuclear spin levels by the Overhauser cross relaxation and subsequent retention of the nuclear polarization in the product.

We report in the present paper a detailed CIDNP study and a correlated CIDEP study of the photolysis of *p*-fluoranil in dioxane solution.

Experimental

p-Fluoronil (Aldrich) and 2,6-di-*tert*-butylphenol were purified by vacuum sublimation. Dioxane (Fisher spectrograde) was dried by passing through an alumina column immediately before use. Sample solutions of fluoranil in dioxane were approximately 10^{-2} *M* in concentration. Chemically induced dynamic nuclear polarization spectra were recorded with a Bruker HX60 spectrometer using a ^{19}F probe modified for irradiation. The light source was a 1 kW super pressure mercury lamp equipped with a water filter. The chemical shifts reported are referred to external trifluoroacetic acid inserted into the sample tube by means of a sealed capillary tubing. Apparatus for CIDEP study has been described previously (3).

Results and Discussions

A typical CIDNP spectrum taken during the photolysis of *p*-fluoranil in dioxane solution at room temperature is shown in Fig. 1*a*. After prolonged irradiation of a more concentrated solution of *p*-fluoranil in dioxane, the spectrum of the products is shown in Fig. 1*b*. These CIDNP observations can be readily explained by the Kaptein's rules at high field (7) according to the reaction Scheme 1.

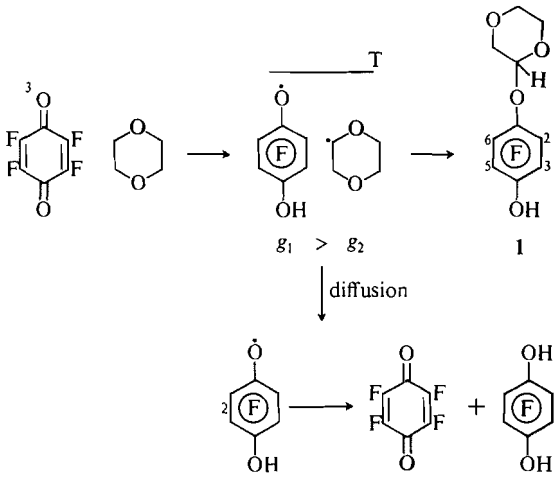

SCHEME 1

Can. J. Chem. Downloaded from www.nrcresearchpress.com by 210.87.254.5 on 09/05/12
For personal use only.

From the esr measurements it was found that the *g*-value for the semiquinone radical is greater than that of the dioxane radical. The ^{19}F hyperfine coupling constants for the semiquinone radical are (−)3.8 and (+)14.1 G for the *meta* and *ortho* fluorines, respectively. The signs of the coupling constants are obtained from an INDO calculation and are consistent with the assignments reported in literature (8).

Recombination product similar to **1** in the photoreduction of *p*-quinones by xanthene in carbon tetrachloride solution has been observed to exhibit CIDNP (9). In the present system, the recombination of the semiquinone and the dioxane radicals could also lead to two other isomeric products:

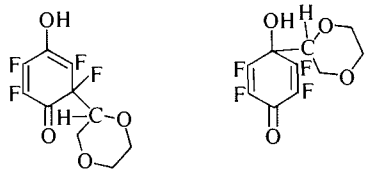

However, the product spectrum in Fig. 1*b* can be assigned to the product structure **1** which has a simple first order A_2X_2 ^{19}F pattern (represented by lines 2,3,4,5 in Fig. 1*b*). The major doublet splitting is due to the coupling of the *ortho* fluorines with $J_{23} = J_{65} = 18$ MHz in **1**. Since the *ortho* coupling signs are usually negative (10), the application of the Kaptein's rules for the cage recombination product **1** would predict a CIDNP multiplet effect with an *E*/*A* pattern which is consistent with the experimental observation. Thus, we conclude that apart from self-disproportionation, the other major reaction of the semiquinone radicals is the 'cage' recombination with the counter radical and that the major combination product is **1**. In a conventional kinetic esr study, only the semiquinone radicals diffused from the primary cage would be observed and these diffused radicals would indeed decay by a second-order kinetics via self-disproportionation.

The self-disproportionation of the semiquinone radicals leads to the so-called 'escaped products' which are the hydroquinone and the *p*-quinone. The experimental observation (Fig. 1*a*) shows that the hydroquinone (line 1) is in the emissive mode and during the photolysis the parent peak of the *p*-fluoranil was found to exhibit diminished absorption, due to the emission from the escaped product *p*-fluoranil. At first we thought that the polarization in the escaped product could result from the initial nuclear polarization generated in the semiquinone radicals. However, a referee has pointed out that such a mechanism requires that the nuclear T_1 must be relatively long compared to the chemical lifetime of the radical undergoing disproportionation. The referee further pointed out in our present system the minimum lifetime of the radical is about 2 ms, which would be much longer than a reasonable T_1 value for the ^{19}F relaxation. The short T_1 for ^{19}F in this case can be inferred from the experimental fact that CIDEP was not observed in the semiquinone radical because of rapid electron relaxation. Under such conditions, the referee suggested that the 'escape' radical polarization could be transferred to the products via the following exchange (scavenging) reactions:

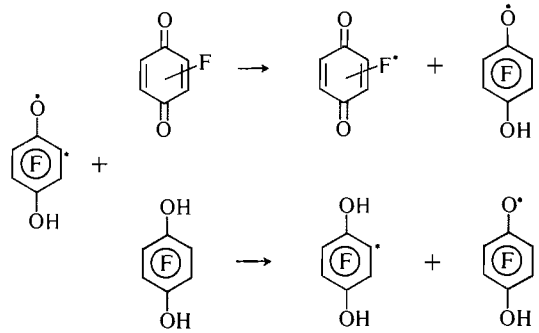

These exchange reactions are expected to be very fast so that the second exchange reaction with hydroquinone would require only a trace of hydroquinone initially produced unpolarized via self-disproportionation. Since neither of these exchange reactions causes a net loss of semiquinone radicals, they would not be detected by esr kinetic measurements.

In CIDEP study of the photoreduction of *p*-fluoranil in dioxane, it was expected that similar to other quinones, the electron polarization of the radicals would come mainly from the phototriplet mechanism (5, 11). However, in the formulation of the triplet model, we have emphasized that the rate of abstraction by the polarized triplet quinone must be comparable

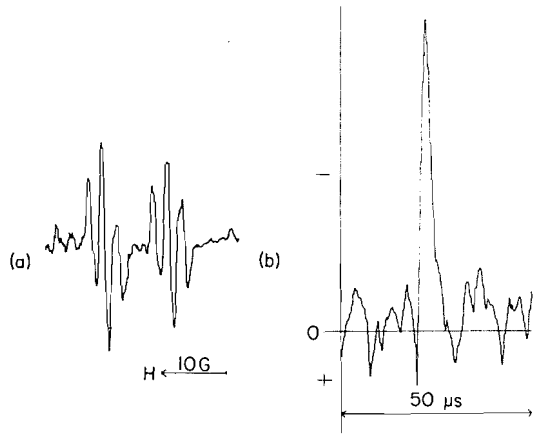

FIG. 2. (*a*) Electron spin resonance spectrum of the phenoxy radical using 2 MHz modulation; (*b*) The time dependence of esr intensity of the phenoxy radical observed during the 5 ns pulse laser photolysis of *p*-fluoranil and 2,6-di-*tert*-butyl phenol in dioxane. The (+) sign indicates absorption and the (−) sign emission.

or faster than the depolarization rate of the triplet (11). In the present system, no electron polarization was observed and this can be attributed to the much slower abstraction rate of the triplet *p*-fluoranil from the dioxane molecule. The spin–lattice relaxation time of the tetrafluorosemiquinone radical may also be shorter than the proton analog. It was therefore necessary to introduce a more efficient hydrogen-donor in the photoreduction. When 2,6-di-*tert*-butylphenol was added to the dioxane solution of *p*-fluoranil, the corresponding phenoxy radical was observed in strongly emissive mode (Fig. 2). However, polarization was still too weak for observation in the fluorosemiquinone radical. It was further established that in the phenoxy radical, all hyperfine lines exhibit emission, as expected from the phototriplet model (11). Since it was difficult to observe the polarization from the counter semiquinone radical, total emission spectra of the one phenoxy radical could still arise from the Δg effect, according to the radical-pair theory. Nevertheless, in the present system both the fluorosemiquinone radical and the phenoxy radical have identical *g*-values (2.0048 ± 0.0003), it follows that the phototriplet mechanism must be mainly responsible for the totally emissive polarization of the phenoxy radical. Thus the CIDEP study supported the scheme in Scheme 1 in that the abstraction reaction involves the triplet *p*-fluoranil and that the resulting radical-pair is initially a triplet pair.

We have also carried out CIDNP study of the photoreduction of *p*-fluoranil by fluorohydroquinone at low field (5–500 G). In a previous low field study (3*b*) of the photoreduction of *p*-quinones, we were mainly interested in the escaped products. Here we extend the study to cover the cage recombination products. In general, $S-T_{\pm}$ mixing becomes efficient at low fields. Since nuclei are flipped during $S-T_{\pm}$ transitions, the consequence is that at low fields the polarization of the recombination products generally will not be opposite in sign to that of the escaped products. Since calculations on the CIDNP of recombination products at low fields have not been formally presented, it is perhaps worthwhile to report them here.

The calculations are mainly based on Lawler's formulism (12) of a dynamic reaction:

$$R \xrightarrow{t_0\,t_1} E \longrightarrow D \xrightarrow{t_2\,t_3} E \longrightarrow D$$
$$\downarrow$$
$$C$$

where R is the initial reactants, E is the encounter pair, D is the diffused pair, and C is the combination product. The density operators $\hat{\rho}^D$ and $\hat{\rho}^S$, for the diffused radical-pair and the scavenged product, respectively, satisfy the equation of motion:

$$[1] \qquad \frac{d}{dt}\hat{\rho}^D = -i[\hat{\Omega}\hat{\rho}^D] - 1/\tau_S(\hat{\rho}^D)$$

$$[2] \qquad \frac{d}{dt}\hat{\rho}^S = 1/\tau_S(\hat{\rho}^D)$$

where $\hat{\Omega}$ is the radical-pair Hamiltonian operator and the commutator describes the time evolution. The term $\hat{\rho}^D/\tau_S$ describes the kinetics of the disappearance of D and the formation of S.

During the encounter interval t_{23}, a radical-pair in the singlet state can react to form products but a radical-pair in the triplet state cannot. This 'bleeding' of the singlet state during encounter interval t_{23} thus represents the formation of product C. The CIDNP intensity, $I_{jk}{}^C$, of an nmr transition $|j\rangle \rightarrow |k\rangle$ in the product C can be approximated by (3*b*).

$$I_{jk}{}^C \propto (\phi_j - \phi_k)|\langle j|\hat{\mu}_\perp|k\rangle|^2$$

The probability ϕ_I of finding the product C in a nuclear state $|I\rangle$ is related to the elements of

Can. J. Chem. Downloaded from www.nrcresearchpress.com by 210.87.254.5 on 09/05/12
For personal use only.

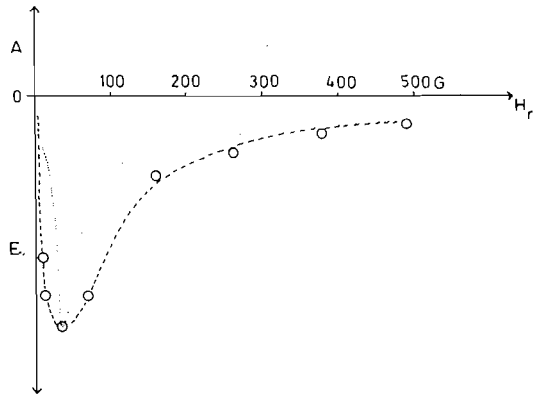

FIG. 3. The experimental (--○--) and theoretical (···) curves of the field dependent CIDNP intensity of the *p*-fluoranil during photoreduction by fluorohydroquinone.

the density operator $\hat{\rho}^D$ according to the following equation:

$$\phi_I = \lambda Z_R \langle \rho_{SI,SI}{}^D(t_2) \rangle$$

$$= P \sum_{i,\alpha,\beta} \frac{U_{iI,\alpha}\, U_{iI,\beta}}{1 + (|\omega_{\alpha\beta}|\tau_S)^2} \times$$

$$P_{\alpha\beta} \sqrt{\frac{\pi|\omega_{\alpha\beta}|\tau_D}{2}} (1 + |\omega_{\alpha\beta}|\tau_S)$$

where λ is the probability of a singlet radical-pair reacting during an encounter, Z_R is the number of nuclear states in R, P is the probability of at least one encounter, and all other symbols are described previously (3*b*).

The field-dependent CIDNP intensity of the photoreduction of *p*-fluoroanil by fluorohydroquinone was observed experimentally and plotted between 0 and 500 G, as shown in Fig. 3. The calculated CIDNP intensity is also included in Fig. 3. The calculations were made on four nuclei including the two *ortho* and two *meta* fluorines. The following parameters were used: $J = -0.44 \times 10^9$ rad/s; $P = 0.8$; $\lambda = 0.95$; $g = 2.0048$; $\Delta g = 0$; $\tau_S = 0.25 \times 10^{-4}$ s; $\tau_D = 1 \times 10^{-11}$ s; $A_{ortho}{}^F = +14.1$ G; $A_{meta}{}^F = -3.8$ G.

It is apparent from Fig. 3 that the experimental curve fitted very nicely with the theoretical curve. We therefore conclude that in the present system at very low fields, the $S-T_{\pm}$ mixing is so efficient that it becomes the dominant mechanism in the CIDNP observation.

Acknowledgments

This research is supported by the National Research Council of Canada and the School of Graduate Studies and Research. We thank Dr. Scott Nee for some computational assistance. We are particularly grateful to a referee who suggested the mechanism of the 'escape' polarization.

1. H. M. VYAS and J. K. S. WAN. Int. J. Chem. Kinet. **6**, 125 (1974).
2. S. K. WONG, W. SYTNYK, and J. K. S. WAN. Can. J. Chem. **50**, 3052 (1972).
3. (*a*) H. M. VYAS, S. K. WONG, B. B. ADELEKE, and J. K. S. WAN. J. Am. Chem. Soc. **97**, 1385 (1975); (*b*) D. A. HUTCHINSON, H. M. VYAS, S. K. WONG, and J. K. S. WAN. Mol. Phys. **29**, 1767 (1975).
4. K. Y. CHOO and J. K. S. WAN. J. Am. Chem. Soc. **97**, 7127 (1975).
5. B. B. ADELEKE and J. K. S. WAN. To be published.
6. H. M. VYAS and J. K. S. WAN. Chem. Phys. Lett. **34**, 470 (1975).
7. R. KAPTEIN. Chem. Commun. 732 (1971).
8. A. HUDSON and J. W. LEWIS. J. Chem. Soc. B, 531 (1969); W. E. GEIGER and W. M. GULICK. J. Am. Chem. Soc. **91**, 4657 (1969).
9. K. MARUYAMA, T. OTSUKI, A. TAKUWA, and S. ARAKAWA. Bull. Chem. Soc. Jpn. **46**, 2470 (1973).
10. E. F. MOONEY. An introduction to ^{19}F nmr spectroscopy. Heydon & Son, Ireland. 1970. p. 45.
11. S. K. WONG, D. A. HUTCHINSON, and J. K. S. WAN. J. Chem. Phys. **58**, 985 (1973); J. Am. Chem. Soc. **95**, 622 (1973).
12. R. G. LAWLER. Prog. Nucl. Magn. Reson. Spectrosc. **9**, 145 (1973).

Can. J. Chem. Downloaded from www.nrcresearchpress.com by 210.87.254.5 on 09/05/12
For personal use only.

The reactions of atomic oxygen with methanol and ethanol[1]

CYNTHIA M. OWENS[2] AND JOHN M. ROSCOE[3]

Department of Chemistry, Acadia University, Wolfville, Nova Scotia B0P 1X0

Received September 3, 1975

CYNTHIA M. OWENS and JOHN M. ROSCOE. Can. J. Chem. **54**, 984 (1976).

The reactions of $O(^3P)$ with CH_3OH and C_2H_5OH were studied as a function of temperature. The absolute rate constants for these reactions fit the following expressions:

$$O + CH_3OH \quad \log k = 9.16 \pm 0.03 - (12.8 \pm 1.2)/RT$$

$$O + C_2H_5OH \quad \log k = 8.62 \pm 0.05 - (6.3 \pm 1.7)/RT$$

(Activation energies are in kJ/mol. Rate constants are in l mol^{-1} s^{-1}.) The data support abstraction of the α-H atom as the primary step. The α-C—H bond in ethanol is apparently weaker than that in methanol, and this alters the nature of subsequent steps in the mechanisms for these reactions. The presence of oxygen alters the stoichiometric coefficients for these reactions and produces the corresponding carboxylic acid.

CYNTHIA M. OWENS et JOHN M. ROSCOE. Can. J. Chem. **54**, 984 (1976).

Les réactions de $O(^3P)$ avec le CH_3OH et le C_2H_5OH ont été étudiées en fonction de la température. Les constantes absolues de vitesse de ces réactions peuvent être exprimées par les expressions suivantes:

$$O + CH_3OH \quad \log k = 9.16 \pm 0.03 - (12.8 \pm 1.2)/RT$$

$$O + C_2H_5OH \quad \log k = 8.62 \pm 0.05 - (6.3 \pm 1.7)/RT$$

(Les énergies d'activation sont exprimées en kJ/mol. Les constantes de vitesse sont exprimées en l mol^{-1} s^{-1}.) Les résultats impliquent que la perte d'un atome α-H est l'étape première. La liaison α-C—H semble être plus faible en le C_2H_5OH que dans le CH_3OH et par conséquent les mécanisms pour les deux réactions ont des étapes secondaire différentes. La présence d'oxygène abaisse les constantes stoichiométriques et conduit à la formation de l'acide carboxylique correspondant.

While the reactions of atomic oxygen with hydrocarbons have been extensively studied, very little attention appears to have been paid to the corresponding reactions of polar compounds such as alcohols. Our interest in the reactions of atomic oxygen with alcohols arose as a result of oxygen atom participation in the reactions of alcohols with active nitrogen (1).

While some information is available on the mechanism of oxygen atom attack on alcohols (2–5), only two kinetic investigations have been reported (3, 6). The rate constants reported by LeFevre *et al.* (6) are approximately an order of magnitude higher than those of Avramenko *et al.* (3), and large differences exist in both the preexponential factor and activation energy. Neither group determined the stoichiometric coefficient for their reaction, and absolute rate constants are therefore unavailable. Aside from the quantitative discrepancies among existing data, the reaction mechanism postulated by Avramenko *et al.* (3) is different from that postulated by Kato and Cvetanović (4, 5). The work reported here attempts to resolve some of the discrepancies among existing data for the reactions of atomic oxygen with methanol and ethanol, and presents absolute rate constants for these reactions.

Experimental

The reactions were studied in a conventional flow system similar to that described previously (1). The apparatus was modified slightly for the stoichiometric measurements by placing a molecular leak in the observation zone so that consumption of atoms and alcohol, and formation of reaction products, could be monitored simultaneously at the same reaction time. Stable species could be measured via this molecular leak using a CEC model 21-104 single focussing mass spectrometer.

The mass spectrometer was operated at sufficiently low ionizing voltages to minimize interference by fragmentation

[1]This paper is dedicated to Professor C. A. Winkler of McGill University on the occasion of his sixty-fifth birthday by one of his former students (J.M.R.).

[2]Present address: Department of Chemistry, University of Windsor, Windsor, Ontario.

[3]To whom correspondence should be addressed.

Can. J. Chem. Downloaded from www.nrcresearchpress.com by 210.87.254.42 on 09/05/12
For personal use only.

TABLE 1. Stoichiometric coefficients

Reaction	No O_2		Excess O_2		
	[ROH]/[O]	Δ[O]/Δ[ROH]	$[O_2]/[O]$	[ROH]/[O]	Δ[O]/Δ[ROH]
O + CH_3OH	17.0	2.0	91.1	30.7	1.0
	13.7	1.6	91.1	16.1	1.0
	10.9	1.6	91.1	14.2	1.3
	6.54	2.4	91.1	9.22	1.1
	5.64	1.9	91.1	5.34	1.2
	3.24	1.9	91.1	4.61	1.4
	1.65	2.0	91.1	2.03	1.3
	—	—	91.1	0.786	1.5
		Ave. 1.9±0.2			Ave. 1.2±0.2
O + C_2H_5OH	23.2	1.7	85.1	34.1	0.67
	19.9	1.5	85.1	27.1	0.67
	19.2	1.6	85.1	22.6	0.69
	17.4	1.3	85.1	22.2	0.65
	15.0	1.8	85.1	21.0	0.65
	11.0	1.5	85.1	20.9	0.69
		Ave. 1.6±0.1			Ave. 0.67±0.01

products. While no measurable contribution was found at *m/e* 18 for formic acid or acetic acid at concentrations typical of those under actual reaction conditions, small contributions were found from methanol and ethanol and appropriate corrections were made when calculating the yield of water. The presence of a small excess of NO used to produce the NO_2 emission for monitoring O atom concentrations produced too great an interference at *m/e* 30 to permit measurement of formaldehyde.

Oxygen atoms were produced by NO titration of N atoms formed in a microwave discharge through N_2 (7, 8). The O atom concentration was monitored by measuring the intensity of the NO_2 emission produced by a small excess of NO added to the gas stream (9). The method was calibrated by measuring the intensity of the emission when O atoms were made in varying concentrations. The intensity varied linearly with the amount of NO added in excess of the titration end point for a constant O atom concentration, and also varied linearly with O atom concentration for a constant excess of NO.

Nitrogen, NO, and the alcohols were purified as outlined previously (1). Oxygen was purified by passing it at atmospheric pressure through a furnace packed with oxidized copper turnings and heated to 400 °C, and then through a trap cooled in Dry Ice and acetone. This treatment was necessary to remove traces of hydrocarbons and water. The purified O_2 was then metered through a needle valve and entered the reaction vessel downstream from the discharge but upstream from the reactant inlet. In this way, possible interference by singlet oxygen formed in a discharge through O_2 was avoided.

The method of kinetic analysis has been described previously (1, 10). It may be easily shown that in addition to compensating for first order atom recombination, the method also corrects for gradual drift of the NO concentration. Both the Arrhenius parameters and the rate constants were calculated by weighted least squares with weights $y^2/\sigma^2(y)$ where $y = k$ for the Arrhenius expression and y = intensity in the pseudo first order analysis.

Results and Discussion

Kinetics

The stoichiometric coefficients for the reactions studied here are presented in Table 1. These values were obtained at long reaction times (about 200 ms) by simultaneous measurement of O atom and alcohol consumption. These stoichiometric coefficients were used to convert the experimental rate constants to the absolute values recorded in Table 2 and Fig. 1.

The data in Table 2 indicate that the pre-exponential factor for O + C_2H_5OH is smaller than for O + CH_3OH. This would be consistent with the postulate (4, 5) that the O atom

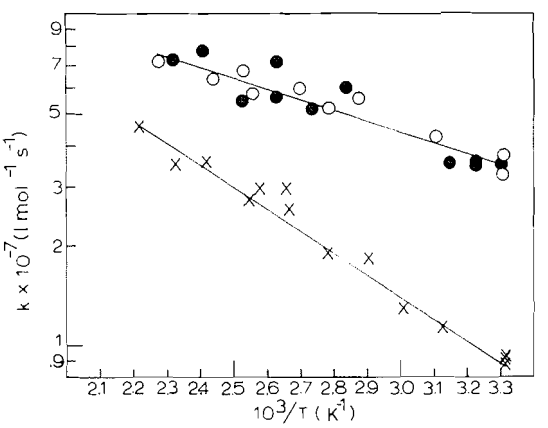

FIG. 1. Arrhenius plots for O + CH_3OH in absence of O_2, ×; O + C_2H_5OH in the absence of O_2, ○; O + C_2H_5OH in the presence of excess O_2, ●. All plots use absolute rate constants.

Can. J. Chem. Downloaded from www.nrcresearchpress.com by 210.87.254.42 on 09/05/12
For personal use only.

TABLE 2. Absolute rate constants*

Pressure (Torr)	Velocity ($m\ s^{-1}$)	$[ROH] \times 10^6$ ($mol\ l^{-1}$)	$[O] \times 10^7$ ($mol\ l^{-1}$)	Temperature (K)	$k_{abs} \times 10^{-7}$ ($l\ mol^{-1}\ s^{-1}$)
$O + CH_3OH$					
1.07	9.45	1.14	1.00	451	4.56
1.07	8.78	1.50	1.25	430	3.46
1.06	8.47	1.34	1.26	413	3.60
1.06	8.04	1.39	1.23	392	2.73
1.75	5.35	1.94	1.92	388	2.99
1.00	7.57	1.29	1.20	376	2.26
1.76	5.42	1.69	1.60	374	2.57
1.00	7.19	1.26	1.20	359	1.88
1.00	6.89	1.23	1.21	344	1.82
1.04	6.68	1.19	1.18	332	1.29
1.17	6.88	1.44	1.34	320	1.12
1.17	6.62	1.72	1.60	301	0.866
1.17	6.65	1.85	1.54	301	0.870
1.05	7.83	2.49	1.81	301	0.770
$\log k = 9.16 \pm 0.03 - (12.8 \pm 1.2)/RT$; correlation coefficient = 0.99					
$O + C_2H_5OH$ (no O_2)					
1.35	8.33	0.890	0.566	439	6.75
1.35	7.78	0.954	0.606	410	5.93
1.35	7.49	0.968	0.629	395	6.34
1.31	7.72	1.21	1.17	390	5.42
1.15	7.89	1.68	1.29	371	6.00
1.31	7.13	1.32	1.28	360	4.91
1.31	6.87	1.37	1.33	347	5.25
1.32	6.30	1.18	1.10	322	3.95
1.28	6.09	1.39	1.05	302	3.54
1.28	6.09	1.71	1.54	302	3.12
$O + C_2H_5OH$ (excess O_2)					
1.36	8.26	1.03	0.251	431	7.34
1.36	7.95	1.07	0.273	415	7.84
1.36	7.52	1.13	0.215	396	5.54
1.36	7.22	1.18	0.200	380	5.67
1.28	7.77	1.34	0.254	380	7.32
1.28	7.46	1.39	0.221	365	5.18
1.28	7.20	1.40	0.316	352	6.04
1.29	6.32	1.12	0.175	317	3.57
1.29	6.21	1.12	0.205	310	3.50
1.28	5.99	0.929	0.115	301	3.50
1.28	5.99	0.911	0.112	301	3.48
$\log k = 8.62 \pm 0.05 - (6.3 \pm 1.7)/RT$; correlation coefficient = 0.93†					

*Activation energies are in $kJ\ mol^{-1}$. All rate constants are within two standard deviations of the regression line.

†This expression was fitted to the combined data for C_2H_5OH.

abstracts the α-H atom, since there are fewer α-hydrogens in ethanol than in methanol and they are also less accessible in ethanol than in methanol. The same data indicate that the activation energy for $O + C_2H_5OH$ is less than that for $O + CH_3OH$. This suggests that the α-C—H bond in ethanol is weaker than that in methanol, which is consistent with other values of these bond energies (11). In methanol, the electron-withdrawing effect of the OH is distributed among three C—H bonds, while in ethanol it is distributed mainly between the two α-C—H bonds. This is offset to some extent by electron donation from the methyl group in ethanol, but the net effect seems to be bond weakening.

The kinetic parameters for $O + CH_3OH$ may be compared with those of Avramenko *et al.* (3) and of Timmons and co-workers (6). Our rate constants are at least an order of

Can. J. Chem. Downloaded from www.nrcresearchpress.com by 210.87.254.42 on 09/05/12
For personal use only.

TABLE 3. Product yields*

	No O_2		Excess O_2			
	$[H_2O]$	[RCH:O]	$[O_2]$	$[H_2O]$	[RCH:O]	[RC(:O)OH]
Reaction	Δ[O]	Δ[O]	Δ[O]	Δ[O]	Δ[O]	Δ[O]
$O + CH_3OH$	0.082	—	74.5	0.31	—	0.16
	0.072	—	74.5	0.21	—	0.14
	0.085	—	74.5	0.27	—	0.16
	0.082	—	74.5	0.19	—	0.13
	0.078	—	74.5	0.26	—	0.17
	Ave. 0.080±0.004			0.25±0.04		0.15±0.02
$O + C_2H_5OH$	0.87	0.28	71.2	3.3	0.75	0.061
	0.98	0.22	71.2	3.5	0.89	0.063
	1.2	0.24	71.2	4.0	0.89	0.061
	1.2	0.28	71.2	3.5	0.78	0.065
	1.1	0.19	71.2	3.5	0.91	0.069
	—	0.26	71.2	—	0.81	0.063
	—	0.30	71.2	—	0.73	—
	—	0.24	71.2	—	0.88	—
	Ave. 1.1±0.1	0.25±0.03		3.6±0.2	0.83±0.06	0.064±0.002

*[ROH]/[O] ranged from 11.0 to 37.0 in these experiments.

magnitude larger than those reported by Avramenko, and our activation energy is also much smaller. Others have experienced difficulty in reproducing Avramenko's results both quantitatively and qualitatively (5, 6), and this extends to reactions other than those reported here (12). Some potential sources of this discrepancy have also been discussed elsewhere (5, 12).

An apparent printing error in ref. 6 resulted in two values of the activation energy for $O + CH_3OH$ being reported. To determine the correct value, their rate constants were subjected to *y*-weighted least squares analysis. This gave an activation energy of 11.4 ± 2.3 kJ mol^{-1}. The preexponential factor obtained was (1.70 ± 0.66) × 10^{12} cm^3 mol^{-1} s^{-1} which is the same as that reported (6) and suggests that our analysis of the data is probably correct. These recalculated values are in excellent agreement with our values of 12.8 ± 1.2 kJ mol^{-1} and (1.44 ± 0.12) × 10^{12} cm^3 mol^{-1} s^{-1}, in spite of the quite different experimental methods used.

Reaction Mechanisms

From Table 1, it is clear that O_2 alters the stoichiometry of both $O + CH_3OH$ and $O + C_2H_5OH$. These reactions are best considered separately.

$O + CH_3OH$

The following mechanism has been suggested for the reaction of O atoms with methanol (5):

[1] $O + CH_3OH \rightarrow CH_2OH + OH$

[2] $OH + CH_3OH \rightarrow CH_2OH + H_2O$

[3*a*] $2CH_2OH \rightarrow CH_3OH + H_2C{:}O$

[3*b*] $2CH_2OH \rightarrow HOCH_2CH_2OH$

The yields of H_2O in Table 3 indicate that reaction 2 can account for only about 8% of the OH radicals formed in [1], and another loss route is needed for OH. Furthermore, it is impossible to obtain a stoichiometric coefficient of 1.9 (Table 1) from this mechanism without placing undue weight on reaction 3*a*. The importance of [3*a*] could not be assessed directly because of interferences in the mass spectrometric analysis as noted in the experimental section. A possible solution to this problem is to invoke the reaction

[4] $O + OH \rightarrow O_2 + H$

which has been postulated to be important in the overall reaction under similar conditions (6). It is known to be fast (13–15), with absolute rate constant about 10^{10} l mol^{-1} s^{-1} and effectively no activation energy. The use of [4]

Can. J. Chem. Downloaded from www.nrcresearchpress.com by 210.87.254.42 on 09/05/12
For personal use only.

Can. J. Chem. Downloaded from www.nrcresearchpress.com by 210.87.254.42 on 09/05/12
For personal use only.

in place of [2] provides the alternative source of H_2O

[5a] $H + CH_3OH \rightarrow CH_3 + H_2O$

[5b] $H + CH_3OH \rightarrow CH_2OH + H_2$

Under conditions similar to those in our experiments, it was found that $k_{5a}/k_{5b} = 7/3$ (16).

A decision as to the relative importance of [2] and [5a] can be made from the product yields in the presence of O_2 (Table 3). These data were used to calculate the relative weights of the steps in the mechanism listed in Table 4, taking the relative weight of reaction 1 as unity. The H_2O yield in the presence of O_2 was not used in these calculations for reasons that will be clear later. Instead, the disproportionation/combination ratio for CH_2OH calculated in the absence of O_2 was combined with the measured yield of formic acid to calculate the yield of H_2O which was then compared with the experimental value. It was assumed that the formic acid was formed in the reaction

[6] $O_2 + CH_2OH \rightarrow H_2CO_2 + OH$

This reaction is not meant to be an elementary one, and may well result from formation of $HOCH_2O{-}O\cdot$ followed by elimination of OH and rearrangement. Similar reactions have been proposed in studies of the oxidation of organic substrates (17–20).

It will be noted that in Table 4 the relative weight for [5a] + [5b] increases from 0.23 in the absence of O_2 to 1.09 when O_2 is added. Assuming that all the H produced in [4] reacts via [5], the weight for [5] should be unity in the absence of O_2. We interpret this discrepancy as indicating that about 77% of the H atoms formed in [4] are lost at the wall.

In the presence of O_2, the weight of [5] should be 1.35 if all the H formed in [4] were removed by [5]. The lower value of 1.09 is again interpreted as a loss of 20% of the H atoms at the wall. This lower value of H atom loss may be a result of poisoning of the wall by water and by formic acid. Water is known to be a good inhibitor of heterogeneous H atom recombination, and it is possible that formic acid is also strongly adsorbed although its properties as a recombination inhibitor are not clear. It may also be significant that in the presence of O_2, the O atom signal returned to its initial value sluggishly when the CH_3OH flow was turned off, while it returned to its initial value quite readily in the absence of O_2. This kind of behaviour is also typical of altered wall conditions.

TABLE 4. Relative reaction weights

	Relative weights			
	No O_2		Excess O_2	
Reactions	(a)	(b)	(a)	(b)
[1]	1	1	1	1
[2]	0.15	0	0.01	0
[3a]	0.18	0.18	0.12	0.14
[3b]	0.97	0.35	0.62	0.27
[4]	0.85	1.0	0.08	1.0
[5a]	0	0.16	0	0.76
[5b]	0	0.07	0	0.33
[6]	0	0	0.16	0.35

	No O_2		Excess O_2	
$[H_2O]/\Delta[O]$	(a)	(b)	(a)	(b)
Measured	0.080	0.080	0.25	0.25
Calculated	—	—	0.009	0.32

O + C_2H_5OH

The following mechanism has been suggested for the reaction of O atoms with ethanol (4):

[11] $O + C_2H_5OH \rightarrow CH_3CHOH + OH$

[12] $OH + C_2H_5OH \rightarrow CH_3CHOH + H_2O$

[13a] $2CH_3CHOH \rightarrow C_2H_5OH + CH_3CH{:}O$

[13b] $2CH_3CHOH \rightarrow CH_3CH(OH)CH(OH)CH_3$

This mechanism accounts satisfactorily for the observed yield of H_2O (Table 3). Any intervention by reaction 4 as in the methanol reaction would decrease the yield of H_2O below the measured value. These results suggest that OH reacts much more readily with C_2H_5OH than with CH_3OH. This is consistent with the observed lower activation energy for $O + C_2H_5OH$ compared with $O + CH_3OH$ since OH presumably abstracts the α-H atom. It seems reasonable to suggest a lower limit of about 10^{10} l mol^{-1} s^{-1} for k_{12} since k_{12} must be at least as large as k_4 to give $H_2O/\Delta O = 1.1 \pm 10\%$ under our experimental conditions.

The mechanism outlined above predicts a larger yield of acetyldehyde than is observed.

Can. J. Chem. Downloaded from www.nrcresearchpress.com by 210.87.254.42 on 09/05/12
For personal use only.

Since acetaldehyde reacts readily with O atoms (12, 21), the following reactions should probably be included.

[14] $O + CH_3CH{:}O \rightarrow CH_3C{:}O + OH$

[15] $CH_3C{:}O + C_2H_5OH \rightarrow CH_3CHOH + CH_3CH{:}O$

[16] $2CH_3C{:}O \rightarrow CH_3C(:O)C(:O)CH_3$

The mechanism consisting of reactions 11 through 16 accounts satisfactorily for the measured yields and stoichiometric coefficient and gives acceptable balance of all free radicals. It may be relevant that the reactions

[17] $O + CH_3CHOH \rightarrow OH + CH_3CH{:}O$

[18] $OH + CH_3CHOH \rightarrow H_2O + CH_3CH{:}O$

were unsatisfactory as sources of acetaldehyde. Mechanisms in which either or both of these reactions were used consistently predicted too large a yield of acetaldehyde.

The addition of O_2 to the $O + C_2H_5OH$ reaction increases the yields of H_2O and acetaldehyde (Table 3), decreases the stoichiometric coefficient (Table 1), and produces acetic acid (Table 3). The acetic acid is assumed to arise from

[19] $CH_3CHOH + O_2 \rightarrow CH_3C(:O)OH + OH$

The general explanation of these effects is presumably similar to that advanced for the $O + CH_3OH$ reaction, but the available experimental data do not allow a quantitative treatment of this system, because of the potentially greater number of reactions involved.

It is perhaps surprising that the reactions of CH_3OH and of C_2H_5OH with O atoms are not satisfactorily described under our experimental conditions by a single mechanism. This is apparently due to the lower activation energy for abstraction of the α-H atom from ethanol compared to methanol. This evidently prevents $OH + CH_3OH$ from competing with $O + OH$ under our conditions. The difference between our results and those of ref. 4 are likely a result of two substantial differences in experimental conditions. At the lower pressures used in our work, heterogeneous reactions may be much more important than in ref. 4, and the much larger excess of CH_3OH over O in ref. 4 may well have allowed $OH + CH_3OH$ to compete successfully with $OH + O$, thereby altering the yields and stoichiometry of the $O + CH_3OH$ reaction. Because of this, our results should not be construed as being inconsistent with their results. Of greater importance is our conclusion that abstraction of the α-H atom is the initial step in the reactions of both alcohols with O atoms, in agreement with the results of refs. 4–6 and in contradiction of Avramenko's interpretation (3).

Acknowledgments

Financial support for this work was provided by the National Research Council of Canada. The assistance of Mr. Walter MacKay in some of the experiments is gratefully acknowledged.

1. JOHN M. ROSCOE and SHARON G. ROSCOE. Can. J. Chem. **51**, 3671 (1973).
2. P. HARTECK and U. KOPSCH. Z. Phys. Chem. (Leipzig), B**12**, 327 (1931).
3. L. I. AVRAMENKO, R. V. KOLESNIKOVA, and N. L. KIZNETSOVA. Izv. Akad. Nauk SSSR Otd. Khim. Nauk, 599 (1961).
4. A. KATO and R. J. CVETANOVIĆ. Can. J. Chem. **45**, 1845 (1967).
5. A. KATO and R. J. CVETANOVIĆ. Can. J. Chem. **46**, 235 (1968).
6. HENRY F. LEFEVRE, JAMES F. MEAGHER, and RICHARD B. TIMMONS. Int. J. Chem. Kinet. **4**, 103 (1972).
7. G. B. KISTIAKOWSKY and G. G. VOLPI. J. Chem. Phys. **27**, 1141 (1957).
8. F. KAUFMAN and J. R. KELSO. J. Chem. Phys. **27**, 1209 (1957).
9. F. KAUFMAN. Prog. React. Kinet. **1**, 1 (1961).
10. A. A. WESTENBERG and N. DEHAAS. J. Chem. Phys. **46**, 490 (1967).
11. J. A. KERR. Chem. Rev. **66**, 465 (1966).
12. H. E. AVERY and R. J. CVETANOVIĆ. J. Chem. Phys. **43**, 3725 (1965).
13. F. P. DELGRECO and F. KAUFMAN. Discuss. Faraday Soc. **33**, 128 (1962).
14. M. A. A. CLYNE and B. A. THRUSH. Proc. R. Soc. Ser. A, **275**, 544 (1963).
15. A. A. WESTENBERG, N. DEHAAS, and J. M. ROSCOE. J. Phys. Chem. **74**, 3431 (1970).
16. W.-K. ADERS and H. GG. WAGNER. Z. Phys. Chem. **74**, 224 (1971).
17. A. FISH. Q. Rev. **18**, 243 (1964).
18. G. E. ZAIKOV, C. D. KAZANCHEVA, and Z. K. MAEZUS. Teor. Eksp. Khim. **2**, 204 (1966).
19. B. D. BOSS and R. N. HAZLETT. Can. J. Chem. **47**, 4175 (1969).
20. DAVID R. KEARNS. Chem. Rev. **17**, 395 (1971).
21. R. D. CADLE and J. W. POWERS. J. Phys. Chem. **71**, 1702 (1967).

Free radicals by mass spectrometry, XLVII. Ionization potentials and ionic heats of formation of C_5–C_7 alkyl radicals[1]

F. P. Lossing

Division of Chemistry, National Research Council of Canada, Ottawa, Canada K1A 0R9

AND

Allan Maccoll

Christopher Ingold Laboratory, University College, 20 Gordon St., London, England WC1H OAJ

Received September 19, 1975

F. P. Lossing and Allan Maccoll. Can. J. Chem. **54**, 990 (1976).

Using an energy-resolved electron beam, ionization potentials have been measured for a number of C_5–C_7 isomeric alkyl radicals, produced by pyrolysis of nitrite intermediates. Values for primary radicals, which could not be produced in sufficient yield, are estimated by extrapolation from lower members of the series. Ionic heats of formation and hydride ion affinities are reported.

F. P. Lossing et Allan Maccoll. Can. J. Chem. **54**, 990 (1976).

Utilisant appel à un faisceau d'électrons, résolu quand à l'énergie, on a pu mesurer les potentiels d'ionisation d'un certain nombre de radicaux alcoylés C_5 à C_7 qui avaient été produits par pyrolyse de nitrites intermédiaires. Dans le cas des radicaux primaires, qui ne peuvent pas être produits en quantités suffisantes, on a évalué ces potentiels en extrapolant à partir des premiers termes de la série. On rapporte aussi les chaleurs de formation ionique et les affinités des ions hydrures.

[Traduit par le journal]

Introduction

Reliable heats of formation data for fragment ions are essential to our understanding of the ionization and dissociation processes leading to the formation of mass spectra. Much of the existing data has been obtained from low energy-resolution measurements, or from dissociative ionization threshold measurements for which the identity of the fragment ion, aside from its formula, is unknown. From recent work (1, 2), in which heats of formation of even-electron hydrocarbon ions made by ionizing the corresponding neutral free radicals have been compared with heats of formation derived from fragment ion appearance potentials, it is clear that major structural rearrangements to produce the more stable isomers of a given fragment ion can take place close to the enthalpy minimum for the dissociation. For this reason the thermochemistry of alkyl fragment ions derived from dissociative ionization thresholds does not exhibit a clear separation into primary, secondary, and tertiary ions. Thermochemical data obtained by direct ionization of free radicals of known structure, although subject to errors of a different kind, are free from complications resulting from ionic rearrangements, since the ionization energy measured is that required to form the ion on a time-scale much shorter than that required for changes in internuclear distance, and is, of course, unaffected by the subsequent rearrangements of the ion. The ionization potential so measured will usually be lower than the vertical value, and may approximate the adiabatic value, depending on the shapes of the potential energy curves for the radical and ion, and on the experimental sensitivity. These factors have been clearly explained by Morrison (3).

The ionization potentials and ionic heats of formation for C_1–C_4 alkyl radicals obtained in this way have been reported (4). The present work was undertaken to extend these measurements to higher alkyl radicals in the range C_5–C_7.

Experimental

Ionization efficiency curves were obtained as described earlier (4) using an energy-resolved electron beam from a double-hemispherical energy selector, coupled to a quadrupole ion filter. The initial portions of the ionization efficiency curves were scanned repeatedly over a 0.8 V range and the data were stored and analyzed using a

[1]NRCC No. 15144.

Can. J. Chem. Downloaded from www.nrcresearchpress.com by 210.87.254.6 on 09/05/12
For personal use only.

TABLE 1. Heats of formation of C_3–C_7 alkyl ions from radical ionization potentials

Radical	IP (V)	$\Delta H_f(R)$ (kcal/mol)	$\Delta H_f(R^+)$ (kcal/mol)	Hydride ion affinity $D(R^+—H^-)$† (kcal/mol)
Primary				
1-C_3H_7	8.10*	21.0	208	268
1-C_4H_9	8.01*	16.0	201	266
iso-C_4H_9	8.01*	14.0	199	266
1-C_5H_{11}	(7.94 est.)	10.9	~194	~264
neo-C_5H_{11}	7.91	5.6	188	263
1-C_6H_{13}	(7.92 est.)	6.0	~189	~263
1-C_7H_{15}	(7.90 est.)	1.0	~183	~263
Secondary				
2-C_3H_7	7.55*	18.1	192	252
2-C_4H_9	7.41*	12.5	183	248
2-C_5H_{11}	7.41	7.4	179	248
2-C_6H_{13}	7.38	3.0	173	248
2-C_7H_{15}	(7.35 est.)	−2.0	~168	~247
Tertiary				
t-C_4H_9	6.93*	7.5	167	234
t-C_5H_{11} (2Me 2-C_4H_9)	6.85	3.1	161	233
t-C_6H_{13} (2Me 2-C_5H_{11})	6.82	−1.9	155	231
t-C_7H_{15} (2Me 2-C_6H_{13})	6.79	−6.6	150	231

*Reference 4.
†$\Delta H_f(H^-)$ = 34.7 kcal/mol.

mini-computer (2). Energy thresholds were calibrated against H_2O and Kr standards. The electron beam had a full width at half maximum of about 0.07 eV. The free radicals were produced by thermal decomposition of the appropriate nitrites (5) at low pressure:

$$RCH_2ONO \rightarrow \dot{R} + CH_2O + NO$$

Results and Discussion

Ionization potentials were measured for neopentyl, 2-pentyl, 2-hexyl, 2-methyl 2-butyl (*tert*-pentyl), 2-methyl 2-pentyl (*tert*-hexyl), and 2-methyl 2-hexyl (*tert*-heptyl) radicals. The results are given in Table 1, along with values obtained earlier (4) for propyl and butyl radicals for comparison. Owing to their thermal instability at the temperature of pyrolysis of the nitrites, an adequate yield could not be obtained for 1-pentyl, 1-hexyl, 1-heptyl, and 2-heptyl radicals. Since ionization potentials decrease quite slowly with carbon number for alkyl radicals above C_4, it is possible to estimate these values by extrapolation within about ±0.06 V. Estimated ionization potentials for four radicals are given in Table 1. The heats of formation of the neutral radicals were calculated from the bond dissociation energies D(primary-H) = 98 kcal/mol, D(secondary-H) = 95 kcal/mol, and D(tertiary-H) = 92 kcal/mol (6). The ionic heats of formation obtained from the combined quantities are probably uncertain to ±3 kcal/mol.

The trends in stabilization of the alkyl ions as a function of substitution and carbon number are more easily seen in terms of hydride ion affinities $D(R^+—H^-)$ than from the ionic heats of formation,[2] which decrease with increasing carbon number along with the heats of formation of the hydrocarbons. The hydride ion affinities, given in Table 1, decrease rapidly with carbon number to a nearly constant value for each of the three types of ion at about C_4.

The difference in stabilization between primary and secondary ions of the same carbon number is about 16 kcal/mol, and the difference between secondary and tertiary is about the same within experimental error. Values for

[2]This is a special case of the heterolytic bond dissociation (7).

Can. J. Chem. Downloaded from www.nrcresearchpress.com by 210.87.254.6 on 09/05/12
For personal use only.

tertiary pentyl and hexyl ions are in reasonable agreement (± 2 kcal/mol) with those reported recently by Solomon and Field (8) from hydride ion transfer equilibria. However, our results indicate that the extra 14.2 kcal/mol stabilization found by these authors for the 2,4-dimethyl-3-pentyl (tertiary) ion does not have a counterpart in the 2-methyl-2-hexyl (tertiary) ion, which has a hydride ion affinity consistent with the other tertiary alkyl ions in Table 1.

Although a detailed discussion will not be given here, it is of interest to compare the $\Delta H_f(R^+)$ values from Table 1 with those derived from fragment ion appearance potentials. The most reliable set of appearance potential data for these ions is undoubtedly the photoionization data of Steiner, Giese, and Inghram (9). From these results it is clear that $-CH_3$ group loss from straight-chain hydrocarbons corresponds in most cases to formation of secondary alkyl ions at the dissociation threshold. Rearrangements involving formation of tertiary ions are less common.

1. F. P. Lossing. Can. J. Chem. **50**, 3973 (1972).
2. F. P. Lossing and J. C. Traeger. Int. J. Mass. Spectr. Ion Phys. **19**, 9 (1976).
3. J. D. Morrison. MTP review of chemistry, Ser. 1. Vol. 5. *Edited by* A. Maccoll. Butterworths. 1972. p. 25.
4. F. P. Lossing and G. P. Semeluk. Can. J. Chem. **48**, 955 (1970).
5. F. P. Lossing and J. B. de Sousa. J. Am. Chem. Soc. **81**, 281 (1959).
6. D. M. Golden and S. W. Benson. Chem. Rev. **69**, 125 (1969).
7. A. Maccoll. The transition state. Special Publication No. 16, The Chemical Society, London, 1962. p. 160.
8. J. J. Solomon and F. H. Field. J. Am. Chem. Soc. **97**, 2625 (1975).
9. B. Steiner, C. F. Giese, and M. G. Inghram. J. Chem. Phys. **34**, 189 (1961).

Can. J. Chem. Downloaded from www.nrcresearchpress.com by 210.87.254.6 on 09/05/12
For personal use only.

Derivatives of 2-pyrazolin-5-one. IV.[1] Preparation and properties of two spiro[benzothiazoline-2,4′-[2]pyrazoline] derivatives

RONALD T. COUTTS, ABDEL-MONAEM EL-HAWARI, AND NORMAN J. POUND

Faculty of Pharmacy and Pharmaceutical Sciences, University of Alberta, Edmonton, Alberta T6G 2H7

AND

RUDOLPH A. ABRAMOVITCH

Department of Chemistry, University of Alabama, University, Alabama 35486, U.S.A.

Received September 15, 1975

RONALD T. COUTTS, ABDEL-MONAEM EL-HAWARI, NORMAN J. POUND, and RUDOLPH A. ABRAMOVITCH. Can. J. Chem. **54**, 993 (1976).

Reduction of 3-methyl-4-(2-nitrophenylthio)-1-phenyl-2-pyrazolin-5-one (**2***a*) with sodium borohydride and palladium–charcoal gave two products which are identified as 3′-methyl-1′-phenylspiro[benzothiazoline-2,4′-[2]pyrazoline]-5′-one (**3***a*) and 4-(2-mercaptophenylamino)-3-methyl-1-phenyl-2-pyrazolin-5-one (**4***a*). Evidence is presented in support of a reaction mechanism in which the spiro compound **3***a* is formed first and is then further reduced to the thiol **4***a*.

Reduction of the 1,3-diphenyl-4-(2-nitrophenylthio)-2-pyrazolin-5-one (**2***b*) with the same reducing agent proceeded in a similar manner and diphenyl products **3***b* and **4***b*, analogous to the spiro compound **3***a* and the thiol **4***a*, respectively, were formed.

Some chemical properties of the thiol **4***a* were investigated; it formed a dimethyl derivative, a diacetate, and a tribenzoate.

Reduction of the pyrazolones **2***a* and **2***b* with zinc and ammonium chloride produced the same spirobenzothiazolines **3***a* and **3***b*.

RONALD T. COUTTS, ABDEL-MONAEM EL-HAWARI, NORMAN J. POUND et RUDOLPH A. ABRAMOVITCH. Can. J. Chem. **54**, 993 (1976).

La réduction de la méthyl-3 (nitro-2 phénylthio)-4 phényl-1 pyrazoline-2 one-5 (**2***a*) par le borohydrure de sodium et le palladium sur charbon conduit à deux produits que l'on a identifié comme étant la méthyl-3′ phényl-1′ spiro[benzothiazoline-2,4′-pyrazoline-2]one-5′ (**3***a*) et la (mercapto-2 phénylamino)-4 méthyl-3 phényl-1 pyrazoline-2 one-5 (**4***a*). On présente des données qui supportent un mécanisme réactionnel dans lequel un composé de type spiro **3***a* est formé dans une première étape pour être ensuite réduit en thiol **4***a*.

La réduction de la diphényl-1,3 (nitro-2 phénylthio)-4 pyrazoline-2 one-5 (**2***b*) par le même agent réducteur conduit de la même manière à deux produits diphénylés **3***b* et **4***b* analogues respectivement au composé spiro **3***a* et au thiol **4***a*.

On a examiné quelques propriétés chimiques du thiol **4***a*; il forme un dérivé diméthylé, un diacétate et un tribenzoate.

Le réduction des pyrazolones **2***a* et **2***b* par le zinc et le chlorure d'ammonium conduit aux mêmes spirobenzothiazolines **3***a* et **3***b*.

[Traduit par le journal]

Palladium–charcoal catalyzed sodium borohydride reductions of α-(*o*-nitrophenylthio) aliphatic acids (1) and esters (2,3) produce cyclic hydroxamic acids which are formed via hydroxylamine intermediates. A similar reduction (4) of the pyrazolone **1***a* yielded the corresponding hydroxylamine **1***b* as the major product, together with a small amount of the amine **1***c*. It was of interest to us to extend these reduction studies to see whether catalyzed sodium borohydride reductions of the related pyrazolones **2***a* and **2***b* would produce cyclic *N*-hydroxylated products. Hydroxylamines, however, were not isolated; instead, the reaction followed an unexpected pathway.

Pyrazolones **2***a* and **2***b* are soluble in aqueous sodium hydroxide. A solution of **2***a* in this solvent was reduced with sodium borohydride

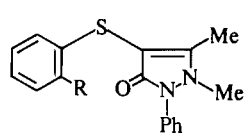

1 *a* R = NO_2
b R = NHOH
c R = NH_2

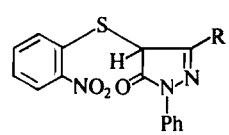

2 *a* R = Me
b R = Ph

[1]For part III, see ref. 17.

Can. J. Chem. Downloaded from www.nrcresearchpress.com by 210.87.254.40 on 09/05/12
For personal use only.

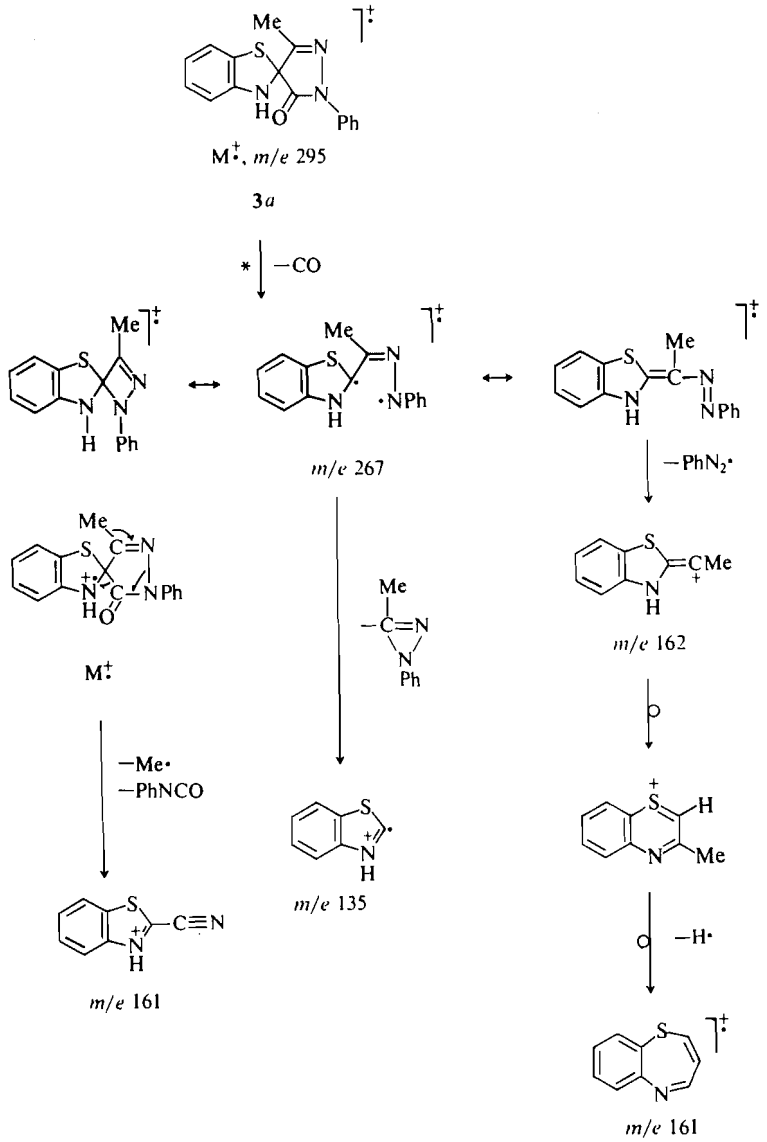

SCHEME 1

in the presence of palladium–charcoal. On completion of the reaction, the filtrate was acidified with dilute acetic acid. The cream-colored amorphous product was soluble initially in 95% ethanol but, on standing, a precipitate separated from solution as a pale yellow crystalline solid (product *A*) which was only sparingly soluble in ethanol. Concentration of the mother liquor remaining after removal of product *A* led to the separation, in variable yields, of the second reduction product (product *B*).

Product *B* ($C_{16}H_{13}N_3OS$; M^+ *m/e* 295) was a pale yellow crystalline compound and was identified first. Its ir spectrum confirmed the presence of a carbonyl and an NH grouping in the structure. Its pmr spectrum displayed signals attributable to an uncoupled methyl group, an NH function, and nine aromatic protons. The presence of carbonyl absorption at 1705 cm^{-1} and the insolubility of the compound in sodium hydroxide solution indicated that the pyrazolone ring in product *B* was incapable of tautomerism and therefore lacked

Can. J. Chem. Downloaded from www.nrcresearchpress.com by 210.87.254.40 on 09/05/12
For personal use only.

Can. J. Chem. Downloaded from www.nrcresearchpress.com by 210.87.254.40 on 09/05/12
For personal use only.

a hydrogen atom at C-4. These properties are in contrast with those of the starting material **2***a* which was soluble in sodium hydroxide solution and showed no carbonyl stretching in the ir (5). Compound **2***a* presumably exists in the solid state as the enol tautomer.

These data suggested that compound *B* was 3′-methyl-1′-phenylspiro[benzothiazoline-2,4′-[2]pyrazoline]-5′-one, **3***a*. Mass spectral evidence supported this structure. Major fragment ions present in the spectrum had *m/e* 267, 162, 161, and 135, identified by accurate measurements as $C_{15}H_{13}N_3S$, C_9H_8NS, a mixture of C_9H_7NS and $C_8H_5N_2S$, and C_7H_5NS respectively. Plausible fragmentation pathways are suggested (Scheme 1).

Product *A* ($C_{16}H_{15}N_3OS$; M^+, *m/e* 297) was soluble in aqueous sodium hydroxide but not in sodium carbonate solution. Its equivalent weight was determined titrimetrically to be 148 and indicated the presence of two acidic groupings, both of which were phenolic and/or enolic. It formed a dimethyl derivative ($C_{18}H_{19}N_3OS$; M^+ *m/e* 325) when treated with dimethyl sulfate. Benzoylation of *A* produced a tribenzoate ($C_{37}H_{27}N_3O_4S$; M^+, *m/e* 609) and acetylation with acetic anhydride in pyridine converted *A* to a diacetate, ($C_{20}H_{19}N_3O_3S$; M^+ *m/e* 381). The ir spectrum of the dimethyl derivative showed carbonyl absorption at 1670 cm^{-1}. In contrast, the carbonyl stretching band of compound *A* was located at 1626 cm^{-1}.

Product *A* was readily oxidized when solutions of it were allowed to stand in contact with air. When *A*, for example, was suspended in ethanol with stirring, the compound slowly entered solution, then a yellow crystalline solid, identical with product *B* (**3***a*), slowly precipitated. Similarly, when *A* was dissolved in DMSO-d_6 in order to record its pmr spectrum, the trace had to be recorded rapidly, otherwise a mixture of *A* and *B* was indicated. Eventually complete conversion of *A* to *B* occurred in this solvent. This facile conversion indicated that *A* and *B* had structural features in common.

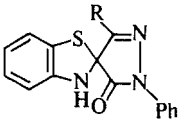

3 *a* R = Me
b R = Ph

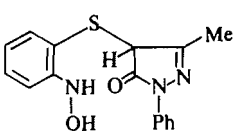

5

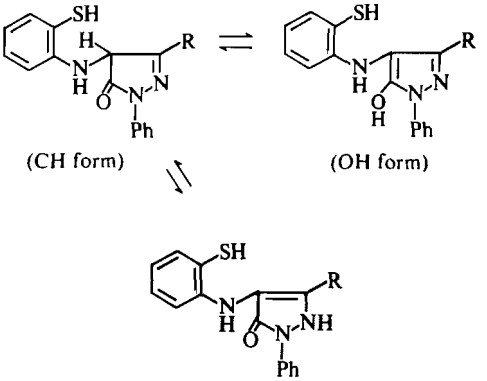

(CH form) (OH form)

(NH form)

4 *a* R = Me
b R = Ph

Based on all these findings and on corroborating evidence which is described later, the structure of product *A* is concluded to be 4-(2-mercaptophenylamino)-3-methyl-1-phenyl-2-pyrazolin-5-one, **4***a*, which can exist in three tautomeric forms. The presence of a strongly bonded carbonyl absorption band at 1626 cm^{-1} suggested that in the solid state, the CH- and NH-forms dominate.

The presence of the SH group in product *A* was suspected initially from its ir spectrum which showed a weak band at 2600 cm^{-1}, and was clearly demonstrated in the mass spectrum. Its presence was also inferred from the mass spectra of the dimethyl, diacetyl, and tribenzoyl derivatives of *A* which are discussed later. The mass spectrum of *A* was very similar to that of *B*. The base peak resulted from the expulsion of a hydrogen molecule from *A* prior to ionization, or from the molecular ion of *A*, to give an ion corresponding to that of molecule *B*. Subsequent fragmentations paralleled those of molecule *B*. The mass spectrum of *A* also had three diagnostic ions of *m/e* 297, 279, and 264 which were absent from the spectrum of *B*. Accurate mass measurements identified each of these ions, and fragmentation pathways which explain the formation of each ion are suggested in Scheme 2. Attempts to prepare a deuteroderivative of *A* resulted only in the formation of deuterated *B*.

Possible mechanisms for the formation of the thiol **4***a* by reduction of the (*o*-nitrophenylthio)pyrazolone **2***a* in basic solution are proposed in Scheme 3. It is known (6) that the

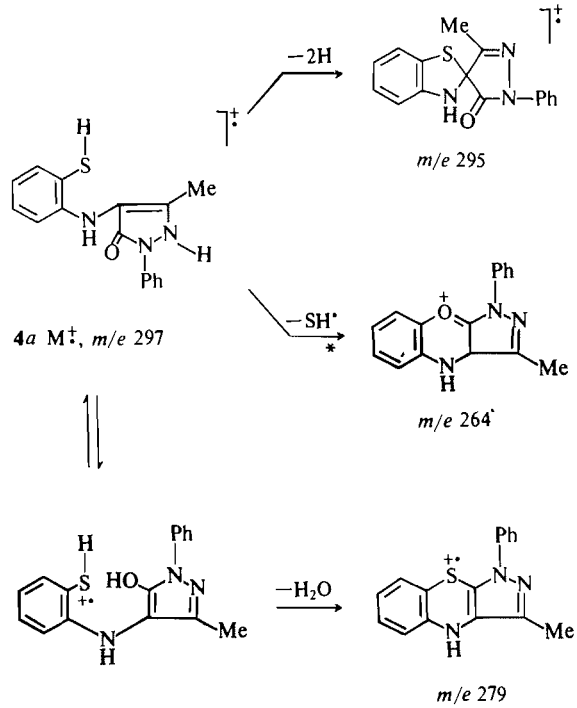

SCHEME 2

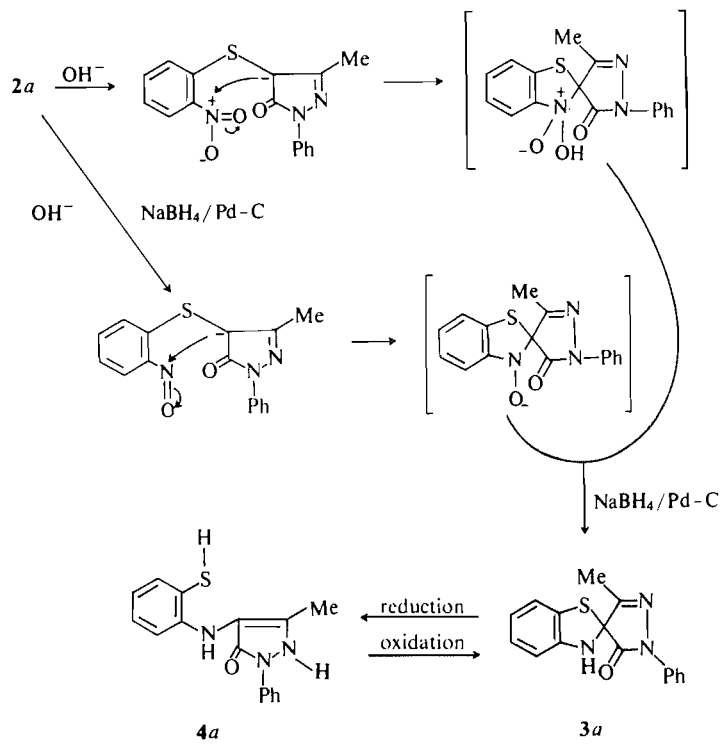

SCHEME 3

Can. J. Chem. Downloaded from www.nrcresearchpress.com by 210.87.254.40 on 09/05/12
For personal use only.

Can. J. Chem. Downloaded from www.nrcresearchpress.com by 210.87.254.40 on 09/05/12
For personal use only.

nitro group can provide an electrophilic centre for cyclization reactions of this type. The same two products, **3***a* and **4***a*, are also isolated, however, when **2***a* is reduced with zinc and ammonium chloride in aqueous ethanol. This suggests an alternative mechanism in which the hydroxylamine **5** is first formed and then dehydrates to the spiro compound **3***a*. In order to verify the assumption that the spirobenzothiazoline **3***a* is obtained first then further reduced to compound **4***a*, a sample of the former was reduced with sodium borohydride and palladium–charcoal in a mixture of dioxane and aqueous sodium hydroxide. Compound **4***a* was the main product isolated.

Attempts to methylate the thiol **4***a* with diazomethane resulted only in its oxidation to **3***a*. However, when an alkaline solution of **4***a* was treated with dimethyl sulfate, 2,3-dimethyl-4-(2-methylthiophenylamino)-1-phenyl-3-pyrazolin-5-one, **6**, was formed. Methylation at N-2 of the pyrazolone nucleus was indicated by the pmr spectrum (N-CH_3 at δ 3.03 (7)), and the ir carbonyl absorption band at 1670 cm^{-1} which is expected only when the pyrazolone ring exists in the NH-form (8,9). 3-Methyl-1-phenyl-2-pyrazolin-5-one, **7**, is methylated at N-2 with dimethyl sulfate in a similar manner to give antipyrene, **8***a*, (10,11). The pmr spectrum of **6** had two other methyl singlets at δ 2.14 and δ 2.39. The former is assigned to the C-Me group since the equivalent group in **4***a* was detected at δ 2.04. The signal at δ 2.39 is therefore assigned to the S-Me protons.

The mass spectrum of the dimethylated product **6** was consistent with the proposed structure. The base peak was located at *m/e* 56. This ion, which corresponds to $MeC{\equiv}\overset{+}{N}Me \leftrightarrow Me\overset{+}{C}{=}NMe$, is present in the spectra of anti-

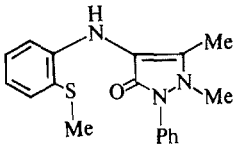

6

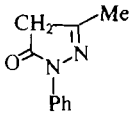

7

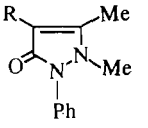

8 *a* R = H
b R = NMe_2

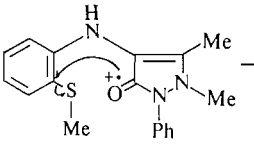

6 $M^{+\cdot}$, *m/e* 325

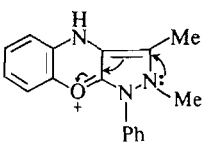

10 *m/e* 278

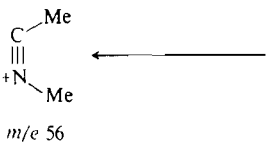

m/e 56

SCHEME 4

pyrene **8***a*, aminopyrene **8***b*, and the *N*-methylpyrazolones **9***a* and *b* (7). The fact that *S*-methylation had occurred was also substantiated by the mass spectrum which showed the molecular ion at *m/e* 325 ($C_{18}H_{19}N_3OS$), an abundant $(M - 47)^+$ fragment ion ($C_{17}H_{16}N_3O$) and an appropriate metastable ion at *m/e* 237.9, all of which indicated a direct loss of an SMe radical from the molecular ion. A possible structure of this $(M - 47)^+$ fragment is depicted in Scheme 4. Such a structure could give rise to the *m/e* 56 ion. The loss of OMe or SMe radicals from aromatic ethers or thioethers is not a common fragmentation pathway but might be expected if it leads to the formation of a cyclic ion such as **10** which permits extensive charge delocalization. Similar *ortho* effects with aromatic ethers have been reported (12,13).

Benzoylation of the thiol **4***a* with benzoyl chloride in aqueous sodium hydroxide gave a semisolid which was separated by column

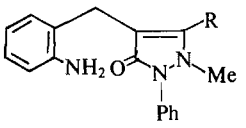

9 *a* R = Me
b R = Ph

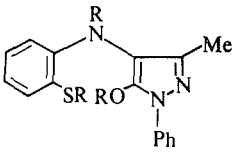

11 R = COPh

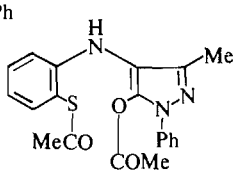

12

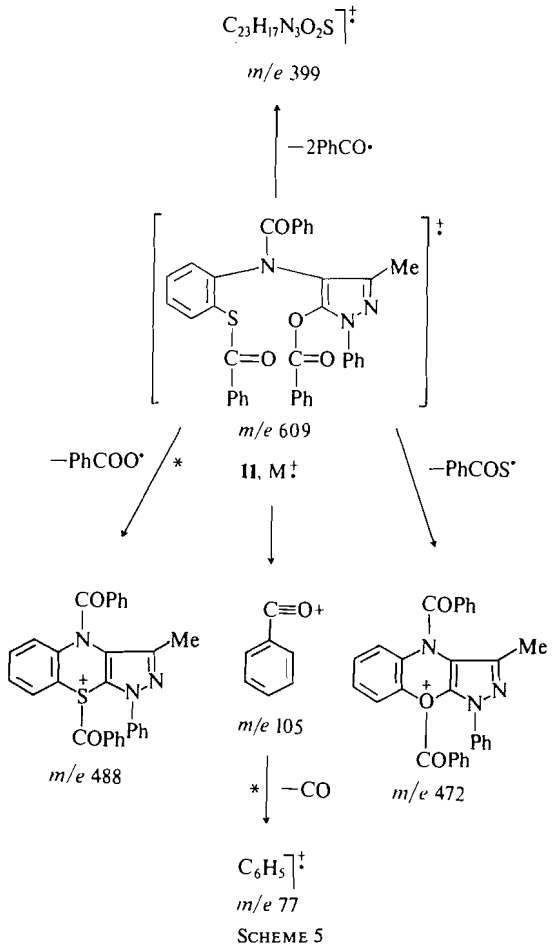

SCHEME 5

chromatography into several dark oils, one of which solidified when triturated with petroleum ether. This product is identified as 4-[*N*-benzoyl-*N*-(2-benzoylthiophenyl)amino]-5-benzoyloxy-3-methyl-1-phenylpyrazole, **11**. That *O*-benzoylation had occurred was deduced from the ir spectrum (ν_{max} 1758 cm^{-1}) and the mass spectrum which had a strong fragment ion (*m/e* 488) and a strong metastable ion (*m/e* 391.0), both of which resulted from the expulsion of a benzoyloxy radical from the molecular ion. Benzoylation of both the NH and SH functions was apparent from the absence of any NH or SH absorption bands in the ir spectrum. In addition, the CO absorption band at 1679 cm^{-1} can be attributed to both *S*-benzoyl and *N*-benzoyl functions (14–16). Additional diagnostic fragment ions were present in the mass spectrum of **11** and are identified in Scheme 5.

Attempts to acetylate **4***a* with acetic anhydride or acetyl chloride were unsuccessful and resulted only in the isolation of the spirobenzothiazoline, **3***a*. A diacetate was obtained when **4***a* was treated with acetic anhydride in pyridine. From its ir, pmr, and mass spectral behavior, this compound is identified as 5-acetyloxy-3-methyl-4-(2-acetylthiophenylamino)-1-phenylpyrazole, **12**. Its ir spectrum displayed NH absorption at 3368 cm^{-1} and two carbonyl absorption bands at 1720 (SCOMe) and 1788 (OCOMe) cm^{-1}. Alkyl thiolesters of this type are known to absorb near 1710 cm^{-1} (16). As required by structure **12**, its pmr spectrum contained three methyl signals and a signal due to one D-exchangeable NH proton. The mass spectrum of **12** was also consistent with the proposed structure; the molecular ion (*m/e* 381) fragmented by expelling two successive ketene molecules. The loss of a molecule of acetic acid from both the molecular ion and the (M − 42) ion was also demonstrated.

The pyrazolone **2***b* was then reduced with the sodium borohydride–palladium–charcoal system in 10% sodium hydroxide solution. Products analogous to those obtained by reducing the methyl analog **2***a* were formed. The two reduction products isolated are identified as 1,3-diphenyl-4-(2-mercaptophenylamino)-2-pyrazolin-5-one, **4***b*, and 1′,3′-diphenylspiro[benzothiazoline-2,4′-[2]pyrazoline]-5′-one, **3***b*. The latter compound is believed to be formed by the oxidation of the thiol **4***b* during crystallization since the ir spectrum of the initial crude reduction product was devoid of any carbonyl absorption near 1700 cm^{-1}.

Compound **4***b* ($C_{21}H_{17}N_3OS$) was soluble in aqueous sodium hydroxide. Its ir and mass spectra (M^+, *m/e* 359) were similar to those of the methyl analog **4***a* and consistent with the proposed structure. The molecular ion fragmented mainly by the loss of a hydrogen molecule yielding the spirobenzothiazoline **3***b*. Two minor but diagnostic fragment ions were also present and were due to the expulsion from the molecular ion of a molecule of water and an SH radical. These ions are analogous to the (M − 18) and (M − 33) ions proposed earlier for the methyl analog **4***a*.

The spirobenzothiazoline **3***b* was obtained only in minor quantities during crystallization of the thiol **4***b* but it was isolated in good yield

Can. J. Chem. Downloaded from www.nrcresearchpress.com by 210.87.254.40 on 09/05/12
For personal use only.

Can. J. Chem. Downloaded from www.nrcresearchpress.com by 210.87.254.40 on 09/05/12
For personal use only.

when **4***b* was treated with cold acetic acid. Its identification was based on a correct elemental analysis and its spectral characteristics which were similar to those observed for the methyl analog **3***a*.

In a final attempt to prepare cyclic hydroxylamines, the pyrazolones **2***a* and **2***b* were reduced under nitrogen in aqueous ethanol with zinc and ammonium chloride. This resulted in good yields of the spirobenzothiazolines **3***a* and **3***b*. When this reduction of **2***a* was prolonged, the thiol **4***a* was obtained as the major product.

Experimental

Infrared spectra were recorded for Nujol mulls with a Beckman IR-10 spectrophotometer. Proton magnetic resonance spectra were recorded with a Varian A60 spectrometer, with tetramethylsilane as internal standard, and mass spectra were measured with an A.E.I. MS9 spectrometer at 70eV (direct insertion technique). Melting points (capillary) are uncorrected. Deuterated compounds were prepared by repeated crystallization of the non-labelled precursor from dioxane–D_2O.

Reduction of 3-Methyl-4-(2-nitrophenylthio)-1-phenyl-2-pyrazolin-5-one, **2***a*

(*i*) A solution of sodium borohydride (1.0 g) in water (20 ml) was added to a suspension of 10% palladium–charcoal (0.10 g) in water (10 ml). To this, a solution of the title compound (5) (2.0 g) in 10% aqueous sodium hydroxide (50 ml) was added dropwise with stirring over a period of 30 min. Nitrogen was bubbled through the reaction mixture during the addition and for a further 15 min. The mixture was filtered, and the filtrate was cooled in ice and acidified with dilute acetic acid. A copious cream-colored product (1.9 g), mp 140–146 °C, precipitated. Crystallization from ethanol gave 4-(2-mercaptophenylamino)-3-methyl-1-phenyl-2-pyrazolin-5-one (**4***a*, product *A*) (0.65 g); mp 215–217 °C; equiv. wt. 148 (excess 0.1 *N* NaOH/0.1 *N* HCl, methyl orange); ir ν_{max} 2100–3300 (br with weak maxima at 2600, 2660, and 3070 (OH, SH)), 3370 (NH), 1626 (CO) cm^{-1}; pmr (DMSO-d_6) δ 2.09 (3H, s, CH_3), 6.30–8.10 (12H, m, aromatic protons and 2 or 3 protons which exchanged with D_2O, *i.e.* NH, SH, and pyrazolone proton). Mass spectrum *m/e* (% relative abundance) 297.0919 (60) (calcd. for $C_{16}H_{15}N_3OS$: 297.0921), 295.0779 (100) (calcd. for $C_{16}H_{13}N_3OS$: 295.0780), 279.0823 (7) (calcd. for $C_{16}H_{13}N_3S$: 279.0830), 264.1138 (9) (calcd. for $C_{16}H_{14}N_3O$: 264.1136). *Anal.* calcd. for $C_{16}H_{15}N_3OS$: C 64.62, H 5.08, N 14.13; found: C 64.78, H 4.91, N 14.39.

When the mother liquor remaining after the removal of the above product **4***a* was concentrated and allowed to stand, pale yellow needles of product *B* (0.25 g), mp 153–154 °C (from ethanol), separated. This was 3′-methyl-1′-phenylspiro[benzothiazoline-2,4′-[2]pyrazoline]-5′-one, **3***a*. Infrared ν_{max} 3275 (NH), 1705 (CO) cm^{-1}; pmr ($CDCl_3$) δ 2.22 (3H, s, CH_3), 4.98 (1H, br s, exchanged with D_2O, NH), 6.50–8.21 (9H, m, aromatic protons). Mass spectrum *m/e* (% relative abundance) 295.0781 (100) (calcd. for $C_{16}H_{13}N_3OS$: 295.0780), 267.0831 (94) (calcd. for $C_{15}H_{13}N_3S$: 267.0831), 250.0563 (36) (calcd. for $C_{15}H_{10}N_2S$: 250.0565), 162.0377 (31) (calcd. for C_9H_8NS: 162.0378), 161.0300 (12) (calcd. for C_9H_7NS: 161.0300), 161.0177 (8) (calcd. for $C_8H_5N_2S$: 161.0174), 135.0146 (65) (calcd. for C_7H_5NS: 135.0143). *Anal.* calcd. for $C_{16}H_{13}N_3OS$: C 65.06, H 4.44, N 14.23; found: C 65.23, H 4.18, N 14.16.

(*ii*) To a hot solution of **2***a* (1.0 g) in 60% aqueous ethanol (100 ml) was added a solution of ammonium chloride (0.20 g) in water (10 ml), followed by zinc dust (1.0 g), and the mixture was heated under reflux for 3 h under nitrogen. The mixture was filtered and the filtrate was evaporated *in vacuo*. The residue was dissolved in boiling ethanol and filtered. On cooling a yellow solid (0.10 g), mp 212–214 °C, precipitated from the filtrate. It was identical (ir, mass spectrum) to the thiol **4***a* described immediately above.

The mother liquor remaining after the removal of **4***a* was cooled and from it the spiro[benzothiazoline-2,4′-[2]pyrazolone] (**3***a*, 0.46 g) slowly deposited as dark yellow needles, mp 153–154 °C. Its ir spectrum was identical to that of product *B* described in preparation *i*.

Reduction of 1,3-Diphenyl-4-(2-nitrophenylthio)-1-phenyl-2-pyrazolin-5-one, **2***b*

(*i*) The title compound (5) (2.0 g) was reduced with sodium borohydride and 10% palladium–charcoal in the manner described in the reduction of **2***a*, method *i*. Acidification of the filtrate gave a flocculent yellow solid which was crystallized from ethanol. A yellow solid (0.52 g), mp 211–212 °C precipitated first. This was 1,3-diphenyl-4-(2-mercaptophenylamino)-2-pyrazolin-5-one, **4***b*; ir ν_{max} 2300–3400 (br (OH) with maxima at 3060 (SH) and 3360 (NH)), 1627 (CO) cm^{-1}; mass spectrum *m/e* (% relative abundance) 359.1090 (80) (calcd. for $C_{21}H_{17}N_3OS$: 359.1090), 357 (87), 341.0984 (10) (calcd. for $C_{21}H_{15}N_3OS$: 341.0987), 329 (77), 328 (91), 326 (16), 135 (100). *Anal.* calcd. for $C_{21}H_{17}N_3OS$: C 70.17, H 4.77 N 11.69; found: C 70.03, H 4.86, N 12.14.

When the mother liquor remaining after the removal of **4***b* was concentrated and cooled, 1′,3′-diphenylspiro-[benzothiazoline-2,4′-[2]pyrazoline]-5′-one (**3***b*, 0.47 g), mp 185–186 °C, precipitated as dark yellow needles; ir ν_{max} 3373 (NH), 1715 (CO) cm^{-1}; pmr ($CDCl_3$) δ 5.01 (1H, br s, exchanged with D_2O, NH), 6.50–8.30 (14H, m, aromatic protons); mass spectrum *m/e* (% relative abundance) 357.0935 (64) (calcd. for $C_{21}H_{15}N_3OS$: 357.0936), 329.0987 (80) (calcd. for $C_{20}H_{15}N_3S$: 329.0987), 328.0907 (100) (calcd. for $C_{20}H_{14}N_3S$: 328.0908), 254.0516 (26) (calcd. for $C_{14}H_{10}NOS$: 254.0514), 135.0143 (76) (calcd. for C_7H_5NS: 135.0143). *Anal.* calcd. for $C_{21}H_{15}N_3OS$: C 70.57, H 4.23, N 11.76; found: C 70.51, H 4.28, N 11.55.

(*ii*) Ammonium chloride (0.2 g) in water (10 ml) was added to a solution of title compound (1.0 g) in 60% aqueous ethanol (70 ml). To this, zinc dust (1.0 g) was added and the mixture was stirred under nitrogen for 10 h at room temperature, then filtered. The filtrate was evaporated *in vacuo*, dissolved in hot ethanol, and refiltered. Cooling yielded golden-yellow needles (0.61 g), mp 185–186 °C, identified (ir and mixture mp with authentic sample) as the spiro(benzothiazoline)pyrazoline, **3***b*, described immediately above.

Can. J. Chem. Downloaded from www.nrcresearchpress.com by 210.87.254.40 on 09/05/12
For personal use only.

2,3-Dimethyl-4-(2-methylthiophenylamino)-1-phenyl-2-pyrazolin-5-one, 6

Dimethyl sulfate (1.0 ml) was added dropwise, with stirring, to an ice-cold solution of the thiol **4***a* (1.0 g) in 10% aqueous sodium hydroxide, and stirring was continued for 2 h. A gummy precipitate separated. It was dissolved in chloroform and the chloroform solution was washed with 10% aqueous sodium hydroxide then with water. Evaporation of the dried ($CaCl_2$) extract gave a brown solid which crystallized from ethanol yielding the title compound (0.47 g) as pale brown needles, mp 161–162 °C; ir ν_{max} 3335 (NH), 1670 (CO) cm^{-1}; pmr ($CDCl_3$) δ 2.14 (3H, s, C-CH_3), 2.39 (3H, s, S-CH_3), 3.03 (3H, s, N-CH_3), 6.12 (1H, br s, exchanged with D_2O, NH), 6.40–7.65 (9H, m, aromatic protons); mass spectrum *m/e* (% relative abundance) 325.1240 (34) (calcd. for $C_{18}H_{19}N_3OS$: 325.1249), 278.1287 (19) (calcd. for $C_{17}H_{16}N_3O$: 278.1293), 56 (100). *Anal.* calcd. for $C_{18}H_{19}N_3OS$: C 66.46, H 5.85, N 12.92; found: C 66.83, H 6.16, N 12.68.

4-[N-Benzoyl-N-(2-benzoylthiophenyl)amino]-5-benzoyloxy-3-methyl-1-phenylpyrazole, 11

Benzoyl chloride (2.0 ml) was added dropwise, with stirring, to an ice-cold solution of the thiol **4***a* (1.0 g) in 10% aqueous sodium hydroxide (40 ml) and stirring was continued for 1 h at room temperature. The semisolid which precipitated was dissolved in chloroform. The dried ($CaCl_2$) extract was chromatographed on a silica gel column (benzene–chloroform, 1:2 v/v) and yielded a brown solid (0.61 g) which was crystallized twice from benzene–petroleum ether (40–60 °C) to give the title compound as a pale brown solid; mp 105–107 °C; ir ν_{max} 1679 and 1758 (CO) cm^{-1}; mass spectrum *m/e* (% relative abundance) 609.1724 (12) (calcd. for $C_{37}H_{27}N_3O_4S$: 609.1723), 488 (40), 472 (4), 399 (5), 211 (4), 105 (100), 77 (36). *Anal.* calcd. for $C_{37}H_{27}N_3O_4S$: C 72.89, H 4.46, N 6.89; found: C 72.67, H 4.51, N 6.99.

5-Acetyloxy-3-methyl-4-(2-acetylthiophenylamino)-1-phenylpyrazole, 12

A solution of the thiol **2***a* (0.5 g) in pyridine (5.0 ml) and acetic anhydride (5.0 ml) was stirred at 5 °C for 15 min, then added with stirring to cold (5 °C) water (40 ml). The title compound (0.46 g) precipitated as a yellow solid, mp 104–108 °C. It was insoluble in dilute sodium hydroxide solution. Attempts to crystallize this product from various solvents resulted in decomposition. Infrared ν_{max} 3368 (NH), 1788 ($OCOCH_3$), 1720 ($SCOCH_3$) cm^{-1}; pmr ($CDCl_3$) δ 2.15 (3H, s, CH_3), 2.22 (3H, s, CH_3), 2.44 (3H, s, CH_3), 6.22 (1H, br s, NH), 6.50–8.20 (9H, m, aromatic protons); mass spectrum *m/e* (% relative abundance) 381 (M^+, 3), 339 (17), 321 (3), 297 (20), 295 (64), 279 (30), 267 (75), 135 (100). *Anal.* calcd. for $C_{20}H_{19}N_3O_3S$: C 62.97, H 5.02, N 11.02; found: C 63.35, H 4.89, N 11.00.

Reduction of 3'-Methyl-5'-phenylspiro[benzothiazoline-2,4'-[2]pyrazolin]-5'-one, 3a

A solution of the title compound (1.0 g) in a mixture of dioxane (15 ml) and 10% aqueous sodium hydroxide (15 ml) was reduced with sodium borohydride and palladium–charcoal in the manner described for the reduction of **2***a*, method *i*. The filtrate, to which ice had been added, was acidified with dilute acetic acid and the pale yellow solid which precipitated was dissolved in ethanol. From this solution, a yellow product (0.13 g), mp 211–214 °C slowly precipitated, and was identical (ir, mass spectrum) to 4-(2-mercaptophenylamino)-3-methyl-1-phenyl-2-pyrazolin-5-one, **4***a*. Concentration of the mother liquor yielded yellow crystals (0.36 g), mp 152–154 °C, the ir spectrum of which was identical to that of the title compound.

Oxidation of 4-(2-Mercaptophenylamino)-3-methyl-1-phenyl-2-pyrazolin-5-one, 4a

A sample (0.3 g) of the title compound was suspended in ethanol (15 ml) and left exposed to the atmosphere at room temperature for 48 h, during which time it entered solution. The yellow solution turned brown, then yellow needles (0.18 g), mp 153–154 °C, slowly separated. This product was found (ir, pmr, mixture mp) to be the spiro-(benzothiazoline)pyrazolone **3***a*.

Acknowledgments

The authors thank the Medical Research Council of Canada for an operating grant, MT-2993, (to R.T.C.), and for the award of a studentship (to N.J.P.). They also thank Dr. A. M. Hogg and his associates at the Department of Chemistry, University of Alberta, Edmonton, for providing the mass spectral data, and Mr. W. Dylke of the Faculty of Pharmacy and Pharmaceutical Sciences, University of Alberta, Edmonton, for recording the pmr data and determining elemental analyses.

1. R. T. COUTTS, D. L. BARTON, and E. M. SMITH. Can. J. Chem. **44**, 1733 (1966).
2. R. T. COUTTS, H. W. PEEL, and E. M. SMITH. Can. J. Chem. **43**, 3221 (1965).
3. R. T. COUTTS and E. M. SMITH. Can. J. Chem. **45**, 975 (1967).
4. R. T. COUTTS and N. J. POUND. Can. J. Chem. **48**, 1859 (1970).
5. R. T. COUTTS, K. W. HINDMARSH, and N. J. POUND. Can. J. Chem. **44**, 2105 (1966).
6. J. D. LOUDON and G. TENNANT. Q. Rev. London, **18**, 389 (1964).
7. R. T. COUTTS and A.-M. EL-HAWARI. Can. J. Chem. **53**, 3637 (1975).
8. K. NAKANISHI. Infrared absorption spectroscopy. Nankodo, Tokyo. 1962. p. 42.
9. G. A. NEWMAN and P. J. S. PAUWELS. Tetrahedron, **25**, 4605 (1969).
10. R. H. WILEY and P. WILEY. Pyrazolones, pyrazolidones, and derivatives. Interscience, New York. 1964.
11. K. BODENDORF and H. RAAF. Ann. **592**, 26 (1955).
12. J. CABLE, S. A. KAGAL, and J. K. MACLEOD. Org. Mass Spectrom. **6**, 301 (1972).
13. R. T. COUTTS and J. L. MALICKY. Org. Mass Spectrom. **7**, 985 (1973).

14. R. A. NYQUIST and W. J. POTTS. Spectrochim. Acta, **7**, 514 (1959).
15. A. W. BAKER and G. W. HARRIS. J. Am. Chem. Soc. **82**, 1923 (1960).
16. L. J. BELLAMY. Advances in infrared group frequencies. Methuen, London. 1968. p. 123.
17. R. T. COUTTS, A.-M. EL-HAWARI, and D. F. BIGGS. Can. J. Chem. **53**, 3645 (1975).

Can. J. Chem. Downloaded from www.nrcresearchpress.com by 210.87.254.40 on 09/05/12
For personal use only.

The crystal structure of potassium trichloro(2,6-lutidine)platinum(II)

R. MELANSON AND F. D. ROCHON

Département de chimie, Université du Québec à Montréal, C.P. 8888, Montréal, Québec H3C 3P8

Received September 11, 1975

R. MELANSON and F. D. ROCHON. Can. J. Chem. **54**, 1002 (1976).

The molecular and crystal structure of potassium trichloro(2,6-lutidine)platinum(II) has been determined by X-ray diffraction. The complex salt forms monoclinic crystals, $a = 6.941$, $b = 24.301$, $c = 11.168$ Å, $\beta = 141.58°$, $Z = 4$, and space group $P2_1/c$. Positional and anisotropic thermal parameters were refined by full matrix least squares calculations to $R = 0.038$ and $R_w = 0.034$.

The coordination around the platinum atom is planar. The Pt—Cl bond lengths are 2.301, 2.299, and 2.302 Å and the Pt—N bond length is 2.011 Å. The 2,6-lutidine ring lies almost perpendicular to the coordination plane of the platinum atom (81.6°). The $PtCl_3$ moieties are packed around the potassium ions, which are surrounded by four chlorine atoms at distances smaller than 3.15 Å forming a distorted tetrahedron.

R. MELANSON et F. D. ROCHON. Can. J. Chem. **54**, 1002 (1976).

La structure moléculaire et cristalline du trichloro(lutidine-2,6) platinate(II) de potassium a été déterminée par diffraction des rayons-X. Le sel complexe cristallise dans le système monoclinique, $a = 6.941$, $b = 24.301$, $c = 11.168$ Å, $\beta = 141.58°$, $Z = 4$ et le groupe spatial $P2_1/c$. Les coordonnées et les facteurs thermiques anisotropes ont été affinés par la méthode des moindres carrés à matrice entière jusqu'à $R = 0.038$ et $R_w = 0.034$.

La coordination autour de l'atome de platine est plane. La longueur des liaisons Pt—Cl est 2.301, 2.299 et 2.302 Å et celle de Pt—N est 2.011 Å. Le ligand lutidine-2,6 est presque perpendiculaire au plan de coordination du platine (81.6°). Les groupements $PtCl_3$ sont entassés autour de l'ion potassium. Ce dernier est entouré de quatre atomes de chlore à des distances inférieures à 3.15 Å formant une géométrie tétraédrique déformée.

Introduction

Recently, some platinum complexes of amines were found effective against tumors (ref. 1 and references cited therein). It has been shown that *cis*-$[Pt(NH_3)_2Cl_2]$ forms interstrand cross-linking in DNA (2). The main chemotherapic limitations of the known compounds are their kidney toxicity (3) and their insolubility. It has been suggested that complexes of the type *cis*-[Pt(amine)(amine′)Cl_2] would be worth investigating. In order to prepare this kind of complexes, the monobase $[Pt(amine)Cl_3]^-$ has to be synthesized first. Recently we have developed a simple method for the synthesis of the latter compound (4). We report here the structure of the complex salt K[Pt(2,6-lutidine)-Cl_3].

Experimental Section

Crystal Data

$KPtCl_3C_7H_9N$ fw = 447.71

Monoclinic $P2_1/c$, $a = 6.941(4)$, $b = 24.301(8)$, $c = 11.168(7)$ Å, $\beta = 141.58(3)°$, $Z = 4$, $V = 1170.6(0.98)$ Å^3, $\rho_c = 2.540$ g/cm^3, $\rho_o = 2.52(2)$ g/cm^3 (flotation), λMoKα = 0.71069 Å, μMoKα = 135.84 cm^{-1}, $T = 22$ °C.

The complex salt K[Pt(2,6-lutidine)Cl_3] was synthesized by the method already described (4) and the crystals were recrystallized from water.

A set of precession photographs showed that the $h0l$, $l = 2n + 1$ and $0k0$, $k = 2n + 1$ reflections are systematic absences indicating the $P2_1/c$ space group. The cell parameters were obtained by least squares refinement from the setting angles of 15 automatically centered reflections on a Syntex P$\bar{1}$ diffractometer using graphite monochromatized MoKα radiation.

Collection and Reduction of Intensity Data

The intensity data were collected from a crystal measuring 0.59 × 0.11 × 0.12 mm elongated along the a axis, and bounded by the faces $\{\bar{1}00\}$, $\{10\bar{1}\}$, $\{010\}$, $\{0\bar{1}0\}$, $\{\bar{1}02\}$, and $\{10\bar{2}\}$. A total of 3408 independent reflections were measured in the region of $2\theta < 60°$ by the $2\theta/\theta$ scan technique using MoKα radiation. The data collection was done at a variable speed (24 to 1 deg min^{-1}) depending on the intensity of the reflection (Syntex $2\theta/\theta$ autocollection program). Most of the reflections were measured at a speed of 1 deg min^{-1}. A 2θ scan range of 1.2° below Kα_1 and 1.2° over Kα_2 was selected. The background time to scan time ratio was 0.40. During the data collection, three standard reflections (2,0,0; 0,10,0; and 0,0,4) were measured after every 47 reflections. Their variations were less than 2.5% from their respective means. The measurements reduced to a set of 3327 independent reflections after taking out the systematically absent reflections. The reflections for which the intensity was less than 2.5 $\sigma(I)$

Can. J. Chem. Downloaded from www.nrcresearchpress.com by 210.87.254.6 on 09/05/12
For personal use only.

Can. J. Chem. Downloaded from www.nrcresearchpress.com by 210.87.254.6 on 09/05/12
For personal use only.

TABLE 1. Final structure parameters[a] and estimated standard deviation[b] ($\times 10^4$)

Atom	x	y	z	U_{11}	U_{22}	U_{33}	U_{12}	U_{13}	U_{23}
Pt	2596.0(10)	1614.2(1)	2544.0(6)	403.3(18)	311.1(30)	457.4(17)	−4.7(16)	353.1(15)	−7.6(17)
K	7604(7)	2486(1)	2548(5)	552(12)	437(12)	821(15)	−17(14)	474(12)	−0(15)
Cl_1	2730(6)	1583(1)	4668(4)	629(15)	449(15)	571(14)	22(12)	507(13)	−7(12)
Cl_2	2690(11)	2560(1)	2590(7)	1133(24)	326(12)	1097(21)	−31(19)	969(21)	−15(19)
Cl_3	2449(6)	1593(1)	413(4)	623(15)	470(15)	593(14)	22(13)	517(14)	46(12)
N	2486(23)	787(2)	2493(15)	477(36)	389(30)	522(37)	−47(42)	426(33)	9(43)
C_1	−217(27)	526(5)	1345(19)	574(66)	568(60)	752(76)	−275(53)	551(65)	−324(60)
C_2	−294(35)	−43(6)	1333(21)	799(90)	718(90)	822(88)	−265(74)	696(83)	−196(68)
C_3	2332(47)	−342(4)	2397(24)	1247(105)	509(60)	849(76)	−211(90)	928(85)	−298(77)
C_4	5039(32)	−80(4)	3558(17)	1001(93)	359(60)	600(63)	223(58)	708(74)	171(51)
C_5	5144(25)	500(4)	3599(13)	689(63)	449(60)	425(46)	96(42)	514(52)	−8(43)
C_6	6901(26)	862(6)	134(20)	376(57)	897(90)	708(78)	−227(58)	382(61)	−264(68)
C_7	8061(27)	807(5)	4854(17)	524(61)	688(90)	603(66)	37(53)	464(59)	120(60)

[a]The anisotropic thermal parameters are in the form $\exp[-2\pi^2(U_{11}h^2a^{*2} + U_{22}k^2b^{*2} + U_{33}l^2c^{*2} + 2U_{12}hka^*b^* + 2U_{13}hla^*c^* + 2U_{23}klb^*c^*)]$.
[b]Standard deviations are given in parentheses.

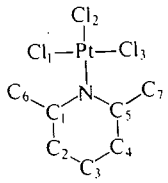

FIG. 1. Atom identification in complex anion [Pt(2,6-lutidine)Cl_3]$^-$.

were considered as unobserved. The standard deviation $\sigma(I)$ was calculated as already described (5). An absorption correction based on the equations of the crystal faces was applied to the 1870 independent observed reflections. The transmission factors varied from 0.202 to 0.289. The data were then corrected for the Lorentz and polarization effects. The scattering factors for platinum, potassium, chlorine, nitrogen, and carbon were those of Cromer and Waber (6) and those of Stewart *et al.* were used for hydrogen (7). The anomalous dispersion terms (8) of platinum ($\Delta f' = -2.05$, $\Delta f'' = 8.43$), potassium ($\Delta f' = 0.21$, $\Delta f'' = 0.30$), and chlorine ($\Delta f' = 0.15$, $\Delta f'' = 0.19$) were included in the calculations.

Structure Determination

The platinum atom was easily located from the three-dimensional Patterson map. The positions of all other atoms, except the hydrogen atom, were obtained by structure factor and Fourier map calculations. The refinement of the parameters was carried out by full matrix least squares calculations. In the early stages of refinement, unit weight was assigned to all observed reflections. Individual weights w according to the equation $1/w = a + bF_o + cF_o^2$ were later calculated. The values of a, b, and c were adjusted to make the distribution of $w|\Delta F|^2$ constant with respect to $|F_o|$ and $\sin\theta/\lambda$ ($a = 40.0$, $b = -0.45$, and $c = 0.0015$). An isotropic secondary extinction correction (9) was also introduced. The hydrogen atoms on the three aromatic carbons were fixed at the calculated positions, while those on the terminal methyl groups could not be localized. The refinement of the scale factor, the coordinates and anisotropic temperature factors of all nonhydrogen atoms converged to $R = \sum(|F_o| - |F_c|)/\sum|F_o|$ of 0.038 and a weighted residual $R_w = [\sum w(|F_o| - |F_c|)^2/\sum w|F_o|^2]^{1/2}$ of 0.034.[1] The standard deviation of an observation of unit weight is 0.961. The final difference Fourier map using all observed reflections only showed peaks lower than 0.8 e/Å^3 (in the platinum environment). The refined parameters are given in Table 1.

The calculations were performed with a CDC 6400 computer. The programs used have already been described (5).

Results and Discussion

The structure consists of an arrangement of the complex anion [Pt(2,6-lutidine)Cl_3]$^-$ and of K^+. The atoms were labelled according to Fig. 1.

[1]The structure factor table is available, at a nominal charge, from the Depository of Unpublished Data, CISTI, National Research Council of Canada, Ottawa, Canada K1A 0S2.

TABLE 2. Bond distances and bond angles in the [Pt(2,6-lutidine)Cl_3]$^-$ ion

Bond	Distance (Å)	Bonds	Angle (deg)
Pt—Cl_1	2.301(4)	Cl_1—Pt—Cl_2	91.8(2)
Pt—Cl_2	2.299(2)	Cl_1—Pt—Cl_3	176.8(2)
Pt—Cl_3	2.302(5)	Cl_1—Pt—N	88.0(4)
Pt—N	2.011(6)	Cl_2—Pt—Cl_3	91.3(2)
N—C_1	1.34(2)	Cl_2—Pt—N	179.6(4)
N—C_5	1.36(2)	Cl_3—Pt—N	88.8(4)
C_1—C_2	1.38(2)	Pt—N—C_1	119(1)
C_2—C_3	1.37(3)	Pt—N—C_5	119(1)
C_3—C_4	1.34(3)	C_1—N—C_5	121(1)
C_4—C_5	1.41(1)	N—C_1—C_2	120(2)
C_5—C_7	1.47(2)	N—C_1—C_6	119(1)
C_1—C_6	1.50(3)	C_1—C_2—C_3	120(2)
		C_2—C_3—C_4	119(2)
		C_3—C_4—C_5	120(2)
		C_4—C_5—N	119(1)
		N—C_5—C_7	119(1)

A stereoscopic view of the complex anion is shown in Fig. 2. The bond distances and angles are listed in Table 2. Three chlorine and one nitrogen atoms form the square planar coordination expected for Pt(II) complexes. The weighted best plane was calculated through the five atoms. The deviation from this plane are: Pt, −0.0001; Cl_1, 0.0014; Cl_2, 0.0023; Cl_3, 0.0014; and N, 0.0101 Å. The angles around platinum are close to the expected 90 and 180°.

The Pt—Cl bond lengths (2.301, 2.299, and 2.302 Å) are normal (10–16). The Pt—N distance of 2.011 (7) Å is also normal (5, 11, 14, 16, 17) and agrees well with the expected value (the radius sum is 2.02 Å). It is identical to the Pt—N distances found in *cis*- and *trans*-[$PtCl_2(NH_3)_2$], 2.01 and 2.05 Å (14).

The bond lengths within the aromatic ring vary from 1.34 to 1.41 Å and the angles are all 120°. The structure of a 1:1 complex of 2,6-lutidine with urea has been determined (18). The structure of 2,6-lutidine is very similar in both complexes even if it is difficult to compare the molecular dimensions, since in the case of the organic complex, they were determined from two projections and only a few crystallographic data.

The 2,6-lutidine ring is planar and lies almost perpendicular to the $PtCl_1Cl_2Cl_3N$ plane (81.6°) as is shown in Figs. 2 and 3.

Figure 3 illustrates the packing in the K[Pt-(2,6-lutidine)Cl_3] crystal. It consists of alternate layers of [Pt(lutidine)Cl_3]$^-$ anions and potas-

Can. J. Chem. Downloaded from www.nrcresearchpress.com by 210.87.254.6 on 09/05/12
For personal use only.

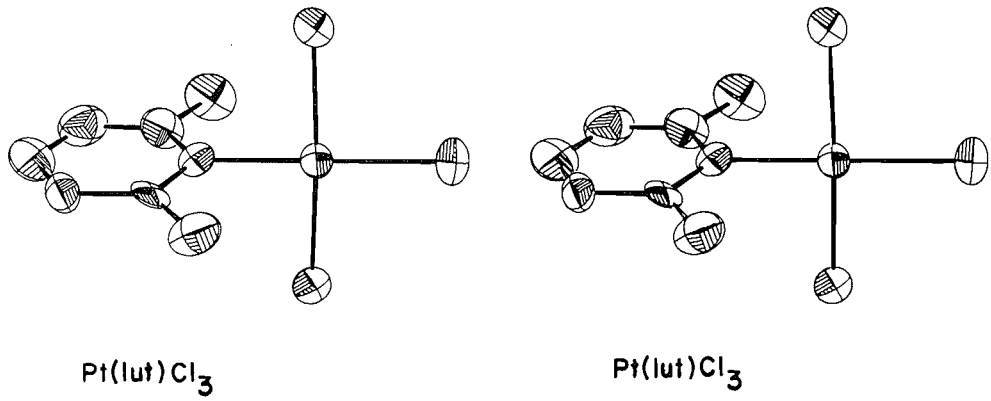

FIG. 2. Stereoscopic view of $[Pt(2,6\text{-lutidine})Cl_3]^-$.

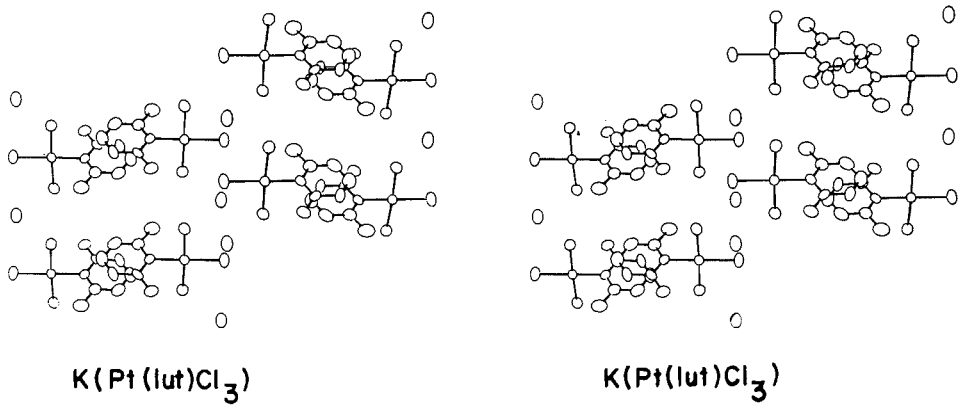

FIG. 3. Packing in the $K[Pt(2,6\text{-lutidine})Cl_3]$ crystal.

TABLE 3. The K—Cl distances and related angles

Atoms	Distance (Å)	Atoms[a]	Angle (deg)
$K—Cl_1$	3.143(6)	$Cl_1—K—Cl_1^1$	161.8(2)
$K—Cl_1^1$	3.141(5)	$Cl_1—K—Cl_3^2$	91.9(2)
$K—Cl_3^2$	3.134(6)	$Cl_1—K—Cl_3^3$	93.1(2)
$K—Cl_3^3$	3.114(5)	$Cl_1^1—K—Cl_3^2$	92.7(2)
		$Cl_1^1—K—Cl_3^3$	87.9(2)
		$Cl_3^2—K—Cl_3^3$	161.7(2)

[a]Coordinates x, y, z except: $^1x-1, \frac{1}{2}-y, z-\frac{1}{2}$; $^2x-1, y, z$; $^3x, \frac{1}{2}-y, \frac{1}{2}+z$.

sium cations parallel to the *ac* plane. The $PtCl_3$ moieties are packed around the potassium ions. Each potassium ion is surrounded by four chlorine atoms at distances smaller than 3.15 Å, defining a distorted tetrahedral geometry (Table 3).

Acknowledgments

Grateful acknowledgments are made to the National Research Council of Canada for financial support, to Dr. Pi-Chang Kong for the synthesis of the analysed compound, and to Johnson Matthey & Co. Limited for the loan of potassium chloroplatinite.

1. B. ROSENBERG. Platinum Met. Rev. **15**, 42 (1971).
2. P. HORACEK and J. DROBNIK. Biochim. Biophys. Acta, **254**, 341 (1971).
3. M. J. CLEARE. Coord. Chem. Rev. **12**, 349 (1974).
4. PI-CHANG KONG and F. D. ROCHON. J. Chem. Soc. Chem. Commun. 599 (1975).
5. R. MELANSON, J. HUBERT, and F. D. ROCHON. Can. J. Chem. **53**, 1139 (1975).
6. D. T. CROMER and J. T. WABER. Acta Crystallogr. **18**, 104 (1965).
7. R. F. STEWART, E. R. DAVIDSON, and W. T. SIMPSON. J. Chem. Phys. **42**, 3175 (1965).

Can. J. Chem. Downloaded from www.nrcresearchpress.com by 210.87.254.6 on 09/05/12
For personal use only.

8. D. T. CROMER. Acta Crystallogr. **18**, 17 (1965).
9. P. COPPENS and W. C. HAMILTON. Acta Crystallogr. Sect. A, **26**, 71 (1970).
10. R. MELANSON and F. D. ROCHON. Can. J. Chem. **53**, 2371 (1975).
11. C. J. L. LOCK, R. A. SPERANZINI, and J. POWELL. Can. J. Chem. **54**, 53 (1976).
12. R. H. B. MAIS, P. G. OWSTON, and A. M. WOOD. Acta Crystallogr. Sect. B, **28**, 393 (1972).
13. J. A. J. JARVIS, B. T. KILBOURN, and P. G. OWSTON. Acta Crystallogr. Sect. B, **27**, 366 (1971).
14. G. R. DAVIES, W. HEWERTSON, R. H. B. MAIS, P. G. OWSTON, and C. G. PATEL. J. Chem. Soc. 1873 (1970).
15. T. G. APPLETON, H. C. CLARK, and L. E. MANZER. Coord. Chem. Rev. **10**, 335 (1973).
16. C. PEDONE and E. BENEDETTI. J. Organometal. Chem. **29**, 443 (1971).
17. J. W. CARMICHAEL, N. CHAN, A. W. CORDES, C. K. FAIR, and D. A. JOHNSON. Inorg. Chem. **11**, 1117 (1972).
18. J. D. LEE and S. C. WALLWORK. Acta Crystallogr. **19**, 311 (1965).

Can. J. Chem. Downloaded from www.nrcresearchpress.com by 210.87.254.6 on 09/05/12
For personal use only.

Can. J. Chem. Downloaded from www.nrcresearchpress.com by 210.87.254.40 on 09/05/12
For personal use only.

Canadian Journal of Chemistry

Published by
THE NATIONAL RESEARCH COUNCIL OF CANADA

Journal canadien de chimie

Publié par
LE CONSEIL NATIONAL DE RECHERCHES DU CANADA

Volume 54 Number 7 April 1, 1976

Volume 54 numéro 7 1 avril 1976

Metastable ion studies. VI. The identification of $C_2H_5N^{+\cdot}$ ion structures from their characteristic kinetic energy releases

JOHN L. HOLMES and JOHAN K. TERLOUW[1]

Chemistry Department, University of Ottawa, Ottawa, Canada K1N 6N5

Received October 15, 1975

JOHN L. HOLMES and JOHAN K. TERLOUW. Can. J. Chem. **54**, 1007 (1976).

Metastable peaks for the fragmentation $C_2H_5N^{+\cdot} \rightarrow C_2H_4N^+ + H^\cdot$ have been studied in the first field-free region of a double focussing mass spectrometer. Isomeric structures of $C_2H_5N^{+\cdot}$ ions derived from a variety of precursor molecules were characterised by their metastable peak shape and kinetic energy release. The identifications were aided by appropriate deuterium labelling experiments. Four isomeric ions

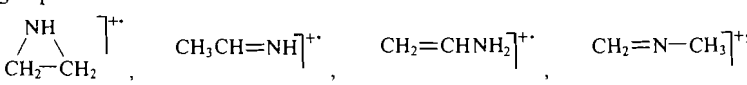

(a) (b) (c) (e)

were shown to retain their structural identity within the ion energy and lifetime ranges observable in these experiments. Ion (a), generated from aziridine was found to be indistinguishable from its open chain isomer $CH_2—NH=CH_2]^{+\cdot}$ (d).

The results closely parallel those previously found for the isoelectronic $C_2H_4O^{+\cdot}$ ions, but the differences in characteristic kinetic energy release are smaller. A simple deuterium exchange labelling experiment may be necessary for the unequivocal identification of $C_2H_5N^{+\cdot}$ ion structures.

JOHN L. HOLMES et JOHAN K. TERLOUW. Can. J. Chem. **54**, 1007 (1976).

On a étudié les pics métastables dus à la fragmentation $C_2H_5N^{+\cdot} \rightarrow C_2H_4N^+ + H^\cdot$ dans la première région libre de champ d'un spectromètre à double focalisation. On a caractérisé les structures isomères des ions $C_2H_5N^{+\cdot}$ dérivés d'une grande variété de molécules précurseurs par la forme de leurs pics métastables et par la libération d'énergie cinétique. Les identifications furent facilitées par des expériences impliquant des molécules marquées au deutérium dans des positions appropriées. On a montré que les quatres ions isomères

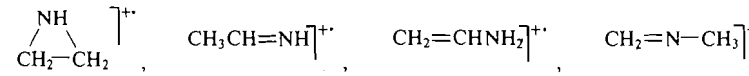

(a) (b) (c) (e)

maintiennent leur identité structurale à l'intérieur des énergies ioniques et des périodes de temps de vie observables dans ces expériences. On a trouvé que l'ion (a), généré à partir de l'aziridine, ne peut pas être distingué de son isomère en chaîne ouverte $CH_2—NH=CH_2]^{+\cdot}$ (d).

Les résultats obtenus sont très parallèles à ceux observés antérieurement pour les ions isoélectroniques $C_2H_4O^{+\cdot}$; toutefois les différences dans les libérations d'énergie cinétique caractéristique sont plus faibles. Il pourrait être nécessaire d'effectuer une simple expérience d'échange isotopique du deutérium pour prouver d'une façon non équivoque les structures ioniques des $C_2H_5N^{+\cdot}$.

[Traduit par le journal]

[1]Permanent address: Analytical Chemistry Laboratory, University of Utrecht, Croesestraat 77A, Utrecht, The Netherlands.

Can. J. Chem. Downloaded from www.nrcresearchpress.com by 210.87.254.40 on 09/05/12
For personal use only.

Introduction

In a previous paper (1) the structures of fragmenting $C_2H_4O^{+\cdot}$ ions were established from metastable peaks examined under conditions of good energy resolution. Three isomeric structures

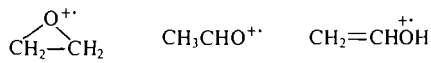

(a) (b) (c)

were shown to be stable within the microsecond time-frame. Each isomer generated a characteristic first field-free region metastable peak for H atom loss, (^{1}m*), thus providing a powerful method for ion structure determination.

With the aid of deuterium labelling, it was shown that the acetaldehyde ion (b) exclusively loses its α-C—H atom, while it is the hydroxylic H atom that is lost from the vinyl alcohol ion (c). In addition, it was argued that a ring opened form of ethylene oxide ($\overset{+}{C}H_2—O—\dot{C}H_2$, (d)) probably exists as a fourth separate stable species.

In this paper, results are reported for a similar study of the $C_2H_5N^{+\cdot}$ ion (*m/e* 43). It is isoelectronic with $C_2H_4O^{+\cdot}$ and in view of the similarity with which oxygen and nitrogen atoms direct mass spectral decompositions, we were interested to see whether the analogous nitrogen-containing ions are stable. Such an analogy certainly exists between the $C_2H_5O^+$ and $C_2H_6N^+$ ions which have been subject to several investigations (2, 3). The $C_2H_5N^+$ ion, although an important fragment ion in the mass spectra of many nitrogen-containing compounds, has only been investigated by conventional labelling studies (4–6).

In the present work, the chosen probe reaction again was H· loss because the associated intense ^{1}m* peak was found to be characteristic of the structure of the $C_2H_5N^{+\cdot}$ ion.

Results and Discussion

Reference Ions

Some reasonable structural forms for the $C_2H_5N^{+\cdot}$ ion are:

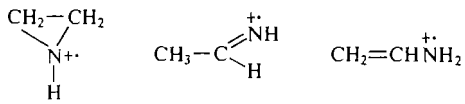

(a) (b) (c)

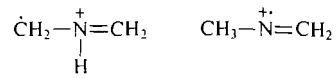

(d) (e)

Of these, only (a) has a stable neutral counterpart, aziridine. (b) is the analogue of the acetaldehyde ion, but no neutral species is available that can serve as a reference ion. The only oxygen-containing compounds which produced acetaldehyde type ions (although as a minor component, together with (c) type ions) were compounds which generated $C_2H_5O^+$ ions having the protonated acetaldehyde structure (*e.g.* isopropanol, diethylether, etc.) (1). The behaviour of analogous nitrogen-containing compounds will be discussed below.

Ion (c) is the analogue of ionized vinyl alcohol; this does not exist as a stable neutral species but several classes of oxygen-containing compounds (*e.g.*, *n*-butanal and higher homologues, ethyl vinyl ether, cyclobutanol, etc.) were found to generate this ion (1), which is the most stable form of $C_2H_4O^{+\cdot}$ (7). The corresponding nitrogen-containing compounds, with the exception of cyclobutylamine, are either unstable or not readily available. For cyclobutylamine it is reasonable to propose that the *m/e* 43 ions (base peak) in its mass spectrum have the vinylamine structure (c):

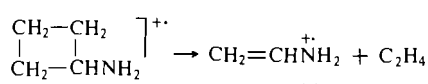

(c)

Ion (a) might be produced by loss of H_2 from the molecular ion of dimethylamine (*cf.* H_2 loss from dimethylether (1)) and this structure has already been assigned to $C_2H_5N^{+\cdot}$ ions generated in the mass spectra of pyrrolidine and piperidine (4–6). Finally, ion structure (e) has no oxy-analogue. It has been proposed that such ions are generated from *N*-methylpiperidine (4, 5) and trimethylamine (2).

In the discussion which follows, it will be argued that ions a/d, b, c, and e exist as stable entities within the framework imposed by observations of H atom loss in the microsecond time scale. As in the previous work (1), the experimental evidence is based upon the shapes of the appropriate ^{1}m* peaks and the effects of deuterium labelling.

TABLE 1. $T_{0.5}$ values (meV) for H· loss from $C_2H_5N^{+\cdot}$ ions generated from various precursor molecules

Precursor compound	Ion type	$T_{0.5}$	$T_{0.5}$ (Deuterated compounds)					
Cyclobutylamine	c	400	(45 → 43+D·	420	44 → 43+H·	390	44 → 42+D·	415)
Isopropylamine	c[a]	360	(45 → 43+D·	400	44 → 43+H·	330	44 → 42+D·	390)
n-Propylamine	c[a]	380	(45 → 43+D·	395	44 → 43+H·	345	44 → 42+D·	390)
Ethylamine	c[a]	360	(45 → 43+D.	410	44 → 43+H·	345	44 → 42+D·	[b])
Ethylamine-α,α'-d_2			(44 → 43+H·	360	44 → 42+D·	200)		
Diethylamine	c,b(2:3)	280	(44 → 43+H·	230	44 → 42+D·	415	43 → 42+H·	[b])
Diethylamine-α,α'-d_4			(44 → 43+H·	375	44 → 42+D·	195	45 → 44+H·	370)
Aziridine	a/d	255	(44 → 43+H·	245	44 → 42+D	315)		
Dimethylamine	a/d	265	(44 → 43+H·	265	44 → 42+D	[b])		
Dimethylamine-d_6	a/d		(47 → 45+D·	265	47 → 46+H	285)		
Pyrrolidine	a/d	265	(44 → 43+H·	265	44 → 42+D	[b])		
Piperidine	a/d	290						
4-Methylpiperidine	a/d	255	(44 → 43+H·	275	44 → 42+D	[b])		
N-Methylpiperidine	e	130						
Trimethylamine	e	140						
N,*N*-Dimethylformamide	e	145						

[a]A minor contribution from (b) is also present (see text).
[b]Obscured by other fragmentations.

Ion (c)

The $^1m^*$ peak for the fragmentation $C_2H_5N^{+\cdot} \rightarrow C_2H_4N^+ + H^\cdot$ in cyclobutylamine is a dished peak with a $T_{0.5}$ value of 400 meV (T_h = 195 meV).[2] The peak shape remained unchanged at low electron energy, indicating that it is non-composite. Another and more sensitive test is based upon the possible separation of components by specific deuterium labelling (1).

Deuteration of the sample (by D_2O exchange) showed that metastable $C_2H_3D_2N^{+\cdot}$ ions, *m/e* 45, lost *only* D· as did the analogous $C_2H_3DO^{+\cdot}$ ion from cyclobutanol. $T_{0.5}$ = 420 meV (see Table 1) is very similar to that of the unlabelled compound ($T_H/T_D \cong 1.05$) and is consistent with the $43 \rightarrow 42 + H^\cdot$ $^1m^*$ peak being noncomposite. This result is compatible with a vinylamine structure for $C_2H_3D_2N^{+\cdot}$, *i.e.*

$$CH_2{=}CH{-}ND_2^{+\cdot} \rightarrow \overbrace{CH_2CHND}^{+} + D^\cdot$$

However, a minor second component could still be present, especially if its characteristic energy release were close to that of the proposed (c) species. We therefore also examined the neighbouring transitions[3] $44 \rightarrow 43 + H^\cdot$ (which could arise from the process $CH_3{-}CH{=}\overset{+\cdot}{N}H \rightarrow CH_3{-}\overset{+}{C}{\equiv}ND + H^\cdot$) and $44 \rightarrow 42 + D^\cdot$. Their associated half-height energy releases were 390 and 415 meV respectively.

We conclude that no second structure is present and that these transitions originate from the presence of only vinylamine ions generated by the N-d_1 compound:

$$CH_2{=}CH{=}\overset{+\cdot}{N}\begin{matrix}D\\H\end{matrix} \quad (m/e\ 44) \rightarrow \begin{cases} \overbrace{CH_2CHNH}^{+} + D^\cdot \quad (m/e\ 42) \\ \overbrace{CH_2CHND}^{+} + H^\cdot \quad (m/e\ 43) \end{cases}$$

Although there is at most only a small isotope effect on $T_{0.5}$ there is an appreciable isotope effect on the abundance; ($^1m^*$(peak area)$44 \rightarrow 43$)/($^1m^*$ $44 \rightarrow 42$) = 3.9.

Ion (b)

Other nitrogen containing analogues of oxy-compounds that exclusively generated vinyl alcohol ions were not available. However, in a recent collisional activation study (3) it was proposed that $C_2H_6N^+$ ions of the protonated acetaldimine structure are stable species. If their (m* confirmed) H· loss parallels that of the corresponding $C_2H_5O^+$ ion (1), a mixture of vinylamine (c) and acetaldimine (b) type ions

[2]T_h indicates the energy release calculated from the width of a dished peak at its upper extremeties. $T_{0.5}$ is the energy release calculated from the peak width at half-height.

[3]It is essential to make sure that no interference occurs from other neighbouring transitions. Fortunately the only intense metastable peak found in the unlabelled compound is H· loss from $C_2H_5N^{+\cdot}$ ions.

Can. J. Chem. Downloaded from www.nrcresearchpress.com by 210.87.254.40 on 09/05/12
For personal use only.

Can. J. Chem. Downloaded from www.nrcresearchpress.com by 210.87.254.40 on 09/05/12
For personal use only.

could be generated, *i.e.*

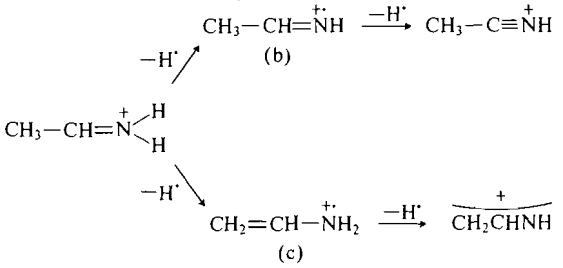

Some support for this proposal is to be found in the CA study where it was stated that "loss of a single H atom to form *m/e* 43 occurs *mainly* from the carbon atoms". The production of (b) type ions may therefore be a minor process as is observed in the dissociation of the analogous $C_2H_5O^+$ ion (1).

The first compound investigated in this context was isopropylamine. Loss of $CH_3^\cdot$ from the molecular ion generates an intense peak at *m/e* 44 of structure $CH_3—CH=\overset{+}{N}H_2$. The energy release for the probe reaction was found to be lower (Table 1) than that of the vinylamine species from cyclobutylamine. Although this lower value can *a priori* result from slightly different internal energy contents of the ions, a deuteration experiment indicated that a minor second component with a lower $T_{0.5}$ value is involved. Exchange deuteration showed that both of the fragmentations $45 \rightarrow 43 + D^\cdot$ (N-d_2 compound) and $44 \rightarrow 42 + D^\cdot$ (N-d_1 compound) had $T_{0.5}$ values compatible with those found for cyclobutylamine; however, $T_{0.5}$ for $44 \rightarrow 43 + H^\cdot$ was significantly lower (see Table 1). These observations are in accord with the above proposal that the major part of the dissociating $C_2H_5N^{+\cdot}$ ions have the vinylamine (c) structure, but that some contribution from acetaldimine (b) ions is also present. Note that these ions appear at *m/e* 44 ($CH_3—CD=\overset{+}{N}D$) in the labelled compound. If they behave like acetaldehyde ions, the α-C—H atom will be lost and therefore their only fragmentation will be $44 \rightarrow 43 + H^\cdot$; this metastable peak will be a composite of (c) ($CH_2=CH—\overset{+\cdot}{N}DH$ from N-d_1 isopropylamine, $T_{0.5} \cong 400$ meV) and (b) ($CH_3—CH=\overset{+\cdot}{N}D$, $T_{0.5} < 330$ meV) type ions. It was estimated from summations of (b) and (c) in various proportions (see below) that about 20% of the metastable $C_2H_5N^{+\cdot}$ ions could have the (b) structure. (In isopropanol 15% of the $C_2H_4O^{+\cdot}$ ions have the acetaldehyde structure (1).) An accurate value of $T_{0.5}$ for (b) cannot be obtained from these data.

n-Propylamine yielded similar results. Its *m/e* 44 ions have the initial structure $CH_2—CH_2—\overset{+}{N}H_2$ but CA evidence (3) indicates that isomerisation to $CH_3—CH=\overset{+}{N}H_2$ could occur. (Note that (c) type ions can be generated from the initial ion.) The $T_{0.5}$ value (see Table 1) indicates that the major component is the vinylamine ion (c) but the slightly but significantly lower $T_{0.5}$ value for the transition $44 \rightarrow 43 + H^\cdot$ in the labelled compound again points to the presence of (b) type ions, ~10%, based on peak summations.

The third compound investigated in this series was ethylamine (see Table 1); its behaviour was very similar to that of isopropylamine. Proper examination of the minor (b) type component requires a very high degree of N-*d* labelling. However this is difficult to achieve via an exchange deuteration performed in the mass spectrometer and we therefore investigated the compound $CH_3CD_2NH_2$. This compound has been studied before (9). It almost exclusively loses $D^\cdot$ generating the protonated acetaldimine ion $CH_3—CD=\overset{+}{N}\begin{smallmatrix}H\\H\end{smallmatrix}$ at *m/e* 46. If this ion behaves as proposed above, two different ions will be formed at *m/e* 44, the (c) type ions $CH_2=CD—\overset{+\cdot}{N}H_2$ and the (b) type ions $CH_3—CD=\overset{+\cdot}{N}H$. The (c) ions will only lose a $H^\cdot$ atom, while the (b) type ions should exclusively lose the $D^\cdot$ atom. As predicted, the $^1m^*$, $44 \rightarrow 43 + H^\cdot$ is that for (c) type ions, while the $^1m^*$, $44 \rightarrow 42 + D^\cdot$ had a much lower $T_{0.5}$ value (200 meV) which can therefore with some confidence be assigned to acetaldimine, (b) type ions. From trial and error summations of the metastable peak profiles for (b) and (c) it was estimated that ~20% of the $C_2H_5N^{+\cdot}$ ions from unlabelled ethylamine had the former structure. The ratio of the metastable peak areas $44 \rightarrow 43$ and $44 \rightarrow 42$ was 9:1; this however contains an unknown isotope effect.

These results parallel those obtained with ethanol where a ratio of (c):(b) = 8:1 was found. Structural assignment of the components and an accurate estimation of their abundance is how-

Can. J. Chem. Downloaded from www.nrcresearchpress.com by 210.87.254.40 on 09/05/12
For personal use only.

ever much easier for $C_2H_4O^{+\cdot}$ ions where there is a much greater difference between the characteristic energy releases of the two components.

Apart from alcohols, it was also found (1) that a mixture of (b) and (c) ions could be generated via the $C_2H_5O^+$ ion produced from simple ethers and we therefore examined diethylamine as a representative compound.

$T_{0.5}$ for the probe reaction was 280 meV, close to that for species (a) or (d) $\dot{C}H_2—\overset{+}{N}H=CH_2$ (see below). It seems improbable that the latter is formed from this compound[4] and so the $^1m^*$ was examined at reduced electron energy. $T_{0.5}$ became significantly lower (225 meV at nominal 30 eV) indicating the possible presence of a composite metastable peak. Exchange deuteration permitted a separation into two fragmentations; $44 \rightarrow 42 + D^\cdot$, with a $T_{0.5}$ (see Table 1) appropriate for (c) type ions and a second more intense metastable peak $44 \rightarrow 43 + H$ with $T_{0.5} = 230$ meV, which could be a composite of mainly (b) with some (c).

The formation of the (c) ion can satisfactorily be explained by the following scheme, which can also account for the observation of a contribution of (c) ions in the transition $44 \rightarrow 43 + H$ even with a high degree of exchange labelling. Although this mechanism explains the formation of both (b) and (c) ions it is difficult to understand why the $C_2H_6N^+$ ions in this compound generate the (b) type ion in such abundance.

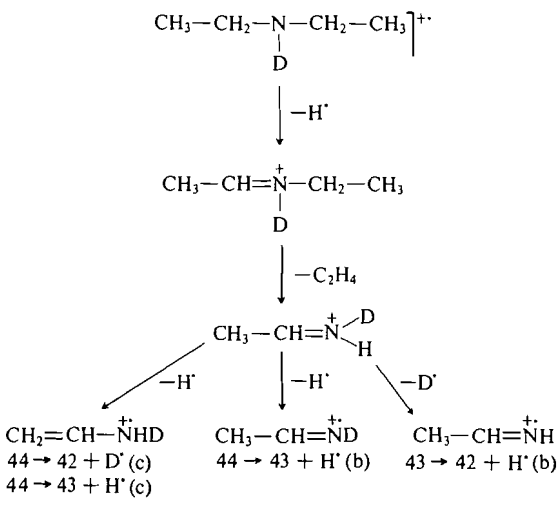

In order to discover whether a second mechanism exists for the formation of (b) type ions and to isolate the pure H loss metastable peak for (b) for its unequivocal identification, the mass spectrum of $CH_3CD_2NHCD_2CH_3$ was examined. The peak of high intensity at *m/e* 44 (C_2H_6N) was not only shifted to *m/e* 45 (60%) but also to *m/e* 46 (40%). The partial shift to *m/e* 45 is consistent with the mechanism previously proposed. The presence of the appropriate $^1m^*$'s showed that it was formed by loss of D·, followed by loss of $CD_2=CH_2$. This supports the postulated protonated acetaldimine structure $CH_3—CD=\overset{+}{N}H_2$ and this ion will account for the C_2H_5N type transitions $44 \rightarrow 43 + H^\cdot$ (from $CH_2=CD—\overset{+\cdot}{N}H_2$, (c)) and to a minor extent for $44 \rightarrow 42 + D^\cdot$ (from $CH_3—CD=\overset{+\cdot}{N}H$, (b)).

The shift to *m/e* 46, however, clearly shows that $C_2H_6N^+$ ions of an (initially) different structure are also generated, most probably by simple bond cleavage from the molecular ion:

$$CH_3—CD_2—\overset{+\cdot}{N}H—CD_2—CH_3 \rightarrow CH_3—CD_2—\overset{+}{N}H + \dot{C}D_2—CH_3$$
(*m/e* 46)

D· loss from this ion could explain the relatively high abundance of (b) type ions:

$$CH_3—CD_2—\overset{+}{N}H \xrightarrow{D^\cdot} CH_3—CD=\overset{+\cdot}{N}H$$
(b) (*m/e* 44)

$$CH_3—CD=\overset{+\cdot}{N}H \xrightarrow{D^\cdot} CH_3—C\equiv\overset{+}{N}H + D^\cdot \; (44 \rightarrow 42 + D^\cdot)$$

The CA study (3) indicated that the nondissociating ions isomerise

$$CH_3—CD_2—\overset{+}{N}H \rightarrow CH_3—CD=\overset{+}{N}HD$$

This hypothesis was confirmed by our observations (see Table 1). Not only was a (c) type metastable peak found for the transition $44 \rightarrow 43 + 1$ (intensity, $I = 50$ (arbitrary units)) but the intense $^1m^*$ for $44 \rightarrow 42 + D^\cdot$ ($I = 100$) was a (b) type component characterized by an energy release in excellent agreement with that found in $CH_3CD_2NH_2$. Note that the characteristic energy release of ion (b) is derived from loss of a D atom; $T_{0.5}$ for H atom loss may not be identical.

However, a *partial* isomerisation of the $C_2H_4D_2N$ ions at *m/e* 46 into the structure

[4]For example, by consecutive loss of two CH_3 radicals. This possibility was indeed effectively ruled out by examining the mass spectrum of $CH_3CD_2NHCD_2CH_3$; no *m/e* 51 ions are present.

$CH_3—CD=\overset{+}{N}HD$ (which will *mainly* form vinylamine ions at *m/e* 45 ($CH_2=CD—\overset{+}{N}DH$)), must occur, because a fairly intense metastable peak for the process $45 \rightarrow 44 + H^{\cdot}$ ($I = 70$) with a (c) type energy release[5] was also observed. The accompanying transition $45 \rightarrow 43 + D^{\cdot}$ was also observed but the peak is distorted by loss of H_2 from $CH_3CDNH_2\rceil^+$.

Summation of the observed peaks for (b) and (c) in a ratio of 3:2 produced a peak closely similar to that for the unlabelled compound.

Ions (a) and (d)

A third type of ion that can be identified by its characteristic energy release is the molecular ion of aziridine 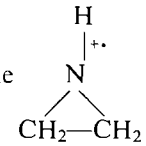 (a). Loss of H$^{\cdot}$ therefrom generated an intense, steep-sided metastable peak having a small dish and $T_{0.5}$ of 255 meV. It appeared to be noncomposite because the peak's shape remained unchanged at low electron energy and moreover, following an exchange deuteration the probe reaction became $44 \rightarrow 43 + H^{\cdot}$ with the same energy release. Thus the loss of a H atom attached to carbon is the major process for the metastable ions, but a small loss of D$^{\cdot}$ (~5%) was also observed (transition $44 \rightarrow 42 + D^{\cdot}$, $T_{0.5} = 315$ meV). Ions of higher energy, *i.e.* those dissociating in the ion source, lose both H and D in about equal proportions (10, 11).

Although (a) type aziridine ions clearly behave differently from (b) and (c) ions, it is not known whether the C—H atom is lost from an intact ring or the ring opened structure $\dot{C}H_2—\overset{+}{N}H=CH_2$ (d). The same energy release, peak shape, and shift upon exchange deuteration were found for the $C_2H_5N^{+\cdot}$ ions derived from dimethylamine. A similar small loss of D in CH_3NDCH_3 could not be detected because of interference from the intense metastable peak for the fragmentation $C_2H_6N^+ \rightarrow C_2H_4N^+ + H_2$ in unlabelled material. A study of CD_3NHCD_3, however, showed that loss of a C—H atom still is the major process ($47 \rightarrow 45 + D^{\cdot}$, $T_{0.5} = 285$ meV). There is thus no significant isotope effect on the energy release for loss of H/D bonded to carbon, whereas there is a small isotope effect for H/D bonded to nitrogen. The simplest interpretation of the results is that C—H and N—H fragmentations are competing processes, the former having a lower activation energy. The results cannot be satisfactorily explained on the basis of atom scrambling.

Three other compounds, piperidine, 4-methylpiperidine, and pyrrolidine were also found to generate a/d ions. For pyrrolidine, structure (d) was proposed from a study of labelled compounds (6). However, it was also concluded in this study (6) that H loss from this ion involves only the H atom attached to *nitrogen*. Our results on pyrrolidine-N-*d* show that the ions fragmenting in the ion source lose both types of hydrogen atom to an almost equal extent (compare aziridine) while the metastable ions almost exclusively[6] lose the carbon H atom.

Ion (e)

Finally, there is evidence for the existence of a fifth stable ionic species. Deuterium labelling studies had resulted in the following structure being proposed (5) for the $C_2H_5N^{+\cdot}$ ion (base peak) from *N*-methylpiperidine: $CH_3—N=CH_2\rceil^{+\cdot}$ (e). The translational energy release in the very intense metastable peak for H$^{\cdot}$ loss had $T_{0.5} = 130$ meV, much lower than that found for the other isomers, indicating the presence of a new species. It was furthermore concluded in the study described in ref. 5 that the H atoms of the methyl group are not lost and so the reaction will be:

$$CH_3—N=CH_2\rceil^{+\cdot} \rightarrow CH_3—\overset{+}{N}\equiv CH + H^{\cdot}$$

Two more compounds were found also to generate this ion (e), *N*,*N*-dimethylformamide and trimethylamine. The latter clearly produces

[5]The $^1m^*$ intensity for H$^{\cdot}$ loss from C_2H_6N ions is less than 0.1 of the corresponding C_2H_5N dissociation. Interference from H$^{\cdot}$ loss of the C_2H_5DN component in *m/e* 45 is therefore negligible.

[6]The % contribution of D atom loss can only be estimated but it must be <5%. In the unlabelled compound part of the *m/e* 43 ions are C_3H_7 ions, generated by HCN loss from (M—H) (6). In the N-*d* labelled compound this ion is shifted to *m/e* 44 (C_3H_6D) (exact mass measurements and shift of the transition $70 \rightarrow 43 + 27$ to $71 \rightarrow 44 + 27$). It gives rise to an intense m* for H_2 loss (20% of $44 \rightarrow 43 + 1$, $T_{0.5} = 400$ meV) that interferes with the detection of a small contribution of the transition $44 \rightarrow 42 + D^{\cdot}$.

Can. J. Chem. Downloaded from www.nrcresearchpress.com by 210.87.254.40 on 09/05/12
For personal use only.

these ions by the following pathway (8):

$$(CH_3)_3\overset{+\cdot}{N} \xrightarrow[-H^{\cdot}]{*} CH_3-\overset{CH_3}{\overset{|}{\underset{+}{N}}}=CH_2 \xrightarrow[-CH_3^{\cdot}]{*} CH_3-N=CH_2\rceil^{+\cdot}$$

although a second route via the $C_2H_6N^+$ ion (initially $CH_3-\overset{+}{N}-CH_3$) is also possible. Generation of the ion in *N,N*-dimethylformamide probably occurs mainly via the *m/e* 44 ions (base peak):

$$\begin{matrix} CH_3 & O^{+\cdot} \\ \diagdown & // \\ N-C & \\ \diagup & \diagdown \\ CH_3 & H \end{matrix} \xrightarrow[-\dot{C}HO]{*} CH_3-\overset{+}{N}-CH_3 \xrightarrow[-H^{\cdot}]{*} CH_3-N=CH_2\rceil^{+}$$

Both compounds show $T_{0.5}$ values for the probe reaction close to that found for *N*-methylpiperidine (see Table 1). Their shape is however slightly different from that found for *N*-methylpiperidine, in that both peaks have significantly wider skirts. We believe that this is caused by the presence of a minor second component, which we have not unequivocally identified.

Conclusions

$C_2H_5N^{+\cdot}$ ions generated from a variety of precursor molecules display characteristic differences in kinetic energy release in their metastable peaks for loss of an H atom. The following stable isomeric ions were thus identified:

$\begin{matrix} NH \\ / \quad \backslash \\ CH_2-CH_2 \end{matrix}\rceil^{+\cdot}$ (a) $T_{0.5} = 260 \pm 15$ meV

$CH_3CHNH\rceil^{+\cdot}$ (b) $T_{0.5} = 200 \pm 10$ meV

$CH_2CHNH_2\rceil^{+\cdot}$ (c) $T_{0.5} = 390 \pm 20$ meV

$CH_2NHCH_2\rceil^{+\cdot}$ (d) indistinguishable from (a)

$CH_2NCH_3\rceil^{+\cdot}$ (e) $T_{0.5} = 140 \pm 10$ meV

In contrast with the behaviour of the oxy-analogues, differences in peak shape were relatively small, rendering more difficult the direct identification of a composite metastable peak. Separation of components could, however, be achieved by appropriate deuterium labelling experiments.

It must be emphasized that the identification of isomeric ion structures from studies of a single fragmentation depend upon such structures being nonfreely interconverting in the internal energy range and time scale of such observations. This technique is poorly applicable to hydrocarbons (12) where isomerisation prior to fragmentation predominates but the method appears to hold considerable promise for hetero-atom containing ions.

Experimental

The metastable peak measurements were performed with an A.E.I.-G.E.C. MS 902S instrument using the procedure described in ref. 1. All compounds, except for $CH_3CD_2NH_2$ (97% d_2 species), which was obtained from $LiAlD_4$ reduction of acetonitrile (13), were obtained commercially and, if necessary, were purified by preparative gas chromatography. Compounds were admitted to the ion source via a Granville-Phillips variable leak; sample pressure *ca.* 5×10^{-7} torr. Energy release values were calculated in the usual way with a main beam energy spread correction of 1.3 V (1). For most measurements the reproducibility of the half-height width of the metastable peak was ± 0.5 V at an acceleration potential of 6000 V.

Acknowledgements

We wish to thank Dr. R. Renault for the gift of CD_3NHCD_3 (95% d_6 species) and $CH_3CD_2NHCD_2CH_3$ (95% d_4 species).

This work was financially supported by the National Research Council of Canada. One of us (J.K.T.) thanks the Netherlands Organisation for the Advancement of Pure Research (Z.W.O.) for a Fellowship during the tenure of which this work was completed.

1. J. L. Holmes and J. K. Terlouw. Can. J. Chem. **53**, 2076 (1975).
2. F. W. McLafferty, R. Kornfeld, W. F. Haddon, K. Levsen, P. F. Bente III, S. C. Tsai, and H. D. R. Schuddemage. J. Am. Chem. Soc. **95**, 3886 (1973).
3. K. Levsen and F. W. McLafferty. J. Am. Chem. Soc. **96**, 139 (1974).
4. H. Budzikiewicz, C. Djerassi, and D. H. Williams. Mass spectrometry of organic compounds. Holden-Day Inc., San Francisco. 1967. Chapt. 8.
5. A. M. Duffield, H. Budzikiewicz, D. H. Williams, and C. Djerassi. J. Am. Chem. Soc. **87**, 810 (1965).
6. A. M. Duffield, H. Budzikiewicz, and C. Djerassi. J. Am. Chem. Soc. **87**, 2920 (1965).
7. J. L. Holmes, F. P. Lossing, and J. K. Terlouw. In preparation.

Can. J. Chem. Downloaded from www.nrcresearchpress.com by 210.87.254.40 on 09/05/12
For personal use only.

8. G. HVISTENDAHL and K. UNDHEIM. Org. Mass Spectrom. **3**, 821 (1970).
9. J. E. COLLIN, M. J. FRANSKIN, and D. HYATT. Bull. Soc. R. Sci. Liège, **36**, 318 (1967).
10. Q. N. PORTER and R. J. SPEAR. Org. Mass Spectrom. **3**, 1259 (1970).
11. V. K. POTAPOV, O. A. YUZHAKOVA, KH. KHAFIZOV, and R. G. KOSTYANOVSKII. Dokl. Akad. Nauk SSSR, **203**, 379 (1972).
12. J. L. HOLMES and J. K. TERLOUW. Org. Mass Spectrom. **10**, 787 (1975).
13. L. S. TRZUPEK, E. R. STEDRONSKY, and G. M. WHITESIDES. J. Org. Chem. **37**, 3300 (1972).

Can. J. Chem. Downloaded from www.nrcresearchpress.com by 210.87.254.40 on 09/05/12
For personal use only.

On the oxidative dimerization of 2,3-dialkylindoles[1]

VINOD DAVE AND E. W. WARNHOFF
Department of Chemistry, University of Western Ontario, London, Ontario N6A 5B7

Received October 6, 1975

VINOD DAVE and E. W. WARNHOFF. Can. J. Chem. **54**, 1015 (1976).

The oxidative dimerization of 3-alkyl-2-methylindoles to **1** has been found to occur with several primary 3-alkyl and one secondary 3-alkyl groups. A tertiary 3-alkyl group prevents dimerization of the intermediate 3-hydroxyindolenine. These new dimers undergo the same acid-catalyzed rearrangement as **1***a*.

VINOD DAVE et E. W. WARNHOFF. Can. J. Chem. **54**, 1015 (1976).

On a trouvé que la dimérisation oxydante des alkyl-3 méthyl-2 indoles en **1** se produit avec plusieurs groupes alkyl-3 primaires et un groupe alkyl-3 secondaire. Un groupe alkyl-3 tertiaire empêche la dimérisation de l'intermédiaire hydroxy-3 indolénine. Ces nouveaux dimères subissent le même réarrangement acido-catalysé que subit le composé **1***a*.

[Traduit par le journal]

Sometime ago we (2) and others (3) determined the structure and stereochemistry of the oxidative dimerization product **1***a* from 2,3-dimethylindole (**4***a*). McLean and Dmitrienko (4) have shown that 2-methyl-3-ethylindole (**4***b*) forms an analogous product, **1***b*. These bisindolines were found to arise by dimerization of two molecules of the 3-hydroxyindolenine **2**, probably produced by reaction of the initially formed 3-hydroperoxyindolenine **3** with the indole **4**. To explore further the generality of this reaction we have examined the effect of changing the alkyl substituents, and the results are reported in this paper. In an accompanying paper (5) are described some new reactions discovered during preparation of one of the requisite indoles.

Considerable evidence was already available that any alkyl group other than methyl at C-2 caused other reactions (*e.g.* oxidation or rearrangement) to predominate over dimerization of the 3-hydroxyindolenine (4). Thus, the 3-methyl-2-ethyl derivative **2***c* underwent oxidation to the oxindole **8** (4); the 2,3-diethyl derivative **2***d* was not reported to dimerize (6); 3-methyl-2-isopropylindole, **4***e*, gave only monomeric products of further oxidation of **3***e* (7); and 2-benzyl-3-phenylindole, **4***f*, did not give a product of type **1** (8). We have further confirmed that even in the absence of oxygen, 3-methyl-2-ethyl-3-hydroxyindolenine, **2***c*, gave no evidence of dimer **1***c* in the mixture of products formed on standing.

On the other hand, if the alkyl group at C-2 is methyl, the alkyl group at C-3 can be varied without preventing dimerization. Thus, dimers were obtained by the usual procedure (see Experimental) from 3-*n*-propyl-, 3-*i*-propyl-, 3-*n*-butyl-, and 3-*n*-amyl-2-methylindoles (**4***g–j*), and these dimers were accompanied by minor amounts of the yellow indoxyls **6***g–j* from rearrangement of the dimers. In the case of 2-methyl-3-benzylindole, **4***k*, the indoxyl **6***k* was the major product. The structures postulated for the new dimers are based on their ^{1}Hmr and mass spectra and on their acid-catalyzed rearrangement products **6** and **7** which were analogous to those observed for the 2,3-dimethyl derivative **1***a* (9).[2]

Only when the 3-alkyl group became as bulky as *tert*-butyl was no dimer obtained from the hydroxyindolenine **2***l*, the product being instead the indoxyl **5***l* from rearrangement. This steric effect is not surprising because the initial dimerization step leading to **9***l* would have brought adjacent methyl and *tert*-butyl groups into eclipse on the indoline ring. The steric effect observed in this reaction can be compared to that in the related acid-catalyzed dimerization of 3-alkylindoles in which either a 3-isopropyl or a 3-*tert*-butyl group is reported to prevent dimerization (10).

[1]Organic nitrogen chemistry. 12. For paper 11 see ref. 1.

[2]In the ^{1}Hmr spectra of dimers **1***g–j* no splitting of the tetrahydrofuran CH_2 signal was observed at 60 MHz as found for **1***a*. See also ref. 4, p. 3643.

Can. J. Chem. Downloaded from www.nrcresearchpress.com by 210.87.254.6 on 09/05/12
For personal use only.

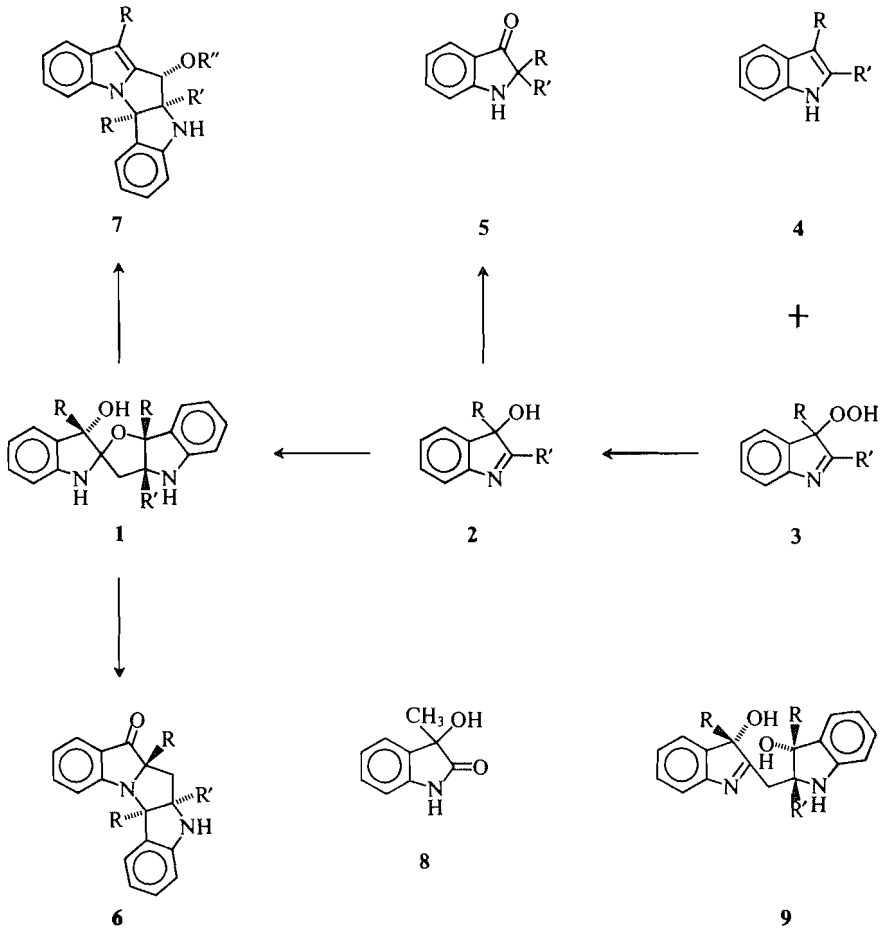

	R	R′
a	Me	Me
b	Et	Me
c	Me	Et
d	Et	Et
e	Me	*i*-Pr
f	Ph	$PhCH_2$

	R	R′
g	*n*-Pr	Me
h	*i*-Pr	Me
i	*n*-Bu	Me
j	*n*-Am	Me
k	$PhCH_2$	Me
l	*t*-Bu	Me

Experimental

Materials and apparatus were the same as in ref. 9 except for the following. Infrared spectra were taken on Beckman IR-20A and Acculab 4 instruments. Ultraviolet spectra were recorded on a Cary Model 118 spectrometer. Chemical shifts for aromatic protons and undecipherable aliphatic protons in ^1H nmr spectra are not reported. Preparative thick layer plates contained 20 g of Merck GF_{254} silica gel on a 20 × 20 cm plate unless otherwise specified. Petroleum ether refers to the fraction of bp 30–60 °C unless otherwise specified. The following abbreviations have been used: b = broad, s = singlet, d = doublet, q = quartet, m = multiplet, sh = shoulder, Ph = phenyl, and Ac = acetyl.

Indoles

The 2,3-disubstituted indoles used in the present work were prepared by refluxing a solution of the appropriate ketone (0.05 mol) and phenylhydrazine hydrochloride (0.04 mol) in glacial acetic acid (30 ml) for 3 h. The cooled reaction mixture was dissolved in ether and washed first with 10% aqueous HCl, then with 5% aqueous NaOH, and finally with water. The dried organic solution was concentrated, and the crude indole was either distilled or, in the case of solids, recrystallized from ether – petroleum ether. Purity was checked by tlc and ^1Hmr spectroscopy. Physical constants are reported in Table 1.

The distilled 2-methyl-3-*tert*-butylindole on standing became purple from air oxidation of a minor contaminant arising from traces of 2-neopentylindole (see following

Can. J. Chem. Downloaded from www.nrcresearchpress.com by 210.87.254.6 on 09/05/12
For personal use only.

TABLE 1. Physical constants of indoles prepared

Ketone	Indole (yield)	Physical constants	
		Experimental	Literature
2-Pentanone	2-Methyl-3-ethylindole(63%)	bp 115.5–116 °C/0.8 torr	bp 120 °C/1 torr (11*a*)
3-Pentanone	2-Ethyl-3-methylindole(68%)	mp 62–65 °C	mp 64–66 °C (4)
2-Hexanone	2-Methyl-3-*n*-propylindole(50%)	bp 123.5–124 °C/0.8 torr	bp 131–135 °C/1.1 torr (11*b*)
4-Methyl-2-pentanone	2-Methyl-3-isopropylindole(64%)	bp 120–121 °C/0.7 torr	bp 120 °C/0.8 torr (11*a*)
2-Heptanone	2-Methyl-3-*n*-butylindole(81%)	bp 130–131 °C/0.8 torr	bp 124–127 °C/1 torr (11*c*)
4,4-Dimethyl-2-pentanone	2-Methyl-3-*tert*-butylindole(35%)	bp 136–138 °C/0.8 torr	bp 134–136 °C/0.5 torr (11*d*)
2-Octanone	2-Methyl-3-*n*-amylindole(72%)	bp 144.5–145 °C/0.9 torr	bp 205–206 °C/23 torr (11*e*)
4-Phenylbutanone	2-Methyl-3-benzylindole(80%)	mp 117–119 °C	mp 116 °C (11*f*)

paper). Pure 2-methyl-3-*tert*-butylindole was obtained by chromatography of this material on silica gel.

Hydroxyindolenine Dimers

These dimers were prepared by aerial oxidation of the 2,3-dialkylindoles in $CHCl_3$ solution in an open vessel for several days (with occasional addition of $CHCl_3$ to maintain volume) and were separated from unreacted indole and other products by preparative layer chromatography on silica gel in benzene–ether (80:20 to 95:5) mixtures. All of the dimers had ir absorption at 3370 and 3500 cm^{-1} for NH and OH bonds. The uv spectra of all of the dimers were virtually identical with λ_{max} (MeOH) 242 (16 000) and 297 nm (4700).

2-Methyl-3-ethyl Dimer **1***b*

From 2.0 g of crude oxidation product was obtained 1.3 g (59%) of dimer. Three recrystallizations from $CHCl_3$ – petroleum ether (bp 60–80 °C) gave pure **1***b*, mp 157–160 °C (lit. (4) 157–160 °C); δ ($CDCl_3$) 0.90 (t, 3H, J = 7 Hz, $CH_3(CH_2)$), 1.12 (t, 3H, J = 7 Hz, $CH_3(CH_2)$), 1.37 (s, 3H, CH_3), 2.35 (s, 2H, CH_2), 3.20 (s, 1H, OH, exch. D_2O), 3.80 (b s, 1H, NH, exch. D_2O), and 4.90 ppm (b s, 1H, NH, exch. D_2O); *m/e* 350 (molecular ion).

2-Methyl-3-n-propyl Dimer **1***g*

From 290 mg of crude oxidation product was obtained 97 mg (30%) of dimer. Three recrystallizations from ether – petroleum ether gave pure **1***g*, mp 142–145 °C, δ ($CDCl_3$) 1.34 (s, 3H, CH_3), 2.37 (s, 2H, CH_2), 3.23 (s, 1H, OH, exch. D_2O), 3.80 (b s, 1H, NH, exch. D_2O), and 4.90 ppm (b s, 1H, NH, exch. D_2O); *m/e* 378 (molecular ion). *Anal.* calcd. for $C_{24}H_{30}N_2O_2$ (378.5): C 76.16, H 7.99, N 7.40; found: C 76.23, H 7.85, N 7.05.

2-Methyl-3-n-butyl Dimer **1***i*

From 2.0 g of crude oxidation product was obtained 937 mg (43%) of dimer.[3] Recrystallization from ether – petroleum ether gave pure **1***i*, mp 112–117 °C (dec.), δ ($CDCl_3$) 1.34 (s, 3H, CH_3), 2.33 (s, 2H, CH_2), 3.23 (s, 1H, OH, exch. D_2O), 3.80 (b s, 1H, NH, exch. D_2O), and 4.80 ppm (b s, 1H, NH, exch. D_2O); *m/e* 406 (molecular ion). *Anal.* calcd. for $C_{26}H_{34}N_2O_2$ (406.6): C 76.81, H 8.43, N 6.89; found: C 76.40, H 8.58, N 6.40.

2-Methyl-3-n-amylindole Dimer **1***j*

From 1.2 g of crude oxidation product was obtained 746 mg (57%) of dimer. Four recrystallizations from ether – petroleum ether gave pure **1***j*, mp 113–114 °C, δ ($CDCl_3$) 1.34 (s, 3H, CH_3), 2.38 (s, 2H, CH_2), 3.27 (s, 1H, OH, exch. D_2O), and two NH peaks so broadened as to be almost merged in the baseline; *m/e* 434 (molecular ion); osmometric mol. wt. ($CHCl_3$) 419. *Anal.* calcd. for $C_{28}H_{38}N_2O_2$ (434.6): C 77.38, H 8.81, N 6.45; found: C 77.20, H 8.81, N 6.36.

2-Methyl-3-isopropyl Dimer **1***h*

This compound, an unstable oil, was not obtained by this simple procedure, and the oxidation of **4***h* is described separately below.

Rearranged Acetates **7** *(Ac for R″)*

The hydroxyindolenine dimers were rearranged to alcohols **7** (R″ = H) by treatment of the dimer (100 mg) in acetone (1 ml) with 0.1 *N* aqueous HCl (0.3 ml) at room temperature overnight. The products were isolated by preparative layer chromatography on silica gel in benzene–ether mixture (85:15 to 95:5). For characterization the liquid alcohols **7** (H for R″) (50 mg) were converted into the crystalline acetates **7** (Ac for R″) by treatment with acetic anhydride (0.2 ml) in pyridine (0.5 ml) at room temperature for 5 h. They were purified by preparative layer chromatography on silica gel in benzene–ether mixtures (100:0 to 90:10). All of the acetates had ir absorption at 3380–3360 (NH) and 1720–1730 cm^{-1} (C=O). The uv spectra of all of the acetates were virtually the same with λ_{max} (MeOH) 228 (40 000), 294 (9500), and 305 nm (8500).

2-Methyl-3-ethyl Acetate **7***b (Ac for R″)*

From 102 mg of chromatographed acid-rearrangement product **7***b* (H for R″) was obtained 70 mg of *O*-acetate **7***b* (Ac for R″). Three recrystallizations from ether – petroleum ether gave colourless granules of pure **7***b* (Ac for R″), mp 163–166 °C, δ ($CDCl_3$) 0.78 (t, 3H, J = 7 Hz, $CH_3(CH_2)$), 1.20 (t, 3H, J = 7 Hz, $CH_3(CH_2)$), 1.38 (s,

[3]A second product, the indoxyl **6***i*, was also found, and its isolation is described under a separate heading.

Can. J. Chem. Downloaded from www.nrcresearchpress.com by 210.87.254.6 on 09/05/12
For personal use only.

Can. J. Chem. Downloaded from www.nrcresearchpress.com by 210.87.254.6 on 09/05/12
For personal use only.

3H, CH_3), 2.12 (s, 3H, $CH_3C{=}O$), 2.72 (q, 2H, J = 7 Hz, $CH_2(CH_3)$),[4] and 6.33 ppm (s, 1H, C*H*OAc), NH not apparent; *m/e* 374 (molecular ion). *Anal.* calcd. for. $C_{24}H_{26}N_2O_2$ (374.5): C 76.98, H 7.00; found: C 77.60, H 6.74.

2-Methyl-3-n-propyl Acetate 7g (Ac for R″)

From 100 mg of the dimer **1***g* was obtained 30 mg of rearrangement product **7***g* (H for R″) which gave 22 mg of *O*-acetate **7***g* (Ac for R″). Two recrystallizations from $CHCl_3$ – petroleum ether (bp 60–80 °C) and two from MeOH – petroleum ether (bp 60–80 °C) gave pure **7***g* (Ac for R″), mp 179–181 °C; δ ($CDCl_3$) 0.81–0.94 (m, 6H, $2CH_3(CH_2)$), 1.34 (s, 3H, CH_3), 2.08 (s, 3H, $CH_3C{=}O$), ~2.10 (b, 1H, NH, exch. D_2O), 2.56–2.70 (m, 4H, $2CH_2$—Et), and 6.24 ppm (s, 1H, C*H*OAc); *m/e* 402 (molecular ion). *Anal.* calcd. for $C_{26}H_{30}N_2O_2$ (402.5): C 77.58, H 7.51; found: C 77.56, H 7.66.

2-Methyl-3-isopropyl Acetate 7h (Ac for R″)

From 85 mg of crude dimer **1***h* rearrangement product was obtained 25 mg of **7***h* (H for R″) which gave 21 mg of *O*-acetate **7***h* (Ac for R″). Two recrystallizations from $CHCl_3$ – petroleum ether (bp 60–80 °C) gave colourless small needles of pure **7***h* (Ac for R″), mp (subl.) 180 °C, δ ($CDCl_3$) 0.84 (d, 3H, J = 7 Hz, CH_3—CH), 1.21 (d, 3H, J = 7 Hz, CH_3—CH), 1.32 (d, 6H, J = 7 Hz, CH_3—(CH)—CH_3), 1.49 (s, 3H, CH_3), 2.16 (s, 3H, $CH_3C{=}O$), 3.12–3.62 (8 lines, 2H, J = 7 Hz, 2 overlapping C*H*Me_2s), 4.00 (b s, 1H, NH, exch. D_2O), and 6.51 ppm (s, 1H, C*H*OAc); m/*e* 402 (molecular ion). *Anal.* calcd. for $C_{26}H_{30}N_2O_2$ (402.5): C 77.58, H 7.51; found: C 77.80, H 7.61.

2-Methyl-3-n-butyl Acetate 7i (Ac for R″)

From 100 mg of dimer **1***i* was obtained 54 mg of rearrangement product 7*i* (H for R″) which gave 30 mg of *O*-acetate **7***i* (Ac for R″). Four recrystallizations from $CHCl_3$ – petroleum ether (bp 60–80 °C) gave colourless small needles of pure **7***i* (Ac for R″), mp 166–168 °C, δ ($CDCl_3$) 0.81–0.94 (m, 6H, $2CH_3(CH_2)$), 1.38 (s, 3H, CH_3), 2.11 (s, 3H, $CH_3C{=}O$), 2.30 (b, 1H, NH, exch. D_2O), 2.60–2.75 (m, 4H, $2CH_2$-*n*-Pr), and 6.27 ppm (s, 1H, C*H*OAc); *m/e* 430 (molecular ion). *Anal.* calcd. for $C_{28}H_{34}N_2O_2$ (430.6): C 78.10, H 7.96; found: C 77.98, H 8.00.

2-Methyl-3-n-amyl Acetate 7j (Ac for R″)

From 100 mg of dimer **1***j* was obtained 43 mg of rearrangement product 7*j* (H for R″) which gave 26 mg of *O*-acetate **7***j* (Ac for R″). Two recrystallizations from $CHCl_3$ – petroleum ether (bp 60–80 °C) gave colourless granules of 7*j* (Ac for R″), mp 151–153 °C, δ ($CDCl_3$) 0.77–0.90 (m, 6H, $2CH_3(CH_2)$), 1.35 (s, 3H, CH_3), ~2.0 (b, 1H, NH, exch. D_2O), 2.08 (s, 3H, $CH_3C{=}O$), 2.59–2.73 (m, 4H, $2CH_2$-*n*-Bu), and 6.25 ppm (s, 1H, C*H*OAc); *m/e* 458 (molecular ion). *Anal.* calcd. for $C_{30}H_{38}N_2O_2$ (458.6): C 78.56, H 8.35; found: C 78.49, H 8.29.

2-Methyl-3-isopropyl-3-hydroperoxyindolenine, 3h

When 2-methyl-3-isopropylindole (1.2 g) was air-oxidized in $CHCl_3$ solution, no dimer **1***h* was isolated, but instead the indolenine hydroperoxide (239 mg) was found. Two recrystallizations from ether – petroleum ether gave pure **3***h*, mp 119.5–120 °C (dec.), ν_{max} ($CHCl_3$) 3100–3400 cm^{-1} (OH); λ_{max} (MeOH) 218 (23 000), 257 (3300), and 290 nm (2300); λ_{inf} (MeOH) 213 (20 000) and 224 nm (16 000); δ ($CDCl_3$) 0.50 (d, 3H, J = 7 Hz, CH_3CH), 1.22 (d, 3H, J = 7 Hz, CH_3CH), 2.26 (b s, 3H, $CH_3C{=}$), ~2.30 (pattern hidden by $CH_3C{=}$, 1H, C*H*Me_2), and 9.90 ppm (b s, 1H, OOH, exch. D_2O); *m/e* 205 (molecular ion). *Anal.* calcd. for $C_{12}H_{15}NO_2$ (205.3): C 70.22, H 7.37; found: C 69.13, H 7.26.[5]

2-Methyl-3-isopropyl-3-hydroxyindolenine, 2h

A solution of indole **4***h* (500 mg) in petroleum ether (bp 60–80 °C) (10 ml) was allowed to stand in an open beaker overnight. The precipitate was filtered and washed with cold petroleum ether (bp 60–80 °C); yield 45 mg. Three recrystallizations from ether – petroleum ether gave colourless needles of hydroxyindolenine **2***h*, mp subl. 120 °C; ν_{max} ($CHCl_3$) 3100–3600 cm^{-1} (OH); λ_{max} (MeOH) 218 (21 000), 255 (3200), and 290 nm (2000); λ_{inf} (MeOH) 213 (19 000) and 224 nm (15 000); δ ($CDCl_3$) 0.41 (d, 3H, J = 7 Hz, CH_3—CH), 1.20 (d, 3H, J = 7 Hz, CH_3—H), 1.94 (s, 3H, $CH_3C{=}$), 2.18 (septet, 1H, C*H*Me_2), and 4.50 ppm (b s, 1H, OH, exch. D_2O); *m/e* 189 (molecular ion). *Anal.* calcd. for $C_{12}H_{15}NO$ (189.3): C 76.16, H 7.99; found: C 76.23, H 8.03.

When a solution of the hydroxyindolenine (200 mg) in $CHCl_3$ was allowed to stand in an open beaker for two weeks, the crude product after preparative layer chromatography gave an unstable oil (85 mg) which was judged to be *dimer* **1***h* by the result of its acid-catalyzed rearrangement (see below).

Dimeric Indoxyls, 6

2-Methyl-3-n-butylindoxyl, 6i

A second, more polar band from the preparative plate separation of dimer **1***i* gave 497 mg (21%) of yellow oily indoxyl **6***i*. Rechromatography and acetylation gave the *N*-acetyl indoxyl **6***i* (NAc for NH) which was chromatographed and recrystallized from ether – petroleum ether to give yellow granules of **6***i* (NAc for NH), mp 112–114 °C, ν_{max} ($CHCl_3$) 1685 (indoxyl C=O) and 1645 cm^{-1} (acetamide C=O); λ_{max} (MeOH) 240 (36 000), 257 (20 000), 290 (3500), 320 (1400), and 405 nm (2400); δ ($CDCl_3$) 1.49 (s, 3H, CH_3), 2.29 (s, 2H, CH_2), and 2.47 ppm (s, 3H, $CH_3C{=}O$); *m/e* 430 (molecular ion). *Anal.* calcd. for $C_{28}H_{34}N_2O_2$ (430.6): C 78.10, H 7.96; found: C 77.96, H 7.81.

2-Methyl-3-benzylindoxyl, 6k

Chromatography of the crude product (500 mg) of air oxidation of 2-methyl-3-benzylindole, **4***k*, gave as the major product a yellow oil (130 mg). Rechromatography and two recrystallizations from ether – petroleum ether gave lemon yellow needles of the dimeric indoxyl **6***k*, mp 154–156 °C, ν_{max} ($CHCl_3$) 3360 (NH) and 1690 cm^{-1} (indoxyl C=O); λ_{max} (MeOH) 238 (28 000), 305 (4700), and 410 nm (2100); δ ($CDCl_3$) 1.17 (s, 3H, CH_3), 2.21 (s, 2H, CH_2), and 2.92–3.82 ppm (6 lines, 4H, 2 overlapping PhCH_2), NH not apparent; *m/e* 456 (molecular ion).

[4]The quartet from the second —$CH_2(CH_3)$ was split further, presumably by the —C*H*OAc methine hydrogen.

[5]The low carbon value is presumably due to decomposition of the sensitive peroxide.

Anal. calcd. for $C_{32}H_{28}N_2O$ (456.6): C 84.18, H 6.18; found: C 84.00, H 6.29.

Air oxidation of **4***k* in various other solvents also failed to yield the dimer **1***k* itself. The following attempts to prepare the hydroxyindolenine **2***k* for dimerization studies also failed: (*a*) catalytic oxygenation with Pt, (*b*) oxygenation of the indole Grignard reagent, (*c*) hydrolysis of the 3-chloroindolenine, and (*d*) acetoxylation of indole **4***k*.

Oxidation of 2-Methyl-3-tert-butylindole, 4l

(*a*) When indole **4***l* was oxidized in $CHCl_3$ solution by air there was no evidence of formation of dimer **1***l*. The major product was yellow 2-methyl-2-*tert*-butylindoxyl, **5***l*, mp 130–137 °C; δ ($CDCl_3$) 1.00 (s, 9H, *tert*-Bu), 1.29 (s, 3H, CH_3), and 4.65 ppm (b s, 1H, NH, exch. D_2O); *Mol. Wt.* calcd. for $C_{13}H_{17}NO$: 203.130; found (mass spectrometry): 203.131 (molecular ion). Hydroxyindolenine **2***l* was also isolated from this reaction (mp and ^{1}Hmr).

(*b*) When a solution of indole **4***l* (750 mg, freshly chromatographed) in petroleum ether (15 ml) was stirred in an open beaker at room temperature, solid precipitated within 2 h. After 6.5 h the solid was filtered and washed with cold petroleum ether. Two recrystallizations from ether – petroleum ether gave 25 mg of colourless needles of *2-methyl-3-tert-butyl-3-hydroxyindolenine*, **2***l*, mp subl. 130 °C, ν_{max} ($CHCl_3$) 3100–3600 cm^{-1} (OH); λ_{max} (MeOH) 220 (23 000), 255 (3200), and 285 nm (2800); λ_{Inf}(MeOH) 215 (20 000) and 226 nm (17 000); δ ($CDCl_3$) 1.00 (s, 9H, *tert*-Bu), 2.08 (s, 3H, $=CCH_3$), and 3.75 ppm (b s, 1H, OH, exch. D_2O); *m/e* 203 (molecular ion). *Anal.* calcd. for $C_{13}H_{17}NO$ (203.3): C 76.81, H 8.43; found: C 76.67, H 8.42.

When a solution of hydroxyindolenine **2***l* in $CHCl_3$ (or benzene or ethyl acetate) was allowed to stand for several days, tlc and ^{1}Hmr showed the only product to be the monomeric indoxyl **5***l*.

Acknowledgements

We thank Ms. Heather Schroeder for the 100 MHz ^{1}Hmr spectra, Mr. D. Hairsine for the mass spectra, and the National Research Council of Canada for financial support.

1. V. Dave and E. W. Warnhoff. Tetrahedron, **31**, 1255 (1975).
2. V. Dave and E. W. Warnhoff. Chem. Commun. 919 (1970); Can. J. Chem. **49**, 1911 (1971).
3. (*a*) G. Berti, A. Da Settimo, G. Di Colo, and E. Nannipieri. J. Chem. Soc. C, 2703 (1969); (*b*) S. McLean, E. K. Strøm-Gundersen, K. S. Dichmann, J. K. Fawcett, and S. C. Nyburg. Tetrahedron Lett. 2645 (1970).
4. S. McLean and G. Dmitrienko. Can. J. Chem. **49**, 3642 (1971).
5. V. Dave and E. W. Warnhoff. Can. J. Chem. This issue.
6. E. Leete. J. Am. Chem. Soc. **83**, 3645 (1961).
7. H. H. Wasserman and M. B. Floyd. Tetrahedron Lett. 2009 (1963).
8. F. Y. H. Chen and E. Leete. Tetrahedron Lett. 2013 (1963).
9. V. Dave and E. W. Warnhoff. Can. J. Chem. **49**, 1911 (1971) **49**, 1921 (1971).
10. G. F. Smith and A. E. Walters. J. Chem. Soc. 940 (1961).
11. (*a*) A. H. Jackson and P. Smith. Tetrahedron, **24**, 2227 (1964); (*b*) A. R. Bader, R. J. Bridgwater, and P. R. Freeman. J. Am. Chem. Soc. **83**, 3319 (1961); (*c*) V. F. Martynov and I. A. Kastron. J. Gen. Chem. U.S.S.R. (Engl. transl.), **28**, 2119 (1958); (*d*) S. David and P. Régent. Bull. Soc. Chim. Fr. 101 (1964); (*e*) N. P. Buu-Hoi and R. Royer. Recl. Trav. Chim. Pays-Bas, **66**, 305 (1947); (*f*) S. Kuroda. J. Pharm. Soc. Jpn. **493**, 1313 (1923); Chem. Abstr., **17**, 3031 (1923).

Can. J. Chem. Downloaded from www.nrcresearchpress.com by 210.87.254.6 on 09/05/12
For personal use only.

New reactions of 2-substituted indoles[1]

VINOD DAVE AND E. W. WARNHOFF
Department of Chemistry, University of Western Ontario, London, Ontario N6A 5B7

Received October 6, 1975

VINOD DAVE and E. W. WARNHOFF. Can. J. Chem. **54**, 1020 (1976).

2-Alkyl (or aryl) indoles react readily with phenylhydrazine in hydrochloric–acetic acid to give *o*-aminophenylpyrazoles **7**, if the 2-substituent is of small or moderate size, or else 3-aminoindoles, if the 2-substituent is sufficiently bulky. The 3-aminoindoles readily undergo oxidative dimerization to indolylidene aminoindoles **4** ⇌ **4′**. Evidence is provided for the mechanisms of formation of these two kinds of products.

VINOD DAVE et E. W. WARNHOFF. Can. J. Chem. **54**, 1020 (1976).

Lorsque le substituant en position 2 est de grosseur petite ou moyenne, les alkyl-2 (ou aryl) indoles réagissent facilement avec la phénylhydrazine dans un mélange acide chlorhydrique – acide acétique pour conduire aux *o*-aminophénylpyrazoles **7**; toutefois si le substituant en position 2 est suffisamment volumineux, la réaction conduit aux amino-3 indoles. Les amino-3 indoles subissent facilement une dimérisation oxydante pour conduire aux indolylodènes aminoindoles **4** ⇌ **4′**. On fournit des preuves pour les mécanismes de formation de ces deux sortes de produits.

[Traduit par le journal]

In the course of preparing 2-methyl-3-*tert*-butylindole, **1**, by the Fischer method to study its possible oxidative dimerization as described in an accompanying paper (1), it was noticed that the colourless distilled product on standing in air turned a permanganate-purple colour. Investigation of the purple product, formed in 0.6–0.8% yield, revealed two previously unreported reactions of 2-substituted indoles (Scheme 1) which are the subject of this paper.

The molecular formula, $C_{26}H_{31}N_3$, and the simple ^{1}Hmr spectrum of the purple compound suggested a symmetrical structure incorporating two molecules of an indole plus an additional nitrogen atom which would have to be provided by a molecule of phenylhydrazine. Since pure

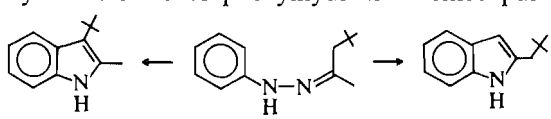

1 **2** **3*e***

2-methyl-3-*tert*-butylindole, **1**, did not give any purple compound under the reaction conditions ($PhNHNH_2 \cdot HCl$ in refluxing glacial HOAc containing concentrated aqueous HCl), 2-neopentylindole, **3*e***, a minor product from the alternative cyclization of phenylhydrazone **2**, was possibly involved. This minor product **3*e*** became the only product when boron trifluoride etherate was used as catalyst to cyclize the phenylhydrazone.[2] When 2-neopentylindole was treated with phenylhydrazine hydrochloride in refluxing acetic–hydrochloric acids, the purple compound was indeed formed as the major product (>60%) after exposure of the crude product to air. It was also found that 2-*tert*-butylindole and 2-phenylindole gave the same kind of intensely coloured product under the same conditions. The most likely structure for all three of the products was **4**,[3] and this was proved for the phenyl substituted derivative **4*f*** by establishing its identity with the known product of condensation of 3-amino-2-phenylindole, **10**, with 3-imino-2-phenylindolenine, **11**. The magnetic equivalence of the two neopentyl groups of **4*e*** and the two *tert*-butyl groups of **4*d*** in the ^{1}Hmr spectra is attributed to tautomerization (**4** ⇌ **4′**) and *syn–anti* isomerization about the central nitrogen atom. The

[1]Organic nitrogen chemistry. 13. For paper 12 see ref. 1.

[2]Such reversals of the direction of cyclization of phenylhydrazones have been ascribed to differences in steric effects at the transition states for possible cyclizations depending on whether a proton or a Lewis acid is complexed to the nitrogen atom of the phenylhydrazone (2).

[3]The formulas shown are not intended to imply the actual geometry of the molecules. The preferred geometry is presumably the best compromise between maximization of π-delocalization and minimization of steric hindrance. Inspection of Stuart–Briegleb models suggests that the preferred geometry of **4*d*–*f*** is certainly noncoplanar.

Can. J. Chem. Downloaded from www.nrcresearchpress.com by 210.87.254.105 on 09/05/12
For personal use only.

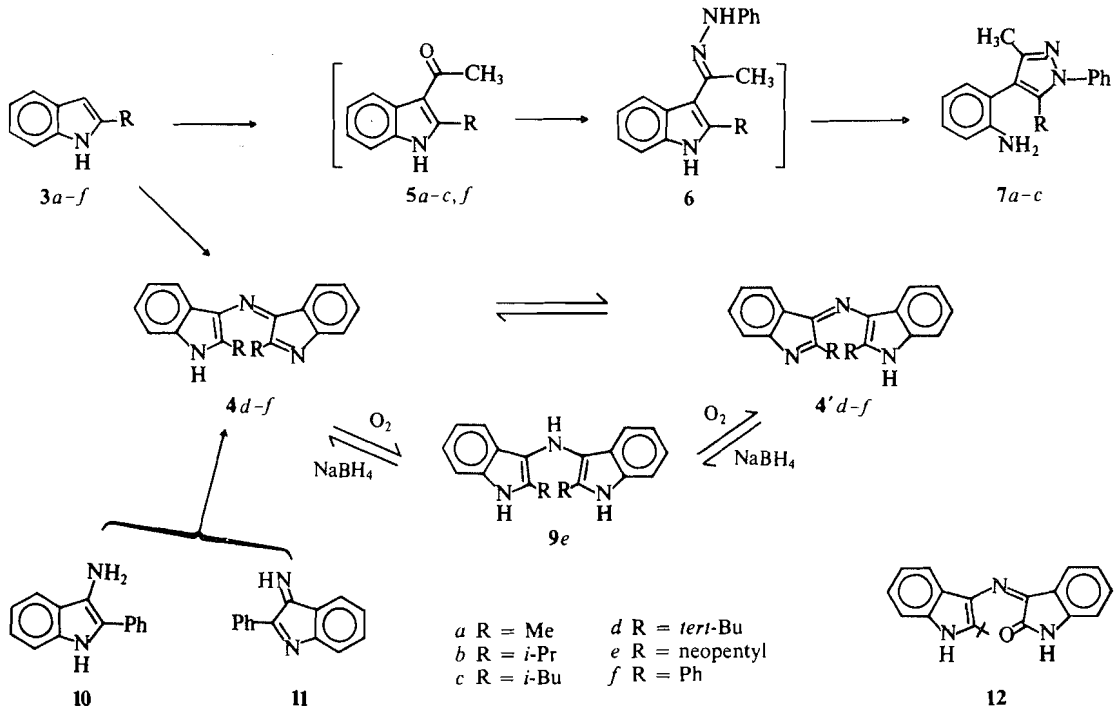

3a-f 5a-c,f 6 7a-c 4d-f 10 11 12

SCHEME 1

presence of some dynamic process(es) was apparent from the ^{13}Cmr spectrum of **4***e* because the sp^2-carbon signals had almost vanished in the baseline.

Although there are several ways in which the blue-purple compounds[4] might have arisen, an important clue to the actual path of its formation (Scheme 2) was provided by the observation that mild acetylation of the crude product from both 2-neopentylindole and 2-phenylindole gave high yields of the corresponding 3-acetamido-2-substituted indole (**16***e* and **16***f*) plus acetanilide.[5] Therefore, the product of the reaction is the 3-amino-2-substituted indole **15** which is slowly air oxidized to the indolenine-imine **17** (a well precedented reaction). Since the air oxidation would require the free base **15**, it is understandable that **15** is not oxidized while protonated in the strongly acidic reaction medium. Then, as soon as **17** is formed, it reacts with a molecule of the amine **15** to produce via **18** the purple compound **4** in another well-precedented reaction.[6] The presumed initial product in the reaction sequence is **14** which would be formed by acid-catalyzed addition of phenylhydrazine to the 2-substituted indole (**3** → **13** → **14**) followed by an elimination reaction in which the N—N bond is broken with aniline as the leaving group. It is recognized that reversible protonation of **3** at C-3 is the faster initial process, but the product-forming cation is apparently **13**, which could arise either by hydride migration in the C-3 protonated cation or else by a slower direct protonation at C-2. A radical mechanism, attack of phenylhydrazine radicals on **3**, is not con-

[4]These compounds are aza-analogues of the cations from **8** and Fischer's rosindoles (3), and as such they would be expected to have similar colours. In acidic methanol, protonation causes considerable change in the uv–visible spectrum causing the purple colour to become a clear blue.

[5]The ^{1}Hmr spectra of both 3-acetamido derivatives show evidence of hindered rotation. For the neopentyl compound **16***e* both the CH_2 group and the acetyl CH_3 group occur as pairs of singlets which only merge at ~130 °C (see Experimental).

[6]In the acid reaction with the *tert*-butyl derivative **3***d* which can lose a relatively stable tertiary cation, at some stage before formation of **4***d*, an intermediate is partially dealkylated and oxidized because the oxindole derivative **12** is formed as well as **4***d*.

Can. J. Chem. Downloaded from www.nrcresearchpress.com by 210.87.254.105 on 09/05/12
For personal use only.

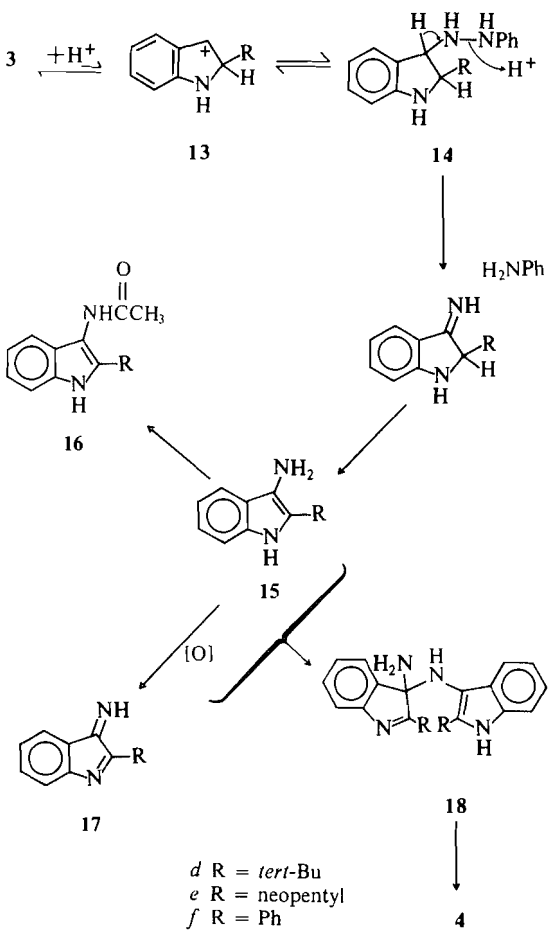

SCHEME 2

sistent with the fact that the same product **15** is formed in the absence of oxygen. Although acid-catalyzed cleavage of hydrazines is not unusual, a close analogy for the **14** → **15** reaction was provided in the present work by the demonstration that two *N*,*N*′-benzylphenylhydrazines (**19**, R = H, CH_3) were cleaved to aniline and imine under the same acidic conditions. The addition–elimination sequence is quite sensitive to acid strength and solvent since reflux of 2-neopentylindole, **3***e*, with phenylhydrazine and acetic acid alone gave no purple compound **4***e*, although reflux of **3***e* with phenylhydrazine, acetic acid, and water did give a small amount of **4***e*. Nor was any **4***e* formed when the reaction with **3***e* was carried out in alcoholic solvents ($PhNHNH_2 \cdot HCl$ – concentrated aqueous HCl – MeOH or $PhNHNH_2 \cdot HCl$ – concentrated aqueous HCl – EtOH).

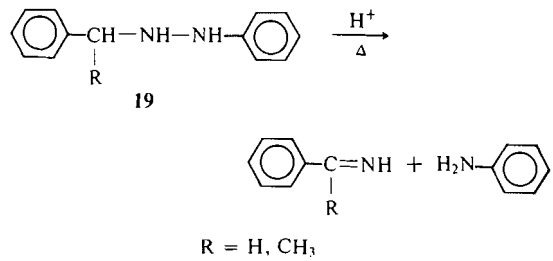

R = H, CH_3

In contrast, 2-alkylindoles bearing smaller alkyl groups (methyl, isopropyl, or isobutyl) did not give any of the intensely coloured product **4**, but instead yielded substituted pyrazoles **7** as the major products. The presence of an aminophenyl group in the pyrazole **7***a* from 2-methylindole was proved by deamination to 3,5-dimethyl-1,4-diphenylpyrazole **7***a* (H for NH_2); the other structures are assigned by analogy. The pyrazole results from electrophilic attack of acetic acid at the 3-position of the indole to produce the 3-acetyl derivative **5** which is then converted into the phenylhydrazone **6**. Subsequently, the phenylhydrazone **6** is transformed into the pyrazole **7** under the acidic conditions as has been observed in the reaction of 3-acylindoles with hydrazine (4). In agreement with this proposed sequence it was found that 3-acetyl-2-methylindole, **5***a*, did form the pyrazole **7***a* under the reaction conditions ($PhNHNH_2 \cdot HCl$ in refluxing glacial HOAc containing concentrated aqueous HCl).

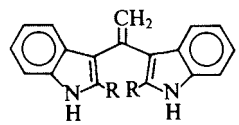

8*a*, *f*

A minor product in the reaction with 2-methylindole was the vinylidene condensation product **8***a* which presumably arises from reaction of 3-acetyl-2-methylindole with another molecule of 2-methylindole; the same compound **8***a* can be prepared by reaction of 2-methylindole with acetyl chloride at room temperature (5). As noted elsewhere (5), 2-phenylindole also gives a similar bis condensation product with boiling acetyl chloride. Although there has been some question about the structures of these compounds (5–8), in the present work they were unambiguously proved to be **8***a* and **8***f* by the changes in

Can. J. Chem. Downloaded from www.nrcresearchpress.com by 210.87.254.105 on 09/05/12
For personal use only.

Can. J. Chem. Downloaded from www.nrcresearchpress.com by 210.87.254.105 on 09/05/12
For personal use only.

the ^{1}Hmr spectra ($C{=}CH_2 \rightarrow CH{-}CH_3$) observed on hydrogenation (see Experimental).

The difference in the reaction of the 2-*tert*-butyl-, 2-neopentyl-, and 2-phenylindoles on the one hand, and the 2-methyl-, 2-isopropyl-, and 2-isobutylindoles on the other hand, can be rationalized in terms of steric hindrance at C-3. In the absence of serious hindrance at C-3, acetylation, which leads to pyrazoles, is the faster reaction. When the rate of acetylation at C-3 is slowed sufficiently by the bulkier 2-substituents, the addition of phenylhydrazine at C-3 (**13** → **14**) (a reaction less subject to steric hindrance), which leads to the bisindolylamine derivatives now becomes the relatively faster reaction. This interpretation is supported by the fact that, in contrast to 2-methylindole, 2-neopentylindole does not react with acetyl chloride at room temperature to yield **8***e*. Moreover, 2-neopentylindole reacts with refluxing acetic anhydride to give the 3-acetylindole more slowly than does 2-methylindole.

Finally, the two reactions of 2-substituted indoles described in this work also constitute side reactions during the preparation of indoles by the Fischer cyclization since the reaction medium is one commonly used for this indole synthesis. Should the extent of these side reactions prove bothersome, they can be suppressed by preforming the phenylhydrazone, by avoiding carboxylic acid solvents, and by avoiding, if possible, the use of such strong acids as hydrochloric. On the other hand, the reaction of certain indoles with phenylhydrazine may be a useful method for preparation of 3-aminoindoles.

Experimental

General methods and reagents are the same as in refs. 1 and 9, except for the following. Accurate mass determinations were carried out on a MAT 311A instrument.

N-Acetylphenylhydrazine, mp 128–130 °C, δ ($CDCl_3$, 60 °C) 1.90 ppm (s, 3H, $CH_3C{=}O$), which was formed as one of the products in each of the reactions described below (tlc evidence), was not isolated and purified from all reactions, and it is not mentioned further.

Reaction of 2-Methylindole with Phenylhydrazine

A solution of 2-methylindole (2.3 g) (10) (bp 115–118 °C/3 torr, δ ($CDCl_3$) 2.30 (s, 3H, CH_3) and 6.13 ppm (b s, 1H, =CH)), $PhNHNH_2 \cdot HCl$ (2.3 g), glacial HOAc (13 ml), and concentrated HCl (2.3 ml) was stirred (magnetic bar) and refluxed for 5 h. After distillation of most of the acid under reduced pressure, the residue was dissolved in ether and washed with 5% aqueous $NaHCO_3$ and with water. The organic layer was dried and concentrated to give a yellowish-brown oil (2.4 g).

The crude product was separated on four preparative layer plates with benzene–ether (90:10) into four bands, one orange and three colourless but visible under uv light. The band moving with the solvent front gave recovered *2-methylindole* as a colourless solid (538 mg).

The orange band at R_f 0.73 gave a pale yellow oil (744 mg) which was rechromatographed on two preparative plates to produce an off-white solid (144 mg). Two recrystallizations from acetone – petroleum ether gave almost colourless *1,1-bis(2-methyl-3-indolyl)ethylene*, **8***a*, (63 mg) which soon acquired a pink colour on standing in air, mp 190–195 °C, identical in all respects (mp, mixture mp, tlc, and spectra) with an authentic specimen (see below).

The colourless band at R_f 0.45 gave a pale yellow oil (1.4 g, 38%) which crystallized on trituration with petroleum ether. Three recrystallizations of 100 mg of the solid from ether – petroleum ether (activated carbon treatment) gave *3,5-dimethyl-1-phenyl-4-(o-aminophenyl)-pyrazole*, **7***a*, as colourless granules (15 mg), mp 82–84 °C, ν_{max} ($CHCl_3$) 3360 and 3440 cm^{-1} (NH_2); λ_{max} (MeOH) 241 (19 000) and 295 nm (4400); δ ($CDCl_3$) 2.20 (s, 3H, CH_3), 2.23 (s, 3H, CH_3), and 3.70 ppm (b s, NH_2, exch. D_2O); *Mol. Wt.* calcd. for $C_{17}H_{17}N_3$ (*m/e*): 263.1421; found (mass spectrometry): 263.1421.

The band at R_f 0.21 gave a colourless solid which after three recrystallizations from acetone – petroleum ether yielded pure *3-acetyl-2-methylindole* (**5***a*, 56 mg), mp 197–200 °C identical in all respects with an authentic specimen (see below).

1,1-Bis(2-methyl-3-indolyl)ethylene, **8***a*

This compound was prepared by the reaction of 2-methylindole (150 mg) and AcCl (1.5 ml) at *room temperature* according to the procedure of Borsche and Groth (5). The crude pinkish solid (135 mg), mp 189–195 °C, was recrystallized twice from acetone – petroleum ether to give off-white crystals of **8***a*, mp 190–195 °C, ν_{max} ($CHCl_3$) 3470 cm^{-1} (NH); λ_{max} (MeOH) 223 (76 000) and 270 nm (25 000); δ ($CDCl_3$) 2.16 (s, 6H, $2CH_3$), 5.50 (s, 2H, vinylogous enamine, $=CH_2$, exch. D_2O), and 7.70 ppm (b s, 2H, NH, exch. D_2O); *m/e* 286 (molecular ion). The reported melting point varies from 192.5 to 208 °C (5, 6, 11).

1,1-Bis(2-methyl-3-indolyl)ethane

To a mixture of 5% Pd/C (15 mg) and MeOH (1 ml) saturated with H_2 was added with stirring a solution of the vinylidene compound **8***a* (30 mg) in MeOH (1 ml). After 6 h the product was isolated by filtration and evaporation. Two recrystallizations from acetone – petroleum ether gave off-white not quite pure crystals (5 mg) of the dihydro compound **8***a* ($CH{-}CH_3$ for $C{=}CH_2$), mp 170–180 °C (dec.), ν_{max} ($CHCl_3$) 3450 cm^{-1} (NH); δ ($CDCl_3$) 1.90 (d, 3H, J = 8 Hz, (CH)—CH_3), 2.23 (s, 6H, 2 indole-CH_3), and 4.62 ppm (q, 1H, J = 8 Hz, CH—(CH_3)); *m/e* 288 (molecular ion). The melting point reported for this compound varies from 191 to 210 °C (6, 12).

1,1-Bis(2-phenyl-3-indolyl)ethylene, **8***f*[7]

This compound was prepared by the reaction of 2-

Can. J. Chem. Downloaded from www.nrcresearchpress.com by 210.87.254.105 on 09/05/12
For personal use only.

phenylindole (80 mg) and AcCl (3 ml) (blue colour) at *reflux* for 4 h according to the procedure of Borsche and Groth (5). The crude product was chromatographed on two preparative plates with benzene – petroleum ether (bp 60–80 °C) (75:25). The band at R_f 0.38 gave an almost colourless solid (32 mg) which after two recrystallizations from acetone – petroleum ether afforded off-white crystals of **8***f*, mp 244–246 °C (lit. (5) 247 °C),[7] ν_{max} (Nujol) 3400 cm^{-1} (NH); λ_{max} (MeOH) 242 (70 000) and 306 nm (30 000); δ ($CDCl_3$, 60 °C) 5.66 (s, 2H, vinylogous enamine, $=CH_2$, exch. D_2O) and 7.54 ppm (b s, 2H, NH, exch. D_2O); *m/e* 410 (molecular ion).

When the hydrochloride corresponding to **8***f*, but prepared by Majer's method (*13*), was treated with aqueous NaOH the vinylidene compound **8***f* was regenerated.

1,1-Bis(2-phenyl-3-indolyl)ethane

The hydrogenation of **8***f* (18 mg) was carried out as for the 2-methyl analogue **8***a* except that tetrahydrofuran was used as solvent. The crude product was chromatographed on a thick plate (10 g of silica gel) with benzene – petroleum ether (75:25). The band at R_f 0.47 yielded colourless oily **8***f* ($CHCH_3$ for $C{=}CH_2$) (12 mg), δ ($CDCl_3$) 1.88 (d, 3H, J = 8 Hz, (CH)—CH_3) and 4.94 ppm (q, 1H, J = 8 Hz, CH—(CH_3)); *m/e* 412 (molecular ion).

Reaction of 3-Acetyl-2-methylindole with Phenylhydrazine

3-Acetyl-2-methylindole, **5***a*, was prepared by refluxing 2-methylindole (200 mg) in Ac_2O (3 ml) for 4 h according to the procedure of Borsche and Groth (5). The crude product was recrystallized thrice (activated carbon treatment) from $CHCl_3$ – petroleum ether (bp 60–80 °C) to give colourless crystals (30 mg), mp 198–200 °C (lit. (14) 200 °C), ν_{max} (Nujol) 3100–3200 (b, NH) 1630 (sh), and 1615 cm^{-1} (C=O); λ_{max} (MeOH) 213 (44 000), 240 (18 000), 265 (14 000), and 299 nm (14 000); δ ($CDCl_3$, 60 °C) 2.62 (s, 3H, CH_3 or $CH_3C{=}O$) and 2.72 ppm (s, 3H, $CH_3C{=}O$ or CH_3); *m/e* 173 (molecular ion).

A solution of 3-acetyl-2-methylindole (**5***a*, 40 mg), $PhNHNH_2 \cdot HCl$ (40 mg), glacial HOAc (1 ml), and concentrated HCl (0.2 ml) was refluxed for 5 h. After distillation of the acid at reduced pressure, the residue was dissolved in ether and washed with 5% aqueous $NaHCO_3$ and water. Evaporation of the dried ether solution left an amber oil (42 mg) which was chromatographed on a thick layer plate (10 g of silica gel) in benzene–ether (65:35). The band at R_f 0.46 yielded *3,5-dimethyl-1-phenyl-4-(o-aminophenyl)pyrazole*, **7***a*, as a colourless oil (20 mg) identical (^{1}Hmr and ir spectra and tlc) with the pyrazole obtained from the reaction of 2-methylindole and $PhNHNH_2 \cdot HCl$ in HOAc.

When MeOH was substituted for HOAc in this reaction, the same compound **7***a* was obtained.

[7]In ref. 5 the incorrect structure **i** was assigned to this compound.

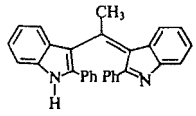

i

Deamination of 3,5-Dimethyl-1-phenyl-4-(o-aminophenyl)-pyrazole, 7a

To a stirred (magnetic bar) solution of the amino compound **7***a* (125 mg) in concentrated HCl (2 ml) at 5 °C was added a solution of $NaNO_2$ (250 mg) in water (2 ml) during 5 min. After 0.5 h at 5 °C, H_3PO_2 (50%, 1 ml) was added, and the mixture was stirred at 0 °C for 6 h., then neutralized with NaOH pellets, and finally extracted with ether. The crude product (100 mg) from the water-washed and dried ether layer was chromatographed on a preparative layer plate in benzene–ether (75:25). The band at R_f 0.68 furnished *3,5-dimethyl-1,4-diphenylpyrazole* as an almost colourless oil (85 mg), ir no NH absorption; λ_{max} (MeOH), 252 nm (18 000); δ ($CDCl_3$) 2.20 (s, 3H, CH_3) and 2.28 ppm (s, 3H, CH_3); *m/e* 248 (molecular ion). The analytical sample was evaporatively distilled at 155 °C/0.1 torr. *Anal.* calcd. for $C_{17}H_{16}N_2$ (248.3): C 82.22, H 6.49, N 11.28; found: C 82.08, H 6.32, N 11.46.

Reaction of 2-Isopropylindole with Phenylhydrazine

A solution of 2-isopropylindole (2.0 g) (15) (bp 118–120 °C/0.8 torr, mp 70–73 °C (lit. (15) 73–74 °C), δ ($CDCl_3$) 1.23 (d, 6H, J = 7 Hz, $(CH_3)_2CH$), 3.00 (septet, 1H, J = 7 Hz, $CHMe_2$), and 6.11 ppm (b s, 1H, =CH)), $PhNHNH_2 \cdot HCl$ (2.0 g), glacial HOAc (12 ml), and concentrated HCl (1.5 ml) was stirred (magnetic bar) and refluxed for 5 h. Work-up as for the reaction with 2-methylindole gave a brown oily solid (2.3 g) which was chromatographed on four preparative plates with benzene–ether (90:10). The band at the solvent front gave recovered *2-isopropylindole*. The band at R_f 0.23 gave an almost colourless oil (252 mg) which solidified. Three recrystallizations from ether – petroleum ether (activated carbon treatment) gave colourless crystals of *3-methyl-5-isopropyl-1-phenyl-4-(o-aminophenyl)pyrazole*, **7***b*, mp 122–125 °C, ν_{max} ($CHCl_3$) 3380 and 3460 cm^{-1} (NH_2); λ_{max} (MeOH) 231 (22 000) and 290 nm (4600); δ ($CDCl_3$) 1.01 (d, 3H, J = 6 Hz, CH_3—($CHCH_3$)), 1.12 (d, 3H, J = 6 Hz, (CH_3CH)—CH_3), 2.00 (s, 3H, CH_3), 2.90 (septet, 1H, J = 6 Hz, CH—(CH_3)$_2$), and 3.50 ppm (b s, 2H, NH_2, exch. D_2O); *m/e* 291 (molecular ion). *Anal.* calcd. for $C_{19}H_{21}N_3$ (291.4): C 78.32, H 7.26, N 14.42; found: C 78.15, H 7.31, N 14.47.

Reaction of 2-Isobutylindole with Phenylhydrazine

A solution of 2-isobutylindole (1.8 g) (16) (bp 120–122 °C/0.7 torr; δ ($CDCl_3$) 0.93 (d, 6H, J = 7 Hz, $(CH_3)_2CH$)), 2.20 (septet, 1H, J = 7 Hz, CH), 2.57 (d, 2H, J = 6 Hz, (CH)—CH_2), and 6.17 ppm (b s, 1H, =CH)), $PhNHNH_2 \cdot HCl$ (1.8 g), glacial HOAc (12 ml), and concentrated HCl (1.8 ml) was stirred (magnetic bar) and refluxed for 5 h. Work-up as for the reaction with 2-methylindole gave a yellowish brown oil (1.7 g) which was chromatographed on four preparative layer plates in benzene–ether (90:10). The band at R_f 0.82 gave recovered *2-isobutylindole* as a colourless oil (1.1 g). The faintly purple band at R_f 0.32 gave a viscous oil (630 mg) which soon turned pink in the air. Rechromatography of this oil on two preparative plates gave *3-methyl-5-isobutyl-1-phenyl-4-(o-aminophenyl)pyrazole*, **7***c*, as an amber oil (416 mg) which failed to crystallize, ν_{max} ($CHCl_3$) 3380 and 3460 cm^{-1} (NH_2); λ_{max} (MeOH) 240 (18 000) and 295 nm (3800); δ ($CDCl_3$) 0.58 (d, 6H, J = 6 Hz, $(CH_3)_2CH$), 1.60 (m, 1H, CH), 2.17 (s, 3H,

Can. J. Chem. Downloaded from www.nrcresearchpress.com by 210.87.254.105 on 09/05/12
For personal use only.

CH_3), 2.55 (d, 2H, (CH)CH_2), and 3.60 ppm (b s, 2H, NH_2, exch. D_2O); *m/e* 305 (molecular ion).

Acetylation of the aminophenyl group of **7***c* (50 mg) with Ac_2O (0.3 ml) and pyridine (1 ml) at room temperature for 3 h gave a crude product which on thick layer chromatography in benzene–ether (75:25) yielded a colourless solid (35 mg). Two recrystallizations from ether – petroleum ether (activated carbon treatment) gave colourless granules (30 mg) of the *monoacetyl derivative* **7***c*, (NHAc for NH_2), mp 123–125 °C, ν_{max} ($CHCl_3$) 3360 (NH) and 1675 cm^{-1} (amide C=O); λ_{max} (MeOH) 246 nm (21 000); δ ($CDCl_3$) 0.59 (d, 6H, J = 6 Hz, (CH_3)$_2$-CH), 2.05 (s, 3H, CH_3C=O or =CCH_3), 2.13 (s, 3H, =CCH_3 or CH_3C=O), and 2.5 ppm (m, 3H, CH_2 and CH); *m/e* 347 (molecular ion). *Anal.* calcd. for $C_{22}H_{25}N_3O$ (347.5): C 76.05, H 7.25, N 12.09; found: C 75.93, H 7.11, N 12.25.

Reaction of Pinacolone with Phenylhydrazine

A solution of pinacolone (2.5 g), $PhNHNH_2 \cdot HCl$ (2.5 g), and glacial HOAc (15 ml) was stirred (magnetic bar) and refluxed for 5 h. Work-up as for the reaction with 2-methylindole gave the crude product (1.8 g) which became bluish purple on standing open to the air for 1 day. The products were separated by chromatography on four preparative plates in benzene–ether (90:10). The pale yellow band at R_f 0.91 gave oily *2-tert-butylindole* (490 mg), δ ($CDCl_3$) 1.30 (s, 9H, *tert*-Bu), and 6.13 ppm (s, 1H, =CH), NH not apparent.

The blue band at R_f 0.62 gave a deep bluish-purple solid (111 mg). Two recrystallizations from $CHCl_3$ – petroleum ether (bp 60–80 °C) gave deep blue granules (42 mg) of *2-tert-butyl-3-(2'-tert-butyl-3'H-indol-3'-ylidene)aminoindole*, **4***d*, mp 235–250 °C (dec. with partial sublimation), ν_{max} ($CHCl_3$) 3470 cm^{-1} (NH); λ_{max} (MeOH) 231 (44 000), 260 (12 000), 340 (7600), and 550 nm (10 000); λ_{max} (MeOH + 2 drops of 0.1 *N* HCl) 218 (36 000), 285 (14 000), 298 (12 000), and 615 nm (18 000); δ ($CDCl_3$) 1.55 ppm (s, 18H, 2*tert*-Bu); *Mol. Wt.* calcd. for $C_{24}H_{27}N_3$: 357.2204; found (mass spectrometry): 357.2202.

The reddish brown band on the base line of the preparative plates yielded a brick red solid (230 mg). Rechromatography on silica gel in benzene–ether (50:50) and then on alumina plates in ether–MeOH (97.5:2.5) gave a purple solid (43 mg) which after two recrystallizations from $CHCl_3$ – petroleum ether (bp 60–80 °C) furnished the pure purple *oxindole derivative* **12**, mp 270–280 °C (dec. with sublimation), ν_{max} (Nujol) 3300–3100 (NH) and 1710 cm^{-1} (amide C=O); λ_{max} (MeOH) 230 (55 000), 253 (21 000), 290 (12 000), and 510 nm (7000); δ (DMSO-d_6) 1.46 (s, 9H, *tert*-Bu), 10.78 (b s, 1H, NH, exch. D_2O), and 11.20 ppm (b s, 1H, NH, exch. D_2O); *m/e* 317 (molecular ion). *Anal.* calcd. for $C_{20}H_{19}N_3O$ (317.4): C 75.69, H 6.03, N 13.24; found: C 75.97, H 6.44, N 12.56.

When $NaBH_4$ (10 mg) was added to a solution of oxindole **12** (4 mg) in MeOH (0.5 ml) the purple colour faded (presumably due to reduction of the imine) and then reappeared on standing (presumably air oxidation). Oxindole **12** (3 mg) was recovered from the solution.

A mixture of the di-*tert*-butyl bluish-purple compound **4***d* (3 mg), $PhNHNH_2 \cdot HCl$ (3 mg), glacial HOAc (0.5 ml), and concentrated HCl (2 drops) was stirred and refluxed for 5 h. Work-up gave a yellow oil (3.5 mg) which on standing in air overnight became purple. Thin layer chromatography in benzene–ether (50:50) showed the complete absence of starting material **4***d* and a purple spot having the same R_f as the mono-*tert*-butyloxindole **12**.

2-Neopentylindole, **3***e*

A solution of 4,4-dimethyl-2-pentanone (230 mg) and $PhNHNH_2$ (200 mg) in MeOH (2 ml) was refluxed for 0.5 h. After distillation of volatile material at reduced pressure, BF_3 etherate (2 ml) was added to the residual phenylhydrazone, and the solution was refluxed for 3 h. The BF_3 etherate was removed at reduced pressure, and the residue was dissolved in ether. The ethereal solution was washed with 5% aqueous $NaHCO_3$ and water. Concentration of the dried solution left a yellow oily solid (337 mg) whose ^{1}Hmr spectrum showed it to be free of **1**. Chromatography on a preparative plate in benzene–petroleum ether (bp 60–80 °C) (75:25) gave a band at R_f 0.65 which yielded a colourless solid (216 mg, 63%). Two recrystallizations from ether – petroleum ether gave colourless crystals of pleasant smelling *2-neopentylindole*, **3***e*, mp 102–104 °C, ν_{max} ($CHCl_3$) 3450 cm^{-1} (NH); λ_{max} (MeOH) 220 (42 000), 280 (10 000), and 288 nm (8500); δ ($CDCl_3$) 0.98 (s, 9H, *tert*-Bu), 2.54 (s, 2H, CH_2), and 6.34 ppm (b s, 1H, =CH); *m/e* 187 (molecular ion). *Anal.* calcd. for $C_{13}H_{17}N$ (187.3): C 83.37, H 9.15; found: C 83.22, H 9.12.

Reaction of 2-Neopentylindole with Phenylhydrazine

A solution of 2-neopentylindole (50 mg), $PhNHNH_2 \cdot HCl$ (50 mg), glacial HOAc (2 ml), and concentrated HCl (0.2 ml) was stirred (magnetic bar) and refluxed for 5 h. Work-up as for the 2-methylindole reaction gave a yellowish brown oil (85 mg) which turned permanganate-purple on standing in air overnight.[8] Chromatography on a preparative plate (10 g of silica gel) in benzene–ether (90:10) gave a colourless band (R_f 0.82) of recovered 2-neopentylindole, (**3***e*, 38 mg) and a purple band (R_f 0.43) of oily solid (12 mg). Recrystallization from $CHCl_3$–petroleum ether (bp 60–80 °C) yielded permanganate-purple granules (7 mg) of *2-neopentyl-3-(2'-neopentyl-3'H-indol-3'-ylidene)aminoindole*, **4***e*,[9] mp 201–203 °C, ν_{max} ($CHCl_3$) 3440 cm^{-1} (NH); λ_{max} (MeOH) 225 (67 500), 260 (22 500), 340 (7500), and 530 nm (15 000); λ_{max} (MeOH + 2 drops 0.1 *N* HCl) 223 (63 000), 283 (22 000), 295 (19 000), and 590 nm (33 000); δ ($CDCl_3$) 1.04 (s, 18H, 2 *tert*-Bu) and 2.92 ppm (s, 4H, $2CH_2$); *m/e* 385 (molecular ion); osmometric mol. wt. ($CHCl_3$) 390. *Anal.* calcd. for $C_{26}H_{31}N_3$ (385.6): C 81.00, H 8.10, N 10.90; found: C 80.77, H 8.13, N 10.47.

Addition of $NaBH_4$ to a solution of **4***e* in MeOH discharged the purple colour, but it reappeared on standing. Work-up gave back the purple **4***e*.

[8]If the distilled yellowish brown oily product is sealed in a tube away from oxygen, there is no change in colour until the tube is opened, whereupon it becomes purple within a few hours.

[9]One of the authors found that the compound caused irritation of the nasal mucous membrane even in quite low concentration.

Can. J. Chem. Downloaded from www.nrcresearchpress.com by 210.87.254.105 on 09/05/12
For personal use only.

When **3***e* was refluxed with $PhNHNH_2$ in glacial HOAc, the product after work-up did not turn purple on exposure to air.

From a reaction of 4,4-dimethyl-2-pentanone (2.5 g) with $PhNHNH_2 \cdot HCl$ (2.5 g) in glacial HOAc (15 ml) was obtained after work-up and distillation 900 mg of indole fraction which on standing in petroleum ether (bp 60–80 °C) deposited the purple compound **4***e* and also acetanilide.

Acetylation of 2-Neopentylindole–Phenylhydrazine Reaction Product

The crude yellowish product from reaction of 2-neopentylindole (**3***e*, 100 mg) and $PhNHNH_2 \cdot HCl$ (100 mg) carried out as described in the previous experiment was immediately acetylated at room temperature with Ac_2O (1 ml) and pyridine (1 ml) for 1.5 h under a nitrogen atmosphere. Evaporation of Ac_2O and pyridine at room temperature (0.1 torr) left a pale yellow oily solid (103 mg) which after washing with ether and two recrystallizations (activated carbon treatment) from $CHCl_3$ – petroleum ether (bp 60–80 °C) gave 22 mg of colourless plates of *3-acetamido-2-neopentylindole*, **16***e*, mp 199–201 °C, ν_{max} (Nujol) 3200–3600 (NH) and 1650 cm^{-1} (amide C=O); λ_{max} (MeOH) 222 (33 000), 281 (8600), and 288 nm (7600); δ ($CDCl_3$) 0.94 and 1.00 (both s, 9H total, CMe_3 of two rotamers), 1.62 (s, 1H, NH, exch. D_2O), 1.83 and 2.20 (both s, 3H total, CH_3C=O of two rotamers), and 2.44 and 2.57 ppm (both s, 2H total, CH_2-*tert*-Bu of two rotamers); in pyridine solution all three sets of double peaks had merged by 120 °C; *m/e* 244 (molecular ion); osmometric mol. wt. ($CHCl_3$) 260, 268. *Anal.* calcd. for $C_{15}H_{20}N_2O$ (244.3): C 73.74, H 8.25; found: C 73.49, H 8.32.

The mother liquors from the above purification were chromatographed on a silica gel thick plate developed with benzene–ether (75:25). The uv visible band at R_f 0.87 gave 10 mg of recovered **3***e*, and the uv visible band at R_f 0.22 furnished 58 mg of oily solid which was washed with ether. Two recrystallizations from $CHCl_3$ – petroleum ether (bp 60–80 °C) gave 17 mg of colourless plates of **16***e* (to bring the total yield to 34%),[10] mp 198–200 °C.

The mother liquors from the above two recrystallizations were chromatographed on a silica gel plate developed three times with benzene–ether (75:25). The band (under uv) at R_f 0.58 gave 27 mg of solid which was recrystallized twice (activated carbon treatment) from ether – petroleum ether to afford 14 mg (22%) of colourless *acetanilide*, mp 110–112 °C, identical with an authentic specimen.

Reaction of 2-Phenylindole with Phenylhydrazine

A solution of 2-phenylindole (165 mg) (17) (mp 185–187 °C, δ ($CDCl_3$) 6.75 ppm (b s, 1H, =CH)), $PhNHNH_2 \cdot HCl$ (165 mg), glacial HOAc (2.5 ml), and concentrated HCl (0.5 ml) was stirred (magnetic bar) and refluxed for 5 h. Work-up as for the reaction with 2-methylindole gave a yellowish-brown oily solid (200 mg) which turned blue on standing in air for 2 days. Chromatography on two preparative plates in benzene–ether (90:10) gave two main bands. The band at the solvent front gave recovered *2-phenylindole*. The blue band at R_f 0.41 was extracted and rechromatographed on two preparative plates in benzene–ether (90:10, four developments). The blue band at R_f 0.60 yielded a solid (66 mg, 31%) which was recrystallized thrice from aqueous pyridine to furnish blue-black crystals of *2-phenyl-3-(2′-phenyl-3′H-indol-3′-ylidene)aminoindole*, **4***f*, mp 320–330 °C (dec.) (lit. (18) 338 °C); ν_{max} (Nujol) 3100 cm^{-1} (b, NH); λ_{max} (MeOH) 241 (40 000), 260 (40 000), 330 (18 000), and 570 nm (12 000); λ_{max} (MeOH + 2 drops of 0.1 *N* HCl) 230 (43 000), 291 (36 000), 360 (15 000), and 645 nm (27 000); *Mol. Wt.* calcd. for $C_{28}H_{19}N_3$: 397.1578; found (mass spectroscopy): 397.1573.

2-Phenyl-3-(2′-phenyl-3′H-indol-3′-ylidene)aminoindole, **4***f*

(*a*) An authentic sample of **4***f* was prepared by the method of Schmitt and co-workers (18*a*). 3-Oximino-2-phenylindole (19) was reduced (20) with Zn and concentrated HCl to 3-amino-2-phenylindole (**10**, 50 mg) which was then condensed with 3-imino-2-phenylindolenine (**11**, 50 mg) (19) in glacial HOAc (1 ml) at room temperature for 1h. The greenish-blue solution was concentrated under vacuum and the residue dissolved in $CHCl_3$. Evaporation of the washed (5% aqueous $NaHCO_3$, water) and dried $CHCl_3$ solution left a blue solid (78 mg). Two recrystallizations from $CHCl_3$ followed by two more recrystallizations from aqueous pyridine gave blue-black crystals of **4***f*, mp 320–330 °C (dec.) identical in all respects (mp, mixture mp, ir, uv, ^{1}Hmr) with the material from the reaction of 2-phenylindole and $PhNHNH_2 \cdot HCl$.

(*b*) Compound **4***f* was also prepared by air oxidation of 3-amino-2-phenylindole alone. A solution of **10** (25 mg) in $CHCl_3$ (5 ml) was stirred in an open vessel for 2 days. Chromatography of the dark product on a silica gel plate (10 g) with benzene–ether (95:5) gave a dark blue band from which was isolated 6 mg of crystals of **4***f* identical (tlc, mp, mixture mp, and ir) with the material prepared in (*a*) and in the previous experiment.

Acetylation of 2-Phenylindole–Phenylhydrazine Reaction Product

The crude product from reaction of 2-phenylindole (100 mg) and $PhNHNH_2 \cdot HCl$ (100 mg) carried out as described above was immediately acetylated at room temperature as above for the neopentylindole reaction. The partially solid yellow product was chromatographed on a silica gel plate developed with benzene–ether (50:50). The uv–visible band at R_f 0.89 gave 10 mg of recovered **3***f*, and the uv–visible band at R_f 0.42 gave 66 mg of colourless oily solid. Two recrystallizations (activated carbon treatment) from $CHCl_3$ – petroleum ether (bp 60–80 °C) gave 36 mg of almost colourless crystals of *3-acetamido-2-phenylindole*, **16***f*, mp 198–202 °C, identical with the authentic sample prepared as described below. Thin layer chromatography of the recrystallization mother liquors revealed a spot with the same R_f as acetanilide.

An authentic specimen of **16***f* was prepared by acetylation at room temperature of 25 mg of **10***f* prepared as described in ref. 19. Thick layer chromatography and recrystallization from $CHCl_3$ – petroleum ether (bp 60–80 °C) gave 8 mg of colourless crystals of *3-acetamido-*

[10]The actual yield is considerably higher because the only compounds detected by tlc and ^{1}Hmr in the crude product were **16***e* and acetanilide.

Can. J. Chem. Downloaded from www.nrcresearchpress.com by 210.87.254.105 on 09/05/12
For personal use only.

2-phenylindole, **16***f*, mp 198–200 °C (lit. (21) mp 202–203 °C), ν_{max} ($CHCl_3$) 3300–3500 (NH) and 1670 cm^{-1} (amide (C=O); λ_{max} (MeOH) 222 (33 000), 280 (8800), and 288 nm (7900); δ ($CDCl_3$) 1.79 and 2.21 (both s, total 3H, $CH_3C{=}O$ of two rotational isomers; both peaks broaden as the temperature is raised) and 6.80 ppm (b, 1H, NH, exch. D_2O); *m/e* 250 (molecular ion).

From reaction of a vacuum-degassed mixture of **3***f* (50 mg), $PhNHNH_2 \cdot HCl$ (50 mg), HOAc (1 ml), and concentrated aqueous HCl (0.2 ml) in a sealed tube at 150 °C for 5 h was obtained 37 mg of **16***f* by acetylation and chromatography.

*Acidic Cleavage of N,N'-Benzylphenylhydrazine (**19**, R = H)*

A solution of benzaldehyde phenylhydrazone (300 mg) in EtOAc (8 ml) was hydrogenated at atmospheric pressure in the presence of 5% palladium-on-carbon catalyst (50 mg) for 1.5 h. Filtration and evaporation of solvent left 300 mg of faintly yellow liquid *N,N'*-benzylphenylhydrazine which was dissolved in HOAc (2 ml) – concentrated HCl (0.5 ml) and refluxed for 5 h. The reaction mixture was divided into two equal portions which were treated as in (*a*) and (*b*) below.

(*a*) After neutralization of the acid with aqueous NaOH, the mixture was extracted with ether. The organic layer was washed with water, dried, and concentrated at atmospheric pressure. The residual oil was acetylated at room temperature with Ac_2O (1.5 ml) and pyridine (1.5 ml) for 1.5 h. The oil left after distillation of Ac_2O and pyridine was chromatographed on a silica gel plate developed with benzene–ether (50:50). The band (under uv) at R_f 0.32 gave 10 mg (~100% based on unreacted starting material) of *acetanilide*, mp 110–112 °C after two recrystallizations from ether – petroleum ether, identical with an authentic specimen. The band (under uv) at R_f 0.68 furnished 170 mg of *N-acetyl-N-benzyl-N'-phenylhydrazine*, mp 88–90 °C after two recrystallizations from ether – petroleum ether, which was identical with an authentic specimen prepared by acetylation (Ac_2O–pyridine) of the hydrogenation product of benzaldehyde phenylhydrazone, mp 89–90 °C (lit. (22) mp 91 °C), ν_{max} ($CHCl_3$) 3340 (NH) and 1655 cm^{-1} (amide C=O); δ ($CDCl_3$) 2.18 (s, 3H, $CH_3C{=}O$), 4.72 (very broad, 2H, $PhCH_2N$, sharpens to s at 80 °C), and 5.60 ppm (s, 1H, NH, exch. D_2O); *m/e* 240 (molecular ion).

(*b*) The other half of the reaction mixture was treated with acidic 2,4-dinitrophenylhydrazine solution in MeOH. The MeOH was evaporated and the residue triturated with water. The resulting solid was filtered and chromatographed on a silica gel plate developed with benzene. The yellow band at R_f 0.74 gave 6 mg (40% based on unreacted starting material) of *benzaldehyde-2,4-dinitrophenylhydrazone*, mp 238–240 °C after two recrystallizations from $CHCl_3$ – petroleum ether (bp 60–80 °C), identical with an authentic specimen.

*Acidic Cleavage of N,N'-α-Phenylethylphenylhydrazine (**19**, R = CH_3)*

Acetophenone phenylhydrazone (300 mg, mp 102–104 °C (lit. (23) mp 105 °C) was hydrogenated in EtOAc as described above for benzaldehyde phenylhydrazone. The resulting phenylhydrazine (**19**, R = CH_3) (δ ($CDCl_3$) 1.36 (d, 3H, J = 6 Hz), 3.98 (q, 1H, J = 6 Hz), and 3.4–4.2 ppm (broad lump, 2NH)) was refluxed with acid and worked-up as described for the *N,N'*-benzylphenylhydrazine reaction.

(*a*) From the acetylated portion of the hydrolysate was obtained 10 mg of *acetanilide*, mp 110–112 °C after one recrystallization from ether – petroleum ether, and 45 mg of *acetyl N,N'-α-phenylethylphenylhydrazine*, mp 114–115 °C after three recrystallizations from ether – petroleum ether, identical with an authentic specimen, mp 114–116 °C (lit. (24), mp 118 °C); δ ($CDCl_3$, 80 °C) 1.47 (d, 3H, J = 6 Hz) and 5.94 ppm (q, 1H, J = 6 Hz); *m/e* 254 (molecular ion).

(*b*) From the other half of the hydrolysate was obtained, after one recrystallization from $CHCl_3$ – petroleum ether (bp 60–80 °C), 13 mg of *acetophenone-2,4-dinitrophenylhydrazone*, mp 245–247 °C (lit. (25) mp 248–249 °C).

Acknowledgements

We would like to thank Dr. S. K. Wong (U.W.O.), Dr. R. J. Highet (N.I.H., U.S.A.), and Mr. D. Hairsine (U.W.O.) for the mass spectra, Ms. Heather Schroeder for the 100 MHz ^{1}Hmr spectra, and the National Research Council of Canada for financial assistance.

1. V. Dave and E W. Warnhoff. Can. J. Chem. This issue.
2. R. E. Lyle and L. Skarlos. Chem. Commun. 644 (1966).
3. E. Fischer and P. Wagner. Ber. **20**, 815 (1887).
4. C. Alberti. Gazz. Chim. Ital. **87**, 729 (1958); **87**, 736 (1958); **87**, 751 (1958); **87**, 762 (1958).
5. W. Borsche and H. Groth. Ann. **549**, 238 (1941).
6. A. K. Kiang and F. G. Mann. J. Chem. Soc. 594 (1953).
7. J. E. Saxton. J. Chem. Soc. 3592 (1952).
8. C. T. Bahner, H. Kinder, and L. Gutman. J. Med. Chem. **8**, 397 (1965).
9. V. Dave and E. W. Warnhoff. Can. J. Chem. **49**, 1911 (1971).
10. C. F. H. Allen and J. Van Allan. Org. Syn., Col. Vol. **3**, 597 (1967).
11. A. Angeli and G. Marchetti. Gazz. Chim. Ital. **64**, 359 (1934).
12. E. Fischer. Ann. **242**, 372 (1887).
13. J. R. Majer. Tetrahedron, **9**, 111 (1960).
14. K. T. Potts. J. Org. Chem. **26**, 4719 (1961).
15. H. Illy and L. Funderburk. J. Org. Chem. **33**, 4283 (1968).
16. M. A. Verley and J. Beduwe. Bull. Soc. Chim. Fr. **37**, 189 (1925).
17. W. E. Noland, K. R. Rush, and L. R. Smith. J. Org. Chem. **31**, 65 (1966).
18. (*a*) J. Schmitt, M. Langlois, and C. Perrin. Bull. Soc. Chim. Fr. 1234 (1969); (*b*) M. Colonna, P. Bruni, and G. Guerra. Gazz. Chim. Ital. **99**, 3 (1969).
19. R. J. Richman and A. Hassner. J. Org. Chem. **33**, 2548 (1968).

20. H. P. PATEL and J. M. TEDDER. J. Chem. Soc. 4593 (1963).
21. HUANG-HSINMIN and F. G. MANN. J. Chem. Soc. 2911 (1949).
22. O. SCHLENK. J. Prakt. Chem. **78**, 49 (1908).
23. E. FISCHER. Ber. **17**, 576 (1884).
24. P. GRAMMATICAKIS. C.R. Acad. Sci. Paris Ser. C, **204**, 1262 (1937).
25. Y. R. NAVES. Helv. Chim. Acta, **32**, 2171 (1949).

Can. J. Chem. Downloaded from www.nrcresearchpress.com by 210.87.254.105 on 09/05/12
For personal use only.

Syntheses, structural and conformational assignments, and conversions of pyridine and triazolopyridine nucleosides[1]

BRIAN MAURICE LYNCH[2] AND SURESH CHANDRA SHARMA[3]
Organic Chemistry Laboratory, Saint Francis Xavier University, Antigonish, Nova Scotia B0H 1C0

Received July 31, 1975

BRIAN MAURICE LYNCH and SURESH CHANDRA SHARMA. Can. J. Chem. **54**, 1029 (1976).

Regioselective and stereoselective routes to 2- and/or 4-substituted *vic*-triazolo(4,5-*b*)pyrid-5-ones have been established, and series of 4- and 2-β-D-ribofuranosyl derivatives have been prepared as candidate substrates for, and potential inhibitors of, the enzymes of polynucleotide synthesis. Structural assignments were made by comparison of spectroscopic properties (pmr, uv) with those of appropriate model compounds, and on the bases of proton chemical shift and coupling constant patterns in the ribose moieties, it is proposed that 4-β-D-ribofuranosyl-*vic*-triazolo(4,5-*b*)pyrid-5-ones adopt conformations with 'high *anti*' sugar–base torsional angles. A facile ribofuranose → ribopyranose conversion is observed with a 2-β-D-ribofuranosyl-*vic*-triazolo(4,5-*b*)pyrid-5-one.

BRIAN MAURICE LYNCH et SURESH CHANDRA SHARMA. Can. J. Chem. **54**, 1029 (1976).

On a établi des méthodes régiosélectives et stéréosélectives pour conduire aux *vic*-triazolo-(4,5-*b*) pyridones-5 substituées en positions 2 et/ou 4; on a préparé des séries de dérivés de β-D-ribofurannosyles substitués en positions 2 et 4 comme substrats possibles pour, et comme inhibiteur potentiel de la synthèse, des enzymes responsables de la synthèse de polynucléotides. On a fait les attributions de structure par comparaison des propriétés spectroscopiques (rmp et uv) avec celles de composés modèles appropriés; sur la base des déplacements chimiques et des patrons des constantes de couplage dans la portion ribose on propose que la β-D-ribofurannosyl-4 *vic*-triazolo(4,5-*b*) pyridones-5 adopte une conformation avec des angles de torsion sucre–base 'élevés en *anti*'. Avec la β-D-ribofurannosyle-2 *vic*-triazolo(4,5-*b*) pyridone-5 on observe une conversion facile du ribofurannose en ribopyrannose.

[Traduit par le journal]

Introduction

Certain pyridine (3-deazapyrimidine) nucleosides exhibit antibacterial and antileukemic activities (1, 2), and bicyclic unnatural nucleoside species with the sugar moiety in the six-membered ring (including nucleosides of oxazolo-(4,5-*b*)pyrimidines (3), pyrrolo(2,3-*d*)pyrimidines (4), thiazolo(5,4-*d*)pyrimidines (5), pyrido(2,3-*d*)-pyrimidines (6), and quinazolines (7)) have shown significant biochemical and chemotherapeutic activities.

The present work forms part of a program of exploration of stereospecific and regioselective syntheses of unnatural nucleosides, and is concerned with each of the above general classes, where appropriately substituted pyridines or pyridine nucleosides are used as precursors of

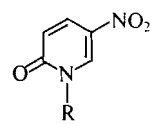

1

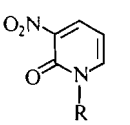

2

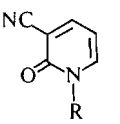

3

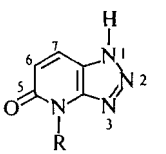

4

a R = H
b R = β-D-ribofuranosyl
c R = β-D-(2,3,5-tri-*O*-acetylribofuranosyl)
d R = β-D-(2,3,5-tri-*O*-benzoylribofuranosyl)
e R = CH_3
f R = $CH_2 \cdot C_6H_5$

4-substituted *vic*-triazolo(4,5-*b*)pyridines, and the species obtained are subjected to further alkylations and/or ribosylations. The primary objective of this synthetic program is to obtain a set of positionally isomeric nucleosides with markedly

[1]Presented in part at the 54th Canadian Chemical Conference of the Chemical Institute of Canada, Halifax, Nova Scotia, June, 1971.

[2]Author to whom requests for reprints should be addressed.

[3]Professional Research Associate.

Can. J. Chem. Downloaded from www.nrcresearchpress.com by 210.87.254.40 on 09/05/12
For personal use only.

Can. J. Chem. Downloaded from www.nrcresearchpress.com by 210.87.254.40 on 09/05/12
For personal use only.

different geometrical and steric constraints on preferred sugar–base torsional angles, providing test compounds for the postulated restriction of the enzymes of polynucleotide synthesis to nucleoside phosphate substrates possessing *anti* conformations (8–11).

Results and Discussion

(a) Syntheses and Conversions

The 2-pyridone nucleosides **1***b*, **2***b*, and **3***b* were obtained by treatment of the trimethylsilyl derivatives of the precursor species **1***a*, **2***a*, and **3***a* with tetra-*O*-acetyl-β-D-ribofuranose (12) in refluxing 1,2-dichloroethane in the presence of anhydrous tin(IV) chloride (13, *cf.* 14–16), followed by deacetylation with ammonia-saturated methanol. The tri-*O*-benzoylribofuranose species **1***d* was similarly obtained from 1-*O*-acetyl-2,3,5-tri-*O*-benzoyl-β-D-ribofuranose (17), and **1***b* was accessible from the reaction of 1-bromo-2,3,5-tri-*O*-acetylribofuranose (18) with the trimethylsilyl derivative of **1***a*, without catalysis by the tin(IV) species.

The compounds **1***a*–**1***f* were converted into the corresponding 4-substituted *vic*-triazolo(4,5-*b*)-pyrid-5-ones **4***a*–**4***f*, using the successive substitution and cyclization effected by azide ion in aprotic dipolar media (a route established by Fox and co-workers (19)). The intermediate addition-cyclization product **5** in the conversion **1***b* → **4***b* may be isolated from the reaction mixture (see Experimental), and yields **4***b* on acid treatment. The yields of **4***b* obtained via deblocking of the species **4***c* and **4***d*, using the protected nucleosides

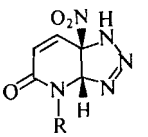

5

R = β-D-ribofuranosyl

1*c* and **1***d*, were significantly better than for the direct conversion of **1***b* into **4***b*.

Further treatment of the trimethylsilyl derivatives of several compounds of general structure **4** with tetra-*O*-acetyl-β-D-ribofuranose under tin(IV) catalysis efficiently introduces the triacetylribofuranose moiety selectively into the 2-position of the *vic*-triazolo(4,5-*b*)pyridone nucleus, yielding the compounds **6***c*–**6***f*. Deblocking of **6***c* provided the hygroscopic bis-riboside **7***b*, and deblocking of **6***e* provided **7***e*. Remarkably, attempted reacetylation of **7***e* resulted in a ribofuranosyl → ribopyranosyl conversion, yielding the species **8**.

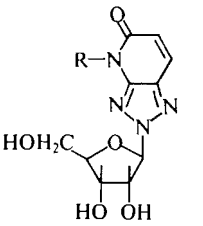

7

a R = H
b R = β-D-ribofuranosyl
c R = β-D-(2,3,5-tri-*O*-acetylribofuranosyl)
d R = β-D-(2,3,5-tri-*O*-benzoylribofuranosyl)
e R = CH_3
f R = $CH_2 \cdot C_6H_5$

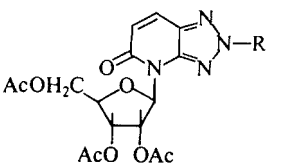

6

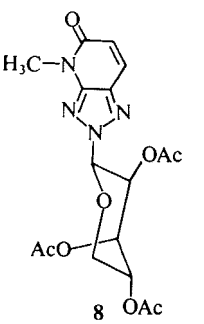

8

a R = H
b R = β-D-ribofuranosyl
c R = β-D-(2,3,5-tri-*O*-acetylribofuranosyl)
d R = β-D-(2,3,5-tri-*O*-benzoylribofuranosyl)
e R = CH_3
f R = $CH_2 \cdot C_6H_5$

To provide model reference compounds, the parent *vic*-triazolo(4,5-*b*)pyrid-5-one **4***a* was dimethylated in basic media, and the 4-methyl compound **4***e* similarly methylated, yielding a mixture of three dimethylated species in the ratio (as estimated from integration of the characteristic triazole *N*-methyl proton signals) 1:0.27:0.02, identified (see section *b* below) respectively as the 2,4-,1,4-, and 3,4-species **10**, **11**, and **12**; **10** and **11** were separable by sublimation under reduced pressure.

(b) Structure Assignments

If 1-substituted-5-nitro-2-pyridones are employed as starting materials, the cyclization route assures definition of the 4-substituted *vic*-

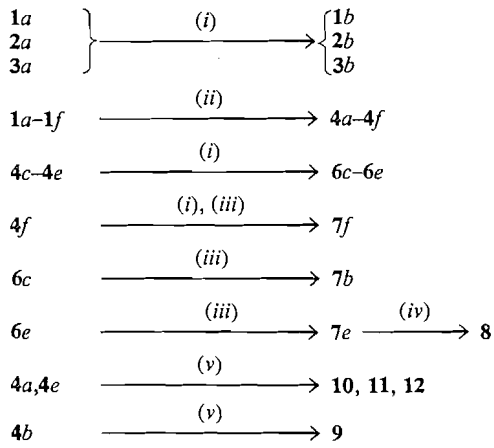

FIG. 1. Flow sheet of reactions and conversions: (*i*) treatment with 1,2,3,5-tetra-*O*-acetyl-β-D-ribofuranose in $C_2H_4Cl_2$ with $SnCl_4$; (*ii*) annelation with azide ion in aprotic dipolar solvent; (*iii*) deblocking with NH_3–CH_3OH or $NaOCH_3$–CH_3OH; (*iv*) acetylation with Ac_2O–pyridine; (*v*) methylation with CH_3I–Na_2CO_3.

triazolo(4,5-*b*)pyrid-5-one structure, but further alkylations (including ribosylations) could occur at each position in the triazole ring, and unequivocal identification and separation of related species has offered considerable difficulties (*cf.* 20–23).

The structures of the compounds cited in section *a* were established using pmr spectroscopy and electronic spectroscopy, with reference to the patterns shown by the model compounds **10** and **11** (see Tables 1 and 2). The structure assignment to compound **11**, mp 201–203 °C, was made using the nuclear Overhauser effect (24, 25). This compound showed an 11% increase in signal intensity for the low field pyridone 7-proton (δ 7.97) on irradiation of the triazole

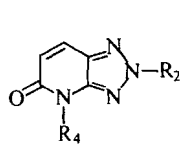

9 $R_2 = CH_3$
R_4 = β-D-ribofuranosyl
10 $R_2 = R_4 = CH_3$

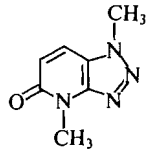

11

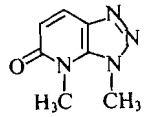

12

N-methyl signal (δ 4.22), requiring its formulation as the 1,4-dimethyl species.

The predominant methylation product from **4***a* and **4***e*, species **10**, mp 134 °C, showed no Overhauser enhancement of the pyridone *N*-methyl signal (δ 3.49) when the triazole *N*-methyl signal (δ 4.28) was irradiated, thus ruling out the 3,4-dimethyl species **12** and requiring assignment as the 2,4-dimethyl compound. The third isomer from the methylation, formed in smallest proportion, is then assigned as the 3,4-dimethyl compound **12**, and the low field positions of each of the two *N*-methyl signals in this compound (by comparison with the other isomers) may be attributed to steric compression or steric polarization influences.

With the structures **10** and **11** as reference points, the presence of a triazole *N*-methyl signal at δ 4.27 defines the structure of the methylation product of compound **4***b* as the 2-methyl-4-β-D-ribofuranosyl compound **9**. Further, the occurrence of the pyridone *N*-methyl signals in the δ 3.47–3.53 region in the triacetylribosyl compounds and the ribosyl derivative obtained from **4***e* (compounds **6***e*, **8**, and **7***e*), rather than in the δ 3.61 region, suggests the 2,4-substitution pattern. Further nuclear Overhauser effect experiments supported the suggestion that introduction of the blocked ribosyl species in the tin(IV) catalysed conversions of the compounds occurs selectively at the 2-position. Tests for enhancement of the H-1′ signal by irradiation of the pyridone 7-proton, or by irradiation of the protons of the 4-substituent, gave null results for the compounds **6***c*–**6***f*.

Since some abnormal relaxation effect could cast some doubt on the null results from the nOe experiments, we also made comparisons of the electronic spectra of the compounds **10** and **11** with the various ribosylated derivatives (see Table 2). Compound **10** (the 2,4-dimethyl compound) shows two discrete intense maxima above 300 nm; compound **11** shows a single peak in this region. All the compounds obtained by introduction of a methyl or blocked ribosyl species into a 4-substituted *vic*-triazolo(4,5-*b*)-pyrid-5-one show spectral patterns resembling **10**, but not **11**, and are confirmed as 2-substituted species. The slight but significant bathochromic and hyperchromic effects in the 2,4- *vs.* 1,4-species are consistent with previous findings (26–28) that 'extended' N-substituted species (of

Can. J. Chem. Downloaded from www.nrcresearchpress.com by 210.87.254.40 on 09/05/12
For personal use only.

TABLE 1. Proton magnetic resonance spectra of *vic*-triazolo(4,5-*b*)pyrid-5-ones*

Species	Chemical shifts for protons (ppm) 6-	7-	1′	Others	Coupling constants (Hz) $J_{1'2'}$
4*a*	6.53	8.07			
4*b*	6.58	8.07	6.38		6.50
4*c*	6.55	8.05	6.45		3.70
4*d*	6.58	8.10	6.78		0.0
4*e*	6.52	7.95		4-Me 3.53	
4*f*	6.65	8.08		4-Benzyl 5.33 (CH_2), 7.33 (C_6H_5)	
5	5.98 (J_{67} = 9.0 Hz)	7.78	6.55		7.50
6*c* (in $CDCl_3$)	6.70	7.83	6.57, 6.29		2.90, 3.40
6*e*	6.67	8.03	6.43	4-Me 3.53	2.50
6*f*	6.63	8.02	6.48	4-Benzyl 5.32 (CH_2), 7.40 (C_6H_5)	2.00
7*b* (in D_2O)	6.64	7.92	6.44, 6.18		2.60, 4.80
7*e*	6.63	8.01	5.97	4-Me 3.51	3.70
7*f*	6.68	8.07	5.95	4-Benzyl 5.27 (CH_2), 7.33 (C_6H_5)	3.40
8	6.65	8.01	6.15	4-Me 3.47	7.30
9	6.53	8.01	6.28	2-Me 4.27	4.80
10	6.53	7.92		2-Me 4.28, 4-Me 3.49	
11	6.55	7.97		1-Me 4.22, 4-Me 3.61	
12	6.37	7.89		3-Me 4.38, 4-Me 3.79	

*Unless otherwise stated, all spectra are for *ca.* 5% w/v solutions in DMSO-d_6, and all J_{67} values are 9.5 ± 0.1 Hz.

type **10**) show more intense and longer wavelength maxima than isomers with an N-substituent adjacent to an azine ring.

In assignments of anomeric configurations to unnatural ribofuranosides, small $J_{1'2'}$ couplings (less than 4 Hz) may be regarded as strongly indicative of *trans*-hydrogens (29), and thus of a β-configuration. The bicyclic species **4***b*, **5** and **9** show H-1′ couplings much greater than this, but since these compounds derive from the compound **1***b* (with $J_{1'2'} \simeq 0$ and thus unambiguously β), they are almost certainly β-species. There is the unlikely possibility that stereospecific anomerization occurs under the influence of the azide nucleophile, and to eliminate this, we converted **4***b* into its isopropylidene derivative. These species commonly show decreased $J_{1'2'}$ values as compared with the parent ribofuranoside, and it has been shown (30–32) that the chemical shift difference between the methyl groups of such derivatives may be used to confirm configurations (a difference >0.18 ppm is diagnostic of a β configuration (31)). The isopropylidene derivative of **4***b* showed methyl signals at δ 1.35 and 1.67, with $J_{1'2'}$ = 3.50 Hz, and is clearly β.

For the series of peracetylated ribosides (**4***c*, **6***e*, **6***f*) $J_{1'2'}$ is less than in the deblocked species (**4***b*, **7***e*, **7***f*) (see Table 1); yet in the course of attempted reacetylation of the deblocked riboside **6***e* using acetic anhydride – pyridine at room temperature, an isomeric product distinct from **7***e* was obtained, showing a large $J_{1'2'}$ (7.3 Hz). From the close correspondence of the comparable ^{13}C nmr ribose carbon signals in the

TABLE 2. Electronic absorption spectra of *vic*-triazolo(4,5-*b*)pyrid-5-ones (in methanol)

Species	λ_{max} (nm)	log ε
10	312	4.20
	302	4.19
	238	3.67
11	308	4.02
	249	3.66
6*c*	312	4.13
	301	4.17
	234	3.84
6*e*	313	4.30
	304	4.32
	239	3.87
7*e*	312	4.34
	304	4.35
	233	3.90
8	311	4.18
	302	4.18
	245	3.60
9	312	4.20
	303	4.22
	235	3.90

Can. J. Chem. Downloaded from www.nrcresearchpress.com by 210.87.254.40 on 09/05/12
For personal use only.

TABLE 3. ^{13}C nmr spectra of 4-methyl-2-(β-D-2,3,5-tri-*O*-acetylribofuranosyl)-*vic*-triazolo(4,5-*b*)pyrid-5-one (**6***e*), 4-methyl-2-(β-D-2,3,4-tri-*O*-acetylribopyranosyl)-*vic*-triazolo(4,5-*b*)pyrid-5-one (**8**) and 1,2,3,5-tetraacetyl-β-D-ribofuranose and 1,2,3,4-tetraacetyl-β-D-ribopyranose

	^{13}C chemical shifts (ppm)			
^{13}C assignment	**6***e*	Tetraacetyl-ribofuranose	**8**	Tetraacetyl-ribopyranose
Acetyl carbonyls	170.0	170.0	169.85	169.55
	169.6	169.3	169.2	169.4
	169.4	169.1	168.6	169.2
		168.6		168.4
Pyridine ring C-2	161.3		161.2	
C-6	148.5		148.2	
C-4	130.9		130.8	
C-5	129.2		129.2	
C-3	124.6		124.7	
Ribose ring C-1′	93.6	98.2	86.4	90.9
C-4′	80.1	79.4	67.6	67.3
C-3′	73.5	74.2	67.0	66.3
C-2′	70.6	70.6	65.6	66.2
C-5′	62.8	63.6	63.0	62.6
N-Methyl	29.3		29.2	
Acetyl methyls	20.3	20.9 20.33	20.4	20.7 20.65
		20.55 20.31	20.1	20.6 20.55

compound **7***e* and its isomeric deblocking → reacetylation product to those of tetraacetylribofuranose and tetraacetylribopyranose models (see Table 3), it is clearly evident that conversion into the pyranose species **8** has occurred (assignments of nuclei in Table 3 are based upon the ^{13}C spectra of the parent sugars (33) and some nucleosides (34), and standard ranges for pyridine ring atoms and for acetyl carbonyl and methyl groups (35)). The high value of $J_{1'2'}$ (7.3 Hz) in **8** establishes that the configuration of the ribopyranose moiety remains β, since α-pyranose nucleoside species are characterized by small values (*ca.* 2 Hz, *cf.* Montgomery and Thomas (36)). Although it is well known (37) that the pyranose form of ribose species is favored thermodynamically, and there are precedents for furanose → pyranose conversions with azapurine nucleosides (36), the ease of conversion in the present example is noteworthy, and suggests that careful continued monitoring of isomeric structures in nucleoside conversions is appropriate.

Finally, the β-ribofuranosyl configurations are tentatively assigned to the 2-substituted derivatives **6***c*–**6***f*, **7***b*, **7***e*, and **7***f*, since the $J_{1'2'}$ values for the peracetylated precursors **6** (from which the nucleosides are obtained by deblocking), are uniformly less than 4 Hz (Table 1, *cf.* Stevens and Fletcher (29)).

(c) Suggested Conformational Preferences: Sugar–Base Torsional Relationships

The interpretation given below relies largely upon the definitive discussions by Altona and Sundaralingam (38, 39). The unusual structural features in the nucleoside **4***b*, where the sugar–base link is sited between an amide carbonyl and the conjoined triazole ring, might be expected to impose conformational restraints, which should be evident in differences in the pmr spectra of the ribose protons in **4***b* as compared with species possessing fewer constraints (*cf* ref. 8).

Changes by comparison with 'normal' ribosides might include: (*i*) a change in the ribose conformation towards the S-conformation (C-(2′)-*endo*, C(3′)-*exo*, $^2T_3$ (38, 39)), since for this conformation, the base moiety adopts a quasi-equatorial site, so that bulky groups in the base then interact least with the ribose 3′-, 4′-, and 5′-substituents (40); this should be evident in high values for the coupling constant $J_{1'2'}$; (*ii*) increases in the coupling constant $J_{2'3'}$ from values characteristic of *anti* nucleosides (4.8–5.5 Hz) (39) towards the range 6.0–6.4 Hz, as observed for the analogously substituted nucleo-

Can. J. Chem. Downloaded from www.nrcresearchpress.com by 210.87.254.40 on 09/05/12
For personal use only.

TABLE 4. The pmr spectra of various ribosides related to 4-β-D-ribofuranosyl-*vic*-triazolo(4,5-*b*)pyrid-5-one*

Species	Chemical shifts (ppm)					Coupling constants (Hz)	
	H-1′	2′	3′	4′	5′,5″	$J_{1'2'}$	$J_{2'3'}$
4*b*	6.38	4.80	4.23	3.90	3.67	6.50	6.00
1*b*	5.95	4.03			3.77	≃0	≃5.0
5	6.55	5.00				7.50	6.00
Uridine	5.80	4.05	4.00	3.85	3.63	4.50	
Inosine	5.85	4.52	4.17	3.95	3.60	5.50	5.00
Adenosine	5.90	4.65	4.13	4.00	3.60	6.00	4.80
6-Azauridine	5.91	4.25	4.03	3.77	3.50	3.50	4.00
8-Azaxanthine, 3-riboside (36)	6.12					7.00	
3-Ribosyladenine (45)	5.95					7.00	
3-Ribosylhypoxanthine (45)	5.98					6.00	
2,4-Dioxo-1-β-D-ribofuranosylpyrido-(2,3-*d*)pyrimidine (6)	6.56					3.50	
1-β-D-Ribofuranosylquinazoline-2,4-dione (8)†	6.55	4.93	4.54	4.22	4.10		

*All original spectra are for 5% w/v solutions in DMSO-d_6. Missing entries indicate that proton signals were not readily resolved (for current work), or that the data were not presented (literature data).
†Values with respect to external TMS capillary.

sides orotidine (41) and β-cyanuric acid riboside (42); (*iii*) downfield shifts in the H-1′ and H-2′ resonances (as compared with the monocyclic **1***b*, assumed to adopt an *anti* conformation), associated with deshielding of these nuclei by the carbonyl and triazole functions. Table 4, which includes comparisons of **4***b* with several related ribosides, shows that each of these proposed features appears in the pmr spectra of **4***b* (and of the intermediate **5**): the coupling constants $J_{1'2'}$ and $J_{2'3'}$ have high values; H-1′ is deshielded by 0.43 ppm, and H-2′ by 0.77 ppm as compared with **1***b*. Dreiding molecular models for 'high-*anti*' (intermediate *anti-syn*) (43) conformations for **4***b* (see Fig. 2) indicate that both H-1′ and H-2′ will be under the deshielding influences of either the carbonyl group or the unshared pair of the nitrogen at position 3. We suggest that each of the structures A and B of Fig. 2 will be energy minima among the torsional range for **4***b*.

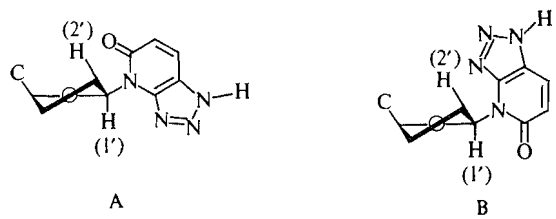

FIG 2. Hydrogen and oxygen atoms other than those of the ribose skeleton are omitted for clarity.

(d) Prognosis for Future Work

We are now engaged in syntheses of the nucleoside phosphates of the newly available ribosyl species, and plan to evaluate these as substrates for polynucleotide phosphorylases (8–11). The synthesized ribosides are also being supplied to the University of Alberta Cancer Research Unit for evaluation as inhibitors of the enzymes of purine synthesis. We hope to extend our nmr studies, using ^{13}C–H vicinal couplings to verify the proposed sugar–base torsional relationships (*cf.* ref. 44).

Experimental

General

Melting points were determined using a Fisher–Johns apparatus or a Kofler Heizbank. Most of the proton magnetic resonance spectra were recorded with a Varian A-60D instrument using DMSO-d_6 as solvent, while the nuclear Overhauser effect (nOe) experiments were made using a Varian HA-100. The ^{13}C magnetic resonance spectra were obtained for deuteriochloroform solutions using a Varian XL-100 spectrometer in the Fourier transform mode with full proton decoupling. All chemical shifts (proton and ^{13}C) are expressed in parts per million downfield from internal tetramethylsilane. Infrared spectra (potassium chloride disks) were measured on a Beckman Acculab 4 instrument, and electronic absorption spectra with a Beckman Acta III spectrophotometer. Column chromatographic separations used Fluka Type 507C neutral alumina, Brockmann activity 1. Specimens for elemental analyses were dried at 65 °C/0.2 torr for at least 6 h and were analysed using a Hewlett–Packard

Can. J. Chem. Downloaded from www.nrcresearchpress.com by 210.87.254.40 on 09/05/12
For personal use only.

Can. J. Chem. Downloaded from www.nrcresearchpress.com by 210.87.254.40 on 09/05/12
For personal use only.

Model 185 CHN Analyser. All extracts were dried over anhydrous sodium sulfate and evaporations were effected below 35 °C under reduced pressure. Known compounds referred to in the tables and in details of experiments were commercial materials, whose physical properties accorded with literature values.

2-Pyridone Nucleosides

(a) 5-Nitro-1-β-D-ribofuranosyl-2-pyridone, ***1b***

Method i — 5-Nitro-2-pyridone (3.0 g) in hexamethyldisilazane (40 ml) was heated under reflux with a catalytic amount (10 mg) of ammonium sulfate for 4 h, with precautions for exclusion of moisture. Excess solvent was removed under reduced pressure and the residue, without further purification, was dissolved in 1,2-dichloroethane (100 ml) and 1,2,3,5-tetra-*O*-acetyl-β-D-ribofuranose (6.25 g) and tin(IV) chloride (1.0 ml) were added. The mixture was heated under reflux for 8 h and allowed to stand at room temperature for a further 12 h. 1,2-Dichloroethane (50 ml) was added to the reaction mixture, which was washed successively with aqueous sodium carbonate and with water, and the organic phase was dried. Concentration under reduced pressure yielded an oil whose pmr spectrum was consistent with formulation as the tri-*O*-acetyl species **1***c*. The oil was treated at 0 °C for 4 days with methanol (225 ml) presaturated with ammonia at 0 °C. Concentration of the solution under reduced pressure, followed by crystallization from water, provided 5-nitro-1-β-D-ribofuranosyl-2-nitropyridone **1***b* (4.83 g, 80%), mp 225 °C. *Anal.* calcd. for $C_{10}H_{12}N_2O_7$: C 44.12, H 4.44, N 10.29; found: C 43.70, H 4.50, N 10.30. The pmr spectra: δ 5.95 (s, 1H, H-1′), 6.52 (d, 1H, J = 9.5 Hz, H-3), 8.15 (dd, 1H, J = 9.5 and 3.3 Hz, H-4), 9.66 (d, 1H, J = 3.3 Hz, H-6).

Method ii — 5-Nitro-2-pyridone (1.50 g) was converted into its trimethylsilyl derivative as above, and was treated with 1-bromo-2,3,5-tri-*O*-acetylribofuranose (18) (3.25 g) in 1,2-dichloroethane (100 ml). The mixture was heated under reflux for 6 h and left at room temperature overnight. Deacetylation as in method *i* and crystallization from water provided **1***b* (2.11 g, 70%) mp and mixture mp 225 °C.

(b) 5-Nitro-1-β-D-(2,3,5-tri-O-benzoylribofuranosyl)-2-pyridone, ***1d***

The trimethylsilyl derivative, prepared as above from 5-nitro-2-pyridone (2.80 g) was treated with 1-acetyl-2,3,5-tri-*O*-benzoyl-β-D-ribofuranose (17) (9.50 g) in 1,2-dichloroethane (100 ml) and the mixture was heated under reflux for 8 h in the presence of tin(IV) chloride (1.0 ml). After working up as in method *i* above, and crystallization from ethanol, the product **1***d* was obtained (8.37 g, 72%), mp 178–180 °C. *Anal.* calcd. for $C_{31}H_{24}N_2O_{10}$: C 63.69, H 4.14, N 4.79; found: C 64.06, H 4.20, N 4.43. The pmr spectra: δ 6.28 (s, 1H, H-1′), 6.57 (d, 1H, J = 9.5 Hz, H-3), 8.17 (dd, 1H, J = 9.5 and 2.9 Hz, H-4), 9.17 (d, 1H, J = 2.9 Hz, H-6). **1***d* afforded the deblocked nucleoside **1***b* in quantitative yield on treatment with ammonia saturated methanol.

(c) 3-Nitro-1-β-D-ribofuranosyl-2-pyridone, ***2b***

3-Nitro-2-pyridone **2***a* (1.50 g), on ribosylation following method *i* above, yielded the product **2***b* (1.50 g, 51%), mp 225–228 °C. *Anal.* found: C 44.30, H 4.38, N 10.38. The pmr spectra: δ 6.00 (d, 1H, J = 2.0 Hz, H-1′), 6.50 (t, 1H, J = 7.0 Hz, H-5), 8.20 (dd, 1H, J = 7.0 and 2.3 Hz, H-4), 8.48 (dd, 1H, J = 7.0 and 2.3 Hz, H-6).

(d) 3-Cyano-1-β-D-ribofuranosyl-2-pyridone, ***3b***

3-Cyano-2-pyridone (0.70 g), mp 222–225 °C, was ribosylated following the procedure of method *i* above, yielding **3***b* (0.70 g, 48%), mp 220–222 °C, after crystallization from ethanol. *Anal.* calcd. for $C_{11}H_{12}N_2O_5$: C 52.38, H 4.80, N 11.11; found: C 52.69, H 4.81, N 11.10. The pmr spectra: δ 6.08 (d, 1H, J = 2.0 Hz, H-1′), 6.54 (t, 1H, J = 7.5 Hz, H-5), 8.49 (dd, 1H, J = 7.5 and 2.5 Hz, H-6 or H-4), 8.64 (dd, 1H, J = 7.5 and 2.5 Hz, H-4 or H-6).

Annelation Reactions Yielding Triazolopyridones

4-β-D-Ribofuranosyl-vic-triazolo(4,5-b)pyrid-5-one, ***4b***

To the nucleoside **1***b* (8.15 g) in dimethyl sulfoxide (50 ml) was added sodium azide (2.40 g) and the mixture was heated at 115–117 °C for 24 h (stirring). The cooled solution was diluted with chloroform (200 ml) and the resulting semisolid was collected by decantation, dissolved in the minimum quantity of methanol, and applied to a neutral alumina column (100 g, moistened with chloroform). Elution with methanol followed by evaporation under reduced pressure yielded the intermediate **5** (1.63 g), mp 254–256 °C (shrinks at 235 °C) after crystallization from water. This material showed no azide absorption in the 2000–2500 cm^{-1} region; pmr spectra, see Table 1. Crystallization from 1 *M* hydrochloric acid yielded **4***b*, mp 263–265 °C (dec.). *Anal.* calcd. for $C_{10}H_{12}N_4O_5$: C 44.78, H 4.51, N 20.89; found: C 44.83, H 4.56, N 20.63. For pmr spectra, see Table 1.

4-β-D-(2,3,5-Tri-O-acetylribofuranosyl)-vic-triazolo-(4,5-b)pyrid-5-one, ***4c***

To the nucleoside **1***c* (13.50 g) in *N*,*N*-dimethylformamide (50 ml) was added sodium azide (5.20 g), and the mixture was heated at 110 °C for 24 h, and concentrated under reduced pressure (0.8 torr). The residue was extracted with chloroform (3 × 100 ml), washed with 1 *M* hydrochloric acid and with water, and the organic extract was dried and the solvent removed. The residual oil (8.70 g) was dissolved in ethyl ether (150 ml); slow evaporation of the ether yielded **4***c* as light yellow crystals (5.37 g, 40%), mp 223–224 °C. *Anal.* calcd. for $C_{16}H_{18}N_4O_8$: C 48.73, H 4.60, N 14.21; found: C 48.87, H 4.36, N 14.49. For pmr spectra, see Table 1. Deblocking with ammonia saturated methanol afforded the nucleoside **4***b* quantitatively.

4-β-D-(2,3,5-Tri-O-benzoylribofuranosyl)-vic-triazolo-(4,5-b)pyrid-5-one, ***4d***

The nucleoside derivative **1***d* (5.90 g) in *N*,*N*-dimethylformamide (50 ml) was heated with sodium azide (2.40 g) at 88–90 °C (stirring) for 24 h. The solvent was removed under reduced pressure (0.5 torr) and the residue was neutralized with 2 *M* hydrochloric acid. The product was isolated by extraction with chloroform (3 × 75 ml). Evaporation of the extract followed by crystallization from ethyl ether yielded **4***d* (5.49 g, 93%), mp 157–159 °C. *Anal.* calcd. for $C_{31}H_{24}N_4O_8$: C 64.13, H 4.17, N 9.65; found: C 64.34, H 4.41, N 9.29. For pmr spectra, see Table 1. Deblocking with 0.5 *M* methanolic sodium methoxide afforded **4***b* quantitatively.

Can. J. Chem. Downloaded from www.nrcresearchpress.com by 210.87.254.40 on 09/05/12
For personal use only.

4-Benzyl-vic-triazolo(4,5-b)pyrid-5-one, 4f

1-Benzyl-5-nitro-2-pyridone (16.5 g) in *N,N*-dimethylformamide (75 ml) was heated with sodium azide (9.40 g) at 93 °C for 18 h and at 103 °C for 30 h. The product was isolated by acidification with 1 *M* hydrochloric acid, collection, and crystallization from aqueous ethanol, yielding **4***f* (14.96 g, 92%), mp 231–232 °C. *Anal.* calcd. for $C_{12}H_{10}N_4O$: C 63.71, H 4.46, N 24.76; found C 63.60, H 4.30, N 24.80. For pmr spectra, see Table 1.

Nucleoside Syntheses from 4-Substituted Triazolopyridones

2,4-Bis(β-D-2,3,5-tri-O-acetylribofuranosyl)-vic-triazolo-(4,5-b)pyrid-5-one, 6c

The peracetylated triazolopyridone nucleoside **4***c* (0.80 g) was heated under reflux with hexamethyldisilazane (15 ml) and a catalytic amount of ammonium sulfate for 3 h, with precautions for exclusion of moisture. After removal of the excess of hexamethyldisilazane, the residue was dissolved in 1,2-dichloroethane (50 ml) and reacted with 1,2,3,5-tetra-*O*-acetyl-β-D-ribofuranose (0.68 g) and tin(IV) chloride (0.5 ml) by heating under reflux for 8 h. Chloroform (50 ml) was added and the organic layer was shaken successively with water, saturated aqueous sodium hydrogen carbonate, and water. After drying and concentration, followed by crystallization from methanol, the product **6***c* was obtained, mp 63–65 °C (1.40 g, 85%). *Anal.* calcd. for $C_{27}H_{32}N_4O_{15}$: C 49.70, H 4.94, N 8.58; found: C 50.03, H 5.26, N 8.25. For pmr spectra, see Table 1.

2-β-D-2,3,5-Tri-O-acetylribofuranosyl-4-β-D-2,3,5-tri-O-benzoylribofuranosyl-vic-triazolo(4,5-b)pyrid-5-one, 6d

The tribenzoyl derivative **4***d* (2.50 g) was heated under reflux for 18 h in hexamethyldisilazane (35 ml) as for **6***c* above. Excess solvent was removed under reduced pressure, and the residue was dissolved in 1,2-dichloroethane (80 ml); 1,2,3,5-tetra-*O*-acetyl-β-D-ribofuranose (1.34 g) was added, together with tin(IV) chloride (0.5 ml), and the mixture was heated under reflux for 8 h. Work-up as for **6***c* gave crude material, which was purified by crystallization from ethanol, yielding 1.0 g (28%) of **6***d*, mp 66–68 °C. *Anal.* calcd. for $C_{42}H_{38}N_4O_{15}$: C 60.14, H 4.57, N 6.68; found: C 60.48, H 4.93, N 6.54.

4-Methyl-2-β-D-2,3,5-tri-O-acetylribofuranosyl-vic-triazolo(4,5-b)pyrid-5-one, 6e

The trimethylsilyl derivative prepared from 4-methyl-*vic*-triazolo(4,5-*b*)pyrid-5-one **4***e* (19) (1.50 g) by treatment with excess of hexamethyldisilazane, was reacted with 1,2,3,5-tetra-*O*-acetyl-β-D-ribofuranose (3.05 g) and tin(IV) chloride (0.5 g) in 1,2-dichloroethane (50 ml) under reflux for 6 h, and left at room temperature for 18 h. The product was isolated after removal of inorganic materials in the usual manner, and crystallized from petroleum, bp 60–65 °C, as colorless needles, mp 52–53 °C. *Anal.* calcd. for $C_{17}H_{20}N_4O_8$: C 50.00, H 4.94, N 13.72; found: C 50.04, H 5.02, N 13.59. For pmr spectra, see Table 1; ^{13}C nmr spectra, see Table 3.

2,4-Bis-β-D-ribofuranosyl-vic-triazolo(4,5-b)pyrid-5-one, 7b

The bistriacetylribofuranose derivative **6***c* (1.0 g) was dissolved at 0 °C in methanol (75 ml) presaturated with ammonia at 0 °C, and the solution was allowed to stand at 0 °C for 18 h. Evaporation of the solvent gave a colorless solid, which was crystallized from water and recrystallized from methanol, yielding 0.71 g of material, mp 135–137 °C. The compound was too hygroscopic for satisfactory elemental analysis, but the pmr spectra support the assigned structure (see Table 1).

4-Methyl-2-β-D-ribofuranosyl-vic-triazolo(4,5-b)pyrid-5-one, 7e

The 4-methyl-2-triacetylribofuranose derivative **6***e* (2.50 g) was treated with freshly prepared sodium methoxide in methanol (from 0.50 g sodium in methanol (50 ml)) at 21 °C for 20 h. The solution was neutralized by passage through Amberlite resin IRC-50(H), and concentration of the solution gave the deacetylated nucleoside **7***e*, which was crystallized from 2-propanol to give needles (1.48 g, 86%), mp 135–137 °C. *Anal.* calcd. for $C_{11}H_{14}N_4O_5$: C 46.81, H 5.00, N 19.85; found: C 47.08, H 4.83, N 19.66. For pmr spectra, see Table 1.

4-Benzyl-2-β-D-ribofuranosyl-vic-triazolo(4,5-b)pyrid-5-one, 7f

4-Benzyl-*vic*-triazolo(4,5-*b*)pyrid-5-one **4***f* (3.45 g) was converted into the trimethylsilyl derivative by treatment with excess of hexamethyldisilazane, and dissolved in 1,2-dichloroethane (100 ml) when 1,2,3,5-tetra-*O*-acetyl-β-D-ribofuranose (4.52 g) and tin(IV) chloride (0.7 ml) were added. The reaction mixture was heated under reflux for 8 h and left at 21 °C for 16 h. After the usual isolation procedure, a viscous oil (6.70 g, 90% based on the assumption that the triacetylribofuranose moiety had been introduced) was obtained. The oil (5.0 g) was dissolved in freshly prepared sodium methoxide in methanol (0.8 g sodium in methanol (70 ml)) and left at room temperature for 16 h. The solution was neutralized by passage through Amberlite resin IRC-50(H), and the product isolated on concentration was crystallized from methanol – ethyl ether, yielding needles of **7***f* (2.88 g, 78% based on the 5.0 g portion), mp 191–193 °C. *Anal.* calcd. for $C_{17}H_{18}N_4O_5$: C 56.98, H 5.06, N 15.63; found: C 56.75, H 5.00, N 15.69. For pmr spectra, see Table 1.

4-Methyl-2-β-D-(2,3,4-tri-O-acetylribopyranosyl)-vic-triazolo(4,5-b)pyrid-5-one, 8

To 4-methyl-2-β-D-ribofuranosyl-*vic*-triazolo(4,5-*b*)-pyrid-5-one **7***e* (0.22 g) in dry pyridine (10 ml) was added acetic anhydride (1.0 g) and the reaction mixture was left at 21 °C for 64 h. The solution was concentrated under reduced pressure (4 torr), and the solid thus obtained was treated three times with ethanol (15 ml portions) with successive evaporation under reduced pressure, and finally crystallized from ethanol, providing the triacetylribopyranose species **8** (0.29 g, 91%), mp 185–186 °C. *Anal.* found: C 50.25, H 5.25, N 13.81. For pmr spectra, see Table 1; ^{13}C nmr spectra, see Table 3.

Methylations of Triazolopyridone Species

(*a*) Methylation of *vic*-triazolo(4,5-*b*)pyrid-5-one, **4***a*. To the above-named compound **4***a* (19) (0.50 g) in methanol (100 ml) was added methyl iodide (0.5 ml) and potassium carbonate (0.50 g) and the mixture was set aside at 21 °C for 16 h. The solution was concentrated and the residue was extracted into chloroform (3 × 50 ml), the extract was dried, and the solvent removed yielding a mixture of dimethylated species: the 2,4-dimethyl compound **10**, the 1,4-dimethyl compound **11**, and the 3,4-dimethyl compound **12**, in the ratios 1.00:0.27:0.02 as estimated by pmr spectroscopy, total yield 0.53 g (88%).

Can. J. Chem. Downloaded from www.nrcresearchpress.com by 210.87.254.40 on 09/05/12
For personal use only.

The compounds **10** and **11** were separated by sublimation at 1 torr: **10** sublimed at 105 °C, and **11** at 165 °C. 2,4-Dimethyl-*vic*-triazolo(4,5-*b*)pyrid-5-one, **10**, had mp 134 °C. *Anal.* calcd. for $C_7H_8N_4O$: C 51.21, H 4.91, N 34.13; found: C 51.19, H 4.69, N 34.44. 1,4-Dimethyl-*vic*-triazolo(4,5-*b*)pyrid-5-one, **11**, had mp 201–203 °C. *Anal.* found: C 51.46, H 5.32, N 34.10. For pmr and electronic spectra, see Tables 1 and 2.

(*b*) Methylation of 4-methyl-*vic*-triazolo(4,5-*b*)pyrid-5-one, **4***e*. Methylation of this species (1.0 g) in methanol (95 ml) with methyl iodide (1.0 g) in the presence of potassium carbonate (1.0 g) under the same conditions as for (*a*) above provided a similar mixture of dimethylated species (**10**, **11**, **12**) in the same ratio as above (total yield 0.82 g, 75%). The isomers **10** and **11** were separated by sublimation as above and characterized by mp, mixture mp, and pmr spectra.

(*c*) Methylation of 4-β-D-ribofuranosyl-*vic*-triazolo-(4,5-*b*)pyrid-5-one. The above named species **4***b* (1.00 g) in water (5 ml) was added to a mixture of potassium carbonate (1.00 g), methyl iodide (1.00 ml), and methanol (10 ml). The reaction mixture was set aside for 18 h, solvents were removed under reduced pressure, and the residue was crystallized from water, providing 2-methyl-4-β-D-ribofuranosyl-*vic*-triazolo(4,5-*b*)pyrid-5-one **9** (0.72 g, 76%), mp 210–211 °C. *Anal.* found: C 47.12, H 4.85, N 19.89. For pmr spectra, see Table 1; electronic spectra, see Table 2.

Acknowledgements

Particular thanks are due to Dr. A. G. McInnes and Mr. D. G. Smith of the Atlantic Regional Laboratory, National Research Council of Canada, for the nuclear Overhauser effect measurements, and for ^{13}C nmr data. This study was assisted by grants-in-aid from the National Cancer Institute of Canada, the National Research Council of Canada, and the Saint Francis Xavier University Council for Research.

1. B. L. Currie, R. K. Robins, and M. J. Robins. J. Heterocycl. Chem. **7**, 323 (1970).
2. A. Bloch, G. Dutschman, B. L. Currie, R. K. Robins, and M. J. Robins. J. Med. Chem. **16**, 294 (1973).
3. K. Ikeda, T. Sumi, K. Yokoi, and Y. Mizuno. Chem. Pharm. Bull. **21**, 1327 (1973).
4. M. W. Winkley. J. Chem. Soc. C, 1869 (1970).
5. C. L. Schmidt, W. J. Rusho, and L. B. Townsend. Chem. Commun. 1515 (1971).
6. B. H. Rizkalla, A. D. Broom, M. G. Stout, and R. K. Robins. J. Org. Chem. **37**, 3795 (1972).
7. M. G. Stout and R. K. Robins. J. Org. Chem. **33**, 1219 (1968).
8. M. P. Schweizer, E. B. Banta, J. T. Witkowski, and R. K. Robins. J. Am. Chem. Soc. **95**, 3770 (1973).
9. A. M. Kapuler, C. Monny, and A. M. Michelson. Biochim. Biophys. Acta, **217**, 18 (1970).
10. A. M. Kapuler and E. Reich. Biochemistry, **10**, 4050 (1971).
11. M. Ikehara, I. Tazawa, and T. Fukui. Biochemistry, **8**, 736 (1969).
12. R. D. Guthrie and S. C. Smith. Chem. Ind. 547 (1968).
13. L. Y. Foo and B. M. Lynch. Efficient syntheses of ribosides. Abstracts, 54th Annual Meeting, Canadian Chemical Conference of the Chemical Institute of Canada, Halifax, Nova Scotia, June, 1971.
14. R. U. Lemieux and W. P. Shyluk. Can. J. Chem. **31**, 528 (1953).
15. U. Niedballa and H. Vorbruggen. Angew. Chem. Int. Ed. Engl. **9**, 461 (1970).
16. U. Niedballa and H. Vorbruggen. J. Org. Chem. **39**, 3654 (1974).
17. J. D. Stevens, R. K. Ness, and H. G. Fletcher. J. Org. Chem. **33**, 1806 (1968).
18. H. M. Kissman, C. Pidacks, and B. R. Baker. J. Am. Chem. Soc. **77**, 18 (1955).
19. H. U. Blank, I. Wempen, and J. J. Fox. J. Org. Chem. **35**, 1131 (1970).
20. J. Elguero and S. Mignonac-Mondon. Bull. Soc. Chim. Fr. 2916 (1972).
21. Y. Mizuno, M. Ikehara, T. Itoh, and K. Saito. J. Org. Chem. **28**, 1837 (1963).
22. K. B. de Roos and C. A. Salemink. Recl. Trav. Chim. **90**, 1181 (1971).
23. P. C. Jain, S. K. Chatterjee, and N. Anand. Indian J. Chem. **3**, 84 (1965).
24. P. A. Hart and J. P. Davis. J. Am. Chem. Soc. **91**, 512 (1969).
25. P. A. Hart and J. P. Davis. J. Am. Chem. Soc. **93**, 753 (1971).
26. G. R. Revankar and L. B. Townsend. J. Heterocycl. Chem. **7**, 117 (1970).
27. S. Senka, K. Hirota, and G. N. Yang. Chem. Pharm. Bull. **20**, 391 (1972); **20**, 399 (1972).
28. R. A. Earl, R. J. Pugmire, G. R. Revankar, and L. B. Townsend. J. Org. Chem. **40**, 1822 (1975).
29. J. D. Stevens and H. G. Fletcher. J. Org. Chem. **33**, 1799 (1968).
30. E. J. Reist, D. F. Calkins, and L. Goodman. J. Org. Chem. **32**, 169 (1967).
31. J. L. Imbach, J. L. Barascut, B. L. Kam, B. Rayner, C. Tamby, and C. Tapiero. J. Heterocycl. Chem. **10**, 1069 (1973).
32. J. L. Barascut, C. Tamby, and J. L. Imbach. J. Carbohydr. Nucleosides, Nucleotides. **1**, 77 (1974).
33. L. D. Hall and L. F. Johnson. Chem. Commun. 509 (1967).
34. A. J. Jones, D. M. Grant, M. W. Winkley, and R. K. Robins. J. Am. Chem. Soc. **92**, 4079 (1970).
35. J. B. Stothers. Carbon-13 NMR spectroscopy. Academic Press, New York. 1972.
36. J. A. Montgomery and H. J. Thomas. J. Org. Chem. **36**, 1962 (1971).
37. C. T. Bishop and F. P. Cooper. Can. J. Chem. **41**, 2743 (1963).
38. C. Altona and M. Sundaralingam. J. Am. Chem. Soc. **94**, 8205 (1972).
39. C. Altona and M. Sundaralingam. J. Am. Chem. Soc. **95**, 2333 (1973).
40. D. Suck and W. Saenger. J. Am. Chem. Soc. **94**, 6520 (1972).

41. F. E. HRUSKA. J. Am. Chem. Soc. **93**, 1795 (1971).
42. H. DUGAS, B. J. BLACKBURN, R. DESLAURIERS, and I. C. P. SMITH. J. Am. Chem. Soc. **93**, 3468 (1971).
43. P. SINGH and D. J. HODGSON. J. Am. Chem. Soc. **96**, 5276 (1974).
44. R. U. LEMIEUX, T. L. NAGABHUSAN, and B. PAUL. Can. J. Chem. **50**, 773 (1972).
45. C. G. TINDALL, R. K. ROBINS, R. L. TOLMAN, and W. HUTZENLAUB. J. Org. Chem. **37**, 3985 (1972).

Can. J. Chem. Downloaded from www.nrcresearchpress.com by 210.87.254.40 on 09/05/12
For personal use only.

The synthesis of chasmanine: aromatic intermediate

SHY-FUH LEE, GANESH M. SATHE, WING WAH SY, PAK-TSUN HO, AND KAREL WIESNER
Natural Products Research Center, University of New Brunswick, Fredericton, New Brunswick E3B 5A3

Received October 14, 1975

SHY-FUH LEE, GANESH M. SATHE, WING WAH SY, PAK-TSUN HO, and KAREL WIESNER. Can. J. Chem. **54**, 1039 (1976).

The stereospecific total synthesis of the pentacyclic tetrasubstituted intermediate **39** is described. The conversion of this material to the delphinine type alkaloid chasmanine **IV** by the method worked out recently by the same group (1) is envisaged.

SHY-FUH LEE, GANESH M. SATHE, WING WAH SY, PAK-TSUN HO et KAREL WIESNER. Can. J. Chem. **54**, 1039 (1976).

On décrit une synthèse totale stéréospécifique de l'intermédiaire pentacyclique tétrasubstitué **39**. On envisage la conversion, par une méthode dont les détails ont été décrits récemment par le même groupe, de ce composé en chasmanine **IV**, un alcaloide du type de delphinine.

[Traduit par le journal]

Introduction

We have recently completed and reported (1) a simple stereospecific conversion of compound **I** to the chasmanine model **II**. All the steps of this process proceeded under mild conditions and in high yield and we felt that they could be applied without major modification to compound **III** with a suitably blocked nitrogen. This would lead very simply to the fully substituted, naturally occurring delphinium alkaloid chasmanine **IV** (2).

In the present communication we wish to report the stereospecific synthesis of the intermediate **III (39)** in which the R group is formyl.[1] The route to compound **39** resembled in principle our synthesis of the aromatic intermediate **V** for napelline (3). There were, however, some important differences. The relatively simple substitution pattern of napelline did not do justice to our synthetic method which can provide automatically all the substituents of a delphinine type alkaloid. It should be noted that both in the process **I** → **II** and in the synthesis of **39** all the substituents materialize stereospecifically in the correct positions simultaneously with the construction of the skeleton.

[1]The first step of the model sequence **I** → **II** and of the planned sequence **III** → **IV** is a Birch reduction of the anisole ring. If this process is applied to **39** the formyl is lost and may be replaced by a *N*-acetyl group which in turn may be reduced to the *N*-ethyl of chasmanine in the last step of the synthesis. The Birch reduction followed by acetylation and treatment with acid to the corresponding *N*-acetyl-α,β-unsaturated ketone has been already successfully performed on compound **39**.

The position of the aromatic methoxyl in compound **39** had an unfavorable effect on the direction of the aziridine rearrangement, a key

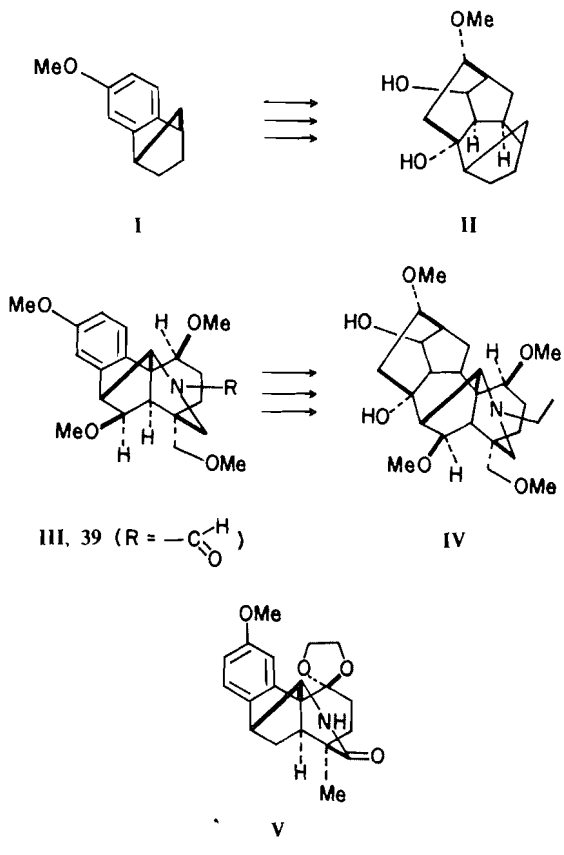

SCHEME 1

Can. J. Chem. Downloaded from www.nrcresearchpress.com by 210.87.254.42 on 09/05/12
For personal use only.

Can. J. Chem. Downloaded from www.nrcresearchpress.com by 210.87.254.42 on 09/05/12
For personal use only.

step in the synthesis. This was corrected by the introduction of the bridgehead methoxyl, which helped to steer the rearrangement in the desired direction. A detailed discussion of the various factors influencing the direction of aziridine rearrangements may be found in the first paper of this series (4).

Discussion

The starting materials for the present synthesis were the compounds **7** and **16** both of which we have previously reported (4, 5). However, both these compounds were now prepared by fundamentally improved methods.

The known (6) methoxy indanone **1** was converted to the enol ether **2**, and the anion of this material, prepared by the action *n*-butyllithium in tetrahydrofuran, was carboxylated with carbon dioxide at −70 °C. The acid **3** was thus obtained in a yield of 82% after crystallization. It was converted into the methyl ester **4** by esterification with gaseous hydrochloric acid in methanol. We have previously prepared compounds **3** and **4** by a less efficient method (4) and the identity of our present materials with the reference samples was established by mixture melting points and spectral data.[2]

The conversion of the ester **4** via the intermediates **5** and **6** to the tricyclic ester **7** was described previously (4). This process has now been improved and is recorded in the Experimental.

Reduction of the ester **7** with lithium aluminum hydride and oxidation of the resulting primary alcohol **8** with dicyclohexylcarbodiimide in dimethyl sulfoxide yielded 89% of the aldehyde **9**. The stage was thus set for the attachment of the side chain **16** by a Grignard reaction.

The bromide **16** was prepared on a large scale by a very simple method starting from commercially available homoallyl alcohol. Tritylation of this material gave the ether **11** which was converted to the crystalline epoxide **12** by perbenzoic acid.

The opening of the epoxide ring in methanolic sodium methoxide yielded quantitatively the methoxy alcohol **13**. The preparation of the primary alcohol **15** was completed by benzylation of **13** with sodium hydride and benzyl chloride in dioxane, followed by the treatment of the product **14** with 90% acetic acid at 45 °C for 24 h. The overall yield of the alcohol **15** from the starting material **10** was 58%. The conversion of **15** to the bromide **16** was performed as reported previously (5).

The attachment of the side chain to the aldehyde **9** was carried out as in the previously reported cases (3, 5). Compound **9** was added to an excess of the Grignard reagent prepared from the bromide **16** and the oily diastereoisomeric mixture **17** was isolated in a 90% yield.

Oxidation of **17** with chromium trioxide in pyridine yielded the oily ketone **18** which behaved as a homogeneous product in spite of the fact that a mixture of two epimers was expected. The conversion of compound **18** to the diketone **19** was performed in one step. Compound **18** was treated with a large excess of benzenesulfonylazide in glacial acetic acid and a small amount of *p*-toluenesulfonic acid. The *exo*-benzenesulfonylaziridine which was formed under these conditions immediately rearranged as indicated by the arrows in formula **18***b*.

We have discussed in our first paper (4) the influence of the ketone and bridgehead methoxyl on the steering of the aziridine rearrangement in the desired direction. The bridgehead methoxyl clearly works by accelerating the desired rearrangement (see arrow in **18***b*) and the ketone by retarding the competing one leading to compound **20**. Nevertheless, the combined influence of these two groups did not suffice to eliminate completely the formation of this by-product. In fact, compounds **19** and **20** were obtained in a total yield of 80% and a ratio of 3:2. This is due to the powerful enhancement of the rearrangement leading to **20** by the aromatic methoxyl.

The third device which we have described for dealing with this situation (4), *i.e.*, the replacement of the aromatic methoxyl by the electron-withdrawing mesyloxy group and the conversion of this group into a methoxyl at a later stage of the synthesis eliminates the undesirable rearrangement completely. However, preliminary experiments along these lines have shown that the additional operations required completely consume the yield gain in the rearrangement step and thus represent only profitless extra work.

The conversion of the diketone **19** to the diketolactam **33** (via the intermediates **21** through

[2]Spectral data for all compounds are recorded in the Experimental. Spectral data are mentioned in the Discussion only in specially relevant cases to conserve space.

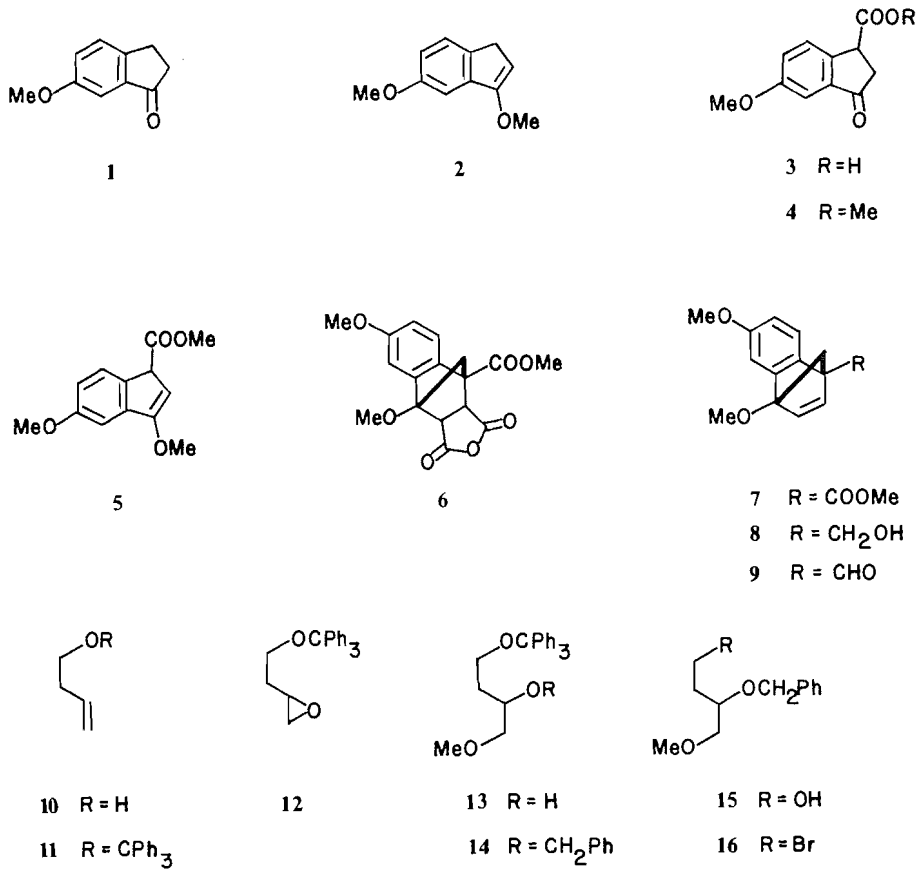

SCHEME 2

32) proceeded precisely by the methods which we have worked out previously (3) in the synthesis of compound **V**. Consequently, we shall comment in the Discussion only briefly on some of the small differences which we have encountered. The details of all the steps are recorded in the Experimental. Lithium aluminum hydride reduction and acetylation of **19** gave the diastereoisomeric mixture **21**. For analytical purposes we were able to separate it by preparative thin layer chromatography (tlc) into two groups of diastereoisomers with the acetoxyl marked by the arrow in formula **21** *endo* and *exo*.

In spite of the stereochemical inhomogeneity the partial hydrolysis of **21** to **22** proceeded as previously reported (3). Hydrogenolysis of **22** gave **23** and this material was oxidized to **24**. For characterization the diketone **24** was resolved by preparative tlc into two homogeneous crystalline epimers. All the intermediates in the synthesis from this point on were mixtures of two epimers and they were separated only on a small scale for characterization purposes. In compound **33** finally the last uncontrolled asymmetric center was removed and a homogeneous product resulted.

A minor improvement of the process was achieved in the degradation of the homoaldehyde **27** to the ester **31**. The aldehyde **27** was converted to the enol ether **30** via the acetal intermediates **28** and **29**. Compound **30** was oxidized with periodate–permanganate and the resulting carboxylic acid was immediately, without purification, esterified with diazomethane to the crystalline epimeric esters **31**.

As we have already pointed out all the uncontrolled asymmetric centers were finally eliminated and the diketolactam **33** was reached *stereospecifically*. This crucial intermediate was beautifully crystalline (mp 253 °C) and all its spectral

Can. J. Chem. Downloaded from www.nrcresearchpress.com by 210.87.254.42 on 09/05/12
For personal use only.

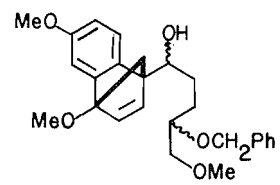

17

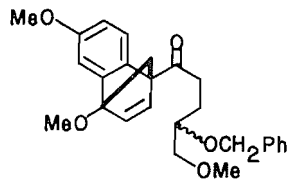

18

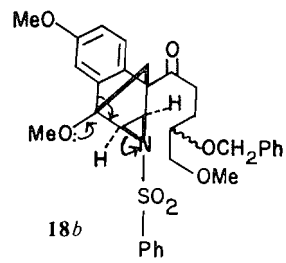

18*b*

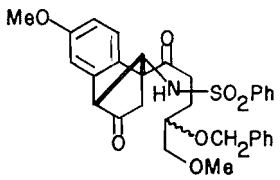

19

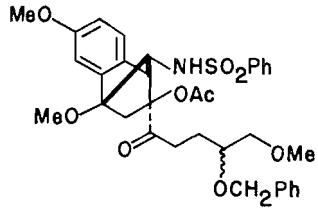

20

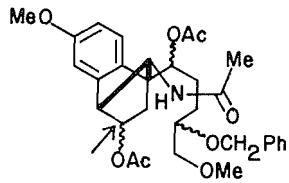

21

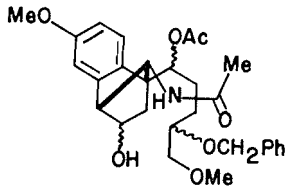

22

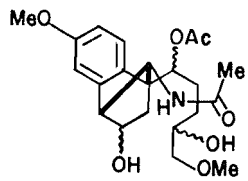

23

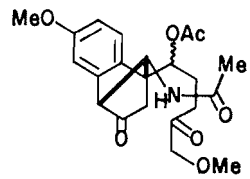

24

SCHEME 3

characteristics were analogous to those of the similar compound prepared in our synthesis of napelline (3).

In the infrared spectrum (ir) it showed carbonyl maxima at 1750, 1700, and 1667 cm^{-1} corresponding to the five- and six-membered ketones and the lactam. In the nuclear magnetic resonance (nmr) spectrum two sharp singlets (3H each) at τ = 6.20 and 6.62 ppm indicated the presence of the aromatic and primary methoxyls.

Reduction of the diketo lactam **33** with lithium tri-*tert*-butoxyaluminohydride yielded quantitatively and stereospecifically the dihydroxy lactam **34**. The same material was also obtained when the identical reduction conditions were applied to the β-epimer of the hydroxyketo lactam **32**. The β-configuration of the ring A hydroxyl in compound **34** is best demonstrated by nmr spectra of the two epimeric hydroxy ketones **32** (*cf.* 3). The aromatic hydrogen marked by the arrow in formula **32** is in close proximity of the ring A substituent in the α-epimer and is deshielded by it (d, 1H, τ = 2.39 ppm). In the β-epimer this hydrogen shows a signal at τ = 2.69 ppm. The nmr spectrum of compound **34** shows signals at τ = 5.50 (m, 1H, proton deshielded by the ring A hydroxyl), 5.78 (d, 1H, proton deshielded by the ring B *exo*-hydroxyl), 6.20 (s, 3H, aromatic methoxyl), 6.65 (s, 3H, primary methoxyl), and 2.93 ppm (d, 1H, aromatic proton marked by arrow in formula **34**).

Acetylation of compound **34** with acetic anhydride and *p*-toluenesulfonic acid yielded a mixture of two products: the amorphous diacetoxy derivative **35** and the crystalline lactone **36**, which not unexpectedly was produced by an acid-catalyzed acyl migration. The ir spectrum of this last material shows a carbonyl peak at 1775 cm^{-1} indicating clearly the presence of a

Can. J. Chem. Downloaded from www.nrcresearchpress.com by 210.87.254.42 on 09/05/12
For personal use only.

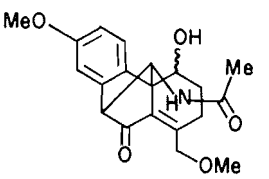

25

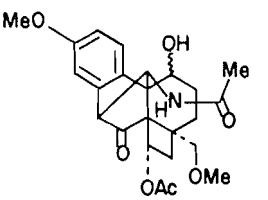

26

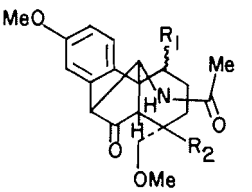

27 R_1 = OH, R_2 = CH_2CHO

28 R_1 = OH, R_2 = $CH_2CH(OMe)_2$

29 R_1 = OAc, R_2 = $CH_2CH(OMe)_2$

30 R_1 = OAc, R_2 = $CH{=}CH(OMe)$

31 R_1 = OAc, R_2 = COOMe

SCHEME 4

γ-lactone. Treatment of the lactone **36** with methanolic potassium hydroxide at room temperature gave quantitatively the lactame **34**. The characterization of the lactone **36** corroborated the *exo* configuration of the ring B hydroxyl in compound **34** by the most rigorous of stereochemical methods, *i.e.*, ring formation.

Compound **34** was now methylated with methyl iodide and sodium hydride in anhydrous dioxane, and the oily tetramethoxy-*N*-methyl lactam **37** was obtained in a yield of 62% after careful purification (*cf.* 5). Its nmr spectrum showed methoxy group singlets, 3H each, at τ = 6.20, 6.60, 6.65, and 6.69 ppm and a singlet, 3H, at τ = 7.05 ppm assigned to the *N*-methyl group.

Reduction of the lactam **37** to the amine **38** with lithium aluminum hydride was uneventful. In the nmr spectrum of **38** the *N*-methyl group singlet shifted to τ = 7.64 ppm and the ir of this product revealed the absence of the lactam carbonyl.

Finally oxidation of **38** to the *N*-formyl derivative **39** with potassium permanganate in acetic acid by the method which we have used previously (5) proceeded in a yield of 86%.

A carbonyl peak in the ir of **39** at 1658 cm^{-1} and a singlet, 1H, at τ = 1.84 ppm in the nmr spectrum of this product demonstrated the presence of the formyl group.

The stereospecific synthesis of the pentacyclic polysubstituted intermediate **39** is thus complete

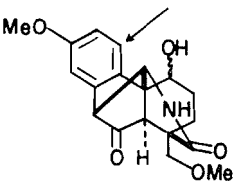

32

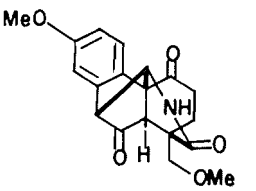

33

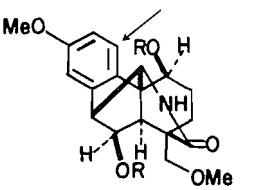

34 R = H

35 R = Ac

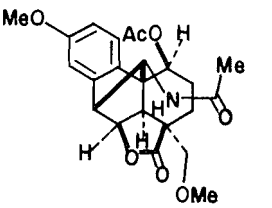

36

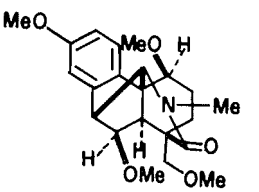

37

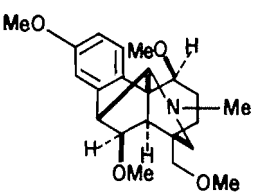

38

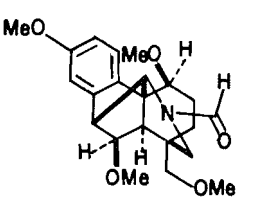

39

SCHEME 5

Can. J. Chem. Downloaded from www.nrcresearchpress.com by 210.87.254.42 on 09/05/12
For personal use only.

by a procedure which certainly makes it possible to prepare several grams of this material.

Such an amount should be more than sufficient to synthesize by our published method (1) enough racemic chasmanine to allow resolution into optical antipodes.

Experimental

Preparation of the Enol Ether **2**

Trimethyl orthoformate (50 ml), absolute methanol (50 ml), and saturated methanolic hydrogen chloride (5 ml) were added in sequence to a solution of 6-methoxy-1-indanone **1** (50 g) (6) in anhydrous benzene (750 ml). The solution was stirred at room temperature for 18 h, after which time trimethyl orthoformate (15 ml) and saturated methanolic hydrogen chloride (2 ml) were added and the reaction mixture was kept at room temperature for another 2 days. The solution was evaporated to dryness *in vacuo* and the enol ether **2** was obtained in a quantitative yield as an oil homogeneous in tlc. It was used immediately for the subsequent step. *Mol. Wt.* calcd. for $C_{11}H_{12}O_2$: 176; found (mass spectroscopy): 176. Spectral data: ir ($CHCl_3$) 1610 cm^{-1} (enol ether); nmr ($CDCl_3$) τ 4.74 (t, 1H, vinylic proton), 6.14 and 6.17 (2s, 6H, 2 methoxyls), 6.77 ppm (2d, 2H, benzylic protons).

Preparation of the Keto Ester **4**

A solution of compound **2** (50 g) in absolutely anhydrous tetrahydrofuran (800 ml) was cooled to −70 °C (acetone – dry ice) and *n*-butyllithium (328 ml of 1.9 *M* in hexane) was added dropwise with stirring under nitrogen. After the addition was completed the stirring was continued for 2 h, after which time carbon dioxide gas was passed through the solution at a moderate rate. After 6 h the mixture turned dark yellow and was poured into ice water (2000 ml) and washed with chloroform (2 × 700 ml). The aqueous layer was collected, acidified with 10% aqueous hydrochloric acid, and extracted with chloroform (3 × 800 ml). The chloroform solution was dried and evaporated to dryness. The pure acid **3** (48 g, 82%) was obtained by recrystallization from chloroform–ether and melted at 145 °C. *Anal.* calcd. for $C_{11}H_{10}O_4$: C 64.07, H 4.89; found: C 63.95, H 4.93. Spectral data: ir ($CHCl_3$) 1710 cm^{-1} (ketone and carboxyl); nmr ($CDCl_3$) τ 5.84 (2d, 1H, benzylic proton), 6.17 (s, 3H, aromatic methoxyl), 7.00 ppm (t, 2H, methylenic protons).

The acid **3** (40 g) was dissolved in saturated methanolic hydrogen chloride (400 ml) and heated under reflux for 8 h. Evaporation of the solvent and crystallization from benzene–hexane yielded the keto ester **4** (40.6 g, 100%), mp 74 °C. *Anal.* calcd. for $C_{12}H_{12}O_4$: C 65.44, H 5.49; found: C 65.46, H 5.55. Spectral data: ir ($CHCl_3$) 1750, 1725 cm^{-1} (ester, ketone); nmr ($CDCl_3$) τ 5.87 (2d, 1H, benzylic proton), 6.17 (s, 3H, aromatic methoxyl), 6.27 ppm (s, 3H, ester methoxyl).

Preparation of the Enol Ether **5** *from the Keto Ester* **4**

Comopund **4** was converted to the enol ether **5** by the procedure described above for the preparation of **2**. The product **5** was obtained in a quantitative yield as an oil homogeneous in tlc. *Mol. Wt.* calcd. for $C_{13}H_{14}O_4$: 234.0892; found (high resolution mass spectroscopy): 234.0887. Spectral data: ir (CCl_4) 1745, 1625 cm^{-1} (ester, enol ether); nmr (CCl_4) τ 4.75 (d, J = 2 Hz, 1H, vinylic proton), 5.82 (d, J = 2 Hz, 1H, benzylic proton), 6.14 and 6.19 (2s, 6H, 2 methoxyls), 6.34 ppm (s, 3H, ester methoxyl).

The Diels–Alder Adduct **6**

A solution of the enol ether **5** (53 g) and an excess of maleic anhydride (35 g) in xylene (60 ml) was heated under nitrogen to 175 °C (oil bath temperature) for 6 h. After cooling, the solvent and excess maleic anhydride were removed *in vacuo*. Analysis by tlc showed the reaction mixture to consist of two components in a ratio 95:5. The *endo* adduct **6** (49 g) was first isolated by fractional crystallization from acetone. The mother liquid was then subjected to column chromatography on silica gel. Elution with 15% acetone in *n*-hexane gave another 8.4 g of the same product and further elution yielded 2.4 g of the *exo* adduct **6**. The total yield was 79%. The *endo* adduct **6** melted at 203 °C after recrystallization from acetone. *Anal.* calcd. for $C_{17}H_{16}O_7$: C 61.44, H 4.85; found: C 61.33, H 4.89. *Mol. Wt.* calcd. for $C_{17}H_{16}O_7$: 332; found (mass spectroscopy): 332. Spectral data: ir ($CHCl_3$) 1870, 1790 (anhydride), 1740 cm^{-1} (ester); nmr ($CDCl_3$) τ 5.72 (q, J = 9 Hz, 2H,), 6.09 (s, 3H, aromatic methoxyl), 6.20 (s, 3H, ester methoxyl), 6.40 (s, 3H, bridgehead methoxyl), 7.49 ppm (q, 2H, J = 8 Hz, 2H, apex protons).

The *exo* adduct **6** melted at 155 °C after recrystallization from acetone. *Anal.* calcd. for $C_{17}H_{16}O_7$: C 61.44, H 4.85; found: C 61.38, H 4.90. *Mol. Wt.* calcd. for $C_{17}H_{16}O_7$: 332; found (mass spectroscopy): 332. The mass spectra of both isomers were practically identical. Spectral data: ir ($CHCl_3$) 1875, 1790 (anhydride), 1740 cm^{-1} (ester); nmr ($CDCl_3$) τ 6.04 (s, 3H, aromatic methoxyl), 6.15 (s, 3H, ester methoxyl), 6.37 (s, 3H, bridgehead methoxyl), 6.69 (q, 2H, J = 8 Hz,), 7.68 ppm (q, J = 10 Hz, 2H, apex protons).

Decarboxylation of the Adduct **6**

The mixture of the *endo* and *exo* adducts **6** (40 g) was dissolved in anhydrous diglyme (800 ml) and bis(triphenylphosphine)nickel dicarbonyl (100 g) was added. The solution was heated under reflux in a nitrogen atmosphere at 210 °C for 6 h. The solvent was distilled off under reduced pressure, the residue was dissolved in ether, and the black precipitate was removed by filtration. After evaporation of the ether the residue was subjected to chromatography on silica gel. Elution with 8% acetone in *n*-hexane yielded the oily olefin **7** (27.8 g, 81%), homogeneous in tlc. *Mol. Wt.* calcd. for $C_{15}H_{16}O_4$: 260.1049; found (high resolution mass spectroscopy): 260.1041. Spectral data: ir (film) 1740 (ester), 1612 cm^{-1} (double bond); nmr ($CDCl_3$) τ 3.33 (m, 2H, vinylic protons), 6.18 (s, 3H, aromatic methoxyl), 6.27 (s, 3H, ester methoxyl), 6.50 (s, 3H, bridgehead methoxyl), 7.38 ppm (q, J = 6 Hz, 2H, apex protons).

Can. J. Chem. Downloaded from www.nrcresearchpress.com by 210.87.254.42 on 09/05/12
For personal use only.

Can. J. Chem. Downloaded from www.nrcresearchpress.com by 210.87.254.42 on 09/05/12
For personal use only.

*Reduction of the Ester **7** to the Primary Alcohol **8***

A solution of **7** (50 g) in anhydrous ether (300 ml) was added dropwise to a stirred suspension of $LiAlH_4$ (12 g) in anhydrous ether (500 ml) at 0 °C and stirring was continued for a further 2 h at room temperature. After careful addition of wet ether (1000 ml) and 10% aqueous sodium hydroxide (10 ml) the white precipitate was filtered off and the filtrate was dried over anhydrous magnesium sulfate. Evaporation of the solvent yielded 44.5 g of the pure alcohol **8** as a colorless oil homogeneous in tlc. *Mol. Wt.* calcd. for $C_{14}H_{16}O_3$: 232; found (mass spectroscopy): 232. Spectral data: ir ($CHCl_3$) 3650 cm^{-1} (hydroxyl); nmr ($CDCl_3$) τ 3.34 (m, 2H, vinylic protons), 5.74 (s, 2H, protons deshielded by hydroxyl), 6.20 (s, 3H, aromatic methoxyl), 6.44 (s, 3H, bridgehead methoxyl), 7.64 ppm (2d, 2H, apex protons).

*Preparation of the Aldehyde **9***

Trifluoroacetic acid (16 ml) was added dropwise to a solution of compound **8** (43 g), *N,N'*-dicyclohexylcarbodiimide (114 g), anhydrous dimethyl sulfoxide (320 ml) and pyridine (30 ml) in dry benzene (700 ml). The solution was stirred at room temperature overnight and diluted with ether (800 ml). Methanolic oxalic acid (46 g in 100 ml) was added slowly with cooling and stirring. The white precipitate was filtered off and the filtrate was washed several times with saturated aqueous sodium chloride. The organic layer was dried and evaporated to dryness. Chromatography of the residue on silica gel (10% ether in benzene) gave 38 g (89.2%) of the oily aldehyde **9** which behaved homogeneously in tlc. *Mol. Wt.* calcd. for $C_{14}H_{14}O_3$: 230.0943; found (high resolution mass spectroscopy): 230.0940. Spectral data: ir ($CHCl_3$) 2845, 2725, 1725 cm^{-1} (aldehyde); nmr ($CDCl_3$) τ −1.02 (s, 1H, aldehyde proton), 3.14 (m, 2H, vinylic protons), 6.17 (s, 3H, aromatic methoxyl), 6.40 (s, 3H, bridgehead methoxyl), 7.27 ppm (q, 2H, apex protons).

*The Trityl Ether **11***

Commercially available 3-buten-1-ol, **10** (100 g) was dissolved in pyridine (500 ml) and cooled to −10 °C. Trityl chloride (436 g) was added in portions to the stirred solution, and stirring was continued at room temperature for 3 days. After removal of the white precipitate by filtration, most of the solvent was evaporated *in vacuo* and the residue was dissolved in ether. The solution was washed with 5% aqueous hydrochloric acid, aqueous sodium bicarbonate, and with water, dried, and evaporated to dryness. The crude product was purified by a short column chromatography on silica gel, (50% hexane in benzene), to yield pure **11** (390 g, 90%) as an oil homogeneous in tlc. *Mol. Wt.* calcd. for $C_{23}H_{22}O$: 314; found (mass spectroscopy): 314. Spectral data: ir ($CHCl_3$) 1635 cm^{-1} (double bond); nmr ($CDCl_3$) τ 2.67 (m, 15H, phenyl protons), 4.10 (m, 1H, vinylic proton), 4.87, 5.10 (m, 2H, vinylic protons), 6.85 (t, 2H, $—CH_2—O—$), 7.65 ppm (q, 2H, methylenic protons).

*Preparation of the Epoxide **12***

Perbenzoic acid (2500 ml, 0.6 *M* in chloroform) was added dropwise to a stirred mixture of the olefin **11** (390 g) and anhydrous sodium carbonate (120 g) in chloroform (1000 ml) and stirring at room temperature was continued for 12 h. The reaction mixture was filtered, the filtrate was washed several times with 5% aqueous potassium carbonate, and with water. Evaporation of the dried solvent and crystallization of the crude product from hexane gave the pure epoxide **12** in a quantitative yield (mp 89 °C). *Anal.* calcd. for $C_{23}H_{22}O_2$: C 83.60, H 6.71; found: C 83.70, H 6.89. Spectral data: nmr ($CDCl_3$) τ 2.67 (m, 15H, phenyl protons), 6.74 (t, 2H, $—CH_2—O—$), 6.97 (m, 1H, $>C\overset{O}{<}C<^{H}$), 7.40 (q, 2H, $H_2C\overset{O}{<}C<$), 8.20 ppm (q, 2H, methylenic protons).

*Preparation of Compound **14***

A solution of the epoxide **12** (400 g) and sodium methoxide (100 g) in absolute methanol (1200 ml) was heated under reflux in a nitrogen atmosphere for 24 h. The solvent was evaporated *in vacuo*, the residue dissolved in ice water and the resulting aqueous solution was extracted with ether. The extract was washed with water, dried, and evaporated to dryness. The oily alcohol **13** was obtained in a quantitative yield and behaved homogeneously in tlc. It was benzylated without further purification. Spectral data: ir ($CHCl_3$) 3500 cm^{-1} (hydroxyl); nmr ($CDCl_3$) τ 6.00 (m, 1H, proton unshielded by hydroxyl), 6.67 ppm (s, 3H, primary methoxyl).

To a solution of the above material (300 g) in anhydrous dioxane (2500 ml) sodium hydride (69.6 g, 57% suspension in oil) was added in portions and the reaction mixture was heated under reflux for 5 h. At this point benzyl chloride (118 g) was added dropwise and the reflux was continued for another 15 h. The reaction mixture was concentrated under reduced pressure, poured into ice water, and extracted with ether. The extract was dried, evaporated to dryness, and the residue was distilled *in vacuo* (bp 108–114 °C/2 torr) to give the pure compound **14** in a quantitative yield as an oil homogeneous in tlc. *Mol. Wt.* calcd. for $C_{31}H_{32}O_3$: 452; found (mass spectroscopy): 452. Spectral data: nmr ($CDCl_3$) τ 2.67 (m, 20H, phenyl protons), 5.44 (q, 2H, benzylic protons), 6.67 ppm (s, 3H, methoxyl).

*1-Methoxy-2-benzyloxy-4-hydroxybutane, **15***

A solution of compound **14** (274 g) in 90% aqueous acetic acid (500 ml) was heated to 45 °C for 24 h. The solvent was removed under reduced pressure and the residue was diluted with hexane. The white precipitate was filtered off, the filtrate was washed with dilute aqueous sodium bicarbonate and water, dried over anhydrous magnesium sulfate, and evaporated to dryness. Distillation of the residue *in vacuo* (bp 122–125 °C/1 torr) yielded pure **15** (101 g, 80%) as a colorless oil, homogeneous in tlc. The product was identified by ir, nmr, and tlc, with an authentic sample (5). *Mol. Wt.* calcd. for $C_{12}H_{18}O_3$: 210.2156; found (high resolution mass spectroscopy): 210.2154. Spectral data: ir ($CHCl_3$) 3500 cm^{-1} (hydroxyl); nmr ($CDCl_3$) τ 2.65 (br s, 5H, phenyl protons), 5.37 (q,2 H, benzylic protons), 6.28 (t, 2H, protons deshielded by hydroxyl), 6.70 ppm (s, 3H, methoxyl).

*Preparation of the Secondary Alcohol **17***

A small portion (5 ml) of a solution of 1-methoxy-2-benzyloxy-4-bromobutane **16** (180 g, six-fold excess) in anhydrous tetrahydrofuran (1200 ml) was added to a warm stirred mixture of magnesium turnings (15.8 g) and a few iodine crystals in anhydrous tetrahydrofuran

Can. J. Chem. Downloaded from www.nrcresearchpress.com by 210.87.254.42 on 09/05/12
For personal use only.

(100 ml) under nitrogen. As soon as the color of iodine had disappeared, the remaining solution of **16** was added very slowly at 85 °C (oil bath temperature) under nitrogen. After the addition was completed, reflux was maintained for 1 h. A solution of the aldehyde **9** (30 g) in absolute tetrahydrofuran (800 ml) was then added dropwise with stirring and reflux was continued for another 3 h. After cooling, the reaction mixture was poured into a cold 10% aqueous ammonium chloride solution (1000 ml) and extracted with ether (3 × 1000 ml). The combined extracts were dried, evaporated to dryness, and the oily residue was chromatographed on silica gel. The alcohol **17** was eluted with 20% ether in benzene (50 g, 90%). *Mol. Wt.* calcd. for $C_{26}H_{32}O_5$: 424; found (mass spectroscopy): 424. Spectral data: ir ($CHCl_3$) 3615, 3640 cm^{-1} (hydroxyl); nmr ($CDCl_3$) τ 3.02 (m, 2H, vinylic protons), 5.34 (q, 2H, benzylic protons), 6.24 (s, 3H, aromatic methoxyl), 6.44 (s, 3H, bridgehead methoxyl), 6.60 ppm (s, 3H, primary methoxyl).

*Oxidation of the Alcohol **17** to the Ketone **18***

A solution of the alcohol **17** (50 g) in methylene dichloride (500 ml) was added dropwise to a stirred solution of the chromium trioxide – pyridine complex (150 g) in the same solvent (1500 ml) and the mixture was stirred at room temperature overnight. Next morning it was diluted with ether (500 ml) and the brown precipitate was removed by filtration. The filtrate was then washed with 5% aqueous hydrochloric acid (4 × 500 ml), 10% aqueous sodium bicarbonate (2 × 500 ml), and finally with water. The organic layer was dried over anhydrous magnesium sulfate and evaporated to dryness. Chromatography of the residue on silica gel and elution with 5% ether in benzene yielded 44 g (88%) of the ketone **18** as a colorless oil, homogeneous in tlc. *Mol. Wt.* calcd. for $C_{26}H_{30}O_5$: 422.2093; found: (high resolution mass spectroscopy): 422.2093. Spectral data: ir ($CHCl_3$) 1710 cm^{-1} (ketone); nmr ($CDCl_3$) τ 3.04 (m, 2H, vinylic protons), 5.40 (q, 2H, benzylic protons), 6.27 (s, 3H, aromatic methoxyl), 6.47 (s, 3H, bridgehead methoxyl), 6.64 ppm (s, 3H, primary methoxyl).

Aziridine Formation and Rearrangement

Compound **18** (24 g), a large excess of benzenesulfonyl azide (60 g), glacial acetic acid (110 ml), *p*-toluenesulfonic acid (0.48 g) and anhydrous benzene (20 ml), were stirred under nitrogen at room temperature for 10 days. The mixture was diluted with chloroform (2000 ml), washed with saturated aqueous sodium bicarbonate (5 × 100 ml) and several times with water, dried, and evaporated to dryness.

Analysis by tlc (ethyl acetate – benzene, 3:8) indicated the presence of two compounds in a ratio of 3:2. The oily product was separated by column chromatography on silica gel. Elution with 15% ethyl acetate in benzene gave the diketone **19** (15.4 g) and further elution with the same solvent yielded compound **20** (10 g). Compound **19** was oily and homogeneous in tlc; compound **20** crystallized and melted at 170 °C. The total yield was 80%.

Compound **19**. *Mol. Wt.* calcd. for $C_{31}H_{33}O_7NS$: 563.1978; found (high resolution mass spectroscopy): 563.1973. Spectral data: ir ($CHCl_3$) 3370 (NH), 1756 (five-membered ketone), 1710 (side chain ketone), 1350, 1160 cm^{-1} (sulfonyl); nmr ($CDCl_3$) τ 3.94 (d, J = 6 Hz, 1H, —NH), 5.40 (q, 2H, benzylic protons), 5.87 (d, J = 6 Hz, 1H, apex proton), 6.27 (s, 3H, aromatic methoxyl), 7.64 ppm (s, 3H, side chain methoxyl).

Compound **20**. *Anal.* calcd. for $C_{34}H_{39}O_9NS$: C 64.03, H 6.16, N 2.20; found: C 63.74, H 6.23, N 2.22. Spectral data: ir ($CHCl_3$) 3410 (NH), 1740 (acetate), 1712 cm^{-1} (ketone); nmr ($CDCl_3$) τ 5.50 (q, 2H, benzylic protons), 6.27 (s, 3H, aromatic methoxyl), 6.67 (s, 3H, bridgehead methoxyl), 6.70 (s, 3H, side chain methoxyl), 7.90 ppm (s, 3H, acetoxy methyl).

*Conversion of Compound **19** to the Diastereoisomeric Mixture **21***

The diketone **19** (12.0 g) and $LiAlH_4$ (12 g) were refluxed under nitrogen in anhydrous dioxane (300 ml) for 20 h. The mixture was then cooled with ice, and methanol (5 ml) followed by 10% aqueous sodium hydroxide (4 ml) were added dropwise. The white precipitate was filtered off and washed with ether (4 × 100 ml), and tetrahydrofuran (2 × 100 ml). The combined filtrates were evaporated to dryness and the residue was acetylated with acetic anhydride (10 ml) and pyridine (100 ml) at 45 °C overnight. Most of the solvent was removed *in vacuo* and the residue was dissolved in chloroform (800 ml). The solution was washed with dilute hydrochloric acid, aqueous sodium bicarbonate, and with water. After drying over anhydrous sodium sulfate, evaporation of the solvent gave a yellow residue which was subjected to chromatography on silica gel. Elution with chloroform–methanol (99:1) yielded 8.12 g (70%) of the mixture **21** as a colorless oil.

When this mixture was examined by tlc on silica gel (methanol–chloroform 4:96), it was possible to resolve it into two groups of diastereoisomers which were epimers with respect to the ring B acetoxyl. For analytical purposes, the two groups of epimers were separated by preparative tlc.

exo-Epimers: *Mol. Wt.* calcd. for $C_{31}H_{39}O_8N$: 553.2676; found (high resolution mass spectroscopy): 553.2677. Spectral data: ir ($CHCl_3$) 3460 (NH), 1737 (acetate), 1678 cm^{-1} (amide); nmr ($CDCl_3$) τ 3.80 (d, J = 8 Hz, 1H, —N—H), 4.54 (m, 1H, proton deshielded by acetoxyl), 5.20 (m, 1H, proton deshielded by acetoxyl), 5.47 (t, 2H, benzylic protons), 5.80 (d, J = 16 Hz, 1H, apex proton), 6.20 (s, 3H, aromatic methoxyl), 6.70 (s, 3H, primary methoxyl), 7.90 (s, 6H, acetoxy methyls), 8.00 ppm (s, 3H, —N—C—CH_3).

endo-Epimers: *Mol. Wt.* calcd. for $C_{31}H_{39}O_8N$: 553.2676; found (high resolution mass spectroscopy): 553.2677. The mass spectra of both epimers were practically identical. Spectral data: ir ($CHCl_3$) 3460 (NH), 1735 (acetate), 1678 cm^{-1} (amide); nmr ($CDCl_3$) τ 4.00 (d, J = 7 Hz, 1H, —N—H), 4.50 (m, 2H, protons deshielded by acetoxyls), 5.40 (q, 2H, benzylic protons), 6.20 (s, 3H, aromatic methoxyl), 6.56 (s, 3H, primary methoxyl), 7.90 (s, 3H, side chain acetoxy methyl), 8.00

Can. J. Chem. Downloaded from www.nrcresearchpress.com by 210.87.254.42 on 09/05/12
For personal use only.

(s, 3H, —N—C—CH_3), 8.17 ppm (s, 3H, ring B endo acetoxy methyl shielded by the aromatic ring, *cf.* ref. 5).

*Selective Hydrolysis of the Diacetate **21** to the Hydroxy Acetate **22***

A solution of the diacetate **21** (7.5 g) in methanolic potassium carbonate (750 ml, p*H* 8.5) was stirred at room temperature for 5 h. After this time the solution was neutralized with 5% aqueous hydrochloric acid (2.5 ml) and poured into saturated aqueous sodium chloride (700 ml). The mixture was then extracted with chloroform (5 × 400 ml) and the extract was dried over anhydrous magnesium sulfate. After evaporation of the chloroform, the residue was chromatographed on silica gel and gave the hydroxy acetate **22** (5.9 g, 85%) as a waxy material. For analysis, the two groups of epimers were separated by preparative tlc on silica gel.

exo-Epimers: *Mol. Wt.* calcd. for $C_{29}H_{37}O_7N$: 511.2570; found (high resolution mass spectroscopy): 511.2571. Spectral data: ir ($CHCl_3$) 3620 (hydroxyl), 3430 (NH), 1730 (acetate), 1674 cm^{-1} (amide); nmr ($CDCl_3$) τ 4.60 (m, 1H, proton deshielded by acetoxyl), 5.40 (t, 2H, benzylic protons), 6.27 (s, 3H, aromatic methoxyl), 6.67 (s, 3H, primary methoxyl), 6.94 (br s, 1H, benzylic bridgehead proton), 7.97 (s, 3H, acetoxy methyl), 8.07

ppm (s, 3H, —N—C—CH_3).

endo-Epimers: *Mol. Wt.* calcd. for $C_{29}H_{37}O_7N$: 511.2570; found (high resolution mass spectroscopy): 511.2571. Spectral data: ir ($CHCl_3$) 3588 (hydroxyl), 3462 (NH), 1735 (acetate), 1675 cm^{-1} (amide); nmr ($CDCl_3$) τ 4.50 (m, 1H, proton deshielded by acetoxyl), 5.40 (q, 2H, benzylic protons), 6.21 (s, 3H, aromatic methoxyl), 6.64 (s, 3H, primary methoxyl), 7.94 (s, 3H,

acetoxy methyl), 8.04 ppm (s, 3H, —N—C—CH_3).

*Preparation of the Diol **23***

Compound **22** (5 g) was hydrogenated in methanol (250 ml) with 10% palladium-on-charcoal (1.5 g) at atmospheric pressure and room temperature for 6 h. The catalyst was removed by filtration on celite and the solvent was evaporated under reduced pressure. The diol **23** (3.45 g, 85%) was obtained as a foam. The analytical samples of the two groups of epimers were obtained by preparative tlc on silica gel.

exo-Epimers: *Mol. Wt.* calcd. for $C_{22}H_{31}O_7N$: 421; found (mass spectroscopy): 421. Spectral data: ir ($CHCl_3$) 3620 (hydroxyl), 3430 (NH), 1735 (acetate), 1675 cm^{-1} (amide); nmr ($CDCl_3$) τ 4.47 (m, 1H, proton deshielded by acetoxyl), 6.24 (s, 3H, aromatic methoxyl), 6.64 (s, 3H, primary methoxyl), 6.87 (br s, 1H, benzylic bridgehead proton), 7.49 (s, 3H, acetoxy methyl), 8.04 ppm (s, 3H,

—N—C—CH_3).

endo-Epimers: *Mol. Wt.* calcd. for $C_{22}H_{31}O_7N$: 421; found (mass spectroscopy): 421. Both groups of epimers have identical mass spectra. Spectral data: ir ($CHCl_3$) 3600 (hydroxyl), 3462 (NH), 1740 (acetate), 1675 cm^{-1} (amide); nmr ($CDCl_3$) τ 4.40 (m, 1H, proton deshielded by acetoxyl), 6.20 (s, 3H, aromatic methoxyl), 6.64 (s, 3H, primary methoxyl), 7.90 (s, 3H, acetoxy methyl), 8.00 ppm

s, 3H, —N—C—CH_3).

*Oxidation of the Diol **23** to the Diketone **24***

A solution of the diol **23** (3 g) in dry methylene chloride (30 ml) was added dropwise at room temperature to a stirred solution of the chromium trioxide – pyridine complex (12 g) in the same solvent (130 ml). The mixture was stirred at room temperature for 2 days after which time it was diluted with ether (200 ml) and the brown precipitate was filtered off. The filtrate was washed with dilute aqueous hydrochloric acid (2 × 200 ml), 10% aqueous sodium bicarbonate, and water. After drying the solvent was evaporated and chromatography of the residue on silica gel gave 2.4 g (80%) of the crystalline diketone **24**. This material was a mixture of two epimers in a ratio 4:1. For analytical purposes, a portion of the mixture was separated by preparative tlc and the pure epimers were recrystallized from ether. The major α-epimer melted at 83 °C, while the minor β-epimer melted at 228 °C.

α-Epimer: *Anal.* calcd. for $C_{22}H_{27}O_7N$: C 63.29, H 6.52, N 3.37; found: C 63.34, H 6.63, N 3.36. Spectral data: ir ($CHCl_3$) 3450 (NH), 1750 (five-membered ketone), 1730 (ketone and acetate), 1678 cm^{-1} (amide);

nmr ($CDCl_3$) τ 3.32 (d, J = 7 Hz, 1H, —N—H), 4.34 (2d, 1H, proton deshielded by acetoxyl), 5.10 (d, J = 7 Hz,

1H, apex proton), 5.96 (s, 2H, —C—CH_2—OCH_3), 6.24 (s, 3H, aromatic methoxyl), 6.54 (s, 3H, primary methoxyl),

7.90 (s, 3H, acetoxyl), 8.00 ppm (s, 3H, —N—C—CH_3).

β-Epimer: *Anal.* calcd. for $C_{22}H_{27}O_7N$: C 63.29, H 6.52, N 3.37; found: C 63.27, H 6.63, N 3.29. The mass spectra of both epimers were identical. Spectral data: ir ($CHCl_3$) 3450 (NH), 1750 (five-membered ketone), 1730 (ketone and acetate), 1678 cm^{-1} (amide); nmr ($CDCl_3$) τ 3.46 (d, J = 8 Hz, 1H, —N—H), 4.40 (t, 1H, proton deshielded by acetoxyl), 5.35 (d, J = 8 Hz, 1H, apex

proton), 5.97 (s, 2H, —C—CH_2—OCH_3), 6.20 (s, 3H, aromatic methoxyl), 6.57 (s, 3H, primary methoxyl), 7.87

(s, 3H, acetoxyl), 7.94 ppm (s, 3H, —N—C—CH_3).

*Preparation of the α,β-Unsaturated Ketone **25***

A solution of the diketone **24** (9.05 g) and potassium carbonate (9 g) in absolute methanol (900 ml) was heated under reflux in a nitrogen atmosphere for 8 h. The reaction mixture was carefully neutralized with dilute hydrochloric acid, most of the solvent was removed *in vacuo* and water (600 ml) was added. The mixture was extracted with chloroform (3 × 200 ml) and the combined extracts

Can. J. Chem. Downloaded from www.nrcresearchpress.com by 210.87.254.42 on 09/05/12
For personal use only.

were dried and evaporated to dryness. The crude product was crystallized from chloroform–ether and gave 6.2 g (80%) of the unsaturated ketone **25**. For analysis, samples of the α- and β-epimers were obtained by preparative tlc and recrystallized from chloroform ether.

α-Epimer, mp 230 °C: *Anal.* calcd. for $C_{20}H_{23}O_5N$: C 67.21, H 6.48, N 3.91; found: C 67.04, H 6.45, N 3.96. Spectral data: ir ($CHCl_3$) 3600 (hydroxyl), 3440 (NH), 1720 (conjugated five-membered ketone), 1658 cm^{-1} (conjugated double bond and amide); uv λ_{max} (EtOH) 240 nm (ε 14 280); nmr ($CDCl_3$) τ 2.57 (d, J = 9 Hz, 1H, proton *meta* to methoxyl), 3.17 (d, J = 3 Hz, 1H, proton *ortho* to methoxyl), 3.34 (q, J = 9 Hz, J = 3 Hz, 1H, proton *ortho* to methoxyl), 5.59 (2d, J = 13 Hz, 2H, —C=C—CH_2—OCH_3), 6.27 (s, 3H, aromatic methoxyl), 6.50 (br s, 1H, benzylic bridgehead proton), 6.74 (s, 3H, primary methoxyl), 7.97 ppm (s, 3H, —N—C(=O)—CH_3).

β-Epimer, mp 136 °C: *Anal.* calcd. for $C_{20}H_{23}O_5N$: C 67.21, H 6.48, N 3.91; found: C 66.80, H 6.43, N 4.19. The mass spectra of both epimers were identical. Spectral data: ir ($CHCl_3$) 3600 (hydroxyl), 3450 (NH), 1720 (conjugated five-membered ketone), 1658 cm^{-1} (conjugated double bond and amide); uv λ_{max} (EtOH) 242 nm (ε 14 470); nmr ($CDCl_3$) τ 3.00 (d, J = 8 Hz, 1H, proton *meta* to methoxyl), 3.14 (d, J = 2.5 Hz, 1H, proton *ortho* to methoxyl), 3.34 (q, J = 8 Hz, J = 2.5 Hz, 1H, proton *ortho* to methoxyl), 5.78 (2d, J = 13 Hz, 2H, —C=C—CH_2—OCH_3), 6.14 (br s, 1H, benzylic bridgehead proton), 6.24 (s, 3H, aromatic methoxyl), 6.77 (s, 3H, primary methoxyl), 8.00 ppm (s, 3H, —N—C(=O)—CH_3).

Photoaddition of Vinyl Acetate to the Enone ***25***

A solution of the enone **25** (8.75 g) and vinyl acetate (200 ml) in freshly distilled tetrahydrofuran (250 ml) was irradiated in a nitrogen atmosphere at −78 °C for 2 h with a 200 W Hanovia mercury lamp through a pyrex filter. After evaporation of the vinyl acetate and of the solvent, the crude product was crystallized from ether to yield 9.7 g, (89%) of the adduct **26**. A small portion of this material was separated by preparative tlc. Both epimers were recrystallized from ether.

α-Epimer, mp 224 °C: *Anal.* calcd. for $C_{24}H_{29}O_7N$: C 64.99, H 6.59, N 3.15; found: C 64.86, H 6.63, N 3.04. Spectral data: ir ($CHCl_3$) 3500 (hydroxyl), 3425 (NH), 1750 (five-membered ketone), 1738 (acetate), 1670 cm^{-1} (amide); nmr ($CDCl_3$) τ 2.94 (d, J = 8 Hz, 1H, —NH), 4.57 (q, 1H, proton deshielded by acetoxyl), 5.67 (d, J = 8 Hz, 1H, apex proton), 6.17 (s, 3H, aromatic methoxyl), 6.34 (br s, 1H, benzylic bridgehead proton), 7.20 (s, 3H, primary methoxyl shielded by benzene ring), 7.84 (s, 3H, acetoxy methyl), 8.14 ppm (s, 3H, —N—C(=O)—CH_3).

β-Epimer, mp 159 °C: *Anal.* calcd. for $C_{24}H_{29}O_7N$: C 64.99, H 6.59, N 3.15; found: C 65.03, H 6.65, N 3.18. The mass spectra of both epimers were identical. Spectral data: ir ($CHCl_3$) 3500 (hydroxyl), 3425 (NH), 1750 (five-membered ketone), 1740 (acetate), 1670 cm^{-1} (amide); nmr ($CDCl_3$) τ 3.36 (d, 1H, —NH), 4.60 (q, 1H, proton deshielded by acetoxyl), 5.70 (d, 1H, apex proton), 6.17 (s, 3H, aromatic methoxyl), 7.10 (s, 3H, primary methoxyl shielded by benzene ring), 7.80 (s, 3H, acetoxy methyl), 8.10 ppm (s, 3H, —N—C(=O)—CH_3).

Preparation of the Aldehyde ***27***

The photoadduct **26** (5.0 g) was saponified in 1% methanolic potassium hydroxide (150 ml) at room temperature (for 4 h). The reaction mixture was poured into water, extracted with chloroform, the extract was washed with water, dried over anhydrous magnesium sulfate, and evaporated to dryness. The crude product was purified by chromatography on silica gel and gave 4.01 g (88%) of the aldehyde **27** as a foam. A portion of this material was separated by preparative tlc. Both epimers were foams and homogeneous in tlc in several solvent systems.

α-Epimer: *Mol. Wt.* calcd. for $C_{22}H_{27}O_6N$: 401.1838; found (high resolution mass spectroscopy): 401.1833. Spectral data: ir ($CHCl_3$) 3500, 3350 (hydroxyl, NH), 2700 (aldehyde), 1745 (five-membered ketone), 1715 (aldehyde), 1675 cm^{-1} (amide); nmr ($CDCl_3$) τ 0.04 (t, 1H, aldehyde proton), 2.24 (d, J = 7 Hz, 1H, —N—H), 5.85 (d, J = 7 Hz, 1H, apex proton), 6.19 (s, 3H, aromatic methoxyl), 7.38 (s, 3H, primary methoxyl shielded by benzene ring), 7.94 ppm (s, 3H, —N—C(=O)—CH_3).

β-Epimer: *Mol. Wt.* calcd. for $C_{22}H_{27}O_6N$: 401.1838; found (high resolution mass spectroscopy): 401.1834. Both epimers had identical mass spectra. Spectral data: ir ($CHCl_3$) 3500, 3442 (hydroxyl, NH), 2707 (aldehyde), 1748 (five-membered ketone), 1715 (aldehyde), 1675 cm^{-1} (amide); nmr ($CDCl_3$) τ 0.17 (t, 1H, aldehyde proton), 2.50 (d, J = 8 Hz, 1H, —N—H), 5.90 (d, J = 8 Hz, 1H, apex proton), 6.20 (s, 3H, aromatic methoxyl), 7.24 (s, 3H, primary methoxyl shielded by benzene ring), 8.00 ppm (s, 3H, —N—C(=O)—CH_3).

Preparation of the Acetal ***29***

A solution of the aldehyde **27** (2.03 g), trimethyl orthoformate (9.6 ml), and *p*-toluenesulfonic acid (54 mg) in anhydrous peroxide free dioxane (60 ml) was stirred at room temperature for 5 h. After this time pyridine (3 ml) was added and the solution was evaporated to dryness *in vacuo*. The unstable hydroxy acetal **28** was immediately acetylated with acetic anhydride (4.5 ml) and pyridine (30 ml) at room temperature overnight and worked up in the usual manner. The crude material was chromatographed on silica gel and gave 1.99 g (80%) of the oily acetal **29**. For analysis, the two epimers were separated by preparative tlc.

α-Epimer: *Mol. Wt.* calcd. for $C_{26}H_{35}O_8N$: 489.2046; found (high resolution mass spectroscopy): 489.2041. Spectral data: ir ($CHCl_3$) 3445 (NH), 1740 (five-membered

Can. J. Chem. Downloaded from www.nrcresearchpress.com by 210.87.254.42 on 09/05/12
For personal use only.

ketone and acetate), 1685 cm^{-1} (amide); nmr ($CDCl_3$) τ 5.07 (t, 1H, proton deshielded by acetoxyl), 5.47 (t, 1H, —*CH*(OCH_3)$_2$), 6.20 (s, 3H, aromatic methoxyl), 6.70 and 6.72 (2s, 6H, acetal), 7.42 (s, 3H, primary methoxyl shielded by benzene ring), 7.92 (s, 3H, acetoxy methyl), 8.00 ppm (s, 3H, —N(—C(=O)—CH_3)—).

β-Epimer: *Mol. Wt.* calcd. for $C_{26}H_{35}O_8N$: 489.2046; found (high resolution mass spectroscopy): 489.2047. The mass spectra of both epimers were identical. Spectral data: ir ($CHCl_3$) 3446 (NH), 1740 (five-membered ketone and acetate), 1683 cm^{-1} (amide); nmr ($CDCl_3$) τ 4.27 (br s, 1H, proton deshielded by acetoxyl), 5.37 (t, 1H, —*CH*(OCH_3)$_2$), 6.20 (s, 3H, aromatic methoxyl), 6.67 and 6.70 (2s, 6H, acetal), 7.44 (s, 3H, primary methoxyl shielded by benzene ring), 7.90 (s, 3H, acetoxy methyl), 8.00 ppm (s, 3H, —N(—C(=O)—CH_3)—).

Preparation of the Enol Ether 30

A solution of compound **29** (470 mg) and pyridine (825 mg) in *p*-xylene (24 ml) was refluxed under nitrogen for 36 h, after which time the solvent was removed *in vacuo* and the enol ether **30** (460 mg, 100%) was obtained as an unstable oil. It had to be used immediately for the subsequent step. *Mol. Wt.* calcd. for $C_{25}H_{31}O_7N$: 457; found (mass spectroscopy): 457. Spectral data: ir ($CHCl_3$) 3400 (NH), 1740 (five-membered ketone and acetate), 1687 (amide), 1650 cm^{-1} (enol ether); nmr ($CDCl_3$) τ 3.69 (d, J = 13 Hz, 1H, vinylic proton), 4.57 (d, J = 13 Hz, 1H, vinylic proton), 5.07 (t, 1H, proton deshielded by acetoxyl), 6.47 (s, 3H, —CH=CH—O*CH*$_3$), 6.20 (s, 3H, aromatic methoxyl), 7,34 (s, 3H, primary methoxyl shielded by benzene ring), 7.92 (s, 3H, acetoxyl), 8.00 ppm (s, 3H, —N(—C(=O)—CH_3)—).

Preparation of the Keto Ester 31

A solution of the enol ether **30** (900 mg) in acetone (20 ml) was added dropwise to a stirred solution of sodium metaperiodate (2.42 g), potassium carbonate (600 mg), and potassium permanganate (80 mg) in acetone (60 ml) and water (30 ml). The mixture was stirred at room temperature for 48 h. The acetone was then removed *in vacuo*, the residue poured into water (200 ml) and the aqueous solution washed with ether. The aqueous layer was acidified with dilute hydrochloric acid, and extracted with chloroform (5 × 150 ml). After drying over anhydrous magnesium sulfate and evaporation of the chloroform, the white solid material (840 mg) was dissolved in methylene chloride (30 ml) and treated with excess diazomethane. Evaporation of the solvent and crystallization of the crude product from ether gave the keto ester **31** (610 mg, 70%). The two epimers were separated for analytical purposes by preparative tlc and recrystallized from ether.

α-Epimer, mp 224 °C: *Anal.* calcd. for $C_{24}H_{29}O_8N$: C 62.73, H 6.36, N 3.05; found: C 62.83, H 6.40, N 2.96. *Mol. Wt.* calcd. for $C_{24}H_{29}O_8N$: 459; found (mass spectroscopy): 459. Spectral data: ir ($CHCl_3$) 3430 (NH), 1750 (five-membered ketone), 1740 and 1733 (acetate and ester), 1683 cm^{-1} (amide); nmr ($CDCl_3$) τ 4.97 (t, 1H, proton deshielded by acetoxyl), 6.22 (s, 3H, aromatic methoxyl), 6.29 (s, 3H, —C(=O)—OCH_3), 6.80 (q, 2H, —C(H)—*CH*$_2$—OCH_3), 7.50 (s, 3H, primary methoxyl shielded by benzene ring), 7.92 (s, 3H, acetoxyl), 8.04 ppm (s, 3H, —N(—C(=O)—CH_3)—).

β-Epimer, mp 210 °C: *Anal.* calcd. for $C_{24}H_{29}O_8N$: C 62.73, H 6.36, N 3.05; found: C 62.63, H 6.39, N 3.03. *Mol. Wt.* calcd. for $C_{24}H_{29}O_8N$: 459.1893; found (high resolution mass spectroscopy): 459.1908. Both epimers had identical mass spectra. Spectral data: ir ($CHCl_3$) 3436 (NH), 1750 (five-membered ketone), 1742 and 1738 (acetate and ester), 1683 cm^{-1} (amide); nmr ($CDCl_3$) τ 4.27 (br s, 1H, proton deshielded by acetoxyl), 6.20 (s, 3H, aromatic methoxyl), 6.24 (s, 3H, —C(=O)—OCH_3), 6.90 (q, 2H, —C(H)—*CH*$_2$—OCH_3), 7.44 (s, 3H, primary methoxyl shielded by benzene ring), 7.90 (s, 3H, acetoxyl), 8.00 ppm (s, 3H, —N(—C(=O)—CH_3)—).

Ring Closure to the Keto Lactam 32

A solution of the keto ester **31** (795 mg) in absolute methanol (60 ml) was added to a solution of sodium methoxide prepared by dissolving sodium metal (600 mg) in absolute methanol (210 ml). The resulting mixture was heated under reflux in a nitrogen atmosphere for 48 h. After evaporation of the solvent under reduced pressure, the residue was dissolved in water, acidified with dilute HCl, and extracted with chloroform (3 × 150 ml). The combined extracts were dried and evaporated to dryness. The product was crystallized from chloroform and yielded 471 mg (80%) of the keto lactam **32**. For analytical purposes, the two epimers were again separated by preparative tlc and recrystallized from chloroform.

α-Epimer, mp 180 °C: *Anal.* calcd. for $C_{19}H_{21}O_5N$: C 69.36, H 6.46, N 4.08; found: C 69.47, H 6.24, N 3.98. *Mol. Wt.* calcd. for $C_{19}H_{21}O_5N$: 343.1420; found (high resolution mass spectroscopy): 343.1415. Spectral data: ir (KBr) 3460 (OH and NH), 1750 (five-membered ketone), 1640 cm^{-1} (lactam); nmr (DMSO-d_6) τ 2.39 (d, 1H, —N(H)—H), 2.39 (d, J = 8 Hz, 1H, proton *meta* to methoxyl), 3.19 (d, J = 1 Hz, 1H, proton *ortho* to methoxyl), 3.21 (q, J = 8 Hz, 1 Hz, 1H, proton *ortho* to methoxyl), 6.24 (s, 3H, aromatic methoxyl), 6.63 ppm (s, 3H, primary methoxyl).

β-Epimer, mp 246 °C: *Anal.* calcd. for $C_{19}H_{21}O_5N$: C 69.36, H 6.46, N 4.08; found: C 69.47, H 6.24, N 3.98. *Mol. Wt.* calcd. for $C_{19}H_{21}O_5N$: 343.1420; found (high resolution mass spectroscopy): 343.1421. Spectral data: ir (KBr) 3500 and 3475 (OH and NH), 1750 (five-membered ketone), 1646 cm^{-1} (lactam); nmr (DMSO-d_6) τ 2.20 (d, 1H, —N(H)—H), 2.69 (d, J = 8 Hz, 1H, proton

Can. J. Chem. Downloaded from www.nrcresearchpress.com by 210.87.254.42 on 09/05/12
For personal use only.

meta to methoxyl), 3.10 (d, J = 1 Hz, 1H, proton *ortho* to methoxyl), 3.20 (q, J = 8 Hz, 1 Hz, 1H, proton *ortho* to methoxyl), 6.20 (s, 3H, aromatic methoxyl), 6.65 ppm (primary methoxyl).

*Reduction of the β-Hydroxy Keto Lactam **32** to the Diol **34***

Excess lithium tri-*tert*-butoxyaluminum hydride (300 mg) was added to a solution of the β-epimer **32** (100 mg) in anhydrous tetrahydrofuran (30 ml) and the reaction mixture was stirred at room temperature for 2 days. Water was then added and the aqueous solution was extracted with chloroform (4 × 50 ml). Drying and evaporation of the chloroform gave the diol **34** as a foam in a quantitative yield. It behaved homogeneously in tlc in several solvent systems. *Mol. Wt.* calcd. for $C_{19}H_{23}O_5N$: 345.1576; found (high resolution mass spectroscopy): 345.1584. Spectral data: ir ($CHCl_3$) 3500, 3350 (OH and NH), 1667 cm^{-1} (lactam); nmr ($CDCl_3$) τ 5.50 (m, 1H, proton deshielded by ring A hydroxyl), 5.78 (d, J = 8 Hz, 1H, proton deshielded by ring-B *exo*-hydroxyl), 6.20 (s, 3H, aromatic methoxyl), 6.65 ppm (s, 3H, primary methoxyl).

*Oxidation of Compound **32** to the Diketone **33***

The mixture of epimers **32** (830 mg) was oxidized at 0 °C with the Jones reagent in acetone (100 ml) for 1 h. The solvent was then removed under reduced pressure and the reaction mixture was poured into water. The product was extracted with chloroform (3 × 100 ml), the chloroform solution was washed with water, dried over anhydrous magnesium sulfate, and evaporated to dryness. The crude material was crystallized from chloroform and gave the pure diketone **33** (740 mg, 80%) as white crystals. It behaved homogeneously in tlc in several solvent systems. An analytical sample was prepared by recrystallization from chloroform–ether and melted at 253 °C. *Anal.* calcd. for $C_{19}H_{19}O_5N$: C 66.85, H 5.61, N 4.10; found: C 66.78, H 5.59, N 4.09. *Mol. Wt.* calcd. for $C_{19}H_{19}O_5N$: 341.1263; found (high resolution mass spectroscopy): 341.1255. Spectral data: ir (KBr) 3300 (NH), 1750 (five-membered ketone), 1700 (six-membered ketone), 1667 cm^{-1} (lactam); nmr (DMSO-d_6) τ 6.20 (s, 3H, aromatic methoxyl), 6.62 ppm (s, 3H, primary methoxyl).

*Reduction of the Diketone **33** to the Diol **34***

The diketone **33** was subjected to a reduction by the same procedure used in the preparation of the diol **34** from the β-epimer **32**. Work-up gave the identical diol **34** in a quantitative yield.

*Acetylation of Compound **34***

A mixture of the diol **34** (30 mg), and *p*-toluenesulfonic acid (5 mg) in acetic anhydride (2 ml) was stirred at room temperature for 24 h. The solvent was evaporated *in vacuo* and the residue was dissolved in chloroform and washed with dilute aqueous sodium bicarbonate and water. After drying over magnesium sulfate, evaporation gave a mixture of compounds **35** and **36**. After separation by preparative tlc on silica gel, 20 mg of the oily diacetate **35** and 9 mg of the crystalline lactone **36** (mp 222 °C) were obtained. The total yield was 92%.

Diacetate **35**: *Mol. Wt.* calcd. for $C_{23}H_{27}O_7N$: 429.1788; found (high resolution mass spectroscopy): 429.1778. Spectral data: ir ($CHCl_3$) 3440 (NH), 1738 (acetate), 1667 cm^{-1} (lactam); nmr ($CDCl_3$) τ 4.34 (t, 1H, proton deshielded by ring-A acetoxyl), 5.17 (d, J = 8 Hz, 1H, proton deshielded by ring-B acetoxyl), 6.20 (s, 3H, aromatic methoxyl), 6.75 (s, 3H, primary methoxyl), 7.94 (s, 3H, acetate), 8.10 ppm (s, 3H, acetate).

Lactone **36**: *Mol. Wt.* calcd. for $C_{23}H_{27}O_7N$: 429.1788; found (high resolution mass spectroscopy): 429.1788. Spectral data: ir ($CHCl_3$) 3480 (NH), 1775 (lactone), 1738 (acetate), 1692 cm^{-1} (amide); nmr ($CDCl_3$) τ 4.34 (t, 1H, proton deshielded by ring-A acetoxyl), 5.17 (d, 1H, proton deshielded by lactone), 6.20 (s, 3H, aromatic methoxyl), 6.75 (s, 3H, primary methoxyl), 7.94 (s, 3H, acetate), 8.02 ppm (s, 3H, $-\overset{|}{N}-\overset{\overset{O}{\|}}{C}-CH_3$).

*Conversion of Compound **36** to **34***

Compound **36** (9 mg) was dissolved in 1% methanolic potassium hydroxide (5 ml) and the mixture was stirred at room temperature for one week. The usual work-up yielded quantitatively the diol **34**.

*Methylation of Compound **34** to **37***

A mixture of compound **34** (232 mg) and sodium hydride (280 mg, 57% oil suspension) in anhydrous dioxane (20 ml) was refluxed under nitrogen for 2½ h. After cooling to room temperature, excess methyl iodide (1 ml) was added and the solution was refluxed for another 2 h. The mixture was then filtered through celite, the filtrate was diluted with ether, washed with water, dried over anhydrous magnesium sulfate, and evaporated to dryness. The crude product was purified by preparative tlc on silica gel and yielded 160 mg (62%) of the oily methylation product **37**. *Mol. Wt.* calcd. for $C_{22}H_{29}O_5N$: 387.2046; found (high resolution mass spectroscopy): 387.2045. Spectral data: ir ($CHCl_3$) 1633 cm^{-1} (tertiary amide); nmr ($CDCl_3$) τ 6.20 (s, 3H, aromatic methoxyl), 6.60, 6.65, and 6.69 (3s, 9H, 3 methoxyls), 7.07 ppm (s, 3H, $-\overset{|}{N}-CH_3$).

*Preparation of the Amine **38***

Lithium aluminum hydride (400 mg) was added to the lactam **37** (400 mg) dissolved in anhydrous dioxane. The mixture was heated under reflux for 20 h and worked up in the usual manner. The crude product was purified by preparative tlc on silica gel. The pure tertiary amine **38** (253 mg, 66%) was an oil homogeneous in tlc in several systems. *Mol. Wt.* calcd. for $C_{22}H_{31}O_4N$: 373.2253; found (high resolution mass spectroscopy): 373.2239. Spectral data: ir ($CHCl_3$) no amide absorption; nmr ($CDCl_3$) τ 6.20 (s, 3H, aromatic methoxyl), 6.60, 6.65, and 6.69 (3s, 9H, 3 methoxyls), 7.64 ppm (s, 3H, $-\overset{|}{N}-CH_3$).

*Preparation of the N-Formyl Derivative **39***

A mixture of the amine **38** (225 mg), potassium permanganate (200 mg), acetic acid (2.4 ml) and acetone (56 ml) was stirred at room temperature for 15 min. The excess of potassium permanganate was then destroyed with sodium sulfite and sulfuric acid, most of the solvent was evaporated *in vacuo*, and the residue was dissolved in ether and washed with water. The ether extract was dried

over anhydrous magnesium sulfate and evaporated to dryness. Separation by preparative tlc yielded 155 mg of the *N*-formyl compound **39** and 46 mg of the tertiary lactam **37**, both oily and homogeneous in tlc. The total yield was 86%. *Mol. Wt.* calcd. for $C_{22}H_{29}O_5N$: 387.2046; found (high resolution mass spectroscopy): 387.2036. Spectral data: ir ($CHCl_3$) 1658 cm^{-1} (formamide); nmr

($CDCl_3$) τ 1.84 (s, 1H, —N—C—H), 6.20 (s, 3H, aromatic methoxyl), 6.60, 6.65, and 6.69 ppm (3s, 9H, three methoxyls).

Acknowledgements

We wish to thank the National Research Council of Canada, Ottawa, and the Hoffmann – La Roche Company, Vaudreuil, Quebec, for the generous support of this synthetic study.

1. K. Wiesner, P. T. Ho, W. C. Liu, and M. N. Shanbhag. Can. J. Chem. **53**, 2140 (1975).
2. S. W. Pelletier, Z. Djarmati, and S. Lajsic. J. Am. Chem. Soc. **96**, 7817 (1974).
3. K. Wiesner, P. T. Ho, D. Chang, Y. K. Lam, C. S. J. Pan, and W. Y. Ren. Can. J. Chem. **51**, 3978 (1973).
4. K. Wiesner, P. T. Ho, R. C. Jain, S. F. Lee, S. Oida, and A. Philipp. Can. J. Chem. **51**, 1448 (1973).
5. K. Wiesner, E. W. K. Jay, T. Y. R. Tsai, C. Demerson, L. Jay, T. Kanno, J. Krèpinský, A. Vilim, and C. S. Wu. Can. J. Chem. **50**, 1925 (1972).
6. H. O. House and C. B. Hudson. J. Org. Chem. **35**, 647 (1970).

Can. J. Chem. Downloaded from www.nrcresearchpress.com by 210.87.254.42 on 09/05/12
For personal use only.

The lithium–indium system[1]

W. A. ALEXANDER, L. D. CALVERT, R. H. GAMBLE, AND K. SCHINZEL
Division of Chemistry, National Research Council of Canada, Ottawa, Canada K1A 0R9

Received September 2, 1975

W. A. ALEXANDER, L. D. CALVERT, R. H. GAMBLE, and K. SCHINZEL. Can. J. Chem. **54**, 1052 (1976).

A re-examination of the Li–In system, based on thermal and X-ray diffraction analysis of 42 alloys, shows it to be more complex than originally reported. This complexity is more consistent with the analogous Li–Tl and Li–Ga systems. The solid solubility of Li in In is about 1.5 at% Li, while that of In in Li appears to be very low. The homogeneous Li–In phase extends from about 46 at% to between 55 and 63 at% Li, depending on the temperature. Of the 11 new phases, 5 with the nominal compositions Li_7In_4, Li_2In, Li_8In_3, Li_3In, and $Li_4In(\lambda)$ are stable at room temperature, while Li_5In_2, $Li_{73}In_{27}(\eta)$, $Li_{11}In_4$, $Li_4In(\kappa)$, Li_6In and $Li_{12}In$ occur at higher temperatures.

W. A. ALEXANDER, L. D. CALVERT, R. H. GAMBLE et K. SCHINZEL. Can. J. Chem. **54**, 1052 (1976).

Un réexamen du système Li–In basé sur des analyses thermiques et de diffraction de rayons-X de 42 alliages montre que ce système est beaucoup plus complexe qu'il n'avait été rapporté originalement. Cette complexité est en accord avec celle des systèmes analogues du Li–Tl et Li–Ga. La solubilité à l'état solide du Li dans l'In est approximativement 1.5 at% de Li, alors que celle de In dans Li semble être très basse. La phase homogène du Li–In va d'environ 46 at% jusqu'à 55 et 63 at% de Li dépendant de la température. Des onzes nouvelles phases observées, 5 avec des compositions nominals de Li_7In_4, Li_2In, Li_8In_3, Li_3In et $Li_4In(\lambda)$ sont stables à la température de la pièce alors que Li_5In_2, $Li_{73}In_{27}(\eta)$, $Li_{11}In_4$, $Li_4In(\kappa)$, Li_6In et $Li_{12}In$ existent uniquement à des températures plus élevées.

[Traduit par le journal]

Introduction

As part of a study of reactive metal phase diagrams, the lithium–indium system has been investigated. There is only one previous study by Grube and Wolf (1) in 1935, which showed one equiatomic compound. This was carried out using 0.6 g samples with a very limited supply of indium. Hansen and Anderko (2) revised the Grube and Wolf diagram. The analogous Li–Tl and Li–Ga systems each show five compounds according to Hansen and Anderko (2) and Yatsenko *et al.* (3), respectively, a conspicuous difference without any apparent reason. Graham and Raynor (4) briefly present the results of lattice parameter measurements, and report a solid solubility of up to 14% lithium in indium. The equiatomic phase LiIn was found by Zintl and Brauer (5) in 1933 to have the NaTl type structure; other work on the LiIn phase has been reported (6–8, 12, 13).

Experimental

High purity metals were used to prepare the alloys; 99.98% Li from Koch-Light Laboratories, England, with the natural isotope ratios, 99.999% In from Cominco, Canada. All operations with the metals and the alloys were carried out in an argon atmosphere dry box. Charges were calculated to produce about 15 ml of cast alloy. The X-ray powder sample preparations were carried out in a small 'dry box', which could be flushed more effectively. The argon supply for the dry boxes and for the cooling curve apparatus was passed through: (*a*) Drierite, (*b*) B.T.S. Cu–CuO catalyst from B.A.S.F. Canada, for O_2 and H_2 removal, (*c*) a molecular sieve to remove water, and (*d*) a Ca turnings furnace at 650 °C to remove N_2. The melting vessel and cooling curve apparatus are described in ref. 9. A port permitted transfer of the melting vessel between a large dry box and the furnace of the cooling curve apparatus without any exposure of the charge to air. The cooling and heating curves were recorded on a Hartmann-Braun 6 point recorder with a sensitivity of ±0.2 °C. The cooling or heating rate was held constant automatically and usually was set at about 0.6 °C per min. Platinum/platinum–rhodium thermocouples were calibrated in pure metals and provided with electrical shielding. A stainless steel block formed the reference body for the differential signal. The melt vessel was made from type 416 stainless steel, an iron – 12% chromium type, because a preliminary test showed that Ni contamination occurred with ordinary stainless steel. After removal from the mold, samples were taken from the top and bottom of each alloy, and the ingots were stored in the atmosphere of the dry box in two concentric rubber-stoppered glass test tubes, sealed by rubber cement.

X-Ray diffraction photographs were taken of annealed

[1]NRCC No. 15116.

Can. J. Chem. Downloaded from www.nrcresearchpress.com by 210.87.254.6 on 09/05/12
For personal use only.

Can. J. Chem. Downloaded from www.nrcresearchpress.com by 210.87.254.6 on 09/05/12
For personal use only.

alloy powders in 114 mm diameter Debye–Scherrer cameras, using nickel filtered copper radiation or lithium fluoride monochromated copper K_α radiation, (λ = 1.54060 Å).

The powders were annealed in threaded mild steel tubes closed with an Allen screw. These tubes were sealed inside Pyrex glass ampoules under argon at a pressure sufficient to give 1 atm at the annealing temperature. This technique prevented the lithium vapor attacking the glass ampoules causing them to crack, which occurred frequently when the alloys were simply wrapped in iron foil. The argon atmosphere annealing gave more efficient quenching than vacuum annealing, and reduced the loss of Li. Some samples quenched for X-ray examination were stored at solid CO_2 temperatures to test the possibility of changes at room temperature. X-Ray powder samples were inspected microscopically before and after exposure to check for decomposition of the alloy.

At least two cooling curves were recorded for each alloy, and in most cases a heating curve was recorded as well. The main arrests on the cooling curves were reproducibly observed, though less accurately so on the heating curve, while shorter arrests were often observed at somewhat variable temperatures.

The errors in thermocouple calibration, temperature measurement, reading of charts, etc., are estimated at ±1.5 °C for the liquidus arrests, and ±0.5 °C for peritectic and more pronounced arrests. The temperature gradient in the furnace was about ±0.8 °C from the mean in the 500–600 °C range, while in the alloy it was only about ±0.3 °C. The apparatus error was checked by observing the melting points of the 'pure' metals; observed values were: In, 156.3 °C and Li, 180.5 °C, while literature values are: In, 156.4 °C(2) and Li, 180 °C(3).

Metallographic examination of some high lithium alloys was attempted, but the high reactivity of the intermediate phases prevented simple polishing and examination of these alloys in air.

Forty-three alloys were prepared and examined, with attention being given to the production of homogeneous ingots. Samples from the top and from the bottom of each ingot were analysed, and the results are shown in Table 1.[2] Portions of the annealed alloy powders or pieces used to prepare X-ray specimens were analysed in most cases, but the total lithium plus indium was usually only 96–98 wt%. X-Ray examination of two rather highly oxidized alloy powders showed that the oxidation product under our experimental conditions is mainly LiOH. Assuming this to be true in all cases and that the LiOH acts as an inert diluent, all analytical results were recalculated to give the proportions of lithium and indium as metals in the alloys. The resulting changes were insignificant for the massive ingots, but with few exceptions amounted to 1 to 3% in the case of the powders.

Results

The liquidus arrests from thermal analysis are plotted in Fig. 1 as circles, and the most pronounced and reproducible solid state arrests are shown as squares. The numerical values are given in Table 2. In the rest of the paper all percentage compositions are atomic percent. The average of 11 lower Li peritectic arrests is 158.7 °C, while the range is 158.0 to 158.9 °C. Thus the peritectic reaction is only about 2.4 °C above the melting point of indium, while the composition as shown by the projection of the liquidus line is about 0.4% Li. A probable arrangement of the phase boundaries, similar to that of Grube and Wolf (1), is given in the insert in Fig. 1; this is supported by the estimate of a solubility of the order of 1.5% lithium in indium from X-ray data. In general the solidus and solid state arrests were reproducible, and supported the phase boundary arrangement shown in Fig. 1. The liquidus curve is very close to that of Grube and Wolf (1) (Fig. 1), although from our data the maximum is more rounded, and the peritectic reaction to give α plus β occurs at a lower Li content.

The main evidence for the solid phase compositions and transformations indicated in Fig. 1 above 46% Li, is the X-ray diffraction patterns of alloy powders annealed at various temperatures up to 480 °C, and samples from ingots held at room temperature up to about 2 years. With improved annealing, quenching, and sampling techniques, excellent photographs were produced in nearly all attempts. Those photographs which showed the presence of three phases were rejected as having failed to reach equilibrium, and those in which the lines of indium appeared in alloys with greater than 50% lithium were discarded as having decomposed. Of the 229 acceptable X-ray diffraction observations, 30 did not fit in exactly with the phase arrangement suggested in Fig. 1. Of these, 23 are plotted as "*X*" in Figs. 2 and 3, while 7 two phase points are plotted just outside the suggested two-phase regions. The phases and their compositions are listed in Table 8.

X-Ray Diffraction Observations

Preliminary photographs were taken using specimens from the $\alpha + \beta$ phase field, stored at room temperature for some months. These photographs showed either the pattern of indium with a lattice parameter equal to that of pure In, or the pattern of a mixture of β plus In plus

[2]Tables 1, 2, 5–7, and 9 are available, at a nominal charge, from the Depository of Unpublished Data, CISTI, National Research Council of Canada, Ottawa, Canada K1A 0S2.

Can. J. Chem. Downloaded from www.nrcresearchpress.com by 210.87.254.6 on 09/05/12
For personal use only.

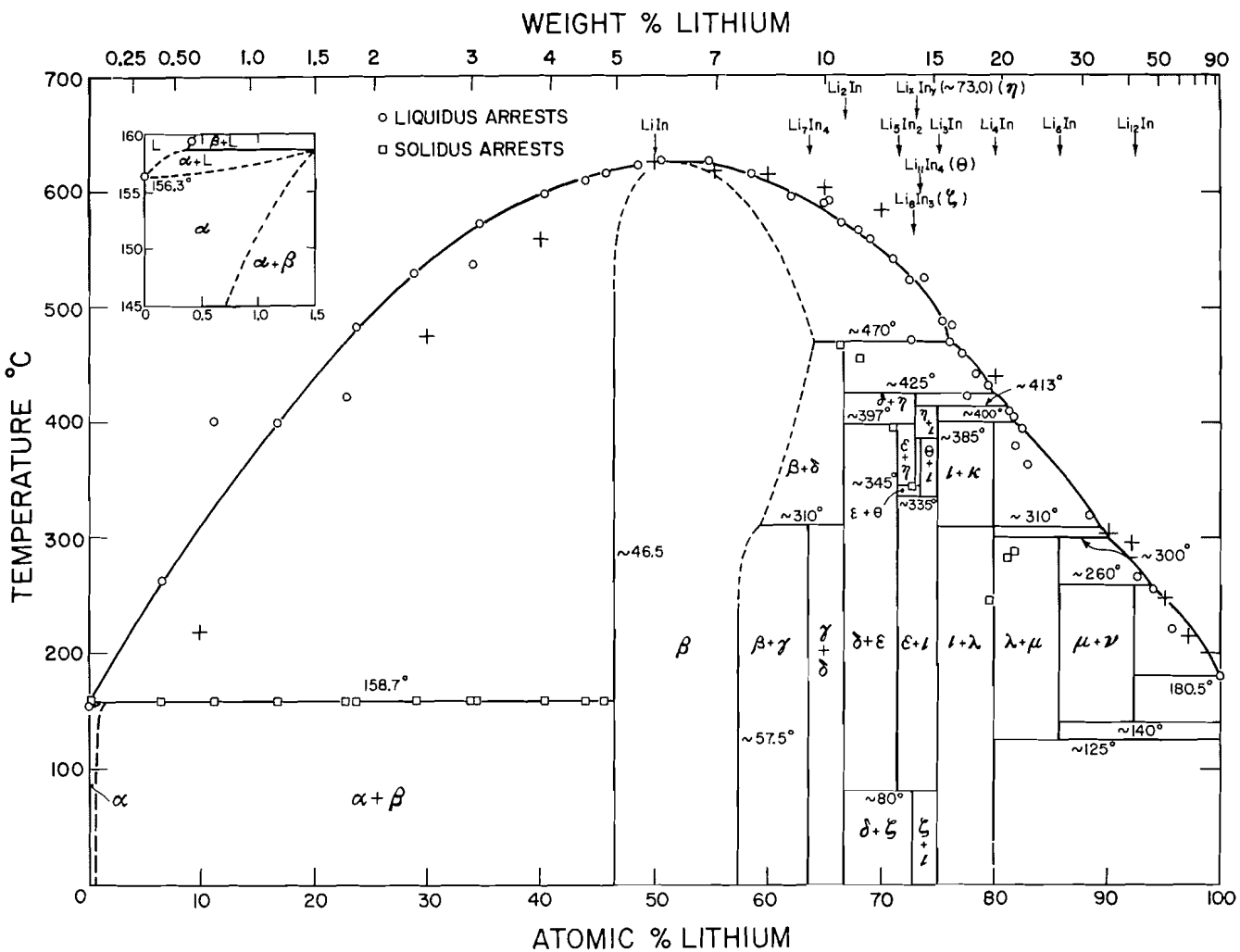

FIG. 1. The LiIn diagram with thermal arrest data; + liquidus arrests of Grube and Wolf (1).

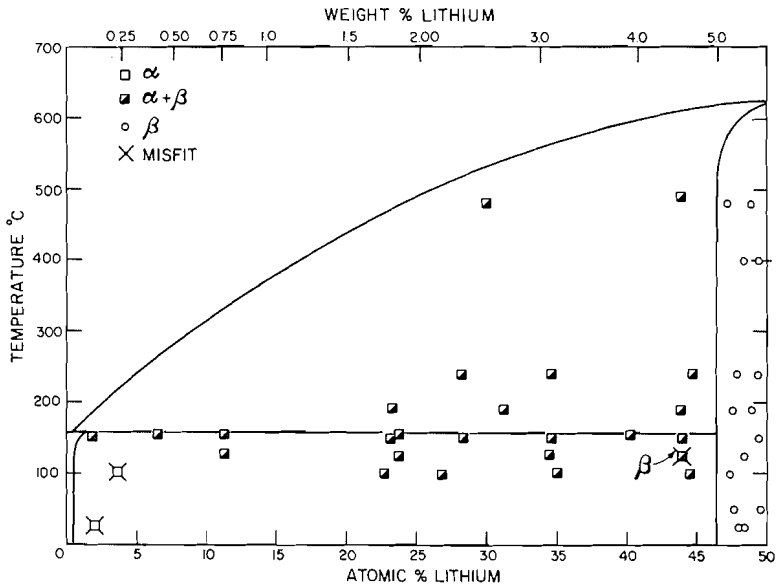

FIG. 2. X-Ray diffraction data for low lithium alloys.

abnormally dark backgrounds. Fresh filings were then prepared, annealed in an argon atmosphere to provide more efficient quenching, quenched, and stored in Dry Ice until photographed. They were found to give the expected β and In patterns in the two-phase field. It should be noted that many high Li content alloy powders gave patterns with the pure In lattice parameter; we assume chemical breakdown of the X-ray powder specimens. In contrast, the massive ingots are quite stable for at least 2–3 years. In some tests in which the prepared X-ray specimens in their capillaries were re-annealed, the dark background disappeared and the β pattern re-appeared; in others the pure indium pattern plus background persisted. We assume that this indicates that in some cases an amorphous precipitate of β was responsible for the background, and in the others that the background was due to an amorphous precipitate of the reaction product with air and water vapour, which is largely lithium hydroxide plus some 10% lithium nitride. Even with the improved techniques some samples showed evidence of decomposition and were rejected. Contrary to expectation, relatively few Li-rich alloys showed evidence of decomposition, such as a white powder and/or small metallic spheres.

In Solid Solution Range

The results of the X-ray diffraction examination of alloys with up to 50% Li are shown in Fig. 2. The pattern of the β phase, InLi, which has the NaTl (B32) type structure, was observed in samples from a nominal 6.5% Li alloy ingot, where the actual X-ray samples analysed at 1.8 and 3.7% Li, respectively. These samples were annealed at 155, 150, and 100 °C. The β phase pattern was also observed in all alloys with higher Li content up to 65% Li. This finding is contrary to that of Graham and Raynor (4), who reported a solid solution up to 13½% Li in In without observing the β phase. They mention "the presence of relatively intense backgrounds", and discuss various possible sources of error. No alloy ingots were successfully prepared by us with less than 6.5% Li.

On our preliminary films with intense backgrounds, the presence of the β phase was not detected. In later films with clean backgrounds, including monochromatised films with virtually no background, although the presence of the β phase was not detected in the front reflection region, the β lines (751 + 555), (822 + 660) were clearly visible in the back reflection region of adequately annealed samples. It is not probable that these lines were indexed by Graham

Can. J. Chem. Downloaded from www.nrcresearchpress.com by 210.87.254.6 on 09/05/12
For personal use only.

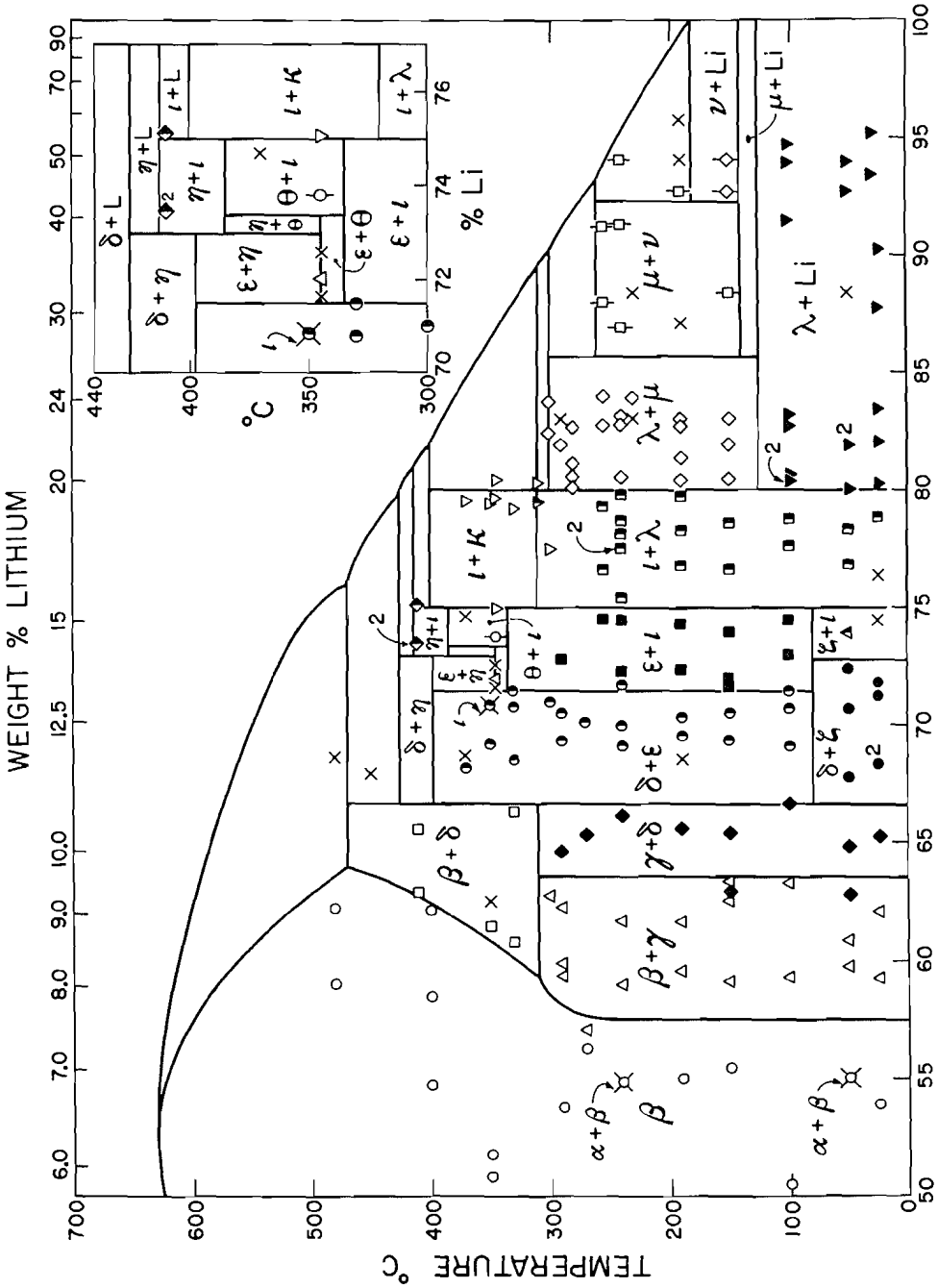

FIG. 3. X-Ray diffraction data for high lithium alloys: ×, misfit points; 2, two coincident points. Note: The plot makes no distinction between patterns where only one phase is seen and those where two phases are recognizable. Thus the symbols in any phase field, except for most of the β area, generally represent two-phase patterns in the centre of the field or single phase patterns close to a boundary. A few symbols belonging to one phase field occur in an adjacent field but within the limits of experimental error. *cf.* Tables 5–7.

Can. J. Chem. Downloaded from www.nrcresearchpress.com by 210.87.254.6 on 09/05/12
For personal use only.

TABLE 3. Lattice parameters of 0–50 at% Li alloys

Section[a]	Alloy number	At% Li[d]	Annealing temperature (°C)	Lattice parameters (Å)[f] a	c
Pure indium	1	0	25	3.2525[b] ±0.0003	4.9459[b] ±0.0003
In–Li solid solution + β phase	3	3.69	100	3.2589	4.9141
	3	1.82	150	3.2585	4.9179
	6	13.74	25	3.2578	4.9157
	9	23.28	190	3.2578	4.9154
				3.2583[c] ±0.0003	4.9158[c] ±0.002
β phase + In–Li solid solution	5	35.84	50	6.7714	
	5	34.75	150	6.7714	
	6	13.74	25	6.7701	
	7	(23.8)[e]	50	6.7713	
	9	30.8	25	6.7726	
	10	(43.9)[e]	125	6.7712	
β phase + liquid	9	23.28	190	6.7715	
	10	(43.9)[e]	190	6.7710	
	10	(43.9)[e]	240	6.7711	
	23	44.0	190	6.7712	
				6.7712[c] ±0.0002	

[a]The major constituent is listed first.
[b]Averages of eight samples.
[c]Averages of four samples; precision of c value is low because line 116 was not observed.
[d]Analyses of X-ray powder samples.
[e]Analyses of DTA alloy ingots.
[f]Samples were examined at room temperature after quenching from the annealing temperature.

and Raynor as indium lines; more probably the intense background prevented detection of the β phase pattern, and accounted for Graham and Raynor's conclusion. Their reported values, from ref. 4, p. 1361, Fig. 3, *viz.*, $a = 3.2533$, $c = 4.9354$ Å, in the body centred description, $I4/mmm$, correspond to a somewhat lower lithium content that those reported here, *cf.* Table 3. There is no direct evidence for the solid solution limit in the present work, but if one assumes a linear relation between the volume of In and of Li, then one can derive a solubility of the order of 1½%, *cf.* Table 3.

We believe that the values for a and c reported by Graham and Raynor (4) are consistent with our observations, and that it is reasonable to assume that they observed the same patterns as we did, but did not detect the presence of the β phase due to the intense backgrounds on their films. It is our contention that their results (ref. 4, p. 1361, Fig. 3) fall into two groups: three results showing some Li in solution, (a and c values given above), and three results (plotted at 7 to 15% Li) which are actually from the α + β phase field with values of $a = 3.2533$ Å and $c = 4.9370$ Å, not very different from those observed in our work, though implying a smaller Li content.

β Phase Region

The β phase has the NaTl structure (5); on X-ray evidence it has a wide range of solid solution.

The β phase lattice parameters derived from two-phase alloys containing In and β are listed in Table 3. We conclude that the indium-rich β solid-solution line is vertical in the solidus region and up to 240 °C ($a = 6.7712$ Å). Somewhere between 240 and 480 °C the line appears to curve towards higher Li content (alloy #10 annealed at 480 °C, $a = 6.7721$). At low temperatures, the limit lies between 45% Li (alloy 23, Table 1, $a = 6.7712$ Å) and 47.5% Li (alloy 31, $a = 6.7926$), *cf.* Tables 3 and 4.

The evidence for the Li-rich β phase boundary in the solidus region is meagre below 200 °C,

Can. J. Chem. Downloaded from www.nrcresearchpress.com by 210.87.254.6 on 09/05/12
For personal use only.

Can. J. Chem. Downloaded from www.nrcresearchpress.com by 210.87.254.6 on 09/05/12
For personal use only.

TABLE 4. Lattice parameters of single phase β alloys

Alloy number	At% Li[a]	Annealing temperature (°C)	a (Å)[e]
31	47.26	480	6.7862
31	48.5	400	6.7864
31	48.5	400	6.7864
31	47.62	190	6.7905
31	48.1	25	6.7890
31	48.1	25	6.7926[c]
31	48.1	25	6.7908
31	48.1	25	6.7919
12	48.9	480	6.7878
12	49.1	100	6.7917
12	48.6	50	6.7917
12	48.46	25	6.7921
12	49.1	25	6.7924
13	(54.8)[b]	400	6.7835
13	51.8	350	6.7760
13	56.3	270	6.7683
13	55.1	190	6.7666
14	59.1	480	6.7580
14	(58.6)[b]	400	6.7641
14	50.9	350	6.7496
14	59.3	100	6.7738
15	(62.2)[b]	400	6.7392
32	(65.1)[b]	400	6.7388
32	62.6	350	6.7333[d]

[a]Analyses of X-ray powder samples.
[b]Analyses of DTA alloy ingots.
[c]Maximum.
[d]Minimum.
[e]σ = 0.0003 Å. Samples were examined at room temperature after quenching from the annealing temperature.

because the β patterns in two-phase alloys in the 55–60% Li region usually lacked measurable back-reflection lines, despite long term annealing. The single phase field at 25 °C and up to 280 °C extends to between 55% Li (alloy 13, β phase only detected) and 59.5% Li (alloy 14, Table 1, $\beta + \gamma$ phase observed). Above 280 °C this limit bends toward higher Li contents, reaching a maximum of about 63% Li at ~480 °C (alloy 32, β phase only detected).

Lattice parameters of single phase β alloys range from 6.7926 to 6.7333, Table 4. In addition, a number of lattice parameter measurements in the range 6.7333 to 6.7392 were recorded from two-phase alloys, $\beta + \delta$ or $\beta + \gamma$.

The observed values of 6.7926 to 6.7333, which are not directly correlated with the compositions of analysed alloys annealed at a range of temperature because of a lack of reproducibility (see below), indicate a rising then falling value in the β field, and should be compared with the values obtained from the analysed samples in the In + β or liquid + β fields. These parameters average 6.7713, a value not at all consistent with the single phase β values of 6.7862, 6.7864, 6.7905, 6.7926, 6.7908 in Table 4 for alloy 31, annealed at various temperatures. The same comparison on the Li-rich side is much less certain, but in this case also much lower lattice parameters (6.7316 to 6.7388) are observed in the two-phase region than in the homogeneous single phase alloys quite close in composition.

A number of alloys in the β phase field showed either broadened lines or doubled lines equivalent to two patterns, each of the B32 type, with lattice parameters within the range given above. Sometimes an alloy gave a high lattice parameter, in the 6.793 . . . range from one sample, and also a low lattice parameter, in the 6.734 . . . range, for a second sample from the same ingot; or even occasionally from separate X-ray samples taken from the same lot of annealed alloy powder. It seems possible that there are two phases in this region below about 300 °C, β and β', both with the NaTl (B32) type structure, and additional complications due to transitional or metastable phases are not ruled out. There is evidence to suggest that these phases, once formed, are difficult to anneal out. Evidently much further work is required to resolve these points. The extensive lattice parameter studies necessary to establish the β phase boundaries in detail were not undertaken.

Kuriyama (12) in a report on the preparation of single crystals of the β phase gave a small graph based on six measurements, which shows a maximum in the lattice parameter *vs.* composition curve. Our early results, as stated above, showed a similar maximum with similar but not identical values. More extensive measurements did not reproduce these values, the variations being many times the standard deviation of the measurements (Table 4), and revealed the complexity described above.

Li-rich Phases

X-Ray diffraction results used to deduce the phase relations from 50 to 100% Li, are plotted in Fig. 3. The observed Debye–Scherrer powder patterns are given in Table 9. The β phase is observed together with the γ phase in alloys above 57% Li, *cf.* Tables 6 and 7, and below 63% Li, alloy 32 between 25 and 350 °C. Above this temperature the β phase is observed to-

Can. J. Chem. Downloaded from www.nrcresearchpress.com by 210.87.254.6 on 09/05/12
For personal use only.

gether with the δ phase in the range up to 63% Li (alloy 32, Table 1). The composition of γ is not well established, nor is its temperature range. The composition of δ is reasonably established; it exists from 25 °C up to its melting point at ~470 °C. The composition of γ is suggested at 63.6% and of δ at about 66.7% Li.

The ζ phase was first considered to occur at about 350–400 °C because of earlier observations of its pattern in photographs of quenched samples annealed at these temperatures. Later, we considered it more likely that this phase is stable from room temperature up to somewhere between 50 and 100 °C, since it was observed more recently in several alloys annealed at 25 and at 50 °C, and was not observed at 100 nor up to 330 °C. We believe the ζ pattern at 345 °C is due to inefficient quenching, allowing the ζ phase to form partially during cooling, and that the low temperature annealings had reached equilibrium, *cf.* ref. 4, p. 1355 and ref. 7, p. 179. The alternative is that the high temperature ζ phase is readily retained to room temperature, and that the room temperature and 50 °C anneals were not sufficient to reach equilibrium, so that the ζ phase was still present. It appears probable that the ζ phase transforms to the ϵ phase with increase in temperature, since the same alloys show ζ at 50 °C and ϵ at 100 °C and above. On the other hand, one should note that the high temperature structure of other phases is successfully retained on quenching, *e.g.* the κ phase.

The range of essentially single phase observations is shown in Table 5.[3] Mean values of the compositions were calculated, rejecting values greater than two standard deviations from the mean. Two-phase observations are listed in Table 6 and 'misfit' values in Table 7; nearly one-half of the latter are small deviations. It will be seen from Table 6 that some of the two-phase regions in Fig. 3 were not found in the photographs. The evidence for the composition assigned to the ϵ phase is not strong, but more confidence may be placed in the compositions at the ι and κ–λ phases. With one exception, the compositions observed for the ι phase lie reasonably close together. The κ phase compositions are all close together, but there is a considerable scatter in the λ observations, as some five points lie more than two standard deviations from the mean.

The composition, 4:1 suggested for the structure κ–λ could be just as well given as 22:5 (81.5% Li) because of the strong resemblance of the κ X-ray films to the pattern of the $Li_{22}Pb_5$ structure type (10). All but three lines of the κ phase could be indexed on a face-centred-cubic cell of the $Li_{22}Pb_5$ type and an extrapolation against $\frac{1}{2}(\cos^2\theta/\sin\theta + \cos^2\theta/\theta)$ gave $a = 20.071$ (± 0.005) and $M_{20} = 2.8$ which is not a satisfactory value. A calculation based on the $Li_{22}Pb_5$ type gave reasonable agreement for the stronger lines of the κ pattern but nevertheless the existence of three lines which could not be indexed on the face-centred cell but could be on a primitive cubic cell indicated that although there was a strong resemblance between the structure of the κ phase and that of $Li_{22}Pb_5$, some modification would be required. No satisfactory trial structure was obtained. The existence of the low-temperature–high-temperature modifications is indicated by the reversible transformations of three alloys near this composition. The compositions suggested for the other phases are chosen from simple atomic ratios, fitted to the observed X-ray data.

The ratio for ι is possibly 7:2, (77.8% Li), rather than 3:1, because of its resemblance to the Li_7Pb_2 pattern (11). Although the ι pattern resembles that of Li_7Pb_2, no trial structure based on Li_7Pb_2 gave a satisfactory agreement. Many attempts were made to index the patterns of all the other phases, but while it was always possible to find cells which indexed all or most of the lines, they were not convincing because it is well-known that Debye–Scherrer powder patterns are usually not accurate enough to support a trial indexing without the support of a trial structure and no satisfactory trials were obtained.

The phases μ and ν are drawn over a limited temperature range, since they were not observed above or below these limits. The terminal solubility of indium in lithium was not estimated.

Conclusions

From X-ray evidence there are seven phases stable at room temperature, *viz.*, α, β, γ, δ, ζ, ι, and λ. The phases ϵ, η, θ, κ, μ, and ν appear to be

[3]These specimens gave essentially one pattern, indicating the presence of only one major phase; small amounts of another phase would not have been detected.

TABLE 8. Phases indicated in Li–In system

Phase	Potential formula	Composition, % Li	
		Formula	Mean observed
α	(Solid solution)	—	—
β	LiIn	50	46.5–63
γ	Li_7In_4	63.6	63.6
δ	Li_2In	66.7	66.8
ϵ	Li_5In_2	71.5	71.8
ζ	Li_8In_3	72.8	71.9
η	Li_xIn_y	—	—
θ	$Li_{11}In_4$	73.4	—
ι	Li_3In	75.0	75.8
κ	Li_4In	80.0	80.7
λ	Li_4In	80.0	80.7
μ	Li_6In	85.7	85.5
ν	$Li_{12}In$	92.3	92.6

stable only at higher temperatures, and their existence is inferred from X-ray data with some support from cooling curve arrests. The arrangement of the phases in the area of η and θ is tentative, simply indicating a complex structure in this region.

This work has confirmed and extended the liquidus data of Grube and Wolf (1). The discovery of 11 phases (Li_7In_4, Li_2In, Li_5In_2, Li_8In_3, $Li_{73}In_{27}$, $Li_{11}In_4$, Li_3In, $Li_4In(\kappa,\lambda)$, Li_6In, $Li_{12}In$) in the high lithium region has removed the apparent anomaly between the In–Li and the In–Ga and In–Tl systems. The solid solubility of Li in In is low ($\approx 1\frac{1}{2}\%$) and of In in Li is very small.

Acknowledgments

We have had valuable assistance from the Analytical Section of the Chemistry Division, particularly Mr. J. A. H. Desaulniers and Mr. E. C. Goodhue, in the numerous analyses of ingots and of X-ray powder samples. One of us, K.S., acknowledges assistance in the form of a National Research Council of Canada Postdoctoral Fellowship.

1. G. GRUBE and W. WOLF. Z. Elektrochem. **41**, 675 (1935).
2. M. HANSEN and K. ADNERKO. Constitution of binary alloys. McGraw-Hill Book Co., Inc., New York. 1958. p. 859.
3. S. P. YATSENKO, K. A. CHUNTONOV, S. I. ALYAMOVSKII, and E. N. DIEVA. Izv. Akad. Nauk SSSR, Met. 185 (1973).
4. J. GRAHAM and G. V. RAYNOR. Phil. Mag. **2**, 1354 (1957).
5. E. ZINTL and G. BRAUER. Z. Phys. Chem. Abt. B, **20**, 245 (1933).
6. A. SCHNEIDER and O. HILMER. Z. Anorg. Allg. Chem. **286**, 97 (1956).
7. H. E. SCHONE and W. D. KNIGHT. Acta Metall. **11**, 179 (1963).
8. W. KLEMM and H. FRICKE. Z. Anorg. Allg. Chem. **282**, 162 (1955).
9. W. A. ALEXANDER, L. D. CALVERT, A. DESAULNIERS, H. S. DUNSMORE, and D. F. SARGENT. Can. J. Chem. **47**, 611 (1969).
10. A. ZALKIN and W. J. RAMSAY. J. Phys. Chem. **62**, 689 (1958).
11. A. ZALKIN and W. J. RAMSAY. J. Phys. Chem. **60**, 234, 1275 (1956).
12. K. KURIYAMA. J. Cryst. Growth, **23**, 160 (1974).
13. W. PAULY, A. WEISS, and H. WITTE. Z. Metallkd. **59**, 554 (1968).

Can. J. Chem. Downloaded from www.nrcresearchpress.com by 210.87.254.6 on 09/05/12
For personal use only.

The photochemistry of some *cis*-dihalo rhodium(III) complexes

JAMES SELLAN AND ROBERT RUMFELDT
Department of Chemistry, University of Windsor, Windsor, Ontario N9B 3P4

Received August 14, 1975

JAMES SELLAN and ROBERT RUMFELDT. Can. J. Chem. **54**, 1061 (1976).

The photochemistry of *cis*-$[Rh(cyclam)X_2]^+$ (where X = Cl, Br, or I) and *cis*-$[Rh(en)_2Cl_2]^+$ have been studied. Whilst only halide aquation is observed for the cyclam complexes, amine aquation is the principal reaction mode for the ethylenediamine complex. In each case, the photosensitivity was greater for charge transfer excitation than ligand field excitation. Although this wavelength dependence was also exhibited for the corresponding *trans* complexes, the dependence on the leaving group which was $\phi(Cl^-) < \phi(Br^-) < \phi(I^-)$ for the *trans* complexes is completely reversed for *cis*-$[Rh(cyclam)X_2]^+$ where $\phi(Cl^-) = 0.37 > \phi(Br^-) = 0.32 \gg \phi(I^-) = 0.03$ for ligand field excitation.

The behaviour of *cis*-$[Rh(en)_2Cl_2]^+$ and *cis*-$[Rh(cyclam)I_2]^+$ is seen to be consistent with the preferential amine activation predicted by the photochemical model proposed by Zink. The change in photospecificity observed with *cis*-$[Rh(cyclam)Cl_2]^+$ and *cis*-$[Rh(cyclam)Br_2]^+$ is interpreted as the result of distortion from effective tetragonal symmetry which causes the repulsive energy to become progressively more localized in the metal–halide bond.

JAMES SELLAN et ROBERT RUMFELDT. Can. J. Chem. **54**, 1061 (1976).

On a étudié la photochimie du *cis*-$[Rh(cyclam)X_2]^+$ (où X = Cl, Br ou I) et *cis*-$[Rh(en)_2Cl_2]^+$. Alors que l'on n'observe que l'aquation de l'halogénure dans les complexes du cyclame, l'aquation de l'amine est la principale réaction qui s'effectue pour le complexe de l'éthylènediamine. Dans chaque cas, la photosensibilité est plus grande pour l'excitation par transfert de charge que pour l'excitation par champ de ligand. Quoique l'on aie observé cette dépendance sur la longueur d'onde dans le cas des complexes correspondants *trans*, la dépendance sur le nucléofuge qui était $\phi(Cl^-) < \phi(Br^-) < \phi(I^-)$ pour les complexes *trans* est complètement renversée pour le *cis*-$[Rh(cyclam)X_2]^+$ où $\phi(Cl^-) = 0.37 > \phi(Br^-) = 0.32 \gg \phi(I^-) = 0.03$ pour l'excitation par champ de ligand.

Il semble que le comportement du *cis*-$[Rh(en)_2Cl_2]^+$ et du *cis*-$[Rh(cyclam)I_2]^+$ est en accord avec l'activation préférentielle de l'amine prédite par le modèle photochimique proposé par Zink. On interprète le changement dans la photospécificité observée avec les *cis*-$[Rh(cyclam)Cl_2]^+$ et *cis*-$[Rh(cyclam)Br_2]^+$ comme résultant d'une distorsion de la symétrie tétragonale effective qui amène l'énergie répulsive à devenir progressivement plus localisée dans le lien métal–halogénure.

[Traduit par le journal]

Introduction

We have recently reported (1) the results of the photolysis of a series of rhodium(III) haloamines. Whilst the photoreactions of the *trans* complexes were accurately predicted by Zink's model (2), the *cis* complexes exhibited an apparently inconsistent behaviour. Thus, the photolysis of *cis*-$[Rh(en)_2Cl_2]^+$ was characterized by the anti-thermal ethylenediamine aquation whereas the analogous complex, *cis*-$[Rh(cyclam)Cl_2]^+$, (cyclam = 1,4,8,11-tetraazocyclotetradecane) exhibited chloride aquation exclusively. In principle, if a *cis* complex possessed tetragonal symmetry then Zink's model would predict that the strongest ligand on the weak field axis would be preferentially labilized. Therefore, the ethylenediamine aquation in the photolysis of *cis*-$[Rh(en)_2Cl_2]^+$ constituted the normal reaction, while the *cis*-$[Rh(cyclam)Cl_2]^+$ represented the exceptional case.

The relatively high intensity of the *d–d* bands in the spectrum of *cis*-$[Rh(cyclam)Cl_2]^+$ suggested a significant distortion from tetragonal symmetry (1) and it seems apparent that the change in photospecificity must in some way be related to this distortion. Assuming that the lowest electronically excited state within a manifold is the photoactive state, then for either ligand field (lf) or charge transfer (ct) excitation this state will correlate with a configuration in which either a metal nonbonding electron (lf) or a ligand nonbonding electron (ct) has been excited to the lowest open orbital. Although this can be readily identified as a σ^*-antibonding

Can. J. Chem. Downloaded from www.nrcresearchpress.com by 210.87.254.5 on 09/05/12
For personal use only.

TABLE 1. Electronic spectra of some $[Rh(amine)X_2]^+$ complexes[a]

Transition[b]		Frequency				
		cis complexes				
Term	Orbital	(cyclam)Cl_2	(cyclam)Br_2	(cyclam)I_2	$(en)_2Cl_2$	*trans*-[Rh(cyclam)I_2]$^+$
$^1A_1 \rightarrow {}^3T_1$	$\pi^* \rightarrow \sigma^*$	—	—	20 700 (110)	—	18 200 (18)
$^1A_1 \rightarrow {}^1T_1$	$\pi^* \rightarrow \sigma^*$	28 300 (223)	27 400 (236)	24 840 (1 090)	28 640 (143)	21 740 (200)
$^1A_1 \rightarrow {}^1T_2$	$\pi^* \rightarrow \sigma^*$	33 500 (294)	32 400 (800)	33 300 (4 400)	34 240 (133)	—
$^1A_1 \rightarrow {}^1T_1$	$\pi^{nb} \rightarrow \sigma^*$	48 600 (36 300)	43 400 (19 000)	38 480 (12 600)	52 200 (29 800)	28 230 (11 300)
ct	—	—	47 700 (22 000)	41 600 (18 200)	—	36 400 (31 400)
ct	—	—	51 300 (19 300)	44 720 (14 500)	—	42 020 (3 800)
ct	—	—	—	50 040 (27 900)	—	46 800 (6 000)

[a]Frequency in cm^{-1}, extinction coefficient (M^{-1} cm^{-1}) in parentheses.
[b]Terms refer to pseudo-octahedral symmetry.

orbital, the low symmetry of the complex makes it extremely difficult to predict in which bond the destabilization will become localized. The relatively high yield of Cl^- could be interpreted as reflecting a high degree of Cl^- specificity inherent in the wavefunction for the photoactive state. Alternately, because the stereorigidity of the cyclam ligand renders the individual amine nitrogens effectively inert, Cl^- aquation may be efficient since it represents the only available reaction mode which could respond to the overall destabilizing effects of the excited state.

If the latter explanation was valid and the increased photosensitivity of diiodo complexes observed with the *trans* complex is also considered then in prospect a quantum yield near unity could be anticipated for the potentially more photolabile *cis*-[Rh(cyclam)I_2]$^+$. The present investigation was undertaken to explore this possibility and to further explore the influence of structural distortion on the photochemistry of Rh(III) complexes.

Results and Discussion

The data given in Table 1 summarizes the spectra of the complexes used in this study. Although the *cis* complexes formally belong to C_{2v} symmetry, the transitions should approximate an octahedral scheme since the low symmetry components would be unlikely to effect a measurable term splitting. Thus, the transitions have been assigned according to their octahedral parentage.

In the case of the iodo complexes the appearance of the observable lf triplet bands permitted direct irradiation into this band. Otherwise, the exciting radiation was chosen to correspond to the first spin allowed lf band. The ultraviolet irradiations were all at the fixed wavelength of 254 nm. This achieved virtually selective excitation to the first ct state in the chloro and bromo complexes but in the case of *trans*-[Rh(cyclam)I_2]$^+$ the radiation would be absorbed principally by the second ct band, whilst for *cis*-[Rh(cyclam)I_2]$^+$ there would be an almost equal distribution between the first and second ct bands. The yield data are listed in Table 2.

TABLE 2. Product yields from the photolysis of Rh(III) complexes

Complex	Wavelength (nm)	Quantum yield of halide
cis-[Rh(cyclam)Cl_2]$^+$	254	0.47 ± 0.02
	400[a]	0.37 ± 0.02
cis-[Rh(cyclam)Br_2]$^+$	254	0.34 ± 0.02
	400[a]	0.32 ± 0.02
cis-[Rh(cyclam)I_2]$^+$	254	0.05 ± 0.002
	400[a]	0.03 ± 0.002
	480	0.02 ± 0.002
trans-[Rh(cyclam)I_2]$^+$	254	0.18 ± 0.01
	400	0.14 ± 0.01
	460[a]	0.14 ± 0.01
	550	0.15 ± 0.01
cis-[Rh(en)$_2$$Cl_2$]$^+$	254[b]	0.1

[a]First allowed lf band.
[b]Reference 8. $\phi(-H^+) = 0.4$.

With the exception of *cis*-[Rh(en)$_2$$Cl_2$]$^+$ which has been described previously (1), the photoreactions proceed by halide aquation with complete isomeric retention in the hydrolysed complex. In each case, ct excitation produces larger yields than lf excitation, indicating a lack of any significant internal conversion between the ct and lf states. On the other hand, the lack of a wave-

Can. J. Chem. Downloaded from www.nrcresearchpress.com by 210.87.254.5 on 09/05/12
For personal use only.

Can. J. Chem. Downloaded from www.nrcresearchpress.com by 210.87.254.5 on 09/05/12
For personal use only.

length dependence in lf region observed for the iodo complexes is consistent with efficient intersystem crossing (3, 4) and supports the assumption that the lowest excited state within a manifold will be the dominant photoactive state (2).

The outstanding feature of the data in Table 2 is the complete reversal from the order of photosensitivities observed for the *trans* complexes (1). However, a similarity can be identified between the photochemistry of $[Rh(NH_3)_5X]^{2+}$ (4) and *cis*-$[Rh(cyclam)X_2]^+$ since in both cases with lf excitation $\phi(Cl^-) > \phi(Br^-) > \phi(I^-)$. In each of these series of complexes a halide ligand is nominally *trans* to an amine nitrogen but while the NH_3 is potentially labile, the cyclam nitrogen would be substitution stable. The NH_3 yields observed with $[Rh(NH_3)_5X]^{2+}$ would merely correspond to deactivation in *cis*-$[Rh(cyclam)X_2]^+$. In this context the reactions of $[Rh(NH_3)_5I]^{2+}$ for which $\phi(I^-) = 0.01$ and *cis*-$[Rh(cyclam)I_2]^+$ for which $\phi(I^-) = 0.03$ are seen to be very similar. Although the comparison between the bromo complexes is not as close, the chloro complexes compare favorably, particularly if allowance is made for the possible retarding influence of the larger positive charge of the pentaammine complex. Overall, the similarity between the two sets of complexes is quite remarkable.

The behaviour of $[Rh(NH_3)_5X]^{2+}$ was explained by Kelly and Endicott (4) by proposing two distinct photoactive states of similar energy but different geometry. The relative energies of these two states would determine which ligand is preferentially activated and the magnitude of the gap would determine the degree of selectivity. This explanation is easily adapted to the *cis* complexes since the low symmetry field would lift the degeneracy of the ^3E state (the lowest electronically excited state in either D_{4h} or C_{4v} symmetry); however, the splitting would be too small (5) to allow resolution of the resultant states even in the rare cases when the ^3E state is spectroscopically prominent. Nevertheless, the invisible quality of these states does not diminish the theoretical fact of their existence and their possible role in determining the photochemical reaction coordinates.

The practical difficulty lies in attempting to describe such states and thereby derive some rationale for the type of behaviour exhibited by the series of *cis* complexes. Thus, it is not possible to anticipate which of the two possible reaction modes will dominate. For example, in the halopentaammine series the change from halide to ammine aquation occurs between the chloro and bromo complexes, whereas for *cis*-$[Rh(cyclam)X_2]^+$ the apparent change occurs between the bromo and iodo complexes. Similarly the reversal in photospecificity between *cis*-$[Rh(en)_2Cl_2]^+$ and *cis*-$[Rh(cyclam)Cl_2]^+$ would be unexpected.

The model proposed by Zink (2) employs the fundamental assumption that the lowest excited level will be the dominant photoactive level and therefore is essentially not at variance with the proposal of Kelly and Endicott. In addition, Zink provides a method for predicting the photoreaction by comparing the energy of the lowest MO to the energies of the *trans* donor orbitals. If the energy of the MO is greater than that of the ligand orbital, destabilization will occur in that metal–ligand bond. Specific labilization should depend upon the energy difference between the two ligands with the stronger ligand being preferentially activated. Applying Zink's model to the two potentially active states proposed by Kelly and Endicott leads to the conclusion that it will be the lower state that possesses the highest degree of photospecificity, whilst the upper state will become progressively less discriminating (and important) as its energy increases.

On this basis, the photoreactions of *cis*-$[Rh(en)_2Cl_2]^+$ and *cis*-$[Rh(cyclam)I_2]^+$ can be regarded as normal (*i.e.* predictable). The result with the *cis*-$[Rh(cyclam)I_2]^+$ is particularly significant because it establishes that when the activated ligand is inert then the complex remains inert and does not transfer its reactivity to a secondary reaction mode. Thus the relatively large yields of Cl^- and Br^- cannot be considered as the result of a blockage of a primary reaction mode due to the cyclic structure of the cyclam ligand system. Consequently, the Cl^- and Br^- yields must derive from a process of specific labilization which is determined by some factors unique to these complexes.

Judging from a comparison of the spectra of *cis*-$[Rh(en)_2Cl_2]^+$ and *cis*-$[Rh(cyclam)Cl_2]^+$, the change from amine to halide aquation appears related to a structural distortion in the complex. Figure 1 illustrates two possible *cis* structures with that shown by (*a*) representing the tetra-

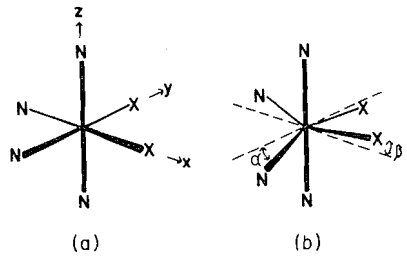

FIG. 1. Structure of *cis*-$[Rh(N)_4X_2]^+$ where (*a*) represents the pseudotetragonal form and (*b*) represents the distorted structure.

gonal symmetry proposed for *cis*-$[Rh(en)_2Cl_2]^+$. The structure represented by (*b*) illustrates the type of distortion likely for a cyclam-containing complex. Based on model structures, the strain of the cyclam ring would be minimized by an opening of the N—Rh—N bond angles. However, unless this is also accompanied by a contraction of the X—Rh—X angle then whatever advantage might have accrued due to release of the cyclam ring strain would be offset by the repulsion encountered by the closing of the N—Rh—X angles.

Thus, the X—Rh—X angle may be critical to the photospecificity, since a lack of contraction would favour structure (*a*) which would lead to adherence to the prediction of Zink's model. Of the three *cis*-$[Rh(cyclam)X_2]^+$ complexes, the diiodo complex would obviously be the least susceptible to contraction of the X—Rh—X angle and its relative inactivity is accurately predicted by Zink's model. In contrast, the higher electronegativity of the chloro ligands would reduce the valence electron density at the metal thereby facilitating a contraction of the X—Rh—X angle with the result that *cis*-$[Rh(cyclam)Cl_2]^+$ should approximate structure (*b*).

If for simplicity it is assumed that the major effects are restricted to the *xy* plane of Fig. 1*a* then the distortion can be represented by the angles α and β of Fig. 1*b*. In order to estimate the anti-bonding character of the critical planar *d*-orbitals (d_{xy} and $d_{x^2-y^2}$) the variation in the individual ligand–metal overlap integrals were computed as a function of the distortion angles α and β. According to this simplified scheme when $\alpha = \beta = 0$, the lowest open σ*-antibonding MO will correlate almost exclusively with the $d_{x^2-y^2}$ orbital while the d_{xy} will remain either

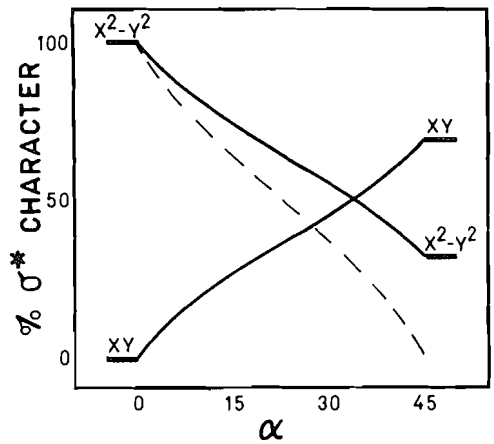

FIG. 2. The variation in σ*-antibonding character of the $d_{x^2-y^2}$ and d_{xy} orbitals as a function of the distortion in the in-plane bond angle. The solid curve represents the overall effects for an assumed relationship of $\alpha = 3\beta$ and the broken line represents the effect for an isolated Rh—N bond.

nonbonding or weakly π*-antibonding. As α or β increases $d_{x^2-y^2}$ will decrease in σ*-antibonding character while d_{xy} will increase. Taking account of the limitations imposed by ligand–ligand repulsion the most probable distortion would correspond to $\alpha > \beta$ and Fig. 2 was constructed to illustrate the effects for an arbitrary relationship of $\alpha = 3\beta$. Under these conditions it is seen that until an extreme distortion is reached the $d_{x^2-y^2}$ orbital will remain higher in energy than the d_{xy} orbital. Figure 2 also shows (the broken line) that the $d_{x^2-y^2}$ contribution to the Rh—N bond decreases more rapidly than the overall σ*-antibonding character of the $d_{x^2-y^2}$ orbital decreases. Therefore, for the type of distortion suggested, the $d_{x^2-y^2}$ orbital will remain a predominantly Rh—Cl σ*-antibonding orbital while the d_{xy} orbital is growing in Rh—N σ*-antibonding character. Under these circumstances the lowest electronically excited state would correspond to an electron transfer from the d_{xy} to $d_{x^2-y^2}$ orbital. Since this would tend to stabilize the planar Rh—N by effectively depopulating an orbital having Rh—N σ*-antibonding character and destabilize the Rh—Cl bond, the natural result is the preferential labilization of the chloride ligand.

As in the case of the *trans* complexes, ct excitation results in each case in a larger yield. This could reflect an inherently more reactive

Can. J. Chem. Downloaded from www.nrcresearchpress.com by 210.87.254.5 on 09/05/12
For personal use only.

precursor state (*i.e.* through more efficient competition with quenching processes) or a higher degree of preferential labilization. Because of the inert nature of the cyclam ligand, we cannot experimentally distinguish between the two possibilities. However, when the respective lf and ct excited state configurations are compared it is seen that the $d_{x^2-y^2}$ orbital is common to both as the lowest acceptor orbital but they differ in their donor orbitals. Thus, we conclude that the photospecificity is controlled principally by the antibonding properties generated by population of the lowest unoccupied orbital and the interpretation of the uv photolyses should be essentially the same as that proposed for the photolyses in the lf region.

The present study reveals the uncertainty that must attend any attempt to predict the photoreactions of complexes possessing effective low symmetry. Although all four *cis* complexes considered here can possess no higher than C_{2v} symmetry, their photochemical behaviour is consistent with tetragonal symmetry in two cases but nontetragonal symmetry in the other two cases. Since the degree of distortion required to define a complex as effectively nontetragonal is unknown, then susceptible systems such as *cis* complexes may be expected to exhibit *unpredictable* behaviour.

Experimental

The irradiation procedures and analytical techniques employed are essentially the same as previously described (1). The preparation complexes used in this study were by methods described in the literature (6, 7) except that the perchlorate salts were prepared. The purity of the complexes was determined by comparison of their absorption spectra with published data (6).

Acknowledgments

The authors wish to acknowledge the financial assistance of the National Research Council of Canada and for the award of a scholarship to J.S. We are also grateful to Drs. C. S. Lin and B. R. McGarvey for their helpful discussions.

1. JAMES SELLAN and ROBERT RUMFELDT. Can. J. Chem. **54**, 519 (1976).
2. (*a*) J. I. ZINK. J. Am. Chem. Soc. **94**, 8039 (1972); Mol. Photochem. **5**, 151 (1973); Inorg. Chem. **12**, 1018 (1973); **12**, 1957 (1973).
3. T. R. THOMAS and G. A. CROSBY. J. Mol. Spectrosc. **38**, 118 (1971).
4. T. L. KELLY and J. F. ENDICOTT. J. Am. Chem. Soc. **94**, 278 (1972).
5. C. J. BALLHAUSEN. Introduction to ligand field theory. McGraw-Hill, New York. 1962. pp. 106–108.
6. E. J. BOUNSALL and S. R. KOPRICH. Can. J. Chem. **48**, 1481 (1970).
7. E. J. BOUNSALL. Ph.D. Thesis. Imperial College, University of London, London, England. 1964.
8. M. MUIR and W. HUANG. Inorg. Chem. **12**, 1831 (1973).

Can. J. Chem. Downloaded from www.nrcresearchpress.com by 210.87.254.5 on 09/05/12
For personal use only.

Recherches en série hétérocyclique. XXVI. Etude de la condensation de l'azidoacétate d'éthyle sur le thiophènedicarbaldéhyde-2,3: nouvelle voie d'accès à des thiéno[2,3-*c*] et -[3,2-*c*] pyridines et pyridones

MICHEL FARNIER, SAMRETH SOTH ET PIERRE FOURNARI

Laboratoire de Polarographie Organique associé au C.N.R.S., Chimie des Hétérocycles, Faculté des Sciences Gabriel - 21000 Dijon, France

Reçu le 2 octobre 1975

MICHEL FARNIER, SAMRETH SOTH et PIERRE FOURNARI. Can. J. Chem. **54**, 1066 (1976).

L'azidoacétate d'éthyle se condense sur le thiophènedicarbaldéhyde-2,3 dont les deux groupes formyle sont libres ou dont l'un a été bloqué à l'état d'acétal diéthylique pour, après cyclisation, conduire respectivement à des thiéno[2,3-*c*] et-[3,2-*c*] pyridines et pyridones. La structure des produits intermédiaires est précisée par spectroscopie rmn et un processus réactionnel est proposé.

MICHEL FARNIER, SAMRETH SOTH, and PIERRE FOURNARI. Can. J. Chem. **54**, 1066 (1976).

Ethyl azidoacetate was reacted with thiophene-2,3-dialdehyde, in which the two formyl groups are free or in which one of them is blocked as the diethyl acetal, to yield, after cyclization, thieno[2,3-*c*] and -[3,2-*c*] pyridines and pyridones, respectively. The structures of the intermediate products were established by nmr; a reaction scheme is proposed.

[Journal translation]

Introduction

Les travaux de Hemetsberger *et al.* (1) ont montré que l'azidoacétate d'éthyle se condensait sur des aldéhydes aromatiques ou homoaromatiques. Par cyclisation du produit ainsi obtenu on accolait un cycle pyrrolique au cycle initial, le composé formé comportant un groupe carboxylate d'éthyle en α de l'azote pyrrolique. Nous avons appliqué cette réaction à des monoaldéhydes thiophéniques (2), sélénophéniques et pyrroliques (3) et accédé ainsi à des systèmes comportant un cycle pyrrolique orthocondensé à l'hétérocycle de départ. Il nous a paru intéressant de chercher à étendre la réaction de Hemetsberger aux dialdéhydes thiophéniques et nous indiquerons tout d'abord les résultats obtenus lorsque le thiophènedicarbaldéhyde-2,3 est mis en oeuvre.

Résultats

L'action de l'azidoacétate d'éthyle sur ce dialdéhyde apparaît sur le schéma 1. Bien qu'un gros excès de réactif (8 mol pour 1 mol de dialdéhyde **1**) soit utilisé, les deux produits de monocondensation **3** et **4** se forment en proportion non négligeable (20 à 25% au total), le rendement global de la condensation étant assez faible (18%). Le mélange obtenu est analysé par chromatographie sur acide silicique. Le produit **2** est aisément isolé mais tous nos essais de séparation des isomères **3** et **4** se sont révélés infructueux.

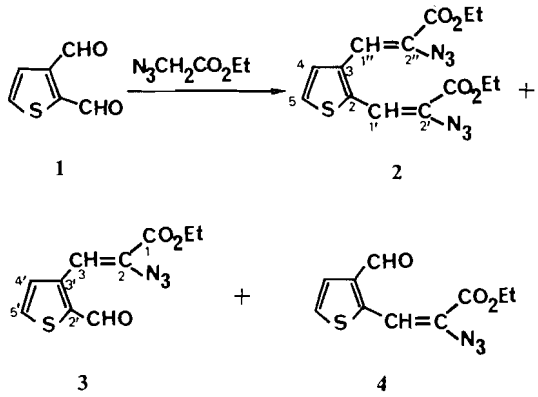

SCHÉMA 1

Pour obtenir uniquement chacun des produits **3** et **4** nous avons mis en oeuvre les deux acétals diéthyliques du thiophènedicarbaldéhyde-2,3: les synthèses réalisées au départ de ces composés, **5** et **6** sont regroupées sur le schéma 2.

Les acétals aldéhydes **5** et **6** conduisent aux produits attendus, respectivement **7** et **8**, avec un rendement de l'ordre de 65%. L'action du chlorure d'hydrogène sur les composés **7** et **8** libère le groupe formyle (rendement environ 80%) et les isomères **3** et **4** sont ainsi obtenus

Can. J. Chem. Downloaded from www.nrcresearchpress.com by 210.87.254.6 on 09/05/12
For personal use only.

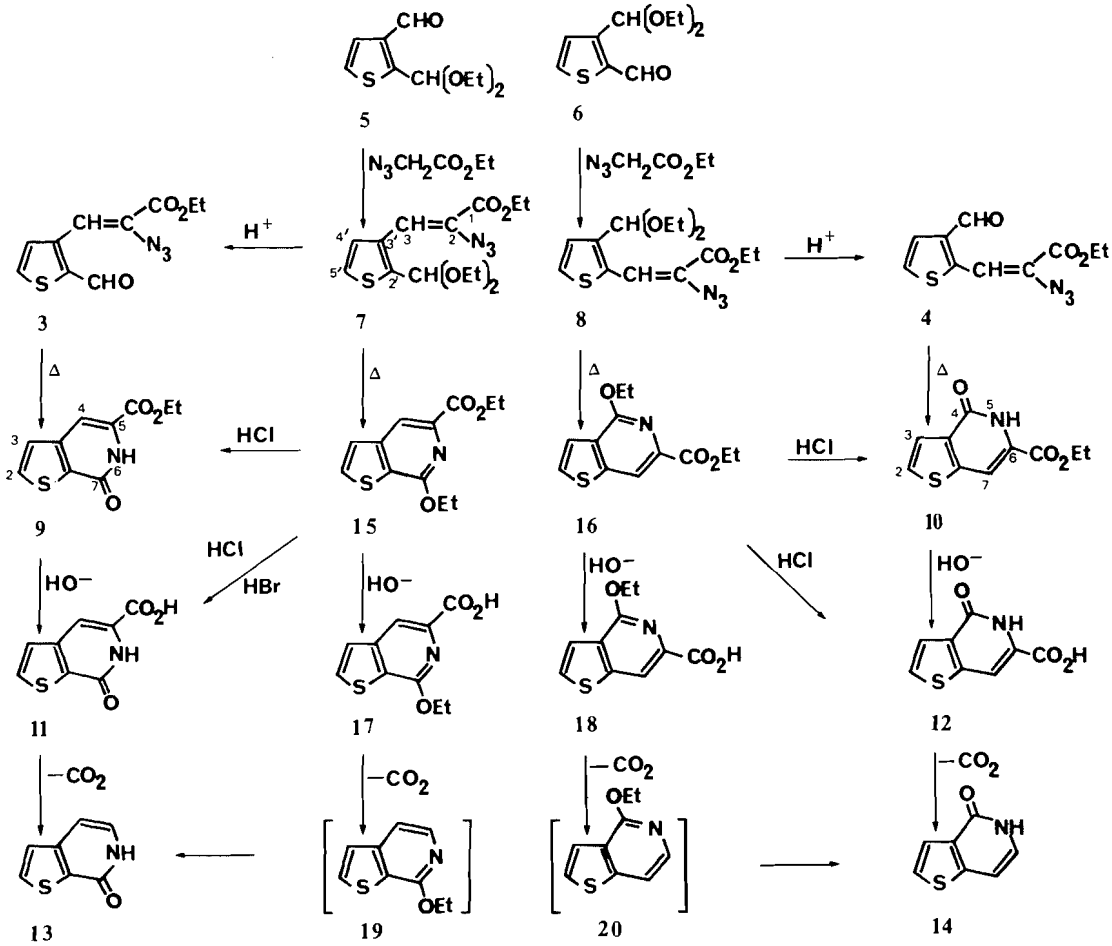

SCHÉMA 2

avec un rendement général voisin de 50%.

La cyclisation du composé **3** donne naissance (rendement 81%) à la thiéno[2,3-*c*]pyridone substituée **9**. Cette cyclisation intéresse donc le groupe formyle et non le sommet β' du cycle thiophénique: ce résultat rejoint ceux observés (1*b*, 2, 3) lors de la cyclisation du produit de condensation de l'azidoacétate d'éthyle sur les aldéhydes-3 hétérocycliques. Par hydrolyse alcaline de l'ester **9** on accède quantitativement à l'acide **11** qui, par décarboxylation (poudre de cuivre – quinoléine), donne naissance (rendement 40%) à la thiéno[2,3-*c*]pyridone **13**.

Le comportement du produit **4** est tout à fait analogue à celui exposé pour son isomère **3** et la thiénopyridone **14** est obtenue par l'intermédiaire de l'ester **10** et de l'acide **12** (rendement général des transformations **4** → **14**, 39%).

La cyclisation du dérivé **7** en la thiéno[2,3-*c*] pyridine éthoxylée **15** s'effectue avec un rendement plus faible (49%) que lorsqu'on opère au départ du composé **3** présentant un carbonyle libre. L'hydrolyse du produit **15** a été réalisée en milieu acide et en milieu basique. Dans le premier cas, et lorsqu'on opère en présence de chlorure d'hydrogène, les thiénopyridones **9** et **11** apparaissent simultanément (proportions relatives, 30 et 70%; rendement général, 82%); lorsqu'on utilise le bromure d'hydrogène, seul se forme **11** (rendement quantitatif). Ces résultats confirment que la forme lactame des deux composés **9** et **11** est très hautement favorisée. Lorsqu'on traite l'ester éther **15** par une solution aqueuse de potasse, on accède quantitativement à l'acide **17**. La décarboxylation de ce dernier composé a été réalisée dans la quinoléine en

Can. J. Chem. Downloaded from www.nrcresearchpress.com by 210.87.254.6 on 09/05/12
For personal use only.

Can. J. Chem. Downloaded from www.nrcresearchpress.com by 210.87.254.6 on 09/05/12
For personal use only.

opérant en présence soit de poudre de cuivre, soit de chromite de cuivre activé par du baryum: dans les deux cas on isole la thiéno[2,3-*c*]pyridone **13** et non la thiénopyridine éthoxylée **19**. Cette thiénopyridine éthoxylée étant par ailleurs connue (4), le fait qu'elle ne soit pas isolée au cours de la transformation n'est donc pas dû à son instabilité éventuelle mais aux conditions opératoires mêmes: le proton qui apparaît au cours de la décarboxylation doit libérer la forme lactime qui par tautomérie conduit à la thiénopyridone **13**.

Le comportement du composé **8** est tout à fait analogue à celui de son isomère **7** et finalement la thiéno[3,2-*c*]pyridone **14** est parallèlement obtenue par l'intermédiaire de **20** en décarboxylant l'acide **18**.

Notons par ailleurs que nous avons cyclisé le mélange des composés **3** et **4** obtenu lors de la condensation de l'azidoacétate d'éthyle sur le dialdéhyde **1**. La cyclisation donne naissance à un mélange des thiénopyridones **9** et **10** (proportions relatives environ 60 et 40%; rendement global 40%) aisément séparables par chromatographie.

Nous avons également étudié le comportement du dérivé disubstitué **2** vis à vis de la chaleur (schéma 3).

La cyclisation donne curieusement naissance à un mélange d'esters de thiénopyridines **21** et **22** (proportions relatives 20 et 80%, rendement global 65%). L'hydrolyse alcaline de ces esters conduit aux acides **23** et **24** avec un rendement de l'ordre de 90%. Par décarboxylation des acides **23** et **24** (quinoléine–cuivre), on isole respectivement la thiéno[2,3-*c*]pyridine **25** (rendement 41%) et la thiéno[3,2-*c*]pyridine **26** (rendement 57%).

Les thiénopyridones **13** et **14** et les thiénopyridines **25** et **26** ont déjà été préparées par d'autres voies (5–9).[1] En revanche les intermédiaires que nous avons utilisés n'étaient pas connus: la structure de chacun d'eux découle de celle du produit final isolé et a été précisée par analyse des spectres rmn.

Spectroscopie de résonance magnétique nucléaire

Les caractéristiques rmn des produits non cyclisés sont indiquées tableau 1. L'attribution

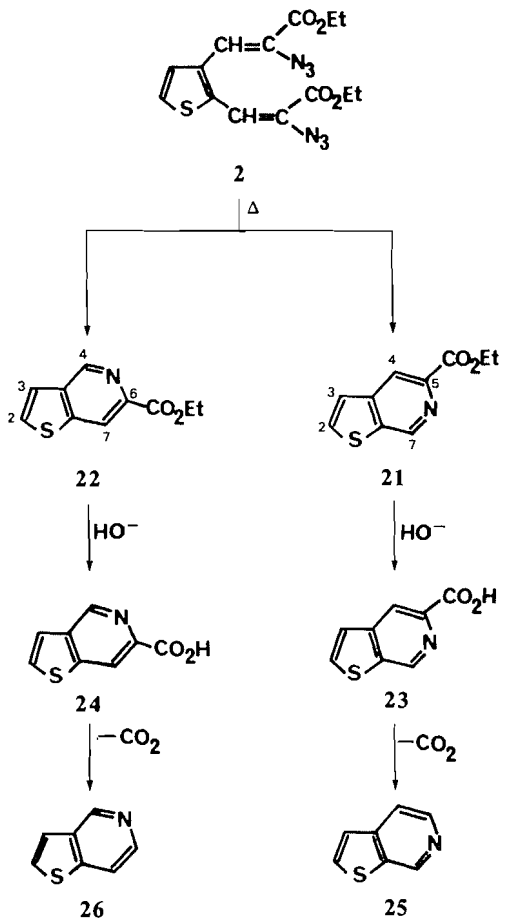

SCHÉMA 3

qui figure sur ce tableau pour les protons thiophéniques $H_{4(ou\ 4')}$ et $H_{5(ou\ 5')}$ a été effectuée compte tenu du déblindage général des protons α thiophéniques par rapport aux protons β et des incréments apportés en série thiophénique (11) par un groupe formyle ou azidoacrylate d'éthyle. A noter que les caractéristiques observées ne permettent pas de déterminer la configuration spatiale de chacun des composés étudiés; l'étude nous paraît cependant confirmer que la condensation ne conduit qu'à un seul des isomères géométriques théoriquement possibles.

En dehors de celles des thiéno[2,3-*c*] et -[3,2-*c*] pyridines **25** et **26** qui ont fait l'objet d'une étude rmn approfondie (12), les caractéristiques rmn de toutes les autres thiénopyridines et pyridones synthétisées apparaissent au tableau 2. Celles des thiénopyridones **13** et **14**, déjà reportées par

[1]Pour une revue d'ensemble sur les thiénopyridines, voir la réf. 10.

TABLEAU 1. Caractéristiques rmn des thiophènes disubstitués (solvant $CDCl_3$)

	Déplacement chimique des protons (ppm)*										
			Exocycliques								
	Du cycle thiophénique		$CH{=}C(N_3)CO_2CH_2CH_3$ (a) (b) (c)				$CH(OCH_2CH_3)_2$ (d) (e) (f)				
Composé	$H_{4(4')}$	$H_{5(5')}$	(a)		(b)	(c)	(d)	(e)	(f)	CHO	Constantes de couplage (Hz) $J_{45(4'5')}$
2	d	d	s	s	q	t					
	7.44	7.87	7.08	7.28	4.38	1.39					5.2
3	d	d	s		q	t				s	
	7.67	7.94	7.50		4.42	1.38				9.96	5.1
4	s	s	s		q	t				s	
	7.43	7.43	7.96		4.41	1.39				10.05	
7	d	d	s		q	t	s	q	t		
	7.22	7.84	7.26		4.39	1.33	5.86	3.65	1.22		5.2
8	d	d	s		q	t	s	q	t		
	7.14	7.36	7.57		4.39	1.36	5.72	3.62	1.22		5.1

*s, singulet; d, doublet; t, triplet; q, quadruplet.

Eloy et Deryckere (4, 5), sont indiquées tableau 2 pour conforter les attributions proposées.

Notons que pour les composés étudiés on retrouve les caractéristiques morphologiques signalées (12) pour les thiéno[2,3-*c*] et -[3,2-*c*] pyridines, en particulier l'existence des couplages J_{47} et J_{37}. Pour les composés **9**, **11**, **13**, **15** et **17** l'attribution des signaux des protons thiophéniques à H_2 ou à H_3 a été effectuée par référence aux résultats observés pour les thiénopyridines **21**, **23** et **25** pour lesquelles ne se pose aucun problème. Enfin, signalons que, pour les composés **15** et **16**, si les protons méthyléniques sont assignés de façon certaine soit au groupe OC_2H_5 soit au groupe $CO_2C_2H_5$, il n'en est pas de même pour les protons méthyliques de ces mêmes groupements.

Mécanisme réactionnel

La connaissance de la structure des divers produits obtenus nous a incités à tenter de préciser le mécanisme responsable de la formation, assez surprenante, des thiénopyridines et pyridones.

Le passage **7** → **15** est symbolisé sur le schéma 4. Après départ classique d'azote moléculaire, l'atome d'azote déficient en électrons attaque la liaison carbone–hydrogène et l'inclusion dans le cycle formé d'un doublet de l'amidure conduit à l'élimination d'un groupe éthoxy.

Lors de la cyclisation **3** → **9** (voir schéma 5),

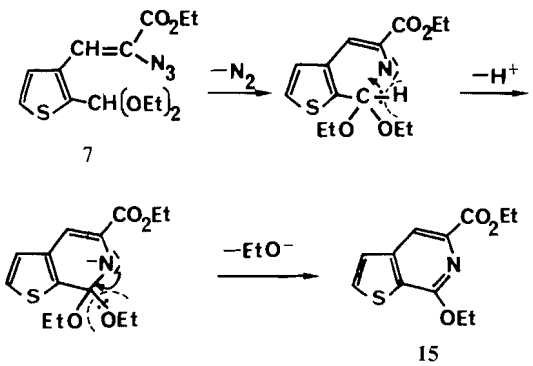

SCHÉMA 4

on passerait par l'intermédiaire d'une hydroxypyridine qui par prototropie donnerait naissance à la pyridone correspondante.

Un mécanisme analogue interviendrait dans le cas de la transformation **2** → **21** et **22** (voir schéma 6), mais l'appel d'électrons intéresserait les électrons π d'un groupe acrylate d'éthyle. Ce processus implique le départ de cyanoformiate d'éthyle. Nous avons vérifié la validité de l'hypothèse envisagée en mettant en évidence la présence de cet ester cyané en quantité proche de la stoechiométrie (par rapport au nombre de moles de thiénopyridines formées).

Expérimentalement on observe que le composé **22** est environ quatre fois plus abondant que son isomère **21**; ce résultat peut s'interpréter par

Can. J. Chem. Downloaded from www.nrcresearchpress.com by 210.87.254.6 on 09/05/12
For personal use only.

TABLEAU 2. Caractéristiques rmn des thiénopyridines et pyridones

Composé	Solvant	Déplacement chimique des protons (ppm)*										Constantes de couplage (Hz)		
		Du cycle thiénopyridinique						Exocycliques						
		H_2	H_3	H_4	H_5	H_6	H_7	$CO_2C_2H_5$		OC_2H_5				
9	$CDCl_3$	d 7.82	d 7.37	s 7.54				q 4.47	t 1.42			J_{23} 5.0		
10	$CDCl_3$	d 7.49	2d 7.74				d 7.54	q 4.44	t 1.41			J_{23} 5.4	J_{37} 0.7	
11	DMSO-d_6	d 8.13	d 7.54	s 7.50								J_{23} 4.8		
12	DMSO-d_6	d 7.87	2d 7.61				d 7.69					J_{23} 5.0	J_{37} 0.7	
13	DMSO-d_6	d 8.03	d 7.39	d 6.73	d 7.29							J_{23} 5.1	J_{45} 6.5	
14	DMSO-d_6	d 7.62	2d 7.53			d 7.30	2d 6.87					J_{23} 5.1	J_{67} 6.8	J_{37} 0.7
15	$CDCl_3$	d 7.72	d 7.42	s 8.21				q 4.46	t 1.49	q 4.70	t 1.44	J_{23} 5.3		
16	$CDCl_3$	s 7.52	s 7.52				s 8.17	q 4.44	t 1.45	q 4.65	t 1.40			
	DMSO-d_6	d 8.04	2d 7.60				d 8.37	q 4.45	t 1.45	q 4.65	t 1.39	J_{23} 5.4	J_{37} 0.8	
17	DMSO-d_6	d 8.17	d 7.63	s 8.24						q 4.62	t 1.44	J_{23} 5.3		
18	DMSO-d_6	d 8.04	2d 7.59				d 8.49			q 4.64	t 1.43	J_{23} 5.4	J_{37} 0.8	
21	$CDCl_3$	d 7.87	2d 7.54	d 8.62			m 9.26	q 4.56	t 1.47			J_{23} 5.2	J_{47} 1.0	J_{37} 0.8
22	$CDCl_3$	d 7.77	2d 7.57	d 9.21			m 8.71	q 4.57	t 1.47			J_{23} 5.3	J_{47} 0.9	J_{37} 0.8
23	DMSO-d_6	d 8.24	2d 7.72	d 8.55			m 9.29					J_{23} 5.1	J_{47} 1.0	J_{37} 0.8
24	DMSO-d_6	d 8.18	2d 7.78	d 9.23			m 8.84					J_{23} 5.1	J_{47} 0.9	J_{37} 0.8

*m, multiplet.

la plus grande stabilité ou la plus grande réactivité des intermédiaires obtenus selon *B*.

Partie expérimentale

Les analyses élémentaires ont été effectuées par le Laboratoire Central de Microanalyses du C.N.R.S. Les spectres rmn ont été relevés sur un appareil JEOL C 60 HL en utilisant le TMS comme référence interne. Les chromatogrammes en phase gazeuse ont été obtenus à l'aide d'un appareil Aerograph Autoprep A-700. Les caractéristiques de la colonne utilisée étaient les suivantes: phase stationnaire SE 30 à 20% sur Chromosorb WAW 45–60 mesh; longueur 10 pieds; diamètre extérieur $\frac{3}{8}$ po; température 100 °C; débit du gaz vecteur (He) 30 cm³/min.

Matières premières

Les dérivés thiophéniques de départ (thiophènedicarbaldéhyde-2,3 **1**, thiophènedicarbaldéhyde-2,3 diéthylacétal-2 **5**, thiophènedicarbaldéhyde-2,3 diéthylacétal-3 **6**) ont été préparés par les méthodes citées en réfs. 13 et 14.

Condensation de l'azidoacétate d'éthyle sur le thiophènedicarbaldéhyde-2,3 diéthylacétal-2

A une solution d'éthanolate de sodium (1.84 g (0.08 at. g) de Na dans 60 cm³ d'éthanol absolu), on ajoute goutte à goutte et à 0 °C une solution de 4.28 g (0.02 mol) de l'aldéhyde acétal **5** et 10.32 g (0.08 mol) d'azidoacétate d'éthyle dans 50 cm³ d'éthanol absolu. L'addition terminée, l'agitation est maintenue 2 h à 0 °C. Après avoir évaporé 80% du solvant, on verse sur une solution glacée de chlorure d'ammonium et on extrait à l'éther. La phase

Can. J. Chem. Downloaded from www.nrcresearchpress.com by 210.87.254.6 on 09/05/12
For personal use only.

Can. J. Chem. Downloaded from www.nrcresearchpress.com by 210.87.254.6 on 09/05/12
For personal use only.

éthérée est lavée à l'eau à neutralité, séchée ($MgSO_4$) et évaporée. L'huile résiduelle est éluée sur colonne d'acide silicique désactivé par le benzène. On recueille, après évaporation du solvant et séchage de l'huile obtenue, 4.3 g (66%) d'azido-2 (diéthylacétal-2′ thiényl-3′)-3 acrylate d'éthyle, **7**.

Condensation de l'azidoacétate d'éthyle sur le thiophènedicarbaldéhyde-2,3 diéthylacétal-3

On opère comme précédemment mais au départ de l'aldéhyde acétal **6**. Après chromatographie (éluant chloroforme), on obtient 4.2 g (65%) d'azido-2 (diéthylacétal-3′ thiényl-2′)-3 acrylate d'éthyle, **8**.

Les composés **7** et **8** ne peuvent être isolés à l'état de pureté analytique car tout essai de purification, soit par distillation, soit par chromatographie phase gazeuse, entraîne leur cyclisation.

Azido-2 (formyl-2′ thiényl-3′)-3 acrylate d'éthyle 3

A température ambiante, on maintient 5 min sous agitation 4.3 g du composé **7** dans 30 cm^3 d'une solution d'acide chlorhydrique 5 *N*. Il se forme un précipité. On ajoute alors 40 cm^3 de chloroforme et laisse l'agitation se poursuivre durant 10 min. Après décantation, la phase aqueuse est extraite au chloroforme. Les phases chloroformiques sont lavées à l'eau à neutralité, séchées ($MgSO_4$) et évaporées. Après recristallisation dans un mélange benzène–hexane (1:2), on recueille 2.7 g (81%) du produit **3**, pf 128–129 °C. *Anal.* calc. pour $C_{10}H_9N_3O_3S$: C 47.80, N 16.72, O 19.11, S 12.76; trouvé: C 48.02, N 16.44, O 19.21, S 12.60.

Azido-2 (formyl-3′ thiényl-2′)-3 acrylate d'éthyle 4

La coupure du groupe acétal de **8** est réalisée comme indiqué ci-dessus pour **7**. On isole ainsi le composé **4** avec un rendement de 75%, pf 136 °C. *Anal.* calc. pour $C_{10}H_9N_3O_3S$: C 47.80, N 16.72, O 19.11, S 12.76, trouvé: C 47.68, N 16.38, O 19.00, S 12.85.

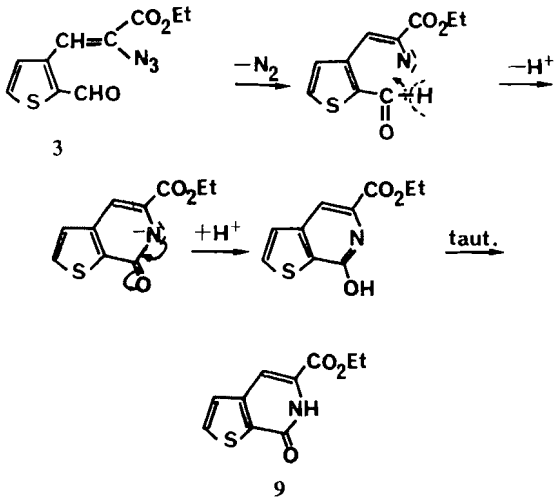

SCHÉMA 5

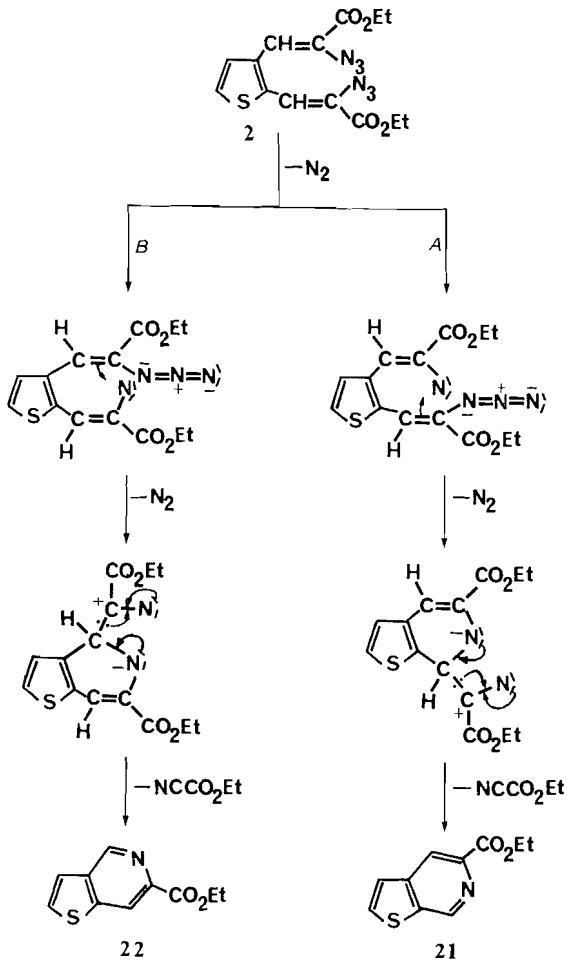

SCHÉMA 6

Oxo-7 dihydro-6,7 thiéno[2,3-c]pyridinecarboxylate-5 d'éthyle 9

Sous agitation, on porte 2 h à reflux 43 g du composé **3** dans 1200 cm^3 de xylène. Le xylène est éliminé par distillation et le résidu obtenu est repris par l'éther. Le précipité formé est recristallisé dans un mélange éthanol–eau (3:1). On isole ainsi 31 g (81%) de la thiénopyridone **9**, pf 181 °C. *Anal.* calc. pour $C_{10}H_9NO_3S$: C 53.81, H 4.06, N 6.28, O 21.55, S 14.30; trouvé: C 53.94, H 4.13, N 6.19, O 21.69, S 14.11.

Oxo-4 dihydro-4,5 thiéno[3,2-c]pyridinecarboxylate-6 d'éthyle 10

La cyclisation du dérivé **4** est réalisée comme indiqué pour son isomère **3**. Au départ de 35 g du composé **4** et après recristallisation dans l'éthanol, on obtient 28 g (90%) de la thiénopyridone **10**, pf 196 °C.

Anal. calc. pour $C_{10}H_9NO_3S$: C 53.81, H 4.06, N 6.28, O 21.55, S 14.30; trouvé: C 54.06, H 4.17,6.3 N 6, O 21.38, S 14.14.

Can. J. Chem. Downloaded from www.nrcresearchpress.com by 210.87.254.6 on 09/05/12
For personal use only.

Ethoxy-7 thiéno[2,3-c]pyridinecarboxylate-5 d'éthyle ***15***

Le produit **7** (10 g) dissous dans 200 cm³ de xylène est porté 90 min à reflux sous agitation. Le xylène est ensuite éliminé par distillation et le résidu élué sur acide silicique par le mélange benzène–acétone (20:1). Après recristallisation dans l'éther de pétrole, on isole 3.8 g (49%) de l'éthoxy thiénopyridine **15**, pf 77 °C. *Anal.* calc. pour $C_{12}H_{13}NO_3S$: C 57.35, H 5.21, N 5.57, O 19.10, S 12.76; trouvé: C 57.89, H 5.23, N 5.54, O 18.73, S 12.91.

Ethoxy-4 thiéno[3,2-c]pyridinecarboxylate-6 d'éthyle ***16***

L'éthoxy thiénopyridine **16** (pf 75 °C) est préparée avec un rendement de 36% selon un mode opératoire identique à celui utilisé pour l'obtention de son isomère **15**. *Anal.* calc. pour $C_{12}H_{13}NO_3S$: C 57.35, H 5.21, N 5.57, O 19.10, S 12.76; trouvé: C 57.06, H 5.18, N 5.81, O 18.99, S 12.84.

Hydrolyse alcaline des esters ***9***, ***10***, ***15*** *et* ***16***

L'hydrolyse alcaline des esters **9**, **10**, **15** et **16** est réalisée quantitativement selon un même mode opératoire décrit dans un cas particulier. On porte 4 h à reflux 4.46 g de l'ester **9** et 2.24 g de potasse dans 20 cm³ d'eau. Après retour à la température ambiante, on acidifie par une solution glacée d'acide chlorhydrique 5 *N*. Le précipité qui apparaît est essoré, lavé à l'eau glacée à neutralité et séché. On obtient 3.9 g d'acide oxo-7 dihydro-6,7 thiéno-[2,3-*c*]pyridinecarboxylique-5 **11**, pf 333 °C.

Acide oxo-4 dihydro-4,5 thiéno[3,2-*c*]pyridinecarboxylique-6 **12**, pf 335 °C.

Acide éthoxy-7 thiéno[2,3-*c*]pyridinecarboxylique-5 **17**, pf 165 °C.

Acide éthoxy-4 thiéno[3,2-*c*]pyridinecarboxylique-6 **18**, pf 170 °C.

Hydrolyse acide des éthoxy esters ***15*** *et* ***16***

(a) Action de HBr sur l'éthoxy ester ***15***

On porte 45 min à reflux 500 mg du composé **15** dans 20 cm³ d'acide bromhydrique à 40%. Le précipité formé après retour à température ambiante est essoré, lavé à l'eau glacée à neutralité et séché. On obtient ainsi quantitativement l'acide **11**.

(b) Action de HCl sur l'éthoxy ester ***15***

L'ester **15** (500 mg) dans 20 cm³ d'acide chlorhydrique 5 *N* est chauffé 90 min à 70–75 °C. Le précipité qui apparaît à température ambiante, filtré, lavé au chloroforme puis à l'eau glacée, enfin séché fournit 220 mg (57%) d'acide **11**.

Les phases aqueuses acides sont extraites au chloroforme. Les phases chloroformiques sont ensuite lavées à l'eau glacée à neutralité, séchées et évaporées. Après recristallisation, on isole 110 mg (25%) d'ester **9**.

(c) Action de HCl sur l'éthoxy ester ***16***

On opère comme en (*b*) et obtient ainsi au départ de 500 mg du dérivé **16**, 310 mg (80%) d'acide **12** et 18 mg (4%) d'ester **10**.

Décarboxylation des acides ***11***, ***12***, ***17*** *et* ***18***

La décarboxylation de ces acides a été réalisée par deux voies en opérant dans la quinoléine en présence soit de poudre de cuivre, soit de chromite de cuivre activé par du baryum.

(a) Quinoléine – poudre de cuivre

Le mode opératoire est décrit dans le cas de la décarboxylation de l'acide **11**. Une suspension de 1.95 g d'acide **11** et 2 g de poudre de cuivre dans 60 cm³ de quinoléine est chauffée 2 h à 200–210 °C. Puis on élimine le cuivre par filtration et la quinoléine par distillation sous 0.05 torr. Le résidu obtenu est chromatographié sur acide silicique (éluant benzène–acétone (3:2)). On obtient, après recristallisation dans l'eau, 600 mg (40%) d'oxo-7 dihydro-6,7 thiéno[2,3-*c*]pyridine **13**, pf 195 °C.

Cette même thiénopyridine **13** est obtenue (33%) en décarboxylant l'acide **17** par chauffage à reflux (1 h) dans la quinoléine.

L'oxo-4 dihydro-4,5 thiéno[3,2-*c*]pyridine **14**, pf 212 °C (litt. (5) pf 213–214 °C) est isolée de la même façon au départ soit de l'acide **12** (rendement 43%), soit de l'acide **18** (rendement 30%).

(b) Quinoléine – chromite de cuivre

Les acides **17** et **18** conduisent aux thiénopyridones **13** et **14** (rendements respectifs 25 et 20%) en opérant 30 min à 220 °C, mais les acides **11** et **12** ne permettent pas, par cette méthode, d'isoler ces mêmes thiénopyridones.

Condensation de l'azidoacétate d'éthyle sur le thiophènedicarbaldéhyde-2,3

On opère comme pour la condensation sur l'aldéhyde acétal **5**, mais en maintenant la température à −10 °C. Le résidu finalement obtenu après extraction de la phase aqueuse au chloroforme puis évaporation de ce solvant, est élué sur colonne d'acide silicique par le benzène. Au départ de 0.05 mol du dialdéhyde **1**, on obtient: (*i*) après recristallisation dans le mélange benzène–hexane (1:5) 2.55 g (14%) de (azido-2′ éthoxycarbonyl-2′ vinyl)-2 (azido-2″ éthoxycarbonyl-2″ vinyl)-3 thiophène **2**, pf 130 °C; *Anal.* calc. pour $C_{14}H_{14}N_6O_4S$: C 46.40, H 3.89, O 17.66, S 8.85; trouvé: C 46.60, H 3.92, O 17.69, S 9.08; et (*ii*) 500 mg (4%) de mélange des deux composés monocondensés **3** et **4** identifiés par chromatographie sur couche mince. La rmn montre que ce mélange contient environ 60% de composé **3** et 40% de composé **4**. Cette proportion est voisine de celle que l'on observe en cyclisant le mélange obtenu, puis en séparant les thiénopyridones **9** et **10** par chromatographie sur colonne d'acide silicique (éluant chloroforme–acétone (10:1)).

Cyclisation du dérivé dicondensé **2**

On chauffe 2 h à 120 °C 10 g du composé **2** dans 500 cm³ de xylène. Par distillation sous 1 atm, on recueille d'abord la fraction qui passe au dessous de 139 °C. On élimine ensuite la totalité du xylène et le résidu obtenu est chromatographié sur colonne d'acide silicique (éluant chloroforme–acétone (20:1)). On isole, après recristallisation dans l'éther de pétrole (*i*) 800 mg (14%) de thiéno-[2,3-*c*]pyridinecarboxylate-5 d'éthyle **21**, pf 78 °C; *Anal.* calc. pour $C_{10}H_9NO_2S$: C 57.95, H 4.38, N 6.76 O 15.44, S 15.47; trouvé: C 57.50, H 4.45, N 6.86, O 15.32, S 15.48; et (*ii*) 2.95 g (51%) de thiéno[3,2-*c*]pyridinecarboxylate-6 d'éthyle **22**, pf 65 °C; *Anal.* calc. pour $C_{10}H_9NO_2S$: C 57.95, H 4.38, N 6.76, O 15.44, S 15.47; trouvé: C 58.06, H 4.38, N 6.77, O 15.42, S 15.47.

La fraction qui a été initialement recueillie (p. éb <139 °C), analysée par chromatographie en phase gazeuse préparative, permet de récupérer 1.45 g (80% par rapport au nombre de mol de thiénopyridines formées) de cyanoformiate d'éthyle identifié à un échantillon commercial (même temps de rétention, même spectre ir).

*Hydrolyse alcaline des esters **21** et **22***

Les acides **23** et **24** sont obtenus selon le même procédé décrit dans le cas de l'isomère **23**. On porte 4 h à reflux 3.105 g d'ester **21** et 1.68 g de potasse dans 15 cm^3 d'eau. Puis, à 0 °C, on acidifie jusqu'à p*H* 3 par une solution d'acide chlorhydrique 5 *N*. Le précipité formé est essoré, lavé à l'eau glacée à neutralité, et séché. On obtient 2.47 g (92%) d'acide thiéno[2,3-*c*]pyridinecarboxylique-5 **23**, pf 240 °C.

Acide thiéno[3,2-*c*]pyridinecarboxylique-6 **24**, pf 204 °C.

*Décarboxylation des acides **23** et **24***

On chauffe 1 h à 205 °C une suspension de 1 g d'acide **24**, 1 g de poudre de cuivre dans 15 cm^3 de quinoléine. Après retour à température ambiante, la quinoléine est éliminée en éluant sur acide silicique par le mélange benzène–acétone (3:1). Après recristallisation dans le pentane, on isole 430 mg de thiéno[3,2-*c*]pyridine **26**, pf 46 °C, (litt. (5, 6, 9) pf 42–45 °C).

L'acide **23** décarboxylé dans les mêmes conditions (solvant d'élution, benzène–acétone–hexane (3:2:2)) fournit la thiéno[2,3-*c*]pyridine **25**, pf 54–55 °C (litt. (5, 6, 9) pf 54–58 °C).

1. (*a*) H. Hemetsberger, D. Knittel et H. Weidmann. Monatsh. Chem. **101**, 161 (1970); (*b*) H. Hemetsberger et D. Knittel. Monatsh. Chem. **103**, 194 (1972).
2. S. Soth, M. Farnier et P. Fournari. Bull. Soc. Chim. Fr. 2511 (1975).
3. K. N. Java, S. Soth, M. Farnier et C. Paulmier. C.R. Acad. Sci. Ser. C, **281**, 793 (1975).
4. F. Eloy et A. Deryckere. Bull. Soc. Chim. Belg. **79**, 407 (1970).
5. F. Eloy et A. Deryckere. Bull. Soc. Chim. Belg. **79**, 301 (1970).
6. W. Herz et L. Tsai. J. Am. Chem. Soc. **75**, 5122 (1953).
7. C. Hansch, W. Carpenter et J. Todd. J. Org. Chem. **23**, 1924 (1958).
8. L. H. Klemm, J. Shabtai, D. R. McCoy et W. K. T. Kiang. J. Heterocycl. Chem. **5**, 883 (1968); **6**, 813 (1969).
9. S. Gronowitz et E. Sandberg. Ark. Kemi, **32**, 217 (1970).
10. S. W. Schneller. Int. J. Sulfur Chem. Part B, **7**, 309 (1972).
11. M. Farnier, S. Soth et P. Fournari. Can. J. Chem. **54**, 1074 (1976).
12. S. Gronowitz et E. Sandberg. Ark. Kemi, **32**, 269 (1970).
13. R. Guilard et P. Fournari. Bull. Soc. Chim. Fr. 1437 (1971).
14. P. Pastour, P. Savalle et P. Eymery. C.R. Acad. Sci. Ser. C, **260**, 6130 (1965).

Can. J. Chem. Downloaded from www.nrcresearchpress.com by 210.87.254.6 on 09/05/12
For personal use only.

Recherches en série hétérocyclique. XXVII.[1] Etude de la condensation de l'azidoacétate d'éthyle sur les thiophènedicarbaldéhydes-2,5, -2,4 et -3,4

MICHEL FARNIER, SAMRETH SOTH ET PIERRE FOURNARI

Laboratoire de Polarographie Organique associé au C.N.R.S., Chimie des Hétérocycles, Faculté des Sciences Gabriel - 21000 Dijon, France

Reçu le 2 octobre 1975

MICHEL FARNIER, SAMRETH SOTH et PIERRE FOURNARI. Can. J. Chem. **54**, 1074 (1976).

L'azidoacétate d'éthyle réagit avec les thiophènedicarbaldéhydes-2,5, es-2,5, -2,4 et -3,4 pour conduire à des produits de mono- et de dicondensation. La cyclisation des dérivés thiophéniques ainsi obtenus donne naissance soit à des thiénopyrroles substitués, soit à des systèmes comportant deux noyaux pyrroliques orthocondensés à un cycle thiophénique, soit enfin à des thiéno[3,4-*c*]pyridones et pyridines. La structure des composés obtenus au cours des diverses synthèses réalisées est précisée par spectroscopie rmn.

MICHEL FARNIER, SAMRETH SOTH, and PIERRE FOURNARI. Can. J. Chem. **54**, 1074 (1976).

Ethyl azidoacetate reacts with 2,5-, 2,4-, and 3,4-thiophenedialdehydes to yield products of both mono- and dicondensation. Cyclization of the thiophene derivatives thus obtained leads to substituted thienopyrroles, to systems involving two pyrrole rings orthocondensed to one thiophene ring, or to thieno[3,4-*c*]pyridones and pyridines. The structures of the compounds obtained from various syntheses were established by nmr.

[Journal translation]

Introduction

Alors que la réaction de Hemetsberger et Knittel (2) appliquée à un monoaldéhyde thiophénique conduit à un thiénopyrrole (2, 3), nous avons indiqué dans l'article précédent (1) qu'au départ du thiophénedicarbaldéhyde-2,3, on accédait à des thiénopyridines et pyridones. Ces résultats sont certainement dûs au fait que l'azidoacrylate d'éthyle substitué, formé après action de l'azidoacétate d'éthyle peut interagir soit avec le groupe formyle qui reste libre, soit avec un deuxième groupe azidoacrylate d'éthyle introduit par dicondensation, ces interactions étant d'autant plus aisées que les substitutions intéressent deux atomes de carbone cycliques vicinaux et qu'aucun sommet α, plus réactif qu'un sommet β, n'est en position favorable pour la formation d'un cycle pyrrolique.

Pour les trois dialdéhydes thiophéniques isomères, ces diverses caractéristiques ne peuvent être présentes simultanément et, *a priori*, les structures des produits finaux devaient ou pouvaient être différentes de celles auxquelles conduit le dialdéhyde-2,3; aussi avons-nous cherché à préciser le comportement de chacun de ces dialdéhydes lorsqu'on l'oppose à l'azidoacétate d'éthyle et nous envisagerons successivement les résultats obtenus au départ des dialdéhydes-2,5, -2,4 et -3,4.

[1]Pour la partie XXVI voir la réf. 1.

Résultats

Synthèses en série 2,5

Pour le dialdéhyde-2,5, aucune des interactions envisagées précédement ne peut intervenir et la nature des produits finalement obtenus au départ du dialdéhyde $\alpha\alpha'$ devait donc raisonnablement être différente de celle du dialdéhyde $\alpha\beta$; c'est effectivement ce qui est observé, les diverses synthèses réalisées figurant au schéma 1.

Dans les mêmes conditions opératoires que celles utilisées dans le cas du dialdéhyde-2,3 (8 mol d'azidoacétate d'éthyle pour une mol de dialdéhyde), le dialdéhyde **1** donne un produit de monocondensation **2** et un de dicondensation **3** (proportions relatives 9 et 91%, rendement global 45%). La cyclisation du composé **2** conduit normalement au dérivé disubstitué correspondant du thiéno[3,2-*b*]pyrrole, **4** composé déjà préparé par une autre voie (4); quant à celle du produit **3**, elle permet, par l'intermédiaire du diester **5** et du diacide **6**, l'accès au 4*H*,5*H*-thiéno[3,2-*b*:4,5-*b'*]dipyrrole **7**, le rendement global de la transformation **3** → **7** étant de 26%.

Can. J. Chem. Downloaded from www.nrcresearchpress.com by 210.87.254.6 on 09/05/12
For personal use only.

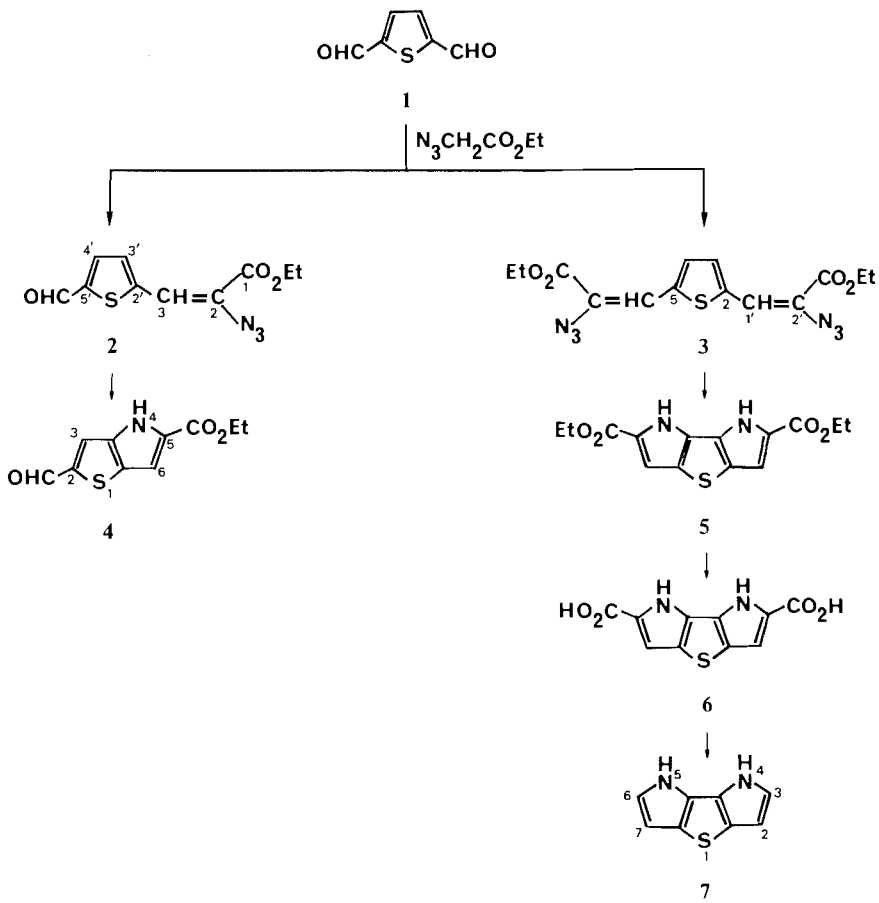

SCHÉMA 1

Synthèses en série 2,4

Les remarques relatives au dialdéhyde-2,5 sont également valables pour le dialdéhyde-2,4; on devait donc s'attendre à l'obtention finale de produits analogues à ceux signalés dans le cas précédent; l'expérience vérifie parfaitement ces prévisions et les résultats que nous avons observés sont indiqués sur le schéma 2.

La condensation de l'azidoacétate d'éthyle sur le dialdéhyde **8** donne naissance à un mélange de trois produits: deux de monocondensation **9** et **10** et un de dicondensation **11** (proportions relatives et respectives 18, 4 et 78%, rendement général 36%). Les transformations réalisées au départ des produits **9**, **10** et **11** analogues à celles signalées précédemment, conduisent directement aux thiénopyrroles disubstitués **12** et **13** et, par l'intermédiaire du diester **14** et du diacide **15**, au 2*H*,5*H*-thiéno[2,3-*b*:4,5-*b*']dipyrrole **16**, le rendement global de la transformation **11** → **16** étant de 15%. A noter que le composé **13** est identique au produit principal de la formylation de l'ester éthylique en 5 du thiéno[2,3-*b*]pyrrole (3).

Synthèses en série 3,4

Le dialdéhyde-3,4 peut, comme l'isomère 2,3, être considéré comme un dialdéhyde *ortho*, mais les positions α thiophéniques sont libres. Compte tenu des observations précédentes on pouvait envisager une compétition entre une cyclisation intéressant le noyau thiophénique et une cyclisation résultant de l'interaction des substituants en 3,4. Le schéma 3, qui regroupe les résultats obtenus en série 3,4, confirme ces prévisions.

De même que dans le cas des trois autres dialdéhydes, la réaction de condensation au départ du dialdéhyde **17**[2] se traduit par la

[2]L'étude de la condensation de l'azidoacétate d'éthyle sur le dialdéhyde-3,4 a fait l'objet d'une publication préliminaire (5).

Can. J. Chem. Downloaded from www.nrcresearchpress.com by 210.87.254.6 on 09/05/12
For personal use only.

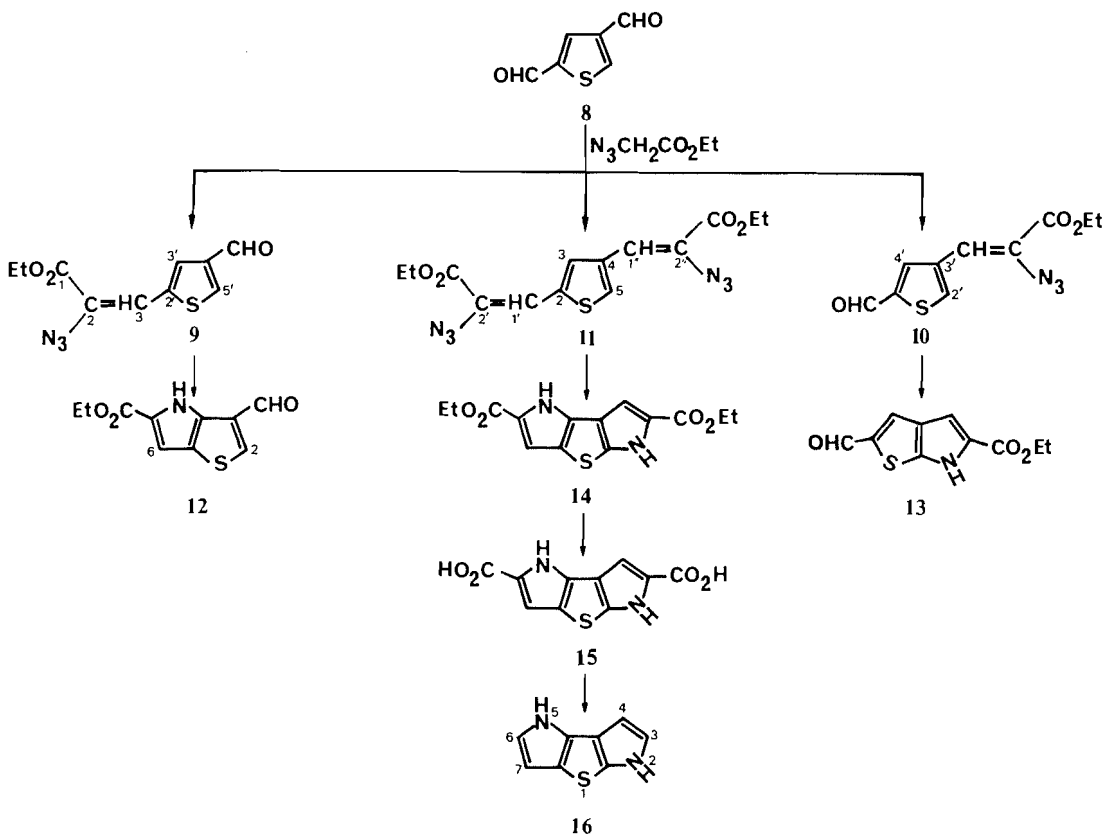

SCHÉMA 2

formation simultanée d'un produit de monocondensation **18** et d'un de dicondensation **19** (proportions relatives et respectives 47 et 53%, rendement général 28%). La cyclisation de chacun des produits obtenus intéresse d'une part le (ou les) atome(s) de carbone en α du (ou des) groupe(s) azidoacrylate d'éthyle, d'autre part l'un de ces groupes et le groupe porté par le carbone β' voisin. Le produit de monocondensation conduit donc (et ainsi que nous l'avons noté dans une précédente publication (3)) au dérivé disubstitué **20** du thiéno[2,3-*b*]pyrrole et à un ester éthylique **21** d'une thiéno[3,4-*c*]pyridone (proportions relatives 90 et 10%, rendement global 76%).

L'ester **21** donne naissance, via l'acide **24**, à la thiéno[3,4-*c*]pyridone **25**, stable, le rendement du passage **21** → **25** étant voisin de 20%. Parallèlement, le produit de dicondensation **19** conduit respectivement aux esters **22** et **23** en proportions sensiblement équimoléculaires et avec un excellent rendement (92%). On accède ainsi à un ester **23** de la thiéno[3,4-*c*]pyridine, ester parfaitement stable alors qu'il a déjà été signalé (6) que la thiéno[3,4-*c*]pyridine correspondante ne peut être conservée que sous forme de picrate. Le diester **22** conduit normalement, par l'intermédiaire du diacide **26**, au 2*H*,7*H*-thiéno-[2,3-*b*:5,4-*b'*]dipyrrole **27** avec un rendement de 25%.

Notons par ailleurs que nous avons pu obtenir un monoester éthylique du thiénodipyrrole **27** en opérant de la façon suivante (voir schéma 4): le thiéno[2,3-*b*]pyrrolecarbaldéhyde-3 **28**, dérivé de **20**, (3) se condense, mais avec un faible rendement, sur l'azidoacétate d'éthyle pour conduire à l'azide **29** dont la cyclisation conduit à l'ester **30**, mais cette voie d'accès au système hétérocyclique fondamental **27** est nettement moins favorable que celle indiquée sur le schéma 3. A noter, de plus, que l'aldéhyde **28** est le seul des quatre aldéhydes thiéno[2,3-*b*]pyrroliques à se

Can. J. Chem. Downloaded from www.nrcresearchpress.com by 210.87.254.6 on 09/05/12
For personal use only.

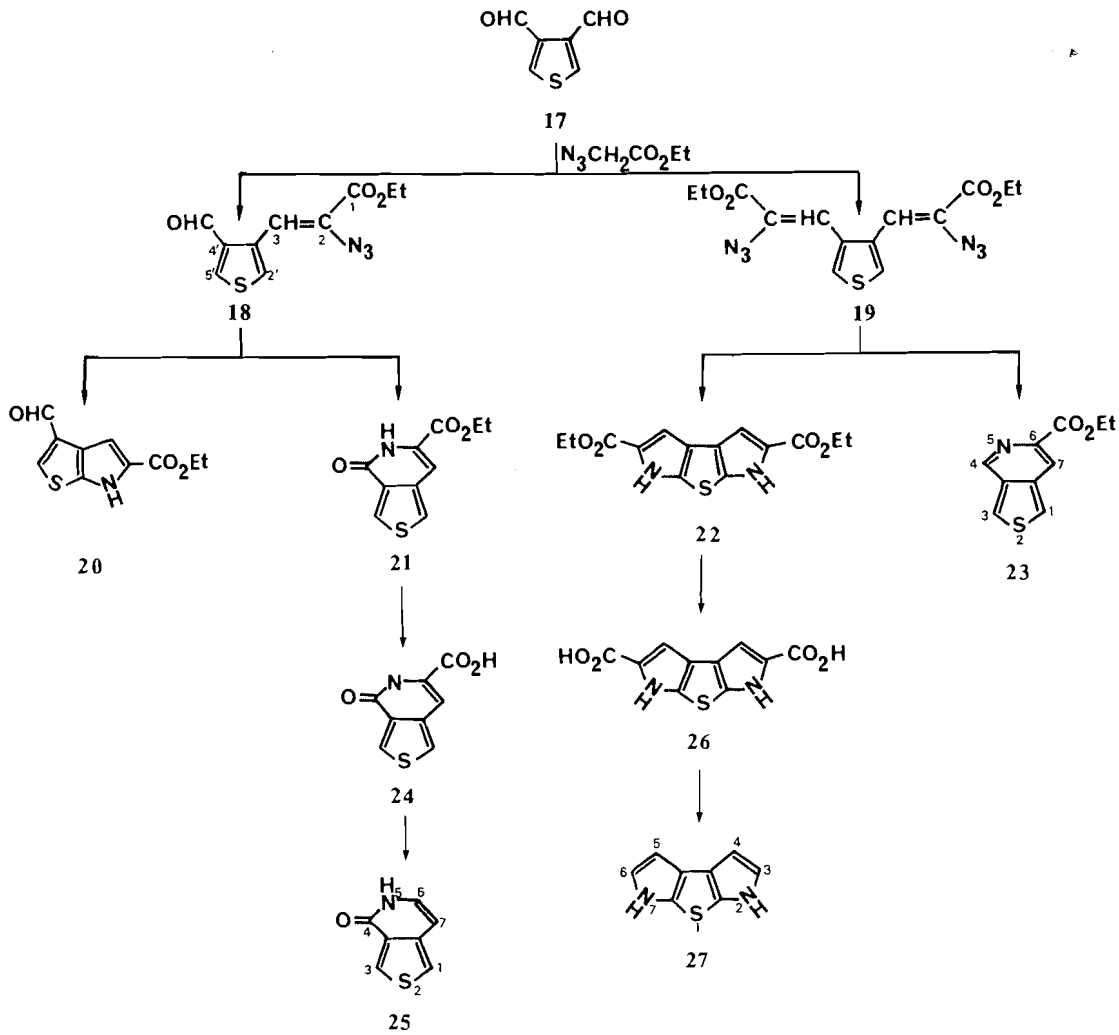

SCHÉMA 3

condenser sur l'azidoacétate d'éthyle dans les conditions opératoires utilisées.

De l'ensemble des études réalisées au départ des dialdéhydes thiophéniques nous paraissent se dégager les observations générales suivantes.

(*i*) Alors que pour des monoaldéhydes thiophéniques le rendement de la réaction de condensation est relativement élevé (50 à 70%), il n'atteint jamais 50% pour les dialdéhydes. La présence d'un second groupe formyle défavorise donc la condensation; cet effet est davantage marqué lorsque les deux groupes formyle sont en *ortho*: des implications stériques interviennent alors certainement.

(*ii*) En ce qui concerne les réactions de cyclisation, la facilité de formation d'un cycle pyrrolique n'est pratiquement pas affectée par la présence d'un groupe formyle; parmi les dérivés bicondensés, c'est le dérivé porteur de groupes azidoacrylate d'éthyle en positions 2,4 qui se cyclise le plus difficilement. Ce résultat est vraisemblablement imputable au fait que les systèmes éthyléniques présentent des configurations ou des conformations peu adaptées à une bicyclisation conduisant à des "enroulements" dans des sens différents.

Spectroscopie de résonance magnétique nucléaire

Dans le tableau 1 nous avons groupé les caractéristiques observées pour les produits de

Can. J. Chem. Downloaded from www.nrcresearchpress.com by 210.87.254.6 on 09/05/12
For personal use only.

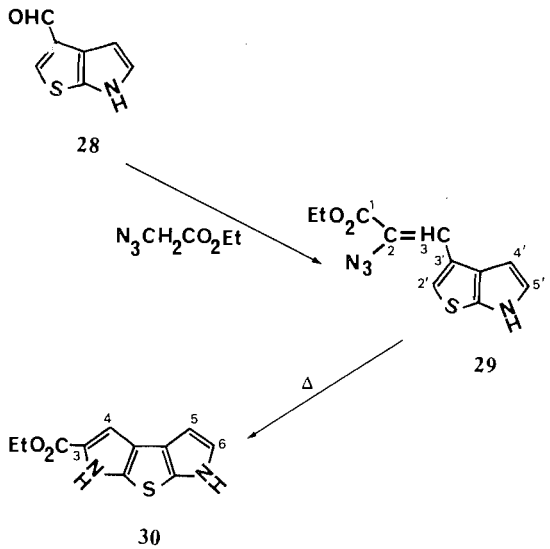

SCHÉMA 4

mono- et de dicondensation des dialdéhydes-2,5, -2,4 et -3,4 et nous y avons fait figurer également, aux fins de comparaison, celles relatives aux dérivés de condensation **31** et **32** des aldéhydes α et β thiophéniques.

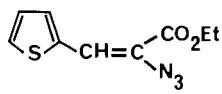

31

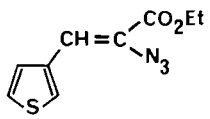

32

Les caractéristiques rmn des dérivés **31** et **32** ont déjà été signalées (2): par rapport aux résultats indiqués par Hemetsberger et Knittel, les valeurs qui figurent au tableau 1 sont concordantes pour tous les protons thiophéniques du composé **31**, mais celles relatives aux protons $H_{4'}$ et $H_{5'}$ de son isomère **32** sont inversées. L'ensemble des couplages observés nous paraît confirmer l'assignation donnée au tableau 1.

En ce qui concerne les produits de mono- et de dicondensation des dialdéhydes-2,5, -2,4 et -3,4, l'attribution des signaux observés tant pour les protons thiophéniques que pour les protons vinyliques n'est généralement pas immédiate. Elle a été réalisée compte tenu: (*i*) du déblindage général des protons α thiophéniques par rapport aux protons β; (*ii*) des incréments de glissement chimique apportés tant par un groupe formyle (7) que par un groupe azidoacrylate d'éthyle (et en appliquant la règle d'additivité des incréments); et (*iii*) enfin, du fait que le proton vinylique du groupe azidoacrylate d'éthyle résonne très généralement vers 6.9 ppm lorsque ce groupe est fixé en position β du soufre et vers 7.1 ppm lorsqu'il est en position α.

Ainsi, la généralisation de cette dernière constatation permet, pour le dérivé dicondensé **11**, d'attribuer le singulet à 7.08 ppm à $H_{1'}$ et celui à 6.82 ppm à $H_{1''}$.

Notons enfin que la structure du dérivé **10** (et par voie de conséquence celle de son isomère **9**) découle de l'identité de l'ester aldéhyde **13** et d'un produit de formylation du thiéno[2,3-*b*]-pyrrolecarboxylate-5 d'éthyle.

La structure des divers dérivés thiophéniques disubstitués étant parfaitement définie, les filiations chimiques qui conduisent aux composés comportant deux ou trois cycles orthocondensés sont sans ambiguïté sauf en ce qui concerne la série 3,4 où il existe deux possibilités de cyclisation. Dans ce cas la spectroscopie rmn permet d'établir la structure des composés obtenus. Nous avons rassemblé dans le tableau 2 l'ensemble des caractéristiques rmn des hétérocycles orthocondensés synthétisés.

Les valeurs qui figurent au tableau 2 nous paraissent appeler les quelques remarques suivantes. Dans le cas du thiénodipyrrole **16**, si les protons α des cycles pyrroliques sont aisément distingués des protons β, un problème se pose pour l'attribution des signaux de H_3 et H_6 d'une part et de H_4 et H_7 d'autre part. Or, les glissements chimiques des protons α sont très voisins (et il en est de même de ceux des protons β). Ceci rejoint les résultats observés par exemple (8) pour les *N*-benzylthiéno[2,3-*b*]- et thiéno[3,2-*b*]-pyrroles. Il en résulte que le signal assigné au tableau 2 à H_3 pourrait l'être à H_6 et réciproquement, et il en est de même pour H_4 et H_7. En ce qui concerne les constantes de couplage, les valeurs relevées sont conformes à celles attendues. Comme le laissaient prévoir les résultats obtenus pour les thiéno[2,3-*c*]- et -[3,2-*c*]pyridines (9), on observe un couplage à longue distance J_{37} pour les thiéno[3,4-*c*]pyridones **21**, **24** et **25**. Pour la thiéno[3,4-*c*]pyridine **23** (pour laquelle l'attribution des signaux à H_1 et H_3 est

Can. J. Chem. Downloaded from www.nrcresearchpress.com by 210.87.254.6 on 09/05/12
For personal use only.

TABLEAU 1. Caractéristiques rmn (solvant $CDCl_3$) des composés du type

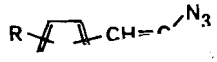

iques

Composé										Constantes de couplage (Hz)		
							I_2CH_3 (c)	CHO				
2							t 1.37	s 9.97	$J_{3'4'}$ 3.7	$J_{33'}$ 0.6	
3							t 1.38				
9							t .38	s 9.94	$J_{3'5'}$ 1.3	$J_{35'}$ 0.7	
10	s 8.1						t 39	s 9.97			
11				.,75	7.08	6.82 q 4.34	t 1.37				
18	d 8.09			m 8.31		d 7.82 q 4.38	t 1.39	d 9.94	$J_{2'5'}$ 2.7	$J_{35'}$ 0.75	$J_{5'\text{-CHO}}$ 0.5
19	s 8.23			s 8.23		s 6.92 q 4.37	t 1.40				
31		m 7.27	2d 7.00	m 7.44		m 7.12 q 4.34	t 1.36		$J_{3'5'}$ 1.2 $J_{33'}$ 0.5–0.6	$J_{3'4'}$ 3.6 $J_{35'}$ 0.7	$J_{4'5'}$ 4.8
32	m 7.86		2d 7.47	2d 7.29		M 6.94 q 4.35	t 1.38		$J_{2'4'}$ 1.2 $J_{32'}$ 0.6–0.7	$J_{2'5'}$ 2.8	$J_{4'5'}$ 4.8

*s, singulet; d, doublet; t, triplet; q, quadruplet; m, multiplet; M, massif.

incertaine) apparaissent deux couplages supplémentaires J_{14} et J_{47}.

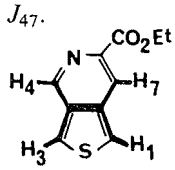

23

Ces mêmes caractéristiques se manifestent également sur les spectres des isomères [2,3-*c*] et [3,2-*c*] (1, 9). Signalons enfin que sur les spectres des thiénodipyrroles **7**, **16** et **27**, relevés dans le DMSO-d_6 sans ajout de D_2O, on note la présence de couplages $J_{H_\alpha\text{-NH}} = 2.4$ à 2.6 Hz et $J_{H_\beta\text{-NH}} = 1.9$ à 2.2 Hz.

Partie expérimentale

Les analyses élémentaires ont été effectuées par le Laboratoire Central de Microanalyses du C.N.R.S. A noter qu'il est difficile d'obtenir des résultats analytiques successifs concordants pour les composés thiophéniques dicondensés **3**, **11** et **19** et pour le composé monocondensé **29** qui se dégradent assez rapidement. C'est la raison pour laquelle aucun résultat analytique n'est indiqué pour les dérivés **3** et **29**. Les spectres rmn ont été relevés sur un appareil JEOL C 60 HL en utilisant le TMS comme référence interne. Les spectres de masse ont été obtenus à l'aide d'un appareil LKB 9000 (température de la source 300 °C; tension d'accélération 70 eV) et les spectres uv sur un appareil Beckman DK 2.

Matières premières

Les thiophènedicarbaldéhydes-2,5, -2,4 et -3,4 de départ ont été préparés selon les méthodes décrites dans la littérature (10).

Can. J. Chem. Downloaded from www.nrcresearchpress.com by 210.87.254.6 on 09/05/12
For personal use only.

TABLEAU 2. Caractéristiques rmn des produits comportant deux ou trois cycles orthocondensés

Composé	Déplacement chimique des protons (ppm)*										Constantes de couplage (Hz)			
	Cycliques							Exocycliques						
	H_1	H_2	H_3	H_4	H_5	H_6	H_7	$CO_2C_2H_5$		CHO				
4‡			d 7.98			d 7.17		q 4.35	t 1.34	s 10.00	J_{36} 0.7			
5		s 7.12					s 7.12	q 4.31	t 1.32					
6		s 7.11					s 7.11							
7†		d 6.35	d 6.87			d 6.87	d 6.35				J_{23} 2.8			
12		s 8.61				s 7.22		q 4.32	t 1.34	s 10.11				
14†				s 7.10			s 7.10	q 4.31	t 1.34					
15†				s 7.12			s 7.12							
16†			d 6.95	d 6.28		d 6.82	d 6.36				J_{34} 3.0	J_{67} 3.0		
21	d 7.60		2d 8.30				M 7.29	q 4.39	t 1.38		J_{13} 3.1	J_{37} 0.7		
22				s 7.06	s 7.06			q 4.27	t 1.31					
23	2d 7.93		2d 8.14	m 9.19			m 8.40	q 4.49	t 1.45		J_{13} 3.0	J_{14} 0.9–1.0	J_{37} 1.0	J_{47} 1.0
24	d 7.98		2d 8.40				M 7.31				J_{13} 3.0	J_{37} 0.7		
25†	d 7.68		2d 8.36			d 6.90	2d 6.53				J_{13} 3.0	J_{37} 0.7	J_{67} 7.5	
26†				s 7.11	s 7.11									
27†			d 6.92	d 6.32	d 6.32	d 6.92					J_{34} 2.9			
30†				s 6.99	d 6.37	d 6.92		q 4.26	t 1.30		J_{56} 2.9			

*Solvant DMSO-d_6 sauf pour les composés **21** et **23** ($CDCl_3$).
†Ajout de D_2O.
‡Valeurs en bon accord avec celles de Gale *et al.* (4).

Condensation de l'azidoacétate d'éthyle sur le thiophènedicarbaldéhyde-2,5

A une solution d'éthanolate de sodium (3.68 g (0.16 at. g) de Na dans 100 cm³ d'éthanol absolu), on ajoute goutte à goutte, à −10 °C et sous agitation une solution de 2.8 g (0.02 mol) du dialdéhyde **1** et 20.64 g (0.16 mol) d'azidoacétate d'éthyle dans 80 cm³ d'éthanol absolu. L'addition terminée, l'agitation est maintenue 1½ h à −10 °C. Le mélange réactionnel est versé dans une solution glacée de chlorure d'ammonium et extrait à l'éther. La phase éthérée est lavée à l'eau, séchée et le solvant est évaporé jusqu'à obtention d'environ 10 cm³ de solution. Le produit dicondensé **3** qui précipite est isolé par filtration et le filtrat est élué par le benzène sur colonne d'acide silicique. On récupère ainsi à nouveau un peu de produit dicondensé **3** et le dérivé monocondensé **2**. Finalement on obtient: (*i*) après recristallisation dans un mélange éther–hexane (1:2), 3.0 g (41%) de bis(azido-2′ éthoxycarbonyl-2′ vinyl)-2,5 thiophène **3**, pf 134 °C; et (*ii*) après recristallisation dans un mélange benzène–hexane (1:3), 200 mg (4%) d'azido-2 (formyl-5′ thiényl-2′)-3 acrylate d'éthyle **2**, pf 138 °C. *Anal.* calc. pour $C_{10}H_9N_3O_3S$: C 47.80, N 16.72, O 19.11, S 12.76; trouvé: C 47.97, N 16.53, O 19.34, S 12.61.

Can. J. Chem. Downloaded from www.nrcresearchpress.com by 210.87.254.6 on 09/05/12
For personal use only.

Can. J. Chem. Downloaded from www.nrcresearchpress.com by 210.87.254.6 on 09/05/12
For personal use only.

Condensation de l'azidoacétate d'éthyle sur le thiophènedicarbaldéhyde-2,4

On opère comme décrit ci-dessus mais au départ de 0.02 mol du dialdéhyde **8** et en maintenant la température à 0 °C. Après addition, on continue l'agitation 2 h à 0 °C puis 1 h à température ambiante. Le résidu obtenu après extraction et évaporation du solvant est chromatographié sur acide silicique (éluant benzène). On isole après recristallisation: (*i*) 2.0 g (28%) de (azido-2′ éthoxycarbonyl-2′ vinyl)-2 (azido-2″ éthoxycarbonyl-2″ vinyl)-4 thiophène **11**, pf 110 °C (solvant de recristallisation éther–hexane (1:3)); *Anal.* calc. pour $C_{14}H_{14}N_6O_4S$: C 46.40, H 3.89, N 23.20, S 8.85; trouvé: C 46.60, H 3.84, N 23.25, S 8.96; (*ii*) 65 mg (1.3%) d'azido-2 (formyl-5′ thiényl-3′)-3 acrylate d'éthyle **10**, pf 84 °C (solvant de recristallisation éther–pentane (1:4)); *Anal.* calc. pour $C_{10}H_9N_3O_3S$: C 47.80, H 3.61, N 16.72, O 19.11, S 12.76; trouvé: C 47.93, H 3.55, N 16.74, O 19.10, S 12.62; et (*iii*) 330 mg (6.6%) d'azido-2 (formyl-4′ thiényl-2′)-3 acrylate d'éthyle **9**, pf 60 °C (solvant de recristallisation pentane); *Anal.* calc. pour $C_{10}H_9N_3O_3S$: C 47.80, N 16.72, O 19.11, S 12.76; trouvé: C 47.65, N 16.43, O 19.12, S 12.87.

Condensation de l'azidoacétate d'éthyle sur le thiophènedicarbaldéhyde-3,4

La condensation est réalisée selon le mode opératoire général décrit pour le dialdéhyde-2,5, mais avec les modifications suivantes: on opère à 0 °C et on extrait au chloroforme. Au départ de 1.4 g du dialdéhyde **17** et après chromatographie sur acide silicique (éluant benzène) et recristallisation dans des mélanges benzène–hexane, on obtient: (*i*) 540 mg (15%) de bis(azido-2′ éthoxycarbonyl-2′ vinyl)-3,4 thiophène **19**, pf 140 °C; *Anal.* calc. pour $C_{14}H_{14}N_6O_4S$: C 46.40, N 23.20, O 17.66, S 8.85; trouvé: C 46.46, N 23.13, O 17.83, S 8.78; et (*ii*) 330 mg (13%) d'azido-2 (formyl-4′ thiényl-3′)-3 acrylate d'éthyle **18**, pf 121 °C, déjà obtenu par nous-mêmes par une autre voie (3).

*Cyclisation des produits de monocondensation **2**, **9**, **10** et **18***

Nous avons déjà signalé (3) les modalités et les résultats de la cyclisation du dérivé **18**. Celle des composés **2**, **9** et **10** a été effectuée selon le même procédé décrit dans le cas de l'isomère **2**.

*(a) Cyclisation du produit **2***

On porte 1 h à reflux 1 g du composé **2** dans 100 cm³ de xylène. Le xylène est ensuite éliminé par distillation et le résidu obtenu est élué sur acide silicique par le mélange chloroforme–acétone (20:1). Après recristallisation dans le benzène, on isole 670 mg (75%) de formyl-2 thiéno-[3,2-*b*]pyrrolecarboxylate-5 d'éthyle **4**, pf 177 °C (litt. (4) pf 181–181.8 °C).

*(b) Cyclisation du produit **9***

Au départ de 1 g du composé **9**, on obtient, après recristallisation dans l'hexane, 620 mg (70%) de formyl-3 thiéno[3,2-*b*]pyrrolecarboxylate-5 d'éthyle **12**, pf 86 °C. *Anal.* calc. pour $C_{10}H_9NO_3S$: C 53.81, H 4.06, N 6.27, O 21.50, S 14.36; trouvé: C 53.56, H 4.09, N 6.40, O 21.23, S 14.34.

*(c) Cyclisation du produit **10***

A partir de 200 mg du composé **10** et après élimination du xylène par distillation, un solide apparaît. Il est recristallisé directement dans un mélange benzène–hexane (3:1) et on isole 90 mg (51%) de formyl-2 thiéno[2,3-*b*]-pyrrolecarboxylate-5 d'éthyle **13**, pf 168 °C. Ce composé est identifié à l'un des produits de formylation (3) de l'ester éthylique en 5 du thiéno[2,3-*b*]pyrrole.

*Cyclisation des dérivés dicondensés **3**, **11**, et **19***

*(a) Cyclisation de **3***

Le composé **3** (21.7 g) dans 1 litre de xylène est porté 1 h à reflux. Par refroidissement la solution abandonne 14.0 g (76%) de 4*H*,5*H*-thiéno[3,2-*b*:4,5-*b*′]dipyrroledicarboxylate-3,6 de diéthyle **5**, pf 254 °C. *Anal.* calc. pour $C_{14}H_{14}N_2O_4S$: C 54.89, H 4.60, N 9.15, O 20.89, S 10.47; trouvé: C 54.74, H 4.52, N 9.39, O 20.71, S 10.22.

*(b) Cyclisation de **11***

A 250 cm³ de xylène chauffés à ébullition, sont ajoutés, sous agitation et par petites portions (en 10 min environ), 5 g du composé **11**. Après addition on agite encore 10 min et on élimine par distillation environ 80% du xylène. Le solide qui précipite par refroidissement est recristallisé dans un mélange éthanol–eau (3:1) et on obtient 1.8 g (43%) de 2*H*,5*H*-thiéno[2,3-*b*:4,5-*b*′]dipyrroledicarboxylate-3,6 de diéthyle **14**, pf 294–295 °C. *Anal.* calc. pour $C_{14}H_{14}N_2O_4S$: C 54.89, H 4.60, N 9.15, O 20.89, S 10.47; trouvé: C 54.97, H 4.71, N 9.31, O 20.78, S 10.34.

*(c) Cyclisation de **19***

On porte 400 cm³ de xylène à reflux, puis en 15 min environ on introduit, par fractions et sous agitation, 10 g du dérivé **19**. L'addition terminée, on maintient le reflux durant 20 min. Le précipité qui apparaît par refroidissement est séché et on isole ainsi 3.95 g (47%) de 2*H*,7*H*-thiéno[2,3-*b*:5,4-*b*′]dipyrroledicarboxylate-3,6 de diéthyle **22**, pf 309 °C. *Anal.* calc. pour $C_{14}H_{14}N_2O_4S$: C 54.89, N 9.15, O 20.89, S 10.47; trouvé: C 55.00, N 9.13, O 20.66, S 10.41.

Le xylène est ensuite éliminé par distillation et le résidu obtenu est élué sur acide silicique par le mélange chloroforme–acétone (9:1). On obtient après recristallisation dans un mélange benzène–hexane (1:4), 2.6 g (45%) de thiéno[3,4-*c*]pyridinecarboxylate-6 d'éthyle **23**, pf 108 °C. *Anal.* calc. pour $C_{10}H_9NO_2S$: C 57.95, N 6.76, O 15.44, S 15.47; trouvé: C 57.79, N 6.61, O 15.42, S 15.25.

*Hydrolyse des diesters **5**, **14** et **22***

L'hydrolyse alcaline des esters **5**, **14** et **22** est effectuée quantitativement selon le même mode opératoire décrit dans un cas particulier. Le diester **5** (6.12 g) et 4.48 g de potasse dans 60 cm³ d'eau sont portés 6 h à reflux. A température ambiante, on acidifie par une solution d'acide chlorhydrique 5 *N*. Le précipité obtenu est lavé à l'eau glacée jusqu'à neutralité et séché. On obtient 5 g d'acide 4*H*,5*H*-thiéno[3,2-*b*:4,5-*b*′]dipyrroledicarboxylique-3,6 **6**, pf (déc.) >360 °C.

Acide 2*H*,5*H*-thiéno[2,3-*b*:4,5-*b*′]dipyrroledicarboxylique-3,6 **15**, pf (déc.) >360 °C.

Acide 2*H*,7*H*-thiéno[2,3-*b*:5,4-*b*′]dipyrroledicarboxylique-3,6 **26**, pf (déc.) >360 °C.

*Décarboxylation des diacides **6**, **15** et **26***

*(a) Décarboxylation du diacide **6***

On chauffe 35 min à 130 °C, 2.5 g du diacide **6** et 750 mg de chromite de cuivre (activé par du baryum) dans 40 cm³ de quinoléine. Puis on refroidit rapidement par un

bain d'eau glacée et on verse dans 500 cm³ d'éther. La phase éthérée est isolée, lavée par une solution d'acide chlorhydrique 0.2 *N* puis à l'eau à neutralité et séchée. Après évaporation de l'éther et recristallisation dans un mélange benzène–hexane (3:2), on isole 570 mg (35%) de 4*H*,5*H*-thiéno[3,2-*b*:4,5-*b'*]dipyrrole **7**, pf 195 °C; λ_{max} (EtOH) 224 (ϵ 5800), 263 (15 600), 272 (17 900), 282 nm (14 500); spectre de masse, M^+ 162 (100%), 161 (17), 135 (47). *Anal.* calc. pour $C_8H_6N_2S$: C 59.23, H 3.73, N 17.27, S 19.77; trouvé: C 59.34, H 3.92, N 17.20, S 19.64.

(b) Décarboxylation du diacide ***15***

On opère comme pour l'isomère **6**. Au départ de 1 g du diacide **15** et après recristallisation dans un mélange benzène–hexane (1:1), on obtient 220 mg (34%) de 2*H*,5*H*-thiéno[2,3-*b*:4,5-*b'*]dipyrrole **16**, pf 140 °C; λ_{max} (EtOH) 214 (ϵ 14 800), 230 (14 500), 255 nm (10 100); spectre de masse, M^+ 162 (100%), 161 (35), 135 (37). *Anal.* calc. pour $C_8H_6N_2S$: C 59.23, H 3.73, N 17.27, S 19.77; trouvé: C 59.19, H 3.60, N 17.24, S 19.53.

(c) Décarboxylation du diacide ***26***

En opérant comme décrit pour l'isomère **6**, on isole au départ de 1.6 g du diacide **26**, 260 mg (25%) de 2*H*,7*H*-thiéno[2,3-*b*:5,4-*b'*]dipyrrole **27**, pf 113 °C (benzène–hexane (1:1); λ_{max} (EtOH) 208 nm (ϵ 22 700); spectre de masse, M^+ 162 (100%), 161 (50), 135 (23). *Anal.* calc. pour $C_8H_6N_2S$: C 59.23, H 3.73, N 17.27, S 19.77; trouvé: C 59.48, H 3.89, N 17.43, S 19.49.

Acide oxo-4 dihydro-4,5 thiéno[3,4-c]pyridinecarboxylique-6 ***24***

On chauffe 90 min à 60–70 °C, 700 mg d'ester **21** et 350 mg de potasse dans 10 cm³ d'eau. Après avoir acidifié par une solution d'acide chlorhydrique 5 *N* et lavé à l'eau glacée le précipité obtenu, on isole quantitativement l'acide **24**, pf (déc.) 324–325 °C.

Oxo-4 dihydro-4,5 thiéno[3,4-c]pyridine ***25***

Une suspension de 500 mg d'acide **24** et 250 mg de chromite de cuivre (activé par du baryum) dans 7 cm³ de quinoléine est portée 1 h à 195 °C. La quinoléine est ensuite éliminée par distillation sous 0.05 torr et le résidu obtenu élué sur colonne d'acide silicique par le mélange benzène–acétone (2:1). Après recristallisation dans l'eau, on obtient 80 mg (21%) de la thiénopyridone **25**, pf 200 °C. *Anal.* calc. pour C_7H_5NOS: C 55.61, H 3.33, N 9.27, O 10.58, S 21.21; trouvé: C 55.68, H 3.39, N 9.32, O 10.70, S 21.41.

Condensation de l'azidoacétate d'éthyle sur le 6H-thiéno[2,3-b]pyrrolecarbaldéhyde-3, ***28***

On opère comme décrit pour la condensation sur le thiophènedicarbaldéhyde-2,5 mais en maintenant la température à 0 °C. Le résidu finalement obtenu au départ de 1.51 g d'aldéhyde **28** (et de 5.16 g d'azidoacétate d'éthyle) est chromatographié sur acide silicique (éluant chloroforme–acétone (20:1)). On récupère ainsi 380 mg de l'aldéhyde **28** de départ et on obtient, après recristallisation dans un mélange benzène–hexane (1:3), 350 mg (18%) d'azido-2 (thiéno[2,3-*b*]pyrrolyl-3′)-3 acrylate d'éthyle **29**, pf 150 °C; rmn (DMSO-d_6, D_2O) δ 1.33 (t, 3H), 4.31 (q, 2H), 6.53 (d, $J_{4'5'}$ = 2.9 Hz, $H_{4'}$), 6.99 (s, H_3), 7.09 (2d, $J_{4'5'}$ = 2.9 et $J_{2'5'}$ = 1.1 Hz, $H_{5'}$), 7.72 (s élargi, $H_{2'}$).

2H,7H-Thiéno[2,3-b:5,4-b']dipyrrolecarboxylate-3 d'éthyle ***30***

On chauffe 1 h à 100 °C 1 g du composé **29** dans 100 cm³ de xylène. Le solvant est éliminé par distillation et le résidu obtenu élué sur acide silicique par le mélange chloroforme–acétone (20:1). Après recristallisation dans le mélange éthanol–eau (1:2), on isole 350 mg (39%) de l'ester **30**, pf 201 °C. *Anal.* calc. pour $C_{11}H_{10}N_2O_2S$: C 56.39, H 4.30, N 11.96, O 13.66, S 13.69; trouvé: C 56.29, H 4.05, N 12.04, O 13.52, S 13.52.

1. M. Farnier, S. Soth et P. Fournari. Can. J. Chem. **54**, 1066 (1976).
2. H. Hemetsberger et D. Knittel. Monatsh. Chem. **103**, 194 (1972).
3. S. Soth, M. Farnier et P. Fournari. Bull. Soc. Chim. Fr. 2511 (1975).
4. W. W. Gale, A. N. Scott et H. R. Snyder. J. Org. Chem. **29**, 2160 (1964).
5. M. Farnier, S. Soth et P. Fournari. C.R. Acad. Sci. Ser. C, **277**, 1149 (1973).
6. L. H. Klemm, W. O. Johnson et D. V. White. J. Heterocycl. Chem. **7**, 463 (1970); **9**, 843 (1972).
7. (*a*) R. Guilard. Thèse. Université de Dijon. 1971. p. 10; (*b*) S. Gronowitz et R. A. Hoffman. Ark. Kemi, **16**, 539 (1961).
8. R. K. Olsen et H. R. Snyder. J. Org. Chem. **30**, 184 (1965).
9. S. Gronowitz et E. Sandberg. Ark. Kemi, **32**, 269 (1970).
10. M. Robba, B. Roques et M. Bonhomme. Bull. Soc. Chim. Fr. 2495 (1967).

Can. J. Chem. Downloaded from www.nrcresearchpress.com by 210.87.254.6 on 09/05/12
For personal use only.

Recherches en série hétérocyclique. XXVIII.[1] Synthèse de bipyrroles

MICHEL FARNIER, SAMRETH SOTH ET PIERRE FOURNARI

Laboratoire de Polarographie Organique associé au C.N.R.S., Chimie des Hétérocycles, Faculté des Sciences Gabriel - 21000 Dijon, France

Reçu le 2 octobre 1975

MICHEL FARNIER, SAMRETH SOTH et PIERRE FOURNARI. Can. J. Chem. **54**, 1083 (1976).

La réduction par le nickel de Raney de diesters de thiénodipyrroles se traduit par une désulfuration. Par traitement des diesters bipyrroliques ainsi obtenus on accède aux trois systèmes fondamentaux; les bipyrroles-2,2′, -2,3′ et -3,3′.

MICHEL FARNIER, SAMRETH SOTH, and PIERRE FOURNARI. Can. J. Chem. **54**, 1083 (1976).

Raney nickel reduction of the diesters of thieno dipyrroles proceeds by a desulfuration. Treatment of the dipyrrole diesters thus obtained leads to three fundamental systems; 2,2′-, 2,3′-, and 3,3′-dipyrroles.

[Journal translation]

Introduction

Alors que les trois bithiophènes sont connus de longue date, le seul bipyrrole qui, à notre connaissance, ait été isolé est le bipyrrole-2,2′ (2, 3). Un certain nombre de ses dérivés de substitution ont également été synthétisés (2, 4–11). L'intérêt porté à la série des bipyrroles-2,2′ tient entre autres au fait que le méthoxy-4 bipyrrole-2,2′ carbaldéhyde-5 est le précurseur de prodigiosines (11–13), composés qui revêtent une importance certaine en biochimie. Par contre, en série 2,3′ seuls deux dérivés hautement substitués ont été décrits (14) et aucun représentant de la série 3,3′ ne paraît avoir été signalé. Notons enfin que si un seul bipyrrole non substitué a été obtenu les trois isomères ont déjà fait l'objet d'études théoriques tant du point de vue conformation (15) que du point de vue spectroscopie électronique (16).

Le fait que ni le bipyrrole-2,3′, ni le bipyrrole-3,3′ n'aient été synthétisés nous semble tenir essentiellement au fait que les monohalogénopyrroles, précurseurs potentiels de ces composés, sont très instables (17). Il paraissait cependant intéressant *a priori* de disposer des deux isomères du bipyrrole-2,2′ aux fins de pouvoir tenter de dégager l'influence de la structure sur l'activité chimique ou biochimique de leurs dérivés.

Dans l'article précédent, nous avons indiqué les voies d'accès à des produits de substitution de thiénodipyrroles et aux systèmes fondamentaux. Or, on sait (18) que le cycle thiophénique subit aisément une désulfuration lorsqu'on traite un composé comportant un tel cycle par le nickel de Raney. Cette caractéristique, qui s'est révélée contraignante dans la synthèse de certains thiénopyrroles substitués (19), pouvait *a priori* être mise à profit pour l'accès aux bipyrroles au départ de thiénodipyrroles. Mais ces derniers composés n'ont pu être isolés qu'en quantités relativement faibles, aussi nous avons préféré opérer sur les diesters $\alpha\alpha'$ accessibles dans de meilleures conditions.

Résultats

Les synthèses réalisées sont indiquées sur le schéma 1. La réduction désulfurante des trois diesters thiénodipyrroliques **1**, **2** et **3** s'effectue avec des rendements de l'ordre de 70–80%. Les diesters bipyrroliques ainsi obtenus, **4**, **5** et **6**, sont hydrolysés quantitativement en les diacides correspondants **7**, **8** et **9**. La bis décarboxylation de ces acides donne naissance aux trois bipyrroles **10**, **11** et **12** avec un rendement variant de 30 à 45%. Par cette voie, on passe donc d'un diester de thiénodipyrrole au bipyrrole correspondant avec un rendement général de l'ordre de 30%.

A noter, qu'assez curieusement, la nature du produit de départ n'a pratiquement aucune influence sur la facilité de la transformation.

La structure des bipyrroles et des intermédiaires découle directement des transformations réalisées. Les caractéristiques rmn observées pour chacun des produits synthétisés sont groupées dans le tableau 1.

[1]Pour la partie XXVII voir la réf. 1.

Can. J. Chem. Downloaded from www.nrcresearchpress.com by 210.87.254.42 on 09/05/12
For personal use only.

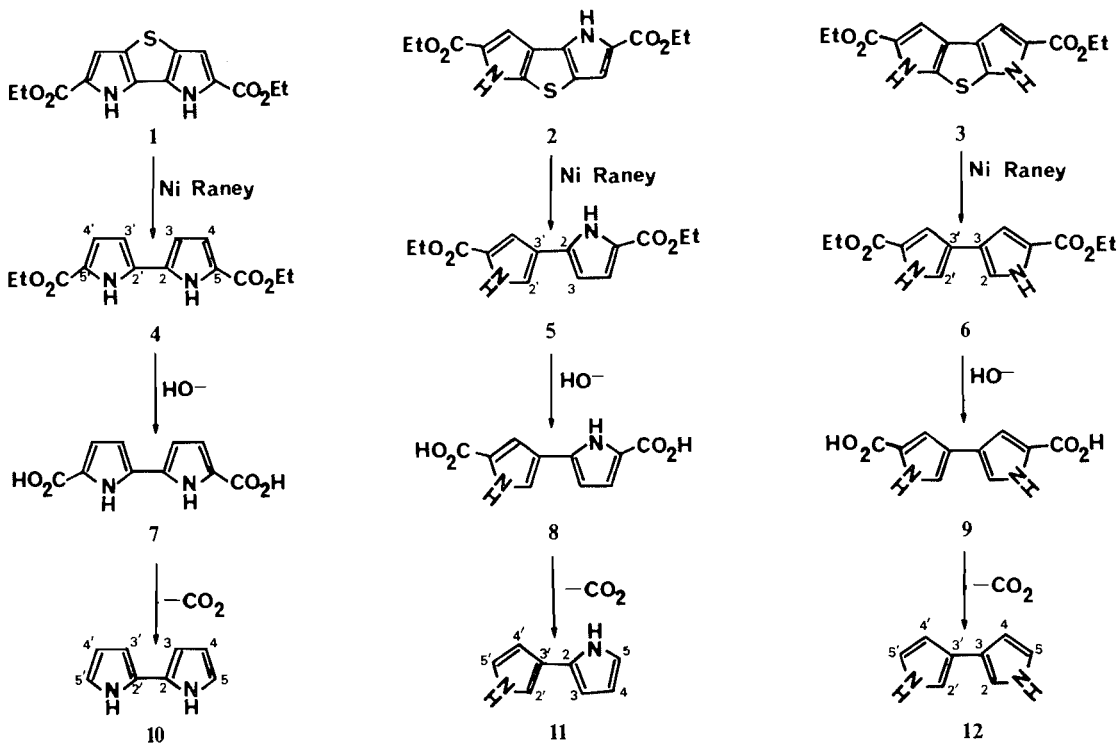

SCHÉMA 1

Notons tout d'abord que le bipyrrole-2,2′ a déjà été étudié en rmn protonique en opérant en solution dans le dioxyde de soufre liquide (3) et très récemment (13) en rmn du ^{13}C en utilisant le DMSO-d_6 comme solvant. Dans ce solvant, et en présence d'eau lourde, on obtient un spectre de type ABX pour les protons de ce bipyrrole. Dans les mêmes conditions le bipyrrole-3,3′ fournit un spectre de type AMX et le bipyrrole-2,3′ la superposition de deux systèmes, un système ABX pour les protons H_3, H_4 et H_5 et un système AMX pour les protons $H_{2'}$, $H_{4'}$ et $H_{5'}$. Dans le cas de ce dernier bipyrrole, les deux mêmes types de couplage apparaissent pour H_5 et $H_{4'}$ et l'attribution des signaux observés à chacun de ces deux protons est effectuée en considérant (par référence aux résultats obtenus pour les deux autres bipyrroles) le proton H_5 comme étant le plus déblindé.

De façon générale, on ne constate qu'une faible différence de glissement chimique entre les protons α des bipyrroles et du pyrrole lui-même étudié dans le même solvant (20), et il en est de même pour les protons β. Par ailleurs, il existe une très bonne concordance entre les constantes de couplage observées pour les bipyrroles et pour le pyrrole (20). L'attribution des signaux observés pour les divers protons du cycle bipyrrolique des diesters **4**, **5** et **6** et des diacides **7**, **8** et **9** a été réalisée compte tenu du déblindage général des protons α par rapport aux protons β dans l'hétérocycle non substitué, et des incréments apportés par un groupe carboxylate d'éthyle en série pyrrolique (20).

En spectrométrie de masse, on note, comme pour les bithiophènes (21), une grande similitude des spectres des trois bipyrroles. Comme pour le bipyrrole-2,2′ (11), le pic moléculaire (*m/e* 132) des bipyrroles-2,3′ et -3,3′ est le pic de base et il est accompagné entre autres de pics importants à $M - 1$ (*m/e* 131), $M - 27$ (*m/e* 105) et $M - 28$ (*m/e* 104). Les spectres des trois isomères ne se différencient que par quelques minimes variations de l'intensité relative des pics.

En revanche, les trois spectres uv sont nettement différents. Celui du bipyrrole-2,2′ a déjà été décrit (2, 8). Les résultats que nous avons obtenus pour ce composé sont en excellente concordance avec les données de la littérature. Milun et Trinajstic (16) ont indiqué les caracté-

Can. J. Chem. Downloaded from www.nrcresearchpress.com by 210.87.254.42 on 09/05/12
For personal use only.

TABLEAU 1. Caractéristiques rmn des bipyrroles (solvant DMSO-d_6)*

Composé	Déplacement chimique des protons (ppm)										Constantes de couplage (Hz)
	Des cycles bipyrroliques								Exocycliques		
	H_2	H_3	H_4	H_5	$H_{2'}$	$H_{3'}$	$H_{4'}$	$H_{5'}$	$CO_2CH_2CH_3$		
4		d 6.64	d 6.79			d 6.64	d 6.79		q 4.27	t 1.30	$J_{34(3'4')}$ 3.8
5†		d 6.35	d 6.76		d 7.58		d 7.27		q 4.27	t 1.31	J_{34} 3.8 $J_{2'4'}$ 1.7
6†	d 7.28		d 7.00		d 7.28		d 7.00		q 4.27	t 1.31	$J_{24(2'4')}$ 1.7
7†		d 6.63	d 6.80			d 6.63	d 6.80				$J_{34(3'4')}$ 3.8
8†		d 6.38	d 6.84		d 7.55		d 7.24				J_{34} 3.9 $J_{2'4'}$ 1.7
9†	d 7.23		d 6.95		d 7.23		d 6.95				$J_{24(2'4')}$ 1.7
10		m 6.26	m 6.05	m 6.71		m 6.26	m 6.05	m 6.71			$J_{34(3'4')}$ 3.4 $J_{35(3'5')}$ 1.5 $J_{45(4'5')}$ 2.6
11†		m 6.04	m 5.99	m 6.60	2d 6.95		2d 6.25	2d 6.71			J_{34} 3.4 J_{35} 1.8 J_{45} 2.5 $J_{2'4'}$ 1.6 $J_{2'5'}$ 2.1 $J_{4'5'}$ 2.7
12†	2d 6.81		2d 6.13	2d 6.67	2d 6.81		2d 6.13	2d 6.67			$J_{24(2'4')}$ 1.6 $J_{25(2'5')}$ 2.0 $J_{45(4'5')}$ 2.7

*d, doublet; t, triplet; q, quadruplet; m, multiplet.
†Ajout de D_2O.

ristiques des spectres électroniques qui découlent d'une étude théorique des trois bipyrroles. Les résultats expérimentaux sont en assez bonne concordance avec leurs prévisions.

Partie expérimentale

Les analyses élémentaires ont été effectuées par le Laboratoire Central de Microanalyses du C.N.R.S. Les spectres rmn ont été relevés sur un appareil JEOL C 60 HL en utilisant le TMS comme référence interne. Les spectres de masse ont été obtenus à l'aide d'un appareil LKB 9000 (température de la source 300 °C; tension d'accélération 70 eV) et les spectres uv sur un appareil Beckman DK2. Les diesters de thiénodipyrroles **1**, **2** et **3** ont été préparés comme décrit dans l'article précédent (1).

*Réduction des diesters de thiénodipyrroles **1**, **2** et **3***

*(a) Réduction du composé **1***

A une suspension de nickel de Raney (préparée à partir de 50 g d'alliage) dans 500 cm³ d'acétone, on ajoute 1.53 g du diester **1** et on chauffe 4 h à reflux. A température ambiante, le catalyseur est éliminé par filtration et le solvant évaporé. Le précipité obtenu fournit, après recristallisation dans un mélange éthanol–eau (5:1), 1.06 g (77%) de bipyrrole-2,2′ dicarboxylate-5,5′ de diéthyle **4**, pf 242 °C. *Anal.* calc. pour $C_{14}H_{16}N_2O_4$: C 60.86, H 5.84, N 10.14, O 23.16; trouvé: C 60.82, H 5.96, N 9.95, O 23.10.

*(b) Réduction du composé **2***

On ajoute 2 g du diester **2** à une suspension de nickel de Raney (obtenue au départ de 130 g d'alliage) dans 600 cm³ d'acétone et on chauffe 1½ h à reflux. Le résidu obtenu après évaporation de l'acétone est élué sur colonne d'acide silicique par le mélange benzène – acétate d'éthyle (2:1). Après recristallisation dans un mélange éthanol–eau (1:1), on isole 1.3 g (72%) de bipyrrole-2,3′ dicarboxylate-5,5′ de diéthyle **5**, pf 170 °C. *Anal.* calc. pour $C_{14}H_{16}N_2O_4$: C 60.86, H 5.84, N 10.14, O 23.16; trouvé: C 60.99, H 5.87, N 10.43, O 23.19.

*(c) Réduction du composé **3***

Le mode opératoire est analogue à celui décrit en (*a*). Au départ de 3.06 g du diester **3**, on obtient 2.25 g (82%) de bipyrrole-3,3′ dicarboxylate-5,5′ de diéthyle **6**, pf 224 °C. *Anal.* calc. pour $C_{14}H_{16}N_2O_4$: C 60.86, H 5.84, N 10.14, O 23.16; trouvé: C 60.60, H 5.68, N 10.06, O 23.44.

*Hydrolyse alcaline des diesters **4**, **5** et **6***

Les diacides **7**, **8** et **9** sont obtenus quantitativement par hydrolyse des diesters **4**, **5** et **6** en opérant comme décrit ci-dessous dans le cas de l'isomère **7**. On chauffe 9 h à reflux 1.38 g du diester **4** et 1.12 g de potasse dans 15 cm³ d'eau. A température ambiante, on acidifie par une solution glacée d'acide chlorhydrique 5 *N*. Le précipité formé est essoré, lavé à l'eau glacée et séché. On isole ainsi 1.1 g d'acide bipyrrole-2,2′ dicarboxylique-5,5′ **7**, pf (déc.) >360 °C.

Can. J. Chem. Downloaded from www.nrcresearchpress.com by 210.87.254.42 on 09/05/12
For personal use only.

Acide bipyrrole-2,3′ dicarboxylique-5,5′ **8** (reflux 2 h), pf (déc.) 218 °C.

Acide bipyrrole-3,3′ dicarboxylique-5,5′ **9** (reflux 7 h), pf (déc.) >360 °C.

*Décarboxylation des diacides **7**, **8** et **9***

*(a) Décarboxylation du diacide **7***

On chauffe 35 min à 140 °C une suspension de 1 g du diacide 7 et 300 mg de chromite de cuivre (activé par du baryum) dans 25 cm^3 de quinoléine. A température ambiante, on verse dans de l'éther. La phase éthérée est filtrée pour éliminer le catalyseur, traitée par une solution d'acide chlorhydrique *N*, puis lavée à l'eau à neutralité, enfin séchée. Après évaporation de l'éther et recristallisation dans un mélange benzène–hexane (3:1), on isole 240 mg (40%) de bipyrrole-2,2′ **10**, pf 188 °C (litt. (2, 3) pf 187–190 °C); spectre de masse M^+ 132 (100%), 131 (40), 105 (28), 104 (50).

*(b) Décarboxylation du diacide **8***

De même, au départ de 1 g du diacide **8** (conditions opératoires 1 h à 140 °C) et après recristallisation dans un mélange benzène–hexane (1:1), on obtient 270 mg (45%) de bipyrrole-2,3′ **11**, pf 103 °C; λ_{max} (EtOH) 205 (ϵ 16 300), 213 (ép 15 300), 232 (11 000), 257 (13 400), 279 nm (ép 6500); spectre de masse M^+ 132 (100%), 131 (36), 105 (32), 104 (59). *Anal.* calc. pour $C_8H_8N_2$: C 72.70, H 6.10, N 21.20; trouvé: C 72.53, H 6.25, N 21.09.

*(c) Décarboxylation du diacide **9***

Le diacide **9** (1 g) (conditions opératoires 30 min à 170 °C) fournit, après recristallisation dans un mélange benzène–hexane (2:1), 180 mg (30%) de bipyrrole-3,3′ **12**, pf 116 °C; λ_{max} (EtOH) 206 (ϵ 19 700), 237 nm (6100); spectre de masse M^+ 132 (100%), 131 (31), 105 (28), 104 (65). *Anal.* calc. pour $C_8H_8N_2$: C 72.70, H 6.10, N 21.20; trouvé: C 72.30, H 6.09, N 21.19.

1. M. Farnier, S. Soth et P. Fournari. Can. J. Chem. **54**, 1074 (1976).
2. H. Rapoport et K. G. Holden. J. Am. Chem. Soc. **84**, 635 (1962).
3. H. Rapoport et N. Castagnoli. J. Am. Chem. Soc. **84**, 2178 (1962).
4. R. Grigg, A. W. Johnson et J. W. F. Wasley. J. Chem. Soc. 359 (1963).
5. E. Bullock, R. Grigg, A. W. Johnson et J. W. F. Wasley. J. Chem. Soc. 2326 (1963).
6. H. Rapoport, N. Castagnoli et K. G. Holden. J. Org. Chem. **29**, 883 (1964).
7. H. Rapoport et J. Bordner. J. Org. Chem. **29**, 2727 (1964).
8. R. Grigg et A. W. Johnson. J. Chem. Soc. 3315 (1964).
9. J. Bordner et H. Rapoport. J. Org. Chem. **30**, 3824 (1965).
10. H. Bauer. Chem. Ber. **100**, 1704 (1967).
11. W. R. Hearn, M. K. Elson, R. H. Williams et J. Medina-Castro. J. Org. Chem. **35**, 142 (1970).
12. (*a*) H. H. Wasserman, J. E. McKeon, L. A. Smith et P. Forgione. Tetrahedron Suppl. **8**, 647 (1966); (*b*) R. J. Cushley, D. R. Anderson, S. R. Lipsky, R. J. Sykes et H. H. Wasserman. J. Am. Chem. Soc. **93**, 6284 (1971); (*c*) H. H. Wasserman, R. J. Sykes, P. Peverada, C. K. Shaw, R. J. Cushley et S. R. Lipsky. J. Am. Chem. Soc. **95**, 6874 (1973).
13. R. J. Cushley, R. J. Sykes, C. K. Shaw et H. H. Wasserman. Can. J. Chem. **53**, 148 (1975).
14. (*a*) H. Kondo et S. Ohno. J. Pharm. Soc. Jpn. **71**, 693 (1951); Chem. Abstr. **46**, 8086a (1952); (*b*) A. J. Castro, D. D. Giannini et W. F. Greenlee. J. Org. Chem. **35**, 2815 (1970).
15. V. Galasso et N. Trinajstic. Tetrahedron, **28**, 4419 (1972).
16. M. Milun et N. Trinajstic. Spectrosc. Lett. **6**, 329 (1973).
17. M. Farnier et P. Fournari. J. Heterocycl. Chem. **12**, 373 (1975).
18. (*a*) D. S. Matteson et H. R. Snyder. J. Org. Chem. **22**, 1500 (1957); (*b*) V. I. Shvedov, L. B. Altukhova, Y. I. Trofimkin et A. N. Grinev. Khim. Geterosikl. Soedin. 1577 (1972).
19. S. Soth, M. Farnier et P. Fournari. Bull. Soc. Chim. Fr. 2511 (1975).
20. P. Fournari, M. Farnier et C. Fournier. Bull. Soc. Chim. Fr. 283 (1972).
21. Q. N. Porter et J. Baldas. Mass spectrometry of heterocyclic compounds. Wiley-Interscience, New York. 1971. p. 248.

Can. J. Chem. Downloaded from www.nrcresearchpress.com by 210.87.254.42 on 09/05/12
For personal use only.

A proton magnetic resonance relaxation study of molecular motions in trimethylamine-borane

T. T. ANG[1] AND B. A. DUNELL

Department of Chemistry, The University of British Columbia, Vancouver, British Columbia V6T 1W5

Received August 13, 1975

T. T. ANG and B. A. DUNELL. Can. J. Chem. **54**, 1087 (1976).

Proton magnetic resonance spin–lattice relaxation times T_1 have been measured for trimethylamine-borane from 120 to 380 K, a few degrees above the melting point. Minima in T_1 at 157 and 259 K are attributed to threefold reorientation of each of the three methyl groups and the borane group and to threefold reorientation of the whole molecule about the B—N axis, respectively. Activation energies for these processes were found to be 3.3 and 6.7 kcal/mol. Abrupt changes in T_1 at 350 and 360 K correspond exactly with heat capacity transitions observed by other workers. The time constant for the decay of the free induction signal (FID curve) changes by two orders of magnitude at 360 K. Having a value of some 3 ms above 360 K, it shows that there must be rapid diffusion as well as molecular tumbling in the highest temperature solid phase.

T. T. ANG et B. A. DUNELL. Can. J. Chem. **54**, 1087 (1976).

On a mesuré les temps de relaxation spin–réseau T_1 de la résonance magnétique nucléaire du proton du complexe triméthylamine-borane a des températures allant de 120 à 380 K, soit quelques degrés au-dessus du point de fusion. On attribue respectivement les minima de T_1 à 157 et 259 K à une réorientation ternaire de chacun des trois groupes méthyles et du groupe borane et une réorientation ternaire de la molécule entière autour de l'axe B—N. On a trouvé que les énergies d'activation pour ces processus sont de 3.3 et 6.7 kcal/mol. Les changements abruptes dans T_1 à 350 et 360 K correspondent exactement aux transitions de capacité calorifiques observées par d'autres chercheurs. La constante de temps pour la décomposition du signal d'induction libre (courbe FID) change par deux ordres de grandeur à 360 K. Puisque l'on a une valeur de quelque 3 ms au-dessus de 360 K, ceci démontre qu'il doit y avoir une diffusion rapide de même qu'un retournement moléculaire dans la phase solide de plus haute température.
[Traduit par le journal]

Introduction

Molecular motion in solid trimethylamine-borane was studied a few years ago by continuous wave nmr methods by Yim and Gilson (1). The proton magnetic resonance relaxation study which this paper reports is complementary to this earlier work, and in general agreement with it. We have measured activation energies for the reorientation of the three-spin groups attached to nitrogen and for a threefold reorientation of the whole molecule. Our observations of the behaviour of the molecule in its higher temperature solid phases differ somewhat from those of Yim and Gilson.

Experimental

The compound was prepared as one of a series of borane adducts in our own laboratory. We hope to report the results of measurements on related compounds soon.

[1]Visiting Scientist. Permanent address: School of Chemical Sciences, Universiti Sains Malaysia, Penang, Malaysia.

Diborane (2, 3) was produced by allowing boron trifluoride etherate (Aldrich) to drop into an excess of a solution of sodium borohydride (Matheson, Coleman, Bell) in previously dried diglyme and the product was condensed in a vessel in liquid nitrogen. The diborane was vaporized at dry ice – acetone temperature and condensed at liquid nitrogen temperature in a vessel containing previously dried trimethylamine (Matheson). The desired product was produced in a moderately vigorous reaction when the vessel was slowly warmed to dry ice – acetone temperature. Excess of either reactant was removed at room temperature through a vacuum line and the product sealed off under vacuum. The trimethylamine-borane was purified by sublimation at 65 °C in order to sharpen the phase transitions that occur in the solid some 6 and 16 deg below the melting point.

Spin–lattice relaxation times were obtained at 30 MHz from a Bruker BKR-322s pulse spectrometer using a π–τ–$\pi/2$ pulse sequence, phase sensitive detection, and a Bruker box-car integrator. The decay of magnetization, as indicated by the function $(I_0 - I_z(t)/2I_0)$, was exponential with time throughout the temperature range studied.

Free induction decays and solid echoes were recorded at some higher temperatures. The time required for the FID to decrease in intensity by a factor e was taken as a measure of T_2 and was a useful qualitative indicator of the existence of phase changes. Where a solid echo was

Can. J. Chem. Downloaded from www.nrcresearchpress.com by 210.87.254.42 on 09/05/12
For personal use only.

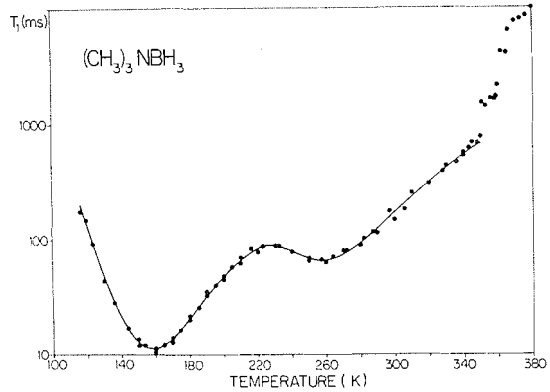

FIG. 1. Spin–lattice relaxation time, T_1, of trimethylamine-borane as a function of temperature. The solid line is calculated from eq. 6′ and the parameters in Table 1.

recorded it was fitted to

$$I/I_0 = 1 - M_2t^2/2$$

for the first 15 or 20 μs from the maximum of the echo, where M_2 is the second moment and $t = 0$ at the maximum (4). Accumulation of pulse data was made possible by a small computer system interfaced with the Bruker spectrometer by Burnell and the departmental electronics shop.

Results and Analysis

The proton spin–lattice relaxation time of trimethylamine-borane is shown as a function of temperature in Fig. 1. There are two minima in T_1, one of 11 ms at 157 K, which we attribute to simultaneous reorientation of the three methyl groups and the borane group, the other of 65 ms at 259 K, which we attribute to a motion of the molecule as a whole, most probably a reorientation of the trimethylamine moiety about the threefold B—N axis. The sudden changes in T_1 at 350 and 360 K correspond to thermal transitions observed at 350.1 and 360.4 K in the heat capacity measurements of Good and co-workers (5) and mentioned by Yim and Gilson (1), who noted a surprising increase in second moment at 358 K. The sudden increase in T_1 at 366 K corresponds to melting. It may be noted that the two transitions before melting were observed clearly only in a sample which was purified by sublimation.

Since the decay of magnetization was found to be exponential under all observed conditions, we can ignore cross-correlation effects in the groups of three spins (6). We can also conclude that, although there are significant dipolar interactions between the borane protons and the boron atom contributing to the rate of proton relaxation to the lattice, the cross-relaxation effects between protons and the boron spins are very small because non-exponential behaviour is absent. Calculation of a theoretical value of $(T_1^{IS})^{-1}$ within the BH_3 group shows that it is about 15 times smaller than the intra-BH_3 value of $(T_1^{II})^{-1}$, where I represents ^1H and S represents ^{10}B and ^{11}B, and T_1^{IS} and T_1^{II} are the relaxation times that appear in the coupled differential equations for relaxation in a cross-relaxing heteronuclear system (7).

Yim and Gilson (1) found a second moment above 200 K which was compatible with reorientation of the CH_3 and BH_3 groups about their C_3 axes and simultaneously a reorientation of the trimethylamine moiety about the B–N axis (a C_3' motion). The relaxation rate for a methyl proton involved in such a combined motion can be written as (8)

$$[1]\quad (T_1^{-1})_{\text{intra } CH_3} = \gamma^4\hbar^2 r_{HH}^{-6}\left[\frac{2}{15}f(\tau_c) + \frac{2}{15}f(\tau_{c2}) + \frac{19}{60}f(\tau_{c5})\right]$$

where

$$f(\tau) = \tau/(1 + \omega_H^2\tau^2) + 4\tau/(1 + \omega_H^2\tau^2)$$

τ_c is the correlation time for the C_3 motions, τ_{c2} the correlation time for the C_3' motion,

$$\tau_{c5}^{-1} = \tau_c^{-1} + \tau_{c2}^{-1}$$

and it has been assumed that the angles at the nitrogen atom are tetrahedral. We assume throughout that correlation times have an Arrhenius type of dependence on temperature,

$$\tau_c = \tau_c^0 \exp(E/RT)$$

When $\omega\tau_c \ll 1$, intergroup contributions to the rate of relaxation of a methyl proton can be determined in the manner of Albert, Gutowsky, and Ripmeester (9) as

$$[2]\quad (T_1^{-1})_{\text{intergroup}} = \frac{27}{20}\gamma^4\hbar^2 r_{*1}^{-6} f(\tau_{c2}) + \frac{27}{80}\gamma^4\hbar^2 r_{*2}^{-6} f(\tau_{c2})$$

where r_{*1} is the distance between the centres of the C_3 rotation of the methyl protons and r_{*2} is the distance between the centres of the C_3 rotation of the protons of a methyl group and of the borane group. The second term in [2] arises from the C_3' reorientation of an 'average' interproton

Can. J. Chem. Downloaded from www.nrcresearchpress.com by 210.87.254.42 on 09/05/12
For personal use only.

Can. J. Chem. Downloaded from www.nrcresearchpress.com by 210.87.254.42 on 09/05/12
For personal use only.

vector from the centre of rotation of methyl protons to the centre of rotation of the borane protons. This vector makes an angle $\Delta \approx 35°$ with the C_3' axis, and the coefficient 27/80 is the value of

$$3 \times \tfrac{3}{2}I(I+1)[\tfrac{2}{5}\sin^2\Delta\cos^2\Delta + \tfrac{1}{10}\sin^4\Delta]$$

for

$$\Delta = 35°$$

The initial factor 3 accounts for the fact that each methyl proton interacts with 3 borane protons, and the origin of the trigonometric factor is shown explicitly in ref. 10.

The borane group is assumed to have only C_3 reorientation, and the rate of relaxation of a borane proton through this motion can be divided into a contribution due to proton–proton interactions,

$$[3] \qquad (T_1^{-1})_{\text{HH in BH}_3} = \frac{9}{20}\gamma^4\hbar^2 r_{\text{HH}}^{-6} f(\tau_c)$$

where r_{HH} is here the interproton distance in borane, and a contribution due to proton–boron interactions. This has the form of $1/T_1^{II}$ in the equations for the two-spin heteronuclear relaxation (7), namely

$$[4] \quad (T_1^{-1})_{BH} = \gamma_I^2\gamma_S^2\hbar^2 S(S+1)[(1/12)J^{(0)}(\omega_I - \omega_S) + (3/2)J^{(1)}(\omega_I) + (3/4)J^{(2)}(\omega_I + \omega_S)]$$

where I = ^{1}H, S = ^{10}B or ^{11}B, and $J^{(n)}$ is the Fourier transform of the autocorrelation function of the time dependent perturbation Hamiltonian. If we assume tetrahedral angles about boron, the functions $J^{(n)}$ become

$$J^{(1)}(\omega) = 0.119 r_{BH}^{-6}\tau_c/(1+\omega^2\tau_c^2)$$
$$J^{(2)}(\omega) = 4J^{(1)}(\omega)$$
$$J^{(0)}(\omega) = 6J^{(1)}(\omega)$$

where 0.119 is the value of

$$(2/5)\sin^2\Delta\cos^2\Delta + (1/10)\sin^4\Delta$$

for

$$\Delta = 70.5°$$

The average rate of relaxation of protons in the molecule is, then,

$$[5] \quad T_1^{-1} = (3/4)(T_1^{-1})_{CH_3} + (1/4)(T_1^{-1})_{BH_3} = 0.75([1]+[2]) + 0.25([3]+[4])$$

In evaluating [4] allowance must be made for the fact that the two isotopes of boron, ^{10}B and ^{11}B, have a natural abundance of 0.1883 and 0.8117 and have resonant frequencies of

$$\omega = 2.025 \times 10^7\ \text{s}^{-1} \quad \text{and} \quad 6.049 \times 10^7\ \text{s}^{-1}$$

in the Zeeman field which gives a proton Larmor frequency of 30 MHz. Equation 5 can be written as

$$[6] \qquad T_1^{-1} = Ah(\tau_c) + Bf(\tau_{c2}) + Cf(\tau_{c5})$$

where

$$h(\tau_c) = \sum_{i=1}^{6} a_i\tau_c/(1+\omega_i^2\tau_c^2)$$

with

$$\omega_i = \omega_H,\ 2\omega_H,\ \omega_H - \omega_{^{10}B},\ \omega_H + \omega_{^{10}B},\ \omega_H - \omega_{^{11}B},\ \text{and}\ \omega_H + \omega_{^{11}B}$$

The a_i are obtained from [1], [3], and [4]. Ideally A should be unity, but it is allowed to deviate from the theoretical value to obtain a good fit of [6] to the experimental points. Theoretical values of B and C are obtained from [1] and [2]. If

$$\tau_{c2} \gg \tau_c$$

at every temperature, we have the simplification that

$$\tau_{c5} = \tau_c$$

and the nonlinear least squares fitting routine obtains the best parameters much more readily.[2] The simplified form is

$$[6'] \qquad T_1^{-1} = Ah'(\tau_c) + Bf(\tau_{c2})$$

where in $h'(\tau_c)$,

$$a_1' = a_1 + C$$

and

$$a_2' = a_2 + 4C$$

The best fit coefficients for [6'] showed that τ_{c2} was in fact much greater than τ_c at each temperature. At 350 K

$$\tau_{c2}/\tau_c = 11$$

and the ratio increases rapidly with decreasing temperature so that at 250 K the ratio is 80. The

[2]Program written by P. Sampson, Health Science Computing Facility, University of California at Los Angeles, Los Angeles, California.

Can. J. Chem. Downloaded from www.nrcresearchpress.com by 210.87.254.42 on 09/05/12
For personal use only.

TABLE 1. Proton spin–lattice relaxation parameters for $(CH_3)_3NBH_3$

Parameter	Value*
A (expt.)	1.22 ± 0.03
A (theory)	1.00
$[h'(\tau_c)]_{max}$ (theory)	$73.1\ s^{-1}$
$(T_1)_{min}$ (theory)	13.7 ms
$(T_1)_{min}$ (expt.)	11.2 ± 0.2 ms
τ_c°	$(8.6 \pm 0.9) \times 10^{-14}$ s
E	3.34 ± 0.05 kcal/mol
B (expt.)	$(1.62 \pm 0.05) \times 10^9\ s^{-2}$
B (theory)	$2.52 \times 10^9\ s^{-2}$
τ_{c2}°	$(7.3 \pm 1.6) \times 10^{-15}$ s
E_2	6.74 ± 0.16 kcal/mol

*Experimental error given is one standard deviation in the least squares fit.

best fit parameters for the experimental points to [6′] are given in Table 1.

A theoretical value for the low temperature minimum in T_1 is the reciprocal of the maximum in $h'(\tau_c)$. If the B—H bond length is taken as 1.20 Å (11), the C—H bond length as 1.10 Å, and all angles as tetrahedral,

$$[h'(\tau_c)]_{max} = 73.1\ s^{-1}$$

and correspondingly

$$(T_1)_{min} = 13.7\ ms$$

For an isolated BH_3 group reorienting about its C_3 axis, the minimum in T_1 would be 8.1 ms using the above geometry, or 9.0 ms using the parameters obtained by Bryan and Kuczkowski (12) for $(CH_3)_3PBH_3$, *viz.*,

$$B—H = 1.212\ Å$$

and

$$\angle HBH = 113°$$

Use of these parameters would worsen the agreement between 13.8 ms and the observed 11.2 ms by very little. We find our conclusions to be in agreement with those of Yim and Gilson that at low temperature the CH_3 and BH_3 groups undergo C_3 reorientation at essentially the same frequency. The temperature at which

$$\tau_c^{-1} = \gamma\sqrt{M_2}$$

where M_2 is the mid-value of the second moment transition due to C_3 motion, is predicted from our results to be 92 K for

$$M_2 = 25\ G^2$$

This is within a few degrees of the temperature observed by Yim and Gilson.

A theoretical value for the parameter B in [6′] is obtained by summing the coefficients of $f(\tau_{c2})$ in [1] and [2]. If r_{*1} is taken as 3.01 Å and r_{*2} as 3.13 Å (B—N = 1.59 Å, B—H = 1.20 Å, C—N = 1.47 Å, C—H = 1.10 Å, and tetrahedral angles),

$$B = 2.52 \times 10^9\ s^{-2}$$

a value which is not in good agreement with the experimental value

$$B = 1.62 \times 10^9\ s^{-2}$$

A threefold reorientation of the molecule about a C—N bond would give a maximum contribution of $21.9\ s^{-1}$ to the relaxation rate. That value can be compared with the experimental contribution of

$$B_{expt}[f(\tau_c)]_{max} = 12.2\ s^{-1}$$

Isotropic tumbling of the molecule would make a maximum contribution of $32.6\ s^{-1}$ to the relaxation rate

$$(\text{or} \quad B = 3.53 \times 10^9\ s^{-2})$$

and isotropic tumbling plus C_3' motion would give a maximum contribution of about $6\ s^{-1}$ to the relaxation rate

$$(\text{or} \quad B \approx 0.8 \times 10^9\ s^{-2})$$

The C_3' motion about C—N, or any motion involving isotropic tumbling, gives poorer agreement with the experimental results than the C_3' motion about B—N. The observed second moment of 3.1 G^2 between 220 and 320 K (1) is also incompatible with the involvement of isotropic tumbling in the higher temperature motional process. Thus we agree with Yim and Gilson's assignment of a threefold reorientation of the $(CH_3)_3N$ moiety about B—N as the most probable motion giving rise to the second transition in second moment and the second T_1 minimum. The temperature at which

$$\tau_{c2}^{-1} = \gamma\sqrt{M_2}$$

where

$$M_2 = 5\ G^2$$

is the midvalue of the second transition in second moment, is predicted from our results to be 157 K, which is in reasonable agreement with the experimental value (1) of about 165 K.

The discontinuous character of the changes in T_1 and in heat capacity (5) at 350 and 360 K indicates that we are dealing with phase transitions in the solid. It is not possible, however, to determine the nature of the molecular motions in the higher temperature phases from the T_1 values. Between 335 and 350 K, the time constant T_2 for the approximately exponential FID curves increases from about 20 to 32 μs and then falls to 24 μs at 352 K and 26 μs at 358 K. The FID curves also change shape in the higher temperature phase, decaying more rapidly than an exponential decay. Above 360 K there is a large increase in T_2, measured from the again approximately exponential FID, to about 3 ms. Here the FID is essentially that of a liquid, and the molecular motion in this highest temperature solid phase must involve rapid diffusion and isotropic molecular tumbling. We find no conclusive evidence of the increase in second moment reported by Yim and Gilson (1), and in particular not at 358 K.

Acknowledgements

We are grateful to the National Research Council of Canada for a grant-in-aid of this research. We also thank Drs. E. E. Burnell and A. Storr for helpful advice and assistance, and Dr. J. A. Ripmeester for a valuable discussion on relaxation in heteronuclear systems and communication of some work before publication.

1. C. T. YIM and D. F. R. GILSON. Can. J. Chem. **48**, 515 (1970).
2. H. C. MILLER and E. L. MUETTERTIES. Inorg. Synth. **10**, 82 (1967).
3. K. M. BISWAS and A. H. JACKSON. J. Chem. Soc. C, 1667 (1970).
4. J. G. POWLES and J. H. STRANGE. Proc. Phys. Soc. (London), **82**, 6 (1963).
5. W. D. GOOD, H. L. FINKE, S. S. TODD, and D. R. DOUSLIN. U. S. Bureau of Mines, Bartlesville, Technical Report AD635296. 1966.
6. L. K. RUNNELS. Phys. Rev. **134**, A28 (1964).
7. A. ABRAGAM. The principles of nuclear magnetism. Oxford, England. 1961. p. 294.
8. M. B. DUNN and C. A. MCDOWELL. Mol. Phys. **24**, 969 (1972).
9. S. ALBERT, H. S. GUTOWSKY, and J. A. RIPMEESTER. J. Chem. Phys. **56**, 3672 (1972).
10. B. A. DUNELL and S. E. ULRICH. J. Chem. Soc. Faraday Trans. II, **69**, 377 (1973).
11. Interatomic distances, Chem. Soc. Spec. Publ. No. 11, 1958, and No. 18, 1965.
12. P. S. BRYAN and R. L. KUCZKOWSKI. Inorg. Chem. **11**, 553 (1972).

Can. J. Chem. Downloaded from www.nrcresearchpress.com by 210.87.254.42 on 09/05/12
For personal use only.

^{60}Co γ radiolysis of reduced glutathione in aerated solutions at pH values between 1–7.0

MANOHAR LAL

Chemistry Division, Bhabha Atomic Research Centre, Trombay, Bombay - 400 085

Received August 14, 1975

MANOHAR LAL. Can. J. Chem. **54**, 1092 (1976).

G-values for the formation of oxidised glutathione (GuS—SGu), glutathione sulphinic acid ($GuSO_2H$), γ-glutamylalanylglycine (GuH), γ-glutamylserylglycine (GuOH), and hydrogen peroxide and G(—GuSH) have been estimated in the γ-radiolysis of aerated reduced glutathione solutions at pH values between 1–7.3. The results show excellent material balance for the radiolytic amino products. Oxygen is necessary for the production of both glutathione sulphinic acid and γ-glutamylserylglycine in the radiolysis of glutathione. Product yields increase with increasing GuSH concentration and reflect the occurrence of a small chain reaction. Although the spectrum of amino products is identical to the corresponding products from cysteine radiolysis under similar conditions, their yields are very much different. It is significant, that there is no evidence for the scission of the peptide chain, at any of the GuSH concentrations and pH's; thus the —SH group of glutathione is the site of attack of the primary species.

A reaction mechanism, which explains most of the experimental results has been put forward. A rate expression for G(—GuSH) has been evaluated and it is found that the experimental and calculated G(—GuSH) are in good agreement.

MANOHAR LAL. Can. J. Chem. **54**, 1092 (1976).

On a estimé les valeurs de G pour la formation du glutathion oxydé (GuS—SGu), de l'acide glutathion sulfinique ($GuSO_2H$), de la γ-glutamylalanylglycine (GuH), de la γ-glutamylserylglycine (GuOH) et de peroxyde d'hydrogène et G(—GuSH); ces valeurs ont été déterminées par la radiolyse-γ d'une solution aérée de glutathion réduit à des valeurs de pH allant de 1–7.3. Les résultats montrent une excellente balance de matériel pour les produits aminés de radiolyse. De l'oxygène est nécessaire pour la production de l'acide glutathion sulfinique et de la γ-glutamylsérylglycine lors de la radiolyse du glutathion. Les rendements en produits augmentent avec une augmentation de la concentration du GuSH et ces résultats réflètent la présence d'une petite réaction en chaîne. Quoique les spectres des produits aminés soient identiques à ceux des produits correspondants de la radiolyse de la cystéine dans des conditions similaires, les rendements sont toutefois très différents. Il est important de noter qu'aucun résultat n'indique qu'il y a une scission de la chaîne peptidique à aucune des concentrations du GuSH et à aucun des pH; ces résultats indiquent que le groupe —SH du glutathion est le site de l'attaque des espèces primaires.

Un mécanisme de réaction qui explique la plupart des résultats expérimentaux est proposé. On évalue l'équation de vitesse pour G(—GuSH) et on trouve que les valeurs expérimentales et calculées pour G(—GuSH) sont en bon accord.

[Traduit par le journal]

Introduction

The study of the effect of ionizing radiations on the sulphydryl amino acid, cysteine has been of considerable interest during the past several years (1–9). However, not much attention has been paid to an equally important radioprotective compound, the tripeptide-reduced glutathione (GuSH), which represents a simple and a convenient model containing the amino acid cysteine (CySH), as it would occur in a protein. Dale and Davies (10) as early as in 1951, studied the liberation of hydrogen sulphide by the X-irradiation of cysteine and glutathione. Armstrong and co-workers (11) in 1969 investigated the γ-radiolysis of reduced glutathione in air-free solutions and elucidated the mechanism.

To understand the effect of radiations on proteins and enzymes, it is a prerequisite to know the radiolytic mechanisms of simpler molecules (cysteine and glutathione), which form the primary constituents of these macromolecules. As a first step towards this, we have recently reported the results and mechanism of cysteine radiolysis in aerated solutions at pH = 0 and 5.5 (12, 13). This paper presents a detailed study on the γ-radiolysis of reduced glutathione in aerated

Can. J. Chem. Downloaded from www.nrcresearchpress.com by 210.87.254.105 on 09/05/12
For personal use only.

Can. J. Chem. Downloaded from www.nrcresearchpress.com by 210.87.254.105 on 09/05/12
For personal use only.

solutions at various pH's. For convenience the following symbols have been used. The tripeptide reduced glutathione, GuSH;

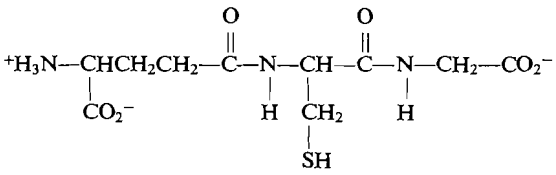

oxidised glutathione, GuS—SGu; γ-glutamylalanylglycine, GuH; γ-glutamylserylglycine, GuOH; glutathione sulphinic acid, $GuSO_2H$.

Experimental

Details of experimental procedures have already been reported (12, 13). Reduced glutathione (procured from E. Merck Co., Germany) solutions were prepared just before irradiation in triple distilled water and analysed for radiolytic amino products using Technicon's auto-analyser immediately after irradiation. The residual glutathione was analysed without fixing the —SH group by iodoacetic acid (11).

Glutathione sulphinic acid was prepared according to the method reported earlier (14). γ-Glutamylserylglycine was prepared from reduced glutathione (15). This compound was not actually synthesized, but the *S*-methylglutathione treated with cyanogen bromide in tris buffer at pH = 8 (according to ref. 15) on amino acid analysis with a Beckman 121 Autoanalyser[1] gave a peak which coincides exactly with peak 3, designated as γ glutamylserylglycine in the γ-irradiated reduced glutathione solutions (see Fig. 1). Although γ-glutamylserylglycine peak reported in ref. 15 was unconfirmed, later studies by Awad[2] revealed the amino acid composition of γ-glutamylserylglycine to have the following molar proportions (glycine 1.00, glutamic acid 0.85, and serine 0.85). γ-Glutamylalanylglycine was prepared by the reduction of reduced glutathione with Raney Nickel. Oxidised glutathione (grade III) which is used as standard was procured from Sigma Chemical Co.

As the natural pH of the reduced glutathione is 3.3, the pH of the solution was adjusted by means of sodium hydroxide. For studies at pH = 1, 10^{-1} M perchloric acid solution in triple distilled water was used. Dose rate of the ^{60}Co source used was $\sim 2 \times 10^{17}$ eV ml^{-1} min^{-1}.

Results and Discussion

Since thermal hydrolysis occurs in 1 N $HClO_4$ solutions (pH = 0) of reduced glutathione, as reported by Armstrong and co-workers (11), the radiolysis was investigated at pH = 1, 3.3, and 5.5. The thermal hydrolysis was not observed at these pH's. Figure 1 *a–d* gives a set of chromatograms for 10^{-3} M aerated acidic reduced glutathione solutions for various doses of γ-irradiation. Figure 1*a* for unirradiated solution gave only three peaks (numbers 2, 5, and 6). These peaks are marked in the order of increasing elution time in the amino acid analysis. Peak 2 appears to be due to some impurity and does not interfere with any of the radiolytic products. Peaks 5 and 6 respectively were identified as reduced and oxidised glutathione, the latter being present in very small amounts in reduced glutathione. Figures 1 *b–d* are for irradiated (increasing γ-dose) solutions and show six peaks. It can be seen that peaks 2, 5, and 6 in the irradiated reduced glutathione solutions coincide well with those for unirradiated solutions. Peaks 1, 3, and 4 were identified as due to glutathione sulphinic acid, γ-glutamylserylglycine, and γ-glutamylalanylglycine respectively.

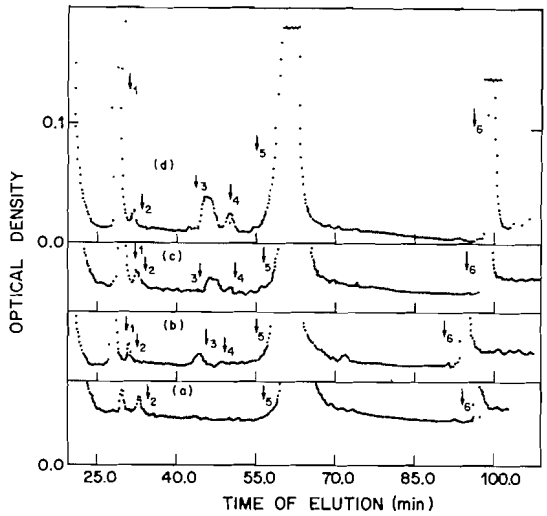

FIG. 1. Chromatograms due to 10^{-3} M aerated, reduced glutathione in 0.1 N perchloric acid solutions: (*a*) unirradiated; (*b*) irradiated to a γ-dose of 2.0×10^{18} eV/5 ml; (*c*) irradiated to a γ-dose of 5.0×10^{18} eV/5 ml; (*d*) irradiated to a γ-dose of 1.0×10^{19} eV/5 ml. Peak 1, glutathione sulfinic acid; peak 2, impurity; peak 3, γ-glutamylserylglycine; peak 4, γ-glutamylalanylglycine; peak 5, reduced glutathione; peak 6, oxidised glutathione.

G-values for the products at all the glutathione concentrations were estimated from the initial slopes of the best straight lines through the yield–dose plots and are presented in Table 1. Each value in Table 1 is an average of at least

[1]The amino acid analysis of the above preparation was carried out by the courtesy of Dr. K. J. Stevenson, Department of Chemistry, University of Calgary, Calgary, Alberta.

[2]W. M. Awad, unpublished results.

Can. J. Chem. Downloaded from www.nrcresearchpress.com by 210.87.254.105 on 09/05/12
For personal use only.

TABLE 1. Product yields in γ-irradiated reduced glutathione in aerated solutions*

[GuSH] (mol/l)	pH	$G(H_2O_2)$	G(GuH) a	G(GuH) a.f.	G(GuOH) a	G(GuOH) a.f.	$G(GuSO_2H)$ a	$G(GuSO_2H)$ a.f.	G(GuS—SGu) a	G(GuS—SGu) a.f.	G(—GuSH) a	G(—GuSH) a.f.	$2G$(GuS—SGu) + G(GuH) + G(GuOH) + $G(GuSO_2H)$
1×10^{-3}	1.0	0.96 (4.6)	0.1	0.9	0.8 ±0.1	0.0	5.4±0.5 (1.0)	0.0	2.2 ±0.4 (4.6)	3.2	10.5±1.0 (10.6)	7.3	10.7
4×10^{-3}	1.0	0.96 (5.1)	0.1	—	0.95±0.1	—	6.8±0.8 (1.4)	0.0	5.1 ±0.5 (6.8)	—	17.6±2.0 (15.3)	—	18.0
1×10^{-2}	1.0	1.2 (5.7)	0.15	—	1.1 ±0.1	0.0	7.0±0.8 (0.2)	0.0	7.2 ±0.8 (8.5)	—	21.0±2.0	—	23.45
1×10^{-3}	3.3	0.96	0.1	1.5	1.0 ±0.1	0.0	3.8±0.5	0.0	1.25±0.15	3.0	7.4±0.5	7.5	7.35
4×10^{-3}	3.3	1.35	0.2	—	1.2 ±0.1	0.0	4.5±0.7	0.0	3.2 ±0.5	—	11.9±1.0	—	12.1
1×10^{-2}	3.3	1.68	0.5	—	1.6 ±0.1	0.0	4.5±0.5	0.0	6.1 ±0.5	—	18.5±1.0	—	18.7
4×10^{-3}	5.5	—	0.26 (0.15)	—	1.85±0.15 (1.5)	0.0	2.4±0.3 (0.9)	0.0	4.5 ±0.5 (8.5)	—	13.1±1.0 (18.0)	—	13.5
4×10^{-3}	7.3	—	—	—	2.4 ±0.2	0.0	1.8±0.3	0.0	7.3 ±0.7	—	17.3±1.5	—	18.8

*a, aerated; a.f., air free. Numbers in parentheses are the yields of the corresponding products from cysteine under similar conditions.

Can. J. Chem. Downloaded from www.nrcresearchpress.com by 210.87.254.105 on 09/05/12
For personal use only.

7–10 independent observations. The product yields in the γ-radiolysis of GuSH in air-free solutions (11) are also given and the yields of the corresponding products from cysteine radiolysis (12, 13) under identical conditions, are shown in parentheses for comparison.

The following observations can be made from the results presented in Table 1

(*i*) Since oxidised glutathione, glutathione sulphinic acid, γ-glutamylalanylglycine, and γ-glutamylserylglycine are the only radiolytic amino products, the material balance requires that

$$G(\text{—GuSH}) = 2(\text{GuS—SGu}) + G(\text{GuSO}_2\text{H}) + G(\text{GuOH}) + G(\text{GuH})$$

The data given in columns 12 and 14 of Table 1 are consistent with this.

(*ii*) There is an increase in the product yields with increasing glutathione concentrations. G(—GuSH) are high when compared with air-free solutions. This is indicative of a small chain reaction.

(*iii*) It is interesting that G(GuS—SGu) in 10^{-3} M aerated solutions at pH = 1 and 3.3 are considerably lower than the G(GuS—SGu) in air-free solutions.

(*iv*) At a particular glutathione concentration: (*a*) G(GuOH) increases with increasing pH. (*b*) $G(\text{GuSO}_2\text{H})$ decreases drastically with increasing pH. This is similar to the results of cysteine radiolysis. (*c*) Starting with pH = 1, both G(GuS—SGu) and G(—GuSH) decrease first with increasing pH = 3.3. However with further increase in pH there is an increase in G(GuS—SGu) and G(—GuSH).

(*v*) GuOH and GuSO_2H are the major products in aerated solutions whereas these products are absent in air-free solutions.

(*vi*) G(GuOH) at pH = 1 is of the order of 1, but the corresponding product CyOH in aerated-cysteine radiolysis is absent at this pH.

(*vii*) $G(\text{GuSO}_2\text{H})$ are very much higher, and G(GuS—SGu) are lower than the analogous products CySO_2H and CyS—SCy under exactly similar conditions of cysteine radiolysis.

The rate constant of hydrated electron at neutral pH with reduced glutathione is equal to 3.2×10^9 l mol^{-1} s^{-1} (16) and 3.4×10^9 l mol^{-1} s^{-1} (17) and the rate constant of hydroxyl radical with GuSH at pH = 1 is equal to 8.8×10^9 l mol^{-1} s^{-1} (18). These are at least 10–20 times higher than the respective rate constants of e_{aq}^- and OH radicals with other simple peptides. This suggests that SH group present in glutathione is much more reactive than the other groups present in peptides and as in cysteine the mode of breakdown is the fission of —SH. The excellent material balance observed for the radiolytic aminoproducts and the lack of the scission of the peptide linkage further confirms this. Although the radiolytic products are similar to those of the analogous products from the cysteine radiolysis, their product yields are quite different (see Table 1). SH group being the focal point of the chemical change in both cases, the general pattern of the reaction mechanism must be similar to that of the cysteine.

In view of this, a probable reaction mechanism which explains most of the results is suggested below:

$$H_2O \rightsquigarrow H,\ e_{aq}^-,\ OH,\ H_2,\ \text{and}\ H_2O_2$$

Initiation

[1] $\text{GuSH} + \text{H} \rightarrow \text{GuS} + \text{H}_2$

[2] $\text{GuSH} + \text{H} \rightarrow \text{Gu} + \text{H}_2\text{S}$

[3] $\text{GuSH} + e_{aq}^- \xrightarrow{\text{H}^+} \text{Gu} + \text{H}_2\text{S}$

[4] $\text{GuSH} + \text{Gu} \rightarrow \text{GuH} + \text{GuS}$

[5] $\text{GuSH} + \text{OH} \rightarrow \text{GuS} + \text{H}_2\text{O}$

[6] $e_{aq}^- + \text{H}^+ \rightarrow \text{H}$

[7] $\text{H (or } e_{aq}^-) + \text{O}_2 \rightarrow \text{HO}_2 \text{ (or } \text{O}_2^-)$

Propagation

[8] $\text{GuSH} + \text{HO}_2 \text{ (or } \text{O}_2^-) \xrightarrow{\text{H}^+} \text{GuS} + \text{H}_2\text{O}_2$

[9] $\text{GuS} + \text{O}_2 \rightarrow \text{GuSO}_2$

[10*a*] $\text{GuS—SGu} + \text{HO}_2 \text{ (or } \text{O}_2^-)$

[10*b*] $\text{GuSH} + \text{GuSO}_2 \rightarrow \text{GuSO}_2\text{H} + \text{GuS}$

[10*c*] $\text{GuSOOH} + \text{GuS}$

[11] $\text{Gu} + \text{O}_2 \rightarrow \text{GuO}_2$

[12] $3\text{GuSH} + \text{GuO}_2 \rightarrow 3\text{GuS} + \text{GuOH} + \text{H}_2\text{O}$

Termination

[13] $\text{GuSO}_2 + \text{GuSO}_2 \rightarrow \text{GuSO}_2\text{SGu} + \text{O}_2$; $\text{GuSO}_2\text{SGu} + \text{GuSH} \rightarrow \text{GuS—SGu} + \text{GuSO}_2\text{H}$

[14] $\text{GuSO}_2 + \text{HO}_2 \text{ (}\text{O}_2^-\text{)} \xrightarrow{\text{H}^+} \text{GuSO}_2\text{H} + \text{O}_2$

[15] $2\text{HO}_2 \text{ (or } \text{O}_2^-) \rightarrow \text{H}_2\text{O}_2$

Can. J. Chem. Downloaded from www.nrcresearchpress.com by 210.87.254.105 on 09/05/12
For personal use only.

Reactions 1–6 have been proposed by Armstrong and co-workers (11) in the γ-radiolysis of air-free glutathione solutions. Reactions similar to 8–13 have earlier been reported in the pulse and γ-radiolysis of cysteine solutions (9, 12, 13). Reaction 14 in the present case has been included so as to explain the high yields of $GuSO_2H$ at low pH's. It would be worthwhile to compare the results of the γ-radiolysis of glutathione in air-free solutions with aerated solutions. From Table 1, columns 10 and 11, it is observed that G(GuS—SGu) for 10^{-3} M aerated reduced glutathione solutions at pH = 1 and 3.3 are considerably lower, when compared with air-free solutions. The reason for this may be, that in air-free solutions, the fate of GuS radicals produced during radiolysis is only the dimerization to disulphide (11), whereas in aerated solutions, the radical GuS reacts with oxygen to give $GuSO_2$ (reaction 9), which further reacts either with GuSH (reaction 10) and/or HO_2 (or O_2^-) (reaction 14) or with itself (reaction 13) to give either $GuSO_2H$ or GuS—SGu. It is difficult at this stage to pinpoint which of the reaction paths (and to what extent) radical $GuSO_2$ follows. However, as GuS—SGu yields at pH = 1 and 3.3 are lower in aerated solutions, it can be inferred that the dimerisation of $GuSO_2$ radicals (reaction 13) and reaction 10*a* are not the prominent reactions.

This point is further strengthened from the comparison of the reduced glutathione and cysteine radiolysis results in aerated solutions. The results of Table 1 show that $G(GuSO_2H)$ is much higher (column 8) and G(GuS—SGu) is lower (column 10) than the corresponding product yields from cysteine radiolysis under identical conditions. This observation suggests that either there must be some reaction (reaction 14) other than reactions 10*b* or 13 which may be responsible for the formation of $GuSO_2H$ or the glutathione sulphenyl hydroperoxide formed from reaction 10*c* undergoes complete internal rearrangement (12, 19) to give increased $GuSO_2H$ and makes reaction 10*c* an important reaction in this system. The reaction of glutathione sulphenyl hydroperoxide with glutathione (similar to reaction 7 of ref. 12)

[16] $GuSOOH + GuSH \rightarrow GuS—SGu + H_2O_2$

may not be important because it gives rise to GuS—SGu and H_2O_2. That the reactions 10*a* and 13 are less prominent and 10*b*, 10*c*, and 14 are more prominent here, is reflected from the low yields of hydrogen peroxide (as compared to aerated cysteine radiolysis results) (12).

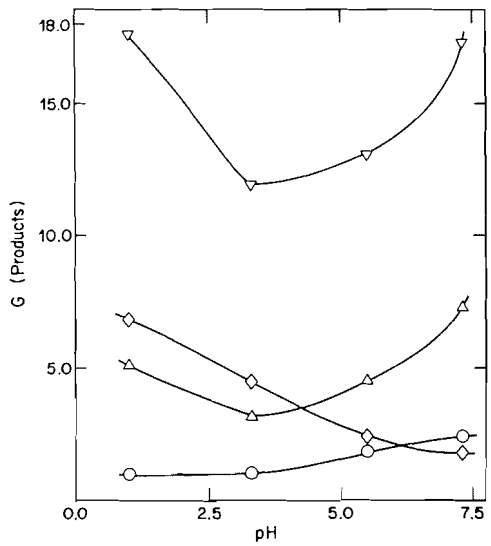

FIG. 2. Effect of pH on the G-values of the products in the γ-radiolysis of aerated reduced glutathione: ▽, G(—GuSH); ◇, $G(GuSO_2H)$; △, G(GuS—SGu); ○, G(GuOH).

The rate constant ratio $k_1/k_2 = 2.8 \pm 0.4$ for reduced glutathione reported by Armstrong and co-workers (11) is significantly lower than that of $k_1/k_2 = 3.5 \pm 0.4$ for cysteine (11). This tends to increase the formation of Gu radicals, which react more favourably with oxygen (to give GuO_2 radical) than with GuSH (to give GuH) and show the preference of reaction 11 over reaction 4 (see Table 1, column 4). GuO_2 further reacts with GuSH to give γ-glutamylserylglycine.

The product yields for 4×10^{-3} M aerated glutathione solutions plotted against pH are presented in Fig. 2. This shows that as the pH increases, the GuOH increases, whereas $GuSO_2H$ progressively decreases. The increase in GuOH is understandable and can be explained on the basis of competition between reactions 3 and 6. As the pH increases reaction 6 becomes unimportant (at pH = 5.5) and the hydrated electron reacts according to reaction 3. Thus, as the pH increases, more Gu radicals are produced to react with oxygen and give GuO_2 radicals and finally GuOH. At pH = 7.3 almost all the hydrated electrons give rise to GuOH (=2.4). The decrease in $GuSO_2H$ with increasing pH can be explained, as discussed earlier in this paper, on the basis of competition between reactions

10*a* and 10*b* or 10*c*, 13, and 14. At high acidities reactions 10*b*, 10*c*, and 14 may be more prominent and the chain is propagated through reactions 10*b* and 10*c* (giving rise to $GuSO_2H$) whereas at low acidities reactions 10*a* and 13 are prominent and the chain is propagated through reaction 10*a* (giving rise to higher GuS—SGu). It is difficult to explain the lowering of the G(GuS—SGu) and G(—GuSH) at pH = 3.3 (see Fig. 2). It appears that the chain propagation at this pH is minimal.

Following a steady state treatment and considering the above reaction scheme, it can be seen that

$$[17]\quad G(\text{—GuSH}) = \tfrac{1}{2}G_{OH} + G(\text{GuS—SGu}) + G(H_2O_2) + 2G(\text{GuOH}) + G(\text{GuH}) + G(GuSO_2H) - G_{H_2O_2} - \tfrac{1}{2}G_H - \tfrac{1}{2}G_{e_{aq}^-} + \frac{G_H + \dfrac{G_{e_{aq}^-}}{1 + \dfrac{k_3[\text{GuSH}]}{k_6[H^+]} + \dfrac{k_7[O_2]}{k_6[H^+]}}}{1 + \dfrac{k_7[O_2]}{[k_1 + k_2]\,[\text{GuSH}]}} + \frac{G_{e_{aq}^-}}{1 + \dfrac{k_7[O_2]}{k_3[\text{GuSH}]} + \dfrac{k_6[H^+]}{k_3[\text{GuSH}]}}$$

Substituting the experimental yields of the products, the yields of the primary species (20), known rate constants (21), and the concentrations used in this study in expression 17 G(—GuSH) has been calculated and compared in Table 2.

It can be seen from Table 2 that there is good agreement between the calculated and experimental yields. Thus the radiolytic oxidation of glutathione can be considered to be initiated by reactions 1–7, propagated by reactions 8–12, and terminated by reactions 13–15.

TABLE 2. Comparison of experimental and calculated G(—GuSH)

[GuSH] (mol/l)	pH	G(—GuSH) Calculated	G(—GuSH) Experimental
1×10^{-3}	1.0	10.0	10.5±1.0
4×10^{-3}	1.0	15.7	17.6±2.0
1×10^{-2}	1.0	18.7	21.0±2.0
1×10^{-3}	3.3	7.35	7.4±0.5
4×10^{-3}	3.3	11.85	11.9±1.0
1×10^{-2}	3.3	16.9	18.5±1.0
4×10^{-3}	5.5	12.4	13.7±1.0

Acknowledgements

The author wishes to express his thanks to Dr. M. D. Karkhanavala, Head, Chemistry Division and Dr. K. N. Rao for discussion and keen interest in this work. Thanks are also due to Professor D. A. Armstrong, University of Calgary, Calgary, Alberta for many helpful discussions.

1. (*a*) D. A. ARMSTRONG and V. G. WILKENING. Can. J. Chem. **42**, 2631 (1964); (*b*) V. G. WILKENING, MANOHAR LAL, M. ARENDS, and D. A. ARMSTRONG. Ca. J. Chem. **45**, 1209 (1967); (*c*) V. G. WILKENING, MANOHAR LAL, M. ARENDS, and D. A. ARMSTRONG. J. Phys. Chem. **72**, 185 (1968).
2. (*a*) A. EL. SAMAHY, M. L. WHITE, and C. N. TRUMBORE. J. Am. Chem. Soc. **86**, 3177 (1964); (*b*) A. AL-THANNON, R. M. PETERSON, and C. N. TRUMBORE. J. Phys. Chem. **72**, 2395 (1968).
3. P. MARKAKIS and A. L. TAPPEL. J. Am. Chem. Soc. **82**, 1613 (1960).
4. MANOHAR LAL. Radiat. Eff. **2**, 225 (1970).
5. T. C. OWEN and M. T. BROWN. J. Org. Chem. **34**, 1161 (1969).
6. J. E. PACKER. J. Chem. Soc. 2320 (1963).
7. J. E. PACKER and R. V. WINCHESTER. Chem. Commun. 826 (1968).
8. J. E. PACKER and R. V. WINCHESTER. Can. J. Chem. **48**, 417 (1970).
9. J. P. BARTON and J. E. PACKER. Int. J. Radiat. Phys. Chem. **2**, 159 (1970).
10. W. M. DALE and J. W. DAVIES. Biochem. J. **48**, 129 (1951).
11. MANOHAR LAL, D. A. ARMSTRONG, and META WIESER. Radiat. Res. **37**, 246 (1969).
12. MANOHAR LAL. Radiat. Eff. **22**, 49 (1974).
13. MANOHAR LAL. Radiat. Eff. **22**, 237 (1974).
14. D. H. CALAM and S. G. WALEY. Biochem. J. **85**, 417 (1962).
15. W. M. AWAD, JR. and P. E. WILCOX. Biochem. Biophys. Res. Commun. **17**, 709 (1969).
16. R. BRAAMS. *In* Pulse radiolysis. Academic Press, New York. 1965.
17. MORTON Z. HOFFMAN and E. HAYON. J. Phys. Chem. **77**, 990 (1973).
18. G. E. ADAMS, J. W. BOAG, J. CURRANT, and B. D. MICHAEL. *In* Pulse radiolysis. Academic Press, New York. 1965.
19. B. SHAPIRO and L. ELDJARN. Radiat. Res. **3**, 393 (1955).
20. B. H. J. BIELSKI and A. O. ALLEN. Int. J. Radiat. Phys. Chem. **1**, 155 (1969).
21. M. ANBAR and P. NETA. Int. J. Appl. Radiat. Isot. **18**, 493 (1967).

Can. J. Chem. Downloaded from www.nrcresearchpress.com by 210.87.254.105 on 09/05/12
For personal use only.

Milieux hyperbasiques: préparation et alkylation de carbanions en α d'amides *N,N*-disubstitués. Application à la synthèse de la *d,l*-pipéritone

PIERRE HULLOT, THÉRÈSE CUVIGNY, MARC LARCHEVÊQUE ET HENRI NORMANT

Laboratoire de Synthèse Organique, Université Pierre et Marie Curie, Laboratoire associé au C.N.R.S. n° 239, tour 44–45, 4, place Jussieu 75230 Paris Cédex 05

Reçu le 22 juillet 1975

PIERRE HULLOT, THÉRÈSE CUVIGNY, MARC LARCHEVÊQUE et HENRI NORMANT. Can. J. Chem. **54**, 1098 (1976).

Les carbanions en α d'amides *N,N*-disubstitués sont obtenus avec d'excellents rendements par action des "dialkylamidures activés" en solution dans le HMPT. Ils réagissent avec les dérivés mono ou polyhalogénés pour conduire à des amides substitués fonctionnels ou non. L'addition ultérieure d'organo lithiens permet d'obtenir des cétones alkylées régiosélectivement. La réaction est utilisée pour préparer la dicétone-1,5 intermédiaire de synthèse de la *d,l*-pipéritone.

PIERRE HULLOT, THÉRÈSE CUVIGNY, MARC LARCHEVÊQUE, and HENRI NORMANT. Can. J. Chem. **54**, 1098 (1976).

The anions α to *N,N*-disubstituted amides can be conveniently prepared by treatment with very powerful bases, "activated dialkylamides" in HMPT. These anions may react with various electrophiles especially with halogenated compounds. The use of functional halides (chloro or bromo compounds) affords functional amides. Lithiated amides are very useful intermediates in organic synthesis because they give regiospecific alkyl ketones by reacting with organo lithium compounds. In this way, we succeeded in obtaining the 1,5-diketone which was cyclised by intramolecular aldolization into *d,l*-piperitone.

La métallation directe, en milieu aprotique, des composés à méthylène activé dérivés des acides carboxyliques, nécessite l'emploi de bases particulièrement puissantes. Après avoir étudié le cas des esters et des nitriles nous envisageons maintenant celui des amides *N,N*-dialkylés (1, 2).

Synthèse de divers amides N,N-disubstitués

Le pK_a d'un amide aliphatique est de l'ordre de 30 alors qu'il n'est que de 22 à 25 pour les esters et les nitriles. Ceci explique les difficultés rencontrées jusqu'ici par les quelques auteurs qui ont étudié la métallation des amides, et seuls les carbanions d'amides qui possèdent en α un groupe susceptible de les stabiliser (C_6H_5, C≡N, COC_6H_5) sont facilement accessibles. L'amidure de sodium dans l'ammoniac liquide convient bien pour les amides RCH_2CONMe_2 (R = H ou Me) (3) mais dans le benzène ou le toluène à reflux les résultats ne sont satisfaisants que si R = H (4). L'amidure de lithium ne réagit pas (3), excepté le cas des β-lactames (5*a*); le butyllithium est un agent médiocre (5*b*) et si le dérivé lithié du trithiane, plus difficilement accessible, lui est supérieur, les rendements en dérivé alkylé sont parfois très faibles (5*b*).

Nous savons préparer depuis quelques années au laboratoire des bases extrêmement puissantes: les "dialkylamidures de lithium activés", obtenus aisément par simple agitation du métal dans une solution benzène–amine–HMPT (6, 7). Nous avons constaté que ces amidures étaient supérieurs à la plupart des bases, la présence de HMPT permettant non seulement d'accélérer la réaction d'arrachement du proton et de former ainsi divers carbanions à très basse température, mais également de favoriser les réactions ultérieures d'alkylation (2, 8–10).

Ces amidures "activés" ont conduit aux carbanions attendus, quel que soit l'amide *N,N*-disubstitué mis en oeuvre et l'encombrement de ce dernier (1, 2, 11).

Divers essais de métallation du *N,N*-diméthylformamide $HCONMe_2$ nous ont montré que les "amidures activés" peu encombrés (dérivés de la diéthylamine ou de la morpholine) provoquent une transamination mais qu'un amidure plus encombré (obtenu à partir de la diisopropylamine) conduit bien au carbanion instable **1** dont la formation vient d'être signalée (12, 13).

$$O{=}\bar{C}{-}N(R)_2$$

1

Can. J. Chem. Downloaded from www.nrcresearchpress.com by 210.87.254.5 on 09/05/12
For personal use only.

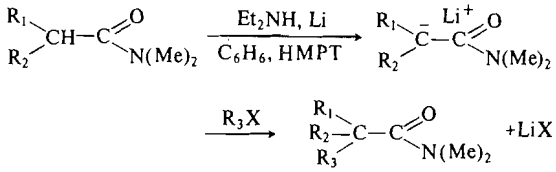

R_1 et R_2 = H ou alkyle

Le tableau 1 résume quelques essais.

Les amides linéaires même ramifiés mènent au carbanion sans difficulté. L'isobutyramide *N*,*N*-dialkylé a été plus particulièrement étudié car la ramification portée par le carbone siège de la réaction pouvait entraver celle-ci. La durée de la métallation est plus longue (1–2 h) et nécessite une température un peu plus élevée (−20 à +15 °C). Les carbanions obtenus, par suite de la présence de l'atome d'azote, sont plus stables que ceux des esters. Cette stabilité dépend bien sûr des substituants et augmente avec l'encombrement.

Les alkylations se font à basse température après dilution du milieu par du THF. On observe que: (*i*) les groupes R portés par l'azote n'affectent pas le cours de la réaction (tableau 1, essais 5 et 10); et (*ii*) la présence du HMPT permet de

TABLEAU 1. Alkylation de $R_1R_2\bar{C}$—$CON(Me)_2$ par R_3X

Essai	R_1	R_2	R_3X	Amide	Rendement[a] (%)
1	H	H	$C_6H_{13}Br$	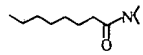	82
2	H	H	CH_2=CH—CH_2Br	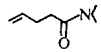	75
3	H	H	HC≡C—CH_2Br	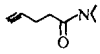	42
4	H	CH_3	$C_6H_{13}Br$	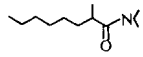	93
5[b]	H	C_2H_5	$C_6H_{13}Br$	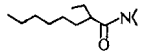	87
6	H	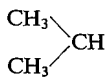	CH_3Br		70
7	H	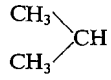	CH_2=CH—CH_2Br	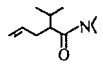	92
8	CH_3	CH_3	CH_3Br		81
9	CH_3	CH_3	C_4H_9Br	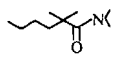	86
10[c]	CH_3	CH_3	C_4H_9Br	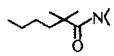	84
11	CH_3	CH_3	C_4H_9Cl	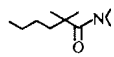	62
12	CH_3	CH_3	CH_3—CH_2—$CHBrCH_3$		58
13	CH_3	CH_3	CH_2=CH—CH_2Br	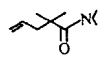	80
14	CH_3	CH_3	HC≡C—CH_2Br	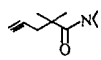	68

[a] En produits distillés.
[b] Amide *N*-méthyl *N*-phényl.
[c] Amide *N*,*N*-diéthyl.

Can. J. Chem. Downloaded from www.nrcresearchpress.com by 210.87.254.5 on 09/05/12
For personal use only.

TABLEAU 2. Synthèse d'amides ω-halogénés

Essai	R_1	R_2	Dérivé halogéné	Amide obtenu	Rendement[a] (%)
1	H	H	$CH_2{=}CCl{-}CH_2I$	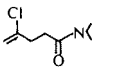	41
2	H	H	$Cl(CH_2)_3Br$	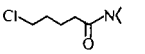	85
3	H	H	$ClCH_2CH(CH_3)CH_2Br$	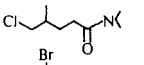	68
4	H	H	$CH_2{=}CBrCH_2Br$	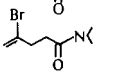	82
5	H	CH_3	$Cl(CH_2)_4Br$	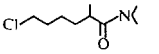	77
6[b]	H	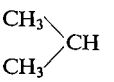	$BrCH_2{-}CBr{=}CH_2$	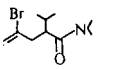	69
7			$Cl(CH_2)_4Br$	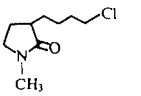	68
8			$Cl(CH_3)_3Br$	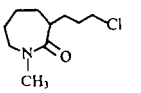	70

[a]En produits distillés.
[b]Amide *N,N*-diéthyl.

condenser des halogénures peu réactifs: ainsi le chlorure de butyle donne un rendement de 62% (essai 11 du tableau 1), résultat remarquable comparé aux essais effectués avec le dérivé du trithiane (rendement inférieur à 5% à partir du *N,N*-diméthylacétamide et du chlorure de butyle) (5).

Cette condensation n'a lieu cependant qu'à température relativement élevée (+15 °C) et cette différence de réactivité permet de réaliser des alkylations sélectives: les halogénures chlorobromés mènent aux amides ω-chlorés purs (voir tableau 2).

Le tableau 3 regroupe quelques essais effectués sur des lactames. On peut noter qu'avec la *N*-méthyl pyrrolidone une bis métallation suivie d'alkylation conduit au dérivé bis méthylé (tableau 3, essai 2). Le rendement est de 82% alors qu'il n'est que de 45% lorsqu'on emploie l'amidure de sodium dans l'ammoniac liquide (3). Des publications récentes décrivent des synthèses analogues en traitant la *N*-méthyl pipéridone-2 par les dialkylamidures usuels, mais la réaction nécessite l'emploi de dérivés halogénés très réactifs (14).

Applications des amides N,N-disubstitués: synthèse de la pipéritone

Disposant ainsi d'une bonne méthode de synthèse d'amides diversement substitués, nous avons envisagé quelques applications.

La réduction des amides conduit rapidement aux aldéhydes, alcools ou amines mais nous nous sommes plus particulièrement attachés à la préparation de cétones alkylées régiosélectivement.

En effet, l'alkylation directe des énolates de cétones mène rarement à un produit pur exempt d'isomère et si l'alkylation des énamines (15) des sels magnésiens d'imines (16) ou des carbanions lithiés des imines (17) fournit un composé unique, elle se fait toujours, lorsque la cétone est dissymétrique, du côté le moins encombré (composé **2**).

Par contre la condensation sur une fonction trivalente d'un organométallique tel que le méthyllithium permet d'accéder aux méthyl cétones du type **3**. En fait, on sait que seuls les acides et les amides permettent d'isoler les cétones avec des rendements satisfaisants. Ainsi, le *N,N*-diméthyl isobutyramide traité par le butyllithium ou le chlorure de butylmagnésium

Can. J. Chem. Downloaded from www.nrcresearchpress.com by 210.87.254.5 on 09/05/12
For personal use only.

TABLEAU 3. Alkylation de lactames

Essai	Lactame	Dérivé halogéné	Lactame alkylé	Rendement[a] (%)
1		CH_3Br		73
2[b]		$2CH_3Br$		82
3		$C_6H_5CH_2Cl$		82
4		CH_3CH_2Br		93
5		C_4H_9Br	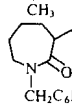	70

[a]En produits distillés.
[b]Métallation avec 2 Et_2NLi.

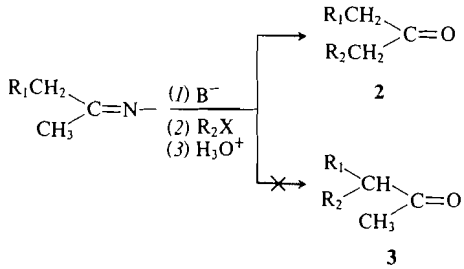

nous a conduits à la méthyl-2 heptanone-3 avec des rendements respectifs de 87 et 82%.

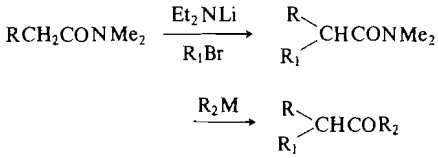

Nous avons appliqué cette méthode à la synthèse de la *d,l*-pipéritone, cétone terpénique utilisée dans la chimie des parfums et qu'on trouve dans diverses essences de menthe.

Cette synthèse passe par la préparation d'une dicétone-1,5 **6** qui est ensuite cyclisée par aldolisation interne. Les amides conduisent immédiatement à une telle cétone. Il suffit de condenser un halogénure convenablement choisi sur l'isovaléramide. Le dichloro-1,3 butène-2 commercial, convient bien puisque le carbone sp^2 porteur du chlore est en fait un carbonyle à l'état potentiel.

Nous avons donc traité l'isovaléramide par le diéthyl amidure de lithium activé vers −20 °C; la condensation du dihalogénure est effectuée à −50 °C et conduit après hydrolyse à l'amide chloré vinylique **4**.

L'addition stoechiométrique de méthyllithium, préalablement dosé (18) à −20 °C mène à la cétone chlorée **5**. En milieu acide sulfurique concentré froid elle donne la dicétone-1,5 attendue **6**. Cette dernière n'est pas isolée mais cyclisée directement par simple dilution du milieu acide qui est ensuite chauffé à 90 °C.

Cette cyclisation en milieu acide fournit un produit pur alors qu'en milieu basique il est souillé de 5% d'impureté. Il est vraisemblable que dans ce dernier cas il y a équilibre entre les deux isomères **7** et **8**[1]. On sait en effet que l'équilibre thermodynamique est de 92:8 et qu'il s'établit environ 30 fois plus vite en milieu basique qu'en milieu acide (19). Un chauffage prolongé en milieu acide fait d'ailleurs apparaître la même impureté qu'en milieu basique.

Cette synthèse rapide de la *d,l*-pipéritone illustre bien l'une des possibilités offertes par

[1]Nous remercions le Dr. James S. Roberts (Université de Stirling) qui nous a aimablement communiqué le spectre rmn du composé **8** ainsi que le Professeur G. J. Martin (Université de Nantes) qui nous a aidés à interpréter le spectre de la pipéritone.

Can. J. Chem. Downloaded from www.nrcresearchpress.com by 210.87.254.5 on 09/05/12
For personal use only.

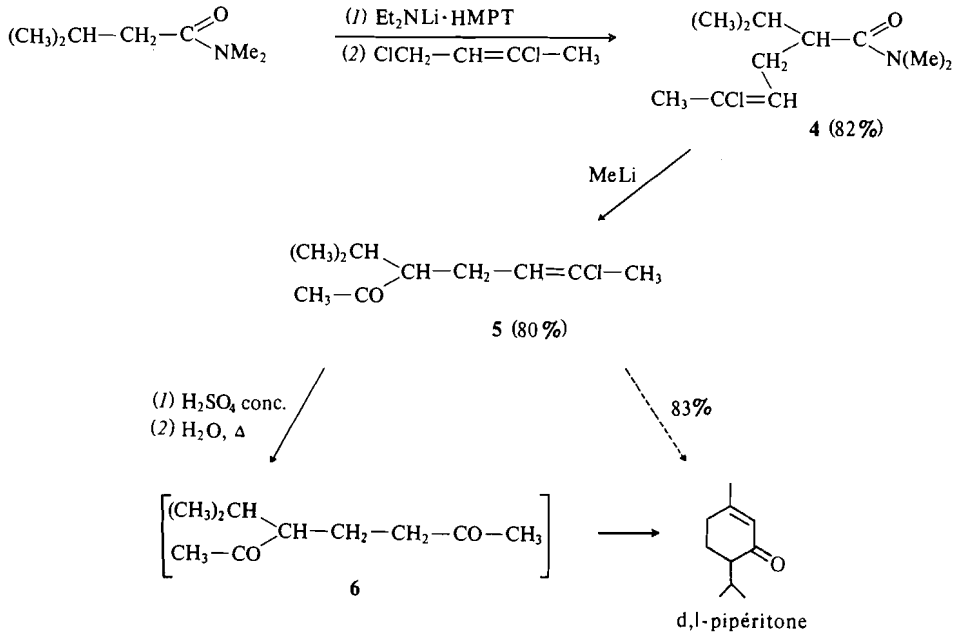

notre nouvelle méthode d'alkylation des amides *N,N*-disubstitués. Dans un prochain mémoire nous examinerons la formation des hydroxy-amides (note préliminaire, réf. 20).

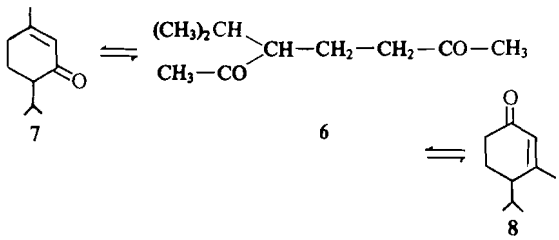

Partie expérimentale

La structure des divers amides a été confirmée par ir et rmn. Les spectres infrarouges ont été effectués sur un spectrophotomètre Perkin-Elmer 457 sous forme de film. Les spectres rmn ont été enregistrés sur un appareil Perkin-Elmer R 12 à 60 MHz, en utilisant le CCl_4–TMS comme solvant. La pureté des produits a été contrôlée par chromatographie en phase gazeuse sur colonne SE 30 de 3 m et les produits ont été analysés.

Préparation de diéthylamidure de lithium

Dans un tétracol de 250 ml on introduit sous argon: 10 ml de HMPT, 10 ml de benzène et 4 g (0.055 mol) de diéthylamine. On ajoute alors 0.055 at. g. de lithium martelé, le milieu devient rapidement rouge foncé; la température est maintenue à 20 °C à l'aide d'un bain d'eau. Le lithium disparaît en 2-3 h.

Métallation et alkylation du N,N-diméthylacétamide

Le diéthylamidure de lithium dilué de 10 ml d'éther ou de THF pour éviter la prise en masse est refroidi à −60 °C. On introduit 0.05 mol d'amide dilué d'un égal volume d'éther ou de THF. Le milieu devient rapidement violet, on laisse revenir la température à −50 °C pendant 30 min. Le dérivé halogéné (0.055 mol) dilué dans 80 ml de THF est introduit à −60 °C. On observe une décoloration rapide de la solution qui devient jaune. On laisse revenir à température ambiante toute la nuit.

Métallation et alkylation des amides linéaires, ramifiés ou cycliques

On opère comme précédemment en introduisant l'amide à −20 °C, puis la température est ramenée progressivement à +15 °C, pendant 1½ h. Le carbanion peut être alors alkylé à −60 °C. Les dérivés insaturés sont hydrolysés au bout de 2–3 h à −50 °C, pour les autres composés on revient à température ambiante la nuit et hydrolyse. Après extraction à l'éther, la couche organique est séchée au sulfate de magnésium, on chasse sous vide les solvants, puis on distille sous pression réduite le résidu.

Purification

Dans certains cas, la distillation ne permet pas de séparer le HMPT de l'amide alkylé. La chromatographie sur colonne d'alumine fournit un produit pur. L'élution se fait à l'aide de solutions hexane–éther (20:80), puis 50:50 et pour finir à l'éther pur. Le HMPT reste fixé sur la colonne.

Tableau 1

Les amides de départ ont été obtenus par action du chlorure d'acide sur la diméthylamine anhydre, la diéthylamine ou la *N*-méthylaniline.

Essai 1—p éb: 135 °C/17 torr; ir: 1640 cm^{-1} (C=O); rmn: δ 2.83 et 2.97 (6H, d, NMe_2), 2.21 (2H, t, CH_2CO).

Essai 2—p éb: 110 °C/20 torr (litt. (21) 88 °C/10 torr); ir: 1655 (C=C), 1640 (C=O), 910 cm^{-1} (CH_2=); rmn: δ 6.17 à 5.46 (1H, m, CH=), 5.17 à 4.73 (2H, m, CH_2=), 3.01 et 2.86 (6H, d, NMe_2).

Can. J. Chem. Downloaded from www.nrcresearchpress.com by 210.87.254.5 on 09/05/12
For personal use only.

Can. J. Chem. Downloaded from www.nrcresearchpress.com by 210.87.254.5 on 09/05/12
For personal use only.

Essai 3—p éb: 120 °C/17 torr; ir: 3250 (C≡H), 2120 (C≡C), 1640(C=O), 745 cm^{-1}(C≡H), rmn: δ 3.01 et 2.86 (6H, d, NMe_2), 2.43 (4H, m, CH_2), 2.06 (1H, m, C≡CH).

Essai 4—p éb: 120 °C/0.01 torr; ir: 1645 cm^{-1} (C=O); rmn: δ 3.04 et 2.9 (6H, d, NMe_2), 2.82 à 2.45 (2H, m, CH_2—CO).

Essai 5—p éb: 102 °C/0.01 torr; ir: 1650 cm^{-1} (C=O); rmn: δ 7.26 (5H, m, C_6H_5), 3.2 (3H, s, NCH_3), 2.2 (1H, m, CH).

Essai 6—p éb: 90 °C/16 torr (litt. (5) 96–98 °C/18 torr); ir: 1640 cm^{-1} (C=O); rmn: δ 2.98 et 2.90 (6H, d, NMe_2), 2.33 (1H, m, CHCO), 1.81 (1H, m, CH), 1.25 à 0.74 (9H, m, CH_3).

Essai 7—p éb: 108 °C/15 torr; ir: 1640 (C=O), 910 cm^{-1} (CH_2=); rmn: δ 6 à 5.3 (1H, m, CH=), 5.15 à 4.73 (2H, m, CH_2=), 3 et 2.87 (6H, d, NMe_2), 2.1 (1H, m, CH—CO).

Essai 8—p éb: 45 °C/0.01 torr (litt. (22) 85.5 °C/13 torr); ir: 1625 (C=O), 1395, 1375 cm^{-1} (*tert*-butyl); rmn: δ 2.95 (6H, s, NMe_2), 1.22 (9H, s, CH_3).

Essais 9 et 11—p éb: 110 °C/17 torr (litt. (21) 61–62 °C/0.7 torr); ir: 1630 cm^{-1} (C=O); rmn: δ 2.97 (6H, s, NMe_2), 1.75 à 1.05 (6H, m, CH_2), 1.18 (6H, s, CH_3), 0.94 (3H, m, CH_3). *Anal.* calc. pour $C_{10}H_{21}NO$: C 70.12, H 12.36, N 8.18; trouvé: C 70.04, H 12.30, N 8.28.

Essai 10—p éb: 116 °C/17 torr; ir: 1633 cm^{-1} (C=O); rmn: δ 3.35 (4H, q, NCH_2).

Essai 12—p éb: 113–115 °C/17 torr; ir: 1625 cm^{-1} (C=O); rmn: δ 2.95 (6H, s, NMe_2), 1.09 (6H, s, CH_3), 1 à 0.65 (6H, m, CH_3).

Essai 13—p éb: 98 °C/15 torr (litt. (21) 75–80 °C/4 torr); ir: 1625 (C=O), 910 cm^{-1} (CH_2=); rmn: δ 6.1 à 5.5 (1H, m, CH=), 5.15 à 4.75 (2H, m, CH_2=), 2.96 (6H, s, NMe_2), 2.24 et 2.35 (2H, d, CH_2), 1.18 (6H, s, CH_3) (réf. 21). *Anal.* calc. pour $C_9H_{17}NO$: C 69.63, H 11.04, N 9.02; trouvé: C 69.84, H 11.09, N 9.08.

Essai 14—p éb: 113 °C/16 torr; ir: 3270 (C≡H), 2120 (C≡C), 1625 cm^{-1} (C=O); rmn: δ 3.02 (6H, s, NMe_2), 2.44 (2H, d, CH_2), 1.95 (1H, m, CH). *Anal.* calc. pour $C_9H_{15}NO$: C 70.55, H 9.87, N 9.14; trouvé: C 70.32, H 9.98, N 9.25.

Tableau 2

Essai 1—p éb: 65 °C/0.01 torr; ir: 1655 (C=C), 1640 (C=O), 883 (CH_2=), 615 cm^{-1} (Cl); rmn: δ 5.22 et 5.09 (2H, d, CH_2=), 2.97 et 2.83 (6H, d, NMe_2), 2.6 (4H, m, CH_2).

Essai 2—p éb: 130 °C/23 torr; ir: 1640 (C=O), 650, cm^{-1} (Cl); rmn: δ 3.55 (2H, t, CH_2Cl), 3.01 et 2.86 (6H, d, NMe_2), 2.3 (2H, t, CH_2CO), 1.97 à 1.61 (4H, m, CH_2).

Essai 3—p éb: 82 °C/0.01 torr; ir: 1640 (C=O), 680 et 615 cm^{-1} (Cl); rmn: δ 3.53 et 3.44 (2H, d, CH_2Cl), 3.01 et 2.86 (6H, d, NMe_2), 2.31 (2H, t, CH_2CO), 1.08 et 0.97 (3H, d, CH_3).

Essai 4—p éb: 67 °C/0.01 torr; ir: 1655 (C=C), 1640 (C=O), 890 (CH_2=), 555 cm^{-1} (Br); rmn: δ 5.63 et 5.32 (2H, d, CH_2=), 3.01 et 2.86 (6H, d, NMe_2), 2.6 (4H, m, CH_2). *Anal.* calc. pour $C_7H_{12}BrNO$: C 40.79, H 5.88, Br 38.77, N 6.79; trouvé: C 40.80, H 6.02, Br 38.45, N 7.03.

Essai 5—p éb: 150–155 °C/15 torr; ir: 1640 (C=O), 650 cm^{-1} (Cl); rmn: δ 3.51 (2H, t, CH_2Cl), 3.05 et 2.9 (6H, d, NMe_2), 1.1 à 2 (6H, m, CH_2), 1.06 et 0.96 (3H, d, CH_3).

Essai 6—p éb: 80 °C/0.01; ir: 1655 (C=C), 1633 (C=O), 890 (CH_2=C), 560 cm^{-1} (Br); rmn: δ 5.55 et 5.3 (2H, d, CH_2=), 3.35 (4H, m, NCH_2), 2.75 (2H, m, CH_2—CBr).

Essai 7—p éb: 105 °C/0.01 torr; ir: 1685 (C=O), 660 cm^{-1} (Cl); rmn: δ 3.44 (2H, m, CH_2Cl), 3.29 (2H, m, NCH_2), 2.78 (3H, s, NCH_3). *Anal.* calc. pour $C_9H_{16}ClNO$: C 56.98, H 8.50, Cl 18.69, N 7.38; trouvé: C 56.91, H 8.57, Cl 18.51, N 7.48.

Essai 8—p éb: 105–111 °C/0.01 torr; ir: 1640 (C=O), 650 cm^{-1} (Cl); rmn: δ 3.56 (2H, t, CH_2Cl), 3.30 (2H, m, NCH_2), 2.98 (3H, s, NCH_3).

Tableau 3

Le *N*-méthyl caprolactame et le *N*-benzyl caprolactame ont été obtenus par action de l'hydrure de sodium en milieu THF sur le caprolactame, suivie d'une alkylation par l'iodure de méthyle, ou le chlorure de benzyle.

Essai 1—p éb: 100 °C/17 torr; ir: 1680 cm^{-1} (C=O); rmn: δ 3.25 (2H, q, NCH_2), 2.75 (3H, s, NCH_3), 1.15 et 1.03 (3H, d, CH_3).

Essai 2—p éb: 47 °C/0.01 torr (litt. (2) 72–73 °C/20 torr, (23) 87 °C/20 torr); ir: 1680 cm^{-1} (C=O); rmn: δ 3.25 (2H, t, NCH_2), 2.74 (3H, s, NCH_3), 2.02 (1H, m, CH), 1.8 (2H, t, CH_2), 1.03 (6H, s, Me_2) (litt. (2) 3.26 (2H, t, NCH_2), 2.73 (3H, s, NCH_3), 1.83 (1H, t, CH_2), 1.25 (6H, s, Me_2)).

Essai 3—p éb: 115 °C/0.01 torr; ir: 3030, 1600, 750 (C_6H_5), 1675 cm^{-1} (C=O); rmn: δ 7.18 (5H, s, C_6H_5), 3.1 (2H, m, NCH_2), 2.65 (2H, m, $CH_2C_6H_5$).

Essai 4—p éb: 120 °C/16 torr; ir: 1640 cm^{-1} (C=O); rmn: δ 3.7 à 3.12 (2H, m, NCH_2), 2.95 (3H, s, NCH_3), 0.99 et 0.87 (3H, d, CH_3).

Essai 5—p éb: 145 °C/0.1 torr; ir: 3015, 1600, 730, 700 (C_6H_5), 1640 cm^{-1} (C=O); rmn: δ 7.14 (5H, s, C_6H_5), 4.44 (2H, d, $NCH_2C_6H_5$), 3.22 (2H, m, NCH_2), 2.32 (1H, m, CH), 0.93 (3H, m, CH_3). *Anal.* calc. pour $C_{17}H_{25}NO$: C 78.76, H 9.65, N 5.40; trouvé: C 78.45, H 9.61, N 5.44.

Préparation de la méthyl-2 heptanone-3

(a) Par action du butyllithium

A 0.055 mol de butyllithium dans l'éther refroidi à −20 °C, on ajoute sous argon 0.050 mol de *N*,*N*-diméthyl isobutyramide dilué d'un égal volume d'éther. On agite 3 h puis on revient à température ambiante et hydrolyse à −10 °C par une solution de chlorure d'ammonium saturée. Après avoir extrait à l'éther et séché sur sulfate de magnésium, les solvants sont chassés sous vide et le résidu distillé sous pression réduite: rendement 87%.

(b) Par action du chlorure de butylmagnésium

A 0.15 mol de réactif de Grignard dans le THF, on ajoute à température ambiante 0.075 mol d'amide dilué dans le THF. On agite 13 h puis porte 4 h à 60 °C, refroidit et hydrolyse par une solution d'acide chlorhydrique 2 *N*: p éb: 47 °C/15 torr; rendement: 82%. Les spectres ir et rmn sont identiques à ceux d'un échantillon authentique.

Synthèse de la d,l-pipéritone

Composé 4

Le *N*,*N*-diméthyl isovaléramide (0.05 mol) est métallé par le diéthylamidure de lithium à −20 °C comme décrit précédemment.

Le dichloro-1,3 butène (0.06 mol) dilué dans 100 ml de THF est introduit à −60 °C et on laisse revenir la température à −50 °C. On hydrolyse à −50 °C 2 h après la

fin de l'addition. On extrait à l'éther, sèche la couche organique sur sulfate de magnésium, chasse sous vide les solvants puis distille sous pression réduite: p éb: 70 °C/-0.02 torr; liquide jaune clair: 8.95 g (0.041 mol); rendement: 82%; ir: 1640 (C=O), 825 (CH=), 625 cm^{-1} (Cl); rmn: δ 5.41 (1H, t, CH=), 3 et 2.88 (6H, d, NMe_2), 2.31 (2H, m, CH_2—CH=), 2.04 (3H, pic large, CH_3CCl), 0.88 (6H, 2d, CH_3). *Anal.* calc. pour $C_{11}H_{20}ClNO$: C 60.67, H 9.25, Cl 16.28, N 6.43; trouvé: C 60.96, H 9.32, Cl 16.42, N 6.50.

Composé **5**

A 0.022 mol de méthyllithium dans l'éther refroidi à −20 °C on ajoute sous argon 0.020 mol d'amide chloré **4**. On agite 3 h à −20 °C puis on revient 30 min à température ambiante. On hydrolyse à −10 °C par une solution saturée de chlorure d'ammonium. Après traitement usuel on distille sous pression réduite: p éb: 50 °C/-0.01 torr; liquide incolore: 3 g; rendement 80%; ir: 1705 (C=O), 615 cm^{-1} (Cl); rmn: δ 5.4 (1H, m, CH=), 2.2 (2H, m, CH_2), 2.05 (6H, 2s, CH_3CO et CH_3CCl), 0.9 (6H, 2d, CH_3). *Anal.* calc. pour $C_{10}H_{17}ClO$: C 63.64, H 9.08, Cl 18.79; trouvé: C 63.85, H 9.25, Cl 18.96.

d,l-Pipéritone **7**

Une solution composée de 2 g de cétone chlorée **5** (0.010 mol) et de 12 ml d'hexane est additionnée goutte à goutte à 8 ml d'acide sulfurique concentré refroidi à 0 °C. Dès le début de l'addition on note un dégagement d'acide chlorhydrique, le milieu devient beige. Au bout de 40 min on hydrolyse par 30 ml d'eau glacée (on refroidit à l'aide d'un bain à −40 °C). On revient à température ambiante et porte à 90 °C pendant 3 h. Après extraction à l'éther et lavage à la soude diluée, la couche organique est séchée sur sulfate de magnésium, on chasse sous vide les solvants puis distille sous pression réduite: p éb: 55 °C/0.01 torr; n_D^{22}: 1.4845 (litt. (19) p éb 111 °C/15 torr, n_D^{22} 1.4847); liquide incolore, d'odeur mentholée: 1.35 g; rendement: 83%; ir: 1665 (C=O), 870 cm^{-1} (CH=); rmn: δ 5.69 (1H, q, CH=), 1.9 (3H, d, CH_3), 0.84 (6H, 2d, CH_3); spectre de masse: pic de masse *m/e* 152, principal fragment: *m/e* 82, autres pics: *m/e* 110, 95, 39, 41, 54, 137. Ce spectre identique au spectre décrit dans la littérature (24) confirme la structure de la *d,l*-pipéritone.

1. TH. CUVIGNY et H. NORMANT. C.R. Acad. Sci. Paris, C, **268**, 1380 (1969).
2. TH. CUVIGNY et H. NORMANT. Organometal. Chem. Syn. **1**, 237 (1971).
3. P. G. GASSMAN et B. L. FOX. J. Org. Chem. **31**, 982 (1966).
4. H. L. NEEDLES et R. E. WHITFIELD. J. Org. Chem. **31**, 989 (1966).
5. (*a*) T. DURST, R. VAN DEN ELZEN et R. LEGAULT. Can. J. Chem. **52**, 3206 (1974); (*b*) D. N. CROUSE et D. SEEBACH. Chem. Ber. **101**, 3113 (1968).
6. H. NORMANT, TH. CUVIGNY et D. REISDORF. C.R. Acad. Sci. Paris, C, **268**, 521 (1969).
7. H. NORMANT et TH. CUVIGNY. Organometal. Chem. Syn. **1**, 223 (1971).
8. M. LARCHEVÊQUE, P. MULOT et TH. CUVIGNY. J. Organometal. Chem. C, **57**, 33 (1973).
9. M. LARCHEVÊQUE, A. DEBAL et TH. CUVIGNY. Bull. Soc. Chim. Fr. 1710 (1974).
10. M. LARCHEVÊQUE, G. VALETTE, TH. CUVIGNY et H. NORMANT. Synthesis, 256 (1975).
11. TH. CUVIGNY, P. HULLOT, M. LARCHEVÊQUE et H. NORMANT. C.R. Acad. Sci. Paris, C, **278**, 1105 (1974).
12. B. BANHIDAI et U. SCHÖLLKOPF. Ang. Chem., Int. Ed. Engl. **12**, 836 (1973).
13. R. R. FRASER et P. R. HUBERT. Can. J. Chem. **52**, 185 (1974).
14. B. M. TROST et R. A. KUNZ. J. Org. Chem. **39**, 2475 (1974); P. DESLONGCHAMPS, U. O. CHERIYAN et D. R. PATTERSON. Can. J. Chem. **53**, 1682 (1975).
15. G. STORK, A. BRIZZOLARA, H. LANDESMAN, J. SZMUSZKOVICZ et R. TERRELL. J. Am. Chem. Soc. **85**, 207 (1963).
16. G. STORK et S. R. DOWD. J. Am. Chem. Soc. **85**, 2178 (1963).
17. TH. CUVIGNY, M. LARCHEVÊQUE et H. NORMANT. Ann. Chem. 719 (1975).
18. S. C. WATSON et J. F. EASTHAM. J. Organometal. Chem. **9**, 165 (1967).
19. R. N. LACEY. J. Chem. Soc. 1639 (1960).
20. TH. CUVIGNY, P. HULLOT, M. LARCHEVÊQUE et H. NORMANT. C.R. Acad. Sci. Paris, C, **279**, 569 (1974).
21. C. F. HOBBS et H. WEINGARTEN. J. Org. Chem. **33**, 2385 (1968).
22. H. C. BROWN et A. TSUKAMOTO. J. Am. Chem. Soc. **86**, 1089 (1964).
23. R. LUKES et V. DEDEK. Chem. Listy, **51**, 2139 (1957).
24. A. F. THOMAS, B. WILLHAM et J. H. BOWIE. J. Chem. Soc. B, 392 (1967).

Can. J. Chem. Downloaded from www.nrcresearchpress.com by 210.87.254.5 on 09/05/12
For personal use only.

Structure de la mycosporine (P 310)[1]

JEAN FAVRE-BONVIN ET NOËL ARPIN

Département de Biologie Végétale, Service de Phytochimie et de Phytophysiologie, Université Claude Bernard - Lyon I (Laboratoire associé au CNRS n°44); 43 boulevard du 11 novembre 1918, 69621 - Villeurbanne, France

ET

CHRISTIAN BREVARD

Société Brüker, 34, rue de l'Industrie, 67160, Wissembourg, France

Reçu le 20 octobre 1975

JEAN FAVRE-BONVIN, NOËL ARPIN et CHRISTIAN BREVARD. Can. J. Chem. **54**, 1105 (1976).

La structure **1** (méthoxy-2 bis(hydroxyméthyl)méthylamino-3 hydroxy-5 hydroxyméthyl-5 cyclohexène-2 one-1) a été attribuée à la mycosporine (P 310), substance isolée de *Stereum hirsutum* (Willd. ex Fr.) Fr.; ce résultat découle de l'analyse des spectres (uv, ir, sm et rmn de ^{1}H et ^{13}C) du produit naturel et de ses dérivés.

JEAN FAVRE-BONVIN, NOËL ARPIN, and CHRISTIAN BREVARD. Can. J. Chem. **54**, 1105 (1976).

The structure **1** (2-methoxy-3-bis(hydroxymethyl)methylamino-5-hydroxy-5-hydroxymethyl-2-cyclohexen-1-one has been attributed to mycosporine (P. 310), a product isolated from *Stereum hirsutum* (Willd. ex Fr.) Fr.; this result is derived from the uv, ir, ms, and nmr of ^{1}H and ^{13}C spectral analysis of the natural product and its derivatives.

Introduction

Etudiant le cycle de développement de divers champignons phytopathogènes, Leach et coll. misent en évidence, de 1961 à 1969 (1, 2), la nécessité de la lumière ultraviolette pour induire la reproduction sexuée comme asexuée des espèces envisagées. Parallèlement il remarqua que les extraits aqueux des mycéliums irradiés en ultraviolet présentaient une très intense absorption en uv avec un maximum à 310 nm (3). Par la suite trois substances furent isolées, absorbant toutes trois à 310 nm, et désignées P 310 A, P 310 B, P 310 C, cette dernière nettement plus abondante (2). Cependant Trione et Leach ne donnèrent que très peu d'informations relatives à la structure de ces composés photo-induits et bien que d'autres chercheurs (4–7) aient isolé à nouveau ce type de substances, ils restèrent en deçà des indications déjà fournies (2).

Dans une note préliminaire (Arpin, Thivend et Favre-Bonvin, à paraître) nous relatons la présence, abondante, de P 310 dans les carpophores de *Stereum hirsutum*; nous avons comparé (spectres uv, ir, sm, rmn et chromatographie) la substance isolée avec le P 310 extrait de *Nectria galligena* par Dehorter:[2] les deux composés se révèlent identiques en tous points.

Nous rapportons et discutons ici l'ensemble des informations chimiques, essentiellement obtenues par des méthodes spectrales, qui nous ont conduits à la structure **1** (schéma 1) pour P 310.

Comme se composé a été isolé de spores à plusieurs reprises, nous proposons de donner à cette molécule ou méthoxy-2 bis(hydroxyméthyl)-méthylamino-3 hydroxy-5 hydroxyméthyl-5 cyclohéxène-2 one-1 le nom de mycosporine.

Résultats et discussion

La mycosporine, composé blanc de consistance pâteuse à la température ambiante, présente une réaction positive avec la dinitro-2,4 phénylhydrazine; elle réagit également avec le chlorure ferrique (coloration rouge brun). Le spectre uv se caractérise par une bande d'absorption unique à 310 nm (fig. 1) ce qui, *a priori*, n'apporte guère d'indication sur le chromophore car les substances actuellement connues pour présenter un tel spectre (dimère de la thymine et son produit de déshydratation (8), zéatine (9)) s'avèrent nettement différentes par ailleurs.

Au plan de la spectrométrie ir, trois bandes

[1]Recherches chimiotaxinomiques sur les Champignons. XXXI. Pour XXX voir: Substances photoabsorbantes de *Stereum hirsutum* (Willd. ex Fr.) Fr.; isolement de P 310 par N. Arpin, S. Thivend et Jean Favre-Bonvin. A paraître.

[2]M. Dehorter, Université de Lille, France, a bien voulu nous transmettre un échantillon de P 310: nous l'en remercions très chaleureusement.

Can. J. Chem. Downloaded from www.nrcresearchpress.com by 210.87.254.6 on 09/05/12
For personal use only.

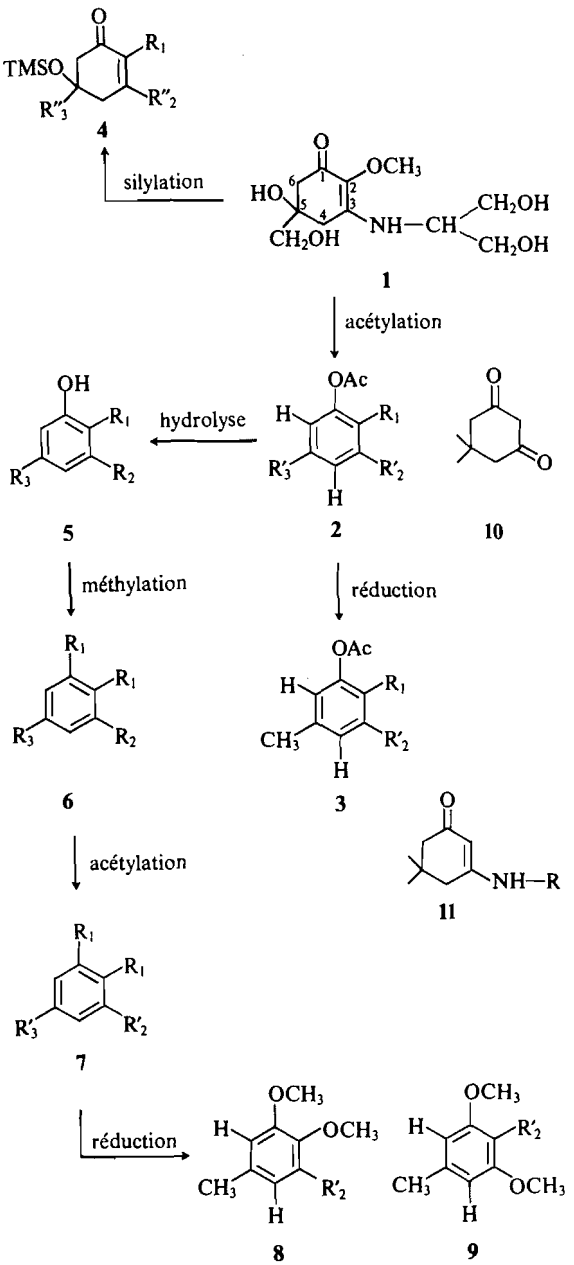

$R_1 = OCH_3$

$R_2 = NH—CH—(CH_2OH)_2$ $R_3 = CH_2OH$
$R'_2 = NH—CH—(CH_2OAc)_2$ $R'_3 = CH_2OAc$
$R''_2 = NH—CH—(CH_2OTMS)_2$ $R''_3 = CH_2OTMS$

SCHÉMA I

sont à signaler: une à 1610 cm^{-1} pouvant correspondre à un carbonyle très influencé, une autre, importante, à 1540 cm^{-1} et enfin une bande hydroxyle, également intense, à 3330 cm^{-1}.

En spectrométrie de masse on observe, dans tous les cas, un pic à *m/e* 243 (243.1103, 243.1106 pour $C_{11}H_{17}NO_5$); ce pic provient de la déshydratation du produit naturel dont le pic moléculaire très faible (et souvent inexistant) se situe à *m/e* 261 correspondant à $C_{11}H_{19}NO_6$. L'existence pour le dérivé tétra-triméthylsilylé d'un pic moléculaire intense à *m/e* 549 confirme la valeur *m/e* 261 pour le pic moléculaire du produit naturel et par le fait la très facile déshydratation. C'est en fait l'étude détaillée des spectres de rmn ^1H et ^{13}C du produit naturel et de ses dérivés acétylés qui nous a conduits à la structure de la mycosporine.[3]

Tout d'abord signalons l'existence, dans tous ces spectres, d'un signal méthoxyle (figs 1–4 et tableau 1).

L'important déblindage observé par rapport au déplacement chimique moyen d'un méthoxyle (5 ppm) en ^{13}C semblerait indiquer un fort encombrement stérique au niveau des positions de substitution adjacentes à ce groupe méthoxyle. De tels effets ont déjà été observés dans des anisoles *ortho*-disubstituées (réf. 10, p. 203–204).

La présence d'un groupement C=O est évidente en ^{13}C où le signal se situe à une valeur de 186.2 ppm (pyridine) (187.9 ppm dans D_2O); dans le spectre de ^{13}C non découplé, ce signal apparaît sous forme d'un triplet indiquant un couplage à longue distance avec les protons d'un CH_2 vicinal: la constante de couplage de 4.1 Hz, est en bon accord avec les valeurs déjà obtenues dans la littérature. Le blindage important de ce carbonyle implique la présence d'une cétone α,β insaturée. Les déplacements chimiques des cétones, peu sensibles aux effets inductifs de substituants en α de ce groupe fonctionnel sont par contre affectés très nettement par des formes mésomères du genre:

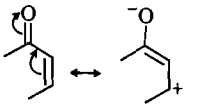

[3]Nous avons grandement bénéficié dans ce domaine de l'expérience, des suggestions et conseils de M. Robert Mottet (Société Rhone-Poulenc): nous tenons à lui exprimer ici toute notre reconnaissance.

Can. J. Chem. Downloaded from www.nrcresearchpress.com by 210.87.254.6 on 09/05/12
For personal use only.

Can. J. Chem. Downloaded from www.nrcresearchpress.com by 210.87.254.6 on 09/05/12
For personal use only.

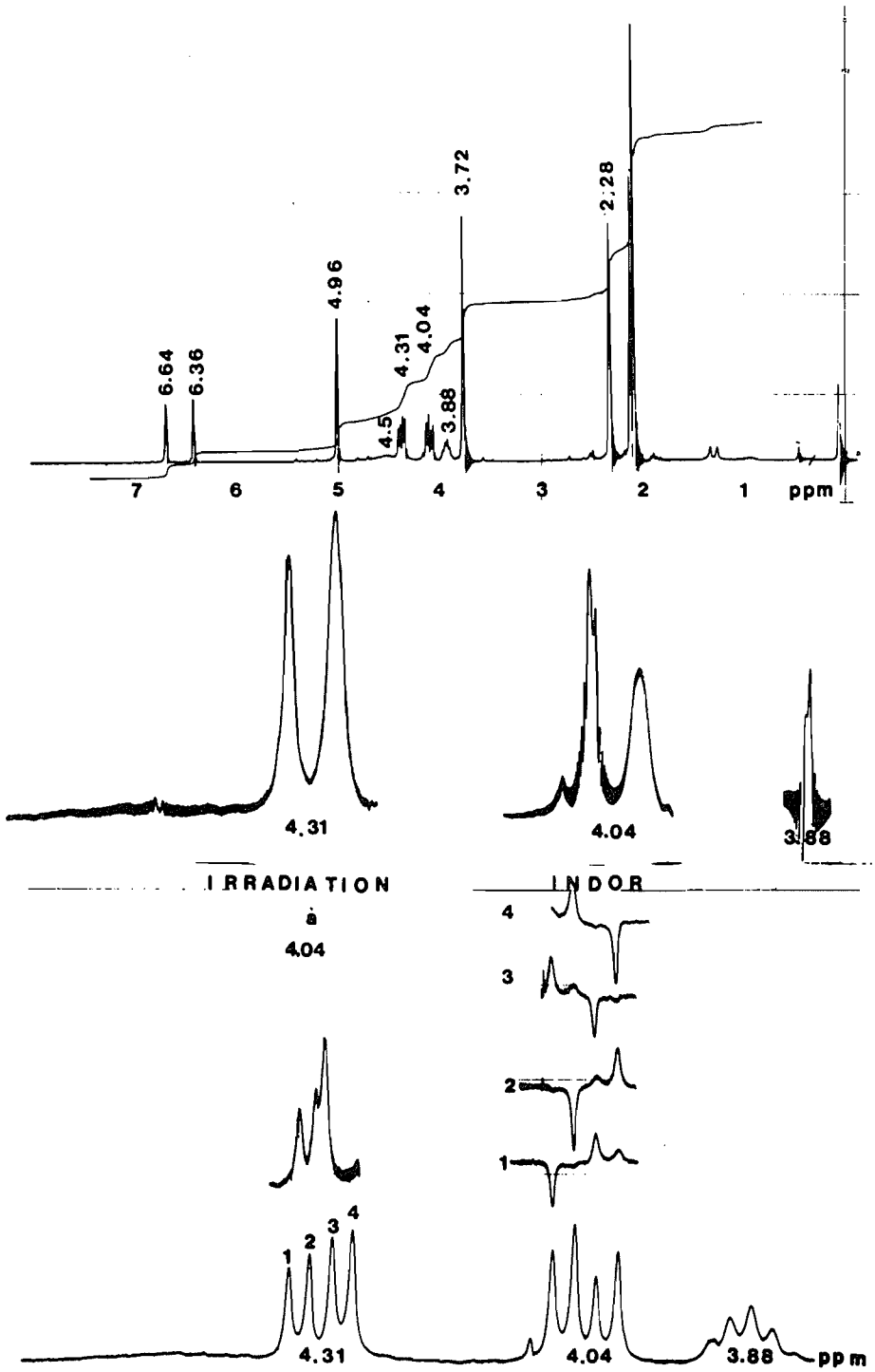

FIG. 1. Spectres de rmn ^1H à 250 MHz de l'acétate **2** (CCl_4); agrandissements, découplages et INDOR.

TABLEAU 1. Valeurs des déplacements chimiques (ppm) des ^{13}C de la mycosporine, **1**, et de l'acétate **2**

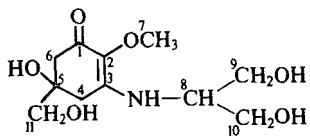

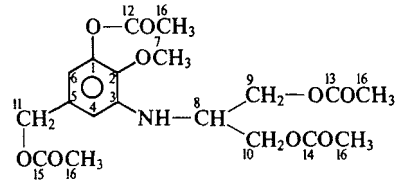

C	D_2O	Figure off res.[a]	Pyridine	C	$CDCl_3$	Figure off res.[a]
1	187.9[b]	s	186.2	1	143.1[c]	s
2	132.5	s	131.5	2	140.6[c]	s
3	160.5	s	153.4	3	138.0[c]	s
4	35.9	t	34.9	4	108.4	d
5	74.5	s	72.7	5	132.2[c]	s
6	45.4	t	46.3	6	111.2	d
7	61.5	q	58.8	7	59.9	q
8	55.8	d	56.5	8	50.8	d
9	63.7	t	62.1	9	62.8	t
10	63.7	t	62.3	10	62.8	t
11	70.0	t	69.4	11	65.7	t
				12	168.1	s
				13	170.1	s
				14	170.1	s
				15	170.1	s
				16	20.0	q

[a]s, singulet; d, doublet; t, triplet; q, quadruplet.
[b]Donne un triplet (J très faible) dans un spectre non découplé.
[c]Valeurs attribuées arbitrairement.

diminuant la déficience de charge électronique au niveau du C oxygéné. Les pics à 132.5 et 160.5 ppm (D_2O) et 131.5 et 153.4 ppm (pyridine) correspondent respectivement aux C-2 et C-3 (réf. 10, p. 193).

Les quatre hydroxyles silylables, déjà détectés par sm sont parfaitement confirmés en rmn de ^1H où s'observent deux signaux O—TMS, dans le rapport 3:1, ce qui indique déjà nettement l'existence d'un hydroxyle particulier, légèrement plus blindé sous forme de TMS que les trois autres. Ces trois hydroxyles s'acétylent aisément: on observe alors deux signaux à 2.07 et 2.10 ppm ($CDCl_3$) dans le rapport 2:1 (fig. 2). Il existe donc deux acétyles parfaitement identiques, un autre légèrement plus déblindé, dérivant tous trois d'alcools primaires, compte-tenu du déplacement chimique des trois signaux —CH_2O— (*ca.* 4 ppm) observé dans les spectres du produit naturel.

Les expériences de découplage de spin et d'INDOR réalisées sur le dérivé tétraacétylé **2** (CCl_4) apportent la preuve de la présence d'un groupement isopropanediol (schéma 2).

Après irradiation du —CH à 970 Hz (3.88 ppm, fig. 1), les deux quadruplets centrés à 4.04 et 4.31 ppm se résolvent chacun en un doublet (J = 11.2 Hz): les protons H_A et $H_{A'}$ sont donc

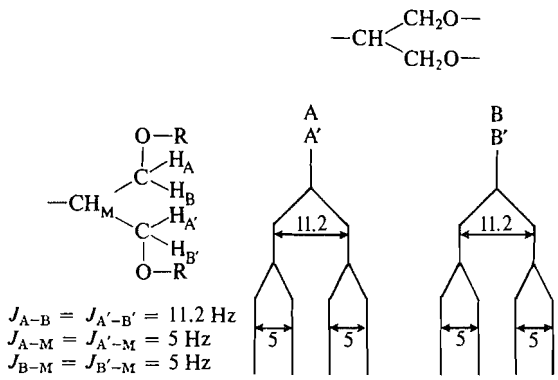

$J_{A-B} = J_{A'-B'} = 11.2$ Hz
$J_{A-M} = J_{A'-M} = 5$ Hz
$J_{B-M} = J_{B'-M} = 5$ Hz

SCHÉMA 2

Can. J. Chem. Downloaded from www.nrcresearchpress.com by 210.87.254.6 on 09/05/12
For personal use only.

Can. J. Chem. Downloaded from www.nrcresearchpress.com by 210.87.254.6 on 09/05/12
For personal use only.

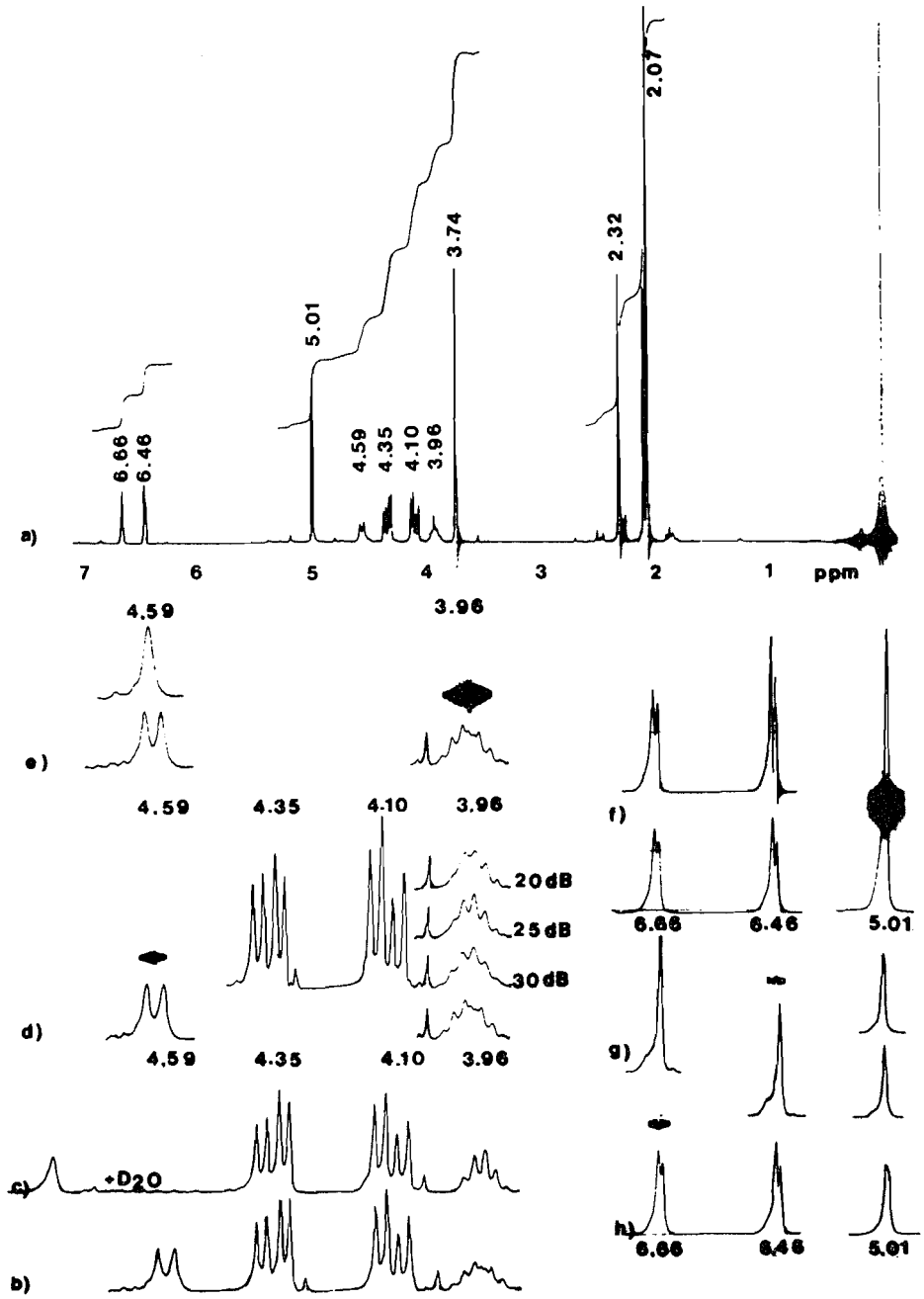

FIG. 2. Spectres de rmn ^1H à 250 MHz de l'acétate **2** ($CDCl_3$); agrandissements et découplages.

isochrones comme le sont également H_B et $H_{B'}$; chacun de ces couples étant dédoublé par H_M on comprend ainsi la présence de deux quadruplets.

Le troisième acétyle (2.10 ppm) dérive d'un autre CH_2OH résonant ici à *ca.* 5 ppm (figs 1 et 2) alors que dans le produit naturel son déplacement chimique se situe à 4 ppm (pyridine deutériée; avec D_2O ce CH_2OH se trouve plus blindé que le —OCH_3, fig. 3).

En fait d'autres modifications notables sur-

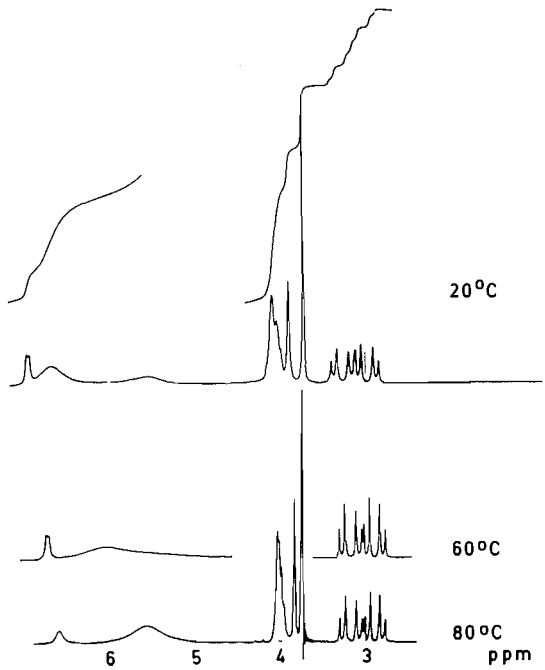

FIG. 3. Spectres de rmn ^1H à 250 MHz de la mycosporine **1** (pyridine) à différentes températures.

viennent par acétylation comme le montre à l'évidence la comparaison des spectres de rmn du produit naturel et des acétates.

Tout d'abord on note dans le produit naturel **1** la présence de deux C—CH_2—C formant chacun un système AB (double doublet) avec dans tous les cas une constante de couplage de 17 Hz (fig. 3).

Or ces quatre protons ($2CH_2$) disparaissent totalement dans les spectres de rmn des divers acétates préparés; corrélativement, deux protons éthyléniques résonant à 6.46 et 6.66 ppm ($CDCl_3$) apparaissent dans **2**. On montre aisément par irradiation (fig. 2*g* et *h*) que ces deux protons se trouvent couplés l'un à l'autre, en position *méta* (J = 2 Hz). De plus on constate (figs 1 et 2) la présence d'un quatrième acétyle, fortement déblindé (2.32 ppm, $CDCl_3$), correspondant à un acétate énolique ou phénolique (1770 cm^{-1}) tandis que disparaît le C=O, comme le montre le spectre de rmn du ^{13}C de **2**.

Ainsi donc l'acétylation provoque le fort déblindage d'un —CH_2OH, la disparition des deux C—CH_2—C, celle du C=O et la formation corrélative de deux protons éthyléniques et d'un —OAc. Par ailleurs le pic moléculaire du tétra-

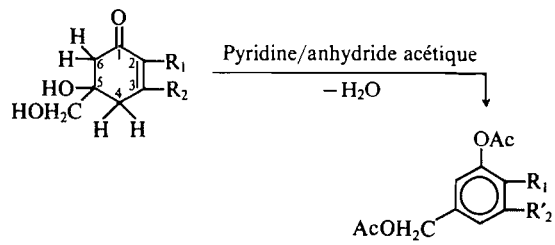

SCHÉMA 3

acétate **2** se situe à m/e 411 (au lieu de m/e attendu à 429): tous ces changements sont compatibles avec une aromatisation selon le schéma 3.

L'aromatisation résulte donc d'un double phénomène de déshydratation au niveau de l'OH tertiaire et d'énolisation. Cette dernière réaction met en jeu le CH_2 le plus déblindé de **1** dont les quatre signaux disparaissent par addition de NaOD (D_2O). Compte tenu de la présence du groupement isopropanediol, l'enchaînement proposé explique parfaitement la formation d'un dérivé tétra-triméthylsilylé (avec un —OTMS plus blindé que les trois autres) et celle d'un dérivé tétraacétylé (avec un acétate nettement plus déblindé que les trois autres). De tels mécanismes d'aromatisation ont déjà été mentionnés pour diverses molécules d'origine fongique: flavomannine (11), diméthyl-6,6′ flavomannine (12), asperflavine (13), tétrangomycine (14) etc.

La réduction de **2** provoque la formation du triacétate **3** (M à m/e 353). Le CH_2—OAc ainsi réduit (CH_3 à 2.26 ppm, CCl_4) se trouve porté par le C-5: on observe en effet (figs 2 et 4) les couplages du CH_2OAc dans **2** d'une part et de CH_3 dans **3** d'autre part avec les deux protons aromatiques (H-4 et H-6). Les expériences de découplage (figs 2*f–h* et 4) réalisées sur les H aromatiques comme sur CH_2OAc ou CH_3 confirment cet emplacement sans ambigüité. Ce carbone 5 porte également l'OH tertiaire silylable (et très facilement éliminé par déshydratation); il est asymétrique ce qui explique le pouvoir rotatoire de **1**.

Nous avons jusqu'ici rendu compte des 6 oxygènes et de 18 des 19 hydrogènes indiqués par la mesure de masse à haute résolution (1CO, $1CH_2OH$, $2CH_2$, $1CH_2OH—\underset{|}{CH}—CH_2OH$, $1OCH_3$, 1OH tertiaire); le dernier proton appartient à une amine secondaire exocyclique comme l'indiquent les spectres de rmn du produit naturel

Can. J. Chem. Downloaded from www.nrcresearchpress.com by 210.87.254.6 on 09/05/12
For personal use only.

Can. J. Chem. Downloaded from www.nrcresearchpress.com by 210.87.254.6 on 09/05/12
For personal use only.

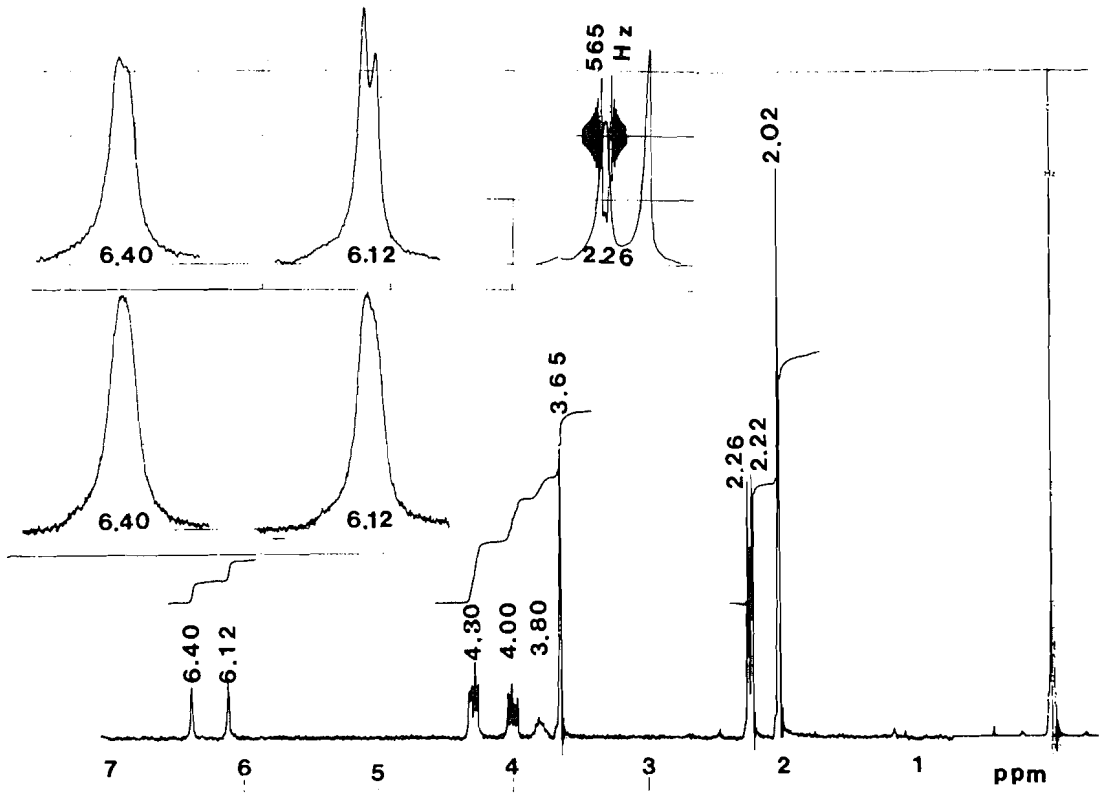

FIG. 4. Spectre de rmn ^{1}H à 250 MHz de l'acétate **3** (CCl_4); agrandissements et découplages.

(7.02 ppm, pyridine, fig. 3) et des acétates (*ca.* 4.5 ppm, figs 1 et 2).

Alors qu'en solution dans CCl_4 on n'observe qu'une bande large pour cet NH, l'utilisation de $CDCl_3$ fait apparaître un doublet dû à la liaison avec le CH du groupement isopropanediol comme le démontrent clairement les expériences de découplage (irradiations et échange avec D_2O) représentées sur la figure 2*a–e*: l'irradiation à 3.96 ppm (fig. 2*e*) provoque la disparition du doublet du *NH*, l'irradiation à 4.59 ppm, comme l'échange avec D_2O, entraînent l'affinement des raies du multiplet à 3.96 ppm. (On tend ainsi vers une figure identique au schéma théorique obtenu par ordinateur pour le seul couplage $-CH\langle^{CH_2-}_{CH_2-}$). Signalons ici que l'H du NH facilement échangeable par D_2O au niveau des acétates ne l'est pas du tout dans le produit naturel. Or il a été souvent constaté (Steglich, communication personnelle) que l'H d'un amide (cas de la mycosporine **1**, vinylogue d'amide), contrairement à celui d'une amine (cas des acétates) se révèle difficilement échangeable.

La présence des 11C est parfaitement démontrée en rmn de ^{13}C (tableau 1); quatre parmi ceux-ci ne portent aucun H: C-1 (C=O) et C-5 (porteur de CH_2OH et OH) déjà étudiés, auxquels il faut joindre 2C reliés entre eux par une double liaison et porteur en outre chacun d'un des deux substituants R_1 (OCH_3) et R_2 ($-NH-CH=(CH_2OH)_2$) dont il convient de préciser l'emplacement; à ces neuf carbones s'ajoutent les $2CH_2$.

Les dérivés **11** obtenus par condensation du dimédon **10** (15) avec des amines primaires, se caractérisent par une absorption uv au voisinage de 280 nm sous forme de pic unique (15, 16); ces vinylogues d'amide se singularisent en outre par des bandes d'absorption en ir à 3250 et 1610 cm^{-1} (15). Comme l'effet bathochrome résultant de la substitution d'un —H par $-OCH_3$ sur une double liaison conjuguée avec un C=O est sensiblement le même (30–35 nm) en α ou en β de ce carbonyle (17) il était difficile de lever par uv

Can. J. Chem. Downloaded from www.nrcresearchpress.com by 210.87.254.6 on 09/05/12
For personal use only.

l'indétermination concernant la position respective de R_1 et R_2. Le choix de la position 2 pour $-OCH_3$ résulte de l'étude par rmn du dérivé **8**, obtenu par l'intermédiaire des composés **5–7**, dans lequel l'acétate phénolique est remplacé par un méthyle. On observe *deux* signaux $-OCH_3$ et *deux* signaux (élargis) pour les protons aromatiques ce qui élimine l'hypothèse d'une structure symétrique **9** pour l'acétate et justifie bien la formule **1** proposée pour le produit naturel.

Signalons enfin que la résonance des CH_2 endocycliques diffère selon la nature du solvant utilisé: dans la pyridine on note un élargissement sensiblement égal de tous les signaux (bien visibles à 80 °C, fig. 3), alors que dans D_2O le proton le plus blindé de chaque CH_2 se trouve élargi par couplage à longue distance. Des expériences actuellement en cours doivent permettre de comprendre ces données et d'aborder ainsi la stéréochimie de la mycosporine, ce qui fera l'objet d'une note ultérieure.

Partie expérimentale

Nous avons décrit dans la note précédente (Arpin, Thivend et Favre-Bonvin, à paraître) les méthodes utilisées pour l'extraction et la purification de la mycosporine.

Mycosporine ***1***: uv λ_{max} (H_2O) 310 nm (ϵ 27 270); ir (KBr) 3340, 1610, 1540, 1450, 1400, 1265, 1185, 1120, 1075, 1040 et 980 cm^{-1}; sm *m/e* à 261 (1%), 243.1103 (20%, $C_{11}H_{17}NO_5$, calc. 243.1106), 212.0927 (100%, $C_{10}H_{14}NO_4$, calc. 212.0922), 194 (10%), 182 (4%); rmn (fig. 3) δ_{pyr} 20 °C 2.97 (d, 1H, J = 17 Hz), 3.18 (d, 1H, J = 17 Hz), 3.25 (d, 1H, J = 17 Hz), 3.46 (d, 1H, J = 17 Hz), 3.82 (s, 3H), 4 (s, 2H), 4.06–4.3 (m, 5H), 5.06 (large signal, 1H), 6.76 (large signal, 3H), 7.02 (d, 1H); rmn ^{13}C tableau 1, $[\alpha]_{365}^{20}$ −121.

Acétylation et silylation ont été conduites selon les techniques usuelles, en milieu pyridinique – anhydride acétique pour la première, HMDS et TMCS pour la seconde. L'acétate **2** a été hydrolysé par chauffage à l'ébullition pendant quelques minutes en présence d'HCl *N*. Les composés **2** et **7** ont été réduits en **3** et **8** respectivement par hydrogénation en présence de charbon palladié (à 10%) à la température ambiante et à la pression atmosphérique en solution éthanolique. Enfin la méthylation de **5** en **6** a été réalisée à l'aide du diazométhane dans le méthanol.

La pureté du produit naturel a été contrôlé par chromatographie sur couche mince de gel de silice et par chromatographie en phase gazeuse (sous forme de dérivé TMS sur une colonne de 3 m remplie de Gas Chrom Q 80–100 mesh imprégné à 4% d'OV-1). La purification des acétates sur colonne de gel de silice (solvant $CHCl_3$) a été suivie par CPG (colonne de 2 m remplie de Gas Chrom Q imprégné à 5% de SE 52). L'appareil utilisé était un Girdel 3000 équipé d'un détecteur à ionisation de flamme.

Les acétates de P 310 obtenus en quantités suffisantes sont des liquides à la température ambiante, à l'exception de l'acétate réduit, **3**, qui cristallise dans l'éthanol absolu sous forme d'aiguilles blanches.

Dérivé silylé ***4***: uv *cf.* **1**; sm (% de *m/e* 549) *m/e* à 549 (100%, M^+), 534 (24%), 531 (32%), 446 (50%), 420 (88%), 356 (10%), 338 (4%), 266 (3%), 248 (12%).

Acétate ***2***: uv λ_{max} (MeOH) 212, 252, 292 nm; ir (KBr) 3350, 2900, 1755,1745, 1605, 1590, 1515, 1450, 1360, 1220, 1125, 1040, 990, 960 et 885 cm^{-1}; sm (% de *m/e* 278) *m/e* à 411.1531 (63%, M^+, $C_{19}H_{25}NO_9$, calc. 411.1529, 369 (3%), 352 (5%), 338.1248 (25%, $C_{16}H_{20}NO_7$, calc. 338.1240), 310 (3%), 296 (15%), 278.1029 (100%, $C_{14}H_{16}NO_5$, calc. 278.1027), 254 (20%), 236 (33%), 218 (8%), 212 (44%), 204 (10%), 194 (12%), 170 (56%), 162 (15%); rmn (250 MHz, figs 1 et 2); δ_{CDCl_3} 2.07 (s, 6H), 2.10 (s, 3H), 2.32 (s, 3H), 3.74 (s, 3H), 3.96 (m, 1H), 4.10 (q, 2H, J_1 = 11.25 Hz, J_2 = 5 Hz), 4.35 (q, 2H, J_1 = 11.25 Hz, J_2 = 5 Hz), 4.59 (d, 1H), 5.01 (s, 2H), 6.46 (d, 1H, J = 2 Hz), 6.66 (d, 1H, J = 2 Hz); rmn ^{13}C tableau 1.

Acétate ***3***: uv *cf.* **2**; ir (KBr) 3350, 2900, 1775, 1740, 1605, 1590, 1500, 1450, 1370, 1250, 1225, 1200, 1115, 1090, 1030, 1020, 990, 885, 850, 810 et 780 cm^{-1}; sm (% de *m/e* 280) *m/e* à 353.1471 (80%, M^+, $C_{17}H_{23}NO_7$, calc. 353.1473), 296 (9%), 280.1184 (100%, $C_{14}H_{18}NO_5$, calc. 280.1184), 238.1092 (55%, $C_{12}H_{16}NO_4$, calc. 238.1079), 196 (22%), 178 (25%), 146 (32%); rmn (250 MHz, fig. 4) δ_{CCl_4} 2.02 (s, 6H), 2.22 (s, 3H), 2.26 (s, 3H), 3.65 (s, 3H), 3.8 (m, 1H), 4 (q, 2H), 4.3 (m, 3H), 6.12 (1H), 6.4 (1H). *Anal.* calc. pour $C_{17}H_{23}O_7N$: C 57.58, H 6.56, O 31.69, N 3.96; trouvé: C 57.54, H 6.79, O 31.47, N 3.90.

Méthyl acétate ***7***: rmn (100 MHz) δ_{CDCl_3} 2.03 (s, 6H), 2.07 (s, 3H), 3.52 (s, 3H), 3.75 (s, 3H), 3.97–4.41 (m, 5H), 4.5 (1H), 4.97 (s, 2H), 6.33 (1H), 6.40 (1H).

Méthyl acétate réduit ***8***: rmn (100 MHz) δ_{CDCl_3} 2.06 (s, 6H), 2.27 (s, 3H), 3.76 (s, 3H), 3.83 (s, 3H), 3.90–4.5 (m, 6H), 6.20 (1H), 6.26 (1H).

Les spectres de rmn de ^1H ont été enregistrés d'une part sur des appareils Cameca (250 MHz) à Paris et Marseille et sur un Varian HA-100 à Lyon, ceux de ^{13}C sur une Brüker HX-90E à Wissembourg. Les spectres de masse et les mesures en haute résolution ont été réalisées sur un appareil AEI MS-902 du Centre de Spectrométrie de Masse de Lyon.

Remerciements

Nous tenons à exprimer nos plus vifs remerciements à Mme Crepaux (Société Cameca Paris) et à Mlle Noailly (Fac. Pharmacie de Marseille) pour l'enregistrement des spectres de rmn à 250 MHz.

Nous remercions également M. les Docteurs Anker (I.N.S.A. de Lyon), Buchecher (Université de Trondheim), Chopin, (Université de Lyon), Steglich (Université de Berlin) et Thommen (Hoffmann – La Roche, Bâle) pour la lecture critique de ce manuscrit.

1. C. M. Leach. Can. J. Bot. **39**, 705 (1961); **40**, 151 (1962); **40**, 1577 (1962).

2. E. J. TRIONE et C. M. LEACH. Phytopathology, **59**, 1077 (1969).
3. C. M. LEACH. Can. J. Bot. **43**, 187 (1965).
4. G. VAN DEN ENDE et J. J. CORNELIS. Neth. J. Plant Pathol. **76**, 183 (1970).
5. B. DEHORTER. Thèse 3ème cycle, Université de Lille, 59650 Villeneuve d'Ascq., France. 1972.
6. R. E. HITE. Plant Dis. Rep. **57**, 760 (1973).
7. K. K. TAN et H. A. S. EPTON. Trans Br. Mycol. Soc. **63**, 157 (1974).
8. A. J. VARGHESE et S. Y. WANG. Science, **160**, 186 (1968).
9. D. S. LETHAM, J. S. SHANNON et I. R. C. MCDONALD. Tetrahedron, **23**, 479 (1967).
10. J. B. STOTHERS. Carbon 13 NMR spectroscopy. Academic Press, London. 1972.
11. J. ATHERTON, B. W. BYCROFT, J. C. ROBERTS, P. ROFFEY et M. E. WILCOX. J. Chem. Soc. C, 2560 (1968).
12. W. STEGLICH, E. TÖPFER-PETERSEN, W. REININGER, K. GLUCHOFF et N. ARPIN. Phytochem. **11**, 3299 (1972).
13. J. F. GROVE. J. Chem. Soc. Perkin Trans I, 2406 (1972).
14. M. P. KUNTSMANN et L. A. MITSCHER. J. Org. Chem. **31**, 2920 (1966).
15. B. HALPERN et L. B. JAMES. Aust. J. Chem. **17**, 1282 (1964).
16. P. CRABBE, B. HALPERN et E. SANTOS. Tetrahedron, **24**, 4299 (1968).
17. A. I. SCOTT. Interpretation of the ultraviolet spectra of natural products. *In* International series of monographs on organic chemistry. Vol 7. Pergamon Press. 1964. p. 58.

Can. J. Chem. Downloaded from www.nrcresearchpress.com by 210.87.254.6 on 09/05/12
For personal use only.

The effect of ultrasound on water in the presence of dissolved gases

ERIC L. MEAD, RONALD G. SUTHERLAND, AND RONALD E. VERRALL[1]

Department of Chemistry and Chemical Engineering, University of Saskatchewan, Saskatoon, Saskatchewan S7N 0W0

Received August 11, 1975

ERIC L. MEAD, RONALD G. SUTHERLAND, and RONALD E. VERRALL. Can. J. Chem. **54**, 1114 (1976).

Sonolysis of water at 447 kHz causes a decrease in the p*H*. The products formed depend to some extent on the nature of the dissolved gases; products observed are hydrogen peroxide, nitrous and nitric acid. The yield of hydrogen peroxide follows the order O_2 > air > Ar > N_2. In the case of total acid (nitrous and nitric) the yield follows the order air > N_2 > Ar > O_2. Nitrogen fixation occurs in the presence of Ar and O_2 because of the presence of small amounts of N_2 either as an impurity in the dissolved gases, or as residual air in the incompletely degassed water.

An attempt was made by using the Fricke dosimeter to obtain information on the relative chemical activity of cavitation.

ERIC L. MEAD, RONALD G. SUTHERLAND et RONALD E. VERRALL. Can. J. Chem. **54**, 1114 (1976).

La sonolyse de l'eau à 447 kHz produit une diminution du p*H*. Les produits formés dépendent, jusqu'à un certain point, de la nature des gas dissous; les produits observés sont le peroxyde d'hydrogène et les acides nitreux et nitrique. Le rendement en peroxide d'hydrogène suit l'ordre O_2 > air > Ar > N_2. Dans le cas de l'acide total (nitreux et nitriques), le rendement suit l'ordre air > N_2 > Ar > O_2. La fixation de l'azote se produit en présence d'Ar et d'O_2 à cause de la présence de faibles quantités de N_2 soit sous forme d'impureté dans les gas dissous ou sous forme d'air résiduel si l'eau n'a pas été complètement dégasée.

On a fait un essai pour utiliser le dosimètre de Fricke afin d'obtenir de l'information concernant l'activité chimique active de cavitation.

[Traduit par le journal]

Can. J. Chem. Downloaded from www.nrcresearchpress.com by 210.87.254.5 on 09/05/12
For personal use only.

Introduction

Chemical transformation can be effected both in pure liquids and solutions by an ultrasonic field. An ultrasonic wave passing through a ilquid medium can induce the phenomenon of "cavitation"; this occurs when rapidly alternating increases and decreases in the pressure overcome the liquid cohesive forces to form holes or cavities in the liquid (1, 2). These cavities are then filled by dissolved gases or by vapour from the liquid. Subsequent collapse of the bubbles produces large amplitude shock waves and large increases of local temperature. Electrical discharges are also believed to occur.

Chemical reactions may then be induced either in the cavity itself or via the high energy intermediates produced when the cavity collapses. The maximum pressure attainable under conditions of adiabatic collapse have been estimated to be *ca.* 1×10^5 atm with temperatures reaching 10^4 K (3–5). Thermolytic reactions are to be expected under these conditions in the vapour phase within the cavity. Other authors (6, 7) have suggested that reactions occurring in the cavity are aided by electrical discharges due to charge separation on the surface of the bubbles.

In aqueous solution there is evidence (8–11) that the lifetime of chemically active radicals produced by sonolysis is larger than the lifetime of the cavitation bubble and so these chemically active species which are formed in the vapour phase of the cavity (the temperature of a hot gas bubble will be greater than 2000 K) migrate and are available to trigger chemical reactions. It has also been shown (1, 12–14) that the presence of certain gases can alter the secondary reaction of these radicals. Reports of studies of cavitation-induced chemical reactions in pure organic liquids are few, but recent work by Diedrich *et al.* (15) indicates such reactions can readily occur in the case of several substituted benzenes.

The nature of the products obtained when water is insonated have been found to be dependent on the acoustical power (12, 13), design of the

[1]To whom all correspondence should be addressed.

Can. J. Chem. Downloaded from www.nrcresearchpress.com by 210.87.254.5 on 09/05/12
For personal use only.

insonation cell (12), temperature (16), external pressure (12), and on the nature of the dissolved gas (1, 12–14). Hydrogen peroxide is the major product, other minor products such as molecular hydrogen (12), ozone (17), and nitrous and nitric acids (13, 18, 19), have been reported. There is only one report (13) of an investigation of the variation of p*H*, as a function of insonation time, of water saturated with various gases. In view of our studies on the effect of sonolysis of heterocyclic bases in aqueous media and possible effects of minor products such as nitrous and nitric acid on our reactions it seemed necessary to reinvestigate the effect of ultrasound on water saturated with gases such as nitrogen, oxygen, and argon. As well it was thought that the results would be useful in shedding light on the mechanism of sono-chemical reactions of solutes in aqueous solutions.

Experimental

Irradiations were conducted with an ultrasonic generator (Macrosonics Multisons MC500-1) with a continuously variable output from 10 to 10^4 kHz at 0 to 500 W. The sound source was a cobalt barium titanate transducer, Model HFS-450, operating with maximum efficiency at 447 kHz with rated average power output of 50 W. The insonation vessel was similar in design and construction materials to that used by Spurlock and Reifsneider (14). The cell cap was fitted with two outlets and a demountable sampling tube which permitted aliquots of the solution to be examined as well as the addition and removal of gases to and from the reaction vessel. A plexiglass ring (1 cm high) was used to support and position the cell reproducibly over the transducer. It was fitted with a tube to force cooling water across the face of the cell. The temperature inside the cell was kept relatively constant by circulating the water effecting the sound coupling between the source and insonation vessel through a constant temperature bath (25 ± 0.2 °C). The temperature inside the cell was monitored by means of a potentiometer using a copper–constantan thermocouple with an ice-point reference. Temperatures were always recorded immediately after insonation to assure that values recorded were not affected by anomalous interaction between the thermocouple and the ultrasonic field.

The total acoustic power absorbed by the system during the insonation process is not an accurate measure of the energy available for chemical reactions since only a small fraction (20) of the total acoustic energy is used for the formation of free radicals. We employed the Fricke dosimeter in an attempt to gain some information on the relative chemical activity of cavitation or the rate at which available energy is deposited by cavitation. The change in optical density of the aerated dosimeter solutions was a linear function of the insonation time up to 6 min. However, at longer times the yields of Fe^{3+} deviated from linearity due to a degassing of the solution by the cavitation process. The latter was corroborated by the fact that saturating the solution with oxygen prior to insonation extended the linear yield of Fe^{3+} up to 8 min. The production of nitrous acid in the air-saturated water caused a time dependent oxidation of Fe^{2+} to Fe^{3+}. Quenching of the solution with sulfamic acid immediately after insonation reduced the error in the measurement of the Fe^{3+} yield.

The water used throughout this study was prepared from singly distilled water which was subsequently passed through a 12 in. column of activated charcoal (8–12 mesh), two Illco-way ion exchange resin columns, and a 30 in. column of Fisher analytic grade Amberlite MB-1 resin (Rexyn 300 H-OH). This water was then distilled from alkaline permanganate in an all glass still under pure nitrogen atmosphere. The p*H* of the water was normally between 6.5 and 7.0 with a specific conductivity less than 1.0×10^{-6} mhos at 25 °C. The water obtained was then transferred to a high vacuum all glass system and the water degassed in a large conical vessel in three or more successive freeze, evacuate, and thaw cycles. The lack of trapped gases gave rise to a virtually transparent solid phase of water. Aliquots (50 ml) of the degassed water were transferred under vacuum to the insonation cell and saturated *in situ* by bubbling the gas through the water for 10 min.

The p*H* of insonated solutions was measured by means of a glass electrode using a calomel electrode as reference. p*H* was recorded directly on a Beckman Expandomatic SS-2 p*H* meter. The p*H* measurement was carried out in a separate compartment connected to the insonation cell. The insonated solution was displaced into the p*H* measuring compartment by means of a positive pressure of the saturating gas. The design of the apparatus was such that the electrodes were always kept wet between p*H* determinations.

Canada Liquid Air gases were used in all experiments. They had the following specifications: argon contained <10 ppm O_2, <2 ppm H_2, <23 ppm N_2, <10 ppm H_2O, <0.5 ppm CO_2, and <0.5 ppm CH_4; nitrogen contained <20 ppm O_2, <10 ppm H_2O, and 80 ppm Ar; and oxygen contained <10 ppm H_2O, and 4990 ppm N_2 and Ar combined.

The rate of hydrogen peroxide formation was measured using a catalyzed colorimetric procedure (21). Two solutions (*A*: 1 g NaOH, 33 g KI, 0.1 g $(NH_4)_6Mo_7O_{24}.H_2O$ in 500 ml H_2O; *B*: 10 g potassium acid phthalate in 500 ml H_2O) were mixed 1:1 just prior to the determination, and subsequently mixed in a 1:1 ratio with a 5 ml aliquot of the insonated sample. The color intensity was measured at 350 nm in a 1 cm cell using a Beckman DB-G spectrophotometer.

Nitric acid was determined by cadmium–copper reduction to nitrite following the procedure of Wood *et al.* (22). Nitrous acid was determined by the same method with the following changes: the reduction step was eliminated and the sulphanilimide solution contained half the acid concentration of that used for the nitric acid determinations. Both tests were insensitive to the presence of hydrogen peroxide up to 0.5×10^{-3} mol l^{-1}.

The concentrations of H_2O_2, HNO_2, and HNO_3 for each insonation experiment were calculated directly from a calculation factor based on Beer's Law. These factors

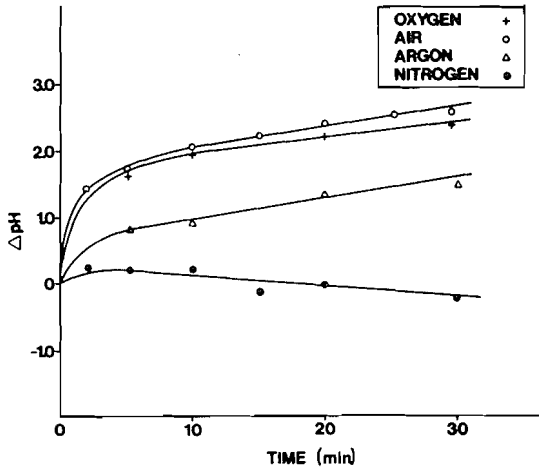

FIG. 1. Variation in the pH of distilled water with insonation time in the presence of various gases. ΔpH = pH(initial) − pH(final).

were obtained from freshly prepared standards analyzed spectrophotometrically and concurrently with the unknown samples. The concentrations of these standard solutions were chosen to cover the range of experimental concentrations obtained for each product. The root-mean-square deviation of the calculation factors are a measure of the precision of the analyses and were found to be ±0.50, ±0.37, and ±0.60% for H_2O_2, HNO_2, and HNO_3, respectively, based on 50 determinations of standards for each product.

The average deviations of the experimental results, based on at least three runs for each time interval in the presence of a particular saturating gas, were ±5.3, ±3.0, and ±4.1% for H_2O_2, HNO_2, and HNO_3, respectively. Blank analyses were carried out on all distilled degassed water samples prior to insonation. Only in the case of HNO_2 was a small residual of $<10^{-7}$ M found and it was subtracted from the results.

Results

Figure 1 shows the effect of ultrasonic irradiation of the pH of water saturated with a single gas or air. ΔpH = pH(initial) − pH(final) so that a positive ΔpH corresponds to a decrease in pH. Solution pH decreased in the presence of oxygen, argon, and air. Although scatter in the data is greatest in the case of nitrogen, it is apparent that after a small initial decrease in pH, it remains unchanged at longer insonation times.

The results of the influence of dissolved gases on the production of hydrogen peroxide in insonated water are shown in Fig. 2. Values of the initial slopes obtained from a least squares analysis of the data appear in Table 1. Figures 3 and 4 show the results of nitrous and nitric acid

TABLE 1. Rate studies of the formation of products from water by ultrasonic irradiation at 25 °C

	Initial rate of formation[a] (mol l^{-1} min^{-1})			
Product	Air	O_2	N_2	Ar
H_2O_2	2.1×10^{-5}	3.0×10^{-5}	4.1×10^{-7}	7.9×10^{-6}
HNO_2	2.2×10^{-5}	5.6×10^{-9}	1.5×10^{-6}	3.2×10^{-8}
HNO_3	6.0×10^{-6}	1.3×10^{-7}	4.3×10^{-7}	1.5×10^{-7}

[a]Estimated error ±20%.

formation, respectively, as a function of insonation time and values of the initial rate data are given in Table 1.

An attempt was made to obtain an estimate of the energy deposited during the cavitation process. Todd (23) has shown that a value of $U(Fe^{3+})_{O_2} = 3.9 \pm 0.1$, where U is defined as the number of molecules or radicals reacting per 100 eV of chemico-acoustic energy, may be applicable to cavitation. From the chemical dosimeter results and using this value of U, the chemico-acoustic energy absorbed was calculated to be 11 700 rad min^{-1} for the insonation conditions employed in this work. Todd, using a different type of generator and transducer, has reported a value of 9600 rad min^{-1} for the frequency range 250–1000 kHz.

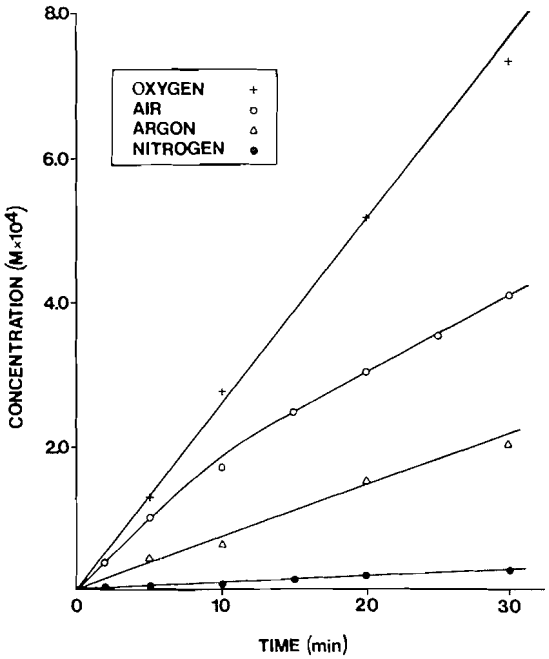

FIG. 2. Concentration of H_2O_2 produced as a function of insonation time.

Can. J. Chem. Downloaded from www.nrcresearchpress.com by 210.87.254.5 on 09/05/12
For personal use only.

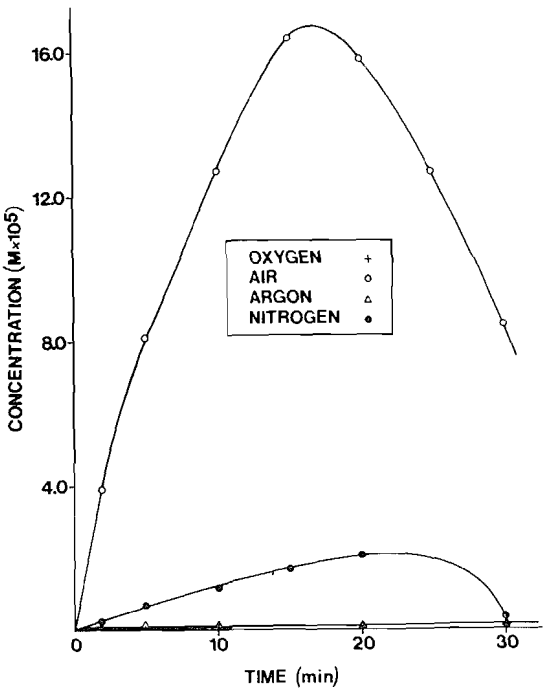

FIG. 3. Concentration of HNO_2 produced as a function of insonation time.

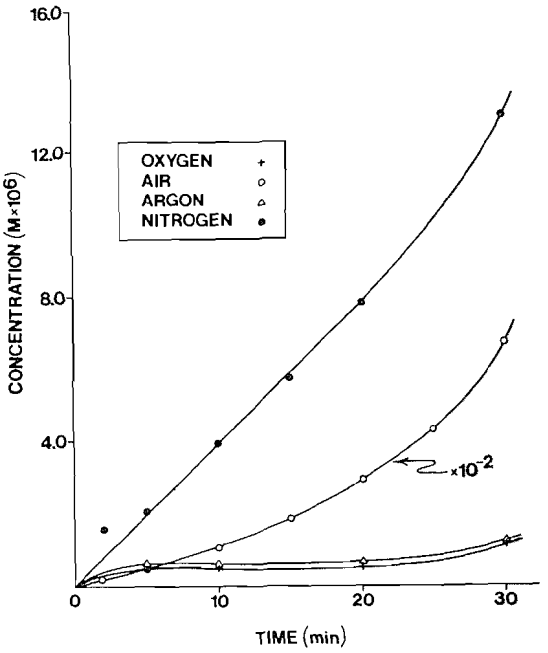

FIG. 4. Concentration of HNO_3 produced as a function of insonation time.

In a single experiment water saturated with hydrogen gas was insonated for 30 min. The following results were obtained: $\Delta pH = -0.15$; $[H_2O_2] = 2.6 \times 10^{-6}\ M$; $[HNO_2] = 1 \times 10^{-9}\ M$; and $[HNO_3] = 1.7 \times 10^{-7}\ M$. These product yields were smaller than in the case of other gases for a comparable period of insonation.

The fact that measurable concentrations of nitrous and nitric acid were observed in the case of experiments carried out in the supposed absence of N_2, *i.e.*, O_2, Ar, and H_2 saturated water, is evidence of either incompletely degassed water or residual nitrogen present in the gases used. The latter argument may be used in the case of oxygen (see Experimental section) but it cannot be advanced in the case of Ar. It seems probable that in the case of argon the difficulty lies in obtaining thoroughly degassed water. Nevertheless, the results in Table 1 show that at any given time shortly after the start of insonation, the total amount of nitrogen fixed as nitrous or nitric acid in solutions saturated with O_2 or Ar is *ca.* 0.1 and 6.4×10^{-3} times less than for solutions saturated with N_2 or air, respectively.

Discussion

Sonochemistry is a very complex process and the reactions proposed to account for the observed products in this work are conjectural in view of the somewhat simple experiments reported in this work.

The nature of the energy transported by the molecules entering the cavities, *i.e.*, either electrical or thermal, is not well understood. It appears, however, that dissolved gases admitted to the cavity (with water vapor) can react in primary and secondary reactions (20). The primary reaction is the formation of H and OH radicals (10, 11), reaction 1

[1] $$H_2O \rightarrow H + OH$$

It is also conceivable that atomic nitrogen and oxygen can be produced (reactions 2 and 3) at the high temperatures and pressures predicted to arise during the collapse of a cavity

[2] $$N_2 \rightarrow 2N$$

[3] $$O_2 \rightarrow 2O$$

Nitrogen fixation (24, 25) can occur in the cavity via reaction 4

[4] $$N + O \rightarrow NO$$

Can. J. Chem. Downloaded from www.nrcresearchpress.com by 210.87.254.5 on 09/05/12
For personal use only.

Can. J. Chem. Downloaded from www.nrcresearchpress.com by 210.87.254.5 on 09/05/12
For personal use only.

If the cavity collapse were to occur irreversibly because of heat transport processes, then temperature and pressure conditions would be lower than those predicted on the basis of a reversible process. Using a lower limit of 2000 K, thermodynamic calculations from data in ref. 26, and assuming the temperature independence of ΔH^0, show the magnitude of the estimated equilibrium constants for reactions 1 to 4 are still large enough to provide sufficient concentrations of intermediates.

Another primary mechanism has been suggested (20) in which inert gases penetrating into a cavity can contribute to the transfer of electron excitation energy to water molecules as shown in the following reactions.

$$[5] \qquad Ar \rightarrow Ar^*$$

$$[6] \qquad Ar^* + H_2O \rightarrow H_2O^* + Ar$$

$$[7] \qquad H_2O^* \rightarrow H + OH$$

where * refers to an excited molecule.

Other reactions that can occur either in the vapor phase or in the liquid phase also depend on the dissolved gas. For example, a gas such as O_2 can probably take part in radical transformation reactions, reaction 8

$$[8] \qquad H + O_2 \rightarrow HO_2$$

A brief rationalization of the observed results for the nitrogen containing acids and hydrogen peroxide follows.

Nitrous and Nitric Acid

Nitric oxide can be converted to nitrous acid in the gas phase by reaction 9

$$[9] \qquad OH + NO + M \rightarrow HNO_2 + M$$

Preliminary results (27) from rate constant studies of this reaction in the presence of argon as a "third body" give a value of $2.5\text{–}4.0 \times 10^{-31}$ $cm^6\ s^{-1}$ for the third order rate constant at 298 K. On the other hand, since reaction 9 relies on the prior formation of NO in the same cavitation, it is likely that the second order reaction of OH radicals with NO in the bulk of the solution may be the more predominant source of HNO_2.

The initial rate data, Table 1, shows that the rate of formation of total acid follows the order air > N_2 > Ar > O_2. Initially all solutions showed a decrease in pH with increasing insonation time which is to be expected on the basis of increased nitric acid production. However, the order in the decrease of pH with respect to the dissolved gas does not correlate with that for the acid production in the presence of these same gases. The initial rate data also show HNO_2 is the major acid component formed during the insonation of water saturated with air and nitrogen, whereas HNO_3 is the major acid product arising from insonation in the presence of oxygen and argon. The very small amounts of nitric oxide that are present in these latter solutions could be readily converted to NO_2 by means of atomic oxygen produced during cavitation (28). The NO_2 can be converted to nitric acid in a reaction scheme similar to reaction 9.

Nitrogen fixation in the absence of O_2, *i.e.*, in the presence of N and Ar, may take place subsequent to the formation of atomic nitrogen and hydroxyl radicals as follows:

$$[10] \qquad N + OH \rightarrow NOH$$

$$[11] \qquad NOH + OH \rightarrow NO + H_2O$$

$$[12] \qquad NOH + HO_2 \rightarrow NO + H_2O_2$$

Figures 3 and 4 show, for the case of air- and nitrogen-saturated water at insonation times greater than *ca.* 15–20 min, that the nitrous acid production goes through a maximum while the concentration of HNO_3 shows a greater increase. This could indicate that HNO_2 is scavenging the OH radicals and will also lead to a suppression of the formation of H_2O_2. The slight reduction in H_2O_2 formation with increasing insonation time (Fig. 2) seems to substantiate this argument.

It is not known to what degree the effect of the production of pernitrous acid, formed from the reaction of H_2O_2 and HNO_2 under acid conditions, may have on the concentrations of these products. The long time yields of nitric acid reported here are of the same order of magnitude as reported elsewhere (13). Data for insonation times less than 10 min were not previously reported (13).

Hydrogen Peroxide

The relative magnitude of the initial yields of H_2O_2, Fig. 2, in the presence of the various gases follows the order O_2 > air > Ar > N_2 in agreement with previously reported results (13, 14). The mechanism whereby H_2O_2 is produced sonolytically has been the subject of some controversy (9, 17). The use of hydroxyl radical scavengers to study the diminution of H_2O_2

produced has led to opposing views on whether the H_2O_2 is formed in the vaporous cavity or in the liquid phase. Evidence for the formation of the hydrated electron in an ultrasonic field has been presented by Margulis and Mal'tsev (29). As well, Lippitt *et al.* (30) have shown that hydroperoxyl radicals, HO_2, are produced during insonation of aqueous solutions.

The following series of reactions (31, 32) likely contribute to the formation of H_2O_2.

[13] $$OH + OH + M \rightarrow H_2O_2 + M$$

[14] $$O + H_2O + M \rightarrow H_2O_2 + M$$

[15] $$H + O_2 + M \rightarrow HO_2 + M$$

[16] $$OH + H_2O_2 \rightarrow HO_2 + H_2O$$

[17] $$HO_2 + HO_2 \rightarrow H_2O_2 + O_2$$

Reaction 13 will predominate in the absence of O_2 and of reducing agents. The small amount of hydrogen peroxide produced in the case of N_2-saturated water may arise because of a suppression of reaction 15 in the absence of O_2 and the scavenging effect of HNO_2.

It is conceivable that other pathways could be suggested which would account for the observed products. The results do raise several points, however. While the existence of oxidizing species in an ultrasonic field has been well documented, little has been done in the way of using this process for the oxidative treatment of organic compounds in waste water (33, 34). The low efficiency of the conversion sequence: electrical energy → acoustic energy → chemical effects precludes the use of this method as a primary treatment. However, it may have potential use on a synergetic basis in the conversion of low concentrations of pollutants (35). Finally, it would be of interest to determine whether there is indeed a preponderence of nitrite and nitrate ion concentrations, or, of bacteria that injest and convert these ions via metabolic pathways, in river systems downstream from spillways and hydroelectric generators. Water turbulence and hence the probability of the occurrence of cavitation will be greatest at these points.

Acknowledgement

The authors acknowledge support of this work from the Research Corporation and the National Research Council of Canada.

1. E. I. El'piner. Ultrasound: physical, chemical and biological effects. *Edited by* Consultants Bureau, New York, N.Y. 1964.
2. H. G. Flynn. *In* Physical acoustics. Vol. 1B. *Edited by* W. P. Mason. Academic, New York. 1964. pp. 57–172.
3. R. Rayleigh. Phil. Mag. **34**, 94 (1917).
4. B. E. Noltingk, E. A. Neppiras. Proc. Phys. Soc. London, Sect. B, **63**, 674 (1950); E. A. Neppiras and B. E. Noltingk. Proc. Phys. Soc. London, Sect. B, **64**, 1032 (1951).
5. M. E. Fitzgerald, V. Griffing, and J. Sullivan. J. Chem. Phys. **25**, 926 (1956).
6. Y. I. Frenkel. Zh. Fiz. Khim. **14**, 305 (1940).
7. M. Degrois and P. Baldo. Ultrasonics, **12**, 25 (1974).
8. M. Del Duca, E. Yeager, M. O. Davies, and F. H. Hovorka. J. Acoust. Soc. Am. **30**, 301 (1958).
9. A. Weissler. J. Am. Chem. Soc. **81**, 1077 (1959).
10. T. K. Saksena and W. L. Nyborg. J. Chem. Phys. **53**, 1722 (1970).
11. M. Anbar and I. Pecht. J. Phys. Chem. **68**, 1460 (1964).
12. M. Haïssinsky, R. Klein, and P. Rivayrand. J. Chem. Phys. **59**, 611 (1962).
13. H. Süss and H. Hanke. Pharm. Zentralhalle, **106**, 86 (1967).
14. L. A. Spurlock and S. B. Reifsneider. J. Am. Chem. Soc. **92**, 6112 (1970).
15. G. K. Diedrich, P. Kruus, and L. M. Rachlis. Can. J. Chem. **50**, 1743 (1972).
16. M. Haïssinsky and R. Klein. J. Chim. Phys. **65**, 326 (1968).
17. M. Anbar and I. Pecht. J. Phys. Chem. **68**, 352 (1964).
18. M. S. Levinson, G. S. Komolova, and F. A. Gurevich. Izvest. Sibir. Otdel. Akad. Nauk SSSR, **8**, 114 (1959).
19. M. S. Levinson and B. G. Kovrov. Izvest. Sibir. Otdel. Akad. Nauk SSSR, **12**, 67 (1960).
20. M. A. Margulis. Sov. Phys. Acoust. **15**, 135 (1969).
21. A. O. Allen, C. J. Hochanadel, J. A. Ghormley, and T. W. Davis. J. Phys. Chem. **56**, 575 (1952).
22. E. D. Wood, F. A. J. Armstrong, and F. A. Richards. J. Mar. Biol. Assoc. U.K. **47**, 23 (1967).
23. J. H. Todd. Ulstrasonics, **8**, 234 (1970).
24. A. Virtanen and N. Ellfolk. J. Am. Chem. Soc. **72**, 1046 (1950).
25. A. V. Sokol'skaya and I. E. El'piner. Sov. Phys. Acoust. **3**, 313 (1957).
26. Selected Values of Chemical Thermodynamic Properties, Circular of NBS No. 500. United States Government Printing Office, Washington, D.C. 1952.
27. J. G. Anderson and F. Kaufman. Chem. Phys. Lett., **16**, 375 (1972).
28. S. W. Benson. The foundations of chemical kinetics. McGraw-Hill, New York. 1960. Chapt. 12.
29. M. A. Margulis and A. N. Mal'tsev. Russ. J. Phys. Chem. **42**, 1412 (1968).
30. B. Lippitt, J. M. McCord, and I. Fridovich. J. Biol. Chem. **247**, 4688 (1972).
31. I. G. Draganic and Z. D. Draganic. The radiation chemistry of water. Academic Press Inc., New York. 1971.

Can. J. Chem. Downloaded from www.nrcresearchpress.com by 210.87.254.5 on 09/05/12
For personal use only.

32. R. S. DIXON. Radiat. Res. Rev. **2**, 237 (1970).
33. Y. Y. LUR'E, P. F. KANDZAS, and A. A. MONIKA. Chem. Abstr. **58**, 8423a (1963).
34. L. LLIBOUTY. Macrosonics corporation technical report. Part IV. Macrosonics Corp., Carternet, N.J. 1965.
35. G. V. SMITH. University of Illinois water resources center research report No. 36, Urbana, Illinois. 1970.

Can. J. Chem. Downloaded from www.nrcresearchpress.com by 210.87.254.5 on 09/05/12
For personal use only.

Urea – boron trihalide adducts. IV. Ionic–covalent equilibria in the tetramethylthiourea–BF_3 and tetramethylselenourea–BF_3 systems and the influence of $B_2F_7^-$ formation

J. Stephen Hartman,[1] Gary J. Schrobilgen, and Peter Stilbs
Department of Chemistry, Brock University, St. Catharines, Ontario L2S 3A1

Received July 29, 1975

J. Stephen Hartman, Gary J. Schrobilgen, and Peter Stilbs. Can. J. Chem. **54**, 1121 (1976).

Tetramethylthiourea and tetramethylselenourea form 1:1 BF_3 adducts which are partially converted to ionic structures (donor)$_2BF_2^+.BF_4^-$ in solution. The degree of ionization is small except at low temperatures when BF_3 is in excess; ionization is essentially complete at −90 °C when a sufficient excess of BF_3 is present. Formation of $B_2F_7^-$ from BF_4^- and BF_3 at low temperatures is responsible for this. Hence under these conditions the 1:1 adduct is replaced by (donor)$_2BF_2^+.B_2F_7^-$. The existence of ionic adducts is further confirmed by the identification of BF_3Cl^- and $BF_2Cl_2^-$ in the mixed-halogen system tetramethylthiourea–BF_3–BCl_3.

Methyl group nonequivalence in the proton spectrum below −70 °C indicates restricted rotation about the central C—N bonds of coordinated tetramethylthiourea.

J. Stephen Hartman, Gary J. Schrobilgen et Peter Stilbs. Can. J. Chem. **54**, 1121 (1976).

La tétraméthylthiourée et la tétraméthylsélénourée forment des complexes 1:1 avec BF_3; en solution, ces complexes se transforment partiellement en structures ioniques (donneur)$_2BF_2^+.BF_4^-$. Le degré d'ionisation est faible excepté à basse température quand le BF_3 est en excès; l'ionisation est complète à −90 °C quand un excès suffisant de BF_3 est présent. La formation de $B_2F_7^-$ à partir de BF_4^- et de BF_3 à basse température est responsable pour ce résultat. Donc dans ces conditions les complexes 1:1 est remplacé par (donneur)$_2BF_2^+.B_2F_7^-$. On confirme l'existence des complexes ioniques par l'identification de BF_3Cl^- et $BF_2Cl_2^-$ dans la système halogénés mixtes tétraméthylthiourée–BF_3–BCl_3.

Le fait que l'on observe la non-équivalence des groupes méthyles dans le spectre rmn à des températures plus basses que −70 °C indique qu'il y a empêchement à la rotation autour des liens centraux C—N de la tétraméthylthiourée coordonnée.

[Traduit par le journal]

Introduction

Our investigations of the 1:1 boron trifluoride adducts of tetramethylurea (TMU) and dialkylureas demonstrated that oxygen was the donor site (1, 2). We also found that under appropriate conditions redistribution to give ionic adducts (TMU)$_2BF_2^+.BX_4^-$ takes place (3). We now report extension of our studies to BF_3 adducts of tetramethylthiourea (TMTU) and tetramethylselenourea (TMSeU).

Boron trifluoride adducts of bases with the urea structure **1** are of interest for a number of reasons. The existence of more than one potential donor site allows the possibility of linkage isomerism. Although ureas donate from oxygen, in TMTU and TMSeU the doubly bonded donor atom is a "soft donor" (4), and BF_3, a "hard acceptor" (4), might interact more strongly with the hard nitrogen donor site. There is also the possibility of formation of adducts of other than 1:1 stoichiometry, as in the diprotonation of TMU in which oxygen and one of the nitrogens are donors (5). A further interesting feature is the unusual rearrangement from ionic to covalent adducts which was observed in the TMU–BF_3 system (3) and merited further investigation. Also if sulfur (selenium) is the donor in TMTU (TMSeU), restricted rotation is likely to be observed in the adducts, as in BF_3 and $SbCl_5$ adducts of alkylureas (2, 6). Restricted rotation has been observed in uncomplexed thio- and selenoureas having fewer alkyl substituents (7) but not in TMTU or TMSeU (8).

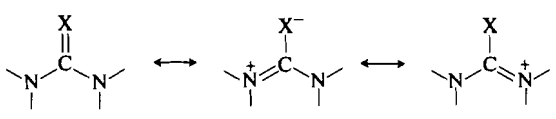

1a **1b** **1c**

A previous study by Greenwood and Robinson was not conclusive but was interpreted as indi-

[1]To whom correspondence should be addressed.

Can. J. Chem. Downloaded from www.nrcresearchpress.com by 210.87.254.40 on 09/05/12
For personal use only.

Can. J. Chem. Downloaded from www.nrcresearchpress.com by 210.87.254.40 on 09/05/12
For personal use only.

cating nitrogen donation in *N,N'*-dialkylthiourea – boron trihalide adducts (9). We now report firm evidence for sulfur donation and for the presence of a second adduct of other than 1:1 stoichiometry.

Experimental

Boron trifluoride, methylene chloride, and the nmr reference compounds were purified as described previously (1). Deuterochloroform (Merck, Sharp and Dohme) and dichlorofluoromethane (Matheson) were trap-to-trap distilled under high vacuum, the initial cut being rejected.

Commercial tetramethylthiourea (Aldrich) was found to contain significant quantities of bis(dimethylthiocarbonyl) sulfide and bis(dimethylthiocarbonyl) disulfide (verified by comparison of the mass spectrum and ^1H nmr spectrum with the spectra of commercial samples of the two impurities (Eastman)). Vacuum sublimation of tetramethylthiourea at room temperature onto a −78 °C cold finger removed these impurities and resulted in a white solid, mp 78.0–78.5 °C (lit. 78 °C).

Tetramethylselenourea was prepared according to Jensen *et al.* (10) by heating finely ground phosphorus pentaselenide (K & K Laboratories) with an excess of tetramethylurea in an evacuated sealed tube. The mixture was heated for one week at 70–80 °C and then transferred to a vacuum line where most of the excess tetramethylurea was removed by vacuum distillation at room temperature. The residue was stirred with hexane, previously dried and distilled over P_2O_5, and filtered. On recrystallization twice from hexane at −78 °C, very light pink crystals were obtained. The crystals were dried under vacuum for 1 h and then sublimed at 50 °C onto a Dry Ice – acetone cold finger. The resulting white solid, mp 78.5–79.0 °C (lit. (10) 78–79 °C), was stored in sealed ampoules under vacuum until used. All manipulations involving the selenourea were carried out in a dry oxygen-free atmosphere.

The nmr samples were prepared on a high-vacuum system by condensation of known amounts of BF_3 from a calibrated volume directly into 5 mm od precision Pyrex sample tubes containing a degassed solution of the base (approximately 1 *M*). The solvents used were methylene chloride, dichlorofluoromethane, and mixtures of the two, and the more recent samples contained deuterochloroform to provide a deuterium lock signal. Solvent variation caused negligible change in proton chemical shifts but addition of deuterochloroform caused changes of up to 1 ppm in some of the fluorine chemical shifts. After condensing in small quantities of TMS and $CFCl_3$ (and hexafluorobenzene in recent samples), the samples were sealed off under vacuum with the contents still at liquid nitrogen temperature, then allowed to warm to −78 °C or room temperature.

The CW nmr instrumentation has been described previously (1). Fourier transform spectra were obtained on a Bruker WP-60 multinuclear nmr spectrometer operating at 60 MHz (protons) and 56.4 MHz (fluorine-19). The transformed spectra contained 4K points. In signal averaging a sufficient delay (~10 s) was introduced between pulses to allow the spin system to return to thermal equilibrium and thus eliminate intensity distortions in the peaks.

Results

The most detailed studies were carried out on the TMTU–BF_3 adduct system. The TMSeU–BF_3 system is very similar. These systems differ from the TMU–BF_3 system (1, 3) in that the donor–acceptor bond lifetime is much shorter. Exchange of adduct with excess TMTU is rapid on the proton nmr time scale and even at −90 °C no free-TMTU peak could be detected at δ 3.01 when BF_3 was present. Very fast exchange between adduct and excess donor is typical of sulfur–donor and selenium–donor adducts with BF_3 (11–13).[2] The present systems also differ from the TMU–BF_3 system in that the adducts remain appreciably soluble in the presence of excess BF_3, allowing extension of the study to low-temperature excess-acid conditions where especially interesting results are obtained.

The TMTU–BF_3 System: ^1H Spectra

Room temperature proton spectra of TMTU–BF_3 solutions contained a single major peak having a chemical shift which varied almost linearly with the acid–base ratio up to 1:1 proportions, as shown in Fig. 1. At 1:1 acid–base proportions and in excess-BF_3 samples a new signal appeared at δ 3.30, just to low field of the main peak. Increasing the excess of BF_3 over TMTU increased the size of this new peak. In all excess-BF_3 solutions relative peak areas were highly dependent on temperature.

Figure 2 shows spectra of a typical excess-BF_3 solution. Between +7 and −40 °C the relative area of the low-field peak varies inversely with the absolute temperature (Fig. 3). Below −40 °C further broadening of the overlapping peaks made even an approximate measurement of relative areas impossible. By −70 °C the broad signal separated into two signals at δ 3.20 and δ 3.37 (Fig. 2). These had equal areas except in excess-TMTU samples as described below. The two signals apparently arise from an amide-type restricted rotation about the central C—N bond (14) in the adduct species. Although two adduct species are evidently present, as shown by spectra above −40 °C, only one pair of equal-area peaks is seen at −90 °C. There is sufficient peak broadening at −90 °C to prevent resolution of closely spaced peaks. The slow-exchange signal shape is

[2]J. S. Hartman and C. V. Raman, unpublished results.

Can. J. Chem. Downloaded from www.nrcresearchpress.com by 210.87.254.40 on 09/05/12
For personal use only.

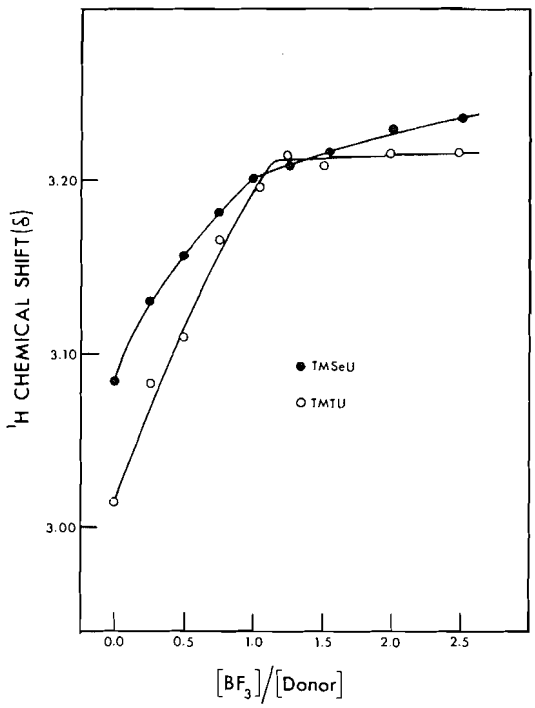

FIG. 1. Variation of the 37 °C chemical shift of the major (high-field) proton peak in TMTU–BF_3 and TMSeU–BF_3 solutions with the acid–base ratio.

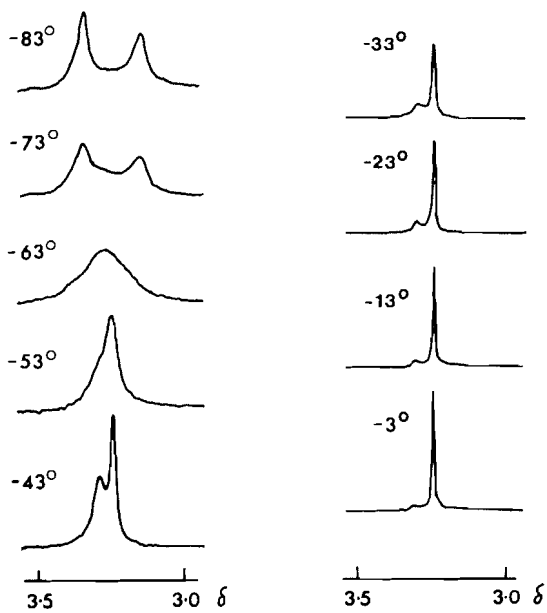

FIG. 2. 60 MHz proton spectra of a methylene chloride solution of TMTU and BF_3 in the molar ratio 1:2, at various temperatures.

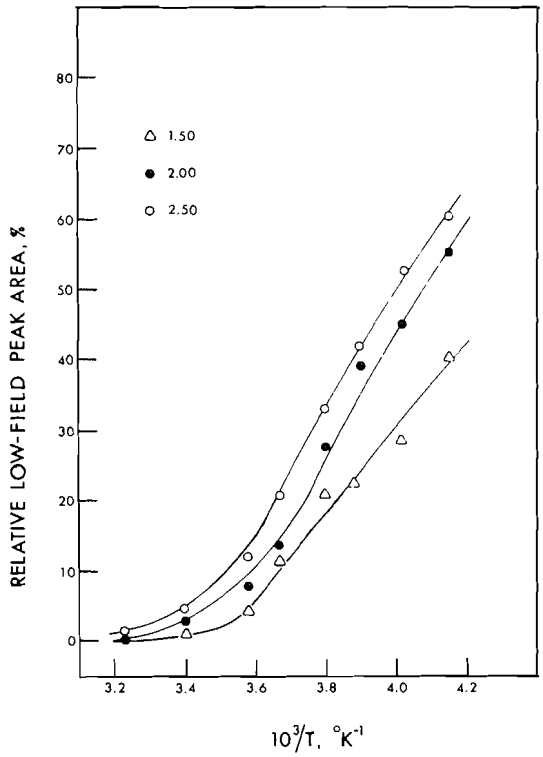

FIG. 3. Temperature-dependence of the relative areas of ^{1}H peaks in solutions having ratios of BF_3 to TMTU of 1.50:1, 2.00:1, and 2.50:1. The low-field peak area is given as a percentage of total peak area.

strikingly similar to previously reported TMU–$SbCl_5$ spectra (6).

When TMTU was in slight excess the −90 °C spectrum appeared to be a superposition of the two equal-area adduct peaks and an additional peak, *i.e.*, the higher-field peak was larger than the lower-field peak. Only a single −90 °C peak was observed when a greater excess of TMTU was present. This is in accord with rapid exchange between free and complexed TMTU and with C—N bond rotation occurring more rapidly when the molecule is not complexed.

The new adduct species which is favoured by excess BF_3 and low temperatures equilibrates with the 1:1 adduct in a few minutes at low temperatures. Thus rapid warming of a sample from −78 to −27 °C gave an initial −27 °C spectrum with an abnormally large peak of the new adduct species, but after 2 min the normal −27 °C relative peak areas were established. At this temperature the *cis–trans* interconversion in

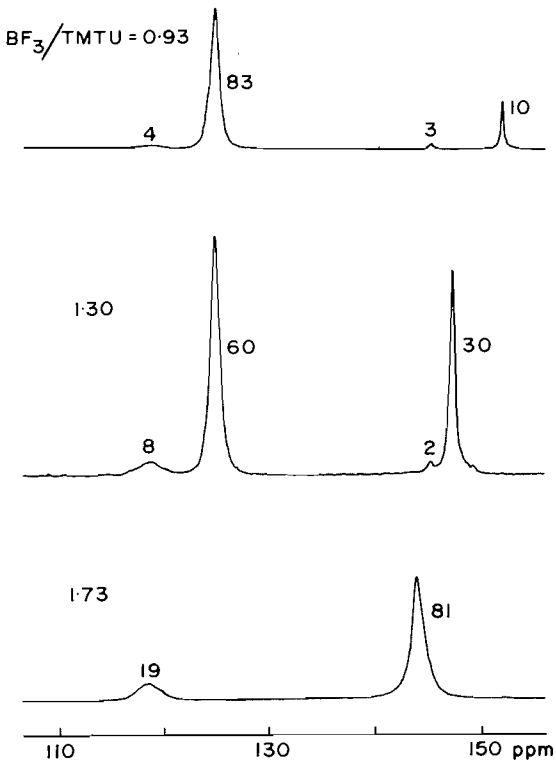

FIG. 4. ^{19}F spectra (−90 °C) of TMTU–BF_3 solutions showing changes with the BF_3/TMTU ratio. The total donor concentration is about 1 *M*. The numbers on the peaks are relative peak areas. The small peak at 145 ppm is due to an impurity. (FT spectra, 64 scans, 56.4 MHz).

the adduct is already rapid on the nmr time scale (lifetime $\ll 10^{-2}$ s), and thus the rates of the two processes observed differ by several orders of magnitude.

The TMTU–BF_3 System. ^{19}F Spectra

All of the samples gave only a single exchange-averaged ^{19}F peak at room temperature. Spectra at −90 °C were more informative. When the ratio of BF_3 to TMTU was 1:1 or less there was one major −90 °C peak at 126 ppm assigned to TMTU.BF_3 and also two much smaller peaks in an approximate 1:2 ratio at 119 and 152 ppm (Fig. 4*a*). The smaller broad peak at 119 ppm is assigned to $(TMTU)_2BF_2^+$. The sharper peak at 152 ppm is assigned to BF_4^-, and this assignment was confirmed by growth of this peak and the appearance of no new peaks on addition of *n*-$Bu_4N^+.BF_4^-$. A small impurity peak was present at 145 ppm in many samples, and tended to be larger in samples with a greater excess of donor.

As an excess of BF_3 was introduced the −90 °C spectra showed pronounced changes parallelling the ^1H spectral changes described above. As the proportion of excess BF_3 increased the TMTU.BF_3 peak diminished and finally disappeared when the BF_3:TMTU ratio increased past 1.5:1 (Fig. 4). At the same time the peak which in excess-base samples had been assigned to BF_4^- increased greatly in size and shifted to lower field, indicating chemical exchange between BF_4^- and a new species. Unlike BF_3 adduct systems of simpler donors (15), no free-BF_3 peak appeared in the 124 ppm region. The 119 ppm peak increased somewhat in relative size and its chemical shift remained constant. Coalescence of peaks at higher temperatures prevented studies over the temperature range covered in the proton spectra. The disappearance of the TMTU.BF_3 peak past 1.5:1 proportions indicates that the second adduct species has the stoichiometry 2TMTU.3BF_3.

Further support for our peak assignments comes from a comparison of ^{19}F spectra of the TMTU and TMSeU adduct systems. Figure 5 shows equivalent excess-BF_3 spectra in the two systems. In both systems the high-field peak has essentially the same chemical shift, indicating that the same species, not containing the donor molecule, is present in both systems. The major and minor low-field peaks are assigned to major and minor sulfur– and selenium–donor species as in Table 1. Each selenium–donor species absorbs 8–10 ppm to low field of the corresponding sulfur–donor species, in excellent agreement with a known pair of simple BF_3 adducts: $Me_2S.BF_3$, 139.3 ppm (11); $Me_2Se.BF_3$, 130.5 ppm.[2]

Additional correlations support our assignments. Thus

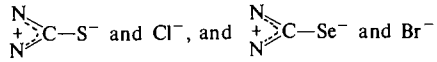

are pairs of isoelectronic donors, and the similarity of ^{19}F chemical shifts of (*i*) TMTU.BF_3 and BF_3Cl^- (124.6 ppm (16)) and (*ii*) TMSeU.BF_3 and BF_3Br^- (113.8 ppm (16)) is striking. Also the shift to low field of the $D_2BF_2^+$ ^{19}F resonance, compared to the D.BF_3 resonance, follows the regular trend 3.1, 6.0, 8.5 ppm in the series of donors TMU (3), TMTU, TMSeU.

Can. J. Chem. Downloaded from www.nrcresearchpress.com by 210.87.254.40 on 09/05/12
For personal use only.

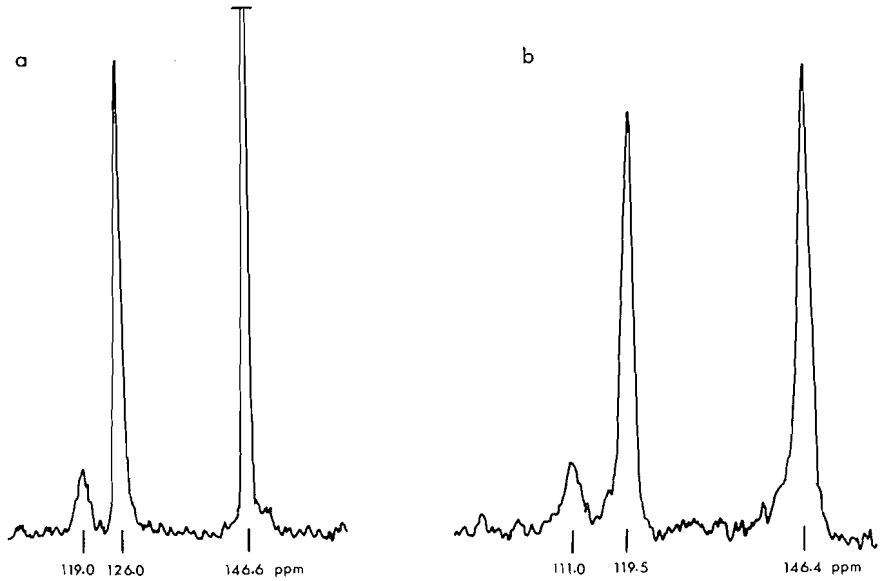

FIG. 5. ^{19}F spectra (−90 °C) of methylene chloride solutions of (*a*) TMTU and BF_3; (*b*) TMSeU and BF_3, in the mole ratio 1:1.25. (CW spectra, 56.4 MHz).

Although chemical exchange involving BF_4^- is rapid on the nmr time scale at −90 °C in excess-BF_3 samples, it becomes slow at extremely low temperatures. Spectra of dichlorofluoromethane solutions of TMTU (~0.3 *M*) and a small excess of BF_3, at temperatures down to −150 °C, showed that the highest-field −90 °C peak (~147 ppm) was an exchange-averaged peak. Below −90 °C this peak broadened and appeared to shift to higher field, and at −150 °C it was replaced by two peaks, still broad and partially overlapping, at 152.0 and 153.3 ppm. Clearly a further resonance must be present at lower field to give the weighted average in the 147 ppm region at −90 °C, but this was not resolved at −150 °C. We have recently shown that the ^{19}F spectrum of $B_2F_7^-$ at −155 °C consists of a doublet (151.4 ppm, J_{FBF} = 95 Hz) for the six terminal fluorines and a broad bridging-fluorine signal at 117 ppm, and that when BF_4^- as well as $B_2F_7^-$ is present the BF_4^- resonance occurs at 153.5 ppm at −150 °C in this solvent (17). Thus the high-field −150 °C ^{19}F peaks observed in the present work arise from $B_2F_7^-$ and BF_4^-; exchange is still too fast at −150 °C to allow resolution of the low-field bridging-fluorine peak or the doublet fine structure of the terminal-fluorine peak of $B_2F_7^-$. Thus $B_2F_7^-$ is formed in excess-BF_3 solutions of TMTU at low temperatures, and we can formulate the excess-BF_3-containing adduct as $(TMTU)_2BF_2^+.B_2F_7^-$.

TABLE 1. Nuclear magnetic resonance parameters

Species	Chemical shifts ^1H[a]	Chemical shifts ^{19}F[b]	$J_{^{11}B-^{19}F}$ (Hz)
TMTU	3.01		
TMTU.BF_3	3.20	126.0	
$(TMTU)_2BF_2^+$	3.30	119.0	
TMTU.BF_2Cl[c]		109.8	64
TMTU.$BFCl_2$[c]		101.7	88
TMTU.BCl_3	3.30		
BF_4^-		152.0[d]	1
BF_3Cl^-[e]		125.6	23
$BF_2Cl_2^-$[e]		105.1	56
$B_2F_7^-$ (terminal fluorine)		152.0[f]	
TMSeU	3.08		
TMSeU.BF_3	3.21	119.5	
$(TMSeU)_2BF_2^+$	3.32	111.0	

[a] 37 °C; methylene chloride solution; ppm to low field of internal TMS; ±0.01 ppm.
[b] −90 °C; methylene chloride solution unless otherwise specified; ±0.6 ppm; shifts are appreciably affected by the presence of $CDCl_3$.
[c] Tentative assignment.
[d] Chemical shift in $CHFCl_2$ is 153.3 ppm at −150 °C.
[e] Previous value (16): BF_3Cl^-, 124.6 ppm, J = 25.2 Hz; $BF_2Cl_2^-$, 104.1 ppm, J = 54.2 Hz.
[f] $CHFCl_2$ solution. Previous value 151.4 ppm (17).

The TMTU–BF_3–BCl_3 System

This was investigated briefly to provide further confirmation that TMTU forms ionic species.

Can. J. Chem. Downloaded from www.nrcresearchpress.com by 210.87.254.40 on 09/05/12
For personal use only.

Can. J. Chem. Downloaded from www.nrcresearchpress.com by 210.87.254.40 on 09/05/12
For personal use only.

Freshly prepared solutions of TMTU, BF_3, and BCl_3 in an approximate 1:0.4:0.4 molar ratio, which had not been heated above −70 °C, gave −90 °C ^{19}F signals at about 105, 110, and 126 ppm, and a large BF_4^- signal at 152 ppm. After brief warming to room temperature there was a marked decrease in the size of the BF_4^- peak, an increase in the size of the other peaks, and a new peak appeared at about 102 ppm. Spectra at −50 °C showed splittings due to ^{11}B–^{19}F coupling on some of the peaks and allowed identification of BF_3Cl^- and $BF_2Cl_2^-$ (16) by comparison with literature values (Table 1). The chemical shift of BF_3Cl^- is very similar to that of TMTU.BF_3 but the fine structure is characteristic of BF_3Cl^- and not of TMTU.BF_3.

The identification of these anions proves that TMTU forms cationic species. When equal amounts of fluorine and chlorine were present much of the fluorine appeared to be present in BF_4^- and BF_3Cl^-, suggesting that the neutral and cationic species are enriched in chlorine. The nonrandom distribution of fluorine and chlorine at equilibrium is not surprising in view of other studies of sulfur–donor adducts (11–13). The remaining ^{19}F peaks in the TMTU–BF_3–BCl_3 system are tentatively assigned to TMTU.BF_2Cl and TMTU.$BFCl_2$ as in Table 1, although $(TMTU)_2BFCl^+$ cannot be excluded at present. Above −40 °C all of the ^{19}F peaks coalesced.

The TMSeU–BF_3 System

This system is very similar to the TMTU–BF_3 system. Proton spectra show similar rapid exchange between excess donor and the 1:1 adduct, but the donor–acceptor bond is appreciably weaker in this case; the smooth curve without a break at 1:1 proportions in the plot of TMSeU chemical shift *vs.* acid–base ratio (Fig. 1) indicates considerable dissociation of the adduct at room temperature. Again a second small ^1H peak appears at lower field (δ 3.32) when BF_3 is in excess, and under excess BF_3 conditions the relative areas of the proton peaks show a similar dependence on the acid–base ratio and on temperature. However, the relative area of the low-field peak varies inversely with absolute temperature in a higher temperature range (+38 to −10 °C), and toward −40 °C the relative peak areas seem to be approaching a constant value. In excess-base samples the major ^{19}F peak (TMSeU.BF_3) appears at 118 ppm, with the smaller peaks appearing at 110 ppm ($(TMSeU)_2BF_2^+$) and 152 ppm (BF_4^-). An excess-acid ^{19}F spectrum is shown in Fig. 5.

Colour variations support the presence in solution of two different TMSeU-containing adduct species. Methylene chloride solutions of TMSeU were a very pale yellow colour. As BF_3 was added up to 1:1 proportions this colour deepened in intensity, but beyond 1:1 proportions it diminished again. In excess-TMSeU samples lowering the temperature caused little colour change. When excess BF_3 was present, however, the intensity of the colour decreased reversibly with decreasing temperature. When there was a large excess of BF_3 over TMSeU the solutions became colourless below −40 °C, indicating that essentially all of the TMSeU was incorporated into the colourless adduct. By analogy with the TMTU–BF_3 system the coloured species is TMSeU.BF_3 and the colourless species is $(TMSeU)_2BF_2^+$.

Discussion

All of the behaviour of the TMTU–BF_3 and TMSeU–BF_3 adduct systems can be explained in terms of the following reaction scheme, in which D represents TMTU or TMSeU:

[1] $$D + BF_3 \rightleftharpoons D.BF_3$$

[2] $$2D.BF_3 \rightleftharpoons D_2BF_2^+ + BF_4^-$$

[3] $$BF_4^- + BF_3 \rightleftharpoons \left[[F_3B\!-\!F\!-\!BF_3]\right]^-$$

Reaction 1 is well established in a wide range of BF_3 adducts. Reaction 2 has been established for TMU (3) and several lines of evidence presented above confirm it for TMTU and TMSeU. Reaction 3 has not previously been shown to affect a BF_3 adduct system; our attempts to confirm it in this work have led to the direct observation of $B_2F_7^-$ at extremely low temperatures (17). Reactions 2 and 3 together are the key to the unusual behaviour of the TMTU–BF_3 system. Equilibrium in reaction 2 lies well to the left. At −90 °C,

$$K = \frac{[D_2BF_2^+][BF_4^-]}{[D.BF_3]^2} \approx 6 \times 10^{-3}$$

as determined from integration of ^{19}F peak areas of an excess-TMTU solution. However at low temperatures when excess BF_3 is present, BF_4^- is

Can. J. Chem. Downloaded from www.nrcresearchpress.com by 210.87.254.40 on 09/05/12
For personal use only.

removed from the system according to reaction 3, and this forces reaction 2 to the right. Thus when there is a sufficient excess of BF_3 and a sufficiently low temperature the simple 1:1 adduct TMTU.BF_3 disappears.

The equilibrium in reaction 3 is very temperature-dependent. Dissociation of $B_2F_7^-$ occurs as the temperature increases (18), assisted by the pronounced decrease in solubility of BF_3 (Fig. 2 of ref. 18) and the resulting shift of BF_3 to the gas phase. Release of BF_4^- as dissociation proceeds shifts reaction 2 to the left, thus accounting for the pronounced and reversible temperature-dependence observed in the proton spectra of excess-BF_3 solutions of TMTU and TMSeU.

It is of interest that, given $B_2F_7^-$ formation, it is possible to form an excess-BF_3-containing adduct, yet have only one donor–acceptor linkage per donor molecule. $B_2F_7^-$ has previously been shown to stabilize an excess-BF_3-containing adduct in a special case involving fluoride abstraction from the Lewis base (19). Additional unstable BF_3-containing anions analogous to $B_2F_7^-$,

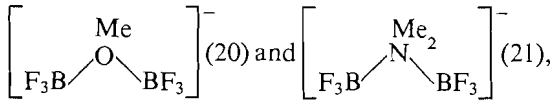

(20) and
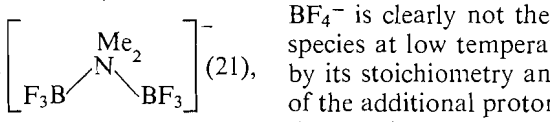

(21),

have been reported previously.

Of the following plausible excess-BF_3-containing adduct species, only **5** is consistent with our results. Nitrogen donation and the covalent

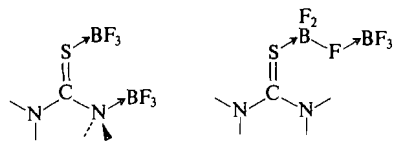

2 **3**

(*A*) Covalent structures (1:2 stoichiometry)

4 TMTU.BF_2^+.BF_4^- 1:2 stoichiometry
5 $(TMTU)_2BF_2^+.B_2F_7^-$ 2:3 stoichiometry
6 TMTU.$BF_2^+.B_2F_7^-$ 1:3 stoichiometry

(*B*) Ionic structures (sulfur donation)

structures **2** and **3** are excluded by a number of features of the ^1H and ^{19}F spectra as described above. A further confirmation of sulfur donation in the TMTU adducts is the similarity of the ^1H coalescence temperature for C—N bond rotation with that observed for the *S*-methyl cation of TMTU (22).

The absence of **2**, although diprotonation of thiourea and selenourea in very strong acids apparently gives structures analogous to **2** (5), may be a result of steric hindrance when BF_3 is the Lewis acid, or of the existence of the additional ($B_2F_7^-$) mode of association which is not possible in protonation. Structure **3** would be plausible on the basis of the existence of similar fluorine bridging in $B_2F_7^-$ (17) but its presence should not be dependent on a particular structure of donor molecule and could not explain why excess BF_3 is incorporated only when certain donors are involved.

The alternative ionic structures **4** and **6** require a trigonal boron cation, of which only one example seems to be firmly established (23). The existence of trigonal boron cations D.BF_2^+ along with the counterion BF_4^- was postulated by Gutmann and Imhof on the basis of room temperature conductivity and nmr studies of BF_3 adducts of phosphoryl compounds (24) but the evidence seems insufficient to confirm this. In our low-temperature work **4** is excluded since BF_4^- is clearly not the anion in the excess-BF_3 species at low temperatures. **6** is excluded both by its stoichiometry and by the nonobservation of the additional proton and fluorine resonances that would be expected from the trigonal-boron cation. We exclude the possibility of the D.BF_2^+ cation being the only cation (*i.e.*, reaction 4

[4] $$2D.BF_3 \rightleftharpoons D.BF_2^+ + BF_4^- + D$$

replacing reaction 2) on the basis of: (*i*) the stoichiometry of the $B_2F_7^-$ salt which would be 1:3 rather than 2:3; (*ii*) the absence of any appreciable dependence of the ionic–covalent equilibrium on the concentration of uncomplexed donor; (*iii*) the absence of the expected ^{19}F peak at much lower field (*cf.* BF_2Cl, 73.5 ppm (15)); and (*iv*) the rarity of trigonal-boron cations (23) as compared to tetrahedral-boron cations (25).

Although we exclude the trigonal-boron cation D.BF_2^+ under the conditions we have studied, this type of cation might well be important under other conditions, *i.e.*, (*i*) with stronger donors capable of π bonding to boron, or (*ii*) in the presence of a very large excess of BF_3, in which case two donor molecules would be less likely to remain coordinated to a single boron atom.

Complex boron cations including many of structure $D_2BH_2^+$ are well known (25), and a few

Can. J. Chem. Downloaded from www.nrcresearchpress.com by 210.87.254.40 on 09/05/12
For personal use only.

of structure $D_2BX_2^+$ (X = F, Cl) have been prepared (26). There have been reports of reactions analogous to reaction 2 with BCl_3 adducts (27). However, reaction 2 does not occur to any appreciable extent in the case of BF_3 adducts of simple donors such as $Me_2C{=}O$ or Me_2O (15), even under the "forcing conditions" that cause a complete conversion to ionic species in the TMTU–BF_3 system; instead, the BF_3 beyond 1:1 proportions remains uncomplexed (15). The tendency of bases with the urea type of structure to allow ionic as well as covalent BF_3 adducts to form seems to be a result of the especially favourable stabilization of positive charge through delocalization which is possible in these structures:

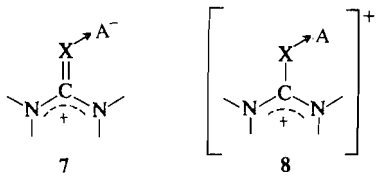

7 8

Thus the NCN unit stabilizes the positive charge on the donor at a site far removed from the donor atom, and this apparently allows a second donor molecule to become attached to the same boron atom without an unfavourable buildup of too much positive charge adjacent to boron. Other cases of spontaneous equilibration between covalent and ionic BF_3 adducts are to be expected where there is a similar delocalization of positive charge over the donor. In accord with this, we have found that hexamethylphosphoramide, where a similar charge delocalization is possible, also gives both covalent and ionic adducts, apparently according to reaction 2 (28); however, the system behaves very differently under excess-BF_3 conditions.

Unfortunately ionization of adducts leads to lowered solubility in nondonor solvents in most cases. The irregular solubility behaviour which has been noted in many studies of boron trihalide adducts may be a result of differing tendencies to form insoluble ionic adducts. Some cases in which initially-soluble adducts become insoluble on long standing would be consistent with a slow conversion of covalent to ionic structures. In the present work we are fortunate that the ionic species are sufficiently soluble.

We have attributed the splitting of the TMTU.BF_3 methyl resonance at low temperatures to restricted rotation about the central C—N bonds. The *S*-methyl cation of TMTU, unlike TMTU.BF_3, shows further splittings of the ^1H resonances at the lowest temperatures due to slowed *cis–trans* isomerization about the central C—S bond (22). (This complication was not observed by later workers, however (29).) Slowed *cis–trans* isomerization of BF_3 about the C—S bond is a possible alternative explanation of the splitting of the TMTU.BF_3 methyl resonance. However, there are strong grounds for discarding this alternative. (*i*) Restricted rotation about C—N bonds is well established in some uncomplexed thioureas (7), and the barrier to rotation is expected to increase substantially on complexation as the resonance forms **1***b* and **1***c* increase in importance (2). (*ii*) The absence of a separate free TMTU peak when excess TMTU is present indicates a rapid breaking and reforming of the donor–acceptor bond, as has been observed with other sulfur donors (11–13), and this reaction provides an additional mechanism whereby BF_3 could interchange rapidly between *cis* and *trans* positions. (*iii*) ^1H coalescence temperatures for *cis–trans* isomerization of BF_3 about C=O in ketone.BF_3 adducts can be as low as −120 °C (30), well outside the temperature range studied in the present work. Complexed thioureas, with large contributions from **1***b* and **1***c*, should have even lower barriers to *cis–trans* isomerization of BF_3 about the formally double-bonded sulfur than are observed about C=O in the ketone complexes.

Further work is in progress to determine the scope and limitations of these reactions.

Acknowledgements

We thank the National Research Council of Canada for financial support, Dr. J. M. Miller for helpful discussions, and the Department of Chemistry, McMaster University, for the use of CW ^{19}F nmr facilities.

1. J. S. Hartman and G. J. Schrobilgen. Can. J. Chem. **50**, 713 (1972).
2. J. S. Hartman and G. J. Schrobilgen. Can. J. Chem. **51**, 99 (1973).
3. J. S. Hartman and G. J. Schrobilgen. Inorg. Chem. **13**, 874 (1974).
4. R. G. Pearson. J. Chem. Educ. **45**, 581 (1968) and references cited therein.
5. G. A. Olah, A. M. White, and D. H. O'Brien. Chem. Rev. **70**, 561 (1970); Carbonium ions. Vol. 4. *Edited*

by G. A. Olah and P. von R. Schleyer. Wiley-Interscience, New York, 1973. Chapt. 31, especially pp. 1767–1770.
6. G. Olofsson, P. Stilbs, T. Drakenberg and S. Forsén, Tetrahedron, **27**, 4583 (1971).
7. R. H. Sullivan and E. Price. Org. Magn. Reson. **7**, 143 (1975); W. Walter, E. Schaumann, and H. Rose. Tetrahedron, **28**, 3233 (1972); M. L. Filleux-Blanchard and A. Durand-Couturier. Bull. Soc. Chim. Fr. 4710 (1972); A. M. Giuliani. J. Chem. Soc. Dalton Trans. 492 (1972); D. R. Eaton and K. Zaw. Can. J. Chem. **49**, 3315 (1971).
8. K. A. Jensen and J. Sandström. Acta Chem. Scand. **23**, 1911 (1969).
9. N. N. Greenwood and B. H. Robinson. J. Chem. Soc. A, 511 (1967).
10. K. A. Jensen, G. Felbert, and B. Kägi. Acta Chem. Scand. **20**, 281 (1966).
11. M. J. Bula and J. S. Hartman. J. Chem. Soc. Dalton Trans. 1047 (1973).
12. M. J. Bula, J. S. Hartman, and C. V. Raman. J. Chem. Soc. Dalton Trans. 725 (1974).
13. M. J. Bula, J. S. Hartman, and C. V. Raman. Can. J. Chem. **53**, 326 (1975).
14. W. E. Stewart and T. H. Siddall III. Chem. Rev. **70**, 517 (1970).
15. (*a*) R. J. Gillespie and J. S. Hartman. Can. J. Chem. **46**, 2147 (1968); (*b*) M. J. Bula, D. E. Hamilton, and J. S. Hartman. J. Chem. Soc. Dalton Trans. 1405 (1972).
16. J. S. Hartman and G. J. Schrobilgen. Inorg. Chem. **11**, 940 (1972).
17. J. S. Hartman and P. Stilbs. Chem. Commun. 566 (1975).
18. S. Brownstein and J. Paasivirta. Can. J. Chem. **43**, 1645 (1965).
19. S. Fleming, M. K. Lupton, and K. Jekot. Inorg. Chem. **11**, 2534 (1972).
20. D. F. Shriver and M. J. Biallas. J. Am. Chem. Soc. **89**, 1078 (1967).
21. R. J. Ronan, J. W. Gilje, and M. J. Biallas. J. Am. Chem. Soc. **93**, 6811 (1971).
22. H. Kessler and D. Liebfritz. Tetrahedron Lett. 427 (1969).
23. G. E. Ryschkewitsch and J. W. Wiggins. J. Am. Chem. Soc. **92**, 1790 (1970).
24. V. Gutmann and J. Imhof. Inorg. Chim. Acta, **4**, 171 (1970).
25. G. E. Ryschkewitsch. *In* Boron hydride chemistry. *Edited by* E. L. Muetterties. Academic Press, 1975. Chapt. 6; O. P. Shitov, S. L. Ioffe, V. A. Tartakovskii, and S. S. Novikov. Russ. Chem. Rev. **40**, 905 (1970); H. Nöth. Prog. Boron Chem. **3**, 211 (1970).
26. N. E. Miller and E. L. Muetterties. J. Am. Chem. Soc. **86**, 1033 (1964); N. Wiberg and J. W. Buchler. Chem. Ber. **96**, 3000 (1963).
27. C. D. Schmulbach and I. Y. Ahmed. Inorg. Chem. **11**, 228 (1972); V. Gutmann and J. Imhof. Monatsch. Chem. **101**, 1 (1970); N. N. Greenwood and K. Wade. J. Chem. Soc. 1130 (1960); J. R. Blackborow, M. N. S. Hill, and S. Kumar. J. Chem. Soc. Dalton Trans. 411 (1974).
28. J. S. Hartman and P. Stilbs. To be published.
29. P. Hansen and D. A. R. Williams. J. Chem. Soc. Perkin Trans. II, 2162 (1973).
30. V. Henriksson and S. Forsén. Chem. Commun. 1229 (1970).

Can. J. Chem. Downloaded from www.nrcresearchpress.com by 210.87.254.40 on 09/05/12
For personal use only.

Urea – boron trihalide adducts. V.[1] Effects of acid strength on restricted rotation in adducts of tetramethylurea and 1,1-bis(dimethylamino)ethylene

J. Stephen Hartman[2] and Ronald R. Yetman
Department of Chemistry, Brock University, St. Catharines, Ontario L2S 3A1

Received September 4, 1975

J. Stephen Hartman and Ronald R. Yetman. Can. J. Chem. **54**, 1130 (1976).

Boron trihalide adducts of tetramethylurea (**1**) and of 1,1-bis(dimethylamino)ethylene (**2**) show similar complexation shifts and restricted rotation about the central C—N bonds. Rotation becomes more hindered as the Lewis acid strength increases in the series $BF_3 < BCl_3 < BBr_3$. A large high-field complexation shift of the CH_2 protons of **2** corresponds to loss of the olefinic structure on formation of the BF_3 adduct.

J. Stephen Hartman et Ronald R. Yetman. Can. J. Chem. **54**, 1130 (1976)

Les complexes des trihalogénures de bore avec la tétraméthylurée (**1**) et le bis(diméthylamino-1,1)éthylène (**2**) présentent des déplacements de complexation et des rotations empêchées autour du lien central C—N qui sont semblables. La rotation devient plus empêchée à mesure que la force de l'acide de Lewis augmente dans la série $BF_3 < BCl_3 < BBr_3$. Il y a un fort déplacement de complexation vers les hauts champs pour les protons CH_2 de **2**; ceci correspond à une perte de la structure oléfinique lors de la formation de l'adduit avec BF_3.

[Traduit par le journal]

Introduction

Although proton spectra of tetramethylurea (TMU, **1**) or its BF_3 adduct show no evidence of restricted rotation about the central C—N bonds down to −100 °C (2), restricted rotation has been detected in the TMU.$SbCl_5$ adduct (3) and in dialkylurea–BF_3 adducts (4). This confirms that oxygen is the donor site. We now report ^1H nmr studies of restricted rotation in the heavier boron trihalide adducts of TMU and in the oxygen-replaced analogue of TMU, 1,1-bis-(dimethylamino)ethylene (**2**). The adducts of **2** show some additional interesting features.

Results and Discussion

Room temperature proton chemical shifts of **1** and **2** and their adducts are given in Table 1. In both series of adducts the *N*-methyl resonance shows the expected complexation shift to low field, which becomes larger as the Lewis acid strength increases in the order $BF_3 < BCl_3 < BBr_3 < BI_3$ (5). Changes in chemical shifts along the series of adducts of both bases are very similar (Fig. 1). They are however much less than those of the corresponding Me_3N adducts (5), also shown in Fig. 1, and this is apparently a result of the greater charge delocalization that is

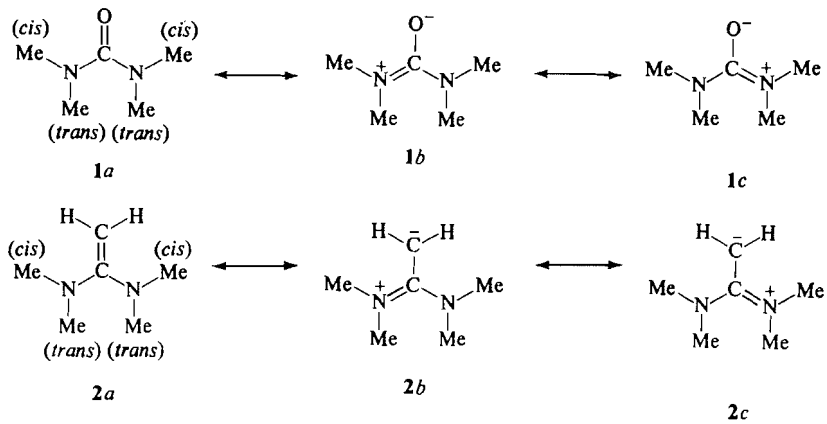

[1]For Part IV, see ref. 1.
[2]To whom all correspondence should be addressed.

Can. J. Chem. Downloaded from www.nrcresearchpress.com by 210.87.254.105 on 09/05/12
For personal use only.

Can. J. Chem. Downloaded from www.nrcresearchpress.com by 210.87.254.105 on 09/05/12
For personal use only.

TABLE 1. Proton chemical shifts of adducts[a]

Adduct with	TMU (*N*-Methyl)	1,1-Bis(dimethylamino)ethylene *N*-Methyl	1,1-Bis(dimethylamino)ethylene CH_2
[b]	2.75	2.54	3.15
BF_3	3.02	3.12	2.00[c]
BCl_3	3.18	3.23	2.75[c]
BBr_3	3.22	3.28	3.21[c]
BI_3[d]	3.26	3.33	3.67[c]

[a]In ppm to low field of internal tetramethylsilane; 35 °C.
[b]Uncomplexed tetramethylurea and 1,1-bis(dimethylamino)ethylene.
[c]Broad resonance; sharpened by ^{11}B decoupling; singlets for BCl_3, BBr_3, and BI_3 adducts, but a complex multiplet for the BF_3 adduct.
[d]The BI_3 adduct of 1,1-bis(dimethylamino)ethylene decomposes rapidly in the absence of excess BI_3.

possible in the adducts of **1** and **2**, as well as of diminished base strength.[3]

^1H spectra of the BCl_3, BBr_3, and BI_3 adducts of both **1** and **2** show evidence of restricted rotation about the central C—N bonds as summarized in Table 2. Except for TMU.BI_3, the *N*-methyl peak splits into two peaks of equal area at low temperatures. The coalescence temperatures are unaffected by the presence of excess base but show a pronounced drop in the presence of excess boron trihalide, as observed previously

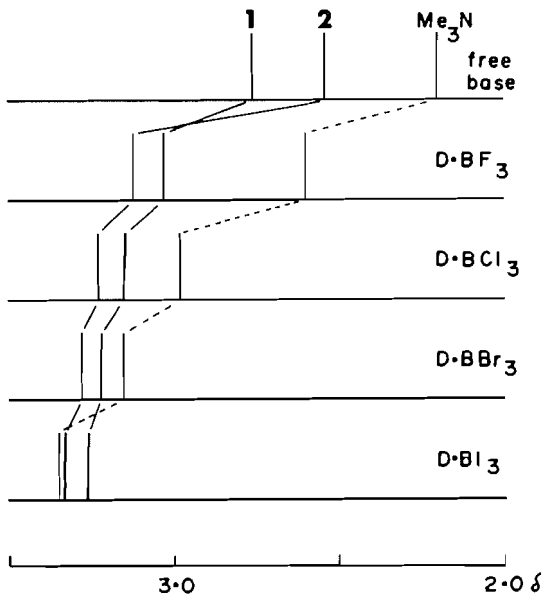

FIG. 1. Trends in boron trihalide complexation shifts of *N*-methyl protons of tetramethylurea (**1**), 1,1-bis-(dimethylamino)ethylene (**2**), and trimethylamine.

[3]Displacement studies show that the order of base strength is TMU < **2** < Me_3N.

TABLE 2. *N*-Methyl peak coalescence in adducts of tetramethylurea (**1**) and 1,1-Bis(dimethylamino)ethylene (**2**)

Compound	Relative chemical shift of *N*-methyl peaks at −90 °C (ppm)	Coalescence temperature (°C)
1.BF_3	[a]	—
1.BCl_3	0.05	−61
1.BBr_3	0.04	−56
1.BI_3	[b]	—
1.$SbCl_5$[c]	0.11	−46
2.BF_3	[a]	—
2.BCl_3	0.12	−45
2.BBr_3	0.11	−43
2.BI_3	0.06	−73

[a]No broadening or separation into two peaks down to −100 °C.
[b]Broadened at low temperatures but no separation into two peaks.
[c]Reference 3.

with TMU.$SbCl_5$ (3). With TMU.BI_3 only a broadening of the *N*-methyl peak was observed at low temperatures, and this may be due to a very small chemical shift difference between the two peaks. Neither free **1** or **2** or their BF_3 adducts showed any evidence of slowed rotation about the central C—N bonds down to −100 °C. The observation of restricted rotation in TMU.BCl_3 and TMU.BBr_3 confirms oxygen donation in these adducts, and the similar behaviour of the adducts of **2** indicates that the CH_2 carbon is the donor site:

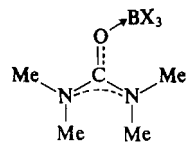

3

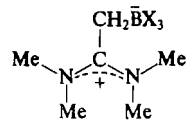

4

The enhancement of the barrier to rotation in ureas on complexation is attributed to the increased contribution of the mesomeric forms **1***b* and **1***c* in the adducts (4), and a similar enhancement of mesomeric forms **2***b* and **2***c* should occur in complexes of **2**. Donation by carbon rather than nitrogen can be interpreted as vinylogous nitrogen donation, and the same interpretation can be applied to oxygen donation in ureas.

There is an anomalously large *N*-methyl complexation shift between **2** and its BF_3 adduct (0.58 ppm, compared with 0.28 ppm for TMU and 0.40 ppm for Me_3N). A discontinuity between **2** and its adducts appears much more strikingly in the CH_2 complexation shifts (Fig. 2) and confirms that **2** undergoes a pronounced

Can. J. Chem. Downloaded from www.nrcresearchpress.com by 210.87.254.105 on 09/05/12
For personal use only.

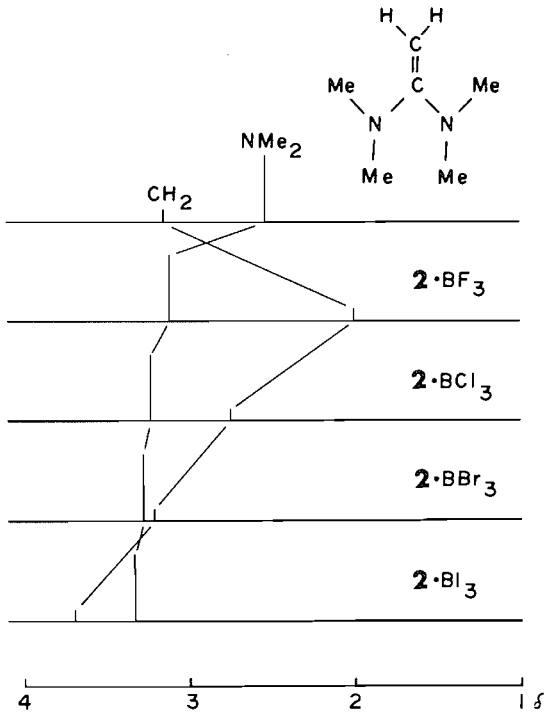

FIG. 2. Trends in proton complexation shifts of adducts of 1,1-bis(dimethylamino)ethylene.

structural change on adduct formation. The contributions of 2*b* and 2*c* in the free base are minor but apparently not negligible since the CH_2 protons (δ 3.15) absorb to high field of the usual olefinic range (δ 3.6–5.5). It is well established that mesomeric forms analogous to 2*b* and 2*c* are important in polarized ethylenes (6). Structure 2*a*, unlike 1*a*, must become negligible in the adducts since it cannot function as a σ donor from the CH_2 carbon, and thus the parent compound for the adducts can be considered to be the hypothetical zwitterion $2b \leftrightarrow 2c$. The CH_2^- resonance of the zwitterion would occur at very high field, and the apparent anomaly in complexation shifts disappears when the system is considered in this way.

Thus the complexation shifts of **2** are consistent with the CH_2 carbon being the donor and undergoing a change of hybridization (sp^2 to sp^3) on complexation. The large changes in CH_2 chemical shift as the Lewis acid strength increases from BF_3 to BI_3 (Fig. 2) are expected for protons directly attached to the donor site. Further confirmation of CH_2 donation comes from a pronounced broadening of the CH_2 resonance in the adducts, and its sharpening again on ^{11}B decoupling. This indicates a large coupling to ^{11}B, and hence proximity to boron. In contrast the *N*-methyl resonances were not appreciably broader in the adducts than in free **2** and were unaffected by ^{11}B decoupling.

Enediamines such as **2** readily undergo addition β to nitrogen (7). Compound **2** itself is a reasonably strong base, protonating on the CH_2 carbon to give the tetramethylacetamidinium ion **5** (8). Complexation to the boron trihalides

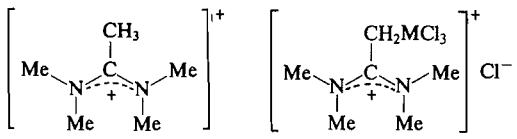

5 **6**

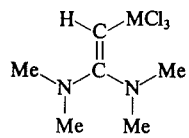

7

is directly analogous. In a study of the reaction of **2** with MCl_4 (M = Si, Ge, Sn), Weingarten and Wager formulated the initial product as the immonium salt **6** (9). We exclude this in the boron trihalide adducts because of (*i*) the similarities in chemical shifts between corresponding adducts of **1** and **2** (Fig. 1) and (*ii*) the ^{19}F spectrum of the BF_3 adduct (single peak, 146.5 ppm; $TMU.BF_3$, 149.2 ppm (2)) which shows no evidence of a fluorine being removed.

Adducts of **2** are subject to further reactions which have no analogy in the TMU adducts. Thus, **6** is reported to react to give organometallic enediamines **7** by loss of HCl (9). There is nmr evidence for formation of a second species from the boron trihalide adducts as well, in the presence of uncomplexed **2**, by loss of a proton from **4**:

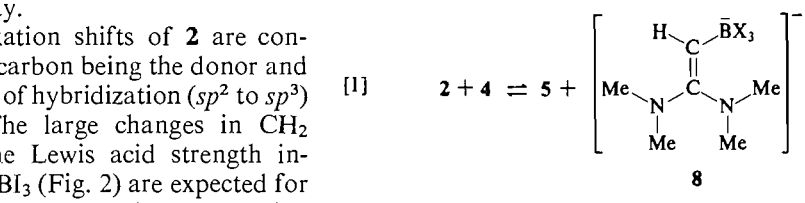

[1] **2** + **4** ⇌ **5** + **8**

Evidence for **8** (X = F) is provided by ^{19}F spectra of solutions of the BF_3 adduct. On standing a

Can. J. Chem. Downloaded from www.nrcresearchpress.com by 210.87.254.105 on 09/05/12
For personal use only.

second ^{19}F resonance (1:1:1:1 quartet, 137.1 ppm, $J_{^{11}B-^{19}F}$ 51.7 Hz) increases in size. This has nmr parameters very similar to those of the (vinyl)BF_3^- anion (138 ppm, J 51.8 Hz (10)) and very different from those of (vinyl)BF_2 (88.6 ppm, J 67 Hz (11)), indicating that the new species is **8** (X = F) rather than a neutral species analogous to **7**. Proton nmr is consistent with reaction 1. Thus with all boron trihalide adducts of **2** the peaks due to **5** increase in size on allowing the samples to stand at room temperature, and an additional small broad proton resonance, apparently arising from the olefinic proton of **8**, sharpens on ^{11}B decoupling.

A further complication, to be expected by the analogy with urea adducts, is an equilibration between ionic and covalent adducts (1, 12).

[2] $$2(\text{donor}).BX_3 \rightleftharpoons (\text{donor})_2BX_2^+ + BX_4^-$$

Small additional peaks in some samples of adducts of **2** indicate that such a reaction does occur to a small extent. Thus adducts of **2** show a number of analogies to adducts of tetramethylurea, in addition to showing unique features due to the presence of protons on the donor site and their activation by complex formation.

Ureas coordinate to metal ions as well as to the boron trihalides. The similarity in coordination behaviour of **1** and **2** in the present work suggests that enediamines might also form analogous metal complexes in a wide range of systems. If so, the presence of both ^1H and ^{13}C nmr labels at the donor site would make such complexes especially suitable for nmr studies. Investigations of this possibility are in progress.

Experimental

The methods of nmr sample preparation and the purification of the boron trihalides and methylene chloride have been described previously (13). Tetramethylurea (Aldrich) was used without further purification. 1,1-Bis-(dimethylamino)ethylene (**2**) was synthesized by the method of Brederick and co-workers (14). The mass spectrum included a parent ion peak at m/e 114 and a base peak at m/e 70. The proton nmr spectrum consisted of two singlets of relative intensity 6:1 at δ 2.54 and δ 3.15 respectively; these chemical shifts showed negligible variation with temperature (~0.06 ppm between −90 °C and +80 °C). Protonation of **2** occurs readily to give **5** (8) having two proton resonances of relative intensity 4:1 at δ 3.33 and δ 2.55; the larger (*N*-methyl) resonance was barely resolved into a 1:3:3:1 quartet by long-range coupling (0.37 Hz) to the *C*-methyl protons. Small peaks corresponding to **5** were often present in proton spectra of adducts of **2**.

Both **1** and **2** give adducts of 1:1 stoichiometry with the boron trihalides, as shown by relative areas of ^1H peaks due to free base and adduct in samples having a wide range of acid–base ratios. As with TMU.BF_3 (2), separate peaks due to free and complexed base are observable to room temperature. The adducts of **2** show evidence of further reactions, as discussed elsewhere in this paper. The BI_3 adducts of both **1** and **2** were much less soluble and also more prone to decomposition than the other adducts; these were prepared and studied directly in nmr tubes at low temperatures without ever being warmed to room temperature. All of the adducts appear to be more stable in the presence of excess boron trihalide.

The BF_3, BCl_3, and BBr_3 adducts of **2** could be prepared as viscous oils on a high vacuum system by condensing excess boron trihalide on top of a solution of 1 g of **2** in 5 ml of methylene chloride, and allowing the mixture to warm and react. The solvent and excess boron trihalide were then removed by pumping under high vacuum. However, as in previous work with TMU.BF_3 (12), nmr spectra indicated that the adducts were not pure, but that a further reaction had occurred to a small extent, apparently to give small amounts of ionic adducts (12) and small amounts of **5**. Mass spectra of the adducts did not give parent ion peaks. Instead, all of the peaks of uncomplexed **2** were obtained as well as peaks corresponding to BX_2^+, $C_2H_5NBX_2^+$, and to loss of HX and HX + CH_4 from the adducts.

The nmr instrumentation has been described previously (2). ^{11}B decoupling of ^1H spectra was carried out on a Varian Associates A-60 nmr spectrometer (2) equipped with an NMR Specialties HD-60 heteronuclear decoupler. An HP 4204A decade oscillator was used to drive at 30 Hz a Waveteck 141 Voltage Controlled Generator used to tune the HD-60 side bands, thus providing pseudo "noise" decoupling over a 3 kHz bandwidth.

Acknowledgements

We thank the National Research Council of Canada for financial support of this work and for the award of a scholarship (to R.R.Y.). Thanks are also due to Dr. J. M. Miller for help with the ^{11}B decoupling experiments and to Drs. P. Bickart and M. S. Gibson for helpful discussions.

1. J. S. Hartman, G. J. Schrobilgen, and P. Stilbs. Can. J. Chem. This issue.
2. J. S. Hartman and G. J. Schrobilgen. Can. J. Chem. **50**, 713 (1972).
3. G. Olofsson, P. Stilbs, T. Drakenberg, and S. Forsén. Tetrahedron, **27**, 4583 (1971).
4. J. S. Hartman and G. J. Schrobilgen. Can. J. Chem. **51**, 99 (1973).
5. B. Benton-Jones, M. E. A. Davidson, J. S. Hartman, J. J. Klassen, and J. M. Miller. J. Chem. Soc. Dalton, 2603 (1972).
6. J. Sandström. Endeavour, **33**, 111 (1974); I. Wennerbeck and J. Sandström. Org. Magn. Reson. **4**, 783 (1972); H-O. Kalinowski, H. Kessler, and A. Walter. Tetrahedron, **30**, 1137 (1974); R. F. Hobson and L. W. Reeves. J. Phys. Chem. **77**, 419 (1973).

7. A. G. COOK. Enamines. Synthesis, structures and reactions. Marcel Dekker, New York. 1969.
8. J. D. WILSON, C. F. HOBBS, and H. WEINGARTEN. J. Org. Chem. **35**, 1542 (1970).
9. H. WEINGARTEN and J. S. WAGER. Synth. Inorg. Met. Org. Chem. **1**, 123 (1971).
10. S. L. STAFFORD. Can. J. Chem. **41**, 806 (1963).
11. T. D. COYLE and F. G. A. STONE. J. Am. Chem. Soc. **82**, 6223 (1960).
12. J. S. HARTMAN and G. J. SCHROBILGEN. Inorg. Chem. **13**, 874 (1974).
13. M. J. BULA, D. E. HAMILTON, and J. S. HARTMAN. J. Chem. Soc. Dalton, 1405 (1972).
14. H. BREDERICK, F. EFFENBERGER, and H. P. BEYERLIN. Chem. Ber. **97**, 3081 (1964).

Can. J. Chem. Downloaded from www.nrcresearchpress.com by 210.87.254.105 on 09/05/12
For personal use only.

^{1}H nuclear magnetic resonance conformational study of medium-sized rings: 3,4-dihydro-1,6-benzodiazocine-2,5-diones

JOSÉ ELGUERO, ALAIN FRUCHIER, GEORGES LLOUQUET, AND CLAUDE MARZIN

Laboratoire de synthèse et d'étude physicochimique d'hétérocycles azotés, Université des Sciences et Techniques du Languedoc, 34060 Montpellier Cédex, France

Received October 1, 1975

JOSÉ ELGUERO, ALAIN FRUCHIER, GEORGES LLOUQUET, and CLAUDE MARZIN. Can. J. Chem. **54**, 1135 (1976).

From a ^{1}H nmr study it has been possible to show that the eight-membered ring of the *N,N'*-disubstituted 3,4-dihydro-1,6-benzodiazocine-2,5-diones has a boat conformation, the interconversion barrier of which is slightly over 100 kJ/mol.

JOSÉ ELGUERO, ALAIN FRUCHIER, GEORGES LLOUQUET et CLAUDE MARZIN. Can. J. Chem. **54**, 1135 (1976).

Une étude rmn protonique nous a permis de déterminer que le cycle à huit chaînons des dihydro-3,4 benzodiazocine-1,6 diones-2,5 *N,N'*-disubstituées possède une conformation bateau dont la barrière d'interconversion est légèrement supérieure à 100 kJ/mol.

Introduction

Lately the boat conformation of *N,N'*-disubstituted dibenzo[*b,f*][1,4]diazocine-6,11-diones and dibenzo[*b,f*][1,5]diazocine-6,12-diones has been demonstrated (1, 2). We have found that the 3,4-dihydro-1,6-benzodiazocine-2,5-diones **1***b* and **2***b* also have a boat conformation.

1*a* $R_1 = R_3 = R_6 = H$
1*b* $R_3 = H$, $R_1 = R_6 = CH_3$
1*c* $R_3 = R_6 = H$, $R_1 = CH_3$
2*a* $R_1 = R_6 = H$, $R_3 = CH_3$
2*b* $R_1 = R_3 = R_6 = CH_3$

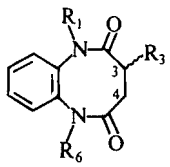

Experimental

Preparation of 3,4-Dihydro-1,6-benzodiazocine-2,5-dione, 1a

The procedure of Paudler and Zeiler (16) has been modified. Condensation of *o*-phenylenediamine and diethyl succinate in the presence of NaH was performed in anhydrous THF at room temperature; mp 264 °C (DMF) (lit. (16) mp 264–265 °C) (40%).

Preparation of 3-Methyl-4-hydro-1,6-benzodiazocine-2,5-dione, 2a

This compound has been obtained by refluxing *o*-phenylenediamine with an excess (1:3) of 2-methyl dimethyl succinate in DMF in the presence of NaH for 2 h; mp 205 °C (ethanol) (45%).

Preparation of Compounds 1b, 2b, and 1c

Methylation reactions of **1***a* and **2***a* were carried out with dimethyl sulfate in the presence of 20% NaOH at room temperature for 2 h; **1***b*, mp 218 °C (ethanol) (lit. (17) mp 218 °C) (10%); **2***b*, mp 176 °C (ethanol) (35%). Monomethylation of compound **1***a* has been performed using a great excess of diester at room temperature, the reaction being stopped after 5 min; mp 230 °C (ethanol) (10%).

Results and Discussion

The proton spectrum of **1***b* in $CDCl_3$ at 30 °C exhibits only one signal for the two *N*-methyl groups, an AA'BB' system for the aromatic protons and another AA'BB' system for the protons in positions 3 and 4. The low frequency AA' part of the latter system is slightly broadened and becomes sharper by irradiation of the *N*-methyl group signal. This interaction, ^5J, too small to be measured, shows that the protons A and A' are fixed to two different carbons. The fact that the nmr spectrum of the ethanic protons appears as an AA'BB' system and not as an A_4 or ABCD one shows that the ring inversion is slow on the nmr time scale at room temperature and that the ethanic fragment has an eclipsed or a staggered conformation. Librational motions around the C_3—C_4 bond having a low activation energy do not remove the isochrony of the A–A' and B–B' pairs. Four conformations can correspond to these observations (Fig. 1): two of C_s symmetry, boat *B* and chair *C*, and two of C_2 symmetry, staggered twist *Ts* and eclipsed twist *Te*.

The analysis of the AA'BB' system is not evident because of the apparent lack of transitions in the spectra at 60, 100, as well as 220

Can. J. Chem. Downloaded from www.nrcresearchpress.com by 210.87.254.105 on 09/05/12
For personal use only.

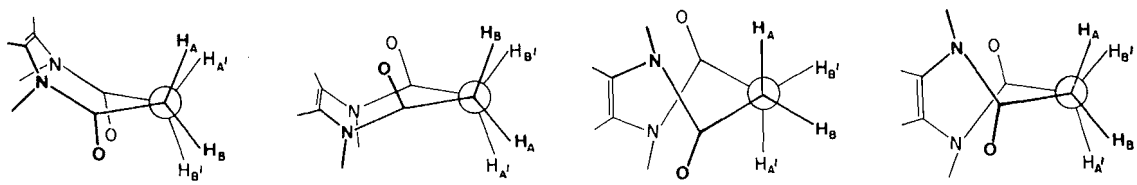

Boat *B* Chair *C* Staggered twist *Ts* Eclipsed twist *Te*

FIG. 1. Possible conformations of 3,4-dihydro-1,6-benzodiazocine-2,5-diones.

TABLE 1. Calculated and experimental ratios of vicinal coupling constants for the conformations of Fig. 1

Conformation	φ^a	$\Delta\varphi^b$	$J_{AA'}/J_{BB'}$	$J_{AA'}/J_{AB'}$ or $J_{BB'}/J_{A'B}$
B, C	0°	0°	1.0	3.7
Ts	180°	0°	5.4	5.4
Te	120°	0°	1.0	0.3
			Experimental	
			1.0	2.4[c]
			Calculated (6)	
	0°	23°	1.0	2.4

[a]Dihedral angle between the H_A–C_3–C_4 and C_3–C_4–H'_A planes.
[b]Libration angle.
[c]Mean value between $J_{AA'}$ and $J_{BB'}$: 11.9 Hz.

MHz:[1] each half spectrum has only 9 transitions instead of 12. Two reasons are accountable for that. Firstly, one experimental line is due to two overlapping theoretical transitions. This was observed when we varied $\Delta\delta_{AB}$ by working at different concentrations and by adding a lanthanide chelate ($Eu(fod)_3$) which complexes on the amidic oxygen (3, 4) to the $CDCl_3$ solution. Secondly, the antisymmetric AB subspectrum has a very small splitting indicating that the parameter $M = J_{AA'} - J_{BB'}$ is close to zero. Then trial parameters can be obtained and successive iterations give a spectrum which is superimposable on the experimental one at 100 MHz. The parameters obtained with LAOCN 3 (5) have been used to simulate spectra at 60 and 220 MHz and at different concentrations, and the agreement with the experimental values is very good. In $CDCl_3$ with a concentration of 60 mg/ml, the values are: $\delta_A = 2.26$ ppm, $\delta_B = 2.60$ ppm, $J_{AB} = J_{A'B'} = -13.9$ Hz, $J_{AB'} = J_{A'B} = 5.0$ Hz, $J_{AA'} = 12.1$ Hz and $J_{BB'} = 11.7$ Hz.

To determine the conformation of medium-sized rings, it is better to use the ratio of vicinal coupling constants than the constants themselves (6). Listed in Table 1 are calculated values of these ratios for the conformations *B*, *C*, *Ts*, and *Te*, together with the experimental ones. It is obvious that only the conformations *B* and *C* agree with the experiment. The method we described (6) allows one to calculate the libration dihedral angle $\Delta\varphi$. The value found, 23°, is probably, as in the case of 2-pyrazolines, overestimated.

In order to choose between these possibilities, we have calculated the effects of the benzene ring[2] and of the carbonyl group[3] on the chemical shifts of the protons in positions 3 and 4 in these two conformations. The calculated differences of chemical shifts between protons A and B are as follows: chair *C* 0.32 ppm, boat *B* 0.29 ppm.

[1]We thank the Canadian 220 MHz NMR Centre for the 220 MHz nmr spectrum.

[2]For the protons above the benzene ring we have used the dipolar model of Johnson and Bovey (7) and for the other ones the quantic model of Haigh and Mallion (8).

[3]The anisotropy of the carbonyl groups has been calculated from a dipolar model (9, 10), the dipole center being taken on the oxygen atom. The values of $\Delta\chi$ have been taken from ref. 11. The molecular coordinates have been calculated using a program from Schachtschneider (12).

Can. J. Chem. Downloaded from www.nrcresearchpress.com by 210.87.254.105 on 09/05/12
For personal use only.

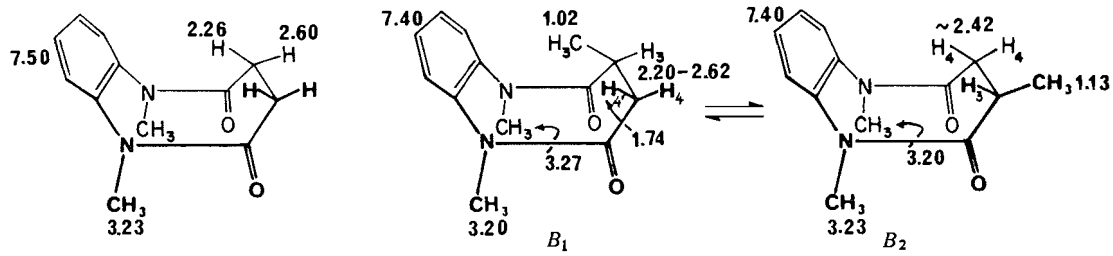

1*b* 2*b*

As the experimental difference is 0.30 to 0.34 ppm depending on the concentration, these calculations do not allow a choice between a chair or a boat conformation. But the presence of a small coupling constant between the *anti* periplanar protons of the *N*-methyl groups and two protons in 3 and 4 positions shows that the amidic parts of the diazocinedione ring are planar (13, 14). This is the case only in the boat conformation in which the two protons A and A′ above the benzene ring appear at lower frequencies than the two other ones.

The nmr spectrum of compound **2***b* shows the presence of an equilibrium between two conformations at ambient temperature in $CDCl_3$. From the result found for **1***b*, these two conformations must be B_1 and B_2. The protons in positions 3 and 4 appear as a complex system: only the proton H'_4 of B_1 appears at a lower frequency because of the effect of the benzene ring and of the *cis* methyl group (15).[4] Thus B_1 is the kinetic product of the methylation reaction (about 70%); but this equilibrium is displaced with time and temperature so that when thermodynamic equilibrium is reached, B_1 exists only at 20%. The existence of such a direct equilibration shows that the free energy of activation for the boat–boat equilibrium is above 96 kJ/mol. But if the spectrum of compound **2***b* is taken in α-chloronaphthalene at temperatures above 180 °C, the three *N*-methyl group signals coalesce (the two expected *N*-methyl signals have an accidental isochrony) and the *C*-methyl signals and those of protons in positions 3 and 4 are broadened; unfortunately, it has not been possible to obtain spectra above 200 °C. But the observation of this phenomenon shows that the boat–boat interconversion becomes fast above 180 °C and that the free activation energy must have a value between 100 and 105 kJ/mol. In the case of compound **1***b*, the same behaviour is observed: the AA′BB′ system of the protons in positions 3 and 4 is broadened in α-chloronaphthalene above 180 °C. Thus the free activation energy for the interconversion can be estimated to be over 100 kJ/mol.

For compound **1***c*, the spectrum taken in α-chloronaphthalene shows a broadening of the ABCD system of protons in positions 3 and 4 above 120 °C. A complete analysis could not be performed because the compound decomposes above 140 °C. However it can be concluded that the free activation energy for the boat–boat interconversion of this compound is smaller than that of compounds **1***b* and **2***b*. In the case of the di-NH compounds **1***a* and **2***a*, the spectrum shows that a rapid boat–boat interconversion occurs at ambient temperature (presence of an A_4 system for the protons in positions 3 and 4 of **1***a*, and presence of only one C-methyl signal in **2***a*).

Thus, even if quantitative values cannot be given, it can be concluded that the boat–boat interconversion in 3,4-dihydro-1,6-benzodiazocine-2,5-diones depends greatly on the interaction between the *N*-substituents and the *ortho*-phenyl protons.

[4]The signal given by the methyl group in position 3 of B_2 appears as a broad doublet because the H_3 proton to which it is coupled is itself strongly coupled to H_4 and H'_4 appearing at identical frequencies.

1. W. D. Ollis and J. F. Stoddart. J. Chem. Soc. Chem. Commun. 571 (1973).
2. G. Llouquet. Thèse de Spécialité. U.S.T.L. Montpellier, France. 1975.
3. C. Beaute, Z. W. Wolkowski, and N. Thoai. Chem. Commun. 700 (1971).
4. R. A. Fletton, G. F. H. Green, and J. E. Page. Chem. Commun. 1134 (1972).
5. S. M. Castellano and A. A. Bothner-by. *In* Computer programs for chemistry. Vol. I. *Edited by* D. F. Detar. Benjamin, New York. 1968.

Can. J. Chem. Downloaded from www.nrcresearchpress.com by 210.87.254.105 on 09/05/12
For personal use only.

6. J. ELGUERO and A. FRUCHIER. An. Quim. Spain, **70**, 141 (1974).
7. C. E. JOHNSON and F. A. BOVEY. J. Chem. Phys. **29**, 1012 (1958).
8. C. W. HAIGH and R. B. MAILLON. Org. Magn. Reson. **4**, 203 (1972).
9. G. J. KARABATSOS, G. C. SONNISCHEN, N. HSI, and D. J. FENOGLIO. J. Am. Chem. Soc. **89**, 5067 (1967).
10. J. W. APSIMON, P. V. DEMARCO, D. W. MATHIESON, W. G. CRAIG, A. KARIM, L. SAUNDERS, and W. B. WHALLEY. Tetrahedron, **26**, 119 (1970).
11. J. W. APSIMON, J. ELGUERO, A. FRUCHIER, D. MATHIEU, and R. PHAN-TAN-LUU. Can. J. Chem. **52**, 2296 (1974).
12. J. H. SCHACHTSCHNEIDER, Shell Development Co. Project No. 31450, Tech. Rep. No. 231–64. (1964).
13. C. D. POULTER and R. B. DICKSON. Tetrahedron Lett. 2255 (1971).
14. D. B. DAVIES and M. ABUKHALED. Tetrahedron Lett. 2829 (1973).
15. J. ELGUERO and A. FRUCHIER. Bull. Soc. Chim. Fr. 496 (1970).
16. W. W. PAUDLER and A. G. ZEILER. J. Org. Chem. **34**, 2138 (1969).
17. J. L. AUBAGNAC, J. ELGUERO, and R. ROBERT. Bull. Soc. Chim. Fr. 2868 (1972).

Can. J. Chem. Downloaded from www.nrcresearchpress.com by 210.87.254.105 on 09/05/12
For personal use only.

A re-examination of the nitrobenzene – 2,2,4-trimethyl pentane system in the consolute region and of the thermodynamical considerations concerning the value of ε' at the consolute point

R. HALLIWELL,[1] D. A. HUTCHINSON, AND R. MCINTOSH

Department of Chemistry, Queen's University, Kingston, Ontario K7L 3N6

Received July 21, 1975

R. HALLIWELL, D. A. HUTCHINSON, and R. MCINTOSH. Can. J. Chem. **54**, 1139 (1976).

Failure to find maxima in ε' and ε'' for aniline–cyclohexane in the consolute region by Lubezky and McIntosh (8) led to re-examination of the system nitrobenzene – 2,2,4-trimethyl pentane for which anomalous values of ε' and ε'' have been reported. Earlier results by Lubezky and McIntosh (6) could not be repeated. A re-examination of thermodynamical arguments was then undertaken and the conclusion reached that these do not predict anomalous values of ε'.

R. HALLIWELL, D. A. HUTCHINSON et R. MCINTOSH. Can. J. Chem. **54**, 1139 (1976).

Le fait qu'il a été impossible pour Lubezky et McIntosh (8) de trouver des maxima dans les ε' et ε'' pour le système aniline cyclohexane dans la région consolutée nous a amené à réexaminer le système nitrobenzène – triméthyle-2,2,4 pentane pour lequel les valeurs anormales de ε' et de ε'' ont été rapportées. On n'a pas pu répéter les résultats antérieurs de Lubezky et McIntosh (6). On a donc entrepris un réexamen des arguments thermodynamiques et on est arrivé à la conclusion que ces arguments ne prédisent pas des valeurs anormales pour ε'.

[Traduit par le journal]

Introduction

There has been interest in the dielectric properties of binary liquid systems which are close to the critical solution temperature for a number of years. One of the earliest workers, Piekara (1), studied the nitrobenzene–hexane system. He observed that the dielectric constant ε' increased with decreasing temperature and that there was a discontinuity in $d\varepsilon'/dt$ at the temperature that the system passed from a single phase to a two-phase state. He also noted that for mixtures having the critical concentration $d\varepsilon'/dt$ was not a constant above the critical temperature, but that $|d\varepsilon'/dt|$ decreased with decreasing temperature. Similar results for systems consisting of a polar and a nonpolar liquid have been reported by Lomova and Shakhparonov (7) and Lubezky and McIntosh (8).

Semenchenko (2), however, has argued that quite general thermodynamical considerations suggest that there must be a maximum in the dielectric constant at the critical solution temperature, or consolute point. The magnitude of the maximum should be large since Semenchenko predicts its occurrence at the critical temperature and composition on the basis of the relation

$$\left(\frac{\partial E}{\partial D}\right)_{mpT} = \frac{1}{\varepsilon} = 0$$

He examined a number of polar–nonpolar (3) systems including nitrobenzene–hexane and found that there are maxima in both the dielectric constant ε' and the dielectric loss ε''. Similar results have been reported by Quinn and Smyth (4) and Ripley and McIntosh (5) for the system nitrobenzene – 2,2,4-trimethyl pentane. There is also an anomalous result on the same system by Lubezky and McIntosh (6); whereas no maximum was observed in ε' at the consolute (critical) point, a maximum was observed for mixtures with nitrobenzene concentrations less than the critical concentration and at a temperature above that at which discrete layers form.

More recently there have been several theoretical treatments based on the assumption of density fluctuations in submicroscopic regions. Systems consisting of a mixture of nonpolar

[1]Postdoctoral Fellow 1974–1975. Present address: Building Research, National Research Council of Canada, Ottawa, Canada K1A 0R6.

Can. J. Chem. Downloaded from www.nrcresearchpress.com by 210.87.254.6 on 09/05/12
For personal use only.

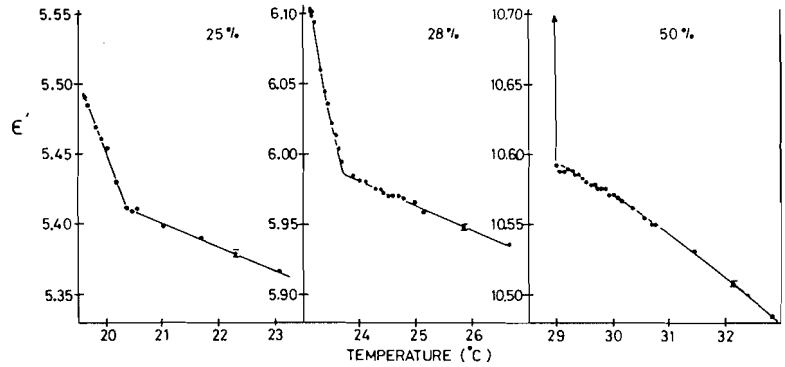

FIG. 1. Dielectric constant for 25%, 28%, and 50% nitrobenzene in 2,2,4-trimethyl pentane at 60 kHz. The break in the curves coincides with phase separation.

liquids were considered by Kim and Mazur (9), who showed that there will be a maximum for ε' at the consolute point but that this maximum is very small (of the order of one part in a thousand or smaller). This prediction is very different from that made by Semenchenko. Snider (10), however, was unable to make a definite statement about the behaviour of ε' for polar–nonpolar systems because of uncertainty in the precise functional behaviour of the osmotic compressibility with electric field in the critical region.

It is apparent that the behaviour of ε' near the consolute point has not been defined, either from an experimental or a theoretical point of view. The present work involves a re-examination of the anomalous results of Lubezky and McIntosh (6) for the nitrobenzene–2,2,4-trimethyl pentane system and of the basic thermodynamical arguments proposed by Semenchenko (2) for the existence of a maximum of ε' at the consolute point.

Experimental

The electronic circuitry, dielectric cell, and measurement procedures for frequencies less than 100 kHz were the same as those already described by Lubezky and McIntosh (6). At higher frequencies a coaxial cell containing a variable condenser as an integral part of the cell, in the manner used by Hartshorn and Ward (11), was used in a resonant circuit. In each case the high potential lead consisted of a thin wire which was surrounded for an appreciable depth by the dielectric contained within the plates of the cell. Changes in the fringing field would only occur because of an alteration of the height of the liquid which would be small over the range of temperature employed.

Reagent grade nitrobenzene, obtained from Fisher Scientific Company, was first dried over calcium chloride, then over phosphorus pentoxide, and finally distilled under vacuum to reduce any danger of decomposition. The purified liquid was then stored over type 4A molecular sieve in a sealed container until used.

Spectranalyzed grade 2,2,4-trimethyl pentane, also from Fisher Scientific Company, was first dried over anhydrous calcium sulphate and then distilled. The purified liquid was stored over type 4A molecular sieve in a sealed container until used.

To prevent contamination with water, the mixtures were prepared and loaded into the dielectric cell under an atmosphere of dry nitrogen in a dry box.

A series of experiments was carried out at frequencies ranging from 20 kHz to 35 MHz for mixtures containing 25%, 28%, and 50% nitrobenzene by weight. The sensitivity to contamination was also tested by exposing previously dried mixtures to the laboratory atmosphere, and by preparing mixtures from reagents that had not been previously dried or purified.

Results and Discussion

The results of measurements of the dielectric constant ε' and dielectric loss ε'' at 60 kKz for liquid mixtures containing 25%, 28%, and 50% nitrobenzene are shown in Figs. 1 and 2. These compositions were selected as they were in the range where the largest effects had been observed earlier by Lubezky and McIntosh or corresponded closely with the critical or consolute concentration (6). Figure 3 shows ε' for 25% and 50% mixtures at higher frequencies. Each figure shows the relative uncertainty in the measurements by an error bar for one point of the diagram.

Can. J. Chem. Downloaded from www.nrcresearchpress.com by 210.87.254.6 on 09/05/12
For personal use only.

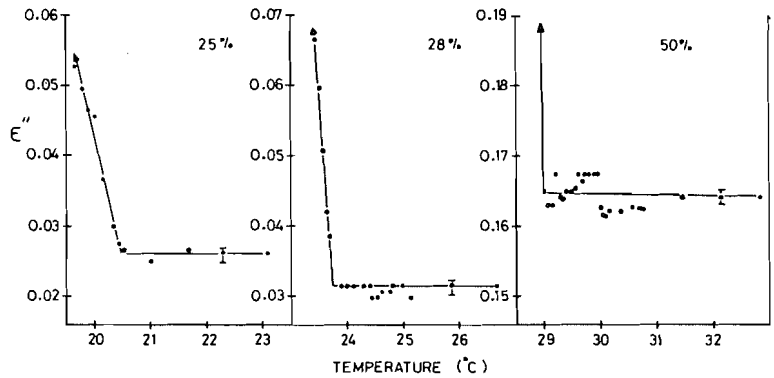

FIG. 2. Dielectric loss for 25%, 28%, and 50% nitrobenzene in 2,2,4-trimethyl pentane at 60 kHz. The break in the curve coincides with phase separation.

The results all show the same feature of no maximum in ε' above the temperature at which the mixture separates into two phases. The behaviour of ε' below the phase separation temperature depends on both the particular mixture under consideration and the geometry of the cell. Mixtures which were exposed to the laboratory atmosphere or prepared with reagents which were not purified gave similar results, although there was some shifting of the temperature of phase separation (8).

Despite the variation of a number of experimental parameters it was not possible to reproduce the results of Lubezky and McIntosh for the nitrobenzene – 2,2,4-trimethyl pentane system in this frequency range. If the experimental uncertainties quoted by Lubezky and McIntosh are applied to their experimental data it is immediately apparent that the observed maxima are not sufficiently well defined to be considered significant. As a consequence it is concluded that the published results for this system are incorrect. For the one case, that of 25% nitrobenzene, where the maximum observed by Lubezky and McIntosh may be significant, the amplitude of the observed peak is an order of magnitude less than that observed by Quinn and Smyth (4) for the same system. Unfortunately Quinn and Smyth did not examine the case of critical concentration so that it is not possible to make further comparison with the results of Lubezky and McIntosh. It is also not possible to say anything about the validity of the results of Ripley and McIntosh (5), although there is some uncertainty about the manner in which the temperature of phase separation was determined.

The analysis of Snider is not able to give an *a priori* answer to the question of a maximum in ε' at the consolute point, but depends on the experimentally determined functional form of the

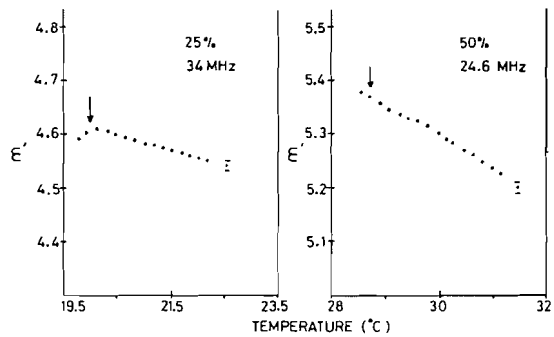

FIG. 3. Dielectric constant for 25% and 50% nitrobenzene in 2,2,4-trimethyl pentane at 34 MHz and 24.6 MHz. The arrow denotes the temperature at which phase separation occurred. Relative values only are recorded and as may be seen from Fig. 1, absolute values may be greater by a factor of approximately two.

Can. J. Chem. Downloaded from www.nrcresearchpress.com by 210.87.254.6 on 09/05/12
For personal use only.

Can. J. Chem. Downloaded from www.nrcresearchpress.com by 210.87.254.6 on 09/05/12
For personal use only.

osmotic compressibility. Since such a maximum is unambiguously predicted by Semenchenko, and experimentally this maximum appears to be rather elusive, it was considered worthwhile to re-examine the thermodynamical arguments which led Semenchenko to this conclusion.

For the thermodynamic description of a dielectric in an electric field, it is convenient to include the following modes of energy transfer between the system and surroundings: heat, pressure–volume work, mass transfer, and electrical work. In such a situation the well known condition for phase stability reads

$$[1] \qquad \delta U - T_{ext}\delta S + p_{ext}\delta V - \zeta_{1\,ext}\delta m_1 - \zeta_{2\,ext}\delta m_2 - \Phi_{ext}\delta Q \geqslant 0$$

The subscript 'ext' denotes the surroundings; the absence of this subscript indicates that the property refers to the system. The remaining notation is: U, internal energy; T, temperature; S, entropy; p, pressure; V, volume; ζ_j, chemical potential, per unit mass, of component j; m_j, mass of component j; Φ, potential difference (Φ_{ext} is the potential difference between the terminals of a large external cell); and Q, charge on capacitor.

If T, p, ζ_1, ζ_2, and Φ are identical for the system and surroundings, [1] remains valid; then it is a criterion for the stability of a phase described by T, p, ζ_1, ζ_2, and Φ against a variation δU, δS, δm_1, δm_2, δQ. It is possible (12) to rewrite $\Phi\delta Q$ as

$$[2] \qquad \Phi\delta Q = \frac{1}{4\pi}\int d^3x\ \boldsymbol{E}.\delta\boldsymbol{D}$$

the integral is over all space.

The system consists of the dielectric, the capacitor, and the surrounding fields. A constant volume is chosen and the volume is large enough to encompass the region of space with non-zero fields. If the system is defined in this manner, then [1] with the aid of [2] becomes

$$[3] \qquad \delta u - T\delta s - \zeta_1\delta\rho_1 - \zeta_2\delta\rho_2 - \frac{1}{4\pi}\boldsymbol{E}.\delta\boldsymbol{D} \geqslant 0$$

where u, s, ρ_1, and ρ_2 respectively refer to the energy, entropy, and masses per unit volume. For the geometry of a parallel plate or coaxial cylindrical plate capacitor, with an isotropic dielectric, the inner product $\boldsymbol{E}.\delta\boldsymbol{D}$ simply leaves $E\delta D$.

The properties of the consolute point, a critical point, are of particular interest. In the region of two phase separation, the variables T, ζ_1, ζ_2, and E are the same in coexisting phases for a vertical parallel plate capacitor or vertical coaxial cylindrical capacitor. For a horizontal parallel plate capacitor T, ζ_1, ζ_2, and D are the same in coexisting phases. Since the experiments in this study were done with a vertical coaxial cylindrical capacitor, the former case is of more interest.

The auxiliary function

$$[4] \qquad f^D = u - Ts - \zeta_1\rho_1 - \zeta_2\rho_2$$

is useful for a discussion of the dielectric constant at the consolute point. Whereas u has simple first order partial derivatives when expressed as a function of s, ρ_1, ρ_2, and D, f^D has simple first order partial derivatives when expressed as a function of T, ζ_1, ζ_2, and D; the partial derivatives are

$$[5] \qquad \left(\frac{\partial f^D}{\partial T}\right)_{\zeta_1\zeta_2 D} = -s \qquad \left(\frac{\partial f^D}{\partial \zeta_1}\right)_{TD\zeta_2} = -\rho_1$$
$$\left(\frac{\partial f^D}{\partial \zeta_2}\right)_{TD\zeta_1} = -\rho_2 \qquad \left(\frac{\partial f^D}{\partial D}\right)_{T\zeta_1\zeta_2} = \frac{E}{4\pi}$$

If one rewrites [4] as

$$u = f^D + Ts + \zeta_1\rho_1 + \zeta_2\rho_2$$

and substitutes this result into [3], and retains all terms up to and including second order in δT, $\delta\zeta_1$, $\delta\zeta_2$, and δD, then with the help of [5] one obtains the result

$$\frac{1}{2}\overbrace{\delta T\ \delta\zeta_1\ \delta\zeta_2\ \delta D}\begin{pmatrix} \frac{\partial s}{\partial T} & \frac{\partial s}{\partial \zeta_1} & \frac{\partial s}{\partial \zeta_2} & 0 \\ \frac{\partial \rho_1}{\partial T} & \frac{\delta \rho_1}{\partial \zeta_1} & \frac{\delta \rho_1}{\partial \zeta_2} & 0 \\ \frac{\partial \rho_2}{\partial T} & \frac{\partial \rho_2}{\partial \zeta_1} & \frac{\partial \rho_2}{\partial \zeta_2} & 0 \\ 0 & 0 & 0 & \frac{1}{4\pi}\frac{\partial E}{\partial D} \end{pmatrix}\begin{pmatrix} \delta T \\ \delta\zeta_1 \\ \delta\zeta_2 \\ \partial D \end{pmatrix} \geqslant 0$$

If $\delta T = \delta\zeta_1 = \delta\zeta_2 = 0$, it is then apparent for a stable phase that

$$\left(\frac{\partial E}{\partial D}\right)_{T\zeta_1\zeta_2} \geqslant 0 \qquad [6]$$

Since T, ζ_1, ζ_2, and E are identical for coexistent phases, whereas s, ρ_1, ρ_2, and D differ in coexistent phases, it then can be said that

$$\left(\frac{\Delta E}{\Delta D}\right)_{T\zeta_1\zeta_2} = 0 \qquad [7]$$

for coexistent phases. In [7], $T\zeta_1\zeta_2$ identify the coexistent phases (three intensive variables are required); ΔE and ΔD are the respective differences for the electric field and the dielectric displacement.

The critical phase may be approached along a path through the region of single phase stability, provided that such a path contains the point representing the critical phase. For all phases on such a path, [6] is valid. Also the critical phase may be approached by considering pairs of coexistent phases in the two-phase region. As the critical phase is approached, the coexistent phases become more alike and the process terminates with the single critical phase. For all pairs of coexistent phases, [7] is valid. In order that the critical phase be simultaneously the limiting situations for which [6] and [7] are valid, one concludes that

$$\left(\frac{\partial E}{\partial D}\right)_{T\zeta_1\zeta_2} = 0 \qquad [8]$$

for the critical phase. This paragraph has outlined Gibbs' concept of the critical phase (13): the critical phase is the limit of single phase stability and it is also the limit of the coexistence of two phases.

A similar treatment of the auxiliary functions

$$f^s = u - \zeta_1\rho_1 - \zeta_2\rho_2 - \frac{1}{4\pi}ED$$

$$f^{\rho_1} = u - Ts - \zeta_2\rho_2 - \frac{1}{4\pi}ED$$

$$f^{\rho_2} = u - Ts - \zeta_1\rho_1 - \frac{1}{4\pi}ED$$

yields the respective results

$$\left(\frac{\partial T}{\partial s}\right)_{\zeta_1\zeta_2 E} = 0 \qquad [9a]$$

Can. J. Chem. Downloaded from www.nrcresearchpress.com by 210.87.254.6 on 09/05/12
For personal use only.

[9b] $$\left(\frac{\partial \zeta_1}{\partial \rho_1}\right)_{T\zeta_2 E} = 0$$

[9c] $$\left(\frac{\partial \zeta_2}{\partial \rho_2}\right)_{T\zeta_1 E} = 0$$

for the critical phase. It is important to note that the derivatives in [8] and [9] have the following properties in common: the dependent variable is the same in coexistent phases, the variable with respect to which the differentiation is performed is in general different in the coexistent phases, and the variables which are held fixed are the same in coexistent phases. The derivative which defines the dielectric constant does not have these properties.

The reciprocal of the dielectric constant ε' is defined by

$$\frac{1}{\varepsilon'} = \left(\frac{\partial E}{\partial D}\right)_{Tpx_2}$$

where x_2 is the mole fraction of component 2. The chain rule allows one to write

$$\frac{1}{\varepsilon'} = \left(\frac{\partial E}{\partial D}\right)_{T\rho_1\rho_2} + \left(\frac{\partial E}{\partial \rho_1}\right)_{TD\rho_2}\left(\frac{\partial \rho_1}{\partial D}\right)_{Tpx_2} + \left(\frac{\partial E}{\partial \rho_2}\right)_{TD\rho_1}\left(\frac{\partial \rho_2}{\partial D}\right)_{Tpx_2}$$

Since $(\partial\rho_1/\partial D)_{Tpx_2}$ and $(\partial\rho_2/\partial D)_{Tpx_2}$ are likely to be small, one has the approximate result

[10] $$\frac{1}{\varepsilon'} \simeq \left(\frac{\partial E}{\partial D}\right)_{T\rho_1\rho_2}$$

Clearly this result is quite different from [8]; ρ_1 and ρ_2 are not the same in coexistent phases. No apparent simple connection exists between [8] and [10]; thus thermodynamic arguments have little to say about the dielectric constant of a critical phase. Although the auxiliary function

$$a = u - Ts$$

can be used to infer that $1/\varepsilon' \geqslant 0$ in the region of single phase stability, little of relevance can be said about

$$\left(\frac{\Delta E}{\Delta D}\right)_{T\rho_1\rho_2}$$

in the two-phase region. The phases for which ρ_1 and ρ_2 are the same (if such a pair of phases exists) are not coexistent phases. Thus the previous arguments which lead up to [8] are not valid in this case.

Further comments can be made about [8] and [9]. From the method of Jacobians one can write

[11a] $$0 = \left(\frac{\partial E}{\partial D}\right)_{T\zeta_1\zeta_2} = \frac{\partial(ET\zeta_1\zeta_2)}{\partial(DT\zeta_1\zeta_2)} = \frac{\partial(ET\zeta_1\zeta_2)}{\partial(Ds\rho_1\rho_2)} \Big/ \frac{\partial(DT\zeta_1\zeta_2)}{\partial(Ds\rho_1\rho_2)}$$

[11b] $$0 = \left(\frac{\partial T}{\partial s}\right)_{\zeta_1\zeta_2 E} = \frac{\partial(ET\zeta_1\zeta_2)}{\partial(Es\zeta_1\zeta_2)} = \frac{\partial(ET\zeta_1\zeta_2)}{\partial(Ds\rho_1\rho_2)} \Big/ \frac{\partial(Es\zeta_1\zeta_2)}{\partial(Ds\rho_1\rho_2)}$$

[11c] $$0 = \left(\frac{\partial \zeta_1}{\partial \rho_1}\right)_{T\zeta_2 E} = \frac{\partial(ET\zeta_1\zeta_2)}{\partial(ET\rho_1\zeta_2)} = \frac{\partial(ET\zeta_1\zeta_2)}{\partial(Ds\rho_1\rho_2)} \Big/ \frac{\partial(ET\rho_1\zeta_2)}{\partial(Ds\rho_1\rho_2)}$$

[11d] $$0 = \left(\frac{\partial \zeta_2}{\partial \rho_2}\right)_{T\zeta_1 E} = \frac{\partial(ET\zeta_1\zeta_2)}{\partial(ET\zeta_1\rho_2)} = \frac{\partial(ET\zeta_1\zeta_2)}{\partial(Ds\rho_1\rho_2)} \Big/ \frac{\partial(ET\zeta_1\rho_2)}{\partial(Ds\rho_1\rho_2)}$$

Can. J. Chem. Downloaded from www.nrcresearchpress.com by 210.87.254.6 on 09/05/12
For personal use only.

Each numerator on the right hand side of [11] consists of the same fourth order determinant whereas each denominator consists of a different third order determinant. Thus, one can readily make the inference that

$$[12] \qquad \frac{\partial(ET\zeta_1\zeta_2)}{\partial(Ds\rho_1\rho_2)} = 0$$

for the critical phase. In this determinant, it is important to note that the 'numerator variables' are the same in coexistent phases whereas the 'denominator variables' differ in coexistent phases. Unfortunately, the determinant

$$\frac{\partial(ETpm_1m_2)}{\partial(DsVm_1m_2)}$$

upon which Semenchenko based his conclusions does not have these properties. Also the determinant

$$[13] \qquad \frac{1}{\varepsilon'} \simeq \left(\frac{\partial E}{\partial D}\right)_{T\rho_1\rho_2} = \frac{\partial(ET\rho_1\rho_2)}{\partial(DT\rho_1\rho_2)}$$

which would arise from [10] lacks these properties. Moreover, [13] bears no simple relationship to [12], so once more little can be said about ε' for the critical phase.

Finally, if the experimental arrangement consisted of a horizontal parallel plate capacitor, one would work with the auxiliary energy function

$$f^E = u - Ts - \zeta_1\rho_1 - \zeta_2\rho_2 - \frac{1}{4\pi}ED$$

The preceding analysis and results would then remain valid if E and D were interchanged and also if $1/\varepsilon'$ were replaced by ε' itself. Thus the same sort of indefinite conclusions about ε' at the critical point would be obtained.

Conclusions

On the basis of these experiments it is possible to state that there is no maximum in the dielectric constant at the consolute point for the system nitrobenzene–2,2,4-trimethyl pentane in the frequency range 20 kHz to 34 MHz. Furthermore it is shown that there is no reason based on thermodynamical arguments to expect such a maximum. It is concluded that the question of existence of a maximum in ε' will be resolved only by careful experimentation rather than by general arguments of this kind.

Acknowledgments

The authors acknowledge with thanks the benefits arising from useful discussions with Dr. N. S. Snider. Also, financial support from the National Research Council of Canada is gratefully acknowledged.

1. A. Piekara. Phys. Rev. **42**, 448 (1932).
2. V. K. Semenchenko. Zhur. Fiz. Khim. **25**, 121 (1951).
3. K. V. Arkhangelskii and V. K. Semenchenko. Zhur. Fiz. Khim. **41**, 1303 (1967) (Russ. J. Phys. Chem. **41**, 692 (1967)).
4. R. G. Quinn and C. P. Smyth. J. Chem. Phys. **39**, 3285 (1963).
5. B. D. Ripley and R. McIntosh. Can. J. Chem. **39**, 526 (1961).
6. I. Lubezky and R. McIntosh. Can. J. Chem. **51**, 545 (1973).
7. N. N. Lomova and M. I. Shakhparonov. Dokl. Akad. Nauk. SSSR, **134**, 632 (1960).
8. I. Lubezky and R. McIntosh. Can. J. Chem. **52**, 3176 (1974).
9. S. K. Kim and P. Mazur. Physica, **71**, 579 (1974).
10. N. S. Snider. J. Chem. Phys. **55**, 3994 (1971).
11. L. Hartshorn and W. H. Ward. J. Inst. Electr. Eng. **79**, 597 (1936).
12. L. D. Landau and E. M. Lifshitz. Electrodynamics of continuous media. Pergamon Press Ltd., London. 1960. p. 47.
13. J. W. Gibbs. The scientific papers of J. Willard Gibbs. Dover Publications, New York. 1961. p. 130.

Can. J. Chem. Downloaded from www.nrcresearchpress.com by 210.87.254.6 on 09/05/12
For personal use only.

^{13}C kinetic isotope effects and reaction coordinate motions in transition states for S_N2 displacement reactions

WARREN EDWARD BUDDENBAUM AND VERNON JACK SHINER, JR.

Department of Chemistry, Indiana University, Bloomington, Indiana 47401

Received March 4, 1975[1]

WARREN EDWARD BUDDENBAUM and VERNON JACK SHINER, JR. Can. J. Chem. **54**, 1146 (1976).

Reaction coordinate motions and ^{13}C kinetic isotope effects at 25 °C have been calculated for the S_N2 reactions of methyl iodide with iodide, cyanide, and chloride ions and for the S_N2 reaction of benzyl bromide with hydroxide ion using transition state models characterized by single interaction force constant, F_{12}, between the bond being formed and the bond being broken. The isotope effect calculations show that the dependence of calculated ^{13}C isotope effects on transition state symmetry found by Willi and Sims *et al.* holds true for reaction barriers corresponding to small values of ν_L, while the symmetry dependence observed by Bron holds true for barriers corresponding to large values of ν_L. ν_L was also found to have a strong influence on the reaction coordinate motions of the transition states. In particular, for the methyl iodide reactions an increase in ν_L increases the distortion of the methyl group in the direction expected for a classical S_N2 reaction. Finally, reaction coordinate motions were used to show that the model proposed by Bron for the borderline region between S_N1 and S_N2 reaction mechanisms predicts an *increase* in the ^{13}C kinetic isotope effect with decreasing total bond order and not the *decrease* suggested by Bron.

WARREN EDWARD BUDDENBAUM et VERNON JACK SHINER, JR. Can. J. Chem. **54**, 1146 (1976).

On a calculé les mouvements des coordonnées de la réaction et les effets isotopiques cinétiques du ^{13}C à 25 °C pour les réactions S_N2 de l'iodure de méthyle avec les ions iodure, cyanure et chlorure et pour la réaction S_N2 du bromure de benzyle avec l'ion hydroxyde en utilisant des modèles d'états de transition caractérisés par une constante de force pour une seule interaction, F_{12}, entre le lien qui se forme et le lien qui se brise. Les calculs d'effet isotopique montrent que la dépendance des effets isotopiques de ^{13}C sur la symétrie des états de transition qui a été trouvée par Willi et par Sims *et al.* prévaut pour des barrières à la réaction correspondant à de petites valeurs de ν_L, alors que la dépendance sur la symétrie observée par Bron prévaut dans les cas où les barrières à la réaction correspondent à des valeurs élevées de ν_L. On a aussi trouvé que ν_L a une influence importante sur les mouvements des coordonnées de la réaction des états de transition. En particulier, pour les réactions de l'iodure de méthyle, une augmentation de ν_L augmente la distorsion du groupe méthyle dans la direction attendue pour une réaction S_N2 classique. Finalement, on a utilisé les mouvements des coordonnées de réaction pour montrer quelle modèle proposé par Bron pour la région intermédiaire entre les mécanismes de réaction S_N1 et S_N2 prédit une *augmentation* de l'effet isotopique cinétique du ^{13}C avec une diminution de l'ordre total de liaison et non pas une *diminution* telle que sugérée par Bron.

[Traduit par le journal]

Theoretical considerations lead to the prediction that primary hydrogen kinetic isotope effects should depend on transition state symmetry and that maximum values should be shown by symmetrical transition states (1–7). Experimental studies of several reaction series have supported this prediction in that each series shows a maximum isotope effect when the environment of the transferred hydrogen in the product is most similar to its environment in the reactant (8). Some years ago, Fry (9) extended this concept to carbon isotope effects. He suggested that an S_N2 displacement reaction at saturated carbon (10–12) can be viewed as the transfer of a carbon (C*) fragment between two groups, X and Y [1]. Therefore, by analogy with hydrogen transfer, carbon kinetic isotope

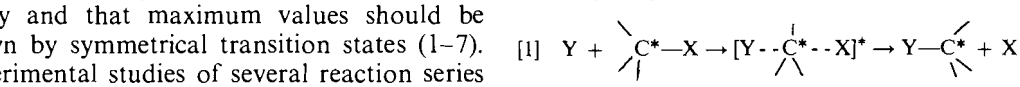

[1]

effects for such displacements should also depend on transition state symmetry. Although no experimental study which illustrates such a variation of carbon isotope effects with transition state symmetry has yet been reported,[2]

[1]Revision received December 22, 1975.

[2]Footnote added in proof. See the work of Yamataka and Ando, ref. 44, for present data that appear to show that the ^{14}C isotope effect for S_N2 displacements of a series of benzyl arenesulfonates goes through a maximum.

Can. J. Chem. Downloaded from www.nrcresearchpress.com by 210.87.254.6 on 09/05/12
For personal use only.

Can. J. Chem. Downloaded from www.nrcresearchpress.com by 210.87.254.6 on 09/05/12
For personal use only.

Willi (13) and later Sims *et al.* (14) found support for Fry's suggestion in detailed model calculations. Recently, however, Bron (15) has published calculations using a different S_N2 reaction model which, contrary to the previous studies (13, 14) do not show a maximum in the carbon isotope effects; instead k_{12}/k_{13} was predicted to vary monotonically from reactant-like to product-like transition states. As yet no explanation for the differing predictions of these calculations has been offered. More specifically, we would like to know the range and limitations of the application of each of these two different kinds of models for S_N2 reactions.

We have been utilizing kinetic isotope effect theory (for recent reviews see ref. 16) in an analysis of some ^{13}C, $^{35}Cl/^{37}Cl$, and deuterium kinetic isotope effects for the bimolecular displacement reaction, methyl iodide plus chloride ion in dimethylformamide (17). During this model study we have examined these earlier calculations (13–15) and the calculated ^{13}C kinetic isotope effects for two other closely related S_N2 displacement reactions, methyl iodide plus cyanide ion (18) and methyl iodide plus iodide ion (19). In this paper we report some results of this analysis and comment upon some questions concerning the properties of the transition states for S_N2 displacement reactions as inferred from kinetic isotope effect studies.

Results and Discussion

When one employs Eyring's transition state theory (20) for the calculation of kinetic isotope effects (k_1/k_2) on reaction 1 above, one obtains (21–23) eq. 2 where the subscripts 1 and 2

$$[2] \qquad k_1/k_2 = \frac{\tau_1\kappa_1 Q_1^{*} Q_{Y_2} Q_{CX_2}}{\tau_2\kappa_2 Q_2^{*} Q_{Y_1} Q_{CX_1}}$$

refer to the light and heavy isotopic forms respectively; the τ_i's are tunnelling corrections that express the probability that complexes with less energy than the potential energy barrier for the reaction will nevertheless form products; the κ_i's are transmission coefficients which express the probability that transition states once attained will yield products; the Q_i's are partition functions summed over all the energy levels of the reactants, Y and CX; and the Q_i^{*}'s are partition functions for the transition states which are special in that they are summed over all the energy levels of the transition state except that corresponding to ν_L, the frequency associated with reaction coordinate motion in the transition state, *i.e.*, that degree of freedom in the transition state complex corresponding to motion across the maximum of the potential energy barrier for the reaction (20*a*).

ν_L is imaginary (or zero) since its value depends in part upon the degree of curvature of the potential energy barrier. Its value also depends upon the masses and extents of displacement of the atoms which are involved in the reaction coordinate motion. The chief result of this mass dependence is that ν_L can be sensitive to isotopic substitution in the reactants. An isotope effect on ν_L can give rise to a tunnelling isotope effect (τ_1/τ_2) on k_1/k_2 (23); but, more importantly, the isotope effect on ν_L, ν_{1L}/ν_{2L}, is the high temperature or classical limit of the kinetic isotope effect itself (21). That is, eq. 2 can be written as eq. 3,

$$[3] \qquad k_1/k_2 = (\nu_{1L}/\nu_{2L})(TDF)$$

where *TDF* approaches one at high temperatures and is termed the temperature dependent factor of k_1/k_2 since it contains all of the temperature dependence of the isotope effect. ν_{1L}/ν_{2L} is, of course, independent of temperature and in discussions of the temperature dependence of k_1/k_2 is sometimes termed the temperature independent factor, *TIF* (see for example ref. 24). Clearly, it is the existence of the reaction coordinate degree of freedom and its associated imaginary frequency, ν_L, that distinguishes transition state complexes from normal molecules.

In general, the evaluation of eqs. 2 and 3 requires knowledge of (*1*) the structure of the reactants and of the transition state and (*2*) the potential energy surface of the reacting system in those regions near the reactants and the transition state in sufficient detail to carry out a rotational–vibrational analysis of the two states (16, 20–25). For the reactants the required structural and potential energy data for these analyses can be obtained from spectral observations or estimated by analogy to other stable molecules (25–27); however, because of the difficulty of theoretical calculations of potential energy surfaces (23, 28, 29), most of our information about transition state properties in

Can. J. Chem. Downloaded from www.nrcresearchpress.com by 210.87.254.6 on 09/05/12
For personal use only.

general (23, 28) and about S_N2 reactions in particular (29) has been inferred from the fitting of transition state models to experimental data (a recent illustration is contained in ref. 30).

The chief limitation of such model calculations is that the number of parameters needed to describe a transition state is too large for all of the parameters to be uniquely fitted by the experimental data, and as a result the investigator is forced to assume values for many of the properties of a model before any attempt to fit the model to the experimental data can be carried out. Thus the reliability or 'correctness' of transition state properties as inferred from model calculations is subject to considerations of the 'correctness' or the relative chemical and physical reasonableness of all the properties of the model. In the case of model calculations of carbon kinetic isotope effects in S_N2 reactions only three of the four basic types of properties of transition states have been subject to such considerations. These are (*1*) the structure of the transition state, (*2*) the potential energy force constants for the transition state, and (*3*) the magnitude of the imaginary frequency, ν_L. The reaction coordinate motion and its influence on the calculated isotope effects has not been examined separately. One immediate consequence of this neglect is that several models reported previously have reaction coordinate motions which do not appear to correspond to that expected for a displacement reaction, *i.e.*, the transfer of the carbon fragment from the group X to the group Y (9–12). In addition, previous discussions of reaction coordinates have dealt with atom transfer or with the transfer of groups containing no internal degrees of freedom, as, for example, the transfer of a methyl group as a rigid group of mass 15 (3, 4, 6).

Calculation of k_1/k_2, ν_L, and the Reaction Coordinate Motion of a Transition State Model

The kinetic isotope effects reported in the following sections were calculated via eq. 2 in a manner very similar to that employed in the previous calculations of kinetic isotope effects in displacement reactions, in that we have neglected any isotope effects on the transmission (8, 16) and the tunnelling (23) coefficients in eq. 2 and have evaluated the partition functions in this equation in the rigid rotor–harmonic oscillator approximation (16, 31) using a program supplied by Wolfsberg and Stern (32).

The Wolfsberg and Stern program uses a modification of the Schachtschneider and Snyder computer program (33) for the Wilson **FG**-matrix solution (25) of the harmonic vibrational problem to determine the required vibrational energy levels of the reactants and of the transition state model from an input of the structure (bond distances and angles), the masses of the atoms, and a quadratic (harmonic) vibrational potential function for each molecular species. The Wilson **FG**-matrix program also determines for the transition state model the frequency, ν_L, of the required (20–22) aperiodic distortion of the assumed structure of the transition state. *It is this atomic motion that we have identified in the following sections as the reaction coordinate motion associated with each calculation of ν_L and k_1/k_2 (34–36).*

We have expressed these motions in terms of the cartesian displacements from their equilibrium position, ΔX(atom), ΔY(atom), ΔZ(atom), of each of the atoms of the transition state involved in the motion (25, 27). In general this will include all N atoms of the model. This is because the above recipe for identifying the reaction coordinate motion requires that these infinitesimal displacements be subject to the conditions (25) in eq. 4

$$[4] \qquad \sum^{N} M(\text{atom})\Delta X(\text{atom}) = 0$$

$$\sum^{N} M(\text{atom})\Delta Y(\text{atom}) = 0$$

$$\sum^{N} M(\text{atom})\Delta Z(\text{atom}) = 0$$

where M (atom) is the atomic mass of the atom; *i.e.*, there is no displacement of the center of mass of the transition state model in the reaction coordinate motion. This means the reported magnitudes of the displacements are arbitrary and it is the relative values and relative signs of the displacements that describe the reaction coordinate motion for a given calculation. Or, alternatively, the values of these displacements can be viewed as a description of the transition state model that will, in general, have a different dependence than k_1/k_2 and ν_L on the absolute and relative values of the input parameters for the transition state. The correlation of changes

Can. J. Chem. Downloaded from www.nrcresearchpress.com by 210.87.254.6 on 09/05/12
For personal use only.

in k_1/k_2 and in the reaction coordinate motion which results from changes in the input parameters in what we mean by the influence of reaction coordinate motion on calculated kinetic isotope effects.

As a first step in determining such a correlation for kinetic isotope effects in the methyl iodide plus chloride ion reaction (17) we (*a*) reproduced the k_1/k_2 calculations of Willi (13), Sims *et al.* (14), and Bron (15); (*b*) determined as described above the reaction coordinate motions associated with each k_1/k_2; and (*c*) examined these motions in terms of the model used by each investigator in his discussion of the k_1/k_2's. The results of this analysis, supplemented by similar calculations on data reported in two additional papers by Willi on S_N2 reactions of methyl iodide (18, 19), then served as a guide for our methyl iodide–chloride calculations.

In addition we determined for each model those parts of the input potential function, *i.e.*, those diagonal and off-diagonal force constants, whose values determine the value of ν_L of each calculation. This was necessary because previous work on reaction coordinates (34–36) shows that these same force constants which generate ν_L also determine the reaction coordinate motion. To make this determination we used standard matrix techniques (25, 33) to transform the quadratic potential function, V^*, eq. 5,

$$[5] \qquad V^* = V_0 + \tfrac{1}{2}\sum_i \sum_j \bar{F}_{ij}\Delta X_i \Delta X_j$$

where V_0 is a constant,

$$\bar{F}_{ij} = \left(\frac{d^2V}{dX_i dX_j}\right)_{V_0}$$

and the ΔX_i are the set of displacement coordinates used in the previous calculations (13–15, 18, 19) into

$$[6] \qquad V^* = V_0 + \tfrac{1}{2}\sum_i^M \sum_j^M F_{ij}\Delta S_i \Delta S_j$$

where

$$F_{ij} = \left(\frac{d^2V}{dS_i dS_j}\right)_{V_0}$$

and the ΔS_i are a common set of M valence coordinates involving only changes in the distance between bonded atoms and in the included angles between these bonds. In all cases (13–15, 18, 19) the resulting V^* had the form

$$[7] \qquad V^* = V_0 + \tfrac{1}{2}\sum_{i=1}^{M} F_{ii}\Delta S_i^2 + F_{12}\Delta S_1 \Delta S_2$$

where ΔS_1 is a change in the length of the bond being broken (CX), ΔS_2 is a change in the bond being formed (CY), and F_{12} is an interaction force constant that couples the displacements in these two bonds. Consequently we have restricted ourselves in this paper to S_N2 transition states with V^* of this form and will discuss the influence of a more general V^* in a future paper.

A Symmetrical S_N2 Transition State

The first transition states we will consider in this study of the influence of reaction coordinate motion on calculated S_N2 ^{13}C kinetic isotope effects are those for the bimolecular exchange reaction of methyl iodide and iodide ion (19). This system was chosen for three reasons. First, of all the S_N2 reactions of methyl iodide the one with iodide ion has the transition state with the highest degree of molecular symmetry (29) and is, therefore, the reaction which best serves as a reference point for a consideration of the influence of symmetry on isotope effects. Secondly, as a consequence of this symmetry (25–27) the transition state for this reaction can be described by fewer input parameters, *i.e.*, force constants, bond distances, and angles, than the transition states for any other S_N2 reaction of methyl iodide. Finally, the deuterium and ^{13}C kinetic isotope effects for this reaction have already been the subject of detailed model calculations by Willi (19) in which k_1/k_2 and ν_{1L}/ν_{2L} were determined for a rather complete set of ICH_3I^- transition state models. The reader is referred to the original paper for details of the structure and force fields used in the Willi calculations; however, in brief, the transition states were assumed to have D_{3h} symmetry with the CI bond distances being 10% longer than that in methyl iodide although Willi shows that the actual length of these bonds has little influence on the results. In the models we will consider here, all but three of the transition state's force constants were assigned values by analogy to stable molecules containing sp^2 carbons. These three constants were CI bond stretching (F_{CI}), interaction between the two CI bonds (F_{12}), and HCI valence angle deformation

Can. J. Chem. Downloaded from www.nrcresearchpress.com by 210.87.254.6 on 09/05/12
For personal use only.

TABLE 1. Calculated deuterium and ^{13}C isotope effects on rates and ν_L for the reaction $CH_3I + I^-$ at 25 °C[a]

Number[b]	F_ρ[c]	F_{HCI}[c]	ν_{HL}[d]	ν_{HL}/ν_{DL}	k_H/k_D[e]	ν_{12L}/ν_{13L}	k_{12}/k_{13}
3	—[f]	0.25	0	1.090	1.121	1.031	1.047
21	4.0	0.25	496*i*	1.063	1.066	1.034	1.054
15	6.0	0.25	710*i*	1.045	1.033	1.036	1.058
25	8.0	0.25	878*i*	1.033	1.014	1.037	1.061
24	—[f]	0.27	0	1.090	1.062	1.031	1.047
22	8.0	0.27	878*i*	1.032	1.056	1.037	1.062

[a]Taken in part from ref. 19.
[b]Identification number in ref. 19.
[c]Units: mdyn/Å.
[d]Units: cm^{-1}.
[e]per D.
[f]Formula in eq. 10 not used, F_{12} set equal to F_{CI} so that $\nu_L = 0$ will hold (see refs. 19 and 34).

(F_{HCI}). Willi set limits on the value of F_{CI} and F_{12} by assuming that the potential function for the two CI bonds could be written as eq. 8 where ρ

$$[8] \quad 2V^* = F_{CI}'(\Delta r_1^2 + \Delta r_2^2) - F_\rho \rho^2 + \ldots$$

is the arithmetic mean of the increase in length (Δr_1) of one CI bond and the decrease in length ($-\Delta r_2$) of the other CI bond, F_ρ is the force constant for the coordinate ρ, and F_{CI}' measures the restoring forces within each CI bond (19). Comparison of eq. 8 with the potential function expressed in terms of F_{12} gives eq. 9 which

$$[9] \quad 2V^* = F_{CI}(\Delta r_1^2 + \Delta r_2^2) + 2F_{12}\Delta r_1 \Delta r_2 + \ldots$$

yields equations for F_{CI} and F_{12} in terms of two parameters, F_{CI}' and F_ρ, eq. 10. Willi determined

$$[10] \quad F_{CI} = F_{CI}' - \tfrac{1}{4}F_\rho \text{ and } F_{12} = \tfrac{1}{4}F_\rho$$

that for a reaction barrier of 20 kcal/mol and F_{CI}' equal to 1 mdyn/Å the upper limit for F_ρ would be about 8 mdyn/Å.[3]

Table 1 gives the ν_L and the calculated deuterium (k_H/k_D per D) and ^{13}C (k_{12}/k_{13}) isotope effects taken from ref. 19 and reproduced in this work for the special case, $\nu_L = 0$, and for selected values of F_ρ. The maximum value of F_ρ, calculations 22 and 25, gives a ν_L of about 900*i* cm^{-1}.[4] As pointed out by Willi as ν_L increases (calculations 3, 21, 15, and 25) the two calculated isotope effects change in opposite directions, k_{12}/k_{13} increasing from 1.047 to 1.061 and k_H/k_D decreasing from 1.121 to 1.014. Willi also noted that these trends in the isotope effects are paralleled by the changes in the *TIF*'s (ν_{HL}/ν_{DL} and ν_{12L}/ν_{13L}) and suggested that they are, therefore, due in part to a change in the reaction coordinate motions of the hydrogens and carbon with changes in ν_L. This suggestion is supported by the data in Table 2 where we have listed the Wilson **FG**-matrix calculation of the atomic motions associated with each ν_L in Table 1 in terms of the cartesian displacement along the ICI bond axis (*X*-axis) where the sign of the ΔX's has been chosen so that the entering group, I_Y, moves toward the center of mass, *i.e.*, $\Delta X(I_Y) > 0$. Clearly each motion listed in Table 2 is asymmetric (34) in that as one CI bond distance, ΔR_{CI_X}, increases the other ΔR_{CI_Y}, decreases, the relative bond changes being such that the I---I distance remains a constant, *i.e.*, ΔR_{CI_X} equals ΔR_{CI_Y} and $\Delta X(I_Y)$ equals $\Delta X(I_X)$.

When ν_L is zero, calculations 3 and 24, the CH_3 fragment is transferred as a rigid planar structure, *i.e.*, $\Delta X(C) = \Delta X(H_1) = \Delta X(H_2) = \Delta X(H_3)$, and one therefore obtains the same ν_{12L}/ν_{13L} as when the CH_3 group is treated as a mass point. However, in contrast to the atom transfer case (34–36) where an increase in ν_L

[3]In this calculation F_{CI} can be negative. In a more recent calculation (28*e*) Willi employs a potential function which utilizes only positive F_{CI}'s and yields isotope effects and a maximum value of ν_L close to those obtained in this earlier study (19).

[4]The correct value of ν_L is as yet unknown. In *ab initio* calculations of the potential energy surfaces for the exchange reactions, methyl chloride plus chloride (29*a*) and methyl fluoride plus fluoride (29*b*), the energy of the XCH_3X^- complex was lower than the sums of the energy of the separated CH_3X and X^- and it was suggested that any activation barrier arises from solvation effects (29*f*). More recent *ab initio* calculations find a barrier height of 8 kcal/mol for the gas phase reaction CH_3F plus F^- (24*d*); however, the curvature of the barrier was not determined.

TABLE 2. Cartesian displacements in the reaction coordinate motions for the transition states in Table 1

Number[a]	ν_L[b]	$\Delta X(I_Y)$[c, d]	$\Delta X(C)$	$\Delta X(H)$[e]	$\Delta X(I_X)$[f]
3	0	0.015	−0.251	−0.251	0.015
21	496*i*	0.015	−0.263	−0.194	0.015
15	710*i*	0.015	−0.270	−0.154	0.015
25	878*i*	0.015	−0.273	−0.128	0.015
24	0[g]	0.015	−0.251	−0.251	0.015
22	878*i*[g]	0.015	−0.273	−0.123	0.015
24′	—[h]	0.015	−0.242	−0.242	0.015
22′	—[h]	0.015	−0.262	−0.123	0.015

[a]Identification number in ref. 19 and Table 1.
[b]Units: cm^{-1}.
[c]*X*-axis parallel to ICI axis. Sign of ΔX chosen so that I_Y and C move towards each other. Only displacements along this *X*-axis are observed.
[d]Entering iodide ion.
[e]Same for each of the three hydrogens of the CH_3 group.
[f]Leaving iodide ion.
[g]Effect of change in HCI bending force constant.
[h]Displacement of $I^{13}CH_3I^-$ species.

does not change ν_{12L}/ν_{13L}, k_{12}/k_{13}, or the reaction coordinate motion, here a non-zero value of ν_L leads to different carbon and hydrogen displacements with corresponding changes in the respective *TIF*'s. Although only displacements parallel to the *X*-axis occur, the increase in ν_L introduces into the reaction coordinate motion not only HCI deformation but also motion in all the valence coordinates of the complex. This results in an overall motion that looks like that expected for a reaction coordinate in an S_N2 displacement, *i.e.*, the CH bond distances and the HCI_Y angles increase and the HCH and HCI_X angles decrease as the CI_Y bond distance approaches that in methyl iodide. One result of the inclusion of HCI bending in the reaction coordinate is to make the isotope effects on ν_L sensitive to the value of F_{HCI}. This can be seen by comparing calculations 3 and 25 with calculations 24 and 22 in Table 1. Finally, comparison of the displacements in the ^{13}C species (calculation 22′) indicates that the substitution of ^{13}C for ^{12}C in a symmetrical transition state only affects the displacement of the carbon, and not that of any of the other atoms.

An Asymmetrical S_N2 Transition State

As an example of a reaction which would be expected to have an asymmetrical transition state, *i.e.*, $R_{CX} \neq R_{CY}$, we will next consider Willi's calculations of the ^{13}C kinetic isotope effects in the bimolecular reaction of methyl iodide with cyanide ion (18). The transition state structure used above was employed in the calculations with the exception that the forming bond length was shortened to that expected for a CC single bond and that I was replaced with a CN group whose bond distance was set equal to that in cyanide ion (18). Essentially the same sp^2 force constants were also used; however, because of the assumed lower molecular symmetry of the transition state there are six force constants that must be assigned values: F_{CI}, F_{CC}, F_{12}, F_{HCI}, F_{HCC}, and F_{CN}. We will only consider models where the first three are varied according to formulas similar to those used above, eq. 10,

$$[11] \qquad \begin{aligned} F_{CC} &= F_{CC}' - \tfrac{1}{4}F_\rho \\ F_{CI} &= F_{CI}' - \tfrac{1}{4}F_\rho \\ F_{12} &= \tfrac{1}{4}F_\rho \end{aligned}$$

where for F_{CC}' equal to 2.0 and F_{CI}' equal to 1.0 a maximum value for F_ρ of 10 mdyn/Å is obtained.[3] The calculated isotope effects on ν_L and on the rate are given in Table 3. As in the case of the symmetrical transition state for the exchange reaction, the changes in ν_{12L}/ν_{13L} parallel those in the k_{12}/k_{13}'s; however, in this *asymmetric* reaction an increase in ν_L does not necessarily lead to an increase in the carbon isotope effect. For example, in calculations 50 and 81 k_{12}/k_{13} decreases from 1.069 to 1.066 as ν_L increases from 768*i* to 805*i* cm^{-1}, but in calculation 82 where ν_L is 570*i* cm^{-1}, k_{12}/k_{13} is smaller than when ν_L is zero. The reason for this becomes clear when one examines the

Can. J. Chem. Downloaded from www.nrcresearchpress.com by 210.87.254.6 on 09/05/12
For personal use only.

TABLE 3. Calculated ^{13}C isotope effects on rates and ν_L for the reaction $CH_3I + CN^-$ at 18 °C[a]

Number[b]	F_ρ[c]	F_{CI}[c]	F_{CC}[c]	F_{12}[c]	ν_{12L}[d]	ν_{12L}/ν_{13L}	k_{12}/k_{13}
41	—[e]	0.2	0.2	0.2	0	1.030	1.058
27	—[f]	0.2	0.2	1.5	606*i*	1.032	1.066
50	7.2	−0.8	0.2	1.8	768*i*	1.034	1.069
81	—[f]	0.2	−0.8	1.8	805*i*	1.032	1.066
56	10.0	−1.5	−0.5	2.5	1016*i*	1.035	1.071
96	—[f]	−2.0	−2.0	2.7	1209*i*	1.034	1.070
82	—[f]	2.0	−1.0	1.2	570*i*	1.023	1.051

[a]Taken in part from ref. 18.
[b]Identification number in ref. 18.
[c]Units: mdyn/Å.
[d]Units: cm^{-1}.
[e]Formulae in eq. 11 not used, F_{12} set equal to $\sqrt{F_{CI}F_{CC}}$ so that $\nu_L = 0$ would hold (refs. 18 and 34).
[f]F_{CI}, F_{CC}, and F_{12} arbitrarily chosen (see ref. 18).

TABLE 4. Normalized cartesian displacements in the reaction coordinates for the transition states in Table 3[a]

Number[b]	ν_{12L}[c]	ΔX(CN)[d,e]	ΔX(C*)	ΔX(H)[f]	ΔX(I)	θ[g]
41	0	0.008	−0.073	−0.073	0.008	−45
27	606*i*	0.046	−0.099	−0.063	0.007	−36
27′	—[h]	0.045	−0.092	−0.060	0.007	−36
50	768*i*	0.037	−0.098	−0.052	0.007	−38
81	805*i*	0.063	−0.104	−0.051	0.005	−33
56	1016*i*	0.045	−0.105	−0.040	0.007	−37
96	1209*i*	0.057	−0.109	−0.033	0.006	−35
82	570*i*	0.083	−0.080	−0.049	−0.001	−26

[a]The eigenvector inverse for ν_L was normalized, (see ref. 26, p. 52) before cartesian coordinates were calculated.
[b]Identification number in ref. 18.
[c]Units: cm^{-1}.
[d]X-axis parallel to ICCN axis. Sign of ΔX chosen so that CN group moves toward carbon. There are no displacements in Y and Z directions.
[e]Displacement of N same as C, $\Delta R_{CN} = 0$.
[f]Displacement of each of the methyl H's the same.
[g]θ = arctan $\Delta R_{CI}/\Delta R_{CCN}$ (see text).
[h]Motion of $NC^{13}CH_3I^-$ isomeric complex.

normalized cartesian displacements given in Table 4.[5] As before only displacements along the ICCN axis occur and the overall motion with respect to the CC and CI bonds is still asymmetric, but now the displacements of the entering and leaving groups are sensitive to ν_L. Thus we see that for the same ΔX(C*) (calculations 27 and 50) the smaller displacement of the CN group in 50 leads to an increase in ν_{12L}/ν_{13L}, *i.e.*, the effective mass of motion in 50 is smaller than in 27 and the substitution of mass 13 for mass 12 has a greater effect. The opposite is true for calculations 41 through 82. The effect of ν_L on the relative motions of the carbon and hydrogens of the CH_3 is the same as observed before in that as ν_L increases, the HCC angles, etc., of the transition state change in the direction expected for formation of the methyl cyanide product. However, there is no change in the CN bond distance in any of these reaction coordinates.

In the case of an asymmetrical reaction such as this, the transition state for the reaction is often described as being either product-like or reactant-like. In general such a characterization of a transition state is based upon a calculated or assumed knowledge of the value of one or more of the properties of the transition state and a judgement of how product-like (or reactant-

[5]The eigenvector inverse for ν_L was normalized to one before the cartesian coordinates were calculated. See ref. 26, p. 52.

Can. J. Chem. Downloaded from www.nrcresearchpress.com by 210.87.254.6 on 09/05/12
For personal use only.

TABLE 5. Comparison of single interaction force constant methods for the generation of ν_L in S_N2 transition states of differing bond order[a]

Reaction	Reference	F_{CX}	F_{CY}	F_{12}
$CH_3I + OH^-$	13	$n_1 F_{CI}^0$	$n_2 F_{CO}^0$	$F_{CI}F_{CO} - F_{12}^2 = d \leqslant 0$
Benzyl chloride + oxygen	14	$n_1 F_{CCl}^0$	$n_2 F_{CO}^0$	$F_{12} \geqslant +\sqrt{F_{CCl}F_{CO}}$
Benzyl bromide + oxygen	15	$-Xn_1 F_{CBr}^0$	$(1 - X)n_1 F_{CO}^0$	$F_{12} = 4n_1 - 2$

[a]See text for definition of symbols.

like) these values are. For example, in calculation 41 in Table 3 the value of F_{CI} is 0.2 mdyn/Å which is to be compared with the 2.3 value it has in methyl iodide and the zero value it will have in the product; therefore, based on F_{CI} this transition state was very product-like. Initially, it was assumed that if one property of a transition state was product-like (or reactant-like) it meant all of the properties of the transition state would be product-like (or reactant-like) (23); however, theoretical calculations of potential energy surfaces (7, 28, 29) suggest that the timing of structural and bonding changes during a reaction step can be such that some parameters of a transition state may still be reactant-like even though others might have assumed product-like values. Thus the fact that F_{CC} in calculation 41 is very reactant-like while F_{CI} is product-like does not mean that transition state 41 is unsuitable for the CH_3I/CN^- reaction; but rather it means that Willi has assumed that in this reaction bond breaking occurs faster or is more important than bond formation. Willi made the same assumption for calculation 27 in Table 3 except here the magnitude of F_{12} and therefore of ν_L is larger. This change clearly affects the reaction coordinate motion and the question arises as to whether this change in F_{12} makes the motion for calculation 27 more product-like or less product-like than that for calculation 41. In the next section we will show that it seems to make the motion more reactant-like.

Reaction Coordinates and the Product-like (Reactant-like) Character of S_N2 Transition States

In the approach employed by Willi (13), Sims *et al.* (14), and Bron (15) for the calculation of carbon isotope effects in S_N2 reactions no single transition state structure is used but instead a series of structures of differing reactant-like (product-like) character are considered. Following Johnston (23) and others (5), the reactant-like character of a transition state is measured by the bond order of the bond being broken in the reaction. The central assumptions (see comments above) of this approach are that (*1*) the sum of bond orders, n_1 for the bond being broken (C*—X) and n_2 for the bond being formed (Y—C*), around the atom being transferred remains a constant, n_t, throughout the reaction process (23); (*2*) the bond distances and bond angles are calculable from the assigned bond orders by, for example, Pauling's rule (38); and (*3*) the force constants of the transition state are also calculable from the assumed bond orders (39) subject to the constraint that the required imaginary (or zero) frequency for the transition state is obtained.

This approach makes no explicit assumptions about the reaction coordinate motions of the transition states, and, therefore, we can use it to determine if these motions have a dependence on n_1 or n_t that we might use to measure the product-like (or reactant-like) character of an S_N2 transition state. More importantly, we are interested in the conditions under which this dependence for S_N2 displacement differs from that for atom transfer (1–8).

When one examines the reaction coordinate motions of the S_N2 transition states employed in such constant bond order calculations in terms of the reaction coordinate motions discussed above one finds that they have many features in common. Moreover, it appears that these common features result from the manner in which the frequency ν_L is generated. Since these methods differ from those discussed above (compare with eqs. 10 and 11) they are summarized in Table 5. We will show their influence on the carbon isotope effect by the application of each method to the same reacting system, the reaction of methyl chloride and iodide ion (17), using where possible common reactant and transition state models. The structure and

Can. J. Chem. Downloaded from www.nrcresearchpress.com by 210.87.254.6 on 09/05/12
For personal use only.

Can. J. Chem. Downloaded from www.nrcresearchpress.com by 210.87.254.6 on 09/05/12
For personal use only.

TABLE 6. Definition of geometry and force field of reactant and transition states for the $CH_3Cl + I^-$ reaction

State	Geometry	Force field[a, b]
Reactant[c] CH_3Cl	$r_{CH} = 1.095$ $r_{CCl} = 1.78$ Tetrahedral	$F_{CH} = 4.970$ $F_{CCl} = 3.390$ $F_{HCH} = 0.468$ $F_{HCCl} = 0.566$
Product[c] CH_3I	$r_{CH} = 1.095$ $r_{CI} = 2.139$ Tetrahedral	$F_{CH} = 4.970$ $F_{CI} = 2.310$ $F_{HCH} = 0.450$ $F_{HCI} = 0.444$
Transition state[d] $I\cdots CH_3\cdots Cl$	$r_{CH} = 1.095$ $r_{CCl} = 1.78 - 0.6 \log n_1$ $r_{CI} = 2.139 - 0.6 \log n_2$ $\alpha_{HCCl} = 110°n_1 + 70°n_2$	$F_{CH} = 4.970$ $F_{HCH} = 0.459$ $F_{CI} = 2.310n_2$ $F_{CCl} = 3.386n_1$ $F_{HCI} = 0.444n_2$ $F_{HCCl} = 0.566n_1$

[a]Units: stretching force constants are mydn/Å and bending mdyn Å/rad^2.
[b]Atomic weights: C.R.C. Handbook of Chemistry and Physics, 53rd ed.
[c]C_{3v} symmetry: total of 10 internal valence coordinates (ref. 40).
[d]C_{3v} symmetry: total of 14 internal valence coordinates.

TABLE 7. Calculated ^{13}C isotope effects and reaction coordinates for the reaction $CH_3Cl + I^-$ at 25 °C for $\nu_L = 0$ as a function of CCl bond order (n_1)

n_1(CCl)	F_{12}[a]	ν_{12L}/ν_{13L}	k_{12}/k_{13}	ΔX(I)[b]	ΔX(CH)[c]	ΔX(Cl)	θ[d]
1.00	0.0	1.007	1.006	0.047	−0.120	−0.120	0
0.85	0.999	1.004	1.030	0.046	−0.168	−0.094	−20
0.70	1.281	1.020	1.043	0.043	−0.200	−0.069	−28
0.60	1.370	1.024	1.050	0.039	−0.221	−0.046	−34
0.50	1.398	1.028	1.056	0.033	−0.239	−0.015	−39
0.405[e]	1.373	1.030	1.059	0.023	−0.247	0.023	−45
0.30	1.281	1.027	1.055	0.008	−0.232	0.071	−52
0.15	0.999	1.013	1.039	−0.016	−0.164	0.127	−63
0.00	0.0	1.001	1.010	−0.038	−0.038	0.151	−90

[a]$F_{12} = \sqrt{F_{CCl}F_{Cl}}$; units, mdyn/Å.
[b]X-axis parallel to ICCl axis. There were no displacements in Y and Z directions. Sign of ΔX is such that CH_3 is transferred toward I.
[c]Displacement of hydrogen same as carbon.
[d]θ = arctan $\Delta R_{CCl}/\Delta R_{Cl}$ (see text).
[e]Value of n_1 when $F_{CCl} = F_{Cl}$.

bond order–force constant relationships we have employed for these basic models are given in Table 6. These models are very similar to the constant bond order models used previously (5, 13–15, 40) but it should be noted that none of these transition states will fit all the kinetic isotope data for the methyl iodide–chloride ion system (17).

The first calculations we will consider will be those for $\nu_L = 0$ and for total bond order, $n_t = 1 = n_1 + n_2$, with $F_{12} = +(F_{CCl}F_{Cl})^{1/2}$ (see Table 5) where the force constants for the Cl and the CCl bonds are given in Table 6. The F_{12}'s, the *TIF*'s, the ^{13}C isotope rate effects, and the reaction coordinate displacements for selected values of n_1 are shown in Table 7. As was observed by Sims *et al.* (14) the ^{13}C isotope effect for such a calculation goes through a maximum which in the case of methyl chloride plus iodide ion occurs at $n_1 = 0.405$. The ν_{12L}/ν_{13L}, the k_{12}/k_{13}'s and the CH_3 groups' displacement also go through maxima at this

Can. J. Chem. Downloaded from www.nrcresearchpress.com by 210.87.254.6 on 09/05/12
For personal use only.

value of n_1. It should be noted that at this value of n_1, F_{Cl} equals F_{CCl} and that F_{12} is not at its maximum value.

Here again for $v_L = 0$ the CH_3 group is transferred as a rigid structure in an asymmetric motion. A convenient measure of this asymmetry is θ

$$\theta = \arctan \Delta R_{CX}/\Delta R_{CY} \quad [12]$$

where $\Delta R_{CX}/\Delta R_{CY}$ is the relative displacement in the CX and CY bonds in the reaction coordinate for the transition state and tan θ is therefore the slope in the R_{CX}–R_{CY} plane of the reaction path at the transition state. This is illustrated in Fig. 1 which is *not* a potential energy surface but is a plot (solid line) of the locus of the geometries of the transition states (R_{CCl}, R_{Cl}) in Table 6 for the various values of n_1. As indicated by Table 7 and Fig. 1, θ will vary from 0 to $-90°$. For a very reactant-like transition state (point *A* on Fig. 1), the CH_3Cl group moves as a rigid structure towards the iodide ion, the slope at point *A* is near zero and the value of θ in Table 7 is near zero. For a very product-like transition state (point *B* in Fig. 1), a rigid CH_3I group moves away from the chloride ion, the slope approaches infinity, and θ approaches $-90°$. In the case of the symmetrical transition state (point *C*) θ is $-45°$ and the slope is -1. Thus based on the criteria of θ, the transition states for the methyl iodide plus CN ion (Table 4) where the θ's in column 7 vary from $-45°$ in calculation 41 to $-26°$ in calculation 82 are all more reactant-like than the symmetrical case (calculation 41).

Although the overall motion in each transition state in Table 7 is asymmetric we observe that the relative directions of the motion of the Cl and I atoms change twice; from $n_1 = 1$ until $n_1 = 0.5$ these two atoms move toward each other; from $n_1 = 0.5$ until $n_1 = 0.15$ they move in the same direction; and then from $n_1 = 0.15$ to zero they move again in opposite directions. Thus the differences in the reaction coordinate motions of the individual atoms in calculations 41 and 27 (Table 4) also appear to classify transition state 27 as more reactant-like than 41 in that in 27 the CN moves toward I while in 41 the two groups move in the same direction.

These results are to be contrasted with the reaction coordinates obtained when these calculations are repeated with $v_L = 0$ generated

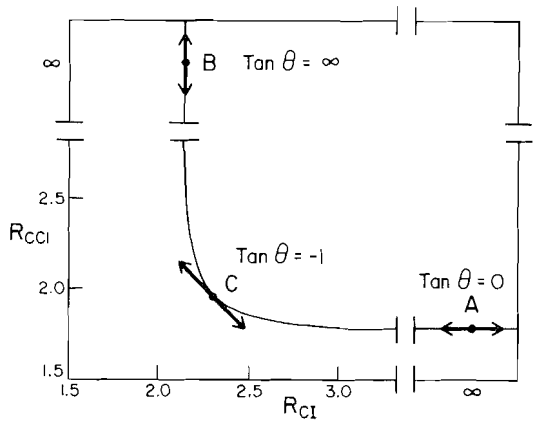

FIG. 1. Plot of the locus of transition state structures in R_{CX}–R_{CY} space as a function of bond order.

using $F_{12} = -\sqrt{F_{CCl}F_{Cl}}$; *i.e.*, $d = 0$ in Table 5. These coordinates are given in Table 8 where the $\Delta X(I)$'s are set equal to those in the first calculations (Table 7). Clearly there are several differences. First of all, at no value of n_1 are I and Cl displaced in the same direction. Secondly, in these calculations the displacement of the CH_3 group goes through a minimum and not the maximum observed in Table 7. These two observations are a consequence of the fact that all of these reaction coordinate motions are symmetric in that ΔR_{CX} always has the same sign as ΔR_{CY}; *i.e.*, θ for each n_1 is positive. These θ's are shown in column 6 of Table 8. They each have the same value but the opposite sign in comparison with the corresponding coordinates in Table 7; therefore, these motions do not represent changes in structure along the solid line in Fig. 1 but are changes in structure off the solid line. In particular at $n_1 = 0.405$ (point *C*, Fig. 1) this symmetric motion is perpendicular or normal to the locus of structures used in constant bond order calculations and therefore does not appear to be a reasonable reaction coordinate for an S_N2 displacement reaction.

As seen from Table 5, Bron's generation of v_L differs from that of Willi (13) and Sims *et al.* (14) in that (*a*) he uses a constant interaction constant, F_{12}, for all values of n_1 with a given n_t while the other calculations use a variable value of F_{12} and (*b*) he uses a negative force constant for the CX bond. We will consider the effect of a constant F_{12} first. Table 9 shows the effect of a constant F_{12} on v_L, the carbon isotope

TABLE 8. Calculated reaction coordinates for the reaction $CH_3Cl + I^-$ for $\nu_L = 0$ and F_{12} negative[a]

n_1(CCl)	F_{12}[a]	ΔX(I)[b]	ΔX(CH)[b, c]	ΔX(Cl)[b]	θ[d]
1.00	0.00	0.047	−0.121	−0.121	0
0.85	−0.999	0.046	−0.083	−0.130	20
0.70	−1.281	0.043	−0.067	−0.126	28
0.60	−1.370	0.039	−0.053	−0.117	34
0.50	−1.398	0.033	−0.041	−0.101	39
0.405[e]	−1.373	0.023	−0.025	−0.072	45
0.30	−1.281	0.008	−0.007	−0.025	52
0.15	−0.999	−0.016	0.000	0.054	63
0.00	0.00	−0.038	−0.038	0.151	90

[a] $F_{12} = -\sqrt{F_{CCl}F_{Cl}}$; units mdyn/Å; compare with Table 7.
[b] X-axis parallel to ICCl axis. No displacements in Y and Z. Sign and value of ΔX(I) set equal to that in Table 7.
[c] Displacement of hydrogen same as carbon.
[d] θ = arctan $\Delta R_{CCl}/\Delta R_{Cl}$ (see text).
[e] Value of n_1 when $F_{CCl} = F_{Cl}$.

TABLE 9. Effect of constant interaction constant on ^{13}C isotope effects and reaction coordinates as a function of CCl bond order on $CH_3Cl + I^-$ at 25 °C

F_{12}[a]	n_1	ν_L[b]	k_{12}/k_{13}	ΔX(I)[c]	ΔX(C)	ΔX(H)	ΔX(Cl)	θ[d]
1.398	1.0	230i	1.039	0.044	−0.197	−0.185	−0.074	−27
	0.7	119i	1.047	0.041	−0.213	−0.209	−0.056	−32
	0.405	79i	1.059	0.022	−0.247	−0.245	0.025	−45
	0.0	371i	1.051	−0.004	−0.212	−0.175	0.102	−56
2.000	1.0	371i	1.053	0.038	−0.232	−0.199	−0.040	−35
	0.7	358i	1.060	0.031	−0.249	−0.212	−0.006	−41
	0.405	406i	1.063	0.018	−0.254	−0.205	0.041	−47
	0.0	534i	1.060	0.004	−0.238	−0.166	0.082	−53
6.000	1.0	1095i	1.072	0.020	−0.271	−0.111	0.030	−46
	0.7	1126i	1.073	0.018	−0.271	−0.100	0.038	−47
	0.405	1159i	1.073[e]	0.015	−0.270	−0.092	0.046	−48
	0.0	1207i	1.073	0.012	−0.267	−0.083	0.056	−49

[a] Units: mdyn/Å.
[b] Units: cm^{-1}.
[c] X-axis parallel to ICCl axis. No displacements in Y and Z directions. Signs of ΔX chosen so that CH_3 group moves toward I.
[d] θ = arctan $\Delta R_{CCl}/\Delta R_{Cl}$ (see text).
[e] Maximum value of 1.0732 between 0.4 and 0.5.

effect, and the reaction coordinate motions in Table 7. The first value of F_{12} (1.398) is the smallest that will force all the transition states to have an imaginary (or zero) frequency. As a result ν_L is larger for very product-like and reactant-like transition states than it is for nearly symmetrical transition states. We know of no evidence or rationale in the literature to lead us to expect this behavior for the value of ν_L. Rather the calculations of Johnston (42) indicate that the curvature of the barrier is less for product-like or reactant-like transition states than it is for symmetrical ones. However, the data in Table 9 are of interest since they show the effect of increasing F_{12} to values greater than $+\sqrt{F_{CCl}F_{Cl}}$ on transition states of different molecular symmetry, *i.e.*, different n_1, in terms of not only the calculated kinetic isotope effects but also in terms of other parameters that describe the transition state model. For example, an increase in F_{12} makes the value of θ approach −45° from both the product and reactant sides. Moreover, this change in θ is reflected in the increase in k_{12}/k_{13} as well as an increase in the

Can. J. Chem. Downloaded from www.nrcresearchpress.com by 210.87.254.6 on 09/05/12
For personal use only.

TABLE 10. Effect of variable interaction constant on ^{13}C isotope effects and reaction coordinates as a function of bond order and constant curvature ($F_0 = -0.6$) $CH_3Cl + I^-$ at 25 °C

n_1(CCl)	F_{12}[a]	ν_{HL}[b]	k_{12}/k_{13}	ΔX(I)[c]	ΔX(C)	ΔX(H)	ΔX(Cl)	θ[d]
1.00	1.547	263*i*	1.043	0.042	−0.207	−0.191	−0.065	−30
0.85	1.814	306*i*	1.053	0.037	−0.232	−0.207	−0.037	−36
0.70	1.960	346*i*	1.060	0.031	−0.248	−0.214	−0.008	−41
0.60	2.003	368*i*	1.062	0.027	−0.253	−0.213	0.010	−43
0.50	2.006	386*i*	1.063	0.026	−0.255	−0.211	0.026	−45
0.405	1.973	396*i*	1.063	0.018	−0.254	−0.207	0.041	−47
0.30	1.893	400*i*	1.062	0.013	−0.249	−0.201	0.056	−49
0.15	1.685	389*i*	1.059	0.005	−0.236	−0.191	0.079	−53
0.00	1.321	348*i*	1.050	−0.006	−0.206	−0.174	0.106	−57

[a] $F_{12} = \sqrt{(F_{Cl} - F_0)(F_{CCl} - F_0)}$; $F_0 = -0.6$; units: mdyn/Å.
[b] Units: cm^{-1}.
[c] X-axis parallel to ICCl axis. No displacement in Y and Z directions. Sign of ΔX chosen such that CH_3 moves toward I.
[d] θ = arctan $\Delta R_{CCl}/\Delta R_{Cl}$ (see text).

displacement of the carbon. These shifts become more pronounced as F_{12} is increased to 2 mdyn/Å (a value near that used by Bron for $n_t = 1$) and then to the extreme value of 6 mdyn/Å where the isotope effects[6] and the ΔX(C)'s become nearly constant regardless of the variation of the force field with n_1. Note, however, that the other ΔX(atoms)'s still have a dependence on n_1. In particular, the degree of distortion of the transferred methyl group still depends on n_1.

Table 10 gives the isotope effects and reaction coordinates when we follow the example of Willi and vary F_{12} with n_1. For these calculations we employed the formula [13] where F_0 is the

$$[13] \quad F_{12} = +\sqrt{(F_{Cl} - F_0)(F_{CCl} - F_0)}$$

negative eigenvalue of the **F** matrix for the transition state's force field. Buddenbaum and Yankwich (34) have related F_0 to the curvature of the barrier at the transition state along the reaction coordinate via Willi's d (Table 5). This formula gives essentially the same results as does Willi's but we feel it has the advantage of holding the curvature (F_0) at the potential energy maximum constant for all values of n_1. This is not the case with Willi's formula (34). The value of F_0 used in the construction of Table 10 was −0.6 mdyn/Å and was chosen to give an F_{12} equal to about 2 mdyn/Å at $n_1 = 0.5$ in order to make a more direct comparison with the constant F_{12} calculations in Table 9. As can be seen in Table 10 the ν_L now go through a maximum leading to a more pronounced maximum in the isotope effect. Since it is likely that the curvature will be less for product-like (or reactant-like) transition states than for the symmetrical transition states (41) the use of an F_0 that varies with n_1 should lead to a more pronounced maximum than obtained in Table 10. It should be pointed out that as F_0 is increased the resultant F_{12} calculated by eq. 13 approaches a constant value independent of n_1; therefore, in this limit the same behavior for k_{12}/k_{13} and ΔX(C) as in Table 9 is observed. An important point about the data in Table 10 is that $\theta = -45°$ now occurs at $n_1 = 0.5$. A future paper will discuss the consequences of this observation for the calculation of S_N2 kinetic isotope effects.

Bron used models for the aqueous solvolysis of benzyl bromide that employed negative force constants for the CBr bond (Table 5). Let us now consider the effect of a negative F_{CX} on the reaction coordinate motions for S_N2 displacements. This study will be presented as part of a set of calculations dealing with the influence of total bond order on S_N2 kinetic isotope effects.

The Influence of Total Bond Order on S_N2 Kinetic Isotope Effects

Bron (15) considered the influence of total bond order, n_t, on the ^{13}C kinetic isotope effects for displacement reactions and has suggested that as n_t decreases the S_N2 transition states

[6] The effect of ν_L on k_1/k_2 for the triatomic case as a function of n_t has been commented upon by several workers (3–5).

Can. J. Chem. Downloaded from www.nrcresearchpress.com by 210.87.254.6 on 09/05/12
For personal use only.

Can. J. Chem. Downloaded from www.nrcresearchpress.com by 210.87.254.6 on 09/05/12
For personal use only.

TABLE 11. Calculated ^{13}C isotope effects and reaction coordinates for the reaction benzyl bromide + O^- at 25 °C as a function of total bond order, n_t[a]

n_t	n_1(CBr)	ν_{HL}[b]	k_{12}/k_{13}	ΔX(O)[c]	ΔX(C*)	ΔX(H)	ΔX(C)	ΔX(Br)	θ[d]
1.0	0.8	822*i*	1.051	0.040	−0.267	−0.098	−0.007	0.036	−45
	0.6	670*i*	1.049	0.002	−0.261	−0.122	−0.007	0.043	−49
	0.4	525*i*	1.042	−0.041	−0.245	−0.144	−0.014	0.050	−55
	0.2	395*i*	1.030	−0.076	−0.223	−0.160	−0.022	0.056	−62
0.45	0.8	245*i*	1.024	−0.128	−0.175	−0.158	−0.035	0.061	−79
	0.6	205*i*	1.015	−0.143	−0.156	−0.145	−0.043	0.062	−87
	0.4	165*i*	1.008	−0.148	−0.146	−0.139	−0.054	0.063	90
	0.2	116*i*	1.002	−0.147	−0.136	−0.135	−0.071	0.064	87
0.10	0.8	306*i*	0.987	−0.208	−0.070	−0.058	−0.010	0.055	48
	0.6	298*i*	0.986	−0.207	−0.072	−0.060	−0.011	0.055	47
	0.4	290*i*	0.986	−0.206	−0.074	−0.062	−0.012	0.056	45
	0.2	282*i*	0.985	−0.204	−0.077	−0.064	−0.013	0.056	46
0.01	0.8–0.2	339*i*	0.9811–0.9816	−0.211	−0.063	−0.050	−0.008	0.054	52

[a]Bron's models were recalculated (ref. 15)
[b]Units: cm^{-1}.
[c]*X*-axis parallel to BrCO axis. Some displacements in *Y* and *Z* directions; all less than 10% of ΔX displacement. Sign of ΔX chosen so that CH_3 group moves toward oxygen.
[d]θ = arctan $\Delta R_{C\text{-}Br}/\Delta R_{CO}$ (see text).

TABLE 12. Effect of variable interaction constant on ^{13}C isotope effects and reaction coordinates as a function of total bond order, n_t, for reaction $CH_3Cl + I^-$ at 25 °C

n_t	n_1	$(k_{12}/k_{13})_0$[a]	ν_L[b]	k_{12}/k_{13}	ΔX(I)[c]	ΔX(C)	ΔX(H)	ΔX(Cl)	θ[d]
0.5	1.0	1.018	317*i*	1.056	0.034	−0.241	−0.215	0.023	−44
	0.6	1.051	382*i*	1.063	0.022	−0.255	−0.209	0.026	−45
	0.4	1.058	397*i*	1.063	0.017	−0.253	−0.206	0.044	−47
	0.0	1.013	427*i*	1.058	0.003	−0.232	−0.186	0.084	−53
0.01	1.0	1.033	397*i*	1.060	0.016	−0.251	−0.211	0.048	−51
	0.6	1.053	441*i*	1.062	0.015	−0.253	−0.199	0.048	−51
	0.4	1.058	439*i*	1.063	0.015	−0.253	−0.198	0.049	−51
	0.0	1.030	431*i*	1.064	0.015	−0.253	−0.196	0.050	−53

[a] ^{13}C isotope effect when $\nu_L = 0$. Reaction coordinate same as in Table 7.
[b] Units: cm^{-1}.
[c] X-axis parallel to ICCl axis. No displacements in Y and Z directions. Sign of ΔX chosen such that CH_3 group moves toward I.
[d] θ = arctan $\Delta R_{CCl}/\Delta R_{CI}$ (see text).

approach those for S_N1 reactions.[7] We have reproduced all the transition state models used by Bron to calculate ^{13}C isotope effects in the benzyl bromide plus oxygen reaction as a function of n_t. The properties of a selected number of these transition states are given in Table 11. In contrast to the previous models we no longer have C_{3v} symmetry at the transferred carbon, and since the hydrogens and the benzyl carbon will be displaced to different extents with respect to the X or OCBr axis, there are now some displacements perpendicular to the X or OCBr axis. These are all less than 10% of the ΔX displacement and are not shown in this table.

When $n_t = 1.0$ the *net effect* of a *negative* F_{CBr} and a *constant* F_{12} is to yield transition states in which ν_L decreases monotonically from $1000i$ cm^{-1} at $n_1 = 1$ to about $200i$ cm^{-1} at $n_1 = 0$. The monotonic decrease in k_{12}/k_{13} reflects this trend as do the monotonic changes in $\Delta X(C^*)$ and θ. In particular the value of θ suggests that all these transition states are product-like in the R_{CBr}–R_{OC} plane, *i.e.*, θ is between −90° and −45°. When n_1 is reduced to 0.45, the magnitude of ν_L decreases as do the isotope effects and the $\Delta X(C^*)$'s; however, we note that for $n_1 = 0.4$, θ is positive, *i.e.*, the reaction coordinate motion is symmetric stretch, not asymmetric stretch. The reason for this is that for $n_t = 0.5$ the formulas used by Bron make F_{12} negative which when coupled with a negative F_{CBr} leads at $n_1 = 0.45$ and $n_1 = 0.4$ to a change in the character of the reaction coordinate motion. All of the remaining reaction coordinates in Table 11 are also symmetric stretch and thus appear unreasonable for displacement reaction transition states.

In order to assess the influence of total bond order, n_t, on isotope effect calculations employing an F_{12} calculated from eq. 13, we determined the effect of n_t on the methyl chloride–iodide model calculations above. The results for $n_t = 0.5$ and 0.01 are given in Table 12. These data are to be compared with the data in Table 7. The $(k_{12}/k_{13})_0$ entry in Table 12 is for the $\nu_L = 0$ case. Since the reaction coordinates for ν_L equal zero are independent of n,[8] the coordinates for these entries are the same as those in Table 7. Figure 2*A* shows a plot of $(k_{12}/k_{13})_0$ for various values of n_1 as a function of n_t. These curves show that for $\nu_L = 0$, n_t has no effect on the maximum isotope effect at $n_1 = 0.405$ while at other n_1's the isotope effect increases as n_t decreases. This, of course, must be due to an increase in *TDF*.

Figure 2*B* shows the influence of n_1 and n_t on the isotope effect when F_0 is −0.6 mdyn/Å and an imaginary ν_L is obtained. The data for these calculations, given in the right-hand columns of Table 12, are to be compared with

[7] As Bron has pointed out, such a model for an S_N1 reaction would only apply if no intermediates were involved in the reaction (15). It is now known that the S_N1 category includes a rather large family of mechanistic possibilities (11, 12). At least three intermediates, the tight ion pair, the solvent separated ion pair, and the free carbonium ion, have been identified as being kinetically significant in some reactions.

[8] Since $n_1 = n_t X$ and $n_2 = n_t(1 - X)$ where X varies from one to zero, the ratio of F_{CI} and F_{CCl} and therefore the ratio of ΔR_{CI} to ΔR_{CCl} is independent of n_t for ν_L equal zero. See ref. 34.

Can. J. Chem. Downloaded from www.nrcresearchpress.com by 210.87.254.6 on 09/05/12
For personal use only.

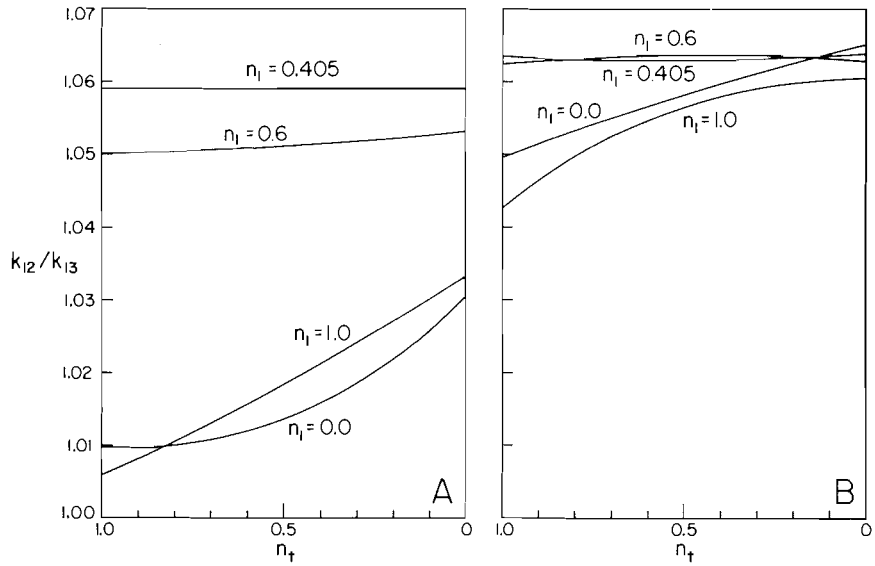

FIG. 2. Effect of total bond order (n_t) and CCl bond order (n_l) on calculated ^{13}C kinetic isotope effects in the S_N2 reaction $CH_3Cl + I^-$. (*A*) $\nu_L = 0$ ($F_0 = 0$); (*B*) ν_L = imaginary ($F_0 = -0.6$ mdyn/Å).

the data in Table 11. These data show that the effect of large F_0 to make the carbon isotope effect independent of n_l is general for all values of n_t.

In summary, the reaction coordinate motions for all of these latter calculations are asymmetric and the overall effect of the n_t model is to predict larger isotope effects for n_t small, *i.e.*, for a loosening of the reacting bonds around the carbon. Thus the experimental observations (43 and A. Fry in ref. 7, Chap. 6) of small ^{13}C isotope effects in S_N1 reactions cannot be explained by this model; although better agreement could possibly obtain if the force constants of the non-reacting bonds to the carbon are increased (43).

Conclusion

The reaction coordinate motion associated with the imaginary (or zero) frequency, ν_L, of a transition state was found to be a useful criterion for the analysis of kinetic isotope effect calculations. In particular, it was shown that the model proposed by Bron for the borderline region between S_N2 and S_N1 reaction mechanisms predicts an *increase* in the ^{13}C kinetic isotope effect with decreasing total bond order and not the *decrease* suggested by Bron.

The contributions of different atoms to the reaction coordinate motion were found to provide useful insight for examining the interrelationships between the magnitude of a ν_L generated by a single interaction force constant and the calculated ^{13}C isotope effects in transfers of a group having internal structure. In such cases, it was found that changes in the isotope effects can be correlated with distortions in the group being transferred. In the case of models for the reaction of methyl chloride plus iodide ion this distortion was found to be that expected of the classical representation of the S_N2 reaction mechanism. A more direct method for producing this distortion through the use of multiple interaction force constants (34–36) is currently being investigated.

Acknowledgment

This work was supported by funds from NSF Grant GP 32854.

1. F. H. WESTHEIMER. Chem. Rev. **61**, 265 (1961).
2. E. R. THORNTON. J. Org. Chem. **27**, 1943 (1962).
3. A. V. WILLI and M. WOLFSBERG. Chem. Ind. 2097 (1964).
4. J. BIGELEISEN. Pure Appl. Chem. **8**, 217 (1964).
5. R. MORE O'FERRALL and J. KOUBA. J. Chem. Soc. B, 985 (1967).
6. W. J. ALBERY. Trans. Faraday Soc. **63**, 200 (1967).
7. E. R. THORNTON and E. F. THORNTON. *In* Isotope effects in chemical reactions. *Edited by* C. J. Collins

Can. J. Chem. Downloaded from www.nrcresearchpress.com by 210.87.254.6 on 09/05/12
For personal use only.

and N. S. Bowman. Van Nostrand Reinhold Co., New York. 1971. pp. 238–246.
8. R. P. BELL. Chem. Soc. Rev. **3**, 513 (1974), and references cited therein.
9. A. FRY. Pure Appl. Chem. **8**, 409 (1964).
10. C. K. INGOLD. Q. Rev. **11**, 1 (1957).
11. V. J. SHINER, Jr. *In* Isotope effects in chemical reactions. *Edited by* C. J. Collins and N. S. Bowman. Van Nostrand Reinhold Co., New York. 1971.
12. S. WINSTEIN, B. APPEL, R. BAKER, and A. DIAZ. Chem. Soc. Spec. Publ. 19. 1965.
13. A. V. WILLI. Z. Naturforsch. Teil A, **21**, 1385 (1966).
14. L. B. SIMS, A. FRY, L. T. NETHERTON, J. C. WILSON, K. D. REPPOND, and S. W. CROOK. J. Am. Chem. Soc. **94**, 1364 (1972).
15. J. BRON. Can. J. Chem. **52**, 903 (1974).
16. W. A. VAN HOOK. *In* Isotope effects in chemical reactions. *Edited by* C. J. Collins and N. S. Bowman. Van Nostrand Reinhold Co., New York. 1971; M. Wolfsberg. Acc. Chem. Res. **5**, 225 (1972), and references cited therein.
17. A. C. MACCOLL, V. J. SHINER, JR., and A. G. LOUDEN. Unpublished results.
18. A. V. WILLI. Z. Naturforsch. Teil A, **21**, 1377 (1966).
19. A. V. WILLI. Can. J. Chem. **44**, 1889 (1966).
20. (*a*) S. GLASSTONE, K. LAIDLER, and H. EYRING. The theory of rate processes. McGraw-Hill, New York. 1941; (*b*) K. LAIDLER and A. TWEEDALE. Adv. Chem. Phys. **21**, 113 (1971).
21. (*a*) J. BIGELEISEN and M. G. MAYER. J. Chem. Phys. **15**, 261 (1947); (*b*) J. BIGELEISEN and M. WOLFSBERG. Adv. Chem. Phys. **1**, 15 (1958).
22. L. MELANDER. Isotope effects on reaction rates. Ronald Press, New York. 1960.
23. H. S. JOHNSTON. Gas phase reaction rate theory. Ronald Press, New York. 1966. Chap. 2 and 10.
24. C. R. TURNQUIST, J. W. TAYLOR, E. P. GRIMSRUD, and R. C. WILLIAMS. J. Am. Chem. Soc. **95**, 4133 (1973), and references cited therein.
25. E. B. WILSON, JR., J. E. DECIUS, and P. R. CROSS. Molecular vibrations. McGraw-Hill Book Company, Inc., New York. 1955.
26. P. GANS. Vibrating molecules. Chapman and Hall Ltd., London. 1971. Chap. 6.
27. T. SHIMANOUCHI and I. NAKAGAWA. Annu. Rev. Phys. Chem. **23**, 217 (1972).
28. (*a*) M. KRAUSS. Annu. Rev. Phys. Chem. **21**, 39 (1970); (*b*) T. F. GEORGE and J. ROSS. Annu. Rev. Phys. Chem. **24**, 263 (1973); (*c*) T. CARRINGTON. Acc. Chem. Res. **7**, 20 (1974); (*d*) J. W. MCIVER, JR. Acc. Chem. Res. **7**, 72 (1974).
29. (*a*) A. M. WOOLEY and M. S. CHILD. Mol. Phys. **19**, 625 (1970); (*b*) G. BERTHIER, D. J. DAVID, and A. VEILLARD. Theor. Chim. Acta, **14**, 329 (1969); (*c*) C. D. RITCHIE and G. A. CHAPPELL. J. Am. Chem. Soc. **92**, 1819 (1970); (*d*) A. DEDIEU and A. VEILLARD. J. Am. Chem. Soc. **94**, 6730 (1972); (*e*) A. V. WILLI, Z. Phys. Chem. N.F. **66**, 317 (1969); (*f*) P. CREMASCHI, A. GAMBA, and M. SIMONETTA. Theor. Chim. Acta, **25**, 237 (1972).
30. R. C. WILLIAMS and J. W. TAYLOR. J. Am. Chem. Soc. **96**, 3721 (1974).
31. M. WOLFSBERG. Annu. Rev. Phys. Chem. **20**, 449 (1969).
32. M. WOLFSBERG and M. J. STERN. Pure Appl. Chem. **8**, 225 (1964); **8**, 325 (1964).
33. J. G. SCHACHTSCHNEIDER and R. G. SNYDER. Spectrochim. Acta, **19**, 177 (1965).
34. W. E. BUDDENBAUM and P. E. YANKWICH. J. Phys. Chem. **71**, 3136 (1967).
35. R. W. KIDD and P. E. YANKWICH. J. Chem. Phys. **60**, 610 (1974).
36. G.-J. WEI and P. E. YANKWICH. J. Chem. Phys. **60**, 3619 (1974).
37. B. L. CRAWFORD and W. H. FLETCHER. J. Chem. Phys. **19**, 141 (1951); **20**, 977 (1952).
38. L. PAULING. J. Am. Chem. Soc. **69**, 542 (1947).
39. R. M. BADGER. J. Chem. Phys. **3**, 710 (1935); **2**, 128 (1934).
40. S. R. HARTSHORN and V. J. SHINER, JR. J. Am. Chem. Soc. **94**, 9002 (1972).
41. H. S. JOHNSTON, W. A. BONNER, and D. J. WILSON. J. Chem. Phys. **26**, 1002 (1957).
42. H. S. JOHNSTON. Adv. Chem. Phys. **3**, 131 (1960).
43. A. J. KRESGE, N. N. LICHTIN, K. N. RAO, and R. E. WESTON, JR. J. Am. Chem. Soc. **87**, 437 (1965).
44. H. YAMATAKA and T. ANDO. Tetrahedron Lett. 1059 (1975).

Can. J. Chem. Downloaded from www.nrcresearchpress.com by 210.87.254.6 on 09/05/12
For personal use only.

Chemical relaxations in micellar solutions by ultrasonic spectroscopy. II. Sodium heptylsulfate and hexylammonium chloride solutions

DOUGLAS A. W. ADAIR, VINCENT C. REINSBOROUGH, AND HAYDEN M. TRENHOLM

Chemistry Department, Mount Allison University, Sackville, New Brunswick E0A 3C0

AND

JOHN P. VALLEAU

Lash Miller Chemical Laboratories, University of Toronto, Toronto, Ontario M5S 1A1

Received September 24, 1975

DOUGLAS A. W. ADAIR, VINCENT C. REINSBOROUGH, HAYDEN M. TRENHOLM, and JOHN P. VALLEAU. Can. J. Chem. **54**, 1162 (1976).

Ultrasonic absorptions have been measured by the pulse technique for the dilute and concentrated micellar range for Na heptylsulfate and hexylammonium chloride solutions. The dilute micellar range was also investigated for the Li, K, Rb, and Cs heptylsulfate systems. Single-valued relaxations were found in each system. The relaxation frequencies increased linearly with concentration in the concentrated micellar range but in the dilute range were relatively constant. The relaxation behaviour was interpreted in terms of monomer exchange between micelles.

DOUGLAS A. W. ADAIR, VINCENT C. REINSBOROUGH, HAYDEN M. TRENHOLM et JOHN P. VALLEAU. Can. J. Chem. **54**, 1162 (1976).

Faisant appel à la méthode des pulsations, on a mesuré les absorptions ultrasoniques de solutions diluées et concentrées en micelles de solutions d'heptylsulfate de sodium et de chlorure d'hexylammonium. On a aussi examiné des solutions micellaires diluées du système heptylsulfate de Li, de K, de Rb et de Cs. On a trouvé des valeurs uniques de relaxation dans chacun des systèmes. Les fréquences de relaxation augmentent d'une façon linéaire avec la concentration dans des solutions concentrées en micelles mais dans des solutions diluées elles sont relativement constantes. On interprète le comportement de relaxation en terms d'échange de monomère entre micelles.

[Traduit par le journal]

Introduction

Chemical relaxation studies by various techniques have shown that usually two well separated, single-valued relaxation frequencies can be detected in micellar systems (1, 2). The faster process, studied almost exclusively by the ultrasonic technique ($10^{-6} - 10^{-9}$ s), is generally assumed to involve some exchange equilibrium between monomer and micelle (2–5). Investigators, however, are not agreed on which model of micelle dissociation–association can best explain the observed facts, in particular the concentration dependence of the relaxation frequency f_c. In concentrated micellar solutions, f_c is found to increase linearly with concentration but in dilute micellar solutions, *i.e.* from the c.m.c. (critical micelle concentration) to roughly twice the c.m.c., f_c has been reported by other workers to remain approximately constant (5) or to decrease in linear fashion from the high concentration values to either a finite number (2) or to zero (3). A different model must be invoked in each case. The main purpose of the present investigation is to examine in detail for chemical relaxations a representative anionic surfactant system and a cationic surfactant system over the entire micellar region.

The accurate pulse technique employed is confined to micellar systems consisting of surfactants of short hydrocarbon length (6–8 carbon atoms) because of the narrow frequency range of operation (10–150 MHz). Thus, sodium heptylsulfate and hexylammonium chloride were chosen as the two key surfactants. The dilute micellar range for the other alkali metal heptylsulfates (Li, K, Rb, Cs) was also examined ultrasonically to confirm the earlier finding that the counterion had little effect upon the relaxation parameters and the dilute solution behaviour (5).

Experimental

The pulse technique and the preparation, purification, and analysis of the alkali metal heptylsulfates were

Can. J. Chem. Downloaded from www.nrcresearchpress.com by 210.87.254.105 on 09/05/12
For personal use only.

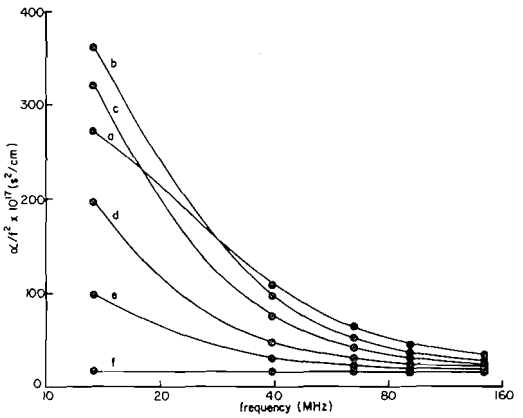

FIG. 1. Ultrasonic absorption in Na heptylsulfate solutions at 40 °C in the 10–150 MHz range. The circles represent the experimental data while the curves have been fitted to reaction 2. The concentrations of the solutions are (*a*) 0.9790 *m*, (*b*) 0.5795 *m*, (*c*) 0.4447 *m*, (*d*) 0.3233 *m*, (*e*) 0.2729 *m*, (*f*) 0.2000 *m*.

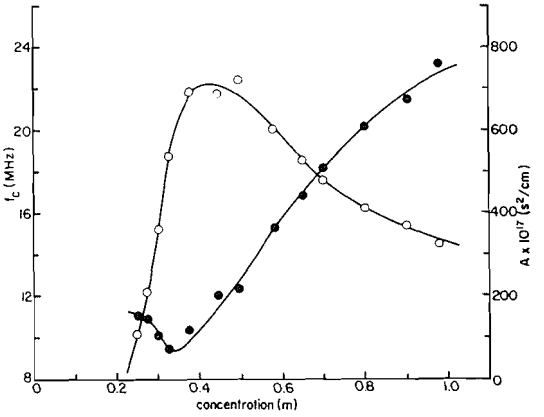

FIG. 2. Relaxational parameters f_c (closed circles) and A (open circles) for Na heptylsulfate solutions at 40.0 °C.

described previously (5). Impurities are now known to affect relaxation frequencies in the neighbourhood of the c.m.c. (6). Special care was then taken to ensure the highest purity. After three re-crystallizations (one from butanol and two from water), the surfactants were analyzed by Epton's method involving titration against standard cetylpyridinium bromide solutions (7). Only when the analyses recorded purities in excess of 99% was it deemed reasonable to proceed.

Hexylammonium chloride was supplied by Eastman Kodak and these solutions were thermostatted at 25.0 °C. The operating temperature of all the other solutions was 40.0 °C so that comparison might be made more easily with the previous work (5).

Results

Ultrasonic absorptions (α/f^2) in the aqueous sodium heptylsulfate system are shown in Fig. 1. To avoid confusion, data for only six of the twelve solutions studied are represented. The closed circles are the experimental points while the curves have been fitted according to the equation for a single relaxation

$$[1] \qquad \frac{\alpha}{f^2} = \frac{A}{1 + (f/f_c)^2} + B$$

where A and B are parameters representing the contribution to the absorption from the relaxation and the background respectively. The relaxation frequency f_c along with A and B were found by a least-squares computer fit for each concentration.

Table 1 lists the values of f_c, A, B, and the standard deviation of the experimental points from the fitted curve for each solution that showed excess sound absorption in the Li, Na, K, Rb, and Cs heptylsulfate and the hexylammonium chloride systems. The values of f_c for the sodium heptylsulfate system are plotted in Fig. 2 and for the hexylammonium chloride system in Fig. 3. The A curves for the same two surfactants are shown in Figs. 2 and 4.

The c.m.c.'s, as determined by the linear extrapolation of the A curve to zero excess absorption (5), were as follows: LiC_7 0.24 *m*, NaC_7 0.22 *m*, KC_7 0.21 *m*, RbC_7 0.21 *m*, CsC_7 0.21 *m* (all at 40 °C) and 0.89 *m* for hexylammonium chloride (at 25 °C). The only literature c.m.c. value for these surfactants is 0.9 *m* for hexylammonium chloride (8).

No excess absorption was obtained for solutions less concentrated than the c.m.c.

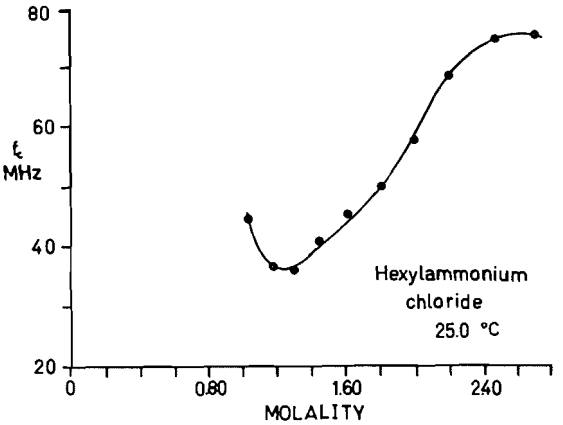

FIG. 3. Relaxation frequencies f_c of hexylammonium chloride solutions at 25.0 °C as a function of concentration.

Can. J. Chem. Downloaded from www.nrcresearchpress.com by 210.87.254.105 on 09/05/12
For personal use only.

Can. J. Chem. Downloaded from www.nrcresearchpress.com by 210.87.254.105 on 09/05/12
For personal use only.

TABLE 1
(*a*) Relaxational parameters for heptylsulfate solutions at 40 °C

Solute	Concentration (m)	$10^{17} A$ ($cm^{-1} Hz^{-2}$)	$10^{17} B$ ($cm^{-1} Hz^{-2}$)	f_c (MHz)	Standard deviation $\times 10^{17}$
LiC_7	0.201	—	16.0	—	—
	0.2372	18.9	16.2	20.1	0.04
	0.2549	37.2	16.5	16.9	0.10
	0.2749	96.6	17.2	13.5	0.20
	0.2996	212	16.7	12.0	0.35
	0.3399	359	17.5	11.7	0.22
	0.3784	472	18.1	11.7	0.24
	0.4986	545	20.0	13.4	0.65
	0.5980	441	20.7	16.7	0.69
NaC_7	0.16; 0.18; 0.20	—	16.5	—	—
	0.2501	107.7	17.0	11.1	0.46
	0.2729	205	17.1	10.9	0.30
	0.2991	362	18.1	10.1_5	0.44
	0.3233	541	18.5	9.44	0.52
	0.3765	692	18.1	10.3_5	0.66
	0.4447	687	18.8	12.0	0.33
	0.4963	722	20.1	12.3	0.23
	0.5795	604	20.0	15.2	0.37
	0.6499	524	21.7	16.8_5	0.55
	0.7023	480	21.8	18.2	0.41
	0.7965	412	23.5	20.2	0.92
	0.9066	369	24.7	21.5	0.98
KC_7	0.17; 0.20	—	16.0	—	—
	0.2491	211	16.3	10.7	0.27
	0.2747	385	16.7	9.9_5	0.38
	0.2999	722	18.3	8.1	0.23
	0.3473	778	17.3	9.9	0.13
	0.4000	723	17.6	12.0	0.61
RbC_7	0.15; 0.18	—	16.0	—	—
	0.2249	58.2	16.2	12.1_5	0.34
	0.2500	173	15.6	11.0	0.48
	0.2750	342	15.4	10.1_5	0.59
	0.2998	499	16.3	9.7	0.50
	0.3887	857	17.8	10.2	0.17
CsC_7	0.14; 0.17	—	15.0	—	—
	0.2240	57.6	15.2	14.0	0.08
	0.2500	179	15.8	11.0	0.51
	0.2751	384	15.8	9.0_5	0.68
	0.2999	723	17.5	7.3_7	0.53
	0.3500	840	18.7	8.4	0.24

Discussion

The excess ultrasonic absorptions observed in the dilute micellar range of the alkali metal heptylsulfate solutions were similar to that obtained in the corresponding octyl and hexyl systems (5) and must be related to micellization in some manner. The actual alkali metal employed as counterion was found to make little difference to the relaxation parameters with the mean f_c in dilute micellar solution ranging from 11.9 MHz in Na heptylsulfate solutions to 8.9 MHz in Cs heptylsulfate solutions. There is thus little likelihood that the counterion plays a significant role in the mechanism responsible for the relaxation.

The concentration dependence of f_c showed a minimum at roughly 0.35 m in sodium heptylsulfate solutions at 40 °C. Rassing, Sams and Wyn-Jones (4) have obtained ultrasonic data for this system at 25 °C and our results are in agreement in the concentrated micellar range (taking into account the temperature difference).

TABLE 1 (*Concluded*)
(*b*) Relaxational parameters for hexylammonium chloride solutions at 25 °C

Concentration (*m*)	10^{17} *A* (cm^{-1} Hz^{-2})	10^{17} *B* (cm^{-1} Hz^{-2})	f_c (MHz)	Standard deviation $\times 10^{17}$
0.22; 0.37	—	20.7	—	—
0.62	—	21.6	—	—
0.696	—	23.3	—	—
1.027	77	30.0	50.0	0.7
1.168	343	51.2	36.6	0.3
1.294	499	56.0	36.1	0.9
1.442	686	47.1	40.9	2.3
1.612	756	53.2	45.1	0.8
1.813	716	65.0	49.9	5.1
2.00	661	63.3	57.8	2.0
2.20	595	53.9	68.4	7.3
2.49	510	61.2	74.5	2.8
2.72	460	78.5	75.2	0.9

However, in the dilute micellar region, these authors did not detect any minima but found instead that the relaxation frequencies continued to decrease in linear fashion to an extrapolated f_c value of zero or near-zero at the c.m.c.

Our results show minima in f_c for all surfactant systems investigated to date. Since the error in measuring α/f^2 of the order of 80–200 $\times$ 10^{-17} s^2 cm^{-1} could be appreciable, it is difficult to say whether close to the c.m.c. the f_c values are in fact increasing. For example, in a 1.00 *m* hexylammonium chloride solution (c.m.c. is 0.89 *m* in this sytem), the f_c that led to the minimum standard deviation was 45 MHz. If 25 MHz had been chosen instead, the average standard deviation would have increased from 1.0 $\times$ 10^{-17} to 1.6 $\times$ 10^{-17} s^2 cm^{-1} which is still a reasonable fit. As a result, even though all systems always show a smoothly increasing f_c on approaching the c.m.c. from the high concentration side, we shall content ourselves with saying that in the dilute micellar range, the relaxation frequency remains constant within experimental error. This was the conclusion of our previous work with hexyl and octylsulfates (5).

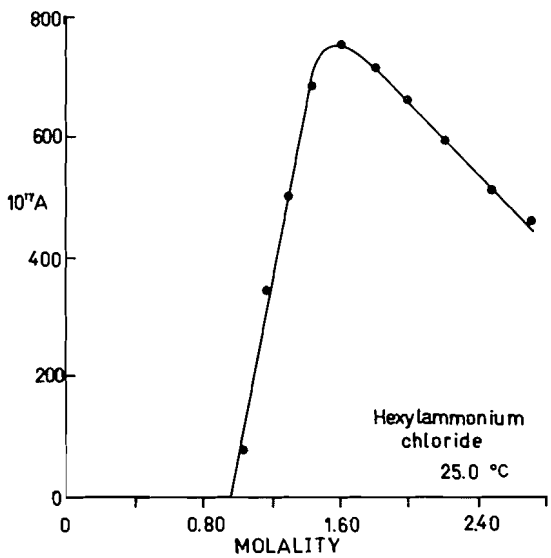

FIG. 4. Plot of *A* *vs.* molality for hexylammonium chloride solutions at 25.0 °C.

The minimum in f_c curve for the hexylammonium chloride solutions at 25 °C was 36.0 MHz and it occurred roughly at 1.30 *m*. These results must be treated with more respect than the heptylsulfate data since the relaxation frequencies for this system (30–75 MHz) fell well within the experimental range of the pulse apparatus employed. The f_c results for the sodium heptylsulfate system are open to the criticism that the f_c's in dilute solution were just at the edge of the experimental range, *i.e.* only the upper half of the relaxation curve was under observation. However, excellent fit of the results to single relaxation curves (*cf.* Fig. 1) and the systematic behaviour of the relaxation parameters (especially the relative constancy in *B*) tend to confirm the adequacy of the analysis.

To eliminate the possibility that the observed concentration patterns in f_c and *A* were simply

Can. J. Chem. Downloaded from www.nrcresearchpress.com by 210.87.254.105 on 09/05/12
For personal use only.

Can. J. Chem. Downloaded from www.nrcresearchpress.com by 210.87.254.105 on 09/05/12
For personal use only.

artifacts of our apparatus, the hexylammonium chloride system was re-investigated at 27 °C on the ultrasonic set-up at Carleton University over the frequency range 10.6–52.8 MHz. Within experimental error, no differences in behaviour were noted.

Previously, we had proposed a rather rough theoretical treatment to account for our results. It still appears to have relevance since no more sophisticated model has been successful. It considers that the chemical relaxation is associated with one of the stepwise equilibria represented by:

$$[2] \qquad m + M_n \underset{k_d}{\overset{k_a}{\rightleftharpoons}} M_{n+1}$$

where m represents the monomeric surfactant ion and M_n and M_{n+1} represents the micelles formed from n and $(n + 1)$ monomers respectively. The kinetic equation for this process should thus be

$$[3] \qquad 2\pi f_c = k_d + k_a([m] + [M_n])$$

which reduces to

$$[4] \qquad 2\pi f_c \approx k_d + k_a(\text{c.m.c.})$$

when the usual assumptions $[m] \gg [M_n]$ and $[m] \approx$ c.m.c. are made.

Above the c.m.c., the solution will contain monomers at an almost constant concentration and n-mers having a rather narrow range of n defining the "micelle size". If the ultrasonic absorption is due to monomer addition/subtraction reactions like [2], it will certainly be dominated by those large values of n for which the n-mer concentration is relatively large. The effect of increasing the total surfactant concentration should not be dramatic since the distribution ratio would change only minimally ($[M_{n+1}]/[M_n] \approx [m]$). Thus, we can expect the same reactions as before to be responsible for the absorption. Therefore, the overall relaxation frequency should probably shift little with concentration while the magnitude of the absorption should increase fairly rapidly with and be roughly proportional to the total micelle concentration. The slight decrease in f_c observed in the dilute micellar range may simply be due to a decrease in the monomer concentration.

This model has more difficulty with the more concentrated micellar region in which f_c is seen to increase linearly with concentration. At the same time, A undergoes a maximum in the curve in the neighbourhood of the f_c minimum and appears to be decreasing gradually to a more or less constant value. The concentration marking the beginning of this more concentrated micellar zone may be the so-called "second c.m.c." (9). For short-chained surfactants, the second c.m.c. may simply indicate the end of a transition range of micelle formation (10).

The ultrasonic data would receive a ready explanation if in the dilute micellar range micelles of a uniform size are being formed so that f_c remains constant and A increases linearly with the increase in the number of these micelles. Beyond the second c.m.c., a differently-shaped or larger-sized micelle becomes energetically more feasible (11) and this new micelle does not absorb sound in this frequency range. Consequently, as the original micelles continue to dissociate with increasing surfactant concentration, A decreases. The increase in f_c could result from k_d in eq. 4 becoming greater reflecting the increasing instability of the original micelles. At this stage, eq. 4 retains only qualitative significance as the monomer concentration must be being altered in some fashion by the appearance of the new micelle or range of micelles. At present, conductivity, viscosity, and density measurements are being conducted in this transitional region to shed further light on these micellar phenomena.

Acknowledgments

We are grateful to the National Research Council of Canada for financial support, to Dr. Peeter Kruus of Carleton University for kindly making available his ultrasonic instrumentation and Mr. David J. Williams for technical assistance.

1. N. MULLER. J. Phys. Chem. **76**, 3017 (1972).
2. J. LANG, C. TONDRE, R. ZANA, R. BAUER, H. HOFFMANN, and W. ULBRICHT. J. Phys. Chem. **79**, 276 (1975).
3. P. J. SAMS, E. WYN-JONES, and J. RASSING. Chem. Phys. Lett. **13**, 233 (1972).
4. J. RASSING, P. J. SAMS, and E. WYN-JONES. J. Chem. Soc. Faraday II, **70**, 1247 (1974).
5. D. A. W. ADAIR, V. C. REINSBOROUGH, N. PLAVAC, and J. P. VALLEAU. Can. J. Chem. **52**, 429 (1974).
6. H. HOFFMANN. Chemical and biological applications of relaxation spectrometry. Series C, Vol. 18. NATO Advanced Study Institutes Series. *Edited by* E. Wyn-Jones. D. Reidel, Dordrecht-Holland. 1975. p. 181.

7. S. R. EPTON. Trans. Faraday Soc. **44**, 226 (1948).
8. P. MUKERJEE and K. J. MYSELS. Critical micelle concentrations of aqueous surfactant systems. National Bureau of Standards (U.S.) NSRDS-NBS 36, Washington. 1971. p. 184.
9. P. EKWALL and P. STENIUS. Acta Chem. Scand. **27**, 1767 (1967).
10. G. M. MUSBALLY, G. PERRON, and J. E. DESNOYERS. J. Colloid Interface Sci. **48**, 494 (1974).
11. F. REISS-HUSSON and V. LUZZATI. J. Colloid Interface Sci. **21**, 534 (1966).

Can. J. Chem. Downloaded from www.nrcresearchpress.com by 210.87.254.105 on 09/05/12
For personal use only.

Crystal and molecular structure of (salicylaldehydato)diphenylboron

STEVEN J. RETTIG AND JAMES TROTTER

Department of Chemistry, University of British Columbia, Vancouver, British Columbia V6T 1W5

Received September 11, 1975

STEVEN J. RETTIG and JAMES TROTTER. Can. J. Chem. **54**, 1168 (1976).

Crystals of (salicylaldehydato)diphenylboron are orthorhombic, $a = 11.6548(5)$, $b = 16.2983(5)$, $c = 8.0806(2)$ Å, $Z = 4$, space group $Pna2_1$. The structure was solved by direct methods and was refined by full-matrix least-squares procedures to a final R of 0.051 for 1386 reflections with $I \geq 3\sigma(I)$. The BO_2C_3 ring has a distorted 'sofa' conformation. Bond lengths in the molecule (those not involving hydrogen atoms have been corrected for thermal motion) are: C—O, 1.263(4) and 1.334(4), B—O, 1.500(4) and 1.574(4), C—B, 1.603(5) and 1.610(5), C—C(salicylaldehyde), 1.368–1.423(5–8), C—C(phenyl), 1.352–1.413(5–11), and weighted mean C(sp^2)—H, 0.96 Å.

STEVEN J. RETTIG et JAMES TROTTER. Can. J. Chem. **54**, 1168 (1976).

Les cristaux du salicylaldéhydato diphénylbore sont orthorhombiques, $a = 11.6548(5)$, $b = 16.2983(5)$, $c = 8.0806(2)$ Å, $Z = 4$, groupe d'espace $Pna2_1$. On a résolu la structure par des méthodes directes et on l'a affinée par la méthode des moindres carrés (matrice complète) jusqu'à une valeur finale de R de 0.051 pour 1386 réflexions avec $I \geq 3\sigma(I)$. Le cycle BO_2C_3 a la conformation "sofa" croisée. Les longueurs de liaisons dans la molécule (celles n'impliquant pas les atomes d'hydrogène ont été corrigées pour les mouvements thermiques) sont C—O 1.263(4) et 1.334(4), B—O 1.500(4) et 1.574(4), C—B 1.603(5) et 1.610(5), C—C (salicylaldéhyde), 1.368–1.423(5–8), C—C(phényl), 1.352–1.413(5–11), et la valeur moyenne du C(sp^2)—H est de 0.96 A.

[Traduit par le journal]

Introduction

The crystal structures of a number of organoboron compounds containing intramolecular N → B interactions have now been determined. Among these compounds are the ethanolamine esters of the boron acids (**1**, **2**, and **3**) (1–5). We now report the structure of the salicylaldehyde ester of diphenylborinic acid (**4**) which contains an intramolecular O→B interaction.

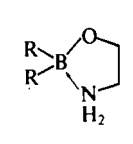

1

a R = C_6H_5
b R = *p*-FC_6H_4

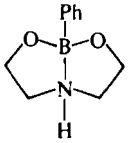

2

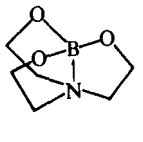

3

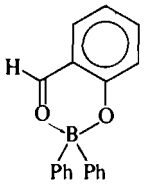

4

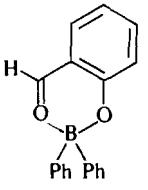

5

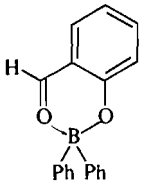

6

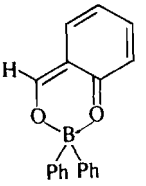

7

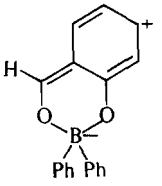

8

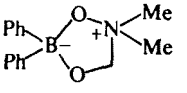

9

Experimental

(Salicylaldehydato)diphenylboron was prepared as previously described (6, 7). Recrystallization from 100% ethanol gave bright yellow-orange needles elongated along *c*. The crystal chosen for study was mounted with *c* parallel to the goniostat axis and had dimensions of *ca.* 0.35 × 0.35 × 0.6 mm. Unit-cell and space group data were obtained from film and diffractometer measurements. The unit-cell parameters were refined by a least-squares treatment of $\sin^2\theta$ values for 16 reflections measured on a diffractometer with Cu K_α radiation. Crystal data are: $C_{19}H_{15}BO_2$ f.w. = 286.1 Orthorhombic, $a = 11.6548(5)$, $b = 16.2983(5)$, $c = 8.0806(2)$ Å, $V = 1534.9(1)$ Å^3, $\rho_m = 1.24$ (flotation in aqueous KI), $Z = 4$, $\rho_c = 1.2381(1)$ g cm^{-3}, $F(000) = 664$ (22 °C, Cu K_α, $\lambda = 1.5418$ Å, $\mu = 6.3$ cm^{-1}). Absent reflections: $0kl$, $k + l \neq 2n$ and $h0l$, $h \neq 2n$, space group $Pna2_1$ (C_{2v}^9, No. 33).

Intensities were measured on a Datex-automated General Electric XRD 6 diffractometer, with a scintillation

Can. J. Chem. Downloaded from www.nrcresearchpress.com by 210.87.254.105 on 09/05/12
For personal use only.

Can. J. Chem. Downloaded from www.nrcresearchpress.com by 210.87.254.105 on 09/05/12
For personal use only.

counter, Cu K_α (nickel filter and pulse height analyser), and a θ–2θ scan at 2° min^{-1} over a range of (1.80 + 0.86 tan θ) deg in 2θ, with 10 s background counts being measured at each end of the scan. Data were measured to 2θ = 146° (minimum interplanar spacing 0.81 Å). The intensity of the check reflection, measured every 40 reflections throughout the data collection, decreased slowly to a value which was 80% of the initial count by the end of the data collection. Lorentz and polarization corrections and check reflection scaling were applied, and the structure amplitudes were derived. No absorption correction was made in view of the low value of μ. Of the 1649 independent reflections measured, 257 had intensities less than $3\sigma(I)$ above background where $\sigma^2(I) = S + B + (0.06S)^2$ with S = scan count and B = time-averaged background count. These reflections were given zero weight in the refinement but were included in the structure factor calculations.

Structure Analysis

The systematic absences allow space groups $Pna2_1$ or *Pnam*. The noncentrosymmetric space group $Pna2_1$ was indicated by the *E*-statistics. The structure was solved by direct methods, 225 reflections with normalized structure factor $|E| \geq 1.40$ being used in the symbolic addition procedure for noncentrosymmetric crystals (8). Four sets of phases were generated by a computer program which determines phases using the tangent formula (9, 10). One set of phases was outstanding in that it had the lowest value of *Rk* (0.16) and the greatest number of phases determined (225). The highest 22 peaks on an *E*-map calculated from this set of phases accounted for the 22 non-hydrogen atoms in the molecule.

Two cycles of isotropic followed by two cycles of anisotropic full-matrix least squares refinement of the non-hydrogen atoms gave *R* 0.079. A difference map at this point gave positions for all 15 hydrogen atoms, which were included in all subsequent cycles of refinement with isotropic thermal parameters. The entire structure was refined for 4 cycles giving a final *R* of 0.051 and R_w of 0.065 for 1386 reflections with $I \geq 3\sigma(I)$ (6 reflections which had $|F_o| - |F_c| > 3\sigma(F)$ were removed from the data set in the final stages of refinement).

The least-squares refinement was based on the minimization of $\sum w[|F_o| - |F_c/(1 + gI)|]^2$ where g is the extinction parameter and I the uncorrected intensity. The final value of g was 6.4×10^{-8}. The scattering factors of ref. 11 were used for the non-hydrogen atoms and those of ref. 12 for the hydrogen atoms. Anomalous scattering factors from ref. 13 were used for the non-hydrogen atoms. The anisotropic thermal parameters employed in the refinement are U_{ij} in the expression:

$$f = f^0 \exp\,[-2\pi^2(U_{11}h^2a^{*2} + U_{22}k^2b^{*2} + U_{33}l^2c^{*2} + 2U_{12}hka^*b^* + 2U_{13}hla^*c^* + 2U_{23}klb^*c^*)]$$

where f^0 is the tabulated scattering factor and f is that corrected for thermal motion. The weighting scheme: $w = 1/\sigma^2(F)$ where $\sigma^2(F)$ is derived from the previously defined $\sigma^2(I)$ gave uniform average values of $w(|F_o| - |F_c|)^2$ over ranges of $|F_o|$ and was employed in the final stages of refinement.

The absolute configuration of the molecule (for the particular crystal used) has been determined through the anomalous scattering of the non-hydrogen atoms. Enantiomorph A is represented by the coordinates in Table 1 referred to a right-handed axial system and enantiomorph B, the mirror image of A, was generated by changing the z coordinates of A to $1 - z$. Both enantiomorphs were refined and Hamilton's test (14) applied to the resulting *R* factor ratios. These ratios (B/A) and the % probabilities that A is the correct enantiomorph are: 1.0007 (75%) for *R* (all data), 1.0012 (90%) for *R* (3σ data), 1.0001 (indeterminate) for R_w (all data), and 1.0006 (50%) for R_w (3σ data). The figures quoted above represent a marginal indication that enantiomorph A is correct.

On the final cycle of refinement the mean parameter shift was 0.03σ and no parameter shift was larger than 0.27σ. The mean error in an observation of unit weight was 1.54. The final positional and thermal parameters appear in Tables 1 and 2, respectively. Measured and

TABLE 1. Final positional parameters (fractional × 10^4, H × 10^3) with estimated standard deviations in parentheses

Atom	*x*	*y*	*z*
O(1)	6867(2)	4232(1)	3633
O(2)	5298(2)	4573(1)	5574(5)
C(1)	6516(3)	3455(2)	3667(6)
C(2)	5549(3)	3231(2)	4598(6)
C(3)	5146(4)	2409(3)	4534(8)
C(4)	5700(5)	1839(3)	3593(8)
C(5)	6647(5)	2082(3)	2663(8)
C(6)	7059(4)	2877(3)	2671(7)
C(7)	4938(3)	3846(2)	5450(7)
C(8)	6566(3)	5717(2)	4397(6)
C(9)	5773(4)	6303(2)	4881(6)
C(10)	5890(4)	7121(3)	4373(7)
C(11)	6789(4)	7366(3)	3452(8)
C(12)	7598(4)	6808(3)	2953(7)
C(13)	7480(3)	5993(2)	3424(7)
C(14)	7372(3)	4638(2)	6602(6)
C(15)	6963(4)	4702(3)	8224(6)
C(16)	7695(7)	4622(3)	9567(8)
C(17)	8855(7)	4483(4)	9304(11)
C(18)	9259(4)	4429(3)	7757(12)
C(19)	8530(3)	4500(3)	6403(8)
B	6556(3)	4789(2)	5036(6)
H(3)	455(4)	230(2)	518(6)
H(4)	538(5)	126(4)	367(11)
H(5)	712(4)	170(3)	192(7)
H(6)	771(4)	302(3)	200(8)
H(7)	414(4)	376(3)	588(6)
H(9)	516(3)	610(2)	537(6)
H(10)	527(4)	743(3)	464(8)
H(11)	690(5)	787(4)	308(10)
H(12)	829(5)	688(4)	214(10)
H(13)	814(4)	559(3)	309(8)
H(15)	609(4)	482(3)	834(8)
H(16)	738(5)	470(4)	1068(11)
H(17)	919(6)	453(4)	1018(12)
H(18)	1001(4)	434(2)	750(6)
H(19)	886(4)	439(3)	539(8)

Can. J. Chem. Downloaded from www.nrcresearchpress.com by 210.87.254.105 on 09/05/12
For personal use only.

TABLE 2. Final thermal parameters and their estimated standard deviations
(*a*) Anisotropic thermal parameters ($U_{ij} \times 10^3$ Å^2)

Atom	U_{11}	U_{22}	U_{33}	U_{12}	U_{13}	U_{23}
O(1)	59(1)	43(1)	40(1)	−3(1)	12(1)	−4(1)
O(2)	39(1)	46(1)	54(2)	0(1)	4(1)	1(1)
C(1)	58(2)	47(2)	33(2)	−2(1)	−4(2)	0(2)
C(2)	49(2)	49(2)	43(2)	1(1)	−4(2)	1(2)
C(3)	75(3)	55(2)	64(3)	−11(2)	7(3)	2(2)
C(4)	99(3)	48(2)	70(3)	−11(2)	0(3)	−7(2)
C(5)	105(4)	49(2)	71(3)	8(2)	13(3)	−12(2)
C(6)	77(3)	60(2)	50(3)	3(2)	7(2)	−9(2)
C(7)	41(2)	51(2)	53(2)	−2(1)	0(2)	3(2)
C(8)	47(2)	42(2)	31(2)	−1(1)	−7(1)	0(1)
C(9)	53(2)	49(2)	50(2)	2(2)	1(2)	0(2)
C(10)	85(3)	48(2)	61(3)	20(2)	−10(3)	−6(2)
C(11)	87(3)	44(2)	63(3)	−8(2)	−12(3)	6(2)
C(12)	71(3)	56(2)	60(3)	−11(2)	−2(2)	14(2)
C(13)	47(2)	50(2)	54(2)	−1(1)	1(2)	8(2)
C(14)	47(2)	30(1)	37(2)	0(1)	0(2)	3(1)
C(15)	77(3)	59(2)	36(2)	5(2)	2(2)	0(2)
C(16)	152(6)	62(3)	38(3)	−9(3)	−17(3)	0(2)
C(17)	123(5)	64(3)	83(5)	−28(3)	−62(5)	22(3)
C(18)	52(3)	68(3)	136(6)	−14(2)	−35(3)	35(4)
C(19)	43(2)	57(2)	65(3)	0(2)	1(2)	17(2)
B	38(2)	44(2)	34(2)	3(1)	4(2)	−1(2)

(*b*) Isotropic thermal parameters ($U \times 100$)

Atom	U (Å^2)	Atom	U (Å^2)	Atom	U (Å^2)
H(3)	5(1)	H(9)	5(1)	H(15)	9(2)
H(4)	13(2)	H(10)	8(2)	H(16)	10(2)
H(5)	7(1)	H(11)	11(2)	H(17)	13(3)
H(6)	8(2)	H(12)	11(2)	H(18)	6(1)
H(7)	6(1)	H(13)	8(2)	H(19)	7(2)

calculated structure factors have been placed in the Depository of Unpublished Data.[1]

The thermal motion has been analysed in terms of the rigid-body modes of translation, libration, and screw motion (15) using the computer program MGTLS. Rigid-body analyses were successful for the three groups: C(1)–C(8), B, O(1), O(2), and C(14) (r.m.s. ΔU_{ij} = 0.0042 Å^2), C(8)–C(13), and B (r.m.s. ΔU_{ij} = 0.0030 Å^2), and C(14)–C(19), and B (r.m.s. ΔU_{ij} = 0.0043 Å^2). The root-mean-square standard deviation in the individual U_{ij} is 0.0024 Å^2. All bond distances not involving hydrogen atoms have been corrected for libration (16, 17) and appear along with the uncorrected distances in Table 3. Changes in the bond angles were not significant thus only the uncorrected angles appear in Table 4.

Results and Discussion

Figure 1 shows a general view of the molecule and crystallographic numbering scheme and Fig. 2 shows the packing arrangement viewed down *c*. Intraannular torsion angles defining the conformation of the six-membered BOCCCO ring are listed in Table 5 and some weighted least-squares mean planes in Table 6. Nonbonded inter- and intramolecular contacts are given in Table 7.

The expected O→B interaction is indeed present in this structure. The resulting six-membered BOCCCO ring has a somewhat distorted sofa conformation. The boron atom is displaced 0.33 Å from the mean plane of the other five atoms. The five atom segment [O(1),O(2),C(1),C(2),C(7)] is itself significantly nonplanar but all five atoms are within ±0.06 Å of the mean plane. This arrangement is unlike that in related Cu, Ni, and Pt complexes (18–22) wherein the metal atom is co-planar with the salicylaldehyde ligand. The geometry

[1]The structure factor table is available, at a nominal charge, from the Depository of Unpublished Data, CISTI, National Research Council of Canada, Ottawa, Canada K1A 0S2.

TABLE 3. Bond lengths (Å) with estimated standard deviations in parentheses
(*a*) Non-hydrogen atoms

Bond	Distance		Bond	Distance	
	Uncorrected	Corrected		Uncorrected	Corrected
O(1)—C(1)	1.332(4)	1.334	C(8)—B	1.599(5)	1.603
O(1)—B	1.496(4)	1.500	C(9)—C(10)	1.401(6)	1.405
O(2)—C(7)	1.261(4)	1.263	C(10)—C(11)	1.346(7)	1.353
O(2)—B	1.569(4)	1.574	C(11)—C(12)	1.371(7)	1.380
C(1)—C(2)	1.403(5)	1.407	C(12)—C(13)	1.389(6)	1.393
C(1)—C(6)	1.392(6)	1.396	C(14)—C(15)	1.398(6)	1.413
C(2)—C(3)	1.421(5)	1.423	C(14)—C(19)	1.378(5)	1.393
C(2)—C(7)	1.409(5)	1.413	C(14)—B	1.602(5)	1.610
C(3)—C(4)	1.364(7)	1.368	C(15)—C(16)	1.386(8)	1.396
C(4)—C(5)	1.393(8)	1.397	C(16)—C(17)	1.388(11)	1.403
C(5)—C(6)	1.380(6)	1.382	C(17)—C(18)	1.339(11)	1.352
C(8)—C(9)	1.386(5)	1.395	C(18)—C(19)	1.391(8)	1.400
C(8)—C(13)	1.399(5)	1.407			

(*b*) Bonds involving hydrogen atoms

Bond	Distance	Bond	Distance
C(3) —H(3)	0.89(4)	C(12)—H(12)	1.04(7)
C(4) —H(4)	1.02(6)	C(13)—H(13)	1.05(5)
C(5) —H(5)	1.03(5)	C(15)—H(15)	1.04(5)
C(6) —H(6)	0.96(6)	C(16)—H(16)	0.98(8)
C(7) —H(7)	1.00(5)	C(17)—H(17)	0.81(9)
C(9) —H(9)	0.88(4)	C(18)—H(18)	0.91(5)
C(10)—H(10)	0.91(5)	C(19)—H(19)	0.92(6)
C(11)—H(11)	0.89(7)		

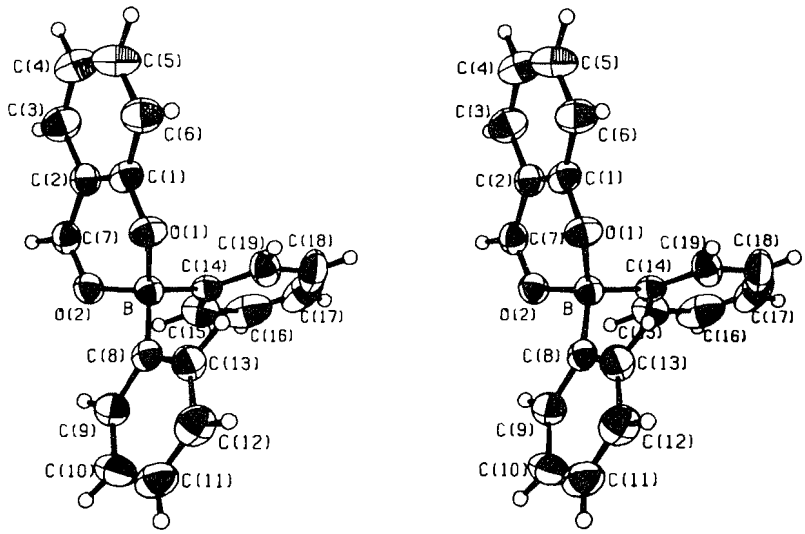

FIG. 1. A stereo view of the (salicylaldehydato)diphenylboron molecule. 50% ellipsoids are shown for the non-hydrogen atoms.

Can. J. Chem. Downloaded from www.nrcresearchpress.com by 210.87.254.105 on 09/05/12
For personal use only.

Can. J. Chem. Downloaded from www.nrcresearchpress.com by 210.87.254.105 on 09/05/12
For personal use only.

TABLE 4. Bond angles (deg) with estimated standard deviations in parentheses

(*a*) Non-hydrogen atoms

Bonds	Angle (deg)	Bonds	Angle (deg)
C(1) —O(1) —B	119.1(3)	C(10)—C(11)—C(12)	120.0(4)
C(7) —O(2) —B	120.0(3)	C(11)—C(12)—C(13)	119.1(4)
O(1) —C(1) —C(2)	120.4(3)	C(8) —C(13)—C(12)	122.5(4)
O(1) —C(1) —C(6)	119.5(4)	C(15)—C(14)—C(19)	117.1(4)
C(2) —C(1) —C(6)	119.9(3)	C(15)—C(14)—B	121.8(3)
C(1) —C(2) —C(3)	119.5(4)	C(19)—C(14)—B	120.9(4)
C(1) —C(2) —C(7)	118.9(3)	C(14)—C(15)—C(16)	121.1(5)
C(3) —C(2) —C(7)	121.4(4)	C(15)—C(16)—C(17)	119.7(6)
C(2) —C(3) —C(4)	120.4(5)	C(16)—C(17)—C(18)	119.8(5)
C(3) —C(4) —C(5)	118.8(4)	C(17)—C(18)—C(19)	121.0(5)
C(4) —C(5) —C(6)	122.7(4)	C(15)—C(19)—C(18)	121.3(5)
C(1) —C(6) —C(5)	118.7(4)	O(1) —B —O(2)	107.5(3)
O(2) —C(7) —C(2)	122.6(3)	O(1) —B —C(8)	109.1(3)
C(9) —C(8) —C(13)	116.4(3)	O(1) —B —C(14)	111.2(3)
C(9) —C(8) —B	123.8(3)	O(2) —B —C(8)	107.9(3)
C(13)—C(8) —B	119.4(3)	O(2) —B —C(14)	107.6(3)
C(8) —C(9) —C(10)	120.5(4)	C(8) —B —C(14)	113.3(3)
C(9) —C(10)—C(11)	121.4(4)		

(*b*) Angles involving hydrogen atoms

Bonds	Angle (deg)	Bonds	Angle (deg)
C(2) —C(3) —H(3)	116(3)	C(12)—C(11)—H(11)	115(4)
C(4) —C(3) —H(3)	124(3)	C(11)—C(12)—H(12)	130(3)
C(3) —C(4) —H(4)	115(4)	C(13)—C(12)—H(12)	111(3)
C(5) —C(4) —H(4)	126(4)	C(8) —C(13)—H(13)	120(3)
C(4) —C(5) —H(5)	125(3)	C(12)—C(13)—H(13)	117(3)
C(6) —C(5) —H(5)	113(3)	C(14)—C(15)—H(15)	116(4)
C(1) —C(6) —H(6)	121(3)	C(16)—C(15)—H(15)	123(4)
C(5) —C(6) —H(6)	120(3)	C(15)—C(16)—H(16)	119(4)
O(2) —C(7) —H(7)	114(3)	C(17)—C(16)—H(16)	122(4)
C(2) —C(7) —H(7)	123(3)	C(16)—C(17)—H(17)	109(6)
C(8) —C(9) —H(9)	114(3)	C(18)—C(17)—H(17)	130(6)
C(10)—C(9) —H(9)	125(3)	C(17)—C(18)—H(18)	124(3)
C(9) —C(10)—H(10)	113(3)	C(19)—C(18)—H(18)	115(3)
C(11)—C(10)—H(10)	126(3)	C(14)—C(19)—H(19)	123(3)
C(10)—C(11)—H(11)	125(4)	C(18)—C(19)—H(19)	115(3)

TABLE 5. Intra-annular torsion angles (deg) six-membered BOCCCO ring

Bond	Angle (deg)
B —O(1)	38.5(3)
O(1)—C(1)	−23.9(4)
C(1)—C(2)	−2.0(4)
C(2)—C(7)	8.6(4)
C(7)—O(2)	10.6(4)
O(2)—B	−32.3(4)

of the salicylaldehyde portion of the molecule is similar to that of the metal complexes (18–22) as well as that of the free aldehyde (23). Bond lengths in the molecule suggest that resonance forms **5**–**8** are the most important contributors to the structure.

The two B—O bonds, B—O(1), 1.500(4), and B—O(2), 1.574(4) Å, are significantly different. These distances are similar to those found for the related compound **9** (24) of 1.506(7) and 1.556(8) Å. The shorter B—O(1) bond at 1.500(4) Å is longer than the mean B—O single bond distance of 1.477 Å in compounds **1** and **2** (1–3).

Both phenyl rings are planar within experimental error. For each phenyl group the B atom is significantly displaced from the mean plane while all substituent hydrogen atoms lie

Can. J. Chem. Downloaded from www.nrcresearchpress.com by 210.87.254.105 on 09/05/12
For personal use only.

TABLE 6. (*a*) Equations of weighted least-squares planes in the form $lX + mY + nZ = p$ where X, Y, and Z are orthogonal coordinates with respect to a, b, and c; deviations of atoms from the planes are also given

Plane	χ^2	Equation	Deviations of atoms from plane (Å)					
			Atom	Deviation	Atom	Deviation	Atom	Deviation
1, C(8)–C(13)	7.6	$-0.5321X - 0.1859Y - 0.8266Z = -8.7362$	C(8)	0.002(4)	C(9)	−0.008(5)	C(10)	0.011(6)
			C(11)	−0.005(6)	C(12)	−0.003(6)	C(13)	0.002(5)
			H(9)	0.11(5)	H(10)	0.12(6)	H(11)	0.03(7)
			H(12)	0.09(7)	H(13)	−0.06(6)	B	−0.138(5)
2, C(14)–C(19)	2.9	$0.1627X + 0.9865Y - 0.0158Z = 8.7726$	C(14)	−0.002(3)	C(15)	0.004(4)	C(16)	−0.003(5)
			C(17)	−0.004(6)	C(18)	0.005(5)	C(19)	−0.001(4)
			H(15)	0.03(5)	H(16)	0.05(6)	H(17)	0.12(7)
			H(18)	0.01(5)	H(19)	−0.10(5)	B	0.106(5)
3, C(1)–C(6)	14.2	$-0.5971X + 0.2342Y - 0.7672Z = -5.4812$	C(1)	−0.008(4)	C(2)	0.002(4)	C(3)	0.009(6)
			C(4)	−0.011(6)	C(5)	−0.001(6)	C(6)	0.011(5)
			O(1)	0.066(2)	C(7)	0.134(5)	H(3)	−0.02(5)
			H(4)	−0.06(8)	H(5)	−0.02(5)	H(6)	0.03(6)
			H(7)	0.39(5)	O(2)	0.085(3)		

(*b*) Dihedral angles between planes

Planes	Angle (deg)
1–2	104.9
1–3	24.8
2–3	81.6

Can. J. Chem. Downloaded from www.nrcresearchpress.com by 210.87.254.105 on 09/05/12
For personal use only.

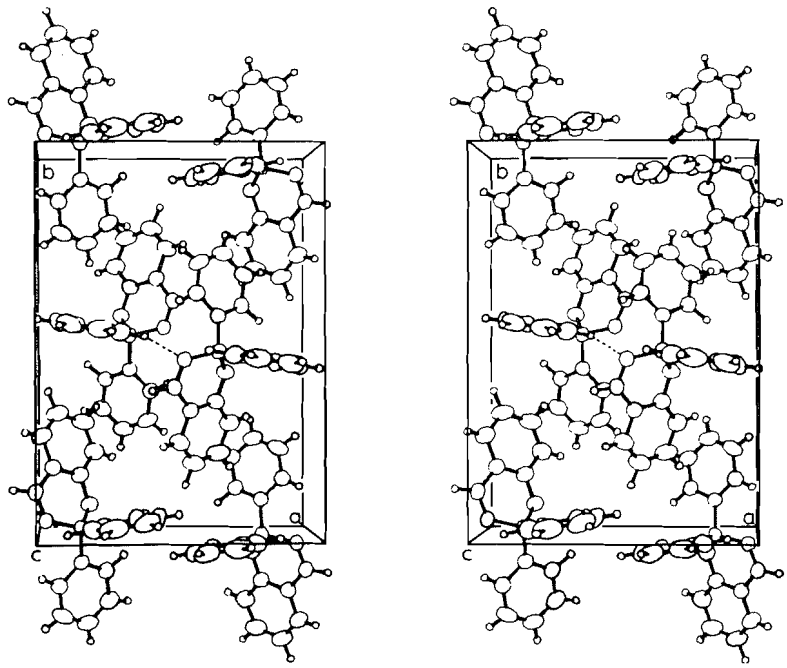

FIG. 2. The crystal structure viewed down *c*.

TABLE 7
(*a*) Selected intramolecular contacts and intermolecular distances (Å)

Intramolecular contacts		Intermolecular distance*	
Atoms	Distance	Atoms	Distance
O(1)...C(13)	2.962(4)	C(12)...H(7)[1]	2.79(5)
O(1)...C(19)	2.993(6)	H(13)...H(18)[2]	2.22(7)
C(1)...C(14)	3.215(5)		
C(7)...C(14)	3.253(5)		
C(3)...H(7)	2.73(5)		
C(7)...H(3)	2.57(4)		

(*b*) C—H...O interactions (distances in Å and angles in deg)*

	Distance			
D—H...A	H...A	D...A	∠DHA	∠XAH
C(16)—H(16)...O(1)[3]	2.58(8)	3.483(7)	154(5)	112, 125(1)
C(15)—H(15)...O(2)[4]	2.62(6)	3.457(5)	137(4)	95, 107(1)
C(15)—H(15)...O(2)	2.45(6)	2.898(5)	105(4)	111, 82(1)
C(9)—H(9)...O(2)	2.50(4)	2.928(5)	111(3)	155, 80(1)

*Superscripts refer to atoms at positions: [1] $1-x, 1-y, z-\frac{1}{2}$; [2] $2-x, 1-y, z-\frac{1}{2}$; [3] $x, y, 1+z$; [4] $1-x, 1-y, \frac{1}{2}+z$.

Can. J. Chem. Downloaded from www.nrcresearchpress.com by 210.87.254.105 on 09/05/12
For personal use only.

in their respective mean planes. The dihedral angles defining the orientations of the phenyl rings are: O(2)[B–C(8)]C(9), −24.6, O(1)[B–C(8)]C(13), 45.5, O(2)[B–C(14)]C(15), 27.4, and O(1)[B–C(14)]C(19), −40.2°.

The B—C(phenyl) distances in the related ethanolamine complexes (1–3) range from 1.613(2) to 1.623(5) Å with a weighted mean value of 1.618(4) Å while the two B—C distances in the present structure are 1.603(5) and 1.610(5) Å. These distances appear to be slightly shorter than in the ethanolamine complexes while the structure **9** (24), which also has two weak B—O bonds, has two B—C bonds which are longer than those in the ethanolamine complexes (1.624(7) and 1.639(8) Å). The C–C distances in the phenyl rings have a mean value of 1.393 Å but the individual values, which range from 1.352(11) to 1.413(6) Å, are significantly different. Corresponding bond lengths and angles in the two phenyl rings are equal within experimental error (going from C(8) to C(13) in the first ring and from C(14) to C(15) in the other).

The distribution of C—H distances in this structure is bimodal with seven short bonds ranging from 0.81(9) to 0.92(6) Å and eight longer bonds ranging from 0.96(6) to 1.05(5) Å. The weighted mean values are 0.89(3) and 1.02(3) Å respectively and the overall mean value of 0.96 Å is as expected for X-ray data. The bond angles involving hydrogen atoms (see Table 4*b*) are as expected.

The packing arrangement, shown in Fig. 2, displays some interesting features. There appears to be a network of weak C—H...O interactions present in the structure. There are four unique interactions (listed in Table 7), one of which involves O(1). The arrangement at O(2) is interesting in that H(15) is involved in two separate interactions (one intramolecular and one intermolecular) with the bonding $p\pi$ orbital of O(2). The other interaction involves H(9) and the sp^2 hybridized lone pair of O(2). All other intermolecular distances correspond to normal van der Waals interactions.

Acknowledgments

We thank the National Research Council of Canada for financial support and the University of British Columbia Computing Centre for assistance.

1. S. J. Rettig and J. Trotter. Can. J. Chem. **51**, 1288 (1973).
2. S. J. Rettig and J. Trotter. Acta Crystallogr. **B30**, 2139 (1974).
3. S. J. Rettig and J. Trotter. Can. J. Chem. **53**, 1393 (1975).
4. Z. Taira and K. Osaki. Inorg. Nucl. Chem. Lett. **7**, 509 (1971).
5. (*a*) R. Mattes, D. Fenske, and K. F. Tebbe. Chem. Ber. **105**, 2089 (1972); (*b*) H. Follner. Mh. Chem. **104**, 477 (1973).
6. F. Umland and C. Schleyerbach. Angew. Chem. **77**, 426 (1965).
7. I. Bally, A. Arsene, M. Bacescu-Roman, and A. T. Balaban. Tetrahedron Lett. 3929 (1965).
8. J. Karle and I. L. Karle. Acta Crystallogr. **21**, 849 (1966).
9. J. Karle and H. Hauptman. Acta Crystallogr. **9**, 635 (1965).
10. (*a*) M. G. B. Drew. Private communication. (*b*) M. G. B. Drew, D. H. Templeton, and A. Zalkin. Acta Crystallogr. **B25**, 261 (1969).
11. D. T. Cromer and J. B. Mann. Acta. Crystallogr. **A24**, 321 (1968).
12. R. F. Stewart, E. R. Davidson, and W. T. Simpson. J. Chem. Phys. **42**, 3175 (1965).
13. D. T. Cromer and D. Liberman. J. Chem. Phys. **53**, 1891 (1970).
14. W. C. Hamilton. Acta Crystallogr. **18**, 502 (1965).
15. V. Schomaker and K. N. Trueblood. Acta Crystallogr. **B24**, 63 (1969).
16. D. W. J. Cruickshank. Acta Crystallogr. **9**, 747 (1956); **9**, 754 (1956).
17. D. W. J. Cruickshank. Acta Crystallogr. **14**, 896 (1961).
18. A. J. McKinnon, T. N. Waters, and D. Hall. J. Chem. Soc. 3290 (1964).
19. J. A. Bevan, D. P. Graddon, and J. F. McConnell. Nature, **199**, 373 (1963).
20. A. J. McKinnon, T. N. Waters, and D. Hall. J. Chem. Soc. 425 (1965).
21. J. M. Stewart, E. C. Lingafelter, and J. D. Breazeale. Acta Crystallogr. **14**, 888 (1961).
22. M. R. Truter and R. C. Watling. J. Chem. Soc. (A), 1955 (1967).
23. P. Bourre-Maladiere. C. R. Acad. Sci. Paris, **237**, 825 (1953).
24. S. J. Rettig, J. Trotter, and W. Kliegel. Can. J. Chem. **52**, 2531 (1974).

Can. J. Chem. Downloaded from www.nrcresearchpress.com by 210.87.254.6 on 09/05/12
For personal use only.

Canadian Journal of Chemistry

Published by
THE NATIONAL RESEARCH COUNCIL OF CANADA

Journal canadien de chimie

Publié par
LE CONSEIL NATIONAL DE RECHERCHES DU CANADA

Volume 54 Number 8 April 15, 1976

Volume 54 numéro 8 15 avril 1976

Reaction rates of electrons in liquid methanol and ethanol: effects of pressure[1]

GERALD L. BOLTON,[2] MAURICE G. ROBINSON,[3] AND GORDON R. FREEMAN
Chemistry Department, University of Alberta, Edmonton, Alberta T6G 2G2

Received November 26, 1975

GERALD L. BOLTON, MAURICE G. ROBINSON, and GORDON R. FREEMAN. Can. J. Chem. **54**, 1177 (1976).

The value of the rate constant k_1 for the reaction $e^-_{solv} \rightarrow RO^-_{solv} + H$, [1], at 295 K and 1 bar is $\leq 1.4 \times 10^5\ s^{-1}$ in methanol and $\leq 8 \times 10^4\ s^{-1}$ in ethanol. The respective volumes of activation averaged between 1 bar and 2 kbar are $\Delta V_1^* \leq -21$ and $\leq -22\ cm^3\ mol^{-1}$. A high concentration of potassium hydroxide (1 *M*) or water (5 *M*) decreases the apparent value of k_1 somewhat but has little or no effect on the value of ΔV_1^*. The effect of pressure on the rate constant of $e^-_{solv} + S \rightarrow$ product, [2], was also measured for a series of solutes that displays a wide range of reactivity. Experimental values of ΔV_2^* depend on the relative contributions of the effects of solvent density on the reactant diffusion rates, the concentrations of the actual reacting species, and the relative energies of the reactant and intermediate states. For reactions whose rates are near the diffusion controlled limit, $k_2 \approx 10^{10}\ M^{-1}\ s^{-1}$ in methanol and ethanol, the values of ΔV_2^* are positive and similar to those for the diffusion of simple ions. ΔV^* (e^-_{solv} diffusion) $\approx 4\ cm^3\ mol^{-1}$ in methanol and $6\ cm^3\ mol^{-1}$ in ethanol. Cadmium chloride is apparently not completely dissociated in alcohols, and $k(e^-_{solv} + CdCl_2) < k(e^-_{solv} + CdCl^+) < k(e^-_{solv} + Cd^{2+})$. For a series of compounds with lower rate constants there is a correlation between log k_2 and ΔV_2^*, the latter being negative for very low values of k_2. The products of electron capture by benzene, toluene, ethyl acetate, and possibly acetonitrile appear to be stabilized by protonation: $e^-_{solv} + S \rightleftharpoons S^-_{solv}$, [3, −3],; $S^-_{solv} + ROH \rightarrow SH + RO^-_{solv}$, [4]. The results indicate that the decomposition of e^-_{solv} in a pure alcohol occurs by protonation of the electron site, $e^-_{solv} + ROH \rightarrow H + RO^-_{solv}$, [4′], rather than by electron transfer to an alcohol molecule followed by decomposition of the anion.

GERALD L. BOLTON, MAURICE G. ROBINSON et GORDON R. FREEMAN. Can. J. Chem. **54**, 1177 (1976).

La valeur de la constante de vitesse k_1 pour la réaction $e^-_{solv} \rightarrow RO^-_{solv} + H$, [1], (à 295 K et 1 bar) est de $\leq 1.4 \times 10^5\ s^{-1}$ dans le méthanol et $\leq 8 \times 10^4\ s^{-1}$ dans l'éthanol. Les volumes d'activation respectifs, moyens entre 1 bar et 2 kbar, sont $\Delta V_1^* \leq -21$ et $\leq -22\ cm^3\ mol^{-1}$. Une concentration élevée d'hydroxyde de potassium (1 *M*) ou d'eau (5 *M*) diminue un peu la valeur apparente de k_1 mais a peu ou pas d'effet sur la valeur de ΔV_1^*. On a aussi mesuré l'effet de la pression sur la constante de vitesse de $e^-_{solv} + S \rightarrow$ produits, [2], pour une série de solutés qui montrent une grande différence de réactivité. Les valeurs expérimentales ΔV_2^* dépendent des contributions relatives des effets de densité de solvants des taux de diffusion des réactifs, des concentrations des espèces qui réagissent de faits et des énergies relatives des réactifs et des états intermédiaires. Pour les réactions dont les vitesses sont près de la limite contrôlée par la diffusion,

[1]Financially assisted by the National Research Council of Canada.
[2]Holder of National Research Council of Canada and Province of Alberta Fellowships, 1970–1974.
[3]Present address: Chemistry Department, Royal Roads Military College, Victoria, British Columbia.

$k_2 \approx 10^{10}\ M^{-1}\ s^{-1}$ dans le méthanol et l'éthanol, les valeurs de ΔV_2 sont positives et semblables à celles trouvées pour la diffusion d'ions simples. $\Delta V^{\neq}$ (e^-_{solv} diffusion) $\approx 4\ cm^3\ mol^{-1}$ dans le méthanol et $6\ cm^3\ mol^{-1}$ dans l'éthanol. Il semble que le chlorure de cadmium n'est pas complètement dissocié dans les alcools et $k(e^-_{solv} + CdCl_2) < k(e^-_{solv} + CdCl) < k(e^-_{solv} + Cd^{2+})$. Pour une série de composés avec des constantes de vitesse plus basses il existe une corrélation entre log k_2 et $\Delta V_2^{\neq}$; cette dernière valeur est négative pour des très faibles valeurs de k_2. Les produits de capture d'électron par le benzène, le toluène, l'acétate d'éthyle et possiblement par l'acétonitrile semblent être stabilisés par protonation: $e^-_{solv} + S \rightleftharpoons S^-_{solv}$, [3, −3]; $S^-_{solv} + ROH \rightarrow SH + RO^-_{solv}$, [4]. Les résultats indiquent que la décomposition de e^-_{solv} dans les alcools purs se produit par protonation du site électronique $e^-_{solv} + ROH \rightarrow H + RO^-_{solv}$, [4'], plutôt que par un transfert d'électron à une molécule d'alcool processus qui serait suivi par une décomposition d'anion.

[Traduit par le journal]

Introduction

Studies of the influence of pressure on the rate of a reaction provide information about the parameters that limit the reaction rate (1). A change in rate with pressure can be related to a change of volume $\Delta V^{\neq}$ on going from the initial to the transition state. This "activation volume" is the sum of changes resulting from solvent rearrangement (mainly due to electrostriction) and rearrangement of the reactants themselves.

Most pressure studies of electron reactions in alcohols have involved competition kinetics (2, 3). Such measurements yield the value of the difference between the activation volumes of the reactions in competition. Separate values for individual reactions would be more useful. In ethanol at 298 K the value $\Delta V_1^{\neq} = -16\ cm^3/mol$, averaged between 1 bar and 5.2 kbar, has been measured for reaction 1 by pulse radiolysis (4).

[1] $$e^-_{solv} \rightarrow RO^-_{solv} + H$$

This large negative volume of activation correlates with the large negative entropy of activation, $\Delta S_1^{\neq} = -21\ cal\ deg^{-1}\ mol^{-1}$ (5), and is attributed to the increased electrostriction that results when the relatively diffuse charge cloud of e^-_{solv} is condensed onto the oxygen atom to form RO^-_{solv}. It is the difference between the solvation energies of e^- and RO^- that drives reaction 1. The disappearance of an electron "cavity", if one exists in alcohols, would also contribute to the negative $\Delta V_1^{\neq}$.

The present article reports values of $\Delta V^{\neq}$ for a number of electron reactions in methanol and ethanol.

Experimental

Materials

Certified ACS Spectroanalyzed methanol from Fisher Scientific Co. and Commercial Grade methanol (5 ppm carbonyl, 20 ppm acid, and 70 ppm water) from Monsanto Co. ultimately gave longer half lives for e^-_{solv} than did Reagent Spectrophotometric Grade methanol from Baker Chemical Co. The first two sources were therefore used. Purification was done in a grease free Pyrex apparatus that was maintained at a slight positive pressure of flowing ultra high purity (UHP) argon which escaped through U-tubes containing mercury. Sulfuric acid (1.0 ml/l) and 2,4-dinitrophenylhydrazine (1.5 g/l) were added to the methanol. The solution was gently refluxed for at least 15 h, then slowly distilled through a 1 m column packed with glass helices. Receivers were rinsed several times with fresh distillate before being used to collect the middle fraction.

An alternative purification used the same apparatus and procedure, but the methanol was treated with 1 g/l each of sodium and sodium borohydride.

Methanol purified by either or both of the methods was nearly odorless and gave similar electron half lives. Treated methanol was stored under UHP argon in Pyrex flasks with stoppers wrapped in Parafilm "M". No deterioration in purity occurred over several months.

Absolute Reagent Grade ethanol from U.S. Industrial Chemical Co. had reported maximum impurity levels of 50 ppm water, 5 ppm methanol, and <1 ppm of benzene, halogen compounds, or carbonyl compounds. Treatment by either of the methods used for methanol gave no increase in electron half life, and occasionally decreased it by about 20%. Contact with oxygen or moisture was avoided by fitting the ethanol bottle with a Pyrex syphon fitted with a Teflon stopcock. The bottle was maintained under about 100 torr excess pressure of UHP argon. This ethanol was the same brand as that used in earlier studies (6, 7).

Water was triply distilled (7).

The reagents and solutes were Reagent Grade unless otherwise mentioned: acetone (spectro ACS, Eastman Organic Co.); acetonitrile and ethyl acetate (spectroquality, Matheson, Coleman and Bell Co.); argon (UHP, Matheson Co.); benzene (research grade, Phillips Petroleum Co.); cadmium chloride (Baker Chemical Co.); *n*-hexane (99%, Fisher Scientific Co.); naphthalene (Eastman Organic Co.); nitrobenzene, potassium hydroxide, and toluene (Fisher Scientific Co.); perchloric acid (70 wt%, Baker and Adamson Co.); potassium and dry sodium (BDH Chemicals Co.); sodium borohydride (98%, Fisher Scientific Co.); sulfuric acid (Canadian Industries Ltd.).

Can. J. Chem. Downloaded from www.nrcresearchpress.com by 210.87.254.6 on 09/05/12
For personal use only.

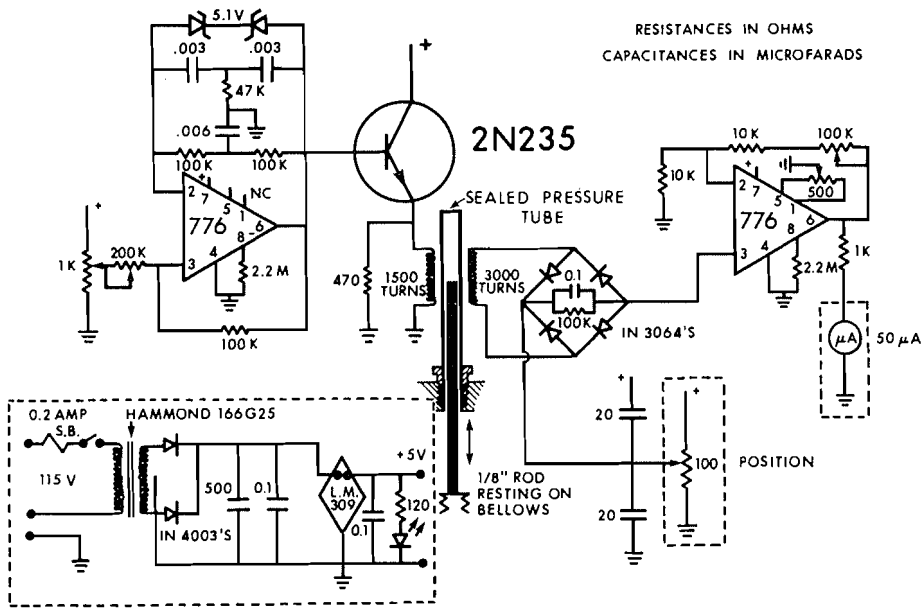

FIG. 1. Schematic diagram of the bellows compression indicator. The components within the dotted lines were together in a metal box placed by the Heise gauge, such that the microammeter could be viewed by a television monitor. The rest of the components were in another box that was pierced at the center of the transformer coils, so that it could be slipped over tube that housed the movable rod (see text).

The UHP argon was passed through a 1 m column of Oxisorb G (Messer Griesheim GMBH Industriegase). Benzene and toluene were distilled under vacuum onto freshly prepared sodium–potassium alloy (~30 wt% Na) and stirred overnight, then distilled into 10 ml Pyrex bulbs and sealed under vacuum for storage. Naphthalene was sublimed under vacuum. Nitrobenzene was distilled in an atmosphere of argon, retaining the middle 50% fraction. Sodium and potassium were cut under *n*-hexane and dried in a stream of argon before use. The other materials were used as received.

Pressure System

The pressure system is described in detail in ref. 8. The system that had been used with a 90 MeV linear accelerator (4) had to be considerably refined for successful use with the much lower energy electron beam from a 2 MeV van de Graaff accelerator.

The air driven fluid pump (Haskel Engineering and Supply Co., 75 000 psi rated) was regulated so that it would not pressurize the system over 2.6 kbar (38 000 psi). This was necessary to protect the thin "electron window" in the irradiation cell. The driving gas was nitrogen (Liquid Carbonic Canadian Corp.) and the pressurizing fluid was Bayol 35 (Imperial Oil Co.). The valves and fittings were 100 000 psi rated (American Instruments Co.). Several valves were fitted with slow-syn driving motors (Superior Electric Co.) for remote operation.

To obtain accurately the same pressure in different experiments the system was pressurized beyond the desired value, then some of the pressure was released through a controlled leak. The leak was made from an Aminco high pressure union (Cat. no. 45-12957) and a short piece of $\frac{1}{4}$ in. steel rod containing a shallow file mark on the surface.

A factory calibrated 100 000 psi Heise gauge was used for pressure measurement. It was viewed by closed circuit television.

The filling and pressurizing system for the optical cell were of the same general design as that in ref. 4. In addition, a bellows-compression indicator was used to guard against destruction of the bellows by over-compression. The indicator used the induction change created when an iron rod moved in the cores of two transformer coils. The $\frac{1}{8} \times 6$ in. iron rod rested on the top of the bellows (and was moved up and down by it) and extended into a 4 in. piece of $\frac{3}{8}$ in. od antimagnetic stainless steel (304) pressure tubing that extended from the top of the pressurizing bomb. The upper end of this tubing was sealed. The transformer coils were wound to slip over the tubing. The electronic circuitry is shown in Fig. 1. The microammeter was placed near the Heise gauge such that it could be read on the television monitor.

The optical cell is shown in Fig. 2. The sapphire windows (American Instruments Co., part no. A4-62065) were fixed to the caps with a thin layer of Elmer's epoxy (Borden Chemical Co.). The electron window was fabricated from a 2×25 mm disc of Vascomax Maraging steel hardened to 57 Rockwell C. The central portion (9.0 mm diameter) of the disc was thinned to 0.71 mm to allow the electron beam to pass. This "electron window" withstood pressures greater than 3 kbar. Many pressure cycles caused the window to become brittle, necessitating periodic replacement to avoid failure.

Can. J. Chem. Downloaded from www.nrcresearchpress.com by 210.87.254.6 on 09/05/12
For personal use only.

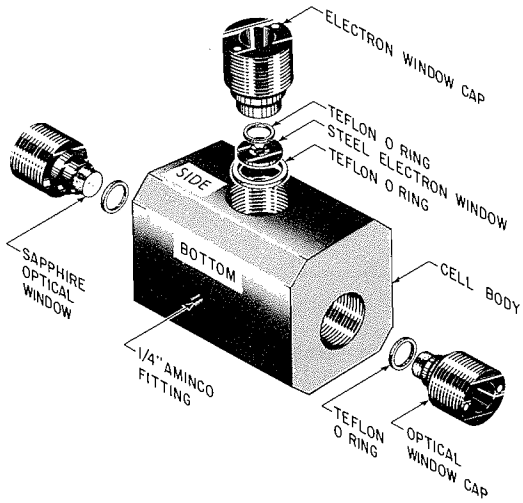

FIG. 2. High pressure optical cell. The cell body of 410 stainless steel was not heat treated. It was 12.5 cm long. The electron and optical window caps of 416 stainless steel were heat treated to 36 Rockwell C hardness. A small amount of Loc-Lube (Burrell Corp.) was used on the cap threads to prevent their fusing to the cell body under pressure.

The van de Graaff electron window was protected against failure of the cell electron window by interposing a rubber-lined steel shutter, which opened for 1 s to allow passage of an electron pulse.

The effect of pulse dose on electron half life at 1 bar was measured in a 1.0 cm Suprasil cell.

Optical System

The optical system was the same as that reported earlier (7). However, the Xe arc lamp housing (Oriel Optics Corp., model C-60-50) contained a Pyrex filter in front of the quartz lens to remove light with $\lambda < 320$ nm. This prevented ozone formation in the room. The lamp power supply was an SRL 40-50 Sorenson obtained from Raytheon Co.

Sample Preparation and Handling

Samples were prepared as in ref. 7. The high pressure optical cell was rinsed and filled as in ref. 4. The sample temperature was 295 ± 1 K. The temperature increased or decreased a few degrees upon compression or decompression, respectively, but returned to 295 ± 1 K within 3 min of a pressure change.

Irradiation

The van de Graaff accelerator was run at 2.2 MeV. The dose delivered during a 1.0 μs pulse was 1×10^{17} eV/g. Each pulse was monitored by a secondary emission chamber, calibrated with the absorption of e^-_{solv} in water at $\lambda = 718$ nm, using $G\epsilon = 5.1 \times 10^4$ electron (100 eV M cm)$^{-1}$ (7).

Liquid Densities

The solution concentrations and absorbed dose/cm^3 increased with pressure, due to the increasing solvent density. The densities of the alcohols at different pressures were calculated by multiplying the values at 1 bar by the appropriate ratios from ref. 9.

Results

Reaction rates were determined from the first order decay rates of the e^-_{solv} spectrum at $\lambda = 600$–700 nm, which was near the absorption maximum at all pressures (4). There was no detectable variation of decay rate with wavelength in the region scanned.

Effect of Pressure on e^-_{solv} Decomposition Rate

The first order decay constants of e^-_{solv} in methanol and ethanol increase with increasing pressure (Fig. 3). Addition of 1 mM potassium hydroxide to methanol decreased the decay rate significantly. Further addition up to 69 mM had negligible effect, but the rate decreased again at very high hydroxide concentration (Fig. 3*A*). The behavior in ethanol was similar (Fig. 3*B*).

The potassium hydroxide contained 13 wt% water, so the molar concentrations of the latter were half those of the former. It was therefore necessary to measure the effect of water. Addition of 0.1 M water to ethanol had a negligible effect on the electron decomposition rate, but 0.5 M and larger concentrations caused the rate to decrease somewhat (Fig. 4).

The water contained a few μM of electron scavenging impurities (estimated by assuming a second order rate constant of $\sim 1 \times 10^{10}$ M^{-1} s^{-1}) and the e^-_{solv} half life in 55.6 M water corresponded to a first order decomposition rate constant of 4.8×10^4 s^{-1}.

The magnitude of the pressure effect decreased with increasing water concentration (Fig. 4).

Effect of Pulse Dose

The half lives of e^-_{solv} in neutral and basic methanol at 1 bar and 295 ± 1 K were measured at different pulse doses. The pulse lengths were 30 ns, 100 ns, or 1.0 μs and the doses ranged from 0.3 to 33×10^{16} eV/cm^3. The electron half life decreased with increasing pulse dose (Fig. 5*A*). The presence of base had little effect at low doses and decreased the dose effect at high doses.

The half lives extrapolated to zero dose were 5 μs in methanol and ~ 9 μs in ethanol (Fig. 5*B*), corresponding to first order decay constants of 1.4×10^5 and 8×10^4 s^{-1}, respectively.

Can. J. Chem. Downloaded from www.nrcresearchpress.com by 210.87.254.6 on 09/05/12
For personal use only.

Can. J. Chem. Downloaded from www.nrcresearchpress.com by 210.87.254.6 on 09/05/12
For personal use only.

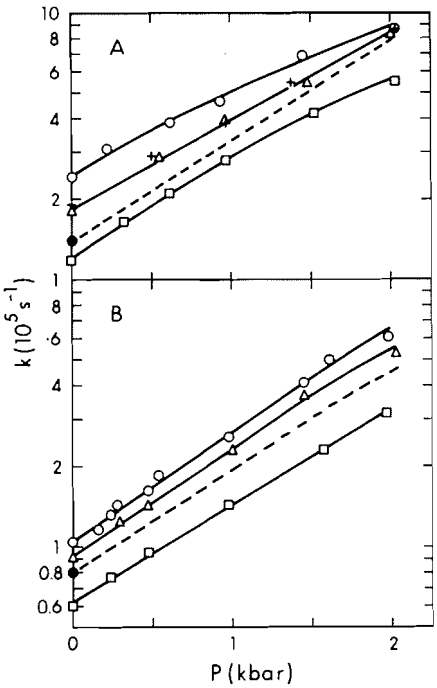

FIG. 3. Effect of pressure on the decay rates of e^-_{solv} in neutral and basic methanol (*A*) and ethanol (*B*) at 295 ± 1 K. $k = 0.693/t_{1/2}$, where $t_{1/2}$ = half life. The concentrations of KOH in methanol were: zero (○), 1.0 m*M* (△), 69 m*M* (+), and 0.90 *M* (□). Those in ethanol were zero (○), 13 m*M* (△), and 0.98 *M* (□). ● represents the value extrapolated to zero pulse dose in 0–10 m*M* base. The dashed lines are estimates of the zero dose values.

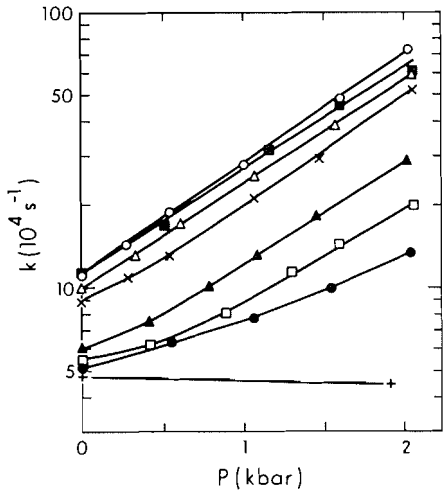

FIG. 4. Effect of water on the e^-_{solv} decay rate in ethanol at 295 ± 1 K and different pressures. $k = 0.693/t_{1/2}$. $[H_2O]$ = 0.0 *M* (○), 0.10 *M* (■), 0.50 *M* (△), 1.0 *M* (×), 3.0 *M* (▲), 5.0 *M* (□), 10.0 *M* (●), 55.6 *M* (+).

Effect of Pressure on k (e^-_{solv} + S)

The effects of pressure on the rates of reaction of e^-_{solv} with scavengers S were measured for a number of compounds that were chosen to display a wide range of rate constants.

Pseudo first order decay constants were measured for different concentrations of a given solute. The value of the second order rate constant k_2 for reaction 2 was determined from

[2] $$e^-_{solv} + S \rightarrow \text{product}$$

the slope of a plot of the pseudo first order constants against the concentration of S. From 4 to 15 concentrations were used to determine k_2 at each pressure. The molar concentrations were adjusted for change in solvent density with pressure (9).

The nature and quality of the results are illustrated by the study of acetonitrile in ethanol. Plots of the pseudo first order decay constants against acetonitrile concentration are shown in Fig. 6. Values of k_2 obtained from the slopes of these lines are plotted against the pressure in Fig. 7. In contrast with the results in Fig. 3, k_2

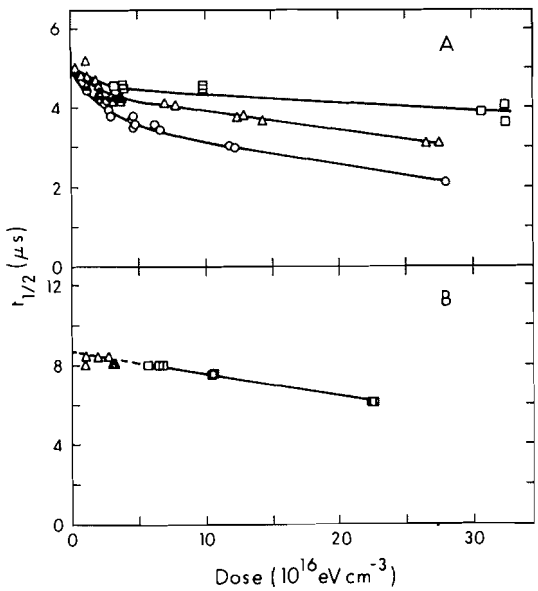

FIG. 5. Effect of pulse dose on the half life of e^-_{solv} in alcohols at 1 bar and 295 ± 1 K. (*A*) Methanol: neutral (○), 1 m*M* $NaOCH_3$ (△), 31 m*M* $NaOCH_3$ (□); (*B*) ethanol: 4 m*M* $NaOC_2H_5$ (△), 10 m*M* KOH (□).

Can. J. Chem. Downloaded from www.nrcresearchpress.com by 210.87.254.6 on 09/05/12
For personal use only.

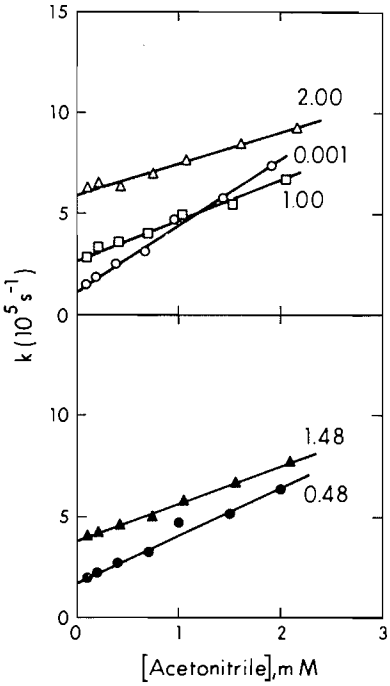

FIG. 6. Plots of e^-_{solv} pseudo first order decay rate constants against acetonitrile concentration in ethanol. $k = 0.693/t_{1/2}$. The numbers labelling the curves are the pressures in kbar.

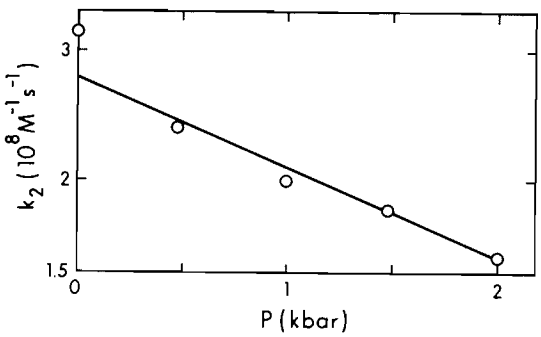

FIG. 7. Plot of k_2 against pressure for acetonitrile in ethanol.

for acetonitrile decreases with increasing pressure.

With $k_2 = 3 \times 10^8$ M^{-1} s^{-1} at 1 bar, acetonitrile does not react at the diffusion controlled rate. The apparent value of k_2 could therefore have been enhanced by the presence of an impurity that had a higher rate constant. Although spectroquality acetonitrile from Matheson, Coleman and Bell Co. has been reported to be of very high purity (10), with the major impurity being 0.04 wt% water, the possible influence of contamination by acrylonitrile was checked. The value of k_2 for acrylonitrile in ethanol at 1 bar was measured to be 7×10^9 M^{-1} s^{-1} (using only one solution and the pure solvent). The optical absorbancy coefficient of acrylonitrile in acetonitrile at 197 nm was found to be 1×10^4 M^{-1} cm^{-1}.[4] The concentration of the former in our acetonitrile was $\sim 2 \times 10^{-5}$ M, so it did not contribute appreciably to the observed k_2. Other possible impurities are benzene, ammonia, and acetic acid (11). None were in high enough concentration to affect the results. Thus the observed value of k_2 was attributed to acetonitrile itself.

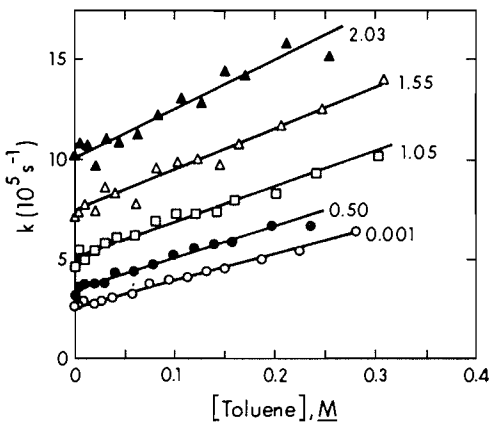

FIG. 8. Plots of e^-_{solv} pseudo first order decay rate constants against toluene concentration in methanol. $k = 0.693/t_{1/2}$. The numbers labelling the curves are the pressures in kbar.

The value of the volume of activation $\Delta V^{\neq}$ was calculated from the slope of a plot of log k against P, using

$$\Delta V^{\neq} = -\frac{2.3RT \log (k_a/k_b)}{P_a - P_b} \text{ cm}^3 \text{ mol}^{-1}$$

where R is the gas constant, T is the absolute temperature, and the k_a and k_b are rate constants at pressures P_a and P_b, respectively. The slope of the line in Fig. 7 corresponds to $\Delta V_2^{\neq} = +7$ cm^3 mol^{-1} for acetonitrile in ethanol.

Scavengers that had a negative volume of activation are illustrated by toluene in methanol (Figs. 8 and 9), for which $\Delta V^{\neq} = -7$ cm^3 mol^{-1}.

The effects of pressure on k_2 for a number of other solutes are collected in Figs. 10 and 11.

[4]Unicam 1700 spectrophotometer, slit 0.25 mm, 0.8 nm band pass, 1.0 cm cells.

Can. J. Chem. Downloaded from www.nrcresearchpress.com by 210.87.254.6 on 09/05/12
For personal use only.

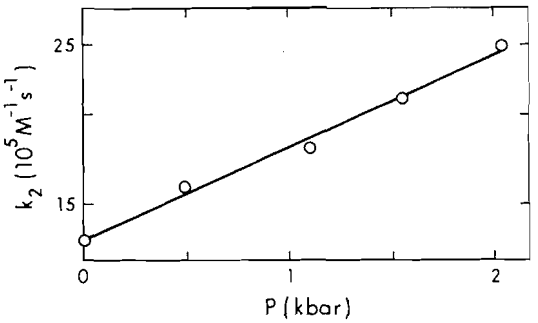

FIG. 9. Plot of k_2 against pressure for toluene in methanol.

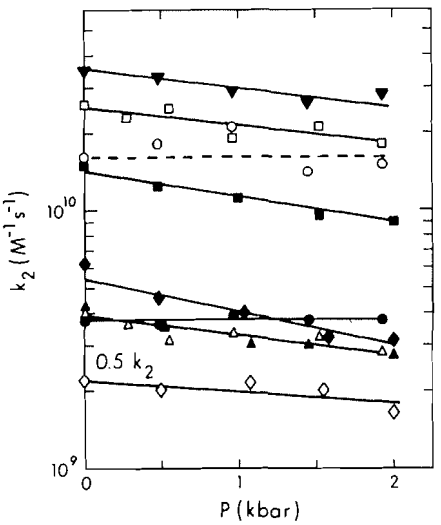

FIG. 10. Plots of k_2 against pressure for perchloric acid (▼), nitrobenzene (□, ■), cadmium chloride (○, ●), naphthalene (◊, ♦), and acetone (△, ▲). The open points are for methanol solvent and the filled points for ethanol.

The values of k_2 at 1 bar and $\Delta V_2^{\neq}$ are listed in Table 1. Increasing pressure enhances the reaction rates of benzene and toluene, has little or no effect on those of ethyl acetate and cadmium chloride, and diminishes those of acetonitrile, naphthalene, acetone, nitrobenzene, and acid.

Judging from the electron half lives in the acid solutions before and after a pressure cycle, acid was removed from solution by reaction at higher pressures. Corrections were applied for this effect in ethanol, but the reaction was sufficiently rapid in methanol that reliable values of k_2 could not be obtained. The reaction was presumably ester formation. The effect was not observed with other scavengers.

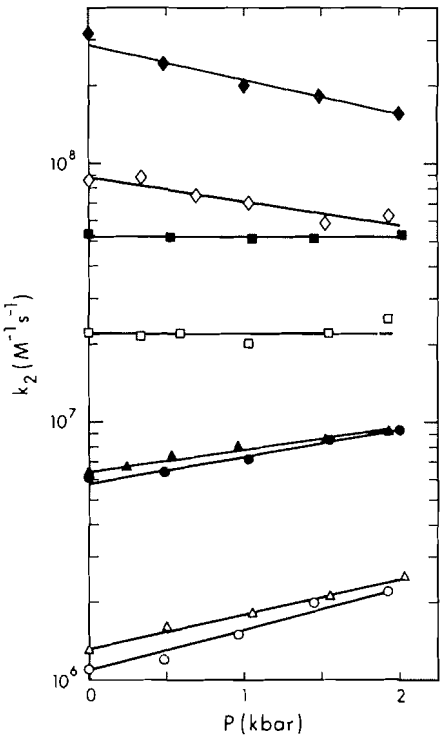

FIG. 11. Plots of k_2 against pressure for ethyl acetate (□, ■), acetonitrile (◊, ♦), toluene (△, ▲), and benzene (○, ●). The open points are for methanol solvent and the filled points for ethanol.

Discussion

Effect of Pressure on e^-_{solv} Decomposition Rate

Measurement of the rate constant of reaction 1 is complicated by the simultaneous occurrence of reaction 2, where S includes impurities and radiolysis products such as ROH_2^+ and radicals formed during the radiation pulse. Addition of 10^{-3}–10^{-2} *M* base to the alcohol causes ROH_2^+ to be neutralized in $\sim 10^{-8}$ s, thereby preventing it reacting by reaction 2. Furthermore, the volume of activation of reaction 1 is more negative than that of reaction 2 (2–4), so interference by the latter diminishes with increasing pressure.

The values of k for a series of pressures in Fig. 3 were determined on a single sample. Although the pulse doses were relatively small, the amount of acetaldehyde that accumulated in the ethanol (6) caused a measurable increase in k. The value of k at 1 bar after a run was typically $\sim 40\%$ greater than that at the beginning of a

TABLE 1. Rate constants k_2 at 1 bar and volumes of activation $\Delta V_2^{\neq}$ for (e^-_{solv} + S) reactions in alcohols at 295 ± 1 K

	Methanol			Ethanol		
S	Concentration range (10^{-4} M)	k_2 (M^{-1} s^{-1})	$\Delta V_2^{\neq}$ (cm^3 mol^{-1})[a]	Concentration range (10^{-4} M)	k_2 (M^{-1} s^{-1})	$\Delta V_2^{\neq}$ (cm^3 mol^{-1})[a]
Acetone	0.1–1.1	4×10^9	4	0.1–1.9	4×10^9	4
Acetonitrile	5–70	8.6×10^7	5	1–40	3.2×10^8	7
Acid, perchloric				0.1–0.5	3.5×10^{10}	4 ± 2
Acrylonitrile				0 and 1	7×10^9	—
Benzene	500–2500	1.1×10^6	−8	60–700	6.1×10^6	−6
Cadmium chloride	0.02–0.10	1.6×10^{10}	0 ± 3	0.05–0.4	3.6×10^9	0
Ethyl acetate	10–100	2.2×10^7	0	10–150	5.3×10^7	0
Naphthalene	0.1–1.2	4.4×10^9	2	0.2–1.4	6×10^9	7 ± 2
Nitrobenzene	0.01–0.11	2.6×10^{10}	4	0.02–0.2	1.5×10^{10}	5
Toluene	100–3000	1.3×10^6	−7	100–700	6.4×10^6	−5
Solvent		$\leq 1.4\times10^5$[b]	≤ -21		$\leq 8\times10^4$[b]	≤ -22

[a] ±1 cm^3 mol^{-1} unless otherwise stated.
[b] k_1, s^{-1}.

run. A correction could be applied for accumulated dose in a sample. Methanol samples displayed the same values of k at 1 bar before and after a run, presumably because the formaldehyde product rapidly reacts with the alcohol to form dimethoxymethane.

The curves in Fig. 3 for the slightly basic alcohols were extrapolated to zero pulse dose by using Fig. 5 and assuming $\Delta V_2^{\neq} - \Delta V_1^{\neq} \approx 25$ cm^3 mol^{-1} when S is a free radical.

The dashed lines in Fig. 3 represent the values of k corrected to zero pulse dose and to zero accumulated acetaldehyde. The slopes represent lower limits of the magnitude of $\Delta V_1^{\neq}$, which are -21 cm^3 mol^{-1} in methanol and -22 cm^3 mol^{-1} in ethanol. If the alcohols contained significant amounts of impurities capable of reacting with electrons, the values of k_1 would be lower and $\Delta V_1^{\neq}$ would be more negative. Hence, $k_1 \leq 1.4 \times 10^5$ s^{-1} with $\Delta V_1^{\neq} \leq -21$ cm^3 mol^{-1} in methanol and $k_1 \leq 8 \times 10^4$ s^{-1} with $\Delta V_1^{\neq} \leq -22$ cm^3 mol^{-1} in ethanol at 295 K. These values of k_1 at 1 bar agree with those of Baxendale and Wardman (12), but are lower than other estimates (4, 13, 14).

The degree of confidence in these values of $\Delta V_1^{\neq}$ is enhanced somewhat by noting that the various manipulations did not have a large effect (Table 2). The increase in $\Delta V^{\neq}$ (decrease in absolute magnitude) caused by adding large amounts of water to ethanol was caused mainly by the occurrence of reaction 2 with trace impurities in the water. This explains the curvature of the lines in Fig. 4; in the sample containing 5 M water reaction 2 dominates at low pressures and reaction 1 at high pressures.

The value of $\Delta V_1^{\neq}$ is insensitive to relatively high concentrations of water in ethanol. Although k_1 is two orders of magnitude smaller in water, 890 s^{-1} (15), than in the alcohols, $\Delta V_1^{\neq}$ has similar values in the two kinds of liquid. An estimate from competition kinetics gave $\Delta V_1^{\neq} = -14.3$ cm^3 mol^{-1} in water at 298 K and pressures between 2.7 and 8.7 kbar (16), which compares with -13 cm^3 mol^{-1} in ethanol at 298 K and pressures between 2.1 and 5.2 kbar (4). The magnitude of the latter value is somewhat low (not negative enough), because the ethanol contained a trace of electron scavenging impurity ($k = 1.2 \times 10^5$ s^{-1} at 1 bar in the alcohol containing 5 mM sodium hydroxide (4)).

The magnitude of $\Delta V_1^{\neq}$ decreases with increasing pressure. The earlier work with ethanol (4) indicated average values of -19 cm^3 mol^{-1} between 1 bar and 1 kbar, and -15 cm^3 mol^{-1} between 1 and 3 kbar. The former value is in reasonable agreement with the present more accurate determination of $\Delta V_1^{\neq} \leq -22$ cm^3 mol^{-1}.

Combining the present value $\Delta V_2^{\neq} = 4$ cm^3 mol^{-1} for nitrobenzene and acetone in methanol (Table 1) with results from an earlier study of competition kinetics (3) gives $\Delta V_1^{\neq} = -17$ cm^3 mol^{-1} at 1 bar in methanol. This is in reasonable agreement with the present more accurate value $\Delta V_1^{\neq} \leq -21$ cm^3 mol^{-1}.

Can. J. Chem. Downloaded from www.nrcresearchpress.com by 210.87.254.6 on 09/05/12
For personal use only.

TABLE 2. Effect of base and water on the rate and activation volume of e^-_{solv} decomposition in alcohols at 295 ± 1 K

Solvent	[KOH][a,b] (M)	[H_2O][a,b] (M)	k[a] (10^5 s^{-1})	$\Delta V^{\neq}$[c] (cm^3 mol^{-1})
CH_3OH	0	0	2.4 (1.4)[d]	−18 (−21)[d]
	0.001	0	1.8	−19
	0.005	0.002	2.0	−18
	0.021	0.010	1.8	−18
	0.069	0.033	1.9	−19
	0.90	0.42	1.2	−20
C_2H_5OH	0	0	1.1 (0.8)[d]	−23 (−22)[d]
	0.013	0.006	0.9	−22
	0.98	0.46	0.6	−21
	0	0	1.1	−23
	0	0.10	1.1	−21
	0	0.50	1.0	−21
	0	1.0	0.89	−22[e]
	0	3.0	0.61	−21[e]
	0	5.0	0.55	−19[e]
	0	10.0	0.52	−14[e]
	0	55.6	0.48	+0.8[e]

[a]At 1 bar.
[b]KOH contains 13 wt% H_2O, so [H_2O] = 0.47[KOH].
[c]Averaged between 1 bar and 1.5 kbar, unless otherwise mentioned.
[d]Corrected for pulse dose and accumulated products.
[e]Calculated from the slope at high pressure only. The results are affected by the reaction of electrons with an impurity.

Effect of Pressure on k_2

The reactions are divided into two categories for discussion, (*a*) those with $k_2 > 10^9$ M^{-1} s^{-1} and (*b*) those with $k_2 < 10^9$ M^{-1} s^{-1}.

(*a*) The more efficient reactions in alcohols have rate constants in the vicinity of 10^{10} M^{-1} s^{-1}. There is no obvious correlation between the magnitudes of k_2 at 1 bar and $\Delta V_2^{\neq}$ for these reactions (Fig. 12). However, all the volumes of activation are positive except those for cadmium chloride, which are zero. The volume of activation for a diffusion controlled reaction is the weighted average of those for the diffusion of the reactants. The volume of activation for diffusion of simple ions such as sodium and bromide is positive; it is 5 cm^3 mol^{-1} in methanol, 2 cm^3 mol^{-1} smaller than that for viscous flow (17). By analogy the volume of activation for diffusion of simple ions in ethanol would be about 6 cm^3 mol^{-1} (2). These are similar to the values of $\Delta V_2^{\neq}$ for the faster reactions, with the exception of cadmium chloride which is discussed below. It therefore appears that the volume of activation of diffusion of solvated electrons in alcohols is similar to that for the diffusion of simple ions. This is consistent with the low, ion-like mobilities of electrons in the alcohols (18–20). The present and earlier (2, 3) results suggest that $\Delta V^{\neq}(e^-_{solv}$ diffusion) ≈ 4 cm^3 mol^{-1} in methanol and 6 cm^3 mol^{-1} in ethanol.

The value $\Delta V_2^{\neq} = 0$ for cadmium chloride is unusual. The reaction of electrons with Cd^{2+} ions in water is essentially diffusion controlled, with $k_2 = 5.2 \times 10^{10}$ M^{-1} s^{-1} at room temperature (21). The value of k_2 decreases progressively

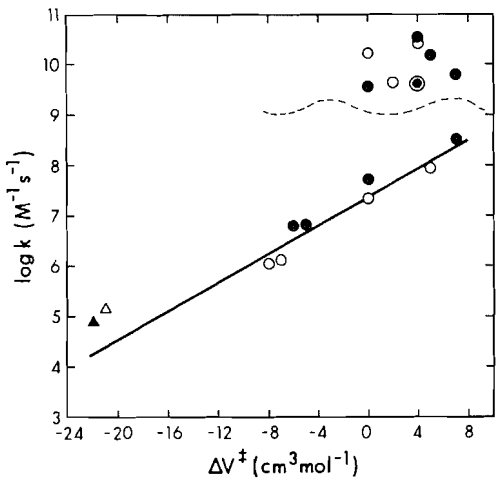

FIG. 12. Plot of log k at 1 bar against $\Delta V^{\neq}$ for electron reactions in methanol (open points) and ethanol (closed points) at 295 ± 1 K. ○, ●, k_2; △, ▲, k_1. The values are taken from Table 1.

Can. J. Chem. Downloaded from www.nrcresearchpress.com by 210.87.254.6 on 09/05/12
For personal use only.

Can. J. Chem. Downloaded from www.nrcresearchpress.com by 210.87.254.6 on 09/05/12
For personal use only.

on going to methanol, $1.6 \times 10^{10}\ M^{-1}\ s^{-1}$, and ethanol, $3.6 \times 10^{9}\ M^{-1}\ s^{-1}$. The rate constants do not correlate with the solvent viscosities, which are equal for water and ethanol at 1 bar. The change in k_2 is in the wrong direction to be attributed to a simple influence of the decreasing dielectric constant on the interaction between Cd^{2+} and e^-_{solv}. The results suggest that cadmium chloride is progressively less dissociated in solvents with lower dielectric constants,

$$CdCl_2 \rightleftharpoons CdCl^+ + Cl^- \rightleftharpoons Cd^{2+} + 2Cl^-$$

and that the electron rate constants are higher with the more highly charged cadmium species,

$$k_2(e^-_{solv} + CdCl_2) < k_2(e^-_{solv} + CdCl^+) < k_2(e^-_{solv} + Cd^{2+})$$

Dissociation of electrolytes is favored by increasing pressure, due to the associated increasing dielectric constant (22–24) and decreasing volume (9). The former reduces the coulombic interaction between the free ions, while the latter operates in the same direction as the electrostriction and enhances the ion solvation energies. The observed lack of pressure dependence of k_2 for cadmium chloride in both alcohols (Fig. 10) may be the result of a decrease in the real values of k_2 for the cadmium species, due to decreasing diffusion coefficients, and a compensating increase in the concentrations of Cd^{2+} and $CdCl^+$ due to increasing dissociation constants. The real values of $\Delta V_2^{\neq}$ for the cadmium ions would therefore be positive, in accord with those for the other efficient electron scavengers.

Each of the fast reactions appears to be a simple electron transfer, and all have positive volumes of activation that are at least partly related to the diffusion rates.

(*b*) For the reactions that have lower rate constants there is a correlation between the values of log k_2 at 1 bar and those of $\Delta V_2^{\neq}$ (Fig. 12). A two step mechanism is proposed for the formation and stabilization of the scavenging product.

$$[3,-3] \qquad e^-_{solv} + S \rightleftharpoons S^-_{solv}$$

$$[4] \qquad S^-_{solv} + ROH \rightarrow SH + RO^-_{solv}$$

The negative ions of benzene, ethyl acetate, and so on appear to be inherently unstable, but the electron capture may be stabilized by protonation of the anion. The step [3,−3] could make either a positive or negative contribution to the observed volume of activation. The contribution of reaction 4 is likely to be zero or negative.

Reaction 4 is pseudo first order, because ROH is the solvent, so we write k_4' [ROH] = k_4.

The overall kinetics of reaction 3,−3 and 4 have two limiting cases. When $k_{-3} \ll k_4$, the observed electron capture rate constant $k_2 = k_3$ and $\Delta V_2^{\neq} = \Delta V_3^{\neq}$. This condition appears to apply for acetonitrile. When $k_{-3} \gg k_4$, then $k_2 = k_3k_4/k_{-3}$ and $\Delta V_2^{\neq} = \Delta V_3^{\neq} - \Delta V_{-3}^{\neq} + \Delta V_4^{\neq} = \Delta V_3 + \Delta V_4^{\neq}$, where ΔV_3 is the actual volume change of the system on going from (e^-_{solv} + S) to S^-_{solv}. This condition appears to apply to benzene and toluene. Ethyl acetate is an intermediate case.

The equilibrium [3,−3] is shifted towards the right if increasing the pressure on the system diminishes the degree of instability of the anion. The instability indicates that the energy state of S^-_{solv} lies above that of e^-_{solv}. If increasing the pressure lowers the energy of S^-_{solv} more than that of e^-_{solv}, the energy gap is decreased and the anion is less unstable (Fig. 13). In this case the value of (k_3/k_{-3}) increases with pressure and makes a negative contribution to the observed volume of activation. On the other hand, if increasing pressure widens the energy gap, the equilibrium constant would decrease and make a positive contribution to the observed volume of activation.

The magnitudes of the rate constants (Table 1) indicate that the energy gap for the various solutes decreases in the order benzene ≈ toluene > ethyl acetate > acetonitrile. The gas phase electron affinity of benzene is negative (25), consistent with the proposed gap, but values for the other compounds are not known. The negative volumes of activation for benzene and toluene are also consistent with the observation of reversible growth and shrinkage of esr signals from their anions in alkali metal – ether solutions upon cooling and warming, respectively (26). The solvent density increases with cooling and with pressure, enhancing electrostriction.

Protonation of the anion has a negative volume of activation due to enhanced electrostriction if the alkoxide ion is more strongly solvated than the S^-. However, the degree to which reaction 4 contributes to the observed $\Delta V_2^{\neq}$ depends on the relative rates of reactions −3 and 4.

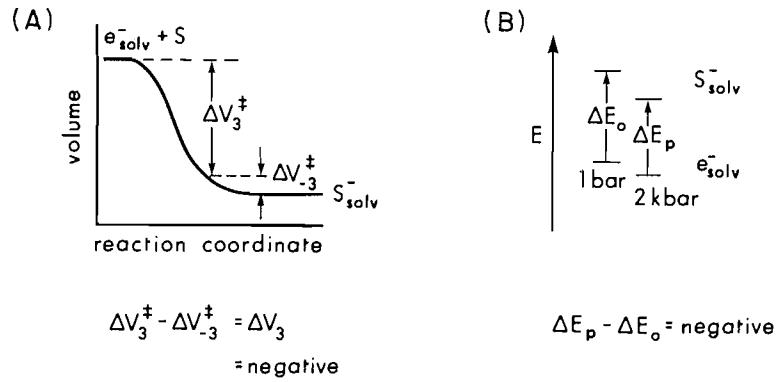

FIG. 13. Schematic diagrams for a system such as $e^-_{solv} + C_6H_6$. (*A*) Volume of the system along the reaction coordinate. (*B*) Effect of pressure on the relative energy states of e^-_{solv} and S^-_{solv}.

$e^-_{solv} + ROH \rightarrow H + RO^-_{solv}$

It is informative to treat the reaction of the electron with the solvent as a proton transfer reaction analogous to reaction 4. This would correspond to the transfer of a proton from one of the —OH groups in the first coordination sphere of e^-_{solv} to the site of the electron, and would be the protonation of the solvated electron. The decomposition reaction 1 of e^-_{solv} has previously been thought to occur by electron transfer to an ROH molecule, which then decomposes to $RO^-_{solv} + H$. The nature of the intermediate anion has never been clear. The transition state of the proton transfer mechanism is less difficult to imagine, since it is somewhat analogous to that for the autoionization of the solvent.

Considering reaction 1 to be analogous to reaction 4 and recalling that $k_2 = (k_3/k_{-3})k_4$, it is interesting to plot k_1 and $\Delta V_1^{\ddagger}$ in Fig. 12. The points for both alcohols lie somewhat above the extrapolation of a correlation line drawn for benzene and other inefficient scavengers. This would be expected, since $(k_3/k_{-3}) < 1$ for inefficient scavengers. Furthermore, the point for reaction 1 in ethanol lies below that for reaction 1 in methanol, whereas the reverse is true for reaction 2 with the inefficient scavengers. The fact that k_2 for benzene, etc. in methanol is smaller than the analogous constant in ethanol is attributed to (k_3/k_{-3}) being lower in the solvent for which the energy state of e^-_{solv} is lower. The optical excitation energy of e^-_{solv} is greater in methanol than in ethanol (5), so the energy gap for reaction 3 might be expected to be greater in the former solvent (Fig. 13*B*).

The coherence of the above picture supports the suggestion that reaction 1 occurs by proton transfer, rather than by electron transfer.

Acknowledgements

We would like to express our appreciation to the personnel of the Chemistry Department Machine and Electronics Shops and the Radiation Research Center for construction of vital parts of the equipment.

1. K. J. LAIDLER. Chemical kinetics. McGraw-Hill, London. 1965. Chapt. 5.
2. K. N. JHA and G. R. FREEMAN. J. Chem. Phys. **57**, 1408 (1972).
3. K. N. JHA and G. R. FREEMAN. J. Am. Chem. Soc. **95**, 5891 (1973).
4. M. G. ROBINSON, K. N. JHA, and G. R. FREEMAN. J. Chem. Phys. **55**, 4933 (1971).
5. K. N. JHA and G. R. FREEMAN. J. Chem. Phys. **51**, 2846 (1969).
6. S. M. S. AKHTAR and G. R. FREEMAN. J. Phys. Chem. **75**, 2756 (1971).
7. K. N. JHA, G. L. BOLTON, and G. R. FREEMAN. J. Phys. Chem. **76**, 3876 (1972).
8. G. L. BOLTON. Ph.D. Thesis, University of Alberta, Edmonton, Alberta. 1974.
9. P. W. BRIDGMAN. The physics of high pressure. G. Bell and Sons, London. 1958.
10. M. WALTER and L. RAMALEY. Anal. Chem. **45**, 165 (1973).
11. J. F. COETZEE. Pure Appl. Chem. **13**, 429 (1966).
12. J. H. BAXENDALE and P. WARDMAN. Chem. Commun. 429 (1971).
13. K. N. JHA and G. R. FREEMAN. J. Chem. Phys. **48**, 5480 (1968).
14. J. W. FLETCHER, P. J. RICHARDS, and W. A. SEDDON. Can. J. Chem. **48**, 1645 (1970).
15. E. J. HART, S. GORDON, and E. M. FIELDEN. J. Phys. Chem. **70**, 150 (1966).

Can. J. Chem. Downloaded from www.nrcresearchpress.com by 210.87.254.6 on 09/05/12
For personal use only.

16. R. R. HENTZ and R. J. KNIGHT. J. Chem. Phys. **52**, 2456 (1970).
17. W. STRAUSS. Aust. J. Chem. **10**, 277 (1957).
18. P. FOWLES. Trans. Faraday Soc. **67**, 428 (1971).
19. R. A. VERMEER and G. R. FREEMAN. Can. J. Chem. **52**, 1181 (1974).
20. J.-P. DODELET and G. R. FREEMAN. Can. J. Chem. **53**, 1263 (1975).
21. J. H. BAXENDALE, E. M. FIELDEN, and J. P. KEENE. Proc. R. Soc. London, Ser. A, **256**, 320 (1965).
22. I. M. KOLTHOFF and S. BRUCKENSTEIN. *In* Treatise on analytical chemistry. Part I, Vol. I. *Edited by* I. M. Kolthoff, P. J. Elving, and E. B. Sandell. Interscience Publishers, New York. 1959. Chapt. 13.
23. S. KYROPOULOS. Z. Phys. **40**, 507 (1926).
24. W. E. DANFORTH, JR. Phys. Rev. **38**, 1224 (1931).
25. G. BRIEGLEB. Angew. Chem. Int. Ed. Engl. **3**, 617 (1964).
26. T. R. TUTTLE, JR. and S. I. WEISSMAN. J. Am. Chem. Soc. **80**, 5342 (1958).

Can. J. Chem. Downloaded from www.nrcresearchpress.com by 210.87.254.6 on 09/05/12
For personal use only.

Synthesis and vibrational spectra of lead(II) thiocyanate complexes[1]

ANTHONY D. BARANYI, RAMESH MAKHIJA, AND MARIO ONYSZCHUK
Department of Chemistry, McGill University, Montreal, Quebec H3C 3G1

Received October 20, 1975

ANTHONY D. BARANYI, RAMESH MAKHIJA, and MARIO ONYSZCHUK. Can. J. Chem. **54**, 1189 (1976).

The preparation, properties, and vibrational spectra are reported for the following complexes of lead(II) thiocyanate with mono- and bidentate ligands: $Pb(NCS)_2 \cdot 2py$, $Pb(NCS)_2 \cdot phen$, $Pb(NCS)_2 \cdot 2phen$, $Pb(NCS)_2 \cdot tmen$, $Pb(NCS)_2 \cdot en$, $Pb(NCS)_2 \cdot 2en$, $Pb(NCS)_2 \cdot 2dmso$, and $Pb(NCS)_2 \cdot 2dma$. Assignments are made for the ν(CN), ν(CS), and δ(NCS) vibrational bands of the thiocyanate group and the results are discussed in terms of the type of coordination of NCS with lead(II). Values are consistent with bridge-bonded and/or N-bonded thiocyanate. Infrared and Raman spectra of the complexes $Pb(NCS)_2 \cdot bipy$ and $Pb(NCS)_2 \cdot 4tu$ are re-examined and new assignments are made which support bridge-bonded and/or N-bonded NCS contrary to previous reports of S-bonded NCS.

ANTHONY D. BARANYI, RAMESH MAKHIJA et MARIO ONYSZCHUK. Can. J. Chem. **54**, 1189 (1976).

On rapporte la préparation, les propriétés et les spectres de vibration des complexes suivants du thiocyanate de plomb(II) avec des ligands mono- et bidentates: $Pb(NCS)_2 \cdot 2py$, $Pb(NCS)_2 \cdot phen$, $Pb(NCS)_2 \cdot 2phen$, $Pb(NCS)_2 \cdot tmen$, $Pb(NCS)_2 \cdot en$, $Pb(NCS)_2 \cdot 2en$, $Pb(NCS)_2 \cdot 2dmso$ et $Pb(NCS)_2 \cdot 2dma$. On a effectué les attributions pour les bandes de vibration ν(CN), ν(CS) et δ(NCS) du groupe thiocyanate et on discute des résultats en terme du type de coordination du NCS avec le plomb(II). Les valeurs suggèrent que les thiocyanates sont pontés et/ou liés par l'azote. On a réexaminé les spectres infrarouges et Raman des complexes $Pb(NCS)_2 \cdot bipy$ et $Pb(NCS)_2 \cdot 4tu$ et on propose de nouvelles attributions qui suggèrent que les NCS sont pontés et/ou liés par l'azote; cette conclusion est contraire aux rapports antérieurs qui indiquaient que le NCS est lié par le soufre.

[Traduit par le journal]

Introduction

Few complexes of lead(II) thiocyanate, $Pb(SCN)_2$, are known. The X-ray crystal structures of 1,7,10,16-tetraoxa-4,13-diazacyclooctadecane lead(II) thiocyanate (1), $Pb(SCN)_2 \cdot C_{12}H_{26}N_2O_4$, 4,7,13,16,21,24-hexaoxa-1,10-diazabicyclo[8.8.8]-hexacosane lead(II) thiocyanate (2), $Pb(SCN)_2 \cdot C_{18}H_{36}N_2O_6$, and bis-dimethylsulfoxide lead(II) isothiocyanate (25), $Pb(NCS)_2 \cdot 2[(CH_3)_2SO]$ have been described. Infrared spectra have been reported for $Pb(SCN)_2 \cdot 4tu$ (3), $Pb(SCN)_2 \cdot$(2,2′-bipy) (4), and $2Pb(SCN)_4 \cdot$(4,4′-bipy) (4).[2]

Our interest in the modes of metal–thiocyanate coordination (*e.g.*, M—NCS, M—SCN, M—NCS—M) prompted this study of the vibrational spectra and structures of complexes of $Pb(SCN)_2$ with various Lewis base ligands. The complexes $Pb(SCN)_2 \cdot 4tu$ and $Pb(SCN)_2 \cdot$(2,2′-bipy) were also synthesized to re-examine their spectra and test the previous conclusion that thiocyanate is S-bonded in these complexes (4).

Experimental

Materials

Lead(II) thiocyanate was prepared by standard methods (5). Dimethylacetamide (dma), dimethylsulfoxide (dmso), tetramethylethylenediamine (tmen), ethylenediamine (en), and pyridine (py) were dried over molecular sieves. Thiourea (tu), 2,2′-bipyridyl (bipy), and 1,10-phenanthroline (phen) were used directly.

Physical Measurements

Infrared spectra (4000–250 cm^{-1}) were recorded on a Perkin-Elmer 521 spectrophotometer. Samples were examined as Nujol mulls using CsI plates. Raman spectra (3000–30 cm^{-1}) were recorded on a Jarrell-Ash 25-300 spectrophotometer. Samples were sealed in capillary tubes and cooled to −40 °C with nitrogen gas. Far infrared spectra (400–30 cm^{-1}) were recorded on a Hitachi FIS-3 spectrophotometer. Samples were examined as Nujol mulls sealed between thin polyethylene films (Dow Handi-Wrap). Vibrational bands of the NCS group were distinguished from ligand bands by preparing the anal-

[1]This paper is dedicated to Professor C. A. Winkler of McGill University on the occasion of his sixty-fifth birthday by one of his former students (M.O.).

[2]Throughout this paper coordinated thiocyanate is written SCN if it is S-bonded and NCS if it is N-bonded as proposed or confirmed in the reference cited.

TABLE 1. Analytical results for complexes of $Pb(NCS)_2$

Complex	Pb		C		H		N		Melting and/or decomposition temperature (°C)
	Found	Calcd.	Found	Calcd.	Found	Calcd.	Found	Calcd.	
$Pb(NCS)_2 \cdot 2py$	44.59	43.04	27.89	29.91	2.04	2.08	10.63	11.63	110
$Pb(NCS)_2 \cdot 2dmso$	42.75	43.21	15.21	15.02	3.37	2.50	5.72	5.84	104
$Pb(NCS)_2 \cdot bipy$	43.16	43.22	29.04	30.04	1.46	1.67	11.32	11.68	225
$Pb(NCS)_2 \cdot phen$	42.20	41.15	32.14	33.25	1.76	1.60	10.56	11.10	232
$Pb(NCS)_2 \cdot 2phen$	30.03	30.13	44.29	45.15	2.39	2.34	11.81	12.15	252
$Pb(NCS)_2 \cdot 2en$	47.09	46.73	15.71	16.24	3.74	3.61	17.92	18.94	82
$Pb(NCS)_2 \cdot en$	54.23	54.03	12.23	12.53	1.90	2.10	14.22	14.61	124–134
$Pb(NCS)_2 \cdot tmen$	49.08	48.71	20.85	22.57	3.41	3.76	12.37	13.17	140
$Pb(NCS)_2 \cdot 2dma$	41.30	41.65	20.37	24.14	3.00	3.65	9.08	11.26	94
$Pb(NCS)_2 \cdot 4tu$	34.81	33.01	10.32	11.50	2.08	2.50	21.61	22.30	100

ogous lead(II) halide complexes for each ligand and performing a band by band comparison of the spectra. In most cases the NCS bands were found with ease. Coordination of the ligands were verified by examining the frequency shifts of the ligand vibrations most directly involved with coordination.

Melting points were measured in duplicate in sealed capillary tubes. None of the complexes melt sharply. The values recorded in Table 1 are the temperatures at which melting and/or decomposition begins. All complexes are hygroscopic and decompose slowly when exposed to air. The pyridine, ethylenediamine (1:2), and dimethylacetamide complexes are the least stable and decompose slowly while being stored at 25 °C, even under an atmosphere of nitrogen. Poor elemental analyses were obtained because of their low stabilities. These three complexes can be recrystallized from solutions in their parent ligand but not from any other common polar or non-polar solvent. All other complexes in Table 1 are also insoluble in common polar or non-polar solvents. The fact that they could not be recrystallized made it impossible to obtain analytically pure samples in a few cases in spite of repeated attempts and careful purification of reagents.

Analyses for C, H, and N were done by Chemalytics Inc., Tempe, Arizona. Lead was analyzed in duplicate gravimetrically as $PbSO_4$ promptly after preparation of a complex, the sample of which was transferred to a weighing vial in a nitrogen-filled dry-box.

X-Ray powder diffraction patterns were taken with a Debye–Scherrer camera using Ni-filtered CuK_α radiation (λ = 1.5418 Å). Single-crystal measurements were obtained from rotation, Weissenberg, and precession photographs using Ni-filtered CuK_α radiation.

Preparation of $Pb(NCS)_2 \cdot phen$, $Pb(NCS)_2 \cdot 2phen$, $Pb(NCS)_2 \cdot en$, $Pb(NCS)_2 \cdot bipy$, and $Pb(NCS)_2 \cdot 4tu$

Stoichiometric amounts of the ligands (*e.g.*, 3.6 g, 20 mmol phenanthroline) were dissolved in absolute ethanol (100 ml) to which $Pb(SCN)_2$ (3.23 g, 10 mmol) was added. The mixture was stirred for periods ranging from 1 h to 3 days, and then filtered under dry nitrogen. The products (*e.g.*, $Pb(NCS)_2 \cdot 2phen$) were subsequently dried under a vacuum at 25 °C for 6 h. Analytical data are given in Table 1.

Preparation of $Pb(NCS)_2 \cdot 2en$, $Pb(NCS)_2 \cdot tmen$, $Pb(NCS)_2 \cdot 2py$, and $Pb(NCS)_2 \cdot 2dmso$

Lead(II) thiocyanate (3.23 g, 10 mmol) was added to an excess of the pure ligand (*e.g.*, 50 ml dmso) and heated to about 50 °C until $Pb(SCN)_2$ dissolved completely. Excess absolute ethanol, benzene, or hexane was added until a precipitate formed. The product (*e.g.*, $Pb(NCS)_2 \cdot 2dmso$, 4.5 g, 94% yield) was then filtered and dried as before. Crystals were also grown by allowing the saturated solution of ligand and $Pb(SCN)_2$ to stand for several days. $Pb(NCS)_2 \cdot 2py$ was dried by suction under dry nitrogen

Preparation of $Pb(NCS)_2 \cdot 2dma$

A slurry of $Pb(SCN)_2$ (3.23 g, 10 mmol) and dry acetone (20 ml) was heated to 50 °C and stirred. Dimethylacetamide was added dropwise until a clear solution resulted. Absolute ether (100 ml) was added slowly until a white precipitate formed. The product (4.6 g, 93% yield) was filtered and dried with suction in a nitrogen-filled dry-box.

Results and Discussion

Infrared and Raman absorption frequencies of the thiocyanate group are collected in Table 2, while far infrared and low-frequency Raman bands are listed in Table 3. Correlations of thiocyanate bonding type with ranges of the thiocyanate fundamental frequencies, as summarized in Table 4 (6), have been used successfully in a variety of transition metal complexes for which X-ray data is available (6, 7). However, the validity of these criteria has been severely questioned because overlapping ranges lead to ambiguous answers in some cases, and the factors causing vibrational shifts are uncertain. Accordingly, Norbury (6) has urged caution in the use of vibrational data for deciding thiocyanate bonding modes, while emphasizing the need for X-ray crystal structure determinations.

TABLE 2. Vibrational frequencies (cm^{-1}) of the NCS group

	ν(CN)		ν(CS)		δ(NCS)[a]	
	Infrared	Raman	Infrared	Raman	Infrared	Raman
K^+NCS^-	2053 s		744 w		483, 470, 459	
Pb $(SCN)_2$	2058 s, 2045 m	2037 m	753 m	765 m	470, 461, 455	478, 466
$Pb(NCS)_2 \cdot$bipy	2050 s, 2007 s	2053 s, 2038 w, 2012 w	749 w	753 w	472, 469, 457	473, 465
$Pb(NCS)_2 \cdot 2$py	2100 s, 2054 s, 2009 s	2094 s, 2061 s, 2037 w, 2021 w, 2003 m	758 w	762 w, 723 m	476, 454, 443	498, 473, 458, 444
$Pb(NCS)_2 \cdot$phen	2046 s	2075 s, 2036 w	743 w	762 w, 750 w	474, 470, 456	470
$Pb(NCS)_2 \cdot 2$phen	2083 s, 2054 s, 2021 w	2085 m, 2070 w, 2058 w, 2053 m, 2040 w, 2025 m	754 w, 745 w	Fluorescence interferes	484, 470, 455	470, 460, 455
$Pb(NCS)_2 \cdot$tmen	2062 s, 2017 m	2058 s, 2035 w	Ligand interferes		Ligand interferes	
$Pb(NCS)_2 \cdot$en	2060 s, 2018 s	2053 s, 2040 s, 2015 s	765 w, 756 w	769 w, 763 w	481, 468, 459	471
$Pb(NCS)_2 \cdot 2$en	2072 s, 2044 s	2076 m, 2053 s, 2012 s	765 w	770 w, 752 sh, 742 m, 730 w	468	Fluorescence interferes
$Pb(NCS)_2 \cdot 2$dmso	2051 s	2055 s, 2032 m	781 w	785 m, 758 w	468, 461	466, 460
$Pb(NCS)_2 \cdot 2$dma	2097 s, 2079 s, 2056 s	2084 s, 2038 w	749 w	754 s	472, 459, 457	468, 459
$Pb(NCS)_2 \cdot 4$tu	2064 s, 1965 s	2062 s, 2036 s, 1995 w, 1972 m	796 w	800 m, 760 m	472	507

[a]All bands are weak.

TABLE 3. Low frequency bands (cm^{-1})

Compounds	Infrared	Raman
$Pb(NCS)_2$	278 w; 230 w, b; 175 m, b; 130 sh, m; 76 s, b; 38 w	185 m, sh; 152 m, b; 134 w, sh; 102 s; 74 s; 44 s; 30 s
$Pb(NCS)_2 \cdot 2py$	196 s, b; 114 m; 92 w, sh; 80–70 s, b; 60 m, sh	391 w; 360 vw; 198 w; 187 w; 163 w, sh; 150 w; 115 w, sh; 100 w, sh; 69 vs; 50 m; 42 m; 28 s
$Pb(NCS)_2 \cdot bipy$	345 m; 250 w; 210 m; 157 m; 126 sh, w; 90–80 vs, b	350 s; 240 m; 220 w; 187 s; 168 s; 153 m; 137 sh; 115 s; 85 m; 56 w; 38 s
$Pb(NCS)_2 \cdot phen$	264 m; 157 s; 148 m, b; 106 s; 83 s, b; 36 w	271 m; 260 sh; 255 w; 185 vw; 174 vw; 155 w; 125 sh; 115 w; 90 m; 62 s; 36 s; 30 w
$Pb(NCS)_2 \cdot 2phen$	298 w, 271 sh; 266 m; 254–251 m, b; 243 m, 152–149 s, b; 112 s, b; 81–77 s, b; 40 w	274 m; 265 sh; 253 m; 235 w; 153 w; 108 sh; 79 m; 55 sh; 44 s
$Pb(NCS)_2 \cdot tmen$	370 m; 302 vw; 269 vw; 194–186 m, b; 100–96 s, b	374 w; 153 m; 145 w; 135 sh; 128 sh; 115 s; 100 s; 71 m; 53 m; 42 m
$Pb(NCS)_2 \cdot en$	383 w; 270 w, b; 203 w, sh; 162 m, sh; 125 m, b; 102 s; 86 w; 73 w, sh; 55 s; 38 vs	384–376 m, vb; 270 vw; 184–176 m, b; 126 m, sh; 104–97 s, b; 77 m, sh
$Pb(NCS)_2 \cdot 2en$	366 m, b; 277 w, b; 120–100 s	378 s; 295–290 m, b; 198 m, b; 175 w; 67 w; 55 m; 35 s
$Pb(NCS)_2 \cdot 2dmso$	392 s; 342 s; 308 m; 280 vw; 120–106 vs, b	400 w; 342 s; 310 s; 195 w; 135 m; 102 sh; 79 sh; 56 sh; 43 s
$Pb(NCS)_2 \cdot 2dma$	340 m, 212 s, b; 188–170 m, vb; 140 w, sh; 116–106 s, b; 100–95 s, b; 74 sh	188 w; 156 m; 129 w; 100 s; 78 w; 71 m; 53 sh; 42 s; 27 s
$Pb(NCS)_2 \cdot 4tu$	226 sh; 202 sh; 178–174 s, b; 140 s, b; 106 w, sh; 45 w, b	188 w; 156 m; 129 w; 100 s; 78 w; 71 m; 53 sh; 42 s; 27 s

Of the complexes listed in Table 2, the crystal and molecular structure of only $Pb(NCS)_2 \cdot 2dmso$ has been determined (25). Its Pb—N bond distances (2.45, 2.42 Å) indicate appreciable covalent character in a six-coordinate, thiocyanate-bridged polymeric structure. Although crystalline $Pb(SCN)_2$ also has bridging thiocyanate groups, its Pb—N bond distances (2.687, 2.781 Å) suggest the predominance of ionic bonding (8). Surprisingly, both compounds have essentially the same CN stretching frequencies.

TABLE 4. Correlation of bonding type with thiocyanate frequencies (6)

Bonding type	ν(CN) (cm^{-1})	ν(CS) (cm^{-1})	δ(NCS) (cm^{-1})
NCS^-	2053	746	486, 471
M—NCS	2100–2050	870–820	485–475
M—SCN	2130–2085	760–700	470–430
M—NCS—M	2165–2065	800–750	470–440

However, they differ appreciably in the frequencies of their CS stretching vibrations. As evident from Table 4, the higher value of 781 cm^{-1} correlates well with the bridged structure of $Pb(NCS)_2 \cdot 2dmso$.

The other complexes in Table 2 are probably also thiocyanate-bridged polymeric chains with stronger N- than S-bonding and six-coordinate lead. The CN and CS stretching frequencies of these complexes are consistent with a bridged polymeric structure, as are their physical properties such as insolubility in common solvents and failure to melt sharply. None of the complexes have a CS stretching frequency appreciably below 750 cm^{-1} which would be indicative of a thiocyanate S-bonded structure. The thiocyanate deformation frequencies, δ(NCS), of most complexes are not significantly different from those of $Pb(SCN)_2$, and the absence of bands below 450 cm^{-1} is consistent with the absence of predominantly S-bonded thiocyanate. Unfortunately, overlap of the regions characteristic of

thiocyanate bridge bonding and terminal N-bonding (Table 4) makes the discrete assignment of one structure or the other impossible for our complexes on the basis of vibrational data alone.

In an attempt to explain the coordinating properties of the thiocyanate group, Kharitonov *et al.* (9) made a semi-empirical analysis which showed that for terminal N-bonded thiocyanate groups values of ν(CN) and ν(CS) increase linearly with the force constant K_{MN} of the M—NCS bond. However, the value of ν(CS) increases more rapidly than that of ν(CN). Calculations for the bridged structure revealed an increase in ν(CN) of about the same magnitude as for the terminal N-bonded case. They concluded that other factors needed to be considered to explain the large change in ν(CN) found experimentally for bridged transition metal thiocyanates. However, calculations were done only for strongly bridged structures.

The lack of change in the ν(CN) and ν(CS) frequencies upon complexation of $Pb(SCN)_2$ may be due to the relatively small Pb—NCS force constants. While the Pb—N bond in $Pb(NCS)_2 \cdot 2dmso$ is shorter and has more covalent character than in $Pb(SCN)_2$, it is still longer than the sums of the covalent radii of Pb and N (8). The use of force constants calculated by Kharitonov *et al.* (9) allows us to make the following comparisons. Whereas $Pb(NCS)_2 \cdot 2dmso$ has ν(CN) = 2051 cm^{-1} and ν(CS) = 781 cm^{-1}, Kharitonov *et al.* (9) calculated ν(CN) = 2057 cm^{-1} and ν(CS) = 778 cm^{-1} for K_{MN} = 1.0 mdyn $Å^{-1}$ and mass 200 for the N-bonded thiocyanate. The observation of ν(CN) = 2058 and 2045 cm^{-1} and ν(CS) = 753 cm^{-1} in $Pb(SCN)_2$ compares favorably with the calculation by Kharitonov *et al.* (9) of ν(CN) = 2051 cm^{-1} and ν(CS) = 761 cm^{-1} for $K_{MN} = K_{SM}$ = 0.5 mdyn $Å^{-1}$ and mass 200. Although frequencies of other complexes can be fitted to the calculated values, it is not justifiable to do this in the absence of crystal structure data.

Ligand vibrations most diagnostic of coordination, listed and assigned in Table 5, agree with literature reports for other metal complexes. Because of the large number of bands and the low symmetry of the complexes, no attempt is made to assign the far infrared and Raman bands listed in Table 3. The low symmetry of the complexes is clearly evident from their X-ray powder diffraction patterns,[3] each of which consisted of sharp and well-defined lines. Comparisons of *d*-spacings and relative intensities confirm that none of the complexes are isomorphous. Attempts were made to obtain the single-crystal X-ray structure of $Pb(NCS)_2 \cdot 2en$, but because of its slow decomposition in the X-ray beam only rotation and Weissenberg photographs were taken. These were good enough to show that crystals are orthorhombic with cell dimensions $a \approx b = 14.9 \pm 0.1$ Å, and $c = 36.0 \pm 0.1$ Å. Unfortunately the crystals were not stable long enough in the X-ray beam to allow the recording of precession photographs and collection of intensity data necessary to solve the structure.

It is now necessary to discuss those of our vibrational measurements and assignments which differ from previous reports. Tramer (18) observed two bands at 2042 and 2095 cm^{-1} in the infrared spectrum of crystalline $Pb(SCN)_2$ in a KBr disc and he assigned them to the CN stretching vibrations of N-bonded and S-bonded thiocyanate, respectively. Our repeated attempts with a wide range of concentrations of $Pb(SCN)_2$ in Nujol mulls failed to reveal bands other than those at 2058 and 2045 cm^{-1} in the infrared and at 2037 cm^{-1} in the Raman spectrum. Likewise, Mokuolu and Speakman (8) did not observe a band higher than 2055 cm^{-1} in their infrared spectrum of $Pb(SCN)_2$ in KBr disc form. Perhaps the 2095 cm^{-1} band reported by Tramer (18) is due to exchange of thiocyanate with KBr or to a thiocyanate impurity.

Czakis-Sulikowska and Kusnik (3) assigned the strong band at 725 cm^{-1} in the infrared spectrum of $Pb(SCN)_2 \cdot 4tu$ to the thiocyanate CS stretching vibration. They also proposed that thiocyanate was S-bonded in the complex on the basis that this frequency occurs in the region characteristic of S-bonded thiocyanates (19). We believe that this strong band is actually due to the CS stretching vibration of coordinated thiourea because similar strong bands have been observed in the spectra of thiourea complexes of Sn(II) (20) and a variety of transition metal ions

[3]Tables of *d*-spacings and relative intensities may be obtained, at a nominal charge, from the Depository of Unpublished Data, CISTI, National Research Council of Canada, Ottawa, Canada K1A 0S2.

TABLE 5. Ligand coordination frequencies (cm^{-1})

Observed	Free ligand	Assignment	Reference	Observed	Free ligand	Assignment	Reference
$Pb(NCS)_2 \cdot 2py$	Py			$Pb(NCS)_2 \cdot bipy$	bipy		
1591, 1588	1580	Ring stretch	10	1596, 1588	1579	Ring stretch	10
1003, 998	992	Ring breathing	10	1568, 1557	1553	Ring stretch	10
622, 616	605	Ring bending	10	1011, 1006	991	Ring breathing	10
412	405	Ring torsion	10	644, 625	651, 618	Ring bending	10
				410	398	Ring torsion	10
$Pb(NCS)_2 \cdot phen$	phen			$Pb(NCS)_2 \cdot 2phen$	phen		
1514	1500	Ring stretch	11	1511	1500	Ring stretch	11
1099	1087	Ring vibration	11	1198, 1193	1087	Ring vibration	11
418	408	Ring breathing	11	416	408	Ring breathing	11
$Pb(NCS)_2 \cdot en$	en			$Pb(NCS)_2 \cdot 2en$	en		
1000, 958	1104, 980	N—C—C—N stretch	12	996, 960	1104, 980	N—C—C—N stretch	12
$Pb(NCS)_2 \cdot tmen$	tmen			$Pb(NCS)_2 \cdot 4tu$	tu		
1077, 1042	1104	C—N stretch	13	1400, 1372	1412	C=S stretch	14
1020, 1005	1040	C—N stretch	13	720	732	C—S, N—C—N stretch	15
$Pb(NCS)_2 \cdot 2dmso$	dmso			$Pb(NCS)_2 \cdot dma$	dma		
1021	1042	S=O stretch	16	1600	1662	C=O, C=N stretch	17
712	695, 666	C—S stretch	16				
393	382	C—S sym. def.	16				
345	333	C—S—O antisym. stretch	16				

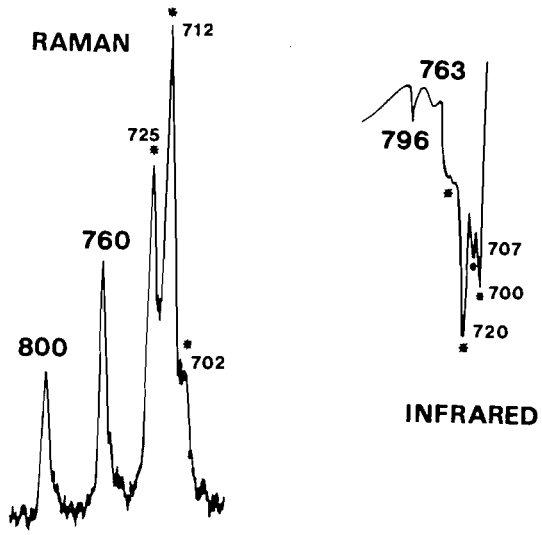

FIG. 1. Vibrational bands (cm^{-1}) of $Pb(NCS)_2 \cdot 4tu$ in the ν(CS) region. (Ligand bands are designated by an asterisk.)

(21). By measuring the infrared spectrum of $Pb(NCS)_2 \cdot 4tu$ in a thick Nujol mull, we observed a weak band at 796 cm^{-1} which we assign to the thiocyanate CS stretching vibration (Fig. 1). This mode produces bands of medium intensity at 800 and 760 cm^{-1} in the Raman spectrum. These frequencies are in the range usually associated with bridged or N-bonded thiocyanate complexes (Table 4). The CN stretching frequency at 2064 cm^{-1} is also compatible with bridging thiocyanate groups (6), although the presence of N-bonded thiocyanate cannot be excluded. Thus neither CN nor CS stretching frequencies are consistent with S-bonded thiocyanate or the presence of thiocyanate ions.

The single-crystal X-ray diffraction photographs of $Pb(NCS)_2 \cdot 4tu$ obtained by Boeyens and Herbstein (22) proved to be so complicated that they have not yet been interpreted. Our own measurements reveal that the crystals are tetragonal, space group $P4/mcc$ or $P4cc$, cell dimensions of $a = b = 10.53 \pm 0.05$ Å, $c = 8.03 \pm 0.05$ Å, and the [001] rotation photograph of the diffuse layer shows diffuse lines corresponding to an interplanar distance of 12.0 ± 0.1 Å. A Weissenberg photograph of a diffuse layer shows a similar tetragonal structure indicating the presence of long-range disorder with short-range order similar to that reported for $Pb(NO_3)_2 \cdot 6tu$ (22). Thus, both diffraction and vibrational measurements are not sufficiently definitive to show the coordination about Pb(II). Considering that both thiocyanate and thiourea frequently behave as bridging ligands, Pb(II) in $Pb(NCS)_2 \cdot 4tu$ probably has a coordination number greater than six. High values have been reported in such thiourea complexes as: (*i*) $PbCl_2 \cdot 2tu$ in which Pb(II) is seven-coordinate with both thiourea molecules and one chlorine atom bridging (23), (*ii*) $Pb(NO_3)_2 \cdot 6tu$ and $Pb(ClO_4)_2 \cdot 6tu$ which are presumed to have eight-coordinate Pb(II) (22), and (*iii*) $Pb(HCOO)_2 \cdot 2tu \cdot H_2O$ which has three bridging sulphur atoms and five oxygen atoms in a distorted dodecahedral arrangement around Pb(II) (24).

For $Pb(SCN)_2 \cdot bipy$, Czakis-Sulikowska and Kusnik (3) observed a band at 2080 cm^{-1} which they attributed to the CN stretching vibration of S-bonded thiocyanate because this frequency is at the lower limit of the range for such bonding (19). We observed the CN stretching frequencies at 2050 and 2007 cm^{-1} in the infrared, and at 2053, 2038, and 2012 cm^{-1} in the Raman spectrum; no higher frequency bands were found. The CS stretching frequency, observed by Czakis-Sulikowska and Kusnik (3) at 749 cm^{-1} and confirmed by us at the same position, is on the borderline of the regions associated with bridge-bonded and S-bonded thiocyanate (6). The CN and CS stretching frequencies taken together, like those of $Pb(NCS)_2 \cdot 4tu$, strongly suggest the presence of bridge-bonded and/or N-bonded thiocyanate rather than S-bonded tihocyanate.

Acknowledgments

The financial support of the National Research Council of Canada and le Gouvernement du Québec, Ministère de l'Education, is gratefully acknowledged. We are also grateful to Professor Gabrielle Donnay for the use of X-ray equipment and assistance in the interpretation of the data.

1. B. METZ and R. WEISS. Acta Crystallogr. Sect. B, **29**, 1088 (1973).
2. B. METZ and R. WEISS. Inorg. Chem. **13**, 2094 (1974).
3. D. M. CZAKIS-SULIKOWSKA and B. KUSNIK. Rocz. Chem. **43**, 1363 (1969).
4. D. M. CZAKIS-SULIKOWSKA, J. RADWANSKA-DOCZEKALSKA, and A. GRECKA. Rocz. Chem. **47**, 2345 (1973).
5. G. BRAUER. Preparative inorganic chemistry. Academic Press, New York. 1963. p. 769.

6. A. H. NORBURY. Adv. Inorg. Chem. Radiochem. **17**, 231 (1975).
7. T. A. BAILEY, S. L. KOZAK, T. W. MICHELSON, and W. N. MILLS. Coord. Chem. Rev. **6**, 407 (1971).
8. J. A. A. MOKUOLU and J. C. SPEAKMAN. Acta Crystallogr. Sect. B, **31**, 172 (1975).
9. YU. YA. KHARITONOV, G. TSINTSADZE, and M. A. PORAI-KOSHITS. Russ. J. Inorg. Chem. **10**, 427 (1965).
10. J. S. STRUKL and J. L. WALTER. Spectrochim. Acta, Part A, **27**, 209 (1971).
11. A. A. SCHILT and R. C. TAYLOR. J. Inorg. Nucl. Chem. **9**, 211 (1959).
12. A. SABITINI and S. CALIFANO. Spectrochim. Acta, **16**, 667 (1960).
13. S. C. JAIN and R. RIVEST. Inorg. Chim. Acta, **3**, 552 (1969).
14. M. NISHIKAWA, H. MIMA, and T. KANZAWA. Chem. Pharm. Bull. **10**, 1199 (1961).
15. C. N. R. RAO, R. VENHATARAGHAVAN, and T. R. KASTURI. Can. J. Chem. **42**, 36 (1964).
16. W. D. HORROCKS, JR. and F. A. COTTON. Spectrochim. Acta, **17**, 134 (1961).
17. G. DURGAPRASAD, D. N. SATHYANARAYAN, C. C. PATEL, H. S. RANDHAWA, A. GOEL, and C. N. R. RAO. Spectrochim. Acta, Part A, **28**, 2311 (1972).
18. A. TRAMER. J. Chim. Phys. **59**, 232 (1962).
19. J. LEWIS, R. S. NYHOLM, and P. W. SMITH. J. Chem. Soc. 4590 (1961).
20. J. E. CASSIDY, W. MOSER, J. D. DONALDSON, A. JELEN, and D. G. NICHOLSON. J. Chem. Soc. A, 173 (1970).
21. L. D. DREMYATSKAYA, N. B. LYUBIMOVA, and S. D. BESKOV. Russ. J. Phys. Chem. **43**, 470 (1969).
22. J. C. A. BOEYENS and F. H. HERBSTEIN. Inorg. Chem. **6**, 1408 (1967).
23. M. NARDELLI and G. FAVA. Acta Crystallogr. **12**, 727 (1959).
24. I. GOLDBERG and F. H. HERBSTEIN. Acta Crystallogr. Sect. B, **29**, 246 (1973).
25. A. D. BARANYI, M. ONYSZCHUK, S. FORTIER, and G. DONNAY. To be published.

Electrochemical reduction of 1,3-diketones in hydroorganic medium. Preparation of 1,2-cyclopropanediols

JOSEPH ARMAND AND LINE BOULARES

Laboratoire de Physicochimie des Solutions, Université Paris VI, 8, Rue Cuvier 75230 Paris Cédex 05, France

Received July 21, 1975

JOSEPH ARMAND and LINE BOULARES. Can. J. Chem. **54**, 1197 (1976).

The electrochemical reduction of 1,3-diketones $C_6H_5—CO—CR_1R_2—CO—R_3$ (R_1 = H, CH_3; R_2 = CH_3, $CH_2C_6H_5$; R_3 = CH_3, C_6H_5) in an hydroorganic medium corresponds to a bielectronic process and leads to 1,2-cyclopropanediols which, in most cases, are obtained in good yields. The polarographic results are presented and the mechanisms are discussed.

JOSEPH ARMAND et LINE BOULARES. Can. J. Chem. **54**, 1197 (1976).

La réduction électrochimique des dicétones-1,3, $C_6H_5—CO—CR_1R_2—CO—R_3$ (R_1 = H, CH_3; R_2 = CH_3, $CH_2C_6H_5$; et R_3 = CH_3, C_6H_5), dans un milieu hydroorganique correspond à un processus biélectronique et conduit aux cyclopropanediols-1,2 qui sont obtenus dans la plupart des cas avec de bons rendements. On présente les résultats polarographiques et on discute des mécanismes.

[Traduit par le journal]

Introduction

In a preceeding paper (1), we described the polarographic behaviour of 1,3-diphenyl-1,3-propanediones with an halogeno, acetoxy, or amino group on the 2-position. This led us to investigate the electrochemical reduction in hydroorganic medium of β-diketones such as $R_1COC(R_2)(R_3)COR_4$ (R_1, R_2, R_3, R_4 = alkyl or aryl).

Polarography and electrolysis of 1,3-diphenyl-1,3-propanediones and 1-phenyl-1,3-butanediones

2,2-Dimethyl-1,3-diphenyl-1,3-propanedione, 3, and 2-Methyl-1,3-diphenyl-1,3-propanedione, 2

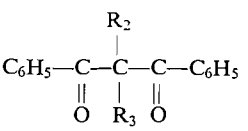

1 $R_2 = R_3 = H$
2 $R_2 = H$, $R_3 = CH_3$
3 $R_2 = R_3 = CH_3$

The electrochemical reduction of **1** has been reported in several papers (2–5). In a water–ethanol medium the polarograms of **1** show one, two, or three waves according to the p*H* (4). The first monoelectronic wave corresponds to the dimerization in eq. 1, while the second wave is

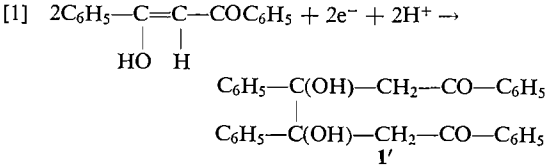

[1] $2C_6H_5—C(HO)=C(H)—COC_6H_5 + 2e^- + 2H^+ \rightarrow$ $C_6H_5—C(OH)—CH_2—CO—C_6H_5$ | $C_6H_5—C(OH)—CH_2—CO—C_6H_5$ **1′**

assigned to the reduction of the dimer **1′** into a cyclic tetrol, as in eq. 2. In solution, compound **1**

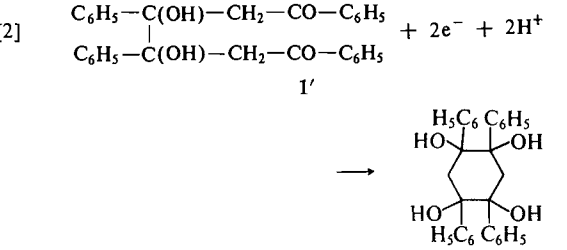

[2] $C_6H_5—C(OH)—CH_2—CO—C_6H_5$ | $C_6H_5—C(OH)—CH_2—CO—C_6H_5$ **1′** $+ 2e^- + 2H^+ \rightarrow$ 1,2,3,4-tetrol (H_5C_6, C_6H_5, HO, OH)

is in an enolic form $\mathbf{1}_E$ (6) and most probably it is this enolic species which is reduced at the electrode, as the formation of **1′** by preparative electrolysis shows that the behaviour of **1** is analogous to that of benzalacetophenone $C_6H_5—CH=CH—CO—C_6H_5$ (2).

As unenolizable 1,3-diphenyl-1,3-propanediones had never been investigated, we became interested in the behaviour of 2,2-dimethyl-1,3-diphenyl-1,3-propanediones, **3**.[1]

In the p*H* range where it is stable (p*H* 1–10) **3** presents a 2e cathodic wave (by reference to benzil at p*H* 1); this wave is distorted at p*H* higher than 4.5; its $E_{1/2}$ varies with the p*H* as shown in Fig. 1. Electrolysis in dilute solutions ($C = 10^{-3}$ *M*, CH_3OH 50%) consumes about 2 electrons per molecule at p*H* 3.7 (E =

[1]In DMSO, it was shown that the electrochemical reduction of **3** gives a radical anion which slowly decomposes into several products amongst which is isobutyrophenone (8).

Can. J. Chem. Downloaded from www.nrcresearchpress.com by 210.87.254.40 on 09/05/12
For personal use only.

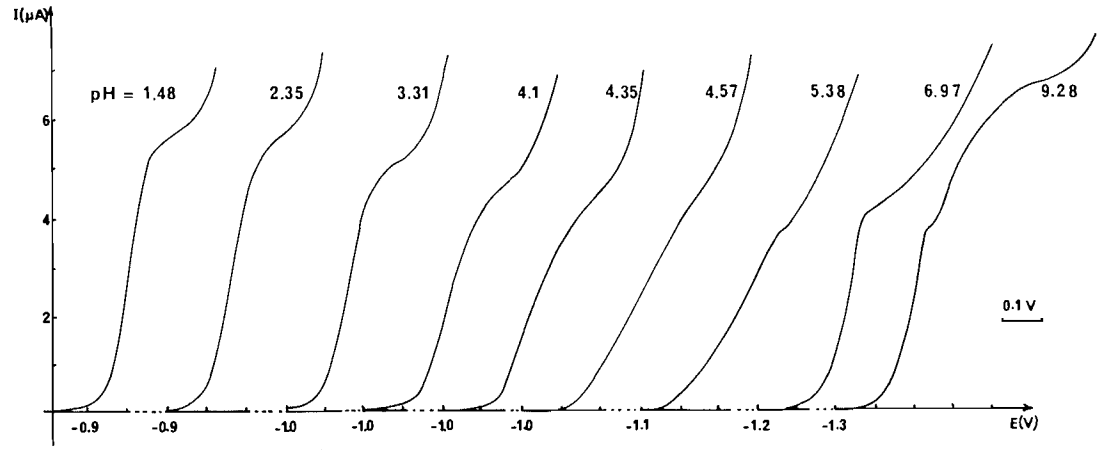

FIG. 1. Polarograms of **3**, C_6H_5—CO—$C(CH_3)_2$—CO—C_6H_5 (CH_3OH 50%, $C = 10^{-3}$ *M*).

-1.25 V) as well as at p*H* 7.15 ($E = -1.50$ V); the electrolyzed solutions show a 2e anodic wave ($E_{1/2} = -0.15$ V at p*H* 7.15). Preparative electrolysis carried out with 600 mg of **3** at p*H* 3.7 gives the *cis*-3,3-dimethyl-1,2-diphenyl-1,2-cyclopropanediol, **4**, in 80% yield. Compound **4** shows the same anodic wave which was observed during the coulometries of **1**. This wave corresponds to the oxidation of **4** into **3**, and the reduction scheme is shown in eq. 3.

[3] $C_6H_5—CO—C(CH_3)_2—CO—C_6H_5 + 2e^- + 2H^+$

3

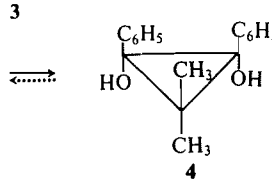

4

Between p*H* 1 and 10 a 2e wave is seen for **2** which is p*H* dependent (Fig. 2). Coulometry at p*H* 3.72 ($C = 2 \times 10^{-3}$ *M*, CH_3OH 50%, $E = -1.25$ V) indicates the consumption of 2e per molecule and the resulting solution gives a 2e anodic wave ($E_{1/2} = 0.00$ V at p*H* 3.7, $E_{1/2} = -0.27$ V at p*H* 7.0) (Fig. 3). Preparative electrolysis with 1 g of **2** at p*H* 3.7 gives 80% of one of the three isomers (one of the two *meso* or the *d,l*) of 1,3-diphenyl-2-methyl-1,2-cyclopropanediol **5**. Spectral data allow us to assign the structure of *r*-1-methyl-*t*-2,*t*-3-diphenyl-*c*-2,*c*-3-cyclopropanediol to **5**. Compound **5** shows the same anodic wave which was observed in the course of dilute electrolysis of **2**: this wave is related to the oxidation of **5** to **2**. Thus, the reduction scheme is as described in eq. 4.

[4] $C_6H_5—CO—CH(CH_3)—CO—C_6H_5 + 2e^- + 2H^+$

2

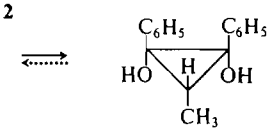

5

1-Phenyl-1,3-butanedione and some 2-Substituted Derivatives

The polarographic behaviour of 1-phenyl-1,3-butanedione, **6**, has been investigated in a water–ethanol medium by Zuman and coworkers (7). Between p*H* 1 and 5, **6** gives a 2e wave i_1; at p*H* higher than 5, i_1 decreases at the expense of wave i_2 with a more negative $E_{1/2}$; i_2 in its turn is replaced by a more negative wave i_3. The sum of the wave heights $i_1 + i_2 + i_3$ remains close to 2e to p*H* 10. In the 3–8 p*H* range, preparative electrolysis gives the 4-hydroxy-4-phenyl-2-butanone C_6H_5—CHOH—CH_2—CO—CH_3 **7** with a 'good' undetermined yield. Compound **7** is obtained as an oil after evaporation of the electrolyzed solution, etheral extraction, washing of the etheral solution with a dilute sodium hydroxide solution, and evaporation of ether. The purpose of washing of the etheral extracts with sodium hydroxide solutions is to separate **6** from **7**. The authors point out that between p*H* 6 and 9, during the electrolysis of dilute solutions, an anodic wave can be observed ($E_{1/2} = -0.15$ V at p*H* 6.9, $E_{1/2} = -0.34$ V at p*H* 9.3). On the contrary the oil isolated from preparative electrolysis does not show an anodic wave. The compound responsible for the anodic wave is ignored in the discussion;

Can. J. Chem. Downloaded from www.nrcresearchpress.com by 210.87.254.40 on 09/05/12
For personal use only.

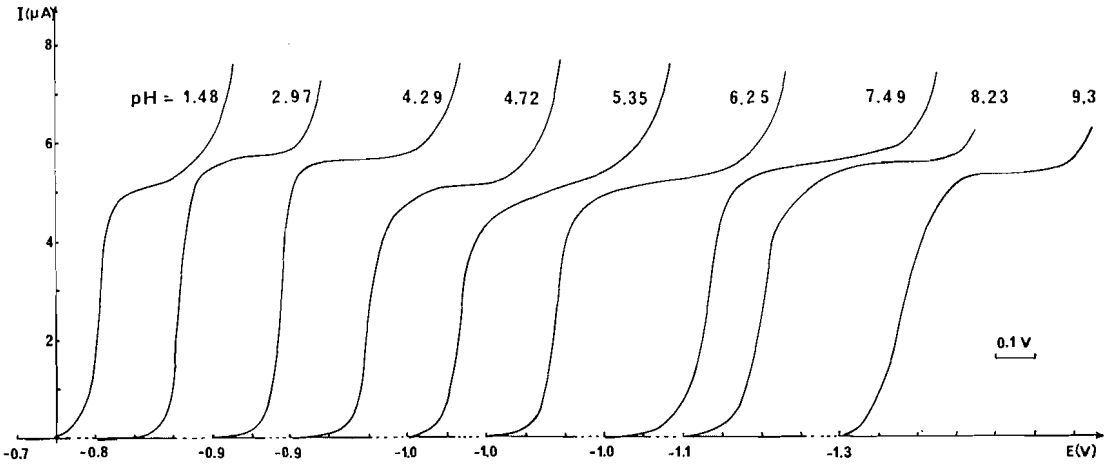

FIG. 2. Polarograms of **2**, C_6H_5—CO—$CH(CH_3)$—CO—C_6H_5 (CH_3OH 50%, $C = 10^{-3}$ *M*).

the three waves i_1, i_2, and i_3 are all assigned to the overall reduction scheme in eq. 5. The

[5] $C_6H_5COCH_2COCH_3 + 2e^- + 2H^+ \rightarrow C_6H_5CHOHCH_2COCH_3$

reduced species are different for the three waves: i_1 corresponds to the reduction of a biprotonated form, i_2 to that of a monoprotonated form, and i_3 to the reduction of the neutral molecule. Without detailing their arguments further, the authors state that the diketo form is reduced and not the enol form. The enolic tautomer, which accounts for about 40% of the product in the medium used, would be transformed into diketone as this last species is reduced. This last point seems quite plausible because, as we have already seen in the case of **1**, if the enolic form was reduced, **6** should behave as benzalacetophenone C_6H_5 CH=CHCOCH$_3$. Benzalacetophenone (2) is known to show a one electron wave leading to the reduction into an ε-diketone (eq. 6). The presence of an anodic wave during

[6] $2C_6H_5CH{=}CHCOCH_3 + 2e^- + 2H^+ \rightarrow$

C_6H_5—CH—CH_2—$COCH_3$

|

C_6H_5—CH—CH_2—$COCH_3$

the electrolysis of dilute solutions of **6** in addition to the preceding results (1) suggest at least a partial yield of a 1,2-cyclopropanediol. Therefore the investigation of compounds of the type C_6H_5—CO—$C(R_1)(R_2)$—CO—CH_3 was undertaken.

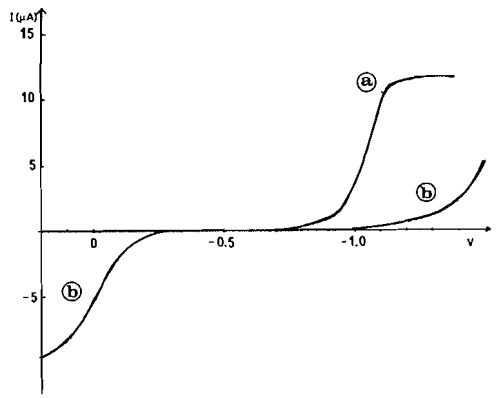

FIG. 3. Electrolysis of C_6H_5—CO—$CH(CH_3)$—CO—C_6H_5, **2** (p*H* = 3.72, 50% CH_3OH, $C = 2 \times 10^{-3}$ *M*, *V* = 200 ml, $E = -1.25$ V) (*a*) before electrolysis, (*b*) at the end of the electrolysis.

1-Phenyl-1,3-butanedione **6**

Electrolysis of dilute solutions of **6** were performed to measure the height of the anodic wave described by ref. 7. These electrolyses were carried out under argon: (*a*) at p*H* 3.80 ($C = 2 \times 10^{-3}$ *M*, CH_3OH 20%, $E = -1.25$ V), an anodic wave is observed at the end of the electrolysis ($E_{1/2} = -0.10$ V) and its height reaches about 20% of the initial wave of **6**; (*b*) at p*H* 7.23 ($C = 2 \times 10^{-3}$ *M*, CH_3OH 50%, $E = -1.60$ V) the anodic wave ($E_{1/2} = -0.08$ V) reaches about 30% of the sum of the waves $i_1 + i_2 + i_3$ of **6**; (*c*) at p*H* 6.58 ($C = 2 \times 10^{-3}$ M, CH_3OH 20%, $E = -1.60$ V) the height of the anodic wave ($E_{1/2} = -0.05$ V) is about 50% of the total height of waves $i_1 + i_2$ of **6** (Fig. 4). The uv spectrum at completion of the electrolysis

Can. J. Chem. Downloaded from www.nrcresearchpress.com by 210.87.254.40 on 09/05/12
For personal use only.

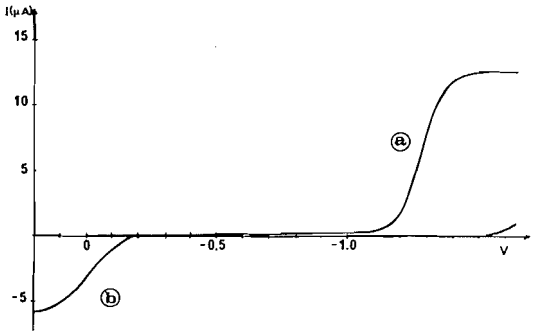

FIG. 4. Electrolysis of C_6H_5—CO—CH_2—CO—CH_3, **6** (p*H* = 6.58, 20% CH_3OH, $C = 2 \times 10^{-3}$ *M*, *V* = 200 ml, $E = -1.60$ V) (*a*) before electrolysis, (*b*) end of the electrolysis.

shows the complete disappearance of the absorption of the C_6H_5CO— and C_6H_5—C(OH)=CH— groups. As in the case of ref. 7, 2e are consumed per molecule in our electrolysis. The results obtained in addition to those discussed above suggest a yield of about 50% of 1 2-cyclopropanediol in dilute solutions at p*H* 6.58. Thus, cyclopropanediol is not isolated from preparative electrolysis either because it is oxidized into **6** and washed away with sodium hydroxide or because it is transformed during the treatment of the etheral extracts with sodium hydroxide and eliminated with the aqueous layer (a transformation cyclopropanediol → C_6H_5-$CHOHCH_2COCH_3$ does not seem very likely).

1-Phenyl-2-methyl-1,3-butanedione, ***8***

Between p*H* 1 and 8, compound **8**, C_6H_5—CO—$CH(CH_3)$—CO—CH_3, shows a p*H* dependent 2e wave ($C = 10^{-3}$ *M*, 50% CH_3OH).

p*H*	$E_{1/2}$(V)	p*H*	$E_{1/2}$(V)
1.50	−0.95	5.35	−1.24
2.70	−1.07	7.18	−1.35
3.80	−1.18	8.43	−1.46
4.70	−1.23		

Coulometry at p*H* 7.4 ($C = 2 \times 10^{-3}$ *M*, CH_3OH 50%, $E = -1.50$ V) consumes about 2e per mol and at the end, the solution presents an anodic wave ($E_{1/2} = -0.12$ V) the height of which is about 75% of that of the wave of **8**. At p*H* 3.74 electrolysis in dilute solution ($C = 2 \times 10^{-3}$ *M*, CH_3OH 50%, $E = -1.30$ V) also gives a compound with an anodic wave. By changing the p*H* of the electrolyzed solution from 3.74 to 7.4 an anodic wave is observed ($E_{1/2} = -0.12$ V); its height is about 70% of the height of the wave of **8** at p*H* 7.4.

1-Phenyl-2,2-dimethyl-1,3-butanedione, ***9***

Between p*H* 1 and 8 C_6H_5—CO—$C(CH_3)_2$—CO—CH_3, **9**, presents a p*H* dependent 2e wave ($C = 10^{-3}$ *M*, 50% CH_3OH). Coulometry at

p*H*	$E_{1/2}$(V)	p*H*	$E_{1/2}$(V)
1.51	−0.98	5.03	−1.41
2.31	−1.06	5.90	−1.45
3.11	−1.15	7.74	−1.45
4.16	−1.32		

p*H* 7.95 ($C = 2 \times 10^{-3}$ *M*, CH_3OH 50%, $E = -1.55$ V) consumes 2e per mol and the electrolyzed solution shows an anodic wave ($E_{1/2} = -0.08$ V), the height of which is about 65% of the height of the wave of **9**. At p*H* 3.82 electrolysis ($C = 2 \times 10^{-3}$ *M*, CH_3OH 50%, $E = -1.25$ V) also gives a compound with an anodic wave: by changing the p*H* to 7.9 an anodic wave with $E_{1/2} = -0.08$ V is observed, the height of which is about 60% of the height of the wave of **9**. Preparative electrolysis carried out with 1 g at p*H* 3.7 gives 80% of a 50:50 mixture of the two isomers of 1,1,2-trimethyl-3-phenyl-2,3-cyclopropanediol, **10** [7].

[7] C_6H_5—CO—$C(CH_3)_2$—CO—CH_3 + $2e^-$ + $2H^+$ →

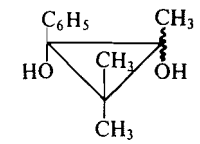

10

1-Phenyl-2-benzyl-2-methyl-1,3-butanedione, ***11***

At p*H* 3.7, **9** gives a 2e wave with $E_{1/2} = -1.16$ V. Electrolysis in dilute solution at this p*H* ($C = 1.5 \times 10^{-3}$ *M*, CH_3OH 50%, $E = -1.30$V) consumes 2e per mol and the resulting solution shows an anodic wave ($E_{1/2} = -0.05$ V at p*H* 7) the height of which is, at p*H* = 7, about 30% of the height of the wave of **11**. Preparative electrolysis carried out at p*H* 3.7 with 400 mg of **11** gives an oil. The nmr spectrum and the easy oxidation into **11** indicate a mixture of the isomers of 1,3-dimethyl-2-phenyl-3-benzyl-1,2-cyclopropanediol **12** [8].

Can. J. Chem. Downloaded from www.nrcresearchpress.com by 210.87.254.40 on 09/05/12
For personal use only.

Can. J. Chem. Downloaded from www.nrcresearchpress.com by 210.87.254.40 on 09/05/12
For personal use only.

[8] 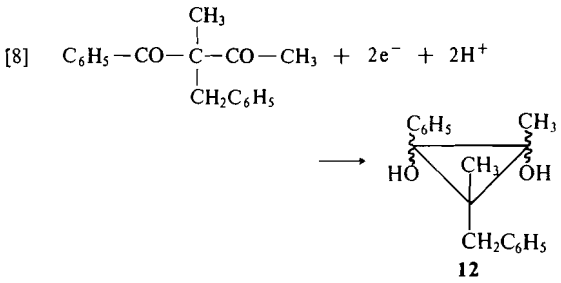

12

Discussion: Reduction Mechanism

Besides the β-diketones already mentioned, some cyclic β-diketones have been investigated by electrochemistry. Thus, 2-phenyl-1,3-indanedione is reduced in hydroorganic medium according to ref. 19 as in eq. 9. The scheme shows

[9] 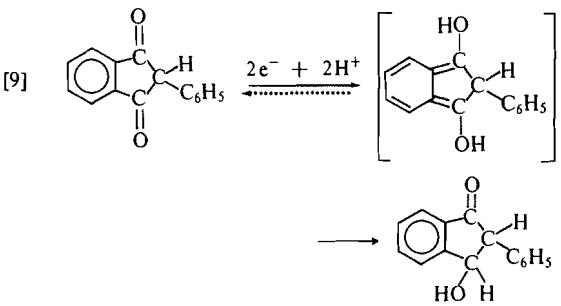

that this compound behaves as an α-diketone (reduction into an enediol followed by a rearrangement into an α-ketol). This is not surprising as this compound is a vinylogue of α-diketone. In alcoholic medium the schemes shown in eqs. 10 and 11 were demonstrated (20).

[10] 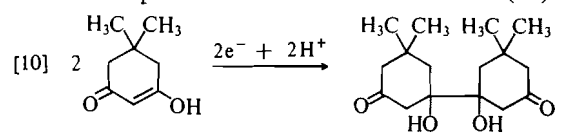

[11] 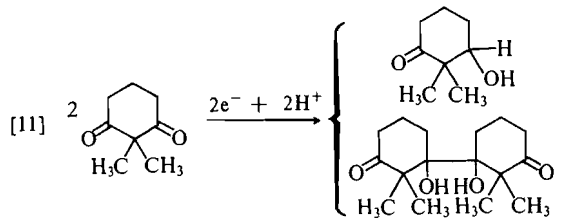

In aprotic medium, the first derivatives of 1,2-cyclopropanediols were obtained by electrochemical reduction (9) as illustrated in eqs. 12 and 13. In protic medium the results described in the literature show that when the β-diketone is enolizable and when it is reduced as an enol it

[12] 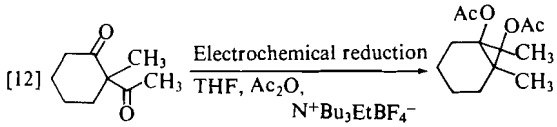

[13] 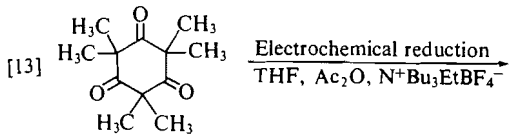

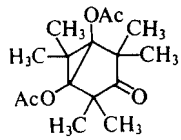

behaves as an α-ethylenic ketone; the reduction is monoelectronic and gives an ε-diketone. When the diketo form is reduced the reduction proceeds, at least partially, as a simple ketone; a β-ketol (19, 20) and a pinacol (20) can be isolated. Our results show that 1,2-cyclopropanediols are obtained in some cases.

Derivatives **2**, **3**, **9** and **11** do not give alcohol or pinacol; if they had been formed they would have been isolated together with the 1,2-cyclopropanediol and detected by nmr. In the case of **6**, the results of Zuman (7), as well as our own, indicate the simultaneous formation of 1,2-cyclopropanediol and of alcohol.

In an acidic or a neutral protic medium, the overall first step of the reduction mechanism for the compounds investigated is shown in eq. 14.

[14] 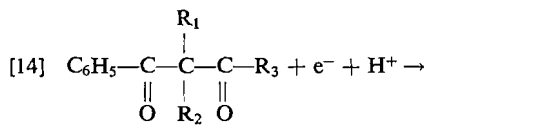

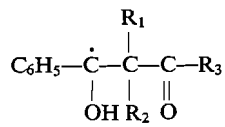

Two routes are then possible as shown in eqs. 15 and 16. Reaction 15 could be operative when $R_3 = C_6H_5$ as the group $-C(=O)-C_6H_5$ is electroreducible but not in the case when $R_3 = CH_3$ as the aliphatic ketones are not electroreducible in hydroorganic medium. Reaction 16 seems more likely as it explains the formation of both the alcohol and the 1,2-cyclopropanediol; this last

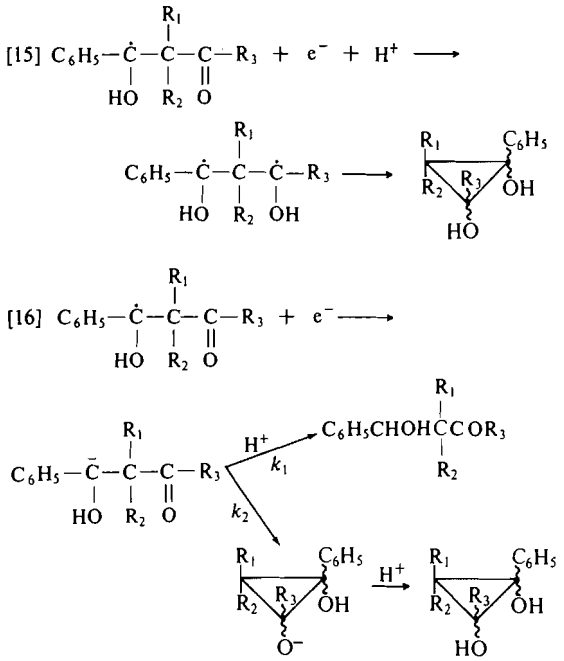

compound would be obtained through a nucleophilic attack of the carbanion on the β-carbonyl group. The alcohol–cyclopropanediol ratio depends on the relative values of reaction rates k_1 and k_2 which, in turn, depend on the nature of R_1, R_2, and R_3.

Conclusion

It is shown that in hydroorganic medium the β-diketones such as $C_6H_5—CO—\underset{\displaystyle R_1}{\overset{|}{C}}—CO—$ show a 2e polarographic wave which corresponds to a reduction to a 1,2-cyclopropanediol. Previous to this investigation, three 1,2-cyclopropanediols had been synthesized: Rausch and Priddy (10) had reduced cyclic β-diketones by alkaline metals in liquid ammonia; these same authors and, simultaneously, Curphey and McCartney (11, 12) had shown that the 1,2-cyclopropanediols were the expected intermediates in the Clemmensen reduction of β-diketones; finally a cyclopropanediol was obtained by reduction of a β-diester by sodium in liquid ammonia (13).

The method used in this paper, the electrochemical reduction in hydroorganic medium, yields cyclopropanediols easily and in fair yields. Thus, it complements the other methods which can be used in a limited number of cases only.

Experimental

The techniques and apparatus used have already been described (14). All the potentials are given by reference to the saturated calomel electrode.

Preparation of Compounds ***2***, ***3***, ***7***, ***8***, ***9***, *and* ***11***

$C_6H_5—CO—C(CH_3)_2—CO—C_6H_5$, **3**, is prepared by a Friedel–Crafts reaction between the dichloride of 2,2-dimethyl malonic acid and benzene according to ref 15; $(CH_3)_2C(COCl)_2$ is obtained by reaction of $SOCl_2$ with malonic acid according to ref. 16; mp = 96 °C. $C_{17}H_{16}O_2$ nmr ($CDCl_3$): 6 protons, CH_3 s at 1.67 ppm; 10 protons, C_6H_5, centered at 7.4 and 7.8 ppm; uv (CH_3OH): 248 nm (ε 18 200), 280 nm (ε 2200).

The preparation of $C_6H_5—CO—CH(CH_3)—CO—C_6H_5$, **2**, and its physicochemical properties have been described in a recent paper (1).

$C_6H_5—CO—CH_2—CO—CH_3$ is an analytical E.G.A. product.

$C_6H_5—CO—CH(CH_3)—CO—CH_3$ is prepared by the reaction of the sodium salt of **6** with CH_3I according to ref. 17; bp 130–134 °C/11 torr $C_{11}H_{12}O_2$ nmr ($CDCl_3$): (*a*) diketone: 2.7 protons, $CH_3—\underset{\displaystyle |}{\overset{|}{CH}}—$, d at 1.43 ppm; 0.9 protons, $CH_3—\underset{\displaystyle |}{\overset{|}{C}}—H$, q at 4.56 ppm, $J_{CH_3—CH} = 7$ Hz; 3 protons, $CH_3—CO$, s at 2.17 ppm; 5 protons, C_6H_5, m centered at 7.7 and 8.1 ppm; (*b*) enol : 0.1 protons, $—\underset{\displaystyle HO}{\overset{|}{C}}=\underset{\displaystyle CH_3}{\overset{|}{C}}—CO$, s at 16.63 ppm, disappears on the addition of D_2O; 0.3 protons, $—\underset{\displaystyle HO}{\overset{|}{C}}=\underset{\displaystyle CH_3}{\overset{|}{C}}—CO—$, s at 1.9 ppm. This spectrum shows that the enol accounts for about 10% of the product. Ultraviolet (CH_3OH): 246 nm (ε 10 800), 285 nm (ε 1700).

$C_6H_5—CO—C(CH_3)_2—CO—CH_3$, **9**, is prepared by the reaction of the sodium salt of $C_6H_5—CO—CH(CH_3)—CO—CH_3$, **8**, with CH_3I according to ref. 6; bp 84 °C/2 torr. $C_{12}H_{14}O_2$ nmr ($CDCl_3$): 6 protons, $—C(CH_3)_2—$, s at 1.47 ppm; 3 protons, $—CO—CH_3$, s at 2.08 ppm; 5 protons, C_6H_5 m 7.35–7.90 ppm; uv (CH_3OH): 243 nm (ε 9600), 275 nm (ε 1200).

$C_6H_5—CO—C(CH_3)(CH_2C_6H_5)—CO—CH_3$, **11**, is prepared by reaction of the sodium salt of **8** with $C_6H_5CH_2Br$ according to ref. 18; mp 105–106 °C. $C_{18}H_{18}O_2$ nmr ($CDCl_3$): 3 protons, $—CO—C(CH_3)—CO$, s at 1.37 ppm; 3 protons, $—CO—CH_3$, s at 2.10 ppm; 2 protons, $—C(CH_2—C_6H_5)—CO—$, d at 3.44 ppm; 10 protons, $—C_6H_5$, m at 6.85–8.05 ppm.

Preparative Electrolysis

Electrolysis of **3**, $C_6H_5—CO—C(CH_3)_2—CO—C_6H_5$: 250 ml of solution are prepared from 125 ml of methanol, 75 ml of a 0.5 *M* solution of citric acid, 30 ml of a 0.5 *M* solution of Na_2HPO_4, and water. 200 ml of this solution and 600 mg of **3** are used to fill the cathodic compartment while the remainder is used in the anodic compartment; p*H* = 3.70, *E* = −1.25 V. After consumption of 500 C

Can. J. Chem. Downloaded from www.nrcresearchpress.com by 210.87.254.40 on 09/05/12
For personal use only.

Can. J. Chem. Downloaded from www.nrcresearchpress.com by 210.87.254.40 on 09/05/12
For personal use only.

(2e per mol corresponds to 460 C), the current drops to 2 mA and the solution is filtered and poured into 200 ml of deoxygenated water. The aqueous solution is extracted with 2 × 100 ml of ether; the etheral extracts are dried over Na_2SO_4 and evaporated to give an oil which crystallizes into a white solid, **4**; 480 mg, 80% yield, mp 132 °C. $C_{17}H_{18}O_2$: mol. wt. 254 by mass spectrometry at 10 eV and 235 by cryometry in C_6H_6; nmr ($CDCl_3$): 3 protons, $—CH_3(a)$, s at 1.07 ppm; 3 protons, $—CH_3(b)$, s at 1.37 ppm; 2 protons, —OH, s at 3.27 ppm which disappear on the addition of D_2O; 10 protons, $—C_6H_5$, s at 7.25 ppm. After a few days in the $CDCl_3$ solution **4** is reoxidized by air into **3**. Ultraviolet (CH_3OH) shoulder around 235 nm (ε 7000). On the basis of these data the formula illustrated is assigned to **4**. Indeed, **4** is obtained from **3** by a reduc-

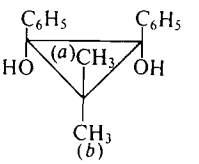

tion involving 2 electrons per molecule and **4** can be entirely reoxidized to **3**. The nmr spectrum gives evidence of two nonequivalent $—CH_3$ groups. The uv spectrum shows the disappearance of the C_6H_5CO group (absence of a strong band at 250 nm) and the absence of conjugation with $—C_6H_5$. This assignment also relies on the results published by Reusch and Priddy (10): by reduction (Li + NH_3) of a cyclic β-diketone they isolated a 1,2-cyclopropanediol which is easily reoxidized into a β-diketone. The compound which is obtained is the pure *cis* derivative, as in nmr the methyl groups give two singlets of three protons each.

Electrolysis of **2**, $C_6H_5—CO—CH(CH_3)—CO—C_6H_5$

A solution is prepared as in the case of **3**. Compound **2** (1 g) is reduced in 200 ml of this solution; p*H* = 3.70 at *E* = −1.25 V. After consumption of 750 C (2e per mol correspond to 800 C) the current decreases to 1 mA. The solution is worked up as in the case of **3** to give a white solid which is dried over P_2O_5 and washed with deoxygenated CCl_4. A yield of 800 mg of **5** is obtained (80%); mp 122 °C (dec.). $C_{16}H_{16}O_2$ mol. wt. 240 by mass spectrometry at 10 eV and 220 by cryometry in benzene; nmr ($CDCl_3$): 3 protons, —CH—C*H*$_3$, d at 1.26 ppm; 1 proton, —C*H*—CH_3, q at 2.03 ppm, $J_{CH—CH_3} = 6.5$ Hz; 2 protons, —O*H*, s at 3.17 ppm which disappears on the addition of D_2O; 10 protons, $—C_6H_5$, s at 7.1 ppm; uv (CH_3OH): shoulder around 230 nm (ε 8000). These results agree with the formula of one of the three isomers of 1,2-diphenyl-3-methyl-1,2-cyclopropanediol; its physicochemical properties are similar to those of **4**. Only one of the three possible isomers is obtained (one of the two *meso* or the *d,l*) as a single quadruplet is observed for C*H*—CH_3 and a single doublet for the methyl. In fact, this isomer is one of the two *meso* isomers as these signals are not split when the nmr spectrum is recorded in the presence of the chiral complex tris[(2,2,2-trifluoro-1-hydroxyethylidene)3-*d*-camphorato]europium. The chemical shift of the methyl group (δ = 1.26 ppm) is lower (Δδ = −0.11 ppm) than the chemical shift of $—CH_3(b)$ of **4** and higher (Δδ = +0.19 ppm) than the chemical shift of $—CH_3(a)$ of **4**. Moreover, the substitution of methyl by H in the 1,1-dimethylcyclopropane (22) leads to a decrease of the chemical shift (Δδ = −0.09 ppm) of the remaining methyl: $\delta_{CH_3}(CDCl_3) = 1.04$ ppm for the 1,1-dimethylcyclopropane and $\delta_{CH_3}(CDCl_3) = 0.95$ ppm for the methylcyclopropane prepared according to ref. 21. These results lead to the conclusion that the methyl of **5** has the same position as the $CH_3(b)$ of **4**; thus **5** is the *r*-1-methyl-*t*-2,*t*-3-diphenyl-*c*-2,*c*-3-cyclopropanediol.

Electrolysis of $C_6H_5—CO—C(CH_3)_2—CO—CH_3$, ***9***

Compound **9** (1 g) is dissolved in 200 ml of a solution prepared as in the case of **3**; p*H* = 3.74, *E* = −1.25 V. After 950 C (*i* = 1 mA) (2e per mol corresponds to 1065 C) the solution is worked up as described before to give an oil (500 mg, yield 50%), the properties of which are in agreement with those of a mixture of the two isomers of 2,3,3-trimethyl-1-phenyl-1,2-cyclopropanediol (*cis* and *trans* diols). The nmr spectrum ($CDCl_3$): 3 protons, $—CH_3(a)$, s at 0.93 ppm, $—CH_3(b)$, (s) at 1.00 ppm; 3 protons, $—CH_3(c,d)$, s at 1.23 ppm; 3 protons, $—CH_3(e)$, s at 1.33 ppm and $—CH_3(f)$, s at 1.55 ppm; 5 protons,

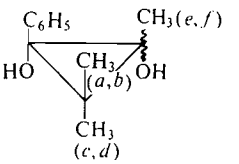

$—C_6H_5$, s at 7.20 and 7.28 ppm. The chloroformic solution is entirely reoxidized by air after three days to give **9**.

Electrolysis of $C_6H_5—CO—C(CH_3)(CH_2C_6H_5)—CO—CH_3$, ***11***

Compound **11** (420 mg) is electrolyzed in 200 ml of the usual solution; p*H* = 3.70, *E* = −1.30 V. After 290 C (*i* = 1 mA) (2e per mol corresponds to 310 C) the solution is worked up as usual to give 200 mg (48% yield) of an oil, the properties of which show that it is a mixture of the four pairs of stereoisomers of 1-methyl-2-phenyl-3-benzyl-3-methyl-1,2-cyclopropanediol. The nmr spectrum ($CDCl_3$): 6 protons, $—CH_3$, 8 s at 0.73, 0.80, 1.17, 1.23, 1.43, 1.53, 1.63, and 1.73 ppm; 4 protons, $—CH_2$ and —OH, multiplets between 2.6 and 3.2 ppm; 10 protons, $—C_6H_5$, m 7.0–7.8 ppm. The chloroform solution of the cyclopropanediols is reoxidized by air into **11** in 4 days.

1. J. Armand and L. Boulares. Bull. Soc. Chim. Fr. 711 (1975).
2. R. Pasternak. Helv. Chim. Acta, **31**, 753 (1948).
3. R. H. Philp, R. L. Flurry, and R. A. Day. J. Electrochem. Soc. **111**, 328 (1964).
4. D. H. Evans and E. C. Woodbury. J. Org. Chem. **32**, 2158 (1967).
5. R. C. Buchta and D. H. Evans. J. Electrochem. Soc. **117**, 1494 (1970).
6. R. A. Morton, A. Hassan, and T. C. Calloway. J. Chem. Soc. 883 (1934).
7. G. Nisli, D. Barnes, and P. Zuman. J. Chem. Soc. B, 778 (1970).
8. R. C. Buchta and D. H. Evans. J. Org. Chem. **35**, 2844 (1970).
9. T. J. Curphey, C. W. Amelotti, T. Playhoff, R. L. McCartney, and J. H. Williams. J. Am. Chem. Soc. **91**, 2817 (1969).

10. W. REUSCH and D. B. PRIDDY. J. Am. Chem. Soc. **91**, 3677 (1969).
11. D. B. PRIDDY and W. REUSCH. Tetrahedron Lett. 5291 (1969).
12. T. J. CURPHEY and R. L. MCCARTNEY. Tetrahedron Lett. 5295 (1969).
13. F. CHEN and C. ALSWORTH. J. Am. Chem. Soc. **94**, 4037 (1972).
14. J. ARMAND and L. BOULARES. Bull. Soc. Chim. Fr. 366 (1975).
15. J. SMEDLEY. J. Chem. Soc. 1492 (1910).
16. E. ROHSTEIN and R. W. SAVILLE. J. Chem. Soc. 1961 (1949); FREUND and FLEISHER. Ann. **373**, 291 (1910); **399**, 182 (1913).
17. C. WEYGAND and H. FORKEL. Ber. **61**, 687 (1928).
18. L. I. SMITH and J. R. HOLUM. J. Am. Chem. Soc. **78**, 3240 (1956).
19. D. ZACHAROVA-KALAVSKA, I. ZELENSKY, and A. PERJESSY. Coll. Czech. Chem. Commun. **36**, 2716 (1971), and references therein.
20. E. KARIV and E. GILEADI. Coll. Czech. Chem. Commun. **36**, 476 (1971).
21. N. DEMJANOFF. Ber. **28**, 21 (1895).
22. T. STRZALKO and J. SEYDEN-PENNE. C.R. Acad. Sc. C, **269**, 604 (1969).

Can. J. Chem. Downloaded from www.nrcresearchpress.com by 210.87.254.40 on 09/05/12
For personal use only.

Substituent effects on polarographic reduction of some photographic color intermediates

AHMAD S. SHAWALI[1]
Department of Chemistry, Faculty of Science, University of Kuwait, Kuwait
AND
BAHGAT E. EL-ANADOULI
Department of Chemistry, Faculty of Science, University of Cairo, Egypt

Received September 5, 1975

AHMAD S. SHAWALI and BAHGAT E. EL-ANADOULI. Can. J. Chem, **54**, 1205 (1976).

Polarographic reduction of two series of benzoylacetanilides has been investigated in 40% (by volume) ethanolic Britton–Robinson buffers. One series (*A*) contains substituents on the anilide moiety, and the second (*B*) has substituents on both the anilide and benzoyl moieties. Polarographic controlled-potential electrolysis data indicate that the electroactive species in both series is the protonated form $(ArCOCH_2CONHAr')H^+$. The reduction half-wave potentials of anilides of series *A* were found to be independent of the nature of the substituent, whereas those of series *B* show a good linear relationship when plotted *vs.* the σ substituent constant of the substituent on the benzoyl moiety ($\rho = 0.284$, $r = 0.995$). Values of the acid dissociation constants of the keto (K_1) and enol (K_2) tautomers of the anilides of series *A* were calculated; unlike their $E_{1/2}$ values, the pK_1 data show a linear correlation with the Hammett substituent constant, σ. The pK_2 values show, however, little variation with σ.

AHMAD S. SHAWALI et BAHGAT E. EL-ANADOULI. Can. J. Chem. **54**, 1205 (1976).

On a étudié, dans des tampons Britton–Robinson à 40% (par volume) d'éthanol, la réduction polarographique de deux séries de benzoylacétanilide. Une série (*A*) contient des substituants sur la portion anilide et l'autre (*B*) a des substituants à la fois sur les portions anilide et benzoyle. Les données électrolytiques, obtenues par polarographie à potentiel contrôlé, indiquent que l'espèce électroactive dans chaque série est la forme protonée $(ArCOCH_2CONHAr')H^+$. Les potentiels de réduction de demi-vague des anilides de la série *A* sont indépendants de la nature du substituant alors que ceux de la série *B* montrent une bonne relation linéaire avec la constante σ du substituant de la portion du benzoyle ($\rho = 0.284$; $r = 0.995$). On a calculé les valeurs pour les constantes de dissociation acide des tautomères céto (K_1) et énol (K_2) des anilides de la série *A*; par opposition avec leurs valeurs $E_{1/2}$, les données de pK_1 montrent une bonne corrélation linéaire avec la constante de Hammett σ du substituant. Les valeurs de pK_2 montrent toutefois très peu de variation avec σ.

[Traduit par le journal]

Introduction

Benzoylacetanilides (**1**) are important intermediates in the color photographic process (1). Though their chemistry has been extensively studied (2), their polarographic reduction has received no attention. The mechanism of the electrochemical reduction of the related ester, namely ethyl benzoylacetate, has recently been reported (3), and the elucidation of the structure–reactivity–potential relationship in a series of substituted ethyl benzoylacetates is well summarized in a recent publication (4). In the present communication we report the polarographic and spectrophotometric properties of two series of substituted benzoylacetanilides. In one series (*A*) the substituents are placed on the anilide ring, and the second series (*B*) contains substituents on both the anilide and benzoyl moieties. Our goal was on one hand to investigate the scheme of the

$$XC_6H_4COCH_2CONHC_6H_4Y$$

1

polarographic reduction of such a class of compounds, and on the other hand to examine the susceptibility of the electrode process to substituent effects. It was also of interest to isolate the acid dissociation constants of the keto (K_1) and enol (K_2) tautomers of benzoylacetanilides (eqs. 1 and 2 respectively) and to follow the substituent effects on such equilibria.

[1]Author to whom all inquiries should be addressed.

Can. J. Chem. Downloaded from www.nrcresearchpress.com by 210.87.254.40 on 09/05/12
For personal use only.

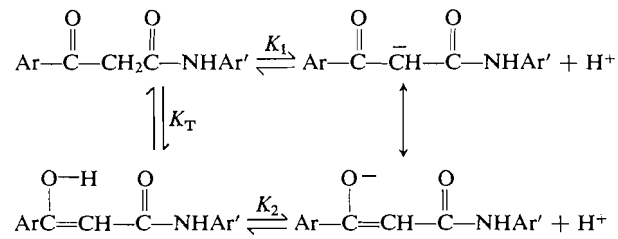

[1]

[2]

Results and Discussion

Polarographic current–potential curves, obtained with a dropping mercury electrode, dme, for each anilide show one cathodic wave, whose height decreases as the pH increases (Fig. 1). The plot of wave i_1 against pH has the shape of a dissociation curve (Fig. 2). The polarographic dissociation constants, pK', computed from the current–pH data are given in Table 1. Within the pH range 3–10, the wave i_1 was proportional to the square root of the height of the mercury column, h, and at p$H > 10$ it became independent of h. Furthermore, the wave i_1 was found to be directly proportional to the anilide concentration.

The polarographic half-wave potentials of all benzoylacetanilides investigated in this study are shifted by about 60 mV/pH towards more negative values. The linear $E_{1/2}$ *vs.* pH plots, Fig. 3, were practically parallel, showing that the value of αn remains approximately constant within the reaction series. Logarithmic analysis of potential *vs.* current data (Fig. 4) also substantiates the consistency of αn within the series (5).

The controlled-potential electrolysis of the parent benzoylacetanilide (**1**, X = Y = H) at pH 6.5 shows a linear plot of log i *vs.* time, t. From this plot, a value of two was obtained for the number of electrons transferred in the electrode process given by wave i_1. The product obtained from a large scale electrolysis of this parent anilide was identified as 3-hydroxy-3-phenylpropionanilide.

The polarographic results described above, in particular the change of wave height and half-wave potential with pH, indicate that the electrochemical reaction is first order with respect to

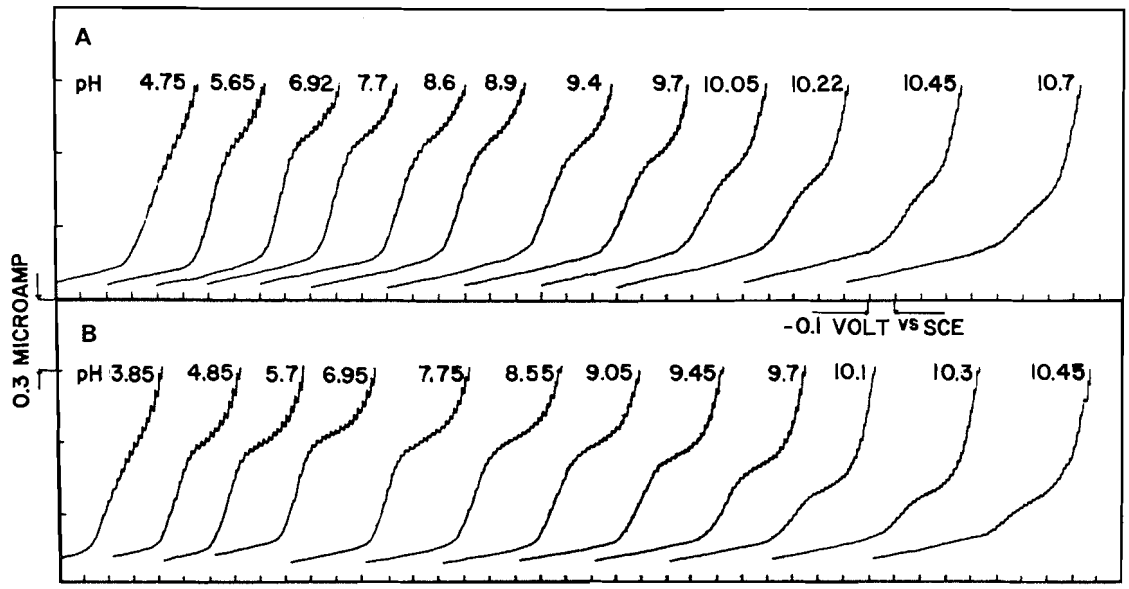

FIG. 1. Polarographic curves of *p*-anisoylacet-*p*-bromoanilide (*A*) and benzoylacet-*p*-toluidide (*B*) at different *p*H's.

Can. J. Chem. Downloaded from www.nrcresearchpress.com by 210.87.254.40 on 09/05/12
For personal use only.

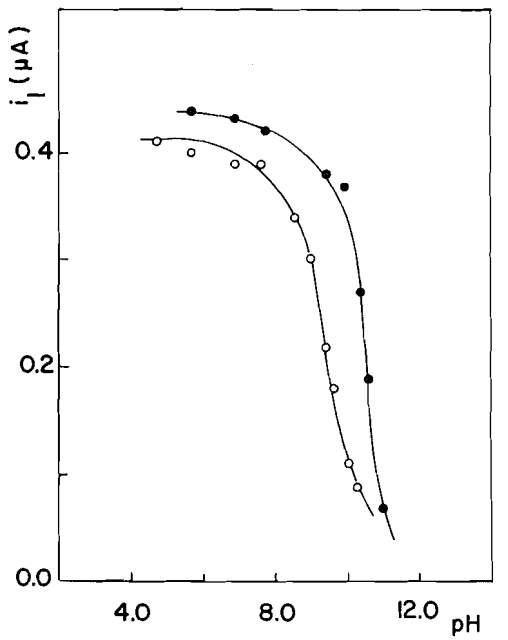

FIG. 2. Dependence of the polarographic limiting current (i_l) of benzoylacet-*p*-bromoanilide and *p*-anisoylacet-*p*-toluidide on p*H*. ○ $C_6H_5COCH_2CONHC_6H_4Br$-*p*, ● *p*-$MeOC_6H_4COCH_2CONHC_6H_4Me$-*p*.

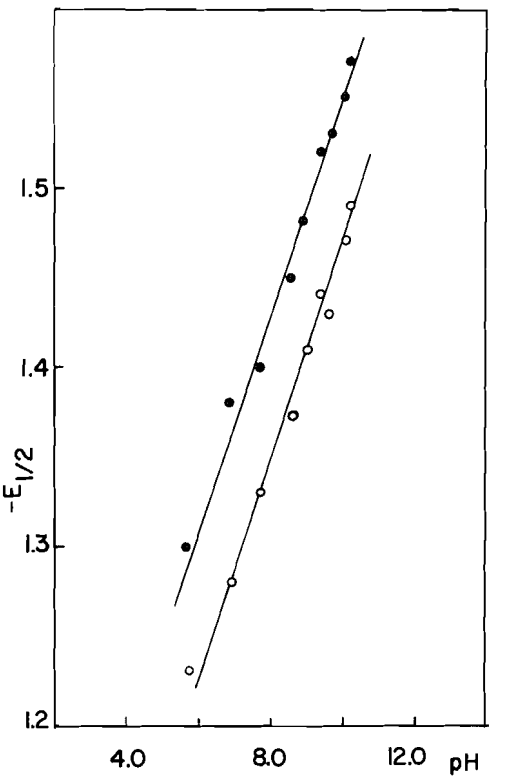

FIG. 3. Dependence of the half-wave potentials ($E_{1/2}$) of anisoylacet-*p*-bromoanilide and benzoylacet-*p*-chloroanilide on p*H*. ○ $C_6H_5COCH_2CONHC_6H_4Cl$-*p*, ● *p*-$MeOC_6H_4COCH_2CONHC_6H_4Br$-*p*.

protons, and it can be rationalized by eqs. 3–5.

[3] $ArCOCH_2CONHAr' \; H^+ \underset{k_p}{\overset{k_d}{\rightleftharpoons}} (ArCOCH_2CONHAr')H^+ \quad K' = \frac{k_d}{k_p}$

[4] $(ArCOCH_2CONHAr')H^+ + 2e^- \rightarrow ArC\bar{O}HCH_2CONHAr'$

[5] $ArC\bar{O}HCH_2CONHAr' + H^+ \rightleftharpoons ArCHOHCH_2CONHAr'$

The reduction wave corresponds to the reduction of the monoprotonated form of the keto anilide. Because the protonation at the electroactive group or another centre in the molecule affects the wave height and half-wave potential in a similar way, polarography does not enable one to distinguish between the various sites of protona-

TABLE 1. Typical polarographic data and the polarographic dissociation constants, pK'. of aroylacetarylamides, $XC_6H_4COCH_2CONHC_6H_4Y$

		p*H* 5.70		p*H* 7.70		p*H* 9.60		
X	Y	$E_{1/2}$(v)	i_l(μA)	$E_{1/2}$(v)	i_l(μA)	$E_{1/2}$(v)	i_l(μA)	pK'
H	*p*-MeO	1.26	0.42	1.32	0.40	1.42	0.27	10.20
H	*p*-Me	1.26	0.39	1.33	0.34	1.51	0.24	9.60
H	*m*-Me	1.25	0.40	1.35	0.40	1.44	0.26	9.45
H	H	1.20	0.43	1.32	0.44	1.46	0.21	9.40
H	*p*-Cl	1.22	0.43	1.33	0.41	1.43	0.20	9.25
H	*p*-Br	1.24	0.40	1.30	0.39	1.43	0.18	9.20
p-MeO	*p*-Me	1.30	0.44	1.40	0.43	1.55	0.37	10.60
p-MeO	*p*-Br	1.32	0.44	1.42	0.42	1.53	0.32	10.20
p-Cl	*p*-Me	1.20	0.38	1.27	0.38	1.38	0.16	9.30

Can. J. Chem. Downloaded from www.nrcresearchpress.com by 210.87.254.40 on 09/05/12
For personal use only.

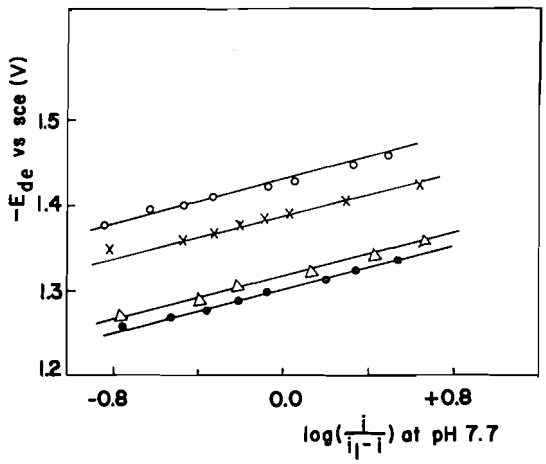

FIG. 4. Logarithmic analysis for some aroylacetarylamides at pH 7.70. ● $C_6H_5COCH_2CONHC_6H_4Br$-p, △ $C_6H_5COCH_2CONHC_6H_4OCH_3$-$p$, × p-$CH_3OC_6H_4COCH_2CONHC_6H_4Br$-$p$, ○ p-$CH_3OC_6H_4COCH_2CONHC_6H_4CH$-$p$.

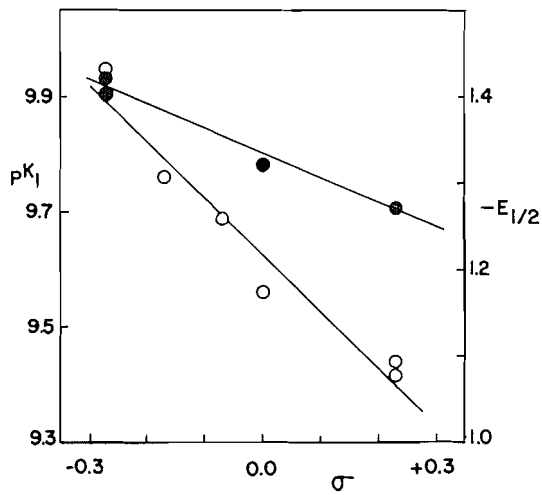

FIG. 5. Dependence of the acid dissociation constant (pK_1), and half-wave potentials ($E_{1/2}$ at pH 7.70) on the Hammett substituent constant σ. ○ pK_1 values, ● $E_{1/2}$ (*vs.* sce).

tion. However, the variation of the pK' value with substituent (Table 1) appears to indicate that the monoprotonated anilide molecule probably bears the proton on the more basic amide group. This might also account for the finding that the pK' value (9.40) found for benzoylacetanilide in this study is larger than that reported for the monoprotonated forms of benzoylacetone (pK' = 8.45) and ethyl benzoylacetate (pK' = 6.55) (3). The half-wave potential of the wave is shifted towards more negative potentials with increasing pH, because the reestablishment of equilibrium 3 precedes the two electron uptake [4]. At p$H > 6$ the rate of protonation with the rate constant k_p is no longer sufficient to transform all the unprotonated keto anilide into the monoprotonated form. This leads to a sharp decrease in i_l at high pH as in Fig. 2. The decrease of wave i_l with pK' 9.30–10.20 (Table 1) corresponds to the decrease of the rate of the process 3 at the electrode surface. Because the thermodynamic pK of equilibrium 3 can be expected to be equal to zero or negative, it can be deduced that process 3 which governs the height of wave i_l is a surface reaction rather than a volume reaction (3). It is assumed that the enol form of each anilide does not participate in the electrode process. This presumption is valid as the reduction potential of styrene derivatives is too negative to show a distinct wave in the accessible potential range. However, this does not exclude the involvement of the equilibria in eqs. 1 and 2. Such equilibria exist as competitive equilibria in the bulk. Independence of limiting current at p$H > 10$ indicates that the wave i_l becomes kinetically controlled by the rate of process 3. This observation does not mean that at p$H < 10$ the current is proportional to the concentration of the keto form in the bulk, only that the rate of protonation of the keto form is faster than that of the transport (diffusion).

The half-wave potentials for the anilides of series A do not show any noticeable change with substituent (Table 1). This finding is not unexpected in view of the insulation of electronic effects by the —CH_2CONH— grouping. The half-wave potentials of the anilides of series B are a linear function of the Hammett substituent constant, σ, of the group on the benzoyl moiety (Fig. 5). The equation of the regression line obtained is

$$E_{1/2} = 0.284\sigma - 1.33 \quad r = 0.995$$

This result implies that the electrode process is susceptible only to the electronic effects of substituents on the benzoyl moiety of the molecule. The ρ value of 0.284 obtained for series B is of the same order of magnitude as that predicted (ρ = 0.30) from the ρ–E relationship for a system where the unsubstituted compound is reduced at −1.32 V (5).

Can. J. Chem. Downloaded from www.nrcresearchpress.com by 210.87.254.40 on 09/05/12
For personal use only.

TABLE 2. Separation of dissociation constants of the keto (K_1) and enol (K_2) forms of benzoylacetarylamides, $C_6H_5COCH_2CONHC_6H_4Y$

Y	σ	pK^*	pK_T	pK_1	pK_2
p-MeO	−0.27	10.04	0.896	9.95	9.09
p-Me	−0.17	9.84	0.721	9.76	9.04
m-Me	−0.07	9.74	0.606	9.69	9.06
H	0.00	9.66	0.590	9.56	8.97
p-Cl	+0.23	9.56	0.509	9.44	8.93
p-Br	+0.23	9.53	0.553	9.42	8.87

Values of the acid dissociation equilibria (K_1 and K_2) of the keto and enol tautomers of benzoylacetanilides (eqs. 1 and 2 respectively) are not directly accessible to measurement. They can be calculated, however, from the overall acid dissociation constant, K^*, and the tautomeric equilibrium constant, K_T, defined by eqs. 6 and 7, respectively.

$$[6] \qquad K^* = \frac{[\text{carbanion-enolate}][H^+]}{[\text{keto form}][\text{enol form}]}$$

$$[7] \qquad K_T = \frac{[\text{enol form}]}{[\text{keto form}]}$$

The values of K^* and K_T constants are related to the dissociation constants K_1 and K_2 by the equations

$$[8] \qquad K^* = \frac{K_1K_2}{K_1 + K_2} = \frac{K_1}{1 + K_T}$$

$$[9] \qquad K_T = K_1/K_2$$

Because of the kinetic character of the wave pointed out above, it is not possible to use the polarographic constants, pK', so obtained, for calculation of the equilibrium constants K_1 and K_2. Accordingly, to calculate the latter constants, the overall acid dissociation constants, K^*, of the keto anilides studied were determined spectrophotometrically, and their previously reported K_T constants (2*c*) were used.

At pH > 8 solutions of each anilide containing 60 vol% ethanol give an intense absorption peak at 250–280 nm. With increasing pH, the height of this peak decreases and simultaneously another peak at 305–360 nm increases. Values of pK^* calculated from the pH-absorbance data obtained are given in Table 2. From these pK^* values and the corresponding pK_T values, the equilibrium constants pK_1 and pK_2 were evaluated. The results of the computation are given in Table 2. The data indicate that the enol form acting as the *O*-acid is stronger than the *C*-acid of the keto form, in agreement with existing views on acid strength.

A comparison of the numerical values for the acidity constants pK^* and pK_1 in Table 2 and the polarographic constants, pK', in Table 1 shows that they are similar. It should be indicated that in spite of the similarity of the numerical values of pK_1 and pK', these values have nothing in common since they correspond to different processes (eqs. 1 and 3 respectively). This is further indicated by the kinetic character of the wave i_1 at pH > 10. Were the dissociation equilibrium 1 the process governing the height of wave i_1, the current would be diffusion controlled, and not kinetically controlled as observed. The similarity of the values of pK^* and pK_1 is probably due to the small values of K_T. In aqueous ethanol the keto form predominates so that [enol] ≪ [keto], then, according to eq. 8, the measured value of pK^* would be close to pK_1.

Like their half-wave potentials, the pK_2 constants of anilides of series *B* exhibit no noticeable change with substituents (Table 2). This insensitivity of the enol tautomer of such series might be due to the weak transmission of electronic effects through the —CH=CHCONH— bridge. In contrast to pK_2, the pK_1 equilibrium data show a reasonable correlation (r = 0.946) with the substituent constant σ (Fig. 5). The equation that fits the data best is pK_1 = 9.63 − 1.008σ.

Experimental

Aroylacetarylamides, **1**, were synthesized by the method described for benzoylacetanilide employing the appropriately substituted amine (6). The anilides were crystallized to constant melting point and were then dried *in vacuo*. Stock solutions (10^{-3} *M*) were prepared in EtOH. The Britton–Robinson buffers were prepared as previously described (10). All chemicals used were of AnalaR grade. Infrared spectra were determined on a Unicam SP1000 spectrophotometer employing KBr discs. Solution elec-

Can. J. Chem. Downloaded from www.nrcresearchpress.com by 210.87.254.40 on 09/05/12
For personal use only.

tronic spectra were recorded on a Unicam SP8000 spectrophotometer. The polarograms were recorded using a pen-recording polarograph LP 60 (Laboratorni Pristorje, Prague). A digital Radiometer pH meter, type 63, equipped with a combined glass electrode type GK2311C was used for measuring the pH. The pH readings were calibrated before and checked after each measurement using standard Radiometer aqueous buffers of pH's 4.01 ± 0.01 and 7.00 ± 0.01.

Polarography

Polarographic i *vs.* E curves were recorded in solutions placed in a cell in which is immersed a calomel electrode of surface area 12.5 cm^2 and a dropping mercury electrode with t = 3.7 s and m = 1.8 mg/s at a mercury head of 59 cm and 0.00 V. The junction between the two half cells is accomplished through a sintered glass disc of porosity G4 sealed into the wall of the polarographic cell.

Ethanolic buffer solution (15 ml, 34% (v/v)) containing 0.3 ml gelatin solution (0.5%) were transferred into the cell and deaerated by a stream of nitrogen for 2 min, then 1.5 ml of the anilide stock solution were added. After deaeration for a further 45 s, the polarographic curve was recorded, and then the apparent pH of the test solution was measured. All buffer solutions were checked for impurities.

Controlled-potential Electrolysis

The determination of the number of electrons transferred in the electrode process was carried out coulometrically following the method of Lingane (7) and using a cell similar to that described by Manousek and Zuman (9). In each run, 34% ethanolic buffer solution (31.5 ml) was stirred with a stream of hydrogen for 30 min, the emf was adjusted to a value of 0.3 V more than $E_{1/2}$ of the anilide used, and electrolysis was continued for 30 min. Then the emf was readjusted to a value of 0.1 V more than $E_{1/2}$ of the anilide and 3.5 ml of anilide stock solution were added and electrolysis was continued while a stream of hydrogen was passed through. The changes of the limiting current with time were determined by recording the polarogram at selected intervals during a period of 2 h. The number of electrons (n) transferred was calculated using eq. 10,

$$[10] \qquad n = i_0/2.3CFv(\mathrm{d}\log i/\mathrm{d}t)$$

where i_0 is the current at t = 0, when $C = C_0$, v is the volume in litres of the solution, and (d log i/dt) the slope of the plot of log i *vs.* t.

Preparative Electrolysis

The reaction mixtures obtained from five controlled-potential electrolysis experiments were combined, the solvent was evaporated under reduced pressure, and the residue left was extracted three times with ether. The combined ether extracts were washed with dilute aqueous NaOH solution, dried over magnesium sulfate, filtered, and the ether was finally removed. The white solid left was collected and its mp and spectra were measured. The product obtained from controlled-potential electrolysis of the parent anilide proved to be 3-hydroxy-3-phenylpropionanilide, mp 160 °C (mmp 160–162 °C) (8); ν (KBr) 3500–3300 (OH), 1680 (anilide CO) cm^{-1}; λ_{max} (EtOH) (log ϵ) 244 (5.034), 210 (4.927) nm.

*Spectrophotometric Acid Dissociation Constants, K**

These were determined by recording the spectra of solutions of keto anilides (10^{-5}–10^{-4} M) in 40% (v/v) aqueous ethanolic buffers (μ = 0.1). The experimental procedure and calculations are the same as previously reported (*2a*, *d*).

Acknowledgments

We wish to thank Prof. P. Zuman for his interest and helpful comments. The authors also express their thanks to a referee for many helpful comments in the preparation of the final form of this paper.

1. C. E. K. Mees. The theory of the photographic process. Macmillan, New York. 1969.
2. (*a*) P. van Brandt, E. de Hoffmann, and A. Bruylants. Bull. Soc. Chim. Biol. Belg. **73**, 783 (1962); (*b*) A. S. Shawali, M. M. Naoum, and S. A. Ibrahim. Bull. Chem. Soc. Jpn. **45**, 2504 (1972); (*c*) A. S. Shawali and B. A. Akrawi. Indian J. Chem. **12**, 1074 (1974); (*d*) E. Pelizzetti and C. Verdi. J. Chem. Soc. Perkin Trans. II, 808 (1973); (*e*) A. Syamal. Z. Naturforsche. Teil B, **26**, 320 (1971).
3. G. Nisli, D. Barnes, and P. Zuman. J. Chem. Soc. B, 764, (1970); 778 (1970).
4. S. Singer and P. Zuman. J. Org. Chem. **39**, 836 (1974).
5. P. Zuman. Substituent effects in organic polarography. Plenum Press, New York. 1967.
6. C. J. Kibler and A. Weissenberger. Organic synthesis. Coll. Vol. 3, 108 (1955).
7. J. J. Lingane. J. Am. Chem. Soc. **67**, 1916 (1945); G. A. Gilbert and A. K. Rideal. Trans. Faraday Soc. **47**, 396 (1951).
8. C. R. Hauser. Chem. Ind. (London), **43**, 1789 (1965).
9. O. Manousek and P. Zuman. Collect. Czech. Chem. Commun. **29**, 17 (1964).
10. H. T. S. Britton. Hydrogen ions. Vol. 1, 4th ed. Chapman and Hall. 1955. p. 365; H. T. S. Britton. J. Chem. Soc. 458, 1456 (1931).

Can. J. Chem. Downloaded from www.nrcresearchpress.com by 210.87.254.40 on 09/05/12
For personal use only.

^{13}C nuclear magnetic resonance studies. 55.[1] A comparison of the stereochemical dependence of γ- and δ-substituent effects on ^{13}C shieldings in several norbornanols and norbornenols

J. B. STOTHERS, C. T. TAN, AND K. C. TEO
Department of Chemistry, University of Western Ontario, London, Ontario N6A 5B7

Received October 9, 1975

J. B. STOTHERS, C. T. TAN, and K. C. TEO. Can. J. Chem. **54**, 1211 (1976).

The ^{13}C nmr spectra of a series of 50 methyl substituted norbornanols have been determined to gain further insight into the nature of stereochemical effects on the shieldings of carbons having closely neighboring substituents. The relatively rigid norbornyl skeleton permits examination of a variety of orientations of substituents separated by three and four bonds, the γ and δ interactions, respectively. While methyl carbons close to γ substituents exhibit upfield shifts, as is well established, methyl carbons close to δ substituents are significantly deshielded. Even more striking shifts are found for the carbons bearing these closely lying groups. The penultimate carbons in a fragment having a δ interaction between terminal groups show deviations of up to +11 ppm from the shieldings predicted by simple additivity. For fragments having a corresponding γ interaction, the penultimate carbons absorb as much as −10 ppm from the values expected by additivity. These deviations have considerable potential for stereochemical assignments and offer a challenge for theoretical interpretation.

Some norbornenols and the acetates of several of the norbornanols were also included in this series and the latter shieldings are compared briefly with those observed for the parent alcohols.

J. B. STOTHERS, C. T. TAN et K. C. TEO. Can. J. Chem. **54**, 1211 (1976).

On a déterminé les spectres rmn du ^{13}C d'une série de 50 norbornanols substitués par des méthyles afin d'obtenir une meilleure compréhension de la nature des effets stéréochimiques sur les blindages de carbones possédant des substituants dans les positions adjacentes. Le squelette relativement rigide du norbornyle permet d'examiner une variété d'orientations des substituants séparés par trois et quatre liens, à savoir les interactions γ et δ. Alors que les carbones des méthyles près des substituants γ présentent des déplacements vers les hauts champs, comme il a été bien établi, les carbones des méthyles près des substituants δ sont déblindés d'une façon très significative. On trouve des déplacements encore plus frappants pour les carbones portant ces groupes installés très près. Les avant-dernier carbones dans un fragment ayant une interaction δ entre les groupes terminaux montrent des déviations allant jusqu'à +11 ppm par rapport au blindage que l'on peut prédire par additivité simple. Pour les fragments possédant une interaction γ correspondante, les avant-dernier carbones absorbent à des valeurs aussi grande que −10 ppm par rapport aux valeurs attendues par l'additivité. Ces déviations possèdent un potentiel considérable pour l'attribution des stéréochimies et offrent un défi pour des interprétations théoriques.

On a aussi inclus quelques norbornénols et des acétates de plusieurs norbornanols dans cette série et on compare brièvement les blindages de ces derniers avec ceux obtenus avec les alcools correspondants.

[Traduit par le journal]

Introduction

It is well established that ^{13}C shieldings are markedly sensitive to molecular geometry and this feature renders ^{13}C nmr to be a valuable aid for stereochemical assignments (1). Probably the most widely recognized aspect is the variation of the shieldings for carbons vicinal to other carbons or substituents as a function of the dihedral angle relating the two groups. In a wide variety of systems it is found that a carbon involved in a *gauche* or eclipsed 1,4-nonbonded interaction is more strongly shielded than its counterpart in an *anti* orientation. Also, the carbons bearing the *gauche* or eclipsed groups are shielded relative to their absorption positions for the *anti* arrangement. In other words, all carbons in the fragment involved in the *gauche* interaction are shielded relative to the corresponding carbons in a fragment lacking the close approach of the

[1]For part 54 see ref. 15; part 53 see ref. 24; part 52 see ref. 25.

Can. J. Chem. Downloaded from www.nrcresearchpress.com by 210.87.254.6 on 09/05/12
For personal use only.

Can. J. Chem. Downloaded from www.nrcresearchpress.com by 210.87.254.6 on 09/05/12
For personal use only.

terminal groups, although certain *anti* heteroatoms tend to shield the γ-carbon (2). These are the γ effects and it may be noted that the shielding tendencies are larger for sp^3 than for sp^2 carbons. More recently, significant deshielding trends have been found for carbons with closely neighboring δ substituents, *i.e.* separated by four bonds, typical of which are *syn*-axial groups (3); the other orientations for groups separated by four bonds appear to lead to weak shielding effects.

Substituted bicyclic systems such as the norbornanes, are very useful models to investigate the shielding variations produced by these steric interactions of substituents since the relatively rigid skeleton holds the groups in fairly well defined positions and a variety of orientations can be studied for groups separated by three and four bonds. Consequently, several extensive ^{13}C studies of norbornyl systems have been reported (4, 5), with attention mainly directed toward the effects of substituents on the skeletal carbon shieldings of monosubstituted derivatives. Recently we examined a series of methyl substituted norcamphors focussing our attention on the methyl and carbonyl shieldings as a function of their relative orientations (5). These compounds readily provided a series of methylnorbornanols with which the interactions of hydroxyl and methyl groups can be investigated and we wish to present these results in this paper. From these data it is apparent that shifts of as much as 10–11 ppm occur for the carbons bearing the sterically crowded γ and δ nuclei upon comparison of the observed shieldings with those predicted on the basis of simple additivity of substituent effects. If the γ and δ nuclei are well separated, however, the observed shieldings agree well with the predicted values. In the sterically crowded cases, the deviations from predictions are in opposite directions for the two types of interaction, upfield for γ nuclei and downfield for δ nuclei. For the latter the shifts are much larger than those found for the terminal carbons and have potential for stereochemical elucidations. Some of the compounds included in this series have been reported previously (4); these were reexamined to obtain data for the entire series under closely similar conditions, namely, 10–20% solutions in deuteriochloroform, for internal consistency.

Results

The ^{13}C shieldings of the norbornan-2-ols (**1**, **2**) and several monomethyl derivatives **3**–**20** examined in this study are listed in Table 1. Some of these compounds had been examined previously (4*a*, *b*, *d*) and, in general, there is reasonable agreement between the different sets of data in view of the different solvents and referencing methods used. The data reported relative to CS_2 (4*a*) were converted to the TMS scale with the factor 192.8 ppm. The present results tend toward higher field by 0.2–1.1 ppm, except for the carbinyl carbon shieldings which are 0.0–0.5 ppm less shielded, indicating the presence of small, but significant solvent effects. Our assignments concur generally with the earlier ones with the exception of C-3 and C-7 for *endo*-2-norbornanol (**2**) which Lippmaa *et al.* (4*d*) reversed from those of Roberts and coworkers (4*a*); the latter assignment was confirmed by deuterium exchange at the α-position of norcamphor before reduction to **2**. For *exo*-3-methyl-*exo*-2-norbornanol (**7**) we find the methyl absorption at 13.4 ppm, or 6.5 ppm upfield from the value reported by Roberts' group (4*a*). However, in their study the 3-methyl-2-norbornanols **5**–**8** were examined as mixtures while in the present case each of the four isomers was examined individually, permitting unequivocal identification of the methyl signals.

From the shieldings of the 2-methyl (5), 1- and 7-methyl (4*a*), and 2-hydroxyl derivatives of norbornane relative to those for norbornane, substituent effects at the various skeletal carbons can be obtained as listed in Table 2. For the 1- and 7-methyl derivatives, the norbornane data obtained in the same study (4*a*) were used. Also, inspection of the entire set of data indicated that the C-5 and C-6 assignments for *exo*-2-methylnorbornane and those for C-3 and C-7 in *endo*-2-methylnorbornane should be reversed from our earlier assignments (5). With these substituent effects, one can predict the shieldings for the array of methylnorbornanols **3**–**20** for comparison with those observed as assigned in Table 1. In each case, off-resonance decoupled spectra distinguished the methyl, methylene, methine, and quaternary signals and the characteristic signal at δ_C 70–80 clearly revealed the carbinyl absorption. For many of these compounds, the signals were readily assigned from the expected

TABLE 1. ^{13}C shieldings* of some monomethylnorbornanols

Compound	Substitution Me	Substitution 2-OH	C-1	C-2	C-3	C-4	C-5	C-6	C-7	Me
1	—	*exo*	44.2	74.7	42.2	35.4	28.1	24.4	34.4	
2	—	*endo*	42.5	72.9	39.4	37.2	29.9	20.0	37.6	
3	1	*exo*	47.4	77.3	43.1	35.9	30.3	33.1	40.1	16.1
			(−4.1)	(−4.4)	(−0.6)	(−0.9)	(0.7)	(1.7)	(−1.2)	
4	1	*endo*	47.8	77.6	40.6	36.8	31.3	26.9	44.4	18.4
			(−2.0)	(−2.3)	(−0.3)	(−1.8)	(−0.1)	(−0.1)	(−0.1)	
5	*endo*-3	*exo*	45.4	82.5	46.6	40.9	21.0	25.0	36.5	15.0
			(−0.2)	(−1.0)	(0.0)	(0.1)	(0.4)	(0.0)	(0.2)	
6	*exo*-3	*endo*	43.2	81.8	45.8	43.8	30.1	19.4	34.4	20.1
			(0.1)	(−1.2)	(−0.4)	(−0.1)	(−0.2)	(0.3)	(0.3)	
7	*exo*-3	*exo*	44.8	76.5	43.2	42.8	29.2	24.6	31.9	13.4
			(0.0)	(−8.4)	(−5.8)	(0.7)	(0.7)	(1.1)	(1.0)	
8	*endo*-3	*endo*	43.5	72.2	36.5	42.2	21.8	19.7	36.7	10.2
			(−0.4)	(−9.5)	(−7.3)	(−0.4)	(−0.6)	(−0.9)	(−2.8)	
9	*exo*-5	*exo*	44.8	74.1	42.5	42.0	34.9	34.3	30.7	21.9
			(0.0)	(0.3)	(−0.1)	(−0.1)	(0.0)	(−0.3)	(−0.2)	
10	*endo*-5	*exo*	45.5	74.6	34.8	40.7	32.4	33.3	36.2	16.9
			(−0.1)	(0.7)	(0.1)	(−0.1)	(−0.1)	(0.1)	(−0.1)	
11	*exo*-6	*exo*	51.1	74.6	41.3	35.7	38.1	31.3	31.2	21.4
			(0.2)	(−0.5)	(0.0)	(−0.3)	(−0.2)	(0.1)	(0.3)	
12	*endo*-6	*exo*	49.4	69.0	42.9	36.8	36.8	31.5	36.5	16.9
			(−0.2)	(1.8)	(0.1)	(0.0)	(−0.1)	(2.7)	(0.2)	
13	*exo*-5	*endo*	43.0	72.1	40.3	43.5	36.3	30.2	34.1	22.4
			(−0.1)	(0.1)	(0.5)	(−0.4)	(−0.4)	(0.0)	(0.0)	
14	*endo*-5	*endo*	43.7	73.3	31.5	42.7	34.3	27.6	39.5	16.3
			(−0.2)	(−0.2)	(−0.4)	(0.1)	(0.0)	(−1.2)	(−1.6)	
15	*exo*-6	*endo*	49.2	72.8	38.5	37.9	40.0	25.3	34.3	21.8
			(0.0)	(−0.5)	(0.0)	(0.1)	(−0.1)	(−1.5)	(0.2)	
16	*endo*-6	*endo*	47.0	76.4	39.4	39.1	37.9	35.4	40.0	19.4
			(−0.9)	(11.0)	(−0.6)	(0.5)	(−0.8)	(11.0)	(0.7)	
17	*anti*-7	*exo*	48.5	75.4	43.4	39.5	25.3	22.2	39.6	11.9
			(0.1)	(−0.2)	(0.3)	(−0.1)	(0.1)	(0.7)	(−0.4)	
18	*syn*-7	*exo*	48.2	76.3	39.9	41.0	28.7	26.5	43.7	13.5
			(−0.2)	(+4.5)	(0.6)	(1.4)	(−0.3)	(1.2)	(+3.7)	
19	*endo*-2	*exo*	49.3	77.9	48.7	37.0	27.9	24.0	37.4	25.8
			(−0.3)	(−1.2)	(−2.3)	(0.2)	(−0.8)	(7.1)	(1.1)	
20	*exo*-2	*endo*	48.4	77.2	47.0	37.3	28.3	22.0	38.7	30.4
			(−0.8)	(−2.5)	(−2.6)	(−0.5)	(−0.7)	(1.6)	(4.6)	

*In ppm from internal TMS in $CDCl_3$ solutions. Values in parentheses are ($\delta_C^{obsd} - \delta_C^{calcd}$), where δ_C^{calcd} was obtained by assuming simple additivity of substituent effects (see text).

substituent effects but for those having closely neighboring substituents there are pronounced differences between the observed and predicted shieldings. The differences, $\delta_C^{obsd} - \delta_C^{calcd}$, are given in parentheses in Table 1. There is a distinct pattern for the compounds having the large deviations from additivity, however, and this is discussed in the next section.

The data for several di- and trimethyl derivatives **21–42** are collected in Table 3. Again, off-resonance decoupled spectra identified the absorptions for the various carbon types and the carbinyl signals were characterized by their position. The assignments for isoborneol (**33**) and borneol (**34**) had been obtained previously from shift reagent studies (6). Our data agree well with those reported for **34** in CCl_4 (6*b*) but there are much larger differences between our results and those given for **33** in CCl_4 (6*b*), with an average difference of 2 ppm for the skeletal carbons, perhaps indicating a referencing error. To test for additivity of substituent effects, shieldings for **21–28** were estimated from the values for the appropriate dimethylnorbornane (5) and

Can. J. Chem. Downloaded from www.nrcresearchpress.com by 210.87.254.6 on 09/05/12
For personal use only.

TABLE 2. Substituent effects* of methyl and hydroxyl groups on the skeletal shieldings of bicyclo[2.2.1]heptanes

Substituent	Orientation	α C-2	β C-1	β C-3	γ C-4	γ C-6	γ C-7	δ C-5	Reference
2-Methyl	*exo*	6.8	6.7	10.2	0.6	0.4	−3.5	−0.9	5†
	endo	4.4	5.4	8.8	1.4	−7.5	1.9	0.6	5‡
2,2-Dimethyl		6.8	11.3	17.1	2.0	−5.1	−0.1	−1.4	4*a*
2-Methyl-Δ^5	*exo*	7.9	6.5	10.0	0.5	1.8	−3.7	0.7	5
	endo	7.9	5.4	9.1	1.3	−3.1	1.6	1.5	5
2-Hydroxyl	*exo*	45.1	7.9	12.6	−0.9	−5.2	−3.9	−1.5	
	endo	43.3	6.2	9.8	0.9	−9.6	−0.7	0.3	
2-Hydroxyl-Δ^5	*exo*	47.7	8.3	12.3	−1.1	−1.7	−2.9	5.0	
	endo	47.7	6.3	13.0	1.1	−4.1	−0.3	4.8	

	C-1	C-2	C-7	C-3	C-4	
1-Methyl	7.3	7.0	6.9	1.5	1.4	4*a*

	C-7	C-1	C-2,3	C-5,6	
7-Methyl	5.6	4.2	−2.9§	0.9‖	4*a*

	C-1	C-7	C-2	C-4	C-6	C-3	C-5	
1,7-Methyl	7.4	9.0	3.2§	5.2	8.0‖	1.7§	−0.5‖	4*d*

*$\Delta\delta^X = \delta_C RX - \delta_C RH$, where RH = hydrocarbon (in ppm); positive values indicate downfield shifts.
†Original assignments for C-5 and C-6 are interchanged.
‡Original assignments for C-3 and C-7 are interchanged.
§ *syn* with respect to the 7-methyl.
‖ *anti* with respect to the 7-methyl.

the effects of the hydroxyl group (Table 2). For **29–31**, **36**, **37**, and **42**, the effects of the dimethyl substituents (Table 2) were combined with the shieldings of **1** and **2**; the predicted values were generated in this way because the appropriate hydrocarbons were not available to us, but the shielding effects of the dimethyl substituents could be obtained from a self-consistent set of data (*4a*, *d*). For **38–41**, the effects of the lone methyl group were combined with the observed values for the appropriate 3,3-dimethylnorbornan-2-ol (**36** and **37**) to examine the deviations from additivity for monomethyl substitution at C-1 and C-6. The differences, $\delta_C^{obsd} - \delta_C^{calcd}$, from each of these comparisons are listed in parentheses in Table 3. As found for the monomethyl derivatives, appreciable deviations from additivity occur for those compounds having closely neighboring substituents and the deviations follow patterns consistent with those for the less highly substituted cases. These patterns are discussed in detail in the next section.

The shielding results for some norbornen-2-ols, **43–50**, are collected in Table 4 and the differences, $\delta_C^{obsd} - \delta_C^{calcd}$, are given in parentheses for **45–48**, the 3-methyl derivatives. The calculated values were obtained using the present data for the effects of a 2-hydroxyl group on the norbornene shieldings and our earlier data for the methylnorbornenes (5); these substituent effects are included in Table 2.

The preparative method used for many of the alcohols gave initially the corresponding acetate which was subsequently hydrolyzed to the desired alcohol. The ^{13}C spectra of these acetates were recorded to examine the differences between acetoxyl and hydroxyl substitution for comparison with the known trends in acyclic and monocyclic systems (refs. 7 and 8, and for a general discussion see ref. 9). In each case the acetoxyl signals appeared in nearly the same positions, δ_C 21.2 ± 0.3 (CH_3) and 170.5 ± 0.3 (C=O). In general the norbornyl carbons were little affected by acetylation of the hydroxyl group, only the carbinyl carbon and its immediate neighbors exhibited significant shifts. The shifts caused by acetylation are listed in Table 5 for the 22 acetates examined.

Discussion

The norbornane skeleton is an attractive model system with which to examine geometric

Can. J. Chem. Downloaded from www.nrcresearchpress.com by 210.87.254.6 on 09/05/12
For personal use only.

TABLE 3. ^{13}C shieldings* of some di- and trimethylnorbornanols

	Substitution									Methyl	
Compound	Me	2-OH	C-1	C-2	C-3	C-4	C-5	C-6	C-7	5-Me	6-Me
21	*exo*-5-*exo*-6	*exo*	52.9 (0.5)	74.8 (0.0)	42.5 (0.2)	43.5 (−0.1)	38.5 (0.1)	34.5 (0.2)	28.4 (−0.4)	(15.4)	(15.3)
22		*endo*	50.7 (0.0)	72.7 (0.3)	40.2 (0.7)	45.2 (−0.2)	40.2 (0.0)	28.9 (−1.4)	31.6 (0.4)	(15.8)	(15.2)
23	*endo*-5-*exo*-6	*exo*	52.4 (0.1)	74.8 (0.6)	34.3 (0.5)	(41.5) (0.0)	(42.7) (0.2)	(40.7) (0.7)	33.4 (0.4)	15.5	20.2
24		*endo*	50.2 (0.4)	73.2 (0.4)	30.9 (0.1)	43.5 (0.2)	44.6 (0.3)	33.4 (−2.2)	36.4 (0.2)	14.8	20.6
25	*exo*-5-*endo*-6	*exo*	50.5 (0.2)	69.0 (2.7)	43.4 (0.5)	(43.4) (0.1)	(43.9) (0.2)	(41.7) (2.9)	33.2 (0.2)	20.9	15.5
26		*endo*	47.9 (−0.7)	75.8 (11.3)	40.8 (0.7)	(45.2) (0.1)	(45.8) (0.3)	(44.3) (9.9)	36.2 (0.0)	21.2	17.7
27	*endo*-5-*endo*-6	*exo*	51.2 (0.2)	69.0 (2.1)	35.2 (0.8)	42.4 (0.2)	33.3 (0.0)	33.3 (3.7)	35.9 (0.1)	(11.8)	(11.3)
28		*endo*	48.2 (−1.1)	76.2 (11.1)	31.1 (0.5)	43.8 (0.2)	(35.1) (0.0)	(35.5) (10.3)	38.8 (−0.2)	11.6	14.2
										1-Me	7-Me
29	1-*anti*-7	*exo*	48.6 (−3.0)	78.3 (−4.3)	42.2 (0.5)	40.4 (−0.2)	30.4 (0.6)	27.4 (−0.2)	42.3 (−1.1)	13.8	10.0
30		*endo*	49.4 (−0.5)	78.5 (−2.4)	40.2 (1.3)	41.6 (−0.8)	28.5 (−3.1)	24.0 (0.8)	46.6 (0.0)	16.1	10.5
31	1-*syn*-7	*exo*	48.1 (−3.2)	78.3 (0.4)	40.6 (−3.3)	41.1 (0.5)	28.6 (1.0)	35.3 (2.9)	47.3 (3.9)	14.1	11.4
32		*endo*	48.4 (−1.5)	76.1 (0.0)	38.3 (−2.8)	41.2 (−1.2)	29.7 (0.3)	28.6 (0.6)	49.5 (2.9)	16.2	10.1
33	7,7	*exo*	51.4	77.6	41.9	44.4	27.5	25.7	45.7		22.2 22.4
34	1,7,7	*exo*	46.3	79.7	40.5	45.1	27.3	34.0	48.9	11.4	20.2 20.5
35		*endo*	49.5	77.2	39.0	45.2	28.3	26.0	48.0	13.3	18.7 20.2
											3-Me
36	3,3	*exo*	46.3 (0.1)	83.9 (−7.9)	42.8 (−6.2)	48.0 (1.3)	25.1 (2.1)	23.9 (0.9)	35.2 (0.9)		23.2(*exo*) 26.2(*endo*)
37		*endo*	44.1 (−0.4)	80.5 (−9.5)	38.0 (−8.2)	48.4 (−0.1)	24.7 (−0.1)	18.3 (−0.3)	33.9 (−3.6)		30.6(*exo*) 20.2(*endo*)
38	1,3,3	*exo*	49.1	86.2	43.5	48.4	25.6	33.8	40.9	17.1	23.1(*exo*) 26.3(*endo*)
39		*endo*	49.2	85.1	39.1	48.0	26.2	25.2	41.1	19.5	30.8(*exo*) 20.2(*endo*)
										6-Me	
40	3,3-*exo*-6	*endo*	51.1	80.6	37.4	49.3	34.8	24.1	29.7	21.7	30.6(*exo*) 19.7(*endo*)
41	3,3-*endo*-6	*endo*	49.5	83.9	37.4	48.6	33.2	31.8	35.5	18.9	31.1(*exo*) 20.0(*endo*)
42	6,6	*endo*	52.7	76.1	37.1	38.3	47.8	33.2	37.2	33.2(*exo*) 28.8(*endo*)	

*In ppm from internal TMS in $CDCl_3$ solutions. Values in parentheses are ($\delta_C^{obsd} - \delta_C^{calcd}$), where δ_C^{calcd} was obtained by assuming simple additivity of substituent effects (see text).

effects on ^{13}C shieldings since a variety of well-defined orientations for neighboring substituents are available by simple synthesis. The present series provides several examples of two different arrangements involving methyl and hydroxyl groups. As the first set, one can consider the various orientations of vicinal substituents, while the second set are those having the methyl

Can. J. Chem. Downloaded from www.nrcresearchpress.com by 210.87.254.6 on 09/05/12
For personal use only.

TABLE 4. ^{13}C shieldings* of some norbornen-2-ols

Compound	Substitution: Me	Substitution: 2-OH	C-1	C-2	C-3	C-4	C-5	C-6	C-7	Methyl
43		*exo*	50.1	72.3	36.9	40.7	140.2	133.5	45.6	
44		*endo*	48.2	72.3	37.6	42.9	140.0	131.1	48.2	
45	*exo*-3	*exo*	50.6	72.6	36.8	47.9	141.9	133.6	42.6	14.8
			(0.0)	(−9.7)	(−8.0)	(0.7)	(−0.1)	(−0.6)	(0.7)	
46		*endo*	48.7	81.1	44.9	49.3	141.1	131.5	44.9	19.4
			(0.1)	(−1.2)	(−0.6)	(−0.1)	(−0.7)	(−0.3)	(0.4)	
47	*endo*-3	*exo*	51.4	80.2	44.6	46.4	137.4	134.1	47.2	18.1
			(0.0)	(−1.2)	(−0.2)	(0.3)	(0.3)	(−0.9)	(0.0)	
48		*endo*	49.4	73.6	38.7	47.0	138.6	132.9	48.3	13.1
			(0.0)	(−7.8)	(−6.8)	(−1.3)	(1.7)	(0.3)	(−1.5)	
49	3,3	*exo*	51.8	80.1	40.6	52.9	138.9	133.0	45.8	24.2(*exo*) 28.3(*endo*)
50		*endo*	49.7	81.3	41.9	54.1	141.1	131.7	44.4	29.9(*exo*) 22.2(*endo*)

*In ppm from internal TMS in $CDCl_3$ solutions. Values in parentheses are $(\delta_C^{obsd} - \delta_C^{calcd})$, where δ_C^{calcd} were obtained by assuming simple additivity of substituent effects (see text).

TABLE 5. Substituent effects* of the acetyl group in norbornyl acetates

Parent alcohol	Substitution: Me	Substitution: 2-OAc	β C-2	γ C-1	γ C-3	δ C-4	δ C-6	δ C-7	ε C-5	Methyl
1	—	*exo*	2.8	−2.6	−2.5	0.1	0.0	0.9	0.2	
9	*exo*-5	*exo*	2.8	−1.9	−2.7	0.1	−0.2	0.9	0.0	−0.1
10	*endo*-5	*exo*	2.9	−2.7	−2.1	0.1	0.0	0.8	−0.1	0.0
11	*exo*-6	*exo*	2.7	−3.1	−2.6	0.1	0.1	0.7	0.1	−0.1
12	*endo*-6	*exo*	4.3	−2.7	−2.4	0.0	0.2	0.8	0.0	0.0
25	*exo*-5-*endo*-6	*exo*	4.2	−2.8	−2.6	−0.2	0.0	0.8	0.2	0.0(5,6)
23	*endo*-5-*exo*-6	*exo*	2.7	−3.1	−2.6	0.0	−0.2	0.7	0.3	0.0(5) −0.1(6)
17	*anti*-7	*exo*	2.8	−2.9	−2.7	0.0	−0.2	0.8	0.0	−0.2
29	1-*anti*-7	*exo*	1.8	−0.9	−2.0	0.0	−0.3	1.2	−0.3	0.0(1) −0.1(7)
18	*syn*-7	*exo*	2.2	−2.7	−1.6	0.3	−0.3	0.2	−0.1	−0.5
31	1-*syn*-7	*exo*	1.3	−0.5	−1.8	0.0	−0.2	0.5	−0.2	0.0(1) −0.4(7)
43		*exo*	2.7	−2.7	−2.3	0.0	−0.5	0.7	0.8	
45	*exo*-3	*exo*	2.8	−2.7	−0.4	0.0	−0.4	0.8	0.0	0.3
47	*endo*-3	*exo*	1.8	−2.9	−2.5	−0.3	0.8	0.3	0.8	−0.2
49	3,3	*exo*	1.9	−2.7	0.5	0.0	−0.6	0.6	1.0	0.0(*exo*) −0.4(*endo*)
2		*endo*	2.8	−2.2	−2.3	−0.5	1.0	−0.6	−0.4	
13	*exo*-5	*endo*	3.5	−2.3	−2.8	−0.7	0.9	−0.3	−0.4	−0.2
15	*exo*-6	*endo*	2.6	−2.5	−2.6	−0.8	1.0	−0.5	−0.5	−0.2
44		*endo*	2.6	−2.3	−3.0	−0.6	0.6	−0.5	−1.7	
46	*exo*-3	*endo*	1.7	−2.6	−3.2	−0.6	0.6	−0.7	−2.2	0.0
48	*endo*-3	*endo*	2.6	−1.5	−0.5	0.0	0.7	−1.2	−2.3	0.1
50	3,3	*endo*	1.7	−2.5	0.5	−0.3	0.7	0.1	−2.7	−0.6(*exo*) −0.1(*endo*)

*$\Delta\delta = \delta_C^{ROCOCH_3} - \delta_C^{ROH}$ in ppm; downfield shifts are positive.

and hydroxyl groups separated by four bonds. In a preceding part of this series (5) we focussed attention on the variation of methyl shieldings as a function of the dihedral angle (ϕ) relating a methyl carbon to another methyl or the carbonyl oxygen in several norcamphors, *i.e.* a number of

Can. J. Chem. Downloaded from www.nrcresearchpress.com by 210.87.254.6 on 09/05/12
For personal use only.

TABLE 6. Methyl ^{13}C shieldings of some methylnorbornanes*

Substitution	$\delta_C^{CH_3}$	Reference	Substitution	$\delta_C^{CH_3}$	Reference
1-Methyl	21.0	4*a*	7-Methyl	12.7	4*a*
exo-2-Methyl	22.3	5	1,7-Dimethyl	10.7(7-Me) 18.6(1-Me)	4*d*
endo-2-Methyl	17.4	5			
2,2-Dimethyl	31.6(*exo*) 27.2(*endo*)	4*a*	1,7,7-Trimethyl	15.8(1-Me) 19.2(7-Me)	4*a*

*In ppm from TMS; data from ref. 4*a* converted using the factor 192.8 ppm.

vicinal interactions, for which it was found that the methyl shielding increased as the dihedral angle decreased in the range, 0–120°. Although the norbornyl skeleton may be twisted by as much as 14° from C_{2v} symmetry (10) the approximate dihedral angles between vicinal substituents provide a guide to the relative steric crowding. To examine the effect of the vicinal hydroxyl group, the methyl shieldings may be compared with those for the corresponding carbons in the appropriate methylnorbornane and the required data are listed in Table 6. Although all of these results were not determined under the same conditions, we have found that the methyl shieldings seem the least sensitive to solvent effects and there is generally good agreement, 0.0–0.3 ppm, between values measured in $CDCl_3$ (5) and in dioxane (4*a*). In any event we are seeking trends rather than specific values and the consistency of these indicates that the reference data in Table 6 are valid.

For the simplest cases, **5**–**8**, there are two different dihedral angles relating the methyl carbon and the hydroxyl group, 0° and 120°. For **5** and **6**, with $\phi \sim 120°$, the methyl carbons are shielded by 2.3 ppm relative to the values for the corresponding methylnorbornanes; for **7** and **8**, with $\phi \sim 0°$, the upfield shifts are 8.9 and 7.6 ppm, respectively. In the norbornenols **45**–**48** comparable shifts are found for the methyl carbons: $\phi \sim 120°$, −1.2 (**47**), −2.2 (**46**); $\phi \sim 0°$, −6.8 (**45**), −6.2 ppm (**48**). In the 3,3-dimethyl derivatives **36**–**41**, one of the geminal methyls is eclipsed, or nearly so, with the hydroxyl while the other has $\phi \sim 120°$ and the upfield shifts average 7.6 and 0.9 ppm, respectively, for the two orientations. Clearly there is a distinct sensitivity of the methyl shielding to ϕ but it may be noted that there is a variation of nearly 2 ppm within each group. The alcohols bearing a 1-methyl group provide examples with two other orientations of the methyl and hydroxyl groups; an *endo*-2-hydroxyl has $\phi \sim 90°$ and for an *exo*-2-hydroxyl, $\phi \sim 30°$. For the first group (**4**, **30**, **32**, **35**, and **39**) with $\phi \sim 90°$, the upfield shifts average 2.3 ppm; the corresponding shift for the second group (**3**, **29**, **31**, **34**, and **38**) with $\phi \sim 30°$ is 4.5 ppm. Again there is variation within each group but only ~1 ppm, possibly because skeletal twist does not alter the dihedral angle between groups on C-1 and C-2 as much as that between substituents on C-2 and C-3. Nevertheless, a trend is clear with the methyl shielding increasing as the dihedral angle decreases. This is entirely in accord with the general trend exhibited by vicinal substituents (1, 5, 9) and has been well-defined in a variety of alicyclic hydrocarbons (11). These effects, known as the γ-effects have been ascribed (12) to steric polarization produced by the close approach of the terminal nuclei in the γ fragment, the unit containing the vicinal substituents.

In this series, there are several examples having a variety of different orientations of methyl and hydroxyl groups separated by four bonds. This array of δ interactions can be subdivided into four basic types, **51**–**54**, recognizing that the **a** and **b** orientations are not strictly equivalent but are closely similar. The simplest examples and the methyl shifts, relative to the parent hydrocarbon are as follows: **11**, −0.9 ppm (**51a**); **12**, −0.5 ppm (**52a**); **15**, −0.5 ppm (**53a**), **17**, −0.8 ppm (**53b**); **16**, +2.0 ppm (**54a**), **18**, +0.8 ppm (**54b**). The methyl carbon is slightly shielded if well separated from the hydroxyl group but is deshielded if the methyl and hydroxyl groups are close neighbors as in **54**. The latter arrangements are analogous to a *syn*-axial disposition of substituents in cyclo-

Can. J. Chem. Downloaded from www.nrcresearchpress.com by 210.87.254.6 on 09/05/12
For personal use only.

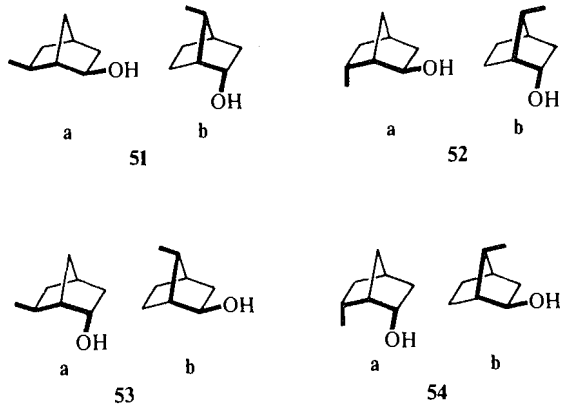

hexane systems and to the $g(+)g(-)$ conformation in acyclic cases. Earlier, from the results cited above and corresponding trends in some *trans*-decalols and steroids, we drew attention to these deshielding *syn*-axial interactions (3). Comparable shifts are found for the terminal methyl carbons in highly substituted acyclic hydrocarbons which have substantial populations in $g(+)g(-)$ conformations (13). Larger deshielding effects occur for the methyl carbons in a variety of polycyclic aromatic hydrocarbons having *peri* methyl groups (14). Thus, it appears that the interaction of substituents in *syn*-axial, or equivalent orientations, tend, in general, to deshield the terminal carbons in a δ fragment and the present series allows further definition of the effects accompanying these steric perturbations.

Of the dimethyl derivatives, **21** and **23** have the **51a** arrangement and the 6-methyl carbons are shielded by 0.4 and 0.9 ppm, respectively, but the 7-methyl shift in **30** (**51b**) is only −0.2 ppm. The 6- and 7-methyl carbons in several other cases exhibit average upfield shifts of 0.5 ppm and can be grouped as follows: **25** and **27** (**52a**); **32** (**52b**); **22**, **24**, and **40** (**53a**); **29** (**53b**). Thus, in all of the examples, orientations **51**–**53** exhibit a small shielding effect at the appropriate methyl carbon. Additional examples of the '*syn*-axial' arrangement **54a** include **26**, **28**, and **41** which exhibit downfield methyl shifts of 1.8, 2.4, and 1.5 ppm, respectively. It is interesting that in **42** both geminal methyls at C-6 are deshielded by 1.6 ppm. Similarly in **34** both geminal methyls at C-7 are deshielded; the shifts are 1.0 and 1.3 ppm but assignments are uncertain. In **31**, the 7-methyl is deshielded by 0.7 ppm. These latter examples contain arrangement **54b**. The smaller shifts for this group relative to those found for the 6-methyl carbons in **54a** may be due to the somewhat larger separation between the methyl and hydroxyl groups.

Closer inspection of the data for the compounds having '*syn*-axial' interactions reveals much more striking trends (Tables 1 and 3) which we have described in preliminary form recently (15). The differences between the observed shieldings and those estimated by additivity for the skeletal carbons are particularly large for the carbons bearing the terminal nuclei in the crowded δ fragment. For **16**, **26**, **28**, and **41** these differences are in the range 9.1–11.3 ppm whereas the differences for the remaining carbons in these compounds are <1.3 ppm and average 0.5 ppm. Clearly, the carbons bearing these interacting substituents are substantially deshielded. A similar trend is found for **18** but the deviations from additivity for the substituted carbons are smaller (3.7 and 4.5 ppm), possibly reflecting the effect of a less severe interaction, as was indicated by the methyl shifts. These deviations may be compared with those found for the other δ arrangements. For **51a**, the observed and predicted shieldings are in excellent agreement as in **11**, **21**, and **23**; similarly for **53a**, there is good agreement in **15**, **22**, **24**, and **40** with the exception of C-6 which is consistently shielded by 1–2 ppm. For the **52a** examples, both C-2 and C-6, the substituted carbons, are deshielded by 1.8–3.7 ppm as in **12**, **25**, and **27** while the remaining deviations are less than 0.6 ppm. In each of these cases, the interaction involves a single methyl and the hydroxyl whereas in **42** the *syn*-axial interaction involves the methyl of a geminal pair at C-6 and it was noted above that both methyls are deshielded. The substituted carbons are also substantially deshielded but less than those in **16**, **26**, **28**, and **41**, namely, by 6.4 and 8.3 ppm. Nevertheless, there is a clear trend; in compounds having a *syn*-axial or equivalent interaction between δ substituents, the carbons bearing the substituents are appreciably deshielded. It follows that the magnitude of these deviations from additivity should be useful in the interpretation of spectra of more complex systems in stereochemical terms.

In contrast to the effects of closely neighboring δ substituents, the deviations from additivity for the carbons bearing closely neighboring γ substituents are negative, *i.e.* these carbons are

Can. J. Chem. Downloaded from www.nrcresearchpress.com by 210.87.254.6 on 09/05/12
For personal use only.

Can. J. Chem. Downloaded from www.nrcresearchpress.com by 210.87.254.6 on 09/05/12
For personal use only.

more shielded by the γ interaction than predicted by simple additivity. Examples having eclipsed vicinal methyl and hydroxyl groups at C-2 and C-3 include **7**, **8**, **36**, **37**, **45**, and **48** for which the substituted carbons show deviations of 5.8–9.7 ppm upfield from the predicted values. Alteration of these deviations by increasing the dihedral angle is illustrated by the results for **3** and **38** with $\phi \sim 30°$ between the 1-methyl carbon and the hydroxyl group for which the deviations lie in the range 4.1–4.7 ppm; in **4** and **39** with $\phi \sim 90°$ the corresponding deviations are 2.0–2.4 ppm. In addition it can be noted that the remaining skeletal shieldings are in generally good agreement with those predicted by simple additivity. For **5**, **6**, **46**, and **47** in which $\phi \sim 120°$, there are no pronounced deviations from additivity. Clearly the shielding effects within a γ fragment are exactly opposite those in a δ fragment for those cases in which the terminal nuclei of these fragments closely approach each other. For both types of interaction, the marked deviations from additivity are essentially restricted to the carbons in the fragment containing the closely neighboring substituents.

With these trends in mind it is interesting to examine the deviations found for the 1,7-dimethyl derivatives **29–32**. For **29**, the largest deviations occur for C-1 and C-2 and are readily attributed to the γ interaction between the 1-methyl and hydroxyl groups. Its counterpart having a *syn*-7-methyl, **31**, has a positive deviation for C-7, negative for C-1, and essentially none for C-2. The latter presumably arises because of opposing shifts caused by the γ effect of the bridgehead methyl and the δ effect of the *syn*-7-methyl. Since the '*syn*-axial' perturbations in the other examples have essentially no effect at the central carbon of the δ fragment (see **16**, **18**, **26**, **28**, **41**, and **42**), C-1 can be expected to shift upfield because of the γ interaction. The downfield shift for C-7 is readily ascribed to the δ interaction of its methyl with the *exo*-hydroxyl group. In **31**, however, C-3 and C-6 also show appreciable deviations, $\sim$3 ppm, in opposite directions. Perhaps these changes occur because of skeletal twist to minimize the *syn*-methyl–hydroxyl and methyl–methyl interactions, thereby enhancing the shielding at C-3 and reducing that of C-6. The observed deviations at C-1, -2, and -7 in **30** and **32** can be interpreted similarly. For example, one expects both the γ and δ interactions in **32** to give smaller shifts than those for **31** because $\phi \sim 90°$ between the bridgehead methyl and the *endo*-hydroxyl and the δ interaction is **52b**. These effects could cancel at C-2 while shielding C-1 and deshielding C-7. In both **30** and **32** one of the methylene carbons has a deviation of -3 ppm which could arise from a skeletal twist which enhances the shielding effect of the 7-methyl at one of the *syn*-methylene carbons.

Apart from C-6 and C-7 in *endo*-5-methyl-*endo*-2-norbornanol (**14**), the deviations for the 5-methyl derivatives **9**, **10**, **13**, and **14** average 0.2 ppm, indicating that these substituents are acting essentially independently. The deviations of -1.2 and -1.6 ppm for the two centres in **14** may arise because of a skeletal twist to minimize an interaction between the two *endo*-substituents. It is interesting that the methyl carbon in **14** is slightly shielded (-1.1 ppm) as is the corresponding methyl in **24** which also has the 5-methyl and hydroxyl groups *endo*. The other 5-methyl carbons exhibit little difference (<0.5 ppm) from their shieldings in the corresponding hydrocarbons.

To summarize, marked shielding effects arise from steric interactions of closely neighboring substituents. For groups separated by four bonds the *syn*-axial or equivalent orientation deshields the carbons bearing the substituents by as much as 11 ppm. This trend is in direct contrast to the upfield shifts found for carbons bearing closely neighboring vicinal substituents. Although comparable shifts are produced at the terminal nuclei in the latter cases, the terminal nuclei in δ fragments exhibit much less distinctive shifts, albeit in the opposite direction. The marked deshielding of the substituted carbons in *syn*-axial arrangements, however, should prove useful in the interpretation of spectra of more complex systems.

Experimental

Spectra

The ^{13}C spectra were recorded with a Varian XL-100-15 system operating in the Fourier transform mode. Solutions (10–15% w/v) in deuteriochloroform containing a few drops of TMS were examined in 5 mm tubes. Line positions were measured relative to TMS to ± 1 Hz or better and the precision of the chemical shifts is ± 0.05 ppm. The purity of several samples was checked by proton spectra obtained on Varian T-60 and HA-100 instruments

Can. J. Chem. Downloaded from www.nrcresearchpress.com by 210.87.254.6 on 09/05/12
For personal use only.

Materials

Norcamphor was the starting material for the preparation of **1** and **2**, by reduction with $NaBH_4$, of **20** and **3** following the literature method (16), of **29** and **31** according to Hatfield and Huntsman (17), as well as of **5–8** by methylation (18) followed by reduction with $NaBH_4$. Alcohols **5–8** were also prepared from **45–48** by hydrogenation over a PtO_2 catalyst in ether or ethanol. Unsaturated acetates of alcohols **43–50** were obtained by the Diels–Alder reaction of cyclopentadiene with vinyl acetate or the enol acetates of propanal or isobutyraldehyde (5). Samples of the individual acetates were separated by preparative gc and hydrolyzed to furnish the desired alcohols; **43** was also prepared by hydroboration of norbornadiene (19). Hydrogenation of **49** and **50** over PtO_2 gave **36** and **37** respectively; the latter were also obtained from camphenilone. From the two 5-methyl- and three 5,6-dimethylnorbornenes (5), **9–12**, **21**, **23**, **25**, and **27** were generated by hydroboration. For those cases in which mixtures are formed, separation was accomplished by preparative gc of the mixtures after acetylation; subsequent hydrolysis of the individual acetates provided samples of the alcohols. Oxidation of these alcohols with CrO_3–pyridine in CH_2Cl_2 (20) gave the corresponding ketones which were reduced to the *endo*-alcohols **13–16**, **22**, **24**, **26**, and **28** with lithium trimethoxyaluminum hydride in tetrahydrofuran (21). Reduction of 1-methylnorcamphor, the santenones, fenchone, and the 7,7-dimethyl and 6,6-dimethylnorcamphors in the same way gave **4**, **30**, **32**, **39**, **33**, and **42**, respectively. Borneol (**35**) and isoborneol (**34**) were commercial products and a sample of **19** was kindly supplied by J. A. Berson.

In an examination of the lead tetraacetate decarboxylation of the 3-methylnorbornane-2-carboxylic acids (22), after the method of Corey and Casanova (23), it was found that the product mixture contained the acetates of **5–7**, **17**, and **18**. Preparative gc on a Carbowax 4000 column at 175 °C gave essentially pure samples of the **5**, **6**, and **17** acetates and a mixture of the **7** and **18** acetates, judged to be ~4:1 from the ^1H and ^{13}C spectra. These acetates and the corresponding alcohols obtained by hydrolysis were identified by their proton and ^{13}C spectra since authentic samples of **5–7** were available (as described above). The data for **17** and **18** were distinctly different from those for **5–16**, the other possible monomethyl derivatives which could give rise to a doublet for the methyl group in the proton spectrum as observed for **17** and **18**. The carbinyl absorption for **17** and **18** closely resembled that for **29** and **31**, respectively, as expected since there will be negligible vicinal coupling between the bridgehead proton and the 2-*endo* proton in **17** and **18**.

Acknowledgments

We wish to thank Prof. J. A. Berson for kindly supplying authentic samples of **5**, **7**, **19**, and **20** and Ms. J. L. Gough, C. Ferriera, and I. Grikis for technical assistance. We are grateful to the National Research Council of Canada for financial support.

1. N. K. Wilson and J. B. Stothers. *In* Topics in stereochemistry. Vol. 8. *Edited by* E. L. Eliel and N. L. Allinger. Wiley–Interscience, New York. 1974.
2. E. L. Eliel, W. F. Bailey, L. D. Kopp, R. L. Willer, D. M. Grant, R. Bertrand, K. A. Christensen, D. K. Dalling, M. W. Duch, E. Wenkert, F. M. Schell, and D. W. Cochran. J. Am. Chem. Soc. **97**, 322 (1975).
3. S. H. Grover, J. P. Guthrie, J. B. Stothers, and C. T. Tan. J. Magn. Reson. **10**, 227 (1973).
4. (*a*) J. B. Grutzner, M. Jautelat, J. B. Dence, R. A. Smith, and J. D. Roberts. J. Am. Chem. Soc. **92**, 7107 (1970); (*b*) H.-J. Schneider and W. Bremser. Tetrahedron Lett. 5197 (1970); (*c*) T. I. Pehk, E. T. Lippmaa, N. A. Belikova, and A. F. Plate. Dokl. Akad. Nauk. SSSR, **195**, 885 (1970); (*d*) E. Lippmaa, T. Pehk, J. Paasivirta, N. Belikova, and A. Plate. Org. Magn. Reson. **2**, 581 (1970); (*e*) K. Tori, T. Tsushima, H. Tanida, K. Kushida, and S. Satoh. Org. Magn. Reson. **6**, 324 (1974); (*f*) N. H. Werstiuk, R. Taileffer, R. A. Bell, and B. G. Sayer. Can. J. Chem. **50**, 2146 (1972); (*g*) S. H. Grover and J. B. Stothers. Can. J. Chem. **53**, 589 (1975).
5. J. B. Stothers, C. T. Tan, and K. C. Teo. Can. J. Chem. **51**, 2893 (1973).
6. (*a*) J. Briggs, F. A. Hart, G. P. Moss, and E. W. Randall. Chem. Commun. 364 (1971); (*b*) O. A. Gansow, M. R. Willcott, and K. E. Lenkinski. J. Am. Chem. Soc. **93**, 4295 (1971).
7. E. Lippmaa and T. Pehk. Esti NSV Tead. Akad. Toim Keem. Geol. **17**, 210 (1968).
8. M. Christl, H. J. Reich, and J. D. Roberts. J. Am. Chem. Soc. **93**, 3463 (1971).
9. J. B. Stothers. Carbon-13 NMR spectroscopy. Academic Press, New York. 1972. Chap. 5.
10. C. Altona and M. Sundaralingam. J. Am. Chem. Soc. **92**, 1995 (1970).
11. D. K. Dalling and D. M. Grant. J. Am. Chem. Soc. **89**, 6612 (1967); **94**, 5318 (1972); **96**, 1827 (1974); D. K. Dalling, D. M. Grant, and E. G. Paul, J. Am. Chem. Soc. **95**, 3718 (1973).
12. D. M. Grant and B. V. Cheney. J. Am. Chem. Soc. **89**, 5315 (1967).
13. J. G. Batchelor. J. Magn. Reson. **18**, 212 (1975).
14. N. K. Wilson and J. B. Stothers. J. Magn. Reson. **15**, 31 (1974); M. L. Caspar, J. B. Stothers, and N. K. Wilson. Can. J. Chem. **53**, 1958 (1975).
15. J. B. Stothers, C. T. Tan, and K. C. Teo. J. Magn. Reson. **20**, 570 (1975).
16. J. A. Berson, J. S. Walia, A. Remanick, S. Suzaki, P. Reynolds-Warnhoff, and D. Willner. J. Am. Chem. Soc. **83**, 3986 (1961).
17. L. D. Hatfield and W. D. Huntsman. J. Org. Chem. **32**, 844 (1967).
18. E. J. Corey, R. Hartmann, and R. A. Vatakencherry. J. Am. Chem. Soc. **84**, 2611 (1962).
19. G. Zweifel, K. Nagase, and H. C. Brown. J. Am. Chem. Soc. **84**, 183 (1962).
20. R. Ratcliffe and R. Rodehorst. J. Org. Chem. **35**, 4000 (1970).
21. E. C. Ashby, J. P. Sevenair, and F. R. Dobbs. J. Org. Chem. **36**, 197 (1971).

22. J. B. STOTHERS and K. C. TEO. Can. J. Chem. This issue.
23. E. J. COREY and J. CASANOVA. J. Am. Chem. Soc. **85**, 165 (1963).
24. P. A. W. DEAN, D. G. IBBOTT, and J. B. STOTHERS. Can. J. Chem. **54**, 166 (1976).
25. A. STOESSL and J. B. STOTHERS. Can. J. Chem. **53**, 3359 (1975).

Can. J. Chem. Downloaded from www.nrcresearchpress.com by 210.87.254.6 on 09/05/12
For personal use only.

Oxidative decarboxylation of the 3-methyl-2-carboxynorbornanes with lead tetraacetate[1]

J. B. STOTHERS AND K. C. TEO

Department of Chemistry, University of Western Ontario, London, Ontario N6A 5B7

Received October 9, 1975

J. B. STOTHERS and K. C. TEO. Can. J. Chem. **54**, 1222 (1976).

The mixtures of isomeric acetates produced by oxidative decarboxylation of the four 3-methylnorbornane-2-carboxylic acids with lead tetraacetate in benzene have been characterized. The composition of these products depends primarily on the configuration of the methyl group in the starting material. The results are compared with those found for the $Pb(OAc)_4$ decarboxylation of the norbornane-, bornane-, and 2,3,3-trimethylnorbornane-2-carboxylic acids. The formation of the products is interpreted in terms of competitive cationic and S_Ni substitution.

J. B. STOTHERS et K. C. TEO. Can. J. Chem. **54**, 1222 (1976).

On a caractérisé les mélanges d'isomères d'acétates produits par la décarboxylation oxydante de quatre acides méthyl-3 norbornanecarboxyliques-2 par le tétraacétate de plomb dans le benzène. La composition de ces produits dépend principalement de la configuration du groupe méthyle dans le produit de départ. On a comparé les résultats avec ceux obtenus pour la décarboxylation par le tétraacétate de plomb des acides norbornane-, bornane- et triméthyl-2,3,3 norbornanecarboxyliques-2. On interprète la formation des produits en termes d'une compétition entre des réactions de substitution cationique et S_Ni.

[Traduit par le journal]

In the course of an investigation of stereochemical effects on ^{13}C nmr shieldings of norbornyl systems (1), we wished to examine several monomethyl derivatives of 2-norbornanol. A potential route to the 7-methyl members of this series appeared to be via lead tetraacetate decarboxylation of the 3-methylnorbornane-2-carboxylic acids (**1**–**4**) since this oxidative decarboxylation of other norbornanecarboxylic acids (2, 3) leads, through cationic intermediates, to norbornyl acetates with skeletal rearrangement. For example, the bornane-2-carboxylic acids gave bornyl, isobornyl, and 2,3,3-trimethylnorbornyl acetates, among other products (3), and it may be noted that the composition of the acetate mixture was independent of the orientation of the carboxyl group in the starting material. Initially, the acids, as lead(IV) carboxylates, lose carbon dioxide to form radicals which, in addition to undergoing typical radical reactions, may be converted to lead(IV) alkyls. The organolead derivatives then decompose by (*a*) heterolysis to carbonium ions and lead(II) derivatives, (*b*) a cyclic S_Ni process to give the acetates, and (*c*) *cis*-elimination to give the alkenes (3*b*). Path *a* can lead to acetates having a rearranged skeleton. Thus, it was anticipated that formation of the 3-methylnorbornyl cation from acids **1**–**4** could yield mixtures of the 3-methyl- and 7-methyl-2-norbornyl acetates. This was found to be the case and, furthermore, the composition of the mixture of acetates obtained depended markedly on the initial orientation of the methyl group in the acid. Acids **1** and **2**, having an *exo*-3-methyl group, gave the same mixture of five acetates (**5**–**9**), while a mixture of essentially two acetates (**6** and **9**) was obtained from the decarboxylation of **3** and **4**.

The decarboxylations were carried out at reflux temperature in benzene containing pyridine as described by Corey and Casanova (2) using a 2:1 molar ratio of lead tetraacetate – carboxylic acid. Only the acetate portion of the product was isolated and, as in the original work, the yields were variable (20–44%) in different runs; the compositions of the product mixtures, however, were reproducible according to gas chromatographic (gc) analysis. The reactions were complete in approximately 2 h and it was found that reaction times up to 8 h did not alter the product composition. Preparative gc was used to separate these mixtures into their component acetates. Although we were unable to separate **7** and **9** completely (formed in a 4:1

[1]Part 56 of ^{13}C nmr studies; for part 55 see ref. 1.

Can. J. Chem. Downloaded from www.nrcresearchpress.com by 210.87.254.42 on 09/05/12
For personal use only.

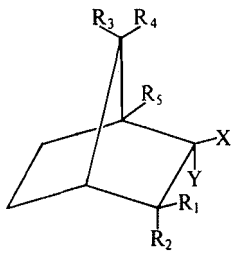

	X	Y	R_1	R_2	R_3	R_4	R_5
1	COOH	H	Me	H	H	H	H
2	H	COOH	Me	H	H	H	H
3	COOH	H	H	Me	H	H	H
4	H	COOH	H	Me	H	H	H
5	H	OAc	Me	H	H	H	H
6	OAc	H	H	Me	H	H	H
7	OAc	H	Me	H	H	H	H
8	OAc	H	H	H	Me	H	H
9	OAc	H	H	H	H	Me	H
10	OAc	H	H	H	Me	H	Me
11	OAc	H	H	H	H	Me	Me
12	H	OAc	H	Me	H	H	H

ratio from **1** and **2**) it was possible to obtain a sample enriched in **9** by gc. The individual acetates were identified by their ^{13}C and ^{1}H spectra aided by those of authentic samples of acetates **5–7** which were on hand from other preparative routes (1). As further proof of identity of these acetates, the various samples were hydrolyzed to the corresponding alcohols and their ^{13}C and ^{1}H spectra recorded for comparison with those of authentic samples of the alcohols from **5–7**. Acetates **10** and **11** were also available, having been prepared by acid-catalyzed rearrangement of 2,3-dimethyl-*endo*-2-norbornanol as described by Hatfield and Huntsman (4).

The total acetate product from each acid **1–4** was examined by gc. The chromatograms of the products from **1** and **2** had four distinct bands which were separable by preparative gc. Similarly two major fractions were collected from the products of **3** and **4**. Proton spectra of each fraction were recorded and the methyl and carbinyl patterns compared with those for acetates **5–7**. It was found that the first and second fractions from **1** and **2** were **5** and **6**, respectively, while the third fraction was a mixture of two acetates with **7** as the predominant component. The carbinyl proton absorptions for the minor component of fraction three and for the fourth fraction did not correspond to those for **5–7** or to that for *endo*-3-methyl-*endo*-2-norbornyl acetate, **12**, a sample of which was available from other work (1). These proton data are collected in Table 1. The first fraction of the products from **3** and **4** was similarly identified as **6** while the second major fraction exhibited a proton spectrum identical to that of the fourth fraction from **1** and **2**. This acetate was shown to be **8** from its proton and ^{13}C spectra. In the former the carbinyl absorption at 4.57 ppm was a doublet of doublets with spacings of 7.6 and 2.5 Hz while the methyl absorption was a doublet ($J \sim 7$ Hz) centered at 0.87 ppm. These patterns are very similar to the corresponding absorptions for **10**, its 1-methyl derivative (Table 1), and clearly show the presence of an *exo*-acetoxyl group. In the ^{13}C spectrum, the presence of two methylene signals at 22.3 and 25.3 ppm established that the methyl group cannot be at C-1, -4, -5, or -6, since methyl substitution at any one of these carbons would deshield a geminal methylene carbon by 7–10 ppm (1) whereas the two methylene signals are 2–3 ppm upfield from the corresponding signals for norbornyl acetate (Table 2). This upfield shift is entirely consistent with the γ effect expected for *anti*-7-methyl substitution on the norbornyl skeleton (5). These data, therefore, identified this acetate as **8**. The ester initially collected as the minor part (~20%) of the third fraction

TABLE 1. Characteristic proton absorptions* of acetates **5–12**

		—CH(—OAc)					—CH(OAc)—		
Acetate	CH_3	δ	Multiplicity†	Width‡	Acetate	CH_3	δ	Multiplicity†	Width‡
5	1.03_5	4.46	t	7.0	**8**	0.87	4.57	d(d)	10.1
6	1.03	4.04	t	4.2	**9**	1.05_5	4.60	t	12.0
7	0.84	4.70_5	d	7.5	**10**	0.79	4.51	d(d)	10.2
12	0.82	4.97	d(d)	15.5	**11**	0.94	4.51	t	12.2

*Chemical shifts in ppm from TMS for $CDCl_3$ solutions; methyl doublets had spacings of ~7 Hz.
†Apparent multiplicity: t, triplet; d, doublet.
‡Spacing in Hz of outermost bands in each multiplet.

Can. J. Chem. Downloaded from www.nrcresearchpress.com by 210.87.254.42 on 09/05/12
For personal use only.

TABLE 2. ^{13}C shieldings* of norbornyl acetate and 7–9

Acetate	C-1	C-2	C-3	C-4	C-5	C-6	C-7	CH_3	OAc —CO—	OAc CH_3
Norbornyl	41.6	77.5	39.7	35.5	28.3	24.4	35.3	—	170.5	21.2
8	45.6	78.2	40.7	39.5	25.3	22.0	40.4	11.7	170.5	21.3
9	45.5	78.5	37.3	40.7	28.6	26.2	43.9	13.0	170.6	21.4
7	42.3	78.9	42.3	43.2	29.0	24.5	32.9	13.9	170.8	21.4

*In ppm from internal TMS for $CDCl_3$ solutions.

from **1** and **2** was obtained as the predominant component (~65%) in a sample collected by preparative gc from a portion of the third band in the product from **1** and **2**. The carbinyl proton pattern at 4.60 ppm closely resembled that for **11** at 4.51 ppm (Table 1) while its methyl doublet appeared at 1.055 ppm. Its ^{13}C spectrum (Table 2) contained two methylene signals at 26.2 and 28.6 ppm which are slightly downfield from the most shielded methylene carbons in norbornyl acetate. These signals rule out methyl substitution at C-1, -4, -5, and -6 but are entirely consistent with *syn*-7-methyl substitution leading to structure **9** for this ester. The product from **3** and **4** also contained small amounts (~4%) of another acetate having carbinyl absorption at 4.71 ppm as a doublet of doublets with spacings of 7 and 4 Hz. This material was not isolated or identified but it cannot be a 1-, 5-, or 6-methylnorbornyl-2-*exo*-acetate since its carbinyl absorption differs from that for each of these esters (6). Gas chromatography also indicated the presence of small amounts ($\leq$3%) of the mixture of **7** and **9** in the total product from **3** and **4**. The product compositions from each of the 3-methylnorbornanecarboxylic acids are listed in Table 3.

TABLE 3. Product distribution* in the acetate fraction from decarboxylations of **1–4**

Acid	Acetates **5**	**6**	**8**	**7** and **9**	Other†
1	13	5	5	76‡	—
2	13	11	5	71‡	—
3	—	71	25	—	4
4	—	72	21	3(?)	4

*Given as % of total acetate fraction as determined by gc and ^1H nmr; estimated precision ±3%.
†Unidentified ester (see text).
‡Estimated ratio ~4:1 from the carbinyl and methyl proton absorptions.

Although the yields of acetates were variable in different runs, averaging 30%, the conversion of acids **1–4** to acetates was somewhat higher than those found for the bornane- and 2,3,3-trimethylnorbornane-2-carboxylic acids (3*b*) but lower than those we have obtained from norbornane-*endo*-2-carboxylic acid (~50%). From Table 3, it is apparent that the product composition depends primarily on the orientation of the methyl group in the starting material and is essentially independent of the carboxyl orientation. The latter feature is consistent with the results for other norbornane derivatives (2, 3). In each case, the major product was the *exo*-2-acetoxy-3-methyl derivative having the methyl orientation unchanged from the starting material and approximately 20% of the product was the 7-methyl derivative formed by a Wagner–Meerwein shift in the initial 3-methylnorbornyl cation, *i.e.* *exo*-3 → *anti*-7 and *endo*-3 → *syn*-7. Acetate **5** may arise through a cyclic S_Ni process akin to that suggested for the formation of bornyl acetate from the bornanecarboxylic acids (3*b*). The absence of an *endo*-acetate from **3** and **4** is consistent with the findings for the 2,3,3-trimethylnorbornyl system (3*b*) and may be attributed to steric hindrance because of the *endo*-3-methyl group. In each case, the product contained small amounts of esters having the 3-methyl orientation changed from that initially present, *i.e.* **6** from **1** and **2**; **7** from **3** and **4**, behavior which would appear to require 6,2-hydride shifts. However, 5-methyl-2-norbornyl acetates were not detected and authentic samples of each of the four isomers were available for comparison of spectral data. Thus, the behavior of the presumed 3-methylnorbornyl cationic species formed by lead tetraacetate decarboxylation of **1–4** is distinctly different from that formed under solvolytic conditions, as has been elegantly characterized by Berson and co-

Can. J. Chem. Downloaded from www.nrcresearchpress.com by 210.87.254.42 on 09/05/12
For personal use only.

Can. J. Chem. Downloaded from www.nrcresearchpress.com by 210.87.254.42 on 09/05/12
For personal use only.

workers (7). The formation of significant amounts of acetates with rearranged skeletons supports the premise of cationic intermediates since a methylnorbornyl radical would not be expected to rearrange by analogy with the bornyl radical which is not subject to skeletal change at these temperatures (8). Nevertheless, the initial intermediate seems most likely to be the 3-methylnorbornyl radical (*exo*-methyl from **1** and **2**; *endo*-methyl from **3** and **4**), the formation of which readily accounts for the finding that **1** and **2** gave the same products while **3** and **4** gave a different mixture of acetates. Each of the crude products contained toluene, confirming that methyl radicals are generated, presumably in the formation of the initial intermediate. Formation of an organolead intermediate, from the initial radical, which then decomposes primarily by an S_Ni mechanism, but in part by heterolysis, could account for the observed mixtures of acetates. This interpretation is entirely analogous to that of Gream and co-workers (3*b*, *c*) for the other norbornane derivatives examined.

Experimental

Materials

The 3-methylnorbornanecarboxylic acids, prepared as described by Alder and Günzl (9), had the following melting points: **1**, mp 111–113 °C, (lit. (9) mp 114–115 °C); **2**, mp 67–69 °C (lit. (9) mp 69–70 °C); **3**, mp 36–39 °C (lit. (9) mp 38–39 °C); **4**, mp 57–59 °C (lit. (9) mp 57–58 °C).

Typical Decarboxylation Procedure

A mixture of the acid (0.308 g, 2.0 mmol) and lead tetraacetate (1.84 g, 4.1 mmol) in dry benzene (8 ml) containing pyridine (0.478 g, 6.0 mmol) was vigorously stirred at reflux temperature for the required period of time (2, 4, or 8 h). After cooling to room temperature, brine (20 ml) was added, followed by ether (20 ml), and, upon stirring, a brown precipitate formed which was removed by filtration through Celite. The Celite was washed twice with ether (2 × 10 ml). The ethereal layer was separated and washed successively with 6 *M* HCl (15 ml), 10% sodium carbonate (10 ml), brine (4 × 15 ml), and then dried over magnesium sulfate. After concentration by careful evaporation on a rotary evaporator under reduced pressure, a crude product (20–44% yield) was obtained which was analyzed by gc using a 20% Carbowax 4000 column (Chromosorb W 60/80, 6.5 mm × 3.03 m). These chromatograms were described above but it should be noted that in each case a band of very short retention time followed the benzene band; it was shown to be toluene by nmr spectroscopy. Preparative gc furnished samples of the separate bands from each product mixture. For those prepared from **1** and **2**, collection of part of the band containing **7** and **9** gave a sample enriched in **9**. Mass spectral analysis of each fraction showed the parent peak to have *m/e* of 168, confirming that each was a methylnorbornyl acetate. Proton spectra were recorded for each fraction to establish its identity. The spectrum of the third fraction from the reactions of **1** and **2** gave a measure of the ratio of **7**:**9** by integration of the carbinyl and methyl absorptions. ^{13}C spectra of **7**–**11**, were recorded to confirm the structures of **8** and **9**. Samples of each fraction were treated with $LiAlH_4$ in ether to obtain the corresponding alcohols for additional proof of the assigned structure. The ^{13}C spectra of the alcohols derived from **5**–**12** have been described (1). Authentic samples of **5**–**7**, **10**–**12**, and the corresponding alcohols were available from other work as well as samples of the 5- and 6-methyl-2-norbornyl acetates and alcohols (1, 6).

Spectra

Proton spectra were obtained with a Varian HA-100 spectrometer using $CDCl_3$ solutions containing small amounts of TMS. Highly concentrated solutions were employed to obtain high signal:noise for integration and detection of minor components. $CDCl_3$ solutions were also used to record the ^{13}C spectra of **7**–**11** with a Varian XL-100-15 system operating in the Fourier transform mode with proton decoupling. Off-resonance decoupled ^{13}C spectra were also obtained to distinguish the methyl, methylene, methine, and quaternary signals in each spectrum.

Acknowledgements

We wish to thank the National Research Council of Canada for financial support of this work. We are grateful to Inara Grikis for technical assistance, to Mrs. H. Schroeder for recording the 100 MHz proton spectra, and Robert Lazier for mass spectrometric analyses.

1. J. B. Stothers, C. T. Tan, and K. C. Teo. Can. J. Chem. This issue.
2. E. J. Corey and J. Casanova. J. Am. Chem. Soc. **85**, 165 (1963).
3. (*a*) G. E. Gream and D. Wege. Tetrahedron Lett. 503 (1967); (*b*) G. E. Gream, C. F. Pincombe, and D. Wege. Aust. J. Chem. **27**, 603 (1974); (*c*) A. L. J. Beckwith, R. T. Cross, and G. E. Gream. Aust. J. Chem. **27**, 1693 (1974).
4. L. D. Hatfield and W. D. Huntsman. J. Org. Chem. **32**, 844 (1967).
5. J. B. Stothers. Carbon-13 NMR spectroscopy. Academic Press, New York. 1972; N. K. Wilson and J. B. Stothers. *In* Topics in stereochemistry. Vol. 8. *Edited by* E. L. Eliel and N. L. Allinger. Wiley–Interscience, New York. 1974. Chap. 1.
6. C. T. Tan. Ph.D. Thesis, University of Western Ontario, London, Ontario. 1976.
7. J. A. Berson, A. W. McRowe, and R. G. Bergman. J. Am. Chem. Soc. **89**, 2573 (1967); J. A. Berson, R. G. Bergman, J. H. Hammons, and A. W. McRowe. J. Am. Chem. Soc. **89**, 2581 (1967); J. A. Berson, J. H. Hammons, A. W. McRowe, R. G. Bergman, A. Remanick, and D. Houston. J. Am. Chem. Soc. **89**, 2590 (1967).
8. J. A. Berson and C. J. Olsen. J. Am. Chem. Soc. **84**, 3178 (1962).
9. K. Alder and W. Günzl. Chem. Ber. **93**, 809 (1960).

Empirical equations for predicting ^{13}C chemical shifts in nuclear magnetic resonance spectra of certain types of amino acids[1]

JAMES C. MACDONALD, GREGORY G. BISHOP, AND MYTOSK MAZUREK
National Research Council of Canada, Prairie Regional Laboratory, Saskatoon, Saskatchewan S7N 0W9

Received October 22, 1975

JAMES C. MACDONALD, GREGORY G. BISHOP, and MYTOSK MAZUREK. Can. J. Chem. **54**, 1226 (1976).

^{13}C chemical shift data were obtained for amino acids related to glycine which had the following types of substituents on C-2: alkyl, branched chain alkyl, ω-amino alkyl, and ω-guanido alkyl. Such data were obtained for aqueous solutions at a p*H* between the p*K* values of the carboxyl and 2-amino groups (zwitterion form). The data were subjected to graphical and statistical analysis to obtain separate predictive equations for C-1, C-2, and other carbon atoms. Data for the change in chemical shifts on titration with acid were also obtained to aid in ^{13}C assignments and to elucidate configuration.

JAMES C. MACDONALD, GREGORY G. BISHOP et MYTOSK MAZUREK. Can. J. Chem. **54**, 1226 (1976).

On a obtenu des données concernant les déplacements chimiques du ^{13}C pour des acides aminés reliés à la glycine portant les substituants suivants sur le C-2: des groupes alkyles et alkyles ramifiés, des groupes ω-aminoalkyles et des groupes ω-guanidoalkyles. On a obtenu ces données pour des solutions aqueuses à des p*H* entre les valeurs de p*K* des groupes carboxylique et amino-2 (sous la forme de zwitterion). On a soumis les données à une analyse graphique et statistique afin d'obtenir des équations distinctes pour prédire les déplacements pour les C-1, C-2 et des autres atomes de carbone. On a aussi obtenu des données concernant les changements dans les déplacements chimiques lors de la titration par de l'acide; ces données ont été obtenues afin d'aider à l'attribution des déplacements de ^{13}C et pour élucider les configurations.
[Traduit par le journal]

Introduction

The ^{13}C spectra of amino acids are useful not only for studying their properties (1–3), but also as a starting point for the structural determination of compounds derived from amino acids, such as peptides and proteins (4–7), and even complex pyrazinones such as arglecin, deoxyaspergillic acid, and flavacol (8). One method used to assign ^{13}C spectra of amino acids was that using additive parameter terms (9) which, however, were derived from studies on the chemical shifts of entirely different compounds. Hagen and Roberts (10) have noted that the validity of comparing ^{13}C chemical shifts of carboxylic acids in water to shifts for substituted hydrocarbons is questionable because of the very large difference in environment in which the shifts are measured, and the same criticism could apply equally well to amino acids. Indeed, the predicted shifts obtained by Horsley and Sternlicht (9) were not sufficiently accurate to prevent the incorrect assignment of C-3 and C-5 of lysine (later corrected by Christl and Roberts (5)), and they differed from the observed values for alkyl amino acids by as much as 4.6 ppm.

Grant and Paul (11) investigated the ^{13}C chemical shifts of linear and branched alkanes, starting with graphical evaluations and continuing with computation techniques, to obtain predictive shift parameters for these compounds. The purpose of the present work was to follow this systematic method, using ^{13}C chemical shifts for amino acids, to obtain predictive parameters better applicable to linear and branched alkyl amino acids and, if possible, to ω-amino and ω-guanido amino acids as well.

Materials and Methods

^{13}C spectra were obtained at 25.2 MHz with a Varian XLFT-100 nmr spectrometer, using the pulsed Fourier transform mode and an acquisition time of 0.8 s (resolution 1.25 Hz or 0.05 ppm per spectral point). Maximum decoupling power with noise modulation was applied in the region of 100 MHz to remove ^{13}C–H coupling. A stream of air at room temperature was used to cool the sample contained in a 12 mm diameter sample tube. In some cases the air was heated with a Varian variable

[1]NRCC No. 15143.

Can. J. Chem. Downloaded from www.nrcresearchpress.com by 210.87.254.6 on 09/05/12
For personal use only.

Can. J. Chem. Downloaded from www.nrcresearchpress.com by 210.87.254.6 on 09/05/12
For personal use only.

temperature controller to obtain higher sample temperatures. Sample temperatures were measured immediately after obtaining spectra, with decoupling power still applied, by inserting a thermometer prewarmed to the approximate sample temperature into the solution still in place in the probe.

The amino acids were commercial samples, except for DL-2-aminoheptanoic acid, which was prepared as described by Greenstein and Winitz (12). The solvent was H_2O containing 5% D_2O for the heteronuclear lock signal and a small amount of dioxane as an internal reference. ^{13}C chemical shifts were expressed as δ referred to δ TMS = 0 with this reference (δ dioxane − δ TMS = 67.40). In general, the amino acids as supplied were dissolved at 1 *M* concentration or the limit of their solubility in the above solvent and gave a p*H* approximately halfway between the p*K* values of their carboxyl and 2-amino groups (12); if necessary, the p*H* was so adjusted. In the present work, this was defined as the zwitterion form, and the form obtained on acid titration as the cation form; the positive charge on the ω-amino and ω-guanido groups was disregarded in this definition.

To convert the zwitterion to the cation, the amino acid solutions were adjusted with aqueous HCl to a p*H* one unit less than the p*K* of the carboxyl group, or to p*H* 1.0, whichever was less. Conversion to the cation form, therefore, was over 90% for data obtained here.

Calculation Method

The empirical predictive equation was of the type: Y = constant + $X_1P_1 + X_2P_2 + X_3P_3 + \ldots$ etc., where Y was the chemical shift of a certain carbon atom, X_n the number of times a specific structural parameter (see examples below) was applied to this carbon atom, and P_n the value of this parameter. For each case entered in the computation, the variables Y, X_1, X_2, X_3, etc. were known, and the constant and P values were unknown. Calculations were done on groups of cases with an IBM 370 computer and the SPSS multiple linear regression program (13) to obtain the constant and parameter values which were the least-squares fit of Y with the X variables. In order to obtain meaningful results, the program had to be run and the results interpreted in a systematic way. Parameters of the most obvious importance were those concerned with substituents α, β, and γ to the carbon atoms being considered. Their X variables were entered stepwise in the regression first, followed, in the second stage, by stepwise entering of the X variables of the parameters of less obvious importance, such as those concerned with substituents δ to the carbon atom, the type of bonds, and the type of configuration. In our treatment, $2^o(2^o)$, a bond between two secondary carbon atoms, was considered as the 'normal' type bond, and a variable for it was not entered in the regression, although X variables for all other bond types (11) were. The most significant statistical fit was taken as the stage when the standard error of estimate of the regression equation reached a minimum. At this stage, the statistical F values of individual parameters were tested for significance at the 0.05 level (13) and any not significant noted. The regression analysis was repeated with X variables for significant parameters only, to obtain the final statistics and a table of residuals; the latter are observed chemical shift (Y) less chemical shift (Y') predicted by the equation.

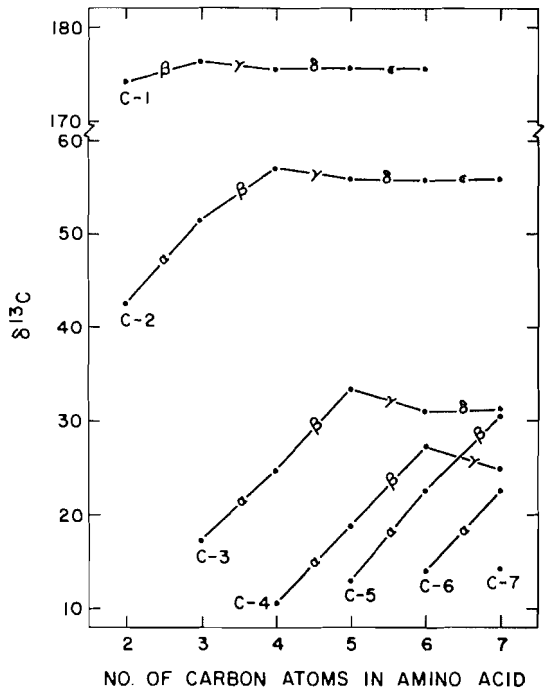

FIG. 1. ^{13}C chemical shifts for C-1 to C-7 of linear alkyl amino acids. The greek letters refer to '*C*' parameters that would be responsible for the change in chemical shift.

Two types of statistics can be obtained from the regression analysis. The F value, multiple correlation coefficient squared (R^2), and standard error of estimate (se) indicate essentially how well the data fit the equation, while the standard deviation of residuals (sd) and range of residuals (rr) indicate how well the equation predicts chemical shifts.

Results and Discussion

Carbons of amino acids were numbered from the carboxyl end (Fig. 1, Tables 1 and 2). Substituents on a branch of the carbon chain were numbered the same way, but given a primed number. For example, the 3-methyl substituent of isoleucine and *allo*-isoleucine was designated as C-4'. Where two methyl groups were in the terminal position (valine, leucine), the one with the lower chemical shift was arbitrarily designated by a primed number.

Solvent, Concentration, and Heating Effects

Other workers (2, 5, 7) have also used H_2O as a solvent for obtaining ^{13}C spectra of amino acids and peptides, and in our experience this solvent had the advantage that stronger signals were obtained for carboxyl and guanido carbon

TABLE 1. Increase in ^{13}C chemical shift in ppm on heating*

Amino acid	Form	Temperature (°C) Lower	Upper	C-1	C-2	C-3	C-4	C-5	Other	
DL-Norvaline	Z	33	92		0.29	0.05	0.04	−0.15		
	C	37	97	−0.53	0.15	0.01	−0.12	−0.19		
L-Valine	Z	32	92		0.26	−0.18	−0.08*B*		C-4′	0.07*A*
	C	37	90	−0.45	0.19	−0.04	−0.13*B*			0.14*A*
L-Leucine	Z	32	92		0.36	0.03	0.07	−0.14*B*	C-5′	0.15*A*
	C	37	89		0.27	0.10	0.06	−0.15*B*		0.15*A*
L-Isoleucine	Z	32	94		0.21	−0.09	0.03*A*	−0.20	C-4′	−0.07*B*
	C	37	97	−0.55	0.14	0.00	0.05*A*	−0.23		−0.15*B*
D-*allo*-Isoleucine	Z	32	93	−0.80	0.48	−0.11	−0.03*B*	−0.17	C-4′	−0.01*A*
	C	36	95	−0.60	0.37	0.07	−0.15*B*	−0.23		0.09*A*
DL-3-Aminoalanine	Z	39	95	−0.47	0.00	0.14				
L-Lysine	Z	35	94	−0.60	0.28	−0.01	0.13	−0.11	C-6	0.18

*Z and C refer to zwitterion and cation forms, respectively. *A* and *B* refer to configuration (see text).

atoms than when D_2O was used as the solvent. Even so, the signal for the carboxyl carbon could not be detected in some spectra. Where comparisons were possible, the chemical shifts obtained here were within 0.6 ppm of those obtained with D_2O as the solvent by Horsley and Sternlicht (9), as recalculated by Stothers (14).

For comparison of changes in chemical shifts on acid titration it was thought best to obtain spectra at the same concentration used for the zwitterion form, even though the amino acid was more soluble in its cation form. This precaution probably was not necessary because there was little difference between spectra of the cation form of 2-aminoheptanoic acid run at two concentrations (0.028 *M*, as used for the zwitterion form, *vs.* 0.5 *M*, maximum solubility of the cation form, maximum discrepancy 0.1 ppm), or between spectra of the cation form of L-leucine run at two concentrations (0.18 *M*, as used for the zwitterion form, *vs.* 1.0 *M*, maximum discrepancy 0.2 ppm). This also suggests that shifts of the zwitterion form of amino acids measured at concentrations below 1.0 *M* because of their low solubility were probably similar to what might be expected if 1.0 *M* solutions could be used.

The use of a high intensity radio-frequency magnetic field for proton decoupling can give rise to appreciable heating effects which would remain undetected unless sample temperatures are measured. This heating effect was most marked for solutions of high ionic strength, and was apparently owing not to proton absorption of energy, but to increased motion of ions caused by the oscillating magnetic field, which motion caused an increase in temperature. For instance, the temperature attained by 5 *M* NaCl in either H_2O or D_2O under the standard cooling conditions and application of full decoupling power was 52–53 °C, as compared to 32–33 °C for H_2O or D_2O alone. Our original intent to measure titration shifts with 1 *M* to 2 *M* excess HCl as the solvent was abandoned because of such heating effects. For data here, done at more moderate p*H* values, the temperatures under standard cooling conditions were 32–33 °C for alkyl amino acids in the zwitterion form and 36–40 °C for the same in the cation form. For the hydrochlorides of ω-amino or ω-guanido amino acids, the temperatures were 35–42 °C for the zwitterion form, and 42–48 °C for the cation form. With linear temperature shifts of the maximum magnitude shown in Table 1, a 10 °C rise in temperature might give a change in chemical shift of approximately −0.13 and +0.08 ppm for C-1 and C-2, respectively, and less than this for other carbon atoms.

Effects of the magnitude mentioned above with respect to either concentration or temperature were not considered serious in the present work, although they might become important in refined studies on the conformation of amino acids.

Can. J. Chem. Downloaded from www.nrcresearchpress.com by 210.87.254.6 on 09/05/12
For personal use only.

TABLE 2. ^{13}C chemical shifts for the zwitterion form of amino acids and change, Δ, for titration with HCl*

Amino acid	C-1	C-2	C-3	C-4	C-5	C-6	C-7	Other
Glycine	173.11	42.55						
Δ	2.46	1.27						
L-Alanine	176.42	51.54	17.20					
Δ	2.92	1.64	0.82					
DL-Butyrine	175.49	56.90	24.71	9.54				
Δ	2.58	1.75	0.47	0.07				
DL-Norvaline	175.73	55.70	33.53	18.79	13.93			
Δ	2.59	1.82	0.75	0.16	0.16			
L-Norleucine	175.63	55.84	31.05	27.28	22.54	13.91		
Δ	2.43	1.82	0.65	0.20	0.13	0.08		
DL-2-Aminoheptanoic acid		55.94	31.34	24.79	31.47	22.51	14.13	
Δ		1.89	0.71	0.25	0.22	0.14	0.09	
L-Valine	174.88	61.40	30.04	18.93*B*				C-4′ 17.59*A*
Δ	2.47	1.94	0.05	0.60*B*				−0.23*A*
L-Leucine	176.17	54.50	40.79	25.08	22.95*B*			C-5′ 21.86*A*
Δ	2.62	1.93	0.92	0.20	0.39*B*			−0.06*A*
L-Isoleucine	174.78	60.60	36.84	25.36*A*	12.05			C-4′ 15.64*B*
Δ	2.42	2.18	0.09	−0.28*A*	0.17			0.52*B*
D-*allo*-Isoleucine	175.24	59.53	36.51	26.36*B*	11.96			C-4′ 14.24*A*
Δ	2.40	1.55	0.18	0.47*B*	0.18			−0.10*A*
DL-3-Aminoalanine	171.74	51.48	40.02					
Δ	2.16	0.66	0.54					
DL-4-Aminobutyrine	173.89	53.54	29.15	37.77				
Δ	2.44	1.96	0.53	0.52				
L-Ornithine	174.74	55.15	28.40	23.81	40.07			
Δ	2.53	1.69	0.58	0.07	0.05			
L-Lysine	175.19	55.51	30.85	22.37	27.38	40.24		
Δ	2.49	1.70	0.62	0.06	0.14	−0.07		
L-Arginine	174.99	55.35	28.56	24.89	41.56			guanido-C 157.58
Δ	2.49	1.69	0.64	0.14	0.10			0.03
L-Homarginine	175.32	55.68	30.98	22.54	28.50	41.83		guanido-C 157.55
Δ	2.58	1.78	0.68	0.17	0.16	0.07		0.05

*A positive Δ value represents an upfield shift (to lesser $\delta^{13}C$) in ppm on titration with acid. *A* and *B* represent relative configuration (see text).

Parameter Variables

Each term in the predictive equations was the product of an X variable and a parameter constant. The definition of the parameter is obvious from the definition of the variable, and only variables found significant are defined below.

Term X_1V. X_1 was a continuous variable, whose value was a pK for the carboxyl group, evaluated by counting the carbon atoms separating the carboxyl and amino groups, and applying simple empirical formulae (12). It had the value 4.83 for carboxylic acids, 2.33 for alkyl amino acids, and 1.40, 1.82, 2.03, or 2.15, for the series of ω-NH_3^+ amino acids from 3-aminoalanine to lysine (Table 2), respectively.

Terms X_2C_α, X_3C_β, X_4C_γ, X_5C_δ. These were integer variables which represented the number of carbon atoms in the α, β, γ, or δ position, respectively, from the carbon atom being considered, excluding the carboxyl carbon from this count, since its total effect, combined with that of the 2-amino group, was included in 'Z' (zwitterion) parameters.

Term $X_6$2°(3°). X_6 had a value other than zero only if the carbon atom being considered was secondary, and had at least one tertiary carbon atom bonded directly to it. In such a

Can. J. Chem. Downloaded from www.nrcresearchpress.com by 210.87.254.6 on 09/05/12
For personal use only.

TABLE 3. Parameter constants

Applicable to	Parameter subscript α	β	γ	δ	Other corrections $2^o(3^o)$	$3^o(2^o)$	$3^o(3^o)$	A	V
C-1					n.a.	n.a.	n.a.	n.a.	3.46
C parameters	n.a.	3.31	−0.80	0.21					
N parameters	n.a.	0	−1.43*	0					
C-2					n.a.	0	0	n.a.	n.a.
C parameters	9.05	5.00	−1.02	0					
N parameters	n.a.	0	−3.06*	0					
C-3 to C-7					−1.07	−2.18	−4.38	−1.19	n.a.
C parameters	8.70	8.70	−2.49	0					
N parameters	26.07	4.73	−5.00	0					
G parameters	27.61	5.99	−4.83	0					
Z parameters	n.a.	9.22	−6.64	0					

*The values for these parameters were based on one case; n.a. means not applicable to, or not available from, the structural comparisons made; a figure of zero indicates that the parameter was not statistically significant.

case, X_6 had a value equal to the number of such tertiary carbon atoms (11). C-2 of most of the amino acids in Table 2 was considered to be a tertiary carbon.

Terms $X_7 3^o(2^o)$, $X_8 3^o(3^o)$. These variables had values other than zero only if the carbon atom being considered was tertiary. X_7 then equalled the number of secondary carbon atoms bonded to the tertiary carbon being considered, and X_8 equalled the number of tertiary carbon atoms bonded to it.

All the following variables were considered as logical variables, having the value 1.0 if the description was true, and 0 if it was false. Terms X_9N_α, $X_{10}N_\beta$, $X_{11}N_\gamma$: the carbon atom being considered was α, β, or γ, respectively, to an ω-NH_3^+ substituent. Terms $X_{12}G_\alpha$, $X_{13}G_\beta$, $X_{14}G_\gamma$: the carbon atom was α, β, or γ, respectively, to an ω-guanido$^+$ substituent. Terms $X_{15}Z_\beta$, $X_{16}Z_\gamma$: the carbon atom was β or γ, respectively, to the carboxyl and 2-amino groups of the amino acid. Term $X_{17}A$: the carbon atom had the 'A' configuration (see text).

In regression analyses, computation of parameter constants was accompanied by computation of their 'standard errors'. In our experience with data of the type above where most of the variables were either discontinuous (integer, from 0 to 3) or logical (0 or 1), these standard errors were of no value in indicating the probable errors between predicted and observed chemical shifts, and therefore have not been supplied in Table 3. The agreement that may be expected for predictions is adequately represented by other statistics given.

Predictive Equation for the C-1 Carboxylate Ion of Amino Acids and Carboxylic Acids

Comparison of data in Fig. 1 indicated that the C_β and C_γ parameter constants for C-1 were much less than those for other carbon atoms of the amino acids. A similar comparison of literature values (14) for carboxylate ions of monocarboxylic acids revealed that C_β and C_γ parameter constants for these were similar to those for the alkyl amino acids. Attempts to fit the ω-NH_3^+-substituted amino acids into the framework of predictions suggested that the major differences between chemical shifts for carboxylate ions in general might be a linear function of their pK, and a calculated pK (12) was used so that predictions for other similar compounds would not require experimental data. A regression analysis on ^{13}C chemical shifts for C-1 of acetate to valerate (14), and glycine to lysine (Table 2) gave the best equation

$$Y' = 165.01 + X_1V + X_3C_\beta + X_4C_\gamma + X_5C_\delta + X_{11}N_\gamma$$

and the values for the parameter constants are given in Table 3. *Statistics*: 17 cases, $F = 3032$, $R^2 = 0.9993$, se = 0.13, sd = 0.11, rr = −0.23 (isoleucine) to +0.23 (*allo*-isoleucine). The equation constant, 165.01, would include a X_2C_α term, but since $X_2 = 1$ for all cases in the regres-

Can. J. Chem. Downloaded from www.nrcresearchpress.com by 210.87.254.6 on 09/05/12
For personal use only.

Can. J. Chem. Downloaded from www.nrcresearchpress.com by 210.87.254.6 on 09/05/12
For personal use only.

sion analysis, the value for C_α could not be determined statistically.

This equation could be used with C-1 of arginine and homoarginine by assuming that pK values are the same as for ornithine and lysine, respectively, and residuals for such a prediction would be 0.22 and 0.14 ppm, respectively. The equation could also be used with C-1 of β-alanine, in which $X_1 = 3.58, X_3 = X_{11} = 1, X_4 = X_5 = 0$. The calculated shift was 179.28; the shift we found experimentally (pH 6.2) was 178.94; the residual was -0.34. This shows that the above equation might be expected to give good results also with ω-amino carboxylic acids.

Predictive Equation for C-2 of Amino Acids

Comparison of the data in Fig. 1 indicated that the C_β and C_γ parameters for C-2 were about 60% of those for C-3, C-4, etc. Linear regression analysis of data for C-2 of amino acids from glycine to homoarginine (Table 2) gave a predictive equation ($F = 531$, se = 0.36) based on variables X_2 to X_4, and X_{11} being significant. The predictive equation was improved by adding a corrective parameter, '*allo*', applicable only to C-2 associated with an *allo* configuration (*i.e.* *allo*-isoleucine) about C-2 and C-3. This parameter was significant at the 0.005 level (F test) whereas bond parameters, or a corresponding 'iso' corrective parameter, were not significant at the 0.05 level. Apparently the effects of configuration and/or conformation about C-2 in the *allo* configuration were sufficiently different from those for other compounds as to require a special corrective parameter, and this parameter may be useful in assigning C-2 in spectra of other 2-amino-3-methyl carboxylic acids of the *allo* configuration. The best equation was

$$Y' = 42.55 + X_2C_\alpha + X_3C_\beta + X_4C_\gamma + X_{11}N_\gamma + \text{'}allo\text{'}$$

The *allo* parameter term was applied only to C-2 of *allo*-isoleucine and had the value -1.05; values for other parameter constants are given in Table 3. *Statistics*: 16 cases, $F = 910$, $R^2 = 0.9978$, se = 0.25, sd = 0.20, rr = -0.43 (ornithine) to $+0.36$ (2-aminoheptanoic acid).

The equation constant, 42.55, would include a Z_α parameter, which in turn would be composed of chemical shift contributions of COO^- and 2-NH_3^+ and the type of bonds to these substituents, but this parameter cannot be determined statistically from the data.

Predictive Equation for C-3 to C-7 of Amino Acids

The C parameter values for these carbons appeared to be similar (Fig. 1), and variables for substituent and bond parameters alone gave moderately good predictive equations for some cases. However, some carbon atoms with exactly the same substituent and bond parameters had different chemical shifts, and are structurally diastereotopic (15) (*eg.* C-4′ of isoleucine and *allo*-isoleucine, or C-4 and C-4′ of valine). If the structures of D- and L-isoleucine, and D- and L-*allo*-isoleucine, whose relative and absolute configurations are known, are written in the Newman projection (16) with the H atoms on C-2 and C-3 eclipsed, then the carbon atom eclipsed by the carboxyl can be designated as having '*A*' configuration, and that eclipsed by the amino group as having '*B*' configuration (3). The carbon atoms designated by *A* and *B* had changes of chemical shift on titration that can be related to those of the diastereotopic methyl groups of valine (3) or leucine. The configuration of leucine can be considered with respect to a Newman projection through the C-2 to C-4 axis, and thus can be related to that of valine.

For the same group in diastereoisomers (isoleucine *vs.* *allo*-isoleucine) or the diastereotopic methyl groups in the same compound (valine or leucine), the carbon atom designated by *B* had a higher chemical shift than that designated by *A* (Table 2). On acid titration, the carbon designated by *B* had a positive Δ value, while that of *A* had a negative or approximately zero Δ value (Table 2). In our regression analysis of alkyl amino acids, the term for the *A* parameter was significant, that for the *B* parameter was not, and the predictive equation had an $F = 3326$, se = 0.31.

In the next stage of regression analysis, data for 2,ω-diamino acids were included with those for alkyl amino acids, along with extra variables for N parameters. The predictive equation was poorer, with $F = 746$, se = 0.58. The largest residuals were those for the ω-carbons of 3-aminoalanine (residual -1.73) and 4-aminobutyrine ($+1.72$). It seemed probable that the close proximity of the ω-amino group and the

Can. J. Chem. Downloaded from www.nrcresearchpress.com by 210.87.254.6 on 09/05/12
For personal use only.

zwitterion caused deviations in substituent parameter values, so these two cases were deleted from the regression analysis, to give a predictive equation with $F = 2259$, se = 0.31.

With deletion of the two cases just mentioned, the predictive equation obtained from data for amino acids from alanine to homoarginine (Table 2) was

$$Y' = -0.84 + \text{sum of terms containing variables } X_2 \text{ to } X_4, X_6 \text{ to } X_{17}$$

The parameter constants are given in Table 3. *Statistics*: 45 cases, $F = 2379$, $R^2 = 0.9992$, se = 0.30, sd = 0.24, rr = −0.71 (C-4′ of *allo*-isoleucine) to +0.45 (C-5 of isoleucine).

The two cases omitted from the above regression could be predicted within 0.15 ppm with the following assumption. Where a N_α and a Z parameter term were both non zero for the same carbon atom, the variable for the Z parameter should be 0.76 instead of 1.0. This attenuation of Z_β and Z_γ parameter terms for cases in which polar substituents are close together parallels effects observed with C-2, which also has polar substituents close together and shows attenuation of parameter constants (C_β, C_γ, N_β, N_γ, Table 3) as compared to those for C-3 to C-7. The substituent parameters obtained for C-3 to C-7 for amino acids in water were, in general, less in absolute value than those for neat alkanes, as obtained by Grant and Paul (11) and referred to the TMS scale by Stothers (14). This also supports the thesis that high polarity can cause an attenuation of substituent parameter constants. It would seem likely that an adequate theory to explain chemical shifts would have to include competitive effects, as well as additive ones.

Our regression analysis of the data of Grant and Paul (11) for alkanes gave the same predictive equation as theirs. *Statistics*: 53 cases, $F = 3606$, $R^2 = 0.9992$, se = 0.30, sd = 0.26, rr = −0.48 (C-4 of 2-methylpentane) to +0.72 (C-3a of 3-methylpentane). The predictive equations for various carbons of amino acids had statistics (present work) that compared favourably with these.

Conformation with Regard to Temperature and Titration Effects

Theoretical explanations of the branching parameters such as 3°(3°) were not investigated by Grant and Paul (11), but these parameters, together with the '*A*' parameter, would seem most likely to be concerned with the shape of the molecule. Information on conformation of the branched chain alkyl amino acids (*e.g.* rotamer populations) would be of great theoretical interest, and preferably would include not only the relative mole fraction of the three most likely rotamers, but also the chemical shift contribution per unit mole fraction of each with respect to various associated carbon atoms, as explained by Gutowsky and co-workers (17, 18). In favorable cases (18), this type of information has been obtained from the temperature dependence of chemical shifts, with the essential prerequisite that the change in chemical shifts with temperature be large compared with the experimental accuracy. Much of the data in Table 1 (resolution 0.05 ppm/spectral point) did not meet this prerequisite, because changes even for a 50–60 °C temperature rise were relatively small. A second essential prerequisite was that the temperature dependence should result only from changes in the equilibrium proportions of the rotamers, and not be modified by molecular association or solvation effects (18). Considering the nature of amino acids and the solvent used, it seems unlikely that the latter prerequisite would be met. If a temperature dependent solvation effect existed, the chemical shift changes on heating would be greater for carbons bearing polar substituents. This could explain the greater changes obtained for C-1 and C-2 as compared to other carbon atoms (Table 1).

The change of chemical shifts on acid titration for linear alkyl amino acids, or linear ω-substituted amino acids from ornithine to homoarginine (Table 2) were quite regular, with Δ values in the order C-1 (2.4 to 2.9) > C-2 (1.3 to 1.8) > C-3 (0.5 to 0.8) > other carbons (−0.1 to 0.3). In such amino acids a plot of chemical shift *vs.* p*H* could distinguish between C-3 and other carbons, and was used here to confirm assignments for C-3 *vs.* C-5 for 2-aminoheptanoic acid and homoarginine. The above relationship was not applicable to 3-aminoalanine and 4-aminobutyrine, in which the polar substituents are relatively close together, or to branched chain alkyl amino acids. The typically different titration shifts for certain carbon atoms of branched chain alkyl amino acids gives some insight as to their relative configuration (ref. 3, and see

Can. J. Chem. Downloaded from www.nrcresearchpress.com by 210.87.254.6 on 09/05/12
For personal use only.

above). Whether titration shifts could give information on conformation as well is still in reasonable doubt, since interpretations so far (1) did not take into account the essential differences in configuration of the diastereotopic carbon atoms.

Conclusion

The 'state of the art' in the prediction of chemical shifts of amino acids is such that molecular orbital calculations do not satisfactorily account for ^{13}C shift changes on titration (2). Until such time that theory can satisfactorily account for such changes, can be extended to predict chemical shifts as well as these changes, and can be easily applied, empirical methods of assigning chemical shifts by addition of parameter terms will be widely used. The present work emphasizes that parameter constants for carbon atoms attached to polar substituents may be different from those for less polar carbon atoms. The ^{13}C shifts for the latter carbon atoms in amino acids are the more difficult to assign, and the equation for prediction of these shifts should be valuable.

Sample Calculations

The pertinent predictive equations are in the text above, and the parameter constants in Table 3. The parameter variables are determined by inspecting the structure of the amino acid.

Calculation for C-2 of 4-Aminobutyrine

This carbon atom has one carbon α to it, one carbon β to it, and itself is γ to the ω-amino group, so $X_2 = X_3 = X_{11} = 1$, $X_4 = 0$. The equation for C-2 becomes

$$\begin{aligned} Y' &= 42.55 + C_\alpha + C_\beta + N_\gamma \\ &= 42.55 + 9.05 + 5.00 - 3.06 \\ &= 53.54 \end{aligned}$$

Calculation for the Methylene Carbon (C-4) of Isoleucine

This carbon atom has two carbon atoms α to it, two carbon atoms β to it, and itself is γ to the zwitterion carboxyl. It is a secondary carbon atom that has one tertiary carbon atom attached to it, and it has the '*A*' configuration. Accordingly, $X_2 = X_3 = 2$, $X_6 = X_{16} = X_{17} = 1$, and other X variables pertinent to the predictive equation for C-3 to C-7 are 0, so the equation becomes

$$\begin{aligned} Y' &= -0.84 + 2C_\alpha + 2C_\beta + Z_\gamma + 2^\circ(3^\circ) + A \\ &= -0.84 + 2(8.70) + 2(8.70) - 6.64 - 1.07 \\ &\quad - 1.19 \\ &= 25.06 \end{aligned}$$

Calculation for C-4 of Ornithine

This carbon atom has two carbon atoms α to it, and one carbon atom β to it. It is γ to the zwitterion carboxyl and β to the ω-amino group. Accordingly, $X_2 = 2$, $X_3 = X_{16} = X_{10} = 1$, and omitting zero value terms, the appropriate equation is

$$\begin{aligned} Y' &= -0.84 + 2C_\alpha + C_\beta + Z_\gamma + N_\beta \\ &= -0.84 + 2(8.70) + 8.70 - 6.64 + 4.73 \\ &= 23.35 \end{aligned}$$

1. S. Tran-Dinh, S. Fermandjian, E. Sala, R. Mermet-Bouvier, M. Cohen, and P. Fromageot. J. Am. Chem. Soc. **96**, 1484 (1974).
2. A. R. Quirt, J. R. Lyerla, Jr., I. R. Peat, J. S. Cohen, W. F. Reynolds, and M. H. Freedman. J. Am. Chem. Soc. **96**, 570 (1974).
3. J. G. Batchelor and J. Feeney. J. Chem. Soc. Chem. Commun. 503 (1975).
4. W. Voelter, G. Jung, E. Breitmaier, and E. Bayer. Z. Naturforsch. **26**, 213 (1971).
5. M. Christl and J. D. Roberts. J. Am. Chem. Soc. **94**, 4565 (1972).
6. C. Grathwohl and K. Wuthrich. J. Magn. Reson. **13**, 217 (1974).
7. J. R. Lyerla, Jr. and M. H. Freedman. J. Biol. Chem. **247**, 8183 (1972).
8. J. C. MacDonald, G. G. Bishop, and M. Mazurek. Tetrahedron, In press.
9. W. J. Horsley, H. Sternlicht, and J. S. Cohen. J. Am. Chem. Soc. **92**, 680 (1970).
10. R. Hagen and J. D. Roberts. J. Am. Chem. Soc. **91**, 4504 (1969).
11. D. M. Grant and E. G. Paul. J. Am. Chem. Soc. **86**, 2984 (1964).
12. J. P. Greenstein and M. Winitz. Chemistry of the amino acids. John Wiley and Sons, New York. 1961. pp. 486, 501, 2383.
13. N. H. Nie, C. H. Hull, J. G. Jenkins, K. Steinbrenner, and D. H. Bent. SPSS Statistical package for the social sciences. 2nd. ed. McGraw-Hill, New York. 1975. p. 320.
14. J. B. Stothers. Carbon-13 NMR spectroscopy. Academic Press, New York. 1972. pp. 58, 295, 479.
15. A. Ault. J. Chem. Educ. **51**, 729 (1974).
16. IUPAC tentative rules for the nomenclature of organic chemistry. Section E. Fundamental stereochemistry. J. Org. Chem. **35**, 2858 (1970).
17. H. S. Gutowsky. J. Chem. Phys. **37**, 2196 (1962).
18. H. S. Gutowsky, G. G. Belford, and P. E. McMahon. J. Chem. Phys. **36**, 3353 (1962).

Reactions of trifluoromethyl radicals with iodine and nitric oxide

J. C. AMPHLETT AND L. J. MACAULEY
Chemistry Department, Royal Military College of Canada, Kingston, Ontario K7L 2W3

Received September 30, 1974[1]

J. C. AMPHLETT and L. J. MACAULEY. Can. J. Chem. **54**, 1234 (1976).

The reactions 2 and 3 have been studied by competitive methods. Use of previous Arrhenius

[2] $$CF_3 + I_2 \rightarrow CF_3I + I$$

[3] $$CF_3 + NO + M(?) \rightarrow CF_3NO$$

parameters for reaction 2 leads to $k_3 = 1.3 \times 10^{10} \exp -[(700 \pm 100J)/RT]$. Arrhenius parameters of reactions 2 and 3 are compared with those for reactions of other radicals with I_2 and NO.

J. C. AMPHLETT et L. J. MACAULEY. Can. J. Chem. **54**, 1234 (1976).

On a étudié, par des méthodes compétitives, les réactions 2 et 3. Utilisant les paramètres

[2] $$CF_3 + I_2 \rightarrow CF_3I + I$$

[3] $$CF_3 + NO + M(?) \rightarrow CF_3NO$$

d'Arrhénius obtenus antérieurement pour la réaction 2, on peut établir que $k_3 = 1.3 \times 10^{10} \exp -[(700 \pm 100J)/RT]$. On compare les paramètres d'Arrhénius des réactions 2 et 3 avec ceux d'autres réactions de radicaux avec I_2 et NO.

[Traduit par le journal]

Introduction

Previous papers (1–3) have dealt with the determination by competitive methods of Arrhenius parameters for the reactions

$$CF_3 + X_2 \rightarrow CF_3X + X$$

$$CF_3 + HX \rightarrow CF_3H + X$$

where $X_2 = Cl_2$, Br_2, or I_2 and HX = HCl, HBr, or HI. This work has now been extended to include the reactions of CF_3 radicals with I_2 and NO.

Experimental

Materials

Hexafluoroacetone, HFA, was obtained from Peninsular Chemical Research. Analar grade I_2 was purified by vacuum sublimation. NO (Matheson gas products) was passed through 90% H_2SO_4, 50% aqueous KOH, silica gel, and a trap at −80 °C; it was collected in a trap cooled in liquid air and was further purified by several distillations from liquid air to liquid nitrogen. CF_3NO and CF_3I were obtained from Peninsular Chemical Research. Each compound was given several bulb-to-bulb distillations *in vacuo* and the middle cut retained for use. All compounds were spectroscopically pure (infrared and gsc).

Apparatus and Procedure

A conventional high vacuum system was used. The quartz reaction vessel was a cylinder of diameter 5 cm, length 10 cm, located in an oven with temperature held constant to ±0.5 °C. Ace Glass greaseless stopcocks were used in the region of the reaction vessel and I_2 store. The line in this region was heated when I_2 was used. Pressures were measured on a Texas Instruments precision pressure gauge. The light source was a medium pressure 220 W mercury lamp (Oriel Optics Corp.) fitted with a *f*/1.5 condensing lens for parallel light. The filter employed was an aqueous solution containing $NiCl_2$ (89 g/l) and K_2CrO_4 (0.25 g/l) in conjunction with two glass filters. This filter gave a narrow band peaking at 312 nm with 16% transmission. Approximately 20 mmol of HFA were photolysed in the presence of I_2 and NO.

Analysis

Products of the photolysis of HFA with I_2 and NO were first passed through a trap at 0 °C to remove I_2 and then frozen into two Ward stills cooled in liquid air. The total noncondensible gas consisting of NO and CO was measured in a gas burette and was then combusted on CuO at 320 °C. The CO_2 formed was frozen in liquid air and the residual unchanged NO was measured and discarded. The CO_2 was then measured and the sum of the CO_2 + NO was always equal, within experimental error, to the combined CO + NO before combustion. The Ward stills were next warmed to room temperature and the contents analysed by gas–solid chromatography using either a 6 ft × $\frac{1}{8}$ in. column of silica gel at 140 °C. or a 6 ft × $\frac{1}{8}$ in. column of Porapak Q at 100 °C. Analysis for NO_2 was carried out in preliminary experiments using ir spectroscopy and gsc using the Porapak Q column at 30 °C. For the analytical procedure used the minimum

[1]Revision received January 8, 1976.

Can. J. Chem. Downloaded from www.nrcresearchpress.com by 210.87.254.5 on 09/05/12
For personal use only.

Can. J. Chem. Downloaded from www.nrcresearchpress.com by 210.87.254.5 on 09/05/12
For personal use only.

detectable ratio of NO_2–CO was approximately 2:1. Conversions of I_2 and NO were $I_2 \leq 2\%$ and NO $\leq 8\%$.

Results

When HFA is photolysed in the presence of I_2 and NO, the following reactions are expected to occur

[1] $$CF_3COCF_3 + h\nu \rightarrow 2CF_3 + CO$$

[2] $$CF_3 + I_2 \rightarrow CF_3I + I$$

[3] $$CF_3 + NO \rightarrow CF_3NO$$

[4] $$I + I + M \rightarrow I_2 + M$$

Reaction 3 is fast (4) hence the important reactions consuming CF_3 radicals in this system are [2] and [3]. The presence of CF_3I and CF_3NO in the products of the photolysis of HFA with a mixture of I_2 + NO was confirmed by gsc and their ir spectra. However, quantitative analysis of CF_3NO in the presence of NO presents difficulties. Pure CF_3NO can be readily distilled from a Ward still at -150 °C but it is quite involatile at this temperature in the presence of an excess of NO (at least a twofold excess). Since we have $\leq 8\%$ conversion of NO in all our experiments the above situation is present. The infrared spectrum of a gaseous mixture of NO + CF_3NO is simply the sum of the spectra of the separate components, both before and after freezing in liquid nitrogen. The spectrum was unchanged after leaving the mixture for up to 4 h at both liquid nitrogen and room temperature. Also addition of CF_3I in amounts found in our systems showed no effect on the spectrum of the NO and CF_3NO. This seems to indicate that there is no appreciable permanent reaction between CF_3NO and NO under the conditions of our experiments. This is contrary to that found by several other workers (6, 7) and to the reaction CH_3NO + NO which reacts fairly readily at room temperature (5). It is also noted that a mixture of CF_3NO and NO when frozen in liquid nitrogen is a green colour rather than the deep blue of CF_3NO alone. This suggests the possibility of a complex being formed between the two, probably in the liquid phase, which dissociates reversibly at higher temperatures. This would explain the involatility of the mixture at -150 °C. Yakubovich *et al.* (8) showed that a similar reaction occurs between CF_3NO and NO in organic solvents at low temperatures. The product is a complex with the empirical formula $CF_3NO \cdot 2NO$ and it is stable at -100 °C but decomposes at -50 °C. In our case we found that the CF_3NO could be removed from the Ward stills at -90 °C. The thermal decomposition of this complex has been described by Boyer (9). The adduct $CF_3NO \cdot 2NO$ has been isolated, but usually rearranges to a diazonium nitrate and then decomposes, releasing CF_3 and NO_3 radicals [5]. In the presence

[5] $$CF_3NO + 2NO \rightarrow CF_3N(NO)—ONO \rightarrow CF_3N{=}N—ONO_2 \rightarrow CF_3 + N_2 + NO_3$$

of excess nitric oxide a disproportionation would yield nitrogen dioxide [6]. The CF_3 radicals

[6] $$NO_3 + NO \rightarrow 2NO_2$$

would, in part, reform CF_3NO by reaction 3, so that the overall process is the chain disproportionation reaction [7] catalysed by CF_3NO

[7] $$2NO \rightarrow N_2 + NO_2$$

during the warming of the Ward still. In our case no NO_2 was detected, therefore either the above process is negligible or some other complex is formed in the Ward still which decomposes quantitatively on warming the still. We also found that if trace quantities of O_2, NO_2, or CF_3I (in quantities comparable to those found in ref. 7) were introduced into the system, the CF_3NO and NO peaks in the infrared spectrum were reduced and a peak corresponding to NO_2 appeared. The presence of NO_2 was also confirmed by gsc. In all our photolysis reactions no NO_2 or any other extraneous products were detected in the reaction products. The maximum amount of CF_3NO that formed initially and that could have been decomposed by reaction 5 must be $<1\%$.

Hence, reaction products plus unchanged reactants were frozen in Ward stills cooled in liquid air and the CO and uncomplexed NO pumped away or measured. Since it was impossible to separate the products and the reactants, the Ward stills were then warmed to room temperature and the total contents consisting of HFA + CF_3I + CF_3NO + complexed NO were analysed for CF_3I and CF_3NO by gsc. If CF_3I and CF_3NO are formed only by reactions 2 and 3 respectively and if [3] is in its second-order region then

[8] $$R_{CF_3NO}/R_{CF_3I} = k_{NO}[NO]/k_{I_2}[I_2]$$

where k_{I_2} and k_{NO} are the rate constants for

Can. J. Chem. Downloaded from www.nrcresearchpress.com by 210.87.254.5 on 09/05/12
For personal use only.

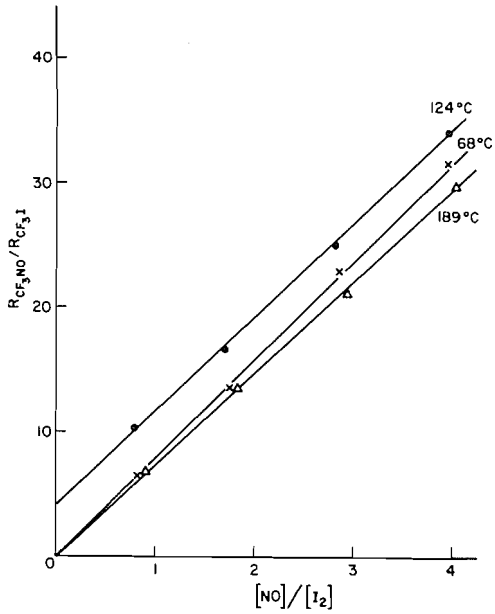

FIG. 1. Variation of R_{CF_3NO}/R_{CF_3I} with $[NO]/[I_2]$; test of eq. 5. To avoid overlap the curve at 124 °C is displaced upwards by 4 scale units.

reactions 2 and 3. If any CF_3I were formed by reaction 9 or CF_3NO removed by reaction 10,

[9] $$CF_3 + I + M \rightarrow CF_3I + M$$

[10] $$2CF_3NO \overset{h\nu}{\rightleftarrows} (CF_3)_2N{-}O{-}NO \rightarrow (CF_3)_2N{-}NO_2$$

then eq. 8 would be invalid. Reaction 9 is unlikely to occur because both reactions 2 and 3 are so fast that the stationary concentration of CF_3 radicals in the system is very low. Reaction 10 is unlikely to occur to any appreciable extent in our systems due to the relatively small concentrations of CF_3NO present.

If eq. 8 is valid, a plot of R_{CF_3NO}/R_{CF_3I} *vs.* $[NO]/[I_2]$ should be a straight line passing through the origin, such plots are shown in Fig. 1 for temperatures of 68, 124, and 189 °C and they indicate that eq. 8 is obeyed.

The slopes of the lines in Fig. 1 yield values of k_{NO}/k_{I_2} which, together with results from other temperatures, are used in an Arrhenius plot shown in Fig. 2. From 28 runs in the range 68–189 °C we obtain by a least-squares method

[11] $$k_{NO}/k_{I_2} = (8.8 \pm 0.20) \exp -[(700 \pm 100J)/RT]$$

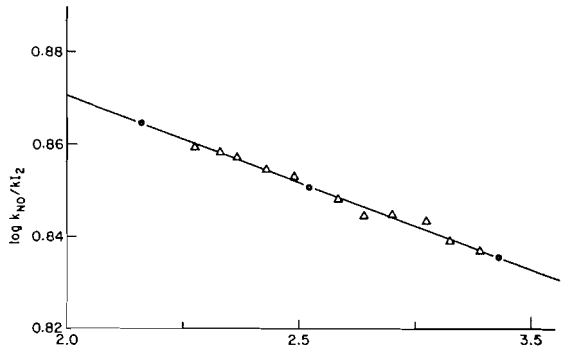

FIG. 2. Arrhenius plot for k_{NO}/k_{I_2}; △ single runs, ● from slopes of curves in Fig. 1.

Discussion

The reaction between the CF_3 radical and NO is of particular interest since very little is known about the rate constants for the reactions of radicals with NO and the variation of these rate constants with temperature.

Using competitive methods we have determined from eq. 11 $E_{NO} - E_{I_2} = 0.700 \pm 0.100$ kJ mol^{-1} $A_{NO}/A_{I_2} = 8.8 \pm 0.2$. Now using 6.8×10^9 l mol^{-1} s^{-1} for the rate of combination of CF_3 radicals[2] we obtain from the results of Amphlett and Whittle (2) $A_{I_2} = 7.5 \times 10^8$ l mol^{-1} s^{-1} and $E_{I_2} = 0.0 \pm 2.0$ kJ mol^{-1} hence, $E_{NO} = 0.7 \pm 2.0$ kJ mol^{-1}, and $A_{NO} = 6.6 \times 10^9$ l mol^{-1} s^{-1}.

The analogous reaction between CH_3 and NO has been studied extensively and most of the previous attempts to measure the rate of combination [12] have been reviewed (12, 13). This

[12] $$CH_3 + NO\,(+M) \rightarrow CH_3NO\,(+M)$$

reaction is an association reaction which will involve a third body at low pressures. However, the pressure region over which this occurs is uncertain. Sleppy and Calvert (14) found the reaction to be second order in the range 150–280 torr with M = neopentane, whereas Hoare (15) found that the reaction was third order up to 200 torr with M = acetone. The high pressure rate constant *i.e.* k_{12} (second order) has recently been studied using spectroscopic methods. Basco

[2]This value of 6.8×10^9 l mol^{-1} s^{-1} for CF_3 combination is an average of the results obtained by Ogawa *et al.* (10) and Basco and Hathorne (11) at 400 K, assuming that the activation energy for CF_3 combination is zero.

Can. J. Chem. Downloaded from www.nrcresearchpress.com by 210.87.254.5 on 09/05/12
For personal use only.

TABLE 1. Test of second-order rate equation for k_{NO}/k_{I_2} at 156 °C

HFA (torr)	NO(Av) (torr)	I_2(Av) (torr)	CF_3NO (μmol)	CF_3I (μmol)	k_{NO}/k_{I_2}
10.1	3.2	9.4	2.50	1.02	7.19
20.2	3.1	9.3	4.90	2.03	7.25
30.1	3.1	9.3	7.45	3.09	7.23
40.0	3.1	9.2	9.73	4.03	7.16
50.1	3.2	9.4	12.14	4.96	7.18
60.1	3.1	9.3	14.48	5.98	7.26
69.9	3.6	9.3	16.84	6.00	7.25
20.1	10.2	2.8	12.85	0.49	7.16
20.2	5.6	5.8	6.47	0.93	7.23
20.1	12.4	1.4	13.53	0.21	7.19

et al. (16) found k_{12}(2nd order) = 2.4 ± 0.2 × 10^9 l mol^{-1} s^{-1}, while Van Den Burgh and Callear (17) obtained k_{12}(2nd order) = 1.00 ± 0.15 × 10^{10} l mol^{-1} s^{-1}. These values are considerably larger than any previously determined values.

We have assumed that in our work reaction 3 is second order. Most of our experiments were carried out with approximately the same quantities of reactants, however at 156 °C we varied the pressure of the HFA from 10–70 torr with no apparent change in the ratio k_{NO}/k_{I_2} (see Table 1). Under these pressure conditions reaction 3 is more likely to be second order than reaction 12 since the number of effective oscillators in CF_3NO should be greater than in CH_3NO because of the lower vibrational frequencies of C—F bonds (18). However, if reaction 3 is actually third order under our conditions, then the calculated second-order rate constant must be less than the true value so that, k_3(2nd order) > 6.6 × 10^9 l mol^{-1} s^{-1}. This is close to the rate constant for combination of CF_3 radicals,[2] 6.8 × 10^9 l mol^{-1} s^{-1}, and is also reasonably close to the collision number Z_3 = 1.7 × 10^{11} l mol^{-1} s^{-1} at 400 K based on collision diameters of 4.0 Å for CF_3 and 3.5 Å for NO. Both these facts provide some support to our assumption that reaction 2 is second order. Furthermore, our value obtained for k_3 (second order) is of the same order of magnitude as the recently obtained (16, 17) values for k_{12} (second order). Our results also indicate that reaction 3 has an activation energy fairly close to zero in the range 68–189 °C which is consistent with the fact that k_3 is similar in magnitude to Z_3.

From our results on the reactions of CF_3 radicals with I_2 and NO, reactions 2 and 3, we find that k_3/k_2 = 6.6 at 300 K for eq. 11. The corresponding reactions 13 and 14 were studied

[13] $$R + NO \rightarrow RNO$$

[14] $$R + I_2 \rightarrow RI + I$$

by Christie and Frost (19) who found that, for R = CH_3, C_2H_5, $CH_3CH_2CH_2$, and $(CH_3)_3CH$, k_{14}/k_{13} = 6, 7, 11, and 22 respectively at room temperature, assuming that reaction 13 is second order. These results are opposite to ours *e.g.* for CF_3 k_{13}/k_{14} = 6.6 whereas for CH_3 k_{13}/k_{14} = 1/6. These results are surprising since one would not normally expect such differences in behaviour between CF_3 and CH_3 radicals especially since Christie estimates that for CH_3 k_{14} = 3.0 × 10^9 l mol^{-1} s^{-1} whereas for CF_3 k_{14} = 7.5 × 10^8 l mol^{-1} s^{-1}. However, using the latest reported values of k_{13} for CH_3 (16, 17) we have k_{13}/k_{14} = 1–3.3.

Acknowledgments

We wish to thank Prof. E. Whittle for helpful discussion. This work was supported by the Defence Research Board Grant No. 9530-110.

1. B. G. TUCKER and E. WHITTLE. Trans. Faraday Soc. **61**, 866 (1965).
2. J. C. AMPHLETT and E. WHITTLE. Trans. Faraday Soc. **62**, 1662 (1966).
3. J. C. AMPHLETT and E. WHITTLE. Trans. Faraday Soc. **63**, 2695 (1967).
4. B. G. TUCKER and E. WHITTLE. Trans. Faraday Soc. **61**, 484 (1965).
5. M. I. CHRISTIE, C. GILBERT, and M. A. VOISEY. J. Chem. Soc. 3147 (1964).
6. A. H. DINWOODIE and R. N. HASZELDINE. J. Chem. Soc. 1675 (1965).
7. JULIAN HEICKLEN. J. Phys. Chem. **70**, 112 (1966).
8. A. V. YAKUBOVICH, S. P. MAKAROV, V. A. GINSBURG, N. F. PRIVEZENTSEVA, and L. L. MARTYNOVA. Dokl. Akad. Nauk. SSSR, **141**, 125 (1961).
9. J. H. BOYER. The chemistry of nitro and nitroso groups. *Edited by* H. Feuer. Interscience. 1969. p. 265.
10. T. OGAWA, G. A. CARLSON, and G. C. PIMENTEL. J. Phys. Chem. **74**, 2090 (1970).
11. N. BASCO and F. G. M. HATHORN. Chem. Phys. Lett. **8**, 291 (1971).
12. E. R. ALLEN and K. W. BAGLEY. Ber. Bunsenges. Phys. Chem. **72**, 227 (1968).
13. J. HEICKLEN and N. COHEN. Adv. Photochem. **5**, 275 (1968).
14. W. C. SLEPPY and J. G. CALVERT. J. Am. Chem. Soc. **81**, 769 (1959).
15. D. E. HOARE. Can. J. Chem. **40**, 2012 (1962).

16. N. BASCO, D. G. L. JAMES, and R. D. SUART. Int. J. Chem. Kinet. **2**, 215 (1970).
17. H. E. VAN DEN BURGH and A. B. CALLEAR. Trans. Faraday Soc. **67**, 2017 (1971).
18. S. W. BENSEN and G. HAUGEN. J. Phys. Chem. **69**, 3898 (1965).
19. M. I. CHRISTIE and J. S. FROST. Trans. Faraday Soc. **61**, 468 (1965).

Can. J. Chem. Downloaded from www.nrcresearchpress.com by 210.87.254.5 on 09/05/12
For personal use only.

The structure and equilibria of a manganese(II) complex of fulvic acid studied by ion exchange and nuclear magnetic resonance[1,2,3]

DONALD S. GAMBLE
Soil Research Institute, Agriculture Canada, Ottawa, Canada
AND
COOPER H. LANGFORD[4] AND JAMES P. K. TONG
Department of Chemistry, Carleton University, Ottawa, Canada KIS 5B6

Received October 9, 1975

DONALD S. GAMBLE, COOPER H. LANGFORD, and JAMES P. K. TONG. Can. J. Chem. **54**, 1239 (1976).

The binding of Mn^{2+} to a well characterized fulvic acid sample is reported based on the competition with K^+ in an ion exchange equilibration. The free energy of binding of $\frac{1}{2}Mn^{2+}$ to fulvic acid is only 1–2 kJ/equivalent more favourable than that for K^+. This suggests an outer sphere electrostatic structure for the complex. The suggestion is confirmed by observation of minimal change in the presence of fulvic acid of the effect of paramagnetic Mn^{2+} on the nmr spectra of water. The interpretation of nmr spectra is supported by comparison with nmr measurements of Mn^{2+} complexes with simple ligands and contrast with nmr measurements on Fe^{3+} – fulvic acid complexing. The latter is confirmed as inner sphere.

DONALD S. GAMBLE, COOPER H. LANGFORD et JAMES P. K. TONG. Can J. Chem. **54**, 1239 (1976).

On rapporte la liaison du Mn^{2+} à un échantillon bien caractérisé d'acide fulvique; les conclusions sont basées sur la compétition avec K^+ dans un équilibre d'échange ionique. L'énergie libre de liaison de $\frac{1}{2}Mn^{2+}$ à l'acide fulvique n'est que de 1 à 2 kJ par équivalent plus favorable que celle pour K^+. Ceci suggère une structure électrostatique de sphère externe pour le complexe. Cette suggestion est confirmée par l'observation qu'en présence de l'acide fulvique il ne se produit qu'un changement minimal de l'effet de Mn^{2+} paramagnétique sur le spectre rmn de l'eau. L'interprétation du spectre rmn est en accord avec la comparaison de mesures rmn de complexes du Mn^{2+} avec des ligands simples et est en opposition avec les spectres rmn de complexes entre le Fe^{3+} et l'acide fulvique. On confirme donc que dans ce dernier cas il s'agit de sphères internes.

[Traduit par le journal]

Introduction

At least two types of reactions have been found between metal ions and fulvic acid. One is outer sphere electrostatic binding of ions by a polyanion without displacement of water from the ion (1). The second is inner sphere chelation at bidentate sites having a salicylic acid type of structure (2–4). There are therefore both outer sphere and inner sphere complexes. It is suspected that Mn^{2+} forms outer sphere complexes with many ligands, possibly including fulvic acid.

The result of this work supports the idea that Mn^{2+} forms outer sphere complexes with fulvic acid. The evidence comes from two experimental methods which are entirely independent of each other: (*1*) $\frac{1}{2}Mn^{2+}$–K^+ ion exchange equilibrium used as a calibrated probe for measuring the complexing equilibria of Mn^{2+} and K^+ with fulvic acid. (*2*) Proton nmr line broadening as a method of studying changes in inner sphere solvation of the paramagnetic ion.

Theory

Cation Exchange Equilibria

A cation exchange equilibrium is used as the calibrated probe with which Mn^{2+} – fulvic acid

---

[1]Presented at the 58th Chemical Conference and Exhibition of the Chemical Institute of Canada, Toronto, Ontario, May 25–28, 1975. Soil Research Institute contribution No. 567.

[2]Supported in part under a research agreement between the Inland Waters Directorate and Carleton University and by NRCC grants and a fellowship to C.H.L. and J.P.K.T. respectively.

[3]We thank Douglas Hindle and Katalin Deczky for substantial and expert experimental assistance.

[4]To whom correspondence should be addressed.

Can. J. Chem. Downloaded from www.nrcresearchpress.com by 210.87.254.105 on 09/05/12
For personal use only.

Can. J. Chem. Downloaded from www.nrcresearchpress.com by 210.87.254.105 on 09/05/12
For personal use only.

complexing may be measured. This necessarily introduces a second cation, K^+, which will generally compete with the Mn^{2+} for organic ligand complexing sites (1). This in turn shifts the ion exchange equilibrium. The calibration procedure must take this into account. The ion exchange reaction is described by [1]

$$\tfrac{1}{2}Mn^{2+} + (K^+) \underset{}{\overset{\bar{K}_x}{\rightleftharpoons}} K^+ + (\tfrac{1}{2}Mn^{2+}) \qquad [1]$$

$$\bar{K}_x = \frac{(m_M)m_K}{m_M(m_K)}$$

The parentheses indicate ion concentrations in the exchanger; m_M is a molality of Mn^{2+} and m_K is a molality of K^+. $\bar{K}_x$ is usually assumed to be a constant in complexing studies by the ion exchange method (5, 6). This may be unjustified in the present case, and is certainly unnecessary. It is sufficient to use instead, the more general assumption

$$\bar{K}_x = \bar{f}_x[(m_M)] \qquad [2]$$

The total concentration of metal ions in the ion exchanger is

$$(C) = (m_K) + (m_M)$$

When this is introduced, [1] may be rearranged to give a function that accounts for both metal ions in solution. [3] gives the resulting empirical calibration function Y, which is a function of only one variable, (m_M).

$$Y \equiv \frac{m_M}{m_K} = \frac{(m_M)}{[(C) - (m_M)]\bar{K}_x} \qquad [3]$$

$$Y = Y[(m_M)]$$

The electrostatic binding of K^+ has been previously demonstrated (1), and outer sphere complexing is being postulated here. This suggests that the problem should be formulated with [4] to [6] where T represents a fulvic acid binding site. In these equations, molalities m have subscripts H, T, and HT, designating respectively the proton, the binding site anion, and the protonated binding site anion.

$$TH \underset{}{\overset{\bar{K}_T}{\rightleftharpoons}} T^- + H^+ \qquad [4]$$

$$\bar{K}_T = \frac{m_T m_H}{m_{TH}}$$

$$T^- + K^+ \underset{}{\overset{\bar{K}_5}{\rightleftharpoons}} T^-\text{---}K^+ \qquad [5]$$

$$\bar{K}_5 = \frac{m_b}{m_T m_K}$$

$$T^- + \tfrac{1}{2}Mn^{2+} \underset{}{\overset{\bar{K}_M}{\rightleftharpoons}} T^-\text{---}\tfrac{1}{2}Mn^{2+} \qquad [6]$$

$$\bar{K}_M = \frac{m_c}{m_T m_M}$$

Examination of the present experimental results indicates that $m_T \approx 0$, within the limits of experimental error. That is, under these experimental conditions, almost none of the carboxyl groups are free from cations. The complexing equilibria must therefore be described by [7] and [8].

$$TH + \tfrac{1}{2}Mn^{2+} \underset{}{\overset{\bar{K}_c}{\rightleftharpoons}} T^-\text{---}\tfrac{1}{2}Mn^{2+} + H^+ \qquad [7]$$

$$\bar{K}_c = \frac{m_c m_H}{m_{TH} m_M}$$

$$TH + K^+ \underset{}{\overset{\bar{K}_b}{\rightleftharpoons}} T^-\text{---}K^+ + H^+ \qquad [8]$$

$$\bar{K}_b = \frac{m_b m_H}{m_{TH} m_K}$$

Let

$$Z = C_M + C_K - C_T + m_{TH} \qquad [9]$$

C_M, C_K, and C_T are the total solution concentrations of $\frac{1}{2}Mn^{2+}$ and K^+ may now be calculated from Z, and the calibration function Y defined in [3]. This is done with [10].

$$m_M = \left(\frac{Z}{\frac{1}{Y} + 1}\right) \qquad [10]$$

$$m_K = \left(\frac{Z}{1 + Y}\right)$$

Appropriate differential equilibrium functions, K, and ΔG_b are calculated from the corresponding $\bar{K}$ functions as previously described (1, 3, 7, 8). ΔG_b differs from ΔG^0 to the extent of a small activity coefficient term (7).

Can. J. Chem. Downloaded from www.nrcresearchpress.com by 210.87.254.105 on 09/05/12
For personal use only.

Nuclear Magnetic Resonance Probes of the Solvation Sphere of Mn^{2+}

The effect of coordination to an organic ligand on the line broadening that a paramagnetic Mn^{2+} ion produces in the solvent (water) nmr signal has been used successfully to explore manganese binding to enzymes (9). The effect depends upon the reduction in T_2, the transverse relaxation time, of protons in the neighbourhood (approximately the inner coordination sphere) of a paramagnetic ion. When those protons exchange rapidly with the bulk of the solution as do water molecules coordinated to Mn^{2+}, the nmr spectrum reveals a single average absorption with one value of T_2 governed by McConnell's equation for fast exchange (10).

$$[11] \qquad 1/T_{2(obs)} = P_M/T_{2M} + P_B/T_{2B}$$

In [11], $T_{2(obs)}$ refers to the experimental relaxation time, P_M and P_B, the probabilities that a proton is to be found in the coordination sphere of the metal ion (M) or the bulk of the solution (B), and T_{2M} and T_{2B} represent the relaxation times characteristic of these two environments. When an inner sphere complex of Mn^{2+} is formed with an organic ligand, the ligand *replaces* coordinated water and consequently *reduces* P_M. If this were the only effect, it would be a straightforward matter to determine the 'chelating' ability of an organic ligand from knowledge of the binding equilibria and $T_{2(obs)}$ as was done for sulfate coordination (11). Unfortunately, the situation can become more complicated. T_{2M} is related to relaxation of the paramagnetic electron (12). The high spin d^5 electron configuration ions like Mn^{2+} and Fe^{3+} have long electron relaxation times in high symmetry environments including octahedral species like $Mn(OH_2)_6^{2+}$. In lower symmetry, with an organic ligand coordinated, splitting of electronic levels can lead to shorter electronic relaxation times which result in longer T_{2M}.

To put this in an experimental context, $1/T_{2M(obs)}$ is proportional to the width at half height, $\Delta\nu_{1/2}$, of the nmr absorption signal for water. The signal is broadened by Mn^{2+}. Addition of an inner sphere complexing ligand may decrease that broadening by either of two mechanisms: (*1*) replacement of H_2O reducing P_M, or (*2*) enhancement of electronic relaxation which lengthens T_{2M}. Results for Mn^{2+} were obtained suggesting a leading role for mechanism (*1*). Contrasting results using Fe^{3+} suggested a leading role for mechanism (*2*). In both cases, evidence on inner *vs.* outer sphere coordination by fulvic acid was obtained.

Experimental

Materials and Equipment

All solutions were prepared from reagent grade chemicals and H_2O redistilled under N_2. The fulvic acid was the Batch FA1 previously described (7, 8). Bio Rad AG50W-X16, 200 to 400 U.S. Mesh Size, was used for all of the ion exchange equilibrations.

Metal ion concentrations were estimated by atomic absorption using a spectrometer calibrated in the usual manner. Reference organic compounds were research grades used without special purification. Nuclear magnetic resonance spectra were recorded using Varian T-60 and HA-100 NMR spectrometers for 60 and 100 MHz spectra respectively. Transverse relaxation times were correlated with the width at half height of absorption bands assuming a Lorentzian line shape and the relation:

$$1/T_{2(obs)} = \pi\Delta\nu_{1/2}$$

where $\Delta\nu_{1/2}$ designates the width at half height of the absorption spectral band.

Procedure and Data Treatment

Stock solutions, standards, analysis solutions, and experimental samples were all prepared gravimetrically. The ion exchange resin was collected and weighed in the dry K^+ form after use. A time study indicated a 4 h equilibration time for Mn^{2+}–K^+ ion exchange with 200–400 U.S. Mesh Size resin at 25.0 °C. The 24 h equilibration time subsequently used included several hours of shaking at room temperature followed by overnight storage in a thermostat at 25.00 ± 0.05 °C.

Six independent runs were used for the Mn^{2+}–K^+ ion exchange calibration curve, with each run having 9 to 12 measurement samples. These samples were prepared from K^+ form resin and $MnCl_2$–KCl stock solution. The equilibration temperature was 25.00 ± 0.05 °C. Initial averaging of the experimental data was done separately for each of the six runs. Empirical curves were calculated in each case for Mn^{2+} concentration in solution as a function of the weight ratio of dry K^+ resin to stock solution, and for Mn^{2+} content of the resin also as a function of this weight ratio. The calculations were done by least squares fitting to polynomials. The ion exchange calibration curve was then calculated with these averaged data from all six runs taken together. A least squares fitted polynomial was again used.

Six independent complexing runs were carried out, with each run having 15 to 19 ion exchange-complexing samples. These samples were prepared from $MnCl_2$ – KCl – fulvic acid stock solutions, and ion exchange resin. The resin was converted to 39 mol% $\frac{1}{2}Mn^{2+}$ form, and 61 mol% K^+ form. The partly converted resin limited the mass transfer of cations which results from ion exchange. This achieved the purpose of limiting the total electrolyte concentration in the complexing solutions. Initial averaging of the solution concentrations of total Mn^{2+} and free

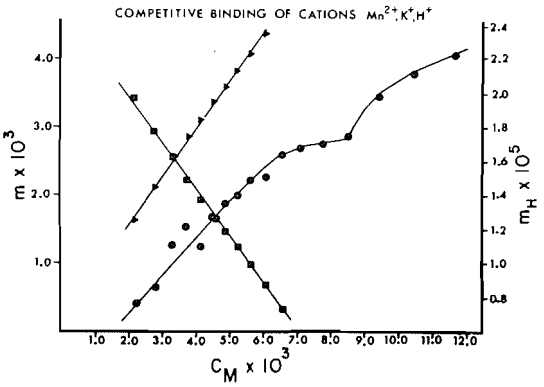

FIG. 1. Competitive binding of the cations Mn^{2+}, K^+, and H^+, as C_M, the concentration of total $\frac{1}{2}Mn^{2+}$, is increased. ▲, molality of complexed $\frac{1}{2}Mn^{2+}$; $\sigma = \pm 15\%$. ■, molality of complexed K^+; $\sigma = \pm 5\%$. ●, molality of free H^+; $\sigma = \pm 56\%$.

H^+, and of the Mn^{2+} content of the resin, were done as described for the calibration runs. For each of the six complexing runs, empirical curves were fitted by least squares for the three solution concentrations, total Mn^{2+}, total K^+, and free H^+, as functions of the Mn^{2+} content of the resin. The interpolated values of the latter were the same as those used for the calibration curve. The $\bar{K}$ and K functions were also calculated for the separate runs, but the two ΔG_b curves were each calculated with data from all six runs taken together.

Results and Discussion

The experimental results of the ion exchange equilibration experiments demonstrate the following important points, some of which are commonly overlooked: (*1*) Figure 1 shows the competitive binding of the three cations by the fulvic acid. Contrary to common practice, the three equilibria are calculated together. (*2*) Figure 2 indicates that $\bar{K}_c$ is a function of two independent variables, in the most general case. Those chosen here to specify the state of the system are X_c, the mole fraction of carboxylates having site-bound $\frac{1}{2}Mn^{2+}$, and X_{TH}, the mole fraction of carboxyl groups still protonated. This verifies experimentally the theoretical conclusion (1, 3, 7) that $\bar{K}_c$ is not a thermodynamic equilibrium constant. It also follows from these results that a 'conditional constant', for which a single numerical value is provided, cannot properly represent the system. (*3*) K_c, from which the $\frac{1}{2}Mn^{2+}$ curve of Fig. 3 is calculated, is defined for an infinitesimal increment of site-bound complex (1, 3, 7). It is found here to be larger than the macroscopically observed $\bar{K}_c$ by a factor of 25

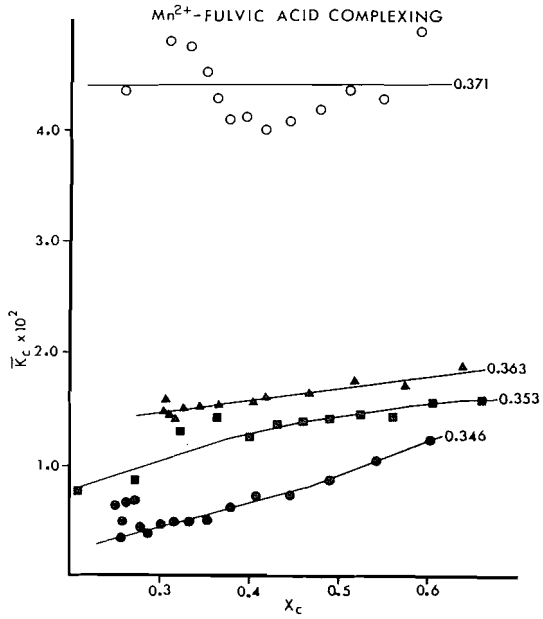

FIG. 2. $\frac{1}{2}Mn^{2+}$ – fulvic acid complexing equilibrium at 25.00 ± 0.05 °C. K_c, $\pm\sigma = 20\%$. ●, $X_{TH} = 0.346 \pm 5\%$. ■, $X_{TH} = 0.353 \pm 5\%$. ▲, $X_{TH} = 0.363 \pm 5\%$. ○, $X_{TH} = 0.371 \pm 5\%$.

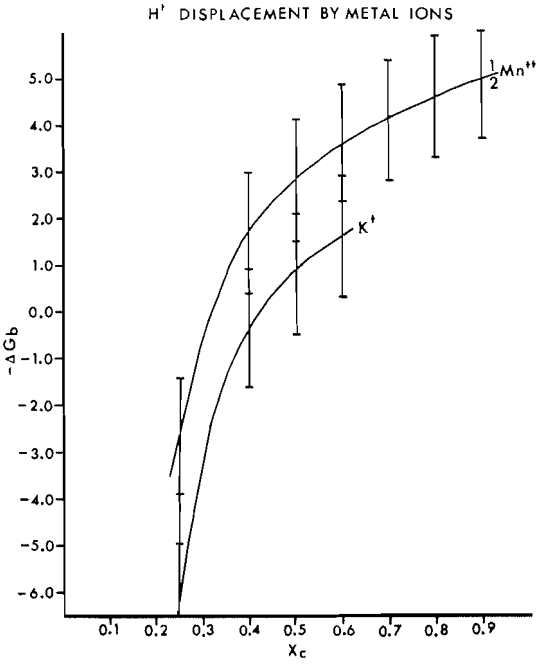

FIG. 3. Equilibrium H^+ displacement by metal ions at 25.00 ± 0.05 °C. $\Delta G_b = \Delta G^0 + \Delta G_\Gamma$, where ΔG_Γ is a small activity coefficient term.

Can. J. Chem. Downloaded from www.nrcresearchpress.com by 210.87.254.105 on 09/05/12
For personal use only.

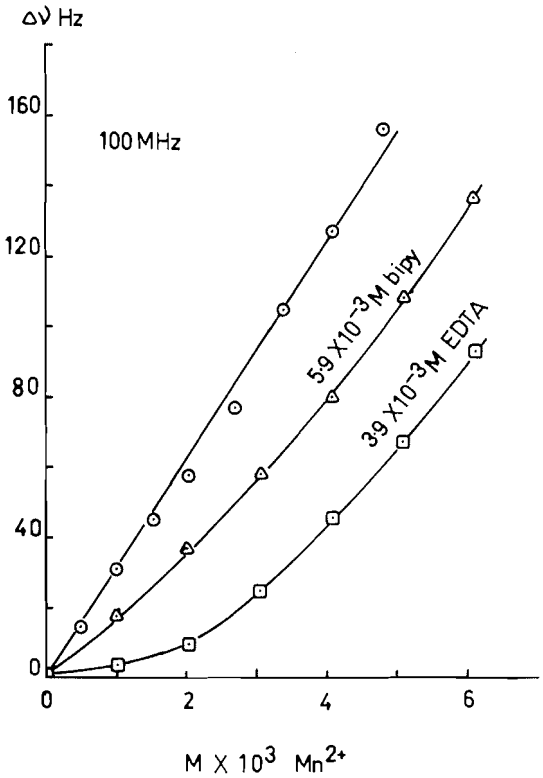

FIG. 4. Water proton nmr line-broadening in Mn^{2+} solutions at 100 MHz. ○, no additives; △, solutions containing 5.9×10^{-3} *M* 2,2-bipyridine; □, solutions containing 3.9×10^{-3} *M* EDTA.

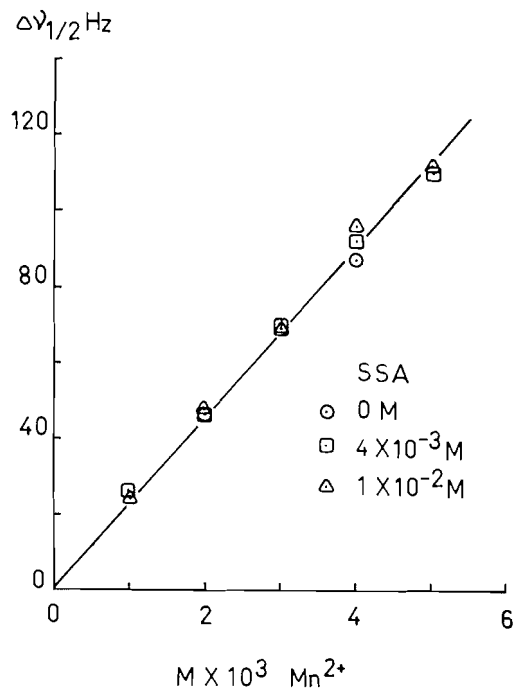

FIG. 5. Water proton nmr line-broadening in Mn^{2+} solutions with SSA added. Data at 60 MHz.

to 250. A comparable effect has been found in previously published Na^+ and K^+ binding results (1). The conceptual distinction between $\bar{K}_c$ and K_c is therefore neither trivial nor academic. (*4*) Figure 3 gives Gibbs free energies for the equilibrium complexing of $\frac{1}{2}Mn^{2+}$ and K^+. These have been calculated from the corresponding differential functions K_c and K_b, and differ from standard Gibbs free energies only to the extent of small activity coefficient terms. The significant point here is that Mn^{2+} is complexed to the fulvic acid with an energy very similar to that of K^+. The difference, in fact, is only about 1 to 2 kJ/equivalent of bound metal ion. This suggests that $\frac{1}{2}Mn^{2+}$ and K^+ are complexed to the fulvic acid in essentially the same way.

Turning to nmr results, we see in Fig. 4 the effect on water proton line width of addition of Mn^{2+} to solutions of several ligands. The paradigm of a complexing agent is EDTA (ethylenediamminetetraacetic acid) which is seen to cause very substantial reduction in water nmr line width as it complexes. (The ligand displaces 5–6 water molecules.) A related case is bipyridine. This uncharged ligand can display a binding constant greater than 10^2 only if it forms inner sphere complexes displacing water. The charge–dipole forces holding an outer sphere would be too weak to account for so large a binding constant. Again, it is evident that water line widths are reduced. Indeed, the change compared to the aquo-Mn^{2+} species is entirely consistent with displacement of one-third of the water molecules by the ligand.

Sulfosalicylic acid, SSA, is a different case shown in Fig. 5. No reduction of the water line width is observed. Since it is known that SSA 'complexes' Mn^{2+}, it must be the case that it is an outer sphere complex that forms with no displacement of coordinated water and correspondingly no change in P_M (see [11]). In Fig. 6, data corresponding to those in Fig. 4 are presented for fulvic acid solutions. It is immediately seen that the closest comparison is with SSA although there is a slight but definite decrease in water line

Can. J. Chem. Downloaded from www.nrcresearchpress.com by 210.87.254.105 on 09/05/12
For personal use only.

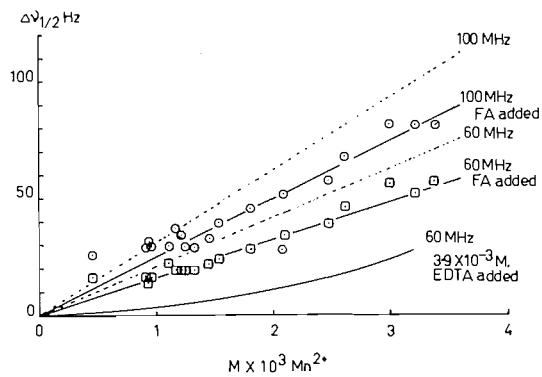

FIG. 6. Water proton nmr line-broadening in Mn^{2+} solutions with various amounts of fulvic acid added. ○, 100 MHz; □, 60 MHz. The dotted lines show where the Mn^{2+}(aq) curves in the absence of fulvic acid appear.

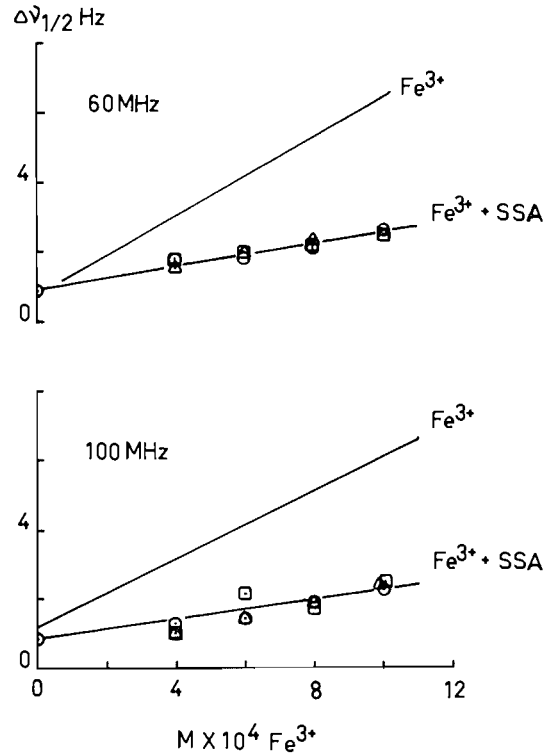

FIG. 7. Water proton nmr line width in Fe^{3+} solutions containing SSA. SSA concentrations: ○ = 1×10^{-3} *M*; △ = 2×10^{-3} *M*; □ = 1×10^{-2} *M*. The intercept is the experimental line width of pure water.

widths. This could be attributed to a small amount of water being displaced from the coordination sphere of Mn^{2+}. However, there is another possibility. It may be that association of $Mn(OH_2)_6^{2+}$ within a fulvic acid 'cage' imposes a slight but significant distortion from octahedral symmetry which changes electron relaxation time (12) enough to cause a slight decrease in line width.

Experiments with Fe(III) provide contrasting evidence supporting the picture given of Mn^{2+} complexing by fulvic acid. In Fig. 7, line widths as a function of ligand concentration are shown for Fe(III) complexes. The important observation is that for small concentrations of SSA, great reductions in line width are observed which cannot be interpreted simply in terms of displacement of water from $Fe(OH_2)_6^{3+}$. It must be true that the ligand substantially alters electron relaxation time and this implies inner sphere coordination (12). The binding of fulvic acid is parallel. Line widths in excess of the machine broadening of pure water could not be accurately estimated. When Fe^{3+} is bound to fulvic acid, the remaining paramagnetic broadening is small. It is clear that the complex is inner sphere 'chelation', but it is impossible to determine the exact number of water molecules displaced.

A referee has pointed out that ΔG^0 values in the literature for typical Mn^{2+} and K^+ complexes further support the postulated outer sphere complexing. Regardless of whether they are outer or inner sphere, K^+ complexes will have primarily electrostatic interactions such as ion-polyion or ion–dipole interactions. On the other hand, a somewhat stronger bond is likely for a Mn^{2+} complex if it is of the inner sphere type. Typical literature values for K^+ complexing are $9.13 \text{ kJ/mol} \lesssim -\Delta G^0 \lesssim 16.6 \text{ kJ/mol}$ (13–16). Some typical values for $\frac{1}{2}Mn^{2+}$ complexes with organic ligands, evidently outer sphere, are $1.8 \text{ kJ/mol} \lesssim -\Delta G^0 \lesssim 21 \text{ kJ/mol}$ (13, 17–21).

If taken separately, neither the comparison of equilibrium free energies nor the nmr method provides conclusive proof of the postulated outer sphere complexing. The two methods are in agreement however, and both are consistent with this conclusion. There may be some slight inner sphere binding, although it is more likely that the outer sphere complex is somewhat unsymmetrical. We conclude that there is strong evidence for $Mn(OH_2)_6^{2+}$ binding electrostatically to anionic outer sphere sites on the fulvic acid in a manner very much more like K^+(aq)

Can. J. Chem. Downloaded from www.nrcresearchpress.com by 210.87.254.105 on 09/05/12
For personal use only.

than Fe(III). In this context, the behaviour of Cu^{2+} would be especially interesting.

1. DONALD S. GAMBLE. Can. J. Chem. **51**, 3217 (1973).
2. DONALD S. GAMBLE, M. SCHNITZER, and I. HOFFMAN. Can. J. Chem. **48**, 3197 (1970).
3. DONALD S. GAMBLE and MORRIS SCHNITZER. *In* Trace metals and metal organic interactions in natural waters. *Edited by* Philip C. Singer. Ann Arbor Science Publishers, Inc. Ann Arbor, Michigan. 1973. Chapt. 9.
4. C. H. LANGFORD and D. S. GAMBLE. Proceedings of the International Conference on Transport of Persistent Chemicals in Aquatic Ecosystems. Ottawa, Canada, 1974.
5. FRIEDRICH HELFFERICH. Ion exchange. McGraw-Hill Book Company, Inc., New York. 1962.
6. Y. MARCUS. *In* Ion exchange. Vol. 1. *Edited by* Jacob A. Marinsky. Marcel Dekker, Inc., New York. 1966. Chapt. 3.
7. DONALD S. GAMBLE. Can. J. Chem. **48**, 2662 (1970).
8. DONALD S. GAMBLE. Can. J. Chem. **50**, 2680 (1972).
9. A. S. MILDVAN and M. COHN. Adv. Enzymol. **33**, 1 (1970).
10. H. M. MCCONNELL. J. Chem. Phys. **28**, 430 (1958).
11. L. S. FRANKEL, T. R. STENGLE, and C. H. LANGFORD. J. Inorg. Nucl. Chem. **29**, 243 (1967).
12. T. J. SWIFT. *In* NMR of paramagnetic molecules. *Edited by* G. N. LaMar, W. DeW. Horrocks, and R. H. Holm. Academic Press, New York. 1973. Chapt. 2.
13. LARS GUNNAR SILLEN and ARTHUR MARTELL. Stability constants of metal–ion complexes. Section II: Organic ligands. Special publication No. 17. The Chemical Society, Burlington House, W.1, London. 1964.
14. REED M. IZATT, J. HOWARD RYTTING, DENNIS P. NELSON, BARRY L. HAYMORE, and JAMES J. CHRISTENSEN. Science, **164**, 443 (1969).
15. H. K. FRENSDORFF. J. Am. Chem. Soc. **93**, 600 (1971).
16. M. S. LEWIS and H. A. SAROFF. J. Am. Chem. Soc. **79**, 2112 (1957).
17. N. C. LI, W. M. WESTFALL, A. LINDENBAUM, J. M. WHITE, and J. SCHUBERT. J. Am. Chem. Soc. **79**, 5864 (1957).
18. K. B. YATSIMIRSKII and T. I. FEDOROVA. Zh. Neorg. Khim. **1**, 2310 (1956).
19. W. P. EVANS and C. B. MONK. J. Chem. Soc. 550 (1954).
20. V. S. K. NAIR and G. H. NANCOLLAS. J. Chem. Soc. 4367 (1961).
21. A. McAuley and G. H. Nancollas. J. Chem. Soc. 2215 (1961).

Can. J. Chem. Downloaded from www.nrcresearchpress.com by 210.87.254.105 on 09/05/12
For personal use only.

Ion pairs and heat capacity of activation for 2,2-disubstituted cyclopropyl bromides

SURENDRA SINGH AND ROSS ELMORE ROBERTSON
Department of Chemistry, The University of Calgary, Calgary, Alberta T2N 1N4

Received July 3, 1975

SURENDRA SINGH and ROSS ELMORE ROBERTSON. Can. J. Chem. **54**, 1246 (1976).

The temperature dependence of the rates of hydrolysis of 2,2-dimethylcyclopropyl bromide, 2,2-*cis*-vinyl-*trans*-methylcyclopropyl bromide and 2,2-*cis*-methyl-*trans*-vinylcyclopropyl bromide have been determined in water. The temperature coefficient of the enthalpy of activation ($\Delta C_p^{\neq}$) for these compounds was determined to be -52, -27 and -37 cal deg^{-1} mol^{-1} respectively. The relative rate ratios for hydrolysis of the 2,2-methylvinylcyclopropyl bromides with respect to the appropriate 2-vinylcyclopropyl bromide isomer indicate a considerable progress towards allyl cations at the transition state in contrast to the indications of the $\Delta C_p^{\neq}$ values.

The $\Delta C_p^{\neq}$ term for such reactions in water depends to an important degree on the external effects of charge development on water structure but is insensitive to internal electrostatic effects. In the three examples of $\Delta C_p^{\neq}$ reported in this study, all tend to show small external effects in spite of evidence which might suggest larger. The differences in $\Delta C_p^{\neq}$ are attributed to the particular shape and charge distribution of the quasi-ion pair.

SURENDRA SINGH et ROSS ELMORE ROBERTSON. Can. J. Chem. **54**, 1246 (1976).

On a déterminé, dans l'eau, la dépendance sur la température des vitesses des hydrolyses du bromure de diméthyl-2,2 cyclopropyle, du bromure de méthyl-2 *trans* vinyl-2 *cis* cyclopropyle et du bromure de méthyl-2 *cis* vinyl-2 *trans* cyclopropyle. On a déterminé que les coefficients de température des enthalpies d'activation ($\Delta C_p^{\neq}$) de ces composés sont respectivement de -52, -27 et -37 cal deg^{-1} mol^{-1}. Les vitesses relatives d'hydrolyse des bromures de méthyl-2 vinyl-2 cyclopropyle par rapport à l'isomère approprié du bromure de vinyl-2 cyclopropyle indiquent qu'il y a un déplacement considérable vers le cation allylique dans l'état de transition et ceci par opposition aux indications des valeurs de $\Delta C_p^{\neq}$.

Le terme $\Delta C_p^{\neq}$ pour de telles réactions dans l'eau dépend beaucoup sur des effets externes impliquant un développement de la charge sur la structure de l'eau; ce terme est toutefois insensible aux effets électrostatiques internes. Dans les trois exemples de $\Delta C_p^{\neq}$ rapportés dans cette étude, malgré les indications qui pourraient suggérer que ces effets sont plus grands tous les cas tendent à montrer l'existence de petits effets externes. On attribue les différences dans les $\Delta C_p^{\neq}$ à la forme et à la distribution de charges particulières dans la quasi paire d'ion.

[Traduit par le journal]

It is well established that the enthalpy of activation, $\Delta H^{\neq}$, for ionogenic reactions in water has a negative temperature coefficient, $\Delta C_p^{\neq}$, which varies with the nature of the displaced group and with mechanism (1). Empirically we observe that this coefficient, $\Delta C_p^{\neq}$, appears to have at least two sources. One, a rather constant value of about -25 to -30 cal deg^{-1} mol^{-1}, seems to be independent of the displaced group, or the solvent, or solvent mixtures (2). The physical significance of this part of $\Delta C_p^{\neq}$ has not been identified.[1] The other major contributor to $\Delta C_p^{\neq}$ for ionogenic reactions in water has been related to the unique nature of the initial state solvation of weakly polar solutes in such systems and to the effect of charge development in breaking down that solvation shell in the activation process (1). Since the stability of the initial state solvation shell is known to be temperature dependent from gas → aqueous solution equilibria studies (5–7), the negative temperature coefficient of $\Delta H^{\neq}$ from this source at least can be rationalized (8). A similar picture has evolved to account for the heat capacity changes found to characterize acid–base equilibria (9, 10).

There is, however, one important difference between the latter ΔC_{pa} values and the majority of $\Delta C_p^{\neq}$ values obtained in kinetic studies. Whereas the acid–base equilibria reflect differences in the solvation of solvent-separated ions, the transition state in kinetic studies has the possibility of various degrees of residual covalency, of charge development, ion pairing, and

[1]For other suggestions in connection with $\Delta C_p^{\neq}$ see refs. 3, 4.

Can. J. Chem. Downloaded from www.nrcresearchpress.com by 210.87.254.6 on 09/05/12
For personal use only.

Can. J. Chem. Downloaded from www.nrcresearchpress.com by 210.87.254.6 on 09/05/12
For personal use only.

ion separation. This point is implicit in the extended rate series of Winstein and co-workers (11) who gave formal extension to the operational S_N1–S_N2 classification as[2]

$$\text{RX} \underset{k_2}{\overset{k_1}{\rightleftharpoons}} \text{R}^{\delta+}\text{X}^{\delta-} \rightleftharpoons \text{R}^+||\text{X}^- \rightleftharpoons \text{R}^+ + \text{X}^- \qquad [\text{I}]$$

$$\downarrow k_{1n} \qquad \downarrow k_{2n} \qquad \downarrow k_{3n} \qquad \downarrow k_{4n}$$

$$\text{P} \qquad \text{P} \qquad \text{P} \qquad \text{P}$$

and thus suggested a more complex framework for a detailed examination of solvation effects. Reaction I may not express exactly the detailed mechanism but as it stands it emphasizes the possibility of varying internal and external interactions as well as other potential complexities (12, 13) and hence, in so far as it is acceptable, provides a model, useful for examining $\Delta C_p^{\neq}$ values. This possibility will not be explored here. In general whether solvolytic reactions in water involve stages beyond the tight ion-pair is doubtful.

Even though the temperature dependence of solvent reorganization is recognized to play an important role in determining the value of ΔC_{pa} and $\Delta C_p^{\neq}$, and even though the evidence from Walden products (14) and from ΔC_{pa} (15) lead to the reasonable conclusion that positive cations such as the trimethylammonium ion break up water structure (14), indications to date support the conclusion that, in general, the cationic moiety at the transition state in the hydrolysis of alkyl halides and related compounds does not seem to have much effect on the surrounding water structure. Since this deduction can have an important bearing on the arguments to be advanced to account for the $\Delta C_p^{\neq}$ values found in this study, some of the supporting evidence for this observation is given in Table 1.

On the basis of α-deuterium isotope effects (20) and general electronic considerations from other sources (21) we expect the isopropyl bromide to have a more ionic transition state than the methyl homologue and this expectation is reflected in the more negative $\Delta C_p^{\neq}$ values (Table 1 entry *A*). These are, admittedly, overall values and it is not readily apparent how the contributions to such values are to be divided between the effect of the positive and the negative charges. However, if we examine Table 1 entry *B* and recognize that the methanesulfonic ion does not appear to have much effect on water structure (22)[3] then it is probable that the positive charge on the isopropyl group at the transition state is either dispersed or shielded from the solvent since in *B* there is no appreciable difference between $\Delta C_p^{\neq}$ values in spite of a probable difference in charge development. Finally in entry *C*, the 3-methyl-2-butyl-methanesulfonate should have as great a positive charge or greater than the 3-methyl-2-butyl bromide which on the basis of the $\Delta C_p^{\neq}$ value tends toward a limiting mechanism ($\Delta C_p^{\neq}$ for *tert*-butyl chloride = -81 cal deg^{-1} mol^{-1}) yet there is no evidence of an enhanced positive charge. Hence, we conclude that the electrostatic influence of the cation on water structure is relatively small. It might be claimed as a possible weakness of this argument, that the transition state for all the sulfonates is reached at an early stage in charge development but at least in *C* the fact that k_H/k_D is about the same for the methanesulfonate as for the bromide would seem to discount such an assertion. From evidence such as given in Table 1 (19), and from kinetic solvent isotope effects (23) we have concluded that in the *majority* of cases the positive charge on the cationic moiety at the transition state for molecules of the type studied to date does not contribute in an important way to $\Delta C_p^{\neq}$.

In a recent paper Ong and Robertson (24) reported that the apparent temperature coefficient of the enthalpy of activation ($\Delta C_p^{\neq}$) in the

TABLE 1. A comparison of $\Delta C_p^{\neq}$ values for hydrolysis in water

Class	Compound	$\Delta C_p^{\neq}$ (cal deg^{-1} mol^{-1})	Reference
A	Methyl bromide	−46	16
	Isopropyl bromide	−59	17
B	Methyl methanesulfonate	−38	18
	Isopropyl methanesulfonate	−35	18
C	3-Methyl-2-butyl bromide	−82	19
	3-Methyl-2-butyl methanesulfonate	−40	19

[2]We have modified the original equation by including $\delta+$ and $\delta-$ in the tight ion-pair since the degree of charge development is uncertain; probably not complete; may and probably does vary from compound to compound.

[3]Reference 22 refers to the tosylate ion but on the basis of $\Delta C_p^{\neq}$ values (1) the same conclusion is justified.

Can. J. Chem. Downloaded from www.nrcresearchpress.com by 210.87.254.6 on 09/05/12
For personal use only.

TABLE 2. Empirical constants* for the interpolation of rates

Compound	A_1	$-A_2$	$-A_3$	T_1–T_2 (°C)†
2,2-Dimethylcyclopropyl bromide	89.0183	9610.9980	25.2472	44–70
2,2-*cis*-Vinyl-*trans*-methylcyclopropyl bromide	58.5116	7978.0069	15.0763	40–72
2,2-*cis*-Methyl-*trans*-vinylcyclopropyl bromide	65.8359	8383.3871	17.4815	40–70

*For the equation $\log_{10} k = A_1 + A_2/T + A_3 \log_{10} T$.
†T_1–T_2 define experimental temperature range.

hydrolysis of *cis*- and *trans*-2-vinylcyclopropyl bromide was about -30 cal deg^{-1} mol^{-1}. This was as unusual[4] a value of $\Delta C_p^{\ddagger}$ for the hydrolysis of a halide in water, as it was unexpected, particularly where some evidence pointed to an ionic mechanism (25). Previous determinations of this temperature coefficient for the hydrolysis of a series of unsaturated halides gave no cause to suspect that the initial state solvation effects could be responsible for such low[5] values (26, 27). Hence, by implication the cause was presumed to lie in some feature of the activation process. Since the work reported by Ong and Robertson was the first study of the hydrolysis of vinylcyclopropyl bromides in water to determine the temperature coefficient of $\Delta H^{\ddagger}$, further work was needed to resolve the apparent anomaly revealed by their results. In that paper we reported rate data and derived parameters for the hydrolysis of *cis*- and *trans*-2-vinylcyclopropyl bromides. Here are given results for the hydrolysis of 2,2-dimethyl and 2,2-methylvinylcyclopropyl bromides. Complementary work on a series of 2,3-dimethylcyclopropyl bromides will be reported at an early date.

Results and Discussion

The solvolytic rate data for the hydrolysis of 2,2-dimethyl and 2,2-methylvinylcyclopropyl bromides were obtained over a range of temperatures by a conductance method which has been described adequately in previous papers (28). Experimental details with regard to synthetic methods follow the discussion. In so far as could be determined the product forming step occurred after the transition state and the resulting alcohols corresponded to the respective allyl cations. The temperature dependence of the rates for each series has been shown to conform to the equation

$$[2] \quad \log_{10} k_1 = A_1 + A_2/T + A_3 \log_{10} T$$

within experimental error. Corresponding constants derived from a least-mean-squares fit, assuming all significant error rests in k, are given in Table 2. These equations permit the calculation of rates at intermediate temperatures and in conjunction with the application of transition state formalism provided for the derivation of apparent values of $\Delta G^{\ddagger}$, $\Delta H^{\ddagger}$, $\Delta S^{\ddagger}$ and $\Delta C_p^{\ddagger}$ (1). The interpretation of the last of these derived terms provided the focus for this paper. Values of these terms together with the related terms from the work of Ong and Robertson (24) are given in Table 3.

It is evident that the values of $\Delta C_p^{\ddagger}$ were not altered by the substitution of the methyl group for β-hydrogen although the rates of hydrolysis were increased significantly:

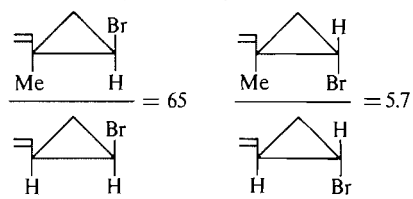

I II

Replacement of the vinyl group by methyl to give 2,2-dimethylcyclopropyl bromide resulted in a more negative value of $\Delta C_p^{\ddagger}$ though the value (-52 cal deg^{-1} mol^{-1}) was still in the "normal" range for primary or secondary halides. Unquestionably, the β-vinyl group resulted in

[4]While exceptional values are known, the majority of $\Delta C_p^{\ddagger}$ values are consistent with the generalization that those halides which would be expected to react by an S_N2 mechanism will have a value of -50 ± 5 cal deg^{-1} mol^{-1} while halides where other evidence would suggest might react by an S_N1 mechanism, yield values between -80 and -100 cal deg^{-1} mol^{-1} (1).

[5]"Low" refers to less negative $\Delta C_p^{\ddagger}$ values.

TABLE 3. Enthalpies, entropies, and heat capacities of activation for the solvolysis in water of 2,2-disubstituted cyclopropylbromides at 50 °C

Compound	$\Delta H^{\neq}$ (kcal mol^{-1})	$\Delta S^{\neq}$ (cal deg^{-1} mol^{-1})	$\Delta C_p^{\neq}$ (cal deg^{-1} mol^{-1})
2,2-Dimethylcyclopropyl bromide	27.120 ± 0.02	6.56 ± 0.05	−52 ± 2
2,2-*cis*-Vinyl-*trans*-methylcyclopropyl bromide	26.230 ± 0.02	4.14 ± 0.06	−27 ± 4
2,2-*cis*-Methyl-*trans*-vinylcyclopropyl bromide	26.549 ± 0.01	5.10 ± 0.02	−37 ± 2
trans-2-Vinylcyclopropyl bromide	26.360 ± 0.10	1.29 ± 0.03	−35 ± 2*
cis-2-Vinylcyclopropyl bromide	27.960 ± 0.28	0.85 ± 0.08	−27 ± 4*

*Reference 24.

TABLE 4. Summary of $\Delta C_p^{\neq}$ values and relative rates for the hydrolysis of a series of unsaturated halides

Compound	$\Delta C_p^{\neq}$ (cal deg^{-1} mol^{-1})	Relative rates (40 °C)	Reference
Allyl chloride	50 ± 1	1	26
β-Methylallyl chloride	49 ± 5	8	34
α-Methylallyl chloride	92 ± 3	720	34
trans-γ-Methylallyl chloride	82 ± 3	620	34
cis-γ-Methylallyl chloride	66 ± 1	50	34

significantly more positive values of $\Delta C_p^{\neq}$.

In searching for a possible explanation for the "abnormal" $\Delta C_p^{\neq}$ values which characterize the hydrolysis of β-vinyl substituted cyclopropyl bromides (Table 3) we note that the effect of such substitution is to enhance the rate relative to the unsubstituted parent compound.[6]

Substitution of a methyl group for a β-hydrogen in such compounds has a further accelerating effect on concerted disrotatory ring opening which differs depending on the configuration of the leaving group (29). Such changes in the relative rate ratios are consistent with the explanation that in case [I] there is relief of steric strain whereas in the other [II] there is an increase in the non-bonded interaction in the activation process. In neither case can the effect of the β-methyl on the rate of hydrolysis be considered large.

Furthermore we note that β-methyl substitution makes no difference in the values of $\Delta C_p^{\neq}$ (Table 3). In all four cases the value of these coefficients indicates that charge development was either very small (24) or was cancelled out in so far as external indications are concerned, *i.e.* in all four examples, the external effects of charge development were insufficient to cause significant modification in the surrounding hydrophobic solvent shell.

The participation hypothesis (30) proposed by Schleyer and co-worker to explain the enhanced reactivity of the cyclopropyl compounds compared to an earlier explanation offered by Roberts and Chambers (31) provided for the possibility of an unusual activation process and hence for the possibility of unusual values of $\Delta C_p^{\neq}$. Participation alone had been found to be associated with more negative rather than less negative values of $\Delta C_p^{\neq}$ (19, 32–34). In the case of the 2,2-dimethyl substituted cyclopropyl bromide, the value of $\Delta C_p^{\neq}$ is not minimal, hence participation alone through σ-bonding is unlikely to be a cause.

Initially the possibility of a temperature-dependent solvation effect analogous to that postulated by Robertson and Rossall (35) was entertained as a possible source of abnormal $\Delta C_p^{\neq}$ values in the system. However the values of $\Delta C_p^{\neq}$ found for a series of allylic compounds (Table 4) as well as the accumulation of data for other cyclopropyl bromides seemed to oppose such an explanation.

The problem inherent in the $\Delta C_p^{\neq}$ values found for the 2-vinyl substituted cyclopropyl

[6]Estimated k_i for cyclopropyl bromide at 100 °C is 1.74×10^{-6} s^{-1}; the 2-*cis* and 2-*trans*-vinylcyclopropyl bromides react 280 and 3000 times faster at the same temperature.

Can. J. Chem. Downloaded from www.nrcresearchpress.com by 210.87.254.6 on 09/05/12
For personal use only.

Can. J. Chem. Downloaded from www.nrcresearchpress.com by 210.87.254.6 on 09/05/12
For personal use only.

bromides was how to rationalize the indications that solvent reorganization was not occurring and the concomitant implication that charge development was minimal with the other evidence in favor of enhanced steric hindrance and release of non-bonded interaction which pointed to considerable degree of charge development at the transition state. Here the operative word is "considerable" and the question follows "why is there not, therefore, considerable solvent reorganization?".

One answer to that question is that while our earlier assumption of a relation existing between charge development at the transition state, solvent reorganization, and $\Delta C_p^{\neq}$ was valid in a general sense, the relationship is neither simple nor necessarily linear.

The apparent paradox created by evidence of ring opening yet negligible evidence of charge development may be rationalized if it is recognized that while the coefficient $\Delta C_p^{\neq}$ is assumed to reflect the effect of charge on water structure, it gives no indication of the degree to which internal electrostatic interactions reduce the effect of charge on the surrounding solvent shell. Thus with the β-vinyl substituted cyclopropyl system an extended conjugated system is in the process of being formed which could result in a tight-ion pair and thus effectively cancel external effects. In line with this proposal is the observation that the 2-*cis* epimer which tends to a sickle-form ion (36) has a more positive value of $\Delta C_p^{\neq}$ than the *trans* isomer both in this work and in the earlier work of Ong and Robertson. The unexpected difference in the $\Delta C_p^{\neq}$ values for the *cis*- and *trans*-crotyl chlorides (Table 4) might be considered as further evidence supporting this interpretation. Such a hypothesis is not advanced as a universal explanation for all "low" $\Delta C_p^{\neq}$ values but it does raise the question as to what the "normal" value of $\Delta C_p^{\neq}$ should be for a tight ion-pair involving a developing halide ion[7] and provides an alternative to the previous suggestion that the transition state was reached at an early stage along the reaction coordinate (24).

The "low" values of $\Delta C_p^{\neq}$ reported here are by no means unique. Thus a whole series of substituted alkyl benzenesulfonates and methanesulfonates gave values of $\Delta C_p^{\neq}$ in the same range as was found for the 2-vinyl and 2,2-vinylmethylcyclopropyl bromides (1). Kohnstam had also reported many similar values of $\Delta C_p^{\neq}$ (2) for hydrolysis of a wide range of reactants in different solvent mixtures where the possibility of contributions from hydrophobic bonding to $\Delta C_p^{\neq}$ was extremely unlikely. The value of $\Delta C_p^{\neq}$ found for the hydrolysis of isopropyl chloride in water is -37 cal deg^{-1} mol^{-1} (17). In view of the more recent information presented here, the tight-ion pair which reduces external solvation effects appears to be a more appropriate model for rationalizing the seemingly contradictory evidence of participation and $\Delta C_p^{\neq}$ value near -30 cal deg^{-1} mol^{-1} for the 2-vinyl and 2,2-methylvinylcyclopropyl bromides. Whether this alternative is significantly different from the suggestion of Ong and Robertson that the transition state occurs at an early stage along the reaction co-ordinate is an open question.

The recognition that the external effects of a tight ion-pair need not reflect the degree of charge development is not restricted to kinetic situations. Thus Ting-Po I and Grunwald (37) show that the LiCl ion-pair does not "freeze" solvent and remains similar to LiCl in the gas phase. This is an extreme example compared to the ion-pairs which presumably is characteristic of the transition states discussed above. In the case of the benzenesulfonic ion, the introduction of a *p*-nitro substituent is claimed to shift the electrical center from near the sulfonate oxygens to the benzene ring (37). This shift appears to have but a small effect on $\Delta C_p^{\neq}$ (1) suggesting either the transition state occurs at an early stage in charge development, or that the charge is dispersed or both, as could be argued both from α-deuterium and kinetic solvent isotope effects. The rather obvious fact stands out that solvation effects whether evaluated in terms of "*m*" values, salt effects or $\Delta C_p^{\neq}$ reflect only the external effects of charge development.

Experimental

The *gem*-dihalides were synthesized by the addition of dibromocarbene to the appropriate olefin. The dibromocarbene was generated from bromoform and potassium *tert*-butoxide according to the procedure described by Van der Kerk (38). The reduction of the *gem*-dibromo compound was carried out following the procedure of Seyferth *et al.* (39).

[7]Values of $\Delta C_p^{\neq}$ in the dimethylcyclopropyl derivatives are now known to cover the range -52 to -145 cal deg^{-1} mol^{-1}.

Can. J. Chem. Downloaded from www.nrcresearchpress.com by 210.87.254.6 on 09/05/12
For personal use only.

1,1-Dibromo-2,2-dimethylcyclopropane

Isobutene (100 g, 1.78 mol, K and K) and potassium *tert*-butoxide (76 g, 0.68 mol, Ventron Alpha Products), were placed in a two litre 3-neck flask. Distilled bromoform (130 g, 0.52 mol, Fisher Scientific) was added dropwise at about −25 °C under nitrogen. The mixture was stirred for 2 h after addition was complete. Then the temperature was raised slowly to 20 °C. The addend was hydrolysed with 250 ml water and the organic layer separated. The aqueous layer was extracted with two 50 ml portions of pentane and the combined organic solutions were dried over anhydrous Na_2SO_4. The solvent was removed under vacuum and then the residue was distilled. The desired product has bp 41–43 °C/8.5–9 mm.

1-Bromo-2,2-dimethylcyclopropane

1,1-Dibromo-2,2-dimethylcyclopropane from the above synthesis (10.8 g, 0.05 mol) was reduced with tri-*n*-butyltin hydride (13.8 g, 0.05 mol) to give 1-bromo-2,2-dimethylcyclopropane (bp 25 °C/33 mm). This product was purified further through glc using 30% QF_1 on 45/60 Chrom W in a 20 ft × $\frac{3}{8}$ in. column. The sample collected was >99.9% pure; nmr (CCl_4) δ (TMS) 2.70 (m, 1H, CHBr), 1.12, 1.24 (2s, 6H, CH_3), 0.60, 0.93 (m, 2H, —CH_2—). Mass spectrum gave parent peaks at *m/e* 148, 150 (1:1), base peak at *m/e* 69 ($C_5H_9^+$) and significant fragments at *m/e* 133 and 135 (M-15), 53 and 41.

1,1-Dibromo-2-methyl-2-vinylcyclopropane

2-Methylbutadiene (50 g, 0.73 mol, Aldrich Chemicals) and potassium *tert*-butoxide (90 g, 0.80 mol, Alpha Products) and 200 ml of dry pentane were placed in a one litre 3-neck flask and kept under a positive pressure of N_2. Freshly distilled bromoform (175 g, 0.69 mol) was added dropwise at −5 °C under N_2. The mixture was stirred overnight after the addition was complete, then hydrolysed with 200 ml of water, and treated as above. The product has bp 45–50 °C/5 mm.

1-Bromo-2-methyl-2-vinylcyclopropane

1,1-Dibromo-2-methyl-2-vinylcyclopropane from above (23 g, 0.09 mol) was reduced with tri-*n*-butyltin hydride (27 g, 0.09 mol) to get 1-bromo-2-methyl-2-vinylcyclopropane. The two isomeric monobromides were separated on a prep-glc column using 30% FFAP column on Chromosorb 60–80, 20 ft × $\frac{3}{8}$ in. Identification of the isomers was made by nmr and mass spectrum.

2,2-cis-Vinyl-trans-methylcyclopropyl bromide

The nmr (CCl_4) δ (TMS) 5.30–5.58 (m, 1H, —CH=), 4.80–5.02 (m, 2H, =CH), 2.78–2.93 (m, 1H, —CHBr), 1.34 (s, 3H, —CH_3), 0.78–0.92 (m, 2H, —CH_2—). Mass spectrum gave parent peak at *m/e* 160, 162 (1:1), base peak at *m/e* 79 and significant fragments at *m/e* 81, 80, 77, 53, 41.

2,2-cis-Methyl-trans-vinylcyclopropyl bromide

The nmr (CCl_4) δ (TMS) 5.56–5.88 (m, 1H, —CH=), 4.90–5.14 (m, 2H, =CH_2), 2.78–2.94 (m, 1H, —CHBr), 1.22 (s, 3H, —CH_3), 0.96–1.12 (m, 2H, —CH_2—). Mass spectrum gave exactly the same peak distribution as the isomer.

Note on Identification of Isomers

It has been found that in most cases the *endo*-proton (*i.e.* the *exo*-isomer) (40, 41) absorbs at a higher field than the *exo*-proton (*i.e. endo*-isomer). This shielding effect is associated with the diamagnetic anisotropy of the carbon–carbon on the same side of the ring at the β-carbon. Meiboom and Snyder (42) reported that the vicinal coupling constant *J-cis* is larger than *J-trans*, an observation supported by the earlier calculations of Karplus (43). The stereochemical assignments made on the basis of nmr spectroscopy were found to be consistent with the kinetic data.

1. R. E. Robertson. Progr. Phys. Org. Chem. **4**, 213 (1967).
2. G. Kohnstam. Adv. Phys. Org. Chem. **5**, 121 (1967).
3. D. H. Everett and W. F. K. Wynne-Jones. Trans. Faraday Soc. **35**, 1380 (1939).
4. J. R. Hullet. Q. Rev. (London), **18**, 227 (1964).
5. H. S. Frank and M. W. Evans. J. Chem. Phys. **13**, 507 (1945).
6. D. D. Eley. Trans. Faraday Soc. 184 (1944).
7. D. N. Glew and E. A. Moelwyn-Hughes. Discuss. Faraday Soc. **15**, 150 (1953).
8. R. E. Robertson. Can. J. Chem. **33**, 1536 (1955).
9. D. H. Everett and W. F. K. Wynne-Jones. Proc. Roy. Soc. **117**A, 499 (1941).
10. D. J. G. Ives and P. D. Marsden. J. Chem. Soc. 649 (1965).
11. S. Winstein, B. Appel, R. Baker, and B. Diaz. Chem. Soc. Special Publ. No. **19**, 109 (1965) and references therein.
12. R. A. Sneen and J. W. Larsen. J. Am. Chem. Soc. **91**, 362 (1969) and subsequent papers.
13. J. M. W. Scott and R. E. Robertson. Can. J. Chem. **50**, 167 (1972).
14. R. L. Kay. Adv. Chem. **73**, 1 (1968).
15. S. Lobo. Ph.D. Thesis, University of Calgary, Calgary, Alberta. 1975.
16. R. L. Heppolette and R. E. Robertson. Proc. Roy. Soc. London, A**252**, 273 (1959).
17. R. L. Heppolette and R. E. Robertson. Can. J. Chem. **44**, 677 (1966).
18. P. W. C. Barnard and R. E. Robertson. Can. J. Chem. **39**, 881 (1961).
19. Y. Inomoto, R. E. Robertson, and G. Sarkis. Can. J. Chem. **47**, 4599 (1969).
20. V. J. Shiner, Jr. *In* Isotope effects in chemical reactions. *Edited by* D. J. Collins and N. S. Bowman. Van Nostrand and Reinhold Co., New York. 1970. Chapt. 2.
21. C. K. Ingold. Structure and mechanism in organic chemistry. Cornell University Press, Ithaca, N.Y. 1953. Chapt. VII.
22. H. M. R. Hoffman. J. Chem. Soc. 6753 (1965).
23. P. M. Laughton and R. E. Robertson. *In* Solute–solvent interactions. *Edited by* J. F. Coetzee and C. D. Ritchie. Marcel Dekker, N.Y. 1969. Chapt. 7.
24. J. H. Ong and R. E. Robertson. Can. J. Chem. **52**, 2660 (1974).
25. W. F. Sliwinski, T. M. Su, and P. v. R. Schleyer. J. Am. Chem. Soc. **94**, 133 (1972).
26. R. E. Robertson and J. M. W. Scott. J. Chem. Soc. 1596 (1961).

27. L. J. BRUBACHER, L. TREINDL, and R. E. ROBERTSON. J. Am. Chem. Soc. **90**, 4611 (1968).
28. R. E. ROBERTSON and S. E. SUGAMORI. J. Am. Chem. Soc. **91**, 7254 (1969).
29. P. v. R. SCHLEYER, W. F. SLINWINSKI, G. W. VAN DINE, U. SCHÖLLKOPF, J. PAUST, and K. FELLENBERGER. J. Am. Chem. Soc. **94**, 125 (1972).
30. P. v. R. SCHLEYER and R. D. NICHOLAS. J. Am. Chem. Soc. **83**, 182 (1961).
31. J. D. ROBERTS and V. C. CHAMBERS. J. Am. Chem. Soc. **73**, 5036 (1951).
32. M. J. BLANDAMER, H. S. GOLINKIN, and R. E. ROBERTSON. J. Am. Chem. Soc. **91**, 2678 (1969).
33. H. S. GOLINKIN, D. M. PARBHOO, and R. E. ROBERTSON. Can. J. Chem. **48**, 1296 (1970).
34. L. J. BRUBACHER, L. TREINDL, and R. E. ROBERTSON. J. Am. Chem. Soc. **90**, 4611 (1968).
35. R. E. ROBERTSON and B. ROSSALL. Can. J. Chem. **49**, 1441 (1971).
36. SURENDRA SINGH. Ph.D. Thesis, University of Calgary, Calgary, Alberta. 1975.
37. TING-PO I and E. GRUNWALD. J. Am. Chem. Soc. **96**, 2387 (1974).
38. G. J. M. VAN DER KERK, J. A. NOLTÉS, and J. G. A. LUIJTEN. J. Appl. Chem. **7**, 366 (1957).
39. D. SEYFERTH, H. YAMAZAKI, and D. ALLESTON. J. Org. Chem. **28**, 703 (1963).
40. W. G. DAUBEN and T. WIPKE. J. Org. Chem. **32**, 2976 (1967).
41. C. K. FAY, J. B. GRUTZNER, L. F. JOHNSON, S. SERNHELL, and P. W. WESTERMAN. J. ORG. Chem. **38**, 3122 (1973).
42. S. MEIBOOM and L. C. SNYDER. J. Am. Chem. Soc. **89**, 1038 (1967).
43. M. KARPLUS. J. Chem. Phys. **30**, 11 (1959).

Can. J. Chem. Downloaded from www.nrcresearchpress.com by 210.87.254.6 on 09/05/12
For personal use only.

The effect of alkene structure upon the rates and product composition of addition of 4-chlorobenzenesulfenyl chloride[1]

GEORGE H. SCHMID, COLEEN L. DEAN, AND DENNIS G. GARRATT
Department of Chemistry, University of Toronto, Toronto, Ontario M5S 1A1

Received November 12, 1975

Can. J. Chem. Downloaded from www.nrcresearchpress.com by 210.87.254.40 on 09/05/12
For personal use only.

GEORGE H. SCHMID, COLEEN L. DEAN, and DENNIS G. GARRATT. Can. J. Chem. **54**, 1253 (1976).

The rates and products of addition of 4-chlorobenzenesulfenyl chloride to 30 mono- and disubstituted alkenes have been determined in 1,1,2,2-tetrachloroethane at 25 °C. The rates of addition span a range of 10^6. No correlation with the extended Taft equation was found with the rates of all 30 compounds. The rate ratio k_c/k_t for addition to nine pairs of isomeric *cis–trans* alkenes ranges from a low of 3.1 for the 2-butenes to a high of 1.57×10^5 for the 2,2,5,5-tetramethyl-3-hexenes. The rate ratio k_c/k_t does not always increase regularly with the increasing size of the substituents which suggests that relief of ground state strain is not important in the rate determining transition state. Greater steric hindrance between the electrophile and the *trans* alkene compared to the *cis* isomer is proposed to account for the results.

GEORGE H. SCHMID, COLEEN L. DEAN et DENNIS G. GARRATT. Can. J. Chem. **54**, 1253 (1976).

On a déterminé, dans le tétrachloro-1,1,2,2 éthane à 25 °C, les vitesses et les produits d'addition du chlorure de chloro-4 benzènesulfényle à 30 alcènes mono- et disubstitués. Les vitesses d'addition s'étalent sur une échelle de vitesse variant par 10^6. On n'a trouvé aucune relation entre l'équation élargie de Taft et les vitesses de réaction des 30 composés. Les rapports de vitesse k_c/k_t pour les additions à neuf paires d'isomères *cis–trans* varient d'une valeur de 3.1 pour les butènes-2 jusqu'à une valeur de 1.57×10^5 pour les tétraméthyl-2,2,5,5 hexènes-3. Les rapports de vitesse k_c/k_t n'augmentent pas d'une façon régulière avec une augmentation du volume des substituants; ces résultats suggèrent que l'élimination des contraintes dans l'état fondamental n'est pas le facteur important dans l'étape déterminante de la réaction. Pour expliquer les résultats on suggère qu'il existe, entre l'électrophile et l'alcène *trans*, un empêchement stérique plus grand qu'avec l'alcène *cis*.

[Traduit par le journal]

Introduction

The addition of arenesulfenyl chlorides to alkenes has been extensively studied by a number of workers (2–5). As a result of these investigations, a mechanism has been proposed involving a rate determining formation of a thiiranium ion which is then attacked by chloride ion in the product determining step. This two-step mechanism is illustrated in Scheme 1.

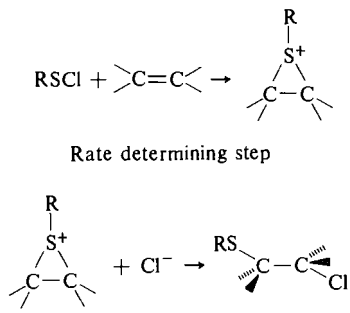

SCHEME 1

A number of workers have studied the influence of the structure of the alkene on the rate of addition of arene- and alkanesulfenyl halides. Beverly and Hogg (6) measured the rate of addition of 2,4-dinitrobenzenesulfenyl chloride to six alkyl substituted olefins. Thaler (7) obtained the relative rates of reaction of a series of alkyl substituted alkenes with methanesulfenyl chloride by means of a series of competitive rate determinations. These results are suspect, however, since it has been shown that the competitive method of obtaining rates of arene- or alkanesulfenyl chloride additions to alkenes suffers from the fact that thermodynamically rather than kinetically controlled product mixtures are often formed (8). Pritzkow and co-workers (9) have

[1]Reactions of sulfenyl chlorides and their derivatives. XIII. For part XII, see ref. 1.

Can. J. Chem. Downloaded from www.nrcresearchpress.com by 210.87.254.40 on 09/05/12
For personal use only.

TABLE 1. The specific rate constants for the addition of 4-chlorobenzenesulfenyl chloride to alkenes in 1,1,2,2-tetrachloroethane at 25 °C

Alkene		k_2 (M^{-1} s^{-1})	Number of runs	k_c/k_t
		Terminal Alkenes		
$CH_2{=}CH_2$	**1**	65 ± 3.0	8	
$CH_3CH{=}CH_2$	**2**	205 ± 18	6	
$C_2H_5CH{=}CH_2$	**3**	248 ± 10	4	
i-$C_3H_7CH{=}CH_2$	**4**	140 ± 2	4	
n-$C_4H_9CH{=}CH_2$	**5**	133 ± 5	3	
t-$C_4H_9CH{=}CH_2$	**6**	95 ± 3	3	
$(CH_3)_2C{=}CH_2$	**7**	550 ± 50	6	
$(C_2H_5)_2C{=}CH_2$	**8**	372 ± 7	3	
$(t$-$C_4H_9)_2C{=}CH_2$	**9**	0.0317 ± 0.0005	4	
$C_2H_5(CH_3)C{=}CH_2$	**10**	611 ± 1	4	
i-$C_3H_7(CH_3)C{=}CH_2$	**11**	420 ± 5	4	
t-$C_4H_9(CH_3)C{=}CH_2$	**12**	147 ± 2	4	
		cis–trans Isomers		
$CH_3CH{=}CHCH_3$	*cis* **13**	1340 ± 100	16	3.1
	trans **14**	434 ± 13	11	
$C_2H_5CH{=}CHC_2H_5$	*cis* **15**	3563	3	9.2
	trans **16**	388	3	
i-$C_3H_7CH{=}CH$-i-C_3H_7	*cis* **17**	990 ± 20	3	9.8
	trans **18**	102 ± 1	2	
t-$C_4H_9CH{=}CH$-t-C_4H_9	*cis* **19**	846 ± 11	2	1.57×10^5
	trans **20**	$5.36 \pm 0.02\times10^{-3}$	2	
$C_2H_5CH{=}CHCH_3$	*cis* **21**	2690 ± 90	3	4.7
	trans **22**	568 ± 9	3	
i-$C_3H_7CH{=}CHCH_3$	*cis* **23**	2624 ± 54	2	8.1
	trans **24**	325 ± 4	2	
t-$C_4H_9CH{=}CHCH_3$	*cis* **25**	1029 ± 27	6	7.5
	trans **26**	162 ± 6	5	
i-$C_3H_7CH{=}CHC_2H_5$	*cis* **27**	2769 ± 62	6	11.3
	trans **28**	245 ± 9	4	
t-$C_4H_9CH{=}CHC_2H_5$	*cis* **29**	1704 ± 40	2	14.1
	trans **30**	121 ± 1	2	

measured the rate of addition of 2,4-dinitrobenzenesulfenyl chloride to a large number of alkenes in acetic acid, by both a direct and a competitive technique.

The data from these studies are insufficient to enable us to establish the major effects of alkyl substituents upon both the rate and products of addition of sulfenyl halides to alkenes. The major problem is that rarely have kinetic data and product compositions been determined under comparable conditions. We wish to report a study of the effect of systematically varying the size and position of alkyl groups on the rate and product determining steps of the addition of 4-chlorobenzenesulfenyl chloride to alkenes.

Results

We have measured the rate of addition of 4-chlorobenzenesulfenyl chloride to 30 mono- and disubstituted alkenes in 1,1,2,2-tetrachloroethane (TCE) at 25 °C by means of the stopped-flow technique using a Durrum–Gibson stopped-flow spectrophotometer. The rate of disappearance of 4-chlorobenzenesulfenyl chloride was followed by measuring the decrease in its absorption at 392.5 nm. The addition was found to exhibit normal second-order kinetics, first-order in alkene and first-order in sulfenyl chloride to 80% completion of the reaction. The rate data are presented in Table 1.

The product compositions were determined by nmr spectroscopy. The basis of this method is that protons α or β to chlorine are considerably deshielded relative to those α or β to sulfur (10, 11). The nmr parameters of the adducts obtained in this study are reported in Table 2. In

TABLE 2. Proton magnetic resonance parameters of 4-chlorobenzenesulfenyl chloride adducts[a]

Alkene	Group assignments						Chemical Shifts (ppm), multiplicity					
	1	2	3	4	5	6	1	2	3	4	5	6
cis-2-Pentene	CH_3CS	CH_2CCl	CH_3CH_2		CHS	CHCl	1.36d	1.95m	1.10t		3.51dq	3.86dt
	CH_3CCl	CH_2CS	CH_3CH_2		CHS	CHCl	1.55d	1.95m	1.01t		3.15dt	4.21dq
trans-2-Pentene	CH_3CS	CH_2CCl	CH_3CH_2		CHS	CHCl	1.35d	1.83m	1.09t		3.30dq	3.90dt
	CH_3CCl	CH_2CS	CH_3CH_2		CHS	CHCl	1.57d	1.83m	1.00t		3.03dt	4.11dq
cis-3-Hexene	CH_3CH_2CS	CH_3CH_2CS	CH_3CH_2CCl	CH_3CH_2CCl	CHS	CCCl	1.00t	1.80m	1.90m	1.07t	3.17m	3.91dt
trans-3-Hexene	CH_3CH_2CS	CH_3CH_2CS	CH_3CH_2CCl	CH_3CH_2CCl	CHS	CHCl	1.00t	1.73dt	1.85dt	1.10t	3.10m	3.90m
cis-4-Methyl-2-pentene	$(CH_3)_2CCS$	CHCS	CH_3CCl		CHS	CHCl	1.00d	2.13m	1.60d		2.90dd	4.35dq
	$(CH_3)_2CCCl$	CHCl	CH_3CS		CHS	CHCl	1.07d	2.13m	1.50d		2.67m	3.70m
trans-4-Methyl-2-pentene	$(CH_3)_2CCS$	CHCS	CH_3CCl		CHS	CHCl	0.95d	2.50m	1.60d		2.98dd	4.16dq
	$(CH_3)_2CCCl$	CHCl	CH_3CS		CHS	CHCl	1.08d	2.50m	1.36d		2.64m	3.73m
cis-4,4-Dimethyl-2-pentene	*t*-BuCS	CH_3CCl			CHS	CHCl	1.13s	1.78d			2.93d	4.60dq
	t-BuCCl	CH_3CS			CHS	CHCl	1.15s	1.42d			3.60dq	3.82d
trans-4,4-Dimethyl-2-pentene	*t*-BuCS	CH_3CCl			CHS	CHCl	1.10s	1.63d			3.28d	4.66dq
	t-BuCCl	CH_3CS			CHS	CHCl	0.98s	1.38d			3.47dq	3.90d
cis-2-Methyl-3-hexene	$(CH_3)_2CCS$	CH_2CCl	CHCS	CH_3CH_2	CHS	CHCl	1.13d	1.93m	1.93m	1.00t	2.96dd	4.10dt
	$(CH_3)_2CCCl$	CH_2CS	CHCCl	CH_3CH_2	CHS	CHCl	1.14d	1.93m	1.93m	0.98t	3.16dt	3.76dd
trans-2-Methyl-3-hexene	$(CH_3)_2CCS$	CH_2CCl	CHCS	CH_3CH_2	CHS	CHCl	1.02d	1.80m	2.34m	0.95t	3.03dd	3.96dt
	$(CH_3)_2CCCl$	CH_2CS	CHCCl	CH_3CH_2	CHS	CHCl	1.13d	1.77m	2.54m	0.93t	3.13dt	3.80dd
cis-2,2-Dimethyl-3-hexene	*t*-BuCS	CH_2CCl	CH_3CH_2		CHS	CHCl	1.15s	1.86m	0.99t		3.01d	4.25dt
	t-BuCCl	CH_2CS	CH_3CH_2		CHS	CHCl	1.17s	1.86m	0.96t		2.91dt	4.27d
trans-2,2-Dimethyl-3-hexene	*t*-BuCS	CH_2CCl	CH_3CH_2		CHS	CHCl	1.06s	1.96m	1.03t		3.38d	4.36dt
	t-BuCCl	CH_2CS	CH_3CH_2		CHS	CHCl	1.10s	1.96m	1.01t		3.45dt	3.97d
cis-2,5-Dimethyl-3-hexene	$(CH_3)_2CCS$	$(CH_3)_2CCCl$	CHCS	CHCCl	CHS	CHCl	1.06d 0.86d	1.06d	2.13m	2.13m	2.95dd	3.85dd
trans-2,5-Dimethyl-3-hexene	$(CH_3)_2CCS$	$(CH_3)_2CCCl$	CHCS	CHCCl	CHS	CHCl	0.95d 0.55d	1.25d 1.08d	2.63m	2.63m	3.03dd	3.90dd
1-Butene	CH_3	CH_2CH	CH_2S	CHCl			1.58	1.9m	3.27m	3.63m		
3-Methyl-1-butene	$(CH_3)_2CH$	$(CH_3)_2CH$	CHCl	CH_2S			1.00d 0.88d	2.10m	3.88m	3.22d		
3,3-Dimethyl-1-butene	$(CH_3)_3C$	CHCl	CH_2S				1.13s	3.77dd	3.30dd 3.06dd			
1-Butene	CH_3	CH_2CH	CH_2Cl	CHS			1.07t	1.9m	3.68m	3.20m		
3-Methyl-1-butene	$(CH_3)_2CH$	$(CH_3)_2CH$	CHS	CH_2Cl			0.98d 1.15d	2.07m	3.12d	3.63m		
3,3-Dimethyl-1-butene	$(CH_3)_3C$	CHS	CH_2Cl				1.06s	2.96dd	3.84dd 3.49dd			
2-Methyl-1-butene	CH_3CH_2	CH_3CH_2	CH_3C	CH_2			1.05t	1.78q	1.60s	3.35s		
2,3-Dimethyl-1-butene	$(CH_3)_2CH$	$(CH_3)_2CH$	CH_3C	CH_2			1.00t	1.65q	1.25s	3.53s		
	$(CH_3)_2CH$	$(CH_3)_2CH$	CH_3C	CH_2			0.98d	2.07m	1.57s	3.35s		
	$(CH_3)_2CH$	$(CH_3)_2CH$	CH_3C	CH_2			1.03d	2.07m	1.13s	3.35q		
2,3,3-Trimethyl-1-butene	$(CH_3)_3C$	CH_3	CH_2									
	$(CH_3)_3C$	CH_3	CH_2				1.12s	1.65s	3.40s			
2-Ethyl-1-butene	CH_3CH_2	CH_3CH_2	CH_2				1.00t	1.85q	3.28s			
	CH_3CH_2	CH_3CH_2	CH_2				0.95	1.40q	3.42s			

[a]Abbreviations: s singlet, d doublet, t triplet, q quartet, m multiplet, dt doublet of triplets, dq doublet of quartets, dd doublet of doublets.

every case it was possible to find at least one nonoverlapping signal from which the isomer distribution could be calculated.

The kinetically controlled product composition was determined by immediate nmr analysis of the reaction mixture. This *in situ* determination of the adduct isomer ratio is necessary because of the known tendency of many β-chlorosulfides to isomerize (3–5).

The thermodynamically controlled product composition was determined by allowing the nmr sample tubes to stand at 25 °C until the product composition, as determined by nmr, remained constant. This technique results in the stereospecific isomerization of regioisomers (5). The kinetically and thermodynamically controlled product compositions are given in Table 3.

In Table 3 we use the designation Markownikoff and *anti*-Markownikoff to distinguish between isomeric adducts. Such nomenclature is confusing for adducts derived from 1,2-dialkyl substituted ethylenes. When both carbons contain an identical number of alkyl groups, we can define the Markownikoff isomer as that one in which the chlorine is bonded to the carbon atom whose sum of Tafts' inductive substituent constant (12), $\sum\sigma^*$, is the more negative. According to this designation the following are isomeric Markownikoff and *anti*-Markownikoff adducts.

The nmr data are consistent with products formed by stereospecific *anti*-addition. Symmetrical *cis–trans* isomeric alkenes each give only one product which differ in their pmr spectra in the expected manner. Unsymmetrical alkenes form two different products whose identity, as established by nmr, are consistent with a pair of Markownikoff and *anti*-Markownikoff

Can. J. Chem. Downloaded from www.nrcresearchpress.com by 210.87.254.40 on 09/05/12
For personal use only.

Can. J. Chem. Downloaded from www.nrcresearchpress.com by 210.87.254.40 on 09/05/12
For personal use only.

Markownikoff adduct	*Anti*-Markownikoff adduct
$C_2H_5CHCHCH_3$ (Cl, SAr)	$C_2H_5CHCHCH_3$ (SAr, Cl)
$(CH_3)_3CCHCHCH(CH_3)_2$ (Cl, SAr)	$(CH_3)_3CCHCHCH(CH_3)_2$ (SAr, Cl)
$(CH_3)_2CCC_2H_5$ (Cl, SAr)	$(CH_3)_2CCHC_2H_5$ (SAr, Cl)

isomers. Furthermore their isomerization serves to establish their relative configuration. The sole examples of nonstereospecific addition occur in the case of the addition of 2,4-dinitrobenzene sulfenyl chloride to *cis*- and *trans*-1-phenylpropenes containing methoxy, isopropoxy, and phenoxy substituents on the ring (1, 13). These alkenes are all capable of forming highly stabilized benzylic cations. Our results as well as previous evidence clearly establishes that the addition of alkane and arenesulfenyl chloride to aliphatic alkenes occurs stereospecifically *anti*.

TABLE 3. Kinetically and thermodynamically controlled products of addition of 4-chlorobenzenesulfenyl chloride to unsymmetrical alkenes in 1,1,2,2-Tetrachloroethane at 25 °C

Alkene		KCP[a] M	KCP[a] aM	TCP[a] M	TCP[a] aM
$CH_3CH{=}CH_2$		38	62	68	32
$C_2H_5CH{=}CH_2$		23	77	70	30
i-$C_3H_7CH{=}CH_2$		0	100	100	0
n-$C_4H_9CH{=}CH_2$		32	68	65	35
t-$C_4H_9CH{=}CH_2$		0	100	>95	<5
$(CH_3)_2C{=}CH_2$		12	88	95	5
$(C_2H_5)_2C{=}CH_2$		41	59	100	0
$(t$-$C_4H_9)_2C{=}CH_2$		0	100	26[b]	59[b]
$C_2H_5(CH_3)C{=}CH_2$		46	54	100	0
i-$C_3H_7(CH_3)C{=}CH_2$		47	53	100	0
t-$C_4H_9(CH_3)C{=}CH_2$		0	100	100	0
$C_2H_5CH{=}CHCH_3$	*cis*	33	67		
	trans	32	68	72	28
i-$C_3H_7CH{=}CHCH_3$	*cis*	0	100	76	24
	trans	17	83	81	19
t-$C_4H_9CH{=}CHCH_3$	*cis*	0	100	100	0
	trans	0	100		
i-$C_3H_7CH{=}CHC_2H_5$	*cis*	10	90	>95	<5
	trans	37	63	>95	<5
t-$C_4H_9CH{=}CHC_2H_5$	*cis*	0	100	85[b]	15[b]
	trans	0	100	93[b]	7[b]

[a]KCP = kinetically controlled product composition; TCP = thermodynamically controlled product composition; M = Markownikoff orientation; aM = *anti*-Markownikoff orientation.
[b]Probably not KCP/TCP.

Discussion

The values of the specific rate constants given in Table 1 span a range of 10^6. In general substituting electron-donating alkyl groups for the hydrogens of ethylene causes an increase in rate. The exceptions are compounds **9** and **20**. This rate increase reaches a maximum when an ethyl group is substituted for hydrogen and then decreases as the size of the alkyl group increases. These data indicate that both polar and steric effects are important in the rate determining transition state.

In order to evaluate the relative importance of these two effects an extended Taft correlation (12) was attempted with all 30 compounds. Such a correlation was unsuccessful. Satisfactory correlations with both the simple and extended Taft equation could be obtained by excluding selected members of the 30 compounds. (Particularly compounds with sterically bulky groups such as *tert*-butyl.) Such correlations with rather limited series of compounds (6, 8) or compounds of similar structure (9) have been previously reported. Similar problems have been encountered in correlating rates of bromination of alkenes with the Taft equations (14).

The failure of the Taft equations to correlate the rate of addition of all 30 alkenes may be due to several reasons. Firstly, the steric constants, E_s, are determined from the hydrolysis of aliphatic esters, a reaction whose steric requirements are quite different from those of the addition of arenesulfenyl halides to alkenes. However, an attempt to improve the correlation by using the steric substituent constants E_s*, obtained by Fellous and Luft (15) for the addition of disiamylborane to alkenes was unsuccessful. A second reason may be that the steric effects of the substituents are not additive, which would be important for large bulky groups.

A third possibility is that there is a change in the structure of the rate determining transition state as the bulk of the alkyl substituents increases. The available evidence is not in accord with this possibility. Addition occurs in an *anti* stereospecific manner in all cases, even for *cis*- and *trans*-1,2-di-*tert*-butylethylene (17). For all unsymmetrical alkenes products with *anti*-Markownikoff as well as Markownikoff orientation are obtained. Furthermore, in the case of disubstituted ethylenes, the effect of the two alkyl substituents is relatively independent of their

Can. J. Chem. Downloaded from www.nrcresearchpress.com by 210.87.254.40 on 09/05/12
For personal use only.

TABLE 4. Rates of addition of 4-chlorobenzenesulfenyl chloride to sets of alkenes containing the same substituents

Alkene		k_2 (M^{-1} s^{-1})	Alkene		k_2 (M^{-1} s^{-1})
$(CH_3)_2C{=}CH_2$	**7**	550 ± 50	$C_2H_5(CH_3)C{=}CH_2$	**10**	611 ± 1
cis-$CH_3CH{=}CHCH_3$	**13**	1340 ± 100	*cis*-$CH_3CH{=}CHC_2H_5$	**21**	2690 ± 90
trans-$CH_3CH{=}CHCH_3$	**14**	434 ± 13	*trans*-$CH_3CH{=}CHC_2H_5$	**22**	568 ± 9
$(C_2H_5)_2C{=}CH_2$	**8**	372 ± 7	*i*-$C_3H_7(CH_3)C{=}CH_2$	**11**	420 ± 5
cis-$C_2H_5CH{=}CHC_2H_5$	**15**	3563	*cis*-$CH_3CH{=}CH$-*i*-C_3H_7	**23**	2624 ± 54
trans-$C_2H_5CH{=}CHC_2H_5$	**16**	388	*trans*-$CH_3CH{=}CH$-*i*-C_3H_7	**24**	325 ± 4
			t-$C_4H_9(CH_3)C{=}CH_2$	**12**	147 ± 2
			cis-$CH_3CH{=}CH$-*t*-C_4H_9	**25**	1029 ± 27
			trans-$CH_3CH{=}CH$-*t*-C_4H_9	**26**	162 ± 6

positions. Thus two alkyl groups substituted on one carbon have about the same effect as when they are substituted on adjacent carbons. The data are summarized in Table 4. Thus the specific rate constants for addition to compounds **7**, **8**, **10**, **11**, and **12** are almost identical to those for addition to their isomeric *trans* alkenes **14**, **16**, **22**, **24**, and **26** respectively. The agreement is not as good with the *cis* isomers and between the 1,1- and 1,2-di-*tert*-butylethylenes. These results are most simply explained by invoking a bridged transition state in both the rate and product determining steps for all the reactions studied here.

While our data did not correlate with established linear free energy relationships it is clear that both polar and steric factors are important in the rate determining transition state. With methyl and ethyl substituents the polar effect is dominant, while as the groups become bulkier the steric effect becomes the dominant one as in the case of the di-*tert*-butylethylenes.

One of the most interesting aspects of this study is the effect on the rate of addition of the position, *cis* or *trans*, of the two alkyl groups of a 1,2-dialkylethylene. The data in Table 1 give the results of the rate of addition to nine pairs of isomeric *cis*–*trans* alkenes. We have found that the addition to the *cis* isomer always occurs faster than to the *trans* isomer. The ratio, k_c/k_t, ranges from a low of 3.1 for the 2-butenes to a high of 1.57×10^5 for the 2,2,5,5-tetramethyl-3-hexenes. These ratios are generally slightly lower than those reported by Pritzkow and co-workers (9) for the addition of 2,4-dinitrobenzenesulfenyl chloride to four isomeric *cis*–*trans* alkene pairs but are still higher than the ratios obtained for the addition of bromine, ISCN, and NOCl.

In general the ratio k_c/k_t given in Table 1 increases with increasing size of the alkyl substituents. This can be best appreciated by collecting the data as shown in Table 5 in which the compounds have been arranged into four series. In the three 1,2-disubstituted ethylene series one alkyl group remains constant while the other is progressively varied from methyl, ethyl, isopropyl, to *tert*-butyl, while in the fourth series the two substituents are identical.

In two of the four series the ratio k_c/k_t increases regularly with increasing size of the substituents. The two exceptions are series one and three. In series one, changing the substituent from isopropyl to *tert*-butyl causes a decrease in

TABLE 5. Variation of k_c/k_t with increasing bulk of the substituents on the alkene

	R			
	CH_3	C_2H_5	*i*-C_3H_7	*tert*-C_4H_9
	Series 1 $RCH{=}CHCH_3$			
k_c/k_t	3.1	5.2	8.1	7.5
ΔH_i^f	−0.75[a]	−0.88[b]	−1.08[c]	−3.92[d]
	Series 2 $RCH{=}CHC_2H_5$			
k_c/k_t	5.2	9.2	11.3	14.2
ΔH_i^f	−0.88[b]	−1.70[c]		−5.12[e]
	Series 3 $RCH{=}CHCH(CH_3)_2$			
k_c/k_t	8.1	11.3	9.8	
ΔH_i^f	−1.08[c]		−1.96[c]	
	Series 4 $RCH{=}CHR$			
k_c/k_t	3.1	9.2	9.8	1.97×10^5
ΔH_i^f	−0.75[a]	−1.70	−1.96[e]	−10.2[e]

[a]Reference 18.
[b]Reference 19.
[c]Reference 20.
[d]Reference 21.
[e]Reference 16.
[f]In kcal/mol for the process *cis* alkene → *trans* alkene with both isomers in the liquid phase at 25 °C.

Can. J. Chem. Downloaded from www.nrcresearchpress.com by 210.87.254.40 on 09/05/12
For personal use only.

k_c/k_t as does a change from ethyl to isopropyl in series three.

Since addition occurs faster to the *cis* than to the *trans* alkene, some of the ground state energy difference between the *cis* and *trans* isomer must be lost in the rate determining transition state. One explanation advanced to explain this observation is that relief of ground state steric strain occurs in the transition state of addition to the *cis* alkene with a consequent increase in rate of addition (14). While this may be a correct explanation for certain electrophilic addition reactions, we do not believe that it adequately explains our results for the following reasons.

In Table 5 are listed the enthalpies of isomerization for the pairs of isomeric *cis–trans* alkenes studied in this paper. In all cases the *trans* is the more stable isomer. The differences in stability range from a low of −0.75 kcal/mol for the 2-butenes to a high of 10.2 kcal/mol for the 2,2,5,5-tetramethyl-3-hexenes. This difference in stability is due to the steric interaction of the alkyl groups in the *cis* isomer. If relief of all or a part of this ground state strain occurs in the rate determining transition state then there should be some correlation between ΔH_i and the k_c/k_t ratio. No clear relationship exists. Particularly surprising is the lack of a much larger change in the k_c/k_t ratio upon substitution of one *tert*-butyl group. For example in series one, the difference in the *cis–trans* ground state enthalpies increases markedly when the substituent is changed from isopropyl to *tert*-butyl yet the k_c/k_t ratio *decreases*. Similarly in series three the k_c/k_t ratio does not parallel the *cis–trans* ground state enthalpy differences.

Further support of this view is obtained from the results of Yates and McDonald (16) who employed a thermochemical–kinetic approach to the transition state structure of the bromination of several geometrically isomeric 1,2-disubstituted ethylenes. They found that in all cases the initial enthalpy difference between starting *cis* and *trans* isomers was *increased* at the bridged bromination transition state. Thus it appears that arguments based upon relief in the transition state of ground state steric strain are incorrect.

It may be possible to account for the faster rate of addition of the *cis* alkene relative to its *trans* isomer on the basis of steric interaction between the incoming electrophile and the alkyl groups on the double bond. In the *cis* alkene the two alkyl groups are located on the same side of the molecule with the result that the path of the electrophile is less hindered relative to the *trans* alkene. In the extreme case with two *tert*-butyl groups, it is possible that the electrophile will be forced out of its usual path, perpendicular to the plane of the alkene, and attack at a more oblique angle. Such an explanation has been proposed to explain the large difference in rates of addition of bromine and arenesulfenyl chloride to *cis*- and *trans*-1,2-di-*tert*-butylethylenes (16, 17).

The rate of addition to the *cis* alkene would be faster if its entropy loss for addition were less than that of the *trans* isomer (16). Such a situation would occur if the alkyl groups of the *cis* isomer have already lost most of their rotational entropy in the ground state. Thus in passing to the transition state they would have less entropy loss. This could be an important effect in alkenes containing large bulky substituents.

The second step of the mechanism involves attack at one of the two carbon atoms of the thiiranium ion. Since the products are all formed by stereospecific *anti*-addition, it is concluded that the transition state in this step is bridged. The kinetically controlled product composition serves to indicate the relative importance of polar and steric factors in this, the product determining step. Examination of the kinetically controlled product distribution in Table 3 shows that generally the amount of *anti*-Markownikoff product obtained by chloride attack at one carbon atom of the thiiranium ion increases with the steric bulk of the substituent on the other carbon atom. This is particularly true for such bulky groups as *tert*-butyl where the steric effect seems to be dominant. These results are in accord with the work of Beverly and Hogg (3) and Mueller and Butler (4).

While we do not completely understand the effects of alkene configuration on the rates and products of addition of arenesulfenyl chloride it is clear that relief of ground state steric strain of the alkene in the rate determining transition state is not important. In the second or product determining step steric rather than polar effects seem to be the more important.

Experimental

All melting and boiling points are uncorrected. Micro-

TABLE 6. Analytical data for sulfenyl chloride adducts

Alkene		Analysis (%) C Calcd.	C Found	H Calcd.	H Found	S Calcd.	S Found
cis-2-Pentene	**21**	53.02	53.01	5.66	5.54	12.87	12.78
trans-2-Pentene	**22**	53.02	53.06	5.66	5.48	12.87	12.74
cis-3-Hexene	**15**	54.76	54.88	6.12	6.01	12.18	12.37
trans-3-Hexene	**16**	54.76	54.79	6.12	6.29	12.18	12.15
cis-4-Methylpentene-2	**23**	54.76	54.66	6.12	6.05	12.18	12.33
trans-4-Methylpentene-2	**24**	54.76	54.72	6.12	6.09	12.18	12.32
cis-4,4-Dimethylpentene-2	**25**	56.32	56.54	6.54	6.30	11.56	11.36
trans-4,4-Dimethylpentene-2	**26**	56.32	56.47	6.54	6.49	11.56	11.59
cis-2-Methylhexene-3	**27**	56.32	56.28	6.54	6.61	11.56	11.36
trans-2-Methylhexene-3	**28**	56.32	56.34	6.54	6.56	11.56	11.55
cis-2,2-Dimethylhexene-3	**29**	57.73	57.55	6.92	6.89	11.01	11.05
trans-2,2-Dimethylhexene-3	**30**	57.73	57.74	6.92	7.01	11.01	10.97
cis-2,5-Dimethylhexene-3	**17**	57.73	57.84	6.92	6.83	11.01	11.15
trans-2,5-Dimethylhexene-3	**18**	57.73	57.61	6.92	6.89	11.01	10.88
Butene-1	**3**	51.07	50.98	5.14	5.13	13.63	13.43
3-Methylbutene-1	**4**	53.02	53.04	5.66	5.63	12.87	12.75
Hexene-1	**5**	54.76	54.71	6.12	6.03	12.13	12.32
2-Ethylbutene-1	**8**	54.76	54.61	6.12	6.00	12.18	12.29
2-Methylbutene-1	**10**	53.02	53.22	5.66	5.49	12.87	12.63
2,3-Dimethylbutene-1	**11**	54.76	54.71	6.12	6.07	12.18	12.06
2,3,3-Trimethylbutene-1	**12**	56.32	56.43	6.54	6.70	11.56	11.55

analyses were carried out by A. B. Gygli Microanalysis Laboratory, Toronto, Ontario.

The olefins were obtained commercially and their purity was verified by glc and nmr.

4-Chlorobenzenesulfenyl chloride was prepared as previously described (5). *1,1,2,2-Tetrachloroethane* was purified as previously described (5).

Kinetics, product composition, and analytical samples were carried out or prepared as previously described (5). The elemental analysis for adducts not previously reported are given in Table 6.

Acknowledgements

Continued financial support from the National Research Council of Canada is gratefully acknowledged. A University of Toronto Special Open Fellowship (1973–1974) and a National Research Council of Canada Postgraduate Scholarship (1974–1976) to one of us (D.G.G.) is also very much appreciated.

1. G. H. SCHMID and V. J. NOWLAN. Can. J. Chem. **54**, 695 (1976).
2. W. L. ORR and N. KHARASCH. J. Am. Chem. Soc. **78**, 1201 (1956).
3. G. M. BEVERLY and D. R. HOGG. Chem. Commun. 138 (1966).
4. W. H. MUELLER and P. E. BUTLER. J. Am. Chem. Soc. **80**, 2075 (1968).
5. G. H. SCHMID, V. M. CSIZMADIA, V. J. NOWLAN, and D. G. GARRATT. Can. J. Chem. **50**, 245 (1972).
6. G. M. BEVERLY and D. R. HOGG. J. Chem. Soc. B, 175 (1971).
7. W. A. THALER. J. Org. Chem. **34**, 817 (1969).
8. G. H. SCHMID and D. G. GARRATT. Can. J. Chem. **51**, 2463 (1973).
9. G. COLLIN, U. JAHNKE, G. JUST, G. LORENZ, W. PRITZKOW, M. RÖLIG, and L. WINGUTH. J. Prakt. Chem. **311**, 238 (1969).
10. J. R. CAVANAUGH and B. P. DAILEY. J. Chem. Phys. **34**, 1093 (1961).
11. B. P. DAILEY and J. N. SCHOOLERY. J. Am. Chem. Soc. **77**, 3977 (1955).
12. R. W. TAFT, JR. Steric effects in organic chemistry. *Edited by* M. S. Newman. John Wiley and Sons, Inc., New York. 1956. Chap. 13.
13. G. H. SCHMID and V. J. NOWLAN. J. Org. Chem. **37**, 3086 (1972).
14. J. E. DUBOIS and G. MOUVIER. Tetrahedron Lett. 1629 (1965).
15. R. FELLOUS and R. LUFT. J. Am. Chem. Soc. **95**, 5593 (1973).
16. K. YATES and R. MCDONALD. J. Org. Chem. **38**, 2465 (1973).
17. C. L. DEAN, D. G. GARRATT, T. T. TIDWELL, and G. H. SCHMID. J. Am. Chem. Soc. **96**, 4958 (1974).
18. E. J. POSEN, F. W. MASON, and F. D. ROSSINI. Natl. Bur. Stand. J. Res. **46**, 106 (1951).
19. S. YA. KARASERA and D. N. ANDREERSKII. Neftekhimiya. **8**, 504 (1968).
20. H. F. BARTOLO and F. D. ROSSINI. J. Phys. Chem. **64**, 1685 (1960).
21. J. D. ROCKENFELLAR and F. D. ROSSINI. J. Phys. Chem. **65**, 267 (1961).

Can. J. Chem. Downloaded from www.nrcresearchpress.com by 210.87.254.40 on 09/05/12
For personal use only.

A simple synthesis of oxazolidine and thiazolidine derivatives of hydroxymethylglyceraldehyde acetonide

GEORGE JUST, BONG YOUNG CHUNG,[1] GERALD ROSEBERY,[2] AND MICHEL DUPRÉ

Department of Chemistry, McGill University, Montreal, Quebec H3C 3G1

Received December 19, 1975

GEORGE JUST, BONG YOUNG CHUNG, GERALD ROSEBERY, and MICHEL DUPRÉ. Can. J. Chem. **54**, 1260 (1976).

Starting from mannitol diacetonide, a simple, high yield preparation of the title compounds is described.

GEORGE JUST, BONG YOUNG CHUNG, GERALD ROSEBERY et MICHEL DUPRÉ. Can. J. Chem. **54**, 1260 (1976).

A partir du diacétonide du mannitol, on décrit une synthèse simple et à rendement élevé des composés mentionnés ci-haut.

Can. J. Chem. Downloaded from www.nrcresearchpress.com by 210.87.254.5 on 09/05/12
For personal use only.

In connection with a synthesis of cephalosporin and oxacephalosporin derivatives, we required a large amount of hydroxymethylglyceraldehyde acetonide, in which the aldehyde group was protected as an oxazolidine or thiazolidine derivative.

We recently reported (1) that **5** could be obtained from mannitol diacetonide (2) **1** via the sequence **1** → **2** → **3** → **4** → **5**. When these reactions were carried out on a large scale, it became apparent that (*i*) the lead tetraacetate oxidation of **1** was unwieldy; (*ii*) the distillation of dioxolane **3** to hydroxyaldehyde **4** could not be scaled up because of polymerization of **4**; (*iii*) that, because of this polymerization, the yield of **4** was low; and (*iv*) that **5** was contaminated with varying amounts (5–50%) of an impurity.

The nature of this impurity became apparent when **5**, containing a particularly large amount of side product, was mesylated. In addition to the expected mesylate **7**, dimesylate **10***b*, mp 74–75 °C, was isolated. Its structure followed from its analytical and nmr data and it obviously was derived from a Cannizzaro reaction occurring during the work-up of **3**, which had involved the removal of methanol in the presence of potassium carbonate and formaldehyde.

Although remaining highly crystalline, it was noted that **3** decomposed at room temperature in a period of several weeks, and that formaldehyde was liberated during that transformation. Based on this information, it was decided to investigate the periodate oxidation of mannitol diacetonide, to use reaction conditions which minimized the undesired Cannizzaro reaction in the transformation of **2** to **3**, and to make use of the equilibrium between **3** and **4** and formaldehyde to trap **4** directly as its oxazolidine derivative **5**.

Initial attempts to cleave mannitol diacetonide with aqueous periodate gave **2** in 10–20% yield

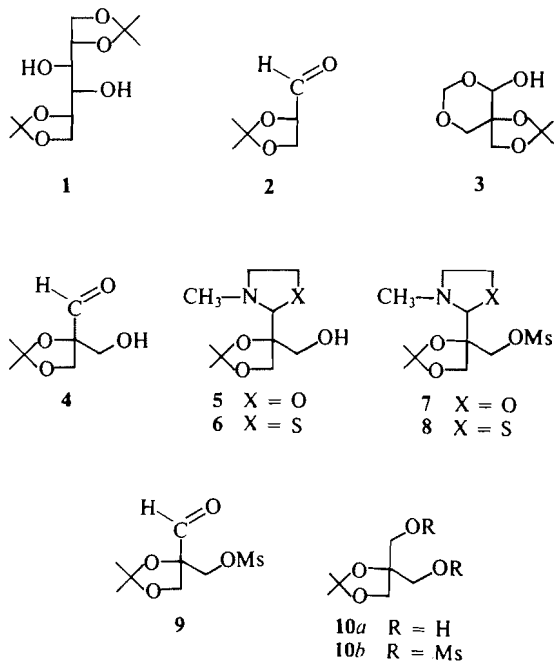

[1]Holder of a National Research Council of Canada Scholarship, 1974–1975.

[2]Holder of a National Research Council of Canada Scholarship, 1970–1973.

Can. J. Chem. Downloaded from www.nrcresearchpress.com by 210.87.254.5 on 09/05/12
For personal use only.

only. A careful study of the reaction indicated that at p*H* 5, mannitol diacetonide had disappeared within 5 min, and that glyceraldehyde acetonide had started decomposing very rapidly due to the slightly acidic conditions. When the periodate reaction was carried out at p*H* 6, the reaction was complete after 30 min with little degradation of **2**. Reaction of the aqueous solution of **2** with aqueous formaldehyde and potassium carbonate for 16 h, followed by methylene chloride extraction, gave pure **3** (1), in 70–80% yield. A benzene solution of **3** was then boiled for 1 h with continuous removal of water with 2 equiv. of *N*-methylethanolamine. Distillation gave a 95% yield of pure oxazolidine **5**, uncontaminated by diol **10***a*. It was converted to its crystalline mesylate **7** in high yield.

Similarly, treatment of **3** with *N*-methylthioethanolamine (3) gave **6** in high yield as a mixture of two epimers. No attempt was made to determine the relative stereochemistry of two epimers of **6**. Mesylation of **6** gave **8**.

Conversion of the oxazolidine function in **7** to the free aldehyde **9** could be effected by treatment with aqueous acetic acid (1). The same aldehyde **9** was obtained from the thiazolidine **8** by hydrolysis with mercuric chloride either in aqueous acetonitrile (4) or tetrahydrofuran. Alternatively, the thiazolidine group could be removed under virtually aprotic conditions by oxidation of **8** at 0 °C with 2 equiv. of *m*-chloroperbenzoic acid in methylene chloride for 5 min. Direct chromatography of the reaction product or washing with aqueous sodium bicarbonate gave the free aldehyde **9** in 70% yield.

Experimental

Melting points were determined on a Gallenkamp block and are uncorrected. Mass spectra were obtained on an AEI-MS-902 mass spectrometer at 70 eV using a direct insertion probe. Microanalyses were carried out by C. Daessle, Montreal.

*Formaldehyde Adduct **3** from Mannitol Diacetonide*

To a solution of 24 g of mannitol diacetonide in 400 ml phosphate buffer (p*H* 6) was added 20.4 g of sodium metaperiodate. The mixture was stirred for 30 min, 23.1 g of potassium carbonate in 70 ml water and 74 ml of aqueous 40% formaldehyde were added, and the mixture stirred overnight at room temperature. Methylene chloride extraction and evaporation gave 25.5 g (73%) of pure **3** (1), mp 89–90 °C.

*Oxazolidine **5** and Thiazolidine **6** from **3***

A solution of 0.1 mol of **3** and 2.2 equiv. of *N*-methylethanolamine in 500 ml benzene was heated to reflux and the benzene slowly distilled off over a period of 2 h. Distillation gave a 90–95% yield of **5** (1), bp 100–103 °C/0.5 torr.

When *N*-methylthioethanolamine was used instead of *N*-methylethanolamine, thiazolidine **6**, bp 98–101 °C/0.05 torr was obtained in 90% yield. *Anal.* calcd. for $C_{10}H_{19}NO_3S$: C 51.49, H 8.21, N 6.01, S 13.72; found: C 51.53, H 8.17, N 6.13, S 13.63; *m/e* 233 (M^+).

*Mesylate **8***

A solution of 11.65 g of **6** and 7.6 g of triethylamine (1.5 equiv.) in 200 ml of methylene chloride was cooled to −50 °C and 6.3 g (1.1 equiv.) of freshly distilled methanesulfonyl chloride in 100 ml of methylene chloride added dropwise over a period of 3 h. The cloudy solution was poured into 300 ml of cold water, separated, and washed twice with cold water. Drying and evaporation gave a quantitative yield of oily mesylate. The oily residue was shaken vigorously with ether, and the solvent pumped off under high vacuum to give a solid. Treatment with ether and filtration after cooling to −10 °C for 2 h gave 14 g (90%) of **8**, mp 65–66 °C (mixture of epimers). *Anal.* calcd. for $C_{11}H_{21}NO_5S_2$: C 42.45, H 6.75, N 4.50, S 20.58; found: C 42.25, H 6.59, N 4.62, S 20.32.

*Aldehyde **9** from **8***

Using Mercuric Chloride

To a solution of 311 mg of **8** in 80% aqueous acetonitrile or tetrahydrofuran (10 ml) was added mercuric chloride (280 mg, 1.1 equiv.). The white milky suspension was refluxed for 1 h and filtered. The filtrate was evaporated *in vacuo* and the residue extracted with benzene. The benzene solution was washed with dilute hydrochloric acid and water, dried over anhydrous sodium sulfate, and evaporated to dryness *in vacuo*, giving 248 mg (96%) of **9** as a white oil.

Using m-Chloroperbenzoic Acid

A solution of 311 mg of **8** in methylene chloride (5 ml) was cooled to 0 °C and *m*-chloroperbenzoic acid (344 mg, 2 equiv.) was added. The mixture was stirred for 5 min and washed with sodium bicarbonate solution. Drying over anhydrous sodium sulfate, evaporation, passing through a silica gel column using ethyl ether as eluant, and evaporation gave 188 mg (72%) of **9** as a white oil. The nmr and ir spectra were the same as those of the product (1) from the acidic hydrolysis of the oxazolidine mesylate. *Anal.* calcd. for $C_8H_{14}O_6S$: C 40.34, H 5.88, S 13.46; found: C 40.10, H 6.11, S 13.35.

Acknowledgements

We wish to thank the National Research Council of Canada and Bristol Laboratories for generous financial support.

1. G. Just and P. Rossy. J. Org. Chem. **38**, 1534 (1973).
2. G. Kohan and G. Just. Synthesis, 192 (1974).
3. D. S. Tarbell and D. P. Cameron. J. Am. Chem. Soc. **78**, 2731 (1956).
4. A. I. Meyers, R. Munavu, and J. Durandetta. Tetrahedron Lett. 3929 (1972).

Constituents of *Nauclea diderrichii*. Part VII. Synthesis of naucleđerine, naucleonine, and naucleonidine; spectroscopic evidence for the structures of 3α-dihydrocadambine and two other constituents

STEWART MCLEAN, GARY I. DMITRIENKO, AND AKOS SZAKOLCAI
Department of Chemistry, University of Toronto, Toronto, Ontario M5S 1A1

Received October 23, 1975

STEWART MCLEAN, GARY I. DMITRIENKO, and AKOS SZAKOLCAI. Can. J. Chem. **54**, 1262 (1976).

Evidence is advanced concerning the structures of six *N. diderrichii* alkaloids, based on synthetic and spectroscopic studies. The synthesis of naucleđerine, **2**, provides support for the structural assignment made earlier. Synthesis has shown that the structures previously assigned to the alkaloids designated ND-305B and ND-363C are incorrect; this, however, has led to revised structures (**19** and **20**) for these alkaloids, now named naucleonine and naucleonidine, respectively, and these have been established by synthesis. Based on this study and an examination of data obtained previously, a tentative proposal is made for the structure **21** of another constituent of the plant, designated ND-363B. Spectroscopic studies have allowed a structure **22** to be advanced for the glycosidic alkaloid, which was shown to be identical with the alkaloid 3α-dihydrocadambine obtained by Brown and Fraser. Based on this study and a reexamination of data reported previously, structure **25** is tentatively proposed for another constituent of the plant, designated ND-370.

STEWART MCLEAN, GARY I. DMITRIENKO et AKOS SZAKOLCAI. Can. J. Chem. **54**, 1262 (1976).

On présente des données, basées sur des études de synthèse et de spectroscopie, concernant la structure de six alcaloïdes *N. diderrichii*. La synthèse de la nauclédérine, **2**, fournit une preuve supplémentaire pour l'attribution de structure proposée antérieurement. On a démontré, par synthèse, que les structures proposées antérieurement pour les alcaloïdes ND-305B et ND-363C ne sont pas correctes. Nos études ont toutefois permis d'attribuer les structures revisées (**19** et **20**) à ces alcaloïdes qui sont maintenant nommés respectivement naucléonine et naucléonidine; ces structures ont maintenant été établies par synthèse. En se basant sur l'étude présente et en réexaminant les données obtenues antérieurement, une structure non-définitive **21** est proposée pour le constituant ND-363B de la plante. Des études spectroscopiques ont permis de proposer la structure **22** pour l'alcaloïde glycosidique; on a montré que cet alcaloïde est identique avec l'alcaloïde 3α dihydrocadambine obtenu par Brown et Fraser. En se basant sur l'étude actuelle et à l'aide d'un réexamen des données obtenues antérieurement, on propose, d'une façon non-définitive, la structure **25** pour le constituant ND-370 de la plante.

[Traduit par le journal]

We have described the isolation of constituents of *Nauclea diderrichii* which, for convenience, we have placed in four categories (1). The structures of all of the members of the first two groups, the simple β-carbolines and the simple pyridines were established with confidence (1*a*). In the third group, the indole-pyridine alkaloids, only naucledine, **1**, was assigned a structure unequivocally, but provisional structures were advanced for other members of the group with varying degrees of confidence (1*b*). Structural assignments to the members of the fourth group, miscellaneous substances, were at best tentative (1*c*). More recently we have published preliminary communications in which we make firm structural assignments to several members of the third and fourth groups (2). We now provide details of these latter assignments and also describe progress in the elucidation of the structures of several other constituents of this plant.

Because of the small amounts of material available from natural sources (1*a*), it has been necessary throughout this study to resort to total synthesis to test and substantiate the structural assignments based on spectroscopic studies. The structure of the first indole-pyridine alkaloid, naucledine, **1**, was established in this way (1*b*), and, of the other members of this group, naucleđerine appeared to be the best candidate for a synthetic attack. The favored structure for naucleđerine was the azepinoindole **2**, but a small

Can. J. Chem. Downloaded from www.nrcresearchpress.com by 210.87.254.42 on 09/05/12
For personal use only.

Can. J. Chem. Downloaded from www.nrcresearchpress.com by 210.87.254.42 on 09/05/12
For personal use only.

number of alternative structures remained possible though unlikely since each was difficult to reconcile with at least one piece of spectroscopic data. One of these, the picolyltetrahydro-β-carboline **3**, which was considered unlikely on the basis of the fragmentation pattern in the mass spectrum of the alkaloid, was disposed of when it was synthesized and shown to be different from the alkaloid. (The mass spectrum of **3** was that expected for the structure.) The synthesis of **3** was accomplished by Bischler–Napieralski cyclization of the amide **5** and sodium borohydride reduction of the dihydro-β-carboline product. The amide **5** was prepared from the dinicotinic acid derivative **6** (X = Cl) (1*a*) by an Arndt–Eistert sequence in which the intermediate diazo ketone **6** (X = CHN_2) was allowed to react with tryptamine in the presence of silver oxide. An interesting feature of the dihydro-β-carboline intermediate is that its nmr spectrum shows that the imine form **4** exists in dynamic equilibrium with the enamine **4***a*; the proton signals indicate that both tautomeric forms are present in substantial amounts in the solution and the addition of D_2O removes all of the signals associated with the mobile hydrogens.

A route to the favored structure, **2**, by acid-catalyzed cyclization of the amino alcohol **7** could be seen but it was considered advisable to explore this approach by attempting the cyclization of the phenyl analog **8**, which seemed to be more readily accessible. This intermediate could, indeed, be prepared by the reaction of tryptamine with styrene bromohydrin or the epoxide derived from it, but under all of the reaction conditions used, significant amounts of the bis product **9** were obtained; attempts to prevent over-reaction left unchanged tryptamine and presented subsequent problems with purification of the product, and the best practical course was found to be the quantitative conversion of tryptamine to **9** with styrene oxide. A route to **8** alone by the reaction of tryptamine with *O*-acetylmandelyl chloride followed by hydrolysis of the ester and reduction of the amide was developed, but this was of little advantage since it was found that polyphosphoric acid converted both **8** and **9** to **10**, the phenyl analog of **2**, with about the same efficiency; it is probable that **9** produced the *N*-substituted derivative of **10**, which underwent dehydration and hydrolysis under the reaction conditions (3). The product **10** was identical with material assigned this structure by Freter (4), and obtained by a different route.

The epoxide precursor, **11**, required for the synthesis of **2** itself was most conveniently pre-

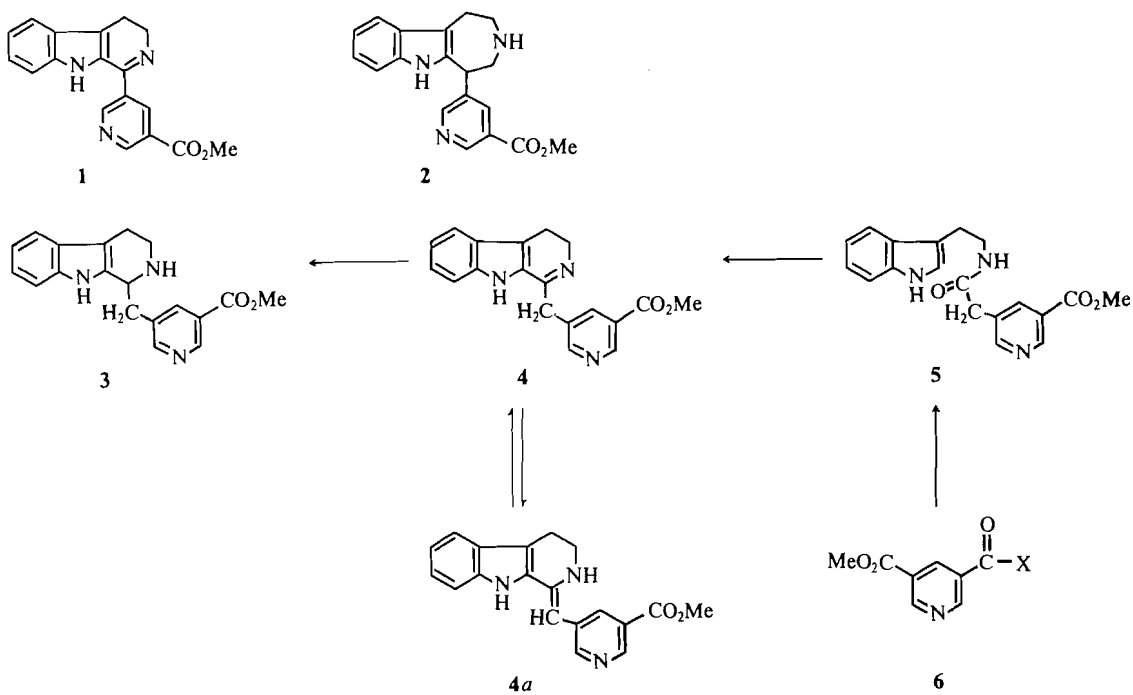

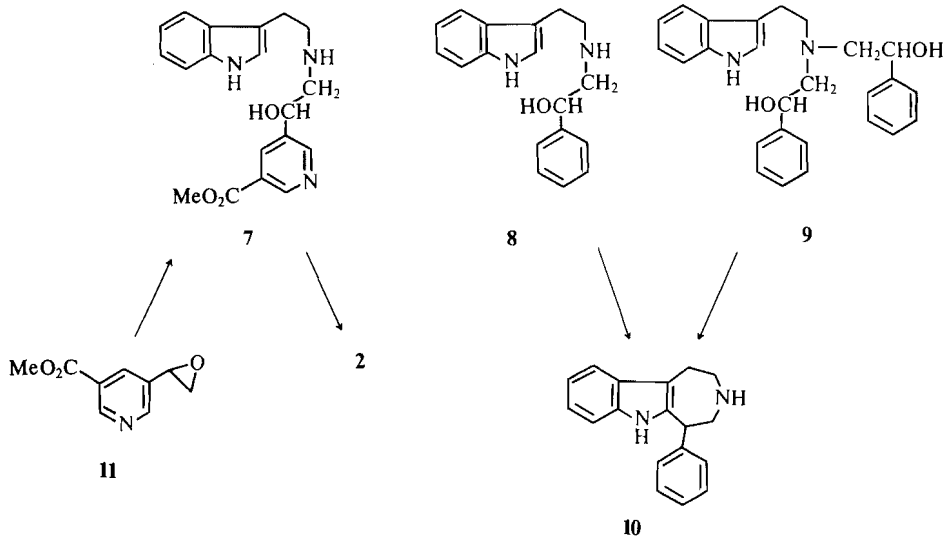

pared from the bromohydrin obtained by treatment of the diazo ketone **6** (X = CHN_2) with hydrobromic acid followed by borohydride reduction of the resulting bromo ketone. A small amount of the epoxide itself was formed in this reduction, but the bulk of the product was bromohydrin which was converted to epoxide by treatment with sodium hydride under mild conditions. The epoxide was obtained crystalline, mp 63.5–64.5 °C, by sublimation (60 °C/0.05 torr) and was stable up to this temperature. (In contrast, the epoxide of 4-vinylpyridine has been described (5) as an unstable liquid.) As in the model series, problems with bis alkylation were found when tryptamine was treated with epoxide **11**, but in this case conditions were found in which acceptable yields of **7** could be isolated, provided that the reaction was carried out batchwise with small amounts of reactants. After numerous attempts, conditions were found in which **7** was cyclized to **2**, albeit in only 5.4% yield. The structural identity of **2** and natural naucleferine was judged from their spectroscopic (ir, uv, nmr, and ms) and tlc characteristics. The natural material melted over a wide range (102–124 °C), and comment has been made about this previously (1*b*); the range observed for the synthetic material (94–108 °C) was similar, but did not serve as a good criterion of identity. Microanalytical values indicated that synthetic **2** retained a molecule of solvent of crystallization, but completely satisfactory and reproducible results could not be obtained with the small amount of material available and, as with natural naucleferine, the best proof of constitution came from a determination of the masses of the parent ion and certain fragment ions in a high resolution mass spectrum.

In an attempt to improve the yield in the cyclization step, the *N*,*O*-diacetyl derivative of **7** was prepared with the intention of selectively hydrolyzing the ester function and leaving the nitrogen protected during the treatment with polyphosphoric acid. A feature of interest in this diacetyl derivative and the corresponding derivatives in the model series is that the nmr spectrum shows two signals for the *N*-acetyl protons, indicative of the existence of two relatively stable rotamers. However, the *N*-acetyl group proved to be unusually susceptible to acid hydrolysis and, by using the nmr spectrometer to monitor the course of the reaction, it could be seen that the hydrolysis of the original *O*-acetyl group was followed by a rapid $N \rightarrow O$-acetyl migration and then further hydrolysis. It seemed most improbable, therefore, that the *N*-acetyl group would provide any protection in the polyphosphoric acid treatment. The *N*-tosyl derivative was also prepared and subjected to cyclization in polyphosphoric acid, but without any improvement in yield.

The isolation of naucleferine, even in small yield, provides strong support for the proposed structure **2**. It is recognized, however, that this sequence does not quite reach the level of a completely unequivocal proof of structure, since

Can. J. Chem. Downloaded from www.nrcresearchpress.com by 210.87.254.42 on 09/05/12
For personal use only.

Can. J. Chem. Downloaded from www.nrcresearchpress.com by 210.87.254.42 on 09/05/12
For personal use only.

the mechanism of the acid-catalyzed cyclization step has not been established. The nature of the electrophilic centre generated in the reaction has not been established, and the possibility exists that an aziridinium intermediate could be formed and lead to rearranged product. In any case, the electrophilic centre may well attack the β-position of the indole generating a six-membered ring, with subsequent Plancher rearrangement of the spiroindolenine providing the azepinoindole (6). Even if this were so, migration of the picolyl substituent to form **2** can be expected rather than the alternative rearrangement. Furthermore, the formation of **10** from **8** and from the precursor used by Freter (4) buttresses its structural assignment and provides firm support for the assignment of **2** to nauclederine, which strongly resembles **10** spectroscopically.

A further member of the indole-pyridine group of alkaloids was the substance referred to by its laboratory designation ND-363C and tentatively assigned structure **12** (X = CO_2Me) as a working hypothesis (1*b*). It was recognized that the sample consisted of a pair of equilibratible epimers and it was postulated that opening and closing the carbinolamine ether (*cf.* **13**) provided a route for the epimerization. However, two pieces of spectroscopic data could not readily be accommodated by this hypothesis: the presence in the nmr spectrum of a τ 8.22 peak, readily removed by addition of D_2O, and the occurrence of an $M - CH_3$ ion as the base peak in the mass spectrum. Another substance, ND-305B, was closely similar in its behavior and was considered to be the decarbomethoxy analog **12** (X = H).

As a test of the structural hypothesis, synthesis of the ring-opened tautomers **13** was undertaken, and the most readily available model was **13** (R = H). γ-Butyrolactone **15** (R = H) reacted smoothly with tryptamine to form the amide **14** (R = H), which was protected as its *O*-acetyl derivative and subjected to Bischler–Napieralski cyclization. Careful hydrolysis of the *O*-acetyl group led to **13** (R = H) which was isolated as a waxy solid. However, this material showed spectroscopic characteristics appropriate for the ring-opened imine form and showed no tendency to cyclize to the carbinolamine ether; in particular, the nmr spectrum showed no evidence for tautomerism and the uv spectrum was that of a typical dihydro-β-carboline in acidic, neutral, and basic media. The same sequence was carried out with the phenylbutyrolactone **15** (R = Ph) and the pyridyl analog **15** (R = 3-pyridyl) which was prepared from ethyl nicotinate by a routine synthetic sequence. In both cases the product existed in the imine form **13**, and it was clear that the equilibrium was not shifted to favor the ring-closed tautomer by an effect associated with either the bulk of the substituent or a special characteristic of the pyridyl group. Clearly the original structural hypothesis was incorrect, and, in particular, **13** (R = 3-pyridyl) was not identical with ND-305B nor did it lead to it.

Because these observations raised questions regarding the proposed tautomerism, the imminium salt **17** (R = H) was prepared by the reaction of harmalan, **16**, with 2-bromoethanol, and when this was treated with aqueous base, it spontaneously formed the ring-closed product **18** (R = H). Two spectroscopic properties of this material were of commanding interest: the mass spectrum showed an $M - CH_3$ base peak and the nmr spectrum showed a three-proton singlet at τ 8.28 which rapidly disappeared when the sample was shaken with D_2O. Clearly the latter observation indicates that some of the enamine tautomer is in equilibrium with the carbinolamine ether. Furthermore, when harmalan was treated with styrene oxide, **18** (R = Ph) was formed directly and this material showed, in addition to the two spectroscopic features just mentioned, the 'doubling' of the nmr spectrum that had been associated in the case of the alkaloids with the existence of a pair of epimers differing in stereochemistry at the point of ring-closure. An explanation for the problematic spectroscopic observations for the alkaloids was immediately apparent, and the true structures of ND-363C and ND-305B were revealed (2*b*).

The obvious synthetic precursor to ND-363C was the epoxide **11** which was already available (see above), and reaction of this with harmalan in refluxing chloroform led to the isolation of a glassy solid in 46% yield which showed tlc behavior identical to that of natural ND-363C. This product did not crystallize, nor could a crystalline derivative be prepared from it, but a sample of the synthetic material that was carefully purified by chromatography gave a satisfactory analysis for the expected formula $C_{21}H_{21}N_3O_3$. The spectroscopic properties, including the p*H* dependence of the uv spectra, of

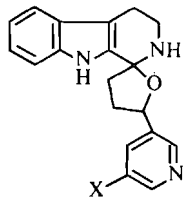

12

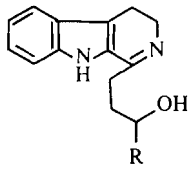

13

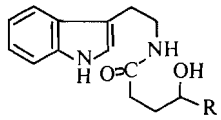

14

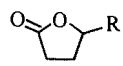

15

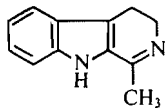

16

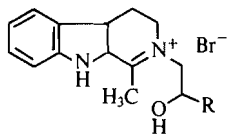

17

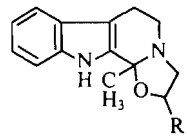

18

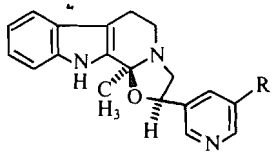

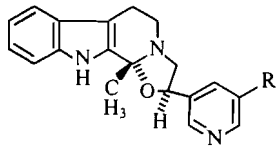

19*a* α-Naucleonine R = H
20*a* α-Naucleonidine R = CO_2Me

19*b* β-Naucleonine
20*b* β-Naucleonidine

natural and synthetic materials corresponded in every important respect, and the differences that were observed could be confidently attributed to the presence of small amounts of impurities in the natural material, which had been difficult to isolate and purify (1*b*). Furthermore, the synthetic material was available in larger quantities than the natural material and its solution spectra showed better resolution.

The precursor required for the synthesis of ND-305B was the epoxide of 3-vinylpyridine, and this was conveniently prepared by treatment of 3-pyridinecarboxaldehyde with dimethyloxosulfonium methylide (7). The oily product darkened rapidly (reference has been made above to the report (5) of the instability of its 4-isomer), and freshly prepared epoxide was used without further purification in the reaction with harmalan. Synthetic ND-305B was obtained in 32% yield; the correspondence between natural and synthetic materials exactly parallels that described for ND-363C. Once again, better resolution could be obtained in the nmr spectrum of synthetic material; the high field methyl signals were, for example, clearly resolved into two singlets, both removed by treatment with D_2O.

Each of the substances ND-305B and ND-363C is, therefore, a pair of epimers based on structure **18**. Although the pairs have not been separated, and they may, in fact, be inseparable in practice, it is convenient now to assign the alkaloids the names naucleonine and naucleonidine (ND-305B and ND-363C, respectively) with the arbitrary designation of relative configuration shown in **19** and **20**.

Attention may now be drawn to a constituent which received the laboratory designation ND-363B since its mass spectrum indicated that it had the same molecular weight as ND-363C; in fact, the two mass spectra appeared to be very similar indeed (8). Most of the other spectroscopic data were also very similar and it was initially thought that ND-363B was an impure sample of ND-363C and it was not, therefore, included in our earlier listing of isolated constituents (1). The nmr spectrum of ND-363B, while not well resolved, resembled that of ND-363C but had the appearance of an out-of-focus picture or one seen with double vision; the 'doubled' spectrum of ND-363C seemed to have 'doubled' again, particularly in some regions. However, the most obvious difference was that ND-363B lacked the τ 8.22 peak of ND-363C, but since there was, at first, no satisfactory

Can. J. Chem. Downloaded from www.nrcresearchpress.com by 210.87.254.42 on 09/05/12
For personal use only.

Can. J. Chem. Downloaded from www.nrcresearchpress.com by 210.87.254.42 on 09/05/12
For personal use only.

explanation for the presence of this peak in the spectrum of ND-363C and it was thought to be caused by some degree of hydration of the molecule, its absence in ND-363B seemed to be associated with the mode of preparation of the sample. It is now clear that this explanation can not be correct since the established structure for naucleonidine, **20**, must be modified more significantly to accommodate the observations. One apparent possibility was that ND-363B was a dimer of the assigned formula that fragmented readily to **20** in the mass spectrometer. The availability of field desorption mass spectrometry offered a means of testing this hypothesis, and when the mass spectrum was obtained by this technique. ions of approximately double the originally assigned mass were indeed found at low operating temperatures, but these disappeared at higher temperatures. With the technique used there is more uncertainty than with electron impact mass spectrometry in determining exact molecular weights; besides the problems associated with calibration of the *m/e* range there is uncertainty concerning the probability of ion–molecule reactions. Nevertheless, the values, *m/e* 741 and 739, assigned to the ions observed in the high mass range are too high to be associated with a simple dimer, but could arise from a homolog of the dimer. Furthermore, there are two ions, *m/e* 364 and 376, in the intermediate mass range that could be associated with a monomeric fragment and its homolog. A reasonable explanation for these observations is that ND-363B has a structure such as **21** in which two molecules of naucleonidine (enamine tautomer) have condensed, *in vitro* or *in vivo*, with a one-carbon unit equivalent to formaldehyde. The mass spectrum would then result from a ready fragmentation effectively reversing the last synthetic step, the complexity of the nmr spectrum would be associated with the diastereoisomeric possibilities implied by **21**, and this would not show the τ 8.22 methyl signals of naucleonidine. The signals for the methylene protons that replace the methyl groups of naucleonidine can not be recognized with confidence in the higher field envelope, but treatment of the sample with D_2O causes a marked reduction in the integrated area of the signals near τ 7.9, as would be expected by analogy with the behavior of naucleonidine. It is clear that

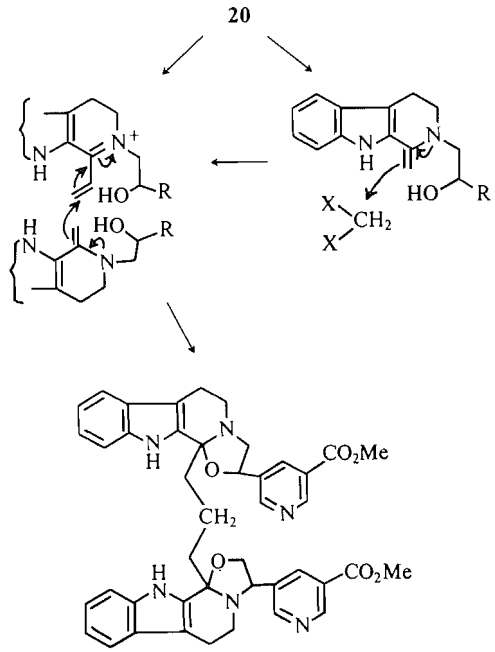

alternative modes of condensation can be suggested and that structure **21** is used to provide a concrete illustration of a plausible type of condensation product.

Among the substances of the fourth group was an amorphous material which was believed to be a glycosidic alkaloid, but it appeared to be too involatile to give a satisfactory mass spectrum and its constitution was not determined (1*c*). This alkaloid has now been assigned structure **22** (2*a*). Acetylation provided an amorphous product which was purified chromatographically and analyzed. While the results were of limited value at this stage, they were compatible with a hypothesis that the product was a pentaacetate with a molecular weight of about 790; when the structure was eventually assigned to the alkaloid, these results were in accord with the calculated values for the pentaacetate of **22**, provided the sample retained a molecule of solvent. Subsequently, when field desorption mass spectrometry became available, the results obtained with the alkaloid itself and its pentaacetate were in accord with the formula $C_{27}H_{34}N_2O_{10}$ assigned to the alkaloid.

The most decisive structural evidence was obtained from the 220 MHz nmr spectra of the

Can. J. Chem. Downloaded from www.nrcresearchpress.com by 210.87.254.42 on 09/05/12
For personal use only.

alkaloid and its pentaacetate. By associating the integrated areas of certain key signals with an appropriate number of protons in a rational way, it was possible to recognize that the spectra indicated that the substance was a monoglycoside of an indolic alkaloid of the expected molecular weight. The features associated with the indolic portion of the molecule, the methyl β-alkoxyacrylate, and the glycosidic part (acetylated in the case of the derivative) could be recognized; correlations are available which give evidence that the latter feature is a β-glucoside (9). A detailed listing of these spectra has already been given (*2a*) and will not be repeated here, but attention can be drawn to the remaining features in the spectra, mainly associated with rings D and E of structure **22**, the portion of the molecule that is presumably of terpenoid origin. The protons associated with the contiguous positions 3, 14, and 15 in the alkaloid could be recognized and specific decoupling experiments showed coupling constants of 10 Hz between H-3 (τ 6.14) and H-14b (τ 8.26) and 9.5 Hz between H-14b and H-15 (τ 6.97) which established the structure and stereochemistry assigned to this portion of the molecule; similar critical values were found for the pentaacetate, but some of the minor details could not be seen as clearly in this spectrum. The features associated with the chain comprised of positions 18, 19, 20, and 21 were, however, more clearly visible in the spectrum of the pentaacetate than in that of the free alkaloid: H-18a (τ 7.04) was coupled, J = 5 Hz, to H-19 (τ 4.60), which was also coupled, J = 6 Hz, to H-18b (τ 6.77) and, J = 1.5 Hz, to H-20 (τ 7.24), which was coupled further, J = 5 Hz, to H-21 (τ 4.50; doublet). Each of these couplings was established by a decoupling experiment, but the coupling between H-15 and H-20 could not be established in this manner because the chemical shifts are not sufficiently different in the alkaloid or its pentaacetate; in the alkaloid, a simple analysis of the spectrum showed that H-15 and H-20 each had an unassigned coupling, J = 6 Hz, and this was, by elimination, considered to be their mutual coupling. The structural and stereochemical features of rings D and E were assigned from these data. It can be noted that, since ring D is seven-membered, the stereochemical features based on coupling constants are not as secure as they would have been for a six-membered ring; furthermore, some of the values which could be measured for both the alkaloid and its acetylated derivative showed differences, presumably associated with conformational effects caused by having either OH or OAc at C-19. The values of $J_{19,20}$ (3.5 Hz) and $J_{20,21}$ (8.5 Hz) were both larger in the unacetylated alkaloid. Nevertheless, we feel that the weight of the evidence favors the assigned structure **22** for the alkaloid.

Brown and Fraser (10) have isolated an alkaloid from *Anthocephalus cadamba* to which they assign structure **22**; they assign structure **23** to a congener, cadambine, which can be interrelated with **22** by chemical transformations. Cadambine contains the interesting oxazolidine feature we have found in naucleonine, **19**, and naucleonidine, **20**, and its oxygen atom bridging the seven-membered ring of cadambine can be expected to lead to greater conformational rigidity. The type of evidence that Brown and Fraser adduce is similar to ours but, since they had both **22** and **23** available, they have taken their stereochemical conclusions further than we have. Nevertheless, the conclusions regarding **22**, which should now be called 3α-dihydrocadambine, were reached independently, and since the identity of samples of the pentaacetate prepared in the two laboratories has been established on the basis of spectroscopic and chromatographic criteria, the evidence and conclusions of both groups are corroborative, and the assignments made are additionally secure.

It may be noted in passing that structure **24** was suggested previously for the indole-pyridine alkaloid nauclechine (*1b*) on independent evidence. Although no further evidence from direct studies of nauclechine is available yet, the assignment of structure **22** to dihydrocadambine makes the assignment of **24** to nauclechine increasingly attractive.

Attention may now be drawn to another alkaloid that was placed in the fourth category and designated ND-370 (*1c*). A considerable amount of spectroscopic data was obtained for this crystalline alkaloid, mp 209–211 °C, which was obtained in very small amounts: the formula $C_{21}H_{26}N_2O_4$ was assigned to it from mass spectrometry, it was clearly an indole alkaloid and its formula suggested that it was derived from a tryptamine unit and a C_9-terpenoid unit.

TABLE 1. Nuclear magnetic resonance spectrum and assignments to ND-370, **25**

Proton§	Chemical shift (τ)	Multiplicity	Coupling constants (Hz)
1†	1.62	broad s	—
5a,b 6a,b	6.8–7.4	m	—
9, 10, 11, 12	2.4–3.0	m	—
14a,b† 15	8.2–8.4	m	—
16a	8.60	dd	$J_{16a,16b} = 12$; $J_{16a,17} = 10$*
16b	8.14	ddd	$J_{16b,16a} = 12$; $J_{16b,17} = 2.5$*; $J_{16b,15} = 3$
17	5.18	dd	$J_{17,16a} = 10$*; $J_{17,16b} = 2.5$*
18a	6.07	d	$J_{18a,18b} = 10.5$*
18b	7.28	m	$J_{18b,18a} = 10.5$*; $J_{18b,19} = 6.5$*
19	5.46	dd	$J_{19,18a} = 6.5$*; $J_{19,20} = 2$*
20	7.93	ddd	$J_{20,15} = 12$; $J_{20,19} = 2$*; $J_{20,21} = 3.5$*
21	5.08	d	$J_{21,20} = 3.5$*
OMe	6.46	s	—
OMe	6.55	s	—

*Coupling constants demonstrated by explicit decoupling experiment (the others are deduced from splitting patterns).
§Integrated areas are in accord with the numbers of protons assigned.
†The addition of D_2O/MeOD removes the signals associated with these protons.

The nmr spectrum, which supplied some of the evidence for the above conclusions, clearly showed the presence of two methoxyl groups in the molecule, but it appeared to be too complex to interpret further in structural terms. The uv spectrum was of interest since it strongly resembled those of naucleonine and naucleonidine,

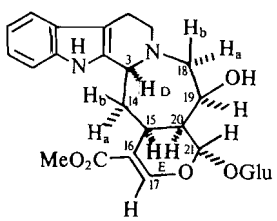

22

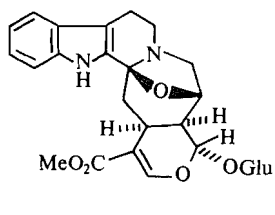

23

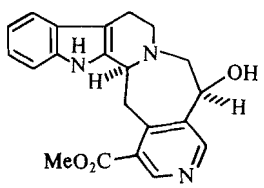

24

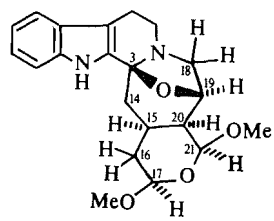

25

particularly with respect to its p*H* dependence. Since the structures of naucleonidine and naucleonine were not established at that time, this information was of limited assistance; however, now that the structures of these alkaloids have been established and the uv characteristics have been associated with the oxazolidine unit, a feature also observed in the case of cadambine (10), it is logical to expect that ND-370 contains this structural unit, and we have reassessed the data obtained previously in the light of this proposal and experience gained with this class of alkaloids. Structure **25** accommodates all of the data presently available and represents a rational hypothesis for the structure of ND-370.

The mass spectrum of ND-370 had been studied in considerable detail (8); the formulae of important fragment ions had been assigned from accurate mass measurements, and a number of metastable ion transitions had been established (1*c*). All of these data are compatible with the fragmentation pattern expected for an ion produced from a molecule of formula **25**. The 100 MHz nmr spectrum had also been examined in considerable detail (8), and it is now shown in convenient form in Table 1. The interpretation

Can. J. Chem. Downloaded from www.nrcresearchpress.com by 210.87.254.42 on 09/05/12
For personal use only.

Can. J. Chem. Downloaded from www.nrcresearchpress.com by 210.87.254.42 on 09/05/12
For personal use only.

of this spectrum in the light of more recent experience is the principal basis on which we have made the assignments shown, leading to the structural proposal **25**; the 220 MHz spectrum was also examined subsequently, but in this case it provided no further structural information, although it did help to reinforce some of the assignments. The assignments to the tryptamine-derived portion of the molecule (H-1–H-12) and the methoxyl groups are straightforward. A key assignment for the rest of the molecule is that of H-19: its chemical shift is appropriate for its environment and it has been shown by decoupling experiments to be coupled to a proton, H-18b, which is part of a methylene group, and to H-20 which is also coupled (demonstrated by decoupling) to H-21 (τ 5.08; at a carbon bearing two oxygen substituents) as well as to another proton (presumed to be H-15). The other proton, H-17, assigned to a carbon bearing two oxygen substituents, is coupled to the protons of a methylene group, H-16a,b, which are coupled to a single proton, H-15. Unfortunately, it has not been possible to disentangle the signals assigned to H-15 and the adjacent methylene group, H-14a,b. The continuous chain encompassing C-18 to C-21 seems well established, and the coupling constants are in accord with a *cis* relationship of the hydrogens at C-19, C-20, and C-21. The data for the C-14 to C-17 chain are less explicit, but, wherever specific assignments can be made, are in accord with the proposed structure. The apparent coupling between H-20 and H-15 is 12 Hz, considerably larger than in cadambine and dihydrocadambine (2*a*, 10), and this leads to difficulties in making stereochemical assignments to the remaining centres that are consistent with the coupling constant data, particularly if the *cis* relationship assigned to the ring fusion in cadambine and dihydrocadambine is assumed to be retained. Although the quality of the data does not allow the structural assignment to be made as securely as was the case with 3α-dihydrocadambine, the proposed structure **25** is an attractive working hypothesis, and the observation that the hydrogens of the methylene group assigned to C-14 can be exchanged with D_2O is what is expected on the basis of precedent, and provides support for the present assignments.

It can now be seen that the alkaloidal constituents of *N. diderrichii* form a substantial array of structural types, many of which seem, at first glance, to bear little chemical resemblance to one another. Nevertheless, closer examination shows that a pattern unfolds which allows the various members to be interconnected by rational and reasonable chemical reactions. These transformations may represent actual steps in the formation of the alkaloids either in a biosynthetic sense or as accidental reactions forming artifacts during the isolation process (1*c*). Although it is possible only to speculate about the reactions, the pattern becomes apparent on examination of Scheme 1.

There is ample evidence to expect that these alkaloids are derived from tryptophan or tryptamine, **26**, and a terpenoid component which in the final pre-alkaloidal stage is represented by secologanin, **27** (11). It is clear that dihydrocadambine, **22**, contains these units structurally intact with only a minimal chemical modification, an oxidation. This oxidation involves transforming the vinyl group to an epoxide equivalent, probably after the initial condensation forming vincoside (11), and reaction of this unit with the amino function can lead to the hydroxylated seven-membered ring. (It seems likely that the alkaloids of *N. latifolia* (12) arise by a sequence corresponding to that outlined below, but without formation of this seven-membered ring; instead, lactamization occurs at a subsequent stage.) A further oxidation would form cadambine, **23**, and obvious modifications would lead to isodihydrocadambine (10) and rubenine, 13, which have been isolated from related species. Hydrolysis of **23** leads to a key intermediate, which can be represented in a formal manner as the carboxydialdehyde **28**: decarboxylation and cyclization in the presence of methanol leads to the ketal **25** (ND-370); reaction of **28** with ammonia or its equivalent, either with or without a decarboxylation step, leads to the dihydropyridines **29** which, by the fragmentation shown can form the pyridines **30** that have been shown to be tautomers of naucleonine and naucleonidine (**19**, **20**); reference has already been made to the formation of **21** from **30** (R = CO_2Me). An alternative opening and rearrangement of **29** (R = CO_2Me) leads to its isomer nauclechine, **24**; alternatively, **24** could be formed from **22** by conversion to the corresponding dihydropyridine, followed by oxidation to the pyridine. The formation of naucledérine, **2**, requires the loss of a two-carbon unit and it is rational to look for this from

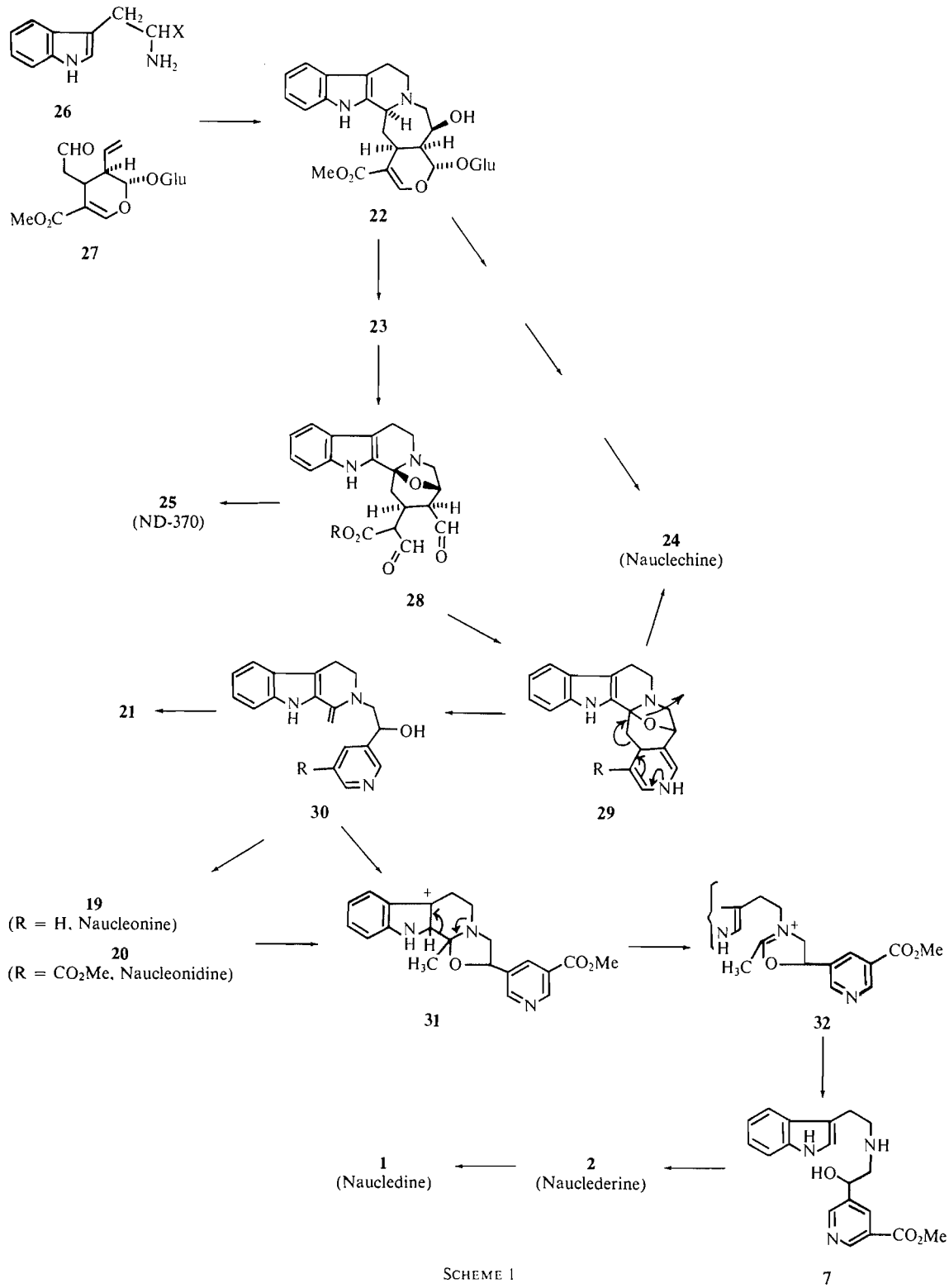

SCHEME 1

Can. J. Chem. Downloaded from www.nrcresearchpress.com by 210.87.254.42 on 09/05/12
For personal use only.

Can. J. Chem. Downloaded from www.nrcresearchpress.com by 210.87.254.42 on 09/05/12
For personal use only.

naucleonidine (or a tautomer) where fragmentation has already opened up such a unit; a suggestion of how this could occur through **31** and **32**, leading to the synthetic precursor **7** of **2**, is offered. Naucledine, **1**, chemically the simplest of the indole-pyridine alkaloids, is almost certainly the one that has suffered the greatest chemical change; it is the only one in which the two-carbon unit at a 3-pyridyl position has been eroded to a single carbon, and it seems probable that it represents an oxidative ring contraction product of naucledérine, **2**. Although other routes to them can certainly be proposed, it is interesting to speculate that some, at least, of the simple β-carboline and pyridine alkaloids isolated from this plant (*1a*) may also have been formed by fragmentation of more complex molecules appearing in Scheme 1.

Experimental

Melting points were determined on a Thomas–Kofler micro hot stage. Spectrometers used were a Perkin-Elmer 237B for ir spectra, a Unicam SP 800A for uv spectra, a Varian HA-100 for routine nmr spectra (100 MHz), a Varian HR-220 (at the Canadian 220 MHz NMR Centre) for 220 MHz nmr spectra, a CEC 21-490 for routine mass spectra, an AEI MS-902 for accurate mass measurements, and a Varian CH5 (at the University of Windsor) for field desorption mass spectra. Unless otherwise indicated, chloroform solutions were used to obtain ir spectra and the wavelengths of significant absorptions are reported in μm, methanol solutions were used to obtain uv spectra (MeOH–HCl or MeOH–KOH means that one drop of 5% hydrochloric acid or aqueous potassium hydroxide was added to the sample cell) and the wavelengths of absorption maxima (λ_{max}) are reported in nm followed by the extinction coefficient (ε) in parentheses, and chloroform-*d* solutions (with tetramethylsilane as internal standard) were used to obtain nmr spectra and chemical shifts are reported on the τ scale followed in parentheses with an indication of the multiplicity of the signal (initial letter abbreviations for singlet, doublet, etc.; the letter is placed in quotation marks when the multiplicity is only apparent) and the number of protons associated with it. Routine mass spectra were determined at 70 eV and the *m/e* values of significant ions are reported followed in parentheses by the height of the peak relative to the base peak (100%). Merck precoated silica gel F254 plates (0.5 mm analytical, 2.0 mm preparative) with a fluorescent indicator were used for tlc unless otherwise indicated; the common elution system 85:14:1 methylene chloride – methanol – concentrated ammonia is abbreviated as m-m-a.

1-(5′-Carbomethoxy-3′-picolyl)tetrahydro-β-carboline **3**

3-Diazoacetyl-5-carbomethoxypyridine, **6** (*X* = CHN_2)

A solution of the acid chloride **6** (X = Cl) (*1a*) (2 g, 10 mmol) in 150 ml of ether was added dropwise with stirring over a period of 15 min to a cold ethereal solution of diazomethane (20 mmol), prepared from bis(*N*-methyl-*N*-nitroso)terephthalimide and distilled. The reaction mixture was stirred under nitrogen for a further 2 h, filtered, and the diazo ketone **6** (X = CHN_2) was obtained in quantitative yield by evaporation of the solvent. An analytical sample (decomposed before melting) was recrystallized from chloroform–ether. *Anal.* calcd. for $C_9H_7N_3O_3$: C 52.68, H 3.44, N 20.48; found: C 52.67, H 3.47, N 20.37. Spectroscopic characteristics: ir 4.72, 5.79, 6.16, 7.37; nmr 0.73 (d, J = 2 Hz, 1H), 0.89 (d, J = 2 Hz, 1H), 1.44 ('t', 2 Hz spacing, 1H), 3.88 (s, 1H), 5.99 (s, 3H); ms 205 (100), 177 (30), 174 (16), 164 (57), 149 (14), 146 (46), 136 (28), 118 (33), 106 (15), 90 (17), 78 (10), 63 (13).

1-(5′-Carbomethoxy-3′-picolyl)dihydro-β-carboline, **4**

The diazo ketone **6** (X = CHN_2) (3.90 g, 19.0 mmol) was added to a stirred solution of tryptamine (3.62 g, 22.6 mmol) in 160 ml of dry dioxane at 55 °C under nitrogen, and freshly prepared silver oxide (1.4 g) was then added in portions over an 18 h period. Stirring was continued for a further 6 h, and during the reaction period the bath temperature was allowed to rise to 100 °C. Filtration and evaporation afforded a brown foam which was dissolved in methanol and passed through a short alumina column. Slow addition of ether caused the tryptamide **5** to separate as an oil (1.83 g, 28% yield) which was collected. Spectroscopic characteristics: ir (CH_3CN) 5.80, 6.00; nmr (DMSO-d_6/$CDCl_3$) −0.55 (br, 1H), 1.00 (d, J = 2 Hz, 1H), 1.33 (d, J = 2 Hz, 1H), 1.78 ('t', 2 Hz spacings, 1H), 1.90 (t, J = 6 Hz, 1H), 2.33–3.10 (complex, 5H), 6.10 (s, 3H), 6.33–6.82 (complex, 4H), 7.12 ('t', 7 Hz spacings, 2H); ms 337 (13), 316 (14), 144 (14), 143 (100), 130 (57); high resolution ms 337.1426 ($C_{19}H_{19}N_3O_3$: 337.1426).

The tryptamide **5** (250 mg, 0.74 mmol) was suspended in 17 ml of freshly distilled phosphorus oxychloride and refluxed for 2 h under nitrogen. Evaporation under reduced pressure afforded a brown residue which was dissolved in dilute acetic acid, filtered, and the filtrate was made basic with dilute aqueous ammonia. A brown solid (200 mg) was obtained by chloroform extraction and evaporation of the chloroform. A concentrated chloroform solution of this solid slowly deposited the dihydro-β-carboline **4** (93 mg, 38% yield) as a yellow solid. An analytical sample, mp 194–203 °C (dec.), was recrystallized from methanol. *Anal.* calcd. for $C_{19}H_{17}N_3O_2$: C 71.45, H 5.37, N 13.16; found: C 71.09, H 5.21, N 12.92. Spectroscopic characteristics: ir (KBr) 5.81; uv 213 (21 700, end absorption), 245 (sh), 324 (10 900), 352 (sh); nmr (8:2 DMSO-d_6/$CDCl_3$) −0.55 (br, 1H), 1.15 (d, J = 2 Hz, 1H), 1.24 (d, J = 2 Hz, 1H), 1.76 ('t', 2 Hz spacings, 1H), 2.34–3.04 (complex, 4H), 3.91 (m, 0.75H), 4.15 (s, 0.75H), 5.82 (s, 0.5H) (the preceding three signals together correspond to 2 protons, addition of D_2O removes all three signals), 6.02 (s, 3H); 6.53 (br, 2H, after addition of D_2O, signal is 't', 6 Hz spacings, 2H), 7.10 ('t', 6 Hz spacings, 2H); ms 319 (3), 318 (4), 317 (3), 316 (3), 168 (8), 145 (12), 138 (12), 131 (5), 130 (9), 106 (31), 105 (28), 87 (7), 85 (63), 83 (100), 77 (20).

A solution of sodium borohydride (29 mg, 0.76 mmol) in 2 ml of methanol was added to a stirred suspension of

Can. J. Chem. Downloaded from www.nrcresearchpress.com by 210.87.254.42 on 09/05/12
For personal use only.

the dihydro-β-carboline (122 mg, 0.38 mmol) in 14 ml of methanol at 5 °C under nitrogen, and 5 ml of diglyme was added to effect solution. After the solution had been stirred at 5 °C for 5.5 h, the tetrahydro-β-carboline **3** was isolated in the usual manner in quantitative yield as a beige solid. Spectroscopic characteristics: ir 290 (sharp), 3.03 (br), 5.80; uv 226 (24 800, end absorption), 275 (6950), 291 (sh); nmr (1:9 DMSO-d_6/$CDCl_3$) −0.14 (br, 1H), 0.97 (d, J = 2 Hz, 1H), 1.33 (d, J = 2 Hz, 1H), 1.76 ('t', 2 Hz spacings, 1H), 2.40–3.07 (complex, 4H), 5.73 (m, 1H), 6.08 (s, 3H), 6.60–7.50 (complex, 6H), 7.76 (br, 1H); ms 321 (3), 320 (15), 319 (64), 318 (59), 317 (57), 316 (17), 304 (11), 258 (10), 172 (15), 171 (100), 129 (13), 115 (14), 85 (10), 83 (17); high resolution ms 321.1466 ($C_{19}H_{19}N_3O_2$: 321.1477).

The Model Phenylhexahydroazepinoindole, ***10***

N,N-Bis(2-phenyl-2-hydroxyethyl)tryptamine, ***9***

Styrene oxide (5.24 g, 43.7 mmol), prepared by treatment of styrene bromohydrin with sodium hydride, was added to molten tryptamine (3.50 g, 21.9 mmol) and stirred at 135 °C for 3 h. Unchanged styrene oxide was removed at 135 °C/0.1 torr. When the melt was allowed to cool, the disubstituted product **9** formed a glassy unstable solid. Spectroscopic characteristics: ir 2.77 (sharp), 2.87 (sharp), 2.84–3.05; nmr 1.73 (br, 1H), 2.40–3.12 (complex, 15H), 5.39 (m, 2H), 6.43 (br, 2H, removed by D_2O), 7.45–6.87 (complex, 8H); ms 364 (8), 232 (13), 144 (16), 143 (26), 132 (15), 131 (13), 130 (42), 129 (22), 120 (14), 118 (13), 117 (11), 107 (16), 106 (70), 105 (98), 104 (35), 103 (28), 102 (11), 91 (46), 90 (15), 89 (12), 78 (24), 77 (100), 76 (14), 69 (14), 64 (15), 57 (27), 56 (14), 55 (28), 52 (14), 51 (48), 50 (27).

N-(2-Phenyl-2-hydroxyethyl)tryptamine, ***8***

The monosubstituted product was prepared as a mixture with the disubstituted product (**8**:**9** of 45:55) by the addition of styrene bromohydrin to an equivalent amount of tryptamine in a boiling solution of sodium bicarbonate in aqueous methanol. The mixture could be separated by tlc with methanol elution. A more convenient preparation is the following. α-Acetoxyphenylacetyltryptamine was prepared from tryptamine and *O*-acetylmandelyl chloride (14) in the usual way. It was obtained in 75% yield as an uncrystallizable semisolid. This material (2.8 g) was refluxed for 6 h in 70 ml of 3% methanolic hydrogen chloride and α-hydroxyphenylacetyltryptamine was obtained in 96% yield. An analytical sample, mp 183.5–185 °C, was obtained by recrystallization from methanol. *Anal.* calcd. for $C_{18}H_{18}N_2O_2$: C 73.45, H 6.16, N 9.52; found: C 73.39, H 6.21, N 9.48. Spectroscopic characteristics: ir (Nujol) 2.97 (sharp), 3.03 (sharp), 3.11 (br), 6.11, 6.49; nmr (DMSO-d_6) −0.83 (br, 1H), 1.95 (m, 1H), 2.23–3.06 (complex, 10H), 3.82 (d, J = 5 Hz, 1H), 5.02 (d, J = 5 Hz, 1H), 6.55 (4 peaks, 7 Hz spacings, 2H), 7.13 (3 peaks, 7 Hz spacings, 2H); ms 294 (2), 276 (18), 220 (11), 144 (20), 143 (100), 132 (11) 130 (49), 77 (15).

The α-hydroxyphenylacetyltryptamine (1.30 g, 4.4 mmol) in 10 ml of dry tetrahydrofuran was added dropwise to a stirred suspension of lithium aluminum hydride (0.59 g, 15.5 mmol) in 40 ml of dry tetrahydrofuran and refluxed under nitrogen for 20 h. Work up by treatment with aqueous sodium hydroxide followed by an acid–base separation provided the hydroxy amine in 55% yield, and an analytical sample, mp 116–117 °C, was obtained by recrystallization from methanol. *Anal.* calcd. for $C_{18}H_{20}N_2O$: C 77.11, H 7.19, N 9.99; found: C 76.83, H 7.03, N 9.89. Spectroscopic characteristics: ir 2.88 (sharp), 3.02 (br); nmr 1.72 (br, 1H), 2.30–3.00 (complex, 9H), 5.32 (dd, J = 8 and 4 Hz, 1H), 6.40 (br, 2H, removed by D_2O), 7.05 (complex, 6H); ms 262 (9), 171 (8), 160 (7), 132 (7), 131 (18), 130 (37), 123 (11), 122 (91), 106 (24), 105 (100), 78 (9), 77 (64), 51 (17), 44 (23), 40 (44).

Diacetyl derivative: ir 5.76, 6.12; nmr 1.6 (br, 1H), 2.4–3.2 (complex, 10H), 3.95 (complex, 1H), 6.2–6.8 (complex, 4H), 7.06 (complex, 2H), 7.97 (s, 4H), 8.11 (s, 2H). (The complexities of the spectrum are attributed to the presence of two rotamers.)

The disubstituted tryptamine **9** (136 mg, 0.36 mmol) was stirred in 4.8 g of polyphosphoric acid at 88 °C under nitrogen for 6.5 h, and then water was added to the hot reaction mixture. After it had cooled, the reaction mixture was made basic with aqueous ammonia, and extracted with methylene chloride. The extract afforded a brown oil which was purified by preparative tlc with m-m-a elution. The product (28 mg, 22% yield) was identical in ir, nmr, and tlc characteristics with a sample of **10** provided by K. Freter (4).

These reaction conditions converted the monosubstituted tryptamine **8**, to **10** in 26% yield.

Naucledérine, ***2***

Chilled 48% hydrobromic acid was slowly added dropwise to freshly prepared 3-diazoacetyl-5-carbomethoxypyridine (**6**, X = CHN_2) with stirring and cooling until a slight excess of the acid was present. The paste obtained was suction filtered and washed with cold acetone, leaving the hydrobromide of the bromo ketone **6** (X = Br) as beige crystals (7.74 g, 77% yield). An analytical sample (darkens but does not melt below 355 °C) was recrystallized from methanol–ether. *Anal.* calcd. for $C_9H_9NO_3Br_2$: C 31.91, H 2.68, N 4.13, Br 47.10; found: C 31.94, H 2.70, N 4.28, Br 46.88. Spectroscopic characteristics: ir (KBr) 3.9 (br), 5.75, 5.77, 5.85; nmr (methanol-d_4) 0.63 (br, 1H), 0.86 (br, 2H), 5.92 (s, 3H), 6.15 (s, 2H).

Sodium borohydride (475 mg, 12.5 mmol) in 20 ml of methanol was added dropwise to a stirred solution of the bromo ketone hydrobromide (4.25 g, 12.5 mmol) in 220 ml of methanol cooled to 1 °C. Stirring was continued at 1 °C for 7 min and then at 25 °C for 25 min. A second portion of sodium borohydride (475 mg, 12.5 mmol) in 20 ml of methanol was then added. Methanol was removed under reduced pressure, water containing a few drops of acetic acid was added to the residue, and the mixture was extracted with methylene chloride. The extract afforded a product which proved to be a mixture of the bromohydrin (68% yield) and the epoxide **11** (85:15). A sample of the bromohydrin was purified by preparative tlc with elution by 95:5 chloroform–methanol and obtained as an amorphous solid. Spectroscopic characteristics: ir 2.80 (sharp), 3.10 (br), 5.80; nmr 0.90 (d, J = 2 Hz, 1H), 1.22 (d, J = 2 Hz, 1H), 1.62 ('t', 2 Hz spacings, 1H), 4.92 ('t', 6 Hz spacings, 1H), 5.25 (br, 1H),

Can. J. Chem. Downloaded from www.nrcresearchpress.com by 210.87.254.42 on 09/05/12
For personal use only.

6.03 (s, 3H), 6.38 (d, J = 6 Hz, 2H); ms 261 (1), 259 (1), 243 (1), 241 (1), 230 (3), 228 (3), 166 (100), 134 (13), 78 (10), 74 (14), 59 (27), 45 (14), 44 (14); high resolution ms 258.9845, 260.9825 (equal intensity) ($C_9H_{10}NO_3Br$: 258.9845, 260.9825).

The mixture of products was not normally separated, but carried forward to the next step, in which it was stirred with a twofold excess of sodium hydride in dry tetrahydrofuran at 25 °C for about 24 h. The reaction mixture was filtered, concentrated to an oil, and partitioned between water and methylene chloride. The organic layer afforded the epoxide **11** (93% yield) as an amorphous solid. Sublimation at 60 °C/0.05 torr provided an analytical sample, mp 63.5–64.5 °C. *Anal.* calcd. for $C_9H_9NO_3$: C 60.33, H 5.06, N 7.86; found: C 60.11, H 5.25, N 7.89. Spectroscopic characteristics: ir 5.80; nmr 0.87 (d, J = 2 Hz, 1H), 1.28 (d, J = 2 Hz, 1H), 1.85 ('t', 2 Hz spacings, 1H), 6.03 (superimposed s and m, 4H), 6.82 (m, J = 5.8 and 4.1 Hz, 1H), 7.18 (m, J = 5.8 and 2.5 Hz, 1H); ms 179 (63), 178 (54), 164 (11), 151 (44), 150 (30), 148 (45), 134 (11), 121 (10), 120 (100), 119 (13), 106 (38), 92 (23), 78 (22), 65 (27), 63 (27), 59 (16).

A solution of the epoxide **11** (550 mg, 3.1 mmol) in 4 ml of methanol was added over a 2 h period to a solution of tryptamine (1.08 g, 6.8 mmol) in 4 ml of refluxing methanol under nitrogen, and reflux was continued for a further 1.5 h. The methanol was removed under reduced pressure and the residue containing mono- and disubstituted products was purified by preparative tlc with m-m-a elution. The major fraction isolated in 46% yield was the amino alcohol **7** which was obtained as an amorphous solid. Spectroscopic characteristics: ir 2.88 (sharp), 3.0 (br), 5.80; nmr 0.94 (d, J = 2 Hz, 1H), 1.10 (br, 1H), 1.32 (d, J = 2 Hz, 1H), 1.72 ('t', 2 Hz spacings, 1H), 2.26–3.17 (complex, 5H), 5.26 (m, 1H, after D_2O treatment, dd, J = 8 and 4 Hz, 1H), 6.02 (s, 3H), 6.60 (br, 2H), 6.9–7.2 (complex, 6H); ms 339 (4), 321 (10), 223 (38), 209 (22), 193 (14), 192 (11), 191 (59), 187 (40), 174 (17), 173 (44), 168 (11), 167 (40), 166 (10), 165 (27), 164 (16), 144 (95), 143 (36), 134 (27), 132 (18), 131 (100), 130 (90), 129 (24), 117 (15), 106 (16), 78 (12), 77 (12), 58(16), 57(14); high resolution ms 339.1583 ($C_{19}H_{21}N_3O_3$: 339:1583).

Diacetyl derivative: ir 2.88 (sharp), 5.81 (br), 6.12; nmr 0.66 (br, 1H), 0.81 (d, J = 2 Hz, 1H), 1.22 (d, J = 2 Hz, 1H), 1.70 ('t', 2 Hz spacings, 1H), 2.12–3.06 (complex, 5H), 3.80 (dd, J = 8 and 4 Hz, 1H), 6.02 (s, 3H), 6.13–6.60 (complex, 4H), 6.72–7.22 (complex, 2H), 7.87 (s, 4H), 8.03 (s, 2H). (The complexities of the spectrum are attributed to the presence of two rotamers.)

The disubstituted tryptamine was isolated as a mixture of diastereoisomers in 8% yield. Spectroscopic characteristics: ir 2.88 (sharp), 2.94 (br), 5.80; nmr 0.90 (br, 2H), 1.16 (br, 1H, removed by D_2O), 1.30 (d, J = 2 Hz, 1H), 1.40 (d, J = 2 Hz, 1H), 1.70 (br, 2H), 2.20–3.14 (complex, 5H), 5.26 (complex, 2H), 5.70 (br, 2H), 6.01 (s, 6H), 6.72–7.43 (complex, 8H).

The hydroxy amine **7** (823 mg, 2.5 mmol) was mixed with 40 g of polyphosphoric acid under nitrogen and stirred at 95 °C for 8 h. The reaction mixture was cooled, made basic with chilled dilute ammonia, and extracted with methylene chloride. The extract afforded a product which was purified by preparative tlc with m-m-a elution. Naucledérine, **2**, (42 mg, 5.4% yield) was obtained as an oil that was recrystallized from methanol to give crystals, mp 94–108 °C. *Anal.* calcd. for $C_{19}H_{19}N_3O_2$: C 71.01, H 5.96, N 13.08; for $C_{19}H_{19}N_3O_2 \cdot H_2O$: C 67.24, H 6.24, N 12.38, for $C_{19}H_{19}N_3O_2 \cdot CH_3OH$: C 67.97, H 6.56, N 11.89; found: C 67.13, H 6.13; by ultramicro analysis: C 67.19, H 6.70, N 11.61. High resolution ms 321.1474 ($C_{19}H_{19}N_3O_2$: 321.1477), 292.1212 ($C_{18}H_{16}N_2O_2$: 292.1212), 279.1132 ($C_{17}H_{15}N_2O_2$: 279.1133).

The ir, uv, nmr, and ms characteristics of the synthetic material and natural naucledérine (1*b*) were identical in all significant aspects; their tlc behavior was identical on silica gel (3 systems) and on alumina.

The Dihydro-β-carbolines, ***13***

1-(3'-Hydroxypropyl)dihydro-β-carboline, ***13*** *(R = H)*

A solution of tryptamine (1.60 g, 10.0 mmol) and γ-butyrolactone, **15** (R = H) (0.92 g, 10.7 mmol) in 2 ml of absolute ethanol was refluxed under nitrogen for 27 h. The solvent was removed on a rotary evaporator and the gummy residue was triturated with carbon tetrachloride, leaving the tryptamide **14** (R = H) as a crystalline solid (2.34 g, 9.5 mmol), mp 67–73 °C. Spectroscopic characteristics: ir 2.89, 3.0, 6.06; uv 229 (9900), 275 (4850), 282 (5250), 291 (4500); ms 246 (4), 228 (4), 160 (11), 143 (55), 131 (45), 130 (100). This was acetylated with acetic anhydride in pyridine at room temperature for 24 h, and converted to the acetate, mp 92–97 °C, in 89% yield. *Anal.* calcd. for $C_{16}H_{20}N_2O_3$: C 66.64, H 6.99, N 9.72; found: C 66.80, H 6.90, N 9.64. Spectroscopic characteristics: ir 2.88, 3.0, 5.78, 6.01; uv 229 (12 450), 275 (4750), 282 (5250), 291 (4400); nmr 1.14 (br, 1H, removed by $NaOD/D_2O$), 2.37–3.13 (complex, 5H), 4.00 ('t', 6.5 Hz spacings, 1H, removed by $NaOD/D_2O$), 6.00 ('t', 6 Hz spacings, 2H), 6.47 (4 peaks, 6.5 Hz spacings, 2H, after $NaOD/D_2O$ treatment, 't', 6.5 Hz spacings, 2H), 7.03 ('t', 6.5 Hz spacings, 2H), 7.80–8.23 (m, 4H), 8.05 (s, 3H); ms 288 (8), 144 (17), 143 (100), 131 (8), 130 (61).

A mixture of the acetoxytryptamide (563 mg, 1.95 mmol) and 4 ml of freshly distilled phosphorus oxychloride was refluxed under nitrogen for 2 h. Excess phosphorus oxychloride was removed under reduced pressure, and the residue was taken up in 100 ml of 20% aqueous acetic acid. The solution was made basic with solid sodium carbonate and extracted with methylene chloride. The extract afforded a brown oil which was subjected to preparative tlc with m-m-a elution, and the product (192 mg, 36% yield) was obtained as an uncrystallizable gum: ir 2.89, 3.06, 5.80; uv 216 (14 600), 229 (14 350), 235 (14 350), 318 (12 450); in MeOH–HCl 215 (14 350), 247 (10 000), 355 (18 500); nmr 2.23–3.07 (m, 4H), 5.63–6.33 (m, 4H), 6.90–7.43 (m, 4H), 7.57–8.24 (m, 2H), 8.03 (s, 3H); ms 270 (8), 210 (71), 209 (100), 184 (55).

The above product (58 mg, 0.21 mmol) was dissolved in 5 ml of 80% aqueous methanol to which potassium bicarbonate (100 mg, 1.0 mmol) was added, and the solution was refluxed under nitrogen for 10.5 h. The methanol was removed on a rotary evaporator and the residue was partitioned between 50 ml of water and 100 ml of methylene chloride, and the aqueous layer was ex-

Can. J. Chem. Downloaded from www.nrcresearchpress.com by 210.87.254.42 on 09/05/12
For personal use only.

tracted with a further 100 ml of methylene chloride. The combined organic layers provided an oil which was purified by preparative tlc with m-m-a elution, and the product **13** (R = H) was obtained as a waxy solid (46 mg, 93% yield). Spectroscopic characteristics: ir 2.88, 3.12; uv 215 (12 500), 236 (11 950), 241 (11 800), 318 (11 900); in MeOH–HCl 214 (12 250), 246 (8300), 353 (19 400); in MeOH–KOH 216 (12 900), 236 (13 000), 314 (13 200); nmr ($CDCl_3/CD_3OD$) 2.23–3.07 (m, 4H), 5.90–6.43 (m, 4H), 6.90–7.40 (m, 2H), 7.80–8.33 (m, 2H); ms 228 (5), 210 (68), 209 (100), 198 (5), 184 (50).

A sample was converted to its hydrochloride salt, mp 186–206 °C (dec.) for analysis. *Anal.* calcd. for $C_{14}H_{17}N_2OCl$: C 63.51, H 6.47, N 10.58; found: C 63.60, H 6.41, N 10.48.

1-(3′-Hydroxy-3′-phenylpropyl)dihydro-β-carboline, ***13*** *(R = Ph)*

A solution of tryptamine (1.60 g, 10.0 mmol) and γ-phenyl-γ-butyrolactone, **15** (R = Ph) (1.74 g, 10.7 mmol) in 2 ml of absolute ethanol was refluxed under nitrogen for 26 h. The solvent was removed on a rotary evaporator and the residue was dissolved in hot methanol and treated with activated charcoal. The clarified solution yielded the tryptamide **14** (R = Ph) as a light yellow gum (3.13 g, 9.6 mmol) that was pure enough for use in the next step. An analytical sample was obtained by tlc with m-m-a elution. *Anal.* calcd. for $C_{20}H_{22}N_2O_2$: N 8.69; found: N 8.44. Spectroscopic characteristics: ir 2.87, 3.0, 6.05; uv 227 (18 150), 275 (5200), 282 (5500), 291 (4700); ms 322 (0.2), 304 (2), 162 (38), 160 (17), 143 (25), 131 (54), 130 (100).

The hydroxytryptamide **14** (R = Ph) was acetylated by stirring it for 18 h with 0.25 ml of acetic anhydride in 1.0 ml of pyridine and 5 ml of methylene chloride under nitrogen. The acetate was obtained in 97% yield as a pale yellow gum: ir 2.87, 3.03, 5.79, 6.03; uv 226 (29 900), 275 (6200), 282 (6600), 291 (5800); nmr 1.0 (br, 1H), 2.2–3.2 (complex, 5H), 4.03 ('t', 6 Hz spacings, 1H), 4.25 ('t', 6 Hz spacings, 1H), 6.47 ('q', 6 Hz spacings, 2H), 7.10 ('t', 6 Hz spacings, 2H), 7.7–8.1 (m, 4H), 8.02 (s, 3H); ms 364 (0.8), 304 (7), 144 (16), 143 (100), 131 (11), 130 (77).

The acetylated material (429 mg) was treated with 5 ml of freshly distilled phosphorus oxychloride in the manner described above. The product was obtained as an uncrystallizable yellow gum (122 mg, 29% yield): ir 2.90, 3.06, 5.78; uv 213 (22 400), 235 (14 200), 318 (11 000); in MeOH–HCl 212 (22 400), 242 (10 250), 356 (15 400); nmr 0.57 (br, 1H), 2.3–3.2 (complex, 9H), 4.20 ('t', 6 Hz spacings, 1H), 6.17 ('t', 8 Hz spacings, 2H), 6.8–8.1 (complex, 6H), 8.03 (s, 3H); ms 346 (2), 288 (9), 287 (29), 286 (100), 285 (73), 284 (13), 210 (6), 209 (32), 184 (49).

The above product (116 mg, 0.34 mmol) was hydrolyzed by refluxing it for 6 h in 5 ml of 80% aqueous methanol containing potassium bicarbonate (100 mg, 1.0 mmol) under nitrogen in the manner described above. The product **13** (R = Ph) was recovered in 83% yield as a yellow oil: uv 216 (18 900), 248 (11 300), 289 (6400), 318 (8500); in MeOH–HCl 214 (18 200), 305 (4700), 352 (12 500); in MeOH–KOH 217 (21 700), 289 (7800), 316 (10 200); nmr ($CDCl_3/CD_3OD$) 2.3–3.1 (complex, 9H), 5.1–5.4 (m, 1H), 6.0–6.5 (m, 2H), 7.0–7.5 (m, 4H), 7.7–8.2 (m, 2H). A sample was converted to its hydrochloride salt, mp 180–220 °C (dec.), for analysis. *Anal.* calcd. for $C_{20}H_{21}N_2OCl$: C 70.47, H 6.21, N 8.22; found: C 70.20, H 6.12, N 8.37.

The Pyridylhydroxypropyl-β-carboline ***13*** *(R = 3-pyridyl)*

A solution of β-nicotinylpropionic acid (15) (2.00 g, 11.2 mmol) in 15 ml of water containing sodium hydroxide (20 mmol) was added dropwise to a stirred ice-cold solution of sodium borohydride (400 mg, 10.8 mmol) in 20 ml of 0.2 *N* sodium hydroxide under nitrogen. Stirring was continued at room temperature for 22 h, and the cooled reaction mixture was neutralized with concentrated sulfuric acid. A further 10 ml of concentrated sulfuric acid was added and the solution was stirred at room temperature for 22 h. The solution was made basic with solid sodium carbonate and extracted with methylene chloride. The extract afforded the lactone **15** (R = 3-pyridyl) in 13% yield as a colorless oil which was suitable for the next step. An analytical sample was purified by microdistillation. *Anal.* calcd. for $C_9H_9NO_2$: C 66.24, H 5.56, N 8.58; found: C 66.02, H 5.65, N 8.46. Spectroscopic characteristics: ir 5.60; uv 211 (6600), 255 (6200), 260 (6900), 266 (4950); nmr 1.23–2.80 (m, 4H), 4.47 ('t', 7 Hz spacings, 1H), 7.0–8.1 (m, 4H); ms 164 (19), 163 (100), 162 (29), 135 (35), 134 (90), 119 (24), 118 (50), 109 (17), 108 (60), 107 (25), 106 (63).

A solution of the pyridylbutyrolactone **15** (R = 3-pyridyl) (198 mg, 1.21 mmol) and tryptamine (198 mg, 1.24 mmol) in 0.5 ml of absolute ethanol was refluxed for 15 h under nitrogen. The solvent was removed on a rotary evaporator, and the oily product was subjected to preparative tlc with m-m-a elution. The tryptamide **14** (R = 3-pyridyl) was obtained as an uncrystallizable colorless gum (206 mg, 0.64 mmol). An analytical sample was prepared by microdistillation. *Anal.* calcd. for $C_{19}H_{21}N_3O_2$: C 70.56, H 6.55, N 13.00; found: C 70.00, H 6.74, N 12.67. Spectroscopic characteristics: ir 2.89, 3.03, 6.05; ms 323 (1), 305 (2), 164 (9) 163 (70), 162 (18), 160 (22), 134 (39), 131 (60), 130 (100), 120 (28), 108 (72), 107 (15), 106 (30).

The hydroxytryptamide **14** (R = 3-pyridyl) (170 mg) was acetylated in the manner described above for **14** (R = Ph). The acetate was recovered in 95% yield as an uncrystallizable colorless gum: ir 2.87, 3.0, 5.79, 6.01; uv 225 (22 900), 262 (5050), 268 (5300), 282 (4700), 291 (3950); nmr 0.73 (br, 1H, removed by $NaOD/D_2O$), 1.3–3.2 (complex, 8H), 3.80 ('t', 6 Hz spacings, 1H, removed by $NaOD/D_2O$), 4.30 (m, 1H), 6.48 (4 peaks, 6 Hz spacings, 2H, after $NaOD/D_2O$ treatment, 3 peaks, 6 Hz spacings, 2H), 7.10 (3 peaks, 6 Hz spacings, 2H), 7.7–8.2 (m, 4H), 8.00 (s, 3H); ms 366 (4), 365 (14), 305 (5), 223 (15), 164 (6), 163 (9), 144 (17), 143 (100), 131 (6), 130 (40).

The acetylated product (169 mg, 0.46 mmol) was treated with 5 ml of phosphorus oxychloride in the manner described above. The product was obtained as a yellow glassy solid (132 mg, 0.38 mmol): ir 2.89, 3.06, 5.80; uv 214 (23 400), 317 (11 700); in MeOH–HCl 212 (17 700), 250 (11 200), 356 (16 700); nmr −0.37 (br, 1H), 1.4–3.0 (complex, 8H), 3.9–4.3 (m, 1H), 5.9–6.3 (m, 2H), 6.8–8.2 (complex, 6H), 8.03 (s, 3H); ms 348 (4), 347 (12),

Can. J. Chem. Downloaded from www.nrcresearchpress.com by 210.87.254.42 on 09/05/12
For personal use only.

289 (65), 288 (54), 287 (52), 286 (50), 211 (20), 210 (100), 209 (19), 168 (100), 167 (40); high resolution ms 347.1634 ($C_{21}H_{21}N_3O_2$: 347.1634).

This acetate (120 mg, 0.37 mmol) was hydrolyzed in the manner described in the preparation of **13** (R = Ph). The product, **13** (R = 3-pyridyl), was recovered as an uncrystallizable glassy yellow solid (103 mg, 0.34 mmol): ir 2.89, 3.12; uv 213 (17 600), 239 (12 700), 243 (12 600), 260 (sh), 268 (sh), 319 (12 000), in MeOH–HCl 213 (17 600), 250 (10 100), 356 (18 100); in MeOH–KOH 213 (22 300), 239 (14 500), 243 (14 300), 260 (sh), 268 (sh), 318 (13 400); nmr ($CDCl_3$/DMSO-d_6) −1.27 (br, 1H), 1.2–3.0 (complex, 8H), 4.8–5.2 (m, 2H), 5.9–6.3 (m, 2H), 6.8–7.5 (m, 4H), 7.6–8.0 (m, 2H).

*Naucleonine, **19**, and Naucleonidine, **20***

*Model compound **18** (R = H)*

A solution of harmalan, **16**, (364 mg, 2 mmol) and 0.5 ml of freshly distilled ethylene bromohydrin (8 mmol) in 8 ml of dry chloroform was refluxed under nitrogen for 16 h. The yellow solid which precipitated was collected, washed with chloroform, and recrystallized from ethanol – ethyl acetate. The hydrobromide **17** (R = H) was obtained as yellow needles (115 mg, 0.37 mmol), mp 233–240 °C (dec.). *Anal.* calcd. for $C_{14}H_{17}N_2OBr$: C 54.38, H 5.54, N 9.06, Br 25.84; found: C 54.57, H 5.78, N 9.04, Br 25.83. Spectroscopic characteristics: ir (Nujol) 3.04, 3.23, 6.18, 6.25, 6.38, 6.46; uv 210 (14 600), 249 (9100), 358 (17 000).

The hydrobromide (114 mg, 0.37 mmol) was suspended in a rapidly stirred mixture of 30 ml of methylene chloride and 30 ml of 5% aqueous potassium hydroxide under nitrogen and the stirring was continued for 1 h. The phases were separated and the aqueous phase was extracted with two 50 ml portions of methylene chloride. The combined organic phases yielded the oxazolidine **18** (R = H) as a pale yellow glass (74 mg, 0.33 mmol): ir 2.90, 3.05; uv 226 (15 300), 248 (6100), 275 (2300), 283 (2400), 291 (2600), 357 (10 000); in MeOH–HCl 211 (14 000), 249 (9700), 357 (20 800); in MeOH–KOH 226 (23 300), 275 (6800), 282 (7000), 291 (5300); nmr 1.01 (s, 1H), 2.3–3.0 (m, 4H), 5.7–6.4 (m, 2H), 6.5–7.8 (complex, 2H), 8.28 (s, 3H, removed by D_2O).

*Model compound **18** (R = Ph)*

A solution of harmalan, **16**, (166 mg, 0.9 mmol) and styrene oxide (233 mg, 1.9 mmol) in 8 ml of chloroform was refluxed under nitrogen for 5 days. Removal of the solvent afforded a yellow oil which was purified by preparative tlc with m-m-a elution. The oxazolidine **18** (R = Ph) was obtained as an oil (166 mg, 0.55 mmol): ir 2.90, 3.04; uv 225 (20 600), 250 (6200), 274 (3800), 282 (3800), 291 (3300), 360 (11 400); in MeOH–HCl 214 (16 600), 250 (10 400), 362 (23 500); in MeOH–KOH 229 (24 900), 275 (8300), 282 (8300), 291 (7100); nmr (areas based on 50:50 mixture of two $C_{20}H_{20}N_2O$ isomers) 1.36 (s, 1H, removed by D_2O), 1.53 (s, 1H, removed by D_2O), 2.4–3.0 (complex, 18H), 4.66 (4 peaks, separations 6, 4, 6 Hz, 1H), 5.12 (4 peaks, separations 6, 1, 6 Hz, 1H), 6.4–7.6 (complex, 12H), 8.21 (s, 3H, removed by D_2O), 8.26 (s, 3H, removed by D_2O); ms 305 (5), 304 (14), 290 (20), 289 (100), 200 (5), 199 (13), 198 (57), 197 (12), 185 (6), 184 (6), 183 (12), 182 (6), 172 (15), 171 (7), 170 (12).

A sample of the picrate, mp 215–230 °C (dec.), was prepared for analysis. *Anal.* calcd. for $C_{26}H_{23}N_5O_8$: C 58.53, H 4.35, N 13.13; found: C 58.48, H 4.17, N 12.88.

*Naucleonine, **19***

Sodium hydride (1.8 g of a 57% dispersion in mineral oil, 43 mmol) was washed with hexane to remove the mineral oil, and then suspended in 30 ml of dry dimethyl sulfoxide stirred under nitrogen. Trimethyloxosulfonium iodide (9.2 g, 42 mmol) was added to the stirred suspension and, when evolution of hydrogen had ceased, a solution of 3-pyridinecarboxaldehyde (3.51 g, 33 mmol) in 20 ml of dimethyl sulfoxide was added dropwise over 15 min. The mixture was heated in an oil bath at 53 °C for 30 min, cooled, and poured into 500 ml of ice water. Extraction with methylene chloride afforded 3-vinylpyridine epoxide as a pale yellow oil (3.72 g) which darkened rapidly on standing. Attempts to purify the epoxide further were unsuccessful because of its instability.

The freshly prepared epoxide (117 mg, 0.97 mmol) and harmalan, **16**, (145 mg, 0.8 mmol) were heated together at 50 °C under nitrogen for 18.5 h. Preparative tlc of the crude reaction mixture with elution by methanol yielded a glassy solid (77 mg, 0.25 mmol) which had the same tlc behavior as natural naucleonine (ND-305B) and very similar spectroscopic characteristics (1*b*). The synthetic naucleonine, **19**, could not be obtained in a crystalline form, but further purification was carried out by tlc with m-m-a elution. *Anal.* calcd. for $C_{19}H_{19}N_3O$: C 74.73, H 6.27, N 13.76; found: C 74.77, H 6.15, N 13.28. Spectroscopic characteristics: ir 2.90 (sharp), 3.1; uv 224 (21 300), 252 (7600), 268 (5400), 281 (4000), 291 (3200), 360 (10 500); in MeOH–HCl 213 (16 500), 251 (11 900), 363 (23 800); in MeOH–KOH 227 (29 700), 269 (8700), 282 (7600), 291 (6400), nmr (areas based on equimolar mixture of **19***a* and **19***b*) 0.96 (s, 1H, removed by D_2O), 1.00 (s, 1H, removed by D_2O), 1.3–2.5 (complex, 8H), 2.5–3.0 (complex, 8H), 4.71 (4 peaks, spacings 6, 3, and 6 Hz, 1H), 5.10 (4 peaks, spacings 6, 1, and 6 Hz, 1H), 6.1–7.6 (complex, 12H), 8.21 (s, 3H, removed by D_2O), 8.24 (s, 3H, removed by D_2O); ms 306 (5), 305 (18), 291 (22), 290 (100), 199 (3), 198 (14), 197 (3), 184 (5), 183 (6), 172 (5), 156 (3), 155 (5), 154 (4), 144 (5), 143 (3), 130 (4), 129 (2), 128 (2), 115 (2), 107 (4), 106 (8), 78 (4), 77 (2); high resolution ms 305.1530 ($C_{19}H_{19}N_3O$: 305.1528).

*Naucleonidine, **20***

A solution of the epoxide of 3-vinyl-5-carbomethoxy pyridine, **11**, (described above) (394 mg, 2.20 mmol) and harmalan, **16**, (377 mg, 2.05 mmol) in 5 ml of chloroform was refluxed under nitrogen for 72 h. Solvent was removed on a rotary evaporator and the brown gum that remained was subjected to tlc with m-m-a elution. A glassy solid (355 mg, 0.98 mmol) was obtained that had the same tlc behavior as naucleonidine (ND-363C) and very similar spectroscopic characteristics (1*b*). The synthetic naucleonidine, **20**, could not be obtained in crystalline form, but further purification was carried out by tlc with m-m-a elution. *Anal.* calcd. for $C_{21}H_{21}N_3O_3$: C 69.40, H 5.83, N 11.56; found: C 69.29, H 5.79, N 11.26. Spectroscopic characteristics: ir 2.90 (sharp), 3.05, 5.80, 5.82 (sh); uv 224 (28 200), 272 (6650), 291 (4450), 360 (5850); in MeOH–HCl 212 (18 950), 250 (10 900), 364 (21 200); in MeOH–KOH 225 (35 100), 273 (10 000), 291 (7250);

Can. J. Chem. Downloaded from www.nrcresearchpress.com by 210.87.254.42 on 09/05/12
For personal use only.

nmr (areas based on equimolar mixture of **20***a* and **20***b*) 0.86 (superimposed signals, 3H, after D_2O treatment, d, J = 2 Hz, 1H), 1.02 (d, J = 2 Hz, 1H), 1.21 (d, J = 2 Hz, 1H), 1.52 (d, J = 2 Hz, 1H), 1.68 ('t', 2 Hz spacings, 1H), 2.20 ('t', 2 Hz spacings, 1H), 2.4–3.0 (complex, 8H), 4.71 (4 peaks, spacings 6, 3, and 6 Hz, 1H), 5.09 (4 peaks, spacings 6, 1, and 6 Hz, 1H), 6.10 (s, 3H), 6.34 (s, 3H), 6.3–7.5 (complex, 12H), 8.22 (s, 6H, removed by D_2O); ms 364 (7), 363 (19), 349 (26), 348 (100), 332 (2), 316 (5), 199 (8), 198 (25), 197 (6), 183 (6), 172 (10), 170 (6), 169 (6), 165 (9), 164 (14), 157 (5), 156 (5), 155 (9), 154 (7), 144 (10), 143 (5), 134 (9), 130 (9), 129 (7), 128 (4), 115 (4), 106 (5), 104 (5), 99 (6), 77 (6); high resolution ms 363.1585 ($C_{21}H_{21}N_3O_3$: 363.1582).

Alkaloid ND-363B

This substance was obtained as a syrup in the tlc fractionation of the *N. diderrichii* extract (1*a*, *b*): ir 2.90 (sharp), 3.1 (br), 5.80, 5.82 (sh); uv (extinction coefficients based on mol. wt. 738) 222 (60 400), 270 (13 850), 279 (sh), 289 (sh), 361 (8300); in MeOH–HCl 222 (end absorption 29 000), 247 (19 600), 265 (sh), 362 (35 600); in MeOH–KOH 223 (71 000), 273 (15 500), 280 (sh), 289 (sh); nmr (integrated areas uncertain, comparison made with naucleonidine (ND-363C) spectrum (1*b*) and comment made only on significant differences) 0.75–2.2 (peaks correspond, but each broadened or doubled, peak at 0.96 removed by D_2O), 4.76 (4 peaks, each split further), 5.03 (3 peaks, each split further), 6.04 (s), 6.08 (s), 6.25 (s), 6.27 (s), 7.9 (broad peak, absent in ND-363C; removed by D_2O; no peak near 8.2); ms 364 (7), 363 (20), 362 (4), 349 (25), 348 (100), 332 (3), 316 (4), 279 (5), 199 (13), 198 (27); metastables 334.0 (calcd. for 363 → 348: 333.6), 287.1 (calcd. for 348 → 316: 286.9); high resolution ms 363.1581 ($C_{21}H_{21}N_3O_3$: 363.1582), 348.1354 ($C_{20}H_{18}N_3O_3$: 348.1348), 316.1089 ($C_{19}H_{14}N_3O_2$: 316.1086); field desorption ms (low temperature) 741 (17), 739 (7), 376 (22), 364 (100), 278 (10); (high temperature) 376 (10), 364 (100), 182 (22), 166 (38).

Dihydrocadambine, **22**

This alkaloid was isolated as a pale brown glass in the tlc fractionation of the *N. diderrichii* extract (1*a*, *b*): ir 2.92 (sh), 3.05 (br, strong), 5.93, 6.12; uv 225 (27 550), 278 (6300); nmr tabulated previously (2*a*); field desorption ms 546. Acetylation with acetic anhydride and pyridine at room temperature and purification by tlc with elution by 96:4 chloroform–methanol provided a syrup: ir 2.89 (sharp), 3.02 (br, medium height), 5.73 (strong), 5.89, 6.10; nmr tabulated previously (2*a*); field desorption ms 756. *Anal.* calcd. for $C_{37}H_{44}N_2O_{15}$: C 58.72, H 5.86, N 3.71, 5Ac 28.48, for $C_{37}H_{44}N_2O_{15}\cdot CH_3OH$: C 57.86, H 6.13, N 3.55, 5Ac 27.29; found: C 57.74, H 6.43, N 3.43, Ac 26.83.

Acknowledgments

This paper is taken from the Ph.D. theses (University of Toronto, 1974) of G.I.D. and A.S. We thank the National Research Council of Canada for support of this investigation and for a scholarship (to G.I.D.). We thank Professor G. W. Wood, University of Windsor, for the field desorption mass spectra.

1. (*a*) S. McLEAN and D. G. MURRAY. Can. J. Chem. **50**, 1478 (1972); (*b*) D. G. MURRAY, A. SZAKOLCAI, and S. McLEAN. Can. J. Chem. **50**, 1486 (1972); (*c*) S. McLEAN and D. G. MURRAY. Can. J. Chem. **50**, 1496 (1972).
2. (*a*) G. I. DMITRIENKO, D. G. MURRAY, and S. McLEAN. Tetrahedron Lett. 1961 (1974); (*b*) G. I. DMITRIENKO, A. SZAKOLCAI, and S. McLEAN. Tetrahedron Lett. 2599 (1974).
3. S. A. FINE, R. F. FREESE, and M. G. GREENE. J. Org. Chem. **38**, 2089 (1973).
4. K. FRETER. Justus Liebigs Ann. Chem. **721**, 101 (1969).
5. F. I. CARROLL. Org. Prep. Proc. Int. **3**, 121 (1971).
6. A. H. JACKSON and A. F. SMITH. Tetrahedron, **24**, 403 (1968); A. H. JACKSON and P. SMITH. Tetrahedron, **24**, 2227 (1968); A. H. JACKSON, B. NAIDOO, and P. SMITH. Tetrahedron, **24**, 6119 (1968).
7. E. J. COREY and M. CHAYKOVSKY. J. Am. Chem. Soc. **87**, 1353 (1965); Org. Synth. Coll. Vol. 5, 755 (1973).
8. D. G. MURRAY. Ph.D. Thesis, University of Toronto, Toronto, Ontario. 1971.
9. F. W. LICHTENTHALER and P. EMIG. Tetrahedron Lett. 577 (1967); G. DESCOTES, F. CHIZAT, and J. C. MARTIN. Bull. Soc. Chim. Fr. 2304 (1970).
10. R. T. BROWN and S. B. FRASER. Tetrahedron Lett. 1957 (1974).
11. A. I. SCOTT. MTP International Review of Science. Organic Chemistry, Series One, Vol. 9. *Edited by* K. F. Wiesner. Butterworths, London. 1973, p. 105.
12. F. HOTELLIER, P. DELAVEAU, and J.-L. POUSSET. Phytochemistry, **14**, 1407 (1975).
13. R. T. BROWN and A. A. CHARALAMBIDES. J. Chem. Soc. Chem. Commun. 765 (1973).
14. F. K. THAYER. Org. Synth. Coll. Vol. 1, 12 (1944).
15. J. C. SHIVERS, M. L. DILLON, and C. R. HAUSER. J. Am. Chem. Soc. **69**, 119 (1947).

Crystal and molecular structure of the salicylaldehydatogallium dimethyl dimer

STEVEN J. RETTIG, ALAN STORR, AND JAMES TROTTER

Department of Chemistry, University of British Columbia, Vancouver, British Columbia V6T 1W5

Received October 10, 1975

STEVEN J. RETTIG, ALAN STORR, and JAMES TROTTER. Can. J. Chem. **54**, 1278 (1976).

Crystals of the salicylaldehydatogallium dimethyl dimer, $[C_7H_5O_2 \cdot GaMe_2]_2$, are triclinic, $a = 9.845(1)$, $b = 8.6892(8)$, $c = 7.4153(6)$ Å, $\alpha = 118.236(5)$, $\beta = 92.46(1)$, $\gamma = 115.81(1)°$, $Z = 1$, space group $P\bar{1}$. The structure was solved by Patterson and Fourier syntheses and was refined by full-matrix least-squares procedures to a final R of 0.050 and R_w of 0.064 for 1644 reflections with $I \geq 3\sigma(I)$. The structure features a five-coordinate gallium atom having distorted trigonal bipyramidal geometry. Monomer units link via the formation of a four-membered Ga_2O_2 ring to form the centrosymmetric dimers. Bond lengths in the molecule are: Ga—O(eq), 1.933(3), Ga—O(ax), 2.127(3) and 2.469(3), Ga—C, 1.944(6) and 1.946(5), C—O, 1.333(4) and 1.231(6), C(ar)—C(sp^2), 1.432(7), mean C—C(ar), 1.395(8), mean C(sp^3)—H, 0.92(4), and mean C(sp^2)—H, 0.93(2) Å. Bonds not involving hydrogen have been corrected for thermal motion.

STEVEN J. RETTIG, ALAN STORR et JAMES TROTTER. Can. J. Chem. **54**, 1278 (1976).

Les cristaux du dimère du diméthyl salicylaldéhydatogallium, $[C_7H_5O_2 \cdot GaMe_2]_2$, sont tricliniques, $a = 9.845(1)$, $b = 8.6892(8)$, $c = 7.4153(6)$ Å, $\alpha = 118.236(5)$, $\beta = 92.46(1)$, $\gamma = 115.81(1)°$, $Z = 1$, groupe d'espace $P\bar{1}$. On a résolu la structure par les synthèse de Patterson et de Fourier et on l'a affinée par la méthode des moindres carrés (matrice complète) jusqu'à une valeur finale de R de 0.050 et de R_w de 0.064 pour 1644 réflexions avec $I \geq 3\sigma(I)$. Dans la structure, on remarque un atome de gallium pentacoordonné possédant une géométrie bipyramidale trigonale déformée. Les unités monomères se lient par la formation de cycle Ga_2O_2 à quatre membres pour former des dimères centrosymétriques. Les longueurs des liaisons dans les molécules sont: Ga—O(eq), 1.933(3), Ga—O(ax), 2.127(3) et 2.469(3), Ga—C, 1.944(6) et 1.946(5), C—O, 1.333(4) et 1.231(6), C(ar)—C(sp^2), 1.432(7), moyenne des C—C(ar), 1.395(8), moyenne des C(sp^3)—H, 0.92(4), et moyenne des C(sp^2)—H, 0.93(2) Å. On a corrigé les liens n'impliquant pas les hydrogènes pour le mouvement thermique.

[Traduit par le journal]

Introduction

Numerous examples of five-coordinate gallium atoms have recently been reported (1–5). The present X-ray analysis provides an additional crystallographic example of this type of coordination for the gallium atom which is novel on two counts. It is the first example not to include nitrogen in the pentacoordination sphere about the metal atom (the gallium is coordinated to three oxygen and two carbon atoms) and it is the first example where the dimer units present in the solid state are not in evidence in either the gas phase or in solution where monomeric constitutions are indicated.

Experimental

Salicylaldehydatogallium Dimethyl $C_7H_5O_2 \cdot GaMe_2$ (6)

The compound was prepared by reacting equimolar amounts of salicylaldehyde and gallium trimethyl in benzene at room temperature. Methane was briskly evolved, and following removal of solvent at the cessation of the reaction, a canary yellow solid product was obtained. This was sublimed under vacuum to yield air sensitive yellow crystals. mp 78 °C; *Anal.* calcd. for $C_7H_5O_2 \cdot GaMe_2$: C 48.9, H 4.98; found: C 48.8, H 4.98. *Mol. Wt.* calcd. for $C_7H_5O_2 \cdot GaMe_2$: 220.9; found (cryoscopy in benzene solution): 221; proton nmr (C_6D_6) τ_{Ga-Me} (singlet) 11.07 ppm ($\tau_{C_6H_6}$) 2.84 ppm).

The low frequency infrared spectrum showed characteristic ν_{Ga-C} bands at 595 and 555 cm^{-1} in addition to bands at 515, 440, 430, and 370 cm^{-1} which may arise from heterocyclic ring modes.

Crystallographic Analysis

The crystal chosen for study was positioned in a capillary tube under a nitrogen atmosphere to avoid the rapid hydrolysis which occurs on contact of the compound with moist air. The capillary was then flame sealed. The crystal was mounted with $-2\,2\,1$ parallel to the goniostat axis and had dimensions of *ca.* 0.45 × 0.60 × 0.80 mm. Unit-cell and space group data were obtained from film and diffractometer measurements. The unit-cell parameters were refined by a least-squares treatment of $\sin^2\theta$ values for 30 reflections measured on a diffractometer with CuK_α radiation. Crystal data are:

$C_{18}H_{22}Ga_2O_4$ fw = 441.8

Triclinic, $a = 9.845(1)$, $b = 8.6892(8)$, $c = 7.4153(6)$

Can. J. Chem. Downloaded from www.nrcresearchpress.com by 210.87.254.105 on 09/05/12
For personal use only.

Can. J. Chem. Downloaded from www.nrcresearchpress.com by 210.87.254.105 on 09/05/12
For personal use only.

Å, $\alpha = 118.236(5)$, $\beta = 92.46(1)$, $\gamma = 115.81(1)°$, $V = 477.7(1)$ Å^3, $Z = 1$, $\rho_c = 1.5357(3)$ g cm^{-3}, $F(000) = 224$ (22 °C, CuK_α, $\lambda = 1.5418$ Å, $\mu = 38.9$ cm^{-1}). Space group $P\bar{1}$ (C_i^1, No. 2).

Intensities were measured on a Datex-automated General Electric XRD 6 diffractometer, with a scintillation counter, CuK_α (nickel filter and pulse height analyser), and a θ–2θ scan at 4° min^{-1} over a range of $(1.80 + 0.86 \tan\theta)$ degrees in 2θ, with 10 s background counts being measured at each end of the scan. Data were measured to $2\theta = 146°$ (minimum interplanar spacing 0.81 Å). The intensity of the check reflection, measured every 50 reflections, decreased uniformly to a value which was 92% of the initial count by the end of the data collection. Lorentz and polarization corrections and check reflection scaling were applied, and the structure amplitudes were derived. No absorption correction was made due to possible uncertainties which would result from the irregular shape of the crystal. Of the 1921 independent reflections measured, 260 had intensities less than $3\sigma(I)$ above background where $\sigma^2(I) = S + B + (0.06S)^2$ with S = scan count and B = time averaged background count. These reflections were given zero weight in the refinement but were included in the structure factor calculations.

The position of the gallium atom was determined from the three-dimensional Patterson function. Two cycles of full-matrix least-squares refinement of the positional and isotropic thermal parameters of the gallium atom gave $R = 0.34$. The positions of the other nonhydrogen atoms were taken from a subsequent difference map. The nonhydrogen atoms were refined isotropically for two cycles and then anisotropically for two cycles giving $R = 0.062$. The hydrogen atom positions were located from a difference map at this point. The entire structure (hydrogen atoms having isotropic thermal parameters) was refined for six cycles giving a final R of 0.050 and R_w of 0.064 for 1644 reflections with $I \geq 3\sigma(I)$ (17 reflections which had $|F_o| - |F_c| > 3\sigma(F)$ were removed from the data set in the final stages of refinement).

The least-squares refinement was based on the minimization of $\sum w[|F_o| - |F_c/(1 + gI)|]^2$ where g is the extinction parameter and I the uncorrected intensity. The final value of g was $1.6(2) \times 10^{-7}$. The scattering factors of ref. 7 were used for the nonhydrogen atoms and those of ref. 8 for the hydrogen atoms. Anomalous scattering factors from ref. 9 were used for the Ga, O, and C atoms. The anisotropic thermal parameters employed in the refinement are U_{ij} in the expression:

$$f = f^0 \exp[-2\pi^2(U_{11}h^2a^{*2} + U_{22}k^2b^{*2} + U_{33}l^2c^{*2} + 2U_{12}hka^*b^* + 2U_{13}hla^*c^* + 2U_{23}klb^*c^*)]$$

where f^0 is the tabulated scattering factor and f is that corrected for thermal motion. The weighting scheme: $w = 1/\sigma^2(F)$ where $\sigma^2(F)$ is derived from the previously defined $\sigma^2(I)$ gave uniform average values of $w(|F_o| - |F_c|)^2$ over ranges of $|F_o|$ and was employed in the final stages of refinement. The mean error in an observation of unit weight was 1.59. On the final cycle of refinement the mean parameter shift was 0.03σ and no parameter shift was greater than 0.17σ. A final difference map showed maximum fluctuations of ± 0.9 e Å^{-3} in the vicinity of the gallium atom. The final positional and thermal parameters appear in Tables 1 and 2 respectively. Measured and calculated structure factors have been placed in the Depository of Unpublished Data.[1] The ellipsoids of thermal motion for the nonhydrogen atoms are shown in Fig. 1. The thermal motion has been analysed in terms of the rigid-body modes of translation (T), libration (L), and screw (S) motion (10) using the computer program MGTLS. The rms standard deviation in the temperature factors U_{ij} is 0.0022 Å^2. The analyses were carried out for all nonhydrogen atoms in the centrosymmetric dimer and in the monomer unit. The latter analysis was successful (rms $\Delta U_{ij} = 0.0056$ Å^2) while the former was not. This indicates that the dimer unit as a whole is not a rigid body and that the thermal motion is better described as independent motions of the monomer units.

TABLE 1. Final positional parameters (fractional $\times 10^4$, Ga $\times 10^5$, H $\times 10^3$) with estimated standard deviations in parentheses

Atom	x	y	z
Ga	60950(6)	39015(6)	38055(8)
O(1)	6504(3)	6615(4)	5761(5)
O(2)	8537(4)	5187(5)	4049(6)
C(1)	9328(4)	8653(6)	6576(7)
C(2)	7846(4)	8421(5)	6768(6)
C(3)	7803(6)	10183(6)	8081(8)
C(4)	9177(7)	12083(7)	9204(9)
C(5)	10635(6)	12313(7)	9032(8)
C(6)	10704(5)	10624(8)	7742(8)
C(7)	9557(5)	7010(8)	5224(9)
C(8)	6198(7)	2613(8)	5301(9)
C(9)	5347(7)	3044(9)	844(9)
H(3)	681(6)	1006(8)	829(8)
H(4)	916(7)	1317(10)	997(9)
H(5)	1157(9)	1358(13)	973(12)
H(6)	1170(7)	1072(9)	750(8)
H(7)	1055(6)	731(8)	520(8)
H(8a)	719(9)	326(12)	621(12)
H(8b)	547(9)	250(13)	595(13)
H(8c)	610(11)	117(16)	437(15)
H(9a)	476(9)	152(14)	−16(12)
H(9b)	480(10)	356(15)	95(13)
H(9c)	598(13)	300(17)	16(17)

The appropriate bond distances and angles have been corrected for libration (11, 12), using shape parameters q^2 of 0.08 for all atoms involved. Both corrected and uncorrected bond lengths appear in Table 3. Changes in the bond angles were not significant, thus only the uncorrected angles appear in Table 4.

Results and Discussion

The structure consists of centrosymmetric dimeric units which contain five-coordinate

[1]The structure factor table is available, at a nominal charge, from the Depository of Unpublished Data, CISTI, National Research Council of Canada, Ottawa, Canada K1A 0S2.

Can. J. Chem. Downloaded from www.nrcresearchpress.com by 210.87.254.105 on 09/05/12
For personal use only.

TABLE 2. Final thermal parameters and their estimated standard deviations

(*a*) Anisotropic thermal parameters ($U_{ij} \times 10^3$, Ga $\times 10^4$ Å^2)

Atom	U_{11}	U_{22}	U_{33}	U_{12}	U_{13}	U_{23}
Ga	681(4)	423(3)	680(4)	293(2)	157(2)	301(2)
O(1)	48(1)	37(1)	96(2)	16(1)	21(1)	32(1)
O(2)	59(2)	61(2)	103(2)	34(1)	23(2)	40(2)
C(1)	52(2)	54(2)	68(2)	20(2)	7(2)	38(2)
C(2)	54(2)	40(2)	68(2)	17(1)	11(2)	32(2)
C(3)	69(3)	43(2)	89(3)	22(2)	20(2)	30(2)
C(4)	89(3)	41(2)	81(3)	16(2)	15(2)	27(2)
C(5)	68(3)	52(2)	81(3)	4(2)	1(2)	32(2)
C(6)	53(2)	69(3)	81(3)	15(2)	5(2)	44(2)
C(7)	51(2)	73(3)	98(3)	33(2)	19(2)	49(3)
C(8)	87(3)	64(3)	85(3)	39(3)	19(3)	48(2)
C(9)	76(3)	79(3)	77(3)	39(3)	22(2)	43(3)

(*b*) Isotropic thermal parameters ($U \times 100$)

Atom	U (Å^2)	Atom	U (Å^2)
H(3)	7(1)	H(8b)	13(3)
H(4)	8(2)	H(8c)	16(3)
H(5)	13(2)	H(9a)	12(2)
H(6)	7(1)	H(9b)	14(3)
H(7)	7(1)	H(9c)	17(4)
H(8a)	11(2)		

gallium atoms having distorted trigonal bipyramidal geometry. The monomer units (containing four-coordinated gallium atoms) predicted by the molecular weight in solution, the mass spectrum, and the structure of the related boron compound salicylaldehydatoboron diphenyl (13), dimerize via formation of centrosymmetric (thus planar) four-membered Ga_2O_2 rings. This type of dimerization also occurs in the molecules $[MeN(CH_2CH_2O)_2GaH]_2$ (3) and $[Me_2NCH_2CH_2OGaR_2]_2$ (R = H and Me) (4). The resulting dimer (**1**) features a nearly planar system of five fused rings.

The trigonal planar phenolic oxygen atom, O(1), bridges the two gallium atoms and occupies an equatorial position on Ga and an axial site on Ga′. O(1)′ occupies an axial position on Ga. (Here and elsewhere in this paper primed atoms refer to atoms related by the center of symmetry at $\frac{1}{2},\frac{1}{2},\frac{1}{2}$ to those whose coordinates are given in Table 1.) The remaining axial position at Ga is taken by O(2) while the other two equatorial sites are occupied by methyl groups. The angular distortion of the trigonal bipyramid is less marked than in the related compounds $[MeN(CH_2CH_2O)_2GaH]_2$ and $[Me_2NCH_2CH_2OGaR_2]_2$ which have five-membered rings (rather than six-membered rings) fused to the Ga_2O_2 rings. The angle between the axial substituents is 164.4(1)° in the present structure compared to angles in the range 150–152° for the ethanolamine complexes (3, 4). The axial–Ga–equatorial angles

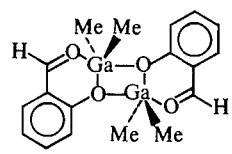

1

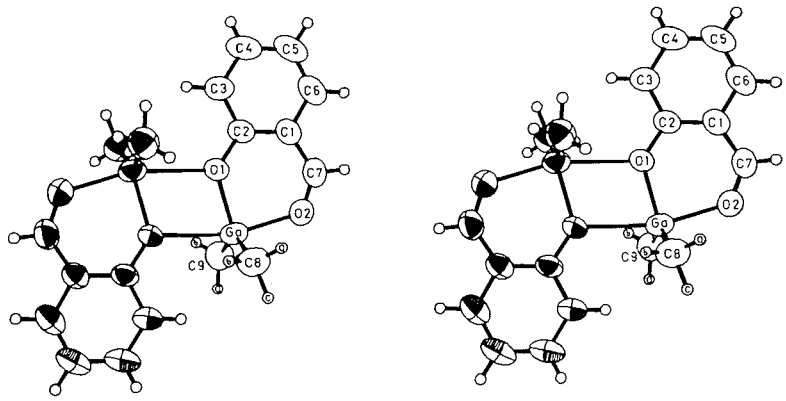

FIG. 1. A stereo view of the salicylaldehydatogallium dimethyl molecule. 50% ellipsoids are shown for the nonhydrogen atoms.

Can. J. Chem. Downloaded from www.nrcresearchpress.com by 210.87.254.105 on 09/05/12
For personal use only.

TABLE 3. Bond lengths (Å) with estimated standard deviations in parentheses

(*a*) Nonhydrogen atoms

Bond	Distance (Å)		Bond	Distance (Å)	
	Uncorrected	Corrected		Uncorrected	Corrected
Ga—O(1)	1.927(3)	1.933	C(1)—C(2)	1.406(6)	1.413
Ga—O(1)′	2.462(3)	2.469	C(1)—C(6)	1.412(6)	1.414
Ga—O(2)	2.120(3)	2.127	C(1)—C(7)	1.428(7)	1.432
Ga—C(8)	1.939(5)	1.946	C(2)—C(3)	1.394(6)	1.400
Ga—C(9)	1.938(6)	1.944	C(3)—C(4)	1.381(6)	1.383
O(1)—C(2)	1.330(4)	1.333	C(4)—C(5)	1.381(9)	1.386
O(2)—C(7)	1.229(6)	1.231	C(5)—C(6)	1.356(8)	1.360

(*b*) Bonds involving hydrogen atoms

Bond	Distance (Å)	Bond	Distance (Å)
C(3)—H(3)	0.96(5)	C(8)—H(8a)	0.91(8)
C(4)—H(4)	0.85(6)	C(8)—H(8b)	0.88(8)
C(5)—H(5)	0.93(8)	C(8)—H(8c)	1.06(10)
C(6)—H(6)	0.98(5)	C(9)—H(9a)	1.00(9)
C(7)—H(7)	0.90(5)	C(9)—H(9b)	0.83(10)
		C(9)—H(9c)	0.82(11)

TABLE 4. Bond angles (deg) with estimated standard deviations in parentheses

(*a*) Nonhydrogen atoms

Bonds	Angle (deg)	Bonds	Angle (deg)
O(1)—Ga—C(8)	111.9(2)	Ga—O(2)—C(7)	125.1(3)
O(1)—Ga—C(9)	110.5(2)	C(2)—C(1)—C(6)	119.5(4)
C(8)—Ga—C(9)	136.6(3)	C(2)—C(1)—C(7)	124.4(4)
O(2)—Ga—O(1)	88.9(1)	C(6)—C(1)—C(7)	116.1(4)
O(2)—Ga—C(8)	94.0(2)	O(1)—C(2)—C(1)	123.1(4)
O(2)—Ga—C(9)	95.7(2)	O(1)—C(2)—C(3)	119.2(4)
O(1)′—Ga—O(1)	75.5(1)	C(1)—C(2)—C(3)	117.7(4)
O(1)′—Ga—C(8)	91.2(2)	C(2)—C(3)—C(4)	121.0(5)
O(1)′—Ga—C(9)	90.5(2)	C(3)—C(4)—C(5)	121.4(5)
O(1)′—Ga—O(2)	164.4(1)	C(4)—C(5)—C(6)	118.7(4)
Ga—O(1)—Ga′	104.5(1)	C(1)—C(6)—C(5)	121.7(5)
Ga—O(1)—C(2)	131.0(3)	O(2)—C(7)—C(1)	127.4(4)
Ga′—O(1)—C(2)	124.5(2)		

(*b*) Angles involving hydrogen atoms

Bonds	Angle (deg)	Bonds	Angle (deg)
C(2)—C(3)—H(3)	119(3)	Ga—C(8)—H(8b)	110(5)
C(4)—C(3)—H(3)	119(3)	Ga—C(8)—H(8c)	117(5)
C(3)—C(4)—H(4)	122(4)	H(8a)—C(8)—H(8b)	112(7)
C(5)—C(4)—H(4)	117(4)	H(8a)—C(8)—H(8c)	95(7)
C(4)—C(5)—H(5)	123(5)	H(8b)—C(8)—H(8c)	109(7)
C(6)—C(5)—H(5)	118(5)	Ga—C(9)—H(9a)	111(4)
C(1)—C(6)—H(6)	117(3)	Ga—C(9)—H(9b)	101(6)
C(5)—C(6)—H(6)	121(3)	Ga—C(9)—H(9c)	116(7)
O(2)—C(7)—H(7)	115(3)	H(9a)—C(9)—H(9b)	115(7)
C(1)—C(7)—H(7)	118(3)	H(9a)—C(9)—H(9c)	84(8)
Ga—C(8)—H(8a)	113(5)	H(9b)—C(9)—H(9c)	129(9)

Can. J. Chem. Downloaded from www.nrcresearchpress.com by 210.87.254.105 on 09/05/12
For personal use only.

TABLE 5

(*a*) Equations of weighted least-squares planes in the form $lX + mY + nZ = p$ where X, Y, Z are orthogonal coordinates (Å) with respect to a, b', and c^*, deviations of atoms from the planes are also given

Plane	Atoms in plane	χ^2	Equation of plane	Deviation of atoms from plane (Å)									
				Atom	Deviation	Atom	Deviation	Atom	Deviation	Atom	Deviation	Atom	Deviation
1	C(1)–C(6)	6.7	$-0.1730X + 0.6103Y$	C(1)	0.005(5)	C(2)	−0.007(4)	C(3)	0.009(6)	C(4)	−0.003(6)	C(5)	−0.002(6)
			$- 0.7731Z = -1.6391$	C(6)	−0.001(6)	O(1)	−0.033(3)	C(7)	0.049(6)	O(2)	0.080(4)	H(3)	−0.04(6)
				H(4)	0.04(7)	H(5)	0.02(9)	H(6)	0.05(6)	H(7)	0.06(6)		
2	Ga, O(1), O(2), C(1), C(2), C(7)	121.4	$-0.2097X + 0.6033Y$	Ga	−0.0005(5)	O(1)	0.012(3)	O(2)	0.030(4)	C(1)	−0.030(5)	C(2)	0.011(4)
			$- 0.7695Z = -1.8280$	C(7)	−0.016(6)	O(1)′	−0.058(3)	Ga′	−0.0455(5)	C(6)	−0.061(6)	C(3)	0.052(6)
				H(7)	−0.04(6)								
3	Ga, Ga′, O(1), O(2), O(2)′, C(1)–C(7), C(1)′–C(7)′	1155.0	$- 0.2211X + 0.6047Y$	Ga	0.0013(5)	O(1)	0.029(3)	O(2)	0.011(4)	C(1)	−0.032(5)	C(2)	0.025(5)
			$- 0.7652Z = -1.8679$	C(3)	0.079(6)	C(4)	0.038(6)	C(5)	−0.028(6)	C(6)	−0.065(6)	C(7)	−0.033(6)
				C(8)	−1.804(7)	C(9)	1.797(7)	H(3)	0.08(6)	H(4)	0.11(7)	H(5)	−0.03(9)
				H(6)	−0.06(6)	H(7)	−0.07(6)	[a]					

[a]With symmetry related atoms displaced in the opposite direction.

(*b*) Dihedral angles between the planes

Planes	Dihedral angle (deg)
1–2	2.2
1–3	2.8
2–3	0.7

Can. J. Chem. Downloaded from www.nrcresearchpress.com by 210.87.254.105 on 09/05/12
For personal use only.

range from 75.5(1)° in the four-membered ring to 95.7(2)° for O(2)—Ga—C(9) and the equatorial angles range from 110.5(2) to 136.6(3)°, the latter being the angle between the methyl groups. The equatorial group is significantly nonplanar with the gallium atom displaced from the O(1)C(8)-C(9) plane 0.1096(6) Å toward O(2).

The Ga_2O_2 ring differs significantly from those in related compounds. The equatorial Ga—O(1) bond length of 1.933(3) Å is intermediate between the values of 1.960(8) Å for $[MeN(CH_2CH_2O)_2GaH]_2$ and 1.911(3) and 1.913(3) Å for $[Me_2NCH_2CH_2OGaR_2]_2$ (R = H and Me respectively) while the axial Ga′—O(1) bond at 2.469(3) Å is considerably longer than the distances of 2.018(2), 2.053(3), and 2.078(3) Å for $[MeN(CH_2CH_2O)_2GaH]_2$ and $[Me_2NCH_2CH_2OGaR_2]_2$ (R = H and Me) respectively. The second axial bond, Ga—O(2), at 2.127(3) Å is also significantly longer than those in the related molecules listed above (3, 4). All of the above mentioned Ga—O bonds involve formally charged oxygen atoms but the oxygen atoms are of three different types. In $[MeN(CH_2CH_2O)_2GaH]_2$ and $[Me_2NCH_2CH_2OGaR_2]_2$ there are alkoxide bridges while in the present structure there is a phenoxide type bridge as well as a dative interaction between the carbonyl oxygen O(2) and the gallium atom. In salicylaldehydatoboron diphenyl both B—O bonds are similarly longer than the usual value of 1.474 Å (see *e.g.* refs. 14–17) and the bond involving the carbonyl oxygen is significantly longer than the other B—O bond (1.574(4) *vs.* 1.500(4) Å). The bond lengths in the salicylaldehyde moiety of the present structure are equal within experimental error to those in salicylaldehydatoboron diphenyl with the exception of those in the aldehyde function. The C(7)—O(2) bond, 1.231(6) Å, is significantly shorter than the value of 1.263(4) Å in salicylaldehydatoboron diphenyl and the C(1)—C(7) bonds (1.432(7) in the present structure and 1.413(5) Å in the boron compound) differ by a possibly significant 2.2σ. The equatorial Ga—C bonds, 1.944(6) and 1.946(5) Å, are slightly, but not significantly, shorter than the values of 1.951(7) and 1.971(6) Å in $[Me_2NCH_2CH_2OGaR_2]_2$ (R = Me). The bond distances and angles involving hydrogen atoms are as expected for X-ray data (see Tables 3 and 4).

The entire dimer (excluding the methyl groups) is roughly, but not rigorously, planar. The largest deviation from this plane is 0.079 Å. Least-squares mean planes through the molecule are given in Table 5. The Ga_2O_2 ring is exactly planar and the aromatic ring, C(1)–C(6), is planar within experimental error. The nonplanarity of the fused ring system as a whole originates in the heterocyclic GaO_2C_3 ring which is significantly nonplanar even though all six atoms lie within ±0.03 Å of the mean plane. Intraannular torsion angles in the GaO_2C_3 ring are listed in Table 6.

TABLE 6. Intra-annular torsion angles (deg). Six-membered GaO_2C_3 ring

Bond	Angle (obsvd.)
Ga—O(1)	1.2(3)
O(1)—C(2)	1.4(5)
C(2)—C(1)	−2.8(6)
C(1)—C(7)	0.1(6)
C(7)—O(2)	3.4(6)
O(2)—Ga	−3.5(4)

The crystal structure consists of well-separated dimer units; the closest nonbonded contact between dimers (O . . . O, 3.360(6) Å) corresponds to a normal van der Waals contact. Table 7 lists intra- and intermolecular nonbonded contacts, including those in the gallium coordination sphere.

The absence of dimer units in both solution (measured cryoscopically in this study and ebullioscopically in ref. 6) and the gas phase can be attributed to the weakness of the long axial Ga—O bonds (2.469(3) Å) which hold the monomer units together in the crystal. This weakness is also reflected in the rigid body thermal analysis. These bonds are presumably ruptured on dissolution of the solid in benzene or in vaporization. The difference between the two Ga—O bonds in the monomer unit is also reflected in the mass spectrum experiment in which the $C_6H_5OGa^+$ ion is apparent (Ga—O(1), 1.933(3) Å) but the $C_7H_6OGa^+$ ion is not (Ga—O(2), 2.127(3) Å).

The mass spectrum of the complex revealed as its strongest signals peaks due to the parent monomer ion minus one methyl group (see Table 8). The relative intensities of the peaks in the doublet signals agree well with those predicted from the isotopic distribution of the metal atoms (^{69}Ga (60%); ^{71}Ga (40%)). The parent

TABLE 7

(*a*) Selected intra- and intermolecular contacts (Å)

Intramolecular		Intermolecular[a]	
Atoms	Distance (Å)	Atoms	Distance (Å)
C(6) . . . H(7)	2.51(5)	O(2) . . . O(2)^{1}	3.360(6)
C(7) . . . H(6)	2.52(6)	O(2) . . . C(7)^{1}	3.385(6)
H(6) . . . H(7)	2.26(8)	C(5) . . . C(7)^{2}	3.485(8)

(*b*) Gallium coordination sphere

Atoms	Distance (Å)	Atoms	Distance (Å)
Ga . . . Ga′	3.485(1)	O(1)′ . . . C(8)	3.166(6)
O(1) . . . O(1)′	2.720(5)	O(1)′ . . . C(9)	3.148(7)
O(1) . . . O(2)	2.837(4)	O(2) . . . C(8)	2.971(7)
O(1) . . . C(8)	3.202(5)	O(2) . . . C(9)	3.010(7)
O(1) . . . C(9)	3.175(7)	C(8) . . . C(9)	3.602(11)

[a]Superscripts refer to atoms at positions: $^{1}2 - x, 1 - y, 1 - z$; $^{2}2 - x, 2 - y, 1 - z$.

TABLE 8. Mass spectrum of salicylaldehydatogallium dimethyl[a]

m/e	Intensity	Assignment
222	4.3	$C_7H_5O_2GaMe_2^+$
220	7.0	
207	68.0	$C_7H_5O_2GaMe^+$
205	100.0	
192	4.3	$C_7H_5O_2Ga^+$
190	7.0	
164	5.6	$C_6H_5OGa^+$
162	8.3	
122	13.3	$C_7H_6O_2^+$
121	2.6	$C_7H_5O_2^+$
101	3.4	$GaMe_2^+$
99	5.0	
71	5.2	Ga^+
69	8.0	

[a]Recorded on a Varian MAT CH4B mass spectrometer at 70 eV with an ion source temperature of approximately 70 °C.

monomer ion itself was detected but at a much lower intensity compared with the strongest signal. No signals due to species with higher mass numbers than the monomer ion were observed in the spectrum but the expected fragmentation of the monomer into lower mass fragments was observed, and the various ions, together with relative intensities and assignments, are collected in Table 8.

Acknowledgments

We thank the National Research Council of Canada for financial support, the University of British Columbia Computing Centre for assistance, Mr. P. Borda for the C and H analyses, and Mr. J. Nip for recording the mass spectrum.

1. M. SHIRO and Q. FERNANDO. Anal. Che m. **43**, 1222 (1971).
2. K. DYMOCK and G. J. PALENIK. Chem. Commun., 884 (1973).
3. S. J. RETTIG, A. STORR, and J. TROTTER. Can. J. Chem. **52**, 2206 (1974).
4. S. J. RETTIG, A. STORR, and J. TROTTER. Can. J. Chem. **53**, 58 (1975).
5. S. J. RETTIG, A. STORR, and J. TROTTER. Can. J. Chem. **53**, 753 (1975).
6. G. E. COATES and R. G. HAYTER. J. Chem. Soc. 2519 (1953).
7. D. T. CROMER and J. B. MANN. Acta Crystallogr. Sect. A, **24**, 321 (1968).
8. R. F. STEWART, E. R. DAVIDSON, and W. T. SIMPSON. J. Chem. Phys. **42**, 3175 (1965).
9. D. T. CROMER and D. LIBERMAN. J. Chem. Phys. **53**, 1891 (1970).
10. V. SCHOMAKER and K. N. TRUEBLOOD. Acta Crystallogr. Sect. B, **24**, 63 (1968).
11. D. W. J. CRUICKSHANK. Acta Crystallogr. **14**, 896 (1961).
12. D. W. J. CRUICKSHANK. Acta Crystallogr. **9**, 747 (1956); **9**, 754 (1956).
13. S. J. RETTIG and J. TROTTER. Can. J. Chem. **54**, 1168 (1976).
14. S. J. RETTIG and J. TROTTER. Can. J. Chem. **51**, 1288 (1973).
15. S. J. RETTIG and J. TROTTER. Acta Crystallogr. Sect. B, **30**, 2139 (1974).
16. S. J. RETTIG and J. TROTTER. Can. J. Chem. **53**, 1393 (1975).
17. S. J. RETTIG and J. TROTTER. In preparation.

Can. J. Chem. Downloaded from www.nrcresearchpress.com by 210.87.254.105 on 09/05/12
For personal use only.

Bis[*o*-phenylenebis(dimethylarsine)]Fe(II) complexes: structure and bonding from ^{57}Fe Mössbauer spectra

G. Michael Bancroft and Gary Cerantola
Chemistry Department, University of Western Ontario, London, Ontario N6A 5B7

Received October 3, 1975

G. Michael Bancroft and Gary Cerantola. Can. J. Chem. **54**, 1285 (1976).

^{57}Fe Mössbauer spectra are reported for neutral $FeX_2(diars)_2$ (X = Cl, Br, I, NCS) complexes and newly prepared cationic $[FeClL(diars)_2]Y$ (L = CO, $P(OMe)_3$, $P(OPh)_3$; Y = $SnCl_3$, BPh_4) compounds. Using partial quadrupole splittings to calculate quadrupole splittings, all compounds are assigned the *trans* structure. From ^{57}Fe centre shifts and quadrupole splittings, diars is found to be an appreciably poorer σ donor than analogous chelating phosphines, and a very similar σ donor and π acceptor to *o*-phenanthroline.

G. Michael Bancroft et Gary Cerantola. Can. J. Chem. **54**, 1285 (1976).

On rapporte les spectres Mössbauer du ^{57}Fe des complexes neutres $FeX_2(diars)_2$ (X = Cl, Br, I, NCS) et des composés cationiques nouvellement préparés $[FeClL(diars)_2]Y$ (L = CO, $P(OMe)_3$, $P(OPh)_3$; Y = $SnCl_3$, BPh_4). Utilisant les couplages quadrupolaires partiels pour calculer les couplages quadrupolaires, on a assigné des structures *trans* à tous les composés. A partir des déplacements des centres de ^{57}Fe et des couplages quadrupolaires, on a trouvé que diars est un donneur σ beaucoup plus faible que les phosphines chélatantes analogues et un donneur σ et un accepteur π très semblable à l'*o*-phénantroline.

[Traduit par le journal]

Introduction

The ligand *o*-phenylenebis(dimethylarsine) (1) (diars) is an extremely versatile complexing agent. It forms complexes with transition metals in which the coordination number of the metal varies from 4 to 8, and in which the oxidation state of the metal varies from 0 to +5 (2). Since the initial preparation of diars complexes of Fe by Nyholm (3), it has been shown that diars forms complexes with Fe in oxidation states from 0 to 4 (4, 5). The $FeX_2(diars)_2^{n+}$ (n = 0, 1, 2) are all low spin (4), and the infrared spectra (6) and electronic spectra (7, 8) have been well characterized. Detailed interpretation of the Mössbauer spectra of the n = 1 and 2 complexes have recently appeared (9, 10), and the Mössbauer spectrum of the n = 0 $FeCl_2(diars)_2$ complex has also been reported (10). The infrared (6), electronic spectra (7, 8), and pmr spectra (5) indicate that all these iron complexes have the *trans* geometry, but no X-ray crystal structures have appeared. Very recently, after the completion of our work, a number of Fe(II) and Fe(III) diars complexes of NO, CO, and CH_3CN have also been prepared (5). Despite all the work on Fe, and other transition metal complexes of diars, the factors governing the extraordinary coordinating power of diars remain obscure.

In this paper, we report the Mössbauer spectra of a number of novel and known Fe(II) diars complexes. We wanted to use the Mössbauer centre shifts and quadrupole splittings to elucidate the bonding properties of diars relative to other known ligands using the treatment previously published (11, 12). After obtaining a relatively small negative partial quadrupole splitting (pqs) value for diars/2 (-0.52 mm s^{-1}), we became very interested in preparing cationic $FeSnCl_3L(diars)_2^+$ compounds so that we could use the Libbey–Bancroft method (13) for obtaining relative signs of Fe and Sn quadrupole splittings, as well as for studying both Fe and Sn Mössbauer parameters as a function of L.

Experimental

Preparations

All compounds were prepared under an atmosphere of nitrogen using standard Schenkware inert atmosphere techniques (14). All solvents were thoroughly degassed before use and purified by standard methods. The ligand *o*-phenylenebis(dimethylarsine) was obtained from Strem Chemicals. The compounds were analyzed by Chemalytics, Inc., Tempe, Arizona, and the results are given in Table 1.

The complexes $FeX_2(diars)_2$ (X = Cl, Br, I, NCS) were prepared by the methods of Nyholm and co-workers (3, 6). Because we wanted to make $FeSnCl_3L(diars)_2$ complexes, our starting material was $FeSnCl_3Cl(diars)_2$.

Can. J. Chem. Downloaded from www.nrcresearchpress.com by 210.87.254.105 on 09/05/12
For personal use only.

TABLE 1. Elemental analyses

Complex	C (%)		H (%)		Halide (%)	
	Calcd.	Found	Calcd.	Found	Calcd.	Found
$FeSnCl_3Cl(diars)_2$	27.02	26.84	3.63	3.52	15.96	15.32
$[FeClCO(diars)_2]SnCl_3$	27.53	27.04	3.52	3.34	15.47	15.24
$[FeClCO(diars)_2]BPh_4$	53.47	53.21	5.18	5.02	3.50	3.67
$[FeClP(OPh)_3(diars)_2]SnCl_3$	39.66	39.21	4.11	4.18	12.32	11.64
$[FeClP(OPh_3)(diars)_2]BPh_4$	57.59	57.17	5.22	5.36	2.74	3.23
$[FeClP(OMe)_3(diars)_2]SnCl_3$	28.63	26.44	4.28	4.05	14.70	13.14
$[FeClP(OMe)_3(diars)_2]BPh_4$	53.31	51.16	5.80	5.84	3.34	3.32

Chloro(trichlorostannyl)bis[o-phenylenebis(dimethylarsine)]iron(II)

$FeCl_2 \cdot 4H_2O$ (0.140 g) and $SnCl_2$ (0.133 g) were dissolved in 16 ml of degassed MeOH. Diars (0.41 g) was then added. A green-blue precipitate appeared almost instantaneously. It was filtered, washed with anhydrous ether, and recrystallized in a *very* small portion of chloroform. Yield 89%. The compound showed great instability in undegassed solvents giving a brilliant red colour. In excess chloroform, it gave a red precipitate which would not analyze.

Chlorocarbonylbis[o-phenylenebis(dimethylarsine)]iron(II) trichlorostannate

$FeSnCl_3Cl(diars)_2$ (0.10 g) was added to about 40 ml of degassed acetone and CO was bubbled through the solution for 30 min. The solution turned orange and there appeared to be a slight trace of white precipitate which was filtered off. An orange precipitate was taken down with degassed 30–60 petroleum ether. The compound was washed with solvent several times and dried *in vacuo*.

Chlorocarbonylbis[o-phenylenebis(dimethylarsine]iron(II) tetraphenylborate

This complex was prepared recently from $FeCl_2(diars)_2$ (5). $FeSnCl_3Cl(diars)_2$ (0.1 g) and $NaBPh_4$ (0.0385 g) were added to about 20 ml of degassed acetone. CO was bubbled through for about 20 min. A small amount of white precipitate (NaCl) appeared at the bottom of the reaction tube after the solution started changing from green to pale orange. The solution was filtered and yellow crystals were taken down with degassed 30–60 petroleum ether. The yellow compound was washed several times with solvent and dried over nitrogen.

The compound could also be made from the reaction of $[FeClCO(diars)_2]SnCl_3$ with $NaBPh_4$ in acetone. It was brought down with methanol.

Phosphite Complexes

These red compounds were prepared from $FeSnCl_3Cl(diars)_2$ in acetone in analogous fashion to the two CO compounds. The $SnCl_3$ compounds were brought down with anhydrous ether, while the BPh_4 complexes were brought down with methanol. The $P(OMe)_3$ complexes did not analyze well, but no significant impurities (at the ~5% level) were detected in the Mössbauer spectra of these two compounds. The poor analyses are probably due to the relative instability of these compounds to air and moisture.

Other Reactions

Other similar cationic reactions were carried out using γ-picoline and dinitrogen. In the former case, a yellow compound was isolated which analyzed for $FeCl_2(diars)_2$. In the latter, an infrared band appeared at 2030 cm^{-1} which seemed to be characteristic of a coordinated N_2. No pure compound has yet been isolated.

Spectra

Infrared spectra were obtained as Nujol mulls on a Beckmann IR-20A spectrometer. The peak positions are believed to be accurate to ± 3 cm^{-1}.

^{57}Fe and ^{119}Sn Mössbauer spectra were recorded at 110 K using an Austin Associates Spectrometer. Centre shifts for the ^{57}Fe spectra are quoted relative to a sodium nitroprusside absorber at room temperature, and the ^{119}Sn centre shift is quoted relative to a $BaSnO_3$ absorber at room temperature. The spectrometer was calibrated with a 99.99% Fe foil. The spectra were fitted with Lorentzian line shapes using Stone's program (Appendix to ref. 15). Statistically acceptable χ^2 values (between 500 and 550) were obtained for all spectra. The Mössbauer spectra of the diarsine compounds give poorer absorptions than those for analogous phosphine complexes (11). These smaller absorptions are probably due to selective absorption of the 14.4 keV γ rays by As. ^{57}Fe absorptions were typically between 2 and 3%, while the ^{119}Sn absorption for $FeSnCl_3Cl(diars)_2$ was less than 1%. For the cationic $SnCl_3$ complexes, satisfactory Sn spectra could not be obtained after numerous attempts, but weak peaks at ~3 mm s^{-1} were discernible. ^{57}Fe spectra were not recorded for the $B\phi_4$ compounds of $P(OPh)_3$ and $P(OMe)_3$.

Results and Discussion

Preparations

The $FeSnCl_3Cl(diars)_2$ complex is analogous to that prepared previously with depe (11) (depe = 1,2-bis(diethylphosphino)ethane), and appears to be an excellent starting material for making cationic compounds. The ^{119}Sn Mössbauer parameters for this compound are characteristic of $SnCl_3$ coordinated to a transition metal (16–18). Combined with the ^{57}Fe Möss-

Can. J. Chem. Downloaded from www.nrcresearchpress.com by 210.87.254.105 on 09/05/12
For personal use only.

TABLE 2. ^{57}Fe (and ^{119}Sn) Mössbauer parameters (mm s^{-1} at 110 K)*

Compound	Centre shift	Quadrupole splitting	
		Observed	Predicted†
trans-$FeCl_2(diars)_2$	0.81 (0.80)‡	0.87 (+0.87)‡	
trans-$FeCl_2(depe)_2$§	0.66	+1.42	
trans-$FeCl_2(depb)_2$§	0.64	1.16	
trans-$FeBr_2(diars)_2$	0.80	0.96	+0.96
trans-$FeI_2(diars)_2$	0.77	0.94	+0.92
trans-$Fe(NCS)_2(diars)_2$	0.64	0.21	+0.04
trans-$FeSnCl_3Cl(diars)_2$	0.65	0.78	+0.62
(^{119}Sn resonance)	2.02	1.97	
trans-$FeSnCl_3Cl(depe)_2$§	0.59	1.34	+1.14
trans-$[FeClCO(diars)_2]SnCl_3$	0.48	0.40	+0.38
trans-$[FeClCO(diars)_2]B\phi_4$	0.45	0.38	+0.38
trans-$[FeClP(OPh)_3(diars)_2]SnCl_3$	0.62	0.55	+0.38
trans-$[FeClP(OMe)_3(diars)_2]SnCl_3$	0.54	0.31	+0.18

*^{57}Fe line widths were always 0.30 ± 0.02 mm s^{-1}. Errors in centre shifts and quadrupole splittings are 0.02 mm s^{-1}. The line widths are typical for Fe^{II} low spin compounds on our equipment (12).

†Predicted quadrupole splitting for *trans* structures. The pqs value for diars/2 is derived from *trans*-$FeCl_2(diars)_2$. All other values are taken from ref. 12.

‡Values in parentheses reported in ref. 10 at 4.2 K. Centre shift value is corrected from Fe standard by adding 0.26 mm s^{-1}.

§Compounds and Mössbauer parameters previously reported in ref. 11: depe = 1,2-bis(diethylphosphino)ethane, depb = *o*-phenylenebis(diethylphosphine).

bauer data, all our evidence suggests that this compound is a *trans* six-coordinate Fe(II) compound.

It was hoped that the large *trans* labilizing influence of $SnCl_3$ (19, 20) would result in cationic $FeSnCl_3L(diars)_2^+$ compounds, especially when stabilized by BPh_4. However, the analyses for the BPh_4 compounds (Table 1) show conclusively that the $[FeClL(diars)_2]BPh_4$ compounds were obtained. For the $SnCl_3$ complexes, three pieces of evidence show conclusively that these are also $FeClL(diars)_2^+$ complexes. First, the Mössbauer parameters for the two CO complexes are identical within error, strongly suggesting that the Fe atoms in both complexes have the same nearest neighbours. Second, the CO infrared stretching frequency observed for both $SnCl_3$ and BPh_4 compounds (1930 cm^{-1}) are the same as that observed by Nappier *et al.* (5) for the $FeClO(diars)_2BPh_4$ compound prepared from $FeCl_2(diars)_2$ and $NaBPh_4$. Third, the ^{119}Sn Mössbauer spectra, although very weak, did indicate lines at ~3 mm s^{-1}, typical of uncoordinated $SnCl_3^-$ (16, 18).

Because of the high *trans* labilizing influence of $SnCl_3$ (19, 20) and the appearance of a NaCl precipitate, it seems likely that in the $NaBPh_4$ reactions the $FeSnCl_3L(diars)_2^+$ compound is formed initially, and gives the $FeClCO(diars)_2^+$ compound via elimination of $SnCl_2$, *i.e.*,

$$FeSnCl_3Cl(diars)_2 + CO \xrightarrow{NaBPh_4} NaCl + [FeSnCl_3CO(diars)_2]BPh_4 \xrightarrow{\text{rapid}} [FeClCO(diars)_2]BPh_4 + SnCl_2$$

Such an elimination of $SnCl_2$ has been postulated in $PtSnCl_3$ chemistry (20).

Structure and Bonding

Previous spectroscopic data (5–8) suggested that both the neutral $FeX_2(diars)_2$ (X = Cl, Br, I, NCS) compounds and the cationic $FeClL(diars)_2^+$ compounds have the *trans* structure. Our quadrupole splittings (Table 2) also strongly suggest that these complexes have the *trans* configuration. The positive sign of the quadrupole splitting and small η for $FeCl_2(diars)_2$ (10) is entirely consistent with a *trans* structure. All partial quadrupole splittings for known neutral ligands are relatively more negative than the halide pqs values (12), and thus any compound of the type *trans*-FeX_2L_4 will have a positive

Can. J. Chem. Downloaded from www.nrcresearchpress.com by 210.87.254.105 on 09/05/12
For personal use only.

Can. J. Chem. Downloaded from www.nrcresearchpress.com by 210.87.254.105 on 09/05/12
For personal use only.

quadrupole splitting and small η.[1] In contrast, the *cis*-FeX_2L_4 analogue would be expected to have a negative quadrupole splitting as observed for *cis*-$FeCl_2(MeOC_6H_4NC)_4$ (22).

The generally good agreement between predicted and observed quadrupole splittings for the other Fe(II) compounds suggests that they also have the *trans* structure. Taking $FeCl_2(diars)_2$ as *trans*, and using the pqs value of Cl ($= -0.30$ mm s^{-1}) (11), the calculated pqs value for diars/2 $= -0.52$ mm s^{-1} ($+0.87 = -1.20 + 4\{diars/2\}$). Using the other pqs values given previously (12), the quadrupole splittings in Table 2 have been calculated. Previously observed (11) quadrupole splittings for the analogous phosphine compounds $FeCl_2(depe)_2$, $FeCl_2(depb)_2$, and $FeSnCl_3Cl(depe)_2$ have been included for comparison. All predicted quadrupole splittings in Table 2 are within 0.20 mm s^{-1} of the observed values (the limit previously suggested as reasonable agreement (12)). Some of the predicted quadrupole splittings are significantly smaller than those observed, but the predicted quadrupole splittings for *cis* structures would be much smaller still, close to one-half of those in Table 2.[2] Thus the agreement between predicted and observed quadrupole splittings for *cis* structures would be much worse than in Table 2 for *trans* species.

It is apparent from Table 2 that diars compounds give significantly smaller quadrupole splittings and larger centre shifts than their phosphine analogues. Thus *trans*-$FeCl_2(diars)_2$ has a centre shift and quadrupole splitting of 0.81 and $+0.87$ mm s^{-1} respectively compared to centre shift and quadrupole splitting values for the phosphine analogue[3] *trans*-$FeCl_2(depb)_2$ of 0.64 and 1.16 mm s^{-1}. The centre shifts for the $FeX_2(diars)_2$ compounds are unusually large for Fe(II) low spin compounds and appear to be the largest yet observed for Fe(II) low spin species. In fact, these centre shifts are above that normally supposed to be the low spin – high spin transition centre shift (11). Using the assumptions and treatment outlined earlier (11, 12), the very large centre shifts for the diars compounds show that diars is a weaker σ donor and/or weaker π acceptor than depb (11) (a weaker $(\sigma + \pi)$ ligand). As discussed earlier (11), both increasing σ donation and π acceptance lead to a smaller centre shift. Indeed, when partial centre shifts (pcs) (11) are derived (Table 3) and compared with a number of other well-known ligands, diars has a slightly more positive pcs than PPh_3 and *o*-phenanthroline (phen), indicating that diars is a slightly weaker $(\sigma + \pi)$ ligand than PPh_3 or phen.

TABLE 3. Comparison of partial centre shift and partial quadrupole splittings (mm s^{-1})

Ligand	Partial centre shift*	Partial quadrupole splitting*
$AsPh_3$	≥ 0.09	-0.51
diars/2	0.08†	-0.52
PPh_3	0.07	-0.53
phen/2	0.07‡	(-0.52)§
depb/2	0.06	-0.59
depe/2	0.06	-0.65
$P(OMe)_3$	0.03	-0.65
RNC	0.00	-0.70

*Values taken from ref. 12, except for the phen/2 values (25) and diars/2 values.
†Value from the average of pcs values calculated from the $FeX_2(diars)_2$ (X = Cl, Br, I, NCS) using centre shift $= 0.22 + \Sigma$pcs (12).
‡Reference 25.
§Derived from the quadrupole splitting for *cis*-$Fe(phen)_2(CN)_2$. See ref. 26 for discussion.

Diars is normally considered (7, 23) to be a slightly stronger field ligand than nitrogen ligands such as NH_3, pyridine, and ethylenediame (en) which give high spin complexes with Fe(II). It is apparent that our correlation of pcs *vs.* position in the spectrochemical series (11) does not hold for diars and the nitrogen ligands. A possible explanation for this "anomaly" may be found in the very low β values found in the electronic spectra of the diars compounds (7).

The quadrupole splitting of $FeCl_2(diars)_2$ relative to $FeCl_2(depb)_2$ indicates that diars is a weaker σ donor and/or stronger π acceptor (a weaker $(\sigma-\pi)$) ligand than depb (11, 12). A comparison of pqs values, which become more negative as $(\sigma-\pi)$ increases, enables a qualitative separation of σ and π effects. As with partial centre shifts, diars has a very similar pqs value to PPh_3 and phen. Thus it can be concluded that diars is a very similar or slightly weaker σ donor and π acceptor ligand to phen and PPh_3. However, the smaller negative pqs value of diars

[1]Possible exceptions to this "rule" might occur when the in-plane bond angles (the As—FeAs angles in these compounds) differ greatly from 90° *and* the quadrupole splitting is small (21).

[2]For compounds of the type FeXY(diars)$_2$, the *cis* quadrupole splitting will always be larger than half of the *trans* quadrupole splitting and $\eta \neq 0$.

[3]The Fe complex of the exact analogue of dmpb (*o*-phenylenebis(dimethylphosphine) has not been made.

relative to depb, along with their pcs values and the general correlation between pcs and pqs values (12), shows that diars and depb are comparable weak π acceptors, while depb is a significantly better donor than diars.

It is interesting to note in proof the very recent Mössbauer results (24) on analogous compounds of Fe^{II} with the phosphine ligand dppen (*cis*-1,2,-bis(diphenylphosphino)ethylene. The centre shifts, quadrupole splittings, pqs (-0.50 mm s^{-1}), and pcs (0.07 mm s^{-1}) indicate that dppen is a slightly better σ donor and π acceptor than diars, yet the Fe dppen compounds of $FeCl_2$, $FeBr_2$, and FeI_2 exhibit high spin forms (as do the analogues of phen).

Acknowledgments

We thank Drs. E. T. Libbey and P. L. Sears for running some of the spectra, and the National Research Council of Canada for financial support.

1. J. Chatt and F. G. Mann. J. Chem. Soc. 610 (1939).
2. F. P. Dwyer and D. P. Mellor (*Editors*). Chelating agents and metal chelates. Academic Press, New York, N.Y. 1964.
3. R. S. Nyholm. J. Chem. Soc. 851 (1950); F. H. Burstall and R. S. Nyholm. J. Chem. Soc. 3570 (1952).
4. G. S. F. Hazeldean, R. S. Nyholm, and R. V. Parish. J. Chem. Soc. A, 162 (1966).
5. T. E. Nappier, R. D. Feltham, J. H. Enemark, A. Kruse, and M. Cooke. Inorg. Chem. **14**, 806 (1975).
6. J. Lewis, R. S. Nyholm, and G. A. Rodley. J. Chem. Soc. 1483 (1965).
7. R. D. Feltham and W. Silverthorn. Inorg. Chem. **7**, 1154 (1968).
8. R. D. Feltham and W. Silverthorn. Inorg. Chem. **9**, 1207 (1970).
9. E. A. Paez, D. L. Weaver, and W. T. Oosterhuis. J. Chem. Phys. **57**, 3709 (1972).
10. W. T. Oosterhuis, D. L. Weaver, and E. A. Paez. J. Chem. Phys. **60**, 1018 (1974).
11. G. M. Bancroft, M. J. Mays, and B. E. Brater. J. Chem. Soc. A, 956 (1970).
12. G. M. Bancroft and E. T. Libbey. J. Chem. Soc. Dalton Trans. 2103 (1973).
13. E. T. Libbey and G. M. Bancroft. Chem. Commun. 503 (1973).
14. D. F. Shriver. The manipulation of air sensitive compounds. McGraw-Hill, New York, N.Y. 1969.
15. G. M. Bancroft, W. K. Ong, A. G. Maddock, R. H. Prince, and A. J. Stone. J. Chem. Soc. A, 1966 (1967).
16. D. E. Fenton and J. J. Zuckerman. Inorg. Chem. **8**, 1771 (1969).
17. G. M. Bancroft and K. D. Butler. J. Chem. Soc. Dalton Trans. 1209 (1972).
18. M. J. Mays and P. L. Sears. J. Chem. Soc. Dalton Trans. 2254 (1974).
19. R. D. Cramer, R. V. Lindsey, C. T. Prewitt, and V. G. Stolberg. J. Am. Chem. Soc. **87**, 658 (1965); J. F. Young, R. D. Gillard, and G. Wilkinson. J. Chem. Soc. 5176 (1964).
20. H. C. Clark, C. Jablonski, J. Halpern, A. Montovani, and T. A. Weil. Inorg. Chem. 1541 (1974) and references therein.
21. R. A. LaRossa and T. L. Brown. J. Am. Chem. Soc. **96**, 2072 (1972).
22. G. M. Bancroft, R. E. B. Garrod, A. G. Maddock, M. J. Mays, and B. E. Prater. Chem. Commun. 200 (1970).
23. T. M. Dunn, R. S. Nyholm, and S. Yamada. J. Chem. Soc. 1564 (1962).
24. W. Levason, C. A. McAuliffe, M. M. Khan, and S. M. Nelson. J. Chem. Soc. Dalton Trans. 1778 (1975).
25. G. M. Bancroft and R. H. Platt. Adv. Inorg. Radiochem. **15**, 59 (1972).
26. G. M. Bancroft and P. L. Sears. Inorg. Chem. **14**, 2716 (1975).

Can. J. Chem. Downloaded from www.nrcresearchpress.com by 210.87.254.105 on 09/05/12
For personal use only.

Reactions of thiyl radicals. XII. Triplet mercury photosensitized decomposition of ethyl sulfide in the gas phase

CONRAD S. SMITH AND ARTHUR R. KNIGHT

Department of Chemistry and Chemical Engineering, University of Saskatchewan, Saskatoon, Saskatchewan S7N 0W0

Received December 12, 1975

CONRAD S. SMITH and ARTHUR R. KNIGHT. Can. J. Chem. **54**, 1290 (1976).

The triplet mercury photosensitized decomposition of ethyl sulfide vapour has been studied at 25 °C. The reaction products include C_2H_4 ($\Phi^0 = 0.075$), C_2H_6 ($\Phi^0 = 0.043$), C_4H_{10} ($\Phi^0 = 0.011$), C_2H_5SH ($\Phi^0 = 0.068$), 4-methyl-3-thiahexane ($\Phi^0 = 0.011$), and $C_2H_5SSC_2H_5$ ($\Phi^0 = 0.175$). The overall decomposition quantum yield is 0.38 at high sulfide pressures. The initial decomposition gives principally ethyl radicals and ethylthiyl radicals; a second step which yields ethylene and ethanethiol may account for up to 20% of the primary process. Comparison of the direct and sensitized decompositions indicates that both likely originate in the triplet manifold of ethyl sulfide.

Primary decomposition quantum yields have been accurately redetermined for the direct, 254 nm, photolysis of methyl sulfide (0.51), methylethyl sulfide (0.46), and ethyl sulfide (0.49).

CONRAD S. SMITH et ARTHUR R. KNIGHT. Can. J. Chem. **54**, 1290 (1976).

On a étudié, à 25 °C, la décomposition photosensibilisée par le mercure à l'état triplet du sulfure d'éthyle en phase vapeur. Les produits de la réaction comprennent: C_2H_4 ($\Phi^0 = 0.075$), C_2H_6 ($\Phi^0 = 0.043$), C_4H_{10} ($\Phi^0 = 0.011$), C_2H_5SH ($\Phi^0 = 0.068$), méthyl-4 thia-4 hexane ($\Phi^0 = 0.011$) et $C_2H_5SSC_2H_5$ ($\Phi^0 = 0.175$). A pression de sulfure élevée, le rendement quantique total pour la décomposition est de 0.38. La décomposition initiale conduit principalement aux radicaux éthyles et éthylthiyles; une deuxième étape, qui conduit à l'éthylène et à l'éthanethiol, implique jusqu'à 20% du processus primaire. Une comparaison des décompositions directe et sensibilisée indique que chacun de ces types de décomposition trouve son origine dans le triplet du sulfure d'éthyle.

On a redéterminé avec précision, les rendements quantiques primaires pour la décomposition directe par photolyse à 254 nm du sulfure de méthyle (0.51), du sulfure de méthyléthyle (0.46) et du sulfure d'éthyle (0.49).

[Traduit par le journal]

Introduction

The direct and sensitized photolysis of several lower molecular weight alkyl sulfides have recently been investigated in this laboratory. Methyl sulfide has been studied in both direct (1) and Hg-sensitized decomposition (2), but only the direct photolysis of ethyl sulfide has been investigated (3).

Although the product distribution is not dramatically different in the direct and sensitized decompositions, there are several significant alterations in relative rates in the two types of system that are worthy of further exploration, most particularly as they affect product yields from which $k_{\text{disproportionation}}/k_{\text{combination}}$ values for thiyl radicals can be computed. We have therefore studied and report here on the triplet mercury photosensitized decomposition of ethyl sulfide.

Another important consideration is that there is no obvious explanation for the very large difference in decomposition quantum yields reported for the direct and sensitized photolysis of these substrates. To permit comparison between the several systems involved, the Φ_D values for methyl sulfide, ethyl sulfide, and methylethyl sulfide in direct photolysis have also been redetermined under conditions designed to eliminate possible difficulties in accurate determination of the actual absorbed intensities.

Experimental

The apparatus and procedures in general have been described previously (2, 3). In the sensitized experiments the light source was a Hanovia 688A45 low pressure resonance lamp, and the light intensity was determined using propane as actinometer. Pre-irradiated propane was photolysed and the rate of hydrogen production measured. The calculated light intensity absorbed, assuming $\Phi(H_2) = 0.58$ (4), was 0.90 μeinstein min^{-1}. The cylindrical reaction cell had a volume of 0.30 l.

Can. J. Chem. Downloaded from www.nrcresearchpress.com by 210.87.254.6 on 09/05/12
For personal use only.

Can. J. Chem. Downloaded from www.nrcresearchpress.com by 210.87.254.6 on 09/05/12
For personal use only.

The quantum yields in the direct photolysis of CH_3SCH_3, $CH_3SC_2H_5$, and $C_2H_5SC_2H_5$ were determined in the following manner. The light source was a Zeiss LX501M high pressure xenon lamp, and the illumination was passed through a Zeiss M4QIIId monochromator set at 2550 Å with slits fully open, giving a band width of *ca.* 80 Å, and thence through a 6 cm × 5 cm od cylindrical cell filled with mercury vapour to remove the 2537 Å line. The absorption cell was mounted in a furnace on an optical bench and was 20 cm long. The absorbance of 13.4 torr diethyl ketone used as actinometer, 50.0 torr of methylethyl sulfide, 60 torr methyl sulfide, and 30.0 torr ethyl sulfide were determined under photolysis conditions to be 22.8, 22.0, 15.8, and 14.8%, respectively. The absorption was monitored during the experiments by a recorder trace of the Zeiss PMQ photomultiplier output. The ketone photolyses were carried out at room temperature. A separate investigation in this apparatus demonstrated that the three sulfides follow Beer's law over the pressure range employed here. The absorbed light intensity in the actinometry experiments was determined to be 3.6×10^{-3} μeinstein min^{-1}.

In previous determinations of the quantum yields in the direct photolysis of methyl sulfide (1) and methylethyl sulfide (5), interference filters were employed to isolate the photolysing wavelengths, 2288 Å. Some preliminary experiments carried out in the present work indicated that although this procedure is adequate for wavelength selection with respect to the sulfide absorption, the combination of strong lines in the lamp emission at longer wavelengths and the small percent transmission of the filter at these wavelengths likely led to incorrect estimation of the fraction of the incident intensity absorbed by the actinometer. The problem is exacerbated by the small absorption coefficient of the ketone at the photolysing wavelength. Thus the previously reported quantum yields for these two systems need to be revised upwards.

Results

The direct photolysis decomposition quantum yields for the three alkyl disulfides were calculated on the basis of the yields of hydrocarbon products. For example, in the case of ethyl sulfide, the equation is

$$[1] \quad \Phi_D = \Phi_{C_2H_4} + \Phi_{C_2H_6} + 2\Phi_{C_4H_{10}} + \Phi_{MTH}$$

where Φ_{MTH} is the value for 4-methyl-3-thiahexane. The calculation can also be done on the basis of the yields of sulfur containing compounds, but those values are less reliable because of the sulfur deficiency generally observed.

The decomposition quantum yields are summarized in Table 1.

The reaction products observed in the mercury photosensitized decomposition of ethyl sulfide vapour are the same as those reported for the direct photolysis, namely ethylene, ethane, butane, ethanethiol, 4-methyl-3-thiahexane (MTH), ethyl disulfide, and 4-methyl-3,5-dithiaheptane (MDTH).

TABLE 1. Decomposition quantum yields in the direct photolysis of alkyl sulfides

Sulfide	Φ_D (direct photolysis)	
	Literature	This work
CH_3SCH_3	0.17*	0.51
$CH_3SC_2H_5$	0.02†	0.46
$C_2H_5SC_2H_5$	0.48‡	0.49

*Reference 1. 2288 Å (Cd-lamp).
†Reference 5. 2288 Å (filtered medium pressure Hg-lamp).
‡Reference 3. 2537 Å (low pressure Hg-lamp).

As is apparent from an analysis of the product rates, however, there is a significant difference in the relative amounts of products from the various recombination and disproportionation processes in the two systems.

Figures 1 and 2 give the rates of formation of the six products whose yield was large enough to determine accurately, as a function of sulfide pressure. In the lower pressure range all products show the rate increase to be expected from increased quenching collision frequency and pressure broadening of the absorption line. Beyond about 10 torr sulfide it would appear that only pressure broadening is a significant factor.

The effect of exposure time was investigated in a series of experiments for which the results are given in Figs. 3 and 4. With respect to the possible role of secondary processes, it is in-

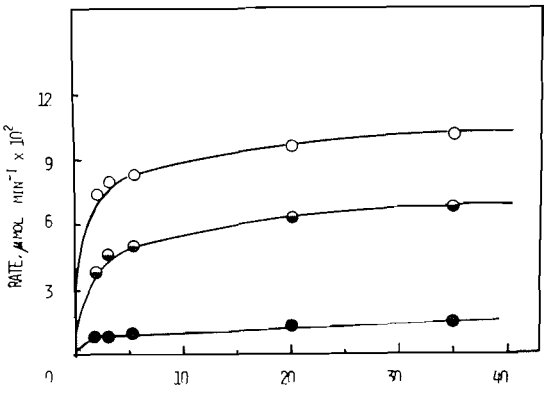

FIG. 1. Rate of formation of C_4H_{10}, ○; C_2H_6, ◒; and MTH, ●; as a function of ethyl sulfide pressure for an exposure time of 10 min.

Can. J. Chem. Downloaded from www.nrcresearchpress.com by 210.87.254.6 on 09/05/12
For personal use only.

TABLE 2. Product quantum yields in the Hg-sensitized decomposition of ethyl sulfide

Pressure (torr)	Quantum yield × 10^2						
	C_2H_4	C_2H_6	C_2H_{10}	C_2H_5SH	MTH	$C_2H_5SSC_2H_5$	Φ_D*
2	5.2	4.2	8.3	4.7	0.8	2.3	27
3	5.5	5.1	8.9	5.2	0.9	13.6	29
5.4	6.0	5.5	9.1	5.4	1.0	14.6	31
20	7.1	7.0	10.7	5.9	1.4	17.3	37
35	7.6	7.6	11.3	5.3	1.6	17.9	39
20†	7.5	4.2	11.0	6.8	1.1	17.5	35

*Calculated from eq. 1.
†Initial quantum yields, determined from time dependence of rates in Figs. 3 and 4.

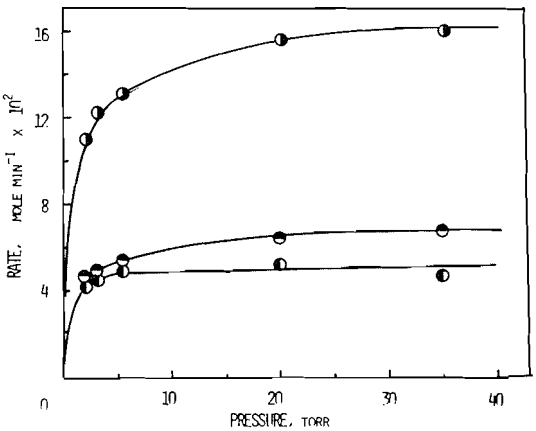

FIG. 2. Rate of formation of C_2H_4, ◓; C_2H_5SH, ◐; and $C_2H_5SSC_2H_5$, ◑; as a function of ethyl sulfide pressure for an exposure time of 10 min.

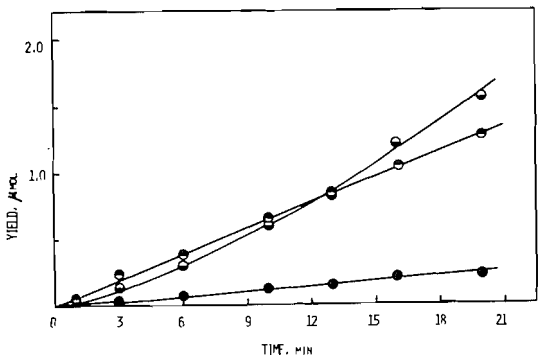

FIG. 3. Yield of C_2H_4, ◓; MTH, ●; and C_2H_6, ◒; as a function of exposure time for 20 torr ethyl sulfide.

structive to note the decrease in the rate of formation of ethanethiol, as well as the decline in $R(C_4H_{10})$ in a manner roughly parallel to the increase in $R(C_2H_6)$.

Table 2 gives the calculated quantum yields for

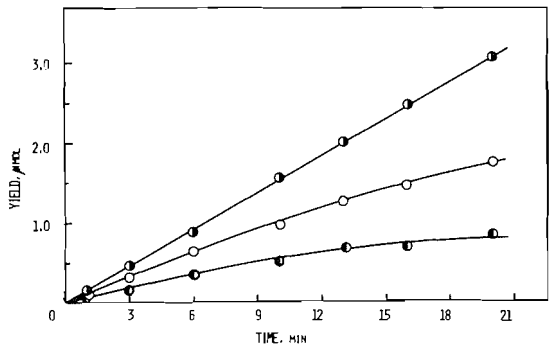

FIG. 4. Yield of C_4H_{10}, ○; C_2H_5SH, ◐; $C_2H_5SSC_2H_5$, ◑; as a function of exposure time for 20 torr ethyl sulfide.

the various reaction products, along with the value of the decomposition quantum yield determined from eq. 1.

The mass balance in carbon and sulfur for the reaction products can be calculated in the following way, A rate for carbon-containing products can be calculated from eq. 2.

$$[2] \quad R_C = 2R_{C_2H_4} + 2R_{C_2H_6} + 4R_{C_4H_{10}} + 2R_{C_2H_5SH} + 4R_{(C_2H_5S)_2} + 6R_{MTH}$$

The analogous expression for the sulfur-containing products is

$$[3] \quad R_S = R_{C_2H_5SH} + R_{MTH} + 2R_{(C_2H_5S)_2}$$

On the basis of the rate so defined there should be an equivalence of R_C and R_S in the ethyl sulfide system. The product MDTH, which could not be determined quantitatively, and the thioacetaldehyde that would result from disproportionation reactions involving C_2H_5S radicals, are not included in the above equations.

Can. J. Chem. Downloaded from www.nrcresearchpress.com by 210.87.254.6 on 09/05/12
For personal use only.

TABLE 3. Calculated R_C and R_S values

Pressure (torr)	Time (min)	Calculated rates (μmol min^{-1})	
		R_C	$4R_S$
2	10	1.03	1.08
3	10	1.14	1.20
5.4	10	1.21	1.28
20	10	1.45	1.51
35	10	1.51	1.54
20	1	1.27	1.37
20	3	1.42	1.43
20	6	1.42	1.44
20	13	1.44	1.49
20	16	1.41	1.45
20	20	1.40	1.43

A deficiency in R_S would therefore be expected if those products were formed at significant rates.

Table 3 lists the values of R_C and $4R_S$ for both the pressure and exposure time series. The agreement with the stoichiometric expectation indicates that the major products of the reaction have been accounted for, and that the MDTH yield and that of CH_3CHS are sufficiently small not to affect the mass balance.

Discussion

The nature of the products observed in this decomposition indicates that the principal primary process is

[4] $C_2H_5SC_2H_5 + Hg\ 6(^3P_1) \rightarrow C_2H_5S + C_2H_5 + Hg^0$

and the occurrence of all observed products can be explained by subsequent reactions of the primary radicals.

Consideration of the relative yields of the various products, however, suggests that a second primary step,

[5] $C_2H_5SC_2H_5 + Hg\ 6(^3P_1) \rightarrow C_2H_5SH + C_2H_4 + Hg^0$

is also involved. In order to determine the extent to which such a process contributes to the observed decomposition on the basis of relative product yields, it is necessary to consider other steps in the overall mechanism in which C_2H_4 and ethanethiol can be produced.

On the basis of the characteristics of sulfide systems previously investigated, it is proposed that the mechanism for the Hg-sensitized decomposition of $C_2H_5SC_2H_5$ consists of reactions 4 and 5 and the reactions:

[6] $2C_2H_5 \rightarrow C_2H_4 + C_2H_6$

[7] $2C_2H_5 \rightarrow C_4H_{10}$

[8] $2C_2H_5S \rightarrow C_2H_5SH + C_2H_4S$

[9] $2C_2H_5S \rightarrow C_2H_5SSC_2H_5$

[10] $C_2H_5 + C_2H_5S \rightarrow C_2H_5SC_2H_5$

[11] $C_2H_5 + C_2H_5S \rightarrow C_2H_4 + C_2H_5SH$

[12] $C_2H_5 + C_2H_5S \rightarrow C_2H_6 + C_2H_4S$

[13] $C_2H_5 + C_2H_5SSC_2H_5 \rightarrow C_2H_6 + C_2H_5S\dot{C}HCH_3$

[14] $C_2H_5S + C_2H_5SSC_2H_5 \rightarrow C_2H_5SH + C_2H_5S\dot{C}HCH_3$

[15] $C_2H_5 + C_2H_5S\dot{C}HCH_3 \rightarrow MTH$

[16] $C_2H_5S + C_2H_5S\dot{C}HCH_3 \rightarrow MDTH$

[17] $C_2H_5 + C_2H_5SH \rightarrow C_2H_6 + C_2H_5S$

The mechanism accounts for all of the observed products and for the time dependence of the ethane and ethanethiol rates. As is apparent from Figs. 3 and 4 as the quantum yield of C_2H_5SH decreases, there is a parallel increase in the ethane yield. In fact, for $t \geq 10$ min, $\Phi_{C_2H_5SH} + \Phi_{C_2H_6}$ is essentially constant at 0.130 $\pm$ 0.004.

Making use of known rate constant ratios, an estimate can be made of the quantum yields of the products in several specific reactions.

Butane is formed in process 7 only. From $\Phi_{C_4H_{10}}$ and the reported (6, 7) value of 0.14 for k_6/k_7, $(\Phi_{C_2H_4})_{[6]} = 0.015$ and thus $(\Phi_{C_2H_4})_{[5,11]} = \Phi_{C_2H_4} - 0.015 = 0.058$, where all calculations are based on initial quantum yields and the subscripts in square brackets indicate specific reaction or reactions in which that yield originates. An alternative estimate of the yields from reactions 5 and 11 can be obtained in the following fashion. If k_8/k_9 is assumed to have the same value as observed in the methylethyl sulfide system (5), *i.e.*, 0.067 at 25 torr sulfide pressure, the thiol yield from sources other than reaction 8 would be $\Phi_{C_2H_5SH} - 0.067\Phi_{C_2H_5SSC_2H_5} = 0.054$. In addition to reactions 5 and 11, ethanethiol could be formed in process 14. However, reaction 13 is considerably more energetically favourable and the observed MTH and MDTH products are more likely to arise from $C_2H_5S\dot{C}HCH_3$ radicals generated principally in reaction 13. On that basis the calculated value of $\Phi = 0.054$ can appropriately be identified as $(\Phi_{C_2H_5SH})_{[5,11]}$. The combined quantum yields of reactions 5 and 11 therefore would be 0.056 $\pm$ 0.002.

Can. J. Chem. Downloaded from www.nrcresearchpress.com by 210.87.254.6 on 09/05/12
For personal use only.

There is no simple way in which the $R_{[5]}/R_{[11]}$ ratio can be extracted from the data. However, if it is assumed that the disproportionation reaction 11 occurs to the same extent as reaction 8 involving two thiyl radicals, this would give $\Phi_{[5]} = 0.056 - 0.012 = 0.044$. With the decomposition quantum yield of 0.35, process 5 would thus contribute between 13 and 16% to the total decomposition. If either of the disproportionation processes contributes more than estimated here, the effect would be to indicate a lower contribution from primary process 5. Conversely, if C_2H_5S radicals are not involved in disproportionation at all, reaction 5 would account for 20% of the primary decomposition. Nevertheless, reaction 5 appears to be an inherently unlikely process compared to reaction 4 and it may be that its contribution is even more minor than these estimates indicate.

Similar limits obtain in any computation of the disproportionation:combination ratio for ethylthiyl radicals. If reaction 4 is the sole primary process, and reactions 8, 11, and 12 occur at approximately equal rates, k_8/k_9 would be (0.068/3)/0.175 or about 0.13.

The k_{dis}/k_{com} ratio for thiyl radicals cannot be inferred directly from thiol:disulfide yield ratios without consideration of other processes or the conditions of the experiment. A self-consistent interpretation of the data obtained in the present work indicates, as has been the case in previously investigated systems, that disproportionation accounts for an order of magnitude of 10% of thiyl radicals formed photochemically at room temperature.

Further insights into the photosensitized decomposition may be gained from a comparison of the product distribution ratios with those observed in the direct photolysis. The relative yields of products with diethyldisulfide as 100, at 20 torr pressure and a moderate exposure time of 30 min are as follows, with values for the direct photolysis in parentheses: C_4H_{10}, 61(62); C_2H_4, 41(48); C_2H_6, 41(78); C_2H_5SH, 32(54); and MTH, 9(19). In the sensitized system the extent of secondary photodecomposition of the disulfide is a function of the relative concentrations of the substrate and $C_2H_5SSC_2H_5$ and their quenching cross-sections. At the relatively low conversions here such a process would be quite unimportant. The alterations in relative rates with time indicated above are related to increasingly effective competition for radical attack by the ethanethiol product. In the direct photolysis, on the other hand, secondary photodecomposition of the product disulfide is important. In both systems, however, the disulfide:ethylene:butane ratios are essentially the same.

The high pressure decomposition quantum yield is somewhat higher (0.49) in the direct photolysis than in the sensitized decomposition (0.39) but this is evidently due in the main to the increased yields of products from secondary abstraction reactions in the former system.

The weight of evidence therefore suggests that when the differences due to secondary reaction effects are factored out, the product distribution is essentially the same in the direct and triplet mercury sensitized decompositions. The chemical decomposition of the sulfide molecule that occurs most likely originates in the triplet manifold of ethyl sulfide in both cases. In that situation, since the originally formed excited state must be singlet, intersystem crossing in the lower molecular weight sulfides would be a highly efficient process. Although no emission studies have yet been carried out on ethyl sulfide, fluorescence cannot be detected in methyl sulfide.[1]

The fact that the quantum yields are significantly less than unity in all these systems could indicate that there is efficient intersystem crossing from T_1 to high, non-dissociative vibrational levels of the ground state, or that processes such as reaction 10 are important, or both. Additional data on the effect of radical scavengers and deactivating addends in these systems will be required to elucidate those matters.

Acknowledgments

The authors are pleased to acknowledge the support of the National Research Council of Canada for this research.

1. P. M. Rao and A. R. Knight. Can. J. Chem. **50**, 844 (1972).
2. D. R. Tycholiz and A. R. Knight. J. Am. Chem. Soc. **95**, 1726 (1973).
3. C. S. Smith and A. R. Knight. Can. J. Chem. **51**, 780 (1973).

[1]Using apparatus and procedures described elsewhere (8) methyl sulfide was irradiated over its entire absorption band and a search made for emission between 2000 and 9000 Å. No emission was observed.

4. T. POLLACK. Ph.D. Thesis, University of Alberta, Edmonton, Alberta. 1971.
5. D. R. TYCHOLIZ and A. R. KNIGHT. Can. J. Chem. **50**, 1734 (1972).
6. D. G. L. JAMES and G. E. TROUGHTON. Trans. Faraday Soc. **65**, 763 (1969).
7. A. C. R. BROWN and D. G. L. JAMES. Can. J. Chem. **43**, 660 (1965).
8. T. OKA, A. R. KNIGHT, and R. P. STEER. J. Chem. Phys. **63**, 2414 (1975).

Can. J. Chem. Downloaded from www.nrcresearchpress.com by 210.87.254.6 on 09/05/12
For personal use only.

Substituent and solvent effects on organic acids: an electrostatic theory[1]

TAKEKI MATSUI[2] AND LOREN G. HEPLER
Department of Chemistry, University of Lethbridge, Lethbridge, Alberta T1K 3M4

Received December 11, 1975

TAKEKI MATSUI and LOREN G. HEPLER. Can. J. Chem. **54**, 1296 (1976).

We have used an electrostatic model as basis for derived equations to represent the effects of substituents and solvents on the thermodynamics of proton transfer reactions. Equations derived in this manner are related to those based on earlier 'internal-environmental' models and are also discussed in relation to recent gas phase acidity work.

TAKEKI MATSUI et LOREN G. HEPLER. Can. J. Chem. **54**, 1296 (1976).

On a utilisé un modèle électrostatique comme base pour dériver des équations qui représentent les effets des substituants et des solvants sur la thermodynamique des réactions de transfert de proton. Les équations dérivées de cette manière peuvent être reliées à celles basées sur les modèles antérieurs 'interne-environnement' et on les discute aussi en termes des travaux récents sur l'acidité en phase gazeuse.

[Traduit par le journal]

We are here concerned with effects of substituents and solvents on the thermodynamic properties for proton transfer reactions of the type represented by

[1] $HAx(s) + Ao^-(s) = Ax^-(s) + HAo(s)$

in which HAo is a reference acid (such as benzoic acid), HAx is a substituted acid of the same class as the reference acid, and 's' indicates that each species is dissolved in some solvent.

The standard state thermodynamic properties for ionization of the reference acid are represented by K_{HAo}, ΔG^0_{HAo}, ΔH^0_{HAo}, and ΔS^0_{HAo}, all referring to solutions in some specified solvent at temperature T. Similarly, K_{HAx}, ΔG^0_{HAx}, ΔH^0_{HAx}, and ΔS^0_{HAx} refer to ionization of a substituted acid.

Many previous investigations of substituent and solvent effects on reactions of type 1 have been described in terms of the Hammett equation that is written here as

[2] $$\log (K_{HAx}/K_{HAo}) = \rho\sigma$$

in which σ is usually taken to depend only on substituent while ρ depends on solvent, temperature, pressure, and reaction type. The Hammett equation, [2], can also be written as

[3] $$\delta\Delta G^0 = -2.3RT\rho\sigma$$

in which

[4] $$\delta\Delta G^0 = \Delta G^0_{HAx} - \Delta G^0_{HAo}$$

The equilibrium constant ratio in [2] and $\delta\Delta G^0$ in [3] and [4] refer to the reaction represented by [1]. Similarly, we have

[5] $$\delta\Delta H^0 = \Delta H^0_{HAx} - \Delta H^0_{HAo}$$

and

[6] $$\delta\Delta S^0 = \Delta S^0_{HAx} - \Delta S^0_{HAo}$$

in which $\delta\Delta H^0$ and $\delta\Delta S^0$ also refer to reactions of type 1.

Several earlier theoretical investigations (1–10) of reactions of type 1 have been carried out in terms of internal (int) and external or environmental (env) contributions to $\delta\Delta G^0$, $\delta\Delta H^0$. and $\delta\Delta S^0$:

[7] $$\delta\Delta G^0 = \delta\Delta G_{int} + \delta\Delta G_{env}$$

[8] $$\delta\Delta H^0 = \delta\Delta H_{int} + \delta\Delta H_{env}$$

[9] $$\delta\Delta S^0 = \delta\Delta S_{int} + \delta\Delta S_{env}$$

Pitzer's (11) statistical thermodynamic considerations lead to $\delta\Delta S_{int} \simeq 0$ for reactions of type 1, except when HAx contains a substituent that is

[1]Part of this work was done while L.G.H. was in Japan as Visiting Professor under the programme of the Japan Society for Promotion of Science. We are both grateful to Professor N. Tokura for providing us with working space in the Department of Applied Chemistry, Faculty of Engineering, Osaka University.

[2]Present address: Technical Research Laboratory, Asahi Chemical Industry, Fuji, Shizuoka, Japan.

Can. J. Chem. Downloaded from www.nrcresearchpress.com by 210.87.254.5 on 09/05/12
For personal use only.

located close to the functional group containing the acidic proton. Equation 9 has therefore been written as

$$[10] \qquad \delta\Delta S^0 = \delta\Delta S_{env}$$

and combined (3, 5–8, 10) with a relationship between $\delta\Delta H_{env}$ and $\delta\Delta S_{env}$ to obtain

$$[11] \qquad \delta\Delta G^0 = \delta\Delta H_{int}\,(1 + \gamma)$$

in which γ is a solute–solvent interaction parameter that depends on solvent, temperature, pressure, and reaction type. This earlier approach (3, 5–8, 10) has been successful in that it has accounted for the general form of the Hammett equation, [2], with ρ dependent on T^{-1} and has also led to $\delta\Delta H_{int}$ proportional to σ. On the other hand, these earlier works have been deficient in that they have not permitted unequivocal evaluation of $\delta\Delta H_{int}$, nor have they provided detailed information about the related parameters ρ and γ. In this paper we move toward some remedies for these earlier deficiences.

Theoretical approaches to understanding substituent and solvent effects on reactions of type 1 have also been based on various electrostatic models, as reviewed by King (12). These approaches can be summarized by

$$[12] \qquad \delta\Delta G^0 = (e\mu_x \cos\phi)\epsilon_{eff}\, c^2$$

in which e represents the magnitude of the electron charge, μ_x represents a point dipole moment associated with the substituent x, ϕ is the angle between the dipole line and the line that can be drawn to connect the dipole with the center of the functional group, ϵ_{eff} represents a dielectric constant that is discussed below, and c is the distance between the substituent dipole μ_x and the proton to be dissociated from HAx(s).

Smallwood (13) took $\epsilon_{eff} = 1.0$; Eucken (14) took ϵ_{eff} to be the ordinary macroscopic dielectric constant of the solvent; Kirkwood and Westheimer (15) calculated ϵ_{eff} as a complicated function of the macroscopic dielectric constant of the solvent and reasonable estimates of the dielectric constant and shape of the cavity containing the solute species. Smallwood's (13) approach overestimates the electrostatic effect, while Eucken's (14) approach underestimates it. There have been several recent applications (16) of the more realistic Kirkwood–Westheimer (16) treatment, and King (12) has provided an excellent review of some earlier applications.

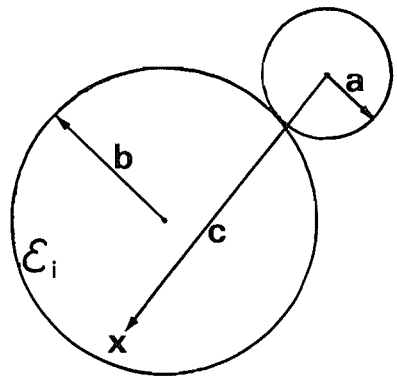

FIG. 1. Symbols have the following meanings: a represents the radius of the functional group; b represents the radius of the aromatic nucleus; c represents the distance from the center of the functional group to the substituent x; and ϵ_i represents the 'dielectric constant' of the 'molecular cavity'. In our equations we use $-q_x$ and $-q_o$ to represent effective charges on the functional group in Ax^- and Ao^-.

Although equations such as [12] have been applied (12, 15, 16) usefully to explanation of a variety of substituent effects on ionization, it should also be noted (17) that equations of this type are generally unable to account for the solvent dependence of the Hammett ρ. Further, equations of type 12 generally lead to the conclusion that $\delta\Delta S^0 \simeq 0$, which is often incorrect.

We begin our new electrostatic treatment by considering the free energy of transfer (ΔG_{tr}) of anions (pictured in Fig. 1) from a hypothetical solvent with dielectric constant ϵ_i to a real solvent with dielectric constant ϵ_s. The difference in these free energies of transfer for the anions Ax^- and Ao^- is

$$[13] \quad \Delta G_{tr}(Ax^-) - \Delta G_{tr}(Ao^-) = -\frac{q_x^2}{2a}\left(\frac{1}{\epsilon_i} - \frac{1}{\epsilon_s}\right) + \frac{q_o^2}{2a}\left(\frac{1}{\epsilon_i} - \frac{1}{\epsilon_s}\right) + \ldots$$

in which terms due to aromatic nucleus–solvent interactions and dipole–solvent interactions are negligible because $b > a$ and $(1 - q) \ll 1$. Because an expression analogous to [13] for the difference in free energies of transfer of HAx and HAo involves only terms that are small compared to those that are written above, we have the following for the free energy of reaction 1 in solvent with dielectric constant ϵ_s:

Can. J. Chem. Downloaded from www.nrcresearchpress.com by 210.87.254.5 on 09/05/12
For personal use only.

Can. J. Chem. Downloaded from www.nrcresearchpress.com by 210.87.254.5 on 09/05/12
For personal use only.

$$[14] \quad \delta\Delta G^0 = \frac{e\mu\cos\phi}{\epsilon_i c^2} - \frac{q_x^2 - q_o^2}{2a\epsilon_i} + \frac{q_x^2 - q_o^2}{2a\epsilon_s}$$

Now we express the relationship between q_x and q_o as

$$[15] \quad q_x = q_o + (\partial q/\partial\mu)\mu$$

and combine with [14] to obtain

$$[16] \quad \delta\Delta G^0 = \frac{e\mu\cos\phi}{\epsilon_i c^2} - \frac{q_o\,\mu(\partial q/\partial\mu)}{a}\left(\frac{1}{\epsilon_i} - \frac{1}{\epsilon_s}\right) + \cdots$$

in which we have omitted relatively small terms that involve $\mu^2(\partial q/\partial\mu)^2$.

Equation 16 is conveniently written and used in terms of the defined (dimensionless, solvent independent) parameter B:

$$[17] \quad B \equiv (c^2 q_o/ae\cos\phi)\,(\partial q/\partial\mu)$$

$$[18] \quad \delta\Delta G^0 = \frac{e\mu\cos\phi}{c^2}\left(\frac{1}{\epsilon_i} - \frac{B}{\epsilon_i} + \frac{B}{\epsilon_s}\right)$$

Combination of [3] and [18] gives

$$[19] \quad \rho\sigma = \left[\frac{e\mu\cos\phi}{2.3R}\right]\left[\frac{\frac{1}{\epsilon_i} - B\left(\frac{1}{\epsilon_i} - \frac{1}{\epsilon_s}\right)}{c^2 T}\right]$$

in which we identify the first term in brackets as proportional to σ and the second term in brackets as proportional to ρ. It is directly clear that the term we identify with σ is dependent only on substituent, as it should be. Over modest ranges of temperature for which we may write (18) $\epsilon_s \simeq \epsilon_o \exp(-T/\theta)$, we find that the term we identify with ρ is nearly proportional to T^{-1}. We therefore conclude that our electrostatic model and the resultant equations [18] and [19] are consistent with the general form and meaning of the Hammett equation.

Now we show the connection between the present electrostatic theory and the earlier (3, 5–8, 10) 'internal-environmental' treatment that led to [11]. We begin by grouping the right-hand side of [18] into solvent independent and solvent dependent terms:

$$[20] \quad \delta\Delta G^0 = \frac{e\mu\cos\phi}{c^2}\left(\frac{1}{\epsilon_i} - \frac{B}{\epsilon_i}\right) + \frac{Be\mu\cos\phi}{\epsilon_s c^2}$$

Making use of [7] with [20], we obtain

$$[21] \quad \delta\Delta G_{int} = (1 - B)\,(e\mu\cos\phi)/c^2\epsilon_i$$

and

$$[22] \quad \delta\Delta G_{env} = (Be\mu\cos\phi)/c^2\epsilon_s$$

Because the right hand side of [21] is temperature independent, we have

$$d\delta\Delta G_{int}/dT = -\delta\Delta S_{int} = 0$$

as previously stated in obtaining [10] from [9]. We therefore also have

$$[23] \quad \delta\Delta H_{int} = (1 - B)(e\mu\cos\phi)/(c^2\epsilon_i)$$

Now combination of [20] with [23] gives us

$$[24] \quad \delta\Delta G^0 = \delta\Delta H_{int}\left[1 + \frac{B\epsilon_i}{(1 - B)\epsilon_s}\right]$$

that is of the same form as [11] obtained previously. We can now identify

$$[25] \quad \gamma = B\epsilon_i/(1 - B)\epsilon_s$$

These equations, [20]–[25], show the relationship between the earlier 'internal-environmental' theory and the present electrostatic model (and can also be applied to other electrostatic theories).

We now use either [18] or [24] to compare $\delta\Delta G^0$ in the gas phase ($\epsilon_s = 1$) with $\delta\Delta G^0$ in solution (ϵ_s) as follows:

$$[26] \quad \frac{\delta\Delta G^0(\text{gas}, \epsilon_s = 1)}{\delta\Delta G^0(\text{sol'n}, \epsilon_s)} = \frac{\epsilon_s(1 - B + B\epsilon_i)}{\epsilon_s(1 - B) + B\epsilon_i}$$

Taking $\epsilon_s = 78$ for water at 25 °C and 'reasonable' ϵ_i values from about 2.5 to about 6, we now find the following: negative B values lead to the ratio in [26] between about -4 and unity; B values from 0 to $\epsilon_s/(\epsilon_s - \epsilon_i)$ lead to the ratio in [26] between unity and $+\infty$; B values greater than $\epsilon_s/(\epsilon_s - \epsilon_i)$ lead to negative values for the ratio in [26]. Recent measurements (19–23) of gas phase acidities have shown that the ratio $\delta\Delta G^0$(gas)/$\delta\Delta G^0$(aqueous solution) ranges from 4 to 10 for various acids–bases (pyridines, phenols, aliphatic carboxylic acids, and benzoic acids). These gas phase results therefore require that B is in the range from about 0.4 to about 0.8.

We have previously identified the second term in brackets in [19] as being proportional to the Hammett ρ. For a particular reaction series in

two solvents x and y with dielectric constants ϵ_x and ϵ_y we obtain from [19]

$$[27] \qquad \frac{\rho_y}{\rho_x} = \frac{1 - B\left(\frac{\epsilon_y - \epsilon_i}{\epsilon_y}\right)}{1 - B\left(\frac{\epsilon_x - \epsilon_i}{\epsilon_x}\right)}$$

Taking values of B in the range specified above and choosing 'reasonable' values of ϵ_i, we can calculate values of the ratio ρ_y/ρ_x. For such high dielectric constant solvents as water and water–alcohol mixtures, these calculated ratios are closer to unity than are the few available experimental values (24). It is possible to improve the agreement between calculated and experimental ρ_y/ρ_x ratios by choosing an unreasonably large value for ϵ_i or by choosing $B > 0.8$. This last choice is inconsistent with the gas phase results. We therefore conclude that the present electrostatic model cannot be quantitatively and simultaneously consistent with the experimental results for aqueous solutions, for other high dielectric constant solutions, and for gas phase acidities. There are no experimental results adequate for testing the model with respect to solutions having low dielectric constants.

In spite of the over-simplifications in this and previous electrostatic theories, it does appear that these approaches are gradually leading to improved understanding of both substituent and solvent effects, and are therefore worth continuing.

Acknowledgments

We are grateful to the National Research Council of Canada and the Japan Society for Promotion of Science for their support. We also thank Dr. L. D. Hansen and Dr. H. P. Hopkins for helpful discussions. Dr. Hansen has pointed out that some electrostatic calculations related to ours have been published (25). Dr. Hopkins has pointed out that there are now useful semi-empirical quantum theoretical calculations that can provide further information related to our equation 15.

1. L. G. Hepler and W. F. O'Hara. J. Phys. Chem. **65**, 811 (1961); L. G. Hepler. J. Am. Chem. Soc. **85**, 3089 (1963).
2. L. G. Hepler. J. Phys. Chem. **68**, 2645 (1964).
3. J. W. Larson and L. G. Hepler. J. Org. Chem. **33**, 3961 (1968).
4. D. J. G. Ives and P. D. Marsden. J. Chem. Soc. 649 (1965).
5. J. W. Larson and L. G. Hepler. *In* Solute–solvent interactions. *Edited by* J. F. Coetzee and C. D. Ritchie, Marcel Dekker, Inc., New York. 1970.
6. L. G. Hepler. Can. J. Chem. **49**, 2803 (1971).
7. P. D. Bolton and L. G. Hepler. Q. Rev. **25**, 521 (1971).
8. L. D. Hansen and L. G. Hepler. Can. J. Chem. **50**, 1030 (1972).
9. C. L. Liotta, E. M. Perdue, and H. P. Hopkins, Jr. J. Am. Chem. Soc. **95**, 2439 (1973); **96**, 7308 (1974).
10. L. G. Hepler and E. M. Woolley. *In* Water: a comprehensive treatise. Vol. 3. *Edited by* F. Franks. Plenum Press, New York. 1973.
11. K. S. Pitzer. J. Am. Chem. Soc. **59**, 2365 (1937).
12. E. J. King. Acid–base equilibria. Pergamon Press, Inc. 1965.
13. H. M. Smallwood. J. Am. Chem. Soc. **54**, 3048 (1932).
14. A. Eucken. Angew. Chem. **45**, 203 (1932).
15. J. G. Kirkwood and F. H. Westheimer. J. Chem. Phys. **6**, 506 (1938).
16. C. F. Wilcox and C. Leung. J. Am. Chem. Soc. **90**, 336 (1968); R. Golden and L. M. Stock. J. Am. Chem. Soc. **94**, 3080 (1972); **88**, 5928 (1966); W. Adcock and M. J. S. Dewar. J. Am. Chem. Soc. **89**, 379 (1967); C. L. Liotta, W. F. Fisher, G. H. Greene, Jr., and B. L. Joyner. J. Am. Chem. Soc. **94**, 4891 (1972).
17. Y. Kondo, T. Matsui, and N. Tokura. Bull. Chem. Soc. Jpn. **42**, 4037 (1969).
18. R. W. Gurney. Ionic processes in solution. McGraw-Hill, New York. 1953. Dover, New York. 1962.
19. M. Taagepera, W. G. Henderson, R. T. C. Brownlee, J. L. Beauchamp, D. Holtz, and R. W. Taft. J. Am. Chem. Soc. **94**, 1369 (1972).
20. R. T. McIver, Jr., and J. H. Silvers. J. Am. Chem. Soc. **95**, 8462 (1973).
21. K. Hiraoka, R. Yamdagni, and P. Kebarle. J. Am. Chem. Soc. **95**, 6833 (1973).
22. R. Yamdagni and P. Kebarle. Can. J. Chem. **52**, 861 (1974).
23. R. Yamdagni, T. B. McMahon, and P. Kebarle. J. Am. Chem. Soc. **96**, 4035 (1974).
24. P. R. Wells. Chem. Rev. **63**, 171 (1963).
25. L. D. Hansen, E. A. Lewis, J. J. Christensen, R. M. Izatt, and D. P. Wrathall. J. Am. Chem. Soc. **93**, 1099 (1971); L. D. Hansen and E. A. Lewis. J. Phys. Chem. **77**, 286 (1973).

Can. J. Chem. Downloaded from www.nrcresearchpress.com by 210.87.254.5 on 09/05/12
For personal use only.

Molecular design to mimic the copper(II) transport site of human albumin: studies of equilibria between copper(II) and glycylglycyl-L-histidine-*N*-methyl amide and comparison with human albumin

THEO P. A. KRUCK, SHOW-JY LAU, AND BIBUDHENDRA SARKAR[1]

The Research Institute of the Hospital for Sick Children, Toronto, Ontario M5G 1X8 and The Department of Biochemistry, University of Toronto, Toronto, Ontario M5S 1A8

Received October 15, 1975

THEO P. A. KRUCK, SHOW-JY LAU, and BIBUDHENDRA SARKAR. Can. J. Chem. **54**, 1300 (1976).

In continuing the investigation of designing the specific Cu(II)-transport site of human serum albumin, the peptide derivative glycylglycyl-L-histidine-*N*-methyl amide was designed to approximate more closely to the native protein. This peptide derivative was synthesized in good yield. The equilibria involved in the binary system, Cu(II)–glycylglycyl-L-histidine-*N*-methyl amide, have been studied, as well as those in the ternary system, L-histidine–Cu(II)–glycylglycyl-L-histidine-*N*-methyl amide. This peptide derivative was found to bind Cu(II) exclusively as a 1:1 complex in the p*H* range 4 to 11, having the same ligand atoms as those for the carboxyl-terminal free peptide and human albumin. However, it was found that glycylglycyl-L-histidine-*N*-methyl amide bound Cu(II) more strongly than did glycylglycyl-L-histidine, the stability constants being log $\beta_{1\text{-}21} = -0.479$ and -1.99 respectively. In the ternary system, only 10% of the mixed complex was detected at p*H* 7, in comparison to 80% found in the case of the carboxyl-terminal free peptide. This finding agrees well with the increased stability of this peptide binary complex. These observations are also consistent with the results obtained from the equilibrium dialysis experiments. The Cu(II) – peptide amide complex has a dissociation constant of 2.07×10^{-17}, indicating a higher binding strength of this peptide derivative for Cu(II) over the native albumin by a factor of 3.

THEO P. A. KRUCK, SHOW-JY LAU et BIBUDHENDRA SARKAR. Can. J. Chem. **54**, 1300 (1976).

Dans le but d'étudier le site de transport spécifique du Cu(II) dans le sérum d'albumine humaine, on a préparé le dérivé peptidique *N*-méthylamide du glycylglycyl-L-histidine qui se rapproche plus de la protéine réelle. On a synthétisé ce dérivé peptidique avec un bon rendement. On a étudié l'équilibre impliqué dans le système binaire Cu(II) plus *N*-méthylamide du glycylglycyl-L-histidine de même que ceux impliqués dans le système ternaire L-histidine–Cu(II)–*N*-méthylamide du glycylglycyl-L-histidine. On a trouvé que ce dérivé peptidique lie le Cu(II) exclusivement sous forme de complexe 1:1 dans la zone de p*H* 4 à 11 et qu'il a les mêmes atomes comme ligands que ceux du peptide possédant la fonction carboxyle terminal libre et que l'albumine humaine. Toutefois on a trouvé que la *N*-méthylamide du glycylglycyl-L-histidine lie le Cu(II) plus fortement que la glycylglycyl-L-histidine; les constantes de stabilité respectives log $\beta_{1\text{-}21}$ sont de -0.479 et -1.99. Dans le système ternaire, à un p*H* de 7, on n'a détecté que 10% d'un complexe mixte; par opposition on en trouve 80% dans le cas du peptide portant un groupe carboxyle terminal libre. Ces données sont en bon accord avec l'augmentation de stabilité de ce complexe peptidique binaire. Ces observations sont aussi en accord avec les résultats obtenus pour des expériences d'équilibre par dialyse. Le complexe Cu(II) – amide peptidique a une constante de dissociation de 2.07×10^{-17} ce qui indique une plus grande force de liaison de ce dérivé peptidique pour le Cu(II) par rapport à l'albumine naturelle et ceci par un facteur de 3.

[Traduit par le journal]

Introduction

As we have previously reported (1, 2), the peptide glycylglycyl-L-histidine, which was designed to mimic the specific Cu(II)-transport site of human albumin, bound Cu(II) in the same manner as did albumin. This small molecule permitted studies which often cannot be applied to large protein molecules (3). A comparative study between this peptide and albumin revealed that, although they bound Cu(II) in the same manner, they functioned differently. The peptide did not bind Cu(II) as strongly as did albumin and the Cu(II)-exchange rate differed in comparison to albumin (2, 4). These studies led to consideration of the improve-

[1]To whom correspondence should be addressed at The Hospital for Sick Children.

Can. J. Chem. Downloaded from www.nrcresearchpress.com by 210.87.254.105 on 09/05/12
For personal use only.

Can. J. Chem. Downloaded from www.nrcresearchpress.com by 210.87.254.105 on 09/05/12
For personal use only.

ment of the design. In the albumin molecule, the carboxyl group close to the Cu(II)-binding imidazole moiety of the third position histidine residue (5) is peptide linked. It was considered that the free carboxyl group close to the Cu(II)-binding imidazole residue of the tripeptide may have a pronounced effect on the binding strength and exchange rate. Thus, the peptide derivative, glycylglycyl-L-histidine-*N*-methyl amide was designed to approximate the native protein more closely. This peptide still excluded all other extraneous sections of the macromolecule not involved in the specific binding of Cu(II).

In this paper, we are reporting the synthesis and the detailed Cu(II)-binding study of the peptide amide. A comparative study was undertaken between albumin and the peptide amide to understand the relative Cu(II)-binding strength. Because of the importance of the albumin–Cu(II)–L-histidine ternary complex in the transportation of Cu(II) in blood (6, 7), the equilibria in the ternary system L-histidine – Cu(II) – glycylglycyl-L-histidine-*N*-methyl amide were investigated.

Experimental Section

Materials

Human serum albumin (Fraction V) was a gift from Connaught Laboratories and purified as described previously to yield Cu(II)-free monomeric albumin (6). The CBZ-glycylglycine *p*-nitrophenyl ester and L-histidine free base were purchased from Nutritional Biochemicals. The L-histidine methyl ester dihydrochloride was obtained from Fluka Chemical Company. Anhydrous monomethyl amine gas was obtained from Matheson of Canada. Dialysis membrane was obtained from Visking Company. The radioisotope $^{67}Cu(II)$ was obtained as previously stated (7). All other reagents were of analytical grade.

Synthesis of Glycylglycyl-L-histidine-N-methyl Amide

To the aqueous solution of L-histidine methyl ester dihydrochloride (9.8 g in 10 ml), 100 ml of $CHCl_3$ was added. The mixture was chilled on salt–ice bath. Then 8 ml (10 *N*) NaOH and 50 g K_2CO_3 were added. The mixture was shaken vigorously and filtered into anhydrous Na_2SO_4. The filtrate was reduced in volume ($\sim$ 20 ml) under reduced pressure. This solution of L-histidine methyl ester was combined with 11.5 g CBZ-glycylglycine *p*-nitrophenyl ester in 1000 ml of $CHCl_3$, and stirred at room temperature for a day. The precipitate was filtered and washed with $CHCl_3$ and then anhydrous ether. The purity of the product, CBZ-glycylglycyl-L-histidine methyl ester (7.5 g) was checked by thin-layer chromatography, mp 198 °C. This compound (6.0 g) was then dissolved in 450 ml 95% EtOH. The ethanolic solution was kept on ice-bath and monomethyl amine gas was passed through until complete conversion (5 h). The mixture was left in cold overnight. The precipitate was filtered and washed with cold EtOH. It was then recrystallized from hot 95% EtOH. Dry weight: 5.0 g, mp 236–237 °C. To 5.0 g of CBZ-glycylglycyl-L-histidine-*N*-methyl amide in 300 ml of MeOH and 20 ml water, 0.36 g of 10% Pd/C was added. Hydrogenation was carried out for 4 h to assure the complete removal of the CBZ-group. It was filtered and the filtrate was dried under reduced pressure. The residue was recrystallized from cold 90% CH_3CN (in water). The purity of the final product (1.7 g) was examined by both thin-layer chromatography and high-voltage electrophoresis. The amino acid ratio of this product after acid hydrolysis gave Gly:His as 2:1.

Stability Constants and Species Distribution

This study involved the use of the technique of analytical potentiometry (8). The 0.1008 *N* NaOH was prepared carbonate-free and stored under argon atmosphere. It was standardized against phthalate (National Bureau of Standards). A solution of 0.1 *N* HCl was standardized against the 0.1008 *N* base. Analytical grade cupric chloride (Fisher Scientific Co.) was dissolved to give 0.1 *M* solution in 10^{-3} *N* HCl and standardized by complexometric titration with EDTA. The peptide solutions were prepared fresh every second day and stored at 4 °C if not in use and the concentrations were established by titrating the imidazole and the amino functional groups (this also provided another check on the purity of the peptide). The accuracy of the p*H* determination is estimated at $\pm$0.05 p*H* units. All calculations were performed on a GE 400 series computer. The proton liberation data and the amounts of unreacted reagents were determined by processing the original titration data by program PLOT-2.[2] These data then were worked up, using programs GUESS-2 and LEASK-2, to obtain the species distribution. A detailed account of the data processing has been reported previously (9–12).

Spectrophotometry

Absorbance measurements were made against appropriate references in cells having 5 cm path length in a Cary model 15 recording spectrophotometer with the cell compartment thermostated to 25 $\pm$ 0.1 °C.

Equilibrium Dialysis

The competitions of the peptide amide and albumin for Cu(II) were carried out in 0.1 *M* *N*-ethylmorpholine–HCl buffer at p*H* 7.53, 6 °C and ionic strength 0.16 by the equilibrium dialysis technique, in the same manner as described previously (7). One half-cell contained the stock solution of Cu(II)–albumin mixed with $^{67}CuCl_2$, the other half-cell contained various amounts of the peptide amide. The molar ratio of the peptide amide to Cu(II)–albumin ranged from 0.25 to 5.0. Radioactivity of $^{67}Cu(II)$ was measured both before and after dialysis.

[2]The earlier versions of Programs PLOT, GUESS, and LEASK have been revised and modified to permit more efficient operation. These programs (PLOT-2, GUESS-2, LEASK-2) are available in both FORTRAN-IV and APL languages. All inquiries regarding these programs should be directed to the author to whom correspondence should be addressed.

Can. J. Chem. Downloaded from www.nrcresearchpress.com by 210.87.254.105 on 09/05/12
For personal use only.

TABLE 1. Sample composition of the system A:H (A = Glycylglycyl-L-histidine-*N*-methyl amide H = proton) titrated in 0.15 *M* NaCl at 25 °C

Sample No.	$C_A \times 10^5$ (moles)	$C_{HCl} \times 10^5$ (moles)
Ligand A variation		
1	0.000	15.000
2	1.754	18.508
3	3.508	22.016

Results

Determination of Complex Species and Stability Constants

Calculations

The general equilibrium between C_M moles of metal ion M, C_H moles of proton H, C_A moles of anionic ligand glycylglycyl-L-histidine-*N*-methyl amide A and C_B moles of anionic ligand L-histidine B, is described in reaction 1.

$$[1] \qquad pM + qH + rA + sB \leftrightarrows M_pH_qA_rB_s$$

where p, q, r, and s are the numbers of moles of M, H, A, and B reacting to form the complex species $M_pH_qA_rB_s$. The stability constant then is represented by β_{pqrs} in terms of concentration at constant ionic strength, temperature and pressure.

$$[2] \qquad \beta_{pqrs} = \frac{M_pH_qA_rB_s}{m^p h^q a^r b^s}$$

where m, h, a, and b are the concentrations of free metal ion, hydrogen ion, completely deprotonated ligand A and B, respectively. One way of accounting for all the species in the system is given in eq. 3

$$[3] \qquad C_M = m + \sum_{pqrs} p\beta_{pqrs} m^p h^q a^r b^s$$

where C_M represents the total metal concentration. Equations 4, 5, and 6 were used to determine the unbound metal and ligands remaining in solution throughout the titration experiments

$$[4] \qquad pM = pM_o + \int_{pH_o}^{pH_i} \partial H_1^+ / \partial C_M \mathrm{d}pH$$

$$[5] \qquad pA = pA_o + \int_{pH_o}^{pH_i} \partial H_1^+ / \partial C_A \mathrm{d}pH$$

$$[6] \qquad pB = pB_o + \int_{pH_o}^{pH_i} \partial H_1^+ / \partial C_B \mathrm{d}pH$$

where subscripts o and i represent the initial and final states of the system throughout the titration. Program PLOT-2 is designed to solve these integral equations. The quantities, $\partial H_1^+/\partial C_M$, $\partial H_1^+/\partial C_A$ and $\partial H_1^+/\partial C_B$ are the intermediate output data of program PLOT-2, representing the molar proton liberation for Cu(II), the peptide amide and L-histidine respectively for the complex systems.

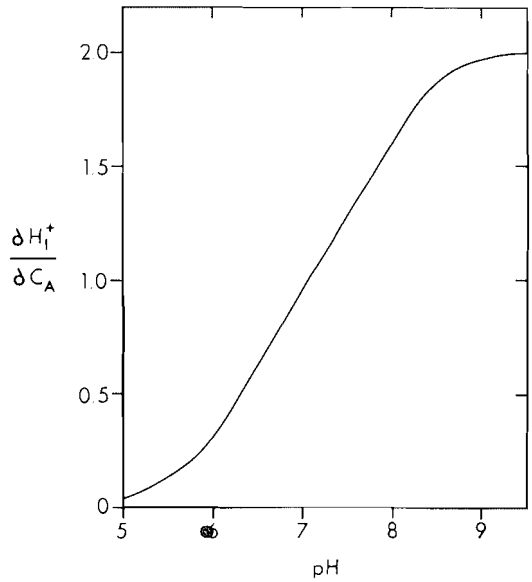

FIG. 1. Proton displacement $\partial H_1^+/\partial C_A$ as a function of pH for the proton – glycylglycyl-L-histidine-*N*-methyl amide system ($C_A = 4.008 \times 10^{-4}$ *M*).

The acid dissociation constants β_{0q1} were determined, using data $\bar{n}_H$ (the average number of bound protons) in eq. 7.

$$[7] \qquad \bar{n}_H = Q - \partial H_1^+ / \partial C_A$$

where Q = maximum number of protons bound to the ligand A throughout the titration range. To obtain values for the proton binding constants β_{0q1}, sets of simultaneous equations, as shown in eq. 8, were solved,

$$[8] \quad \bar{n}_H = \beta_{011}(1 - \bar{n}_H)h + \beta_{021}(2 - \bar{n}_H)h^2$$

To obtain values for the stability constants β_{pqrs} of complex species existing in solution, a matrix was set up, containing the coefficients $m^p h^q a^r b^s$ for all possible combinations of p, q, r, and s of the unknown stability constants β_{pqrs} as shown in eq. 2. This matrix representing simultaneous equations (eq. 3) was solved to obtain values for the unknown β_{pqrs}.

TABLE 2. Comparison of log stability constants (log β_{pqrs} and log β'_{pqrs}) of the complex species $M_pH_qA_rB_s$ (M = Cu(II), A = glycylglycyl-L-histidine-*N*-methyl amide, A′ = glycylglycyl-L-histidine, B = L-histidine) in 0.15 *M* NaCl at 25 °C

p	q	r	s	log β_{pqrs} ($M_pH_qA_rB_s$)	log β'_{pqrs}[a] ($M_pH_qA'_rB_o$)	log β_{pqrs}[b] ($M_pH_pA_oB_s$)	log β'_{pqrs}[c] ($M_pH_qA'_rB_s$)
0	3	1	0	—	17.50	—	—
0	2	1	0	14.47	14.78	—	—
0	1	1	0	8.00	8.04	—	—
1	−2	1	0	−0.479	−1.99	—	—
1	1	0	1	—	—	14.18	—
1	0	0	1	—	—	10.20	—
1	2	0	2	—	—	26.91	—
1	1	0	2	—	—	24.01	—
1	0	0	2	—	—	18.45	—
1	2	1	1	27.75	—	—	28.83
1	1	1	1	—	—	—	23.61
1	0	1	1	—	—	—	17.56
1	−1	1	1	11.31	—	—	11.05
1	−2	1	1	3.02	—	—	1.70

[a]Reference 2.
[b]Reference 11.
[c]Reference 3.

TABLE 3. Sample compositions of the binary system M:A (M = Cu(II), A = glycylglycyl-L-histidine-*N*-methyl amide) titrated in 0.15 *M* NaCl at 25 °C

Sample	$C_M \times 10^5$ (moles)	$C_A \times 10^5$ (moles)	$C_{HCl} \times 10^5$ (moles)
Metal variation			
4	0.000	4.008	23.016
5	0.888	4.008	23.016
6	1.776	4.008	23.016
Ligand A variation			
7	0.888	2.004	19.004
8	0.888	4.008	23.016
9	0.888	5.010	25.020

Proton – Glycylglycyl-L-histidine-N-methyl Amide System

Solutions *1–3* in Table 1 were titrated and the titration curves were processed, using program PLOT-2 to obtain the proton liberation data $\partial H_1^+/\partial C_A$ as a function of p*H*. These are plotted in Fig. 1. Using increments of 0.2 p*H* units, simultaneous sets of equations (eq. 8) were set up and processed by program LEASK-2 to obtain the protonation constants β_{011} and β_{021} of the species HA and H_2A, listed in Table 2.

Proton – Cu(II) – Glycylglycyl-L-histidine-N-methyl Amide System

To determine the unbound metal as a function of p*H*, solutions *4–6* in Table 3 (metal variation) were titrated. The data were digitized and processed by program PLOT-2 to yield p*M* as a function of p*H*. Simultaneously, the molar proton liberation $\partial H_1^+/\partial C_M$ was calculated The results are shown in Fig. 2, curve *1*. To obtain the values for the unbound ligand as a function of p*H* and ensuing metal complexation, solutions *7–9* (ligand variation) were titrated. These data again were digitized and processed by program PLOT-2 to give p*A* as a function of p*H* and an intermediate output $\partial H_1^+/\partial C_A$ as a function of p*H*, the latter being plotted in Fig. 2, curve *2*.

To test for the presence of likely species formed in the metal–ligand system, the following values for p, q, and r were used: $p = 1, 2$; $q = +2, +1, 0, -1, -2$; $r = 1, 2$. In the process of calculating values for β_{pqr} (program

Can. J. Chem. Downloaded from www.nrcresearchpress.com by 210.87.254.105 on 09/05/12
For personal use only.

Can. J. Chem. Downloaded from www.nrcresearchpress.com by 210.87.254.105 on 09/05/12
For personal use only.

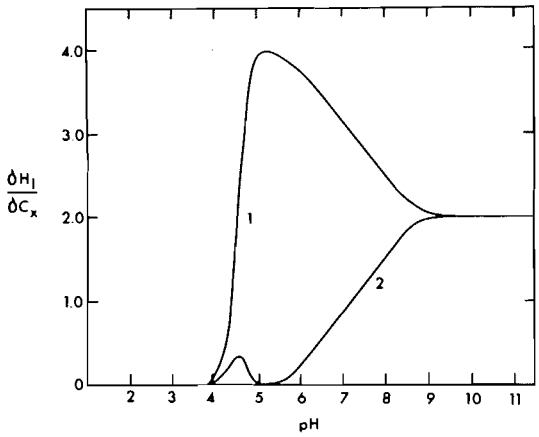

FIG. 2. Proton displacement $\partial H_1^+/\partial C_X$ as a function of pH for the Cu(II) – glycylglycyl-L-histidine-N-methyl amide system. Curve *1*, $\partial H_1^+/\partial C_M$; curve *2*, $\partial H_1^+/\partial C_A$ ($C_M = 1.776 \times 10^{-4}$ M, $C_A = 1.776 \times 10^{-4}$ M).

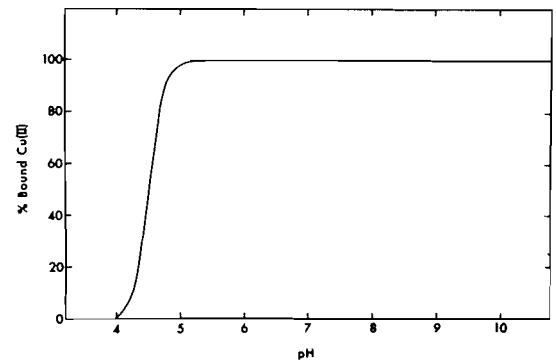

FIG. 3. Species distribution in the system Cu(II) – glycylglycyl-L-histidine-N-methyl amide as a function of pH ($C_M = 1.776 \times 10^{-4}$ M, $C_A = 7.016 \times 10^{-4}$ M).

LEASK-2), it was found that only one complex species $MH_{-2}A$ was required to give a minimum error solution in the pH range 4.0–10.8. The stability constant β_{pqr} is listed in Table 2. The minimum solution β_{pqr} was used to calculate the species distribution (Fig. 3), which gives the amount of the species present in the system as a function of pH.

Proton – Cu(II) – Glycylglycyl-L-histidine-N-methyl Amide – L-Histidine System

To determine the unbound metal as a function of pH, solutions *10–12* in Table 3 (metal variation) were titrated. Data processing with program PLOT-2 yielded pM as a function of pH and the intermediate output $\partial H_1^+/\partial C_M$ as a function of pH. This molar proton liberation

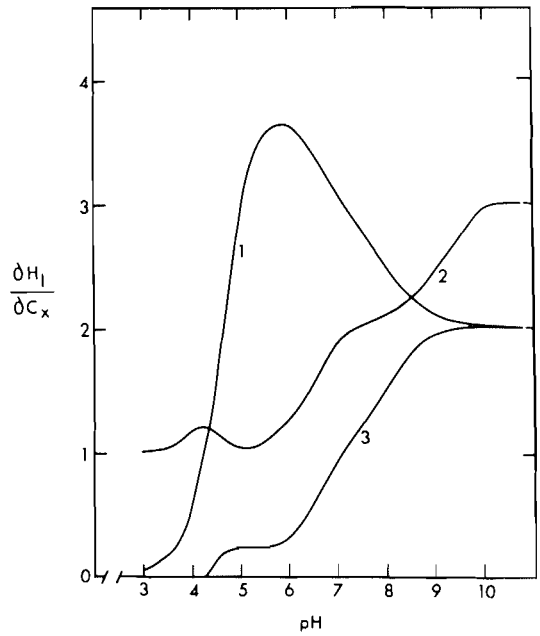

FIG. 4. Proton displacement $\partial H_1^+/\partial C_X$ as a function of pH for the Cu(II) – glycylglycyl-L-histidine-N-methyl amide – L-histidine system. Curve *1*, $\partial H_1^+/\partial C_M$; curve *2*, $\partial H_1^+/\partial C_B$; curve *3*, $\partial H_1^+/\partial C_A$ ($C_M = 1.776 \times 10^{-4}$ M, $C_A = 7.016 \times 10^{-4}$ M, $C_B = 8.016 \times 10^{-4}$ M).

is shown in Fig. 4, curve *1*. To obtain the values for the unbound ligand A (glycylglycyl-L-histidine-N-methyl amide) as a function of pH, solutions *13–15* in Table 4 were titrated. Data processing yielded pA as a function of pH and $\partial H_1^+/\partial C_A$ as a function of pH. The latter data are plotted in Fig. 4, curve *3*. To obtain the values for the unbound ligand B (L-histidine) as a function of pH, solutions *16–18* in Table 4 were titrated. Data processing yielded pB as a function of pH and $\partial H_1^+/\partial C_B$ as a function of pH. The latter data are plotted in Fig. 4, curve *2*.

To test for the presence of likely species formed in the metal ligand system, the following values for p, q, r, and s were used: $p = 1$, $q = +2, +1, 0, -1, -2$; $r = 1, 2$; $s = 1, 2$. Upon solving the binary systems $M_pH_qA_r$ and $M_pH_qB_s$, it was found that no binuclear or polymeric species ($p \neq 1$) were formed. To solve for stability constants for the ternary complex species, all previously determined stability constants for the binary systems were kept invariant and only the stability constants of the ternary species $M_pH_qA_rB_s$ were treated

TABLE 4. Sample compositions of the ternary system M:A:B (M = Cu(II), A = glycylglycyl-L-histidine-*N*-methyl amide, B = L-histidine) titrated in 0.15 *M* NaCl at 25 °C

Sample	$C_M \times 10^5$ (moles)	$C_A \times 10^5$ (moles)	$C_B \times 10^5$ (moles)	$C_{HCl} \times 10^5$ (moles)
Metal variation				
10	0.000	1.754	2.004	24.520
11	0.888	1.754	2.004	24.520
12	1.776	1.754	2.004	24.520
Ligand A variation				
13	0.888	0.877	2.004	22.766
14	0.888	1.754	2.004	24.520
15	0.888	2.631	2.004	26.274
Ligand B variation				
16	0.888	1.754	0.501	19.510
17	0.888	1.754	1.002	20.512
18	0.888	1.754	2.004	22.516

as adjustable parameters. The minimum error solution for the total system permitted only the three following ternary complex species, MH_2AB, $MH_{-1}AB$ and $MH_{-2}AB$, while the majority of Cu(II) was bound to the peptide amide in the complex $MH_{-2}A$ between p*H* 5 and 10. The stability constants β_{pqrs} of the ternary complexes are listed in Table 2, and the species distribution is plotted in Fig. 5.

Spectrophotometry

The sample solution contained M:A in a ratio of 1:4, 0.15 *M* NaCl under anaerobic conditions. The metal concentration was 1.776×10^{-3} *M*. The spectra were taken at various p*H* values and were found to be invariant above neutral p*H*. The spectrum represented in Fig. 6 was taken at p*H* 8.0. The complex $MH_{-2}A$ was found to have $\lambda_{max} = 525$ nm and $\varepsilon_{max} = 103$.

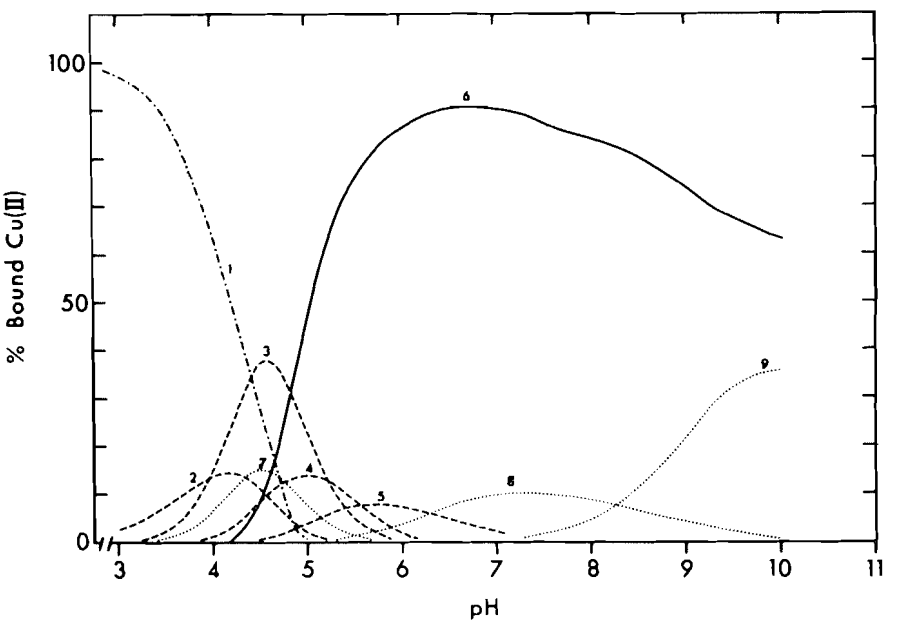

FIG. 5. Species distribution in the ternary system Cu(II) – glycylglycyl-L-histidine-*N*-methyl amide – L-histidine as a function of p*H*. Curve *1*, unbound Cu(II); curve *2*, MHB; curve *3*, MB; curve *4*, MHB_2; curve *5*, MB_2; curve *6*, $MH_{-2}A$; curve *7*, MH_2AB; curve *8*, $MH_{-1}AB$; curve *9*, $MH_{-2}AB$ ($C_M = 1.776 \times 10^{-4}$ *M*, $C_A = 7.016 \times 10^{-4}$ *M*, $C_B = 8.016 \times 10^{-4}$ *M*).

Can. J. Chem. Downloaded from www.nrcresearchpress.com by 210.87.254.105 on 09/05/12
For personal use only.

Can. J. Chem. Downloaded from www.nrcresearchpress.com by 210.87.254.105 on 09/05/12
For personal use only.

TABLE 5. Equilibrium dialysis of the ternary binding system[a]

$[\text{Peptide amide}]_t$ (10^4 M)	[Cu(II)–peptide amide] (10^4 M)	[Peptide amide] (10^4 M)	[Cu(II)–albumin] (10^4 M)	[Albumin] (10^4 M)	K_{eq}	$K_{D,\ Cu(II)\text{–peptide amide}}$ (10^{17} M)
0.76	0.69	0.07	2.21	0.69	3.07	2.15
1.39	1.09	0.30	1.81	1.09	2.46	2.69
2.23	1.67	0.56	1.23	1.67	4.11	1.61
2.74	1.80	0.94	1.10	1.80	3.08	2.15
2.97	1.91	1.06	0.99	1.91	3.48	1.90
5.88	2.37	3.51	0.53	2.37	3.00	2.20
6.67	2.42	4.25	0.48	2.42	2.84	2.32
14.28	2.74	11.54	0.16	2.74	4.20	1.57

[a]The equilibrium dialysis was carried out in 0.1 M N-ethylmorpholine-HCl buffer at pH 7.53, 6 °C, and ionic strength 0.16. Total initial Cu(II)–albumin concentration was kept at 2.90×10^{-4} M, while the peptide amide was varied. Subscript t denotes total peptide amide concentration in the system.

Can. J. Chem. Downloaded from www.nrcresearchpress.com by 210.87.254.105 on 09/05/12
For personal use only.

Comparison of Binding Strength Between Cu(II) – Peptide Amide and Cu(II)–Albumin

The dissociation of Cu(II) – peptide amide and the competition of Cu(II) between the peptide amide and albumin are similar to that expressed previously (2). The dissociation constant for Cu(II) – peptide amide was determined from the equilibrium dialysis data, using ^{67}Cu(II) as a tracer. The results are presented in Table 5. The average value of $K_{D,\ Cu(II)-peptide\ amide}$ is 2.07×10^{-17}.

Discussion

In the glycylglycyl-L-histidine-*N*-methyl amide – Cu(II) system (Fig. 3) we observed the existence of a single species $MH_{-2}A$ over a wide range of p*H* which is indicative of a very high specificity of this peptide amide for the Cu(II) ion. The peptide glycylglycyl-L-histidine-*N*-methyl amide carries four ionizable groups capable of yielding protons. Two of those, the imidazole and amino groups, are titratable in the normal titration range. The results in Fig. 2, curve *1*, show that Cu(II)-complexation starts just past p*H* 4.2 and rapidly reaches a maximum value of four protons per mole of Cu(II) over a range less than 2 p*H* units. This means that, once the first coordination bond is formed, the chelate effect will aid in forming the following coordination bonds to the central Cu(II) ion. Increasing the p*H* from ~6.0 to 6.5, the molar proton liberation reaches 3.5 for a net loss of 0.5 protons. Since the imidazole group has its pK_a established at 6.4, we can conclude that this group is involved in Cu(II) coordination. Upon raising the p*H* to 8, a value of 2.5 protons per mole of Cu(II) is obtained. The pK_a of the amino group was found to be 8.00. This establishes the NH_2-terminal amino group of this peptide amide as a coordinating ligand for the Cu(II) ion. Above p*H* 9, a constant value for $\partial H_1^+/\partial C_M = 2.0$ is reached. These protons originate from coordinating groups with pK_a values beyond the limits of our titration (p*H* 10.8). It has been established that peptide amide protons have p*K* values in excess of 14 (13). Furthermore, it is now well established that Cu(II) ion upon binding to peptides and proteins can displace peptide amide hydrogens (14). Since there are no other ionizable groups capable of dissociating protons, it can be concluded that

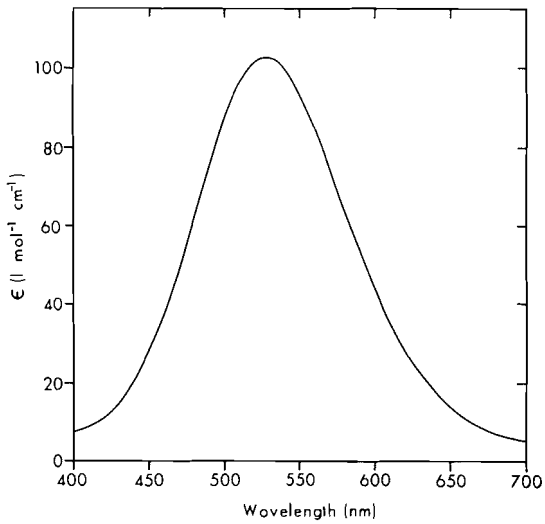

FIG. 6. Visible spectrum of the complex system Cu(II) – glycylglycyl-L-histidine-*N*-methyl amide taken at p*H* 8 ($C_M = 1.776 \times 10^{-3}$ *M*, $C_A = 7.016 \times 10^{-3}$ *M*).

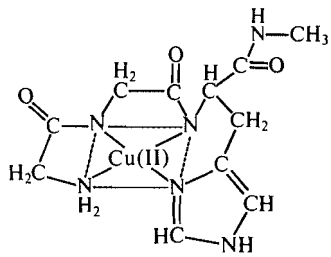

FIG. 7. Proposed solution structure of the complex species $MH_{-2}A$.

two peptide nitrogens are coordinated to the central Cu(II) ion. Sterical examinations show that the first and second peptide nitrogens will occupy two corners of the coordination square, while the amino and imidazole groups occupy the remaining two positions of the square plane as shown in Fig. 7. The observed λ_{max} at 525 nm and ε_{max} of 103 for the Cu(II) – glycylglycyl-L-histidine-*N*-methyl amide complex, are identical to those observed for the Cu(II)–albumin complex and the previously reported complex Cu(II) – glycylglycyl-L-histidine. The proposed structure for the complex $MH_{-2}A$ shows the same coordination geometry as the first Cu(II)-binding site of albumin which has been established earlier, and also identical to the structure which has been established for the neutral Cu(II)-complex of glycylglycyl-L-histidine. The proposed solution structure of $MH_{-2}A$ is

Can. J. Chem. Downloaded from www.nrcresearchpress.com by 210.87.254.105 on 09/05/12
For personal use only.

further confirmed by X-ray crystallographic analysis of the complex (15).

Even though the structures for the complexes of Cu(II) – glycylglycyl-L-histidine-*N*-methyl amide and Cu(II)–glycylglycyl-L-histidine are similar, the former complex ($MH_{-2}A$) shows a higher stability than the latter one ($MH_{-2}A'$), $\log \beta_{1\text{-}21} = -0.479$ and $\log \beta'_{1\text{-}21} = -1.99$ (Table 2). This enhanced stability has to be ascribed to the replacement of the negatively charged carboxyl group by the *N*-methyl amide group which approximates more closely the steric and charge distribution conditions of the NH_2-terminal of the albumin. The results obtained from equilibrium dialysis show that glycylglycyl-L-histidine-*N*-methyl amide exhibits a higher binding strength for Cu(II) than that of the native albumin by a factor of 3. The higher binding strength of the peptide amide is consistent with the observation of the ligand exchange rate of the peptide amide compared to the carboxyl free peptide (16).

The analysis of the ternary system glycylglycyl-L-histidine-*N*-methyl amide – Cu(II) – L-histidine gave additional significant information. Examination of the species distribution, Fig. 5, shows that less ternary complexes (max. ~35%) are formed in this system than was reported for the glycylglycyl-L-histidine–Cu(II)–L-histidine system (max. ~80%) (2). At p*H* 7, we find 10% mixed complex, while in the previously examined system, we had 80% of the Cu(II) bound in the ternary complex form. This finding again is consistent with the fact that this peptide *N*-methyl amide was found to have greatly increased stability over the peptide carrying a free carboxyl group. Since the formation of a ternary Cu(II)-complex involves the formation of at least one coordination bond from L-histidine in the coordination square plane, it would require the removal of at least one of the Cu(II)-coordinating nitrogens of the peptide. Again, with the higher $\beta_{1\text{-}21}$ for the peptide *N*-methyl amide, we would expect lesser amounts of mixed complexes to be formed; we have found this.

Structurally, this new Cu(II) – glycylglycyl-L-histidine-*N*-methyl amide complex mimics the native albumin binding site for the first equivalent of Cu(II). However, this molecule binds Cu(II) with even higher affinity than the natural Cu(II)-specific binding site on albumin. Further studies are underway to delineate this interesting phenomenon.

Acknowledgment

The research was supported by a grant from the Medical Research Council of Canada.

1. B. SARKAR. Proc. Can. Fed. Biol. Soc. **15**, 659 (1972); Proc. 9th International Congr. of Biochemistry. Stockholm, Sweden. 1973. p. 122.
2. S. LAU, T. P. A. KRUCK, and B. SARKAR. J. Biol. Chem. **249**, 5878 (1974).
3. T. P. A. KRUCK and B. SARKAR. Inorg. Chem. **14**, 2383 (1975).
4. S. LAU and B. SARKAR. Can. J. Chem. **53**, 710 (1975).
5. T. PETERS, JR. and F. A. BLUMENSTOCK. J. Biol. Chem. **242**, 1574 (1967).
6. B. SARKAR and Y. WIGFIELD. Can. J. Biochem. **46**, 601 (1968).
7. S. LAU and B. SARKAR. J. Biol. Chem. **246**, 5938 (1971).
8. B. SARKAR and T. P. A. KRUCK. Can. J. Chem. **51**, 3541 (1973).
9. T. P. A. KRUCK and B. SARKAR. Can. J. Chem. **51**, 3549 (1973).
10. T. P. A. KRUCK and B. SARKAR. Can. J. Chem. **51**, 3555 (1973).
11. T. P. A. KRUCK and B. SARKAR. Can. J. Chem. **51**, 3563 (1973).
12. D. W. APPLETON and B. SARKAR. Proc. Nat. Acad. Sci. (USA) **71**, 1686 (1974).
13. D. W. APPLETON, T. P. A. KRUCK, and B. SARKAR. To be published.
14. H. C. FREEMAN. Adv. Protein Chem. **22**, 257 (1967).
15. N. CAMERMAN, A. CAMERMAN, and B. SARKAR. Can. J. Chem. This issue.
16. B. SARKAR, V. RENUGOPALAKRISHNAN, T. P. A. KRUCK, and S. LAU. *In* Environmental effects on molecular structure and properties. *Edited by* B. Pullman and E. Bergmann. D. Reidel Publishing Co., Dordrecht, The Netherlands. 1975. pp. 165–178.

Molecular design to mimic the copper(II) transport site of human albumin. The crystal and molecular structure of copper(II) – glycylglycyl-L-histidine-*N*-methyl amide monoaquo complex

NORMAN CAMERMAN[1]

Department of Biochemistry, University of Toronto, Toronto, Ontario M5S 1A8

AND

ARTHUR CAMERMAN

Departments of Medicine (Neurology) and Pharmacology, University of Washington, Seattle, Washington 98195

AND

BIBUDHENDRA SARKAR

Research Institute, Hospital for Sick Children, Toronto, Ontario M5G 1X8
and Department of Biochemistry, University of Toronto, Toronto, Ontario M5S 1A8

Received October 15, 1975

NORMAN CAMERMAN, ARTHUR CAMERMAN, and BIBUDHENDRA SARKAR. Can. J. Chem. **54**, 1309 (1976).

Glycylglycyl-L-histidine-*N*-methyl amide is a copper-binding tripeptide designed and synthesized to mimic the copper-transport site of human albumin. Reddish-purple crystals of the copper-tripeptide amide complex (Cu–GGHa), grown at physiological p*H*, are triclinic, with cell dimensions $a = 9.990$, $b = 9.986$, $c = 7.682$ Å, $\alpha = 107.40$, $\beta = 91.72$, $\gamma = 96.49°$, space group $P\bar{1}$, Z = two units of Cu–GGHa and two water molecules per cell. The structure was solved by interpretation of a Cu-phased Fourier map containing a great deal of false symmetry, after multiple attempts with direct phasing methods failed. Refinement proceeded to $R = 0.036$. The conformations of the two Cu–GGHa units are virtually identical. Each copper is tetradentate chelated by the amino terminal nitrogen, the next two peptide nitrogens, and a histidyl nitrogen of a single tripeptide molecule in a mildly distorted square planar arrangement. The Cu...N distances range between 1.90–2.05 Å, with N...Cu...N angles of 165 and 176°. An oxygen atom provides a fifth position weaker interaction in each case, with Cu...O distances of 2.61 and 2.88 Å.

NORMAN CAMERMAN, ARTHUR CAMERMAN et BIBUDHENDRA SARKAR. Can. J. Chem. **54**, 1309 (1976).

La glycylglycyl-L-histidine-*N*-méthyle amide est un tripeptide, pouvant fixer le cuivre, qui a été proposée et synthétisée pour mimer les sites de transport du cuivre dans l'albumine humaine. Les cristaux rouge violacé du complexe du cuivre et du tripeptide amide (Cu–GGHa), que l'on a fait croître à un p*H* physiologique, sont tricliniques avec des dimensions de maille $a = 9.990$, $b = 9.986$, $c = 7.682$ Å, $\alpha = 107.40$, $\beta = 91.72$, $\gamma = 96.49°$, groupe d'espace $P\bar{1}$, Z = deux unités de Cu–GGHa et deux molécules d'eau par maille. Après que de multiples essais des méthodes directes eurent fait défaut, on a résolu la structure par une interprétation d'une carte de Fourier phasée par le cuivre et contenant un grand nombre de fausses symétries. On a procédé à l'affinement jusqu'à une valeur de $R = 0.036$. Les conformations des deux unités Cu–GGHa sont pratiquement identiques. Chaque atome de cuivre est chélaté par l'azote du groupe amino terminal, par les azotes des deux peptides suivants et par un azote du groupe hystidyle de la même molécule du tripeptide; le tout est dans un arrangement plan carré légèrement déformé. Les distances Cu...N varient entre 1.90–2.05 Å avec des angles N...Cu...N de 165 et 176°. Dans chaque cas, un atome d'oxygène fournit une cinquième position d'interaction plus faible à des distances Cu...O de 2.61 et 2.88 Å.

[Traduit par le journal]

Introduction

The tripeptide glycylglycyl-L-histidine was designed (1) to achieve a molecule which could adopt a conformation similar to that of the Cu(II) transport site of human serum albumin, and was shown (2) to bind Cu(II) exclusively as a 1:1 complex at physiological p*H*. Although the same ligands were thought to be involved in the coordination to the copper in both the tripeptide–Cu(II) complex and the albumin–

[1]To whom correspondence should be addressed.

Can. J. Chem. Downloaded from www.nrcresearchpress.com by 210.87.254.40 on 09/05/12
For personal use only.

Can. J. Chem. Downloaded from www.nrcresearchpress.com by 210.87.254.40 on 09/05/12
For personal use only.

Cu(II) complex, the binding strength of the peptide complex was lower than that for albumin and the Cu(II) exchange rate was also different (3). The free carboxyl group of the peptide may be partly responsible for the lower binding strength; to eliminate this, and to make the peptide chemically and structurally more similar to the Cu(II) transport site of albumin, the methyl amide of glycylglycyl-L-histidine was synthesized, and was found to have a higher binding affinity for Cu(II) than does the free peptide (4).

There is considerable interest both in the possible use of a peptide such as this as a copper-chelator for rapid removal of Cu(II) in Wilson's disease (5), and in the use of the same concepts in the synthetic design of peptides to emulate active regions of other macromolecules (6). Knowledge of the chemical nature and geometry of the binding is of utmost importance to the furthering of these studies. Therefore, we have determined the three-dimensional structure of the Cu(II) – glycylglycyl-L-histidine-*N*-methyl amide complex (Cu–GGHa) and now present a detailed description of the stereochemistry of the complex.

Experimental Section

Crystals of Cu–GGHa were crystallized from 50% water–acetonitrile; they are reddish-purple chunks with poorly-developed faces. Preliminary photographic and density measurements revealed the crystal cell to be triclinic with two units of Cu–GGHa and two water molecules comprising the asymmetric unit. Unit cell dimensions were determined by least-squares refinement of diffractometer measurements, and crystal data are given in Table 1.

Intensity data were collected on an automated four-circle diffractometer (Zr-filtered Mo radiation) and all independent reflections having 2θ (MoKα) $\leqslant 55°$ (corresponding to a minimum interplanar spacing of 0.77 Å) were measured. The $\theta/2\theta$ scan method was employed, with stationary background radiation measurements taken on both sides of each reflection. Intensities of 3224 reflections (out of a total of 3318 in the range recorded) were greater than twice their standard deviation and these reflections were classified as observed. The crystal used for the data collection was small and absorption corrections were not carried out. The standard geometrical corrections to the intensities were applied, and structure amplitudes $|F|$ and normalized structure amplitudes $|E|$ were derived.

Structure Determination

Because the complex contains an optically-active isomer the space group is necessarily $P1$; the origin was therefore defined as the position of one Cu atom and the coordinates of the second Cu in the asymmetric unit were obtained from the largest peak on an $E^2 - 1$ Patterson map. A three-dimensional Fourier summation, phased on the two coppers, necessarily had a false centre of symmetry halfway between them. Moreover, because the overall conformation of the Cu–GGHa complex is very roughly planar and parallel to the *ab* plane (17 of 21 atoms in one Cu–GGHa unit have z between 0.44–0.55 and 16 of 21 in the other Cu–GGHa have z between −0.03–0.08) the false symmetry produced an image of each Cu–GGHa complex superimposed on the other. This made the Fourier map extremely difficult to decipher. Attempts at finding a histidine ring and solving the structure therefrom failed, possibly both because of the difficulty in unambiguously identifying a ring and the inability of a small fragment of a molecule to effect any significant degree of resolution of the false symmetry in subsequent Fourier summations.

Attempts were then made to get around the problem of false symmetry by finding phases by direct methods. Phases based on the two Cu atoms were calculated for the 250 reflections with the highest $|E|$ values ($3.77 \geqslant E \geqslant 1.57$) and these were refined by use of the tangent formula; however, no phase changes resulted. Phase determination was then initiated with input only of three origin-specifying reflections and three symbolic phases into multiple-solution tangent formula programs. Two programs were used, TANFOR, in which we specified the starting reflections, and MULTAN, in which the program was allowed to determine the best starting set. The results were similar in both cases: both programs produced 32 sets of phases, all sets having virtually identical values of R_{Karle} (0.073) and of other reliability indices. One set of phases from each program, the set with the marginally (but insignificantly) best set of reliability indices, was used to generate an E-map; the two maps were different but equally uninterpretable.

The structure was finally solved by interpretation of the false symmetry-containing Cu-phased Fourier distribution. After a great deal of study, positions were chosen for 12 light atoms around one Cu position, and a new

TABLE 1. Crystal data for copper – glycylglycyl-L-histidine-*N*-methyl amide – H_2O (formula $CuC_{11}H_{16}N_6O_3.H_2O$)

Parameter	Value
Molecular weight	361.85
Crystal system	Triclinic
a (Å)	9.990±0.01
b (Å)	9.986±0.01
c (Å)	7.682±0.01
α (deg)	107.40 ±0.05
β (deg)	91.72 ±0.05
γ (deg)	96.49 ±0.05
Volume of unit cell (Å^3)	724.9
Measured density (g cm^{-3})	1.64
Number of molecules in unit cell	2
Calculated density (g cm^{-3})	1.66
Absorption coefficient, μ(MoKα) (cm^{-1})	15.9
Space group	$P1$
Wavelength, MoKα (Å)	0.7107

Can. J. Chem. Downloaded from www.nrcresearchpress.com by 210.87.254.40 on 09/05/12
For personal use only.

TABLE 2. Fractional atomic coordinates and thermal ($\times 10^5$) parameters. Standard deviations are given in parentheses, $T = \exp(-(\beta_{11}h^2 + \beta_{22}k^2 + \beta_{33}l^2 + 2\beta_{12}hk + 2\beta_{13}hl + 2\beta_{23}kl))$

Atom	x	y	z	β_{11}	β_{22}	β_{33}	β_{12}	β_{13}	β_{23}
Molecule 1									
Cu	1.0	1.0	0.0	486(9)	453(9)	1644(20)	80(7)	−8(10)	439(11)
N1	1.1875(4)	0.9342(4)	−0.0383(6)	638	568	1539	69	−48	409
Cα1	1.2916(6)	1.0554(6)	0.0151(8)	673	1003	1757	262	131	738
C1	1.2344(5)	1.1933(5)	0.0454(6)	618	609	1067	70	130	277
O1	1.3104(4)	1.3081(4)	0.1060(6)	642	682	2643	−129	−1	425
N2	1.1035(4)	1.1769(4)	0.0066(6)	429	560	1391	36	−11	272
Cα2	1.0267(5)	1.2943(5)	0.0254(8)	720	532	1573	202	181	342
C2	0.8812(4)	1.2481(4)	0.0528(6)	573	445	928	81	35	186
O2	0.8005(4)	1.3398(4)	0.0784(6)	625	473	2213	115	88	444
N3	0.8528(4)	1.1144(4)	0.0511(5)	528	530	1123	120	23	373
Cα3	0.7131(4)	1.0629(4)	0.0681(6)	512	446	1380	183	−7	421
C3	0.6735(4)	1.0864(5)	0.2659(6)	507	700	1059	160	15	140
O3	0.5533(4)	1.0800(6)	0.2939(6)	473	2624	1568	341	85	191
N4	0.7697(4)	1.1097(5)	0.3955(6)	529	1021	1394	121	131	412
Cα4	0.7390(7)	1.1328(8)	0.5858(8)	1032	1742	1355	359	490	421
Cβ	0.6772(5)	0.9112(5)	−0.0443(7)	639	794	1356	152	−54	499
C1h	0.7582(5)	0.8061(5)	−0.0006(6)	673	728	905	132	−15	205
N2h	0.8970(4)	0.8295(4)	0.0225(6)	701	475	1519	78	28	365
C3h	0.9345(6)	0.7148(5)	0.0548(8)	793	573	1877	141	197	383
N4h	0.8279(5)	0.6203(4)	0.0505(7)	867	511	2148	168	276	557
C5h	0.7152(6)	0.6770(6)	0.0149(8)	780	736	1911	−1	−88	477
Molecule 2									
Cu	0.3322(1)	0.4242(1)	0.4990(1)	339(8)	617(10)	1169(16)	94(7)	62(9)	393(10)
N1	0.3974(4)	0.2522(4)	0.5492(6)	615	732	1151	83	108	377
Cα1	0.2817(5)	0.1476(5)	0.5423(8)	553	583	1864	38	36	475
C1	0.1484(5)	0.1998(5)	0.5163(7)	496	738	1098	73	71	339
O1	0.0407(4)	0.1170(4)	0.4946(7)	501	1010	3397	−49	−104	1237
N2	0.1619(4)	0.3318(4)	0.5203(6)	428	627	1436	105	16	478
Cα2	0.0457(5)	0.4019(5)	0.5025(7)	497	853	1200	223	41	509
C2	0.0955(5)	0.5433(5)	0.4710(6)	496	690	1074	110	31	287
O2	0.0102(4)	0.6182(4)	0.4417(6)	418	820	2362	112	17	706
N3	0.2293(4)	0.5748(4)	0.4775(5)	437	531	918	94	107	254
Cα3	0.2816(5)	0.7106(5)	0.4545(6)	534	561	869	212	59	171
C3	0.2887(5)	0.7091(5)	0.2548(7)	563	512	1325	40	−78	340
O3	0.2911(5)	0.8221(4)	0.2213(6)	1846	688	1582	226	−71	559
N4	0.2917(5)	0.5885(4)	0.1302(5)	1031	659	869	173	191	346
Cα4	0.3036(7)	0.5787(7)	−0.0603(8)	1494	1356	1011	374	277	696
Cβ	0.4209(5)	0.7671(4)	0.5557(7)	638	294	1247	27	48	−52
C1h	0.5302(5)	0.6733(5)	0.5032(6)	502	621	1007	37	−7	187
N2h	0.5102(4)	0.5293(4)	0.4861(7)	302	700	1783	13	141	408
C3h	0.6283(5)	0.4832(6)	0.4486(8)	576	1032	1797	105	77	631
N4h	0.7216(4)	0.5881(5)	0.4458(7)	382	1124	1900	97	270	441
C5h	0.6616(5)	0.7067(5)	0.4761(7)	461	671	1534	−72	67	117
OW1	0.9812(5)	0.9009(4)	−0.3561(6)	1653	760	1939	−74	71	418
OW2	0.5399(4)	0.3408(6)	0.9249(6)	826	1797	2010	362	221	846
Mean standard deviations of light atom thermal parameters				60	67	120	50	67	73

Can. J. Chem. Downloaded from www.nrcresearchpress.com by 210.87.254.40 on 09/05/12
For personal use only.

TABLE 3. Fractional atomic coordinates for hydrogen atoms

	Molecule 1			Molecule 2		
Atom	x	y	z	x	y	z
H(N1)	1.189	0.875	−0.009	0.456	0.255	0.483
H(N1)	1.163	0.885	−0.150	0.429	0.292	0.644
H(Cα1)	1.340	1.068	0.146	0.289	0.055	0.435
H(Cα1)	1.358	1.043	−0.101	0.291	0.126	0.657
H(Cα2)	1.058	1.378	0.151	−0.007	0.359	0.413
H(Cα2)	1.049	1.308	−0.051	0.020	0.427	0.584
H(Cα3)	0.692	1.114	0.060	0.231	0.764	0.498
H(N4)	0.864	1.113	0.350	0.270	0.495	0.166
H(Cα4)	0.816	1.105	0.682	0.224	0.601	−0.124
H(Cα4)	0.667	1.064	0.605	0.395	0.601	−0.092
H(Cα4)	0.728	1.228	0.680	0.296	0.469	−0.163
H(Cβ)	0.709	0.900	−0.172	0.451	0.843	0.549
H(Cβ)	0.601	0.895	−0.043	0.388	0.795	0.708
H(C3h)	1.032	0.710	0.091	0.651	0.372	0.366
H(N4h)	0.836	0.547	0.056	0.788	0.574	0.427
H(C5h)	0.627	0.629	−0.012	0.686	0.796	0.494
		OW1			OW2	
H	1.047	0.915	−0.397	0.598	0.303	0.897
H	1.012	0.811	−0.387	0.467	0.310	1.018
Standard deviations	0.005	0.006	0.007	0.005	0.006	0.007

Fourier was summed with phases based on the Cu's plus these atoms. Although no improvement of the resolution in the molecule input to the calculations occurred, it was possible to choose a five-membered ring plus three nearby atomic positions around the other Cu, and a new Fourier phased on the Cu's plus 19 light atoms (one of the original 12 refined to an obviously wrong position and so was omitted) showed sufficient new detail to allow one (with imagination) to elucidate most of the structure. Fifteen additional atomic positions were assigned, and a subsequent difference Fourier revealed the remainder of the peptide atoms plus two water molecule oxygens.

Structure Refinement

One cycle of isotropic full-matrix least-squares refinement resulted in a discrepancy index $R = 0.095$, and a further cycle with the copper and oxygen thermal parameters refined anisotropically lowered R to 0.057. A cycle of full anisotropic refinement ($R = 0.052$) was followed by a difference Fourier which allowed assignment of positions for most of the hydrogen atoms. A number of cycles of least-squares, refining (not always concurrently) heavy atom positions and anisotropic thermal parameters and hydrogen positions (hydrogen atoms were assigned thermal parameters of the atoms to which they are bonded), followed by difference Fourier syntheses, gave positions for all hydrogen atoms and led to a discrepancy $R = 0.038$. A final least-squares cycle, refining heavy atom positions and using unit weights rather than statistical weights reduced R to 0.036 and improved the 'goodness-of-fit' parameter, $\{\sum w(F_o - F_c)^2/(m - n)\}^{1/2}$, from 2.3 to 1.4. Apart from diffraction ripples around the Cu's no density above 0.35 electrons was present on a difference Fourier map. Table 2 lists the final positional and thermal parameters for the nonhydrogen atoms, and the hydrogen coordinates are given in Table 3. The observed and calculated structure factors are available.[2] Scattering factors used in the refinement were those of Cromer and Mann (7), with the neutral Cu curve being utilized.

Results and Discussion

Figure 1 is a stereoscopic representation of the structures of the two Cu–GGHa units in the cell shown in similar orientations. The nature of the Cu(II) binding of the Cu–GGHa complex as elucidated in solution (5), is confirmed here; in both molecules, the copper atoms are tetradentate chelated by the terminal amino nitrogen, the next two peptide nitrogens, and a nitrogen of the histidine ring, forming a mildly distorted square plane arrangement. The results of this X-ray analysis further corroborate the spectroscopic, potentiometric, and previous structural evidence that of the various possible metal coordinating atoms in oligopeptides, at $pH > 5$, the imidazole, amino, and peptide nitrogens are the strongest donor atoms for coordinating to Cu(II). Inspection of Fig. 1

[2]Tables of final observed and calculated structure factors are available, at a nominal charge, from the depository of unpublished data, CISTI, National Research Council of Canada, Ottawa, Canada K1A 0S2.

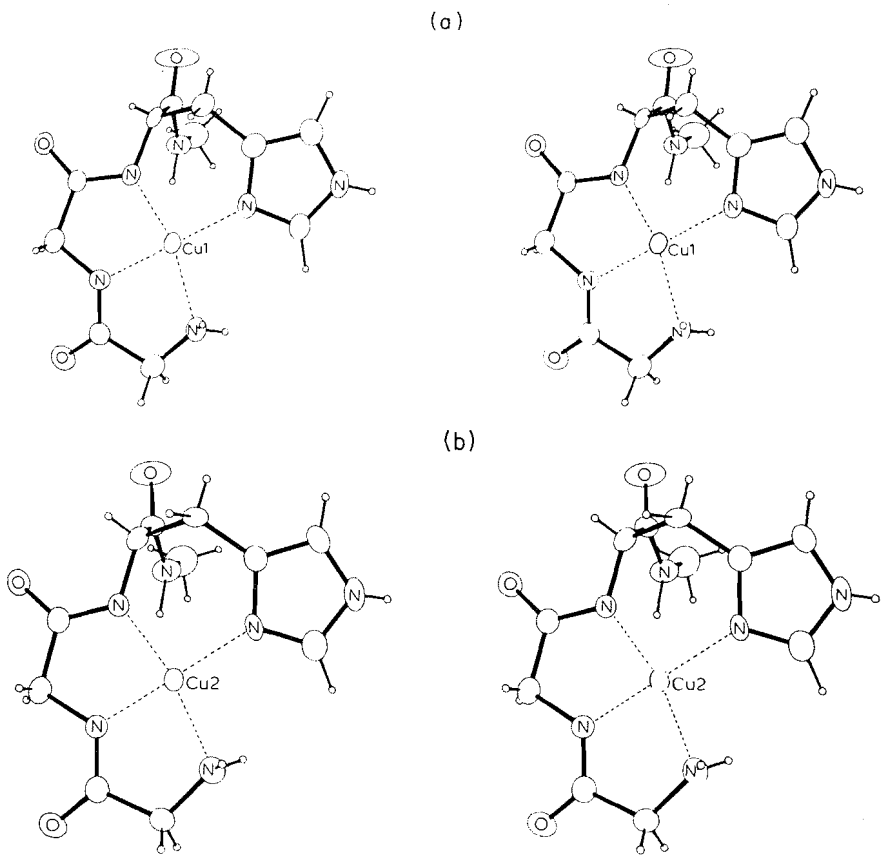

FIG. 1. Stereoscopic drawings of the two crystallographically-independent Cu–GGHa molecules in the unit cell, viewed in similar orientations. (*a*) molecule 1; (*b*) molecule 2.

TABLE 4. Torsion angles (deg). Standard deviations are approximately 0.4–0.6°

		Value				Value	
Bond	Angle	Molecule Cu1	Molecule Cu2	Bond	Angle	Molecule Cu1	Molecule Cu2
N—Cα	ϕ_2	−155.1	−167.9	C—N	ω_1	180.0	−178.4
	ϕ_3	−88.2	−84.1		ω_2	−177.1	−178.0
Cα—C	ψ_1	−4.1	−5.4		ω_3	180.0	−177.6
	ψ_2	−1.1	−3.8	Cα—Cβ	χ_3^1	59.6	57.9
	ψ_3	−19.5	−21.8	Cβ—Clh	$\chi_3^{2,1}$	−46.9	−47.0

shows that the overall conformations of the two crystallographically-independent Cu–GGHa molecules are virtually identical. The torsion angles in the two tripeptides (Table 4) differ by more than 4° in only one angle, and the average difference in all the other corresponding torsion angles is 1.9°.

Bond distances and angles in Cu–GGHa are given in Fig. 2; the values shown are averages of the equivalent parameters in the two independent units (no corresponding parameters differ from the mean by more than 3σ in the two peptide chains). The copper–nitrogen distances range from 1.90 to 2.05 Å, the longest distance being between the Cu(II) and amino nitrogen, and the shortest involving the first peptide nitrogen, which is the only nitrogen occurring in two five-membered chelate rings. The C—N—Cu

Can. J. Chem. Downloaded from www.nrcresearchpress.com by 210.87.254.40 on 09/05/12
For personal use only.

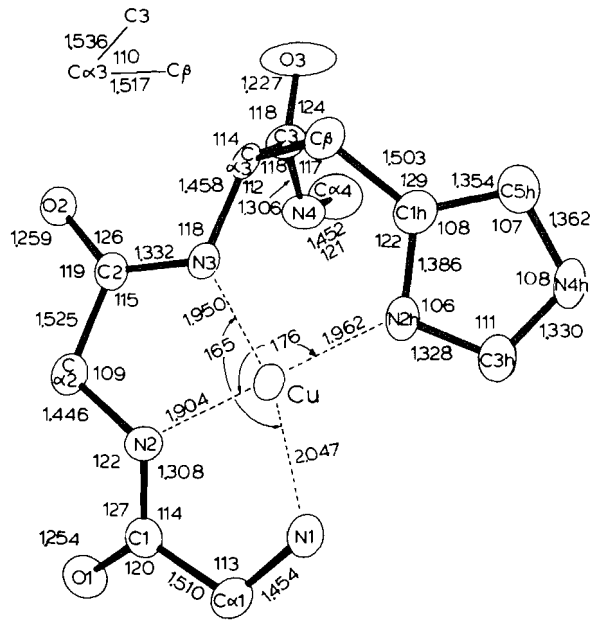

FIG. 2. Bond lengths (Å) and angles (deg) averaged over the two independent Cu–GGHa units. Standard deviations are 0.004 Å and 0.2° for Cu–N bonds and angles, and 0.006 Å and 0.4° for light atom parameters.

angles also vary systematically, with ∠Cα1—N1—Cu = 110°, ∠C1—N2—Cu = 119°, ∠Cα2—N2—Cu = 117°, ∠C2—N3—Cu = 116°, ∠Cα3—N3—Cu = 126°. These distances and angles involving copper and nitrogen atoms are closely consistent with the previously noted (8) crystal-independent trends for interactions between copper and terminal amino nitrogens, peptide nitrogens involved in two five-membered chelate rings, and peptide nitrogens taking part in one five-membered chelate ring, respectively, in other copper–oligopeptide complexes. The copper–imidazole nitrogen distance of 1.962 Å is shorter than that reported in a Cu(gly-L-his) complex (9) and in other earlier structures (10), but is similar to the corresponding length of 1.95 Å in Cu(L-his)(L-thr) (11) and in two complexes of copper with mixed glycine and imidazole ligands (12). The averaged central N...Cu...N angles at the Cu are 82, 84, 95, 99°, going clockwise from N1 (Fig. 1). The bond lengths and angles in the peptide backbone are typical of such molecules and need little comment. The values in the imidazole ring are very similar to those found in the imidazole portions of a bis(histidinato)nickel complex (13). The similar values of the two N—C3h distances in the ring indicate electron delocalization over these bonds. The averaged value of the peptide bonds in Cu–GGHa is 1.315 Å, compared to 1.325 Å found in a high precision structure determination of tri-L-alanine (14) and 1.326 and 1.330 Å determined in neutron diffraction studies of α-glycylglycine (15) and glycylglycine.$HCl.H_2O$ (16). The individual bond lengths and angles involving hydrogens are inaccurate and are not given here; the averages of the N—H and C—H distances are 0.8 and 1.0 Å, respectively.

Figure 3 is a stereoscopic illustration of the contents of one unit cell, and shows the mutual arrangement of the two independent Cu–GGHa molecules. In all the complexes of Cu(II) with amino acids and/or peptides thus far structurally elucidated the coordination about the Cu(II) has been square planar, square pyramidal, or octahedral (10); in Cu–GGHa, the arrangement is square planar, with an oxygen atom weakly interacting with each Cu(II) to form a square pyramid. In the case of Cu1 the oxygen atom is that of a water molecule (Cu...OW1 = 2.61 Å) and for Cu2 the square pyramidal interaction is with a carbonyl oxygen (O1) of another molecule (Cu...O1 = 2.88 Å). This

Can. J. Chem. Downloaded from www.nrcresearchpress.com by 210.87.254.40 on 09/05/12
For personal use only.

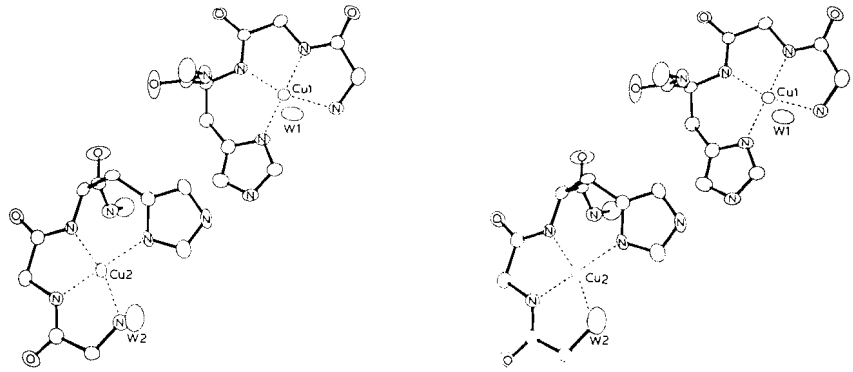

FIG. 3. Stereoscopic drawing illustrating the contents of one asymmetric unit (one unit cell) of Cu-GGHa.

weak fifth coordination of Cu may explain the greater Cu-binding of albumin: an oxygen atom of the protein probably occupies this coordination position when albumin binds Cu(II). The oxygen atom might even conceivably be from the carboxyl side chain of the N-terminal aspartate of albumin; such a possibility could be tested by binding and structural studies of an analogous tripeptide with an N-terminal aspartic acid.

Table 5 gives the atomic displacements from various planes in the Cu–GGHa units. In both cases the deviation of the copper from the square plane is in the direction of the weakly-interacting pyramidal oxygen. The histidyl planes are not coplanar with the square planes, the angles between normals being 20 and 18° for the Cu1–his and Cu2–his planes respectively.

There is intermolecular hydrogen bonding in the Cu–GGHa crystal structure, involving the free (N4) imino hydrogens, the water molecules, and carbonyl oxygens. Each H(N4) forms a hydrogen bond to an O1 carbonyl oxygen, with H...O distances of 2.05 and 1.88 Å and N—H...O angles of 127 and 142° in molecules 1 and 2 respectively (C=O...H angles of 129 and 131°). Water molecule 1 has a hydrogen bond to a carbonyl O2 (H...O2 distance is 1.98 Å, OW1—H...O2 angle is 150°, C2—O2...H angle is 119°), and water molecule 2 interacts

TABLE 5. Atomic displacements (Å) from least-squares planes

	Peptide i = 1		Peptide i = 2		Peptide i = 3	
Atom	Molecule 1	Molecule 2	Molecule 1	Molecule 2	Molecule 1	Molecule 2
C_α^i	−0.004	−0.012	0.018	−0.010	0.001	−0.013
C^i	0.009	0.010	−0.002	0.005	−0.011	0.002
O^i	−0.003	−0.000	−0.008	0.002	0.005	0.005
N^{i+1}	−0.000	0.015	−0.034	0.015	0.008	0.024
C_α^{i+1}	−0.002	−0.013	0.025	−0.012	−0.003	−0.018

	Square plane			Histidyl plane	
Atom	Molecule 1	Molecule 2	Atom	Molecule 1	Molecule 2
N1	0.015	−0.023	C1h	−0.007	0.000
N2	−0.018	0.028	N2h	0.006	−0.007
N3	0.016	−0.025	C3h	−0.003	0.011
N2h	−0.013	0.020	N4h	−0.002	−0.011
Cu*	0.083	0.061	C5h	0.005	0.006
OW*	2.640	−2.726	Cβ*	0.016	−0.078
			Cu*	0.067	0.095

*These atoms were not included in the calculation of the plane.

Can. J. Chem. Downloaded from www.nrcresearchpress.com by 210.87.254.40 on 09/05/12
For personal use only.

with a carbonyl O1 (H...O1 = 1.72 Å, OW2—H...O1 angle = 152°, C1—O1...H angle = 115°). There is also a weak intermolecular contact between H(N4h) on the imidazole ring of molecule 1 and a carbonyl O2 atom, the H...O distance being 2.12 Å. All other intermolecular distances correspond to normal van der Waals separations.

The structural results presented here have confirmed that the Cu(II) coordinating atoms in GGHa are those predicted from potentiometric solution studies (4) of the Cu(II)–peptide system, and have provided the detailed stereochemistry of the complex. These results therefore also support the feasibility of making use of knowledge of macromolecular metal binding to synthesize a simpler peptide with similar binding properties.

Acknowledgments

Support was from the Medical Research Council of Canada, and from the U.S. National Institutes of Health through grants NS-09839 and CA-15879. A.C. is the recipient of Research Career Development Award NS 70801 from the National Institute of Health (NINCDS).

1. B. SARKAR. Proc. Can. Fed. Biol. Soc. **15**, 659 (1972); Proc. 9th. Int. Congr. Biochem., Stockholm, Aktiebolaget Egnellska Boktryckeriet, Stockholm. 1973. p. 122.
2. S. LAU, T. P. A. KRUCK, and B. SARKAR. J. Biol. Chem. **249**, 5878 (1974).
3. S. LAU and B. SARKAR. Can. J. Chem. **53**, 710 (1975).
4. T. P. A. KRUCK, S. LAU, and B. SARKAR. Can. J. Chem. This issue.
5. B. SARKAR. Proc. 3rd Int. Symp. on Wilson's disease. Paris. 1973. p. 5.
6. K. S. N. IYER and B. SARKAR. Peptides: chemistry, structure and biology. *Edited by* R. Walter and J. Meienhofer. Ann Arbor Science Publishers, Ann Arbor, Michigan. 1975. p. 215. V. RENUGOPALAKRISHNAN and B. SARKAR. Peptides: chemistry, structure and biology. *Edited by* R. Walter and J. Meienhofer. Ann Arbor Science Publishers, Ann Arbor, Michigan. 1975. p. 209.
7. D. T. CROMER and J. B. MANN. Acta Crystallogr. Sect. A, **24**, 321 (1968).
8. J. F. BLOUNT, H. C. FREEMAN, R. V. HOLLAND, and G. H. W. MILBURN. J. Biol. Chem. **245**, 5177 (1970).
9. J. F. BLOUNT, K. A. FRASER, H. C. FREEMAN, J. T. SZYMANSKI, and C.-H. WANG. Acta Crystallogr. **22**, 396 (1967).
10. H. C. FREEMAN. Adv. Protein Chem. **22**, 257 (1967).
11. H. C. FREEMAN, J. M. GUSS, M. J. HEALY, R.-P. MARTIN, C. E. NOCKOLDS, and B. SARKAR. Chem. Commun. 225 (1969).
12. J. D. BELL, H. C. FREEMAN, A. M. WOOD, R. DRIVER, and W. R. WALKER. Chem. Commun. 1441 (1969).
13. K. A. FRASER and M. M. HARDING. J. Chem. Soc. A, 415 (1967).
14. J. K. FAWCETT, N. CAMERMAN, and A. CAMERMAN. Acta Crystallogr. Sect. B, **31**, 658 (1975).
15. H. C. FREEMAN, I. C. PAUL, and T. M. SABINE. Acta Crystallogr. Sect. B, **26**, 925 (1970).
16. T. F. KOETZLE, W. C. HAMILTON, and R. PARTHASARATHY. Acta Crystallogr. Sect. B, **28**, 2083 (1972).

Can. J. Chem. Downloaded from www.nrcresearchpress.com by 210.87.254.40 on 09/05/12
For personal use only.

Structure of 2′,3′-dimethyl-3,5-diiodo-D,L-thyronine, a fixed-conformation analogue of the thyroid hormone 3,5,3′-triiodo-L-thyronine

J. KEITH FAWCETT AND NORMAN CAMERMAN
Department of Biochemistry, University of Toronto, Toronto, Ontario M5S 1A8
AND
ARTHUR CAMERMAN
Departments of Medicine (Neurology) and Pharmacology, University of Washington, Seattle, Washington 98195

Received January 20, 1976

J. KEITH FAWCETT, NORMAN CAMERMAN, and ARTHUR CAMERMAN. Can. J. Chem. **54**, 1317 (1976).

The three-dimensional molecular structure of 2′,3′-dimethyl-3,5-diiodo-D,L-thyronine (2′,3′-DMT_2) has been determined by X-ray diffraction in order to establish the conformational characteristics responsible for biological activity in thyroid hormone analogues. Crystals of 2′,3′-DMT_2 hydrochoride hydrate are monoclinic with cell dimensions $a = 29.76$, $b = 6.84$, $c = 24.09$ Å, $\beta = 91.4°$, space group $C2/c$ with $Z = 8$ molecules per cell. The structure was solved by Patterson and Fourier techniques and refined by least squares. The atoms comprising the alanine portion of the molecule are disordered but the conformation of the diphenyl ether rings is clear: the β-ring 2′-methyl and 3′-methyl groups are situated distal to the α-ring. Thus the conformation postulated for this compound in biological tests of fixed-conformation thyromimetics is now structurally supported.

J. KEITH FAWCETT, NORMAN CAMERMAN et ARTHUR CAMERMAN. Can. J. Chem. **54**, 1317 (1976).

On a déterminé, par diffraction de rayon-X, la structure moléculaire tridimentionnelle de la diméthyl-2′,3′ diiodo-3,5 D,L-thyronine (2′,3′-DMT_2) afin d'établir les caractéristiques conformationnelles responsables de l'activité biologique d'hormones analogues à la thyroide. Les cristaux du chlorhydrate hydraté de la 2′,3′-DMT_2 sont monocliniques avec des dimensions de mailles $a = 29.76$, $b = 6.84$, $c = 24.09$ Å, $\beta = 91.4°$, groupe d'espace $C2/c$ et $Z = 8$ molécules par maille. On a résolu la structure par les techniques de Patterson et Fourier et on l'a affinée par moindres carrés. Les atomes formant la partie alanine de la molécule sont désordonnées mais la conformation des cycles diphényles éther est claire: les groupes cycle β méthyl-2′ et méthyl-3′ sont situés distal par rapport au cycle α. On peut donc en conclure que la conformation postulée pour ce composé lors de tests biologiques de thyromimétiques à conformation fixée reçoit maintenant une confirmation structurale.

[Traduit par le journal]

Structural elucidations of the thyroid hormone 3,5,3′-triiodo-L-thyronine (1, 2) (T_3) and other thyroactive analogues which also possess asymmetric β-ring structures (3–5) have revealed these compounds to adopt either one of two molecular conformations: a roughly mutually-perpendicular arrangement of the two aromatic rings, with the β-ring 3′-substituent oriented either proximal or distal to the diiodotyrosyl (α) ring. In order to ascertain the conformation which interacts with biological receptors Jorgensen *et al.* (6, 7) synthesized 2′,3′-dimethyl-3,5-diiodothyronine (2′,3′-DMT_2) and 2′,5′-dimethyl-3,5-diiodothyronine (2′,5′-DMT_2), analogues of T_3 in which the methyl group on the 2′-carbon was postulated from steric considerations to be distal to the α-ring and to prevent β-ring rotation, thus fixing the conformation of 2′,3′-DMT_2 and 2′,5′-DMT_2 to be 3′-methyl group distal and 5′-methyl group proximal to the α-ring respectively. Tests of hormonal potency (6, 7) and protein-binding capacity (8) of these two analogues resulted in the conclusion that biological activity resides primarily in the distal conformation. For the applicability of these conclusions to the naturally occurring hormones it is highly desirable that the three-dimensional structures of the fixed-conformation models be conclusively established. Therefore we have crystallized 2′,3′-DMT_2 (**1**) and determined its structure by X-ray diffraction.

Two samples of 2′,3′-DMT_2 were used.[1]

[1]Two samples of 2′,3′-DMT_2 were kindly supplied by E. C. Jorgensen.

Can. J. Chem. Downloaded from www.nrcresearchpress.com by 210.87.254.42 on 09/05/12
For personal use only.

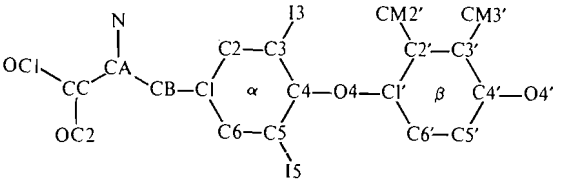

1

Sample 1, thought to be the D-isomer, was crystallized from ethanol – 1 *M* HCl (2/1 v/v), yielding monoclinic laths elongated along *b* with unit-cell parameters $a = 25.95$, $b = 6.75$, $c = 24.27$ Å, $\beta = 105.8°$, $U = 4091$ Å^3, $Z = 8$. Although the sample showed activity in an ord spectrum the systematic absences indicated space group *Cc* or *C*2/*c*, and the Patterson function was solvable only if a *c*-glide was assumed, suggesting that the sample was optically impure. From the Patterson and Fourier syntheses 19 atoms only were located (the α- and β-rings and their immediate substituents) and least squares refinement gave poor bond lengths and angles and $R = 0.22$. Positions for CB, O(4′), CM(2′), and CM(3′) were very poorly defined giving high temperature factors and unsatisfactory bond lengths and angles on refinement. Positions for the atoms of the alanine group could not be assigned.

Because of the contradictions and poor results we turned to sample 2, the DL-isomer, and slow evaporation of the same solvent as for sample 1 gave interesting, optically-uniform groupings of crystals (Fig. 1). Laths were chipped off and sealed in a capillary with mother liquor; cell parameters are $a = 29.76$, $b = 6.84$, $c = 24.09$ Å, $\beta = 91.4°$, U = 4902 Å^3; space group *Cc* or *C*2/*c*, $Z = 8$. Subsequent refinement favours

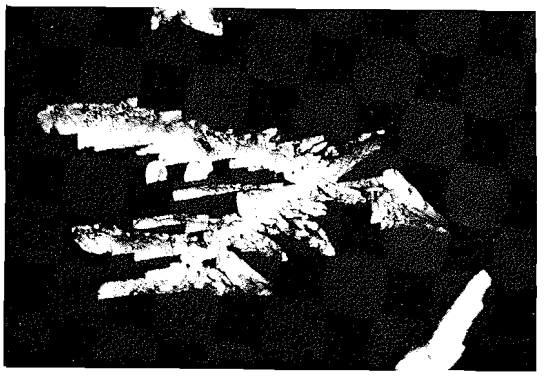

FIG. 1. Crystalline 2′,3′-DMT$_2$ hydrochloride hydrate (magnification approximately 80×).

*C*2/*c* with one molecule of HCl and at least one disordered water of hydration per 2′,3′-DMT$_2$ molecule ($C_{17}H_{17}NO_4I_2 \cdot HCl \cdot H_2O$, mol. wt. = 607.6, $D_x = 1.65$ g cm^{-3}). It is interesting to note that crystals from sample 2 when allowed to stand in air for some days exhibit the X-ray pattern of sample 1, the difference seemingly being due to loss of HCl (and possibly H_2O), since the chlorine position appears to be unoccupied in difference maps calculated for sample 1. In addition, crystals from sample 1, when sealed in capillaries with mother liquor, give diffraction patterns identical to sample 2.

For crystal 2, 2312 unique reflections having $2\theta_{MoK\alpha} \leq 40°$ were measured on an automated four circle diffractometer with zirconium-filtered MoKα (λ = 0.71069 Å) radiation using the 2θ–θ scan technique. The fall-off in net intensity during data collection was 25% (linear correction applied) and was accompanied by small but measurable changes in the *a*, *c*, and β cell parameters (0.02 Å and 0.2°), causing a decrease in cell volume of 0.2%. The 1036 reflections with $I > 2\sigma(I)$ were considered observed and were used for all subsequent calculations. No absorption corrections were applied (μ(MoKα) = 32.8 cm^{-1}).

The iodine positions were close to those for the crystal of sample 1 and Fourier syntheses revealed the α- and β-rings, their immediate substituents, and the Cl^-. The alanine side-chain is thermally and/or statistically disordered but many attempts to sort out the exact nature of the disorder were unsuccessful (including attempts to solve and refine the structure in space group *Cc*). Fourier maps of the alanine region showed only diffuse electron density from which it was impossible to estimate atomic positions. Assignments of positions for CA, N, CC, OC(1), and OC(2) were based on chemical reasonableness and peak heights (1.0–1.7 e/Å^3) from the difference Fourier. Several other peaks in the same region of the difference map had maxima of 0.6–1.0 e/Å^3 but they were diffuse and no chemical sense could be made of them. Attempts to refine positions and thermal parameters for the alanine side-chain resulted in very poor molecular parameters. The other atoms of the molecule and the Cl^- ion, however, refined well to give satisfactory molecular parameters. There was no evidence of disorder in the diaryl ether portion of the molecule and the temperature

Can. J. Chem. Downloaded from www.nrcresearchpress.com by 210.87.254.42 on 09/05/12
For personal use only.

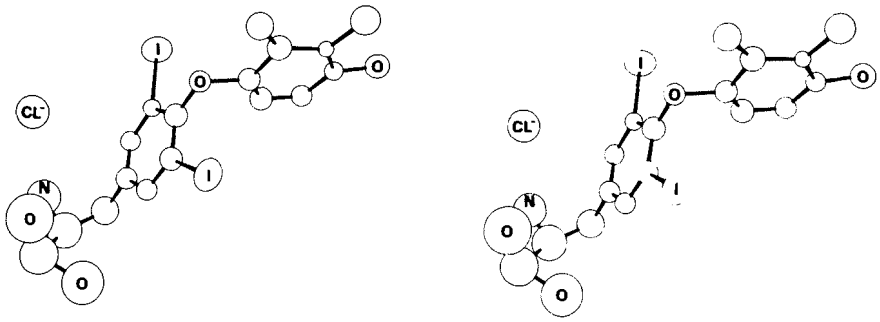

FIG. 2. Stereoscopic drawing of the molecular confirmation of 2′,3′-dimethyl-3,5-diiodo-D,L-thyronine hydrochloride hydrate.

factors and bond lengths and angles of this portion are reasonable. Thus, there is little doubt that the structure and conformation of the α-, β-ring system, which is the primary source of interest, is correct. Full matrix least squares refinement in space group $C2/c$ with the 2 I and Cl^- anisotropic, the 17 C and O atoms of the α- and β-rings and immediate substituents isotropic. and with the other 5 C, N, and O atoms of the alanine side-chain as well as two $\frac{1}{2}$-occupied water oxygens included in the structure factor calculation but not refined gave $R = 0.14$. Unit weights were used. Scattering factors for I, Cl^-, O, N, and C were those of Cromer and Mann (9). No anomalous dispersion corrections were applied. The 1036 observed and calculated structure factors are available.[2] The final positional and thermal parameters are given in Table 1. Although the results from sample 2 are not entirely satisfactory they are considerably better than those for sample 1. The positions of the iodine atoms from sample 1 had esd's 3× those for sample 2. The average aromatic C—C distance for sample 1 was 1.48 Å with a range of 1.19–1.71 Å whereas for sample 2 the average was 1.39 Å with a range of 1.33–1.45 Å. Over the course of a year, many attempts were made to grow better crystals from our limited amount of sample 2 but the crystal used was the best that could be obtained.

A stereoscopic drawing of 2′,3′-dimethyl-3,5-diiodo-D,L-thyronine·HCl is given in Fig. 2. The figure clearly shows that the 3′-methyl group is, as expected, distal to the α-ring. As is the case for thyroid hormone structures, the planes of the phenyl rings are skewed with respect to one another and approach mutual perpendicularity. The angles between the α- and β-rings and the plane of the inter-ring ether linkage (see ref. 3 for a definition of the sense of these angles) are 91 and 20°, respectively, similar to values for thyroid hormones. (See, for example, ref. 10.)

Bond lengths and angles in the α- and β-rings and their immediate substituents are normal, being within 2σ of the expected values ($\langle\sigma$(C—C)$\rangle$ = 0.05 Å, $\langle\sigma(\angle$C—C—C)$\rangle$ = 3.0°). The angle at the ether oxygen is 121°. Short intermolecular contacts between iodine atoms, which may stabilize other thyroid hormone and analogue structures (4), are not present for 2′,3′-DMT_2. In other thyroid hormone·HCl structures (1, 3, 4) the chloride ion accepts hydrogen bonds from the amino nitrogen and water molecules. In 2′,3′-DMT_2 it is the phenolic oxygen which acts as a donor (d(O–Cl^-) = 3.06 Å). There are no identifiable water molecules close to the Cl^- and the closest contact with the poorly-defined amino nitrogen is 3.4 Å.

Despite the severe disorder in the alanine portion of the molecule, the structure determination of 2′,3′-DMT_2 has established the conformational characteristics of the diphenyl–ether system: the 3′-methyl group is distal to the α-ring. Thus the conformational postulations for this part of the molecules used in the biological potency tests are now structurally supported.

[2]A table of observed and calculated structure factors is available, at a nominal charge, from the Depository of Unpublished Data, CISTI, National Research Council of Canada, Ottawa, Canada K1A 0S2.

Acknowledgments

We thank Dr. E. C. Jorgensen for samples of 2′,3′-DMT_2. Support was from the Medical

Can. J. Chem. Downloaded from www.nrcresearchpress.com by 210.87.254.42 on 09/05/12
For personal use only.

Can. J. Chem. Downloaded from www.nrcresearchpress.com by 210.87.254.42 on 09/05/12
For personal use only.

TABLE 1. Atomic coordinates and thermal parameters. Standard deviations are given in parentheses. Those parameters without standard deviations were not refined (positions from difference Fourier synthesis). Anisotropic $T = \exp(-(\beta_{11}h^2 + \beta_{22}k^2 + \beta_{33}l^2 + 2\beta_{12}hk + 2\beta_{13}hl + 2\beta_{23}kl))$

Atom	x	y	z	β_{11}	β_{22}	β_{33}	β_{12}	β_{13}	β_{23}
I(3)	0.4292(1)	0.2995(6)	0.2671(1)	0.0020(1)	0.058(1)	0.0019(1)	−0.0010(2)	0.0002(1)	0.0001(2)
I(5)	0.4453(2)	0.2050(6)	0.5143(1)	0.0037(1)	0.047(1)	0.0019(1)	0.0013(3)	0.0001(1)	−0.0001(2)
Cl(1)	0.3091(6)	0.5687(46)	0.5657(12)	0.0021(3)	0.116(14)	0.0102(11)	0.0021(17)	−0.0008(4)	−0.0118(32)

Atom	x	y	z	B (Å^2)	Atom	x	y	z	B (Å^2)
C(1)	0.3853(13)	0.644(6)	0.4076(16)	4.7(9)	O(4)	0.4557(7)	0.128(3)	0.3839(9)	3.1(5)
C(2)	0.3927(12)	0.569(6)	0.3538(15)	3.8(8)	C(1′)	0.5051(15)	0.139(7)	0.3771(18)	6.0(1.0)
C(3)	0.4168(12)	0.406(6)	0.3482(15)	3.4(8)	C(2′)	0.5242(12)	−0.034(6)	0.3531(15)	3.9(8)
C(4)	0.4321(12)	0.289(6)	0.3927(15)	3.7(8)	C(3′)	0.5691(10)	−0.030(4)	0.3468(12)	2.4(6)
C(5)	0.4237(11)	0.366(5)	0.4454(13)	2.9(7)	C(4′)	0.5921(10)	0.135(5)	0.3726(13)	2.6(6)
C(6)	0.4023(10)	0.542(5)	0.4512(12)	2.8(6)	C(5′)	0.5750(14)	0.303(6)	0.3941(17)	4.8(9)
CB	0.3630(21)	0.839(10)	0.4139(25)	8.5(1.6)	C(6′)	0.5292(16)	0.292(8)	0.3974(20)	7.7(1.2)
CA	0.311	0.855	0.402	15.0	O(4′)	0.6393(10)	0.129(5)	0.3645(13)	7.3(8)
CC	0.290	0.780	0.340	15.0	CM(2′)	0.4917(14)	−0.188(7)	0.3341(18)	5.9(1.0)
N	0.295	0.680	0.427	15.0	CM(3′)	0.5898(16)	−0.204(7)	0.3217(19)	6.2(1.1)
OC(1)	0.325	0.870	0.304	20.0	O(W1)	0.193	0.425	0.464	15.0
OC(2)	0.274	0.585	0.344	20.0	O(W2)	0.309	0.080	0.215	15.0

Research Council of Canada and from the National Institutes of Health grant AM 16417. A.C. is the recipient of Research Career Development Award NS70801 from the National Institute of Neurological and Communicative Disorders and Stroke.

1. A. CAMERMAN and N. CAMERMAN. Acta Crystallogr. Sect. B, **30**, 182 (1974).
2. V. CODY. J. Am. Chem. Soc. **96**, 6720 (1974).
3. N. CAMERMAN and A. CAMERMAN. Can. J. Chem. **52**, 3048 (1974).
4. J. K. FAWCETT, N. CAMERMAN, and A. CAMERMAN. J. Am. Chem. Soc. **98**, 587 (1976).
5. V. CODY and W. L. DUAX. Biochem. Biophys. Res. Commun. **52**, 430 (1973).
6. E. C. JORGENSEN, N. ZENKER, and C. GREENBERG. J. Biol. Chem. **235**, 1732 (1960).
7. E. C. JORGENSEN, P. A. LEHMANN, C. GREENBERG, and N. ZENKER. J. Biol. Chem., **237**, 3832 (1962).
8. G. C. SCHUSSLER. Science, **178**, 172 (1972).
9. D. T. CROMER and J. B. MANN. Acta Crystallogr. Sect. A, **24**, 321 (1968).
10. A. CAMERMAN and N. CAMERMAN. Can. J. Chem. **52**, 3042 (1974).

Can. J. Chem. Downloaded from www.nrcresearchpress.com by 210.87.254.42 on 09/05/12
For personal use only.

Nuclear magnetic resonance and molecular orbital studies of the conformational preferences of the fluoromethyl group in some benzylfluoride derivatives

TED SCHAEFER, J. BRIAN ROWBOTHAM,[1] WILLIAM J. E. PARR,[2] KIRK MARAT, AND ALEXANDER F. JANZEN

Department of Chemistry, University of Manitoba, Winnipeg, Manitoba R3T 2N2

Received August 29, 1975

TED SCHAEFER, J. BRIAN ROWBOTHAM, WILLIAM J. E. PARR, KIRK MARAT, and ALEXANDER F. JANZEN. Can. J. Chem. **54**, 1322 (1976).

The proton magnetic resonance spectra of some benzylfluoride derivatives yield long-range spin–spin coupling constants between ring protons and protons or fluorine nuclei in the fluoromethyl group. In conjunction with the eigenfunctions for a hindered twofold rotor, the couplings over six bonds are used to show that in 3,5-dichlorobenzylfluoride in solution the C—F bond prefers the benzene plane by 260 ± 50 cal/mol; in close agreement with *ab initio* and MINDO/3 molecular orbital calculations. The latter method suggests that in a conformation in which the C—F bond lies in a plane perpendicular to the benzene ring, the C – C – F angle reduces to 107.2° and the C – C – H angles become 116.1°, perhaps due to increased conjugation of the C—F bond or fluorine atom with the π electrons of the ring. The observed barrier is presumably a delicate balance between steric interactions, hyperconjugation or p–p conjugation effects, and dipole–dipole interactions between polarized bonds.

TED SCHAEFER, J. BRIAN ROWBOTHAM, WILLIAM J. E. PARR, KIRK MARAT et ALEXANDER F. JANZEN. Can. J. Chem. **54**, 1322 (1976).

Les spectres rmn du proton de quelques dérivés du fluorure de benzyle permettent d'obtenir les constantes de couplage spin–spin à longue distance entre les protons du cycle et les protons ou le noyau de fluor du groupe fluorométhyle. On a utilisé les constantes de couplage à travers six liens, de concert avec les fonctions eigen d'un rotor binaire empêché, pour démontrer que dans le fluorure de dichloro-3,5 benzyle en solution, le lien C—F préfère le plan du benzène par 260 ± 50 cal/mol. Cette conclusion est en accord avec des calculs d'orbitales moléculaires *ab initio* et MINDO/3. Cette dernière méthode suggère que la conformation dans laquelle le lien C—F se trouve dans le plan perpendiculaire à celui du noyau benzénique, l'angle C–C–F est réduit à 107.2° et l'angle C–C–H devient 116.1° probablement dû au fait qu'il y a une augmentation de la conjugaison du lien C—F ou de l'atome de fluor avec les électrons π du cycle. La barrière que l'on observe est probablement due à une balance délicate entre des interactions stériques, des effets d'hyperconjugaison ou de conjugaison p–p et des interactions dipole–dipole entre les liens polarisés.

[Traduit par le journal]

Introduction

The sixfold barrier to internal rotation in toluene is 14 cal/mol (1,2). Mono- or disubstitution at the methyl carbon atom gives rise to a predominantly twofold barrier. For example, for benzalfluoride *ab initio* molecular orbital (MO) calculations (3) predict a barrier to internal rotation of 180 cal/mol, the conformation with the C—H bond of the difluoromethyl group lying in the benzene plane being more stable. The long-range spin–spin coupling constants between ring protons and protons or fluorine nuclei on the side chain of benzalfluoride and some of its derivatives are stereospecific and their measured magnitudes (4) are consistent with the quantum mechanical calculations.

In this paper some high resolution magnetic resonance parameters are reported for the benzylfluoride derivatives, **1** to **5**. The proton magnetic resonance spectrum of benzylfluoride itself cannot be reliably analyzed at 100 MHz, covering only about 2 Hz under a variety of solvent conditions. This fact is consistent with the calculated (3) π electron densities at the ring carbon atoms, varying as they do by a lesser extent than in toluene. Similarly, an acceptable analysis of the fluorine and proton magnetic resonance spectra of 2,5-dichlorobenzylfluoride could not be obtained.

In this paper it will be assumed that intrinsic substituent effects of the chlorine atoms on the

[1]Research associate, 1974–1975.
[2]Postdoctoral fellow, 1974–1975.

Can. J. Chem. Downloaded from www.nrcresearchpress.com by 210.87.254.5 on 09/05/12
For personal use only.

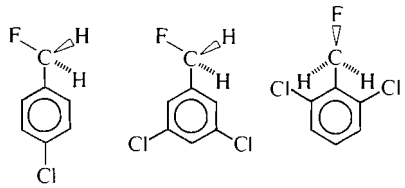

1 2 3

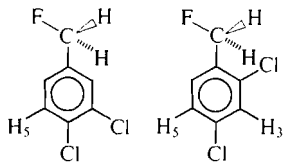

4 5

long-range couplings involving the side chain are small, *i.e.*, they will be neglected when substitution occurs *meta* or *para* to the fluoromethyl group. When substitution occurs at the *ortho* position their bulk will be assumed to determine the preferred conformation of the fluoromethyl group, without necessarily altering the stereospecifically determined magnitude of the long-range couplings (see section 2*b* of the discussion below). In various polynitro derivatives of toluene the long-range couplings are equal to those in toluene (5).

With these assumptions it is possible to deduce both the low energy conformation and the rotational barrier for **2** and, by implication, for **1**, **4**, and benzylfluoride itself, from the long-range couplings. MO calculations of conformational energies and of spin–spin couplings are used as aids in these deductions.

Experimental

The benzylfluoride derivatives, **1** to **5**, were produced from the corresponding benzyl alcohols by reaction with sulfur tetrafluoride. Polymerization of the products under the action of hydrogen fluoride was inhibited by the presence of triethylamine or pyridine in the reaction mixture (6). Typically, 1 g of the alcohol was added to 5 g of CCl_4 and 3 g of cyc-C_6H_{12}. $(CH_3)_3N$ (1 equiv.) was added to the solution in a 25 ml glass vial. SF_4 (1.5 equiv.) was condensed into the solution from a metal vacuum system and the vial was flame-sealed at −196 °C. After 10 min at room temperature the gaseous products were vented and liquid materials were fractionated under reduced pressure. No attempt was made to optimize yields. Product identity was checked by fluorine and proton magnetic resonance spectroscopy and by mass spectrometry. Compounds **2**, **4**, and **5** had boiling points of 82 °C/1 torr, 84 °C/2 torr, and 90 °C/1 torr, respectively.

TABLE 1. Proton chemical shifts*† and spin–spin coupling constants† in 2,4-dichlorobenzylfluoride

Parameter	Methylene protons decoupled	Six-spin analysis
ν_3	705.354(4)	705.792(3)
ν_5	696.463(6)	696.874(4)
ν_6	689.155(6)	689.550(4)
ν_{CH_2}	—	508.108(3)
$^3J_o^{H,H}$	8.282(6)	8.295(4)
$^4J_m^{H,H}$	2.086(7)	2.093(5)
$^5J_p^{H,H}$	0.336(7)	0.324(5)
$^4J^{H,CH_2}$	—	−0.737(4)
$^5J_m^{H_3,CH_2}$	—	0.325(3)
$^5J_m^{H_5,CH_2}$	—	0.425(4)
$^4J_o^{H,CF}$	−0.671(10)	−0.696(7)
$^5J_m^{H_3,CF}$	1.356(8)	1.351(5)
$^5J_m^{H_5,CF}$	0.707(10)	0.709(7)
$^2J^{H,F}$	—	47.174(5)
Error (rms)	0.009	0.014
Largest error	0.016	0.051
Lines assigned	24	127
Transitions calculated	29	167

*In Hz at 100 MHz to low field of internal tetramethylsilane of a 10 mol% solution in benzene-d_6.

†In Hz, the numbers in parentheses corresponding to the standard deviation in the last figure, as given by the least squares program LAME (14).

Degassed 10 to 20 mol% solutions of the benzylfluorides in benzene-d_6, containing internal tetramethylsilane, had their proton magnetic resonance calibrated in the frequency sweep mode of an HA100 spectrometer at sweep rates of 0.02 and 0.01 Hz/s. The chemical shift range was greater in benzene-d_6 than in other common solvents, ensuring more reliable analyses.

INDO–MO–FPT (7, 8), *ab initio* STO-3G (3,9), and MINDO/3 (10, 11) MO computations were performed on a 370/158 computing system.[3] Standard geometries (12) were used in all calculations unless indicated otherwise.

Results and Discussion

(1) Spectral Analysis

The spectra, corresponding to six- and seven-spin systems, were analyzed with the computer program LAME (13, 14). The results of an analytical procedure for one compound, 2,4-dichlorobenzylfluoride, are given in Table 1. The standard deviations in the spectral parameters suggest that the likely error in the coupling constants is 0.02 Hz, which also represents the rms error in the experimental determination of resonance peak frequencies.

[3]The MINDO/3 program was adapted for use with the IBM computer from a version written for a CDC system.

Can. J. Chem. Downloaded from www.nrcresearchpress.com by 210.87.254.5 on 09/05/12
For personal use only.

TABLE 2. Long-range coupling constants* between ring protons and side chain protons and fluorine nuclei in benzylfluoride derivatives†

Parameter	1	2	3	4	5
$^4J_o^{H,CH_\alpha}$	−0.60	−0.67	—	−0.63[2,6]‡	−0.74
$^5J_m^{H,CH_\alpha}$	0.31_5	—	0.34	0.32	0.32_5[3] 0.42_5[5]
$^6J_p^{H,CH_\alpha}$	—	−0.53	−0.16	—	—
$^4J_o^{H,CF}$	−1.67	−1.34	—	−1.58[2] −1.49[6]	−0.70
$^5J_m^{H,CF}$	1.11	—	1.25	1.12	1.35[3] 0.71[5]
$^6J_p^{H,CF}$	—	1.11	−2.43	—	—

*In Hz to an accuracy of 0.02 Hz, numbering of compounds given in text.
†Between 10 and 20 mol% in benzene-d_6 solution.
‡The numbers in parentheses refer to the ring positions.

The full spectral results are not given for all compounds. Rather, those of immediate interest in this paper, the long-range coupling constants between side chain nuclei and ring protons, are reproduced in Table 2. The proton spectral data for **3** have been previously published (15).

(2) Long-range Couplings and Conformational Information

The long-range couplings over six bonds, $^6J_p^{H,CH}$ and $^6J_p^{H,CF}$, depend on a $\sigma-\pi$ electron mechanism (16–19) and apparently are proportional to $\sin^2\theta$, where θ is the angle defined in **6** to **8**. Thus, in toluene and *p*-xylene, $^6J_p^{H,CH_3} = -^7J_p^{CH_3,CH_3}$ should hold for such a coupling mechanism and is found to hold within experimental error (18). Furthermore, INDO calculations display a $\sin^2\theta$ relationship for $^6J_p^{H,CH_3}$ in toluene (19) and for rapid rotation of the methyl group, when $\langle\sin^2\theta\rangle = 0.5$, we find $^6J_p^{H,CH_3} = -0.62$ Hz; in exact, if fortuitous, agreement with experiment (20).

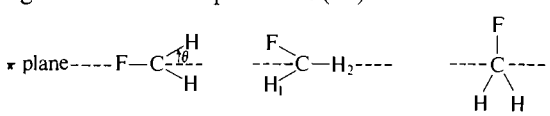

$\theta = 60°$ for H, $\theta = 0°$ for F — **6**

$\theta = 60°$ for H_1, $\theta = 0°$ for H_2 — **7**

$\theta = 30°$ for H, $\theta = 90°$ for F — **8**

If the values of $^6J_p^{H,CH}$ and $^6J_p^{H,CF}$ are known for $\theta = 90°$ and if the average of $\sin^2\theta$ over the motion can be calculated for the hindering potential, the observed couplings must yield both the barrier to rotation and the low energy conformation, which we shall assume to be **6**, **7**, or **8**. Unfortunately, INDO calculations do not necessarily give accurate values of the extremes in ^6J (19), so that recourse must be had to experimental estimates for these quantities. A final assumption, that ^6J vanishes when $\theta = 0°$, is supported by the nonobservable $^6J_p^{H,CH}$ values when the C—H bond of the group R_1R_2C—H is forced to lie in the benzene plane (21).

(a) Calculation of $\langle\sin^2\theta\rangle$ as a Function of Barrier

For barriers to internal rotation as low as 1 to 3 kcal/mol at ambient temperatures, an algorithm based on harmonic oscillators becomes inadequate. Consequently, following the procedure of ref. 22, the hindered rotor problem was solved for a twofold potential using the 11 lowest free rotor eigenfunctions as a basis set. Reduced moments of inertia between 0.4 and 14.0×10^{-38} g cm^2 were employed and the values of $\langle\sin^2\theta\rangle$ were calculated at 305 K (the temperature of the probe) as a function of the hindering potential between 0 and 10 kcal/mol.

The details of the relatively straightforward computations are not given here because the general method is adequately described[4] in ref. 22. The present approach reduces to the results in ref. 22 under the assumptions stated there.

[4]Note, however, that eq. 5 of ref. 22 should carry a multiplier of $1/\sqrt{\pi}$ in the expansion, as should eq. 6; which should also have an additional term equal to $(1/\sqrt{2\pi})\, b_{m\lambda}$. Furthermore, eqs. 8 and 9 should each have a factor of $2/V_0$ multiplied into the second term, *i.e.* into the summation over the level index.

Can. J. Chem. Downloaded from www.nrcresearchpress.com by 210.87.254.5 on 09/05/12
For personal use only.

Can. J. Chem. Downloaded from www.nrcresearchpress.com by 210.87.254.5 on 09/05/12
For personal use only.

(b) $^6J_p^{H,CF}$ *and the Barrier to Rotation*

The simplest treatment is given first, followed by qualifications. $^6J_p^{H,CF}$ is -2.43 Hz in **3** and $\sin^2\theta = 1$ for a rigid form **8**, caused by the presence of bulky chlorine atoms in the *ortho* positions. $^6J_p^{H,CF}$ is -1.11 Hz in **2**, less than $-2.43/2$ Hz. Hence **6** is the conformation of lowest energy in the absence of *ortho* substituents because for **7** and **8** a nonzero barrier entails an observed $^6J_p^{H,CF}$ of greater than $-2.43/2$ Hz. This condition follows because in **7** the coupling would be $-2.43 \times 3/4$ Hz for a rigid conformation and would be -2.43 for a rigid **8**. These two numbers tend towards $-2.43/2$ as the barrier tends to zero, *i.e.*, when $\langle\sin^2\theta\rangle = \frac{1}{2}$.

The ratio of the values of $^6J_p^{H,CF}$ in **2** and **3** is 1.11/2.43 or 0.46. The reduced moment of inertia of **2** is 0.524×10^{-38} g cm^2 and a plot of $\langle\sin^2\theta\rangle$ *vs.* barrier at 305 K then yields a barrier of 220 cal/mol; perhaps in accidental agreement[5] with the *ab initio* value of 250 cal/mol (3) favoring **6**. The derived barrier is insensitive to the reduced moment of inertia, at least within the range of error introduced by the assumption of a rigid internal rotor. The derived barrier is subject to the following *caveats*.

(*i*) If $^6J_p^{H,CF}$ in **3**, having conformation **8**, is reduced by torsional motions, the value of 220 cal/mol is a lower limit; although **6** is still the preferred conformation of **2**. An estimate of any reduction in $^6J_p^{H,CF}$ is made as follows. *Ab initio* calculations on 2,6-dichlorobenzylfluoride, **3**, gave **8** as 0.24 and 12.71 kcal/mol lower in energy than **7** and **6**, respectively. Optimization[6] of the C–C–F angle in **6** and **8** gave 117.2 and 110.5°, respectively, and reduced the energy difference to 6.81 kcal/mol. Such a barrier reduces $^6J_p^{H,CF}$ from its rigid value by at most 5% and recalculation then yields 310 cal/mol.

(*ii*) These two calculations assume that *ortho* substitution by chlorine atoms does not change the magnitude of $^6J_p^{H,CF}$, *i.e.*, intrinsic substituent effects are ignored. If this assumption is dropped one may proceed by adducing evidence for such changes. The ring substituents in benzalfluoride derivatives alter the magnitudes of J^{H,CF_2} somewhat (4). In Table 2, $^4J_o^{H,CF}$ is reduced to 80% of its magnitude on moving from **1** to **2**. A similar change in $^6J_p^{H,CF}$ yields -1.39 Hz for this coupling in **2**. For consistency, $^6J_p^{H,CF}$ in **3** must then change to -3.04 Hz. Of course, these new values of $^6J_p^{H,CF}$ have the same ratio as before and lead to the same barrier as before. If, as seems reasonable, substitution at *ortho* positions has a larger intrinsic effect on the magnitude of $^6J_p^{H,CF}$ than substitution at the *meta* positions, the estimate above is a lower limit to the barrier. If $^6J_p^{H,CF}$ is in fact as large in magnitude as -3.16 Hz, as calculated by INDO–MO in Table 3, the barrier rises to 310 cal/mol.

(*iii*) The calculated values of $^6J_p^{H,CF}$ in Table 3 closely follow a $\sin^2\theta$ relationship, at least between $\theta = 5$ and 85° (convergence was not attained on perturbing the fluorine *s* orbital for $\theta = 0$ and 90°). Comparison of the calculated and observed values in Tables 3 and 2 demonstrates the substantial overestimation of computed values of $^4J_o^{H,CF}$ and $^5J_m^{H,CF}$, suggesting the sufficient severity of the *caveat* in *ii*.

(*iv*) The dependence of $^6J_p^{H,CF}$ on the C–C–F angle is not known. If hyperconjugation is responsible for the transmission of spin state information, $^6J_p^{H,CF}$ will probably decrease as the angle increases. The calculated angle of 110.5° then indicates a reduced $^6J_p^{H,CF}$ in **3** and once more the barrier estimate of 220 cal/mol represents a lower limit. Of course, the calculated angle has only changed by 1° so that any effect on $^6J_p^{H,CF}$ may well be minimal.

(c) Comparison with o-Fluorotoluene

The microwave barrier to internal rotation of the methyl group is 649 cal/mol in *o*-fluorotoluene (23), 567 ± 48 cal/mol in α-d_1-*ortho*-fluorotoluene and 711 ± 40 cal/mol in α-d_2-*ortho*-fluorotoluene (24). This range of values apparently reflects the errors introduced by the approximations in the semirigid model to internal rotation and is not an isotope effect (24). The data for *o*-fluorotoluene are taken as indicative of a small barrier in benzylfluoride and that the value of 260 ± 50 cal/mol derived from $^6J_p^{H,CF}$ is possibly comparable in accuracy to the microwave results.

[5]The INDO–MO method favors **6** over **8** by 2.4 kcal/mol, clearly in disagreement with experiment because $^6J_p^{H,CF}$ would then be -0.4 Hz in **2**, as found from the hindered rotor value for $\langle\sin^2\theta\rangle$.

[6]The cpu time for one geometry was about 40 min, for optimization of the C–C–F angle about 2 h, so that further calculations became too costly.

TABLE 3. Computed long-range coupling constants in Hz in benzylfluoride as given by INDO–MO–FPT

θ*	$^4J_o^{H,CH}$	$^5J_m^{H,CH}$	$^6J_p^{H,CH}$	$^4J_o^{H,CF}$	$^5J_m^{H,CF}$	$^6J_p^{H,CF}$
0(5)	−0.19	0.14	−0.07	−4.01	0.60	−0.08
15	−0.19	0.14	−0.07	−3.63	0.71	−0.27
30	−0.31	0.20	−0.20	−2.91	1.03	−0.84
45	−0.54	0.32	−0.43	−2.66	1.42	−1.61
60	−0.82	0.47	−0.70	−2.90	1.79	−2.39
75	−1.08	0.63	−0.94	−3.28	2.12	−2.97
90(85)	−1.24	0.77	−1.07	−3.46	2.30	−3.16
105	−1.29	0.87	−1.07	−3.45	2.55	
120	−1.20	0.93	−0.93	−3.11	2.62	
135	−1.02	0.95	−0.70	−2.58	2.59	
150	−0.80	0.93	−0.43	−2.02	2.49	
165	−0.60	0.91	−0.21	−1.57	2.37	
180(175)	−0.49	0.89	−0.07	−1.42	2.33	

*θ is measured in degrees and is zero when the C—H (C—F) bond of the side chain lies in the plane of the benzene ring and eclipses the C—H bond in the ring. The angles in parentheses refer to coupling involving fluorine.

(d) $^6J_p^{H,CH}$ and the Barrier to Rotation

The value of $^6J_p^{H,CH}$ in toluene is −1.24 Hz when $\theta = 90°$ (19), as discussed above. Substitution by the electronegative fluorine atom at the methyl carbon polarizes the adjacent C—H bonds and may thereby reduce the magnitude of $^6J_p^{H,CH}$. In molecular orbital terms, the degree of localization of the π type orbitals of the CH_2F group is greater than in the CH_3 group (25). The extent of the reduction in $^6J_p^{H,CH}$ is problematical.

However, if the conclusions about the barrier in **2** reached on the basis of $^6J_p^{H,CF}$ are correct, the value of −0.53 Hz in **2** may be used to predict the maximum magnitude of $^6J_p^{H,CH}$, *i.e.*, when $\theta = 90°$. Remembering that **6** is the low energy form, that $\sin^2\theta$ is decreasing towards 0.5 from 0.75 at its maximum as the barrier decreases, and that the barrier is 250 ± 50 cal/mol, the hindered rotor solutions yield a maximum magnitude in $^HJ_p^{C,H}$ of −1.02 ± 0.02 Hz. Note that $^6J_p^{H,CH}$ is less sensitive than $^6J_p^{H,CF}$ to the size of the barrier because it has a lower magnitude and because it varies by only 25% of its maximum, while $^6J_p^{H,CF}$ varies by 50% of its maximum.

The derived maximum magnitude of −1.02 Hz in **2** is 83% of that observed and calculated for toluene. In Table 3 the INDO value for benzylfluoride is −1.09 Hz, 88% of that in toluene. Similar changes are noted in the calculated β-proton hyperfine coupling constants in the ethyl and β-fluoroethyl radicals (26), in which the corresponding ratio is 90%. The coupling mechanism in these radicals displays the same angular behaviour as that postulated here for **2**.

The calculated value of $^6J_p^{H,CH}$ in Table 3 peaks in magnitude at $\theta = 97°$, a consequence of the dissymmetry introduced by the C—F bond as the fluoromethyl group is rotated about the internal axis. In other words, the calculated $^6J_p^{H,CH}$ is proportional to $\sin^2(\theta - 7)$, behaving in a manner reminiscent of that displayed by the β-proton hyperfine coupling in the β-fluoroethyl radical (26). However, the change in magnitude between $\theta = 90°$ and $\theta = 97°$ is only 0.02 Hz.

*(e) The Apparently Anomalous Values of $^6J_p^{H,CH}$ in **3***

The value of −0.16 Hz in **3** is much too low in magnitude, considering that for **8** more stable than **6** its value should be very near −1.02/4 = −0.26 Hz. If −0.16 Hz is treated as a normal magnitude it follows that the maximum value of $^6J_p^{H,CH}$ is −0.64 Hz and that conformation **6** is still the stable form of **2** with a barrier of at least 3 kcal/mol. This conclusion contradicts the larger observed magnitude of $^6J_p^{H,CF}$ in **2**, as well as the indications from the *ab initio* calculations, and is taken as false.

An explanation of the low magnitude of $^6J_p^{H,CH}$ in **2** goes as follows. In the β-chloroethyl radical, the β-proton hyperfine coupling is anomalously low in magnitude (26–28). This

Can. J. Chem. Downloaded from www.nrcresearchpress.com by 210.87.254.5 on 09/05/12
For personal use only.

Can. J. Chem. Downloaded from www.nrcresearchpress.com by 210.87.254.5 on 09/05/12
For personal use only.

fact is explained (29) by a decrease in the C–C–Cl angle when $\theta = 90°$ and a concomitant increase in the C–C–H angle, bringing the β-proton nearly into the nodal plane of the π-orbital on the methylene group and thereby reducing the hyperfine interaction. The C–C–Cl angle decreases because of the conjugative interaction of the orbitals in the C—Cl bond, or on the chlorine atom, with the $p\pi$ orbitals on the methylene group (26–31).

The present *ab initio* predictions of the C–C–F angle in conformation **8** of benzylfluoride and of **3** are 111.1 and 110.5°, respectively, contrary to the trends indicated for the β-chloroethyl radical. In contrast, MINDO/3 optimization procedures[7] gave the C–C–F angle as 107.2° and the C–C–H angles as 116.1° for benzylfluoride in conformation **8**. If the latter angle were 120°, a zero $^6J_p^{H,CH}$ would be indicated. Therefore the anomalous value of $^6J_p^{H,CH}$ is here attributed to bond angle distortion in **3**; and can perhaps be taken as evidence for such distortion.

The optimization procedure also allowed variation of the C—C, C—F, and C—H bond lengths of the CH_2F group, other geometries being standard. The final (initial) lengths in Å are C—C, 1.485 (1.52); C—F, 1.387 (1.36); C—H, 1.113 (1.09).

Finally, conformation **6** was calculated as 300 cal/mol more stable than **8** for benzylfluoride in the optimized geometry, compared to 570 cal/mol for a standard geometry. The MINDO/3 predictions are therefore consistent with the *ab initio* results and with the conclusions based on $^6J_p^{H,CF}$ for **2**.

(f) The Long-range Couplings over Four and Five Bonds

(i) Proton–Proton Coupling—The average calculated value of $^4J_o^{H,CH}$ in Table 3 is −0.75 Hz, about 0.1 Hz larger in magnitude than that observed in **1**, **2**, and **4**. Of course, there exists a slight preference for $\theta = 60$ and 120° and if the θ dependence of $^4J_o^{H,CH}$ were known, it could be averaged over the eigenfunctions of the hindered rotor problem. The computations indicate a mixture of a σ–π mechanism, giving large magnitudes for out-of-plane conformations, and a σ mechanism, which yields finite couplings for an extended planar arrangement of bonds ($\theta = 180°$); so that the computed values peak around $\theta = 120°$.

In **5** the fluoromethyl rotor samples conformations **9**, **10**, and **11** much more frequently than **12**, which has a relatively high energy according to the *ab initio* calculations above on 2,6-dichlorobenzylfluoride. Furthermore, the conformation of **3** analogous to **11** is only 240 cal/mol above that analogous to **8**, according to these calculations. Accordingly, the value of −0.74 Hz for $^4J_o^{H,CH}$ in **5** is larger in magnitude than in **1**, **2**, and **4**. More precise conformational deductions cannot be reached from $^4J_o^{H,CH}$.

9 **10**

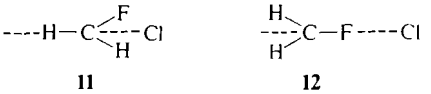

11 **12**

The observed values of $^5J_m^{H,CH}$ in Table 2, are close to the 0.36 Hz measured for toluene (20). The computed values in Table 3 are clearly too large (19) and peak near $\theta = 135°$, again implying contributions from both σ–π and σ mechanisms (19). In **5** the coupling of 0.43 Hz to proton 5 is larger than the 0.33 Hz to proton 3, as expected for a predominance of conformations **9** to **11**.

The INDO overestimates of the magnitudes of $^4J_o^{H,CH}$ and $^5J_m^{H,CH}$ suggest that $^6J_p^{H,CH}$ will hardly be underestimated and thus that the arguments in section 2*d* are reasonable.

(ii) Proton–Fluorine Couplings—The large magnitude of $^4J_o^{H,CF}$ near $\theta = 0°$, as calculated by INDO, exemplifies a negative 'through-space' coupling mechanism (32) dependent on the proximity of the fluorine and hydrogen atoms (33). This interaction drops rapidly in size as the interatomic distance increases. The σ–π mechanism peaks at $\theta = 90°$. The superposition of the two contributions then yields a local minimum near $\theta = 45°$. If the calculations are *qualitatively* correct, then the relatively small, observed magnitude of 0.70 Hz for $^4J_o^{H,CF}$ in **5** implies that **10** is somewhat lower in energy than **9** and **11**. Note that the C—H bond is

[7]Unfortunately, MINDO/3 cannot be used for **3** because it contains a second row element, chlorine, and a first row element, fluorine, other than carbon and hydrogen.

Can. J. Chem. Downloaded from www.nrcresearchpress.com by 210.87.254.5 on 09/05/12
For personal use only.

polarized as $^{+}C—H^{-}$ and that the single C—Cl bond *ortho* to it is polarized as $^{+}C—Cl^{-}$ in **10**, as indicated by both sets of MO calculations, perhaps accounting for a stable form **10**.

The calculated values of $^{5}J_{m}^{H,CF}$ peak in the vicinity of $\theta = 120°$. In **5** the observed coupling is 1.35 Hz to proton 3 and 0.71 Hz to proton 5, emphasizing the importance of conformations in which the C—F bond avoids the vicinity of the *ortho* C—Cl bond.

(g) The ^{13}C Spectrum of **2**

This was measured by R. A. Bell at McMaster University on a Bruker WH-90 spectrometer. The sample was identical to that used in the proton magnetic resonance experiments. The magnitudes of the $^{13}C,^{19}F$ couplings over one, two and three bonds are 171.4, 18.4, and 7.3 Hz, respectively. The deshielding of the ring carbon attached to the CH_2F group is consistent with a preferred in-plane conformation for the fluorine atom, as are the chemical shifts of the *ortho* carbon nuclei.[8]

Acknowledgements

We are grateful to Dr. R. A. Bell for his generosity in measuring and discussing the ^{13}C magnetic resonance spectrum, to Dr. R. E. D. McClung for very helpful communications on the hindered rotor problem, to the University of Manitoba Computer Center for provisions of computing time, and to the National Research Council of Canada for financial support.

1. H. D. Rudolph, H. Dreizler, A. Jaeschke, and P. Wendling. Z. Naturforsch. Teil A, **22**, 940 (1967).
2. W. Caminati, G. Cazzoli, and A. M. Mirri. Chem. Phys. Lett. **31**, 104 (1975).
3. W. J. Hehre, L. Radom, and J. A. Pople. J. Am. Chem. Soc. **94**, 1496 (1972).
4. J. B. Rowbotham, A. F. Janzen, J. Peeling, and T. Schaefer. Can. J. Chem. **52**, 481 (1974).
5. D. G. Gehring and G. S. Reddy. Anal. Chem. **40**, 792 (1968).
6. J. Bernstein, J. S. Roth, and W. T. Miller, Jr. J. Am. Chem. Soc. **70**, 2310 (1948).
7. J. A. Pople and D. L. Beveridge. Approximate molecular orbital theory. McGraw-Hill Book Company, New York, N.Y. 1970.
8. P. A. Dobosh. Program No. 141. Q.C.P.E. University of Indiana, Bloomington, Indiana.
9. Program No. 236. Q.C.P.E. University of Indiana, Bloomington, Indiana.
10. R. C. Bingham, M. J. S. Dewar, and D. H. Lo. J. Am. Chem. Soc. **97**, 1285 (1975).
11. Program No. 279. Q.C.P.E. University of Indiana, Bloomington, Indiana.
12. J. A. Pople and M. S. Gordon. J. Am. Chem. Soc. **89**, 4253 (1967).
13. S. Castellano and A. A. Bothner-By. J. Chem. Phys. **41**, 3863 (1964); LAOCN 3, Mellon Institute, Pittsburgh, Pa. 1966.
14. C. W. Haigh and J. M. Williams. J. Mol. Spectrosc. **32**, 398 (1969).
15. T. Schaefer, C. M. Wong, and K. C. Tam. Can. J. Chem. **47**, 3688 (1969).
16. R. A. Hoffman. Mol. Phys. **1**, 326 (1958).
17. M. Barfield and B. Chakrabarti. J. Am. Chem. Soc. **91**, 4346 (1969).
18. C. J. Macdonald and W. F. Reynolds. Can. J. Chem. **48**, 1002 (1970).
19. R. Wasylishen and T. Schaefer. Can. J. Chem. **50**, 1852 (1972).
20. M. P. Williamson, R. J. Kostelnik, and S. M. Castellano. J. Chem. Phys. **49**, 2218 (1968).
21. H. M. Hutton, J. B. Rowbotham, B. H. Barber, and T. Schaefer. Can. J. Chem. **49**, 2033 (1971).
22. P. B. Ayscough, M. C. Price, and R. E. D. McClung. Mol. Phys. **20**, 41 (1971).
23. J. Susskind. J. Chem. Phys. **53**, 2492 (1970).
24. D. Schwoch and H. D. Rudolph. J. Mol. Spectrosc. **57**, 47 (1975).
25. R. Hoffman, L. Radom, J. A. Pople, P.v.R. Schleyer, W. J. Hehre, and L. Salem. J. Am. Chem. Soc. **94**, 6221 (1972).
26. K. S. Chen, P. J. Krusic, P. Meakin, and J. K. Kochi. J. Phys. Chem. **78**, 2014 (1974).
27. T. Kawamura, D. J. Edge, and J. K. Kochi. J. Am. Chem. Soc. **94**, 1752 (1972).
28. K. S. Chen, I. H. Elson, and J. K. Kochi. J. Am. Chem. Soc. **95**, 5341 (1973).
29. I. Biddles and A. Hudson. Chem. Phys. Lett. **18**, 45 (1973).
30. A. R. Lyons and M. C. R. Symons. J. Chem. Soc. Faraday Trans. 2, **68**, 622 (1972).
31. D. Griller and K. U. Ingold. J. Am. Chem. Soc. **96**, 6715 (1974).
32. K. Hirao, H. Nakatsuji, and H. Kato. J. Am. Chem. Soc. **95**, 31 (1973).
33. T. Schaefer and J. B. Rowbotham. Chem. Phys. Lett. **29**, 633 (1974).

[8]R. A. Bell, private communication.

Spectre de l'indazole en résonance magnétique nucléaire du ^{13}C

JOSÉ ELGUERO, ALAIN FRUCHIER[1] ET MARIA DEL CARMEN PARDO[2]

Laboratoire de Synthèse et d'Etudes physicochimiques d'Hétérocycles azotés, Université des Sciences et Techniques du Languedoc, 34060 Montpellier Cédex, France

Reçu le 26 septembre 1975

JOSÉ ELGUERO, ALAIN FRUCHIER et MARIA DEL CARMEN PARDO. Can. J. Chem. **54**, 1329 (1976).

La synthèse des cinq monodeutério-indazoles a permis l'attribution sans ambiguité en résonance du ^{13}C des sept carbones de l'indazole. Des constantes de couplage ^1J, ^2J et ^3J ont été mesurées sur le spectre obtenu en l'absence d'irradiation des noyaux de ^1H.

JOSÉ ELGUERO, ALAIN FRUCHIER, and MARIA DEL CARMEN PARDO. Can. J. Chem. **54**, 1329 (1976).

Synthesis of all monodeuterio indazole derivatives has allowed the assignment of the seven carbons in the ^{13}C nmr spectrum of indazole. Some ^1J, ^2J, and ^3J coupling constants have been measured from the coupled spectrum.

Introduction

La plupart des noyaux hétérocycliques pentagonaux simples ont fait l'objet d'études en rmn du ^{13}C (voir par exemple réfs 1 et 2). Seuls l'indazole, **1**, et le benzotriazole, **2**, n'ont pas encore été examinés.

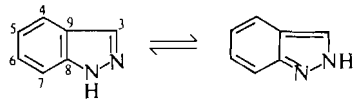

1*a* **1***b*

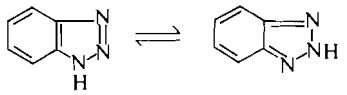

2*a* **2***b*

Dans ce travail nous présentons les résultats concernant l'indazole, **1**, dont tous les dérivés monodeutériés ont été synthétisés afin d'attribuer sans ambiguité les déplacements chimiques de chaque carbone de la molécule fondamentale.

Partie expérimentale

Les spectres rmn ont été enregistrés sur le spectromètre JEOL PS-100-FT du Laboratoire de Mesures Physiques de l'U.S.T.L. avec des solutions de concentrations molaires. Pour la mesure des déplacements chimiques et des constantes de couplage, les largeurs des spectres sont respectivement 5 kHz et 1.25 kHz. Dans le premier cas l'incertitude est de 0.05 ppm et dans le second de 0.3 Hz. Chaque spectre a demandé 500 impulsions à 90° (28 μs) avec un temps de répétition de 2.5 s. Le verouillage champ-fréquence est effectué sur le signal du deutérium du DMSO-d_6 utilisé comme solvant. Le découplage des noyaux de ^1H est obtenu par un bruit de largeur 2.5 kHz tandis que les spectres couplés sont effectués par la technique du "gate decoupling" qui conserve l'effet Overhauser au niveau des atomes de carbone.

Synthèse des deutério-indazoles

La préparation du deutério-3 indazole a déja été décrite (3). Les quatre autres dérivés ont été obtenus à partir des nitro-indazoles correspondants (les nitro-indazoles sont tous commerciaux sauf le nitro-4 qui a été synthétisé selon la réf. 4) par la méthode suivante.

On agite en chauffant un mélange de 0.02 mol de nitro-indazole, 0.09 mol de chlorure stanneux et 30 ml d'acide chlorhydrique (d = 1.19) jusqu'à totale dissolution. On refroidit et alcalinise la solution avec de la soude 20%. On extrait ensuite à l'acétate d'éthyle, sèche la couche organique sur sulfate de sodium anhydre et chasse le solvant. On obtient ainsi, avec un rendement de l'ordre de 90%, l'amino-indazole correspondant dont la pureté est suffisante pour continuer la réaction.

Pour la désamination nitreuse, nous avons adapté la procédure décrite par Newkome et Fishel (5). Dans un ballon à deux tubulures, protégé de l'humidité ambiante et muni d'une agitation magnétique, on dissout 0.015 mol d'amino-indazole dans 30 ml d'acide chlorhydrique deutérié 5 *N* et refroidit vers 0 °C. On ajoute ensuite 2.5 ml d'acide chlorhydrique deutérié 10 *N* et en 15 min une solution de 0.025 mol de nitrite de sodium dans 5.5 ml d'eau lourde. La température doit rester inférieure à 6 °C pendant toute l'addition. On obtient ainsi une solution rouge du sel de diazonium que l'on verse en agitant sur 28 ml d'acide hypophosphoreux deutérié 50% refroidi à 0 °C. Le mélange est agité 3 h à 0 °C et environ 15 h à température ambiante tout en étant protégé de l'humidité. On neutralise ensuite avec de la soude 10%, extrait à l'acétate d'éthyle, sèche sur sulfate de sodium anhydre et évapore le solvant. Par sublimation du résidu entre 100 et 110 °C sous 1 torr, on obtient le deutério-indazole pur avec un rendement compris entre 35 et 45%.

[1]Auteur auquel la correspondance doit être adressée.

[2]Adresse actuelle: Catedra de Quimica Organica, Facultad de Ciencias, Universidad Complutense de Madrid (Espagne).

Can. J. Chem. Downloaded from www.nrcresearchpress.com by 210.87.254.40 on 09/05/12
For personal use only.

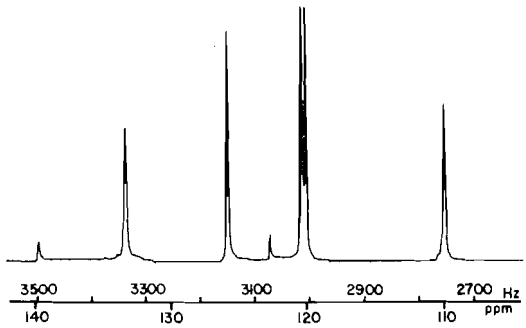

FIG. 1. Spectre de l'indazole lorsque les noyaux ^1H sont irradiés.

L'acide chlorhydrique deutérié se prépare en ajoutant avec précaution de l'eau lourde sur du pentachlorure de phosphore. L'acide chlorhydrique deutérié gazeux est recueilli dans l'eau lourde jusqu'à ce que la solution soit 10 *N*.

Pour préparer l'acide hypophosphoreux deutérié, on élimine, à 40–45 °C sous vide, l'eau d'une solution aqueuse 50%, puis dissout l'acide restant dans une quantité d'eau lourde égale à celle évaporée et recommence l'opération trois ou quatre fois.

Résultats et discussion

Les spectres obtenus avec et sans irradiation des noyaux de ^1H sont représentés dans les figs 1 et 2 respectivement. Tous les dérivés monodeutériés ayant été synthétisés, l'attribution des signaux ne pose pas de problème pour les carbones porteurs d'un atome d'hydrogène. Les déplacements chimiques, en ppm par rapport au TMS (en référence interne), sont donnés dans le tableau 1.

L'effet isotopique de 0.1 ppm vers les fréquences faibles, déja décrit (6, 7), est visible sur tous les carbones adjacents à celui qui porte le deutérium. Il permet d'attribuer sans ambiguité les signaux des carbones C_8 et C_9. L'effet isotopique plus important (6) au niveau du carbone directement lié au deutérium n'a pu être observé par suite de la présence d'indazole non deutérié en faible quantité.

Nous discuterons les déplacements chimiques en fonction du tautomère N(H)-1, **1***a*, seul présent aussi bien à l'état solide (8) qu'en solution (9). On trouve dans la littérature les charges totales de ce tautomère calculées par les méthodes CNDO/2 et CNDO/S (8). Nous avons donc essayé une corrélation avec les déplacements chimiques. En excluant de la régression les carbones C_3, C_4 et C_7, qui occupent une position *péri*, on constate que la méthode CNDO/S donne des résultats plus satisfaisants. Ces derniers sont rassemblés dans le tableau 1. On obtient une pente de -146.4 ppm/e, com-

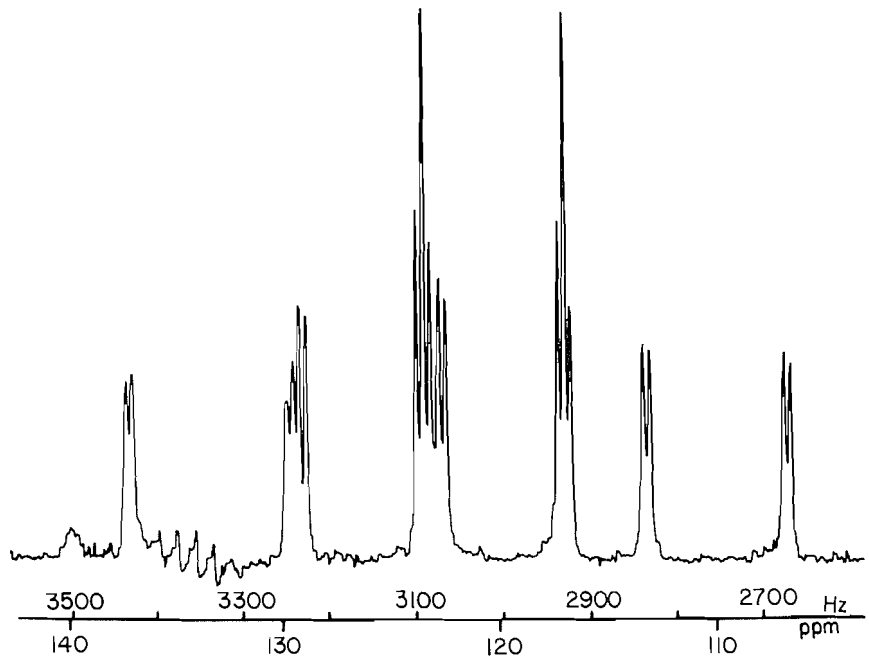

FIG. 2. Spectre de l'indazole non découplé.

Can. J. Chem. Downloaded from www.nrcresearchpress.com by 210.87.254.40 on 09/05/12
For personal use only.

TABLEAU 1. Déplacements chimiques expérimentaux et calculés de l'indazole

Carbone	δ_{exp}	$q(\sigma + \pi)$	δ_{calc}†	Δ‡
3	133.4*	3.9404	134.9	1.5
4	120.4*	3.9938	127.1	6.7
5	120.1	4.0446	119.7	−0.4
6	125.8	3.9966	126.7	0.9
7	110.0*	4.0428	119.9	9.9
8	139.9	3.9098	139.4	−0.5
9	122.8	4.0279	122.1	−0.7

*Ces déplacements chimiques n'ont pas été utilisés dans la régression.
†Ces valeurs sont calculées avec l'équation $\delta = -146.4q + 711.8$.
‡$\Delta = \delta_{calc} - \delta_{exp}$.

parable à celles décrites dans la littérature (10), et un coefficient de corrélation de 0.993. Ces résultats confirment l'attribution des carbones C_8 et C_9. Les carbones *péri* C_4 et C_7 sont déplacés vers les fréquences faibles, comme cela était prévisible d'après les résultats de la littérature (11). Par contre le carbone C_3 est faiblement perturbé.

Les constantes de couplage $^{13}C-^{1}H$ que nous avons pu mesurer sont dans le tableau 2. On notera que la plus grande constante ^{1}J est celle du carbone C_3 (effet de l'atome d'azote voisin (12)) et que les quatre autres sont du même ordre de grandeur. Si les constantes ^{3}J sont normales (13), seul le carbone C_6 présente une interaction ^{2}J de 2 Hz avec H_5. Ce couplage n'est mesurable avec précision que dans le deutério-7 indazole, probablement à cause d'un autre couplage ^{2}J très faible entre le carbone C_6 et H_7 que nous n'avons pu évaluer, même sur le deutério-5 indazole.

TABLEAU 2. Constantes de couplage proton–^{13}C (en Hz) dans l'indazole

	H				
C†	3	4	5	6	7
3	188.0(^{1}J)	7.3(^{3}J)	*	*	*
4	*	162.7(^{1}J)	*	7.6(^{3}J)	*
5	*	*	162.0(^{1}J)	*	7.3(^{3}J)
6	*	7.9(^{3}J)	2.0(^{2}J)	159.9(^{1}J)	*
7	*	*	7.6(^{3}J)	*	163.9(^{1}J)

*Couplages non observés.
†Les signaux correspondants aux carbones 8 et 9 sont trop faibles et élargis pour permettre la mesure des constantes de couplage.

1. J. ELGUERO, C. MARZIN et J. D. ROBERTS. J. Org. Chem. **39**, 357 (1974).
2. R. J. PUGMIRE et D. M. GRANT. J. Am. Chem. Soc. **93**, 1880 (1971).
3. J. ELGUERO, A. FRUCHIER et R. JACQUIER. Bull. Soc. Chim. Fr. 2619 (1967).
4. K. VON AUWERS et P. FRESE. Ber. Chem. B, **58**, 1369 (1925).
5. G. R. NEWKOME et D. L. FISHEL. J. Org. Chem. **31**, 677 (1966).
6. R. A. BELL, C. L. CHAN et B. G. SAYER. J. Chem. Soc. Chem. Commun. 67 (1972).
7. D. LAVER, E. L. MOTELL, D. D. TRAFICANTE et G. E. MACIEL. J. Am. Chem. Soc. **94**, 5335 (1972).
8. A. ESCANDE, J. LAPASSET, R. FAURE, E.-J. VINCENT et J. ELGUERO. Tetrahedron, **30**, 2903 (1974).
9. J. ELGUERO, C. MARZIN, A. R. KATRITZKY et P. LINDA. The tautomerism of heterocycles. Suppl. Vol. 1. Advances in heterocyclic chemistry. Academic Press, New York. Sous presse.
10. J. B. STOTHERS. Carbon-13 NMR spectroscopy. Academic Press, New York. 1972.
11. D. M. GRANT et B. V. CHENEY. J. Am. Chem. Soc. **89**, 5315 (1967).
12. P. LASZLO. Bull. Soc. Chim. Fr. 558 (1966).
13. G. ENGLERT, P. DIEHL et W. NIEDERBERGER. Z. Naturforsch. Teil A, **26**, 1829 (1971).

Can. J. Chem. Downloaded from www.nrcresearchpress.com by 210.87.254.40 on 09/05/12
For personal use only.

The structure of the second coordination sphere of transition metal complexes. V. Nuclear magnetic resonance T_1 measurements

S. O. CHAN AND D. R. EATON

Department of Chemistry, McMaster University, Hamilton, Ontario L8S 4M1

Received October 15, 1976

S. O. CHAN and D. R. EATON. Can. J. Chem. **54**, 1332 (1976).

Proton spin–lattice relaxation times have been measured for several solute and solvent molecules in the presence of paramagnetic chromium(III) acetylacetonate. In each case the T_1 values obtained are considerably shorter than those measured in the absence of the paramagnetic complex. Two models are necessary to describe the results. In the first T_1 is determined by the diffusional correlation time of the solute molecule. This corresponds to a case in which there is no detectable second coordination sphere and leads to the prediction that T_1 will be independent of solute concentration. Acetone, chloroform, and methylene chloride show this behaviour. The second model involves a discrete second coordination sphere and leads to the prediction that above a certain concentration T_1 will vary linearly with solute concentration. Methanol shows this behaviour. Calculations show good agreement with the observed T_1's for a model with a coordination number of 8, a Cr-to-CH_3 separation of 7 Å and an equilibrium constant for displacing solvent (chloroform) of around 10. It is suggested that these results lead to a criterion for second coordination sphere formation compatible with the second coordination sphere requirements for an "interchange" type of ligand exchange mechanism.

S. O. CHAN et D. R. EATON. Can. J. Chem. **54**, 1332 (1976).

On a mesuré les temps de relaxation spin–réseau du proton pour plusieurs molécules de solutés et de solvants en présence d'acétylacétonate de chrome(III) paramagnétique. Dans chaque cas, les valeurs de T_1 obtenues sont beaucoup plus faibles que celles mesurées en l'absence du complexe paramagnétique. Deux modèles sont nécessaires pour décrire les résultats. Dans le premier, T_1 est déterminé par le temps de corrélation de diffusion de la molécule de soluté. Ceci correspond à un cas dans lequel il n'y a pas de sphère de coordination secondaire qui est détectable et ceci conduit à la prédiction que T_1 sera indépendant de la concentration de soluté. L'acétone, le chloroforme et le chlorure de méthylène agissent de cette façon. Le second modèle implique une sphère de coordination secondaire définie et conduit à la prédiction qu'au dessus d'une certaine concentration, T_1 variera d'une façon linéaire avec la concentration de soluté. Le méthanol agit de cette façon. Les calculs sont en bon accord avec les valeurs observées pour T_1 pour un modèle avec un nombre de coordination de 8, une séparation du Cr et du CH_3 de 7 Å et une constante d'équilibre pour le déplacement du solvant (chloroforme) d'environ 10. On suggère que ces résultats conduisent à un critère pour la formation d'une sphère de coordination secondaire qui est compatible avec les nécessités de la sphère de coordination secondaire du mécanisme d'échange de ligand de type "interchange".

[Traduit par le journal]

Introduction

In previous papers in this series (1–4) we have discussed the use of isotropic shifts of nmr resonances, resulting from dipolar interactions with paramagnetic metal complexes, in the study of weak second sphere interactions. The number of complexes available for this type of study is limited by the requirement that the complex have a large magnetic anisotropy if significant shifts are to be observed. The objective of this work is to correlate studies of second sphere structure with the mechanisms of reactions of metal complexes. For this purpose it is desirable to develop techniques of more general applicability than the isotropic shift measurements previously used. In the present paper we report an investigation of the use of proton T_1 measurements for this purpose and demonstrate that this method provides an experimental criterion for the existence of a discrete second coordination sphere. Subsequent papers will demonstrate the importance of second sphere bonding in some catalytic reactions.

The effect of paramagnetic ions or molecules in shortening the spin–lattice relaxation times (T_1) of nuclei in solution has been well documented (5). For weak interactions between a

Can. J. Chem. Downloaded from www.nrcresearchpress.com by 210.87.254.105 on 09/05/12
For personal use only.

Can. J. Chem. Downloaded from www.nrcresearchpress.com by 210.87.254.105 on 09/05/12
For personal use only.

solute and solvent or between two solute molecules the predominant mechanism is dipolar in nature and demands no specific prerequisites such as that of a large magnetic anisotropy as in the case of isotropic shifts. It was realized at an early date that such relaxation effects have potential for studies of weak interactions such as occur in the second coordination sphere of metal complexes. Thus in 1956 Morgan *et al.* (6) reported the effect of a series of Cr(III) complexes on the T_1 of the solvent (water) and deduced a series in which the second coordination sphere of water molecules becomes increasingly less stable. Much of the earlier work in this area has been reviewed in a recent monograph (7). More recent workers have tended to measure the spin–spin relaxation times (T_2) rather than T_1. Thus Stengle and Langford (8) investigated the association of PF_6^- ions with Cr(III)-containing cations by measuring T_2's for the ^{19}F resonances. These ideas were developed by Frankel (9, 10) who deduced the orientation of molecules in the second sphere from the relative decrease in T_2 for different nuclei. Langford and White (11) and Behrendt, Langford, and Stengle (12) developed a method for finding the relative second sphere binding ability of two solvents in a mixed solvent system using T_2 measurements and correlated their results with mechanistic data on the ligand exchange reactions of the same paramagnetic complexes.

In theory, for most of the cases of present interest, T_1 and T_2 are equal. T_2 can be obtained relatively easily from linewidth measurements whereas until recently T_1 required special instrumentation of a type not generally available, *e.g.*, a spin-echo spectrometer. However, the advent of Fourier Transform nmr spectrometers has opened up the possibility of relatively facile T_1 measurements which are in fact probably more reliable than T_2 measurements because they do not involve correction for instrumental broadening of the lines. There is a further important advantage to the use of T_1 measurements: T_2 is affected by processes which occur on a time scale determined by the reciprocal of a chemical shift difference. For a process such as ligand exchange involving a paramagnetic complex this is typically 10^{-3} s. T_1 on the other hand is only affected by processes with a time scale of the order of the reciprocal of the resonance frequency (typically 10^{-8} s) (13). There is therefore the possibility of making both T_1 and T_2 measurements on a system involving ligand exchange. In this case T_1 will not be equal to T_2. In principle T_2 will provide information on the rate of ligand exchange and T_1 on second sphere interactions. If ligand exchange proceeds by an interchange (I) mechanism (14) in which the rate is determined by a step involving interchange of first and second sphere ligands we would expect to be able to correlate the two sets of data.

Before proceeding with an experiment of the type outlined above it seemed prudent first to investigate the effect on T_1 of second sphere interactions with a non-labile complex. For this purpose we chose chromium(III) acetylacetonate as the non-labile paramagnetic complex and methanol as the second sphere ligand. Chromium(III) acetylacetonate has been suggested as a relaxation reagent to reduce the T_1's in ^{13}C nmr spectroscopy (15). Davis and Facker (16) have presented infrared evidence to show that methanol is weakly bound to transition metal β diketonates by hydrogen bonding. Frankel (9) found that the hydroxyl and methyl group T_2's of methanol were both reduced by $Cr(acac)_3$. The effect on the hydroxyl group was 2.4 times greater than that on the methyl group and he inferred that the second sphere methanol molecules were oriented with the hydroxyl group closer to the metal ion. The present measurements were carried out in chloroform which is anticipated to be a less effective second sphere ligand than methanol.

Results

Table 1 presents a set of T_1 measurements on solutions of methanol in deuterochloroform. In the absence of $Cr(acac)_3$ the relaxation time of both types of proton is around 10 s and is relatively insensitive to the methanol concentration. In the presence of 0.01 *M* $Cr(acac)_3$ at low methanol concentration the T_1 for CH_3 is reduced to 0.1 s and that of OH to 0.033 s. The ratio of these relaxation times of 3.0 may be compared with the ratio of 2.4 reported by Frankel for the corresponding T_2's obtained from line width measurements. The dependence of the T_1's on the methanol concentration is shown graphically in Fig. 1. For both the CH_3

TABLE 1. Proton T_1's for methanol*

$[CH_3OH]$ (mol l^{-1})	T_1(s)					
	CH_3 when [Cracac] =			OH when [Cracac] =		
	0	0.005 *M*	0.01 *M*	0	0.005 *M*	0.01 *M*
0.2	10.5	0.198	0.102	9.7	0.064	0.032
0.4		0.201	0.101		0.066	0.035
0.6	10.2		0.100	9.4		0.034
0.8		0.199	0.099		0.060	0.035
1.0	9.9		0.104	9.2		0.032
1.2		0.196	0.099		0.062	0.033
1.5	9.7		0.101	8.9		0.031
1.6		0.205			0.070	
1.8			0.111			0.038
2.0	9.5	0.243	0.125	8.6	0.085	0.042
2.2			0.140			0.046
2.5	9.3	0.305	0.155	8.3	0.100	0.052
3.0		0.361	0.185		0.119	0.062
3.5	8.9	0.428	0.220	7.9	0.141	0.075
4.0	8.7	0.477	0.245	7.7	0.160	0.083

*Solvent $CDCl_3/CHCl_3$. T_1 $CHCl_3$ 0.005 *M* $Cr(acac)_3$ 0.10 s, T_1 0.01 *M* $Cr(acac)_3$ 0.05 s, both independent of CH_3OH concentration.

and the OH protons, T_1 is independent of methanol concentration until the solution is approximately 1.6 *M* in methanol. Thereafter T_1 increases linearly with methanol concentration. A similar set of measurements has been made for solutions 0.005 *M* in $Cr(acac)_3$. These data are included in Table 1. Halving the concentration of paramagnetic complex doubles the T_1's at low concentration and the onset of linear methanol concentration dependence still occurs at 1.6 *M*. A further experiment was performed in mixed $CDCl_3/CHCl_3$ solution in order to measure the solvent relaxation time. Values of 0.05 s (0.1 *M* $Cr(acac)_3$) and 0.1 s (0.05 *M* $Cr(acac)_3$) were obtained which were independent of methanol concentration. In another experiment the T_1's of CH_2Cl_2 and $CHCl_3$ in mixed solvent solutions containing $Cr(acac)_3$ were measured. These T_1's were independent of solvent composition over the full range of compositions from pure chloroform to pure methylene chloride (see Table 2). In contrast to the behaviour of methanol, solutions of acetone in $CDCl_3$ give a T_1 for the solute which is independent of concentration. These data are also contained in Table 2.

In the course of making these T_1 measurements the chemical shifts of the methanol protons were also obtained; these data are shown graphically in Fig. 2. In the absence of $Cr(acac)_3$ the OH proton moves to low field with increasing methanol concentration. This effect has been attributed (17) to increasing association of the methanol due to the intermolecular hydrogen bonding. In the presence of $Cr(acac)_3$ this effect is more pronounced and the plot of OH chemical shift *vs.* methanol concentration apparently shows two distinct linear portions with a break at 1.6 *M*. This concentration is identical with the concentration at which the

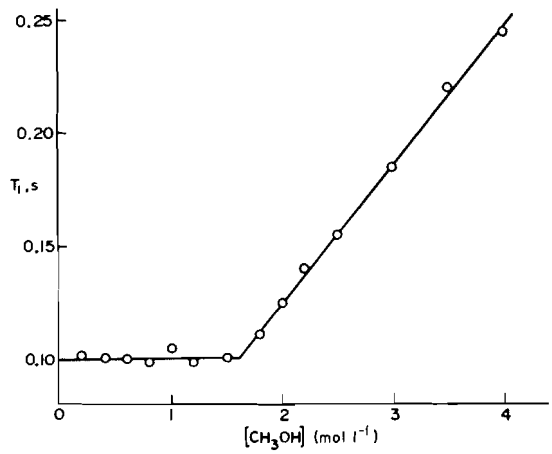

FIG. 1. Dependence of CH_3 T_1 on methanol concentration. Solvent $CDCl_3$ 0.01 *M* $Cr(acac)_3$.

Can. J. Chem. Downloaded from www.nrcresearchpress.com by 210.87.254.105 on 09/05/12
For personal use only.

TABLE 2. Proton T_1's for acetone, chloroform, and methylene chloride*

$[(CH_3)_2CO]$ (mol l^{-1})	T_1 (s)		Mole fraction of $CHCl_3$†	T_1 (s)	
	$(CH_3)_2CO$	$CHCl_3$		$CHCl_3$	CH_2Cl_2
0.1	0.375	—	0	—	0.128
0.2	0.327	0.060	0.1	0.052	0.120
0.3	0.384	—	0.25	0.058	0.118
0.4	0.357	—	0.5	0.048	0.130
0.5	0.364	0.057	0.75	0.055	0.122
0.6	0.378	—	0.9	0.047	0.114
0.7	0.327	—	1.0	0.052	—
0.8	0.354	—			
0.9	0.320	0.063			
1.0	0.339	0.060			
2.0	0.349	0.057			
2.5	0.422	0.051			
3.0	0.392	0.043			
3.5	0.361	—			
4.0	0.353	0.049			

*All solution 0.01 M $Cr(acac)_3$.
†Mole fraction of $CHCl_3$ in $CHCl_3/CH_2Cl_2$ mixture.

T_1's start to increase. There is an indication of a similar break point in the CH_3 chemical shifts but the effect is very much smaller. The temperature dependence of the OH chemical shifts has been examined. The concentration corresponding to the change of slope is quite insensitive to temperature. However, the chemical shifts observed depend strongly on the amount of water present in the sample which leads to some experimental difficulties in reproducing plots from sample to sample. This may be contrasted with the T_1 measurements described above for which the observed T_1 values are insensitive to the amount of water. Because of the above limitation we have not attempted any quantitative analysis of the chemical shift data.

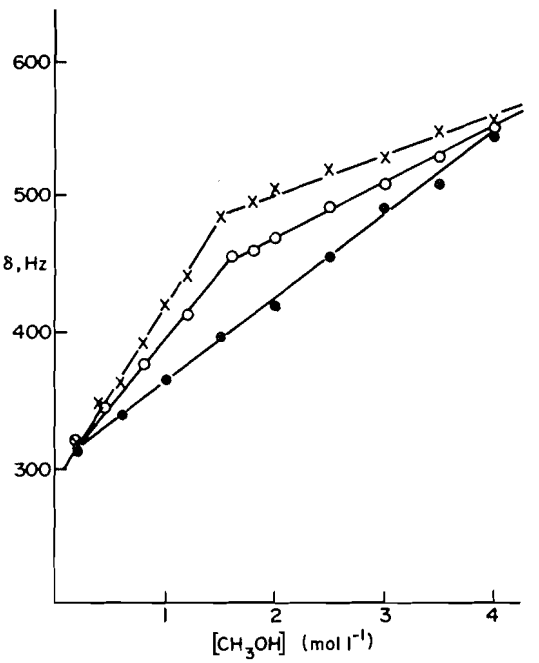

FIG. 2. Chemical shifts of hydroxyl proton of methanol: ●, no $Cr(acac)_3$; ○, 0.005 M $Cr(acac)_3$; ×, 0.01 M $Cr(acac)_3$.

Discussion

It seems very probable that the concentration dependence of the methanol T_1's shown in Fig. 1 reflects some form of second sphere interaction with the $Cr(acac)_3$. The parallel behaviour of the OH chemical shifts suggests further that hydrogen bonding interactions of the type discussed by Davis and Fackler are involved, although the effect of adventitious water complicates the situation. It is therefore desirable to develop a model which will account for this behaviour.

In the absence of any second sphere interaction the effect of the paramagnetic molecules on the proton relaxation of a solvent or solute molecule will be determined by the rate at which the diamagnetic molecule diffuses into the neighbourhood of the paramagnetic complex. Abragam (18) has treated the general problem

Can. J. Chem. Downloaded from www.nrcresearchpress.com by 210.87.254.105 on 09/05/12
For personal use only.

Can. J. Chem. Downloaded from www.nrcresearchpress.com by 210.87.254.105 on 09/05/12
For personal use only.

of relaxation by this type of mechanism and Luz and Meiboom (19) have given specific formulae for a rather similar case involving Co^{2+}. In the latter case the electron spin relaxation time is short and determines the nuclear spin relaxation time. For Cr^{3+} the electron spin relaxation time is relatively long and a small extension of Abragam's formulation leads to the relationship

$$[1] \qquad \frac{1}{T_1} = \frac{4\pi}{45} N\gamma_e^2\hbar^2 S(S+1)\gamma_I^2 \frac{\tau_D}{a^3}$$

In this equation N is the number of molecules of paramagnetic complex contained in 1 cc of solution, a is the radius of the paramagnetic complex, γ_e and γ_I are the magnetogyric ratios of the electron and nucleus respectively, and S is the spin of the metal ion. τ_D is the diffusional correlation time which determines the rate at which the interacting molecule will diffuse to the neighbourhood of the paramagnetic complex. It will be noted that this equation predicts that T_1 will be inversely proportional to the concentration of paramagnetic material but independent of the concentration of diamagnetic molecules. This model therefore satisfactorily accounts for the behaviour of chloroform, methylene chloride, and acetone in the presence of $Cr(acac)_3$ but not for that of methanol. If the reasonable values of $a = 4.5$ Å and $\tau_D = 10^{-10}$ s are assumed, this equation gives $T_1 = 0.049$ s for a 0.01 M solution of $Cr(acac)_3$ which agrees very satisfactorily with the $CHCl_3$ value of 0.05 s.

Consideration of a model involving molecules held in a second coordination sphere requires the definition of several correlation times. τ_S is the average time a ligand such as methanol spends in the second coordination sphere. τ_C is the rotational diffusion time, τ_D is the translational diffusion time encountered above, and τ_r is the average time of rotational tumbling for the complex. These last three correlation times are interrelated. For large molecules $\tau_D \approx 9\tau_C$ and $\tau_r \approx 3\tau_C$. The value of τ_C can be obtained from ^{13}C T_1 measurements on diamagnetic complexes as will be discussed below. We may then define the following situations.

(*a*) $\tau_S \gg \tau_r$. This corresponds to a tight second sphere complex with a well-defined coordination number M and a well-defined T_1 ($T_{1(complex)}$) for protons on a second sphere ligand. $T_{1(obs)}$ will be a function of $T_{1(complex)}$ and $T_{1(free)}$.

(*b*) $\tau_S \ll \tau_r$. In this case there is no measurable second sphere complex formation and $T_{1(obs)}$ is a function of τ_D as discussed above.

(*c*) $\tau_S \approx \tau_r$. This corresponds to a loose second sphere complex. The coordination number n becomes large and poorly defined and $T_{1(obs)}$ will be a complicated function of τ_r and τ_D.

Consider the case of $Cr(acac)_3$ dissolved in a chloroform/methanol mixture in which the interaction of methanol with $Cr(acac)_3$ corresponds to case *a* and the interaction of chloroform to case *b*. The composition of the solvent in the vicinity of $Cr(acac)_3$ will be determined by equilibria such as:

$$Cr(acac)_3(CHCl_3)_{M-m+1}(CH_3OH)_{m-1} + CH_3OH \underset{}{\overset{K_m}{\rightleftharpoons}} Cr(acac)_3(CHCl_3)_{M-m}(CH_3OH)_m + CHCl_3$$

where $m = 1, 2, 3, \ldots, M$ (the coordination number) and K_m is an equilibrium constant. The relaxation time of the methanol in this model will be given by

$$[2] \qquad \frac{1}{T_{1(obs)}} = \frac{[CH_3OH]_C}{[CH_3OH]_0} \cdot \frac{1}{T_{1(complex)}} + \frac{[CH_3OH]}{[CH_3OH]_0} \cdot \frac{1}{T_{1(free)}}$$

where $[CH_3OH]_C$ is the concentration of methanol in the second sphere of the $Cr(acac)_3$ and $[CH_3OH]_0$ is the total concentration of methanol. $[CH_3OH]_C$ can be expressed in terms of the equilibrium constants K_m and it can be shown (see appendix A) that

$$[3] \qquad T_{1(obs)} = \frac{[CH_3OH]_0}{\mu[Cr(acac)_3]_0} T_{1(complex)}$$

where

$$\mu = \frac{\sum_{m=1}^{M} m f^m \prod_{i=1}^{m} K_i}{1 + \sum_{m=1}^{M} f^m \prod_{i=1}^{m} K_i}$$

and

$$f = \frac{[CH_3OH]}{[CHCl_3]}$$

The behaviour of T_1 as a function of methanol concentration therefore depends on the depen-

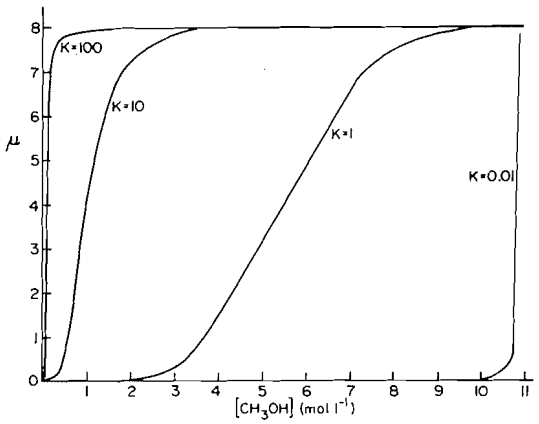

FIG. 3. Dependence of μ on concentration for different values of the equilibrium constant K.

dence of μ on methanol concentration. As a simplifying assumption we assume that all the successive equilibrium constants K_m are equal. Figure 3 shows a set of plots of μ *vs.* $[CH_3OH]_0$ for different values of K. At high $[CH_3OH]_0$ μ reaches a limiting value of M, the coordination number, which was taken to be 8 (see below) for the purpose of the calculations shown in Fig. 3. Therefore at high concentrations of methanol we obtain

$$[4] \qquad T_{1(obs)} = \frac{[CH_3OH]_0}{[Cr(acac)_3]_0} \cdot \frac{T_{1(complex)}}{M}$$

i.e., $T_{1(obs)}$ is proportional to $[CH_3OH]_0$ and the ratio $T_{1(complex)}/M$ can be obtained from the slope of the plot shown in Fig. 1. At lower concentrations of methanol the plots of Fig. 3 show that μ increases with $[CH_3OH]_0$ in an approximately linear manner. In this case eq. 3 shows that $T_{1(obs)}$ will, to a first approximation, be independent of $[CH_3OH]_0$. The model is therefore qualitatively satisfactory.

Further analysis requires a knowledge of $T_{1(complex)}$. For a second sphere complex it is reasonable to assume that T_1 is dominated by dipolar electron spin – nuclear spin interactions. In this case

$$[5] \qquad \frac{1}{T_{1(complex)}} = \frac{4}{3}S(S+1)\left(\frac{g\beta g_N\beta_N}{\hbar r^3}\right)^2\tau_C$$

Utilization of this equation requires a knowledge of τ_C. This quantity may be obtained from the ^{13}C T_1 values of the diamagnetic complex Co(III) acetylacetonate. We assume that the geometry of this compound is closely similar to that of Cr(III) acetylacetonate and that the ^{13}C relaxation times are determined by dipolar interactions with the protons, *i.e.*

$$[6] \qquad \frac{1}{T_1} = \frac{4}{3}I(I+1)\gamma_H{}^2\gamma_C{}^2\hbar\tau_C\sum_{i=1}^{i=a}\frac{1}{b_i{}^6}$$

where b is an internuclear separation between a carbon and a proton. Table 3 gives the ^{13}C T_1 relaxation times and the derived values of τ_C for a 0.2 M solution of $Co(acac)_3$ in $CDCl_3$ and also for a solution 0.2 M in $Co(acac)_3$ and 3.0 M in CH_3OH. It is apparent that the addition of methanol causes a small decrease in the T_1's and a corresponding small increase in τ_C. This is consistent with the existence of a second coordination sphere of methanol molecules surrounding $Co(acac)_3$ as has been deduced for $Cr(acac)_3$. From these results we obtain a value of $\tau_C = 7.7 \times 10^{-11}$ s for use in eq. 5. We may now proceed to calculate values of T_1/M to compare with the experimental value for this quantity. Some results of these calculations are shown in Table 4. Good agreement between experimental and calculated values is obtained for $M = 8$ and r, the Cr atom methyl hydrogen separation, 7 Å. This corresponds rather nicely to the expected internuclear separation in a model with one methanol molecule

TABLE 3. ^{13}C T_1's for Co(III) acetylacetonate*

	Solution A		Solution B	
Carbon	T_1 (s)	τ_C† (s)	T_1† (s)	τ_C† (s)
CH_3	0.23	7.1×10^{-11}	0.22	7.4×10^{-11}
CO	12.5	7.5×10^{-11}	12.0	7.8×10^{-11}
CH	0.67	7.3×10^{-11}	0.62	7.9×10^{-11}

*Solution A, 0.2 M $Co(acac)_3$ in $CDCl_3$. Solution B, 0.2 M $Co(acac)_3$ + 3.0 M CH_3OH in $CDCl_3$.
†Calculated assuming C—C bond length 1.5 Å C—H bond length 1.1 Å.

Can. J. Chem. Downloaded from www.nrcresearchpress.com by 210.87.254.105 on 09/05/12
For personal use only.

TABLE 4. Calculated second sphere relaxation times

r (Å)	$T_{1(complex)}$* (s)	Coordination number, M	$T_{1(complex)}$†/M
5	6.49×10^{-4}	8	8.12×10^{-5}
6	1.95×10^{-3}	8	2.45×10^{-4}
7	5.78×10^{-3}	8	6.48×10^{-4}
8	1.12×10^{-2}	8	1.49×10^{-3}
9	2.29×10^{-2}	8	2.87×10^{-3}
10	4.35×10^{-2}	24	1.80×10^{-3}
11	7.67×10^{-2}	24	3.38×10^{-3}

*Calculated assuming $\tau_C = 7.7 \times 10^{-11}$ s.
†Experimental value of $T_{1(complex)}/M = 6.3 \times 10^{-4}$.

situated on each face of a $Cr(acac)_3$ octahedron. It is not consistent with a diffuse second coordination sphere leading to larger internuclear separations and higher apparent coordination numbers.

From the above ^{13}C relaxation measurements we may also estimate that $\tau_r \approx 2 \times 10^{-10}$ s. The lifetime of a methanol molecule in the second coordination sphere must therefore be greater than this value. An upper limit to this lifetime of perhaps 10^{-2} s may be inferred from the fact that only an average resonance of second coordination sphere and "free solution" methanol is observed.

To summarize the existence of a concentration region in which the T_1 of a potential ligand is proportional to ligand concentration demonstrates the existence of a discrete second coordination sphere with a lifetime greater than τ_r ($\sim 2 \times 10^{-10}$ s in this case). The concentration at which this linear dependence commences is determined by the equilibrium constant K. For the case of methanol and $Cr(acac)_3$ in chloroform discussed above the onset of the linear portion of the T_1 *vs.* concentration plot occurs at approximately 1.6 M. Reference to the curves of Fig. 3 shows that this corresponds to a value of $K \approx 10$, *i.e.*, methanol is approximately a ten times better second sphere ligand than chloroform in this system. This value is consistent with the relative equilibrium constants reported previously for the Co(II) pyrazylborate system (4). In the case of acetone a concentration dependence of T_1 was not observed. We deduce from this either that the lifetime of acetone in the second sphere is less than τ_r, in which case the relaxation is dominated by diffusion, or that the equilibrium constant for second sphere complexation is very small. The former would appear to be the correct interpretation since the curves of Fig. 3 show that for small K's μ is small and varies only slowly with ligand concentration. This would lead to values of $T_{1(obs)}$ larger than those found experimentally (assuming a reasonable value of $T_{1(complex)}$) and to a dependence on ligand concentration. Equation 1 (the diffusion controlled model) predicts no ligand dependence and gives reasonable numerical agreement. In any event the conclusion is that second sphere complexes with acetone are either very weak, very labile or both. The observed independence of T_1 for both chloroform and methylene chloride on the composition of the mixtures of these two solvents leads to the same conclusion regarding their properties as second sphere ligands.

It appears therefore that the existence of a concentration range over which T_1 varies linearly with concentration may be a reasonable criterion for defining a second coordination sphere. Further, it appears that the condition for this criterion, $\tau_S > \tau_r$, is closely similar to the condition for a kinetically significant second coordination sphere (14) leading to the possibility of an I_a or I_d ligand exchange mechanism. We suggest therefore that T_1 measurements may provide a valuable experimental probe for mechanistic studies particularly on non-labile complexes. In principle this experimental method can also be applied to labile complexes. There are however experimental difficulties since if there is fast exchange involving the first coordination sphere of a paramagnetic complex and if the fraction of ligand in the first sphere is substantial the first sphere relaxation time tends to dominate T_1.

Experimental

T_1 measurements were carried out on a Bruker WH90 Fourier Transform instrument. Samples were degassed before making measurements to eliminate the effect of oxygen on the relaxation times. The programme used (Nicolet NIC-27-40713) is based on the usual 180–γ–90 plus sequence. The estimated error in the T_1 measurements is $\pm 5\%$. All T_1 measurements were carried out at 28 °C. The temperature dependence of the methanol chemical shifts briefly reported was obtained from measurements on a Varian HA-100 instrument.

Acknowledgment

We are indebted to the National Research Council of Canada for financial support of this research.

Can. J. Chem. Downloaded from www.nrcresearchpress.com by 210.87.254.105 on 09/05/12
For personal use only.

Can. J. Chem. Downloaded from www.nrcresearchpress.com by 210.87.254.105 on 09/05/12
For personal use only.

Appendix A

Consider the equilibria:

[A1] $$Cr(acac)_3(CHCl_3)_{M-m+1}(CH_3OH)_{m-1} + CH_3OH \overset{K_m}{\rightleftharpoons} Cr(acac)_3(CHCl_3)_{M-m}(CH_3OH)_m + CHCl_3$$

with $m = 1, 2, 3, \ldots, M$. Then

[A2] $$K_m = \frac{[Cr(acac)_3(CHCl_3)_{M-m}(CH_3OH)_m][CHCl_3]}{[Cr(acac)_3(CHCl_3)_{M-m+1}(CH_3OH)_{m-1}][CH_3OH]}$$

The total concentration of complexed methanol is given by

[A3] $$[CH_3OH]_C = \sum_{m=1}^{M} m[Cr(acac)_3(CHCl_3)_{M-m}(CH_3OH)_m]$$

and the total concentration of $Cr(acac)_3$ by

[A4] $$[Cr(acac)_3]_0 = [Cr(acac)_3(CHCl_3)_M] + \sum_{m=1}^{M}[Cr(acac)_3(CHCl_3)_{M-m}(CH_3OH)_m]$$

Substituting [A2] in [A3] and [A4] we obtain [A3*a*] and [A4*a*]

[A3*a*] $$[CH_3OH]_C = [Cr(acac)_3(CHCl_3)_M]\sum_{m=1}^{M} mf'^m \prod_{i=1}^{m} K_i$$

[A4*a*] $$[Cr(acac)_3]_0 = [Cr(acac)_3(CHCl_3)_M]\left\{1 + \sum_{m=1}^{M} f'^m \prod_{i=1}^{m} K_i\right\}$$

where $f' = [CH_3OH]/[CHCl_3]$.

Combining [A3*a*] and [A4*a*] gives

[A5] $$[CH_3OH]_C = \frac{\sum_{m=1}^{M} mf'^m \prod_{i=1}^{m} K_i}{1 + \sum_{m=1}^{M} f'^m \prod_{i=1}^{m} K_i}[Cr(acac)_3]_0$$

For this model

[A6] $$\frac{1}{T_{1(obs)}} = \frac{[CH_3OH]_C}{[CH_3OH]_0}\cdot\frac{1}{T_{1(complex)}} + \frac{[CH_3OH]}{[CH_3OH]_0}\frac{1}{T_{1(free)}}$$

where

$$[CH_3OH]_0 = [CH_3OH]_C + [CH_3OH]$$

Since $[CH_3OH] \approx [CH_3OH]_0$ and $T_{1(free)} \approx 10$ s the second term in [A6] is $\sim 10^{-1}$; $1/T_{1(obs)} \approx 10\text{–}10^2$ and the second term in eq. 6 may be dropped.

Therefore

$$T_{1(obs)} = \frac{[CH_3OH]_0}{[CH_3OH]_C}T_{1(complex)}$$

Substituting eq. A5

$$T_{1(obs)} = \frac{[CH_3OH]_0}{\mu[Cr(acac)_3]_0}T_{1(complex)}$$

where μ is the coefficient of $[Cr(acac)_3]_0$ in [A5].

1. D. R. EATON. Can. J. Chem. **47**, 2645 (1969).
2. D. R. EATON, H. O. OHORODNYK, and L. SEVILLE. Can. J. Chem. **49**, 1218 (1971).
3. D. R. EATON, L. SEVILLE, and J. P. JESSON. Can. J. Chem. **49**, 2751 (1971).
4. D. R. EATON and K. L. CHUA. Can. J. Chem. **51**, 4137 (1973).
5. T. J. SWIFT. *In* NMR of paramagnetic molecules. *Edited by* G. N. LaMar, W. D. Horrocks, and R. H. Holm. Academic Press. 1973.
6. L. O. MORGAN, A. W. NOLLE, R. L. HALL, and J. MURPHY. J. Chem. Phys. **25**, 206 (1956).
7. E. S. AMIS and J. F. HINTON. Solvent effects on chemical phenomena. Vol. 1. Academic Press. 1973.
8. T. R. STENGLE and C. H. LANGFORD. J. Phys. Chem. **69**, 3299 (1965).
9. L. S. FRANKEL. J. Phys. Chem. **73**, 3897 (1969).
10. L. S. FRANKEL. J. Phys. Chem. **74**, 1645 (1970).
11. C. H. LANGFORD and J. F. WHITE. Can. J. Chem. **45**, 3049 (1967).
12. S. BEHRENDT, C. H. LANGFORD, and L. S. FRANKEL. J. Am. Chem. Soc. **91**, 2236 (1969).
13. A. CARRINGTON and A. D. MCLACHLAN. Introduction to magnetic resonance. Harper and Row. 1967.
14. C. H. LANGFORD and H. B. GRAY. Ligand substitution processes. W. A. Benjamin Inc. 1966.
15. G. C. LEVY and U. EDLUND. J. Am. Chem. Soc. **97**, 4482 (1975) and references therein.
16. T. S. DAVIS and J. P. FACKLER. Inorg. Chem. **5**, 242 (1966).
17. J. A. POPLE, W. G. SCHNEIDER, and H. J. BERNSTEIN. High resolution nuclear magnetic resonance. McGraw-Hill. 1959.
18. A. ABRAGAM. The principles of nuclear magnetism. Oxford University Press, Oxford, England. 1961. p. 304.
19. Z. LUZ and S. MEIBOOM. J. Chem. Phys. **40**, 2686 (1964).

Can. J. Chem. Downloaded from www.nrcresearchpress.com by 210.87.254.105 on 09/05/12
For personal use only.

Can. J. Chem. Downloaded from www.nrcresearchpress.com by 210.87.254.42 on 09/05/12
For personal use only.

Canadian Journal of Chemistry

Published by
THE NATIONAL RESEARCH COUNCIL OF CANADA

Journal canadien de chimie

Publié par
LE CONSEIL NATIONAL DE RECHERCHES DU CANADA

Volume 54 Number 9 May 1, 1976

Volume 54 numéro 9 1 mai 1976

Synthetic application of α-hydroxydiazene systems. I. Esters from radical chain reactions of unsaturated compounds with 2-hydroxy-2,5,5-trimethyl-Δ^3-1,3,4-oxadiazoline

PETER KNITTEL AND JOHN WARKENTIN
Department of Chemistry, McMaster University, Hamilton, Ontario L8S 4M1

Received July 21, 1975

PETER KNITTEL and JOHN WARKENTIN. Can. J. Chem. **54**, 1341 (1976).

2-Hydroxy-2,5,5-trimethyl-Δ^3-1,3,4-oxadiazoline (**1**) reacts with acetylenic and olefinic unsaturated systems by addition of the 2-acetoxy-2-propyl group and a hydrogen atom, respectively, to the two atoms forming the multiple bond. The regiochemistry of addition to unsymmetric unsaturated systems is that predicted for a radical chain mechanism, in which the 2-acetoxy-2-propyl radical adds to the multiple bond so as to form the more stable free radical which then abstracts a hydrogen atom from the hydroxyl group of **1**. Polymerization of the unsaturated substrate, as well as abstraction of allylic hydrogen (if any) are competing processes. Yields of adducts, based on **1**, ranged from 80% in reaction with crotonaldehyde to 10% in reaction with cyclohexene.

PETER KNITTEL et JOHN WARKENTIN. Can. J. Chem. **54**, 1341 (1976).

L'hydroxy-2 triméthyl-2,5,5 Δ^3-oxadiazoline-1,3,4 (**1**) réagit avec les systèmes acétyléniques et oléfiniques insaturés par addition du groupe acétoxy-2 propyl-2 et d'un atome d'hydrogène respectivement aux deux atomes formant la liaison multiple. La régiochimie de l'addition à des systèmes insaturés non-symétriques correspond à celle prédite pour un mécanisme radicalaire en chaîne dans lequel les radicaux acétoxy-2 propyl-2 s'additionnent à la liaison multiple de façon à former le radical libre le plus stable qui enlève subséquemment un hydrogène du groupe hydroxyle de **1**. La polymérisation du substrat insaturé de même que l'enlèvement de l'hydrogène allylique (s'il existe) sont des processus qui sont en compétition avec la réaction d'addition. Les rendements d'adduits, basés sur **1**, varient entre 80% pour la réaction avec le crotonaldéhyde jusqu'à 10% pour la réaction avec le cyclohexène.

[Traduit par le journal]

Introduction

The synthesis and novel induced decomposition of 2-hydroxy-2,5,5-trimethyl-Δ^3-1,3,4-oxadiazoline, **1**, was reported recently (1). Evidence for chain decomposition of **1** by radical substitution at the hydroxyl hydrogen included the observation (1) that olefinic substrates react with **1** according to [1]. In this paper we report initial application of that type of reaction

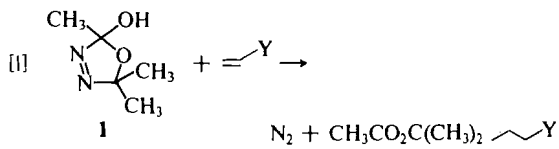

to the synthesis of tertiary acetates.

Can. J. Chem. Downloaded from www.nrcresearchpress.com by 210.87.254.42 on 09/05/12
For personal use only.

Experimental

2-Hydroxy-2,5,5-trimethyl-Δ^3-1,3,4-oxadiazoline, 1

Preparation of **1** from 5,5-dimethyl-Δ^3-1,3,4-oxadiazoline, **2**, and excess methyllithium has been described (1). Addition of **2** in cold ether to excess methylmagnesium iodide in ice-cooled ether, followed by the work-up described in the methyllithium procedure (1), gave **1** of the same quality but in lower yield (60%).

Tertiary Acetates

The following general procedure was used throughout. A solution of **1** (2.0 g, 0.015 mol) in benzene (30 ml) was cooled with ice and stirred vigorously with a magnetic stirrer. The unsaturated compound (2 equiv.) was added all at once, a condenser and drying tube were fitted to the flask, and the reaction mixture was heated to 50–60 °C, with constant stirring, until the pmr spectrum of an aliquot showed that all **1** had reacted (about 4 h). Most of the benzene and excess unsaturated compound were removed by distillation, leaving the product as a crude oil. Isolation of a small, pure sample for spectra and analyses was done by glpc. Large scale preparations and purification by other methods, such as fractional distillation, were not attempted in this exploratory work. Minimum and maximum yields, 10% for cyclohexene and 80% for crotonaldehyde, were estimated by pmr, using the known concentration of an added standard for reference. Effects of other reaction conditions (concentration, temperature, additives, solvents) on yields have not yet been explored.

Nuclear magnetic resonance spectra and analyses of eight tertiary acetates are listed in Table 1. Eight other products of reaction of **1** with olefinic substrates were assigned tertiary acetate structures on the basis of their spectra and analogy, without confirmatory analytical data. Those samples are reported below in the format: olefinic substrate, product, major ir bands (CCl_4), and pmr spectrum (CCl_4, multiplicity symbol and relative integral in parentheses).

tert-Butylacetylene: 2-acetoxy-2,5,5-trimethylhex-3-ene; 1738, 1380, 1360, 1248 cm^{-1}; δ 1.01 (s, 9), 1.47 (s, 6), 1.90 (s, 3), 5.54 (s, 2).

Tetrachloroethylene: 3-acetoxy-3-methyl-1,1,2,2-tetrachlorobutane; 1750, 1661, 1385, 1367, 1240 cm^{-1}; δ 1.72 (s, 6), 1.97 (s, 1), 2.05 (s, 3).

1-(Pyrrolidino)-1-cyclohexene: 1-pyrrolidino-2-(2′-acetoxy-2′-propyl)cyclohexane; 1745, 1640, 1575, 1380, 1355, 1245 cm^{-1}; δ 1.54 (s, 6), 1.40–2.00 (m, 13), 2.08 (s, 3), 2.80–3.30 (m, 5).

N-Phenylmaleimide: 3-(2′-acetoxy-2′-propyl)-*N*-phenyl succinimide; 1725 (br), 1398, 1365, 1248 cm^{-1}; δ 1.58 (s, 3), 1.72 (s, 3), 2.76–2.92 (m, 2), 3.56–3.80 (m, 1), 7.04–7.60 (m, 5).

Maleic anhydride: 3-(2′-acetoxy-2′-propyl)succinic anhydride; δ 1.75 (s, 6), 2.11 (s, 3), 3.10 (d, 2), 3.78 (t, 1).

Norbornadiene: 3-(2′-acetoxy-2′-propyl)tricyclo-[2.2.1.0^{2,6}]heptane; 1740, 1380, 1365, 1252 cm^{-1}; δ 1.46 (s, 3), 1.50 (s, 3), 1.94 (s, 3), 1.04–3.00 (m, 9).

Acrylic acid: 4-acetoxy-4-methylpentanoic acid; 3400–2400, 1740, 1720, 1390, 1370, 1250 cm^{-1}; δ 1.50 (s, 6), 2.00 (s, 3), 2.10–2.85 (m, 4), 10.13 (s, br, 1).

Cyclohexene: 2-acetoxy-2-cyclohexylpropane; 1732, 1379, 1360, 1257 cm^{-1}; δ 1.40 (s, 6), 1.99 (s, 3), 1.06–2.18 (m, 11) and 3,3′-bicyclohexenyl (major product); 3025, 2940, 2865, 2845, 1650 cm^{-1}; δ 1.10–2.30 (m, 14), 5.48–5.88 (m, 4). *Anal.* calcd. for $C_{12}H_{18}$: C 88.88, H 11.12; found: C 88.71, H 11.28.

Discussion

The exploratory work described above demonstrates that the potential of **1** for synthesis is fairly broad. Nucleophilic olefins (enol ethers, enamines) as well as more electrophilic olefins (α,β-unsaturated carbonyl and nitrile systems) add the elements of isopropyl acetate[1] from **1**. A radical chain mechanism (1), with the propagation steps shown in [2] and [3] accounts for both the regiochemistry of addition and the lack of stereospecificity in the addition to dimethyl acetylenedicarboxylate. Vinyl radicals normally lead to both stereoisomeric products (*3a*).

[2] $CH_3CO_2\dot{C}(CH_3)_2 + CH_2{=}CHY \rightarrow$ (**4**)

$CH_3CO_2C(CH_3)_2CH_2\dot{C}HY$ (**5**)

[3] $CH_3CO_2C(CH_3)_2CH_2\dot{C}HY$ (**5**) $+ \mathbf{1} \rightarrow$

$CH_3CO_2C(CH_3)_2CH_2CH_2Y + N_2 + \mathbf{4}$

Stereospecific addition to *tert*-butylacetylene is probably the result of steric hindrance to formation of the *cis* adduct. The observed selectivity of addition to norbornene is also not surprising for *exo* attack on that olefin, by both radicals (4) and electrophiles (5), is well known. Whether or not hydrogen is also added from the *exo* side in this case, where the *exo* substituent already present is large, remains to be tested.

Present limitations in the use of **1** for synthesis include its failure to form adducts, in the sense of [2] and [3], to α-methylstyrene, styrene, ethylazodicarboxylate, azodicarbonamide, *trans*-1,4-dihydroxy-2-butene, *trans*-1,4-dichloro-2-butene, benzalacetophenone, 2-methyl-2-butene, mesityl oxide, hexachlorocyclopentadiene, cyclooctadiene, and stilbene. Major competitive processes known to occur are polymerization (styrenes) and reduction (ethylazodicarboxylate to ethylhydrazodicarboxylate). Abstraction of allylic hydrogen, a major process leading to 3,3′-bicyclohexenyl from cyclohexene, may be the

[1]Addition of isopropyl acetate directly, rather than in its present disguise as **1**, is not a promising alternative. First, simple esters are poor reagents for radical chain addition and second, they add preferentially in the sense $>\dot{C}CO_2CHR_2$ rather than $>CHCO_2\dot{C}R_2$ (2, 3*b*).

Can. J. Chem. Downloaded from www.nrcresearchpress.com by 210.87.254.42 on 09/05/12
For personal use only.

TABLE 1. Analyses and nmr spectra of tertiary acetates

Reactant	Product[a]	pmr[b]	Analysis (%) Calcd. C	Calcd. H	Obsvd. C	Obsvd. H
$CH_3O_2CC{\equiv}CCO_2CH_3$	$CH_3CO_2CH{=}C(CO_2CH_3)C(CH_3)_2O_2CCH_3$[d] ($C_{11}H_{16}O_6$)	1.65 s, 1.76 s, 1.91 s, 1.99 s, 3.80 m, 5.88 s, 6.46 s	54.10	6.56	54.29	6.72
$CH_2{=}CHCN$	$CH_3CO_2C(CH_3)_2CH_2CH_2CN$[e] ($C_8H_{13}NO_2$)	1.55 (s, 6), 2.02 (s, 3), 2.36 (m, 4)	61.93	8.38[f]	60.92	8.35[f]
$CH_3CH{=}CHCHO$	$CH_3CH(CH_2CHO)C(CH_3)_2O_2CCH_3$[g] ($C_9H_{16}O_3$)	0.95 (d, 3), 1.38 (s, 3), 1.46 (s, 3), 1.92 (s, 3), 1.99–2.75 (m, 3), 9.66 (t, 1)	62.79	9.30	61.92	9.32
$CH_2{=}CHCOCH_3$	$CH_3CO_2C(CH_3)_2CH_2CH_2COCH_3$[h] ($C_9H_{16}O_3$)	1.43 (s, 6), 1.98 (s, 3), 2.18 (s, 3), 1.80–2.68 (m, 4)	62.79	9.30	62.96	9.29
$CH_2{=}CHCO_2CH_3$	$CH_3CO_2C(CH_3)_2CH_2CH_2CO_2CH_3$[i] ($C_9H_{16}O_4$)	1.38 (s, 6), 1.88 (s, 3), 1.90–2.42 (m, 4), 3.61 (s, 3)	57.45	8.51	57.17	8.40
$CH_2{=}CHOCH_2CH_3$	$CH_3CO_2C(CH_3)_2CH_2CH_2OCH_2CH_3$[j] ($C_9H_{18}O_3$)	1.17 (t, 3), 1.47 (s, 6), 1.94 (s, 3), 2.02 (t, 2), 3.22–3.63 (m, 4)	62.06	10.34	61.89	10.54
$CH_3O_2CCH{=}CHCO_2CH_3$	$CH_3CO_2C(CH_3)_2CH(CO_2CH_3)CH_2CO_2CH_3$[k] ($C_{11}H_{18}O_6$)	1.54 (s, 6), 1.98 (s, 3), 2.28–3.18 (m, 3), 3.68 (s, 3), 3.74 (s, 3)	53.66	7.32	53.45	7.43
	$C(CH_3)_2O_2CCH_3$[e] ($C_{12}H_{20}O_2$)	1.48 (s, 6), 2.00 (s, 3), 1.00–2.35 (m, 11)	73.47	10.20	73.58	10.41

[a]All products showed the appropriate infrared bands for the ester function (*ca.* 1735 cm^{-1}, the *gem*-dimethyl system (*ca.* 1250 cm^{-1}) and for other strongly-absorbing functional groups, if any.
[b]CCl_4, δ-values, followed by multiplicity symbol and relative integral.
[c]2-Acetoxy-2-(2′-bicyclo[2.2.1]heptyl)propane; probably the *exo* isomer.
[d]Methyl 4-acetoxy-3-carbomethoxy-4-methylpent-2-enoate, *cis–trans* mixture, ratio 2:1. Attempts to separate the isomers by glpc failed and assignment of the structures of the major and minor isomers from spectra of the mixture was not possible.
[e]4-Acetoxy-4-methylvaleronitrile.
[f]Nitrogen: calcd. 9.03, found 8.76.
[g]4-Acetoxy-3,4-dimethylpentanal.
[h]5-Acetoxy-5-methylhexan-2-one.
[i]Methyl-2-acetoxy-2-methylpentanoate.
[j]Ethyl-3-acetoxy-3-methylbutyl ether.
[k]Methyl-2-acetoxy-3-carbomethoxy-2-methylpentanoate.

cause of some other failures. Whether or not the expected adducts were actually formed in some cases but were too unstable to survive, is also not known.

More work will need to be done to improve our understanding of the addition process, and of competitive processes, before the potential of this new method can be fully realized. It may be possible to find selective chain transfer agents (HA) which function like **1** in [3] to decrease the lifetime of adduct radicals (**5**), thereby suppressing polymerization. Such agents would have to react more slowly with **4** than with **5** and the radical A· would have to be capable of abstracting hydrogen from **1** but not of addition to $CH_2{=}CHY$. A reagent meeting those requirements would really be a catalyst for the chain addition of **1**. The outlook for improving yields in the present case is bright, for catalysis of radical chain addition via another α-hydroxydiazene has been achieved by including phenol in the reaction mixture (6).

In summary, the results described suggest that **1**, and other members of the family available from other oxadiazolinones (7) may become valuable reagents for functionalizing alkenes and alkynes by radical chain addition. Synthesis of monodeutero compounds, using hydroxyl deuterated **1** or its analogs, is an obvious extension for which the general approach may be particularly well suited.

Acknowledgment

We are indebted to the National Research Council of Canada for an operating grant from which most of the support for this investigation was drawn.

1. P. KNITTEL and J. WARKENTIN. Can. J. Chem. **53**, 2275 (1975).
2. D. ELAD and R. D. YOUSSEFYEH. Chem. Commun. 7 (1965).
3. P. I. ABELL. Free radicals. Vol. 2. *Edited by* J. K. Kochi. John Wiley and Sons, New York and Toronto. 1973. (*a*) pp. 100–101; (*b*) pp. 95–96.
4. O. L. OSBORNE, T. V. VAN AUKEN, and D. J. TRECKER. J. Am. Chem. Soc. **90**, 5806 (1968).
5. T. G. TRAYLOR. Acc. Chem. Research **2**, 152 (1969).
6. D. W. K. YEUNG and J. WARKENTIN. Can. J. Chem. **54**, 1345 (1976).
7. P. KNITTEL, S. L. LEE, and J. WARKENTIN. Can. J. Chem. **50**, 3248 (1972).

Can. J. Chem. Downloaded from www.nrcresearchpress.com by 210.87.254.42 on 09/05/12
For personal use only.

Synthetic application of α-hydroxydiazene systems. II.[1] Uncatalyzed and phenol catalyzed radical chain hydro-*tert*-butylation of unsaturated compounds with *tert*-butylazodiphenylcarbinol

DOMINIC W. K. YEUNG AND JOHN WARKENTIN
Department of Chemistry, McMaster University, Hamilton, Ontario L8S 4M1

Received July 21, 1975

DOMINIC W. K. YEUNG and JOHN WARKENTIN. Can. J. Chem. **54**, 1345 (1976).

tert-Butylazodiphenylcarbinol **1** decomposes in benzene solution by a chain mechanism involving *tert*-butyl radicals. Many olefinic compounds and azobenzene act as radical traps and are hydro-*tert*-butylated by **1**. The regiochemistry of hydro-*tert*-butylation of unsymmetric alkenes is that expected for a mechanism which involves addition of *tert*-butyl radical so as to form the most stable radical adduct, which subsequently abstracts hydrogen from **1**.

In some cases phenol acts as a catalyst for the hydroalkylation process. The novel catalytic effect of phenol in a radical chain process is attributed to the favourable thermochemistry for induced, concerted decomposition of **1** by radical attack at hydroxyl hydrogen.

DOMINIC W. K. YEUNG et JOHN WARKENTIN. Can. J. Chem. **54**, 1345 (1976).

Le *tert*-butylazodiphénylcarbinol **1** se décompose en solution benzénique par un mécanisme en chaîne impliquant des radicaux *tert*-butyles. Plusieurs composés oléfiniques et l'azobenzène agissent comme piège à radicaux et sont hydro-*tert*-butylés par **1**. La régiochimie de la réaction de l'hydro-*tert*-butylation des alcènes non-symétriques correspond à celle attendue pour un mécanisme qui implique l'addition du radical *tert*-butyle de façon à former l'adduit radicalaire le plus stable suivi par un enlèvement subséquent d'hydrogène à partir de **1**.

Dans quelques cas, le phénol agit comme catalyseur pour le processus d'hydroalkylation. Ce nouvel effet catalytique du phénol dans un processus radicalaire en chaîne est attribué à une thermochimie favorable pour la décomposition induite et concertée de **1** par une attaque radicalaire au niveau de l'hydrogène hydroxylique.

[Traduit par le journal]

Concerted induced decomposition by radical attack at the hydroxyl hydrogen [1] is a recently recognized mechanism in the chemistry of α-hydroxydiazene systems (1–3). The stabilization afforded at the transition state from the heats of

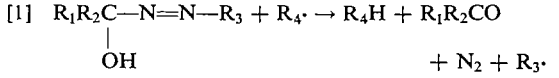

[1] $R_1R_2C(OH)-N=N-R_3 + R_4\cdot \rightarrow R_4H + R_1R_2CO + N_2 + R_3\cdot$

formation of N_2 and of a carbonyl group is sufficient to permit a variety of radicals ($R_4\cdot$), even highly stabilized ones, to abstract hydroxyl hydrogen. In particular, $R_4\cdot$ can be the adduct of $R_3\cdot$ and an alkene or alkyne (1, 3), such as acrylonitrile or dimethylacetylenedicarboxylate. In other words, decomposition of an α-hydroxydiazene in the presence of an unsaturated compound can result in radical chain addition of the groups R_3 and H to that compound (1–3).

In this paper we report the application of *tert*-butylazodiphenylcarbinol, **1**, ($R_1 = R_2 = C_6H_5$, R_3 = *tert*-Bu) as a reagent for radical chain hydro-*tert* butylation of unsaturated compounds.

Methods and Results

tert-Butylazodiphenylcarbinol, **1**, was synthesized from *tert*-butylazodiphenylmethyl acetate as described elsewhere (2). In a typical reaction of **1** with an unsaturated substrate, **1** in benzene was mixed with the substrate (about 4 equiv.) and the resulting solution was heated at 50 °C for 12 h. In some cases the reaction appeared to be over in 4 h or less, as judged visually from the rate of gas evolution (bubbling). In experiments with added phenol, the phenol was introduced all at once before the heating period.

Yields were determined directly by glpc or pmr after addition of a known quantity of an internal standard. Pure samples of products, most of them known compounds, were obtained from the gas chromatograph or by column chromatography. Their identities were readily confirmed by ms, ir, and pmr spectroscopy.

[1]For part I see Knittel and Warkentin (1).

Can. J. Chem. Downloaded from www.nrcresearchpress.com by 210.87.254.42 on 09/05/12
For personal use only.

TABLE 1. Hydro-*tert*-butylation of unsaturated compounds

Reactant	Product	Yield (%)[a]
$CH_2{=}CHCN$	$(CH_3)_3CCH_2CH_2CN$	63(85)[b] (20)[c]
$CH_2{=}CHCOCH_3$	$(CH_3)_3CCH_2CH_2COCH_3$	31(23)[c]
$CH_3CH{=}CHCHO$	$(CH_3)_3CCH(CH_3)CH_2CHO$	32(50)[c]
$CH_2{=}CHCO_2CH_3$	$(CH_3)_3CCH_2CH_2CO_2CH_3$	8(40)[c]
$CH_2{=}C(CH_3)O_2CCH_3$	$(CH_3)_3CCH_2CH(CH_3)O_2CCH_3$	18(12)[c]
	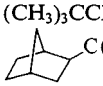	25(0)[c]
$C_6H_5N{=}NC_6H_5$	$C_6H_5NHN(C_6H_5)C(CH_3)_3$	100
$C_6H_5CH{=}CHC_6H_5$ (*trans*)	$C_6H_5CH_2CH(C_6H_5)C(CH_3)_3$[d]	0

[a]Yield of crude product, based on an assay by glpc or nmr.
[b]The bracketed number is the yield of crude product from a run with phenol present, mol ratio phenol : 1 = 0.5.
[c]The number in parentheses is the yield of crude product from a run with phenol present, mol ratio phenol: 1 = 1.0.
[d]Expected but not obtained.

tert-Butyl-1,2-diphenylhydrazine was synthesized by a second route, from *tert*-butyllithium and azobenzene.

Results of small scale reactions of **1** with six olefinic substrates and with azobenzene are gathered in Table 1. Large scale syntheses were not attempted in this exploratory work.

Discussion

Although all substrates listed in Table 1 reacted with **1** in the desired sense, the yields ranged from 100% down to about 20%, based on **1**. The quantitative yield with azobenzene is striking, especially in view of the fact that decomposition of **1** in the presence of *trans*-stilbene did not lead to 1,2-diphenyl-3,3-dimethylbutane. Addition to azobenzene, but not to stilbene, could be attributed to a large dependence of either propagation rate constant on the structure of the unsaturated acceptor molecule. That it is the addition step which is responsible was indicated clearly by the finding that isobutane, which is not formed in reaction of **1** with azobenzene, is a major product of decomposition of **1** in the presence of stilbene. Apparently *tert*-butyl radicals prefer abstraction of hydrogen from **1** over addition to stilbene, even if the latter is present in higher concentration. This could be the result of a low rate constant for addition to stilbene or of reversibility of the addition step. Slow addition or ready reversibility, whichever is applicable, must be attributed in part to steric hindrance in the 1,2-diphenyl-3,3-dimethylbutyl radical. In particular, it is probably difficult to achieve the necessary planarity for benzylic resonance in that radical.

Addition to azobenzene, on the other hand, is probably more facile than addition to stilbene. First, steric hindrance in the adduct radical should be less severe because the bond angles at both nitrogens are expected to be approximately trigonal, on the basis of known angles in diphenylpicrylhydrazyl (4). Second, the adduct radical is stabilized by hydrazyl resonance

$$R{-}\dot{N}{-}\ddot{N}R_2 \leftrightarrow R{-}\bar{\ddot{N}}{-}\overset{+}{N}R_2$$

as well as benzyl resonance. The transition state for addition would have to be product-like to gain most of the available hydrazyl resonance, as a rotation about the N—N bond is required to bring the originally orthogonal lone pair and the π-orbital into conjugation. We have not found estimates or experimental values in the literature for the magnitude of hydrazyl stabilization. That it is large is suggested by the spin density distribution (N_1 = 62%, N_2 = 26%) estimated from the epr splittings of diphenylpicrylhydrazyl (for references and a review of hydrazyl radical chemistry see ref. 5). If hydrazyl resonance is a source of substantial stabilization, as available evidence indicates (5), then even a fraction of it available at the transition state could be sufficient to account for the very different behaviours of azobenzene and stilbene toward *tert*-butyl radicals.

Phenol (and thiophenol) accelerates the chain decomposition of **1** (2) and, in some cases, increases the yield of the addition product (Table 1) from decomposition of **1** in the

Can. J. Chem. Downloaded from www.nrcresearchpress.com by 210.87.254.42 on 09/05/12
For personal use only.

Can. J. Chem. Downloaded from www.nrcresearchpress.com by 210.87.254.42 on 09/05/12
For personal use only.

presence of an alkene. Efficient chain transfer via phenoxy radicals and phenol would decrease the lifetime of an adduct radical, thereby minimizing polymerization, while maintaining (or enhancing)[2] the reaction rate (Scheme 1). Since phenol

$$(CH_3)_3C\cdot + CH_2{=}CHY \rightarrow (CH_3)_3CCH_2\dot{C}HY$$

$$(CH_3)_3CCH_2\dot{C}HY + CH_2{=}CHY \rightarrow \text{Telomer and polymer}$$

$$(CH_3)_3CCH_2\dot{C}HY + ArOH \rightarrow (CH_3)_3CCH_2CH_2Y + ArO\cdot$$

$$ArO\cdot + \mathbf{1} \rightarrow ArOH + (C_6H_5)_2CO + N_2 + (CH_3)_3C\cdot$$

SCHEME 1

can also intercept *tert*-butyl radicals before addition to substrate has occurred, it is not surprising that added phenol can also reduce the yield of addition product (Table 1). The concentration of phenol required for optimizing the yield of adduct is expected to be different for each unsaturated substrate because the rate constants for abstraction from phenol, for polymerization, and for chain termination are structure dependent.

Although optimization experiments still need to be done, the discovery that catalysis can occur appears to be new and important. While it is possible that many free radical reactions are catalyzed by adventitious or unintended H-atom donors, including reactants or products having allylic hydrogens, such catalysis, if it exists, must be hard to demonstrate and control.[3] We are not aware of any other clear cut examples of catalysis by an organic compound in a radical chain addition. Hydrogen bromide catalyses radical addition of thiols to olefins (6), presumably because addition of thiyl radicals is reversible and the reverse reaction is suppressed if an outstanding chain transfer agent like HBr is present.

The reason for the rarity of such catalysis is most easily seen by considering the features which allow phenol to play a catalytic role in the present case. Phenol is a good H-donor to radicals largely because of the resonance stabilization of the phenoxy radical. That stabilization, however, means that phenoxy radicals are very poor at radical substitution and will not normally accomplish the chain transfer step required to complete a catalytic role. Their sluggishness in radical addition and radical substitution steps is, of course, the basis of the normal inhibitory function of phenols in radical processes. Induced decomposition of a hydroxydiazene like **1**, however, is exceedingly exothermic, even if the inducing radical is as stable as phenylthiyl (2), because of the formation of a carbonyl group and of molecular nitrogen. Enough of that favourable enthalpy change is available at the transition state to make the abstraction by phenoxy radicals very efficient. Consequently, phenol acts as a true catalyst.

A general principle can be formulated based on the present results. *For systems* (A—B) *which react with unsaturated substrates by radical chain addition, there may be compounds* (Y—B) *which can act as effective catalysts for the addition of* A—B. *Such catalysis can be expected only if both chain transfer steps*, $Y{-}B + R\cdot \rightarrow Y\cdot + BR$ *and* $AB + Y\cdot \rightarrow A\cdot + YB$, *are very facile*. Although demonstrated catalysis in radical chain addition is currently rare, more examples will probably be found as more 'activated addends', such as α-hydroxydiazenes, are applied as reagents for synthesis.

Experimental

Proton magnetic resonance spectra were obtained with Varian HA-100 or Bruker WH-90 instruments using $CDCl_3$ as solvent and TMS as internal reference. The numbers are δ-values followed, in brackets, by the multiplicity symbol, the apparent coupling constant (J), where appropriate, and the relative integral.

Infrared spectra were obtained with a Beckman-IR5 instrument and mass spectral molecular weights are based on low resolution spectra from a Hitachi RMU-6A instrument.

For gas–liquid partition chromatography, an Aerograph A90-P3 instrument was used with a 10 ft × 0.25 in. column packed with Carbowax 20M (15%) on 60–80 mesh Chromosorb A, at 100–120 °C and with a helium flow rate of 60 ml min^{-1}.

In a typical procedure the unsaturated substrate (*ca.* 0.060 mol) was added to a solution of **1** (mp 74.5–75.5 °C (dec.) (2), 0.40 g, 0.0015 mol) in benzene (3.5 ml). The mixture was stirred or shaken until it was homogeneous before it was heated at 50 °C for 12 h in a septum-stoppered flask vented with a syringe needle.[4] Vigorous gas evolution was observed in all cases either immediately after mixing or soon after heating had started. In most

[2]Rate enhancement is presumably the result of a decreased rate of termination rather than the result of initiation.

[3]We thank a referee for this suggestion.

[4]Reactions of azobenzene with **1** were carried out at 35 °C.

Can. J. Chem. Downloaded from www.nrcresearchpress.com by 210.87.254.42 on 09/05/12
For personal use only.

cases the bubbling stopped well before the end of the 12 h heating period. Bulb-to-bulb distillation under vacuum left behind the benzophenone and telomeric material, if any.

Yields of the first six products (Table 1) were estimated by glpc after addition of *tert*-butylbenzene in known quantity to the distillate. The thermal conductivities of *tert*-butylbenzene and of methylacrylate, determined by injecting a mixture of known composition were found to be the same within experimental error. *tert*-Butylbenzene was used as the standard for the first six products (Table 1) without correction for differences in thermal conductivities, if any.

For reactions of azobenzene with **1** the yield was estimated by pmr after addition of *tert*-butylbromide to a portion of the crude reaction mixture. Only one high field signal was found in addition to that from the bromide and integration indicated a quantitative yield, within experimental error. Isolation of *tert*-butyl-1,2-diphenylhydrazine by extraction into cold aqueous hydrochloric acid was not successful but column chromatography, as described below for the alternative synthesis of that compound, gave material of mp 52–53 °C in 40% yield (isolated).

Individual syntheses are outlined below in the format: olefinic substrate, product, major ir bands (cm^{-1}, $CDCl_3$), and pmr spectrum (δ, $CDCl_3$).

Acrylonitrile: 4,4-dimethylvaleronitrile; 2250 (CN), 1370 (*tert*-Bu) (7); 0.93 (s, 9), 1.61 (t, J = 7.8 Hz, 2), 2.30 (J = 7.8 Hz, 2).

Methyl vinyl ketone: 5,5-dimethylhexan-2-one (mol. wt. 128); 1710 (CO), 1365 (*tert*-Bu); 0.89 (s, 9), 1.64 (t, J = 9.0 Hz, 2), 2.15 (s, 3), 2.48 (t, J = 9.0 Hz, 2). The 2,4-dinitrophenylhydrazone melted at 105–106 °C (lit. (8) mp 105–106 °C).

Crotonaldehyde: 3,4,4-trimethylpentanal (mol. wt. 129); 2820 and 2720 (CHO), 1720 (CO), 1370 (*tert*-Bu); 0.89 and 0.97 (s, *tert*-Bu (s) and one arm of CH_3 (d), total 12), 1.54–2.62 (m, 3), 9.66 (m, 1). The 2,4-dinitrophenylhydrazone (mol. wt. 308) melted at 110 °C (lit. (9) mp 112–112.5 °C).

Methyl acrylate: methyl-4,4-dimethylvalerate; 1730 (CO) 1370 (*tert*-Bu), 1164 (CO_2CH_3); 0.88 (s, 9), 1.36–1.56 (m, 2), 2.10–2.30 (m, 2), 3.50 (s, 3).

Isopropenyl acetate: 2-acetoxy-4,4-dimethylpentane (mol. wt. 158); 1725 (CO), 1370 (*tert*-Bu); 1270 (ester C—O—C); 0.91 (s, 9), 1.20 (d, J = 6.1 Hz, 3), 1.40–1.78 (m, 3), 2.01 (s, 3).

Norbornene: *exo*-2-*tert*-butylbicyclo[2.2.1]heptane; 1367 (*tert*-Bu); 0.87 (s, 9), 0.96–1.60 (m, 9), 2.05–2.30 (m, 2). The pmr spectrum (CCl_4) reported in the literature (10) is in good agreement with ours ($CDCl_3$).

Azobenzene: *tert*-butyl-1,2-diphenylhydrazine (mp 52–53 °C); 1365 (*tert*-Bu); 1.10 (s, 9), 6.50–7.20 (m, 10), NH not seen in pmr spectrum. *Anal.* calcd. for $C_{16}H_{20}N_2$: N 11.67; found: N 11.62.

Independent Synthesis of tert-Butyl-1,2-diphenylhydrazine

The approach was based on the reported (11) reaction between phenyllithium and azobenzene.

A solution of azobenzene (5.5 g, 0.030 mol) in dry benzene (102 ml) was stirred and cooled with ice during addition of *tert*-butyllithium (0.036 mol, 45 ml of 0.8 M solution in pentane) over 10 min. After 10 min more in the ice bath, cold saturated, aqueous NH_4Cl was added. Separation of the benzene layer, extraction of the water layer with ether, drying of the combined organic layers and evaporation of the solvents in a rotary evaporator left a residue which was chromatographed on basic alumina (600 g, 80–200 mesh, Brock, activity grade 1). Elution with petroleum ether – benzene gave a pale yellow crystalline product (10%) which was recrystallized from methanol to mp 54–55 °C. *tert*-Butyl-1,2-diphenylhydrazine is not stable in air. *Anal.* calcd. for $C_{16}H_{20}N_2$: C 80.00, H 8.33, N 11.67; found: C 80.16, H 8.50, N 12.12.

The mass spectrometric mol. wt. (240) and the pmr spectrum matched those of the product from reaction of azobenzene with **1**. Major ir bands matched also, but the material from radical chain addition had additional minor bands attributed to an impurity.

Acknowledgements

We are indebted to the National Research Council of Canada for an operating grant from which most of the support for this investigation was drawn and to Professor S. F. Nelson for helpful correspondence.

1. P. KNITTEL and J. WARKENTIN. Can. J. Chem. This issue.
2. D. W. K. YEUNG and J. WARKENTIN. Can. J. Chem. This issue.
3. P. KNITTEL and J. WARKENTIN. Can. J. Chem. **53**, 2275 (1975).
4. D. E. WILLIAMS. J. Am. Chem. Soc. **89**, 4280 (1967).
5. S. F. NELSEN. Free radicals. Vol. 2. *Edited by* J. K. Kochi. Wiley–Interscience, New York. 1973. pp. 557–559
6. P. S. SKELL and R. G. ALLEN. J. Am. Chem. Soc. **82**, 1511 (1960).
7. D. J. PASTO and C. R. JOHNSON. Organic structure determination. Prentice-Hall, Inc., Englewood Cliffs. N.J. 1969. p. 114.
8. E. H. MAN, F. C. FROSTICK, JR., and C. R. HAUSER. J. Am. Chem. Soc. **74**, 3230 (1952).
9. S. H. POWELL and W. J. WASSERMAN. J. Am. Chem. Soc. **79**, 1937 (1957).
10. J. E. MULVANEY and Z. G. GARLUND. J. Org. Chem. **30**, 917 (1965).
11. P. F. HOLT and B. P. HUGHES. J. Chem. Soc. **764** (1954).

Synthesis and radical decomposition of α-hydroxydiazenes. II.[1] *tert*-Butylazodiphenylcarbinol

DOMINIC W. K. YEUNG AND JOHN WARKENTIN
Department of Chemistry, McMaster University, Hamilton, Ontario L8S 4M1

Received July 21, 1975

DOMINIC W. K. YEUNG and JOHN WARKENTIN. Can. J. Chem. **54**, 1349 (1976).

tert-Butylazodiphenylcarbinol ($Ph_2C(OH)N{=}NCMe_3$, **3**) decomposes in oxygen-free benzene by the unimolecular radical mechanism characteristic of most azo compounds. In benzene or in carbon tetrachloride, with or without air present, decomposition of **3** is also induced by radicals through abstraction of hydroxyl hydrogen in concert with the formation of nitrogen. Radicals which induce decomposition of **3** include trichloromethyl, *tert*-butyl, phenylthiyl, *tert*-butylperoxy and possibly oxygen. The failure of inhibitors like thiophenol to stop chain decomposition of **3** is interpreted in terms of the thermochemistry of induced decomposition.

DOMINIC W. K. YEUNG et JOHN WARKENTIN. Can. J. Chem. **54**, 1349 (1976).

Le *tert*-butylazodiphénylcarbinol ($Ph_2C(OH)N{=}NCMe_3$, **3**) se décompose dans du benzène, sans oxygène, par un mécanisme radicalaire unimoléculaire caractéristique de la plupart des composés azo. Dans le benzène ou dans le tétrachlorure de carbone, en présence ou en absence d'air, on peut aussi induire la décomposition de **3** par les radicaux par l'enlèvement de l'hydrogène de l'hydroxyle en même temps que la formation de l'azote. Les radicaux qui induisent la décomposition de **3** comprennent le trichlorométhyle, le *tert*-butyle, le phénylthiyle, le *tert*-butylperoxy et possiblement l'oxygène. On interprète le fait que des inhibiteurs, comme le thiophénol, n'arrêtent pas la décomposition en chaîne en termes de la thermochimie de la décomposition induite.

[Traduit par le journal]

Introduction

α-Hydroxydiazenes, $R_1N{=}N{-}C(OH)R_2R_3$, were first reported by Schmitz, Ohme, and Schramm (2) who synthesized **1**. Since that time several others of that class, including acyclic and cyclic members have been reported (3–6). Some of these are relatively stable (kinetically) at

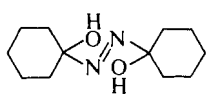

1

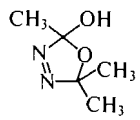

2

ambient and higher temperature while others decompose so rapidly as to preclude convenient purification and isolation. Although the kinetic instability of such systems might be attributed, in part, to stabilization of the transition state for C—N homolysis by the hydroxy substituent(s), the wide range of stabilities of α-hydroxydiazenes suggested that there might be another factor. Evidence for concerted, induced decomposition of **2** by radical attack at the hydroxyl hydrogen was reported recently (1), eq. 1.

[1] 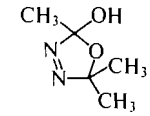 + R· → RH + N_2 + $CH_3CO_2\dot{C}(CH_3)_2$

2

Radicals capable of abstracting hydroxyl hydrogen efficiently from **2** include not only 2-acetoxy-2-propyl, arising from induced decomposition of **2**, but also a variety of radicals resulting from addition of 2-acetoxy-2-propyl to an alkene or alkyne (1, 7). The extraordinary chain transfer ability of **2**, which makes it a useful reagent for synthesis, was attributed to a concerted abstraction mechanism [1] in which part of the heats of formation of N_2 and of a carbonyl group are realized at the transition state to lower the usually high (8) activation energy for H-abstraction from the hydroxyl group.[2]

The potential of **2** and other derivatives of the

[1]For part I see Knittel and Warkentin (1).

[2]Griller and Ingold (8) have recently discussed H-abstraction from the hydroxyl group of alcohols by free radicals. Cyclopropanols are exceptional in their reactivity, which has been accounted for in terms of ring opening in concert with H-abstraction from the hydroxyl group (9).

Can. J. Chem. Downloaded from www.nrcresearchpress.com by 210.87.254.42 on 09/05/12
For personal use only.

Can. J. Chem. Downloaded from www.nrcresearchpress.com by 210.87.254.42 on 09/05/12
For personal use only.

Δ^3-1,3,4-oxadiazolin-2-one family(10)as reagents for radical chain synthesis of small molecules led us to prepare other α-hydroxyazo systems. In this paper we report the synthesis of *tert*-butylazodiphenylcarbinol, **3**, and some of its free radical chemistry.

Results and Discussion

Synthesis

tert-Butylazodiphenylcarbinol, **3**, was synthesized according to Scheme 1. The first step, to benzophenone-*tert*-butylhydrazone via *tert*-butyl Grignard reagent had been reported (11). Oxidation with bromine in cold acetic acid gave the azoacetate, provided that care was taken (Experimental). Conversion of the azoacetate **4** to the lithium derivative of **3** by treatment with methyllithium, followed by acidification, gave **3** as a colorless, crystalline solid.

Spin Trapping

A benzene solution of **3** and nitrosobenzene in an open tube gave a strong, triplet epr signal, a_N = 12.89 G, g = 2.0079. A degassed sample gave a more complex spectrum in which each of the three lines was split into nine lines with intensity ratios 1:2:4:6:6:6:4:2:1. Hyperfine splitting by aryl hydrogens when oxygen is kept out of a sample containing phenyl-*tert*-butyl nitroxide radicals has been reported by others and our values of the hyperfine constants, $a_H^{ortho} = a_H^{para} = 2a_H^{meta} = 1.91$ G, are in good agreement with those in the literature (12, 13). These epr results suggest that **3** decomposes by a radical pathway and that the radical trapped by nitrosobenzene is the *tert*-butyl radical. The products obtained from decomposition of **3** under other conditions (below) serve to confirm that assignment.

Decomposition in Carbon Tetrachloride

In carbon tetrachloride, **3** decomposes spontaneously at room temperature yielding benzophenone, *tert*-butylchloride, and chloroform. Disappearance of **3** and appearance of *tert*-butyl chloride, followed by integrating the *tert*-butyl signals in the pmr spectrum, were first order but the apparent first-order rate constant was not reproducible from run to run (Table 1). That behaviour is inconsistent with rate-determining, unimolecular homolysis of **3** but is expected for a radical chain process, the rate of which can depend strongly on the concentrations of adventitious initiators and/or inhibitors and/or chain transfer agents.

TABLE 1. Kinetics of decomposition of **3** at 35 °C

Initial concentration of **3** (M)	Reaction conditions	$k \times 10^4$ (s^{-1})[a]
0.231	CCl_4, air	25.6
0.231	CCl_4, air	18.2
0.230	CCl_4, air	34.1
0.220	CCl_4, air	36.3
0.228	CCl_4, degassed	0.34
0.198	CCl_4, degassed	0.45
0.253	CCl_4, degassed	0.22
0.238	CCl_4, degassed 0.02 M C_6H_5SH	117
0.243	C_6H_6, degassed	0.093[b]
0.243	C_6H_6, degassed	0.093[b]
0.457	C_6H_6, degassed	[c]
0.457	C_6H_6, degassed	[c]

[a]The first-order rate constant for disappearance of the *tert*-butyl signal of 3 except where otherwise noted.
[b]Apparent first-order rate constant. At the initial concentration of 3 specified only the early points (*ca.* 0.5 $t_{1/2}$) were slightly off a first-order line through the origin. The plot included points representing up to four half-lives.
[c]Between first and three-halves order in 3 but fitting neither.

Disappearance of **3** and appearance of *tert*-butyl chloride, followed by integrating the *tert*-butyl signals in the pmr spectrum, were first order but the apparent first-order rate constant was not reproducible from run to run (Table 1). That behaviour is inconsistent with rate-determining, unimolecular homolysis of **3** but is expected for a radical chain process, the rate of which can depend strongly on the concentrations of adventitious initiators and/or inhibitors and/or chain transfer agents.

One initiator of decomposition of **3** may be oxygen. In carefully degassed carbon tetrachloride solutions, **3** always decomposed more slowly than it did in corresponding undegassed samples prepared from the same batches of **3** and solvent (Table 1). The largest observed rate factor attributed tentatively to initiation by oxygen in air was approximately 165 (Table 1), for solutions of **3** in carbon tetrachloride.

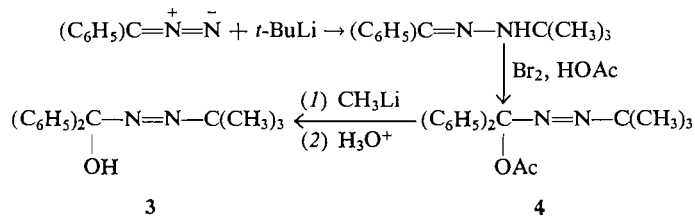

3 **4**

SCHEME 1

First-order chain decomposition of **3** in degassed carbon tetrachloride is consistent with chain termination by reaction of trichloromethyl radicals with *tert*-butyl radicals.

Decomposition in Benzene

Solutions of **3** (0.24 *M*) in benzene gave reproducible first-order kinetics if air was excluded (Table 1), suggesting that decomposition of **3** goes by unimolecular, radical bond scission under those conditions. Higher initial concentrations, however, led to kinetics which fit neither first nor three-halves order. That behaviour can be accounted for in terms of a chain component superimposed on unimolecular decomposition. The most reasonable chain mechanism for decomposition of **3** in benzene is the attack of *tert*-butyl radicals at the hydroxyl hydrogen. The products fit that mechanism well. Benzophenone and isobutane were the only readily detectable products but concentration of the isobutane fraction revealed a small amount (0.9% by glpc; 2% by ms) of isobutene in it. Isobutene could be formed by chain termination involving disproportionation of *tert*-butyl radicals and by disproportionation reactions of a radical pair arising from unimolecular decomposition of **3**, [2]. The former source is more likely

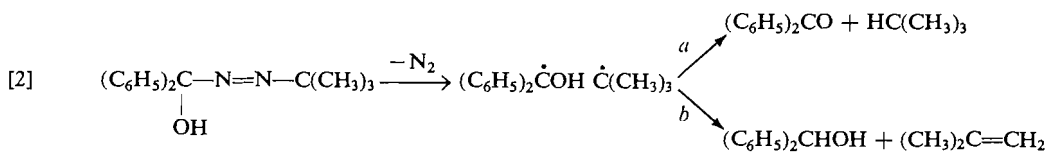

for several reasons. First, disproportionation step *a* [2] is more likely than step *b* on thermochemical grounds since *a* leads to a C=O bond whereas *b* leads to a C=C bond. In support of path *a* and against path *b* is the report that diphenylhydroxymethyl radicals are not spin trapped by 2-methyl-2-nitrosopropane but are converted instead to benzophenone by transfer of the OH hydrogen to the nitroso group (14). Second, the diphenylcarbinol expected from step *b* could not be detected in the benzophenone fraction by either ir or tlc. If essentially all of the isobutane originated from induced decomposition of **3**, as would be the case for a long-chain process, then the decomposition should fit three-halves-order kinetics. Since the observed kinetics is between first and three-halves order in **3**, it appears that chains are short, in the range of concentrations used, and that isobutane arises not only from the induced decomposition but also via path *a* [2].

Mild acceleration of the rate of decomposition of **3** in undegassed benzene solutions may be attributed to several factors. First, initiation by attack of oxygen at the OH group must be considered in view of the fact that 'stable' free radicals like phenylthiyl are chain carriers for decomposition of **3** (see below). Another likely factor is a greater chain length when *tert*-butylperoxy radicals are chain carriers. Peroxy radicals, which are certain to be formed in oxygenated solutions containing alkyl radicals, are known to be better H-abstractors than tertiary radicals like *tert*-butyl. As expected, the pmr spectrum of the product mixture from decomposition of **3** in benzene in the presence of air was complex and included at least four signals slightly downfield from the isobutane doublet. Isobutane was still a major product under conditions of limited oxygen supply (capped nmr tube).

Effect of Thiophenol

Inhibition of chain decomposition of **3** by traces of adventitious impurities is unlikely. Even thiophenol, an excellent inhibitor of many radical chain processes does not inhibit decomposition of **3**. In fact, thiophenol (0.02 *M*) is an effective accelerator of decomposition of **3** in CCl_4 (Table 1). The formation of isobutane (*ca.* 60%) when thiophenol is present (0.02 *M*), but not when it is absent, can only mean that the *tert*-butyl radical abstracts much more efficiently from thiophenol than from carbon tetrachloride, as expected. The resulting phenylthiyl radicals must in turn be efficient at abstracting hydrogen from the hydroxyl group of **3** to account for the high rate. A chain length near 1000 can be calculated if it is assumed that the rate constant for unimolecular decomposition of **3** in carbon tetrachloride containing thiophenol is the same as the rate constant for decomposition of azoacetate **4** in benzene ($k_1^{35°} = 1.20 \times 10^{-6}\ s^{-1}$) and that the thiophenol did not contain initiators.

Can. J. Chem. Downloaded from www.nrcresearchpress.com by 210.87.254.42 on 09/05/12
For personal use only.

Can. J. Chem. Downloaded from www.nrcresearchpress.com by 210.87.254.42 on 09/05/12
For personal use only.

Mechanism and Thermochemistry

Induced decomposition of **3** by relatively stable radicals requires a concerted process, such that some of the heat of formation of nitrogen and of a carbonyl group is realized at the transition state [3]. The enthalpy of the reaction [3], calculated without considering conjugation in benzophenone, is approximately +31 kcal mol^{-1} minus the R—H bond energy.

[3] $(C_6H_5)_2C(OH)—N{=}N—C(CH_3)_3 + R\cdot \rightarrow RH + (C_6H_5)_2CO + N_2 + (CH_3)_3C\cdot$

For the case where R = C_6H_5S [3], ΔH^0 is calculated to be about −50 kcal mol^{-1}. In order to have a thermoneutral abstraction step [3] the radical R· would have to form a R—H bond with a bond energy near 31 kcal mol^{-1}. Such weak bonds are not found in stable molecules and it follows that inhibitors which normally function by forming radicals too stable to serve as chain carriers may be quite useless for inhibiting induced decomposition of **3**. Effective inhibitors which function by addition or substitution reactions with radicals may still be found, but they will have to inhibit decomposition of **3** by virtue of a high activation energy for an exothermic process (eq. 3, R = inhibitor-derived radical). Triphenyl stannane, which inhibits chain decomposition of **2** (1), was found to be ineffective as an inhibitor of **3**.

Experimental

Benzophenone hydrazone was prepared by refluxing benzophenone (100 g, 0.55 mol) with 85% hydrazine hydrate (75 g, 1.28 mol) in absolute ethanol (100 ml) for 24 h. The solution was cooled to room temperature and subsequently to ice temperature. Filtration of the colorless needles and recrystallization from hot 95% ethanol gave 75 g (69%) of hydrazone, mp 96–97 °C (lit. (15) mp 97–98 °C).

Diphenyldiazomethane was prepared by oxidation of benzophenone hydrazone with yellow mercury(II) oxide (16). From 39 g of hydrazone was obtained 35 g (90%) of product, mp 29–30 °C (lit. (16) mp 29–32 °C).

Benzophenone tert-butylhydrazone was synthesized from diphenyldiazomethane and *tert*-butyllithium in a procedure similar to that in the literature (11), based on *tert*-butyl Grignard reagent. Diphenyldiazomethane (4.0 g, 0.021 mol) was dissolved in 10 ml each of benzene and cyclohexane in a 250 ml septum-sealed flask equipped with a stirring bar. The flask was flushed with dry nitrogen and cooled with ice before *tert*-butyllithium (0.024 mol, 25.0 ml of 0.97 *M* reagent in pentane) was added from a syringe during 15 min. The solution turned dark brown and became semisolid. The ice bath was removed and the flask was shaken occasionally during 15 min before anhydrous ether (30 ml) was added to the mixture to dissolve the dark, oily material. Cold, saturated NH_4Cl solution was added slowly until the color of the solution turned to yellow-orange (80–100 ml). The organic layer was separated and the aqueous layer was extracted twice with ether. Drying of the combined organic extracts with anhydrous Na_2SO_4, followed by evaporation of the solvents under vacuum left a yellow-orange oil. Crystallization from aqueous ethanol gave a yellow solid, 77% yield, mp 74–75 °C (lit. (11) mp 73.5–75 °C).

More rapid addition of the *tert*-butyllithium, or increasing the stirring time before work-up, reduced the yield of product, sometimes drastically.

tert-Butylazodiphenylmethyl acetate, available by oxidation of benzophenone *tert*-butylhydrazone with Pb(IV) acetate (17), was also prepared by oxidation with bromine. A solution of benzophenone *tert*-butylhydrazone (1.0 g, 4.0×10^{-3} mol) in glacial acetic acid (50 ml) containing sodium acetate trihydrate (5.4 g) was stirred and cooled with ice while bromine (0.70 g, 4.4×10^{-3} mol) in glacial acetic acid (10 ml) was added in the course of 10–15 min. Ice water (100 ml) was added and the resulting mixture was extracted with methylene chloride until the aqueous layer was colorless. The combined methylene chloride extract was washed, first with water and then with 5% sodium bicarbonate solution, to remove acetic acid. Drying over anhydrous Na_2SO_4, followed by evaporation of solvent with a rotary evaporator, left 0.95 g (77%) of crude product as a yellow oil containing some benzophenone (ν_{CO} 1650 cm^{-1}). The oil was dissolved in pentane from which crystals separated after 5 days in a refrigerator, 35% yield, mp 59–61 °C (lit. (17) mp 61–63 °C).

tert-Butylazodiphenylcarbinol: a solution of *tert*-butylazodiphenylmethyl acetate (3.1 g, 0.010 mol) in 70 ml of anhydrous ether, under dry nitrogen, was cooled to −10 °C. Methyllithium (0.026 mol, 15 ml of 1.7 *M* reagent in ether) was added by drops from a syringe, with stirring, during 10 min. After 15 min more, ice-cold, saturated NH_4Cl solution (50 ml) was added slowly. After separation of the organic layer the aqueous phase was extracted thrice with ether. The ethereal fractions were combined, dried with anhydrous Na_2SO_4, and concentrated (without heating) under reduced pressure with a rotary evaporator. The pale yellow solid which remained was recrystallized from pentane. The yield of the title compound, mp 74.5–75.5 °C. (dec.), was 70%; ir (CCl_4), 3625 and 3340 cm^{-1} (free and bonded OH), 1650 cm^{-1} (CO of benzophenone), increasing in intensity with time as decomposition progressed; Raman (solid), 1587.4 cm^{-1} (N=N); pmr (CCl_4, −12 °C), δ 1.33 (s, 9), 5.92 (s, 1), 7.28–7.66 (m, 10). The signal at 5.92 δ disappeared as a result of shaking the solution with a drop of D_2O before cooling to −12 °C. *Anal.* calcd. for $C_{17}H_{20}N_2O$: C 76.12, H 7.46, N 10.45; found: C 75.88, H 7.55, N 10.30.

Kinetics

Experiments were carried out in nmr tubes at the temperature of the Varian-T60 probe (35 °C). Slow runs were also done with a constant temperature water bath (35.0 ± 0.1 °C) from which tubes were transferred at 1 h

Can. J. Chem. Downloaded from www.nrcresearchpress.com by 210.87.254.42 on 09/05/12
For personal use only.

intervals to the probe for integration. For kinetic runs with oxygen present the tubes were capped while they were in the probe but they were removed at regular intervals for shaking and for venting of accumulated gas. Kinetic runs with oxygen absent were performed using sealed nmr tubes. Solutions in the tubes were put through three or more freeze–pump–thaw cycles (vacuum line pressure < 0.01 torr) before sealing.

About 20 integrals of the *tert*-butyl signals of **3** (δ 1.33) and of *tert*-butyl chloride (δ 1.60) were recorded for runs in CCl_4; the time intervals between integrals ranging from 1 min to 1 h, depending on whether or not air was excluded.

Standard first-order treatment of the data gave straight, least-squares fits to the equation $\ln [a/(a - x)] = kt + c$, with small positive values of c except in the case of concentrated solutions in benzene (above).

Products

The major products from decomposition of **3** in CCl_4 were *tert*-butyl chloride, chloroform, and benzophenone. Isobutane could not be detected by pmr or glpc. *tert*-Butyl chloride and chloroform were identified by pmr and by comparing their retention times on several glpc columns with those of authentic samples. The yields of *tert*-butyl chloride (89%) and chloroform (96%) were estimated by glpc after addition of a weighed quantity of chlorobenzene, which served as a standard. A 10 ft × 0.25 in. column packed with Carbowax 20M (15%) on 60–80 mesh Chromosorb A was used at 110 °C with a helium flow rate of 120 ml/min. Peak areas were estimated by cutting and weighing.

Evaporation of the volatile products at the vacuum pump, addition of a small amount of methanol to the residue, and treatment of the resulting mixture with 2,4-dinitrophenylhydrazine reagent gave benzophenone-2,4-dinitrophenylhydrazone, mp 238 °C (lit. (18) mp 238 °C).

Isobutane, from decomposition of **3** in benzene and in carbon tetrachloride with added thiophenol, was detected in the pmr spectrum as a doublet (J = 6.0 Hz) at δ 0.89. The identity of the product producing that signal was confirmed, both by glpc and by pmr, with solutions prepared by bubbling isobutane (Matheson) into carbon tetrachloride (or benzene).

Yields of isobutane were estimated by calculating that fraction of the total high field integral which was contributed by the isobutane doublet. Reactions in degassed benzene gave isobutane yields near 91%. In CCl_4 with thiophenol (0.02 M) added, the yield of isobutane was 60% and the yield of *tert*-butyl chloride was 40%.

Isobutene from decomposition of **3** in degassed benzene was detected as described below. Spent solutions from several kinetic runs were cooled before the nmr tubes were cut and the contents were transferred to a bulb attached to a vacuum line. The bulb was cooled with liquid N_2 during evacuation and was allowed to warm while another receiver on the line was cooled to receive volatile material from the bulb. Distillate thus collected was then allowed to volatilize into the vacuum line. A sample of the gas was analyzed by ms with a Hitachi RMU6A instrument using 9 eV electrons. The ratio of peaks corresponding to isobutane and isobutene (mass 58 : mass 56) was 100:2. A sample of isobutane (Matheson) gave a negligible signal for mass 56, relative to that for mass 58, at the same instrument settings.

Some of the gas remaining in the vacuum line was condensed into the N_2-cooled gas sampling loop of the gas sampling accessory for the Varian Aerograph A90-P3 gas chromatograph. Simultaneous switching to the injection mode and heating of the loop with hot water injected the sample onto a 10 ft × $\frac{1}{4}$ in. column packed with SE 550 (31%) on firebrick. The same column had been used previously to separate isobutane from the isomeric butenes (19). Instrumental conditions similar to those described (19) led to two signals the areas of which were estimated by triangulation. Injection of a mixture of isobutane and isobutene prepared from authentic samples (Matheson) was carried out to confirm identities.

Acknowledgements

We are indebted to the National Research Council of Canada for an operating grant from which most of the support for this investigation was drawn and to Dr. R. R. Hiatt for valuable criticism.

1. P. KNITTEL and J. WARKENTIN. Can. J. Chem. **53**, 2275 (1975).
2. (*a*) E. SCHMITZ, R. OHME, and S. SCHRAMM. Angew. Chem. Int. Ed. Engl. **2**, 157 (1963); (*b*) E. SCHMITZ, R. OHME, and S. SCHRAMM. Ann. Chem. **702**, 131 (1967).
3. (*a*) J. P. FREEMAN and C. P. RATHJEN. Chem. Commun. 538 (1969); (*b*) J. P. FREEMAN and C. P. RATHJEN. J. Org. Chem. **37**, 1686 (1972).
4. (*a*) S. HÜNIG and J. CRAMER. Angew. Chem. Int. Ed. Engl. **7**, 943 (1968); (*b*) S. HÜNIG and G. BÜTTNER. Angew. Chem. Int. Ed. Engl. **8**, 451 (1969); (*c*) G. BÜTTNER and S. HÜNIG. Chem. Ber. **104**, 1088 (1971); (*d*) G. BÜTTNER and S. HÜNIG. Chem. Ber. **104**, 1104 (1971); (*e*) G. BÜTTNER, J. CRAMER, L. GELDERN, and S. HÜNIG. Chem. Ber. **104**, 1118 (1971).
5. W. NAGATA and S. KAMATA. J. Chem. Soc. C, 540 (1970).
6. P. L. SOUTHWICK, N. LATIF, J. E. KEIJANOWICZ, and J. G. O'CONNOR. Tetrahedron Lett. 1767 (1970).
7. P. KNITTEL and J. WARKENTIN. Can. J. Chem. This issue.
8. D. GRILLER and K. U. INGOLD. J. Am. Chem. Soc. **96**, 630 (1974).
9. (*a*) C. H. DEPUY, H. L. JONES, and D. H. GIBSON. J. Am. Chem. Soc. **90**, 5306 (1968); (*b*) C. H. DEPUY, H. L. JONES, and D. H. GIBSON. J. Am. Chem. Soc. **94**, 3924 (1972).
10. P. KNITTEL, S. L. LEE, and J. WARKENTIN. Can. J. Chem. **50**, 3248 (1972).
11. P. A. S. SMITH, J. M. CLEGG, and J. LAKRITZ. J. Org. Chem. **23**, 1595 (1958).
12. A. K. HOFFMANN, A. M. FELDMAN, and E. GELBLUM. J. Am. Chem. Soc. **86**, 646 (1964).
13. A. MACKOR, TH. A. J. W. WAJER, and TH. J. DEBOER. Tetrahedron Lett. 2155 (1966).

14. I. H. LEAVER and G. C. RAMSAY. Tetrahedron, **25**, 5669 (1969).
15. L. I. SMITH and K. L. HOWARD. Org. Synth. Coll. Vol. 3, 352 (1955).
16. J. B. MILLER. J. Org. Chem. **24**, 560 (1959).
17. D. C. IFFLAND, L. SALISBURY, and W. R. SCHAEFER. J. Am. Chem. Soc. **83**, 747 (1961).
18. A. I. VOGEL. Qualitative organic analysis. Part 2. 2nd Ed. ELBS and Longman, London. 1971. p. 354.
19. J. WARKENTIN and K. E. HINE. Can. J. Chem. **48**, 3545 (1970).

Can. J. Chem. Downloaded from www.nrcresearchpress.com by 210.87.254.42 on 09/05/12
For personal use only.

Isolation and structure of pimaydolide, a cyclodepsipeptide metabolite of *Pithomyces maydicus*[1,2]

D. W. RUSSELL
Biochemistry Department, Dalhousie University, Halifax, Nova Scotia
W. D. JAMIESON AND A. TAYLOR
National Research Council of Canada, Atlantic Regional Laboratory, Halifax, Nova Scotia B3H 3Z1
AND
B. C. DAS
Institut de Chimie des Substances Naturelles, C.N.R.S., 91190, Gif-sur-Yvette, France

Received October 29, 1975

D. W. RUSSELL, W. D. JAMIESON, A. TAYLOR, and B. C. DAS. Can. J. Chem. **54**, 1355 (1976).

A new metabolite has been isolated from cultures of *Pithomyces maydicus*. Evidence is presented that suggests its structure is cyclo(L-2-oxy-3-methylbutyryl-D-valyl-D-leucyl-L-2-oxy-4-methylvaleryl-L-2-oxy-3-methylbutyryl-L-*N*-methylleucyl), **1**.

D. W. RUSSELL, W. D. JAMIESON, A. TAYLOR et B. C. DAS. Can. J. Chem. **54**, 1355 (1976).

On a isolé un nouveau métabolite des milieux de culture du *Pithomyces maydicus*. On présente des données qui suggèrent que sa structure est la suivante soit cyclo(L-oxy-2 méthyl-3 butyryl D-valyl D-leucyl L-oxy-2 méthyl-4 valéryl L-oxy-2 méthyl-3 butyryl L-*N*-méthylleucyl) (**1**).

[Traduit par le journal]

The crude depsipeptide fraction (1) obtained (2) from cultures of *Pithomyces maydicus* on rye grain, was separated into two fractions, one soluble in carbon tetrachloride and an insoluble crystalline material. The former gave sporidesmolide IV (3) and the latter was purified by repeated recrystallization, to constant, integral amino acid composition. The new metabolite was a colorless, crystalline neutral compound, soluble in chloroform, sparingly soluble in other common organic solvents, and insoluble in water. It slowly sublimed when heated above 200 °C and its ord showed no Cotton effect but its cd showed a well defined asymmetric band at λ_{max} 244 nm ($\Delta\epsilon -62°$). It was separated from sporidesmolide IV (3) by tlc on silica gel, using toluene – ethyl acetate – chloroform (1:1:1) as the developing solvent. Elemental analysis and high resolution mass spectroscopy indicated that its molecular formula was $C_{34}H_{59}N_3O_9$. Acid hydrolysis gave valine, leucine, *N*-methylleucine, 2-oxy-3-methylbutyric acid, and 2-oxy-4-methylvaleric acid in the ratios 1:1:1:2.

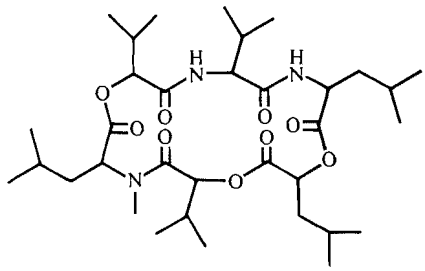

1

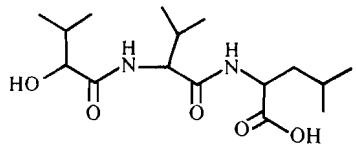

2

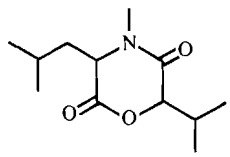

3

Pimaydolide consumed 3 equiv. of alkali on saponification, unlike the sporidesmolides which

[1]NRCC No. 15174.

[2]This work was carried out under the joint scientific agreement between Centre National de la Recherche Scientifique de France and the National Research Council of Canada.

Can. J. Chem. Downloaded from www.nrcresearchpress.com by 210.87.254.40 on 09/05/12
For personal use only.

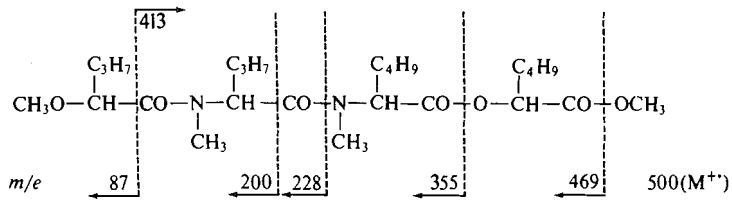

4

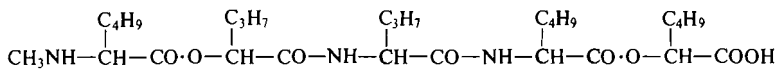

5

required 2 equiv. (3–5). Acidification of the alkaline reaction mixture gave a precipitate which after digestion with chloroform provided sporidesmolic acid A **2** (4). The chloroform mother liquors from sporidesmolic acid A on evaporation and sublimation gave a crystalline sublimate whose elemental analysis and mass spectrum indicated its molecular formula to be $C_{12}H_{21}NO_3$. No indication of higher homologues was found in its mass spectrum. This C_{12} compound was not acidic but it slowly dissolved in dilute alkali. On acid hydrolysis L-2-oxy-3-methylbutyric acid and L-*N*-methylleucine were obtained. Hence, this volatile saponification product is the morpholine-3,6-dione **3**. Another saponification product, L-2-oxy-4-methylvaleric acid was obtained by extraction of the filtrate from the acids insoluble in water, and sublimation of this extract. Thus all the amino and hydroxy acid fragments found in pimaydolide, were obtained in the saponification products and the sequences **2** and **3** (assuming the absence of transannular esterification processes) are present in the metabolite. It is also unlikely, on stoichiometric grounds, that the hydroxy acid residues present in **2** and **3** arise from the same fragment in the metabolite.

The most probable ion reactions of pimaydolide in the mass spectrometer involved the loss of C_3H_6 or C_4H_8 from the hydrocarbon side chains of the depsipeptide ring. The spectrum was searched by a method analogous to that of Biemann *et al.* (9) from the high mass end of the spectrum for ions that had retained these side chains and hence, sequence information. Mass measurement data for such ions are given in Table 1, and the ion reactions are summarized in Scheme 1. Each ion reaction given was observed by focussing the Dupont instrument on the daughter ion and then varying the acceleration voltage. The *m/e* of the parents were then calculated by the product of the *m/e* value of the daughter ion and the inverse of the ratio of the voltage at which it was detected to the voltage of detection of the parent. An abundant ion in the spectrum had *m/e* 611, its formation involving the loss of one of the three isopropyl side chains as C_3H_6. This *m/e* 611 ion then fragmented by the complex reaction

$$C_{31}H_{53}N_3O_9^{+\cdot} \rightarrow C_{30}H_{52}N_3O_8^{+} + \cdot CHO$$

but the subsequent reactions of the product *m/e* 582 ion and its daughters have been demonstrated previously in many analogous systems (6, 8, 9). Thus the first reaction of the ion *m/e* 582 is the loss of 28 mass units shown to arise from a ring carbon by its elemental composition (CO). Subsequently a fragment $C_4H_{10}N$ is lost which is most probably derived from the valine residue in the metabolite. However after further loss of

TABLE 1. Precise mass determinations of the molecular ion and fragment ions of pimaydolide

Ion	Precise mass	
	Found	Calculated
$C_{34}H_{59}N_3O_9$	653.4252	653.4251
$C_{31}H_{53}N_3O_9$	611.3884	611.3881
$C_{30}H_{52}N_3O_8$	582.3857	582.3854
$C_{29}H_{52}N_3O_7$	554.3799	554.3805
$C_{25}H_{42}N_2O_7$	482.2957	482.2991
$C_{24}H_{42}N_2O_6$	454.3039	454.3042
$C_{18}H_{28}NO_6$	354.1919	354.1917
$C_{17}H_{28}NO_5$	326.1981	326.1967

Can. J. Chem. Downloaded from www.nrcresearchpress.com by 210.87.254.40 on 09/05/12
For personal use only.

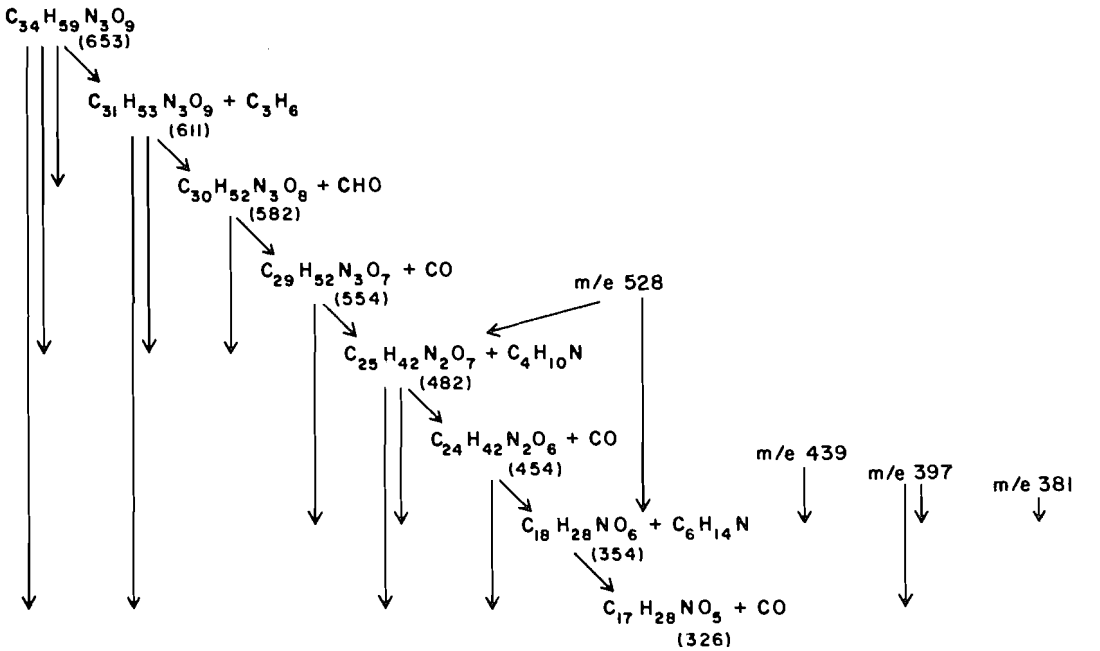

SCHEME 1

CO the next nitrogenous fragment lost, was not $C_5H_{12}N$ as would be expected from the sporidesmolic acid A sequence, but $C_6H_{14}N$. This moiety is therefore fragmented from the other end of the linear ion(s) whose parent is the *m/e* 582 ion. Thus, the *N*-methylleucine residue in pimaydolide is linked to the valine group through a 2-oxy-3-methylbutyryl residue, lost in the ion reactions 653 → 611 → 582 → 554. It follows that the sequence *N*-methylleucyl-2-oxy-3-methylbutyryl-valylleucine is present in pimaydolide, and the complete sequence can be deduced if the morpholine-3,6-dione **3** does not arise by transannular transesterification.

Permethylation of pimaydolide gave a mixture of products (7). When the crude mixture was distilled into the mass spectrometer, at room temperature a molecular ion at *m/e* 386.2781 ($C_{20}H_{38}N_2O_5$ requires 386.2781) was obtained together with abundant ions at *m/e* 355, 200, and 87 (m* ~ 37.3, 200 → 87). In the spectrum of perdeuteriomethylated pimaydolide, measured under the same conditions, ions were observed at *m/e* 398, 364, 206, and 90 (m* ~ 39.1, 206 → 90). These results are consistent with conversion of pimaydolide, in the permethylation reaction to methyl *N,N,O*-trimethylsporidesmolate A.

When the permethylation reaction was allowed to continue for 30 min, a mass spectrum was obtained, at a source temperature of 110 °C, whose most abundant ions had *m/e* 500.3469 ($C_{26}H_{48}N_2O_7$ requires 500.3462), 469, 355.2597 ($C_{19}H_{35}N_2O_4$ requires 355.2597), 228, 200, and 87. Metastable peaks indicating the ion reactions: 500 → 469 (m* ~ 440), 469 → 200 (m* ~ 86), 355 → 228 (m* ~ 147), 228 → 200 (m* ~ 175), 228 → 87 (m* ~ 33) were also observed. An abundant ion *m/e* 413 probably resulted from the loss of 87 mass units from the methoxyl end of the molecule. These data, therefore uniquely define the structure of a second pimaydolide permethylation product as 1-carboxymethyl-3-methylbutyl-*N,N,O*-trimethylsporidesmolate A **4**. The precursor ion experiments allow this sequence to be expanded at the hydroxyl end to the expression **5**, and hence, on stoichiometric grounds to the structure **1** for pimaydolide. This structure is in accord with the nature of the saponification products **2** and **3** and also with the ions observed at 150 °C in the mass spectra of the permethylated and perdeuteriomethylated products at *m/e* 727 (739) and 681 (687); values in parentheses are perdeuteriomethylated species. Further a complete analysis of the formation of ions of *m/e* 356.2433 ($C_{19}H_{34}NO_5$ requires

Can. J. Chem. Downloaded from www.nrcresearchpress.com by 210.87.254.40 on 09/05/12
For personal use only.

Can. J. Chem. Downloaded from www.nrcresearchpress.com by 210.87.254.40 on 09/05/12
For personal use only.

356.2437, 362) and 469.3268 ($C_{25}H_{45}N_2O_6$ requires 469.3278, 478), where all fragmentation possibilities were considered led to the same sequence of hydroxy and amino acids in the depsipeptide ring.[3] Pimaydolide is therefore a structural analogue of sporidesmolide IV in which an amino acid residue (L-valyl) is replaced by the corresponding hydroxy acid residue (L-2-oxy-3-methylbutyryl). This situation is to our knowledge unique, but is of some taxonomic and toxicological importance (10).

Experimental

Melting points were measured on a Köfler hot stage. Infrared spectra were measured for paraffin mulls unless otherwise stated, using a Perkin-Elmer 137B spectrophotometer. Identities were established by comparison of ir spectra. Specific rotations were measured with a Hilger Model A polarimeter; values quoted are the means of at least 10 readings, and the probable error ($0.6754 \times \sigma$) is given. Optical rotatory dispersion and circular dichroism measurements were obtained with a Cary 60 spectropolarimeter. Mass spectra were obtained with Dupont 21-110B and A.E.I. MS-9 instruments. Solid samples were introduced directly into the ion source using a controlled temperature probe (11) at a block temperature of 180–200 °C. Precise mass measurements were made (± 3 ppm) by peak matching and (± 7 ppm) by photoplate measurement. In both cases perfluorokerosene was used as an internal standard. Permethylation and perdeuteriomethylation reactions were carried out by treating pimaydolide (1–3 mg) with excess sodium methylmethylenesulphinate in dimethyl sulphoxide (0.2 ml) and methyl iodide or C[^2H]$_3$I for 1–30 min (see text for exact times). The reaction mixture was diluted with chloroform (1.5 ml) and the solution washed three or four times with water, when it was evaporated and used without further treatment for mass spectroscopy.

Isolation of Pimaydolide from Cultures of Pithomyces maydicus IMI 46232

The organism was grown on rye grain as has been described (1) for *P. chartarum* and after treatment with methanol the grain was extracted 3 times with chloroform. The chloroform extract was treated with charcoal and alumina as previously described (3). The ether insoluble portion (57 g) was dissolved in chloroform (1000 ml), the volume reduced by distillation to 250 ml, and carbon tetrachloride (1750 ml) added. Distillation was continued, with periodic addition of carbon tetrachloride, until all the chloroform was removed. The resulting cloudy solution (2000 ml), allowed to stand at 4 °C for 24 h, furnished an insoluble product (6.8 g). Repetition of this procedure using carbon tetrachloride (500 ml) gave a crude depsipeptide (5.1 g) which, on repeated recrystallization from ethanol (120 ml/g), gave *pimaydolide*, mp (sealed tube) 253–254 °C. *Anal.* calcd. for $C_{34}H_{59}N_3O_9$: C 62.5, H 9.1, N 6.43, O 22.04; found (separate samples): C 62.65, 62.92, 62.07, H 8.91, 8.99, 9.05, N 6.59, 6.07, 6.37, O 22.17, 21.52, $[\alpha]_D^{22}$ +6.2 (*c* 2, $CHCl_3$), $[\phi]_{220}^{20}$ +25 000 (*c* 0.05, trifluoroethanol), λ_{max}(MeOH) 244 nm ($\Delta\epsilon$ −62°), λ_{max} 3.0, 3.1 (N—H), 5.73 (ester CO), 5.95, 6.1 (amide CO), 6.6 (amide II) μm.

Acid Hydrolysis of Pimaydolide

Pimaydolide (6.5 mg) was hydrolyzed in hydrochloric and acetic acids and the amino acid composition determined by paper chromatography of the reconstituted hydrolysate (12, 13). The following amino acids were tentatively identified; valine, leucine, and *N*-methylleucine in the ratio 1.18:1.00:1.03 and in a separate sample, 1.00:1.04:0.99. Ion exchange chromatography gave valine–leucine ratios of 0.95:1.00 and 1.00:0.98 (in separate samples). In another sample run at half speed for *N*-methylamino acids (13, 14) valine, leucine, and *N*-methylleucine in the ratio 1.03:0.92:1.00 were identified by comparison of their elution times with those of standards. Paper chromatograms of ether extracts of the hydrolysates in *tert*-butyl alcohol – 4.25 *N* ammonia (4:1) showed 2 acid spots corresponding in R_F to 2-hydroxy-3-methylbutyric acid and 2-hydroxy-4-methylvaleric acid respectively, the former being the more intense.

Alkaline Hydrolysis of Pimaydolide

A solution of pimaydolide (2.13 g) in chloroform (50 ml) was diluted with ethanol (400 ml) and then concentrated to 200 ml, when sodium hydroxide solution (*N*, 10 ml) was added and the solution evaporated *in vacuo* to 20 ml. Water (50 ml), ethanol (50 ml), and sodium hydroxide (*N*, 25 ml) were added, and after 30 min the solution was titrated with standard hydrochloric acid (3.06 equiv. NaOH/mol). The neutral solution was concentrated at 50 °C/14 torr to 50 ml, filtered, acidified, and kept at 4 °C for 24 h. The precipitate was collected (A) and the filtrate continuously extracted with ether. The extract was evaporated and the residue sublimed (60 °C/14 torr). The sublimate was resublimed 3 times and the final sublimate recrystallized from ether–hexane gave L-2-hydroxy-4-methylvaleric acid (0.24 g, 0.56 mol/mol pimaydolide), mp 79–81 °C, $[\alpha]_D^{22}$ −13.1 ±0.96, (*c* 1.83, H_2O), equivalent, 132, 132 ($C_6H_{12}O_3$ requires 132), Na salt, $[\alpha]_D^{22}$ −24.95 ±1.54 (*c* 1.19, H_2O). This acid (0.199 g) was oxidized with sodium bismuthate (3, 15) and gave isovaleraldehyde-2,4-dinitrophenylhydrazone, 0.121 g, mp 123–124 °C, R_F 0.68, ascending paper (Whatman 3MM) chromatography, stationary phase dimethyl sulphoxide, mobile phase ethyl acetate – hexane (1:9).

The acids (A, 1.58 g) were stirred with chloroform (22 ml) for 30 min, the suspension kept at 4 °C for 6 h and the precipitate dissolved in sodium bicarbonate solution (1%, 80 ml). The solution was acidified, and the precipitate (0.87 g) recrystallized from 20% aqueous acetic acid (30 ml) furnished sporidesmolic acid A (4) (0.75 g), mp 199–200 °C, $[\alpha]_D^{22}$ +60 ±0.3 (*c* 5, HOAc); $[\alpha]_{400}^{22}$ +85, $[\alpha]_{300}^{22}$ +260, $[\alpha]_{250}^{22}$ +651 (*c* 0.1, H_2O); $[\alpha]_{400}^{22}$ +58, $[\alpha]_{277}^{22}$ +118, $[\alpha]_{251}^{22}$ 0, $[\alpha]_{229}^{22}$ −1029, (*c* 0.1, MeOH). The chloroform mother liquors from sporidesmolic acid A were evaporated and the residue digested with small volumes of chloroform. The precipi-

[3]Full details are available, at a nominal charge, from the Depository of Unpublished Data, CISTI, National Research Council of Canada, Ottawa, Canada K1A 0S2.

Can. J. Chem. Downloaded from www.nrcresearchpress.com by 210.87.254.40 on 09/05/12
For personal use only.

tate was filtered, the filtrate evaporated, and the residue sublimed (95 °C/0.05 torr). The sublimate in ether was washed with sodium bicarbonate solution (1%) and water, and sublimed. This sublimate, (mp 32–35 °C, 0.45 g) in hexane (5 ml) was filtered through charcoal (0.2 g) and alumina (0.2 g) and the filtrate and washings combined (8 ml) and kept at −20 °C. *L,L-2-Isopropyl-5-(2'-methylpropyl)-1-methylmorpholine-3,6-dione*, **3**, separated from hexane at −20 °C as needles, mp 38–39 °C, 0.24 g, (0.32 mol/mol pimaydolide). *Anal.* calcd. for $C_{12}H_{21}NO_3$: C 63.41, H 9.31, N 6.16; found: C 63.43, H 9.07, N 6.12. *Exact Mass* calcd. for $C_{12}H_{21}NO_3$: 227.1522; found: 227.1520. λ_{max} 5.7 (lactone CO), 5.92 (lactam CO), 6.79, 7.19, 7.22 μm.

Hydrolysis of the Morpholine-3,6-dione 3

The lactone **3** (0.182 g) in ethanol (5 ml) and water (2.5 ml) was titrated slowly with sodium hydroxide solution (0.1 *N*) to p*H* 9 (Found: 0.799 mequiv., $C_{12}H_{21}NO_3$ requires 0.801 mequiv.). The solution was evaporated, the residue boiled with hydrochloric acid (6 *N*, 80 ml) for 24 h, when the solution was diluted with water (250 ml) and continuously extracted with ether. Sublimation of the extract and recrystallization of the sublimate from ether–hexane gave L-2-hydroxy-3-methylbutyric acid, mp 65–66 °C, 77 mg, $[\alpha]_D^{22}$ +17 ±1.3 (*c* 1.4, $CHCl_3$). The sodium salt in phosphoric acid solution (*M*, 2.05 ml) was treated with sodium bismuthate (0.167 g) (3, 15) for 1 h, when the solution on treatment with 2,4-dinitrophenylhydrazine gave isobutyraldehyde-2,4-dinitrophenylhydrazone (46 mg, mp 185–186 °C). The raffinate from the ether extraction was evaporated, the residue dissolved in water, and the solution treated with Amberlite AG 50W-X12. Evaporation of the aqueous solution gave L-*N*-methylleucine, 63 mg, $[\alpha]_D^{22}$ +24.8 ±2.3 (*c* 1.16, H_2O); +27.4 ±3 (*c* 0.86, 6 *N* HCl). L-*N*-Methylleucine hydrochloride (60 mg) in water (2 ml) was treated with sodium bicarbonate (30 mg), sodium carbonate (70 mg), and 2,4-dinitrofluorobenzene (0.04 ml). The mixture was stirred in the dark for 2 h at 40 °C, extracted with ether and the raffinate acidified with hydrochloric acid (*N*). The mixture was kept 16 h at 4 °C, when the precipitate was collected and recrystallized from carbon tetrachloride, mp 153–154 °C, $[\alpha]_D^{22}$ +583 ±10 (*c* 0.8, 1% $NaHCO_3$). An authentic sample had $[\alpha]_D^{22}$ +585 ±18 under these conditions (16). This 2,4-dinitrophenyl derivative was photolysed for 3 h (17), then kept for 16 h while a stream of nitrogen was passed through the reaction mixture and the volatile products trapped in 2,4-dinitrophenylhydrazine solution. Isovaleraldehyde-2,4-dinitrophenylhydrazone (8.6 mg, mp 123–124 °C) was collected, and the filtrate, extracted with ethyl acetate, gave *N*-methyl-4-nitro-2-nitrosoaniline (7.4 mg, mp (17) 165–169 °C (dec.)) after the extract had been recrystallized from 60% acetone.

Acknowledgment

The support of the Medical Research Council of Canada is gratefully acknowledged.

1. J. Done, P. H. Mortimer, A. Taylor, and D. W. Russell. J. Gen. Microbiol. **26**, 207 (1961).
2. E. Bishop and D. W. Russell. J. Biochem. **19**, 92 (1964).
3. E. Bishop and D. W. Russell. J. Chem. Soc. C, 634 (1967).
4. D. W. Russell. J. Chem. Soc. 753 (1962).
5. W. S. Bertaud, M. C. Probine, J. S. Shannon, and A. Taylor. Tetrahedron, **21**, 677 (1965).
6. C. G. Macdonald, J. S. Shannon, and A. Taylor. Tetrahedron Lett. 2087 (1964).
7. B. C. Das, and E. Lederer. Peptides. *Edited by* H. Nesvadbra. North Holland/American Elsevier, Amsterdam. 1971. p. 254.
8. M. Barber, W. A. Wolstenholme, M. Guinand, G. Michel, B. C. Das, and E. Lederer. Tetrahedron Lett. 1331 (1965).
9. K. Biemann, C. Cone, B. R. Webster, and G. P. Arsenault. J. Am. Chem. Soc. **88**, 5598 (1966).
10. L. G. Atherton, D. Brewer, and A. Taylor. Mycotoxins. *Edited by* I.F.S. Purchase. Elsevier, Amsterdam. 1974. pp. 29.
11. R. D. Grigsby, W. D. Jamieson, A. G. McInnes, W. S. G. Maass, and A. Taylor. Can. J. Chem. **52**, 4117 (1974).
12. D. W. Russell. J. Chromatogr. **4**, 251 (1960).
13. T. K. Audhya and D. W. Russell. J. Chromatogr. **84**, 361 (1973).
14. J. R. Coggins and N. L. Benoiton. J. Chromatogr. **52**, 251 (1970).
15. W. Rigby. J. Chem. Soc. 1907 (1950).
16. Pl. A. Plattner and U. Nager. Helv. Chim. Acta. **31**, 2192 (1948).
17. D. W. Russell. J. Chem. Soc. 2829 (1964).

A new depsipeptide from *Pithomyces chartarum*[1,2]

R. RAHMAN AND A. TAYLOR
National Research Council of Canada, Atlantic Regional Laboratory, Halifax, Nova Scotia B3H 3Z1

B. C. DAS
Institut de Chimie des Substances Naturelles, C.N.R.S., 91190, Gif-sur-Yvette, France

AND

J. A. VERPOORTE
Biochemistry Department, Dalhousie University, Halifax, Nova Scotia

Received October 29, 1975

R. RAHMAN, A. TAYLOR, B. C. DAS, and J. A. VERPOORTE. Can. J. Chem. **54**, 1360 (1976).

Further examination of the pithomycolide fraction of extracts of cultures of *Pithomyces chartarum* has resulted in the isolation of a new depsipeptide, for which the structure cyclo(L-*N*-methylalanyl-L-valyl-D-3-oxy-3-phenylpropionyl-D-3-oxy-3-phenylpropionyl-L-2-oxy-3-methylbutyryl) is proposed.

R. RAHMAN, A. TAYLOR, B. C. DAS et J. A. VERPOORTE. Can. J. Chem. **54**, 1360 (1976).

Un examen plus poussé de la fraction pithomycolide des extraits de culture du *Pithomyces chartarum* nous a permis d'isoler un nouveau depsipeptide pour lequel on propose la structure cyclo(L-*N*-méthylalanyl L-valyl D-oxy-3 phényl-3 propionyl D-oxy-3 phényl-3 propionyl L-oxy-2 méthyl-3 butyryl).

[Traduit par le journal]

In 1960 Synge and White (1) reported the presence of a new natural product containing alanine in extracts of cultures of *Pithomyces chartarum*. They reported that the new metabolite was nontoxic, had mp 244 °C, $[\alpha]$ −95 (HOAc), and that it was probably related to other depsipeptide metabolites (2) of the mould. These cultures were grown on potato–carrot medium but in subsequent large scale production of sporidesmin (3), the fungus was grown on rye grain and relatively large quantities of fractions containing the new depsipeptide were accumulated. An examination of this material was carried out by Briggs *et al.* (4) who were unable to obtain material of similar purity to that of Synge and White (1) by extensive fractional crystallization. From hydrolysates of their purest preparations (mp 242–244 °C (dec.)) Briggs *et al.* isolated L-alanine, L-*N*-methylalanine, L-2-oxy-3-methylbutyric acid, and D-3-hydroxy-3-phenylpropionic acid in the ratios 1:1:1:2. Elemental analysis suggested an empirical formula $C_{15}H_{18}NO_4$ which was expanded to $C_{30}H_{36}N_2O_8$ for the molecular formula on the basis of a molecular ion at *m/e* 552, and consideration of the stoichiometry of the hydrolysis products. These recrystallized preparations were, however, impure because ions at *m/e* 580 were observed in the mass spectra. Briggs *et al.* proposed the structure shown in Fig. 2 (R = Me) for the main component, named pithomycolide, of the depsipeptide mixture, basing the sequence of amino and hydroxy acids on the production of 1.4 mol of cinnamic acid on mild alkaline hydrolysis and the formation of 2-aminopropan-1-ol after treatment of pithomycolide with lithium borohydride, followed by acid hydrolysis.

During work on the isolation of sulphur-containing metabolites of *P. chartarum* (*e.g.* ref. 5) it was found that sporidesmin B (3) could be separated from the pithomycolides by increasing the length of the partition chromatography column used in the purification of sporidesmin (3). A typical separation is shown in Fig. 1*A*. Fractions were combined on the basis of the weight distribution and on the formation of methyl cinnamate after esterification of the products of hydrolysis. Reversed phase chromatography of such fractions (Fig. 1*B*) gave material that contained less than 0.01% S, did not give a positive azide–iodine reaction (6), and on

[1]NRCC No. 15175.

[2]This work was carried out under the joint scientific agreement between Centre National de la Recherche Scientifique de France and the National Research Council of Canada.

Can. J. Chem. Downloaded from www.nrcresearchpress.com by 210.87.254.105 on 09/05/12
For personal use only.

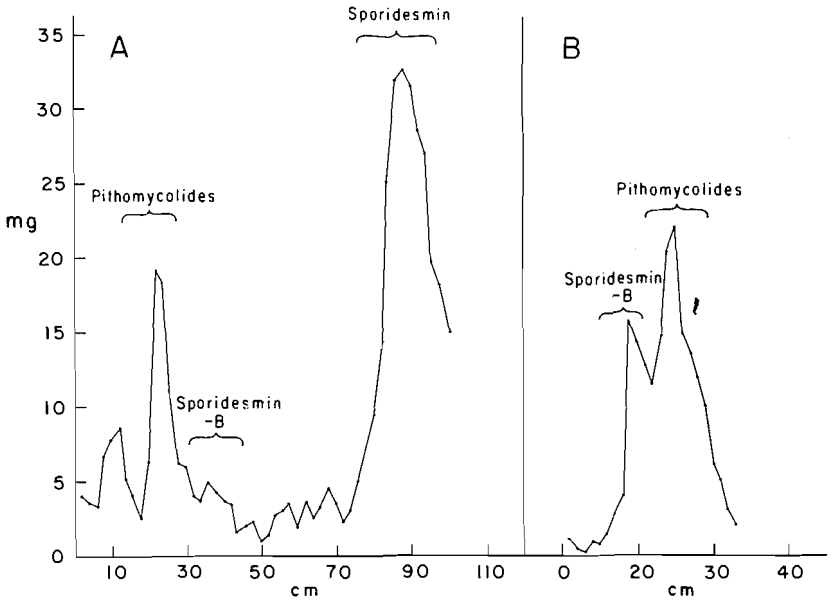

FIG. 1. (*A*) Partition chromatogram of an extract of mycelium of *P. chartarum* on hyflosupercel using the solvents carbon disulphide – methanol – water (5:4:1). (*B*) Reversed phase partition chromatogram of fractions 11–16 from chromatogram *A* using the solvent benzene–chloroform–methanol–water (15:15:23:7).

quantitative amino acid analysis gave (mol%): *N*-methylalanine 47.3, arginine (?) 0.5, glutamic acid 1.5, glycine 0.5, alanine 32.2, cysteine (?) 0.5, valine 17.1, leucine 2.4, and *N*-methylleucine 0.5. Thin layer chromatography on silica gel or high pressure liquid chromatography on porous glass beads separated this mixture into three major zones, which were isolated by preparative tlc. The chemistry and physical properties of each will be discussed in order of increasing R_F.

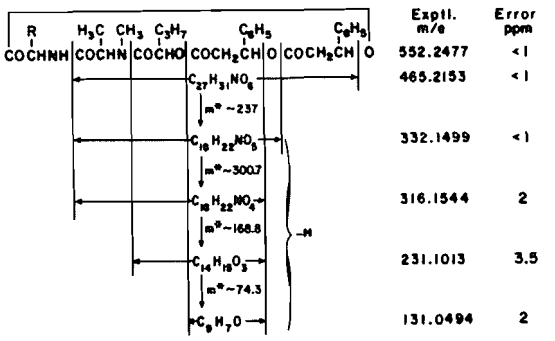

FIG. 2. Fragmentation of pithomycolide (R = Me) and its homologue (R = $^{\beta}$Pr) in the source of the mass spectrometer. The precise mass measurement for the molecular ion of the new depsipeptide is given in the text. Other mass measurements are means of the results from the two compounds; the maximum error is indicated.

The band of R_F = 0.44 (pithomycolide) had physical properties identical with those reported by Synge and White (1). Gas–liquid chromatography of its methanolysis products (7) gave methyl cinnamate as the main peak on the chromatogram. Cinnamic acid and L-2-oxy-3-methylbutyric acid were the only non-nitrogenous acids recovered from hydrolysates. Quantitative analysis of the amino acids in such mixtures gave (mol%); *N*-methylalanine 49.5, alanine 50.1, and valine 0.2. An ion at *m/e* 552.2477 ($C_{30}H_{36}N_2O_8$ requires 552.2471) was shown to be a molecular ion by inserting the experimental values for its abundance together with those of ions 1, 2, and 4 mass units greater into the 'ELAL' algorithm recently reported (8). No ions greater than these were detected. The sequence of ion fragmentations shown in Fig. 2 were deduced from the appearance of metastable ions in the spectra measured on the instrument having Nier–Johnson optics. This sequence was verified by precursor ion experiments run on the instrument having Mattauch–Herzog optics (10). The latter results are given in Table 1 where the numbers in parentheses indicate the relative

Can. J. Chem. Downloaded from www.nrcresearchpress.com by 210.87.254.105 on 09/05/12
For personal use only.

TABLE 1. Ion reactions in the first field free region of the mass spectrometer after electron impact ionisation of pithomycolide

	m/e values				
Daughter ion	465	332	316	231	131
↑	552 (940)	552 (50)	552 (160)		
	510 (40)				
		465 (1600)	465 (200)		
		424 (70)			
		404 (210)	404 (150)		
			388 (60)		
Parent ions		375 (12)		380 (80)	
			361 (180)		
			332 (2)		
				316 (280)	
				288 (890)	288 (1124)
				259 (40)	
					231 (5988)
↓					203 (1421)

extent of the fragmentation of the adjoining parent ion to its daughter in the first field free region of the mass spectrometer. While the relationship of these reactions to the fragmentation process as a whole has not been determined, high figures probably indicate likely fragmentation reactions of the molecule. Thus the loss of an alanine unit (465), then a phenylpropanoid unit (332, 316), then a *N*-methylalanine moiety (231), and finally a valeric acid unit (131) can all be seen to be probable reactions (9).

Two volatile products of the exhaustive methylation of pithomycolide could be selectively distilled into the source of the mass spectrometer. The most volatile showed abundant ions at *m/e* 316, 285, 200, 172 and 87 corresponding to the sequence shown in **1**. The other product had prominent ions at *m/e* 432, 401, 231, and 131 easily accounted for by addition of a cinnamoyl residue to the entity **1** as shown in **2**. These results thus support the structure proposed by earlier workers (4).

The band of $R_F = 0.67$ from the preparative tlc had the ir spectrum shown in Fig. 3*B*; the differences between this spectrum and the spectrum of pithomycolide can be seen in Fig. 3. The uv spectra and cd of the two metabolites were identical. Cinnamic acid and 2-oxy-3-

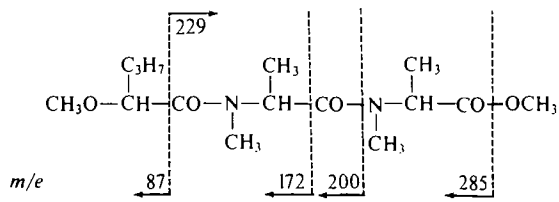

1

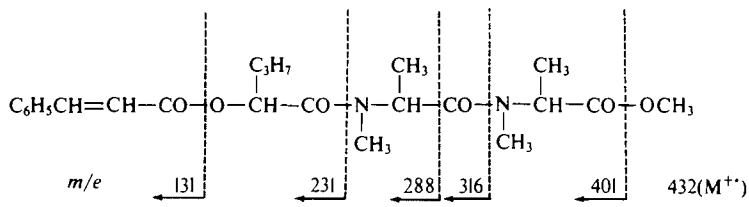

2

Can. J. Chem. Downloaded from www.nrcresearchpress.com by 210.87.254.105 on 09/05/12
For personal use only.

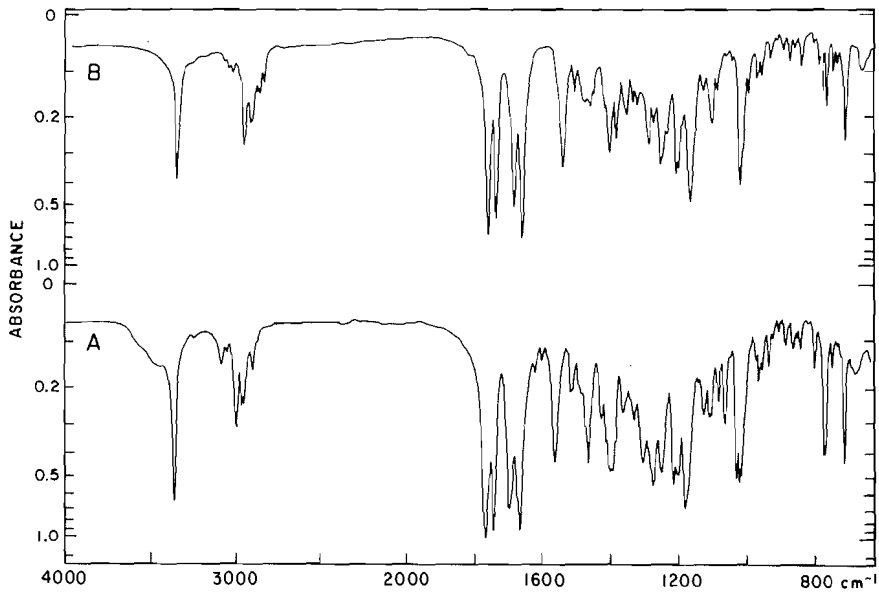

FIG. 3. Infrared spectra of pithomycolide (*A*) and the new depsipeptide (*B*).

methylbutyric acid were found in the ratio 2:1 in hydrolysates, which on quantitative amino acid analysis gave (mol%): *N*-methylalanine 48.2, valine 51, leucine 0.4, *N*-methylleucine 0.3, and alanine 0.1. Further preparative tlc reduced the alanine content of hydrolysates of the major band to $<0.01\%$ but we were unable to remove leucine and *N*-methylleucine from this material chromatographically. The mass spectrum of the recrystallized band of R_F 0.67 was identical with that of the total sporidesmolide fraction (9), with molecular ions at *m/e* 638 and 652. By increasing the temperature of the sample from 250 to 270 °C over a period of 60 min, the spectrum slowly changed and an ion of *m/e* 580 increased in abundance while those at *m/e* 285 and 569 (the most abundant in the spectra of the sporidesmolides) disappeared. From the amino acid and elemental analysis of the sample, the maximum content of sporidesmolides was 0.5%; thus fractional sublimation of the sample removed these entities and gave a sublimate having mp 223–224 °C, which still showed traces of leucine in acid hydrolysates, but on mass spectroscopy gave a molecular ion at *m/e* 580.2781 ($C_{32}H_{40}N_2O_8$ requires 580.2783), with no molecular species of greater mass detectable. These results suggest caution in the interpretation of the mass spectra of mixtures of depsipeptides. The most abundant ions in the mass spectrum of the new depsipeptide were identical with those given in Fig. 2 for pithomycolide. The difference in the two metabolites thus lies in the fragment lost in the formation of the ion *m/e* 465 ($C_{27}H_{31}NO_6$). In the case of pithomycolide this is $C_3H_5NO_2$ and in the new metabolite $C_5H_9NO_2$ corresponding to alanine and valine residues respectively. A volatile product was obtained from the permethylation and perdeuteriomethylation reactions of the new metabolite. Its mass spectrum was closely similar to that described above for the most volatile permethylation product of pithomycolide (**1**). The molecular ion *m/e* 344 was shown to bear three introduced methyl groups because the perdeuteriomethylated product had *m/e* 353. The ion at *m/e* 200 retained only one such group, hence in the fragmentation processes leading to *m/e* 200 one nitrogen and two methyl groups have been lost. Thus the sequence 2-oxy-3-methylbutyryl-*N*-methylalanyl-valine deduced above receives support and the new metabolite can be considered as the valine homologue of pithomycolide. Such a substitution has been reported in the peptidolipin series (11). It is a remarkable coincidence that the most probable ring fission by electron impact occurs at the point that is the source of biological variability.

The band of $R_F = 0.89$ from the preparative tlc appeared to be mainly sporidesmolides from

Can. J. Chem. Downloaded from www.nrcresearchpress.com by 210.87.254.105 on 09/05/12
For personal use only.

Can. J. Chem. Downloaded from www.nrcresearchpress.com by 210.87.254.105 on 09/05/12
For personal use only.

its mass spectrum and amino acid analyses of its hydrolysates. However, the hydrolysates always contained cinnamic acid and *N*-methylalanine; thus the presence of higher homologues of pithomycolide cannot be excluded.

Experimental

Ultraviolet spectra were measured on a Beckman DK-2 instrument, ir on a Perkin-Elmer 521 spectrometer and mass spectra on A.E.I. MS-9 and Dupont 21-110B mass spectrometers. Precise mass measurements were made by the peak matching method, using a suitable ion of known mass in the spectrum of perfluorokerosene. Permethylation reactions were carried out by treating the depsipeptides (1–2 mg) with an excess of sodium methylmethylene sulphinate and methyl iodide in dimethyl sulphoxide for 5 to 20 min. Circular dichroism measurements were obtained on a Cary 60 instrument. Depsipeptides (2 mg) were hydrolysed in a mixture of acetic acid (0.2 ml) and hydrochloric acid (10 *N*, 0.2 ml) for 48 h, at 110 °C. The diluted (×3) acidic solution was extracted with ether and the raffinate evaporated. The water soluble residue was used directly for amino acid analysis using a JEOL JCL-5AH instrument for quantitative work. Qualitative paper chromatography of hydrolysates was done on Whatmann 3MM paper with *tert*-butyl alcohol – ammonia as previously described (2). Gas–liquid chromatography was carried out using Chromosorb W as the support and silicone oil (SAE 30, 5%) as the liquid phase. Helium was the carrier gas (10 l/min) and the column dimensions were 1.5 m × 1.5 mm. High pressure liquid chromatography was run in stainless steel columns (1 m × 1.5 mm) packed with 'Porosil' (Dupont) glass beads and chloroform – ethyl acetate (4:1) was the developing solvent.

Isolation of Pithomycolide and Related Compounds

The crude extract (1.6 g) obtained from cultures of *P. chartarum* on rye grain (3) was dissolved in the bottom phase (5 ml) of the solvents carbon disulphide – methanol – water (5:4:1) and purified Hyflosupercel (2 g) added. The excess solvent was allowed to evaporate at room temperature and the mixture was then packed (12) on a jacketed Hyflosupercel column (45 × 4 cm) prepared as described by Ronaldson *et al.* (3). The column was maintained at 28 °C (±0.1 °C) by pumping water at constant temperature through the jacket. The flow through the column was maintained at 5 ml/min by a head pressure of 0.5 kg cm^{-2}. Fractions were collected as the surface of the upper mobile phase above the column descended each 2 cm. Fractions 11–16 (Fig. 1*A*) were collected from 2 runs of the above column, were combined (150 mg), methyl orange (0.5 mg) added, and chromatographed on a hydrophobic (12) Hyflosupercel column (35 × 1 cm) using the top phase of the solvents chloroform–benzene–methanol–water (15:15:23:7) as the mobile phase. Fractions were collected as before after the appearance of methyl orange in the eluate. Fractions 24–26 (65 mg, Fig. 1*B*) were collected, combined, and applied as a streak of silica gel (Stähl, 40 × 20 × 0.2 cm) and the plate developed with chloroform–ethyl acetate (4:1) until the solvent was 18 mm from the top. The plate was dried at 100 °C for 5 min, cooled, and sprayed with distilled water, when three bands could be seen (R_F 0.44, 0.67, 0.89) under intense illumination (5, 40 W fluorescent tubes). The bands were eluted with ethyl acetate and were rechromatographed in the same way until that of R_F 0.44 contained only traces of valine after hydrolysis, and that of R_F 0.67, alanine. The band having R_F 0.44 recrystallized from benzene–hexane as colorless rods (10.2 mg) mp 243–244 °C, $[\alpha]_D^{25}$ −67, (*c* 0.07, $CHCl_3$), −95 (*c* 0.1, HOAc), λ_{max} (MeOH) 250, 256, 263, 266 nm (ϵ 690, 855, 650, 400), λ(MeOH) 217, 227, 261, 267, ~305 nm ($\Delta\epsilon$ 0, −600, +4.6, +5.2, +0.9°) ir Fig. 3*A*. The band of R_F 0.67 separated from cyclohexane as colorless rods mp 219–220 °C, 4.1 mg, ir Fig. 3*B*. *Anal.* calcd for $C_{32}H_{40}N_2O_8$: C 66.2, H 6.9, N 4.8, O 22.1; found: C 66.0, H 7.3, N 5.1, O 21.8. This material was heated at 260 °C/0.1 torr in a capillary tube when it sublimed as two bands; the most volatile was only detectable with a lens. The tube was cut between the bands and the least volatile band gave colorless rods from cyclohexane mp 223–224 °C, *m/e* 580.2781 ($C_{32}H_{40}N_2O_8$ requires 580.2783), λ_{max} (MeOH) 250, 256, 262, 266 nm (ϵ 630, 670, 555, 380), λ(MeOH) 217, 227, 261, 267 nm ($\Delta\epsilon$ 0, −500, +4.2, +4.5°), ir Fig. 3*B*. The band of R_F 0.89 (35 mg) separated from methanol as needles mp 251–256 °C, $[\alpha]_D^{23}$ −200, (*c*, 0.25, $CHCl_3$), ν_{max} (KBr) 1755, 1675, 1520 cm^{-1}.

1. R. L. M. Synge and E. P. White. N. Z. J. Agric. Res. **3**, 907 (1960).
2. D. W. Russell, R. L. M. Synge, A. Taylor, and E. P. White. J. Chem. Soc. 554 (1962).
3. J. W. Ronaldson, A. Taylor, E. P. White, and R. J. Abraham. J. Chem. Soc. 3172 (1963).
4. L. H. Briggs, L. D. Colebrook, B. R. Davis, and P. W. Le Quesne. J. Chem. Soc. 5626 (1964).
5. R. Hodges, J. S. Shannon, and A. Taylor. J. Chem. Soc. C, 1803 (1966).
6. G. R. Russell. Nature (London), **186**, 788 (1960).
7. S. Safe and D. Brewer. Lipids, **8**, 311 (1973).
8. J. E. Evans and N. B. Jurinski. Anal. Chem. **47**, 961 (1975).
9. C. G. Macdonald, J. S. Shannon, and A. Taylor. Tetrahedron Lett. 2087 (1964).
10. D. W. Russell, W. D. Jamieson, A. Taylor, and B. C. Das. Can. J. Chem. This issue.
11. M. Guinand, M. J. Vacheron, G. Michel, B. C. Das, and E. Lederer. Tetrahedron Suppl. No. 7, 271 (1966).
12. G. A. Howard and A. J. P. Martin. Biochem. J. **46**, 535 (1950).

Crystal structure of β-D-acetyl cellobiose, $C_{28}H_{38}O_{19}$

F. LEUNG, H. D. CHANZY,[1] S. PEREZ, AND R. H. MARCHESSAULT
Department of Chemistry, Université de Montréal, C.P. 6210, Succ. A, Montréal, Québec H3C 3V1

Received September 22, 1975

F. LEUNG, H. D. CHANZY, S. PEREZ, and R. H. MARCHESSAULT. Can. J. Chem. **54**, 1365 (1976).

The crystal structure of β-D-acetyl cellobiose was studied by X-ray crystallography. The crystal data are $a = 31.814(4)$, $b = 19.414(5)$, $c = 5.614(1)$ Å, space group $P2_12_12_1$, $Z = 4$. The structure, solved by direct method, was refined by block-diagonal least-squares to a final R value of 0.075 for 2605 observed reflections. The molecular conformation involves $^4C_1$ pyranose rings with glycosidic torsion angles corresponding to near maximum extension of the molecule. Substantial differences in conformational angles were observed between this molecule and the unacetylated counterpart. The molecules lie along the a-axis of the unit cell.

F. LEUNG, H. D. CHANZY, S. PEREZ et R. H. MARCHESSAULT. Can. J. Chem. **54**, 1365 (1976).

Les cristaux d'acétyl-β-D cellobiose cristallisent dans le groupe spatial $P2_12_12_1$ du système orthorhombique. Les paramètres cristallins sont: $a = 31.814(4)$, $b = 19.414(5)$, $c = 5.614(1)$ Å et $Z = 4$. Les intensités de 3013 réflexions indépendantes ont été mesurées sur un diffractomètre automatique Picker. La structure a été résolue par utilisation des méthodes directes. Un affinement anisotrope a conduit à un facteur de reliabilité final de 0.075. La conformation de la molécule est celle des cycles pyranoses $^4C_1$.

Les angles de torsion glycosidiques sont tels que la molécule est proche de son extension maximum. La comparaison de la conformation de cette molécule avec son homologue non acétylée révèle de notables différences au niveau des angles de torsion. Les molécules sont parallèles à l'axe cristallographique a de la maille cristalline.

Introduction

A classical approach to the solution of polymer crystal structures is to examine a homologous series of oligomers related to the polymer (1). In the case of polysaccharides, this idea has not yet been fully exploited in view of the difficulty of obtaining good single crystals of oligomers. In the cellulose series, it is well known that acetylated oligomers crystallize easily (2). Furthermore cellulose acetate structures are known to be closely related to those of cellulose (3, 4). For this reason, we have undertaken a systematic determination of the structures of oligomers of the cellulose triacetate series as a means of arriving at a fuller understanding of the cellulose structure.

The present work surveys the results of the crystal data on β-D-cellobiose octaacetate. Of prime interest is the ring distortion compared to cellobiose which is introduced by the acetyl substituents and the effect of suppression of the intramolecular hydrogen bond which is present in cellobiose. We are also interested in the effect of acetylation on the values of the torsional angles ϕ, ψ about the bridge oxygen (5).

[1]Present address: CERMAV (CNRS), Domaine universitaire, 38041, Grenoble, Cédex 53, France.

Experimental

The material, which was prepared by a conventional method of cellulose acetolysis, was kindly supplied by M. Vincendon, Centre d'Etudes Nucléaires, Grenoble, France. Crystals suitable for X-ray work were obtained by slow evaporation of acetone and water. The crystals were transparent thin prisms elongated along the chosen crystallographic c-axis. The cell parameters were determined from a least-squares refinement of the angular settings of 12 well centered reflections.

Crystal data are:

$C_{28}H_{38}O_{19}$ fw = 678

$a = 31.814(4)$, $b = 19.414(5)$, $c = 5.614(1)$ Å, $V = 3467.4$ Å^3, $Z = 4$, space group $P2_12_12_1$, $d_{obs} = 1.28$ g cm^{-3}, $d_{calcd} = 1.30$ g cm^{-3}, $F(000) = 1432$ (20 °C; CuKα, $\mu = 9.39$ cm^{-1}).

Intensity data were collected on a Picker FACS-I diffractometer equipped with a graphite monochromator using copper radiation ($\lambda = 1.54178$ Å) within one octant of the sphere limited by $2\theta \leq 120°$. The θ–2θ scanning technique was used throughout the data collection with a scan rate of 1° (2θ) min^{-1} and a minimum scan width of 1.5° (2θ). Background counts of 20 s where taken at each end of the scan range. The intensities of three reflections were monitored as standards every 30 reflections. The data were corrected for Lorentz, polarization, and absorption effects. Of the 3013 measured reflections, 2605 (86%) were considered as observed. These reflections have $I/\sigma(I) \geq 1.96$ where $\sigma(I)$ is the standard deviation estimated from counting statistics (6). The data reduction was performed in the usual manner using the programs of Ahmed, Hall, Pippy, and Huber (7). The atomic scattering factors used for the hydrogen and non-

Can. J. Chem. Downloaded from www.nrcresearchpress.com by 210.87.254.6 on 09/05/12
For personal use only.

TABLE 1

(*a*) Final atomic coordinates and thermal parameters of non-hydrogen atoms. The temperature factor used was $\exp -2\pi^2(U_{11}a^{*2}h^2 + \cdots + 2U_{12}a^*b^*hk + \cdots)$. The standard deviations refer to the last significant digit. The coordinates are in fraction of unit-cell edges $\times 10^4$. All thermal parameters are given $\times 10^3$

Atom	*X*	*Y*	*Z*	U_{11}	U_{22}	U_{33}	U_{12}	U_{13}	U_{23}
O(1)	−836(1)	−6490(1)	−7231(7)	41(1)	63(2)	49(2)	2(1)	0(1)	8(2)
O(2)	−1492(1)	−5556(1)	−7264(6)	54(1)	47(1)	40(1)	−1(1)	6(1)	−0(1)
O(3)	−2294(1)	−6242(2)	−7770(6)	49(1)	78(2)	41(2)	3(1)	−3(1)	−8(2)
O(4)	−2352(1)	−7308(2)	−3898(7)	62(2)	90(3)	53(2)	−28(2)	17(2)	−2(2)
O(5)	−1268(1)	−7335(1)	−5895(7)	52(1)	52(2)	59(2)	−3(1)	−0(2)	8(2)
O(6)	−1751(1)	−8607(2)	−6046(9)	103(3)	63(2)	76(3)	−21(2)	11(3)	4(2)
O(7)	−1442(1)	−5538(2)	−11249(7)	90(3)	81(2)	46(2)	0(2)	8(2)	2(2)
O(8)	−2669(1)	−5704(3)	−5024(9)	69(2)	182(6)	55(2)	33(3)	5(2)	−28(3)
O(9)	−2769(1)	−7741(4)	−6720(11)	80(3)	226(8)	86(3)	−72(4)	1(3)	−27(5)
O(10)	−2151(5)	−9271(6)	−4041(15)	577(26)	350(15)	88(5)	−382(18)	18(10)	3(8)
C(1)	−1201(1)	−6619(2)	−5957(10)	46(2)	51(2)	43(3)	−4(2)	−1(2)	−0(2)
C(2)	−1554(1)	−6283(2)	−7281(9)	44(2)	54(3)	35(2)	−1(2)	6(2)	−1(2)
C(3)	−1972(1)	−6440(3)	−6081(9)	44(2)	66(3)	35(2)	−3(2)	0(2)	−6(2)
C(4)	−2015(1)	−7199(3)	−5588(10)	50(2)	65(3)	45(3)	−12(2)	4(2)	−4(3)
C(5)	−1619(1)	−7487(3)	−4353(11)	62(3)	69(3)	44(3)	−16(3)	−3(3)	8(3)
C(6)	−1625(2)	−8246(3)	−3885(15)	85(4)	78(4)	84(5)	−23(3)	−17(4)	18(4)
C(7)	−1415(1)	−5244(2)	−9391(11)	41(2)	58(3)	49(3)	8(2)	8(2)	6(2)
C(8)	−2621(1)	−5874(3)	−7049(12)	45(2)	80(4)	55(3)	3(2)	−1(2)	−10(3)
C(9)	−2710(2)	−7580(4)	−4734(15)	69(4)	123(6)	77(4)	−45(4)	13(4)	−16(5)
C(10)	−1990(3)	−9129(5)	−5886(16)	195(10)	111(6)	70(5)	−89(7)	2(7)	15(5)
C(11)	−1288(2)	−4525(3)	−9000(14)	63(3)	68(3)	77(4)	−5(3)	6(3)	7(4)
C(12)	−2918(2)	−5756(4)	−9018(14)	64(3)	105(5)	69(4)	23(3)	−17(4)	1(4)
C(13)	−3026(2)	−7630(6)	−2732(20)	89(5)	188(10)	106(7)	−54(6)	37(5)	−10(8)
C(14)	−2139(5)	−9427(6)	−8071(24)	371(24)	154(10)	108(8)	−151(14)	63(13)	−36(9)
O(1′)	828(1)	−6371(2)	−4911(14)	47(2)	78(3)	178(6)	1(2)	−12(3)	−17(4)
O(2′)	540(1)	−7224(2)	−8873(8)	63(2)	88(3)	71(3)	27(2)	14(2)	20(2)
O(3′)	−304(1)	−7700(1)	−7746(7)	63(2)	49(2)	54(2)	5(1)	−9(2)	1(2)
O(5′)	153(1)	−6054(2)	−4293(12)	47(2)	77(2)	134(4)	2(2)	−6(2)	−35(3)
O(6′)	−264(2)	−5089(4)	−1649(15)	122(4)	147(5)	136(6)	14(4)	55(5)	−11(5)
O(7′)	871(2)	−8015(3)	−6766(11)	128(4)	116(4)	75(3)	64(3)	−1(3)	3(3)
O(8′)	−651(2)	−7567(3)	−11199(9)	131(4)	121(4)	58(3)	−18(3)	−25(3)	6(3)
O(9′)	962(2)	−5270(3)	−5620(35)	114(4)	89(4)	466(22)	−26(3)	−66(10)	29(9)
O(10′)	−382(3)	−4352(4)	−4292(25)	256(10)	127(6)	235(12)	−70(7)	34(11)	9(8)
C(1′)	429(1)	−6299(3)	−6099(18)	41(2)	68(3)	139(7)	10(2)	−2(4)	−18(5)
C(2′)	293(1)	−7009(3)	−6867(12)	49(2)	53(3)	66(3)	7(2)	1(3)	−3(3)
C(3′)	−165(1)	−7003(2)	−7724(11)	45(2)	47(2)	54(3)	3(2)	−2(2)	7(2)
C(4′)	−441(1)	−6608(2)	−5999(12)	39(2)	48(2)	63(3)	5(2)	−3(2)	9(3)
C(5′)	−249(1)	−5910(2)	−5264(15)	46(3)	48(3)	108(5)	1(2)	0(3)	−12(3)
C(6′)	−504(1)	−5607(3)	−3270(17)	56(3)	61(3)	121(6)	−1(2)	−8(4)	−46(4)
C(7′)	815(2)	−7742(3)	−8587(13)	61(3)	74(4)	65(4)	22(3)	−3(3)	−12(3)
C(8′)	−560(2)	−7913(3)	−9460(13)	87(4)	71(4)	53(3)	4(3)	−1(3)	−0(3)
C(9′)	1064(2)	−5784(4)	−4799(36)	66(4)	82(5)	314(19)	−9(4)	−36(8)	−27(9)
C(10′)	−260(3)	−4639(7)	−2754(34)	127(8)	205(12)	343(22)	74(8)	157(12)	210(14)
C(11′)	−731(3)	−8619(4)	−8989(19)	115(6)	77(4)	109(7)	− 23(4)	−18(6)	−11(5)
C(12′)	1034(2)	−7911(5)	−10844(16)	92(5)	134(7)	82(5)	48(5)	7(5)	−18(6)
C(13′)	1423(2)	−5921(6)	−2958(34)	92(6)	132(8)	280(18)	−2(5)	−74(10)	−56(12)
C(14′)	−32(3)	−3967(5)	−1179(23)	126(7)	135(8)	157(11)	−77(7)	22(8)	−71(8)

hydrogen atoms were taken from Stewart *et al.* (8) and Cromer and Waber (9), respectively.

The structure was solved by direct methods, employing 480 reflections with $E \geq 1.40$. The correct structure corresponds to the lowest R_{Karl} (0.25) of all 32 phase-sets generated. The TANFOR program (10) was used to perform the tangent-formula iteration. The resulting *E*-map revealed 37 non-hydrogen atoms, the complete molecule was obtained after two successive Fourier maps. After four cycles of full-matrix least-squares refinements of the atomic coordinates and isotropic temperature factors ($R = 0.16$), a difference map indicated the locations of all the non-methyl hydrogen atoms. The rest of the hydrogen atoms were located with successive Fourier difference

Can. J. Chem. Downloaded from www.nrcresearchpress.com by 210.87.254.6 on 09/05/12
For personal use only.

Can. J. Chem. Downloaded from www.nrcresearchpress.com by 210.87.254.6 on 09/05/12
For personal use only.

TABLE 1

(*b*) Atomic coordinates and thermal parameters of hydrogen atoms. The coordinates are in fraction of unit-cell edges $\times 10^3$

Atom	*X*	*Y*	*Z*	*U* (iso)
H(1)	−119(1)	−638(3)	−439(12)	70(18)
H(2)	−155(1)	−645(2)	−893(9)	35(12)
H(3)	−197(1)	−616(2)	−443(11)	55(16)
H(4)	−208(1)	−744(3)	−707(11)	60(17)
H(5)	−158(1)	−726(2)	−278(11)	60(17)
H(6,1)	−184(2)	−830(4)	−271(16)	110(28)
H(6,2)	−133(3)	−823(5)	−342(19)	159(37)
H(11,1)	−147(2)	−426(3)	−841(15)	112(27)
H(11,2)	−122(2)	−432(3)	−1059(14)	94(23)
H(11,3)	−105(2)	−445(3)	−783(15)	92(22)
H(12,1)	−290(3)	−624(5)	−976(21)	158(41)
H(12,2)	−308(3)	−554(4)	−898(20)	135(37)
H(12,3)	−278(2)	−544(4)	−947(18)	144(33)
H(13,1)	−313(2)	−806(4)	−266(18)	131(32)
H(13,2)	−327(3)	−731(4)	−262(21)	149(38)
H(13,3)	−286(2)	−751(4)	−140(16)	139(31)
H(14,1)	−235(2)	−893(4)	−886(17)	134(33)
H(14,2)	−219(2)	−987(5)	−812(22)	151(43)
H(14,3)	−201(1)	−946(2)	−875(10)	42(14)
H(1′)	47(2)	−590(3)	−806(15)	92(24)
H(2′)	30(1)	−740(3)	−550(12)	68(18)
H(3′)	−20(1)	−682(2)	−946(9)	35(13)
H(4′)	−47(1)	−698(3)	−438(12)	67(18)
H(5′)	−12(2)	−555(4)	−669(18)	119(33)
H(6′,1)	−57(2)	−600(3)	−230(15)	87(22)
H(6′,2)	−78(1)	−538(3)	−385(13)	72(20)
H(11′,1)	−100(3)	−864(5)	−876(22)	178(44)
H(11′,2)	−55(3)	−901(5)	−975(24)	182(45)
H(11′,3)	−63(3)	−881(5)	−768(23)	144(39)
H(12′,1)	129(3)	−736(6)	−1118(20)	193(45)
H(12′,2)	109(2)	−842(4)	−1121(16)	115(30)
H(12′,3)	100(2)	−766(5)	−1168(20)	162(39)
H(13′,1)	154(2)	−547(4)	−220(16)	108(28)
H(13′,2)	155(2)	−649(5)	−296(20)	127(38)
H(13′,3)	127(4)	−593(6)	−73(28)	259(62)

syntheses, with the exception of the methyl hydrogens of C(6′) acetate. An 'unusually' short C—O (1.07 Å) in the C(6′) acetate was observed at this stage. A thorough analysis and examination of the intensity data revealed no obvious errors. At this stage, ideal bond lengths and angles were assumed for the position of the C(6′) acetate group and a new refinement cycle was undertaken. However, this yielded the same positions for the atoms in question. No other refinement approaches were tried to solve this anomaly.

Block-diagonal least-squares refinements were used subsequently to adjust the non-hydrogen atomic positions anisotropically and the hydrogen atomic coordinates isotropically. The methyl hydrogens of the C(6′) acetate were excluded in the refinement. The final *R* was 0.075 for 2605 reflections having non-zero intensities. The function minimized was $\sum w(|F_o| - |F_c|)^2$ where w is a weight inversely proportional to the variance derived from the value of $\sigma(I)$: $w = 1/\sigma^2(F)$.

No extinction correction was made. At the end of the refinement, the average shift-to-σ ratio was less than 0.6σ. A final electron density map showed some residual density located around the C(6′) acetate, the extreme fluctuations being 0.60 and −0.55 e A^{-3}. The final positional and thermal parameters are listed in Table 1.

Results and Discussion

The bond lengths, bond angles, and the numbering system of the molecule are shown in Fig. 1 *a* and *b*.[2] The standard deviations of these quantities derived from the calculated esd's of the fractional coordinates amount to 0.015 Å and 0.7° for non-hydrogen atoms bond distances

[2]The structure factor table is available, at a nominal charge, from the Depository of Unpublished Data, CISTI, National Research Council of Canada, Ottawa, Canada K1A 0S2.

Can. J. Chem. Downloaded from www.nrcresearchpress.com by 210.87.254.6 on 09/05/12
For personal use only.

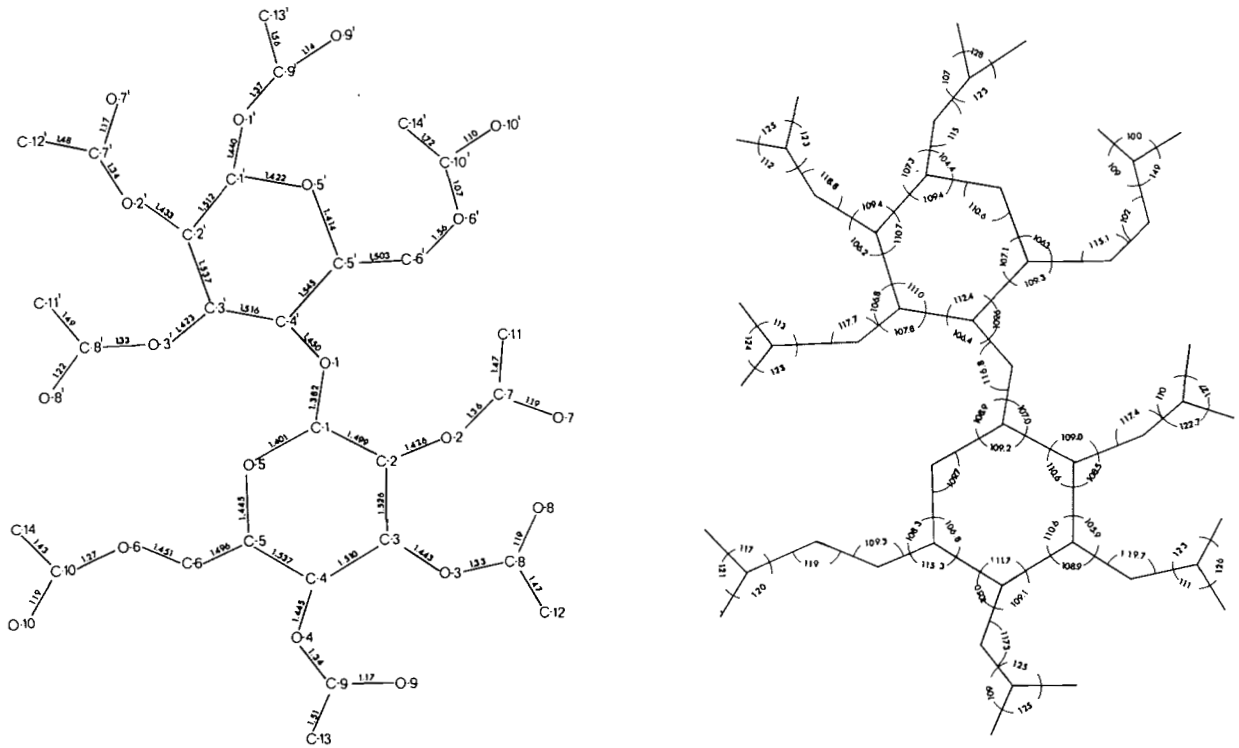

FIG. 1. Bond length, bond angles, and atomic numbering for β-D-acetyl cellobiose. The reader is warned that the standard deviations for bond distances and bond angles within the different acetate groups are 0.02 Å and 1° respectively except for the C(6), C(1′), and C(6′) acetate groups for which the standard deviations average 0.03 Å and 2° for bond distances and angles.

Can. J. Chem. Downloaded from www.nrcresearchpress.com by 210.87.254.6 on 09/05/12
For personal use only.

and angles respectively, when referring to the pyranose rings. These quantities amount to 0.02 Å and 1° for bond distances and angles within the different acetate groups with the exception of the C(6), C(1′), and C(6′) acetate groups for which the standard deviations average 0.03 Å and 2° for bond distances and angles respectively. All bond distances and angles are similar to those found in other carbohydrates (11) with the exception of C(6), C(1′), and particularly C(6′) acetate groups. The latter belongs to the acetate group situated on the 'reducing moiety' of the disaccharide and, as can be seen in Fig. 1, it has a unique environment compared to all other acetate groups in the molecule in that it has no acetate nearest neighbors. It is expected that this would allow the maximum opportunity for disorder or thermal motion which is probably responsible for the abnormal geometry of this group.

The torsional angles of this molecule and those of the β-D-cellobiose are listed in Table 2; since the esd for these angles is about 4°, differences in equivalent angles (Δ) of less than 10° should not be considered significant. Apart from the striking difference in the orientation of the C_6H_2OR groups of the two molecules, significant differences in torsional angles are found in [O(2)—C(2)—C(3)—O(3)] and [O(3)—C(3)—C(4)—O(4)]. Such differences are certainly due to the nonbonded repulsion of the acetate groups on the external part of the ring. Comparison of the same torsional angles in the primed residue fails to show the same large differences.

The relative orientation of contiguous pyranosides is customarily described by the torsional angles around the glycosidic bonds, C(1)—O and O—C(4′). The angles [H(1)—C(1)—O—C(4′)] and [C(1)—O—C(4′)—H(4′)] are denoted as the conformational angles ϕ and ψ respectively (5). For β-D-cellobiose, the (ϕ, ψ) values are (44.6°, −13.7°), the corresponding angles in the acetyl cellobiose are (44.1°, 15.7°). In both cases, the angles were calculated based on the computed hydrogen positions assuming sp^3 hybridization of the carbon atoms and with a C—H bond length of 1.10 Å. The removal of the intramolecular hydrogen bond between O(5)---O(3′) as found in β-D-cellobiose is evidently responsible for the variation of the angle ψ.

A stereoscopic view of the molecule is shown in Fig. 2.

It is interesting to note that the molecules are packed in the unit cell such that their lengths lie

TABLE 2. Comparison of torsion angles for cellobiose and acetyl cellobiose as deduced from X-ray diffraction data

(*a*) Torsion angle about the glucosidic bonds

Bonds	Torsion angle: β-D-Cellobiose (ref. 15)	Torsion angle: β-D-Acetyl cellobiose (This work)	|Δ|
C(1)—O(1)—C(4′)—C(3′)	106.4	133.5	27.1
C(1)—O(1)—C(4′)—C(5′)	−132.3	−103.8	28.5
C(4′)—O(1)—C(1)—O(5)	−76.3	−77.1	0.8
C(4′)—O(1)—C(1)—C(2)	166.5	165.2	1.3

(*b*) Torsion angle for the unprimed residue

(*i*) Endocyclic torsion angles

Bonds	Torsion angle: β-D-Cellobiose (ref. 15)	Torsion angle: β-D-Acetyl cellobiose (This work)	|Δ|
C(1)—O(5)—C(5)—C(4)	59.8	67.7	7.9
C(5)—O(5)—C(1)—C(2)	−65.7	−70.1	4.4
O(5)—C(1)—C(2)—C(3)	63.5	59.3	4.2
C(1)—C(2)—C(3)—C(4)	−57.3	−50.0	7.3
C(2)—C(3)—C(4)—C(5)	51.9	49.2	2.7
C(3)—C(4)—C(5)—O(5)	−51.9	−56.8	4.9

Can. J. Chem. Downloaded from www.nrcresearchpress.com by 210.87.254.6 on 09/05/12
For personal use only.

(*ii*) Exocyclic torsion angles

Bonds	Torsion angle: β-D-Cellobiose (ref. 15)	Torsion angle: β-D-Acetyl cellobiose (This work)	|Δ|
C(1)—O(5)—C(5)—C(6)	179.8	−166.6	13.6
C(5)—O(5)—C(1)—O(1)	176.7	172.5	4.2
O(1)—C(1)—C(2)—C(3)	−179.8	176.9	3.3
O(5)—C(1)—C(2)—O(2)	−171.7	177.6	10.7
O(2)—C(2)—C(3)—C(4)	−179.9	−168.5	11.4
C(1)—C(2)—C(3)—O(3)	178.5	−166.9	14.6
O(3)—C(3)—C(4)—C(5)	176.5	165.7	10.8
C(2)—C(3)—C(4)—O(4)	171.9	162.9	9.0
O(4)—C(4)—C(5)—O(5)	−171.1	−174.1	3.0
C(3)—C(4)—C(5)—C(6)	−168.5	−176.6	8.1
O(1)—C(1)—C(2)—O(2)	−55.0	−64.8	9.8
O(2)—C(2)—C(3)—O(3)	55.9	74.6	18.7
O(3)—C(3)—C(4)—O(4)	−63.5	−80.5	17.0
O(4)—C(4)—C(5)—C(6)	72.3	66.1	6.2
O(5)—C(5)—C(6)—O(6)	48.7	−73.1	121.8
C(4)—C(5)—C(6)—O(6)	168.4	45.9	122.5

(*c*) Torsion angle for the primed residue

(*i*) Endocyclic torsion angle

Bonds	Torsion angle: β-D-Cellobiose (ref. 15)	Torsion angle: β-D-Acetyl cellobiose (This work)	|Δ|
C(1′)—O(5′)—C(5′)—C(4′)	60.9	68.4	7.5
C(5′)—O(5′)—C(1′)—C(2′)	−65.1	−69.8	4.7
O(5′)—C(1′)—C(2′)—C(3′)	57.8	56.6	1.2
C(1′)—C(2′)—C(3′)—C(4′)	−50.7	−45.0	5.7
C(2′)—C(3′)—C(4′)—C(5′)	47.9	43.8	4.1
C(3′)—C(4′)—C(5′)—O(5′)	−51.1	−56.0	4.9

(*ii*) Exocyclic torsion angle

Bonds	Torsion angle: β-D-Cellobiose (ref. 15)	Torsion angle: β-D-Acetyl cellobiose (This work)	|Δ|
C(1′)—O(5′)—C(5′)—C(6′)	−176.2	−176.3	0.1
C(5′)—O(5′)—C(1′)—O(1′)	175.6	174.5	1.1
O(1′)—C(1′)—C(2′)—C(3′)	175.1	168.8	6.3
O(5′)—C(1′)—C(2′)—O(2′)	175.1	174.0	1.1
O(2′)—C(2′)—C(3′)—C(4′)	−170.5	−164.5	6.0
C(1′)—C(2′)—C(3′)—O(3′)	−174.3	−163.8	10.5
O(3′)—C(3′)—C(4′)—C(5′)	168.6	162.6	6.0
C(2′)—C(3′)—C(4′)—O(1′)	165.6	165.6	0
O(1′)—C(4′)—C(5′)—O(5′)	−170.4	−176.0	5.6
C(3′)—C(4′)—C(5′)—C(6′)	−169.7	−168.2	1.5
O(1′)—C(1′)—C(2′)—O(2′)	−67.6	−73.8	6.2
O(2′)—C(2′)—C(3′)—O(3′)	65.8	76.6	10.8
O(3′)—C(3′)—C(4′)—O(4′)	−73.7	−75.6	1.9
O(4′)—C(4′)—C(5′)—C(6′)	71.1	71.7	0.6
O(5′)—C(5′)—C(6′)—O(6′)	70.5	44.6	25.9
C(4′)—C(5′)—C(6′)—O(6′)	−169.3	159.7	31.0

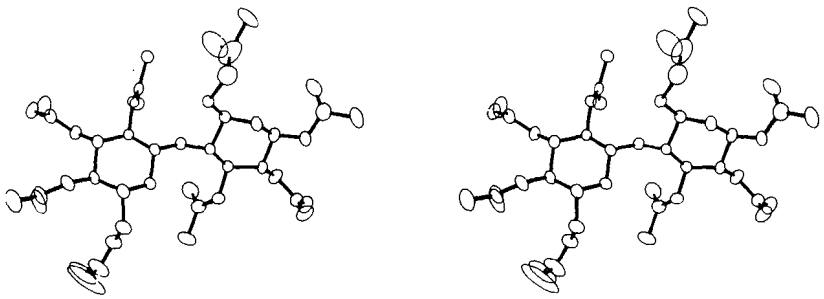

FIG. 2. Stereoscopic view of the molecule of β-D-acetyl cellobiose.

along the longest cell edge, the *a*-axis. The line joining O(4) and O(1′) makes an angle of only 11° with the *a*-axis. This confirms one of the speculations made by Leuck and Mark in 1934 (12) concerning the packing of the molecular chains. It also offers the hope that crystallography of a higher oligomer single crystal of a cellulosic material will lend itself to the basic hypothesis used in all fiber X-ray analysis of polymers *viz.* the macromolecular axis is parallel to one axis of the unit cell. If such a hypothesis can be made, the solution of such a structure by combining packing analysis with a modest amount of diffraction data should be possible.

In the present case, the finding that O(6) and O(6′) are conformationally different with respect to the ring is of significance. Recent high resolution nmr data (13) on cellobiose octaacetate have shown that the protons on C(6) and C(6′) are also conformationally different. On the other hand, in cellulose triacetate a single conformation is found for all the methylene protons (14). From this, we conclude that while C(6) acetates in acetylated cellobiose display two conformational states, a single state obtains for the polymer in solution. It remains to be shown whether the conformational state of the C(6) or of the C(6′) acetate of cellobiose octaacetate or both, is to be found in cellulose acetate. The structure of β,D-cellotriose undecaacetate appears to be the logical model in order to answer this question and this study is underway in our laboratory.

Acknowledgments

This work is part of a long-range program supported by the Echanges France–Québec and the Ministère de l'Education du Québec. One of us (H.C.) benefited from the France–Canada exchange program of the National Research Council of Canada.

1. B. ANDVORD TONNESEN and O. ELLEFSEN. *In* Cellulose and cellulose derivatives. Vol. V, part IV. *Edited by* N. Bikales and L. Segal. Wiley–Interscience, New York. 1971.
2. E. F. DICKEY and M. L. WOLFROM. J. Am. Chem. Soc. **71**, 825 (1949).
3. W. J. DULMAGE. J. Polym. Sci. **26**, 277 (1957).
4. B. S. SPRAGUE, J. L. RILEY, and H. D. NOETHER. Text. Res. J. **28**, 275 (1958).
5. P. R. SUNDARARAJAN and V. S. R. RAO. Biopolymers, **8**, 313 (1969).
6. S. PEREZ and F. BRISSE. Acta Crystallogr. B**32**, 470 (1976).
7. F. R. AHMED, S. R. HALL, M. E. PIPPY, and C. P. HUBER. NRC crystallographic programs for the IBM 360 system. World list of crystallographic computer programs. 2nd ed. Utrecht, Oosthoek. 1966. Appendix, p. 52.
8. R. F. STEWART, E. R. DAVISON, and W. T. SIMPSON. J. Chem. Phys. **42**, 3175 (1965).
9. D. T. CROMER and J. T. WABER. Acta Crystallogr. **18**, 104 (1965).
10. M. DREW. TANFOR program. University of California, Berkeley, California. 1969.
11. G. A. JEFFREY and K. D. ROSENSTEIN. Adv. Carbohydr. Chem. **19**, 17 (1964).
12. GERALD J. LEUCK and H. MARK. J. Am. Chem. Soc. **56**, 1959 (1934).
13. D. GAGNAIRE and M. VINCENDON. Bull. Soc. Chim. Fr. 472 (1965).
14. M. VINCENDON. Thèse de doctorat, CENG, Chemin des Martyrs, Grenoble, France. 1972.
15. S. S. C. CHU and G. A. JEFFREY. Acta Crystallogr. Sect. B, **24**, 830 (1968).

Can. J. Chem. Downloaded from www.nrcresearchpress.com by 210.87.254.6 on 09/05/12
For personal use only.

Base-catalyzed intramolecular displacements on certain 1,2-epoxides

V. SRINIVASAN AND E. W. WARNHOFF
Department of Chemistry, University of Western Ontario, London, Ontario N6A 5B7

Received December 11, 1975

V. SRINIVASAN and E. W. WARNHOFF. Can. J. Chem. **54**, 1372 (1976).

Intramolecular displacement by hydroxyl on the 1,2-epoxide group under basic or neutral conditions has been studied for seven of the stereoisomeric 1,2-diols derived by oxidation of the exocyclic double bond of **1**. In six of the examples (the seventh is ambiguous) the single or largely predominant product is that one of the less strained *cis*-fused isomers which has the fewer unfavourable steric interactions leading to it, without regard to whether the displacement occurs at the secondary or tertiary epoxide carbon.

V. SRINIVASAN et E. W. WARNHOFF. Can. J. Chem. **54**, 1372 (1976).

On a étudié le déplacement intramoléculaire par un hydroxyle du groupe époxyde-1,2; ces études ont été effectuées dans des conditions neutres ou basiques utilisant sept diols-1,2 stéréoisomères obtenus par oxydation de la double liaison exocyclique de **1**. Dans six des exemples, (le septième est ambigu) le seul produit ou le produit largement prédominant est l'isomère, attaché par une jonction *cis*, qui est le moins tendu; l'état de transition conduisant à ce composé présente moins d'interactions stériques non favorables que la réaction de déplacement se produise au niveau des carbones secondaire ou tertiaire de l'époxyde.

[Traduit par le journal]

Some time ago it was shown that base-catalyzed intramolecular displacement in the caryophyllene oxidodiol **10** led exclusively to attack at the tertiary (rather than the secondary) carbon of the oxide to produce glycol **17** (1). It was pointed out that this reaction, if applied to other stereoisomers of **10**, provided a means of probing the relative importance of various factors in an intramolecular S_N2 reaction of an epoxide. Caryophyllene is a convenient molecule because three of the four epoxide stereoisomers of **1** were known, both possible configurations of

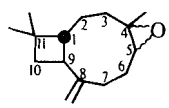

1

the hydroxyl group at C-8 were accessible by suitable choice of oxidizing agent, and finally the structure and stereochemistry of the products were easily discernible. These three points are discussed below, followed by the results for specific compounds.

The two *cis*-oxides **6** and **7** and one *trans*-oxide **3** were known from the work of Barton and co-workers (2) and Ramage and Whitehead (3), and the second *trans*-oxide of structure **1** has recently been found to be a minor product in the epoxidation of caryophyllene (4). The reaction of each of the four oxides with OsO_4 occurred only from the α-side[1] of the molecule, and the resulting 1,2-diol underwent intramolecular cyclization in the reaction medium. With oxides **2** and **7** the reaction of $KMnO_4$ also gave α-attack and the same cyclization product as obtained from OsO_4. The argument for α-hydroxylation is threefold. First, since the hydroxylation reagents must bond to both carbon atoms of the double bond in a five-membered transition state **A**, steric effects will be important.[2] Of the two extreme conformations of the exocyclic methylene group in the two *trans*-oxides, the one with the methylene down has both faces of the double bond strongly hindered toward such reagents, while the conformation with the methylene up has the α-face unshielded although the β-face is hindered by the β-methyl at C-11 and the β-hydrogens at C-1 and C-5. Second, the cyclization products from the two *trans*-oxides have been proved by interrelation to have the same configuration at C-8 (4), and therefore both oxides underwent reaction at the same side of the

[1]The term β refers to substituents on the same side of the molecule as the reference hydrogen atom at C-1, while α refers to those substituents on the side opposite this hydrogen atom.

[2]*Cf.* the ready epoxidation of 1,1-dineopentylethylene with its failure to react with $KMnO_4$ at room temperature (5)

Can. J. Chem. Downloaded from www.nrcresearchpress.com by 210.87.254.5 on 09/05/12
For personal use only.

Can. J. Chem. Downloaded from www.nrcresearchpress.com by 210.87.254.5 on 09/05/12
For personal use only.

double bond. Third, for each of the four epoxides a much more strained stereochemistry is required to fit the structure of the cyclization product if β-attack is assumed. *In toto*, this argument is a convincing one that only α-attack has occurred.

On the other hand, when the two *cis*-oxides

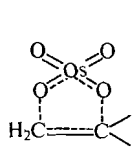

A

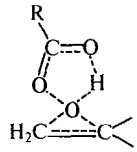

B

and one *trans*-oxide were treated with peracid, the major bisepoxide in each case resulted from reaction at the opposite face of the double bond from that attacked by OsO_4. The proof of this reversal lies in the fact that base-catalyzed ring opening and cyclization of each of the three major bisepoxides gave glycols different from those of the corresponding OsO_4 reactions. The change in the direction of attack is a reflection of the smaller steric requirements for epoxidation (see **B**);[2] α-attack is presumably slowed because the bulkier $-CH_2-$ part (6) of the developing $-O-CH_2-$ group encounters the greater steric hindrance of the C-11 β-methyl and C-10 β-H. Other examples of this reversal of major product depending on whether peracid or $OsO_4/KMnO_4$ is used are known, such as in Scheme 1.

The structures of the transannular glycol cyclization products were easily determined for the caryophyllene molecule because in each of the four conceivable products from a single oxide the combination of hydroxyl group types was different: 1° + 2°, 1° + 3°, 3° + 2°, or 3° + 3°. Hence, the nature of the hydroxyl groups in the product defined the ether ring formed and, therefore, the glycol structure. Once it had been verified that each glycol was not a 1,2-diol by its failure to react with $NaIO_4$, the type of hydroxyl group was determined by mild acetylation and chromic acid oxidation in conjunction with infrared and ^{1}Hmr spectroscopy. The only remaining point of uncertainty, the stereochemistry of the cyclization products, was fixed by the assumption that in each case the 1,2-epoxide ring was opened with inversion at the carbon atom undergoing displacement; this assumption is justified as follows. The C_4,C_5-epoxy group did not open solvolytically in an S_N1 reaction since the 142° diol **10** and the 127° diol **11***a* were stable to long reflux in methanol. However, since these and two other epoxy 1,2-diols did undergo base-catalyzed intramolecular cyclization in methanolic hydroxide, the cyclization must be an S_N2 displacement by an alkoxide ion on the oxide ring with inversion thus required at the reaction center. For the cyclizations that occurred during the course of $KMnO_4$ or OsO_4 hydroxylations, the $KMnO_4$ reactions occurred in an increasingly basic solution and in the case of **3** and **7** the same product was obtained from OsO_4 as from $KMnO_4$. Finally, the $KMnO_4$ and OsO_4 reactions with caryophyllene oxide **3** gave the same 119° glycol **17** obtained by base-catalyzed cyclization of the 142° diol **10** (1); likewise, reaction of OsO_4 with **6** produced the same glycol **20** as hydroxide-catalyzed cyclization of **13***a*.

In the case of the bisepoxides, the oxide from the exocyclic methylene group is opened first. Caryophyllene oxide **3** itself did not react with aqueous KOH at 150 °C, whereas under these conditions its bisepoxide **4** opened and cyclized

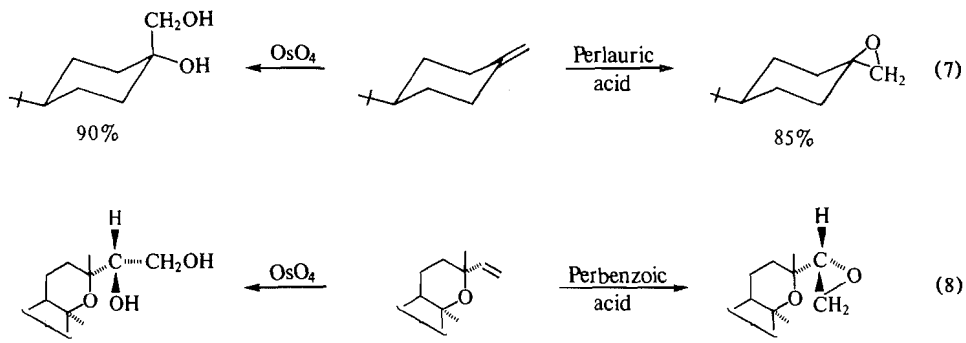

SCHEME 1

TABLE 1. Glycols from oxidation and cyclization of the four caryophyllene monoepoxides **1**

Starting material	Reagent	Glycol mp (°C)	Product from CrO_3	Product from Ac_2O	Nature of OH groups	Glycol structure
trans-Oxide **3** α-1,2-Diol **10** (from **3**)	MnO_4^- or OsO_4 HO^- + MeOH	119	Keto aldehyde	Di Ac	1°,2°	**17**[a]
Bisepoxide **4** (from **3**) β-1,2-Diol **11***a* (from **3**)	HO^- or ϕCH_2O^- HO^- + MeOH	116	Aldehyde **25**	Mono Ac[b]	1°,3°	**18***a*
cis-Oxide-*a* **7**	MnO_4^- or OsO_4	130	Aldehyde **28**	Mono Ac[b]	1°,3°	**21***a*
β-1,2-Diol **15***a* (from **7**)	HO^- + MeOH	227	No reaction	No reaction	3°,3°	**22**
cis-Oxide-*b* **6** α-1,2-Diol **13***a* (from **6**)	OsO_4 HO^- + MeOH	195.5	No reaction	No reaction	3°,3°	**20**
Bisepoxide **5** (from **6**)	ϕCH_2O^-	153	Not done	Mono Ac[b]	1°,3°	**19***a*
trans-Oxide **2**	OsO_4	136	Ketone **23**	Mono Ac[b]	2°,3°	**16**[c]

[a]Details reported in ref. 1.
[b]The monoacetate did not react with CrO_3.
[c]Details reported in ref. 4.

to the 119° glycol **17**. As expected, the primary carbon of the exocyclic epoxide is the point of attack, and in the benzyloxide reactions (see Experimental) the benzyl ethers formed were attached to this primary carbon atom.[3]

As it turned out, each transannular cyclization either gave exclusively one product or else one very predominant product. The product of each reaction together with its hydroxyl group type analysis is summarized in Table 1. The ^{1}Hmr data for the various products and intermediates are summarized in Table 2. The stereochemistry of the products and intermediates is shown in Scheme 2. The 116° glycol **18***a* and the 130° glycol **21***a* were further differentiated from each other (and from the 119° glycol **17** and the 136° glycol **16**) by oxidation of each to a different hydroxy aldehyde **25** and **28**, respectively. Where possible, stereostructural assignments were supported by interconversions. Thus, the two glycols **16** and **17** were correlated by chromic acid oxidation and Wolff–Kishner reduction to the same unsaturated 1,2-diol **31** (1, 4). The monoacetates of the glycols **18***a* and **19***a* were dehydrated to mixtures of the same pair of unsaturated monoacetates **26** and **27**, whereas the monoacetate of glycol **21***a* was dehydrated to a different pair of unsaturated monoacetates **29** and **30**. In the dehydration of the monoacetate **18***b* (but not **19***b* or **21***b*), a third product was formed which proved to be **32***b* resulting from 1,2-hydride shift.[4] Hydrolysis of **32***b* and treatment of the resulting **32***a* with $NaIO_4$ gave diketone **33**.

A priori, each oxido 1,2-diol (or its equivalent bisepoxide) could have given four possible cyclization products depending on whether the primary or the tertiary hydroxyl group attacked the secondary or the tertiary carbon atom of the

[3]The use of a benzyl alcohol solution of hydroxide (instead of aqueous hydroxide) to open the bisepoxides offered the advantages of homogeneity and lower reaction temperature because the more nucleophilic alkoxide in the less polar solvent allowed the reaction temperature to be lowered about 50 °C for the same reaction time. The benzyl ethers were easily hydrogenolyzed under neutral conditions.

[4]Formation of a hydride shift product such as **32***b* from **18***b* only is understandable since the preferred conformation of **18***b* has the worst arrangement of the three for *anti* elimination toward C-3, and therefore a carbonium ion intermediate is more likely for **18***b*, while **19***b* and **21***b* can give concerted *anti* elimination toward C-3. Any carbonium ion generated from **18***b* may be stabilized partly by hydride shift to **i** although π-stabilization by the oxygen atom is offset to some extent by strain introduced by the sp^2-carbon at the bridgehead. In agreement with this interpretation, the endocyclic double bond isomer **27** was the minor component (~15%) of the olefinic acetate product.

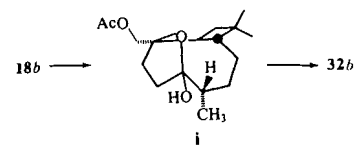

i

Can. J. Chem. Downloaded from www.nrcresearchpress.com by 210.87.254.5 on 09/05/12
For personal use only.

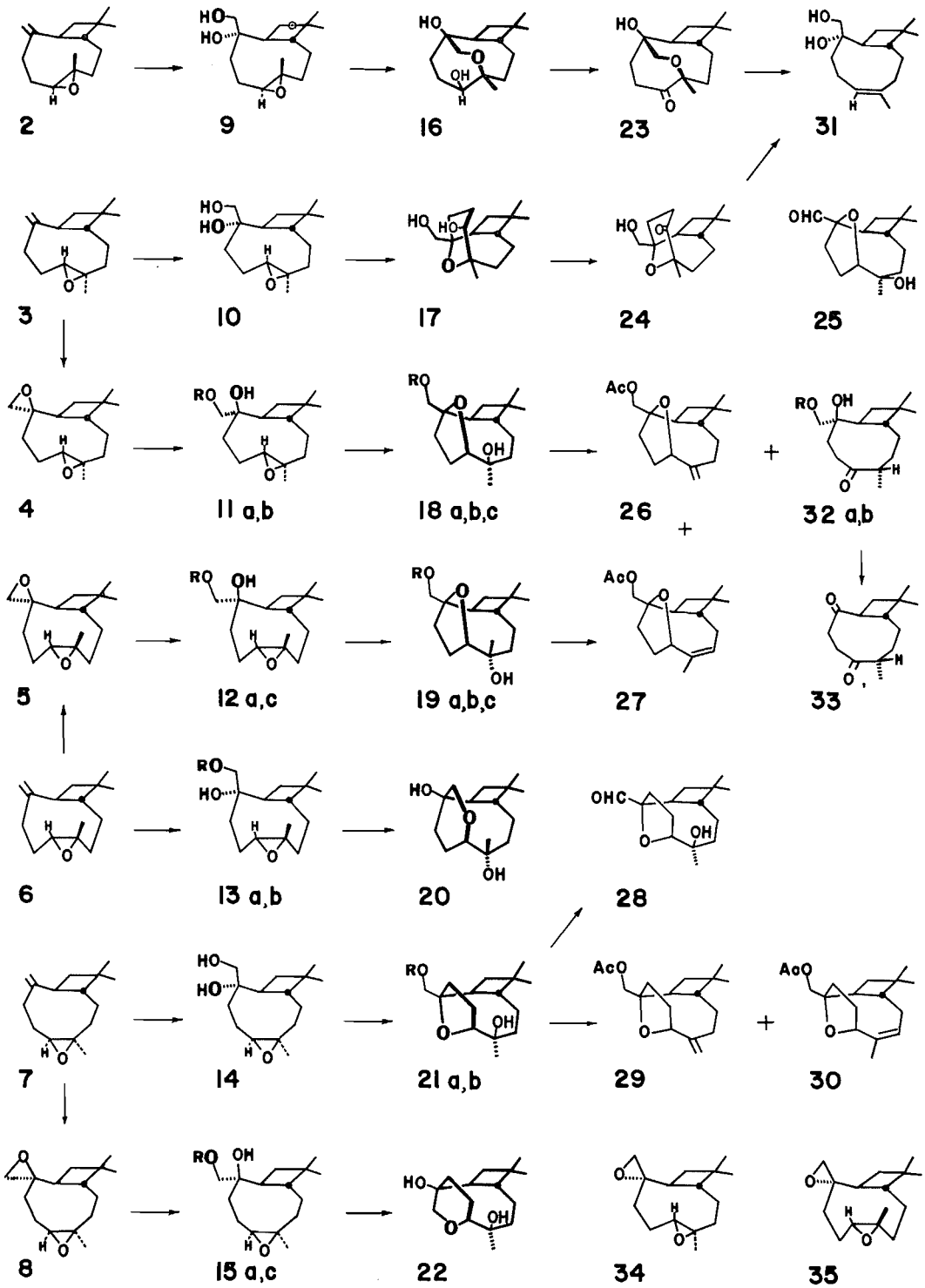

a R = H *b* R = OAc *c* R = $C_6H_5HC_2$

SCHEME 2

Can. J. Chem. Downloaded from www.nrcresearchpress.com by 210.87.254.5 on 09/05/12
For personal use only.

Can. J. Chem. Downloaded from www.nrcresearchpress.com by 210.87.254.5 on 09/05/12
For personal use only.

TABLE 2. ^{1}Hmr data[a]

Compound	C_4-Me[b]	C_5-H[b]	C_8-CH_2[b]	C_{11}-*gem*-diMe[b]	Other peaks
Bisepoxide **4**	1.28	3.06 m	2.52 and 2.64 (J = 5)	0.94	
Bisepoxide **34**	1.36	~2.70 m	2.62 s	0.96	
Bisepoxide **5**	1.28	?	2.60 ($J \approx \delta$)[d]	0.96	
Bisepoxide **35**	1.37	?	?	1.00, 1.03	
Bisepoxide **8**	1.36	~2.95 m	2.58 and 2.72 (J=5)	0.96, 1.00	
1,2-Diol **10**	1.33	2.82 m	3.69 bs	0.97	2.38 b (20H)
1,2-Diol **11***a*	1.30	~3.25 m	3.38 ($J \approx \delta$)[d]	0.96	
1,2-Diol **13***a*	1.24	?	3.23 ($J \approx \delta$)[d]	0.97	
1,2-Diol **15***a*	1.34	2.75 m	3.21 and 3.33 (J=10)	0.98	2.16 b (20H)
1,2-Diol monoacetate **11***b*	1.27	3.24 m	3.72 and 3.88 (J=11)	0.96	2.10 s ($CH_3C{=}O$) 2.24 s (OH)
1,2-Diol monoacetate **13***b*	1.23	2.75 m	3.78 s	0.99	2.07 s ($CH_3C{=}O$) 2.34 b (OH)
Glycol **16**	1.27	?[c]	3.84[d]	0.96, 1.00	?[c]
Glycol **16** monoacetate	1.13	4.95 m	3.78 and 3.92 (J=12)	0.98, 1.00	2.13 s ($CH_3C{=}O$)
Glycol **17**	1.20	3.55 m	3.20 s	1.02	2.89 b (20H)
Glycol **17** diacetate	1.09	4.96 m	3.85 s	1.03	2.05 s ($2CH_3C{=}O$)
Glycol **18***a*	1.00	~3.99 m	3.30 and 3.76 (J=12)	0.95, 0.97	2.94 s (20H)
Glycol monoacetate **18***b*	1.01	4.05 m	4.07 s	0.94, 0.97	2.05 s ($CH_3C{=}O$) 2.54 m (OH)
Glycol **19***a*	1.32	~3.95 m	3.34 and 3.76 (J=12)	0.95, 0.96	1.64 bs (OH)
Glycol monoacetate **19***b*	1.31	~3.95 m	4.08 s	0.95, 0.98	2.04 s ($CH_3C{=}O$) 3.48 bs (OH)
Glycol **20** *in pyridine*	1.53	~4.02 m	3.60 and 4.08 (J=10)	0.98, 1.00	5.06 bs (20H)
Glycol **21***a*	1.31	3.93 m	3.23 and 3.37 (J=11)	0.98	
Glycol monoacetate **21***b*	1.31	4.04 m	3.90 s	1.00	2.05 s ($CH_3C{=}O$) 1.75 bs (OH)
Glycol **22** *in pyridine*	1.62	~3.90 m	3.49 and 3.71 (J=10)	1.00	5.16 bs (20H)
Glycol benzylether **18***c*	1.00	3.96 m	3.43 s	0.93	4.50 s ($ArCH_2O$) 7.25 bs (C_6H_5)
Hydroxy ketone **23**	1.28	—	2.99 and 3.57 (J=12)	1.00	
Hydroxy ketone **24**	1.28	—	3.40 s	1.00	
Hydroxy aldehyde **25**	1.06	4.13 m	9.72 s ($CH{=}O$)	0.94, 0.97	2.58 b (OH)
Hydroxy aldehyde **28** 2,4-DNP	1.36	4.08 m	7.42 s ($CH{=}N$)	1.04	2.88 b (OH)
Dehydration product **26**	4.75 bs and 4.89 bs ($=CH_2$)	~4.17 m	4.17 s	1.00, 0.92	2.10 s ($CH_3C{=}O$)
+ **27**	1.58 bs	?	4.05 and 4.29 (J=7)	0.97	2.07 s ($CH_3C{=}O$) 4.70 m ($=CH-$)
Dehydration product **29** + **30**	4.90 bs ($=CH_2$) 1.72	? ?	3.94 s 3.96[d]	1.00 1.00	2.08 s ($CH_3C{=}O$)
Keto diol monoacetate **32***b*	1.02 d (J=7)	—	3.84 and 3.96 (J=12)	0.91, 0.92	2.08 s ($CH_3C{=}O$)

[a]Chemical shifts are given in ppm from tetramethylsilane (δ) and coupling constants in Hz for $CDCl_3$ solutions unless otherwise specified; s singlet, d doublet, m multiplet, b broad. All methyl groups except one were singlets and no designation is given except for that one.
[b]The carbon atoms of each compound are considered to retain the numbering shown in formula **1**.
[c]Solubility problems prevented observation of this absorption.
[d]Pattern unclear because of weakness of spectrum, or overlapping peaks, or coupling to hydroxyl proton. The chemical shift given is that of the centre of the pattern.

TABLE 3. Analysis of cyclization reactions

Diol cyclized	*cis*-Cyclization actually observed	*cis*-Cyclization NOT observed	Bicyclic system formed	Destabilizing interaction in cyclization NOT observed
9	1° OH → 3° C	3° OH → 2° C	[4.3.2]	C_4-Me ↔ H_β-C_1
10	3° OH → 3° C	1° OH → 2° C	[4.3.1]	C_4Me ↔ H_α-C_9
11*a*	3° OH → 2° C	1° OH → 3° C	[5.2.1]	C_5H_β ↔ H_β-C_1
12*a*	3° OH → 2° C	3° OH → 3° C	[5.2.1]	Torsional and angle strain required to get 3° OH behind 3° C C_1-H_β ↔ 3° OH
13*a*	1° OH → 2° C	1° OH → 3° C	[5.2.2]	None obvious
14	3° OH → 2° C	3° OH → 3° C	[5.2.1]	Torsional and angle strain required to get 3° OH behind 3° C
15*a*	1° OH → 2° C	1° OH → 3° C	[5.2.2]	C_2-H_α ↔ O-CH_2 C_5-H_α ↔ H_2C-O

oxide[5], and it remains to discuss why only one predominant product is formed in each case. One factor is angle strain in the potential cyclization product. Subject only to the provisos of α-hydroxylation by MnO_4^-/OsO_4 and inversion at the epoxide carbon atom undergoing substitution, each of the products actually formed has a *cis* ring fusion in the new bicyclic system. Dreiding models reveal that in each case the corresponding *trans*-fused systems would have much more angle strain, and since two of each of the four possible cyclization products would have a *trans* bicyclic fusion, the activation energy for these two cyclizations is prohibitive. Evidence that this is so is the fact that the benzyl ether **15***c* did not cyclize; its single tertiary hydroxyl group could only give a *trans*-fused product, whichever carbon atom of the epoxide it attacked with inversion.

The factor(s) responsible for deciding which of the remaining two *cis* products is formed is not so obvious. It is not merely so simple as a

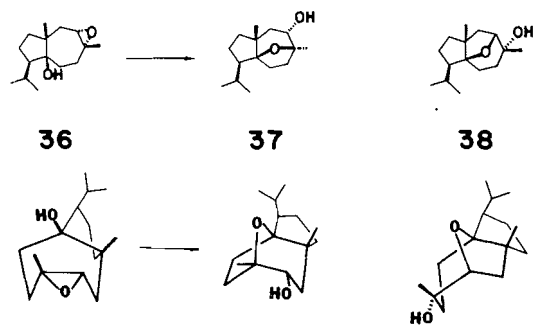

preference for S_N2-attack at the secondary rather than the tertiary carbon atom of the epoxide system as is the general rule for intermolecular examples.[6] Although five of the seven reactions in Table 3 (diols **11***a*, **12***a*, **13***a*, **14**, and **15***a*) do follow this rule, and although in four of these five cases (**12***a*, **13***a*, **14**, and **15***a*) one of the two hydroxyl groups could have given a *cis*-fused product by attack at either the secondary or tertiary oxide carbon atom, nevertheless the

[5]In practice, this was not strictly true. For the two compounds (**7** and **2**) whose reaction with OsO_4 gave only cyclized product directly and no 1,2-diol, it is assumed that the same cyclized product would have resulted from the reaction of 1,2-diol with hydroxide ion. This assumption is supported by the reactions of **3** and **6** which did give the same cyclization product from 1,2-diol plus hydroxide as from the MnO_4^-/OsO_4 reaction.

For the bisepoxide **5** the 1,2-diol **12***a* was not isolated because the benzyl ether **12***c* underwent cyclization to **19***c*. Therefore, only the tertiary hydroxyl group was offered the possibility of reacting in this case.

[6]"Under basic or neutral conditions, the normal isomer (corresponding to attack on the least substituted carbon atom) is nearly always the major or only isolated product" (9).

"In general nucleophiles attack at the less highly substituted carbon atom of the epoxide ring in neutral or basic media, as would be anticipated for a normal S_N2 process" (10).

"As indicated, if one of the carbons in the ethylene oxide ring is less substituted than the other, attack will occur preferentially (sometimes exclusively) at the less substituted carbon" (11).

Can. J. Chem. Downloaded from www.nrcresearchpress.com by 210.87.254.5 on 09/05/12
For personal use only.

Can. J. Chem. Downloaded from www.nrcresearchpress.com by 210.87.254.5 on 09/05/12
For personal use only.

other two reactions (diols **9** and **10**) are anomalous in that a *cis*-fused product of reaction at the *tertiary* carbon atom is formed instead of the alternative *cis*-fused product of reaction at the secondary carbon atom. Thus the diol intermediate **9** in the reaction of **2** with OsO_4 had the option of cyclization to a *cis* bicyclic system either by attack of the tertiary hydroxyl group on the secondary oxide carbon or by attack of the primary hydroxyl group on the tertiary oxide carbon atom; it chose the latter possibility. On the other hand, diol **11***a* was offered the same choice, and it chose the former possibility of attack of tertiary hydroxyl on the secondary oxide position.

The usual situation of secondary attack leading to a less crowded transition state than tertiary attack in intermolecular S_N2 displacements would not necessarily hold for an intramolecular reaction. When the S_N2 transition state leading to each of the possible *cis* products from each of the seven diols is considered by means of both Dreiding and Stuart–Briegleb models, then the observed product from six of the diols (**9**, **10**, **11***a*, **12***a*, **14**, and **15***a*) clearly has the less crowded transition state leading to it. The serious steric interaction destabilizing the other transition state that would have led to the unobserved *cis* product is noted in Table 3. From this analysis, the cyclizations of **9** and **10** are both anomalous because of the C-4 methyl group on the epoxide ring; in the case of **9** this methyl group would be jammed into the β C-1 hydrogen atom in the transition state for the unobserved product, while for **10** this same methyl group would be crowded into the α C-9 hydrogen in the transition state for the unobserved product. For the seventh diol, **13***a*, this analysis did not reveal any obvious difference in steric interactions for attack of the primary hydroxyl on the secondary relative to the tertiary carbon of the epoxide. Conceivably the extra crowding and restriction due to the epoxide C-4 methyl group in the pentacoordinate carbon atom for reaction at tertiary C-4 relative to secondary C-5 is responsible; possibly the lower energy of the chair six-membered ring for reaction at secondary C-5, relative to the seven-membered ring for reaction at tertiary C-4, is reflected in the two transition states.

Such anomalous intramolecular S_N2 openings of epoxide rings are not restricted to the caryophyllene skeleton, and a particularly interesting example occurs in Levisalles and Rudler's conversion of carotol epoxide **36** into daucol **37** with methanolic potassium hydroxide (12). The hydroxyl group situated directly behind the epoxide C—C bond is ideally disposed for S_N2 displacement at either the secondary or tertiary carbon atom, and a five-membered ring would result from reaction at either site. In fact, displacement occurs entirely at the tertiary carbon atom. The probable reason for this result is clearly seen from Dreiding models of both possible products: the product **37** formed is relatively strainless with a chair six-membered ring, whereas the product **38** of reaction at the secondary site would have considerable torsional (and angle?) strain introduced by the *trans*-fusion of the new furan ring to the other five-membered ring. These product differences must be reflected in the transition states for cyclization.

Experimental

General procedures and apparatus are the same as for ref. 1 except for the following. Mass spectra were run on a Varian M-66 instrument. Analyses were done in the laboratories of A. Bernhardt, Mülheim; A. B. Gygli, Toronto; and Chemalytics, Tempe, Arizona. In the general workup procedure ether extracts were washed to neutrality with dilute aqueous HCl, aqueous $NaHCO_3$, and water before being dried and evaporated.

Caryophyllene monoxide, isocaryophyllene, and isocaryophyllene oxides (*-b* and *-a*) were prepared as described previously (1).

The following abbreviations have been used: MeOH for methanol, Py for pyridine, Ac_2O for acetic anhydride, PE for petroleum ether (bp 60–80 °C), and DMF for *N*,*N*-dimethylformamide. Optical rotations are expressed in degrees.

*Attempted Solvolysis of the 142° Diol **10***

A solution of 2 mg of the 142° diol **10**, mp 138–139 °C, in 2 ml of MeOH was refluxed for 160 h. Removal of solvent gave white crystals, mp 137–139 °C, undepressed on admixture with starting material. Thin layer chromatographic examination gave a single spot corresponding in R_f to **10**.

*Caryophyllene Bisepoxide, **4***[7]

To a solution of 3.50 g (15.9 mmol) of pure monoxide **3** in 4 ml of ether was added 75 ml of a solution of monoperphthalic acid in ether (equivalent to 19.3 mmol), and the reaction mixture was kept at ~5 °C for 90 h. Filtration from phthalic acid, washing with aqueous $NaHCO_3$, drying, and evaporation afforded 9.34 g (94%) of colorless

[7]This crystalline bisepoxide is unstable on standing for several months at room temperature; it liquified and gave several tlc spots.

Can. J. Chem. Downloaded from www.nrcresearchpress.com by 210.87.254.5 on 09/05/12
For personal use only.

viscous oil, $[\alpha]_D^{21}$ −72 (*c* 2.13, $CHCl_3$). The nmr spectrum showed (ratio of C_4:Me peaks) the product to be a mixture of **4** and **34** in the ratio of ~65:~35 contaminated with 5–10% of starting material **3**. Six recrystallizations from PE gave 714 mg (19%) of colorless prisms of the major *bisepoxide* **4**, mp 76–77 °C; $[\alpha]_D^{20}$ −69 (*c* 1.71, $CHCl_3$); ν_{max} (CS_2) 3050 and 3030 cm^{-1} (CH and CH_2 of epoxide ring). *Anal.* calcd. for $C_{15}H_{24}O_2$ (236.3): C 76.22, H 10.23; found; C 76.57, H 10.15.

When perbenzoic acid in benzene was used for the epoxidation (7 days, room temperature), the ratio of the bisepoxides **4**:**34** in the product (one tlc spot) was ~80:20. The previously reported bisepoxide was a liquid (**13**).

Base-catalyzed Cleavage of Bisepoxide from Caryophyllene Oxide ***4***

Long Time

A solution of 351 mg of pure bisepoxide **4** and 10 NaOH pellets in 5 ml of benzyl alcohol was heated on a steam bath for 30 h. The yellow reaction mixture was steam distilled to remove excess benzyl alcohol. Extraction of the steam distillation residue with ether gave 677 mg of the benzyl ether **18***c* and excess benzyl alcohol. The crude product was hydrogenolyzed in 6 ml of 95% EtOH containing 146 mg of 5% Pd/C for 24 h. Filtration and evaporation left 349 mg (92%) of glassy **18***a* which crystallized on standing and gave one major tlc spot with two less polar trace contaminants. Three recrystallizations from ether gave colorless granules of *glycol* **18***a*, mp 115–116 °C, $[\alpha]_D^{18}$ −49 (*c* 3.17, $CHCl_3$); ν_{max} ($CHCl_3$) 3480 and 3580 cm^{-1} (OH). The mixture melting point with the 119° glycol **17** was depressed to 90–110 °C. *Anal* calcd. for $C_{15}H_{26}O_3$ (254.4): C 70.83, H 10.30; found: C 70.85, H 10.06.

When a solution of 62 mg of **18***a* and 100 mg of $NaIO_4$ in 3 ml of MeOH and 1 ml of water was allowed to stand at room temperature for 5 h, 56 mg of **18***a* was recovered (tlc, ir, mp, mixture mp).

The same glycol **18***a* was obtained from the reaction of the bisepoxide **4** with aqueous KOH in a sealed tube at 150 °C for 35 h. On the other hand caryophyllene monoxide **3** was recovered unchanged from aqueous KOH in a sealed tube at 150 °C for 29 h (tlc, mp).

Although the other, minor bisepoxide **34** was not isolated, base-catalyzed opening of a mixture of **4** and **34** gave Treibs' 119° glycol **17** in addition to the 116° glycol **18***a* in confirmation of the stereochemical assignments to the two bisepoxides.

Short Time

When 667 mg of a mixture of the two bisepoxides (**4**:**34**, ~65:35) from caryophyllene monoxide **3** and 5 NaOH pellets in 5 ml of benzyl alcohol was heated on a steam bath for only 20 h, there was obtained 657 mg (96%) of crude glycol mixture after steam distillation and hydrogenolysis. Preparative tlc on two thick plates (EtOAc–PE, 15:85) gave 180 mg of recovered bisepoxide mixture and 325 mg (62%) of glycol mixture which was acetylated at room temperature for 24 h with 2 ml of Ac_2O and 2.5 ml of Py. The acetylated product (380 mg, 100%) was recrystallized three times from ether to give 113 mg (30%) of long felted needles of *monoacetate* **11***b*, mp 149–151 °C, $[\alpha]_D^{18}$ −100 (*c* 1.26, $CHCl_3$); ν_{max} 3571, 3509 (OH), and 1739 cm^{-1} (ester C=O). *Anal.* calcd. for $C_{17}H_{28}O_4$ (296.4): C 68.89, H 9.52; found: C 69.02, H 9.84.

When the mother liquor from the first crystallization of **11***c* was concentrated, a crop of 150 mg of >90% pure monoacetate **11***b* was collected.

Saponification of the 151° Monoacetate ***11b***

A solution of 50 mg of monoacetate **11***b* and 0.7 g of KOH in 7 ml of MeOH was refluxed for 1 h. Dilution with water and extraction with ether gave 35 mg (81%) of colorless solid. Two recrystallizations from PE gave 19 mg of colorless felted needles of *1,2-diol* **11***a*, mp 126–127 °C, $[\alpha]_D^{18}$ −121 (*c* 1.46, $CHCl_3$); ν_{max} ($CHCl_3$) 3560 and 3440 cm^{-1} (OH). *Exact mass* calcd. for $C_{15}H_{26}O_3$: 254.1882; found (ms): 254.1886.

$NaIO_4$ Cleavage of the 127° Diol ***11a***

A solution of 12 mg of **11***a* and 25 mg of $NaIO_4$ in 1 ml of MeOH and 1 ml of water was allowed to stand for 2 h. Dilution with water and extraction with ether gave 7 mg of *ketoepoxide* **3** (=O for $=CH_2$), mp 62.5–63 °C after two recrystallizations from PE (bp 30–60 °C), which was identical (mp, mixture mp, ir, tlc) with an authentic sample prepared by $KMnO_4$ oxidation of **3** (3).

Base-catalyzed Isomerization of the 127° Diol ***11a***

A solution of 19 mg of 1,2-diol **11***a* and 4 KOH pellets in 2.5 ml of MeOH was refluxed for 118 h. Dilution with water and extraction with ether gave 9 mg (51%) of colorless solid. Two recrystallizations from ether yielded granules of *glycol* **18***a*, mp 112–114 °C undepressed on admixture with an authentic specimen of **18***a*, mp 115–116 °C.

A solution of 2 mg of 1,2-diol **11***a* in 2 ml of MeOH was refluxed for 120 h. Thin layer chromatography (EtOAc) showed the 2 mg of product to have the same R_f as starting material **11***a* and different from the R_f of glycols **18***a* and **17**.

116° Glycol Monoacetate ***18b***

A solution of 1.0 g of glycol **18***a* and 10 ml of Ac_2O in 10 ml of Py was left at room temperature for 24 h. Dilution with water and extraction with ether gave 1.1 g (94%) of an oil that crystallized on trituration with PE (bp 30–60 °C). Thin layer chromatography (EtOAc) showed the product to consist of over 90% of a monoacetate and 10% of a less polar component (diacetate?). Three recrystallizations from PE gave 800 mg (68%) of colorless needles of monoacetate **18***b*, mp 92–92.5 °C, $[\alpha]_D^{18}$ −44 (*c* 2.11, $CHCl_3$); ν_{max} (CS_2) 3600, 3490 (OH), and 1748 cm^{-1} (ester C=O). *Anal.* calcd. for $C_{17}H_{28}O_4$ (296.4): C 68.89, H 9.52; found: C 69.30, H 9.52.

The attempted oxidation of 74 mg of monoacetate **18***b* with 30 mg of CrO_3 in 1.5 ml of Py at room temperature for 14 h gave 72 mg of recovered **18***b* (tlc, nmr, ir) as the only product.

CrO_3 Oxidation of the 116° Glycol ***18a***

A solution of 300 mg (1.18 mmol) of pure **18***a* in 2 ml of Py was added to the orange complex from 300 mg (3.00 mmol) of CrO_3 and 2 ml of Py. After 24 h at room temperature the reaction mixture was diluted with CH_2Cl_2 and filtered through alumina (neutral IV) to yield 280 mg of oil whose tlc showed two spots of about equal intensity, one corresponding to starting material and the

Can. J. Chem. Downloaded from www.nrcresearchpress.com by 210.87.254.5 on 09/05/12
For personal use only.

other less polar spot from aldehyde **25**. Preparative tlc gave 95 mg of oily *hydroxy aldehyde* **25**, ν_{max} (CS_2) 3600, 3510 (OH), 2810, 2710 (C*H*=O), and 1745 cm^{-1} (CH=O). *Anal.* calcd. for $C_{15}H_{24}O_3$ (252.4): C 71.39, H 9.59; found: C 71.26, H 9.56.

Dehydration of the 116° Glycol Monoacetate ***18b***

The procedure of Hazen and Rosenburg was used (14). To a vigorously stirred (magnetic bar) solution of 355 mg (1.20 mmol) of **18***b* in 4 ml of γ-collidine (freshly distilled) and 5 ml of DMF (freshly distilled from type 4A molecular sieves) cooled to 0 °C was added in small portions, during 1 min, 2.03 g (19.6 mmol) of CH_3SO_2Cl (freshly distilled) containing 105 mg of SO_2. After 15 min the excess CH_3SO_2Cl in the muddy brown mixture was destroyed by addition of water. Extraction of the wine red solution gave after washing (10% aqueous HOAc, water), drying, and evaporation 334 mg (100%) of a pale yellow solid whose tlc (EtOAc–PE, 65:35) had two major spots, R_f 0.80 and 0.60.

Recrystallization from PE gave 120 mg (36%) of the more polar compound, R_f 0.60. Four more recrystallizations from the same solvent gave flocculent needles of the *hydroxy keto acetate* **32***b* (from hydride shift), mp 138–139.5 °C; $[\alpha]_D^{18}$ +50 (*c* 2.06, $CHCl_3$); ν_{max} ($CHCl_3$) 3560 and 3460 (OH), 1725 (ester C=O), and 1700 cm^{-1} (9-ring ketone C=O); *m/e* 296 (molecular ion). *Anal* calcd. for $C_{17}H_{28}O_4$ (296.4): C 68.89, H 9.52; found: C 68.85, H 9.69.

Evaporation of the mother liquors from the first recrystallization left 200 mg of an oil which was chromatographed on a thick plate in EtOAc–PE (65:35). The less polar product, R_f 0.80, was separated and eluted to give 126 mg (38%) of a liquid mixture (single tlc spot) of the double bond isomers **26** and **27** in a ratio of ~85:~15 (nmr spectrum), ν_{max} (CS_2) 3060 (=CH_2), 1735 (ester C=O), and 885 cm^{-1} (=CH_2). *Anal.* calcd. for $C_{17}H_{26}O_3$ (278.4): C 73.35, H 9.41; found: C 72.62, H 9.54.

Degradation of Hydroxy Keto Acetate ***32b***

The hydroxy keto acetate **32***b* (25 mg) was saponified by reflux in 2.5 ml of MeOH containing 3 KOH pellets. Dilution with water and ether extraction gave 20 mg (93%) of keto diol **32***a* whose tlc (EtOAc–PE, 65:35) had two spots R_f 0.20 and R_f 0.25 (second spot from a hemiketal of **32***a*?).

The 20 mg of **32***a* in 1.5 ml of MeOH was allowed to react for 11 h with 25 mg of $NaIO_4$ in 1 ml of water. Dilution with water and extraction with ether gave 14 mg (80%) of liquid *diketone* **33**, R_f 0.70 (EtOAc–PE, 65:35), ν_{max} 1695 cm^{-1} (9-ring ketone C=O); *m/e* 222 (molecular ion).

OsO_4 Oxidation of Isocaryophyllene Oxide-a, ***7***

To a solution of 980 mg (3.85 mmol) of OsO_4 in 5 ml of anhydrous ether was added at room temperature a solution of 840 mg (3.82 mmol) of **7**, mp 73–75 °C, in 6 ml of anhydrous ether. After 6 days the reaction mixture was diluted with ether and saturated with H_2S. Filtration and evaporation of the filtrate left 470 mg of colorless glass. The black precipitate was refluxed with KOH–EtOH–H_2O–mannitol and extracted with ether to yield 200 mg of a dark glass. Thin layer chromatography (EtOAc–PE, 60:40) on the combined product (670 mg, 69%) revealed one major spot and seven faint spots; the nmr spectrum was that of one main product. Chromatography on 20 g of alumina (neutral IV) gave 365 mg (54% of crude) of **21***a* on elution with $CHCl_3$–C_6H_6 (25:75). Three recrystallizations from PE gave 145 mg of colorless needles of *glycol* **21***a*, mp 128.5–130 °C, $[\alpha]_D^{20}$ −2.6 (*c* 3.13, 95% EtOH); ν_{max} (CCl_4) 3420 cm^{-1} (OH). *Anal.* calcd. for $C_{15}H_{26}O_3$ (254.4): C 70.83, H 10.30; found: C 70.36, H 9.99.

Glycol **21***a* was unchanged (mp, tlc, ir) on treatment with $NaIO_4$ in H_2O–MeOH.

From a $KMnO_4$ (2.5 g) oxidation of 1.0 g of *cis*-oxide-*a*, **7**, in 25 ml of acetone and 0.3 ml of water at room temperature there was obtained by filtration and chromatography on alumina (neutral IV) 155 mg (13%) of pure glycol **21***a* in addition to recovered **7** and keto oxide **7** (=O for =CH_2).

CrO_3 Oxidation of the 130° Glycol ***21a***

A solution of 80 mg (0.32 mmol) of **21***a* in 1 ml of Py was added to a slurry of 60 mg (0.60 mmol) of CrO_3 in 2 ml of Py. After 96 h at room temperature the reaction mixture was diluted with CH_2Cl_2 and passed through alumina (neutral IV). Evaporation of the eluate left 51 mg (62%) of *hydroxy aldehyde* **28**, R_f 0.63, contaminated with a minor spot of starting material **21***a*, R_f 0.20, (EtOAc–PE, 65:35). Evaporative distillation at 0.02 torr gave pure **28** as a colorless glass, ν_{max} ($CHCl_3$) 3390 (OH) and 1754 cm^{-1} (—CH=O). The *2,4-dinitrophenylhydrazone* was prepared and recrystallized twice from $CHCl_3$ – 95% EtOH to give small yellow needles, mp 215–218 °C; *m/e* 432 (molecular ion). *Anal.* calcd. for $C_{21}H_{28}N_4O_6$ (432.5): C 58.32, H 6.53; found C 58.56, H 6.62.

130° Glycol Monoacetate ***21b***

A solution of 90 mg of **21***a* and 1 ml of Ac_2O and 2 ml of Py was allowed to stand at room temperature for **24** h. Dilution with water and extraction with ether yielded 112 mg (100%) of colorless oily monoacetate **21***b* which gave a single tlc spot in EtOAc–PE (65:35). A sample was evaporatively distilled at 75–80 °C (0.02 torr) for analysis, $[\alpha]_D^{16}$ −8.0 (*c* 1.80, $CHCl_3$); ν_{max} (CCl_4) 3570 (OH) and 1748 cm^{-1} (ester C=O). *Anal.* calcd. for $C_{17}H_{28}O_4$ (296.4): C 68.89, H 9.52; found: C 68.87, H 9.55.

The attempted oxidation of 46 mg of **21***b* with 20 mg of CrO_3 in 4 ml of Py for 24 h gave as the only product 40 mg of recovered **21***b* (ir, tlc) on passage through alumina (neutral IV) in CH_2Cl_2.

Dehydration of the 130° Glycol Monoacetate ***21b***

According to the procedure of Hazen and Rosenburg (14), there was added in small portions during 1 min 1.14 g (10 mmol) of freshly distilled CH_3SO_2Cl containing 60 mg of SO_2 to a vigorously stirred (magnetic bar) solution (maintained at 0 °C) of 178 mg (0.6 mmol) of pure **21***b* in 3 ml of DMF (freshly distilled from 4A molecular sieves) and 2 ml of freshly distilled γ-collidine. After 15 min the brown reaction mixture was diluted with water and extracted with ether to yield 152 mg (91%) of pale yellow liquid. Thin layer chromatography (EtOAc–PE, 65:35) gave one major spot, R_f 0.85, and a trace of more polar starting material. Preparative tlc in the same solvent system gave 100 mg of a mixture of **29** and **30**, ratio ~85:15, single tlc spot, ν_{max} (CS_2) 3070 (=CH) and 1740 cm^{-1} (ester C=O).

Can. J. Chem. Downloaded from www.nrcresearchpress.com by 210.87.254.5 on 09/05/12
For personal use only.

Epoxidation of Isocaryophyllene Oxide-a, 7

To a solution of 13.56 g (61.6 mmol) of *cis*-oxide-*a* **7** in 50 ml of benzene was added 350 ml of a benzene solution of perbenzoic acid (61.5 mmol) at room temperature. After 7 days the reaction mixture was diluted with ether, washed with aqueous $NaHCO_3$, dried, and evaporated to leave 14.5 g (100%) of pale yellow oil. Thin layer chromatography in EtOAc gave one major spot, R_f 0.80 (different from **7**, R_f 0.90) and one minor (~10%) spot, R_f 0.40. The nmr spectrum was consistent with a single bisepoxide stereoisomer. Rapid chromatography (to minimize rearrangement) on 330 g of alumina (neutral III) gave 5.5 g (38%) of crystalline **8** in the PE eluate and 9.0 g (62%) of a mixture of **8** and a more polar transformation product in the ether eluate. Three recrystallizations of a sample of **8** from PE (bp 30–60 °C) gave colorless crystals of *bisepoxide* **8**, mp 98.5–100 °C, $[\alpha]_D^{18}$ −21 (*c* 2.38, $CHCl_3$); ν_{max} (CS_2) 3010 and 3020 cm^{-1} (epoxide CH). *Anal.* calcd. for $C_{15}H_{24}O_2$ (236.4): C 76.23, H 10.24; found: C 76.04, H 10.32.

Base-catalyzed Cleavage of Bisepoxide 8 from Isocaryophyllene Oxide-a

A solution of 1.68 g (7.1 mmol) of pure **8** and 3.5 g of KOH in 27 ml of benzyl alcohol was heated on a steam bath for 96 h. The light yellow reaction mixture was steam distilled to remove excess benzyl alcohol. The steam distillation residue was extracted with ether to yield 3.5 g of crude benzyl ether **15***c* containing some benzyl alcohol. The crude product was hydrogenolyzed in 100 ml of 95% EtOH containing 3 g of 5% Pd/C on a Parr shaker at room temperature for 40 h. Filtration and evaporation left 1.80 g (100%) of colorless semisolid glycol mixture. Thin layer chromatography (EtOAc–PE, 65:35) gave one major spot R_f 0.25 (~80%) and two minor spots R_f 0.10 and 0.05. Thin layer chromatographic comparison with authentic **21***a*, R_f 0.15, showed that no **21***a* was present.

Chromatography on 50 g of alumina (neutral IV) yielded 1.15 g (60%) of crystalline **15***a*. Three recrystallizations from ether gave rosettes of prisms of *glycol* **15***a*, mp 151–152 °C, $[\alpha]_D^{18}$ −45 (*c* 2.44 $CHCl_3$); ν_{max} ($CHCl_3$) 3570 and 3440 cm^{-1} (OH). *Anal.* calcd. for $C_{15}H_{26}O_3$ (254.4): C 70.83, H 10.30; found: C 70.67, H 10.44.

$NaIO_4$ Cleavage of the 152° Glycol 15a

A solution of 254 mg (1.00 mmol) of **15***a* in 1 ml of MeOH was allowed to react at room temperature with a solution of 255 mg (1.2 mmol) of $NaIO_4$ in 3 ml of water. Dilution with water, and ether extraction yielded 215 mg (98%) of liquid keto oxide **7** (=O for $=CH_2$), single spot on tlc, $[\alpha]_D^{18}$ −79 (*c* 4.46, MeOH) (lit. (3) $[\alpha]_D$ −72). The ir and nmr spectra were identical with those of authentic **7** (=O for $=CH_2$) prepared by $KMnO_4$ oxidation of **7**.

Base-catalyzed Isomerization of the 152° Glycol 15a

A solution of 175 mg (0.68 mmol) of **15***a* in 5 ml of MeOH containing 0.6 g of KOH was refluxed for 168 h. Dilution with water and extraction with ether gave 140 mg (80%) of white solid, major tlc spot (~85%), R_f 0.28, and two minor spots, R_f 0.10 and 0.05. Three recrystallizations from $CHCl_3$ gave clusters of small colorless needles of *glycol* **22**, mp 225–227 °C (sealed capillary), $[\alpha]_D^{18}$ +31 (*c* 1.25, MeOH); ν_{max} 3430 cm^{-1} (OH); *m/e* 254 (molecular ion). *Anal.* calcd. for $C_{15}H_{26}O_3$ (254.4): C 70.83, H 10.30; found: C 70.49, H 10.18.

The attempted acetylation of 18 mg of **22** in 0.5 ml of Py and 0.5 ml of Ac_2O for 24 h at room temperature gave only 17 mg of recovered starting material **22** on work-up.

The attempted oxidation of 12 mg of **22** with 15 mg of CrO_3 in 1 ml of Py for 24 h gave only 11 mg of recovered **22** on work-up (tlc, ir, mp, mixture mp).

When the *acid*-catalyzed isomerization of 9 mg of **15***a* in 1.5 ml of acetone and 0.5 ml of 5% aqueous H_2SO_4 was attempted, the crude product showed four tlc spots and was not investigated further.

OsO_4 Oxidation of Isocaryophyllene Oxide-b (6)

To a solution of 1.00 g (3.94 mmol) of OsO_4 in 5 ml of dry ether was added a solution of 870 mg (3.94 mmol) of isocaryophyllene oxide-*b* (~85% oxide-*b* **6** contaminated with ~15% of oxide-*a* **7**) in 6 ml of dry ether. After 5 days the reaction mixture was diluted with ether and saturated with H_2S. Filtration and evaporation of the filtrate left 398 mg of colorless viscous oil. The black precipitate was refluxed with KOH – 95% EtOH – mannitol and extracted with ether to yield 350 mg of viscous oil. Thin layer chromatography (EtOAc–PE, 65:35) on the combined product (748 mg, 74%) revealed one major spot, R_f 0.45, and three minor more polar spots, R_f 0.25, 0.15, and 0.10. Chromatography on 45 g of alumina (neutral IV) gave 127 mg (17%) of recovered oxide-*b* **6** (eluted by PE) and 361 mg (48%) of crystalline **20** (eluted by benzene–$CHCl_3$). Six recrystallizations of a portion from $CHCl_3$–PE gave colorless felted needles of *glycol* **20**, mp 194–195.5 °C (sealed capillary), $[\alpha]_D^{19}$ −24 (*c* 1.28, MeOH); ν_{max} (KBr) 3300 cm^{-1} (OH); *m/e* 254 (molecular ion). *Anal.* calcd. for $C_{15}H_{26}O_3$ (254.4): C 70.83, H 10.30; found: C 71.15, H 10.44.

Further elution with $CHCl_3$ and preparative tlc with EtOAc gave 85 mg (11%) of 1,2-diol **13***a* and 20 mg (3%) of glycol **21** (from *cis*-oxide-*a* **7**).

The attempted acetylation of 51 mg of 195.5° glycol in 1 ml of Ac_2O and 1 ml of Py for 24 h at room temperature gave 50 mg of recovered starting material, R_f 0.30, contaminated with a less polar carbonyl containing component (~20%, presumably an acetate), R_f 0.65 in EtOAc–PE (65:35).

The attempted oxidation of 48 mg of **20** with 40 mg of CrO_3 in 1 ml of Py gave 35 mg of recovered starting material contaminated with some (~20%) less polar material showing carbonyl ir absorption.

The 195.5° glycol **20** was not cleaved by $NaIO_4$ in MeOH.

$NaIO_4$ Cleavage of the 1,2-Diol 13a

A solution of 15 mg of the 1,2-diol **13***a* in 1 ml of MeOH was allowed to react at room temperature with a solution of 40 mg of $NaIO_4$ in 1 ml of water. Dilution with water and ether extraction yielded 6 mg of an oil whose ir and tlc behavior were identical with that of authentic keto oxide-*b* **6** (=O for $=CH_2$) prepared by $KMnO_4$ oxidation of **6** (3).

1,2-Diol Monoacetate, 13b

A solution of 60 mg of 1,2-diol **13***a* and 1 ml of Ac_2O

Can. J. Chem. Downloaded from www.nrcresearchpress.com by 210.87.254.5 on 09/05/12
For personal use only.

in 1 ml of Py was left at room temperature for 24 h. Dilution with water and extraction with ether afforded 65 mg of an oil which solidified on cooling. Three recrystallizations from PE (bp 30–60 °C) gave crystals of *monoacetate* **13***b*, mp 86–87 °C, $[\alpha]_D^{17}$ +34 (*c* 2.00, $CHCl_3$); ν_{max} (CS_2) 3450 (OH) and 1748 cm^{-1} (ester C=O). *Anal.* calcd. for $C_{17}H_{28}O_4$ (296.4): C 68.89, H 9.52; found: C 69.22, H 9.71.

Base-catalyzed Isomerization of the 1,2-Diol 13a

A solution of 95 mg of a mixture of monoacetates (70% **21***b* and 30% **13***b*) in 5 ml of MeOH containing 0.5 g of KOH was refluxed for 7 days. Dilution with water and extraction with ether gave 80 mg (98%) of an oil whose tlc (EtOAc) showed two spots R_f 0.40, corresponding to **20** from oxide-*b*, and R_f 0.25 corresponding to the 130° glycol **21***a* from oxide-*a*. Separation by chromatography on alumina (neutral IV) gave 12 mg of pure **20**, mp 192–194 °C (sealed capillary) after recrystallization from PE, and 35 mg of pure **21***a*.

Epoxidation of Isocaryophyllene Oxide-b, 6

To a solution of 2.2 g (10 mmol) of *cis*-oxide-*b* **6** (contaminated with ~30% of *cis*-oxide-*a* **7**) in 10 ml of ether at 0 °C was added 30 ml (15 mmol) of an ether solution of monoperphthalic acid. After 7 days at ~5 °C the reaction mixture was worked up as described for the preparation of bisepoxide **8** to yield 2.2 g (93%) of an oil. Thin layer chromatography (EtOAc–PE, 65:35) showed one major spot R_f 0.65 different from starting material, R_f 0.85, and two faint spots R_f 0.20 and 0.10. The nmr spectrum exhibited the C-4 methyl peaks of **5** and **35** in a ratio of ~70:~30 together with the C-4 methyl peak of the bisepoxide **8** from *cis*-oxide-*a*. Since the bisepoxides tended to rearrange readily, the crude bisepoxide mixture was used in the next experiment.

Base-catalyzed Cleavage of Bisepoxide 5 from Isocaryophyllene Oxide-b

A solution of 2.10 g of the crude bisepoxide mixture obtained from the above experiment and 3.5 g of KOH in 30 ml of benzyl alcohol was heated on a steam bath for 96 h. The yellow reaction mixture was steam distilled to remove excess benzyl alcohol. Ether extraction of the steam distillation residue gave 8.40 g of benzyl ether **19***c* containing some benzyl alcohol. The crude product was hydrogenolyzed in 100 ml of 95% EtOH containing 4 g of 5% Pd/C on a Parr shaker at room temperature for 21 h. Filtration and evaporation left 2.30 g (100%) of an oil which solidified on standing. Thin layer chromatography (EtOAc–PE, 65:35) gave a major spot and three minor spots. Recrystallization of the crude glycol mixture from ether–PE afforded 370 mg (16%) of the major spot material. Further recrystallization from ether gave colorless needles of *glycol* **19***a*, mp 152–153 °C, $[\alpha]_D^{18}$ −62 (*c* 1.75, $CHCl_3$); ν_{max} ($CHCl_3$) 3590 and 3440 cm^{-1} (OH). *Anal.* calcd. for $C_{15}H_{26}O_3$ (254.4): C 70.83, H 10.30; found: C 70.57, H 10.10.

Two of the minor components in the crude product were shown to be 1,2-diols by $NaIO_4$ cleavage of the mother liquor material to a mixture of keto oxides **6** (=O for $=CH_2$) and **7** (=O for $=CH_2$). Further amounts of the 153° glycol **19***a* were obtained by chromatography of the $NaIO_4$ product.

When a solution of 20 mg of **19***a* and 27 mg of $NaIO_4$ in 1 ml of MeOH and 1 ml of water was allowed to stand for 24 h at room temperature, 17 mg of starting material **19***a* was recovered.

153° Glycol Monoacetate 19b

A solution of 115 mg of pure **19***a* and 1 ml of Ac_2O in 1 ml of Py was left at room temperature for 24 h. Dilution with water and extraction with ether gave 135 mg (100%) of an oil which solidified. Three recrystallizations from PE (bp 30–60 °C) gave 78 mg of crystals of monoacetate **19***b*, mp 84.5–86 °C, $[\alpha]_D^{18}$ −57 (*c* 0.89, $CHCl_3$); ν_{max} ($CHCl_3$) 3590, 3440 (OH), and 1725 cm^{-1} (ester C=O). *Anal.* calcd. for $C_{17}H_{28}O_4$ (296.4): C 68.89, H 9.52; found: C 68.58, H 9.46.

Dehydration of the 153° Glycol Monoacetate 19b

The reagents and procedure of Hazen and Rosenburg (14) were used as described for the dehydration of the 116° glycol monoacetate **18***b*. To a vigorously stirred solution of 40 mg of monoacetate **19***b* in 3 ml of γ-collidine and 4 ml of DMF cooled to 0 °C was added 115 mg of CH_3SO_2Cl containing 25 mg of SO_2 during 1 min. Work-up as described previously gave 40 mg of a yellow oil whose nmr spectrum showed the product to be an approximately 50:50 mixture of the same two double bond isomers **26** and **27** obtained from the 116° glycol monoacetate **18***b*, ν_{max} (CS_2) 3060 ($=CH_2$), 1740 (ester C=O), 1625 (C=C), and 890 cm^{-1} ($=CH_2$).

Acknowledgment

We would like to thank the National Research Council of Canada for financial support.

1. E. W. Warnhoff and V. Srinivasan. Can. J. Chem. **44**, 2259 (1966).
2. A. Aebi, D. H. R. Barton, and A. S. Lindsey. J. Chem. Soc. 3124 (1953).
3. G. R. Ramage and R. Whitehead. J. Chem. Soc. 4336 (1954).
4. E. W. Warnhoff and V. Srinivasan. Can. J. Chem. **51**, 3955 (1973).
5. P. D. Bartlett, G. L. Fraser, and R. B. Woodward. J. Am. Chem. Soc. **63**, 495 (1941).
6. J. J. Uebel. Tetrahedron Lett. 4751 (1967).
7. H. B. Henbest. Proc. Chem. Soc. 164 (1963).
8. P. Coates, A. K. Goh, P. R. Jeffries, J. R. Knox, and T. G. Payne. Tetrahedron, **24**, 795 (1968).
9. R. E. Parker and N. S. Isaacs. Chem. Rev. **59**, 742 (1959).
10. H. O. House. Modern synthetic reactions. 2nd ed. W. A. Benjamin, Inc., Menlo Park, California. 1972. p. 302.
11. E. S. Gould. Mechanism and structure in organic chemistry. Henry Holt and Co., New York, N.Y. 1959. p. 292.
12. J. Levisalles and H. Rudler. Bull. Soc. Chim. Fr. 2059 (1967).
13. W. Treibs. Ber. **80**, 56 (1947).
14. G. C. Hazen and D. W. Rosenburg. J. Org. Chem. **29**, 1930 (1964).

Enthalpies of formation of $Cr^{3+}(aq)$ and the inner sphere complexes $CrF^{2+}(aq)$, $CrCl^{2+}(aq)$, $CrBr^{2+}(aq)$, and $CrSO_4^{+}(aq)$

INGEMAR DELLIEN[1] AND LOREN G. HEPLER

Department of Chemistry, University of Lethbridge, Lethbridge, Alberta T1K 3M4

Received October 20, 1975

INGEMAR DELLIEN and LOREN G. HEPLER. Can. J. Chem. **54**, 1383 (1976).

We have carried out calorimetric measurements leading to $\Delta H_f^0 = -60$ kcal mol^{-1} for $Cr^{3+}(aq)$. Further calorimetric measurements have led to enthalpies of reaction of $Cr^{3+}(aq)$ with HF(aq), $Cl^-(aq)$, $Br^-(aq)$, and $SO_4^{2-}(aq)$ to form the 'inner sphere' complexes $CrF^{2+}(aq)$, $CrCl^{2+}(aq)$, $CrBr^{2+}(aq)$, and $CrSO_4^{+}(aq)$. Results of our measurements lead to $\Delta H_f^0 = (-60.0 \pm 1.5)$ kcal mol^{-1} for $Cr^{3+}(aq)$, $\Delta H_f^0 = -136.8$ kcal mol^{-1} for $CrF^{2+}(aq)$, $\Delta H_f^0 = -93.7$ kcal mol^{-1} for $CrCl^{2+}(aq)$, $\Delta H_f^0 = -80.1$ kcal mol^{-1} for $CrBr^{2+}(aq)$, and $\Delta H_f^0 = -269.7$ kcal mol^{-1} for $CrSO_4^{+}(aq)$.

INGEMAR DELLIEN et LOREN G. HEPLER. Can. J. Chem. **54**, 1383 (1976).

On a effectué des mesures calorimétriques permettant de déterminer que le ΔH_f^0 du $Cr^{3+}(aq)$ est -60 kcal mol^{-1}. D'autres mesures calorimétriques ont permis d'évaluer les enthalpies des réactions du $Cr^{3+}(aq)$ avec HF(aq), $Cl^-(aq)$, $Br^-(aq)$ et $SO_4^{2-}(aq)$ conduisant à des complexes de "sphère interne" $CrF^{2+}(aq)$, $CrCl^{2+}(aq)$, $CrBr^{2+}(aq)$ et $CrSO_4^{+}(aq)$. Les résultats de nos mesures conduisent aux valeurs de $\Delta H_f^0 = (-60.0 \pm 1.5)$ kcal mol^{-1} pour $Cr^{3+}(aq)$, $\Delta H_f^0 = -136.8$ kcal mol^{-1} pour $CrF^{2+}(aq)$, $\Delta H_f^0 = -93.7$ kcal mol^{-1} pour $CrCl^{2+}(aq)$, $\Delta H_f^0 = -80.1$ kcal mol^{-1} pour $CrBr^{2+}(aq)$ et $\Delta H_f^0 = -269.7$ kcal mol^{-1} pour $CrSO_4^{+}(aq)$.

[Traduit par le journal]

Introduction

The National Bureau of Standards Technical Note 270-4 (1) lists $\Delta H_f^0 = -477.8$ kcal mol^{-1} for $Cr(H_2O)_6^{3+}(aq)$, which corresponds to $\Delta H_f^0 = -477.8 - 6(-68.315) = -67.9$ kcal mol^{-1} for $Cr^{3+}(aq)$ in which no water of hydration is explicitly included. Dellien *et al.* (2) have recently reviewed seven different paths to this enthalpy of formation and have calculated ΔH_f^0 values ranging from -51 to -62 kcal mol^{-1} for $Cr^{3+}(aq)$. We (2) selected $\Delta H_f^0 = -57$ kcal mol^{-1} for $Cr^{3+}(aq)$ and the corresponding $\Delta H_f^0 = -57 + 6(-68.315) = -467$ kcal mol^{-1} for $Cr(H_2O)_6^{3+}(aq)$ as 'best' values. Neither the selection of ref. 2 nor that in ref. 1 can be defended as accurate or reliable. We have therefore undertaken calorimetric measurements to resolve the substantial (17 kcal mol^{-1}) discrepancy between 'reasonable' interpretations of previously published results.

There are also significant gaps and uncertainties in the presently available thermochemical data for some important halide and sulfate complexes of Cr(III) in aqueous solution. We have therefore made calorimetric measurements on some of these species.

It is likely that the substantial discrepancies between the results of earlier investigators are mostly due to chemical difficulties rather than calorimetric errors. We have therefore taken considerable care to identify the chromium species involved in the various calorimetric reactions we have investigated.

Experimental

All calorimetric measurements were made with the LKB 8700 Precision Calorimetry System. The standard 100 ml LKB glass reaction vessel was used with 1 ml glass ampoules for some of the measurements; other measurements were made with a stainless steel bomb calorimeter (from which we could exclude oxygen) identical to that described by Olofsson, Sunner, Efimov, and Laynez (3). All of our calorimetric results refer to 25.00 ± 0.03 °C and are reported in terms of the defined thermochemical calorie (1 cal = 4.184 J).

Solutions of chromous perchlorate were prepared by electrolytic reduction of solutions of chromic perchlorate, as described by Pecsok and Schaefer (4). Concentrations of $Cr^{2+}(aq)$ in final solutions ranged from 0.080 to 0.100 *M*, as determined by reaction with excess I_2 followed by titration with thiosulfate solution.

Our preparations of ferric perchlorate solutions began with $FeCl_3 \cdot 6H_2O$ (BDH Analar), which was dissolved in aqueous perchloric acid. The 'ferric hydroxide' that was precipitated on addition of $NH_3(aq)$ was filtered off, washed, redissolved in perchloric acid, reprecipitated with $NH_3(aq)$, etc., until the resulting ferric perchlorate solution showed no test for chloride with silver nitrate.

[1]On leave from Chemical Center, Physical Chemistry I, University of Lund, Lund, Sweden, 1974–1975.

Can. J. Chem. Downloaded from www.nrcresearchpress.com by 210.87.254.42 on 09/05/12
For personal use only.

Can. J. Chem. Downloaded from www.nrcresearchpress.com by 210.87.254.42 on 09/05/12
For personal use only.

Solutions were standardized with $KMnO_4$ solution after reduction of $Fe^{3+}(aq)$ to $Fe^{2+}(aq)$ with zinc.

A solution of cupric perchlorate was prepared by dissolving CuO (BDH) in perchloric acid. After the solution was filtered, it was standardized by reaction with iodide and thiosulfate.

Stock Ce(IV) perchlorate solution was prepared by dissolving $(NH_4)_2Ce(NO_3)_6$ in warm $HClO_4$. After the solution was cooled and the precipitated ammonium perchlorate removed by filtration, Ce(IV) concentration was determined against $K_4Fe(CN)_6 \cdot 3H_2O$ with ferroin indicator.

Solutions of $CrF^{2+}(aq)$ were prepared according to the procedure of Swaddle and King (5), except that we used somewhat lower concentrations than they did. Spectra of our solutions agreed well with those reported by Swaddle and King (5). Solutions were stored in a refrigerator, with all calorimetric runs and analyses being completed within 36 h of the original preparation. Solutions of $CrCl^{2+}(aq)$ were prepared and handled in similar fashion, as also described by Swaddle and King (5).

Solutions of $CrBr^{2+}(aq)$ were prepared as described by Guthrie and King (6), except that we began with electrolytically prepared solutions of $Cr^{2+}(aq)$ as described above so that we had no $Zn^{2+}(aq)$ in our solutions. Extinction coefficients of our solutions were about 4% larger than values previously reported by Taube and Myers (7). Solutions were stored in the refrigerator, with samples taken out for analyses and calorimetric measurements within a few hours of completion of the preparation.

Solutions of $Cr(SO_4)^+(aq)$ were prepared by reducing cold solutions of $K_2Cr_2O_7$ and H_2SO_4 with H_2O_2, followed by ion exchange separation with Biorad AG 50W $\times$ 8 resin. The spectra of the resulting solutions were similar to that reported by Fogel, Tai, and Yarborough (8), but our extinction coefficients (λ = 590 nm, ϵ = 19.0 M^{-1} cm^{-1}; λ = 420 nm, ϵ = 18.9 M^{-1} cm^{-1}) were larger than theirs. In this connection we note that our extinction coefficients for $Cr^{3+}(aq)$ agree with those of several earlier investigators.

Solutions containing the various inner sphere complexes of Cr(III) were analyzed for chromium spectrophotometrically after oxidation with H_2O_2 in alkaline solution, as described by Haupt (9). A Cary 14 spectrophotometer was used for these and other spectrophotometric measurements. The same instrument was used for observation of various calorimetric solutions to insure that appropriate reactants and products were identical as required for combination of various reaction ΔH values.

Reduction of CrO_3 with H_2O_2 in $HClO_4$ solution led to solutions of chromic perchlorate from which we obtained hydrated crystals of chromic perchlorate after several weeks' storage with concentrated H_2SO_4 in a desiccator. Solutions of $Cr^{3+}(aq)$ prepared by dissolving these crystals in water and perchloric acid were free of dimers as judged by the spectrum around the 267 nm peak and also lower wavelengths.

Results and Calculations

We have measured the enthalpy of reaction of $Cr^{2+}(aq)$ with $Fe^{3+}(aq)$. Our choice of $Fe^{3+}(aq)$ as oxidizing agent was partly based on the suggestion of Ardon and Plane (10) that monomeric $Cr^{3+}(aq)$ is the principal product when $Cr^{2+}(aq)$ is oxidized in one electron transfer reactions. We carried out test tube reactions followed by spectrophotometric analysis of the product solutions to establish that more than 95% of the chromium product was present as the desired monomeric $Cr^{3+}(aq)$. Ardon and Plane (10) had previously used an ion exchange method (probably better than our spectrophotometric method) to show that more than 99% of the chromium was present as monomeric $Cr^{3+}(aq)$ in similar solutions. We therefore represent the calorimetric reaction by

$$[1] \quad Cr^{2+}(aq) + Fe^{3+}(aq) = Cr^{3+}(aq) + Fe^{2+}(aq)$$

Our calorimetric measurements on reaction 1 were carried out with weighed amounts of standardized concentrated ferric perchlorate solution in the ampoule and a slight excess of dilute chromous solution in the bomb calorimetric vessel, with both solutions being 0.5 M in $HClO_4$. Seven measurements led to a *total* $\Delta H = -36.0$ kcal mol^{-1} (average deviation = 0.6 kcal mol^{-1}) for reaction 1 plus the enthalpy of dilution of the ferric perchlorate solution. Separate determination of this enthalpy of dilution (0.31 kcal mol^{-1}) permits us to select $\Delta H^0 = -36.3$ kcal mol^{-1} for the reaction represented by [1]. Because of the electrical symmetry of this reaction, it is reasonable to assume that the effect of the 0.5 M $HClO_4$ on the enthalpy of reaction is small compared to the uncertainty indicated by the average deviation of our results cited above; we have therefore neglected further heats of dilution in arriving at our standard enthalpy of reaction represented by ΔH^0.

Stout and Chisholm (11) have reviewed earlier investigations and have calculated an apparently reliable $\Delta H_f^0 = -94.52$ kcal mol^{-1} for $CrCl_2(c)$. Gregory and Burton (12) have measured the enthalpy of solution of $CrCl_2(c)$ in 1.0 M $Cl^-(aq)$, with a result in fair agreement with an earlier (13) measurement. Combination of these results with our estimated enthalpies of dilution and the ΔH_f^0 of $CrCl_2(c)$ cited above leads to $\Delta H_f^0 = -34.3$ kcal mol^{-1} for $Cr^{2+}(aq)$. These ΔH_f^0 values for $CrCl_2(c)$ and $Cr^{2+}(aq)$ are the same as listed in ref. 1. We therefore use these values for calculations with our ΔH^0 for reaction 1.

Can. J. Chem. Downloaded from www.nrcresearchpress.com by 210.87.254.42 on 09/05/12
For personal use only.

The difference in ΔH_f^0 values listed in ref. 1 for $Fe^{2+}(aq)$ and $Fe^{3+}(aq)$ amounts to 9.7 kcal mol^{-1}. We use this value for subsequent calculations, although it should be noted that there is some evidence (14) that this difference is larger than 9.7 kcal mol^{-1}.

Use of the ΔH_f^0 values cited above with our ΔH^0 for reaction 1 leads to $\Delta H_f^0 = -60.9$ kcal mol^{-1} for $Cr^{3+}(aq)$. We suggest that the total uncertainty in this value is about ± 1.5 kcal mol^{-1}. Choosing a larger difference between ΔH_f^0 values for $Fe^{2+}(aq)$ and $Fe^{3+}(aq)$ would lead to ΔH_f^0 of $Cr^{3+}(aq)$ being less negative than the -60.9 kcal mol^{-1} above.

We have also made calorimetric measurements on the enthalpy of reaction of excess $Cr^{2+}(aq)$ (in the bomb) with $Cu^{2+}(aq)$ (in the ampoule), all in 0.5 *M* $HClO_4$ solution. Duplicate test tube experiments followed by ion exchange separation of products established that the principal calorimetric reaction can be represented by

[2] $Cr^{2+}(aq) + Cu^{2+}(aq) = Cu^{+}(aq) + Cr^{3+}(aq)$

with about 4% of the Cr(III) present as hydrolytic dimers or polymers. Five determinations (adjusted for enthalpy of dilution of cupric perchlorate solution) lead to $\Delta H^0 = -25.9$ kcal mol^{-1} (average deviation = 1.8 kcal mol^{-1}) for reaction 2.

Reference 1 lists $\Delta H_f^0 = 15.48$ kcal mol^{-1} for $Cu^{2+}(aq)$ and $\Delta H_f^0 = 17.13$ kcal mol^{-1} for $Cu^{+}(aq)$. Use of these values with the ΔH_f^0 for $Cr^{2+}(aq)$ cited above and our ΔH^0 for reaction 2 leads to $\Delta H_f^0 = -60.95$ kcal mol^{-1} for $Cr^{3+}(aq)$. We suggest that the uncertainty in this value is about ± 2 kcal mol^{-1}. Use of slightly different (15) ΔH_f^0 values for $Cu^{+}(aq)$ and $Cu^{2+}(aq)$ leads to an insignificantly different ΔH_f^0 of $Cr^{3+}(aq)$.

Oxidation of $Cr^{2+}(aq)$ with $Ag^{+}(aq)$ was tried but found to be unsuited for our purposes because a considerable fraction of the Cr(III) formed was in the form of dimers or hydrolytic polymers rather than the desired $Cr^{3+}(aq)$. Similarly, reduction of Cr(VI) in acidic solution by $H_2O_2(aq)$ leads to solutions containing substantial fractions of Cr(III) in the form of dimeric or larger species. We also note that the species formed by reaction of metallic chromium with aqueous hydrochloric acid depend on purity of the metal, presence or absence of oxygen, and possibly other factors, all sufficiently complicated that we did not choose such reactions as promising for detailed calorimetric investigation.

We have also made calorimetric measurements of the enthalpy of oxidation of monomeric $Cr^{3+}(aq)$ with Ce(IV) in 0.5 *M* $HClO_4$ solution as represented by

[3] $Cr^{3+}(aq) + 3Ce(IV) = Cr(VI) + 3Ce(III)$

Our measurements lead to $\Delta H = -2.2$ kcal mol^{-1} (average deviation = 0.7 kcal mol^{-1}) for this reaction. We have also measured the enthalpy of oxidation of $Fe^{2+}(aq)$ with Ce(IV) in 0.5 *M* $HClO_4$ and found $\Delta H = -28.76$ kcal mol^{-1} (average deviation = 0.06 kcal mol^{-1}) for the reaction that we represent by

[4] $Fe^{2+}(aq) + Ce(IV) = Fe^{3+}(aq) + Ce(III)$

Finally, we have also carried out calorimetric measurements to find that $\Delta H = -2.1$ kcal mol^{-1} (average deviation = 0.4 kcal mol^{-1}) for dissolving $K_2CrO_4(c)$ in our Ce(IV) calorimetric solution and $\Delta H = 0.002$ kcal mol^{-1} for adding water to our Ce(IV) solution, as represented by reactions 5 and 6:

[5] $K_2CrO_4(c) = 2K^{+}(soln) + Cr(VI)$

[6] $H_2O(liq) = H_2O(soln)$

Combination of our enthalpies of reactions 3–6 leads (neglecting enthalpies of dilution) to $\Delta H^0 = 86.18$ kcal mol^{-1} (average deviation = 0.8 kcal mol^{-1}) for the reaction that we represent by

[7] $Cr^{3+}(aq) + 3Fe^{3+}(aq) + 2K^{+}(aq) + 4H_2O(liq) = K_2CrO_4(c) + 3Fe^{2+}(aq) + 8H^{+}(aq)$

We use this result with $\Delta H_f^0 = -335.4$ kcal mol^{-1} for $K_2CrO_4(c)$ from our recent review (2), ΔH_f^0 values for $Fe^{2+}(aq)$ and $Fe^{3+}(aq)$ from ref. 1, and ΔH_f^0 values for $K^{+}(aq)$ and $H_2O(liq)$ from ref. 16 to obtain $\Delta H_f^0 = -56.8$ kcal mol^{-1} for $Cr^{3+}(aq)$. Use of a larger difference between enthalpies of formation of $Fe^{2+}(aq)$ and $Fe^{3+}(aq)$ leads to ΔH_f^0 of $Cr^{3+}(aq)$ more negative than -56.8 kcal mol^{-1}. We also point out that the ΔH_f^0 for $K_2CrO_4(c)$ is related (2) to ΔH_f^0 values for $(NH_4)_2Cr_2O_7(c)$, $CrO_3(c)$, and $Cr_2O_3(c)$, for all of which there may be non-negligible uncertainties. It is therefore impractical to provide an estimate of the uncertainty to be associated with the above $\Delta H^0 = -56.8$ kcal mol^{-1} for $Cr^{3+}(aq)$.

On the basis of uncertainties in our calorimetric results and in various ΔH_f^0 values that we

Can. J. Chem. Downloaded from www.nrcresearchpress.com by 210.87.254.42 on 09/05/12
For personal use only.

have used, we suggest that $\Delta H_f^0 = -60$ kcal mol^{-1} for $Cr^{3+}(aq)$ is the best value that is presently available (as compared to the range from -51 to -67.9 kcal mol^{-1} cited in the Introduction). We also suggest that the uncertainty in this value is about ± 1.5 kcal mol^{-1}. Because some enthalpies of complex formation are known with accuracy considerably better than ± 1.5 kcal mol^{-1} (as discussed later in this paper), we suggest that the value above be written as $\Delta H_f^0 = -60.0$ kcal mol^{-1}. We therefore also adopt $\Delta H_f^0 = -469.9$ kcal mol^{-1} for $Cr(H_2O)_6^{3+}(aq)$ in which we have explicitly included water of hydration.

Now we turn to our investigations of various aqueous complexes of Cr(III). All of our work has been done with 'inner sphere' complexes, such as $CrF(H_2O)_5^{2+}(aq)$. We choose to describe all of our results concisely without specifically indicating the water of hydration; thus we represent the chromic fluoride complex by $CrF^{2+}(aq)$, and similarly for other complexes.

We have measured the enthalpy of oxidation of $CrF^{2+}(aq)$ with Ce(IV) in 0.5 *M* $HClO_4$ to be -12.22 kcal mol^{-1} (average deviation = 0.1 kcal mol^{-1}) and the enthalpy of oxidation of solutions of $Cr^{3+}(aq)$ and HF(aq) to yield an identical final solution to be -12.55 kcal mol^{-1} (average deviation = 0.3 kcal mol^{-1}). Combination of these two results yields $\Delta H = -0.33$ kcal mol^{-1} for the reaction

$$[8] \quad Cr^{3+}(aq) + HF(aq) = CrF^{2+}(aq) + H^+(aq)$$

The only earlier result we can compare with is $\Delta H = 1.3$ kcal mol^{-1} at 86 °C reported by Swaddle and King (5) on the basis of their d ln K/dT results for 1 *M* $LiClO_4$ solutions.

We have measured the enthalpy of oxidation of $CrCl^{2+}(aq)$ with Ce(IV) in 0.5 *M* $HClO_4$ to be -8.42 kcal mol^{-1} (average deviation = 0.2 kcal mol^{-1}) and the enthalpy of oxidation of solutions of $Cr^{3+}(aq)$ and $Cl^-(aq)$ with Ce(IV) to yield identical final solutions to be -2.13 kcal mol^{-1} (average deviation = 0.04 kcal mol^{-1}). Combination of these values leads to $\Delta H = 6.29$ kcal mol^{-1} for the reaction

$$[9] \quad Cr^{3+}(aq) + Cl^-(aq) = CrCl^{2+}(aq)$$

Related earlier investigations have been carried out by King and co-workers (17); our earlier assessment (2) of their results led to $\Delta H = 5$ kcal mol^{-1} for reaction 9, but it is also reasonable to select a larger value in close agreement with our new result.

We have measured the enthalpy of oxidation of $CrBr^{2+}(aq)$ with Ce(IV) in 0.5 *M* $HClO_4$ to be -20.16 kcal mol^{-1} (average deviation = 0.14 kcal mol^{-1}) and the enthalpy of oxidation of solutions of $Cr^{3+}(aq)$ and $Br^-(aq)$ to yield identical final solutions to be -11.23 kcal mol^{-1} (average deviation = 0.07 kcal mol^{-1}). Combination of these values leads to $\Delta H = 8.93$ kcal mol^{-1} for the reaction

$$[10] \quad Cr^{3+}(aq) + Br^-(aq) = CrBr^{2+}(aq)$$

Our ΔH for oxidation of $CrBr^{2+}(aq)$ includes a correction for decomposition of the complex. The amount of such decomposition during the time between analysis and calorimetric reaction was estimated by way of the rate data of Guthrie and King (6); the magnitude of the correction was less than 0.6 kcal mol^{-1} for all runs.

Earlier d ln K/dT results of Espenson and King (18) lead to an enthalpy of reaction 10 (taken to be 5 kcal mol^{-1} in our review (2)) that is significantly smaller than the value we have obtained above.

We have measured the enthalpy of oxidation of $CrSO_4^+(aq)$ (inner sphere complex) by Ce(IV) in 0.5 *M* $HClO_4$ solution to be -10.30 kcal mol^{-1} (average deviation = 0.10 kcal mol^{-1}) and the enthalpy of oxidation of solutions of $Cr^{3+}(aq)$ and ($SO_4^{2-}(aq)$ and $HSO_4^-(aq)$) to yield the same final solution to be -6.65 kcal mol^{-1} (average deviation = 0.03 kcal mol^{-1}). Combination of these results leads to $\Delta H = 3.65$ kcal mol^{-1} for the reaction we represent by

$$[11] \quad Cr^{3+}(aq) + \alpha HSO_4^-(aq) + (1 - \alpha)SO_4^{2-}(aq) = CrSO_4^+(aq) + \alpha H^+(aq)$$

in which α is the fraction of S(VI) that is in the $HSO_4^-(aq)$ form. For the reaction

$$[12] \quad HSO_4^-(aq) = H^+(aq) + SO_4^{2-}(aq)$$

we have taken log $K = -0.75$ and $\Delta H = -5.4$ kcal mol^{-1} (both for 0.5 *M* $HClO_4$ solution) on the basis of many results summarized by Sillén and Martell (19). We combine all of these results to obtain $\Delta H = 7.6$ kcal mol^{-1} for

$$[13] \quad Cr^{3+}(aq) + SO_4^{2-}(aq) = CrSO_4^+(aq) \text{ (inner sphere)}$$

Kinetic results from Fogel, Tai, and Yarborough (8) show that dissociation of $Cr(SO_4)^+(aq)$ complexes is negligible in our solutions

TABLE 1. Enthalpies of formation (298 K)

Ion	ΔH_f^0 (kcal mol^{-1})
Cr^{3+}(aq)	−60.0
CrF^{2+}(aq)	−136.8
$CrCl^{2+}$(aq)	−93.7
$CrBr^{2+}$(aq)	−80.1
$CrSO_4^+$(aq)	−269.7

during the time between completion of the preparation and completion of the calorimetric measurements. Their results (8) also show that outer sphere association of Cr^{3+}(aq) with SO_4^{2-}(aq) is negligible (less than 0.2%) in our solutions. Fogel *et al.* (8) have previously reported $\Delta H = 7.2$ kcal mol^{-1} for this reaction, based on their equilibrium constants over the temperature range 48 to 84 °C in 1 *M* $NaClO_4$ solution.

Our enthalpies of reactions 8–10 and 13 have been combined with our ΔH_f^0 of Cr^{3+}(aq) and ΔH_f^0 values for HF(aq), Cl^-(aq), Br^-(aq), and SO_4^{2-}(aq) from ref. 16 to obtain the ΔH_f^0 values for CrF^{2+}(aq), $CrCl^{2+}$(aq), $CrBr^{2+}$(aq), and $CrSO_4^+$(aq) (all inner sphere complexes) that are listed in Table 1.

Acknowledgments

We are grateful to the National Research Council of Canada for support of this research. In addition, I.D. thanks Bokelunska resestipendiet and Per Westlings minnesfond for travel grants.

1. D. D. WAGMAN, W. H. EVANS, V. B. PARKER, I. HALOW, S. M. BAILEY, and R. H. SCHUMM. National Bureau of Standards Technical Note 270-4. U.S. Government Printing Office, Washington, D.C. 1969.
2. I. DELLIEN, F. M. HALL, and L. G. HEPLER. Chem. Rev. In press.
3. G. OLOFSSON, S. SUNNER, M. EFIMOV, and J. LAYNEZ. J. Chem. Thermodyn. **5**, 199 (1973).
4. R. L. PECSOK and W. P. SCHAEFER. J. Am. Chem. Soc. **83**, 62 (1961).
5. T. W. SWADDLE and E. L. KING. Inorg. Chem. **4**, 532 (1965).
6. F. A. GUTHRIE and E. L. KING. Inorg. Chem. **3**, 916 (1964).
7. H. TAUBE and H. MYERS. J. Am. Chem. Soc. **76**, 2103 (1954).
8. N. FOGEL, J. M. J. TAI, and J. YARBOROUGH. J. Am. Chem. Soc. **84**, 1145 (1962).
9. G. W. HAUPT. J. Res. Natl. Bur. Stand. **48**, 414 (1952).
10. M. ARDON and R. A. PLANE. J. Am. Chem. Soc. **81**, 3197 (1959).
11. J. W. STOUT and R. C. CHISHOLM. J. Chem. Phys. **36**, 979 (1962).
12. N. W. GREGORY and T. R. BURTON. J. Am. Chem. Soc. **75**, 6054 (1953).
13. F. R. BICHOWSKY and F. D. ROSSINI. The thermochemistry of the chemical substances. Reinhold Publishing Corp., New York. 1936.
14. J. W. LARSON, P. CERUTTI, H. K. GARBER, and L. G. HEPLER. J. Phys. Chem. **72**, 2902 (1968).
15. L. M. GEDANSKY, E. M. WOOLLEY, and L. G. HEPLER. J. Chem. Thermodyn. **2**, 561 (1970).
16. D. D. WAGMAN, W. H. EVANS, V. B. PARKER, I. HALOW, S. M. BAILEY, and R. H. SCHUMM. National Bureau of Standards Technical Note 270-3. U.S. Government Printing Office, Washington, D.C. 1968.
17. C. F. HALE and E. L. KING. J. Am. Chem. Soc. **71**, 1779 (1967); R. J. BALTISBERGER and E. L. KING. J. Am. Chem. Soc. **86**, 795 (1964); H. S. GATES and E. L. KING. J. Am. Chem. Soc. **80**, 5011 (1958); K. SCHUG and E. L. KING. J. Am. Chem. Soc. **80**, 1089 (1958).
18. J. H. ESPENSON and E. L. KING. J. Phys. Chem. **64**, 380 (1960).
19. L. G. SILLÉN and A. E. MARTELL. Stability constants of metal-ion complexes. Special Publ. No. 17. The Chemical Society, London. 1964; L. G. SILLÉN and A. E. MARTELL. Stability constants of metal-ion complexes, Supplement No. 1. Special Publ. No. 25. The Chemical Society, London. 1971.

Can. J. Chem. Downloaded from www.nrcresearchpress.com by 210.87.254.42 on 09/05/12
For personal use only.

Concerning the influence of inert gas adsorption on the infrared spectrum of OH groups on powdered silica

J. G. ROTH AND M. J. DIGNAM
Department of Chemistry, University of Toronto, Toronto, Ontario M5S 1A1

Received December 9, 1975

J. G. ROTH and M. J. DIGNAM. Can. J. Chem. **54**, 1388 (1976).

McDonald's study of the absorption band at 3749 cm^{-1}, due to the O—H stretching vibration of hydroxyl groups on outgassed powdered silica, revealed substantial changes in center frequency and band area upon adsorption of Ar. The main features of these changes are accounted for here using an optical model for porous adsorbent–adsorbate systems due to Dignam, Rao, and Roth. The possibility of using the measured change in band intensity on adsorbing an inert gas, as a general indicator of the orientational distribution of the adsorbed species responsible for the band, is noted.

J. G. ROTH et M. J. DIGNAM. Can. J. Chem. **54**, 1388 (1976).

L'étude de McDonald, sur la bande d'absorption à 3749 cm^{-1}, due à la vibration de fréquence O—H des groupes hydroxyles sur des silices en poudre et dégasées, révélait que des changements importants dans le centre de fréquence et dans la surface de la bande se produisent lorsqu'il y a adsorption de Ar. Les principales caractéristiques de ces changements peuvent être expliquées en utilisant un modèle optique, dû à Dignam, Rao et Roth, pour des systèmes poreux adsorbant–adsorbé. On note la possibilité d'utiliser les changements mesurés dans l'intensité des bandes lorsqu'il y a adsorbtion d'un gaz inerte comme un indicateur général de la distribution des orientations des espèces adsorbées responsables pour ces bandes.

[Traduit par le journal]

Introduction

Infrared spectroscopy of species adsorbed on powdered specimens has been the subject of considerable interest for some time. Comprehensive reviews have been given by Little (1) and Hair (2). Results have been interpreted almost exclusively in chemical terms, rather than optical terms. Thus shifts in the frequency of an absorption band are ascribed to chemical interactions of the various species with each other and with the surface. Similarly, changes in peak intensities following adsorption are generally interpreted in terms of changes in the population of the adsorbed species.

Optical models of porous adsorbent–adsorbate systems have been presented (3) based on the scattering and extinction properties of particles and cavities coated with anisotropic films (4). These have been tested against data for CO adsorbed on various alkali halides (5) and it was found that local field effects (*i.e.* phenomena purely optical in nature), could explain most of the spectroscopic features observed and previously explained in terms of special adsorption sites, *i.e.* chemical interactions (6). The purpose of the present publication is to reexamine, in the light of the above optical models, the data obtained by McDonald (7) for OH groups on powdered silica glass.

McDonald studied the absorption band at 3749 cm^{-1} due to the oxygen–hydrogen stretching vibration of the free hydroxyl groups on outgassed powdered silica glass and the effects on the spectrum of adsorbing various gases. Figure 1 shows the results obtained using argon as the adsorbing gas. The dotted curve represents the spectrum obtained for the outgassed silica. The dashed curve was obtained following admission of argon to the cell at 135 torr and 83 K. The solid line is the spectrum obtained when argon was allowed to condense into the transmission cell at 73 K. An interpretation of these results will now be attempted.

Theory

A set of equations has been derived (3) for the chemical extinction coefficient of a porous adsorbent–adsorbate system consisting of a random isotropic distribution of coated spherical particles of random size, but with particle size and separation small compared to the wavelength of light in question. Defining the chemical extinc-

Can. J. Chem. Downloaded from www.nrcresearchpress.com by 210.87.254.5 on 09/05/12
For personal use only.

Can. J. Chem. Downloaded from www.nrcresearchpress.com by 210.87.254.5 on 09/05/12
For personal use only.

tion coefficient of the adsorbed species, β_a, according to

$$[1] \qquad \beta_a = (1/L) \log_{10} (I_t^0/I_t)$$

where I_t and I_t^0 are the transmitted light intensities with and without adsorbate respectively, and L the thickness of the specimen, the following equation for β_a was derived for this model:

$$[2] \quad \beta_a = \frac{AC_s \left(\frac{\epsilon_s}{\epsilon_a}\right)\left(\frac{2\pi}{3}\right)\left[\left(\frac{2\epsilon_a^2}{\epsilon_s^2}\right) \mathrm{Im}\,(-\gamma_t) + \mathrm{Im}\,(-\gamma_n)\right]}{2.303\lambda_0}$$

where A is the surface area per unit volume of the adsorbent, ϵ_s and ϵ_a the substrate and ambient dielectric constants respectively (assumed real valued), λ_0 the wavelength *in vacuo*, and Im denotes the imaginary part of the function. C_s is a constant which depends on (ϵ_s/ϵ_a) and the relative pore volume but is close to unity for all reasonable choices of these (3). In deriving [2], the adsorbed film was treated as uniaxial with its optic axis coincident with the local normal to the surface to allow for possible non-isotropic molecular orientation. Defining ϵ_n and ϵ_t as the complex dielectric tensor components for the film in the directions normal to and tangent to the surface respectively, then γ_n and γ_t are defined according to

$$[3] \qquad \gamma_t = d(\epsilon_t/\epsilon_a - 1)$$

and

$$[4] \qquad \gamma_n = d(1 - \epsilon_a/\epsilon_n)$$

where d is the effective thickness of the film. They characterize the optical properties of the molecular layer and are 4π times the polarization relative to the ambient phase in the t (tangential to the surface plane) or n (normal) direction per unit adsorbent area divided by the t or n component of the field that would obtain in the absence of the adsorbate (8).

Dignam and Moskovits (8) derived the following expressions relating γ_u, u = n, t, to the components of the mean polarizability, α_u, u = n, t, of the adsorbed species relative to the ambient:

$$[5] \qquad \gamma_t = \frac{4\pi N\alpha_t}{1 - \theta_t\left(\frac{4\pi}{3}\right)\left(\frac{N}{a}\right)\alpha_t}$$

$$[6] \qquad \gamma_n = \frac{4\pi N\alpha_n}{1 + \theta_n\left(\frac{8\pi}{3}\right)\left(\frac{N}{a}\right)\alpha_n}$$

where N is the mean surface concentration of the adsorbed species. The θ's express the correlation between the polarizability of a molecule at a point on the surface and the field at that point due to the other molecules on the surface. In the analysis below, we assume these quantities to be uncorrelated, and hence set the θ's to unity. Any error introduced by this assumption will probably be small for the cases studied here (8). The quantity a is related to the pair distribution function, $f(r)$, (*i.e.* the expectation value of the number of molecules within a distance r of any given molecule divided by the corresponding number for a random distribution of points on a plane) through

$$[7] \qquad a = 8/\left\{9\int_0^\infty [f(r)/r^2]\mathrm{d}r\right\}$$

It was also shown that if the adsorbed molecules are treated as randomly distributed hard discs of diameter d', then at low coverage $a = (4/3)d'$ while for a close packed square planar array, $a = 0.935d'$ with a being about 20% smaller for a hexagonal close packed array. Thus for a random distribution of adsorbed species, all of diameter d', a varies from $(4/3)d'$ at low coverage to about $0.9d'$ at full coverage. In the following treatment we make the simplifying approximations (*i*) that a is constant, independent of the concentration and composition of the adsorbed layer, and (*ii*) that $\theta_n = 1 = \theta_t$.

The difference in the sign of the terms in the denominators of [5] and [6] arises from the fact that for a tangentially oriented external field, the field due to the induced dipole moments augments the external field, while for a normally oriented external field, the opposite is the case.

If pre-adsorbed species (*e.g.* OH groups) occupy only a fraction of the surface area, with subsequently adsorbed species (*e.g.* Ar) occupying some or all of the remaining area, then on making simplifying approximations (*i*) and (*ii*), the following substitutions into [5] and [6] may be made.

$$[8] \qquad N\alpha_u \leftarrow N\alpha_u + N''\alpha_u''$$

where u = n, t; α and α'' are the components of the mean polarizability tensors of the adsorbed

Can. J. Chem. Downloaded from www.nrcresearchpress.com by 210.87.254.5 on 09/05/12
For personal use only.

hydroxyl radicals, and the adsorbed 'inert' gas molecules respectively; and N and N'' are the corresponding concentrations per unit area.

Assuming that the 'inert' gas molecules do not absorb near the spectral region of interest, α_u'' will be constant and real valued. The components of the polarizability of the hydroxyl radicals can be represented approximately by Lorentzian functions:

$$[9] \qquad \alpha_u = \alpha_u^{\infty} + \frac{s_u}{1 - \left(\frac{\omega}{\omega'}\right)^2 + i\Gamma\frac{\omega}{\omega'}}$$

where u = n, t; α_u^{∞} is the high frequency contribution; s_u is the oscillator strength; ω' is the center frequency; and Γ is the line width. Both of these last two quantities are assumed to be the same for the normal and tangential components since only a single ir absorption band is involved. The relative values of the oscillator strength can be calculated from a knowledge of the orientational distribution of the related transition dipole moment. Thus, for example, if the transition dipole moment makes an average angle θ with the surface normal,

$$[10] \qquad s_n = \cos^2\theta\, s$$

$$[11] \qquad s_t = \tfrac{1}{2}\sin^2\theta\, s$$

where s is the oscillator strength of the transition and

$$[12] \qquad s_n + 2s_t = s$$

For the isotropic case, the dipole is equally likely to be oriented normal to the surface or in one of the two orthogonal tangential directions, and $s_t = s_n$. No simple relationship will in general exist between the high frequency contributions, but for the isotropic case they will be equal.

Substituting [8] into [5] and [6], and expressing the results as Lorentzian functions gives

$$[13] \qquad \gamma_u = \gamma_u^{\infty} + \frac{S_u}{1 - \left(\frac{\omega}{\omega_u}\right)^2 + i\Gamma_u\left(\frac{\omega}{\omega_u}\right)}$$

where

$$[14] \qquad \gamma_u^{\infty} = \frac{4\pi N\alpha_u^{\infty}}{1 - K_u\left(\frac{4\pi}{3}\right)\left(\frac{N}{a}\right)\alpha_u^{\infty}}$$

$$[15] \qquad S_u = \frac{4\pi N s_u}{\left[1 - K_u\left(\frac{4\pi}{3}\right)\left(\frac{N}{a}\right)\alpha_u^{\infty}\right]\left[1 - K_u\left(\frac{4\pi}{3}\right)\left(\frac{N}{a}\right)(\alpha_u^{\infty} + s_u)\right]}$$

$$[16] \qquad \frac{\Gamma}{\Gamma_u} = \frac{\omega_u}{\omega'} = \left[\frac{1 - K_u\left(\frac{4\pi}{3}\right)\left(\frac{N}{a}\right)(\alpha_u^{\infty} + s)}{1 - K_u\left(\frac{4\pi}{3}\right)\left(\frac{N}{a}\right)\alpha_u^{\infty}}\right]^{1/2}$$

with u = n, t; $K_t = 1$; and $K_n = -2$.

Substituting [8] and [9] into [5] and [6] and assuming $K_u(4\pi/3)(N/a)\alpha_u^{\infty}$ and similar terms are small compared to unity, gives the following expressions for the frequency shift on adsorption of the 'inert' gas:

$$[17] \qquad \frac{\omega_t'' - \omega_t}{\omega'} = -\tfrac{1}{2}\left[\left(\frac{4\pi}{3}\right)\left(\frac{N}{a}\right)s_t\right]^2\frac{N''\alpha_t''}{Ns_t}$$

$$[18] \qquad \frac{\omega_n'' - \omega_n}{\omega'} = -2\left[\left(\frac{4\pi}{3}\right)\left(\frac{N}{a}\right)s_n\right]^2\frac{N''\alpha_n''}{Ns_n}$$

where ω_n'' (u = n, t) is the center frequency with the 'inert' gas adsorbed, and ω_u that for the outgassed silica. Thus the normal component is, in general, shifted more than the tangential, both being shifted to lower frequencies.

Another quantity of interest is the peak absorbance, which for a Lorentzian function is given approximately by S/Γ. It can be shown by similar calculations that when the 'inert' gas is added to the surface, the peak absorbance due to the tangential component increases while that due to the normal component decreases.

For the case of the gas condensed in the cell, [5] and [6] can be applied directly, except that the polarizability of the hydroxyl radical must be replaced by its effective polarizability in the condensed gas. It is assumed that the condensed gas does not perturb the polarizability of the radical except that the effective polarizability must be calculated for the new ambient. This is achieved as follows. The effective polarizability, α_a, of a spherical particle of radius R in an ambient medium of dielectric constant ϵ_a is given by

$$[19] \qquad \alpha_a = R^3(\epsilon - \epsilon_a)/2\epsilon_a + \epsilon)$$

Can. J. Chem. Downloaded from www.nrcresearchpress.com by 210.87.254.5 on 09/05/12
For personal use only.

where ϵ is the dielectric constant of the medium composing the particle. The macroscopic dielectric tensor components for the OH radical are calculated using [19], which with the ambient assumed to be vacuum, gives

$$[20] \qquad \epsilon_u = [1 + 2\alpha_u/R^3]/[1 - \alpha_u/R^3]$$

where u = n, t; while substituting [20] back into [19], keeping R fixed, gives

$$[21] \qquad \alpha_u^c = R^3[\epsilon_u - \epsilon_c]/[\epsilon_u + 2\epsilon_c]$$

as the effective polarizability in the new ambient, where ϵ_c is the dielectric constant of the condensed phase.

Calculations and Results

Equations 2, 5, 6, 8, and 9, along with values for the physical parameters, can now be used in an attempt to reproduce the data of Fig. 1. The results presented in Fig. 2 were generated as follows. First the normal component of the polarizability tensor for the OH radical was assumed Lorentzian (as given by [9]) with the tangential component represented by a real valued constant. The parameters were then chosen to more or less duplicate McDonald's result for the outgassed silica (dotted line in Fig. 1*A*). The values so chosen were approximately those discussed below for the more detailed analysis of the hydroxyl–argon system. The frequency shifts resulting from adsorption and then condensation of argon could be adjusted somewhat by changing certain parameters in accordance with [17] and [19] but significant line broadening could not be produced. Results are also shown in Fig. 2 using the same parameters as above except that the OH radicals were assumed to lie parallel, rather than normal, to the local surface. The resulting frequency shifts are approximately correct, but again no broadening is obtained.

A further attempt was made to duplicate the results of McDonald by mixing the normal and tangential modes as given by [10] and [11] and the results are shown in Fig. 1. The powdered silica substrate was assumed to be 0.5 mm thick, with sample density per unit beam area of 10 mg/cm² and a surface area of 200 m²/g, as given by McDonald (7). This gave a volume fraction,

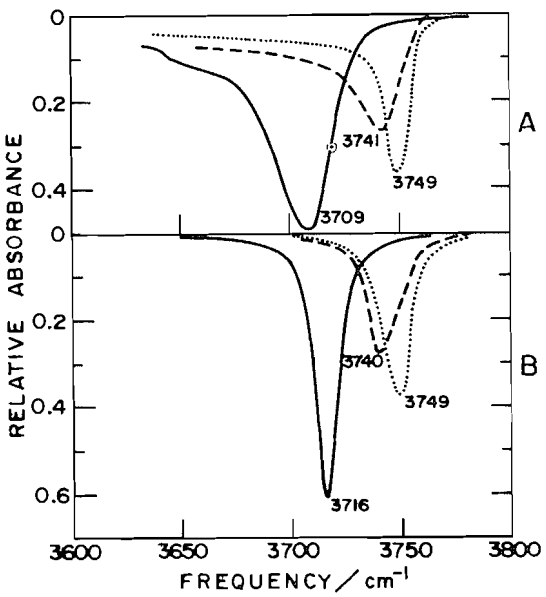

FIG. 1. Infrared spectrum for OH groups on powdered silica: *A*, McDonald's results (7); *B*, calculated curves. The three curves correspond to results for: · · · ·, outgassed silica; ---, Ar adsorbed at 135 torr and 83 K; —, and Ar condensed in the cell at 73 K.

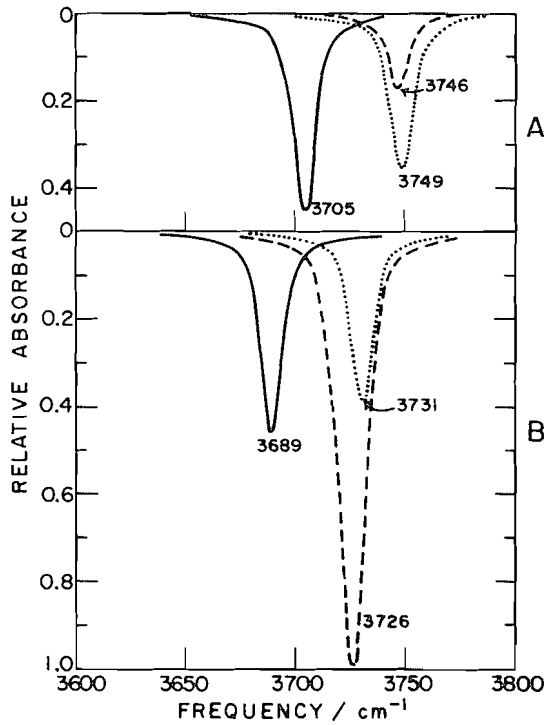

FIG. 2. Infrared spectrum for OH groups on powdered silica calculated assuming the OH groups to be oriented: *A*, normal to the surface, *B*, tangential to the surface. The three curves are identified as in Fig. 1.

Can. J. Chem. Downloaded from www.nrcresearchpress.com by 210.87.254.5 on 09/05/12
For personal use only.

V, of 0.087 and surface area per unit volume, A, of 0.4 μm^{-1}. The dielectric constant of the particles was assumed to be that of fused silica (9) and the ambient was assumed to be vacuum. The hydroxyl radicals on the outgassed silica were assumed to form a layer of one-eighth full coverage, based on 8 per nm^2 (10), and the layer was assumed to be 0.26 nm thick, estimated as the sum of the radius of liquid water and the covalent radius of oxygen (11). The polarizability as given by [9] was then adjusted to best duplicate McDonald's spectrum for the outgassed surface using [2], and assuming 80% loss due to scattering, as McDonald observed. The parameter values that gave the best agreement were: a high frequency polarizability of 0.85×10^{-24} cm^3, a center frequency, $\omega'/2\pi c$, of 3741 cm^{-1}, and a relative line width, Γ, of 0.003, the same set applying for both components. The strength in the normal direction, s_n, was 0.15×10^{-24} cm^3, with the strength in the tangential direction being 60% of this value, this proportion being chosen to give the best fit to the spectrum resulting from adsorbing one monolayer of Ar. This corresponds to a mean angle for the O—H axis of about 50° to the surface normal (from [10] and [12]). The oscillator strength and concentration per unit area appear essentially as a product, making the strength and coverage factor one adjustable parameter. In all, five adjustable parameters were used to fit all three spectra: the center frequency, the line width, the ratio of strengths, the strength of the normal mode, and the high frequency polarizability, the last two being essentially scaling parameters.

For monolayer coverage, argon atoms were assumed to occupy all remaining surface sites, and have an isotropic polarizability of 1.65×10^{-24} cm^3 (7), unperturbed from the gas state. The substitution [8] was made and the result was a band shifted to 3740 cm^{-1} compared to the observed value 3741 cm^{-1} and a width at half height of 19 cm^{-1} as compared to the observed 24 cm^{-1}. The peak intensity decreased to about the same extent as observed by McDonald. The broadening in the calculated spectrum is due mainly to the superposition of the normal and tangential contributions to the absorption band. For outgassed silica the tangential mode does not contribute significantly to the calculated spectrum (Fig. 1), but does make a significant contribution following adsorption of one monolayer of Ar (see Fig. 2).

For the spectrum resulting after argon is condensed in the cell, [20] and [21] were used to calculate the polarizability of the OH radicals relative to the new ambient. This resulted in a shift of 33 cm^{-1} (compared to the observed shift 40 cm^{-1}), but a narrowing of the band to 12 cm^{-1} at half height (compared to a broadening to 30 cm^{-1}). The calculated narrowing occurs because the tangential component again does not contribute significantly to the band. Calculations for krypton and xenon show similar agreement, while the calculations for nitrogen, oxygen and methane do not agree with McDonald's results.

Discussion

McDonald attributed the observed line broadening and frequency shifts to the formation of weak hydrogen bonds between surface hydroxyls and the adsorbed molecules. This bonding was assumed to perturb the hydroxyl radical and alter the stretching frequency. He attempted to correlate the frequency shifts with adsorbate polarizabilities, the noble gases giving a smooth relationship, but not nitrogen, oxygen, and methane. The relatively large effect of these last three gases was attributed by Frohnsdorff and Kingston (12) to interactions with the large quadrupole moments of these molecules. While these explanations are probably correct for nitrogen, oxygen, and methane, the results for the noble gases (where any hydrogen bonding would be considerably weaker) can be largely accounted for on the basis of the purely optical effects treated here. The present treatment specifically neglected perturbations to the OH radicals on adsorption of the 'inert' gas. We do not claim that there are in fact no such perturbations present in these systems. On the contrary, it is likely that the broadening observed on condensing argon into the cell is due largely to van der Waals interactions leading to phonon broadening. The conclusion we wish to draw from our calculations is that it is necessary to take into account the effects of altering the dielectric environment of surface species, in addition to considering effects due to chemical interactions.

Finally, we point out the usefulness of results, such as those presented by McDonald, for

determining the orientation of chemisorbed species. If the transition dipoles of the chemisorbed molecules for a particular band are oriented in a direction normal to the surface, adsorbing a monolayer of an 'inert' gas would result in a decrease in the area of the band, whereas if they are tangentially oriented, an increase would result (see Fig. 2). The 'inert' gas would, of course, have to be one that did not interact significantly with the chemisorbed species, and should have a high polarizability.

1. L. H. LITTLE. Infrared spectra of adsorbed species. Academic Press, London. 1966.
2. M. L. HAIR. Infrared spectroscopy in surface chemistry. Marcel Dekker, New York. 1967.
3. M. J. DIGNAM, B. RAO, and J. ROTH. J. Chem. Soc. Faraday Trans II, **69**, 804 (1973).
4. J. ROTH and M. J. DIGNAM. J. Opt. Soc. Am. **63**, 308 (1973).
5. B. RAO and M. J. DIGNAM. J. Chem. Soc. Faraday Trans II, **70**, 492 (1974).
6. R. GEVIRZMAN, Y. KOZIROVSKY, and M. FOLMAN. Trans. Faraday Soc. **65**, 2206 (1960).
7. R. S. MCDONALD. J. Am. Chem. Soc. **79**, 850 (1957).
8. M. J. DIGNAM and M. MOSKOVITS. J. Chem. Soc. Faraday Trans. II, **69**, 56 (1973).
9. A.I.P. Handbook (1963).
10. R. K. ILER. The colloid chemistry of silica and silicates. 1955. p. 235.
11. F. A. COTTON and G. WILKINSON. Advanced inorganic chemistry. Interscience, New York. 1966.
12. G. J. C. FROHNSDORFF and G. I. KINGTON. Trans. Faraday Soc. **55**, 1172 (1959).

Can. J. Chem. Downloaded from www.nrcresearchpress.com by 210.87.254.5 on 09/05/12
For personal use only.

The thermal (dark) decomposition of 2-(2′,4′-dinitrophenylamino)-2-deoxy-D-glucose (DNP-glucosamine) in alkaline borate buffer

R. O. OKOTORE[1]

Department of Biological Sciences, University of Lagos, Lagos, Nigeria

Received November 12, 1974[2]

R. O. OKOTORE. Can. J. Chem. **54**, 1394 (1976).

The thermal lability of 2-(2′,4′-dinitrophenylamino)-2-deoxy-D-glucose (DNP-glucosamine) in alkaline borate buffer is reported. This was dependent on borate ion concentration at constant p*H*. Of the many reaction products, 2,4-dinitroaniline was isolated and identified by spectroscopic and other means. It was formed in 20% yield. A mechanism of reaction is suggested.

R. O. OKOTORE. Can. J. Chem. **54**, 1394 (1976).

On a établi la labilité thermique du (dinitro-2′,4′ phénylamino)-2 déoxy-2 D-glucose dans des tampons alcalins de borate. A p*H* constant, cette propriété dépend de la concentration en ions borates. De tous les produits de la réaction, on a pu isoler et identifier la dinitro-2,4 aniline par spectroscopie ainsi que d'autres méthodes. Ce composé se forme avec un rendement de 20%. On suggère un mécanisme pour cette réaction.

[Traduit par le journal]

Introduction

The amino sugars occur as components of mucopolysaccharides, mucoids, and glycoproteins. Identification of naturally occurring hexosamines, especially glucosamine and galactosamine (chondrosamine) have been accomplished as the hydrochlorides, the benzyloxycarbonyl chloride derivatives (1), as various Schiff bases (2, 3), and by X-ray diffraction (4). Numerous colorimetric methods for their determination have also been reported, (5–7).

The first quantitative estimation of these hexosamines in a natural product, blood group substances, carried out by Annison *et al.* employed the *N*-2,4-dinitrophenyl derivatives, (8). Chromatography of these derivatives on alkaline borate buffered Celite columns led to a successful separation of glucosamine from galactosamine. However, the colour of the DNP-glucosamine band on these columns faded continuously during chromatography resulting in variable and consistently low recoveries of DNP-glucosamine as compared to DNP-galactosamine which was stable. It was inferred from this observation that DNP-glucosamine probably underwent decomposition. This paper reports a detailed investigation on the nature of thermal (dark) decomposition of DNP-glucosamine in alkaline borate buffer.

[1]Formerly, Department of Biochemistry, Dalhousie University, Halifax, Nova Scotia.

[2]Revision received December 15, 1975.

Experimental

All chemicals used in this study were of analytical reagent grade and were not further purified.

D-Glucosamine hydrochloride and fluoro-2,4-dinitrobenzene were obtained from Koch-Light Laboratories Limited, Colnbrook, Bucks., England. Cellulose powder, MN 300, silica gel H (without binder), silica gel G (15% $CaSO_4$), and silica gel powder (chromatographic grade) were products of E. Merck A.G. Darmstadt, Germany.

Ultraviolet–visible spectra were recorded with a Unicam SP 800 spectrophotometer, and occasionally with a wavelength calibrated Carl Zeiss PMQ II spectrophotometer, using silica cuvettes, with a 1.00 cm light path. Wavelengths are accurate to within ± 2 Å. Unless otherwise stated, solutions for ultraviolet spectrophotometry were prepared by diluting aliquots from the reaction mixture with distilled water.

Infrared spectra were measured with a Perkin-Elmer Infra-cord spectrophotometer; paraffin mulls were used except where otherwise stated.

Preparation of DNP-glucosamine

DNP-D-glucosamine was prepared by a modification of the method of Lloyd and Stacey (9). D-Glucosamine hydrochloride (25.0 g) was dissolved in water (250 ml) and stirred vigorously with fluoro-2,4-dinitrobenzene (13.9 ml) followed by acetone (125 ml) in a dark bottle during the rapid addition of sodium carbonate (12.9 g), previously dissolved in water (250 ml).

Stirring was continued for 18 h at room temperature. The mixture was concentrated under reduced pressure on a water bath initially at 30–40 °C, but was not further heated. After 2–3 h the heavy yellow suspension which formed was carefully decanted through a filter, leaving a

Can. J. Chem. Downloaded from www.nrcresearchpress.com by 210.87.254.6 on 09/05/12
For personal use only.

Can. J. Chem. Downloaded from www.nrcresearchpress.com by 210.87.254.6 on 09/05/12
For personal use only.

gum adhering to the flask. The solid on the filter was washed with a little cold water and dried *in vacuo* over concentrated sulphuric acid to give a yellow solid (24 g). The filtrate and washings were combined, stored at 4 °C overnight, and filtered. In most preparations a further 1–2 g thus obtained, was combined with the main product.

The combined material was boiled with water (300 ml) and the boiling extract decanted from an oily residue. The decantate was boiled with charcoal (5 g) and filtered while hot. The filtrate, cooled at 4 °C overnight, yielded a crystalline product (7.81 g). The dried product was extracted at room temperature with acetone (170 ml) in which it was almost completely soluble. The filtered extract was diluted with an equal volume of benzene. After storage at 4 °C overnight, the bright yellow crystals of DNP-D-glucosamine were collected, washed with benzene, and dried *in vacuo* (H_2SO_4). Yield 5.45 g; mp 199–201 °C (uncorrected), (lit. (9) 194–196 °C; (8) 201–203 °C (uncorrected)); $[\alpha]_D^{23}$ +60.5 ± 2 (*c* 0.08 in 80% v/v EtOH). (lit. (9) +63.70; (10) +50); R_f = 0.80 (system A) (lit. (9) 0.8).

The mother liquors contained mainly the required product (tlc) but were not worked up. The product, as obtained above, was used for the experiments to be described. It recrystallized from water without change in melting point or specific rotation.

Spectrophotometric Analysis

Solutions of DNP-D-glucosamine were prepared in standard volumetric flasks made of actinic glass and kept in a dark cupboard for the specified period of incubation (see results). Aliquots (50 μl) were withdrawn from the incubating solution at ½ h intervals into other flasks and diluted with distilled water to 10 ml. The ultraviolet spectrum of this diluted solution was recorded. The ratio E_{360}/E_{295} was the index for monitoring the rate of decomposition.

Solvent Systems

The following solvent systems were employed: (*A*) *n*-butanol–ethanol–water (4:1:5 v/v) upper phase; (*B*) ethyl acetate – absolute alcohol – water (188:12:1 v/v).

Results

The ultraviolet absorption spectrum of DNP-D-glucosamine in absolute alcohol is shown in Fig. 1. The λ_{max} and λ_{min} were at 352 nm and 295 nm respectively. The molar absorptivity, ϵ, was 19 600. The spectra of DNP-D-glucosamine solutions in the p*H* range 1–8, kept in the dark during a 24 h incubation period or even for 5 days, were similar. There was no evidence of decomposition.

DNP-D-glucosamine in Alkaline Buffer Systems

Solutions of DNP-D-glucosamine (0.01 *M*) were prepared in three different buffer systems, (0.05 *M*): phosphate–KOH, boric acid–borate, and bicarbonate–carbonate at p*H* 9.5.

Each test solution was sampled at intervals.

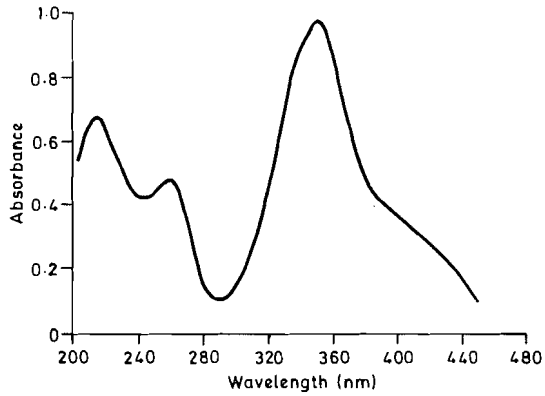

FIG. 1. The ultraviolet spectrum of DNP-D-glucosamine (50 μ*M*) in absolute alcohol. The path length was 1 cm.

The plot of E_{360}/E_{295} against the period of incubation for the sample (0.01 *M*) and also at higher concentration (0.03 *M*) in the bicarbonate–carbonate buffer at p*H* 9.5 is depicted in Fig. 2.

At p*H* 8.5, this ratio was 6.05 for freshly prepared solutions in all three buffer systems. This value decreased to 4.0 after one day incubation for solutions in borate buffer only, but it was fairly constant in the remaining two systems. At p*H* 9.0, the ratio decreased to 4.0 within 90 min incubation, changing to 1.5 after one day.

Effect of pH

Solutions of DNP-D-glucosamine (0.01 *M*)

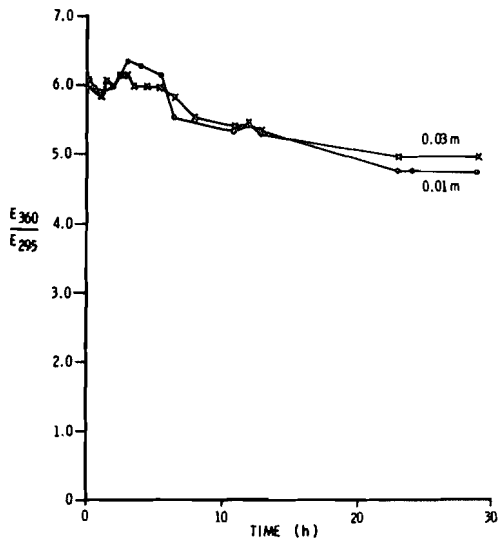

FIG. 2. DNP-D-glucosamine in bicarbonate–carbonate buffer (0.05 *M*) at p*H* 9.5.

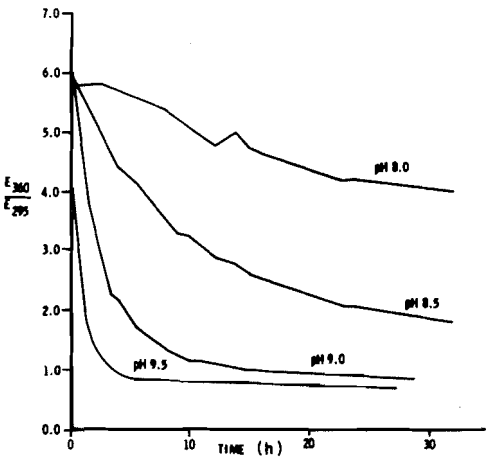

FIG. 3. Decomposition of DNP-D-glucosamine in borate buffer (0.2 *M*) as a function of p*H*.

were prepared in borate buffers of four different p*H* values, *viz.* 8.0, 8.5, 9.0, and 9.5 and then sampled at intervals. In each case the ratio E_{360}/E_{295} was plotted against time, (Fig. 3). The initial reaction was fastest at p*H* 9.5.

Effect of Borate Concentration

Solutions (0.01 *M*) of DNP-D-glucosamine were prepared in borate buffers of different molarities, *viz.* 0.025, 0.05, 0.10, and 0.20 *M* at p*H* 9.5, then sampled at intervals.

The times at which the bathochromatic shift occurred in the spectra of these solutions respectively were 24, $4\frac{1}{2}$, 3, and 2 h after incubation. This suggested that the reaction was dependent on the borate concentration.

Effect of DNP-D-glucosamine Concentration

Solutions of DNP-D-glucosamine, approximately 0.01, 0.03, and 0.05 *M* in 0.20 *M* borate buffer at p*H* 9.5 were stored and sampled at intervals. The plot of E_{360}/E_{295} against time is shown in Fig. 4. The most rapid decrease in E_{360}/E_{295} took place in the most dilute solution.

Investigation of the Reaction Products

The results of the experiments described above led to the conclusion that the best condition for the rapid thermal decomposition of DNP-glucosamine was to incubate it in borate buffer, 0.2 *M*, p*H* 9.5.

Solutions of DNP-D-glucosamine in the alkaline borate buffer after decomposition had occurred were yellow but little colour was extracted into ethyl acetate. However, in the presence of excess D-mannitol, added after decomposition, most of the colour was extracted into the organic phase. Acidification of the aqueous layer and further extraction with ethyl acetate led to the total removal of the yellow colour. Thin layer chromatography of the ethyl acetate layer in solvent system *B* (cellulose layers) gave three yellow spots, R_f 0.91, 0.65, and 0.28. In a semipreparative run, the three bands were eluted with 95% ethanol, and were found to contain roughly equal quantities of material by weight. Only the product from the fastest moving band, R_f 0.91 was homogenous in several solvent systems. The other two bands, R_f 0.65 and 0.25 respectively were inhomogenous. They were not further investigated.

The infrared spectrum of the product extracted from the chromatographically pure band, R_f 0.91, was diagnostic. It had two N—H stretching absorptions at 2.91 μm and 3.03 μm characteristic of a primary amine (—NH_2). The diffuse absorption in the region 3.0–3.3 μm characteristic of —OH stretching absorptions from the sugar portion of the starting material was absent which suggested that the scission of the carbohydrate (C—N) bond had occurred. This product (mp 178–180 °C) was identified as 2,4-dinitroaniline. An authentic sample of 2,4-dinitroaniline (mp 180 °C) caused no depression of the melting point of the product (mixture mp 179–180 °C). The infrared spectrum of the authentic sample of

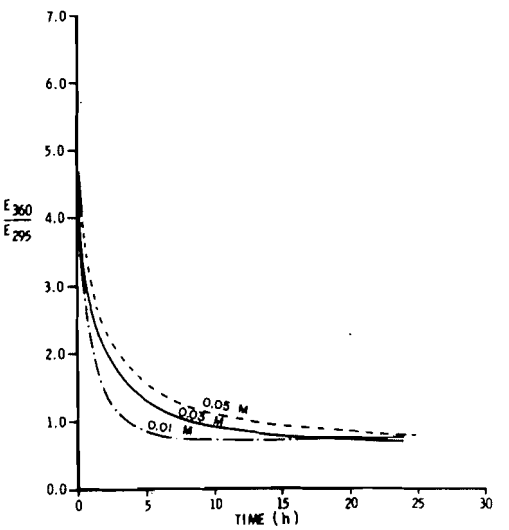

FIG. 4. Decomposition of DNP-D-glucosamine in borate buffer (0.2 *M*) at p*H* 9.5 as a function of DNP-D-glucosamine concentration.

Can. J. Chem. Downloaded from www.nrcresearchpress.com by 210.87.254.6 on 09/05/12
For personal use only.

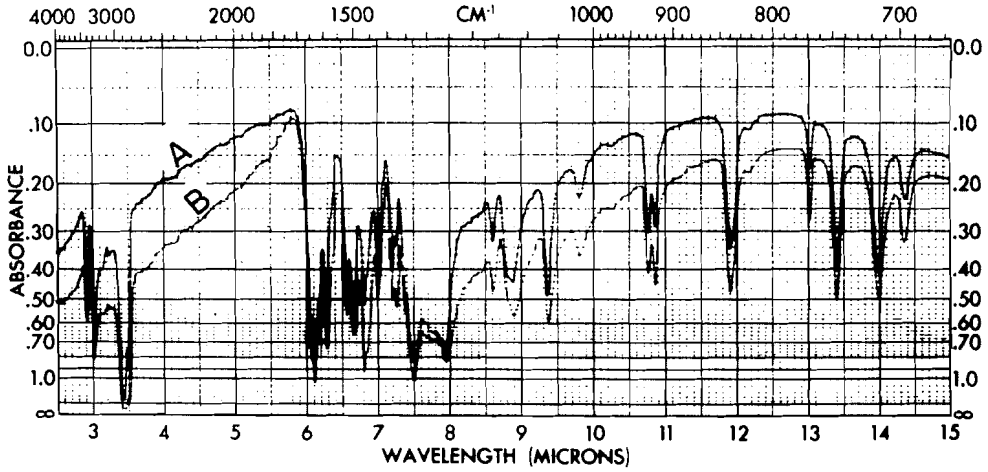

FIG. 5. The infrared spectra of authentic 2,4-dinitroaniline (*A*) and the isolated chromatographically pure component (*B*).

2,4-dinitroaniline and that of the isolated product were indistinguishable (Fig. 5). Its ultraviolet spectrum was indistinguishable from that of an authentic sample of 2,4-dinitroaniline (Fig. 6).

Yield of 2,4-Dinitroaniline from the Reaction Mixture

In separate experiments, it was established that only the product identified above as 2,4-dinitroaniline was extractable with benzene from the reaction mixture. The λ_{max} for this compound in benzene was 330 nm and the absorbance was proportional to the dinitroaniline concentration in the range 1.0–11 μg/ml.

A solution (0.01 *M*) of DNP-D-glucosamine in borate buffer (0.2 *M*, p*H* 9.5) was sampled at intervals for the content of 2,4-dinitroaniline present therein. The amount of the latter formed as a function of time is shown in Fig. 7. The yield was at a maximum after 4 h of incubation and constituted roughly 20% of the starting material.

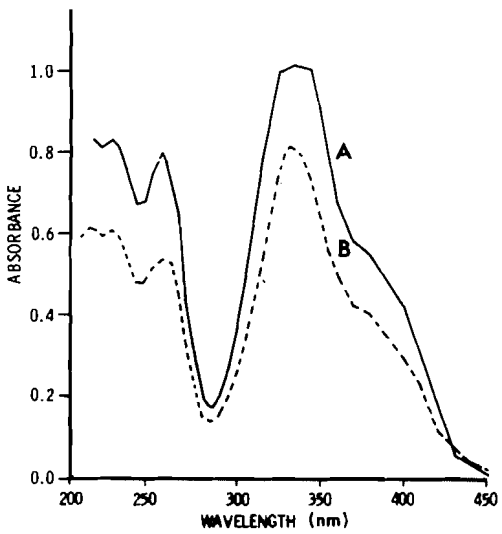

FIG. 6. The ultraviolet spectra of 2,4-dinitroaniline (0.0014%) solution in absolute alcohol (*A*) and isolated component, 0.001% solution in absolute alcohol (*B*).

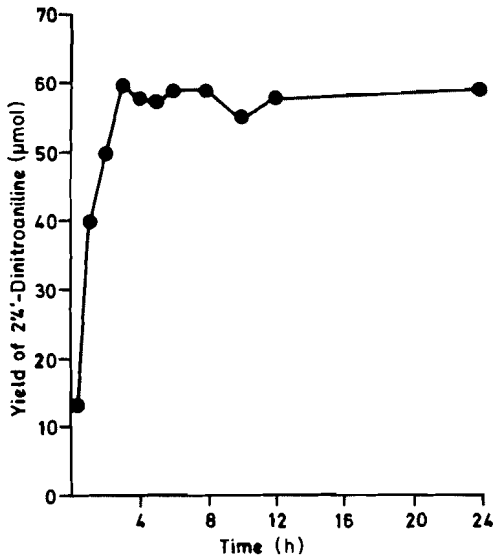

FIG. 7. Rate of formation of the isolated component, (2,4-dinitroaniline) from DNP-D-glucosamine in borate buffer (0.2 *M*) at p*H* 9.5 as a function of time.

Can. J. Chem. Downloaded from www.nrcresearchpress.com by 210.87.254.6 on 09/05/12
For personal use only.

Can. J. Chem. Downloaded from www.nrcresearchpress.com by 210.87.254.6 on 09/05/12
For personal use only.

Discussion

Glucosamine is recovered almost quantitatively from its DNP derivative by alkaline hydrolysis with an anion exchange resin in the hydroxide form, the other product being 2,4-dinitrophenol (9). Also, amino acids are commonly recovered from their DNP derivatives by hydrolysis with hot ammonium hydroxide in a sealed tube. Both reactions presumably involve attack of a hydroxide ion on the aromatic carbon and require a high concentration of hydroxyl ion. Both DNP-glucosamine and DNP-amino acids are reasonably stable at alkaline p*H*, not too far removed from neutrality. In the present work, however, little decomposition of the carbohydrate derivative occurred in phosphate (p*H* 9.0) or carbonate (p*H* 9.5) buffers. Moreover, the decomposition that occurred in borate was not accompanied by any detectable amount of 2,4-dinitrophenol. Accordingly, an explanation for the instability of DNP-glucosamine in alkaline borate solutions cannot be sought in a simple attack of hydroxide ion of the type encountered at high p*H*.

Borate forms a complex with *cis*-1,2-diol structures (11). These groupings are absent in DNP-glucosamine which is presumably in the pyranose form like DNP-galactosamine, (9) so no possibility of borate complexation exists.

However, Good and Bessman, (12), in their study of the effect of borate on the Morgan–Elson reaction, (13) found that the chromogens obtained were furan derivatives of type **1**. It is supposed that their precursor is the furanose form of *N*-acetylglucosamine. The yield of these chromogens increased when borate was present in the medium. To explain this, they postulated that *N*-acetylglucosamine formed a 3,5-borate complex in the furanose form thus disturbing the pyranose–furanose equilibrium in favour of the latter. Strong support for the concept was obtained by a study of molecular models and, from the work of Mazurek and Perlin (14).

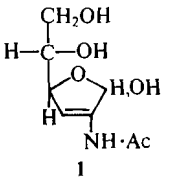

1

Paper electrophoresis of DNP-D-glucosamine in alkaline buffer systems (boric acid – borate, bicarbonate–carbonate) at p*H* 9.5 (Table 1), provide support for the existence of such a complex. In the borate buffer DNP-D-glucosamine behaved like glucose to form complexes with a resultant net negative charge, hence the migration towards the anode (15).

TABLE 1. Electrophoretic behaviour of DNP-D-glucosamine in alkaline buffer systems at p*H* 9.5*

Compound	Distance migrated from the origin (mm)†	
	Boric acid – borate buffer	Bicarbonate–carbonate buffer
Glucose	+15	−7
Glucosamine	−6	−10
DNP-D-glucosamine	+2.0	−3
2,4-Dinitrophenol	+19	+19

*The electrophoretic run was carried out at 115 V for 30 min on Whatman 1 mm (15 × 8 cm) strips. The chromatograms were stained with alkaline silver nitrate reagent and also ninhydrin reagent for the detection of glucose and glucosamine respectively.
†Migration directions: +, towards anode; −, towards cathode.

Thus, the results of this investigation may then be interpreted, if not explained, by postulating that it is the 3,5-borate complex of 2-(2′4′-dinitrophenylamino)-2-deoxy-D-glucofuranose, which suffers alkaline degradation. In a typical example of this complex, **2**, there is the possibility of hydrogen bond formation between the free borate hydroxyl group and the imino group of the dinitrophenylamino moiety. This might promote the scission of the (sugar) carbon–nitrogen linkage, by creating a better leaving group (*i.e.* an incipient 2,4-dinitroaniline molecule) on attack of hydroxyl ions at C-2 as shown in **2**. It is suggested that borate increases the rate at which the furanose borate complex is formed, while the hydroxyl ions increase the rates of both complex formation and decomposition.

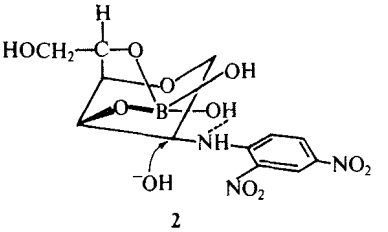

2

The alternative plausible mechanism that may explain the elimination of 2,4-dinitroaniline as suggested by one of the referees would involve the formation of a Schiff base as an intermediate. The arrangement to the Schiff base via an enol could arise if a furanose 3,5-borate complex such

as **3** is in equilibrium with a higher percentage of *aldehydo* sugar than is the uncomplexed pyranose.

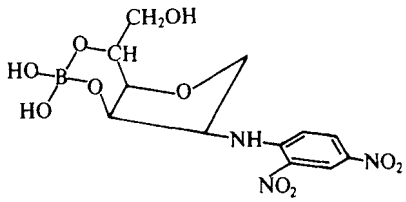

3

However, neither glucose, mannose, nor fructose and especially organic acids of lower molecular weight could be detected among the products of reaction. These observations suggest that decomposition by such a route is unlikely. The results of colour reactions suggest that elimination of 2,4-dinitroaniline may be accompanied by formation of 2,5-anhydro-D-mannose, a reaction involving inversion at C-2. This anhydro sugar is unstable in alkaline solution, being converted essentially into a single unknown product (16). The speculation as to the mechanisms is best deferred until the sugar moiety produced on release of the dinitroaniline is characterised. Work is in progress on this aspect.

Acknowledgements

I am grateful to Professor D. W. Russell, Department of Biochemistry, Dalhousie University, Halifax, Nova Scotia, for his interest, guidance, and helpful discussions. The financial support of the Canadian Government (Commonwealth Scholarship Award) is gratefully acknowledged.

1. E. CHARGAFF and M. BOVARNICK. J. Biol. Chem. **118**, 421 (1937).
2. A. NEUBERGER. Biochem. J. **32**, 1435 (1938).
3. Z. E. JOLLES and W. T. J. MORGAN. Biochem. J. **34**, 1183 (1940).
4. G. BLIX, L. SVENNERHOLM, and I. WERNER. Acta Chem. Scand. **4**, 717 (1950).
5. L. A. ELSON and W. T. J. MORGAN. Biochem. J. **27**, 1824 (1933).
6. N. F. BOAS. J. Biol. Chem. **204**, 553 (1953).
7. Y. C. LEE and R. MONTGOMERY. Arch. Biochem. Biophys. **93**, 292 (1961).
8. E. F. ANNISON, A. T. JAMES, and W. T. J. MORGAN. Biochem. J. **48**, 471 (1951).
9. P. F. LLOYD and M. STACEY. Tetrahedron, **9**, 116 (1960).
10. P. W. KENT. Research, **3**, 427 (1950).
11. J. BOESEKEN. Adv. Carbohydr. Chem. **4**, 189 (1949).
12. T. A. GOOD and S. P. BESSMAN. Anal. Biochem. **9**, 253 (1964).
13. W. T. J. MORGAN and L. A. ELSON. Biochem. J. **38**, 988 (1934).
14. M. MAZUREK and A. S. PERLIN. Can. J. Chem. **41**, 2403 (1963).
15. A. B. FOSTER. Adv. Carbohydr. Chem. **12**, 81 (1957).
16. B. C. BERA, A. B. FOSTER, and M. STACEY. J. Chem. Soc. **1**, 4531 (1956).

Can. J. Chem. Downloaded from www.nrcresearchpress.com by 210.87.254.6 on 09/05/12
For personal use only.

The hydrolysis of maleimide in alkaline solution

REMIGIO GERMANO BARRADAS, STEPHEN FLETCHER, AND JOHN DOUGLAS PORTER
Department of Chemistry, Carleton University, Ottawa, Canada K1S 5B6

Received October 14, 1975

REMIGIO GERMANO BARRADAS, STEPHEN FLETCHER, and JOHN DOUGLAS PORTER. Can. J. Chem. **54**, 1400 (1976).

The hydrolysis of maleimide has been investigated in the p*H* range 8.5–14. Polarographic limiting currents were well-defined, so that the bulk concentration of reactant during reduction could be clearly followed as a function of time. Logarithmic analysis of derived data indicated an arrest in the rate of reaction at circa p*H* 12, and a reaction scheme is proposed to explain this. In this scheme, the neutral maleimide molecule exists in equilibrium with its anion, and both of these species may undergo hydrolysis at the appropriate p*H*. From derived rate equations, the pK_a of maleimide was found to be 10.0, whilst estimates of the rates of hydrolysis were also calculated.

REMIGIO GERMANO BARRADAS, STEPHEN FLETCHER et JOHN DOUGLAS PORTER. Can. J. Chem. **54**, 1400 (1976).

On a étudié l'hydrolyse de la maléimide à des p*H* allant de 8.5–14. Les courants limitants en polarographie sont bien définis; on peut donc en conclure que l'on peut mesurer la concentration globale du réactif durant la réaction en fonction du temps. L'analyse logarithmique des données dérivées indique qu'un arrêt de la vitesse de la réaction se produit aux environs d'un p*H* de 12 et on propose un mécanisme réactionnel pour expliquer ce résultat. Dans ce schéma, la molécule de la maléimide neutre existe en équilibre avec son anion et ces deux espèces peuvent subir une hydrolyse à un p*H* approprié. A l'aide des équations de vitesse qui ont été établies, on a trouvé que le pK_a de la maléimide est de 10.0 alors qu'on a aussi calculé des estimés pour les vitesses d'hydrolyse.

[Traduit par le journal]

Introduction

During electrochemical investigations, it has been observed that maleimide and its derivatives undergo hydrolysis in alkaline, aqueous media (1). This observation is confirmed in the present work, where accurate measurement of the hydrolysis rate of the parent maleimide has been achieved using polarography. By conducting the investigation in the p*H* range 8.5–14 several interesting features were revealed. An overall reaction scheme is postulated which reasonably describes the experimental behaviour, and from this the corresponding rate equations are deduced.

These equations are in agreement with the conclusions of Tirouflet *et al.* (2, 3), who showed that phthalimide and its derivatives undergo a similar hydrolysis in aqueous, ethanolic media.

It is also shown that an estimate of the pK_a of maleimide can be determined from derived data, as well as the rate constants for the hydrolysis of both the neutral molecule and its anion.

Experimental

All experiments were performed in aqueous, alkaline buffers. Because of the broad p*H* range covered, three separate buffer systems had to be employed; these are listed in Table 1. Water was distilled twice before use. The maleimide was a commercial product (Aldrich Chemicals) mp 92–94 °C. All other reagents were of ANALAR quality.

TABLE 1. Composition of buffer at various p*H* values

Buffer composition	p*H* range
$NaHCO_3$/NaOH	8.5–10
Na_2HPO_4/NaOH	10 –12
KCl/KOH	12 –14

All potentials are quoted relative to the saturated calomel reference electrode (s.c.e.). The cell used in polarography was undivided and was equipped with a luggin reference probe and a dropping mercury electrode (h = 38.7 cm, t = 0.96 s, m = 6.07 mg s^{-1}). Short drop-times were utilized in order to obtain the maximum number of data points. Deoxygenation was accomplished, as was stirring, by flushing the apparatus with a stream of nitrogen purified by the method of Meites (4). Mercury was checked for purity before use by mass spectrometry. All polarization data were recorded on a Beckman 1005 y–t recorder.

Because of the complex cell design used, thermostats could not be employed. Therefore the test solutions were allowed to equilibrate to room temperature (22 °C), and

Can. J. Chem. Downloaded from www.nrcresearchpress.com by 210.87.254.40 on 09/05/12
For personal use only.

Can. J. Chem. Downloaded from www.nrcresearchpress.com by 210.87.254.40 on 09/05/12
For personal use only.

accurate measurement was verified *in situ* with a Comark electronic thermometer to ensure that all solutions were at identical temperatures. During the course of the measurements, the laboratory temperature varied no more than ± 1 °C from 22 °C, whilst the cell temperature remained virtually constant at 22.0 °C.

Results

Figure 1 shows a typical polarogram run at pH 8.54 in a $NaHCO_3/NaOH$ buffer solution, initially 0.026 M in maleimide. Two distinct waves are observed with well-defined limiting currents. These arise because of the reaction (1):

[1] 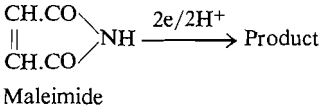

Maleimide

Limiting currents were found to be proportional to the concentration of the reducible species in the bulk of solution, in accordance with the Ilkovič equation:

$$[2] \qquad i_{\lim} = 607nD^{1/2}m^{2/3}t^{1/6}C^{b}$$

Consequently, the bulk concentration of maleimide (C^b) could be followed by measurement of the total wave-height as a function of time.

Maleimide samples from a stock solution were injected into a series of buffers in the polarographic cell, and deoxygenated for 30 s. It was observed in all cases that

$$[3] \qquad i = i_{t=0} \exp(-\bar{K}t)$$

where $\bar{K}$ is a constant at a given pH. Thus plots of ln i *vs.* t are linear with intercept ln ($i_{t=0}$) and gradients of $-\bar{K}$. Some of these are shown in Fig. 2. Small corrections had to be made for background currents, because the product of hydrolysis generated a two-electron wave at more negative potentials. Its Tafel region therefore coincided with the limiting current region of the maleimide wave proper. However, such corrections were easy to perform by allowing the hydrolysis to go to completion, and then measuring the background current at $t \rightarrow \infty$.

Figure 3 plots polarographic limiting currents as a function of pH. These values were obtained by applying least-square analyses to the data of Fig. 2, and extrapolating back to $t = 0$ s. It is clear that a virtually constant limiting current is observed below pH 12, whilst above this value the data steadily increase from circa 33 to 54 μA at pH 14.

The graph of log $\bar{K}$ *vs.* pH showed a most interesting phenomenon (Fig. 4). As the pH range is ascended (region A) the rate of hydrolysis increases, but reaches an arrest in

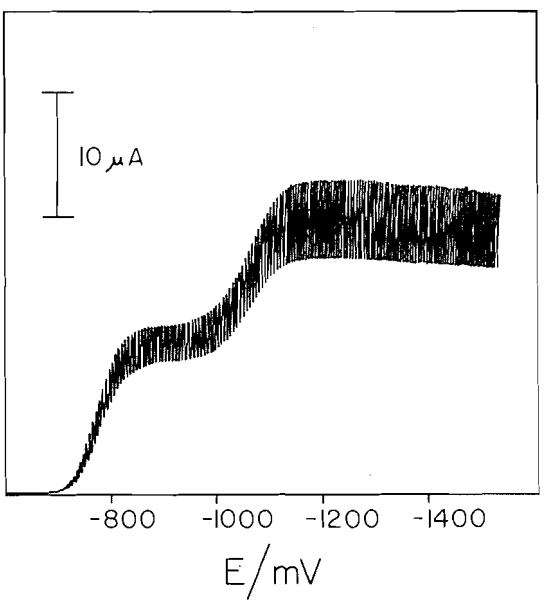

FIG. 1. Typical polarogram of maleimide in alkaline solution, several minutes after injection of sample. Initial concentration 0.026 M, pH 8.54 ($NaHCO_3/NaOH$ buffer).

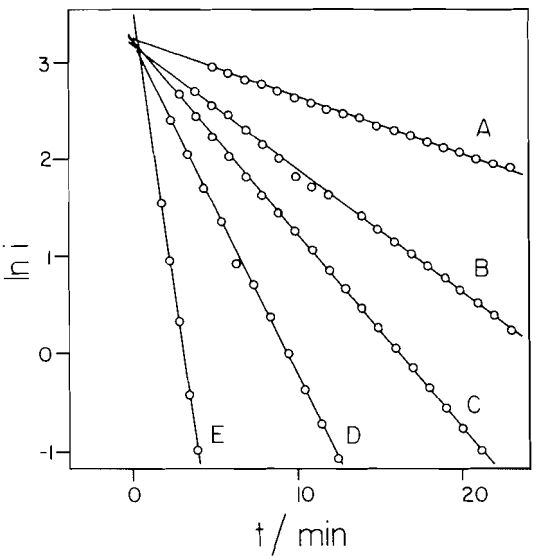

FIG. 2. Diminution of polarographic limiting currents *vs.* time. (*A*) pH 9.48, (*B*) pH 9.89, (*C*) pH 10.31, (*D*) pH 11.60, (*E*) pH 14.05.

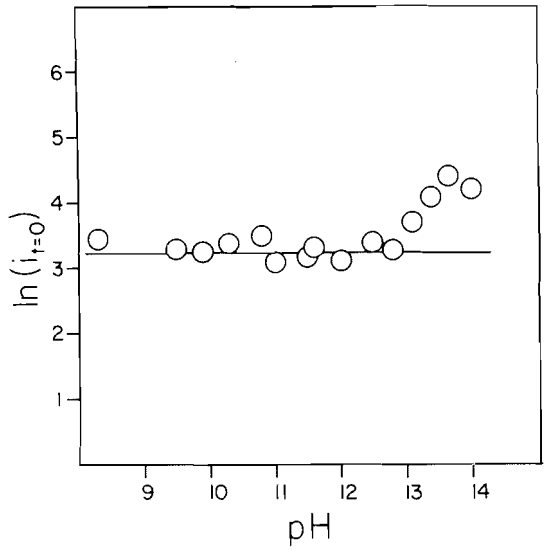

FIG. 3. Computed values of overall polarographic limiting currents at $t = 0$ s *vs.* p*H*.

region B. Finally, in region C, the reaction rate once more increases rapidly. In both of the limiting cases the reaction approaches first order in $[OH^-]$.

Figure 6 shows the reaction order plot in protons for the electrochemical reduction of maleimide. Note the changes of gradient at p*H*'s 7 and 10. Below p*H* 7 the maleimide accepts a proton prior to reaction, whilst in the p*H* range 7 to 10 the neutral molecule is reduced. Finally, above p*H* 10, it is the anion which predominates in the bulk of solution. The system thus behaves in classical fashion; the more protonated molecule reduces at the least negative potentials. In consequence, the reactive species in the vicinity of the electrode can be readily identified at a given p*H*.

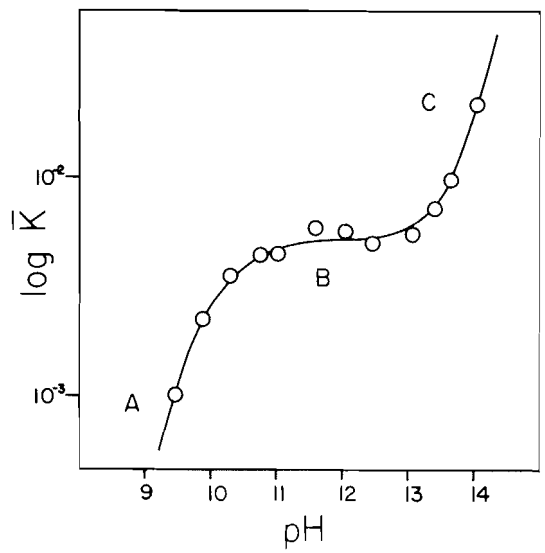

FIG. 4. Reaction order plot for the overall hydrolysis rate constant ($\bar{K}$) as a function of p*H*.

Discussion

In the light of the electrochemical data described above, the following reaction scheme is postulated to explain the hydrolysis mechanism

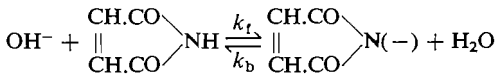

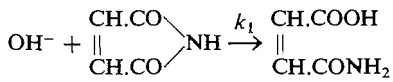

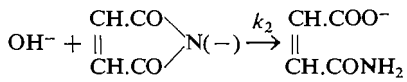

Such a reaction scheme has been previously reported for the hydrolysis of phthalimides (2, 3). We now present a rigourous derivation of the corresponding rate equation.

If we assume that any back reaction is negligible, and that the reactants are at equilibrium throughout the reaction, then we may write

$$[7] \quad \frac{d[A]}{dt} = k_b[B] - k_1[A][OH^-] - k_f[A][OH^-]$$

$$[8] \quad \frac{d[B]}{dt} = k_f[A][OH^-] - k_f[B] - k_2[B][OH^-]$$

where [A] and [B] represent the concentrations of maleimide and its anion respectively. Because of the equilibrium, the disappearance of B will affect the concentration of A, and vice versa. In consequence, we see:

$$[9] \quad \frac{d[A + B]}{dt} = \frac{d[A]}{dt} + \frac{d[B]}{dt}$$
$$= - k_1[A][OH^-] - k_2[B][OH^-]$$

Taking k_b to be a pseudo first-order rate constant, incorporating a term in $[H_2O]$, then we may describe the concentration of A at any time in terms of [B] according to

Can. J. Chem. Downloaded from www.nrcresearchpress.com by 210.87.254.40 on 09/05/12
For personal use only.

Can. J. Chem. Downloaded from www.nrcresearchpress.com by 210.87.254.40 on 09/05/12
For personal use only.

[10] $$k_f[A][OH^-] = k_b[B]$$

Substituting in [9] allows us to eliminate [B], so that

[11] $$\frac{d[A]}{dt} = \frac{-k_1[A][OH^-] - k_2\frac{k_f}{k_b}[A][OH^-]^2}{1 + \frac{k_f}{k_b}[OH^-]}$$

Polarographically, we may only measure $d[A]/dt$ because the neutral molecule reduces more easily than the anion. The anion must always accept a proton before electron transfer takes place. In effect, the increasingly negative reduction potentials above pH 10 merely reflect a diminution in the concentration of species A. Now by simple integration

[12] $$\frac{[A]}{[A]_{t=0}} = \exp\left[\frac{-k_1[OH^-] - k_2\frac{k_f}{k_b}[OH^-]^2}{1 + \frac{k_f}{k_b}[OH^-]}t\right]$$
$$= \exp(-\bar{K}t)$$

Computed values of $\bar{K}$ from this equation were then superimposed iteratively on the experimental data until the best fit was obtained. This is shown as the smooth curve in Fig. 4. The resulting values of the rate constants were

$$k_1 = 47\ M^{-1}\ s^{-1} \pm 5\%$$
$$k_2 = 10^{-2}\ M^{-1}\ s^{-1} \pm 10\%$$
$$\frac{k_f}{k_b} = 10^4 \pm 5\%$$

The errors were estimated by standard deviation of the experimental data from the best-fitted curve. The error associated with k_2 is somewhat greater than that of k_1, presumably because of the short time-scale required for its measurement.

The pK_a of maleimide is thus 10.0, and a useful check of this is as follows: the limiting hydrolysis rate at low pH (i.e. in region A, Fig. 4) is given by

[13] $$\text{Rate}_{lim} = \frac{-d[A]}{dt} = k_1[A][OH^-]$$

whilst the observed rate is

[14] $$\text{Rate}_{obs} = \bar{K}[A] = \frac{k_1[OH^-]}{1 + \frac{k_f}{k_b}[OH^-]}[A]$$
as $[OH^-]^2 \to 0$

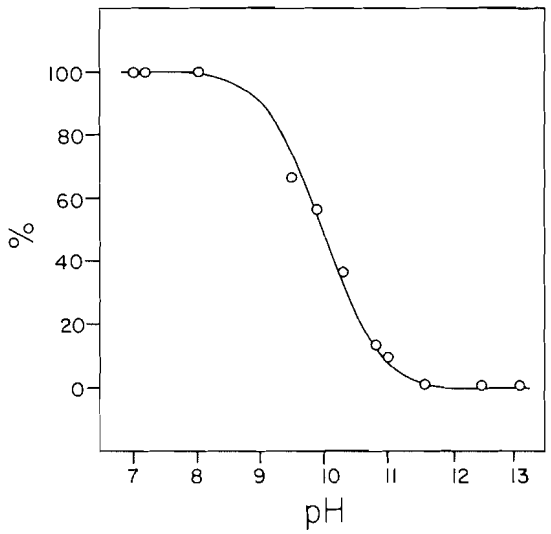

FIG. 5. Dissociation curve for the equilibrium between maleimide and its anion.

The ratio of these two rates, plotted *vs.* pH, is a dissociation curve, since

[15] $$\text{Ratio} = \frac{\text{Rate}_{obs}}{\text{Rate}_{lim}}$$
$$= \frac{1}{1 + \frac{k_f}{k_b}[OH^-]}$$
$$= \frac{[A]}{[A] + [B]}$$

provided the equilibrium constant is independent of concentration. The result is shown in Fig. 5, assuming k_1 is 47 M^{-1} s^{-1}. Once again, the pK_a is 10.0. Furthermore, the experimental points coincide with the theoretical shape for a simple dissociation reaction.

The curve shown in Fig. 3 is also explained by the outlined mechanism. Presumably, the diffusion coefficient of maleimide and its anion are not identical, so that i_{lim} in the Ilkovič equation would necessarily be expected to vary with pH. Changes in solution composition will also affect D, as well as producing changes in the surface tension of the dropping mercury electrode. However, such changes will not affect the derived values of $\bar{K}$, because of the differential nature of the analysis used.

The product of hydrolysis at all pH's has a

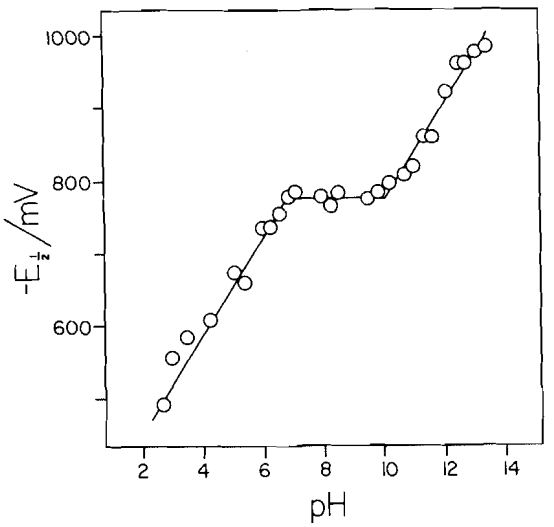

FIG. 6. Reaction order plot in protons for the electrochemical reduction of maleimide.

well-defined 2-electron reduction wave at potentials more negative than maleimide, and was readily shown by mass spectroscopy and nmr to be the half-amide rather than the fully hydrolysed product (singlet, $\delta = 6.8$, $m/e = 115.09$, mp 152 °C).

In consequence, we deduce that the rate-determining step is the cleavage of the carbon–nitrogen bond;

[16]

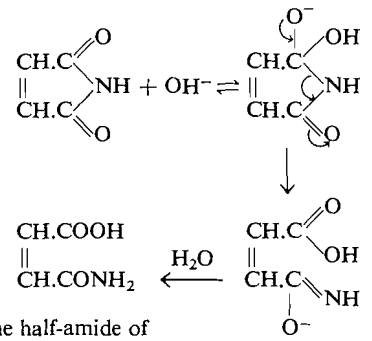

Finally, it is interesting to compare the derived pK_a with the polarographic pK'. The pK' is obtained by plotting the reduction half-wave potential as a function of pH (Fig. 6). A change in reaction mechanism occurs at pH 10 because in the bulk of solution the reactive species becomes the anion rather than the neutral maleimide molecule.

For $pH < pK'$

[17]

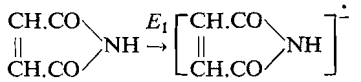

$E_1 \neq f(pH)$

For $pH > pK'$

[18]

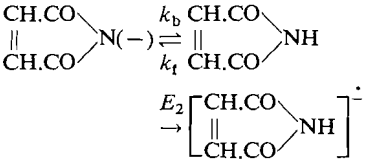

$E_2 = f(pH)$

Nevertheless, at the electrode surface the electron transfer still takes place into the neutral molecule as described earlier. Consequently, it is clear that the mechanism deduced electrochemically validates the assumptions made concerning the structures of the reactive species in the bulk of solution in [4], [5], and [6].

Conclusions

The rates of hydrolysis of maleimide and its anion have been calculated to be 47 M^{-1} s^{-1} and 10^{-2} M^{-1} s^{-1}, respectively. The reaction scheme proposed is consistent with both electrochemical and kinetic data, and the reaction pathway is found to be identical to that deduced by Tirouflet *et al.* (2, 3) for the hydrolysis of phthalimide derivatives.

The pK_a of maleimide has also been determined from the experimental data, and a rigorous proof of the rate equation has been described.

Acknowledgement

This work has been supported by a research grant from the National Research Council of Canada.

1. A. NĚMĚCKOVÁ, M. MATUROVÁ, M. PERGÁL, and F. ŠANTAVÝ. Coll. Czech. Chem. Commun. **26**, 2749 (1960).
2. J. TIROUFLET, R. ROBIN, and M. GUYARD. Bull Soc. Chim. Fr. 571 (1956).
3. J. TIROUFLET and E. LE TROUIT. Comptes Rendu, **241**, 1053 (1955).
4. L. MEITES. Polarographic techniques. Interscience, New York. 1965.

Can. J. Chem. Downloaded from www.nrcresearchpress.com by 210.87.254.40 on 09/05/12
For personal use only.

Structure of radicals produced by γ-radiolysis. Part 5. Radicals derived from some aliphatic alkene molecules

R. E. LINDER AND D. L. WINTERS
Department of Chemistry, West Virginia University, Morgantown, West Virginia 26506
AND
A. CAMPBELL LING[1]
Nuclear Chemistry Facility, San Jose State University, San Jose, California 95192

Received September 30, 1974[2]

R. E. LINDER, D. L. WINTERS, and A. CAMPBELL LING. Can. J. Chem. **54**, 1405 (1976).

Adamantane isolation matrices have been used to determine the structure of radicals produced by room temperature γ-radiolysis of certain selected alkene systems. The molecules studied include linear 1-ene homologues, linear 2-ene homologues, 2-methylpropene (2MPr), 2-methylbutene-1 (2MB1), 3-methylbutene-1 (3MB1), 2-methylbutene-2 (2MB2), 2-methylpentene-1 (2MP1), 2-methylpentene-2 (2MP2), 4-methylpentene-2 (4MP2), 2,3-dimethylbutene-2 (DMB2), 3,3-dimethylbutene-1 (33DMB), and 2,4,4-trimethylpentene-1 (TMPE). The general mode of reaction is allylic radical formation, with one isomer predominating, and structures have been either confirmed or assigned for the radicals derived from butene-1, butene-2, 2MPr, 2MB1, 2MB2, 2MP1, 4MP2, DMB2, and a listing of hfsc values have been obtained for each radical studied.

R. E. LINDER, D. L. WINTERS et A. CAMPBELL LING. Can. J. Chem. **54**, 1405 (1976).

On a utilisé des matrices isolantes d'adamantane pour déterminer la structure des radicaux produits par la radiolyse γ, à température de la pièce, de certains systèmes choisis d'alcène. Les molécules étudiées comprennent des homologues linéaires d'alcènes en position 1, des homologues d'alcènes en position 2, le méthyl-2 propène (2MPr), le méthyl-2 butène-1 (2MB1), le méthyl-3 butène-1 (3MB1), le méthyl-2 butène-2 (2MB2), le méthyl-2 pentène-1 (2MP1), le méthyl-2 pentène-2 (2MP2), le méthyl-4 pentène-2 (4MP2), le diméthyl-2,3 butène-2 (DMB2), le diméthyl-3,3 butène-1 (33DMB) et le triméthyl-2,4,4 pentène-1 (TMPE). Le mode général de réaction implique la formation d'un radical allylique dans lequel un isomère prédomine; on a confirmé ou attribué les structures des radicaux dérivant du butène-1, du butène-2, 2MPr, 2MB1, 2MB2, 2MP1, 4MP2, DMB2 et on a obtenu une liste des valeurs hfsc pour chacun des radicaux étudiés.

[Traduit par le journal]

Introduction

Radiolysis studies of alkenes have occupied the attention of many investigators in the past. Problems associated with resolution of electron spin resonance (esr) signals from solid samples have precluded entirely unambiguous assignments of radical structures in many cases, and controversies still exist as to the nature of the predominant radical species produced from various alkenes and their homologous and isomeric molecules. Adamantane isolation techniques are well established as an alternate investigatory method for attacking such problems, and can often provide data unavailable by other means (1). Even at room temperatures, esr resolution from radicals trapped in adamantane ($C_{10}H_{16}$) and perdeuterated adamantane ($C_{10}D_{16}$) is far superior to other matrix isolation techniques, and can approach that achieved in liquid phase studies, with FWHM line-widths that can be as small as 0.4 G in $C_{10}D_{16}$ matrices.

Previous studies of alkenes in condensed phases seem to indicate that radiolysis produces preferential formation of allyl radicals. Stabilized by electron delocalization, allylic radical species have been seen in rigid glassy and polycrystalline matrices at low temperatures. Identification of such allylic radicals has often come by comparison with concurrent liquid phase studies, where unambiguously produced radical species can be seen clearly, and only rarely can the solid state spectrum be directly attributed to any one particular structure. Smith and West (2) have used adamantane isolation methods to examine both alkane and alkene solutes, and they report that

[1]To whom correspondence should be addressed.
[2]Revision received January 2, 1976.

Can. J. Chem. Downloaded from www.nrcresearchpress.com by 210.87.254.42 on 09/05/12
For personal use only.

Can. J. Chem. Downloaded from www.nrcresearchpress.com by 210.87.254.42 on 09/05/12
For personal use only.

radiolysis of alkane solutes in $C_{10}H_{16}$ at 77 K produces a radical derived from $C_{10}H_{16}$ initially. On warming towards room temperature, this adamantyl radical disappears and is replaced by a radical derived from the alkane solute. A similar sequence of changes was observed by Ling and Kevan when 2-methyltetrahydrofuran was subject to γ-radiolysis while held in $C_{10}D_{16}$ matrices (3). This behaviour may be contrasted with that observed from γ-radiolysis of alkene solutes in $C_{10}H_{16}$, where Smith and West (2) report that both an alkyl radical and a radical derived from adamantane are observed at low temperatures, and on warming, both disappear to yield an allyl radical. The allylic species therefore appears to be the high temperature stable product from alkenes.

Among other studies reported are: radiolyses of polycrystalline pure phase alkenes (4), radiolyses of glassy pure phase alkenes (5), and radiolyses of some selected alkene derivatives held in adamantane (1*a*, 1*e*, 2, 6). It is of interest to note that abstraction reactions induced by chemical agents, *e.g.* *tert*-butoxy radicals (7), and kinetically hot methyl radicals (4), produce qualitatively identical results to those seen following radiolytically induced abstraction. This seems to indicate that the radiation induced abstraction process occurs through abstraction by a second molecule, *i.e.* a bimolecular process rather than a radiolytically induced unimolecular process. This is in accord with the data presented by Smith and West (2), where the adamantyl radical disappears and a solute radical appears.

For alkenes held as solutes in solid inert isolation matrices, H-atom addition to the alkene should provide a competitive pathway for radical production. Such addition has been noted for aliphatic alkene molecules (1*a*, 6) and aromatic systems (1*b*) held in adamantane, together with radiolyses of pure-phase aromatic alkenes (8). Addition of H atoms has also been studied following H-atom bombardment of thin films of alkenes held at low temperatures (see a series of reports, from, among others, ref. 9), together with the elegant experimental technique developed by Bennett and Mile (10), which utilizes both H-atom bombardment and adamantane isolation methods to provide superior esr resolution from solid state trapped radicals. Also pertinent to this study are photolyses of polycrystalline pure-phase alkenes (11), photolyses of alkenes held in inert-gas isolation matrices (12) where allenyl radical formation was noted for conjugated-ene systems, and photolyses of alkenes and chloro-olefins held in adamantane matrices (1*e*).

Experimental

Adamantane ($C_{10}H_{16}$), perdeuterated adamantane ($C_{10}D_{16}$), alkenes, and other incidental chemicals were supplied from standard commercial sources. Experimental techniques for incorporating liquid solutes into adamantane matrices have been adequately described previously, together with details of radiation sources (1*c*, 6*a*, 13). A Varian Associates E.3 Electron Spin Resonance Spectrometer was used throughout these studies, typically operated at 3380 ± 100 G, 0.5–50 mW microwave power, and 0.1 to 2 G modulation at 100 kHz. Computer simulations were executed by an IBM 360/75 computer and CalComp Plotter accessory using a Fortran IVG program written by one of us (14).

Results and Discussion

Adamantane isolation techniques provide simple experimental procedures that can, in general, yield excellently resolved esr signals from a variety of radicals trapped at room temperature. It is not necessary, even, to irradiate and monitor samples while under vacuum, although exposure to the atmosphere can lead to H-atom scavenging by oxygen and thus curtailment of H-atom addition processes in alkenes and alkynes, and exposure to the atmosphere can shorten the lifetime of the observed radical. Wood and co-workers (1*b*) have reported marked differences in the ratio of H-atom abstraction to H-atom addition in aniline and other aromatic alkene derivatives when samples are X-irradiated in vacuum or in oxygen atmospheres. Whether significant H-atom addition occurs, and thus whether H-atom scavenging can be seen, appears to depend on the relative size of the π-cloud in the molecule; since we cannot see H-atom addition in cyclopentene, but can see it in cyclopentadiene (6*a*), and can only see H-atom addition in some furan and thiophene derivatives but not all (15). Radical lifetimes at room temperature exposed to the atmosphere can exceed 10^3 min, and are rarely less than 10 min (1*c*). Observed Lorentzian line-widths can be as small as 0.4 G FWHM, and *ca.* 0.6 G peak-to-peak in first derivative presentations, for $C_{10}D_{16}$ matrices; allylic and allenylic radical species seem to exhibit a markedly smaller line-

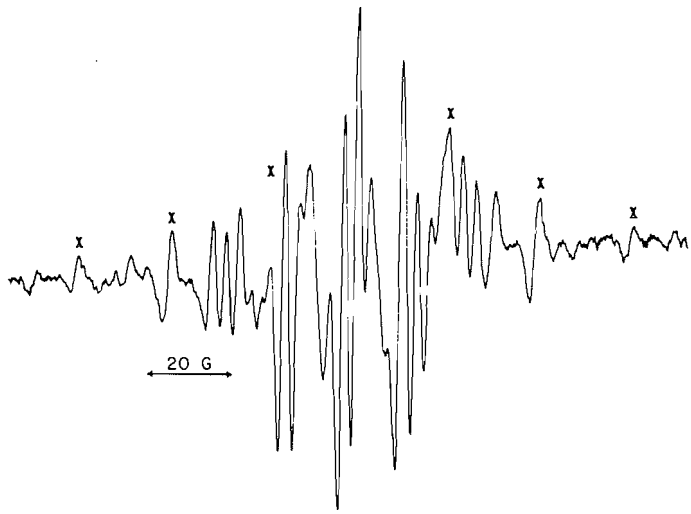

FIG. 1. First derivative esr spectrum obtained by γ-radiolysis of 2-methylpropene held in an adamantane matrix at room temperature. Lines marked X show contribution to spectrum from the *tert*-butyl radical formed by H· addition reactions.

width and correspondingly enhanced esr resolution when compared to alkyl radicals (15). Thus, hyperfine coupling constants and assignments of structure to a radical via esr spectrometry can often be determined as unambiguously as for liquid phase studies, and esr resolution from adamantane matrices is far superior to that achieved in any other solid matrices.

2-Methylpropene (2MPr)

The first derivative esr spectrum obtained following γ-radiolysis of 2MPr in $C_{10}H_{16}$ at room temperature is shown in Fig. 1, and exhibits features characteristic of at least two radicals. The spectrum is basically asymmetric, and exhibits two clearly distinct line-widths. The central portion of the spectrum, the predominant radical, is characterized by a line-with of *ca.* 1 G (peak-to-peak in first derivative), and a hyperfine pattern of $3 \times 3 \times 4$ lines with hyperfine splitting constants (a^H values) of 13.8 (2 protons), 14.7 (2), and 3.2 G (3), respectively.[3] These a^H values are typical of allylic species (16), and may be compared to those obtained by Kochi and Krusic (16*b*) for a radical obtained by *tert*-butoxy initiated H-atom abstraction from 2MPr (13.82, 14.68, and 3.19 G, respectively), and by Volman and co-workers (1*e*) by direct photolysis of the requisite chloro-olefin held in adamantane (13.8, 14.7, and 3.2 G).

This spectrum is assigned to radical **1**, where

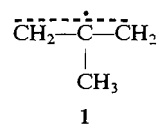

1

each proton of the $\cdot\cdot\cdot CH_2$ group are non-equivalent. However, this assignment fails to account for all of the clearly discernible lines in the spectrum shown in Fig. 1. A second radical species produces an overall wider spectrum, with line-widths of >2 G, and is characterized by a single a^H value of 22.7 G. We attribute this spectrum to the *tert*-butyl radical obtained by H-atom addition to 2MPr. Lines 2, 3, 4, 7, 8, 9 of the 10-line spectrum are marked X in Fig. 1, lines 1 and 10 cannot be distinguished from background noise due to relative intensity factors. Fessenden and Schuler (17) report a_β^H (9) = 22.72 G for a *tert*-butyl radical produced by a continuous flow liquid phase radiolysis experiment at sub-ambient temperatures.

2-Methylbutene-1 (2MB1) and 2-Methylpentene-1 (2MP1)

Structurally related to 2MPr are 2MB1 and 2MP1, the latter being of intrinsic interest to radiation chemists for its use as an isolation matrix and/or positive charge scavenger. Data

[3] *cf.* values of 14.81 (2 protons), 13.90 (2), and 4.06 (1) G, were noted for the allyl radical itself by Kochi *et al.* (see Table 1).

Can. J. Chem. Downloaded from www.nrcresearchpress.com by 210.87.254.42 on 09/05/12
For personal use only.

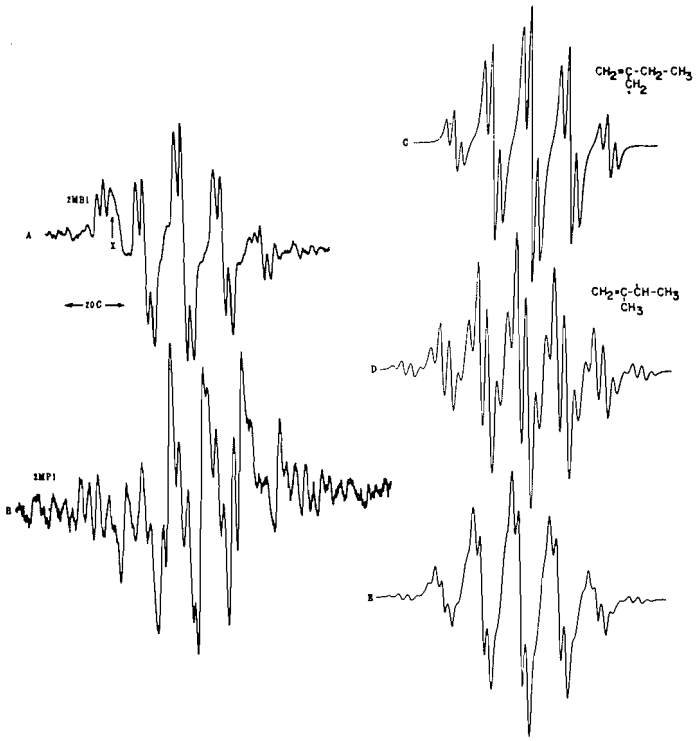

FIG. 2. First derivative esr spectra obtained at room temperature from γ-radiolysis of 2-methylbutene-1 and 2-methylpentene-1 at room temperature held in adamantane matrices; (*A*) experimental spectrum for 2MB1; (*B*) experimental spectrum for XMP1; (*C*) computer simulation of esr spectrum for radical **2**; (*D*) computer simulation of esr spectrum for radical **3**; (*E*) computer spectrum containing 80/20 contributions from radicals **2**/**3**, respectively. The arrow and X in (*A*) indicate probable interference from a radical derived from the adamantane matrix.

from room temperature radiolyses of 2MB1 and 2MP1 held in adamantane matrices are shown in Fig. 2 *A* and *B*, respectively. It is clear from an examination of these spectra that line resolution is poor, and that the two spectra are probably not related to each other directly, and therefore the radicals derived from each molecule differ structurally in fundamental geometry.

The expected radical species from 2MB1 is either **2** or **3** if we assume that allylic H-atom

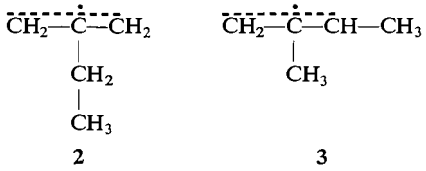

2 **3**

abstraction will occur; the corresponding allylic structures from 2MP1 are shown in **4** and **5**.

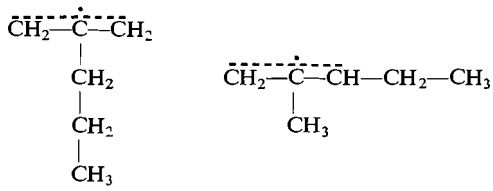

4 **5**

Computer simulation of esr spectra using a variety of hyperfine coupling constants and differing line-widths appears to indicate that radical **2** (with $a^{H}(2) = 14.2$, $a^{H}(2) = 13.5$, and $a^{H}(2) = 2.75$ G, and Lorentzian peak-to-peak line-widths of 1.6 G) is a major contributor to the observed spectrum in Fig. 2*A*. The computer simulation of **2** is shown in Fig. 2*C*. A corresponding simulation of **3** (with $a^{H}(2) = 14.0$, $a^{H}(1) = 14.5$, $a^{H}(3) = 13.5$, and $a^{H}(3) = 3.2$ G, peak-to-peak line-width of 1.7 G) is shown in Fig. 2*D*, and exhibits a basic septet of quartets

Can. J. Chem. Downloaded from www.nrcresearchpress.com by 210.87.254.42 on 09/05/12
For personal use only.

Can. J. Chem. Downloaded from www.nrcresearchpress.com by 210.87.254.42 on 09/05/12
For personal use only.

pattern. This is noticeably different to the experimentally observed spectrum from 2MB1 shown in Fig. 2*A*, and thus **3** cannot be a major component from γ-radiolysis of 2MB1. However, the observed resolution is too poor to distinguish small contributions less than 20% of **3** to the experimentally observed spectrum, and we show a computer simulation in Fig. 2*E* that exhibits a 20% contribution of **3** with **2** which might be interpreted as providing a slightly better fit than **2** alone to the experimental spectrum.

In view of the relative magnitude of γ-coupling constants in aliphatic alkenes and alkanes, we would not expect the spectrum from **4** to differ significantly from that seen from **2**. Any possible γ-coupling will contribute primarily to line-broadening, and will not change the hyperfine pattern observed under the conditions of our experiments. We, therefore, discount **4** as a major contributor to the experimentally observed spectrum from 2MP1 shown in Fig. 2*B*.

Structure **5** is similar to **3** and will produce a qualitatively similar pattern. Computer simulation of **5** (with $a^{H}(2) = 14.0$, $a^{H}(2) = 13.5$, $a^{H}(1) = 14.5$, and $a^{H}(3) = 3.2$ G, 1.7 G line-width peak-to-peak Lorentzian shape) produces a basic sextet of quartets visually similar to the septet of quartets produced by **3** and shown in Fig. 2*D*, and in our opinion matches the observed spectrum in more detail than does a simulation based on structure **4**. Thus we believe that the predominant contributor to the experimentally observed spectrum produced by γ-radiolysis of 2MP1 in adamantane is **5**, but contributions from **4** cannot be entirely ignored.

Consideration of radical structures formed by H-atom addition can be discounted on several points. Of the two possible radicals that H-atom addition would produce from 2MB1, and the equivalent two radicals from 2MP1, one of each pair has already been unequivocably identified by us previously (18). Since 2MB1 and 2MP1 would lead to isopentyl and 2-methylpentyl radicals, respectively, each of which has been identified previously. Neither of the experimentally observed spectra in Fig. 2 *A* and *B* have any points of similarity to those seen from isopentyl and 2-methylpentyl radicals, respectively. Equally, other possible alkyl radicals would lead to esr spectra that are too wide overall to match observed spectra. Finally, although the resolution exhibited in Fig. 2 *A* and *B* is generally poor, observed line-widths are less than 2 G (peak-to-peak first derivative), and generally alkyl radicals exhibit line-widths that are *ca.* 2.5 G, or broader. We conclude that alkyl or alkenyl radical species with a saturated spin-center do not contribute significantly to our observed spectra, and that under the conditions of our experiment neither H-atom abstraction at sites removed from the ene-group (*i.e.* non-allylic abstraction) nor H-atom addition to the ene-group, occur to any observable extent for 2MB1 or 2MP1 in our systems at room temperature. This is in agreement with the data from Smith and West (2), who indicate that the alkyl radical formed from alkenes initially at low temperatures in adamantane is unstable at room temperatures.

2-Methylbutene-2 (2MB2) and 2-Methylpentene-2 (2MP2)

Data from room temperature γ-radiolysis of 2MB2 held in $C_{10}H_{16}$ matrices are shown in Fig. 3*C*. By analogy with the results above, two possible allylic radicals can be formed, structures **6** and **7**. Structure **6** is identical with **3** derived from 2MB1.

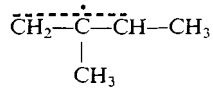

6

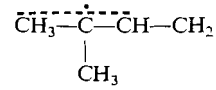

7

Computer simulations of first-derivative esr spectra from **6** and **7** are shown in Fig. 3 *A* and *B*, respectively. The parameters chosen for **6** are identical to those used for **3** ($a^{H}(2) = 14.0$, $a^{H}(1) = 14.5$, $a^{H}(3) = 13.5$, $a^{H}(3) = 3.2$ G, 1.7 G peak-to-peak first derivative line-width). The parameters chosen for **7** were: $a^{H}(3) = 15.5$, $a^{H}(3) = 12.25$, $a^{H}(1) = 14.0$, $a^{H}(1) = 13.3$, and $a^{H}(1) = 3.5$ G, with a peak-to-peak first derivative line-width of 1.7 G. Comparison of the experimentally observed spectrum shown in Fig. 3*C* with the simulations in 3*A* and 3*B* appears to support the hypothesis that **7** is the predominant species contributing to the experimental spectrum. As for 2MB1, contributions from the other possible allylic species cannot be discounted, and we show a computer simulation containing 20% contribution of **6** to **7**. The simulated composite spectrum provides a slightly better fit to the experimentally observed spectrum, but is far from being an unambiguous assignment of the data. Again, as for 2MB1,

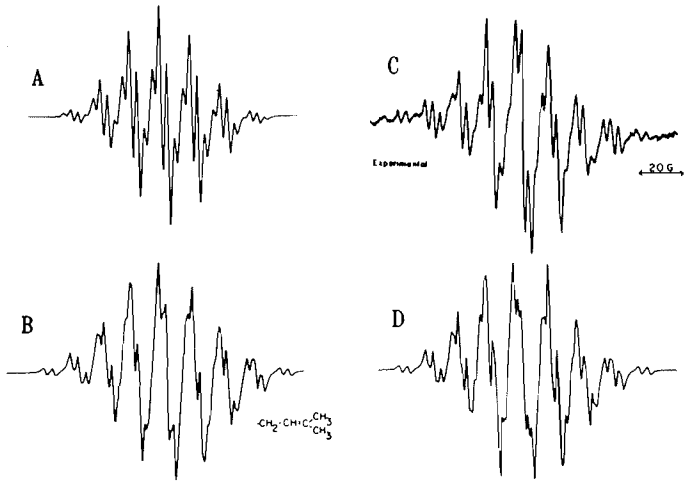

FIG. 3. First derivative esr spectra for the radicals derived from 2-methylbutene-2 by γ-radiolysis in adamantane at room temperature; (*A*) computer simulation of radical **6**; (*B*) computer simulation of radical **7**; (*C*) experimentally observed spectrum from 2MB2; (*D*) computer simulation comprising 20/80 contributions of **6**/**7**, respectively.

there are no data supporting the formation of alkyl radicals from H-atom addition under these conditions, and non-allylic H-atom abstraction in 2MB2 is structurally impossible.

The esr spectrum obtained via room temperature γ-radiolysis of 2MP2 in adamantane (not shown) was poorly resolved, and the resolution could not be improved. The observed spectrum did not respond to microwave power saturation techniques to enhance one radical species at the expense of another, and a rational assignment of structure for the radical derived from 2MP2 cannot be made at this time.

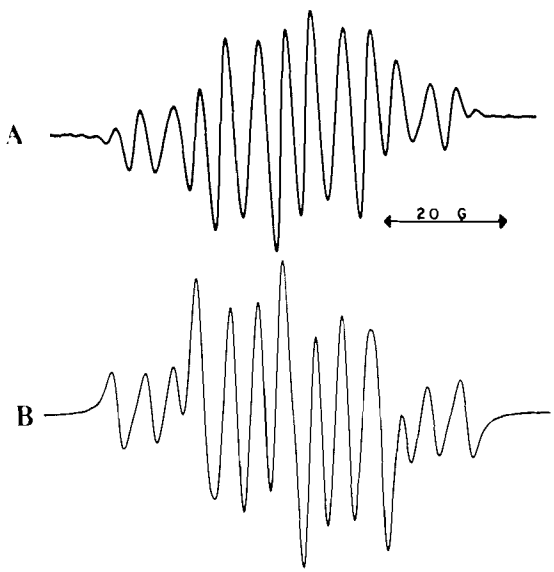

FIG. 4. First derivative esr spectra obtained from room temperature γ-radiolysis of 4-methylpentene-2 held in an adamantane matrix; (*A*) experimentally observed spectrum, (*B*) computer simulation of esr spectrum based on structure **6**.

4-Methylpentene-2 (4MP2)

The lack of satisfactory data from 2MP2 prompted the examination of an isomer, 4MP2. The experimental first derivative esr spectrum obtained by γ-radiolysis of 4MP2 in adamantane at room temperature is shown in Fig. 4*A*. *Prima-facie* evidence from overall spectrum width together with hyperfine coupling constant values appears to rule out any possibility of an alkyl radical, and thus denies the possibility of a radical formed by non-allylic abstraction or H-atom addition under our conditions. The two possible allylic structures derived from 4MP2 are radicals **8** and **9**. Radical **9** resembles that derived from

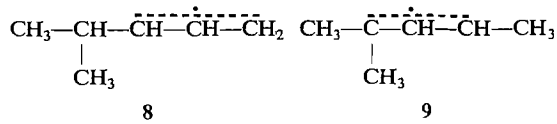

8 **9**

2MB2 (radical **7**) except that one terminal allylic proton in **7** has been replaced by a methyl group in **9**. Thus the expected allylic terminal methyl coupling of *ca.* 14 ± 2 G will replace a single

Can. J. Chem. Downloaded from www.nrcresearchpress.com by 210.87.254.42 on 09/05/12
For personal use only.

Can. J. Chem. Downloaded from www.nrcresearchpress.com by 210.87.254.42 on 09/05/12
For personal use only.

proton with a similar coupling, and the expected overall spectrum width from the radical derived from 4MP2 should be considerably wider than that derived from 2MB2 if the radical has structure **9**. In fact, the experimental spectrum from 4MP2 (*ca.* 65 G total) is considerably narrower than that seen from 2MB2 (*ca.* 115 G). For this reason, and our failure to simulate the experimental spectrum using **9** as a structural basis, we reject **9** as a predominant contributor to the experimental spectrum. Radical **8**, however, is simply the allyl radical itself with one β-proton, and will be a very narrow overall spectrum more closely resembling the experimentally observed spectrum. The observed spectrum is deceptively simple, suggesting that several coupling constants are closely matching, leading to severe line-broadening and line-overlapping, and markedly altering relative intensities of lines observed. Computer simulations of the observed spectrum using **8** as a basis were not totally successful, but we show one such simulation that provides reasonable agreement with the experimental spectrum using $a^H(1) = 14.5$, $a^H(2) = 13.7$, $a^H(1) = 10.0$, and $a^H(1) = 3.8$ G, and a first derivative peak-to-peak line-width of 2.3 G. It is probable that the two methyl groups of the isopropyl moiety will contribute a γ-coupling of *ca.* 0.2–0.4 G which will lead to a marked increase in line-width compared to other allylic radicals. This is reflected in simulations where a 2.3 G line-width is used for 4MP2 compared to 1.6 or 1.7 G used for other systems above.

2,3-Dimethylbutene-2 (DMB2)

Of particular interest to this study of radiolysis effects in aliphatic alkene systems is the compound DMB2, since the hydrogen atoms in this molecule are all equivalent, and there is only one possible radical structure that can result from H-atom abstraction, radical **10**. The experimental first derivative esr spectrum obtained by γ-radiolysis of DMB2 at room temperature in adamantane is shown in Fig. 5. The resultant spectrum in $C_{10}H_{16}$ is well resolved and almost totally symmetrical, indicating that one species predominates, and can be interpreted as an

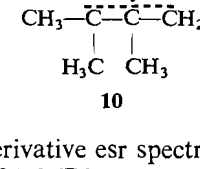

10

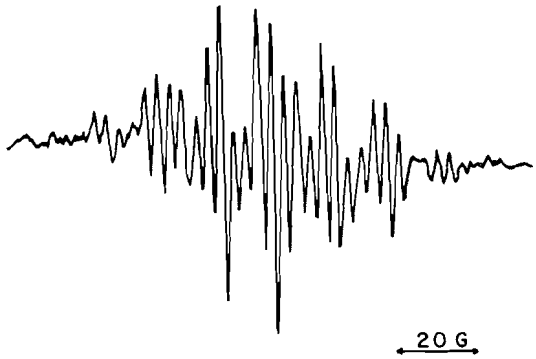

FIG. 5. Experimentally observed first derivative esr spectrum obtained from room temperature γ-radiolysis of 2,3-dimethylbutene-2 held in an adamantane matrix.

allylic radical with a^H value of 15.5 (3 protons), 12.25 (3), 13.5 (1), 14.5 (1), and 3.2 (3) G, and peak-to-peak line width of 1.3 G. These constants can be compared to those noted for the DMB2-cation radical seen by Dessau (19), where a nine-line spectrum characterized by one coupling constant of 16.6 G was observed in the liquid, and attributed to equivalent coupling to four methyl groups.

Linear 1-Alkenes

Experimental first derivative esr spectra obtained by γ-radiolysis of butene-1, hexene-1, heptene-1, and nonene-1 held in adamantane matrices, are shown in Fig. 6. A marked qualitative difference in spectra is noted for nonene-1, characterized by a distinct loss of resolution from line-broadening. This is possible *prima-facie* data affording an estimate of the "size" of trapping sites accessible to solutes held in an adamantane matrix, line-width broadening being attributed to a curtailment of isotropic tumbling mobility by steric factors. Octene-1 (not shown) yielded an equally ill-resolved spectrum, with considerable asymmetry, compared to 1-heptene and smaller homologues.

In general, the spectra are asymmetric about their centers, a good indication that two, or more, radicals with different *g*-values are contributing to the observed spectrum. However, for 1-alkenes, only one possible allylic radical can be formed, structure **11**, where R may be H, CH_3,

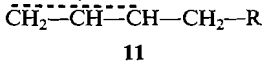

11

or larger hydrocarbon moieties. On this basis,

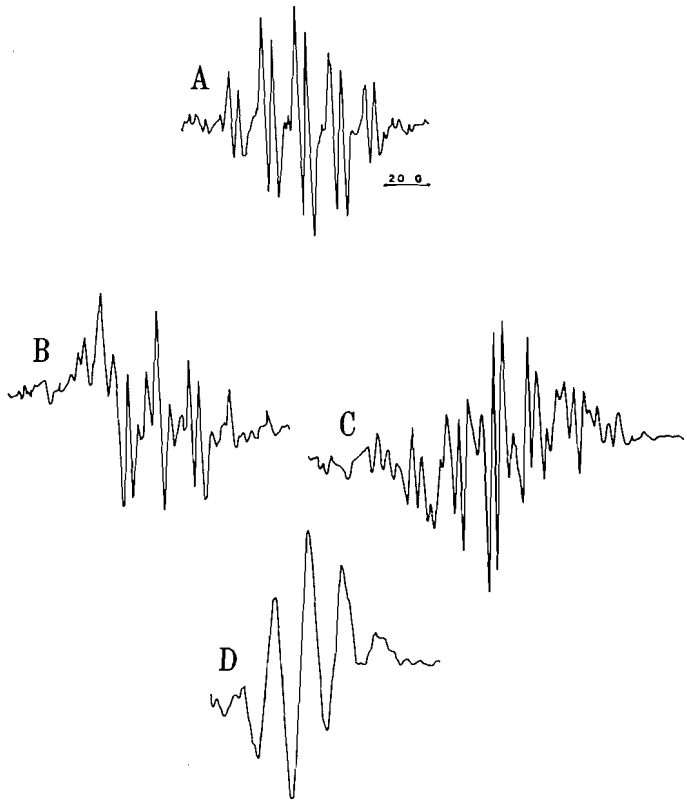

FIG. 6. Experimentally observed first order esr spectra obtained by γ-radiolysis of 1-alkenes held in adamantane matrices at room temperatures; (*A*) butene-1; (*B*) hexene-1; (*C*) heptene-1; (*D*) nonene-1.

butene-1 (B1) can only lead to a radical similar to that obtained from butene-2 (discussed below), and indeed the experimental spectrum obtained from either system are identical. Equally, since the group R in **11** is so far removed from the spin-center (except where R = H), the esr spectra obtained from all 1-alkenes should be virtually identical (line-width and resolution factors permitting). It is immediately obvious from Fig. 6 that this state of affairs does not obtain. It is probable that allylic H-atom abstraction will occur for smaller molecular weight 1-alkenes, such as butene-1 and pentene-1, but that random non-allylic abstraction occurs for the larger molecules such as hexene-1 and heptene-1.

Equally, in view of the data from other alkenes above, and from previous studies, it does not seem probable that H-atom addition will occur in these alkenes under the conditions of our experiments. Moreover, the coupling constants noted for these esr spectra (shown in Fig. 6) are typical of allylic species (apparent a^{H} values of *ca.* 12–14 G, with closely spaced doublets or multiplets of *ca.* 3 G). In view of these observations, we must conclude that some form of ene-group isomerization is occurring to yield different allylic species from each homologue. This could be initiated by non-allylic abstraction at a point well removed from the ene-group, an internal cyclization process (intramolecular radical addition), followed by rearrangement of the cyclized intermediate to a different linear radical with an allylic structure. Such cyclization processes have been noted for alkene radicals in solution, and the strong cage effect operating in $C_{10}H_{16}$ matrices will be equally conducive to such reactions. In view of the linear structure of the radicals, the allylic species expected in each case by direct allylic-abstraction would contain a lone central proton, and each radical would differ in the nature of the

Can. J. Chem. Downloaded from www.nrcresearchpress.com by 210.87.254.42 on 09/05/12
For personal use only.

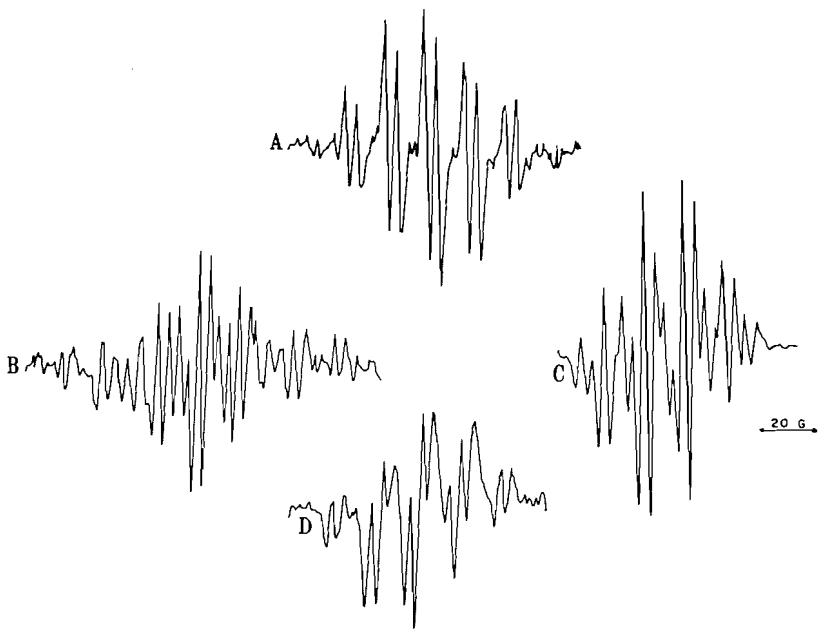

FIG. 7. First derivative esr spectra obtained by γ-radiolysis of alkene-2 in adamantane matrices; (*A*) butene-2; (*B*) pentene-2; (*C*) hexene-2; (*D*) heptene-2.

terminal allylic groups. This would produce a spectrum characterized by a multiple set of doublets, these can be seen clearly for B1, but are either obscured or absent from the other spectra. In support of this latter conjecture, there is no reason to suppose that if cyclization and subsequent rearrangement does occur, and which is probably unlikely in B1 for steric reasons, that the resultant final radical could not equally well contain a short side chain involving a methyl or ethyl moiety. Thus, the resultant allylic species from the higher homologues may not exhibit a lone central allylic proton, and no doublet pattern may be observable. We have been unable to simulate any of the spectra shown in Fig. 6 on the basis of direct allylic abstraction, except for butene-1 which is discussed in the next section, and we are unable at this time to account for the observed spectra in terms of other linear allylic isomers produced by isomerization processes.

Linear 2-Alkenes

Experimental first derivative esr spectra obtained by γ-radiolysis of butene-2, pentene-2, hexene-2, and *cis*-heptene-2, held in adamantane matrices at room temperatures are shown in Fig. 7. The spectra are all reasonably well resolved, more symmetrical about their centers than spectra from the corresponding 1-alkenes, and are characterized by a small doublet splitting (*ca.* 3.5 ± 0.5) for each homologue and which is typical of allylic radicals with one lone central proton. If allylic H-atom abstraction predominates as usual, then whichever allylic H-atom is removed, the resulting radicals will each contain such a lone central proton, and the overall radical will differ only in the nature and conformation of the end group to the allyl-system as different homologues are considered.

As was noted above, the experimental spectrum from 2-butene (B2) was identical to that obtained from 1-butene, and the best fit to the experimental data was obtained with a^H values of 13.8 (2 protons), 14.5 (3), 14.2 (1), and 3.8 (1) G, with a peak-to-peak Lorentzian linewidth of 2.0 G. These values are similar to those obtained by other workers (20).

Since the spectra from 2-alkenes do not match those from the corresponding 1-alkenes to any extent, it is probable that the predominant species contributing to the observed spectra is a radical with structure **12**, where R = H for butenyl, and

$$CH_3—\dot{C}H—CH—CH—R$$

12

Can. J. Chem. Downloaded from www.nrcresearchpress.com by 210.87.254.42 on 09/05/12
For personal use only.

TABLE 1. Hyperfine splitting constants for radicals derived from some aliphatic alkenes by γ-radiolysis at room temperature

Precursor molecule[a]	Text identity	hfsc values (G) and radical structures postulated	Line-width[b] (G)	Reference
Allene[c]		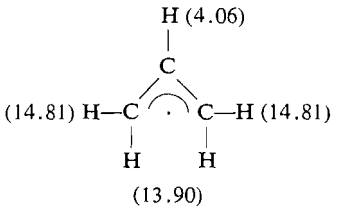 (13.90)		7
2MPr	1	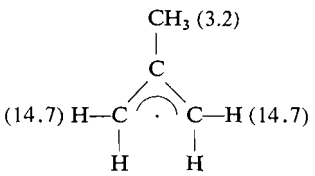 (13.8) (80%)	1.8	1*e* 7 16*b*
		$\cdot C(CH_3)_3$ (22.7) (20%)	2.0	17
B1 and B2		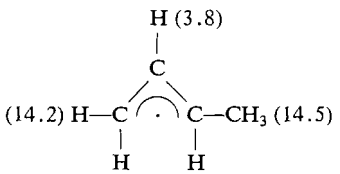 (13.8)	2.0	7
2MB1	2	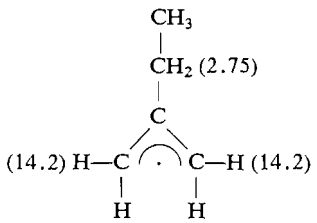 (13.5) (80%)	1.6	This work
		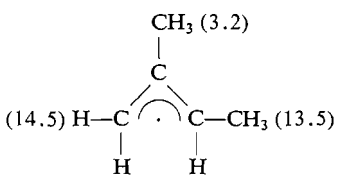 (14.0) (20%)	1.7	This work

Can. J. Chem. Downloaded from www.nrcresearchpress.com by 210.87.254.42 on 09/05/12
For personal use only.

TABLE 1 (*Continued*)

Precursor molecule[a]	Text identity	hfsc values (G) and radical structures postulated	Line-width[b] (G)	Reference
2MB2	**7**	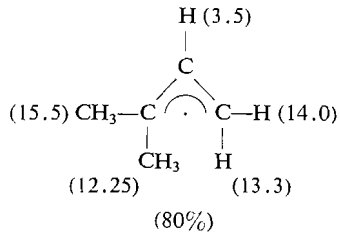	1.7	This work
	6	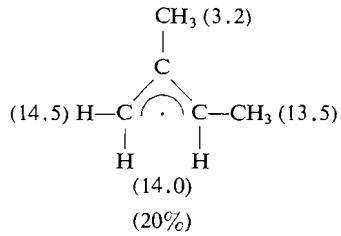	1.7	This work
2MP1	**5**	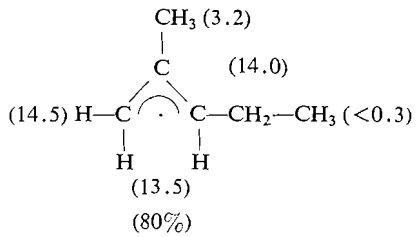	1.7	This work
4MP2	**8**	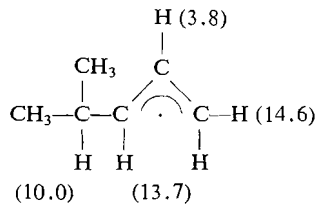	2.3	This work
DMB2	**10**	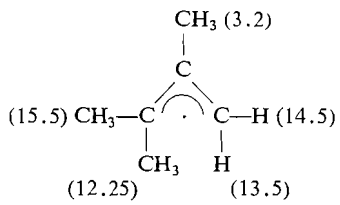	1.3	This work
Linear 1-enes	**11**	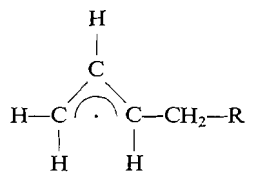	*ca.* 2.2	This work

Can. J. Chem. Downloaded from www.nrcresearchpress.com by 210.87.254.42 on 09/05/12
For personal use only.

TABLE 1 (*Concluded*)

Precursor molecule[a]	Text identity	hfsc values (G) and radical structures postulated	Line-width[b] (G)	Reference
Linear 2-enes	**12**	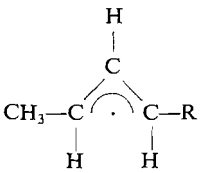 R = CH_3, CH_3CH_2, . . .	*ca.* 2.2	This work

[a]See text for identification of abbreviations used.
[b]Peak-to-peak Lorentzian first derivative line-width.
[c]Liquid phase studies by Kochi *et al.* (7)

R = CH_3, CH_3CH_2—, etc. for pentenyl, hexenyl, and higher homologues, respectively. It is certain that the radical is allylic, and since the spectra have coincident centers (within the experimental errors) they are all structurally similar with regard to the environment of the unpaired electron. The coupling constants found exclude the possibility of alkyl radical formation from H-atom addition, or internal cyclization (which has been noted for liquid phase studies). Nevertheless, despite the noted resolution accessible to us, and the apparent simplicity of observed spectra, we have been unable to successfully simulate the observed spectra for homologues higher than butenyl. Experimental work involving spin-trapping techniques, and further computer-based analyses, are currently in progress.

Other Experimental Systems

Other alkenes examined in this study were 3-methylbutene-1 (3MB1), 3,3-dimethylbutene-1 (33DMB), and 2,4,4-trimethylpentene-1 (TMPE). These compounds were selected since, for 3MB1, the only allylic hydrogen is also a tertiary hydrogen atom, and this should have led to "reinforcement" of the one radical that should be formed, by analogy with previous data from alkanes (18) and the above studies for alkenes; equally, 33DMB was of interest in that it has no allylic hydrogen atom to lose, whereas TMPE has only one accessible allylic atom. Unfortunately, the spectra obtained from each of these systems, even that from 3MB1, were poorly resolved, and quite unassignable to a structure for the radical observed.

Summary

Data obtained from radiolysis of alkene molecules held in adamantane matrices at room temperature are shown in Table 1. Assignments of esr hfsc values to *cis/trans* conformers in allylic systems have been made on the basis of the results obtained by Kochi and Krusic (7, 16*b*), they have not been confirmed by specific labelling experiments, and must be regarded as tentative. The predominant radical in each case is allylic, and there is little evidence for H-atom addition in these systems under the conditions of our experiments except for 2MPr where the symmetrical and relatively stable *tert*-butyl radical has been detected. Where the formation of more than one allylic species is possible, the predominant species detected appears to be the more symmetrical of the possible isomeric radicals. Although radical life-times for allylic species at room temperature in adamantane were comparable to those obtained for us by alkyl radicals (1*c*, 6*a*, 18) and heterocyclic radicals (3, 15) (*ca.* 10–100 min), it is interesting to note that the experimentally observed peak-to-peak first derivative line-widths (Lorentzian) for allylic radicals in adamantane at room temperature are significantly smaller (*ca.* 1.3–2.3 G) than those observed for alkyl radicals (2.0–2.8 G), and are comparable to those observed for substituted benzene radicals (21), heterocyclic radical systems (15), and other delocalized or partially delocalized systems (1*c*). Moreover, use of perdeuterated adamantane matrices did not lead to any noticeable increase in esr spectral resolution for allylic systems, although substantial reductions in experimental line-widths had been observed for other species by this method (3, 15).

Acknowledgments

Material included in this report was taken in part from that submitted by D. L. Winters in

Can. J. Chem. Downloaded from www.nrcresearchpress.com by 210.87.254.42 on 09/05/12
For personal use only.

partial fulfillment of the requirements for the M.S. degree (W.V.U. 1974). We thank the Research Corporation, Dreyfus Foundation, and American Cancer Society, for partial support of this work.

1. (*a*) D. R. Gee and J. K. S. Wan. Can. J. Chem. **49**, 20 (1971); (*b*) S. DiGregorio, M. B. Yim, and D. E. Wood. J. Am. Chem. Soc. **95**, 8457 (1973); (*c*) M. E. Manzuk, D. L. Winters, G. J. Hyfantis, and A. C. Ling. Int. J. Radiat. Biol. **26**, 51 (1974); (*d*) D. M. Camaioni, H. F. Walter, J. E. Jordan, and D. W. Pratt. J. Am. Chem. Soc. **95**, 7978 (1973); (*e*) T. Richerzhagen, P. Svedja, and D. H. Volman. J. Phys. Chem. **77**, 1819 (1973).
2. D. R. Smith and P. West. AECL-3776 and 3851, Progress reports of Chemistry and Materials Division, Chalk River Nuclear Laboratories, Atomic Energy of Canada Limited, Chalk River, Ontario.
3. A. C. Ling and L. Kevan. J. Phys. Chem. To be published.
4. P. B. Ayscough and H. E. Evans. Trans. Faraday Soc. **60**, 801 (1964).
5. D. R. Smith and J. J. Pieroni. J. Phys. Chem. **70**, 2379 (1966) and references therein.
6. (*a*) R. E. Linder and A. C. Ling. Can. J. Chem **50**, 3982 (1972); (*b*) A. R. McIntosh, D. R. Gee, and J. K. S. Wan. Spectrosc. Lett. **4**, 217 (1971).
7. P. J. Krusic and J. K. Kochi. J. Am. Chem. Soc. **92**, 4110 (1970); J. Am. Chem. Soc **90**, 7157 (1968); and references therein :
8. D. Campbell, M. C. R. Symons, and G. S. P. Verma. J. Chem. Soc. (A), 2480 (1969).
9. (*a*) R. Klein and M. D. Scheer. J. Phys. Chem. **67**, 1874 (1963) and references therein; (*b*) C. U. Morgan and co-workers. J. Am. Chem. Soc. **92**, 3309 (1970) and references therein.
10. J. E. Bennett and B. Mile. J. Chem. Soc. Faraday Trans. I, **69**, 1398 (1973).
11. C. P. Poole, and R. S Anderson. J. Chem. Phys. **31**, 346 (1959).
12. P. H. Kasai and D. McLeod. J. Am. Chem. Soc. **95**, 4801 (1973) and references therein.
13. (*a*) G. J. Hyfantis and A. C. Ling. Can. J. Chem. **52**, 1206 (1974); (*b*) G. J. Hyfantis and A. C. Ling. Chem. Phys. Lett. **24**, 335 (1974).
14. A. C. Ling. J. Chem. Educ. **51**, 174 (1974).
15. D. L. Winters and A. C. Ling. Can. J. Chem. In press.
16. (*a*) P. Smith, R. A. Kaba, and P. B. Wood. J. Phys. Chem. **78**, 117 (1974); (*b*) J. K. Kochi and P. J. Krusic. J. Am. Chem. Soc. **92**, 4110 (1970).
17. R. W. Fessenden and R. H. Schuler. J. Chem. Phys. **39**, 2147 (1963).
18. S. W. Kanick, R. E. Linder, and A. C. Ling. J. Chem. Soc. (A). 2971 (1971).
19. R. M. Dessau. J. Am. Chem. Soc. **92**, 6356 (1970).
20. D. R. Smith, F. Okenka, and J. J. Pieroni. Can. J. Chem. **45**, 833 (1967).
21. D. L. Winters and A. C. Ling. Unpublished work.

Can. J. Chem. Downloaded from www.nrcresearchpress.com by 210.87.254.42 on 09/05/12
For personal use only.

Macroscopic viscosity and the dielectric relaxation of some substituted benzenes

S. C. SRIVASTAVA AND J. CROSSLEY[1]

Department of Chemistry, Lakehead University, Thunder Bay, Ontario P7B 5E1

Received December 24, 1975

S. C. SRIVASTAVA and J. CROSSLEY. Can. J. Chem. **54**, 1418 (1976).

Microwave dielectric constants and losses, and viscosities (η) have been obtained for acetophenone, anisole, bromobenzene, and *p*-dimethoxybenzene in *n*-heptane, *n*-hexadecane, paraffin oil, and three *n*-heptane + paraffin oil mixtures between 15 and 60 °C. The dielectric results have been analyzed for mean relaxation times (τ_0). Plots of ln $\tau_0 T$ against ln η for bromobenzene are compared with those for the other solutes in an attempt to determine the effect of contributions from intramolecular relaxation processes. The results suggest that measurements employing several solvents at one temperature provide a better insight into mechanisms of dipole reorientation than those with one solvent at several temperatures.

S. C. SRIVASTAVA et J. CROSSLEY. Can. J. Chem. **54**, 1418 (1976).

On a obtenu les constantes et les pertes diélectriques de microonde ainsi que les viscosités (η) de l'acétophénone de l'anisole, du bromobenzène et du *p*-diméthoxy-benzène dans le *n*-heptane, le *n*-hexadécane, l'huile de paraffine et trois mélanges de *n*-heptane et d'huile de paraffine entre 15 et 60 °C. On a analysé les résultats diélectriques afin d'établir les temps de relaxation moyen τ_0. On a comparé la courbe de ln $\tau_0 T$ en fonction de ln η pour le bromobenzène avec celles des autres solutés dans un effort pour déterminer l'effet des contributions des processus de relaxations intramoléculaires. Les résultats suggèrent que les mesures faisant appel à plusieurs solvants à une température fournissent une meilleure vue des mécanismes de réorientation de dipole que ceux dans un solvant à plusieurs températures.

[Traduit par le journal]

Introduction

The effect of increasing macroscopic viscosity upon the dielectric relaxation of some *n*-alkylbromides and alkanones was examined in an earlier paper (1). It was evident that additional, more systematic, studies were required before any conclusions, regarding the possibility of employing viscous solvents to provide some insight into mechanisms of dipole reorientation, could be reached.

The Debye (2) equation

$$[1] \qquad \tau = 4\pi\eta a^3/kT = 3\eta V/kT$$

in which a is the radius of a spherical molecule of volume V in a homogeneous fluid of viscosity η, k is the Boltzmann constant and T is the absolute temperature, gives relaxation times, τ, in reasonable agreement with experiment only when the volume of the solute is about three times greater than that of the solvent (3). In the majority of cases, however, relaxation times calculated from eq. 1 are considerably longer than the experimental values. This is especially true for small spherical solute molecules and for viscous solvents. Several modifications of the Debye equation have been put forward (4), but it is seldom possible to predict, with any certainty, the relaxation time of a polar molecule from molecular dimensions and the viscosity of the medium.

Kalman and Smyth (5) found that the empirical relationship

$$[2] \qquad \tau = \text{constant} \times \eta^x/T$$

satisfactorily represented their data for polar solutes in the viscous Nujol solvent over a small temperature range. It can be shown (6) that, for a particular solute–solvent system, the ratio of the activation energy for dielectric relaxation to that for viscous flow $n(\Delta H_\tau^{\neq}/\Delta H_\eta^{\neq})$ should equal x, provided the entropies of activation for the two processes are the same. Higasi (7) finds that x is close to zero for small spherical solute molecules and approaches unity for large nonspherical solute molecules. Furthermore, the x value for benzophenone, which relaxes by whole

[1]To whom correspondence to be addressed. Present address: Edward Davies Chemical Laboratories, University College of Wales, Aberystwyth, Dyfed, U.K. SY23 1NE.

Can. J. Chem. Downloaded from www.nrcresearchpress.com by 210.87.254.42 on 09/05/12
For personal use only.

Can. J. Chem. Downloaded from www.nrcresearchpress.com by 210.87.254.42 on 09/05/12
For personal use only.

molecule rotation, is almost twelve times that for diphenylether, a molecule of similar shape and size which relaxes primarily by a fast intramolecular process. Thus the parameter x should provide some insight into the mechanisms of dipole reorientation.

The majority of relaxation time – viscosity studies have been confined to the relatively small viscosity changes possible with the conventional nonpolar solvents, or, by small temperature variations. Grubb and Smyth (5) employed Nujol (paraffin oil) to separate the two relaxation processes, overall molecular rotation and intramolecular rotation, for some aromatic ethers. A more systematic approach has been made by Balogun and Cumper (9) who used benzene + liquid paraffin mixtures to obtain a wide range of solvent viscosities. They made their measurements at several temperatures and were thus able to obtain $\Delta H_\tau^{\neq}$, $\Delta H_\eta^{\neq}$, and x values. Unfortunately, they did not include nonrigid aromatic compounds amongst their solutes, and benzene may not have been a particularly good solvent for diluting the paraffin oil, since it interacts quite significantly with many polar molecules (10). In addition, paraffin oil is a mixture of aliphatic hydrocarbons which are of course molecularly quite different from benzene.

This paper reports dielectric relaxation time and viscosity data for both rigid and nonrigid substituted benzenes in *n*-heptane, *n*-hexadecane, paraffin oil, and paraffin oil + *n*-heptane mixtures between 15 and 60 °C. Kalman and Smyth x values (eq. 2) are obtained from (*i*) temperature variations for a given solution and (*ii*) viscosity variations, produced by using different solvents, at fixed temperatures.

Experimental

The apparatus and procedure used to determine the dielectric constant (ϵ') and the dielectric loss (ϵ'') at 35, 24, 16, 9.3, 2.5, 1.9, 1.5, and 0.98 GHz have been described previously (11, 12). Low frequency dielectric constants (ϵ_0) were measured at 2 MHz using a WTW Dipolmeter. The solution viscosities (η) were measured using calibrated Ubbelohde type viscometers and density bottles. All the chemicals were dried prior to their use. Each solute was dissolved (about 0.2 to 0.4 mol l^{-1}) in pure *n*-heptane, pure *n*-hexadecane, pure paraffin oil (p.o.), and paraffin oil + *n*-heptane mixtures made up in the following percentages by volume: (*i*) 75% paraffin oil + 25% *n*-heptane (p.o.75), (*ii*) 85% paraffin oil + 15% *n*-heptane (p.o.85), and (*iii*) 95% paraffin oil + 5% *n*-heptane (p.o.95).

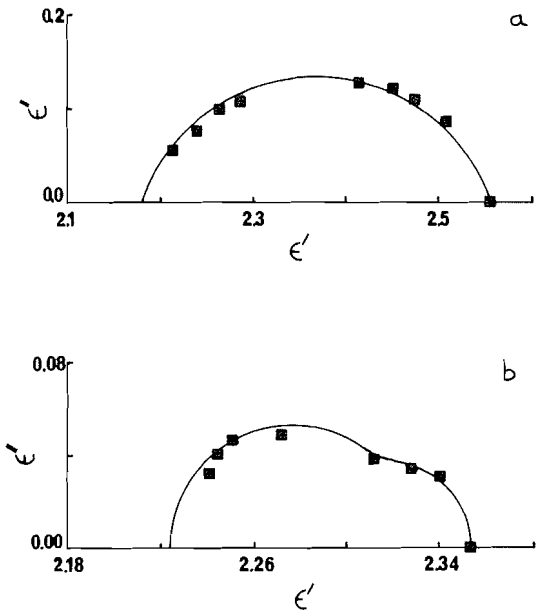

FIG. 1. Cole–Cole plots for (*a*) acetophenone and (*b*) anisole in paraffin oil at 25 °C. The frequencies are: 35.11, 23.98, 16.20, 9.31, 2.5, 1.9, 1.5 (0.98 for acetophenone only) and 0.002 GHz.

Results

Cole–Cole plots (13) for all the acetophenone, bromobenzene, *p*-dimethoxybenzene, and the majority of the anisole solutions were quite symmetrical (Fig. 1*a*). The anisole in pure paraffin oil solutions showed some indication of separation into two dispersion regions (Fig. 1*b*). Mean relaxation times (τ_0), Cole–Cole distribution parameters (α) and high frequency dielectric constants (ϵ_∞) were determined for all the solutions, by a computer fit of the experimental ϵ', ϵ'', and ϵ_0 data to the Cole–Cole equations as described previously (14). The errors involved in this type of analysis have been discussed in detail (14). Previous work has shown that the dielectric absorptions of the anisole and *p*-dimethoxybenzene solutions contain contributions from two relaxation processes (8, 15, 16). In view of the distribution of relaxation times observed for bromobenzene, which has only one relaxation process, however, we have refrained from analyzing the data for the other systems in terms of two discrete relaxation times.

The mean relaxation times, Cole–Cole distribution parameters, and viscosities are listed in Table 1.

Can. J. Chem. Downloaded from www.nrcresearchpress.com by 210.87.254.42 on 09/05/12
For personal use only.

Enthalpies of activation for dielectric relaxation ($\Delta H_\tau^{\neq}$) and viscous flow ($\Delta H_\eta^{\neq}$) were obtained from ln $\tau_0 T$ against $1/T$ (Fig. 2) and ln η against $1/T$ plots respectively. The values are presented in Table 2.

Values of x in the Kalman and Smyth equation

TABLE 1. Relaxation times, distribution parameters, and solution viscosities for polar solutes in several nonpolar solvents

Solvent	T (°C)	τ_0 (ps)	α	η (cP)	τ' (ps)	τ'' (ps)	$10^{24} \times \frac{\tau_0 kT}{3\eta}$
				Bromobenzene			
Heptane	15	7.3	0.00	0.479	7.9	7.9	20
	25	7.1	0.00	0.435	7.0	7.1	22
	40	6.1	0.00	0.389	6.1	5.9	23
	60	4.9	0.00	0.324	4.9	4.8	23
p.o.75	15	26	0.14	16.2	27	28	2.2
	25	20	0.17	10.3	21	21	2.7
	40	16	0.09	6.39	15	17	3.7
	60	11	0.14	3.89	11	12	4.4
p.o.85	15	41	0.27	42.2	40	39	1.3
	25	28	0.24	23.6	29	28	1.6
	40	21	0.16	12.8	21	21	2.4
	60	14	0.15	6.84	14	14	3.2
p.o.95	15	47	0.22	69.0	47	47	0.91
	25	34	0.30	39.4	35	33	1.2
	40	24	0.12	19.9	24	25	1.8
	60	17	0.17	9.80	16	16	2.6
p.o.	15	64	0.27	183	64	66	0.47
	25	43	0.33	87.3	46	43	0.65
	40	34	0.15	39.2	31	32	1.24
	60	20	0.18	16.9	21	20	1.83
				Anisole			
Heptane	15	6.0	0.11	0.479	6.1	6.4	17
	25	5.7	0.07	0.431	5.5	6.2	18
	40	5.0	0.05	0.374	4.9	5.1	19
	60	4.1	0.06	0.316	4.2	4.0	20
Hexadecane	15	13	0.11	3.46	14	11	4.9
	25	11	0.12	2.43	10	9.3	6.0
	40	8.2	0.10	1.84	7.7	7.3	6.4
	60	5.2	0.15	1.38	5.8	5.3	10
p.o.75	15	16	0.19	9.44	16	15	2.2
	25	12	0.22	7.16	13	12	2.2
	40	9.6	0.16	4.63	9.0	9.1	3.0
	60	6.1	0.20	3.01	6.4	6.0	3.1
p.o.85	15	20	0.20	20.7	19	19	1.3
	25	14	0.26	14.3	14	14	1.3
	40	8.6	0.29	8.33	9.3	10	1.5
	60	6.6	0.24	4.75	6.0	6.6	2.1
p.o.95	15	23	0.23	41.7	22	24	0.73
	25	16	0.29	27.8	17	17	0.78
	40	13	0.21	15.0	12	12	1.2
	60	7.4	0.24	7.97	7.6	7.2	1.4
p.o.	15	28	0.24	83.9	27	29	0.44
	25	20	0.28	50.3	21	19	0.55
	40	14	0.23	23.4	13	13	0.84
	60	7.1	0.31	11.7	9.0	7.7	0.93

TABLE 1 (*Concluded*)

Solvent	T (°C)	τ_0 (ps)	α	η (cP)	τ' (ps)	τ'' (ps)	$10^{24} \times \frac{\tau_0 kT}{3\eta}$
				Acetophenone			
Heptane	15	9.7	0.05	0.48	9.6	9.8	27
	25	8.4	0.06	0.43	8.2	8.6	27
	40	6.7	0.08	0.37	6.6	6.9	26
	60	5.4	0.14	0.32	5.3	5.3	26
Hexadecane	25	19	0.09	2.81	19	17	9.1
	40	14	0.08	2.08	14	13	9.8
	60	9.5	0.11	1.49	9.4	9.3	9.8
p.o.75	15	34	0.19	14.2	33	33	3.1
	25	26	0.16	9.68	26	27	3.6
	40	19	0.13	6.07	19	19	4.5
	60	13	0.11	3.75	13	13	5.4
p.o.85	15	49	0.22	32.0	49	45	2.0
	25	36	0.21	20.7	36	36	2.4
	40	25	0.18	11.7	25	25	3.0
	60	16	0.13	6.53	16	16	3.8
p.o.95	15	63	0.23	77.6	65	61	1.1
	25	49	0.23	43.8	47	47	1.5
	40	31	0.21	21.6	31	31	2.0
	60	19	0.16	10.6	20	19	2.8
p.o.	15	77	0.24	186	82	84	0.55
	25	61	0.21	89.4	57	62	0.93
	40	40	0.21	41.7	38	40	1.4
	60	24	0.16	18.2	25	23	2.0
				p-Dimethoxybenzene			
Heptane	25	6.1	0.27	0.432	6.1	6.6	20
	40	5.0	0.38	0.375	5.0	5.1	19
	60	3.9	0.32	0.318	3.9	3.9	19
Hexadecane	25	12	0.21	2.93	11.6	11.5	5.6
	40	8.1	0.22	2.04	8.6	8.7	5.8
	60	6.6	0.27	1.46	6.4	6.7	6.9
p.o.75	15	30	0.32	15.1	28	31	2.7
	25	22	0.20	10.5	2.3	17	2.9
	40	14	0.20	6.61	17	13	3.1
	60	14	0.24	4.06	13	9.7	5.2
p.o.85	15	35	0.20	37.8	33	34	1.2
	25	24	0.18	23.7	25	21	1.4
	40	16	0.20	13.2	17	16	1.7
	60	12	0.20	7.09	12	12	2.7
p.o.95	15	37	0.42	103	36	37	0.47
	25	28	0.20	70.5	30	29	0.53
	40	23	0.18	33.0	21	21	1.0
	60	14	0.23	14.7	15	15	1.5
p.o.	15	40	0.34	204	36	40	0.26
	25	27	0.19	109	30	33	0.34
	40	21	0.20	48.2	23	24	0.63
	60	19	0.22	20.6	17	17	1.4

were obtained from plots of $\ln \tau_0 T$ against $\ln \eta$ (Fig. 3) by two methods:

(*a*) Linear regression analysis of the points for a given solution at the four temperatures using the relationship

$$[3] \qquad \ln \tau_0 T = \ln A + x' \ln \eta$$

Can. J. Chem. Downloaded from www.nrcresearchpress.com by 210.87.254.42 on 09/05/12
For personal use only.

TABLE 2. The effect of temperature on the dielectric relaxation and viscosity for polar solute – nonpolar solvent solutions

Solvent	$\Delta H_\eta^{\ddagger}$ (kcal mol^{-1})	$\Delta H_\tau^{\ddagger}$ (kcal mol^{-1})	$\frac{\Delta H_\tau^{\ddagger}}{\Delta H_\eta^{\ddagger}}$	x'	$10^8 \times A$	$10^{24} \times \frac{Ak}{3}$
			Bromobenzene			
Heptane	1.65	1.48	0.89	0.86	22.9	10.5
p.o.75	6.01	3.04	0.51	0.50	1.92	0.88
p.o.85	7.66	3.75	0.47	0.49	1.76	0.81
p.o.95	8.29	3.75	0.45	0.45	1.59	0.73
p.o.	10.05	4.10	0.41	0.40	1.43	0.66
			Anisole			
Heptane	1.77	1.18	0.67	0.56	3.48	1.60
Hexadecane	3.80	3.15	0.83	0.79	5.65	2.60
p.o.75	4.92	3.92	0.80	0.65	2.07	0.95
p.o.85	6.31	3.95	0.63	0.66	1.50	0.69
p.o.95	7.10	3.97	0.56	0.56	1.04	0.48
p.o.	8.46	4.60	0.54	0.49	0.85	0.39
			Acetophenone			
Heptane	1.64	1.85	1.13	1.10	97.8	45.0
Hexadecane	3.51	3.04	0.87	0.90	13.8	6.36
p.o.75	5.74	3.43	0.60	0.59	3.03	1.39
p.o.85	6.86	4.07	0.59	0.60	2.79	1.28
p.o.95	8.63	4.45	0.52	0.53	2.15	0.99
p.o.	10.40	3.90	0.38	0.45	1.78	0.82
			p-Dimethoxybenzene			
Heptane	1.73	1.91	1.10	1.10	72.3	33.3
Hexadecane	4.00	2.72	0.68	0.70	4.09	1.88
p.o.75	5.65	2.75	0.49	0.50	2.08	0.96
p.o.85	7.09	3.82	0.54	0.54	1.62	0.75
p.o.95	8.56	3.34	0.39	0.39	1.02	0.47
p.o.	9.87	3.91	0.40	0.26	0.87	0.40

(*b*) Linear regression analysis of the points for a solute in each of the solvents, at a given temperature, using the relationship

$$[4] \qquad \ln \tau_0 T = \ln B + x'' \ln \eta$$

The constants A and B in the above equations are dependent upon the solute and solvent, and replace $3V/k$ in the Debye equation. Values of A and B have been determined from the intercepts of the $\ln \tau_0 T$ against $\ln \eta$ plots by methods (*a*) and (*b*), respectively. In order to assess the linearity of these plots relaxation times τ' and τ'' calculated from x' and A, and, x'' and B respectively are compared with the experimental τ_0 values in Table 1.

Discussion

Dielectric relaxation times for rigid polar molecules of the same shape measured in the same solvent at the same temperature are found to be proportional to their molecular volumes (17). For acetophenone, anisole, bromobenzene, and *p*-dimethoxybenzene the calculated molecular volumes (18) are 121, 108, 107, and 132 $\times$ 10^{-24} cc, respectively. The τ_0 values (Table 1) for anisole and *p*-dimethoxybenzene, especially in the more viscous solvents, are significantly shorter than those for the rigid bromobenzene. Consequently, the dielectric absorption of the two ethers must, in accord with earlier measurements (8, 15, 16), contain contributions from an intramolecular relaxation process, *i.e.* methoxy group rotation. It has been suggested (19) that acetyl group rotation makes a significant contribution to the dielectric absorption of acetophenone. However, the mean relaxation times for acetophenone and bromobenzene are very nearly in the same ratio as their molecular volumes.

Table 1 gives the molecular volumes ($\tau_0 kT/3\eta$) for the polar solutes calculated from the experi-

Can. J. Chem. Downloaded from www.nrcresearchpress.com by 210.87.254.42 on 09/05/12
For personal use only.

Can. J. Chem. Downloaded from www.nrcresearchpress.com by 210.87.254.42 on 09/05/12
For personal use only.

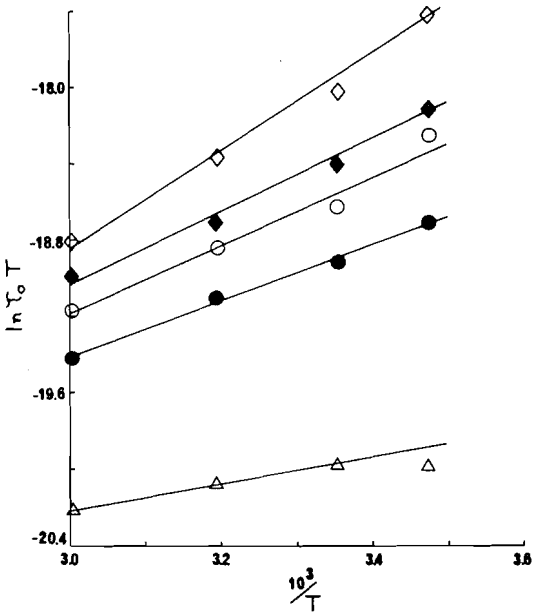

FIG. 2. Plots of ln $\tau_0 T$ against $1/T$ for bromobenzene in heptane △; p.o.75 ●; p.o.85 ○; p.o.95 ◆; and p.o. ◇.

mental τ_0 and solution viscosity values. These calculated volumes are much smaller than the true values, and they decrease markedly with increased viscosity, which illustrates the inadequacy of the Debye equation and the use of a macroscopic viscosity for these systems.

The $\Delta H_\eta^{\neq}$ values (Table 2) increase with increased viscosity and are similar to those reported for benzene + paraffin oil solutions by Balogun and Cumper (9). In contrast, the $\Delta H_\tau^{\neq}$ values do not increase markedly with increased viscosity for the heptane + paraffin oil solutions. Plots of ln $\tau_0 T$ against ln η for a given solution at the different temperatures are linear (Fig. 3) and the slopes x' are, as predicted (6), very similar to the respective n values. The relaxation times, τ', calculated from the slopes and intercepts of these plots are in excellent agreement with the experimental τ_0 values. For all the solutes, n and x' (Table 2) tend to decrease with increased solvent viscosity and follow the same trend as those obtained by Balogun and Cumper (9). The values in paraffin oil are quite similar to those reported, for 1-chloronaphthalene (0.38) and isoquinoline (0.43) in Nujol, by Kalman and Smyth (5). A comparison of the n and x' data in Table 2 for anisole and p-dimethoxybenzene with corresponding data for bromobenzene reveals that they are not sensitive indicators of contributions from intramolecular relaxation processes. Volumes ($AK/3$ in Table 2) calculated from the intercepts of the ln $\tau_0 T$ against ln η plots are, of course independent of temperature. However, they are considerably smaller than the true values and they decrease with increased solvent viscosity. Obviously some additional parameter(s) must be contained in the A values in order to obtain better agreement. The A, and thus $AK/3$, values in pure paraffin oil are the only ones in Table 2 which reflect the contribution that intramolecular rotation makes to the dielectric absorption of the two ethers. In addition, the A value for acetophenone in paraffin oil is larger than that for bromobenzene which suggests that acetophenone behaves essentially as a rigid molecule. It is clear, however, that n, x', and A do not provide any appreciable

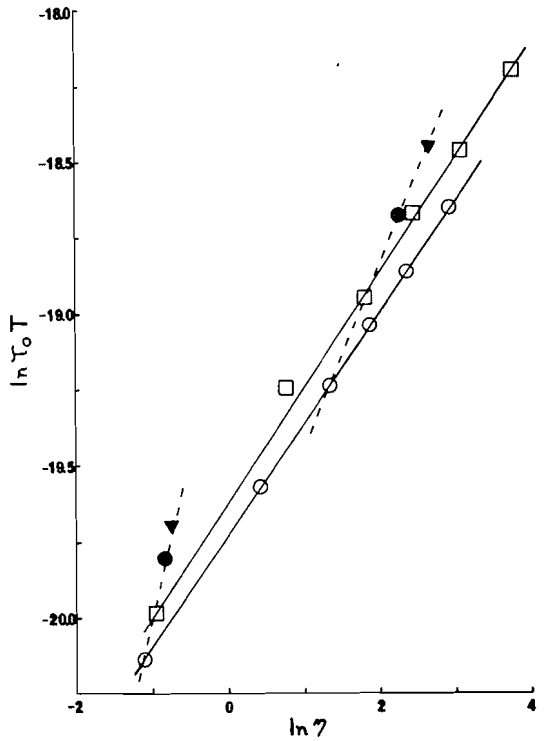

FIG. 3. Plot of ln $\tau_0 T$ against ln η for acetophenone in several solvents at 15 °C, ▼; 25 °C, ●; 40 °C, □; and 60 °C, ○. The solid lines are drawn through the points, for each of the six solvents, at a fixed temperature (slope x''). The broken lines are drawn through the points for the n-heptane and p.o.75 solutions at four temperatures (slope x').

TABLE 3. The effect of solvent on the dielectric relaxation for polar solute – nonpolar solvent solutions

Solute	T (°C)	x''	$10^8 \times B$	$10^{24} \times \frac{Bk}{3}$
Bromobenzene	15	0.36	1.53	0.70
	25	0.34	1.35	0.62
	40	0.37	1.43	0.66
	60	0.36	1.25	0.58
Anisole	15	0.29	0.87	0.40
	25	0.24	0.68	0.31
	40	0.23	0.57	0.26
	60	0.18	0.38	0.17
Acetophenone	15	0.36	1.94	0.89
	25	0.37	1.92	0.88
	40	0.37	1.71	0.79
	60	0.37	1.46	0.67
p-Dimethoxy-benzene	15	0.10	1.07	0.49
	25	0.29	0.96	0.44
	40	0.32	0.95	0.44
	60	0.36	1.02	0.47

insight into the mechanisms of dielectric absorption in these systems.

Table 3 lists the slopes (x''), intercepts (B), and volumes ($Bk/3$) obtained from ln $\tau_0 T$ against ln η plots for each of the solutes at fixed temperatures, *i.e.* both τ_0 and η are increased by increasing the solvent viscosity. Again the calculated relaxation times, τ'', are in good agreement with those determined by experiment. The x'' values for a particular solute are, with the exception of *p*-dimethoxybenzene, relatively independent of temperature and, of course, the solvent. Higasi (7) obtained x'' values of 0.20, 0.23, and 0.31 for the rigid molecules *o*-dichlorobenzene, isoquinoline, and 1-chloronaphthalene respectively, although he did not indicate the viscosity range. Crossley (1) obtained x'' values of about 0.27 for a number of alkylbromides and alkanones in paraffin oil + heptane mixtures at 25 °C. The x'' and B values for the nonrigid anisole and *p*-dimethoxybenzene are clearly smaller than those for the rigid bromobenzene. The ratio of the B values for acetophenone and bromobenzene is about 1.25 compared with 1.14 for their molecular volumes, which further indicates that acetyl group rotation does not significantly contribute to the dielectric absorption of acetophenone.

The results in Tables 2 and 3 suggest that dielectric measurements of a polar solute in a series of different viscosity solvents may provide a better insight into the mechanisms of dipole reorientation than measurements with one solvent at several temperatures. It will be interesting to note whether these conclusions are substantiated by measurements on polar solutes of a different shape and size.

Acknowledgement

We wish to thank the National Research Council of Canada for providing a grant which supported this work.

1. J. CROSSLEY. J. Chem. Phys. **61**, 866 (1974).
2. P. DEBYE. Trans. Faraday Soc. **30**, 679 (1934).
3. R. J. MEAKINS. Trans. Faraday Soc. **54**, 1160 (1958).
4. K. H. ILLINGER. Progress in dielectrics. *Edited by* J. B. Birks and J. Hart. Heywood, London, 1962. Vol. 4.
5. O. F. KALMAN and C. P. SMYTH. J. Am. Chem. Soc. **82**, 783 (1960).
6. J. P. SHUKLA, D. D. SHUKLA, and M. C. SAXENA. J. Phys. Chem. **73**, 2187 (1969).
7. K. HIGASI. Dielectric relaxation and molecular structure. Research Institute of Applied Electricity, Sapporo. 1961.
8. E. L. GRUBB and C. P. SMYTH. J. Am. Chem. Soc. **83**, 4873 (1962).
9. G. A. BALOGUN and C. W. N. CUMPER. J. Chem. Soc. Faraday II, 1172 (1973).
10. J. CROSSLEY and C. P. SMYTH. J. Am. Chem. Soc. **91**, 2482 (1969).
11. W. F. HASSELL, M. D. MAGEE, S. W. TUCKER, and S. WALKER. Tetrahedron, **20**, 2137 (1964).
12. S. E. KEEFE and E. H. GRANT. Rev. Sci. Instrum. **39**, 1800 (1965).
13. K. S. COLE and R. H. COLE. J. Chem. Phys. **9**, 341 (1941).
14. J. CROSSLEY, S. P. TAY, and S. WALKER. Adv. Mol. Relax. Processes. **6**, 69 (1974).
15. D. B. FARMER and S. WALKER. Can. J. Chem. **47**, 4645 (1969).
16. W. E. VAUGHAN, S. B. W. ROEDER, and T. PROVDER. J. Chem. Phys. **39**, 701 (1963).
17. W. F. HASSELL and S. WALKER. Trans. Faraday Soc. **62**, 2695 (1966).
18. J. T. EDWARD. Chem. Ind. (London). 774 (1956).
19. D. B. FARMER, P. F. MOUNTAIN, and S. WALKER. J. Phys. Chem. **77**, 714 (1973).

Can. J. Chem. Downloaded from www.nrcresearchpress.com by 210.87.254.42 on 09/05/12
For personal use only.

Alkylation of the dimethylglyoximato ligands in reduced cobaloxime

RICHARD B. SILVERMAN[1]
Department of Chemistry, Harvard University, Cambridge, Massachusetts 02138
AND
D. DOLPHIN[2]
Department of Chemistry, The University of British Columbia, Vancouver, British Columbia V6T 1W5

Received September 8, 1976

RICHARD B. SILVERMAN and D. DOLPHIN. Can. J. Chem. **54**, 1425 (1976).

Cobalt(II) cobaloximes can undergo atom transfer reactions with certain alkyl halides to give the corresponding alkyl cobalt(III) cobaloximes. However, in the presence of powerfully electrophilic alkyl halides, such as chloromethyl methyl ether, reaction at the periphery, and not at the cobalt, occurs to give dimethylglyoxime-*O*-methoxymethyl ether.

RICHARD B. SILVERMAN et D. DOLPHIN. Can. J. Chem. **54**, 1425 (1976).

Les cobaloximes de cobalt(II) peuvent subir des réactions de transferts d'atomes avec certains halogénures d'alkyle pour conduire aux cobaloximes correspondantes de cobalt(III) alkylé. Toutefois en présence d'halogénures d'alkyle très électroaffinitaires, tel que le méthoxychlorométhane, une réaction à la périphérie, et non pas au niveau du cobalt, se produit pour conduire à l'éther diméthylglyoxime-*O*-méthoxyméthyle.

[Traduit par le journal]

In the presence of certain alkyl halides cobalt(II) cobaloximes are known to undergo atom transfer reactions (1). Thus the reaction of two equivalents of pyridine(bisdimethylglyoximato)cobalt(II) with benzyl bromide, in benzene, yields equal amounts of bromo- and benzyl-(pyridine)cobaloxime (2) (reaction 1, Scheme 1), and such reactions are favored when the intermediates are 'stable' organic radicals, such as the benzyl radical.

We wish to report here a novel reaction of pyridine(bisdimethylglyoximato)cobalt(II) with a highly reactive alkyl halide, chloromethyl methyl ether, in which an ionic, rather than radical, pathway leads to preferential alkylation of the ligand rather than of the cobalt. When chloromethyl methyl ether was added to a solution of pyridine(bisdimethylglyoximato)cobalt(II), in deoxygenated dry benzene, a blue solid slowly precipitated. Addition of this blue solid to water gave a pink solution containing a white precipitate. Anhydrous cobalt(II) chloride is a blue complex which turns red upon hydration, and this suggested that the reaction had produced inorganic cobalt and a modified ligand (reaction 2, Scheme 1). This was confirmed when the white solid was shown to be identical to a sample of dimethylglyoxime-*O*-methoxymethyl ether, prepared by monoalkylation of sodium dimethylglyoxime with chloromethyl methyl ether.

No reaction occurred when chloromethyl

[1]National Institutes of Health Predoctoral Trainee, 1971–1974.

[2]To whom correspondence should be addressed.

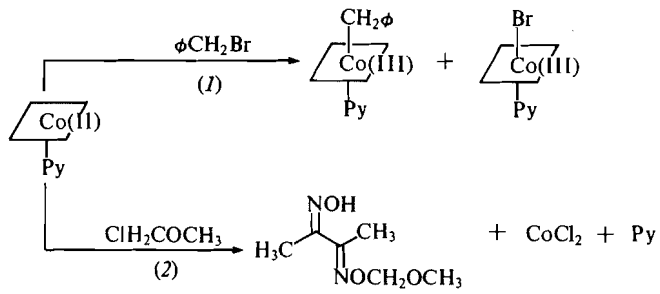

SCHEME 1

Can. J. Chem. Downloaded from www.nrcresearchpress.com by 210.87.254.6 on 09/05/12
For personal use only.

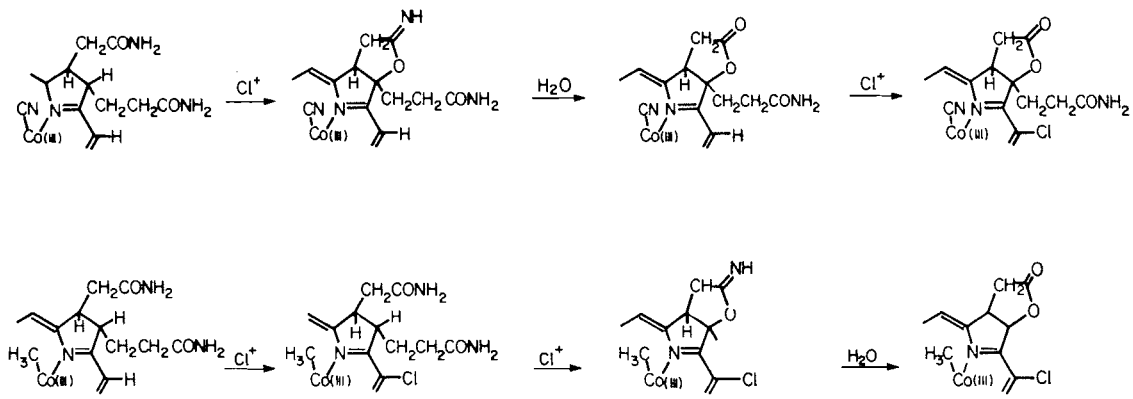

SCHEME 2

methyl ether was added to bromo- or methyl-(pyridine)cobaloximeCo(III), in methanol, methylene chloride, or benzene. Thus the cobalt needs to be in a lower oxidation state in order for ligand *O*-alkylation to occur, indicating that the greater electron density of the divalent cobalt must be transmitted into the ligand system, which renders the glyoxime oxygens more nucleophilic. The rate of *O*-alkylation is then faster than the cobalt-atom transfer reaction and destruction of the complex occurs.

Similar observations have been made with the cobalamins, for which the cobaloximes are frequently used as model compounds (3). Thus reactions at the periphery of the corrin nucleus may be modified by varying the electron density of the trivalent cobalt (4). When cyanocobalamin was treated with an equivalent of chloramine T, cyclization of the ring B acetamide side chain, of the corrin nucleus, occurred to give the stable fused lactone upon hydrolysis, and then the further action of chloramine T brought about substitution at C_{10} of the corrin nucleus to give the chloro-lactone (Scheme 2). The reaction of methylcobalamin, however, took a different course. The first equivalent of chloramine T caused substitution at C_{10} with no lactonization, and excess chloramine T was required to bring about lactonization (Scheme 2).

O-Protonation of the dimethylglyoxime ligand has been suggested by numerous authors (5, 6) and crystalline *O*-protonated alkylcobaloximes have been recently reported (7), indicating that the increased electron density on cobalt, when supplied by a carbanion as axial ligand (*i.e.* in the alkyl-cobalamins and -cobaloximes), can be transmitted to the periphery of both the corrin and cobaloxime ligands.

Experimental

Melting points were determined in a Thomas–Hoover capillary melting point apparatus and are uncorrected. The ir spectra (KBr) were determined with a Perkin-Elmer 457A Grating Infrared Spectrometer. The pmr spectra were determined on a Varian Associates A-60 spectrometer with tetramethylsilane as internal standard and deuterio-chloroform as solvent; chemical shifts are expressed on the δ-scale.

Dimethylglyoxime-O-methoxymethyl Ether

To dimethylglyoxime (2.32 g, 0.02 mol) in boiling methanol (50 ml) was added solid sodium methoxide (1.1 g, 0.02 mol). After a few minutes, chloromethyl methyl ether (1.5 ml, 0.02 mol) was added. The reaction mixture was cooled to room temperature, the white solid which precipitated was removed by filtration, and the solvent evaporated. The yellow residual oil was extracted with benzene and the solvent was evaporated to give a yellow oily solid. The color was removed and crystallization induced by stirring in water; a white solid was collected and washed with water. Recrystallization of the solid from ether – petroleum ether, then from *n*-hexane gave the product as shiny white needles (0.84 g, 26%) mp 87–87.5 °C, ν 1470, 1456, 1433, 1393, 1368 (note that dimethylglyoxime exhibits two bands at 1428 and 1364 cm^{-1}); pmr 2.08 (s, 3H), 2.12 (s, 3H), 3.48 (s, 3H), 5.23 (s, 2H), 9.10 (bs, 1H). *Anal.* Calcd. for $C_6H_{12}N_2O_3$: C 44.99, H 7.55, N 17.49. Found: C 44.99, H 7.59, N 17.22.

Reactions between Pyridine(bisdimethylglyoximato)-cobalt(II) and Chloromethyl Methyl Ether

Pyridine(bisdimethylglyoximato)cobalt(II) (8) (0.74 g, 2.0 mmol) was flushed with argon for 30 min, then deoxygenated dry benzene (15 ml) was added. When all the solid had dissolved, deoxygenated chloromethyl methyl ether (0.45 ml, 6.0 mmol) was added through a syringe. After stirring for 2 h, the blue solid (0.75 g) formed was collected by filtration and was stirred in

Can. J. Chem. Downloaded from www.nrcresearchpress.com by 210.87.254.6 on 09/05/12
For personal use only.

water (5 ml), giving a white solid in a pink solution. After recrystallization from ether – petroleum ether, then from *n*-hexane, long white needles were obtained (mp 87.5–88 °C), having identical nmr and ir spectra as dimethylglyoxime-*O*-methoxymethyl ether. A mixture melting point was undepressed.

Acknowledgment

This work was supported by the United States National Institutes of Health and the National Research Council of Canada.

1. D. Dodd and M. D. Johnson. J. Organomet. Chem. **52**, 1 (1973).
2. J. Halpern and P. F. Phelan. J. Am. Chem. Soc. **94**, 1881 (1972).
3. G. N. Schrauzer. Acc. Chem. Res. **1**, 97 (1968).
4. D. Dolphin, A. W. Johnson, and R. Rodrigo. Ann. N. Y. Acad. Sci. **112**, 590 (1964).
5. Y. A. Simonov, A. A. Dvorkin, O. A. Boloya, A. V. Dblov, and T. A. Minovskii. Dokl. Akad. Nauk. SSR, **210**, 615 (1973).
6. R. D. Gillard and G. Wilkinson. J. Chem. Soc. 6041 (1963).
7. A. L. Crumbliss and P. L. Gaus. Inorg. Chem. **14**, 486 (1975).
8. G. N. Schrauzer and R. J. Windgassen. Chem. Ber. **99**, 602 (1966).

Can. J. Chem. Downloaded from www.nrcresearchpress.com by 210.87.254.6 on 09/05/12
For personal use only.

A stereochemical investigation of substituted ethylene sulfites via ^{13}C nuclear magnetic resonance

GERALD W. BUCHANAN[1]
Department of Chemistry, Carleton University, Ottawa, Canada K1S 5B6
AND
DESMOND G. HELLIER
Department of Chemistry, Westfield College, London NW3 7ST, England

Received December 30, 1975

GERALD W. BUCHANAN and DESMOND G. HELLIER. Can. J. Chem. **54**, 1428 (1976).

^{13}C nmr chemical shifts for ethylene sulfite and 17 derivatives are presented. From the magnitudes of the γ shifts and the tenets of conformational analysis, support is gained for the existence of twist-envelope conformations in solution. Pseudorotational paths are suggested which do not involve inversion at the sulfur atom.

GERALD W. BUCHANAN et DESMOND G. HELLIER. Can. J. Chem. **54**, 1428 (1976).

On rapporte les déplacements chimiques en résonance magnétique nucléaire du ^{13}C du sulfite d'éthylène et de 17 de ses dérivés. En se basant sur les amplitudes des déplacements et sur les principes de l'analyse conformationnelle, on est porté à croire à l'existence, en solution, de conformations enveloppe tordue. On suggère des chemins de pseudorotation qui n'impliquent pas une inversion au niveau de l'atome de soufre.

[Traduit par le journal]

Introduction

The conformational analysis of cyclic sulfites is an area of current interest in several laboratories. For ethylene sulfites, physical methods such as infrared (ir) spectroscopy (1), ^1H nmr (2–6), and electron diffraction (7) have been applied to the problem.

The early ir data (1) for ethylene sulfite were interpreted in terms of a conformational equilibrium in solution as depicted in Scheme 1.

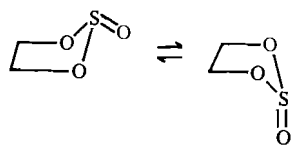

SCHEME 1

Subsequently, variable temperature proton nmr work (2, 3) led to the postulate of a 'non-inverting' ring with a pseudo axial preference for the S=O bond. On the basis of ^1H nmr chemical shift additivity relationships and a similar solvent and concentration dependence of the S=O stretching frequency, methyl and phenyl-substituted ethylene sulfites were deemed to possess similar geometries to the parent compound (4, 5). The most recent nmr work (6) which presents a detailed analysis of vicinal couplings, suggests the existence of twist-envelope forms which are interconverted by rapid pseudorotatory paths not involving inversion at sulfur (Scheme 2). By contrast, an electron diffraction

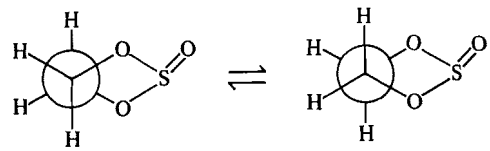

SCHEME 2

study (7) has indicated an essentially planar structure for the ethylene sulfite ring.

For trimethylene sulfites (8) and thiane-oxides (9) it has been found that ^{13}C nmr is a valuable method for conformational analysis, as the chemical shifts are highly sensitive to the stereochemistry of the S=O bond. Since ^1H decoupled ^{13}C spectra are first order the application of this technique to the ethylene sulfite problem seems

[1]Author to whom correspondence should be addressed.

Can. J. Chem. Downloaded from www.nrcresearchpress.com by 210.87.254.6 on 09/05/12
For personal use only.

TABLE 1. ^{13}C chemical shifts of ethylene sulfites (δ_c from TMS ± 0.1)*

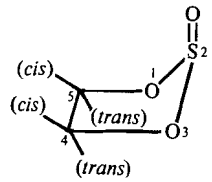

Compound*	Position											
	C-4	C-5	4-CH_3 (*cis*)	4-CH_3 (*trans*)	4-CH_2-X† (*cis*)	4-CH_2-X† (*trans*)	5-CH_3 (*cis*)	5-CH_3 (*trans*)	C-quat.	C-*o*	C-*m*	C-*p*
1	67.6	67.6										
2	76.5	72.9		17.8								
3	80.2	70.9	18.7									
4	89.2	75.6	26.4	26.4								
5	80.5	85.4		15.9			18.0					
6	78.5	78.5		14.4				14.4				
7	81.2	81.2	16.2				16.2					
8	90.7	80.6	25.5	22.7				13.5				
9	88.7	86.1	25.8	23.2			15.7					
10	91.0	91.0	24.2	23.8			24.2	23.8				
11	79.3	69.5				42.9						
12	81.4	70.4			43.7							
13	77.9	68.9				66.8			158.2	114.9	129.7	122.0
14	79.9	70.0			68.6				158.2	114.9	129.7	122.0
15	80.9	73.5							134.7	126.6	129.0	129.4
16	85.6	71.4							134.1	127.5	129.0	129.4
17	84.8	84.8							132.6	126.8	128.6	128.1
18	86.9	86.9							133.3	127.5	128.3	128.0

*0.05–0.10 *M* solutions in $CDCl_3$.
†For compounds **11** and **12** X = Cl; for compounds **13** and **14** X = OPh.

attractive. Herein we present ^{13}C data for ethylene sulfite and 17 substituted derivatives, in which comparison with trends found in the trimethylene sulfites permits some useful conformational deductions.

Results and Discussion

^{13}C chemical shifts for the materials examined as $CDCl_3$ solutions are presented in Table 1. Assignments are based on well established trends of alkyl substitution (10), selective ^1H decoupling using published ^1H data (4, 5), and single frequency off-resonance decoupling (SFORD) experiments.[2]

Before embarking on a detailed discussion of the ethylene sulfite data, it is necessary to recall the major stereochemical features of the ^{13}C shifts for trimethylene sulfites (8). Initially, the 'γ' shift is a useful indicator of the interaction of an axial S=O bond with *syn*-axial H's, **I**(ax), and results in a shielding of the γ carbon of *ca.* 9 ppm relative to the case where the S=O is equatorial, **I**(eq). Replacement of a *syn*-axial H

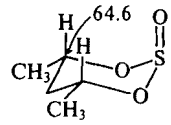

I (ax)

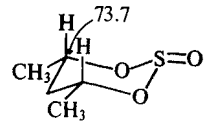

I (eq)

by a carbon results in the loss of the major part of the 'γ' shift as indicated in **II**(ax) and **II**(eq).

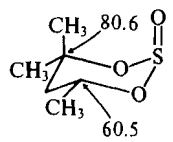

II (ax)

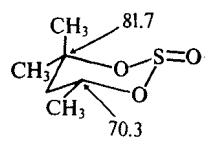

II (eq)

[2]Specifically, relative assignments of C-4 and C-5 in **2–4**, **8**, **9**, **11**, **12**, **15**, and **16** were made by off-resonance decoupling. For **5**, **13**, and **14** selective ^1H decoupling permitted unambiguous assignments, since the ^1H spectra of these materials have been analyzed (4, 5).

Can. J. Chem. Downloaded from www.nrcresearchpress.com by 210.87.254.6 on 09/05/12
For personal use only.

Can. J. Chem. Downloaded from www.nrcresearchpress.com by 210.87.254.6 on 09/05/12
For personal use only.

A second, albeit less dramatic, result, is the so-called 'δ' shift (11) in which a methyl group which is *syn*-axial, **III**(ax), to an S=O bond experiences a minor deshielding effect relative to its equatorial counterpart.

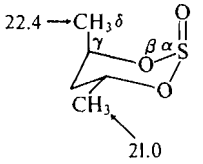

III (ax)

With these findings as a background it is interesting to compare shifts for the epimeric 4-methyl ethylene sulfites **2** and **3**. For **2**, having the CH_3 *trans* to the S=O, the preferred conformation is suggested (6) to be that depicted as **2***a* in which the CH_3 is essentially equatorial and the C-4 H is axial. (Newman projection along C-4–5 bond.) In isomer **3**, however, there will be

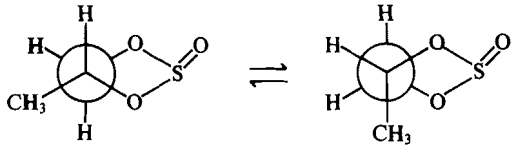

2*a* **2***b*

repulsive van der Waals interactions between the *cis* CH_3 hydrogens and the S=O function which will force the conformational equilibrium toward **3***b*. Also *gauche* CH_3- - -O interactions will destabilize **2***b* and **3***a*.

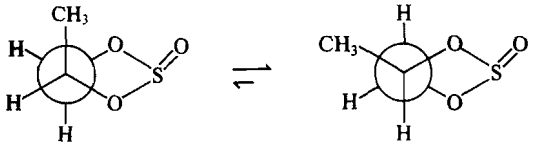

3*a* **3***b*

The 'γ' shifts for **2** and **3** are consistent with these conformational arguments. For **2**, C-4 is shielded by 3.7 ppm relative to C-4 of **3**, since the H on C-4 is *syn*-axial to the S=O in **2***a*. Conversely, C-5 of **2** is deshielded relative to this position in **3** by *ca.* 2 ppm since C-5 of **3***b* bears a H which is *syn*-axial to the S=O bond. The minor 'δ' shift for the CH_3 of **3** (0.9 ppm) may arise from the contribution of conformer **3***a*. An alternative argument which is more satisfying from the energetic point of view, is that the CH_3 of **2** is preferentially *shielded* compared to **3** due to the contribution from **2***b*. In **2***b* there is a *gauche* CH_3- - -O interaction which is known to cause increased shielding at carbon (12). Quantitatively, the ^1H data (6) led to a suggestion that the preference for **2***a* is *ca.* 60% and for **3***b* is *ca.* 95%. The ^{13}C data are qualitatively supportive.

In the *gem*-dimethyl derivative **4** it is somewhat surprising that there is no shift difference between the CH_3 groups. From previous arguments the preferred rotamer should be **4***a* in which the axial CH_3 has no steric compression with the S=O. The *gauche* CH_3- - -O interaction

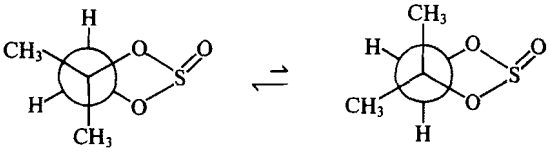

4*a* **4***b*

is expected to shield the axial CH_3 in **4***a* (12), however, no effect is observed.

For the *trans*-vicinal dimethyl compound **5**, again viewing the Newman projection along the C-4–C-5 bond, it has been proposed (6) that a conformer similar to **5***a* should dominate. To relieve the *gauche* CH_3- - -CH_3 interaction in **5***a*, it has been suggested on the basis of vicinal couplings (6) that the molecule may assume an intermediate geometry as indicated in **5***c*. The

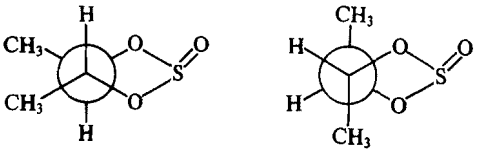

5*a* **5***b*

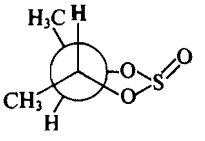

5*c*

upfield γ shift at C-4 relative to C-5 is in qualitative agreement with a quasi-axial H on C-4, and the quasi-axial CH_3 at C-5 is evidenced by its deshielding relative to the C-4 CH_3 group.

Comparing the other vicinal dimethyl isomers **6** and **7**, the substitution of two CH_3 groups *trans*, **6**, and *cis*, **7**, to the S=O bond produces in each case rotamers that are equivalent by symmetry. The shielding γ effect for C-4,5 of **6**

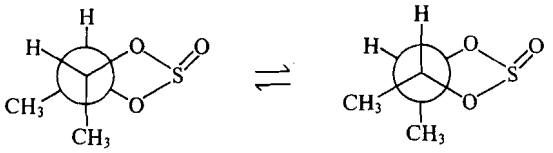

6*a* 6*b*

(2.7 ppm) and the deshielding δ effects for the CH_3's of **7** are consistent with earlier arguments.

The possible staggered twist-envelope forms for the trimethyl compounds **8** and **9** are illustrated in Scheme 3. In order to suggest preferred forms, a value of 1.1 kcal/mol (6) is used for each *syn*-axial CH_3- - -S=O interaction, 0.3 kcal/mol for each CH_3- - -O *gauche* interaction (13) and 0.8 kcal/mol for each CH_3- - -CH_3 *gauche* interaction (13).

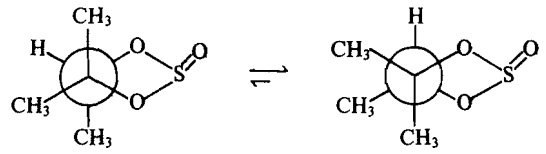

8*a* 8*b*

1.1 + 0.8 + 2(0.3) = 2.5 2(0.8) + 0.3 = 1.9

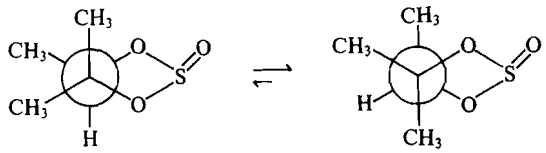

9*a* 9*b*

1.1 + 2(0.8) + 0.3 = 3.0 1.1 + 0.8 + 2(0.3) = 2.5

SCHEME 3

On this basis, substantial preferences (*ca.* 0.5 kcal/mol) are predicted for conformers **8***b* and **9***b* respectively. The C-5 chemical shifts of 80.6 in **8** and 86.1 in **9** are in accord with a *syn*-axial H- - -S=O in **8**, as in **8***b*. It is interesting to note that the C-5 CH_3 shift in **8** of 13.5 ppm is the most shielded of any methyl resonance in these compounds. The presence of two *gauche* CH_3- - -CH_3 interactions in **8***b*, which are known to cause increased shielding (14), no doubt account for this. For **9** the C-5 CH_3 group resonates at 15.7 ppm. Presumably this follows from the preponderance of conformer **9***b* in which there is a deshielding *syn*-axial CH_3- - -S=O interaction (δ effect) in addition to the CH_3- - -O and CH_3- - -CH_3 *gauche* interactions.

In the tetramethyl system **10** the CH_3's *cis* to the S=O are deshielded by only 0.4 ppm relative to the *trans* groupings. The presence of the two *cis*-CH_3's may be sufficient to cause the ethylene sulfite ring to distort such that the S=O bond becomes equatorial or at least pseudo axial. thereby decreasing the δ effect.

By analogy with **2** and **3**, the preferred rotamers of **11** and **12** are presumably **11***a* and **12***b* respectively.

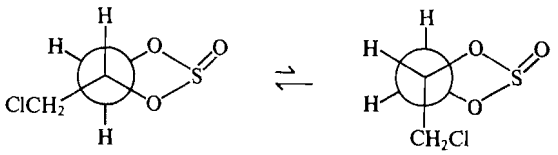

11*a* 11*b*

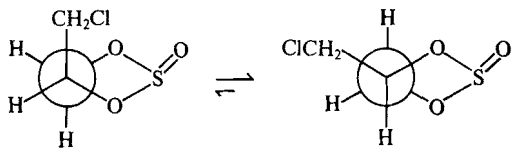

12*a* 12*b*

The 'γ' shifts at the C-4 position of **11** *vs.* **12** are in agreement with an axial H at C-4 of **11**. Also the minor shielding effect (0.8 ppm) observed for the CH_2—Cl carbon of **11** reflects the greater contribution which **11***b* makes to the time averaged geometry of **11** relative to the contribution of **12***a* to **12**. Similar arguments apply to the results for **13** and **14** (X = OPh in Table 1). The only apparent anomalies in the comparison of ^{13}C data for **11**–**14** with **2** and **3** are the C-5 chemical shifts. In **3** it was argued that the predominance of **3***b* in which there is a *syn*-axial H- - -S=O interaction shields the C-5 of **3** relative to **2**. For the corresponding compounds **12** and **14** C-5 becomes slightly deshielded (*ca.* 1 ppm) relative to **11** and **13** respectively. Apparently replacement of a methyl hydrogen by a larger Cl or OPh group introduces a further (unaccountable at present) perturbation.

For the 4-phenyl isomers **15** and **16**, the shifts at C-4 and C-5 are in accord with the trends noted for the corresponding methyl compounds **2** and **3**, thereby supporting the case for the predominance of conformers **15***a* and **16***b* respectively, in solution.

Can. J. Chem. Downloaded from www.nrcresearchpress.com by 210.87.254.6 on 09/05/12
For personal use only.

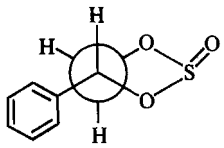

15*a*

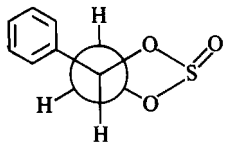

16*b*

Compounds **17** and **18**, having the vicinal phenyl groups *trans* and *cis* to the S=O bond respectively, exhibit γ effects at C-4,5 of similar magnitude to the analogous dimethyl isomers **6** and **7**. Accordingly one can suggest similar solution conformations for these systems. In conclusion it is evident that the ^{13}C γ shifts provide useful information regarding ethylene sulfite conformations. Support for the concept of twist-envelope forms in which there are rapid pseudorotation paths, not involving conformation inversion at sulfur, is gained.

Experimental

Spectra

The ^{13}C chemical shifts were determined using previously described procedures (15).

Materials

Syntheses and physical data for all sulfites described have been reported earlier (4–6).

Acknowledgement

G. W. Buchanan thanks the National Research Council of Canada for financial support and Mrs. V. Paré for technical assistance.

1. P. B. de la Mare, W. Klyne, D. J. Millen, J. G. Pritchard, and D. Watson. J. Chem. Soc. 1813 (1956).
2. H. Finegold. J. Phys. Chem. **72**, 3244 (1968).
3. H. Finegold. J. Phys. Chem. **73**, 4020 (1969).
4. C. H. Green and D. G. Hellier. J. Chem. Soc. Perkin Trans. II, 243 (1973).
5. C. H. Green and D. G. Hellier. J. Chem. Soc. Perkin Trans. II, 1966 (1973).
6. C. H. Green and D. G. Hellier. J. Chem. Soc. Perkin Trans. II, 190 (1975).
7. B. A. Arbuzov, V. A. Naumov, N. M. Zaripov, and L. D. Pronicheva. Dokl. Akad. Nauk S.S.S.R. **198**, 1333 (1970).
8. G. W. Buchanan, J. B. Stothers, and G. Wood. Can. J. Chem. **51**, 3746 (1973).
9. G. W. Buchanan and T. Durst. Tetrahedron Lett. 1683 (1975).
10. J. B. Stothers. Carbon-13 NMR spectroscopy. Academic Press, New York, N.Y. 1972. p. 57.
11. S. H. Grover, J. P. Guthrie, J. B. Stothers, and C. T. Tan. J. Magn. Reson. **10**, 227 (1973).
12. G. W. Buchanan, D. A. Ross, and J. B. Stothers. J. Am. Chem. Soc. **88**, 4301 (1966).
13. N. L. Allinger, S. J. Angyal, E. L. Eliel, and G. A. Morrison. Conformational analysis. Wiley-Interscience, New York. 1965, pp. 437–439.
14. D. M. Grant and E. G. Paul. J. Am. Chem. Soc. **86**, 2984 (1964).
15. G. W. Buchanan, C. Reyes-Zamora, and D. E. Clarke. Can. J. Chem. **52**, 3895 (1974).

Can. J. Chem. Downloaded from www.nrcresearchpress.com by 210.87.254.6 on 09/05/12
For personal use only.

Etude par résonance magnétique nucléaire des propriétés acides de l'éthyltrifluoroacétoacétate d'uranium(IV)

J. PARIS ET G. FOLCHER

CEN-Saclay, Commissariat à l'Energie Atomique, B.P. 2, 91190 Gif-sur-Yvette, France

Reçu le 21 février 1975[1]

J. PARIS et G. FOLCHER. Can. J. Chem. **54**, 1433 (1976).

Le composé $(CF_3COCHCOOC_2H_5)_4U$ a été préparé. Les déplacements chimiques des protons du groupe éthyle sont très importants et ont été trouvés très sensibles aux interactions avec le solvant. Leur étude a permis d'établir certaines corrélations avec d'autres grandeurs physiques accessibles par ailleurs. Ces déplacements peuvent être interprétés comme résultant de la variation de la répartition des électrons non appariés de l'uranium entre le chélatant et la base.

J. PARIS and G. FOLCHER. Can. J. Chem. **54**, 1433 (1976).

The compound $(CF_3COCHCOOC_2H_5)_4U$ has been prepared. The chemical shifts of the ethyl protons are very important and were found to be very sensitive to interactions with the solvent. From their study certain correlations were established with physical quantities available elsewhere. These displacements can be interpreted as resulting from the variation of the sharing of the non-paired electrons of uranium between the chelate and the base.

[Journal translation]

Introduction

Il a été montré (1) que les β dicétonates d'uranium(IV) présentent des propriétés de réactifs conformationnels. Cet effet met en évidence des interactions de type acide base entre ces chélates et les molécules capables de se comporter comme des donneurs. Une bonne connaissance de ces interactions ainsi que des composés d'addition formés permettrait une meilleure utilisation de ces réactifs. Les propriétés acides d'un nombre important de molécules présentant une acidité de Lewis ont été étudiées par ir (2–6). Il est plus difficile d'accéder aux acidités des ions métalliques engagés dans des chélates par cette méthode. Les déplacements chimiques d'un proton appartenant à un acide ont été utilisés (7–9) pour apprécier la force des liaisons formées dans le composé d'addition. La difficulté avec les déplacements d'origine paramagnétique réside dans l'ambiguité de l'interprétation des résultats. En effet, le déplacement est la somme d'un terme de pseudocontact dépendant des propriétés géométriques de la molécule et d'un terme de contact dépendant de la délocalisation des électrons du métal et il est difficile de prévoir comment la stabilité du composé formé va influer sur chacun de ces termes.

Il a été montré (10) que dans le cas de l'association des chélates de nickel avec des anilines substituées les déplacements chimiques de contact des protons des bases varient largement.

Dans l'exemple particulier que nous avons choisi nous nous sommes intéressés aux protons du chélate et nous nous sommes efforcés d'établir des relations simples entre ces déplacements chimiques et la force des liaisons que ce composé peut établir avec diverses bases.

L'analyse des relations entre la nature de la base et la stabilité des produits d'addition a été interprêtée en s'appuyant sur la théorie de Drago et Wayland (11) qui permet de déterminer les parts relatives de covalence et des interactions électrostatiques dans ces composés d'addition.

Partie expérimentale

Le composé est préparé de même façon que les β dicétonates d'uranium (1). On mélange une solution aqueuse d'U^{IV} à pH 1 avec HTFEA ($CF_3COCH_2COOC_2H_5$) et on agite pendant 15 min. Le précipité qui se forme lentement est filtré, lavé à l'eau et recristallisé dans le benzène. On obtient ainsi un solide vert, contrairement aux autres β dicétonates d'uranium. Le composé se détériore lentement si on le laisse exposé à l'air humide, mais conserve son aspect si on le maintient en dessicateur.

Les spectres sont obtenus sur un appareil Varian NV14. On opère en général sur des solvants non deutériés.

Résultats

La fig. 1 représente le spectre de résonance du

[1]Revision reçue le 15 décembre 1975.

Can. J. Chem. Downloaded from www.nrcresearchpress.com by 210.87.254.42 on 09/05/12
For personal use only.

Can. J. Chem. Downloaded from www.nrcresearchpress.com by 210.87.254.42 on 09/05/12
For personal use only.

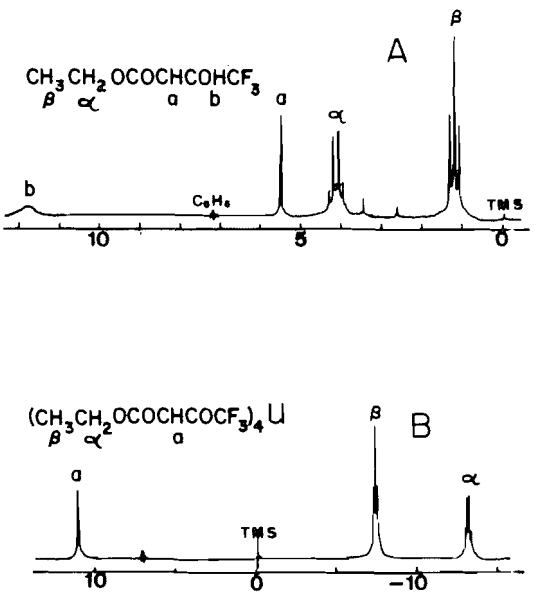

FIG. 1. Spectre rmn du proton pour: *A* le trifluoroacétylacétone; *B* le trifluoroacétylacétate d'uranium(IV) (en solution dans le CCl_4 à 20% de benzène).

proton de HTFEA et de $(TFEA)_4U$ dans CCl_4. On identifie sans difficulté les pics attribuables au radical éthyle et au proton méthylénique. Il est à noter que le déplacement chimique du groupement éthyle est plus important que pour des composés semblables (12) et apparaissant à plus de 7 ppm vers les hauts champs, il peut être observé même dans des solvants protonés.

La tableau 1 présente les valeurs des déplacements chimiques des protons du groupe éthyle $\Delta\delta_\alpha$ et $\Delta\delta_\beta$ ainsi que du proton méthylénique $\Delta\delta_m$.

TABLEAU 1. Déplacements chimiques des protons du trifluoacétylacétate d'uranium pour différentes bases

Base	$\Delta\delta_\alpha$	$\Delta\delta\beta$	$\Delta\delta_m$
Hexane	17.70	9.10	—
Benzène	17.43	8.93	−5.57
p-Xylène	17.23	8.83	−5.68
β,β′-Dichloroethylether	17.23	8.84	−6.39
Mesitylène	17.03	8.73	—
Acétonitrile	15.67	8.07	−6.25
Acétone	14.43	7.43	−6.92
Dioxane	13.60	7.13	—
Pyridine	12.38	6.42	−8.82
Aniline	12.38	6.40	−8.05
Dimethylformamide	11.27	5.90	—
Triisobutylphosphate	10.43	5.37	−5.75
Triisobutylamine	11.37	5.92	—

Pour les trois cas $\Delta\delta$ représente la différence en ppm entre les fréquences de résonance des protons du HTFEA et du $(TFEA)_4U$. La partie diamagnétique du déplacement est négligeable devant la partie paramagnétique comme l'a montré Wiedenheft (12) en comparant des β dicétonates de thorium et d'uranium. $(TFEA)_4U$ étant dissout dans le composé B avec lequel il forme un composé d'addition, nous considérerons que l'équilibre

$$(TFEA)_4U + B \rightleftarrows (TFEA)_4UB$$

est entièrement déplacé vers le composé d'addition et qu'il n'existe pas de $(TFEA)_4U$ libre. Par ailleurs, on n'a pas déterminé avec chacune des bases la stoechiométrie du composé d'addition mais il a été vérifié, par ailleurs, (1) que les β dicétonates d'U^{IV} ne donnaient que la stoechiométrie 1:1 avec diverses bases fortes. En effet, le déplacement chimique de la base varie linéairement avec le rapport molaire [U]/[Base], ce qui est en accord avec les conclusions de Reuben (13). La linéarité de cette courbe jusqu'à des valeurs du rapport molaire de 0.7 (1) montre que la constante est élevée.

Dans le cas de bases faibles comme le benzène nous pensons que le très gros excès de ces molécules par rapport à celles du composé d'uranium implique que peu de molécules de ce composé sont libres. Nous faisons l'hypothèse que la stoechiométrie est conservée.

Des mesures à température variable ont également été faites dans deux cas extrêmes: celui du benzène et celui de la pyridine. La fig. 2 montre

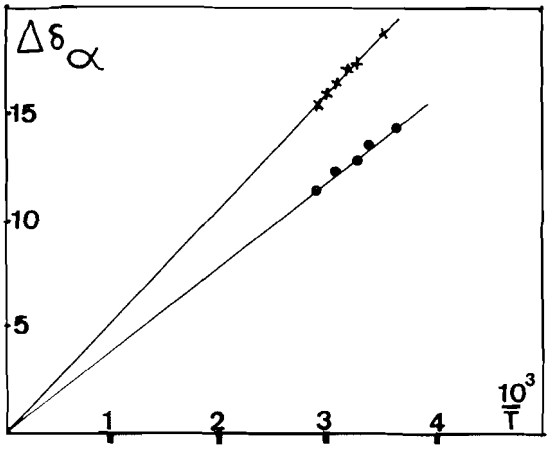

FIG. 2. Déplacements chimiques des protons du quadruplet en fonction de l'inverse de la température: × benzène, ● pyridine.

que les déplacements sont linéaires en I/T pour les protons du groupe éthyle et que l'extrapolation à $I/T = 0$ conduit à un déplacement sensiblement nul ce qui n'est pas vérifié sur d'autres chélates tels que $(BTFA)_4U$ (BTFA = $C_6H_5COCHCOCF_3$).

Enfin, nous nous sommes assurés que l'uranium était bien lié aux oxygènes cétoniques et non à l'oxygène adjacent au groupe éthyle. Le spectre ir de $(TFEA)_4U$, dans KBr ne montre pas de bandes attribuables à un C=O non complexé (attendue à 1720 cm^{-1}) et on trouve bien les fréquences C=O complexé à 1630 et 1580 cm^{-1}, fréquences voisines de celles rapportées par Grinberg *et al.* (14) et Yoshimura *et al.* (15) pour plusieurs β dicétones d'U^{IV}.

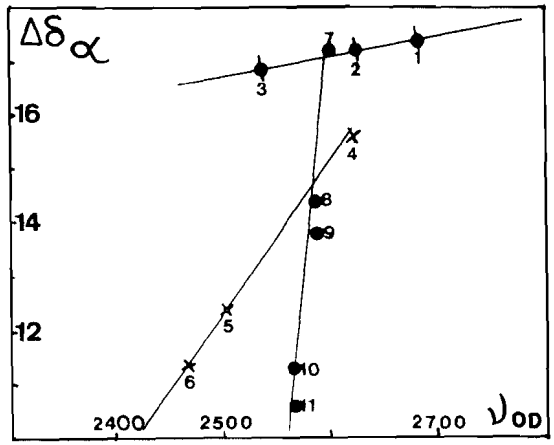

FIG. 3. Déplacements chimiques des protons du quadruplet en fonction de la fréquence infrarouge de la liaison OD du méthanol pour (*1*) le benzène; (*2*) le xylène; (*3*) la diméthylaniline; (*4*) l'acétonitrile; (*5*) la pyridine; (*6*) la triisobutylamine (*7*) le dichloroéthylether; (*8*) l'acétone; (*9*) le dioxane; (*10*) le diméthyl formamide; (*11*) le triisobutylphosphate.

Discussion

Propriétés acides

Le déplacement chimique des protons du chélate est l'indice sensible des interactions de ce chélate avec le solvant. La question est de savoir comment cette mesure se relie à la basicité du solvant et quelle indication elle donne sur l'acidité du chélate.

Les bases provoquant un déplacement chimique provoquent aussi un déplacement des fréquences de vibration d'acides tels que le méthanol, le pyrrole, l'acide cyanhydrique. Si on reporte le $\Delta\delta$ des protons en fonction du $\Delta\nu$ variation de la fréquence de vibration de la liaison X—H chaque valeur étant prise pour une base donnée, on constate qu'il y a une certaine corrélation dans le cas méthanol suivant la nature du donneur (fig. 3). Dans le cas du pyrrole, $\Delta\delta$ et $\Delta\nu$ varient dans le même sens, quelle que soit la base considérée et la nature de l'atome donneur. Cette remarque suggère que l'on ne peut pas définir les interactions acide–base par un seul paramètre, mais qu'il convient de les mesurer par un couple de paramètres conformément à la théorie de Drago et Wayland (11). Selon cette théorie, on peut représenter un acide par deux paramètres E_A et C_A et une base par deux paramètres E_B et C_B, de sorte que l'enthalpie de formation de l'adduit s'écrive

$$-\Delta H = E_A E_B + C_A C_B$$

Les valeurs $E_A = 1$, $C_A = 1$ ont été arbitrairement affectées à l'iode. Les valeurs de E_B et C_B ont été déterminées pour un nombre important de bases par des mesures calorimétriques. Il a été montré sur de nombreux exemples qu'il y a une bonne corrélation entre ΔH et $\Delta\nu_X$-H (16).

Si on compare le comportement du pyrrole et celui de $(TFEA)_4U$ par rapport à toutes les bases, on constate que $\Delta\delta$ est proportionnel à $\Delta\nu_X$-H (tableau 2). Comme $\Delta\nu_X$-H est proportionnel à l'enthalpie de formation de l'adduit, donc à la quantité $E_pE_B + C_pC_B$ (p correspondant au pyrrole) quel que soit E_B et C_B. $\Delta\delta$ devra donc s'exprimer sous une forme analogue $RE_B + SC_B$ avec $R/S = E_p/C_p$. Ceci montre que $\Delta\delta$ est proportionnel à l'enthalpie de formation de l'adduit et que les paramètres E_u et C_u sont proportionnels à ceux du pyrrole. Le rapport E/C est de 8.6 (17) pour le pyrrole. On doit attendre une valeur voisine pour l'uranium dans le chélate. Cette valeur peut être comparée à la valeur obtenue dans le cas analogue de l'hexafluoroacétylacétonate de cuivre $E/C = 2.42$ (17). Elle confirme le fait que l'U^{4+} se présente dans la classification de Pearson (18) comme un accepteur plus dur que Cu^{2+} lequel occupe une position intermédiaire (19).

Le cas des interactions avec les hydrocarbures aromatiques peut être souligné, Caldow et Thomson (4) ont montré, dans le cas de l'interaction de l'acide cyanhydrique avec les cycles aromatiques, que l'on pouvait relier $\Delta\nu$ de HCN

Can. J. Chem. Downloaded from www.nrcresearchpress.com by 210.87.254.42 on 09/05/12
For personal use only.

TABLEAU 2. Paramètres de Drago et déplacements chimiques pour les protons du trifluoroacétylacétate d'uranium

Base	C^e	E^e	$\Delta\delta_{calc.}{}^a$	$\Delta\delta_{exp.}{}^b$
Benzène	0.681	0.525	3.28	3.87
p-Xylène	1.78	0.416	3.20	4.07
Mesitylène	2.19	0.574	4.30	4.27
Acétone	2.33	0.987	6.76	6.87
p-Dioxane	2.38	1.09	7.29	7.70
Acétonitrile	1.34	0.886	5.62	5.63
DMF	2.48	1.23	8.14	10.03
Pyridine	6.40	1.17	9.76	8.92
TBP[c]	6.55	0.838	8.80	10.87
Triisobutylamine[d]	11	1	12.10	9.93

[a]Les valeurs sont calculées en prenant les meilleures valeurs pour E_u et C_u.
[b]Les valeurs expérimentales sont les déplacements mesurés par rapport au composé supposé gazeux. Le meilleur accord est obtenu en prenant 21.3 ppm pour le composé sans interaction. Les calculs sont faits sur les déplacements des protons notés "α" (fig. 1).
[c]Les valeurs de E et C sont celles de la triméthylphosphine.
[d]Les valeurs de E et C sont celles de la triethylamine.
[e]Les valeurs de C et E sont extraites de l'article de Drago (17).

avec les paramètres de Taft $\sum(\sigma_I + \sigma_R)$ des cycles. La fig. 4 montre qu'une corrélation analogue est observée entre les paramètres de Taft et les déplacements des protons de notre chélate. Cette corrélation démontre l'existence d'interaction entre les hydrocarbures aromatiques et le chélate d'uranium. Cette interaction se faisant suivant l'axe perpendiculaire du cycle. On peut aussi en déduire que dans le cas de la diméthylaniline la liaison se fait par le cycle et non par l'azote.

Déplacements chimiques

Les déplacements chimiques paramagnétiques des protons de $(CF_3COCHCOOC_2H_5)^-$, lié à l'uranium(IV) par rapport à un chélate où l'ion central serait diamagnétique, sont dus à deux types d'interaction: contact et pseudocontact.

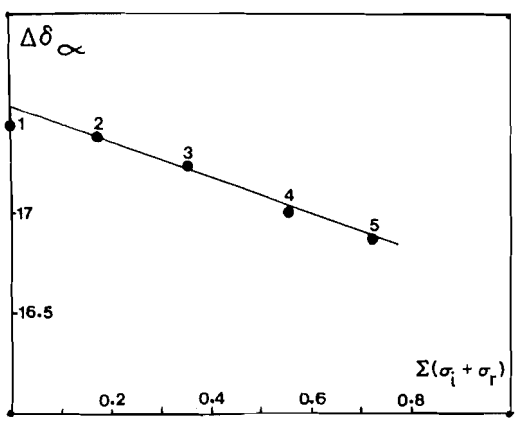

FIG. 4. Déplacements chimiques des protons du quadruplet en fonction des paramètres de Taft pour (*1*) le benzène; (*2*) le toluène; (*3*) le xylène; (*4*) le mésitylène; (*5*) la diméthylaniline.

Les déplacements de contacts sont calculés par l'expression

$$\frac{\Delta H}{H} = -A_i \frac{\gamma_e}{\gamma_H} \frac{g\beta S(S+1)}{6kT}$$

où A_i est la constante de couplage hyperfin, γ_e et γ_H les rapports gyromagnétiques de l'électron et du proton et g la valeur moyenne du facteur spectroscopique. La partie du pseudocontact peut se mettre sous la forme

$$\frac{\Delta H}{H} = \frac{\beta^2}{kT} F$$

conforme à la variation linéaire en I/T du déplacement mesuré fig. 2, où F est une fonction des positions des atomes dans le chélate du type de l'éq. 21, calculée par Kurland et McGarvey (20). Dans le cas de l'uranium, elle n'aurait pas nécessairement la forme en

$$\frac{3\cos^2\theta - 1}{R_i^3}$$

de McConnell et Robertson (21) en symétrie axiale.

Nous observons donc les protons du groupe éthyle donnant un quadruplet et un triplet et le proton méthylénique qui donne un singulet. Le fait que chaque type de proton du ligand ne donne qu'une position de résonance (1, 12, 22, 23) s'explique généralement par un échange

Can. J. Chem. Downloaded from www.nrcresearchpress.com by 210.87.254.42 on 09/05/12
For personal use only.

Can. J. Chem. Downloaded from www.nrcresearchpress.com by 210.87.254.42 on 09/05/12
For personal use only.

rapide des ligands entre diverses positions possibles.

Pour une base donnée, les déplacements des protons en α et β de l'oxygène s'écrivent

$$\Delta\delta_\alpha = K\frac{gA_\alpha}{kT} + \frac{\beta^2}{kT}F_\alpha$$

$$\Delta\delta_\beta = K'\frac{gA_\beta}{kT} + \frac{\beta^2}{kT}F_\beta$$

K et K' sont deux constantes et F_α F_β les valeurs de la fonction F correspondantes aux positions des protons en α et en β de l'oxygène.

Lorsque la base change, on doit s'attendre à une variation des facteurs g,A ainsi que des paramètres géométriques du chélate, donc de la fonction F.

On constate (fig. 5) que $\Delta\delta_\alpha$ et $\Delta\delta_\beta$ varient proportionnellement. Ce résultat pourrait être obtenu si les deux termes des $\Delta\delta$ étaient proportionnels à une même quantité, par exemple la densité de spin non apparié, mais alors le déplacement du proton méthylénique serait aussi proportionnel à $\Delta\delta_\alpha$ et $\Delta\delta_\beta$, ce qui n'est pas le cas. La proportionnalité de $\Delta\delta_\alpha$:$\Delta\delta_\beta$ peut être obtenue dans certains cas si l'un des termes est négligeable devant l'autre. Si le terme de contact est négligeable

$$\frac{\Delta\delta_\alpha}{\Delta\delta_\beta} = \frac{F_\alpha}{F_\beta}$$

Ce rapport peut rester constant si la géométrie des divers adduits est la même, quelle que soit la base, mais la variation des $\Delta\delta$ serait alors uniquement fonction de facteurs de la forme $(g_\perp - g_\parallel)$ et la corrélation avec la basicité serait fortuite.

Si le terme de pseudocontact est négligeable, on a

$$\frac{\Delta\delta_\alpha}{\Delta\delta_\beta} = \frac{A_\alpha}{A_\beta}$$

A_α/A_β décrit la répartition de spin non apparié sur les groupes CH_2 et CH_3, rapport qu'il est raisonnable de supposer constant.

Dans cette hypothèse, $\Delta\delta$ varie comme le produit gA. La variation du déplacement due à g ne semble pas raisonnable, étant donné l'importance de cette variation. Or, on a vu qu'il y a proportionnalité entre $\Delta\delta$ et la fonction de Taft (*cf.* fig. 4) qui chiffre la densité électronique d'un cycle participant à la liaison avec

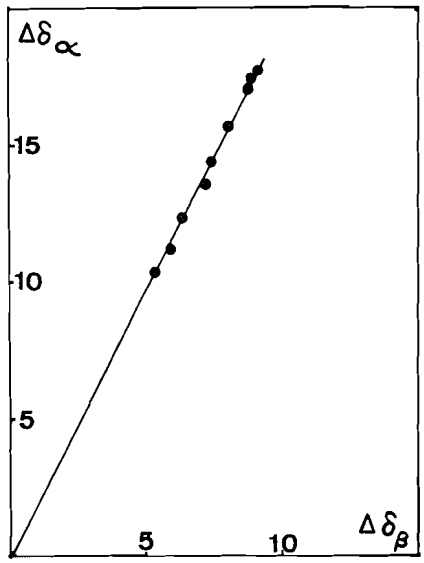

FIG. 5. Déplacements chimiques des protons du quadruplet en fonction de ceux du triplet pour toutes les bases utilisées.

l'uranium dans le chélate. On peut alors avancer l'hypothèse selon laquelle les valeurs de A qui dépendent de la densité de spin des électrons f de l'uranium susceptibles de se délocaliser sur les atomes du chélatant diminuent quand cette densité de spin peut aussi se délocaliser vers la molécule basique de l'adduit.

Ce résultat rejoint celui de Berus *et al.* (10) qui ont montré, sur des β dicétonates de nickel, que quand la force de la base croît, la densité d'électron non apparié sur cette base croît. Cette croissance se fait donc au détriment de la densité d'électrons non appariés sur le chélatant.

De plus, Schwendiman et Zink qui ont mesuré la susceptibilité magnétique et les déplacements de chélate d'europium dans divers solvants, plus ou moins donneurs, n'ont pas trouvé des corrélations très nettes entre ces deux quantités (24).

Ils interprètent, par contre, leurs résultats plutôt par l'intervention du déplacement de pseudocontact. Wiedenheft (12) explique aussi la majeure partie des déplacements d'un chélate d'uranium par le pseudocontact. Nous pensons que le cas du chélate $(TFEA)_4U$ est différent. En effet, si on admet une structure antiprismatique pour les chélates d'uranium(IV) (25), l'angle moyen que fait la chaîne éthyle avec l'axe de l'antiprisme est voisin d'une valeur qui annule $3\cos^2\theta - 1$.

Le cas du proton méthylénique est différent et l'absence de proportionnalité entre son déplacement et celui des protons de la chaîne éthyle signifie que contact et pseudocontact apportent tous deux des contributions comparables. En effet, dans la structure antiprismatique, sa position est telle que pour lui $3\cos^2\theta - 1$ est maximum.

L'ensemble des résultats obtenus nous permet donc d'avancer l'hypothèse d'un déplacement d'origine essentiellement de contact pour les protons de la chaîne éthyle, déplacement fortement fonction du partage de la densité de spin de l'uranium(IV) entre le chélatant et les molécules basiques formant un adduit.

Remerciements

Ce travail a été effectué dans le Service EPCP du Département de Génie Isotopique. Nous tenons à remercier M. Rigny pour les discussions fructueuses que nous avons eues sur ce sujet.

1. G. Folcher, J. Paris, P. Plurien, P. Rigny et E. Soulie. Chem. Commun. 3, 1974.
2. W. Wordy et S. C. Stanford. J. Chem. Phys. **9**, 204 (1941).
3. L. J. Bellamy, H. E. Hallam et R. L. Williams. Trans. Faraday Soc. **54**, 1120 (1958).
4. G. L. Caldow et H. W. Thomson. Proc. R. Soc. London, A, **254**, 1 (1960).
5. J. A. Pollin et R. L. Werner. Nature, 206, (1965).
6. W. Lesch et R. Ulbrich. Z. Naturforsch. Teil A, **23**, 1939 (1968).
7. D. P. Eyman et R. S. Drago. J. Am. Chem. Soc. **88**, 1617 (1966).
8. T. Gramstad et E. D. Bercker. J. Mol. Struct. **3**, 253 (1970).
9. F. L. Slejko, R. S. Drago et D. G. Brown. J. Am. Chem. Soc. **94**, 9210 (1972).
10. E. I. Berus, P. V. Schastnev, V. A. Barkharsh et Y. U. N. Molin. Zh. Strukt. Khim. **14**, 34 (1975).
11. R. S. Drago et G. B. Wayland. J. Am. Chem. Soc. **87**, 3571 (1965).
12. C. Wienenheft. Inorg. Chem. **8**, 1175 (1969).
13. S. Reuben. Prog. Nucl. Magn. Reson. Spectrosc. **9**, 1 (1975).
14. A. A. Grinberg, G. I. Petshak et G. S. Lozhkina. Radiokhimiya, **13**, 904 (1971).
15. T. Yoshimura, C. Miyake et S. Imoto. Bull Chem. Soc. Jpn. **46**, 2096 (1973).
16. M. D. Joeston et R. S. Drago. J. Am. Chem. Soc. **84**, 3817 (1962).
17. R. S. Drago. Struct. Bonding, **15**, 73 (1973).
18. R. G. Pearson. J. Am. Chem. Soc. **85**, 3533 (1963).
19. S. Ahrland. Struct. Bonding, **5**, 118 (1968).
20. R. J. Kurland et B. R. McGarvey. J. Magn. Reson. **2**, 286 (1970).
21. H. M. McConnell et R. E. Robertson. J. Chem. Phys. **29**, 1361 (1958).
22. J. H. Siddal, W. E. Stewart et D. G. Karraker. Chem. Phys. Lett. **3**, 498 (1969).
23. A. C. Adams et E. M. Larsen. J. Am. Chem. Soc. **85**, 3508 (1963).
24. D. Schwendiman et J. I. Zink. Inorg. Chem. **11**, 3051 (1972).
25. L. Wolf et H. Barnighausen. Acta Crystallogr. **13**, 778 (1960).

Can. J. Chem. Downloaded from www.nrcresearchpress.com by 210.87.254.42 on 09/05/12
For personal use only.

Medium effects on tetraalkylammonium ions in aqueous acid solutions

TOMASZ A. MODRO, WILLIAM F. REYNOLDS, AND KEITH YATES
Department of Chemistry, University of Toronto, Toronto, Ontario M5S 1A1

Received February 4, 1976

TOMASZ A. MODRO, WILLIAM F. REYNOLDS, and KEITH YATES. Can. J. Chem. **54**, 1439 (1976).

Medium effects upon ^1H and ^{13}C chemical shifts have been determined for some tetraalkylammonium ions in 0–10 *M* aqueous solutions of H_2SO_4, $HClO_4$, and H_3PO_4. The observed effects are very weak in magnitude, thus justifying the choice of tetraalkylammonium ions as reference standards for studies of ionic species in aqueous solutions of strong acids. The trends in the observed low-field shifts are interpreted in terms of changes in cation hydration and in hydrogen bonding between alkyl hydrogens and acid anions.

TOMASZ A. MODRO, WILLIAM F. REYNOLDS et KEITH YATES. Can. J. Chem. **54**, 1439 (1976).

On a déterminé les effets du milieu sur les déplacements chimiques du ^1H et du ^{13}C pour quelques ions tétraalkylammonium dans des solutions aqueuses de 0–10 *M* en H_2SO_4, $HClO_4$ et H_3PO_4. Les effets observés sont de très faible amplitude ce qui justifie le choix des sels des ions tétraalkylammonium comme produits de référence pour des études d'espèces ioniques dans des solutions aqueuses d'acides forts. On interprète les tendances observées dans les déplacements à bas champs en termes de changements dans l'hydratation du cation et dans les liens hydrogènes entre les hydrogènes des groupes alkyles et les anions des acides.
[Traduit par le journal]

A knowledge of the behavior of activity coefficients of cationic species is of primary importance in studies of acid–base equilibria and acid–catalyzed reactions in nondilute solutions.[1] In the acidity function approach, the medium dependence of the activity coefficients of the indicator base (f_B) and its conjugate acid (f_{BH^+}) provide a key to the understanding of the very individual behavior of different classes of organic bases in their protonation equilibria. For acid–catalyzed reactions it has been demonstrated (2) that it is possible to determine the acidity–activity coefficient dependence for the transition state of the rate-determining reorganization of the protonated substrate for some reactions in strongly acidic media. In this case, the activity coefficient under consideration, $f_{S^\ddagger}$, also involves an ionic system and its behavior can be directly compared with those of various stable cationic species of related structure. Since the activity coefficients of single ions are experimentally inaccessible, the generally accepted approach introduced by Boyd (3) involves the use of standard reference ions, and presents the ion activity coefficient relative to the reference ion, *i.e.*

$$f_{Z^+}{}^* \equiv f_{Z^+}/f_{X^+}$$

where X^+ is the standard reference cation. The most commonly used reference cation is the tetraethylammonium ion (TEA^+) which is expected to be relatively free of medium-dependent specific solute–solvent interactions.[2] This rather intuitive choice can be, in principle, tested experimentally by examining medium effects on the TEA^+ ion in aqueous solutions of strong acids and comparing them with similar effects on some structurally related ions. It is known (1) that the activity coefficients of some tetraalkylammonium ions, relative to that of TEA^+, vary significantly with a change of acidity for aqueous solutions of H_2SO_4. This can be considered, however, only as a measure of the differences in the free energy of the ion studied and the reference ion for a given medium and provides no information concerning absolute values of the changes in ion–medium interactions with the change in medium composition.

Most physical techniques such as solubility or distribution measurements only yield information about the sum of the cation and anion interactions with the medium. By contrast, measurements of nuclear magnetic resonance

[1]For a recent review of this topic see ref. 1.

[2]Recently determined (4) hydronium ion activities in aqueous solutions of strong acids are also expressed relative to the standard reference ion (TEA^+):

$$a_{H^+}{}^* \equiv a_{H^+}/f_{TEA^+}$$

Can. J. Chem. Downloaded from www.nrcresearchpress.com by 210.87.254.6 on 09/05/12
For personal use only.

Can. J. Chem. Downloaded from www.nrcresearchpress.com by 210.87.254.6 on 09/05/12
For personal use only.

shifts can provide information not only about the interaction of a specific ion with the medium, but even about the interactions of individual atoms within the molecule. Both ^1H (5) and ^{13}C (6) chemical shifts are sensitive to medium effects. In this investigation, we have determined and compared medium effects upon ^1H and ^{13}C chemical shifts for TEA^+ and other tetraalkylammonium ions in aqueous solutions of sulfuric, perchloric, and phosphoric acids. These medium-induced shifts are interpreted in terms of solvent–solute interactions, particularly with respect to the relative hydration of tetraalkylammonium ions and to the involvement of alkyl hydrogen atoms in weak hydrogen bonding with acid anions.

Experimental

Materials

Tetramethylammonium fluoroborate (Aldrich Chem. Co.) and tetraethylammonium fluoroborate (Ozark-Mahoning Co.) were used as supplied. Methyltriethylammonium fluoroborate was synthesized by methylation of triethylamine with trimethyloxonium fluoroborate (7); yield 96%, dec. 320 °C. *Anal.* calcd. for $C_7H_{18}BF_4N$: C 41.41, H 8.94, N 6.90; found: C 41.23, H 8.85, N 7.07. Tetramethylammonium and tetraethylammonium pentacyanopropenides were prepared according to Middleton *et al.* (8). All solutions were prepared by diluting the appropriate concentrated acid or dissolving the salt in distilled water. The concentrations of aqueous solutions of acids were determined from their densities; densities were measured with a DMA 02C digital precision density meter at 25.0 °C.

Chemical Shift Measurements

Proton magnetic resonance spectra were run on a Varian HA-100 spectrometer operating in the frequency sweep mode. Chemical shifts were measured relative to external TMS (coaxial tube). They were taken as the centers of gravity of multiplets, and each value represents the mean of at least two determinations. Most experiments were performed at a 0.050 *M* concentration of the tetraalkylammonium salt. ^{13}C nmr spectra were obtained on a Varian CFT-20 spectrometer operating in the pulsed Fourier transform mode. Chemical shifts were measured relative to external 1,4-dioxane (20% v/v in D_2O, coaxial tube). Tetraalkylammonium salt concentrations were 0.20 *M*.

Magnetic Susceptibility Correction

The true chemical shift relative to the chemical shift in pure water was calculated as

$$\Delta\delta(\text{true}) = \Delta\delta(\text{observed}) + \tfrac{2}{3}\pi(\chi_v^{H_2O} - \chi_v^{sol}) \times 10^6$$

where $\Delta\delta$(observed) is a measured difference between chemical shifts in a given solution and in water (in ppm); $\chi_v^{H_2O} = -0.719 \times 10^6$ (9) is the volume magnetic susceptibility of water, and χ_v^{sol} the corresponding susceptibility of the medium. Values of χ_v^{sol} were calculated from the specific magnetic susceptibilities χ_s and densities, since $\chi_v = \chi_s \times d$. For aqueous solutions of sulfuric (10), phosphoric (11), and perchloric (12) acids values of χ_s were available in the literature. For aqueous solutions of the salts, the values of χ_s were calculated from the equation (13):

$$-\chi_s = \chi_s^{H_2O} - (\chi_m - M\chi_s^{H_2O})c/1000$$

where $\chi_s^{H_2O} = -0.720 \times 10^{-6}$ is the specific susceptibility of water, χ_m is a molar magnetic susceptibility of a salt, *M* is the salt's molecular weight, and *c* is a concentration of salt, expressed in moles per 1000 g of solution. The following values of χ_m were used: $NaClO_4$, -39.0×10^{-6} (13); $NaHSO_4$, -43.8×10^{-6} (14); NaH_2PO_4, -45.72×10^{-6} (15).

TABLE 1. Activity coefficients of TMA^+ at 25.0 °C

Acid concentration (*M*)	$\log f_{TMA^{+*}}$[a] $HClO_4$	H_3PO_4
1.0	−0.30	−0.02
2.0	−0.02	−0.03
3.0	0.40	−0.02
4.0	0.74	0.00
5.0	1.12	0.03
6.0	1.52	0.08
7.0	1.92	0.14
8.0	2.32	0.19
9.0		0.22
10.0		0.23

[a] $f_{TMA^{+*}} = (f_{\pm(TMA^+PCP^-)}/f_{\pm(TEA^+PCP^-)})^2$.

Activity Coefficient Measurements

All activity coefficients were determined by the solubility method, as described previously (4), and are collected in Table 1. Values of $f_{TMA^{+*}}$ in aqueous H_2SO_4 and f_{PCP^-} in aqueous H_2SO_4 and $HClO_4$ were taken from ref. 1.

Results and Discussion

Carbon and proton chemical shifts of tetramethyl-, tetraethyl-, and methyltriethylammonium ions have been determined in aqueous solutions of sulfuric, perchloric, and phosphoric acids, and their monosodium salts. Medium effects are expressed as the difference in magnetic resonance frequency (in ppm) between a given medium and in water; downfield shifts are shown as positive. All data have been corrected for the changes in the bulk magnetic susceptibility of the medium. The observed differences are essentially independent of the concentration of the ammonium salt (in a range of 0.002–0.020 *M*) and of the nature of the counterion (BF_4^- or pentacyano-

Can. J. Chem. Downloaded from www.nrcresearchpress.com by 210.87.254.6 on 09/05/12
For personal use only.

propenide, PCP^-);[3] we therefore ascribe these effects to the interactions between the tetraalkylammonium cation and the medium. For all systems, the trends found in aqueous solutions of acids are followed by similar trends in the solutions of the monosodium salts of these acids; the latter values are believed to be less reliable because of the possibly lower accuracy of magnetic susceptibility corrections in these media. The nuclei of individual groups in the methyltriethylammonium ion show the chemical shift changes similar to those for the corresponding groups in the TMA^+ and TEA^+ ions. In consequence, we will focus our attention mainly on the medium effects on chemical shifts observed for TMA^+ and TEA^+ ions in aqueous sulfuric, perchloric, and phosphoric acids.

In the first place it should be emphasized that the medium effects observed for tetraalkylammonium ions in aqueous acids are extremely weak in nature. For such a dramatic change in medium composition, as from pure water to 10 *M* solution of strong acids, the differences in ^1H chemical shifts do not exceed a value of 0.13 ppm, and those in ^{13}C chemical shift a value of 0.48 ppm. This is in sharp contrast with the value of $\Delta\delta_H = 2.27$ ppm found for the TMA^+ ion in chloroform and 1-bromonaphthalene solutions (16). Similarly, $\Delta\delta_C = 4.24$ ppm for chloroform when the solvent is changed from cyclohexane to hexamethylphosphorotriamide (17). Thus our results suggest that the tetraalkylammonium ions represent good reference ions for studies in strongly acidic aqueous solutions.

The differences in ^{13}C chemical shifts for all carbons in TMA^+ and TEA^+ ions are presented in Figs. 1 and 2. While the observed shifts are small, there are certain patterns of deshielding effects which we believe can be interpreted in terms of solution interactions. We suggest that the observed deshielding effects result mainly from two types of medium–solute interactions, being of different relative importance for different atoms in the tetraalkylammonium ion. The first 'general' effect involves a decrease in the availability of water and consequent decrease in the hydration of the positively charged nitrogen. This should result in decreased shielding (low-field shift), assuming that hydration increases shielding by effectively neutralizing part of the positive charge on nitrogen. When the water

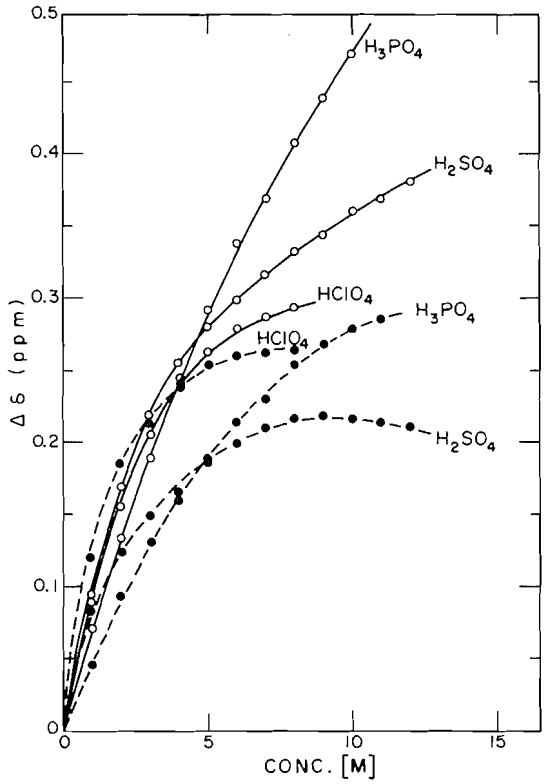

FIG. 1. ^{13}C chemical shifts of R_4N^+ as a function of acid concentration. ○, tetramethylammonium ion; ●, α-carbons in the tetraethylammonium ion.

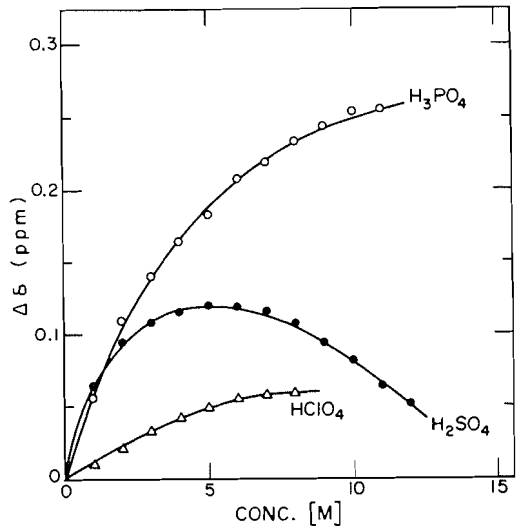

FIG. 2. ^{13}C chemical shift of the β-carbons in tetraethylammonium ion as a function of acid concentration.

[3]This observation itself supports Boyd's assumption (3) that in a dilute aqueous solution of a salt behavior of the ion should be independent of the counterion.

Can. J. Chem. Downloaded from www.nrcresearchpress.com by 210.87.254.6 on 09/05/12
For personal use only.

molecules are subsequently replaced by anions of the mineral acid, the effective solvation (and in consequence shielding effects) is most likely decreased because of the steric hindrance for the approach of the bulky anion to the close proximity of the positive center. The next 'specific' interactions can probably be best described in terms of weak hydrogen bonding between the acid anion and the alkyl hydrogen atoms in the tetraalkylammonium ions. Hydrogen bonding to C—H bonds is known to cause low-field shifts for both ^{13}C and ^{1}H nuclei (17). The net changes in the external shielding factors can be therefore represented for the aqueous solutions of an acid AH as:

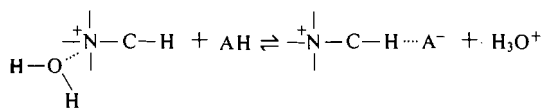

Since the effect related to the removal of water increases the $-I$ effect of the ammonium nitrogen, it is expected to influence mostly the shielding of α-carbon atoms; β-carbons should be much less sensitive to the changes of the effective charge at the positive center. The second type of interaction should depend on the degree of the negative charge delocalization in the acid anion and should decrease in the order: $H_2PO_4^- > HSO_4^- > ClO_4^-$, with all anions being superior to H_2O (decrease in hydrogen bonding donor ability). This effect should be more important for the methyl groups than for the sterically hindered methylene hydrogens in the TEA^+ ion. The above interpretation is consistent with the observed chemical shift behavior. For the methylene carbons in the TEA^+ ion (Fig. 1), if we ignore the hydrogen bonding effects, the low-field shift results primarily from the decrease in the hydration of the positive center. At acid concentrations below 5 *M*, this effect increases in the order $H_3PO_4 < H_2SO_4 < HClO_4$, following the order of the decrease in water activity in these media (18). These deshielding effects tend to level off at higher acid concentrations, probably due to the removal of most of the water molecules from the solvation shell of the ammonium cation (in H_3PO_4 some increase in $\Delta\delta$ values is observed at high concentrations, probably as a result of some H-bonding effect due to the $H_2PO_4^-$ ions). The acid concentrations at which the levelling of the plots occurs correspond to a similar value of $\log a_{H_2O}$ (*ca.* -0.5) in these media.

For the TMA^+ ion (Fig. 1), the above effect can be superimposed with the additional deshielding due to the C—H···A^- hydrogen bonding. The latter interactions should be of least importance for the $HClO_4$ system,[4] and in fact the $\Delta\delta$ plots for TMA^+ and C_α in TEA^+ (Fig. 1) in aqueous $HClO_4$ are almost identical. In sulfuric and phosphoric acid, the deshielding at low acid concentration is presumably mainly due to decreased hydration. However, at high acidity, hydrogen bonding should become increasingly important. Above 5 *M*, low-field shifts are in the order $H_3PO_4 > H_2SO_4 > HClO_4$, consistent with increasing acid anion hydrogen bonding.

The medium dependence of the chemical shift for the β-carbon of the TEA^+ ion (Fig. 2) is essentially different from that of the α-carbon; the low-field shift decreases sharply in the order $H_3PO_4 > H_2SO_4 > HClO_4$ over almost the total range of acidities. This remains in agreement with the expected order of hydrogen bonding abilities of the conjugate bases of these acids and indicates that in the case of atoms in a β-position to the positive center, this type of interaction plays a major role in determining the shielding effects of the medium. Analogous behavior, reflecting the relative extent of the C—H···A^- hydrogen bonding in H_3PO_4, H_2SO_4, and $HClO_4$, is also observed for the variation of the values of $\Delta\delta$ for all hydrogens in TMA^+ and TEA^+ ions (as well as in the methyltriethylammonium ion) in these media. Although the pmr chemical shifts differences are smaller in magnitude, and therefore less reliable, the observed trends can again be interpreted in terms of the hydrogen bonding to the medium and they support conclusions drawn from the results obtained for the carbon chemical shift data. Figure 3 shows the typical variation of the $\Delta\delta$ values for protons of the methyl groups in the TEA^+ ion. There is a close parallel between Figs. 2 and 3, except that the ^{13}C chemical shifts are approximately twice as large as the ^{1}H chemical shifts. This supports the

[4]Harmon *et al.* (19) demonstrated the existence of cation C—H to anion hydrogen bonding in the solid state even for tetramethylammonium perchlorate; these effects should be still stronger for bisulfate and dihydrogenphosphate anions because of the lower degree of charge delocalization.

Can. J. Chem. Downloaded from www.nrcresearchpress.com by 210.87.254.6 on 09/05/12
For personal use only.

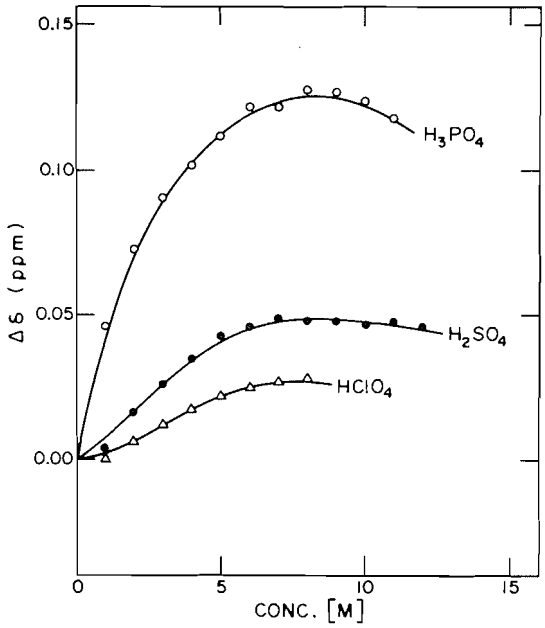

FIG. 3. ^1H chemical shift of the β-hydrogens in tetraethylammonium ion as a function of acid concentration.

model of specific acid anion hydrogen bonding since it has been shown that ^{13}C chemical shifts in $CHCl_3$ are almost exactly two times as sensitive to hydrogen bonding interactions as the corresponding ^1H chemical shifts (17).

In terms of the relative magnitude of medium effects on the chemical shifts, TMA^+ ion exhibits rather higher sensitivity to the changes in medium composition than the TEA^+ ion (*cf.* Fig. 1). This is probably a consequence of the higher hydration requirements of the small tetramethylammonium ion as compared with the case of the relatively shielded tetraethylammonium ion. The difference in hydration requirements of these two cations are also reflected in the relative values of the free energies of transfer of these ions from pure water to aqueous solutions of strong acids. Figure 4 presents the behavior of the TMA^+ ion activity coefficient relative to that of the TEA^+ ion ($f_{TMA^+}{}^* \equiv f_{TMA^+}/f_{TEA^+}$) for aqueous H_2SO_4, H_3PO_4, and $HClO_4$ solutions. In all media, when the acid concentration increases, *i.e.* water availability decreases, the TMA^+ ion shows a salting-out (relative destabilization) effect, decreasing in the order $HClO_4 > H_2SO_4 > H_3PO_4$. Since perchloric acid removes water from the medium most effectively, and the compensating solvation of the tetraalkylammonium ion by the acid anion is in this case lowest (because of the highest degree of charge delocalization in the ClO_4^- anion), the salting-out effect is most pronounced in this medium. On the contrary, in phosphoric acid, water activity decreases slowly and the $H_2PO_4^-$ anion is a relatively good solvating species. Thus, the difference between the behavior of TMA^+ and TEA^+ ions is small.

According to the proposed model, the transfer of the tetraalkylammonium ion from pure water to a solution of strong acid results in the removal of water molecules from close proximity to the positive charge and in the formation of weak hydrogen bonds between alkyl hydrogens and anions of an acid. For the tetraethylammonium ion, the first effect is assumed to be responsible for the α-carbon down-field shifts; the second type of interaction determines the down-field shifts of the β-carbons. In the tetramethylammonium system the observed shift changes are the consequence of both effects, superimposed on each other. If this is true, the variation of the sum of the $\Delta\delta$ values for both α- and β-carbon atoms in the TEA^+ ion should, to a first approximation, be similar to that of the $\Delta\delta$ values for the TMA^+ ion. Such a plot is presented in Fig. 5; in fact, up to at least a 7 *M* concentration of acids, the change in $\sum\Delta\delta$ are strikingly similar to those for the TMA^+ ion (Fig. 1). For a given acidity the total chemical shifts for the TEA^+ ion are slightly larger than those for TMA^+; this could be expected since the 'general' effects are

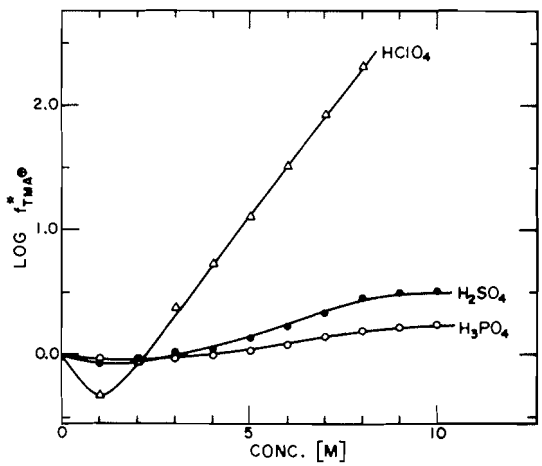

FIG. 4. Activity coefficient behavior of tetramethylammonium ion in aqueous acids.

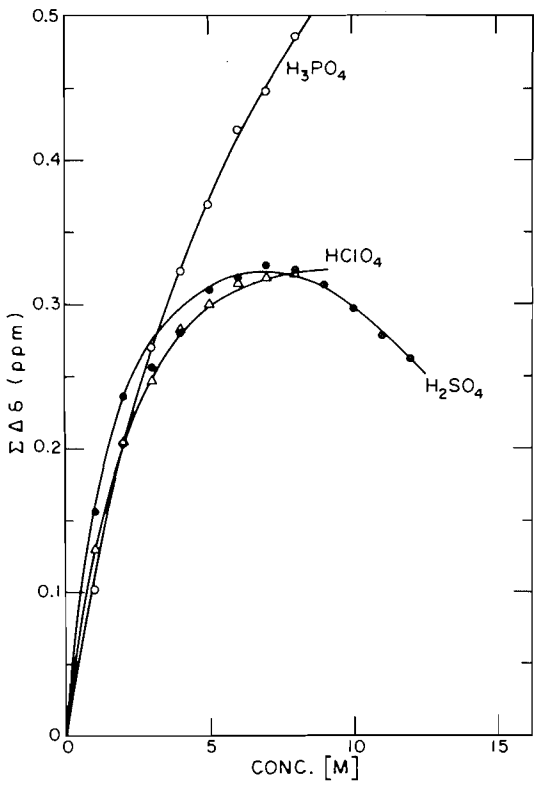

FIG. 5. Sum of the ^{13}C chemical shifts for α- and β-carbons in tetraethylammonium ion as a function of acid concentration.

probably operating to some extent with respect to the β-carbons, and 'specific' effects contribute also to the deshielding of α-carbons.

In conclusion, we believe that the medium effects observed fully justify the choice of tetraalkylammonium ions as reference standards for studies of the behavior of ionic species in strongly acidic aqueous solutions. The magnitude of these effects indicates that the absolute variation of the tetraalkylammonium ion activity coefficients with acid concentration cannot be large. This allows the value of f_{Z^+}* for any ionic species to reflect reasonably well only the behavior of the Z^+ ion. Our results indicate that the TEA^+ ion fulfils the requirements for an 'ideal' reference ion better than the TMA^+ ion, since the latter shows a higher demand for solvation by water molecules, and therefore higher sensitivity to the changes in medium composition.

1. K. YATES and R. A. MCCLELLAND. Prog. Phys. Org. Chem. **11**, 323 (1974).
2. R. A. MCCLELLAND, T. A. MODRO, M. F. GOLDMAN, and K. YATES. J. Am. Chem. Soc. **97**, 5223 (1975).
3. R. H. BOYD. J. Am. Chem. Soc. **85**, 1555 (1963).
4. T. A. MODRO, K. YATES, and J. JANATA. J. Am. Chem. Soc. **97**, 1492 (1975).
5. P. LASZLO. *In* Progress in NMR spectroscopy. Vol. 3. Pergamon Press, New York. 1967.
6. (*a*) G. C. LEVY and G. L. NELSON. Carbon 13 nuclear magnetic resonance for organic chemists. Wiley-Interscience, New York. 1972; (*b*) I. B. STOTHERS. Carbon 13 NMR spectroscopy. Academic Press, New York. 1972.
7. G. WITTIG, G. KOENGL, and K. CLAUS. Ann. **593**, 127 (1955).
8. W. J. MIDDLETON, E. L. LITTLE, D. D. COFFMAN, and V. E. ENGELHART. J. Am. Chem. Soc. **80**, 2795 (1958).
9. J. W. EMSLEY, J. FEENEY, and L. H. SUTCLIFFE. High resolution NMR spectroscopy. Vol. 1. Pergamon Press. New York. 1965. p. 605.
10. A. PACAULT and J. CHEDIN. Bull. Soc. Chim. Fr. **17**, 766 (1950).
11. A. T. ZDUKOS, A. A. VISHNYAKOVA, and M. N. NABIEV. Uzb. Khim. Zh. **13**, 7 (1969).
12. O. E. FRIVOLD and N. G. OLSEN. Avh. Nor. Vidensk.-Akad. Oslo. Mat.-Naturvidensk. Kl. **7**, 1 (1944).
13. O. E. FRIVOLD and H. SOGN. Ann. Phys. **23**, 413 (1935).
14. M. B. KENNEDY, M. W. LISTER, R. MARSON, and R. B. POYNTZ. Can. J. Chem. **51**, 674 (1973).
15. International critical tables. Vol. VI. McGraw-Hill, New York. 1929. p. 360.
16. R. P. TAYLOR and I. D. KUNTZ. J. Am. Chem. Soc. **92**, 4813 (1970).
17. R. L. LICHTER and J. D. ROBERTS. J. Chem. Phys. **74**, 912 (1970).
18. J. F. BUNNETT. J. Am. Chem. Soc. **83**, 4956 (1961); K. L. ELMORE, C. M. MASON, and J. H. CHRISTENSEN. J. Am. Chem. Soc. **68**, 2528 (1946).
19. K. M. HARMON, J. GENNICK, and S. L. MADEIRA. J. Phys. Chem. **78**, 2585 (1974).

Can. J. Chem. Downloaded from www.nrcresearchpress.com by 210.87.254.6 on 09/05/12
For personal use only.

Olefin cycloadditions to 2′,3′,5′-triacetyluridine

JAMES L. CHARLTON AND HOI KIONG LAI
Department of Chemistry, University of Manitoba, Winnipeg, Manitoba R3T 2N2

Received September 17, 1975

JAMES L. CHARLTON and HOI KIONG LAI. Can. J. Chem. **54**, 1445 (1976).

Photocycloadditions of 2′,3′,5′-triacetyluridine to tetramethylethylene, isopropenyl acetate, 1,1-diethoxyethylene, and vinylene carbonate are described. The rearrangement of the vinylene carbonate adduct to 2′,3′,5′-triacetyl-5-formylmethyluridine followed by oxidation to the 5-carboxymethyl or decarbonylation to the 5-methyl (ribothymidine) derivative is also described.

JAMES L. CHARLTON et HOI KIONG LAI. Can. J. Chem. **54**, 1445 (1976).

On décrit les cycloadditions de la triacétyl-2′,3′,5′ uridine au tétraméthyléthylène, à l'acétate d'isopropényl, au diéthoxy-1,1 éthylène et au carbonate de vinylène. On décrit aussi le réarrangement de l'adduit du carbonate de vinylène en triacétyl-2′,3′,5′ formyl-5 méthyluridine qui après oxydation ou décarbonylation conduit aux dérivés carboxyméthyl-5 ou méthyl-5 (ribothymidine).

[Traduit par le journal]

Introduction

Despite the fact that many authors (1) have studied the photodimerizations of pyrimidine nucleosides such as uridine and thymidine, there has been little investigation of simple photoadditions with olefins. Shugar and co-workers have prepared the ethylene adduct of 2′-deoxyuridine and the propylene and 1-hexene adducts of uridine as part of a larger study involving 5-alkyl pyrimidine nucleosides (2).

The fact that photocycloaddition had been demonstrated suggested the possibility of preparing a variety of 5,6-substituted pyrimidine nucleosides. These adducts might be useful for biological studies themselves, but more importantly they might also be used as intermediates in the synthesis of other less common but naturally occurring nucleosides. Unfortunately the addition of asymmetrical olefins across the 5,6 double bond of a nucleoside such as uridine might lead to as many as eight different stereoisomers. Although this might make complete product characterization impossible, earlier work by Swenton *et al.* on dimethyluracil had shown the addition to be somewhat stereoselective (3). We also hoped that selection of the symmetrical olefin tetramethylethylene would allow complete characterization of at least this one adduct.

It was the primary purpose of this work to demonstrate the feasibility of photocycloaddition of 2′,3′,5′-triacetyl uridine to a variety of olefins. Secondly we have attempted the specific synthesis of the naturally occurring nucleosides, 5-carboxymethyluridine and ribothymidine from uridine, via a vinylene carbonate adduct. The use of vinylene carbonate for carrying out this type of transformation was first described for α,β-unsaturated ketones by Wiesner and co-workers (4) and later for uracil by Bergstrom and Agosta (5).

Results and Discussion

The photochemistry of uridine has been largely studied in aqueous solution as the compound is not particularly soluble in organic solvents. Uridine has also been reported to photoreact with hydroxylic solvents such as alcohol and water to give either addition to the 6 position and/or photoreduction (1). Since we wished to avoid these side reactions, all experiments were carried out on 2′,3′,5′-triacetyluridine in ethyl acetate, a solvent we found convenient for the photoreactions. Irradiation of 2.0×10^{-2} *M* solutions of triacetyluridine in ethyl acetate containing an olefin (2% by volume) resulted in complete disappearance of the uridine chromophore after a few hours. The irradiations were carried out using a water cooled quartz vessel and a low pressure mercury lamp (2537 Å). The olefins tetramethylethylene, isopropenyl acetate, 1,1-diethoxyethylene, and vinylene carbonate were successfully added. With diphenylacetylene no reaction could be detected. In each case the adducts could be separated from the olefin by silica gel chromatography and the yield of crude

Can. J. Chem. Downloaded from www.nrcresearchpress.com by 210.87.254.40 on 09/05/12
For personal use only.

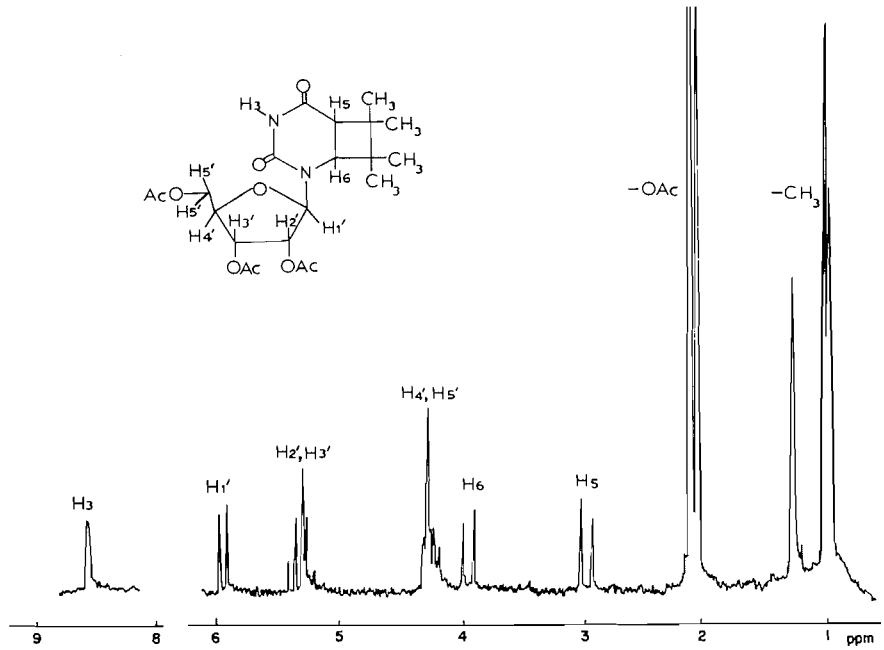

FIG. 1. Triacetyluridine–tetramethylethylene adduct III.

product in most cases was nearly quantitative. Elemental analyses and mass spectra were consistent with 1:1 adducts in each case. The fact that the uridine chromophore at 257 nm (ethyl acetate) disappeared indicated saturation of the 5,6 double bond and additional evidence for this was gathered from nuclear magnetic resonance (nmr) spectra of the crude adducts. Although these spectra were complicated, indicating a mixture of isomers, they showed the lack of the typical uridine H_5 and H_6 absorption.

Separation of the isomeric product mixture was accomplished only in the case of the tetramethylethylene adduct. Careful chromatography led to the differentiation of three isomers. Two of these isomers were obtained pure and gave satisfactory elemental analyses and mass spectra. The presence of the third isomer was determined from the nmr spectrum of a mixed fraction. The spectrum of one of the pure isomers is illustrated in Fig. 1 with the proton assignments. The other isomers exhibited similar spectra and the data can be found in the experimental section. From these spectra it was clear that the compounds were 1:1 adducts formed at the uridine 5,6 double bond. The H_5 to H_6 coupling in two of the isomers was 9.8 Hz, characteristic of a *cis* hydrogen coupling (3). The third isomer had an H_5 to H_6 coupling of 13.3 Hz more indicative of a *trans* fused ring system (3, 6).

Having demonstrated the ready accessibility of the 5,6-uridine adducts we attempted to convert one of them, the vinylene carbonate adduct, to other known uridine derivatives. Dissolution of the vinylene carbonate adduct in absolute ethyl alcohol containing 2% triethylamine resulted in the appearance of a single new spot on thin layer chromatography (tlc) after 15 min. An nmr spectrum of the residue left after evaporation of the solvent was most consistent with the formation of 5-carboxymethyl triacetyluridine. From tlc and nmr it is estimated that the crude product is more than 90% pure. The compound could likewise be obtained by simply stirring the vinylene carbonate adduct in ethanol (95%) for 2 days although the presence of impurities is evident on tlc. Material recovered from tlc gave a satisfactory elemental analysis and had an ultraviolet (uv) maximum at 260 nm typical of the uridine chromophore. Evidently the aldehyde expected from rearrangement of the adduct is very susceptible to air oxidation.

5-Carboxymethyluridine had been isolated previously from wheat and yeast tRNAs (7) and the synthesis described here represents a considerable improvement in yield over the more

Can. J. Chem. Downloaded from www.nrcresearchpress.com by 210.87.254.40 on 09/05/12
For personal use only.

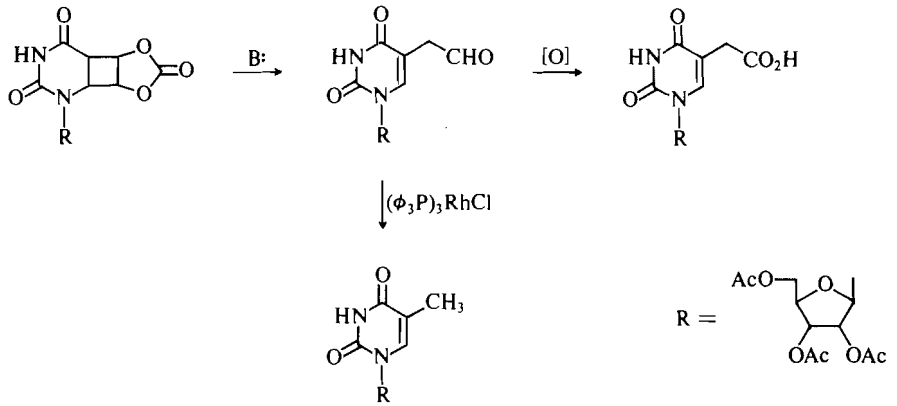

classical approach described in the literature (8).

The decarboxylation of 5-carboxymethyluridine to ribothymidine has also been described (8) but the yield was very low (5). Since tristriphenyl phosphine rhodium chloride (TPRC) has been used to decarbonylate aldehydes (9) we attempted to isolate the aldehyde intermediate. It was found that stirring the vinylene carbonate adduct in 10^{-4} *M* KOH in 95% ethanol for 0.5 h gave the largest yield of a compound running at R_f 0.45 on tlc. Attempted characterization of this material was unsuccessful but immediate treatment of the eluted material with TPRC gave up to 40% yields of 2′,3′,5′-triacetylribothymidine. The product was identified by comparison of both itself and its hydrolysis product to authentic samples.[1]

It is hoped that further investigations of the methods and intermediates described here will lead to synthetic routes to other known nucleosides.

Experimental

Photocycloadditions were carried out by irradiating a 2×10^{-2} *M* solution of 2′,3′,5′-triacetyluridine in ethyl acetate containing 2% by volume of the olefin. The source was a low pressure mercury arc (Ultraviolet Products Inc. PCQXI) and the reaction vessel a Hanovia 450 W lamp jacket (No. 19434). Tap water (*ca.* 10 °C) was circulated through the jacket.

Column chromatography was carried out on silica gel (Camag DSF-5), which was also used for tlc separations.

Ultraviolet spectra were recorded on a Cary-14 recording spectrometer and mass spectra (ms) obtained on a Finnigan 1015 mass spectrometer at an ionization energy of 70 eV. The reported mass ratios are precise only to ±2%. (Mass plus one peaks are often observed in this instrument presumably due to chemical ionization in some cases.) Nuclear magnetic resonance spectra were recorded in deuteriochloroform on a Varian A56-60 or HA-100 spectrometer. Chemical shifts are reported in ppm relative to tetramethylsilane. Melting points are uncorrected. The elemental analyses were carried out by Chemalytics Inc., Tempe, Arizona.

2′,3′,5′-Triacetyluridine

Uridine (1.0 g, Sigma Chemicals) was dissolved in dry pyridine (10.0 ml). Distilled acetic anhydride (40.0 ml) was then added and the solution stirred for 15 h. Methanol (20 ml) was added cautiously and the solution warmed on a steam bath for 30 min. Evaporation *in vacuo* and recrystallization from ether–hexane gave a quantitative yield of triacetyluridine, mp 126–128 °C (lit. (10) 128–130 °C). The nmr exhibited typical vinyl absorption at δ 5.75 (1H, d, J = 8.0 Hz) and 7.48 (1H, d, J = 8.0 Hz).

2′,3′,5′-Triacetyluridine – Isopropenyl Acetate Adduct

The triacetyluridine and isopropenyl acetate (Eastman Kodak) were irradiated for 3 h (see general procedure). Evaporation of the solvent followed by tlc (eluant benzene – ethyl acetate 50:50) gave a band at R_f 0.23. The band was eluted and after treatment with charcoal and evaporation gave 90% yield of solid residue, based on the triacetyluridine. Mass spectrum: *m/e* (relative intensity) 471 (<1), 371 (36), 259 (>100), 191 (21), 139 (>100), 115 (66), 113 (100), 97 (>100). *Anal.* calcd. for $C_{20}H_{26}N_2O_{11}$: C 51.11, H 5.57, N 5.95; found: C 51.38, H 5.67, N 5.78.

1,1-Diethoxyethylene

1,1-Diethoxyethylene was prepared by the method of McElvain and Kundiger (11) in 60% yield.

2′,3′,5′-Triacetyluridine–1,1-Diethoxyethylene Adduct

The triacetyluridine and 1,1-diethoxyethylene were irradiated for 3 h (see general procedure). Evaporation of the solvent and tlc (eluant benzene – ethyl acetate 50:50) gave one major product, R_f 0.62, 49% yield based on triacetyluridine. Mass spectrum: *m/e* (relative intensity) 441 (7, M – OEt), 259 (70), 157 (100), 139 (>100), 116 (>100), 112 (93); nmr δ 1.11–1.40 (8H, m), 2.15 (9H, 3s), 2.40 (2H, m), 3.50 (4H, q), 4.24 (4H, m), 5.50 (1H, m), 5.80 (1H, m), 6.18 (1H, br), 8.58 (1H, br). *Anal.* calcd. for $C_{21}H_{30}N_2O_{11}$: C 51.85, H 6.22, N 5.76; found: C 51.63, H 6.20, N 5.70.

[1]A sample of ribothymidine was provided by K. K. Ogilvie, McGill University, Montreal, Quebec.

Can. J. Chem. Downloaded from www.nrcresearchpress.com by 210.87.254.40 on 09/05/12
For personal use only.

2',3',5'-Triacetyluridine – Vinylene Carbonate Adduct

The triacetyluridine and vinylene carbonate were irradiated for 3 h (see general procedure). Evaporation of the solvent gave a glassy solid which, on dissolution in benzene, gave a low yield of white crystals having mass spectral peaks at *m/e* 173 and 86 (vinylene carbonate dimer?). The remainder was chromatographed on silica gel using benzene – ethyl acetate as eluant. After the vinylene carbonate one fraction was collected to give 90% yield of product based on triacetyluridine. Mass spectrum: *m/e* (relative intensity) 457 (3), 384 (6), 371 (6), 310 (36), 259 (>100), 250 (75), 191 (100), 139 (>100), 97 (>100). *Anal* calcd. for $C_{18}H_{20}N_2O_{12}$: C 47.37, H 4.42, N 6.14; found: C 47.70, H 4.80, N 5.75.

2',3',5'-Triacetyluridine–Tetramethylethylene Adduct

Triacetyluridine and tetramethylethylene (Aldrich Chemicals) were irradiated for 2 h (see general procedure). Evaporation of the solvent gave a glassy solid. Column chromatography of 1.19 g of the crude product on 70 g of silica gel (DSF-5) using benzene – ethyl acetate as eluant gave three compounds. In order of elution these were characterized as follows.

Compound I, recrystallized from ether–hexane to give white crystals, had mp 59–61 °C. Mass spectrum: *m/e* (relative intensity) 455 (2), 396 (15), 371 (15), 259 (>100), 139 (100), 84 (77); nmr δ 1.05 (3H, s), 1.08 (3H, s), 1.21 (6H, s), 2.08 (9H, s), 2.56 (1H, d, J = 13.3 Hz), 3.75 (1H, d, J = 13.3 Hz), 4.05–4.41 (3H, m), 4.82 (1H, d, J = 13.03 Hz), 6.06 (2H, m), 7.48 (1H, s). *Anal.* calcd. for $C_{21}H_{30}N_2O_9$: C 55.50, H 6.65, N 6.16; found: C 55.23, H 6.69, N 5.93.

Compound II was obtained only in a mixture with III (see below). Its nmr spectrum was obtained by ignoring the contribution of III; nmr δ 1.02 (6H, s), 1.10 (3H, s), 1.25 (3H, s), 2.10 (9H, s), 2.95 (1H, d, J = 9.8 Hz), 4.00 (1H, d, J = 9.8 Hz), 4.10–4.38 (3H, m), 5.12 (1H, t, $J_{2'3'}$ = 5.8 Hz), 5.30 (1H, t, $J_{2'3'}$ = 5.8 Hz), 5.79 (1H, d, J = 5.6 Hz), 8.78 (1H, s).

Compound III could be recrystallized from ether–hexane, mp 48–53 °C. Mass spectrum: *m/e* (relative intensity) 455 (1), 371 (1.5), 259 (21), 139 (100), 113 (52), 97 (>100), 84 (>100); nmr δ 0.96 (3H, s), 1.00 (6H, s), 1.22 (3H, s), 2.06 (3H, s), 2.11 (6H, s), 2.96 (1H, d, J = 9.8 Hz), 3.92 (1H, d, J = 9.8 Hz), 4.15–4.36 (3H, m), 5.14 (1H, t, $J_{2'3'}$ = 5.8 Hz), 5.35 (1H, $J_{2'3'}$ = 5.8 Hz), 5.95 (1H, d, J = 5.6 Hz), 8.61 (1H, s). *Anal.* calcd. for $C_{21}H_{30}N_2O_9$: C 55.50, H 6.65, N 6.16; found: C 55.29, H 6.71, N 5.91.

5-Carboxymethyl-2',3',4'-triacetyluridine

The triacetyluridine – vinylene carbonate adduct (100 mg) was dissolved in absolute ethanol (25 ml) and triethylamine (0.5 ml) then added. The solution was stirred at 70 °C for 15 min then evaporated to dryness *in vacuo*. Dissolution in ethyl acetate followed by extraction with 1 *N* HCl removed traces of triethylamine. Thin layer chromatography (solvent ethyl acetate – benzene (75:25)) gave a single compound (R_f 0.25) which, after elution and treatment with charcoal, recrystallized from ether–hexane, mp 84–89 °C; uv λ_{max} (EtOAc) 260 nm; ms *m/e* (relative intensity) 413 (<1), 384 (55), 310 (100), 259 (>100); nmr δ 2.10 (9H, s), 3.43 (2H, s), 4.34 (3H, m), 5.30 (2H, m), 6.04 (1H, d), 7.46 (1H, s), 9.69 (1H, s), 9.77 (1H, s). *Anal.* calcd. for $C_{17}H_{20}N_2O_{11}$: C 47.67, H 4.71, N 6.54; found: C 47.89, H 4.86, N 6.13.

2',3',5'-Triacetylribothymidine

The vinylene carbonate – triacetyluridine adduct (230 mg) was dissolved in 95% ethanol (20 ml). A solution of KOH (0.2 ml, 0.1 *N*) was added. After 30 min acetic acid was added to neutralize the base and the solution then evaporated *in vacuo*. The residue was chromatographed on thin layer plates (solvent ethyl acetate – benzene (75:25)) and the material at R_f 0.45 eluted. This was evaporated to dryness and promptly dissolved in benzene – 95% ethanol (10 ml : 2 ml). Tristriphenylphosphine rhodium chloride (460 mg) was added and the mixture refluxed 3 h. The rhodium complex was separated by filtration, the solvent evaporated, and the residue triturated with ethyl acetate to leave a residue of triphenylphosphine oxide. Thin layer chromatography of the extract (solvent ethyl acetate – benzene (90:10)) gave 76 mg (39%); uv λ_{max} (EtOH) 266 nm; ms *m/e* (relative intensity) 384 (<1), 324 (3), 311 (2), 259 (100), 208 (17), 204 (23), 157 (100), 139 (>100). nmr δ 1.9 (3H, s), 2.15 (9H, s), 4.30 (3H, m), 5.35 (2H, m), 5.96 (1H, m), 7.2 (1H, s), and 9.6 (1H).

Ribothymidine

2',3',5'-Triacetylribothymidine (36 mg) was dissolved in 15% NH_4OH (3 ml) in methanol. The solution was stirred overnight at room temperature. Thin layer chromatography (solvent tetrahydrofuran) gave 10 mg; uv λ_{max} (EtOH) 266 nm (lit. (12) 267 nm); ms *m/e* 258, 155, 133, 125, and 97 (identical to literature (12)).

1. A. A. Lamola. Pure Appl. Chem. **34**, 281 (1973).
2. E. Krajewska and D. Shugar. Science, **173**, 453 (1971); Acta Biochim. Pol. **19**, 207 (1972); E. Sztumpf-Kulikowska and D. Shugar. Acta Biochim. Pol. **21**, 73 (1974).
3. J. S. Swenton, J. A. Hyatt, J. M. Lisy, and J. Clardy. J. Am. Chem. Soc. **96**, 4885 (1974).
4. P. T. Ho, S. F. Lee, D. Chang, and K. Wiesner. Experientia, **27**, 1377 (1971).
5. D. E. Bergstrom and W. C. Agosta. Tetrahedron Lett. 1087 (1974).
6. P. J. Nelson, D. Ostrem, J. D. Lassila, and O. L. Chapman. J. Org. Chem. **34**, 811 (1969).
7. M. W. Gray and B. G. Lane. Biochim. Biophys. Acta, **134**, 234 (1967); Biochemistry, **7**, 3441 (1968); T. D. Tumaitis and B. G. Lane. Biochim. Biophys. Acta, **224**, 391 (1970).
8. G. A. Ivanovics, R. J. Rousseau, and R. K. Robins. Physiol. Chim. Phys. **3**, 489 (1971).
9. M. C. Baird, C. J. Nyman, and G. Wilkinson. J. Chem. Soc. A, 348 (1968).
10. D. M. Brown, A. R. Todd, and S. Varadarajan. J. Chem. Soc. 2388 (1956).
11. S. M. McElvain and D. Kundiger. Organic synthesis. Wiley and Sons Inc., New York. 1964. p. 506.
12. R. Hall. The modified nucleosides of nucleic acids. Columbia University Press, New York. 1971. p. 162.

Can. J. Chem. Downloaded from www.nrcresearchpress.com by 210.87.254.40 on 09/05/12
For personal use only.

The assignment of ^{1}H and ^{13}C chemical shifts for dihydro-3(2*H*)-furanone derivatives by means of specific ^{2}H labelling experiments and $^{13}C\{^{1}H\}$ decoupling experiments

PATRICK M. BURKE, WILLIAM F. REYNOLDS, JANET C. L. TAM, AND PETER YATES
Lash Miller Chemical Laboratories, University of Toronto, Toronto, Ontario M5S 1A1

Received September 8, 1975

PATRICK M. BURKE, WILLIAM F. REYNOLDS, JANET C. L. TAM, and PETER YATES. Can. J. Chem. **54**, 1449 (1976).

The ^{1}H nmr spectrum of dihydro-2,2,5,5-tetramethyl-3(2*H*)-furanone (**1**) in 80% sulfuric acid shows a time-dependent decrease in the intensity of the lower-field *gem*-dimethyl signal relative to the upper-field *gem*-dimethyl signal. This is interpreted as involving reversible opening of **1** to 2-hydroxy-2,5-dimethyl-4-hexen-3-one, resulting in deuterium exchange at the C-5 methyl groups of **1**. The lower-field *gem*-dimethyl signal of **1** in this medium is therefore assigned to these methyl groups. A similar relationship between the methyl proton signals of **1** in organic solvents has been demonstrated by (*i*) synthesis of **1**-d_8 (**8**), (*ii*) comparison of the ^{1}H nmr spectra of **1** and its 2,2- and 5,5-dimethyl analogs, and (*iii*) observation of long range coupling in the spectrum of **1**. Assignment of ^{13}C chemical shifts for **1** has been made based on proton-coupled spectra, showing that the signal of the C-5 methyl carbons appears at *ca.* 4 ppm towards lower field than that of the C-2 methyl carbons. Both the ^{1}H and ^{13}C chemical shift assignments for **1** were confirmed from $^{13}C\{^{1}H\}$ spectra using low power single frequency ^{1}H decoupling, demonstrating the utility of this technique for the assignment of chemical shifts.

PATRICK M. BURKE, WILLIAM F. REYNOLDS, JANET C. L. TAM et PETER YATES. Can. J. Chem. **54**, 1449 (1976).

Le spectre rmn du ^{1}H de la dihydrotétraméthyl-2,2,5,5 (2*H*) furannone-3 (**1**) dans l'acide sulfurique à 80% montre que le rapport des intensités des signaux dus aux groupes *gem*-diméthyles apparaissant respectivement à champ faible et fort diminue en fonction du temps. On interprète ce résultat en faisant l'hypothèse qu'il se produit une ouverture réversible de **1** conduisant à l'hydroxy-2 diméthyl-2,5 hexène-4 one-3 et provoquant un échange de deutérium au niveau des groupes méthyles en C-5 de **1**. On attribue donc le signal à champ faible, dû au *gem*-diméthyle de **1** et observé dans ce milieu, à ces groupes méthyles. On démontre à l'aide des résultats suivants qu'une relation semblable existe entre les protons des groupes méthyles de **1** dans des solvants organiques: (*i*) par une synthèse de **1**-d_8 (**8**), (*ii*) par comparaison du spectre rmn du ^{1}H de **1** avec ceux de ses analogues diméthylés en 2,2 et en 5,5 et (*iii*) par l'observation d'une constante de couplage à longue distance dans le spectre de **1**. On a fait l'attribution des déplacements chimiques du ^{13}C dans **1** en se basant sur un spectre, où les protons sont couplés, montrant que le signal des groupes méthyles en C-5 apparaît à un champ d'environ 4 ppm plus faible que celui des carbones du groupe méthyle en C-2. Les déplacements chimiques de ^{1}H et ^{13}C de **1** ont pu être confirmés à partir des spectres $^{13}C\{^{1}H\}$ utilisant un découplage de ^{1}H à fréquence unique de faible intensité; on démontre ainsi l'utilité de cette technique pour l'attribution des déplacements chimiques.

[Traduit par le journal]

Several years ago in the course of an investigation of the reaction of dihydro-2,2,5,5-tetramethyl-3(2*H*)-furanone, **1**, with sulfuric acid we concluded that, contrary to original anticipation, the signal arising from the C-5 methyl groups in the ^{1}H nmr spectrum of **1** in carbon tetrachloride occurs at lower field than that of the C-2 methyl groups (1). A similar conclusion was reached in respect to the hydrogen atoms at the C-5 and C-2 positions of the parent dihydro-3(2*H*)-furanone, **2**, on the basis of direct examination of its spectrum (2).[1] Subsequently, an analysis of the ^{1}H nmr spectra of several dihydro-3(2*H*)-furanones was based on the 'rule' that the signals of C-5 protons and methyl groups occur on the low-field side of the corresponding C-2 signals (4), although some of the assignments are not without ambiguity. We discuss now the evidence that led to our original conclusion together with recent corroborative evidence from more de-

[1] *Cf.* ref. 3.

Can. J. Chem. Downloaded from www.nrcresearchpress.com by 210.87.254.6 on 09/05/12
For personal use only.

Can. J. Chem. Downloaded from www.nrcresearchpress.com by 210.87.254.6 on 09/05/12
For personal use only.

tailed ^{1}H nmr studies and related observations from ^{13}C nmr studies.

The ^{1}H nmr spectrum of **1** in carbon tetrachloride shows two six-proton singlets at δ 1.18 and 1.32, attributable to the two *gem*-dimethyl groups and a singlet at δ 2.40, arising from the C-4 protons.[2] The spectrum of **1** in 80% sulfuric acid shows corresponding signals at δ 1.42, 1.51, and 2.87,[3] which are attributed to the protonated

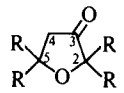

1 R = CH_3
2 R = H

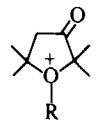

3 R = H
4 R = D

species **3**. A very similar spectrum was observed for a freshly prepared solution of **3** in 80% deuterosulfuric acid – deuterium oxide (δ 1.40, 1.49, 2.85),[3] attributable to the deuterated species **4**. As expected, this spectrum changed rapidly with time and after 20 min the methylene proton signal was no longer detectable due to deuterium–hydrogen exchange at C-4 to give **5**. Unexpectedly, however, after the solution had stood for 40 h a small diminution (10%) in the intensity of the signal at δ 1.49 relative to that at 1.40 could be detected; after 5 days the ratio of the intensities of the two signals had become 1:2.

The most probable route for the exchange of the protons of one of the *gem*-dimethyl groups appeared to be that shown in Scheme 1, in which **5** undergoes reversible conversion to an acyclic intermediate **6** that results in incorporation of deuterium into the *gem*-dimethyl groups at C-5. The occurrence of such ring opening is corroborated by the observation that treatment of **1** with 96% sulfuric acid followed by quenching in water leads to products that include compound **7**, corresponding to **6** (1). Scheme 1 necessarily implies that in sulfuric acid solution the C-5 methyl signal appears at lower field than the C-2 methyl signal.

To investigate whether a similar circumstance holds in solution in carbon tetrachloride, compound **8** was synthesized from **7** by the route shown in Scheme 2. Deuteration of **7**, which

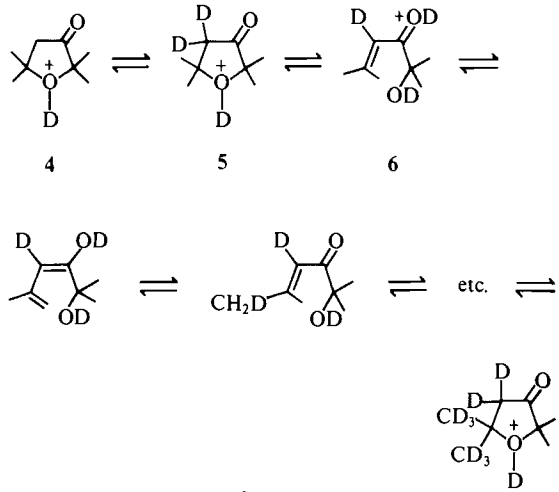

4 **5** **6**

SCHEME 1

could readily be followed by ^{1}H nmr spectroscopy, resulted in almost complete conversion to **9**, which cyclized to **8** in the presence of a catalytic amount of *p*-toluenesulfonic acid in chloroform. The ^{1}H nmr spectrum of **8** in carbon tetrachloride shows a strong signal at δ 1.18 with weak residual signals at δ 1.32 and 2.40, lending strong support to the assignment of the signal of **1** at δ 1.18 to the C-2 methyl protons.

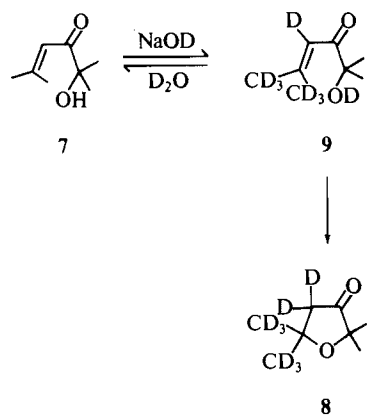

7 **9** **8**

SCHEME 2

Further support for this assignment was obtained by comparison of the methyl ^{1}H chemical shifts for **1** with those for compounds **10** and **11** (see Table 1) and the observation that the low-field methyl signal of **1** is split into a triplet ($J = \pm 0.3$ Hz) due to long range coupling to the methylene protons. Since ^4J coupling is normally greater than ^5J coupling (6) this supports the assignment of the low-field signal to the C-5 methyl groups.

[2]The spectrum of **1** in chloroform reported in ref. 4 must clearly include a typographical error as one of the *gem*-dimethyl signals is listed as occurring at δ 3.86.

[3]Tetramethylammonium chloride was used as an internal standard, and assigned a value of δ 3.10 relative to tetramethylsilane (*cf.* ref. 5).

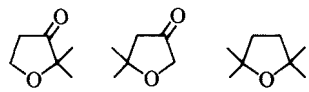

10 11 12

Assignment of the ^{13}C chemical shifts of **1** was initially based on proton-coupled spectra. In addition to ^1J splittings (which are listed in Table 1), the methylene carbon and the methyl carbon signals all show splittings of *ca.* 4 Hz, characteristic of vicinal H–C–C–C coupling (7). The septet splitting for the CH_2 signal is assigned to $^{13}CH_2$–C(CH_3)$_2$ coupling, the tetrad splitting for the high-field methyl signal is assigned to $^{13}CH_3$–C–$^{12}CH_3$ coupling within a pair of methyl groups, while the sextet splitting of the low-field methyl signal is attributed to a combination of $^{13}CH_3$–C–$^{12}CH_3$ and $^{13}CH_3$–C–CH_2 coupling, assuming these two coupling constants are nearly equal in magnitude.

The above ^1H and ^{13}C chemical shift assignments for **1** were confirmed from $^{13}C\{^1H\}$ spectra obtained using low power single frequency ^1H decoupling (see Experimental for details of decoupling power level for each experiment). Irradiation in the proton region at δ 1.10 (high-field methyl ^1H signal)[4] collapsed the high-field ^{13}C methyl signal to a singlet while leaving the low-field ^{13}C methyl signal as a close-spaced quartet ($J_{C-H} \sim 5$ Hz), due to partial decoupling of the directly bonded ^{13}C–^1H coupling. Similarly irradiation at δ 1.25 (low-field methyl ^1H signal) collapsed the low-field ^{13}C methyl signal to a singlet while leaving the high-field methyl signal as a partially collapsed quartet. These experiments confirm that the low-field ^{13}C and ^1H methyl signals are due to the same methyl group.

Irradiation with very low power[5] at δ 2.43 (CH_2 chemical shift) collapsed the sextet splitting of the low-field methyl signal to a quartet, corresponding to removal of the $^{13}CH_3$–C–CH_2 coupling. Similarly, very low power irradiation at δ 1.25 would be expected to remove both $^{13}CH_3$–C–$^{12}CH_3$ and $^{13}CH_2$–C(CH_3)$_2$ vicinal coupling. As expected, the methylene carbon septet splitting was removed while the low-field methyl sextets collapsed to triplets, corresponding to the residual $^{13}CH_3$–C–CH_2 coupling to the methylene hydrogens. These two experiments confirm that the low-field methyl groups are coupled to the methylene group and thereby confirm that these groups are β to one another. These experiments demonstrate the usefulness of low power single frequency decoupling of individual C–H coupling constants for assignment of ^{13}C spectra. Selective decoupling experiments of this type allow assignment of all ^{13}C–^1H coupling constants, with the assignment of chemical shifts for individual carbons and protons following logically from the splitting patterns.

TABLE 1. ^1H and ^{13}C chemical shifts for dihydro-3-furanone derivatives[a]

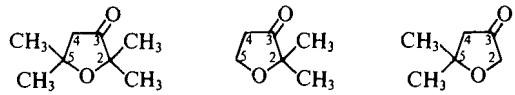

1 10 11

Compound	1	10	11
C(2)H_2	—	—	3.89
C(4)H_2	2.40	2.42[b]	2.23
C(5)H_2	—	4.05[b]	—
C(2)-CH_3	1.18	1.17	—
C(5)-CH_3	1.32	—	1.33
C(2)	80.8	79.1	70.2
C(3)	218.8	217.5	216.1
C(4)	48.4 ($^1J_{C-H}$ = 132 Hz)	35.9	49.5
C(5)	76.1	61.5	80.1
C(2)-CH_3	26.3 ($^1J_{C-H}$ = 128 Hz)	22.3	—
C(5)-CH_3	30.1 ($^1J_{C-H}$ = 126 Hz)	—	27.2

[a]In ppm to low field of internal tetramethylsilane: ^1H spectra were recorded in CCl_4 and ^{13}C spectra in $CDCl_3$.
[b]Triplet J = 7 Hz.

Comparison of the ^1H nmr spectrum of **1** with that of 2,2,5,5-tetramethyltetrahydrofuran, **12** (δ 1.15 (6H), 1.75 (4H)), shows that the overriding effect of the introduction of the carbonyl group on the methyl proton signals is to cause a downfield shift of the C-5 methyl proton signal ($\Delta\delta$ 0.17); there is little effect on the C-2 methyl proton signal ($\Delta\delta$ 0.03).

A corresponding effect has been observed in the ^1H nmr spectrum of **13**, the carbocyclic analog of **1**. The spectrum of **13** in carbon tetrachloride shows two six-proton singlets at δ 1.05 and 1.10 and two two-proton singlets at δ 1.75 and 2.15. Assignment of the methyl signals was accomplished by the synthesis of the trideutero derivative **14** by conjugate addition of

[4]Proton chemical shift in acetone-d_6 (see Experimental).
[5]At very low power ^1J couplings were unaffected and only vicinal splittings were changed; multiplicities quoted here refer specifically to the latter splittings.

Can. J. Chem. Downloaded from www.nrcresearchpress.com by 210.87.254.6 on 09/05/12
For personal use only.

methyl-d_3-magnesium iodide to 3,5,5-trimethyl-2-cyclopentenone, **15**. The spectrum of **14** shows high-field signals at δ 1.05 and 1.10 in the ratio of 2:1, demonstrating that the corresponding signals in the spectrum of **13** arise from the C-2 and C-4-methyl groups, respectively. Thus, as in the case of **1**, the distal methyl signal occurs at lower field than the proximal methyl signal, although the chemical shift difference is smaller in the case of **13**.

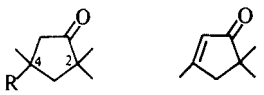

13 R = CH_3 **15**
14 R = CD_3

The ^{13}C chemical shift difference for the C-2 and C-5 methyl groups in **1** probably primarily reflects the γ effect of the carbonyl oxygen since C-4 in 2-pentanone occurs at -5.1 ppm (high field) relative to C-4 in *n*-pentane while the corresponding shift for C-5 is only -0.2 ppm (8). The ^1H chemical shift difference may primarily reflect the electric field effect (9) of the polar C=O group. Since this field acts nearly directly along the bond axes of the C-5 methyl groups but more nearly at right angles to those of the C-2 methyl groups, one would expect a greater low-field shift for the C-5 methyl protons, consistent with the shift changes in **1** relative to **12** (*vide supra*). Since the field effect is an order of magnitude greater for ^{13}C chemical shifts (10), this could also partially account for the ^{13}C chemical shift difference. Finally, the ^1H chemical shift difference could be at least partly due to the anisotropic magnetic susceptibility of the carbonyl group. However, it is impossible to estimate this contribution with certainty, both because of uncertainty concerning the molecular conformation and because the various reported $\Delta\chi$ values for the carbonyl group (11–13) lead to completely contradictory conclusions concerning the relative effects on C-2 and C-5 methyl groups in **1**.

Experimental

Melting and boiling points are uncorrected. Vapour phase chromatographic analyses were carried out on an F and M Model 500 apparatus with helium as the carrier gas at a flow rate of 35–45 ml/min. The following 0.25-in. columns were used: 10% Carbowax 1500 on 60–80 mesh Chromosorb P (6 ft) and 10% neopentylglycol sebacate (NPGS) on 60–80 mesh Chromosorb P (8 ft). Preparative vpc separations were carried out on an F and M Model 770 apparatus with helium as the carrier gas at a flow rate of 1.5–2 litre/min and two 4-ft × 0.75-in. columns of 10% NPGS on 60–80 mesh Chromosorb W.

2-Hydroxy-2,5-dimethyl-4-hexen-3-one, **7**

2-Acetoxy-2,5-dimethyl-4-hexen-3-one was prepared by the method of Lozac'h (14). It was obtained as a colorless liquid, bp 56 °C/0.75 torr) (lit. (14) bp 96–97 °C/14 torr); λ_{max} (CCl_4) 5.75, 5.90, 6.15 μm; $^H\delta$ (CCl_4) 1.39 (s, 6H), 1.91 (br s, 3H), 1.98 (s, 3H), 2.09 (br s, 3H), 6.10 (m, 1H). Hydrolysis of the acetate (14) gave **7** as a colorless liquid, bp 42 °C/0.9 torr, n_D^{25} 1.4668 (lit. bp 81 °C/16 torr, n_D^{20} 1.461). This sample was contaminated with 3,5,5-trimethyl-2-cyclopentenone (1); purification by vpc (Carbowax, 120 °C) gave pure **7**; λ_{max} (CCl_4) 2.90, 5.97, 6.18 μm; λ_{max} 240 nm (ϵ 12 600); $^H\delta$ (CCl_4) 1.27 (s, 6H), 1.96 (d, J = 1.5 Hz, 3H), 2.18 (d, J = 1.5 Hz, 3H), 3.75 (br s, 1H), 6.20 (m, 1H).

Dihydro-2,2,5,5-tetramethyl-3(2H)-furanone-d_8, **8**

Compound **7** (500 mg) was allowed to stand for 3 days in D_2O containing a catalytic amount of KOH (20 mg). The solution was extracted with ether (2 × 10 ml), the extract was dried ($MgSO_4$), and the ether was evaporated; the ^1H nmr spectrum of the product showed a strong signal at δ 1.27 (s), and only weak signals corresponding to the other signals in the spectrum of **7**. This product was dissolved in CCl_4 (5 ml) containing *p*-toluenesulfonic acid (30 mg) and the solution was boiled under reflux for 2 days. The solution was diluted with chloroform (15 ml), washed with water (15 ml), and dried, and the solvent was evaporated under reduced pressure. Vapour phase chromatographic analysis (NPGS, 100 °C) showed the presence of five compounds; a sample of **8** was collected by vpc as a colorless liquid λ_{max} (CCl_4) 4.5–4.7, 5.71 μm; $^H\delta$ (CCl_4) 1.18 (s, 6H), 1.32 (s, 1.5H), 2.40 (s, 0.8H).

Dihydro-2,2-dimethyl-3(2H)-furanone, **10**

Compound **10** was prepared by the general method of Gianturco and co-workers (15). To a suspension of sodium hydride (9.60 g) in ether (200 ml) was added methyl 2-hydroxy-2-methylpropionate (23.6 g) with stirring. After the evolution of hydrogen had stopped, the ether was removed under reduced pressure, and a solution of methyl acrylate (18.92 g) in DMSO (100 ml) was added in one batch to the residue cooled in an ice-water bath. Stirring with cooling was continued for 15 min, and then the solution was stirred at room temperature for 30 min. The solution was filtered, poured into excess ice-cold dilute sulfuric acid, and extracted with ether (3 × 200 ml). The combined extracts were washed with saturated aqueous NaCl and dried (Na_2SO_4), and the solvent was evaporated under reduced pressure. The residual oil was distilled to afford 4-carbomethoxy-2,2-dimethyl-3(2*H*)-furanone (9.73 g, 37%) as a colorless liquid, bp 68–69 °C/0.5 torr; λ_{max} (CCl_4) 5.66, 5.74 μm. This keto ester (9.73 g) was heated with boiling 10% sulfuric acid (100 ml) under reflux for 1 h under nitrogen. The solution was extracted with ether (3 × 100 ml), and the combined extracts were washed consecutively with aqueous $NaHCO_3$ and saturated aqueous NaCl, and dried ($MgSO_4$). The solvent was removed by distillation at

Can. J. Chem. Downloaded from www.nrcresearchpress.com by 210.87.254.6 on 09/05/12
For personal use only.

Can. J. Chem. Downloaded from www.nrcresearchpress.com by 210.87.254.6 on 09/05/12
For personal use only.

atmospheric pressure; distillation of the residual oil gave **10** as a colorless liquid (4.22 g, 67%), bp 70–71 °C; λ_{max} (CCl_4) 5.68 μm.

*Dihydro-5,5-dimethyl-3(2H)-furanone, **11***

Compound **11** was prepared by the method of Gianturco and co-workers (15). It was obtained as a colorless liquid; λ_{max} (CCl_4) 5.68 μm.

*3,5,5-Trimethyl-2-cyclopentenone, **15***

Compound **15** was prepared by the method of Sargent (16), which gives a mixture of **15** and 3,4,4-trimethyl-2-cyclopentenone. These were readily separated by preparative vpc (NPGS, 120 °C). Compound **15** was the compound with the lower retention time and was obtained as a colorless liquid, n_D^{20} 1.4670; λ_{max} (CCl_4) 5.84, 6.15 μm; λ_{max} (EtOH) 229 nm (ε 12 600); $^{H}\delta$ (CCl_4) 1.05 (s, 6H), 2.09 (d, J = 1.5 Hz, 3H), 2.48 (br s, 2H), 5.78 (m, 1H).

*2,2,4,4-Tetramethylcyclopentanone, **13***

Compound **13** was prepared by the method of Slomp *et al.* (17). It was obtained as a colorless liquid, bp 72–74 °C/35 torr, n_D^{23} 1.4300 (lit (17) bp 165.4 °C, n_D^{20} 1.4305); λ_{max} (CCl_4) 5.74 μm; $^{H}\delta$ (CCl_4) 1.05 (s, 6H), 1.10 (s, 6H), 1.75 (s, 2H), 2.15 (s, 2H). It was also prepared by conjugate addition of methylmagnesium iodide to **15** in the presence of Cu_2Cl_2 (*cf.* preparation of **14**).

*2,2,4,4-Tetramethylcyclopentanone-d_3, **14***

Trideuteromethylmagnesium iodide was prepared by addition of trideuteromethyl iodide (Merck, Sharpe and Dohme: 1.6 g) in dry ether (30 ml) to magnesium turnings (240 mg). Cuprous chloride (10 mg) was added and the mixture was cooled to 0–5 °C in an ice bath. A solution of compound **15** (1.10 g) in ether (40 ml) was added with stirring, and the reaction mixture was allowed to come to room temperature overnight. Water (5 ml) and 20% sulfuric acid (2.5 ml) were added, and the ethereal layer was separated and washed with aqueous 5% $NaHCO_3$ (20 ml) and water (2 × 20 ml). The ethereal solution was dried ($MgSO_4$) and the ether was evaporated. The resulting yellow oil (830 mg) was separated into three approximately equal fractions by preparative vpc (NPGS, 120 °C). The middle fraction afforded **14** as a colorless liquid: λ_{max} (CCl_4) 4.50, 4.82, 5.75 μm; $^{H}\delta$ (CCl_4) 1.65 (s, 6H), 1.10 (s, 3H), 1.75 (s, 2H), 2.12 (s, 2H).

*Tetrahydro-2,2,5,5-tetramethylfuran, **12***

Compound **12** was prepared by a modification of the method of Gillis and Beck (18). 2,5-Dimethyl-2,5-hexanediol (20 g) and anhydrous DMSO (128 g) were heated together at 155–165 °C for 22 h. The reaction mixture was distilled at 85–135 °C through a 10-in. Vigreux column. Separation of the entrained water gave a colorless liquid (14.5 g), which was dried (Na_2SO_4). A stream of nitrosyl chloride was passed through the liquid until a permanent green color was produced. It was then distilled under reduced pressure over potassium carbonate to give **12**.

Nuclear Magnetic Resonance Spectra

^{1}H spectra were recorded on T-60 and HA-100 spectrometers, using 0.5 M solutions in CCl_4 with tetramethylsilane as internal reference. ^{13}C spectra were obtained on an XL-100-15 spectrometer operating in the pulsed Fourier transform mode. Most ^{13}C spectra were recorded for 0.5 M solutions in $CDCl_3$. Specific decoupling experiments for **1** were performed using the neat liquid with 20% (v/v) acetone-d_6 added to provide the deuterium lock signal. The ^{1}H spectrum of this solution was measured on an HA-100 to provide accurate ^{1}H chemical shifts for specific decoupling. Specific single frequency decoupling of direct methyl ^{13}C–^{1}H couplings was carried out with a decoupler power level, $\gamma H/2\pi$ = 500 Hz. Selective decoupling of vicinal ^{13}C–C–C–^{1}H couplings was carried out using decoupler power levels in the range 15–30 Hz. Decoupler power levels were measured by the method of Pachler (19).

Acknowledgement

We thank the National Research Council of Canada for support of this research.

1. P. M. Burke. Ph.D. Thesis, University of Toronto, Toronto, Ontario. 1966.
2. J. H. S. Weiland, H. Dijkstra, and A. B. Pik. Recl. Trav. Chim. Pays-Bas, **82**, 651 (1963).
3. N. S. Bhacca, D. P. Hollis, L. F. Johnson, and E. A. Pier. NMR spectra catalog. Vol. 2, Varian Associates, Palo Alto. 1963. Spectra 438 and 439; D. H. Williams and I. Fleming. Spectroscopic methods in organic chemistry. McGraw-Hill, London. 1966, pp. 117–120.
4. M. Anteunis and M. Vandewalle. Spectrochim. Acta, Part A, **27**, 2119 (1971).
5. N. C. Deno, H. C. Richey, Jr., N. Friedman, J. O. Hodge, J. J. Houser, and C. U. Pittman, Jr. J. Am. Chem. Soc. **85**, 2991 (1963).
6. M. Barfield and B. Chakrabarti. Chem. Rev. **69**, 759 (1969).
7. J. B. Stothers. Carbon-13 NMR spectroscopy. Academic Press, New York. 1972. Chapt. 10.
8. D. M. Grant and E. G. Paul. J. Am. Chem. Soc. **86**, 2984 (1964); B. V. Cheney. Ph.D. Thesis, University of Utah, Salt Lake City, Utah. 1966.
9. A. D. Buckingham. Can. J. Chem. **38**, 300 (1960).
10. J. G. Batchelor, J. H. Prestegard, R. J. Cushley, and S. R. Lipsky. J. Am. Chem. Soc. **95**, 6358 (1973).
11. J. A. Pople. J. Chem. Phys. **37**, 60 (1962).
12. R. F. Zurcher. *In* Progress in NMR spectroscopy. Vol. 2. *Edited by* J. W. Emsley, J. Feeney, and L. H. Sutcliffe. Pergamon Press, Oxford. 1967, p. 205.
13. J. W. ApSimon, P. V. Demarco, D. W. Mathieson, W. G. Craig, A. Karim, L. Saunders, and W. B. Whalley. Tetrahedron, **26**, 119 (1970).
14. W. Lozac'h. Bull. Soc. Chim. Fr. 416 (1944).
15. M. A. Gianturco and P. Friedel. Can. J. Chem. **43**, 2121 (1965); M. A. Gianturco, P. Friedel, and A. S. Giammarino. Tetrahedron, **20**, 1763 (1964).
16. H. Sargent. J. Org. Chem. **7**, 154 (1942).
17. G. Slomp, Jr., M. Inatome, C. E. Bowers, J. M. Derfer, K. W. Greenlee, and C. E. Boord. J. Org. Chem. **25**, 514 (1960).
18. B. T. Gillis and P. E. Beck. J. Org. Chem. **28**, 1388 (1963).
19. K. G. R. Pachler. J. Magn. Reson. **7**, 442 (1972).

The interrelation between polarographic half-wave potentials and the energies of electronic excited states

RAFIK O. LOUTFY
Xerox Research Centre of Canada Ltd., 2480 Dunwin Drive, Mississauga, Ontario L5L 1J9
AND
RAOUF O. LOUTFY
Noranda Research Centre, 240 Hymus Boulevard, Point Claire, Quebec H9R 1G5

Received October 15, 1975

RAFIK O. LOUTFY and RAOUF O. LOUTFY. Can. J. Chem. **54**, 1454 (1976).

The polarographic half-wave oxidation and reduction potentials, singlet and triplet energies of a series of (*i*) monocyclic aza-aromatics, (*ii*) polycyclic aza-aromatics and their *N*-oxides, (*iii*) condensed aromatic hydrocarbons, and (*iv*) substituted benzene derivatives are reported. The interrelation between the spectroscopic and electrochemical data is developed and discussed in regard to theoretical and experimental parameters. A linear free-energy relationship between the triplet energies and the absolute difference between the oxidation and reduction potentials of the first three series was found. These correlations were utilized to estimate the triplet energies of other molecules in the series, to predict the true half-wave oxidation potential of some heteroaromatic *N*-oxides and to compute the coulomb repulsion integral. No correlation between $E_T(\pi,\pi^*)$ and $(E_{1/2}{}^{ox} - E_{1/2}{}^{R})$ for substituted benzenes was found. The various reasons for this deviation were discussed.

RAFIK O. LOUTFY et RAOUF O. LOUTFY. Can. J. Chem. **54**, 1454 (1976).

On rapporte les potentiels d'oxydation polarographique à demi vague et les potentiels de réduction ainsi que les énergies singulet et triplet d'une série (*i*) de composés aza-aromatiques monocycliques, (*ii*) de composés aza-aromatiques polycycliques ainsi que de leurs *N*-oxydes, (*iii*) d'hydrocarbures aromatiques condensés et (*iv*) de dérivés benzéniques substitués. On développe une interrelation entre les données spectroscopiques et électrochimiques et on les discute en fonction de paramètres théoriques et expérimentaux. On a trouvé une relation linéaire d'énergie libre entre les énergies des états triplets et les différences absolues entre les potentiels d'oxydation et de réduction des trois premières séries. On a utilisé ces corrélations pour estimer les énergies triplets des autres molécules de la série afin de prédire les valeurs réelles des potentiels d'oxydation à demi-vague pour quelques *N*-oxydes de composés hétéro-aromatiques et pour calculer l'intégrale de répulsion coulombienne. On n'a trouvé aucune relation entre $E_T(\pi,\pi^*)$ et $(E_{1/2}{}^{ox} - E_{1/2}{}^{R})$ pour les dérivés benzéniques substitués. On discute des diverses raisons pour cette déviation.

[Traduit par le journal]

Introduction

Recent years have seen the development of the use of electrochemical redox potential data to interpret photochemical reactions in which the excited states undergo electron or charge transfer processes (1, 2). In order to understand these processes, it is necessary to know not only the excitation energy of the electrons, but also the oxidation and reduction potentials of the interacting molecules, which provide a convenient method of determining the absolute position of energy levels of these molecules. A desire to develop the connection between spectroscopic and electrochemical data (3, 4) prompted us to examine the polarographic redox potentials and the singlet and triplet energies of a series of aza-heterocyclics, aromatic hydrocarbons, and substituted benzenes.

The objective of this study is to establish the relationship between the triplet excitation energy and the absolute difference in the electrochemical oxidation and reduction potential for the compounds studied. These correlations were utilized to: (*a*) predict the triplet energies (E_T) of other molecules in the series with transitions which are inaccessible or undetectable by experimental spectroscopy, (*b*) estimate the true half-wave oxidation potential ($E_{1/2}{}^{ox}$) of molecules which are difficult to measure because of experimental limitation, and (*c*) estimate the coulomb repulsion integral, J_{12}. It is interesting to compare the J_{12} term as predicted from simple electrochemical

Can. J. Chem. Downloaded from www.nrcresearchpress.com by 210.87.254.40 on 09/05/12
For personal use only.

Can. J. Chem. Downloaded from www.nrcresearchpress.com by 210.87.254.40 on 09/05/12
For personal use only.

data with that obtained using semi-empirical molecular orbital theories.

Results and Discussion

A full understanding of the relation between electrochemical and spectral data requires careful examination of both with regard to theoretical and experimental parameters. This will be discussed below.

The single configuration formula for the singlet and triplet excitation energy, E_S and E_T respectively, can be given as (5)

$$[1] \qquad E_S = \epsilon_1 - \epsilon_2 - J_{12} + 2K_{12}$$

$$[2] \qquad E_T = \epsilon_1 - \epsilon_2 - J_{12}$$

where ϵ_1 and ϵ_2 are the energies of the highest occupied and the lowest vacant molecular orbital respectively, J_{12} is the coulomb repulsion integral, and K_{12} is the exchange integral.

$$[3] \quad J_{12} = \iint \psi_1^2(1) \frac{e^2}{r_{12}} \psi_2^2(2) \delta\tau_1 \delta\tau_2$$

$$[4] \quad K_{12} = \iint \psi_1(1)\psi_2(1) \frac{e^2}{r_{12}} \psi_1(2)\psi_2(2) \delta\tau_1 \delta\tau_2$$

The exchange integral, also named overlap integral, K_{12}, depends on the overlap density of the atomic orbitals ψ_1 and ψ_2; *i.e.* on the volume to which the electron is confined. The molecular orbital calculation of the diagonal elements J_{12} and K_{12} involves computation of $N^4/8$ integrals, where N is the number of the valence electrons. Applying the zero differential overlap approximation the number of integrals can be reduced to $N^2/2$. For instance, at least 648 integrals must be computed for benzene. Calculation of these parameters for large molecules becomes impractical and the coulomb and exchange integrals in terms of atomic orbitals are usually evaluated by means of empirical or semi-empirical procedures rather than computation. However, a distinction must be made between the energy of the lowest vacant molecular orbital of a molecule when occupied by an electron after excitation and the energy of the empty orbital in closed shell configuration. This difference, in the case of a singlet excited state $(-J_{12} + 2K_{12})$ could be as large as 0.4 eV.

Maccoll (6) was the first to point out that the reversible polarographic half-wave oxidation and reduction potentials could be related to the energy of the highest occupied (ϵ_1) and lowest vacant (ϵ_2) molecular orbitals, respectively. The orbital energies are also related to the gas phase ionization potential (IP) and electron affinity (EA) of the molecule (7). In practice, the half-wave potentials, for reversible reactions, are set equal to the standard potentials, E^0, however, the full expression (7) is

$$[5] \quad E_{1/2} = E^0 - \frac{RT}{F} \ln f_R/f_0 + \frac{RT}{F} \ln (D_R/D_0)^{1/2}$$

where f_R, f_0 are the activity coefficients of the ions and neutral molecules and D_R, D_0 are their diffusion coefficients. The estimated error involved in neglecting these terms is less than 10 mV. Thus

$$[6] \qquad E_{1/2}{}^R = \epsilon_2 + C$$

$$[7] \qquad E_{1/2}{}^{ox} = \epsilon_1 + C$$

where C is a constant which includes the potential of the reference electrode on the absolute scale, and ϵ_1 and ϵ_2 correspond to the energy of the highest occupied and lowest vacant molecular orbital in solution.

Substituting [6] and [7] into [1] and [2], the singlet and triplet excitation energy can be given simply as

$$[8] \qquad E_S = E_{1/2}{}^{ox} - E_{1/2}{}^R - J_{12} + 2K_{12}$$

$$[9] \qquad E_T = E_{1/2}{}^{ox} - E_{1/2}{}^R - J_{12}$$

The relation between the energy levels of molecules as determined by electrochemical, spectroscopic, and molecular orbital measurements is schematically shown in Fig. 1.

According to [9], a linear relationship should exist between the absolute difference between the oxidation and reduction potential and the triplet excitation energy for a series of closely related molecules provided that the coulomb repulsion integral is constant or varies in a regular manner within the series. Similarly, and according to [8], the existence of a linear free-energy relationship between the redox properties of series of molecules and their singlet excitation energy is expected, provided that the term $(-J_{12} + 2K_{12})$ is constant. Equation 8 can be written in the form:

$$[10] \qquad E_S = (E_{1/2}{}^{ox} - E_{1/2}{}^R) + k$$

We recently reported (4) a linear relationship between the singlet excitation energy and the

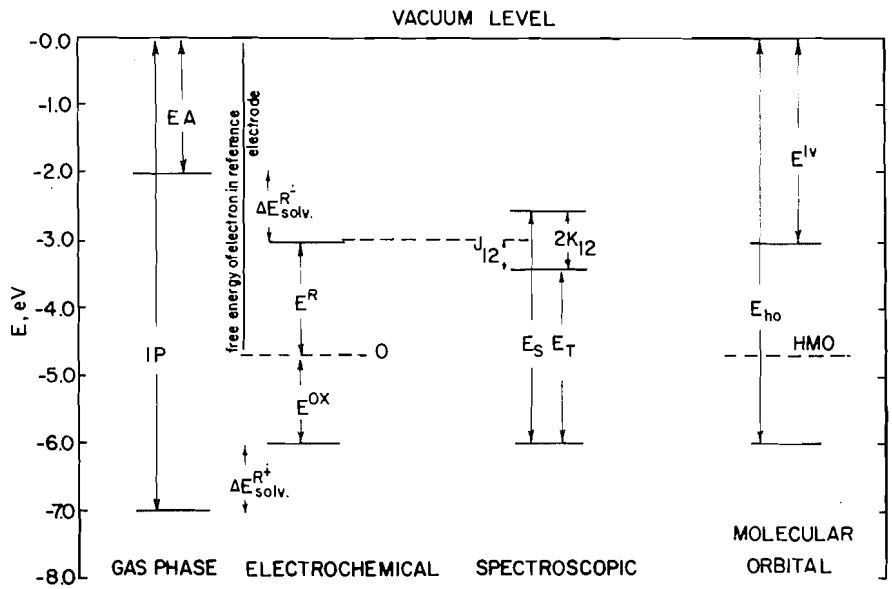

FIG. 1. Relation between gas phase, electrochemical, spectroscopic, and quantum mechanically calculated molecular energy levels.

absolute difference in electrochemical oxidation and reduction potential for over 50 dye molecules. The determined value of the constant k was found to be 0.35 eV (*cf.* eq. 15).

Monocyclic Aza-aromatics

The electronically excited triplet states of *N*-heterocyclics have recently been the subject of extensive investigation because of their important role in photobiological reactions (8).

Innes (9) measured the n,π^* triplet energies of pyridine, pyrimidine, pyrazine, pyradazine, and 1,3,5-triazine while Tabner and Yardle (10) studied their electroreduction. The reduction process has been shown to be one-electron transfer forming radical anions. The half-wave reduction potentials and the singlet and n,π^* triplet energies of the above compounds are given in Table 1. From the results in Table 1, it can be shown that the n,π^* triplet energy of monocyclic aza-aromatic compounds are linearly related to the absolute difference between the oxidation and reduction potentials of these compounds (see Fig. 2). The equation for the regression line is

$$[11] \quad E_T(n,\pi^*) = 0.88(E_{1/2}{}^{ox} - E_{1/2}{}^{R}) - 0.54$$

The deviation of the slope from the expected unity can be mainly attributed to small but systematic variation in J_{12} along the series. However, J_{12} apparently is dependent on the

TABLE 1. Electrochemical data, triplet and singlet energies of monocyclic aza-aromatics

Number	Compound	$E_T(n,\pi^*)$ (eV)[a]	E_S (eV)[b]	$2K_{12}$ (eV)	J_{12} (eV)	$-E_{1/2}{}^{R}$ (V)[c]	$E_{1/2}{}^{ox}$ (V)[d]	$E^{ox} - E^{R}$ (V)	E_T calcd. (eV)[e]
1	Pyridine	3.68	4.265	0.585	1.29	2.76	2.21	4.97	3.82
2	Pyrimidine	3.63	3.83	0.20	1.11	2.35	2.39	4.74	3.62
3	Pyrazine	3.32	3.79	0.47	1.08	2.17	2.23	4.40	3.32
4	Pyridazine	3.08	3.32	0.24	1.03	2.22	1.89	4.11	3.07
5	*sym*-Triazine	3.26	3.91	0.65	1.08	2.05	2.29	4.34	3.27

[a]Reference 9.
[b]Reference 11.
[c]Reference 10. The reduction potentials were measured in DMF *vs.* Ag/AgCl reference electrode.
[d]Calculated from the ionization potential. See ref. 12.
[e]Calculated using [11].

Can. J. Chem. Downloaded from www.nrcresearchpress.com by 210.87.254.40 on 09/05/12
For personal use only.

Can. J. Chem. Downloaded from www.nrcresearchpress.com by 210.87.254.40 on 09/05/12
For personal use only.

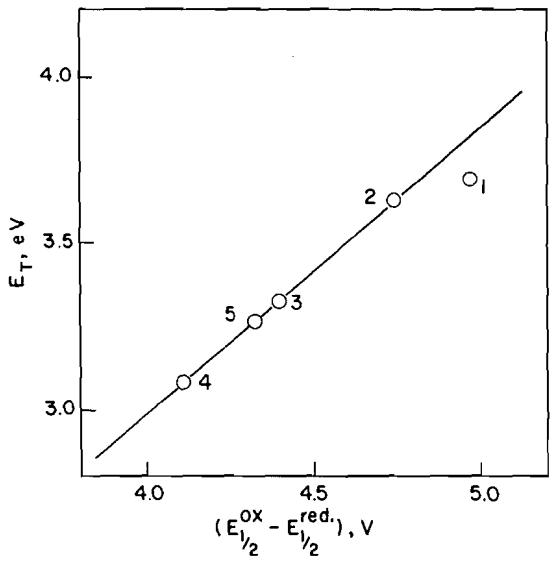

FIG. 2. Relationship between the n,π^* triplet energies of monocyclic *N*-heteroaromatics and the absolute difference between their oxidation and reduction potentials.

magnitude of the redox difference, which can be written as

$$[12] \qquad J_{12} = a + b(E_{1/2}^{ox} - E_{1/2}^{R})$$

where a and b are constants, characteristic of each series of closely related molecules. Substituting from [12] in [9] gives

$$[13] \qquad E_T = (1 - b)[E_{1/2}^{ox} - E_{1/2}^{R}] - a$$

For this series of monocyclic aza-aromatic the value of the constants a and b are found to be 0.54 and 0.12, respectively. The singlet–triplet splittings

$$2\left\langle \psi n \psi \pi^* \left| \frac{e^2}{r_{12}} \right| \psi \pi^* \psi n \right\rangle$$

for the above monocyclic aza-aromatic compound are also shown in Table 1. The values of the exchange integral Kn,π^* vary from 0.2 for primidine to 0.65 eV for *sym*-triazine. Kn,π^* depend on the overlap integral between the n-orbital and the π^*-orbitals and since these orbitals are orthogonal, the exchange integral will be generally small and highly dependent on the charge distribution in the molecule and the orbital hybridization of the heteroatom. No correlation between the singlet energies of these molecules and their redox parameters is expected due to the large variation in the exchange integral (see eq. 8). The average coulomb repulsion integral J_{12} for the monocyclic aza-aromatic calculated from [9] or [12] was found to be 1.12 ± 0.1 eV.

In Table 1 we show a comparison between the experimental E_T(n,π^*) and those calculated using [11]. The agreement is quite good.

Polycyclic Aza-aromatics

The lowest excited triplet states of monocyclic aza-aromatics are due to n–π^* transitions as we have discussed. However, in the case of polycyclic aza-aromatics, the lowest excited states are of the π,π^* type and thus expected to show different reactivity, lifetime, and S–T splitting.

The electroreduction and oxidation potential of 15 poly *N*-heterocyclic compounds are given in Table 2 together with their π,π^* singlet and the triplet energies of 7 of them. A plot of the absolute difference between the oxidation and reduction potentials of the polyaza-aromatics *vs.* their triplet and singlet energies is shown in Fig. 3. An excellent linear free-energy relationship was obtained. The equations for the linear regressions are:

$$[14] \qquad E_T = 0.90(E_{1/2}^{ox} - E_{1/2}^{R}) - 0.687$$

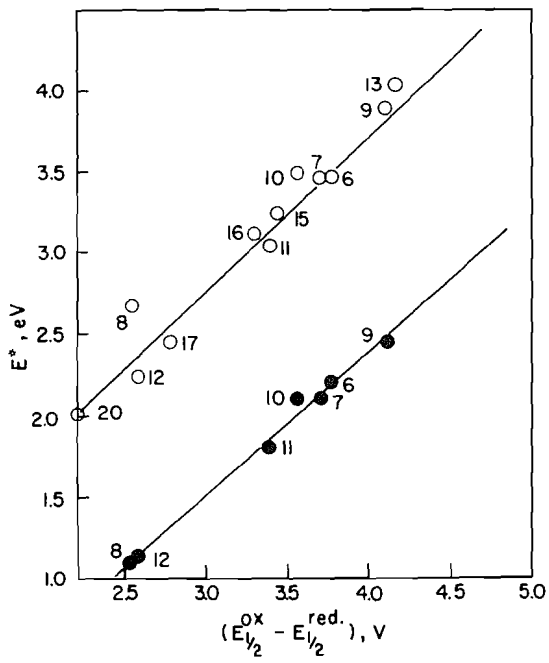

FIG. 3. Plots of the difference between the oxidation and reduction potentials of polycyclic aza-aromatics against the π,π^* singlet (○) and triplet energies (●).

TABLE 2. Electrochemical data, triplet and singlet energies, S–Tsplitting, and coulomb repulsion integral of polycyclic aza-aromatics

Number	Compound	$E_T(\pi,\pi^*)$ (eV)[a,b]	$E_S(\pi,\pi^*)$ (eV)[a]	$2K_{12}$ (eV)	J_{12} (eV)	$-E_{1/2}{}^R$ (V)[c]	$E_{1/2}{}^{ox}$ (V)[c]	$E^{ox}-E^R$ (V)	E_T calcd. (eV)
6	Quinoline	2.71	3.96	1.25	1.05	2.03	1.73	3.76	2.70
7	Isoquinoline	2.61	3.96	1.35	1.09	2.13	1.57	3.70	2.64
8	Acridine	1.60	3.18	1.58	0.94	1.54	1.00	2.54	1.60
9	Pyridine-*N*-oxide	2.97	4.39	1.32	1.13	2.30	1.80	4.10	3.00
10	Isoquinoline-*N*-oxide	2.61	4.00	1.39	0.94	1.95	1.60	3.55	2.51
11	Quinoline-*N*-oxide	2.31	3.543	1.233	1.07	1.84	1.54	3.38	2.35
12	Acridine-*N*-oxide	1.62	2.74	1.12	0.96	1.30	1.28	2.58	1.63
13	Pyrazine-*N*-oxide	—	4.53	(1.48)[d]	(1.10)	1.84	2.31	4.15	3.05
14	Pyrimidine-*N*-oxide	—	4.64	(1.48)	(1.12)	1.93	2.35	4.28	3.16
15	Quinoxaline-*N*-oxide	—	3.75	(1.35)	(1.02)	1.456	1.97	3.426	2.40
16	Phenanthridine-*N*-oxide	—	3.62	(1.35)	(1.02)	1.81	1.48	3.29	2.27
17	Phenazine-*N*-oxide	—	2.94	(1.14)	(0.97)	1.02	1.75	2.77	1.80
18	Pyrazine di-*N*-oxide	—	3.87	(1.54)	(1.02)	1.615	1.74	3.356	2.33
19	Quinoxaline di-*N*-oxide	—	3.02	(1.15)	(0.97)	1.247	1.598	2.845	1.87
20	Phenazine di-*N*-oxide	—	2.51	(1.22)	(0.90)	0.851	1.344	2.195	1.29

[a]Reference 13.
[b]Reference 14.
[c]References 15 and 26. The oxidation and reduction potentials were measured in acetonitrile *vs.* SCE.
[d]Values in parentheses are estimated.

[15] $$E_S = (E_{1/2}{}^{ox} - E_{1/2}{}^R) + 0.30$$

The average π,π^* singlet–triplet splitting was found to be $\sim$1.30 eV, which is larger than the corresponding value of $n \rightarrow \pi^*$ transitions, however, of the same magnitude as that found for aromatic hydrocarbons. The coulomb repulsion integral

$$\left\langle \psi\pi\psi\pi^* \left| \frac{e^2}{r_{12}} \right| \psi\pi\psi\pi^* \right\rangle$$

for the polycyclic aza-aromatics was found to be 1.02 ± 0.10 eV. It is interesting to note that the coulomb repulsion integral for both series of aza-aromatics is quite similar. However, for this series of polyaza-aromatics the values of the constants *a* and *b* are 0.687 and 0.10, respectively (*cf.* eqs. 14 and 12).

In Table 2 the triplet energies calculated from [14] are listed for comparison with the experimentally measured triplet energies. The calculated triplet energies are also given for the eight heterocyclic *N*-oxides for which an experimental value has not yet been obtained.

Previously the determination of the triplet energies of organic compounds has relied on measuring emission spectra (phosphorescence) in solid matrices at low temperature (16) or from singlet–triplet absorption techniques, phosphorescence excitation (17), or oxygen-intensification (18). However, in general, reported triplet energies are scarce compared to the singlet energies of organic compounds. A correlation of the type presented in this paper could be regarded as a useful method for estimating the triplet energies of compounds with transitions which are inaccessible or undetectable by experimental spectroscopy. In addition, the interrelation between electrochemical and spectroscopic data could be utilized to estimate the coulomb repulsion integrals (see column 6 in Table 2) which is usually difficult to compute.

The term $(-J_{12} + K_{12})$ for polyaza-aromatic compound was found to be 0.30 eV (see eq. 15). This represents the difference between the energy of the lowest vacant molecular orbital when it is occupied by an electron after excitation compared to being empty in closed shell configuration.

Recent advances in electronic instrumentation have made possible the development of techniques for studying fast electrochemical reactions. Among these techniques are cyclic voltammetry and pulse polarography which enable accurate measurement of redox potentials even in cases where the electrolysed organic compound produces a short-lived reactive intermediate. However, generally follow-up chemical reaction or irreversible electron transfer processes complicate

Can. J. Chem. Downloaded from www.nrcresearchpress.com by 210.87.254.40 on 09/05/12
For personal use only.

TABLE 3. Electroreduction, triplet and singlet energies, and the calculated oxidation potential of poly-*N*-hetero aromatic hydrocarbons

Number	Compound	E_T (eV)[a]	E_S (eV)[a]	$\Delta(S-T)$ (eV)	$-E_{1/2}^R$ (V)[b]	$E^{ox}-E^{Rc}$ calcd.	$E_{1/2}^{ox}$ calcd.
21	Quinoxaline	2.63	3.345	0.715	1.80	3.69	1.87
22	2-Methylquinoline	2.71	3.93	1.22	2.20	3.77	1.57
23	4-Methylquinoline	2.70	3.90	1.20	2.25	3.76	1.51
24	6-Methylquinoline	2.64	3.87	1.23	2.19	3.70	1.51
25	8-Methylquinoline	2.61	3.81	1.20	2.22	3.66	1.44
26	2,6-Dimethylquinoline	2.62	(3.987)[d]	1.37	2.31	3.68	1.37
27	5,6-Benzoquinoline	2.71	3.56	0.85	2.20	3.77	1.57
28	7,8-Benzoquinoline	2.69	3.53	0.84	2.23	3.75	1.52
29	3,4-Benzoquinoline	2.66	3.51	0.85	—	3.72	—
30	3-Methylisoquinoline	2.503	(3.84)	1.34	2.28	3.55	1.27
31	Phenazine	1.93	2.78	0.85	1.20	2.91	1.71
32	Phenanthroline	2.738	3.655	0.92	2.12	3.81	1.69
33	Dibenzophenazine	2.28	3.15	0.87	1.35	3.30	1.95
34	Dibenzoquinoxaline	2.85	3.41	0.56	1.78	3.93	2.13

[a]Reference 14.
[b]Reference 19.
[c]Calculated using [14].
[d]Values in parentheses are estimated.

the measurements. Also, in many cases experimental restrictions imposed by the type of material investigated on the selection of solvents and electrolytes limits the positive potential range which make $E_{1/2}^{ox}$ inaccessible. These oxidation potentials could be estimated from experimentally measured values of E_T and $E_{1/2}^R$, utilizing [14]. In Table 3, the electroreduction potentials, π,π^* singlet and triplet energies of 14 polyaza-aromatics are listed. The oxidation potentials of these materials were calculated using [14] by substituting the measured values of the triplet energies and reduction potentials. The true oxidation potentials are of interest to electrochemists studying the rate of heterogeneous electron transfer.

Aromatic Hydrocarbons

Watson and Matsen (20) were the first to point out that a correlation could exist between the energy of the lowest excited singlet state of polycyclic aromatic hydrocarbons and the corresponding half-wave reduction and oxidation potentials. Examples are now well established (2, 21–26). Condensed aromatic hydrocarbons are one of the most widely studied group of compounds in spectroscopy. Hence, the triplet states of aromatic molecules continue to receive considerable attention from both the experimental and theoretical viewpoints. The interrelation between the electrochemical data and triplet energies may be extended to cover aromatic hydrocarbons. Table 4 contains the electrochemical oxidation and reduction potentials, π,π^* singlet and triplet energies of 13 aromatic hydrocarbons. A plot of $(E_{1/2}^{ox}-E_{1/2}^R)$ for the polycyclic aromatic hydrocarbons against their π,π^* triplet energies is shown in Fig. 4. A linear

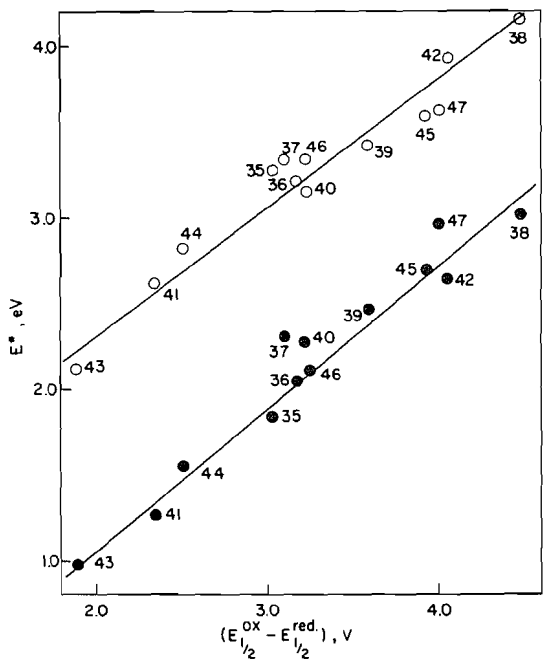

FIG. 4. The relation between $(E_{1/2}^{ox}-E_{1/2}^R)$ of aromatic hydrocarbons and their triplet (●) and singlet energies (○).

Can. J. Chem. Downloaded from www.nrcresearchpress.com by 210.87.254.40 on 09/05/12
For personal use only.

TABLE 4. Electrochemical oxidation and reduction potentials, $\pi \rightarrow \pi^*$ singlet and triplet energies, and the calculated repulsion integrals for aromatic hydrocarbons

Number	Compound	E_T (eV)[a]	E_S (eV)[a]	$2K_{12}$ (eV)	J_{12} (eV)	$-E^R$ (V)[b]	E^{ox} (V)[c]	$E^{ox}-E^R$ (V)	E_T[d] calcd.	$m_m - m_{m+1}$ (β)
35	Anthracene	1.84	3.27	1.43	1.20	1.95	1.09	3.04	1.96	0.83
36	1,2-Benzanthracene	2.05	3.20	1.15	1.13	2.00	1.18	3.18	2.07	0.904
37	1,2-Benzpyrene	2.31	3.33	1.02	0.80	2.10	1.01	3.11	2.02	0.742
38	Biphenyl	3.00	4.16	1.16	1.49	2.58	1.91	4.49	3.15	1.41
39	Chrysene	2.47	3.42	0.95	1.13	2.25	1.35	3.60	2.42	1.04
40	1,2,5,6-Dibenzanthracene	2.27	3.16	0.89	0.96	2.04	1.19	3.23	2.12	0.948
41	Naphthacene	1.27	2.62	1.35	1.08	1.58	0.74	2.35	1.39	0.59
42	Naphthalene	2.64	3.93	1.29	1.43	2.53	1.54	4.07	2.80	1.236
43	Pentacene	0.98	2.12	1.14	0.92	1.36	0.54	1.90	1.03	0.439
44	Perylene	1.55	2.82	1.27	0.97	1.67	0.85	2.52	1.54	0.695
45	Phenanthrene	2.69	3.59	0.90	1.25	2.44	1.50	3.94	2.70	1.21
46	Pyrene	2.10	3.34	1.24	1.15	2.09	1.16	3.25	2.13	0.89
47	Triphenylene	2.96	3.62	0.66	1.05	2.46	1.55	4.01	2.75	1.368

[a]Reference 11.
[b]Reference 27. The reduction potentials were measured in acetonitrile *vs.* SCE.
[c]Reference 15. The oxidation potentials were measured in DMF *vs.* SCE.
[d]Calculated using [16].

free energy relationship was obtained. The equation for the linear regression is

$$[16] \quad E_T(\pi,\pi^*) = 0.82(E_{1/2}{}^{ox} - E_{1/2}{}^{R}) - 0.52$$

The average value for the exchange and coulomb integrals of the aromatic hydrocarbons is found to be 1.12 ± 0.3 eV, while the values of the constants a and b were found to be 0.52 and 0.18, respectively.

The energy of the highest occupied (ϵ_{ho}) and lowest vacant (ϵ_{lv}) molecular orbitals of the aromatic hydrocarbons can be given as $\epsilon_{ho} = \alpha_0 + m_m\beta$ and $\epsilon_{lv} = \alpha_0 + m_{m+1}\beta$ respectively (28). Hoijtink (29) has shown that the half-wave oxidation potentials of aromatic hydrocarbons give a good linear correlation with the energy coefficient, m_m, of the highest occupied molecular orbitals. Similarly the half-wave reduction potentials were found to linearly relate to the energy coefficient, m_{m+1}, of the lowest vacant molecular orbitals (28), see [6] and [7]. For alternate hydrocarbons the m-values of the ho and lv MO's differ only in sign; hence a plot of polarographic reduction potentials *vs.* oxidation potentials should, and was, found to give a straight line (29). Consequently, we would expect that the triplet energies of aromatic hydrocarbons should be related to either the oxidation or reduction potentials. Such linear correlations are indeed obtained (see Fig. 5). The slopes were found to be close to two as would be expected.

The relation between the singlet transition energies and the Hückel molecular orbital (HMO) energy difference, $(m_m - m_{m+1})$ has been reviewed by Streitwieser (28). We also found an excellent linear correlation between the triplet energies of aromatic hydrocarbons and the HMO calculated energy difference (Fig. 6). The slope of this line corresponds to the resonance integral $\beta = 2.11$ eV.

Benzene Derivatives

The existence of linear free energy relationship between triplet energies and electrochemical data of series for closely related molecules depends on the assumption that the coulomb repulsion integral is constant or varies regularly along the series. It was found that the average value of J_{12} for condensed aromatics and aza-aromatics π,π^* transition in solution is about 1.12 eV. To test the generality of this treatment we examined the electrochemical redox potentials and triplet and singlet energies of a series of halogenated and other benzene derivatives. The data are listed in Table 5. No correlation was found between the absolute difference of oxidation and reduction potentials of substituted benzenes and their triplet or singlet energies. The deviation from the correlation predicted by [9] could be due to

Can. J. Chem. Downloaded from www.nrcresearchpress.com by 210.87.254.40 on 09/05/12
For personal use only.

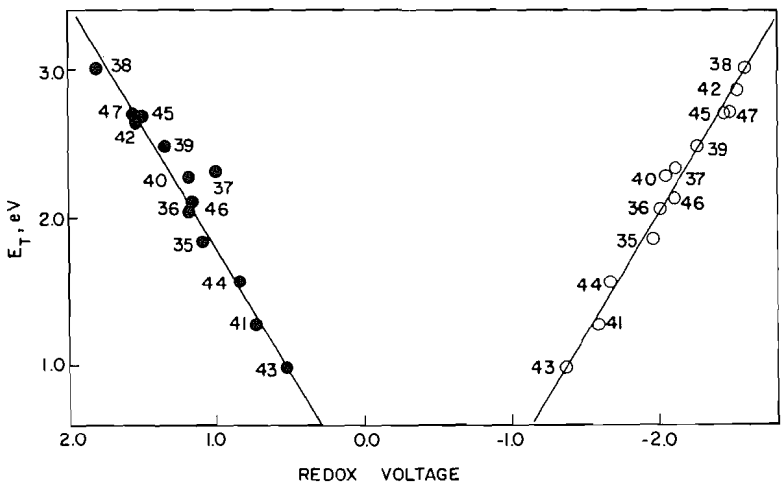

FIG. 5. Plot of $E_T(\pi,\pi^*)$ of aromatic hydrocarbons against their half-wave oxidation (●) and reduction (○) potentials.

variation in the coulomb repulsion integral within the series in a manner not predicted by [12] or a number of other possible reasons. Substituting one to six halogen atoms for hydrogen atoms in the benzene ring causes a marked change in the charge distribution in the ground and excited state of the molecule. A considerable charge transfer between the ring π-system and the substituents will profoundly affect the overlap integral and thus, the value of J_{12} will be highly dependent on the perturbation of the charge distribution caused by the substituent. If one assumes that the deviation is mainly due to irregular variation in J_{12}, it is possible to calculate this term using [9]. As expected, the J values vary irregularly along the series. Comparison between the repulsion integral estimated from [9] with calculated values might verify the assumption that the deviation from linearity is indeed due to the variation of J. This comparison will be discussed later.

Another factor which might contribute to the

TABLE 5. Electrochemical data, $\pi\rightarrow\pi^*$ singlet and triplet energies, and the calculated repulsion integrals of some benzene derivatives

Number	Compound	E_T (eV)[a]	E_S (eV)[a]	$-E^R$ (V)[b]	E^{ox} (V)[c]	$E^{ox} - E^R$ (V)	J_{12} (eV)
48	Benzene	3.65	4.71	2.80	2.18	4.98	1.33
49	Fluoro-	3.66	4.67	2.69	2.40	5.09	1.43
50	Chloro-	3.58	4.61	2.64	2.37	4.63	1.43
51	Bromo-	3.50	4.55	2.35	2.28	4.63	1.13
52	Trifluoromethyl-	3.62	4.69	2.54	2.68	5.22	1.60
53	Cyano-	3.37	4.42	2.30	2.70	5.00	1.63
54	*m*-Difluoro-	3.56	4.69	2.64	2.52	5.16	1.60
55	*p*-Difluoro-	3.45	4.46	2.68	2.49	5.17	1.72
56	*o*-Difluoro-	3.59	4.66	2.62	2.50	5.12	1.63
57	1,2,4,5-Tetrafluoro-	3.49	4.54	2.40	2.51	4.91	1.42
58	Pentafluoro-	3.31	4.46	2.35	2.78	5.13	1.82
59	Hexafluoro-	3.22	4.28	2.11	2.86	4.97	1.75
60	Hydroxy-	3.55	4.42	2.10	1.34	3.44	−0.11
61	Amino-	3.32		1.66	1.00	2.66	−0.66
62	Methyl-	3.57	4.71	2.80	1.98	4.78	1.21

[a]Reference 30.
[b]References 31 and 15. The reduction potentials were measured in DMF *vs.* SCE.
[c]References 12 and 15. The oxidation potentials were measured in AN *vs.* SCE. For compounds **52–59** E^{ox} were calculated from $E^{ox} = 0.6031P - 3.15$.

Can. J. Chem. Downloaded from www.nrcresearchpress.com by 210.87.254.40 on 09/05/12
For personal use only.

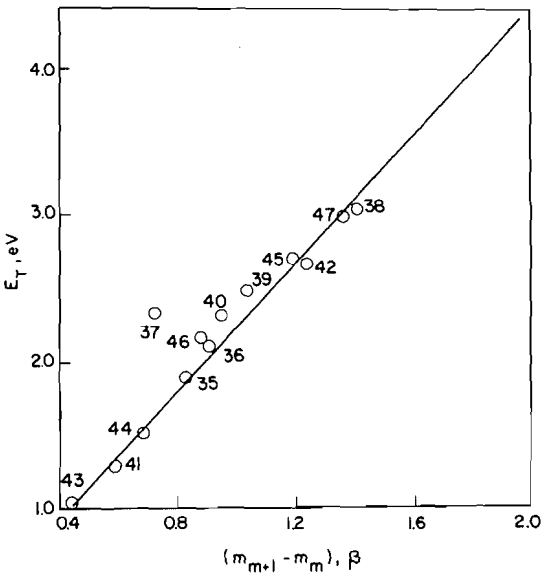

FIG. 6. Plot of $E_T(\pi,\pi^*)$ of aromatic hydrocarbons against the HMO coefficient energy difference $(m_{m+1} - m_m)$.

deviation could be inaccuracies in the reported triplet energies of benzene derivatives. Most benzene derivatives exhibit a structureless phosphorescence spectrum (30*b*) from which the triplet energies were calculated from the intercept of the plot of emission intensity *vs.* wavelength. In another report (32) the phosphorescence emission maximum of fluorobenzene derivatives were found to be shifted about 3000 cm^{-1} to the red of the 0–0 band. In addition, the nature of the triplet transition for benzene derivatives having strong electron donating substituents, might be different from those having strong electron withdrawing substituents (due to charge transfer to or from the π-ring). Thus both inaccurate measurement as well as possible variations in the nature of the triplet states of benzene derivatives could contribute to the absence of a correlation between E_T and electrochemical data.

A final possible reason could be that most benzene derivatives exhibit irreversible reduction waves (31*b*) making the accuracy of $E_{1/2}{}^R$ doubtful. Also, the oxidation potential of compounds **52–59** were calculated from the corresponding ionization potentials assuming that the solvation energy of the radical cation is constant. However, when the ionization potential is very large, an indication that the electrons are very strongly bound to the core in the gas phase, solvation of the ion can be very strong. As a result the solvation energy is expected to be larger for benzene derivatives with higher IP's. It should be mentioned here that bigger aromatic hydrocarbons are not expected to show such dependence since the solvation energy of large ions having well delocalized electrons could remain independent of IP and EA.

Repulsion Integrals

The numerical calculations of the electronic structures and spectra of polyatomic molecules are very complicated and a difficult problem. Semi-empirical procedures are widely used to calculate and understand the electronic states of molecules. A number of purely semi-empirical theories, in which various assumptions were made to simplify computation, were reviewed by Jaffe (33). One of the questions raised by these semi-empirical theories concerns the repulsion integral, $\langle\psi_i\psi_j|g|\psi_i\psi_j\rangle$, where g is the repulsion operator. The coulomb repulsion integral given in terms of Hartree–Fock LCAO-MO wave functions, eq. 4, may be expanded in terms of atomic orbitals to give the expression:

$$[17] \quad J_{ij} = \sum_u\sum_v\sum_r\sum_s C_{iu}C_{iv}C_{jr}C_{js} \times \iint\phi_u(1)\phi_v(1)|g|\phi_r(2)\phi_s(2)$$

Pariser–Parr and Pople introduced the zero differential overlap approximation (ZDO) (34). According to the ZDO method only the one-center and two-center coulomb repulsion integrals remain to be evaluated and then J_{ij} in terms of the MO's can be written as follows

$$[18] \quad J_{ij} = \sum_u\sum_r C_{iu}{}^2C_{jr}{}^2\gamma_{ur}$$

The coulomb integrals in terms of AO's may be evaluated by empirical or semi-empirical procedures. The one-center repulsion integral γ_{uu}, estimated semi-empirical by Pariser (35), is given by

$$[19] \quad \gamma_{uu} = IP_u - EA_u = 10.5\ eV$$

where IP_u and EA_u are the valence state ionization potential and electron affinity of the neutral carbon atom. This semi-empirical relation was recently justified by Freed (36). He also showed that the true two-center repulsion integrals γ_{ur} are in semi-quantitative agreement with their empirical counterparts.

Table 6 shows a comparison between the

Can. J. Chem. Downloaded from www.nrcresearchpress.com by 210.87.254.40 on 09/05/12
For personal use only.

TABLE 6. Comparison between the semi-empirically calculated coulomb repulsion integral and that estimated from electrochemical and spectroscopic data

Compound	J_{12} MO[a]	J_{12} Calculated[b]
Benzene	1.20	1.33
Pyrene	1.30	1.15
Anthracene	1.34	1.20

[a]References 37 and 38.
[b]Calculated from [9].

coulomb repulsion integral predicted from electrochemical/spectroscopic data and that evaluated using the above relationships (37) for benzene, pyrene, and anthracene. The reasonable agreement verifies the validity of estimating the coulomb repulsion integral from electrochemical and spectroscopic data.

In summary: the interrelations between electrochemical and spectroscopic data measured in solution were developed and utilized to estimate the triplet energies for compounds in which this transition is either inaccessible or unobservable by experimental spectroscopy. The true oxidation potentials were calculated for a number of aza-aromatics. A deviation in the relationship between $E_T(\pi,\pi^*)$ and the absolute difference between oxidation and reduction potential of benzene derivatives was attributed to variation of the coulomb repulsion integral in this series.

Acknowledgements

The authors wish to thank Dr. J. H. Sharp and Dr. J. Duff, Xerox Research Centre of Canada Ltd., for discussing and exercising their critical faculties on our manuscript.

1. A. WELLER and K. ZACHARIASSE. *In* Molecular luminescence. *Edited by* E. C. Lim. Benjamin, New York. 1969. p. 895.
2. R. F. LARGE. Photographic sensitivity. *Edited by* R. J. Cox. Academic Press, New York. 1973. p. 241.
3. R. O. LOUTFY and R. O. LOUTFY. J. Phys. Chem. **77**, 336 (1973); **76**, 1650 (1972).
4. R. O. LOUTFY and J. H. SHARP. Photogr. Sci. Eng. In press.
5. R. DITCHFIELD, J. E. DEL BENE, and J. A. POPLE. J. Am. Chem. Soc. **94**, 703 (1972).
6. A. MACCOLL. Nature, **163**, 178 (1949).
7. M. E. PEOVER. Electroanal. Chem. **2**, 40 (1967).
8. (*a*) A. A. LAMOLA and T. YAMANE. Proc. Natl. Acad. Sci. U.S.A. **58**, 443 (1967); (*b*) A. J. VARGHESE. Photochem. Photobiol. **15**, 113 (1972); (*c*) D. W. WHILLAMS and H. E. JOHNS. J. Am. Chem. Soc. **93**, 1358 (1971).
9. K. K. INNES. J. Mol. Spectrosc. **122**, 125 (1971).
10. B. J. TABNER and J. R. YARDLE. J. Chem. Soc. A, 381 (1968).
11. P. S. EGEL and B. M. MONROE. Adv. Photochem. **8**, 302 (1970).
12. L. L. MILLER, G. D. NORDBLOM, and E. A. MAYEDA. J. Org. Chem. **37**, 916 (1972).
13. H. V. DRUSHEL and A. L. SOMMERS. Anal. Chem. **38**, 10 (1966).
14. T. KUBOTA, M. YAMAKAWA, and Y. MIZUNO. Bull. Chem. Soc. Jpn. **45**, 3282 (1972).
15. C. K. MANN and K. K. BARNES. Electrochemical reactions in non-aqueous systems. Marcel Dekker, Inc., New York. 1970.
16. G. N. LEWIS and M. KASHA. J. Am. Chem. Soc. **66**, 2108 (1944).
17. D. R. KEARNS and W. A. CASE. J. Am. Chem. Soc. **88**, 5087 (1966).
18. D. F. EVANS. J. Chem. Soc. 1351 (1957); 3885 (1957).
19. B. J. TABNER and J. R. YARDLE. Reaction of molecules at electrodes. *Edited by* N. S. Hush. Wiley-Interscience, New York. 1971. p. 283.
20. A. T. WATSON and F. A. MATSEN. J. Chem. Phys. **18**, 1305 (1950).
21. F. A. MATSEN. J. Chem. Phys. **24**, 602 (1956).
22. B. CASE, N. S. HUSH, R. PARSONS, and M. E. PEOVER. J. Electroanal. Chem. **10**, 360 (1965).
23. M. E. PEOVER. Trans. Faraday Soc. **58**, 1656 (1962); **58**, 2370 (1962); **60**, 479 (1964).
24. M. E. PEOVER. Electrochim. Acta, **13**, 1083 (1968) and references cited therein.
25. R. D. HOLM, W. R. CARPER, and J. A. BLANCHER. J. Phys. Chem. **71**, 3960 (1967).
26. H. MIYAZAKI, T. KUBOTA, and M. YAMAKAWA. Bull. Chem. Soc. Jpn. **45**, 780 (1972).
27. K. SASAKI and W. J. NEWBY. J. Electroanal. Chem. **20**, 137 (1969).
28. A. STREITWIESER, JR. Molecular orbital theory for organic chemists. Wiley and Son Inc., N.Y. 1961.
29. G. H. HOIJTINK. Recl. Trav. Chim. Pays-Bas, **77**, 555 (1958).
30. (*a*) S. P. MCGLYNN, T. AZUMI, and M. KINOSHITA. Molecular spectroscopy of the triplet state. Prentice-Hall, New Jersey. 1969. p. 286; (*b*) D. PHILLIPS. J. Photochem. **1**, 97 (1972); (*c*) H. H. PERKAMPUS and H. R. VOLLBRECHT. Spectrochim. Acta, Part A, **27**, 2173 (1970).
31. (*a*) G. G. YAKOBSON and V. P. PETROV. Sib. Chem. J. **2**, 75 (1965); (*b*) B. H. CAMPBELL. Anal. Chem. **44**, 1659 (1972).
32. J. E. KENT, M. F. O'DWYER, and R. J. STEPHENS. Chem. Phys. Lett. **10**, 201 (1971).
33. H. H. JAFFE. Acc. Chem. Res. **2**, 136 (1969).
34. N. MATAGA and T. KUBOTA. Molecular interactions and electronic spectra. Marcel Dekker Inc., N.Y. 1970. Chapt. 2. p. 68.
35. R. PARISER. J. Chem. Phys. **21**, 568 (1963).
36. K. FREED. Chem. Phys. Lett. **24**, 275 (1974).
37. N. S. HUSH and J. A. POPLE. Trans. Faraday Soc. **51**, 600 (1955).
38. J. N. MURRELL and J. TANAKA. Mol. Phys. **4**, 363 (1964).

Can. J. Chem. Downloaded from www.nrcresearchpress.com by 210.87.254.40 on 09/05/12
For personal use only.

Geometry and rotational barriers in 1,3,5-triphenylpentadienyllithium by ^1H and ^{13}C nuclear magnetic resonance[1]

D. H. HUNTER, R. E. KLINCK,[2] R. P. STEINER,[3] and J. B. STOTHERS

Department of Chemistry, University of Western Ontario, London, Ontario N6A 5B7

Received September 29, 1975

D. H. HUNTER, R. E. KLINCK, R. P. STEINER, and J. B. STOTHERS. Can. J. Chem. **54**, 1464 (1976).

Variable temperature studies of ^1H and ^{13}C spectra have been employed to establish the geometry of 1,3,5-triphenylpentadienyllithium in tetrahydrofuran solution. These data show that the anion exists in both W and S forms, which are of comparable energy, and interconversion between the two S forms is more rapid than W $\rightleftharpoons$ S. This represents one of the few reported measurements of the barrier to rotation about an internal bond in a delocalized carbanion.

D. H. HUNTER, R. E. KLINCK, R. P. STEINER et J. B. STOTHERS. Can. J. Chem. **54**, 1464 (1976).

On a utilisé des études à température variable des spectres rmn du ^1H et du ^{13}H pour établir la géométrie du triphényl-1,3,5 pentadiénylllithium en solution dans le tétrahydrofuranne. Ces données montrent que l'anion existe dans les deux formes W et S qui sont d'énergie comparable et l'interconversion entre les deux formes S est plus rapide que l'interconversion W $\rightleftharpoons$ S. Ces données correspondent à une des quelques valeurs rapportées pour la barrière à la rotation autour d'un lien interne dans un carbanion délocalisé.

[Traduit par le journal]

Introduction

A number of open-chain delocalized carbanions have been examined and characterized in solution by ^1H nmr spectroscopy (for a review see ref. 1), *e.g.*, allyl, pentadienyl, heptatrienyl, and nonatetraenyl. These investigations also included a variety of alkyl, vinyl, and aryl substituted derivatives. In several cases, specific geometries have been assigned on the basis of proton–proton coupling constants and symmetry. Examples pertinent to the present study include pentadienyllithium (2), 1-phenylallyllithium (3), 1,3-diphenylallyllithium (4), and 1,5-diphenylpentadienyllithium (5) whose proposed geometries are shown in Scheme 1. Each of these exists predominantly in the W form. Variable temperature ^1H nmr studies (6) have been made on some systems including those shown (except 1,5-diphenylpentadienyllithium). These spectra indicated that there are appreciable barriers to rotation around the terminal bonds (labelled *a* in Scheme 1) as well as around the bonds to the phenyl ring and the magnitudes of these barriers or the coalescence temperatures have been determined. However, observation and measurement of barriers around inner bonds (labelled *b* in Scheme 1) have been much less frequent.

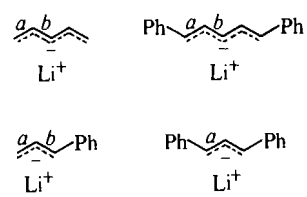

SCHEME 1

Two geometries of 2-methylpentadienyllithium have been observed by proton nmr (2) and the rate of rotation around the 2,3-bond was estimated for the coalescence temperature (−5 °C). A combination of ^1H and ^{13}C nmr spectroscopies has been used to identify more than one geometry of some methyl substituted open-chain pentadienyl anions (1,6). Although it was possible to obtain evidence for the presence of minor amounts of S shapes along with the predominant W form in some cases, barriers could not be estimated. Proton nmr has revealed two geometries for 7-oxoheptatrienyl potassium due to restricted rotation around the 3,4-bond (7).

[1]Part 57 in the series ^{13}C nmr studies; for part 56 see ref. 12.

[2]Present address: Urbana College, Urbana, Ohio, 43078, U.S.A.

[3]Present address: Dept. of Chemistry, University of Utah, Salt Lake City, Utah, 84112, U.S.A.

Can. J. Chem. Downloaded from www.nrcresearchpress.com by 210.87.254.42 on 09/05/12
For personal use only.

Can. J. Chem. Downloaded from www.nrcresearchpress.com by 210.87.254.42 on 09/05/12
For personal use only.

There are very few cases for which quenching of the carbanion has been used to assist in the assignment of geometry. Nonetheless the products from quenching some pentadienyl anions (5, 6, 8) indicated the presence of minor amounts of the S form along with the major W shape.

As part of a study of the electrocyclization of aza-substituted pentadienyl anions, we had occasion to prepare and study 1,3,5-triphenylpentadienyllithium, **1**. The application of variable temperature ^1H and ^{13}C nmr as well as quenching experiments have allowed direct observations of both S and W shapes with the S form predominating. The barrier to rotation around the inner bond has been estimated and it has been shown that direct interconversion of S shapes is not only possible but extremely facile.

Experimental

Spectra

Proton spectra were obtained with a Varian HA-100 spectrometer using tetrahydrofuran-d_8 solutions of the anion (0.2 and 0.4 *M*) prepared in sealed tubes as described below. The same solutions were employed initially for ^{13}C spectra using a Varian XL-100-15 system operating in the Fourier transform mode. The lower field solvent signal served as the ^2H lock signal. For both ^1H and ^{13}C spectra the probe temperature was monitored before and after the collection of each spectrum with a thermocouple placed in a sample tube containing toluene. The two concentrations were examined over the temperature range of +50 to −90 °C initially at 10 °C intervals. These spectra revealed the approximate coalescence temperatures which were more precisely determined by examining spectra obtained at 2–3 °C intervals in the appropriate regions. These experiments were done twice for each solution. To obtain better ^{13}C spectra, a comparable solution (0.4 *M*) was prepared in a 12 mm tube and two sets of data over the range +50 to −77 °C were obtained, initially at 10 °C intervals and then at 2 °C intervals near the coalescence temperatures.

To aid the assignments for the ^{13}C spectrum of the anion at ambient temperature some selective decoupling experiments were performed and a proton-coupled spectrum was obtained with the usual gated-decoupling technique.

Preparation of 1,3,5-Triphenylpentadienyllithium, 1

The following is a typical procedure. Into an nmr tube attached to a one-necked reaction vessel was added 308 mg (1.07 mmol) of 1,3,5-triphenyl-1,3-pentadiene (2), either *trans,trans* or as a mixture with *trans,cis* (9). After evacuating the vessel and introducing an argon atmosphere, 348 mg (2.5 mmol) of 2,2,6,6-tetramethylpiperidine (TMP) was added to the reaction bulb and degassed. To the TMP at −20 °C was added 1 ml (2 mmol) of *n*-butyllithium (2 *M* in hexane, Ventron). After warming to room temperature, the solvent and the excess TMP were removed at 0.03 torr.

To the reaction bulb was added the appropriate volume of THF-d_8 (dried with Na/K alloy) by bulb-to-bulb distillation at 0.03 torr. After the base solution was warmed to room temperature, the solution was tipped onto the pentadienes and the nmr tube sealed.

Preparation of 1,5,5-Trideuterio-1,3,5-triphenyl-1,3-pentadienes, 2-d_3

A 100 mg (0.3 mmol) sample of 1,3,5-triphenyl-*trans*, *trans*-1,3-pentadiene, **2**, was sealed in a degassed, evacuated tube with 2 ml of 0.59 *M* potassium methoxide in methanol-*O*-*d* (10). After heating at 100 °C for 2.5 days, the tube was opened and the contents poured into an excess of D_2O. After extraction with ether, the dienes were purified by thick layer chromatography using silica gel and 10% ether–pentane.

A proton nmr spectrum indicated a 3:1 mixture of *trans,trans*-**2** and *trans,cis*-**2**, respectively. Signals due to the 1- and 5-protons were not observed, indicating ≥90% exchange.

Results and Discussion

Solutions of 1,3,5-triphenylpentadienyllithium (**1**) in tetrahydrofuran-d_8 were prepared by reacting 1,3,5-triphenyl-*trans,trans*-1,3-pentadiene (*trans,trans*-**2**) or a mixture of *trans,trans*-**2** and *trans,cis*-**2** with lithium 2,2,6,6-tetramethylpiperidide in THF-d_8. Besides using ^1H and ^{13}C nmr to characterize the deep blue solution of **1**, the products of quenching with acetic acid were also identified. The reaction of **1** in THF at ambient temperature with acetic acid yielded a mixture of 46% of *trans,trans*-**2** and 54% of *trans,cis*-**2**. Quenching with D_2O yielded the same mixture which analyzed for 94%-d_1 and 6%-d_0 material.

Proton Nuclear Magnetic Resonance Results

Variable temperature proton spectra were obtained using two solutions of **1** in THF-d_8

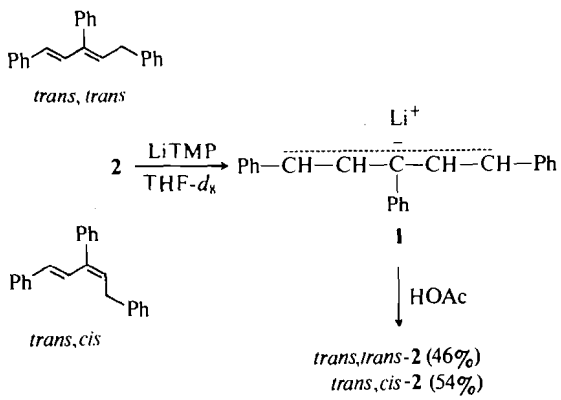

SCHEME 2

TABLE 1. Spectral parameters for the AB spectra observed for **1**

Temperature (°C)	ν_A(ppm)	ν_B(ppm)	J_{AB}(Hz)
+50	5.31	6.60	15.0
−60	4.95	6.4[a]	15.0
	5.48	6.7[a]	15.0

[a]Shielding determined by decoupling experiments.

(0.2 and 0.4 *M*) over the temperature range +50 to −90 °C. Precipitation because of decreased solubility and deterioration of the lock signal determined the lower temperature limit while concern over the stability of **1** determined the upper limit. Changes in the nmr spectra proved to be reversible and reproducible with no observable differences in behaviour of the 0.2 and 0.4 *M* solutions.

The ambient temperature (+32 °C) spectrum was characterized by a complex multiplet in the 6.1–7.1 ppm region assigned to the aromatic protons. The four protons on the pentadienyl chain appeared as an AB system with δ_A near 5.3 ppm and δ_B near 6.6 ppm amid the aryl proton absorption. The latter assignment (see Table 1) was established by proton–proton decoupling experiments.

The signals near 5.3 ppm were assigned to the protons on carbon-1 and -5 of the pentadienyl chain on the basis of the hydrogen-deuterium exchange experiment. A sample of *trans,trans*-**2** was treated with $KOCH_3$–$DOCH_3$ which resulted in 1,5,5-trideuterio-**2** as a mixture of geometrical isomers. Reaction of this material with LiTMP gave 1,5-dideuterio-**1** whose proton nmr spectrum showed the absence of signals near 5.3 ppm and the collapse of the doublet near 6.6 ppm to a singlet.

Upon lowering the temperature, the spectrum of **1** changed markedly and the variations in the region near 5.3 ppm proved to be of greatest diagnostic value. The doublet observed at +32 °C gradually broadened and collapsed into a single broad band (T_c −15°) and then reappeared in the range −40 to −60 °C as two doublets centered at 4.9 and 5.5 ppm (Fig. 1). Both the integrated intensities and the peak positions were consistent with relative populations of 1:2.1 favoring the lower field signal. These doublets were analyzed as the high field halves of two AB spectra and this assignment

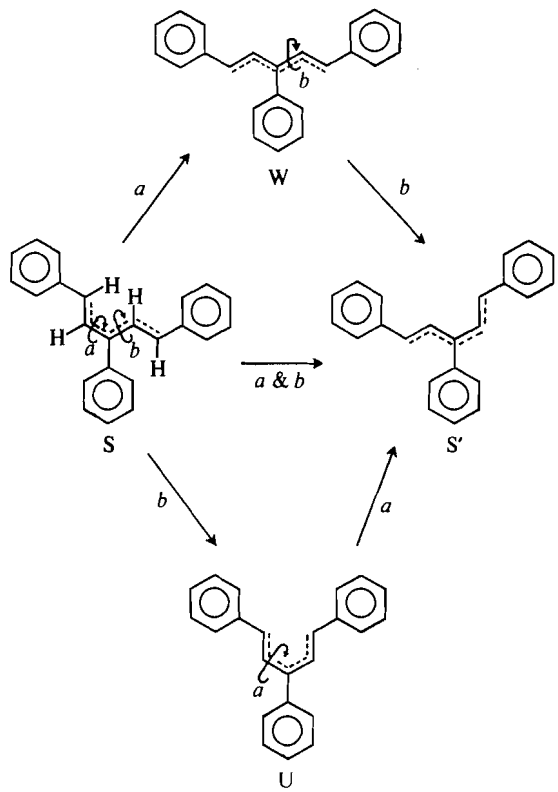

SCHEME 3

was corroborated by decoupling experiments to locate the low field halves (Table 1). On further cooling the less intense doublet near 4.9 ppm was essentially unaffected while that near 5.5 ppm appeared to collapse into a single broad band near −80 °C. Unfortunately, spectra could not be obtained below −90 °C and thus the slow exchange limit for this second rate process could not be observed.

If planar or near-planar conformations are assumed for the pentadienyl chain in **1**, there are three forms available: W, S, and U. If the phenyl rings are placed on these chains to minimize nonbonded interactions then the geometries shown (Scheme 3) should be the most stable. The U form is expected to be the least likely of the three as has been verified for the unsubstituted pentadienyllithium (2,6). Thus the W and S forms are considered to be the major contributors on the basis of nonbonded interactions although in this specific case nmr does not allow a distinction between U and W.

The signals in the 5.0–5.5 ppm region arise

Can. J. Chem. Downloaded from www.nrcresearchpress.com by 210.87.254.42 on 09/05/12
For personal use only.

Can. J. Chem. Downloaded from www.nrcresearchpress.com by 210.87.254.42 on 09/05/12
For personal use only.

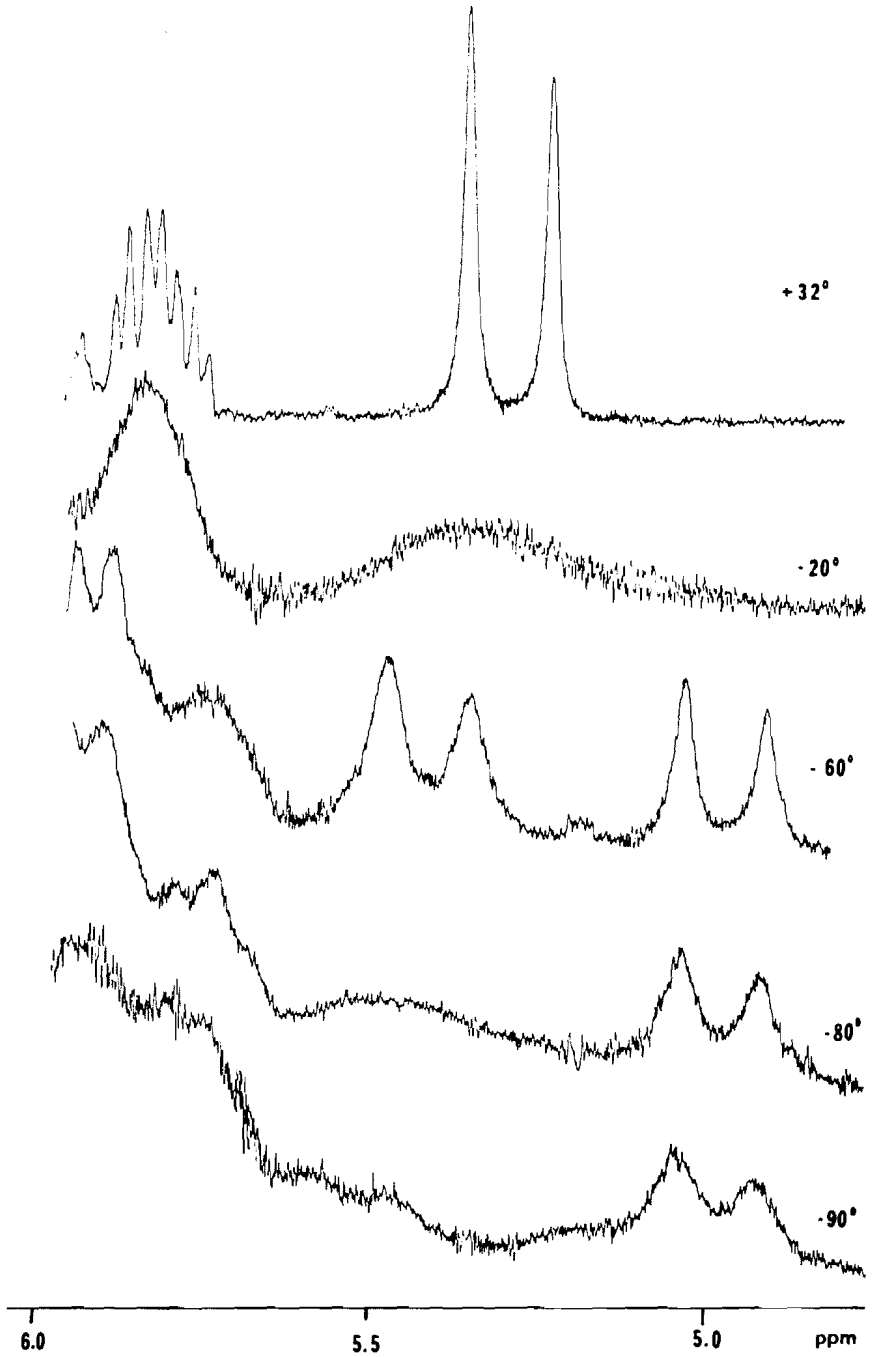

FIG. 1. The effect of temperature on the signals arising from protons at positions 1 and 5 in **1**.

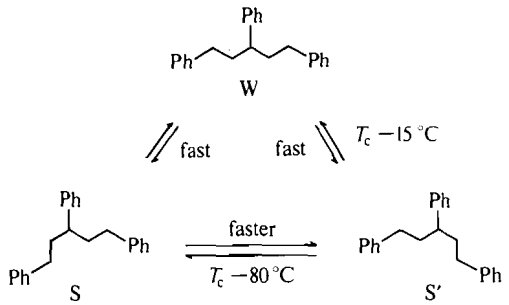

FIG. 2. Mechanistic scheme consistent with the variable temperature ^1H and ^{13}C nmr results.

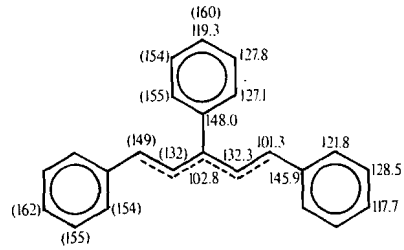

FIG. 3. ^{13}C shieldings and one-bond coupling constants, J_{CH}, (Hz, in parentheses) observed for **1** at 32 °C. The shieldings are given in ppm relative to TMS assuming that the THF-d_8 shieldings are 25.3 and 67.4 ppm.

from the protons at the 1- and 5-positions on the pentadienyl chain. In the three shapes considered, these protons have a *trans*-vicinal neighbor which is consistent with the observed 15.0 Hz coupling constants (1,11). The low temperature nmr results show that (*i*) there is more than one environment available for these protons, (*ii*) there is interchange between these environments and (*iii*) these environments are not equally probable (*i.e.*, the 2.1:1 ratio at 60 °C). Thus, there is dynamic interconversion between two or more forms in solution. Interconverting S shapes would exhibit equally intense doublets at −60 °C. Since these are in a ratio of 2.1:1 it is concluded that the W and S forms are present in unequal amounts.

The observation of a single doublet in the 5.0–5.5 ppm region for the S form could arise in two ways: a coincidence of signals or a rapid interconversion of S forms but not via the W form. The latter explanation is favored since lowering the temperature from −60 to −80 °C results in coalescence of the more intense doublet at 5.5 ppm. This observation is permissive evidence that the ratio of S:W forms is 2.1:1. The overall scheme (Fig. 2) that emerges has the W ⇌ S interconversion characterized by coalescence at a higher temperature (−15 °C) than the S ⇌ S′ interconversion ($T_c \sim -80$ °C), indicating the existence of a low energy direct interconversion of S forms.

Carbon Nuclear Magnetic Resonance Results

In an attempt to obtain independent evidence bearing on the shape of **1** in solution, variable temperature ^{13}C spectra were examined using 0.2 and 0.4 *M* samples of **1** in THF-d_8. The signal assignments for the ambient temperature spectrum (Fig. 3) were made on the basis of the proton-coupled spectrum and selective decoupling experiments. Again, variable temperature studies over the range +50 to −80 °C revealed a number of characteristic changes in the spectra which were reversible and reproducible. The region that proved to be of greatest diagnostic value contained the signals near 100 ppm assigned to carbons 1, 3, and 5 of the pentadienyl chain. The overlap of the signals due to carbons 2, 3, 4, 5, and 6 of the phenyl rings and carbons 2 and 4 of the pentadienyl chain was sufficient to discourage analysis of their temperature dependent behaviour. The signals of carbon-1 of the phenyl rings were sufficiently separate from the remainder of the aromatic carbons but the terminal phenyl signals were only slightly separated at low temperature. The central phenyl was more useful and provided results consistent with carbons 1, 3, and 5 of the pentadienyl chain.

As illustrated in Fig. 4, above ambient temperature at the fast-exchange limit, two signals appeared in the ratio 2:1 readily assigned to C-1, C-5 (101.3 ppm), and C-3 (102.8 ppm). As the temperature was lowered, these signals broadened and collapsed into a broad band at −9 °C to reemerge as four peaks near −40 °C. Upon further cooling to −70 °C, the signal at 103.8 ppm disappeared while the other three remained. As indicated in Fig. 4, the peaks at 106.3 and 101.3 ppm can be associated with the C-3 signal at 102.8 ppm in the spectrum at +51 °C and the signals at 103.8 and 94.9 ppm to the high temperature C-1,C-5 signal at 101.3 ppm.

As deduced from the proton results, the carbon spectra are consistent with the presence

Can. J. Chem. Downloaded from www.nrcresearchpress.com by 210.87.254.42 on 09/05/12
For personal use only.

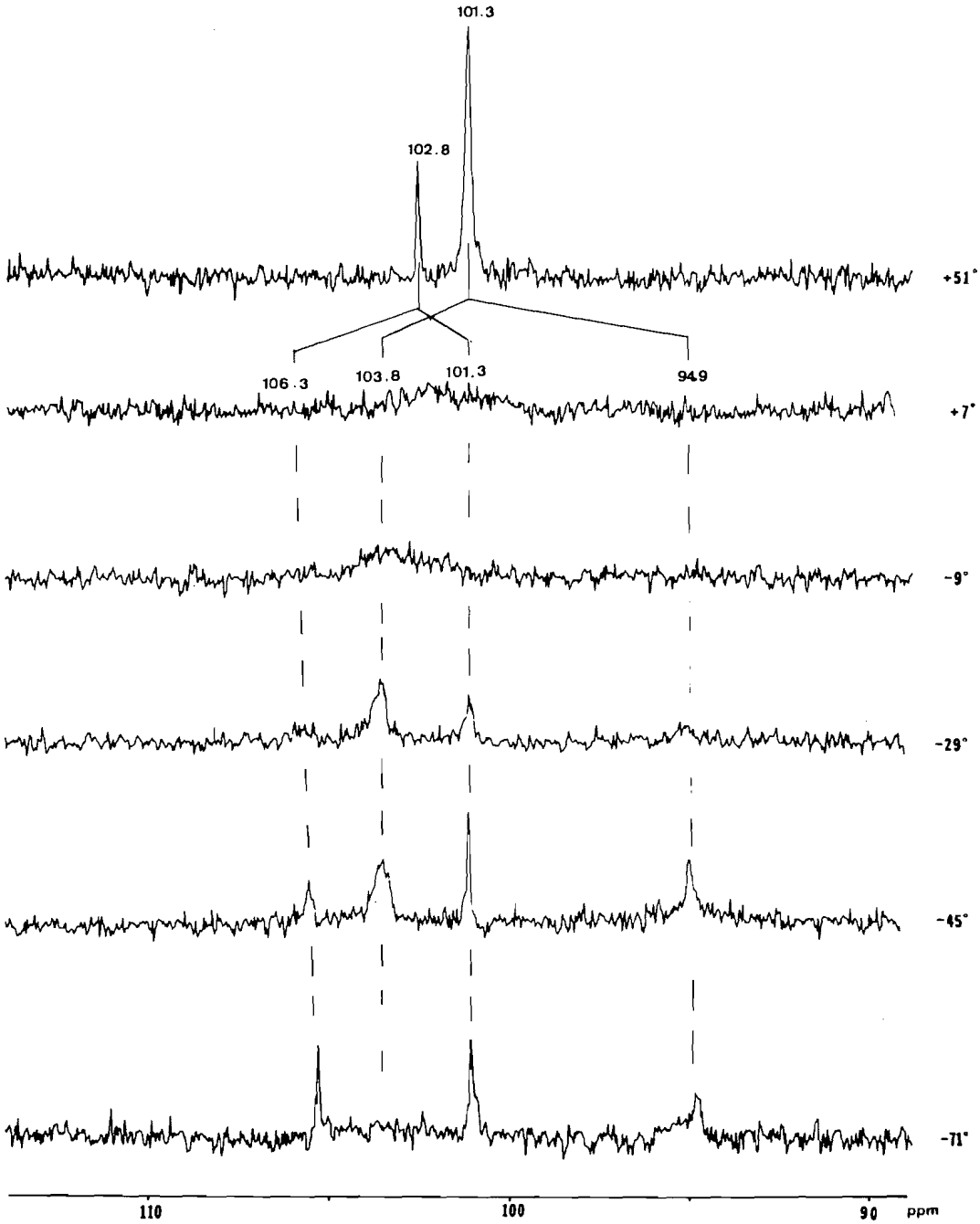

FIG. 4. The effect of temperature on the ^{13}C signals for C-1, -5, and -3 in **1**. The shieldings (ppm from TMS) are given for +32 and +51 °C. Only the signal near 106.3 ppm showed an appreciable temperature dependence.

Can. J. Chem. Downloaded from www.nrcresearchpress.com by 210.87.254.42 on 09/05/12
For personal use only.

Can. J. Chem. Downloaded from www.nrcresearchpress.com by 210.87.254.42 on 09/05/12
For personal use only.

of two interconverting forms, presumably the W and S. Although the exact position of the signal near 106.3 ppm is temperature sensitive, the ratio of the W and S shapes can be estimated from the ratio of the change in signal positions due to coalescence. This corresponds to a ratio of 2.4:1 in reasonable agreement with the 2.1:1 ratio obtained from the proton spectrum. Thus the signals at 106.3 ppm (carbon-3) and 94.9 ppm (carbons-1 and -5) arise from the minor form and the signals at 103.8 ppm (carbons-1 and -5) and 101.3 ppm (carbon-3) from the major form.

The absorptions attributed to the major form should represent the average values for $S \rightleftharpoons S'$ if the interpretation of the proton spectra is valid. Slowing the $S \rightleftharpoons S'$ interconversion (Fig. 2) could result in collapse of the C-1, C-5 signal but that for C-3 should remain unaffected. This feature is unique to the S form and is corroborated by the change noted at -70 °C. Thus both the ^{13}C and ^{1}H nmr results are consistent with the scheme illustrated in Fig. 2.

Mechanism of the Geometrical Interconversion

The nmr observations can be interpreted in terms of a mechanism involving rotations in the delocalized anion itself. In this picture, the lower $\Delta G^{\ddagger}$ for $S \rightleftharpoons S'$ than for $S \rightleftharpoons W$ corresponds to a lower barrier for bond rotation process '*b*' than process '*a*' (see Scheme 3). The 1,3-hydrogen, phenyl interactions involving the central aryl ring in the S form can be relieved by process '*b*' while process '*a*' seems to lack a similar driving force. The precise route followed for the $S \rightleftharpoons S'$ interconversion is not clear except that a planar U form seems to be an unlikely intermediate. While nmr shows the presence of both the W and S shapes, the absence of a third geometry suggests that the U shape is the highest energy species available. Nonetheless the $S \rightleftharpoons S'$ interconversion probably proceeds through a twisted U-shape. An examination[4] of the anticipated transition states for $S \rightleftharpoons W$ interconversion and $S \rightleftharpoons U$ interconversion also suggests that the latter (*trans*, *trans*-1,3-diphenylallyl like) may well be lower in energy than the former (*trans*,*cis*-1,3-diphenylallyl like).

The foregoing argument has neglected any influence of the cation whose possible perturbations are difficult to assess. We have no direct evidence to show whether **1** exists as an ion-pair or a dissociated ion except that the nmr behaviour is the same for both concentrations examined.

The combination of ^{1}H and ^{13}C coalescence phenomena allow an estimation of activation parameters for the $S \rightleftharpoons W$ interconversion although T_c is difficult to gauge for the carbon signals. From the carbon T_c of -5 °C and the proton T_c of -15 °C, $\Delta H^{\ddagger} = 13$ kcal/mol and at both temperatures $\Delta G^{\ddagger} = 12$ kcal/mol. Certainly, within experimental error, $\Delta S^{\ddagger} = 0$.

Integrated intensities and observed line positions gave a ratio of 2.1–2.4 for the relative amounts of S and W forms, respectively. After correcting for the twofold degeneracy of the S form, it appears that the S and W forms must have nearly identical $\Delta H_{\text{formation}}$ values. A comparison of the interactions in the two forms seems to suggest that the central phenyl ring must be twisted out of the plane to minimize its 1,3-non-bonded interactions in the W form.

Summary

The combination of variable temperature ^{1}H and ^{13}C spectra has shown that (*i*) **1** exists in both W and S forms, (*ii*) the W and S forms have comparable energy, (*iii*) the $S \rightleftharpoons S'$ interconversion is more rapid than $S \rightleftharpoons W$ and (*iv*) these rotational processes in the delocalized anion account entirely for the observed results.

Acknowledgments

We are grateful to the National Research Council of Canada for financial support of this study. We thank Inara Grikis for technical assistance and Mrs. H. Schroeder for her careful determinations of the 100 MHz proton spectra.

1. D. H. HUNTER. Isotopes in carbanion rearrangements. *In* Isotopes in molecular rearrangements. *Edited by* E. Buncel and C. C. Lee. Elsevier, Amsterdam. 1975.
2. R. B. BATES, D. W. GOSSELINK, and J. A. KACZYNSKI. Tetrahedron Lett. 205 (1967).
3. V. R. SANDEL, S. V. MCKINLEY, and H. H. FREEDMAN. J. Am. Chem. Soc. **90**, 495 (1968).
4. (*a*) H. H. FREEDMAN, V. R. SANDEL, and B. P. THILL. J. Am. Chem. Soc. **89**, 1762 (1967); (*b*) J. W. BURLEY

[4]The authors wish to thank R. B. Bates for this suggestion.

and R. N. YOUNG. J. Chem. Soc. Perkin Trans. II, 1843 (1972); (*c*) R. J. BUSHBY and G. J. FERBER. Tetrahedron Lett. 3701 (1974).
5. S. BRENNER and J. KLEIN. Isr. J. Chem. **7**, 735 (1969).
6. W. T. FORD and M. NEWCOMB. J. Am. Chem. Soc. **96**, 309 (1974).
7. H. KLOOSTERZEIL and J. A. A. VAN DRUNEN. Recl. Trav. Chim. **89**, 667 (1970).
8. (*a*) R. B. BATES, D. W. GOSSELINK, and J. A. KACZYNSKI. Tetrahedron Lett. 199 (1967); (*b*) R. B. BATES, S. BRENNER, C. M. COLE, E. W. DAVIDSON, G. D. FORSYTHE, D. A. MCCOMBS, and A. S. ROTH. J. Am. Chem. Soc. **95**, 926 (1973).
9. D. H. HUNTER and R. P. STEINER. To be published.
10. A. E. STREITWIESER, JR., L. VERBIT, and P. STANG. J. Org. Chem. **29**, 3706 (1964).
11. D. A. HUTCHISON, K. R. BECK, R. A. BENKESER, and J. B. GRUTZNER. J. Am. Chem. Soc. **95**, 7075 (1973).
12. J. B. STOTHERS and K. C. TEO. Can. J. Chem. **54**, 1222 (1976).

Can. J. Chem. Downloaded from www.nrcresearchpress.com by 210.87.254.42 on 09/05/12
For personal use only.

The conversion of phthalideisoquinolines into spirobenzylisoquinolines and rhoeadine precursors

HERBERT L. HOLLAND, MICHAEL CURCUMELLI-RODOSTAMO, AND DAVID B. MACLEAN

Department of Chemistry, McMaster University, Hamilton, Ontario L8S 4M1

Received October 28, 1975

HERBERT L. HOLLAND, MICHAEL CURCUMELLI-RODOSTAMO, and DAVID B. MACLEAN. Can. J. Chem. **54**, 1472 (1976).

Treatment of hydrastine with *p*-nitrophenylchloroformate in the presence of diethylisopropylamine resulted in opening of the isoquinoline ring with the formation of an ene-lactone carbamate. The latter compound rearranged upon treatment with methanolic sodium methoxide to an indan-1,3-dione carbamate which gave, on basic hydrolysis, the corresponding amine. This was ring closed to a spirobenzylisoquinoline. In addition, acid-catalysed dehydration of the amino indandione led to the formation of two isomeric benzazepines, synthetic precursors of the rhoeadine alkaloids. The predominately formed isomer has a substitution pattern identical with that of the rhoeadines.

HERBERT L. HOLLAND, MICHAEL CURCUMELLI-RODOSTAMO et DAVID B. MACLEAN. Can. J. Chem. **54**, 1472 (1976).

La réaction de l'hydrastine avec le chloroformate de *p*-nitrophényle en présence de diéthylisopropylamine conduit à l'ouverture du cycle isoquinoléine et à la formation d'un carbamate de ène-lactone. Ce dernier composé se réarrange par traitement avec du méthylate de sodium en milieu méthanolique pour fournir un carbamate d'indandione-1,3 qui par hydrolyse basique conduit à l'amine correspondante. Cette amine peut être cyclisée en spirobenzylisoquinoléine. De plus la déshydratation acido catalysé de l'amino-indandione conduit à la formation de deux benzazépines isomères qui sont des précurseurs de synthèse des alkaloïdes rhoéadines. L'isomère formé d'une façon prédominante a un patron de substitution identique à celui des rhoéadines.

[Traduit par le journal]

The functionality inherent in the phthalideisoquinolines, **1**, and their availability in nature and by synthesis (see refs. 2–4 and for a recent review, ref. 1), makes them useful starting materials for the synthesis of other isoquinoline alkaloids. The facile conversion of narcotine, **1***a*, into narceine **2** (5) by treatment of narcotine methiodide with aqueous base demonstrates the ease with which the C-1–N bond may be cleaved when the heteroatom is quaternized. Reactions of this type may be used to functionalize both C-1 and C-1′ of the phthalideisoquinoline system. The formation of an ene-lactone, as shown in Scheme 1, through the treatment of

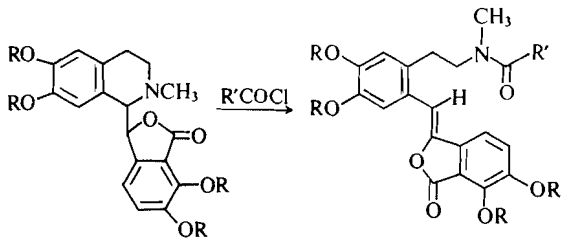

SCHEME 1

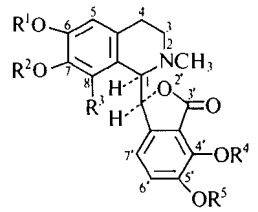

1 *a*; $R^1 + R^2 = CH_2$, $R^3 = OCH_3$, $R^4 = R^5 = CH_3$
b; $R^1 + R^2 = R^4 + R^5 = CH_2$, $R^3 = H$
(Absolute stereochemistry is not necessarily implied)

a phthalideisoquinoline with acyl halides is one such example. This approach has been used in the conversion of a phthalideisoquinoline to a rhoeadine alkaloid. The ene-lactone derived from the reaction of bicuculline, **1***b*, with

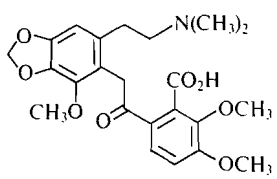

2

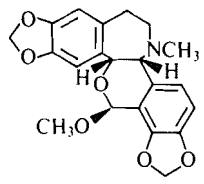

3

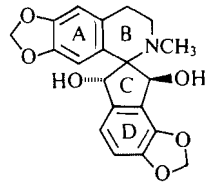

4

phenyl chloroformate was converted in a series of steps into the alkaloid rhoeadine **3** (6).

Ene-lactones such as that shown in Scheme 1 may be readily rearranged by treatment with methanolic methoxide to the corresponding indan-1,3-diones, as shown in Scheme 2 (7).

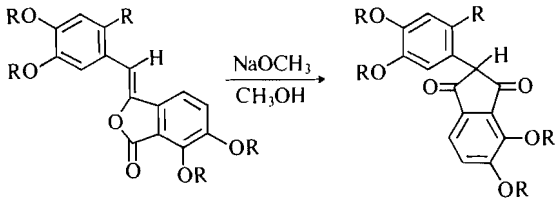

SCHEME 2

This approach has been used in a successful synthesis of the spirobenzylisoquinoline alkaloid ochrobirine, **4** (7). The ene-lactone derived from a phthalideisoquinoline already possesses the aminoethyl side chain necessary for the elaboration of ring **B** of the spirobenzylisoquinoline system, and corresponding indanones have been successfully cyclised to spirobenzylisoquinolines (8) (Scheme 3). The precursor shown in Scheme 3 has also been converted into the rhoeadine system by condensation of the indanone carbonyl at nitrogen, forming a benzazepine system, followed by oxidative transformations of ring C (9).

The indanones from which the spirobenzylisoquinoline (7) and rhoeadine (8) alkaloids were obtained were produced by *de novo* synthesis. We now report that analogous indandiones may be obtained from phthalideisoquinolines in high yield. The key step is the base catalysed rearrangement of the enelactone derived from a phthalide to give an indan-1,3-dione. The latter was then converted both to the spirobenzylisoquinoline and to the benzazepine systems in high yield. The overall sequence is shown in Scheme 4.

Treatment of β-hydrastine, **5**, with a variety of acyl chlorides led to the formation of the ene-lactone system. The choice of an N-pro-

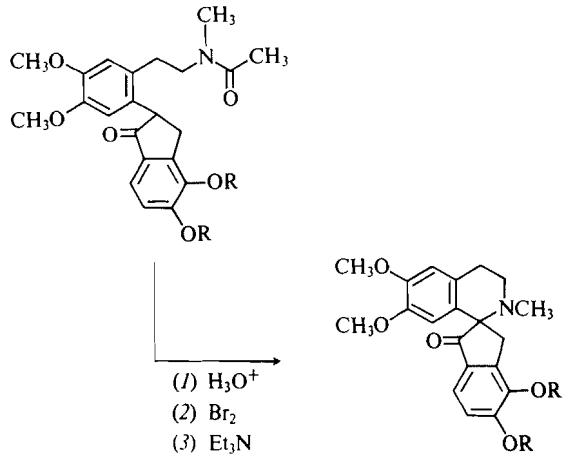

SCHEME 3

tecting group was dictated by the following considerations; firstly, it should be stable to the basic conditions employed in the benzylidenephthalide → indanedione rearrangement, and secondly, it should be easily removable under conditions which would not affect the product **8**. The *p*-nitrophenylcarbamyl group was found to fulfill these requirements, and treatment of β-hydrastine with *p*-nitrophenylchloroformate in the presence of a base produced the ene-lactone **6** in 88% yield. Treatment of **6** with methanolic sodium methoxide resulted in nearly quantitative conversion to the indanedione **7**. Spectral analysis of both **6** and **7** confirmed the structures shown in Scheme 4. Compound **6** showed infrared absorption (ν_{max} 1770 cm^{-1}) characteristic of a five-membered lactone system, and **7** had infrared absorption at 1710 and 1740 cm^{-1} attributable to the indan-1,3-dione carbonyl groups. An interesting feature of the pmr spectrum of **7** is a duality of many of the major peaks attributable to restricted rotation about the amide linkage; such an effect was not observed in **6**.

Removal of the protecting group by basic hydrolysis gave the amine **8** in high yield. Compound **8** was obtained as red crystals which were insoluble in most organic solvents and which did not show the presence of the distinctive indan-1,3-dione carbonyl absorption in the infrared spectrum. This was attributed to the crystallisation of **8** in the zwitterionic form, **12**. The dipolar character of **8** was confirmed by spectral data (see Experimental). However the

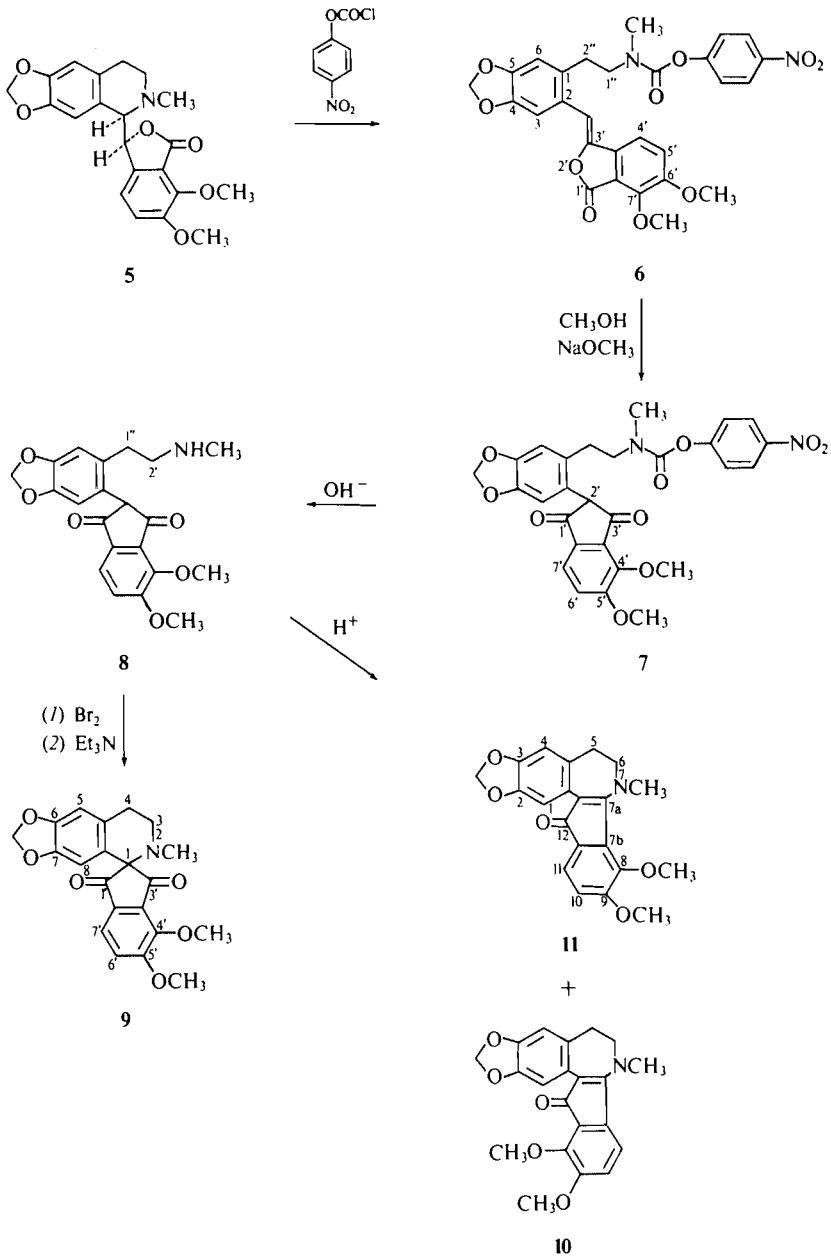

SCHEME 4

hydrochloride obtained from **8** exhibited both pmr and ir (ν_{max} 1705, 1740 cm^{-1}) spectral data consistent with the structure shown in Scheme 4.

As anticipated, **8** was readily transformed to the spirobenzylisoquinoline **9** by bromination at C-2′ followed by treatment of the bromide with triethylamine (8). Compound **9** exhibited spectral properties entirely analogous with spirobenzylisoquinolines of known structure (7, 8). In particular, the pmr spectrum of **9** was characteristic of a spirobenzylisoquinoline (2, 7, 8). The resonances at δ 5.95 and 6.62 were assigned to the C-8 and C-5 hydrogens, respectively, by comparison with the spectra of

analogous alkaloids (2, 7). The overall yield from phthalideisoquinoline to spirobenzylisoquinoline was 75%.

Treatment of **8** with *p*-toluenesulfonic acid in boiling toluene resulted in the formation of the enamino ketones **10** and **11** in unequal amounts. The skeletal structures of **10** and **11** were confirmed by analysis of data presented in the Experimental section. Their pmr spectra are both very similar to that reported for the analogous tetramethoxy enamino ketone (9). The observation of a single carbonyl stretch in the infrared spectrum of both **10** and **11**, and mass spectral data for both compounds, strengthen the structural assignments. The isomers **10** and **11** were differentiated through nuclear Overhauser experiments. Irradiation at the *N*-methyl frequency (δ 3.34) of **10** produced a 23% enhancement of the lower field portion of the AB quartet (δ 6.63 and 7.0). The signals at δ 7.0 are therefore assignable to the C-8 hydrogen. Similar irradiation of **11** at δ 3.14 caused no appreciable signal enhancement in the aromatic region of the spectrum.

The signals caused by the isolated aromatic hydrogens at C-1 and C-4 of **10** and **11** were assigned by double irradiation experiments. In both cases, the higher field singlet (δ 6.46 in **10** and 6.52 in **11**) was broader than that at lower field, and sharpened considerably on irradiation at the C-5 hydrogens (δ 2.90 in **10** and 2.96 in **11**). The aromatic singlets at higher field are therefore assigned to the C-4 hydrogens, and the broadening to long range coupling with the C-5 hydrogens.

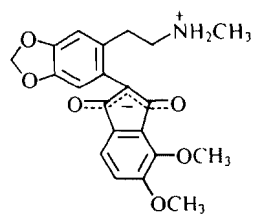

12

We therefore conclude that the structures of **10** and **11** are as shown. The predominant isomer **10** has an oxygenation pattern corresponding to that of the natural rhoeadines and analogues of **10** have been converted into rhoeadine alkaloids (9). Accordingly, the reactions of Scheme 4 constitute a formal conversion of a phthalideisoquinoline into a rhoeadine alkaloid, providing an alternative to the published procedure (6). The concurrent formation of **10** and **11** provides a convenient route both to natural rhoeadine alkaloids and to analogues oxygenated at C-8 and C-9.

The application of the reactions of Scheme 4 to phthalideisoquinolines should prove to be general. It is therefore anticipated that this sequence of reactions will be of general utility in the synthesis of both the spirobenzylisoquinoline and rhoeadine alkaloid types.

Experimental

Apparatus, Materials, and Methods

Melting points were determined on a Kofler block and are uncorrected. Infrared spectra were recorded with KBr pellets on a Beckman IR 5 spectrophotometer. The pmr spectra were obtained at 100 MHz on a Varian HA 100 instrument, using deuteriochloroform as solvent and tetramethylsilane as internal standard. Chemical shifts are reported in ppm (δ) from TMS, the symbols, s (singlet), d (doublet), t (triplet), and m (multiplet) being used in reporting the spectra. Mass spectra were routinely run on all samples using a C.E.C. 21-110B instrument. Merck silica gel F-254 was used for tlc.

Microanalyses were performed by Gygli Microanalytical Laboratory, Toronto.

p-Nitrophenyl[2-[(6′,7′-dimethoxphthalidylidene)methyl]-4,5-(methylenedioxy)phenethyl]methylcarbamate, 6

p-Nitrophenylchloroformate (10.0 g) was added to a stirred solution of β-hydrastine, **5** (8.7 g), and diisopropylethylamine (3.3 g) in benzene (200 ml) and the mixture stirred at room temperature for 20 h. The solvent was removed under reduced pressure and diisopropylethylamine (5.3 g) and dimethyl sulfoxide (33 ml) were added to the residue. The resulting solution was heated on a steam bath for 5 h, cooled, poured onto ice water, and extracted with chloroform. The extract was dried and evaporated to give a residue, which on crystallization from acetonitrile, afforded **6** (11.0 g, 88%), mp 205–207 °C. The analytical sample was recrystallized from the same solvent, mp 206–208 °C. Infrared ν_{max} 1720, 1770 cm^{-1}; pmr δ 2.8–3.6 (m, 4H, C-1″ and C-2″ H's), 2.92 (s, 3H, NCH_3), 3.79 (s, 3H, OCH_3), 4.03 (s, 3H, OCH_3), 5.87 (s, 2H, OCH_2O), 6.66 and 6.70 (s, each 1H, aromatic and benzylidene H's), 7.07, 7.43 (ABq, 2H, J = 8.5 Hz, C-4′ and C-5′ H's), 7.24, 8.17 (ABq, 4H, J = 9.0 Hz, *p*-nitrophenyl H's), 7.74 (s, 1H, aromatic H); ms (*m/e*, %), 548(55), 518(23), 410(100). *Anal.* calcd. for $C_{28}H_{24}N_2O_{10}$: C 61.31, H 4.41, N 5.11; found: C 61.42, H 4.29, N 5.01.

p-Nitrophenyl[2-(4′,5′-dimethoxy-1′,3′-dioxo-2′-indanyl)-4,5-(methylenedioxy)phenethyl]methylcarbamate, 7

A methanolic solution of sodium methoxide (1 *M*, 20 ml) was added to a stirred suspension of **6** (10 g) in methanol (500 ml) under nitrogen, and the resulting red solution refluxed for 4 h. The solution was then evaporated and ice water added to the residue. The aqueous solution was washed with ether, acidified, and then extracted with chloroform. The extract was washed, dried, and evaporated

and the residue crystallized from methanol. Recrystallization from chloroform–methanol afforded the title compound (9.5 g, 95%), mp 189–191 °C. Infrared ν_{max} 1710, 1725, 1740 cm^{-1}; pmr δ 2.88 (m, 2H, C-2″ H's), 2.98, 3.02 (each s, total 3H, NCH_3), 3.56 (m, 2H, C-1″ H's), 3.96 (s, 3H, OCH_3), 4.02 (s, 3H, OCH_3), 4.38, 4.56 (each s, total 1H, C-2′ H), 5.83 (s, 2H, OCH_2O), 6.24 6.26 (each s, total 1H, aromatic H), 6.71, 6.77 (each s, total 1H, aromatic H), 7.19, 7.72, and 7.21, 7.76 (each ABq, total 2H, J = 8 Hz, C-6′ and C-7′ H's), 7.29, 7.35 and 8.12, 8.19 (each ABq, total 4H, J = 9 Hz, *p*-nitrophenyl H's); ms (*m/e*, %), 548(10), 410(100). *Anal.* calcd. for $C_{28}H_{24}N_2O_{10}$: C 61.31, H 4.41, N 5.11; found: C 61.15, H 4.61, N 5.19.

2-[2′-(2″-Methylaminoethyl)-4′,5′-methylenedioxy]-4,5,dimethoxyindan-1,3-dione, 8, 12

A solution of **7** (1 g) in aqueous sodium hydroxide (1 *M*, 25 ml) and dimethyl sulfoxide (25 ml) was heated on a steam bath for 3 h. Water was then added and the solution acidified (HCl) and washed with ether. Ammonia was added to the aqueous solution until p*H* 8 was reached, and the solution then extracted with chloroform. The extract was washed with a saturated solution of NaCl and the washings back-extracted with chloroform. The combined extract was dried and evaporated to yield a residue which was crystallized from ethanol to yield 0.68 g (98%) of red crystals of the zwitterion **12**, mp 229–230 °C. Infrared ν_{max} 1420–1600 (br), 2400–3200 (br); pmr (DMSO-d_6, D_2O) δ 2.70 (t, 2H, C-1″ H), 3.20 (t, 2H, C-2″ H), 3.38 (s, 3H, NCH_3), 3.72 (s, 3H, OCH_3), 3.80 (s, 3H, OCH_3), 5.90 (s, 2H, OCH_2O), 6.62 (s, 1H, aromatic H), 6.70, 6.82 (ABq, 2H, J = 8 Hz, C-6 and C-7 H's), 6.82 (s, 1H, aromatic H); ms (*m/e*, %) 383(1), 381(2), 365(100), 350(18), 340(15). *Anal.* calcd. for $C_{21}H_{21}NO_6$: C 65.79, H 5.52, N 3.65; found: C 65.91, H 5.72, N 3.49.

Hydrochloride

Dry HCl was passed through a suspension of **12** (40 mg) in chloroform (0.5 ml) until solution was complete. The hydrochloride separated on standing at room temperature, mp 168–170 °C. Infrared ν_{max} $CHCl_3$, 1705, 1740 cm^{-1}; pmr δ 2.66 (m, 2H, C-1″ H), 3.20 (m, 5H, C-2″ H and NCH_3), 3.94 (s, 3H, OCH_3), 4.00 (s, 3H, OCH_3), 4.88 (s, 1H, C-2 H), 5.80 (s, 2H, OCH_2O), 6.12 (s, 1H, aromatic H), 6.70 (s, 1H, aromatic H), 7.28, 7.68 (ABq, 2H, J = 8 Hz, C-6 and C-7 H's), 9.0–9.4 (br s, 2H, $-\overset{+}{N}H_2$). *Anal.* calcd. for $C_{21}H_{22}NO_6Cl$: C 60.07, H 5.28, N 3.34, Cl 8.44; found: C 59.93, H 5.49, N 3.38, Cl 8.55.

6,7-Methylenedioxy-1,2,3,4-tetrahydroisoquinoline-1-spiro-2′-(4′,5′-dimethoxyindan-1′,3′-dione), 9

A solution of bromine (0.45 g) in acetic acid (5 ml) was added to a stirred solution of **12** (1 g) in acetic acid (25 ml) under nitrogen. The solution was immediately evaporated under reduced pressure at room temperature and the oily residue dissolved in chloroform (20 ml). Triethylamine (2 ml) was then added, and the solution evaporated. Crystallization of the residue from ether yielded 0.84 g of **9**, mp 149–151 °C. Concentration of the mother liquors yielded a further 0.1 g, mp 147–150 °C. Recrystallization of the combined material from ether gave 0.9 g (91%) of **9**, mp 150–152 °C. Infrared ν_{max} 1705, 1740 cm^{-1}; pmr δ 2.36 (s, 3H, NCH_3), 2.8–3.4 (m, 4H, C-3 and C-4 H's), 4.01 (s, 3H, OCH_3), 4.06 (s, 3H, OCH_3), 5.79 (s, 2H, OCH_2O), 5.95 (s, 1H, C-8H), 6.62 (s, 1H, C-5H), 7.38, 7.80 (ABq, 2H, C-6′ and C-7′ H's); ms (*m/e*, %), 381(100), 366(31), 352(40), 338(19), 324(54). *Anal.* calcd. for $C_{21}H_{19}NO_6$: C 66.13, H 5.02, N 3.67; found: C 66.21, H 5.16, N 3.54.

6,7-Dihydro-10,11-dimethoxy-2,3-methylenedioxy-7-methylbenz[d]indeno[1,2-b]azepin-12(5H)-one, 10, and 6,7-dihydro-8,9-dimethoxy-2,3-methylenedioxy-7-methylbenz[d]indeno[1,2-b]azepin-12(5H)-one, 11

p-Toluenesulfonic acid (350 mg) was added to a solution of **12** (1.0 g) in toluene (200 ml) and the mixture refluxed under a Dean–Stark trap for 4 h. The solution was cooled, washed with saturated sodium bicarbonate, and then dried and the solvent evaporated. Crystallization of the residue from anhydrous ether gave purple crystals of **10** contaminated with a small amount of **11**. Recrystallization from ether gave pure **10** (0.32 g, 34%), mp 188–189 °C. Infrared ν_{max} 1650 cm^{-1}; pmr δ 2.90 (m, 2H, C-5 H's), 3.34 (s, 3H, NCH_3), 3.68 (m, 2H, C-6 H's), 3.81 (s, 3H, OCH_3), 3.98 (s, 3H, OCH_3), 5.84 (s, 2H, OCH_2O), 6.46 (s, 1H, C-4 H), 6.63, 7.0 (ABq, 2H, J = 8 Hz, C-9 and C-8 H's respectively), 7.56 (s, 1H, C-1 H); ms (*m/e*, %), 365(100), 350(11), 336(4), 335(2). *Anal.* calcd. for $C_{21}H_{19}NO_5$: C 69.03, H 5.24, N 3.83; found: C 69.18, H 5.34, N 3.71.

The mother liquors from the crystallization of **10** were evaporated and the residue chromatographed on silica gel. Stepwise gradient elution from chloroform to 10% dioxan in chloroform gave **11** (0.12 g from ether, 14%), followed by **10** (0.28 g from ether, total 0.60 g, 63%). Compound **11** had the following properties: mp 185–187 °C; ir ν_{max} 1660 cm^{-1}; pmr δ 2.96 (m, 2H, C-5 H's), 3.14 (s, 3H, NCH_3), 3.74 (m, 2H, C-6 H's), 3.79 (s, 3H, OCH_3), 3.88 (s, 3H, OCH_3), 5.87 (s, 2H, OCH_2O), 6.52 (s, 1H, C-4 H), 6.72, 7.24 (ABq, 2H, J = 8 Hz, C-10 and C-11 H's), 7.71 (s, 1H, C-1 H); ms (*m/e*, %), 365(100), 350(5), 336(3), 335(4). *Anal.* calcd. for $C_{21}H_{19}NO_5$: C 69.03, H 5.24, N 3.83; found: C 69.32, H 5.48, N 3.78.

Acknowledgments

We thank the National Research Council of Canada for financial support.

We are also grateful to Dr. Kurt L. Loening of the Chemical Abstracts Service for providing the names of compounds **6** and **7**.

1. M. SHAMMA. The isoquinoline alkaloids. Academic Press, New York. 1972. p. 359.
2. V. SMULA, N. E. CUNDASAWMY, H. L. HOLLAND, and D. B. MACLEAN. Can. J. Chem. **51**, 3287 (1973); and references therein.
3. M. SHAMMA and V. ST. GEORGIEV. Tetrahedron Lett. 2339 (1974).
4. T. KAMETANI, S. HIRATA, M. IHARA, and K. FUKUMOTO. Heterocycles, **3**, 405 (1975).

5. C. R. ADDINALL and R. T. MAJOR. J. Am. Chem. Soc. **55**, 2153 (1933).
6. W. KLÖTZER, S. TEITEL, and A. BROSSI. Helv. Chim. Acta, **54**, 2057 (1971); **55**, 2228 (1972); W. KLÖTZER, S. TEITEL, J. F. BLOUNT, and A. BROSSI. J. Am. Chem. Soc. **93**, 4321 (1971); Monatsh. Chem. **103**, 435 (1972).
7. N. E. CUNDASAWMY and D. B. MACLEAN. Can. J. Chem. **50**, 3028 (1972).
8. S. O. DE SILVA, K. ORITO, R. H. MANSKE, and R. RODRIGO. Tetrahedron Lett. 3243 (1974).
9. K. ORITO, R. H. MANSKE, and R. RODRIGO. J. Am. Chem. Soc. **96**, 1944 (1974).

Fragmentation and rearrangement processes in the mass spectra of perhalogenoaromatic compounds. Part X.[1] Pentafluorophenyl dimethyl derivatives of group V

TIMOTHY R. B. JONES AND JACK M. MILLER[2]

Department of Chemistry, Brock University, St. Catharines, Ontario L2S 3A1

AND

J. LOWELL PETERSON AND DEVON W. MEEK

Department of Chemistry, Ohio State University, Columbus, Ohio 43210

Received July 17, 1975

TIMOTHY R. B. JONES, JACK M. MILLER, J. LOWELL PETERSON, and DEVON W. MEEK. Can. J. Chem. **54**, 1478 (1976).

A comprehensive low-resolution study of the mass spectra of the compounds $C_6F_5M(CH_3)_2$, where M = N, P, As, is described, fragmentation pathways being assigned with the aid of normal metastable ions and mass analyzed ion kinetic energy spectra (mikes). A comparison of these spectra has re-affirmed the absence of halogen transfer processes for atoms such as N which are incapable of providing the necessary vacant orbitals apparently prerequisite in the mechanisms. The influence of increased coordination to phosphorus and effects on halogen transfer processes are discussed with respect to the mass spectra of the compounds $C_6F_5PX(CH_3)_2$, X = O, S, Se and the gold adducts $C_6F_5P(CH_3)_2 \cdot AuX$, X = Cl, Br, I.

TIMOTHY R. B. JONES, JACK M. MILLER, J. LOWELL PETERSON et DEVON W. MEEK. Can. J. Chem. **54**, 1478 (1976).

On décrit une étude complète, à basse résolution, des spectres de masse des composés $C_6F_5M(CH_3)_2$, où M = N, P, As; on attribue les modes de décomposition à l'aide des ions métastables normaux et des spectres d'énergie cinétique des ions analysés par masse (mikes). Une comparaison de ces spectres a permis de conclure à l'absence de processus de transfert d'halogène pour des atomes tels que l'azote qui sont incapables de fournir les orbitales vacantes nécessaires et qui sont apparemment prérequises dans les mécanismes. On discute aussi de l'influence de l'augmentation de coordination au phosphore et des effets sur les processus de transfert d'halogènes sur les spectres de masse des composés $C_6F_5PX(CH_3)_2$, X = O, S, Se et des adduits de l'or $C_6F_5P(CH_3)_2 \cdot AuX$, X = Cl, Br, I.

[Traduit par le journal]

Introduction

In recent publications, we have regarded the presence of available, empty orbitals on the Group IV (1–3), V (4–6), and VI (7) heteroatoms of perfluoroaromatic derivatives as a necessity for the operation of halogen transfer processes in the electron impact mass spectra of such compounds. We have now investigated the mass spectra of *N,N*-dimethylpentafluoroaniline, dimethylpentafluorophenyl phosphine, and dimethylpentafluorophenyl arsine using both normal metastable analysis and modified mikes (8) to achieve elucidation of the relevant fragmentation pathways.

Possible suppression of the halogen transfer phenomenon was investigated in the mass spectra of pentafluorophenyl phosphine oxide, sulfide, and selenide as well as the phosphine adducts $C_6F_5P(CH_3)_2 \cdot AuX$ (X = Cl, Br, I).

A large number of mass spectral studies of organic derivatives of Group V have been reported in the last decade, especially compounds of nitrogen and phosphorus. Fluoroaromatic derivatives have been limited to $(3\text{-}FC_6H_4)_3P$ and $(4\text{-}FC_6H_4)_3P$, $(C_6F_5)_3M$, $(C_6F_5)_2(C_6H_5)M$, and $(C_6F_5)(C_6H_5)_2M$ (6) (M = P, As, Sb) all of which are quite symmetrically substituted. A number of trends have been noted with respect to ion abundances. It is quite apparent that the M—C bond strength in both alkyl and aryl substituted compounds is weakened as one moves down the series, *i.e.*, N > P > As > Sb > Bi. This trend also reflects the tendency

[1]For Part IX, see ref. 7*b*.

[2]To whom correspondence should be addressed.

Can. J. Chem. Downloaded from www.nrcresearchpress.com by 210.87.254.6 on 09/05/12
For personal use only.

TABLE 1. Partial mass spectra of $C_6F_5M(CH_3)_2$ (M = N, P, As)

Ion	M			Ion	M		
	N	P	As		N	P	As
$C_6F_5M(CH_3)_2^+$	31.0	21.8	9.7	$C_7F_3H^+$	—	1.0	0.5
$C_6F_5MC_2H_5^+$	35.1	0.2	—	$C_7F_3^+$	—	0.3	0.2
$C_6F_5MCH_3^+$	1.4	6.8	10.3	$C_7F_2H_3^+$	0.1	1.6	2.3
$C_6F_5MCH^+$	6.4	14.4	4.9	$C_7F_2H_2^+$	0.2	0.4	0.2
$C_6F_5MH^+$	1.4	1.2	0.5	$C_7F_2H^+$	—	1.1	0.4
$C_6F_5M^+$	2.4	0.2	2.2	$C_6F_5H^+$	0.7	1.9	0.8
$C_6F_4MCH_2^+$	0.2	1.9	0.6	$C_6F_5^+$	1.4	0.1	—
$C_6F_4M^+$	—	0.4	0.7	$C_6F_4H^+$	0.6	0.2	—
$C_6F_3MC_2H_4^+$	—	—	3.3	$C_6F_4^+$	—	0.3	—
$C_6F_3MCH^+$	0.2	0.4	2.3	$C_6F_3^+$	—	−0.3	1.4
$(CH_3)_2M^+$	0.1	0.9	3.9	$C_6F_2H^+$	—	1.0	0.9
$C_2H_5M^+$	0.3	0.2	0.2	$C_6F_2^+$	—	1.1	1.5
$C_2H_4M^+$	0.9	1.0	1.9	$C_5F_4H^+$	0.2	0.4	2.9
CH_3M^+	—	0.8	1.8	$C_5F_3H_2^+$	—	−0.2	—
CH_2M^+	—	4.5	4.9	$C_5F_3^+$	0.6	0.9	—
CH_3MF^+	—	3.1	3.3	$C_5F_2H^+$	0.4	1.3	0.9
MF_2^+	—	6.0	2.2	$C_5F_2^+$	—	0.5	1.5
MF^+	—	0.2	1.1	C_5HF^+	—	—	0.2
$C_7F_5H_2^+$	2.5	9.5	7.5	C_5F^+	—	—	0.9
$C_7F_4H_3^+$	1.4	0.9	2.4	$C_3F_3^+$	0.2	1.1	0.6
$C_7F_4H_2^+$	0.2	0.2	0.2	$C_3F_2H^+$	0.1	1.4	0.4
$C_7F_4H^+$	0.1	0.8	1.1	$C_2F_3^+$	0.1	—	0.3
$C_7F_3H_3^+$	0.1	1.8	1.3	$C_2FH_2^+$	—	—	1.1
$C_7F_3H_2^+$	0.1	1.8	1.2	CF_3^+	0.2	Masked by PF_2	0.8

for multiple bonding to carbon which is so evident in the spectra of amines and much less common for the other Group V atoms.

Recently, Henrick *et al.* (9) reported their observations concerning the mass spectra of a number of organic derivatives of Group V, including the series $C_6H_5E(CH_3)_2$ (E = N, P, As, Sb). The above general trends were noted as well as some interesting details particular to each E atom, which we will discuss further in our comparisons.

Experimental

N,N-dimethylpentafluoroaniline was prepared by the method of Allen *et al.* (10). Its purity was confirmed by gc/ms analysis before use. All other compounds in this study were prepared according to procedures previously published.[3]

[3]The other compounds used in this study were prepared according to procedures adapted from those of similar compounds. For example, $C_6F_5P(CH_3)_2$ and $C_6F_5As(CH_3)_2$ were prepared from (pentafluorophenyl)-magnesium bromide and $(CH_3)_2PCl$ and $(CH_3)_2AsI$, respectively (11*a*). The phosphine oxide, sulfide, and selenide derivatives were prepared by treating solutions of $C_6F_5P(CH_3)_2$ with air, sulfur, and potassium selenocyanate respectively. Detailed experimental conditions are contained in ref. 11*b*.

Mass spectra were obtained on an AEI-MS30 double beam mass spectrometer at 70 eV with an accelerating voltage of 4 kV, resolution ≃1000 and a source temperature of 180 °C. Samples were admitted to beam 1 via the AGHIS or solid probe while PFK (high boiling) was admitted via a gas-liquid probe into beam 2 to serve as a chemical mass marker, simultaneously recorded but not interfering with the spectrum under investigation. Mass analyzed ion kinetic energy spectra were obtained by techniques previously described (8). Metastable transitions were assigned with the aid of a FORTRAN computer program BMETAST. In cases where more than one ion composition was possible, high resolution data were employed to distinguish between the various choices.

Assignment of mikes transitions were usually supported by normal metastable evidence. In those cases where no normal metastable species could be detected, the peak assignments were made on the basis of the most intense daughter ion in the region under scrutiny. In addition, normal metastables could often be observed on suppression of the normal ion spectrum (8). The apparent doublet nature of the normal ion beam in the mike spectra (Fig. 1) is an instrument artifact due to saturation of the amplifiers, the plots being attenuated at the X-Y recorder, rather than by electron multiplier gain.

Results and Discussion

The Spectra of $(CH_3)_2M(C_6F_5)$ (M = N, P, As)

The partial mass spectra of the species under discussion are shown in Table 1 as a percentage

Can. J. Chem. Downloaded from www.nrcresearchpress.com by 210.87.254.6 on 09/05/12
For personal use only.

Can. J. Chem. Downloaded from www.nrcresearchpress.com by 210.87.254.6 on 09/05/12
For personal use only.

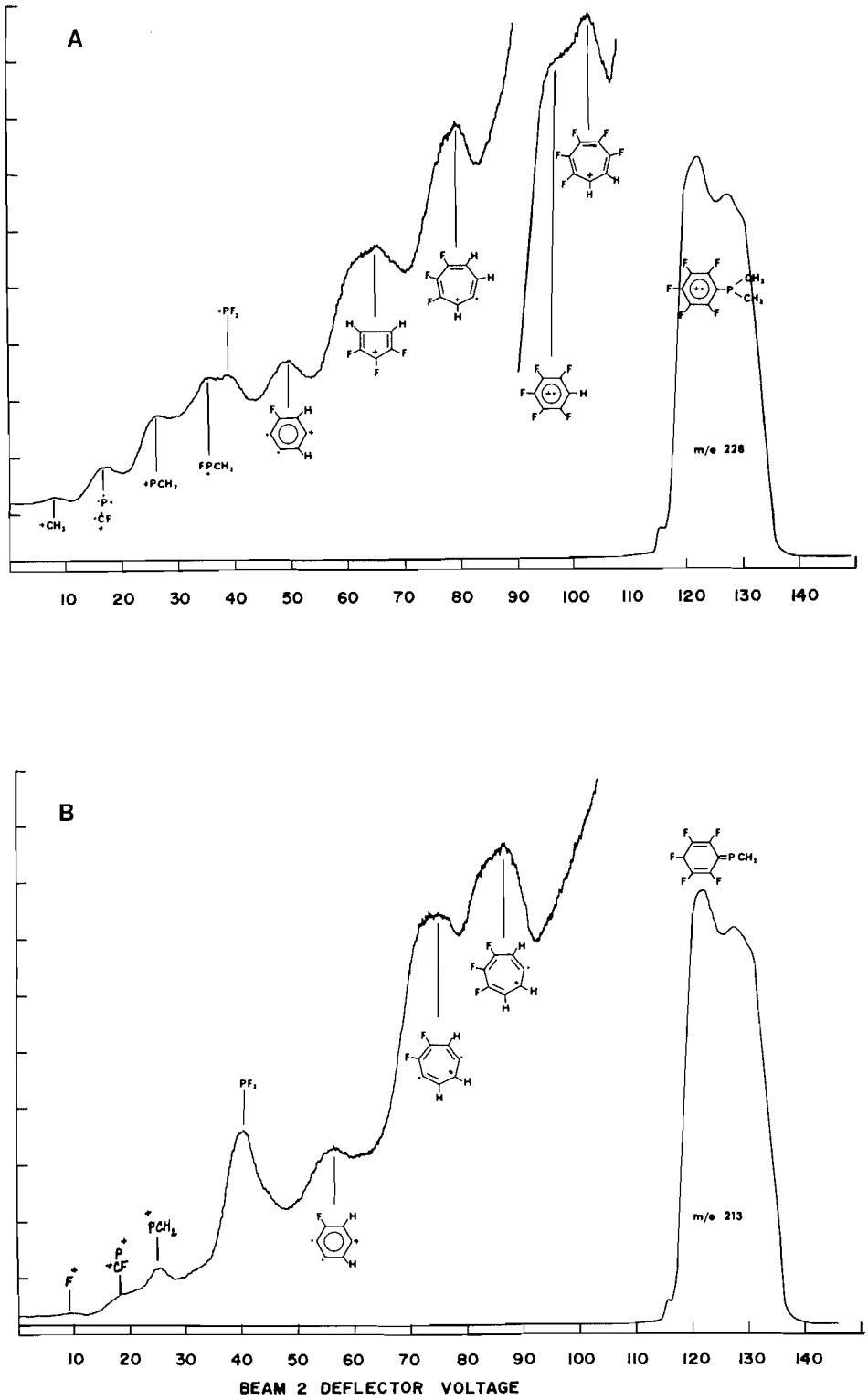

Can. J. Chem. Downloaded from www.nrcresearchpress.com by 210.87.254.6 on 09/05/12
For personal use only.

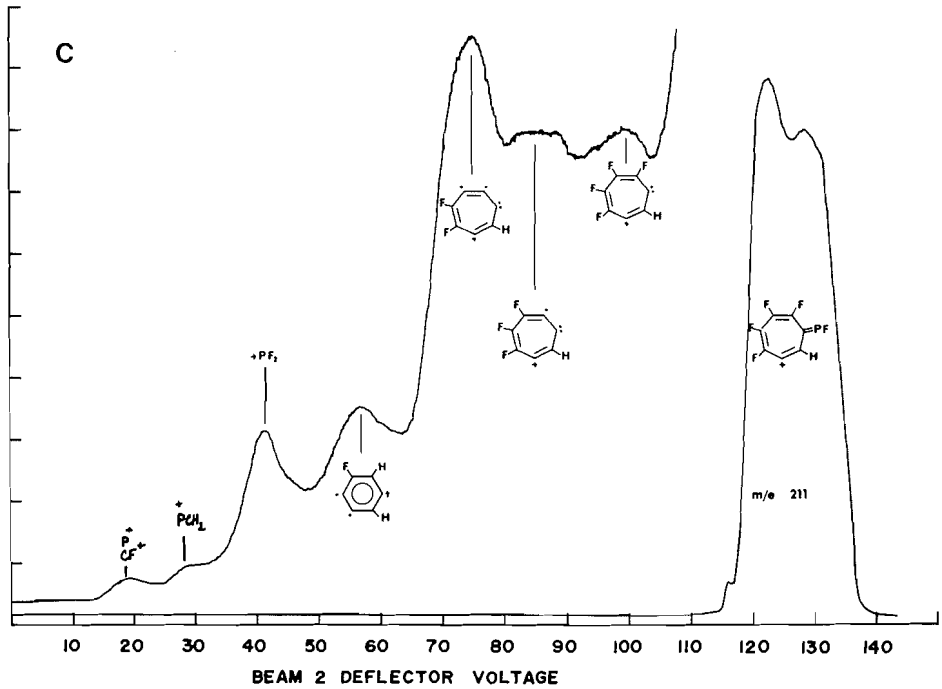

FIG. 1. Mass analyzed ion kinetic energy mike spectra of (*A*) $[C_6F_5P(CH_3)_2]^+$, (*B*) $[C_6F_5PCH_3]^+$, (*C*) $[C_6F_5PCH]^+$.

of the total positive ion current, summed over all isotopic contributions due to a particular species. The observed normal metastables as well as the mike spectra enable us to assign the partial fragmentation schemes shown (Scheme 1). Typical mikes voltage scans are shown in Fig. 1 for three of the prominent ions in the spectrum of $C_6F_5P(CH_3)_2$.

The decreasing abundance of the parent ions through N, P, and As can be regarded as a simple weakening of the C—M bond but one cannot ignore other arguments related to π-electron withdrawal/donation involving the pentafluorophenyl ring (12). Nitrogen, with its greater ability to share electronic charge through π-donation into the ring system, thus facilitating resonance distribution of the positive charge during ionization, would be expected to give a more abundant parent species. Aside from the fact that phosphorus and arsenic are more polarizable, "softer" heteratoms and should therefore, in themselves, be able to stabilize a positive charge to a somewhat larger extent, the π-withdrawal effects of these atoms is more significant than back-donation to the C_6F_5 ring, resulting in preferential C—M cleavage. This aspect of "hard" nitrogen *vs.* "soft" phosphorus or arsenic is clearly evident in the fragmentation pathway of the $C_6F_5\dot{M}CH_3$ ion shown below where route *A* is preferred for M = N, the

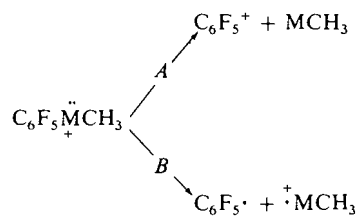

ring carrying all of the positive charge after cleavage while route *B* is more important for M = P, As, the charge tending to remain with the "softer" heteratom fragment. This is also consistent with the order expected in consideration of the respective ionization potentials.

The high abundance of $C_6F_5\dot{M}C_2H_5$ in the spectrum of the amine is a result of the typical α-cleavage observed with all alkyl substituted amines, usually forming a significant part of the breakdown process. Since this latter process is initiated by a radical site on M, it is not sur-

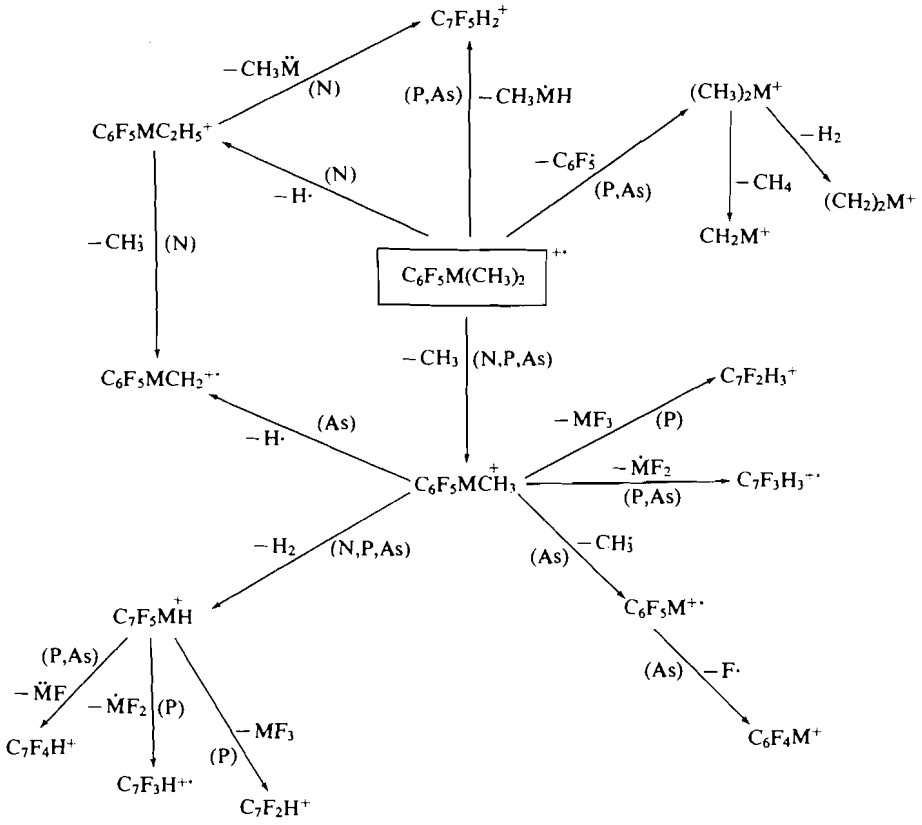

SCHEME 1

prising that the more polarizable phosphorus and arsenic centers do not give significant ions resulting from loss of a proton. The comparison presented in Table 2 indicates the α-cleavage process is also very important in the mass spectrum of *N*,*N*-dimethylaniline. A significant

TABLE 2. Partial mass spectra of $C_6X_5N(CH_3)_2$ (X = H*, F) (in % relative intensity)

	X	
Ion$^+$	H	F
$C_6X_5N(CH_3)_2$	74	87
$C_6X_5NC_2H_5$	100	100
$C_6X_5NCH_2$	13	10
C_6X_5NCH	10	18
C_6X_5	23	4
C_2H_4N	8	3

*From MSDC EIGHT PEAK INDEX, Vol. 1, Compound #D0015.

observation is the effect of C_6F_5 substitution on the operation of the pathway *C*. The Table 2 indicates a two-fold increase in abundance for

$$C_6X_5\dot{N}{\equiv}CH \xrightarrow{C} C_6X_5^+ + HCN$$

$C_6X_5\dot{N}{\equiv}CH$ when X = F reflecting the increased electronegativity of C_6F_5 over C_6H_5 and its subsequent resistance to formation of the $C_6F_5^+$ moiety.

The base peaks in the spectra of the phosphine and arsine are the molecular ion and $(P{-}CH_3)^+$ ions respectively, a behaviour identical to that observed by Henrick *et al.* (9) for the dimethylphenyl phosphine and arsine. These ions reflect the relative weakening of the M—C bond in support of the general trend previously mentioned.

A rather surprising feature of these spectra is the high abundance of the ion formulated as

Can. J. Chem. Downloaded from www.nrcresearchpress.com by 210.87.254.6 on 09/05/12
For personal use only.

Can. J. Chem. Downloaded from www.nrcresearchpress.com by 210.87.254.6 on 09/05/12
For personal use only.

$C_6F_5\dot{M}CH$, which arises from sequential loss of $CH_3\cdot$ and H_2. Facile multiple bonding to carbon predicts **1** as a stable structure for M = N, but **2** and **3** seem more plausible as structures for M = P or As particularly in view of the facile loss of MF and M from these derivatives.

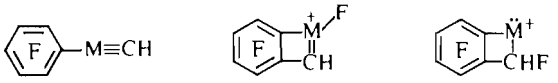

1 **2** **3**

The formation of this ion roughly parallels a similar pathway described for the trimethyl derivatives (13, 14), *e.g.*, in the mass spectrum of $(CH_3)_3P$, the base peak is $(CH_3)_2\dot{P}^+$ which then loses H_2 to give the ion $CH_2{=}\dot{P}{=}CH_2$, the second most intense species in the spectrum. Similarly, $C_2H_4N^+$ and $C_2H_4As^+$ are prominent ions in the mass spectra of $(CH_3)_3N$ and $(CH_3)_3As$ respectivlly. The fact that the $C_7F_5\dot{M}H$ ion is most abundant in the case of the phosphine can be explained in terms of differences in fragmentation pathways. The arsine favours consecutive loss of methyl radicals in the initial stages of fragmentation while for the amine it is suppressed by the much higher abundance of the M^+ and $(M{-}H)^+$ species.

A distinct difference in the spectra of dimethylphenyl phosphine and arsine and their fluorine analogues is the rather high abundance of the $C_6H_4\dot{M}$ ion. The corresponding $C_6F_4\dot{M}$ ions are observed in low abundance, probably a result of pathways involving fluorine abstraction processes. As has been observed in many other cases (1–4), loss of central atom fluorides (PF, PF_2, PF_3, AsF, and AsF_2) neutral species leads to a variety of fluorocarbon ions. No evidence for fluorine transfer phenomena was detected in the spectrum of $C_6F_5N(CH_3)_2$. Any fluorocarbon ions observed in this spectrum resulted from prior loss of C_xH_yN species. For both the arsine and phosphine, however, ions of the form $C_xF_y^+$ and $C_xF_yH_z^+$ carry approximately 40% of the total positive ion current, many of these being formed by direct loss of a central atom fluoride (see Scheme 1). Of the other possible routes to formation of these ions, there is one transition, depicted schematically in Scheme 2, which results in a rather odd rearrangement common to both phosphine and

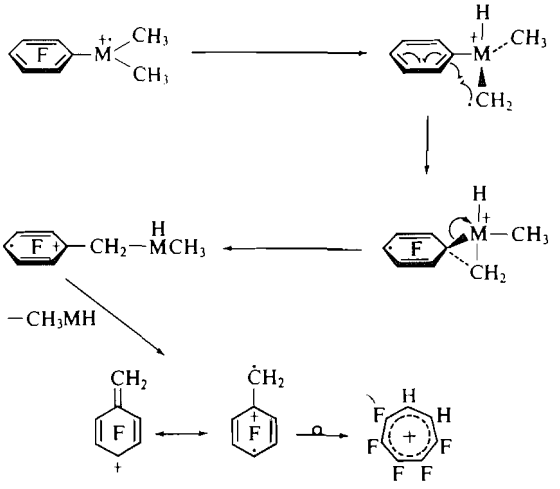

SCHEME 2

arsine. The $C_7F_5H_2^+$ ion is also formed in the spectrum of the amine, but in two steps:

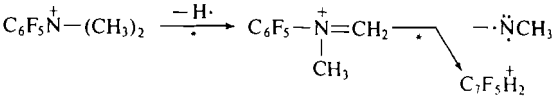

The driving force in the rearrangement depicted in Scheme 2 is apparently the formation of the stable tropylium ion species, which is usually prominent in substituted aromatics.

The arsine spectrum exhibits some features which either are not observed or are of significantly lower abundance for the amine and phosphine. The first is the presence of a highly abundant $^+\ddot{A}s(CH_3)_2$ ion, the formation of which indicates the capacity of the polarizable arsenic for carrying a positive charge since no $C_6F_5^+$ is observed in this spectrum. Two other fragment ions which are significant only in the arsenic spectrum are shown in Scheme 3. The most favourable structures appear to be those where multiple bonds to arsenic do not exist.

No such species were observed in the spectrum of $C_6H_5As(CH_3)_2$, obviously because favourable fragmentation pathways (H_2 *vs.* HF losses) were not available to this molecule. There were, however, quite significant amounts of the ion **4** formed in all three spectra, **4***b* being the preferred structure in the case of arsenic (9).

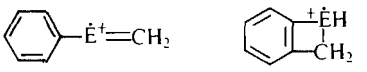

4*a* **4***b*

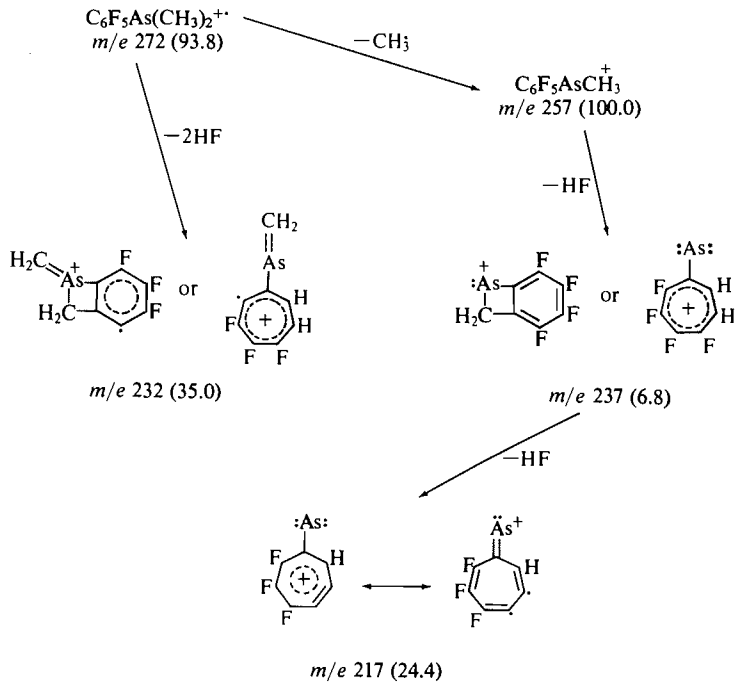

SCHEME 3

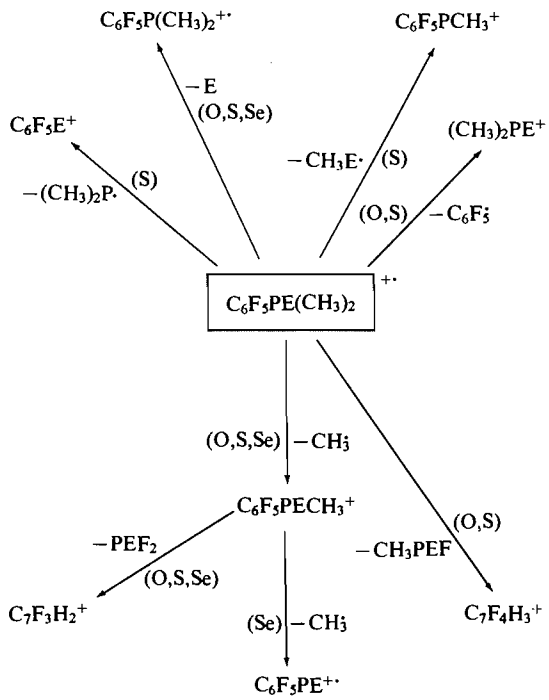

SCHEME 4

The Mass Spectra of $C_6F_5P(E)(CH_3)_2$ (E = O, S, Se)

The partial mass spectra of these compounds are shown in Table 3 and their postulated fragmentation pathways in Scheme 4. A large number of normal metastable ions was observed for the oxide in contrast to both sulfide and selenide. As one might predict from the strengths of the P=E bond, the abundance of PX-containing ions follows the pattern E = O > E = S > E = Se. Indeed, the primary fragmentation pathways also reflect this order. The selenide initially loses a Se atom, the resulting phosphine moiety giving rise to fragments characteristic of the phosphine spectrum. Apart from the parent ion, phosphorus–selenium bonded fragments are of quite low abundance. In contrast, the major pathway in breakdown of the oxide and sulfide occurs via initial cleavage of a P—CH_3 bond.

Fluorocarbon ions of the type $C_xF_yH_z^+$ are still of some importance, especially the tropylium species such as $C_7F_5H_2^+$. As one might expect, the abundance of these ions increases with decreasing P=E bond strength. This appears to be a direct result of the tendency towards a

Can. J. Chem. Downloaded from www.nrcresearchpress.com by 210.87.254.6 on 09/05/12
For personal use only.

TABLE 3. Partial mass spectra of $(CH_3)_2PE(C_6F_5)$ (E = O, S, Se)

Ion	E			Ion	E		
	O	S	Se		O	S	Se
$C_6F_5PE(CH_3)_2^+$	9.2	11.1	9.8	$C_7F_3H_3^+$	0.5	0.7	1.5
$C_6F_5PE(CH_3)^+$	15.7	6.5	1.6	$C_7F_3H_2^+$	2.1	1.5	2.7
$C_6F_5PE^+$	0.3	1.2	0.3	$C_7F_3H^+$	0.1	0.7	1.2
$C_6F_5E^+$	0.1	3.2	0.4	$C_7F_3^+$	0.3	0.4	0.9
$(CH_3)_2PE^+$	6.9	5.1	0.9	$C_7F_2H_3^+$	0.2	0.9	2.1
$(CH_3)PEF^+$	4.1	1.8	—	$C_7F_2H_2^+$	0.1	0.4	0.4
PE^+	6.5	6.5	—	$C_7F_2H^+$	0.4	1.2	0.4
E^+	—	—	2.4	$C_6F_5H^+$	0.2	0.4	0.5
$C_6F_5P(CH_3)_2^+$	0.3	2.3	8.0	$C_6F_5^+$	—	0.2	0.1
$C_6F_5PC_2H_5^+$	0.2	2.2	4.3	$C_6F_4^+$	1.5	0.4	0.2
$C_6F_5PCH_3^+$	0.5	1.3	3.5	$C_6F_3^+$	1.7	0.5	0.3
$C_6F_5PCH_2^+$	—	0.3	4.7	$C_6F_2H^+$	1.7	1.9	1.8
$C_6F_5PCH^+$	0.6	2.8	5.2	$C_5F_3^+$	1.6	1.6	1.1
$C_6F_5PH^+$	0.2	—	3.2	$C_5F_2H^+$	0.7	1.2	1.4
CH_3PF^+	1.1	2.5	1.9	$C_5F_2^+$	0.7	0.9	0.6
$(CH_3)_2P^+$	1.6	3.9	2.5	C_5HF^+	0.2	0.5	0.6
$C_2H_5PF^+$	1.2	2.7	0.8	C_4F^+	2.0	—	—
$C_2H_4P^+$	2.5	2.5	1.9	$C_3F_3^+$	0.9	—	1.2
CH_3P^+	1.1	—	1.1	$C_3F_2H_3^+$	—	1.7	0.6
CH_2P^+	2.2	—	3.1	$C_3F_2H_2^+$	0.7	1.0	0.1
PF_2^+/CH_3^+	5.7	5.7	2.6	$C_3F_2H^+$	1.2	1.7	1.2
$C_7F_5H_2^+$	1.2	4.1	7.0	$C_2F_3^+$	4.1	0.4	0.3
$C_7F_4H_3^+$	2.4	1.4	1.5	$C_2F_2H^+$	4.9	—	0.1
$C_7F_4H^+$	0.4	0.8	1.0				
$C_7F_4^+$	0.8	—	1.3				

more simple phosphine-type breakdown as one descends the series, E = O, S, Se. There seems to be no obvious influence on the fluorine transfer process even though the phosphorus is in a four-coordinate state initially. The transition,

$$C_6F_5P(CH_3)_2 \xrightarrow{-CH_3PF} C_7F_4H_3^+$$

is important in the spectrum of both oxide (E = O) and sulphide (E=S). The nature of the phosphoryl bond in such an ionized state, whether or not it involves a $d\pi$–$p\pi$ component, must allow for some flexibility to enable further overlap of empty phosphorus *d*-orbitals with available fluorine *p*-orbitals if fluorine migration is to take place.

The Mass Spectra of the Complexes $C_6F_5(CH_3)_2P{\cdot}AuX$ (X = Cl, Br, I)

Studies of these compounds revealed no evidence for any fluorine exchange with the gold atom. The spectra are almost devoid of peaks corresponding to gold-containing species, the most intense species being the phosphine and its fragments (I_2 and I are important fragments where X = I). The parent ion and some gold-containing species are listed in Table 4.

One noteworthy species appearing in all of these spectra is that corresponding to a halogen transfer to phosphorus, *i.e.*, $C_6F_5PX(CH_3)_2^+$ (X = Cl, Br) and $C_6F_5P(CH_3)X^+$ (X = Br, I). This is obviously a very peculiar fragment arising from rapid expulsion from the parent ion of a gold atom.

TABLE 4. The partial mass spectra of $C_6F_5P(CH_3)_2{\cdot}AuX$ (X = Cl, Br, I) (fragments arising from $C_6F_5P(CH_3)_2$ are not included)

Ion	Relative intensity* for X =		
	Cl	Br	I
$C_6F_5P(CH_3)_2{\cdot}AuX^{+\cdot}$	1.04	0.73	0.10
$C_6F_5P(CH_3)_2{\cdot}Au^+$	1.79	4.41	0.16
$C_6F_5P(CH_3)_2X^+$	2.01	1.09	—
$C_6F_5P(CH_3)X^{+\cdot}$	—	0.52	0.53
$C_6F_5P(CH_3)_2^{+\cdot}$	100.00	100.00	93.70
X^+	—	5.18	100.00

*Base peak in spectrum given as 100% relative intensity.

Can. J. Chem. Downloaded from www.nrcresearchpress.com by 210.87.254.6 on 09/05/12
For personal use only.

TABLE 5. Abundance of even and odd electron species

(*a*) $C_6F_5M(CH_3)_2$

		M		
	Electron ions	N	P	As
Even	$C_xF_yH_zM^+$	51.6	43.5	41.6
	$C_xF_yH_z^+$	9.0	24.2	29.7
Odd	$C_xF_yH_zM^+$	38.0	24.7	21.4
	$C_xF_yH_z^+$	1.4	7.6	7.3

(*b*) $C_6F_5P(E)(CH_3)_2$

		E		
	Electron ions	O	S	Se
Even	$C_xF_yH_zPE^+$	36.2	26.9	3.3
	$C_xF_yH_zP^+$	17.2	27.4	32.9
	$C_xF_yH_z^+$	28.3	22.6	26.7
Odd	$C_xF_yH_zPE^+$	11.4	14.3	14.2
	$C_xF_yH_zP^+$	1.4	3.0	15.7
	$C_xF_yH_z^+$	5.2	5.8	7.2

Again, this emphasizes the ability of the central atom to proceed with halogen abstraction even when some of its empty, available orbitals are supposedly engaged in other bonding. Admittedly, the examples offered here are of quite low abundance, but considering the unfavourable processes involved, it is amazing that these species are detected at all.

Conclusions

We have re-affirmed our previous statements (3, 5) concerning fluorine transfer to nitrogen in that no MF_n^+ species were detected in the spectrum of $C_6F_5M(CH_3)_2$ where M = N while such moieties are common to the spectra of both phosphine and arsine. This lends further support to the premise (15) that vacant heteroatom *p* or *d* orbitals are required for such rearrangements to occur. Although fluorine migration from C_6F_5— to a metal atom has been observed even when not directly bonded (4, 7), no evidence could be found in these systems for a similar participation of gold. However, halogen transfer to phosphorus from the metal atom was observed to a small extent while fluorine transfer to phosphorus still occurs in the tetrahedral phosphine oxide, sulphide, and selenide despite the $d\pi$–$p\pi$ character of the P—E (E = O, S, Se) bonds in these compounds. The distribution of even and odd electron ions varies (Table 5) for the $C_6F_5(CH_3)_2M$ and $C_6F_5(CH_3)_2P(E)$ (E = O, S, Se). For the former even electron species increase for heavier ions, while in the latter the reverse is true as X becomes heavier. Phosphorus-containing ions are more abundant for $(CH_3)_2PC_6F_5$ than in the corresponding P=O, P=S, or P=Se derivatives.

It is also clear that the heteroatom, in spite of the presence of pentafluorophenyl groups, controls the course of fragmentation to a significant extent. This work further demonstrates the great utility of metastable-defocussed experiments in the elucidation of fragmentation pathways.

Acknowledgments

The authors wish to thank the National Research Council of Canada (J.M.M.) and the U.S. National Science Foundation (D.W.M.) for financial support.

1. J. M. MILLER. Can. J. Chem. **47**, 1613 (1969).
2. T. CHIVERS, G. F. LANTHIER, and J. M. MILLER. J. Chem. Soc. A, 2556 (1971).
3. S. C. COHEN, A. G. MASSEY, G. F. LANTHIER, and J. M. MILLER. Org. Mass Spectrom. **8**, 235 (1974).
4. J. M. MILLER. J. Chem. Soc. A, 828 (1967).
5. G. F. LANTHIER and J. M. MILLER. Org. Mass Spectrom. **6**, 89 (1972).
6. A. T. RAKE and J. M. MILLER. J. Chem. Soc. A, 1881 (1970); Org. Mass Spectrom. **3**, 237 (1970).
7. (*a*) S. C. COHEN, A. G. MASSEY, G. F. LANTHIER, and J. M. MILLER. Org. Mass Spectrom. **6**, 373 (1972); (*b*) G. F. LANTHIER, J. M. MILLER, and A. J. OLIVER. Can. J. Chem. **51**, 1945 (1973).
8. J. M. MILLER, J. ROSS, J. RUSTENBERG, and G. L. WILSON. Anal. Chem. **45**, 627 (1973); J. M. MILLER and G. L. WILSON. Int. J. Mass Spectrom. Ion Phys. **12**, 225 (1973); J. M. MILLER and G. L. WILSON. Anal. Chem. **47**, 191 (1975).
9. K. HENRICK, M. MICKIEWICZ, N. ROBERTS, E. SHEWCHUCK, and S. WILD. Aust. J. Chem. **28**, 1473 (1975).
10. J. ALLEN, J. BURDON, and J. C. TATLOW. J. Chem. Soc. 6329 (1965).
11. (*a*) J. L. PETERSON and D. W. MEEK. Inorg. Synth. **16**, 180 (1975). (*b*) J. L. PETERSON. Ph.D. Thesis. Ohio State University, Columbus, Ohio. 1973.
12. M. G. HOGBEN, R. S. GAY, and W. A. G. GRAHAM. J. Am. Chem. Soc. **88**, 3457 (1966).
13. Y. WADA and R. W. KISER. J. Phys. Chem. **68**, 2290 (1964).
14. D. ALLEN, J. C. TEBBY, and D. H. WILLIAMS. Tetrahedron Lett. 2361 (1965).
15. R. G. CAVELL and R. C. DOBBIE. Inorg. Chem. **7**, 101 (1968).

Can. J. Chem. Downloaded from www.nrcresearchpress.com by 210.87.254.6 on 09/05/12
For personal use only.

Solubilities of the silver halides in benzonitrile and trichloroacetonitrile mixtures with propylene carbonate

MARK SALOMON

Power Sources Technical Area, U.S. Army Electronics Technology and Devices Laboratory (ECOM), Fort Monmouth, New Jersey 07703

Received October 8, 1975

MARK SALOMON. Can. J. Chem. **54**, 1487 (1976).

The complex solubilities of the silver halides, AgCl, AgBr, and AgI, have been determined in benzonitrile and trichloroacetonitrile mixtures with propylene carbonate. The results are compared with previous work in acetonitrile and propionitrile and are discussed in relation to the solvent effect on ion solvation.

MARK SALOMON. Can. J. Chem. **54**, 1487 (1976).

On a déterminé les solubilités complexes d'halogénures d'argent, AgCl, AgBr et AgI, dans des mélanges de benzonitrile et de trichloroacétonitrile avec le carbonate de propylène. On compare les résultats avec ceux obtenus antérieurement dans l'acétonitrile et le propionitrile et on les discute en fonction des effets de solvant sur la solvatation des ions.

[Traduit par le journal]

Can. J. Chem. Downloaded from www.nrcresearchpress.com by 210.87.254.5 on 09/05/12
For personal use only.

Introduction

The present paper is a continuation of our studies on the effect of solvent on the complex solubilities of the silver halides (1). The complex equilibria studied are

$$[1] \qquad AgX \rightleftharpoons Ag^+ + X^- \qquad K_{s0}$$

$$[2] \qquad Ag^+ + nX^- \rightleftharpoons AgX_n^{1-n} \qquad \beta_n$$

and

$$[3] \qquad AgX + X^- \rightleftharpoons AgX_2^- \qquad K_{s2}$$

where X is Cl, Br, and I. These equilibria were studied in benzonitrile (BnN) and mixed solutions of trichloroacetonitrile (TCAN) in propylene carbonate (PC). The magnitude of K_{s0} and K_{s2} are of particular interest as they relate to the relative stabilities of the Ag^+ and X^- ions in a given solvent. BnN and TCAN were chosen for the present study since similar data exist for acetonitrile (AN) and propionitrile (PN) and comparisons can be made on the effects on the above equilibria by the substituent R in R—C≡N.

Experimental

Materials

Tetrapropylammonium perchlorate, chloride, bromide, and iodide (TPAP, TPACl, TPABr, and TPAI, respectively) and PC were purified as described earlier (1). Trichloroacetonitrile was distilled at 765 mm from CaO under argon. The middle third, collected at 84–86 °C was transferred to a VAC argon-filled dry box (O_2 and H_2O content ≤1 ppm). Benzonitrile was distilled under vacuum twice from type 4A molecular sieve and P_2O_5. In each distillation, the middle 3/5 fraction was collected at ~10 torr and 29–32 °C. All solvents were stored in the dry box. Three PC/TCAN mixtures were prepared in the dry box and their densities determined pycnometrically at 25 ± 1 °C. The concentrations of these mixed solvents are: [TCAN] = 1.496 *M*, 3.990 *M*, and 5.895 *M* (or, on a mole fraction basis, x_{TCAN} = 0.131, 0.362, and 0.565). All electrolyte solutions were maintained at a constant ionic strength of 0.0500 *M* with the exception of the PC/TCAN (5.895 *M*) solutions which were 0.0250 *M*. TPAP was used to adjust the ionic strengths.

Method

The solubility and stability constants were obtained from potentiometric titration data. The titrant was 50 m*M* $AgClO_4$ in all the solvents except in the PC/TCAN (5.895 *M*) solutions where the titrant was 25 m*M* $AgClO_4$. The indicator electrode was a coiled Ag wire and the reference electrode was a silver wire in 50 or 25 m*M* $AgClO_4$ and was separated from the titrate by a salt bridge (see ref. 1 for further details). The titration cell (a three-necked 100 ml flask with ST-joints) and 10–15 ml of TPAX + TPAP solution[1] was fitted with a Gilmont 2 ml microburet, removed from the dry box and placed in a water bath at 25 ± 0.1 °C. Magnetic stirring was maintained throughout the titrations. A Doric model DS-100 integrating microvoltmeter was used for the emf measurements in the 1.496 and 3.990 *M* TCAN solutions. The emf's for the other solutions were measured with an Orion model 801 p*H* meter. Both instruments are reproducible to within ±0.1 mV.

Results

The experimental concentrations[1] used to calculate the equilibrium constants are C_X, C_{Ag},

[1]Complete set of tabular data containing concentrations and emf's is available, at a nominal charge, from the Depository of Unpublished Data, CISTI, National Research Council of Canada, Ottawa, Canada K1A 0S2.

Can. J. Chem. Downloaded from www.nrcresearchpress.com by 210.87.254.5 on 09/05/12
For personal use only.

TABLE 1. Experimental equilibrium constants[a]

Solvent	Debye–Hückel A ($M^{1/2}K^{3/2}$)	Salt	$-\log K_{s0}$	$\log \beta_2$	$\log \beta_3$	$\log K_{s2}$	$\log \beta_{43}$
BnN	2.802	AgCl	15.50±0.01	17.12±0.02	19.1±0.1	1.62±0.03	
		AgBr	15.87±0.01	17.12±0.01		1.26±0.01	
		AgI	17.12±0.03	18.08±0.01		0.96±0.03	20.7±0.1
PC/TCAN	0.824	AgCl	19.56±0.03	20.20±0.05		0.64±0.05	
1.496 *M*		AgBr	20.25±0.02	20.66±0.01		0.41±0.03	
PC/TCAN	1.214	AgCl	19.94±0.04	20.15±0.01		0.21±0.04	
(3.990 *M*)		AgBr	20.00±0.01	20.10±0.01		0.10±0.01	
PC/TCAN	1.931	AgCl	19.91±0.04	20.23±0.02		0.32±0.04	
(5.895 *M*)		AgBr	20.29±0.03	20.21±0.02	22.2±0.1	−0.08±0.03	

[a]Based on the molar scale at 25 ± 0.1 °C.

TABLE 2. Standard equilibrium constants[a]

Solvent	Salt	log K_{s0}^0	log β_2^0	log K_{s2}^0
BnN	AgCl	−16.1	17.8	1.6
	AgBr	−16.5	17.8	1.3
	AgI	−17.8	18.7	1.0
PC/TCAN (1.496 *M*)	AgCl	−19.8	20.5	0.6
	AgBr	−20.5	20.9	0.4
PC/TCAN (3.990 *M*)	AgCl	−20.4	20.6	0.2
	AgBr	−20.4	20.5	0.1
PC/TCAN (5.895 *M*)	AgCl	−20.2	20.5	0.3
	AgBr	−20.5	20.5	−0.1
AN[b]	AgCl	−13.2	13.7	0.5
	AgBr	−13.7	13.8	0.1
	AgI	−14.5	14.0	−0.5
PN[c]	AgCl	−15.3	17.0	1.7
	AgBr	−16.0	17.3	1.3
	AgI	−17.1	18.3	1.2
PC[d]	AgCl	−20.2	21.2	1.0
	AgBr	−20.6	20.9	0.3
	AgI	−20.8	22.1	1.3

[a]Units based on the molar scale at 25 °C.
[b]Reference 3.
[c]Reference 4.
[d]Reference 1*a*.

and $[Ag^+]$. C_X and C_{Ag} are the total halide and silver concentrations and the silver ion concentrations were obtained from the Nernst relation

$$[4] \qquad E = E' + (RT/F) \ln [Ag^+]$$

In eq. 4, E is the measured emf and E' is a formal potential since it contains contributions from nonideality and a liquid junction. E' is assumed to remain constant because of the use of a constant ionic strength medium. The emf values were generally stable to within ± 0.5 mV and E' values, determined from the titration data in the region where $C_{Ag} > C_X$, had standard deviations of 1–2 mV.

The stability constants, β_n, were calculated by an iterative least squares method (1). The standard deviations of the β_n's were calculated by Sillén's pit-mapping method (2). The K_{s0} values are averages calculated by a Newton–Raphson iteration for each point in the saturated solution. The refined equilibrium constants and their standard deviations are given in Table 1. In Table 2 the equilibrium constants corrected for activity effects are given along with data for AN (3), PN (1), and PC (4). The activity coefficients used to obtain K^0 values were calculated from the Davies equation (5)

$$[5] \qquad \log \gamma_\pm = -\frac{A\mu^{1/2}}{1 + \mu^{1/2}} + 0.3A\mu$$

In eq. 5, μ is the ionic strength and the Debye–Hückel A factors are given in Table 1. The dielectric constants of the mixed solvents were assumed to be a linear function of the mole fraction. Pure PC and TCAN have dielectric constants of 64.4 (6) and ~7.8 (7), respectively. Standard deviations are not included in Table 2 but are expected to be about 10% higher than the experimental values because of the uncertainty in the use of eq. 5 and the neglect of the possibility of ion-pairing.

Several experimental points were omitted in the least squares refinement of the β's as they gave rise to abnormally large standard deviations.[1] These points usually occurred just prior to precipitation of AgX (*i.e.* at $C_{Ag}/C_X \simeq 0.5$). In the AgI–BnN system, a series of points in the region $C_{Ag}/C_I = 0.40$ to 0.68 were omitted. If, as suggested by L'Her and co-workers (8), this region is governed by the equilibrium

$$[6] \qquad 2AgI_2^- + Ag^+ \rightleftharpoons Ag_3I_4^- \qquad K_{43}$$

then a value of β_{43} ($\beta_{43} = K_{43}\beta_2^2$) can be calculated from

$$[7] \quad E = D - 0.059 \times \{2 \log (3 - 4x) - \log (2x - 1)\}$$

and

$$[8] \quad D = E' + 0.059 \times \{\log K_{43} - \log C_{Ag} - \log 2\}$$

Can. J. Chem. Downloaded from www.nrcresearchpress.com by 210.87.254.5 on 09/05/12
For personal use only.

TABLE 3. Single ion free energies of transfer from water to an organic solvent[a]

Solvent	ΔG_t^0(ion)							
	Li^{+d}	Rb^{+d}	Ag^+	Cl^-	Br^-	I^-	$AgCl_2^-$	AgI_2^-
AN	9.2[b]	3.9[b]	−3.5	8.2	5.4	1.4	1.5	−6.6
PN	8.5[b]	3.7[b]	−2.0	9.5	7.0	3.5	1.2	−4.7
BnN	10.6[b]	4.6[b]	−1.2	7.6	4.4	3.5	1.6	−5.2
PC/TCAN (1.496 *M*)			5.3	8.4	5.9		1.4	
PC/TCAN (3.990 *M*)			6.1	8.3	5.0		2.0	
PC/TCAN (5.895 *M*)			6.1	8.1	5.2		1.6	
PC	2.8[c]	−3.8[c]	5.5	8.7	5.9	1.0	1.3	−8.2

[a]ΔG_t^0 values at 25 °C in kcal/mol.
[b]Reference 9.
[c]Reference 10.
[d]Molal scale; all other data are based on the molar scale.

In eq. 7, $x = C_{Ag}/C_I$ and K_{43} values were calculated from the region where $0.5 < x \leqslant 0.68$ (see Table 1).

No experiments were carried out for the AgI system in PC/TCAN because TPAI reacted with the nitrile to give I_2. In addition, no experiments were carried in pure TCAN because $AgClO_4$ is insoluble in this solvent (TPACl is quite soluble). PC was chosen as the co-solvent for TCAN mixtures because it is known (1) to be a poor solvator for Ag^+ and X^- and any change in solvation properties upon TCAN addition would be easily discernible. This has been demonstrated previously (1) where small additions of tetrahydrothiophene and SO_2 to PC and PN resulted in large changes in ΔG_t^0(ion) values. The difference in solvation properties of the solvents listed in Table 2 can be determined by comparing the free energies of transfer of the individual ions (ΔG_t^0(ion)) from water to the organic solvent. The ΔG_t^0(ion) values were evaluated using the extra-thermodynamic assumption (1) $\Delta G_t^0(AgCl_2^-) = -\Delta G_t^0(AgBr_2^-)$. The ΔG_t^0(ion) values obtained using this assumption are generally within 2 kcal/mol, and of correct sign, to those obtained by more conventional methods (20, 21) with the exception of the iodide systems. The origin of the discrepancy in $\Delta G_t^0(I^-)$ values is not known, but in view of the agreement for the other ions, trends are easily discernible. For more accurate ΔG_t^0(ion) values, other works should be consulted (20, 21). The free energies of transfer of the individual ions, along with those obtained by Coetzee *et al.* (9) for $\Delta G_t^0(Li^+$ and $Rb^+)$ are given in Table 3.

Discussion

The data in Table 3 strongly suggest that AN, PN, and BnN behave as typical class 'b' (11) or 'soft' (12) Lewis bases. This is somewhat surprising since nitrogen, having the highest electronegativity next to oxygen and fluorine, would be expected to behave as a class 'a' or 'hard' donor which is the case for TCAN.

In order to determine those factors which govern the basicity of the nitrogen, CNDO/2 (13) calculations were carried out for AN, PN, BnN, and TCAN. Standard bond lengths and angles were taken from ref. 13 and the results for the electron distributions and populations at the cyano group are given in Fig. 1 and Table 4, respectively. The CNDO results for R—C≡N show that a major effect of R on the nitrogen in —C≡N is in the π bond and the lone-pair electrons. Comparison with the total atom densities (Fig. 1) suggests (13, 14) that

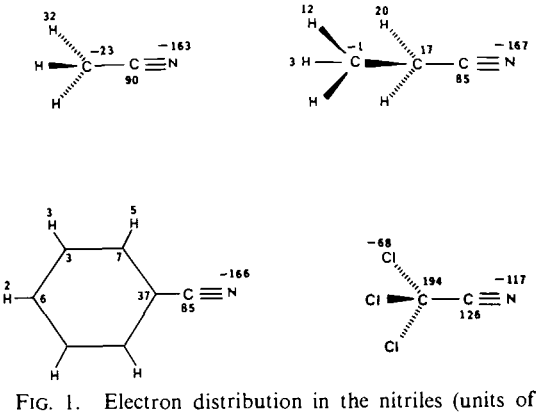

FIG. 1. Electron distribution in the nitriles (units of 10^{-3} electrons).

Can. J. Chem. Downloaded from www.nrcresearchpress.com by 210.87.254.5 on 09/05/12
For personal use only.

TABLE 4. Bond population of the cyano group[a]

	Bond population					
	Carbon			Nitrogen		
Molecule	$2s$	$2p_x$	$2p_y + 2p_z$[d]	$2s$[b]	$2p_x$[c]	$2p_y + 2p_z$[d]
AN	1.086	0.946	1.878	1.650	1.339	2.174
PN	1.091	0.947	1.877	1.650	1.336	2.181
BnN	1.085	0.947	1.883	1.647	1.334	2.185
TCAN	1.064	0.904	1.906	1.651	1.324	2.142

[a]In electron units, C≡N bond taken as the x-axis. All orbitals are atomic orbitals.
[b]σ-Bond density.
[c]Lone-pair density.
[d]π-Bond density.

there is considerable hyperconjugation in AN, PN, and BnN. The effect on the lone-pair electron density at nitrogen by Cl substitution in the methyl group is an inductive rather than a hyperconjugative effect. The present results for $\Delta G_t^0(Ag^+)$ and Coetzee's results for $\Delta G_t^0(Li^+)$ and $\Delta G_t^0(Rb^+)$ are complimentary to these results. A CNDO/2 calculation on the CH_3CN-Li^+ interaction (15) has shown that there is considerable charge transfer from the cyano-carbon which suggests that the charge density at the α-carbon also plays a major role in cation solvation since accumulation of positive charge on both the cyano and α-carbons would lead to instability. This is evident from the data in Table 3 and the atom densities in Fig. 1 which show that the charge on the α-carbon decreases (becomes more positive) as R is varied from CH_3 to CCl_3.

There is still the question why the nitriles in general behave as soft bases. The essential difference between hard and soft bases is that the latter are highly polarizable and tend to coordinate more strongly with highly polarizable (soft) acids (11, 12). However Rb^+ and Cs^+ may be regarded as soft acids (12) since their polarizabilities are 1.8 and 2.8 Å^3, respectively, as compared to 1.8 Å^3 for Ag^+ (16). The data in Table 3 show that Ag^+ is considerably more stable than Rb^+ (and Cs^+ as discussed in ref. 9*b*) so that other factors must be involved. Chatt and co-workers (11) have proposed that the soft acids are stabilized by π bonding since all metallic soft acids possess a large number of low energy *d*-electrons. The back donation of 4*d* electrons into low lying *p*-orbitals on sulfur has been suggested previously (1, 21, 22) to explain the large negative values of $\Delta G_t^0(Ag^+)$ in the transfer from water to several sulfur-containing solvents. The back-donation of 4*d* electrons from Ag^+ into the π^* orbital of R—C≡N appears to be significant for several reasons. It would explain the increased stability of Ag^+ over the larger alkali metal cations which do not have low lying *d*-orbitals. The back-bonding effect would also reduce the positive charge at the cyano and α-carbons which is opposite to the effect produced by the hard Li^+. Another factor contributing to the reduction of positive charge on the cyano-carbon and to the stability of the N–cation bond is that the nitrogen apparently undergoes a rehybridization upon coordination (17, 18). This occurs by a destabilization of the π orbitals and by stabilization of the σ orbital in the C≡N link and an increase in the *p*-character of the lone-pair orbital on nitrogen. This effect results in an increase in the C≡N force constant. Back-donation from the metal into the π^* orbital results in further destabilization of the π orbitals which tends to weaken the C≡N link and hence offset the strengthening by σ stabilization (18*b*). The importance of back-bonding when soft acids are involved can be inferred from the fact (18) that the increase in the C≡N force constant is smallest when the nitrogen coordinates with a soft Lewis acid and largest with a hard acid. The solvent effect on $\Delta G_t^0(Ag^+)$ thus appears to be due to electronic effects rather than steric or dielectric (solvent structure) effects. For example, in the series AN, PN, BnN, TCAN, $\Delta G_t^0(Ag^+)$ decreases in the same way that the lone-pair electron density on the nitrogen decreases. Steric hindrance would also appear to be of minor importance since Ag^+ forms linear complexes of the type $Ag(L)_2^+$.

Can. J. Chem. Downloaded from www.nrcresearchpress.com by 210.87.254.5 on 09/05/12
For personal use only.

Anions in AN tend to have no effect on the C≡N frequency but do lower the C—H stretching frequency and therefore suggests that the anion–AN interaction occurs at the methyl protons rather than at the cyano-carbon (19). For anion solvation in TCAN, there is a weak interaction which probably occurs at the cyano-carbon. The nature of the reaction of I^- with TCAN was not pursued.

1. (*a*) M. SALOMON and B. K. STEVENSON. J. Phys. Chem. **77**, 3002 (1973); (*b*) M. SALOMON. J. Phys. Chem. **79**, 429 (1975); **79**, 2000 (1975).
2. L. G. SILLÉN. Acta Chem. Scand. **16**, 159 (1962).
3. M. K. CHANTOONI and I. M. KOLTHOFF. J. Phys. Chem. **77**, 1 (1973).
4. (*a*) J. N. BUTLER. Adv. Electrochem. **7**, 77 (1970); (*b*) J. COURTOT-CORPEX and M. L'HER. Bull. Soc. Chim. Fr. 675 (1969).
5. C. W. DAVIES. Ion association. Butterworths, London, 1962.
6. A. K. COVINGTON and T. DICKINSON. The physical chemistry of organic solvent systems. Plenum Press, London. 1973.
7. M. DAVIES and D. G. JENKINS. J. Chem. Soc. 2374 (1954).
8. J.-Y. CABON, M. L'HER, and M. LE DEMEZET. C. R. Acad. Sci. Ser. C, **280**, 819 (1975).
9. (*a*) J. F. COETZEE, J. M. SIMON, and R. J. BERTOZZI. Anal. Chem. **41**, 766 (1969); (*b*) J. F. COETZEE, D. K. MCGUIRE, and J. L. HEDRICK. J. Phys. Chem. **67**, 1814 (1963).
10. M. SALOMON. J. Phys. Chem. **74**, 2519 (1970).
11. S. AHRLAND, J. CHATT, and N. R. DAVIES. Q. Rev. (London), **12**, 265 (1958).
12. R. G. PEARSON. J. Am. Chem. Soc. **85**, 3533 (1963).
13. J. A. POPLE and D. L. BEVERIDGE. Approximate molecular orbital theory. McGraw-Hill, N.Y. 1970.
14. J. A. POPLE and M. GORDON. J. Am. Chem. Soc. **89**, 4253 (1967).
15. A. GUPTA and C. N. R. RAO. J. Phys. Chem. **77**, 2888 (1973).
16. B. E. CONWAY. Electrochemical data. Elsevier, Amsterdam. 1952.
17. J. C. EVANS and G. Y.-S. LO. Spectrochim. Acta, **21**, 1033 (1965).
18. (*a*) K. F. PURCELL and R. S. DRAGO. J. Am. Chem. Soc. **88**, 919 (1966); (*b*) K. F. PURCELL. J. Am. Chem. Soc. **89**, 247 (1967); **89**, 6139 (1967).
19. J. F. COETZEE and W. R. SHARPE. J. Solution Chem. **1**, 77 (1972).
20. C. M. CRISS and M. SALOMON. The physical chemistry of organic solvent systems. *Edited by* A. K. Covington and T. Dickinson. Plenum Press, London. 1973.
21. B. COX, G. R. HEDWIG, A. J. PARKER, and D. W. WATTS. Aust. J. Chem. **27**, 477 (1974).
22. (*a*) A. J. PARKER. Search, **4**, 426 (1973); (*b*) D. A. OWEN, A. J. PARKER, and J. W. DIGGLE. J. Am. Chem. Soc. **96**, 2682 (1974).

Can. J. Chem. Downloaded from www.nrcresearchpress.com by 210.87.254.5 on 09/05/12
For personal use only.

Erratum: Mercury(I) chemistry. Part I. Complexes of the mercurous ion with some arenes

PHILIP A. W. DEAN, DAVID G. IBBOTT, AND J. B. STOTHERS
Department of Chemistry, University of Western Ontario, London, Ontario N6A 5B7
Received March 23, 1976
(Ref.: Can. J. Chem. **54**, 166 (1976))

The sentence commencing on line 1, left column, on page 169 should read "Analysis in terms of the formation of both 1:1 and 2:1 complexes gave the parameters listed in Table 2".

Erratum: The heat of formation of N_2H_2 and the proton affinity of N_2

C. WILLIS, F. P. LOSSING, AND R. A. BACK
Division of Chemistry, National Research Council of Canada, Ottawa, Canada K1A 0R6
Received March 8, 1976
(Ref.: Can. J. Chem. **54**, 1 (1976))

On page 2, column 2, the sentence in lines 1 and 2 should read: From our value, a mean N—H bond energy of 34 kcal/mol is obtained.

Can. J. Chem. Downloaded from www.nrcresearchpress.com by 210.87.254.105 on 09/05/12
For personal use only.

COMMUNICATIONS

The total synthesis of coccinelline and precoccinelline

WILLIAM A. AYER AND KIMIAKI FURUICHI
Department of Chemistry, University of Alberta, Edmonton, Alta., Canada T6G 2G2

Received February 12, 1976

WILLIAM A. AYER and KIMIAKI FURUICHI. Can. J. Chem. **54**, 1494 (1976).

The synthesis of the ladybug defensive substances precoccinelline and coccinelline, starting from 2,6-lutidine, is described.

WILLIAM A. AYER et KIMIAKI FURUICHI. Can. J. Chem. **54**, 1494 (1976).

On décrit la synthèse à partir de la lutidine-2,6 des substances défensives des coccinelles soit la precoccinelline et la coccinelline.

[Traduit par le journal]

Recently we have described the synthesis from 2,4,6-collidine of the ladybug defensive substances myrrhine (**1**) hippodamine (**2**), and convergine (**3**) (1). The key step in the synthesis of these substances involved the cyclization of the ketoaldehyde **4***a* (which is isolated as the carbinolamine ketol **5***a*) to furnish the ketones **6***a* and **7***a*. Removal of the oxygen function from **6***a* provided myrrhine (**1**), and from **7***a*, hippodamine (**2**). The ketone **8**, a potential precursor of precoccinelline (**9**) and thus also of coccinelline (**10**), could not be obtained from **4***a* (1). Coccinelline (**10**) (2) is the major defensive substance of several species of Coccinellidae (ladybugs) (3) and thus its synthesis remained a challenge. As noted previously (1) the ketone **7***b* (=**11**), potentially available from the ketoaldehyde **4***b*, is an attractive precursor of precoccinelline (**9**). We now report the synthesis of **11** (= **7***b*) and its transformation to precoccinelline (**9**) and coccinelline (**10**).

The synthesis of **4***b* followed the same pathway as the synthesis of **4***a* except that 2,6-lutidine was utilized as starting material rather than 2,4,6-collidine. Treatment of the monolithium

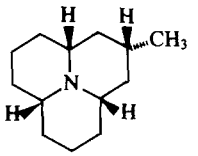

1

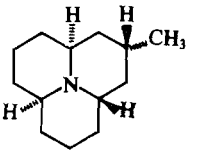

2
3 *N*-oxide of **2**

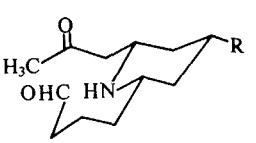

4*a* R = CH_3
4*b* R = H

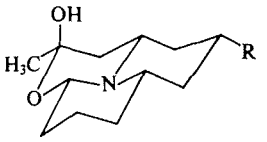

5*a* R = CH_3
5*b* R = H

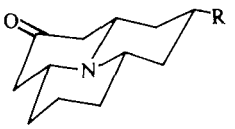

6*a* R = CH_3
6*b* R = H

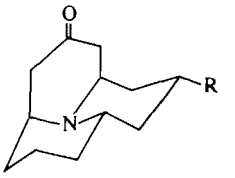

7*a* R = CH_3
7*b* R = H

derivative of 2,6-lutidine (1 equiv.) with β-bromopropionaldehyde dimethyl acetal (1 equiv.) (4) in ether in the presence of excess 2,6-lutidine (2 equiv.) gave the acetal **12**,[1] bp 85–90 °C/0.3 torr, in 76% yield (based on alkylating agent). Treatment of an ether solution of **12** with phenyllithium, followed by the slow (over 4 h) addition of an ethereal solution of acetonitrile (1 equiv.) (1) provided after work-up the crude ketone **13** which was immediately transformed (ethylene glycol – benzene – *p*-toluenesulfonic acid) to the diacetal **14** (bp 110–120 °C/0.1 torr)[1]. The overall

[1]All new compounds reported, with the exception of **16**, gave satisfactory combustion analyses. Nuclear magnetic resonance, ir, and mass spectra were obtained on all new compounds and are completely consistent with the structures formulated.

Can. J. Chem. Downloaded from www.nrcresearchpress.com by 210.87.254.40 on 09/05/12
For personal use only.

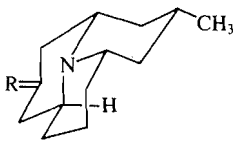

8 R = O
9 R = H, H

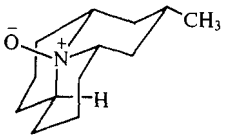

10

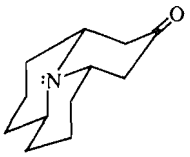

11

yield of **14** from **12** was 48%, with 27% of **12** (as the ethylene acetal) recovered.

Reduction of **14** using sodium – isoamyl alcohol followed by careful chromatography over silicic acid gave the *cis* piperidine **15** (bp 135–140 °C/0.05 torr, hydrochloride mp 118–119 °C)[1] in 63% yield. The *trans*-isomer of **15** was isolated in 25% yield. The stereochemistry of the major product was assigned on the basis of: (*1*) its mode of formation (thermodynamically favored product); (*2*) a comparison of its cmr spectrum with that of the *trans*-isomer (*cf.* ref. 1); (*3*) trans-

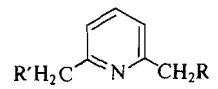

12 R′ = H
R = $CH_2CH_2CH(OCH_3)_2$
13 R′ = $COCH_3$
R = $CH_2CH_2CH(OCH_3)$
14 R′ = —C(=O)—CH_3
R = CH_2CH_2CH(dioxolane)

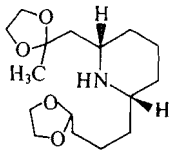

15

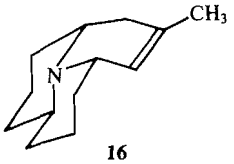

16

formation to the carbinolamine ketol **5***b*. Hydrolysis of **15** with 5% aqueous hydrochloric acid gave the ketol **5***b* (mp 87–88.5 °C)[1] which shows OH absorption and strong Bohlmann bands in the ir, a methyl signal at δ 1.48 (s, 3H) in the pmr and at δ 30.3 in the cmr, and thus must have the structure and stereochemistry shown in **5***b* (*cf.* **5***a*, ref. 1).

Cyclization of **5***b* (closed form of **4***b*) using pyrrolidine (1 equiv.) and acetic acid (2 equiv.) in refluxing tetrahydrofuran (1) gave a 1:1 mixture of ketones **6***b* and **7***b* (= **11**) in 86% yield. The mixture of ketones was separated by chromatography over silicic acid (eluant $CHCl_3$–MeOH–$NHMe_2$, 100:10:1); **6***b* (bp 75–80 °C/0.2 torr)[1] shows carbonyl absorption at 1730 cm^{-1} and *strong Bohlmann bands* in the ir; **7***b* (= **11**) (mp 82–84 °C)[1] shows carbonyl absorption at 1710 cm^{-1} and *no Bohlmann bands*.

Treatment of ketone **7***b* with methyllithium in ether followed by dehydration of the resulting carbinol with thionyl chloride in methylene chloride yielded the air sensitive olefin **16** (pmr, δ 1.66 (bs, 3H), 5.15 (bs, 1H)) which was hydrogenated (Pt, CH_3OH, room temperature, 1 atm) to give precoccinelline **9** (27% yield from **7***b*), identical (ir, pmr, ms, tlc) with an authentic sample.[2] Oxidation of synthetic precoccinelline with *m*-chloroperbenzoic acid in methylene chloride gave coccinelline (**10**), mp 205–210 °C (dec.), hydrochloride mp 215–220 °C (dec.), identical (mp, ir, ms, tlc) with an authentic sample.[2]

Treatment of ketone **6***b* with methyllithium followed by dehydration ($SOCl_2$–CH_2Cl_2) and hydrogenation gave myrrhine (**1**).

Acknowledgement

We wish to thank the National Research Council of Canada for financial support.

1. W. A. Ayer, R. Dawe, R. A. Eisner, and K. Furuichi. Can. J. Chem. **54**, 473 (1976).
2. R. Karlsson and D. Losman. Chem. Commun. 626 (1972).
3. J. M. Pasteels, C. Deroe, B. Tursch, J. C. Braekman, D. Daloze, and C. Hootele. J. Insect Physiol. **19**, 1771 (1973).
4. A. Kirrmann, M. Goudard, and M. Chahidzadeh. Bull. Soc. Chim. Fr. **2**, 2148 (1935).

[2]We wish to thank Prof. B. Tursch for samples and spectra of precoccinelline and coccinelline.

Can. J. Chem. Downloaded from www.nrcresearchpress.com by 210.87.254.40 on 09/05/12
For personal use only.

Canadian Journal of Chemistry

Published by
THE NATIONAL RESEARCH COUNCIL OF CANADA

Volume 54 Number 10 May 15, 1976

Journal canadien de chimie

Publié par
LE CONSEIL NATIONAL DE RECHERCHES DU CANADA

Volume 54 numéro 10 15 mai 1976

Can. J. Chem. Downloaded from www.nrcresearchpress.com by 210.87.254.42 on 09/05/12
For personal use only.

Reaction rates of electrons in liquid methanol and ethanol: Effect of temperature: Kinetics of electron reactions prior to solvation[1]

GERALD L. BOLTON,[2] KAMAL N. JHA, AND GORDON R. FREEMAN
Chemistry Department, University of Alberta, Edmonton, Alberta T6G 2G2

Received December 30, 1975

GERALD L. BOLTON, KAMAL N. JHA, and GORDON R. FREEMAN. Can. J. Chem. **54**, 1497 (1976).

The rate constants of [2] $e^-_{solv} + S \rightarrow$ product, and [3] $e^-_{solv} + ROH \rightarrow H + RO^-_{solv}$ were measured at temperatures from about 180 to 360 K. For a given scavenger S in methanol and ethanol, the ratio of k_2 values in the two solvents, k_M/k_E, equalled 0.2 for the least efficient scavenger benzene and increased towards 2 for the most efficient scavengers. The ratio equalled unity for $k_2 \approx 5 \times 10^9\ M^{-1}\ s^{-1}$. The activation energy E_2 was greatest for benzene (6.0 kcal/mol in both alcohols) and decreased to 3.0 ± 0.2 kcal/mol for the efficient scavengers. Inefficient scavengers appear to react by a two step mechanism, [8,−8] $e^-_{solv} + S \rightleftharpoons S^-_{solv}$, [9] S^-_{solv} (+ ROH) $\rightarrow X^-_{solv}$ + product, with the observed $k_2 = k_9 \exp(-\Delta G_8^0/RT)$. Arrhenius plots of k_3 appear to bend in the temperature region near 235 K in both alcohols, but the observed effect is probably magnified by reaction of a residual impurity. Reaction rates of 'presolvation electrons' with high concentrations of scavengers vary less from scavenger to scavenger and from solvent to solvent and with temperature than do rates of solvated electron reactions. This is attributed to the higher energy of presolvation compared to solvated electrons. An earlier nonhomogeneous kinetics model of solvated electron reactions in spurs is extended to include reactions of presolvation electrons. Between the time when the energy of a secondary electron in an alcohol has been degraded to the region where the electron is scavengeable by phenol, and the time when the electron makes its first diffusive jump in the solvated state, the electron encounters an average of ≥30 molecules.

GERALD L. BOLTON, KAMAL N. JHA et GORDON R. FREEMAN. Can. J. Chem. **54**, 1497 (1976).

On a mesuré, à des températures allant de 180 à 360 K, les constantes de vitesse pour $e^-_{solv} + S \rightarrow$ produits [2] et $e^-_{solv} + ROH \rightarrow H + RO^-$ [3]. Pour un piège donné, S, dans le méthanol et l'éthanol, le rapport des valeurs k_2 dans les deux solvants, k_M/k_E, est égal à 0.2 pour le benzène qui est le piège le moins efficace et augmente jusqu'à une valeur d'approximativement 2 pour les pièges les plus efficaces. Le rapport est égal à un lorsque $k_2 \approx 5 \times 10^9\ M^{-1}\ s^{-1}$. L'énergie d'activation, E_2, est maximale pour le benzène (6.0 kcal/mol dans chaque alcool) et diminue jusqu'à 3.0 ± 0.2 kcal/mol pour les pièges les plus efficaces. Il semble que les pièges inefficaces réagissent par un mécanisme à deux étapes $e^-_{solv} + S \rightleftharpoons S^-_{solv}$ [8,−8], S^-_{solv} (+ ROH) $\rightarrow X^-_{solv}$ + produits [9], alors que la constante observée pour $k_2 = k_9 \exp(-\Delta G_8^0/RT)$. Il semble que les courbes d'Arrhénius pour k_3 ne sont plus linéaires près de 235 K pour chacun des alcools; cet effet est probablement amplifié par la réaction d'une impureté résiduelle. Les vitesses de réaction des 'électrons de présolvatation' avec des concentrations élevées de pièges varient moins d'un piège à l'autre et d'un solvant à l'autre et avec la température que les vitesses de réaction des électrons solvatés. On attribue ce résultat à l'énergie plus élevée des 'électrons de présolvatation' par opposition aux électrons solvatés. On étend un modèle cinétique nonhomogène proposé antérieurement pour les réactions d'électrons solvatés

de façon à inclure les réactions des 'électrons de présolvatation'. Entre le moment où l'énergie d'un électron secondaire dans un alcool s'est dégradé vers la région où l'électron peut être piégé par le phénol et le temps où l'électron fait son premier saut de diffusion dans l'état solvaté, l'électron rencontre une moyenne de ≥ 30 molécules.

[Traduit par le journal]

Can. J. Chem. Downloaded from www.nrcresearchpress.com by 210.87.254.42 on 09/05/12
For personal use only.

Introduction

In a recent study of the effect of pressure on the rates of solvated electron reactions with a wide variety of solutes in alcohols, it was found that for rate constants below $10^9\ M^{-1}\ s^{-1}$ the magnitude and direction of the pressure effect correlate with the magnitude of the rate constant (1). The volume of activation decreases algebraically with the log of the rate constant at 295 K. Electron reaction with inefficient scavengers is endoergic and increasing the pressure lowers the free energy barrier by altering the relative solvation energies of the participating species. For rate constants greater than $10^9\ M^{-1}\ s^{-1}$ there is no simple correlation with the volume of activation, except that all are positive (1).

The volumes of activation for both efficient and inefficient scavengers tend to be lower in methanol than in ethanol, which hints at a previously unsuspected solvent effect.

The search to identify parameters that affect electron reactivity has been extended by measuring temperature coefficients of a number of reactions in methanol and ethanol. The reaction with the solvent itself (2–4) has been reinvestigated.

It has also been noted that electrons in alcohols and water may react with high concentrations of scavengers at relative rates that are different from those in dilute solutions (5–10). Electrons generated in concentrated solutions may react before becoming solvated. The relative reactivity with different scavengers is a function of the electron energy state. The kinetics of the reactions prior to solvation may be described by extension of a stochastic model for reaction of ions and electrons in spurs (11). The extended model is presented and applied in this article.

Experimental

The materials and techniques were the same as those reported earlier (12), with the following additions.

[1]Financially assisted by the National Research Council of Canada, Ottawa, Canada.

[2]Holder of National Research Council of Canada, 1971–1974 and Province of Alberta Fellowships, 1970–1971.

Materials

Reagent grade phenol from B.D.H. Chemicals Ltd. was melted under vacuum in a modified sublimation apparatus. Sodium–potassium alloy was then added with vigorous stirring. After reaction was complete part of the phenol was sublimed, then transferred into an alcohol under an atmosphere of ultrahigh purity argon to make a stock solution.

Dosimetry, SEM

The secondary emission monitor SEM (13, 14) originally contained 0.001 in. thickness aluminum foils. The emission per unit dose varied with beam current density and the characteristics changed with time due to slow oxidation of the foils. These problems were overcome by using 0.0001 in. thickness Havar foils instead of aluminum. Havar is a high strength, cobalt base alloy. The foils were obtained from Hamilton Watch Co., Precision Metals Division. The advantages of the Havar foils for use in SEM were their low mass/cm^2 and their resistance to oxidation.

Current that passed from the center foil during a radiation pulse was collected by an integrator during a 200 μs time window centered on the beam pulse. The integrator then fed into a digital readout.

$KSCN/O_2$ Dosimetry

Oxygen-saturated aqueous solutions of potassium thiocyanate are convenient to use for dosimetry in pulse radiolysis spectroscopy (12, 13). The optical absorption maximum of the transient $(SCN)_2^-$ lies at 478 $\pm$ 4 nm, independent of temperature from 293 to 332 K (12), and the response time is $<1\ \mu$s. However, there is some doubt about the G value and molar extinction coefficient ϵ_{478} of the transient $(SCN)_2^-$ ion (12, 15, 16). Values of $G\epsilon_{478}$ were therefore measured at different thiocyanate concentrations, using the Fricke dosimeter as a standard with $G(Fe^{3+}) = 15.6$ and $\epsilon_{304}(Fe^{3+}) = 2150\ M^{-1}\ cm^{-1}$ at 295 K (17). Fricke dosimeter solutions containing 5, 10, and 50 mM Fe^{2+} gave the same results within experimental error ($\pm 4\%$ due to fluctuations in the analyzing light intensity during the 3 s response time of the Fricke solutions). Each 100 ns pulse of 1.7 MeV electrons delivered $\sim 3 \times 10^{16}$ eV/g to the sample.

The value of $G\epsilon_{478}$ was relatively constant at 2.0×10^4 to 2.1×10^4 for thiocyanate concentrations between 1 and 10 mM (Fig. 1). The decrease at lower concentrations was probably due to incomplete scavenging of the OH radicals in the bulk solution by SCN^-. The increase at high concentrations is attributed to the beginning of OH radical scavenging in spurs. The G value of $(SCN)_2^-$ is equal to that of OH radicals that react with SCN^-. It is commonly assumed that the yield of OH that escapes reaction in the spurs in pure water is equal to the solvated electron free ion yield (18), which is $G(e^-_{solv})_{fi} = 2.7 \pm 0.1$ (18–21). From the shape of the curve in Fig. 1 we take $G\epsilon_{478} = 2.1 \times 10^4$ to correspond to $G(OH)_{scavenged} =$

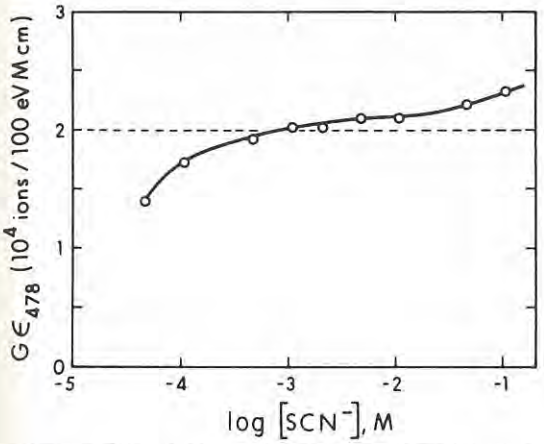

FIG. 1. Plot of $G\epsilon_{478}$ against potassium thiocyanate concentration in oxygen saturated aqueous solutions at 295 K.

$G((SCN)_2^-) = 2.8 \pm 0.1$, whence $\epsilon_{478} = 7500\ M^{-1}\ cm^{-1}$ with an over-all uncertainty of about 500 $M^{-1}\ cm^{-1}$. This agrees satisfactorily with earlier values (12, 15, 16), but points out the relatively large magnitude of the uncertainty.

Thus, for thiocyanate concentrations within a factor of two of 5 mM one may use $G((SCN)_2^-) = 2.8 \pm 0.1$ and $\epsilon_{478} = 7500 \pm 500\ M^{-1}\ cm^{-1}$.

Dosimetry for pulse radiolysis spectroscopy is ultimately based upon the Fricke dosimeter (20). The difficulty of using that system accurately in the pulse mode brings into question the validity of quoting extinction coefficients of radiolysis intermediates to three significant figures (12, 20). For example, a realistic statement of the value of ϵ_{720} for solvated electrons in water is $(1.9 \pm 0.1) \times 10^4\ M^{-1}\ cm^{-1}$.

Results

Decomposition of e^-_{solv}

The first order rate of decay of solvated electrons in methanol was measured at temperatures ranging from 180 to 350 K. An Arrhenius plot of the rates is not linear (Fig. 2). Making the alcohol basic (1 mM KOH) and reducing the pulse dose decreased the decay rate at each temperature, but the shapes of the Arrhenius plots remained similar (Fig. 2). Extrapolation of the decay rate to zero pulse dose from measurements over the range 2×10^{17} to 2×10^{16} eV/g did not remove the bend in the plot. The apparent activation energies in the high temperature region range from 4.1 kcal/mol in the neutral alcohol at high pulse dose to 4.5 kcal/mol in basic alcohol extrapolated to zero dose. Those in the low temperature region are all about 2.1 kcal/mol.

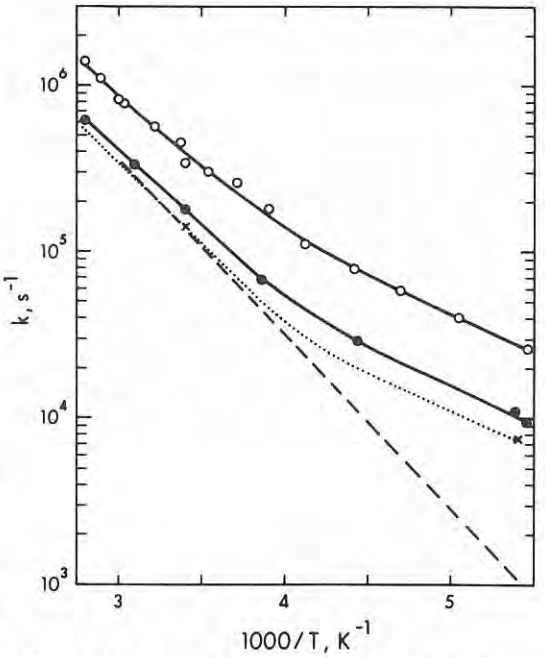

FIG. 2. Arrhenius plots of first order decomposition rates of e^-_{solv} in methanol. ○, neutral methanol, 1 μs pulse dose 9×10^{16} eV/g. ●, 1 mM KOH, 0.1 μs pulse dose 3×10^{16} eV/g. ×, 1 mM KOH, extrapolated to zero dose. The dashed line was calculated from the Arrhenius parameters reported in ref. 4.

The behavior in ethanol was similar (Fig. 3). At the lowest temperatures an initial portion of the observed decay was relatively fast and corresponded to the end of the geminate neutralization reaction (3). For consistency this portion was excluded from the calculations. The recorded values of k refer to the first order decay of the 'free ion' solvated electrons (3). The experimental value of the activation energy in basic ethanol was 5.1 kcal/mol at high temperatures and 3.0 kcal/mol at low temperatures.

A geminate neutralization portion was not apparent in methanol under the conditions used. The solvated electron decay plots were simple first order.

$k(e^-_{solv} + S)$

The effects of temperature on the rates of reaction of solvated electrons with scavengers were measured for a number of compounds that were chosen to display a wide range of rate constants. The nature and quality of the results are illustrated by those for nitrobenzene. Pseudo first order decay constants of e^-_{solv} were measured for

Can. J. Chem. Downloaded from www.nrcresearchpress.com by 210.87.254.42 on 09/05/12
For personal use only.

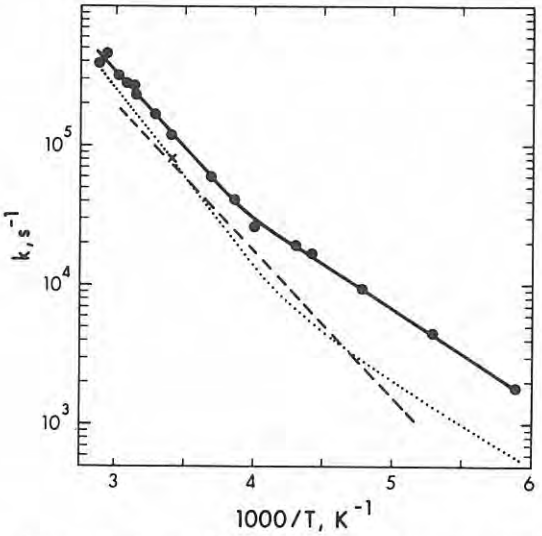

FIG. 3. Arrhenius plots of first order decomposition rates of e^-_{solv} in ethanol. ●, 1 m*M* KOH, 1 μs pulse dose 9×10^{16} eV/g. ×, 1 m*M* KOH, extrapolated to zero dose; the dotted line is an estimate. The dashed line was calculated from the Arrhenius parameters reported in ref. 4.

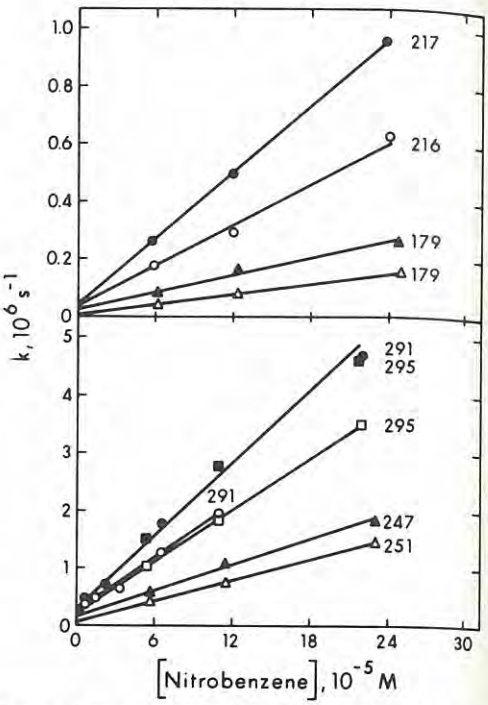

FIG. 4. Pseudo first order decay rates of solvated electron decay in nitrobenzene solutions in methanol (closed points) and ethanol (open points). The numbers labelling the lines indicate the temperature in K.

different concentrations of the solute at a given temperature. The value of the second order rate constant k_2 was obtained from the slope of a plot of the pseudo first order constants against the concentration of scavenger (Fig. 4). Three to six concentrations were used at each temperature. The molar concentrations were adjusted for the change in solvent density with temperature.

The log of k_2 was plotted against the inverse of the temperature to determine the activation energy. The points for nitrobenzene in methanol indicate that the Arrhenius plot is slightly convex towards the T^{-1} axis (Fig. 5). The same is true for some of the other solutes in methanol and ethanol (Figs. 5 and 6), but the experimental scatter prevents drawing the curvature with confidence. Straight lines were therefore used to obtain average values of the activation energies.

Values of the Arrhenius pre-exponential factor A_2 and activation energy E_2 are collected in Table 1: $k_2 = A_2 \exp(-E_2/RT)$. Differences in the values of k_2 at 295 K are reflected to similar extents by differences in log A_2 and in E_2, although no simple correlation between these parameters is evident from the present results (Table 1).

TABLE 1. Values of k_2 at 295 K and of the Arrhenius parameters A_2 and E_2 in methanol and ethanol solvents

	Methanol				Ethanol			
Solute	Concentration range (10^{-4} *M*)	k_2 (M^{-1} s^{-1})	log A_2	E_2 (kcal/mol)	Concentration range (10^{-4} *M*)	k_2 (M^{-1} s^{-1})	log A_2	E_2 (kcal/mol)
Perchloric acid	0.4–1	5.4×10^{10}	13.1	3.2	0.4–1	3.3×10^{10}	13.4	4.0
Nitrobenzene	0.1–2	2.3×10^{10}	12.5	2.9	0.1–2	1.5×10^{10}	12.4	3.0
Acetone	1–7	4.3×10^{9}	11.7	2.7	1–10	4.7×10^{9}	11.8	2.9
Naphthalene	2–8	3.0×10^{9}	11.9	3.2	2–8	4.3×10^{9}	12.0	3.2
Phenol	1000–4000	$\sim1.0\times10^{7}$	10.3	4.5	1000–4000	5×10^{7}	10.9	4.4
Benzene	2000–16000	1.2×10^{6}	10.5	6.0	1000–5000	6.4×10^{6}	11.2	6.0

Can. J. Chem. Downloaded from www.nrcresearchpress.com by 210.87.254.42 on 09/05/12
For personal use only.

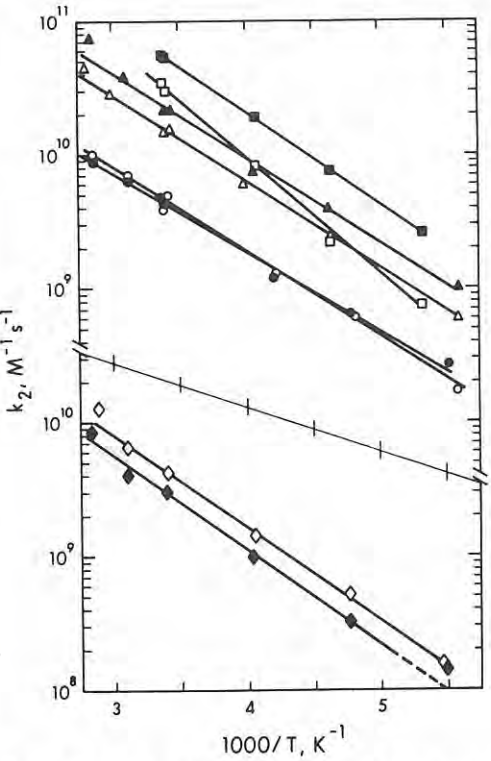

FIG. 5. Arrhenius plots of second order rate constants for reaction of e^-_{solv} with solutes: □, perchloric acid; △, nitrobenzene; ○, acetone; ◇, naphthalene. The closed points refer to methanol solvent, while the open points refer to ethanol.

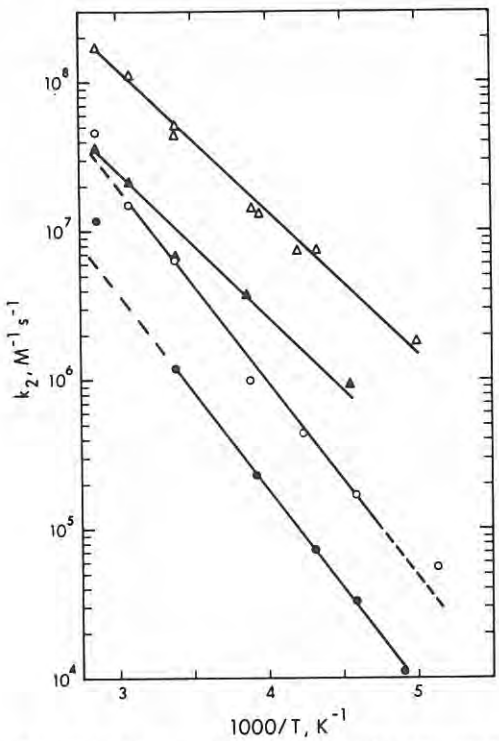

FIG. 6. Arrhenius plots of second order rate constants for reaction of e^-_{solv} with phenol (△) and benzene (○). The closed points refer to methanol solvent, while the open points refer to ethanol.

Scavenging of Electrons Prior to their Solvation

The low concentrations (≤ 1 mM) of nitrobenzene and other efficient scavengers used in these experiments increased the rate of decay of solvated electrons but did not affect the initial yield of solvated electrons formed during the radiation pulse. The initial optical absorbance A_i, corrected for decay during the pulse, was the same in the presence and absence of 1 mM scavengers. However, high concentrations of benzene and phenol were required to scavenge the solvated electrons, because the values of k_2 are relatively small for these compounds (Table 1). The high concentrations of benzene and phenol also reduced the initial optical absorbance (Fig. 7). Plots of (A_i/A_{i0}) against mole fraction N_s of scavenger are shown in Fig. 8; A_{i0} is the initial absorbance when $N_s = 0$. The values of A_i were corrected for decay that occurred during the 0.1 μs pulse due to scavenging of solvated electrons

$$[1] \quad A_i = A_p\left\{\frac{t_{1/2}}{0.069}[1 - \exp(-0.069/t_{1/2})]\right\}^{-1}$$

where A_p is the absorbance at the end of the pulse and $t_{1/2}$ is the decay half-life after the pulse, in μs. At 234 K in ethanol an initial rapid portion of the observed decay was due to the end of the geminate neutralization reaction. For consistency this portion was excluded from the value of A_i by first order extrapolation of the longer half-life portion to the end of the pulse.

Phenol is only twice as effective as benzene in reducing A_i, whereas it is eight times as effective as benzene in scavenging solvated electrons (Table 1).

Discussion

Decomposition of e^-_{solv}

Solvated electrons can react with many species S, including the other radiolysis intermediates ROH_2^+ and neutral free radicals.

$$[2] \quad e^-_{solv} + S \rightarrow \text{Product}$$

Can. J. Chem. Downloaded from www.nrcresearchpress.com by 210.87.254.42 on 09/05/12
For personal use only.

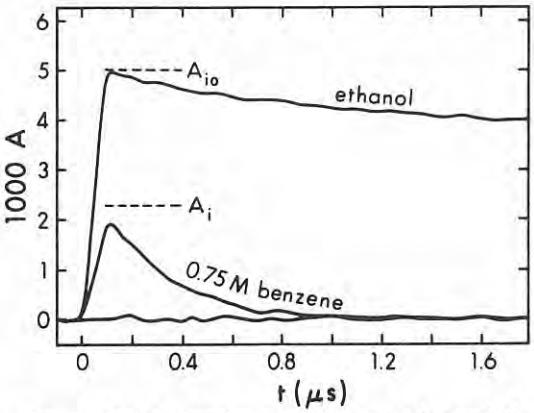

FIG. 7. Optical absorbance at 690 nm during and after a 100 ns pulse of 1.7 MeV electrons in ethanol and ethanol containing 0.75 M benzene. T = 295 K. Dose = 1.8×10^{16} eV/cm³. A_i and A_{i0} represent the initial absorbances corrected for decay during the pulse.

The contribution of ROH_2^+ can be removed by making the alcohol basic, and that of the neutral radicals can be reduced by decreasing the magnitude of the dose delivered in the pulse. These effects are illustrated in Fig. 2. The objective was to make contributions of [2] negligible so that k_3 could be measured

$$[3] \qquad e^-_{solv} + ROH \rightarrow H + RO^-_{solv}$$

Reactions 2 and 3 are each pseudo first order. At high temperatures the activation energy of [3] is greater than that of [2]. The difference at low temperatures is unclear.

Baxendale and Wardman (4) reported Arrhenius parameters for [3], but unfortunately did not publish the experimental plots. The dashed line in Fig. 2 corresponds to their parameters for electrons in methanol, $\log k_3(s^{-1}) = 8.7 - (4830/4.6T)$. The present results extrapolated to zero pulse dose agree with those of Baxendale and Wardman at high but not at low temperatures. The main question is whether or not the Arrhenius plot for k_3 is truly linear. The differences between the three experimental curves in Fig. 2 correspond to reactions with average activation energies of 2.7–2.8 kcal/mol, similar to those for the efficient scavengers listed in Table 1. To straighten out our lowest curve would require a residual impurity reaction that had an activation energy of 1.6 kcal/mol, which is significantly lower than any of the observed values. The curvature might be partly due to an artifact, but the earlier reported linearity (4) is questionable.

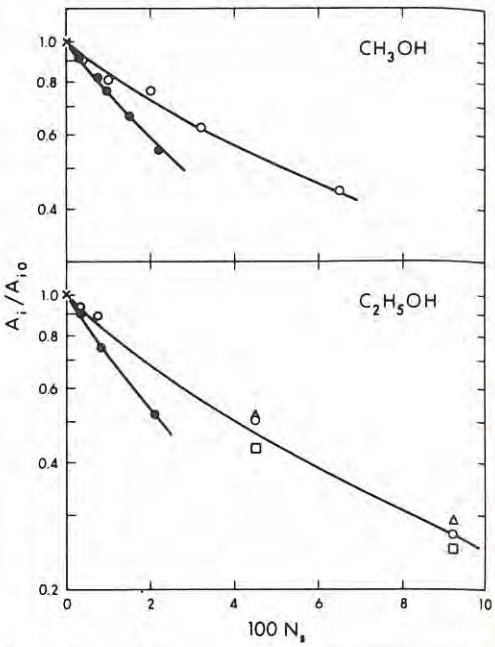

FIG. 8. Effect of benzene (○) and phenol (●) on the initial optical absorbance A_i of solvated electrons after a 100 ns pulse of radiation in methanol and ethanol. A_{i0} is the initial absorbance in the absence of scavenger and N_s is the mol fraction of scavenger. ○, 295 K; △, 257 K; □, 234 K; ×, A_i/A_{i0} = 1.0 for each set. The values of A_i were corrected for decay during the pulse due to scavenging of solvated electrons, using k_2 from Table 1. The curves were calculated from eq. 14, using the parameter values in Table 2.

The zero pulse dose curve for basic ethanol was estimated from the experimental values by assuming that the reaction of solvated electrons with neutral free radicals has the same activation energy as that with acetone, E_2 = 2.9 kcal/mol (Table 1). The magnitude of the dose correction was set by the difference between the experimental and extrapolated points at 294 K ($1000/T$ = 3.40, Fig. 3). The resulting Arrhenius curve is bent, with high and low temperature activation energies of 5.8 and 3.3 kcal/mol, respectively. The magnitudes of the rate constants are in reasonable agreement with those of Baxendale and Wardman (4), but the question of linearity remains.

$k(e^-_{solv} + S)$

A distinct solvent effect occurs in scavenger reaction rates. For the most reactive solutes perchloric acid and nitrobenzene, the rate constants are greater in methanol than in ethanol

Can. J. Chem. Downloaded from www.nrcresearchpress.com by 210.87.254.42 on 09/05/12
For personal use only.

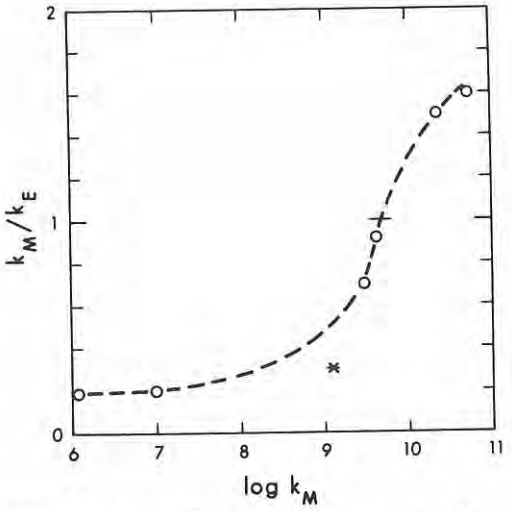

FIG. 9. Ratio of rate constants for a given solute in methanol and ethanol, k_M/k_E, plotted against the rate constant in methanol, k_M at 295 K (○). The point × refers to biphenyl and was estimated from data from two different laboratories (27, 28).

Fig. 5). For the least reactive solutes phenol and benzene, the reverse is true (Fig. 6). Inversion of the relative rates occurs at a rate constant near $5 \times 10^9\ M^{-1}\ s^{-1}$ (Fig. 9).

The diffusion coefficient of electrons in methanol appears to be about double that in ethanol at 298 K (22, 23), in agreement with the ratio of rate constants for reactions that are nearly diffusion controlled ($k > 1 \times 10^{10}\ M^{-1}\ s^{-1}$, Fig. 9). Inversion of the relative rates for less efficient scavengers is attributed to the relative energy levels of solvated electrons in the two liquids. Judging from the optical absorption spectra, the solvation energy of electrons in methanol is about 4 kcal/mol greater than that in ethanol (12). Benzene, which has the lowest rate constant in the present series, has a negative electron affinity in the gas phase (ref. 24, p. 16); formation of the transition state anion is therefore probably endoergic. This is reflected in the higher activation energy and lower frequency factor of the benzene rate constant (Table 1). The lower frequency factor is attributed to a negative entropy change associated with a solvent rearrangement or reaction that is required to stabilize the electron capture product. Mechanisms derived from pressure studies (1, 25, 26) are consistent with this result. For benzene the steps are (1, 7),

[4,−4] $e^-_{solv} + C_6H_6 \rightleftharpoons C_6H_6^-{}_{solv}$

[5] $C_6H_6^-{}_{solv} + ROH \rightarrow \dot{C}_6H_7 + RO^-_{solv}$

while for phenol they appear to be (25, 26)

[6,−6] $e^-_{solv} + C_6H_5OH \rightleftharpoons C_6H_5OH^-_{solv}$

[7] $C_6H_5OH^-_{solv} \rightarrow C_6H_5O^-_{solv} + H$

The pseudo first order reactions 5 and 7 are aided by an increase of solvation energy on going from an anion that has the charge delocalized over an aromatic ring to an anion with the charge localized on an oxygen atom. The increased solvation energy involves solvent rearrangement with a negative entropy change, and hence a reduced Arrhenius A factor.

In general, electron capture by inefficient reactants may be represented as follows

[8,−8] $e^-_{solv} + S \rightleftharpoons S^-_{solv}$

[9] $S^-_{solv}\ (+ ROH) \rightarrow X^-_{solv} + \text{Product}$

where X^-_{solv} is an anion that derives either from S^-_{solv} or the solvent. The observed capture rate constant k_2 is then

[10] $k_2 = k_8k_9/k_{-8} = k_9 \exp(-\Delta G_8^0/RT)$

As the energy gap between e^-_{solv} and S^-_{solv} decreases (Fig. 10) the value of k_2 increases; the participation of [9] gradually becomes less necessary. This behavior may be illustrated by comparing the reactions of benzene and biphenyl. The electron affinity of the latter is less negative than that of the former (24); ΔG_8^0 appears to be positive for benzene and zero or negative for biphenyl. As a result the two steps [8] and [9] have been observed separately for biphenyl (27) but not for benzene. For biphenyl in methanol at

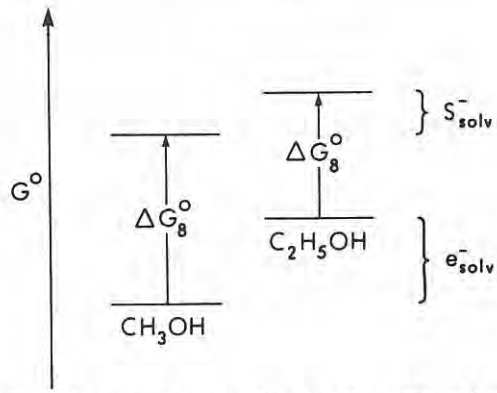

FIG. 10. Schematic sketch of free energy changes during electron capture by inefficient reactants such as benzene in methanol and ethanol.

Can. J. Chem. Downloaded from www.nrcresearchpress.com by 210.87.254.42 on 09/05/12
For personal use only.

Can. J. Chem. Downloaded from www.nrcresearchpress.com by 210.87.254.42 on 09/05/12
For personal use only.

~298 K, $k_8 = 1.3 \times 10^9\ M^{-1}\ s^{-1}$ (28) and $k_9 = 1.7 \times 10^6\ s^{-1}$ (27), while the corresponding values in ethanol (27) are $4.3 \times 10^9\ M^{-1}\ s^{-1}$ and $4.4 \times 10^5\ s^{-1}$.

Scavenging of Electrons Prior to their Solvation

During earlier investigations in which hydrogen yields were measured as a function of solute concentration (25, 26), the scavenging of electrons prior to their solvation was masked by the occurrence of reactions such as [7] and by those of hydrogen atoms. The decrease in initial absorbance A_i caused by high concentrations of benzene and phenol might be attributed to enhancement of geminate neutralization at the expense of the free ion yield, or to capture by the solute of electrons before they are observable in the solvated state. Phenol, which is highly polar, reduces A_i more readily than does benzene, which is nonpolar. If the reduction of A_i had been due to enhancement of geminate neutralization, the nonpolar solute should have been the more effective (29). The behavior is therefore attributed to electron scavenging. The scavenging curves (Fig. 8) are calculable by nonhomogeneous kinetics (11, 30).

Earlier studies of charge scavenging in spurs focussed mainly on effects at lower concentrations of solutes. Under those circumstances the probability of reaction between the solute and electrons before solvation was negligible (31), and for the sake of simplicity was not included in the published formulations (11, 30). However, inclusion of this reaction probability is not difficult.

The reaction cross section of electrons with molecules in the liquid phase depends on the electron energy, on the nature of the reactant molecule, and on the solvent. In general, scavenging may be possible during the last few collisions of the epithermal electron prior to localization. Reaction may also occur in the initial localization site if it contains a scavenger molecule. In liquids that form deep traps, electrons that are initially in shallow traps might migrate and react before settling into the equilibrium solvated state. However, the energy dependence of the reaction cross section is not known. Integration over this series of events may be approximately done by assuming that the presolvation electron,[3] in the energy range where reaction is probable, encounters a number m_{ps} of molecules and that the average probability of reaction per encounter with a scavenger molecule is f_{ps}.

By analogy with the earlier formalism (11), the probability ϕ_{ps} that a presolvation electron does not react with a solute that is present at mole fraction N_s is

$$[11] \qquad \phi_{ps} = (1 - f_{ps}N_s)^{m_{ps}} = A_i/A_{i0}$$

The value of m_{ps} is not the same for all electrons generated in a sample. It has a minimum equal to the number of molecules in the initial solvation shell, say 6, and the value may increase in a random way depending on the speed with which the electron settles into the solvated state. The encounters are counted from the time the electron energy has been degraded to the region where the electron is scavengeable. As the epithermal electron skitters through the liquid prior to localization, let the probability be P that it *does not* become localized at any given collision. The probability that it *does* become localized during m collisions is $(1 - P^m) = [1 - \exp(m \ln P)]$. The distribution function of the number of collisions that an electron undergoes in its reactive state prior to localization is

$$[12] \qquad F(m) = \mathrm{d}(1 - P^m)/\mathrm{d}m = -P^m \ln P$$

The value of P is not known, so it is used as an adjustable parameter. If the electron can migrate from an initial shallow trap before settling into a deeper solvated state the resulting increase in m can be accounted for by appropriately decreasing the assumed value of P. Including the initial solvation shell one obtains:

$$[13] \qquad m_{ps} \approx 6 + m$$

The probability that an electron is not scavenged prior to solvation is therefore

$$[14] \qquad A_i/A_{i0} = \phi_{ps} = \sum_{m=0}^{\infty} F(m)(1 - f_{ps}N_s)^{6+m}$$

$$= -(\ln P)(1 - f_{ps}N_s)^6 \int_0^{\infty} [P(1 - f_{ps}N_s)]^m \mathrm{d}m$$

Both P and f_{ps} are adjustable parameters, al-

[3]A referee has pointed out that the term 'presolvated electron' is ambiguous. The literal meaning of presolvated can be either 'before solvation' or 'solvated in advance'. For brevity we adopt the inelegant term 'presolvation electron'; it is used to refer to electrons in all states and at all times before they are observable in the solvated state. It includes electrons in the initial site of solvation.

TABLE 2. Parameters for scavenging presolvation electrons, eq. 14*

Solvent	Solute	f_{ps}
CH_3OH	C_6H_6	0.44
	C_6H_5OH	0.82
C_2H_5OH	C_6H_6	0.55
	C_6H_5OH	1.0

*P = 0.97, number of molecules in initial solvation shell = 6.

though limitations may be placed on one or the other of them in a given series of systems.[4]

The curves in Fig. 8 were calculated from [14], using the parameter values in Table 2. A preliminary fit was obtained by putting $f_{ps} = 1$ in each system and finding the appropriate value of P. On the assumption that the value of P should be nearly the same in both alcohols, the largest of the four preliminary values was chosen for all, and the values of f_{ps} in the other three systems were adjusted to give agreement between calculated and experimental values of A_i/A_{i0}. The value of $P = 0.97$ corresponds to an average m_{ps} of about 30.

The variations in f_{ps} are in the same direction as those in k_2 (Table 1) but are an order of magnitude smaller. On going from benzene to phenol f_{ps} increases by a factor of two, while k_2 increases eight-fold. Upon changing these two solutes from methanol to ethanol solvent f_{ps} increases by only 20%, while k_2 increases five-fold. The higher energy of presolvation electrons compared to solvated electrons increases their reactivity with 'endoergic scavengers' such as benzene and phenol, and thereby decreases the variation of reactivity with solute and solvent. This also explains the relatively small temperature dependence of the scavenging of presolvation electrons (Fig. 8), in marked contrast with the temperature coefficient of the corresponding solvated electron reactions (Table 1).

If the value of m_{ps} were the same for all electrons generated in a sample, [11] would be used instead of [14]. The experimental values of $(f_{ps}N_s)$ are much smaller than unity, so [11] would reduce to [15].

$$[15] \quad \log (A_i/A_{i0}) = m_{ps} \log (1 - f_{ps}N_s) \approx -m_{ps}f_{ps}N_s/2.3$$

The effect of widening the distribution of m_{ps} values is to make a plot of log (A_i/A_{i0}) against N_s somewhat convex towards the N_s axis. The minimum value of m_{ps} in the present work was arbitrarily chosen as 6. It could as well be 10 or more, depending on the reactivity of the electrons as they skitter into localized states and then settle into solvated states. Increasing the value of the minimum m_{ps} would decrease the minimum required value of P and decrease the deviation from linearity of a plot of log (A_i/A_{i0}) against N_s.

This model offers a realistic interpretation of the recently observed logarithmic dependence of A_i on the concentration of scavenger and its variation from solvent to solvent (32, 33), and of other similar results (34). The value of f_{ps} depends upon both the scavenger and the solvent, while that of m_{ps} depends mainly on the solvent when the mole fraction of solute is small.

It may be mentioned that the 'initial encounter pair' treatment of electron scavenging in concentrated solutions (35) is similar to the stochastic model (11).

The possibility of scavenging presolvation electrons affects the earlier treatment of scavenging kinetics (11, 30) simply by reducing the number of electrons that reach the solvated state. The total probability that an electron will be scavenged before being neutralized or reacting with the solvent is

$$[16] \quad \Phi = (1 - \phi_{ps}) + \phi_{ps} \int_0^\infty F(y)\Phi_y dy$$

where $F(y)dy$ is the fraction of thermalized electron–ion pairs that have initial intrapair distances between y and $y + dy$, and

$$[17] \quad \Phi_y = \phi_y^{fi} + (1 - \phi_y^{fi})[1 - (1 - fN_s)^{1.4\times10^7 \epsilon y^3 \beta}]$$

where $\phi_y^{fi} = \exp(-\xi^2/\epsilon kTy)$, $\xi = 4.8 \times 10^{-10}$ esu, ϵ is the dielectric constant of the liquid, k is Boltzmann's constant, T is the absolute temperature, f is the encounter efficiency of the reaction between *solvated* electrons and the scavenger, and β is an adjustable parameter that relates to the relative motions of the electron, its parent positive ion and the scavenger molecules (11, 30). The value of f may be different from that of f_{ps}. For benzene and phenol, $f < f_{ps}$.

Acknowledgement

We would like to thank the staff of the Radiation Research Center for aid with the electronics.

[4]Program written by Jean-Pol Dodelet.

Can. J. Chem. Downloaded from www.nrcresearchpress.com by 210.87.254.42 on 09/05/12
For personal use only.

1. G. L. BOLTON, M. G. ROBINSON, and G. R. FREEMAN. Can. J. Chem. **54**, 1177 (1976).
2. J. W. FLETCHER and G. R. FREEMAN. Can. J. Chem. **45**, 635 (1967).
3. K. N. JHA and G. R. FREEMAN. J. Chem. Phys. **51**, 2846 (1969).
4. J. H. BAXENDALE and P. WARDMAN. Chem. Commun. 429 (1971).
5. W. H. HAMILL. J. Chem. Phys. **49**, 2446 (1968).
6. W. H. HAMILL. J. Phys. Chem. **73**, 1341 (1969).
7. S. KHORANA and W. H. HAMILL. J. Phys. Chem. **74**, 2885 (1970).
8. H. B. STEEN. J. Phys. Chem. **74**, 4059 (1970).
9. R. K. WOLFF, M. J. BRONSKILL, and J. W. HUNT. J. Chem. Phys. **53**, 4211 (1970).
10. H. B. STEEN, O. KAALHUS, and M. KONGSHAUG. J. Phys. Chem. **75**, 1941 (1971).
11. G. R. FREEMAN. J. Chem. Phys. **43**, 93 (1965); **46**, 2822 (1967).
12. K. N. JHA, G. L. BOLTON, and G. R. FREEMAN. J. Phys. Chem. **76**, 3876 (1972).
13. C. J. KARZMARK. Rev. Sci. Instrum. **35**, 1646 (1964).
14. Radiation dosimetry: Electrons with initial energies between 1 and 50 MeV. International Commission on Radiative Units and Measurements. Report No. 21, Washington, D.C. 1972. Chapt. 4.
15. G. E. ADAMS, J. W. BOAG, J. CURRANT, and B. D. MICHAEL. *In* Pulse radiolysis. *Edited by* M. Ebert, J. P. Keene, A. J. Swallow, and J. H. Baxendale. Academic Press, London. 1965. p. 117.
16. (*a*) J. H. BAXENDALE, P. L. T. BEVAN, and D. A. SCOTT. Trans. Faraday Soc. **64**, 2389 (1968). (*b*) J. H. BAXENDALE. Private communication.
17. N. W. HOLM and R. J. BERRY (*Editors*). Manual of radiation dosimetry. Marcel Dekker, New York. 1970.
18. L. M. DORFMAN and G. E. ADAMS. NSRDS-NBS 46, U.S. Govt. Printing Office, Washington, D.C. 1973.
19. M. HAISSINSKI. J. Chim. Phys. **62**, 1149 (1965).
20. E. M. FIELDEN and E. J. HART. Radiat. Res. **32**, 564 (1967).
21. J. C. RUSSELL and G. R. FREEMAN. J. Chem. Phys. **48**, 90 (1968).
22. P. FOWLES. Trans. Faraday Soc. **67**, 428 (1971).
23. R. A. VERMEER and G. R. FREEMAN. Can. J. Chem. **52**, 1181 (1974).
24. G. R. FREEMAN. Radiat. Res. Rev. **1**, 1 (1968).
25. K. N. JHA and G. R. FREEMAN. Can. J. Chem. **51**, 2033 (1973).
26. K. N. JHA and G. R. FREEMAN. J. Am. Chem. Soc. **95**, 5891 (1973).
27. L. M. DORFMAN and M. S. MATHESON. Progr. React. Kinet. **3**, 237 (1965).
28. A. K. PIKAEV, G. K. SIBIRSKAYA, and S. A. KABAKCHI. Dokl. Phys. Chem. Proc. Adac. Sci. USSR, **198**, 554 (1971).
29. G. R. FREEMAN and J. M. FAYADH. J. Chem. Phys. **43**, 86 (1965).
30. J.-P. DODELET and G. R. FREEMAN. Can. J. Chem. **50**, 2729 (1972).
31. L. G. WALKER. Ph.D. Thesis, University of Alberta, Edmonton, Alberta. 1967.
32. G. L. BOLTON. Ph.D. Thesis, University of Alberta, Edmonton, Alberta. 1974.
33. (*a*) Y. K. LAM. Ph.D. Thesis, University of Toronto, Toronto, Ontario. 1974. (*b*) Y. K. LAM and J. W. HUNT. Int. J. Radiat. Phys. Chem. **7**, 317 (1975).
34. H. OGURA and W. H. HAMILL. J. Phys. Chem. **78**, 504 (1974).
35. G. CZAPSKI and E. PELED. J. Phys. Chem. **77**, 893 (1973).

Can. J. Chem. Downloaded from www.nrcresearchpress.com by 210.87.254.42 on 09/05/12
For personal use only.

The catalytic hydrodesulfurization of thiophenes. VIII. Benzothiophene and 2,3-dihydrobenzothiophene

E. FURIMSKY AND C. H. AMBERG
Department of Chemistry, Carleton University, Ottawa, Canada K1S 5B6

Received December 5, 1975

E. FURIMSKY and C. H. AMBERG. Can. J. Chem. **54**, 1507 (1976).

The hydrodesulfurization of benzothiophene (BT) and 2,3-dihydrobenzothiophene (DHBT) has been examined over a commercial cobalt molybdate on alumina and over an unsupported MoS_2 catalyst promoted with Co. The results, in particular the appearance of styrene among the products, support cleavage of the hetero-ring in BT as the initial step in the reaction sequence under our low-pressure conditions. Ethylbenzene is the predominant product from both BT and DHBT, although increasingly significant amounts of DHBT are dehydrogenated to BT with rising temperature.

E. FURIMSKY et C. H. AMBERG. Can. J. Chem. **54**, 1507 (1976).

On a étudié la réaction d'hydrodésulfurisation du benzothiophène (BT) et du dihydro-2,3 benzothiophène (DHBT) en présence d'un catalyseur commercial de molybdate de cobalt sur l'alumine et d'un catalyseur de MoS_2 sans support mais activé par du Co. Les résultats obtenus, et en particulier la formation de styrène, suggèrent que la réaction initiale, à basse pression, implique un bris de l'hétérocycle du BT. Quoique des quantités de plus en plus grandes de BT se forment, à partir du DHBT, à mesure que la température augmente, l'éthylbenzène est le produit majeur que l'on parte du BT ou du DHBT.

[Traduit par le journal]

Introduction

The mechanism of the catalytic hydrodesulfurization of aromatic sulfur compounds is complex and a number of questions remain unanswered. In the case of thiophene, earlier work in this series (1) strongly supported C—S bond scission rather than ring hydrogenation as the primary reaction in the hydrogenolysis sequence, the first product being 1,3-butadiene or one of its acetylenic precursors. These experiments were carried out in a microreactor under steady-state conditions. Several unsupported MoS_2 catalysts were used, as well as a supported cobalt molybdate and a chromia catalyst, all fully sulfided.

Benzothiophene (BT) has been studied by Givens and Venuto (2) using cobalt molybdate in the oxidic rather than the sulfided form. At 400 °C and low H_2 flow rates only ethylbenzene (EB) was found, but at high flow rates about 2% of 2,3-dihydrobenzothiophene (DHBT) appeared as an additional product. After a series of experiments in which DHBT was employed as a reactant, these authors concluded that the following equilibrium is established between BT and DHBT, and that the desulfurization reaction leading to EB drains this equilibrium in an irreversible manner. From their data they were unable to exclude either BT or DHBT as a possible source of the desulfurized product. Schuit and Gates have stated in their important review article (3) that hydrogenated benzothiophenes (unsubstituted and alkyl-substituted) are formed rapidly from benzothiophenes, and hence, that the former may indeed be intermediates in desulfurization reactions, although they are too short-lived to be identifiable. Bartsch and Tanielian (4) have recently investigated the hydrogenolysis of BT on supported cobalt molybdate over a wide temperature range, and estimated the value of the activation energy to be approximately 5 kcal mol^{-1}. Their catalyst had

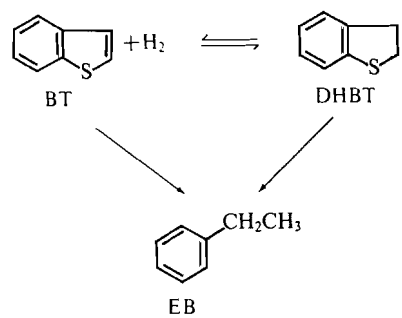

SCHEME 1

Can. J. Chem. Downloaded from www.nrcresearchpress.com by 210.87.254.105 on 09/05/12
For personal use only.

Can. J. Chem. Downloaded from www.nrcresearchpress.com by 210.87.254.105 on 09/05/12
For personal use only.

been prereduced and sulfided in a $H_2 + H_2S$ mixture.

As part of our comparative study of unsupported and supported catalysts, and also to accumulate additional information on reactants of higher molecular weight, we have undertaken a study of BT desulfurization on supported cobalt molybdate (catalyst G) and unsupported MoS_2 activated with Co [$Co/(Co + Mo) = 0.25$, catalyst M]. We have recently compared these catalysts (5) and shown that catalyst G, which has a high surface area of about 240 m^2/g, exhibits higher catalytic activity per gram than does catalyst M, which has a low surface area of about 5 m^2/g. However, when activities were expressed in terms of reaction rates per unit surface area (mol m^{-2} s^{-1}), catalyst M was about 20 times more active than catalyst G. This suggests that a higher concentration of active sites is available on catalyst M, even if part of the alumina support were to remain exposed. Lipsch and Schuit (6) have estimated that no less than 20% of the alumina surface is covered in a typical 'cobalt molybdate' catalyst, so that activities expressed per m^2 of *active* surface would still differ by at least a factor of four. In order to obtain more information about the role of DHBT in the hydrodesulfurization of BT, special attention was paid also to DHBT as a reactant.

Experimental

Materials

Benzothiophene (Aldrich) was purified by molecular still. 2,3-Dihydrobenzothiophene was prepared from BT using the method of Bordwell and McKellin (7). Thiophene (Eastman) was purified by preparative gas chromatography, and ethylbenzene (Phillips) and styrene (Eastman) were used as supplied.

Catalysts

(*i*) Catalyst G, Girdler G 35A, through 65 mesh, was prepared from crushed pellets. This is a 'cobalt molybdate' supported on alumina.

(*ii*) Catalyst M was prepared by impregnation of MoS_2 (Anachemia) with $Co(NO_3)_2$ in liquid ammonia as described elsewhere (5). Composition: $Co/(Co + Mo) = 0.25$. This catalyst had exhibited higher activity per unit surface area than any other catalyst over the whole range of Co compositions.

Apparatus and Procedure

The basic design of the microcatalytic reactor was that described in previous work (1). A stream of hydrogen near atmospheric pressure was passed through the reactor and the analytical glc column, with hydrogen serving both as a reactant and as the carrier gas. Samples of the reactants (thiophene, BT, DHBT, EB, and STY) were fed to the stream through an injection port. Because of poor separation of BT and DHBT in hydrogen, the procedure for the reactions of DHBT had to be varied. Products containing these compounds were therefore trapped out and introduced into the analytical column in a helium stream.

The reactant conversions and product yields were analyzed using a 6-ft squalane on fire brick column (25% w/w).

Results and Discussion

In the hydrodesulfurization of BT on catalyst G, EB was found as the only product other than H_2S. DHBT, which had been suggested as an intermediate in the desulfurization of BT (3), was not found under the present experimental conditions. In the reaction of BT, more BT was apparently consumed than would be expected from the yield of EB. This is attributed to the adsorption of BT on the catalyst surface; it became significant especially below 300 °C. At this temperature the conversion of a 3-μl pulse of BT on 115 mg of the fresh catalyst was 19.2% and this conversion decreased to almost zero after six successive pulses. When the same catalyst had been subsequently reheated to 400 °C and kept at that temperature in a stream of hydrogen for 1 h, then cooled back to 300 °C, the original conversion was regained. At 400 °C the conversion of successive pulses did not change. This demonstrates that the discrepancy was due entirely to adsorption rather than polymerization or coking; or, less likely, that it was due to a hydrocarbon residue removed by hydrogenation at 400 °C. When a 2-μl pulse of EB was injected at 300 °C onto the same amount of catalyst, all of the EB was recovered from the microreactor.

The products from the reaction of DHBT on catalyst G consisted of EB and BT. The appearance of BT as a product shows that dehydrogenation had taken place as well as desulfurization. The product distribution–temperature relation is shown in Fig. 1 in the form of an Arrhenius plot. Curve *1* in the figure shows the amount of DHBT consumed, while curve *2* shows the yield of EB. These amounts are equal only at temperatures higher than 300 °C. Below this limit, the amount of DHBT consumed is larger than the yield of EB, just as in the case of BT.

In the desulfurization of both BT and DHBT

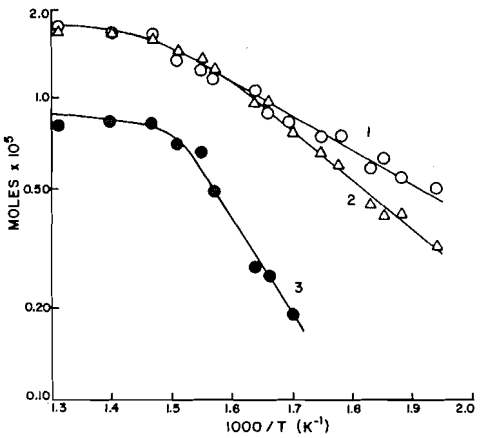

FIG. 1. Arrhenius plot of the conversions of 3-μl pulses of 2,3-dihydrobenzothiophene. Hydrogen flow rates: 30 ml min^{-1}; pressure: near atmospheric. (*1*) moles of DHBT desulfurized; (*2*) yield of EB in moles; and (*3*) yield of BT in moles.

on catalyst M, STY was formed as an additional product. The results in Table 1 show that the relative yield of STY in the desulfurization products is smaller with larger amounts of catalyst, probably due to longer residence of STY in the catalyst bed resulting in increased hydrogenation. The experience with catalyst M suggests that STY cannot be completely ruled out as a product on catalyst G, either. Failure to find it in that case would have to be attributed to its high rate of hydrogenation. Such a high rate was indeed confirmed after 3 μl of STY had been injected into the microreactor, and complete hydrogenation of STY to EB was observed even on as little as 30 mg of catalyst G. On the other hand, when pure STY (1 μl) was injected over 50 mg of catalyst M, 22% was hydrogenated to EB, while over 159 mg of this catalyst the conversion increased only to 48%. When pure EB was injected under the same conditions, no reaction was observed. After hydrogen had been replaced by helium, no conversion of BT whatsoever was

TABLE 1. The amount of styrene in desulfurization products over catalyst M (3-μl pulses of pure reactants in a stream of H_2; flow rate: 30 ml min^{-1}; pressure near atmospheric)

Weight of catalyst (mg)	Reactant	Temperature (°C)	Desulfurization (%)	Styrene (%)
50	BT	373	3	23
	BT	416	5	29
	DHBT	373	20	33
	DHBT	417	28	36
159	BT	415	16	18
	DHBT	371	43	14
	DHBT	427	48	17

observed on the catalyst, while DHBT was converted completely giving predominantly dehydrogenation, and to a small extent also desulfurization, products. Results from these experiments have been summarized in Table 2.

The temperature dependence of the conversion of BT and DHBT is shown in Table 3. The 'activation energies' were calculated from plots similar to those in Fig. 1. Here, two methods were employed: *A*, in which the amount of BT and DHBT desulfurized was used, and *B*, in which the yields of the desulfurization products were used in the calculations. The difference in values obtained by these methods (BT: 5.2 and 11.6 kcal mol^{-1} for *A* and *B* respectively; DHBT: 5.0 and 7.5 kcal mol^{-1}) must arise from the adsorption of reactants, as discussed above. The higher of the two values (*i.e.* method *B*) must be regarded as being more meaningful. Thus, in order to measure the EB yield on an optimally clean surface, care was taken at low temperatures to determine each conversion value on a fresh catalyst. The situation was different on catalyst M, where the activation energies for BT (12.2 and 11.9 kcal mol^{-1}) and DHBT (7.0 and 7.6 kcal mol^{-1}) were similar for both these methods, showing that the adsorption of reactants on the

TABLE 2. Reaction of DHBT in helium at 400 °C using 3-μl pulses (flow rate: 300 ml; pressure: near atmospheric)

Catalyst		Dehydrogenation	Desulfurization	Composition of desulfurization products	
Type	Amount (mg)			EB	STY
G	77	90	10	69	31
M	136	85	15	46	54

Can. J. Chem. Downloaded from www.nrcresearchpress.com by 210.87.254.105 on 09/05/12
For personal use only.

Can. J. Chem. Downloaded from www.nrcresearchpress.com by 210.87.254.105 on 09/05/12
For personal use only.

TABLE 3. Temperature coefficients of the pulse reactions of BT, DHBT, and T over catalysts G and M

Reactant	Catalyst	Method*	'Activation energy' (kcal mol^{-1})
BT	G	A	5.2
		B	11.6
BT	M	A	12.2
		B	11.9
DHBT	G	A	5.0
		B	7.5
		'Yield of BT'	14.8
DHBT	M	A	7.0
		B	7.6
T	G	A	15.6
	M	A	12.3

*Method *A*: from amount of organosulfur compound consumed. Method *B*: from yield of desulfurization products.

low surface area catalyst is not very important. Temperature coefficients were calculated in the straight-line regions between 250 and 400 °C in all cases.

The temperature change of the yield of BT (curve 3 in Fig. 1) was used to estimate the 'activation energy' of dehydrogenation of DHBT. The slope is steeper than the others, thus giving a higher activation energy for dehydrogenation (14.8 kcal mol^{-1}) as compared to desulfurization. This indicates that with increasing temperature the rate of dehydrogenation becomes increasingly important in comparison with that of desulfurization.

For comparison thiophene (T) was also investigated on both these catalysts. Surprisingly, on catalyst M the 'activation energy' was 12.3 kcal mol^{-1}, a value which is similar to that for BT. The Arrhenius plot for this catalyst gave a good straight line in contrast to that on catalyst G, where the line curved downwards at low temperatures, thus making an estimate of activation energy inaccurate. The value of about 16 kcal mol^{-1} is higher than that on catalyst M and the difference, if real, could be explained by assuming adsorption of some products on the surface of catalyst G at low temperatures.

It would appear, then, that the adsorption of both reactants and products on the catalyst surface, especially that of catalyst G, plays a significant role in determining the value of the temperature coefficient ('activation energy'). Moreover, the effect of hydrogen cannot be ignored, although insufficient data are available at present. According to Lipsch and Schuit (8), the adsorption of hydrogen on a supported cobalt molybdate catalyst increases from 220 °C to a maximum at about 550 °C, and then decreases again with a further rise in temperature. This could be an additional factor affecting the temperature coefficient of desulfurization. The effect of hydrogen on unsupported MoS_2 catalysts is not well understood. However, because of the negligible adsorption of organic materials on catalyst M, it is safe to say that the values of the 'activation energies' we have determined over this catalyst from the temperature dependence of the conversions are that much more realistic. Finally, the unexpectedly similar values of the activation energies for BT and T are consistent with the possibility that the two reactants desulfurize by similar initial steps in the reaction sequence.

Before discussing the mechanism of the hydrodesulfurization of BT we wish to summarize some relevant facts observed so far. Apart from the possible similarities in the behaviour of T and BT to which we have referred in the above discussion on activation energies, the observation of STY among the products in the desulfurization of BT and DHBT supports the mechanism involving direct C—S bond scission without an intermediate hydrogenation of the thiophene ring. The tendency of DHBT to dehydrogenate extensively, especially at higher temperatures, does not rule out BT as the source of desulfurization products even in the hydrodesulfurization of DHBT. On the basis of these observations, several reaction routes can be proposed to explain the formation of STY in the desulfurization of BT on catalyst M. For the sake of completeness, routes involving reactions of DHBT are also shown.

Reaction route *a* suggests participation of the β-hydrogen of the thiophene ring in C—S bond cleavage, and formation of product **1**. The very low stability to be expected of such a product rules out any chance of its detection. Some support for this route can be found in the observation of Givens and Venuto (2) of a marked decrease of the desulfurization rate of BT, when the β-hydrogen had been substituted by a methyl group. Route *b* involves C—S bond cleavage with the participation of hydrogen reactant as the initial step. Similarly, here the detection of

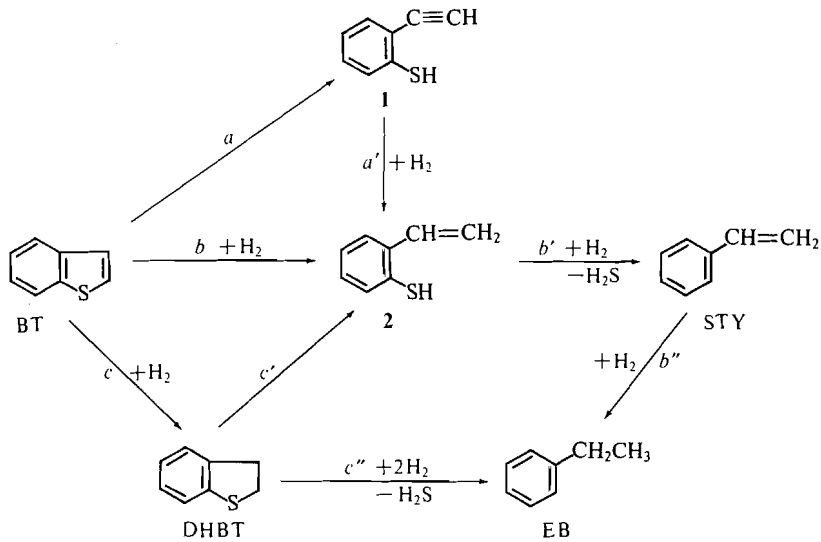

SCHEME 2

product **2** is difficult due to the very high rate of desulfurization of thiophenol derivatives. Route *c* involves the intermediate ring saturation of the hetero-ring in BT. Under the present experimental conditions, however, DHBT tended to dehydrogenate on both our catalysts, thus rendering improbable this particular step, at least under those conditions.

The formation of STY beside EB in the desulfurization of DHBT on catalyst M indicates that, for this reactant, migration of one of the β-hydrogens with subsequent C—S bond cleavage (route *c''*) takes place as well. The results obtained with DHBT under helium on both our catalysts, where both EB and STY were found as products, lend some further support to this route. In that case EB can be formed either directly from DHBT via route *c''*, or by hydrogenation of STY produced in reaction sequence *c'*–*b'*.

The position of equilibrium between BT and DHBT may have an effect on the mechanism of hydrodesulfurization of BT. One of the factors affecting the equilibrium is the concentration of hydrogen. One would expect that, with an increase in concentration, the equilibrium will shift towards DHBT. This may explain the occurrence of DHBT among the products at very high H_2 flow rates in the desulfurization of BT as observed by Givens and Venuto (2). Similarly, in the proposed mechanism, the routes most affected by an increase in H_2 pressure are *b* and *c*. The stability of DHBT compared to that of intermediate **2** can be expected to increase with an increase in H_2 pressure. As the result of such an equilibrium shift DHBT would become a direct source of EB in the desulfurization of BT. Thus, for a complete understanding of the mechanism of hydrodesulfurization of BT it becomes essential to conduct experiments at high H_2 pressures over a sufficiently wide temperature region. Work at moderately high pressures has recently been undertaken by de Beer *et al.* (9); their results appear to be consistent with the above.

Acknowledgements

We thank Mr. Gary Harris for technical assistance and The National Research Council of Canada for financial support.

1. S. Kolboe and C. H. Amberg. Can. J. Chem. **44**, 2623 (1966).
2. E. N. Givens and P. B. Venuto. Am. Chem. Soc. Div. Pet. Chem. Prepr. **15**, A183 (1970).
3. G. C. A. Schuit and B. C. Gates. Am. Inst. Chem. Eng. J. **19**, 417 (1973).
4. R. Bartsch and C. Tanielian. J. Catal. **35**, 353 (1974).
5. E. Furimsky and C. H. Amberg. Can. J. Chem. **53**, 2542 (1975).
6. J. M. J. G. Lipsch and G. C. A. Schuit. J. Catal. **15**, 174 (1969).
7. F. G. Bordwell and W. H. McKellin. J. Am. Chem. Soc. **72**, 1985 (1950).
8. J. M. J. G. Lipsch and G. C. A. Schuit. J. Catal. **15**, 179 (1969).
9. V. H. J. de Beer, J. G. J. Dahlmans, and J. G. M. Smeets. J. Catal. In press.

Can. J. Chem. Downloaded from www.nrcresearchpress.com by 210.87.254.105 on 09/05/12
For personal use only.

Condensation of *cis*-9-methyl-2-decalone with cyclic β-amino esters: synthesis and X-ray crystallography of perhydroazacyclopentaanthracenes and perhydroazabenzanthracenes

RONALD B. KELLY, BARRY A. BECKETT, IJAZ MUMTAZ, ERIC STANLEY, AND PETER S. WHITE
Department of Chemistry, University of New Brunswick, Saint John, New Brunswick E2L 4L5

Received October 9, 1975

RONALD B. KELLY, BARRY A. BECKETT, IJAZ MUMTAZ, ERIC STANLEY, and PETER S. WHITE. Can. J. Chem. **54**, 1512 (1976).

Condensation of *cis*-9-methyl-2-decalone, **9**, with ethyl 2-pyrrolidineacetate, **10**, afforded a mixture of two isomeric vinylogous amides, **11**. Oxidation of either one pure isomer, **11***a*, or the mixture **11** to the same pyridone, **12**, revealed that the two condensation products were stereoisomeric at a single carbon atom and not structural isomers. Reduction of **11***a* afforded the amino ketone **13**. The structures assigned to **11**, **12**, and **13** are based on X-ray crystallographic analysis of **13**.

Similarly, condensation of **9** with ethyl 2-piperidineacetate, **14**, afforded the isomers **15***a* and **15***b* both of which were oxidized to the same pyridone, **16**. Reduction of **15***a* afforded **17**. The structures assigned to **15**, **16**, and **17** are based on X-ray crystallographic analysis of **17**.

RONALD B. KELLY, BARRY A. BECKETT, IJAZ MUMTAZ, ERIC STANLEY et PETER S. WHITE. Can. J. Chem. **54**, 1512 (1976).

La condensation de la méthyl-9 décalone-2 *cis*, **9**, avec le pyrolidineacétate-2 d'éthyle, **10**, conduit à un mélange de deux amides vinylogues isomères, **11**. L'oxydation soit d'un isomère pur, **11***a*, ou du mélange **11** conduisant à la meme pyridone, **12**, révèle que les deux produits de condensation sont des stéréoisomères au niveau d'un seul atome de carbone et non pas des isomères structuraux. La réduction de **11***a* conduit à l'amino cétone **13**. Les structures attribuées à **11**, **12** et **13** sont basées sur une analyse de diffraction de rayon-X de **13**.

De la même manière, la condensation de **9** avec la piperidineacétate-2 d'éthyle, **14**, conduit aux isomères **15***a* et **15***b* qui peuvent être tous les deux oxydés en pyridone, **16**. La réduction de **15***a* conduit à **17**. On a attribué les structures **15**, **16** et **17** grâce à l'analyse de **17** par diffraction des rayons-X.

[Traduit par le journal]

Introduction

Communications from various sources (*e.g.* ref. 1) have described condensations of cyclic ketones with amino acid esters to give cyclic enamino ketones (*e.g.* **3**). The mechanism of such condensations, which are performed in the presence of an acid catalyst, presumably involves the initial formation of an enamine, **1**, which undergoes intramolecular acylation to produce an iminium salt, **2**. The latter is then transformed into a cyclic, conjugated enamino ketone, **3**, by abstraction of a proton (Scheme 1).

The ability to perform condensations of this type suggests the intriguing possibility of forming the 14-aza- and the D-homo-14-azasteroidal nuclei in a single step from simple, readily available starting materials. For example, the condensation of a 9-methyl-2-decalone, **4**, with 2-pyrrolidineacetate, **5**, could, conceivably, give **7** which possesses the 14-azasteroidal nucleus. On the other hand, there also exists the possibility of the condensation of **4** and **5** producing **8**, a structural isomer of **7** with an azacyclopentaanthracene skeleton (Scheme 2).

The ratio of structurally isomeric enamino ketones of type **7** and **8** in the product is dependent upon the relative extent of the participation of the two possible enamines (**6***a* and *b*) in the cyclization which leads to the final products. In the case of *trans*-9-methyl-2-decalones, it might be expected that the 'nonsteroidal' isomer **8** would predominate because of the tendency of *trans*-2-decalones to enolize in the direction away from the ring junction (refs. 1*f*, 2, and references cited therein). This tendency leads to the expectation that enamines of type **6***b*, leading to **8**, would be favoured in the case of *trans*-2-decalones.

With *cis*-9-methyl-2-decalones no such speculations can be entertained with any degree of

Can. J. Chem. Downloaded from www.nrcresearchpress.com by 210.87.254.105 on 09/05/12
For personal use only.

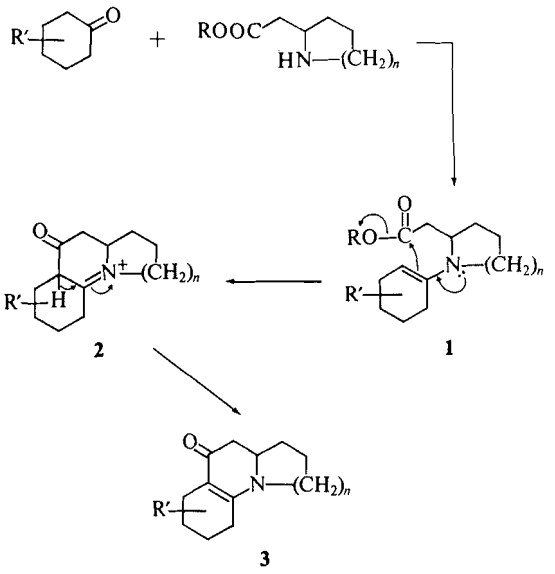

SCHEME 1

confidence because of the combined effects of conformational flexibility and steric factors (1*f*, 2). As a matter of fact, the nmr spectrum of the pyrrolidine enamine of *cis*-9-methyl-2-decalone, **9**, shows signals for two different vinylic protons

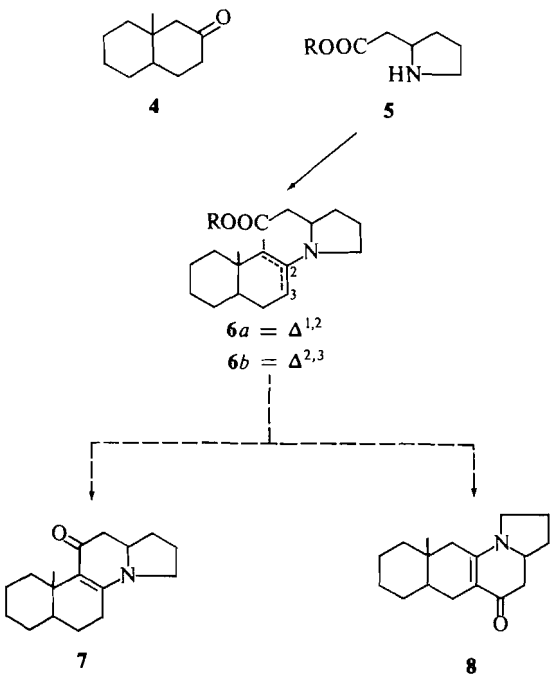

SCHEME 2

indicating the presence of both the possible enamines.

From the above considerations it appeared that the chances of obtaining enamino ketones possessing the 14-aza- and the D-homo-14-azasteroidal nuclei were better with *cis*-9-methyl-2-decalone, **9**, than with the *trans*-isomer. Accordingly, our efforts have been concentrated on an investigation of the condensation of *cis*-9-methyl-2-decalone with ethyl 2-pyrrolidineacetate, **10**, and ethyl 2-piperidineacetate, **14**.

Synthetic Studies

Condensation of *cis*-9-methyl-2-decalone, **9**, with ethyl 2-pyrrolidineacetate, **10**, in refluxing toluene in the presence of a catalytic amount of trifluoroacetic acid afforded a crystalline product in 67% yield. The course of this and similar condensations could be conveniently monitored by the increasing intensity of an absorption maximum in the uv spectrum at *ca.* 340 nm. Although tlc and vpc suggested that the product was a single compound, the appearance of two methyl singlets in the nmr spectrum attested to the presence of two compounds.

These compounds were intractable to separation by chromatographic methods but a pure compound (**11***a*, mp 170 °C) was isolated in 42% yield by fractional crystallization; the remainder (25%) was, like the crude product, a mixture, **11**, of two compounds. Structures **11**, **12**, and **13** are based on an X-ray crystallographic analysis of the latter (*vide infra*). In agreement with the structure **11** assigned to the condensation product, both the mixture **11** and the pure compound **11***a* exhibited spectral properties[1] attributable (3) to a vinylogous amide (ν_{max} 1600 and 1545 cm^{-1}; λ_{max} 340 nm).

Oxidation of either the pure condensation product **11***a* or the mixture **11** with mercuric acetate afforded, in 78% yield, the same crystalline pyridone **12**. The spectral properties of the oxidation product were in agreement with the assigned structure (ν_{max} 1640 and 1530 cm^{-1}; λ_{max} 266 nm; nmr δ 6.13 (vinylic proton)). This result shows that the two products present in the condensation product **11** are C-12 stereoisomers

[1]Spectral data for all compounds are in agreement with assigned structures. Only data pertinent to the discussion will be given in this section; for further details see Experimental.

Can. J. Chem. Downloaded from www.nrcresearchpress.com by 210.87.254.105 on 09/05/12
For personal use only.

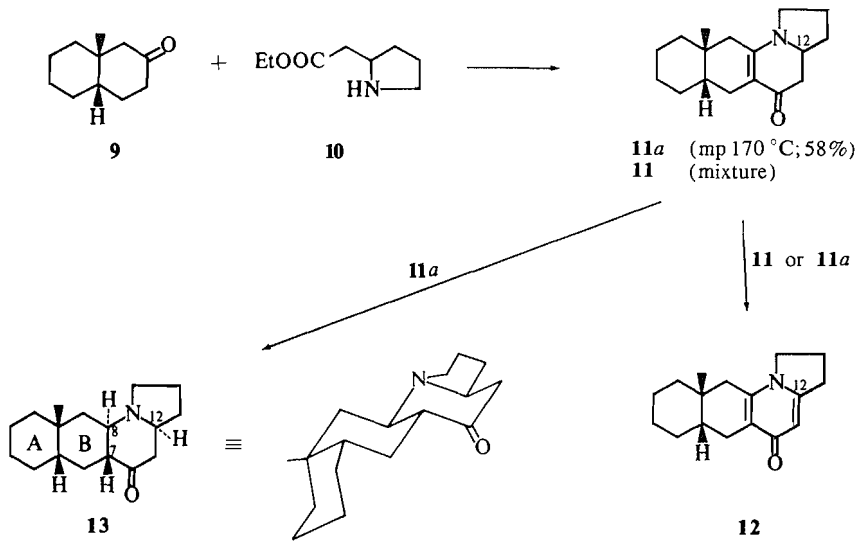

SCHEME 3

and not structural isomers of the type **7** and **8**.

Reduction of the pure condensation product **11***a* with lithium in liquid ammonia followed by equilibration with base afforded a crystalline amino ketone (ν_{max} 1708 cm^{-1}) in 47% yield (36% of starting material recovered). An X-ray crystallographic analysis (*vide infra*) revealed that the amino ketone had the 'non-steroidal' structure represented by **13**. It follows, then, that the structures assigned to the condensation product **11** and to the derived pyridone **12** are valid. Thus, only compounds possessing the 'non-steroidal' azacyclopentaanthracene skeleton were obtained (Scheme 3).

Simultaneously with the work described above, the condensation of *cis*-9-methyl-2-decalone, **9**, with ethyl 2-piperidineacetate, **14**, was studied in a parallel series of experiments (Scheme 4). The condensation, employing conditions similar to those used in the above case, afforded two crystalline products. The major product, **15***a* (mp 224 °C), was obtained in 51% yield while the minor product, **15***b* (mp 165 °C), was obtained in 17% yield. The spectral properties of the two products were in accord with the presence of a vinylogous amide group (3) (ν_{max}, two bands between 1615 and 1610 cm^{-1} and 1560 and 1550 cm^{-1}; λ_{max} *ca.* 330 nm). The structures assigned to the condensation products and to the derived compounds **16** and **17** are again based on X-ray crystallographic analysis (of **17**, *vide infra*). Therefore, in analogy with the previously described sequence, only compounds with the 'non-steroidal', azabenzanthracene skeleton were forthcoming.

Oxidation of either of the condensation products **15***a* or *b* with mercuric acetate afforded, in 67% yield, the same crystalline pyridone **16** (ν_{max} 1625 and 1558 cm^{-1}; λ_{max} 266 nm; nmr δ 6.08 (vinylic proton)). The two products are therefore C-12 stereoisomers and not structural isomers.

Reduction of the major condensation product **15***a* with lithium in liquid ammonia, followed by equilibration with base, afforded a crystalline amino ketone (1710 cm^{-1}) in 67% yield. X-ray crystallographic analysis showed unequivocally that the amino ketone had the structure represented by **17**, hence, the structures assigned to the precursors **15** and **16**.

The differences in the steric configurations at C-7, C-8, and C-12 relative to the angular methyl group in the amino ketones **13** and **17** are noteworthy since these compounds were obtained by reduction of the corresponding enamino ketones, **11***a* and **15***a* respectively, with lithium in liquid ammonia. These differences are likely due to fundamental differences in the stereoelectronic conformations of the transition states encountered during the reduction (4). The nature of the transition states, hence the stereochemistry and the conformations of the products, may in turn be controlled by the stereoconfiguration at C-12 of the precursor enamino ketones **11***a* and **15***a*.

Can. J. Chem. Downloaded from www.nrcresearchpress.com by 210.87.254.105 on 09/05/12
For personal use only.

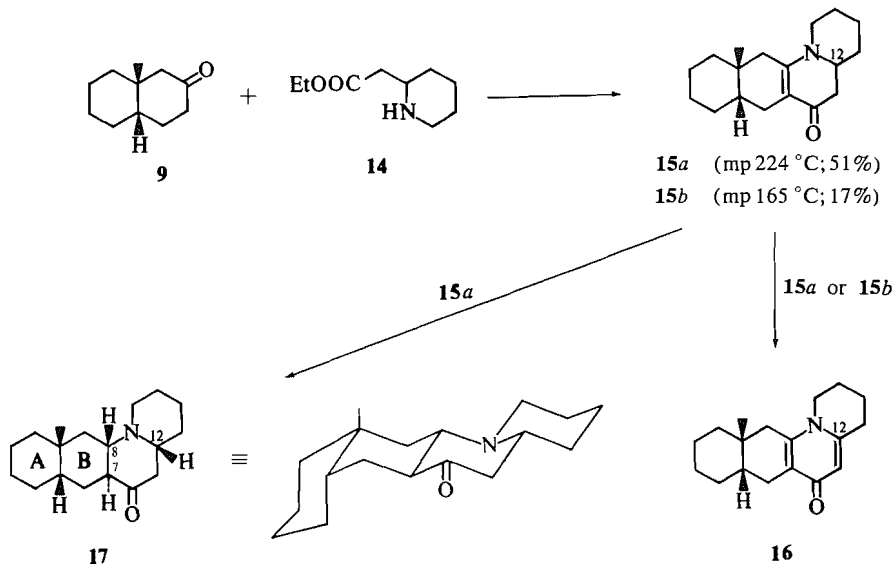

SCHEME 4

It is also appropriate to point out at this stage that the structures of **13** and **17**, as determined by X-ray crystallography (*vide infra*), have different conformations of the *cis*-fused A/B ring system; the remaining conformational features of these molecules follow from the particular A/B conformation which is present. Conformational drawings of **13** and **17** are provided in Schemes 3 and 4 (*cf.* Figs. 1 and 2).

It is apparent that application of the approach described herein to the selected starting materials does not provide compounds possessing the 14-aza- and the D-homo-14-azasteroidal nuclei. However, it is conceivable that control of regio- and stereochemical factors could result in the production of such compounds. The failure to obtain these compounds does not detract from the potential utility of the approach in other aspects of synthetic chemistry.

X-ray Crystallographic Analysis

The structures of the two compounds **13** and **17** have been solved by X-ray techniques. Preliminary Weissenberg photographs taken of both compounds were used to establish space group and approximate cell dimensions.

The final atomic coordinates and temperature factors are given in Tables 1 and 2 in which the hydrogen atoms are numbered after the carbon atom to which they are bonded. Figs. 1 and 2 (9)

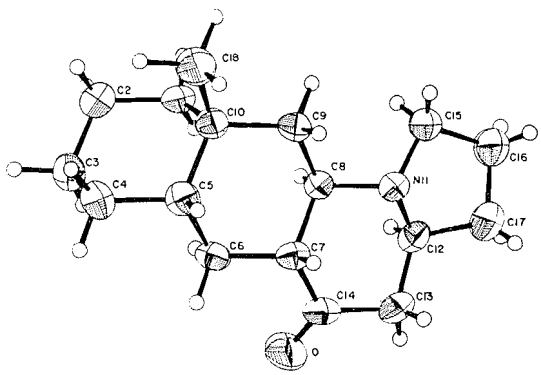

FIG. 1. ORTEP (9) plot of compound **13**, thermal elipsoids drawn with 50% probability.

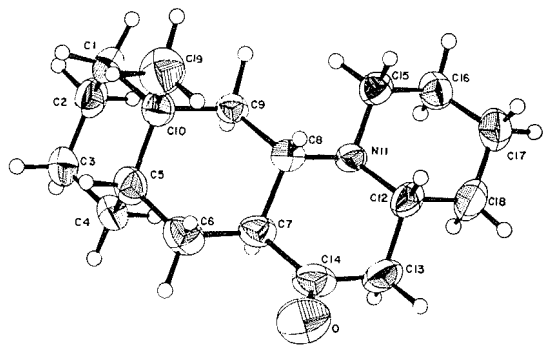

FIG. 2. ORTEP (9) plot of compound **17**, thermal elipsoids drawn with 50% probability.

Can. J. Chem. Downloaded from www.nrcresearchpress.com by 210.87.254.105 on 09/05/12
For personal use only.

TABLE 1

(*a*) Final parameters and estimated standard deviations (e.s.d.'s) $\times 10^4$ for compound **13**.
t.f. = $\exp[-2\pi^2(a^{*2}U_{11}h^2 + b^{*2}U_{22}k^2 + c^{*2}U_{33}l^2 + 2a^*b^*U_{12}hk - 2a^*c^*U_{13}hl - 2b^*c^*U_{23}hl)]$

Atom	x	y	z	U_{11}	U_{22}	U_{33}	U_{12}	U_{13}	U_{23}
C(1)	8808(3)	5927(2)	1269(3)	470(19)	392(17)	614(22)	40(15)	82(16)	−75(16)
C(2)	157(3)	5946(3)	1479(4)	511(21)	578(22)	699(24)	81(17)	136(18)	−34(19)
C(3)	672(3)	6905(3)	2213(4)	425(19)	657(24)	714(25)	3(17)	119(17)	3(20)
C(4)	237(3)	7038(3)	3503(3)	481(20)	622(22)	665(25)	−45(18)	−4(17)	−52(20)
C(5)	8881(3)	7030(2)	3303(3)	472(18)	508(20)	409(18)	−5(15)	65(14)	14(16)
C(6)	8357(3)	8029(2)	2654(3)	528(19)	399(18)	523(21)	−80(15)	89(15)	−78(15)
C(7)	7017(3)	8053(2)	2427(3)	524(19)	396(18)	425(18)	5(15)	145(15)	−24(15)
C(8)	6482(2)	7133(2)	1590(3)	398(17)	380(17)	445(18)	19(14)	104(14)	2(15)
C(9)	6980(3)	6136(2)	2240(3)	484(19)	374(17)	503(21)	−26(14)	123(16)	24(15)
C(10)	8341(3)	6057(2)	2554(3)	436(18)	380(17)	444(19)	10(13)	65(14)	55(14)
N(11)	5187(2)	7173(2)	1393(3)	419(15)	421(15)	558(17)	35(12)	99(12)	−20(13)
C(12)	4702(3)	8113(2)	719(3)	490(20)	528(20)	571(21)	117(16)	105(16)	−11(17)
C(13)	5130(3)	9056(2)	1550(4)	635(24)	481(20)	759(26)	162(17)	155(19)	−11(19)
C(14)	6460(3)	9051(3)	1881(4)	679(24)	360(19)	753(26)	9(18)	130(20)	−82(19)
C(15)	4546(3)	6339(3)	604(4)	439(21)	557(21)	823(27)	−7(16)	32(18)	−70(19)
C(16)	3293(3)	6764(3)	125(4)	488(23)	773(30)	1242(38)	53(20)	−9(22)	−187(27)
C(17)	3385(3)	7908(3)	413(4)	519(22)	732(28)	1064(33)	151(19)	86(21)	−62(25)
C(18)	8649(3)	5091(3)	3428(4)	601(23)	518(22)	844(28)	33(18)	46(20)	258(21)
O	7042(3)	9784(2)	1664(4)	812(20)	453(15)	1790(33)	−48(15)	94(20)	196(19)

(*b*) Final parameters (e.s.d.'s) $\times 10^3$ for compound **13**

Atom	x	y	z	U	Atom	x	y	z	U
H(1A)	845(3)	531(2)	77(3)	49(9)	H(9B)	669(2)	607(2)	307(3)	61(9)
H(1B)	849(2)	649(2)	64(2)	40(7)	H(12)	496(2)	817(2)	−14(3)	42(8)
H(2A)	34(3)	590(3)	53(3)	79(10)	H(13A)	497(3)	969(3)	111(3)	67(10)
H(2B)	48(2)	536(2)	203(3)	43(8)	H(13B)	483(3)	899(2)	245(3)	68(9)
H(3A)	45(2)	753(2)	166(3)	57(8)	H(15A)	459(3)	575(3)	121(3)	76(10)
H(3B)	156(3)	684(2)	242(3)	66(10)	H(15B)	490(3)	615(3)	−17(3)	77(10)
H(4A)	63(2)	647(2)	415(3)	57(9)	H(16A)	277(4)	642(4)	67(4)	124(15)
H(4B)	54(3)	766(2)	400(3)	67(10)	H(16B)	296(4)	658(4)	−70(4)	98(16)
H(5)	871(2)	699(2)	422(3)	48(8)	H(17A)	295(3)	834(3)	−33(4)	96(13)
H(6A)	857(2)	813(2)	181(3)	47(8)	H(17B)	307(3)	807(2)	119(3)	66(10)
H(6B)	866(2)	863(2)	315(3)	53(8)	H(18A)	830(3)	447(3)	289(3)	80(10)
H(7)	678(2)	795(2)	325(3)	52(8)	H(18B)	837(3)	519(3)	433(4)	105(12)
H(8)	668(2)	720(2)	67(3)	37(8)	H(18C)	953(3)	499(3)	379(3)	94(11)
H(9A)	664(2)	556(2)	171(3)	41(7)					

present perspective views of the two molecules and indicate the numbering scheme used and Figs. 3 and 4 give bond lengths.[2]

Experimental

X-ray Analysis

Unit-cell and space group data were obtained from Weissenberg photographs. Both compounds **13** and **17** exhibited systematic absences corresponding to the space group $P2_1/c$. Final cell dimensions were obtained by a least-squares fit of 12 well centered reflections on a Picker FACS-1 diffractometer. The relevant crystallographic data for the two compounds are:

*Compound **13***

$C_{17}H_{27}NO$ f.w. = 261.4

Monoclinic, $P2_1/c$, $a = 11.527(4)$, $b = 12.943(5)$, $c = 10.268(4)$ Å, $\beta = 101.45(2)°$, $V = 1531.9$ Å^3, $\rho_c = 1.13$, $Z = 4$, (20 °C; MoKα, $\lambda = 0.71069$ Å); crystal size, $0.60 \times 0.36 \times 0.24$ mm; $\mu = 0.74$ cm^{-1}.

*Compound **17***

$C_{18}H_{29}NO$ f.w. = 275.4

Monoclinic, $P2_1/c$, $a = 12.106(4)$, $b = 7.678(2)$, $c = 17.324(6)$ Å, $\beta = 98.27(3)°$, $V = 1593.5$ Å^3, $\rho_c = 1.15$, $Z = 4$, (20 °C; MoKα, $\lambda = 0.71069$ Å); crystal size, $0.50 \times 0.36 \times 0.36$ mm; $\mu = 0.75$ cm^{-1}.

[2]Complete tables of observed and calculated structure factors are available, at a nominal charge, from the Depository of Unpublished Data, CISTI, National Research Council of Canada, Ottawa, Canada K1A 0S2.

Can. J. Chem. Downloaded from www.nrcresearchpress.com by 210.87.254.105 on 09/05/12
For personal use only.

Can. J. Chem. Downloaded from www.nrcresearchpress.com by 210.87.254.105 on 09/05/12
For personal use only.

TABLE 2

(*a*) Final parameters (e.s.d.'s) $\times 10^4$ for compound **17**

t.f. = $\exp[-2\pi^2(a^{*2}U_{11}h^2 + b^{*2}U_{22}k^2 + c^{*2}U_{33}l^2 + 2a^*b^*U_{12}hk + 2a^*c^*U_{13}hl + 2b^*c^*U_{23}kl)]$

Atom	x	y	z	U_{11}	U_{22}	U_{33}	U_{12}	U_{13}	U_{23}
C(1)	9049(3)	9166(5)	447(2)	409(21)	711(28)	772(28)	−70(20)	19(19)	−136(23)
C(2)	9046(3)	9878(5)	3300(3)	505(28)	610(26)	873(30)	−132(21)	155(21)	3(27)
C(3)	9357(3)	8491(5)	2757(2)	501(23)	795(29)	759(27)	−49(22)	210(20)	−1(27)
C(4)	8582(3)	6935(5)	2755(2)	499(22)	612(25)	609(27)	7(20)	182(18)	−48(20)
C(5)	8586(3)	6168(5)	3570(2)	431(21)	518(27)	731(26)	108(18)	73(18)	26(20)
C(6)	7805(3)	4603(5)	3549(2)	748(26)	436(22)	778(27)	129(27)	197(21)	40(20)
C(7)	6583(3)	5139(4)	3393(2)	642(24)	325(19)	548(24)	−35(18)	172(20)	−17(18)
C(8)	6260(3)	6517(4)	3967(2)	524(22)	351(20)	382(19)	−1(17)	75(16)	61(17)
C(9)	7076(3)	8039(4)	4002(2)	485(20)	377(20)	465(20)	−33(17)	75(16)	−26(16)
C(10)	8325(3)	7530(5)	4165(2)	444(21)	541(23)	516(23)	43(19)	22(16)	−13(19)
N(11)	5091(2)	7067(3)	3724(1)	469(17)	393(16)	431(16)	−78(14)	104(13)	−57(14)
C(12)	4326(3)	5591(4)	3765(2)	568(22)	577(25)	455(21)	−190(20)	108(17)	21(19)
C(13)	4604(4)	4089(5)	3242(2)	836(31)	536(26)	721(28)	−292(24)	165(23)	−145(22)
C(14)	5798(4)	3596(5)	3390(2)	899(32)	415(26)	676(26)	−75(24)	226(23)	−77(21)
C(15)	4785(3)	8506(5)	4211(2)	489(20)	540(23)	536(22)	−19(19)	140(17)	−46(19)
C(16)	3598(3)	9110(6)	3975(2)	531(23)	759(29)	654(26)	53(22)	128(20)	15(23)
C(17)	2782(3)	7620(6)	4017(2)	487(24)	1069(36)	765(29)	−72(25)	145(21)	−68(27)
C(18)	3110(3)	6131(6)	3539(2)	567(25)	871(32)	714(28)	−237(24)	80(21)	−71(25)
C(19)	8592(3)	6839(6)	5004(2)	740(28)	995(36)	605(26)	69(27)	−75(21)	110(25)
O	6124(3)	2130(4)	3510(2)	1212(27)	342(16)	1484(31)	−63(18)	358(22)	20(19)

(*b*) Final parameters (e.s.d.'s) $\times 10^3$ for compound **17**

Atom	x	y	z	U	Atom	x	y	z	U
H(1A)	877(3)	1007(4)	447(2)	32(10)	H(12)	443(2)	516(4)	431(2)	6(8)
H(1B)	984(3)	899(4)	434(2)	35(10)	H(13A)	412(3)	306(5)	331(2)	37(11)
H(2A)	829(3)	1034(4)	313(2)	38(10)	H(13B)	444(3)	444(5)	269(2)	46(11)
H(2B)	961(2)	1091(4)	336(2)	27(9)	H(15A)	535(2)	954(4)	419(2)	16(8)
H(3A)	931(3)	889(5)	220(2)	39(10)	H(15B)	487(2)	818(4)	479(2)	21(9)
H(3B)	1017(3)	809(4)	292(2)	30(10)	H(16A)	353(3)	951(5)	340(2)	59(11)
H(4A)	777(2)	733(4)	253(2)	12(8)	H(16B)	344(3)	1011(5)	434(2)	45(11)
H(4B)	878(3)	611(5)	235(2)	54(12)	H(17A)	196(3)	798(5)	382(2)	49(12)
H(5)	934(2)	582(4)	375(2)	12(9)	H(17B)	278(3)	728(4)	456(2)	35(10)
H(6A)	794(3)	403(4)	406(2)	28(10)	H(18A)	266(3)	516(5)	357(2)	46(11)
H(6B)	794(3)	371(5)	311(2)	53(12)	H(18B)	304(3)	644(5)	295(2)	45(12)
H(7)	643(2)	564(4)	286(2)	7(9)	H(19A)	812(3)	570(5)	507(2)	52(12)
H(8)	635(2)	593(4)	449(2)	6(8)	H(19B)	936(3)	642(6)	510(2)	69(14)
H(9A)	694(2)	864(3)	350(1)	0(7)	H(19C)	846(3)	787(5)	539(2)	67(14)
H(9B)	695(3)	892(4)	444(2)	30(10)					

Intensities were measured on the diffractometer using graphite monochromated MoKα radiation. A θ–2θ scan at a rate of 1° m^{-1} was used with a base range of 2° corrected for dispersion of the Kα doublet. A stationary background count of 20 s was made on both sides of each reflection. A standard reflection monitored every 20 reflections showed no systematic intensity change for either compound. After correction for background, reflections with a net intensity of less than 15 counts were classified as unobserved. Data were collected to $2\theta = 50°$ for compound **13** and to $2\theta = 45°$ for compound **17**, resulting in 2647 allowed unique reflections, of which 1334 were considered unobserved, for compound **13**; for compound **17** there were 2086 allowed unique reflections of which 737 were considered unobserved.

Both structures were solved by multi-solution direct methods using the program MULTAN (5). In each case

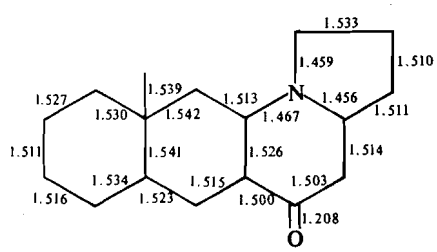

FIG. 3. Bond lengths (Å) for compound **13**. C—H bonds are not shown.

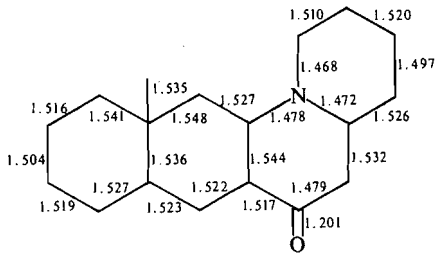

FIG. 4. Bond lengths (Å) for compound **17**. C—H bonds are not shown.

the solution with the best 'combined figure of merit' calculated by the program was used to produce an *E*-map. These maps were searched for the highest peaks and the program FRAGMENT (6) was used to identify possible molecules, consistent with expected bond angles and distances. The *E*-map for compound **13** gave a fragment of 22 peaks from which the 19 non-hydrogen atoms in the molecule could easily be identified. The *E*-map for compound **17** also gave a fragment of 22 peaks, however, in this case it was not possible to unambiguously identify the molecule. The problem was resolved by one cycle of least-squares refinement after which the two erroneous peaks were immediately obvious. In both cases chemical information was used to place the oxygen and nitrogen atoms.

The X-ray 72 suite of programs (7) was used for refinement of the structures, scattering factors used were those given in the International Tables for Crystallography (8). Initial least-squares refinement of the non-hydrogen atoms with isotropic thermal parameters resulted in agreement indices of 0.19 for compound **13** and 0.16 for compound **17**. At this point all the hydrogen atoms for both compounds were located in difference Fourier maps and their inclusion in the refinements reduced the agreement indices to 0.14 and 0.10 respectively. Cruickshank's weighting scheme (7) was used for further refinement, the parameters being adjusted so that the average $w\Delta^2$ was similar for groups of reflections analysed in terms of $|F|$ and sin θ. The quantity minimized was $\sum w(|F_o| - |F_c|)^2$ for observed reflections only. Inclusion of anisotropic temperature factors for the non-hydrogen atoms gave final agreement indices of 0.049 for compound **13** and 0.052 for compound **17**.

Instrumentation, Methods, and Materials

Melting points were determined on a Fisher-Johns apparatus and are uncorrected. The ir spectra were recorded on a Perkin-Elmer model 237 B spectrophotometer and uv spectra were determined with a Perkin-Elmer Coleman model 124 instrument. The nmr spectra were recorded with a Varian T-60 instrument; chemical shifts were expressed in ppm (δ-values) downfield from the signal for tetramethylsilane which is used as an internal standard.

Vapour phase chromatography was performed on a Hewlett-Packard model 5750 instrument fitted with a stainless steel column (6 × ⅛ in.) packed with 10% of UC-W98 (silicone gum rubber) on diatoports (80–100 mesh). The tlc was carried out on silica gel GF-254 procured from Brinkman Instruments (Canada) Ltd.

Petroleum ether refers to the fraction with boiling point range 30–60 °C. Brine refers to a saturated solution of sodium chloride.

*Condensation Products **11** and **11a***

A solution of 500 mg of *cis*-9-methyl-2-decalone, **9** (10), 374 mg of ethyl 2-pyrrolidineacetate (11) and 0.11 ml of trifluoroacetic acid in 5.3 ml of toluene was refluxed under a nitrogen atmosphere for 27 h. Water formed during the initial stages of the reaction was removed by molecular sieve (Linde, type 4A) in a Soxhlet adaptor. The course of the reaction was monitored by the increasing intensity of an adsorption maximum at *ca.* 340 nm. The cooled reaction solution was treated with 70 ml of cold, 1 *M* sodium carbonate solution and the product was extracted into benzene.

The product, obtained by evaporation of the benzene extracts, on crystallization from ether afforded 387 mg (67%) of crystalline **11**, mp 145–158 °C. This crystalline material gave rise to a single spot on silica gel tlc and a single peak on vpc. The nmr spectrum exhibited two methyl singlets at δ 0.90 and δ 0.94 demonstrating the presence of two compounds.

Successive recrystallizations from ether afforded 259 mg (42%) of a single compound **11***a*, mp 169–170 °C; λ_{max} (EtOH) 340 nm (ϵ 14 970); ν_{max} ($CHCl_3$) 1600 and 1545 cm^{-1} (vinylogous amide); nmr ($CDCl_3$), δ 0.90 (s, 3H, methyl). *Anal.* calcd. for $C_{17}H_{25}NO$: C 78.72, H 9.71, N 5.39; found: C 78.52, H 9.96, N 5.34.

The mother liquors afforded 102 mg of crystalline material (mp 157–163 °C), with uv and ir spectra identical with those of **11***a*. There were, however, two methyl singlets in the nmr spectrum at δ 0.90 and δ 0.94 indicating the presence of two compounds.

*Pyridone **12***

A solution of 100 mg of **11***a*, 124 mg of mercuric acetate, and 146 mg of the disodium salt of ethylenediamine tetraacetic acid in 10.2 ml of 55% acetic acid was heated at 65–70 °C for 26 h (12). After cooling, the reaction mixture was made basic by careful addition of 1 *M* sodium carbonate solution and extracted with methylene chloride. Evaporation of the extracts *in vacuo* afforded the crude product.

Purification of the crude product by tlc on silica gel with 7% of methanol in ether as solvent and subsequent crystallization from benzene–ether afforded 78 mg (78%) of **12**, mp 191 °C; λ_{max} (EtOH) 266 nm (ϵ 12 360); ν_{max} ($CHCl_3$) 1640 and 1530 cm^{-1} (pyridone (13)); nmr ($CDCl_3$), δ 0.96 (s, 3H, methyl), 6.2 (s, 1H, vinylic proton). *Anal.* calcd. for $C_{17}H_{23}NO$: C 79.34, H 9.01, N 5.44; found: C 79.03, H 9.15, N 5.68.

Oxidation of the mixture **11** of condensation products, as above, afforded the same pyridone **12** in 78% yield. The identity of the two pyridones was established by mixture melting point (no depression), identity of uv, ir, and nmr spectra and identical behavior on tlc (silica gel) in a variety of solvents.

*Amino Ketone **13***

A solution of 91 mg of condensation product **11***a* in 1.0 ml of dry tetrahydrofuran was added to a solution of 78 mg of lithium in 30 ml of liquid ammonia. After

Can. J. Chem. Downloaded from www.nrcresearchpress.com by 210.87.254.105 on 09/05/12
For personal use only.

Can. J. Chem. Downloaded from www.nrcresearchpress.com by 210.87.254.105 on 09/05/12
For personal use only.

stirring on a dry ice – acetone bath for 90 min, excess reagent was destroyed by the addition of solid ammonium chloride and the ammonia was allowed to evaporate at room temperature. To the residue was added 60 ml of ice water and the aqueous solution was extracted with benzene. Evaporation of the extracts yielded an oil which was refluxed with 20 ml of 1 *M* methanolic potassium hydroxide for 2 h. After removal of most of the solvent by evaporation *in vacuo*, 50 ml of water was added and the aqueous solution was extracted with benzene. Evaporation of the extracts *in vacuo* afforded 86 mg of oil.

The oil was separated into two fractions by tlc on silica gel with 0.5% methanol in ether as solvent. One fraction (33 mg, 36%) was found to be starting material. The second fraction, on crystallization from pentane, afforded 43 mg (47%) of amino ketone **13**, mp 79 °C; ν_{max} ($CHCl_3$) 1708 cm^{-1} (ketone); nmr ($CDCl_3$), δ 1.00 (s, 3H, methyl). *Mol. Wt.* calcd. for $C_{17}H_{27}NO$: 261, found: 261.

Ethyl 2-Piperidineacetate ***14***

This ester was prepared as follows (*cf.* ref. 14). A solution of 1.25 g of 2-pyridylacetic acid hydrochloride in 500 ml of glacial acetic acid was hydrogenated over a platinum catalyst (from 1.0 g of platinum oxide) at room temperature and at 8 atm for 7 h. The catalyst was removed by filtration and the volume of the filtrate was reduced to 90 ml whereupon the product crystallized. Recrystallization from acetic acid afforded 1.149 g (89%) of 2-piperidineacetic acid hydrochloride mp 185 °C (lit. (14*b*) mp 185 °C). A solution of 1.0 g of 2-piperidineacetic acid hydrochloride in 50 ml of absolute ethanol was saturated with dry hydrochloric acid while cooling on an ice-salt bath. The solvent was evaporated *in vacuo*, replaced with another 50 ml portion of absolute ethanol, and saturation with dry hydrochloric acid was repeated. Evaporation of the solvent *in vacuo* and crystallization of the residue from ethanol–ether afforded 1.04 g (88%) of ethyl 2-piperidineacetate hydrochloride, mp 146 °C. *Anal.* calcd. for $C_9H_{18}NO_2Cl$: C 52.05, H 8.74, N 6.74; Found: C 52.19, H 9.19, N 6.66.

A solution of 910 mg of the ethyl ester hydrochloride in 50 ml of cold 1 *N* sodium carbonate solution was extracted with three 50-ml portions of ether. The ether extracts were washed with 50 ml of ice water, dried, and evaporated *in vacuo*. Distillation of the residue (bp 97–98 °C/9 torr) afforded 602 mg of **14** as a colorless oil which gave a *picrate*, mp 125 °C (lit. (14*a*) mp 125 °C).

Condensation Products ***15a*** *and* ***15b***

A solution of 1.00 g of ethyl 2-piperidineacetate, **14**, 2.00 g of *cis*-9-methyl-2-decalone, **9** (10), and 0.4 ml of trifluoroacetic acid in 10 ml of dry toluene was refluxed, under an atmosphere of nitrogen, for 6 days. Water formed in the initial stages was removed by molecular sieve (Linde, type 4A) in a Soxhlet adaptor. The course of the reaction was monitored by the increasing intensity of an absorption maximum at *ca.* 330 nm. To the cooled reaction mixture was added 150 ml of 1 *M* sodium carbonate solution and the aqueous mixture was extracted with benzene.

Evaporation of the extracts yielded a crude product which was separated into two fractions by tlc on silica gel with 5% methanol in ether as solvent. Crystallization of one fraction from methylene chloride – ether afforded 816 mg (51%) of **15***a*, mp 224 °C; λ_{max} (EtOH) 330 nm (ϵ 14 000); ν_{max} ($CHCl_3$) 1615 and 1560 cm^{-1} (vinylogous amide); nmr ($CDCl_3$), δ 0.90 (s, 3H, methyl). *Anal.* calcd. for $C_{18}H_{27}NO$: C 79.07, H 9.94, N 5.12; found: C 79.18, H 10.03, N 5.05.

The second fraction, on crystallization from methylene chloride – ether, afforded 272 mg (17%) of **15***b*, mp 165 °C; λ_{max} (EtOH) 334 nm (ϵ 13 980); ν_{max} ($CHCl_3$), 1610 and 1550 cm^{-1} (vinylogous amide); nmr ($CDCl_3$), δ 0.90 (s, 3H, methyl). *Anal.* calcd. for $C_{18}H_{27}NO$: C 79.07, H 9.94, N 5.12; found C 79.40, H 10.07, N 5.18.

Pyridone ***16***

Oxidation of 80 mg of condensation product **15***a* by the procedure described previously for the oxidation of **11** and **11***a* to **12** afforded 70 mg (88%) of pyridone **16**, mp 242 °C; λ_{max} (EtOH) 266 nm (ϵ 11 200); ν_{max} ($CHCl_3$) 1625 and 1558 cm^{-1} (pyridone (13)); nmr ($CDCl_3$), δ 0.95 (s, 3H, methyl), 6.08 (s, 1H, vinylic proton). *Anal.* calcd. for $C_{18}H_{25}NO$: C 79.66, H 9.29, N 5.16; found: C 79.36, H 9.20, N 5.44.

Oxidation of condensation product **15***b*, as above, afforded in 87% yield, the same pyridone **16**. Identity of the two oxidation products was established by mixture melting point (no depression), identity of uv, ir, and nmr spectra, and identical behavior on tlc (silica gel) in a variety of solvents.

Amino Ketone ***17***

Reduction of 235 mg of the condensation product **15***a* by the procedure used to obtain the amino ketone **13** afforded 230 mg of oil. Purification of the oil by tlc on silica gel with ether as solvent afforded 157 mg (67%) of amino ketone **17**, mp 108 °C; ν_{max} ($CHCl_3$), 1710 cm^{-1} (ketone); nmr ($CDCl_3$), δ 1.03 (s, 3H, methyl). *Anal.* calcd. for $C_{18}H_{29}NO$: C, 78.49, H 10.61, N 5.09; found: C 78.69, H 10.53, N 5.41.

Acknowledgments

We thank the National Research Council of Canada for financial support.

1. (*a*) M. I. MUMTAZ. M.Sc. Thesis, University of New Brunswick, Saint John, N.B. 1974; (*b*) N. A. NELSON, J. E. LADBURY, and R. S. P. HSI. J. Am. Chem. Soc. **80**, 6633 (1958); (*c*) W. SOBOTKA, W. N. BEVERUNG, G. G. MUNOZ, J. C. SIRCAR, and A. I. MEYERS. J. Org. Chem. **30**, 3667 (1965); (*d*) Z. HORII, K. MORIKAWA, H. TAMURA, and I. NINOMIYA. Chem. Pharm. Bull. Jpn. **14**, 1399 (1966); (*e*) Z. HORII, K. MORIKAWA, C. IWATA, and I. NINOMIYA. Chem. Pharm. Bull. Jpn. **16**, 1686 (1968); (*f*) M. AKIBA and S. OHKI. Chem. Pharm. Bull. Jpn. **18**, 2195 (1970); (*g*) M. AKIBA and S. OHKI. Chem. Pharm. Bull. Jpn. **21**, 40 (1973).
2. M. KUEHNE. J. Am. Chem. Soc. **83**, 1492 (1961); and references cited therein.
3. F. BOHLMANN, E. WINTERFELDT, O. SCHMIDT, and W. REUSCHE. Ber. **94**, 1774 (1961); F. BOHLMANN and O. SCHMIDT. Ber. **97**, 1854 (1964); N. H. CROMWELL, F. A. MILLER, A. R. JOHNSON, R. L. FRANK, and D. WALLACE. J. Am. Chem. Soc. **71**, 3337 (1949); G. O. DUDEK J Org. Chem. **30**, 548 (1965).

4. G. STORK and S. D. DARLING. J. Am. Chem. Soc. **86**, 1761 (1964).
5. G. GERMAIN, P. MAIN, and M. M. WOOLFSON. Acta Crystallogr. Sect. A, **27**, 368 (1971).
6. M. J. H. KOCH. Acta Crystallogr. Sect. A, **30**, 67 (1974).
7. J. M. STEWART. X-Ray 72. University of Maryland Computer Science Center, College Park, Maryland. Technical Report TR-192. 1972.
8. International tables for X-ray crystallography. The Kynoch Press, Birmingham. 1952.
9. C. K. JOHNSON. Oak Ridge National Laboratory, Technical Report ORNL-3794. 1965.
10. R. P. LINSTEAD, A. F. MILLIDGE, and A. L. WALPOLE. J. Chem. Soc. 1140 (1937).
11. Z. HORII, K. MORIKAWA, and I. NINOMIYA. Chem. Pharm. Bull. Jpn. **17**, 2230 (1969).
12. J. KNABE. Arch. Pharm. **292**, 416 (1959); J. KNABE. Arch. Pharm. **293**, 121 (1960); J. KNABE and G. GRUND. Arch. Pharm. **296**, 854 (1963); J. KNABE and H. ROLOFF. Ber. **97**, 3452 (1964).
13. A. R. KATRITZKI and R. A. JONES. J. Chem. Soc. 2947 (1960).
14. (*a*) G. R. CLEMO, W. M. MORGAN, and R. RAPER. J. Chem. Soc. 1743 (1935); (*b*) F. MOLL. Arch. Pharm. **301**, 230 (1968).

Can. J. Chem. Downloaded from www.nrcresearchpress.com by 210.87.254.105 on 09/05/12
For personal use only.

Influence of remote substituents on ionization potential. Part II.[1] Enamines

R. S. BROWN

Department of Chemistry, University of Alberta, Edmonton, Alberta T6G 2E1

Received December 16, 1975

R. S. BROWN. Can. J. Chem. **54**, 1521 (1976).

Electronic interactions in vinylamines can be divided into $n_N-\pi$ conjugation, and effects arising as a consequence of the electron-withdrawing abilities ($-I$) of both the nitrogen and π-system. Dehydroquinuclidine represents an ideal model which minimizes $n_N-\pi$ conjugation, and exhibits a pe spectrum which indicates that both the n_N and π-orbitals are stabilized by about 0.4 eV relative to quinuclidine and bicyclooctene respectively. This stabilization is proposed to be a consequence of $-I$ effects of each group and/or rehybridization of the nitrogen. Similar inductive effects are assumed to operate in enamines which do not prohibit $n_N-\pi$ interaction. In these cases, strong conjugative effects are operative in addition to the $-I$ effects.

R. S. BROWN. Can. J. Chem. **54**, 1521 (1976).

On peut diviser les interactions électroniques des vinylamines en conjugaison $n_N-\pi$ et en effets dérivant des propriétés électroaffinitaires ($-I$) à la fois de l'azote et du système π. La dihydroquinuclidine représente un modèle idéal qui minimise la conjugaison $n_N-\pi$ et qui montre un spectre pe indiquant que les orbitales π et n_N sont stabilisées respectivement par environ 0.4 eV par rapport à la quinuclidine et au bicyclooctène. On propose que cette stabilisation provient des effets $-I$ de chaque groupe et/ou de la réhybridisation de l'azote. On fait l'hypothèse que des effets inductifs semblables sont en opération dans les énamines qui n'empêchent pas les interactions $n_N-\pi$. Dans ces cas, des effets de conjugaison très puissants sont en opération en plus des effets $-I$.

[Traduit par le journal]

Enamines have become progressively important as synthetic intermediates since their utility was first demonstrated by Stork *et al.* in 1954 (2). Their ability to undergo electrophilic additions at both carbon and nitrogen has been ascribed to resonance forms such as **1** and **2** which formally place high electron density at either end of the three-atom four-electron system (for a compendium of leading references on this feature and its chemical consequences see ref. 3).

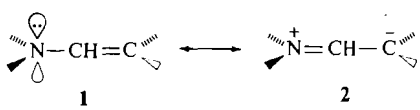

1 **2**

The enamine nitrogen can, in principle, exert two opposing effects on the double bond, an electron-withdrawing inductive effect ($-I$) and an electron-releasing conjugative interaction ($+R$). In most enamines both effects operate simultaneously, and the physical properties of the molecule will reflect the summation of the two. In terms of electrophilic addition to the carbon end of the enamine, the conjugative

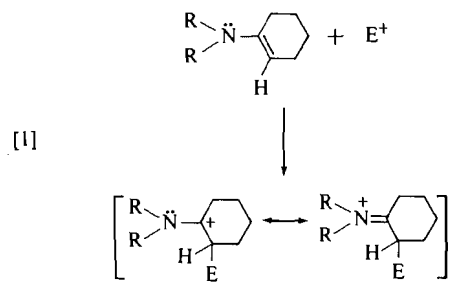

[1]

abilities of the amine will far outweigh the $-I$ effect as illustrated in eq. 1.

Recognizing the possible opposing influences of the nitrogen on the π-system, we felt such systems were particularly suited to study by photoelectron spectroscopy (pes). In order to individually assess the contribution of the opposing $-I$ and $+R$ effects to the total character of the molecule, a model compound was chosen in which one of the effects is minimized relative to the other. Since conjugative interactions depend markedly upon coplanarity of orbitals for maximum effect while inductive interactions do not (4) the best model would be one in which the nitrogen lone pair (n_N) is

[1]For part I, see ref. 1.

Can. J. Chem. Downloaded from www.nrcresearchpress.com by 210.87.254.5 on 09/05/12
For personal use only.

3 4

perpendicular to the π-system. Such an arrangement is provided in the simple system 1-azabicyclo[2.2.2]oct-2-ene or dehydroquinuclidine, **3** (5). Determination of the ionization potential (IP) of the π-bond in **3** will provide an estimate of the $-I$ effect of the adjacent nitrogen. With this value in hand, one can turn to an analysis of the pe spectra of 1-(*N*,*N*-dimethylamino)cyclohexene, **5**, and 1-(*N*,*N*-dimethylamino)cyclopentene, **7**, in which both $+R$ and $-I$ effects are operating in concert.

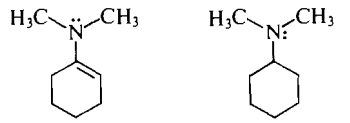

5 6

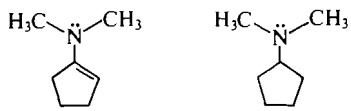

7 8

Experimental

The pe spectra were determined under conditions similar to those described before (1). Dehydroquinuclidine, **3**, was prepared according to published procedure (*5b*). Compounds **5** and **7** were prepared by the method of Blanchard (6), while the saturated analogues **6** and **8** were obtained via a procedure described by Mousseron *et al.* (7). All physical constants agreed with those published and spectral data were consistent with the assigned structures.

Results and Discussion

The pe spectra for compounds **3** and **5–8** are presented in Figs. 1 and 2 respectively, while the corresponding data and assignments are presented in Table 1.

Dehydroquinuclidine, **3**, was first prepared by Grob *et al.* (5) as a vinylamine in which no resonance interaction of n_N and the π-bond is possible. Several chemical and physical properties of **3** reflect reactivity atypical of regular enamines. For example, **3** is relatively stable in either aqueous acid or base (5) while typical enamines such as **5** and **7** rapidly hydrolyse in aqueous media to the corresponding ketones and

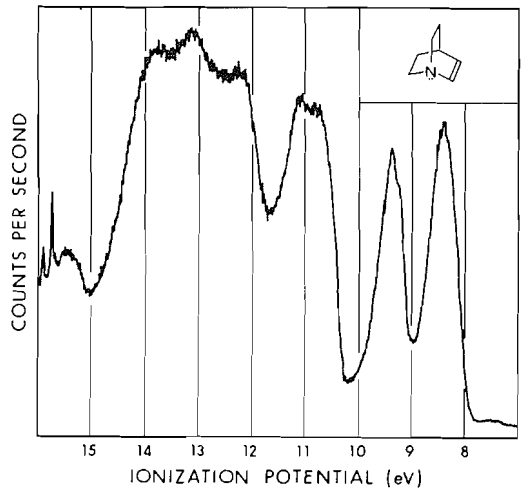

FIG. 1. The pe spectrum of dehydroquinuclidine using argon as an internal calibrating gas.

secondary amine. Treatment of **3** with methyl iodide results in exclusive *N*-alkylation, while enamines such as the pyrrolidine enamine of cyclohexanone react with methyl iodide to form a quaternary salt which may be decomposed by water to yield 70% 2-methylcyclohexanone (2). Grob *et al.* have concluded that **3** is 1.13 p*K* units weaker a base than quinuclidine in aqueous solution at 25 °C, and have attributed this feature to $(-I)$ electron-withdrawal of the double bond. While it is certain that basicity in aqueous solutions is subject to solvation effects (8), in the gas phase where such effects are absent, dehydroquinuclidine, **3**, may be very close in basicity to quinuclidine. For example in aqueous solution quinuclidine, **5**, is about 2200 times as strong a base than benzoquinuclidine, **9**, but in the gas phase they possess equal basicity within experimental error (8).

For systems in which both the $-I$ and $+R$ effects are operative, Stamius and Maas (9) have determined the base strengths of the morpholine, piperidine, and pyrrolidine enamines of isobutyraldehyde in aqueous solution at 25 °C, and concluded that they are 30–200 times weaker bases than the corresponding saturated amines and 200–1000 times weaker than the secondary amines from which they were formed. Un-

9 10

Can. J. Chem. Downloaded from www.nrcresearchpress.com by 210.87.254.5 on 09/05/12
For personal use only.

Can. J. Chem. Downloaded from www.nrcresearchpress.com by 210.87.254.5 on 09/05/12
For personal use only.

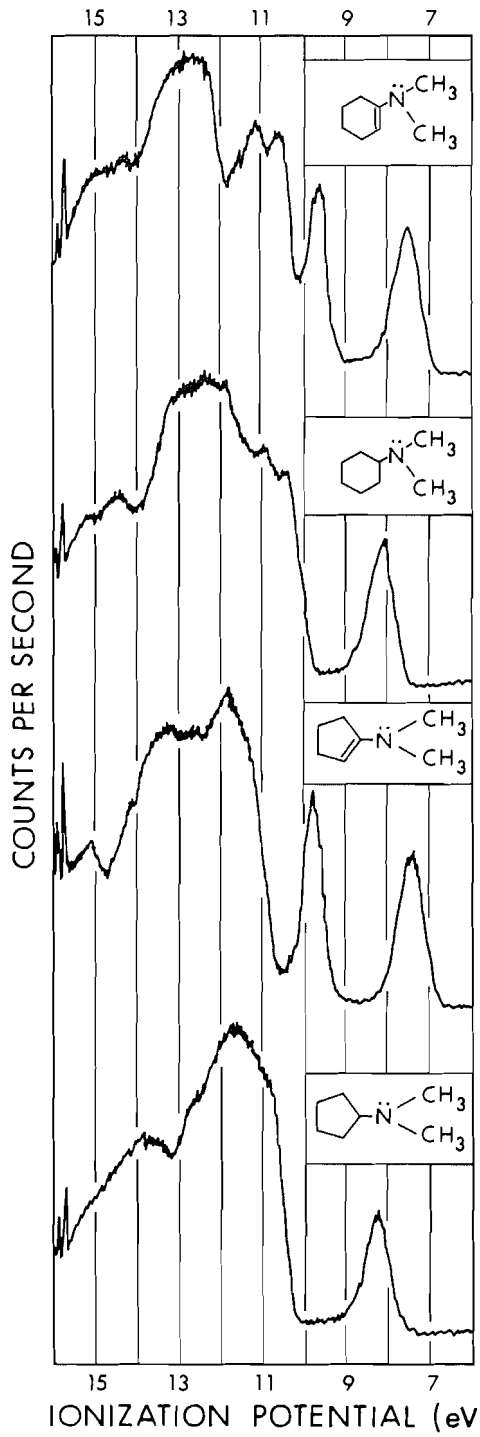

FIG. 2. The pe spectra of 1-(*N*,*N*-dimethylamino)cyclohexene, **5**, *N*,*N*-dimethylaminocyclohexane, **6**, 1-(*N*,*N*-dimethylamino)cyclopentene **7**, and *N*,*N*-dimethylaminocyclopentane, **8**, using argon as an internal calibrating gas.

doubtedly such enamines again show strong solvation effects in water but in chloroform solution, the base strength of several enamines has been shown to be 10–30 times weaker than secondary amines from which they were derived (10). In these cases, the base weakening has been attributed to both the inductive effect of the double bond and the mesomeric delocalization illustrated in **1** and **2** (9, 10).

Photoelectron Spectra

Assuming the validity of Koopmans' theorem (11), when one compares the π-bond energy of **3**, with that of the carbocyclic analogue bicyclo-[2.2.2]oct-2-ene, **10**, the former appears to be stabilized relative to the latter by 0.36 eV (9.41 eV *vs.* 9.01 eV (12)). In principle, stabilization of the π-bond in dehydroquinuclidine relative to **10** could be a consequence of the $-I$ effect of nitrogen and/or a conjugative interaction of the π-orbital with an appropriate combination of empty coplanar antibonding N—C orbitals. The latter effect could effectively lower the π-bond level as illustrated in **11**, but is suspected to be

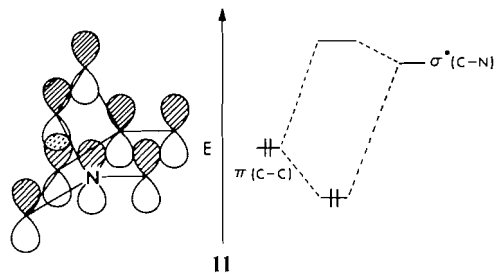

11

minimal or nonexistent in related systems (1) and therefore probably contributes little to the molecule at hand.[2]

Interestingly, the n_N orbital of **3** has been lowered in energy by (8.44 eV − 8.02 eV = 0.42 eV) relative to quinuclidine, **4**. This stabilization is undoubtedly due to the presence of the π-bond and can, in principle, arise from the greater inductive effect (13) of the adjacent sp^2 hybridized carbons relative to the sp^3 hybridized carbons in quinuclidine. The pe spectrum of benzoquinuclidine, **9**, also shows a marked stabilization of

[2]CNDO/2 calculations on dehydroquinuclidine indicate that the orbital comprised mainly of π-character possesses no contribution of the type suggested in **11**. In fact the π-molecular orbital in dehydroquinuclidine appears extensively delocalized and contains contributions from the coplanar σ-framework.

Can. J. Chem. Downloaded from www.nrcresearchpress.com by 210.87.254.5 on 09/05/12
For personal use only.

TABLE 1. Ionization potential data for compounds **3–8** derived from pe spectroscopy

Compound	Vertical IP (eV) and Assignment	
Dehydroquinuclidine **3**	8.44(n_N)[a], 9.41(π),	10.70(σ)[b]
Quinuclidine **4**[c]	8.02(n_N),	10.45(σ)[b]
1-(*N*,*N*-Dimethylamino)cyclohexene **5**	7.56($n_N - \pi$), 9.70($n_N + \pi$),	10.66(σ)
N,*N*-Dimethylaminocyclohexane **6**	8.09(n_N),	10.40(σ)
1-(*N*,*N*-Dimethylamino)cyclopentene **7**	7.46($n_N - \pi$), 9.76($n_N + \pi$),	11.25(σ)
N,*N*-Dimethylaminocyclopentane **8**	8.34(n_N),	10.86(σ)

[a]Adiabatic IP (taken as the onset potential) is 8.02 eV.
[b](σ) defines the first maximum of the broad envelope ascribed to the ionization of the σ-bonds.
[c]Reference 24.

the n_N orbital, relative to **4**, also caused by the presence of the aromatic ring (IP_V n_N = 8.35 eV (14)).

An alternative explanation which may account for the lowering of the n_N orbital of **3** relative to **4** might involve a sterically imposed rehybridization of the nitrogen in **3** to generate an n_N orbital of larger *s*-character than that in **4**. Morishima and co-workers (15) have demonstrated a linear relationship between the IP_V of the n_N orbital of cyclic amines, and percent *s*-character. The question reduces to one of whether the presence of π-bond in **3** constrains the nitrogen sufficiently to account totally for the lowering of n_N.

Intuitively, it seems peculiar that two connected electron-withdrawing groups should *lower* the energy of the outermost occupied orbital on each group. One may well expect that, if simple inductive arguments hold, the excess electron density acquired by nitrogen from its neighbors would be reflected in a reduction of the IP of n_N. That such a reduction is not observed suggests additional factors which complicate the situation. The stabilization of the outermost orbitals of two electron-withdrawing groups by the presence of each other is not a unique phenomenon restricted to **3**. In fact, an assessment of some IP data for propenes substituted at the allylic position by an electronegative group reveals the same general shifts of the n_x and π-orbitals as shown above. For the examples given in Table 2, homoconjugative interactions between n_x and the π-bond would not be expected to produce the observed shifts. In these noncyclic molecules, sterically imposed rehybridization of the type demonstrated by Morishima and co-workers (15) cannot be important, since such geometric restriction is absent. However, inductive effects can account for the observed trends. Unfortunately the charge redistribution which results from the introduction of groups of differing electronegativity will probably be closely associated with some rehybridization which allows the molecule to reach its lowest possible energy.

This aspect of substituent effects was originally discussed by Walsh in 1947 (16) who suggested the following rule: "If a group X attached to carbon is replaced by a more electronegative group Y, then the carbon valency toward Y has more *p*-character than it had toward X". Later Bent (17) in applying this generalization to atoms containing lone pairs reformulated the rule as: "Atomic *s*-character concentrates in orbitals directed toward electropositive substituents". If lone pairs are considered to be directed toward highly electropositive groups (17, 18), then increasing the electronegativity of groups X attached to atom N puts more *p*-character into the N—X bonds, and conversely more *s*-charac-

TABLE 2. Vertical ionization potentials of 3-substituted propenes

Compound	Vertical IP (eV)	
	π-(C—C)	Substituent n
Propene	10.01[a]	
1-Propanol		10.50[b]
Allyl alcohol	10.22[c]	10.99[c]
1-Chloropropane		10.88[d]
Allyl chloride	10.38[c]	11.21[c]
1-Bromopropane		10.34[d,e]
Allyl bromide	10.20[c]	10.62[c,e]
Allyl fluoride	10.60[c]	12.43[c]

[a]Reference 25.
[b]Reference 26.
[c]Reference 27.
[d]Reference 28.
[e]Average of $P_{3/2}$, $P_{1/2}$ splitting.

12

ter into the lone pair, thus lowering its energy. Hence, it is entirely conceivable that one cannot separate the $-I$ effect from inductively induced rehybridization because one effect is a consequence of the other. If such effects are operative in the open-chain systems, they may also be evident in the bicyclic system as well. For the remainder of the discussion, we will attribute the lowering of the n_N orbital in **3** relative to **4** to the $-I$ effect of the π-bond, regardless of whether the exact cause is electronegativity or induced rehybridization.

With the inductive effects of each group on the other qualitatively evaluated, we can now apply these data to enamines **5** and **7** in which delocalization is *not* prohibited by the stereochemical relationships of the groups. Inductive effects such as those present in dehydroquinuclidine must also be operative in conjugated enamines although they are undoubtedly altered by changes in bond length and substitution.

Conjugative interaction between n_N and π in both **5** and **7** preclude orbital assignments which may be classified simply as the nitrogen lone pair or π-bond (14). Rather, as has been clearly discussed by Hoffmann (19), when two orbitals of different energy interact, the lower energy one becomes stabilized by "mixing into itself the higher one in a bonding way, while the upper orbital mixes into itself the lower one in an antibonding way" and becomes destabilized. Thus in enamines **5** and **7** where such interaction is possible, the highest occupied molecular orbital (homo) can be represented as $(n_N - \pi)$ while the second highest MO is represented as $(n_N + \pi)$. An energy level diagram illustrating this point is shown in Fig. 3.

Figure 3 depicts two situations for both **5** and **7** before and after conjugative interaction. In the

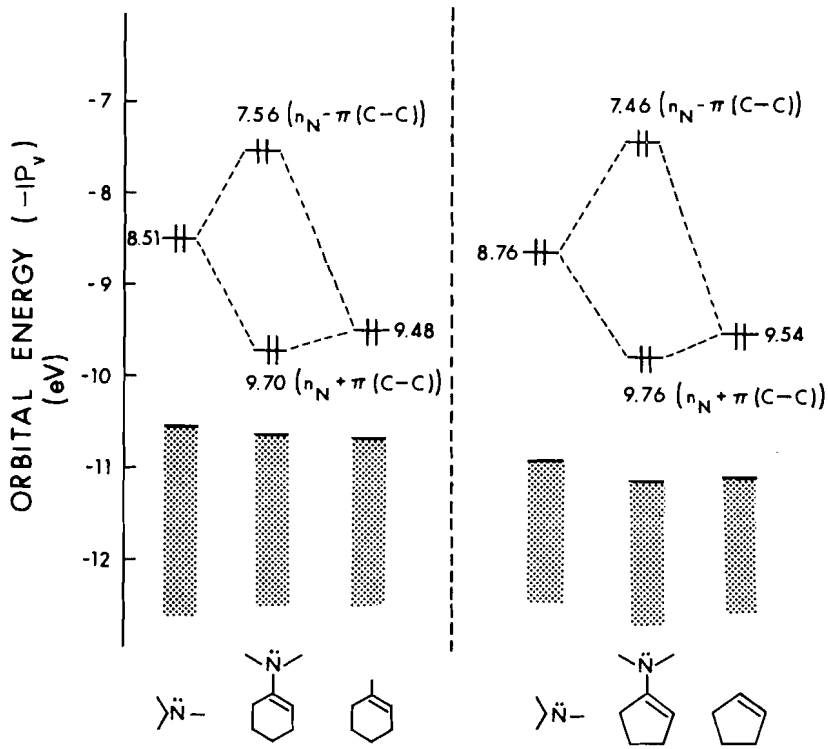

FIG. 3. An energy level diagram illustrating the conjugative interaction between n_N and $\pi_{(C-C)}$ in enamines **5** and **7**. Energy levels are assumed to be equal to $-IP_v$ (9). Values of the levels of the noninteracting units were derived from suitable models corrected for the inductive effects of the substituents (see text). The shaded areas represent the broad envelope ascribed to ionization of the σ-orbitals.

Can. J. Chem. Downloaded from www.nrcresearchpress.com by 210.87.254.5 on 09/05/12
For personal use only.

Can. J. Chem. Downloaded from www.nrcresearchpress.com by 210.87.254.5 on 09/05/12
For personal use only.

absence of delocalization, the starting n_N level for **5** will simply be that of *N,N*-dimethylaminocyclohexane, **6**, modified by the $-I$ effect introduced by the presence of the double bond (-8.09 eV -0.42 eV). Similarly the $\pi_{(C-C)}$ level will be that of unsubstituted cyclohexene (20) modified by the $-I$ effect of the nitrogen (-9.12 eV -0.36 eV). These $-I$ effects of each group upon the other can at least be qualitatively assessed by a comparison of the observed pe values for the orbitals of dehydroquinuclidine, quinuclidine (21), and bicyclo[2.2.2]oct-2-ene (12). Allowing the two orbitals to interact causes a substantial increase in their separation relative to the non-interactive case. The splitting observed between $n_N - \pi$ and $n_N + \pi$ in **5** and **7** is 2.31 eV and 2.30 eV respectively.[3]

It can be shown (23) from a simple LCAO model that when two orbitals (n_N and π) of differing energy interact, the final separation of the two can be given as:

$$\Delta E = ((n_N - \pi)^2 + 4\beta^2)^{1/2}$$

where

$$\beta = \int(n_N H \pi)d\tau$$

Using basis orbitals obtained as above, one can calculate that $\beta(n_N, \pi) = 0.59$ and 0.65 eV for **5** and **7** respectively. Thus the resonance interaction of the two moieties in both enamines is substantial and probably equal. One has no means of assessing whether the interaction in **5** and **7** is optimized, but it certainly will be decreased as the n_N orbital approaches a perpendicular orientation to the double bond. Some chemical reactivity consequences of the lack of coplanarity of orbitals were demonstrated by Opitz *et al.* (24) for the pyrrolidine enamines of cycloheptanone, cyclooctanone, and cyclononanone.

Alkylation of 1-pyrrolidinocycloheptene with ethyl iodide produces 41% *C*- and 53% *N*-alkylation while similar conditions produce only *N*-alkylation for the eight- and nine-membered rings. Presumably geometric restrictions prevent optimum interaction of n_N and π in the latter systems, and if present should be easily monitored by pe spectroscopy.[4]

Conclusion

From the above study one can see that the enamine nitrogen can exert two opposing effects on the adjacent double bond, a $-I$ effect and a $+R$ effect. These effects can be distinguished from each other by recognizing that maximum conjugative interactions require coplanarity of the interacting orbitals. In the absence of such conjugation the electronegativity of nitrogen results in inductive withdrawal of electron density from the π-bond forcing the latter to higher binding potential. Observation of increased binding potential for n_N of dehydroquinuclidine relative to quinuclidine leads one to assess the consequences of the introduction of a π-orbital on the IP of the nitrogen lone pair in the absence of conjugation. If Koopmans' theorem holds and molecules **3** and **4** do not experience widely differing relaxation effects on ionization, then the reasons for the above observation may be associated with the inductive withdrawal of electron density from n_N to the π-system and/or 'inductively induced' rehybridization. The exact reasons are as yet unclear but are certainly deserving of further study.

Acknowledgments

The author gratefully acknowledges the financial support of the University of Alberta and the National Research Council of Canada.

1. R. S. Brown. Can. J. Chem. **54**, 000 (1976).
2. G. Stork, R. Terrell, and J. Szmuszkovicz. J. Am. Chem. Soc. **76**, 2029 (1954).
3. A. G. Cook (*Editor*). Enamines. Marcel Dekker, New York. 1969.

[3]A recent study (22) has shown that the $n_N - \pi$ and $n_N + \pi$ levels in 2-methyl-2-azabicyclo[3.2.1]octa-3-ene are separated by 2.77 eV. It is difficult to compare this separation with those found here because the substitution of the double-bond differs.

[4]Note added in proof—We have subsequently determined the pe spectra of the dimethyl enamines of cycloheptanone and cyclooctanone to test for such restriction of conjugative interaction. For the former (IP_V ($n_N - \pi$) = 7.57 eV; ($n_N + \pi$) = 9.50 eV) the splitting is 1.93 eV while that for the latter (IP_V ($n_N - \pi$) = 7.50 eV; ($n_N + \pi$) = 9.55 eV) is 2.05 eV. While this splitting is less than that found for enamines **5** and **7**, it still suggests that appreciable interaction is present in the seven- and eight-membered rings of this series. Further work is still required in the pyrrolidino series to determine if the difference in chemical reactivity for these systems is a consequence of differences in conjugative interactions.

4. (*a*) A. R. BASSINDALE, C. EABORN, D. R. M. WALTON, and D. J. YOUNG. J. Organometal. Chem. **20**, 49 (1969); (*b*) W. H. HANSTEIN, H. J. BERWIN, and T. G. TRAYLOR. J. Am. Chem. Soc. **92**, 7476 (1970); (*c*) J. P. MAIR and D. W. TURNER. Discuss. Faraday Soc. **54**, 149 (1972); (*d*) J. P. MAIR and D. W. TURNER. J. Chem. Soc. Faraday Trans II, **69**, 196 (1973).
5. (*a*) C. GROB, A. KAISER, and E. RENK. Chem. Ind. (London), 598 (1957); (*b*) C. GROB, A. KAISER, and E. RENK. Helv. Chim. Acta, **40**, 2170 (1957).
6. E. P. BLANCHARD. J. Org. Chem. **28**, 1397 (1963).
7. M. MOUSSERON, R. JACQUIER, and R. ZAGDOWN. Bull. Soc. Chim. Fr. 197 (1952).
8. R. W. TAFT. Proton transfer reactions. *Edited by* E. F. Hall and V. Gold. Chapman and Hall Ltd., London. 1975.
9. (*a*) E. J. STAMIUS and W. MAAS. J. Org. Chem. **30**, 2156 (1965); (*b*) E. J. STAMIUS and W. MAAS. J. Org. Chem. **30**, 2160 (1965).
10. G. STORK, A. BRIZZOLARA, H. LANDESMAN, J. SZMUSZKOVICZ, and R. TERRELL. J. Am. Chem. Soc. **85**, 207 (1963).
11. T. KOOPMANS. Physica, **1**, 104 (1934).
12. (*a*) P. BISCHOF, J. A. HASHMALL, E. HEILBRONNER, and V. HORNUNG. Helv. Chim. Acta, **54**, 783 (1971); (*b*) E. HEILBRONNER. Isr. J. Chem. **10**, 143 (1972).
13. R. S. MULLIKEN. J. Am. Chem. Soc. **72**, 4500 (1950).
14. J. P. MAIER and D. W. TURNER. J. Chem. Soc. Faraday Trans. II, **69**, 521 (1973).
15. K. YOSHIKAWA, M. HASHIMOTO, and I. MORISHIMA. J. Am. Chem. Soc. **96**, 288 (1974).
16. (*a*) A. D. WALSH. Discuss. Faraday Soc. **2**, 18 (1947); (*b*) A. D. WALSH. Trans. Faraday Soc. **42**, 56 (1946); (*c*) A. D. WALSH. Trans. Faraday Soc. **43**, 60 (1947).
17. H. A. BENT. Chem. Rev. **61**, 275 (1961).
18. C. C. LEVIN. J. Am. Chem. Soc. **97**, 5469 (1975).
19. R. HOFFMANN. Acc. Chem. Res. **4**, 1 (1971).
20. P. BISCHOF and E. HEILBRONNER. Helv. Chim. Acta, **53**, 1677 (1970).
21. P. BISCHOF, J. A. HASHMALL, E. HEILBRONNER, and V. HORNUNG. Tetrahedron Lett. **46**, 4025 (1969).
22. G. LAUR, W. SCHÄFER, and A. SCHWEIG. Tetrahedron Lett. 3939 (1975).
23. G. G. PITT. J. Organometal. Chem. **61**, 49 (1973).
24. G. OPITZ, H. MILDENBERGER, and H. SUHR. Ann. **649**, 47 (1961).
25. P. MASCLET, D. GROSJEAN, G. MOUVIER, and J. DUBOIS. J. Elect. Spectr. **2**, 225 (1973).
26. M. B. ROBIN and N. A. KUEBLER. J. Electron Spectrosc. Relat. Phenom. **1**, 13 (1972).
27. G. W. MINES and H. W. THOMPSON. Spectrochim. Acta, **29**, 3177 (1973).
28. K. KIMURA, S. KATSUMATA, Y. ACHIBA, H. MATSUMOTO, and S. NAKAGURA. Bull. Chem. Soc. Jpn. **46**, 373 (1973).

Can. J. Chem. Downloaded from www.nrcresearchpress.com by 210.87.254.5 on 09/05/12
For personal use only.

Effect of aging on properties of polynuclear hydroxyaluminum cations[1]

ROBERT C. TURNER[2]

Soil Research Institute, Research Branch, Canada Department of Agriculture, Ottawa, Canada K1A 0C6
and
Department of Soil Science, Saskatchewan Institute of Pedology, University of Saskatchewan, Saskatoon, Saskatchewan S7N 0W0

Received August 21, 1975

ROBERT C. TURNER. Can. J. Chem. **54**, 1528 (1976).

Very slow partial neutralization of 5×10^{-4} to 6×10^{-2} *M* solutions of $AlCl_3$ and $Al(ClO_4)_3$, using either finely ground dolomite or NH_3 as the base, resulted in the formation of polynuclear hydroxyaluminum cations without the appearance of any solid phases. Certain properties of the polynuclear cations did not change and no solids formed during an aging period of two years. The properties of the polynuclear cations examined were their rate of reaction with 8-hydroxyquinoline and hydrolysis constants using formulas suggested in the literature. In contrast, the concentration of the polynuclears decreased, although very slowly, during aging. This decrease was accompanied by the appearance of a second type of polynuclear hydroxyaluminum cation, which apparently has the same OH/Al mole ratio but is much less reactive than the first type.

ROBERT C. TURNER. Can. J. Chem. **54**, 1528 (1976).

La neutralisation partielle, très lente, de solutions 5×10^{-4} à 6×10^{-2} *M* de $AlCl_3$ et $Al(ClO_4)_3$, utilisant soit de la dolomite en poudre fine ou de l'ammoniac comme base, conduit à la formation de cations hydroxyaluminium polynucléaires sans l'apparition de phases solides. Certaines propriétés des cations polynucléaires ne changent pas et aucun solide ne se forme durant une période de vieillissement de deux ans. Les propriétés des cations polynucléaires qui ont été examinées sont leur vitesse de réaction avec l'hydroxy-8 quinoléine et leur constante d'hydrolyse utilisant des formules suggérées dans la littérature. Par opposition, la concentration des cations polynucléaires diminue, quoique très lentement, durant le processus de vieillissement. Cette diminution est accompagnée par l'apparition d'un second type de cations hydroxyaluminium polynucléaires qui a apparamment le même rapport molaire OH/Al mais qui est beaucoup moins réactif que le premier type.

[Traduit par le journal]

Introduction

It was concluded by Turner (1) and Smith (2) that three forms of Al existed in partially neutralized aqueous solutions or more properly suspensions. This conclusion was based on the observation of different rates of reaction with 8-hydroxyquinoline (1) and ferron (2). The first reaction was instantaneous for all practical purposes, which led to the assumption that the reaction was with mononuclear Al cations. The second was a pseudo-first order process leading to the assumption that the solution contained polynuclear hydroxyaluminum cations. The third form was thought to be composed of solids, from the observation that it reacted very slowly or not at all after a few hours aging. There is some disagreement, however, concerning the effect of aging and degree of neutralization on properties of the polynuclear cations. Turner and Ross (3) stated that the specific rate constant for the reaction between them and 8-hydroxyquinoline, using the standard procedure (4), was 0.16 min^{-1} and that this rate constant was independent of degree of neutralization and length of time of aging of the polynuclear cations. They concluded that the polynuclear cations do not hydrolyze and polymerize upon standing, that is, only the initial solid phases progress to gibbsite.

Smith (2), on the other hand, claimed that the rate constant decreased with increasing degree of neutralization and, at least in some cases, with length of time of aging. Smith (2) concluded from his results, largely on the basis of the changes in the magnitude of the rate constant, that the polynuclear cations grow and eventually become gibbsite.

Smith's (2) conclusion supports the theory

[1]Contribution No. 534 S.R.I. and No. R165 Saskatchewan Institute of Pedology.

[2]Present address: Department of Soil Science, Saskatchewan Institute of Pedology, University of Saskatchewan, Saskatoon, Saskatchewan S7N 0W0.

Can. J. Chem. Downloaded from www.nrcresearchpress.com by 210.87.254.6 on 09/05/12
For personal use only.

Can. J. Chem. Downloaded from www.nrcresearchpress.com by 210.87.254.6 on 09/05/12
For personal use only.

expressed by Hsu and Bates (5) for the development of crystalline aluminum hydroxides. Patterson and Tyree (6), however, as late as 1973, suggest that further work similar to that done by Smith (2) and Bilinski and Tyree (7) should be done to decide the equilibrium state to which hydrolyzed aluminum solute species are tending.

The exact formula for the polynuclear cations is not known. Some of the formulae that have been suggested are: $Al_6(OH)_{15}^{3+}$ (8); $Al_8(OH)_{20}^{4+}$ (9); $Al_{13}(OH)_{32}^{7+}$ (10); $Al_{14}(OH)_{34}^{8+}$ (11). It is not possible, therefore, to calculate unequivocally the concentration of the polynuclear cations from a knowledge of the concentration of Al present as polynuclear cations. It is possible, however, to calculate their concentration assuming any particular formula.

From the foregoing, it is obvious that the question of whether or not the properties of the polynuclear cations change with degree of neutralization and aging is of prime importance. Furthermore, using the standard procedure (4) for determining the concentration of Al present as polynuclear cations, it is possible to calculate their concentration based on any one of the formulae suggested. The calculated concentration will depend, of course, on the formula chosen. From the calculated concentration of the polynuclear cations along with p*H* and Al^{3+} concentration it is possible to calculate a concentration-dependent hydrolysis constant for the formula chosen. The only assumption implied is that only one species exists in the solution. The effect of degree of neutralization and length of time of aging can then be determined. If the degree of neutralization and/or aging affect the calculated hydrolysis constant for the particular formula assumed one can be reasonably sure that the formula is not the correct one or the polynuclear cations are changing with degree of neutralization and/or aging.

The objective in the work reported here was to prepare solutions containing polynuclear cations but without the formation of any solid phases. If this could be done no gibbsite should form, if Turner and Ross are correct, the concentration of the polynuclear cations should remain constant indefinitely and properties of the polynuclear cations could be studied over an unlimited length of time. The properties selected for study were: (*a*) the rate of reaction between them and 8-hydroxyquinoline and (*b*) the hydrolysis constants for their formation assuming each of the following formulae in turn: $Al_6(OH)_{15}^{3+}$ (8); $Al_8(OH)_{20}^{4+}$ (9); $Al_{13}(OH)_{32}^{7+}$ (10); and $Al_{14}(OH)_{35}^{7+}$. The justification for using the fourth arose from observations made during this study.

Experimental

The procedures followed for partially neutralizing Al salt solutions without the formation of any solid phases were based on the idea that the polynuclear cation would form at an ion activity product, $(Al)(OH)^3$, lower than that at which the solids could form (3). In particular, the base was introduced at a rate such that the formation of the polynuclear cations would maintain the ion activity product less than that required for the formation of the initial solid phases. The chemicals used were reagent grade with the exception of dolomite, which was a natural product. The Ca/Mg mole ratio of the dolomite was unity and it had the theoretical CO_2 content. It was ground to pass a 100 mesh sieve. X-Ray analysis of oriented samples was done with a Phillips diffractometer using Fe-filtered Co radiation. In the dialysis experiments the solutions were placed in dialysis bags and the bags were then suspended in double distilled H_2O. A continuous flow of water was maintained outside the bag and the bag was agitated intermittently over a 24 h period.

Procedure A

Finely ground dolomite, which has a relatively slow rate of dissolution, was added to solutions of $AlCl_3$ or $Al(ClO_4)_3$ and the solutions were stirred vigorously with a magnetic stirrer for 5 days. The solutions were then filtered through No. 42 Whatmann filter papers and CO_2-free air was bubbled through the filtrates for several hours with the object of removing carbonic acid. The solutions were stored in ground glass stoppered Erlenmeyer flasks with gentle stirring at 25 °C. Over an extended length of time, the p*H*, total and dialyzable Al and the rate of reaction between 8-hydroxyquinoline and the Al in solution by the standard method (4) were determined periodically. The concentration of mononuclear Al was assumed to be that which reacted instantaneously and the concentration of Al present as the polynuclear cations that which reacted via the pseudo-first order reaction with 8-hydroxyquinoline.

Procedure B

The Al salt solutions were placed in Teflon reaction vessels and stirred vigorously with magnetic stirrers. Air which had passed through a succession of scrubbers containing NaOH, H_2SO_4, lithasorb, and H_2O was bubbled through a column of a solution of *N* NH_4Cl to which NaOH had been added. The mixture of CO_2-free air and NH_3 was led into Teflon reaction vessels over the surface of the salt solutions. There was another outlet to allow the air–NH_3 mixture to pass out of the reaction vessels. The concentration of NaOH in the NH_4Cl solutions governed the concentration of NH_3 in the air that was led into the containers. The concentration of NH_3 was adjusted so that it required a month or more to reach 80% neutralization. The solutions, after neutralization to the

TABLE 1. Effect of aging on the specific rate constant for reaction between the hydroxyaluminum polynuclear cations and 8-hydroxyquinoline

Salt	Concentration	Base	Degree neutralization	Number of dtns.	Days aged	Correlation coefficient[a]	Mean specific rate constant	Standard deviation[b]
$AlCl_3$	10^{-2}	Dolomite	0.81	24	553	+0.09	0.160	0.010
$AlCl_3$	10^{-2}	Dolomite	0.79	10	651	+0.60[c]	0.161	0.005
$AlCl_3$	10^{-2}	Dolomite[d]	0.79	12	214[e]	−0.22	0.167	0.010
$AlCl_3$	10^{-2}	Dolomite	0.55	17	730	+0.34	0.166	0.010
$AlCl_3$	10^{-2}	Dolomite	0.29	15	530	+0.44	0.170	0.021
$AlCl_3$	10^{-2}	Dolomite	0.13	13	356	−0.13	0.162	0.023
$Al(ClO_4)_3$	6×10^{-2}	$CaCO_3$	0.81	7	465[f]	−0.20	0.157	0.013
$AlCl_3$	5×10^{-4}	Dolomite	0.75	18	445	−0.31	0.155	0.009
$AlCl_3$	5×10^{-4}	Dolomite	0.52	12	646	−0.30	0.163	0.010
$AlCl_3$	5×10^{-4}	Dolomite	0.32	12	432	−0.53[c]	0.162	0.017
Total with procedure A				121	—	+0.02	0.162	0.014
$AlCl_3$	10^{-2}	NH_3	0.81	16	558	−0.20	0.164	0.007
$AlCl_3$	10^{-2}	NH_3	0.75	12	581	−0.03	0.164	0.008
$AlCl_3$	10^{-2}	NH_3	0.46	15	589	+0.47[c]	0.164	0.007
$Al(ClO_4)_3$	10^{-2}	NH_3[g]	0.83	11	66[h]	+0.05	0.170	0.016
$AlCl_3$	5×10^{-4}	NH_3	0.79	6	107	−0.17	0.156	0.009
$AlCl_3$	5×10^{-4}	NH_3	0.54	10	110	−0.12	0.161	0.007
Total with procedure B				59		+0.06	0.163	0.003

[a]Correlation coefficient for regression of rate constant on days aging.
[b]Standard deviation.
[c]Significant at $P_{0.05}$ level.
[d]Seeded with synthetic gibbsite after 224 days aging.
[e]Polynuclears absent after 214 days but solid showed only a trace of gibbsite after 517 days aging.
[f]Polynuclears absent after 465 days aging but the solid did not show a very strong gibbsite pattern after 837 days aging.
[g]NH_3 added in 24 h.
[h]Strong gibbsite pattern after 66 days aging.

degree desired, were stored in closed Teflon bottles at 25 °C with gentle stirring. The same determinations were made as with Procedure A.

Three variations of procedures A and B were made to show the effect of initial solid phases, which crystallize to gibbsite during aging, on the properties of systems containing polynuclear cations. The variation with procedure B was to increase the concentration of NH_3 to the extent that 80% neutralization was attained in 24 h. It was not possible to increase the rate of dissolution of the dolomite so one variation with procedure A was to replace the dolomite with $CaCO_3$, which dissolves much more rapidly. A second variation with procedure A was to divide a solution, which had been 79% neutralized and aged 224 days, into two. To one was added a small amount of synthetic gibbsite and then both solutions were aged for a further 517 days.

Results and Discussion

When procedure A or B was used, the presence of solids could not be detected in any of the systems at any time during more than 2 years aging. All of the Al passed through a 25 nm millipore filter and diffused readily across a dialysis membrane regardless of the total Al concentration, which varied from 5×10^{-4} to 6×10^{-2} M, or degree of neutralization, which varied from 0.04 to 0.81. Thus the first objective of the work, to prepare the polynuclear cations without the formation of any solid phases, was successful. On the other hand, when dolomite was replaced with $CaCO_3$, which dissolves much more rapidly, solids formed and gibbsite was eventually identified in the suspensions. The X-ray diffraction patterns of the oriented specimens for the various samples of gibbsite were never very strong, however, even after 837 days aging. With the rapid addition of NH_3, so that the desired degree of neutralization was attained in 24 h, solids were formed and after three weeks aging exhibited strong X-ray diffraction patterns.

Table 1 is a summary of the results showing the effect of degree of neutralization and aging on the specific rate constant for each reaction between the polynuclear cations and 8-hydroxyquinoline. The rate constants were calculated using the method of linear least squares for the best fit of the natural log of the concentration of Al as polynuclear cations remaining to react *vs.*

Can. J. Chem. Downloaded from www.nrcresearchpress.com by 210.87.254.6 on 09/05/12
For personal use only.

Can. J. Chem. Downloaded from www.nrcresearchpress.com by 210.87.254.6 on 09/05/12
For personal use only.

time. The concentration remaining to react was calculated as the concentration that had reacted at $t = \infty$ minus that which had reacted at $t = t$. Since there was no measurable reaction between 30 and 50 min for all experiments during the first 4 weeks of aging, $t = 30$ min was used as $t = \infty$ for all the subsequent experiments. In calculating the line of best fit, $t = 2$ min was taken as zero time for two reasons: (*a*) the reaction with the dimer $Al_2(OH)_2^{4+}$, although not instantaneous, is very rapid and is complete in 2 min (12); and (*b*) with low concentrations of Al and relatively high degrees of neutralization using dolomite as the base (procedure A), there was a small but definite induction period, probably caused by the presence of carbonates. In three cases the correlation coefficient for the regression of the specific rate constant on number of days aged was significant at the $P_{0.05}$ level (Table 1). In two of these cases, however, one with procedure A and one with procedure B, the correlations were positive while in the other it was negative. When all of the results by either procedure A or B were combined, the correlation coefficient between the rate constant and length of time of aging was not significant even at the $P_{0.50}$ level. Similarly, the results in Table 1 show no significant effect of degree of neutralization on the specific rate constant. There were differences between individual pairs but, as with the effect of aging, the differences were obviously caused by experimental error. When all of the results by procedure A were combined the mean specific rate constant was 0.162 min^{-1} and the corresponding mean by procedure B was 0.163 min^{-1}. With the three special experiments, which were made to show the effect of the formation of solid hydroxyaluminum phases on the polynuclear cations, the experimental error was relatively large because many of the determinations were made with rather low concentrations of polynuclear cations. The mean value for the specific rate constant with these experiments was 0.166 min^{-1}. From these results, it can be concluded that the polynuclear cations do not increase in size and complexity with length of time of aging or degree of neutralization, when the rate of reaction with 8-hydroxyquinoline is the criterion used to characterize them.

Hydrolysis constants $K_{c(n,m)}$ were calculated, assuming in turn that $Al_6(OH)_{15}^{3+}$, $Al_8(OH)_{20}^{4+}$, $Al_{13}(OH)_{32}^{7+}$, or $Al_{14}(OH)_{35}^{7+}$ was the formula for the polynuclear cations, for all experiments in which procedures A and B were used. The subscript c in the K_c's denotes that they are not thermodynamic hydrolysis constants, *i.e.* they depend largely on concentrations rather than activities. The K_c's are defined by the equation

$$[1] \qquad K_{c(n,m)} = \frac{[Al_m(OH)_n^{(3m-n)+}](H^+)^n}{[Al^{3+}]^m}$$

where square brackets and parentheses denote concentrations and activities, respectively.

The calculated pK_c's were the same regardless of whether procedure A or B was used. Table 2 shows the pK_c's for $Al_{13}(OH)_{32}^{7+}$ and $Al_6(OH)_{15}^{3+}$. Those for $Al_8(OH)_2^{4+}$ and $Al_{14}(OH)_{35}^{7+}$ were calculated but are not shown in the table because the two shown are sufficient to illustrate everything necessary for interpretations. Results from another investigation, in which NaOH was the base used, are included in Table 1. In that investigation, the degree of neutralization was only 0.04 so that no solid phases were formed. It seemed legitimate, therefore, to include them here.

The magnitude of the pK_c's were not affected by the length of time of aging of the polynuclear cations, as shown by the very small standard deviations for each experiment. This evidence supports the conclusion reached with the reaction rate studies (Table 1), *i.e.* the polynuclear cations do not increase gradually in size and complexity with length of time of aging.

The effect of degree of neutralization on the calculated pK_c's is not consistent. The $pK_{c(15,6)}$'s were higher for the very low degrees of neutralization (0.04) than for the higher ones, for a given total Al concentration or ionic strength. The calculated $pK_{c(20,8)}$'s were also affected in the same way by the degree of neutralization but to a lesser extent. The $pK_{c(32,13)}$'s and $pK_{c(35,14)}$'s however, were not affected by the degree of neutralization. The formula $A_{13}(OH)_{32}^{7+}$ has an OH/Al mole ratio somewhat less than 2.5, whereas the others have this ratio equal to 2.5. It was for this reason that $Al_{14}(OH)_{35}^{7+}$ was also considered. Since $pK_{c(35,14)}$ was also independent of degree of neutralization, it appears that the affect of degree of neutralization on $pK_{c(15,6)}$ and $pK_{c(20,8)}$ was because the formulas $Al_6(OH)_{15}^{3+}$ and $Al_8(OH)_{20}^{4+}$ do not have enough Al atoms per polynuclear cation to represent the formula

TABLE 2. Effect of aluminum concentration and degree of neutralization on calculated hydrolysis constants and on [Al](OH)^3 when no solids were formed

Concentration (M)	Degree of neutralization	Days aged	N^a	$pK_{c(32,13)}$	$pK_{c(15,6)}$	p[Al](OH)^3
6×10^{-2}	0.70	613	13	104.98 ± 0.29^b	50.49 ± 0.14^b	31.94
6×10^{-2}	0.44	687	11	104.76 ± 0.33	50.56 ± 0.23	32.03
10^{-2}	0.81	555	24	103.27 ± 0.93	50.10 ± 0.44	31.82
10^{-2}	0.81	706	15	103.34 ± 0.35	50.10 ± 0.19	31.95
10^{-2}	0.79	620	9	103.65 ± 0.66	50.24 ± 0.33	31.85
10^{-2}	0.75	581	12	103.14 ± 0.59	50.00 ± 0.28	31.89
10^{-2}	0.55	672	18	103.61 ± 0.47	50.21 ± 0.25	32.08
10^{-2}	0.46	586	14	103.06 ± 0.49	50.01 ± 0.22	32.15
10^{-2}	0.29	538	15	103.58 ± 0.50	50.44 ± 0.27	32.16
10^{-3c}	0.04	30	10	103.40 ± 0.13	51.47 ± 0.09	32.17
5×10^{-4c}	0.04	30	10	103.08 ± 0.13	51.55 ± 0.13	32.16
10^{-4c}	0.04	30	10	103.76 ± 0.70	51.77 ± 0.31	31.97
10^{-3d}	0.04	30	10	101.15 ± 0.16	50.44 ± 0.12	32.38
5×10^{-4}	0.79	107	6	101.13 ± 1.03	49.85 ± 0.47	31.90
5×10^{-4}	0.72	485	17	100.56 ± 0.54	49.66 ± 0.25	32.03
5×10^{-4}	0.54	112	10	100.59 ± 1.11	49.61 ± 0.51	32.16
5×10^{-4}	0.52	647	12	100.77 ± 0.42	49.77 ± 0.21	32.16
5×10^{-4}	0.40	677	14	101.04 ± 0.30	49.99 ± 0.15	32.21
5×10^{-4d}	0.04	30	10	100.85 ± 0.09	50.72 ± 0.06	32.37
10^{-4d}	0.04	30	10	100.60 ± 0.08	50.60 ± 0.06	32.24

[a]Number of determinations made periodically during aging.
[b]Standard deviations.
[c,d]Included from another investigation. NaOH as base. Aged 30 days and then 10 replicate determinations. (*c* adjusted to ionic strength 0.06.)

for them. On the strength of the fact that $pK_{c(32,13)}$ and $pK_{c(35,14)}$ were not affected by the degree of neutralization, it can be concluded that the polynuclear cations do not increase in size and complexity with degree of neutralization, a conclusion that is again in agreement with the results from the rate of reaction studies (Table 1).

It has been shown so far that it is possible to prepare polynuclear hydroxyaluminum cations without the formation of any solid phases, and these polynuclear cations do not increase gradually in size and complexity with degree of neutralization or length of time of aging. There remains the question of whether or not, under these conditions, the polynuclear cations remain at constant concentration regardless of length of time of aging.

It can be seen by the results in Table 3, which are representative of 18 such individual experiments, that there was a positive correlation between length of time of aging and concentration of mononuclear Al cations and a negative correlation between length of time of aging and either pH or concentration of polynuclear hydroxyaluminum cations. The regressions, however, were small. On the basis of the calculated linear regression equation, the changes for a two year period of aging were 0.03 and 0.09 pH units, 0.13×10^{-3} and 0.17×10^{-3} in concentrations of mononuclears and 3.21×10^{-3} and 3.94×10^{-3} in concentrations of polynuclears for procedures A and B, respectively. These small changes in the concentration of mononuclear cations and pH, which resulted in very little change in [Al](OH)^3, showed that the polynuclear cations were not hydrolysing to a higher OH/Al mole ratio, as would have been the case if gibbsite were being formed. These results are entirely different from those obtained when neutralization was rapid enough to form the initial solid phases.

In one experiment in which 83% neutralization with NH_3 was attained in 24 h, the pH started at 5.22 and decreased to 3.96, the concentration of mononuclear cations increased from 0.04×10^{-3} to 1.69×10^{-3} M, the Al present as polynuclear cations decreased from 8.12×10^{-3} to 0.17×10^{-3} M, the Al present as solids increased from 0.54×10^{-3} to 6.84×10^{-3} M and p[Al](OH)^3 increased from 31.02 to 32.91 during an aging period of only 101 days. The Al present as solids in the systems was calculated assuming it was equal to the total Al in the system less that in the mononuclear and poly-

Can. J. Chem. Downloaded from www.nrcresearchpress.com by 210.87.254.6 on 09/05/12
For personal use only.

TABLE 3. Effect of aging 81% neutralized approximately 10^{-3} *M* $AlCl_3$ on p*H* and concentrations of Al as mononuclear and polynuclear Al cations

Days aged	Procedure A[a] pH	Al as monos[b] $\times 10^3$ *M*	Al as polys[b] $\times 10^3$ *M*	[Al](OH)^3	Procedure B[a] pH	Al as monos[b] $\times 10^3$ *M*	Al as polys[c] $\times 10^3$ *M*	[Al](OH)^3
4	4.64	0.183	9.95	31.91	4.64	0.289	10.26	31.71
30	4.62	0.195	9.47	31.94	—	—	—	—
56	4.66	0.210	9.34	31.79	4.62	0.310	10.16	31.74
108	4.65	0.246	9.03	31.75	4.57	0.338	9.93	31.84
173	4.63	0.265	8.83	31.78	4.56	0.360	9.50	31.84
234	4.66	0.250	8.44	31.71	4.51	0.380	9.33	31.96
258	4.63	0.265	8.41	31.78	—	—	—	—
277	—	—	—	—	4.52	0.385	8.87	31.92
320	4.62	0.284	8.19	31.78	4.50	0.400	8.61	31.97
398	—	—	—	—	4.52	0.430	8.05	—
423	4.60	0.283	7.78	31.84	—	—	—	—
468	4.61	0.318	7.47	31.76	4.52	0.420	7.81	31.88
554	4.62	0.313	7.25	31.73	4.52	0.430	7.33	31.89
672	—	—	—	—	4.53	0.460	7.01	31.88
740	—	—	—	—	4.53	0.460	6.40	31.88
790	4.63	0.313	6.22	31.70	—	—	—	—
Standard deviation[d]	0.02	0.009	0.19	—	0.02	0.009	0.19	—
r[e]	−0.47	0.847	−0.99	—	−0.65	0.95	−0.99	—

[a]Means over 7 day period.
[b]Mononuclear Al cations.
[c]Polynuclear Al cations
[d]Pooled standard deviations.
[e]Correlation coefficients on days aged.

nuclear cations. The correctness of this assumption was verified, however, at 0, 11, and 32 days aging by determining the nondialyzable Al present in the systems. In another similar experiment, in which the degree of neutralization was only 0.35 and the length of time of aging was extended to 326 days, the p*H* decreased from 4.09 to 3.59, the concentration of mononuclear cations increased from 5.76×10^{-3} to 6.23×10^{-3} *M*; the Al present as polynuclear cations decreased from 4.08×10^{-3} *M* to nil, the Al present as solids increased from 0.16×10^{-3} to 3.77×10^{-3} *M* and p[Al](OH)^3 increased from 32.00 to 33.44. The X-ray analyses of the solids showed strong gibbsite diffraction patterns after only 3 weeks aging.

The results in Table 3, which are characteristic of all the experiments, using procedures A and B, show without a doubt that the concentration of the polynuclears decreases although extremely slowly, with length of time of aging. The fact that the p*H*, concentration of the mononuclears, and p[Al](OH)^3 changed very little over the same aging period, compared with the corresponding changes when the initial solid phases were formed, showed that the polynuclears were not hydrolyzing to gibbsite. In fact, it was found that, as these polynuclears that react with 8-hydroxyquinoline with a specific rate constant of 0.16 min^{-1} disappeared, a new type of polynuclear hydroxyaluminum cation appeared. This second type of polynuclear is adsorbed by cation exchangers in an exchangeable form. Furthermore, they will react with 8-hydroxyquinoline, with the standard method (4), via a pseudo-first order reaction but at a very slow rate. The specific rate constant for this second type of polynuclears is roughly 1/300th of that with the first type. This will be dealt with in detail in a later paper.

1. R. C. TURNER. Can. J. Chem. **47**, 2521 (1969).
2. R. W. SMITH. Am. Chem. Soc. Adv. Chem. Ser. **106**, 250 (1971).
3. R. C. TURNER and G. J. ROSS. Can. J. Chem. **48**, 723 (1970).
4. R. C. TURNER and W. SULAIMAN. Can. J. Chem. **49**, 1683 (1971).
5. PA HO HSU and T. F. BATES. Mineral. Mag. **33**, 749 (1964).
6. J. H. PATTERSON and S. Y. TYREE, JR. J. Colloid Interface Sci. **43**, 389 (1973).

Can. J. Chem. Downloaded from www.nrcresearchpress.com by 210.87.254.6 on 09/05/12
For personal use only.

7. H. BILINSKI and S. Y. TYREE, JR. Am. Chem. Soc. Adv. Chem. Ser. **106**, 235 (1971).
8. C. BROSSET, G. BIEDERMANN, and L. G. SILLEN. Acta Chem. Scand. **8**, 1917 (1954).
9. E. MATIJEVIC, K. G. MATHIA, R. H. OTTERWILL, and M. KERKER. J. Phys. Chem. **65**, 826 (1961).
10. J. AVESTON. J. Chem. Soc. 4438 (1965).
11. D. D. MACDONALD, P. BUTLER, and D. OWEN. J. Phys. Chem. **77**, 2474 (1973).
12. R. C. TURNER. Can. J. Chem. **53**, 2811 (1975).

Can. J. Chem. Downloaded from www.nrcresearchpress.com by 210.87.254.6 on 09/05/12
For personal use only.

Trajectory study of atomic recombination reactions. VII. Recombination of I and Br atoms[1]

D. T. CHANG[2] AND GEORGE BURNS

Lash Miller Chemical Laboratory, University of Toronto, Toronto, Ont., Canada M5S 1A1

Received December 4, 1975

D. T. CHANG and GEORGE BURNS. Can. J. Chem. **54**, 1535 (1976).

Classical 3-D trajectory investigation of bromine and iodine atom recombination reactions in He, Ar, and Xe, performed earlier, are extended, using an improved sampling technique, to include a larger number of trajectories and a wider temperature range (200–1500 K). The three body potential energy surfaces used were assumed to be nearly additive, but otherwise were defined by the existing molecular beam and spectroscopic data and contained essentially no arbitrary parameters. The agreement between computed and experimental rate constants is reasonable, and is best if the third body is heavy and reaction proceeds via a bound complex, such as IXe. Orbiting inert gas – recombining atom intermediate dimers, XM*, where X = I or Br, contribute to the overall recombination reaction via $XM^* + X \rightarrow X_2 + M$ reaction, provided M is heavy. If M = He, this reaction path is negligible at all temperatures studied, again provided that X = I or Br.

D. T. CHANG et GEORGE BURNS. Can. J. Chem. **54**, 1535 (1976).

On a étendu les études classiques de trajectoire en 3-D des atomes de brome et d'iode pour leurs réactions de recombinaison dans He, Ar et Xe qui avaient été effectuées antérieurement; cette extension qui a été faite afin d'inclure un plus grand nombre de trajectoires et un intervalle de température plus grand (200–1500 K) a été réalisée en faisant appel à une méthode d'échantillonnage améliorée. On fait l'hypothèse que les surfaces d'énergie potentielle, pour trois corps, qui ont été utilisées sont additives; elles ont toutefois été définies autrement par des données antérieures provenant de la spectroscopie et d'études de fais ceaux moléculaires et ne contiennent essentiellement aucun paramètre arbitraire. L'accord entre les constantes de vitesse calculées et expérimentales est raisonable; il est meilleur si le troisième corps est lourd et si la réaction se produit par l'intermédiaire d'un complexe lié tel que IXe. Des dimères intermédiaires, à savoir des dimères orbitant de gaz inerte et de l'atome recombinant, XM* (Xe = I ou Br), contribuent à la réaction de recombinaison globale par l'intermédiaire de $XM^* + X \rightarrow X_2 + M$; M doit toutefois être lourd. Si M = He et X = I ou Br, cette trajectoire réactionnelle est négligeable à toutes les températures étudiées.

[Traduit par le journal]

Introduction

Recombination of iodine and bromine atoms in inert gases has been studied previously (1–6) using classical 3-D trajectory technique and Monte Carlo method of sampling. Two dynamical mechanisms were considered in these calculations: the classically *b*ound, or radical–molecule, *c*omplex (BC) mechanism

$$X + M \leftrightharpoons XM$$

$$XM + X \rightarrow X_2 + M$$

and the *e*nergy *t*ransfer (ET) mechanism

$$X + X \rightleftharpoons X_2^*$$

$$X_2^* + M \rightarrow X_2 + M$$

Here the XM is a classically bound intermediate (1) and X_2^* is an orbiting quasidimer (3, 7) with a positive total energy. More recently (5, 6) XM quasidimers, XM*, were also included in calculations. This reaction path involves unbound orbiting states of the radical–molecule complex XM, and it can be referred to as the *q*uasi-*r*adical–*m*olecule *c*omplex mechanism (QRMC). Since QRMC and ET mechanisms involve collisions of three unbound particles, QRMC + ET mechanism can be referred to (6) as a *t*riple *c*ollision (TC) mechanism.

Previous calculations yielded (1–6) theoretical rate constants in fair agreement with experiment; furthermore, detailed dynamical information on

[1]Research sponsored, in part, by the Air Force Office of Scientific Research, Air Force Systems Command, USAF, under grant No. A75-2856. The United States Government is entitled to reproduce and distribute reprints for Government purposes, notwithstanding any copyright notation hereon.

[2]Present address: Singer Simulation Products, Silver Springs, Maryland 20904.

recombination reactions was obtained. In addition, 3-D trajectory study of bromine and iodine molecule dissociation (8, 9) further extended understanding of halogen recombination–dissociation reactions.

Since the above mentioned work (1–4) was completed, it became possible, using the molecular beam technique, to determine (10–12) the interaction potentials between the recombining atom and an inert gas. This removed an important uncertainty in potential energy surfaces, which affected significantly (1) the magnitude of rate constants and the reaction dynamics of recombination–dissociation reactions. At the same time, it became possible to extend the temperature range over which halogen recombination–dissociation reactions could be studied experimentally. Thus, iodine recombination was recently studied (13) at 200 K, while measurements of the dissociation rate of Br_2 were extended (9) to 3000 K. All these facts meant that a meaningful comparison between experimental and previous trajectory (1–6) rate constants could not always be easily made. This situation was further complicated by the discovery that computation (5, 6) of the XM* + X QRMC two-body rate coefficients, k_2^{eq}, involved an error in the weighting factor.

In the present work, new molecular beam (11, 12) data were used to determine XM potentials and the above mentioned error removed. The recombination rate constants for Br and I atoms in He, Ar and Xe were computed at 200, 300, 600, 1000, and 1500 K and compared with experimental data, as well as, whenever possible, with earlier trajectory studies.

Results

(a) Potential Energy Surfaces

Modified additive three-body potential (1) B was used throughout these calculations. The potential energy parameters for XM dimers (Table 1) were consistent with parameters ($\epsilon_\infty^{IKr} = 0.45$ kcal/mol (11) and $\epsilon_\infty^{INe} = 0.33$ kcal/mol (12)), obtained by using the molecular beam technique (11, 12).[3] The σ values were derived (1–6) from the corresponding ϵ_∞ values using Herschbach–Johnston's (14–16) empirical relationship, while ϵ_∞^{IAr}, ϵ_∞^{IXe}, and ϵ_∞^{BrAr} were identical to those used (5, 6) previously. All values of ϵ_∞^{XM} are internally consistent, *i.e.* they satisfy reasonably well the relationship

$$\epsilon^{ij} = \epsilon^{il}(\epsilon^{jj}/\epsilon^{ll})^{0.5}$$

where i represents X and j, l represent different M. Some uncertainty in ϵ_∞ remains because the molecular beam data (11, 12) do not satisfy precisely the above relationship, which is known to be not exact. For the purpose of trajectory calculations, in the case of X_2* dimer, the maximum internuclear separation was taken to be equal to 8 Å, independent of internal energy or angular momentum.

TABLE 1

(*a*) Interaction potentials used for iodine†

M	ϵ_∞^{IM}	σ_∞^{IM}	ϵ_∞^{XeM}	σ_∞^{XeM}
He	0.2 (2.1)	3.08	0.094	3.328
Ar	0.6 (1.9)	3.55	0.323	3.752
Xe	0.7 (1.6)	3.90	0.439	4.100

† ϵ in kcal mol^{-1}, σ in Å. Number in parentheses is the ratio $\epsilon_\infty^{IM}/\epsilon_\infty^{XeM}$.

(*b*) Interaction potentials used for bromine†

M	ϵ_∞^{BrM}	σ_∞^{BrM}	ϵ_∞^{KrM}	σ_∞^{KrM}
He	0.15 (1.8)	2.88	0.083	3.081
Ar	0.6 (1.8)	3.32	0.284	3.506
Xe	0.7 (1.8)	3.62	0.386	3.853

† ϵ in kcal mol^{-1}, σ in Å. Number in parentheses is the ratio $\epsilon_\infty^{BrM}/\epsilon_\infty^{KrM}$.

(b) Equilibrium Recombination Rate Coefficients

The equilibrium recombination rate coefficients (Tables 2 and 3) can be written (5) as the sum of contributions from the three (BC, QRMC, ET) mechanisms:

$$k_r^{eq} = \sum_i k_{ri}^{eq} = \sum_i K_i k_{2i}^{eq}$$

where K is the equilibrium constant for the dimers and k_2^{eq} is (1, 2) the two-body equilibrium rate coefficient. The overall electronic degeneracy factor for each mechanism was taken to be 1/16. Whenever the potential parameters, used previously (5), are the same as those used now, values of K_i obtained here agree well with earlier results (5). Present K_i results for iodine case are presented in Tables 4 and 5.

The computational procedures for evaluating k_2^{eq} were described (1, 2, 5, 6) previously. For each third body at each temperature, enough

[3]We are grateful to Professor Lee for permitting us to use his experimental findings prior to publication.

TABLE 2. Equilibrium one way flux rate coefficients, k_r^{eq} (in 10^7 l^2 mol^{-2} s^{-1}), for iodine†

M	Mechanism	k_r^{eq} 200 K	300 K	600 K	1000 K	1500 K
He	BC	10.2 (400, 48)	5.3 (400, 35)	0.92 (600, 20)	0.57 (800, 24)	0.37 (800, 22)
	QRMC	0.24 (600, 2)	0.13 (600, 1)	0.26 (600, 3)	0 (600, 0)	0.02 (600, 1)
	ET	120.9 (2200, 176)	121.0 (2200, 144)	129.5 (3000, 147)	126.2 (3000, 115)	132.5 (3000, 102)
Ar	BC	203.0 (800, 201)	98.3 (800, 159)	22.9 (1200, 124)	12.7 (600, 56)	5.1 (600, 33)
	QRMC	7.3 (600, 10)	4.2 (600, 8)	6.3 (600, 15)	4.8 (600, 20)	2.7 (600, 15)
	ET	65.9 (1200, 158)	71.9 (1200, 142)	82.2 (2400, 232)	91.5 (2400, 198)	89.3 (2400, 161)
Xe	BC	329.3 (800, 196)	178.0 (800, 180)	51.9 (1200, 187)	19.7 (800, 76)	10.7 (600, 46)
	QRMC	46.0 (600, 37)	37.7 (600, 38)	15.2 (600, 28)	13.1 (600, 34)	6.8 (600, 26)
	ET	27.1 (1200, 101)	31.0 (1800, 142)	38.8 (2400, 195)	53.0 (2400, 200)	49.8 (2400, 158)

†The first figure in the parentheses indicates the number of trajectories which were run; the second figure indicates the number of trajectories which actually led to recombination. In all trajectory calculations the initial separation between the incoming atom and the dimer was taken to be 12.5 Å, while the maximum impact parameter was taken to be 8 Å. In cases of QRMC and ET mechanisms, all trajectories with positive p_r values were omitted. See ref. 3.

TABLE 3. Equilibrium one way flux rate coefficients, k_r^{eq} (in 10^7 l^2 mol^{-2} s^{-1}), for bromine†

M	Mechanism	k_r^{eq} 200 K	300 K	600 K	1000 K	1500 K
He	BC	5.0 (400, 40)	3.1 (400, 28)	1.8 (400, 31)	0.25 (400, 8)	0.07 (400, 5)
	QRMC	1.1 (600, 10)	0.20 (600, 3)	0.12 (600, 3)	0.07 (600, 3)	0.05 (600, 4)
	ET	103.6 (2400, 162)	96.6 (2400, 127)	100.9 (2400, 96)	115.6 (3000, 114)	106.2 (3000, 95)
Ar	BC	137.7 (800, 137)	62.1 (800, 139)	14.4 (400, 41)	8.5 (400, 38)	3.6 (400, 22)
	QRMC	17.4 (600, 24)	19.4 (600, 35)	7.4 (600, 26)	4.3 (600, 23)	2.6 (600, 20)
	ET	59.3 (1200, 136)	60.3 (2400, 226)	63.0 (2400, 187)	68.2 (2400, 164)	71.6 (2400, 140)
Xe	BC	326.1 (800, 211)	159.4 (800, 177)	57.3 (800, 120)	20.5 (400, 45)	10.0 (400, 31)
	QRMC	43.5 (600, 36)	33.8 (600, 36)	21.3 (600, 40)	14.1 (600, 41)	9.6 (600, 38)
	ET	29.0 (600, 53)	34.1 (2400, 209)	39.4 (2400, 183)	42.7 (2400, 165)	38.8 (2400, 136)

†The first figure in the parentheses indicates the number of trajectories which were run; the second figure indicates the number of trajectories which actually led to recombination. In all trajectory calculations the initial separation between the incoming atom and the dimer was taken to be 11 Å, while the maximum impact parameter was taken to be 8 Å. In cases of QRMC and ET mechanisms, all trajectories with positive initial p_r values were omitted. See ref. 3.

TABLE 4. Equilibrium constants for IM dimers (l mol^{-1}), I + M $\rightleftharpoons$ IM

System	ϵ (kcal mol^{-1})	σ (Å)	Mechanism	k^{eq} 200 K	300 K	600 K	1000 K	1500 K
IHe	0.2	3.08	BC	5.6857×10^{-2}	3.0399×10^{-2}	1.0584×10^{-2}	4.8923×10^{-3}	2.6562×10^{-3}
			QRMC	9.3345×10^{-2}	5.4098×10^{-2}	2.0394×10^{-2}	9.7286×10^{-3}	5.3656×10^{-3}
IAr	0.6	3.55	BC	5.3261×10^{-1}	2.6396×10^{-1}	8.7060×10^{-2}	3.9613×10^{-2}	2.1365×10^{-2}
			QRMC	5.2568×10^{-1}	3.3793×10^{-1}	1.4293×10^{-1}	7.1630×10^{-2}	4.0521×10^{-2}
IXe	0.7	3.90	BC	9.4143×10^{-1}	4.5379×10^{-1}	1.4691×10^{-1}	6.6515×10^{-2}	3.5803×10^{-2}
			QRMC	8.1202×10^{-1}	5.3341×10^{-1}	2.3157×10^{-1}	1.1742×10^{-1}	6.6836×10^{-2}

trajectories were run for the dominant mechanism to obtain the rate coefficient with a standard deviation of less than 15% (the latter was defined as

$$\%\ \text{S.D.} = [P(1 - P)/N]^{1/2}/P \times 100$$

where P is the probability of recombination obtained from trajectory calculations, and N is the number of trajectory runs). Enough trajectories were also run for the other two mechanisms, to ensure that the overall rate coefficient would still have a less than 15% standard deviation.

In agreement with previous studies (3–6), it

TABLE 5. Equilibrium constants for I_2^* dimers $I + I \leftrightharpoons I_2^*$ (ref. 5)†

T (K)	$\langle u \rangle$ (kcal mol^{-1})	$\langle t \rangle$ (10^{-12} s)	K	%S.D.
200	0.39	2.62[2]	4.231×10^{-1}	2.06
300	0.59	2.33	4.290×10^{-1}	2.03
600	1.17	1.83	3.976×10^{-1}	1.84
1000	1.95	1.56	3.843×10^{-1}	1.75
1500	2.95	1.36	3.763×10^{-1}	1.73

†D_e = 35.863 kcal mol^{-1}, R_e = 2.667 Å, a = 1.859 Å^{-1}, $\langle u \rangle$ = average relative kinetic energy, $\langle t \rangle$ = lifetime of I_2^*.

was found that BC mechanism predominates at lower temperatures and in the case of stronger X–M interactions. At higher temperatures and for lighter third bodies (weak X—M bond), the ET mechanism predominates (3–6), so that if M = He, the ET mechanism is important at all temperatures studied.

For recombination of both Br and I atoms, the contribution of the QRMC mechanism to k_r^{eq} amounts to <1% for He, <15% for Ar and <20% for Xe at all temperatures. The general trend is that for a given X the contribution from the QRMC mechanism increases with the atomic weight of the third body. Furthermore, the contribution from the QRMC mechanism increases as atomic number of recombining atom decreases. This result differs from our earlier studies (5, 6), and is due to elimination of the sampling error which occurred earlier. It follows from the present results that the QRMC mechanism should be important in recombination of light atoms, such as hydrogen, and in some cases may be predominant, as for the 2H + He reaction. For the 2H + Xe reaction the contribution from the QRMC mechanism will be larger than from the ET mechanism. However, for this particular system either BC or QRMC mechanism could be predominant. Which of these two mechanisms will be the most important will depend on strength of H—Xe bond.

Whenever a comparison between previous (1–6) and present results is possible, the agreement in k_r^{eq} was found to be good. Thus, for the 2Br + He reaction, present k_r^{eq} (ET) agrees within about 10% with earlier (3) studies, even though ϵ_∞^{BrHe} used previously (3), is 2.5 higher than ϵ_∞^{BrHe} used now. For the 2Br + Ar (Xe) reaction, the agreement with an earlier study (3) is particularly good at 1500 K. This occurs because recombination via the ET mechanism is not sensitive to ϵ_∞^{XM}, if it is reasonably small, and if the temperature is reasonably high.

(c) Nonequilibrium Correction Factor

The steady-state recombination rate constant (the observable) can be written (5) as a sum of contributions from the three mechanisms:

$$k_r = \sum_i k_{ri}^{eq} f_i$$

where f is the nonequilibrium correction factor (2), *i.e.* the fraction of molecules formed that does not redissociate on subsequent collisions. The calculated nonequilibrium correction factors were listed in Tables 6 and 7. Also listed in the tables were the sample size of the nascent molecules subjected to successive collisions, their corresponding mechanism (10), the number of collisions required to establish the steady state, and the number of molecules remaining at the steady state. As previously (5, 6), an absorbing barrier was placed at $-3kT$ below the dissociation limit and, consequently, molecules with internal energy below this boundary were assumed to be 'permanently' recombined. In a number of cases, the same nascent ensemble was used twice. In such cases, the initial configurations and relative velocities of successive collisions were selected differently. The results, thus obtained, agreed with each other to within 10%. However, there remains some additional uncertainty, since nascent ensembles might not be sufficiently large.

Present calculations of nonequilibrium correction factors are more extensive than those published (2–6) previously. In some cases, a meaningful comparison between present and previous work can be made. Thus, for the case of the 2Br + Ar reaction, the f(ET) factors, obtained (3) previously, agree within 10–20% with present results. The same can be said about the f(ET)

TABLE 6. Redissociation correction factors, f, for iodine†

M	T (K)	N‡	n§	M¶ Bound	M¶ Meta	f
He	200	176 (ET)	56	63	1	0.42
	300	144 (ET)	60	58	1	0.54
	600	147 (ET)	60	43	3	0.34
	1000	115 (ET)	57	31	0	0.28
	1500	102 (ET)	77	22	1	0.23
Ar	200	201 (BC)	11	156	0	0.77
	300	159 (BC)	13	113	0	0.66
		142 (ET)	10	58	0	0.50
	600	232 (ET)	19	80	0	0.39
	1000	198 (ET)	28	71	0	0.43
	1500	161 (ET)	35	44	1	0.32
Xe	200	196 (BC)	7	148	0	0.69
	300	180 (BC)	9	118	0	0.64
	600	187 (BC)	16	91	0	0.50
		195 (ET)	12	67	0	0.46
	1000	200 (ET)	17	51	0	0.31
	1500	158 (ET)	14	43	0	0.33

†An absorbing barrier was placed at $-3kT$ below the dissociation limit.
‡N is the number of nascent molecules subjected to successive collisions.
§n is the number of successive collisions needed to establish the steady state.
¶M is the number of molecules remained at the steady state.

TABLE 7. Redissociation correction factors, f for bromine†

M	T (K)	N‡	n§	M¶ Bound	M¶ Meta	f
He	200	162 (ET)	40	61	0	0.45
	300	127 (ET)	44	52	0	0.50
	600	96 (ET)	67	42	0	0.49
	1000	114 (ET)	72	47	1	0.46
	1500	95 (ET)	79	34	1	0.44
Ar	200	187 (BC)	14	145	0	0.76
	300	139 (BC)	12	89	0	0.63
		226 (ET)	11	91	0	0.49
	600	187 (ET)	14	73	0	0.46
	1000	164 (ET)	25	53	0	0.36
	1500	140 (ET)	33	53	0	0.48
Xe	200	211 (BC)	9	170	0	0.79
	300	177 (BC)	12	124	0	0.69
	600	120 (BC)	24	73	0	0.58
		183 (ET)	15	67	0	0.42
	1000	165 (ET)	13	45	0	0.33
	1500	136 (ET)	23	39	0	0.37

†An absorbing barrier was placed at $-3kT$ below the dissociation limit.
‡N is the number of nascent molecules subjected to successive collisions.
§n is the number of successive collisions needed to establish the steady state.
¶M is the number of molecules remained at the steady state.

factor for $2I + Ar$ reaction, which was also carefully studied (5) previously.

(d) Calculated Observable Rate Constants

The calculated steady-state observable rate constants were compared with experimental data (17–20), as well as, whenever possible, with earlier calculations (Figs. 1–6). The agreement with earlier calculations is very good (Figs. 1 and 4). The experimental rate constants agree

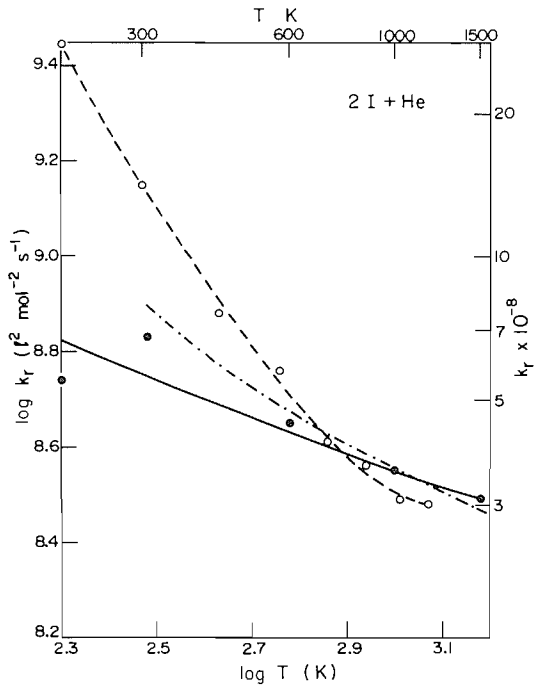

FIG. 1. Recombination rate constants for $2I + He \rightleftarrows I_2 + He$ reaction as a function of temperature. Open circles, dashed line: experimental results from refs. 13 and 20; solid line and solid circles: present work; dot–dashed line, k_r^{ET} (ϵ_∞^{IHe} = 0.5 kcal/mol) from ref. 5.

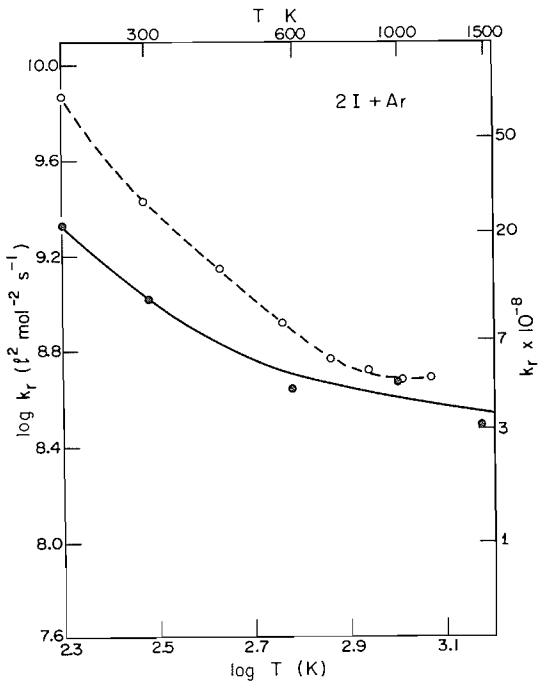

FIG. 2. Recombination rate constant for the $2I + Ar \rightleftarrows I_2 + Ar$ reaction as a function of temperature. Open circles, dashed line: experimental results from refs. 13 and 20; solid line and solid circles: present work.

with calculated results within a factor of better than four. In the intermediate temperature range, *i.e.* between about 600 and 1000 K, the agreement is excellent, and for the case of Xe and Ar, the temperature coefficient of the recombination rate constant is in a reasonable agreement with experiment. However, in the case of I and Br in He, calculated rate constants fail to reproduce experimental temperature dependence of the rate constants, and for iodine in Xe and Ar, the recombination rate constants at 200 K are significantly lower than experimental results.

It was shown previously (1) that it is possible to obtain a good agreement between computed and experimental rate constants, simply by making adjustments of parameters, such as ϵ_∞^{XM}, which define the potential energy surface of the recombination reaction. However, this approach does not seem justifiable to us, because it would bring us in conflict with recent molecular beam data (11, 12). Since potential energy surfaces used contain no significant arbitrary parameters, the agreement between theory and

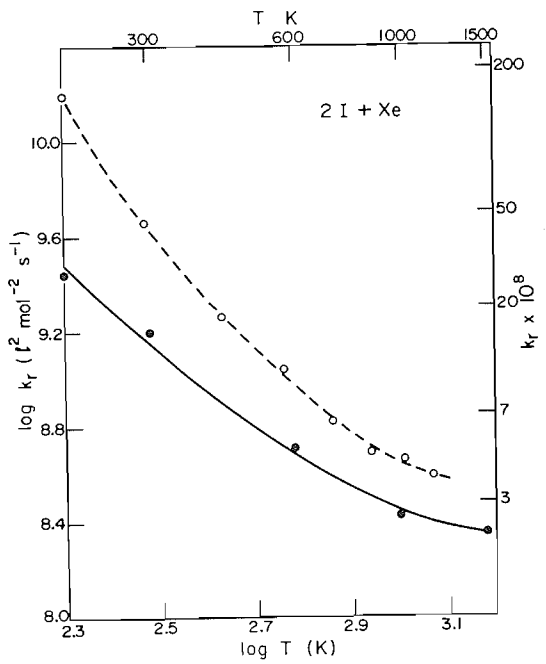

FIG. 3. Recombination rate constant for the $2I + Xe \rightleftarrows I_2 + Xe$ reaction as a function of temperature. Open circles, dashed line: experimental results from refs. 13 and 20; solid circles and solid line: present work.

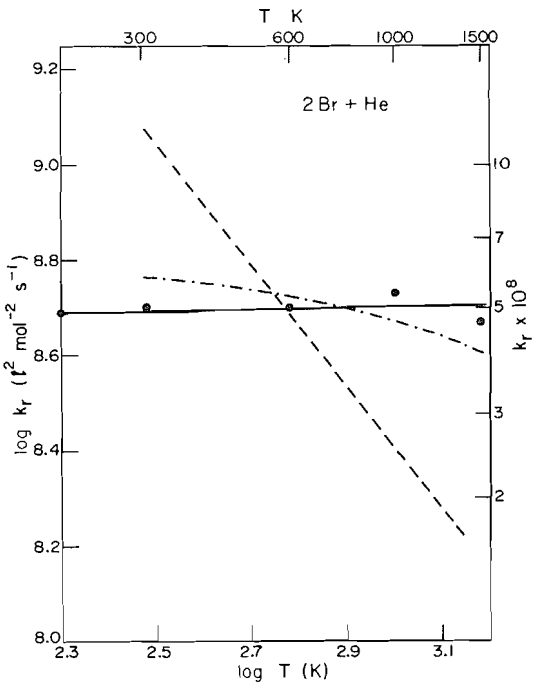

FIG. 4. Recombination rate constant for the 2Br + He $\rightleftarrows$ Br_2 + He reaction as a function of temperature. Dashed line: experimental results from ref. 16; solid circles and solid line: present work; dot-dashed line k_r^{ET} (ϵ_∞^{BrHe} = 0.5 kcal/mol), ref. 3.

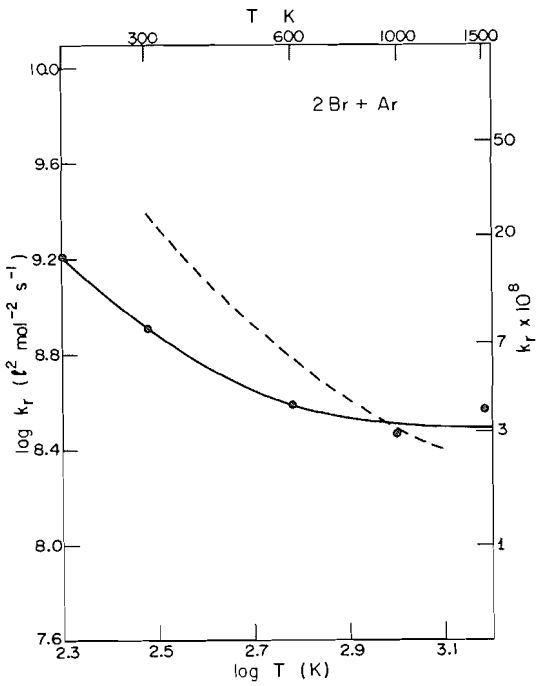

FIG. 5. Recombination rate constant for the 2Br + Ar $\rightleftarrows$ Br_2 + Ar reaction as a function of temperature. Dashed line: experimental work from ref. 16; solid line and solid circles: present work.

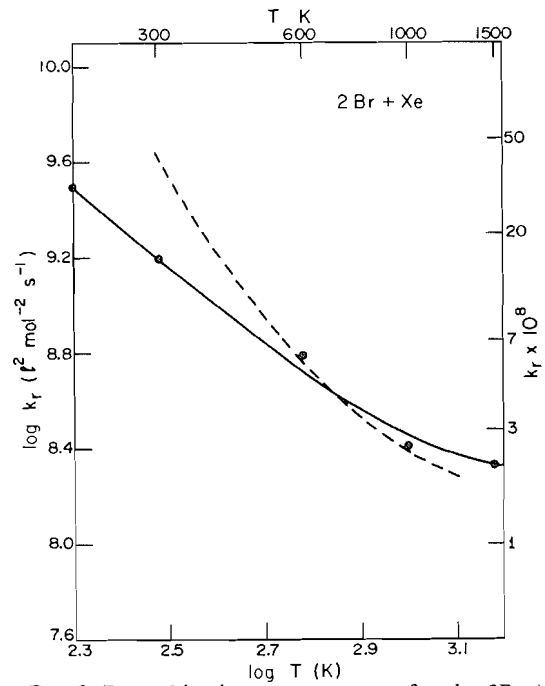

FIG. 6. Recombination rate constants for the 2Br + Xe $\rightleftarrows$ Br_2 + Xe reaction as a function of temperature. Dashed line: experimental work from ref. 19; solid line and solid circles: present work.

experiment is gratifying. The discrepancies between theory and experiment for cases in which the TC mechanism predominates (*i.e.* Figs. 1 and 4) may be due to the fact that in such cases we deal with a genuine collision of three unbound particles. In the present work, whenever the TC mechanism is used, the three-body collision is approximated by two two-body collisions. Preliminary calculations, for 2I + He system, at 1500 K, indicate that such an approximation may change the rate constant by at least 30%. More careful methods of studying genuine three body collisions of unbound particles, using trajectory calculations, are now being developed in our laboratory.

Another discrepancy between computed and experimental rate constants appears to occur at lowest temperatures, where recombination may proceed predominantly via the BC mechanism. This discrepancy may be due, in part, to participation of electronically excited states of X_2 in the overall recombination reaction. In this connection it may be noted that much needed low temperature (*i.e.* below 300 K) recombination

rate constants are still difficult to obtain for Br and I atoms (13).

Acknowledgements

We would like to acknowledge the support of the Air Force Office of Scientific Research, USAF and the National Research Council of Canada.

1. A. G. Clarke and George Burns. J. Chem. Phys. **55**, 4717 (1971).
2. A. Gelb, R. Kapral, and George Burns. J. Chem. Phys. **56**, 4631 (1972).
3. A. G. Clarke and George Burns. J. Chem. Phys. **56**, 4636 (1972).
4. A. G. Clarke and George Burns. J. Chem. Phys. **58**, 1908 (1973).
5. W. H. Wong and George Burns. J. Chem. Phys. **58**, 4459 (1973).
6. W. H. Wong and George Burns. J. Chem. Phys. **59**, 2974 (1973).
7. S. K. Kim and J. Ross. J. Chem. Phys. **42**, 263 (1965).
8. W. H. Wong and George Burns. Proc. Roy. Soc. London, A**341**, 105 (1974).
9. R. K. Boyd, George Burns, D. T. Chang, R. G Macdonald, and W. H. Wong. 15th Symposium (International) on Combustion, The Combustion Institute. 1975. p. 731.
10. R. W. Bickes, B. Lantzsch, J. P. Toennies, and K. Walaschewski. Discuss. Faraday Soc. **55**, 167 (1973).
11. M. J. Cardillo, M. S. Chow, and E. F. Greene. Division of Physical Chemistry, 163rd ACS Meeting, April, 1972. Paper 77.
12. Y. T. Lee. Private communication.
13. H. W. Chang and George Burns. J. Chem. Phys. **64**, 349 (1976).
14. H. S. Johnston. Gas phase reaction rate theory. Ronald, New York. 1966. p. 72.
15. D. R. Herschbach and V. W. Laurie. J. Chem. Phys. **35**, 458 (1961).
16. H. S. Johnston. J. Am. Chem. Soc. **86**, 1643 (1964).
17. J. K. K. Ip and George Burns. J. Chem. Phys. **51**, 3414 (1969).
18. J. A. Blake and George Burns. J. Chem. Phys. **46**, 745 (1969).
19. S. K. Chang, A. G. Clarke, and George Burns. J. Chem. Phys. **54**, 1835 (1971).
20. J. K. K. Ip and George Burns. J. Chem. Phys. **56**, 3155 (1972).

Highly excited 1*sns* states of the helium atom

MARY KURIYAN AND HUW O. PRITCHARD
Centre for Research in Experimental Space Science, York University, Downsview, Ontario M3J 1P3

Received November 21, 1975

MARY KURIYAN and HUW O. PRITCHARD. Can. J. Chem. **54**, 1543 (1976).

Variational calculations are reported on the 1*sns* singlet and triplet states of the helium atom, up to and including $n = 26$. By suitable choice of terms in the expansion for the wave function, significant economies in computer time are possible, and we quote an example of a 12-term uncorrelated wave function which gives a lower energy than Pekeris' 220-term correlated wave function. The problems of extending these calculations to much higher n (*e.g.* $n > 100$) to include states of astrophysical interest are enumerated.

MARY KURIYAN et HUW O. PRITCHARD. Can. J. Chem. **54**, 1543 (1976).

On rapporte des calculs variationnels des états 1*sns* singulet et triplet de l'atome d'hélium jusqu'à une valeur de $n = 26$. En choisisant correctement les termes pour l'expansion de la fonction d'onde, des économies substantielles en temps d'ordinateur sont possibles et on met en évidence un exemple d'une fonction d'onde non corrélée de 12 termes qui donne une énergie plus basse que la fonction corrélée de 220 termes de Pekeris. On énumère aussi les problèmes inhérents à l'extension de ces calculs à des nivaux beaucoup plus élevés de n (*e.g.* $n > 100$) de façon à inclure les états intéressants en astrophysique.

[Traduit par le journal]

Introduction

The recent discovery of very highly excited states of the helium atom in Orion and in other stars (1–4) presents a formidable challenge to computational quantum theory. Some of the states involved are, for example, 1*s*110*l*, 1*s*135*l*, 1*s*160*l*, and so on, where *l*, the azimuthal quantum number, is unspecified. When *l* is large, as it is in all these observed spectra, the singlet–triplet splitting will be infinitesimal, and the estimation of the energies of these states using the hydrogen-like approximation is trivial, *i.e.* assuming that the nucleus plus the 1*s* electron looks like a simple hydrogen core to the distant second electron. However, any two-electron calculation, which would be necessary to describe adequately the properties of 1*sns*, 1*snp*, or 1*snd* states (where the singlet–triplet splittings are significant), would be very difficult indeed, and it is towards this problem that we address ourselves in this paper.

Laboratory observation of excited 1*snl* states of helium extends only up to 1*s*15*f*, 1*s*17*s*, 1*s*21*d*, and 1*s*22*p* (5) and variational calculations have terminated at 1*s*17*s* (ref. 6, see however ref. 20 below and discussion thereof), which Pekeris regards as about the limit of feasibility of his methods with present-day computers.

The difficulty with any variational calculation is twofold. Firstly, depending upon whether one is interested in the singlet or the triplet state, one requires either the nth or the $(n - 1)$th eigenvalue of the secular determinant. But it is a matter of common practical experience (7–12) that as n increases, it becomes progressively more difficult to achieve a given accuracy for the energy of the target state. As it were, the 'rubbish' contained in the original basis set is the most easily projected out for the ground state, less easily for the first excited state, less so still for the second excited state, and so on; thus, the highest eigenvalues and their corresponding eigenvectors may be constructed essentially only from the 'rubbish' that is contained in the basis set, and these solutions bear no resemblance whatever to any real state of the system. For example, if one chooses to perform a calculation on a simple atom or molecule using a rather uninspired choice of N basis functions (N, say, about 20) then typically, of the order of $N/2$ of the calculated eigenvalues will be bound, and of the order of $N/4$ of the calculated eigenvalues could be regarded as being recognisable approximations to real states of the system. Thus, if one is interested in moderately large n, N may have to be very large, of the order of $4n$. We shall see below, however, that if the components of the basis set are chosen in an intelligent way, rather

Can. J. Chem. Downloaded from www.nrcresearchpress.com by 210.87.254.6 on 09/05/12
For personal use only.

Can. J. Chem. Downloaded from www.nrcresearchpress.com by 210.87.254.6 on 09/05/12
For personal use only.

than by the 'natural' methods often used in variational calculations, one can get exceedingly good approximations to the energies of $1sns$ states of helium when $N \simeq n + 3$.

The second major problem is that as n increases, the exponential decay characteristics of the parts of the wave function representing the two electrons become more and more dissimilar (the $1s$ electron will give rise to an exponential term in the wave function rather like e^{-2r_1} whereas the ns electron will be best described by a term rather like $e^{-r_2/n}$ as n becomes large). Thus the wave function must give each electron a different exponential dependence if it is going to allow efficient computations for excited states. But as n becomes large, the dynamic range of the necessary two-electron integrals becomes so large that it cannot be accommodated on a computing machine operating with numbers of fixed exponent length; this, therefore, is the more serious limitation for us. To some extent, this difficulty would be eased by considering $1snl$ states where $l = n - 1$, but the complexity of the integrals themselves becomes considerably greater (10).

The Wave Functions

The trial wave function used in this work is

$$[1]\quad \psi = \sum_{ijk} c_{ijk}\zeta^{(i+j+k)} \times \{r_1^i r_2^j r_{12}^k \exp[\zeta(ar_1 + br_2 + cr_{12})] \pm r_2^i r_1^j r_{12}^k \exp[\zeta(ar_2 + br_1 + cr_{12})]\}$$

and details of the computation of the necessary two-electron integrals and matrix elements are available in earlier papers (9–11). This form of wave function has certain attractive features (13, 14). In particular, it allows each electron to have a different exponential dependence, and the advantages of this flexibility are now well established (6, 9, 10). Furthermore, if c is regarded as a disposable parameter (9), it gives rise to some 'free' correlation even if powers of r_{12} are excluded from the wave function (*i.e.* $k = 0$ only). It has been argued, however (15), that c should not be regarded as disposable, but that ζc should be kept fixed at the value of $\frac{1}{2}$ in order to force the r_{12} cusp to have the correct form (9, 15); it turns out below that adherence to this view represents a severe handicap if one is interested in the *energies* of excited states rather than the ground state, *cf.* also Table 1 of ref. 10.

Computational Procedure

The secular problem was solved by the Choleski–Householder–Bisection technique which we have described previously (16), making use of the Sturm-sequence property of the bisection procedure to locate either the nth or the $(n - 1)$th eigenvalue, for a singlet or a triplet state respectively. The calculated energy of the target state was minimised with respect to the disposable parameters in the wave function *i.e.* ζ, a, b, and c for the given basis set. The computational strategy then separates into three phases: (*i*) how to guess the appropriate values of all the disposable parameters; (*ii*) how to select members of the basis set in the most efficient manner; (*iii*) how to extend the methods to very high n. The answer to (*i*) turns out to be almost trivial and most of the present discussion will be concerned with item (*ii*), and to some extent with item (*iii*).

Selection of Members of the Basis Set

In using a wave function like eq. 1, it is natural to choose the basis functions by taking permutations of the indices i, j, and k in a systematic manner. Thus with 8 terms, one can include all permutations up to r_a ($a \equiv 1$, 2, or 12), 27 terms cover all permutations up to r_a^2, 64 terms up to r_a^3, and so on. This turns out to be a very ineffective way of attacking the excited-state problem because if we single out, for example, the $1s8s$ state, the part of the wave function which describes the motion of the excited electron must have seven nodes in it, and it is very difficult to construct a function having the correct nodal behaviour from functions which only go up to r_a^2 or r_a^3. To demonstrate the strength of this difficulty, it is possible to get very good approximations to the energy of the $1s8s\ ^3S$ state by choosing an 8-term wave function which has the natural capability of giving the required number of nodes *i.e.* all terms in $r_1^0 r_2^j r_{12}^0$, $j = 0, 1, ..., 7$, or $r_1^0 r_2^0 r_{12}^k$, $k = 0, 1, ..., 7$; such functions will be designated by the shorthand terminology $\sum(ijk)$ *i.e.* $\sum_{j=0}^{7}(0j0)$ or $\sum_{k=0}^{7}(00k)$ respectively. The former function is rather more efficient, and even with $c = 0$, *i.e.* no 'free' correlation, it gives a lower energy than Winkler and Porter's 165-term wave function (17). Extending the function up to 12 terms (*i.e.* to $j = 11$) gives a much lower energy even than Pekeris' 220-term wave function (18), as shown in Table 1.

Can. J. Chem. Downloaded from www.nrcresearchpress.com by 210.87.254.6 on 09/05/12
For personal use only.

TABLE 1. Comparison of energies (in atomic units) of the $1s8s$ triplet state of the helium atom calculated with correlated wave functions, and with uncorrelated $\sum(0j0)$ wave functions

Source	Number of terms	Condition	Energy (a.u.)
Winkler and Porter (17)	165	Correlated	−1.9896
Equation 1	8	Uncorrelated	−2.008387
Pekeris (18)	220	Correlated	−2.008414
Equation 1	12	Uncorrelated	−2.008419
Pekeris (6)	2300	Correlated	−2.008427

This behaviour is consistent with an observation of Pekeris (18) that in his method "the first time the root of the $1sns$ state appears is at $\omega_{min} = n - 1$ for singlet states, and at $\omega_{min} = n - 2$ for triplet states"; here $\omega = (a + b + c)$ where he considers polynomials containing $r_1^a \cdot r_2^b\, r_3^c$ in the perimetric coordinates r_1, r_2, and r_3.[1]

At this stage, the choice of the disposable parameters becomes very simple. As we had found previously (9, 10), the best value of ζ was always two; furthermore, for states higher than $1s3s$, the best value of a was always minus one, and for states higher than $1s8s$, the best value of c was always 0. Thus, in practice, there is really only one disposable parameter, b.

There is another very interesting (and in hindsight perhaps rather obvious) point about choosing terms for triplet wave functions. For high target states ($n > 20$), it is relatively disadvantageous to include the first term (000) in the expansion for ψ (*i.e.* $r_1^0\, r_2^0\, r_{12}^0$) and for a fixed expansion length, it is always better to substitute for this an extra ($0j0$) term. This effect is easily rationalised by reference to a different form of wave function, namely a product of hydrogen-like orbitals, where we found the effect is very marked. When talking about singlet states, one has to include the $1s^2$ configuration in the calculation, but when talking about triplet states, it is a hindrance to have the (unwanted) $1s^2$ configuration in the basis set, and the best compromise the variational procedure can achieve in trying to project out this invalid configuration is poorer (for the same number of terms) than if it is consciously excluded.

[1]We thank a referee for adding the comment that Winkler and Porter's wave functions contain no factors of powers of r_a, which of course explains why their calculations gave good results for low-lying states, but not for higher ones because they cannot reproduce the appropriate nodal behaviour. Another example of this effect, also drawn to our attention by the second referee, is the reasonably good representation of $1sns$ states of Ne IX and Ar XVII, (up to $n = 23$ and 24 respectively) using a basis set consisting of only 25 hydrogen-like functions (23), although the effect is not so marked for lower values of Z.

Results

Table 2 compares some energies of correlated wave functions for the states $1s4s$ to $1s8s$ inclusive, using a 24-term wave function of the form

$$[2] \qquad \sum_{j=0}^{12}(0j0) + \sum_{k=1}^{11}(00k)$$

This illustrates another point about selection of terms in the wave function. In general, for a given expansion length, it is better to go to higher single powers in r_2 or r_{12} than to use terms which couple non-zero powers of r_2 and r_{12}. Also, it is always preferable to include another term in j or k rather than in i; in other words, any departures of the functional form of the inner electron from a $1s$ orbital are taken care of automatically by the r_{12} or the $e^{cr_{12}}$ parts of the function. Table 2 shows that in general these 24-term functions give better energies than Winkler and Porter's 165-term functions (17), and also better energies than Pekeris' 220-term calculations (18) for triplet states above $1s5s$ (but not for singlet states).

Since we would like to direct our attention to very high $1sns$ states, it now becomes clear that the most efficient functions for a given expansion length N are uncorrelated and of the general type

$$[3] \quad Na \equiv \sum_{j=0}^{N-1}(0j0) \qquad \text{or} \qquad Nb \equiv \sum_{j=1}^{N}(0j0)$$

Table 3 shows the results of such calculations with $N = 25$ or 26, yielding approximations for all states up to $1s26s$. The termination of our calculations at this point is not due to restrictions of storage space or machine time (these calculations take about 3 min per case on an IBM 370/158 in quadruple-length arithmetic, and this time could probably be halved if a determined attempt were made to optimise all stages of the calculation). The termination at this point is caused, in fact, because as n increases, the optimum numerical magnitude of the non-

Can. J. Chem. Downloaded from www.nrcresearchpress.com by 210.87.254.6 on 09/05/12
For personal use only.

TABLE 2. Energies (in atomic units) of $1sns$ states of the helium atom using correlated wave functions of order $N = 24$, in comparison with other similar calculations

State	$-b$	c	Energy: This work ($N=24$)	Winkler and Porter (17) ($N=165$)	Pekeris (18) ($N=220$)	Pekeris and co-workers (6) ($N=2300$)
4^1S	0.25	0.005	−2.033487	−2.033580	−2.033563	−2.033587
5^1S	0.19	0.005	−2.021116	−2.02105	−2.021150	−2.021177
6^1S	0.136	0.006	−2.014518	−2.0134	−2.014536	−2.014563
7^1S	0.104	0.001	−2.010593	−2.0085	−2.010600	−2.010625
8^1S	0.088	0.005	−2.008065	−1.9910	−2.008068	−2.008093
4^3S	0.13	0.003	−2.036505	−2.03649	−2.036512	−2.036512
5^3S	0.13	0.002	−2.022616	−2.02242	−2.022618	−2.022619
6^3S	0.12	0.001	−2.0153755	−2.0146	−2.0153754	−2.0153774
7^3S	0.099	0.001	−2.0111287	−2.0095	−2.0111239	−2.0111299
8^3S	0.090	0	−2.0084263	−1.9896	−2.0084140	−2.0084271

TABLE 3. Energies (in atomic units) for uncorrelated wave functions for singlet and triplet $1sns$ states of the helium atom

Configuration	Singlet N^*	Singlet $-b$	Singlet Energy	Triplet N^*	Triplet $-b$	Triplet Energy
$1s2s$	26*a*	0.50	−2.1434493	25*a*	0.28	−2.1742455
$1s3s$	26*a*	0.40	−2.0605732	25*a*	0.28	−2.0684847
$1s4s$	26*a*	0.30	−2.0333007	25*a*	0.24	−2.0364364
$1s5s$	26*a*	0.25	−2.0210330	25*a*	0.24	−2.0225826
$1s6s$	26*a*	0.20	−2.0144808	25*a*	0.16	−2.0153573
$1s7s$	26*a*	0.17	−2.0105742	25*a*	0.14	−2.0111176
$1s8s$	26*a*	0.15	−2.0080588	25*a*	0.12	−2.0084190
$1s9s$	26*a*	0.11	−2.0063445	25*a*	0.10	−2.0065959
$1s10s$	26*a*	0.10	−2.0051244	25*a*	0.10	−2.0053067
$1s11s$	26*a*	0.081	−2.0042247	25*a*	0.065	−2.0043617
$1s12s$	26*a*	0.070	−2.0035430	25*a*	0.060	−2.0036483
$1s13s$	26*a*	0.061	−2.0030139	25*a*	0.055	−2.0030967
$1s14s$	26*a*	0.054	−2.0025952	26*a*	0.050	−2.0026613
$1s15s$	26*a*	0.046	−2.0022579	26*a*	0.045	−2.0023117
$1s16s$	26*a*	0.042	−2.0019825	26*a*	0.043	−2.0020267
$1s17s$	26*a*	0.037	−2.0017545	26*a*	0.038	−2.0017913
$1s18s$	26*a*	0.035	−2.0015637	26*a*	0.036	−2.0015946
$1s19s$	26*a*	0.031	−2.0014024	26*a*	0.032	−2.0014286
$1s20s$	26*a*	0.029	−2.0012648	26*a*	0.030	−2.0012872
$1s21s$	26*a*	0.026	−2.0011464	26*a*	0.027	−2.0011655
$1s22s$	26*a*	0.025	−2.0010440	25*b*	0.025	−2.0010600
$1s23s$	26*a*	0.023	−2.0009545	25*b*	0.023	−2.0009682
$1s24s$	26*a*	0.022	−2.0008762	25*b*	0.022	−2.0008881
$1s25s$	26*a*	0.020	−2.0008066	25*b*	0.021	−2.0008150
$1s26s$	26*a*	0.019	−2.0007417	25*b*	0.020	−2.0007520

*For definition of *Na* or *Nb*, see eq. 3.

linear parameter b decreases, and so the integrals for high powers of r_2 become very large. The integrals themselves are generated by a recursion formula (Appendix I of ref. 10) and, apart from a trivial scaling by $\zeta^6/8\pi^2$, are built up starting from a pair of δ-functions. The results shown in Table 3 start by building up the integrals from 0 or 10^{-75} instead of 0 or 1 as the appropriate values of the δ-function, and the integrals overflow, *i.e.*, become greater than 10^{+78} for $N > 26$, $(-b) < 0.02$. Consequently, without a disproportionate amount of programming effort, Table

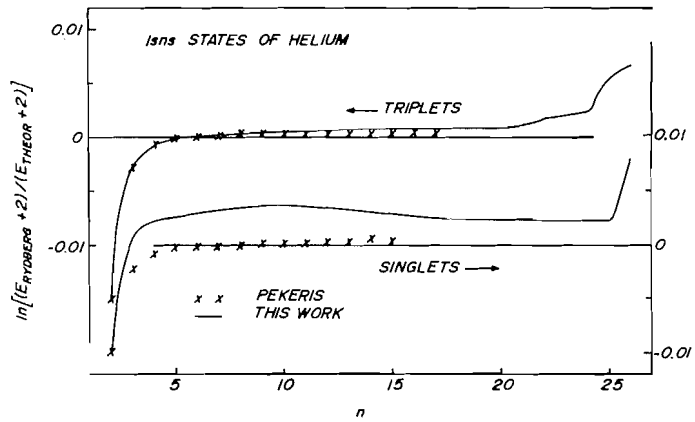

FIG. 1. Comparison of present results for excited singlet and triplet $1sns$ states of the helium atom, and of those of Pekeris, with the Rydberg approximation. The vertical axis represents the logarithm of the ratio of the Rydberg to the computed ionisation potential for the state in question.

3 represents the limit of this method using an IBM computer, although other machines are not so restricted.

Up as far as 15^1S or 17^3S, the reliability of the energies given in Table 3 is easily assessed by comparison with Pekeris' 2300-term solutions, whence it is seen that our singlet levels are about 1.2 cm^{-1} too high, and our triplet levels about 0.2 cm^{-1} too high; in fact, our *uncorrelated* 26-term wave function for 17^3S actually gives a lower energy than Pekeris' 2300-term (method C) wave function! In an attempt to assess the likely accuracy of the energies for higher states, we have constructed in Fig. 1 a graphical comparison between our values, Pekeris' values, and the Rydberg-type formulae for the energies of these states, *viz.*

$$[4] \qquad J_{\text{Rydberg}} = E_{\text{Rydberg}} + 2 = -\tfrac{1}{2}(n+\delta)^{-2} \text{ a.u.}$$

where $\delta = -0.298$ for triplets and $\delta = -0.140$ for singlets (ref. 19, p. 143). Thus, the binding energy of the second electron (*i.e.* $J = (E + 2)$ a.u.) for both our own and Pekeris' calculations is compared with the appropriate Rydberg formula. This diagram suggests that if the Rydberg formula is assumed to be reliable beyond $1s16s$, our singlet binding energies are probably accurate to within about 0.25% *i.e.* 1.2 cm^{-1} at $1s15s$, 0.45 cm^{-1} at $1s25s$. Similarly, until about $1s21s$, our triplet binding energies would seem to be accurate to within 0.04% *i.e.* 0.16 cm^{-1} at $1s17s$ and about 0.10 cm^{-1} at $1s21s$; thereafter, there is a suggestion of a slight deterioration to about 0.16 cm^{-1} at $1s24s$, with $1s25s$ and $1s26s$ being less accurate.

Since this work was completed, a paper reaching rather similar conclusions has been published by Birss and Senn (20) on the ^3S states of helium. Using 51 configurations constructed from a Slater basis set having principal quantum numbers up to $N = 25$, good eigenvalues were obtained up to and including $1s23s$. This again demonstrates the principle that the basis functions need to have sufficient flexibility to describe the nodal properties of the wave functions, in which case target states of very high n are relatively easily represented; thus, the importance of selecting the members of the basis set comes out of their work also. To the number of decimal places quoted by them, there is exact agreement with our results for all levels except $1s23s$, where we estimate that our likely error is 0.16 cm^{-1}. considerably less than the discrepancy (3.3 cm^{-1}) between the two calculations. We also note that for the low-lying triplet states, $1s2s$ to $1s5s$ inclusive, our uncorrelated energies listed in Table 3 are slightly lower than the values they quote for the Hartree–Fock limit.

Towards States of Astrophysical Interest

There is no fundamental reason why the calculation described in this paper could not be extended to higher values of n; likewise the parallel calculations of Birss and Senn. All of the states observed to date could be treated adequately by the solution of matrices of the order

Can. J. Chem. Downloaded from www.nrcresearchpress.com by 210.87.254.6 on 09/05/12
For personal use only.

TABLE 4. Singlet–triplet splittings (in MHz) of some very highly excited $1sns$, $1snp$, and $1snd$ states of the helium atom, estimated either from separate Rydberg-formulae energies for the states in question, or from the $An^{-3} + Bn^{-5}$ formula for the splittings themselves

	^1S–^3S		^1P–^3P	^1D–^3D	Frequency
n	Rydberg formula	$An^{-3}+Bn^{-5}$ formula	$An^{-3}+Bn^{-5}$ formula	$An^{-3}+Bn^{-5}$ formula	of the $n\alpha$ transition
85	1700	1780	870	8.3	10526
109	810	840	410	3.9	5011
134	435	450	220	2.1	2074
158	270	275	135	1.3	1652

of (at most) 200, which is not prohibitive (6, 18, 21). However, if one is limited to the range of numbers from 10^{-75} to 10^{+75}, as we are with our IBM computer, Table 3 represents the limit to this approach, more or less, without a very significant increase in programming effort.

However, Fig. 1 demonstrates that in all probability, the energies of these highly excited states will be well represented by simple Rydberg formula such as eq. 4, and it follows automatically from this conclusion that the original assignments of these observed spectra using the hydrogen-like approximation must be correct. Thus, it is only for two-electron properties of these states that such computational athletics would be required. At the present time, the two-electron property most amenable to observation is the singlet–triplet splitting, which is relatively large for S, P, and D states. We can estimate these splittings in two ways, one by calculating separately the approximate energies of the singlet and the triplet states using eq. 4 and the other using Chang and Poe's suggestion that the singlet–triplet splittings themselves should be well represented by a formula (22) of the kind $An^{-3} + Bn^{-5}$. These two estimates agree very well indeed for S states as shown in Table 4: also listed in Table 4 are the frequencies of some observed $n\alpha$ (*i.e.* $1s(n+1)l \rightarrow 1sn(l \pm 1)$) transitions, and the singlet–triplet splittings for P and D states calculated by the Chang and Poe formula; for F states, the splittings are all less than 0.1 MHz, whereas the width of the 109α line is about 0.3 MHz, and consequently these splittings are not tabulated.

It would seem that the 109α line is the one most likely to show satellites due to a singlet–triplet splitting, first because the lower the value of n, the greater the fraction of the atoms will be in states of low l, and second because this line is one of the strongest so far observed. At $n \approx 110$, roughly[2] one atom in 6000 will be in the $l = 0$ state at thermodynamic equilibrium, 3 in $l = 1$, 5 in $l = 2$, and 7 in 6000 *i.e.* $\sim 0.1\%$ in $l = 3$. Now, since transition probabilities for $nl \rightarrow (n-1)(l-1)$ transitions decrease somewhat as l increases (ref. 19, p. 266), lines corresponding to transitions from $1s110f \rightarrow 1s109d$ should be no less than about 0.1% of the total intensity in the 109α line, which might be just above observable, and according to Table 4, should occur roughly 2 MHz on either side of the 109α line itself. The P and S splittings would be much larger, and much harder to find, but would occur roughly 200 and 600 MHz on either side of the main line, respectively: the latter estimate takes into account the fact that for n in the range of 10–20, the separation between $1snp\ ^3P$ and $1sns\ ^1S$ is about half the separation between $1sns\ ^1S$ and $1sns\ ^3S$, and it is assumed that this pattern persists to high n.

Acknowledgment

This work was supported by the National Research Council of Canada.

1. A. E. LILLEY, P. PALMER, H. PENFIELD, and B. ZUCKERMAN. Nature, **211**, 174 (1966).
2. P. PALMER, B. ZUCKERMAN, H. PENFIELD, A. E. LILLEY, and P. G. MEZGER. Nature, **215**, 40 (1967).
3. P. PALMER, B. ZUCKERMAN, H. PENFIELD, A. E. LILLEY, and P. G. MEZGER. Astrophys. J. **156**, 887 (1969).
4. A. K. DUPREE and L. GOLDBERG. Ann. Rev. Astron. Astrophys. **8**, 231 (1970).
5. W. C. MARTIN. J. Phys. Chem. Ref. Data, **2**, 257 (1973).

[2]Assuming that all $1s110l$ states have the same energy, whence we need not know the temperature.

Can. J. Chem. Downloaded from www.nrcresearchpress.com by 210.87.254.6 on 09/05/12
For personal use only.

6. Y. ACCAD, C. L. PEKERIS, and B. SCHIFF. Phys. Rev. A**4**, 516 (1971).
7. H. SHULL and P-O. LÖWDIN. Phys. Rev. **110**, 1466 (1958).
8. H. O. PRITCHARD and F. H. SUMNER. J. Phys. Chem. **65**, 641 (1961).
9. H. O. PRITCHARD. J. Chem. Phys. **40**, 1496 (1964).
10. H. O. PRITCHARD and A. WALLIS. J. Chem. Phys. **42**, 3548 (1965).
11. A. WALLIS, D. L. S. MCELWAIN, and H. O. PRITCHARD. J. Chem. Phys. **50**, 4543 (1969).
12. A. M. ERMOLAEV. J. Phys. B**7**, 1611 (1974).
13. K. E. BANYARD and G. L. SEDDON. J. Chem. Phys. **58**, 1132 (1973).
14. P. CAVALIERE, G. FERRANTE, R. GERACITANO, and L. LOCASCIO. J. Chem. Phys. **63**, 624 (1975).
15. C. F. LEBEDA and D. M. SCHRADER. J. Chem. Phys. **49**, 2549 (1968).
16. D. L. S. MCELWAIN, A. WALLIS, and H. O. PRITCHARD. Int. J. Quantum Chem. **3**, 711 (1969).
17. P. WINKLER and R. N. PORTER. J. Chem. Phys. **61**, 2038 (1974).
18. C. L. PEKERIS. Phys. Rev. **127**, 509 (1962).
19. H. A. BETHE and E. E. SALPETER. Quantum mechanics of one and two electron atoms. Academic Press Inc., New York. 1957.
20. F. W. BIRSS and P. SENN. J. Chem. Phys. **63**, 1276 (1975).
21. T. ASHTON, D. L. S. MCELWAIN, and H. O. PRITCHARD. Can. J. Chem. **51**, 237 (1973).
22. T. N. CHANG and R. T. POE. Phys. Rev. A**10**, 1981 (1974).
23. P. S. C. WANG and F. WEINHOLD. J. Chem. Phys. **57**, 1738 (1972).

Can. J. Chem. Downloaded from www.nrcresearchpress.com by 210.87.254.6 on 09/05/12
For personal use only.

Calculation of electro-optical parameters, a new approach. Part III. Applications to X_2CZ molecules (X = H, F, Cl, Br and Z = O, S)

P. L. PRASAD AND SURJIT SINGH[1,2]

Structural Chemistry Group, Department of Chemistry, Indian Institute of Technology, Madras 600036, India

Received August 18, 1975

P. L. PRASAD and SURJIT SINGH. Can. J. Chem. **54**, 1550 (1976).

Calculations of electro-optical parameters by the modified first order approximation (MFOA) method have been extended to X_2CZ (X = H, F, Cl, Br; Z = O, S) molecules with a view to investigate the transferability of these parameters. The diagonal and cross elements of the bond moment derivative matrix have been evaluated. Unique values of μ_{C-X} are obtained for the A_1 species. The bond moment derivatives are found to be transferable among A_1 and B_1 species. Transferability of the μ_{C-Z} in B_1 and B_2 species is obtained for thiocarbonyl halides. Bond moment derivatives with respect to angle deformations are not found to be very significant whereas other cross elements of the bond moment derivative matrix are found to be of high magnitude.

P. L. PRASAD et SURJIT SINGH. Can. J. Chem. **54**, 1550 (1976).

Faisant appel à une approximation du premier ordre modifié, on a étendu des calculs de paramètres électro-optiques à des molécules X_2CZ (X = H, F, Cl, Br; Z = O, S); le but de cette étude était d'évaluer la transfèrabilité de ces paramètres. On a évalué les éléments diagonaux et croisés de la matrice dérivée du moment des liasons. On a obtenu des valeurs uniques de μ_{C-X} pour les espèces A_1. On a trouvé que les dérivés du moment de lien sont transferables entre les espèces A_1 et B_1. On obtient une transfèrabilité du μ_{C-Z} dans les espèces B_1 et B_2 pour les halogénures de thiocarbonyles. On trouve que les dérivés du moment de lien par rapport aux angles de déformations ne sont pas importantes; toutefois les autres éléments croisés de la matrice des dérivés du moment des liasons sont importants.

[Traduit par le journal]

Introduction

In the previous two papers (1, 2) it was shown how the electro-optical parameters in polyatomic molecules can be evaluated using a modified first order approximation (MFOA) method. In this approximation the cross elements of the bond moment derivatives matrix are represented in terms of the ratios of the **L** matrix elements and the diagonal elements. Applications of the new approach to the calculations of these parameters have been demonstrated for the A_1 species of nitromethane (2).

Infrared band intensities and simple calculations of electro-optical parameters have been reported for X_2CZ molecules (where X = H, F, Cl, Br and Z = O, S), by Hopper *et al.* (3) and by Hisatsune and Eggers (4). Recently Bruns *et al.* (5) have performed CNDO molecular orbital calculations on these molecules and, with the correct sign combinations thus determined, carried out the calculations of bond moments and their derivatives. It was found that the bond moments and their derivatives evaluated were transferable neither in the same molecule among vibrations of different symmetry species nor among the set of molecules considered.

We thought it of interest to carry out the MFOA calculations on these molecules to determine whether or not they lead to transferable electro-optical parameters.

Calculations

Infrared band intensities of the H_2CO molecule have been reported by Hisatsune and Eggers (4). Because of the band overlap in the spectrum of H_2CO, a simulation technique was applied recently by Jalsovszky (6) and improved band intensities were determined. Duncan (7) has reported a refined set of force constants. The **L** matrix of H_2CO was calculated using Duncan's force field (7) and the optimum geometry (Table 1) calculated using the force method by Kanakavel *et al.* (8). Employing the improved band intensity data of Jalsovszky (6) and the **L** matrix of Table 1, $\partial\mu/\partial S_j$ values were calculated for all

[1]CIDA/NRCC Research Associate at University of Calgary, Calgary, Alberta, 1974–1975.

[2]To whom all correspondence should be addressed.

Can. J. Chem. Downloaded from www.nrcresearchpress.com by 210.87.254.40 on 09/05/12
For personal use only.

TABLE 1. Geometry and L matrices for H_2CO

Geometry	A_1 species			B_1 species	
$r_{C=O} = 1.20$Å $r_{C-H} = 1.10$Å $\angle HCH = 116°$	0.3653	0.0602	−0.0932	1.0564	−0.0095
	−0.0093	−1.0229	−0.0153	−0.1622	1.0635
	0.7695	0.0856	1.4325		

TABLE 2. Comparison of experimental $\partial\mu/\partial S_j$ values with CNDO values

A_1 species				B_1 species		
Sign combination of $\partial\mu_z/\partial Q_i$	$\partial\mu_z/\partial S_1$	$\partial\mu_z/\partial S_2$	$\partial\mu_z/\partial S_3$	Sign combination of $\partial\mu_x/\partial Q_i$	$\partial\mu_x/\partial S_4$	$\partial\mu_x/\partial S_5$
−−+	−3.29	0.96	0.13	−+	−1.21	0.34
−+−	−2.08	−1.31	−0.48	++	1.31	0.36
+++	2.07	−0.99	0.46			
−++	−3.29	−1.33	0.11			
CNDO	−3.45	0.57	0.06	CNDO	−1.20	0.57

TABLE 3. Bond moments and their derivatives calculated by MFOA[a]

	A_1 species			B_1 species[b]		B_2 species
Molecule	$\frac{\partial\mu_{C-Z}}{\partial r_{C-Z}}$	$\frac{\mu_{C-X}}{r_{C-X}}$	$\frac{\partial\mu_{C-X}}{\partial r_{C-X}}$	$\frac{\partial\mu_{C-X}}{\partial r_{C-X}}$	$\frac{\mu_{C-Z}}{r_{C-Z}}$	$\frac{\mu_{C-Z}}{r_{C-Z}}$
H_2CO	−3.05	0.15	0.39	0.22	1.58	0.61
F_2CO	−2.11	−2.21	−1.44	1.12	5.58	4.99
Cl_2CO	−3.82	−0.98	−1.10	0.81	4.73	2.26
				0.51	4.98	
Br_2CO	−4.82	−0.55	−0.69	−0.29	2.85	1.38
F_2CS	0.58	−1.76	−3.10	1.96	2.56	2.51
				1.64	3.12	
Cl_2CS	−1.83	−1.17	−2.36	1.95	2.01	2.15
				1.55	2.71	

[a]The $\partial\mu/\partial S_i$ values used are of the same sign combination of $\partial\mu/\partial Q_i$ as preferred in ref. 5.
[b]Two sets of values in this species correspond to the two sign combinations of $\partial\mu/\partial Q_i$ which are compatible with the CNDO values (ref. 5) Bending symmetry coordinates are scaled by 1 Å.

possible sign combinations of $\partial\mu/\partial Q_i$ and are given in Table 2. A comparison of these values with the CNDO values obtained by Bruns *et al.* (5) shows that the −−+ combination agrees with experimental values (Table 2). The $\partial\mu/\partial S_j$ values from the − − + combination of Table 1 have been used for further calculations on H_2CO. The necessary **L** matrices and band intensity data for other molecules are taken from ref. 3.

A_1 Species

Equations for the evaluation of electro-optical parameters by MFOA for X_2YZ type molecules have been given for the A_1 species previously (1, 2). In the present calculations those equations are used by suitably replacing X by H, F, Cl, Br; Y by C; and Z by O or S. The values for μ_{C-X}, $\partial\mu_{C-X}/\partial r_{C-X}$, and $\partial\mu_{C-Z}/\partial r_{C-Z}$ for H_2CO, F_2CO, Cl_2CO, Br_2CO, F_2CS, and Cl_2CS are given in Table 3. To give an example of the use of the **L**

Can. J. Chem. Downloaded from www.nrcresearchpress.com by 210.87.254.40 on 09/05/12
For personal use only.

matrix for cross elements of the bond moment derivatives matrix (for explanation, see refs. 1 and 2) the following relationships may be examined for H_2CO.

$$\frac{\partial r_{C-O}}{\partial r_{C-H}} = \frac{0.0602}{-\left(\frac{1.0229}{\sqrt{2}}\right)} \qquad \frac{\partial r_{C-H}}{\partial r_{C-O}} = \frac{\frac{1}{\sqrt{2}}(-0.0093)}{0.3653} \qquad \frac{\partial r_{C-O}}{\partial \theta} = \frac{-0.0932}{\frac{2}{\sqrt{6}}(1.4325)}$$

$$\frac{\partial r_{C-H}}{\partial \theta} = \frac{\frac{1}{\sqrt{2}}(-0.0152)}{\left(\frac{2}{\sqrt{6}}\right)(1.4325)} \qquad \frac{\partial \theta}{\partial r_{C-O}} = \frac{\frac{2}{\sqrt{6}}(0.7695)}{0.3653} \qquad \frac{\partial \theta}{\partial r_{C-H}} = \frac{\frac{2}{\sqrt{6}}(0.0856)}{\frac{1}{\sqrt{2}}(-1.0229)}$$

Similar relationships for other molecules can be given using the **L** matrix elements of ref. 3.

B_1 Species

The equilibrium dipole moment of the molecule X_2YZ along the x-axis can be written as follows:

$$\mu_x = \mu_{Y-Z} \cos 90 + \mu_{Y-X_1} \cos (\beta_1 - 90) - \mu_{Y-X_2} \cos (\beta_2 - 90)$$

In a normal vibration of this class the angles are assumed to change as shown in Fig. 1*a*. A small increment in μ_x due to this vibration can be written as follows:

$$\mu_x + \Delta\mu_x = -\mu_{Y-Z} \sin \frac{\Delta\beta}{2} + (\mu_{Y-X_1} + \Delta\mu_{Y-X_1}) \cos \left(\beta_1 - 90 + \frac{\Delta\beta}{2}\right)$$

$$-(\mu_{Y-X_2} - \Delta\mu_{Y-X_2}) \cos \left(\beta_2 - 90 - \frac{\Delta\beta}{2}\right)$$

With the approximation that $\sin (\Delta\beta/2) = \Delta\beta/2$ and that the product of two small terms like $\Delta\mu \cdot \Delta\beta$ can be neglected, we get the following equation:

$$\Delta\mu_x = -\mu_{Y-Z}\frac{\Delta\beta}{2} - \mu_{Y-X_1} \sin (\beta_1 - 90)\frac{\Delta\beta}{2} + \Delta\mu_{Y-X_1} \cos (\beta_1 - 90) - \mu_{Y-X_2} \sin (\beta_2 - 90)\frac{\Delta\beta}{2}$$

$$+ \Delta\mu_{Y-X_2} \cos (\beta_2 - 90)$$

Since $Y-X_1$ and $Y-X_2$ bonds and angles β_1, β_2 are equivalent, this equation can be written as follows:

$$\Delta\mu_x = -\mu_{Y-Z}\frac{\Delta\beta}{2} + \mu_{Y-X} \cos \beta \cdot \Delta\beta + 2\Delta\mu_{Y-X} \sin \beta$$

Hence

$$[1a] \qquad \frac{\Delta\mu_x}{\Delta r_{Y-X}} = \frac{\partial\mu_x}{\partial r_{Y-X}} = -\tfrac{1}{2}\mu_{Y-Z}\frac{\partial\beta}{\partial r_{Y-X}} + \mu_{X-Y} \cos \beta \frac{\partial\beta}{\partial r_{Y-X}} + 2\frac{\partial\mu_{Y-X}}{\partial r_{Y-X}} \sin \beta$$

and

$$[1b] \qquad \frac{\partial\mu_x}{\partial\beta} = -\tfrac{1}{2}\mu_{Y-Z} + \mu_{X-Y} \cos \beta + 2\frac{\partial\mu_{Y-X}}{\partial\beta} \sin \beta$$

These expressions are used to evaluate electro-optical parameters in B_1 species. For example, using MFOA (1, 2), the ratios $\partial\beta/\partial r$ and $\partial\mu_{C-H}/\partial\beta$ for H_2CO can be given as follows:

$$\frac{\partial\beta}{\partial r} = -\frac{0.1622}{1.0564}$$

Can. J. Chem. Downloaded from www.nrcresearchpress.com by 210.87.254.40 on 09/05/12
For personal use only.

and

$$\frac{\partial \mu_{C-H}}{\partial \beta} = \frac{\partial \mu_{C-H}}{\partial r_{C-H}} \frac{\partial r_{C-H}}{\partial \beta} = \left(\frac{-0.0095}{1.0635}\right) \frac{\partial \mu_{C-H}}{\partial r_{C-H}}$$

With these approximations, the eqs. 1*a* and 1*b* are left with three unknowns, namely, $\partial \mu_{Y-Z}/\partial r_{Y-Z}$, $\partial \mu_{Y-X}/\partial_{Y-X}$, and μ_{Y-X}. Since μ_{Y-X} has already been evaluated from A_1 species of vibrations, and assuming the transferability of this parameter, the other two parameters $\partial \mu_{Y-X}/\partial r_{Y-X}$ and μ_{Y-Z} can be evaluated. Bond moments μ_{Y-Z} and their derivatives thus evaluated for all the molecules considered are given in Table 3.

B_2 Species

In the literature (3, 5) $\partial \mu_y/\partial S_6$ has been equated either to μ_{Y-X} or μ_{Y-Z} depending on whether the YX_2 frame distorts with respect to a fixed Y—Z bond or vice versa. However, it seems to be more appropriate if it is assumed that both the XYX frame and the Y—Z bonds are distorted by $\Delta\delta/2$ each, the total distortion being $\Delta\delta$, as shown in Fig. 1*b*.

The dipole moment of the planar X_2YZ molecule along the *y*-axis can be given as follows:

$$\mu_y = \mu_{Y-Z} \cos 90 + 2\mu_{Y-X} \cos \theta/2 \cdot \cos 90 \qquad (\theta = \angle XYX)$$

For a small increment, $\Delta\mu_y$, along the *y*-axis, this equation can be written as follows:

$$\mu_y + \Delta\mu_y = (\mu_{Y-Z} + \Delta\mu_{Y-Z}) \cos\left(90 - \frac{\Delta\delta}{2}\right) + 2(\mu_{Y-X} + \Delta\mu_{Y-X}) \cos\theta/2 \cdot \cos\left(90 - \frac{\Delta\delta}{2}\right)$$

$$\Delta\mu_y = \mu_{Y-Z} \frac{\Delta\delta}{2} + 2\mu_{Y-X} \cos\theta/2 \cdot \frac{\Delta\delta}{2}$$

Hence

[2] $$\frac{\Delta\mu_y}{\Delta\delta} = \frac{\partial\mu_y}{\partial\delta} = \tfrac{1}{2}(\mu_{Y-Z} + 2\mu_{Y-X} \cos\theta/2)$$

Again μ_{Y-X} of the A_1 species is transferred to this equation and the value of μ_{Y-Z} is evaluated. These values for all the molecules considered are given in Table 3.

Discussion

The dipole moments of the C—X bond for all these molecules were evaluated for an A_1 symmetry species. As can be noticed from Table 3, the bond moment decreases in the series $F_2CO > Cl_2CO > Br_2CO > H_2CO$ and $F_2CS > Cl_2CS$. The bond moments can also be calculated roughly by invoking Pauling's (9) relationships on percentage ionic character and electronegativities. The μ/r values

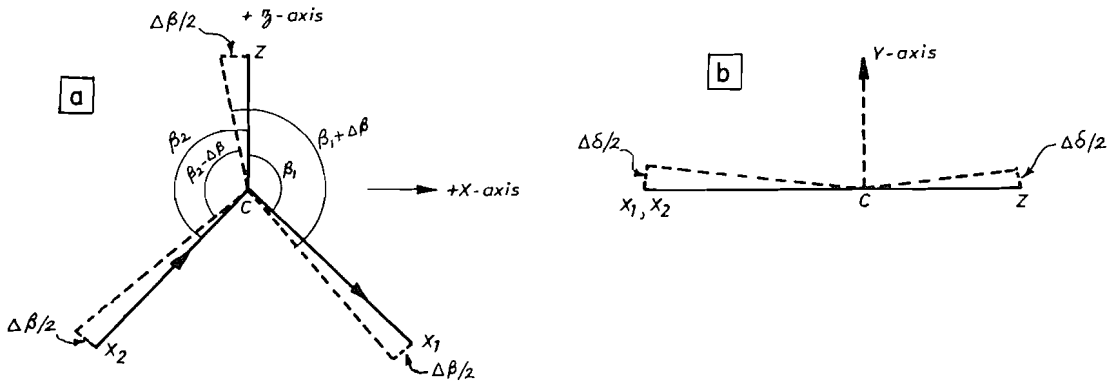

FIG. 1. Distortion of the equilibrium geometry of X_2CZ molecules during (*a*) B_1 and (*b*) B_2 vibrations.

Can. J. Chem. Downloaded from www.nrcresearchpress.com by 210.87.254.40 on 09/05/12
For personal use only.

TABLE 4. Bond moments and their derivatives after inclusion of rehybridisation moments[a]

Molecule	A_1 species			B_1 species		B_2 species
	$\frac{\partial\mu_{C-Z}}{\partial r_{C-Z}}$	$\frac{\mu_{C-X}}{r_{C-X}}$	$\frac{\partial\mu_{C-X}}{\partial r_{C-X}}$	$\frac{\partial\mu_{C-X}}{\partial r_{C-X}}$	$\frac{\mu_{C-Z}}{r_{C-Z}}$	$\frac{\mu_{C-Z}}{r_{C-Z}}$
H_2CO	−2.0408	0.4563	0.2973	−0.5767	0.0969	0.6801
F_2CO	−1.3508	−1.5679	−1.1861	1.2822	4.0599	2.2418
Cl_2CO	−2.8696	−0.5630	−1.3441	1.3892 1.0846	3.9573 4.2092	1.6530
F_2CS	0.2426	−1.0558	−2.1486	1.7651 1.4482	1.6883 2.2479	2.7195
Cl_2CS	−1.9455	−0.6485	−2.4926	2.4961 2.0993	0.9095 1.6003	−0.3040

[a]Rehybridisation moments were obtained from R. E. Bruns by private communication.

for isolated C—X bonds thus calculated are found to be 2.07, 0.34, 0.12, and 0.19 for X = F, Cl, Br, and H respectively. Whereas C—F and C—H bond moments obtained by Pauling's relationships agree well with the values obtained by MFOA, the C—Cl and C—Br bond moments are comparable only as to order of magnitude. The trend in the values of bond moments for C—F, C—Cl, C—Br is, however, similar. The experimental values of bond moments for C—F (10) and C—Cl (11) are fairly close to the values obtained by these calculations.

The bond moment derivatives $\partial\mu_{C-O}/\partial r_{C-O}$ and $\partial\mu_{C-S}/\partial r_{C-S}$ are found only in the A_1 species. These values are found to increase in the series $F_2CO < Cl_2CO < Br_2CO$ and $F_2CS < Cl_2CS$. The value in H_2CO is found to be in between that of Cl_2CO and Br_2CO. Further $\partial\mu_{C-O}/\partial r_{C-O}$ is found to be greater than $\partial\mu_{C-S}/\partial r_{C-S}$ both in fluorinated and chlorinated derivatives. These trends are similar to the trends observed in the bond moment derivatives calculated by Bruns *et al.* (5). Unlike the conclusion drawn by Hopper *et al.* (3), $\partial\mu_{C-O}/\partial r_{C-O}$ is not a characteristic of C=O bond.

The values of $\partial\mu_{C-X}/\partial r_{C-X}$ were found in A_1 and B_1 species and are found to be transferable within an error of 0.3 except in F_2CS where the difference is 1.1. The values are found to decrease in the series $F_2CO > Cl_2CO > Br_2CO > H_2CO$ and $F_2CS > Cl_2CS$ as observed in the case of μ_{C-X} values. The $\partial\mu_{C-X}/\partial r_{C-X}$ is found to be less in X_2CO molecules than in X_2CS molecules, similar to what is observed in the values of Hopper *et al.* (3) and of Bruns *et al.* (5). A general conclusion can be drawn from these values that, whereas $\partial\mu_{C-X}/\partial r_{C-X}$ decreases in the series $F_2CO > Cl_2CO > Br_2CO > H_2CO$, the $\partial\mu_{C-Z}/\partial r_{C-Z}$ values increase. Further $\partial\mu_{C-X}/\partial r_{C-X}$ in the X_2CO molecule is less than in X_2CS molecules whereas $\partial\mu_{C-O}/\partial r_{C-O}$ in various X_2CZ molecules is greater than the corresponding $\partial\mu_{C-S}/\partial r_{C-S}$ values.

The μ_{C-O} and μ_{C-S} values are found in B_1 and B_2 symmetry species and are found to decrease in the series $F_2CO > Cl_2CO > Br_2CO > H_2CO$ and $F_2CS > Cl_2CS$. The values seem to be transferable in B_1 and B_2 symmetry species for F_2CS and Cl_2CS molecules but are not found to be transferable in all X_2CO molecules. Whereas the bond moments are comparable in A_1 species, their derivatives do not seem to be transferable in the set of molecules considered.

Orville-Thomas proposed rehybridisation theory (12) for acquiring transferability of bond moment parameters among different symmetry species of the same molecule. The bond moment parameters are calculated by MFOA including rehybridisation moments obtained by Bruns *et al.* (5) by CNDO calculations. These values are listed in Table 4. As can be noticed the $\partial\mu_{C-X}/\partial r_{C-X}$ values obtained after inclusion of rehybridisation moments are transferable in A_1 and B_1 species within an error of 0.1. As mentioned previously (2) the difference in parameters obtained before and after including rehybridisation contributions will give the hybridisation contributions of individual bonds. It is interesting to note that the hybridisation contributions to C—X bonds, *i.e.* the differences in values of

Can. J. Chem. Downloaded from www.nrcresearchpress.com by 210.87.254.40 on 09/05/12
For personal use only.

TABLE 5. Final values of bond moments and total dipole moments for all molecules[a]

Molecule	$\frac{\mu_{C-Z}}{r_{C-Z}}$	$\frac{\mu_{C-X}}{r_{C-X}}$	μ_z	CNDO
H_2CO	−1.58	0.15	−1.72	−1.94
F_2CO	−3.85	−2.21	−1.10	−0.77
Cl_2CO	−2.26	−0.98	−0.67	−0.41
Br_2CO	−1.38	−0.55	−0.46	—
Cl_2CS	−2.14	−1.18	−1.31	−0.57
F_2CS	−2.51	−1.76	−1.34	−0.95

[a]To calculate total dipole moments μ_{C-X}/r_{C-X} values are taken from A_1 species for all molecules and μ_{C-Z}/r_{C-Z} values are taken from B_2 species except for F_2CO and H_2CO. For F_2CO, μ_{C-O}/r_{C-O} is approximated as 3.85 and for H_2CO μ_{C-O}/r_{C-O} is taken from the B_1 species.

μ_{C-X} of Tables 3 and 4, are found to be −0.84, −0.74, −0.94, and −0.90 in F_2CO, Cl_2CO, F_2CS, and Cl_2CS, respectively. The constancy of this value might indicate that the hybridisation contributions to C—F and C—Cl bonds in both carbonyl and thiocarbonyl halides are the same. However, inclusion of rehybridisation moments did not improve the transferability of μ_{C-O}. The total dipole moments of all these molecules calculated are given in Table 5 where they are compared with CNDO values.

Using $\partial\mu_{C-Z}/\partial r_{C-Z}$ and $\partial\mu_{C-X}/\partial r_{C-X}$ values of A_1 species (Table 3), the cross elements of these bond moment derivatives can be calculated; for example,

$$\frac{\partial\mu_{C-Z}}{\partial r_{C-X}} = \frac{\partial\mu_{C-Z}}{\partial r_{C-Z}} \cdot \frac{\partial r_{C-Z}}{\partial r_{C-X}}$$

and

$$\frac{\partial\mu_{C-Z}}{\partial\theta} = \frac{\partial\mu_{C-Z}}{\partial r_{C-Z}} \cdot \frac{\partial r_{C-Z}}{\partial\theta}$$

The derivatives $\partial r_{C-Z}/\partial r_{C-X}$, $\partial r_{C-Z}/\partial\theta$, etc. are approximated by the ratios of **L** matrix elements as mentioned earlier in the text. It should be remembered that, since C—X_1 and C—X_2 transform into each other and constitute a symmetry coordinate in the A_1 irreducible representation, $\partial\mu_{C-Z}/\partial r_{C-X_1}$ will be equal to $\partial\mu_{C-Z}/\partial r_{C-X_2}$ and $\partial\mu_{C-X_1}/\partial R_j$ will be equal to $\partial\mu_{C-X_2}/\partial R_j$, where R_j is any other internal coordinate. The values of cross derivatives thus calculated are given in Table 6. The values of cross derivatives of bond moments, especially derivatives with respect to bond angle deformation, are small compared to diagonal derivatives as found earlier (2). The values of $\partial\mu_{C-Z}/\partial r_{C-X}$ and $\partial\mu_{C-X}/\partial r_{C-Z}$ are found to increase in the order $F_2CO > Cl_2CO > Br_2CO$. In general the cross derivatives of bond moments of H_2CO are not in line with those of other molecules.

The dipole moment of any bond X—Y is written as $\mu_{X-Y} = \epsilon \cdot r_{X-Y}$ where ϵ is the effective charge and r_{X-Y} is the bond length. The bond moment derivative can be written as follows:

$$\frac{\partial\mu_{X-Y}}{\partial r_{X-Y}} = \frac{\partial\epsilon}{\partial r_{X-Y}} \cdot r_{X-Y} + \epsilon$$

$$= \frac{\partial\epsilon}{\partial r_{X-Y}} \cdot r_{X-Y} + \frac{\mu_{X-Y}}{r_{X-Y}}$$

The difference between the bond moment and its derivative will reflect the change in ionic character of the bond during vibration and is known as the delocalisation moment (13).

$$\frac{\partial\epsilon}{\partial r_{X-Y}} \cdot r_{X-Y} = \frac{\partial\mu_{X-Y}}{\partial r_{X-Y}} - \frac{\mu_{X-Y}}{r_{X-Y}}$$

TABLE 6. Cross derivatives of bond moments calculated by MFOA

Molecule	$\partial\mu_{C-Z}/\partial r_{C-X}$	$\partial\mu_{C-Z}/\partial\theta$	$\partial\mu_{C-X}/\partial r_{C-Z}$	$\partial\mu_{C-X}/\partial\theta$
H_2CO	0.25	0.24	−0.01	−0.01
F_2CO	−0.45	0.07	0.52	−0.17
Cl_2CO	−0.31	0.04	0.37	−0.18
Br_2CO	−0.12	0.10	0.23	−0.24
F_2CS	0.47	−0.09	1.82	−0.08
Cl_2CS	0.61	0.00	1.03	−0.39

Can. J. Chem. Downloaded from www.nrcresearchpress.com by 210.87.254.40 on 09/05/12
For personal use only.

TABLE 7. Comparison of bond moment derivatives calculated by MFOA with literature values

Molecule	$\partial\mu_{C-Z}/\partial r_{C-Z}$			$\partial\mu_{C-X}/\partial r_{C-X}$		
	Hopper *et al.* (3)	Bruns *et al.* (5)	MFOA	Hopper *et al.* (3)	Bruns *et al.* (5)	MFOA
H_2CO	−3.55	−3.45	−3.25	−1.22	−0.80	0.39
F_2CO	−4.13	−5.44	−2.10	−4.67	−5.53	−1.44
Cl_2CO	−4.70	−7.03	−3.82	−3.01	−1.89	−1.10
Br_2CO	−5.30	—	−4.83	−2.07	—	−0.69
F_2CS	−3.07	−4.64	0.58	−6.15	−9.71	−3.10
Cl_2CS	−3.70	−4.93	−1.83	−4.63	−4.11	−2.36

Thus the values of this parameter for all molecules are given below:

Molecule	$\frac{\partial\epsilon}{\partial r_{C-X}}\cdot r_{C-X}$
F_2CO	0.76
H_2CO	0.24
Cl_2CO	−0.12
Br_2CO	−0.13
F_2CS	−1.34
Cl_2CS	−1.19

The trend in values of this parameter in X_2CS and X_2CO molecules can be compared with the electronegativity difference of C—X bonds. The difference in electronegativity for C—X bonds is in the order C—F > C—Cl > C—Br > C—H. But in the series of values of $(\partial\epsilon/\partial r_{C-X})\cdot r_{C-X}$, as can be seen from above, the value for C—H comes next to C—F bond. This might indicate that the percentage of charge migration during vibration is greater for H_2CO than for Cl_2CO and Br_2CO. The change in the sign of these values is due to the fact that the magnitude of $\partial\mu_{C-X}/\partial r_{C-X}$ is greater than μ_{C-X}/r_{C-X} for all molecules except for F_2CO.

Finally it is interesting to compare the various relationships among the bond moment derivatives of these molecules given by Hopper *et al.* (3) and Bruns *et al.* (5). The values of the bond moment derivatives of refs. 3 and 5 and from the present calculation are compared in Table 7. From this table we can notice that semiempirical CNDO calculations predict that $\partial\mu_{C-S}/\partial r_{C-S}$ is smaller than $\partial\mu_{C-O}/\partial r_{C-O}$ by 1.0 and 2.1 in F_2CZ and Cl_2CZ molecules, respectively. Our values predict a difference of 2.6 and 2.0. This difference becomes 1.0 in both the F_2CZ and Cl_2CZ molecules after including rehybridisation moments (Table 4). The magnitudes of $\partial\mu_{C-F}/\partial r_{C-F}$ and $\partial\mu_{C-Cl}/\partial r_{C-Cl}$ in A_1 species are greater by 1.6 and 1.2 in thiocarbonyl halides than in carbonyl halides, whereas Hopper *et al.* (3) predict them to be greater by 1.5 and 1.6, respectively. The prediction of Hopper *et al.* (3) and Bruns *et al.* (5), that the difference between $\partial\mu_{C-F}/\partial r_{C-F}$ and $\partial\mu_{C-Cl}/\partial r_{C-Cl}$ of carbonyl halides is equal to the corresponding difference in thiocarbonyl halides, is more readily apparent from the values from the present calculation by MFOA in Table 7. From this table it is interesting to note that, even though the magnitudes of the bond moment derivatives calculated by MFOA differ considerably from values of Hopper *et al.* (3) and Bruns *et al.* (5), the values of differences among the derivatives mentioned above, in all calculations, are comparable.

Conclusion

The calculations show that it is possible to evaluate the full set of electro-optical parameters using the MFOA method. Transferability of $\partial\mu_{C-X}/\partial r_{C-X}$ parameters has been achieved in A_1 and B_1 species for all molecules considered, whereas transferability of μ_{C-Z}/r_{C-Z} was achieved only for the thiocarbonyl halides. The magnitudes of the cross derivatives compared to the diagonal derivatives clearly show that the former cannot be ignored and explain why the zero order approximation will not yield transferable values. The main advantage of the MFOA method is that the bond moments and derivatives can easily be calculated even for bigger molecules.

Acknowledgements

We are thankful to Dr. R. E. Bruns, Instituto de Quimica, Universidade Estadual de Compinas,

Can. J. Chem. Downloaded from www.nrcresearchpress.com by 210.87.254.40 on 09/05/12
For personal use only.

Brasil for kindly providing us with his CNDO calculations of rehybridisation moments. Also our thanks are due to members of the Structural Chemistry Group for helpful discussions. The authors acknowledge helpful discussions with Professor P. J. Krueger of the University of Calgary, Calgary, Alberta.

1. P. L. PRASAD and SURJIT SINGH. Chem. Phys. Lett. **31**, 535 (1975).
2. P. L. PRASAD and SURJIT SINGH. Chem. Phys. Lett. **32**, 265 (1975).
3. M. J. HOPPER, J. W. RUSSELL, and J. OVEREND. J. Chem. Phys. **48**, 3765 (1968); Spectrochim. Acta, **28**, 1215 (1972).
4. I. C. HISATSUNE and D. F. EGGERS. J. Chem. Phys. **23**, 487 (1955).
5. R. E. BRUNS and R. K. NAIR. J. Chem. Phys. **58**, 1849 (1973); R. E. BRUNS. J. Chem. Phys. **58**, 1855 (1973); R. E. BRUNS and W. B. PERSON. J. Chem. Phys. **58**, 2585 (1973).
6. G. JALSOVZSKY. J. Mol. Struct. **19**, 783 (1973).
7. J. L. DUNCAN. Chem. Phys. Lett. **23**, 597 (1973).
8. M. KANAKAVEL, J. CHANDRASEKHAR, S. SUBRAMANIAN, and SURJIT SINGH. To be published.
9. L. PAULING. The nature of the chemical bond. IIIrd ed. Cornell University Press, New York. 1960.
10. J. W. SMITH. Electric dipole moments. Butterworth Scientific Publications, London. 1955.
11. J. W. STRALEY. J. Chem. Phys. **23**, 2183 (1955).
12. W. J. ORVILLE-THOMAS. J. Mol. Struct. **19**, 761 (1973).
13. W. B. PERSON. Spectrochim. Acta, **20**, 771 (1964).

Can. J. Chem. Downloaded from www.nrcresearchpress.com by 210.87.254.40 on 09/05/12
For personal use only.

Tautomeric equilibrium study of thiazolidine-2-thione. Transition metal complexes of the deprotonated ligand

CARLO PRETI AND GIUSEPPE TOSI
Istituto di Chimica Generale ed Inorganica, University of Modena, 41100 Modena, Italy

Received December 16, 1975

CARLO PRETI and GIUSEPPE TOSI. Can. J. Chem. **54**, 1558 (1976).

The complexes of deprotonated thiazolidine-2-thione (ttz) with many transition metals have been prepared. Probable structures have been proposed for the complexes on the basis of chemical analysis, spectral data (infrared and visible), and magnetic susceptibility measurements. The ligand field parameters have been evaluated and are in keeping with the proposed structures.

CARLO PRETI et GIUSEPPE TOSI. Can. J. Chem. **54**, 1558 (1976).

On a préparé les complexes de la thiazolidinethione-2 (ttz) déprotonée avec plusieurs métaux de transition. On a proposé des structures probables pour les complexes en se basant sur l'analyse chimique, des données spectrales (infrarouge et visible) et des mesures de susceptibilité magnétique. On a évalué les paramètres de champs de ligand et ceux-ci sont en accord avec les structures proposées.

[Traduit par le journal]

The complexing properties of the HNCS group with metal ions have been studied for some time in our laboratory (1, 2). The thiazolidine-2-thione forms a variety of interesting complexes with transition metal ions being coordinated through either the nitrogen or the sulphur of the ring or the exocyclic sulphur of the thioketo group (refs. 3 and 4 and literature cited therein).

This ligand exhibits thiol–thione isomerism involving —N=C—SH and —NH—C=S groups in a thiol–thione equilibrium

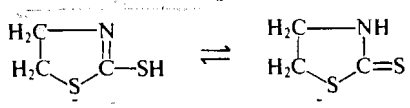

Thiol form Thione form

It has been demonstrated from the ir spectra that the ligand exists in the solid state as a hydrogen-bonded thioamide complex, which partially breaks down in carbon tetrachloride solution (5). The ir spectra do not show a ν(SH) peak in the region of 2500 cm^{-1} nor ν(C=N) at 1700 to 1590 cm^{-1}, but show a strong absorption around 3400 cm^{-1} corresponding to the ν(NH) stretch (6).

Complexation is achieved either by the replacement of a proton by the metal or direct coordination with the ligand acting as monodentate, or by formation of a chelate structure involving both sulphur and nitrogen atoms. Polymeric structures involving bridging ligand are also possible.

The present paper deals with the investigation of the structural aspects of the complexes of deprotonated thiazolidine-2-thione with metal ions like Zn(II), Cd(II), Hg(II), Co(II), Ni(II), Cu(I), Pd(II), Pt(II), Ag(I), Ir(III), and Mn(II). Tentative structures have been proposed for the complexes on the basis of spectral and magnetic susceptibility data and the results of chemical analyses.

Results and Discussion

Table 1 lists the new complexes obtained, together with the analytical results, room temperature magnetic moments, and other physical properties. The band energies from the solid state electronic spectra are listed in Table 2. The most important ir bands in the range 4000 to 50 cm^{-1} are given in Table 3.

The complexes are powdery and insoluble in the most common organic solvents; this last fact suggests that they are polymeric with coordination of more than one ligand molecule to the metal atom. The general insolubility of the complexes precludes their study by such means as nmr, molecular weight, and molar conductivity measurements.

Magnetic and Visible Spectral Studies

The reflectance spectrum of the inner cobalt

Can. J. Chem. Downloaded from www.nrcresearchpress.com by 210.87.254.42 on 09/05/12
For personal use only.

TABLE 1. Analytical data and other physical properties

Compound	Colour	Found % C	Found % H	Found % X	Required % C	Required % H	Required % X	μ (B.M.)	Dec. point (°C)
$Zn(ttz)_2$	White	23.2	2.7	22.0	23.9	2.7	21.7	dia.	270–272
$Cd(ttz)_2$	White	20.8	2.6	32.4	20.7	2.3	32.2	dia.	180–183
$Hg(ttz)_2$	White	16.5	2.1	45.7	16.5	1.8	45.9	dia.	160–162
$Co(ttz)_2 \cdot H_2O$	Turquoise	23.0	3.1	18.6	23.0	3.2	18.8	4.2	>350
$Ni(ttz)_2$	Brown	24.6	3.1	19.9	24.4	2.8	19.9	1.2	255–260
Cuttz	Pale yellow	20.3	2.2	7.7*	19.8	2.2	7.7*	dia.	225–230
$Pd(ttz)_2$	Orange	21.4	2.4	31.0	21.0	2.4	31.0	dia.	255–257
$Pt(ttz)_2$	Hazel-brown	16.9	2.0	45.0	16.7	1.9	45.2	dia.	>350
Agttz	White	15.9	1.9	6.2*	15.9	1.8	6.2*	dia.	188–190
$Au(ttz)_2$†	Pale yellow	16.7	2.2	45.0	16.6	1.9	45.5	dia.	165–167
$Ir(ttz)_3$	Orange-yellow	19.6	2.7	7.7*	19.8	2.6	7.7*	dia.	158–160
$Mn(ttz)_2 \cdot H_2O$	White	23.7	3.4	9.1*	23.3	3.3	9.1*	—	>350

*X = nitrogen for copper, silver, manganese, and iridium derivatives; = metal for all the remaining complexes.
†N% found 6.5; required 6.5.

TABLE 2. Electronic spectra and ligand field parameters

Compound	*d–d* transitions	Wave number	Ligand field* Parameter	Ligand field* Value (cm^{-1})
$Co(ttz)_2 \cdot H_2O$	$^4A_2(F) \rightarrow {}^4T_1(P)$	16 400	Dq	436
	$^4A_2(F) \rightarrow {}^4T_1(F)$	7 575	B'	716
	$^4A_2(F) \rightarrow {}^4T_2(F)$	4 410†	β	0.74
$Ni(ttz)_2$	Charge transfer	23 260		
	$^1A_g \rightarrow {}^1B_{3g}$	20 950		
	$^1A_g \rightarrow {}^1B_{1g}$	16 660sh		
$Pd(ttz)_2$	$^1A_g \rightarrow B_{1g}$	23 800	Δ_1	25 900
$Ir(ttz)_3$	$^1A_{1g} \rightarrow {}^1T_{2g}$	32 000	Δ	29 530
	$^1A_{1g} \rightarrow {}^1T_{1g}$	26 450	B'	371
	$^1A_{1g} \rightarrow {}^3T_{1g}$	21 050	β	0.56
$Mn(ttz)_2 \cdot H_2O$	$^6A_1 \rightarrow {}^4E_g(^4D)$	28 735	Dq	567
	$^6A_1 \rightarrow {}^4E_g, {}^4A_{1g}(^4G)$	24 200	B	647
	$^6A_1 \rightarrow {}^4T_{1g}(^4G)$	20 830	C	3 546

*B is taken to be 967 and 660 cm^{-1} for Co^{2+} and Ir^{3+} free ions, respectively.
†Calculated value.

derivative shows two bands at 7 575, ν_2 and 16 400 cm^{-1}, ν_3 indicating a tetrahedral configuration. It is reasonable to suppose its structure to be that of an infinite polymer with the ligand forming bridges between cobalt ions. A similar structure has been suggested for dibenzimidazolatocobalt(II) and diimidazolatocobalt(II) (7, 8). Using the values of ν_2 and ν_3, the ligand field parameters Dq and B' have been evaluated (Table 2).

By comparison of Dq values reported for CoL_4 groups (9) we can see that the complex $Co(ttz)_2 \cdot H_2O$ shows a Dq value that is, using the 'law of the average environment', typical of a CoS_2N_2 chromophore.

The magnetic moment is 4.2 B.M. Since the orbital contribution in the tetrahedral cobalt(II) is much less than that of the octahedral, tetrahedral cobalt(II) complexes have generally values of magnetic moments in the range 4.3–4.7 B.M. (10). The magnetic moment of $Co(ttz)_2 \cdot H_2O$ is a bit lower than that expected for a tetrahedral geometry and this value could be attributed to the S—C—N chains which form part of a mobile π-electron system present in the ligand in polymeric complexes.

Can. J. Chem. Downloaded from www.nrcresearchpress.com by 210.87.254.42 on 09/05/12
For personal use only.

TABLE 3. Infrared absorption bands (cm^{-1})

Compounds	Thio-amide I	Thio-amide II	Thio-amide III	ν(CS) sym. and asym.	ν(M—N)	ν(M—S)	Other bands
ttz	1490s	1245m	990s	690s,650vs	—	—	434ms,290m,94m
$Zn(ttz)_2$	1500vs	1250m	970vs	— ,680ms	230vs	325vs	437s,304sh,96mw
$Cd(ttz)_2$	1480vs	1250m	970vs	— ,670ms	200vs	260m	433s,302sh,97mw
$Hg(ttz)_2$	1500vs	1270m	965m	760m,680m	200ms,185m	331vs,225s	430s,298w,95m
$Co(ttz)_2 \cdot H_2O$	1495vs	1260ms	975vs	750m,690s	270ms,248m	381ms,322ms	434ms,294mw,96m
$Ni(ttz)_2$	1500s	1250m	980ms	720m,664m	261m	365s,327ms	434m,295m,98w
Cuttz	1520vs	1250m	960s	720mw,660mw	226m	330mw	430ms,284w,94w
$Pd(ttz)_2$	1510vs	1250ms	970vs	— ,683m	303s,263s	378s,368s	434ms,286ms,95w
$Pt(ttz)_2$	1510vs	1250ms	970s	720m,685m	257s,227s	370w	435m,282w,96mw
Agttz	1518vs	1250m	970vs	— ,665m	313vs	242vs	430s,290w,100w
$Au(ttz)_2$	1570vs	1245m	985vs	730mw,660m	282mw	267m	428ms,295w,98w
$Ir(ttz)_3$	1525s	1260m	990m	700m,660m	296ms,277m	312m,306m	435ms,290sh,96w
$Mn(ttz)_2 \cdot H_2O$	1565vs	1250mw	950m	750m,665mw	219m,211m	305m,264ms	430m,284m,98m

The nickel complex $Ni(ttz)_2$, already reported in a previous paper (11) but not studied in detail, is considered in this paper for a more accurate examination. The μ value of this compound is 1.2 B.M. It is noteworthy that the electronic spectrum is indicative of a stereochemistry with a predominantly planar environment (Table 2); thus on the basis of electronic and ir spectral studies (see below) a planar polymeric structure is proposed for the nickel complex (12–15). Being a spectrum of low resolution it is not possible to obtain meaningful bonding parameters.

The copper derivative which resulted is diamagnetic and the analytical results support the formulation of the type Cuttz. Repeated syntheses and elemental analyses gave reproducible results. This fact of the reduction of copper(II) to copper (I) by the ligand is in keeping with the observations on the previously reported complexes of copper with ttz which resulted in products always containing copper(I) (16, 17). No *d–d* transitions have been observed in the electronic spectrum of this complex.

Basson and du Preez (18) have prepared a complex of copper with ttz of stoichiometry $Cu(ttz)_2$, yellow and slightly paramagnetic, 0.79 B.M. The fact that copper remains in the complex in 2+ oxidation state is quite surprising. Any attempt to prepare the complex in the same way as reported by these authors failed and we have obtained only a derivative whose elemental analyses fit well with a Cu(I) complex. Even if our analytical results were incorrect, we should have found in the electronic spectrum the typical transitions of copper(II) and moreover a peak around 375 nm explaining the completely quenching of the paramagnetism (19, 20). We could propose for the copper derivative the following forms: (*a*) a four-ring structure with the copper(I) coordinated through the sulphur and the nitrogen atoms in polymeric materials; (*b*) a salt-like structure with the copper(I) replacing a hydrogen ion; (*c*) a polymeric structure with sulphur bridges in which the copper(I) achieves its maximum coordination number. This question is considered further after the discussion of the ir spectra.

The Pd(II) and Pt(II) ions, with d^8 configuration, have square planar arrangements of ligand molecules around them in a large number of their complexes. In the electronic spectrum of the palladium(II) derivative, recorded in the solid state as a Nujol mull, only the band at 23 800 cm^{-1} can be considered a *d–d* transition of the type $^1A_g \rightarrow {}^1B_{1g}(x^2 - y^2 \rightarrow xy)$. The value of Δ_1, by the standard treatment, is 25 900 cm^{-1} (13); this is what one should expect in the square planar geometry. Assignments have not been possible in the case of the platinum(II) derivative.

The solid state electronic spectrum confirms an octahedral configuration of the central atom in the $Ir(ttz)_3$ derivative. The two observed absorption bands are in the ranges expected for the two spin-allowed transitions from the ground state $^1A_{1g}$. The ratio of the energies of ν_2 and ν_1 is 1.20. The ligand field parameters Δ, B', and β

Can. J. Chem. Downloaded from www.nrcresearchpress.com by 210.87.254.42 on 09/05/12
For personal use only.

Can. J. Chem. Downloaded from www.nrcresearchpress.com by 210.87.254.42 on 09/05/12
For personal use only.

have been calculated by means of the equations

$$\nu_1 = \Delta - 4B' + 86(B')^2/\Delta$$

$$\nu_2 = \Delta + 12B' + 2(B')^2/\Delta$$

and are reported in Table 2.

The B' value is of the order of 56% of the free ion value, suggesting a considerable orbital overlap in the complex. The value of Δ is higher than those found for the iridium dithiocarbamates (22) and could be indicative of an octahedral symmetry with iridium–sulphur and iridium–nitrogen bonds in polymeric materials.

Working with manganese(II) we have obtained the compound $Mn(ttz)_2 \cdot H_2O$. The energies of the ${}^6A_1 \rightarrow {}^4E,{}^4A_1({}^4G)$ and ${}^6A_1 \rightarrow {}^4E({}^4D)$ transitions are independent of Dq, depending only on B and C. The values of B and C have been obtained using the expressions

$${}^4E,{}^4A_1({}^4G) = 10B + 5C = 24\,200$$

$${}^4E({}^4D) = 17B + 5C = 28\,735$$

These values of B and C have then been used together with the ${}^6A_1 \rightarrow {}^4T_{1g}({}^4G)$ transition in solving the secular equations of Tanabe and Sugano (23) to evaluate the value of Dq and are reported in Table 2.

Zinc(II), cadmium(II), and mercury(II) do not show *d–d* transitions and therefore the stereochemistry of their complexes cannot be derived from diffuse reflectance spectra. Most of the complexes of these metals with a 1:2 metal: ligand ratio reported in the literature are tetrahedral, therefore we can propose these diamagnetic derivatives $Zn(ttz)_2$, $Cd(ttz)_2$, and $Hg(ttz)_2$ a tetrahedral arrangement of the ligand molecules in polymeric structures.

The silver(I) complex is diamagnetic and a linear structure is proposed for this derivative.

Infrared Spectra

The coordination mode of the ligand can be distinguished by an analysis of the positions and intensities of the thioamide bands and of the bands due to the prevailing contribution of ν(C—S) symmetric and antisymmetric (Table 3). The directions of the shifts in the position of all the bands in the spectra of the complexes are the same; this fact indicates that the bonding pattern in all the complexes must be similar.

The infrared spectra of the complexes do not display the bands due to ν(NH) and δ(NH), thus indicating the absence of the imino-hydrogen in these compounds. The thioamide I, observed at 1490 cm^{-1} in the ligand, is shifted at higher wave numbers in the complexes; this fact clearly indicates that the nitrogen atom is involved in the coordination to the metal. Band II experiences a blue shift of about 10 cm^{-1} indicating that the bond order of C=N is increased and showing that the metal atom is bonded to the exocyclic sulphur; band III shows a red shift of about 20 cm^{-1}.

Thioamide I has a predominant contribution from δ(CH) + ν(C···N), band II has a predominant contribution from ν(C···N) + δ(CH) + ν(C···S), while band III has a contribution from ν(C···N) + ν(C···S). According to literature data (24–26), the shifts above reported are clearly indicative of simultaneous metal–nitrogen and metal–sulphur bonds. The sulphur atom in the ring is clearly not involved in the coordination, being the stretchings due to the prevailing contribution of ν(C—S) symmetric and antisymmetric shifted towards higher energies. These results agree very well with the conclusions from the electronic spectra.

Further confirmation of —N and —S bondings to the metals in the complexes is obtained by the low-frequency spectral absorptions. In the spectra of N-bonded and S-bonded complexes, absorptions due to ν(M—N) and ν(M—S) are present in the range 350 to 150 cm^{-1}. In our ir spectra new bands are present in the low frequency region, Table 3, which are tentatively assigned to ν(M—N) and ν(M—S) in good accord with literature data (11, 27–36).

In the case of $Co(ttz)_2 \cdot H_2O$ and $Mn(ttz)_2 \cdot H_2O$ complexes, bands due to ν(OH) and δ(HOH) are present at 3500 cm^{-1} (broad) and 1600 cm^{-1} (broad), clearly indicating the presence of lattice water. Twisting, wagging, and rocking vibrational modes of the coordinated water are absent in the expected ranges.

In light of the ir results we propose for all the complexes here reported polymeric structures with the ligands linked to the metal ions through the sulphur and nitrogen atoms; the insolubility of these derivatives in water and even in organic solvents points to a polymeric intermolecular linkage.

Can. J. Chem. Downloaded from www.nrcresearchpress.com by 210.87.254.42 on 09/05/12
For personal use only.

Experimental

Purification of the Ligand

The commercially available ttz has been purified by repeated recrystallizations from hot water, mp 106–107 °C (lit. 106–107 °C (37)).

Preparation of the Complexes

Method A

An aqueous solution of the metal chloride or nitrate or acetate, maintained at a p*H* value lower than that of precipitation of the correspondent hydroxide, has been treated with an aqueous/ethanol solution of the ligand in the metal:ligand stoichiometrical ratio of 1:1, 1:2, and 1:3 depending on the oxidation number of the starting metal. The p*H* value has been checked by a p*H* meter Polymetron 42B during preparation. The chloride, nitrate, or acetate ions were never present in the resulting complexes.

Method B

The metal salts were dissolved in ethanol and added dropwise to a stirred solution of ttz in a mixture of ethanol and dimethylsulfoxide in the ratio 20:3.

The complexes obtained have been purified by means of repeated washing with ethanol and dried over P_4O_{10}.

Infrared Measurements

The ir spectra have been recorded in the range 4000 to 50 cm^{-1} with Perkin Elmer 457 and 225 and Hitachi–Perkin Elmer FIS3 spectrophotometers. The spectra in the range 4000 to 400 cm^{-1} were measured for KBr discs or $CHCl_3$ solution. Far ir spectra were measured for Nujol mulls supported between polyethylene sheets. Atmospheric water was removed from the spectrophotometer housing by flushing with dry nitrogen.

Ultraviolet–Visible Spectra

The electronic spectra have been recorded with a Shimadzu MPS-50L spectrophotometer in the solid state in the range 4 000 to 35 000 cm^{-1}.

Magnetic Susceptibility Measurements

These were carried out by Gouy's method at room temperature. Molecular susceptibilities were corrected for diamagnetism of the component atoms by use of the Pascal's constants.

Acknowledgements

We thank Mr. G. Pistoni for elemental analyses and the National Research Council (C.N.R.) of Italy for financial support.

1. C. Preti and G. Tosi. Can. J. Chem. **54**, 85 (1976).
2. C. Preti and G. Tosi. J. Inorg. Nucl. Chem. In press.
3. C. Preti and G. Tosi. Can. J. Chem. **52**, 2845 (1974).
4. C. Preti and G. Tosi. J. Chem. Soc. (Dalton Transaction). In press.
5. M. St. C. Flett. J. Chem. Soc. 347 (1953).
6. L. H. Little and R. H. Ottewill. Can. J. Chem. **40**, 2110 (1962).
7. M. Goodgame and F. A. Cotton. J. Am. Chem. Soc. **84**, 1543 (1962).
8. W. J. Eilbeck, F. Holmes, and A. E. Underhill. J. Chem. Soc. (A), 757 (1967).
9. B. P. Kennedy and A. B. P. Lever. Can. J. Chem. **50**, 3488 (1972).
10. B. N. Figgis and J. Lewis. Prog. Inorg. Chem. **6**, 192 (1964).
11. D. De Filippo and C. Preti. J. Chem. Soc. (A), 1904 (1970).
12. O. Siimann and J. Fresco. J. Am. Chem. Soc. **92**, 2652 (1970).
13. A. R. Latham, V. Ascall, and H. B. Gray. Inorg. Chem. **4**, 788 (1965).
14. A. B. P. Lever. Inorganic electronic spectroscopy. Elsevier, New York, 1968.
15. G. Marcotrigiano, G. C. Pellacani, and C. Preti. J. Inorg. Nucl. Chem. **36**, 3709 (1974).
16. D. De Filippo, F. Devillanova, C. Preti, E. F. Trogu, G. Verani, and P. Viglino. Can. J. Chem. **51**, 1172 (1973).
17. C. Preti and G. Tosi. Can. J. Chem. **53**, 177 (1975).
18. W. D. Basson and A. L. du Preez. J. Chem. Soc. (Dalton Transaction), 1708 (1974).
19. S. Yamada, H. Nakamura, and R. Tsuchida. Bull. Chem. Soc. Jpn. **31**, 303 (1958).
20. S. Yamada, H. Nishikawa, and R. Tsuchida. Bull. Chem. Soc. Jpn. **33**, 1278 (1960).
21. S. I. Shupack, E. Billig, R. J. H. Clark, R. Williams, and H. B. Gray. J. Am. Chem. Soc. **86**, 4594 (1964).
22. G. Marcotrigiano, G. C. Pellacani, C. Preti, and G. Tosi. Bull. Chem. Soc. Jpn. **48**, 1018 (1975).
23. Y. Tanabe and S. Sugano. J. Phys. Soc. Jpn. **9**, 753 (1954).
24. K. Jensen and P. H. Nielsen. Acta Chem. Scand. **20**, 597 (1966).
25. B. Singh and R. Singh. J. Inorg. Nucl. Chem. **34**, 3449 (1972).
26. B. Singh and K. P. Thakur. J. Inorg. Nucl. Chem. **36**, 1735 (1974).
27. J. R. Ferraro. Low frequency vibrations of inorganic and coordination compounds. Plenum Press, New York. 1971.
28. D. M. Adams. Metal–ligand and related vibrations. E. Arnold, London. 1967.
29. I. S. Ahuja. J. Inorg. Nucl. Chem. **29**, 2091 (1967).
30. J. A. Weaver, P. Hambright, P. T. Talbert, E. Kang, and A. T. Thorpe. Inorg. Chem. **9**, 268 (1970).
31. C. D. Flint and M. Goodgame. J. Chem. Soc. (A), 1718 (1967).
32. C. Preti and D. De Filippo. J. Chem. Soc. (A), 1901 (1970).
33. C. Postmus, J. R. Ferraro, and W. Wozniak. Inorg. Chem. **6**, 2030 (1967).
34. D. M. L. Goodgame, M. Goodgame, P. J. Hayward, and G. W. Rayner-Canham. Inorg. Chem. **7**, 2447 (1968).
35. D. M. L. Goodgame, M. Goodgame, and G. W. Rayner-Canham. Inorg. Chim. Acta, **3**, 399 (1969).
36. R. J. H. Clark and C. S. Williams. Inorg. Chem. **4**, 350 (1965).
37. R. C. Weast (*Editor*). Handbook of chemistry and physics. 49th ed. The Chemical Rubber Co., Cleveland, Ohio. 1968–1969. p. *C*565.

Studies on di-μ-thiocyanato dithiocyanato nickel(II) diisothiocyanato tin(IV) or titanium(IV) and related complexes

P. P. SINGH AND S. B. SHARMA

Chemistry Department, Maharani Lal Kunwari College, Balrampur (U.P.), India

Received July 31, 1975

P. P. SINGH and S. B. SHARMA. Can. J. Chem. **54**, 1563 (1976).

$NiM(NCS)_6$, $[NiL_4][M(NCS)_6]$, and $[NiL_6][M(NCS)_6]$ (M = Sn(IV), Ti(IV); L = pyridine (py), 3-cyanopyridine (cpy), nicotinamide (nia), ethylnicotinate (ent), and ethylenediamine (en)) have been prepared and characterised by elemental analysis, magnetic moment, and infrared and electronic spectral studies. These studies suggest a thiocyanate bridged structure for $NiM(NCS)_6$ and a cationic–anionic structure for $[NiL_4][M(NCS)_6]$ and $[NiL_6][M(NCS)_6]$.

P. P. SINGH et S. B. SHARMA. Can. J. Chem. **54**, 1563 (1976).

On a préparé et caractérisé par analyse élémentaire, moment magnétique et études spectrales infrarouge et électronique les complexes $NiM(NCS)_6$, $[NiL_4][M(NCS)_6]$ et $[NiL_6][M(NCS)_6]$ (M = Sn(IV), Ti(IV); L = pyridine (py), cyano-3 pyridine (cpy), nicotinamide (nia), nicotinate d'éthyle (ent) et éthylènediamine (en)). Ces études suggèrent qu'il existe une structure pontée par le thiocyanate dans le $NiM(NCS)_6$ et une structure cationique–anionique dans le $[NiL_4][M(NCS)_6]$ et le $[NiL_6][M(NCS)_6]$.

[Traduit par le journal]

Introduction

In this article we are presenting the synthesis and structure of a new class of hexathiocyanates. These are of the general formula $NiM(NCS)_6$, $[NiL_4][M(NCS)_6]$, and $[NiL_6][M(NCS)_6]$ (M = Sn(IV), Ti(IV); L = a number of pyridine derivatives and ethylenediamine).

Experimental

Materials and Manipulations

Tin(IV) and titanium(IV) chlorides were purified by the method of Hildebrand and Caster (1). Reagent grade anhydrous nickel(II) chloride and potassium thiocyanate (BDH) were used after drying in vacuum for 24 h. Ethylenediamine (en) and pyridine (py) (BDH) were purified by double distillation. Nicotinamide (nia) (BDH) was crystallized from alcohol and dried in vacuum. Ethylnicotinate (ent) and 3-cyanopyridine (cpy) were synthesized by standard methods (2), from nicotinic acid and nicotinamide respectively, and were purified by distillation under reduced pressure. Solvents were purified and strictly dried by known methods. All reactions were carried out in a dry box flushed with nitrogen.

Preparation of the Complexes

The whole apparatus (Fig. 1) along with the required chemicals was placed in a dry box flushed with nitrogen. Tin(IV) chloride (1.3 g, 5 mmol), finely powdered potassium thiocyanate (2.9 g, 30 mmol), stringently dried acetonitrile (50 ml), and a teflon-coated magnetic stirring bar were placed in the flask A. The whole mass was stirred for 12 h at room temperature. The stop cocks (C and D) were closed and the apparatus was removed from the dry box, and inverted. The stop cock D was connected to the vacuum pump, when quick filtration took place. The residue (KCl) remained on the sintered disc (E) and the filtrate came into the flask B. The apparatus was again transferred to the dry box. Anhydrous nickel(II) chloride (0.65 g, 5 mmol) was added to the filtrate in flask B along with a Teflon-coated magnetic stirrer. The flask A and the disc arm (F) were replaced by fresh components. The stirring was done for 2 h, and the apparatus was brought out of the dry box and inverted. The filtration was done as described above, potassium chloride on the disc was rejected and the filtrate preserved in the flask A.

Following a similar procedure, about a dozen solutions in different flasks A were prepared. Solvent from one of the flasks was evaporated by vacuum, when yellowish green crystals separated. This was $NiSn(NCS)_6$.

To the various other flasks, ligands in 1:4 or 1:6 molar ratio were added and stirred for 6 h. In each case solid complexes were formed which were filtered, washed with the solvent and dried in vacuum.

$NiTi(NCS)_6$, $[NiL_4][Ti(NCS)_6]$, and $[NiL_6][Ti(NCS)_6]$ were prepared by a similar procedure.

Physical Measurements

The infrared spectra of ligands, metal hexathiocyanates, and complexes were recorded on a Perkin-Elmer model 621 or 457 spectrophotometer in the range 4000–200 cm^{-1}. Samples were run as Nujol mulls using CsI plates. Spectra of soluble ligands were also recorded in solution. Infrared spectral data are included in Tables 1 and 2.

Electronic spectra were obtained on a Cary-14 spectrophotometer between 1700–300 nm. Samples were run as their methanol, ethanol, or acetone solutions and as Nujol mulls. Electronic spectral data are included in Table 3.

Magnetic susceptibility measurements were made at

Can. J. Chem. Downloaded from www.nrcresearchpress.com by 210.87.254.42 on 09/05/12
For personal use only.

Can. J. Chem. Downloaded from www.nrcresearchpress.com by 210.87.254.42 on 09/05/12
For personal use only.

TABLE 1. Assignment of infrared spectral bands and fundamental species of $NiM(NCS)_6$ (ref. 20)[1]

Schematic description	C_{2v} Species	No.	Assignment of species	Band positions (cm^{-1}) $NiSn(NCS)_6$	Band positions (cm^{-1}) $NiTi(NCS)_6$
NCS pseudo antisymm. st. degenerate (ν(CN))	$3A_1+2B_1+B_2$	1	A_1+B_2(terminal N-bonded)	2050m	2060mb
		2	A_1+B_1(terminal S-bonded)	2120s	2120sh
		3	A_1+B_1(bridged)	2160s	2160s
NCS pseudo symm. st. degenerate (ν(CS))	$3A_1+2B_1+B_2$	4	A_1+B_2(terminal N-bonded)	770m	767m
		5	A_1+B_1(terminal S-bonded)	722m	720m
		6	A_1+B_1(bridged)	760sh, 740sh	760sh, 735sh
M—NCS deformation A* (δ(MNC))	$2A_1+B_1+B_2$	7	A_1+B_2(terminal N-bonded)	500m	495m
		8	A_1+B_1(bridged)	—	—
Ni—SCN deformation A* (δ(NiSc))	$2A_1+2B_1$	9	A_1+B_1(terminal N-bonded)	—	—
		10	A_1+B_1(bridged)	435sh	430sh
M—NCS and Ni—SCN deformation B* (δ(NCS)) and (δ(SCN))	$3A_1+2B_1+B_2$	11	A_1+B_2(terminal N-bonded)	482w	480m
		12	A_1+B_1(bridged)	455s	456s
		13	A_1+B_1(terminal S-bonded)	420w	420w
M—N_4 degenerate stretch (ν(M—N))	$2A_1+B_1+B_2$	14	A_1+B_2(terminal N-bonded)	307s	305sb
		15	A_1+B_1(bridged)	290sh	280sh
Ni—S_4 degenerate stretch (ν(Ni—S))	$2A_1+2B_1$	16	A_1+B_1(terminal S-bonded)	270sh	275sh
		17	A_1+B_1(bridged)	245w	250w
M—N_4 deformation (δ(NMN))	$A_1+B_1+B_2$	18	—	—	—
Ni—S_4 deformation (δ(SNiS))	A_1+B_1	19	—	—	—

[1] A* involves M—N—C—S deformation and B* involves M—N—C—S deformation (20) st. = stretch, symm. = symmetric, s = strong, m = medium, w = weak, sh = shoulder.

Can. J. Chem. Downloaded from www.nrcresearchpress.com by 210.87.254.42 on 09/05/12
For personal use only.

TABLE 2. Assignments of infrared spectral bands and fundamental species of cationic–anionic complexes

Complexes	Assignments of bands due to $M(NCS)_6^{2-}$ anion					Assignments of bands due to the coordinated cation NiL_x^{2+}, ν(NiL) (ν_7)		
	ν(CN) (ν_1) T_{1u} (O_h)	ν(CS) (ν_2) T_{1u} (O_h)	δ(MNC) (ν_3) T_{1u} (O_h)	δ(NCS) (ν_4) T_{1u} (O_h)	ν(MN) (ν_5) T_{1u} (O_h)	E_u (D_{4h})	T_{1u} (O_h)	T_2 (T_d)
$[Ni(py)_4][Sn(NCS)_6]$	2085sb	805s	485s	470m	320mb	270sh, 235w	—	—
$[Ni(en)_2][Sn(NCS)_6]$	2055sb	810m	487sh	480s	310sb	260wb	—	—
$[Ni(ent)_4][Sn(NCS)_6]$	2055sb	810m	480s	470sh	315sb	255wb	—	—
$[Ni(py)_4][Ti(NCS)_6]$	2080sb	785m	480m	465sh	310mb	265wb	—	—
$[Ni(ent)_4][Ti(NCS)_6]$	2050sb	815m	478m	455sh	320mb	245w	—	—
$[Ni(py)_6][Sn(NCS)_6]$	2075sb	790mb	480s	470sh	320mb	—	265mb	—
$[Ni(nia)_6][Sn(NCS)_6]$	2080sb	795s	482s	470sh	307sh, 295s	—	285mb	—
$[Ni(cpy)_6][Sn(NCS)_6]$	2075sb	805s	483s	475m	305sh, 285mb	—	235wb	—
$[Ni(py)_6][Ti(NCS)_6]$	2075sb	800m	485m	465sh	292sh, 285mb	—	240wb	—
$[Ni(en)_3][Ti(NCS)_6]$	2080sb	810m	480sh	470mb	310mb	—	—	—
$[Ni(nia)_6][Ti(NCS)_6]$	2075sb	807s	480s	460m	300sb	—	260sh	—
$[Ni(cpy)_6][Ti(NCS)_6]$	2080sb	810s	483m	475m	302sh, 290mb	—	255w	—

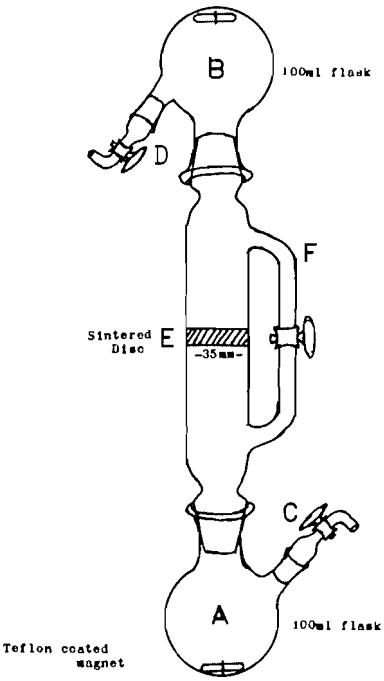

FIG. 1. Apparatus for the preparation of $NiM(NCS)_6$, $[NiL_4][M(NCS)_6]$, and $[NiL_6][M(NCS)_6]$ (M = Sn(IV), Ti(IV)).

room temperature by Gouy's method using $HgCo(NCS)_4$ as standard. The diamagnetic corrections were made by the method outlined by Figgis and Lewis (3). Magnetic moment data are included in Table 3.

Molar conductance of the complexes were determined in alcohol with the help of a Philips conductivity bridge model PR-9500. Molar conductance data are included in Table 4.

Results and Discussion

$NiSn(NCS)_6$ and $NiTi(NCS)_6$

(*i*) The infrared absorption bands assigned to C—N stretching mode are observed at 2160, 2120, 2050, and 2080 cm^{-1}. The positions of these bands indicate the presence of both bridged and terminal thiocyanates (4, 6, 16, 17). The position and number of bands in C—S stretching and NCS bending regions as presented in Table 1 also support the presence of both terminal and bridging thiocyanates (7, 9, 16, 17).

(*ii*) The electronic spectra of the complexes in solid phase show the presence of three bands at about 9 100, 14 600, and 25 000 cm^{-1} (Table 3), due to the transitions $^3A_{2g} \rightarrow {}^3T_{2g}$, $^3A_{2g} \rightarrow {}^3T_{1g}(F)$, and $^3A_{2g} \rightarrow {}^3T_{1g}(P)$, respectively. The positions of these bands are typical of nickel(II) in octahedral environment (10). The colour and Bohr magneton values also favour an octahedral geometry for nickel(II). The Dq values suggest a weak interaction between nickel(II) and thiocyanate ion. Similarly, the Racah parameter (B') indicates less orbital overlap.

(*iii*) On the basis of the above observations we can tentatively propose the following structure (Fig. 2). In these complexes the sulphur end of thiocyanate has been shown attached to nickel(II) and the nitrogen end, to tin(IV) or titanium(IV) according to H.S.A.B. theory (11). The octahedral configuration by nickel(II) and tin(IV) or titanium(IV) is perhaps achieved by weak attachment of thiocyanates at the axial position, similar to nickel(II) in $NiHg(SCN)_4$ (12).

(*iv*) If the proposed structure is correct, the complexes will belong to the C_{2v} point group. Assuming this point group, the number of normal modes along with their species have been calculated (Table 5). The comparison of the observed and calculated number of bands indicates that our proposed structure is correct.

TABLE 3. Electronic spectral band assignments, spectral parameters, and magnetic moment of Ni(II) octahedral complexes

Complexes	ν_1 (cm^{-1}) $^3A_{2g} \rightarrow {}^3T_{2g}$	ν_2 (cm^{-1}) $^3A_{2g} \rightarrow {}^3T_{1g}(F)$	ν_3 (cm^{-1}) $^3A_{2g} \rightarrow {}^3T_{1g}(P)$	$10Dq$ (cm^{-1})	B' (cm^{-1})	β	μ_{eff} (B.M.)
$NiSn(NCS)_6$	9 100	14 600	25 000	8 900	860	0.83	3.3
$NiTi(NCS)_6$	9 090	14 500	24 970	8 820	867	0.83	3.2
$[Ni(py)_6][Ti(NCS)_6]$	9 320	15 300	25 800	9 450	855	0.82	3.1
$[Ni(nia)_6][Ti(NCS)_6]$	9 780	15 625	25 800	9 672	827	0.79	3.2
$[Ni(en)_3][Ti(NCS)_6]$	9 980	16 130	25 950	10 160	773	0.74	2.9
$[Ni(py)_6][Sn(NCS)_6]$	9 230	15 420	25 780	9 485	850	0.82	3.1
$[Ni(cpy)_6][Ti(NCS)_6]$	9 430	15 450	25 640	9 538	832	0.80	3.0
$[Ni(cpy)_6][Sn(NCS)_6]$	9 380	15 500	25 770	9 560	840	0.81	3.2
$[Ni(nia)_6][Sn(NCS)_6]$	9 380	15 715	25 840	9 752	820	0.79	2.9
$[Ni(en)_3][Sn(NCS)_6]$	10 115	16 193	25 970	10 220	767	0.74	2.9

Can. J. Chem. Downloaded from www.nrcresearchpress.com by 210.87.254.42 on 09/05/12
For personal use only.

Can. J. Chem. Downloaded from www.nrcresearchpress.com by 210.87.254.42 on 09/05/12
For personal use only.

TABLE 4. Analytical results and molar conductance data

Complexes	Colour	Melting point (°C)	% Nickel		% Tin or titanium		% Thiocyanate		% Sulphur		Molar conductance (λ_M) (mhos cm^{-2} mol^{-1})	
			Obs.	Calc.	Obs.	Calc.	Obs.	Calc.	Obs.	Calc.	$M/512$	$M/1020$
$NiSn(NCS)_6$	Green	165(dec.)	11.1	11.2	21.1	22.4	64.6	66.3	35.8	36.6	58.5	72.8
$[Ni(py)_4][Sn(NCS)_6]$	Greenish yellow	230	8.0	7.1	13.0	14.0	39.9	41.3	21.2	22.8	68.7	84.9
$[Ni(py)_6][Sn(NCS)_6]$	Blue	280(dec.)	6.8	6.9	10.9	11.8	33.1	34.8	20.1	19.2	71.9	91.7
$[Ni(en)_2][Sn(NCS)_6]$	Greenish yellow	240(dec.)	10.0	9.1	19.0	18.3	51.8	53.6	28.2	29.7	68.7	93.7
$[Ni(ent)_4][Sn(NCS)_6]$	Yellow	175(dec.)	5.8	5.2	9.8	10.5	29.4	30.8	17.8	17.1	74.8	98.9
$[Ni(nia)_6][Sn(NCS)_6]$	Blue	170	6.0	5.0	10.0	9.4	26.9	27.7	14.9	15.2	65.3	92.3
$[Ni(cpy)_6][Sn(NCS)_6]$	Blue	200	6.4	5.1	10.6	10.0	28.9	30.3	15.7	16.7	66.5	102.9
$NiTi(NCS)_6$	Yellowish green	150(dec.)	13.3	12.9	9.9	10.5	74.8	76.5	40.9	42.2	55.4	87.6
$[Ni(py)_4][Ti(NCS)_6]$	Light green	180	8.5	7.6	6.1	6.2	44.1	45.1	23.1	24.9	70.1	90.3
$[Ni(py)_6][Ti(NCS)_6]$	Blue	150(dec.)	6.0	6.3	5.8	5.2	35.9	37.4	19.0	20.7	81.9	96.8
$[Ni(en)_3][Ti(NCS)_6]$	Blue	160(dec.)	10.1	9.3	7.8	7.6	55.2	54.8	31.2	30.2	69.8	91.2
$[Ni(ent)_4][Ti(NCS)_6]$	Yellow	180(dec.)	5.7	5.6	4.6	4.5	31.9	32.8	17.9	18.1	85.2	101.4
$[Ni(nia)_6][Ti(NCS)_6]$	Blue	155	5.4	5.0	4.4	4.0	28.5	29.9	16.7	16.2	68.8	102.5
$[Ni(cpy)_6][Ti(NCS)_6]$	Blue	210(dec.)	6.0	5.5	4.7	4.5	31.6	32.2	18.4	17.9	74.5	90.9

Can. J. Chem. Downloaded from www.nrcresearchpress.com by 210.87.254.42 on 09/05/12
For personal use only.

TABLE 5. Calculated normal modes of different point groups and their fundamental species[1]

Complexes or ions	Point group	Vibrational species	M—NCS and M—L st. species	No. of ir active st. species	M—NCS and M—L_x def. or bend. species	No. of ir active def. species
$NiM(NCS)_6$	C_{2v}	$19\underline{A}_1+A_2+14\underline{B}_1+6\underline{B}_2$	$10\underline{A}_1+7\underline{B}_1+6\underline{B}_2$	20	$9\underline{A}_1+A_2+7\underline{B}_1+3\underline{B}_2$	19
$M(NCS)_6^{2-}$	O_h	$3A_{1g}+3E_g+2T_{1g}+6\underline{T}_{1u}+3T_{2g}+3T_{1u}$	$3A_{1g}+3E_g+3\underline{T}_{1u}$	3	$3T_{2g}+3\underline{T}_{1u}+3T_{2u}$	3
NiL_4^{2+}	D_{4h}	$A_{1g}+B_{1g}+B_{2g}+2\underline{E}_u$	$A_{1g}+B_{1g}+\underline{E}_u$	1	$B_{2g}+\underline{E}_u$	1
NiL_6^{2+}	O_h	$A_{1g}+E_g+T_{2g}+2\underline{T}_{1u}+T_{2u}$	$A_{1g}+E_g+\underline{T}_{1u}$	1	$T_{2g}+\underline{T}_{1u}+T_{2u}$	1

[1]st. = stretching; def. = deformation; bend. = bending.

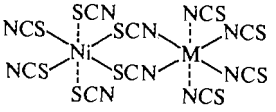

M = Sn(IV), Ti(IV)

FIG. 2. Di-μ-thiocyanato dithiocyanato nickel(II) diisothiocyanato tin(IV) or titanium(IV).

(*v*) Unlike polymeric bridged tetrathiocyanates (12), these complexes are sharp melting and soluble in polar organic solvents. This shows that they are perhaps monomeric in nature. Attempts to find out the molecular weight were not successful as the complexes get solvated with the solvent molecules, and probably a species of the type $[Ni(Solv)_6][M(NCS)_6]$ is formed. The formation of such a species is justified by the molar conductance and infrared spectral measurements. The complexes in ethanol have molar conductance values equivalent to 1:1 electrolyte and the solution spectra show the presence of only nitrogen bonded thiocyanates.

$[NiL_4][M(NCS)_6]$ and $[NiL_6][M(NCS)_6]$
(L = nia, ent, py, cpy; M = Sn(IV), Ti(IV))

(*i*) The infrared spectra of these complexes, show the presence of only one band in C—N stretching region. The position of this band indicates that thiocyanate is nitrogen bonded. The position and number of bands in C—S stretching and NCS bending regions also support the presence of only nitrogen bonded thiocyanates (5, 9, 13).

(*ii*) The colour and magnetic moment values of $[NiL_6][M(NCS)_6]$ show that the nickel(II) in these complexes is in octahedral configuration. The position of the electronic spectral bands and various ligand field parameters as presented in Table 3, also support the octahedral configuration of nickel(II) in these complexes. The *Dq* values of this series of complexes are higher than $NiSn(NCS)_6$ and $NiTi(NCS)_6$, showing greater interaction of ligands with the metal ion. The *Dq* values also vary from ligand to ligand. This shows that the ligands (L) are attached to nickel(II) and not to tin(IV) or titanium(IV). The complexes $[NiL_4][M(NCS)_6]$ are diamagnetic and yellow in colour. This shows that nickel(II) in these complexes is in the square planar geometry. The electronic spectral band positions also support this configuration of nickel(II).

(*iii*) The molar conductance values of these complexes in ethanol are typical of 1:1 electrolyte (Table 4).

(*iv*) On the basis of the above results we can propose a cationic–anionic type of formula for these complexes. The cation will consist of nickel(II) with four or six ligand molecules, and the anion, of tin(IV) or titanium(IV) with six isothiocyanate ions. Hence the complexes can be formulated as $[NiL_4][M(NCS)_6]$ and $[NiL_6][M(NCS)_6]$ (M = Sn(IV), Ti(IV)).

Since the thiocyanate is nitrogen bonded it will prefer Sn(IV) or Ti(IV) for coordination according to H.S.A.B. theory (11).

(*v*) We have assumed D_{4h} point group for $[NiL_4]^{2+}$, O_h for $[NiL_6]^{2+}$ and $[M(NCS)_6]^{2+}$ and have calculated the number of normal modes and their species, the results of which, along with the observed number are presented in Tables 2 and 5. The comparison of calculated and observed number of bands also supports the proposed formulae.

Conclusions

(*i*) The $MPt(SCN)_6$ (14) and $MHg(SCN)_4$ (5, 6, 12, 15), (M = Fe, Co, Ni, Zn, Pb) have generally a polymeric thiocyanate bridged structure. $NiM(NCS)_6$ (M = Sn(IV), Ti(IV)) however, appear to be monomeric in nature.

(*ii*) The thiocyanate bridging in $NiM(NCS)_6$ is perhaps the weakest of all known tetra or hexathiocyanates.

(*iii*) It has been shown recently (18, 19) that the thiocyanate bridge in $MM'(NCS)_4$ is weak when M and M′ belong to class *a* type metals and the bridge is stable if one of the two metals belongs to class *b* type metals. On reaction with bases the thiocyanate bridge is ruptured more easily when both M and M′ belong to class *a* type, and with difficulty when one of them belongs to class *b* type of metal. It has also been shown that in the presence of ligands of weak basicity the bridge is not ruptured even when both M and M′ are class *a* type (18). The thiocyanate bridge in $NiM(NCS)_6$, however, appears to be very weak as it breaks even in polar solvents like ethanol or acetonitrile.

Acknowledgements

The authors gratefully acknowledge the financial support of U.G.C. New Delhi and instru-

Can. J. Chem. Downloaded from www.nrcresearchpress.com by 210.87.254.42 on 09/05/12
For personal use only.

mentation facilities by University of Montreal, Montreal, Quebec.

1. J. H. HILDEBRAND and J. M. CASTER. J. Am. Chem. Soc. **54**, 3592 (1932).
2. A. I. VOGEL. Text book of practical organic chemistry. 3rd. ed. Longmans Publications, London, 1965. p. 849.
3. B. N. FIGGIS and J. LEWIS. Modern coordination chemistry. *Edited by* J. Lewis and R. G. Wilkins. Interscience Publishers Inc., New York. 1960. p. 403.
4. J. CHATT and L. A. DUNCANSON. Nature, **178**, 997 (1956).
5. R. A. BAILEY, S. L. KOZAK, T. W. MICHELSEN and W. N. MILLS. Coord. Chem. Rev. **6**, 407 (1971).
6. J. L. BURMEISTER. Coord. Chem. Rev. **1**, 205 (1966).
7. A. TURCO and C. PECILE. Nature (London), **191**, 66 (1961).
8. J. LEWIS, R. S. NYHOM, and P. W. SMITH. J. Chem. Soc. 4590 (1961).
9. A. SABATINI and I. BERTINI. Inorg. Chem. **4**, 959, 1665 (1965).
10. A. B. P. LEVER. Inorganic electronic spectroscopy. Elsevier Publishers. New York. 1968. p. 344.
11. R. G. PEARSON. J. Chem. Educ. **45**, 581 (1968), **45**, 643 (1968).
12. D. FORSTER and D. M. L. GOODGAME. Inorg. Chem. **4**, 715 (1965); **4**, 823 (1965).
13. H. BHOLAND. E. TIED, and E. ZENKER. J. Less-Common Met. **15**, 89 (1968).
14. A. TRAMER. J. Chim. Phys. **59**, 232 (1962).
15. HISAYA OKY, EISHIN KYUNO, and RYOKICHI TSUCHIYA. Bull. Chem. Soc. Jpn. **41**, 2357 (1968).
16. R. MAKHIJA, L. PAZDERNICK and R. RIVEST. Can. J. Chem. **51**, 437 (1973).
17. P. P. SINGH, U. P. SHUKLA, R. RIVEST, and R. MAKHIJA. J. Inorg. Nucl. Chem. **37**, 679 (1975).
18. P. P. SINGH and S. A. KHAN. Inorg. Chim. Acta, **14**, 143 (1975).
19. P. P. SINGH and J. N. SETH. Inorg. Chim. Acta, **16**, 227 (1975).
20. G. L. CARLSON. Spectrochim. Acta, **18**, 1529 (1962).

Can. J. Chem. Downloaded from www.nrcresearchpress.com by 210.87.254.42 on 09/05/12
For personal use only.

Réarrangement thermique comparé de vinylaziridines *cis* et *trans*

J. C. POMMELET ET J. CHUCHE

Laboratoire de Chimie Organique Physique, Faculté des Sciences, B.P. 347, 51062 - Reims Cédex, France

Reçu le 21 juillet 1975

J. C. POMMELET et J. CHUCHE. Can. J. Chem. **54**, 1571 (1976).

La synthèse stéréospécifique d'aziridines diéthyléniques **3***a–d* et de phénylvinylaziridines **3***e–g cis* et *trans* est réalisée à partir des époxydes **1***a–g* correspondants.

La divinylaziridine **3***a cis* n'est pas stable à température ordinaire; le réarrangement de Cope de la dipropénylaziridine **3***c cis* donne la dihydroazépine **4***c cis*. La thermolyse des divinylaziridines **3***a–d trans* conduit aux dihydroazépines, celle des phénylvinylaziridines au pyrrolines-2. Les résultats sont comparés à ceux obtenus en série époxydique.

J. C. POMMELET and J. CHUCHE. Can. J. Chem. **54**, 1571 (1976).

The stereospecific syntheses of the *cis*- and *trans*-diethylenic aziridines **3***a–d* and phenylvinylaziridines **3***e–g* was achieved with the corresponding epoxides **1***a–g* as starting materials.

cis-Divinylaziridine, **3***a*, is not stable at ordinary temperatures; the Cope rearrangement of *cis*-dipropenylaziridine, **3***c*, yields *cis*-dihydroazepine, **4***c*. Thermolysis of the *trans*-divinylaziridines **3***a–d* leads to the dihydroazepines while that of the phenylvinylaziridines yields 2-pyrrolines. The results are compared with those obtained in the epoxide series.

[Journal translation]

Introduction

Le réarrangement thermique de cycles à trois chaînons insaturés (époxydes, X = O; cyclopropanes, X = CH_2; R′ = ϕ ou vinyle) a fait l'objet de nombreux travaux. Dans tous les cas, les systèmes *cis* **A** et *trans* **B** se coupent sous l'effet de la chaleur selon la liaison C—C (schéma 1).

La nature des produits de transposition dépend à la fois de R′ et de X. Quand R′ = vinyle: (*i*) le réarrangement de Cope des isomères *cis* **A** conduit dans tous cas au cycle à sept chaînons (cycloheptatriène (1–3) ou dihydrooxépine (4, 5)); (*ii*) la nature de l'atome X influe sur le réarrangement des isomères *trans* **B**: le divinylépoxyde *trans* (X = O) donne à la fois **C** et **D** (4–6), le divinylcyclopropane (X = CH_2) ne conduit qu'à **C** (7). Pour R′ = phényle, on note dans tous les cas: (*i*) l'isomérisation *cis–trans* (**A** $\rightleftarrows$ **B**); (*ii*) la formation de cycle à cinq chaînons **D** (phényl-4 cyclopentène (8) ou dihydrofuranne (9)).

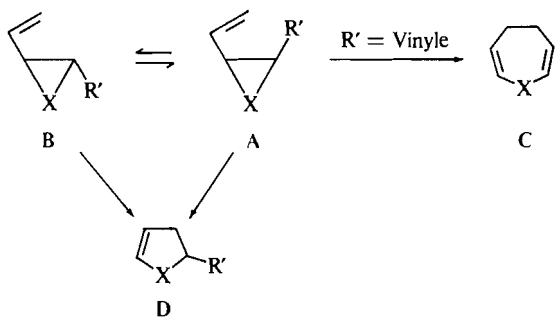

X	R′	Référence
CH_2	Vinyl	1, 2, 3, 7
CH_2	ϕ	8
O	Vinyl	4, 5, 6
O	ϕ	9

SCHÉMA 1

En série azotée (X = N—R″) peu de travaux ont été réalisés jusqu'ici. Ainsi Stogryn et Brois ont vainement tenté d'isoler l'éthyl-1 divinyl-2,3 aziridine *cis* et de réarranger l'aziridine *trans* (10) (comme la divinyl-1,2 aziridine (11), la divinyl-2,3 aziridine *cis* se réarrange à température ordinaire (12)). Enfin récemment, un exemple de réarrangement de phénylvinylaziridine *cis* a été publié par Borel *et al.* (13).

Ces travaux ont été entrepris en vue de préparer et d'isoler la divinyl-2,3 aziridine *cis* connue pour être instable (10), de réaliser l'étude cinétique et d'étudier la stéréochimie de son réarrangement, de réaliser pour la première fois l'isomérisation thermique de divinylaziridines *trans* et de la comparer à la thermolyse des phénylvinylaziridines.

Résultats

Le principal obstacle à l'étude des divinylaziridines réside dans leur mode de préparation.

Can. J. Chem. Downloaded from www.nrcresearchpress.com by 210.87.254.40 on 09/05/12
For personal use only.

Can. J. Chem. Downloaded from www.nrcresearchpress.com by 210.87.254.40 on 09/05/12
For personal use only.

TABLEAU 1. Déplacement chimique en ppm des protons des aminoalcools par rapport au TMS (solvant CCl_4)

Aminoalcool	H_a	H_b	R″	R′	R	$J_{a,b}$ (Hz)	$J_{b,c}$ (Hz)
2*a thréo*	3.81 m	2.69 m	2.31 s	—[a]	—[a]	8.0	7.0
érythro	4.06 m	2.92 2d	2.36 s			4.2	7.2
2*b érythro*	3.9 m	3.32 2d	1.09 s	—[a]	—[a]	4.5	7.0
2*c thréo*	3.69 m	2.59 m	2.28 s	—[a]	1.71 m	8.0	—[b]
érythro	3.90 m	2.8 2d	2.32 s		1.73 m	4.2	7.5
2*d érythro*	3.76 m	3.20 m	1.07 s	—[a]	1.70 m	4.5	6.7
2*e thréo*	4.35 d	3.01 2d	2.4 s	7.35 s	—[a]	8.0	7.2
2*f thréo*	3.94 d	3.1 m	1.08 s	7.20	—[a]	8.2	7.5
érythro	4.47 d	3.44 2d	1.08 s	7.20		4.7	7.2
2*g thréo*	3.94 d	3.0 m	1.07 s	7.20 s	1.53 m	8.2	—[b]
érythro	4.43 d	3.38 2d	1.07 s	7.20 s	1.55 m	4.7	6.7

[a]Protons éthyléniques: entre 4.8 et 6.2 ppm.
[b]Impossible à déterminer.

En 1965, Stogryn et Brois (10) ont tenté la synthèse de l'éthyl-1 divinyl-2,3 aziridine *cis* selon une méthode dérivée du procédé Wenker (14).

Des méthodes récemment décrites (15, 16) nous ont permis de synthétiser de façon stéréospécifique des vinylaziridines *cis* et *trans* diversement substituées sur l'atome d'azote, à partir des époxydes correspondants *cis* et *trans* déjà préparés (4, 17).[1] Les époxydes sont convertis intermédiairement en α-aminoalcools.

α-Aminoalcools

L'époxyde est transformé en amino-alcool par simple aminolyse avec l'amine primaire correspondante (schéma 2). La réaction est stéréospécifique. Les isomères **1***a–g cis* conduisent aux aminoalcools **2***a–g thréo*, les isomères **1***a–g trans* aux aminoalcools **2***a–g érythro*.

Ces aminoalcools sont caractérisés par leur spectre de rmn; conformément à la littérature (19, 20) la constante de couplage $J_{a,b}$ est plus faible pour les composés *érythro* (*érythro* $\simeq$ 4.5 Hz; *thréo* $\simeq$ 8 Hz); le déplacement chimique du proton H_a est également plus faible pour le diastéréoisomère *thréo* (20, 21) (*cf.* tableau 1). Enfin, quand R′ = ϕ (**2***e–g*), l'ouverture de l'époxyde est régiosélective; la base attaque toujours le carbone portant le groupement vinyle: le proton H_a apparaît alors sous forme d'un doublet (tableau 1).

Il est possible d'accéder séparément à chacun des diastéréoisomères **2***a–g*, excepté à **2***c thréo*. Ne pouvant disposer de dipropénylépoxyde **1***c cis* pur (4), nous avons préparé un mélange de **2***c thréo* et *érythro*; une cristallisation fractionnée n'a pas permis d'isoler l'isomère *thréo* pur.

Aziridines 3a–g

La cyclisation par la dibromotriphénylphosphine d'α-aminoalcools en aziridines se réalise aisément à température ordinaire; une inversion de configuration accompagne la réaction (15). Nous avons appliqué cette méthode aux aminoalcools **2***a,c,e* (*cf.* Partie expérimentale) et travaillé à température ordinaire sauf dans le cas

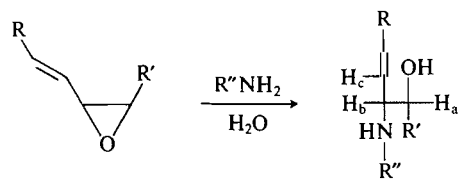

1*a–g cis* **2***a–g* thréo

a R = H; R′ = —CH=CH_2; R″ = Me
b R = H; R′ = —CH=CH_2; R″ = *t*-Bu
c R = Me; R′ = —CH=CH—Me; R″ = Me
d R = Me; R′ = —CH=CH—Me; R″ = *t*-Bu
e R = H; R′ = ϕ; R″ = Me
f R = H; R′ = ϕ; R″ = *t*-Bu
g R = Me; R′ = ϕ; R″ = *t*-Bu

SCHÉMA 2

[1]Les divinylépoxydes **1***a cis* et *trans* ont été préparés en utilisant l'éther anhydre comme solvant; le rendement en est amélioré (respectivement 54 et 50% au lieu de 33 et 8% (4)).

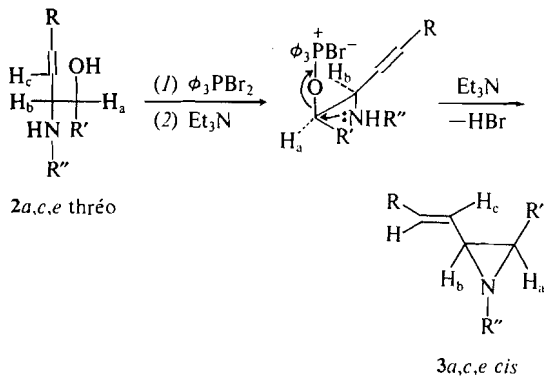

SCHÉMA 3

de **2***a thréo* pour lequel la cyclisation a été effectuée à −15 °C. Dans tous les cas, nous avons isolé l'isomère attendu; la réaction est stéréospécifique (schéma 3).

Une modification a été apportée récemment à cette méthode (16); elle consiste à remplacer formellement la dibromo par la dichlorotriphénylphosphine; elle a l'avantage, tout en étant stéréospécifique, d'être beaucoup plus générale et de donner en particulier de bien meilleurs rendements (15, 16) (tableau 6); cette réaction a été appliquée aux aminoalcools **2***b,c,d,f,g*; les aminoalcools *thréo* conduisent aux aziridines *cis*, les aminoalcools *érythro* aux aziridines *trans*. Ces aziridines ont été caractérisés par leur spectre de rmn (*cf.* tableau 2).

Nous n'avons pas fait d'étude particulière concernant le phénomène d'inversion de l'azote dans ces aziridines. Dans le cas des aziridines diéthyléniques **3***a–d trans* les protons H_a et H_b se présentent en rmn sous la forme d'un ou de deux signaux selon qu'on se trouve au dessus ou au dessous de la température de coalescence (voir schéma 4).

Pour les aziridines **3***a* et **3***c trans* (R″ = CH_3) les spectres sont mal résolus à température ordinaire; par contre, à −15 °C nous sommes en présence des deux invertomères: deux groupes de quatre raies à 1.7 à 1.9 ppm, protons *syn* par rapport à CH_3 et à 2.20–2.30 ppm, protons *anti* (22, 23).

Conformément à la littérature (24–26) le remplacement d'un groupement méthyle par un radical *tert*-butyle abaisse la température de coalescence; ainsi, pour les aziridines **3***b* et **3***d trans* (R″ = *tert*-Bu) l'inversion de l'azote est rapide à température ordinaire (un seul multiplet en rmn pour H_a et H_b).

Enfin, dans le cas de la divinylaziridine *cis* **3***a* (schéma 5) on n'observe qu'un seul signal pour les protons H_a et H_b (1.92 ppm; champs forts);

TABLEAU 2. Déplacement chimique en ppm des protons des aziridines **3***a–g* par rapport au TMS (solvant CCl_4)

Aziridine	H_a	H_b	R	R′	R″	$J_{a,b}$ (Hz)
3*a cis*[a]	1.92 m		—[d]	—[d]	2.37 s	—
3*a trans*[a]	2.29 2d[c]	1.88 2d[b]	—[d]	—[d]	2.40 s	2.8
3*b trans*	2.35 m		—[d]	—[d]	1.09 s	—
3*c cis*[e]	1.75 m sous R		1.70 m	—[d]	2.32 s	—
3*c trans*[a]	2.18 2d[f]	1.7–1.8	1.75 m	—[d]	2.34 s	3.0
3*d trans*	2.25 m		1.69 m	—[d]	1.06 s	—
3*e cis*	2.67 d	2.18 m	—[d]	7.30	2.55 s	6.5
3*f cis*	2.90 d	2.40	—[d]	7.20	1.05 s	6.5
trans	2.84 d	2.50 2d[g]			1.14 s	2.2
3*g cis*	2.82 d	2.36 m	1.53 2d[h]	7.21	1.05 s	6.2
3*g trans*	2.77 d	2.46 m	1.71 m	7.20	1.15 s	2.5

[a]Spectre enregistré à −15 °C.
[b]$J_{a,b}$ = 2.8 Hz; $J_{b,c}$ = 6 Hz.
[c]$J_{a,b}$ = 2.8 Hz; $J_{a,c'}$ = 8 Hz.
[d]Protons éthyléniques entre 4.8 et 6.3 ppm.
[e]Mélange d'aziridines 3*c cis* + *trans*.
[f]$J_{a,b}$ = 3.0 Hz; $J_{a,c'}$ = 8.7 Hz.
[g]$J_{a,b}$ = 2.2 Hz; $J_{b,c}$ = 9.0 Hz.
[h]J_{d,CH_3} = 6.1 Hz; J_{c,CH_3} = 1.2 Hz.

Can. J. Chem. Downloaded from www.nrcresearchpress.com by 210.87.254.40 on 09/05/12
For personal use only.

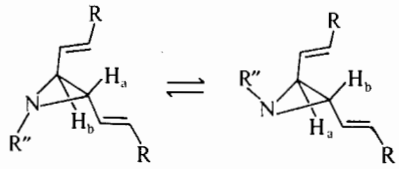

3*a* et *c trans*: R = H ou CH_3; R″ = CH_3
3*b* et *d trans*: R = H ou CH_3; R″ = *t*-Bu

SCHÉMA 4

il est vraisemblable que nous sommes en présence d'un seul invertomère, les protons H_a et H_b étant *syn* par rapport au méthyle (22, 23). Par analogie, nous supposons la conformation de **3***c cis* bloquée (les signaux de H_a et H_b sont confondus avec celui du méthyle éthylénique).

La constante de couplage $J_{a,b}$ ne peut être déterminée dans le cas des aziridines **3***a,c cis* et **3***b,d trans* (les protons H_a et H_b ont même déplacement chimique). Dans tous les autres cas (**3***a,c trans*, **3***e–g cis* et *trans*), conformément à ce qui a déjà été trouvé (22, 23, 27, 28), la constante de couplage $J_{a,b}$ des isomères *cis* est supérieure à celle des isomères *trans*. Le réarrangement plus aisé des aziridines *cis* confirme ces attributions de structure.

Stabilité thermique et réarrangement des divinylaziridines **3***a et c cis*

La méthyl-1 divinyl-2,3 aziridine **3***a cis* a été préparée, isolée et caractérisée à −15 °C; celle-ci n'est pas stable à température ordinaire; à +40 °C elle se réarrange en quelques minutes en donnant la méthyl-1 dihydro-4,5 azépine **4***a* (12) (schéma 6).

L'étude cinétique de son réarrangement a été réalisée en rmn et en solution dans le benzène (12) (voir Partie expérimentale). Les paramètres d'activation ainsi déterminés ($\Delta H^{\ddagger} = 18.5 \pm 1.5$ kcal mol^{-1}; $\Delta S^{\ddagger} = -3.8 \pm 5.0$ cal deg^{-1} mol^{-1}) montrent que ce composé a une instabilité comparable à celle du divinylcyclopropane *cis* isolé récemment à +5 °C (3).

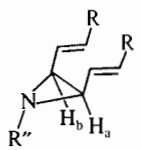

3*a* et *c cis* R = H ou CH_3
R″ = CH_3

SCHÉMA 5

Comme en série époxydique (4), la présence sur la double liaison d'un méthyle en position β augmente la stabilité thermique de l'aziridine. Ainsi, contrairement à la divinylaziridine, la dipropénylaziridine **3***c cis* est stable à 40 °C; elle se réarrange quantitativement en 1 h à 80 °C en dihydroazépine **4***c*. L'énergie d'activation plus importante dans le cas de **3***c cis* est certainement due à l'interaction des méthyles en position éclipsée dans l'état de transition bateau de ce réarrangement de Cope (4). (rmn tableau 3; $J_{2,3} = J_{6,7} = 9.5$ Hz; constantes de couplage *cis*).

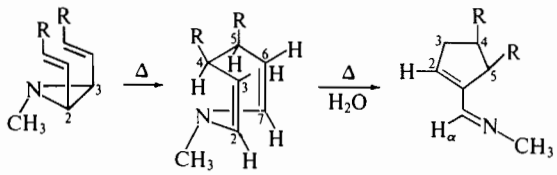

3*a* et *c cis* **4***a* et *c cis* **5***a* et *c cis*

3*a*: R = H; **3***c*: R = CH_3

SCHÉMA 6

La dihydroazépine **4***c* peut présenter l'isomérie *cis–trans*; il ne se forme en fait qu'un seul isomère (un seul doublet pour les méthyles en rmn; *cf.* tableau 3). Par chauffage à 100–150 °C en présence d'eau, la dihydroazépine **4***c* conduit selon un processus déjà décrit (10) à l'aldimine cyclopenténique **5***c* de structure *cis* (29) (rmn, Partie expérimentale; trois pics pour les méthyles à 0.87, 0.99 et 1.11 ppm). Aussi, comme en série époxydique (4), le réarrangement de la dipropénylaziridine **3***c cis* est stéréospécifique; il ne se forme que l'isomère **4***c cis*.

Réarrangement des divinylaziridines trans et des phénylvinylaziridines cis et trans

En 1965, Stogryn et Brois ont chauffé en tube scellé l'éthyl-1 divinyl-2,3 aziridine *trans*; ces auteurs notent qu'il ne se forme pas de produit de transposition (10) (pas de dihydroazépine). Ceci nous a incités à reprendre l'étude thermique des divinylaziridines *trans* et à comparer leur comportement à celui des phénylvinylaziridines analogues.

Le réarrangement de phénylvinylaziridines *cis* a été effectué récemment (13, 30, 31). Il conduit dans tous les cas à une pyrroline-2; la réaction est presque toujours stéréospécifique.

Il était intéressant de réaliser la thermolyse de

Can. J. Chem. Downloaded from www.nrcresearchpress.com by 210.87.254.40 on 09/05/12
For personal use only.

TABLEAU 3. Déplacement chimique en ppm des protons de **4***a* et *c*. Référence interne TMS (solvant CCl_4)

Composé	N—CH_3	H_2 et H_7	H_3 et H_6	R	H_4 et H_5	$J_{2,3}$ et $J_{6,7}$ (Hz)
4*a*	3.0 s	5.62 d	4.47 m	2.32 m		9.5
4*c*	3.0 s	5.55 d	4.37 2d[a]	0.92 d[b]	2.53 m	9.5

[a] $J_{3,4}$ = 6 Hz.
[b] J_{4,CH_3} = 7 Hz.

phénylvinylaziridines *trans* et de savoir en particulier si, comme en série époxydique (9), la stéréochimie de la pyrroline est indépendante de la configuration *cis* ou *trans* de l'aziridine de départ.

Nous avons réarrangé les divinylaziridines **3***a–d trans* et les phénylvinyl **3***f,g cis* et *trans*. Les essais en phase liquide et en tube scellé effectués avec les aziridines **3***c,e* se sont révélés infructueux (polymérisation). Les réarrangements ont été réalisés en régime dynamique: le produit passe rapidement en phase vapeur dans une colonne de verre chauffée électriquement (4).

La thermolyse des aziridines diéthyléniques effectuée à 250 °C pour **3***a,b trans* et 300 °C pour **3***c,d trans*, conduit dans tous les cas à la dihydroazépine (rmn, voir tableau 3 et Partie expérimentale, tableau 9).

Pour les aziridines **3***a,c* (R″ = CH_3), il y a polymérisation partielle des produits; par contre, dans le cas de **3***b,d* (R″ = *tert*-Bu) la réaction est particulièrement propre; à côté des dihydroazépines **4***b,d* (40 à 50% du produit brut de réaction) se forment deux autres produits **X** et **Y** qui n'ont pu être ni séparés, ni identifiés (schéma 7). Le spectre de rmn nous permet de conclure à l'absence de pyrroline-2; ceci n'exclue pas toutefois la formation d'une pyrroline instable qui se décomposerait rapidement (voir plus loin l'instabilité de telles pyrrolines). Les dihydroazépines **4***a–d* n'ayant pu être séparées, la stéréochimie au niveau des carbones C_4 et C_5 n'a pu être établie avec certitude; toutefois, les doubles liaisons sont *cis* ($J_{2,3} = J_{6,7} = 9.5$ Hz).

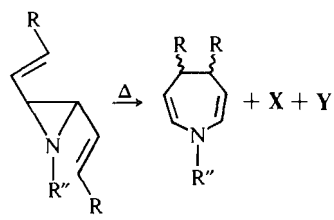

3*a–d trans* **4***a–d*

SCHÉMA 7

La thermolyse des phénylvinylaziridines **3***f–g* a été réalisée entre 240 et 300 °C. On note (*i*) que les isomères **3***f,g trans* se transposent à des températures plus basses que les isomères **3***f,g cis* (**3***f,g trans*: 240 °C; **3***f,g cis*: 300 °C); (*ii*) qu'en aucun cas, il n'y a d'isomérisation *cis–trans* ou *trans–cis* de l'aziridine; et (*iii*) enfin, qu'il se forme dans tous les cas la pyrroline-2 **6** (schéma 8).

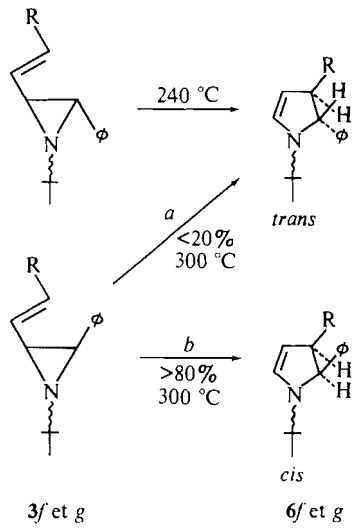

3*f* et *g* **6***f* et *g*

f R = H; *g* R = CH_3

SCHÉMA 8

Dans le cas de **3***g trans*, la réaction est stéréospécifique: il ne se forme que l'isomère **6***g trans*; elle ne l'est pas dans le cas de **3***g cis*; à côté de l'isomère **6***g cis* on trouve un faible pourcentage de l'autre isomère (moins de 20% de **6***g trans*). Les pyrrolines **6** sont instables à température ordinaire, notamment **6***g cis* qui se décompose en moins d'une heure. Un comportement semblable a été observé avec le *tert*-butyl-1 phényl-3

Can. J. Chem. Downloaded from www.nrcresearchpress.com by 210.87.254.40 on 09/05/12
For personal use only.

TABLEAU 4. Déplacement chimique en ppm des protons des pyrrolines-2 **6**, et des dihydrofurannes **7** par rapport au TMS (solvant CCl_4)

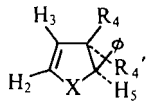

6*f* et *g* X = N-*t*-Bu
7*f* et *g* X = O
f $R_4 = R_4' = H$
cis g $R_4 = Me$ $R_4' = H$
trans g $R_4 = H$ $R_4' = Me$

Hétérocycle	H_2	H_3	H_5	CH_3	J_{H_4,H_5} (Hz)
6*f*	6.17 m	4.1 m	4.48 2d[a]	—	—[a]
6*g cis*[e]	6.07 2d[b]	4.46[c]	4.50 d	0.44 d[d]	11
6*g trans*	6.12 2d[b]	4.48 2d[c]	3.77 d	1.07 d	7.5
7*f*[j]	6.39 q	4.86 q	5.45 q[f]	—	—[f]
7*g cis*[j]	6.38 2d[g]	5.05 t[h]	5.42 d	0.55 q[i]	9.8
7*g trans*[j]	6.38 2d[g]	5.05 t[h]	4.86 d	1.20 d[i]	8.1

[a] $J_{H_5,R_4} = 8.5$ Hz; $J_{H_5,R_4'} = 11.5$ Hz.
[b] $J_{2,3} = 4.0$ Hz; $J_{2,4} = 1.6$ Hz.
[c] $J_{3,4} = 2.3$ Hz.
[d] $J_{R_4,R_4'} = 7.5$ Hz.
[e] Spectre enregistré à −17 °C.
[f] $J_{H_5,R_4} = 8.8$ Hz; $J_{H_5,R_4'} = 10.6$ Hz.
[g] $J_{2,3} = 2.8$ Hz; $J_{2,4} = 2.6$ Hz.
[h] $J_{3,4} = 2.6$ Hz.
[i] $J_{R_4,R_4'} = 7.1$ Hz.
[j] Référence 9.

dihydro-2,3 pyrrole (30, 31). Les pyrrolines **6***f*,*g* sont identifiées par rmn (tableau 4).

Il existe une analogie entre ces spectres de rmn et ceux des dihydrofurannes **7** correspondants (*i*) le méthyle de l'isomère **6***g cis* résonne à champs plus forts que celui de l'isomère **6***g trans*; (*ii*) la constante de couplage J_{H_4,H_5}, plus grande pour l'isomère **6***g cis*, confirme la stéréochimie des pyrrolines **6***g*; et (*iii*) la différence de déplacement chimique entre les protons H_5 de **6***f* et de **6***g trans* est importante (0.7 ppm); elle est pratiquement nulle entre les protons H_5 de **6***f* et de **6***g cis*.

Discussion

Le réarrangement des vinyl-2 aziridines **3***f*,*g* en pyrrolines-2 **6***f*,*g* entraîne nécessairement la rupture de la liaison C—C du cycle; il n'existe à notre connaissance que peu d'exemples de réarrangements de ce type (13, 30–32).

Les résultats obtenus avec les phénylpropényl-aziridines **3***g* diffèrent fondamentalement de ceux observés en série époxydique (9): alors que les phénylpropénylépoxydes *cis* et *trans* conduisent au même dihydrofuranne **7***g cis*, la stéréochimie de la pyrroline-2 **6***g* dépend de la configuration *cis* ou *trans* de l'aziridine de départ.

Pour rendre compte des résultats expérimentaux, trois mécanismes peuvent être envisagés: un mécanisme biradicalaire, un mécanisme sigmatropique-1,3, un mécanisme par ylures.

Le mécanisme radicalaire peut être exclu car il ne permet pas d'expliquer la stéréospécificité des rearrangements (9).

Mécanisme sigmatropique

Nous avons représenté schéma 9, la stéréochimie attendue pour la pyrroline-2 formée à partir de l'aziridine **3***g cis* ou *trans*. La molécule d'aziridine est supposée dans une conformation *gauche* de façon à ce que les pyrrolines formées possèdent une double liaison *cis* (4).

En admettant que la réaction s'effectue par un mécanisme à symétrie permise ($\pi_s^2 + \sigma_a^2$ ou $\pi_a^2 + \sigma_s^2$) dans le cas de **3***g trans* (33), les résultats sont en bon accord avec la théorie; par contre, avec **3***g cis*, nous sommes obligés de faire appel à une compétition entre deux

Can. J. Chem. Downloaded from www.nrcresearchpress.com by 210.87.254.40 on 09/05/12
For personal use only.

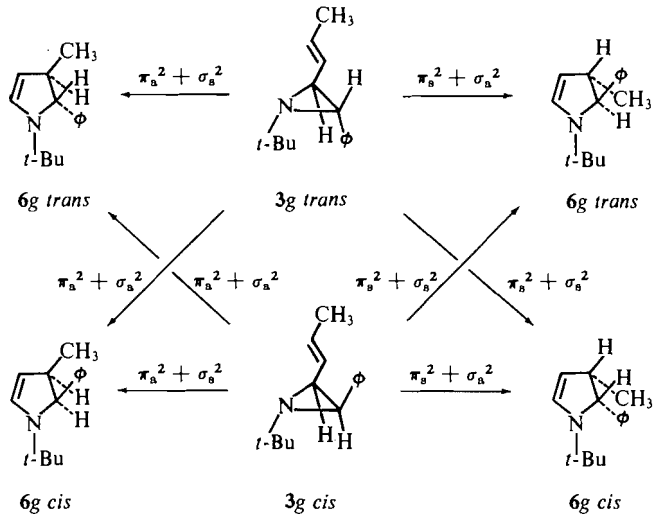

SCHÉMA 9

mécanismes permis ($\pi_s^2 + \sigma_a^2$ ou $\pi_a^2 + \sigma_s^2$) et interdit ($\pi_s^2 + \sigma_s^2$ ou $\pi_a^2 + \sigma_a^2$) pour expliquer les résultats.

Des exemples de compétition entre ces deux mécanismes ont déjà été décrits dans le cas de réactions sigmatropiques-1,3 (34, 35). Cependant, il nous semble difficile d'interpréter la différence de comportement des deux isomères et en particulier la température d'isomérisation plus élevée dans le cas de **3***g cis*.

Mécanisme par ylures

L'ouverture thermique conrotatoire de certaines aziridines conduit par rupture de la liaison C—C à des ylures d'azométhine (36); leur existence a été prouvée en piégeant ces intermédiaires avec des dipolarophiles (37, 38). L'isomérisation de ces ylures a été démontrée; elle explique notamment l'isomérisation *cis–trans* des triphényl-1,2,3 aziridines (39).

Pour chaque isomère **3***f,g cis* et **3***f,g trans*, deux modes d'ouverture sont possibles; nous avons représenté schéma 10 les ylures d'azométhine ainsi obtenus. La fermeture électrocyclique disrotatoire des ylures **8** et **10** qui possèdent des carbones terminaux voisins, permet d'expliquer la stéréospécificité de ces réarrangements (100% de **6***g trans*, 80% de **6***g cis*). De plus, ce mécanisme rend compte de la température de transposition plus élevée pour **3***g cis*. En effet, dans l'état de transition conduisant aux ylures, une interaction stérique importante entre le groupement *tert*-butyle et l'un des substituants vinyle ou phényle se développe dans le cas de l'isomère *cis*; cette interaction est inexistante lors de la formation de l'ylure **8** à partir de **3***g trans*. Bien que l'étude cinétique de cette réaction n'ait pas été réalisée, il est vraisemblable que l'énergie d'activation est plus élevée pour l'isomère *cis* que pour l'isomère *trans* (40).

Pour interpréter la formation de 20% de composé **6***g trans* à partir de **3***g cis*, il est nécessaire de faire intervenir une isomérisation des ylures d'azométhine. Alors qu'en série époxydique cette isomérisation accompagne la formation de dihydrofuranne (on observe en particulier une isomérisation *cis–trans* ou *trans–cis* de l'époxyde), dans les exemples étudiés ici, elle semble beaucoup plus difficile, ce qui correspond à une plus grande stabilité des ylures d'azométhine par rapport aux ylures de carbonyle (18).

La stabilité des ylures **8**, **9**, **10** et **11** dépend de leur encombrement stérique; ainsi, nous pensons que la stabilité de ces ylures décroît dans l'ordre **8** > (**10** et **11**) > **9**; dans **9** l'encombrement est maximum; **3***g trans* doit donc donner préférentiellement l'ylure **8**. La formation stéréospécifique de **6** *trans* exclue l'isomérisation de **8** en **10** à 240 °C. Par contre, une isomérisation de l'ylure **10** autour de la liaison C—N conduit à un ylure **8** plus stable (aucun substituant en interaction avec le groupement *tert*-butyle (40)); une

Can. J. Chem. Downloaded from www.nrcresearchpress.com by 210.87.254.40 on 09/05/12
For personal use only.

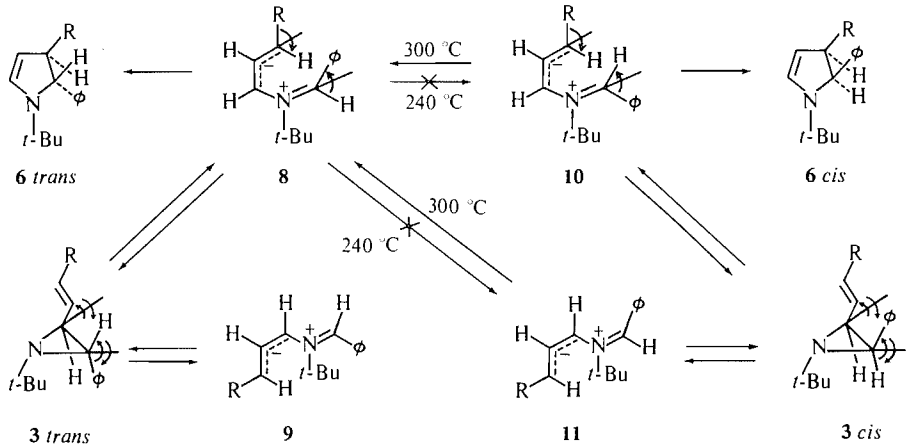

f R = H; *g* R = CH_3

SCHÉMA 10

isomérisation de **10** en **8** est donc possible. Dans ces conditions, bien que le réarrangement à 240 °C de **3***g trans* soit entièrement stéréospécifique, il est concevable qu'à 300 °C celui de **3***g cis* conduise à un mélange de **6***g cis* et **6***g trans*.

De plus, l'absence de **3***g trans* lors de l'isomérisation de **3***g cis*, même pour des taux de conversion faibles, (constatée également dans une série analogue (30, 31)) indique qu'à partir de l'ylure **8**, la vitesse de formation de **6** *trans* est plus rapide que celle de **3** *trans*. Nos résultats sont en bon accord avec ceux présentés par D. Borel *et al.* (31).

Réarrangement des divinyl aziridines trans

En série divinylique, l'ouverture conrotatoire de **3***a–d trans* (schéma 11) donne préférentiellement l'ylure **12**; celui-ci peut conduire par électrocyclisation conrotatoire (système à 8*e*) à la dihydroazépine **4** *trans*. La formation de pyrroline-2 à partir de **12** n'a pas été constatée mais n'est pas à exclure.

La stéréochimie de l'azépine n'ayant pu être déterminée, nous ne pouvons écarter la possibilité d'isomérisation *trans–cis* de l'aziridine. L'isomérisation **12** → **13** suivie de la fermeture électrocyclique conrotatoire à **4***e* conduirait à l'aziridine *cis* qui s'isomériserait immédiatement en azépine **4** *cis* (4).

Conclusion

Au cours de ce travail, nous avons effectué la synthèse et le réarrangement de divinyl et de phénylvinylaziridines *cis* et *trans*. En particulier la divinyl-2,3 aziridine *cis* (R = CH_3) a été isolée pour la première fois; elle a une instabilité comparable à celle du divinylcyclopropane *cis*. Le réarrangement de Cope de la dipropénylaziridine *cis* est stéréospécifique et donne la dihydroazépine *cis*.

La thermolyse des aziridines diéthyléniques *trans* conduit aux dihydroazépines, celle des phénylvinylaziridines à des pyrrolines-2 dont la stéréochimie dépend de la configuration *cis* ou *trans* de l'aziridine de départ. Le réarrangement des phénylvinylaziridines est très stéréospécifique et ne n'accompagne pas d'une isomérisation géométrique.

Bien que les résultats stéréochimiques ne permettent pas d'exclure la possibilité d'un mécanisme sigmatropique à symétrie permise (ou interdite) les réarrangements s'interprètent bien en supposant la formation intermédiaire d'ylures d'azométhine.

Nous avons pu montrer qu'il existe une très grande différence de comportement thermique entre les phénylvinylaziridines et les phénylvinylépoxydes. La présence d'un substituant sur l'hétéroatome modifie la stabilité des ylures d'azométhine comparativement à celle des ylures de carbonyle correspondants et explique les résultats expérimentaux.

Partie expérimentale

Les points de fusion sont pris sur un appareil Büchi. Les spectres de rmn sont enregistrés sur un spectrographe Varian A 60 A le TMS servant de référence interne; les

Can. J. Chem. Downloaded from www.nrcresearchpress.com by 210.87.254.40 on 09/05/12
For personal use only.

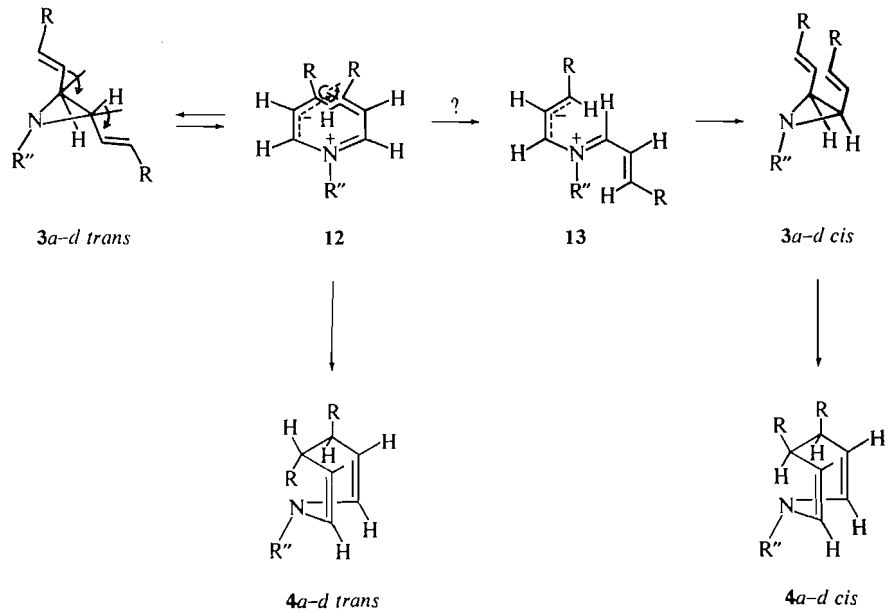

SCHÉMA 11

déplacements chimiques sont exprimés en parties par million (ppm), les constantes de couplage en Hertz (Hz); les abréviations utilisées sont les suivantes: s singulet, d doublet, t triplet, m multiplet.

Préparation des aminoalcools 2a–g

Les aminoalcools sont préparés à partir des époxydes (4, 17) selon un mode opératoire déjà décrit (10), et sont purifiés soit par distillation, soit par recristallisation. Rendements et caractéristiques physiques, voir Tableau 5.

Préparation des aziridines 3a, c et e par la méthode Okada et al. (15)

Dipropénylaziridine 3c trans

La réaction est effectuée avec 0.04 mol de dibromotriphénylphosphine, 0.04 mol (6.20 g) d'aminoalcool **2***c érythro*, 0.08 mol (8.08 g) de triéthylamine (solvant acétonitrile). Le procédé est calqué sur celui d'Okada (15). En fin de réaction, on filtre le précipité de bromure de triéthylamonium, on concentre la solution d'acétonitrile, on extrait le résidu quatre à cinq fois au pentane. On concentre la solution de pentane, filtre le précipité d'oxyde de triphénylphosphine, puis chasse entièrement le pentane. On distille enfin sur potasse. On recueille 0.88 g d'aziridine **3***c trans*.

Aziridines 3a et 3e cis

Le mode opératoire est le même; toutefois, dans le cas de **3***a cis*, on maintient la température vers −15 °C (bain méthanol à −15 °C, filtrations à froid, extraction avec du pentane préalablement refroidi). Rendements, voir tableau 6.

TABLEAU 5. Préparation des aminoalcools **2***a–g*

Aminoalcool	Rendement (%)	pf ou p éb (°C)
2*a thréo*	75	55/0.05 torr
2*a érythro*	55	44
2*b érythro*	80	50/0.03 torr
2*c érythro* + *thréo*	85	88/2 torr
2*c érythro*	80	65
2*d érythro*	90	78/0.3 torr
2*e thréo*	95	≃125
2*f érythro* + *thréo*	67	90/0.2 torr
2*g thréo*	30	—
2*g érythro*	92	—

TABLEAU 6. Synthèse des aziridines $\mathbf{3}_{a-g}$ *cis* et *trans*

Aziridine	Rendement (%)	Aziridine	Rendement (%)
3*a cis*[a]	≃20	**3***d trans*[b]	35
3*a trans*[a]	22	**3***e cis*[a]	20
3*b trans*[b]	40	**3***f cis* + *trans*[b]	60
3*c cis* + *trans*[b]	37	**3***g cis*[b]	35
3*c trans*[a,b]	15[a]	**3***g trans*[b]	53
	36[b]		

[a]Méthode, Okada *et al.* (15).
[b]Méthode, Appel et Kleinstück (16).

TABLEAU 7. Déplacement chimique des protons de **3***a cis* et de **4***a* (solvant benzène)

Composé	N—CH_3	H_2	H_3	H_4
3*a cis*	2.12 s	1.74 m		—
4*a*	2.52 s	5.54 d[a]	4.62 m	2.42 m

[a]$J_{2,3} = J_{6,7} = 9.5$ Hz.

Can. J. Chem. Downloaded from www.nrcresearchpress.com by 210.87.254.40 on 09/05/12
For personal use only.

TABLEAU 8. Déplacement chimique des protons de **5***a* et *c* (solvant CCl_4)

Aldimine	H_α	H_2	N—CH_3	R_4	R_5
5*a*	7.95 m	5.98 m	3.28 m	(R = H)	(R = H)
5*c*	7.98 m	6.0 m	3.34 m	(R = CH_3) d[a] 0.87–0.99	(R = CH_3) d[a] 0.99–1.11

[a] $J_{H_5,R_5} = J_{H_4,R_4} = 7$ Hz.

TABLEAU 9. Déplacement chimique des protons de **4***b* et *d* (solvant CCl_4)

Composé	N-*t*-Bu	H_2 et H_7	H_3 et H_6	R	H_4 et H_5	$J_{2,3}$ et $J_{6,7}$ (Hz)
4*b*	1.18 s	5.98 d	4.48 m	2.27 m		9.5
4*d*	1.27 s	5.94 d	4.36 2d[a]	0.96 d[b]	2.21 m	9.5

[a] $J_{3,4} = 5$ Hz.
[b] $J_{4,CH_3} = 6.5$ Hz.

Synthèse des aziridines **3***b–d, f, et g par la méthode Appel et Kleinstiick (16)*

Dipropénylaziridine **3***c trans*

Dans un réacteur de 100 cm^3 sont introduits 30 cm^3 d'acétonitrile et 4.23 g (0.027 mol) de **2***c érythro*. On ajoute successivement 8.23 g (0.031 mol) de triphénylphosphine, 2.76 g (0.027 mol) de triéthylamine et 4.2 g (0.027 mol) de tétrachlorure de carbone. On agite le tout pendant 24 h et on extrait comme précédemment. Après distillation sur potasse sèche, on recueille 1.4 g d'aziridine **3***c trans*.

Aziridines **3***b, d, f et g*

Le mode opératoire est identique. Rendements, voir tableau 6.

Réarrangement du divinylaziridine **3***a cis: étude cinetique*

Les dosages sont réalisés en rmn; on suit la disparition des pics à 1.74 ppm (protons H_2 et H_3 de **3***a cis*) et l'apparition des signaux à 2.42 et 2.52 ppm, correspondant au N—CH_3 et aux protons H_4 et H_5 de **4***a* (voir tableau 7). Les résultats sont parus dans une note préliminaire (12).

Réarrangement du dipropénylaziridine **3***c cis*

La transposition du dipropénylaziridine *cis* a été réalisée en tube scellé et en solution dans le CCl_4 avec un mélange des aziridines **3***c* enrichi à 80% d'isomère *cis*.

Transpositions de **4***a et c en aldimine* **5***a et c*

Ces transpositions sont effectuées en tube scellé. La dihydroazépine **4** est chauffée dans un mélange CCl_4, H_2O à 100 °C pendant 1 h pour **4***a*, 150 °C pendant 5 min pour **4***c cis*. Dans les deux cas le réarrangement en aldimine-cyclopentènique **5** est quantitatif (rmn, voir tableau 8).

Transpositions des aziridines **3***a–d trans et* **3***f–g cis et trans*

Elles sont effectuées dans un tube de verre de 18 mm de diamètre et 750 mm de hauteur, thermostatée à la température désirée et rempli de billes de verre calibrées. Le vide est réalisé à l'intérieur du tube. Une solution d'aziridine dans le CCl_4 est alors introduite goutte à goutte (une goutte toutes les 30 s). Les produits sont condensés à la sortie et analysés en rmn avant et après transvasement sous pression réduite.

Remerciements

Nous tenons à remercier M. le Professeur Vessière, Mme Y. Gelas-Mialhe et M. D. Borel pour les fructueuses discussions et la communication de leurs résultats.

1. (*a*) E. VOGEL. Angew. Chem. **72**, 4 (1960); (*b*) E. VOGEL, K. H. OTT et K. GAJEK. Liebigs Ann. Chem. **644**, 172 (1961).
2. (*a*) W. VON DOERING et W. R. ROTH. Tetrahedron, **19**, 715 (1963); (*b*) W. VON DOERING et W. R. ROTH. Angew. Chem. Int. Ed. Engl. **2**, 115 (1963).
3. J. M. BROWN, B. T. GOLDING et J. J. STOFKO. Chem. Commun. 319 (1973).
4. J. C. POMMELET, N. MANISSE et J. CHUCHE. Tetrahedron, **28**, 3929 (1972); et références citées.
5. E. VOGEL et H. GUNTHER. Angew. Chem. Int. Ed. Engl. **6**, 385 (1967).
6. (*a*) V. VOKOV, H. TOKUNAGA et R. J. CRAWFORD. Can. J. Chem. **51**, 3718 (1973); (*b*) J. C. PALADINI et R. J. CRAWFORD. Can. J. Chem. **52**, 2098 (1974).
7. (*a*) M. ARAI et R. J. CRAWFORD. Can. J. Chem. **50**, 2158 (1972); (*b*) C. ULLENIUS, P. W. FORD et J. E. BALDWIN. J. Am. Chem. Soc. **94**, 5910 (1972); (*c*) J. E. BALDWIN et C. ULLENIUS. J. Am. Chem. Soc. **96**, 1542 (1974).
8. E. N. MARVELL et C. LIN. Tetrahedron Lett. 2679 (1973).
9. J. C. PALADINI et J. CHUCHE. Bull. Soc. Chim. Fr. 197 (1974).

Can. J. Chem. Downloaded from www.nrcresearchpress.com by 210.87.254.40 on 09/05/12
For personal use only.

10. E. L. STOGRYN et S. J. BROIS. J. Org. Chem. **30**, 88 (1965).
11. E. L. STOGRYN et S. J. BROIS. J. Am. Chem. Soc. **89**, 605 (1967).
12. J. C. POMMELET et J. CHUCHE. Tetrahedron Lett. 3897 (1974).
13. D. BOREL, Y. GELAS-MIALHE et R. VESSIÈRE. C. R. Acad. Sci. Paris Sér. C, **278**, 1393 (1974).
14. H. WENKER. J. Am. Chem. Soc. **57**, 2328 (1935).
15. I. OKADA, K. ICHIMURA et R. SUDO. Bull. Chem. Soc. Jpn. **43**, 1185 (1970).
16. R. APPEL et R. KLEINSTUCK. Chem. Ber. **107**, 5 (1974).
17. J. C. PALADINI et J. CHUCHE. Bull. Soc. Chim. Fr. 190 (1974).
18. E. F. HAYES et A. K. Q. SIU. J. Am. Chem. Soc. **93**, 2090 (1971).
19. M. T. MAURETTE, A. GASET, R. MATHIS et A. LATTES. Bull. Soc. Chim. Fr. 398 (1975).
20. M. E. MUNCK, M. K. MEILAHN et P. FRANKLIN. J. Org. Chem. **33**, 3480 (1968).
21. J. J. CANCEILL, J. J. BASSELIER et J. JACQUES. Bull. Soc. Chim. Fr. 190 (1963).
22. S. J. BROIS. Tetrahedron, **26**, 227 (1970).
23. G. BOUTEVILLE, Y. GELAS-MIALHE et R. VESSIÈRE. Bull. Soc. Chim. Fr. 3264 (1971); et références citées.
24. S. J. BROIS. J. Am. Chem. Soc. **89**, 4242 (1967).
25. A. T. BOTTINI et J. D. ROBERTS. J. Am. Chem. Soc. **80**, 5203 (1958).
26. F. A. L. ANET et J. M. OSYANY. J. Am. Chem. Soc. **89**, 352 (1967).
27. O. C. DERMER et G. E. HAM. Ethylenimine and other aziridines. Academic Press, New York and London. 1969. p. 100.
28. (*a*) S. J. BROIS. J. Org. Chem. **27**, 3522 (1962); (*b*) S. L. MANATT, D. D. ELLEMANN et S. J. BROIS. J. Am. Chem. Soc. **87**, 2220 (1965).
29. J. C. GAUTIER, S. RISSE et J. WIEMANN. Ann. Chim. **5**, 435 (1970).
30. D. BOREL. Thèse de 3ème Cycle. Clermont-Ferrand. 1974.
31. D. BOREL, Y. GELAS-MIALHE et R. VESSIÈRE. Can. J. Chem. **54**, 0000 (1976).
32. P. G. MENTE et H. W. HEINE. J. Org. Chem. **21**, 3076 (1971).
33. R. B. WOODWARD et R. HOFFMANN. Angew. Chem. Int. Ed. Engl. **8**, 829 (1969).
34. (*a*) J. A. BERSON. Acc. Chem. Res. **5**, 406 (1972); (*b*) J. A. BERSON et P. B. DERVAN. J. Am. Chem. Soc. **95**, 269 (1973).
35. J. A. BERSON et L. SALEM. J. Am. Chem. Soc. **94**, 8917 (1972).
36. R. HUISGEN, W. SCHEER, G. SZEIMIES et H. HUBER. Tetrahedron Lett. 397 (1966).
37. R. HUISGEN, W. SCHEER et H. HUBER. J. Am. Chem. Soc. **89**, 1753 (1967).
38. R. HUISGEN et H. MADER. J. Am. Chem. Soc. **93**, 1777 (1971).
39. (*a*) J. H. HALL et R. HUISGEN. Chem. Commun. 1187 (1971); (*b*) J. H. HALL, R. HUISGEN, C. H. ROSS et W. SCHEER. Chem. Commun. 1188 (1971).
40. E. PADWA, D. DEAN, A. MAZZU et E. VEGA. J. Am. Chem. Soc. **95**, 7168 (1973).

Can. J. Chem. Downloaded from www.nrcresearchpress.com by 210.87.254.40 on 09/05/12
For personal use only.

Utilisation de la méthode de Wittig pour la synthèse de vinyl-2 aziridines N-substituées

DANIEL BOREL, YVONNE GELAS-MIALHE ET ROGER VESSIÈRE[1]

Groupe de Recherche de Chimie Organique 2, U.E.R. Sciences Exactes et Naturelles, Université de Clermont-Ferrand, B.P. 45, 63170 Aubiere, France

Reçu le 21 juillet 1975

DANIEL BOREL, YVONNE GELAS-MIALHE et ROGER VESSIÈRE. Can. J. Chem. **54**, 1582 (1976).

Plusieurs vinyl-2 aziridines sont préparées par action de phosphoranes sur des acyl-2 aziridines N-substituées. L'étude des spectres de rmn des produits ainsi obtenus permet de préciser leur stéréochimie au niveau du cycle et de la double liaison. La géométrie de l'acyl-2 aziridine de départ est conservée chez la vinyl-2 aziridine formée.

DANIEL BOREL, YVONNE GELAS-MIALHE, and ROGER VESSIÈRE. Can. J. Chem. **54**, 1582 (1976).

Several 2-vinylaziridines were prepared by treating N-substituted 2-acylaziridines with phosphoranes. The stereochemistry of the ring and the double bond of the products was established from a study of their nmr spectra. The geometry of the starting material 2-acylaziridine is conserved in the 2-vinylaziridine formed.

[Journal translation]

La littérature signale trois grandes méthodes de synthèse des vinyl-2 aziridines: (*i*) l'addition d'un nitrène à un composé diénique (1); (*ii*) la réduction d'oximes α,β-insaturées (2*a* et 2*b*) ou leur réaction sur les organomagnésiens (2*c*); et (*iii*) une modification de la synthèse de Wenker appliquée à des aminoalcools éthyléniques (3).

Par ailleurs, Hortmann et Koo (4) ont récemment montré qu'il était possible de préparer quelques vinyl-2 aziridines secondaires par traitement par une base forte de méthyl-2 aza-1 bicyclobutanes. Exception faite pour ce dernier procédé, dans toutes ces méthodes le cycle aziridine est créé sur un système éthylénique convenablement choisi.

[1] 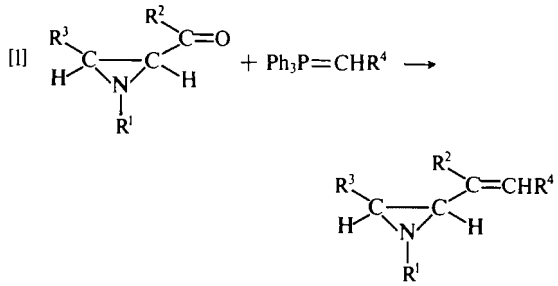

Nous proposons ici un procédé dans lequel la double liaison est créée sur une molécule possédant le cycle aziridine par application de la réaction de Wittig à des acyl-2 aziridines [1].

A notre connaissance aucune vinylaziridine n'avait été préparée par ce procédé; la seule réaction mentionnée dans la littérature (5) conduit à la formation d'une imine [2].

[2] 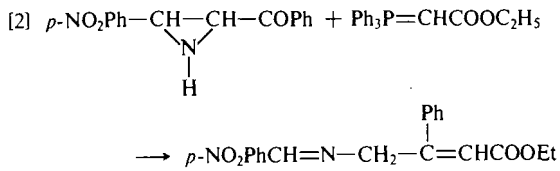

Résultats

Les acyl-2 aziridines **1** à **9** utilisées pour cette étude (tableau 1) ont été préparées par la méthode de Cromwell et Hoeksema (6) et sont pour la plupart connues; leur spectre de rmn permet de préciser leur stéréochimie (*cf.* Partie expérimentale). L'action sur ces dérivés de divers phosphoranes permet d'accéder aux vinyl-2 aziridines **10** à **23** avec des rendements en produits purs généralement compris entre 30 et 60%.

Dans les expériences 1 à 9, 11 et 12, un seul isomère de la vinyl-2 aziridine attendue a été isolé. Par contre, dans les expériences 10, 13 et 14, deux vinyl-2 aziridines isomères sont formées

[1]Ce travail fait partie de la thèse de 3ème Cycle de D. Borel (N° 421, Université de Clermont-Fd, octobre 1974); il a fait l'objet d'une note préliminaire (10) et d'un exposé aux Journées d'études sur la chimie des aziridines (Nice, décembre 1974).

Can. J. Chem. Downloaded from www.nrcresearchpress.com by 210.87.254.105 on 09/05/12
For personal use only.

Can. J. Chem. Downloaded from www.nrcresearchpress.com by 210.87.254.105 on 09/05/12
For personal use only.

TABLEAU 1. Vinylaziridines préparées par réaction de Wittig sur les acyl-2 aziridines 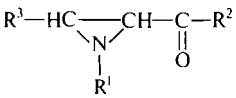

N° exp.	Acylaziridine					Phosphorane	Vinylaziridine		
	Composé	R^1	R^2	R^3	Stéréochimie[a]		Composé	Stéréochimie[a]	Rdt (%)
1	**1**	$C(CH_3)_3$	CH_3	H		$Ph_3P{=}CH_2$	**10**		
2	**2**	$C(CH_3)_3$	Ph	H		$Ph_3P{=}CH_2$	**11**	*trans*	50
3	**3**	CH_2Ph	Ph	H		$Ph_3P{=}CH_2$	**12**	*trans*	33
4	**4**	$C(CH_3)_3$	H	H		$Ph_3P{=}CH{-}COOC_2H_5$	**13**	*trans*	77
5	**5***a*	CH_2Ph	Ph	CH_3	*R*S**	$Ph_3P{=}CH_2$	**14***a*	*R*S**	50[b]
6	**6**	$CH(CH_3)_2$	CH_3	Ph	*R*S** 67%+*R*R** 33%	$Ph_3P{=}CH_2$	**15***a*	*R*S**	12
7	**7**	cC_6H_{11}	Ph	Ph	*R*S** 77%+*R*R** 23%	$Ph_3P{=}CH_2$	**16***a*	*R*S**	60[b]
8	**8***a*+**8***b*	$CH(CH_3)_2$	Ph	Ph	*R*S** 50%+*R*R** 50%	$Ph_3P{=}CH_2$	**17***a*	*R*S**	16
9	**8***a*	$CH(CH_3)_2$	Ph	Ph	*R*S**	$Ph_3P{=}CH_2$	**17***a*	*R*S**	56
10	**8***b*	$CH(CH_3)_2$	Ph	Ph	*R*R**	$Ph_3P{=}CH_2$	**17***b*+**17***b'*	*R*R* trans*+*R*R* cis*	51
11	**9***a*	CH_2Ph	Ph	Ph	*R*S**	$Ph_3P{=}CH_2$	**18***a*	*R*S**	48
12	**9***a*	CH_2Ph	Ph	Ph	*R*S**	$Ph_3P{=}CHCl$	**19***a*	*R*S**	30
13	**9***a*	CH_2Ph	Ph	Ph	*R*S**	$Ph_3P{=}CHPh$	**20***a*+**21***a*	*R*S* Z*+*R*S* E*	36
14	**9***a*	CH_2Ph	Ph	Ph	*R*S**	$Ph_3P{=}CH{-}CH_3$	**22***a*+**23***a*	*R*S* Z*+*R*S* E*	41
15	**9***b*	CH_2Ph	Ph	Ph	*R*R**	$Ph_3P{=}CH_2$	Non isolée[c]		

[a] *R*R** et *R*S** définissent la stéréochimie au niveau des carbones du cycle, *E* et *Z* au niveau de la double liaison, *cis* et *trans* par rapport au groupe vinyle et au substituant de l'azote.
[b] Rendement en produit brut.
[c] Le seul produit isolé est l'imine Ph—CH=N—CH(Ph)CH=C(Ph)CH_3, **24**.

dans les rapports suivants:

Expérience 10 **17***b*:**17***b*′ = 33:67
Expérience 13 **20***a*:**21***a* = 50:50
Expérience 14 **22***a*:**23***a* = 75:25

Aucune vinylaziridine n'a été isolée dans la réaction entre le méthylènetriphénylphosphorane et la cétone **9***b*, le seul produit formé a été identifié à l'imine **24** [3].

[3] 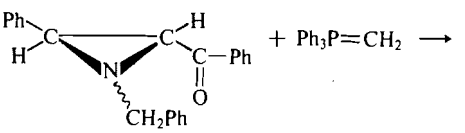

9*b*

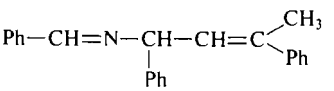

24

Dans les conditions expérimentales adoptées cette réaction n'est pas totale; la stéréochimie de la cétone récupérée n'est pas modifiée par rapport à celle de la cétone de départ.

Enfin, l'aziridine **9***a* ne réagit pas sur l'éthoxycarbonylméthylènetriphénylphosphorane.

Stéréochimie

L'identification des vinylaziridines obtenues et, dans la plupart des cas, la détermination de leur stéréochimie, ont été réalisées par étude de leur spectre de résonance magnétique nucléaire (tableau 2).

Stéréochimie au niveau du cycle

La vitesse d'inversion de l'atome d'azote étant, en général, relativement faible chez les aziridines, les dérivés 1,2-disubstitués peuvent donc se présenter sous deux formes diastéréoisomères *cis* et *trans* selon la position relative des deux substituants par rapport au plan du cycle. Pour les composés 1,2,3-trisubstitués, qui possèdent trois centres asymétriques, quatre formes isomères doivent être prises en considération (schéma 1).

La position relative des substituants fixés sur les carbones 2 et 3 est déduite de la valeur du couplage vicinal $J_{2,3}$ laquelle est de l'ordre de 5 à 7 Hz pour une relation *cis* et de 2 à 3 Hz pour une disposition *trans* (7). Par ailleurs, lorsque la vitesse d'inversion de l'atome d'azote est lente, la position relative du substituant R^1 porté par l'azote peut être également déterminée au moyen des données rmn; en effet, le phénomène d'anisotropie diamagnétique causé par la liaison N—R^1 est plus important sur les protons *syn* par rapport à R^1 que sur les protons *anti*; en conséquence, les premiers résonnent à champ plus fort que les seconds (8). En outre, l'effet sur les protons *syn* est d'autant plus faible que plus important est l'encombrement de R^1 (7).

Pour l'aziridine **11**, le spectre rmn des protons du cycle apparaît sous forme d'un seul motif ABX non modifié dans l'intervalle de température −57 − +120 °C; compte tenu des résultats précédemment acquis pour d'autres aziridines fonctionnalisées en position 2 (7 et 9), il est probable que l'inversion de l'atome d'azote chez le dérivé **11** est très lente dans ce domaine de température; la réaction ne fournit donc qu'un seul des deux invertomères pour lequel la valeur du glissement chimique des protons du cycle conduit à lui attribuer la configuration *trans* (R^1 et groupe vinyle en *trans*).

L'analyse du spectre de rmn de l'aziridine **12** permet, pour les mêmes raisons, de lui attribuer également la configuration *trans*.

La stéréochimie de l'aziridine **13** ne peut être précisée avec certitude. En effet, son spectre de rmn pourrait correspondre à celui d'un composé de configuration *cis*, le proton H-3 étant déplacé vers les champs faibles par rapport au proton H-3′. Toutefois, une telle structure semble thermodynamiquement peu stable en raison des importantes interactions stériques développées entre les substituants de l'azote et du carbone 2 et

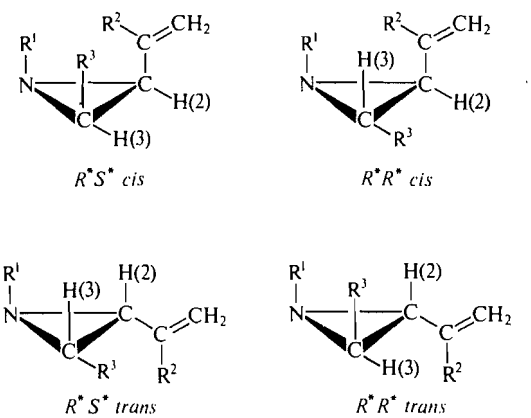

*R*S* cis* *R*R* cis*

*R*S* trans* *R*R* trans*

SCHÉMA 1

Can. J. Chem. Downloaded from www.nrcresearchpress.com by 210.87.254.105 on 09/05/12
For personal use only.

Can. J. Chem. Downloaded from www.nrcresearchpress.com by 210.87.254.105 on 09/05/12
For personal use only.

TABLEAU 2. Spectres de rmn de 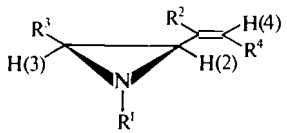

Composé	Solvant	R^1	R^2	R^3	R^4	δ H-2	δ H-3	δ H-4 et δ H-4′	δ R^1	δ R^2	δ R^4	δ R^3	$J_{2,3}$	$J_{4,4'}$	$J_{2,4}$
10	CCl_4	$C(CH_3)_3$	CH_3	H-3	H-4′	1.2 à 2.4 m		4.75 m et 4.92 m	0.95 s	1.60 d $J=1$ Hz					
11	$CDCl_3$	$C(CH_3)_3$	Ph	H-3′	H-4′	2.40 dd	1.50 dd	5.44 m	1.03 s	7.20 à 7.70		2.80 dd	$J_{2,3}=6.4$ $J_{2,3'}=3.0$ $J_{3,3'}=1.2$		
12	$CDCl_3$	CH_2Ph	Ph	H-3′	H-4′	2.32 dd	1.72 d	5.41 s	3.60 AB et 7.00 à 7.60	7.00 à 7.60		2.90 d	$J_{2,3}=6.2$ $J_{2,3'}=3.0$ $J_{3,3'}<1.0$		
13	$CDCl_3$	$C(CH_3)_3$	H	H-3′	COOEt	2.23 m	1.88 dd	5.75 à 7.40 m	1.00 s	5.75 à 7.40 m	1.27 t et 4.18 q	1.61 dd	$J_{2,3}=6.5$ $J_{3,3'}<1.0$ $J_{2,3'}=3.0$		
14*a*	$CDCl_3$	CH_2Ph	Ph	CH_3	H-4′	2.40 d	1.97 dq	5.43 m et 5.57 m	3.63 AB et 7.10 à 7.60	7.10 à 7.60		1.12 d $J=5$	6.2	1.6	<1
15*a*	$CDCl_3$	$CH(CH_3)_2$	CH_3	Ph	H-4′	2.16 dd	2.65 d	4.73 m et 4.96 m	1.16 dd et 1.70 m	1.41 m		7.10 à 7.40	6.8		0.5
16*a*	CCl_4	C_6H_{11}	Ph	Ph	H-4′	2.92 m		5.48 m	1.00 à 1.80	7.10 à 7.60		7.10 à 7.60			
17*a*	$CDCl_3$	$CH(CH_3)_2$	Ph	Ph	H-4′	2.56 d	2.90 d	5.42 m	1.18 d et 1.88 m	7.00 à 7.50		7.00 à 7.50	6.6		<1
17*b*	$CDCl_3$	$CH(CH_3)_2$	Ph	Ph	H-4	3.56 d	3.63 d	5.61 m	1.22 d et 0.93 d 1.70 m	7.15 à 8.20		7.15 à 8.20	2.7		0.5

Can. J. Chem. Downloaded from www.nrcresearchpress.com by 210.87.254.105 on 09/05/12
For personal use only.

TABLEAU 2 (*Suite et fin*)

Composé	Solvant	R^1	R^2	R^3	R^4	δ H-2	δ H-3	δ H-4 et δ H-4′	δ R^1	δ R^2	δ R^4	δ R^3	$J_{2,3}$	$J_{4,4'}$	$J_{2,4}$
17*b*′	$CDCl_3$	$CH(CH_3)_2$	Ph	Ph	H-4	3.08 m		5.61 m	1.15 d et 0.83 d 2.20 m	7.15 à 8.20		7.15 à 8.20			
17*b*′	CD_3COCD_3	$CH(CH_3)_2$	Ph	Ph	H-4	Pic simple centré à 3.05		5.55 m	1.12 d et 0.76 d 2.22 m	7.15 à 8.20		7.15 à 8.20			
18*a*	$CDCl_3$	CH_2Ph	Ph	Ph	H-4′	2.75 d	3.05 d	5.40 m	3.80 s et 7.00 à 7.50	7.00 à 7.50		7.00 à 7.50	6.6		
19*a*	$CDCl_3$	CH_2Ph	Ph	Ph	Cl	2.67 dd	2.96 dd	6.21 d	3.73 s et 6.80 à 7.50	6.80 à 7.50		6.80 à 7.50	6.0		1.5
20*a*	$CDCl_3$	CH_2Ph	Ph	Ph	Ph	3.20 dd	2.88 d	6.53 d	3.80 AB et 7.00 à 7.60	7.00 à 7.60	7.00 à 7.60	7.00 à 7.60	6.4		2
21*a*	$CDCl_3$	CH_2Ph	Ph	Ph	Ph	2.70 d	2.96 d	6.88 m	3.75 AB et 7.00 à 7.60	7.00 à 7.60	7.00 à 7.60	7.00 à 7.60	6.4		<1
22*a*	$CDCl_3$	CH_2Ph	Ph	Ph	CH_3	Pic simple centré à 2.80		5.65 q	3.70 AB et 7.00 à 7.50	7.00 à 7.50	1.62 d $J=7.4$ Hz	7.00 à 7.50			<1
23*a*	$CDCl_3$	CH_2Ph	Ph	Ph	CH_3	2.60 dq	2.92 d	5.90 dq	3.70 AB et 7.00 à 7.50	7.00 à 7.50	1.45 dd $J=7.4$ Hz $J=1.0$ Hz	7.00 à 7.50	6.5		1

Can. J. Chem. Downloaded from www.nrcresearchpress.com by 210.87.254.105 on 09/05/12
For personal use only.

il est peut-être plus raisonnable de penser que la configuration de la molécule est *trans*, le déblindage du proton *syn* du cycle pouvant se justifier par la compression stérique exercée par le groupement *tert*-butyle (7–9).

Les spectres de rmn des aziridines **12** et **13** effectués à température ambiante sont analogues à ceux enregistrés à 120 °C, l'énergie disponible à cette température est donc insuffisante pour provoquer l'inversion de l'atome d'azote.

La multiplicité des signaux attribués aux protons H-2 et H-3 dans le spectre de rmn de l'aziridine **10** n'a pu être établie, il ne nous est donc pas possible de préciser la géométrie de ce composé.

Chez les aziridines 1,2,3-trisubstituées **14***a*, **15***a*, **17***a*, **18***a*, **19***a*, **20***a*, **21***a* et **23***a*, la valeur de la constante de couplage $J_{2,3}$ comprise entre 6 et 6.8 Hz permet de leur attribuer la configuration *R*S**. Chez le dérivé **17***b*, la valeur $J_{2,3} = 2.7$ Hz correspond à une configuration *R*R**.

Ces résultats montrent que la géométrie de l'acyl-2 aziridine de départ (*cf.* tableau 1) est conservée chez la vinyl-2 aziridine obtenue.

Un seul signal est observé pour les protons H-2 et H-3 sur le spectre de rmn du composé **22***a* quel que soit le solvant utilisé ($CDCl_3$, CD_3CO-CD_3, C_6H_6, CS_2); par ailleurs, l'addition de sel d'europium à une solution de ce dérivé dans $CDCl_3$ ne provoque aucun déplacement des différents signaux du spectre. Il ne nous a donc pas été possible de déterminer chez ce dérivé la valeur de la constante $J_{2,3}$. Toutefois, l'acylaziridine utilisée pour la préparation du dérivé **22***a* étant de configuration *R*S**, il semble raisonnable, compte tenu des résultats précédents, d'attribuer également à la vinylaziridine **22***a* la configuration *R*S**. Pour la même raison, nous avons attribué la stéréochimie *R*S** au composé **16***a* bien que la multiplicité des signaux correspondant aux protons H-2 et H-3 ne soit pas observable.

Sur le spectre de l'aziridine **17***b'* les signaux affectés aux protons du cycle sont mal résolus; il semble toutefois raisonnable de considérer **17***b* et **17***b'* comme les deux invertomères de l'isopropyl-1 (phényl-1 vinyl)-2 phényl-3 aziridine *R*R**. Le proton H-3 de l'isomère **17***b'* résonne à champ plus fort que celui de **17***b*; en conséquence, chez **17***b'* H-3 est en *syn* par rapport au substituant R^1. L'aziridine **17***b'* est donc de configuration *cis*, **17***b* étant l'invertomère *trans*. La constante d'équilibre $K_{éq}$ est égale à 2, ce qui correspond à une énergie libre ΔG_0 de -0.4 kcal mol^{-1}.

Le spectre de rmn des dérivés *R*S** **15***a*, **16***a*, **18***a*, **22***a* et **23***a* n'est pas modifié dans une zone de température comprise entre -85 et $+100$ °C. Le spectre des composés **14***a*, **17***a*, **19***a*, **20***a* et **21***a* réalisé à 100 °C est analogue à celui enregistré à température ambiante. Comme pour les aziridines 1,2-disubstituées **11** à **13**, nous pensons que l'inversion de l'azote est bloquée, la réaction conduisant au seul isomère *trans*.

Stéréochimie au niveau de la double liaison

Chez l'aziridine **20***a*, le signal du proton H-2 est situé à champ faible par rapport à celui de son isomère **21***a*. Les modèles moléculaires montrent que le proton H-2 se trouve dans le plan du substituant R^4 = Ph lorsque la double liaison est de configuration *Z*; cette situation doit entraîner un déplacement du signal H-2 vers les champs faibles. En conséquence, les substituants de la double liaison doivent être en relation *Z* dans l'aziridine **20***a* et *E* dans l'isomère **21***a*.

Sur le spectre de rmn du composé **23***a*, on observe un couplage homoallylique $^5J = 1$ Hz, couplage qui n'apparaît pas sur le spectre de son isomère **22***a*; ce couplage indique une disposition transoïde des protons concernés dans l'isomère **23***a*, donc une configuration *E* au niveau de la double liaison, l'isomère **22***a* ayant la structure *Z*.

Aucun élément du spectre de rmn ne nous permet de préciser la configuration de la double liaison des vinylaziridines **13** et **19***a*.

Partie expérimentale

Les spectres de résonance magnétique nucléaire ont été enregistrés à l'aide d'un appareil Varian A 60 ou Varian T 60 en utilisant le tétraméthylsilane comme référence interne. Les déplacements chimiques sont exprimés en ppm et les constantes de couplage en Hz. Les spectres infrarouge ont été effectués sur un spectrophotomètre Perkin-Elmer 157. Les chromatographies sur colonne ont été réalisées sur gel de silice (7734 – Merck).

Préparation des acylaziridines

tert-Butyl-1 acétyl-2 aziridine ***1***

Obtenue à partir de l'α-chlorovinylméthylcétone selon réf. 7: rdt 35%; p éb 65–67 °C/12 torr; ir 1700 cm^{-1} (C=O); rmn (CCl_4) 0.98 (s, $C(CH_3)_3$), 1.87 (s, $COCH_3$), 1.70–2.30 (m, CH_2 cycle).

tert-Butyl-1 formyl-2 aziridine ***4***

Préparée selon Duhamel *et al.* (11): rdt 89%; p éb 54–60 °C/19 torr; rmn ($CDCl_3$) 1.00 (s, $C(CH_3)_3$), 1.90–2.40 (m, CH_2 cycle), 8.95 (d, CHO, $J = 4.5$ Hz).

Can. J. Chem. Downloaded from www.nrcresearchpress.com by 210.87.254.105 on 09/05/12
For personal use only.

Acylaziridines ***2***, ***3***, *et* ***5–9***

Obtenues selon Cromwell et coll. (6, 12).

Tert-butyl-1 benzoyl-2 aziridine ***2***—Résonance magnétique nucléaire ($CDCl_3$) 1.05 (s, $C(CH_3)_3$), 1.97 (dd, H-3), 2.08 (dd, H-3′), 3.11 (dd, H-2), 7.00–8.20 (m, C_6H_5); $J_{2,3}$ = 6, $J_{2,3'}$ = 2.8, $J_{3,3'}$ = 1.8 Hz.

Benzyl-1 benzoyl-2 aziridine ***3***—Résonance magnétique nucléaire ($CDCl_3$) 1.80 (dd, H-3), 2.30 (dd, H-3′), 2.92 (dd, H-2), 3.57 (spectre AB, N—CH_2), 7–8 (m, C_6H_5); $J_{2,3}$ = 6.5, $J_{2,3'}$ = 3, $J_{3,3'}$ = 2 Hz.

Benzyl-1 benzoyl-2 méthyl-3 aziridine ***5a***—Obtenue sous forme de solide: pf 71–73 °C; rdt 55%; rmn ($CDCl_3$) 1.20 (d, CH_3, J = 6 Hz), 2.27 (dq, H-3), 3.02 (d, H-2, $J_{2,3}$ = 7 Hz), 3.68 (spectre AB, N—CH_2), 7.00–7.60 (m, C_6H_5).

Isopropyl-1 acétyl-2 phényl-3 aziridine ***6***—La rmn du produit brut montre qu'il est constitué d'un mélange de deux stéréoisomères *R*R** et *R*S** que nous n'avons pas séparés: rmn ($CDCl_3$) (*i*) isomère *R*R** (33%) 0.92 (dd, $C(CH_3)_2$), 1.87 (m, N—CH), 1.68 (s, $COCH_3$), 3.32 (m, H-2 et H-3), 7.30 (m, C_6H_5); (*ii*) isomère *R*S** (67%) 1.21 (dd, $C(CH_3)_2$), 1.87 (m, N—CH), 2.31 (s, $COCH_3$), 2.90 (spectre AB, H-2 et H-3, $J_{2,3}$ = 7 Hz), 7.30 (m, C_6H_5).

Cyclohexyl-1 benzoyl-2 phényl-3 aziridine ***7***—Obtenue sous forme de solide, pf 97–98 °C (CH_3OH), mélange des deux isomères *R*R** et *R*S** lesquels n'ont pas été séparés (*R*S**:*R*R** = 77:23): rmn (C_6H_6) 1–2 (m, C_6H_{11}), 2.83 (spectre AB, H-2 et H-3 de l'isomère *R*S**, J = 7 Hz), 3.6 (spectre AB, H-2 et H-3 de l'isomère *R*R**, J = 2.5 Hz), 7–8 (m, C_6H_5).

Isopropyl-1 benzoyl-2 phényl-3 aziridines ***8a*** *et* ***8b***—Obtenues sous forme d'huile, mélange des isomères *R*S** (50%) et *R*R** (50%) en accord avec réf. 13. Les deux isomères ont été séparés par chromatographie sur colonne (éluant benzène – heptane – acétate d'éthyle 38:12:50). rmn (C_6H_6) (*i*) isomère *R*S** **8***a* 1.05 (d) et 1.15 (d, $C(CH_3)_2$), 1.50 (m, N—CH), 2.85 (spectre AB, H-2 et H-3, J = 7 Hz), 6.80–8.00 (m, C_6H_5); (*ii*) isomère *R*R** **8***b* 0.92 (d) et 1.12 (d, $C(CH_3)_2$), 3.20 (m, N—CH), 3.49 (d) et 3.67 (d, H-2 et H-3, J = 2.5 Hz), 6.80–8.00 (m, C_6H_5).

Benzyl-1 benzoyl-2 phényl-3 aziridines ***9a*** *et* ***9b***—Le produit brut est un mélange des deux stéréoisomères *R*R** et *R*S** séparés selon Cromwell *et al.* (12) et identifiés par leur spectre de rmn (14): isomère *R*S** **9***a* pf 103 °C; rmn ($CDCl_3$) 3.31 (s, H-2 et H-3), 3.87 (spectre AB, N—CH_2), 7.30 à 8.00 (m, C_6H_5); isomère *R*R** **9***b* pf 53–55 °C; rmn ($CDCl_3$) 3.68 (s, H-2 et H-3), 4.10 (spectre AB, N—CH_2), 7.10 à 8.10 (m, C_6H_5).

Vinylaziridines

Préparation des dérivés ***10–12***, ***14–18*** *et* ***20–23***

Les ylures de phosphore, non stables dans les conditions normales, sont préparés "in situ" par action du *n*-butyllithium sur le sel de phosphonium.

Le mode opératoire adopté est inspiré de celui utilisé par Wittig et Schöllkopf (15).

Dans un réacteur muni d'un agitateur et traversé constamment par un courant d'azote, on place le sel de phosphonium et 200 ml d'éther anhydre. On ajoute, à l'aide d'une ampoule à brome et sous atmosphère d'azote, le *n*-butyllithium en solution dans l'hexane à raison de 1.5 à 2 mol par mol de sel. La solution est ensuite agitée pendant 4 h à température ordinaire. On introduit alors 0.75 mol de cétone par mol de sel de phosphonium; la solution se décolore et un précipité apparaît. Le mélange est chauffé à reflux pendant environ 4 h, puis ramené à température ambiante. On ajoute de l'eau et extrait à l'éther. Les phases éthérées sont séchées sur sulfate de magnésium et évaporées. Les produits obtenus sont alors purifiés.

tert-Butyl-1 isopropényl-2 aziridine ***10***—La réaction effectuée à partir de 0.14 mol (50 g) de bromure de triphénylméthylphosphonium et de 0.1 mol (14.1 g) de *tert*-butyl-1 acétyl-2 aziridine conduit à un liquide dont la composition est déterminée par rmn. Il contient 40% de cétone de départ et 60% de *tert*-butyl-1 isopropényl-2 aziridine. Ces deux produits sont séparés par cpv préparative sur colonne DEGS (95 °C): rmn *cf.* tableau 2; ir (CCl_4) 1640 cm^{-1} (C=C). *Anal.* calc. pour $C_9H_{17}N$: C 77.70, H 12.23, N 10.07; trouvé: C 77.60, H 12.07, N 10.16.

tert-Butyl-1 (phényl-1 vinyl)-2 aziridine ***11***—Le produit brut est purifié par chromatographie sur colonne, cyclohexane – acétate d'éthyle 9:1: rmn *cf.* tableau 2; ir ($CDCl_3$) 1600, 1640, 1680 cm^{-1} (C=C + C_6H_5).

Benzyl-1 (phényl-1 vinyl)-2 aziridine ***12***—Le produit brut est purifié par chromatographie sur colonne, cyclohexane – acétate d'éthyle 8:2: rmn *cf.* tableau 2; ir (pur) 1600, 1680, 1700 cm^{-1} (C=C + C_6H_5).

Benzyl-1 (phényl-1 vinyl)-2 méthyl-3 aziridine ***14a***—Elle est isolée par chromatographie sur colonne, cyclohexane – acétate d'éthyle 8:2: rmn *cf.* tableau 2; ir (pur) 1590, 1610, 1690 cm^{-1} (C=C + C_6H_5).

Isopropyl-1 isopropényl-2 phényl-3 aziridine ***15a***—Elle est purifiée par chromatographie sur colonne, benzène–heptane 3:1: rmn *cf.* tableau 2; ir ($CDCl_3$) 1590, 1640, 1690 cm^{-1} (C=C + C_6H_5).

Cyclohexyl-1 (phényl-1 vinyl)-2 phényl-3 aziridine ***16a***—Ce composé est purifiée par chromatographie sur colonne, benzène–heptane 3:1: rmn *cf.* tableau 2; ir (CCl_4) 1600, 1630 cm^{-1} (C=C + C_6H_5).

Isopropyl-1 (phényl-1 vinyl)-2 phényl-3 aziridines ***17a***, ***17b*** + ***17b′***—La réaction réalisée au départ d'isopropyl-1 benzoyl-2 phényl-3 aziridine (**8***a* 50% + **8***b* 50%) conduit à un produit qui est purifié par recristallisation (méthanol); il constitue l'aziridine **17***a* pure: pf 94 °C; rmn *cf.* tableau 2; ir (CCl_4) 1600, 1630 cm^{-1} (C=C + C_6H_5). *Anal.* calc. pour $C_{19}H_{21}N$ C 86.69, H 7.98, N 5.31: trouvé: C 86.53, H 8.01, N 5.41.

L'aziridine **17***a* peut être également obtenue à partir de la cétone **8***a* pure.

Le produit brut formé dans la réaction de la cétone **8***b* pure sur le méthylènetriphénylphosphorane est purifié par chromatographie sur colonne, cyclohexane – acétate d'éthyle 9:1. Son spectre de rmn montre qu'il constitue un mélange des deux aziridines **17***b* et **17***b′*: rmn *cf.* tableau 2; ir (pur) 1600, 1625, 1665 cm^{-1} (C=C + C_6H_5).

Benzyl-1 (phényl-1 vinyl)-2 phényl-3 aziridine ***18a***—Le produit brut obtenu est purifié par recristallisation (C_2H_5OH 70%). pf 54 °C; rmn *cf.* tableau 2; ir (CCl_4): 1600, 1620 cm^{-1} (C=C + C_6H_5). *Anal.* calc. pour $C_{23}H_{21}N$ C 88.74, H 6.75, N 4.50; trouvé: C 87.23, H 6.74, N 4.86.

Benzyl-1 (phényl-1 styryl)-2 phényl-3 aziridines ***20a*** *et* ***21a***—Le spectre de rmn du produit brut montre qu'il est constitué d'un mélange des deux aziridines isomères **20***a* et **21***a* en quantité égale. Leur séparation est réalisée par chromatographie sur colonne, benzène–cyclohexane 1:2: rmn *cf.* tableau 2; ir ($CDCl_3$) **20***a* + **21***a* 1600, 1610, 1670 cm^{-1} (C=C + C_6H_5).

Can. J. Chem. Downloaded from www.nrcresearchpress.com by 210.87.254.105 on 09/05/12
For personal use only.

Benzyl-1 (phényl-1 propène-1 yl)-2 phényl-3 aziridines ***22a*** *et* ***23a***—Le produit brut est formé d'un mélange des deux aziridines **22***a* (75%) et **23***a* (25%); elles sont séparées par chromatographie sur colonne ou sur plaque, benzène–cyclohexane 1:2: rmn *cf.* tableau 2; ir ($CDCl_3$) **22***a* + **23***a* 1600, 1640 cm^{-1} (C=C + C_6H_5).

Préparation de la benzyl-1 (chloro-2 phényl-1 vinyl)-2 phényl-3 aziridine ***19a***

Le chlorométhylènetriphénylphosphorane est fabriqué selon la méthode décrite par Seyferth *et al.* (16).

On place 0.11 mol (30 g) de triphénylphosphine dans un réacteur de 500 ml équipé d'un agitateur et traversé par un courant d'azote. On ajoute 200 ml d'éther sec et 0.13 mol (11 g) de chlorure de méthylène. Le mélange étant refroidi à −30 à −40 °C, on ajoute lentement et sous agitation vigoureuse 0.1 mol de *n*-butyllithium en solution dans l'hexane, puis, après retour à température ambiante, 0.1 mol (31.3 g) de benzyl-1 benzoyl-2 phényl-3 aziridine; on maintient l'agitation 4 h à température ambiante puis 2 h à reflux. Après avoir filtré, lavé les phases éthérées à l'eau jusqu'à neutralité et évaporé le solvant, on recueille 6 g de produit brut que l'on purifie par chromatographie sur colonne, benzène–cyclohexane 1:2. Il est identifié, par rmn, à la benzyl-1 (chloro-2 phényl-1 vinyl)-2 phényl-3 aziridine **19***a*: rmn *cf.* tableau 2; ir ($CDCl_3$) 1600, 1700 cm^{-1} (C=C + C_6H_5).

Préparation de la tert-butyl-1 (éthoxycarbonyl-2 vinyl)-2 aziridine ***13***

L'éthoxycarbonylméthylènetriphénylphosphorane est obtenu selon un mode opératoire décrit (17).

A une solution aqueuse de 0.1 mol (42.9 g) de bromure d'éthoxycarbonylméthylènetriphénylphosphonium dans 1 litre d'eau, on ajoute une lessive de soude, goutte à goutte, sous agitation, jusqu'à réaction alcaline de la phénolphtaléine. Le phosphorane précipite alors en un produit visqueux que l'on sépare de l'eau et recristallise dans un mélange éther de pétrole – acétate d'éthyle, pf 117 °C (litt. (17) pf = 116–117 °C).

Dans un réacteur muni d'un système d'agitation contenant 0.02 mol (7.5 g) d'éthoxycarbonylméthylènetriphénylphosphorane en solution dans 25 ml de benzène anhydre, on ajoute goutte à goutte 0.02 mol (2.6 g) de *tert*-butyl-1 formyl-2 aziridine; ce mélange est agité 3 h à température ambiante. On évapore le solvant et reprend par de l'éther de pétrole. L'oxyde de triphénylphosphine précipite. On filtre, évapore le solvant et obtient 3 g de produit pur identifié à la *tert*-butyl-1 (éthoxycarbonyl-2 vinyl)-2 aziridine **13**: rmn *cf.* tableau 2; ir ($CDCl_3$) 1720 cm^{-1} (C=O), 1650 cm^{-1} (C=C).

Action du méthylènetriphénylphosphorane sur l'aziridine ***9b****. Obtention de l'imine* ***24***

Selon le mode opératoire utilisé pour la préparation des vinyl-2 aziridines, on fait réagir 0.02 mol de phosphorane (préparé à partir de 0.02 mol de bromure de triphénylméthylènephosphonium et 10 ml de solution 0.2 *M* de *n*-BuLi dans l'hexane) sur 6.3 g (0.02 mol) de benzyl-1 benzoyl-2 phényl-3 aziridine *R*R** **9***b*. On obtient 8 g de produit brut dont la rmn nous montre qu'il est constitué de 43% d'oxyde de triphénylphosphine, 19% de cétone de départ et 38% d'imine.

Imine **24** Ph—CH(a)=N(b)—CH(Ph)(c)—CH(d)=C(Ph)CH_3:

rmn ($CDCl_3$) 2.20 (d, CH_3), 5.45 (d, CH(Ph)), 6.25 (dq, CH=C), 8.45 (s, CH=N), 7–8 (C_6H_5); $J_{b,c}$ = 9, $J_{c,d}$ = 1.2 Hz; ir ($CHCl_3$) 1600, 1630, 1660 cm^{-1} (C=C + C_6H_5).

Remerciements

Nous remercions vivement M. le Professeur J. Chuche et M. J. C. Pommelet pour la communication de leurs résultats et les fructueuses discussions que nous avons eues ensemble.

1. (*a*) K. Hafner, W. Kaiser et R. Puttner. Tetrahedron Lett. 3953 (1964); (*b*) A. G. Anastassiou. J. Am. Chem. Soc. **87**, 5512 (1965); (*c*) A. Mishra, S. N. Rice et W. Lwowski. J. Org. Chem. **33**, 481 (1968); (*d*) P. Scheiner. J. Org. Chem. **32**, 2628 (1967); Tetrahedron, **24**, 2757 (1968); (*e*) R. S. Atkinson et C. W. Rees. Chem. Comm. 1230 (1967); (*f*) R. S. Atkinson et C. W. Rees. J. Chem. Soc. C, 772 (1969); (*g*) D. J. Anderson, T. L. Gilchrist, D. C. Horwell et C. W. Rees. J. Chem. Soc. C, 576 (1970); (*h*) T. L. Gilchrist, C. W. Rees et S. Stanton. J. Chem. Soc. C, 3036 (1971); (*i*) L. Hoesch et A. S. Drieiding. Chimia, **26**, 629 (1972); (*j*) M. P. Sammes et A. Rahman. J. Chem. Soc. Perkin Trans. 1, 344 (1972).
2. (*a*) G. Ricart, D. Couturier et C. Glacet. C. R. Acad. Sci. Sér. C, **277**, 519 (1973); (*b*) L. Ferrero, M. Rouillard, M. Decouzon et M. Azzaro. Tetrahedron Lett. 131 (1974); (*c*) R. Chaabouni et A. Laurent. Synthesis, Sous presse.
3. (*a*) E. L. Stogryn et S. J. Brois. J. Org. Chem. **30**, 88 (1965); (*b*) E. L. Stogryn et S. J. Brois. J. Am. Chem. Soc. **89**, 605 (1967); (*c*) A. Sauleau, J. Sauleau, H. Bouget et J. Huet. C. R. Acad. Sci. Sér. C, **279**, 473 (1974); (*d*) J. C. Pommelet et J. Chuche. Can. J. Chem. Sous presse.
4. A. G. Hortmann et J.-Y. Koo. J. Org. Chem. **39**, 3781 (1974).
5. A. W. Heine, G. B. Lowrie III et K. C. Irving. J. Org. Chem. **35**, 444 (1970).
6. N. H. Cromwell et H. Hoeksema. J. Am. Chem. Soc. **71**, 708 (1949).
7. G. Bouteville, Y. Gelas-Mialhe et R. Vessière. Bull. Soc. Chim. Fr. 3264 (1971); et réf. citées.
8. S. J. Brois. Tetrahedron, **26**, 227 (1970).
9. J. L. Pierre, P. Baret et P. Arnaud. Bull. Soc. Chim. Fr. 3619 (1971).
10. D. Borel, Y. Gelas-Mialhe et R. Vessière. C. R. Acad. Sci. Sér. C, **278**, 1393 (1974).
11. L. Duhamel, P. Duhamel et P. Siret. Bull. Soc. Chim. Fr. 2640 (1973).
12. N. H. Cromwell, N. G. Barker, R. A. Wankel, P. J. Wanderhorst, W. Olson et J. H. Anglin, Jr. J. Am. Chem. Soc. **73**, 1044 (1951).
13. J. W. Lown, G. Dallas et T. Maloney. Can. J. Chem. **47**, 3557 (1969).
14. A. E. Pohland, R. C. Badger et N. H. Cromwell. Tetrahedron Lett. 4369 (1965).
15. G. Wittig et U. Schöllkopf. Org. Synth. **40**, 66 (1960).
16. D. Seyferth, S. O. Grim et T. O. Read. J. Am. Chem. Soc. **83**, 1617 (1961).
17. O. Isler, H. Gutmann, M. Montavon, R. Ruegg, G. Ryser et P. Zeller. Helv. Chim. Acta, **40**, 1242 (1957).

Isomérisation thermique de vinyl-2 aziridines N-substituées

DANIEL BOREL, YVONNE GELAS-MIALHE ET ROGER VESSIÈRE[1]

Groupe de Recherche de Chimie Organique 2, U.E.R. Sciences Exactes et Naturelles, Université de Clermont-Ferrand, B.P. 45, 63170 Aubiere, France

Reçu le 21 juillet 1975

DANIEL BOREL, YVONNE GELAS-MIALHE et ROGER VESSIÈRE. Can. J. Chem. **54**, 1590 (1976).

L'isomérisation thermique de vinyl-2 aziridines diversement substituées sur le cycle et la double liaison est étudiée. La nature des produits formés dépend de celle des substituants en position 1 et 3. Lorsque le carbone 3 du cycle porte un groupement phényle, la thermolyse conduit, dans la plupart des cas, à une Δ-2 pyrroline. Avec les aziridines non substituées ou alkylées en 3 la réaction évolue, selon la nature du substituant de l'azote, soit vers une imine éthylénique, soit vers un mélange de Δ-2 et Δ-3 pyrrolines. Des mécanismes permettant l'interprétation des résultats expérimentaux sont proposés.

DANIEL BOREL, YVONNE GELAS-MIALHE, and ROGER VESSIÈRE. Can. J. Chem. **54**, 1590 (1976).

The thermal isomerization of 2-vinylaziridines, variously substituted on the ring and the double bond, has been studied. The nature of the products formed depends on the nature of the substituents in positions 1 and 3. If the ring carbon-3 carries a phenyl substituent, the thermolysis yields, in most cases, a Δ-2-pyrroline. With unsubstituted or 3-alkylaziridines the reaction proceeds, depending on the nature of the substituent on the nitrogen, either to an ethylene imine or to a mixture of Δ-2- and Δ-3-pyrrolines. Mechanisms to interpret the experimental results are proposed.

[Journal translation]

Plusieurs auteurs (1) ont montré que les vinyl-2 aziridines constituaient des substrats susceptibles de conduire par isomérisation thermique à des pyrrolines-3. La réaction est généralement justifiée par une rupture thermique de la liaison C—N selon un processus comparable à celui invoqué dans l'isomérisation des vinylcyclopropanes en cyclopentènes. Toutefois, la nature des substituants portés par le cycle aziridine peut modifier l'évolution classique de la réaction (1*c–g*, 2–4).

Disposant de plusieurs vinylaziridines (5) diversement substituées sur le cycle, il était, dès lors, intéressant d'étudier leur comportement thermique.

Résultats

Les conditions dans lesquelles les réactions d'isomérisation ont été effectuées sont précisées dans le tableau 1, ainsi que les produits que nous avons obtenus. Ces derniers ont été identifiés principalement par leurs spectres de rmn (*cf.* Partie expérimentale).

L'examen du tableau 1 montre que l'évolution de la réaction est considérablement affectée par la nature des substituants du cycle aziridine.

(*i*) Lorsque le carbone C-3 de l'aziridine porte un groupement phényle et lorsque la double liaison n'est pas substituée en position 2, l'isomérisation conduit à un seul produit identifié à une pyrroline-2 normalement stable (expériences 1–3).

(*ii*) Les aziridines dont le carbone C-3 porte un hydrogène ou un groupement méthyle et dont le substituant de l'azote possède des hydrogènes sur le carbone α s'isomérisent dans les mêmes conditions en un seul produit identifié à une imine β,γ-éthylénique (expériences 4–6).

(*iii*) L'aziridine **11**, non substituée en position 3 et portant sur l'azote le groupement *tert*-butyle, s'isomérise plus difficilement que les composés précédents en conduisant à un mélange de pyrroline-2 **30** et de pyrroline-3 **31**. Ces produits ont été identifiés sur le spectre de rmn du mélange et n'ont pas pu être séparés. Ils sont, en effet, instables: si on les abandonne quelques jours à température ambiante, ils se transforment en deux nouveaux produits qui ont pu être séparés. Le spectre de rmn de l'un d'eux est identique à celui décrit dans la littérature (9) pour le *N-tert*-butyl phényl-3 pyrrole **32**. Le

[1]Ce travail fait partie de la thèse de 3ème Cycle de D. Borel (N° 421, Université de Clermont-Fd, octobre 1974); il a fait l'objet d'une note préliminaire (10) et d'un exposé aux Journées d'études sur la chimie des aziridines (Nice, décembre 1974).

Can. J. Chem. Downloaded from www.nrcresearchpress.com by 210.87.254.105 on 09/05/12
For personal use only.

Can. J. Chem. Downloaded from www.nrcresearchpress.com by 210.87.254.105 on 09/05/12
For personal use only.

second composé constitue vraisemblablement le (*N*-méthylidène *tert*-butylamino)-1 phényl-1 cyclopropane **33**.

(*iv*) Lorsque le système vinylique de l'aziridine porte un substituant en position 2, la pyrroline-2 peut présenter les configurations *cis* et *trans*. Les résultats que nous avons observés montrent que la stéréosélectivité de l'isomérisation des aziridines dépend de la géométrie de leur double liaison (expériences 8–10). Les pyrrolines-2 obtenues sont stables et constituent les produits cinétiques des réactions de thermolyse. En effet, le rapport **34***a*:**34***b* ne varie pas au cours de la thermolyse du composé **21***a* (expérience 9) et, quel que soit le degré d'avancement de la réaction de thermolyse de l'aziridine **20***a* (expérience 8), seule la pyrroline-2 **34***b* est présente dans le mélange réactionnel. En conséquence, dans les conditions adoptées pour la thermolyse des aziridines **20***a* et **21***a*, une éventuelle isomérisation *cis–trans* des pyrrolines-2 **34***a* et **34***b* doit être exclue. De même, au cours du réarrangement thermique du composé **23***a* (expérience 10) seule la pyrroline-2 **35***a cis* est formée, nous n'avons jamais détecté de pyrroline-2 *trans* quel que soit le degré d'avancement de cette réaction.

(*v*) La géométrie de la double liaison de la vinyl-2 aziridine semble également influencer l'évolution de la réaction: l'aziridine **23***a* de configuration *E* se réarrange en pyrroline-2 **35***a* (expérience 10) alors que son isomère **22***a Z* conduit à l'amine diénique **36** (expérience 11).

Nous avons vérifié que le réarrangement thermique de toutes ces vinylaziridines n'était, ni précédé, ni accompagné d'une isomérisation de l'aziridine de départ, tant au niveau du cycle qu'au niveau de la double liaison. En effet, lorsque les réactions sont arrêtées avant leur terme, on constate que la géométrie de l'aziridine récupérée n'est pas modifiée par rapport à celle du produit de départ.

Discussion des résultats

Formation des pyrrolines-2

La formation des pyrrolines-2 implique la rupture de la liaison C—C du cycle aziridine, rupture favorisée par la présence d'un groupement phényle sur le carbone C-3. Plusieurs mécanismes peuvent alors être envisagés.

Mécanisme radicalaire

A l'image du réarrangement thermique des

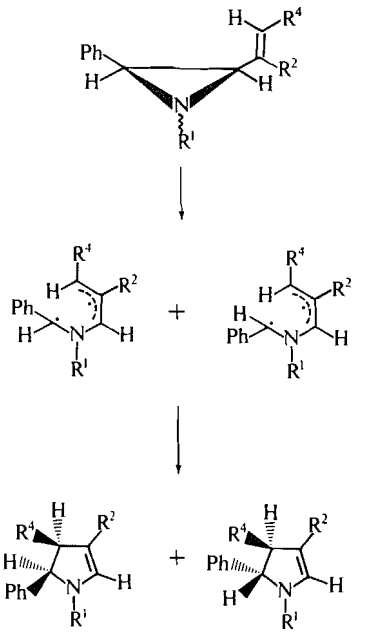

SCHÉMA 1

vinylcyclopropanes, on peut penser que l'isomérisation des vinyl-2 aziridines implique une rupture radicalaire du cycle (schéma 1).

La réaction devrait alors conduire à un mélange des deux pyrrolines-2 isomères quelle que soit la configuration de la double liaison de la vinyl-2 aziridine de départ. Un tel mécanisme ne permet donc pas de justifier la stéréospécificité de l'isomérisation des aziridines **20***a* et **23***a* qui conduit respectivement aux seules pyrrolines **34***b trans* et **35***a cis*.

Mécanisme ionique

Huisgen *et al.* (6) ont montré que les aziridines pouvaient s'ouvrir en ylure d'azométhine selon un processus conrotatoire.

L'ouverture de l'aziridine **23***a* doit alors conduire à un ylure *trans* susceptible de présenter quatre conformations; sa cyclisation en pyrroline-2 ne peut être réalisée que si les deux atomes de carbone entre lesquels s'établit la liaison σ ne sont pas trop éloignés l'un de l'autre, ce qui est uniquement réalisé pour la conformation représentée dans la schéma 2.

La fermeture électrocyclique de l'ylure vraisemblablement disrotatoire (7) doit alors conduire à la pyrroline **35***a cis*.

Au départ de l'aziridine **21***a*, la cyclisation disrotatoire de l'ylure doit être plus difficile en

TABLEAU 1. Thermolyse des vinyl-2 aziridines

Exp. N°	Aziridines	Conditions opératoires: Temps (h)	Conditions opératoires: Température (°C)	Produits obtenus
1	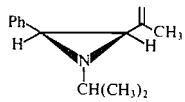 **15***a*	2	160	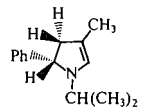 **25**
2	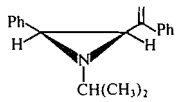 **17***a*	2	160	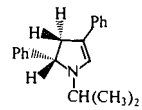 **26**
3	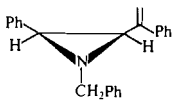 **18***a*	2	160	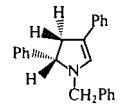 **27**
4	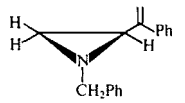 **12**	2	160	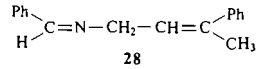 **28**
5	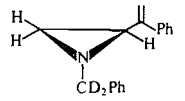 **37**	2	160	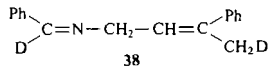 **38**
6	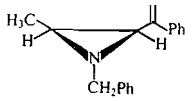 **14***a*	2	160	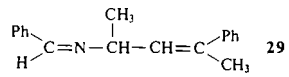 **29**
7	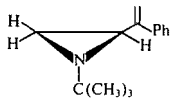 **11**	2	200	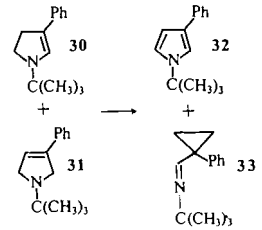 **30** **31** **32** **33**
8	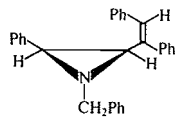 **20***a*	2	100	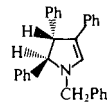 **34***b*
9	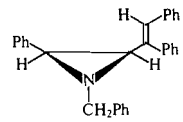 **21***a*	2	100	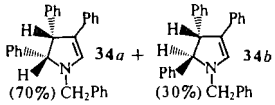 **34***a* + **34***b* (70%) (30%)
10	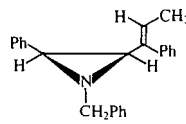 **23***a*	2	150	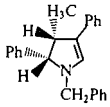 **35***a*
11	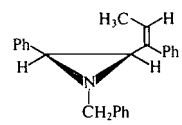 **22***a*	2	150	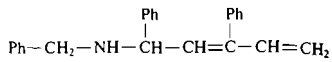 **36**

Can. J. Chem. Downloaded from www.nrcresearchpress.com by 210.87.254.105 on 09/05/12
For personal use only.

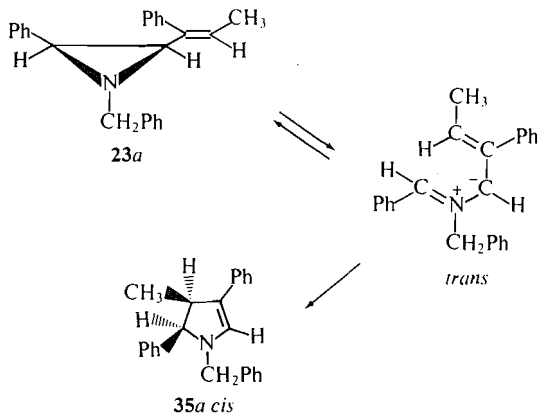

SCHÉMA 2

raison de l'interaction exercée par les deux groupements phényle dont l'approche est *syn*; la cyclisation de l'ylure *trans* peut alors être compétitive avec son isomérisation en ylure *cis* dont la cyclisation conduit à la pyrroline-2 *trans* **34***b* (schéma 3).

Dans cette hypothèse, l'isomérisation de l'aziridine **21***a* n'est pas stéréospécifique, ce qui est en accord avec nos résultats expérimentaux.

Le même raisonnement appliqué à l'aziridine **20***a* conduit à penser que son réarrangement est stéréospécifique. En effet, la cyclisation de l'ylure *trans* doit être plus rapide que son isomérisation en ylure *cis* très encombré (schéma 4).

Nos résultats sont en accord avec cette hypothèse, l'isomérisation de l'aziridine **20***a* conduit à l'unique pyrroline **34***b trans*.

Réaction concertée. Sigmatropie-1,3

Le mécanisme sigmatropique-1,3 à symétrie permise a été proposé par Woodward et Hoffmann (8) pour l'isomérisation du vinylcyclopropane en cyclopentène. Aucune expérience n'a permis à ce jour d'infirmer ou de confirmer cette hypothèse. S'il en est ainsi, la migration sigmatropique-1,3 fait intervenir un processus suprafacial–antarafacial $\pi_s^2 + \sigma_a^2$ ou $\pi_a^2 + \sigma_s^2$; dans ce mécanisme, la thermolyse d'une vinylaziridine *R*S** de configuration *E* sur la double liaison doit être stéréospécifique et conduire à une pyrroline-2 *cis*. Un tel processus ne permet donc pas de rendre compte de nos résultats expérimentaux concernant l'aziridine **21***a*. Par ailleurs et comme nous le verrons par la suite, il n'est pas possible dans ce cadre de justifier l'influence d'un groupe phényle fixé sur le carbone 3 sur le déroulement de la réaction.

*Isomérisation de l'aziridine **11***

Ce composé ne porte sur l'atome d'azote ou sur l'atome de carbone 3 aucun substituant capable d'abaisser l'énergie de rupture des liaisons carbone–azote ou carbone–carbone. Ces deux ruptures semblent donc également probables. Nos résultats expérimentaux montrent qu'elles ont effectivement lieu; en effet, les deux pyrrolines correspondant aux deux ruptures possibles de l'aziridine sont formées en égale

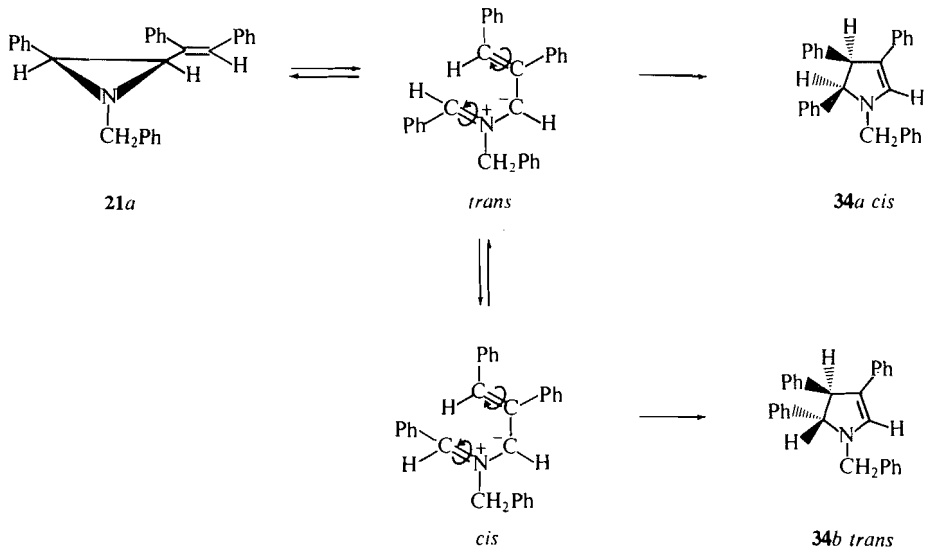

SCHÉMA 3

Can. J. Chem. Downloaded from www.nrcresearchpress.com by 210.87.254.105 on 09/05/12
For personal use only.

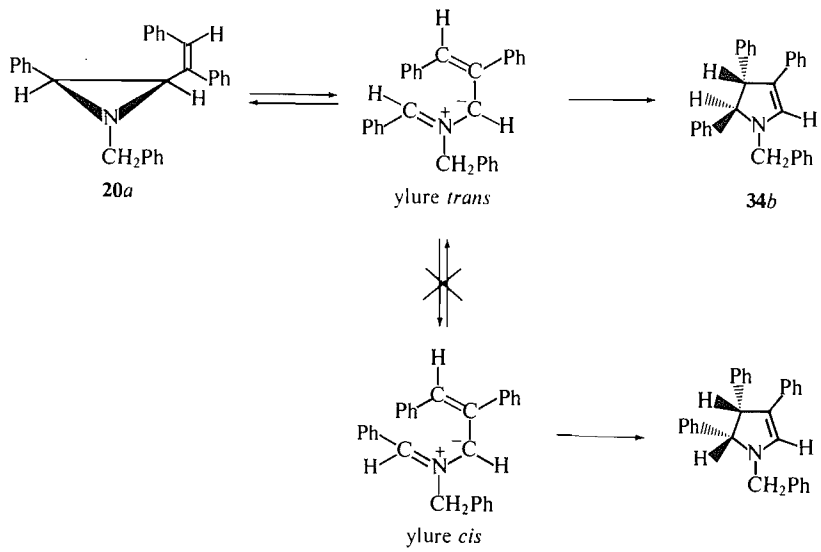

SCHÉMA 4

quantité. Il est difficile de préciser le caractère radicalaire ou ionique de ces deux réactions.

La formation du (*N*-méthylidènealkylamino)-1 cyclopropane **33** à partir de la pyrroline-2 **30** constitue un nouvel exemple de transposition sigmatropique-1,3 en série hétérocyclique (schéma 5).

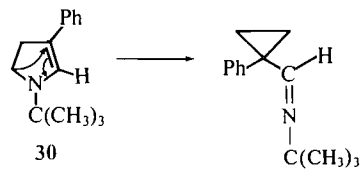

SCHÉMA 5

Formation des imines 28 et 29

Les aziridines **12** et **14***a* dont la thermolyse conduit aux imines **28** et **29** ne possèdent pas sur le carbone 3 de substituants susceptibles d'abaisser l'énergie de rupture de la liaison C—C ou C—N. Par contre, les hydrogènes du méthylène du groupe benzyle porté par l'azote peuvent donner lieu à une migration sigmatropique-1,5 (schéma 6).

L'isomérisation de l'aziridine deutériée **37** en imine deutériée **38** est en faveur d'une telle hypothèse (*cf.* tableau 1). Ce mécanisme implique une relation *cis* pour les substituants vinyle et benzyle, or nous avons indiqué que les aziridines **12** et **14***a* étaient de configuration *trans* à température ambiante (5), la formation des imines **28** et **29** impose donc une inversion de l'azote antérieure à l'isomérisation.

Ce mécanisme permet, par ailleurs, de justifier la formation de l'imine **24** dans la réaction entre le méthylènetriphénylphosphorane et la cétone **9***b* *R***R** signalée dans le mémoire précédent (réf. 5, exp. 15, tableau 1). Cette réaction aurait dû permettre d'accéder à la vinylaziridine **18** pour laquelle il est logique d'admettre par analogie avec les dérivés **17***b* et **17***b*′ un équilibre entre les deux formes *cis* et *trans* à température ambiante (schéma 7).

Une migration sigmatropique-1,5 d'hydrogène chez l'aziridine **18***b* *cis* conduit à l'imine **24**, seul produit isolé. Ce résultat indique que le produit primaire de la réaction entre le méthylènetriphénylphosphorane et la cétone **9***b* (réf. 5, exp. 15, tableau 1) est la vinylaziridine **18***b* dont une fraction au moins est de structure *cis*.

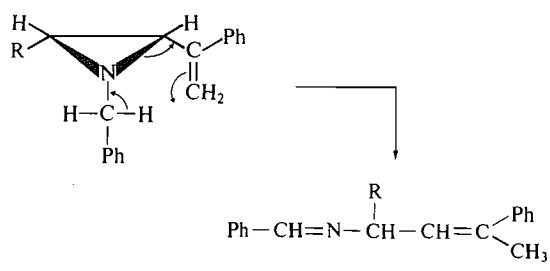

SCHÉMA 6

Can. J. Chem. Downloaded from www.nrcresearchpress.com by 210.87.254.105 on 09/05/12
For personal use only.

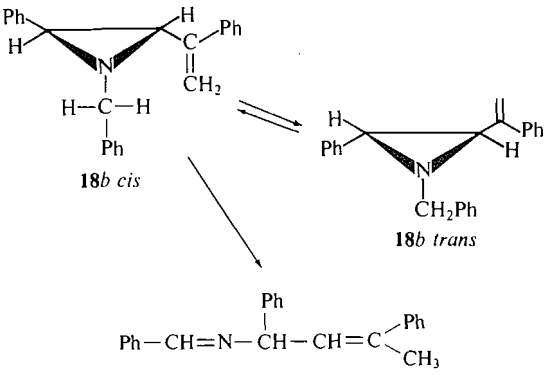

SCHÉMA 7

Obtention de l'amine diénique ***36***

La formation de l'amine diénique **36** au départ de l'aziridine ***22a*** fait vraisemblablement intervenir un processus de migration 1,5 d'hydrogène analogue à celui proposé par Rees et coll. (*1e*) (schéma 8).

Ce processus doit nécessiter une énergie d'activation inférieure à celle mise en jeu dans la réaction conduisant à la pyrroline-2 par rupture de la liaison C—C du cycle aziridine.

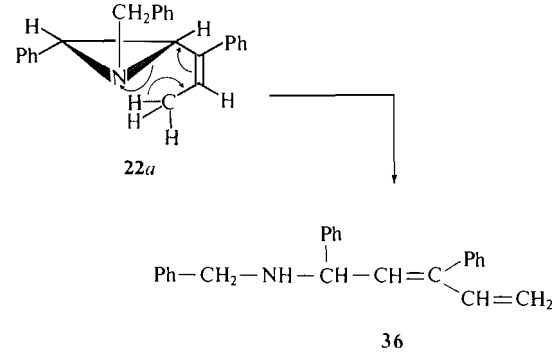

SCHÉMA 8

Conclusion

Au cours de ce travail nous avons montré que la thermolyse des vinylaziridines pouvait conduire à divers produits dont la structure dépend essentiellement des substituants portés par l'hétérocycle de départ. Selon leur nature et leur position sur le cycle aziridine ou sur la double liaison, ils orientent l'isomérisation vers la formation de pyrrolines-2, de pyrrolines-3, d'imines β,γ-éthyléniques ou d'amines diéniques. Ces résultats sont en bon accord avec ceux présentés dans la réf. 11.

Partie expérimentale

Les spectres de résonance magnétique nucléaire ont été enregistrés à l'aide d'un appareil Varian A 60 ou Varian T 60 en utilisant le tétraméthylsilane comme référence interne. Les déplacements chimiques sont exprimés en ppm et les constantes de couplage en Hz. Les spectres infrarouge ont été effectués sur un spectrophotomètre Perkin-Elmer, les spectres de masse sur un appareil Varian Mat CH5 (énergie d'ionisation 70 eV). Les chromatographies sur colonne ont été réalisées sur gel de silice (7734 – Merck).

La préparation des vinylaziridines est décrite dans le mémoire précédent (5).

Préparation de l'aziridine deutériée ***37***

La benzylamine deutériée nécessaire pour préparer ce produit est obtenue par réduction de l'amide benzoïque avec le deutérure de lithium aluminium.

Cette benzylamine deutériée réagit sur l'α,β-dibromopropiophénone selon le mode opératoire décrit précédemment (5) pour conduire à la benzyl-1 benzoyl-2 aziridine deutériée en α de l'azote.

L'action du méthylènetriphénylphosphorane sur cette cétone conduit à l'aziridine **37** dont la purification est effectuée par chromatographie sur colonne, cyclohexane – acétate d'éthyle 80:20: rmn ($CDCl_3$) 1.71 (dd, H-3), 1.89 (dd, H-3'), 2.31 (dd, H-2, $J_{2,3} = 6.5$, $J_{2,3'} = 3.5$, $J_{3,3'} = 0.5$ Hz), 5.37 (s, $=CH_2$), 7.15 à 7.70 (m, 10H C_6H_5).

Réarrangement thermique des vinyl-2 aziridines ***11***, ***12***, ***14a***, ***15a***, ***17a***, ***18a***, ***20a***, ***21a***, ***22a*** *et* ***23a***

Un échantillon de 0.2 g de vinylaziridine pure ou en solution dans du chlorobenzène est chauffé pendant un temps déterminé dans une ampoule scellée sous vide. Le produit brut est ensuite analysé et identifié à l'aide des spectres ir, de rmn et de masse.

Isomérisation de l'isopropyl-1 isopropényl-2 phényl-3 aziridine ***15a***

Chauffée à 160 °C pendant 2 h, elle se transforme, avec un rendement quantitatif, en isopropyl-1 méthyl-3 phényl-5 pyrroline-2, **25**: rmn *cf.* tableau 2.

Isomérisation de l'isopropyl-1 (phényl-1 vinyl)-2 phényl-3 aziridine ***17a***

Après chauffage à 160 °C pendant 2 h, on obtient, avec un rendement quantitatif, l'isopropyl-1 diphényl-3,5 pyrroline-2, **26**: rmn *cf.* tableau 2; ir ($CDCl_3$) 1600, 1620, 1660 cm^{-1} (C=C + C_6H_5). *Anal.* calc. pour $C_{19}H_{21}N$: C 85.60, H 9.25, N 5.12; trouvé: C 84.90, H 9.15, N 4.99.

Isomérisation de la benzyl-1 (phényl-1 vinyl)-2 phényl-3 aziridine ***18a***

Si l'on chauffe cette aziridine à 160 °C durant 2 h, on forme, avec un rendement quantitatif, la benzyl-1 diphényl-3,5 pyrroline-2, **27**: rmn *cf.* tableau 2; ir ($CDCl_3$ 1600, 1620, 1670 cm^{-1} (C=C + C_6H_5). *Anal.* calc. pour $C_{23}H_{21}N$: C 88.74, H 6.75, N 4.50; trouvé: C 85.48, H 6.42, N 5.26.

Isomérisation de la benzyl-1 (phényl-1 vinyl)-2 aziridine ***12***

Après 2 h de chauffage à 160 °C, on obtient, avec un

Can. J. Chem. Downloaded from www.nrcresearchpress.com by 210.87.254.105 on 09/05/12
For personal use only.

Can. J. Chem. Downloaded from www.nrcresearchpress.com by 210.87.254.105 on 09/05/12
For personal use only.

TABLEAU 2. Spectres de rmn ($CDCl_3$) des pyrrolines-2

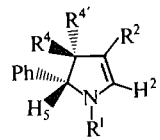

Composé	R^1	R^2	R^4	$R^{4'}$	δ R^1	δ H-2	δ R^2	δ R^4	δ $R^{4'}$	δ C_6H_5	δ H-5	$J_{2,4}$	$J_{4,5}$	$J_{4',5}$	$J_{4,4'}$	$J_{2,4'}$
25	$CH(CH_3)_2$	CH_3	H-4	H-4′	1.80 à 3.20 m 0.92 d et 1.08 d	5.72 t	1.65 s	2.50 à 3.20 m		7.10 à 7.40 m	4.25 dd	1	11.5	10		
26	$CH(CH_3)_2$	Ph	H-4	H-4′	2.30 à 3.50 m 1.10 d et 0.95 d	6.68 t	7.00 à 7.50	3.20 2dd	2.60 2dd	7.00 à 7.50	4.48 dd	1	11.8	10.8	14	
27	CH_2Ph	Ph	H-4	H-4′	3.82 AB $J=15$ 6.80 à 7.60 m	6.48 t	6.80 à 7.60	3.18 2dd	2.68 2dd	6.80 à 7.60	4.28 dd	1	12	10	14	
34*b*	CH_2Ph	Ph	Ph	H-4′	3.92 AB $J=14$ 7.00 à 8.00 m	6.85 d	7 à 8	7 à 8	4.35[a]	7 à 8	4.10[b]		9			0.5
34*a*	CH_2Ph	Ph	H-4	Ph	3.85 AB $J=13.5$ 6.95 à 7.60	6.85 d	6.95 à 7.60	4.30[a]	6.95 à 7.60		4.65[b]	<1	10			
35*a*	CH_2Ph	Ph	H-4	CH_3	3.85 AB $J=14$ 6.70 à 7.70	6.55 s	6.70 à 7.70	3.30 dq	0.68 d	6.70 à 7.70	4.40 d	<0.5	9.5		7	

[a]Partie A du spectre AB que donnent les protons H-4 (ou H-4′) et H-5.
[b]Partie B du spectre AB.

Can. J. Chem. Downloaded from www.nrcresearchpress.com by 210.87.254.105 on 09/05/12
For personal use only.

rendement quantitatif, la *N*-benzylidène(phényl-3 butène-2 yl) amine, **28**: rmn (*cf.* tableau 3).

*Isomérisation de la benzyl-1 (phényl-1 vinyl)-2 méthyl-3 aziridine **14a***

Par chauffage à 160 °C pendant 2 h, on forme, avec un rendement quantitatif, la *N*-benzylidène(méthyl-1 phényl-3 butène-2 yl) amine, **29**: rmn *cf.* tableau 3.

*Isomérisation de l'aziridine deutériée **37***

Cette aziridine, en solution dans du chlorobenzène, est chauffée pendant 2 h à 160 °C. L'analyse du spectre de rmn de la solution montre qu'elle est uniquement constituée de l'imine **38**: rmn (C_6H_5Cl) $Ph—CD=N—CH_2—CH=C<^{Ph}_{CH_2D}$ **38**, 4.32 (d, 2H, J = 6.5 Hz, $N—CH_2$), 6.05 (m, 1H, —CH=), 1.97 (s pic large, 2H, $—CH_2D$).

*Isomérisation de la tert-butyl-1 (phényl-1 vinyl)-2 aziridine **11***

Un échantillon est chauffé 2 h à 200 °C. Une rmn faite immédiatement après l'isomérisation montre que le produit brut est formé uniquement de deux produits que nous n'avons pu séparer mais que nous avons identifiés à la *tert*-butyl-1 phényl-3 pyrroline-2, **30**, et à la *tert*-butyl-1 phényl-3 pyrroline-3, **31**: rmn ($CDCl_3$) de la pyrroline-2 **30**, 1.09 (s, $C(CH_3)_3$), 6.65 (pic large, —CH=), 2.50 à 3.40 (spectre A_2B_2, $—CH_2—CH_2—$), 6.70 à 7.40 (m, C_6H_5); rmn ($CDCl_3$) de la pyrroline-3 **31**, 1.08 (s. $C(CH_3)_3$), 3.60 à 4.10 (spectre $A_2'B_2'$, $—CH_2—N—CH_2—$), 6.05 (t, J = 1 Hz, —CH=), 6.70 à 7.40 (m, C_6H_5).

Ce mélange, abandonné 20 jours à température ambiante, est alors constitué de deux nouveaux composés que nous avons séparés par chromatographie sur couche mince (benzène – acétate d'éthyle 9:1) et identifiés à l'aide de leurs spectres ir et de rmn.

tert-Butyl-1 phényl-3 pyrrole **32**: rmn ($CDCl_3$) (son spectre est analogue à celui décrit dans la littérature (9)), 7.20 à 7.60 (m, 5H), 7.12 (t, J = 2 Hz, 1H), 6.84 (t, J = 2 Hz, 1H), 6.45 (t, J = 2 Hz, 1H), 1.51 (s, 9H); ir 1600, 1700, 1725 cm^{-1} ($C=C + C_6H_5$).

(*N*-méthylidène *tert*-butylamino)-1 cyclopropane **33**: rmn ($CDCl_3$) 8.30 (s, —CH=N), 7.20 à 7.90 (m, C_6H_5), 2.30 à 3.80 (spectre $A_2'B_2'$, $—CH_2—CH_2—$), 1.30 (s, $C(CH_3)_3$); ir 1600, 1640, 1680 cm^{-1} ($C=N + C_6H_5$).

Spectre de masse d'un mélange des composés **30**, **31** et **32**: *m/e* 201 (33, $M^{+\cdot}$), 200 (7, $M^{+\cdot} - H^{\cdot}$), 199 (25, $M^{+\cdot}$), 186 (100, $M^{+\cdot} - \dot{C}H_3$), 184 (4, $M^{+\cdot} - \dot{C}H_3$), 144 (47, $M^{+\cdot} - \dot{C}(CH_3)_3$), 143 (80, $200 - \dot{C}(CH_3)_3$ et $M^{+\cdot} - (CH_3)_2C=CH_2$), 142 (4, $M^{+\cdot} - \dot{C}(CH_3)_3$), 117 (15, $144 - HCN$ et $143 - CH\equiv CH$), 116 (10, $144 - CH_2=CH_2$), 115 (25, $143 - \dot{C}H=NH$), 91 (10, $C_7H_7^+$), 84 (2, $144 - Ph—C\equiv CH$), 77 (2, $C_6H_5^+$), 51 (5, $C_4H_3^+$), 41 (33, $143 - Ph—C\equiv CH$).

*Isomérisation des benzyl-1 (phényl-1 styryl)-2 aziridines **20a** et **21a***

*Aziridine **20a***—Après 2 h de chauffage à 100 °C on obtient, avec un rendement quantitatif, un produit identifié à la pyrroline-2 *trans* **34***b*. Spectre de masse; 387 (30, $M^{+\cdot}$), 310 (6, $M^{+\cdot} - \dot{C}_6H_5$), 296 ($M^{+\cdot} - Ph—\dot{C}H_2$), 208 (30, $310 - Ph—C\equiv CH$), 194 (6, $296 - Ph—C\equiv CH$), 191 (21), 179 (21), 178 (23), 149 (20), 118 (5, $310 - Ph—CH—\underset{\diagdown\!\!/}{\underset{CH}{C}}—Ph$), 117 (3, $310 - Ph—\dot{C}H_2 -$

TABLEAU 3. Spectres de rmn ($CDCl_3$) des imines $Ph—\underset{a}{CH}=N—\underset{b}{\overset{R^3}{\overset{|}{C}}}H—\underset{c}{CH}=C<^{R^2}_{CH_3\ d}$

Composé	δH_a	δH_b	δH_c	δH_d	δR^3	δR^2	δC_6H_5	$J_{b,c}$	$J_{c,d}$	J_{H_b,R^3}
24	8.45 s	5.45 d	6.25 dq	2.20 d		7.00 à 8.00 m		9	1.2	
28	8.21 s	4.35 d	5.65 à 6.25 m	2.01 d		6.80 à 7.90 m		7.1	0.8	
29	8.28 s	4.38 dq	6.15 dq	2.02 d	1.42 d	6.80 à 7.90 m		8	0.8	6.5

Ph—C≡CH), 116 (3, 296 − Ph—CH=CH—Ph), 115 (14, 310 − Ph—CH=N—CH_2—Ph), 106 (57, 310 − 2Ph—C≡CH), 105 (54, 106 − H·), 104 (7, 296 − Ph—CH—C—Ph), 91 (100, $C_7H_7^+$), 77 (47, $C_6H_5^+$)

CH

51 (20, $C_4H_3^+$): rmn *cf.* tableau 2.

Aziridine ***21a***—Chauffée pendant 2 h à 100 °C, cette aziridine conduit, avec un rendement quantitatif, à un mélange constitué de 70% de benzyl-1 triphényl-3,4,5 pyrroline-2 *cis* **34***a* et de 30% de benzyl-1 triphényl-3,4,5 pyrroline-2 *trans* **34***b* que nous n'avons pas tenté de séparer. Spectre de masse du mélange: 387 (10, $M^{+\cdot}$), 310 (1, $M^{+\cdot} - \dot{C}_6H_5$), 296 (3, $M^{+\cdot}$ − Ph—$\dot{C}H_2$), 208 (13, 310 − Ph—C≡CH), 194 (7, 296 − Ph—C≡CH), 179 (10), 178 (11), 118 (6, 310 − Ph—CH—C—Ph),

CH

117 (5, 310 − Ph—$\dot{C}H_2$ − Ph—C≡CH), 116 (2, 296 − Ph—CH=CH—Ph), 115 (5, 310 − Ph—CH=N—CH_2—Ph), 106 (100, 310 − 2Ph—C≡CH), 105 (72, 106 − H·), 104 (6, 296 − Ph—CH—C—Ph), 91 (100, $C_7H_7^+$), 77 (80,

CH

$C_6H_5^+$), 51 (45, $C_4H_3^+$): rmn de la pyrroline-2 **34***a* *cf.* tableau 2.

Isomérisation des benzyl-1 (phényl-1 propène-1 yl)-2 phényl-3 aziridines ***23a*** *et* ***22a***

Aziridine ***23a***—Par chauffage à 150 °C pendant 2 h, ce dérivé se réarrange quantitativement en benzyl-1 diphényl-3,5 méthyl-4 pyrroline-2 **35***a* que nous avons identifiée grâce à son spectre de rmn, *cf.* tableau 2; ir ($CDCl_3$) 1600, 1640, 1670 cm^{-1} (C=C + C_6H_5).

Aziridine ***22a***—Chauffé dans les mêmes conditions que le précédent, ce composé fournit de façon quantitative la *N*-benzyl (diphényl-1,3 pentadiène-2,4 yl) amine **36** identifiée par son spectre de rmn; ir ($CDCl_3$) 3400 cm^{-1} (N—H); 1610, 1700 cm^{-1} (C=C + C_6H_5): rmn ($CDCl_3$) Ph—CH_2—NH—CH(Ph)—CH=C(Ph)—CH=CH_2 6.80 à 7.70 (m, 19H, C_6H_5 + CH= + CH_2=), 4.20 (m, 1H, N—CH), 3.70 (s, 2H, N—CH_2), 2.40 (pic large, 1H, N—H).

Remerciements

Nous remercions vivement M. le Professeur J. Chuche et M. J. C. Pommelet pour la communication de leurs résultats et les fructueuses discussions que nous avons eues ensemble.

1. (*a*) A. Mishra, S. N. Rice et W. Lwowski. J. Org. Chem. **33**, 481 (1968); (*b*) R. S. Atkinson et C. W. Rees. Chem. Commun. 1230 (1967); (*c*) L. Hoesch et A. S. Dreiding. Chimia, **26**, 629 (1972); (*d*) T. L. Gilchrist, C. W. Rees et E. Stanton. J. Chem. Soc. C, 3036 (1971); (*e*) T. L. Gilchrist, C. W. Rees et E. Stanton. J. Chem. Soc. C, 778 (1969); (*f*) R. S. Atkinson et C. W. Rees. Chem. Commun. 631 (1968); (*g*) P. G. Mente, H. W. Heine et G. R. Scharoubim. J. Org. Chem. **33**, 4547 (1968); P. G. Mente et H. W. Heine. J. Org. Chem. **21**, 3076 (1971).
2. P. Scheiner. J. Org. Chem. 2628 (1967); Tetrahedron, 2757 (1968).
3. (*a*) E. L. Stogryn et S. J. Brois. J. Org. Chem. **30**, 88 (1965); (*b*) E. L. Stogryn et S. J. Brois. J. Am. Chem. Soc. **89**, 605 (1967).
4. J. C. Pommelet et J. Chuche. Tetrahedron Lett. 3897 (1974).
5. D. Borel, Y. Gelas-Mialhe et R. Vessière, Can. J. Chem. Mémoire précédent.
6. (*a*) R. Huisgen, W. Scheer et H. Huber. J. Am. Chem. Soc. **89**, 1753 (1967); (*b*) Angew. Chem. Int. Ed. Engl. **8**, 602 (1969).
7. J. Elguero. Bull. Soc. Chim. Fr. 1925 (1971).
8. R. B. Woodward et R. Hoffmann. Angew. Chem. Int. Ed. Engl. **8**, 781 (1969).
9. A. Padwa, F. Albrecht, P. Singa et E. Vega. J. Am. Chem. Soc. **93**, 2928 (1971).
10. D. Borel, Y. Gelas-Mialhe et R. Vessière. C. R. Acad. Sci. Paris, **278**, 1393 (1974).
11. J. C. Pommelet et J. Chuche. Can. J. Chem. This issue.

Can. J. Chem. Downloaded from www.nrcresearchpress.com by 210.87.254.105 on 09/05/12
For personal use only.

Reduction of nitrobenzene with sodium and lithium naphthalenide

NORMAN L. HOLY
Department of Chemistry, Western Kentucky University, Bowling Green, KY, U.S.A. 42101

Received January 6, 1976

NORMAN L. HOLY. Can. J. Chem. **54**, 1599 (1976).

Reduction of nitrobenzene with sodium or lithium naphthalenide results in formation of azobenzene and azoxybenzene in modest yields. With sodium naphthalenide, azoxybenzene formation is favored; use of lithium naphthalenide results in enhanced azobenzene yields. Reduction of azoxybenzene with naphthalenide results in azobenzene and a variety of fragmentation products. Hydrazobenzene was the only product formed upon azobenzene formation.

NORMAN L. HOLY. Can. J. Chem. **54**, 1599 (1976).

La réduction du nitrobenzène par les naphtalures de sodium ou de lithium conduit à la formation, avec des rendements modestes, d'azobenzène et d'azoxybenzène. Avec le naphtalure de sodium, la formation de l'azoxybenzène est favorisée; l'utilisation du naphtalure de lithium conduit à des rendements plus élevés en azobenzène. La réduction de l'azoxybenzène avec les naphtalures conduit à l'azobenzène et à une variété de produits de fragmentation. La réduction de l'azobenzène conduit uniquement à la formation de l'hydrazobenzène.

[Traduit par le journal]

Introduction

Aromatic radical anions have proven to be valuable reducing agents for some functional groups (1). Sodium naphthalenide (NaN), for example, is nearly as powerful a reducing agent as metallic sodium and has the advantage, compared to the metal, of homogeneity. Reductions are rapid at room temperature or below. The principal disadvantages of this approach to reduction are: (*1*), deprotonation may occur in compounds having pK_a's of approximately 33 or lower and (*2*), separating the naphthalene and/or its derivatives from other products is, at best, often tedious. Nevertheless, alkali metal naphthalenides have been used to reduce *inter alia* sulfonate esters (2), sulfonamides (3), ethers (4), and nitrogen (5), as well as initiate 'living polymer' reactions (6). In this paper the results of nitrobenzene reduction are reported.

Discussion

Treatment of nitrobenzene in THF at −10 °C with sodium or lithium naphthalenide was followed by quenching with ice water after 2–5 min and adding a standard (phenyl ether) for glpc analysis (3% SE-30 and 5% QF-1). The results are found in Table 1. Use of sodium naphthalenide eventuates principally in the formation of azoxybenzene, whereas lithium naphthalenide leads to higher yields of azobenzene. The balance of the nitrobenzene was apparently converted to polymer as this product did not migrate on a silica gel tlc plate with 10% chloroform: 90% petroleum ether, conditions under which azobenzene had a R_f value of 0.8, azoxybenzene, 0.7.

When azoxybenzene is treated with sodium or lithium naphthalenide the product distribution again reflects a metal effect. The yield of azobenzene is appreciably higher from lithium naphthalenide than that resulting from use of the sodium salt, a trend consistent with observations noted for nitrobenzene reduction (Table 2).

Reduction with sodium naphthalenide (NaN/azoxybenzene = 4.0) eventuates in at least 18 products. With the exception of azobenzene, none of these substances was detected from among the nitrobenzene reduction products. Three of the products were isolated after separation by column chromatography followed by repeated preparative thin-layer purifications: identified were *o*-anilinoazobenzene (16%), *p*-anilinoazobenzene (7%), and 2,2′-dianilinoazobenzene (6%) by comparison with literature data.

Upon treatment of azobenzene with sodium naphthalenide the only product formed was hydrazobenzene. With 2.5 equivalents of reducing agent the yield was virtually quantitative. An assessment of the yield of this product formed upon reduction of azoxybenzene was not attempted in view of the known facile conversion

TABLE 1. Reduction of nitrobenzene with sodium and lithium naphthalenide[a]

Experiment	MN	[MN]/[$PhNO_2$]	% Azobenzene	% Azoxybenzene	[$PhNO_2$]
1	NaN	8.0	1	24	—
2	NaN	6.0	4	36	—
3	NaN	4.0	14	50	—
4	NaN	3.0	18	40	—
5	NaN	2.0	2	24	5
6	NaN	1.0	Trace	10	30
7	LiN	8.0	9	18	—
8	LiN	7.0	30	20	—
9	LiN	6.0	20	21	—
10	LiN	5.0	18	18	—
11	LiN	4.0	18	15	—
12	LiN	3.0	14	14	—
13	LiN	2.0	2	13	4
14	LiN	1.0	Trace	0.5	28

[a]Yields based on nitrobenzene.

TABLE 2. Reduction of azoxybenzene with sodium and lithium naphthalenide

Experiment	MN	[MN]/[azoxybenzene]	% Azobenzene	% Azoxybenzene
1	NaN	4.0	3	—
2	NaN	2.0	8	15
3	NaN	1.5	25	18
4	LiN	4.0	77	—
5	LiN	2.0	60	23
6	LiN	1.5	50	38

of hydrazobenzene to azobenzene in the presence of oxygen (7). Since this product has a very distinct color reaction (deep purple) to phosphomolybdic acid (in ethanol) developer, it was readily apparent that hydrazobenzene was indeed formed upon the reduction of azoxybenzene with both sodium and lithium naphthalenides, but that it was present in only trace amounts. Also, the yield of azobenzene in Table 2 actually represents the sum of the azobenzene produced directly plus that due to air oxidation of the hydrazobenzene.

While this work was in progress a paper was published by Kalyanaraman and George on the reduction of nitrobenzene with various alkali metals (8). Sodium and potassium were largely ineffective; lithium reduction resulted in azobenzene (34%), 2-anilinoazobenzene (12%), 2,2′-dianilinoazobenzene (0.5%), 2,4′-dianilinodibenzopyridazine, and polymeric azo compounds. Formation of azobenzene was proposed to proceed via the steps outlined in the following scheme.

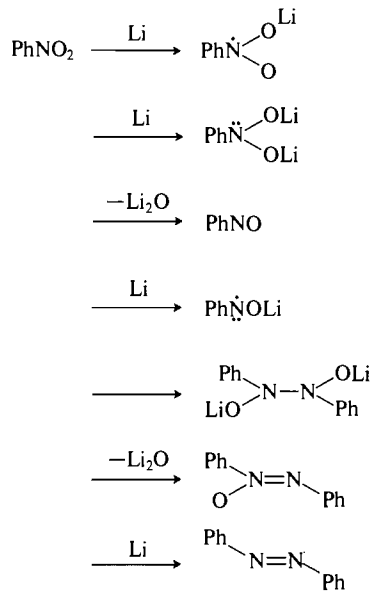

Our results are consistent with this scheme. We do observe, however, differences in product distributions. Azoxybenzene was totally absent

from their products; this was attributed to the low reduction potential of azoxybenzene (9). But in our study azoxybenzene was the major product of nitrobenzene reduction using sodium naphthalenide; its formation is explicable as a kinetic effect. Kalyanaraman and George observed that azobenzene was the sole product of the reduction of azobenzene with metallic lithium, whereas a variety of products were formed from naphthalenide reduction. Thus, naphthalenide directly cleaves the azoxy linkage without intermediate reduction to the azo structure. Cleavage of the azo linkage does not occur and the sole product formed derives from simple reduction. The enhanced yields of azobenzene resulting from use of lithium naphthalenide are consistent with a leaving group effect in which lithium oxide cleaves more readily than sodium oxide, thus directing the reduction into the azobenzene manifold.

Experimental

All melting points were taken with a Fisher-Johns melting point apparatus and are uncorrected. Infrared spectra were determined on a Perkin-Elmer Model 710 infrared spectrometer. Nuclear magnetic resonance spectra were recorded on a Varian A60A spectrometer using TMS as an internal standard. Gas–liquid phase chromatographic results were obtained on a Varian 200, using 5 ft × ¼ in. columns packed with 3% SE-30 on Varaport 30 (100/120 mesh) and 5% QF-L on Chromosorb W (60/30 mesh). Mass spectra were recorded on a Perkin-Elmer U6 at the University of Kentucky, ionizing voltage 70 eV.

Starting Materials

Tetrahydrofuran was purified by distillation under nitrogen from benzophenone sodium ketyl. Reagent grade nitrobenzene was purified by distillation. Reagent grade azobenzene and azoxybenzene were recrystallized from 95% ethanol before use. Reagent grade naphthalene was used directly. 'Baker Analyzed' sodium metal was cleaned of oxide coating before use. Lithium metal was used directly.

General Procedure for the Reduction of Nitrobenzene, Azoxybenzene, and Azobenzene with Sodium and Lithium Naphthalenide

The naphthalenides were prepared by adding finely divided portions of the metals to a 10% *M* excess of naphthalene in dry, deoxygenated THF at −10 °C under nitrogen. The mixture was stirred for 12–15 h before the total base concentration was determined by removing three 5 ml aliquotes, quenching them in 50 ml portions of water and titrating with standard hydrochloric acid to a phenophthalein endpoint. Naphthalenide concentrations were maintained at *ca.* 0.1 *M* so the optical density of the solution was sufficiently low to permit convenient measurement of volumes.

The reactions were performed by cooling 15 ml of THF containing *ca.* 1 g of nitrobenzene, azoxybenzene, or azobenzene to −10 °C with an ice–salt bath. A nitrogen atmosphere was maintained. The requisite amount of naphthalenide was then added via syringe over *ca.* 20 s. After stirring for 2 min the reactions were quenched with ice water and the p*H* adjusted to 7–8 with 3.0 *M* hydrochloric acid. For glpc samples a weighed quantity of phenyl ether was added, the water layer separated, the THF evaporated off on a rotary evaporator and the residue dissolved in ethyl ether and dried over sodium sulfate. This procedure led to less tailing than if the THF solution was used directly. Samples were analyzed on both 3% SE-30 and 5% QF-1 columns against prepared standards using knowns from commercial sources.

The products of azobenzene reduction were quenched with degassed water and analyzed by spotting a silica gel tlc plate, eluting with chloroform in a nitrogen atmosphere and comparing the results with known azobenzene and hydrazobenzene.

Reaction of Azoxybenzene with Sodium Naphthalenide

To a 200 ml THF solution of sodium naphthalenide (11 g, 86 mmol, naphthalene; 1.84 g, 80 mmol, sodium) at −10 °C was added dropwise a solution of 3.96 g (20 mmol) of azoxybenzene in 50 ml of THF over a 5 min period. After stirring for an additional 2 min, ice water was added and the p*H* adjusted to 7–8 with 3.0 *M* hydrochloric acid. Separation of the phases was followed by extraction of the aqueous layer with ethyl ether. The combined organic portions were washed with water, dried over anhydrous magnesium sulfate and evaporated to yield 16.0 g of red solid. Chromatography on a 20 × 20 cm silica gel thin layer plate with chloroform followed by spraying with phosphomolybdic acid (saturated in 95% ethanol), without heating, revealed at least 18 products.

The red solid was chromatographed on a 4.5 × 80 cm column, packed with 1200 g of Matheson, Coleman and Bell activated alumina. Elution with 10% chloroform gives: 90% petroleum ether (bp 60–90 °C) 0.98 g (18%) of crude 2-anilinoazobenzene, mp 45–52 °C. After two silica gel tlc purifications, eluting with chloroform, there was obtained 0.87 g (16%) of 2-anilinoazobenzene, mp 52–54 (lit. (8) 56 °C). Infrared (CCl_4) 3400 (NH) and 1450 (N=N); uv (95% ethanol), $_{max}$285 nm (25 000), 316 (31 000), and 450 (10 000); ms (273).

Further elution of the chromatographic column with 10% chloroform: 90% petroleum ether, followed by two preparative silica gel thin layer separations with chloroform, gave 0.38 g (7%) of 4-anilinoazobenzene, mp 80–81 °C (lit. (10) 82 °C). Infrared (CCl_4) 3400 (NH) and 1450 (N=N); ms (273).

Further elution of the chromatographic column with 20% chloroform:30% petroleum ether followed by two silica gel separations (chloroform led to 0.44 g (6%) of 2,2′-dianilinoazobenzene, mp 156–157 °C dec. (lit. (8) 158 °C). Infrared (CCl_4) 3400–3200 (NH) and 1455 cm^{-1} (N=N); uv (95% ethanol) 279 nm (32 000) and 310 (16 000); ms (364).

1. N. L. HOLY. Chem. Rev. **74**, 243 (1974).
2. J. R. GANSON, S. SCHULENBERG, and W. D. CLOSSON. Tetrahedron Lett. 4397 (1970). W. D. CLOSSON, P. WRIEDE, and S. BANK. J. Am. Chem. Soc. **88**, 1581 (1966).
3. S. JI, L. B. GORTLER, A. WARING, A. BATTISTI, S. BANK, W. D. CLOSSON, and P. WRIEDE. J. Am. Chem. Soc. **89**, 5311 (1967). W. D. CLOSSON, S. JI, and S. SCHULENBERG. J. Am. Chem. Soc. **92**, 650 (1970).
4. B. ANGELO. Bull. Chem. Soc. Fr. 1091 (1966); G. D. SARGENT. J. Am. Chem. Soc. **92**, 650 (1970).
5. E. E. VAN TAMELEN and D. A. SEELEY. J. Am. Chem. Soc. **91**, 5194 (1969). L. G. BELL and H. H. BRINTZINGER. J. Am. Chem. Soc. **92**, 4464 (1970). E. E. VAN TAMELEN, R. B. FECHTER, S. W. SCHNELLER, G. BOCHE, R. H. GREELEY, and B. AKERMARK. J. Am. Chem. Soc. **91**, 1551 (1969). E. E. VAN TAMELEN, G. BOCHE, and R. GREELEY. J. Am. Chem. Soc. **90**, 1677 (1968). G. HENRICI-OLIVE and S. OLIVE. Angew. Chem. Int. Ed. Engl. **6**, 873 (1967). E. E. VAN TAMELEN, D. SEELEY, S. SCHNELLER, H. RUDLER, and W. CRETNEY. J. Am. Chem. Soc. **92**, 5251 (1970).
6. M. SZWARC. Carbanions, living polymers, and electron transfer processes. Interscience, New York, N.Y. 1968. M. SZWARC. Science, **170**, 23 (1970); Ann., N.Y. Acad. Sci. **155**, 400 (1969); Adv. Chem. Ser. No. 91, 236 (1969); Encycl. Polym. Sci. Technol. **8**, 303 (1968); Am. Chem. Soc. Div. Petrol. Chem. Prepr., **13**(**2**), D77 (1968); **8**(**1**), 22 (1967); Pure Appl. Chem. **12**, 127 (1966).
7. J. W. B. REESOR and G. F. WRIGHT. J. Org. Chem. **22**, 375 (1957); M. V. GEORGE, D. WITTENBERG, and H. GILMAN. J. Am. Chem. Soc. **81**, 361 (1959); M. V. GEORGE, P. B. TALUKDAR, and H. GILMAN. J. Organomet. Chem. **5**, 397 (1966); S. S. DUA and M. V. GEORGE. J. Organomet. Chem. **9**, 413 (1967); **10**, 219 (1967).
8. V. KALYANARAMAN and M. V. GEORGE. J. Org. Chem. **38**, 507 (1973).
9. P. E. IVERSON and H. LUND. Tetrahedron Lett. 4027 (1967).
10. G. M. BADGER, R. G. BUTTERY, and G. E. LEWIS. J. Chem. Soc. 1888 (1954).

Pouvoirs donneur et accepteur des ligands dans les dérivés de $Mo(CO)_6$

CLAUDE BARBEAU ET JACQUES TURCOTTE

Département de Chimie, Université Laval, Québec, Québec G1K 7P4

Reçu le 30 septembre 1975

CLAUDE BARBEAU et JACQUES TURCOTTE. Can. J. Chem. **54**, 1603 (1976).

Un modèle de distribution électronique dans les dérivés de $Mo(CO)_6$ a été élaboré à partir de certaines corrélations entre fréquences d'extension CO. L'utilisation des données spectroscopiques des composés $Mo(CO)_{6-n}L_n$ a permis d'établir une échelle des pouvoirs relatifs donneur et accepteur de plus de 50 ligands.

CLAUDE BARBEAU and JACQUES TURCOTTE. Can. J. Chem. **54**, 1603 (1976).

A model of electron distributions in some $Mo(CO)_6$ derivatives has been constructed from certain correlations among the CO stretching frequencies. The use of spectroscopic data for the compounds $Mo(CO)_{6-n}L_n$ permitted establishing a scale of the relative donor and acceptor powers of more than 50 ligands.

[Journal translation]

Introduction

En vue d'établir une échelle du pouvoir donneur net des ligands présents dans les métaux carbonyle et afin de mettre en évidence certains indices expérimentaux pouvant permettre d'expliquer la stabilité et la facilité de substitution des métaux carbonyle substitués, nous avons étudié les caractéristiques des dérivés de $Mo(CO)_6$ tant du point de vue des fréquences de vibration d'extension CO que de celui des moments dipolaires.

Dans ce premier article nous nous limiterons à démontrer de façon empirique, qu'il est possible d'utiliser un modèle de distribution basé sur les fréquences de vibration CO pour constituer une échelle relative du pouvoir donneur net des ligands et pour caractériser les atomes donneurs selon la répartition des charges dans les groupements CO de symétrie *cis* et *trans*.

Modèle de distribution électronique

A l'aide de données spectroscopiques, Bigorgne (1) a établi les fondements du modèle de distribution électronique dans les dérivés des métaux carbonyle. La principale caractéristique du modèle réside dans la variation du pouvoir donneur net d'un ligand selon le nombre et la qualité des autres ligands coordinés au métal. Ainsi la substitution d'un ou plusieurs CO de $Mo(CO)_6$ par un ligand L, dont le pouvoir donneur net est supérieur à celui de CO, entraîne les charges supplémentaires suivantes pour les différents degrés de substitution: $Mo(CO)_5L$, $(5/5)\delta$; $Mo(CO)_4L_2$, $2 \times (4/5)\delta$; $Mo(CO)_3L_3$, $3 \times (3/5)\delta$; $Mo(CO)_2L_4$, $4 \times (2/5)\delta$; où δ représente le pouvoir donneur net du ligand dans un système hexacoordiné contenant cinq CO. Lors de la substitution d'un groupement CO par L le métal central conserve la même charge que dans $Mo(CO)_6$. Les potentiels énergétiques des ligands L et CO doivent donc varier dans des directions opposées afin de maintenir la même charge sur Mo.

Du modèle proposé par Bigorgne (1) découlent deux relations applicables aux groupements CO: (*I*) La variation de potentiel d'un CO moyen selon le degré de substitution suit une relation linéaire. (*II*) La somme des potentiels des CO varie selon les rapports 1:1.6:1.8:1.6:1 en passant de $M(CO)_6$ à $M(CO)_{6-n}L_n$ ($n = 1$ à 5).

Tout changement dans le potentiel énergétique de CO devrait se manifester au niveau de la liaison CO. Moins rigoureuses que les constantes de force de liaison, les fréquences d'extension CO sont néanmoins de fidèles témoins des variations électroniques au voisinage du métal et elles devraient vérifier les deux relations précédentes.

Le tableau 1 contient tous les composés de $Mo(CO)_{6-n}L_n$ dont les fréquences d'extension CO de $Mo(CO)_5L$ et $Mo(CO)_4L_2$ *cis* ont été mesurées en solution. Parce que seulement un très petit nombre de composés $Mo(CO)_4L_2$ *trans* sont connus, seuls les composés où le ligand est en position *trans* à un groupement CO ont été retenus pour cette étude.

Can. J. Chem. Downloaded from www.nrcresearchpress.com by 210.87.254.6 on 09/05/12
For personal use only.

Can. J. Chem. Downloaded from www.nrcresearchpress.com by 210.87.254.6 on 09/05/12
For personal use only.

TABLEAU 1. Calculs et sommes des écarts entre les fréquences d'extension CO de $Mo(CO)_6$* et de $Mo(CO)_{6-n}L_n$†

Numéro	Composé	ν_{CO}§ (cm^{-1}) $A_1^{(2)}$	$A_1^{(1)}$	B_1	B_2	E	ν_m (cm^{-1}) $CO^{(1)}$	$CO^{(2)}$	$\Delta\nu_m$ (cm^{-1}) $CO^{(1)}$	$CO^{(2)}$	$\sum$ ($\pm 2\ cm^{-1}$)	π	Réference
1	$Mo(CO)_5As(OMe)_3$	2088	1975	2006		1968	1975	2007	11	12	59	0.9	3
	$Mo(CO)_4[As(OMe)_3]_2$	2054	1957	1950	1944		1954	1999	32	20	104	1.6	3
	$Mo(CO)_3[As(OMe)_3]_3$		2001			1928	1952		34		102		3
2	$Mo(CO)_5CN\phi$	2075	1964	2001‡		1964	1964	2001	22	18	94	1.2	4
	$Mo(CO)_4[CN\phi]_2$	2015	1954	1942	1942		1949	1979	38	40	156	1.0	4
	$Mo(CO)_3[CN\phi]_3$		1953			1923	1933		53		159		4
3	$Mo(CO)_5P(SMe)_3$	2078	1963	1999‡		1960	1963	1999	23	20	103	1.2	5
	$Mo(CO)_4[P(SMe)_3]_2$	2035	1951	1937	1929		1944	1982	42	37	158	1.1	5
4	$Mo(CO)_5P(OMe)_3$	2081	1968	1995		1953	1968	1996	18	23	110	0.8	6–10
	$Mo(CO)_4[P(OMe)_3]_2$	2037	1946	1924	1924		1935	1981	51	38	178	1.3	6–8, 11
	$Mo(CO)_3[P(OMe)_3]_3$		1977			1889	1918		68		204		6–10
5	$Mo(CO)_5P(OMe)_2Me$	2078	1967	1998		1953	1967	1996	19	23	111	0.8	12
	$Mo(CO)_4[P(OMe)_2Me]_2$	2031	1940	1940	1921		1940	1976	46	43	178	1.1	12
	$Mo(CO)_3[P(OMe)_2Me]_3$		1970			1891	1917		69		207		12
6	$Mo(CO)_5CNMe$	2071	1960	1997‡		1960	1960	1997	26	22	114	1.2	6, 13
	$Mo(CO)_4[CNMe]_2$	2022	1943	1931	1923		1933	1977	53	42	190	1.3	6, 13
	$Mo(CO)_3[CNMe]_3$		1954			1896	1915		71		213		6, 13
7	$Mo(CO)_5CN$*t*-Bu	2071	1962	1988		1962‖	1962	1966	24	23	116	1.0	14
	$Mo(CO)_4[CN$*t*-Bu$]_2$	2020	1943	1933	1922		1938	1971	48	48	192	1.0	14
	$Mo(CO)_3[CN$*t*-Bu$]_3$		1946			1860	1888		98		294		14
8	$Mo(CO)_5CNEt$	2069	1958	1995‡		1958	1958	1995	28	24	124	1.2	13
	$Mo(CO)_4[CNEt]_2$	2018	1941	1921	1930		1931	1974	55	45	200	1.2	13
	$Mo(CO)_3[CNEt]_3$		1952			1895	1914		72		216		13
9	$Mo(CO)_5PH_3$	2081	1962	1994‡		1950	1962	1994	24	25	124	1.0	15
	$Mo(CO)_4[PH_3]_2$	2040	1946	1925	1897		1935	1968	51	51	204	1.0	15
	$Mo(CO)_3[PH_3]_3$		1971			1892	1918		68		204		16
10	$Mo(CO)_5As(NMe_2)_3$	2082	1960	1994‡		1951	1960	1994	26	24	122	1.1	17
	$Mo(CO)_4[As(NMe_2)_3]_2$	2030	1938	1922	1907		1930	1968	56	51	214	1.1	17
11	$Mo(CO)_5Sb\phi_3$	2074	1955	1989		1955	1955	1993	31	26	135	1.2	9, 18
	$Mo(CO)_4[Sb\phi_3]_2$	2024	1933	1920	1904		1927	1964	59	55	228	1.1	18–20
	$Mo(CO)_3[Sb\phi_3]_3$		1955			1875	1902		84		252		21
12	$Mo(CO)_5As\phi_3$	2076	1952	1989		1945	1952	1989	34	30	154	1.1	9
	$Mo(CO)_4[As\phi_3]_2$	2023	1927	1913	1894		1920	1959	66	60	252	1.1	19, 20, 22
	$Mo(CO)_3[As\phi_3]_3$		1941			1852	1882		104		312		23

Can. J. Chem. Downloaded from www.nrcresearchpress.com by 210.87.254.6 on 09/05/12
For personal use only.

TABLEAU 1 (*Suite*)

Numéro	Composé	ν_{CO}§ (cm^{-1})					ν_m (cm^{-1})		$\Delta\nu_m$ (cm^{-1})		Σ ($\pm 2\ cm^{-1}$)	π	Réference
		$A_1^{(2)}$	$A_1^{(1)}$	B_1	B_2	E	$CO^{(1)}$	$CO^{(2)}$	$CO^{(1)}$	$CO^{(2)}$			
13	$Mo(CO)_5P\phi_3$	2075	1949	1988		1949	1949	1990	37	29	153	1.3	7–9
	$Mo(CO)_4[P\phi_3]_2$	2022	1926	1906	1902		1916	1962	70	57	254	1.2	6–8, 20
	$Mo(CO)_3[P\phi_3]_3$		1949			1850	1883		103		309		11
14	$Mo(CO)_5P\phi_2NPr_2$	2073	1946	1986		1946	1946	1988	40	31	164	1.3	24
	$Mo(CO)_4[P\phi_2NPr_2]_2$	2024	1926	1905	1897		1915	1960	71	59	260	1.2	24
15	$Mo(CO)_5P\phi_2NEt_2$	2073	1947	1987		1947	1947	1989	39	30	159	1.3	24
	$Mo(CO)_4[P\phi_2NEt_2]_2$	2024	1922	1911	1889		1916	1956	70	63	266	1.1	24
16	$Mo(CO)_5SbEt_3$	2069	1943	1986		1947	1943	1986	43	33	175	1.3	18, 25
	$Mo(CO)_4[SbEt_3]_2$	2017	1923	1897	1911		1910	1964	76	55	262	1.3	11, 18
	$Mo(CO)_3[SbEt_3]_3$		1944			1859	1888		98		294		18
17	$Mo(CO)_5P(NMe_2)_3$	2073	1949	1986‡		1942	1949	1986	37	33	169	1.1	17
	$Mo(CO)_4[P(NMe_2)_3]_2$	2022	1917	1903	1900		1910	1961	76	58	268	1.3	17
18	$Mo(CO)_5P\phi_2Bu$	2073	1952	1985		1944	1952	1987	34	32	162	1.1	26
	$Mo(CO)_4[P\phi_2Bu]_2$	2021	1924	1904	1892		1914	1956	72	63	270	1.1	27
19	$Mo(CO)_5PMe_3$	2071	1952	1986‡		1943	1952	1986	34	33	166	1.0	7–9
	$Mo(CO)_4[PMe_3]_2$	2016	1923	1902	1899		1912	1957	74	62	272	1.2	7–9
	$Mo(CO)_3[PMe_3]_3$		1943			1856	1885		101		303		7–10
20	$Mo(CO)_5P(p\text{-tolyl})_3$	2075	1955	1985		1940	1955	1985	31	34	167	0.9	28
	$Mo(CO)_4[P(p\text{-tolyl})_3]_2$	2025	1930	1910	1870		1920	1948	66	71	274	0.9	28
21	$Mo(CO)_5P\phi_2NBu_2$	2073	1947	1988		1947	1947	1988	39	30	163	1.3	24
	$Mo(CO)_4[P\phi_2NBu_2]_2$	2025	1927	1904	1880		1915	1952	71	67	276	1.1	24
22	$Mo(CO)_5As\phi_2CH_2As\phi_2$	2075	1945	1990		1945	1945	1989	41	30	161	1.3	30
	$Mo(CO)_4[As\phi_2CH_2As\phi_2]_2$	2025	1920	1910	1875		1915	1950	71	69	280	1.0	30
	$Mo(CO)_3[As\phi_2CH_2As\phi_2]_3$		1945			1840	1875		111		333		30
23	$Mo(CO)_5P\phi Bu_2$	2072	1949	1982		1942	1949	1985	38	34	176	1.1	26
	$Mo(CO)_4[P\phi Bu_2]_2$	2016	1917	1902	1888		1910	1952	76	67	286	1.1	27
24	$Mo(CO)_5PEt_3$	2069	1945	1980		1944	1945	1984	41	35	181	1.2	7, 8, 10
	$Mo(CO)_4[PEt_3]_2$	2016	1916	1895	1896		1906	1956	80	63	286	1.3	7, 8, 10
	$Mo(CO)_3[PEt_3]_3$		1938			1841	1873		113		339		7, 8, 10
25	$Mo(CO)_5AsEt_3$	2070	1945	1983		1943	1945	1985	41	34	177	1.2	3, 22
	$Mo(CO)_4[AsEt_3]_2$	2015	1915	1904	1886		1910	1951	76	68	288	1.1	3, 22
	$Mo(CO)_3[AsEt_3]_3$		1938			1843	1875		111		333		3, 22

Can. J. Chem. Downloaded from www.nrcresearchpress.com by 210.87.254.6 on 09/05/12
For personal use only.

TABLEAU 1 (*Suite et fin*)

Numéro	Composé	ν_{CO}§ (cm^{-1}) $A_1^{(2)}$	$A_1^{(1)}$	B_1	B_2	E	ν_m (cm^{-1}) $CO^{(1)}$	$CO^{(2)}$	$\Delta\nu_m$ (cm^{-1}) $CO^{(1)}$	$CO^{(2)}$	Σ (± 2 cm^{-1})	π	Réference
26	$Mo(CO)_5PBu_3$	2070	1943	1982‡		1938	1943	1982	43	37	191	1.2	26
	$Mo(CO)_4[PBu_3]_2$	2015	1913	1899	1886		1906	1950	80	69	298	1.2	27
27	$Mo(CO)_5P(m\text{-tolyl})_3$	2070	1950	1983		1940	1950	1983	36	36	180	1.0	28
	$Mo(CO)_4[P(m\text{-tolyl})_3]_2$	2020	1920	1900	1865		1910	1943	76	76	304	1.0	28
28	$Mo(CO)_5P\phi Me_2$	2068	1940	1982		1940	1940	1983	46	36	190	1.3	30
	$Mo(CO)_4[P\phi Me_2]_2$	2011	1912	1895	1878		1903	1945	83	74	314	1.1	30
	$Mo(CO)_3[P\phi Me_2]_3$		1939			1832	1868		118		354		30
29	$Mo(CO)_5NCCH_3$	2085	1931	1994‡		1948	1931	1994	55	25	155	2.2	6
	$Mo(CO)_4[NCCH_3]_2$	2023	1881	1833	1912		1857	1967	129	52	362	2.5	31
	$Mo(CO)_3[NCCH_3]_3$		1915			1783	1827		159		477		6, 31
30	$Mo(CO)_5NC_5H_5$	2074	1922	1987‡		1943	1922	1987	64	32	192	2.0	9
	$Mo(CO)_4[NC_5H_5]_2$	2025	1881	1839	1907		1860	1966	126	53	358	2.3	20, 32
	$Mo(CO)_3[NC_5H_5]_3$		1908			1777	1821		165		495		33
31	$Mo(CO)_5NOC_4H_8$	2074	1915	1988‡		1943	1915	1987	71	32	199	2.2	34
	$Mo(CO)_4[NOC_4H_8]_2$	2009	1870	1817	1890		1844	1950	142	69	422	2.1	34
	$Mo(CO)_3[NOC_4H_8]_3$		1870			1740	1783		203		609		34
32	$Mo(CO)_5NC_4H_9$	2072	1910	1982		1940	1910	1983	76	36	220	2.1	34
	$Mo(CO)_4[NC_4H_9]_2$	2010	1815	1888	1870		1852	1940	134	79	428	1.7	34
33	$Mo(CO)_5P(OEt)_3$	2080	1966	1995		1952	1966	1995	20	24	116	0.8	9
	$Mo(CO)_3[P(OEt)_3]_3$		1971			1889	1916		70		210		7, 8
34	$Mo(CO)_5P(O\phi)_3$	2084	1974	2000		1965	1974	2004	12	15	72	0.8	7–9
	$Mo(CO)_3[P(O\phi)_3]_3$		1994			1922	1946		40		120		7, 8
35	$Mo(CO)_5PCl_3$	2095	2000	2022‡		1986	2000	2022	−14	−3	−26		7, 8
	$Mo(CO)_4[PCl_3]_2$	2072	2003	1993	1985		1998	2028	−12	−9	−42		7, 8
	$Mo(CO)_3[PCl_3]_3$		2040			1990	2009		−23		−69		7, 8, 10
36	$Mo(CO)_5PF_3$	2103	2011	2026		1989	2011	2027	−25	−8	−57		6, 35
	$Mo(CO)_4[PF_3]_2$	2086	2013	2010	1989		2011	2037	−25	−18	−86		6, 35
	$Mo(CO)_3[PF_3]_3$		2064			2011	2029		−43		−126		6, 7, 35

*$Mo(CO)_6$: A_{1g}(2116.7), E(2018.8), T_{1u}(1986.1). (2).

†$CO^{(1)}$ = CO *trans* à L; $CO^{(2)}$ = CO *cis* à L; ν_m = fréquence moyenne calculée selon: $\nu_m CO^{(1)}[Mo(CO)_5L] = A_1^{(1)}$, $[Mo(CO)_4L_2] = (A_1^{(1)} + B_1)/2$, $[Mo(CO)_3L_3] = (2E + A_1^{(1)})/3$, $Mo(CO)_6 = T_{1u} = 1986$ cm^{-1}; $\nu_m CO^{(2)}$ $[Mo(CO)_5L] = (2E + B_1 + A_1^{(2)})/4$, $[Mo(CO)_4L_2] = (B_2 + A_1^{(2)})/2$, $Mo(CO)_6 = (3T_{1u} + 2E + A_{1g})/6 = 2019$ cm^{-1}. $\Delta\nu_m$ = écart entre la fréquence moyenne de Mo(CO) et celle d'un dérivé substitué. Σ = somme des $\Delta\nu_m$; $Mo(CO)_5L$, $\Sigma_1 = 4\Delta\nu_m CO^{(2)} + 1\Delta\nu_m CO^{(1)}$; $Mo(CO)_4L_2$, $\Sigma_2 = 2\Delta\nu_m CO^{(2)} + 2\Delta\nu_m CO^{(1)}$; $Mo(CO)_3L_3$, $\Sigma_3 = 3\Delta\nu_m CO^{(1)}$. $\pi = \Delta\nu_m CO^{(1)}/\Delta\nu_m CO^{(2)}$.

‡Fréquence calculée d'après la relation $B_1 = (A_1^{(2)} + 2E)/3$.

§Les fréquences ont été observées en solution et correspondent à des valeurs moyennes tirées de la littérature.

||Nouvelle attribution compte tenue des composés **6** et **8**.

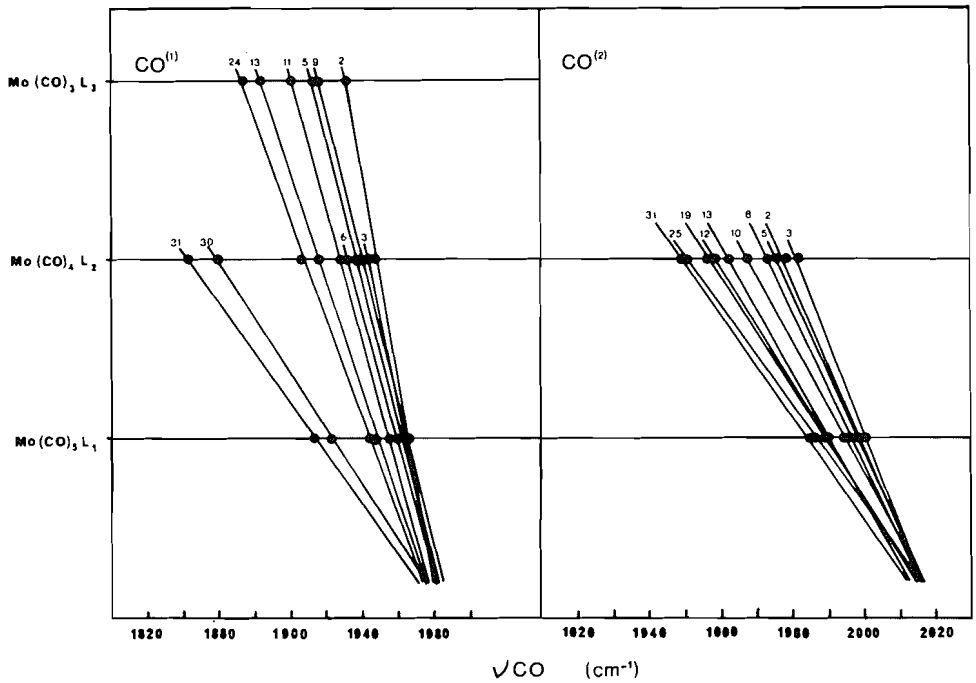

FIG. 1. Convergence des fréquences d'extension CO *cis* et CO *trans* des dérivés $Mo(CO)_{6-n}L_n$.

Pour vérifier la relation (*I*) à l'aide des fréquences d'extension CO, il convient, en premier, de distinguer les CO en position *trans* des ligands de ceux en position *cis*. Dans la partie gauche de la fig. 1 on constate que la fréquence moyenne des CO *trans*, $CO^{(1)}$, varie linéairement selon le degré de substitution et converge vers la fréquence 1985 cm^{-1}, voisine de celle du mode T_{1u} de $Mo(CO)_6$ (1986 cm^{-1}). La partie droite de la fig. 1 présente un faisceau de droites constituées par les fréquences moyennes des CO *cis*, $CO^{(2)}$, qui converge vers 2020 cm^{-1}, fréquence proche de celle du mode E_g de $Mo(CO)_6$ (2019 cm^{-1}). La relation (*I*) étant donc bien suivie par les fréquences CO on peut associer fréquence d'extension CO et potentiel énergétique CO. Les deux valeurs extrapolées de la fig. 1 nous permettent de plus de relier les fréquences des CO *cis* et *trans* de $Mo(CO)_{6-n}L_n$ à des fréquences particulières de $Mo(CO)_6$.

La relation (*II*) est partiellement vérifiée en se servant des fréquences d'extension CO. En effet, la fig. 2 montre que la somme des écarts entre les fréquences d'extension CO de $Mo(CO)_6$ à $Mo(CO)_4L_2$ est souvent 1.6 fois plus élevée que celle entre les fréquences CO de $Mo(CO)_6$ à $Mo(CO)_5L$. La fig. 3 montre d'autre part que beaucoup de composés obéissent au rapport attendu de 1.8 entre la somme des écarts de fréquence CO de $Mo(CO)_6$ à $Mo(CO)_3L_3$ et la somme des écarts de fréquence CO de $Mo(CO)_6$ à $Mo(CO)_5L$.

Il apparaît donc que toute charge nette transférée par le métal aux groupements CO, lors du remplacement d'un CO par un ligand L, est proportionnelle à la somme des écarts de fréquence d'extension CO représentée par $\sum$.

Une étude attentive du tableau 1 et des figs 2 et 3 montre que tous les composés obéissant à la relation (*II*) présentent un rapport $\pi = (\Delta CO^{(1)}/\Delta CO^{(2)})$ voisin de 1.0, valeur théorique attendue lorsque chaque CO reçoit la même fraction de la charge nette apportée par le ligand. Par contre les composés qui s'éloignent le plus des droites de pente 1.6 et 1.8 sont ceux dont la valeur π est de beaucoup supérieure à 1.0. Afin de tenir compte d'une répartition variable dans les CO *cis* et *trans*, nous avons modifié le modèle original de Bigorgne en y introduisant le facteur π.

Modèle modifié

La charge nette résultant d'une substitution et représentée par $\sum$ est répartie selon le facteur

Can. J. Chem. Downloaded from www.nrcresearchpress.com by 210.87.254.6 on 09/05/12
For personal use only.

Can. J. Chem. Downloaded from www.nrcresearchpress.com by 210.87.254.6 on 09/05/12
For personal use only.

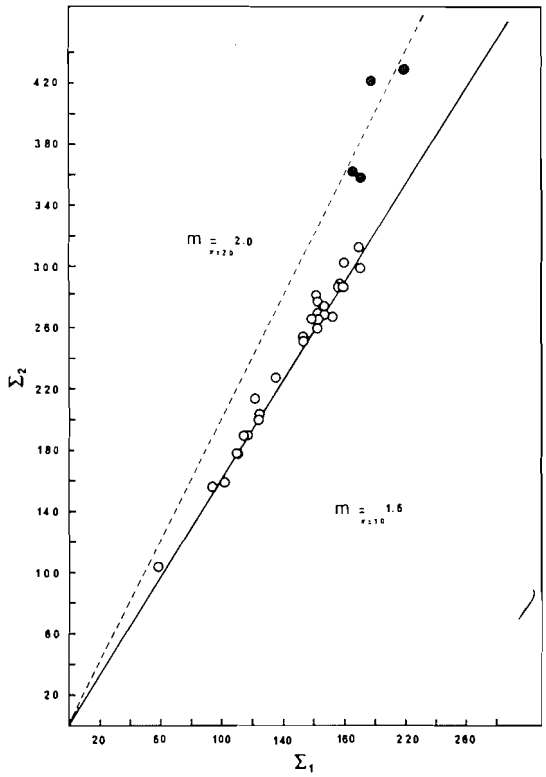

FIG. 2. Relation entre la somme des écarts de fréquence CO des dérivés bisubstitués ($\sum_2$) et la somme des écarts de fréquence CO des dérivés monosubstitués ($\sum_1$).

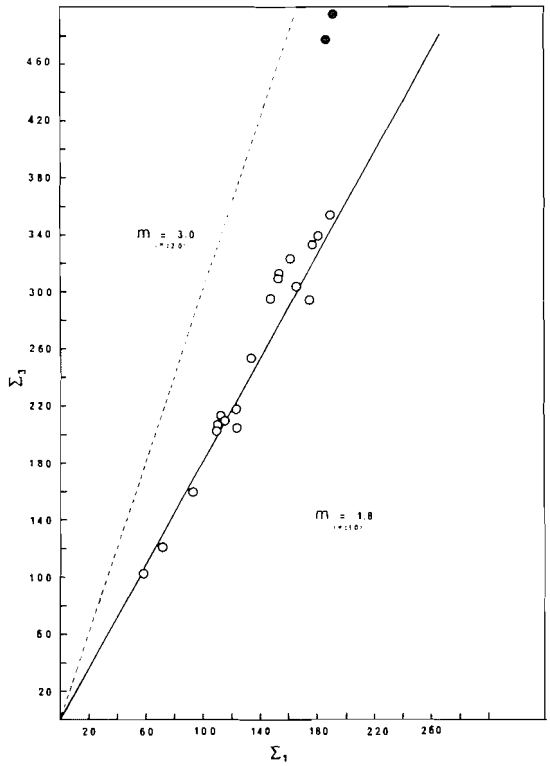

FIG. 3. Relation entre la somme des écarts de fréquence CO des dérivés trisubstitués ($\sum_3$) et la somme des écarts de fréquence CO des dérivés monosubstitués ($\sum_1$).

π entre $CO^{(1)}$ et $CO^{(2)}$. $\sum$ et π sont obtenus en considérant les écarts de fréquence d'extension CO en passant de $Mo(CO)_6$ à $Mo(CO)_{6-n}L_n$. Pour chaque composé $Mo(CO)_{6-n}L_n$ *cis* la charge nette et le facteur de répartition sont les suivants:

$$Mo(CO)_5L \quad \sum_1 = \sum_1^1 + 4\sum_1^2$$
$$\pi = \sum_1^1/\sum_1^2$$
$$Mo(CO)_4L_2 \quad \sum_2 = 2(\sum_2^1 + \sum_2^2)$$
$$\pi = \sum_2^1/\sum_2^2$$
$$Mo(CO)_3L_3 \quad \sum_3 = 3\sum_3^1$$

A l'aide de cette répartition et de la relation (*1*) on tire les relations suivantes:

[1] $$\sum_2^1 = 2\sum_1^1$$

[2] $$\sum_2^2 = 2\sum_1^2$$

[3] $$\sum_3 = 3\sum_1^1$$

[4] $$\sum_2 = 4\sum_1\left(\frac{\pi + 1}{\pi + 4}\right)$$

[5] $$\sum_3 = 9\sum_1\left(\frac{\pi}{\pi + 4}\right)$$

Calculs et discussion

Le tableau 2 démontre clairement que les données spectroscopiques peuvent être utilisées telles quelles pour décrire adéquatement la distribution des charges dans un dérivé de

TABLEAU 2. Vérification des relations du modèle modifié

Relation	Valeur		Nombre de composés
	Théorique	Expérimentale	
1	2	2.0±0.3	32
2	2	2.0±0.2	32
3	3	2.9±0.5	20
4	4	4.0±0.2	32
5	9	8.6±1.2	20

Can. J. Chem. Downloaded from www.nrcresearchpress.com by 210.87.254.6 on 09/05/12
For personal use only.

$Mo(CO)_6$. L'excellent accord entre les valeurs numériques théoriques et expérimentales, pour les composés mono- et bisubstitués (relations [1], [2], [4]), indique que le remplacement de deux CO s'effectue d'une façon similaire au remplacement d'un CO. Compte tenu du plus petit nombre de composés trisubstitués et de l'imprécision sur la valeur $\sum_3$ (largeur de la bande *E*), les valeurs numériques expérimentales des relations [3] et [5] confirment également le rôle distinct des $CO^{(1)}$ et des $CO^{(2)}$ dans la répartition des charges.

Du tableau 1 et des figs 2 et 3 on peut tirer plusieurs observations en utilisant le modèle modifié.

(*1*) La valeur π, dans la plupart des cas, est semblable pour les composés mono- et bisubstitués. Lorsqu'elle varie, on constate très souvent une imprécision dans les fréquences mesurées causée par un chevauchement des bandes d'absorption (**2**, **4**, **5**, **14**, **15**, **21**, **22**, **24**, **28**).

(*2*) Des 32 composés étudiés, seulement 5 (**1**, **4**, **16**, **22**, **30**) présentent une valeur numérique éloignée de 0.3 de la valeur moyenne de 2.0 obtenue pour la relation [2] et 6 composés (**1**, **2**, **4**, **5**, **22**, **29**) s'éloignent de plus de 0.3 de la valeur moyenne de 2.0 associée à la relation [1]. Parmi les 20 composés impliqués par la relation [3], on trouve 14 composés présentant une valeur numérique comprise entre 2.6 et 3.0 tandis que 5 composés (**2**, **4**, **5**, **7**, **16**) montrent une valeur numérique éloignée de plus de 0.6 de la valeur attendue de 3.0.

Il apparait donc que l'on doive accorder plus de confiance aux écarts des $CO^{(2)}$ qu'aux écarts des $CO^{(1)}$ et qu'un certain effet de nivellement se manifeste dans le trisubstitué où les charges reçues par les CO sont souvent moindres que celles calculées selon le modèle.

(*3*) Plus de la moitié des composés monosubstitués possèdent une fréquence de mode $A_1^{(1)}$ mesurée qui est semblable à ± 2 cm^{-1} près de la valeur obtenue selon l'expression $(A_1^{(2)} + 2E)/3$. On peut donc se servir de cette valeur "calculée" pour obtenir l'écart des $CO^{(2)}$ ou pour vérifier les attributions des bandes d'absorption CO du monosubstitué.

(*4*) Les composés dont le ligand contient un groupe OR ou Oϕ (**1**, **3**, **4**, **5**, **33**, **34**) se distinguent par une valeur $\pi < 1.0$, des sommes $\sum$ faibles et un rapport $\sum_3{}^1/\sum_1{}^1$ supérieur à 3.0.

(*5*) Bien qu'il n'existe que très peu de composés où les écarts de fréquence CO soient négatifs (**35**, **36**), on constate que le modèle de distribution peut s'appliquer, de façon approchée, pour les ligands dont le pouvoir donneur net est inférieur à celui de CO.

Echelle des ligands

En utilisant les données du tableau 1 et en tenant compte des désaccords entre valeurs numériques calculées et observées, il est possible de dégager, pour chaque ligand, une somme σ_0 qui représente la valeur moyenne évaluée de l'écart de fréquence CO entre $Mo(CO)_6$ et $Mo(CO)_5L$. σ_0 établit le pouvoir donneur net d'un ligand relatif à CO dans un complexe du type $Mo(CO)_{6-n}L_n$. Dans la plupart des cas σ_0 correspond à $\sum_1$. Cependant, lorsque une ou plusieurs des relations [1] à [5] ne sont pas suivies, la valeur σ_0 sera déduite des données considérées les plus sûres.

Dans le tableau 3 on trouve, outre les ligands des 36 composés du tableau 1, plusieurs autres ligands dont les fréquences CO de leur composé monosubstitué $Mo(CO)_5L$ ont été mesurées en solution. La valeur π_0 représente, soit la moyenne des valeurs π, soit le rapport $\Delta CO^{(1)}/\Delta CO^{(2)}$ jugé le plus sûr.

En comparant toute les données du tableau 3 on peut dégager les observations suivantes:

(*1*) Le pouvoir donneur net des ligands symétriques décroit selon un ordre qui confirme l'importance des effets inductifs. En effet, plus le pouvoir donneur intrinsèque du ligand est élevé, plus grande sera la charge négative distribuée sur les CO.

(*2*) Le facteur π_0 est peu sensible aux groupements attachés à un même atome donneur. Si la répartition entre $CO^{(1)}$ et $CO^{(2)}$ est une indication d'un effet mésomère, on doit conclure que les groupements ont peu d'effet sur le pouvoir accepteur intrinsèque de l'atome principal.

Ces deux constations sont semblables à celles faites sur des dérivés de $Ni(CO)_4$ (40).

(*3*) On observe un rehaussement du pouvoir donneur net parmi les ligands non-symétriques contenant un groupement ϕ.

(*4*) Le facteur π_0 moyen des donneurs P est très voisin de l'unité (1.1). Puisqu'un $CO^{(2)}$ reçoit approximativement la même charge qu'un $CO^{(1)}$, on pourrait conclure que le pouvoir

Can. J. Chem. Downloaded from www.nrcresearchpress.com by 210.87.254.6 on 09/05/12
For personal use only.

TABLEAU 3. Pouvoir donneur net et caractère accepteur des ligands

Numéro	Ligand	σ_0 (± 2 cm^{-1})†	π_0‡	Réference
	$P\phi Et_2$	200*	1.1	36
28	$P\phi Me_2$	190	1.1	
27	P(*m*-tolyl)$_3$	185*	1.0	
26	PBu_3	185*	1.2	
23	$P\phi Bu_2$	175	1.1	
20	P(*p*-tolyl)$_3$	175*	0.9	
24	PEt_3	170	1.2	
	$P\phi(OMe)_2$	170*	1.2	29
	$P\phi_2C_2H_4P\phi_2$	170*	1.2	19
17	$P(NMe_2)_3$	165	1.2	
	$P\phi_2NMe_2$	165	1.1	24
14	$P\phi_2NPr_2$	164	1.2	
19	PMe_3	163	1.1	
21	$P\phi_2NBu_2$	163	1.2	
18	$P\phi_2Bu$	163	1.1	
15	$P\phi_2NEt_2$	158	1.1	
13	$P\phi_3$	151	1.2	
	$PFt\text{-}Bu_2$	125	1.0	37
9	PH_3	122	1.0	
33	$P(OEt)_3$	120*	0.8	
4	$P(OMe)_3$	115*	0.8	
5	$P(OMe)_2Me$	115*	0.8	
3	$P(SMe)_3$	100	1.1	
34	$P(O\phi)_3$	75*	0.8	
	$PF_2t\text{-}Bu$	60*	1.0	37
35	PCl_3	−25*		7, 8
36	PF_3	−55*		6, 35
	$As\phi Me_2$	200*	1.1	29
25	$AsEt_3$	174	1.1	
22	$As\phi_2CH_2As\phi_2$	162	1.1	
12	$As\phi_3$	156	1.1	
	$As(NC_5H_{10})_3$	145*	1.0	3
10	$As(NMe_2)_3$	125*	1.1	
1	$As(OMe)_3$	60*	0.9	
16	$SbEt_3$	155*	1.3	
11	$Sb\phi_3$	135*	1.1	
	EtC≡CEt	210*	1.2	38
	MeC≡CH	190*	1.2	38
	HC≡CH	150*	1.3	38
	$MeHC{=}CH_2$	130*	1.0	38
	$H_2C{=}CH_2$	120*	1.1	38
7	CN*t*-Bu	120*	1.0	
8	CNEt	120*	1.2	
	$H_2C{=}CH\text{-}CH{=}CH_2$	115*	1.1	38
6	CNMe	110*	1.2	
2	CNϕ	95*	1.0	
	$NH_2C_6H_{11}$	235*	2.5	9, 32
32	NC_4H_9	220	1.9	
31	NOC_4H_8	201	2.1	
	NHC_5H_{10}	200*	1.9	9
	NH_2Et	190*	2.0	39
	NH_2Me	190*	2.0	39
	$NHMe_2$	185*	2.1	39
30	NC_5H_5	180*	2.1	
29	$NCCH_3$	150*	2.3	

*± 5 cm^{-1}.
†σ_0 = pouvoir donneur net.
‡$\pi_0 = \Delta\nu_m CO^{(1)}/\Delta\nu_m CO^{(2)}$.

accepteur de l'atome P est semblable à celui de CO.

(*5*) Les donneurs As sont similaires aux donneurs P tant du point de vue donneur (σ_0) qu'accepteur (π_0). Les donneurs Sb paraissent posséder une capacité donneur moindre que les deux précédents.

(*6*) Les donneurs C ressemblent beaucoup aux donneurs P quant à leur pouvoir accepteur ($\pi_0 = 1.1$) mais se révèlent, en général, de moins puissants donneurs.

(*7*) Avec une valeur moyenne π_0 égale à 2.1, les donneurs N se distinguent des autres ligands. Dans les quelques composés comparables, les valeurs σ_0 sont plus élevées avec N qu'avec P.

Des observations précédentes on peut concevoir le mécanisme de répartition suivant: "*La charge introduite par le ligand remplaçant un CO de Mo(CO)$_6$ est répartie également par le métal selon les trois principaux axes. Les pouvoirs accepteurs relatifs de L et CO déterminent la quantité de charges sur CO*$^{(1)}$".

Dans le cas des donneurs N, où la capacité d'accepteur est nulle, toute la charge à distribuer entre N et CO$^{(1)}$ se retrouve sur CO$^{(1)}$ qui possède ainsi le double des charges de CO$^{(2)}$; le facteur π_0 est alors de 2.0. La séparation de charges dans un complexe hexacoordiné sera plus équilibrée si le ligand possède un pouvoir accepteur voisin de celui de CO. Les donneurs P avec $\pi_0 = 1$ pourraient remplacer les CO sans perturbation majeure entre CO$^{(1)}$ et CO$^{(2)}$.

Conclusion

Le modèle de distribution découlant de l'utilisation empirique des données spectroscopiques sur les fréquences d'extension CO permet, entre autres choses, de constituer une échelle du pouvoir donneur net σ_0 des ligands et d'évaluer le pouvoir acceteur π_0 de l'atome donneur. Même si aucune limite de σ_0 applicable à la stabilité des composés n'a pu être observée, le facteur π_0 est apparu de première importance pour des perturbations entre CO. L'article qui suit tentera de quantifier les charges sur les constituants des complexes Mo(CO)$_6$ et Mo(CO)$_{6-n}$L$_n$.

Remerciements

Les auteurs remercient le Ministère de l'Education du Québec pour son aide financière.

1. M. BIGORGNE. J. Organomet. Chem. **2**, 68 (1964).
2. L. H. JONES, R. S. MCDOWELL et M. GOLDBLATT. Inorg. Chem. **8**, 2349 (1969).
3. G. BOUQUET et M. BIGORGNE. Bull. Soc. Chim. Fr. 433 (1962).
4. M. BIGORGNE. Bull Soc. Chim. Fr. 295 (1963).
5. R. MATHIEU, M. LENZI et R. POILBLANC. Inorg. Chem. **9**, 2030 (1970).
6. H. HAAS et R. K. SHELINE. J. Chem. Phys. **47**, 2996 (1967).
7. F. A. COTTON. Inorg. Chem. **3**, 702 (1964).
8. D. BENLIAN et M. BIGORGNE. Bull. Soc. Chim. Fr. 1301 (1962).
9. D. J. DARENSBOURG et T. L. BROWN. Inorg. Chem. **7**, 959 (1968).
10. T. A. MAGEE, C. N. MATTHEWS, T. S. WONG et J. H. WOTY. J. Am. Chem. Soc. **83**, 3200 (1961).
11. R. POILBLANC et M. BIGORGNE. Bull. Soc. Chim. Fr. 4106 (1967).
12. C. E. JONES et K. J. COSKRAN. Inorg. Chem. **10**, 57 (1971).
13. M. BIGORGNE. J. Organomet. Chem. **1**, 101 (1963).
14. R. B. KING et M. S. SARAN. Inorg. Chem. **13**, 74 (1974).
15. F. T. DELBEKE, E. G. CLAYES et G. P. VAN DER KELEN. J. Organomet. Chem. **18**, 391 (1971).
16. C. G. BARLOW et G. C. HOLYWELL. J. Organomet. Chem. **16**, 439 (1969).
17. R. B. KING et T. F. KORENOUWSKI. Inorg. Chem. **10**, 1188 (1971).
18. D. BENLIAN et M. BIGORGNE. Bull. Soc. Chim. Fr. 1583 (1963).
19. J. CHATT, G. J. LEIGH et N. THANKARAJAN. J. Organomet. Chem. **29**, 105 (1971).
20. M. GRAZIANI, F. ZINGALES et U. BELLUCO. Inorg. Chem. **8**, 1582 (1967).
21. C. BARBEAU et J. TURCOTTE. Résultats non-publiés.
22. G. BOUQUET et M. BIGORGNE. Bull. Soc. Chim. Fr. 483 (1963).
23. J. A. BOWDEN, R. COLTON et C. J. COMMONS. Aust. J. Chem. **26**, 655 (1973).
24. L. K. ATKINSON et D. C. SMITH. J. Organomet. Chem. **33**, 189 (1971).
25. J. DALTON, I. PAUL, J. G. SMITH et F. G. A. STONE. J. Chem. Soc. A, 1195 (1968).
26. S. O. GRIM, D. A. WEATHLAND et W. MCFARLANE. J. Am. Chem. Soc. **89**, 5573 (1967).
27. S. O. GRIM et D. A. WEATHLAND. Inorg. Chem. **8**, 1716 (1969).
28. J. A. BOWDEN et R. COLTON. Aust. J. Chem. **24**, 2471 (1971).
29. J. M. JENKINS, J. R. MOSS et B. L. SHAW. J. Chem. Soc. A, 2796 (1969).
30. R. COLTON et C. J. RIX. Aust. J. Chem. **24**, 2461 (1971).
31. B. L. ROSS, J. G. GRASSELLI, W. M. RITCHEY et H. D. KAESZ. Inorg. Chem. **2**, 1023 (1963).
32. C. S. KRAIHANZEL et F. A. COTTON. Inorg. Chem. **2**, 533 (1963).
33. L. W. HOUK et G. R. DOBSON. J. Chem. Soc. A, 317 (1966).
34. G. W. A. FOWLES et D. K. JENKINS. Inorg. Chem. **3**, 257 (1964).
35. J. CLARK et P. I. HOBERMAN. Inorg. Chem. **4**, 1771 (1965).
36. J. CHATT et H. R. WATSON. J. Chem. Soc. 4980 (1961).
37. O. STELZER et R. SCHMUTZLER. J. Chem. Soc. A, 2867 (1971).
38. I. W. STOLZ, G. R. DOBSON et R. K. SHELINE. Inorg. Chem. **3**, 1264 (1963).
39. R. MATHIEU et R. POILBLANC. Inorg. Chem. **11**, 1858 (1972).
40. M. BIGORGNE. J. Inorg. Chem. **26**, 115 (1964).

Can. J. Chem. Downloaded from www.nrcresearchpress.com by 210.87.254.6 on 09/05/12
For personal use only.

Moments dipolaires théoriques des dérivés de $Mo(CO)_6$

CLAUDE BARBEAU ET JACQUES TURCOTTE

Département de Chimie, Université Laval, Québec, Québec G1K 7P4

Reçu le 30 septembre 1975

CLAUDE BARBEAU et JACQUES TURCOTTE. Can. J. Chem. **54**, 1612 (1976).

On démontre qu'il est possible de calculer, *à priori*, les moments dipolaires des dérivés *cis* de $Mo(CO)_{6-n}L_n$. La mesure des moments dipolaires $ArMo(CO)_3$ permet d'obtenir le moment partiel Mo—CO de $Mo(CO)_6$. Une étude comparative des moments dipolaires calculés et mesurés cherche à expliquer les écarts observés.

CLAUDE BARBEAU and JACQUES TURCOTTE. Can. J. Chem. **54**, 1612 (1976).

It is demonstrated that it is possible to calculate, *a priori*, the dipole moments of the *cis*-derivatives of $Mo(CO)_{6-n}L_n$. The partial moment Mo—CO in $Mo(CO)_6$ can be obtained from the measured dipole moments of $ArMo(CO)_3$. Attempts are made to explain the differences observed between the measured and calculated dipole moments.

[Journal translation]

Introduction

Connaissant les pouvoirs relatifs des ligands vis-à-vis le monoxyde de carbone dans les dérivés de $Mo(CO)_6$ (1), il devrait être possible de convertir le pouvoir donneur σ_0 en unités d'électron et ainsi de procéder à des calculs de moments dipolaires théoriques. L'utilisation d'un modèle de distribution électronique relié à l'arrangement géométrique et aux centres de gravité pourrait permettre d'évaluer la charge sur le molybdène et de mettre en évidence une ou plusieurs causes de l'instabilité de certains dérivés.

Partie expérimentale

Les dérivés $ArMo(CO)_3$ ont été obtenus par réaction thermique entre $Mo(CO)_6$ et le donneur aromatique, dans l'éthyle cyclohexane ou l'éther de pétrole (p.é. 90–120 °C), à la température d'ébullition du mélange et selon la technique mise au point par Strohmeier et Gerlach (2).

Les spectres infrarouges ont été enregistrés à l'aide d'un spectromètre Perkin-Elmer 621 à partir de solutions dans le cyclohexane.

Les moments dipolaires résultent de mesures de constante diélectrique et d'indice de réfraction effectuées à 25 °C dans l'appareil et selon la méthode décrits précédemment (3).

Charges et fréquences

Le problème majeur dans tout calcul théorique de moments dipolaires réside dans la localisation des centres de gravité. Alors qu'il est raisonnable de situer le centre de gravité des charges positives sur l'atome donneur d'un ligand L, il est par contre difficile de localiser le centre des charges négatives qui résultent de la présence de ce ligand. La baisse de la fréquence d'extension CO est ordinairement associée à une densité électronique supplémentaire au niveau des orbitales π anti-liantes; il serait alors normal de trouver le centre de gravité des charges négatives le long de l'axe Mo—C—O. Si on situe ce centre à une distance x de Mo, il est possible d'envisager le calcul des moments dipolaires des composés $Mo(CO)_{6-n}L_n$ d'après les équations suivantes:[1]

$$[1]\quad \mu_1 = \mu_0 + \left(\frac{\sigma_0\pi_0}{4+\pi_0}(a+x) + \frac{4\sigma_0}{4+\pi_0}a\right)B$$

$$[2]\quad \mu_2 = \sqrt{2}\left[\mu_0 + \left(\frac{2\sigma_0\pi_0}{4+\pi_0}(a+x) + \frac{2\sigma_0}{4+\pi_0}a\right)B\right]$$

$$[3]\quad \mu_3 = \sqrt{3}\left[\mu_0 + \left(\frac{3\sigma_0\pi_0}{4+\pi_0}(a+x)\right)B\right]$$

$$[4]\quad Z = \frac{(\mu_2/\sqrt{2}) - \mu_0}{\mu_1 - \mu_0} = \frac{2\pi_0(a+x) + 2a}{\pi_0(a+x) + 4a}$$

où μ_0 = moment dipolaire intrinsèque Mo—C—O à la fréquence CO de 1986 cm^{-1}; $\sigma_0\pi_0/(4+\pi_0)$ = charges sur CO *trans* dans $Mo(CO)_5L$, en unités de fréquence $\Delta\nu(1986 - \nu CO^{(1)})$; a = distance en Å entre l'atome donneur du ligand et l'atome Mo; B = facteur de conversion entre les unités de fréquence $\Delta\nu$ et les unités de charges électrostatiques, $\Delta e/\Delta\nu$.

Afin d'obtenir B et x, nous avons utilisé les moments dipolaires des composés $ArMo(CO)_3$,

[1] La représentation géométrique des centres de gravité dans les dérivés $Mo(CO)_{6-n}L_n$ est donnée par Bigorgne (4).

Can. J. Chem. Downloaded from www.nrcresearchpress.com by 210.87.254.40 on 09/05/12
For personal use only.

Can. J. Chem. Downloaded from www.nrcresearchpress.com by 210.87.254.40 on 09/05/12
For personal use only.

tableau 1, lesquels présentent une variation linéaire en fonction de l'écart des fréquences d'extension CO entre $Mo(CO)_6$ et $ArMo(CO)_3$, fig. 1. Une telle corrélation nous permet d'entrevoir une interdépendance des charges nettes portées par un ligand dans un composé $Mo(CO)_{6-n}L_n$ et les valeurs σ_0 attribuées à ce même ligand (1).

Si on considère $ArMo(CO)_3$ comme un dérivé tricarbonyle, son moment dipolaire se décompose en μ_0 et $\mu_{Ar}{}^1$.

$$[5] \qquad \mu_{Ar}{}^C = \sqrt{3}(\mu_0 + \mu_{Ar}{}^1)$$

Cette expression est reliée à l'équation de la droite qui traduit les données du tableau 1 et de la fig. 1:

$$[6] \qquad \mu_{Ar}{}^E = \sqrt{3}(1.77\text{D} + 0.027_4\Delta\nu)$$

En utilisant la valeur 1.77D pour μ_0 dans l'éq. 4 on peut comparer les valeurs Z expérimentale, Z^E, et Z calculée, Z^C, pour différentes distances x.

On constate au tableau 2, que l'accord entre Z^E et Z^C est excellent si on place le centre de gravité des charges négatives apportées par un ligand L à une distance x voisine de 0 Å. Il est important de remarquer que cette décision de placer le centre de gravité des charges supplémentaires négatives sur le métal plutôt que sur l'axe Mo—C—O découle d'un résultat indépendant des charges σ_0 et des distances a.

Pour obtenir B on se sert des éqs 5 et 6 où $\mu_{Ar}{}' = 0.027_4\Delta\nu$. Puisqu'il s'agit d'un tricarbonyle, $\Delta\nu = 3\sigma_0\pi_0/(4 + \pi_0)$ d'où on tire $B = 0.027_4/a$. Dans un composé $ArMo(CO)_3$ la distance Ar–Mo correspond à la normale au plan abaissée sur Mo. Par comparaison avec un composé similaire (5) et les composés analogues du chrome (6), on peut évaluer cette distance à 1.70 ± 0.05 Å, distance à peu près constante de C_6H_6–Mo à $C_6(CH_3)_6$–Mo (6). Le centre de gravité des charges positives étant considéré au centre de gravité du plan de l'aromatique, la distance a, qui correspond à la distance entre le molybdène et un centre situé sur un des axes orthogonaux de $L_3Mo(CO)_3$, est obtenue en effectuant une projection sur l'axe correspondant, *i.e.* $a = 1.7 \times \sqrt{3} = 2.9_4$ Å. B représente le facteur permettant de transformer la baisse de fréquence d'extension CO en unités de charges négatives apportées sur le métal. Dans le cas du molybdène, la valeur B se situe à environ 0.0093 u.e.s. cm^{-1}.

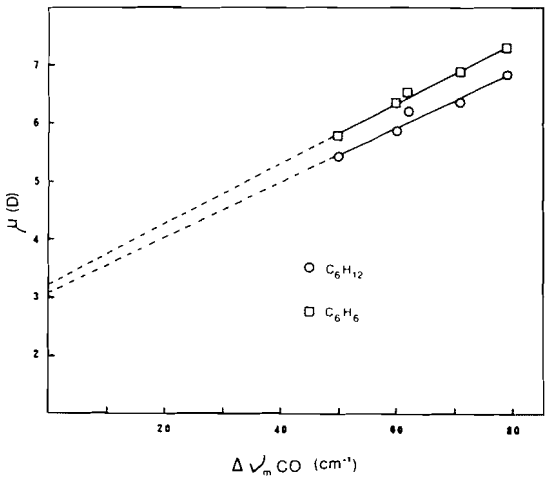

FIG. 1. Détermination du moment dipolaire partiel Mo—CO (μ_0) dans $Mo(CO)_6$ ou ses dérivés.

Le tableau 2 présente quelques valeurs μ_1 calculées pour différents x, selon l'éq. 1 et les valeurs a correspondant aux distances Mo – atome donneur. On observe une bonne concordance entre $\mu_1{}^E$ et $\mu_1{}^C$ pour une distance x voisine de 0.0 Å. Nous estimons que ces derniers résultats joints à ceux des Z^E et Z^C justifient le choix des distances x et a_{Ar}.

Calculs et discussion

En utilisant les valeurs de σ_0 et π_0 obtenues dans l'article précédent (1), nous avons calculé les moments dipolaires μ_1, μ_2 et μ_3 pour les complexes *cis* de l'hexacarbonyle de molybdène dont on connaît au moins un moment dipolaire expérimental (tableau 3).

Sauf pour un cas, tous les moments dipolaires $\mu_1{}^C$ et $\mu_1{}^E$ sont identiques à l'erreur près. Il apparaît évident, par voie de comparaison, que le moment $\mu_1{}^E$ de $Mo(CO)_5P\phi_2NEt_2$ est erroné, sa valeur étant certainement trop faible. Les calculs ont été effectués en plaçant le centre de gravité des charges positives des ligands MX_3 (Sb, As, P et N) sur l'atome donneur M. Lorsque N est lié au carbone par une liaison multiple, l'accord entre $\mu_1{}^E$ et $\mu_1{}^C$ s'obtient seulement si le centre de gravité est situé sur le carbone.

On constate que la plupart des $\mu_2{}^C$ ne sont que peu supérieurs aux $\mu_2{}^E$. En moyenne l'écart

Can. J. Chem. Downloaded from www.nrcresearchpress.com by 210.87.254.40 on 09/05/12
For personal use only.

TABLEAU 1. Moments dipolaires et fréquences CO des composés $ArMo(CO)_3$*

Composé	μ† (D)			μ‡ (D)			νCO (cm^{-1})			
	α	γ'	μ_G' ($\pm$0.05)	α	γ'	μ_G' ($\pm$0.05)	$A_1^{(2)}$ ($\pm$1)	E ($\pm$1)	ν_m ($\pm$2)	$\Delta\nu_m$
$C_6H_6Mo(CO)_3$	30.22	0.51	5.41	46.56	1.19	5.76	1985	1912	1936	50
$C_6H_4(CH_3)_2Mo(CO)_3$	35.56	0.79	5.85	56.75	1.38	6.35	1975	1901	1926	60
$C_6H_3(CH_3)_3Mo(CO)_3$	39.83	0.94	6.21	59.76	1.38	6.51	1972	1900	1924	62
$C_6H_2(CH_3)_4Mo(CO)_3$	40.64	1.10	6.34	67.08	1.48	6.89	1964	1891	1915	71
$C_6(CH_3)_6Mo(CO)_3$	48.85	1.37	6.85	75.57	1.32	7.30	1958	1882	1907	79

†Mesuré dans le cyclohexane à 25 °C.
‡Mesuré dans le benzène à 25 °C.
*$\alpha = d\varepsilon_{12}/df_2$; $\gamma' = dn_{12}^2/df_2$ (3); μ_G' = moment dipolaire calculé d'après la relation modifiée [3] de Guggenheim; $\nu_m = (2E + A_1^{(2)})/3$; $\Delta\nu_m = 1986\ cm^{-1} - \nu_m$.

TABLEAU 2. Influence de la position du centre de gravité des charges négatives sur les moments dipolaires

Ligand	σ_0 (cm^{-1})	π_0	Z^E	Z^C pour x = 1.0a	0.5a	0.2a	0.0a	μ_1^E ($\pm$0.1 D)	μ_1^C (D) pour x = 2.5 Å	2.0 Å	1.0 Å	0.5 Å	0.0 Å
$Sb\phi_3$	135	1.1	0.83	1.03	0.94	0.87	0.82	5.1	5.8	5.7	5.4	5.3	5.2
$As\phi_3$	156	1.1	0.82	1.03	0.94	0.87	0.82	5.4	6.3	6.2	5.9	5.7	5.5
$P\phi_2NPr_2$	164	1.2	0.81	1.06	0.97	0.90	0.85	5.5	6.3	6.2	5.8	5.7	5.6
$NCCH_3$	150	2.3	1.01	1.30	1.19	1.11	1.05	6.8	7.9	7.7	7.2	6.9	6.7

Can. J. Chem. Downloaded from www.nrcresearchpress.com by 210.87.254.40 on 09/05/12
For personal use only.

TABLEAU 3. Comparaison des moments dipolaires calculés μ^C et mesurés μ^{E*}

			$Mo(CO)_5L$			$Mo(CO)_4L_2$ *cis*			$Mo(CO)_3L_3$ *cis*			
Ligand	σ_0 (cm^{-1})	π_0	μ^C (±0.2 D)	μ^E (±0.1 D)	$\Delta\mu$ (D)	μ^C (±0.2 D)	μ^E (±0.1 D)	$\Delta\mu$ (D)	μ^C (±0.2 D)	μ^E (±0.1 D)	$\Delta\mu$ (D)	Réference
$P\phi Et_2$	200	1.1	6.4	—	—	7.9	6.9†	1.0	8.3	—	—	8
$P\phi Me_2$	190	1.1	6.2	—	—	7.7	6.8†	0.9	8.0	—	—	8
$P\phi_2C_2H_4P\phi_2$	170	1.2	5.7	—	—	7.2	7.0	0.2	7.5	—	—	9
$P\phi_2NMe_2$	165	1.1	5.6	—	—	7.0	6.2	0.8	7.4	—	—	9
$P\phi_2NPr_2$	164	1.2	5.6	5.5	0.1	7.0	6.8	0.2	7.3	—	—	9
$P\phi_2NBu_2$	163	1.2	5.6	5.6	0.0	7.0	6.6	0.4	7.3	—	—	9
$P\phi_2NEt_2$	158	1.1	5.4	4.3	1.1	6.8	6.8	0.0	7.2	—	—	9
$P\phi_3$	151	1.1	5.3	5.4	−0.1	6.7	6.3	0.4	7.3	5.2	2.1	7
$As\phi Me_2$	200	1.1	6.6	—	—	8.1	6.8†	1.3	8.5	7.7†	0.8	8
$As\phi_3$	156	1.1	5.5	5.4	0.1	6.9	6.7	0.2	7.3	5.6	1.7	7
$Sb\phi_3$	135	1.1	5.2	5.1	0.1	6.5	6.4	0.1	6.9	6.9	0.0	7
NHC_5H_{10}	200	1.9	6.1	5.9†	0.2	8.6	—	—	10.4	—	—	10
NC_5H_5	180	2.1	6.7	6.4†	0.3	9.6	9.3†	0.3	11.8	—	—	10
$NCCH_3$	150	2.3	6.7	6.8†	−0.1	9.8	9.7†	0.1	12.3	—	—	10

*Mesuré dans le cyclohexane à 25 °C. a = 2.7 Å (Sb), 2.6 Å (As), 2.5 Å (P), 2.35 Å (N), 2.95 Å $\left(N\begin{smallmatrix}\diagup C\\ \diagdown C\end{smallmatrix}\right)$, 3.5 Å (N≡C).

†Mesuré dans le benzène à 20 °C.

$\Delta\mu$ se situe à 0.2 D mais les ligands $M\phi R_2$ sont associés à des valeurs $\Delta\mu$ voisines de 1.0 D.

Quatre des cinq trisubstitués dont les moments dipolaires ont été mesurés présentent un écart $\Delta\mu$ élevé. Il est intéressant de noter que, d'une part la stabilité des complexes $Mo(CO)_3(M\phi_3)_3$ décroît selon l'ordre Sb > As > P (seul $Sb\phi_3$ forme un complexe tétrasubstitué), et que d'autre part $\mu_3{}^C - \mu_3{}^E$ passe de 0.0 D pour $Sb\phi_3$ à 1.7 D pour $As\phi_3$ et à 2.1 D pour $P\phi_3$.

Comme nous l'avions suggéré précédemment (7), toute modification structurale provoquée par des répulsions de nature stérique ou électrostatique suffirait à expliquer une différence $\mu^C - \mu^E$. Les ouvertures angulaires qui ont déjà été observées (11) dans des complexes contenant des groupemenets $P\phi_3$ en position *cis* sont précisément suffisantes pour abaisser le moment dipolaire et justifier le manque de stabilité.

Le moment dipolaire intrinsèque μ_0 traduit la situation des charges portées par le molybdène et le groupement CO dans $Mo(CO)_6$. En situant le centre de gravité des charges négatives au voisinage du carbone, *i.e.* à environ 2 Å du molybdène, μ_0 serait relié à une charge de 0.18 électron. Le monoxyde de carbone agit alors comme accepteur net et la présence de six CO dans $Mo(CO)_6$ entraîne, selon cette approche, une charge positive unitaire (1 +) sur le molybdène.

Selon la fig. 1, l'extrapolation des μ_{Ar} mesurés dans le cyclohexane ou le benzène conduit approximativement à la même valeur μ_0. La pente légèrement supérieure des μ_{Ar} mesurés dans le benzène s'explique par le moment dipolaire additionnel, qui résulte de l'attraction entre une molécule de solvant et la charge positive sur l'aromatique, et dont la grandeur dépend de la charge sur l'aromatique.

Nous pensons avoir démontré qu'il existe une interdépendance simple entre les fréquences d'extension CO et les moments dipolaires, interdépendance qui permet d'expliquer partiellement certaines instabilités et qui permet également de calculer les moments dipolaires à priori. Une étude semblable (12) portant sur les dérivés de $Cr(CO)_6$ et $W(CO)_6$ a permis de tirer les mêmes conclusions.

Remerciements

Nous remercions le Conseil national de la recherche du Canada et le Ministère de l'Education du Québec pour leur aide financière.

1. C. Barbeau et J. Turcotte. Can. J. Chem. Article précédent.
2. W. Strohmeier et K. L. Gerlach. Chem. Ber. **94**, 398 (1961).
3. C. Barbeau, L. Ricard et J. Turcotte. Can. J. Chem. **48**, 1698 (1970).
4. M. Bigorgne et C. Messier. J. Organomet. Chem. **2**, 79 (1964).
5. J. D. Dunitz et P. Pauling. Helv. Chim. Acta, **43** 2188 (1960).
6. M. F. Bailey et L. F. Dahl. Inorg. Chem. **4**, 1298 (1965); M. F. Bailey et L. F. Dahl. Inorg. Chem. **4**, 1314 (1965).
7. C. Barbeau et J. Turcotte. Can. J. Chem. **48**, 3583 (1970).
8. J. M. Jenkins, J. R. Moss et B. L. Shaw. J. Chem. Soc. (A), 2796 (1969).
9. L. K. Atkinson et D. C. Smith. J. Organomet. Chem. **33**, 189 (1971).
10. W. Strohmeier et H. Hellmann. Ber Bunseng. **68**, 481 (1965).
11. C. Barbeau et R. J. Dubey. Can. J. Chem. **52**, 1140 (1974).
12. C. Barbeau et J. Turcotte. Can. J. Chem. A venir.

Can. J. Chem. Downloaded from www.nrcresearchpress.com by 210.87.254.40 on 09/05/12
For personal use only.

Kinetics of radical exchange in the reaction of CF_3 radicals with tin tetramethyl

T. N. BELL AND P. J. YOUNG

Department of Chemistry, Simon Fraser University, Vancouver, British Columbia V5A 1S6

Received December 8, 1975

T. N. BELL and P. J. YOUNG. Can. J. Chem. **54**, 1617 (1976).

The reaction of CF_3 radicals with $SnMe_4$ leads to hydrogen abstraction and also radical exchange.

$$CF_3 + SnMe_4 \leftrightarrows CF_3SnMe_4 \rightarrow CF_3SnMe_3 + Me$$

We propose the exchange reaction proceeds via a five coordinate intermediate. The Arrhenius parameters for the exchange reaction are,

$$\log (k_{ex} \text{ ml mol}^{-1} \text{ s}^{-1}) = 11.60 - 9.32/2.3RT$$

Additional data for the H abstraction reaction

$$CF_3 + SnMe_4 \rightarrow CF_3H + CH_2SnMe_3$$

combined with previous data yields an improved rate constant for abstraction,

$$\log (k_{abst} \text{ ml mol}^{-1} \text{ s}^{-1}) = 12.00 - 7.69/2.3RT$$

T. N. BELL et P. J. YOUNG. Can. J. Chem. **54**, 1617 (1976).

La réaction des radicaux CF_3 avec le $SnMe_4$ conduit à un enlèvement d'hydrogène et aussi à une réaction d'échange de radicaux.

$$CF_3 + SnMe_4 \leftrightarrows CF_3SnMe_4 \rightarrow CF_3SnMe_3 + Me$$

On suggère que la réaction d'échange se produit par un intermédiaire pentacoordonnée. Les paramètres d'Arrhenius pour la réaction d'échange sont

$$\log (k_{échange} \text{ ml mol}^{-1} \text{ s}^{-1}) = 11.60 - 9.32/2.3RT$$

En combinant des données additionnelles pour la réaction d'enlèvement d'hydrogène

$$CF_3 + SnMe_4 \rightarrow CF_3H + CH_2SnMe_3$$

avec des données antérieures on obtient une constante de vitesse améliorée pour la réaction d'élimination d'hydrogène,

$$\log (k_{enlèvement} \text{ ml mol}^{-1} \text{ s}^{-1}) = 12.00 - 7.69/2.3RT$$

[Traduit par le journal]

Introduction

In previous work, formation of methyl-containing products was noted in the reaction of CF_3 radicals with Group IV organometallics and with boron trimethyl (1–3). A radical exchange mechanism was proposed to account for the formation of methyl radicals in these various systems. In the case of tin tetramethyl an estimate was made of the rate constant for exchange at one temperature, and the present work was designed to examine the exchange reaction over a range of temperature in order to establish the conditions for exchange, and also the Arrhenius parameters. During this investigation additional complexities in the system were found. At low temperatures this appeared to involve the reaction of the organometallic compound with excited hexafluoroacetone molecules.

Additional data were obtained on the hydrogen abstraction reaction, which when added to previous data (2) establish more precisely the Arrhenius parameters for that reaction.

Experimental

Materials

The sources of compounds used in this work were hexafluoroacetone (Allied Chemicals) and tetramethyltin (Alfa Inorganics). Each was fractionated in the usual manner, with middle cuts being retained and stored in blackened bulbs.

Can. J. Chem. Downloaded from www.nrcresearchpress.com by 210.87.254.40 on 09/05/12
For personal use only.

Can. J. Chem. Downloaded from www.nrcresearchpress.com by 210.87.254.40 on 09/05/12
For personal use only.

Apparatus

A typical glass vacuum line was used, photolyses being carried out in an Ultrasil cell (illuminated volume 249 ml). The cell was enclosed in a tubular aluminum block furnace, whose temperature was controlled to ±0.5 °C. with an RFL platinum resistance controller.

The light source (P.E.K. 200 W mercury arc) was filtered, using Corning 0-53 and Corning CS7-54 filters. These yielded a band of radiation between 2900 and 3800 Å with a maximum at 3300 Å.

Pressure measurements were made using a Texas Instruments Inc. precision quartz spiral gauge.

Procedures

After reaction, the gases non-condensible in liquid nitrogen (CO, CH_4) were measured using a gas burette and gas chromatography (Porapak Q, 60-80 mesh).

The condensible products were subject to fractionation and those materials volatile at −131 °C were separated from the bulk of reactants, and subjected to quantitative analysis by gas chromatography using an alumina column (5 min at 30 °C, followed by temperature programming at 6 °C min^{-1}). Frequent checks were made to ensure that the volatile compounds of interest to this study were completely removed from the bulk of the product mixture for quantitative analysis.

Results

Hexafluoroacetone photolyses according to the equation

$$HFA \xrightarrow{h\nu} 2CF_3 + CO$$

The primary quantum yield above 200 °C is unity below that temperature the quantum yield falls, the normal useful temperature range of hexafluoroacetone as a source of CF_3 radicals being >100 °C (4).

In the presence of tetramethyltin, the photolysis of HFA leads to the volatile products C_2F_6, CF_3H, CF_2CH_2, CH_4, C_2H_6, CF_3CH_3, together with CO.

This study of the reaction was carried out over a wide temperature range, with complexities being observed at high and low temperature. The results obtained over the various temperature ranges are discussed below.

In a previous paper the formation of CH_3 containing products was ascribed to the reactions of methyl radicals formed in an exchange process involving a five coordinate intermediate (1). The following mechanistic scheme may be written for the reactions of the CF_3 and CH_3 radicals in the presence of $Sn(Me)_4$.

[1] $CF_3 + Sn(Me)_4 \rightleftarrows CF_3Sn(Me)_4 \rightarrow CF_3Sn(Me)_3 + CH_3$

[2] $CF_3 + Sn(Me)_4 \rightarrow CF_3H + CH_2Sn(Me)_3$

[3] $CH_3 + Sn(Me)_4 \rightarrow CH_4 + CH_2Sn(Me)_3$

[4] $CF_3 + CF_3 \rightarrow C_2F_6$

[5] $CH_3 + CF_3 \rightarrow CF_3CH_3^* \xrightarrow{M} CF_3CH_3$

[6] $CF_3CH_3^* \rightarrow CF_2CH_2 + HF$

[7] $CH_3 + CH_3 \rightarrow C_2H_6$

Additional mechanistic complexities occur due to the reactions of the $CH_2Sn(Me)_3$ radicals in combination processes.

We have shown (2, 3, 5–7) that the combination of $CH_2M(Me)_3$ (M = B, Si, Ge, Sn) with CF_3 leads to a vibrationally hot molecule which may stabilize or undergo a facile β fluoro-rearrangement-elimination process, forming additional CF_2CH_2 through reaction 10.

[8] $CF_3 + CH_2Sn(Me)_3 \rightarrow CF_3CH_2Sn(Me)_3^*$

[9] $CF_3CH_2Sn(Me)_3^* \xrightarrow{M} CF_3CH_2Sn(Me)_3$

[10] $CF_3CH_2Sn(Me)_3^* \rightarrow CF_2CH_2 + FSn(Me)^3$

A kinetic analysis to determine $k_{exchange}$, *i.e.* k_1 may be made as follows

$$[11] \quad \frac{R_{ex}}{R_{abst}} = \frac{k_1[CF_3][Sn(Me)_4]}{k_2[CF_3][Sn(Me)_4]} = \frac{\text{Rate formation of } CH_3 \text{ products}}{R_{CF_3H}}$$

$$= \frac{R_{CH_4} + R_{CF_3CH_3} + R_{CF_2CH_2}\,(\text{from [6]}) + 2R_{C_2H_6}}{R_{CF_3H}}$$

A major problem arises from the formation of CF_2CH_2 through reactions 6 and 10 and determining the amount produced from reaction 6, given the difficulty in directly measuring the complementary products HF and $FSnMe_3$. Two alternative approaches are possible.

The first is to use the experimental data for the formation of CF_3CH_3, in conjunction with data by Giles and Whittle (8), on the stabilisation/decomposition ratios of $CF_3CH_3^*$. This suffers from the fact that these ratios are dependent on the third body M. Thus k_5/k_6 = 4.5×10^5 (acetone), 10^6 (HFA), and 1.4×10^6 (cyclo-C_6F_{12}). The third body in our work is HFA + $Sn(Me)_4$.

The second approximation is to estimate the amount of $CF_3CH_3^*$ produced in reaction 5 from a knowledge of the CF_3 and CH_3 radical concentrations. These may be determined from

Can. J. Chem. Downloaded from www.nrcresearchpress.com by 210.87.254.40 on 09/05/12
For personal use only.

a measure of $R_{C_2F_6}$ and $R_{C_2H_6}$ together with the recombination rate constants, k_4 and k_7 (9, 10). The calculated values obtained by this method, assuming a value for $k_5 = 10^{13.34}$ (same as for k_4), were used in the kinetic analysis, as a result of which eq. 11 is written as eq. 12.

$$[12] \quad \frac{R_{ex}}{R_{abst}} = \frac{k_1}{k_2} = \frac{R_{CH_4} + R_{CF_3CH_3}{}^{*}\text{ (calculated)} + 2R_{C_2H_6}}{R_{CF_3H}}$$

The above analysis ignores any loss of CH_3 from the recombination of CH_3 with $CH_2Sn(Me)_3$. There appears no way around this dilemma, it being impossible to measure trace quantities of $CH_3CH_2Sn(Me)_3$ in the presence of relatively large amounts of $Sn(Me)_4$. If, however, this recombination was an important reaction, the experimental results would not be expected to fit eq. 12, to yield an Arrhenius plot with the excellent straight line characteristics as was obtained.

H Abstraction by CF_3

Measurement of CF_3H and C_2F_6 allows a determination of k_2, using a value for $k_4 = 2.3 \times 10^{13}$ ml mol^{-1} s^{-1} (9), thus

$$\frac{k_2}{k_4^{1/2}} = \frac{R_{CF_3H}}{R_{C_2F_6}^{1/2}[Sn(Me)_4]}$$

Results obtained in the present work (Table 1) fit well with previous results (2) for k_2, and are combined with those results in the Arrhenius plot shown in Fig. 1. Least squares analysis of the combined data yields a value

$$\log k_2(\text{ml mol}^{-1}\text{ s}^{-1}) = (12.00 \pm 0.06) - (7.69 \pm 0.11)\text{ kcal}/2.3RT$$

This compares with the previously reported value (2),

$$\log k_2\text{ (ml mol}^{-1}\text{ s}^{-1}) = 11.7 - 7.25/2.3RT$$

determined in the temperature range 25–150 °C.

Radical Exchange

The kinetic data on exchange was obtained in the temperature range 150 to 250 °C; extensive checks showed no dark reaction occurred. The reaction cell was initially cleaned and conditioned by photolysing a mixture of HFA + $SnMe_4$ before obtaining the series of quantitative results in Table 1. The various temperatures used were selected randomly in terms of the sequencing of the experiments, in order to eliminate any concern that there was a systematic changing of the cell conditions with temperature and to give reproducibility in the experimental results.

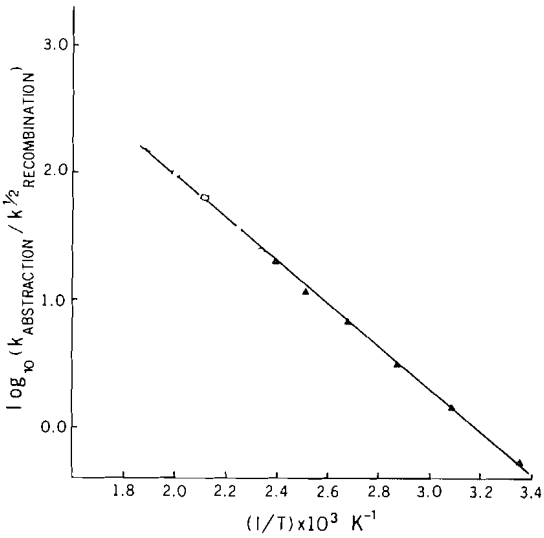

FIG. 1. $\log k_{ab}/k_{recombn}^{1/2}$ *vs.* $1/T$ for $CF_3 + Sn(CH_3)_4$. ▲, Bell and Platt (2); ○, this work.

In the temperature range 150 to 250 °C the CF_3 product ratios $R_{CF_3H}/R_{C_2F_6}^{1/2}$, and the CH_3 product ratios $R_{CH_4}/R_{C_2H_6}^{1/2}$ agreed well with those ratios expected by calculation from the known abstraction and recombination rate constant data (2, 9–11). This agreement is consistent with the requirement of the mechanism proposed, that the products of reaction are a result of the radical reactions 1 to 7, resulting in the kinetic analysis eq. 12.

The results using 10 torr HFA and 10 torr $Sn(Me)_4$ are reported in Table 1, and plotted in Arrhenius form in Fig. 2. A good fit to eq. 12 is observed, and the several results at each temperature are reproducible.

From a least squares analysis of the data and using the amended value obtained for k_2 (see above), the Arrhenius parameters for the exchange reaction 1 are

$$\log A_1 = 11.60 \pm 0.07$$
$$E = 9.32 \pm 0.15\text{ kcal mol}^{-1}$$

Can. J. Chem. Downloaded from www.nrcresearchpress.com by 210.87.254.40 on 09/05/12
For personal use only.

TABLE 1. Exchange and abstraction rate data for the reaction $CF_3 + SiMe_4$[1]

T (C°)	Time (min)	R_{CO}	R_{CH_4}	$R_{C_2H_6}$	$R_{C_2F_6}$	$R_{CF_2CH_2}$	R_{CF_3H}	$R_{CF_3CH_3}$	$R^*_{CF_3CH_3}$	$\frac{R_{CH_4} + 2R_{C_2H_6} + R^*_{CF_3CH_3}}{R_{CF_3H}}$	$k_{ex} \times 10^{-7}$ (ml mol^{-1} s^{-1})	$k_{ab}/k^{1/2}_{recombn}$ (ml$^{1/2}$ mol$^{-1/2}$ s$^{-1/2}$)	Average
156	10	6.380	0.140	0.060	1.060	0.832	9.113	0.245	0.255	0.0565	0.723	23.7	
156	10	—	0.140	0.067	0.987	—	9.220	0.245	0.257	0.0576	0.737	24.8	24.3
156	10	6.760	0.147	0.067	1.033	0.765	9.313	0.252	0.263	0.0584	0.748	24.5	
174	8	11.43	0.225	0.133	1.800	1.917	16.24	0.483	0.490	0.0604	1.11	33.7	
174	8	11.73	0.258	0.125	1.550	1.650	17.18	0.437	0.441	0.0552	1.01	38.4	36.0
174	8	11.35	0.225	0.133	1.517	1.533	15.81	0.442	0.449	0.0595	1.09	35.8	
200	5	12.75	0.440	0.253	1.307	2.027	21.73	0.507	0.574	0.0698	2.05	56.1	
200	6	13.52	0.522	0.233	1.022	1.711	23.24	0.456	0.490	0.0634	1.86	67.8	62.6
200	6	14.62	0.556	0.256	1.378	1.900	25.37	0.556	0.597	0.0655	1.93	63.8	
202	10	9.013	0.400	0.173	0.693	1.380	16.61	0.307	0.345	0.0658	2.01	59.0	
202	10	8.700	0.433	0.167	0.620	1.273	17.35	0.286	0.321	0.0626	1.91	65.2	63.3
202	10	8.513	0.460	0.167	0.580	1.294	16.89	0.288	0.312	0.0654	2.00	65.6	
227	5	16.03	0.893	0.440	1.093	2.800	33.33	0.640	0.692	0.0739	3.37	99.3	
227	5	15.77	0.906	0.440	1.067	2.813	32.52	0.587	0.681	0.0758	3.47	98.1	98.7
227	5	15.28	0.906	0.440	1.053	2.800	32.52	0.640	0.681	0.0758	3.47	98.7	
252	5	17.56	1.347	0.480	0.667	2.360	38.27	0.413	0.563	0.0750	4.96	153	
252	5	18.31	1.613	0.480	0.680	1.907	38.69	0.440	0.570	0.0813	5.37	153	153
252	5	18.03	1.680	0.453	0.640	1.760	37.32	0.400	0.538	0.0837	5.52	152	

[1]In all the above experiments the starting amounts of materials were HFA 10 torr, $SnMe_4$ 10 torr. All R's in mol ml^{-1} s^{-1} $\times 10^{12}$.

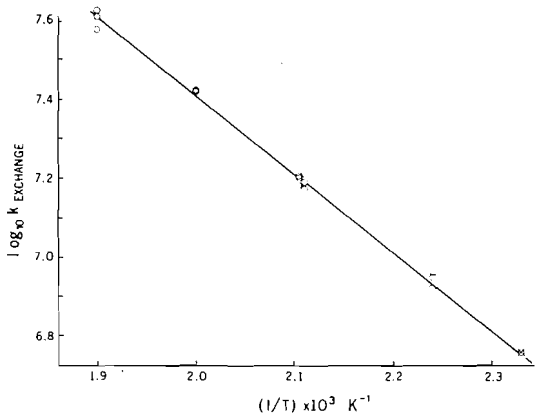

FIG. 2. log k_{ex} *vs.* $1/T$ for $CF_3 + Sn(CH_3)_4$.

Results at Low Temperature

Mixtures of HFA + $Sn(Me)_4$ underwent a noticeable pressure decrease when exposed to the photolysing radiation at temperatures < 100 °C, for the time required (~20 min) for the exchange studies. No dark reaction was, however, observed.

Examination of the cell after photolysis revealed the formation of a non-volatile colourless liquid and a white deposit was formed. The mass spectrum of the non-volatile liquid was consistent with a formula of the type $(Sn(CH_3)_3)_n$, although this is by no means conclusive.

The above complication was not noticed previously by Bell and Platt (2) in their measurements of k_{abst} by CF_3 radicals; however, only short photolysis times (2 min) were used in their work.

Measurement of the CH_4 showed this product to be formed in amount considerably greater than that expected from the stationary state of CH_3 radicals calculated from the C_2H_6 formed. Thus R_{CH_4}(experimental)/R_{CH_4}(calculated) varied up to 40. The results appeared to depend on the condition of the reaction vessel, and were not very reproducible.

The ratio $R_{CF_3H}/R^{1/2}_{C_2F_6}$, however, was consistent with that expected from the rate constant for H abstraction by CF_3 determined by Bell and Platt (2), and was slightly modified by this present work.

Several experiments were carried out to check whether $Sn(Me)_4$ quenched the emission from HFA at 4200 Å (singlet) and 5000 Å (triplet) (12) at these lower temperatures. Strong quenching was in fact observed. Chemical analysis showed that the $Sn(Me)_4$ pressure had a marked effect on the CO yield.

We suggest that the lifetime of excited HFA at temperatures < 100 °C is such as to result in a photosensitized reaction through collisional deactivation by $Sn(Me)_4$, followed by methane production via a non-radical mechanism.

The high temperature pyrolysis (13) of $Sn(Me)_4$ has been reported to yield CH_4 without C_2H_6. If this observation is correct, it suggests the formation of CH_4 intramolecularly.

It is possible that the processes for CH_4 formation are similar in the above cases.

Results at High Temperature

At temperatures above 300 °C the product ratios measured deviated from those expected, in this case those involving the CF_3 radical. Thus, while in the temperature range used for the kinetic results R_{CF_3H}(experimental)/R_{CF_3H} (calculated) is essentially unity, a dark reaction was observed forming CF_3H and CF_2CH_2 at 300 °C.

Discussion

In addition to the work reported here we attempted to measure the rate of exchange for the systems $CF_3 + SiMe_4$, $FSiMe_3$, F_2SiMe_2, F_3SiMe. The reaction was far too slow for quantitative study, H abstraction being the predominant reaction.

This agrees with the qualitative order of reactivity

$$BMe_3 > SnMe_4 \gg GeMe_4 = SiMe_4$$

suggested by Bell and Platt (1).

Grotewold *et al.* (14) measured the rate of exchange,

$$CH_3 + BEt_3 \rightarrow C_2H_5 + CH_3BEt_2$$

obtaining

$$\log k_{ex} = 10.6 - 5200/2.3RT$$

At 150 °C this yields

$$k_{ex} \approx 8 \times 10^7$$

compared with our value for

$$k_{ex}(CF_3 + SnMe_4) \approx 6 \times 10^6$$

suggesting the qualitative order of reactivity above is correct.

Can. J. Chem. Downloaded from www.nrcresearchpress.com by 210.87.254.40 on 09/05/12
For personal use only.

Can. J. Chem. Downloaded from www.nrcresearchpress.com by 210.87.254.40 on 09/05/12
For personal use only.

The competitive process to exchange is H abstraction. Using Grotewold's value for

$$\log k_{abst}(CH_3 + BEt_3) = 12.38 - 7780/2.3RT$$

$$k_{abst}(150\ °C) = 2.3 \times 10^8$$

leads to

$$k_{ex}/k_{abst} = 0.35$$

In the system $CF_3 + SnMe_4$ and using the data in this paper

$$k_{ex}/k_{abst} = 0.05$$

A Factors

The A factor for exchange in the present work, $10^{11.6}$, is slightly less than that for abstraction, $10^{12.0}$, suggestive of a similar and reasonably loose transition state,

$$A_{ex}/A_{abst} = 0.4$$

If exchange is envisaged as proceeding through a five coordinate complex, presumably trigonal bipyramidal, the $6d$ orbital system would be involved. At such high quantum numbers the character of the orbitals is much less prescribed than, for example, in the boron system. Extensive bending vibrational modes might be expected, leading to a loose transition complex.

In the $CH_3 + BEt_3$ system

$$A_{ex}/A_{abst} = 0.02$$

suggestive of a much tighter exchange transition state. The $2p$ orbital would be involved in the formation of the transition state (presumably tetrahedral), and given the well-defined $2p$ orbital character, an important steric contribution might well be expected.

Activation Energies

The formation of this transition complex will involve two enthalpy terms; one exothermic equivalent to a one electron bond being formed, the other endothermic involving the geometrical reorganisation

tetrahedral → trigonal-bipyramidal

It would be useful to calculate these enthalpy terms with a view to comparing this with the competitive H abstraction process.

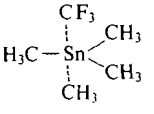

The overall enthalpy of the exchange reaction 1 will be approximately zero on the basis of one Sn—C bond being formed and one broken. The competitive H abstraction process has an overall exothermicity ~2 kcal. The energy diagram for the competitive processes using the experimental energies of activation may be depicted as follows.

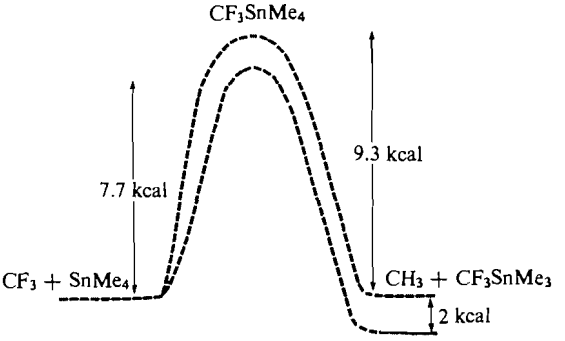

The lower energy of activation for the boron system (5.2 kcal) may well be due to a much higher B—C bond strength relative to the Sn—C system, yielding a greater exothermic contribution to the formation of the transition complex (presumably tetrahedral). Thus, for example, the Sn—C bond energy in $SnMe_4$ has been estimated (14) at 50 kcal mol^{-1}, and that for B—C in BMe_3 at 87 kcal mol^{-1} (16).

Such arguments are clearly speculative at this time.

Acknowledgment

We are grateful to the National Research Council of Canada for financial support.

1. T. N. Bell and A. E. Platt. Chem. Commun. 325 (1970).
2. T. N. Bell and A. E. Platt. Int. J. Chem. Kinet. **2**, 299 (1970).
3. T. N. Bell and A. E. Platt. Int. J. Chem. Kinet. **3**, 307 (1971).
4. D. A. Whytock and K. O. Kutschke. Proc. Roy. Soc. London, A**306**, 503 (1968).
5. T. N. Bell and U. F. Zucker. J. Phys. Chem. **74**, 979 (1970).
6. T. N. Bell and U. F. Zucker. Can. J. Chem. **47**, 1701 (1969).
7. T. N. Bell, R. Berkley, A. E. Platt, and A. G. Sherwood. Can. J. Chem. **52**, 3158 (1974).
8. R. D. Giles and E. Whittle. Trans. Faraday Soc. **61**, 1425 (1965).
9. A. J. Shepp. J. Chem. Phys. **24**, 939 (1956).
10. P. B. Ayscough. J. Chem. Phys. **24**, 944 (1956).

11. T. N. BELL, P. SLADE, and A. G. SHERWOOD. Can. J. Chem. **52**, 1662 (1974).
12. A. GANDINI and K. O. KUTSCHKE. Proc. R. Soc. London, A**306**, 511 (1968).
13. C. E. WARING and W. S. HORTON. J. Am. Chem. Soc. **67**, 540 (1945).
14. J. GROTEWOLD, E. A. LISSI, and J. C. SCAIANO. J. Chem. Soc. (B), 1187 (1971).
15. M. F. LAPPERT, J. SIMPSON, and T. R. SPALDING. J. Organomet. Chem. **17**, 1 (1969).
16. E. L. MUETTERTIES. The chemistry of boron and its compounds. John Wiley and Sons Inc. 1967. p. 502.

Can. J. Chem. Downloaded from www.nrcresearchpress.com by 210.87.254.40 on 09/05/12
For personal use only.

Absolute gas-phase acidities of CH_3NH_2, $C_2H_5NH_2$, $(CH_3)_2NH$, and $(CH_3)_3N$

GERVASE I. MACKAY,[1] RONALD S. HEMSWORTH,[2] AND DIETHARD K. BOHME[3]

Department of Chemistry, York University, Downsview, Ontario M3J 1P3

Received August 13, 1975

GERVASE I. MACKAY, RONALD S. HEMSWORTH, and DIETHARD K. BOHME. Can. J. Chem. **54**, 1624 (1976).

The flowing afterglow technique has been employed in measurements of the rate and equilibrium constants at 296 ± 2 K for reactions of the type

$$H^- + R_1R_2NH \rightleftarrows R_1R_2N^- + H_2$$

and

$$NH_2^- + R_1R_2NH \rightleftarrows R_1R_2N^- + NH_3$$

where R_1 and R_2 may be H, CH_3, or C_2H_5. The equilibrium constant measurements provided absolute values for the intrinsic (gas-phase) acidities of the Brønsted acids CH_3NH_2, $C_2H_5NH_2$, $(CH_3)_2NH$, and $(CH_3)_3N$, the heats of formation of their conjugate bases, and the electron affinities of the corresponding radicals R_1R_2N. Proton removal energies, ΔG^0_{298}/(kcal mol^{-1}), were determined to be 395.7 ± 0.7 for $CH_3NH_2 \rightleftarrows CH_3NH^- + H^+$, 391.7 ± 0.7 for $C_2H_5NH_2 \rightleftarrows C_2H_5NH^- + H^+$, 389.2 ± 0.6 for $(CH_3)_2NH \rightleftarrows (CH_3)_2N^- + H^+$, and >396 for $(CH_3)_3N \rightleftarrows (CH_3)_2NCH_2^- + H^+$. Heats of formation, $\Delta H^0_{f,298}$, were determined to be 30.5 ± 1.5 for CH_3NH^-, 21.2 ± 1.5 for $C_2H_5NH^-$, and 24.7 ± 1.4 for $(CH_3)_2N^-$. Electron affinities (in kcal mol^{-1}) were determined to be 13.1 ± 3.5 for CH_3NH, 17 ± 4 for C_2H_5NH, and 14.3 ± 3.4 for $(CH_3)_2N$. These results quantify earlier conclusions regarding the intrinsic effects of substituents on the gas-phase acidity of amines and provide an experimental assessment of recent molecular orbital calculations of proton removal energies for alkylamines.

GERVASE I. MACKAY, RONALD S. HEMSWORTH et DIETHARD K. BOHME. Can. J. Chem. **54**, 1624 (1976).

On a utilisé la technique de la lueur d'écoulement pour mesurer les vitesses et les constantes d'équilibres à 296 ± 2 K des réactions de type

$$H^- + R_1R_2NH \rightleftarrows R_1R_2N^- + H_2$$

et

$$NH_2^- + R_1R_2NH \rightleftarrows R_1R_2N^- + NH_3$$

où R_1 et R_2 peuvent être H, CH_3 ou C_2H_5. Les mesures des constantes d'équilibres fournissent des valeurs absolues pour les acidités intrinsèques (en phase gaseuse) des acides de Brønsted CH_3NH_2, $C_2H_5NH_2$, $(CH_3)_2NH$ et $(CH_3)_3N$ de même que les chaleurs de formation de leurs bases conjugées et les affinités électroniques des radicaux R_1R_2N correspondants. On a déterminé les énergies ΔG^0_{298}/(kcal mol^{-1}) nécessaires pour enlever les protons; les valeurs s'établissent à 395.7 ± 0.7 pour $CH_3NH_2 \rightleftarrows CH_3NH^- + H^+$, à 391.7 ± 0.7 pour $C_2H_5NH_2 \rightleftarrows C_2H_5NH^- + H^+$ à 389.2 ± 0.6 pour $(CH_3)_2NH \rightleftarrows (CH_3)_2N^- + H^+$ et à >396 pour $(CH_3)_3N \rightleftarrows (CH_3)_2NCH_2^- + H^+$. On a déterminé que les chaleurs de formation, $\Delta H^0_{f,298}$, sont 30.5 ± 1.5 pour CH_3NH^-, 21.2 ± 1.5 pour $C_2H_5NH^-$ et 24.7 ± 1.4 pour $(CH_3)_2N^-$. On a déterminé que les affinités électroniques (en kcal mol^{-1}) sont 13.1 ± 3.5 pour CH_3NH, 17 ± 4 pour C_2H_5NH et 14.3 ± 3.4 pour $(CH_3)_2N$. Ces résultats permettent d'établir d'une façon quantitative les conclusions antérieures se rapportant aux effets intrinsèques des substituants sur l'acidité en phase gaseuse des amines et fournissent une base expérimentale pour des calculs d'orbitales moléculaires récents concernant les énergies d'enlèvement de protons des alkylamines.

[Traduit par le journal]

Introduction

Recent developments in experimental techniques (1), *viz.* pulsed ion cyclotron resonance, pulsed electron beam high-pressure mass spec-

[1]This work was presented by G. I. Mackay in partial fulfilment of the Ph.D. requirements.

[2]Present address: Culham, UKAEA Research Group, Abingdon, Berkshire, England.

[3]Alfred P. Sloan Research Fellow, 1974–1976.

Can. J. Chem. Downloaded from www.nrcresearchpress.com by 210.87.254.105 on 09/05/12
For personal use only.

Can. J. Chem. Downloaded from www.nrcresearchpress.com by 210.87.254.105 on 09/05/12
For personal use only.

trometry, and the flowing afterglow technique, have provided a means of measuring, in the gas phase, rate and equilibrium constants for ion–molecule reactions of the type often encountered in solution. In the case of proton transfer reactions such measurements have proven to be useful for (*i*) the determination of intrinsic molecular properties of acids and their conjugate bases, (*ii*) the experimental assessment of molecular orbital calculations of such properties, and (*iii*) the thermodynamic analysis of the transfer of protonated species from the gas phase to solution. Aliphatic amines represent an important group of acids whose gas-phase acidities have recently been ordered (2) from determinations of the preferred direction of proton transfer reactions of the type

$$[1] \quad R_1R_2N^- + R_3R_4NH \rightleftarrows R_3R_4N^- + R_1R_2NH$$

In this paper we report flowing afterglow measurements of the rate and equilibrium constants at 296 ± 2 K for reactions of the type

$$[2] \quad NH_2^- + R_1R_2NH \rightleftarrows R_1R_2N^- + NH_3$$

$$[3] \quad H^- + R_1R_2NH \rightleftarrows R_1R_2N^- + H_2$$

where R_1 and R_2 may be H, CH_3, or C_2H_5. The equilibrium constant measurements provide absolute values for the intrinsic (gas-phase) acidities of the Brønsted acids CH_3NH_2, $C_2H_5NH_2$, $(CH_3)_2NH$, and $(CH_3)_3N$, the heats of formation of their conjugate bases, and the electron affinities of the corresponding radicals R_1R_2N. These results quantify earlier conclusions (based on measurements of orders of acidity) regarding the intrinsic effects of substituents on the gas-phase acidity of amines (2) and also provide an experimental assessment of recent molecular orbital calculations of proton removal energies for alkylamines (3–5).

Experimental

The experiments were performed with the flowing afterglow technique and are of the type described previously (6). Reactant ions are produced in a flowing plasma either by electron impact or by secondary ionization or ion–molecule reactions. In these experiments the plasma was generated with ionizing electrons having energies in the range 35–70 eV. The filament emission of the electron gun was 0.5 mA.

The neutral reactant is introduced sufficiently downstream of the ion production region to ensure that the reactant ions have undergone enough collisions with the carrier gas (helium was used in the experiments reported here) to become thermalized at the ambient room temperature (296 ± 2 K). The plasma communicates with a quadrupole mass spectrometer through a small orifice mounted at the tip of a sampling nose cone. Rate constants and equilibrium constants for reactions of ions with molecules are determined by measuring changes in ion signals as a function of the addition of neutral reactant molecules.

The gases used were He (Linde, Prepurified Grade, 99.995% He), NH_3 (Matheson, Anhydrous 99.99% min (liquid phase)), H_2 (Linde, Very Dry Grade 99.95% H_2), CH_3NH_2 (Matheson, 98.0% min (liquid phase)), $C_2H_5NH_2$ (Matheson, 98.5% min (liquid phase)), $(CH_3)_2NH$ (Matheson, 99.0% min (liquid phase)), and $(CH_3)_3N$ (Matheson, 99.0% min (liquid phase)).

The determination of the flows of the amines required a separate measurement of their viscosities. The viscosities were determined relative to the well-established values for H_2 and He. For Poiseuille flow through a fixed capillary from a fixed reservoir

$$[4] \quad \frac{\eta_1}{\eta_2} = \left(\frac{\Delta p}{\frac{1}{p}\frac{dp}{dt}}\right)_1 \left(\frac{\Delta p}{\frac{1}{p}\frac{dp}{dt}}\right)_2^{-1}$$

where η is the viscosity, Δp is the pressure drop across the capillary, and p is the pressure in the reservoir. The ratio of viscosities of two pure gases can, therefore, be determined directly from measurements of Δp, p, and the rate of fall of pressure, dp/dt, for the flow of the two gases through a fixed capillary. The viscosities measured for the amines at 296 ± 2 K were: 112 μP for CH_3NH_2, 92.9 μP for $C_2H_5NH_2$, 99.8 μP for $(CH_3)_2NH$, and 96 μP for $(CH_3)_3N$. Independent measurements with gases of known viscosities, *viz.* CO, N_2, and Ar, indicated an accuracy for this method of better than 5%.

All experiments were carried out at a room temperature of 296 ± 2 K.

Data Analysis

The analytical techniques used for the determination of rate and equilibrium constants from the raw flowing afterglow data for reactions of the type

$$[5] \quad A^- + BH \underset{k_r}{\overset{k_f}{\rightleftharpoons}} B^- + AH$$

have been described in detail previously (6). Expressions have been derived for obtaining, from a fit to the decay of the A^- signal, values for k_f when the extent of reverse reaction is negligible (the reaction is far removed from equilibrium) and for k_f and k_r when appreciable back reaction is taking place (the reaction approaches equilibrium). When equilibrium is actually attained the fitting procedure allows a determination only of unique values for the ratio of rate constants, *viz.* k_f/k_r. The expressions developed for these analyses take into account

Can. J. Chem. Downloaded from www.nrcresearchpress.com by 210.87.254.105 on 09/05/12
For personal use only.

the loss of A^- and B^- ions due to ambipolar radial and axial diffusion as well as effects introduced by the neutral gas inlet and sampling port. Equilibrium constants are obtained from the ion signal ratio, $(B^-)/(A^-)$, measured at equilibrium. Mass discrimination factors are deduced from the stoichiometry of reaction 5.

In previous equilibrium studies of reactions of type [5] the reactant gases BH and AH were of high ($\geqslant 99.9\%$) purity and the reactions proceeded generally in the absence of competing and secondary processes. This was often not the case for the systems investigated here. The commercially available amines contained impurities as large as 2% (liquid phase) and in several instances competing and secondary reactions were encountered. Consequently we had to consider in our analysis of some of the data the more general scheme represented by

$$\begin{array}{ccc} A^- + BH & \underset{k_r}{\overset{k_f}{\rightleftharpoons}} & B^- + AH \\ k_f' \downarrow \; BH(XH) & & k_r' \downarrow \; AH(YH) \\ k_f'' \downarrow \; AH(YH) & & k_r'' \downarrow \; BH(XH) \end{array}$$

where XH and YH are impurities present in BH and AH respectively and k' and k'' are the rate constants for competing or secondary reactions. The kinetic equations for this scheme were solved exactly (7); diffusion was neglected. Model calculations incorporating realistic values for the concentrations of the impurities and the various rate constants were performed to indicate the effect of competing as well as secondary reactions on the decay of the reactant ion, $d \ln [A^-]/dF_{BH}$, the rise of the product ion, $d \ln [B^-]/dF_{BH}$, the ratio plot, $d([B^-]/[A^-])/dF_{BH}$, and the mass discrimination plot, $d[A^-]/d[B^-]$, all at various flows of AH, F_{AH}. A number of special cases were considered. The following observations were made for values of $k_f = 1 \times 10^{-9}$ cm^3 molecule^{-1} s^{-1}, $k_r = 1 \times 10^{-11}$ cm^3 molecule^{-1} s^{-1} (*viz.* $K = 100$), $F_{BH} < 10^{19}$ molecule s^{-1}, 10^{17} molecule s^{-1} $< F_{AH} < 10^{20}$ molecule s^{-1}, and a reaction time of 10 ms. These reaction parameters and operating conditions are typical of the experiments whose results are reported in this paper.

(1) Further Reactions of A^- with AH(YH)

In studies of the equilibria for reactions of type [5], AH is added into the reaction region in large excess to that generated by reaction. The AH is usually added upstream of the ionizer since AH often serves as the source gas for A^-. Reactions of A^- with AH or an impurity YH in AH result in a depressed initial A^- signal and give rise to increased curvature in the A^- decay, a shallow maximum in the ratio plot and curvature in the mass discrimination plot whose initial slope will yield a low value for the mass discrimination factor. At sufficiently high values of F_{BH} the A^- signal approaches the unperturbed value and the ratio $[B^-]/[A^-]$ asymtotically approaches the unperturbed ratio. At moderate flows of BH the extent of deviation from the unperturbed behaviour will depend on the relative rates of the proton transfer reaction of A^- with BH and possible reactions of A^- with AH and YH.

For the systems under study and the adopted experimental operating parameters, $k_f[BH] \geqslant 100k_f''[AH]$ and $100k_f''[YH]$ at moderate flows of BH. Under these conditions the apparent values of k_f/k_r (determined from the fit to the A^- decay), K (determined from the ratio plot), and m (determined from the m plot) will be within 90% of the true values.

(2) Further Reactions of B^- with AH(YH)

Competing reactions of B^- with AH(YH) serve as sinks for B^- which may prevent the establishment of equilibrium even at large flows of BH. They lead to decreased curvature in the A^- decay, a maximum in the B^- signal prior to the establishment of an asymptotic value, an asymptotic approach to the unperturbed concentration ratio, $[B^-]/[A^-]$, and curvature in the mass discrimination plot whose initial slope will yield a high value for the mass discrimination factor. The extent of the deviation from the unperturbed behaviour will depend on the relative rates of the proton transfer reaction of B^- with AH and the competing reactions of B^- with AH and YH. For the systems under study and the adopted experimental operating parameters $k_r[AH] \geqslant k_r'[AH]$ and $k_r'[YH]$. Under these conditions the apparent value of k_f/k_r is within 10%, of K is within 1%, and of m is within 20% of the true value.

(3) Further Reactions of both A^- and B^- with AH(YH)

For the special case when $k_f'' = k_r'$ the reactions of B^- with AH(YH) and of A^- with

Can. J. Chem. Downloaded from www.nrcresearchpress.com by 210.87.254.105 on 09/05/12
For personal use only.

AH(YH) act to depress the product and reactant ion signals without altering the shapes of the various ion profiles, *viz.* d ln $[A^-]/dF_{BH}$, d ln $[B^-]/dF_{BH}$, $d([B^-]/[A^-])/dF_{BH}$, and $d[A^-]/d[B^-]$. Differences in these two rate constants of course lead to either case *1* or case *2*.

(4) Further Reactions of A^- with BH(XH)

For the operating conditions and reaction parameters typical of the studies reported here, the occurrence of reactions of A^- with BH and/or reactions of A^- with impurities, XH, does not lead to any characteristic perturbations in the shapes of the decay of A^-, the production of B^-, and the variation of $[B^-]/[A^-]$ with addition of BH(XH). The mass discrimination plot shows curvature at low $[A^-]$ and yields a value for m which is too high. The best fit to the A^- decay and the ratio plot would lead to values for an apparent equilibrium constant approximately equal to $(k_f + k_f')/k_r$ and/or $(k_f + k_f'[XH]/[BH])/k_r$. For the studies reported here $k_f' \leqslant 0.1\, k_f$ and $k_f[BH] \geqslant 0.02k_f'[XH]$, so that the values of the apparent equilibrium constant should be within *ca.* 10% of the value of the true equilibrium constant.

(5) Further Reactions of B^- with BH(XH)

In contrast to competing reactions of A^- with BH(XH), secondary reactions of B^- with BH(XH) can have a marked influence on the shapes of the ion profiles characteristic of the unperturbed equilibrium. The curvature in the A^- decay will be decreased (if $k_r''[BH]$ or $k_r''[XH] > k_r[AH]$ the decay cannot be fitted with the standard analysis), the B^- production will reach a maximum at low additions of BH, the ratio $[B^-][AH]/[A^-][BH]$ will not converge to a constant value, and the sign of the slope of the mass discrimination plot will change at low $[A^-]$.

(6) Further Reactions of both A^- and B^- with BH(XH)

For the special case when $k_r'' = k_f'$ the ratio $[B^-][AH]/[A^-][BH]$ does converge to a constant value which provides a measure of the true equilibrium constant if the mass discrimination factor is known. The sign of the slope of the mass discrimination plot still changes at low $[A^-]$. The slope approaches the true value of m at high $[A^-]$, *viz.* in the limit of little conversion of A^- to B^-. The curvature in the A^- decay is still decreased and the B^- production still reaches a maximum value at low additions of BH. A fit to the curvature in the A^- decay will result in a high value for k_f/k_r.

Results

The extended analysis given above proved to be most valuable for predicting the operating conditions under which the rates of competing and/or secondary reactions were sufficiently depressed to allow an adequate determination of the true rate and equilibrium constants of the proton transfer reaction of interest with the application of the standard analysis. The shapes of the mass discrimination plots as well as, of course, the observed changes in the total mass spectrum proved to be the most sensitive indicators of the presence of competing and/or secondary reactions. In the experiments reported here special care was required to avoid complications which could be introduced by the occurrence of clustering reactions either of the type

$$[6a] \qquad A^- + AH + M \rightleftarrows A^-\cdot AH + M$$

or of the type

$$[6b] \qquad B^- + BH + M \rightleftarrows B^-\cdot BH + M$$

and by the occurrence of reactions with impurities in CH_3NH_2 and $C_2H_5NH_2$. This was accomplished either with a judicious choice of the flows of AH and BH and the reaction time or with a study of the reverse direction of reaction. Complications introduced by clustering reactions of the types

$$[6c] \qquad A^- + BH + M \rightleftarrows A^-\cdot BH + M$$

$$[6d] \qquad B^- + AH + M \rightleftarrows B^-\cdot AH + M$$

and two-body secondary or competing reactions with BH or AH were generally not encountered.

The rate and equilibrium constants determined for the reactions of types [2] and [3] investigated in this study are summarized in Tables 1 and 2. Only those values are included for whose determination the effects of competing and secondary reactions were negligible, so that the standard analysis was applicable. Under less ideal conditions the extended analysis was employed but only to establish further confidence in the results. The results obtained for the individual reactions are described in detail

Can. J. Chem. Downloaded from www.nrcresearchpress.com by 210.87.254.105 on 09/05/12
For personal use only.

TABLE 1. Summary of the experimentally determined values and precisions for $(k_f/k_r)_{ne}$, $(k_f/k_r)_e$ and K at 296 ± 2 K for proton transfer reactions of the type $X^- + YH \rightleftarrows Y^- + XH$ involving H_2, NH_3, and several amines

Reaction	$(k_f/k_r)_{ne}$[a]		$(k_f/k_r)_e$[a]				K[b]			
	N[c]	Forward	N[c]	Forward	N[c]	Reverse	N[c]	Forward	N[c]	Reverse
$NH_2^- + H_2 \rightleftarrows H^- + NH_3$	2	23±2 (8)	2	28±1 (8)			4	27±2 (8)		
$NH_2^- + CH_3NH_2 \rightleftarrows CH_3NH^- + NH_3$					3	2.44±0.18	5	2.25±0.13	3	2.44±0.20
$CH_3NH^- + H_2 \rightleftarrows H^- + CH_3NH_2$	4	13±2					3	11.0±0.2		
$NH_2^- + C_2H_5NH_2 \rightleftarrows C_2H_5NH^- + NH_3$	5	(1.3±0.3)×10³					4	(1.3±0.3)×10³		
$H^- + C_2H_5NH_2 \rightleftarrows C_2H_5NH^- + H_2$			1	65	1	76	1	80	3	83±27
$H^- + (CH_3)_2NH \rightleftarrows (CH_3)_2N^- + H_2$	2	(5.2±1.3)×10³	1	4.8×10³			2	(5.4±1.1)×10³		

[a]Analysis B (6).
[b]Analysis C (6).
[c]N represents the number of experimental determinations.

TABLE 2. Summary of the experimental measurements at 296 ± 2 K of rate constants (in units of 10^{-9} cm^3 molecule^{-1} s^{-1}) and equilibrium constants for proton transfer reactions of the type $X^- + YH \rightleftarrows Y^- + XH$ involving H_2, NH_3, and several amines

Reaction	$k_{forward}$[a]	N[b]	K[c]	N[b]
$NH_2^- + H_2 \rightleftarrows H^- + NH_3$	0.023±0.005 (8)	5	26±6 (8)	8
$NH_2^- + CH_3NH_2 \rightleftarrows CH_3NH^- + NH_3$	≥0.1		2.4±0.4	11
$CH_3NH^- + H_2 \rightleftarrows H^- + CH_3NH_2$	0.20±0.06	4	12±3	7
$NH_2^- + C_2H_5NH_2 \rightleftarrows C_2H_5NH^- + NH_3$	2.6±0.8	5	(1.3±0.4)×10^3	11
$H^- + C_2H_5NH_2 \rightleftarrows C_2H_5NH^- + H_2$	1.1±0.3	4	77±14	6
$H^- + (CH_3)_2NH \rightleftarrows (CH_3)_2N^- + H_2$	4.3±0.9	4	(5.2±1.1)×10^3	5
$NH_2^- + (CH_3)_2NH \rightleftarrows (CH_3)_2N^- + NH_3$	≃3			
$NH_2^- + (CH_3)_3N \rightarrow$	≲0.001			

[a]Values of $k_{forward}$ were determined using either Analysis A or B (6). The limits given along with the mean value represent the estimated accuracy.
[b]N is the number of experiments.
[c]The value for K represents the weighted mean together with its standard error of measurements including one or more of $(k_f/k_r)_c$, $(k_f/k_r)_{nc}$, and K_{ratio} in one or both directions of the reaction (6).

below. An account of the usual sources of error has been given previously (6).

In the remainder of this section the best estimate of a true value is taken to be the mean of a series of measurements. The limits given along with the mean value represent the best estimate of the precision (9).

[7] $NH_2^- + CH_3NH_2 \rightleftarrows CH_3NH^- + NH_3$

Figure 1 shows the variation of the dominant negative ions observed upon the addition of methylamine into a flowing NH_3–He plasma in which NH_2^- is initially a major negative ion. The behaviour shown is representative of the observations made in five separate experiments performed under similar conditions: effective reaction length, L = 60 cm, average flow velocity, $\bar{v}$ = 8.8–8.9 × 10^3 cm s^{-1}, total pressure, p = 0.426–0.452 torr, and flow of NH_3 = 1.19–1.27 × 10^{19} molecule s^{-1}. The ions CN^- and Cl^- which are usual impurity ions detected in the mass spectrum were also monitored but are not included in Fig. 1 as they were observed to be insensitive to the added CH_3NH_2. Helium was used as the buffer gas in all experiments and the NH_2^- ion was produced via electron impact of *ca.* 40 eV on NH_3.

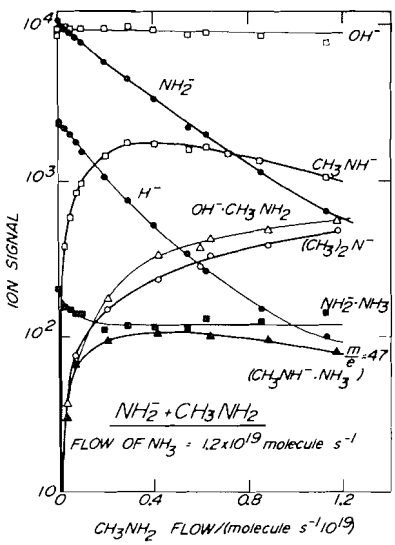

FIG. 1. The variation of the major negative ion signals recorded upon the addition of CH_3NH_2 into a flowing NH_3–He plasma in which NH_2^- is initially a major ion. T = 297 K, p = 0.433 torr, $\bar{v}$ = 8.8 × 10^3 cm s^{-1}, and L = 60 cm.

The decay of the NH_2^- signal and the accompanying increase in the CH_3NH^- signal can be attributed for the most part to the occurrence in the reaction region of the proton transfer reaction 7. For the adopted experimental conditions however, a number of alternate sinks and sources for NH_2^- and CH_3NH^- have to be considered.

Possible alternate sinks for NH_2^- are the displacement reaction

[7a] $NH_2^- + CH_3NH_2 \rightarrow H^- +$ Neutral products

and reactions with the major impurities, *viz.* H_2O, $(CH_3)_2NH$, and $(CH_3)_3N$, which are present in the CH_3NH_2 reactant gas

[8] $NH_2^- + H_2O \rightarrow OH^- + NH_3$

Can. J. Chem. Downloaded from www.nrcresearchpress.com by 210.87.254.105 on 09/05/12
For personal use only.

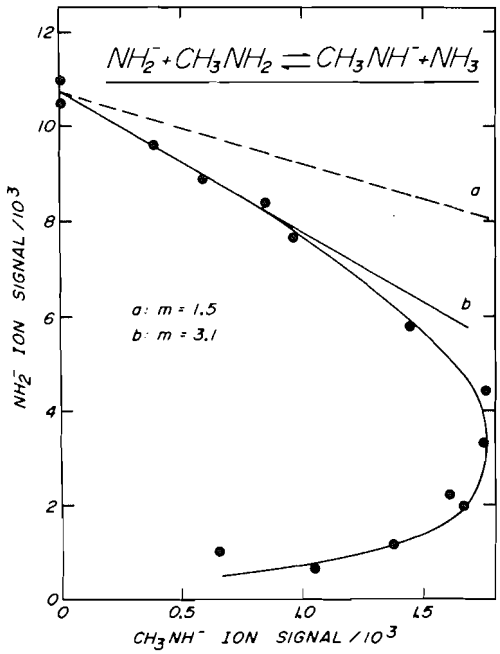

FIG. 2. A plot of the NH_2^- signal against the CH_3NH^- signal as a function of CH_3NH_2 addition for the data shown in Fig. 1. The curvature at low NH_2^- signals is indicative of secondary and/or competing reactions proceeding in either direction. Curve *a* is representative of the mass discrimination plot obtained from a study of the reverse direction of reaction which was observed to be uncomplicated by secondary or competing reactions. Curve *a* is normalized to the initial NH_2^- signal.

[9] $NH_2^- + (CH_3)_2NH \rightarrow (CH_3)_2N^- + NH_3$

Independent experiments which are discussed later in this section indicated that NH_2^- does not react rapidly with $(CH_3)_3N$. There was some evidence for the occurrence of reaction 7*a*; at very low flows of CH_3NH_2 the initial H^- signal actually increases slightly before decaying as a result of further reaction. The reactions with impurities are undoubtedly also occurring to some extent. The observed increase in the $(CH_3)_2N^-$ signal may result, at least in part, from the occurrence of reaction 9. The slight increase in the OH^- signal can be attributed to reaction 8. The ensuing decrease in the OH^- signal results from the three-body association reaction

[10] $OH^- + CH_3NH_2 + M \rightarrow OH^- \cdot CH_3NH_2 + M$

for which the product cluster is readily observed. An analysis of the observed increase in the $OH^- \cdot CH_3NH_2$ signal at low methylamine additions provided a value for $k_{10} \simeq 5 \times 10^{-29}$ cm^6 molecule^{-2} s^{-1}.

A number of reactions appear to be depleting the CH_3NH^- produced from reaction 7. Several secondary reactions with CH_3NH_2 are allowed on the basis of thermodynamic considerations

[11*a*] $CH_3NH^- + CH_3NH_2 \rightarrow NH_2^- + (CH_3)_2NH$

[11*b*] $\rightarrow (CH_3)_2N^- + NH_3$

[11*c*] $\rightarrow H^- +$ Neutral products

[11*d*] $\xrightarrow{M} CH_3NH^- \cdot CH_3NH_2$

One or more of these reactions may be responsible for the observed decrease in the CH_3NH^- signal at large methylamine additions. CH_3NH^- may also be depleted to some extent by proton transfer reactions with the H_2O and $(CH_3)_2NH$ impurities in CH_3NH_2. Finally, a fraction of the CH_3NH^- ions appear to be clustered with NH_3 (which is a fixed quantity in each experiment) as a result of the three-body association reaction

[12] $CH_3NH^- + NH_3 + M \rightarrow CH_3NH^- \cdot NH_3 + M$

An increase in the NH_3 flow was observed to result in an increase in the $CH_3NH^- \cdot NH_3$ production.

Reaction 11*a* represents a possible source of NH_2^- other than reaction '−7'. The proton transfer reaction

[−13] $H^- + CH_3NH_2 \rightarrow CH_3NH^- + H_2$

which accounts for the bulk of the H^- decay, represents an alternate source of CH_3NH^-. The H^- is also depleted to some extent as a result of fast proton transfer reactions with the H_2O and $(CH_3)_2NH$ impurities in methylamine.

The cluster ion $NH_2^- \cdot NH_3$, present in only small amounts in these experiments, appears not to react rapidly with CH_3NH_2. The initial decay in the $NH_2^- \cdot NH_3$ signal can be attributed entirely to the depletion in the reaction region of the precursor ion NH_2^-.

The observations shown in Fig. 1 and the considerations of the foregoing section indicate that the ion chemistry proceeding in the reaction region under the adopted experimental conditions is fairly complex. The mass discrimination plot shown in Fig. 2 provides further evidence of this complex behaviour. Such a plot should be linear with a slope of $-m$ if the proton transfer reaction 7 is the only reaction occurring,

Can. J. Chem. Downloaded from www.nrcresearchpress.com by 210.87.254.105 on 09/05/12
For personal use only.

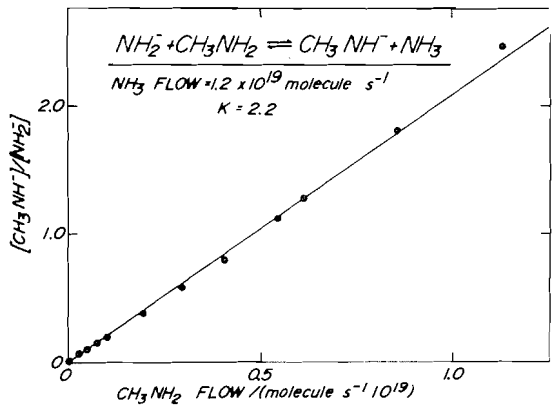

FIG. 3. The observed variation in the ratio of the product to the reactant ion signal corrected for mass discrimination, $[CH_3NH^-]/[NH_2^-]$, with addition of CH_3NH_2 at high back reactant NH_3 flows. T = 297 K, p = 0.433 torr, $\bar{v} = 8.8 \times 10^3$ cm s^{-1}, and L = 60 cm. The mass discrimination factor (m = 1.5) was determined from a study of the reaction in the reverse direction.

and will become non-linear in the presence of secondary and/or competing reactions. The shape of the m plot shown is consistent with the occurrence of competing reactions between NH_2^- and CH_3NH_2 (or impurity) and secondary reactions between CH_3NH^- and CH_3NH_2 (or impurity), cases *4* and *5* in the extended analysis, respectively. The curvature in the m plot of course prevents a direct determination of an accurate value for the mass discrimination factor (the initial slope provides only an upper limit). It was, therefore, decided to adopt the value of $m = 1.5 \pm 0.1$ determined from a study of reaction 7 in the reverse direction under similar sampling conditions. Included in Fig. 2 is a normalized mass discrimination plot obtained from a study of the reaction '−7' which was found to be uncomplicated by secondary and/or competing reactions.

Figure 3 shows the variation of the ratio of the product ion to reactant ion concentrations, $[CH_3NH^-]/[NH_2^-]$, as a function of the neutral reactant CH_3NH_2 flow for the data given in Fig. 1. This behaviour is representative of the observations made in all five experiments. Notwithstanding the complexity of the ion chemistry, the linearity of these ratio plots suggests that equilibrium is readily established, even for the lowest measurable additions of methylamine. The five measurements provided a value of $K = 2.25 \pm 0.13$ which should equal the value of the true equilibrium constant if the rates of secondary and/or competing reactions are not excessive. In order to obtain a measure of the extent of secondary and competing reactions the extended analysis was applied to a fit of the NH_2^- decay, the concomitant rise in the CH_3NH^- signal, and the mass discrimination plot. The extended analysis incorporated the reactions

[14] $NH_2^- + CH_3NH_2$ (impurity) → Products

[15] $CH_3NH^- + CH_3NH_2$ (impurity) → Products

Reactions 14 and 15 represent any or all of the possible competing and secondary reactions described above with methylamine and the impurities therein. The standard analysis which ignores reactions 14 and 15 allowed a fit to the NH_2^- decay only at low flows of CH_3NH_2. However, the extended analysis allowed a fit to the variation of both the NH_2^- and CH_3NH^- ions (and therefore the mass discrimination plot) over the entire range of CH_3NH_2 flows using the values $k_7/k_{-7} = 2.2$, $m = 1.4$, $k_7 = 15k_{14}$ and $k_{-7} = 10k_{15}$. Consequently, it appears that the rates of the competing and/or secondary reactions are not excessive and that the adopted value of m is in fact reasonable so that the value of K determined from the ratio plots should be very nearly equal to (within 10% of) the true value.

[−7] $CH_3NH^- + NH_3 \rightleftarrows NH_2^- + CH_3NH_2$

Reaction '−7' was investigated in order to minimize the complications due to competing and secondary reactions encountered in the study of reaction 7 and so to establish further confidence in the value for the equilibrium constant. The purity of the NH_3 is considerably better than that of CH_3NH_2 so that reactions with impurities present in the forward reactant will be reduced, while reactions with impurities in the methylamine, which is of constant concentration in the reaction region, will be unimportant so long as the rates of depletion of NH_2^- and CH_3NH^- are similar (case *3* in the extended analysis). This then leaves only complications due to any competing and secondary reactions with NH_3 and CH_3NH_2 as potential sources of error. Figure 4 shows the variation of the dominant negative ion signals recorded upon the addition of NH_3 into a CH_3NH_2–He plasma in which CH_3NH^- is initially a major negative ion. This behaviour is representative

Can. J. Chem. Downloaded from www.nrcresearchpress.com by 210.87.254.105 on 09/05/12
For personal use only.

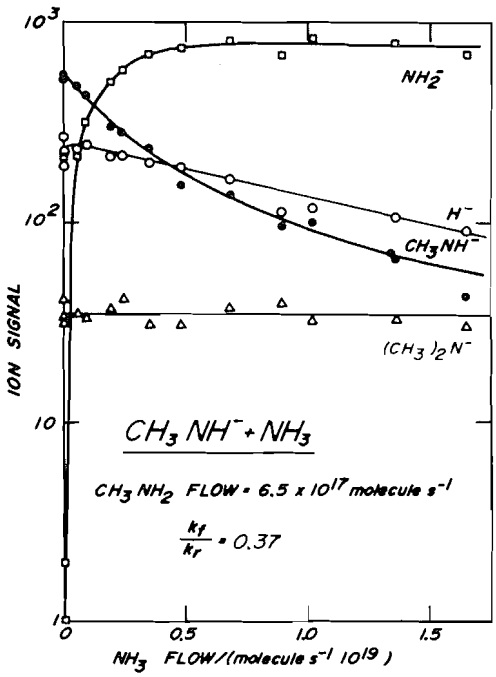

FIG. 4. The variation of the major negative ion signals recorded upon the addition of NH_3 into a flowing CH_3NH_2–He plasma in which CH_3NH^- is initially a dominant negative ion. The curve drawn through the observed CH_3NH^- decay represents a computed fit which yields a value for the ratio of rate constants, k_f/k_r, for the proton transfer reaction $CH_3NH^- + NH_3 \rightleftarrows NH_2^- + CH_3NH_2$. The ion observed at *m/e* 44 is presumed to arise from the $(CH_3)_2NH$ impurity in CH_3NH_2. T = 298 K, p = 0.295 torr, $\bar{v}$ = 9.3 × 10^3 cm s^{-1}, and L = 59 cm.

of the observations made in three separate experiments which were performed over the following range of reaction conditions: L = 59 cm, p = 0.287–0.296 torr, $\bar{v}$ = 9.3–9.4 × 10^3 cm s^{-1}, and CH_3NH_2 flow = 6.5 × 10^{17} – 2.13 × 10^{18} molecule s^{-1}. The usual impurity ions OH^-, CN^-, and Cl^- were also monitored but are not included in Fig. 4 as they were observed not to react rapidly with ammonia. The curvature in the decline of the reactant ion CH_3NH^- and the increase in the NH_2^- signal can be attributed to the occurrence of the proton transfer reaction '−7'. The observation that the $C_2H_6N^-$ ion (*m/e* 44) is insensitive to the addition of NH_3 is strongly suggestive that reaction 11*c*, while thermodynamically allowed, is nevertheless not a significant process at thermal energies. If this reaction were an important source of $(CH_3)_2N^-$ then the loss of its precursor ion CH_3NH^- would result in a corresponding decrease in the signal at *m/e* 44. Most likely the ion at *m/e* 44 observed in both the forward and reverse studies is $(CH_3)_2N^-$ arising from the dimethylamine impurity in the methylamine. Since NH_2^- and CH_3NH^- probably react with $(CH_3)_2NH$ with very similar rate constants the $(CH_3)_2N^-$ signal does not vary as reaction '−7' proceeds.

The H^- ion present in the CH_3NH_2–He plasma is in part a precursor of CH_3NH^- in the reaction region according to reaction '−13' which has a measured rate constant of (1.6 ± 0.5) × 10^{-11} cm^3 $molecule^{-1}$ s^{-1}. Also, Bohme *et al.* (8) have established that H^- reacts with NH_3 according to

$$[-16] \qquad H^- + NH_3 \rightarrow NH_2^- + H_2$$

which has a measured rate constant of (9.0 ± 1.8) × 10^{-13} cm^3 $molecule^{-1}$ s^{-1}. The decay of the H^- in Fig. 4 can therefore be attributed to reaction '−16' and, to a lesser extent, to the reaction of H^- with H_2O impurity in ammonia. Because of reaction '−13' the depletion of H^- by NH_3 contributes indirectly to the loss of CH_3NH^- in the reaction region. The decay of CH_3NH^- will of course also be influenced by any three-body contribution to the reaction of CH_3NH^- with NH_3, *viz.* 12. However, both these contributions to the CH_3NH^- decay were never sufficient to noticeably influence the ratio of rate constants obtained from the fit to the CH_3NH^- decay or the equilibrium constant obtained from the equilibrium ion and neutral concentrations present at the adopted experimental conditions. In all three experiments equilibrium was apparently attained for reaction '−7', already at the smallest additions of ammonia. This is demonstrated by the linearity at the lowest flows of NH_3 in the ratio plot shown in Fig. 5. Furthermore, the mass discrimination plots were observed to be linear over a large range of NH_3 flows. The slopes of these plots were independent of the CH_3NH_2 addition and provided an average value for m = 0.67 ± 0.04. These results also provide a good indication that any further reactions of NH_2^- and CH_3NH^- with CH_3NH_2 (or impurity) and NH_3 (or impurity) do not sufficiently perturb the equilibrium under investigation to prevent the applicability of our standard equilibrium analysis. The three ratio plots yielded a mean value for K_{-7} of 0.41 ± 0.04. Fitting of the CH_3NH^- decay

Can. J. Chem. Downloaded from www.nrcresearchpress.com by 210.87.254.105 on 09/05/12
For personal use only.

Can. J. Chem. Downloaded from www.nrcresearchpress.com by 210.87.254.105 on 09/05/12
For personal use only.

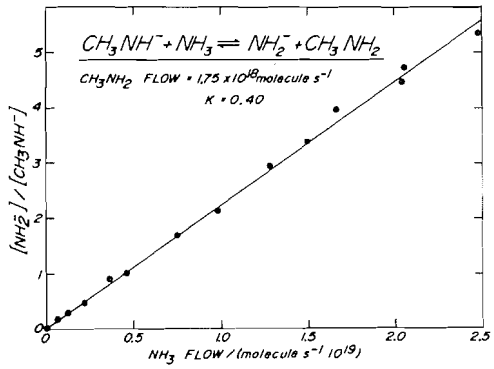

FIG. 5. The observed variation of the ion concentration ratio $[NH_2^-]/[CH_3NH^-]$, with NH_3 addition. The ion signal ratio was corrected for mass discrimination. The linearity of this plot indicates the attainment of equilibrium at all measured NH_3 flows. $T = 297$ K, $p = 0.287$ torr, $\bar{v} = 9.3 \times 10^3$ cm s^{-1}, $L = 59$ cm, and $m = 0.65$.

provided a unique value only for the ratio of rate constants $(k_{-7}/k_7)_e$. The mean value for $(k_{-7}/k_7)_e$ obtained from the three experiments was 0.41 ± 0.03. Fig. 4 includes a fit to the CH_3NH^- decay.

The initial slope in the decay of CH_3NH^- provides a lower limit for k_{-7} of $\sim 4 \times 10^{-11}$ cm^3 $molecule^{-1}$ s^{-1}. This result together with the observation that $k_{-7}/k_7 = 0.41$ provides a lower limit for k_7 of $\sim 1 \times 10^{-10}$ cm^3 $molecule^{-1}$ s^{-1}.

[13] $$CH_3NH^- + H_2 \rightarrow H^- + CH_3NH_2$$

The addition of H_2 to a CH_3NH_2–He plasma in which CH_3NH^- is initially a dominant ion resulted in the ion variation shown in Fig. 6. The entire decay of the CH_3NH^- signal was attributed to the proton-transfer reaction as there was no evidence for other reaction channels. Several alternative (thermodynamically allowed) reaction routes can be envisaged which result in the interconversion of CH_3NH^- and H^-, *viz.*

[17]

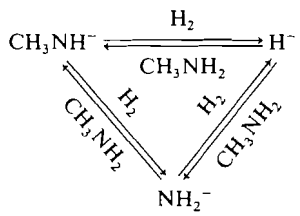

However there was no evidence for the rapid occurrence of these alternate routes; no NH_2^- was observed at low flows of H_2 and CH_3NH_2.

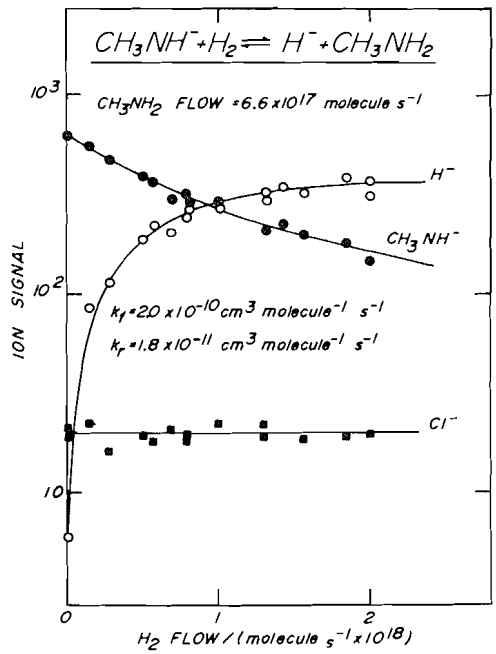

FIG. 6. A determination of the rate constants for the reaction of CH_3NH^- with H_2 from the best fit to the observed decay of CH_3NH^- upon addition of H_2 into a He–CH_3NH_2 plasma. $T = 297$ K, $p = 0.345$ torr, $\bar{v} = 8.3 \times 10^3$ cm s^{-1}, and $L = 60$ cm.

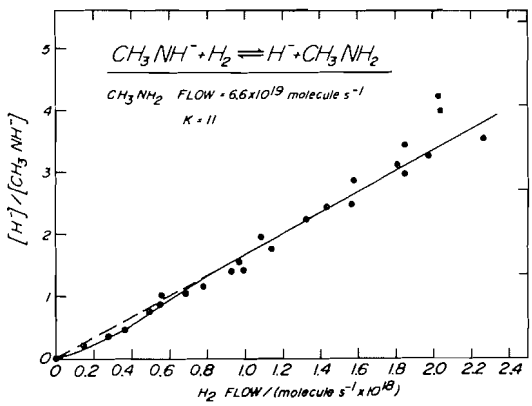

FIG. 7. The observed variation of $[H^-]/[CH_3NH^-]$ with H_2 flow showing the approach to and attainment of equilibrium for the reaction $CH_3NH^- + H_2 \rightleftarrows H^- + CH_3NH_2$. The best straight line through the data points at high H_2 flows yields a value for K of 11. $T = 297$ K, $p = 0.345$ torr, $\bar{v} = 8.3 \times 10^3$ cm s^{-1}, $L = 60$ cm, and $m = 1.4$.

Four separate experiments were performed over a range of flows of CH_3NH_2 from $3.84 \times 10^{17} - 6.6 \times 10^{18}$ molecule s^{-1}, a range of $\bar{v}$ from 8.3–9.1 $\times 10^3$ cm s^{-1}, and reaction lengths,

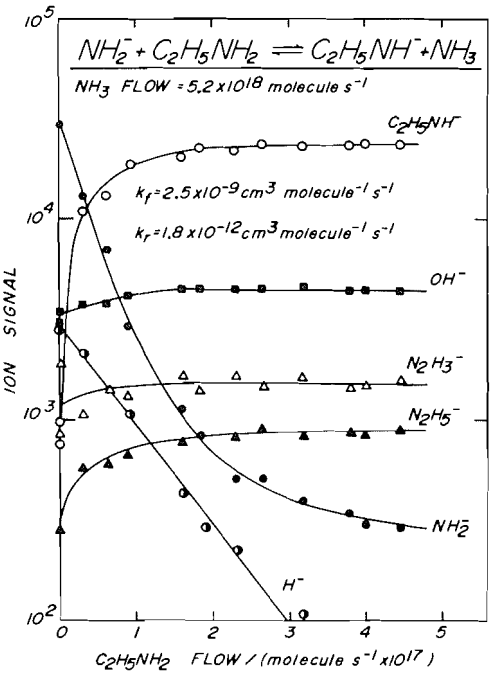

FIG. 8. The variation of the major negative ion signals recorded upon the addition of $C_2H_5NH_2$ into a NH_3–He plasma in which NH_2^- is initially dominant. The solid line drawn through the observed NH_2^- decay represents the best fit which provides the values indicated for the rate constants of the reaction $NH_2^- + C_2H_5NH_2 \rightleftarrows C_2H_5NH^- + NH_3$. $T = 295$ K, $p = 0.398$ torr, $\bar{v} = 8.2 \times 10^3$ cm s^{-1}, and $L = 85$ cm.

$L = 60$ and 84 cm. The total gas pressure, p, had values from 0.287–0.354 torr. Fitting of the four decays of CH_3NH^- using analysis B (6) resulted in unique values for both $k_{13} = (2.0 \pm 0.2) \times 10^{10}$ cm^3 molecule^{-1} s^{-1} and $k_{-13} = (1.6 \pm 0.3) \times 10^{-11}$ cm^3 molecule^{-1} s^{-1} and a mean value for $(k_{13}/k_{-13})_{nc} = 13 \pm 2$. In three of the four experiments equilibrium was established at high flows of H_2. Fig. 7 shows the ratio plot for one of these three experiments. The linear regions in all three ratio plots could be fitted with a value for $K_{13} = 11.0$.

[18] $NH_2^- + C_2H_5NH_2 \rightleftarrows C_2H_5NH^- + NH_3$

Figure 8 shows the variation of the dominant negative ion signals upon addition of $C_2H_5NH_2$ into a NH_3–He plasma in which NH_2^- is initially a major negative ion. Along with the usual unreactive impurity ions, ion signals were monitored at m/e 1, 16, 31, 33, and 44 which were identified as H^-, NH_2^-, $N_2H_3^-$, $N_2H_5^-$, and $C_2H_5NH^-$ respectively.

H^- initially present in the NH_3–He plasma reacts with $C_2H_5NH_2$ according to

[19] $H^- + C_2H_5NH_2 \rightarrow C_2H_5NH^- + H_2$

The $C_2H_5NH^-$ produced in this reaction contributes about 10% to the total $C_2H_5NH^-$ signal. The observed increases in the $N_2H_5^-$ and $N_2H_3^-$ signals can be ascribed either to additional channels for the forward reaction, *viz.*

[18*a*] $NH_2^- + C_2H_5NH_2 \rightarrow N_2H_5^- + C_2H_4$

[18*b*] $\rightarrow N_2H_3^- + C_2H_6$

or to additional channels for the reverse reaction, *viz.*

[−18*a*] $C_2H_5NH^- + NH_3 \rightarrow N_2H_5^- + C_2H_4$

[−18*b*] $\rightarrow N_2H_3^- + C_2H_6$

This latter possibility was however ruled out on the basis of the observed independence of the $C_2H_5NH^-/N_2H_5^-$ and $C_2H_5NH^-/N_2H_3^-$ ion signal ratios on the flow of NH_3. Finally the slight increase in the OH^- signal with $C_2H_5NH_2$ addition can be attributed to the reactions of H^-, NH_2^-, and $C_2H_5NH^-$ with H_2O impurity in $C_2H_5NH_2$ (10).

Five separate experiments were performed over a range of flows of NH_3 from 1.4–7.6 × 10^{18} molecule s^{-1} at total gas pressures, p, in the range 0.334–0.445 torr and effective reaction lengths, L, of 60 and 85 cm. The gas velocity, $\bar{v}$, had values in the range 8.1–8.6 × 10^3 cm s^{-1}. The standard equilibrium analysis adequately reproduced the behaviour of the NH_2^- and $C_2H_5NH^-$ ion signals under these operating conditions. The mass discrimination factor, the ratio of rate constants, and the equilibrium constant were observed to be independent of the flow of NH_3 and $C_2H_5NH_2$. Apparently the rates of the competing and secondary reactions were low enough to leave the equilibrium undisturbed. The application of the standard fitting procedure to the five decays of NH_2^- yielded unique values for $k_{18} = (1.6 \pm 0.1) \times 10^{-9}$ cm^3 molecule^{-1} s^{-1}, $k_{-18} = (1.1 \pm 0.5) \times 10^{-12}$ cm^3 molecule^{-1} s^{-1} and $(k_{18}/k_{-18})_{nc} = (1.3 \pm 0.3) \times 10^3$. The fit to the decay of NH_2^- in one of these experiments is shown in Fig. 8. In four of these experiments and two additional experiments performed at higher flows of NH_3

Can. J. Chem. Downloaded from www.nrcresearchpress.com by 210.87.254.105 on 09/05/12
For personal use only.

Can. J. Chem. Downloaded from www.nrcresearchpress.com by 210.87.254.105 on 09/05/12
For personal use only.

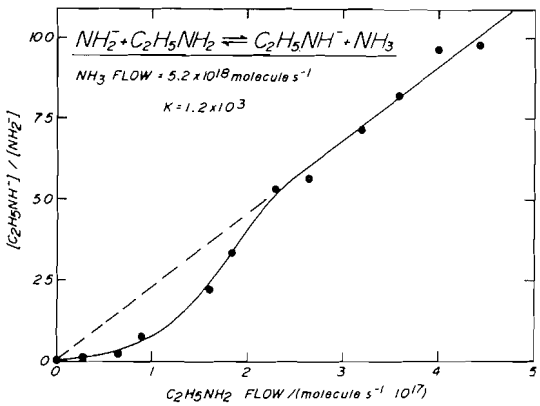

FIG. 9. The observed variation in the ion concentration ratio $[C_2H_5NH^-]/[NH_2^-]$ as a function of $C_2H_5NH_2$ addition showing the approach to and attainment of equilibrium for the reaction $NH_2^- + C_2H_5NH_2 \rightleftarrows C_2H_5NH^- + NH_3$. The best straight line through the points at high $C_2H_5NH_2$ flows yields a value of $K = 1.2 \times 10^3$. $T = 295$ K, $p = 0.398$ torr, $\bar{v} = 8.2 \times 10^3$ cm s^{-1}, $L = 85$ cm, and $m = 1.2$.

(1.9 and 4.4 × 10^{19} molecule s^{-1}) equilibrium was achieved at high flows of $C_2H_5NH_2$ as illustrated in Fig. 9. The slopes of the linear portions in the ratio plots yielded a value for $K_{18} = (1.3 \pm 0.3) \times 10^3$ which is in good agreement with the ratio of rate constants determined with the fitting procedure.

[19] $$H^- + C_2H_5NH_2 \rightleftarrows C_2H_5NH^- + H_2$$

The observed decay of the H^- signal and the accompanying rise in the $C_2H_5NH^-$ signal with addition of $C_2H_5NH_2$ into a NH_3–H_2–He plasma is shown in Fig. 10. The H^- is produced by electron impact on NH_3. Sufficient H_2, which acts as the back reactant in this experiment, was added downstream of the ionizer to remove NH_2^- prior to the reaction region via reaction 16 which also provides an additional source of H^-. The addition of small amounts of $C_2H_5NH_2$ into the reaction region gave rise to sampling effects reminiscent of our experiences with NH_3 (8) and also CH_3NH_2. The sampling effects which are evidenced by the sharp initial increase in the Cl^- signal shown in Fig. 10 discouraged an extensive study of this reaction in this direction. At higher additions of $C_2H_5NH_2$ the ion signals stabilize to reproducible values. The fit to the H^- decay shown in Fig. 10 gave a value for $(k_{19}/k_{-19})_c = (7 \pm 3) \times 10$ whereas the ratio plot shown in Fig. 11 yielded $K_{19} =$

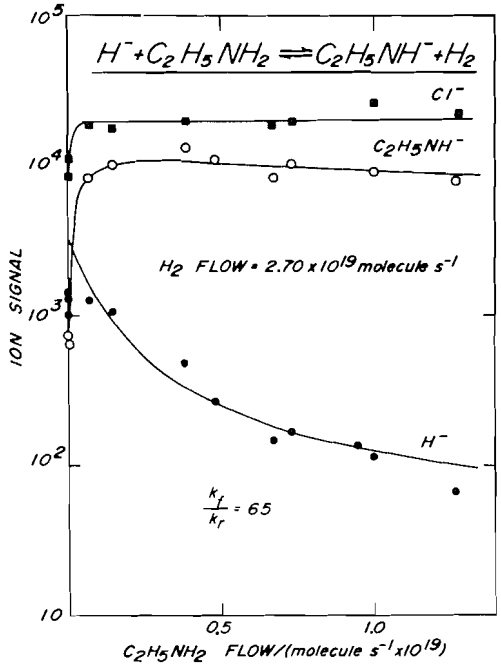

FIG. 10. The variation of major negative ion signals recorded upon the addition of $C_2H_5NH_2$ into a NH_3–H_2–He plasma. The solid line drawn through the observed H^- decay represents the fit which provides the value indicated for k_f/k_r of the reaction $H^- + C_2H_5NH_2 \rightleftarrows C_2H_5NH^- + H_2$. $T = 298$ K, $p = 0.316$ torr, $\bar{v} = 8.4 \times 10^3$ cm s^{-1}, and $L = 59$ cm. The flow of $NH_3 = 5 \times 10^{17}$ molecule s^{-1}.

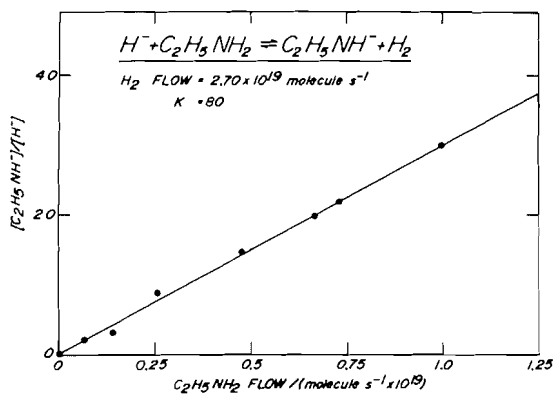

FIG. 11. The observed variation in $[C_2H_5NH^-]/[H^-]$ as a function of $C_2H_5NH_2$ flow for the data shown in Fig. 10. The best straight line through the points yields a value for $K = 80$. $m = 0.4$.

$(8 \pm 3) \times 10$. The large uncertainty in the value for K arises from the uncertainty introduced in the determination of the mass dis-

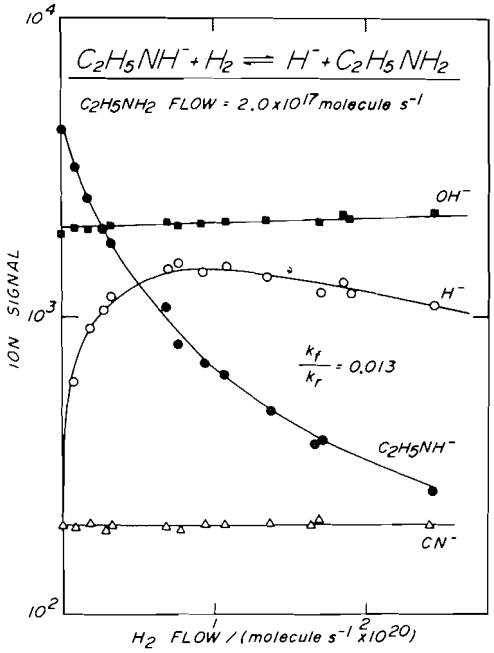

FIG. 12. The variation of the reactant $C_2H_5NH^-$ and product H^- ions upon the addition of H_2 into a $C_2H_5NH_2$–He plasma in which $C_2H_5NH^-$ is initially a dominant ion. The solid line through the $C_2H_5NH^-$ decay is a fit which provides a value for k_f/k_r of 0.013. $T = 298$ K, $p = 0.309$ torr, $\bar{v} = 8.9 \times 10^3$ cm s^{-1}, and $L = 59$ cm.

crimination factor by the unfavourable sampling conditions.

The rate constant for reaction 19 was determined from the earlier studies of reaction 18. In these latter experiments the small amounts of H^- present in the absence of H_2 were observed to react rapidly with $C_2H_5NH_2$ (see Fig. 8) with a rate constant $k_{19} = (1.1 \pm 0.1) \times 10^{-9}$ cm^3 $molecule^{-1}$ s^{-1}.

$$[-19] \quad C_2H_5NH^- + H_2 \underset{k_f}{\overset{k_r}{\rightleftharpoons}} H^- + C_2H_5NH_2$$

The decay of the $C_2H_5NH^-$ signal and the concomitant increase in the product H^- signal observed upon the addition of hydrogen into a $C_2H_5NH_2$–He plasma is shown in Fig. 12. The slight increase in the OH^- signal with H_2 addition may be attributed to the proton transfer reactions of H^- and $C_2H_5NH^-$ with H_2O both of which are rapid at 297 K (10). The water vapour impurity arises from two sources, that present in the back reactant $C_2H_5NH_2$, and that introduced with the H_2. The rate constant for the reaction of H^- with H_2O is almost three times as large as the rate constant for the reaction of $C_2H_5NH^-$ with H_2O so that part of the increase in the OH^- signal will arise from the more rapid reaction of the product H^- with the water vapour present in the back reactant ethylamine. The slight decrease in the H^- signal at large hydrogen flows may be ascribed to the reaction of H^- with the H_2O present in the forward reactant hydrogen. Three experiments were carried out under the following range of conditions: $\bar{v} = 8.4$–8.9 cm^3 s^{-1}, $p = 0.309$–0.316 torr, $L = 59$ and 85 cm, and $C_2H_5NH_2$ flow = 1.75–7.3×10^{17} molecule s^{-1}. The maximum H_2 flow was 2.4×10^{20} molecule s^{-1}. An extended analysis which included the further reaction of both H^- and $C_2H_5NH^-$ with the quoted levels of water impurity in the H_2 and $C_2H_5NH_2$ indicated that the standard analysis of the $C_2H_5NH^-$ decay under these operating conditions should provide values for the rate constants within 10% of the true values for flows of $C_2H_5NH_2$ below $\sim 3 \times 10^{17}$ molecule s^{-1}. Figure 12 shows a fit to the $C_2H_5NH^-$ decay as determined with the standard analysis. This fit provided a value for $k_{-19}/k_{19} = 0.013$. The extended analysis also indicated that the occurrence of the reactions of H^- and $C_2H_5NH^-$ with the H_2O impurities in H_2 and $C_2H_5NH_2$ would not noticeably influence the determination of the equilibrium constant from the equilibrium concentrations present under the chosen operating conditions and that the true value of the mass discrimination factor could be obtained from the data taken at low flows of hydrogen. The ratio plot of the data shown in Fig. 12 is displayed in Fig. 13. It provided a value for $K_{-19} = 0.010$. In all three experiments equilibrium was established already at the lowest flows of H_2 used. The three ratio plots provided a mean value for $K = 0.012 \pm 0.004$.

$$[20] \quad H^- + (CH_3)_2NH \rightleftarrows (CH_3)_2N^- + H_2$$

Figure 14 shows the variation in the major negative ion signals upon the addition of dimethylamine into a NH_3–H_2–He plasma in which H^- is initially a major negative ion. Of the ions monitored in the range *m/e* 1–50, only the ions with *m/e* 1 (H^-) and *m/e* 44 ($(CH_3)_2N^-$) responded significantly to the addition of dimethylamine. Figure 14 also includes the behaviour of the *m/e* 46 (NO_2^-) signal which

Can. J. Chem. Downloaded from www.nrcresearchpress.com by 210.87.254.105 on 09/05/12
For personal use only.

Can. J. Chem. Downloaded from www.nrcresearchpress.com by 210.87.254.105 on 09/05/12
For personal use only.

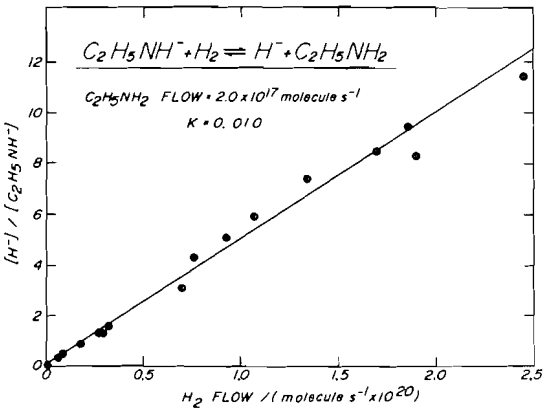

FIG. 13. The variation of the ratio of the product to reactant ion concentrations, $[H^-]/[C_2H_5NH]$, with H_2 addition for the data shown in Fig. 12. m = 2.4.

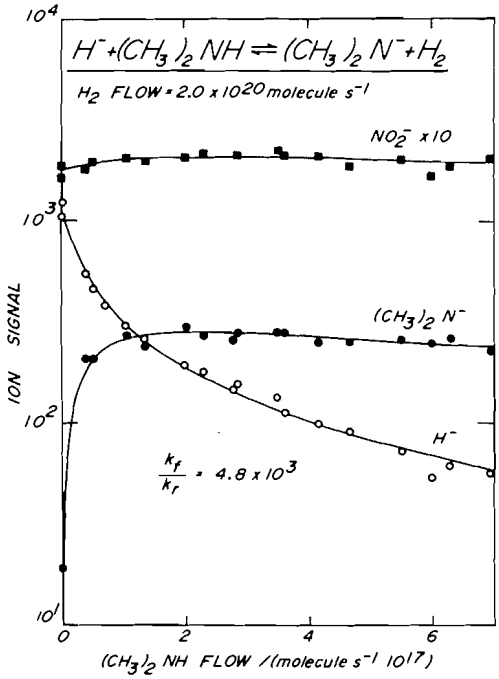

FIG. 14. The determination of the ratio of rate constants for the reaction $H^- + (CH_3)_2NH \rightleftarrows (CH_3)_2N^- + H_2$ from the best fit to the observed decay of H^- upon the addition of $(CH_3)_2NH$ into a NH_3–H_2–He plasma at high fixed H_2 flow. T = 296 K, p = 0.457 torr, $\bar{v}$ = 8.7 × 10^3 cm s^{-1}, and L = 85 cm. The flow of NH_3 = 3.5 × 10^{19} molecule s^{-1}.

typifies the usual behaviour of an unreactive impurity ion.

Three separate experiments were performed over a range of hydrogen flows (1.10 × 10^{18}–

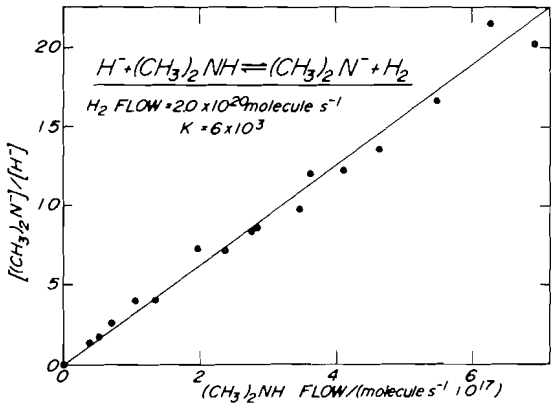

FIG. 15. The variation of the ratio of the product to reactant ion concentrations, $[(CH_3)_2N^-]/[H^-]$, with $(CH_3)_2NH$ addition for the data shown in Fig. 14. m = 3.8.

1.98 × 10^{20} molecule s^{-1}) and $(CH_3)_2NH$ flows (0–7.0 × 10^{17} molecule s^{-1}) sufficiently large to allow the determination of unique values for k_{20} and k_{-20} from a fit to the H^- decay and K_{20} from equilibrium concentrations using the standard analysis. The pressure had values in the range 0.372–0.457 torr, $\bar{v}$ had values in the range 8.2–8.7 × 10^3 cm s^{-1} and L had values of 60 and 85 cm. In two experiments the hydrogen flow was sufficiently low to permit the determination of unique values for k_{20} = (4.30 ± 0.4) × 10^{-9} cm^3 $molecule^{-1}$ s^{-1} and k_{-20} = (8.7 ± 1.2) × 10^{-13} cm^3 $molecule^{-1}$ s^{-1} from fits to the H^- decay. The third experiment, the data for which is shown in Fig. 14, provided only a unique value for the ratio of rate constants k_{20}/k_{-20} = 4.8 × 10^3. One additional experiment was carried out in which hydrogen back reactant was not added. A fit to the exponential decay of the H^- signal provided a value for the forward rate constant k_{20} = 4.2 × 10^{-9} cm^3 $molecule^{-1}$ s^{-1}. In two of the experiments equilibrium was established. One of the ratio plots is shown in Fig. 15. The linear portions of the two ratio plots provided a mean value for K_{20} of (5.4 ± 1.1) × 10^3. Due to the large value of the equilibrium constant no attempt was made to investigate reaction 20 in the reverse direction.

[21] $NH_2^- + (CH_3)_2NH \rightleftarrows (CH_3)_2N^- + NH_3$

One experiment was performed to investigate the proton transfer reaction 21 in a flowing NH_3–He plasma. Due to the large value of the

TABLE 3. Changes in the standard free energy, standard entropy, and standard enthalpy at 298 K for proton transfer reactions of the type $X^- + YH \rightleftarrows XH + Y^-$ involving H_2, NH_3, and several amines

Reaction	$-\Delta G^0_{298}$/(kcal mol^{-1})	ΔS^0_{298}/(eu)	$-\Delta H^0_{298}$/(kcal mol^{-1})
$NH_2^- + H_2 \rightleftarrows H^- + NH_3$	1.9±0.2 (8)	−4.3±0.5 (8)	3.2±0.4 (8)
$NH_2^- + CH_3NH_2 \rightleftarrows CH_3NH^- + NH_3$	0.51±0.10	+0.4±1.6	0.4±0.6
$CH_3NH^- + H_2 \rightleftarrows H^- + CH_3NH_2$	1.5±0.2	−4.5±1.0	2.8±0.5
$NH_2^- + C_2H_5NH_2 \rightleftarrows C_2H_5NH^- + NH_3$	4.2±0.2	+0.8±1.6	4.0±0.7
$H^- + C_2H_5NH_2 \rightleftarrows C_2H_5NH^- + H_2$	2.6±0.2	+5.1±1.0	1.1±0.5
$H^- + (CH_3)_2NH \rightleftarrows (CH_3)_2N^- + H_2$	5.0±0.1	+3.5±1.0	4.0±0.4

equilibrium constant, $\sim 10^5$, and unstable sampling conditions at the required flows of ammonia and dimethylamine, reaction 21 was not studied under equilibrium conditions. From the decay of the NH_2^- ion at moderate $(CH_3)_2NH$ flows it was possible from this one experiment to determine a value for $k_{20} \sim 3 \times 10^{-9}$ cm^3 molecule^{-1} s^{-1}. The conditions under which this experiment was carried out were: $p = 0.367$ torr, $\bar{v} = 8.6 \times 10^3$ cm s^{-1}, $L = 60$ cm, and NH_3 flow $= 2.9 \times 10^{17}$ molecule s^{-1}.

[22] $NH_2^- + (CH_3)_3N \rightleftarrows (CH_3)_2NCH_2^- + NH_3$

An investigation of reaction 22 was carried out again in a NH_3–He plasma in order to assess whether any of the methyl protons were acidic enough to be abstracted by NH_2^-. For large additions of trimethylamine ($\sim 1 \times 10^{19}$ molecule s^{-1}) the NH_2^- ion was observed to decline slowly with an accompanying increase in the ion signals at *m/e* 31, 34, and 44 which were identified as CH_3NH^-, $OH^- \cdot NH_3$, and $(CH_3)_2N^-$ respectively. A careful search was made for the ion $(CH_3)_2NCH_2^-$ (*m/e* 58), which would be the product of reaction 22, for the conditions: $p = 0.336$ torr, $\bar{v} = 8.1 \times 10^3$ cm s^{-1}, $L = 59$ cm, NH_3 flow $= 1.7 \times 10^{18}$ molecule s^{-1}, and $(CH_3)_3N$ flows up to 1×10^{19} molecule s^{-1}. The failure to observe $(CH_3)_2NCH_2^-$ over this range of flows suggests an upper limit to the rate constant for reaction 22 of 1×10^{-12} cm^3 molecule^{-1} s^{-1}. The majority of the observed decay of the NH_2^- signal could therefore be attributed to proton transfer reactions with the impurities H_2O, CH_3NH_2, and $(CH_3)_2NH$ present in the $(CH_3)_3N$. All of these reactions are rapid, and the rate constant for the depletion of NH_2^- determined from the slope of the NH_2^- decay, $k = 3.8 \times 10^{-11}$ cm^3 molecule^{-1} s^{-1}, was consistent with the total rate constant expected from the quoted impurity level of $\sim 1\%$. However, a part of the increase in the *m/e* 44 signal could have been due to the displacement reaction

[22*a*] $NH_2^- + (CH_3)_3N \rightarrow (CH_3)_2N^- + CH_3NH_2$

and/or the reaction

[22*b*] $NH_2^- + (CH_3)_3N \rightarrow C_2H_5NH^- + CH_3NH_2$

Discussion

Table 1 indicates the agreement between the measured ratios of rate constants determined from fits to the primary ion decays (and independent of mass discrimination) and the measured equilibrium ion concentrations (corrected for mass discrimination) together with their observed independence on the direction of approach to equilibrium. These results, together with the observed constancy of the measured ratios of rate constants and equilibrium constants over the range of reaction times and neutral concentrations adopted in these experiments, provide confidence that these measured values represent true equilibrium constants (6, 11). Further confidence is provided by the internal consistency between single-step and multi-step measurements. The equilibrium constant of 26 ± 6 determined directly from a study of the NH_3/H_2 system (8) compares favourably with the equilibrium constants of 29 ± 12 and 17 ± 8 determined indirectly from a study of the NH_3/CH_3NH_2 and CH_3NH_2/H_2 systems and the $NH_3/C_2H_5NH_2$ and $C_2H_5NH_2/H_2$ systems, respectively. The measured equilibrium constants summarized in Table 2 should therefore provide values for changes in the standard Gibbs free energy, ΔG^0_{298}, according to the relation

[23] $\Delta G^0_T = -RT \ln K_T$

Can. J. Chem. Downloaded from www.nrcresearchpress.com by 210.87.254.105 on 09/05/12
For personal use only.

Can. J. Chem. Downloaded from www.nrcresearchpress.com by 210.87.254.105 on 09/05/12
For personal use only.

TABLE 4. Absolute intrinsic acidities of amines at 298 K

$RH \rightleftarrows R^- + H^+$	ΔG^0_{298}/(kcal mol^{-1})
$H_2 \rightleftarrows H^- + H^+$	394.2±0.5 (12)
$NH_3 \rightleftarrows NH_2^- + H^+$	396.1±0.7 (8)
$CH_3NH_2 \rightleftarrows CH_3NH^- + H^+$	395.7±0.7
$C_2H_5NH_2 \rightleftarrows C_2H_5NH^- + H^+$	391.7±0.7
$(CH_3)_2NH \rightleftarrows (CH_3)_2N^- + H^+$	389.2±0.6
$(CH_3)_3N \rightleftarrows (CH_3)_2NCH_2^- + H^+$	>396

The thermodynamics of the proton transfer reactions may be specified further by estimating the standard entropy changes, ΔS^0_{298}, from the known or estimated entropies of the individual species (12) and then calculating the standard enthalpy changes, ΔH^0_{298}, according to the relation

[24] $$\Delta H^0_T = \Delta G^0_T + T\Delta S^0_T$$

The results of these calculations are summarized in Table 3. The entropies of the amide ions CH_3NH^-, $C_2H_5NH^-$, and $(CH_3)_2N^-$ were assumed to be equal to the entropies (13) of the isoelectronic species CH_3OH, C_2H_5OH, and $(CH_3)_2O$ respectively.

ΔG^0_{298} for reactions of types [2] and [3] is a measure of the difference in the intrinsic acidity of the pairs of Brønsted acids H_2 and R_1R_2NH and NH_3 and R_1R_2NH, respectively. Absolute values for the intrinsic acidities of the amines, R_1R_2NH, can therefore be derived from the values of ΔG^0_{298} in Table 3 when reference is made to the well-established intrinsic acidity of H_2. The relative acidity of H_2 and NH_3 has been measured previously (8). The resulting acidities are summarized in Table 4 and the scale of acidities shown in Fig. 16. The order of acidity, *viz.* dimethylamine > ethylamine > methylamine > ammonia is consistent with that first determined by Brauman and Blair (2) with their ion cyclotron resonance and pulsed double-resonance spectroscopy techniques. However, the absolute magnitudes of the differences in acidity show an unexpected pattern. The acidity increase from NH_3 to CH_3NH_2 is only 0.4 kcal mol^{-1} while the corresponding increase from CH_3NH_2 to $(CH_3)_2NH$ is 6.5 kcal mol^{-1}. Furthermore there is a rather large increase of 4.0 kcal mol^{-1} from CH_3NH_2 to $C_2H_5NH_2$.

The observed order of increasing acidity of the amines with increasing alkyl substitution

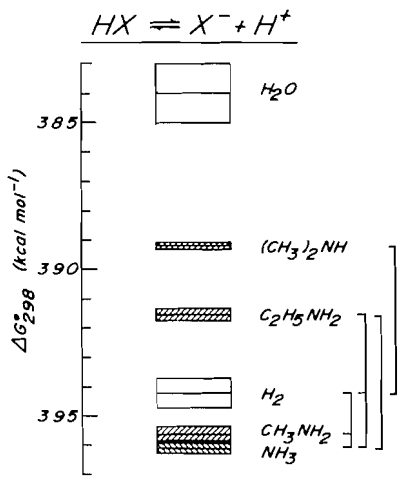

FIG. 16. Scale of intrinsic acidities. The measured relative acidities of pairs of Brønsted acids are represented by the brackets shown on the right hand side. The scale is set by the well established value of the acidity of H_2. The shaded rectangles indicate the experimental uncertainty in acidity relative to the acidity of H_2. The uncertainty in the absolute acidity is indicated for H_2 and H_2O which is included for comparison.

has been rationalized by Brauman and Blair (2) in terms of a model in which the charge localized on the N atom of the conjugate base is stabilized by the alkyl group acting as a polarizable medium. Such a model has also been invoked to explain the acidity orders observed for aliphatic alcohols (14) and monosubstituted carboxylic acids (15), acetylenes (16), and phenols (17). However, a 'first member anomaly' is observed in the latter groups of acids (except *o*-substituted phenols) in the sense that formic acid, acetylene, and phenol have acidities which are unexpectedly large relative to the acidities of the other members of their homologous series. For the acidities of the amines reported in this study the small difference in acidity between NH_3 and CH_3NH_2 compared to the larger differences between CH_3NH_2 and $(CH_3)_2NH$ as well as between CH_3NH_2 and $C_2H_5NH_2$ may also reflect a similar anomaly in that the acidity of NH_3 can be regarded to be unexpectedly large. The first member anomaly has been explained qualitatively in the case of the acetylenes and carboxylic acids in terms of a superimposition in the conjugate base of intrinsic permanent dipole and intramolecular induced dipole effects which act to localize and delocalize respectively the charge on the site in the

TABLE 5. A comparison of experimental and calculated proton affinities (in kcal mol^{-1}) of anions

R^-	Measured[a]	Calculated[b]		
		Hopkinson *et al.* (5)	Radom (4)	Hehre and Pople (3)
H^-	400.4±0.5 (12)	400.5[c]		
NH_2^-	403.6±0.9 (8)	421.9[c]		553.3
CH_3NH^-	403.2±1.0		442.8, 537.5	539.0
$C_2H_5NH^-$	399.4±1.0		439.3, 536.2	
$(CH_3)_2N^-$	396.4±0.9			523.8

[a]PA = ΔH^0_{298} for the reaction $RH \rightleftarrows R^- + H^+$.
[b]PA = ΔE.
[c]ΔE corrected for zero point vibration.

TABLE 6. Standard heats of formation of amide ions, the electron affinities of the corresponding radicals, and pertinent thermochemical information in kcal mol^{-1}. Values determined in this study are underlined

RH	$\Delta H^0_{f,298}(RH)$	$\Delta H^0_{f,298}(R)$	$\Delta H^0_{f,298}(R^-)$	EA(R)
H_2	0	52.100±0.001 (12)	33.2±0.5 (12)	18.9±0.5 (12)
NH_3	−10.97±0.1 (12)	44.3±1.1 (8)	25.4±1.0 (8)	18.9±0.1 (8)
CH_3NH—H	−5.5±0.5 (13)	43.6±2.0 (18)	<u>30.5±1.5</u>	<u>13.1±3.5</u>
C_2H_5NH—H	−11.0±0.5 (13)	38±2[a]	<u>21.2±1.5</u>	<u>17±4</u>
$(CH_3)_2N$—H	−4.5±0.5 (13)	39±2 (18)	<u>24.7±1.4</u>	<u>14.3±3.4</u>

[a]Calculated from $D^0_{298}(C_2H_5NH—H) \simeq D^0_{298}(CH_3NH—H) = 101 \pm 2$ kcal mol^{-1} (2).

anion from which the proton was removed. It is questionable whether a similar explanation is also appropriate in the case of the amines. Further measurements of acidities of other homologous series should provide a more complete and quantitative appreciation of all the factors which influence gas-phase acidity. The only quantitative assessment which is possible at this time is provided by quantum mechanical calculations of proton removal energies.

A number of quantum mechanical calculations of proton removal energies have recently been attempted for amines. Table 5 includes the results of *ab initio* molecular orbital studies reported by Hopkinson *et al.* (5), Radom (4), and Hehre and Pople (3). Although the calculations differ appreciably in quality according to the choice of the basis sets, they all correctly reproduce the observed order of proton affinity of the amide ions in the gas phase. However, the calculated absolute energies for proton removal are consistently higher than the experimental values by as much as ~35%. Better agreement (within ~10%) is obtained with the more extensive basis sets. Differences in intrinsic acidities also appear to be reproduced more accurately with the extensive sets. For example, the measured proton affinity difference of 3.8 ± 2.0 kcal mol^{-1} for $PA(CH_3NH^-)$–$PA(C_2H_5NH^-)$ compares more favourably (in fact remarkably well) with the value of 3.5 kcal mol^{-1} obtained by Radom (4) with the extended 4-31G set than the value of 1.3 kcal mol^{-1} obtained with the minimal STO-3G set.

The experimentally determined values of ΔH^0_{298} given in Table 3 for reactions of types [2] and [3] provide a measure of $\Delta H^0_{f,298}(R_1R_2N^-)$, $EA(R_1R_2N)$, and $PA(R_1R_2N^-)$ according to the relations

$$[25]\quad \Delta H^0_f(R_1R_2N^-) = \Delta H^0_f(R_1R_2NH) - \Delta H^0_f(RH) + \Delta H^0_f(R^-) - \Delta H^0$$

$$[26]\quad EA(R_1R_2N) = \Delta H^0_f(R_1R_2N) - \Delta H^0_f(R_1R_2N^-)$$

$$[27]\quad PA(R_1R_2N^-) = \Delta H^0 + PA(R^-)$$

where R = H or NH_2. The heats of formation of the amide ions and the electron affinities obtained in this manner are given in Table 6 and the proton affinities of the amide ions are summarized in Table 5. The trend in electron affinity with alkyl substitution of the amino radical also supports the notion that polarizable alkyl groups disperse negative charge from a

Can. J. Chem. Downloaded from www.nrcresearchpress.com by 210.87.254.105 on 09/05/12
For personal use only.

Can. J. Chem. Downloaded from www.nrcresearchpress.com by 210.87.254.105 on 09/05/12
For personal use only.

TABLE 7. Rate constants (in units of 10^{-9} cm^3 molecule^{-1} s^{-1}) and apparent activation energies for exothermic proton-transfer reactions involving H_2, NH_3, and several amines in the gas phase at 296 ± 2 K

Reaction	k_{expt}	$k_{capture}$[a]	$k_{expt}/k_{capture}$	E_a[b] (kcal mol^{-1})	$-\Delta H^0_{298}$ (kcal mol^{-1})
$NH_2^- + H_2 \rightarrow H^- + NH_3$	0.023±0.005	1.56[c]	0.015±0.003	2.5±0.1	3.2±0.3
$CH_3NH^- + H_2 \rightarrow H^- + CH_3NH_2$	0.20±0.06	1.52[c]	0.13±0.04	1.2±0.2	2.8±0.4
$NH_2^- + CH_3NH_2 \rightarrow CH_3NH^- + NH_3$	≥0.1	2.04[d]	≥0.05	≤2	0.41±0.45
$H^- + C_2H_5NH_2 \rightarrow C_2H_5NH^- + H_2$	1.1±0.3	7.62[e]	0.14±0.04	1.2±0.2	1.1±0.4
$NH_2^- + C_2H_5NH_2 \rightarrow C_2H_5NH^- + NH_3$	2.6±0.8	2.20[e]	1.2±0.4	0	3.9±0.5
$H^- + (CH_3)_2NH \rightarrow (CH_3)_2N^- + H_2$	4.3±0.8	7.04[f]	0.61±0.14	0.3±0.2	4.0±0.3
$NH_2^- + (CH_3)_2NH \rightarrow (CH_3)_2N^- + NH_3$	~3	1.90[f]	~1.5	0	7.2±0.6

[a]Calculated according to equation 28 in the text.
[b]The uncertainty in E_a reflects only the uncertainty in k_{expt}.
[c]α = 0.79 Å^3 (22).
[d]α = 3.92 Å^3 (22), μ_D = 1.27 D (23), c = 0.169 (21).
[e]α = 5.86 Å^3 (estimated from bond polarizabilities ref. 24), μ_D = 1.22 D (23), c = 0.165 (21).
[f]α = 5.59 Å^3 (estimated from bond polarizabilities, ref. 24), μ_D = 1.03 D (23), c = 0.150 (21).

Can. J. Chem. Downloaded from www.nrcresearchpress.com by 210.87.254.105 on 09/05/12
For personal use only.

charged centre and that larger alkyl groups do so more effectively (2, 4).

Recent room temperature measurements of the rate constants for a large number of exothermic proton-transfer reactions between simple inorganic and organic species proceeding in the gas phase have indicated that the transfer of a proton usually proceeds on nearly every collision, *viz.* that the reaction rate constant usually is very nearly equal to the capture rate constant (19). For reactants having a M.B. energy distribution, current classical theories of ion–molecule interaction predict a capture rate constant given by

$$[28]\quad k_c = 2\pi e\left(\frac{\alpha}{\mu}\right)^{1/2} + C\left(\frac{2\pi e\mu_D}{\mu}\right)\left(\frac{2\mu}{\pi kT}\right)^{1/2}$$

where e is the charge on the ion, μ the reduced mass of the collidants, α is the polarizability and μ_D is the permanent dipole moment of the neutral molecule (20, 21). C is a measure of the extent to which the dipole is oriented with respect to the direction of the approaching ion and can be determined from the ratio $\mu_D/\alpha^{1/2}$ (21). Table 7 presents a comparison of the rate constants measured for the proton transfer reactions investigated in this study with calculated capture rate constants. Although several of these reactions also proceed at essentially the capture rate, the specific rates of the reactions of NH_2^- and CH_3NH^- with H_2 and H^- with $C_2H_5NH_2$ deviate significantly from the predicted capture rate constants. The reasons for these deviations are not understood. Details of the potential energy surfaces for the relevant reaction intermediates (the classical theories of collision completely ignores short-range interactions) are not available. Should the low reaction efficiency be a consequence of the presence of a barrier in the potential energy surface, one can attempt to estimate the magnitude of such a barrier in the traditional Arrhenius manner (25) according to the equation

$$[29]\quad k_{exptl} = k_{capture}\exp(-E_a/RT)$$

where E_a is the apparent Arrhenius activation energy. Table 3 includes values for E_a determined using this equation. Such an approach of course represents a gross oversimplification as a model for including 'chemical' effects in ion–molecule reactions since there are reasons other than an activation energy which can cause a low reaction efficiency. Further insight into these reasons must await measurements of the temperature dependence of the rate constants and detailed calculations of reaction surfaces.

Acknowledgments

The financial assistance of the National Research Council of Canada and the Sloan Foundation is gratefully acknowledged.

1. J. L. Franklin (*Editor*). Ion-molecule reactions. Plenum Press, New York. 1972.
2. J. I. Brauman and L. K. Blair. J. Am. Chem. Soc. **91**, 2126 (1969); **93**, 3911 (1971).
3. W. J. Hehre and J. A. Pople. Tetrahedron Lett. 2959 (1970).
4. L. Radom. Aust. J. Chem. **28**, 1 (1975).
5. A. C. Hopkinson, N. K. Holbrook, K. Yates, and I. G. Csizmadia. J. Chem. Phys. **49**, 3596 (1968).
6. D. K. Bohme, R. S. Hemsworth, H. W. Rundle, and H. I. Schiff. J. Chem. Phys. **58**, 3504 (1973).
7. H. S. Johnston. Gas phase reaction rate theory. The Ronald Press Company, New York. 1966.
8. D. K. Bohme, R. S. Hemsworth, and H. W. Rundle. J. Chem. Phys. **59**, 77 (1973).
9. N. C. Barford. Experimental measurements: precision, error and truth. Addison-Wesley, London. 1967.
10. D. Betowski, J. D. Payzant, G. I. Mackay, and D. K. Bohme. Chem. Phys. Lett. **31**, 321 (1975).
11. D. Betowski, G. Mackay, J. Payzant, and D. Bohme. Can. J. Chem. **53**, 2365 (1975).
12. JANAF Thermochemical tables. 2nd ed. Natl. Stand. Ref. Data Ser. Natl. Bur. Stand. **37** (1971).
13. S. W. Benson, F. R. Cruickshank, D. M. Golden, G. R. Haugen, H. E. O'Neal, A. S. Rodgers, R. Shaw, and R. Walsh. Chem. Rev. **69**, 279 (1969).
14. J. I. Brauman and L. K. Blair. J. Am. Chem. Soc. **92**, 5986 (1970).
15. R. Yamdagni and P. Kebarle. J. Am. Chem. Soc. **95**, 4050 (1973).
16. J. I. Brauman and L. K. Blair. J. Am. Chem. Soc. **93**, 4315 (1971).
17. R. T. McIver, Jr. and J. H. Silvers. J. Am. Chem. Soc. **95**, 8462 (1973).
18. D. K. Sen Sharma and J. L. Franklin. J. Am. Chem. Soc. **95**, 6562 (1973).
19. D. K. Bohme. The kinetics and energetics of proton transfer. *In* Interactions between ions and molecules. *Edited by* P. Ausloos. Plenum Press, New York. 1975.
20. T. Su and M. T. Bowers. J. Chem. Phys. **58**, 3027 (1973).
21. T. Su and M. T. Bowers. Int. J. Mass Spectrom. Ion Phys. **12**, 347 (1973).
22. E. W. Roth and R. B. Bernstein. J. Chem. Phys. **31**, 1619 (1959).
23. R. D. Nelson, D. R. Lide, and A. A. Marjott. Natl. Stand. Ref. Data Ser. Nat. Bur. Stand. **10** (1966).
24. J. O. Hirshfelder, C. F. Curtiss, and R. B. Bird. Molecular theory of gases and liquids. John Wiley and Sons, New York. 1967.
25. H. I. Schiff and D. K. Bohme. Int. J. Mass Spectrom. Ion Phys. **16**, 167 (1975).

Gas-phase reactions of anions with halogenated methanes at 297 ± 2 K

K. TANAKA, G. I. MACKAY, J. D. PAYZANT,[1] AND D. K. BOHME[2]

Department of Chemistry, York University, Downsview, Ontario M3J 1P3

Received September 23, 1975

K. TANAKA, G. I. MACKAY, J. D. PAYZANT, and D. K. BOHME. Can. J. Chem. **54**, 1643 (1976).

The rate constants for a number of exothermic displacement (S_N2) reactions of the type $X^- + CH_3Y \rightarrow Y^- + CH_3X$ where $X^- = H^-$, O^-, C^-, F^-, S^-, Cl^-, OH^-, C_2^-, CN^-, SH^-, S_2^-, C_2H^-, NH_2^-, NO_2^-, CHF^-, CH_2Cl^-, CH_2Br^-, CH_3O^-, CH_3S^-, and CH_3NH^- and Y = F, Cl, and Br, have been measured in the gas phase at 297 ± 2 K using the flowing afterglow technique. These gas-phase measurements provided an opportunity to determine the intrinsic nucleophilic reactivity of 'nude' anions and hence to assess the role of solvation in the kinetics of S_N2 reactions proceeding in solution. Comparisons of the experimental rate constants with rate constants calculated using classical theories of capture indicate that several displacement reactions may possess large *intrinsic* energies of activation, $E_a \gg 2$ kcal mol^{-1}. Correlations were found between apparent activation energies and the heats of reaction. These correlations provided a convenient classification of the various anion nucleophiles. Displacement was observed to compete with proton transfer in reactions involving nucleophiles of high intrinsic basicity and with hydrogen atom transfer and H_2^+ transfer in the reactions of the O^- radical anion.

K. TANAKA, G. I. MACKAY, J. D. PAYZANT et D. K. BOHME. Can. J. Chem. **54**, 1643 (1976).

Utilisant la technique de la lueur d'écoulement on a mesuré, en phase gaseuse, à 297 ± 2 K, les constantes de vitesse d'un certain nombre de réactions de déplacements exothermiques (S_N2) du type $X^- + CH_3Y \rightarrow Y^- + CH_3X$ ou $X^- = H^-$, O^-, C^-, F^-, S^-, Cl^-, OH^-, C_2^-, CN^-, SH^-, S_2^-, C_2H^-, NH_2^-, NO_2^-, CHF^-, CH_2Cl^-, CH_2Br^-, CH_3O^-, CH_3S^- et CH_3NH^- et Y = F, Cl et Br. Ces mesures en phase gaseuse fournissent une occasion de déterminer la réactivité nucléophile intrinsèque d'anions 'nus' et ainsi de déterminer le rôle de la solvatation dans la cinétique des réactions S_N2 se produisant en solution. Une comparaison des constantes de vitesse expérimentales avec les vitesses de réaction calculées en utilisant les théories classiques de capture indiquent que plusieurs réactions de déplacement peuvent posséder de grandes énergies intrinsèques d'activation, $E_a \gg 2$ kcal mol^{-1}. On a trouvé des corrélations entre les énergies d'activation apparentes et les chaleurs de réaction. Ces corrélations fournissent une classification commode des divers anions nucléophiles. On a observé que le déplacement est en compétition avec le transfert de protons dans la réaction impliquant des nucléophiles de basicités intrinsèques élevées et avec le transfert d'atome d'hydrogène et le transfert de H_2^+ dans les réactions de l'anion radical O^-.

[Traduit par le journal]

Introduction

The kinetics of nucleophilic displacement (S_N2) or CH_3^+ transfer reactions of the type

[1] $$X^- + CH_3Y \rightarrow Y^- + CH_3X$$

have been studied extensively in solution in a variety of protic and dipolar aprotic solvents (1). The second-order rate constants for these reactions measured at 25 °C have values generally $< 10^3$ l mol^{-1} s^{-1} ($< 10^{-18}$ cm^3 molecule^{-1} s^{-1}) and are extremely sensitive to the nature of the solvent, being often as much as 10^6 times faster in dipolar aprotic than in protic solvents. The reactions are characterized in solution by activation energies approximately in the range 15–30 kcal mol^{-1}. In order to attain an appreciation of the extent to which solvent determines the kinetics and energetics of such reactions in solution, Moelwyn-Hughes and co-workers (2) were the first to consider the intrinsic interactions between 'nude' ions, X^-, and polar molecules, CH_3Y. They were led to speculate that the solvent was entirely responsible for impeding these reactions in solution and to suppose that such reactions should proceed in the gas phase essentially in the absence of activation energies and with intrinsic rates which would be immeasurably fast. Gas-phase techniques have now become available which in fact allow the measurement of these intrinsic rates (3–5). Early, such measurements indicated

[1]Present address: Department of Chemistry, University of Alberta, Edmonton, Alberta.

[2]Alfred P. Sloan Research Fellow, 1974–1976.

Can. J. Chem. Downloaded from www.nrcresearchpress.com by 210.87.254.105 on 09/05/12
For personal use only.

Can. J. Chem. Downloaded from www.nrcresearchpress.com by 210.87.254.105 on 09/05/12
For personal use only.

that reactions of type [1] involving charge-localized anions could indeed proceed extremely rapidly in the gas phase and that solvation of the anion by one or more solvent molecules did in fact act to reduce the specific rate (3). These results prompted Won and Willi to reopen the discussion of the mechanism of the S_N2 reactions of methyl halides with nucleophiles in solution (6). Later measurements (5, 7) revealed several slow S_N2 reactions and suggested that energy barriers rather than orientation or steric effects were the important rate controlling factors as had been predicted in several molecular orbital calculations (8, 9).

In this paper we report a systematic study of exothermic reactions of type [1] between a variety of anions and the methyl halides CH_3F, CH_3Cl, and CH_3Br at 297 ± 2 K. The study was initiated in part to provide a characterization of the intrinsic behaviour of such reactions so that a comparison of this behaviour with that observed in solution would provide some appreciation of the extent to which the solvent dominates the kinetics and energetics of these reactions in solution.

Experimental

All experiments were performed using a flowing afterglow apparatus whose details of construction and operation have been described previously together with the concomitant data analysis (10). Helium was used as the carrier gas at flows in the range 0.9–2.1 × 10^{16} molecule s^{-1} with resulting average values of the total gas pressure in the range 0.256–0.592 torr. The anions were produced in a flowing plasma of helium containing a suitable parent gas. The plasma was generated with an electron gun operating at a filament emission of 1.0 mA with electron energies in the range 35–70 eV. The anions generated for this study and their parent gases were: H^- (NH_3, CH_4), NH_2^- (NH_3), OH^- (H_2O), CN^- (CH_3NH_2), CH_3O^- (CH_3OH), S^- (H_2S), SH^- (CH_3SH, H_2S), S_2^- (CH_3SH, H_2S), CH_3S^- (CH_3SH), CH_3NH^- (CH_3NH_2), C^- (C_2H_2), C_2^- (C_2H_2), C_2H^- (C_2H_2), O^- (H_2O, air), NO_2^- (air), Cl^- (CCl_4) and F^- (CF_4, CH_3F). The halogenated methanes were introduced sufficiently downstream of the anion production region to ensure that the anions had undergone a sufficient number of collisions (≫ 100) with the helium carrier gas to become thermalized at the ambient room temperature (297 ± 2 K). The effective reaction lengths were in the ranges 59–61 cm and 84–85 cm. The average gas velocity in the reaction region had values in the range 7.8–9.7 × 10^3 cm s^{-1}. Reaction rate constants were determined in the usual manner from measurements of changes in the anion signals as a function of the addition of the halogenated methane into the flowing plasma.

The gases used were He (Linde, Prepurified Grade, 99.995% He), NH_3 (Matheson, anhydrous, ≥99.99% NH_3 (liquid phase)), CH_4 (Matheson, Ultrahigh Purity, ≥99.97% CH_4), H_2O (boiled tap water), CH_3NH_2 (Matheson, ≥98.0% CH_3NH_2 (liquid phase)), CH_3OH (BDH Chemicals), H_2S (Matheson, C.P. Grade, ≥99.5% H_2S (liquid phase)), CH_3SH (Matheson, ≥99.5% CH_3SH (liquid phase)), C_2H_2 (Matheson, Purified, ≥99.6% C_2H_2), CCl_4 (BDH Chemicals), CF_4 (Matheson, ≥99.7% CF_4), CH_3F (Matheson, ≥99.0% CH_3F (liquid phase)), CH_3Cl (Matheson, ≥99.5% CH_3Cl (liquid phase)), and CH_3Br (Matheson, ≥99.5% CH_3Br (liquid phase)).

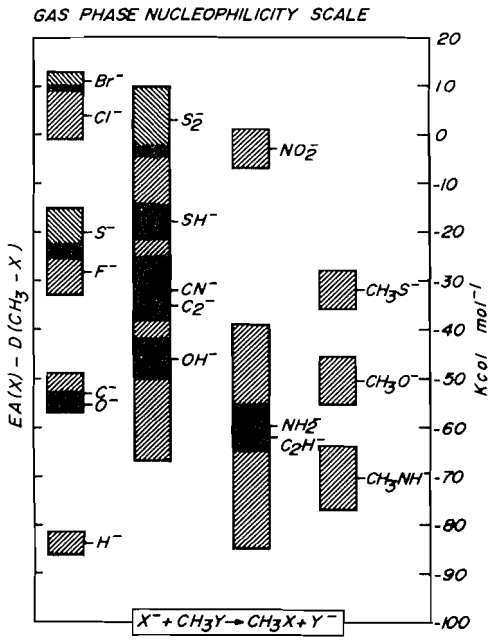

FIG. 1. Scale of thermodynamic nucleophilicity of anions in the gas phase. The width of the shaded areas represents the uncertainty.

Results

Sufficient thermodynamic information is now available to characterize the intrinsic thermodynamic nucleophilicity of many atomic, diatomic, and polyatomic anions in gas-phase reactions of type [I]. For these reactions the intrinsic thermodynamic nucleophilicity is determined by the electron affinity, EA(X), of the nucleophile and the H_3C—X bond strength of the neutral product since the overall standard enthalpy change may be expressed as

$$[2]\quad \Delta H^0 = \mathrm{EA(X)} - D^0(\mathrm{CH_3—X}) - \mathrm{EA(Y)} + D^0(\mathrm{CH_3—Y})$$

Figure 1 provides a scale of the thermodynamic nucleophilicity in the gas phase of most of the anions whose reactions were investigated in this

Can. J. Chem. Downloaded from www.nrcresearchpress.com by 210.87.254.105 on 09/05/12
For personal use only.

TABLE 1. Thermochemical information (in kcal mol^{-1}) employed in the characterization of the intrinsic thermodynamic nucleophilicity of anions in reactions of the type $X^- + CH_3Y \rightarrow Y^- + CH_3X$

X^-	$\Delta H^0_{f,298}(X)$	$EA^0_{298}(X)^a$	$\Delta H^0_{f,298}(X^-)^b$	$D^0_{298}(CH_3—X)^c$	$\Delta H^0_{f,298}(CH_3X)$	$EA^0_{298}(X) - D^0_{298}(CH_3—X)$
H^-	52.100±0.001 (11)	18.9±0.5	33.2±0.5 (11)	102.7±2.0 (12)	−17.90±0.08 (11)	−83.8±2.5
O^-	59.56±0.03 (11)	35.3±0.5	24.3±0.5 (11)	90.5±1.5	3.9±1.0 (13)	−55.2±2.0
C^-	170.89±0.45 (11)	30.4±0.4	140.5±0.8 (11)	83±3	123±3[d]	−53±4
F^-	18.86±0.40 (11)	79.94±0.05	−61.08±0.45 (14)	108±5 (12)	−56±7 (11)	−28±5
S^-	66.29±0.01 (14)	49.4±0.1 (15)	16.9±0.5	69±5 (12)	32.3 (16)	−20±5
Cl^-	28.989±0.02 (14)	84.9±0.5	−55.9±0.5 (11)	81±5 (12)	−20.0±0.5 (14)	4±6
Br^-	26.741 (16)	79.1±0.1 (17)	−52.3±0.5	68±2 (12)	−8.4 (16)	11±2
OH^-	9.492±0.040 (14)	43.81±0.9	−34.32±0.90 (14)	90±3 (12)	−47.96 (16)	−46±4
C_2-	200.2±0.9 (11)	94±20	106±20 (11)	127±12	108±11[e]	−33±32
CN^-	104.0±2.5 (11)	89.5±0.5	14.5±3 (14)	121±5[f] (12)	20.9[f] (16)	−32±6
SH^-	33.4±0.9 (18)	55.0±0.2 (19)	−21.0±1.1	73±3 (12)	−5.34 (16)	−18±3
S_2^-	30.84±0.20 (11)	39.9±0.9 (20)	−9.1±1.1	37±6	29±5[g]	3±7
C_2H^-	118±11 (11, 21)	47±12	71.5±1.1 (22)	109±11	44.32 (16)	−62±23
NH_2^-	44.9±1.7[h]	19.5±0.8 (20)	25.4±0.9 (23)	79±3 (12)	−5.49 (16)	−60±4
NO_2^-	7.91±0.2 (11)	56.4±1.2	−48.45±1.4 (14)	59±3[i] (12)	−17.86[i] (16)	−3±4
CH_3NH^-	43.6±2.0 (24)	13.1±3.5	30.5±1.5 (25)	83.6±3 (26)	−4.41± (16)	−70.5±6.5
CH_3O^-	3.9±1.0 (13)	30.9±2.3	−27.0±1.3[j]	81.4±3 (26)	−43.99 (16)	−50.5±5.3
CH_3S^-	32.3 (16)	44±1	−12±1[j]	76±3	−8.90 (16)	−32±4

[a] $EA^0_{298}(X)$ is calculated from $\Delta H^0_{f,298}(X)$ and $\Delta H^0_{f,298}(X^-)$ unless otherwise indicated.
[b] $\Delta H^0_{f,298}(X^-)$ is calculated from $\Delta H^0_{f,298}(X)$ and $EA^0_{298}(X)$ unless otherwise indicated.
[c] $D^0_{298}(CH_3—X)$ is calculated from the heats of formation of X, CH_3X, and CH_3 (11) unless otherwise indicated.
[d] Calculated from $C_2H_6 \rightarrow CH_3C + 3H$ using a total bond dissociation energy for the three C—H bonds of 300±3 kcal mol^{-1}.
[e] Calculated from $CH_3C_2H \rightarrow CH_3C_2 + H$ assuming that $D^0_{298}(CH_3C_2—H) \simeq D^0_{298}(HC_2—H) = 116 \pm 11$ kcal mol^{-1} determined from the heats of formation of HC_2, H, and C_2H_2 (11).
[f] $CH_3—CN$.
[g] Calculated from $CH_3S_2CH_3 \rightarrow CH_3S_2 + CH_3$ assuming that $D^0_{298}(CH_3S_2—CH_3) \simeq D^0_{298}(S—CH_3)$.
[h] Calculated from $\Delta H^0_{f,298}(NH_2^-)$ and $EA^0_{298}(NH_2)$.
[i] $CH_3—NO_2$.
[j] Unpublished results from this laboratory.

TABLE 2. Measured reaction and calculated capture rate constants (in units of 10^{-9} cm^3 molecule^{-1} s^{-1}) for exothermic reactions of anions with CH_3F in the gas phase at 297 ± 2 K

Anion	N^a	$k_{expt}{}^b$	$k_c{}^c$	$k_{expt}/k_c{}^d$	$-\Delta H^0{}_{298}$/(kcal mol^{-1})
H^-	4	0.015±0.002	7.6	0.0020±0.0004	56±8
O^-	3	1.1±0.1	2.3	0.48±0.09	27±7
C^-	3	⩽0.002	2.5	⩽0.0008	25±9
OH^-	5	0.025±0.002	2.2	0.011±0.003	18±9
C_2^-	3	⩽0.002	2.0	⩽0.001	5±37
CN^-	4	⩽0.003	1.9	⩽0.002	4±11[e]
C_2H^-	3	⩽0.0003	2.0	⩽0.0002	34±28[f]
NH_2^-	3	0.0176±0.0006	2.3	0.0076±0.0015	32±9
CHF^-	1	⩾0.41	1.8	⩾0.23	
CH_3O^-	3	0.014±0.002	1.9	0.0074±0.0016	23±10
CH_3S^-	1	⩽0.001	1.7	⩽0.0006	4±9
CH_3NH^-	1	0.05	1.9	0.03	43±12

[a] N is the number of measurements.
[b] The limits given along with the mean value of the measurements represent the best estimate of the precision (27). The accuracy is estimated to be ±20%.
[c] The capture rate constant is calculated using the Average-Dipole-Orientation Theory (28) with C = 0.23.
[d] The uncertainty in k_{expt}/k_c reflects only the accuracy of k_{expt}.
[e] For the formation of CH_3—CN.
[f] For the formation of CH_3—C≡CH.

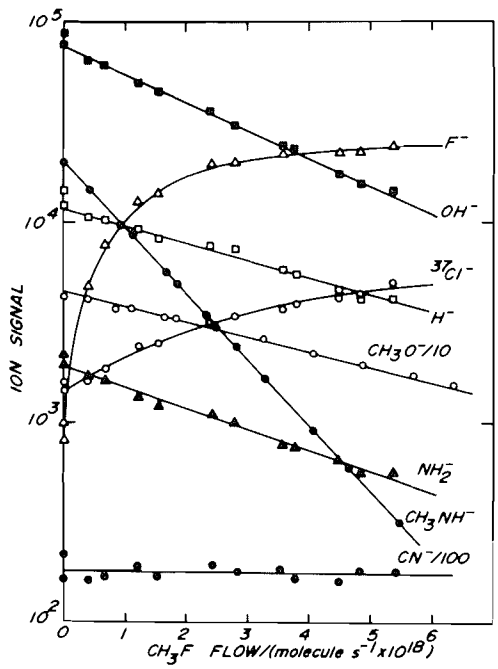

FIG. 2. Summary plot of the variation of anion signals observed as a function of CH_3F flow. T = 297 K, p = 0.331 torr, $\bar{v}$ = 8.1 × 10^3 cm s^{-1}, L = 84 cm, and the flow of NH_3 = 1.4 × 10^{17} molecule s^{-1} (H^-, NH_2^-, OH^-, and CN^-), of CH_3OH ~ 2 × 10^{17} molecule s^{-1} (CH_3O^-), and of CH_3NH_2 = 3.8 × 10^{18} molecule s^{-1} (CH_3NH^-).

study. Table 1 summarizes the thermodynamic information used to calculate these nucleophilicities. H^- is the 'strongest' nucleophile in Fig. 1 in the sense that the displacement of any nucleophile above it on this scale represents the thermodynamically preferred (exothermic) direction of displacement. The experiments reported here were intended to determine the specific rates at 297 ± 2 K for all the exothermic displacements of F^-, Cl^-, and Br^- from CH_3F, CH_3Cl, and CH_3Br respectively, which can be identified in Fig. 1. The measurement of the specific rates was always accompanied by a careful search for product ions since in several instances the displacement reaction was observed to compete with other reaction channels.

Summaries of the rate constant measurements are included in Tables 2, 3, and 4. Sources of error have been described previously (10). The absolute accuracy of the reported rate constants is estimated to be ±20%. A number of the measurements included in Tables 2 and 3 have been reported previously (7).

$X^- + CH_3F$

Figure 2 is representative of the observations of the exothermic displacement reactions of H^-, OH^-, NH_2^-, CH_3O^-, and CH_3NH^- with CH_3F for which the rate constants proved to be measurable. F^- was the only observed product ion in each case. The appearance of the Cl^- ion can be attributed to a chloride impurity (probably CH_3Cl) in CH_3F. The reactions were generally slow, having rate constants in the range 1–6 × 10^{-11} cm^3 molecule^{-1} s^{-1}.

Can. J. Chem. Downloaded from www.nrcresearchpress.com by 210.87.254.105 on 09/05/12
For personal use only.

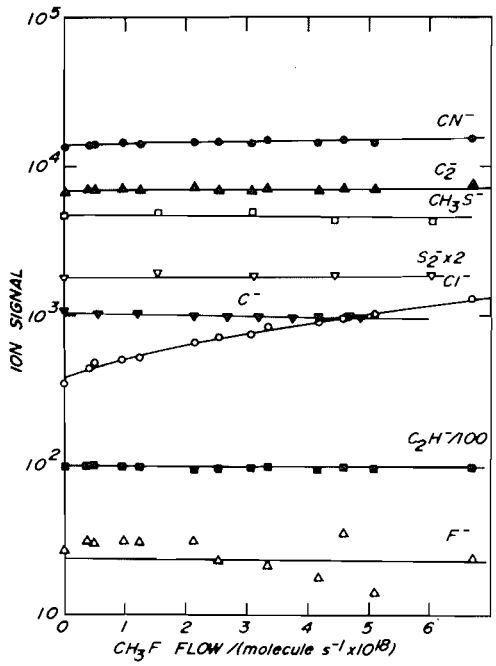

FIG. 3. The variation of anion signals observed as a function of CH_3F flow. $T = 295$ K, $p = 0.411$ torr, $\bar{v} = 8.7 \times 10^3$ cm s^{-1}, $L = 85$ cm, and the flow of $C_2H_2 = 1.5 \times 10^{18}$ molecule s^{-1}. The data of S_2^- and CH_3S^- are taken from another experiment. $T = 297$ K, $p = 0.360$ torr, $\bar{v} = 8.2 \times 10^3$ cm s^{-1}, $L = 85$ cm, and the flow of $CH_3SH = 7.1 \times 10^{17}$ molecule s^{-1}.

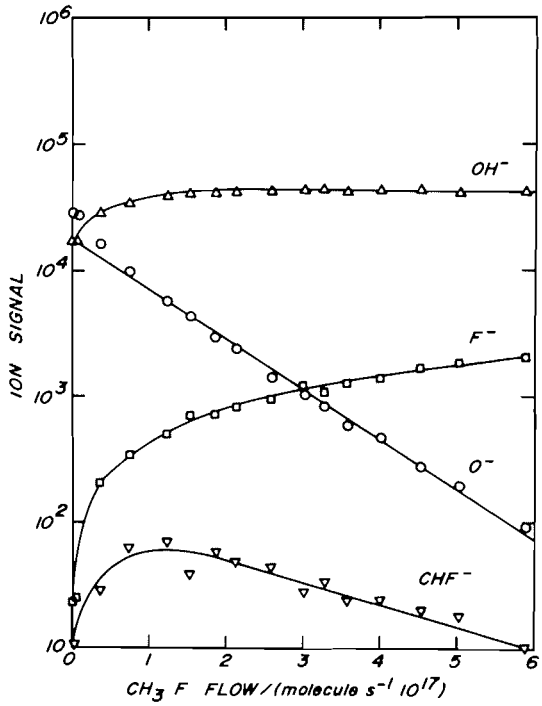

FIG. 4. The variation of the major ion signals observed for the reaction of O^- with CH_3F. $T = 295$ K, $p = 0.409$ torr, $\bar{v} = 8.3 \times 10^3$ cm s^{-1}, $L = 60$ cm, and the flow of $H_2O \sim 2 \times 10^{17}$ molecule s^{-1}.

Figure 3 includes observations of the exothermic reactions of anions with CH_3F with rate constants for which only an upper limit could be determined. Neither the C^-, CN^-, C_2^-, S_2^-, C_2H^-, and CH_3S^- signals nor the F^- signal, whose representative behaviour is included in Fig. 3, were observed to change upon the addition of CH_3F into flowing plasmas containing these ions. The increase in the Cl^- signal again reflects the presence of a chloride impurity in CH_3F.

Figure 4 shows the behaviour of the product ions observed upon the addition of CH_3F into a flowing H_2O–He plasma containing measurable amounts of O^- ions. O^- appears to react with CH_3F in three ways according to

$$[3a] \quad O^- + CH_3F \rightarrow OH^- + CH_2F$$

$$[3b] \quad \rightarrow F^- + CH_3O$$

$$[3c] \quad \rightarrow CHF^- + H_2O$$

Channel 3*a* corresponds to H-atom transfer and channel 3*c* to H_2^+ transfer. The CHF^- ion rapidly reacts further, apparently to produce F^- according to the displacement reaction 4

$$[4] \quad CHF^- + CH_3F \rightarrow F^- + (C_2H_4F)$$

Uncertainties (of at most a factor of three) associated with sampling and detection sensitivities and the further reactions of CHF^- and OH^- with CH_3F precluded a direct determination of the exact branching ratio for reaction 3. However, the H-atom transfer reaction is clearly the dominant channel. A fit to the OH^-, F^-, and CHF^- behaviour which ignored differences in sampling and detection sensitivities provided a branching ratio of approximately 98:1:1 for $OH^-:F^-:CHF^-$.

$X^- + CH_3Cl$

Figure 5 displays typical results observed for the reactions of H^-, F^-, OH^-, CH_3O^-, CN^-, and NO_2^- with CH_3Cl. H^-, F^-, and OH^- are seen to react rapidly to produce Cl^- whereas CN^- and NO_2^- do not react with a measurable rate in spite of the fact that these latter two

Can. J. Chem. Downloaded from www.nrcresearchpress.com by 210.87.254.105 on 09/05/12
For personal use only.

Can. J. Chem. Downloaded from www.nrcresearchpress.com by 210.87.254.105 on 09/05/12
For personal use only.

TABLE 3. Measured reaction and calculated capture rate constants (in units of 10^{-9} cm^3 molecule^{-1} s^{-1}) for exothermic reactions of anions with CH_3Cl in the gas phase at 297 ± 2 K

Anions	N^a	k_{expt} This work[b]	k_{expt} Other values	k_c[c]	k_{expt}/k_c[d]	$-\Delta H^0_{298}$/(kcal mol^{-1})
H^-	2	3.0±0.2	2.5 (4)	8.6	0.35±0.07	88±9
O^-	5	1.7±0.3	2.4 (3)	2.4	0.71±0.14	59±8
C^-	3	0.30±0.04		2.7	0.11±0.02	57±10
F^-	1	1.9	1.8 (4), 0.80±0.09 (5)	2.3	0.83±0.16	32±11
S^-	1	0.030		1.9	0.016±0.003	24±11
OH^-	4	1.5±0.1	1.9 (4)	2.4	0.62±0.13	50±10
C_2^-	3	⩽0.005		2.1	⩽0.002	37±38
CN^-	4	⩽0.0004		2.1	⩽0.0002	36±12[e]
SH^-	6	0.017±0.001		1.9	0.0089±0.0018	22±9
S_2^-	4	⩽0.001		1.6	⩽0.0006	1±13
C_2H^-	4	0.13±0.01	1.2 (7)[f]	2.1	0.062±0.014	66±29[g]
NH_2^-	3	1.5±0.2	2.1 (4)	2.4	0.63±0.13	64±10
NO_2^-	1	⩽0.0010		1.7	⩽0.00059	7±10[h]
CH_2Cl^-	4	0.51±0.04		1.7	0.30±0.06	
CH_3O^-	3	1.3±0.1	1.6 (4)	1.9	0.68±0.14	55±11
CH_3S^-	4	0.11±0.01	0.078±0.012 (5)	1.7	0.065±0.012	36±10
CH_3NH^-	3	1.7±0.1		2.0	0.85±0.17	75±13

[a] N is the number of measurements.
[b] The limits given along with the mean value of the measurements represent the best estimate of the precision (27). The accuracy is estimated to be ±20%.
[c] The capture rate constant is calculated using the Average-Dipole-Orientation Theory (28) with $C = 0.21$.
[d] The uncertainty in k_{expt}/k_c reflects only the accuracy of k_{expt}.
[e] For the formation of CH_3—CN.
[f] The previously reported high value (7) is in error. The origin of this error has been traced to a floating decimal in the data printout. k_{expt} should have been 0.12×10^{-9} cm^3 molecule^{-1} s^{-1}.
[g] For the formation of CH_3—C≡CH.
[h] For the formation of CH_3—NO_2.

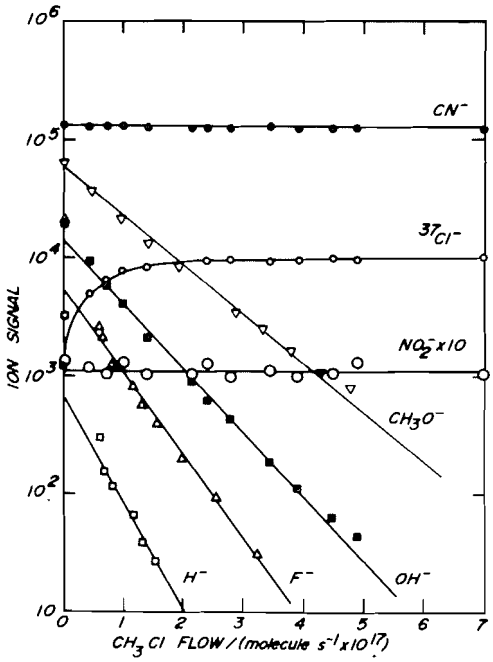

FIG. 5. The variation of anion signals observed as a function of CH_3Cl flow. T = 297 K, p = 0.289 torr, $\bar{v}$ = 8.3 × 10^3 cm s^{-1}, L = 59 cm, and the flow of CH_3F = 1.1 × 10^{17} molecule s^{-1}. H^-, OH^-, NO_2^-, and CN^- are present as impurity ions in this particular experiment. The CH_3O^- decay was taken from another experiment: T = 296 K, p = 0.332 torr, $\bar{v}$ = 8.9 × 10^3 cm s^{-1}, L = 59 cm, and the flow of CH_3OH ~ 4 × 10^{17} molecule s^{-1}.

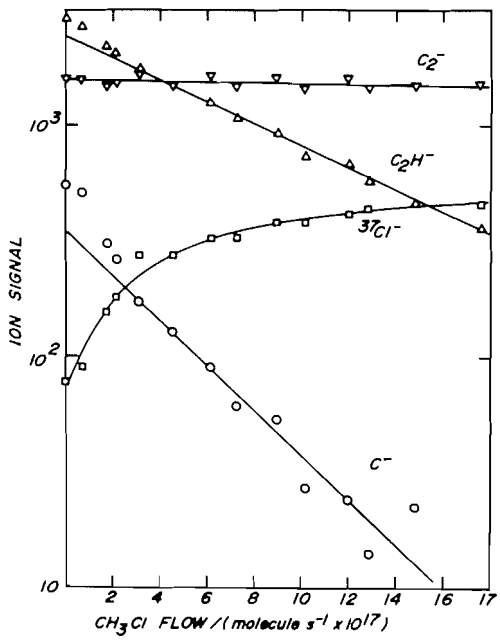

FIG. 6. The variation of carbonaceous anion signals observed as a function of CH_3Cl flow. T = 298 K, p = 0.433 torr, $\bar{v}$ = 8.3 × 10^3 cm s^{-1}, L = 60 cm, and the flow of C_2H_2 = 3.9 × 10^{17} molecule s^{-1}.

reactions are also exothermic. The results obtained for the reactions of the carbonaceous anions C^-, C_2^-, and C_2H^- and the sulfur containing anions S^-, SH^-, S_2^-, and CH_3S^- are shown in Figs. 6 and 7 respectively. A large range in the values of the rate constants for these reactions is again apparent.

Figures 8 and 9 include observations of the reactions of NH_2^- and CH_3NH^-, the two strongest bases of the anions investigated in this study, with CH_3Cl. Since independent experiments indicated that the reactions of OH^- and H^- with CH_3Cl proceed solely by Cl^- displacement, the observed production of CH_2Cl^- in Figs. 8 and 9 can be attributed to the proton transfer reactions

$$[5] \quad NH_2^- + CH_3Cl \rightarrow CH_2Cl^- + NH_3$$

$$[6] \quad CH_3NH^- + CH_3Cl \rightarrow CH_2Cl^- + CH_3NH_2$$

Again only a qualitative assessment could be made of the branching ratio, in this case the extent to which proton transfer competes with Cl^- displacement. Displacement does appear to be the predominant channel with *ca.* 10% of the collisions leading to proton transfer.

CH_2Cl^- is observed to react further with CH_3Cl according to

$$[7] \quad CH_2Cl^- + CH_3Cl \rightarrow Cl^- + (C_2H_5Cl)$$

Figure 10 displays the observation of the reactions of O^- with CH_3Cl

$$[8a] \quad O^- + CH_3Cl \rightarrow Cl^- + CH_3O$$

$$[8b] \quad \rightarrow OH^- + CH_2Cl$$

$$[8c] \quad \rightarrow CHCl^- + H_2O$$

The three channels are analogous to those observed for the reaction of O^- with CH_3F. H-atom transfer is, however, much less dominant with the displacement channel gaining in importance.

$X^- + CH_3Br$

Figures 11–13 are representative of the observations of the exothermic reactions of H^-, C^-, F^-, Cl^-, OH^-, C_2^-, CN^-, SH^-, S_2^-, C_2H^-, NO_2^-, CH_3O^-, and CH_3S^- with CH_3Br for

Can. J. Chem. Downloaded from www.nrcresearchpress.com by 210.87.254.105 on 09/05/12
For personal use only.

Can. J. Chem. Downloaded from www.nrcresearchpress.com by 210.87.254.105 on 09/05/12
For personal use only.

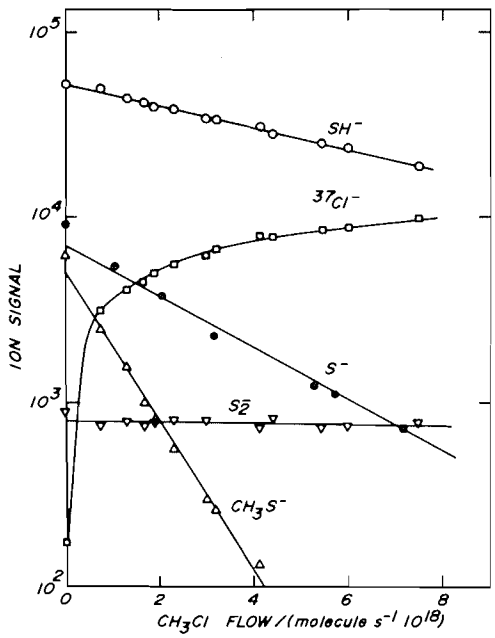

FIG. 7. The variation of sulfur containing anion signals as a function of CH_3Cl flow. T = 296 K, p = 0.347 torr, $\bar{v} = 8.5 \times 10^3$ cm s^{-1}, L = 59 cm, and the flow of $CH_3SH = 7.4 \times 10^{17}$ molecule s^{-1}. The data of S^- are taken from another experiment, T = 297 K, p = 0.336 torr, $\bar{v} = 8.4 \times 10^3$ cm, L = 85 cm, and the flow of $CH_3SH = 1.5 \times 10^{17}$ molecule s^{-1}.

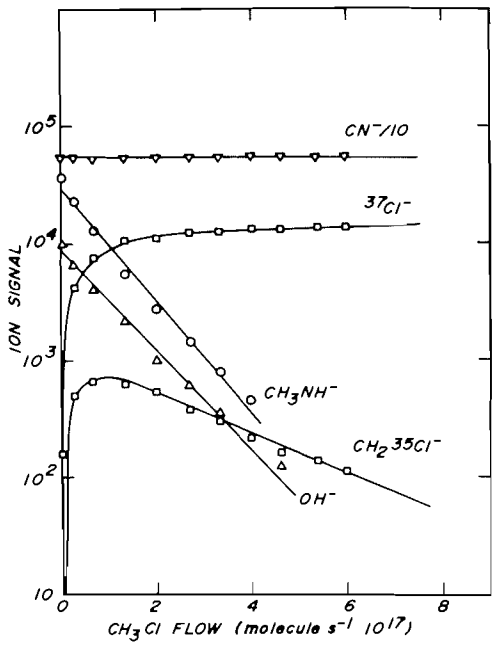

FIG. 9. The variation of the major ion signals observed for the reaction of CH_3NH^- with CH_3Cl. T = 296 K, p = 0.465 torr, $\bar{v} = 9.6 \times 10^3$ cm s^{-1}, L = 60 cm, and the flow of $CH_3NH_2 = 2.6 \times 10^{18}$ molecule s^{-1}.

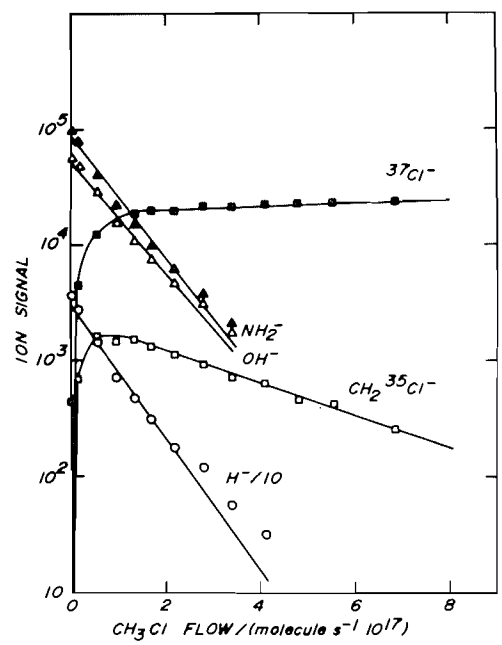

FIG. 8. The variation of the major ion signals observed for the reaction of NH_2^- with CH_3Cl. T = 296 K, p = 0.524 torr, $\bar{v} = 9.5 \times 10^3$ cm s^{-1}, L = 60 cm, and the flow of $NH_3 = 4.3 \times 10^{18}$ molecule s^{-1}.

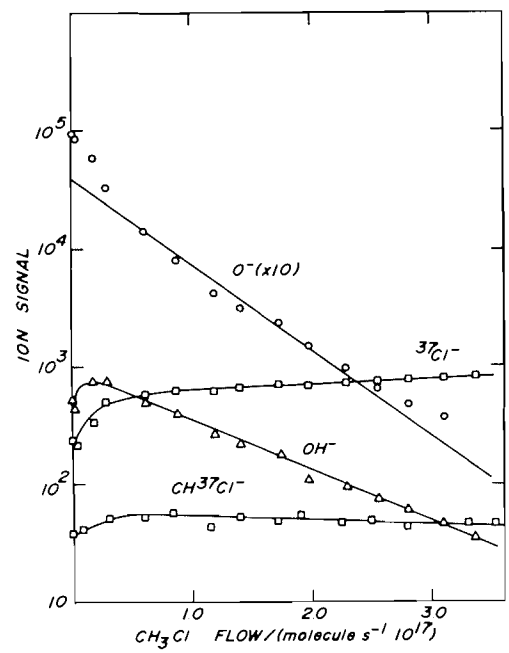

FIG. 10. The variation of the major ion signals observed for the reaction of O^- with CH_3Cl. T = 298 K, p = 0.397 torr, $\bar{v} = 8.2 \times 10^3$ cm s^{-1}, L = 60 cm, and the flow of air $\sim 3 \times 10^{17}$ molecule s^{-1}.

Can. J. Chem. Downloaded from www.nrcresearchpress.com by 210.87.254.105 on 09/05/12
For personal use only.

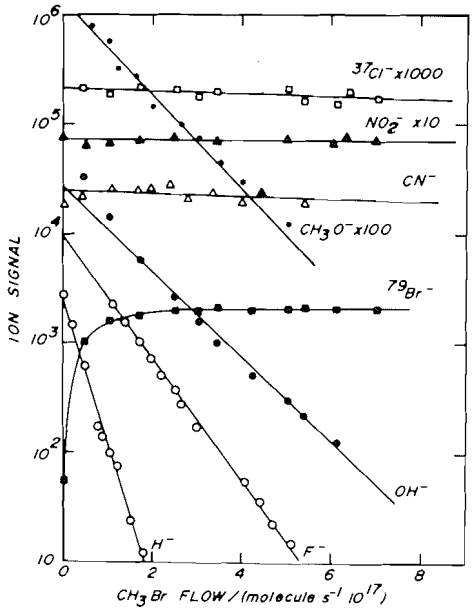

FIG. 11. Summary plot of the variation of anion signals observed as a function of CH_3Br flow. T = 298 K, p = 0.461 torr, $\bar{v}$ = 8.3 × 10^3 cm s^{-1}, L = 60 cm, and the flow of H_2O ~ 5 × 10^{17} molecule s^{-1} (OH^-, Cl^-, and NO_2^-), of CH_3OH ~ 6 × 10^{17} molecule s^{-1} (CH_3O^-), of CF_4 = 1.4 × 10^{17} molecule s^{-1} (F^-), and of NH_3 = 1.3 × 10^{18} molecule s^{-1} (H^- and CN^-).

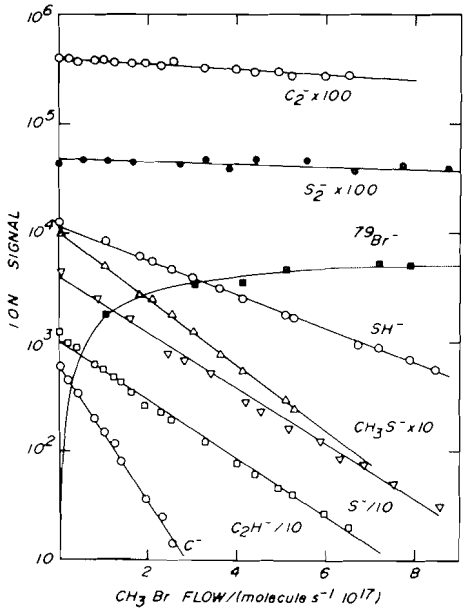

FIG. 12. Summary plot of the variation of anion signals observed as a function of CH_3Br flow. T = 295 K, p = 0.342 torr, $\bar{v}$ = 8.3 × 10^3 cm s^{-1}, L = 85 cm, and the flow of C_2H_2 = 6.6 × 10^{17} molecule s^{-1} (C^-, C_2^-, C_2H^-), of CH_3SH = 4.3 × 10^{17} molecule s^{-1} (S^-, SH^-, CH_3S^-) and of CH_3SH = 2.3 × 10^{18} molecule s^{-1} (S_2^-).

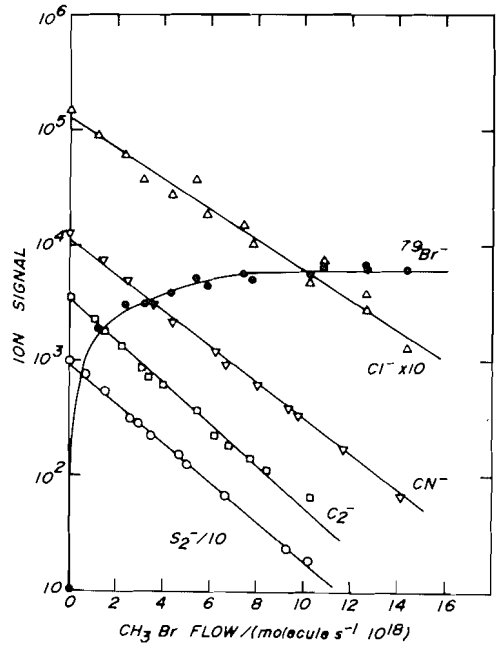

FIG. 13. Summary plot of the variation of anion signals observed as a function of CH_3Br flow. T = 296 K, p = 0.348 torr, $\bar{v}$ = 8.2 × 10^3 cm s^{-1}, L = 85 cm, and the flow of C_2H_2 = 4.6 × 10^{17} molecule s^{-1} (C_2^-), of CH_3SH = 4.9 × 10^{18} molecule s^{-1} (S_2^-), of CH_3NH_2 = 2.4 × 10^{18} molecule s^{-1} (CN^-), and of CCl_4 ~ 5 × 10^{17} molecule s^{-1} (Cl^-).

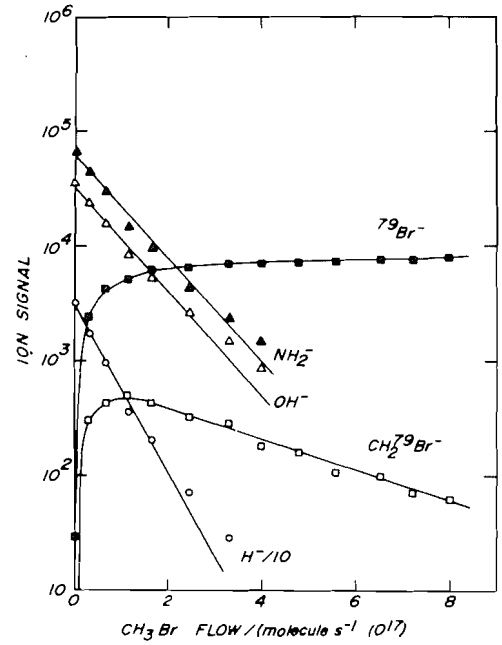

FIG. 14. The variation of the major ion signals observed for the reaction of NH_2^- with CH_3Br. T = 296 K, p = 0.531 torr, $\bar{v}$ = 9.5 × 10^3 cm s^{-1}, L = 61 cm, and the flow of NH_3 = 3.9 × 10^{18} molecule s^{-1}.

Can. J. Chem. Downloaded from www.nrcresearchpress.com by 210.87.254.105 on 09/05/12
For personal use only.

TABLE 4. Measured reaction and calculated capture rate constants (in units of 10^{-9} cm^3 molecule^{-1} s^{-1}) for exothermic reactions of anions with CH_3Br in the gas phase at 297 ± 2 K

Anion	N^a	k_{expt} This work[b]	k_{expt} Other values	k_c[c]	k_{expt}/k_c[d]	$-\Delta H^0_{298}$/(kcal mol^{-1})
H^-	3	3.7±0.6		8.7	0.43±0.09	95±5
O^-	5	1.1±0.1		2.3	0.48±0.09	66±4
C^-	4	1.3±0.2		2.7	0.48±0.11	64±6
F^-	4	1.2±0.1	0.60±0.06 (5)	2.2	0.59±0.09	39±7
S^-	1	0.46		1.8	0.26±0.05	31±7
Cl^-	4	0.021±0.001	0.080±0.010 (5)	1.7	0.012±0.003	7±8
OH^-	4	0.99±0.09		2.3	0.43±0.09	57±6
C_2^-	3	0.032±0.002		2.0	0.016±0.003	44±36
CN^-	4	0.030±0.003		1.9	0.016±0.003	43±8[e]
SH^-	4	0.30±0.02		1.7	0.18±0.03	29±5
S_2^-	1	0.033		1.4	0.024±0.005	8±9
C_2H^-	3	0.52±0.05		1.9	0.26±0.07	73±25[f]
NH_2^-	5	1.1±0.1		2.3	0.48±0.09	71±6
NO_2^-	1	⩽0.001		1.6	⩽0.0006	14±6[g]
CH_2Br^-	3	0.42±0.03		1.3	0.32±0.06	
CH_3O^-	2	1.1±0.1		1.8	0.61±0.11	62±7
CH_3S^-	3	0.52±0.05	0.14±0.02 (5)	1.5	0.35±0.06	43±6
CH_3NH^-	3	1.3±0.1		1.8	0.72±0.14	82±9

[a] N is the number of measurements.
[b] The limits given along with the mean value of the measurements represent the best estimate of the precision (27). The accuracy is estimated to be ±20%.
[c] The capture rate constant is calculated using the Average-Dipole-Orientation Theory (28) with $C = 0.19$.
[d] The uncertainty in k_{expt}/k_c reflects only the accuracy of k_{expt}.
[e] For the formation of CH_3—CN.
[f] For the formation of CH_3—C≡CH.
[g] For the formation of CH_3—NO_2.

Can. J. Chem. Downloaded from www.nrcresearchpress.com by 210.87.254.105 on 09/05/12
For personal use only.

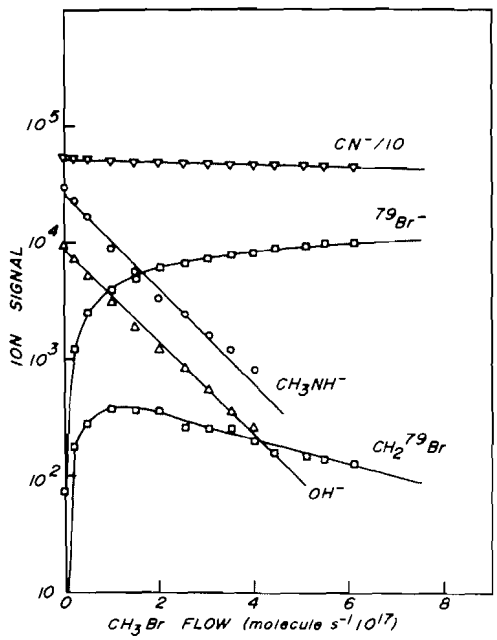

FIG. 15. The variation of the major ion signals observed for the reaction of CH_3NH^- with CH_3Br. T = 296 K, p = 0.459 torr, $\bar{v}$ = 9.7 × 10^3 cm s^{-1}, L = 60 cm, and the flow of CH_3NH_2 = 1.7 × 10^{18} molecule s^{-1}.

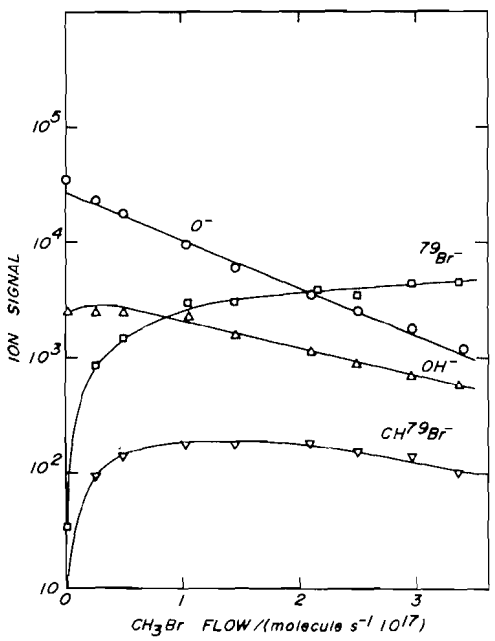

FIG. 16. The variation of the major ion signals observed for the reaction of O^- with CH_3Br. T = 298 K, p = 0.404 torr, $\bar{v}$ = 9.5 × 10^3 cm s^{-1}, L = 60 cm, and the flow of air ~ 5 × 10^{17} molecule s^{-1}.

all of which Br^- was the only observed product channel. A large range in the values of the rate constants for these reactions was again apparent.

The displacement reactions of NH_2^- and CH_3NH^- were again observed to compete with proton transfer as displayed in Figs. 14 and 15. The proton transfer product CH_2Br^- reacts further with CH_3Br according to

[9] $$CH_2Br^- + CH_3Br \rightarrow Br^- + (C_2H_5Br)$$

O^- was observed to react with CH_3Br as shown in Fig. 16 in a manner analogous to the CH_3Cl and CH_3F reactions

[10a] $$O^- + CH_3Br \rightarrow Br^- + CH_3O$$

[10b] $$\rightarrow OH^- + CH_2Br$$

[10c] $$\rightarrow CHBr^- + H_2O$$

The relative magnitude of the Br^- displacement channel is enhanced still further.

Discussion

The results summarized in Tables 2 to 4 revealed several kinetic features which can serve to characterize and classify the intrinsic reactivities of anions towards methyl halides.

(1) The specific rates of exothermic displacement reactions of anions with methyl halides are generally much higher in the gas phase than in solution.

As predicted by Moelwyn-Hughes and coworkers (2), many S_N2 reactions of type [1] do indeed proceed extremely rapidly in the gas phase especially the reactions with CH_3Cl and CH_3Br. The reactions with CH_3F are generally at least ~100 times slower. Table 5 provides a comparison of bimolecular specific rates for several displacement reactions investigated in both the gas phase and solution. It is readily apparent that the specific rates in the gas phase exceed those in solution by many orders of magnitude, *viz.* by factors of $\gtrsim 10^{10}$. This disparity in the magnitude of the specific rates must reflect the effect of solvent on intrinsic reactivity so that one would expect a lowering in the specific rate in the gas phase as a result of the selective solvation of the 'nude' nucleophile by one or more solvent molecules. Such a lowering in specific rate has been observed previously for displacement reactions of 'nude' and solvated alkoxide ions with CH_3Cl (3).

In the gas phase the specific rate of the displacement reactions of type [1] is limited by the

TABLE 5. A comparison of bimolecular specific rates and apparent activation energies for several displacement reactions investigated *in vacuo* and in solution

Reactants $CH_3Y + X^-$	Solution			Gas phase	
	Solvent	$k_{298\,K}$ (cm^3 $molecule^{-1}$ s^{-1})	E_a (kcal mol^{-1})	$k_{297\,K}$ cm^3 $molecule^{-1}$ s^{-1}	E_a[a] (kcal mol^{-1})
$CH_3F + OH^-$	H_2O[b]	9.7×10^{-28}	21.6	$(2.5\pm0.5)\times10^{-11}$	2.7 ± 0.1
$CH_3Cl + OH^-$	H_2O[b]	1.0×10^{-26}	24.3	$(1.5\pm0.3)\times10^{-9}$	0.28 ± 0.14
$CH_3Cl + F^-$	H_2O[b]	2.5×10^{-29}	26.9	$(1.8\pm0.4)\times10^{-9}$	0.15 ± 0.13
$CH_3Br + OH^-$	H_2O[b]	2.3×10^{-25}	23.0	$(9.9\pm2.0)\times10^{-10}$	0.50 ± 0.14
$CH_3Br + F^-$	H_2O[b]	5.6×10^{-28}	25.2	$(1.2\pm0.2)\times10^{-9}$	0.31 ± 0.14
$CH_3Br + Cl^-$	H_2O[b]	8.2×10^{-27}	24.7	$(2.1\pm0.4)\times10^{-11}$	2.6 ± 0.1
	CH_3OH[c]	1.1×10^{-26}			
	DMF[d]	6.7×10^{-22}			
	MeCO[d]	5.3×10^{-21}			

[a]The uncertainty in E_a reflects only the uncertainty in the measured specific rate, 297 K.
[b]Reference 2.
[c]Reference 40.
[d]Reference 1.

collision or capture rate just as the diffusion rate provides an upper limit in solution. The capture rate is readily estimated from current classical theories of collision. For collisions between ions and neutral polar substrates having a Maxwell–Boltzmann energy distribution, the Average-Dipole-Orientation (ADO) theory of Su and Bowers (28) has proven to predict the capture rate at 297 K most adequately (29, 30). According to this theory the capture rate constant is given by

$$[11]\quad k_c = 2\pi e\left(\frac{\alpha}{\mu}\right)^{1/2} + C\left(\frac{2\pi e\mu_D}{\mu}\right)\left(\frac{2\mu}{\pi kT}\right)^{1/2}$$

where e is the charge on the ion, μ the reduced mass of the collidants, α the polarizability and μ_D the permanent dipole moment of the molecule. C is the 'dipole locking' constant which can be determined from the polarizability and permanent dipole moment of the neutral substrate (28). Tables 2, 3, and 4 include values of k_c calculated for all the reactions investigated in this study. Values for μ_D and α were taken from Rothe and Bernstein (31). The ratio $(k_{expt}/k_c)_{297\,K}$ is a measure of the reaction probability per collision. An inspection of the values of k_{expt}/k_c provided in Tables 2, 3, and 4 indicates that whereas many of the reactions proceed essentially upon every collision, a large group of exothermic reactions proceed on at most every 100 collisions.

(2) Many exothermic displacement reactions of anions with methyl halides apparently have activation energies in the gas phase.

Displacement reactions are characterized in solution by large activation energies, $E_a \sim 15$–30 kcal mol^{-1} (see Table 5). These activation energies are usually associated with the work required to break down initial state solvation. Nevertheless, some concern has been expressed regarding the extent to which these observed activation energies reflect intrinsic properties of the reacting systems. Parker has drawn attention to the caution which should be exercised in any attempt to extract such information from solution measurements of specific rates (1). Quantum mechanical calculations of portions of the intrinsic energy surfaces of displacement reactions of type [1] have in fact indicated the presence of what are, in some instances, quite substantial energy barriers (8, 9). The gas-phase (single temperature) measurements reported here can also provide some indication of the possible presence and magnitude of these intrinsic activation energies.

The magnitude of the activation energy can be estimated from the reaction probability per collision, k_{expt}/k_c, in the traditional Arrhenius manner if the following expression is assumed to be approximately valid (32)

$$[12]\qquad k_{expt} = k_c \exp(-E_a/RT)$$

Although such a treatment is a gross oversimplification in that it completely ignores constraints to reaction resulting from short-range interactions, *e.g.* orientation or steric effects, there is some evidence (7) that it is reasonable to a first approximation for displacement re-

Can. J. Chem. Downloaded from www.nrcresearchpress.com by 210.87.254.105 on 09/05/12
For personal use only.

TABLE 6. Apparent activation energies[a] (in kcal mol^{-1}) for exothermic displacement reactions with CH_3F, CH_3Cl, and CH_3Br *in vacuo*

Nucleophile	CH_3F	CH_3Cl	CH_3Br
H^-	3.7±0.1	0.62±0.73	0.50±0.14
C^-	⩾4.2	1.3±0.1	0.43±0.16
F^-		0.1±0.1	0.31±0.10
S^-		2.4±0.2	0.80±0.10
Cl^-			2.6±0.2
OH^-	2.7±0.2	0.28±0.14	0.50±0.14
C_2^-	⩾4.1	⩾3.8	2.5±0.1
CN^-	⩾3.8	⩾5.0	2.4±0.2
SH^-		2.8±0.1	1.0±0.1
S_2^-		⩾4.4	2.2±0.1
C_2H^-	⩾4.5	1.6±0.2	0.80±0.18
NH_2^-	2.9±0.1	0.3±0.1	0.43±0.13
NO_2^-		⩾4.4	⩾4.4
CH_3O^-	2.9±0.1	0.23±0.13	0.29±0.12
CH_3S^-	⩾4.3	1.6±0.1	0.62±0.11
CH_3NH^-	2.1±0.2	0.1±0.1	0.19±0.13

[a]Values underlined correspond to reactions which, within the uncertainty of ΔH^0_{298}, may in fact be endothermic by an amount ⩾ the calculated value for E_a.

actions of type [1]. Nevertheless we recognize that this approach is somewhat speculative and perhaps too enterprising but feel that it is warranted at this stage of development of our knowledge of activation energies in ion–molecule reactions. Clearly the activation energies determined in this manner should be viewed with caution until rate measurements at several temperatures become available. Table 6 summarizes the magnitudes of the apparent activation energies determined using eq. 12. The values range from $\sim 0 - \gtrsim 5$ kcal mol^{-1} and a definite trend in reactivity can be identified. The nucleophiles H^-, F^-, OH^-, CH_3O^-, NH_2^-, and CH_3NH^- appear to react with CH_3Cl and CH_3Br with little or no activation energy ($E_a < 1$ kcal mol^{-1}) whereas their corresponding reactions with CH_3F (excluding $F^- + CH_3F$) exhibit apparent activation energies $2 < E_a < 4$ kcal mol^{-1}. The reactions of the remaining nucleophiles exhibit a similar decrease in apparent activation energy in going from CH_3F to CH_3Cl to CH_3Br with the reactivities of C_2^-, S_2^-, CN^-, and Cl^- remaining low ($E_a > 2$ kcal mol^{-1}) even with CH_3Br.

(3) The nucleophiles may be conveniently classified according to their reactivity and its variation with heat of reaction.

In an attempt to correlate the magnitudes of the apparent activation energies with some simple property of the reacting systems, we have found most useful the empirical expression established about 40 years ago by Evans and Polanyi (33) which relates the activation energy of a reaction to its heat of reaction according to

$$[13] \qquad E_a = \alpha \Delta H + C$$

where $0 < \alpha < 1$ and C is a constant for a homologous series. Expression [13] can be arrived at qualitatively from a consideration of the attractive and repulsive potential energy curves for a series of homologous reactions of varying exothermicity (33, 34). The applicability of the Polanyi relation has been clearly established for a few series of neutral reactions of very closely related compounds (34). However, experimental results for gas-phase ion–molecule reactions which often have no apparent activation energy have not been subjected to such a correlation. M. Polanyi and co-workers did, however, include negative-ion displacement reactions of type [1] amongst the reactions for which relation [13] was developed and in fact attempted to predict activation energies for such reactions proceeding in solution at a time when gas-phase results were unavailable (35).

The Polanyi relation predicts an activation energy which approaches the heat of reaction for highly endothermic processes and becomes negative for sufficiently exothermic reactions. Johnston has developed an analogous empirical expression which constrains the activation energy to approach zero for highly exothermic reactions (36).

Can. J. Chem. Downloaded from www.nrcresearchpress.com by 210.87.254.105 on 09/05/12
For personal use only.

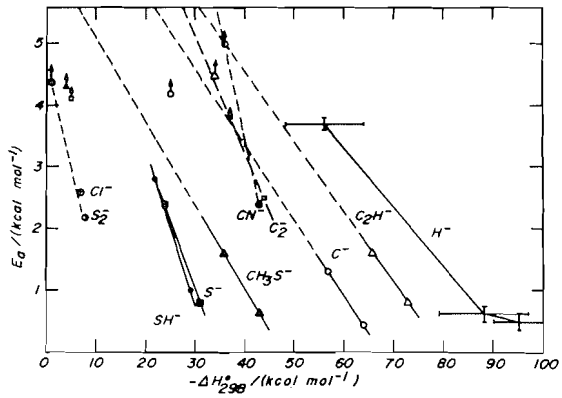

FIG. 17. A plot of the apparent activation energy *vs.* reaction exothermicity for a series of homologous reactions of specific anions with CH_3F, CH_3Cl, and CH_3Br. The uncertainties in E_a and ΔH^0_{298} displayed for the H^- series is approximately representative of the uncertainties associated with the other anion series. The plots for each anion series (excluding the H^- series) assume a linear relationship between E_a and ΔH^0_{298}.

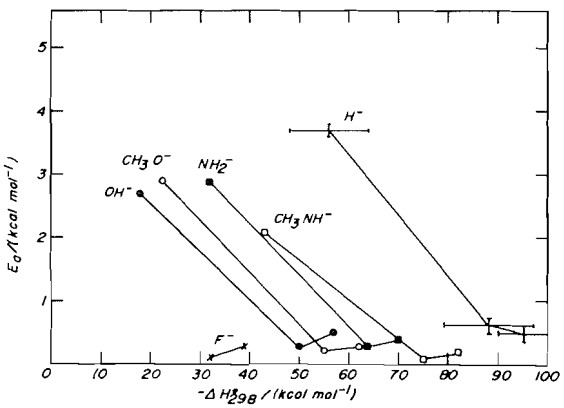

FIG. 18. A plot of the apparent activation energy *vs.* reaction exothermicity for series of homologous reactions of CH_3F, CH_3Cl, and CH_3Br with F^-, OH^-, CH_3O^-, NH_2^-, CH_3NH^-, and H^-, respectively. The uncertainties in E_a and ΔH^0_{298} displayed for the H^- series is approximately representative of the uncertainties associated with the other anion series.

A number of series of homologous reactions can be identified from the reactions investigated in this study. Consider, for example, the homologous series of reactions between a specific anion A^- and the three methyl halides, *viz.*

$$[14] \qquad A^- + CH_3Y \rightarrow CH_3A + Y^-$$

where Y = F, Cl, or Br. For such series of reactions, the exothermicity increases from CH_3F to CH_3Br in accordance with the decrease

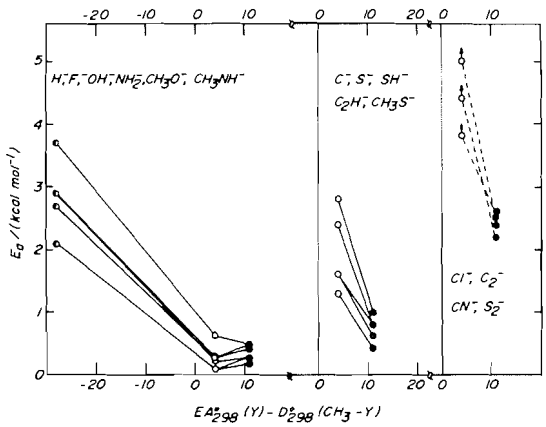

FIG. 19. A classification of nucleophiles according to their Polanyi–Johnston characteristics for series of homologous displacement reactions with CH_3F(◐), CH_3Cl(○) and CH_3Br(●).

in the intrinsic thermodynamic nucleophilicity of the halogen, *viz.* F > Cl > Br, which is largely determined by $D(CH_3—Y)$ since the electron affinities of F, Cl, and Br are very nearly equal. Figures 17 and 18 explore the variations of the apparent activation energies in Table 6 for such series of reactions with exothermicity. The variations generally fit a pattern remarkably consistent with the Polanyi–Johnston expressions which in turn enhances our confidence in the reality of the presence of activation energies in the displacement reactions under study. Those reactions in a homologous series in which a strong bond is broken are generally less probable than those in which the bond is weak. The variations for the S_2^-, SH^-, S^-, CH_3S^-, CN^-, C_2^-, C^-, and C_2H^- series can be fit with the Polanyi relation with values of α in the range 0.1 to 0.3. The variations for the F^-, OH^-, CH_3O^-, NH_2^-, CH_3NH^-, and H^- series are more consistent with an empirical expression of the type derived by Johnston since the apparent activation energies approach zero for the more exothermic reactions with CH_3Cl and CH_3Br. Also one expects, and indeed can observe, a similar accord with the Polanyi–Johnston relations for groups of homologous reactions of a specific halide with a series of homologous anions, *e.g.* S^-, SH^-, CH_3S^-, and S_2^- or NH_2^- and CH_3NH^- or OH^- and CH_3O^-.

A consideration of the magnitudes of the apparent activation energies and their variation

Can. J. Chem. Downloaded from www.nrcresearchpress.com by 210.87.254.105 on 09/05/12
For personal use only.

TABLE 7. Predicted values for the apparent activation energies (in kcal mol^{-1}) of exothermic and thermoneutral displacement reactions with CH_3F and CH_3Cl in the gas phase

$X^- + CH_3Y$	E_a	Other results	$-\Delta H^0_{298}$ (kcal mol^{-1})
$C^- + CH_3F$	5.2		25 ± 10
$F^- + CH_3F$	~3	7.9 (8)[a]	0
$C_2^- + CH_3F$	$\gtrsim 10$		7 ± 37
$CN^- + CH_3F$	$\gtrsim 17$	22 (9)[a]	4 ± 11
$C_2H^- + CH_3F$	5.2		34 ± 28
$Cl^- + CH_3Cl$	$\gtrsim 4.5$	~3.4 (5)[b]	0

[a]Computed heights of energy barriers.
[b]Apparent activation energy deduced from a measured rate constant $k_{298} \sim 6 \times 10^{-12}$ cm^3 $molecule^{-1}$ s^{-1}.

with exothermicity encountered in Figs. 17 and 18 suggests a convenient classification of the nucleophiles into three distinct groups according to Fig. 19 in which the apparent activation energies are plotted against the thermodynamic nucleophilicity of the halogen leaving group.

(*a*) Anions demonstrating high nucleophilicity: H^-, F^-, OH^-, NH_2^-, CH_3O^-, and CH_3NH^-. These anions all demonstrate high reactivity towards CH_3Cl and CH_3Br ($E_a < 1$ kcal mol^{-1}) and low reactivity towards CH_3F ($E_a > 2$ kcal mol^{-1}). Their Polanyi–Johnston characteristics are all of similar shape with α being dependent on exothermicity.

(*b*) Anions demonstrating medium nucleophilicity: C^-, S^-, SH^-, CH_3S^-, and C_2H^-. These anions are distinctly less reactive towards CH_3Cl ($E_a \gtrsim 2$ kcal mol^{-1}) than CH_3Br ($E_a \lesssim 1$ kcal mol^{-1}). Their reactions with CH_3F, when exothermic, appear to have activation energies $\gg 4$ kcal mol^{-1}. α has values in the range 0.1–0.3.

(*c*) Anions demonstrating low nucleophilicity: Cl^-, CN^-, C_2^-, and S_2^-. These anions are distinctly less reactive than the group *b* anions towards CH_3Br ($E_a > 2$ kcal mol^{-1}), CH_3Cl ($E_a > 3$ kcal mol^{-1}), and presumably also CH_3F ($E_a \gg 4$ kcal mol^{-1}). α has values $\gtrsim 0.2$. In each of the three groups the order of leaving group ability (LGA) is $Br^- \gtrsim Cl^- > F^-$.

The empirical correlations established for the three groups of anions allow predictions of values for the apparent activation energies of exothermic and thermoneutral displacement reactions not directly measurable in these experiments. These are summarized in Table 7. For the reactions of F^- and CN^- with CH_3F comparisons can be with the barrier heights computed by Dedieu and Veillard (8) and Bader *et al.* (9). Within the uncertainty of the empirical correlation and its extrapolation the accord between theory and experiment is reasonable. Brauman *et al.* (5) have reported a measured rate constant for the displacement reaction of Cl^- with CH_3Cl which can be reduced to an apparent activation energy $E_a \sim 3.4$ kcal mol^{-1}, in fair agreement with the extrapolated value of $E_a \gtrsim 4.5$ kcal mol^{-1}.

(4) Displacement in the gas phase at 298 K may proceed in competition with other reaction channels.

A variety of channels were observed for the reactions of several anions with methyl halides, *viz.* methyl cation transfer or S_N2, [1*a*], proton transfer, [1*b*], hydrogen atom transfer, [1*c*], and H_2^+ transfer, [1*d*]

$$[1a] \quad X^- + CH_3Y \rightarrow Y^- + CH_3X$$

$$[1b] \quad \rightarrow CH_2Y^- + XH$$

$$[1c] \quad \rightarrow XH^- + CH_2Y$$

$$[1d] \quad \rightarrow CHY^- + H_2X$$

Channel 1*b* becomes exothermic when $PA(X^-) > PA(CH_2Y^-)$, *i.e.* when the intrinsic Brønsted basicity of X^- exceeds that of CH_2Y^-. When the nucleophile, X^-, is a radical anion, the channels 1*c* and 1*d* become viable alternate channels since XH^- and H_2X are now likely to have a significant stability. Channel 1*c* becomes exothermic when the hydrogen-atom affinity of the nucleophile, *viz.* $D(X^-—H)$, exceeds the $H_2YC—H$ bond strength, *i.e.* when

$$[15] \quad D(XH) - EA(XH) + EA(X) > D(H_2YC—H)$$

Can. J. Chem. Downloaded from www.nrcresearchpress.com by 210.87.254.105 on 09/05/12
For personal use only.

Can. J. Chem. Downloaded from www.nrcresearchpress.com by 210.87.254.105 on 09/05/12
For personal use only.

Channel 1*d* becomes exothermic when

$$[16]\quad \Delta H^0_f(X^-) - \Delta H^0_f(H_2X) > \Delta H^0_f(CHY^-) - \Delta H^0_f(CH_3Y)$$

The intrinsic basicity order of the nucleophiles investigated in this study is as follows: $CH_3NH^- > NH_2^- > H^- > OH^- > CH_3O^- > C_2H^- > O^- > F^- > C^- > CH_3S^- > SH^- > CN^- > S^- > NO_2^- > Cl^- > Br^-$.[3] The basicities of C_2^- and S_2^- are not well established but are not likely to be very high. Competing proton transfer channels were observed only for the reactions of CH_3NH^- and NH_2^- with CH_3Cl and CH_3Br. These proton transfer channels are the most exothermic. It appears, therefore, that proton transfer will compete with displacement only if the nucleophile is also a strong base. The possibility remains however that proton transfer will compete only if it is exothermic in accordance with the basicity order $CH_2F^- > CH_3NH^- > NH_2^- > CH_2Cl^-, CH_2Br^- > H^-$. The intrinsic Brønsted acidities of CH_3F, CH_3Cl, and CH_3Br have not been determined previously.

Thermodynamic considerations indicate that, of the radical anions O^-, C^-, S^-, C_2^-, and S_2^-, only O^- is likely to have an H-atom affinity higher than the H_2YC—H bond strength which would explain why H-atom abstraction was observed only for the reactions of this anion. The H_2^+ transfer channel 1*d* is also the most exothermic for the reaction of O^- and was observed only with this anion.

Channels 1*a*, 1*c*, and 1*d* have been previously observed for the reactions of O^- with CH_3Cl by Bohme and Young (3) in a flowing afterglow (FA) experiment and for the reactions of CH_3F (channels 1*c* and 1*d* only), CH_3Cl and CH_3Br by Tiernan and Hughes[4] in a tandem mass spectrometer (tms) experiment at impacting ion energies of 0.3 ± 0.3 eV. The hydrogen atom transfer channel dominates in the reaction of O^- with CH_3F but decreases in importance in the reactions of O^- with CH_3Cl and CH_3Br. It may be of interest to note here that the reaction of O^- with CH_4, a possible fourth member in the homologous series of O^- reactions, has been observed to proceed only by hydrogen atom transfer (39).[4] Both the tms and FA experiments indicate an increasing contribution of the displacement channel to the overall reactions of O^- in progressing from CH_3F to CH_3Br. However, at the higher ion energies of the tms experiments H-atom transfer remains the dominant channel even for the reaction of O^- with CH_3Br. The branching ratio therefore appears to be sensitive to the initial energetics of the reacting system. A measure of the change in branching ratio with ion energy or temperature of the reacting system would no doubt be most instructive in providing further insight into the mechanisms of reactions of this type.

[3]The basicities of $X^- = H^-$, OH^-, O^-, F^-, C^-, SH^-, S^-, Cl^-, and Br^- were computed from known values for IP(H), EA(X) and $D^0_{298}(XH)$ as determined from $\Delta H^0_{f,298}$ (H, X, and XH) see refs. 11, 12, 14, 19, and 37. Measurements from this laboratory have provided values for the basicities of CH_3NH^- (25), NH_2^- (23), C_2H^- (22), and CN^- (38), and the relative basicities of CH_3O^- and CH_3S^-, unpublished results.

[4]T. O. Tiernan and B. M. Hughes, private communication.

Acknowledgments

The financial support of the National Research Council of Canada and the Sloan Foundation is gratefully acknowledged.

1. A. J. Parker. Chem. Rev. **69**, 1 (1969).
2. R. H. Bathgate and E. A. Moelwyn-Hughes. J. Chem. Soc. 2642 (1959).
3. D. K. Bohme and L. B. Young. J. Am. Chem. Soc. **92**, 7354 (1970).
4. L. B. Young, E. Lee-Ruff, and D. K. Bohme. J. Chem. Soc. Chem. Commun. 35 (1973).
5. J. I. Brauman, W. N. Olmstead, and C. A. Lieder. J. Am. Chem. Soc. **96**, 4030 (1974).
6. C. M. Won and A. V. Willi. J. Phys. Chem. **76**, 427 (1972).
7. D. K. Bohme, G. I. Mackay, and J. D. Payzant. J. Am. Chem. Soc. **96**, 4027 (1974).
8. A. Dedieu and A. Veillard. J. Am. Chem. Soc. **94**, 6730 (1972).
9. R. F. Bader, A. J. Duke, and R. R. Messer. J. Am. Chem. Soc. **95**, 7715 (1973).
10. D. K. Bohme, R. S. Hemsworth, H. W. Rundle, and H. I. Schiff. J. Chem. Phys. **58**, 3504 (1973).
11. JANAF thermochemical tables. 2nd ed. Natl. Stand. Ref. Data Ser. Natl. Bur. Stand. **37** (1971).
12. B. deB. Darwent. Natl. Stand. Ref. Data Ser. Natl. Bur. Stand. **31**, (1970).
13. S. W. Benson. Thermochemical kinetics. John Wiley and Sons, Inc., New York, N.Y. 1968.
14. JANAF thermochemical tables. 1974 Suppl. J. Phys. Chem. Ref. Data, **3**, 311 (1974).
15. W. C. Lineberger and B. W. Woodward. Phys. Rev. Lett. **25**, 424 (1970).

16. J. L. FRANKLIN, J. G. DILLARD, H. M. ROSENSTOCK, J. T. HERRON, K. DRAXL, and F. H. FIELD. Ionization potentials, appearance potentials and heats of formation of gaseous positive ions. Natl. Stand. Ref. Data Ser. Natl. Bur. Stand. **26** (1969).
17. R. S. BERRY and C. W. REIMANN. J. Chem. Phys. **38**, 1540 (1963).
18. V. H. DIBELER and S. K. LISTON. J. Chem. Phys. **49**, 482 (1968).
19. L. M. BRANSCOMB. Phys. Rev. **148**, 11 (1966).
20. R. J. CELOTTA, R. A. BENNET, and J. L. HALL. J. Chem. Phys. **60**, 1740 (1974).
21. H. OKABE and V. H. DIBELER. J. Chem. Phys. **59**, 2430 (1973).
22. D. K. BOHME, G. I. MACKAY, H. I. SCHIFF, and R. S. HEMSWORTH. J. Chem. Phys. **61**, 2175 (1974).
23. D. K. BOHME, R. S. HEMSWORTH, and H. W. RUNDLE. J. Chem. Phys. **59**, 77 (1973).
24. D. K. SEN SHARMA and J. L. FRANKLIN. J. Am. Chem. Soc. **95**, 6562 (1973).
25. G. I. MACKAY, R. S. HEMSWORTH, and D. K. BOHME. Can. J. Chem. This issue.
26. K. W. EGGER and A. T. COCKS. Helv. Chim. Acta, **56**, 1516 (1973).
27. N. C. BARFORD. Experimental measurements: precision, error and truth. Addison-Wesley, London. 1967.
28. T. SU and M. T. BOWERS. Int. J. Mass Spectrom. Ion Phys. **12**, 347 (1973).
29. M. T. BOWERS and T. SU. Theory of ion – polar molecule collisions. *In* Interactions between ions and molecules. *Edited by* P. Ausloos. Plenum Press, New York. 1975.
30. D. K. BOHME. The kinetics and energetics of proton transfer. *In* Interactions between ions and molecules. *Edited by* P. Ausloos. Plenum Press, New York. 1975.
31. E. W. ROTHE and R. B. BERNSTEIN. J. Chem. Phys. **31**, 1619 (1959).
32. H. I. SCHIFF and D. K. BOHME. Int. J. Mass Spectrom. Ion Phys. **16**, 167 (1975).
33. M. G. EVANS and M. POLANYI. Trans. Faraday Soc. **34**, 11 (1938).
34. N. N. SEMENOV. Some problems in chemical kinetics and reactivity. Vol. 1. (translated by M. Bondart). Princeton University Press, Princeton, N.J. 1958.
35. R. A. OGG and M. POLANYI. Trans. Faraday Soc. **31**, 604 (1935).
36. H. S. JOHNSTON. Gas phase reaction rate theory. The Ronald Press Company, New York. 1966.
37. H. HOTOP and W. C. LINEBERGER. J. Phys. Chem. Ref. Data. In press.
38. D. BETOWSKI, G. MACKAY, J. PAYZANT, and D. BOHME. Can. J. Chem. **53**, 2365 (1975).
39. D. K. BOHME and F. C. FEHSENFELD. Can. J. Chem. **47**, 2717 (1969).
40. R. ALEXANDER, E. C. F. KO, A. J. PARKER, and T. J. BROXTON. J. Am. Chem. Soc. **90**, 5049 (1968).

Can. J. Chem. Downloaded from www.nrcresearchpress.com by 210.87.254.105 on 09/05/12
For personal use only.

Carbon-13 nuclear magnetic resonance spectra of organic sulfur compounds.[1] Substituent chemical shift (s.c.s.) effects in the 4-thiazoline-2-thione series

I. W. J. STILL[2] AND N. PLAVAC

Department of Chemistry, University of Toronto, Toronto, Ontario M5S 1A1

AND

D. M. MCKINNON AND M. S. CHAUHAN

Department of Chemistry, University of Manitoba, Winnipeg, Manitoba R3T 2N2

Received December 29, 1975

I. W. J. STILL, N. PLAVAC, D. M. MCKINNON, and M. S. CHAUHAN. Can. J. Chem. **54**, 1660 (1976).

^{13}C nmr data have been obtained for a series of 4-thiazoline-2-thiones. Substituent chemical shift (s.c.s.) effects for methyl and phenyl substitution have been collated and are discussed in comparison with s.c.s. effects in other heterocyclic systems. Some attempt has also been made to compare our data with those reported previously for the thiazoles and for some thiones in the isothiazole series.

I. W. J. STILL, N. PLAVAC, D. M. MCKINNON et M. S. CHAUHAN. Can. J. Chem. **54**, 1660 (1976).

On a obtenu des données concernant les spectres rmn du ^{13}C pour une série de thiazoline-4 thiones-2. On a colligé les effets sur les déplacements chimiques de substitutions (s.c.s.) dus à des groupes méthyles ou phényles; on discute de ces effets par comparaison avec d'autres effets s.c.s. dans d'autres systèmes hétérocycliques. On fait aussi quelques efforts afin de comparer nos données avec celles rapportées antérieurement pour les thiazoles et pour quelques thiones de la série isothiazole.

[Traduit par le journal]

Introduction

A relatively large number of papers reporting ^{13}C nmr chemical shift data in a variety of heterocyclic systems has appeared recently (1–4), and the subject has also been reviewed in a recent monograph (5). We ourselves had earlier examined the ^{13}C nmr spectra of a number of isothiazole and benzo[*c*]isothiazole derivatives (6) and Faure *et al.* later reported data independently for a further series of isothiazoles (7).

In our earlier study we had also examined a limited number of isothiazoline-thiones, as part of an investigation aimed at proving (or disproving) the existence of a simple correlation between chemical shift data for C=O and C=S carbon atoms in related series of compounds. We now report the data which we have obtained for a number of 4-thiazoline-2-thione derivatives. In addition to the obvious comparisons to be drawn between the two series of thiones, we have attempted to discuss our data in the light of an earlier study by Faure and co-workers of a large number of simple thiazoles (8).

Experimental

Natural abundance proton decoupled ^{13}C nmr spectra were obtained on a Varian XL-100-15 spectrometer operating at 25.16 MHz in the pulsed Fourier transform mode. The temperature of the probe was 32 ± 3 °C. Spectral widths of 6000 Hz, acquisition times of 0.666 s, and pulse widths of 10 μs (90° pulse = 55 μs) were routinely used. In some cases, pulse delays of 1–10 s were used to intensify quaternary carbons, and in other cases, paramagnetic chromium trisacetylacetonate[3] was used for the same purpose. The spectra were transformed using a Varian 16K-620i computer giving 4096 real points with an accuracy of ± 0.1 ppm. Off-resonance proton decoupled spectra were obtained where deemed necessary. The deuterium of the solvent (chloroform-*d*, or dimethyl sulfoxide-d_6 in one case) was used as lock and primary reference in all cases, and all chemical shifts are measured from TMS (5%) added as internal reference.

Literature references for the preparation of the compounds used in this study, with the two exceptions noted below, are quoted in Table 1. 3-Methylbenzo[*d*]thiazoline-2-thione was obtained commercially (Aldrich Chemical Co.) and used without further purification.

[1]Part IV of a series. For part III see ref. 9.

[2]Author to whom correspondence should be addressed.

[3]$[Cr(AcAc)_3] \approx 17$ mg/2.5 ml of solution.

Can. J. Chem. Downloaded from www.nrcresearchpress.com by 210.87.254.5 on 09/05/12
For personal use only.

Can. J. Chem. Downloaded from www.nrcresearchpress.com by 210.87.254.5 on 09/05/12
For personal use only.

TABLE 1. ^{13}C nmr chemical shifts[a] of 4-thiazoline-2-thiones, and related compounds

Compound	C-2	C-4	C-5	Aromatic C-1	Aromatic *o*-	Aromatic *m*-	Aromatic *p*-	Other	Reference
4-Thiazoline-2-thione, **1**[b]	188.4	128.9	114.0	—	—	—	—	—	15
3-Methyl-4-thiazoline-2-thione, **2**	187.1	132.6	110.9	—	—	—	—	37.5(N-CH_3)	16
3-Methyl-4-thiazolin-2-one	172.2	125.4	101.1	—	—	—	—	32.1(N-CH_3)	See Experimental
3,4-Dimethyl-**1**	187.5	140.1	105.9	—	—	—	—	34.1(N-CH_3) 15.7(C-CH_3)	16
3,5-Dimethyl-**1**	186.5	129.0	124.0	—	—	—	—	37.2(N-CH_3) 12.6(C-CH_3)	17
3,4,5-Trimethyl-**1**	185.0	134.9	117.0	—	—	—	—	34.8(N-CH_3) 13.1[c](C-4-CH_3) 11.6[c](C-5-CH_3)	16
3-Methyl-4-phenyl-**1**	188.1	144.8	108.4	130.7	129.1	129.1	129.9	36.2(N-CH_3)	18
3-Methyl-4-*p*-tolyl-**1**	188.1	145.0	108.1	127.8	129.0	129.7	140.1	36.2(N-CH_3) 21.3(C-CH_3)	[f]
3,4-Diphenyl-**1**	190.1	144.8	109.0	137.8 130.5	129.2[d]	128.8[d]	128.4[d]	—	19
3-Methyl-5-phenyl-**1**	186.7	126.7	129.7	128.4	125.5	129.3	128.7	37.7(N-CH_3)	[f]
3-Methyl-4,5-diphenyl-**1**	186.1	138.9	124.8	130.6[d]	130.4 129.5	128.7 128.2	130.1 130.0	36.5(N-CH_3)	[f]
3-Methylbenzo[*d*]thiazoline-2-thione, **6**	189.0	(141.8[e])	(127.2[e])	—	—	—	—	33.1(N-CH_3) 126.9(C-7) 124.7(C-5) 121.1(C-6) 112.3(C-4)	See Experimental
2-Methylthiothiazole, **3**	166.4	142.6	118.3	—	—	—	—	16.7(S-CH_3)	17
2-Methyl-4-phenylthiazole	165.5	154.9	112.2	134.5	126.3	128.6	127.9	19.1(C-CH_3)	20

[a]All shifts in ppm relative to TMS, in $CDCl_3$, except as noted.
[b]In DMSO-d_6.
[c]These assignments may be reversed.
[d]Substantial overlapping of signals in this region reduces the number of peaks observed.
[e]Although this is a fused ring compound, for convenience these carbons are identified with the C-4 and C-5 positions of a simple thiazole.
[f]D. M. McKinnon and M. H. Hassan, unpublished results.

Can. J. Chem. Downloaded from www.nrcresearchpress.com by 210.87.254.5 on 09/05/12
For personal use only.

3-Methyl-4-thiazolin-2-one

3-Methyl-4-thiazoline-2-thione (1.0 g) was added to a stirred solution of boiling acetone (500 ml) saturated with potassium permanganate, and the reaction mixture stirred for 16 h. Filtration and evaporation of the filtrate afforded a pale yellow oil. Extraction with benzene and reevaporation afforded a product which was contaminated with about 10% of the starting thione. Since we had already recorded the spectrum of the thione, this was not a serious drawback, and no further purification was undertaken.

Results and Discussion

The most obvious feature of the ^{13}C chemical shift data for the 11 representatives of the 4-thiazoline-2-thione series presented in Table 1 is the relatively constant δ value for the C=S(C-2) carbon atom. In the parent compound **1** this is observed at 188.4 ppm. That the thione structure, and not the thiol structure, is indeed the major tautomer present is evident by examining the chemical shift data for the C-2 carbon in the *N*-methyl derivative **2** and its *S*-methyl isomer **3**. The values observed are 187.1 and 166.4 ppm, respectively. Furthermore, the positions of the C-4 and C-5 resonances in **2** are much closer to the analogous signals in compound **1**, than are those of **3**. *N*-Methylation produces a β deshielding effect at C-4 of +3.7 ppm and a γ shielding effect at C-5 of −3.1 ppm. We have recently observed similar effects upon *N*-methylation of 2-pyridinethione (9). The preference for the thione rather than the thiol form in a number of heterocyclic systems is well established (9).

The position of the thione carbon signal in **1** (188.4 ppm), although at relatively high field for a C=S functionality, is very similar to the values of 186.7 and 187.3 ppm which we reported for two 4-isothiazoline-3-thione, **4**, derivatives (6). In part, this must be attributed to the effect of the adjacent N-atom with its electron-releasing capability (sulfur having a much smaller effect). Even in the 3-isothiazoline-5-thione, **5**,

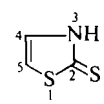

1

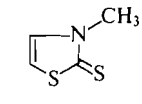

2

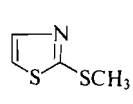

3

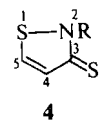

4

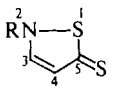

5

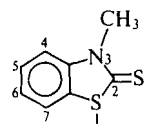

6

TABLE 2. Substituent chemical shift (s.c.s.) effects[a] for methyl and phenyl in the 4-thiazoline-2-thione series

Substituent	s.c.s. effects		
	α	β	γ
4-CH_3	+7.5	−5.0	+0.4
5-CH_3	+13.1	−3.6	−0.6
4-C_6H_5	+12.2	−2.5	+1.0
4-$C_6H_4CH_3(p)$	+12.4	−2.8	+1.0
5-C_6H_5	+18.8	−5.9	−0.4

[a]In ppm; positive values indicate shifts to lower field.

series, where the nitrogen is located in a vinylogous relationship to the C=S, the mean shift observed for the thione carbon was 193.4 ppm. The position of the C=S signal in the present series is relatively insensitive to alkyl or aryl substitution at positions 3, 4, or 5, varying between 185.0 and 190.1 ppm. It was noted, however, that in general the C=S signal tended to drift to higher field with increasing substitution on the ring, *e.g.* δ values of 185.0 in the 3,4,5-trimethyl derivative and 186.1 ppm in the 3-methyl-4,5-diphenyl analogue were observed. Whether this is due to steric compression or electronic factors is uncertain, although the smallness of these effects and the lack of a correlation with substitution patterns suggest that the former is more likely.

The carbonyl analogue of **2**, 3-methyl-4-thiazolin-2-one, is included in Table 1 for comparison. The chemical shift observed for the C=O group at 172.2 ppm is 14.9 ppm upfield from the analogous C=S group. This $\Delta\delta$ value compares closely with the $\Delta\delta$ value of 14.1 ppm observed earlier for both the 2- and 4-pyridones and their respective C=S analogues (9). In comparing the C-4 and C-5 signals in the 4-thiazolin-2-one and 4-thiazoline-2-thione systems, although the individual values differ quite widely, there is a relatively constant difference in $\Delta\delta$ for C-4 and C-5 of 24.3 in the carbonyl compound and 21.7 ppm in the thiocarbonyl compound.

We have been able to compare the substituent chemical shift (s.c.s.) effects for the 4- and 5-methyl substituted 4-thiazoline-2-thiones in Table 1 with the data obtained by Faure and coworkers (8) for 4-methylthiazole and the results recently reported by Gronowitz *et al.* (10) for 2- and 3-methylthiophenes. Our s.c.s. data, for both methyl and phenyl substituted compounds,

Can. J. Chem. Downloaded from www.nrcresearchpress.com by 210.87.254.5 on 09/05/12
For personal use only.

are collected in Table 2. We have earlier reported similar data for the isothiazole and 1,2-dithiole-3-thione systems (6). The α-effect observed at C-4 in our system is +7.5 ppm, which compares with +10.55 ppm in 4-methylthiazole and +10.9 ppm in 3-methylthiophene, or the +12.9 ppm reported for propylene (*vs.* ethylene) by Miyajima *et al.* (11). The β-effect observed in our system for C-4 methyl substitution, −5.0 ppm, on the other hand, is much more similar to those observed in 4-methylthiazole (−5.3) and 3-methylthiophene (−4.3), although still smaller than the −7.4 ppm observed in propylene. Turning to the C-5 methyl substituted 4-thiazoline-2-thione, a much larger α-effect of +13.1 and a smaller β-effect of −3.6 ppm were observed. Faure did not report data for 5-methylthiazole, but the α- and β-effects observed in 2-methylthiophene (10) were +14.2 and −1.4 ppm, respectively. Given the obvious perturbing influence of the ring C=S group in our case, our data seem to correlate reasonably well with those in the model systems chosen.

Fewer model systems are available for comparison with the s.c.s. effects for the 4-phenyl and 5-phenyl substituted analogs (Table 2). The α- and β-effects reported for phenyl substitution in ethylene (11) are +14.4 and −9.5 ppm, respectively. In our 4-phenyl substituted case, both effects are smaller, but in the 5-phenyl compound a very large α-effect of +18.8 ppm may be noted. This presumably reflects the greater ability of the phenyl group at C-5 to accommodate the excess electron density at that position:

As expected, the 4-*p*-tolyl substituent has an effect virtually identical with that of the 4-phenyl group.

We have included the γ-effects for comparison in Table 2, but these are too small to allow any but the most speculative explanations to be advanced.

As a test of the predictive power of the s.c.s. effects in Table 2, we used these values to calculate the expected δ values for the C-4 and C-5 signals in 3,4,5-trimethyl-4-thiazoline-2-thione and 3-methyl-4,5-diphenyl-4-thiazoline-2-thione. The differences between calculated and observed (Table 1) values ranged between 0 and 2.4 ppm. Since no allowance is made for steric crowding, this agreement must be regarded as satisfactory.

The *N*-methyl signals observed in these compounds range from 34.1–37.5 ppm in the methyl series and from 36.2–37.7 ppm in the phenyl series. Substitution in either case at C-5 has virtually no effect on the N—CH_3 chemical shift, whereas the 4-substituted and 4,5-disubstituted analogues reveal shielding effects of up to −2.3 ppm in the methyl series and −1.3 ppm in the phenyl series. It may be noted that the N—CH_3 signal in **2** at 37.5 is deshielded by 5.4 ppm relative to that in its carbonyl counterpart. This difference may be compared with a similar effect of 4.2 ppm in the 2-pyridone/2-pyridinethione analogues (9), and is due to the more effective deshielding cones associated with the thiocarbonyl groups. Dean *et al*, (12), for example, have recently remarked on the distinctive downfield shift (in ^1H nmr) of the α-vinyl proton signal, when O is replaced by S in the part-structure below:

The *C*-methyl signals reported in Table 1 require little comment, except for the fact that the δ values for C-4 and C-5 methyl groups differ by 3.1 ppm, the latter being at higher field. This presumably parallels to some extent the δ values for the C-4 and C-5 positions themselves, and hence the electron density distribution in the ring. The gap between the δ values narrows to 1.5 ppm in the 4,5-dimethyl analogue, but again this may be due to the intervention of steric factors.

Of the remaining compounds in Table 1 which have not been discussed in detail, a few brief comments will suffice. 2-Methyl-4-phenylthiazole was included as a further point of reference to Faure's earlier results and it is interesting, in the light of our earlier comments regarding s.c.s. effects of phenyl and methyl in this heterocyclic system, that the δ values reported by Faure and co-workers (5, 8) for C-2, C-4, and C-5 in 2,4-dimethylthiazole are very similar to those for the analogous carbons in our compound. Substitution at C-2 by CH_3S— or by CH_3— produces very similar α-deshielding effects (+14.2 and +11.8 ppm, respec-

tively), as expected. In the benzo-fused analogue **6** the assignments of the signals due to C-4, C-5, C-6, and C-7 were made using the normal aromatic s.c.s. effects for nitrogen (13) and sulfur (14) substituents, with generally good agreement between calculated and observed values. Little influence is felt by the ring carbon atoms on replacing the N—CH_3 group by N—C_6H_5, except for a deshielding effect of +2.0 ppm on the C=S signal. This probably reflects the competing resonance delocalization possibilities for the nitrogen lone pair electrons.[4]

Acknowledgments

We gratefully acknowledge financial support of this study by the National Research Council of Canada and by the Department of Chemistry, University of Toronto.

1. C. J. TURNER and G. W. H. CHEESEMAN. Org. Magn. Reson. **6**, 663 (1974).
2. W. V. TURNER and W. H. PIRKLE. J. Org. Chem. **39**, 1935 (1974).
3. C. A. KINGSBURY and J. H. LOOKER. J. Org. Chem. **40**, 1120 (1975).
4. S. A. SOJKA. J. Org. Chem. **40**, 1175 (1975).
5. E. BREITMAIER and W. VOELTER. ^{13}C N.m.r. spectroscopy. Methods and applications. Weinheim, Bergatri, and Verlag Chemie. 1974. pp. 182–189.
6. N. PLAVAC, I. W. J. STILL, M. S. CHAUHAN, and D. M. MCKINNON. Can. J. Chem. **53**, 836 (1975).
7. R. FAURE, J.-R. LLINAS, E.-J. VINCENT, and M. RAZMANN. Can. J. Chem. **53**, 1677 (1975).
8. R. GARNIER, R. FAURE, A. BABADJAMIAN, and E.-J. VINCENT. Bull Soc. Chim. Fr. 1040 (1972).
9. I. W. J. STILL, N. PLAVAC, D. M. MCKINNON, and M. S. CHAUHAN. Can. J. Chem. **54**, 280 (1976).
10. S. GRONOWITZ, I. JOHNSON, and A.-B. HÖRNFELDT. Chem. Scr. **7**, 76 (1975).
11. G. MIYAJIMA, K. TAKAHASHI, and K. NISHIMOTO. Org. Magn. Reson. **6**, 413 (1974).
12. F. M. DEAN, J. GOODCHILD, A. W. HILL, S. MURRAY, and A. ZAHMAN. J. Chem. Soc. Perkin Trans. 1, 1335 (1975).
13. G. C. LEVY and G. L. NELSON. Carbon-13 nuclear magnetic resonance for organic chemists. Wiley-Interscience, New York. 1972. p. 81.
14. M. S. CHAUHAN and I. W. J. STILL. Can. J. Chem. **53**, 2880 (1975).
15. R. A. MATHES and A. J. BEBER. J. Am. Chem. Soc. **70**, 1451 (1948).
16. C. M. ROUSSEL, R. GALLO, M. CHANON, and J. METZGER. Bull. Soc. Chim. Fr. 1902 (1971).
17. M. CHANON and J. METZGER. Bull. Soc. Chim. Fr. 2868 (1968).
18. W. J. HUMPHLETT and R. W. LAMON. J. Org. Chem. **29**, 2146 (1964).
19. B. SAHU and B. C. DASH. Indian J. Appl. Chem. **33**, 256 (1970).
20. W. H. MILLS and J. L. B. SMITH. J. Chem. Soc. **121**, 2724 (1922).

[4]We thank one of the referees for this suggestion.

Can. J. Chem. Downloaded from www.nrcresearchpress.com by 210.87.254.5 on 09/05/12
For personal use only.

Can. J. Chem. Downloaded from www.nrcresearchpress.com by 210.87.254.42 on 09/05/12
For personal use only.

Canadian Journal of Chemistry

Published by
THE NATIONAL RESEARCH COUNCIL OF CANADA

Journal canadien de chimie

Publié par
LE CONSEIL NATIONAL DE RECHERCHES DU CANADA

Volume 54 Number 11 June 1, 1976

Volume 54 numéro 11 1 juin 1976

Influence de la nature des ions et sur l'évolution structurale des weberites $A_2B_2O_7$: les weberites $Cd_{2-x}Sr_xSb_2O_7$

G. DESGARDIN, C. ROBERT ET B. RAVEAU

Groupe de Cristallographie et Chimie du Solide, ERA 305, Laboratoire de Chimie Minérale du Solide, Université de Caen, 14032 Caen Cedex, France

Reçu le 12 décembre 1975

G. DESGARDIN, C. ROBERT et B. RAVEAU. Can. J. Chem. **54**, 1665 (1976).

Une nouvelle solution solide $Cd_{2-x}Sr_xSb_2O_7$ ($0 \leq x \leq 2$) de type wébérite est isolée et caractérisée. L'analyse de la structure wébérite, met en évidence pour cette dernière, trois distances métal–oxygène et conduit à proposer un phénomène d'ordre des ions A permettant d'expliquer l'évolution structurale de ces composés.

G. DESGARDIN, C. ROBERT, and B. RAVEAU. Can. J. Chem. **54**, 1665 (1976).

A new series of solid solution $Cd_{2-x}Sr_xSb_2O_7$ ($0 \leq x \leq 2$) of the weberite type has been prepared and characterized. Examination of the weberite structure has revealed the existence of three critical metal–oxygen distances. The proposed ordering of the A ions permits the structural features of these compounds to be explained.

L'étude de l'influence de la nature des ions A et B sur l'évolution structurale des oxydes $A_2B_2O_7$ de type pyrochlore a fait l'objet de nombreux travaux (1–6). Parmi les oxydes de même formulation, les antimonates $A_2Sb_2O_7$ (A = Cd, Ca, Sr) dont la structure de type wébérite (7) est étroitement reliée à celle des pyrochlores (8, 9), mettent en évidence le comportement particulier de l'antimoine à l'état d'oxydation +5: l'étude de l'influence de l'ion B sur l'évolution de la structure des oxydes de type wébérite, montre que la substitution de Sb(V) par des ions de taille voisine (Ta, Nb, Ti) stabilise en effet la structure pyrochlore (5, 10). En revanche, l'influence de la nature des ions A sur l'évolution de la structure wébérite a été peu étudiée à notre connaissance, malgré son importance pour mieux comprendre les stabilités relatives des structures wébérite et pyrochlore. Cependant, le cadmium, en raison de sa structure électronique, se distingue des ions alcalino-terreux par l'existence possible pour la composition $Cd_2Sb_2O_7$ des deux formes wébérite-pyrochlore (9). Le présent travail est donc relatif à l'étude de la substitution dans la wébérite $Cd_2Sb_2O_7$ du cadmium par un ion alcalino-terreux de plus grande taille, le strontium.

Méthode expérimentales

L'étude du système $Cd_2SB_2O_7$–$Sr_2Sb_2O_7$ a été effectuée de deux façons différentes, conduisant à des résultats identiques:

Chauffage à l'air des mélanges d'oxydes CdO, Sb_2O_3 et du carbonate $SrCO_3$

Le préchauffage de ces composés de pureté supérieure à 99.5%, à 650 °C pendant 12 h, permet d'assurer dans un premier temps une oxydation totale de l'antimoine au degré d'oxydation +5. La réaction est ensuite poursuivie par paliers distants de 100 °C, depuis 800 °C jusqu'à 1200 °C. Chaque traitement thermique, dont la durée diminue lorsque la température augmente, est suivi de broyages. On limite ainsi la perte de masse au-delà de 650 °C à moins de 1% de la masse des oxydes CdO ou Sb_2O_3 de départ.

Can. J. Chem. Downloaded from www.nrcresearchpress.com by 210.87.254.42 on 09/05/12
For personal use only.

Chauffage à l'air des mélanges des wébérites $Cd_2Sb_2O_7$ et $Sr_2Sb_2O_7$

Ces mélanges ont été préalablement obtenus suivant le mode opératoire décrit précédemment.

Il faut cependant noter que les composés $Cd_{2-x}Sr_xSb_2O_7$ correspondant à $0.80 < x < 1.2$ sont moins bien cristallisés, quelle que soit la méthode utilisée. Une meilleure cristallisation de ces composés a pu être obtenue pour ces compositions, en traitant les produits préchauffés à 650 °C à l'air, à 1100 °C en tubes de silice scellés sous vide. Les produits obtenus ont été étudiés sur diffractomètre à poudre Philips utilisant un goniomètre horizontal et la raie K_α du cuivre (sans monochromateur).

Résultats et discussion

Caractéristiques structurales des wébérites $Cd_{2-x}Sr_xSb_2O_7$

Dans les conditions précédemment décrites, nous observons un passage continu de la wébérite $Cd_2Sb_2O_7$ à la wébérite $Sr_2Sb_2O_7$ suivant:

$$x\mathrm{SrCO_3} + \mathrm{Sb_2O_3} + (2-x)\mathrm{CdO} + \mathrm{O_2} \rightarrow \mathrm{Cd_{2-x}Sr_xSb_2O_7} + x\mathrm{CO_2}\uparrow$$

ou

$$\frac{x}{2}\mathrm{Sr_2Sb_2O_7} + \frac{2-x}{2}\mathrm{Cd_2Sb_2O_7} \rightarrow \mathrm{Cd_{2-x}Sr_xSb_2O_7}$$

Quelle que soit la valeur de x comprise entre 0 et 2, nous observons une seule phase, qui se présente sous la forme d'une poudre bien cristallisée de couleur blanchâtre.

Les diffractogrammes de ces phases évoluent de façon régulière en fonction du taux de substitution x depuis la wébérite $Cd_2Sb_2O_7$ jusqu'à la wébérite $Sr_2Sb_2O_7$. Ils ont été indexés pour les composés les plus riches en cadmium ($x < 0.60$) et en strontium ($x > 1.20$) dans une maille orthorhombique voisine de celle de la wébérite, et dans une maille quadratique pour les compositions voisines de $x = 1$ ($0.8 < x < 1$). Le composé $CdSrSb_2O_7$, correspondant à $x = 1$, se distingue des autres termes de la solution solide par la relation particulière observée entre ses paramètres ($a = b = c/\sqrt{2}$), permettant son indexation dans une maille cubique d'ordre 2. L'examen de l'évolution des caractéristiques structurales ainsi obtenues (tableau 1, fig. 1) montre que la distorsion orthorhombique de la maille décroît progressivement depuis $x = 0$, jusqu'à $x = 1$, puis croît à nouveau lorsque la teneur en strontium augmente jusqu'à $x = 2$. L'évolution des paramètres de la maille est complexe et fait apparaître deux régions situées de part et d'autre de $CdSrSb_2O_7$: pour $x \leq 1$, les paramètres b et c croissent de façon sensiblement linéaire lorsque x augmente, alors que a diminue, mais très légèrement; pour $x \geq 1$, a et b augmentent alors que c diminue de façon linéaire. Cette rupture dans l'évolution des paramètres au voisinage de $x = 1$, se retrouve, mais de façon moins sensible, dans l'évolution du volume de la maille (fig. 2).

TABLEAU 1. Paramètres des composés $Cd_{2-x}Sr_xSb_2O_7$

x	a (Å)	b (Å)	c (Å)	$c/\sqrt{2}$ (Å)
0	7.34_1*	7.22_2*	10.18_9	7.20_6
0.2	7.33_7	7.25_6	10.25_5	7.25_3
0.4	7.33_6	7.28_1	10.28_3	7.27_2
0.6	7.33_1	7.30_0	10.32_8	7.30_4
0.8	7.33_7	7.33_7	10.37_4	7.33_7
1.0	7.35_6	7.35_6	10.40_1	7.35_6
1.2	7.36_8	7.40_4	10.42_0	7.36_9
1.4	7.38_8	7.46_7	10.40_0	7.35_5
1.6	7.41_0	7.55_3	10.39_1	7.34_9
1.8	7.43_0	7.61_7	10.37_3	7.33_6
2.0	7.45_1	7.68_3	10.36_3	7.32_8

*Les paramètres a et b donnés précédemment par différents auteurs (5, 7), ont été intervertis (voir texte).

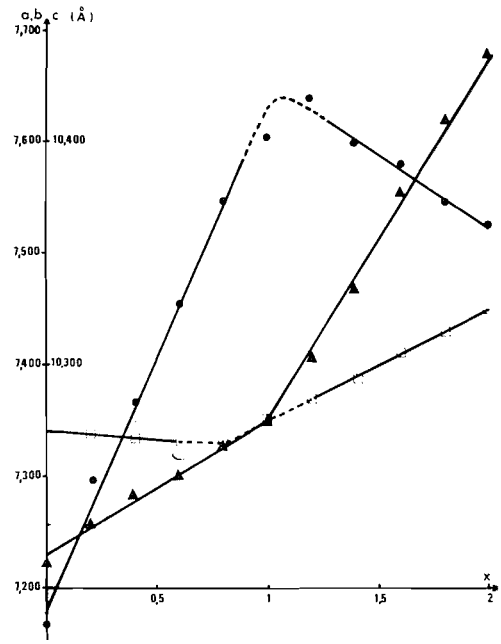

FIG. 1. Evolution des paramètres de la maille orthorhombique des composés wébérites $Cd_{2-x}Sr_xSb_2O_7$. □, a; ▲, b; ●, c.

Can. J. Chem. Downloaded from www.nrcresearchpress.com by 210.87.254.42 on 09/05/12
For personal use only.

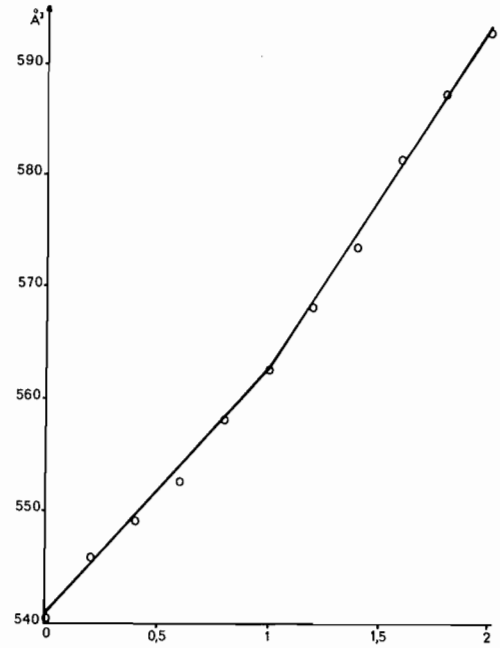

FIG. 2. Evolution du volume de la maille des composés $Cd_{2-x}Sr_xSb_2O_7$.

La wébérite $CdSrSb_2O_7$. Description comparative des réseaux des ions A et B dans les pyrochlores et wébérites $A_2B_2O_7$

L'indexation possible du composé $CdSrSb_2O_7$, dans une maille cubique de paramètre a = 10.401 Å (tableau 2) ne permet pas d'exclure à priori pour cette phase la structure pyrochlore. Cependant, l'existence des réflexions *hkl* telles que 200 et 420 conduit à rejeter le groupe d'espace *Fd3m* des pyrochlores cubiques, et est en faveur d'une structure de type wébérite.

Le réseau des ions métalliques A et B peut être décrit dans les deux structures wébérite et pyrochlore par des plans de composition AB_3, alternant avec des plans A_3B, normaux à la direction $\{111\}_P$ de la maille cubique pyrochlore ou $\{011\}_W$ de la maille orthorhombique wébérite. La description comparative des structures pyrochlore et wébérite en couches de type bronze hexagonal de tungstène, présentée par Pouchard et coll. (11) montre que la distribution des ions A et B dans les plans AB_3, est analogue dans les deux types de structure, aux déformations près du réseau hexagonal (fig. 3*a*).

Cette analogie se retrouve pour les plans A_3B qui peuvent être décrits comme un réseau "anti AB_3" (fig. 3*b*).

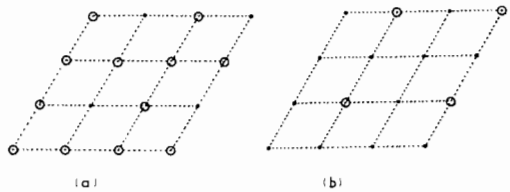

FIG. 3. Description du réseau des ions métalliques A et B dans les structures pyrochlore et wébérite. (Plans $(111)_P$ ou $(011)_W$). (*a*) Arrangement des ions A et B dans les plans A_3B de la structure pyrochlore. La structure wébérite présente un arrangement analogue à de légères déformations près (○ = A; ● = B). (*b*) Arrangement des ions A et B dans les plans AB_3 de la structure pyrochlore. La structure wébérite présente un arrangement analogue à de légères déformations près (○ = A; ● = B).

TABLEAU 2. Indexation de $CdSrSb_2O_7$ dans une maille cubique (a = 10.401 Å)

d_{obs}	I_{obs}*	d_{calc}	*h k l*	d_{obs}	I_{obs}*	d_{calc}	*h k l*
6.00	f	6.005	1 1 1	1.5012	m	1.5012	4 4 4
5.20	tf	5.200	2 0 0	1.354	tf	1.3541	7 3 1–5 5 3
3.68	tf	3.677	2 2 0	1.300	m	1.3001	8 0 0
3.14	f	3.136	3 1 1	1.226	ttf	1.2258	8 8 2–6 6 0
3.0022	TF	3.0024	2 2 2	1.200	ttf	1.2010	7 5 1–5 5 5
2.5997	F	2.6002	4 0 0	1.19304	m^+	1.19307	6 6 2
2.38	ttf	2.3861	3 3 1	1.16278	m^+	1.16278	8 4 0
2.32	tttf	2.3257	4 2 0	1.0615_5	m	1.06151	8 4 4
2.12	tf	2.1230	4 2 2	1.000	tttf	1.00550	9 5 1–7 7 3
2.00	tf	2.0016	5 1 1–3 3 3	1.00086	m	1.00081	10 2 2–6 6 6
1.8383	F	1.8386	4 4 0	0.9193	f^+	0.91933	8 8 0
1.758	tttf	1.7581	5 3 1	0.8822	ttf	0.88220	9 7 3–11 3 3
1.586	ttf	1.5861	5 3 3	0.87908	m^+	0.87904	10 6 2
1.5677	F	1.5679	6 2 2	0.86689	m^-	0.86675	12 0 0–8 8 4

*tf, très faible; f, faible; m, moyenne; F, forte; TF, très forte.

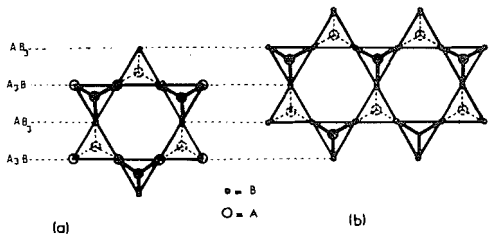

FIG. 4. Dispositions relatives des plans A_3B et AB_3 dans la structure wébérite. (*a*) Les tétraèdres A_3B. (*b*) Les tétraèdres AB_3.

Les deux structures pyrochlore et wébérite, se différencient donc principalement par l'empilement de ces deux types de plans.

Il en résulte que les réseaux de tétraèdres A_4 et B_4 du pyrochlore décrits précédemment par Pannetier et Lucas (12) font place respectivement dans la wébérite à des réseaux de tétraèdres A_3B et AB_3 (fig. 4 *a* et *b*).

Dans ces conditions, il apparaît, compte tenu des caractéristiques structurales présentées par $CdSrSb_2O_7$, deux possibilités quant à la structure de cette phase qui peut être constituée: (*i*) soit de tétraèdres réguliers A_4 et Sb_4 comme dans le pyrochlore; (*ii*) soit de tétraèdres réguliers A_3Sb et ASb_3.

Dans chacune des deux structures, les tétraèdres A_4 et A_3B contiennent respectivement un atome d'oxygène. Ce dernier, situé au barycentre de tétraèdres A_4 dans la structure pyrochlore, ferait apparaître pour $CdSrSb_2O_7$ une distance A—O = 2.2 Å, trop faible pour permettre la présence de strontium dans ces tétraèdres, conduisant à rejeter pour cette phase la possibilité d'une telle structure. En revanche, la présence dans les tétraèdres A_3Sb de la wébérite, de l'ion antimoine de petite taille (Sb—O ≈ 1.96–2 Å) devrait permettre des distances Sr—O convenables.

Un examen plus approfondi de la structure wébérite, et plus particulièrement de l'environnement des ions A, est donc nécessaire pour expliquer l'évolution structurale des composés $Cd_{2-x}Sr_xSb_2O_7$.

Analyse de la structure wébérite: environnement des ions A

L'examen de la structure des composés $A_2B_2X_7$ de type wébérite (fig. 5) fait apparaître d'après les résultats obtenus par Byström (7, 8) pour Na_2MgAlF_7, l'environnement des ions A et B. Les ions B de petite taille présentent la coordinence octaédrique sensiblement déformée, alors que les ions A, occupent deux types de sites de géométrie très différente, notés ici A_I et A_{II} et décrits par les précédents auteurs respectivement comme des sites octaédriques déformés et cubiques déformés.

Les sites A_I

Ils sont en fait caractérisés par une coordinence 2 + (4 + 2). La description récente de la structure wébérite, en couches de type bronze hexagonal présentée par Pouchard et coll. (11) permet de montrer que l'ion A_I est situé au centre d'une bipyramide hexagonale gauche, formée par les octaèdres SbO_6 enchaînés par les sommets. La géométrie de ce site (fig. 6*a*) est donc caractérisée comme dans les pyrochlores $A_2B_2X_7$, par deux distances A_I—O_I courtes, et six distances plus longues (supérieures à 2.50 Å). La coplanéité des oxygènes O_{II} et des ions A_I, B_I, analogue à celle rencontrée dans le bronze hexagonal, fait apparaître quatre distances A_I—O_{II} égales, conduisant à un octaèdre A_IO_6; deux distances A_I—O_{II} plus longues résultent de la forme chaise de l'hexagone oxygène. Ces premières observations laissent penser que les distances A_I—O_I seront des distances critiques très sensibles à la taille des ions A_I.

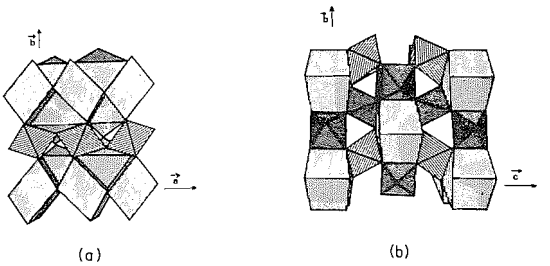

FIG. 5. La structure wébérite: (*a*) suivant le plan 001. (*b*) suivant le plan 100.

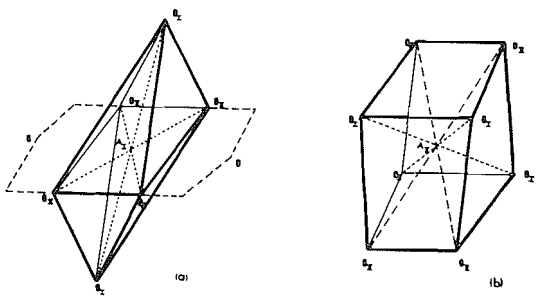

FIG. 6. Géométrie des différents sites des atomes A dans les wébérites $A_2B_2O_7$. (*a*) site A_I, (*b*) site A_{II}.

Can. J. Chem. Downloaded from www.nrcresearchpress.com by 210.87.254.42 on 09/05/12
For personal use only.

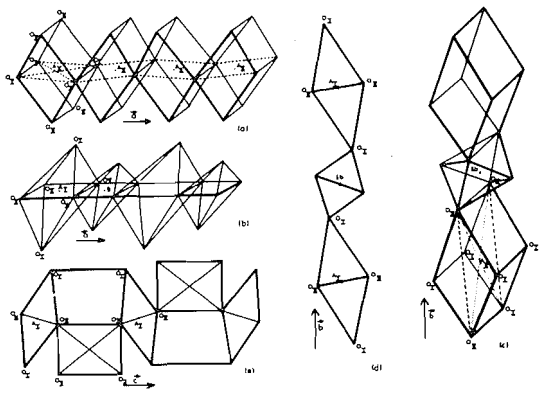

FIG. 7. Enchaînement des différents polyèdres dans la structure wébérite $A_2B_2O_7$. (*a*) Enchaînement des polyèdres $A_{(II)}O_8$ suivant *a*. (*b*) Enchaînement des polyèdres $A_{(I)}O_6$ et BO_6 suivant *a*. (*c*) Enchaînement des polyèdres $A_{(II)}O_8$ et BO_6 suivant *b*. (*d*) Enchaînement des polyèdres $A_{(I)}O_8$ et BO_6 suivant *b*. (*e*) Enchaînement des polyèdres $A_{(I)}O_6$ et $A_{(II)}O_8$ suivant *c*.

Les sites A_{II}

La géométrie de l'environnement des ions A_{II} est trop loin de celle d'un cube pour être considérée comme une déformation de ce dernier. On a en effet une coordinence 4 + 4 correspondant aux plans (A_{II}—O_I) et (A_{II}—O_{II}), (fig. 6*b*), l'angle entre les plans étant voisin de 70° dans $Ca_2Sb_2O_7$ et Na_2MgAlF_7. L'ion A_{II} dans son polyèdre $A_{II}O_8$ est donc situé au centre d'un rectangle avec 4 distances A_{II}—O_{II} égales ou supérieures à 2.60 Å, alors qu'il présente une coordinence voisine de celle d'un carré dans le plan $A_{II}O_I$ avec quatre distances A_{II}—O_I beaucoup plus courtes (voisines de 2.35 A dans $Ca_2Sb_2O_7$). Il est donc à nouveau permis de penser que les distances A_{II}—O_I, seront des distances critiques très sensibles à la taille des ions A_{II}.

Influence de la taille des ions A et B sur l'évolution des paramètres de la wébérite: enchaînement des polyèdres A_IO_6 et $A_{II}O_8$

L'examen de la structure wébérite fait apparaître les remarques suivantes:

(*i*) suivant "*a*", les polyèdres $A_{II}O_8$ sont joints entre eux par leurs côtés parallèles à *c* (fig. 5*a*). Les plans d'oxygènes O_I faisant avec la direction "*a*" (fig. 7*a*) un angle faible et les distances A_{II}—O_I étant des distances critiques, la taille des ions A_{II} pourra avoir une influence notable sur la valeur de *a*.

Par ailleurs, l'enchaînement des polyèdres A_IO_6 et BO_6 (fig. 7*b*), qui mettent en commun leurs côtés normaux à "*a*", montre que la valeur de "*a*" sera liée aux distances O_{II}—O_{II} et par suite dépendra des distances A_I—O_{II} et B—O_{II}.

(*ii*) suivant "*b*" les polyèdres $A_{II}O_8$ et les octaèdres BO_6 mettent en commun leurs côtés parallèles à *c* (fig. 5*a*). Le plan des oxygènes O_{II} fait avec la direction *b* un angle faible (fig. 7*c*) impliquant une contribution notable des distances A_{II}—O_{II} à la valeur de *b*. Cependant, ces distances n'étant pas critiques, le paramètre "*b*" sera peu sensible à la taille de l'ion A_{II}. Il n'en est pas de même pour les polyèdres A_IO_6 joints suivant "*b*" par leurs sommets avec les octaèdres BO_6 (fig. 7*d*): les distances B—O_I et A_I—O_I étant des distances critiques, les tailles des ions A_I et B auront une influence importante sur la valeur de "*b*".

(*iii*) suivant "*c*" les polyèdres $A_{II}O_8$ et A_IO_6 sont joints entre eux par les côtés (fig. 5*b*), de telle sorte que chaque polyèdre A_IO_6 ait ses côtés communs à quatre polyèdres $A_{II}O_8$. On constate que les côtés O_{II}—O_{II} parallèles à "*c*" des polyèdres $A_{II}O_8$ sont mis en commun avec les octaèdres BO_6, et par suite, la distance O_{II}—O_{II} suivant "*c*" dépendra principalement de la taille de B. En revanche, les côtés O_I—O_I des polyèdres $A_{II}O_8$ parallèles à "*c*" dont les sommets appartiennent toujours à deux octaèdres différents, sont indépendants de B, et la variation des distances O_I—O_I qui conduit à un changement d'orientation des polyèdres A_IO_6 (fig. 7*e*), pourra entraîner une variation du paramètre *c*. La distance A_{II}—O_I étant critique, il en résulte que la taille de A_{II} pourra conditionner la valeur de "*c*".

Il faut cependant noter que la taille des ions A et B ne peut être le seul facteur influençant l'évolution structurale de ces composés. La structure électronique de l'ion A peut avoir une influence notable sur les distances A_I—O_{II}. Ainsi, la wébérite $Cd_2Sb_2O_7$ présente une différence entre les paramètres *a* et *b* beaucoup plus faible que celle observée pour la wébérite $Ca_2Sb_2O_7$ malgré les tailles très voisines des ions cadmium et calcium. Ce résultat peut être dû à l'aptitude du cadmium à présenter une coordinence 6 + 2 voisine de celle observée dans les pyrochlores. D'après les valeurs des distances Cd—O observées dans les pyrochlores $Cd_2Nb_2O_7$ et $Cd_2Ta_2O_7$ (9), et des distances Ca—O observées

Can. J. Chem. Downloaded from www.nrcresearchpress.com by 210.87.254.42 on 09/05/12
For personal use only.

Can. J. Chem. Downloaded from www.nrcresearchpress.com by 210.87.254.42 on 09/05/12
For personal use only.

dans $Ca_2Sb_2O_7$ (7), il en résulterait que le remplacement total du calcium par le cadmium dans $Ca_2Sb_2O_7$ devrait conduire à une diminution des distances A_I—O_I et à une augmentation des distances A_I—O_{II}. Ces distances contribuent de façon importante respectivement aux paramètres *b* et *a* de la wébérite. Il s'ensuit que le remplacement total du calcium par le cadmium dans la wébérite $Ca_2Sb_2O_7$ devrait conduire à une diminution de "*b*" et à une augmentation de "*a*". La structure de $Cd_2Sb_2O_7$ n'ayant pas été déterminée, en raison du caractère isoélectronique des ions cadmium et antimoine(V), il est permis de penser que les paramètres donnés précédemment pour cette phase (5, 7) doivent être inversés: $a = 7.341$, $b = 7.222$, $c = 10.189$ Å.

Interprétation de l'évolution structurale des wébérites $Cd_{2-x}Sr_xSb_2O_7$

La plus grande aptitude du cadmium à prendre une coordinence 6 + 2 voisine de celle observée dans les pyrochlores, laisse penser qu'il y aura remplacement préférentiel du cadmium par le strontium dans les sites A_{II}, jusqu'à $x = 1$, conduisant à la wébérite ordonnée $Cd_{(A_I)}Sr_{(A_{II})}Sb_2O_7$, puis au-delà de $x = 1$, il y aura remplacement progressif du cadmium des sites A_I par le strontium. Ce modèle est en excellent accord, compte tenu de l'analyse de la structure wébérite précédente, avec l'évolution des paramètres observée au cours de la substitution (fig. 2).

Pour $x < 1$, le seul remplacement du cadmium par le strontium dans les sites A_{II} doit conduire à une augmentation des distances critiques A_{II}—O_I, sans modifier la géométrie et les dimensions des sites A_I. Il en résulte que seules les distances O_I—O_I parallèles à "*c*" doivent augmenter, entraînant une croissance simultanée des paramètres *b* et *c* par redressement des polyèdres $A_I O_8$ suivant "b" (fig. 7*e*), sans variation notable du paramètre *a*. Au-delà de $x = 1$, le remplacement du cadmium par le strontium dans les seuls sites A_I fait apparaître une augmentation très nette de la distance critique A_I—O_I, d'où la croissance beaucoup plus importante de *b* observée pour $x > 1$ (fig. 1). La substitution du cadmium par le strontium de plus grande taille dans les sites A_I doit également entraîner une augmentation des distances A_I—O_{II}, et par suite, du paramètre "*a*" en accord avec les résultats expérimentaux, évitant ainsi une trop grande

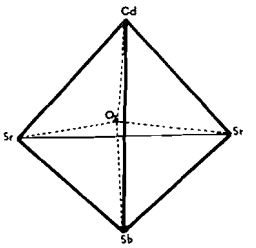

FIG. 8. Environnement de l'oxygène O_I dans le tétraèdre régulier $(CdSr_2Sb)O_I$ correspondant à la composition $CdSrSb_2O_7$.

déformation des octaèdres BO_6. L'augmentation des distances A_I—O_I et A_I—O_{II}, entraîne un accroissement notable des distances O_I—O_I des polyèdres $A_{II}O_8$, dirigées suivant "*a*" (fig. 7*b*). Aucune substitution n'étant effectuée sur les sites A_{II}, les distances A_{II}—O_I restent sensiblement constantes, et par suite, les secondes distances O_I—O_I des polyèdres $A_{II}O_8$ parallèles à "*c*", doivent diminuer, entraînant la décroissance de "*c*" observée pour $x > 1$.

En résumé, il est permis de penser que trois distances critiques doivent influencer principalement l'évolution structurale des wébérites $A_2Sb_2O_7$. Ces trois distances critiques se retrouvent dans le réseau des tétraèdres A_3SbO_I et il en résulte que les tailles relatives des ions présents auront une influence notable sur leur déformation. Le rayon moyen (0.97 Å) des ions métalliques des tétraèdres réguliers $(CdSr_2Sb)O_I$ de la wébérite $CdSrSb_2O_7$, voisin de celui du cadmium (0.95 Å) présent dans les tétraèdres $(Cd_4)O$ des pyrochlores, de volume sensiblement égal, est en accord avec le phénomène d'ordre proposé pour ce composé (fig. 8). Les relations particulières entre les paramètres observées pour les wébérites $Cd_{2-x}Sr_xSb_2O_7$ au voisinage de $x = 1$, semblent donc être dues aux tailles relatives des ions métalliques et ne reflètent pas la symétrie réelle de la structure.

1. F. BRISSE et O. KNOP. Can. J. Chem. **46**, 859 (1968).
2. O. KNOP, F. BRISSE et L. CASTELLIZ. Can. J. Chem. **47**, 971 (1969).
3. R. COLLONGUES, F. QUEYROUX, M. PEREZ, Y. JORBA et J. C. GILLES. Bull. Soc. Chim. Fr. **4**, 1141 (1965).
4. G. DESGARDIN, G. JEANNE et B. RAVEAU. C. R. Acad. Sci. Ser. C, **276**, 851 (1973).
5. G. DESGARDIN, G. JEANNE et B. RAVEAU. C. R. Acad. Sci. Ser. C, **279**, 565 (1974).
6. G. JEANNE, G. DESGARDIN et B. RAVEAU. Mat. Res. Bull. **9**, 1321 (1974).

7. A. BYSTRÖM. Ark. Kemi, Mineral. Geol. **18A**, n° 21 (1944).
8. A. BYSTRÖM. Ark. Kemi, Mineral. Geol. **18B**, n° 10 (1944).
9. F. BRISSE, D. J. STEWART, V. SEIDL et O. KNOP. Can. J. Chem. **50**, 3648 (1972).
10. C. HENAULT, G. DESGARDIN et B. RAVEAU. Rev. Chim. Miner. **12**, 247 (1975).
11. M. VLASSE, J. C. MASSIES, J. P. CHAMINADE et M. POUCHARD. C. R. Acad. Sci. Ser. C, **278**, 1505 (1974).
12. J. PANNETIER et J. LUCAS. Mat. Res. Bull. **5**, 797 (1970).

Can. J. Chem. Downloaded from www.nrcresearchpress.com by 210.87.254.42 on 09/05/12
For personal use only.

Conformation of 2-thiophenesulphonanilides from dipole moment studies

GIUSEPPE C. PAPPALARDO[1] AND SALVATORE GRUTTADAURIA
Istituto di Chimica Generale, Università di Catania, Viale A. Doria, 95125 Catania, Italy
AND
EMANUELE MACCARONE AND GIUSEPPE MUSUMARRA
Istituto di Chimica Industriale, Università di Catania, Viale A. Doria, 95125 Catania, Italy

Received September 30, 1975

GIUSEPPE C. PAPPALARDO, SALVATORE GRUTTADAURIA, EMANUELE MACCARONE, and GIUSEPPE MUSUMARRA. Can. J. Chem. **54**, 1672 (1976).

The electric dipole moments of a number of 2-thiophenesulphonanilides have been measured in benzene solution at 25 °C. The data obtained have been analyzed by the vectorial additive method of calculation. Results of the calculations have shown that the SO_2—NH group prefers the *gauche-syn* conformation in which the N—H bond lies on the plane bisecting the OSO angle. Conformations about the Ph—N bond in the 2′- and 3′-substituted derivatives have also been determined and are discussed.

GIUSEPPE C. PAPPALARDO, SALVATORE GRUTTADAURIA, EMANUELE MACCARONE et GIUSEPPE MUSUMARRA. Can. J. Chem. **54**, 1672 (1976).

On a mesuré, en solution benzénique à 25 °C, les moments dipolaires électriques d'un certain nombre de thiophène-2 sulphonanilides. On a analysé les données obtenues par la méthode de calcul vectoriel additif. Les résultats des calculs montrent que le groupe SO_2—NH préfère la conformation *gauche-syn* dans laquelle le lien N—H se trouve dans le plan bisecteur de l'angle OSO. On a aussi déterminé et on discute des conformations autour des liens Ph—N dans les dérivés substitués en position 2′ et 3′.

[Traduit par le journal]

Introduction

The problem of the spatial structure of the sulphonamido group has not yet been fully resolved. Previous dipole moment measurements for benzenesulphonamides have been interpreted in terms of eclipsed forms (1) or of free rotation about the N—S bond (2). On the other hand, the application of general simplifying rules (3), which are based on theoretical estimates of the repulsive interactions between electron lone pairs and polar bonds, to benzenesulphonamide shows that the *gauche-syn* (**I**, **II**) and the *gauche-anti* (**III**) conformations (Fig. 1) are the energetically most favoured ones. This view is also in agreement with results of X-ray studies on the solid (4), showing that the pertinent atoms are in a *gauche-syn* arrangement. Because of the inherent limitation of the method, however, the N—H orientations in the *gauche-syn* forms indicated by **I** and **II** were indistinguishable.

A definite approach to the resolution of this stereochemical problem has been made by us with the aid of a dipole moment method in the course of studies on a series of 2-thiophenesulphonanilides. We present here the measured dipole moments (benzene, 25 °C) for these molecules, together with an analysis of the relevant data in terms of solution state conformations.

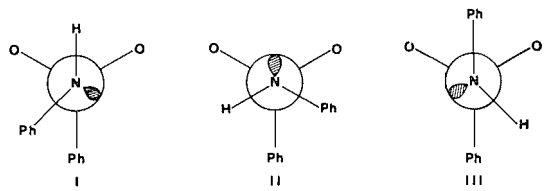

FIG. 1. The possible *gauche* conformations about N—S bond in benzenesulphonamide (Newman projections viewed along the N—S bond).

Experimental

Materials

The formulae and compound numbers of the compounds examined are given in Table 1. The 2-thiophenesulphonanilides **1** (5), **2** (6, 7), **3** and **4** (8), **5** (9), **6** and **13** (10), **7** (11), **8**–**12** (12), **14**–**17** (12), were prepared according to methods described in the literature cited. Com-

[1]Author to whom correspondence should be addressed.

Can. J. Chem. Downloaded from www.nrcresearchpress.com by 210.87.254.40 on 09/05/12
For personal use only.

TABLE 1. Total polarizations ($P_{2\infty}$), molar refractions (R_D), dipole moments (μ), and other parameters for their evaluation, for 2-thiophenesulphonanilides in benzene solution at 25 °C

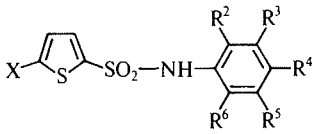

Compound number	α[a]	β[b]	$P_{2\infty}$/cm^3	R_D/cm^3	μ/D
$R^2 = R^3 = R^4 = R^5 = R^6 = H$					
X = H	**1**	10.10	−0.379	507.63	65.1	4.65
X = Cl	**2**	6.72	−0.423	403.34	69.8	4.04
X = Br	**3**	6.32	−0.510	437.29	72.8	4.22
X = I	**4**	6.39	−0.594	497.89	78.1	4.53
X = NO_2	**5**	8.90	−0.473	532.17	71.6	4.74
$R^2 = R^3 = R^5 = R^6 = H$; X = H					
R^4 = Cl	**6**	6.91	−0.423	413.46	69.9	4.10
$R^4 = NO_2$	7	8.52	−0.467	512.18	71.7	4.64
$R^3 = R^4 = R^5 = R^6 = H$; X = H					
$R^2 = CH_3$	**8**	10.05	−0.255	545.43	69.7	4.82
$R^2 = C_2H_5$	**9**	8.88	−0.340	507.85	74.3	4.60
$R^2 = CH(CH_3)_2$	**10**	9.35	−0.226	571.02	79.0	4.90
R^2 = Cl	**11**	11.53	−0.431	650.28	69.7	5.32
$R^2 = NO_2$	**12**	15.48	−1.380	806.47	71.0	5.99
$R^2 = R^4 = R^5 = R^6 = H$; X = H					
R^3 = Cl	**13**	7.27	−0.411	433.28	69.5	4.21
$R^3 = NO_2$	**14**	8.18	−0.475	492.49	71.1	4.54
$R^3 = R^4 = R^5 = H$; X = H					
$R^2 = R^6 = CH_3$	**15**	9.37	−0.329	535.06	74.3	4.74
$R^2 = R^6 = C_2H_5$	**16**	7.67	−0.178	509.96	93.6	4.51
$R^2 = R^6 = CH(CH_3)_2$	**17**	6.63	−0.291	484.47	92.2	4.37

[a] $\alpha = \sum(\epsilon_{12} - \epsilon_{10})/\sum w_2$.
[b] $\beta = \sum(v_{12} - v_{10})/\sum w_2$.

pounds were all purified by recrystallisation to constant mp and constant ϵ_{max} before dipole moment determination. The purity was always ≫99% for each sample, as determined by glc just prior to the dipole moment determination.

Benzene was used as solvent and was purified as previously described (13).

Physical Measurements

Electric dipole moments were determined in benzene solution at 25 ± 0.01 °C. The dielectric constants (ϵ_{12}), specific volumes (v_{12}), and refractive indexes (n_{12}) of solutions at various weight fractions of solute (w_2) were measured using the apparatus and experimental techniques described in detail elsewhere (14). The total solute polarization ($P_{2\infty}$) has been obtained by extrapolation to infinite dilution using the Halverstadt–Kumler method (15). The value of the experimental molar refraction (R_D) for the Na_D line has been used as the electronic and atomic polarization, P_e and P_a, in calculating the dipole moments (μ) from Debye's formula.

The estimated error in μ is ±0.02 D. Duplicate determinations of μ have shown reproducibility of ±0.01 D.

The experimental results are summarized in Table 1.

Method of Calculation

In attempting to interpret the magnitudes of the experimental moments, theoretical dipole moments for the separate conformers **I***a*, **II***a*, **I***b*, **II***b* (Fig. 2) have been calculated by a vectorial additive scheme from the suitable values of the component bond and group moments.

To deduce a reliable set of individual bond moments, the benzenesulphonamide molecule has been chosen as model compound. The basic assumption has been made that this molecule, as solute, adopts the same conformation as in the solid state (4); this is because extremely high rotational energy barriers have been theoretically predicted for rotation about the N—S bond (4). Thus, on this basis, it appears reasonable to consider benzenesulphonamide, even in solution, as a rigid model compound in a conformation of type **I** or **II**. Therefore, its experimental moment

Can. J. Chem. Downloaded from www.nrcresearchpress.com by 210.87.254.40 on 09/05/12
For personal use only.

Can. J. Chem. Downloaded from www.nrcresearchpress.com by 210.87.254.40 on 09/05/12
For personal use only.

(4.77 D (16), in benzene at 25 °C) was given in the form of the sum of the vectors of the moments of the individual fragments. For the calculation the following bond moments were assumed

$$\mu(\text{Ph—N}) = 0.34 \text{ D (17)}$$

$$\mu(\text{H—N}) = 1.30 \text{ D (18)}$$

$$\mu(\text{S=O}) = 3.00 \text{ D (18)}$$

$$\mu(C_{ar}\text{—S}) = 1.30 \text{ D (18)}$$

The chosen values of the interbond angles were those obtained by X-ray structure analysis (4). In this way the unknown μ(N—S) was readily calculated for the two possible structures **I** and **II** using simple trigonometric procedures. Results of the computations show that two values are mathematically admissible for the N—S bond moment when considering benzenesulphonamide in the conformation **I**, *i.e.* μ(N—S) = 1.65 D and μ(S—N) = 5.95 D. The similar calculation based on a **II** type model of benzenesulphonamide provides a value μ(S—N) = 2.15 D.

Three different sets of calculations were thus developed to obtain the total moments, corresponding to the conformations **I** and **II**, for the 2-thiophenesulphonanilides under study, as follows: for the possible conformations **I** the bond moments μ(N—S) = 1.65 D and μ(S—N) = 5.95 D were used to calculate the moments $\mu_{calc}(1)$ and $\mu_{calc}(2)$, respectively; the bond moment value μ(S—N) = 2.15 D was adopted to calculate the total moment $\mu_{calc}(3)$ for the possible conformations of type **II** (Fig. 2). The other bond moments were kept fixed at the values assumed for benzenesulphonamide. The molecular model of 2-thiophenesulphonanilides was oriented relative to the same coordinate axes selected for benzenesulphonamide (Fig. 3).

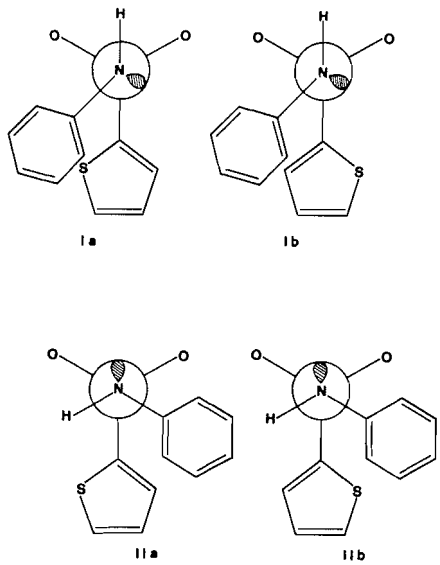

FIG. 2. Possible conformations of 2-thiophenesulphonanilides (Newman projections viewed along the N—S bond).

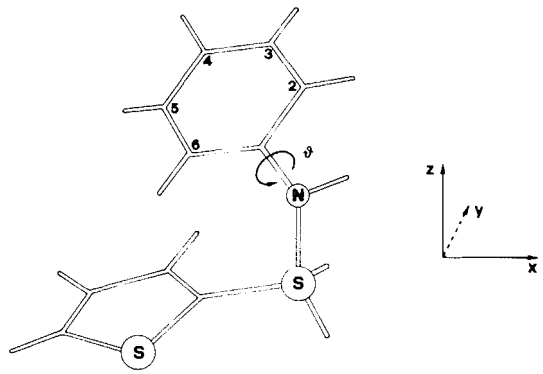

FIG. 3. The molecule of 2-thiophenesulphonanilide in the conformation **I***b* oriented along the coordinate system of axes. The *x*-axis is the perpendicular to the N—S bond on the C_{ar}—S—N—H plane; the *y*-axis is the perpendicular to this plane (and thus to the plane of the paper), with the negative end directed toward the observer; the *z*-axis is coincident with the N—S bond. The same orientation is adopted for the model benzenesulphonamide.

In the calculations the group moments (19)

$$\mu(\text{C—Cl}) = 1.58 \text{ D}$$

$$\mu(\text{C—NO}_2) = 4.01 \text{ D}$$

$$\mu(\text{C—alkyl}) = 0.37 \text{ D}$$

were employed for the substituents in the phenyl ring. For the group moments of the substituents in the thiophene ring the values

$$\mu(C_{ar}\text{—Cl}) = 1.40 \text{ D}$$

$$\mu(C_{ar}\text{—Br}) = 1.16 \text{ D}$$

$$\mu(C_{ar}\text{—I}) = 0.90 \text{ D}$$

$$\mu(C_{ar}\text{—NO}_2) = 4.09 \text{ D}$$

were used, as deduced from experimental data for thiophene and its corresponding 2-substituted derivatives (20). The geometry of the heterocycle was assumed to be that given by microwave

TABLE 2. Theoretical and experimental dipole moments of X- and R[4]-substituted 2-thiophenesulphonanilides

	Conformation						
	I*a*		I*b*		II*a*	II*b*	
Compound	$\mu_{calc}(1)$	$\mu_{calc}(2)$	$\mu_{calc}(1)$	$\mu_{calc}(2)$	$\mu_{calc}(3)$	$\mu_{calc}(3)$	μ_{exp}
1	4.89	4.89	4.84	4.84	5.04	5.19	4.65
2	4.38	4.38	4.24	4.24	3.76	4.19	4.04
3	4.44	4.44	4.31	4.31	3.98	4.34	4.22
4	4.52	4.52	4.41	4.41	4.20	4.51	4.53
5	4.58	4.58	4.31	4.31	1.90	3.20	4.74
6	4.45	5.67	4.07	5.37	4.52	4.93	4.10
7	4.82	7.40	3.98	6.88	4.75	5.47	4.64
15	4.75	5.04	4.62	4.92	4.87	5.09	4.74
16	4.75	5.04	4.62	4.92	4.87	5.09	4.51
17	4.75	5.04	4.62	4.92	4.87	5.09	4.37

spectroscopy (21); the direction of action of its resultant moment (μ_{het}) was taken from the center of the cycle to the heteroatom (22).

Thus, the total moment for the 2-thiophenesulphonanilides **1–5** having no substituents in the phenyl ring was easily calculated for conformations of type **I** by summing the components along the coordinate axes for the benzenesulphonamide moiety to the additional component moments for the thiophene fragment in the rotational isomers *a* (conformation **I***a*) and *b* (conformation **I***b*). The same procedures also apply to determining the total molecular moments for conformations of type **II**, with the difference that, in this case, the components along the *x*, *y*, and *z* axes for the benzenesulphonamide model are those corresponding to the components in form **II**.

When considering the remaining derivative compounds with substituents in the phenyl ring, the additional projections (on the same system of coordinate axes) of the vectors of the group moments (μ_R) were taken into account. A summation of these components was then made individually, with the corresponding components on the *x*, *y*, and *z* axes derived for each conformation considered for the unsubstituted 2-thiophenesulphonanilide, **1**, molecule. In this way, the total moment for conformations **I***a*, **I***b*, **II***a*, and **II***b*, of compounds **8–14** was calculated as a function of the angle θ. This is the rotational angle described by the phenyl ring about the Ph—N axis in a clockwise direction (see Fig. 3) in the molecules in which a 2- or 3-substituent is present. The conformation $\theta = 0°$ was assumed as the one in which the ring plane makes an angle of 90° with the C—N—S plane and the 2- or 3-substituent is on the side of the N—H linkage.

Results of the calculations are summarized in Tables 2 and 3.

Results and Discussion

Table 2 shows that the experimental moment for 2-thiophenesulphonanilide **1** is closer to the calculated values for the conformations **I***a* and **I***b* than for the **II***a* and **II***b* possibilities. On this basis a conformation of type **I** about the N—S bond can be inferred as the more probable for this molecule in solution and its derivative compounds **2–17**. The difference that can be observed between the μ_{exp} and $\mu_{calc}(3)$ values, however, could be considered as not great enough to determine unambiguously the conformation of **1**. On the other hand, results of calculations for molecule **5** permit a more definite discrimination between the **I** and **II** conformations in favour of the former. In the case of this derivative compound **5**, both structures **II***a* and **II***b* can be firmly discounted on the basis of the substantial difference between μ_{exp} and the two $\mu_{calc}(3)$ values. The experimental moment is, in fact, 2.84 D and 1.54 D higher than these calculated moments, and the above deviations considerably exceed the value attributable to the uncertainty of the method of calculation. Furthermore, the good agreement between the measured moment and the $\mu_{calc}(1)$, $\mu_{calc}(2)$ values clearly indicates that this molecule adopts preferentially conformation **I***a* or **I***b*.

In the case of all remaining molecules listed in Table 2 a choice cannot be made between the

Can. J. Chem. Downloaded from www.nrcresearchpress.com by 210.87.254.40 on 09/05/12
For personal use only.

TABLE 3. Values of θ at which μ_{calc} and μ_{exp} agree for R^2- and R^3-substituted 2-thiophenesulphonanilides in the conformations I*a* and I*b*

Compound	Conformation	θ (deg.)
8	I*a*	81, 170.8, 189.2
	I*b*	81.3, 169.4, 190.6
9	I*a*	~180
	I*b*	~180
10	I*a*	±60.3, 159.7, 200.3
	I*b*	±72.2, 132.8, 227.2
11	I*a*	±51.2, 142.8, 217.2
	I*b*	±34.2, 121.3, 238.7
12	I*a*	±68.2, 160.6, 199.4
	I*b*	±81.2, 169.4, 190.6
13	I*a*	±70.4, 162.5, 197.5
	I*b*	132.8, 153.8, 206.2, 227.2
14	I*a*	±65.4, 155.6, 204.4
	I*b*	100.3, 165.4, 194.6, 259.7

I and **II** conformations on the basis of the dipole moment data, all the μ_{calc} values being comparable to the measured moments. The conformation **I**, however, can be reasonably postulated for these compounds by analogy with the **1** and **5** derivatives.

It should be pointed out that for all molecules examined a definite distinction cannot be made between the *a* and *b* forms. This is due to the low value of the thiophene group moment; hence, the difference between the calculated moments for the I*a* and I*b* conformations cannot be considerable.

The possibility that a different system of bond moments leads to the same results occurs for the 2-thiophenesulphonanilides dealt with. There is an exception with the molecules **6** and **7** that permits an evaluation of the appropriate N—S bond moment. By considering that conformation **I** is retained in the compounds **6** and **7**, the expected moments calculated with the 1.65 D bond moment (*i.e.* $\mu_{calc}(1)$) are in better agreement with the experimental than the calculated with 5.95 D ($\mu_{calc}(2)$). It can be therefore concluded that 1.65 D is the effective N—S bond moment and, thus, that the $\mu_{calc}(1)$ values only, are to be considered in the present discussion.

To deduce the orientations of the phenyl group in derivatives **8–14**, the conformational angle θ for each molecule was determined through comparison of measured and calculated dipole moments. Since, in these molecules retention of conformation **I** about the N—S bond can be reasonably assumed, the N—S bond moment of 1.65 D was used in the computations. The values of θ for which there is agreement between μ_{exp} and $\mu_{calc}(1)$ are shown in Table 3. Examination of scale molecular models indicates that the possible conformations in which is $\theta > 180°$ can be eliminated on steric grounds. Further steric considerations suggest the possible values of θ in the range 120–180° correspond to the less hindered positions and thus to the most probable conformations about Ph—N bond in these molecules. The above view is substantiated by results for the derivative compound **9** bearing a bulky alkyl-substituent in the *ortho* position. In this case the experimental moment corresponds only to a single rotational conformation having $\theta \approx 180°$.

In conclusion, the precision of the whole approach appears more convincing when considering that our present findings are in accord with predictions based on the effects of electrostatic influences between the free electron pair and the two polar S—O bonds that may cause an increase of the total energy of the system in conformation **II**. These repulsive effects appear to be lower in conformation **I** which can be furthermore stabilized by some electrostatic attraction operating between the O atoms (negatively charged) of the SO_2 group and the H atom (positively charged) of the NH group. The vector addition scheme of bond moments is, in general, approximate in character. However, as in the present favourable case, essential improvements that enable the method to solve somewhat hard stereochemical problems can be made possible by the use of properly chosen model compounds and selected bond moments. In a recent book (23) that represents the first complete treatment of the topic to date these arguments concerning the conditional validity of the method are widely discussed.

Acknowledgement

This work was supported by the Consiglio Nazionale delle Ricerche (CNR) of Italy.

1. E. SZCZUCKI and K. OKOŃ. Bull. Acad. Pol. Sci. Ser. Sci. Chim. Geol. Geogr. **7**, 75 (1959); Chem. Abstr. **54**, 17303 (1960).
2. N. P. LUSHINA, B. L. LEVASHOVA, and E. N. GUR'YA-

Can. J. Chem. Downloaded from www.nrcresearchpress.com by 210.87.254.40 on 09/05/12
For personal use only.

NOVA. Zh. Strukt. Khim. **10**, 490 (1969); Chem. Abstr. **71**, 90663 (1969).
3. S. WOLFE, A. RAUK, L. M. TEL, and I. G. CSIZMADIA. J. Chem. Soc. B, 136 (1971).
4. B. RÉRAT. Acta Crystallogr. B, **25**, 1392 (1969).
5. L. WEITZ. Ber. **17**, 799 (1884).
6. R. H. CUNDIFF and R. R. ESTES. J. Am. Chem. Soc. **72**, 1424 (1950).
7. H. Y. LEW and C. R. NOLLER. J. Am. Chem. Soc. **72**, 5715 (1950).
8. A. P. TERENT'EV and G. M. KADATSKII. Zh. Obshch. Khim. **21**, 1524 (1951); Chem. Abstr. **46**, 2536 (1952).
9. E. MACCARONE, G. MUSUMARRA, and G. A. TOMASELLI. Ann. Chim. (Italy), **63**, 861 (1973).
10. A. ARCORIA, E. MACCARONE, G. MUSUMARRA, and G. A. TOMASELLI. J. Org. Chem. **38**, 2457 (1973).
11. S. OCCHIPINTI, G. SCARLATA, and M. TORRE. Boll. Sed. Accad. Gioenia Sci. Nat. (Catania) Ser. IV, **11**, 181 (1973).
12. A. ARCORIA, E. MACCARONE, G. MUSUMARRA, and G. A. TOMASELLI. Spectrochim. Acta A, **30**, 611 (1974).
13. A. WEISSBERGER and E. S. PROSKAUER. Organic solvents. Techniques of organic chemistry. Vol. VII. Interscience, New York. 1961.
14. G. C. PAPPALARDO and S. PISTARÀ. J. Chem. Eng. Data, **17**, 2 (1972).
15. I. F. HALVERSTADT and W. D. KUMLER. J. Am. Chem. Soc. **64**, 2988 (1942).
16. W. SCHEELE and W. MEINE. Kolloid-Z. **129**, 39 (1952); Chem. Abstr. **47**, 4674 (1953).
17. C. W. N. CUMPER and A. P. THURSTON. J. Chem. Soc. B, 422 (1971).
18. C. W. N. CUMPER. Tetrahedron, **25**, 3131 (1969).
19. C. P. SMYTH. Dielectric behaviour and structure. McGraw-Hill, New York. 1955. p. 253.
20. R. KESWANI and H. FREISER. J. Am. Chem. Soc. **71**, 218 (1949).
21. B. BAK, D. CHRISTENSEN, W. B. DIXON, L. HANSEN-NYGAARD, J. RASTRUP-ANDERSEN, and M. SCHOTTLÄNDER. J. Mol. Spectrosc. **9**, 124 (1962).
22. G. MARINO. J. Heterocycl. Chem. **9**, 817 (1972).
23. O. EXNER. Dipole moments in organic chemistry. Georg Thieme Verlag, Stuttgart. 1975.

Can. J. Chem. Downloaded from www.nrcresearchpress.com by 210.87.254.40 on 09/05/12
For personal use only.

Formation, mobilité et réactivité d'espèces paramagnétiques adsorbées sur zéolithes H—Y irradiées. Une étude par résonance paramagnétique électronique

JACQUES C. VEDRINE[1] ET JEAN MASSARDIER

Institut de Recherches sur la Catalyse, Centre National de la Recherche Scientifique, 79 Boulevard du 11 novembre 1918, 69626 Villeurbanne, France

ET

ANTOINE ABOU-KAÏS

Facultés des Sciences, Université Libanaise Hadath Liban, et C.N.R.S. Libanais

Reçu le 25 juillet 1975

JACQUES C. VEDRINE, JEAN MASSARDIER et ANTOINE ABOU-KAÏS. Can. J. Chem. **54**, 1678 (1976).

Utilisant le rayonnement γ comme source ionisante il a été possible d'étudier par résonance paramagnétique électronique, les sites d'adsorption et les espèces paramagnétiques adsorbées sur des zéolithes de type H—Y. Les sites d'adsorption sont principalement les atomes d'oxygène du réseau. On a observé que l'hydrogène neutralise les sites ionisés tandis que l'oxygène donne des radicaux de type O_2^- pour lesquels la répartition de densité de spin non apparié est légèrement inéquivalente (43 et 57%). Le monoxyde de carbone donne des espèces de nature C^+O qui réagissent instantanément à 77 K avec l'oxygène en donnant des radicaux de type O_2^- pour lesquels la densité de spin est très inégalement répartie sur les deux atomes ($\frac{1}{4}$, $\frac{3}{4}$). Des radicaux de type $OH^\cdot$ et $NH_2^\cdot$ ont pu être étudiés ainsi que leur mobilité. Ils proviennent de l'ionisation par le rayonnement d'entités H_2O et NH_3 physisorbées, le meilleur rendement étant obtenu pour un recouvrement monocouche. Cette étude permet une approche originale des propriétés adsorbantes des zéolithes.

JACQUES C. VEDRINE, JEAN MASSARDIER, and ANTOINE ABOU-KAÏS. Can. J. Chem. **54**, 1678 (1976).

Use of γ radiation as an ionizing source has been successfully applied to an epr study of adsorption sites and of adsorbed species in the case of H—Y zeolites. Adsorption sites have appeared to be mainly oxygen nuclei from the lattice. It has been observed that molecular hydrogen neutralizes paramagnetic sites while molecular oxygen gives rise to O_2^--type radicals which have nearly equal unpaired spin density on the two nuclei (43 and 57%). Carbon monoxide gives rise to a species assigned to C^+O which reacts very easily at 77 K with molecular oxygen to yield an O_2^--type species for which the spin density distribution is not equivalent on the two oxygen nuclei ($\frac{1}{4}$ and $\frac{3}{4}$). The nature and the mobility of $OH^\cdot$ and $NH_2^\cdot$ radicals have been studied in detail. They arise from the ionization of physisorbed H_2O and NH_3, the better yield being obtained at a monolayer coverage. This study leads to an original approach to the study of the adsorptive properties of zeolites.

Introduction

La résonance paramagnétique électronique (rpe) est une technique précieuse permettant d'obtenir de nombreuses informations sur la structure même d'un matériau solide: directement s'il existe des entités paramagnétiques qui jouent le rôle de "sonde" (1) ou indirectement par introduction de telles entités dans le matériau soit chimiquement soit en ionisant des entités structurales diamagnétiques à l'aide de rayonnements (γ, X, uv). De tels rayonnements sont particulièrement bien adaptés à ces études car ils ont un pouvoir ionisant élevé et ils ne perturbent généralement pas le matériau. Ainsi l'emploi couplé de l'irradiation et de la rpe a permis d'établir des corrélations intéressantes entre l'activité catalytique et la concentration de centres V provenant d'entités silico–aluminates dans une silice–alumine (2), entre l'acidité forte de Brønsted et par conséquent l'activité catalytique due à cette acidité et le piégeage d'atomes d'hydrogène libre ($H^\cdot$) dans des échantillons irradiés de zéolithe (3). De tels centres V sont apparus comme caractéristiques d'entités constituant le réseau lui-même (4) et en relation avec

[1]A qui toute demande concernant ce travail peut être demandée.

Can. J. Chem. Downloaded from www.nrcresearchpress.com by 210.87.254.40 on 09/05/12
For personal use only.

Can. J. Chem. Downloaded from www.nrcresearchpress.com by 210.87.254.40 on 09/05/12
For personal use only.

l'activité catalytique de matériaux tels que les zéolithes (5) ou MgO (6) par exemple.

L'étude de la réactivité de ces entités paramagnétiques vis-à-vis de divers adsorbats ainsi que la détermination éventuelle des espèces intermédiaires d'adsorption présente un grand intérêt dans la compréhension des mécanismes catalytiques. Dans ce domaine, la rpe peut fournir des renseignements très utiles non seulement sur la nature du radical adsorbé mais aussi sur son environnement, sa mobilité, et éventuellement la nature des sites d'adsorption.

L'étude rpe antérieure (3–4) de zéolithes H—Y irradiées à 77 K par les rayons γ a montré qu'il y avait création d'une part d'hydrogène atomique caractérisé par un doublet de séparation 500 Oe et d'autre part de centres V ou "trous d'électron" localisés sur des atomes d'oxygène du réseau pontant des atomes de Si soit à des atomes de Al (centres dits V_1) soit à d'autres atomes de Si (centres dits V_2).

Le but du présent travail est donc d'étudier la réactivité de ces centres et de caractériser pour une zéolithe H—Y les espèces paramagnétiques observées représentatives des espèces diamagnétiques adsorbées sur le solide initial non irradié.

Partie expérimentale

Le matériau utilisé est une zéolithe Linde de type Y dont 87% des ions Na^+ ont été échangés par des cations NH_4^+. La zéolithe ammoniée est traitée à 670 K en lit mince sous oxygène puis sous vide ($p \simeq 10^{-5}$ torr) à cette température pour obtenir un échantillon protoné H—Y sauf spécification différente.

Les échantillons sont placés dans un tube rpe de silice fondue surmonté d'un tube équipé d'une fine membrane de verre, facilement cassable à l'aide de marteaux en verre, pour permettre l'introduction ultérieure d'adsorbat et d'un tube latéral permettant de traiter le solide sous vide avant l'irradiation et que l'on isole par scellement sous vide après le traitement.

L'irradiation a été effectuée à 77 K dans un irradiateur au ^{60}Co pour des doses de l'ordre de 2 Mrad.

L'adsorption des différents composés a été effectuée soit à 77 K (réactivité des centres V) soit à température ambiante (espèces adsorbées). Les adsorbats ont été séchés avec soin sur tamis moléculaire, purifiés des gaz occlus par le traitement suivant répété plusieurs fois "solidification à 77 K, dégazage à 77 K, réchauffement à 295 K". L'ammoniac a aussi été purifié par cryodistillation sous vide. Dans le cas de H_2 et CO les traces d'O_2 ont été soigneusement éliminées par piègeage sur tamis moléculaire à 77 K. Certaines expériences ont été réalisées en présence de molécules enrichies en isotope à spin nucléaire non nul (^{17}O, $I = 5/2$; ^{13}C, $I = 1/2$; D, $I = 1$).

Les mesures rpe ont été effectuées à 77 K avec spectromètre Varian E9 équipé de klystrons de 9.4 (bande X) ou 34.5 (bande Q) GHz.

Resultats expérimentaux

Les centres V, caractérisant les oxygènes du réseau, et de type O^- dans un schéma ionique, ne sont pas stables à la température ambiante de sorte que leur réactivité n'a pu être étudiée que pour des composés ayant une température de liquéfaction peu élevée tels H_2, O_2 et CO. Leur réactivité vis-à-vis d'adsorbats tels H_2O, NH_3, CO_2 etc. n'a pas pu être considérée mais dans de tels cas l'irradiation à 77 K en présence de ces adsorbats permet de surmonter la difficulté.

Réactivité des centres V

Action de l'hydrogène

L'introduction d'hydrogène moléculaire entraîne une diminution dans le rapport 1/2 du signal rpe dû aux centres V mais la forme de ce signal ainsi que le nombre d'H· piégés ne sont pas modifiés tandis qu'aucun autre signal n'apparaît. Si l'irradiation a lieu en présence d'hydrogène le signal dû aux centres V garde une forme identique au cas précédent mais son intensité n'est plus que de 10%, toutes autres propriétés restant égales par ailleurs.

On avait montré antérieurement (4) que la formation de centres V était régie par des équilibres fortement déplacés à gauche comme dans l'éq. 1.

[1] 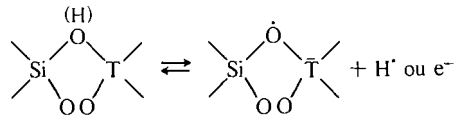 + H· ou e^-

Centres V_1 ou V_2 suivant que T = Al ou Si

Il est donc vraisemblable que l'hydrogène moléculaire se dissocie et neutralise les centres V. L'irradiation en présence d'hydrogène montre que l'hydrogène agit sur les sites diamagnétiques précurseurs des centres V. Ces deux propriétés sont probablement en relation étroite avec les propriétés hydrogénantes (7) et le caractère oxydant de la zéolithe Y.

Action de l'oxygène

L'adsorption d'oxygène sur la zéolithe H—Y irradiée sous vide conduit dès les faibles pressions ($p \simeq 10^{-1}$ torr) à la disparition instantanée du signal dû aux centres V et à l'apparition d'un signal d'intensité comparable correspondant à la superposition de deux signaux (8).

Can. J. Chem. Downloaded from www.nrcresearchpress.com by 210.87.254.40 on 09/05/12
For personal use only.

En utilisant de l'oxygène enrichi en ^{17}O ($I = 5/2$) il avait été montré que l'on a affaire à un radical diatomique de type O_2^- où la densité de spin non apparié est légèrement différente sur les deux atomes d'oxygène avec: $C_x^{I} = 84.5$ et $C_x^{II} = 64.2$ Oe, C_y et C_z étant trop faibles pour être détectés, ce qui correspond à une densité de spin de 56.7 et 43.3%, respectivement, et confère un léger caractère peroxydique aux espèces "oxygène adsorbé". Nous noterons que les paramètres rpe de ces espèces de l'oxygène sont tout à fait distinctes (valeurs principales des tenseurs **g** et **c**) de ceux d'une espèce O_3^- (13) que l'on pourrait attendre de l'action de O_2 sur un centre V de nature O^-. Ceci montre que la liaison entre l'oxygène adsorbé et l'oxygène du réseau (centre V) est très faible, en accord avec l'expérience puisque si l'on désorbe l'échantillon en le réchauffant, les centres V sont restaurés. De plus nous n'avons pas détecté d'interaction superhyperfine due à l'aluminium contrairement à d'autres résultats sur zéolithe Y (9). Cependant, l'observation de deux signaux correspondant à deux valeurs distinctes de g_z (2.032 et 2.022) avait permis de conclure que l'oxygène était adsorbé sur des sites distincts, liés à des cations Si^{4+} et Al^{3+} respectivement (11–12), ce que nous avons reconfirmé.

De plus, lorsque l'oxygène est introduit sur un échantillon de zéolithe Na—Y traité à 670 K, on obtient principalement deux signaux rpe superposés avec les paramètres suivants

$g_z = 2.072$	$g_z = 2.054$
$g_y = 2.0015$	$g_y = 2.0015$
$g_x = 1.9985$	$g_x = 1.9985$

Les valeurs de g_z sont intermédiaires entre celle correspondant à un ion monovalent d'adsorption (2.113, réf. 10) et les valeurs précédentes. Il semble donc que sur une zéolithe Na—Y l'oxygène s'adsorbe sur les mêmes sites que pour les zéolithes H—Y; les ions Na^+ restant à proximité de ces sites.

Action du monoxyde de carbone

Alors que nous avions observé une réactivité instantanée des centres V dès l'introduction d'une faible pression d'oxygène, nous avons constaté qu'il fallait une pression importante ($p \simeq 30$ torr) en oxyde de carbone pour que tous les centres V disparaissent au profit d'autres espèces paramagnétiques (fig. 1*A*). Cette propriété est tout à fait caractéristique de la différence de propriété d'adsorption de la zéolithe vis-à-vis de O_2 et CO.

Lorsque de l'oxyde de carbone enrichi en ^{13}C (90%) est mis en présence de zéolithe H—Y traitée à 670 K on obtient un spectre rpe présentant les paramètres suivants (16)

$g_x = 2.0005 \pm 0.0010$	$C_x = 301 \pm 3$ Oe
$g_y = 2.0015 \pm 0.0010$	$C_y = 255 \pm 3$ Oe
$g_z = 2.0045 \pm 0.0010$	$C_z = 275 \pm 3$ Oe

La décomposition du tenseur hyperfin en ses parties isotrope et anisotrope conduit aux valeurs respectives

$$a = 277 \text{ Oe}$$
$$b_x = 15.3 \text{ Oe}$$
$$b_z = 6.7 \text{ Oe}$$

Les paramètres précédents sont assez délicats à expliquer et nous avions proposé précédemment (16) qu'ils correspondaient à un radical de type CO^+, soumis à un champ cristallin fort dans la zéolithe ce qui conduit à un écart important vis-à-vis d'une symétrie uniaxiale. Un calcul théorique CNDO/SP du radical CO^+ libre donne une valeur du couplage hyperfin isotrope en excellent accord mais le tenseur hyperfin anisotrope est uniaxial (17). Si un tel radical est placé en interaction avec un proton, un écart par rapport à la symétrie uniaxiale a pu être calculé (17) mais demeure nettement inférieur à l'écart expérimental. La perturbation par un proton correspond à un modèle de calcul mais est intéressante à considérer puisque le radical est observé sur une zéolithe protonée. Pour tenter de mettre en évidence une éventuelle influence des protons, nous avons donc effectué une expérience analogue mais en deshydroxylant la zéolithe à 900 K pour éliminer la majeure partie des protons. Le spectre rpe obtenu par action de ^{13}CO sur les centres V est présenté sur la fig. 2. On constate par comparaison avec la fig. 2 de la réf. 16 que le spectre est nettement mieux résolu et présente les paramètres suivants

$g_x = 2.0005 \pm 0.0010$	$C_x = 312 \pm 3$ Oe
$g_y = 2.0015 \pm 0.0010$	$C_y = 267 \pm 3$ Oe
$g_z = 2.0045 \pm 0.0010$	$C_z = 285 \pm 3$ Oe

Le tenseur hyperfin peut également être décomposé en deux tenseurs uniaxiaux selon les axes x et z avec

Can. J. Chem. Downloaded from www.nrcresearchpress.com by 210.87.254.40 on 09/05/12
For personal use only.

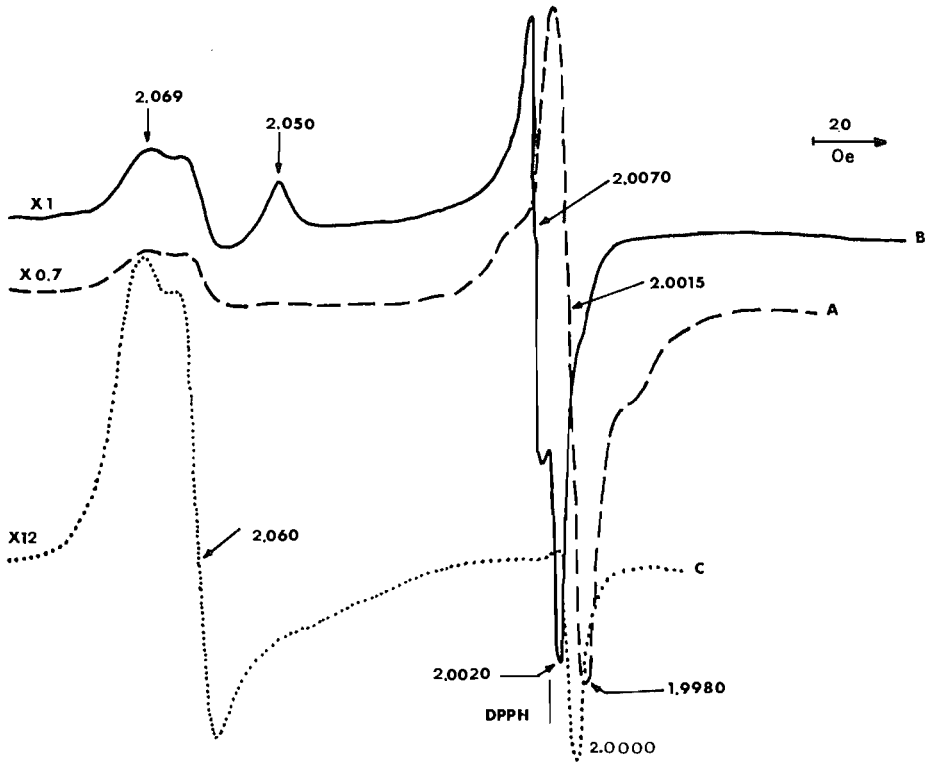

FIG. 1. Spectre rpe à 77 K. (*A*) Adsorption de ^{12}CO (40 torr) à 77 K sur l'échantillon de zéolithe HY-670 K irradié sous vide. (*B*) Adsorption ultérieure à 77 K de $^{16}O_2$ (0.1 torr). (*C*) Réchauffement de l'échantillon B à température ambiante.

$$a = 288 \text{ Oe}$$
$$b_x = 15 \text{ Oe}$$
$$b_z = 6 \text{ Oe}$$

On constate donc que le caractère *s* du radical s'est légèrement accru alors que le caractère *p* n'a pas subi de modifications à la précision des mesures, ce qui montre que la symétrie observée ne dépend pas de la présence de protons. Compte tenu des paramètres rpe, nous proposons le modèle d'adsorption suivant

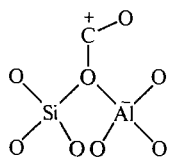

Notons enfin que le radical HCO· (couplage hyperfin de l'ordre de 130 Oe avec l'hydrogène) n'a pas été observé.

Réactivité des espèces CO^+ adsorbées

Lorsque CO est introduit sur la zéolithe

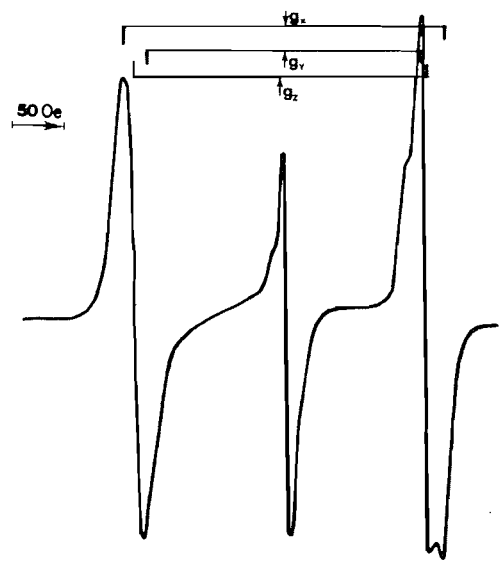

FIG. 2. Spectre rpe à 77 K du radical CO^+ en utilisant du CO enrichi en ^{13}C introduit sur l'échantillon traité à 900 K avant l'irradiation à 77 K.

Can. J. Chem. Downloaded from www.nrcresearchpress.com by 210.87.254.40 on 09/05/12
For personal use only.

irradiée, il avait été observé précédemment (31) que le spectre rpe obtenu était dû à la superposition d'un signal à peu près isotrope attribué au radical CO^+ caractérisé au paragraphe précédent et d'un signal que nous appellerons A, présentant une anisotropie orthorhombique avec:

$$g_z = 2.050 \pm 0.01$$
$$g_y = 2.0070 \pm 0.0005$$
$$g_x = 2.0020 \pm 0.0005$$

et un couplage hyperfin dû au ^{13}C tel que:

$$C_x = 6.7 \text{ Oe}$$
$$C_y = 4.2 \text{ Oe}$$

la valeur de C_z est indéterminée mais faible et probablement du même ordre de grandeur. On peut alors déduire qu'il y a environ 2% de densité de spin de l'électron non apparié qui sont localisés sur l'atome de carbone. Il n'avait alors pas été possible de proposer une attribution satisfaisante à ce signal anisotrope.

Lors de travaux ultérieurs on a pu montrer que des espèces de type $(CO—O_2)^-$ et $(CO_2—O_2)^-$, pour lesquelles l'oxygène avait une nature très peroxydique, c'est-à-dire présentait une très inégale répartition de densité de spin sur les deux noyaux d'oxygène terminaux, pouvaient être obtenues par co-adsorption d'oxygène et de CO ou CO_2 sur TiO_2 (18) et MgO (19) respectivement. Ces derniers résultats nous ont alors suggéré que l'oxyde de carbone utilisé dans le travail (31) contenait des traces d'oxygène qui est alors responsable de l'apparition de l'espèce

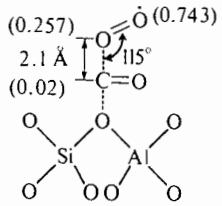

non identifiée *A*. Effectivement en purifiant cet oxyde de carbone nous avons obtenu le radical CO^+ seul étudié dans le paragraphe précédent et par contre, le signal anisotrope *A* est obtenu en introduisant une faible quantité d'oxygène sur le radical CO^+. En adsorbant de l'oxygène moléculaire enrichi en ^{17}O sur l'espèce CO^+, on obtient le spectre hyperfin de la fig. 3 caractéristique d'un radical diatomique pour lequel la densité de spin de l'électron non apparié est très inégalement répartie sur les deux atomes d'oxygène. On a $C_x^{I} = 107$ et $C_x^{II} = 37$ Oe, C_y et C_z sont très faibles pour être détectés, ce qui correspond à une densité de spin de 74.3 et 25.7% sur les deux atomes d'oxygène, donc à un caractère radical peroxy très prononcé.

Compte tenu de l'interprétation donnée dans les références 18 et 19 et la répartition de densité de spin sur l'oxygène et le carbone, le modèle d'adsorption proposé est le suivant où l'angle entre CO et O—O est de l'ordre de 115° et la distance (OC)-(O_2) de l'ordre de 2.1 Å, les chiffres entre parenthèses correspondent à la répartition de la densité de spin non apparié.

Notons aussi l'apparition de raies rpe intenses correspondant à $g_1 = 2.069$, $g_2 = 2.060$ et $g_3 = 2.0000 \pm 0.0005$ (fig. 1*C*) soit $g_{moy} = 2.043$. Ce signal ne présente pas de structure hyperfine due à ^1H ou ^{13}C. L'espèce correspondante n'existe qu'en présence de CO; elle est stable à la température ambiante et ne réagit ni avec l'oxygène ni avec l'oxyde nitrique. Un tel spectre pourrait être attribué à un radical de type O^- (28) situé dans les cages sodalites c'est-à-dire inaccessible aux molécules d'O_2 ou de NO. L'obtention d'un tel radical par action de CO sur les centres V est surprenante et nous pensons que les données tant expérimentales que de rpe ne sont pas suffisantes pour tirer une conclusion définitive. Il est en fait possible que l'action de CO sur des entités diamagnétiques ou sur des impuretés telles que le fer puisse jouer un rôle important.

Les deux espèces d'oxygène adsorbées O_2^- et $CO—O_2^-$ présentent une distribution de densité de spin non apparié très différente. Il nous a paru intéressant de tester leur réactivité chimique. Comme de telles espèces ne sont stables qu'à basse température, nous avons fait agir des gaz tels que H_2, NO et H_2S à 77 K et enregistré les espèces formées par élévation progressive de la température. Nous avons observé que NO réagit facilement à 110 K avec l'espèce $CO—O_2^-$ et à 130 K avec l'espèce O_2^-, en donnant des espèces diamagnétiques. H_2S réagit à plus haute température, mais encore plus facilement avec $CO—O_2^-$ qu'avec O_2^-, 140 et 160 K respectivement, pour donner des radicaux de type SO_2^- (29) ($g_1 = 2.017$, $g_2 = 2.010$ et $g_3 = 2.0025$) qui disparaissent à 200 K sans donner d'espèces paramagnétiques. Les radicaux du soufre n'ont pas été observés (29).

Ces espèces oxygène sont stables thermique-

Can. J. Chem. Downloaded from www.nrcresearchpress.com by 210.87.254.40 on 09/05/12
For personal use only.

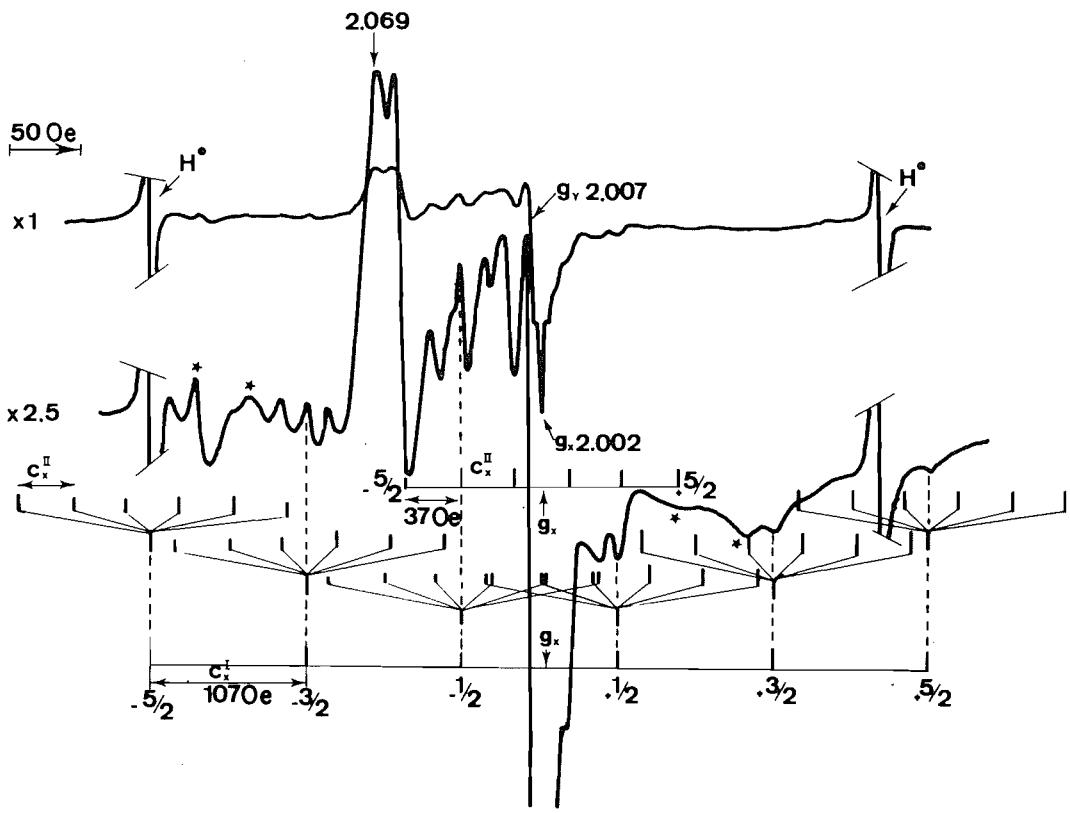

FIG. 3. Espèce formée à 77 K par adsorption d'O_2 enrichi en ^{17}O sur le radical CO^+ de la zéolithe H—Y 670 K. Les étoiles correspondent à des raies existant sur l'échantillon avant l'irradiation.

ment et ne disparaissent qu'à des températures de 200 K. Leur stabilité n'est pas modifiée en présence d'hydrogène. En même temps que les espèces oxygène disparaissent, les centres V les plus stables thermiquement sont restaurés.

En conclusion on peut dire quelles espèces radicalaires de l'oxygène réagissent principalement sur les composés radicalaires tels que NO et ce, d'autant mieux qu'elles présentent un caractère peroxydique plus marqué, comme ceci a été observé par rpe.

Caractérisation d'espèces adsorbées sur zéolithe

Dans ces expériences l'irradiation a lieu en présence de l'adsorbat.

Radical OH°

Le but de ces expériences était de déterminer si l'eau d'une part et les groupements hydroxyles d'autre part pouvaient être ionisés par les rayons γ en espèces paramagnétiques. On a observé un doublet fortement anisotrope (fig. 4) dû au couplage de l'électron célibataire avec un proton

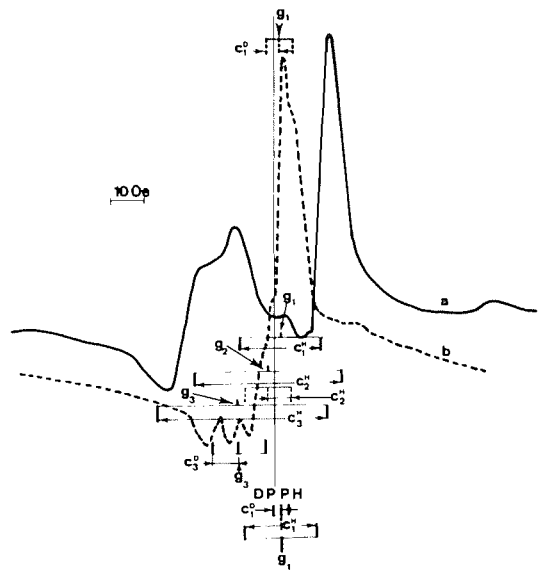

FIG. 4. Spectre rpe à 77 K des radicaux OH° et OD° sur l'échantillon H—Y rehydraté.

Can. J. Chem. Downloaded from www.nrcresearchpress.com by 210.87.254.40 on 09/05/12
For personal use only.

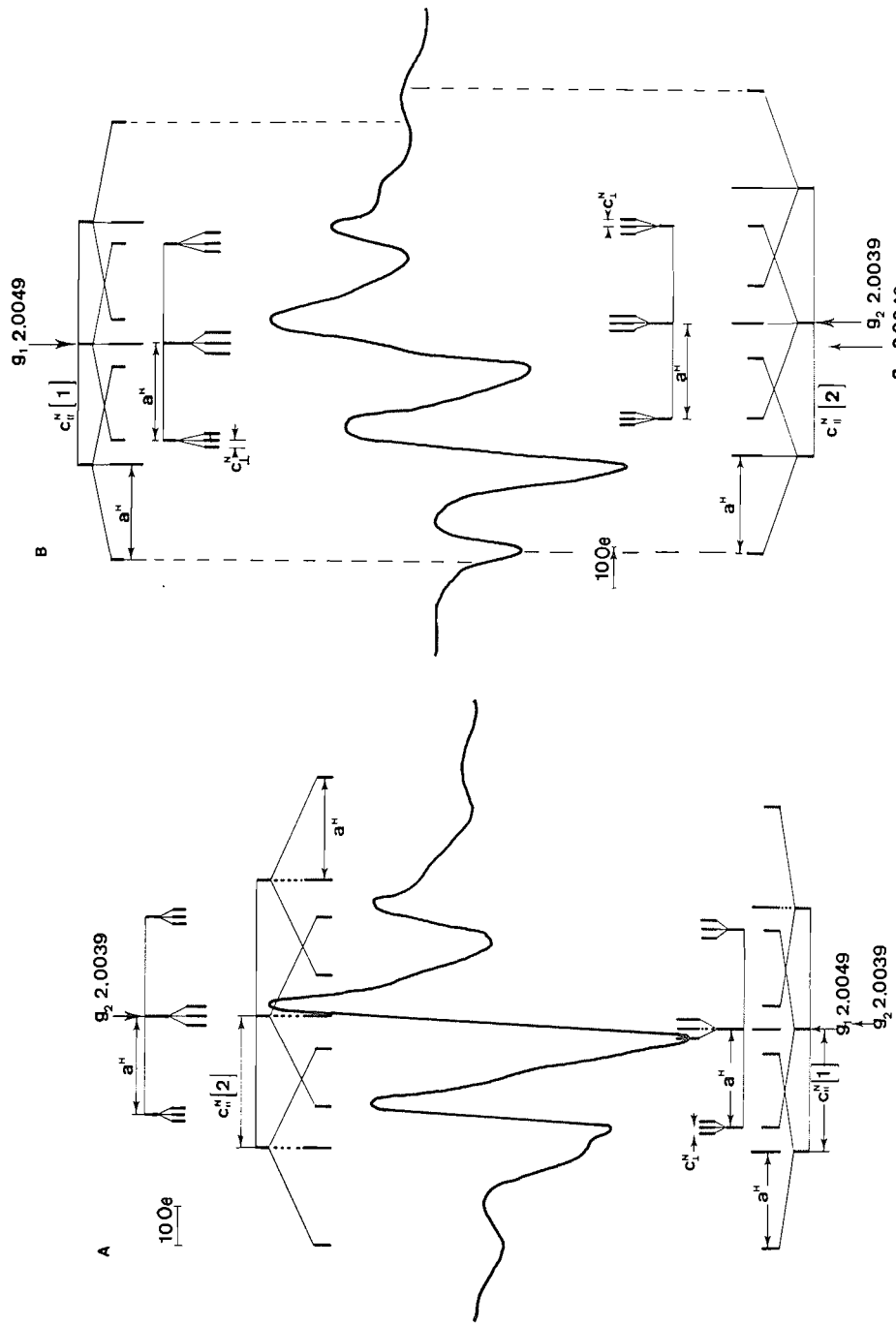

FIG. 5. Spectres en bandes X (*A*) et Q (*B*) des radicaux NH_2' sur zéolithe H—Y ammoniée.

Can. J. Chem. Downloaded from www.nrcresearchpress.com by 210.87.254.40 on 09/05/12
For personal use only.

comme le prouvent les expériences réalisées après échange par l'eau lourde D_2O ($I = 1$ pour D et $\mu H/\mu D \simeq 6.5$). On a pu observer que le radical $OH^\cdot$ n'est obtenu qu'en présence d'eau physisorbée et que son intensité est maximum pour une adsorption de l'ordre de la monocouche. Ses paramètres rpe sont

$$g_1 = 2.0028 \qquad c_1 = -26 \text{ Oe}$$
$$g_2 = 2.0050 \qquad c_2 = -47 \text{ Oe}$$
$$g_z = 2.010 \qquad c_3 = -53 \text{ Oe}$$

La décomposition du tenseur hyperfin donne

$$a = -42 \text{ Oe}$$
$$b_y = -7 \text{ Oe}$$
$$b_z = -9 \text{ Oe}$$

On peut dire que la rotation de ce radical est totalement bloquée ce qui correspond à une adsorption forte. La décomposition du tenseur hyperfin en deux tenseurs uniaxiaux alors qu'on n'en attendrait qu'un peut être expliquée par des liaisons hydrogènes avec les atomes d'oxygène du réseau. Il est à noter que le spectre obtenu est nettement plus anisotrope que celui obtenu dans d'autres matrices (20) et en particulier dans la matrice mère H_2O (21). Ceci montre bien que l'eau est fortement physisorbée dans les zéolithes, en accord avec leur capacité d'adsorption importante.

Notons encore que les groupements hydroxyles structuraux ne donnent pas naissance à des radicaux $OH^\cdot$, la scission sous irradiation ayant probablement lieu entre O et H comme dans l'équilibre 1. Ceci est en relation avec la mobilité des hydrogènes et leur acidité de Brønsted (3).

Radical $NH_2^\cdot$

Les conditions de formation de ce radical sont tout à fait analogues à celles du radical $OH^\cdot$. Il apparait que seul l'ammoniac physisorbé donne naissance à $NH_2^\cdot$ avec une intensité maximum pour des taux de recouvrements voisins de l'unité. Des radicaux de type NH_3^+ (22), dûs à l'ionisation de NH_4^+, n'ont pas été observés.

Les échantillons dégazés à 670 ou 870 K ont été ammoniés à la température ambiante par contact avec la vapeur de NH_3 pendant une nuit. Les spectres les plus caractéristiques et les plus intenses ont été obtenus lorsque l'échantillon est désorbé ensuite entre 300 et 370 K pour éliminer l'excès de NH_3 physisorbé.

Les spectres obtenus (fig. 5) présentent une structure hyperfine à cinq raies caractéristique d'un spectre de poudres. Compte-tenu de travaux utilisant de l'ammoniac enrichi en ^{15}N et ^2H (23, 24) et pour assurer la correspondance entre les spectres en bandes X et Q, nous avons été amenés à décomposer le spectre expérimental en deux signaux sous jacents d'intensité comparable et de paramètres rpe voisins

$$a_{(1)}{}^{H} = a_{(2)}{}^{H} = 24.3 \pm 1 \text{ Oe}$$
$$C_{\parallel}{}^{N}(1) = 30 \pm 1 \text{ Oe}$$
$$C_{\perp}{}^{N}(1) = C_{\perp}{}^{N}(2) = 3 \pm 1.5 \text{ Oe}$$
$$C_{\parallel}{}^{N}(2) = 33.3 \pm 1 \text{ Oe}$$
$$g_{iso}(1) = 2.0049$$
$$g_{iso}(2) = 2.0039$$

on obtient

$$a_{iso}{}^{N}(1) = 12 \text{ Oe } (2.2\%)$$
$$b^{N}(1) = 9 \text{ Oe } (43\%)$$
$$a_{iso}{}^{N}(2) = 13 \text{ Oe } (2.3\%)$$
$$b^{N}(2) = 10 \text{ Oe } (48\%)$$

L'interaction du radical avec des atomes d'Al ($I = 5/2$) ou d'hydrogène ($I = 1/2$) n'a pas été détectée.

L'observation d'une anisotropie hyperfine forte et uniaxiale pour l'azote indique que le radical est adsorbé par l'intermédiaire de son noyau d'azote. La non observation d'anisotropie des hydrogènes de $NH_2^\cdot$ pourrait indiquer une mobilité de ces atomes, par exemple par rotation autour de l'axe d'adsorption. Cependant une telle anisotropie est souvent faible et sa non observation pour des spectres de poudres doit être considérée avec précaution. Notons enfin que $NH_2^\cdot$ piégé dans une matrice inerte (25) ou dans la matrice mère (26) présente un spectre isotrope à neuf raies hyperfines. Le spectre pour les zéolithes montre que le radical est bien adsorbé sur des sites du réseau et sa rotation fortement bloquée probablement du fait de l'existence de liaisons hydrogène avec les atomes d'oxygène du réseau, comme ceci à été observé à un degré moindre sur le Vycor composé à grands pores (30).

Deux types de radicaux ont été envisagés pour interpréter le spectre obtenu. Ceci correspond vraisemblablement à des radicaux adsorbés sur les deux types de sites donnant naissance aux centres V_1 et V_2. Notons en effet que ces centres V ne sont plus détectés lorsque l'ammoniac est adsorbé sur la zéolithe (fig. 5) avant irradiation.

Radical CO_2^-

Par action de CO_2 sur les centres V (type O^-)

on pourrait s'attendre à obtenir des espèces de type CO_3^-. En fait, aucune réactivité n'a été observée, mais ceci peut provenir de la trop faible tension de vapeur de CO_2 à la température de l'expérience (77 K).

Nous avons irradié un échantillon de zéolithe H—Y en présence de CO_2. Le spectre obtenu correspond à la superposition des signaux dûs aux centres V et à un signal que l'on a pu attribuer à CO_2^- à partir du couplage du ^{13}C (15, 27) $a_{iso} \simeq 155$ Oe. Ce dernier signal a une intensité faible par rapport à celle des centres V et nous n'avons pu l'étudier en détail. On peut cependant conclure que CO_2 s'adsorbe sur des sites différents de ceux donnant naissance aux centres V.

Conclusion

La présente étude a permis de caractériser la nature d'espèces adsorbées, leur site d'adsorption, leur mobilité et éventuellement leur réactivité. On a pu montrer que la coadsorption de CO et O_2 modifie fortement la distribution de densité de spin sur la molécule d'oxygène et donc son caractère radicalaire et en conséquence sa réactivité.

Les différentes espèces sont adsorbées sur le solide par des liaisons assez faibles mais néanmoins suffisantes pour bloquer leur mouvement de rotation. Dans le cas de radicaux protonés ($OH^\cdot$, $NH_2^\cdot$) les liaisons hydrogène avec les atomes d'oxygène du réseau bloquent fortement le mouvement du radical et donnent des spectres rpe beaucoup plus anisotropes que ceux obtenus pour les mêmes radicaux piégés dans des matrices inertes ou de leurs molécules mères.

La majorité des adsorbats étudiés s'adsorbent sur les centres précurseurs de centres V donc sur des atomes d'oxygène du réseau ou à proximité immédiate. Seul CO_2 semble s'adsorber différemment.

Remerciements

Les auteurs tiennent à remercier M. G. Wicker pour son aide technique et les Dr. Y. Ben Taarit et P. Meriaudeau pour les fructueuses discussions.

1. H. Dugas. Can. J. Spectrosc. **18**, 110 (1973); M. Che, J. Fraissard et J. C. Vedrine. Bull. Groupe Fr. Argiles, **26**, 1 (1974).
2. J. C. Vedrine, D. Barthomeuf, G. Dalmai-Imelik, Y. Trambouze, B. Imelik et M. Prettre. C.R. Acad. Sci. Paris, Ser. C, **267**, 118 (1968).
3. A. Abou-Kais, J. C. Vedrine, J. Massardier et G. Dalmai-Imelik. J. Chem. Soc. Faraday Trans. 1, **70**, 1039 (1974); J. Catal. **34**, 317 (1974).
4. A. Abou-Kais, J. C. Vedrine et J. Massardier. J. Chem. Soc. Faraday Trans 1, **71**, 1697 (1975).
5. J. H. Lunsford. J. Phys. Chem. **68**, 2312 (1964); K. M. Wang et J. H. Lunsford. J. Catal. **24**, 262 (1972).
6. M. Boudart, A. Delbouille, E. G. Derouane, V. Indovina et A. B. Walters. J. Am. Chem. Soc. **94**, 6622 (1972).
7. Kh. M. Minachev, V. A. Garanin, V. V. Kharlamov et T. A. Isakova. Kinet. Katal. **13**, 1101 (1972); Adv. Chem. **102**, 441 (1971).
8. J. C. Vedrine et C. Naccache. J. Phys. Chem. **77**, 1606 (1973).
9. K. M. Wang et J. H. Lunsford. J. Phys. Chem. **73**, 2069 (1969).
10. P. H. Kasai. J. Chem. Phys. **43**, 3322 (1965).
11. A. A. Gezalov, G. M. Zhabrova, V. V. Nikisha, G. B. Pariisky et K. N. Spiridinov. Kinet. Katal. **9**, 462 (1968).
12. M. Che, C. Naccache et B. Imelik. J. Chim. Phys. **65**, 1301 (1968); J. C. Vedrine, G. Dalmai-Imelik et B. Imelik. Coll. Ampere XV. North Holland Publishers, Amsterdam. 1969. p. 304.
13. A. J. Tench et T. Lawson. Chem. Phys. Lett. **7**, 459 (1970).
14. D. H. Whiffen. J. Chim. Phys. **61**, 1589 (1964).
15. P. Meriaudeau, J. C. Vedrine, Y. Ben Taarit et C. Naccache. J. Chem. Soc. Faraday Trans. 2, **71**, 736 (1975).
16. J. C. Vedrine et C. Naccache. Chem. Phys. Lett. **18**, 190 (1973).
17. N. D. Chuvylkyn, G. M. Zhidomirov et V. B. Kazansky. Chem. Phys. Lett. **26**, 180 (1974).
18. P. Meriaudeau et J. C. Vedrine. J. Chem. Soc. Faraday Trans. 2, **72**, 472 (1976).
19. P. Meriaudeau, Y. Ben Taarit, J. C. Vedrine, C. Naccache et P. de Montgolfier. J. Chem. Soc. Faraday Trans. Soumis pour publication.
20. H. E. Radford. Phys. Rev. **122**, 114 (1961).
21. J. A. McMillan, M. S. Matheson et B. Smaller. J. Chem. Phys. **33**, 609 (1960); S. Siegel, L. H. Faum, S. Skolnik et J. M. Flournoy. J. Chem. Phys. **32**, 1249 (1960); H. C. Box, E. E. Budzinski, K. T. Lilga et H. G. Freund. J. Chem. Phys. **53**, 1059 (1970).
22. T. Cole. J. Chem. Phys. **35**, 1169 (1961).
23. O. I. Brotikovskii, G. M. Zhidomirov, V. B. Kazanskii, A. I. Mashchenko et B. N. Shelimov. Kinet. Katal. **12**, 700 (1971).
24. E. F. Vansant et J. H. Lunsford. J. Phys. Chem. **76**. 2716 (1972).
25. S. N. Foner, E. L. Cochran, V. A. Bowers et C. K. Jen. Phys. Rev. Lett. **1**, 91 (1958).
26. R. Marx et J. Maruani. J. Chim. Phys. **61**, 1604 (1964).
27. K. Sogabe, A. Hasegawa, Y. Yamada and M. Miura. Bull. Chem. Soc. Jpn. **45**, 3362 (1972).
28. C. Naccache. Chem. Phys. Lett. **11**, 323 (1971).
29. Z. Dudzik et M. Bilska-Ziotek. Bull. Acad. Pol. Sci. **23**, 699 (1975).
30. N. Shimamoto, K. Hatano, T. Katsu and Y. Fujita. Bull. Chem. Soc. Jpn. **48**, 18 (1975).
31. A. Abou-Kais. Thèse, Université Claude Bernard, Lyon. 1972.

Can. J. Chem. Downloaded from www.nrcresearchpress.com by 210.87.254.40 on 09/05/12
For personal use only.

Solvolysis rates in aqueous–organic mixed solvents. III. Kinetics of the alkaline solvolysis of monochloroacetate ion in water – *tert*-butyl alcohol solutions

EL-HUSSIENY M. DIEFALLAH[1]
Department of Chemistry, Assiut University, Assiut, Egypt

Received October 20, 1975

EL-HUSSIENY M. DIEFALLAH. Can. J. Chem. **54**, 1687 (1976).

The temperature dependence of the rate of alkaline solvolysis of monochloroacetate ion in water – *tert*-butyl alcohol solutions has been determined. The rates of reaction were first order with respect to both the chloroacetate ion and to the total solvoxide ion concentrations. The reactivity is enhanced, first slowly, and then more rapidly, by increasing the concentration of *tert*-butyl alcohol in the solvent mixtures. The rate of reaction increases with the reciprocal of the dielectric constant of the medium and the plot of log k *vs.* $1/D$ can best be represented by two lines intersecting at a point corresponding to 0.9 water mole fraction. The activation parameters ΔH^* and ΔS^* for the solvolysis reaction showed a minimum at about 0.9 water mole fraction. The significance of these results from the viewpoint of the electrostatic theory and the changing of solvent structure in such mixtures is discussed.

EL-HUSSIENY M. DIEFALLAH. Can. J. Chem. **54**, 1687 (1976).

On a déterminé la dépendance sur la température de la vitesse de solvolyse alcaline de l'ion monochloroacétate dans des solutions d'eau et d'alcool *tert*-butylique. Les vitesses de la réaction sont du premier ordre par rapport à l'ion chloroacétate et par rapport à la concentration totale d'ion solvolysant. La réactivité augmente lentement au début et ensuite plus rapidement à mesure que l'on augmente la concentration d'alcool *tert*-butylique dans les mélanges de solvant. La vitesse de la réaction augmente avec l'inverse de la constante diélectrique du milieu et l'on peut représenter la courbe de log k en fonction de $1/D$ par deux lignes se croisant à un point correspondant à une fraction molaire d'eau de 0.9. Les paramètres d'activation ΔH^* et ΔS^* pour la réaction de solvolyse montrent un minimum lorsque la fraction molaire d'eau est près de 0.9. On discute de l'importance de ces résultats par rapport à la théorie électrostatique et par rapport au changement dans la structure du solvant dans de tels mélanges.

[Traduit par le journal]

Introduction

For many solvolysis reactions carried out in aqueous–organic mixed solvents, the activation enthalpy and entropy pass through an extremum as the solvent composition is varied (1–10). The position and depth of the extrema are dependent upon the substrate and the nonaqueous component of the solvent mixture. If the extrema in the various activation parameters are related to the same physical phenomena, it is expected that the variation of these extrema with changes in the organic component of the solvent mixture should parallel one another (8). For this reason, we have studied the alkaline solvolysis of sodium monochloroacetate in a series of water – *tert*-butyl alcohol solutions covering the composition range 0–50% by weight *tert*-butyl alcohol, in order to test the reality of this expectation and to learn more about solvent effects upon reaction rates. The kinetic study of the alkaline solvolysis of monochloroacetate ion in water–methanol and water–ethanol solutions has been carried out (1, 2). It was demonstrated that the monochloroacetate ion solvolyses in alkaline solution with the operation of an S_N2 mechanism. The reaction yields hydrochloric acid and the corresponding α-solvoxy compound.

Experimental

For all rate determinations, C.P. grade VEB Laborchemie Apolda monochloroacetic acid was used after further recrystallization from benzene. *tert*-Butyl alcohol, reagent grade (obtained from Carlo Erba), was distilled (bp 82.9 °C) and the middle fraction used. Doubly distilled water and the purified alcohol were used to prepare all the solutions. All solvent mixtures used throughout this investigation were mixed by volume, and the mole fractions and weight percentages were calculated making use of the density of the pure components (11). Enough of each solvent mixture was made to complete the series of studies. The rates of reaction were determined by

[1]Present address: Chemistry Department, Faculty of Science, King Abdul-Aziz University, P.O. Box 1540, Jeddah, Saudi Arabia.

Can. J. Chem. Downloaded from www.nrcresearchpress.com by 210.87.254.5 on 09/05/12
For personal use only.

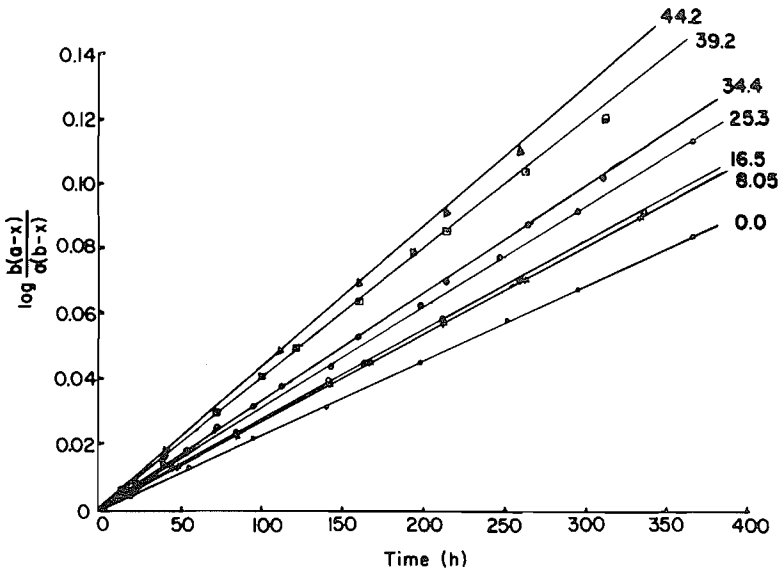

FIG. 1. Second-order plots at 48.0 °C in mixtures of water and *tert*-butyl alcohol. Percent by weight *tert*-butyl alcohol: ●, 0.0; ×, 8.05; ○, 16.5; ⊙, 25.3; ⊗, 34.4; ⊡, 39.2; △, 44.2.

titrimetric methods by comparison of chloride ions liberated with base consumed in the reaction, as has been previously described (1).

The appropriate initial concentration ranges for the kinetic studies of the alkaline solvolysis of sodium monochloroacetate were 0.100–0.020 mol/l for sodium monochloroacetate and 0.200–0.100 mol/l for sodium hydroxide. The reactants in the solvent mixture lead to a clear solution when the *tert*-butyl alcohol in the solvent mixture is less than about 50% by volume. At higher alcohol concentrations, the reaction mixture solutions are turbid due to phase separation which is more noticeable at higher hydroxide concentrations and lower temperatures. Thus, we limited our kinetic runs to solvent mixtures containing less than about 50% by volume *tert*-butyl alcohol. Under these conditions the reaction mixtures were clear and the results were reproducible giving rise to strictly second-order behaviour.

Results and Discussion

The rates of solvolysis reaction follows the second-order expression ($a \neq b$):

$$k = \frac{2.303}{(a-b)t} \log \frac{b(a-x)}{a(b-x)}$$

where x is mol/l reacting in time t, a is the initial concentration of sodium monochloroacetate, b is the initial concentration of base, and k is the specific reaction rate constant. The rate constants were evaluated from the slopes of the straight lines obtained when log $b(a-x)/a(b-x)$ are plotted against time, t. Figure 1 shows typical plots obtained at 48.0 °C in solvent mixtures of water and *tert*-butyl alcohol. Table 1 lists the values of the rate constants obtained at 39.0, 48.0, and 56.0 °C and the medium dielectric constant D of the various solvent mixtures investigated. The rate constants represent the average of at least four determinations. In each solvent mixture, D was calculated from the experimental value for the pure solvents (11) and the composition of the solvent mixture, assuming linear dependence on composition. Figure 2 shows how the second-order rate constants for the reaction vary with solvent composition. It can be seen that the rate of reaction increases in a nonlinear manner as the *tert*-butyl alcohol content of the solvent mixture increases and that the rate first increases slowly up to about 30% by weight *tert*-butyl alcohol and then more rapidly on further increase in the alcohol concentration.

Since the transition state of the solvolysis reaction bears a double negative charge, it is more strongly solvated than the ground state, and it is expected that as the solvent polarity increases the reaction rate increases (12). However, the data in Table 1 shows that this is not true and that the rate of the reaction increases as the dielectric constant of the medium decreases. Moreover, Fig. 3 shows that the plot of log k *vs.* $1/D$ at each specified temperature gave rise to two straight lines intersecting at about 25% by weight *tert*-butyl alcohol (0.9 water mole fraction). These results show that there is no simple

Can. J. Chem. Downloaded from www.nrcresearchpress.com by 210.87.254.5 on 09/05/12
For personal use only.

Can. J. Chem. Downloaded from www.nrcresearchpress.com by 210.87.254.5 on 09/05/12
For personal use only.

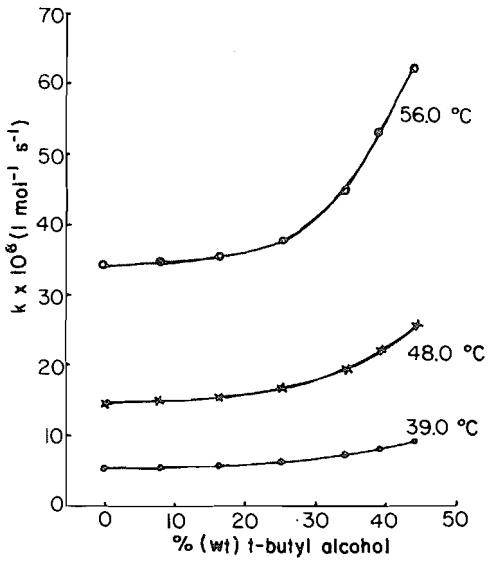

FIG. 2. Dependence of the second-order rate constants on solvent composition.

correlation between the dielectric constant D and the rate constant k and that the values are not even in the same order predicted by simple electrostatic theory. The predictions of the dielectric theory of medium effects sometimes fit and sometimes fail to fit the actual behaviour of polar reactions (13). This failure of the electrostatic picture might be because its general postulates are too simplified and because solvation effects other than those describable in terms of the dielectric constant can be expected to be of similar importance.

The energy of activation of the reaction was calculated from the temperature coefficient of the reaction rates. The enthalpy and entropy of

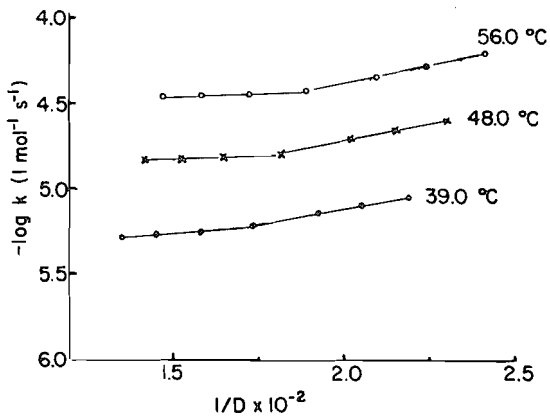

FIG. 3. Dependence of the second-order rate constants on the dielectric constant of the medium.

TABLE 1. Effect of temperature and solvent composition on the rate constants of the alkaline solvolysis of monochloroacetate ion in mixtures of water and *tert*-butyl alcohol

T (°C)	Solvent water – *t*-butyl alcohol (v/v)	Medium dielectric constant	Rate constant $k \times 10^6$ ($l\ mol^{-1}\ s^{-1}$)
39.0	Water	73.8	5.26±0.2
	90.0:10.0	69.0	5.51±0.2
	80.0:20.0	63.4	5.67±0.2
	70.0:30.0	57.8	6.20±0.2
	60.0:40.0	52.0	7.15±0.15
	55.0:45.0	49.0	8.15±0.1
	50.0:50.0	45.6	8.94±0.4
48.0	Water	70.9	14.6±0.4
	90.0:10.0	66.0	15.1±0.2
	80.0:20.0	60.7	15.4±0.2
	70.0:30.0	55.2	16.6±0.2
	60.0:40.0	49.5	19.4±0.4
	55.0:45.0	46.5	22.5±0.6
	50.0:50.0	43.5	25.6±0.6
56.0	Water	68.0	34.4±0.5
	90.0:10.0	63.4	35.1±0.5
	80.0:20.0	58.2	35.7±0.5
	70.0:30.0	53.0	38.1±0.6
	60.0:40.0	47.5	44.9±0.7
	55.0:45.0	44.5	53.3±0.8
	50.0:50.0	41.5	62.4±0.8

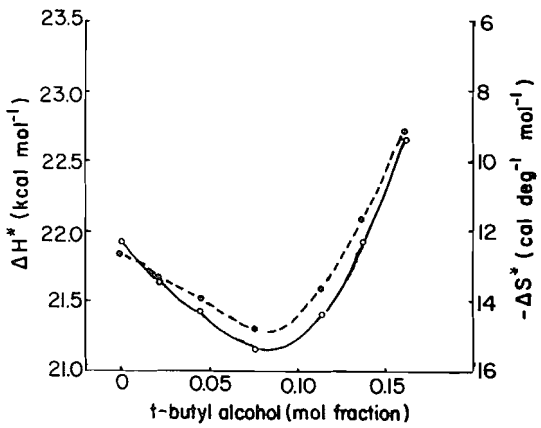

FIG. 4. Dependence of the activation parameters ΔH^* and ΔS^* on solvent composition: ○, ΔH^*; ●, ΔS^*.

activations were calculated from the rate constants using the transition-state theory equations (14):

$$k = \frac{RT}{Nh} e^{-\Delta H^*/RT} e^{\Delta S^*/R}$$

$$\Delta S^* = R \ln \frac{AhN}{eTR}$$

TABLE 2. Activation parameters (at 48.0 °C) for the solvolysis of monochloroacetate ion in water – *tert*-butyl alcohol solvent mixtures

Solvent water – *t*-butyl alcohol (v/v)	Water mole fraction	ΔH^* (kcal/mol)	$-\Delta S^*$ (cal deg^{-1} mol^{-1})	ΔG^* (kcal/mol)
Water	1.0	21.9	12.6	26.0
90.0:10.0	0.979	21.7	13.3	25.9
80.0:20.0	0.955	21.5	13.9	25.9
70.0:30.0	0.924	21.2	14.7	25.9
60.0:40.0	0.887	21.4	13.6	25.8
55.0:45.0	0.864	22.0	11.6	25.7
50.0:50.0	0.839	22.7	9.1	25.6

where A is the frequency factor, R/N is the Boltzmann gas constant, and h is Planck's constant. Table 2 shows the results of the activation parameters calculated at 48.0 °C.

A change in solvent usually affects both the enthalpy and entropy of activation (13). The variation of ΔH^* and ΔS^* with solvent composition is shown in Fig. 4. It is seen that when the concentration of *tert*-butyl alcohol in the solvent mixture is increased, the enthalpy and entropy of activation first decrease to a minimum of about 0.9 water mole fraction, and then increase. It can also be seen that a large entropy is associated with a large enthalpy and a small entropy with a small enthalpy. This is characteristic of reactions involving moderate changes in structure or solvent (13).

The extremum behaviour of the activation enthalpy and entropy has been observed for many solvolytic reactions (1–10) and under a variety of conditions, and seems to reflect a common solvent behaviour (7–10). The appearance of the minimum in aqueous–organic solvent mixtures was explained by Arnett and co-workers (7) on the basis of the behaviour of heats of solution in aqueous alcohols. Both the heat of solution and the enthalpy of activation are related to the same kind of change in solvent structure with changing composition. There is evidence (7, 15–17) which further supports the conclusion that the addition of alcohol to water increases the structuredness of the solution in the water-rich concentration range and that the extremum behaviour may be related to the accompanying solvent reorganization attending the activation process for solvolysis in binary alcohol–water systems (10). In such cases it is concluded that the breakdown of solvent structure as a consequence of charge separation in the activation process parallels the sensitivity to changes in the solvent composition.

The behaviour of variations in ΔH^* and ΔS^* with changes in solvent composition observed in this study is similar to that found for the solvolysis of sodium monochloroacetate in methanol–water and ethanol–water solutions (1, 2). However, in *tert*-butyl alcohol – water solutions, the depth of the ΔH^* minimum relative to pure water is about 0.8 kcal/mol and that for ΔS^* is 2.3 cal deg^{-1} mol^{-1}. This compares with 4 kcal/mol and 12 cal deg^{-1} mol^{-1} for the methanol–water and 1.5 kcal/mol and 4.2 cal deg^{-1} mol^{-1} for ethanol–water solutions. These results indicate that in *tert*-butyl alcohol – water solvent mixtures the activation parameters show relatively little variation with changing solvent composition. The reorganization of solvent molecules during the activation process has relatively less effect on the alkaline solvolysis of monochloroacetate ion in the *tert*-butyl alcohol – water system than in the methanol–water system. Table 3 summarizes the results showing the effect of the size of the alkyl group of the alcohol on the position and depth of the ΔH^* and ΔS^* minima.

In aqueous–organic solvent mixtures, the —OH group of the alcohol is visualized as fitting into the hydrogen-bonded network of the water structure while the water forms a continuous hydrogen-bonded shell about the alkyl group (9). There is evidence (9, 10, 18, 19) for these binary mixtures which supports the conclusion that the relative amount of alcohol compatible with a three-dimensional quasi-aqueous structure is directly dependent on the volume of the alkyl group, *i.e.* extrema being observed at succes-

Can. J. Chem. Downloaded from www.nrcresearchpress.com by 210.87.254.5 on 09/05/12
For personal use only.

TABLE 3. Effect of the size of the alkyl group of the alcohol cosolvent on the position and depth of ΔH^* and ΔS^* minima in the alkaline solvolysis of monochloroacetate ion

Organic cosolvent	Position of ΔS^* or ΔH^* minimum (water mole fraction)	Depth of ΔS^* minimum[a] (cal deg^{-1} mol^{-1})	Depth of ΔH^* minimum[a] (kcal/mol)
Methyl alcohol[b]	0.7	12.0	4.0
Ethyl alcohol[c]	0.8	4.2	1.5
tert-Butyl alcohol[d]	0.9	2.3	0.8

[a]Relative to pure water.
[b]Reference 1.
[c]Reference 2.
[d]This study.

sively lower concentrations of alcohol as the hydrophobic alkyl group increased in volume. Our kinetic results are in agreement with this conclusion. Table 3 shows that the observed minimum is shifted from 0.7 water mole fraction in methanol–water to 0.8 and 0.9 water mole fractions in ethyl alcohol – water and *tert*-butyl alcohol – water solvent mixtures, respectively.

The calculated values of ΔG^* are also listed in Table 2 and it can be seen that they do not change much with solvent composition. This must be due to the linear compensation between ΔH^* and ΔS^*. The plot of ΔH^* *vs.* ΔS^* gave rise to a straight line as shown in Fig. 5. The slope of the straight line, known as the isokinetic or isoequilibrium temperature, equals 270 K. Linear $\Delta H^* - \Delta S^*$ relationships have been observed for many systems (9, 13) and also for the solvolysis of sodium monochloroacetate in methanol–water and ethanol–water solutions (1, 2) and this behaviour is expected if the solvents in a series perform closely similar roles in the reaction (13).

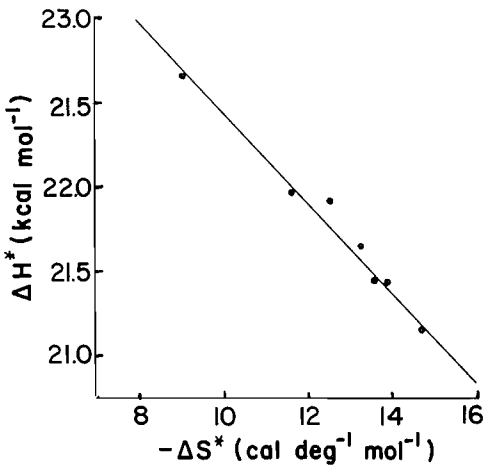

FIG. 5. A plot of ΔH^* *vs.* ΔS^* for the alkaline solvolysis of monochloroacetate ion in a series of water – *tert*-butyl alcohol solvent mixtures.

1. A. M. AZZAM and E.-H. M. DIEFALLAH. Z. Phys. Chem. Leipzig, **91**, 44 (1974).
2. E.-H. M. DIEFALLAH. Paper Ph 3-23 presented at the Fourth Arab Chemical Conference held in Cairo, Egypt, April 26–29, 1975.
3. A. H. FAINBERG and S. WINSTEIN. J. Am. Chem. Soc. **79**, 1597; **79**, 1602 (1957); **79**, 5937 (1957).
4. J. B. HYNE and R. E. ROBERTSON. Can. J. Chem. **34**, 931 (1956).
5. J. B. HYNE and R. WILLS. J. Am. Chem. Soc. **85**, 3650 (1963).
6. J. B. HYNE, R. WILLS, and R. E. WONKKA. J. Am. Chem. Soc. **84**, 2914 (1962).
7. E. M. ARNETT, W. G. BENTRUDE, J. J. BURKE, and P. M. DUGGLEBY. J. Am. Chem. Soc. **87**, 1541 (1965).
8. H. S. GOLINKIN and J. B. HYNE. Can. J. Chem. **46**, 125 (1968).
9. R. E. ROBERTSON and S. E. SUGAMORI. J. Am. Chem. Soc. **91**, 7254 (1969).
10. R. E. ROBERTSON and S. E. SUGAMORI. Can. J. Chem. **50**, 1353 (1972).
11. R. C. WEAST (*Editor*). Handbook of chemistry and physics, 49th ed. Chemical Rubber Co., Cleveland, Ohio. 1968.
12. C. K. INGOLD. Structure and mechanism in organic chemistry. Cornell University Press, Ithaca, N.Y. 1953. Chapt. 7.
13. J. E. LEFFLER. J. Org. Chem. **20**, 1202 (1955).
14. A. A. FROST and R. G. PEARSON. Kinetics and mechanism. 2nd ed. John Wiley & Sons, Inc., New York. 1961. Chapt. 7.
15. H. S. FRANK and M. EVANS. J. Chem. Phys. **13**, 507 (1945).
16. A. BEN-NAIM, J. Phys. Chem. **69**, 1922 (1965).
17. G. L. BERTRAND, F. L. MILLERO, C. WU, and L. G. HEPLER. J. Phys. Chem. **70**, 699 (1966).
18. F. FRANKS and D. J. G. IVES. Q. Rev. Chem. Soc. **20**, 1 (1966).
19. E. M. ARNETT, W. B. KOVER, and J. V. CARTER. J. Am. Chem. Soc. **91**, 4028 (1969).

Can. J. Chem. Downloaded from www.nrcresearchpress.com by 210.87.254.5 on 09/05/12
For personal use only.

Vapour pressures of solid and liquid $NbCl_5$ and $TaCl_5$

DONALD R. SADOWAY AND S. N. FLENGAS

Department of Metallurgy and Materials Science, University of Toronto, Toronto, Ont., Canada M5S 1A4

Received January 12, 1976

DONALD R. SADOWAY and S. N. FLENGAS. Can. J. Chem. **54**, 1692 (1976).

The vapour pressures of solid and liquid $NbCl_5$ and $TaCl_5$ have been measured over the temperature range 425 to 525 K by a quartz Bourdon-type spiral pressure gauge. Enthalpies and entropies of sublimation, fusion, and evaporation as well as melting points and boiling points have been calculated. The present results are compared with those reported in the literature.

DONALD R. SADOWAY et S. N. FLENGAS. Can. J. Chem. **54**, 1692 (1976).

A moyen d'une jauge Bourdon à spirale de quartz, on a mesuré les tensions de vapeur du pentachlorure de niobium et de tantale à l'état solide et liquide, à des températures variant entre 425 et 525 K. Les enthalpies et les entropies de sublimation, de fusion et d'évaporation ont été calculées, ainsi que les températures de fusion et d'ébullition. Les résultats obtenus sont comparés avec les données publiées dans la littérature scientifique.

Introduction

The equilibrium vapour pressures of pure solid and liquid $NbCl_5$ (1–6) and $TaCl_5$ (1–4, 7–10) have been the subject of many investigations. It is evident in Figs. 3 and 4 that the results of various investigations differ greatly. The uncertainties in values of the derived thermodynamic properties such as the enthalpies and entropies of evaporation and of sublimation are even greater since their calculation depends upon an accurate knowledge of the derivative of the logarithm of pressure with respect to the reciprocal of temperature.

In the present investigation the pressures of $NbCl_5$ and $TaCl_5$ vapours, in equilibrium with the pure compounds $NbCl_5$ and $TaCl_5$, respectively, have been measured by a direct method over a temperature range extending below and above their melting points.

The study is part of a research program concerned with the thermodynamic and electrochemical properties of refractory-metal chlorides (11–13).

Experimental

The compounds $NbCl_5$ and $TaCl_5$ were obtained commercially[1] and were certified to be of purity 99.99% and 99.9%, respectively. These were further purified by sublimation in a stream of oxygen-free and dehydrated helium gas saturated with thionyl chloride, as described by Keneshea *et al.* (14). Any oxychloride and water impurities present should react according to

$$MOCl_{3(g)} + SOCl_{2(g)} \rightarrow MCl_{5(g)} + SO_{2(g)}$$

and

$$H_2O_{(g)} + SOCl_{2(g)} \rightarrow 2HCl_{(g)} + SO_{2(g)}$$

where M represents Nb or Ta. The purified compounds were sublimed into glass ampoules which were subsequently sealed under vacuum.

The apparatus for measuring the equilibrium vapour pressures is shown in Fig. 1. It consisted of a Bourdon-type fused quartz spiral.[2] This was enclosed in a quartz chamber in such a way that the salt vapour from the sample entered only the inside of the spiral while air could be admitted to the chamber surrounding the spiral to equilibrate pressures inside and outside the spiral. The gauge served only as a null point detector while the pressure was read directly on a closed-end mercury manometer. The null point of the quartz signal was determined with the aid of a telescope to the nearest 0.2 mm Hg. Mercury levels in the manometer were measured by a cathetometer.

The quartz spiral-type gauge was found to be superior to both the spoon-type Bourdon gauges (15, 16) and the molten tin isoteniscopes (17, 18) used previously in this laboratory because of its ability to sustain large and sudden pressure changes without shattering. This eliminated the need for close supervision of the apparatus since it was no longer necessary to balance the pressures continuously. In addition, because of the compact size of the spiral-type gauge and because it was connected directly to the sample container, the volume of the gas phase was kept to a minimum. Furthermore, the salt sample and its vapour were contained in a closed system. This facilitated conducting experiments over extended time periods with no accompanying material losses.

Heat was supplied by a resistance furnace consisting of

[1]The salts were obtained from Research Organic/Inorganic Chemical Corporation, Belleville, New Jersey, U.S.A.

[2]The Bourdon spiral was manufactured by Worden Quartz Products, Houston, Texas.

Can. J. Chem. Downloaded from www.nrcresearchpress.com by 210.87.254.6 on 09/05/12
For personal use only.

TABLE 1. Measured vapour pressure of $NbCl_5$ and $TaCl_5$

$NbCl_5$				$TaCl_5$			
Sublimation		Evaporation		Sublimation		Evaporation	
Temperature (°C)	Pressure (mm Hg)	Temperature (°C)	Pressure (mm Hg)	Temperature (°C)	Pressure (mm Hg)	Temperature (°C)	Pressure (mm Hg)
153.8	17.1	230.2	485.7	169.3	52.4	236.8	807.8
164.0	30.9	230.1	483.9	185.0	106.6	229.5	672.9
175.5	57.0	240.0	623.2	215.6	425.8	229.1	665.1
182.0	77.1	241.0	638.3	208.7	316.9	226.4	621.3
187.2	99.1	213.6	310.5	201.2	228.2	229.4	672.5
190.0	111.4	235.6	561.7	193.1	161.2	226.4	626.3
191.2	116.2	251.2	813.4	183.4	106.1	224.2	592.0
206.5	247.5	213.6	307.2	219.7	492.5	231.9	723.0
163.0	26.5	209.9	276.1	183.9	111.1	227.6	644.8
158.7	22.3					234.7	777.1

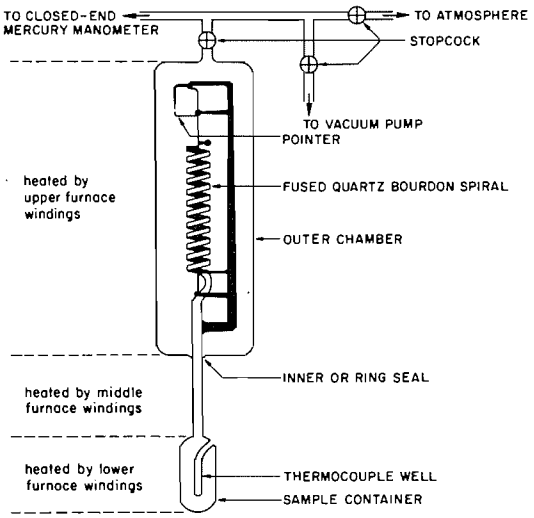

FIG. 1. Apparatus for the measurement of vapour pressure.

three independently controlled nichrome tape windings. The lowest winding heated the sample, while the upper two windings created a temperature profile in the spiral and the tube connecting it to the sample such that condensation of salt in these regions was prevented. The temperature variation in the zone of the furnace occupied by the sample was ± 0.25 K. Temperature was measured by means of a chromel–alumel thermocouple contained in a glass tube immersed in the salt sample. The thermocouple had been calibrated against a certified platinum – 13% rhodium *vs.* platinum standard. Thermal emf's were measured by a volt potentiometer.

In a typical experiment the salt was distilled into the sample container. The system was then sealed under vacuum. Experiments lasted usually a period of three days. During this time the sample was subjected to repeated heating and cooling cycles over the entire temperature range of interest to demonstrate the absence of hysteresis in the Bourdon spiral and to establish the reversibility of the measurements. In each case at the end of the experiment the pressure returned to within 2 to 3 mm Hg of zero.

Results and Discussion

The apparatus was capable of measuring the total vapour pressure in the system. Density measurements of $NbCl_5$ and $TaCl_5$ vapours from 500 K to the critical temperature by Nisel'son *et al.* (19) and by Johnson and Cubicciotti (20) have shown that in the temperature range of the present work the vapour phase may be considered a monomeric ideal gas. Accordingly, in the following thermodynamic calculations fugaci-

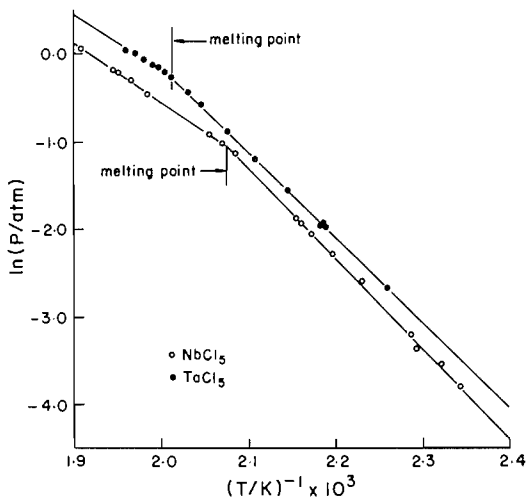

FIG. 2. Temperature dependence of vapour pressure of $NbCl_5$ and $TaCl_5$: results of the present study.

Can. J. Chem. Downloaded from www.nrcresearchpress.com by 210.87.254.6 on 09/05/12
For personal use only.

ties have been replaced by measured vapour pressures.

The pressure measurements are displayed in Table 1. Pressures were measured in mm Hg, and corrections were made for scale expansion, mercury expansion, and gravity (21, 22) to give the corresponding mercury column height under standard conditions, *i.e.* at 273.15 K and an acceleration of free fall of 9.80665 m/s^2. These corrected values appear in the table. Temperatures reported are based on the IPTS-68 (23). In Fig. 2 these data are plotted.

Since the heat capacities of $NbCl_5$ are known (14) it was possible to calculate the complete temperature dependence of its vapour pressure by applying the Σ function method (24). Enthalpy contents of solid and liquid $NbCl_5$ were measured by drop calorimetry by Keneshea *et al.* (14) and the molar heat capacities of solid and liquid $NbCl_5$ are given as 35.35 cal/K and $57.26 - 22.06 \times 10^{-6}\ T^2$ cal/K, respectively.[3]

Werder, Frey, and Guenthard (26) measured the vibrational spectra of solid $NbCl_5$ and calculated the molar heat capacity of the gas from theory based on the harmonic-oscillator rigid-rotator approximation. These results have been fitted herein to the equation

$$[1] \qquad C_{P,\text{gas}} = 31.73 - 2.678 \times 10^5 T^{-2}\ \text{cal/K mol}$$

which is valid in the temperature range 300 to 600 K.

Linear regression of Σ *vs.* $1/T$ yields the following equations for $NbCl_5$:

$$[2] \qquad \Delta H_{\text{sublimation}} = 21651 - 3.62T + 2.678 \times 10^5 T^{-1} \pm 450\ \text{cal/mol}$$

$$[3] \qquad \ln (P_{(s)}/\text{atm}) = 33.116 - 10896T^{-1} - 1.8217 \ln T - 6.738 \times 10^4 T^{-2} \pm 0.029$$

$$[4] \qquad \Delta H_{\text{evaporation}} = 24530 - 25.53T + 2.678 \times 10^5 T^{-1} + 7.340 \times 10^{-6} T^3 \pm 100\ \text{cal/mol}$$

$$[5] \qquad \ln (P_{(l)}/\text{atm}) = 103.801 - 12344T^{-1} - 12.8474 \ln T - 6.738 \times 10^4 T^{-2} + 1.8468 \times 10^{-6} T^2 \pm 0.004$$

Figure 3 shows a comparison of various vapour pressure studies of $NbCl_5$. It may be seen that the results of this investigation are within the range of reported values and agree well with the work performed on this system since 1970 by Johnson *et al.* (5) and Staffansson and Enghag (6).

In the case of $TaCl_5$, heat capacity data could not be found in the literature. However, Schaefer and Kahlenberg (27) have estimated the following values based on the properties of $ZrCl_4$ and $HfCl_4$

$$C_{P,\text{solid}} = 38 - 3 \times 10^5 T^{-2}\ \text{cal/K mol}$$

and

$$C_{P,\text{gas}} = 31.6 - 3.7 \times 10^5 T^{-2}\ \text{cal/K mol}$$

The Σ function analysis of the sublimation vapour pressures yields the following approximate equations for $TaCl_5$

$$[6] \qquad \Delta H_{\text{sublimation}} = 22100 - 6.4T + 7 \times 10^4 T^{-1} \pm 450\ \text{cal/mol}$$

$$[7] \qquad \ln (P_{(s)}/\text{atm}) = 42.180 - 11123T^{-1} - 3.2207 \ln T - 1.761 \times 10^4 T^{-2} \pm 0.024$$

In the absence of any estimate of the heat capacity of molten $TaCl_5$ least-squares analysis of the evaporation vapour pressures gives the following equations

$$[8] \qquad \Delta H_{\text{evaporation}} = 12810 \pm 400\ \text{cal/mol}$$

$$[9] \qquad \ln (P_{(l)}/\text{atm}) = 12.710 - 6.4478 \times 10^3 T^{-1} \pm 0.005$$

[3]The molar heat capacity of $NbCl_5$ was misprinted in eq. 7 of ref. 14 as $57.36 - 22.02 \times 10^{-6} T^2$ cal/K along with the statement that its value is 56.8 cal/K at the melting point. The correct value is $57.26 - 22.02 \times 10^{-6}\ T^2$ with a value of 52.2 at the melting point quoted in the paper. Both errors also appear in the GMELIN handbook (25). These corrections have been confirmed in a private communication by D. Cubicciotti, Stanford Research Institute, Menlo Park, California.

Can. J. Chem. Downloaded from www.nrcresearchpress.com by 210.87.254.6 on 09/05/12
For personal use only.

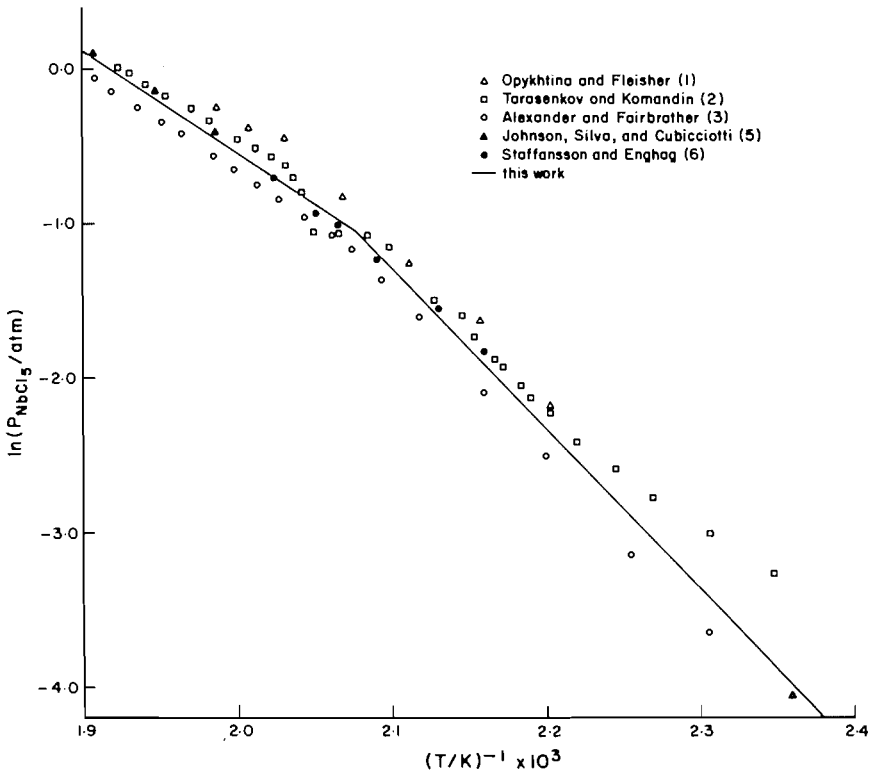

FIG. 3. Temperature dependence of vapour pressure of $NbCl_5$: comparison with other investigations.

Figure 4 compares the pressure results of various investigations of the $TaCl_5$ system. The results of this study agree very well with the recent work by Saeki *et al.* (8).

Table 2 displays calculated values of the boiling point, melting point, and the various enthalpies and entropies of transition of $NbCl_5$. Table 3 compares various determinations of the thermodynamic properties of $NbCl_5$. The results of the present study lie within the range of values reported in the literature for any given property. Noteworthy in Table 3 are the values for the molar enthalpy and entropy of sublimation at 298.15 K which compare well with values reported by Schaefer and Poelert (4) who measured vapour pressures of $NbCl_5$ from 350 to 384 K.

Table 4 shows calculated values of thermodynamic properties of $TaCl_5$. The melting point is determined in this work to be 496.9 K, which is about 2 K higher than that quoted elsewhere.

TABLE 2. Thermodynamic properties of $NbCl_5$*

Temperature	Phase transition	ΔH_T (kcal/mol)	ΔS_T (cal/K mol)
Boiling point: 521.4 K	Liquid–gas	12.77±0.10	24.5±0.1
Mean temperature: 502.3 K	Liquid–gas	13.17±0.10	25.3±0.1
Melting point: 481.5 K	Liquid–gas	13.61±0.10	26.2±0.1
Melting point: 481.5 K	Solid–liquid	6.85±0.55	14.3±1.2
Melting point: 481.5 K	Solid–gas	20.46±0.45	40.5±1.1
Mean temperature: 449.8 K	Solid–gas	20.62±0.45	40.8±1.1
Standard temperature: 298.15 K	Solid–gas	21.47±0.45	43.1±1.1

*All entries in Table 2 were calculated with the use of only [2] through [5]. The mean temperature is defined as the reciprocal of the mean value of T^{-1} for the reported data points.

Can. J. Chem. Downloaded from www.nrcresearchpress.com by 210.87.254.6 on 09/05/12
For personal use only.

Can. J. Chem. Downloaded from www.nrcresearchpress.com by 210.87.254.6 on 09/05/12
For personal use only.

TABLE 3. Comparative values of the thermodynamic properties of $NbCl_5$

(*a*) Sublimation

ΔH_T‡ (kcal/mol)	ΔS_T‡ (cal/K mol)	ΔH_{298} (kcal/mol)	ΔS_{298} (cal/K mol)	Reference
20.0 ±0.8*	39.8±1.8*	20.9†	42.4†	1
18.3 ±0.5*	36.1±1.0*	19.4†	39.1†	2
20.0 ±0.5*	38.9±1.1*	21.0†	41.7†	3
—	—	22.8	46.2	4
18.5	—	19.6	39.4	6
22.00±0.23	43.8†	23.1†	46.8†	28
20.62±0.45	40.7±1.1	21.47±0.45	43.1±1.1	This work

*Analysis of data performed by Schaefer *et al.* (33).
†Analysis of data performed by Schaefer and Poelert (4).
‡T is the mean temperature of the measured vapour pressures.

(*b*) Evaporation

ΔH_T‡ (kcal/mol)	ΔS_T‡ (cal/K mol)	Reference
13.0 ±1.3*	25.4 ±2.7*	1
11.2 ±0.2*	21.6 ±0.5*	2 (Boiling points)
15.0 ±1.7*	29.0 ±3.5*	2 (Static method)
13.2 ±0.05*	25.1 ±0.1*	3
12.77±0.42†	24.6 ±0.8†	5
14.09	27.10	6
12.6 ±0.1	24.3 ±0.3	28
13.69±0.18	—	34
13.17±0.10	25.3 ±0.1	This work

*Analysis performed by Schaefer *et al.* (33).
†These values were calculated herein using only the 3 points of ref. 5 which lie in the temperature range of the present study.
‡T is the mean temperature of the measured vapour pressures.

(*c*) Fusion

ΔH_T* (kcal/mol)	Experimental method	Reference
9.95	Visual synthetic method – phase diagram	35
8.30±0.4	Phase equilibria	34
8.15	Visual synthetic method – phase diagram	36
8.09±0.23	Drop calorimetry	14
6.85±0.55	Vapour pressures	This work

*T is the melting point determined in the respective investigation.

TABLE 4. Thermodynamic properties of $TaCl_5$*

Temperature	Phase transition	ΔH_T (kcal/mol)	ΔS_T (cal/K mol)
Boiling point: 507.3 K	Liquid–gas	—	—
Mean temperature: 502.7 K	Liquid–gas	12.81±0.40	25.3±0.8
Melting point: 496.9 K	Solid–liquid	6.25±0.85	12.5±1.7
Melting point: 496.9 K	Solid–gas	19.06±0.41	37.8±0.9
Mean temperature: 468.2 K	Solid–gas	19.26±0.41	38.2±0.9
Standard temperature: 298.15 K	Solid–gas	20.43±0.41	41.3±0.9

*All entries in Table 4 were calculated with the use of only [6] through [9]. The mean temperature is defined as the reciprocal of the mean value of T^{-1} for the reported data points.

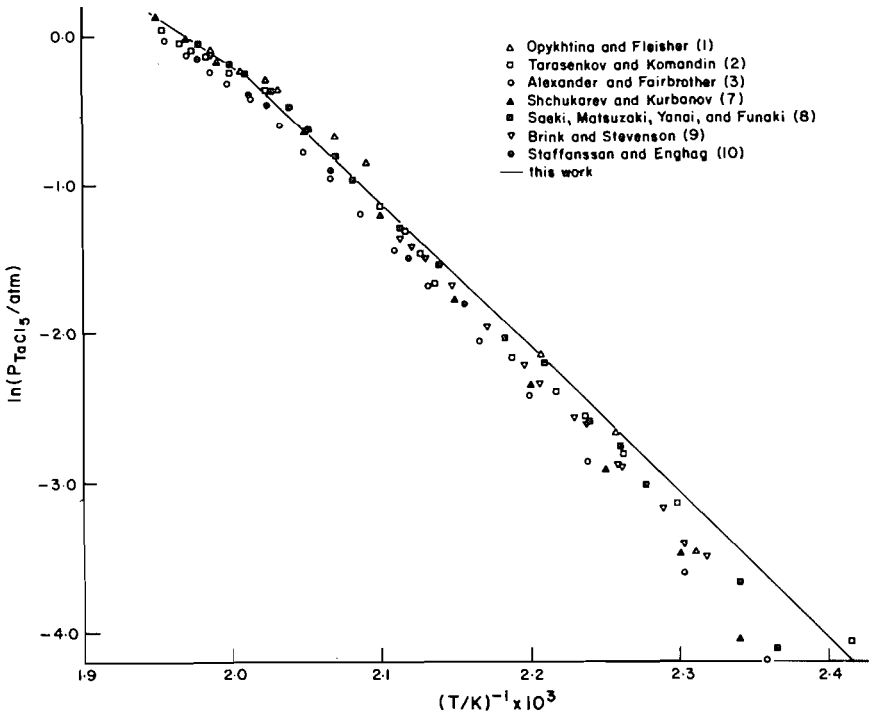

FIG. 4. Temperature dependence of vapour pressure of $TaCl_5$: comparison with other investigations. Data of Saeki *et al.* were estimated herein from Figs. 7 and 8 of ref. 8. Data of Shchukarev and Kurbanov were calculated herein at selected temperatures using equations for the least-squares lines quoted on p. 146 of ref. 7.

The melting point is reported to lie in the range of 488 K (28) to 495 K (29). The boiling point of 507.3 K falls within the reported range of 506 K (28) to 515 K (30, 31). Table 5 compares various determinations of the thermodynamic properties of $TaCl_5$. The enthalpy and entropy of sublimation are lower by approximately 10% than those previously reported. The enthalpy and entropy of evaporation agree well with other studies. The enthalpy of fusion with a value of 6.25 ± 0.85 kcal/mol lies well below the value of 8.6 kcal/mol determined calorimetrically by Dobrotin *et al.* (32). No error limits were quoted in their work.

TABLE 5. Comparative values of the thermodynamic properties of $TaCl_5$

(*a*) Sublimation

ΔH_T‡ (kcal/mol)	ΔS_T‡ (cal/K mol)	ΔH_{298} (kcal/mol)	ΔS_{298} (cal/K mol)	Reference
22.4*	45.2*	23.4†	47.9†	1
20.4*	40.5*	21.5†	43.6†	2
22.4*	44.3*	23.5†	47.3†	3
—	—	22.8	46.4	4
22.7 ±1	45.2±1	23.8	48.3	7
21.63	43.19	—	—	8
21.1 ±0.2	41.9	22.1	44.8	9
20.10	39.80	21.3	42.98	10
19.26±0.41	38.2±0.9	20.43±0.41	41.3±0.9	This work

*Analysis of data obtained by Schaefer *et al.* (33).
†Analysis of data obtained by Schaefer and Poelert (4).
‡T is the mean temperature of the measured vapour pressures.

Can. J. Chem. Downloaded from www.nrcresearchpress.com by 210.87.254.6 on 09/05/12
For personal use only.

(*b*) Evaporation

ΔH_T† (kcal/mol)	ΔS_T† (cal/K mol)	Reference
11.7 ±2.3*	23.0 ±4.7*	1
11.7 ±0.7*	23.0 ±1.4*	2
13.64±0.26*	26.6 ±0.5*	3
14.9 ±1.0	29.3 ±1.0	7
13.71	27.04	8
14.03	27.51	10
13.1 ±0.4	25.9 ±1.3	28
12.81±0.4	25.3 ±0.8	This work

*These values were calculated herein by numerical analysis of the experimental data.
†T is the mean temperature of the measured vapour pressures.

(*c*) Fusion

ΔH_T* (kcal/mol)	Experimental method	Reference
9.15	Visual synthetic method – phase diagram	35
8.6	Calorimetry	32
8.4	Visual synthetic method – phase diagram	36
6.25±0.85	Vapour pressures	This work

†T is the melting point determined in the respective investigations.

Acknowledgement

The financial assistance to one of the authors (D.R.S.) by the National Research Council of Canada in the form of a Postgraduate Scholarship is gratefully acknowledged. As well, the authors cite Mr. R. H. Chappell for his construction of the glassware of the apparatus.

1. M. A. Opykhtina and N. A. Fleisher. Zh. Obshch. Khim. **7**, 2016 (1937).
2. D. N. Tarasenkov and A. V. Komandin. Zh Obshch. Khim. **10**, 1319 (1940).
3. K. M. Alexander and F. Fairbrother. J. Chem. Soc. S223 (1949).
4. H. Schaefer and W. Poelert. Z. Anorg. Allg. Chem. **353**, 78 (1967).
5. J. W. Johnson, W. J. Silva, and D. Cubicciotti. High Temp. Sci. **2**, 20 (1970).
6. L.-I. Staffansson and P. Enghag. Acta Chem. Scand. **27**, 2733 (1973).
7. S. A. Shchukarev and A. R. Kurbanov. Vestn. Leningr. Univ. Ser. Fiz. i Khim. No. 10, 144 (1962).
8. Y. Saeki, R. Matsuzaki, M. Yanai, and K. Funaki. Kogyo Kagaku Zasshi. **71**, 350 (1968).
9. J. M. Brink and F. D. Stevenson. J. Chem. Eng. Data, **17**, 143 (1972).
10. L.-I. Staffansson and P. Enghag. Scand. J. Metall. **2**, 305 (1973).
11. B. Swaroop and S. N. Flengas. Can. J. Chem. **44**, 199 (1966).
12. S. N. Flengas and P. Pint. Can. Metall. Q. **8**, 151 (1969).
13. S. N. Flengas, J. E. Dutrizac, and R. L. Lister. Can. J. Chem. **46**, 495 (1968).
14. F. J. Keneshea, D. Cubicciotti, G. Withers, and H. Eding. J. Phys. Chem. **72**, 1272 (1968).
15. R. L. Lister and S. N. Flengas. J. Electrochem. Soc. **111**, 343 (1964).
16. R. L. Lister and S. N. Flengas. Can. J. Chem. **43**, 2947 (1965).
17. J. E. Dutrizac and S. N. Flengas. Advances in Extractive Metallurgy Symposium. April 17–20, 1967. Institution of Mining and Metallurgy. London. Paper 24.
18. P. Pint and S. N. Flengas. Can. J. Chem. **49**, 2885 (1971).
19. L. A. Nisel'son, A. I. Pustil'nik, and T. D. Sokolova. Russ. J. Inorg. Chem. **9**, 574 (1964). (English translation of Zh. Neorg. Khim. **9**, 1049 (1964).)
20. J. W. Johnson and D. Cubicciotti. High Temp. Sci. **2**, 9 (1970).
21. D. Ambrose. Vapour pressures. *In* Chemical thermodynamics. Vol. I. *Edited by* M. L. McGlashan. The Chemical Society, London. 1973. Chapt. 7.
22. W. G. Brombacher, D. P. Johnson, and J. L. Cross. Mercury barometers and manometers. National Bureau of Standards (United States). Monograph 8. Washington. 1960.
23. R. L. Powell *et al.* Thermocouple Reference Tables Based on the IPTS-68. National Bureau of Standards (United States). Monograph 125. Washington. 1974.
24. L. S. Darken and R. W. Gurry. Physical chemistry of metals. McGraw-Hill, New York. 1953. p. 226.
25. Gmelins Handbuch der anorganischen Chemie. Niob. Teil Bl. System-Nummer 49. Verlag Chemie GmbH, Weinheim. 1970. p. 187.

Can. J. Chem. Downloaded from www.nrcresearchpress.com by 210.87.254.6 on 09/05/12
For personal use only.

26. R. D. WERDER, R. A. FREY, and Hs. H. GUENTHARD. J. Chem. Phys. **47**, 4159 (1967).
27. H. SCHAEFER and F. KAHLENBERG. Z. Anorg. Allg. Chem. **305**, 178 (1960).
28. J. B. AINSCOUGH, R. J. W. HOLT, and F. W. TROWSE. J. Chem. Soc. 1034 (1957).
29. G. L. CARLSON. Spectrochim. Acta, **19**, 1291 (1963).
30. D. GARDNER. U.S. Patent no. 2532295, Dec. 5, 1950. (Chem. Abs. **45**, 1489).
31. Kali-Chemie A.G. (M. Schmeisser and H. Jenkner, inventors). German Patent no. 945757, July 26, 1956. (Chem. Abs. **52**, 20943).
32. R. B. DOBROTIN, A. V. SUVOROV, and YU. V. KONDRAT'EV. Vestn. Leningr. Univ. Ser. Fiz. i Khim. No. 4, 95 (1964).
33. H. SCHAEFER, L. BAYER, and H. LEHMANN. Z. Anorg. Allg. Chem. **268**, 268 (1952).
34. G. MEYER, J. F. OOSTEROM, and W. J. VAN OEVEREN. Rec. Trav. Chim. Pays-Bas, **80**, 502 (1961).
35. L. A. NISEL'SON and G. L. PEREKHREST. Russ. J. Inorg. Chem. **3** (9), 215 (1958). (English translation of Zh. Neorg. Khim. **3**, 2150 (1958).)
36. B. A. VOITOVICH, A. S. BARABANOVA, and N. KH. TUMANOVA. Russ. J. Inorg. Chem. **6** (11), 1286 (1961). (English translation of Zh. Neorg. Khim. **6**, 2545 (1961).)

Can. J. Chem. Downloaded from www.nrcresearchpress.com by 210.87.254.6 on 09/05/12
For personal use only.

cis and *trans* isomers in $R_fFe(CO)_4I$ compounds

KEITH STANLEY[1] AND D. W. MCBRIDE
Department of Chemistry, University of Manitoba, Winnipeg, Man., Canada R3T 2N2

Received March 17, 1975[2]

KEITH STANLEY and D. W. MCBRIDE. Can. J. Chem. **54**, 1700 (1976).

The synthesis and separation of the *cis* and *trans* isomers of Fe(*trans*-σ-CF=CFCF$_3$)(CO)$_4$I is described. The two isomers are identified from the carbonyl region of the infrared spectrum.

KEITH STANLEY et D. W. MCBRIDE. Can. J. Chem. **54**, 1700 (1976).

On décrit la synthèse et la séparation des isomères *cis* et *trans* du Fe(*trans*-σ-CF=CFCF$_3$)-(CO)$_4$I. On a identifié les deux isomères grâce la région carbonyle du spectre infrarouge.
[Traduit par le journal]

Introduction

In the work of Stone and co-workers (1, 2), it was pointed out that compounds of the type $R_fFe(CO)_4I$ can exist in either *cis* or *trans* configurations.

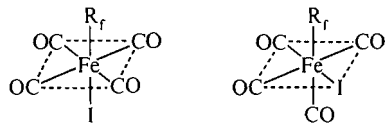

Group theory predicts different C—O stretching patterns in the ir spectrum for these isomers. The *trans* configuration, which has local carbonyl symmetry C_{4v}, is expected to have two ir active carbonyl absorption bands, $A_1 + E$. The *cis* configuration corresponds to the point group C_s (local carbonyl symmetry) which should show four carbonyl absorption bands ($3A' + A''$) in the ir spectrum. Also, some weak ^{13}C—O bands are expected for both these isomers. However, Stone and co-workers did not satisfactorily establish the configuration of the compounds they isolated, (R_f = CF_3, C_2F_5, C_3F_7). We report here the isolation and characterization of the *cis* and *trans* isomers of Fe(*trans*-σ-CF=CFCF$_3$)-(CO)$_4$I.[3]

Experimental

Perfluoroallyl iodide (bp 53–55 °C at 760 mm) was prepared from perfluoroallyl chloride (4) by the method of Miller and Fainberg (5) and stored at 0 °C to reduce decomposition. $Fe_2(CO)_9$ was prepared by the photolysis (sunlight) of neat $Fe(CO)_5$. Prior to use, it was washed with pentane and dried *in vacuo*.

^{19}F nmr spectra were run on a Varian A 56/60A with variable temperature accessory. Samples were prepared under nitrogen and the tube flame sealed under vacuum.

Infrared spectra were recorded on a Perkin-Elmer 337 instrument with an external recorder to obtain expanded scale spectra. The spectra were calibrated with indene and run several times to check reproducibility.

Mass spectra were run on a Hitachi Perkin-Elmer RMU-6D instrument.

Preparation of cis and trans Fe(trans-σ-CF=CFCF$_3$)(CO)$_4$I

All procedures were carried out under nitrogen or *in vacuo*. Perfluoroallyl iodide (1.3 g, 5 mmol) and $Fe_2(CO)_9$ (1 g, 2.7 mmol) were reacted in refluxing pentane for 1 h under nitrogen. The pentane was removed *in vacuo* at room temperature. Still under vacuum (0.01 mm), the reaction flask was then warmed up to 50 °C (hot water bath) and a mixture of red crystals and rust powder sublimed on to the neck of the flask. This material was transferred to a subliming tube (15 cm long, 1 cm i.d.), and resublimed (0.01 mm). The red crystals (mp 61 °C) sublimed higher on the tube than the rust powder (mp 56 °C) which moved just above the level of the hot water. A total yield of 15% was obtained. Sublimation of either compound separately gave a mixture of the two products. Both compounds gave a parent ion at *m/e* 426 with the consecutive loss of four CO groups in the mass spectrum. After a few days *in vacuo* or under nitrogen, both compounds appeared tarnished. Neither isomer could be obtained completely free of the other in respectable quantities; therefore, an elemental analysis of an approximately 1:1 mixture of the isomers was obtained. *Anal.* calcd. for $C_7F_5FeIO_4$: C 19.7, F 22.3, I 29.8; found: C 20.0, F 22.9, I 30.2.

Discussion

Rapid sublimation of the products from the reaction of perfluoroallyl iodide with $Fe_2(CO)_9$ gave two isomers: a rust powder and red crystals.

[1]Present address: Department of Chemistry, Queen's University, Kingston, Ont., Canada K7L 3N6.

[2]Revision received February 23, 1976.

[3]The perfluoropropenyl ligand has a *trans* arrangement of the CF_3 and $Fe(CO)_4I$ groups about the double bond, as shown by the fluorine–fluorine coupling constant $J_{F_A-F_B}$ = 130 Hz (Table 1) (3).

Can. J. Chem. Downloaded from www.nrcresearchpress.com by 210.87.254.105 on 09/05/12
For personal use only.

TABLE 1. ^{19}F nmr and infrared data* for *cis* and *trans* Fe(*trans*-σ-CF=CFCF$_3$)(CO)$_4$I

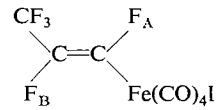

Isomer†	ν(CO) cm^{-1}	δ_{CF_3}‡	δ_{F_A}	δ_{F_B}	$J_{F_A-F_B}$	$J_{F_A-CF_3}$	$J_{F_B-CF_3}$
cis	2141.5 (m) 2093.1 (vs) 2071.4 (s) 2055.0 (w)(^{13}C—O)	66.0	92.5	159.3	130	22	11
trans	2147.2 (w) 2088.2 (vs) 2052.4 (w)(^{13}C—O)	66.2	87.9	161.9	130	22	11

*Infrared spectra in methylcyclohexane, nmr in tetrahydrofuran (10% $CFCl_3$). w = weak, m = medium, s = strong, vs = very strong.
†Both isomers have the C=C vibration at 1640 cm^{-1} (weak).
‡δ values in ppm upfield from $CFCl_3$, J values in Hz.

The ^{19}F nmr spectra (Table 1) show that both compounds contain the σ-perfluoropropenyl ligand. Perfluoroallyl to perfluoropropenyl rearrangements have been observed previously (3) and studied by Goldwhite *et al.* (6) for the compound CF_2=$CClCF_2Mn(CO)_5$ in which a bimolecular process was postulated.

Figure 1 shows the carbonyl region of the infrared spectra for the two compounds isolated. Spectrum A shows ^{12}C—O bands at 2147.2 (A_1) and 2088.2 (E) and a weak band at 2052.4 which can be assigned to a ^{13}C—O vibration. The isomer isolated as red crystals can therefore be identified as *trans*-Fe(*trans*-σ-CF=CFCF$_3$)(CO)$_4$I.

The number of ^{12}C—O bands expected for the *cis* isomer is four. Spectrum B, however, shows only three ^{12}C—O bands and a weak absorption at 2055.0 cm^{-1} which can be assigned to a ^{13}C—O stretch. The 2145.5 cm^{-1} band can be assigned to the A' mode in which there is a symmetric stretching vibration of the pair of carbonyl groups *trans* to one another. The remaining modes $2A' + A''$ must be contained in the 2093.1 cm^{-1} and 2071.4 cm^{-1} bands with

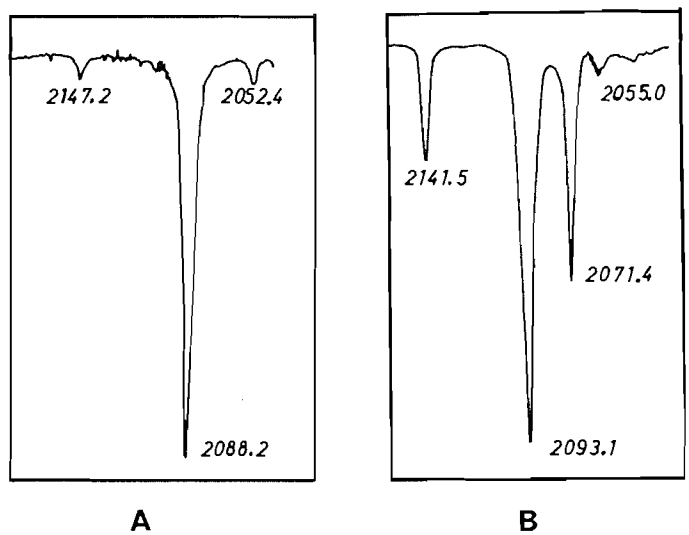

FIG. 1. Infrared carbonyl absorption bands of (*A*) red crystals, *trans*-Fe(*trans*-σ-CF=CFCF$_3$)-(CO)$_4$I, and (*B*) rust powder, *cis*-Fe(*trans*-σ-CF=CFCF$_3$)(CO)$_4$I in methylcyclohexane (expanded spectra calibrated with indene).

Can. J. Chem. Downloaded from www.nrcresearchpress.com by 210.87.254.105 on 09/05/12
For personal use only.

the former, more intense absorption containing two accidentally degenerate vibrations.[4] On this basis, the rust powder was identified as *cis*-Fe(*trans*-σ-CF=CFCF$_3$)(CO)$_4$I.

While both isomers were configurationally stable in the solid form, the preferred species in solution at room temperature was the *cis* isomer. The *trans*-to-*cis* isomerization can be followed by infrared or ^{19}F nmr above 0 °C. The *trans*-to-*cis* half-life at 295 K in THF was approximately 20 min (followed by nmr). At room temperature after several hours a solution which contained pure *trans* initially showed pure *cis* by nmr. Lowering the temperature did not bring about the reappearance of the *trans* form. Raising the temperature resulted in the decomposition of the *cis* isomer to paramagnetic species. It was possible to accomplish the *cis*-to-*trans* conversion by sublimation at 55 °C *in vacuo*.

The isolation of *cis* and *trans* Fe(*trans*-σ-CF=CFCF$_3$)(CO)$_4$I and their identification by infrared spectroscopy suggests that other $R_fFe(CO)_4I$ compounds (R_f = CF_3, C_2F_5, *n*-C_3F_7 (2) and *i*-C_3F_7, *n*-C_7F_{15} (11)) may in fact exist in the two isomeric forms. For instance, the reported carbonyl spectrum (2) of $C_2F_5Fe(CO)_4I$ is 2146(w), 2140(w), 2112(vw), 2087(vs), 2073(sh), and 2056(w) (in tetrachloroethylene). The two high frequency absorption bands especially indicate the presence of both isomers, comparing well with the 2147 cm^{-1} and 2141 cm^{-1} carbonyl bands for *trans* and *cis* Fe(*trans*-σ-CF=CFCF$_3$)(CO)$_4$I respectively. No evidence for both isomers was apparently seen in the ^{19}F nmr spectrum which indicates that special attention must be paid to the isolation and handling of these compounds in solution.

[4]Quasi support for this comes from the infrared spectra of *cis*-$Fe(CO)_4I_2$ (7, 8) and $(CF_2)_4Fe(CO)_4$ (2). It has been observed for both these compounds that two of the ^{12}C—O vibrational frequencies are accidentally degenerate and appear as the most intense band. However, *cis* compounds of the form $(X_3M)Fe(CO)_4X$ (where M is a Group IVB metal and X is H, Cl, Br, or I) do not show this accidental degeneracy and four infrared active ^{12}C—O bands are observed (9, 10).

Acknowledgement

We thank the National Research Council of Canada for financial support and Northern Electric and Alcan for fellowships to K.S.

1. R. B. King, S. L. Stafford, P. M. Treichel, and F. G. A. Stone. J. Am. Chem. Soc. **83**, 3604 (1961).
2. E. Pitcher and F. G. A. Stone. Spectrochim. Acta, **18**, 585 (1962).
3. E. Pitcher and F. G. A. Stone. Spectrochim. Acta, **17**, 1244 (1961).
4. W. J. Cunningham, R. F. Sweeney, and C. Woolf. U.S. Patent 3,047,939, Chem. Abst. **58**, 6693c (1963).
5. W. T. Miller and A. H. Fainberg. J. Am. Chem. Soc. **79**, 4164 (1957).
6. H. Goldwhite, D. G. Rowsell, and C. Valdez. J. Organomet. Chem. **12**, 133 (1968).
7. M. Pankowski and M. Bigorgne. J. Organomet. Chem. **19**, 393 (1969).
8. B. F. G. Johnson, J. Lewis, P. W. Robinson, and J. R. Miller. J. Chem. Soc. A, 1043 (1968).
9. R. Kummer and W. A. G. Graham. Inorg. Chem. **7**, 1208 (1968).
10. B. J. Aylett, J. M. Campbell, and A. Walton. Inorg. Nucl. Chem. Lett. **4**, 79 (1968).
11. R. B. King, R. N. Kapoor, and L. W. Houk. J. Inorg. Nucl. Chem. **31**, 2179 (1969).

Can. J. Chem. Downloaded from www.nrcresearchpress.com by 210.87.254.105 on 09/05/12
For personal use only.

Metabolites of bird's nest fungi. Part 5.[1] The isolation of 1-hydroxy-6-methyl-8-hydroxymethylxanthone, a new xanthone, from *Cyathus intermedius*. Synthesis via photoenolisation

WILLIAM A. AYER AND DAVID R. TAYLOR

Department of Chemistry, The University of Alberta, Edmonton, Alta., Canada T6G 2G2

Received January 23, 1976

WILLIAM A. AYER and DAVID R. TAYLOR. Can. J. Chem. **54**, 1703 (1976).

The structure of 1-hydroxy-6-methyl-8-hydroxymethylxanthone, a new xanthone isolated from the culture broth of *Cyathus intermedius*, has been confirmed by synthesis. Regioselective hydroxylation of the 8-methyl of 1-hydroxy-6,8-dimethylxanthone was achieved via the peroxide formed by reaction of oxygen with the photoenol, and also via bromination of the photoenol. Extraction of the mycelia of *C. intermedius* yielded ergosterol and D-mannitol.

WILLIAM A. AYER et DAVID R. TAYLOR. Can. J. Chem. **54**, 1703 (1976).

On a confirmé par synthèse la structure de l'hydroxy-1 méthyl-6 hydroxyméthyl-8 xanthone, une nouvelle xanthone isolée du milieu de culture du *Cyathus intermedius*. On a effectué l'hydroxylation régiosélective du méthyl-8 de l'hydroxy-1 diméthyl-6,8 xanthone par l'intermédiaire du peroxyde formé par réaction de l'oxygène avec le photoénole et aussi par bromuration du photoénole. L'extraction de mycelles du *C. intermedius* fournit de l'ergostérol et du D-mannitol.

[Traduit par le journal]

We have previously reported on our investigation of the constituents of the rare bird's nest fungus, *Cyathus helenae* Brodie, which provided several novel diterpenes, the cyathins (2, 3). We are engaged in examining other species of this genus and have recently reported (1) on the metabolites of *C. bulleri* Brodie. In this paper, we describe the isolation and synthesis of a new xanthone, **1**, from *C. intermedius*.

C. intermedius was cultured as described for *C. helenae* (4), and, after 30 days, the culture broth was extracted with ethyl acetate. The crude extract was partitioned between Skellysolve B and methanol–water (4:1) and the aqueous methanol phase was then extracted with benzene. Preparative thin layer chromatography (ptlc) of the residue from the benzene phase gave a very small amount of a yellow crystalline compound, $C_{15}H_{12}O_4$, mp 176–178 °C. The uv (5) and ir spectra suggested that the compound was a xanthone. The presence of a sharp, exchangeable, one proton signal at δ 12.68 in the nmr spectrum indicated a strongly chelated hydroxyl at C-1. The fourth oxygen atom was shown to be part of a hydroxymethyl group by the nmr spectrum which displays a two proton doublet at δ 4.98 (J = 7 Hz) coupled to an exchangeable triplet at 4.32. The low field position of the signal for the methylene group when compared to that of benzyl alcohol (δ 4.65) locates the hydroxymethyl at C-8, *peri* to the carbonyl (6). The nmr spectrum further revealed an aromatic methyl group and five aromatic protons. Two of these latter protons are *meta* coupled, while, of the other three, that at lowest field shows coupling to two *ortho* protons which appear as *meta* and *ortho* coupled double doublets. These data are consistent only with structures **1** and **2**. A decision in favour of **1** was made by comparing the chemical shifts of the three mutually coupled aromatic protons with those of the corresponding ones in **3** (7), and this has been confirmed by the synthesis described below.

A simple and direct synthesis of **1** would involve the preferential functionalisation of 1-acetoxy-6,8-dimethylxanthone, **4**, at the C-8 methyl group. It has been shown that *o*-alkyl aromatic carbonyl compounds bearing an aliphatic hydrogen at the γ-position, such as *o*-methylbenzophenones, undergo a reversible photoenolisation on irradiation (8). This process has also been observed in *o*-tolualdehyde (9, 10), 1-methylanthraquinone (11), 3-aroyl-2-benzylchromones (12, 13), and other systems (12, 13), but examples where the expected photoenolisation does not occur are also known (12, 14). These photoenols can be trapped in a Diels–Alder reaction (8, 14, 15) and can also undergo

[1]For part 4, see ref. 1.

Can. J. Chem. Downloaded from www.nrcresearchpress.com by 210.87.254.42 on 09/05/12
For personal use only.

oxidation at the γ-carbon by reaction with oxygen (10, 11, 13, 16) to give peroxides, aldehydes or ketones, and acids. Photooxidation of the dimethylxanthone **4** should therefore yield a peroxide which can be reduced to **5**, thus allowing regioselective hydroxylation of the C-8 methyl of **4**.

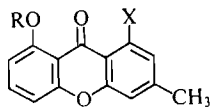

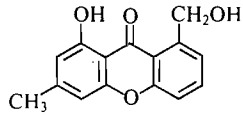

2

1 R = H, X = CH_2OH
4 R = Ac, X = CH_3
5 R = Ac, X = CH_2OH
6 R = H, X = CH_3
8 R = H, X = CHO
9 R = H, X = CO_2H
11 R = Ac, X = CH_2O_2H
12 R = Ac, X = CH_2Br

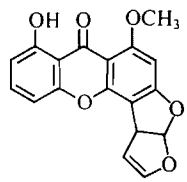

3

1-Hydroxy-6,8-dimethylxanthone, **6**, was synthesised (17) by the condensation of γ-resorcylic acid with 3,5-dimethylphenol catalysed by polyphosphoric acid or phosphorous oxychloride and zinc chloride. We have used the latter method (18) and confirmed that **6** is accompanied by a large amount of 1,6-dihydroxyxanthone-5-carboxylic acid 3,5-dimethylphenyl ester, **7** (17). Acetylation of **6** with acetic anhydride and pyridine at room temperature gave the acetate **4**, mp 133–134 °C.[2] The nmr spectra of both **4** and **6** show the signal for the C-8 methyl at low field (δ 2.79 and 2.80 respectively) as expected (6).

Irradiation of a dilute solution (*cf.* ref. 10) of **4** with a Hanovia medium pressure mercury vapor lamp in cyclohexane in the presence of oxygen gave a major and a minor product (tlc). Reduction of the mixture with triphenylphosphine and ammonolysis of the acetate furnished a mixture which was separated by ptlc into 1-hydroxy-6-methyl-8-hydroxymethylxanthone, **1** (60%), identical with the natural product, and 1-hydroxy-6-methyl-8-formylxanthone, **8** (14%), mp 208–210 °C as well as **6** (7%). No attempt was made to isolate more polar material which might be expected (11, 16) to include the acid **9**. A comparison of the nmr spectra of **1** and **6** reveals that the hydroxymethyl in **1** has replaced the low field (δ 2.80) aromatic methyl in **6** and thus confirms that oxidation had taken place selectively at the C-8 methyl. The structure of the aldehyde **8** follows from its spectral data. In particular, the aldehydic proton occurs at δ 11.16 in the nmr spectrum, reflecting its anisotropic deshielding by the xanthone carbonyl (6), while the methyl gives a singlet at 2.56 as expected for its location at C-6.

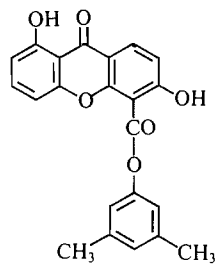

7

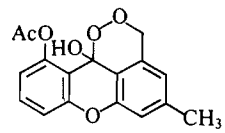

10

The initial oxidation product of a photoenol has been shown, in the few cases in which it has been isolated (10, 13, 16), to be a cyclic peroxide. Evaporation of the solvent after photooxidation of **4** gave a mixture whose nmr spectrum showed that the major constituent was the peroxide **10**. In the nmr spectrum of **10**, the C-8 methylene protons form an AB quartet (J = 16 Hz) at δ 5.23, while the aromatic protons are shifted upfield relative to their positions in **4**. The absence of the xanthone nucleus is further supported by the ir and uv spectra (see Experimental). The peroxide **10** could not be rigorously characterised since attempted purification by ptlc on silica gel resulted in its isomerisation to the hydroperoxide **11** whose spectra corresponded closely with those of **4**, thus confirming the regeneration of the xanthone nucleus. Neither **10** nor **11** show a molecular ion in their mass spectra.

We have also regioselectively brominated **4** on the C-8 methyl. Irradiation of a carbon tetrachloride solution of **4** in the presence of bromine gave, rapidly, mainly one product (tlc). The mass spectrum of the crude product showed it to contain a monobromide (*m/e* 360/362) contaminated with a small amount of a dibromide (*m/e* 438/440/442). The nmr spectrum contains a two proton singlet at δ 5.22 for the C-8 benzylic

[2]The use of sodium acetate and acetic anhydride at reflux temperature (17) gave material of mp 205 °C which was said to be the acetate. The limited nmr data quoted shows it to be different to **4**.

Can. J. Chem. Downloaded from www.nrcresearchpress.com by 210.87.254.42 on 09/05/12
For personal use only.

Can. J. Chem. Downloaded from www.nrcresearchpress.com by 210.87.254.42 on 09/05/12
For personal use only.

protons and only a very weak peak (<0.2H) at 4.45 which could be ascribed to a product with a C-6 bromomethyl (*cf.* PhCH_2Br at δ 4.43 in CCl_4 (19)). The main product from the bromination is thus **12** and crystallisation of the mixture gave pure monobromide **12**, mp 159–162 °C, whose spectral data (see Experimental) fully support the assigned structure. The monobromide **12** is also formed in the presence of galvinoxyl and hence must arise by an ionic bromination of the photoenol (*cf.* ref. 12). Reaction of the crude bromination product with sodium hydrogen carbonate in aqueous tetrahydrofuran gave, in low yield, the natural xanthone **1**.

Xanthones with the carbon skeleton of **1** are, with two exceptions (20), confined to lower plants (21) and are presumed to arise by cleavage of an anthraquinone or anthrone (22, 23) precursor. The carbon atom which originated in the ring (that at C-8 in **1**) is commonly found to occur as an acid or ester (24), but examples have been recently reported in which it is at the oxidation level of an aldehyde (23) and as a hydroxymethyl as in **1** (25).

The mycelia of *C. intermedius* were also extracted but yielded only ergosterol and D-mannitol, both of which have been previously encountered in fungi (ref. 24*a*, pp. 27 and 253).

Experimental

High resolution mass spectra were recorded on an A.E.I. MS-9 mass spectrometer, ir spectra on a Unicam SP1000 grating spectrometer for solutions in $CHCl_3$, uv spectra on a Perkin-Elmer 202 spectrometer for solutions in ethanol, and nmr spectra on a Varian Associates HA-100 spectrometer for solutions in $CDCl_3$ with tetramethylsilane as internal standard, unless stated otherwise.

Preparative thin layer chromatography (ptlc) was carried out on 0.75 mm layers of silica gel PF-254 + 366 (E. Merck AG) and developed with Skellysolve B – acetone (7:3). Bands were detected by viewing under uv light. Skellysolve B refers to Skelly Oil Company light petroleum, bp 62–70 °C. Irradiations were performed in Pyrex flasks using a Hanovia medium pressure mercury vapor lamp (140 W).

*Isolation of 1-Hydroxy-6-methyl-8-hydroxymethylxanthone, **1***

Cyathus intermedius was cultured as described for *C. helenae* (4) and *C. bulleri* (1), and after 30 days the culture broth was extracted with ethyl acetate. The crude extract from 6 l of broth (560 mg) was partitioned between Skellysolve B (50 ml) and methanol–water (4:1, 50 ml). The aqueous methanol layer was then extracted with benzene (50 ml). The residue from the benzene layer (60 mg) was subjected to ptlc (two developments) and the yellow band (green under 254 nm uv light) at R_f 0.55 was isolated by extraction with acetone to give **1** (2.5 mg), yellow needles from acetone – Skellysolve B, mp 176–178 °C; ir 3500, 1649, 1624, 1611, and 1571 cm^{-1}; uv λ_{max} 233 (17 000), 254 (15 500), 262 sh (12 500), 292 (6700), 300 sh (6500), and 363 (3050) nm; with added NaOH, λ_{max} 235 (19 700), 255 (12 000), 264 (12 500), 303 (5700), 310 (5700), and 399 (2700) nm; nmr δ 2.52 (s, 3H, C-6 CH_3), 4.32 (t, J = 7 Hz, 1H, CH_2OH), 4.98 (d, J = 7 Hz, 2H, CH_2OH), 6.83 and 6.94 (dd, J = 1.0 and 8.5 Hz, 1H each, H-2 and H-4), 7.18 and 7.28 (bs, 1H each, H-5 and H-7), 7.62 (t, J = 8.5 Hz, 1H, H-3), and 12.68 (s, 1H, ArO*H*); *m/e* (relative intensities in parentheses) 256.0732 (100) (calculated for $C_{15}H_{12}O_4$: 256.0736), 241 (18), 238 (56), 227 (44), and 210 (61).

*1-Hydroxy-6,8-dimethylxanthone, **6***

A mixture of 3,5-dimethylphenol (1.22 g), γ-resorcylic acid (1.57 g) and zinc chloride (3 g) in phosphorous oxychloride (5 ml) was heated at 80 °C for 3 h. The mixture was cooled, diluted with cold water, and extracted with chloroform. The chloroform solution was washed with aqueous $NaHCO_3$ and water and evaporated to give a gum (1.49 g), shown by tlc to contain two main compounds (approximately 1:1). Crystallisation from acetone yielded the compound of higher R_f, **6**, as yellow needles (158 mg), mp 178–179 °C (lit. (17) 179 °C); ir 1646, 1615 sh, 1604, and 1568 cm^{-1}; uv λ_{max} 234 (30 000), 253 (25 000), 260 sh (19 000), 288 (9500), 302 (9000), and 362 (5000) nm; with added NaOH, λ_{max} 235 (34 000), 257 (19 500), 263 (19 500), 301 sh (8000), 310 (8700), and 389 (5600) nm; nmr δ 2.38 (s, 3H, C-6 CH_3), 2.80 (s, 3H, C-8 CH_3), 6.69 and 6.77 (dd, J = 1.5 and 8.5 Hz, 1H each, H-2 and H-4), 6.84 and 7.00 (bs, 1H each, H-5 and H-7), 7.47 (t, J = 8.5 Hz, 1H, H-3), and 12.97 (s, 1H, ArO*H*); *m/e* 240.0795 (100) (calculated for $C_{15}H_{12}O_3$ 240.0787), 225 (6), 222 (3), 211 (7) and 197 (4). *Anal.* calcd. for $C_{15}H_{12}O_3$: C 75.0, H 5.0; found C 74.9, H 5.0.

The mother liquour gave 1,6-dihydroxyxanthone-5-carboxylic acid 3,5-dimethylphenyl ester, **7**, colourless crystals from methanol, mp 183–185 °C (sealed tube) (lit. (17) 184–186 °C), *m/e* 376 (M^+) whose spectral data were identical with those quoted (17).

*1-Acetoxy-6,8-dimethylxanthone, **4***

A solution of **6** (100 mg) in pyridine (3 ml) and acetic anhydride (5 ml) was set aside at room temperature. The reaction was complete after 4 days (tlc) and the product was isolated by diluting with water and, after 1 h, extraction into chloroform. The acetate **4** crystallised from methanol as colourless needles, mp 133–134 °C; ir 1767, 1659, 1630, 1617, and 1568 cm^{-1}; uv λ_{max} 236 sh (35 000), 241 (36 000), 273 (13 000), 277 sh (12 500), and 340 (6200) nm; nmr δ 2.38 (s, 3H, C-6 CH_3), 2.46 (s, 3H, OAc), 2.79 (s, 3H, C-8 CH_3), 6.88 and 7.06 (bs, 1H each, H-5 and H-7), 6.92 (dd, J = 1.3 and 8.5 Hz, 1H, H-2 or H-4), 7.30 (dd, J = 1.3 and 7.8 Hz, 1H, H-4 or H-2), and 7.61 (dd, J = 7.8 and 8.5 Hz, 1H, H-3); *m/e* 282.0983 (11) (calculated for $C_{17}H_{14}O_4$: 282.0982) and 240 (100). *Anal.* calcd. for $C_{17}H_{14}O_4$: C 72.3, H 5.0; found: C 71.9, H 5.0.

*Synthetic 1-Hydroxy-6-methyl-8-hydroxymethylxanthone, **1***

*(a) Via the Peroxide **10***

A stirred solution of the acetate **4** (31 mg) in cyclo-

Can. J. Chem. Downloaded from www.nrcresearchpress.com by 210.87.254.42 on 09/05/12
For personal use only.

hexane (50 ml) was irradiated while passing oxygen through the solution. After 75 min, tlc showed about 90% conversion of **4** to one major and one minor product. Irradiation was stopped, an excess of Ph_3P added and the solution stirred for 45 min. The solvent was removed *in vacuo* and replaced by a saturated solution of ammonia in methanol. After 1 h at room temperature, the solvent was evaporated and the residue separated by ptlc to give **1**, (17 mg, 60%), mp 176–178 °C (from acetone–water), identical with the natural product by mmp, ir, uv, nmr, and mass spectral comparison. *Anal.* calcd. for $C_{15}H_{12}O_4 \cdot \frac{1}{4}H_2O$: C 69.1, H 4.8; found: C 68.7, H 4.7.

The chromatogram also yielded **6** (2 mg, 7%) and 1-hydroxy-6-methyl-8-formylxanthone, **8** (4 mg, 14%), as yellow crystals, mp 208–210 °C (from methanol); ir 2930, 2850, 1695, 1648, 1618 sh, 1608, and 1575 cm^{-1}; uv λ_{max} 234 (31 000), 256 (22 500), 294 (12 500), and 369 (4750) nm; nmr δ 2.56 (s, 3H, C-6 CH_3), 6.84 (dd, J = 1.0 and 8.2 Hz, 1H, H-2 or H-4), 6.95 (dd, J = 1.0 and 8.4 Hz, 1H, H-4 or H-2), 7.51 (narrow multiplet, 1H, H-5), 7.63 (bs, 1H, H-7), 7.64 (dd, J = 8.2 and 8.4 Hz, 1H, H-3), 11.16 (s, 1H, ArC*H*O), and 12.46 (s, 1H, ArO*H*); *m/e* 254.0582 (24) (calculated for $C_{15}H_{10}O_4$: 254.0579), 226 (100), 198 (12), 197 (7) and 169 (2).

Photooxidation of **4** (10 mg) in cyclohexane (15 ml) as above and evaporation of the solvent at room temperature yielded a mixture which was mainly **10** by nmr; ir (CCl_4) 3480, 1783, 1760 (H-bonded acetate), 1663 (m), and 1615 cm^{-1}; uv (cyclohexane) λ_{max} 213 (14 200), 232 (11 500), 238 sh (11 300), 271 (2900), and 278 (3000); nmr δ 2.35 (s, 3H, C-6 CH_3), 2.39 (s, 3H, OAc), 4.67 (bs, 1H, O*H*), 5.03 and 5.43 (d, J = 16 Hz, 1H each, C-8 CH_2), 6.64 and 6.94 (bs, 1H each, H-5 and H-7), 6.80 and 7.16 (dd, J = 1.5 and 8 Hz, 1H each, H-2 and H-4), and 7.32 (t, J = 8 Hz, 1H, H-3). Attempted purification of the mixture by ptlc gave the hydroperoxide **11**; ir 3700, 3530, 1768, 1657, 1631, 1618, and 1572 cm^{-1}; uv λ_{max} 236 sh (25 300), 241 (26 200), 272 (10 300), 277 sh (9400), and 340 (4300); nmr δ 2.47 (s, 3H, OAc), 2.50 (s, 3H, C-6 CH_3), 5.73 (s, 2H, CH_2O_2H), 6.96 (dd, J = 1.5 and 8 Hz, 1H, H-2 or H-4), 7.23 and 7.37 (bs, 1H each, H-5 and H-7), 7.37 (dd, J = 1.5 and 8 Hz, 1H, H-4 or H-2), 7.66 (t, J = 8 Hz, 1H, H-3), and 8.52 (bs, 1H, CH_2O_2H).

(b) Via the Bromide ***12***

To a stirred solution of the acetate **4** (21 mg) in CCl_4 (4 ml) was added a solution of bromine in CCl_4 (0.46 ml, 25.4 mg/ml) and an excess of solid $NaHCO_3$. After irradiation for 15 min, the solution became colorless and tlc showed almost complete reaction. Filtration, evaporation, and crystallisation from acetone – Skellysolve B gave the bromide **12**, mp 159–162 °C; nmr δ 2.47 (s, 3H, C-6 CH_3), 2.51 (s, 3H, OAc), 5.26 (s, 2H, CH_2Br), 6.96 (dd, J = 1.5 and 7.5 Hz, 1H, H-2 or H-4), 7.20 and 7.22 (d, J = 2 Hz, 1H each, H-5 and H-7), 7.35 (dd, J = 1.5 and 8.0 Hz, 1H, H-4 or H-2), and 7.65 (dd, J = 7.5 and 8.0 Hz, 1H, H-3); *m/e* 362/359.9997 (5) (calculated for $C_{17}H_{13}O_4$ ^{79}Br: 359.9993), 318/320 (27), 281 (4), 239 (100) and 210 (17).

Repeating the bromination in the presence of galvinoxyl (0.01 mol/mol) yielded the same product at the same rate.

The crude bromination product (37 mg) was hydrolysed with $NaHCO_3$ in tetrahydrofuran–water under reflux for 1.5 h. Dilution with water and extraction with $CHCl_3$ gave the crude product (14 mg) which was purified by ptlc to give **1** (3.5 mg), mp 173–176 °C, identical with the natural product by spectral comparison.

Extraction of the Mycelia of C. intermedius

The air dried mycelia (50 g) were blended with ethyl acetate. Filtration and evaporation gave the crude ethyl acetate extract (470 mg). The mycelial residue was then extracted with methanol at room temperature. Partial evaporation of the solvent yielded white crystals of D-mannitol (130 mg), mp 165–166 °C (lit. (26) 166 °C). The hexaacetate, mp 122–123 °C (lit. (26) 125 °C) had $[\alpha]_D$ +20 (lit. (26) +25). The main constituent of the ethyl acetate extract was isolated by ptlc and shown to be ergosterol by comparison with authentic material.

Acknowledgements

We wish to thank Professor H. J. Brodie for the initial culture of *Cyathus intermedius*, J. H. Forsythe for preparing and extracting the liquid cultures, and the National Research Council of Canada for financial support.

1. W. A. Ayer and M. G. Paice. Can. J. Chem. **54**, 910 (1976).
2. W. A. Ayer and H. Taube. Can. J. Chem. **51**, 3842 (1973).
3. W. A. Ayer and L. L. Carstens. Can. J. Chem. **51**, 3157 (1973).
4. A. D. Allbutt, W. A. Ayer, H. J. Brodie, B. N. Johri, and H. Taube. Can. J. Microbiol. **17**, 1401 (1971).
5. A. I. Scott. Interpretation of the ultra-violet spectra of natural products. MacMillan, New York. 1964. p. 158.
6. J. W. ApSimon, P. V. DeMarco, D. W. Mathieson, W. G. Craig, A. Karim, L. Saunders, and W. B. Whalley. Tetrahedron, **26**, 119 (1970); N. S. Bhacca, D. P. Hollis, L. F. Johnson, and E. A. Pier. NMR spectra catalog. Vol. 2. Varian Associates, Palo Alto, California. 1963. No. 650.
7. E. Bullock, J. C. Roberts, and J. G. Underwood. J. Chem. Soc. 4179 (1962).
8. N. C. Yang and C. Rivas. J. Am. Chem. Soc. **83**, 2213 (1961).
9. B. J. Arnold, S. M. Mellows, P. G. Sammes, and T. W. Wallace. J. Chem. Soc. Perkin Trans. I, 401 (1974).
10. D. M. Findlay and M. F. Tchir. J. Chem. Soc. Chem. Commun. 514 (1974).
11. P. Yates, A. C. Mackay, and F. X. Garneau. Tetrahedron Lett. 5389 (1968).
12. K. R. Huffman, M. Loy, and E. F. Ullman. J. Am. Chem. Soc. **87**, 5417 (1965).
13. W. A. Henderson, Jr. and E. F. Ullman. J. Am. Chem. Soc. **87**, 5424 (1965).
14. P. G. Sammes and T. W. Wallace. J. Chem. Soc. Chem. Commun. 562 (1974).
15. N. D. Heindel, E. W. Sarver, and M. A. Pfau. Tetrahedron Lett. 3579 (1968); and references cited therein.

16. N. D. HEINDEL, J. MOLNAR, and M. PFAU. Chem. Commun. 1373 (1970).
17. T. ARUNACHALAN, M. ANCHEL, and M. S. R. NAIR. J. Org. Chem. **37**, 1262 (1972).
18. P. K. GROVER, G. D. SHAH, and R. C. SHAH. J. Chem. Soc. 3982 (1955).
19. G. V. D. TIERS. Table of characteristic NMR shielding values. Minnesota Mining and Manufacturing Company, St. Paul. 1958. p. 10.
20. M. S. R. NAIR, T. C. MCMORRIS, and M. ANCHEL. Phytochemistry, **9**, 1153 (1970); C. E. MOPPETT. Chem. Commun. 423 (1971).
21. O. R. GOTTLIEB. Phytochemistry, **7**, 411 (1968); I. CARPENTER, H. D. LOCKSLEY, and F. SCHEINMANN. Phytochemistry, **8**, 2013 (1969).
22. T. MONEY. Nature, **199**, 592 (1963).
23. J. S. E. HOLKER, R. D. LAPPER, and T. J. SIMPSON. J. Chem. Soc. Perkin Trans. I, 2135 (1974); K. K. CHEXAL, C. FOUWEATHER, J. S. E. HOLKER, T. J. SIMPSON, and K. YOUNG. J. Chem. Soc. Perkin Trans. I, 1584 (1974).
24. (*a*) W. B. TURNER. Fungal metabolites. Academic Press, London. 1971. Chapt. 5; (*b*) T. K. DEVON and A. I. SCOTT. Handbook of naturally occurring compounds. Vol. 1. Academic Press, New York. 1972.
25. A. KAMAL, S. A. HUSAIN, and A. A. QURESHI. Pak. J. Sci. Ind. Res. **14**, 104 (1971); A. KAMAL, S. A. HUSAIN, and A. A. QURESHI. Pak. J. Sci. Ind. Res. **15**, 49 (1972); K. K. CHEXAL, J. S. E. HOLKER, T. J. SIMPSON, and K. YOUNG. J. Chem. Soc. Perkin Trans. I, 543 (1975).
26. L. HOUGH and A. C. RICHARDSON. *In* Rodd's chemistry of carbon compounds. 2nd ed. Vol. 1F *Edited by* S. Coffey. Elsevier, Amsterdam. 1967. p. 22.

Can. J. Chem. Downloaded from www.nrcresearchpress.com by 210.87.254.42 on 09/05/12
For personal use only.

Action of Grignard reagents on hexuronic esters and attempted dehydration of tertiary alcohols to give hex-5-enopyranosides

GERALD O. ASPINALL,[1] OSAMU IGARASHI,[2] THINNAYAM N. KRISHNAMURTHY, AND WALTER MITURA
Department of Chemistry, York University, Downsview, Toronto, Ont. Canada M3J 1P3

AND

MASUO FUNABASHI
Department of Chemistry, Trent University, Peterborough, Ont. Canada K9J 7B8

Received December 5, 1975

GERALD O. ASPINALL, OSAMU IGARASHI, THINNAYAM N. KRISHNAMURTHY, WALTER MITURA, and MASUO FUNABASHI. Can. J. Chem. **54**, 1708 (1976).

The attempted formation of hex-5-enopyranosides from glycosiduronates by the action of Grignard reagents followed by dehydration affords hex-6-enopyranosides or 1,6-anhydrohexopyranoses as major products. ^{13}C nmr spectra of 6,6-di-*C*-substituted hexose derivatives are compared with those of a number of structurally related compounds. The formation of a hex-5-enopyranoside and the selective cleavage of its glycosidic linkage is illustrated by the synthesis and controlled hydrolysis of methyl 6-*O*-(6-deoxy-2,3,4-tri-*O*-methyl-β-L-*arabino*-hex-5-enopyranosyl)-2,3,4-tri-*O*-methyl-β-D-glucopyranoside (**2**).

GERALD O. ASPINALL, OSAMU IGARASHI, THINNAYAM N. KRISHNAMURTHY, WALTER MITURA et MASUO FUNABASHI. Can. J. Chem. **54**, 1708 (1976).

L'essai de formation d'hexèno-5 pyrannosides par l'action de réactif de Grignard sur des glycosiduronates suivie par une déshydratation conduit aux hexèno-6 pyrannosides ou aux anhydro-1,6 hexopyrannoses comme produits principaux. On compare les spectres rmn ^{13}C des dérivés di-*C*-substitués en 6,6 des hexoses avec ceux d'un certain nombre de composés qui leur sont reliés d'une façon structurale. On illustre la formation d'un hexèno-5 pyrannoside et le clivage sélectif de son lien glycosidique par la synthèse et l'hydrolyse contrôlée du méthyl 6-*O*-(6-déoxy-2,3,4-tri-*O*-méthyl-β-L-*arabino*-hex-5-ènopyrannosyl)-2,3,4-tri-*O*-méthyl-β-D-glucopyrannoside (**2**).

[Traduit par le journal]

As part of a series of investigations (1, 2) on the development of procedures for the selective fragmentation of polysaccharides we have examined the formation of hex-5-enopyranosides. In order to explore a method for the modification of hexuronic acid (or ester) units in polysaccharides we attempted to prepare hex-5-enopyranosides by the dehydration of tertiary alcohols formed by the action of Grignard reagents on methyl (methyl 2,3,4-tri-*O*-methyl-α-D-glucopyranosid)uronate (or its β-anomer). These experiments were unsuccessful in their overall objective and the results are described later. However hexuronic acid residues in acidic polysaccharides, which carry permanently (*e.g.* *O*-methyl) or temporarily (*e.g.* *O*-methoxyethyl (3)) stable substituents, may be readily reduced. That such reduction products may be converted into hex-5-enopyranosides which undergo selective acid hydrolysis was shown by the following series of reactions. Methyl 6-*O*-(6-deoxy-6-iodo-2,3,4-tri-*O*-methyl-α-D-galactopyranosyl)-2,3,4-tri-*O*-methyl-β-D-glucopyranoside, **1**, was prepared from methyl 2,2′,3,3′,4,4′-hexa-*O*-methyl-β-melibioside (1) by reaction with triphenylphosphite methiodide (4). Dehydroiodination of the iodo compound **1** proceeded smoothly on heating with DBU (1,5-diazabicyclo[5.4.0]undec-5-ene) in benzene[3] and furnished methyl 6-*O*-(6-deoxy-2,3,4-tri-*O*-methyl-β-L-*arabino*-hex-5-enopyranosyl)-2,3,4-tri-*O*-methyl-β-D-glucopyranoside, **2**. The same product was obtained on treatment of

[1]To whom enquiries should be addressed

[2]On leave (1973–1974) from Ochanomizu University, Research Institute of Food Chemistry, Bunkyo-ku, Tokyo, Japan.

[3]In contrast to the dehydroiodination of 6-deoxy-6-iodo-D-glucopyranosides, which occurs readily at room temperature, the less ready reaction of the D-galactopyranoside probably results from the unfavourable steric interaction in the transition state between the departing iodo and the axially oriented 4-*O*-substituents.

Can. J. Chem. Downloaded from www.nrcresearchpress.com by 210.87.254.105 on 09/05/12
For personal use only.

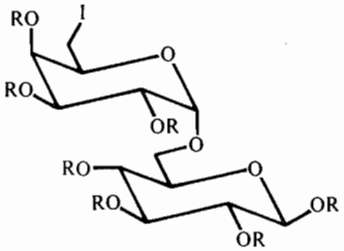

1 R = CH_3

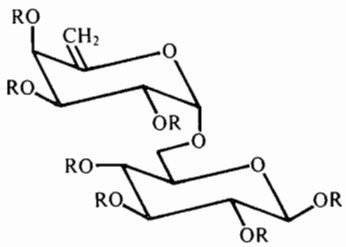

2 R = CH_3

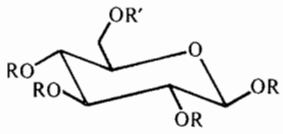

3 R = CH_3, R′ = H
10 R = R′ = CH_3

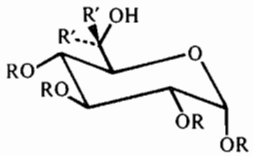

4 R = R′ = CH_3
5 R = CH_3, R′ = Ph

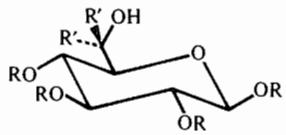

6 R = CH_3, R′ = Ph

the iodo compound **1** with a suspension of silver fluoride in pyridine (5), but, for a reaction to be extended to polysaccharide derivatives, a homogeneous system is preferable. Selective hydrolysis of the hex-5-enopyranoside occurred readily at room temperature by use of a cation-exchange resin as proton source with liberation of methyl 2,3,4-tri-*O*-methyl-β-D-glucopyranoside, **3**, with no detectable further hydrolysis.

Reaction of methyl (methyl 2,3,4-tri-*O*-methyl-α-D-glucopyranosid)uronate with methylmagnesium iodide afforded methyl 7-deoxy-6-*C*-methyl-2,3,4-tri-*O*-methyl-α-D-*gluco*-heptopyranoside, **4**, which, on treatment with thionyl chloride in pyridine gave a mixture of products. Although the mixture was inseparable by glc or tlc, ^{1}H nmr spectroscopy indicated that the hex-6-enopyranoside was the predominant product rather than the desired hex-5-enopyranoside. Methyl 2,3,4-tri-*O*-methyl-6,6-di-*C*-phenyl-α-D-glucopyranoside, **5**, and the anomeric β-D-glycoside, **6**, were prepared by the action of phenylmagnesium bromide on the corresponding methylated hexuronates. Attempts to dehydrate the 6,6-di-*C*-phenyl-α-D-glycoside, **5**, by treatment with thionyl chloride in pyridine (6), by treatment with methanesulfonyl chloride containing sulfur dioxide (7), and by heating in hexamethyl phosphoric triamide (8) gave no recognizable hex-5-enopyranoside. When the 6,6-di-*C*-phenyl-α-D-glycoside, **5**, was heated in methyl sulfoxide at 165 °C for 15 h the sole isolable product (72% yield) was assigned the structure, 1,6-anhydro-2,3,4-tri-*O*-methyl-6,6-di-*C*-phenyl-β-D-glucopyranose, **7**, on the basis of elemental analysis and its ^{1}H and ^{13}C nmr spectra. Similar treatment of the 6,6-di-*C*-phenyl-β-D-glycoside, **6**, also resulted in the formation of the 1,6-anhydro compound **7** but in much lower yield, together with some of the desired methyl 2,3,4-tri-*O*-methyl-6,6-di-*C*-phenyl-β-D-*xylo*-hex-5-enopyranoside, **8**, whose structure was assigned on the basis of spectral data and the formation of benzophenone on ozonolysis. The formation of 1,6-anhydro-β-D-glucopyranose on heating methyl α-D-glucopyranoside in methyl sulfoxide was reported earlier by Fischer (9) but neither this reaction nor the formation of hex-5-enopyranosides as by-products in this procedure holds promise for extension to more complex carbohydrates.

Examination of a molecular model of 1,6-anhydro-2,3,4-tri-*O*-methyl-6,6-di-*C*-phenyl-β-D-glucopyranose, **7**, indicates that the $^1C_4$ conformation **7***a* normally adopted by derivatives of 1,6-anhydro-β-D-glucopyranose (10) would give rise to severe steric repulsions between the 3-*O*-methyl substituent and the *endo* 6-*C*-phenyl group which would be relieved if the ring assumes the ^{1,4}B conformation **7***b*. Support for this contention has been obtained by examination of the ^{13}C nmr spectra of a number of

Can. J. Chem. Downloaded from www.nrcresearchpress.com by 210.87.254.105 on 09/05/12
For personal use only.

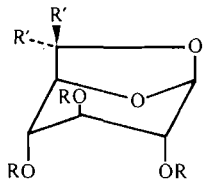

7 R = CH_3, R′ = Ph, *(conformer a)*
11 R = CH_3, R′ = H

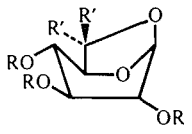

7 conformer *b*

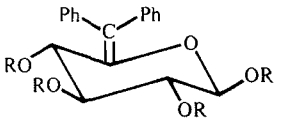

8 R = CH_3

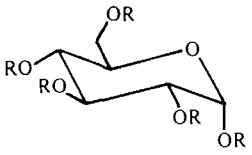

9 R = CH_3

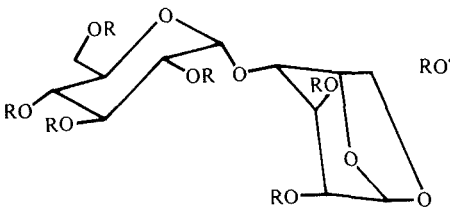

12 R = CH_3

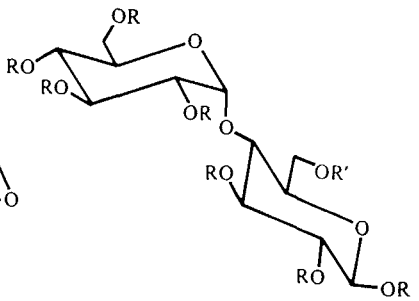

13 R = CH_3, R′ = H
14 R = R′ = CH_3

related compounds. These spectra are summarized in Tables 1 and 2.

First of all, the ^{13}C nmr spectra of the 6,6-di-*C*-substituted D-glucopyranosides **4–6** were compared with those of methyl 2,3,4,6-tetra-*O*-methyl-α- (**9**) and -β- (**10**) D-glucopyranosides, and methyl 2,3,4-tri-*O*-methyl-β-D-glucopyranoside, **3**. With the exception of the C-6 resonances in glycosides **4–6**, which are readily recognized as singlets in the proton undecoupled spectra and, as expected, are shifted downfield, the 6-*C*-substituents showed little effect on the spectra and the other resonances may be assigned with reasonable confidence. The spectrum of the anhydro compound **7** was then compared with that of 1,6-anhydro-2,3,4-tri-*O*-methyl-β-D-glu-

TABLE 1. ^{13}C nmr spectra of D-glucopyranose derivatives

Compound	Assigned resonances* C-1	C-2	C-3	C-4	C-5	C-6	Unassigned resonances	Other data
Me Me_4 α-D-Glc*p* (**9**)	98.2	82.6	84.3	80.6	71.0	72.4		Data from ref. 11
	97.4	81.7	83.4	79.3	69.9	*71.1*		^1J(C1–H1) = 164 Hz
Me 6-deoxy-6-*C*-Me Me_3 α-D-Glc-Hep*p* (**4**)	*97.3*	82.3	84.5	81.3	73.6	*71.9*		^1J(C1–H1) = 166 Hz
Me Me_3 6,6-*C*-Ph_2 α-D-Glc*p* (**5**)	*97.4*	82.0	84.4	82.0	75.0	*78.9*		^1J(C1–H1) = 166 Hz
Me Me_4 β-D-Glc*p* (**10**)	105.0	84.6	87.2	80.5	75.4	72.3		Data from ref. 11
	104.3	83.7	86.6	79.4	74.7	*71.3*		^1J(C1–H1) = 158 Hz
Me 2,3,4-Me_3 β-D-Glc*p* (**3**)	*104.3*	83.7	86.4	79.2	75.2	*61.5*		^1J(C1–H1) = 158 Hz
Me Me_3 6,6-*C*-Ph_2 β-D-Glc*p* (**6**)	*104.7*	84.2	86.8			*79.0*	81.2 79.4	^1J(C1–H1) = 159 Hz
1,6-A Me_3 β-D-Glc*p* (**11**)	*99.6*					*64.9*	79.3 78.7 78.5 73.0	^1J(C1–H1) = 174 Hz
1,6-A Me_3 6,6-*C*-Ph_2 β-D-Glc*p* (**7**)	*101.6*					*87.6*	84.2 82.9 82.5 79.2	^1J(C1–H1) = 176 Hz

*δ Values are relative to tetramethylsilane. Italicized figures indicate resonances unambiguously assigned to C-1 as the most deshielded carbon and to C-6 on the basis of the multiplicity of the signal in the undecoupled spectrum.

Can. J. Chem. Downloaded from www.nrcresearchpress.com by 210.87.254.105 on 09/05/12
For personal use only.

TABLE 2. ^{13}C nmr spectra of maltose derivatives

Compound	Assigned resonances C-1 (C-1′)	C-2 (C-2′)	C-3 (C-3′)	C-4 (C-4′)	C-5 (C-5′)	C-6 (C-6′)	Unassigned resonances		Other data
Me Me_7 β-maltoside (**14**)	104.8 (96.7)	84.9 (82.6)	87.4 (83.9)	73.2 (80.3)	74.7 (71.7)	72.1 (72.2)			Data from ref. 11
Me Me_6 β-maltoside (**13**)	*104.3* (*96.9*)	84.2 (81.8)	86.4 (83.5)	72.2 (79.9)	74.6 (71.5)	*61.1* (*71.1*)			
1,6-A Me_6 β-maltose (**12**)	*100.2* *96.7*	81.8	82.5			*66.1* *71.0*	80.7 75.3 79.3	77.9 70.3 (×2)	^1J(C1–H1) = 174 Hz ^1J(C1–H1) = 168 Hz

copyranose, **10**. Both compounds gave downfield signals, which may be assigned to C-1, which are intermediate between those for C-1 in α- and β-D-glucopyranosides which are present in the $^4C_1$ conformation. These signals for the 1,6-anhydro compounds showed larger $^{13}C1$–H1 couplings (^1J) (~174 Hz) than those of α-D-glucopyranosides (166–168 Hz) and β-D-glucopyranosides (158–160 Hz). Although individual assignments cannot be made for resonances in the spectrum of 1,6-anhydro-2,3,4-tri-*O*-methyl-β-D-glucopyranose, **10**, these resonances (other than that of C-1) appeared at $\delta < 80$ ppm. It is probable, in this case, that the marked downfield shifts which normally accompany *O*-methylation of hydroxyl bearing carbons are largely offset by upfield shifts of the resonances of carbon atoms adjacent to those carrying axial *O*-substituents (11, 12). Similar conclusions may be drawn from a comparison of the spectrum of 1,6-anhydro-hexa-*O*-methyl-β-maltose, **12**, with that of methyl 2,2′,3,3′,4,4′-hexa-*O*-methyl-β-maltoside, **13** (1), and that recently reported for methyl hepta-*O*-methyl-β-maltoside, **14**, (11). In contrast the spectrum of the 6,6-di-*C*-phenyl 1,6-anhydro compound **7** showed resonances for ring carbon atoms (presumably those of C-2, C-3, and C-4) at $\delta > 80$ ppm. The greater deshielding of these carbon nuclei is most readily explained if the pyranose ring in this compound adopts a non-chair (probably a $^{1,4}B$) conformation in which the three *O*-methyl substituents are in pseudo-equatorial orientations.

Experimental

General

Melting points are uncorrected. Optical rotations were measured with a Perkin-Elmer model 141 polarimeter at 20 ± 2°. The ir spectra were measured on a Unicam SP 200 spectrophotometer. ^1H nmr spectra were recorded on JEOL C-60H and Varian A-60, EM-360, and HA-100 spectrophotometers in deuterochloroform with tetramethylsilane as internal standard. ^{13}C nmr spectra were recorded on a Varian CFT-20 FT spectrometer operating at 20 MHz with an 8K 620L-100 computer. Chemical shifts were internally referenced to deuterochloroform and are reported corrected to tetramethylsilane. Mass spectra were recorded on A.E.I. MS 12 and Perkin-Elmer–Hitachi RMU-6 mass spectrometers with ionization potentials of 70 eV. Gas–liquid chromatography was performed with a Hewlett-Packard model 5750 chromatograph using columns of dichlorodimethylsilane-treated Celite coated with (*a*) 5% of neopentylglycol adipate polyester (operating temperature 160–180 °C), (*b*) 3% of silicone gum ECNSS-M (operating temperature 150 °C), and (*c*) 3% of silicone gum XE-60 (operating temperature 130–150 °C). For glc – mass spectrometry columns *b* and *c* were used in a Pye 104 chromatograph attached to the A.E.I. mass spectrometer, or in a Perkin-Elmer 990 chromatograph attached to the Perkin-Elmer–Hitachi mass spectrometer, in both cases via a Watson-Biemann separator.

Thin layer chromatography was performed with Kieselgel HF 254 as the adsorbent and the plates were sprayed with ethanol containing 5% of sulfuric acid and heated at about 150 °C. Solvent systems used for tlc were benzene–acetone (25:3), benzene–methanol (25:3), ethyl acetate – ethanol (10:1), light petroleum – acetone (5:1), and chloroform–acetone (9:1). Column chromatography was carried out on silica gel (Davison grade 950, 60–200 mesh). Light petroleum refers to the fraction of petroleum ether with bp 30–60 °C. Solutions were concentrated at bath temperatures of 50 °C or below.

*Methyl 6-O-6-Deoxy-(6-iodo-2,3,4-tri-O-methyl-α-D-galactopyranosyl)-2,3,4-tri-O-methyl-β-D-glucopyranoside, **1***

Methyl 2,2′,3,3′4,4′-hexa-*O*-methyl-β-melibioside, **1** (2.0 g), was kept in benzene (75 ml) containing triphenylphosphite methiodide (5 g) for 24 h, at which time tlc showed complete disappearance of starting material. The solution was chromatographed on neutral alumina to remove salts, and the benzene eluate was concentrated to a syrup which was further purified by chromatography on silica gel. Recrystallization of the product from ethanol

Can. J. Chem. Downloaded from www.nrcresearchpress.com by 210.87.254.105 on 09/05/12
For personal use only.

Can. J. Chem. Downloaded from www.nrcresearchpress.com by 210.87.254.105 on 09/05/12
For personal use only.

furnished the iodo compound **1** (2.0 g), mp 114–115 °C, $[\alpha]_D$ +72 (*c* 1.4, chloroform); ^{1}H nmr τ 4.92 (d, 1H, $J_{1',2'}$ = 3 Hz, H-1'), 5.83 (d, 1H, $J_{1,2}$ = 7 Hz, H-1), 6.37–6.50, (s, 3H, 7 × OCH_3). *Anal.* calcd. for $C_{19}H_{35}O_{11}I$: C 41.46, H 6.36, I 23.08; found: C 41.63, H 6.21, I 23.33.

*Preparation and Hydrolysis of Methyl 6-O-(6-Deoxy-2,3,4-tri-O-methyl-β-L-arabino-hex-5-enopyranosyl)-2,3,4-tri-O-methyl-β-D-glucopyranoside, **2***

Iodo compound **1** (200 mg) was heated with DBU (0.7 ml) in benzene in a sealed tube at 95 °C for 20 h. The cooled solution was concentrated and the resulting syrup was chromatographed on a column of silica gel with chloroform–acetone (4:1) to give the unsaturated disaccharide **2** (120 mg), $[\alpha]_D$ +47 (*c* 1.1, chloroform); ν_{max} (film) 1640 cm^{-1} (C=C); λ_{max} 208 nm (ϵ 1200 in methanol); ^{1}H nmr τ 4.80 (d, 1H, $J_{1',2'}$ = 3 Hz, H-1'), 5.85 (d, 1H, $J_{1,2}$ = 7 Hz, H-1), 6.39–6.53 (s, 3H, 7 × OCH_3). *Anal.* calcd. for $C_{19}H_{34}O_{10}$: C 54.02, H 8.06; found: C 54.34, H 8.10.

Unsaturated disaccharide **2** (20 mg) in acetone (1 ml) and water (1 ml) was stirred overnight with Dowex 50(H) resin. Thin layer chromatography showed complete disappearance of starting material with formation of a single detectable product. Filtration of the solution and concentration gave a syrup which crystallized from methanol to afford methyl 2,3,4-tri-*O*-methyl-β-D-glucopyranoside, **3** (7 mg), mp and mixture mp 94–95 °C, $[\alpha]_D$ −24 (*c* 1.0, chloroform). In this experiment the second product, 6-deoxy-2,3,4-tri-*O*-methyl-L-*arabino*-hexos-5-ulose, was presumably lost during work-up. In a parallel experiment the formation of 6-deoxy-2,3,4-tri-*O*-methyl-D-*xylo*-hexos-5-ulose on hydrolysis of methyl 6-deoxy-2,3,4-tri-*O*-methyl-α-D-*xylo*-hex-5-enopyranoside was demonstrated by reduction with sodium borohydride and acetylation to give an epimeric pair of 6-deoxy-2,3,4-tri-*O*-methylhexitol diacetates, whose constitutional identities were established by glc – mass spectrometry.

*Methyl 7-Deoxy-6-C-methyl-2,3,4-tri-O-methyl-α-D-gluco-heptopyranoside, **4***

Methyl (methyl 2,3,4,-tri-*O*-methyl-α-D-glucopyranosid)uronate (1.05 g) in ether was added during 20 min to methylmagnesium iodide (from methyl iodide (2 ml) and magnesium 0.5 g)) in boiling ether (25 ml), and the mixture was heated under reflux for 1 h. The cooled reaction mixture was poured into ice water, and, after acidification with dilute sulfuric acid, the ether layer was separated, washed with water, dried, and concentrated to a syrup (550 mg). The aqueous solution was further extracted with chloroform, and the chloroform layer was washed with saturated aqueous sodium chloride, dried, and concentrated to a syrup (360 mg). The combined syrups were separated by preparative layer chromatography using benzene–methanol to give crystalline compound **4** (660 mg), which, after recrystallization from light petroleum had mp 45 °C, $[\alpha]_D$ +167 (*c*. 1.00, dichloromethane); ν_{max} 3700 cm^{-1} (OH); ^{1}H nmr τ 5.23 (d, 1H, $J_{1,2}$ = 4 Hz, H-1), 6.37 (s, 6H), 6.54 (s, 3H) and 6.67 (s, 3H, 4 × OMe), 8.73 (s, 6H, CMe_2). *Anal.* calcd. for $C_{12}H_{24}O_6$: C 54.51, H 9.15; found: C 54.50, H 9.13.

Dehydration of Methyl 7-Deoxy-6-C-methyl-2,3,4-tri-O-methyl-α-D-gluco-heptopyranoside

Thionyl chloride (685 mg) in carbon tetrachloride (5 ml) was added to glycoside **4** (280 mg) in pyridine (3 ml) and carbon tetrachloride (3 ml) at 0 °C and the solution was kept for 30 min. The solution was poured into ice water containing sodium hydrogen carbonate, the mixture was extracted with chloroform, and the chloroform extract was washed with water, and concentrated to a syrup (230 mg). Preparative layer chromatography in benzene–acetone gave a chromatographically homogeneous syrup (180 mg) which gave a single peak on glc; ν_{max} (film) 1650 cm^{-1}; *m/e* 246 (M^+), 215 (M − OCH_3)$^+$, 176 (M − $(CH_3)_2C{=}C{=}O)^+$. The ^{1}H nmr spectrum was consistent with the presence of methyl 7-deoxy-2,3,4-tri-*O*-methyl-6-*C*-vinyl-α-D-*gluco*-heptopyranoside and methyl 7-deoxy 6-*C*-methyl-2,3,4-tri-*O*-methyl-α-D-*xylo*-hex-5-enopyranoside in the ratio of 7:1; τ 8.37 (s, CMe_2), 8.24 (m, CH_3—C=CH_2), 6.40–6.67 (s, 4 × OMe), 5.27 (d, 1H, $J_{1,2}$ = 3.3 Hz, H-1), 5.00 (m, =CH_2).

*Methyl 2,3,4-Tri-O-methyl-6,6-di-C-phenyl-α-D-glucopyranoside, **5***

Methyl (methyl 2,3,4-tri-*O*-methyl-α-D-glucopyranosid)uronate (0.53 g) in ether (25 ml) was added during 20 min to phenylmagnesium bromide (from bromobenzene (1.86 g) and magnesium (0.3 g)) in boiling ether (20 ml), and the mixture was heated under reflux for 1 h. The cooled solution was kept overnight at room temperature and poured into ice water containing dilute sulfuric acid. The ether layer was separated, the aqueous layer was extracted with ether, and the combined ether extracts were washed with water, dried over potassium carbonate, and concentrated to a syrup. The syrup was chromatographed on silica gel (10 g), elution with benzene removing bromobenzene and diphenyl, and elution with benzene–acetone furnishing a syrup (0.63 g). This syrup was purified by preparative layer chromatography using benzene–acetone to give the glycoside **5** (0.51 g) as a syrup, $[\alpha]_D$ +2.5, (*c* 1.51, dichloromethane); ν_{max} (film) 3600 cm^{-1}; ^{1}H nmr τ 5.84 (s, 1H, $J_{4,5}$ = 9.6 Hz, H-5), 5.36 (s, 1H, $J_{1,2}$ = 3.5 Hz, H-1), 5.21 (s, 1H, OH), 2.14–2.90 (m, 10H, 2 × phenyl); *m/e* 388 $(M)^+$, 370 (M − $H_2O)^+$. *Anal.* calcd. for $C_{22}H_{28}O_6$: C 68.00, H 7.26; found: C 68.14, H 7.45.

*Methyl 2,3,4-Tri-O-methyl-6,6-di-C-phenyl-β-D-glucopyranoside, **6***

As described for the α-anomer, **5**, the β-D-glycoside **6** was prepared from the reaction of phenylmagnesium bromide (from bromobenzene (0.93 g) and magnesium (0.144 g)) with methyl (methyl 2,3,4-tri-*O*-methyl-β-D-glucopyranosid)uronate (0.31 g), and was isolated as a syrup (320 mg), $[\alpha]_D$ −116 (*c* 2.7, dichloromethane); ν_{max} (film) 3620 cm^{-1} (OH); ^{1}H nmr τ 6.47, 6.51, 6.93, 7.00 (s, 3H, 4 × OMe), 5.43 (s, 1H, OH), 2.30–2.97 (m, 10H, 2 × phenyl); *m/e* 370 (M − $H_2O)^+$, 356 (M − $CH_3OH)^+$. The glycoside was later obtained as a crystalline solid which, after recrystallization from light petroleum, had mp 84–85 °C. *Anal* calcd. for $C_{22}H_{28}O_6$: C 68.00, H 7.26; found: C 68.30, H 7.30.

*1,6-Anhydro-2,3,4-tri-O-methyl-6,6-di-C-phenyl-β-D-glucopyranose, **7**, and Methyl 2,3,4-Tri-O-methyl-6,6-di-C-phenyl-β-D-xylo-hex-5-pyranoside, **8***

The methyl α-D-glycoside **5** (0.6 g) was heated in methyl sulfoxide (10 ml) at 165 °C for 15 h. The cooled solution was poured into ice water, the mixture was ex-

tracted with chloroform, and the chloroform extract was washed with aqueous 5% sodium chloride, dried, and concentrated to a syrup which crystallized. The crystalline mass was purified by preparative layer chromatography in chloroform–acetone and recrystallization of the major product from methanol gave the 1,6-anhydro compound **7** (0.4 g) mp 124–124.5 °C, $[\alpha]_D$ −120 (*c* 0.95, dichloromethane); ir no absorption at 3600 cm^{-1}; ^1H nmr τ 6.75, 6.59, 6.50 (s, 3H, 3 × OMe), 4.94 (d, 1H, $J_{4,5}$ = 1.2 Hz, H-5), 4.56 (s, 1H, $J_{1,2} = \leq 0.5$ Hz), 2.47–2.90 (m, 10H, 2 × phenyl). *Anal.* calcd. for $C_{21}H_{24}O_5$: C 70.77, H 6.79, OMe 26.10; found: C 70.31, H 6.99, OMe 26.03.

The methyl β-D-glycoside **6** (2 g) was heated in methyl sulfoxide (20 ml) at 165 °C for 15 h. The reaction mixture was worked-up as described above and gave a syrup from which a crystalline mass separated. The crystalline substance was purified by preparative layer chromatography in light petroleum – acetone to give the 1,6-anhydro compound **7** (300 mg), which was identified by mp and mixture mp 123–124 °C and by its ^1H nmr spectrum. The syrupy residue (550 mg) from the above separation was fractionated by preparative layer chromatography in chloroform, and the major component (300 mg), chromatographically homogeneous but not analytically pure, was assigned the structure methyl 2,3,4-tri-*O*-methyl-6,6-di-*C*-phenyl-β-D-*xylo*-hex-5-enopyranoside, **8**; ν_{max} (film) 1630 cm^{-1} (C=C); ^1H nmr τ 6.80 (s, 3H), 6.60 (s, 6H), and 6.47 (s, 3H, 4 × OMe), 2.40–2.90 (m, 10H, 2 × phenyl); *m/e* 370 $(M)^+$. Ozonolysis of the syrup (100 mg) in ethyl acetate, followed by treatment with palladium–charcoal catalyst, furnished a mixture of products from which benzophenone separated and was characterized by mp and mixture mp, and by the identity of its mass spectrum with that of an authentic sample.

1,6-Anhydro-2,2',3,3',4',6'-hexa-O-methyl-β-maltose, 12

1,6-Anhydromaltose (13) (5 g) was methylated with methyl iodide (20 ml) and silver oxide (8 g) in *N,N*-dimethylformamide (30 ml), and after normal work-up the product crystallized from light petroleum to give the hexamethyl ether **12** (3.5 g), mp 62–63 °C; ^1H nmr τ 4.83 (bs, 1H, separation 2 Hz, H-1), 5.08 (d, 1H, $J_{1',2'}$ = 3.5 Hz, H-1'), 6.45–6.70, (s, 3H, 6 × OMe). *Anal.* calcd. for $C_{18}H_{32}O_{10}$: C 52.93, H 7.90, OMe 45.60; found: C 52.71, H 7.80, OMe 45.74.

Acknowledgments

The authors thank the National Research Council of Canada for financial support, Dr. C. E. Holloway for recording ^{13}C nmr spectra, and Dr. C. C. Whitehead for the preparation of 1,6-anhydro-β-maltose hexamethyl ether.

1. G. O. Aspinall, T. N. Krishnamurthy, W. Mitura, and M. Funabashi. Can. J. Chem. **53**, 2182 (1975).
2. G. O. Aspinall and A. S. Chaudhari. Can. J. Chem. **53**, 2189 (1975).
3. M. Curvall, B. Lindberg and J. Lönngren. Carbohydr. Res. **41**, 235 (1975).
4. N. K. Kochetkov and A. I. Usov. Methods Carbohydr. Chem. **6**, 205 (1972).
5. M. G. Blair. Methods Carbohydr. Chem. **2**, 415 (1963).
6. W. S. Allen and S. Bernstein. J. Am. Chem. Soc. **77**, 1028 (1955).
7. G. G. Hazen and D. W. Rosenburg. J. Org. Chem. **29**, 1930 (1964).
8. R. S. Monson. Tetrahedron Lett. 567 (1971).
9. M. H. Fischer. Carbohydr. Res. **8**, 354 (1968).
10. P. L. Durette and D. Horton. Adv. Carbohydr. Chem. Biochem. **26**, 49 (1971).
11. J. Haverkamp, M. J. A. de Bie, and J. F. C. Vliegenthart. Carbohydr. Res. **37**, 111 (1974).
12. W. Voelter, E. Breitmaier, E. B. Rathbone, and A. M. Stephen. Tetrahedron, **29**, 3845 (1973).
13. L. Asp and B. Lindberg. Acta Chem. Scand. **6**, 941 (1952).

Can. J. Chem. Downloaded from www.nrcresearchpress.com by 210.87.254.105 on 09/05/12
For personal use only.

Oligoribonucleotide synthesis. IX.[1] Synthesis of sequences corresponding to the dihydrouridine loop neck region common in several transfer RNA molecules

T. E. ENGLAND AND THOMAS NEILSON
Department of Biochemistry, McMaster University, Hamilton, Ont., Canada L8S 4J9

Received December 11, 1975

T. E. ENGLAND and THOMAS NEILSON. Can. J. Chem. **54**, 1714 (1976).

The syntheses of the oligoribonucleotides GpApGpC, GpCpUpC, and ApGpCpUpC by an improved phosphotriester method are described. These sequences are found in the double-stranded region adjacent to the dihydrouridine loop of several transfer RNAs. Of special significance is the improvement in yields that the activating agent, mesitylenesulfonyl triazolide, provides in coupling reactions involving purine residues.

T. E. ENGLAND et THOMAS NEILSON. Can. J. Chem. **54**, 1714 (1976).

On décrit la synthèse des oligoribonucléotides GpApGpC, GpCpUpC et ApGpCpUpC par une méthode améliorée des phosphotriesters. On trouve ces séquences dans la région de la double hélice adjacente à la boucle dihydrouridine de plusieurs RNA de transfert. Il est important de signaler que les rendements ont été nettement améliorés grâce à l'utilisation de l'agent activant mesitylènesulfonyltriazolide pour les réactions de couplage impliquant des résidus purine.

[Traduit par le journal]

Our interest in the functional role of various regions of the transfer RNA molecule has resulted in the synthesis of oligoribonucleotides whose sequences correspond to specific segments. Subsequent studies involving the participation of these tRNA fragments in protein biosynthesis are intended. Synthesis of a nonaribonucleotide corresponding to the anticodon loop of *E. coli* $tRNA_f^{Met}$ has already been reported (2).

We now describe the synthesis of sequences which correspond to the double-stranded region (Fig. 1, I*b*) adjacent to the dihydrouridine loop of several tRNAs, for example, $tRNA^{Phe}$ (*E. coli*) (ref. 3 and references therein). Heterologous charging studies with yeast phenylalanyl-tRNA synthetase (ligase) (4, 5) indicate this neck region to be a partial recognition site for the enzyme. The duplex formed from these two complementary sequences may allow studies to determine the elements of recognition between the neck and the ligase. Information of this nature should be invaluable in understanding the general problem of nucleic acid – protein interactions of which almost nothing is known.

Since pentamer ApGpCpUpC contains a self-complementary sequence, it could form a duplex which might compete with the desired duplex I*b*. Availability of tetramer GpCpUpC would allow formation of duplex I*c* which would be free from such complications and still approximate to the recognition site. These complementary oligomers, GpCpUpC and GpAp-

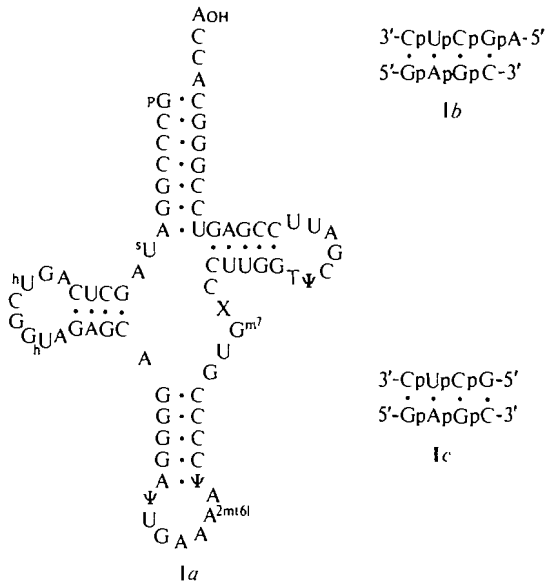

FIG. 1. *E. coli* $tRNA^{Phe}$ in conventional 'cloverleaf' secondary structure; (*b*) and (*c*) two possible duplices from synthetic oligoribonucleotides.

[1]For part VIII see ref. 1.

Can. J. Chem. Downloaded from www.nrcresearchpress.com by 210.87.254.5 on 09/05/12
For personal use only.

Can. J. Chem. Downloaded from www.nrcresearchpress.com by 210.87.254.5 on 09/05/12
For personal use only.

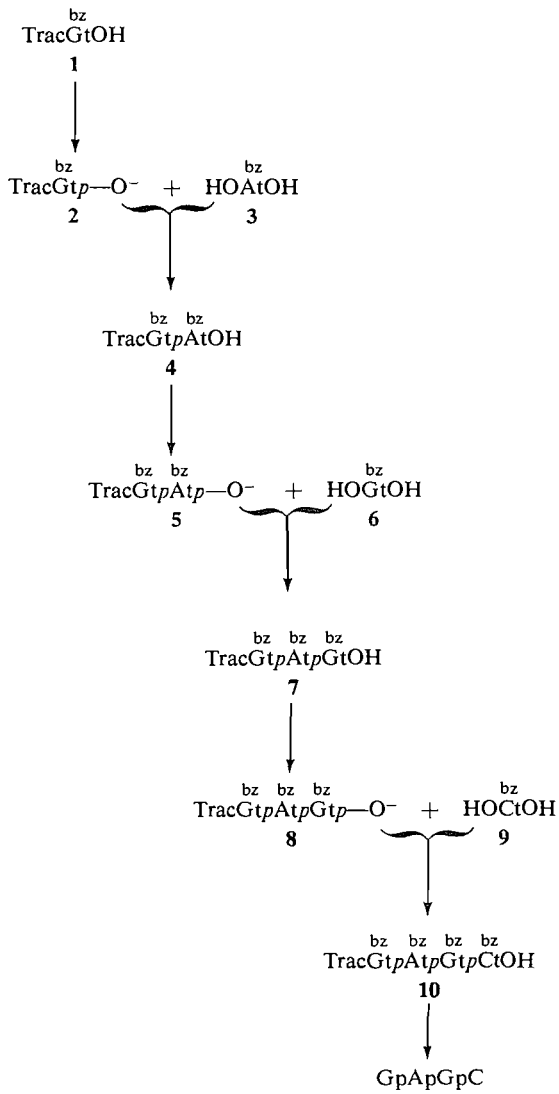

SCHEME 1. Abbreviations are as suggested by the IUPAC–IUB commission. Trac is 5′-*O*-triphenylmethoxyacetyl, t is 2′-*O*-tetrahydropyranyl and bz represents a benzoyl modification of the base amino function. *p*-O⁻ is 3′-*O*-(2,2,2-trichloroethyl) phosphate and *p* between two characters, *e.g.* Gt*p*At, indicates a 3′–5′ (2,2,2-trichloroethyl)phosphotriester internucleotide linkage.

GpC, and ApGpCpUpC and GpApGpC, should make an interesting system for studying the various parameters involved in helix formation (6, 7).

In several other tRNAs, for example, $tRNA^{Phe}$ (yeast) and $tRNA^{Phe}$ (wheat) (3), the sequence in this neck region is $Apm^2GpCpUpC$ instead of ApGpCpUpC. Apparently methylated guanine in this sequence does not affect the association (K_m) of the tRNA with the synthetase but does alter the rate (V_{max}) of aminoacylation (8). Thus duplex **Ib** may be recognized by the readily available phenylalanyl-tRNA synthetase from yeast.

In this communication we report, therefore, the synthesis of the oligoribonucleotides GpApGpC, GpCpUpC, and ApGpCpUpC outlined in Schemes 1, 2, and 3, respectively, using the stepwise phosphotriester method developed in this laboratory (9–11).

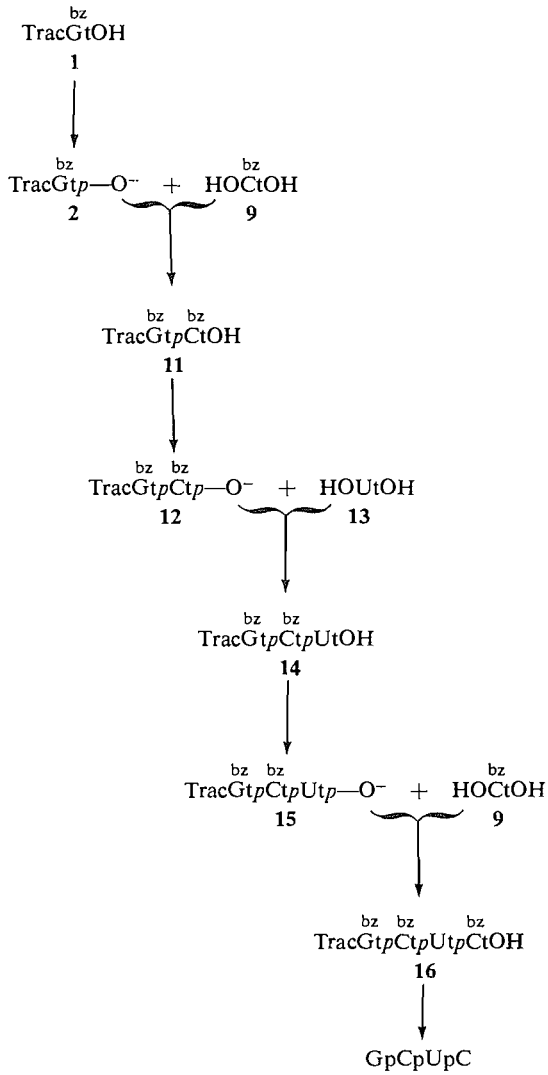

SCHEME 2

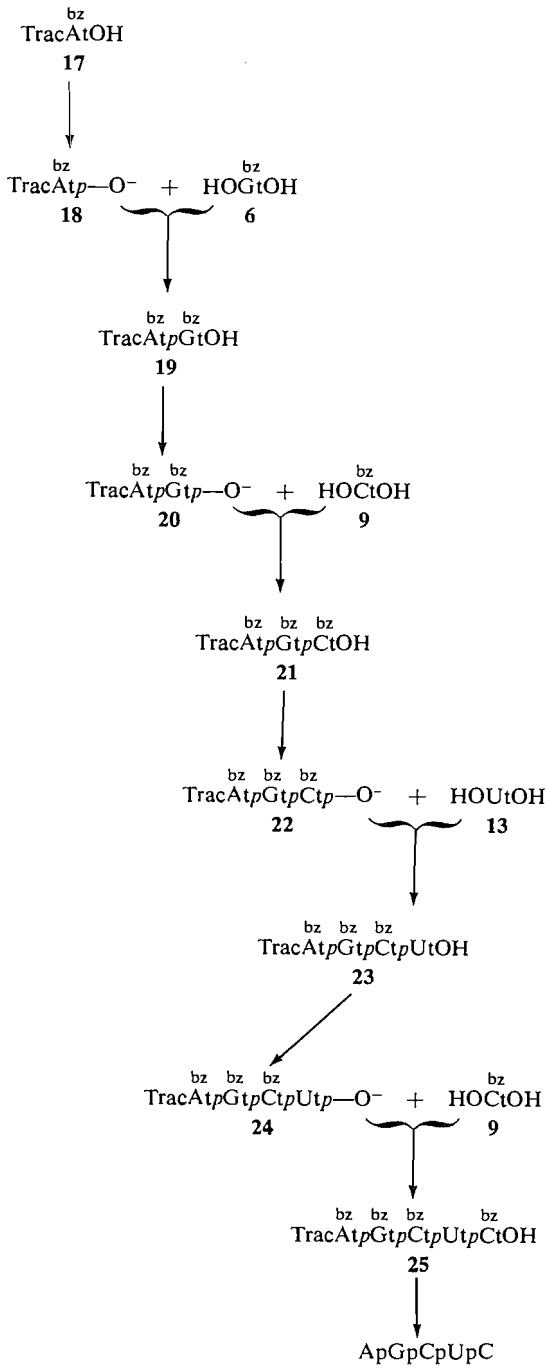

SCHEME 3

Syntheses proceed from the 5′ toward the 3′ end of the oligoribonucleotide. The nucleoside destined to occupy the 5′-terminal position (guanosine in Scheme 1) is protected by 5′-trityloxyacetyl (Trac), 2′-*O*-tetrahydropyranyl (t), and *N*-benzoyl (bz) (except uridine) while its 3′-hydroxyl remains free. Phosphorylation is effected at this 3′-position using mono-2,2,2-trichloroethyl phosphate to give a 3′-nucleotide derivative. The next nucleoside in the sequence (adenosine in Scheme 1) has only 2′-*O*-tetrahydropyranyl and *N*-benzoyl protection, and its 5′-hydroxyl is condensed to the 3′-nucleotide derivative forming a new 3′–5′-phosphotriester internucleotidic linkage. No evidence for the undesirable 3′–3′ linkage has been detected. Apparently the bulky 2′-*O*-tetrahydropyranyl grouping sterically 'shields' the vicinal 3′-hydroxyl from the phosphorylation complex and so forbids 3′–3′ condensation.

Two improvements have been incorporated into our earlier endeavours. First the free mono-2,2,2-trichloroethyl phosphate was employed in place of its corresponding bis(cyclohexylammonium) salt. Traces of cyclohexylamine remaining after exhaustive evaporation from anhydrous pyridine were thought to interfere with coupling by reacting with the phosphorylation complex. Second, TPS was replaced by mesitylenesulfonyl-1,2,4-triazolide (MST) (12) as coupling agent. Arenesulfonyl chlorides appear to attack the N^7 of guanosine derivatives leading to imidazole ring opening in the basic conditions used during deprotection. Loss of guanine residues during later synthesis would have serious consequences leading to a mixture of fragments. Pyridine hydrochloride is not a passive side product, especially towards acid-labile tetrahydropyranyl groups. TPS coupling reactions in pyridine are highly coloured and these colorations seem to associate with products during elution from silica gel columns. MST sidesteps these pitfalls.

The use of free mono-2,2,2-trichloroethyl phosphate and MST has resulted in a greater than 50% increase in yields (Table 1). Of special significance is the improved efficiency in coupling purine residues, for example, **17** with **6**, and **4** with **6**. MST-condensed reactions proceed smoothly to completion without additional quantities of coupling agent, a necessity with similar reactions using TPS. Reaction times were much shorter and coloration considerably reduced.

Investigations into the possibility of using

Can. J. Chem. Downloaded from www.nrcresearchpress.com by 210.87.254.5 on 09/05/12
For personal use only.

TABLE 1. Comparison of TPS and MST as condensing agents in oligoribonucleotide synthesis

Coupling reaction	TPS† yield (%)	MST‡ yield (%)	Improvement (%)
1 + **3** (G + A)*	33	57	73
4 + **6** (GA + G)	17	58	240
8 + **9** (GAG + C)	—	45	—
1 + **9** (G + C)	40	73	83
12 + **13** (GC + U)	50	77	54
14 + **9** (GCU + C)	25	42	68
17 + **6** (A + G)	35	73	108
19 + **9** (AG + C)	40	60	50
21 + **13** (AGC + U)	33	55	67
23 + **9** (AGCU + C)	33	45	36

*G + A represents the following reactions:

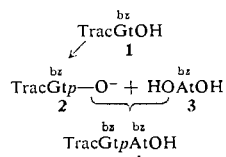

†Phosphorylation with the cyclohexylammonium salt of mono-2,2,2-trichloroethyl phosphate.
‡Phosphorylation with the free acid of mono-2,2,2-trichloroethyl phosphate.

MST to esterify selectively the 5′-hydroxyl group of *N*-benzoyl-2′-*O*-tetrahydropyranyl nucleosides with triphenylmethoxy acetate were undertaken, to thus eliminate TPS entirely from our synthetic scheme. Unfortunately considerable quantities of the 3′-isomer resulted and so TPS-esterification has been retained. These studies do, however, provide some insight into the mechanism of esterification via mixed sulfonyl–carboxylic anhydrides. Apparently the bulky TPS complex cannot approach a hydroxyl vicinal to a tetrahydropyranyl grouping whereas the MS complex can.

General Procedure for Coupling

Phosphorylation of the 3′-hydroxy protected nucleoside or oligonucleotides was accomplished using 2 equiv. of pyridinium mono-2,2,2-trichloroethyl phosphate, previously activated with 4 equiv. of MST. Two to four days were usually sufficient for complete reaction (Table 2) which was monitored by silica gel tlc. For longer sequences 3 or 4 equiv. of activated phosphate were found to be advantageous in certain cases. After quenching with water, the methylene chloride extracted phosphorylated material was reactivated with a fresh 1.2 equiv. of MST and 1.5 equiv. of the next protected nucleoside was added. This second coupling step was normally completed in 3–4 days (Table 2).

The desired oligoribonucleotide could be isolated from the incoming nucleoside derivative and the unreacted sequence bearing a 3′-phosphodiester by silica gel column chromatography. Occasionally the desired sequence and the incoming nucleoside coeluted. This problem could be easily resolved by a 'back-tritylation' reaction (10) and subsequent silica gel chromatography.

Sequences terminating in C residues (**11** and **22**) were more difficult to phosphorylate than sequences of comparable length ending in A, G, or U. An explanation for this observation was not evident as TracC^{bz}tOH itself phosphorylated readily. However, additional equivalents of activated phosphate could overcome this reduced reactivity (Table 2). Sequence TracGt^{bz}pC^{bz}mOH also did not phosphorylate readily (2).

After each addition of each nucleoside derivative to the growing protected sequence, a sample was completely deprotected and sequenced by enzymatic digestion. This procedure confirmed the integrity of the synthetic scheme. Table 3 provides chromatographic data of the various sequences and Table 4 gives the ratios of nucleotide and nucleoside components of the principal oligonucleotides.

Can. J. Chem. Downloaded from www.nrcresearchpress.com by 210.87.254.5 on 09/05/12
For personal use only.

TABLE 2. Summary of the preparation of protected oligoribonucleotides

(*a*) Phosphorylation reactions

Quantity of reactants (mg, with mmol in parentheses)				Product	
No.		Mono-2,2,2-trichloroethyl phosphate	MST	No.	Days to completion
1	500(0.65)	300(1.30)	650(2.59)	**2**	3
17	500(0.68)	305(1.30)	665(2.60)	**18**	2
4	525(0.37)	170(0.74)	370(1.48)	**5**	4
19	500(0.35)	160(0.70)	350(1.41)	**20**	2
14	450(0.23)	160(0.70)	350(1.41)	**15**	5
7	300(0.14)	65(0.29)	145(0.58)	**8**	5
23	220(0.09)	80(0.34)	172(0.69)	**24**	6
11	345(0.25)	115(0.50)	250(1.00)	**12**	<80% after 6 days
11	450(0.32)	220(0.97)	485(1.94)	**12**	2
21	400(0.20)	90(0.39)	195(0.78)	**22**	<75% after 6 days
tz TracCtOH	180(0.25)	115(0.50)	250(1.00)	bz TracCt*p*—O⁻	2

(*b*) Coupling reactions

Reactants				Product		
	Incoming nucleoside					
No. (*ca.* mmol)	Compound	Quantity (mg, with mmol in parentheses)	MST (mg, with mmol in parentheses)	No.	Quantity (mg, with % in parentheses)	Days to completion
2(0.65)	**3**	440(0.97)	195(0.78)	**4**	555(57)	3
2(0.65)	**9**	420(0.97)	195(0.78)	**11**	660(73)	3
18(0.68)	**6**	470(0.99)	180(0.73)	**19**	680(73)	3
5(0.37)	**6**	260(0.56)	110(0.44)	7	450(58)	3
12(0.32)	**13**	160(0.48)	100(0.39)	**14**	475(77)	3
20(0.35)	**9**	195(0.46)	100(0.39)	**21**	370(60)	4
8(0.14)	**9**	95(0.22)	45(0.17)	**10**	175(45)	4
15(0.23)	**9**	150(0.35)	70(0.28)	**16**	250(42)	4
22(0.20)	**13**	95(0.29)	55(0.22)	**23**	275(55)	5
24(0.09)	**9**	75(0.17)	75(0.31)	**25**	125(45)	10

TABLE 3. Experimental data of deprotected sequences

Sequence	R_{Gp}* System A	R_{Gp}* System B	R_{Gp}* System C	Yield (%) for complete deprotection†
GpA	1.53	2.75	0.43	28
GpApG	0.67	0.50	0.56	25
GpApGpC	0.42	0.25	0.80	10
GpC	1.71	3.00	0.54	22
GpCpU	1.33	1.00	0.88	26
GpCpUpC	0.78	0.50	0.96	18
ApG	1.39	2.75	0.44	18
ApGpC	0.92	0.75	0.69	17
ApGpCpU	0.60	0.50	0.90	8
ApGpCpUpC	0.29	0.25	1.08	12

**System A* paper chromatography, ethanol – 1 *M* NH_4OAc, p*H* 7.3 (70:30), Whatman No. 1; *System B* tlc, ethanol – 1 *M* NH_4OAc, p*H* 7.3, (70:30), Avicel F; *System C* paper electrophoresis, 1400 V/95 cm, Whatman No. 1, 0.05 *M* triethylammonium bicarbonate, p*H* 8.0.

†Calculated from spectrophotometric data assuming a 90% hypochromicity factor (10).

Can. J. Chem. Downloaded from www.nrcresearchpress.com by 210.87.254.5 on 09/05/12
For personal use only.

TABLE 4. Enzyme digestion of principal oligoribonucleotides*

Oligomer	Snake venom phosphodiesterase	Bovine spleen phosphodiesterase
GpApGpC	G/pA/pG/pC:1.0/0.9/1.1/1.0	Gp/Ap/C:1.8/1.1/1.0
GpCpUpC	G/pC/pU:1.0/2.1/1.1	Gp/Cp/Up/C:1.0/0.8/1.1/1.0
ApGpCpUpC	A/pG/pC/pU:1.0/1.0/2.2/0.9	Ap/Gp/Cp/Up/C:0.9/1.1/0.8/1.0/1.0

*Enzyme digestion products were separated by paper chromatography in System A.

Modified Deprotection Procedures

The method for complete deprotection was slightly modified from our previous three-step procedure (1, 10). Paper chromatography was used to purify the partially deprotected sequence after the first two steps. At this point only the 2′-*O*-tetrahydropyranyl protecting groups should be present. This isolation permitted easier identification of the completely deprotected sequence after the final step of the deprotection procedure, especially for longer sequences. Yields of the completely deprotected sequences remained low and tended to decrease with increasing length of sequence (Table 3). The procedure is described fully for GpA in the experimental section. Poor yields have also been reported by other workers employing a Zn/Cu couple to cleave the phosphate protecting group, mono-2,2,2-trichloroethyl (13). Alternate deprotection procedures are currently under investigation.

Studies into duplex formation of these complementary sequences and incorporation of a radioactive label are underway.

Experimental

Silica gel (Baker Analyzed Reagent) was used for column chromatography, and Analtech prescored silica gel plates were employed for tlc. The plates were developed in 5 or 10% methanol in methylene chloride mixtures.

The tlc detection was carried out using a ceric sulfate spray (1 g $H_4Ce(SO_4)_4$ in 10% aqueous sulfuric acid solution) and followed by heating the plates at 300–400 °F. Compounds containing a trityl group develop as yellow spots, while others appear as brown spots.

It was essential that moisture be excluded from all coupling reactions. After evaporation *in vacuo* of the pyridine solution, normal pressure was restored with dry nitrogen and *not* atmospheric air. All such evaporations were carried out in the temperature range 30–40 °C.

Emulsions, frequently obtained during methylene chloride extractions of aqueous pyridine solutions, were broken by the addition of a few millilitres of saturated sodium chloride solution.

Protected Nucleosides

Details of the preparation of the various modified nucleosides used in the synthesis have been described previously (1, 9, 11, 14).

Free Acid of Mono-2,2,2-trichloroethyl Phosphate

The free acid of mono-2,2,2-trichloroethyl phosphate was prepared by a modification of Eckstein's procedure for the preparation of the cyclohexylammonium salt (15). Instead of adding cyclohexylamine, the material was acidified with 2 *N* sulfuric acid solution, extracted with diethyl ether and evaporated *in vacuo* to a light yellow oil. During evaporation *in vacuo* from toluene, white crystals separated, mp 119–121 °C (120–121 °C)[2].

N^2-Benzoyl-2′-O-tetrahydropyranyl-5′-O-triphenylmethoxyacetylguanosine-3′-2,2,2-trichloroethyl Phosphate, **2**

(*a*) The bis(cyclohexylammonium) salt of mono-2,2,2-trichloroethyl phosphate (15) (720 mg, 1.62 mmol) was dissolved in anhydrous pyridine (30 ml) with warming and converted to the corresponding pyridinium salt by repetitive evaporation *in vacuo* and solution in pyridine (5 × 30 ml). TPS (980 mg, 3.23 mmol) was added to the above pyridine solution (*ca.* 15 ml) and the solution was then left to stand at room temperature under a nitrogen atmosphere. After 1 h a pyridine solution (*ca.* 5 ml) of TracGtOH^{bz}, **1**, (11) (400 mg, 0.52 mmol) was added to the deep yellow solution of activated phosphate. Thin layer chromatography indicated that the phosphorylation was *ca.* 80% complete (R_F 0.70 → 0.30 in 10% CH_3OH–CH_2Cl_2) after 1 day. Additional TPS (50 mg, 0.17 mmol) was added to complete the reaction in 2 days. Ice (*ca.* 2 g) was added to quench the reaction. After stirring for 30 min the reaction was poured into ice water (*ca.* 75 ml) and extracted with methylene chloride (4 × 30 ml). The combined organic fractions were washed with water (2 × 30 ml) and evaporated *in vacuo* to a brown foam. TracGtp^{bz}—O^-, **2**, was used without further purification.

(*b*) The free acid salt of mono-2,2,2-trichloroethyl phosphate (300 mg, 1.3 mmol) was converted to its pyridinium salt by solution in anhydrous pyridine and repetitive evaporation *in vacuo* (5 × 30 ml). MST (650 mg, 2.59 mmol) (12) was added to this pyridine solution (*ca.* 10 ml) and then left to stand under nitrogen for 1 h. Gentle heating (40 °C) was required to redissolve pyridinium trichloroethyl phosphate which frequently separated. Pyridine solution (*ca.* 5 ml) containing TracGtOH^{bz}, (**1**) (500 mg, 0.65 mmol), was added to the clear solution of activated phosphate. Thin layer chromatography indicated that the phosphorylation was complete (R_F 0.70 → 0.30 in 10% CH_3OH–CH_2Cl_2) in 3 days. The reaction was quenched with ice (*ca.* 2 g), poured into ice water (*ca.* 50 ml), and extracted with methylene chloride (5 × 25 ml). The combined organic extracts were washed

[2]C. B. Reese, personal communication.

Can. J. Chem. Downloaded from www.nrcresearchpress.com by 210.87.254.5 on 09/05/12
For personal use only.

Can. J. Chem. Downloaded from www.nrcresearchpress.com by 210.87.254.5 on 09/05/12
For personal use only.

with water (2 × 40 ml) and evaporated *in vacuo* to a light yellow foam which was used immediately.

N^2-Benzoyl-2′-O-tetrahydropyranyl-5′-O-triphenylmethoxyacetylguanylyl(3′-2,2,2-trichloroethyl-5′)-N^6-benzoyl-2′-O-tetrahydropyranyladenosine, **4**

(*a*) TracGt*p*—O$^-$, **2** (*ca.* 0.52 mmol) prepared above using TPS was repetitively evaporated from anhydrous pyridine (3 × 40 ml, final volume *ca.* 10 ml) and TPS (180 mg, 0.59 mmol) was then added. After 1 h a pyridine solution (5 ml) of the high R_F isomer of HOAtOH, **3** (345 mg, 0.76 mmol), (9) was added. Additional portions of TPS (50 mg, 0.17 mmol) were added on days 3, 4, and 5. After 8 days tlc indicated *ca.* 60% reaction (R_F 0.30 → 0.75 in 10% CH_3OH–CH_2Cl_2). The reaction was quenched with ice (*ca.* 2 g), poured into ice water (*ca.* 75 ml), and extracted with methylene chloride (4 × 30 ml). Combined organic fractions were washed with water (30 ml) and evaporated *in vacuo* to dryness. The last traces of pyridine were removed from the residue by codistillation with toluene (2 × 20 ml) to give a brown foam which was purified by silica gel column chromatography. Elution with 3.0% methanol – methylene chloride yielded a pure fraction of TracGt*p*AtOH, **4** (202 mg), plus a 50% mixed fraction containing TracGt*p*AtOH, **4**, and HOAtOH, **3** (325 mg).

This mixed fraction was dissolved in anhydrous pyridine and repetitively evaporated *in vacuo* (3 × 20 ml). Excess *p*-anisylchlorodiphenylmethane (150 mg, 0.45 mmol) was added to the pyridine solution. After 2 h, contaminating **3** was converted to its 5′-*O*-*p*-methoxytrityl derivative (R_F 0.65 → 0.95 in 10% CH_3OH–CH_2Cl_2). The reaction was quenched with ice (*ca.* 2 g), poured into ice water (40 ml), and extracted with methylene chloride (3 × 25 ml). The combined organic extracts were washed with water (2 × 40 ml) and evaporated *in vacuo* to dryness. Subsequent column chromatography on silica gel yielded further TracGt*p*AtOH, **4** (60 mg). The trityl derivative of **3** was preeluted with 1% methanol – methylene chloride.

The total isolated yield of TracGt*p*AtOH, **4** (262 mg, 0.18 mmol), was 35%.

(*b*) TracGt*p*—O$^-$, **2** (*ca.* 0.65 mmol), prepared above using MST, was repetitively evaporated *in vacuo* from anhydrous pyridine (4 × 30 ml, final volume *ca.* 5 ml) and MST (195 mg, 0.78 mmol) was added. After 1 h a pyridine solution (*ca.* 5 ml) of the high R_F isomer of HOAtOH, **3** (440 mg, 0.97 mmol), was added. Thin layer chromatography indicated the coupling reaction was complete (R_F 0.30 → 0.75 in 10% CH_3OH–CH_2Cl_2) after 2 days. The reaction was quenched and worked-up in the usual manner to give a light yellow foam which was purified by silica gel chromatography. Elution with 3% methanol – methylene chloride gave a pure fraction of TracGt*p*AtOH, **4** (360 mg), and a mixed fraction (475 mg) of **4** and **3**. 'Back tritylation' of the mixed fraction and subsequent silica gel column chromatography gave further quantities (195 mg) of **4**. The total yield of TracGt*p*AtOH, **4** (555 mg), was 57%.

Synthesis of the remaining oligoribonucleotides in Schemes 1, 2, and 3 followed the same procedure as for TracGt*p*AtOH, **4**. Table 2 contains the essential data for those syntheses. Protected sequences longer than trimers did not require 'back tritylation' as these sequences eluted at a higher percentage of methanol – methylene chloride than the incoming nucleoside.

Guanylyl (3′–5′) adenosine (GpA)

TracGt*p*AtOH, **4** (10 mg), was dissolved in anhydrous *N*,*N*-dimethylformamide (1 ml). Zn/Cu couple (*ca.* 20 mg) was added and stirred for 2 h at 50 °C. Thin layer chromatography indicated complete removal of 2,2,2-trichloroethyl (R_F 0.75 → 0.0 in 10% CH_3OH–CH_2Cl_2). Methanolic ammonia (MeOH – concentrated NH_3 1:1) (5 ml) was added and stirring was continued for 72 h at room temperature. Reaction was filtered to remove the Zn/Cu couple which was washed well with dilute aqueous ammonia. The filtrate and washings were evaporated *in vacuo* to reduce the p*H* to *ca.* 9. Chelex 100 (*ca.* 1 g, 100–200 mesh, Na^+ form) was then added to remove Zn and Cu ions. After stirring for 30 min the resin was filtered off and washed well with water. The filtrate was evaporated *in vacuo* to a small volume (<1 ml) and applied to Whatman 3 MM paper. Descending paper chromatography in ethanol – 1 *M* NH_4OAc, p*H* 7.3 (50:50, v/v), yielded a uv absorbing band (R_F 0.85, *ca.* 50 A_{260})[3] that was eluted from the paper with water. The eluate was adjusted to p*H* 2 with a few drops of 2 *N* HCl and stirred at room temperature. The removal of tetrahydropyranyls was followed by Avicel F tlc in ethanol – 1 *M* NH_4OAc, p*H* 7.3 (70:30, v/v) (R_F 0.80 → 0.10). After 48 h the solution was neutralized with dilute ammonia, evaporated *in vacuo* to a small volume (<1 ml), and applied to Whatman 40 paper. Descending paper chromatography in ethanol – 1 *M* NH_4OAc, p*H* 7.3 (50:50, v/v) gave a uv absorbing band (R_F 0.45). This band was desalted by soaking for 1 h in absolute ethanol and 10 min in diethyl ether and then eluted with water (16).

The deprotection procedure yielded GpA (46 A_{260}, 28%) which was characterized by enzymatic digestion. Snake venom phosphodiesterase in NaOAc–$Mg(OAc)_2$ (0.1 *M*, p*H* 8.80) gave the desired products G and pA. Spleen phosphodiesterase in sodium succinate (0.1 *M*, p*H* 6.5) gave the desired products Gp + A. Products of the enzymatic digestion were identified by Avicel F tlc (ethanol – 1 *M* NH_4OAc, p*H* 7.3, (70:30, v/v)).

Similar deprotection procedures were used for all the protected oligoribonucleotides. Enzymic analysis of longer sequences frequently required the use of a second system (Avicel tlc, isobutyric acid – 0.5 *M* NH_4OH, 50:30, v/v, p*H* 4.3).

Acknowledgements

The authors wish to thank Dr. E. S. Werstiuk

[3] A_{260} is the absorbance of the material at 260 nm when dissolved in 1 ml of water.

for frequent helpful discussions. The authors also wish to thank John Hems for the preparation of the free acid of mono-2,2,2-trichloroethyl phosphate. Financial assistance from the Medical Research Council of Canada is acknowledged.

1. T. NEILSON, K. V. DEUGAU, T. E. ENGLAND, and E. S. WERSTIUK. Can. J. Chem. **53**, 1093 (1975).
2. T. NEILSON and E. S. WERSTIUK. J. Am. Chem. Soc. **96**, 2295 (1974).
3. G. DIRHEIMER *et al.* Biochimie, **54**, 127 (1972).
4. B. DUDOCK, C. DIPERI, K. SCILEPPI, and R. RESZELBACH. Proc. Natl. Acad. Sci. **68**, 681 (1971).
5. B. ROE and B. DUDOCK. Biochem. Biophys. Res. Commun. **49**, 399 (1972).
6. S. K. PODDER. Eur. J. Biochem. **22**, 467 (1971).
7. D. B. ARTER, G. C. WALKER, O. C. UHLENBECK, and P. G. SCHMIDT. Biochem. Biophys. Res. Commun. **61**, 1089 (1974).
8. B. ROE, M. MICHAEL, and B. DUDOCK. Nature (London) New Biol. **246**, 135 (1973).
9. T. NEILSON and E. S. WERSTIUK. Can. J. Chem. **49**, 493 (1971).
10. T. NEILSON and E. S. WERSTIUK. Can. J. Chem. **49**, 3004 (1971).
11. T. NEILSON, E. V. WASTRODOWSKI, and E. S. WERSTIUK. Can. J. Chem. **51**, 1068 (1972).
12. N. KATAGIRI, K. ITAKUA, and S. A. NARANG. J. Chem. Soc. Chem. Commun. 325 (1974).
13. J. C. CATLIN and F. CRAMER. J. Org. Chem. **38**, 245 (1973).
14. B. E. GRIFFIN, M. JARMAN, and C. B. REESE. Tetrahedron, **24**, 639 (1968).
15. F. ECKSTEIN. Chem. Ber. **100**, 2228 (1967).
16. R. THACH. Proc. Nuc. Acid Res. **1**, 520 (1966).

Can. J. Chem. Downloaded from www.nrcresearchpress.com by 210.87.254.5 on 09/05/12
For personal use only.

A search for protonated cyclobutane

CHOI CHUCK LEE AND ERIC C. F. KO

Department of Chemistry and Chemical Engineering, University of Saskatchewan, Saskatoon, Sask., Canada S7N 0W0

Received August 22, 1975[1]

CHOI CHUCK LEE and ERIC C. F. KO. Can. J. Chem. **54**, 1722 (1976).

Attempted protonation of cyclobutane with H_2SO_4-*t* or CF_3COOH-*t* failed to give any open chain butyl product as evidence for the formation of protonated cyclobutane. The treatment of cyclobutane with an excess of CF_3SO_3H-*t* in a sealed tube at 75 °C for 3 days followed by hydrolysis did give rise to the four isomeric butyl alcohols containing some T-label in the butyl groups. The upper limit for this ring cleavage, probably via protonated cyclobutane, was about 1%. H–T exchange in the recovered cyclobutane was also observed.

CHOI CHUCK LEE et ERIC C. F. KO. Can. J. Chem. **54**, 1722 (1976).

Des essais de protonation du cyclobutane avec H_2SO_4-*t* ou CF_3COOH-*t* n'ont pas conduit aux produits butyliques en chaînes ouvertes qui auraient pu prouver la formation de cyclobutane protoné. Le traitement du cyclobutane avec du CF_3SO_3H-*t* en excès (en tubes scellés, à 75 °C, pendant 3 jours) suivi d'une hydrolyse conduit à quatre alcools butyliques isomères contenant un peu de marqueur T dans les groupements butyliques. La limite supérieure pour cette coupure de cycle impliquant probablement un cyclobutane protoné est d'environ 1%. On a aussi observé un échange H–T dans le cyclobutane récupéré.

[Traduit par le journal]

Considerable work has been done on protonated cyclopropanes (1–4). The initial definitive evidence for such species was obtained by Baird and Aboderin (5) from the reaction of cyclopropane with D_2SO_4, and these results were subsequently confirmed by the treatment of cyclopropane with H_2SO_4-*t* (6). Protonated cyclobutane intermediates have been suggested as being involved in the mass spectral fragmentation of the butyl cation (7). In the present work, attempts were made to obtain evidence for the existence of protonated cyclobutane under thermochemical conditions. By analogy with the protonation of cyclopropane with H_2SO_4-*t*, the initial experiments were carried out by treating cyclobutane with H_2SO_4-*t*.

It is anticipated that if protonated cyclobutane intermediates were involved in the reaction of cyclobutane with tritiated acids, *n*-butyl products would be formed with the T-label located at C-4 or C-1 and C-4 depending on whether the product is derived from the corner- or edge-protonated species (**1** or **2**), either as a transition state or as an intermediate (Scheme 1). Further equilibration among these protonated species would result in more extensive scrambling of the T-label over the four carbon positions of the *n*-butyl product.

The general experimental approach involved the treatment of cyclobutane with the tritiated acid followed by the hydrolysis of any butyl esters formed in the reaction to the correspond-

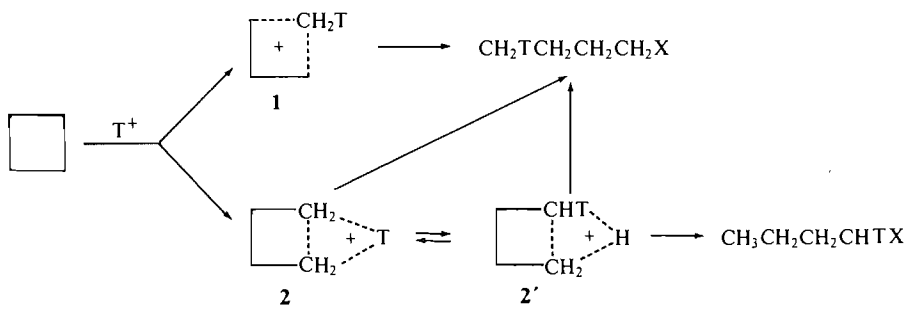

SCHEME 1

[1]Revision received February 27, 1976.

Can. J. Chem. Downloaded from www.nrcresearchpress.com by 210.87.254.42 on 09/05/12
For personal use only.

TABLE 1. Data from the reaction of cyclobutane with CF_3SO_3H-*t*

Cyclobutane (mmol)*	*n*-BuOH† Specific activity (dpm/mmol)	*n*-BuOH† Yield‡ (%)	*sec*-BuOH† Specific activity (dpm/mmol)	*sec*-BuOH† Yield‡ (%)	*iso*-BuOH† Specific activity (dpm/mmol)	*iso*-BuOH† Yield‡ (%)	*t*-BuOH† Specific activity (dpm/mmol)	*t*-BuOH† Yield‡ (%)
18	684 000(70 400)§	0.8	67 900	0.08	62 400	0.07	65 000	0.08
6.3	199 000(20 800)§	1.0	21 100	0.1	16 300	0.07	21 800	0.1

*Amount of cyclobutane in 2.0 ml of CF_3SO_3H-*t*, the specific activity of which was 1.48×10^8 dpm/mmol.
†The alcohols were diluted with inactive carriers (2.0 to 3.5 g), recovered by preparative vpc and assayed as the 3,5-dinitrobenzoate except in the case of *tert*-BuOH which was assayed as sodium *tert*-butoxide.
‡Based on isotope dilution calculations; these yields would be upper limits since part of the activity may be due to exchange.
§The data in the parentheses are the specific activities of $CH_3CH_2CH_2COOH$ from the *n*-BuOH, assayed as the *S*-benzylisothiouronium salt.

ing alcohols. These alcohols were then isolated by preparative vpc with the aid of carriers. Incorporation of the T-label into the butyl groups of the alcohols would suggest the formation of butyl products from cyclobutane, probably via protonated cyclobutane. When cyclobutane was shaken in a sealed tube with H_2SO_4-*t* at temperatures up to 100 °C for several days, there was no detectable T-incorporation to indicate the cleavage of cyclobutane into open chain butyl products, suggesting no solvolytic reaction via protonated cyclobutane.

Some cleavage of cyclobutane to open chain butyl products did occur when cyclobutane was treated with a stronger acid, CF_3SO_3H-*t*. After the heterogeneous mixture of CF_3SO_3H-*t* and cyclobutane was shaken for 3 days at 75 °C, the resulting material was hydrolyzed and the data obtained are summarized in Table 1. Although the conversion of cyclobutane into butyl products, as recorded in Table 1, was no more than about 1%, the incorporation of T-activity into the butyl groups was real and not the result of contamination. If the activities in the various butyl alcohols were simply due to contamination of the added carriers, similar results would have been observed in the experiments with H_2SO_4-*t*, but this was not the case.

The calculation of the yields of butyl products from isotope dilution (illustrated in the experimental section) was based on the assumption that the T-activities in the various solid derivatives of the butyl alcohols (Table 1) were derived from protonation of cyclobutane by the tritiated acid, such as in Scheme 1. The processes in Scheme 1 would give only the *n*-butyl ester which, on hydrolysis, would account for the *n*-BuOH. It is, however, quite probable that, in the CF_3SO_3H medium, any *n*-butyl cation formed during the reaction could also rearrange to the other isomeric butyl cations. Moreover, if H–T exchange were to occur between CF_3SO_3H-*t* and the butyl products, the yields calculated from isotope dilution would be too high since part of the observed activities would have been due to exchange. In order to get some clarification on these points, the effect of CF_3SO_3H-*t* on small amounts of *n*-BuOH was investigated and it was found that under the conditions used in the present studies, some exchange as well as rearrangements to the isomeric alcohols did occur. Moreover, oxidation of the active *n*-BuOH derived from the exchange reaction gave an essentially inactive $CH_3CH_2CH_2COOH$, indicating that the H–T exchange took place at the α-C of *n*-BuOH. The fact that the active *n*-BuOH derived from the protonation experiments lost nearly 90% of its activity upon oxidation to $CH_3CH_2CH_2COOH$ (Table 1) would support the conclusion that some exchange, at the α-C, likely has also occurred during the protonation reaction. However, the magnitudes of the T-activities resulting from exchange, when compared with those in Table 1, suggested that the exchange could account for only a minor part of the observed activities recorded in Table 1. It can, therefore, be concluded that the treatment of cyclobutane with an excess of CF_3SO_3H-*t* did result in a small extent of ring cleavage, probably via protonated cyclobutane, to give an *n*-butyl product. During the reaction, the *n*-butyl cation or product initially formed could also undergo H–T exchange as well as rearrangement to give other isomeric butyl species.

In the early work on protonated cyclopropane by Baird and Aboderin, it was noted that treatment of cyclopropane with D_2SO_4 resulted in the formation of monodeuterocyclopropane (8). Sol-

Can. J. Chem. Downloaded from www.nrcresearchpress.com by 210.87.254.42 on 09/05/12
For personal use only.

Can. J. Chem. Downloaded from www.nrcresearchpress.com by 210.87.254.42 on 09/05/12
For personal use only.

volytic ring cleavage of the cyclopropane was found to occur concurrently with exchange, the rate of solvolysis being about twice that of exchange. When cyclobutane was shaken with excess CF_3SO_3H-*t* at 75 °C for 3 days, the recovered cyclobutane was found to be tritiated, its specific activity being the same as that of the original CF_3SO_3H-*t*. This observation indicated a complete exchange between cyclobutane and CF_3SO_3H-*t* to give a monotritiated cyclobutane. The similarity to the formation of monodeuterocyclopropane in this exchange reaction thus gave further support to the probability of a role for protonated cyclobutane; however, since only a very small amount of ring cleavage was observed (Table 1), the rate of solvolytic cleavage of cyclobutane obviously was much slower than the rate of exchange under the conditions employed.

Since the treatment of cyclobutane with CF_3SO_3H-*t* involved a two-phase heterogeneous system, a homogeneous solution of cyclobutane in an excess of CF_3COOH-*t* in a sealed tube was shaken at 60 °C for 5 days. While the recovered cyclobutane had also undergone exchange, showing a specific activity equalling about 12% of the specific activity of the CF_3COOH-*t*, no tritiated open chain butyl product was detected, indicating no solvolytic ring cleavage. Thus solvolytic cleavage of cyclobutane, probably via protonated cyclobutane, was observed only upon treatment with CF_3SO_3H-*t*. Since the upper limit for the ring cleavage was only about 1%, it is unlikely that processes via protonated cyclobutanes could be major pathways in thermochemical reactions. It is also of interest to note that in the trifluoroacetolysis of 1-butyl-1-^{14}C tosylate (9), the isotopic scrambling results suggested the possibility of some involvement of protonated methylcyclopropane rather than protonated cyclobutane.

Experimental

Tritiated Acids

Essentially 100% H_2SO_4-*t*, CF_3SO_3H-*t*, or CF_3COOH-*t* were prepared by adding H_2O-*t* and the calculated amount of SO_3 (from fuming H_2SO_4), trifluoromethanesulfonic acid anhydride, or trifluoroacetic anhydride to ordinary H_2SO_4, CF_3SO_3H, or CF_3COOH.

Protonation Experiments

The mixture of cyclobutane and an excess of the tritiated acid in a sealed tube was shaken at the desired temperature for different lengths of time. The resulting material was made basic, subjected to hydrolysis, and then worked up in the presence of added isomeric butyl alcohols as carriers. The following is the description of one of the experiments with CF_3SO_3H-*t*.

Cyclobutane (1.01 g, 18 mmol), bp 12–13 °C, prepared from 1,4-dibromobutane (10), was distilled directly into the reaction tube which contained 2.0 ml of CF_3SO_3H-*t* (1.48×10^8 dpm/mmol) and which was cooled in a dry ice – acetone bath. The tube was sealed and the heterogeneous mixture was shaken mechanically in an oil bath at 75 ± 0.2 °C for 3 days. After cooling, the material was made basic with 20 ml of 20% NaOH solution, transferred to a 50 ml flask, and heated under reflux at 75 °C overnight to effect the hydrolysis of any butyl esters that were formed. To the hydrolyzate, inactive carriers (32.7, 32.6, 31.0, and 31.9 mmol of *n*-BuOH, *sec*-BuOH, *iso*-BuOH, and *tert*-BuOH, respectively) were added. The resulting material was extracted with ether, the extract dried over $MgSO_4$, and the alcohols were recovered by vpc using a Pye automatic preparative chromatograph with a 12 ft × $\frac{3}{8}$ in. copper column at 80 °C packed with 20% FFAP on Chromosorb W. The recovered alcohols were converted to the appropriate solid derivatives (Table 1) and assayed for T-activity by a liquid scintillation counter to give the results summarized in Table 1.

The following is an illustration of the isotope dilution calculations. Since the specific activities of the *n*-BuOH before and after isotopic dilution were 1.48×10^8 and 6.84×10^5 dpm/mmol, respectively, and since the amount of *n*-BuOH carrier was 32.7 mmol, if x is the yield of the *n*-BuOH-*t* produced in the protonation reaction, then:

$$1.48 \times 10^8 x = (x + 32.7)6.84 \times 10^5$$

where $x = 0.15$ mmol or $(0.15/18)100 = 0.8\%$.

Effect of CF_3SO_3H-t on n-BuOH

In a typical experiment, 13 mg (0.18 mmol) of *n*-BuOH, corresponding to a 1% yield from the cyclobutane used in one of the protonation experiments, was shaken for 3 days at 75 ± 0.2 °C with 2.0 ml of CF_3SO_3H-*t* (1.48×10^8 dpm/mmol). The resulting material was subjected to basic hydrolysis and then worked up with 28.3, 29.8, 26.4. and 28.7 mmol, respectively, of *n*-BuOH, *sec*-BuOH, *iso*-BuOH, and *tert*-BuOH as carriers. The recovered alcohols, assayed as solid derivatives as in the protonation experiment, were found to be active, the observed activities being 31 800, 4400, 3300, and 6000 dmp/mmol, respectively, for *n*-BuOH, *sec*-BuOH, *iso*-BuOH and *tert*-BuOH. Oxidation of the active *n*-BuOH by alkaline $KMNO_4$ (11) to butyric acid resulted in a loss of essentially all of its T-activity.

H–T Exchange in the Recovered Cyclobutane

A mixture of 1.01 g (18 mmol) of cyclobutane and 2.0 ml of CF_3SO_3H-*t* (1.42×10^7 dpm/mmol) in a sealed tube was shaken at 75 ± 0.2 °C for 3 days as in the protonation experiment. The unreacted cyclobutane was distilled at room temperature into 20 ml of scintillation counting solution (toluene containing PPO and POPOP). The weight of cyclobutane dissolved in the toluene was determined and after appropriate dilution, the specific activity of the recovered cyclobutane was found to be 1.42 and 1.43×10^7 dpm/mmol for duplicate experiments, indicating 100% exchange of one H of the cyclobutane with the CF_3SO_3H-*t*.

In a similar experiment, a homogeneous solution of 0.67 g (12 mmol) of cyclobutane in 2.0 ml of CF_3COOH-*t* (1.86×10^6 dpm/mmol) in a sealed tube was shaken at 60 ± 0.2 °C for 5 days. (One experiment at 75 °C was lost since this temperature was higher than the bp of CF_3COOH and the sealed tube exploded.) From duplicate runs, the recovered cyclobutane showed specific activities of 2.28 and 2.30×10^5 dpm/mmol, corresponding to about 12% exchange of one H in the cyclobutane with the CF_3COOH-*t*.

Acknowledgment

The financial support given by the National Research Council of Canada is sincerely acknowledged.

1. C. J. Collins. Chem. Rev. **69**, 543 (1969).
2. C. C. Lee. Prog. Phys. Org. Chem. **7**, 129 (1970).
3. D. M. Brouwer and H. Hogeveen. Prog. Phys. Org. Chem. **9**, 179 (1972).
4. M. Saunders, P. Vogel, E. L. Hagen, and J. Rosenfeld. Acc. Chem. Res. **6**, 53 (1973).
5. R. L. Baird and A. A. Aboderin. J. Am. Chem. Soc. **86**, 252 (1964).
6. C. C. Lee and L. Gruber. J. Am. Chem. Soc. **90**, 3775 (1968).
7. R. Liardon and L. Gäumann. Helv. Chim. Acta, **54**, 1968 (1971).
8. R. L. Baird and A. Aboderin. Tetrahedron Lett. 235 (1963).
9. C. C. Lee, A. J. Cessna, E. C. F. Ko, and S. Vassie. J. Am. Chem. Soc. **95**, 5688 (1973).
10. K. B. Wiberg and D. S. Connor. J. Am. Chem. Soc. **88**, 4437 (1966).
11. C. C. Lee and I. Y. Zea Ponce. Can. J. Chem. **50**, 3179 (1972).

Can. J. Chem. Downloaded from www.nrcresearchpress.com by 210.87.254.42 on 09/05/12
For personal use only.

Oxidation of olefins by palladium(II). VIII. Kinetics of the oxidation of ethylene by palladium(II) chloride in methanol

HING-BIU LEE AND PATRICK M. HENRY[1]

Guelph–Waterloo Centre for Graduate Work in Chemistry, Guelph Campus, Chemistry Department, University of Guelph, Guelph, Ont., Canada N1G 2W1

Received September 22, 1975

HING-BIU LEE and PATRICK M. HENRY. Can. J. Chem. **54**, 1726 (1976).

The oxidation of ethylene in methanol at 25 °C by palladium(II) chloride plus LiCl, was found to yield mainly $CH_3CH(OCH_3)_2$. If the reaction is run in CH_3OD the acetal is undeuterated. In order to interpret the kinetics the equilibria between Pd(II) and chloride and Pd(II) and C_2H_4 were studied. The equilibria, $PdCl_3(CH_3OH)^- + Cl^- \overset{K_H}{\rightleftharpoons} PdCl_4^{2-}$ and $PdCl_4^{2-} + C_2H_4 \overset{K_1}{\rightleftharpoons} PdCl_3(C_2H_4)^- + Cl^-$, were found to be operative with $K_H = 0.010\ M^{-1}$ and $K_1 = 8.1$ at 25 °C. The value of K_2 for the equilibrium $PdCl_3(C_2H_4)^- + CH_3OH \overset{K_2}{\rightleftharpoons} PdCl_2(C_2H_4)(CH_3OH) + Cl^-$ was found to be less than $10^{-2}\ M$. The ethylene oxidation was studied by gas uptake using quinone to prevent precipitation of Pd(0). The reaction is strongly inhibited by acid and chloride. The acid inhibition by weak acids such as methanesulfonic and acetic depends on the square root of acid concentration which is consistent with a first order acid inhibition. In the $[H^+]$ range from about 10^{-2} to $10^{-5}\ M$ the rate expression is identical to that previously found in water; $-d[C_2H_4]/dt = kK_1[PdCl_4^{2-}][C_2H_4]/[H^+][Cl^-]^2$. The solvent isotope effect $k_{CH_3OH}/k_{CH_3OD} = 1.34$ is much smaller than that found previously in water ($k_{H_2O}/k_{D_2O} = 4.05$). The effect of ionic strength is analogous to that previously found in water. The rate first increases with increasing ionic strength, reaches a maximum at about $\mu = 0.75$ and then gradually decreases. The rate expression and other factors suggest a mechanism analogous to that previously proposed for the aqueous system. This mechanism has the slow step in the reaction involving *cis* insertion of a coordinated methoxide to coordinated ethylene to give a β-methoxyethylpalladium(II) alkyl. Evidence for the mode of decomposition of this alkyl is provided by the oxidation of C_2H_4 in CH_3OD. The resulting dimethyl acetal of acetaldehyde contains no deuterium. This suggests a decomposition step involving Pd(II)-hydride elimination and readdition in the opposite mode to put the Pd(II) on the carbon containing the methoxy group. The Pd(II) is reductively eliminated from this adduct to give Pd(0) and the dimethylacetal product. At $[H^+] < 10^{-5}\ M$ the rate becomes independent of $[H^+]$ and at $[H^+] < 10^{-8}\ M$ the rate actually decreases with decreasing $[H^+]$. The cause of this change in $[H^+]$ dependency is uncertain.

HING-BIU LEE et PATRICK M. HENRY. Can. J. Chem. **54**, 1726 (1976).

On a trouvé que l'oxydation de l'éthylène, dans le méthanol à 25 °C, par le chlorure de palladium(II) en présence de LiCl conduit principalement au $CH_3CH(OCH_3)_2$. Si on effectue la réaction dans le CH_3OD, l'acétal n'est pas deutéré. De façon à interpréter la cinétique, on a étudié l'équilibre entre Pd(II) et le chlorure et Pd(II) et C_2H_4. On a trouvé que les équilibres $PdCl_3(CH_3OH)^- + Cl^- \overset{K_H}{\rightleftharpoons} PdCl_4^{2-}$ et $PdCl_4^{2-} + C_2H_4 \overset{K_1}{\rightleftharpoons} PdCl_3(C_2H_4)^- + Cl^-$, sont des réactions qui se produisent; $K_H = 0.010\ M^{-1}$ et $K_1 = 8.1$ à 25 °C. On a trouvé que la valeur de K_2 pour l'équilibre de $PdCl_3(C_2H_4)^- + CH_3OH \overset{K_2}{\rightleftharpoons} PdCl_2(C_2H_4)CH_3OH) + Cl^-$ est plus faible que $10^{-2}\ M$. On a étudié l'oxydation de l'éthylène par l'absorption de gaz utilisant la quinone pour prévenir la précipitation du Pd(0). La réaction est fortement inhibée par l'acide et le chlorure. L'inhibition acide, par des acides faibles tel que le méthanesulfonique et l'acide acétique, varie avec la racine carré de la concentration de l'acide; ceci est en accord avec une inhibition acide du premier ordre. Lorsque la concentration en H^+ varie entre 10^{-2} et $10^{-5}\ M$, l'expression de vitesse est identique à celle trouvée antérieurement dans l'eau soit $-d[C_2H_4]/dt = kK_1[PdCl_4^{2-}][C_2H_4]/[H^+][Cl^-]^2$. L'effet isotopique du solvant $k_{CH_3OH}/k_{CH_3OD} = 1.34$ est beaucoup plus faible que celui trouvé antérieurement dans l'eau ($k_{H_2O}/k_{D_2O} = 4.05$). L'effet de la force ionique est analogue à celui trouvé antérieurement dans l'eau. La vitesse commence par augmenter avec l'augmentation de la force ionique, elle atteint un maximum aux environs de $\mu = 0.75$ et diminue graduellement. L'expression de vitesse et les autres facteurs suggèrent un mécanisme analogue à celui proposé antérieurement pour le système aqueux. Ce mécanisme

[1]To whom correspondence should be addressed.

Can. J. Chem. Downloaded from www.nrcresearchpress.com by 210.87.254.40 on 09/05/12
For personal use only.

implique une étape déterminante au cours de laquelle il se produit une insertion *cis* d'un méthylate coordonné vers un éthylène coordonnée de façon à produire un alkyle de β-méthoxy-éthylpalladium(II). On obtient des indications concernant le mode de décomposition de cet alkyle par l'oxydation du C_2H_4 dans le CH_3OD. Le diméthyle acétal de l'acétaldéhyde qui en résulte ne contient pas de deutérium. Ceci suggère une étape de décomposition impliquant une élimination de Pd(II)-hydrure et une réaddition dans le mode opposé de façon à obtenir un palladium sur le carbone contenant le groupe méthoxyle. Le palladium(II) est éliminé d'une façon réductrice de cet adduit pour donner du Pd(0) et un produit diméthylacétal. A une concentration de $H^+ < 10^{-5}$ *M* la vitesse devient indépendante de la concentration de H^+ et à $[H^+] < 10^{-8}$ *M*, la vitesse diminue avec une diminution de $[H^+]$. La cause de ce changement de dépendance sur la concentration en H^+ n'est pas connue.

[Traduit par le journal]

Introduction

The field of organic synthesis by palladium(II) catalysis has received considerable study in the last fifteen years (1). The most important example is the oxidation of ethylene by palladium(II) chloride in aqueous solution.

$$[1]\quad C_2H_4 + H_2O + PdCl_4^{2-} \xrightarrow{H_2O} CH_3CHO + Pd(0) + 2HCl + 2Cl^-$$

This oxidation is the basis reaction of the Wacker process for acetaldehyde manufacture from ethylene. Higher olefins are oxidized to mixtures of aldehydes and ketones (1, 2).

The kinetics of the oxidation of olefins by aqueous palladium(II) chloride has been studied by several workers (3–7). All agree that over a wide range of $[H^+]$ and $[Cl^-]$ and at $[PdCl_4^{2-}] < 0.1$ *M* the following rate expression holds for the oxidation of ethylene, propylene, and the butenes,

$$[2]\quad \frac{-\mathrm{d}[\text{olefin}]}{\mathrm{d}t} = \frac{kK[\text{olefin}][PdCl_4^{2-}]}{[H^+][Cl^-]^2}$$

where *K* is the equilibrium constant for π-complex formation.

$$[3]\quad PdCl_4^{2-} + \text{olefin} \overset{K}{\rightleftharpoons} PdCl_3(\text{olefin})^- + Cl^-$$

The equilibrium corresponding to reaction 3 has been detected under several reaction conditions and values of *K* measured (4–10). Thus the rate equation can be written as

$$[4]\quad \frac{-\mathrm{d}[\text{olefin}]}{\mathrm{d}t} = \frac{k'[PdCl_3(\text{olefin})^-]}{[H^+][Cl^-]}$$

Although there is some disagreement about details of some steps, the general mechanism outlined below is accepted by most workers.

$$[5]\quad PdCl_3(RCH{=}CH_2)^- + H_2O \overset{K_1}{\rightleftharpoons} PdCl_2(RCH{=}CH_2)(H_2O) + Cl^-$$

$$[6]\quad PdCl_2(RCH{=}CH_2)(H_2O) + H_2O \overset{K_H}{\rightleftharpoons} PdCl_2(RCH{=}CH_2)(OH)^- + H_3O^+$$

[7]

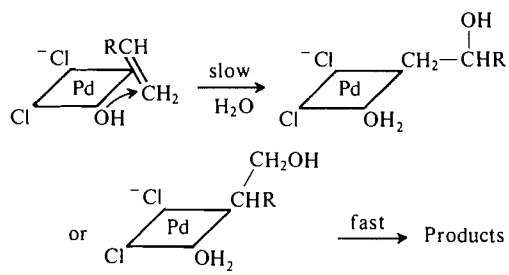

The important feature of the mechanism is the *cis* insertion of the elements of Pd(II) and coordinated OH across the olefinic bond.

Since this original suggestion there have been several reports of both *trans* and *cis* additions of nucleophiles and Pd(II) to olefins (11–16). These results have raised some doubts about the original proposal for the Wacker process. In fact the addition of water to cyclooctadiene to give a stable adduct has very recently been reported to be *trans* (17). Unfortunately with monoolefins in water the carbonyl oxidation products give no information as to stereochemistry. A series of studies on exchange and oxidation reactions in acetic acid indicate that in this solvent addition can be *cis* or *trans* depending on nucleophiles and reaction conditions (12). The intermediates in this solvent, however, are not identical to those in aqueous solution so these differences may not be surprising.

Methanol, however, would be much closer to water than acetic acid and thus oxidation in this solvent might be mechanistically similar to water and there is the possibility in methanol, of re-

Can. J. Chem. Downloaded from www.nrcresearchpress.com by 210.87.254.40 on 09/05/12
For personal use only.

Can. J. Chem. Downloaded from www.nrcresearchpress.com by 210.87.254.40 on 09/05/12
For personal use only.

inforcing kinetic results with stereochemical results. There have already been some stereochemical studies carried out in this solvent. Thus, diolefins are known to react with methanol to give stable adducts by *trans* addition (12, 13) while the oxidation of *cis*- and *trans*-2-butene by palladium(II) chloride in the presence of CO gives carboxylic acid esters whose stereochemistry can best be interpreted in terms of *trans* methoxypalladation (18). However, the kinetics of these processes have not been investigated and the stereochemistry of methoxypalladation of monoolefins in the absence of CO is not known. Because CO forms Pd(II) carbonyl the stereochemistry of methoxypalladation in the presence of CO is likely to be quite different than in its absence.

To our knowledge there has been only one kinetic study of the oxidation of ethylene by palladium(II) chloride in methanol. This study, carried out in the presence of $CuCl_2$ which converted the Pd(0) back to Pd(II), gave the following rate expression at low $[CuCl_2]$ (19)

$$[8] \qquad \frac{-d[C_2H_4]}{dt} = \frac{k[PdCl_4^{2-}][C_2H_4]}{[H^+][Cl^-]}$$

This rate expression was interpreted in terms of a rate determining step which involved attack of methoxide ion on a Pd(II)–ethylene π-complex.

[9] 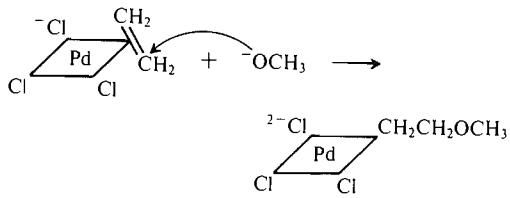

However, in the presence of $CuCl_2$ the actual chloride concentration is uncertain. Therefore, it seemed worthwhile as a first step in a study of the methanol system to determine the rate expression in the absence of $CuCl_2$. This paper describes such a study.

Experimental

Materials

The palladous chloride was purchased from Engelhard Corp. The methanol was of GC-Spectrophotometric quality from J. T. Baker Chemical Co. It was further dried with trimethyl orthoformate. The ethylene (C.P. grade) was purchased from Matheson of Canada, Ltd. All other chemicals were reagent grade. As palladous chloride alone is sparingly soluble in methanol stock solutions of composition 0.2 *M* Li_2PdCl_4 were prepared. Reaction mixtures were prepared by diluting these stock solutions.

Ultraviolet Spectral Study

The spectra were recorded on a Cary 14 or a Cary 118 spectrophotometer at 25 °C. The cell thicknesses were 1, 5, and 10 mm depending on the Pd(II) concentrations.

Kinetic Runs

The rates of oxidation of ethylene were followed by the uptake of ethylene measured in gas burets and creased flask agitated by means of magnetic stirring bars. All reactions were run in the presence of quinone and at a constant ethylene pressure of 1 atm. The temperature of the thermostated bath was kept at 25.0 ± 0.1 °C.

Apart from the initial uptake, a plot of ΔV *vs.* time gave a straight line in all runs until the reoxidant was used up. The solubilities of ethylene were measured by the ethylene uptake of solutions of the same composition as the reaction mixtures but from which the palladium salt was omitted. The reactions were much too slow to be diffusion limited.

Gas Chromatography

Analyses were carried out with a Hewlett-Packard research chromatograph (model H.P. 5750B) using a 6 ft 20% Carbowax 20M column on 60–80 mesh Chromosorb W. Temperature was 68 °C and helium flow rate was 35 ml/min.

Results

The $PdCl_4^{2-}$ and Cl^- Equilibrium

The equilibrium between palladium(II) chloride and LiCl in methanol was studied by uv absorption spectroscopy in the 400–200 nm region at 25 °C. The solutions were adjusted to a constant ionic strength of 2.0 *M* by means of $LiClO_4$.

Stock solutions of composition $PdCl_2 + 2LiCl$ were prepared and their spectra recorded. It was found that addition of more LiCl caused rapid changes in spectra. At [LiCl] > *ca.* 0.4 *M* there was no further change suggesting complete conversion to the final species. The spectra at high chloride was almost identical to K_2PdCl_4. In the presence of an acid such as methanesulfonic acid isosbestic points at lower lithium chloride concentrations (315, 266, and 236 nm) were observed suggesting two species were in equilibrium. The two most logical equilibria are given by reactions 10 and 11.

$$[10] \quad PdCl_4^{2-} + CH_3OH \overset{K_H}{\rightleftharpoons} PdCl_3(CH_3OH)^- + Cl^-$$

$$[11] \quad 2PdCl_4^{2-} \overset{K_D}{\rightleftharpoons} Pd_2Cl_6^{2-} + 2Cl^-$$

TABLE 1. Calculation of K_{II} from spectral data[a]

$[Cl^-]$ (M)	$[Cl^-]^2$ ($M^2 \times 10^4$)	D_i (λ282 nm)	$\frac{P_0}{\Delta D} \times 10^4$	$[PdCl_4^{2-}]^b$ (P_1) ($M \times 10^5$)	$[PdCl_3(CH_3OH)^-]^b$ (P_2) ($M \times 10^5$)	$K_H{}^b$ ($\times 10^2$)
0.100	100.00	0.720	15.0	6.82	0.68	1.00
0.075	56.20	0.700	10.7	6.56	0.94	1.08
0.050	25.00	0.677	8.06	6.26	1.24	0.99
0.030	9.00	0.635	5.56	5.72	1.78	0.93
0.020	4.00	0.587	4.05	5.10	2.40	0.94
0.010	1.00	0.480	2.59	3.71	3.79	1.02
0.005	0.25	0.385	1.95	2.48	5.02	1.01
0.002	0.04	0.250	1.44	1.23	6.27	1.02
						Average 1.00

[a]$[Pd(II)]_t = P_0 = 7.5 \times 10^{-5}$.
[b]Calculated by using $\epsilon_1 = 1.03 \times 10^4\ M^{-1}\ cm^{-1}$ and $\epsilon_2 = 2.58 \times 10^3\ M^{-1}\ cm^{-1}$. Latter value calculated from intercept of plot of $P_0/\Delta D$ *vs.* $[Cl^-]$. Value of K_H calculated from slope of this plot is 0.98×10^{-2}.

If we assume reaction 10 is operative then the following can be written ($P_1 = PdCl_4^{2-}$ and $P_2 = PdCl_3(CH_3OH)^-$; D_i is optical density at $[Cl^-]_i$).

$$[12] \qquad P_0 = P_1 + P_2$$

$$[13] \qquad D_\infty = P_0\epsilon_1 l$$

$$[14] \qquad \begin{aligned} \Delta D &= D_\infty - D_i \\ &= P_0\epsilon_1 l - \epsilon_1 l P_1 - \epsilon_2 l P_2 \\ &= (\epsilon_1 - \epsilon_2) l P_2 \\ &= \Delta\epsilon l P_2 \end{aligned}$$

Now writing the equilibrium and substituting, eq. 15 follows.

$$[15] \qquad K_H = \frac{P_2[Cl^-]}{P_1} = \frac{\Delta D[Cl^-]}{\Delta\epsilon l\left(P_0 - \frac{\Delta D}{\Delta\epsilon l}\right)}$$

This equation can be rearranged to give eq. 16.

$$[16] \qquad \frac{P_0}{\Delta D} = \frac{1}{\Delta\epsilon l} + \frac{[Cl^-]}{K\Delta\epsilon l}$$

Since D_∞ is known ΔD and therefore $P_0/\Delta D$ can be calculated at various $[Cl^-]$. Plots of $P_0/\Delta D$ *vs.* $[Cl^-]$ at several palladium(II) concentrations gave straight lines from which $\Delta\epsilon$ and K could be calculated.

Alternately, if reaction 11 is assumed to be operative the values of K_D can be calculated using various values of ϵ_2 for the $Pd_2Cl_6^{2-}$ species. The lower limit of ϵ_2 can be determined from the optical densities at low $[Cl^-]$. At all values of ϵ_2 the values of K_D vary considerably with both $[Cl^-]$ and total palladium(II) concentration indicating eq. 11 does not represent the true equilibrium.

Some typical data are shown in Table 1. Using ϵ_2 calculated from the intercept of the straight line the values of K_{II} remain constant as $[Cl^-]$ varies. Average value of K_{II} is 1.0×10^{-2} at 25 °C.

In the absence of an acid, isosbestic points were not obtained, indicating that other equilibria are also operative. Attempts have also been made to record the ultraviolet absorption spectra of $PdCl_4^{2-}$ in a series of buffered solutions in methanol, particularly those at low acidities and low chloride concentrations. Because of the rapid decomposition of Pd(II) to Pd(0) under such conditions, the quality of the spectra was not good enough for the calculation of equilibrium constants. However, the spectra do show changes at various acidities, suggesting that an equilibrium such as the one shown below might also be operative.

$$[17] \qquad PdCl_3(MeOH)^- \rightleftharpoons PdCl_3(MeO)^{2-} + H^+$$

Oxidation of Ethylene in Methanol

Ethylene was oxidized by Pd(II) in anhydrous methanol to give dimethylacetal of acetaldehyde and methyl vinyl ether which were analyzed by gas–liquid chromatography (glc). At 25 °C, the major product was the acetal (*ca.* 95% yield, based on the amounts of reoxidant and palladium salt used). The reaction can be made catalytic by adding a reoxidant such as *p*-benzoquinone to the reaction mixture.

$$[18] \qquad Pd(II) + C_2H_4 + CH_3OH \rightarrow Pd(0) + CH_3CH(OCH_3)_2 + CH_2{=}CHOCH_3 + 2H^+$$

Can. J. Chem. Downloaded from www.nrcresearchpress.com by 210.87.254.40 on 09/05/12
For personal use only.

TABLE 2. Determination of equilibrium constants from initial ethylene uptake at high acid concentration[a]

$[Cl^-]_a$	$[PdCl_3(C_2H_4)^-]$	$[PdCl_4^{2-}]$	$[Cl^-]_e$	K[b]
0.6	0.0105	0.0204	0.6108	8.15
0.5	0.0115	0.0195	0.5118	7.87
0.4	0.0128	0.0180	0.4132	7.62
0.3	0.0155	0.0152	0.3160	8.42
0.2	0.0187	0.0120	0.2192	8.86
0.1	0.0218	0.0087	0.1225	7.94
0.05	0.0244	0.0060	0.0752	7.91
				Average 8.10

[a]Conditions: $[Pd]_t = 0.0312\ M$, $[CH_3SO_3H] = 1.0\ M$, $[C_2H_4] = 0.0385\ M$, $\mu = 2.0\ M$, $T = 25.0$ °C. $[Cl^-]_a$ is concentration of NaCl added; $[Cl^-]_e$ is concentration of free chloride at equilibrium.
[b]Average of at least three runs.

[19] Pd(0) + 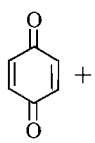 + $2H^+$ ⟶ Pd(II) + 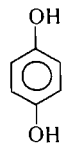

Ethylene π-Complex Formation

The determination of the π-complex formation constant and the kinetic studies described in the next section were carried out using gas uptake measurements.

The reaction of ethylene and palladium(II) chloride in the presence of excess lithium chloride consisted of a very rapid initial ethylene uptake followed by a much slower reaction. At a constant acid concentration, the volume of ethylene initially taken up in excess of solubility requirements decreased with increasing chloride concentration. Since the net ethylene uptake decreased with increasing chloride ion, it is reasonable to assume that a palladium:ethylene π-complex was formed in the initial reaction. Further evidence is provided by the fact that the colour of the solution changed from brown to yellow. Under the conditions used, the major form of the starting material is $PdCl_4^{2-}$ as can be anticipated from the K_H value described above. The reaction can thus be represented by the following equilibrium

$$[20] \quad PdCl_4^{2-} + C_2H_4 \overset{K_1}{\rightleftharpoons} PdCl_3(C_2H_4)^- + Cl^-$$

A 1:2 palladium:ethylene complex is unlikely to be formed here since the corresponding formation constant K_1'

$$[21] \quad PdCl_4^{2-} + 2C_2H_4 \overset{K_1'}{\rightleftharpoons} PdCl_2(C_2H_4)_2 + 2Cl^-$$

did not give constant values at various chloride concentrations.

At high acid concentration (1.0 *M*), the oxidation of ethylene was stopped even at low chloride concentrations (*e.g.*, 0.05 *M*) and the total ethylene uptake equaled to the sum of solubility and that required for π-complex formation. The values of K_1 (Table 2) calculated from these uptake data have an average value of 8.1 at 25 °C.

These data were also treated according to the method of Pestrikov *et al.* (10). Thus, if we assume that the equilibrium represented by [22]

$$[22] \quad PdCl_3(C_2H_4)^- + H_2O \overset{K_2}{\rightleftharpoons} PdCl_2(H_2O)(C_2H_4) + Cl^-$$

is also operative and define $\phi = [C_2H_4]_t/[C_2H_4]$ where $[C_2H_4]_t$ represents the total ethylene concentration (π-complex plus solubility) and $[C_2H_4]$ is the ethylene solubility, it can be readily shown that [23] applies.

$$[23] \quad \frac{[\phi - 1][Cl^-]^2}{[PdCl_4^{2-}]} = K_1[Cl^-] + K_1K_2$$

A plot of the left side of [23] *vs.* $[Cl^-]$ should give a straight line with slope K_1 and intercept K_1K_2. The data in Table 2 do give a straight line plot with intercept near zero. A least squares fit of the data gives a slope of 7.93 with an intercept of 0.046 which corresponds to a K_2 value of 0.006. The correlation coefficient is 0.9972. By dropping various points and refitting the data the maximum intercept consistent with the data can be determined. It appears that an intercept greater than 0.17 is impossible and an intercept higher than 0.09 is very unlikely. This would set a maximum value on K_2 of about 10^{-2} *M*.

At low acid concentrations (<0.1 *M*) where oxidation was usually carried out, the K_1 values could also be calculated from the initial ethylene

Can. J. Chem. Downloaded from www.nrcresearchpress.com by 210.87.254.40 on 09/05/12
For personal use only.

TABLE 3. Determination of equilibrium constants from initial ethylene uptake at low acid concentration[a]

$[Cl^-]_a$	$[PdCl_3(C_2H_4)^-]$	$[PdCl_4^{2-}]$	$[Cl^-]_e$	K^b
0.5	0.0139	0.0170	0.5142	9.11
0.4	0.0157	0.0152	0.4161	9.33
0.3	0.0180	0.0128	0.3184	9.68
0.2	0.0209	0.0099	0.2213	10.18
0.1	0.0239	0.0068	0.1244	9.45
0.075	0.0248	0.0058	0.1004	9.28
0.05	0.0261	0.0045	0.0767	9.28
				Average 9.47

[a]Conditions: $[Pd]_t = 0.0312$ *M*, $[CH_3SO_3H] = 0.1$ *M*, $[C_2H_4] = 0.0461$ *M*, $\mu = 2.0$ *M*, $T = 25.0$ °C.
[b]Average of at least three runs.

TABLE 4. Effect of acidity on π-complex formation[a]

Added Cl^- (*M*)	Net uptake (ml of gas at 25 °C)[b]		
	1 *M* CH_3SO_3H	0.1 *M* CH_3SO_3H	0.1 *M* LiOAc/0.1 *M* HOAc
0.1	13.3	14.6	11.5
0.2	11.4	12.8	10.1
0.3	9.5	11.0	8.5

[a]$[PdCl_4^{2-}] = 0.0312$ *M*, $\mu = 2.0$ *M*. Volume of solution is 25 ml.
[b]Ethylene pressure is 1 atm.

TABLE 5. Rates of oxidation of ethylene at various Li_2PdCl_4 and LiCl concentrations[a]

Initial $[PdCl_4^{2-}]$ (*M*)	Initial $[Cl^-]$ (*M*)	$[PdCl_3(C_2H_4)^-]^b$ ($M \times 10^2$)	$[Cl^-]_{eq}{}^b$ (*M*)	k_{obs} ($M\,s^{-1} \times 10^5$)	k'^c ($M\,s^{-1} \times 10^5$)
0.010	0.100	0.778	0.108	0.47	6.52
0.050	0.100	3.69	0.138	1.61	6.02
0.10	0.100	6.96	0.171	2.55	6.28
0.010	0.200	0.656	0.207	0.192	6.06
0.050	0.200	3.15	0.232	0.846	6.23
0.10	0.200	6.04	0.262	1.46	6.32

[a]All runs at 25 °C under 1 atm of ethylene pressure and 0.1 *M* in CH_3SO_3H.
[b]Calculated using K_1 for eq. 20 = 9.47; these values are the values at equilibrium.
[c]$k' = k_{obs}[Cl^-]_{eq}/[PdCl_3(C_2H_4)^-]$.

uptakes. The results (Table 3) were similar to those presented in Table 2 and the average value of K_1 was 9.47. Because these values are less accurate than those in Table 2 the data were not treated according to the procedure of Pestrikov *et al.* In Table 4 is given the ethylene uptake at various acidities. As can be seen the net (total volume of gas absorbed − volume absorbed due to solubility) uptake decreases to some extent at low $[H^+]$.

Kinetic Studies

All reactions were carried out at 25 °C under 1 atm ethylene pressure. Most are run in the presence of quinone.

(1) Chloride, Olefin and Pd(II) Dependencies

If the rate equation in methanol is analogous to that found in water (eqs. 3 or 4) these dependencies are difficult to separate. Thus the chloride could be inhibiting formation of π-complex via reaction 20 as well as also displaying a second inhibition term. Also since π-complex formation occurs to a significant extent the rate should not be strictly first order in [Pd(II)]. Samples of rate data at three initial $[PdCl_4^{2-}]$ and two initial $[Cl^-]$ are given in Table 5. As can be seen from the final column, the value of k' remains constant when this rate expression is assumed. As a further indication of the second chloride inhibition a plot of $k_{corr}(=k_{obsd}/[PdCl_3(C_2H_4)^-])$

Can. J. Chem. Downloaded from www.nrcresearchpress.com by 210.87.254.40 on 09/05/12
For personal use only.

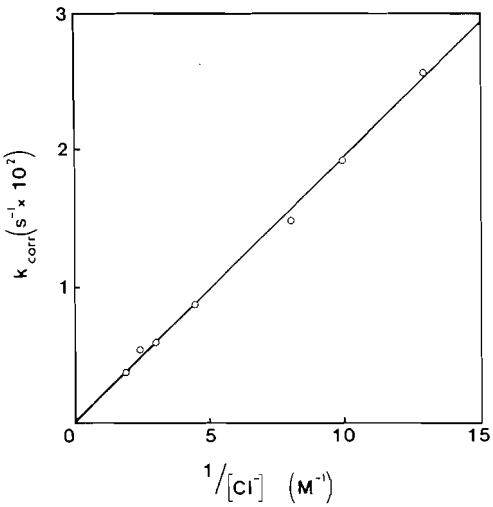

FIG. 1. Plot of k_{corr} *vs.* $1/[Cl^-]$; $[PdCl_4^{2-}] = 0.0312\ M$ and $[CH_3SO_3H] = 0.1\ M$.

vs. $1/[Cl^-]$ at constant acid concentration gives a straight line (Fig. 1).

Thus at constant acid concentration the rate expression is given by eq. 24

$$[24] \qquad \frac{-d[olefin]}{dt} = \frac{k'[PdCl_3(C_2H_4)^-]}{[Cl^-]}$$

This rate expression can alternately be written in terms of initial palladium(II) concentration ($[PdCl_4^{2-}]_{int}$).

$$[25] \qquad \frac{-d[C_2H_4]}{dt} = \frac{k'K[PdCl_4^{2-}]_{int}[C_2H_4]}{(K[C_2H_4] + [Cl^-])[Cl^-]}$$

In this equation as in all other rate expressions the ethylene concentration is the solubility of ethylene in the reaction mixture at 1 atm since all runs are made at 1 atm pressure. The total ethylene concentration is, of course, $[C_2H_4] + [PdCl_3(C_2H_4)^-]$.

In this study the ethylene concentration was not varied but under all conditions the value of $K[C_2H_4]$ in eq. 25 was of the order of magnitude of $[Cl^-]$. However, as demonstrated by Table 5, eq. 25 is obeyed at various $[Pd(II)]_t$, indicating the reaction is first order in $[PdCl_3(C_2H_4)^-]$.

(2) Hydrogen Ion Dependence

The rates of oxidation of ethylene in methanol were strongly inhibited by H^+. Methanesulfonic acid, a moderately weak acid in methanol, was used in these acid dependence runs. If the palladium(II) chloride and ethylene concentrations were kept constant, the reactions were pseudo zero-order. A plot of the rates *vs.* $1/\sqrt{[acid]}$ yielded a straight line within the range of acid concentrations shown in Fig. 2. Since CH_3SO_3H is a weak acid in methanol, $[H^+]$ is proportional to $\sqrt{[acid]}$. Thus the rates of oxidation of ethylene have an inverse first-order dependence on $[H^+]$.

In addition to CH_3SO_3H, CH_3COOH, and $CHCl_2CO_2H$ were also used as acids. It was found that the slope of the plot of k_{obs} *vs.* $1/\sqrt{[acid]}$ depended on the particular acid used. This is expected since the change in $[H^+]$ with [acid] will depend on the K_a of the acid. Thus, at constant $[Cl^-]$ the value of k_{obs} is given by eq. 26 and the slope is equal to $k'/\sqrt{K_a}$.

$$[26] \qquad k_{obs} = \frac{k'}{[H^+]} = \frac{k'}{\sqrt{acid}\sqrt{K_a}}$$

Thus k' = slope $\times$ K_a should be constant for all acids. Using the value of K_a at $\mu = 0$ since the values at $\mu = 2.0$ are not available, the values of k' for CH_3CO_2H and $CHCl_2CO_2H$ are given in Table 6. The values are fairly close considering the high ionic strength. The average k' is 1.84 $\times$

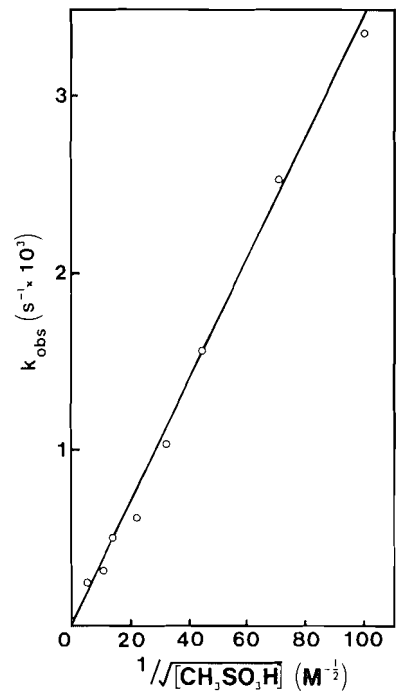

FIG. 2. Plot of k_{obs} *vs.* $1/\sqrt{[CH_3SO_3H]}$; $[PdCl_4^{2-}] = 0.00625\ M$ and $[Cl^-] = 0.48\ M$.

Can. J. Chem. Downloaded from www.nrcresearchpress.com by 210.87.254.40 on 09/05/12
For personal use only.

TABLE 6. Rates of oxidation of ethylene in the presence of various acids[a]

Acid	Slope[b]	K_a[c] ($\mu = 0$)	$\sqrt{K_a}$	k'[e]
CH_3CO_2H	100	2.5×10^{-10}	1.58×10^{-5}	1.58×10^{-3}
$CHCl_2CO_2H$	3.3	4.0×10^{-7}	6.32×10^{-4}	2.1×10^{-3}
CH_3SO_3H	1.0	(3.4×10^{-6})[d]	(1.84×10^{-3})[d]	1.84×10^{-3}[f]

[a]$[Pd(II)] = 0.00625\ M$; $[LiCl] = 0.48\ M$.
[b]Slope of plot of k_{obs} *vs.* $1/\sqrt{\text{acid}}$.
[c]From ref. 20.
[d]Calculated.
[e]$k' = (\text{Slope}) \times (\sqrt{K_a})$.
[f]Average of values for CH_3CO_2H and $CHCl_2CO_2H$.

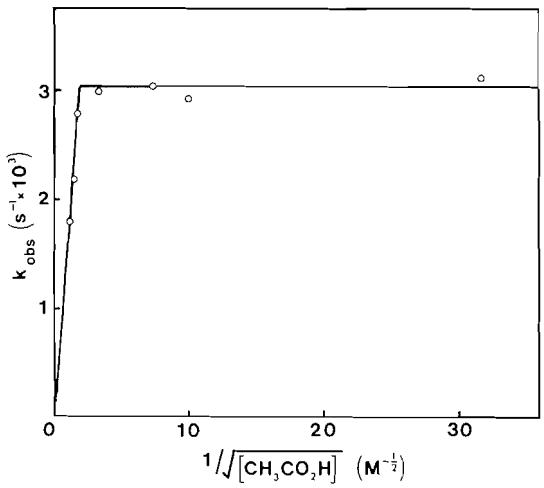

FIG. 3. Plot of k_{obs} *vs.* $1/\sqrt{[CH_3CO_2H]}$; $[PdCl_4^{2-}] = 0.00625\ M$ and $[Cl^-] = 0.48\ M$.

10^{-3}. Using this value to calculate K_a for CH_3SO_3H the value of 3.4×10^{-6} is obtained. The pK_a of CH_3SO_3H in water at 25 °C has been determined to be -1.20 by nmr (21) and -1.86 by Raman spectroscopy (22). The K_a's of many organic acids are in general 10^5 times weaker in methanol than in water (20). Thus, the calculated K_a of CH_3SO_3H is somewhat lower than would have been calculated from its K_a in H_2O.

It was noted that the rates in these runs became independent of acid concentration at low acid concentrations. This is illustrated by the acetic acid runs shown in Fig. 3. The acidity was further decreased by means of buffered solutions such as lithium acetate plus acetic acid. In this range of acidity, rates of oxidation actually decreased with decreasing acidity. Figure 4 shows a plot of rates of oxidation *vs.* $[H^+]$. The straight line indicates the rate expression in this range contains a first-order $[H^+]$ term in the numerator. Since the acidity in this range is varied by changing buffer ratios of LiOAc/HOAc there is the possibility this first-order catalytic term in $[H^+]$ really results from a first-order inhibition term in [LiOAc]. However, this possibility was eliminated by running the reaction at the same buffer ratio but different buffer concentrations. Thus at [LiOAc]/[HOAc] = 0.15 the rates for $[LiOAc] = 1.5 \times 10^{-2}$, 3.0×10^{-2}, and $4.5 \times 10^{-2}\ M$ were 0.262, 0.239, and 0.248 ml/min respectively at $[Pd(II)] = 0.00625\ M$ and $[Cl^-] = 0.48\ M$. If the inhibition were by LiOAc the rate should have decreased by a factor of three in going from the highest to lowest value of [LiOAc]. The overall

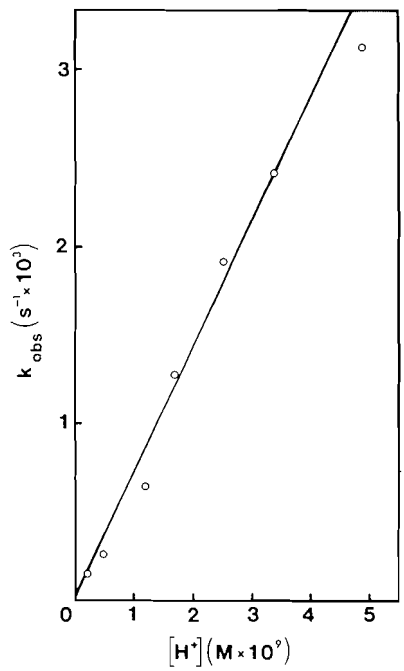

FIG. 4. Plot of k_{obs} *vs.* $[H^+]$ in a LiOAc/HOAc buffer system; $[PdCl_4^{2-}] = 0.00625$ M and $[Cl^-] = 0.48\ M$.

Can. J. Chem. Downloaded from www.nrcresearchpress.com by 210.87.254.40 on 09/05/12
For personal use only.

Can. J. Chem. Downloaded from www.nrcresearchpress.com by 210.87.254.40 on 09/05/12
For personal use only.

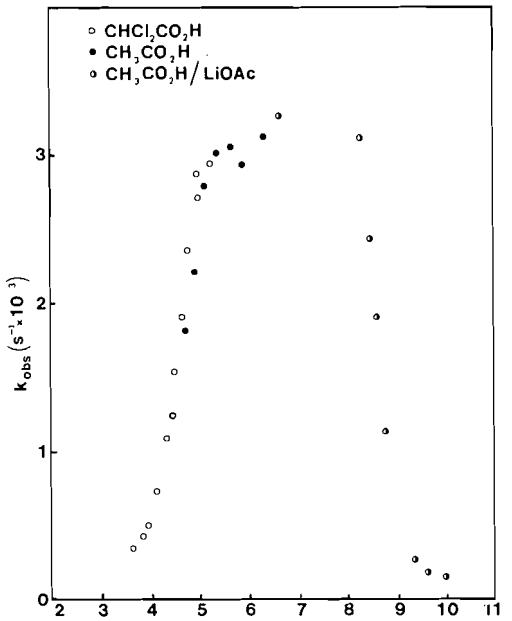

FIG. 5. Plot of k_{obs} *vs.* p*H*; $[PdCl_4^{2-}] = 0.00625$ *M* and $[Cl^-] = 0.48$ *M*.

picture of rates *vs.* acidity was shown in Fig. 5.

(3) Effect of Ionic Strength

The dependence of reaction rates on ionic strength is depicted in Fig. 6. Acids were not used in these runs since the K_a's of the organic acids also varied with ionic strength. The rates reported here have been corrected for the decreasing amount of the active species $PdCl_3(C_2H_4)^-$ as the solubility of ethylene in methanol decreases with increasing ionic strength. The reaction rates reached a maximum at ionic strength in the range 0.5–1.0 *M* and decreased at either high or lower ionic strengths. A similar

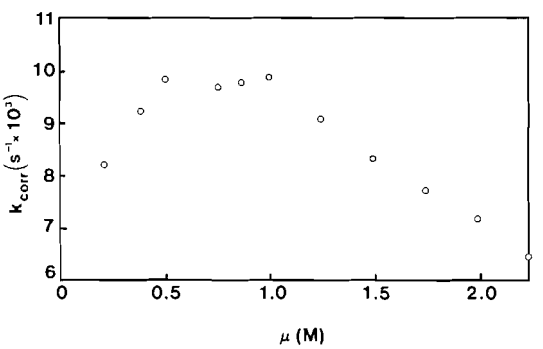

FIG. 6. Variation of k_{obs} with ionic strength in the absence of acid; $[PdCl_4^{2-}] = 0.005$ *M* and $[Cl^-] = 0.2$ *M*.

trend has been previously observed in the water system.

(4) Studies in Methanol-d

The solvent deuterium kinetic isotope effect was determined by measuring the rates of ethylene oxidation in CH_3OD and CH_3OH. The value k_{CH_3OH}/k_{CH_3OD} was 1.34 at 25 °C.

A simple distillation of the reaction products obtained in MeOD yielded an azeotropic mixture enriched in dimethylacetal (*ca.* 5%). The ^1H nmr spectrum (60 MHz) of this sample in CH_3OD showed resonances at τ5.45 q ($J = 5.2$ Hz); 6.70 s, and 8.77 d ($J = 5.2$ Hz) which was identical to that of an authentic sample of dimethylacetal in the same solvent. Integration showed no deuterium is incorporated in the acetal.

Discussion

The complete rate expression for the oxidation of ethylene in methanol catalyzed by Pd(II) in the concentration range; $[Cl^-] = 0.05$–0.5 *M*, Pd(II) = 0.006–0.1 *M*, and $[H^+] = 10^{-2}$–10^{-5} *M*, is

$$[27] \qquad \frac{-d[C_2H_4]}{dt} = \frac{kK_1[PdCl_4^{2-}][C_2H_4]}{[H^+][Cl^-]^2}$$

where the average K_1 is 9 at 25.0 °C and $\mu = 2.0$ *M*. If we assume that the K_a of CH_3SO_3H is *ca.* 10^{-6} then the overall rate constant k is *ca.* 6.2×10^{-7} M^2 s^{-1} at 25.0 °C. In this rate expression all concentrations are equilibrium concentrations. The rate expression can also be written in forms analogous to eqs. 24 and 25.

The rate expression is identical to that found for the aqueous oxidation and differs from the expression previously proposed by Francois which contains only a first-order chloride inhibition term (19). As in the Wacker reaction the chloride inhibition terms are consistent with the prior formation of an ethylene π-complex and its subsequent solvolysis reaction

$$[28] \qquad PdCl_4^{2-} + C_2H_4 \overset{K_1}{\rightleftharpoons} \underset{\mathbf{1}}{PdCl_3(C_2H_4)^-} + Cl^-$$

$$[29] \qquad PdCl_3(C_2H_4)^- + CH_3OH \overset{K_2}{\rightleftharpoons} \underset{\mathbf{2}}{PdCl_2(CH_3OH)(C_2H_4)} + Cl^-$$

The value of K_1 in methanol is similar to that found in water (17.4) (6). The best fit of the data indicated a value of K_2 of 0.006 *M*. However,

Can. J. Chem. Downloaded from www.nrcresearchpress.com by 210.87.254.40 on 09/05/12
For personal use only.

considering the magnitude of the experimental error this value is probably not significantly different from zero. In any case K_2 cannot be much larger.

The proton inhibited term is consistent with either a direct external methoxide attack on **2** or formation of a reactive methoxide species such as **3** by dissociation of a proton from **2**.

[30] $$2 + CH_3O^- \xrightarrow{k_1} \text{Products}$$

[31] $$2 \rightleftharpoons \underset{\mathbf{3}}{[PdCl_2(OCH_3)(C_2H_4)]^-} + H^+$$

The external methoxide ion attack can be ruled out on the basis of rate. If this is the route, the rate expression would be

[32] $$\text{rate} = k_1[\mathbf{2}][MeO^-] = k_1(K_2K_S[\mathbf{1}]/[H^+][Cl^-])$$

where (23)

[33] $$K_S = [H^+][MeO^-] = 2 \times 10^{-17}$$

Substituting the maximum value of 10^{-2} for K_2, one can calculate k_1. It has a value of 3×10^{13} M^{-1} s^{-1} which is *ca.* 10^4 larger than the rate for a diffusion controlled process in solution. This route is thus clearly impossible.

In analogy with the Wacker reaction as well as other Pd(II) catalytic chemistry, the decomposition of **3** almost certainly proceeds through a σ-bonded complex. The π–σ shift of the methoxy-π-complex, **3**, can occur either by attack of methanol on the complex or by internal attack of coordinated methoxide. Although both are consistent with the kinetics but the former seems unlikely. Thus, **3** is of the same charge type as **1**

[34] 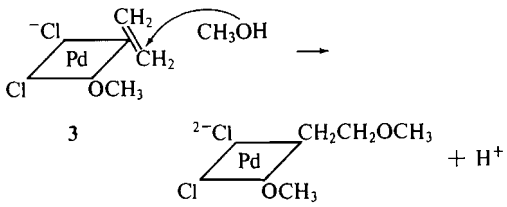

[35] 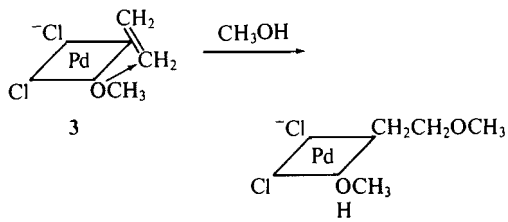

and would be expected to have similar reactivity towards nucleophilic attack. Yet since the concentration of **3** is about 10^{-8} of **1**, **3** would have to be 10^9 more reactive than **1** to attack methanol. This does not seem reasonable. Therefore, the most likely path consistent with the kinetics appears to be internal attack [35].

The reason for the lack of reactivity of **1** or **3** to external methanol attack is probably the negative charge on the complexes. In a series of exchange studies in acetic acid it was found that the reactive species was always a dimeric π-complex which usually underwent external attack (12).

[36] 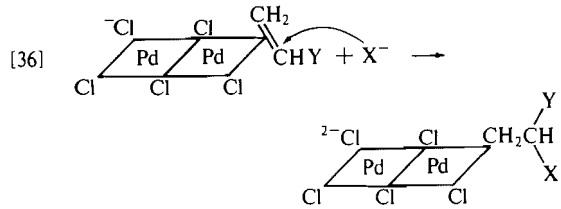

Monomeric π-complexes analogous to **1** were completely unreactive.

[37] 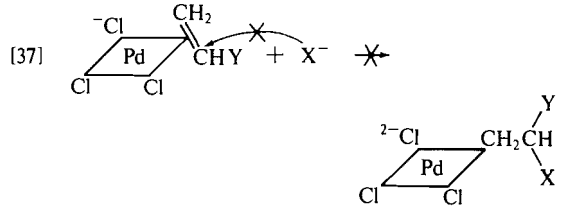

The reason for this large difference in reactivity is believed to result from the smaller negative charge on the Pd(II) complexed to the olefin in the case of the dimeric π-complex. Since, in water and methanol, dimers are not present and the monomers **1** and **3** are unreactive the preferred path is apparently the internal attack of hydroxide or methoxide. Stereochemical studies are presently under way to find evidence for the stereochemistry of addition of the methanol. These studies would either confirm or reject the interpretation of the kinetic data.

In regard to stereochemistry the configuration of the β-substituted acids esters formed from *cis*- or *trans*-2-butene and CO in methanol catalyzed by Pd(II) was interpreted as resulting from initial *trans* methoxypalladation.

[38] 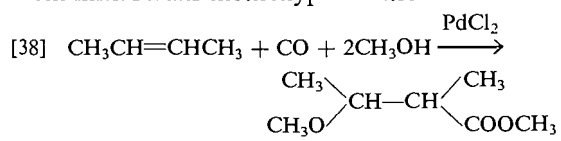

Can. J. Chem. Downloaded from www.nrcresearchpress.com by 210.87.254.40 on 09/05/12
For personal use only.

This interpretation is very likely correct but it should be remembered that the active catalysis is almost certainly a Pd(II) carbonyl and thus quite a different species from the reaction in the absence of CO. Thus, the carbonyl would very likely be a neutral species which would be susceptible to external nucleophilic attack.

The kinetic isotope effect for oxidation of C_2D_4 suggested that the π–σ shift is the slow step in the aqueous reaction (see later discussion). This experiment was not performed in the present study but by analogy with the aqueous oxidation it would be expected to be the rate determining step in the oxidation in methanol.

The solvent isotope effect $k_{CH_3OH}/k_{CH_3OD} = 1.34$ is somewhat smaller than that found in water where $k_{H_2O}/k_{D_2O} = 4.05$. The latter is the ratio found for the dissociation constants of weak acids in these solvents and is thus consistent with the mechanism proposed. To the authors' knowledge no corresponding data for the dissociation of weak acids in CH_3OH and CH_3OD is known. It is, however, reasonable that the solvent isotope effect is smaller for methanol since hydrogen bonding is less important.

The effect of ionic strength on rate shown in Fig. 6 is analogous to that found in water. It is the type of dependence that the dissociation of weak acids displays so this behaviour is consistent with the proposed mechanism.

The effect of acid on reaction rate outlined in Fig. 5 has been previously observed in water (5). In addition a rate maximum has been observed in water at low $[Cl^-]$ when rate was plotted *vs.* $[Cl^-]$. The effect of $[Cl^-]$ at very low $[Cl^-]$ was not tested in the present study but presumably a similar maximum would be observed as in the $[H^+]$ plot.

Two theories have been advanced for these effects. One of the authors has attributed the decrease in rate at low acidities as resulting from the formation of inactive hydroxyl species which are probably polymeric. Other workers were able to fit their data over the entire range of $[H^+]$ and $[Cl^-]$ by the following equation (25):

$$[39] \qquad \text{Rate} = \frac{a[H^+][Cl^-]}{b + [H^+]^2[Cl^-]^3}$$

To account for the form of this equation they postulated the following set of reactions.

[40] $PdCl_4^{2-} + C_2H_4 + 2H_2O \overset{K'}{\rightleftharpoons}$ 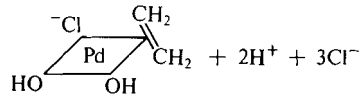 $+ 2H^+ + 3Cl^-$

4

[41] $\mathbf{4} + H^+ + Cl^- \overset{K''}{\rightleftharpoons}$ 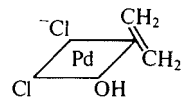

5

[42] $\mathbf{5} \xrightarrow[k']{\text{slow}}$ Products

Assuming the concentration of **5** to be small they arrived at the following rate expression ($[Pd]_t$ = total [Pd(II)]):

$$[43] \qquad \text{Rate} = \frac{k'K'K''[Pd]_t[C_2H_4][H^+][Cl^-]}{K'[C_2H_4] + [H^+]^2[Cl^-]^3}$$

This rate expression is of the same form as [39]. The reason given for the inactivity of **4** relative to **5** is the higher *trans* effect of Cl^- over OH^-. Thus the *trans* chloride would withdraw electron density making the olefin more susceptible to nucleophilic attack.

Now, as pointed out previously, if **4** or any other intermediates in the equilibria are small in concentration these intermediate species are kinetically insignificant. Examination of [43] shows that the reaction becomes acid and chloride catalyzed only when $K'[C_2H_4]$ becomes larger than $[H^+]^2[Cl^-]^3$. However, the $K'[C_2H_4]$ term only becomes significant when appreciable quantities of $PdCl_4^{2-}$ are converted to **4**. This would predict that the equilibrium constant for H-complex formation should increase with decreasing $[H^+]$ and $[Cl^-]$. It has been reported that the equilibrium constant actually *decreases* as the chloride concentration is lowered (7). In the present work it was found that K_1 decreases to some extent at low values of $[H^+]$ (Table 4). This result is inconsistent with the route shown in reactions 40–42.

The other possibility is that at low $[H^+]$ unreactive Pd(II) methoxy species are formed. This theory is supported by the observations of spectral changes of Pd(II) solution in the absence of olefin at low $[H^+]$. However, if this is the case,

the value of K_1 would be expected to also decrease since the unreactive Pd(II) species would not be expected to form π-complexes. As shown in Table 4 the ethylene uptake decreases only a little on going to low $[H^+]$. It is possible that unreactive π-complexes could be formed but at present the cause of the rate retardation has certainly not been definitely established.

The final step to consider is the decomposition step. An important experimental result in relationship to the decomposition step is the finding that C_2H_4 oxidized in CH_3OD gives 1,1-dimethoxyethane which contains no deuterium, a result reported previously in a preliminary form by Moiseev and Vargaftik (26). On the basis of a similar isotope result it was originally proposed that the decomposition step in the aqueous oxidation occurred via a palladium(II) assisted hydride shift from one carbon to the other without the distinct stage of formation of a Pd(II) hydride.

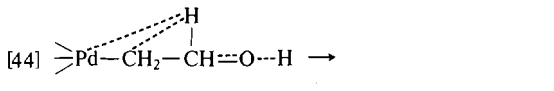

[44] $\rightarrow Pd(0) + CH_3CHO + H^+$

One reason the hydride elimination was not completed was believed due to the fast electronic rearrangement to convert the alcohol to a carbonyl group. In methanol this mechanism would suggest vinyl ethers to be the initial product since an electronic rearrangement to aldehyde is impossible and thus the hydride elimination would be completed. The 1,1-dimethoxyethane would then be formed by addition of methanol across the double bond. If the oxidation was carried out in CH_3OD the 1,1-dimethoxyethane should contain one deuterium.

[45] $CH_2{=}CHOCH_3 + CH_3OD \rightarrow CH_2DCH(OCH_3)_2$

The actual experimental findings that no deuterium is incorporated in the acetal product is inconsistent with this decomposition route.

A more recent proposal involves a Pd(II)-hydride vinyl alcohol complex, **5** (5, 24). The reason that **6** is more reactive towards solvolysis since the incipient carbonium ion is stabilized by the electron donating α-oxygen. There is recent evidence that α-oxygen groups do, in fact, cause the reductive elimination to Pd(0) (27). Furthermore this route is consistent with the deuterium labeling experiment. Thus a decomposition scheme in methanol analogous to that given by [46] and [47] would predict no deuterium incorporation.

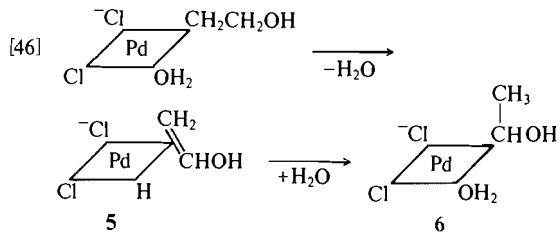

5 **6**

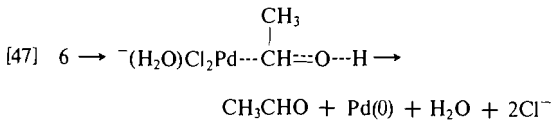

[47] $\rightarrow CH_3CHO + Pd(0) + H_2O + 2Cl^-$

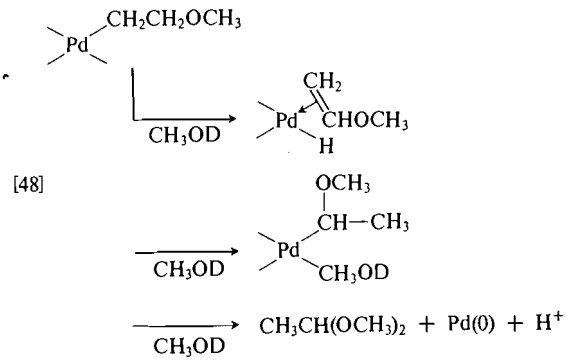

[48] $\rightarrow CH_3CH(OCH_3)_2 + Pd(0) + H^+$

A comment about the slow step of the Wacker reaction is in order. As mentioned earlier it was originally proposed on the basis of a small isotope effect with C_2D_4 ($k_H/k_D = 1.07$), that the hydroxypalladation step was the rate determining step. The reason was based on the fact that a hydride shift occurred in the reaction. Such a shift would be expected to result in a kinetic isotope effect if H is replaced by D. More recently it has been suggested that the decomposition of **6** [47] is rate determining. All previous steps are equilibrium. In this case the small isotope effect can be explained by the fact it is an equilibrium isotope effect which is smaller than a kinetic isotope effect. However, a recent study of the oxidation of 1,2-dideuteroethylene indicates this is not the case (28). If the equilibrium isotope effect is about one the oxidation of CHD=CHD should give equal mixtures of CH_2DCHO and

Can. J. Chem. Downloaded from www.nrcresearchpress.com by 210.87.254.40 on 09/05/12
For personal use only.

CD_2HCDO. Actually the ratio of the first to the second is 1.7 indicating that the isotope effect of 1.07 is *not* an equilibrium isotope effect. This provides evidence that the hydroxypalladation step is, in fact, the slow step of the reaction.

The reason Francois did not detect the second chloride inhibition is, as mentioned in the Introduction, related to the presence of $CuCl_2$ in the reaction mixture. Its presence could either change the mechanism or cause an incorrect calculation of the free $[Cl^-]$ since the equilibria between $CuCl_2$ and Cl^- in methanol is not known. It is of interest, however, that his proposal for direct attack of methoxide ion on the $^-Cl_3Pd(C_2H_4)$ π-complex (reaction 9) can be discarded on kinetic arguments. Thus, if we use the K_1 value for formation of this π-complex (reaction 20) determined in this study and his values for the rate constants, the rate for this attack can be calculated to be 5.5×10^{14} M^{-1} s^{-1} which is 10^5 times faster than a diffusion controlled reaction.

Finally since Francois did not know the correct value of free chloride at low $[CuCl_2]$ there is the possibility his rate expression at high $[CuCl_2]$ which contains a $[CuCl_2]$ term is also incorrect.

Acknowledgement

Acknowledgement is made to the Donors of the Petroleum Research Fund, administered by the American Chemical Society, for the support of this research.

1. (*a*) P. M. MAITLIS. The organic chemistry of palladium. Vols. I and II, Academic Press, New York, N.Y., 1971, a comprehensive review covering literature to end of 1970; (*b*) P. M. HENRY. Adv. Organometal. Chem., **13**, 363 (1974). A review covering literature mainly from 1971 to the end of 1973.
2. J. SMIDT *et al.* Angew. Chem. **71**, 176 (1959).
3. M. N. VARGAFTIK, I. I. MOISEEV, and Y. K. SYRKIN. Dokl. Akad. Nauk SSSR, **139**, 1396 (1961); **147**, 399 (1962).
4. I. I. MOISEEV, M. N. VARGAFTIK, and Y. K. SYRKIN. Dokl. Akad. Nauk SSSR, **153**, 140 (1963).
5. R. JIRA, J. SEDLMEIER, and J. SMIDT. Liebigs Ann. Chem. **693**, 99 (1966).
6. P. M. HENRY. J. Am. Chem. Soc. **86**, 3246 (1964).
7. P. M. HENRY. J. Am. Chem. Soc. **88**, 1595 (1966).
8. I. I. MOISEEV, M. N. VARGAFTIK, and Y. K. SYRKIN. Dokl. Akad. Nauk SSSR, **152**, 147 (1963).
9. S. V. PESTRIKOV, I. I. MOISEEV, and T. N. ROMANOVA, Zh. Neorg. Khim., **10**, 2203 (1965).
10. S. V. PESTRIKOV, I. I. MOISEEV, and B. A. TSVILIKHOVSKAYA. Zh. Neorg. Khim. **11**, 1742 (1966).
11. P. M. HENRY. J. Am. Chem. Soc. **93**, 1494 (1971); **94**, 673 (1972).
12. P. M. HENRY. Acc. Chem. Res. **6**, 16 (1973).
13. J. K. STILLE and R. A. MORGAN. J. Am. Chem. Soc. **88**, 5135 (1966).
14. L. F. HINES and J. K. STILLE. J. Am. Chem. Soc. **94**, 485 (1972).
15. A. Segnitz, P. M. BAILEY, and P. M. MAITLIS. Chem. Commun. 698 (1973).
16. M. C. GALLAZZI, T. L. HANLON, G. VITULLI, and L. PORRI. J. Organomet. Chem. **33**, 645 (1971).
17. J. K. STILLE and D. E. JAMES. J. Am. Chem. Soc. **97**, 674 (1975).
18. J. K. STILLE, D. E. JAMES, and L. F. HINES. J. Am. Chem. Soc. **95**, 5062 (1973).
19. P. FRANCOIS. Ann. Chim. [14] **4**, 371 (1969).
20. B. W. CLARE, D. COOK, E. C. KO, Y. C. MAC, and A. J. PARKER. J. Am. Chem. Soc. **88**, 1911 (1966).
21. A. K. COVINGTON and T. H. LILLEY. Trans. Faraday Soc. **63**, 1749 (1967).
22. J. H. R. CLARKE and L. A. WOODWARD. Trans. Faraday Soc. **63**, 2226 (1966).
23. A. UNMACK, Z. Phys. Chem. **133**, 45 (1928).
24. I. I. MOISEEV, M. N. VARGAFTIK, and Y. K. SIRKIN. Izv. Akad. Nauk SSSR, **139**, 1396 (1961).
25. R. JIRA and W. FREIESLEBEN. Organomet. React. **3**, 1 (1972).
26. I. I. MOISEEV and M. N. VARGAFTIK. Izv. Akad. Nauk SSSR, (Engl. Transl.) 744 (1965).
27. T. HOSOKAWA and P. M. MAITLIS. J. Am. Chem. Soc. **95**, 4924 (1973).
28. P. M. HENRY. J. Org. Chem. **38**, 2415 (1973).

Can. J. Chem. Downloaded from www.nrcresearchpress.com by 210.87.254.40 on 09/05/12
For personal use only.

Formation of *tert*-butyl cation in methane

K. HIRAOKA AND P. KEBARLE
Chemistry Department, University of Alberta, Edmonton, Alta., Canada T6G 2E1

Received January 19, 1976

K. HIRAOKA and P. KEBARLE. Can. J. Chem. **54**, 1739 (1976).

The reactions of CH_3^+ with pure methane in the torr range show an interesting temperature dependence. $C_2H_5^+$ is formed at all temperatures by the well known reaction: $CH_3^+ + CH_4 = C_2H_5^+ + H_2$. In the lowest temperature interval studied (105–125 K) $C_2H_5^+$ adds two CH_4 molecules to give a $C_4H_{13}^+$ species. At higher temperatures only one CH_4 molecule is added on. The resulting $C_3H_9^+$ then reacts with one more CH_4 molecule according to reaction 6.

[6] $$C_3H_9^+ + CH_4 \rightarrow C_4H_{13}^+ \rightarrow t\text{-}C_4H_9^+ + 2H_2$$

The rate constant k_6 is found to be second order and has a positive temperature dependence. An Arrhenius plot gives:

$$k_6 = 9 \times 10^{-13} \exp(-2.1 \text{ kcal mol}^{-1}/RT) \text{ cm}^3 \text{ molecule}^{-1} \text{ s}^{-1}$$

At temperatures above 200 K reaction 6 ceases to occur since $C_3H_9^+$, being unstable at high temperatures, decomposes to $s\text{-}C_3H_7^+ + H_2$.

The reactions were studied using ultra pure methane irradiated with electrons in a pulsed beam high ion source pressure mass spectrometer.

The gas phase reaction mechanism for the formation of $t\text{-}C_4H_9^+$ is found to bear close resemblance to the probable mechanism by which the $t\text{-}C_4H_9^+$ ion is formed from methane dissolved in superacid media.

K. HIRAOKA et P. KEBARLE. Can. J. Chem. **54**, 1739 (1976).

Les réactions du CH_3^+ dans du méthane pur à une pression d'environ une torr varient d'une façon intéressante avec la température. A toutes les températures, il se forme du $C_2H_5^+$ par la réaction bien connue $CH_3^+ + CH_4 \rightleftharpoons C_2H_5^+ + H_2$. Aux températures les plus basses (105–125 K), le $C_2H_5^+$ additionne deux molécules CH_4 pour conduire aux espèces $C_4H_{13}^+$. Aux températures plus élevées, il additionne qu'une molécule CH_4. Le $C_3H_9^+$ qui en résulte réagit alors avec une autre molécule de CH_4 suivant le réaction 6

[6] $$C_3H_9^+ + CH_4 \rightarrow C_4H_{13}^+ \rightarrow t\text{-}C_4H_9^+ + 2H_2$$

On a trouvé que la constante de vitesse k_6 est du deuxième ordre et varie d'une façon positive avec la température. Une courbe d'Arrhénius permet d'établir que

$$k_6 = 9 \times 10^{-13} \exp(-2.1 \text{ kcal mol}^{-1}/RT) \text{ cm}^3 \text{ molecule}^{-1} \text{ s}^{-1}$$

Aux températures plus élevées que 200 K, la réaction 6 cesse de se produire puisque que $C_3H_9^+$ n'est pas stable à haute température et qu'il se décompose en $s\text{-}C_3H_7^+ + H_2$.

On a étudié ces réactions utilisant du méthane ultra pur irradié avec des électrons dans un spectromètre de masse équipé d'une source d'ions à faisceau pulsé fonctionnant à haute pression.

Le mécanisme de la réaction en phase gaseuze pour la formation du $t\text{-}C_4H_9^+$ est semblable au mécanisme probable par lequel l'ion $t\text{-}C_4H_9^+$ se forme à partir du méthane dissout dans un milieu superacide.

[Traduit par le journal]

Introduction

The ion molecule reactions in methane have been studied extensively at low and high pressures and at various temperatures (1–4). The two major primary ions produced by electron impact or other ionizing radiation are CH_4^+ and CH_3^+ roughly in a 1:1 ratio. CH_4^+ reacts by [1] to give CH_5^+ while CH_3^+ gives $C_2H_5^+$ via [2]:

[1] $$CH_4^+ + CH_4 = CH_5^+ + CH_3$$

[2] $$CH_3^+ + CH_4 = C_2H_5^+ + H_2$$

The CH_5^+ ion is totally unreactive towards methane. At low temperatures (5, 6) this ion forms clusters of the type $CH_5^+(CH_4)_n$. Similarly at low temperatures $C_2H_5^+$ forms condensation

Can. J. Chem. Downloaded from www.nrcresearchpress.com by 210.87.254.6 on 09/05/12
For personal use only.

products by the third body dependent reactions [3] and [4].

[3] $C_2H_5^+ + 2CH_4 \rightleftharpoons C_3H_9^+(b) + CH_4$

[4] $C_3H_9^+(b) + 2CH_4 \rightleftharpoons C_4H_{13}^+ + CH_4$

The equilibria [3] were observed (7) between 150–250 K and [4] between 105–125 K.

The product of reaction 3 is written as $C_3H_9^+(b)$ since this species is believed (7) to correspond to protonated propane of structure B, *i.e.* C–C protonated propane. A study (8) of the temperature dependence of the reaction of $C_2H_5^+$ with methane in the temperature interval 240–600 K showed that at these higher temperatures the reaction proceeded as indicated in [5].

[5] $C_2H_5^+ + CH_4 \rightleftharpoons C_3H_9^+(b) \rightarrow C_3H_9(a) \rightarrow s\text{-}C_3H_7^+ + H_2$

The second order rate constant k_5 for the overall reaction leading to s-$C_3H_7^+$ showed positive temperature dependence. The activation energy $E_5 = 2.5$ kcal/mol combined with the heat of formation of $C_3H_9^+(b)$ (obtained via ΔH_3 from the equilibria [3]) lead (8) to an energy barrier of ~9 kcal/mol for the dissociation of $C_3H_9^+(b)$ to s-$C_3H_7^+ + H_2$. As indicated in reaction 5 it was assumed that this dissociation proceeds through the intermediate species $C_3H_9^+(a)$ which is assumed to have the structure A.

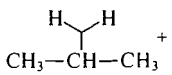

A

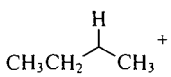

B

Reaction 5 represents a synthesis of s-$C_3H_7^+$ by ion molecule reactions in pure methane involving the primary ion CH_3^+. The present work will describe a somewhat similar reaction also involving CH_3^+ but occurring in the temperature interval 120–200 K by which the *tert*-butyl ion is synthesized. The formation of *tert*-butyl$^+$ from methane, is of interest since it is an example of how a much higher molecular weight product can be obtained in irradiated methane by a temperature dependent process.

The formation of *tert*-butyl$^+$ in gas phase methane described in this work is also of interest in connection with reactions occurring when methane is dissolved in superacids. It will be shown that the gas phase reaction mechanism bears close resemblance to the probable mechanism in solution.

Experimental

The experiments were done with the pulsed electron beam high ion source pressure mass spectrometer with high and low temperature capability which has been described earlier (9).

The methane used was Linde UHP which was further purified by passing it at 1 atm through a 5 Å molecular sieve loaded trap cooled with dry ice. The methane stream before entering the ion source, *i.e.* at pressure in the torr range, was passed through a second 5 Å molecular sieve trap cooled to liquid nitrogen temperature.

The primary ions were produced by an electron pulse of 15 μs duration and there were 15 ms between successive electron pulses. At ~4 torr pressure and the low temperatures used (−150 °C) ion diffusion to the walls is rather slow and an appreciable total ion signal persists even after 15 ms. In order to eliminate the ions before the new pulse was triggered, a 30 V positive voltage pulse of some 200 μs duration was applied to a repeller electrode mounted about 1 cm from the ion exit slit. It was observed that the application of this pulse cut off the ion signal sharply. Evidently the magnitude of the voltage was sufficiently large to cause rapid drift and discharge of the ions on the bottom wall of the ion source.

Results and Discussion

As already mentioned in the introduction, the $C_3H_9^+$ ion formed from $C_2H_5^+$ and CH_4 by reaction 3 can form stable $C_4H_{13}^+$ by addition of CH_4 at low temperatures (reaction 4) or can decompose to s-$C_3H_7^+ + H_2$ at high temperatures (reaction 5). But in the intermediate temperature range 120–200 K this ion seems to engage in a different reaction leading to the formation of t-$C_4H_9^+$. Results from a typical run under these latter conditions are shown in Fig. 1. The time dependence of the ion intensities after the ionizing electron pulse shows two major species, these are the $CH_5^+(CH_4)_n$ ions with $n = 1$ and 2. These ions, derived from CH_5^+ are in equilibrium and have time independent concentrations. The absence of impurities like ethane and propane is also attested by the time invariant $CH_5^+(CH_4)_n$ concentrations since in the presence of such compounds proton transfer would have been rapidly decreasing the $CH_5^+(CH_4)_n$ concentration. The other major ions in Fig. 1 are $C_3H_9^+$ and $C_4H_9^+$. The $C_3H_9^+$ ion decreases with time while the $C_4H_9^+$ ion shows an equivalent increase. This must be due to a reaction converting $C_3H_9^+$ to $C_4H_9^+$. Since the decomposition of $C_3H_9^+$ to $C_3H_7^+ + H_2$ by reaction 5 is too slow

Can. J. Chem. Downloaded from www.nrcresearchpress.com by 210.87.254.6 on 09/05/12
For personal use only.

Can. J. Chem. Downloaded from www.nrcresearchpress.com by 210.87.254.6 on 09/05/12
For personal use only.

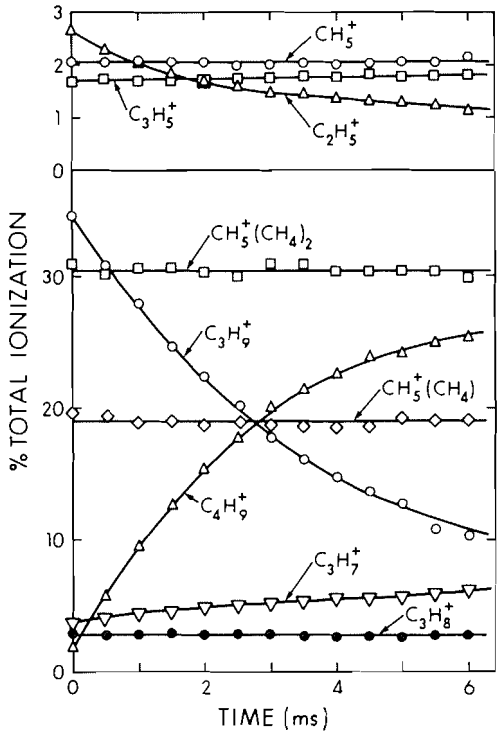

FIG. 1. Normalized ion intensities in function of time after the ionizing electron pulse. Methane pressure 4.3 torr, T = 155 K. Decrease of $C_3H_9^+$ and increase of $C_4H_9^+$ assumed to be due to reaction 6.

(8) at the experimental temperature, the conversion cannot involve $C_3H_7^+$ as intermediate. We conclude therefore that the process responsible should be reaction 6.

[6] $C_3H_9^+(b) + CH_4 \rightleftharpoons C_4H_{13}^+ \rightarrow$
$C_4H_{11}^+ + H_2 \rightarrow t\text{-}C_4H_9^+ + 2H_2$

$C_4H_{13}^+$, instead of being stabilized by collisions, as is the case at lower temperatures, decomposes by loss of hydrogen to yield ultimately t-$C_4H_9^+$. The pressure dependence of the disappearance of $C_3H_9^+$ was examined in several experiments. Logarithmic decay plots of $C_3H_9^+$ at different CH_4 pressure and constant temperature are shown in Fig. 2. The slopes obtained in Fig. 2, equal to the reaction frequency (or pseudo first order rate constant), ν_6, are shown in Fig. 3. This plot of $\nu_6/[CH_4] = k_6$ is constant with CH_4 pressure and shows that reaction 6 is first order in $[CH_4]$, *i.e.* overall second order.

An Arrhenius plot of k_6 values obtained in the temperature interval 120–200 K in which *tert*-butyl$^+$ was the reaction product is shown in Fig. 4. The straight line obtained defines the relationship 7.

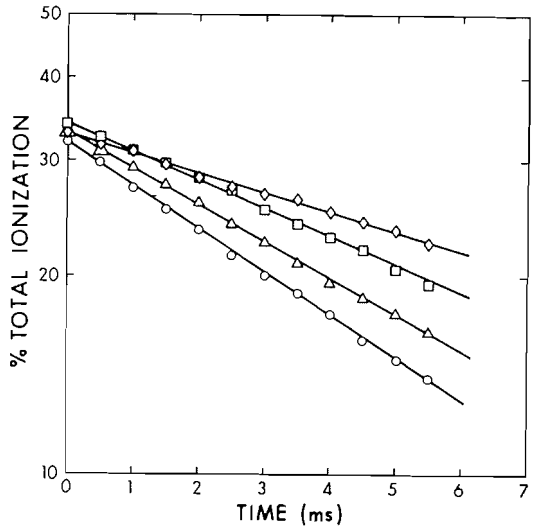

FIG. 2. Plot of log $[C_3H_9^+]$ *vs.* time for different methane pressure and constant temperature of 141 K: ◇, 2.46 torr; □, 3.4 torr; △, 4.9 torr; ○, 5.5 torr methane. Slope taken equal to reaction frequency ν_6.

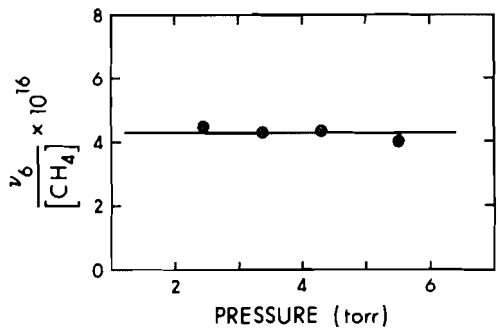

FIG. 3. Plot of $\nu_6/[CH_4]$ based on data of Fig. 2. Independence on pressure shows that $\nu_6/[CH_4] = k_6$, *i.e.* that reaction 6 is first order in methane and first order in $C_3H_9^+$, thus second order.

[7] $k_6 = 9 \times 10^{-13} \exp(-2.1 \text{ kcal mol}^{-1}/RT)$ cm^3 molecule^{-1} s^{-1}

Reaction 6 is seen to have a pre-exponential factor that is lower than Langevin (10^{-9} cm^3 molecule^{-1} s^{-1}) and a positive temperature dependence leading to a small activation energy of 2.1 kcal/mol. The small pre-exponential factor is consistent with the assumption that the reaction proceeds via $C_4H_{13}^+$. While the $C_4H_{13}^+$ might be formed with Langevin collision rates, back dis-

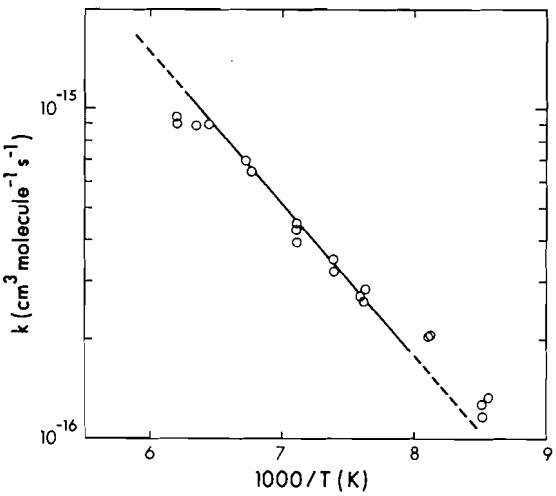

FIG. 4. Arrhenius plot of k_6. Straight line obtained defines relationship: $k_6 = 9 \times 10^{-13}$ exp $(-2.1$ kcal mol$^{-1}/RT$ cm^3 molecule^{-1} s^{-1}).

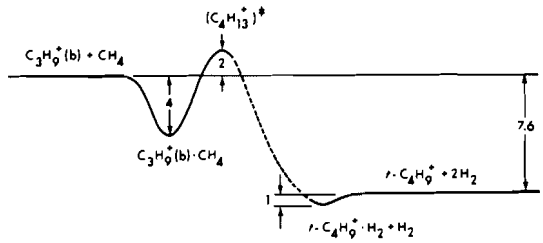

FIG. 5. Schematic representation of potential energy changes involved in reaction 6. Numbers in figure are equal to energy in kcal/mol.

sociation to $C_3H_9^+ + CH_4$ must lead to a lower than Langevin pre-exponential factor for reaction 6. The temperature dependence and parameters of k_6 are close to those for the somewhat similar reaction 5 described earlier (8). These were: $k_5 = 6 \times 10^{-13}$ exp $(-2.5$ kcal mol$^{-1}/RT)$. However, the present reaction 6 has both a higher pre-exponential factor and a lower activation energy such that it is appreciably faster at lower temperatures. The values of k_5 obtained by extrapolating the Arrhenius plot from the region 350 to -35 °C, where k_5 was measured (8), to the present, lower region of the k_6 plot, predicts a value that is about five times lower than the value of k_6.

The $C_4H_9^+$ product of reaction 6 is identified as t-$C_4H_9^+$ on the basis of energetic considerations. Since $\Delta H_f(C_3H_9^+(b)) = 194.5$ kcal/mol (7) only the reaction leading to t-$C_4H_9^+$, whose $\Delta H_f = 169$ kcal/mol (Lossing (10) and Tsang (11)) is exothermic with an enthalpy change $\Delta H_6 = -7.6$ kcal/mol. A reaction leading to s-$C_4H_9^+$ ($\Delta H_f = 183$ kcal/mol) (10) would be endothermic by over 6 kcal/mol, which is much larger than the observed activation energy. All other $C_4H_9^+$ isomers have even higher heats of formation and are therefore also impossible as products.

Available thermochemical information and the present results have been combined in Fig. 5 to obtain a schematic potential energy diagram for reaction 6. The $C_3H_9^+(b)$ and CH_4 interact to form a $C_4H_{13}^+$ adduct. The ~4 kcal/mol energy that is released is based on an approximate determination (7) of $\Delta H_4 \approx -4$ kcal/mol from a Van't Hoff plot of K_4. The $C_4H_{13}^+$ adduct probably should be visualized as a $C_3H_9^+$ of structure B interacting via the most positive hydrogen (*i.e.* the three centre bonded H) with a CH_4 molecule. Before an H_2 molecule can be eliminated a barrier equal to: $-\Delta H_4 + E_6 =$ 6 kcal/mol must be overcome (see Fig. 5). We suspect that after the loss of the first H_2 molecule and before the final products: t-$C_4H_9^+ + 2H_2$ are formed, the system will pass through the stage t-$C_4H_9^+.H_2 + H_2$ indicated on Fig. 5. Recent work (12) from this laboratory has shown that the enthalpy change for reaction 8 is very small ($\Delta H \approx -1$ kcal/mol).

[8] $$t\text{-}C_4H_9^+ + H_2 \rightleftharpoons C_4H_{11}^+(a)$$

The $C_4H_{11}^+(a)$ corresponds to a *tert*-butyl ion interacting with the electrons of the H_2 molecule. This means that once the $C_4H_{11}^+(a)$ ion is formed in the reaction sequence 6 its further dissociation to *tert*-butyl$^+$ and H_2 occurs spontaneously.

The formation of *tert*-butyl$^+$ in methane gas described above is of interest also in connection with carbocation reactions in solution. Olah, in his first communication on chemistry of superacids (13), reported the formation of *tert*-butyl$^+$ resulting from the reactions of methane with "magic acid". The reaction sequence suggested by Olah (13) starting with CH_3^+ and proceeding through $C_2H_5^+$, $C_3H_9^+$, $C_3H_7^+$, to t-$C_4H_9^+$ was nearly identical to the gas phase reaction sequence proposed in the present work. However, Olah assumed that the *tert*-butyl was not formed directly from $C_3H_9^+(b)$ as in reaction 6 but by reaction 9.

[9] $$s\text{-}C_3H_7^+ + CH_4 \rightarrow C_4H_{11}^+ \rightarrow t\text{-}C_4H_9^+ + H_2$$

Can. J. Chem. Downloaded from www.nrcresearchpress.com by 210.87.254.6 on 09/05/12
For personal use only.

The s-$C_3H_7^+$ being formed by the prior decomposition of $C_3H_9^+$(b) to s-$C_3H_7^+ + H_2$. Reaction 9 may seem more appropriate for the superacid solution experiments which were done above room temperature (13) since $C_3H_9^+$(b) is relatively unstable and may decompose to s-$C_3H_7^+ + H_2$ before it has time to engage in reaction 6. Thus earlier work in this laboratory (8) showed that the activation energy for this decomposition (in the gas phase) is only 9 kcal/mol. On the other hand, the present work and earlier experiments (8) showed that in the gas phase s-$C_3H_7^+$ does not react with methane to give *tert*-butyl$^+$, *i.e.* reaction 9 does not occur in the gas phase. We consider it possible that also in solution *tert*-butyl is formed via reaction 6, *i.e.* that the $C_3H_9^+$(b) survives long enough to meet and react with a CH_4 molecule. This could be possible in solution since the $C_3H_9^+$(b) is thermal. In the gas phase the $C_3H_9^+$(b) contains excess energy equal to the exothermicity of the condensation reaction of $C_2H_5^+$ with CH_4 and decomposes to s-$C_3H_7^+ + H_2$ at much lower temperatures (see reaction 5).

In any case it is really interesting that the oligo-condensation of CH_3^+ to t-$C_4H_9^+$ in solution can be also effected in the gas phase at pressures which are only in the torr range, so long as the temperature is kept low and in the right range. The gas phase reactions should be of significance to the solution chemist since in the gas phase the intermediate ions are positively identified and since often the energetics of the reaction sequence can be worked out.

1. F. H. FIELD and M. S. B. MUNSON. J. Am. Chem. Soc. **87**, 3289 (1965).
2. R. M. HAYNES and P. KEBARLE. J. Chem. Phys. **45**, 3899 (1966).
3. S. WEXLER, A. LIFSHITZ, and A. QUATROCHI. *In* Ion molecule reactions in the gas phase. Advances in Chemistry Series 58, Am. Chem. Soc. Washington, D.C. 1966.
4. F. H. FIELD. *In* Ion molecule reactions. *Edited by* J. L. Franklin. Plenum Press, N.Y. 1972.
5. K. HIRAOKA and P. KEBARLE. J. Am. Chem. Soc. **97**, 4179 (1975).
6. F. H. FIELD and D. P. BEGGS. J. Am. Chem. Soc. **93**, 1585 (1971).
7. K. HIRAOKA and P. KEBARLE. Can. J. Chem. **53**, 970 (1975).
8. K. HORAOKA and P. KEBARLE. J. Chem. Phys. **63**, 394 (1975).
9. A. J. CUNNINGHAM, J. D. PAYZANT, and P. KEBARLE. J. Am. Chem. Soc. **94**, 7627 (1972).
10. F. P. LOSSING and G. P. SEMELUK. Can. J. Chem. **48**, 955 (1970).
11. W. TSANG. J. Phys. Chem. **76**, 143 (1972).
12. K. HIRAOKA and P. KEBARLE. J. Am. Chem. Soc. To be published.
13. GEORGE A. OLAH and RICHARD H. SCHLOSBERG. J. Am. Chem. Soc. **90**, 2726 (1968).

Can. J. Chem. Downloaded from www.nrcresearchpress.com by 210.87.254.6 on 09/05/12
For personal use only.

Spectres de résonance paramagnétique électronique de quelques radicaux de type diarylméthyle

P. DEVOLDER

Laboratoire de Physicochimie des états excités, Université des Sciences et Techniques de Lille 1, B.P. 36 – 59650 Villeneuve D'Ascq, France

Reçu le 5 juin, 1975[1]

P. DEVOLDER. Can. J. Chem. **54**, 1744 (1976).

Les spectres de résonance paramagnétique électronique de quelques radicaux de type anthronyle, xanthyle ou thioxanthyle sont obtenus et comparés aux spectres simulés correspondants. Des calculs de densités de spin (méthode de McLachlan) permettent l'attribution de la plupart des constantes de couplage. Certains couplages anormalement élevés sont interprétés à partir des calculs INDO de Pople concernant le radical benzyle.

P. DEVOLDER. Can. J. Chem. **54**, 1744 (1976).

Electron paramagnetic resonance spectra of some anthronyl, xanthyl, or thioxanthyl type radicals are obtained and compared to their simulated spectra. Spin density calculations according to the method of McLachlan give the assignments of most experimental splittings. A few unexpected high splittings are interpreted with Pople's INDO calculations on the twisted benzyl radical.

Introduction

Les radicaux de type diarylméthyle dont les deux groupes phényle sont coplanaires ont fait l'objet d'un grand nombre de travaux tant en spectroscopie de résonance paramagnétique électronique qu'en spectroscopie électronique d'absorption ou de fluorescence. Ces radicaux sont en effet d'une part des modèles plans pour le radical non plan diphénylméthyle (18) et d'autre part sont très directement apparentés au radical benzyle auquel un nombre considérable de travaux théoriques et expérimentaux a été consacré. Les spectre rpe des radicaux xanthyle **1** et anthronyle **2**, rapportés ici, complètent les résultats du radical xanthyle (1) pour ce qui concerne les densités de spin des radicaux plans de type diphénylméthyle. Dans le cas où les groupes phényle ne sont pas coplanaires, comme pour le radical triphénylméthyle par exemple (13, 10), la détermination de l'angle d'équilibre pour lequel effets stériques et de conjugaison se compensent est également d'un grand intérêt. La comparaison des spectres rpe des radicaux **3** et **4** avec celui de **2** permet la mesure de cet angle; en outre, le radical **4** permet de tester la validité du modèle de Pople (14) concernant les constantes de couplage d'un groupe phényle faiblement conjugué.

[1]Revision reçue le 9 février 1976.

Résultats expérimentaux

Formation des radicaux

Le radical xanthyle **1** est préparé par thermolyse de son dimère, le bithioxanthyle (15*b*).

Le radical anthronyle **2** est préparé de même par thermolyse vers 200–250 °C de son dimère, le bianthronyle (15). Au-dessus de 270–280 °C, température de décomposition du bianthronyle, la solution devient verte et le radical **2** disparaît de manière irréversible au profit de **3**.

Luckhurst (5) a observé par ailleurs un spectre moins résolu de **3** par thermolyse de la bianthrone. La bianthrone, dont le thermochronisme (forme verte ⇄ forme jaune) a fait l'objet de nombreux travaux (16), se forme probablement pendant la décomposition du bianthronyle. L'absence du radical **3** par thermolyse ou photolyse du bianthronyle en-dessous de 260 °C exclut la présence de bianthrone en tant qu'impureté. Le radical **3** se forme également par thermolyse de la diazoanthrone catalysée ou non par le cuivre. Dans ce cas, **3** est toujours accompagné d'un radical **3** bis issu de l'attaque du solvant par le carbène formé (15) et la résolution du spectre de **3** diminue fortement quand température ou concentration initiale en diazoanthrone augmentent.

Le radical phénylanthronyle **4** est préparé: (*i*) soit par thermolyse de phénylanthrone (15) vers 120 °C dans l'*ortho*-terphényle ou le *méta*-xylène comme solvants: les constantes de couplage sont ensuite mesurées à la température qui donne la meilleure résolution du spectre compatible avec la diminution d'intensité avec la température; (*ii*) soit par photolyse de phénylanthrone dans le peroxide de tertiobutyle (K&K) vers −20 °C. Les spectres rpe observés avec ces divers solvants diffèrent très légèrement en raison de différences minimes dans les valeurs de a_{ortho}.

Le radical **5** est obtenu par photolyse dans le peroxide

Can. J. Chem. Downloaded from www.nrcresearchpress.com by 210.87.254.6 on 09/05/12
For personal use only.

Can. J. Chem. Downloaded from www.nrcresearchpress.com by 210.87.254.6 on 09/05/12
For personal use only.

TABLEAU 1. Constantes de couplage (en Gauss) des radicaux étudiés:*
$a = \pm 0.10$ G $b = \pm 0.03$ G $c = \pm 0.01$ G

Position du proton	Radical 1	2	3	4	5	
9	11.82	11.86	—	—	—	*a*
1, 8	3.20	3.05	3.01	3.02	3.02	
2, 7	1.07	1.06	0.99	1.01	0.76	
3, 6	3.85	3.54	3.34	3.37	3.52	*b*
4, 5	1.07	0.875	0.80	0.84	0.76	
ortho	—	—	—	1.01 ou 0.84†	0.84‡ 0.25	
méta	—	—	—	0.36	0.07	*c*
para	—	—	—	0.36	0.07	
	Largeur de raie (en Gauss) (expérimentale et simulée)					
	0.14	0.07	0.12	0.06	0.045	

*Conditions expérimentales (solvant et température): **1**, *o*-terphenyl, 300 °C; **2**, *o*-terphenyl, 230 °C; **3**, fluorénone, 150 °C; **4**, *m*-xylène, 20 °C et −50 °C; **5**, peroxide de tertiobutyle, 65 °C.
†20 °C.
‡−50 °C.

de tertiobutyle du xanthène substitué en position 9 correspondant (15*b*).

Appareillage calculs

Le spectromètre rpe est du type Varian V 4502 à modulation de 100 kHz et muni de l'accessoire à température variable Varian.

Une forme de raie Lorentzienne est adoptée pour la simulation des spectres rpe. Le calcul des densités de spin selon la méthode de McLachlan (ML) (7) est effectué en utilisant le formalisme des polarisabilités:

$$\rho_i \text{ ML} = \rho_i \text{ HMO} + \sum_j \pi_{ij}\rho_j \text{ HMO}$$

Pour la liaison 9–9′ on adopte la classique dépendance de l'intégrale d'échange en cos θ. Pour le calcul des contributions a_H* au couplage *ortho* selon la formule proposée par Lunazzi *et al.* (3):

$$a_{H\ ortho} = a_H^* - |a_{para}|$$

avec

$$a_H^* = 507\ \pi\rho_9|\phi_{C_9}[H]|^2 \quad \text{(Gauss)}$$

l'orbitale suivante, de type SCF STO (19) a été adoptée:

$$\phi_{C_9} = 1.74r \exp(-1.57r) \cos\alpha$$

(unités atomiques)

Résultats

Les spectres rpe des radicaux **1**, **2**, **3**, **4** et **5**, ramenés à leurs constantes de couplage, sont rassemblés dans le tableau 1. Des calculs de densité de spin (HMO, McLachlan (7)) permettent de retrouver l'ordre de grandeur

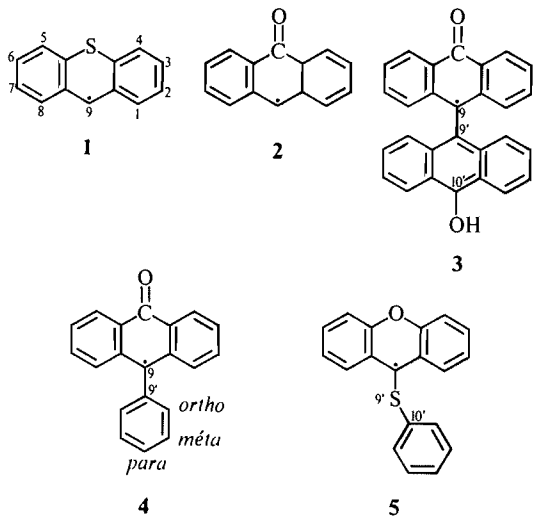

correct des couplages observés (tableau 2). Cependant, l'attribution des constantes de couplage hyperfin aux protons correspondants est établie par analogie avec des radicaux très voisins tels que xanthyle (1), phenylxanthyle (1, 3), phenylthioxanthyle (2), pour lesquels des deutérations sélectives évitent toute ambiguïté.

Cette méthode par extrapolation semble dans notre cas plus judicieuse qu'une interprétation basée sur les calculs de densité de spin: en effet, de tels calculs effectués suivant les méthodes de McLachlan (1–3) ou INDO (2) prévoient toujours $|a_3| < |a_1|$, en contradiction avec l'expérience.

Interprétation et discussion

*Radicaux **1** et **2***

Un spectre très différent de celui enregistré par les auteurs a été attribué par ailleurs (4) au radical **2**. L'extrême similitude des couplages observés pour les radicaux **2**, **3**, **4** d'une part, le bon accord avec les calculs de densité de spin d'autre part, confirme la validité de notre attribution.

La constante de couplage a_9 des radicaux diphénylméthyle et 9-fluorényle substitués ou non a fait l'objet d'une longue controverse: la grande diversité des valeurs de a_9 (pour une revue récente, voir réf. 17) contraste avec la constance relative de a_9 12 ∼ 13 G pour les radicaux **1**, **2** et xanthyle. Nos résultats, en bon accord d'une part avec la valeur récente et définitive de a_9 pour le radical non plan diphénylméthyle (18) d'autre part avec les résultats concernant le radical 9-phénylfluorényle (10) permettent de prévoir une valeur de a_9 de l'ordre de 12 à 13 G pour le radical 9-fluorényle, en désaccord avec les attributions de Dalton et coll.

Can. J. Chem. Downloaded from www.nrcresearchpress.com by 210.87.254.6 on 09/05/12
For personal use only.

TABLEAU 2. Densités de spin expérimentale et calculées selon la méthode de Huckel simple (HMO) et la méthode de McLachlan (ML). Le choix des paramètres semiempiriques nécessaires au calcul (constante Q de McConnell, paramètres h et k des hétéroatomes) est conforme aux références citées

Position du proton	1*			2†			3†			4†			5†		
	Exp.	HMO	ML	Exp.	HMO	ML	Exp.	HMO	ML	Exp.	HMO	ML	Exp.	HMO	ML
9	0.438	0.371	0.538	0.456	0.331	0.466					0.323	0.444			
1, 8	0.118	0.0963	0.144	0.117	0.0881	0.111	0.102	0.0869	0.111	0.098	0.085	0.107	0.125	0.102	0.151
2, 7	0.0396	0.00355	−0.0474	0.0407	0.00536	−0.0346	0.033	0.00362	−0.0346	0.032	0.004	−0.0320	0.032	0.009	−0.0363
3, 6	0.142	0.0927	0.120	0.136	0.0827	0.0981	0.112	0.0833	0.100	0.109	0.081	0.0970	0.147	0.085	0.111
4, 5	0.118	0.00794	−0.0352	0.033	0.0119	−0.0290	0.027	0.00804	−0.0316				0.032	0.032	0.034
ortho							$\rho' < 0.004$	$\rho' < 0.0007$	$\rho' < 0.0011$	0.027	0.009	0.0119	0.010	0.0011	0.0012
méta										0.012	0.00003	−0.00471	0.003	0.0000	−0.0005
para										0.012	0.010	0.0160	0.003	0.0012	0.0014
Constante et paramètres															
Q	27			26			29.7			30.7			24		
h, k	1.6	0.65		1	1.6		0.8	1.6		0.9	1.6		O: $h = 2$ $k = 1.1$		
							85°			70°			S: $h = 1.2$ $k = 0.65$		

*Référence 2.
†Références 1, 5, 21 et 22.

Can. J. Chem. Downloaded from www.nrcresearchpress.com by 210.87.254.6 on 09/05/12
For personal use only.

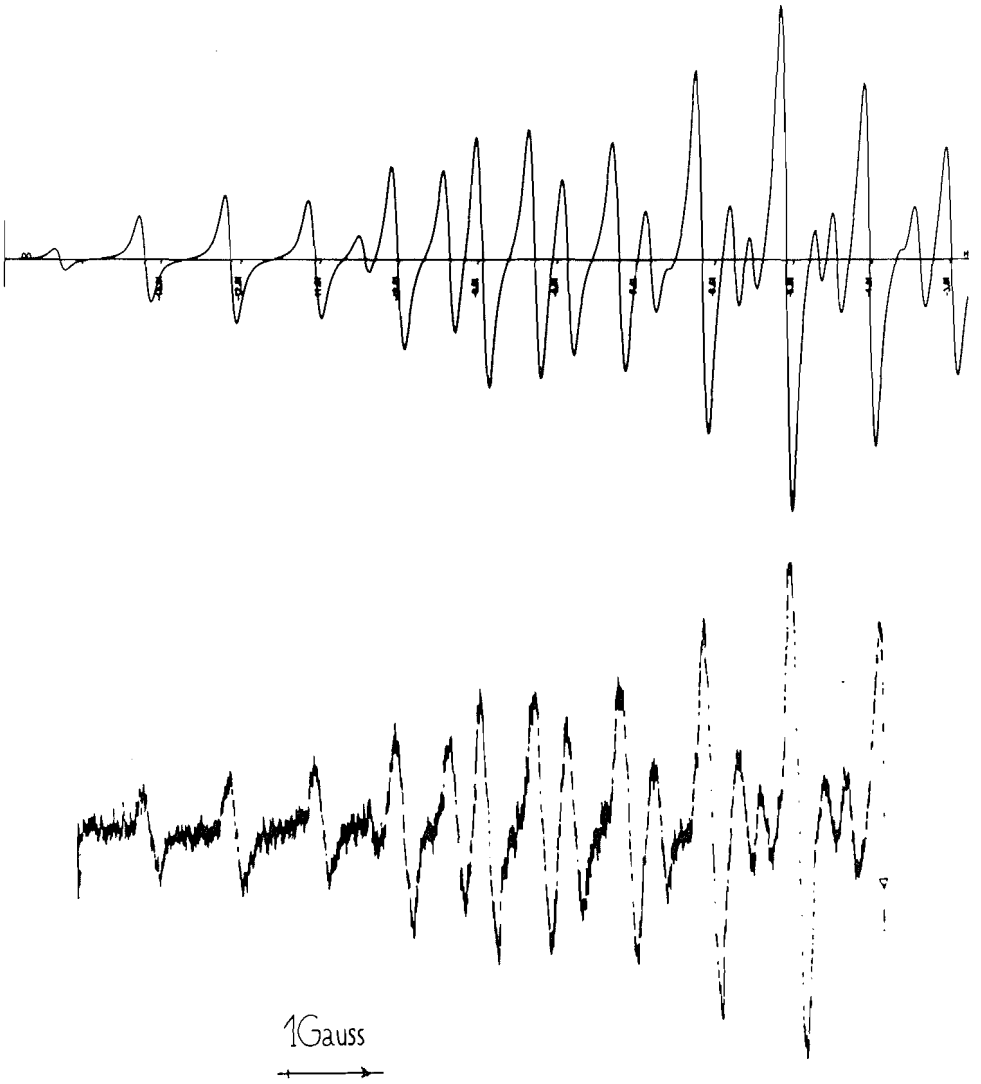

FIG. 1. Spectres expérimental et simulé de **1**.

(8). Notre conclusion se trouve par contre confirmée par les spectres attribués très récemment au radical 9-fluorényle (23, 24).

Radical 3

Le radical **3** a déjà été observé par thermolyse ou photolyse de la bianthrone (5, 6). Bien que nos valeurs des constantes de couplage soient en excellent accord avec celles trouvées par ailleurs, notre attribution en diffère en raison de la remarque suivante: les calculs de densité de spin selon la méthode de McLachlan pour les radicaux de type benzyle (7), di- (9) ou tri- (10) phenylmethyl conduisent toujours à $|a_{ortho}| > |a_{para}|$ en contradiction avec l'expérience. Cette remarque reste valable pour les radicaux xanthyle (1) et phénylthioxanthyle (3).

L'absence de constantes de couplage pour les protons de la moitié du radical contenant le groupement hydroxyle s'explique par l'existence d'un angle de 70/80° entre les deux moitiés de la molécule. On peut en effet calculer que pour un angle de 85°, le couplage maximum dû aux protons du cycle portant OH vaut $a' = 0.03$ G. D'autre part, par comparaison avec le radical **3** ter (6) ($a_{10'} = 0.2$ G) on en déduit que $a' <$

0.05 G. De telles faibles valeurs des couplages ne peuvent donc être détectées eu égard à la largeur de raie (0.12 G).

Radical **4**

La simulation du spectre enregistré à température ambiante ne permet pas de lever l'incertitude

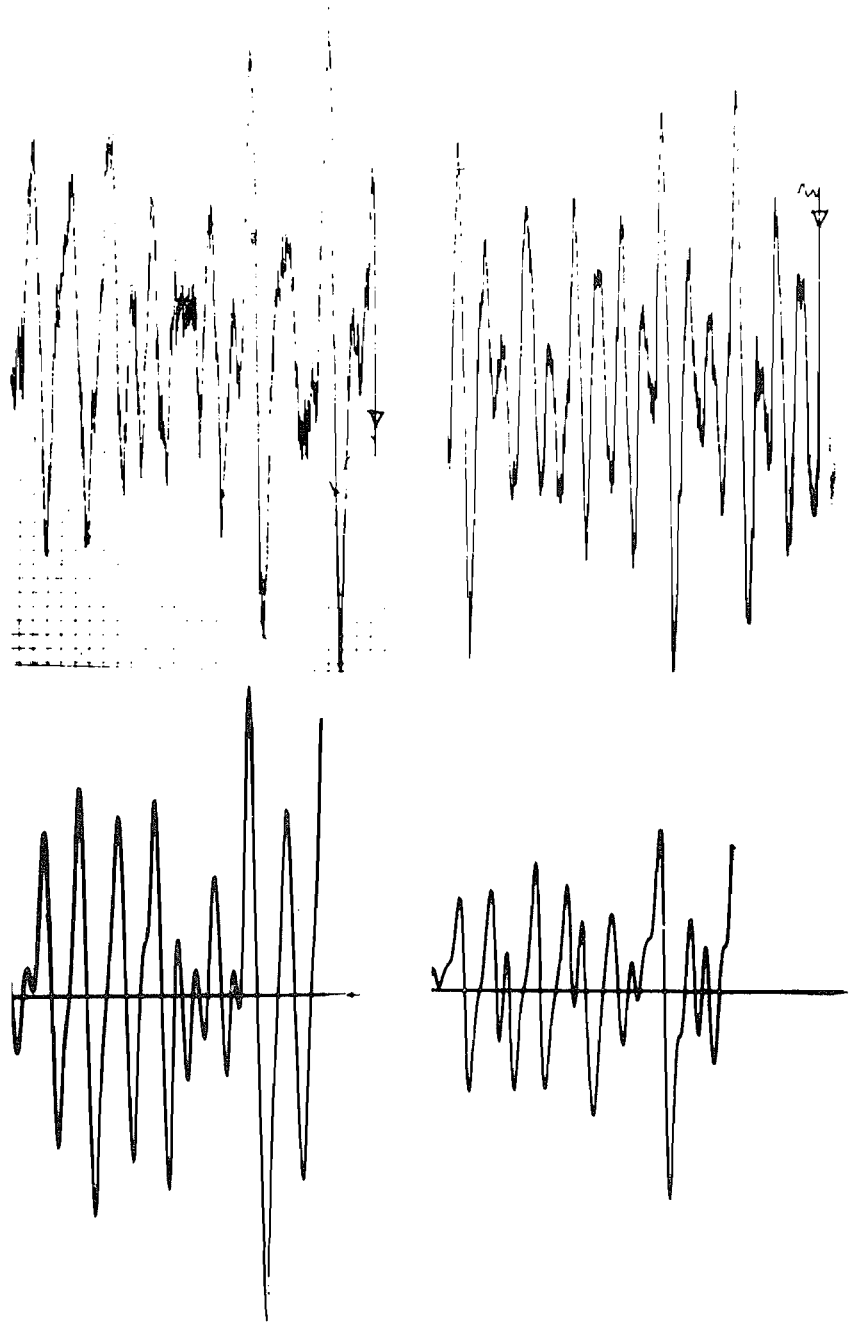

FIG. 2. Partie centrale des spectres expérimental et simulé de **4** à 20 °C (gauche) et à −50 °C (droite).

Can. J. Chem. Downloaded from www.nrcresearchpress.com by 210.87.254.6 on 09/05/12
For personal use only.

portant sur la valeur du couplage *ortho*. Cependant, l'examen du spectre à plus basse température (fig. 2) rend plus probable la valeur a_{ortho} = 0.84 G. L'obtention de valeurs anormalement élevées pour les couplages hyperfins des protons *ortho* est à rapprocher de la situation analogue rencontrée pour les radicaux phenylxanthyle, -thioxanthyle et -sélénoxanthyle (2, 3). De plus, l'équivalence des protons *méta* et *para* est également établie sans ambiguïté pour le radical phenylxanthyle. Une étude ENDOR récente (20) confirme d'ailleurs l'ordre de grandeur des couplages mesurés par rpe (1, 2). La variation avec la température du spectre de **4** semble à priori confirmer le modèle de rotation restreinte proposé par Lunazzi *et al.* (3); on peut en effet

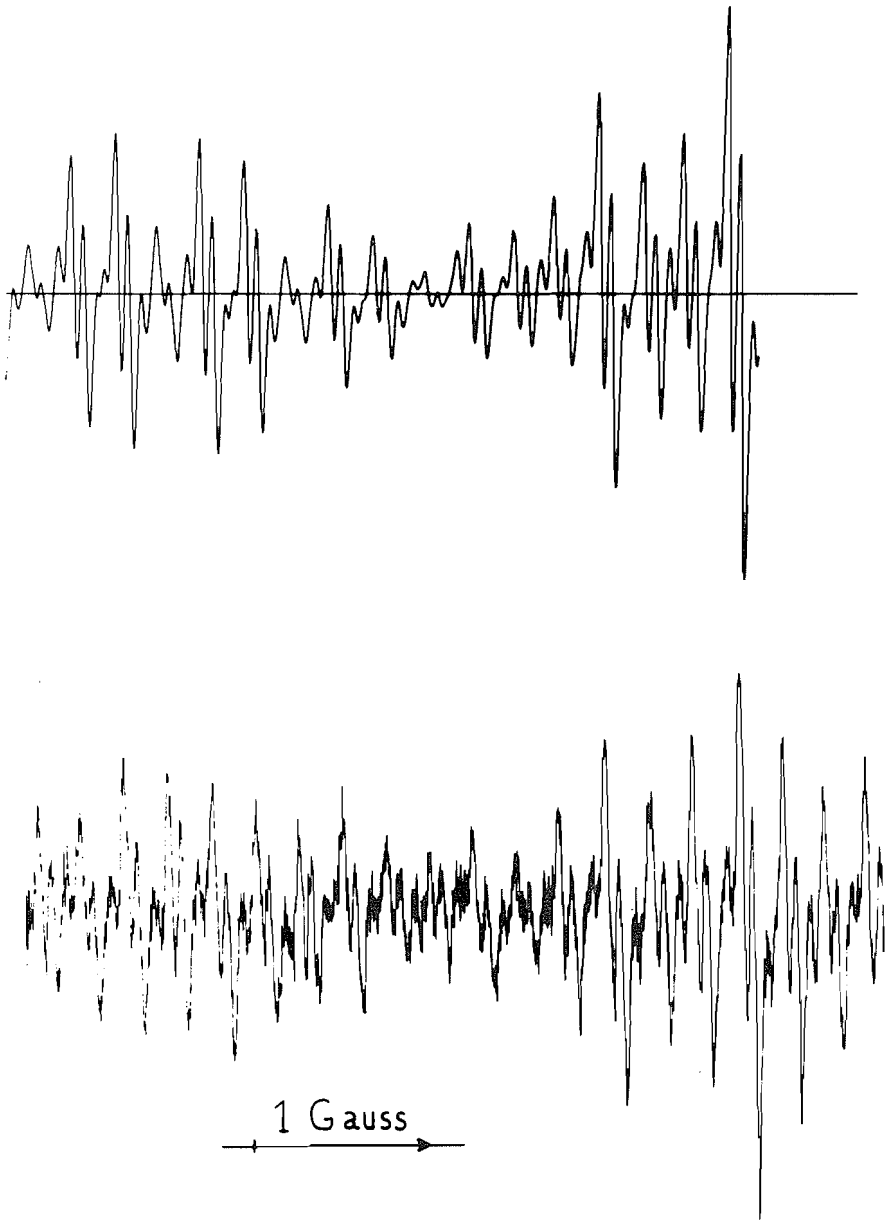

FIG. 3. Spectres expérimental et simulé de **5**.

Can. J. Chem. Downloaded from www.nrcresearchpress.com by 210.87.254.6 on 09/05/12
For personal use only.

Can. J. Chem. Downloaded from www.nrcresearchpress.com by 210.87.254.6 on 09/05/12
For personal use only.

l'expliquer qualitativement par une modification de l'angle du groupe phényle autour de la liaison 9–9′. Cependant, la contribution a_H* provenant du recouvrement de l'orbitale $2p_z$ centrée en C_9 avec les protons *ortho*, calculée selon la méthode de Lunazzi (3), est trop faible pour interpréter nos résultats. Gilbert et coll. (25) concluent de manière identique leur très récente étude rpe des cations 10-phénylphénoxazine et 10-phénylphénothiazine. On doit donc penser plutôt à un mécanisme de type hyperconjugaison, ce qui permettrait d'expliquer qualitativement la variation du couplage avec l'angle de rotation θ autour de la liaison 9–9′. Ce mécanisme a également été proposé pour expliquer les couplages "anormaux" de certains radicaux allyles (11), de type benzyle (12, 27), triarylméthyle (26), xanthyle (28) ou du radical triphénylméthyle (13).

D'autre part, Pople et Beveridge (14) a calculé par la méthode INDO les constantes de couplage du radical benzyle en fonction de l'angle de rotation θ du groupe phényle: sauf pour $a_{méta}$, l'accord avec l'expérience ($\theta = 0$) est satisfaisant. Ce radical benzyle peut servir de modèle pour **4** compte tenu de la réduction de densité de spin en C_9 calculée d'après **2**: $\rho_9 = 0.44$ ($Q = 27$ G). On peut ainsi estimer un ordre de grandeur des couplages *ortho* et *para* en ajoutant les contributions dues à l'interaction σ–π (à partir de $a_{o,p}$ du radical benzyle pour $\theta = 90°$) et à la délocalisation (a_{ML} pour $\theta \neq 90°$). Modèle 1:

$$a_{o,p}(\theta) = \rho_9 a_{\text{benzyle } \theta=90°} + a_{ML}(\theta)$$

Ce calcul améliore très sensiblement l'accord avec l'expérience (tableau 3).

Une autre méthode consiste à utiliser directement les résultats INDO du radical benzyle pour tenir compte de la diminution des constantes de couplages lorsque l'angle θ passe de 0 à θ degrés. A partir des valeurs expérimentales de ce radical benzyle, on peut alors calculer les valeurs correspondantes des couplages pour **4**, ceci pour un angle quelconque: modèle 2:

$$a_{o,m,p}(\theta) = \frac{a_{\text{INDO}}(\theta)}{a_{\text{INDO}}(0°)} \rho_9 a_{o,m,p}$$

(benzyle expérimental)

L'application de cette formule pour $\theta = 75°$ donne d'excellents résultats en *ortho* et *para* (tableau 3).

TABLEAU 3. Constantes de couplage de **4** pour un angle θ de 75°

	|Exp.|	ML ($\lambda = 1.1$)	Modèle 1	Modèle 2
ortho	~0.84	−0.21	−1.24	−0.82
méta	0.36	+0.08	0.69	0.62
para	0.36	−0.19	−0.48	−0.32

Radical 5

Bien que nos résultats soient en bon accord avec ceux de Sevilla et Wincow (1) concernant divers radicaux de type xanthyle, l'existence de couplages observés pour les cinq protons du groupe phényle (donc par l'intermédiaire du soufre) est plus surprenante en raison de l'éloignement du carbone C_9. Signalons cependant que le radical 9-benzylxanthyle montre également de tels couplages (0.14 G et 0.04 G). Pour ce radical **5** très particulier (fig. 3), en négligeant la participation possible des orbitales *d* du soufre, l'ordre de grandeur correct des couplages observés est obtenu en adoptant une intégrale d'échange de $0.26\,\beta_{cc}$ pour la liaison 9′–10′.

1. M. D. SEVILLA et G. WINCOW. J. Phys. Chem. **72**, 3635 (1968); **72**, 3641 (1968).
2. L. LUNAZZI, A. MANGINI, G. PLACUCCI et C. VINCENZI. J. Chem. Soc. Perkin Trans. 1, 2418 (1972).
3. L. LUNAZZI, A. MANGINI, G. PLACUCCI, C. VINCENZI et I. DEGANI. Mol. Phys. **19**, 543 (1970).
4. T. YOSHIDA, Y. VENO et S. WAKABAYASHI. Kogyo Kagaku Zasshi, **72**, 338 (1969).
5. I. AGRANAT, M. RABINOVITZ, H. R. FALLE, G. R. LUCKHURST et J. N. OCKWELL. J. Chem. Soc. B, **294** (1970).
6. L. S. SINGER, I. C. LEWIS, T. RICHERZHAGEN et G. WINCOW. J. Phys. Chem. **75**, 290 (1971).
7. A. D. MCLACHLAN. Mol. Phys. **3**, 233 (1960).
8. (*a*) D. R. DALTON et S. A. LIEBMAN. J. Am. Chem. Soc. **91**, 1194 (1969); (*b*) S. A. LIEBMAN, D. R. DALTON, T. KNUDSEN et G. UNDERWOOD. J. Magn. Reson. **10**, 85 (1973).
9. F. C. ADAM et H. R. FALLE. Can. J. Chem. **44**, 1397 (1966).
10. W. J. VAN DEN HART. Mol. Phys. **19**, 75 (1970).
11. A. BERNDT. Tetrahedron, **25**, 37 (1969).
12. W. J. VAN DEN HOCK, B. A. C. ROUSSEEUW, J. SMIDT, W. G. B. HUYSMANS et W. J. MYS. Chem. Phys. Lett. **13**, 429 (1972).
13. K. SCHREINER, A. BERNDT et F. BAER. Mol. Phys. **26**, 929 (1973).
14. J. A. POPLE et D. L. BEVERIDGE. J. Chem. Phys. **49**, 4725 (1968).
15. (*a*) G. CAUQUIS et G. REVERDY. Tetrahedron Lett. 1493 (1967); (*b*) G. REVERDY. Thèse Grenoble n° AO 8436, 1973.
16. (*a*) G. KORTÜM et K. W. KOCH. Chem. Ber. **100**,

1515 (1967); (*b*) Z. R. GRABOWSKI et M. S. BALASIEWICZ. Trans. Faraday Soc. **64**, 3346 (1968).
17. F. A. NEUGEBAUER et GROH. Tetrahedron Lett. 1005 (1973).
18. A. R. BASSINDALE, A. J. BOWLES, A. HUDSON et R. A. JACKSON. Tetrahedron Lett. 3185 (1973).
19. J. N. MURRELL, S. F. A. KETTLE et J. M. TEDDER. Valence theory. 2leme ed. 1965. p. 32.
20. Y. YAMADA, S. TOYODA et K. OUCHI. J. Phys. Chem. **78**, 2512 (1974).
21. B. J. TABER et J. R. ZDYSIEWICZ. J. Chem. Soc. B, 1659 (1971).
22. R. LUCKHURST. Mol. Phys. **11**, 205 (1966).
23. F. BARIGELLI, G. ORLANDI et G. GIRO. J. Chem. Soc. Faraday Trans. II, **71**, 1436 (1975).
24. A. ATTO. Chem. Phys. Lett. **33**, 477 (1975).
25. D. CLARKE, B. C. GILBERT et P. HANSON. J. Chem. Soc. Perkin Trans. II, 1078 (1975).
26. M. STEIN et A. RIEKER. Tetrahedron Lett. **25**, 2126 (1975).
27. K. SCHREINER et A. BERDT. Angew. Chem. **14**, 366 (1975).
28. E. KRUMBHOLZ, F W. STEUBER, Angew. Chem. **14**, 553 (1975).

Can. J. Chem. Downloaded from www.nrcresearchpress.com by 210.87.254.6 on 09/05/12
For personal use only.

Etude de l'équilibre tautomère des pyrazolinones-4

C. SABATÉ-ALDUY ET J. BASTIDE
Laboratoire de Synthèse Organique, Centre Universitaire, 66025 Perpignan, France

Reçu le 23 avril 1975[1]

C. SABATÉ-ALDUY et J. BASTIDE. Can. J. Chem. **54**, 1752 (1976).

L'étude de l'équilibre cétoénolique de pyrazolinones-4 diversement substituées est effectuée dans plusieurs solvants; ces composés n'existent que sous la forme énolique. Une étude théorique en comparaison avec les pyrazolinones-5 est réalisée.

C. SABATÉ-ALDUY and J. BASTIDE. Can. J. Chem. **54**, 1752 (1976).

The keto-enol equilibria in variously substituted 4-pyrazolinones were studied in several solvents; these compounds exist in the enol form only. An MO theoretical study of these compounds in comparison to the 5-pyrazolinones is reported.

L'équilibre tautomère des pyrazoline-2 ones-5 a fait l'objet de nombreuses publications (1–5) par contre les recherches portant sur les pyrazoline-2 ones-4 sont très limitées.

Nye et Tang (6) ont étudié l'équilibre cétoénolique des pyrazolinones-4 mais tous les composés qu'ils ont analysés sont du même type, disubstitués en 3,5 par des groupes aromatiques. A côté du travail de Nye et Tang on peut noter une publication de Farkas (8) qui traite des pyrazolones substituées par des groupes méthoxycarbonyles et une de Vinokurov (9) qui porte sur la phényl-1 pyrazolinone-4.

Dans le cas des pyrazoline-2 ones-5 deux facteurs influencent d'une façon importante l'équilibre cétoénolique: la nature du solvant dans lequel est étudié le composé et les substituants portés par le cycle.

Nous avons donc étudié l'équilibre cétoénolique des pyrazoline-2 ones-4 en fonction de ces deux paramètres.

Les équilibres tautomères des formes principales de ces composés peuvent être représentés comme suit dans le schéma 1. Les pyrazoline-2 ones-4 étudiées sont indiquées dans le tableau 1.

Les composés **2** à **5** ont été synthétisés par cycloaddition dipolaire-1,3 du diazoacétate d'éthyle sur le sel de sodium du malonate d'éthyle mono substitué. Les composés **1**, **6** et **7** ont été obtenus par hydrolyse et décarboxylation respectivement, des pyrazoline-2 ones-4 **2**, **3** et **4**. Enfin les composés **8** à **11** ont été obtenus par condensation de l'hydrazine sur les époxychalcones et aromatisation ultérieure de l'hydroxy-4 pyrazoline obtenue. La synthèse détaillée de ces différents composés est décrite par ailleurs (10).

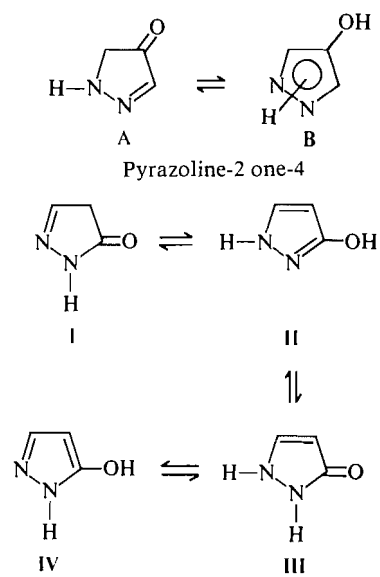

SCHÉMA 1

Caractéristiques spectrales génèrales des différentes formes

Infrarouge

La présence de la forme **A** ou de la forme **B** peut être facilement décelée (pour les composés **1** et **8–11**) par l'existence ou non d'une bande carbonylée (dans le cas d'un composé bloqué sous la forme **A** Nye (6) a observé la bande carbonylée à 1680 cm^{-1}). Pour les autres com-

[1]Revision reçue le 27 février 1976.

Can. J. Chem. Downloaded from www.nrcresearchpress.com by 210.87.254.5 on 09/05/12
For personal use only.

Can. J. Chem. Downloaded from www.nrcresearchpress.com by 210.87.254.5 on 09/05/12
For personal use only.

TABLEAU 1. Les pyrazoline-2 ones-4 étudiées

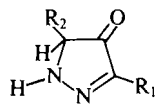

Composé	R_1	R_2	Composé	R_1	R_2
1	H	H	**7**	COC_6H_5	H
2	$CO_2C_2H_5$	$CO_2C_2H_5$	**8**	C_6H_5	C_6H_5
3	$CO_2C_2H_5$	$COCH_3$	**9**	C_6H_5	p-$CH_3OC_6H_4$
4	$CO_2C_2H_5$	COC_6H_5	**10**	C_6H_5	p-$NO_2C_6H_4$
5	$CO_2C_2H_5$	$CH_2C_6H_5$	**11**	C_6H_5	p-ClC_6H_4
6	$COCH_3$	H			

TABLEAU 2. Spectres ir des pyrazolinones-4 (ν, cm^{-1})

Composé	OH—NH	C=O (ester)	R—C=O	Phase
1	3240, 2560			Nujol
	3360			CH_3CN
2	3400, 3230	1725, 1690		Nujol
	3410	1720, 1710, 1690		$CHCl_3$
	3220	1705, 1690		CH_3CN
3	3360, 3200	1680	1660	Nujol
	3400	1680	1660	$CHCl_3$
	3230	1705	1650	CH_3CN
4	3330, 3160	1700	1625	Nujol
	3220	1715	1630	CH_3CN
5	3400, 2600	1700		Nujol
	3515, 3430	1720, 1680		$CHCl_3$
	3270	1720, 1690		CH_3CN
6	3150		1620	Nujol
	3460		1640	CH_3CN
7	3150		1620	Nujol
8	3220, 2450			Nujol
	3300			CH_3CN
9	3200, 2500			Nujol
	3300			CH_3CN
10	3400, 2600			Nujol
11	3200, 2450			Nujol
	3300			CH_3CN

posés cette méthode ne permet pas une détermination certaine du fait de la présence d'autres fonctions carbonylées dans la molécule.

Résonance magnétique nucléaire

La forme **A** devrait présenter une absorption correspondant au proton en position 5 dans la zone 3–5 ppm, alors que la forme **B** devrait présenter un proton hydroxyle dans la région 6–8 ppm.

Ultraviolet

La forme **A** doit présenter une absorption vers 280–290 nm (chromophore —N̈—N=C—C=O) et la forme **B** une absorption vers 235 nm (l'éthoxy-4 pyrazole absorbe à 233 nm (11)).

Ces différentes méthodes peuvent donc permettre d'identifier les formes **A** ou **B** des composés étudiés dans les différents solvants.

Résultats

Les résultats des différentes mesures spectrales sont portés dans les tableaux 2, 3 et 4.

L'analyse des différents résultats obtenus

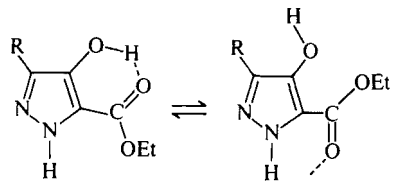

SCHÉMA 2

montre que, quel que soit le solvant employé, les pyrazolinones-4 se présentent toujours sous leur forme énolique hydroxy-4 pyrazoles. En particulier dans le cas des composés substitués en 3 (5), par un groupe méthoxycarbonyle la spectroscopie de rmn permet d'éliminer la forme **A** que la spectroscopie ir pouvait laisser envisager en solution dans le chloroforme.

L'apparition de deux bandes carbonylées dans **5** peut être interprétée par la présence des deux formes chélatées en équilibre (schéma 2). On peut penser que les composés étudiés par Farkas et Flegelova (8) en ir présentent ce même type de chélation et que l'attribution de la deuxième bande carbonyle à la forme **A** est erronée.

Discussion des résultats

Dans le cas des pyrazolinones-5 la forme cétonique apparaît comme la plus stable dans certains solvants, en particulier le chloroforme. Il nous a paru intéressant d'essayer de comprendre pourquoi l'on observait une différence de comportement entre les pyrazolinones-5 et les pyrazolinones-4.

Prenons le cas du modèle fondamental pyrazolinone-5, sa faible solubilité n'a pas permis une

TABLEAU 3. Résonance magnétique nucléaire: déplacements chimiques des pyrazolinones-4 (δ, ppm)

Composé	OH	H_3 et H_5	CH_3	CH_2	Aromatique	Solvant
1	8.2	7.18				CD_3CN
	8.26	7.1				DMS-d_6
		7.16				CD_3OD
2	7.33		1.4(t)	4.46(q)		$CDCl_3$
			1.32(t)	4.31(q)		CD_3CN
			1.29(t)	4.28(q)		DMS-d_6
			1.31(t)	4.38(q)		CD_3OD
3	8.5		1.44(t), 2.6(s)	4.45(q)		$CDCl_3$
			1.34(t), 2.48(s)	4.37(q)		CD_3CN
	9.1		1.29(t), 2.42(s)	4.27(q)		DMS-d_6
			1.28(t), 2.41(s)	4.28(q)		CD_3OD
4	9.15		1.35(t)	4.38(q)		CD_3CN
	7.4, 7.7		1.32(t)	4.31(q)		DMS-d_6
			1.4(t)	4.37(q)		CD_3OD
5	8.36		1.34(t)	4.34(q), 3.94(s)	7.15	$CDCl_3$
			1.21(t)	4.2(q), 3.8(s)	7.08	CD_3CN
	7.18		1.26(t)	4.23(q), 3.82(s)	7.18	DMS-d_6
			1.33(t)	4.32(q), 3.91(s)	7.15	CD_3OD
6	7.78	7.22	2.47(s)			CD_3CN
		7.4	2.3(s)			DMS-d_6
7	7.3, 7.6	7.9, 8.1				DMS-d_6
8	7.32				7.92	CD_3CN
	8.3				7.2, 8.1	DMS-d_6
	7.2, 8				7.2, 8	CD_3OD
9					3.27 (p.x.)	CD_3CN
	8.15				6.9, 8.05	DMS-d_6
	6.8, 7.9				6.8, 7.9	CD_3OD
10	8.7				7.3, 8.35	DMS-d_6
	7.28, 8.15				7.28, 8.15	CD_3OD
11	8.2, 8.6				7.25, 8	DMS-d_6
	7.3, 8				7.3, 8	CD_3OD

Can. J. Chem. Downloaded from www.nrcresearchpress.com by 210.87.254.5 on 09/05/12
For personal use only.

TABLEAU 4. Spectres u.v. (C_2H_5OH, 95%) des pyrazolinones-4

Composé	λ(nm)	log ε	λ(nm)	log ε	λ(nm)	log ε
1	234	3.857				
2	233(e)*	4.274	276	4.230		
3	249(e)	3.991	287	4.124		
4	229	4.518	257	4.472	332(e)	3.958
5	229	4.326	275	4.125		
6	242	4.188	291	4.010		
8	252	4.355	276	4.230	295	4.000
9	259	4.477				
10	262	4.672	333	4.686		
11	260	4.498	302(e)	4.093		

*(e) épaulement.

étude dans tous les solvants, et, dans les solvants utilisés la forme carbonylée n'a pas été mise en évidence. La comparaison des résultats obtenus avec les pyrazolinones substituées par des groupes méthyles permet de penser que cette forme carbonylée peut exister dans les solvants peu polaires.

Solvant	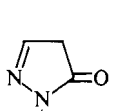	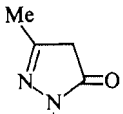	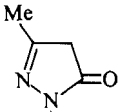
	H	H	Me
$CHCl_3$		I(+ IV)	I
CH_3CN	IV	IV	I(85) + IV(15)

A l'état vapeur la méthyl-3 pyrazoline-2 one-5 se trouve sous forme d'un mélange de **I** et **II** (**I** semblant être en quantité plus importante (12)), on peut donc penser que dans le cas de la pyrazoline-2 one-5 les deux formes sont énergétiquement très voisines.

Dans le cas de la pyrazoline-2 one-4 dans le chloroforme, ce composé n'existe que sous la forme **B** (en spectroscopie uv, il ne présente pas d'absorption au delà de 240 nm); la forme énolique semble donc, d'une façon générale, être énergétiquement plus favorisée que la forme cétonique pour les pyrazolinones-4 et inversement pour les pyrazolinones-5. Dans les deux cas cependant la forme énolique correspond à un système aromatique, un autre facteur doit donc expliquer cette différence de comportement.

Nous avons alors essayé de voir si les calculs théoriques rendaient bien compte de cette différence.

Arriau et coll. (13) ont trouvé pour les pyrazolinones-5 par différentes méthodes de calcul que la forme **I** était la plus stable.

Nous avons étudié les formes **A** et **B** des pyrazolinones-4 et les formes **I** à **IV** des pyrazolinones-5 par la méthode CNDO/2 (14). Les géométries de **I** à **IV** sont celles utilisées par Arriau (13) et celles des pyrazolinones-4 ont été définies par analogie avec celles des pyrazolinones-5.

Les résultats suivants ont été obtenus:

Composé	E_T (u.a.)	Composé	E_T (u.a.)
A	−66.0378	**II**	−66.0470
B	−66.0732	**III**	−66.0302
I	−66.0567	**IV**	−66.0559

Nous voyons que la forme **B** est plus stable que la forme **A** et que **I** est plus stable que **II**, **III** et **IV**. Dans le cas des pyrazolinones-4 la forme énolique **B** est beaucoup plus stable que la forme cétonique **A**; par contre dans le cas des pyrazolinones-5, la forme cétonique **I** est la plus stable mais très légèrement par rapport à la forme énolique **IV** ($\Delta E = 0.5$ kcal/mol). On peut donc penser qu'à l'état gazeux on a un mélange des deux formes cétone et énol.

Ces valeurs sont qualitativement bien en accord avec les résultats expérimentaux; dans le cas des pyrazolinones-5 les interactions avec le solvant sont suffisantes pour déplacer l'équilibre mais elles ne le sont pas dans le cas des pyrazolinones-4. Dans le cycle pyrazolinone-5 la fonction carbonylée est de type amide alors que dans le cas de la pyrazolinone-4 c'est une fonction cétone.

Afin de voir si cette différence au niveau de la fonction carbonylée pouvait être à l'origine de la différence de comportement des deux composés,

Can. J. Chem. Downloaded from www.nrcresearchpress.com by 210.87.254.5 on 09/05/12
For personal use only.

nous avons étudié l'équilibre cétoénolique de l'acétone et de l'acétamide par la méthode CNDO/2; nous avons obtenu les résultats suivants:

ΔE = 190 kcal/mol

ΔE = 320 kcal/mol

La fonction cétone est donc plus facilement énolisable que la fonction amide; ceci peut expliquer la différence de comportement vis-à-vis de l'équilibre cétoénolique entre les pyrazoline-2 ones-5 et les pyrazoline-2 ones-4.

1. J. Elguero, R. Jacquier et G. Tarrago. Bull. Soc. Chim. 3772 (1967); 3780 (1967).
2. A. Maquestiau, Y. Van Haverbeke et R. Jacquerye. Bull. Soc. Chim. Belg. **80**, 17 (1971); **82**, 215 (1973); **82**, 233 (1973).
3. J. Arriau, J. Deschamps, J. Tesseyre, A. Maquestiau et Y. Van Haverbeke. Tetrahedron, **30**, 1225 (1974).
4. H. Dorn. J. Prakt. Chem. **315**, 382 (1973).
5. G. L. Lestina, G. P. Happ, D. P. Maier et T. H. Regan. J. Org. Chem. **33**, 3336 (1968).
6. M. J. Nye et W. P. Tang. Tetrahedron, **28**, 455 (1972); **28**, 463 (1972).
7. M. J. Nye et W. P. Tang. Can. J. Chem. **48**, 3563 (1970).
8. J. Farkas et Z. Flegelova. Tetrahedron Lett. **19**, 1591 (1971).
9. V. G. Vinokurov, V. S. Troitskaya, I. I. Grandberg et Y. A. Pentin. J. Gen. Chem. U.S.S.R. **33**, 2531 (1963).
10. C. Sabaté-Alduy, J. Bastide et P. Berçot. Bull. Soc. Chim. Sous presse.
11. S. N. Groen et J. F. Arens. Recl. Trav. Chim. Pays-Bas, **80**, 879 (1961).
12. A. Maquestiau, Y. Van Haverbeke, A. Bruyère. Bull. Soc. Chim. Belg. **82**, 747 (1973); **87**, 757 (1973); A. Bruyère, Thèse, Mons, Belgique. 1973.
13. J. Deschamps, J. Arriau et P. Parmentier. Tetrahedron, **27**, 5779 (1971).
14. J. A. Pople et G. A. Segal. J. Chem. Phys. **44**, 3289 (1966); Programme QCPE 141, Indiana University, Bloomington, Indiana.

Can. J. Chem. Downloaded from www.nrcresearchpress.com by 210.87.254.5 on 09/05/12
For personal use only.

An improved colorimetric procedure for the analysis of vitamin A

J. A. BLAKE AND J. J. MORAN

Department of Nutrition and Food Science, Faculty of Medicine, University of Toronto, Toronto, Ont., Canada M5S 1A1

Received August 22, 1975

J. A. BLAKE and J. J. MORAN. Can. J. Chem. **54**, 1757 (1976).

Factors affecting the reaction between antimony trichloride and 2,3-dichloropropanol (2,3-DP) with retinol and related compounds were examined. It is shown that purified 2,3-DP with the addition of antimony trichloride produces a stable colour complex with retinol absorbing at 555 nm. A tentative scheme for the reaction mechanism and the possible structure of the complex are also presented.

J. A. BLAKE et J. J. MORAN. Can. J. Chem. **54**, 1757 (1976).

On a examiné les facteurs affectant la réaction du trichlorure d'antimoine et du dichloro-2,3 propanol (2,3-DP) avec le rétinol et d'autres composés qui lui sont reliés. On a montré que l'addition de chlorure d'antimoine à du 2,3-DP provoque la formation, par réaction avec le rétinol, d'un complexe de couleur stable absorbant à 555 nm. On propose un schéma réactionnel et une structure possible pour le complexe.

[Traduit par le journal]

Introduction

Vitamin A and compounds having vitamin A activity are most commonly assayed in food materials or samples of biological origin by; (*1*) bioassay, (*2*) ultraviolet absorption, (*3*) fluorometric analysis, and (*4*) colorimetric analysis.

A large number of related compounds have varying degrees of vitamin A activity. Mild physical or chemical treatment can convert a biologically active compound such as all-*trans* retinol into a compound of low potency like the eleven *cis* isomer. Most physico-chemical tests respond to the different isomers and even to many retinol analogues as if they were all-*trans* retinol. These procedures give an upper limit to the estimate of the amount of vitamin A in a food or biological material. The true vitamin A activity can only be determined by bioassay techniques. These are unfortunately so cumbersome and time-consuming that they have been replaced in most routine testing by the fast, relatively simple, cheap and reliable physico-chemical tests.

Another major difficulty in assaying foods is the presence of carotenoids, food additives, and other materials which interfere with the physico-chemical procedures employed in the analysis. In order to eliminate these interferences extensive chromatographic and extraction purification is necessary in the analysis of most foods. The higher level of vitamin present and the simpler character of most pharmaceutical preparations makes these systems inherently easier to analyze than foods.

The ultraviolet absorption method (measurement of the absorption at the maximum in the vitamin A curve) is an excellent procedure if few interfering compounds are present and if the vitamin is present in relatively high concentration. This method is one of those recommended by the Association of Official Analytical Chemists (AOAC) for the determination of vitamin A in margarine (2). For this purpose it is a difficult but acceptable procedure.

Vitamin A fluoresces strongly near 480 nm with excitation at 330–360 nm. This fluorescence has been little used for quantitative purposes until recently, because of extraneous fluorescence from phytofluene and other fluorescent materials present in many food materials and biological samples. Improved column chromatographic methods of removing the interfering fluorescing compounds have sparked a renewal of interest in the fluorometric procedure (3, 4). This is an excellent, very sensitive research method, especially where the concentration of vitamin A is low, if the interfering compounds can be satisfactorily removed.

Most vitamin A analysis is carried out by colorimetric techniques. Vitamin A reacts with many Lewis acids to produce a transient blue colour (5). In another of the official methods of

Can. J. Chem. Downloaded from www.nrcresearchpress.com by 210.87.254.5 on 09/05/12
For personal use only.

Can. J. Chem. Downloaded from www.nrcresearchpress.com by 210.87.254.5 on 09/05/12
For personal use only.

the AOAC (2), vitamin A in food materials is determined by reacting a vitamin A solution (extracted from the food with nonpolar anhydrous solvents) with a 20–25% solution of antimony trichloride in chloroform. The blue colour produced (λ_{max} = 620 nm) reaches maximum intensity in 5 to 10 s and then rapidly fades. This procedure, which is usually called the Carr–Price (6) method, has the advantage over the ultraviolet technique of being less liable to interference and somewhat more sensitive. Its major disadvantages are: (*1*) it is necessary to take readings of the absorbance within 5 to 10 s of addition of the reagent, (*2*) the poisonous and corrosive nature of the reagent, and (*3*) the development of the colour is affected by traces of water and alcohol. These problems make the method less precise than the ultraviolet technique.

Budowski and Bondi (7) have introduced a second colorimetric procedure. This involves the conversion of vitamin A to anhydrovitamin A with anhydrous ethanolic – HCl or *p*-toluenesulphonic acid. The reaction is very specific for vitamin A but low results are obtained if even small traces of water are present.

A third colorimetric procedure was described by Sobel and Werbin (8). They showed that the reaction of 'activated' 1,3-dichloro-2-propanol (1,3-DP) with vitamin A produces a pink coloured complex which has its absorption maximum at 555 nm and which is stable for 2 to 10 min. The method has never become popular because of the difficulty of reproducibly activating 1,3-DP and because the procedure is less sensitive than the Carr–Price. Sobel and Werbin activated the chemical by vacuum distilling 1,3-DP from a 2.0% solution of antimony trichloride in chloroform. Unfortunately, the 1,3-DP supplied by many commercial sources either cannot be activated by Sobel and Werbin's method or shows only a weak activity with vitamin A.

Penketh (9) has suggested that the activating principle is hydrogen ion. Sobel and Werbin (10) stated that their preparations contained varying amounts of antimony trichloride but that this was not the activating chemical, because direct addition of antimony trichloride did not activate 1,3-DP.

In the study reported here we have concentrated our efforts: (*1*) on improving and understanding the 'activation' of 1,3-DP and the isomer 2,3-dichloro-1-propanol (2,3-DP) and (*2*) on determining the mechanism of the reaction. Our purpose was (*a*) to develop procedures using dichloropropanol compounds which would be more convenient than the common physicochemical methods, and (*b*) to suggest, from a study of the reaction mechanism, other compounds which may give a more intense colour reaction with vitamin A.

Results and Discussion

(a) Preliminary Results with 1,3-DP

When 1 ml of a solution containing less than 150 μg/ml of vitamin A is added to 3 ml of 1,3-DP activated as described by Sobel and Werbin (10), a transient blue colour appears (λ_{max} = 620 nm), but it is replaced within approximately 1 min by a pink colour (λ_{max} = 555 nm). The Carr–Price procedure also produces a blue colour with maximum absorption at 620 nm.

Using the chloramine T method (11) it was found that commercially activated 1,3-DP (glycerol dichlorohydrin for vitamin A analysis from Eastman Kodak, Distillation Products Division) and our own 1,3-DP, activated as described by Sobel and Werbin (10), contained approximately 0.15% reducing material, undoubtedly antimony trichloride. Efforts were concentrated on attempting to activate 1,3-DP by direct addition of antimony trichloride. This was found to be impossible with most commercial samples of 1,3-DP. A pink colour could, however, be developed if the directly activated solution were heated immediately after addition of vitamin A. A sample from BDH described as dichlorohydrin had decomposed slightly and was, therefore, distilled and dried before addition of antimony trichloride. This solution developed a strong pink colour (λ_{max} = 555 nm) when mixed with 30 μg/ml of retinol acetate. Similar distillation of the other samples of 1,3-DP prior to direct addition of antimony trichloride did aid activation but the pink colour produced with retinol acetate was quite weak. An analysis of the dichlorohydrin solution showed that it consisted of an approximately 50:50 mixture of 1,3-DP and 2,3-DP. A sample of 2,3-DP which had been obtained previously, activated readily after distillation. Even crude, undistilled 2,3-DP, prepared as described in the Experimental section,

TABLE 1. Effect of antimony trichloride concentration on absorption and chromophore stability at 555 and 660 nm for retinol–acetate–2,3-DP and retinal–2,3-DP respectively*

Concentration of $SbCl_3$ (gm/100 ml)	Absorbance at 555 nm (retinol acetate)	Time to reach maximum absorption (min)	Absorbance at 660 nm (retinal)	Time to reach maximum absorption (s)
0.1	0.135	6	0.00	—
0.2	0.155	4	0.027	<30
0.5	0.160	2	0.013	<30
1.0	0.190	1	0.104	<30
3.0	0.210	0.6	0.137	<30
10.0	Not measured		0.260	60

*Three millilitres of a solution composed of 90 ml of 1,2-dichloroethane, 10 ml of 2,3-DP, and x g of antimony trichloride were mixed with 1 ml of retinol acetate or retinal in 1,2-dichloroethane. The retinol acetate concentration was 13.2 μg/ml and the retinal 4.64 μg/ml. The temperature was 20 °C.

activated easily, but the colour produced with vitamin A decayed rapidly, probably because of the presence of HCl. Both practical grade 1,3-DP and the 2,3-DP produced from allyl alcohol contain 3–15% impurity before distillation. These impurities, especially in the case of 1,3-DP, appear to inhibit the colour development. Our distillation procedure and Sobel and Werbin's method remove sufficient of these impurities from 1,3-DP to enable it to be activated by antimony trichloride. In Sobel and Werbin's method, the extent of this activation depended partly on the degree of purification achieved and partly on the amount of antimony trichloride carried over in the distillate. According to their own determinations this varied between 0 and 0.67%. Our analysis of several different samples of practical grade 1,3-DP showed that they contained varying amounts of several impurities and their ability to be activated was found to depend inversely on the amount of an impurity which eluted at a retention time of 0.12 relative to 1,3-DP.

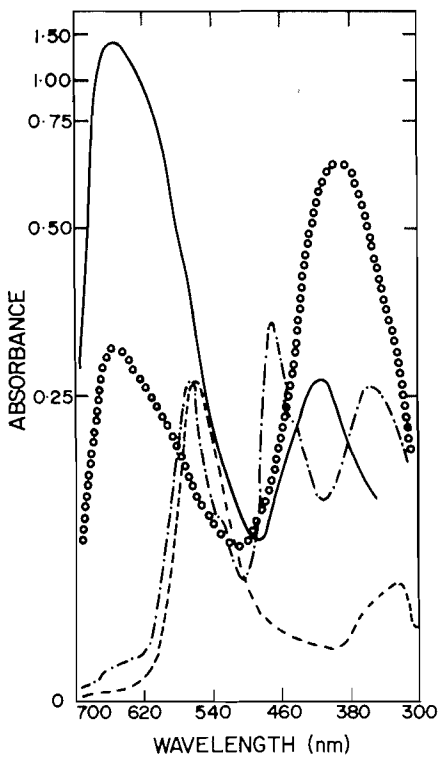

FIG. 1. Spectra of the 2,3-DP – $SbCl_3$ – vitamin A coloured complexes at 32 °C in chloroform: ○, retinal – 2,3-DP – 1% $SbCl_3$; —, retinal – 2,3-DP – 10% $SbCl_3$; - - -, retinol acetate – 2,3-DP – 1% $SbCl_3$; ·····, retinoic acid – 2,3-DP – 1% $SbCl_3$.

Our method of activation is capable of greater reproducibility because it is possible to control much more accurately the removal of impurities and the addition of antimony trichloride. Fortunately, 2,3-DP prepared from allyl alcohol (see Experimental section (*b*) for details) appears to contain few if any inhibiting impurities and it can be activated reproducibly by direct addition of antimony trichloride. In the remainder of this report, we describe the use of 2,3-DP, thus activated, in the analysis of vitamin A.

(b) Studies with 2,3-DP

(i) Effect of Antimony Trichloride Concentration

The dependence of the absorbance at 555 nm of the retinol acetate–2,3-DP chromophore and at 660 nm for the retinal–2,3-DP chromophore is presented in Table 1. The spectra of the vitamin A – 2,3-DP coloured complexes for retinol acetate, retinal, and retinoic acid are presented in Fig. 1. The rise and decay of the

Can. J. Chem. Downloaded from www.nrcresearchpress.com by 210.87.254.5 on 09/05/12
For personal use only.

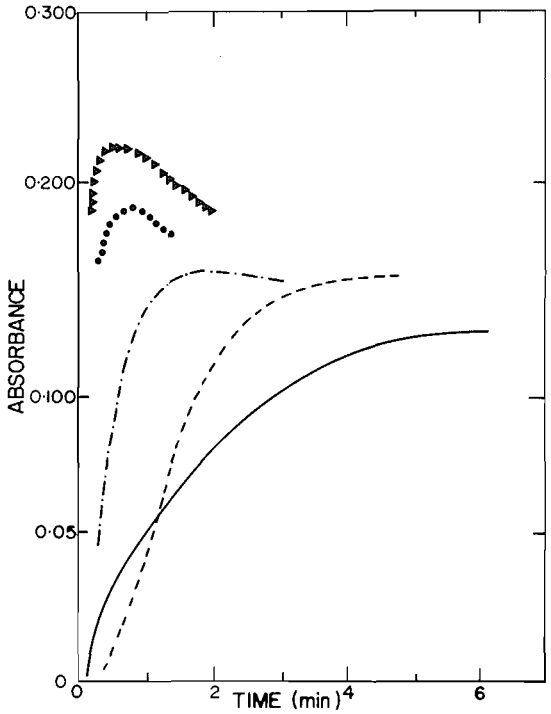

FIG. 2. Rate of change of the absorption at 555 nm as a function of $SbCl_3$ concentration. One millilitre of 13.2 μg/ml retinol acetate in 1,2-dichloroethane was mixed with 3 ml of 90:10:x dichloroethane – 2,3-DP – $SbCl_3$ at 20 °C: —, 0.1% $SbCl_3$; - - -, 0.2% $SbCl_3$; -·-·-, 0.5% $SbCl_3$; ···, 1% $SbCl_3$; ▲, 10% $SbCl_3$.

absorption intensity at 555 nm for retinol acetate are shown in Fig. 2. In earlier work it was found that, in the case of retinol acetate, 1% antimony trichloride was a good compromise between the intensity of colour developed and the rate of decay of absorbance. If maximum sensitivity is not required, possibly 0.5 or even 0.2% is a better choice. Retinol does not react as readily with 2,3-DP so at least a 1% solution is necessary to obtain a satisfactory absorbance value. A 10% solution gives a useful two and one-half fold increase in sensitivity.

(ii) Colour Complexes of Vitamin A Active Compounds

The absorbances relative to retinol acetate of several vitamin A active compounds are presented in Table 2. No absorbance was detected for retinoic acid when a 1% $SbCl_3$ solution was used. If a high concentration of retinoic acid was mixed with a 5% $SbCl_3$ solution, the complex spectrum shown in Fig. 1 was obtained.

TABLE 2. Absorbance of colour complexes of vitamin A compounds*

Compound	Absorbance relative to retinol acetate	Wavelength
Retinol acetate	1.0	555 nm
Retinol palmitate	1.0	555 nm
Retinal	1.6 (3.7)†	660 nm
Retinoic acid	0	

*Three millilitres of a solution composed of 90 ml of 1,2-dichloroethane or chloroform, 10 ml of 2,3-DP, and 1 g of antimony trichloride were mixed with 1 ml of the sample solution. The solvent for the sample was either 1,2-dichloroethane or chloroform and the temperature was 20 °C.
†10% $SbCl_3$ solution.

TABLE 3. Effect of solvent on the 555 nm chromophore*

Solvent	Absorbance at 555 nm / Absorbance at 555 nm in $CHCl_3$
$CHCl_3$†	1.0
Reagent grade $CHCl_3$	0.5
Nitromethane	0
Absolute alcohol	0
Methanol	0
2-Propanol	0
1,2-Dichloroethane	0.93
Carbon tetrachloride	—

*Three millilitres of a solution composed of 90 ml of solvent, 10 ml of 2,3-DP, and 1 g of antimony trichloride were mixed with 1 ml of retinol acetate, in the same solvent. The temperature was 32 °C and the experiments were conducted using a Spectronic Model 20.
†Chloroform was washed and distilled as described by Strohecker and Henning (1).

(iii) Effect of Solvent on the Absorbance at 555 nm

The effects of solvent were quite complex. Results are summarized in Table 3. Addition of 0.5 ml of alcohol per 4 ml of vitamin A – 2,3-DP solution completely prevents colour development. Even the 0.75% alcohol present in reagent grade chloroform severely inhibits colour development. Nitromethane also appears to be an inhibitor.

Carbon tetrachloride is immiscible with 2,3-DP in the proportions employed to construct Table 3. If the concentration of carbon tetrachloride is reduced, *i.e.* by adding 1 ml of retinol acetate in carbon tetrachloride to 3 ml of our standard chloroform–2,3-DP–$SbCl_3$ mixture, the absorbance obtained is identical with that obtained when only chloroform is present. The presence of carbon tetrachloride also appears to suppress the blue absorbance at 620 nm and to slow the reaction rate slightly. The effect of solvent will be

Can. J. Chem. Downloaded from www.nrcresearchpress.com by 210.87.254.5 on 09/05/12
For personal use only.

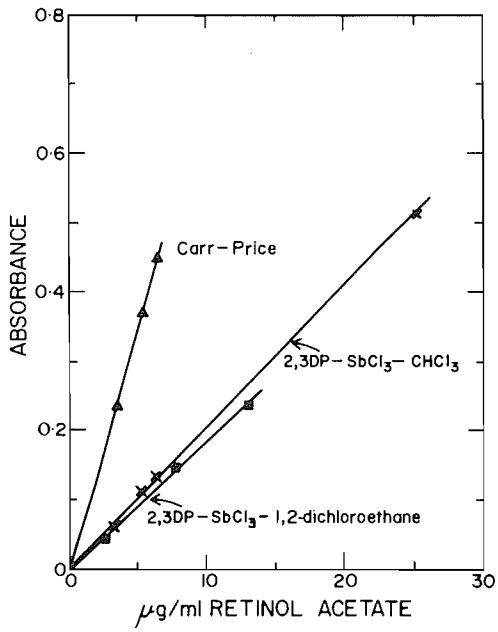

FIG. 3. Comparative Beer–Lambert plots for the Carr–Price and the 2,3-DP procedures ▲, ■. Curves were obtained at 32 °C in a Spectronic 20 and are corrected to a pathlength of 1 cm. In the solution containing 2,3-DP the ratios of solvent 2,3-DP–$SbCl_3$ were 90:10:1. The Carr–Price reagent contained 25 gm/100 ml $SbCl_3$.

further discussed in section (*vii*). Clearly, purified chloroform or 1,2-dichloroethane are the solvents of choice and alcohols should be either avoided or removed from all solvents.

(iv) Beer–Lambert Law Dependence

The Beer-Lambert law plots of retinol acetate in purified chloroform and 1,2-dichloroethane are shown in Fig. 3. The Carr–Price curve is also given. The absorbance of the coloured complex is linear in the concentration range 0–26 μg/ml when the 2,3-DP is diluted 9:1 with solvent. If 2,3-DP is used without dilution, the Beer–Lambert plot is not linear and the absorbance is about one-third less intense. On the basis of the above, the recommended procedure is to add 1 to 3 ml of a vitamin A solution in 1,2-dichloroethane to 3 ml of a 90:10:1 1,2-dichloroethane – 2,3-DP – antimony trichloride solution contained in a spectrophotometer cuvet and to record the maximum absorbance obtained at 555 nm (for retinol acetate).

One of our major goals has not been realized as yet, in that the absorbance is still about 3.5 times less intense than the corresponding Carr–Price absorbance when retinol acetate is assayed. As shown in Table 2, the sensitivity of the reagent for retinal is approximately the same factor higher, so that retinal can be detected by 2,3-DP with approximately the same sensitivity as retinol acetate by the Carr–Price method.

The lower sensitivity of this method for retinol acetate is not actually important in routine analysis. Most pharmaceutical preparations containing vitamin A have such a high level that dilution is necessary before analysis can be employed. Sebrell and Harris (12) show that most food sources of vitamin A contain considerably more than the 3 μg/g of vitamin A for which we found an absorbance of 0.076.

(v) Dependence of the Absorbance at 555 nm on Temperature

The absorbance at 26.5 °C was found to be 13% higher than at 20 °C. To prevent errors due to temperature effects, the procedure is best carried out in a controlled temperature room or a correction table can be prepared if this is not possible. If an instrument like the Spectronic 20 is used, the sample tube should not be inserted into the spectrophotometer until the pink colour appears, as the lamp of the Spectronic 20 noticeably heats the tube.

(vi) Stability of the Reagent

Two samples of reagent prepared by different workers from different samples of allyl alcohol and distilled at different maximum temperatures gave absorbances at 555 nm which differed by only 5% even though one reagent sample had been prepared 3 months before the other.

(vii) Mechanism of the Reaction

The first step in the reaction is certainly the Carr–Price reaction. By omitting the 2,3-DP we found that a strong transient absorption occurs at 620 nm even though the concentration of antimony trichloride is much smaller in our experiments than in the normal Carr–Price procedure. Solvents and the concentration of antimony trichloride markedly affect the absorbance at 620 nm. At antimony trichloride concentrations of less than 0.5% or in the presence of carbon tetrachloride or nitromethane even at 1% antimony trichloride concentration, the 620 nm absorbance is very low and does not vary appreciably with time.

In the presence (or absence) of 2,3-DP two peaks appear immediately at 397 nm with the

Can. J. Chem. Downloaded from www.nrcresearchpress.com by 210.87.254.5 on 09/05/12
For personal use only.

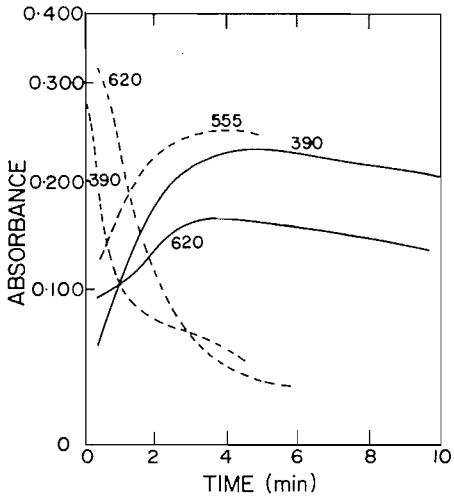

FIG. 4. Effect of 2,3-DP on the rates of change of the absorptions at 390, 620, and 555 nm: —, 3 ml of 1% $SbCl_3$ in $CHCl_3$ + 1 ml of 16.1 mg/ml retinol acetate; - - -, 3 ml of 90:10:1 $CHCl_3$/2,3-DP/$SbCl_3$ + 1 ml of 16.1 μg/ml of retinol acetate. Temperature 8 °C. Rates measured in a Beckman DB spectrophotometer.

hint of a third peak at 355 nm. The antimony trichloride solution absorbs strongly below approximately 370 nm with complete absorption occurring below 350 nm. Thus we could not determine the rate of change of the vitamin A concentration. Edisbury *et al.* (13) and Shantz *et al.* (14) showed that anhydrovitamin A is a product of the Carr–Price reaction. Anhydrovitamin A absorbs at 392, 371, and 351 nm in ethanol (12). The absorptions we obtained at 397 and 375 nm are undoubtedly due to anhydrovitamin A. At 10 °C in the presence of 2,3-DP, absorption at 390 nm was found to fall rapidly whereas in the absence of 2,3-DP it fell very slowly (Fig. 4). On the same time scale the pink colour rose to a maximum when 2,3-DP was present.

The relative values of the 620 and 390 nm absorptions depend on the concentration of antimony trichloride. At antimony trichloride concentrations in excess of 1% the 620 nm absorbance usually exceeds the 390 absorption whereas the reverse is true at lower concentrations of antimony trichloride.

Several different experiments have shown that the absorbance at 390 nm reaches a peak value before the 620 nm absorbance. For instance, 1 ml of a solution containing 9 μg/ml of retinol acetate in carbon tetrachloride was rapidly mixed at 30 °C with 3 ml of a solution containing purified chloroform, 2,3-DP, and antimony trichloride in the ratio 90:10:1. The 390 nm absorbance reached its maximum value in 6 s whereas the 620 nm absorbance took 14 s.

The rate and relative rate of decrease of the absorption at 620 and 390 nm depend on the concentration of antimony trichloride. As already stated, at low concentrations of antimony trichloride the 620 nm absorbance changes very little whereas the 390 nm absorbance decreases gradually from a fairly high value. At higher concentrations with purified chloroform or 1,2-dichloroethane as solvent, both absorptions decrease at approximately the same rate. The disappearance of the 620 and 390 absorptions and the rise of the absorption at 555 nm are best fitted by kinetic equations based on the assumption of reversible first-order kinetics. In the presence of 1% antimony trichloride all forward rate constants measured (k_{620}, k_{390}, k_{555}) agree within 20–30%.

If 0.5 ml of absolute ethanol is added to the reaction mixture after the 620 and 390 nm absorptions have reached their maximum values and the pink complex is present, the absorptions at 620 and 555 nm drop to zero within the mixing time of the chemicals, even at 0 °C. The 390 nm absorption does not change.

The present findings also indicate that a relatively stable complex absorbing at 555 nm is formed in the presence of both antimony trichloride and 2,3-DP. The structure of this complex has not been fully established but can be reasonably assumed to be that given in Fig. 5 by analogy with the known reaction of retinol with ethanol and Lewis acids. Earlier workers have shown that on treatment with anhydrous ethanol – HCl, vitamin A is first converted to anhydrovitamin A (13, 14) and on prolonged treatment, to isoanhydrovitamin A which bears an ethoxy group at 4, 14, or 15. This compound is reported to show absorption peaks at 332, 348, and 366 nm (15), while the Carr–Price complex absorbs at 620 nm (13). Whether or not the complex displays a weaker absorption peak at shorter wavelengths is not reported. Unfortunately, the strong absorption of antimony trichloride in the ultraviolet precludes the possibility of determining unequivocally whether a similar compound is formed between anhydrovitamin A and 2,3-DP in the reaction under study.

Can. J. Chem. Downloaded from www.nrcresearchpress.com by 210.87.254.5 on 09/05/12
For personal use only.

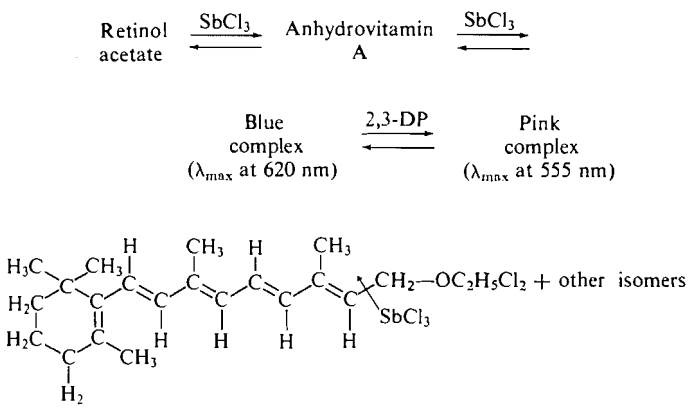

FIG. 5. Proposed reaction mechanism and the postulated structure of the pink complex.

The proposed mechanism for the reaction scheme is shown in Fig. 5. The first step is the conversion of retinol to anhydrovitamin A by antimony trichloride.

Lewis acids interact further with the anhydrovitamin A to form a π-complex with the conjugated system. The strong inductive effect of the chlorine atoms produces a fractional charge separation over the π-complex. The most strongly affected molecular orbital will be the highest occupied orbital (highest energy). Since the long wavelength transition is due to the promotion of an electron from this to the lowest unoccupied molecular orbital, the λ_{max} of the transition will be altered. The effect of the formation of the π-complex will be to destabilize (increase the energy of) the ground state (highest occupied molecular orbital) and to stabilize the excited state (lowest unoccupied molecular orbital). This is brought about by the stabilization of the necessary dipole produced in the optical transition. The decrease in the energy difference between the two states leads to the observed strong bathochromic shift from the ultraviolet to 620 nm.

The slower subsequent addition of 2,3-DP produces the complex shown in Fig. 5 and in effect reduces the conjugation path by a further formal double bond. Since the energy difference between the highest occupied and lowest unoccupied molecular orbital increases with decreasing conjugation path length, interaction with antimony trichloride now gives rise to the transition at 555 nm. Justification for this assumed scheme can be gained from the fact that the Carr–Price complex of vitamin A_2 (with six double bonds in the unperturbed state) absorbs at 693 nm (a shift of 73 nm compared to the retinol complex). If this 73 nm shift is of the right order for addition or subtraction of one double bond then the calculated long wavelength absorption maximum of the Lewis acid complex should be 547 nm. As has already been stated the measured absorption maximum occurs at 555 nm, only 8 nm removed from the calculated value.

Blatz *et al.* (16, 17) postulated extensive *cis–trans* isomerism of retinol in the reaction with Lewis acids leading to the formation of cyclic structures. In view of the known hindrance to rotation due to steric interference between the methyl groups at positions 9 and 13 and the proximal H atoms this is felt to be unlikely though selective *cis–trans* isomerism is obviously possible.

Further Work

Work is proceeding on determining if 2,2′,3,3′-tetrachloro-1-propanol, 2,3-dibromo-1-propanol, and 2,3-diodo-1-propanol have any advantage over 2,3-DP as colorimetric reagents for vitamin A analysis. Isolation of the isoanhydrovitamin A analogue (Fig. 5) is also being attempted.

Chemicals and Experimental Detail

(a) Chemicals

Retinol acetate, 1,3-DP for vitamin A determination, 2,3-dichloro-1-propanol (2,3-DP), allyl alcohol, and antimony trichloride were obtained from Fisher Scientific. Most of the 1,3-DP was manufactured by Eastman Kodak, except for 100 ml from the Baker Chemical Company. Retinol acetate, retinal, retinol, retinoic acid, and retinol palmitate were obtained from the Sigma

Can. J. Chem. Downloaded from www.nrcresearchpress.com by 210.87.254.5 on 09/05/12
For personal use only.

Can. J. Chem. Downloaded from www.nrcresearchpress.com by 210.87.254.5 on 09/05/12
For personal use only.

Chemical Company. Dichlorohydrin was supplied by British Drug Houses (BDH), Chloroamine-T by Eastman Kodak, and chlorine gas by Matheson.

Carbon tetrachloride, nitromethane, 1,2-dichloroethane, absolute ethanol, and chloroform were obtained from Fisher Scientific. Alcohol was removed from the chloroform by the method described by Strohecker and Henning (1).

Chemicals were analyzed on a 6 ft by 0.25 in. 15% EGSS-X on Gas Chrom Q 100–120 mesh column mounted in an F and M 810 gas–liquid chromatograph. A similar DEGS column was also satisfactory.

Absorbance measurements were made in 1 cm quartz cells in a Beckman DB spectrophotometer. In our mechanism studies, the temperature of the cells was controlled to ±1 °C by a Tamson TEZ9 circulator and a Neslab Instrument PBC-4 bath cooler.

(b) Preparation of 2,3-Dichloro-1-propanol (2,3-DP)

Chlorine gas was bubbled through cooled pure allyl alcohol contained in 500 ml gas washing bottles until glc analysis showed that the reaction was complete. Solvents were not used as they were found to be difficult to remove from the 2,3-DP. A temperature programmed run from 110 to 200 °C at a rate of 4 °C/min adequately separated the reaction products on the glc column. The 2,3-DP eluted in approximately 12 min. The chromatogram showed that there were three major impurities and several minor components. Only a trace of 1,3-DP was present. If the reaction was not taken to completion a considerable amount of allyl chloride was detected. If, however, the reaction was continued until the solution turned yellow due to excess chlorine no allyl chloride was found. Presumably one of the other impurities is the completely chlorinated product of allyl chloride.

The solution also contained a considerable amount of HCl either from the cylinder gas or from a side reaction. To purify the 2,3-DP, water was added and the acid was neutralized to p*H* 6–7 with sodium bicarbonate or carbonate. The neutralized solution was separated from the sodium chloride, washed with water, and then dried over anhydrous sodium sulphate. The impurities were distilled from the 2,3-DP at a pressure of a few torr and a maximum temperature of 92 °C. The 2,3-DP darkens above this temperature and rapidly decomposes above 120 °C. The 2,3-DP left in the reaction flask had a slight reddish-brown tinge and was quite viscous.

(c) Carr–Price Procedure

A 25% $SbCl_3$ solution in $CHCl_3$ (3.5 ml) was rapidly added from a wide-mouthed pipet to 1 ml of vitamin A solution contained in a 1.13 cm pathlength Spectronic 20 cell mounted in the spectrometer. Readings were taken at the 'pause' point, 5 s after mixing (temperature 32 °C).

(d) Rate Study Procedure

All chemicals and glassware were cooled to the spectrophotometer's cell temperature in the main tank of the circulator. Nitrogen gas was circulated through the cell compartment of the spectrophotometer to prevent fogging of the cells. Activated 2,3-DP (3 ml) or a total of 3 ml of activated 2,3-DP plus solvent containing the requisite amount of antimony trichloride were placed in a test-tube in the tank of the circulator. A solution of vitamin A in the appropriate solvent (1 ml) was added, the solution agitated for 5–10 s on a vortex mixer and then poured into the precooled sample cell of the double beam spectrophotometer. Mixing was satisfactory at 10 °C but inclusion of air bubbles made results at 0 and −10 °C difficult to obtain.

The blank consisted of all components of the solution except vitamin A. The signal from the spectrophotometer was recorded on a 10 in. Beckman potentiometric recorder.

Acknowledgment

The authors would like to gratefully acknowledge the exploratory work carried out on this project by L. Harris, W. O. Wong, L. S. Chow, and Ms. W. Leung.

1. R. Strohecker and H. M. Henning. Vitamin assay, tested methods. Verlag Chemie GMBH. Weinheim/Bergstr. 1966.
2. W. Horowitz (*Editor*). Official methods of analysis of the Association of Official Analytical Chemists. 11th ed. Washington, D.C. 1970. p. 767.
3. J. N. Thompson, P. Erdody, W. B. Maxwell, and T. K. Murray. J. Dairy Sci. **55**, 1077 (1972).
4. J. W. Erdman, Jr., S. H. F. Hou, and P. A. Lachance. J. Food Sci. **38**, 447 (1973).
5. R. E. Dugan, N. A. Frigerio, and J. M. Siebert. Anal. Chem. **36**, 114 (1964).
6. F. H. Carr and E. A. Price. Biochem. J. **20**, 497 (1926).
7. P. Budowski and A. Bondi. Analyst, **82**, 751 (1957).
8. A. E. Sobel and H. Werbin. J. Biol. Chem. **159**, 681 (1945).
9. D. D. Penketh. Nature, **161**, 893 (1948).
10. A. E. Sobel and H. Werbin. Ind. Eng. Chem. Anal. Ed. **18**, 570 (1946).
11. A. I. Vogel. A textbook of quantitative inorganic analysis. 2nd ed. Longmans, Green and Co., London. 1957. p. 376.
12. W. H. Sebrell, Jr. and R. S. Harris. The vitamins. Vol. 1. 2nd ed. Academic Press, New York and London. 1967. pp. 49–50, 119–120.
13. J. R. Edisbury, A. E. Gillam, I. M. Heilbron, and R. A. Morton. Biochem. J. **26**, 1164 (1932).
14. E. M. Shantz, J. D. Crawley, and N. D. Embree. J. Am. Chem. Soc. **65**, 901 (1943).
15. W. Oroshnik. Science, **119**, 660 (1954).
16. P. E. Blatz and D. L. Pippert. J. Am. Chem. Soc. **90**, 1296 (1968).
17. P. E. Blatz, N. Baumgartner, V. Balasubramaniyan, P. Balasubramaniyan, and E. Stedman. Photochem. Photobiol. **14**, 531 (1971).

The collisional quenching of electronically excited oxygen atoms, $O(2^1D_2)$, by the gases NH_3, H_2O_2, C_2H_6, C_3H_8, and $C(CH_3)_4$, using time-resolved attenuation of atomic resonance radiation

I. S. FLETCHER AND D. HUSAIN

The Department of Physical Chemistry, The University of Cambridge, Lensfield Road, Cambridge CB2 1EP, England

Received December 10, 1975

I. S. FLETCHER and D. HUSAIN. Can. J. Chem. **54**, 1765 (1976).

A kinetic study of electronically excited oxygen atoms, $O(2^1D_2)$, is presented. These optically metastable species were generated by repetitive pulsed irradiation in the Hartley-band continuum and monitored photoelectrically in absorption by time-resolved attenuation of resonance radiation at $\lambda = 115.2$ nm ($O(3^1D_2^0) \leftarrow O(2^1D_2)$). Absolute rate constants for the collisional quenching of $O(2^1D_2)$ are reported for the gases NH_3, H_2O_2, C_2H_6 C_3H_8, and $C(CH_3)_4$. These are found to be respectively (in units of 10^{-10} cm^3 molecule^{-1} s^{-1} at 300 K), 6.3 ± 0.7, 5.2 ± 0.6, 7.3 ± 0.8, 9.5 ± 1.0, and 12.3 ± 1.3. With the exception of a recent measurement for NH_3, these data represent the first absolute measurements for these quenching gases. Further, a general comparison is made between absolute rate measurements using this technique and recent work by Schiff and co-workers using time-resolved emission at $\lambda = 630$ nm ($O(2^1D_2) \rightarrow O(2^3P_2)$) in order to monitor the excited atoms.

I. S. FLETCHER et D. HUSAIN. Can. J. Chem. **54**, 1765 (1976).

On présente une étude cinétique des atomes d'oxygène excités électroniquement, $O(2^1D_2)$. On génère ces espèces optiquement métastable par une irradiation pulsée répétitive dans le continuum de la bande de Hartley et on les détecte photoélectroniquement dans un mode d'absorption par une atténuation résolue dans le temps de la radiation de résonance à $\lambda = 115.2$ nm $O(3^1D_2^0) \leftarrow O(2^1D_2)$). On rapporte les constantes absolues de vitesse pour la désactivation par collision de $O(2^1D_2)$ par les gaz NH_3, H_2O_2, C_2H_6, C_3H_8 et $C(CH_3)_4$. On trouve qu'elles sont respectivement égales à (en unité de 10^{-10} cm^3 molécule^{-1} s^{-1} à 300 K) 6.3 ± 0.7, 5.2 ± 0.6, 7.3 ± 0.8, 9.5 ± 1.0 et 12.3 ± 1.3. À l'exception de la mesure récente pour le NH_3, ces données représentent les premières mesures absolues pour la désactivation par ces gaz. De plus on fait une comparaison générale entre les mesures de vitesses absolues utilisant cette technique et le travail récent de Schiff et de ses collaborateurs utilisant une émission résolue dans le temps à $\lambda = 630$ nm ($O(2^1D_2) \rightarrow O(2^3P_2)$) de façon à mesurer les atomes excités.

[Traduit par le journal]

Introduction

There is extensive and detailed current interest in the collisional behaviour of electronically excited oxygen atoms, $O(2^1D_2)$, 1.967 eV above the $O(2^3P_2)$ ground state (1), both on account of its importance in the chemistry of the stratosphere (2) and the interpretation of the kinetic behaviour within the context of a general framework concerned with the relationship between electronic structure and reactivity (3). In recent years, some emphasis has been given to kinetic studies in which $O(2^1D_2)$ has been monitored directly. Noxon and co-workers (4–6) have employed the weak, magnetic dipole-allowed emission at $\lambda = 630$ nm ($O(2^1D_2) \rightarrow O(2^3P_2)$, $A_{nm} = 1/\tau_e = 6.9 \times 10^{-3}$ s^{-1}) (7) during the continuous photolysis of O_2 and CO_2 in a static system and reported kinetic data for the gases O_2, N_2, CO, and CO_2. Schiff and co-workers (8) employed the observation of the emission in the time-resolved mode following the repetitive flash photolysis of ozone in the Hartley-band continuum (200–320 nm). Very recently, Schiff and co-workers, together with a group at the NOAA Environmental Research Laboratories at Boulder, Colorado (9) have modified this technique in order to effect the photolysis of O_3 by means of a frequency-quadrupled neodymium-YAG laser ($\lambda = 266$ nm). They have reported absolute quenching rate data for $O(2^1D_2)$ with a range of added gases. By contrast, Heidner, Husain, and Wiesenfeld have employed the electric dipole-allowed time-resolved absorption in the vacuum ultraviolet at $\lambda = 115.2$ nm ($O(3^1D_2^0) \leftarrow O(2^1D_2)$) in order to monitor the optically metastable atom following the repetitive flash photolysis of O_3

Can. J. Chem. Downloaded from www.nrcresearchpress.com by 210.87.254.6 on 09/05/12
For personal use only.

Can. J. Chem. Downloaded from www.nrcresearchpress.com by 210.87.254.6 on 09/05/12
For personal use only.

(10–14) and have employed this technique to obtain absolute rate data for a large range of collision partners.

In this paper, we employ the attenuation of resonance radiation method at $\lambda = 115.2$ nm in order to obtain absolute rate data for the removal of $O(2^1D_2)$ with the gases NH_3, H_2O_2, C_2H_6, C_3H_8, and $C(CH_3)_4$. These gases are either important in atmospheric chemistry or in techniques used to obtain rate data for $O(2^1D_2)$. Apart from the very recent work by Schiff and co-workers (9) on NH_3, carried out simultaneously with the present investigation, absolute rate data for these gases have not been reported hitherto.

Experimental

The experimental arrangement was similar to that employed previously (10, 11). Briefly, $O(2^1D_2)$ was generated by the repetitive pulsed irradiation ($E = 64$ J) of ozone in the Hartley-band continuum and monitored photoelectrically in absorption by attenuation of the $\lambda = 115.2$ nm resonance transition, derived from a microwave-powered atomic flow lamp (2% O_2 in He, $p_{\text{total with He}} = 100$ N m^{-2}, incident power = 50–100 W). The flowing reactant system as used in the present arrangement is equivalent to a static system (10, 11). The attenuated signals at $\lambda = 115.2$ nm were detected by means of a solar blind photomultiplier tube (E.M.R. 541G-08-18), mounted at the exit slit of a 1 m concave grating vacuum monochromator (Hilger and Watts), and amplified with a current-to-voltage converter employing a fast-settling operational amplifier (15).

The principal modification to the experimental arrangement employed in previous attenuation studies of $O(2^1D_2)$ (10–14) is the inclusion here of a rapid response precision logarithmic signal converter with a large scale voltage limiter and an a.c.-coupled amplifier with one-directional clamping. This has been described in a previous study on $N(2^2D_J)$ and $N(2^2P_J)$ (16), and a modified circuit, now employed as a regular electronic tool in this laboratory, in a later paper on $C(2^3P_J)$ (17). It is appropriate to note the principal advantages of employing this circuit for measurements on $O(2^1D_2)$, namely, it effectively permits measurements of $\ln(I_0/I_{tr})$ (where the symbols have their usual significance) directly for rapidly decaying signals, including those for relatively weak absorption, and removes the necessity of spreading out the decay signals over a long time base in order to determine the I_0 value. Overall, this system leads to rate data of considerably improved signal-to-noise ratio (16).

Following passage of the amplified photocurrent through the precision logarithmic circuit, the transient signals were digitised and stored in a 200-channel signal averager (Datalab, model 102A). Each kinetic run presented here is, in general, the average of 32 repetitive experiments employing sweep times of 2–50 μs/channel. The contents of the signal averager memory were then punched onto paper tape for subsequent analysis in the University's computer (IBM 370). As previously (10, 11), the numerical data smoothing procedure of Savitsky and Golay (18) was used in order to obtain maximum use of the raw data at low degrees of light absorption. Further, we employ the modified Beer–Lambert law

$$[1] \qquad I_{tr} = I_0 \exp(-\epsilon(cl)^\gamma)$$

where the symbols have their usual significance (19) in order to relate the concentration of $O(2^1D_2)$ to the attenuated and unattenuated signals. The use of this law, in the light of recent studies on eq. 1 by other workers, will be discussed later. For the conditions employed here, previous measurements have yielded $\gamma = 0.41 \pm 0.03$ for this transition (10).

Materials

He, Kr (for the photoflash lamp), O_3, O_2, and CO_2 were employed as previously described (11). Cylinder NH_3 (I.C.I.) was trapped at liquid nitrogen temperatures (−196 °C), degassed by several freeze–pump–thaw (fpt) cycles and fractionally distilled from the temperature of a CO_2/acetone slush (−80 °C) to −196 °C. 'Chemically pure' cylinder propane (Matheson Co.) and ethane (Matheson Co.) were trapped at −196 °C and degassed by several fpt cycles. A similar procedure was employed for neopentane (B.D.H.) except that this material was fractionally distilled from a chloroform slush temperature (−63 °C) to −196 °C. Particular care was taken in the case of hydrogen peroxide. H_2O_2 (Laporte Titanium Ltd.) (mole fraction of H_2O_2 in H_2O = 0.78 from vapour pressure measurements (20)) was transferred to a specially constructed vacuum system with greaseless taps in order to avoid decomposition of the material by standard tap greases. After degassing by fpt cycles, an attempt was made to concentrate further the starting material by careful evaporation. However, this was found to lead to decomposition. The procedure adopted was therefore to carry out rate measurements on $O(2^1D_2)$ with the vapour of the initial material and to correct the observed decays for the vapour pressure of H_2O using the previous measurement for k_{H_2O} reported by Heidner *et al.* (11).

Results and Discussion

An example of the raw data representing $\ln(I_{tr}/I_0)$ at $\lambda = 115.2$ nm resulting from passage through the precision logarithmic amplification circuit and digitising in the signal averager is given in Fig. 1 in order to indicate the nature of the decay of $O(2^1D_2)$ in the presence of ammonia. It can be seen from eq. 1 that $\ln(I_0/I_{tr})$ is a direct linear measure of the concentration of $O(2^1D_2)$. Figure 2 shows typical first-order kinetic plots for the decay of $O(2^1D_2)$ in the presence of varying pressures of NH_3. Inspection of eq. 1 shows that the slopes of such plots are given by $-\gamma k'$ where k' is the overall first-order decay coefficient for $O(2^1D_2)$. k' can then be expressed in the form:

$$[2] \qquad k' = K + k_Q[Q]$$

Can. J. Chem. Downloaded from www.nrcresearchpress.com by 210.87.254.6 on 09/05/12
For personal use only.

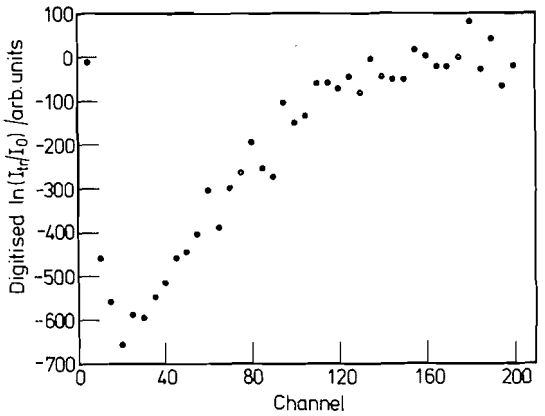

FIG. 1. Digitised time-variation of $\ln(I_{tr}/I_0)$ at λ = 115.2 nm ($O(3^1D_2^0) \rightarrow O(2^1D_2)$) indicating the decay of resonance absorption by $O(2^1D_2)$ in the presence of ammonia. E = 64 J; repetition rate = 0.2 Hz; p_{O_3} = 0.025 N m^{-2}, p_{NH_3} = 0.019 N m^{-2}, $p_{\text{total with He}}$ = *ca.* 2.0 kN m^{-2}; average of 32 experiments; 20% of actual point density represented; sweep rate = 5 μs/channel.

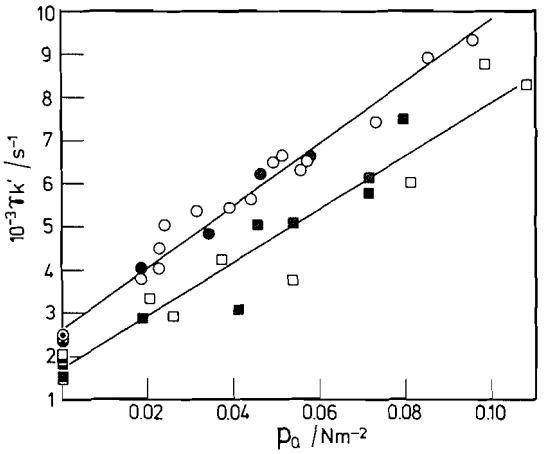

FIG. 3. Plots of pseudo first-order rate coefficients ($\gamma k'$) for the decay of $O(2^1D_2)$ in the presence of NH_3 and C_2H_6. □, ■, NH_3; ○, ●, C_2H_6. $p_{\text{total with He}}$ (kN m^{-2}): ○, ■, *ca.* 2.0; ●, □, *ca.* 3.5 ($\gamma k'$ for NH_3 displaced by -10^3 s^{-1}).

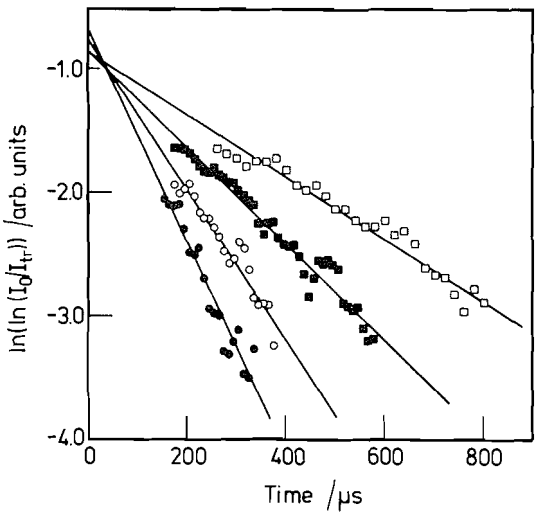

FIG. 2. Typical pseudo first-order plots for the decay of $O(2^1D_2)$ obtained by monitoring the absorption of light at λ = 115.2 nm ($O(3^1D_2) \leftarrow O(2^1D_2)$) in the presence of ammonia. E = 64 J; p_{O_3} = 0.025 N m^{-2}, $p_{\text{total with He}}$ = *ca.* 2.0 kN m^{-2}; p_{NH_3}(N m^{-2}): □, 0.0; ■, 0.019; ○, 0.045; ●, 0.08.

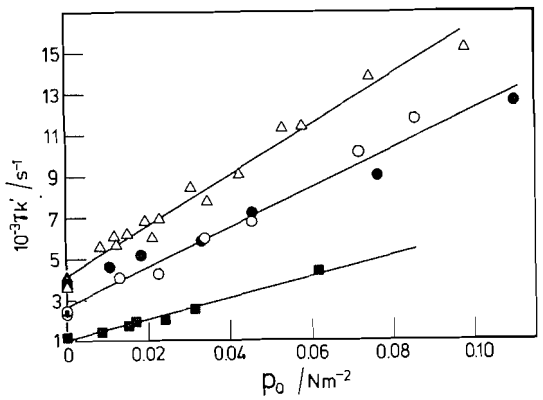

FIG. 4. Plots of pseudo first-order rate coefficients ($\gamma k'$) for the decay of $O(2^1D_2)$ in the presence of H_2O_2, C_3H_8 and $C(CH_3)_4$. ■, H_2O_2; ●, ○, C_3H_8; △, $C(CH_3)_4$. $p_{\text{total with He}}$ (kN m^{-2}): ■, ●, △, *ca.* 2.0; ○, *ca.* 3.5 ($\gamma k'$ for H_2O_2 displaced by -2×10^3 s^{-1}).

where k_Q is the absolute second-order rate constant for the collisional removal of $O(2^1D_2)$ by an added quenching gas, Q, and, in the case of the data of the type given in Fig. 2, k_{NH_3}. K represents first-order decay contributions to k' other than by Q, comprising collisional removal by the products of photolysis, weak spontaneous emission, diffusion and removal by O_3 itself. K is taken to be a constant in a given series of kinetic runs in which [Q] alone is varied. Figures 3 and 4 indicate the linear variation of $\gamma k'$ with [Q] for the gases NH_3, H_2O_2, C_2H_6, C_3H_8, and $C(CH_3)_4$, the slopes of these plots, with the above measured value of γ, yielding the absolute values of k_Q. Measurements were also carried out on O_2 and CO_2 in order to check consistency with previous measurements by this technique but which did not employ the precision logarithmic converter.

TABLE 1. Absolute rate constants ($10^{10}\,k_Q$, cm^3 molecule^{-1} s^{-1}, 300 K) for the collisional removal of $O(2^1D_2)$

Q	$10^{10}\,k_Q$ This work[a]	Schiff and co-workers (9)[b]	Clark and Noxon (6)[c]	Cvetanović (2)[d]
NH_3	6.3 ±0.7	3.4 ±0.3		~4
H_2O_2	5.2 ±0.6			~5
C_2H_6	7.3 ±0.8			4.8 ±0.9
C_3H_8	9.5 ±1.0			8.0 ±1.5
$C(CH_3)_4$	12.3 ±1.3			12.3 ±2.3
O_2	0.53±0.06	0.41±0.05	0.6	0.74±0.15
	0.7 ±0.05 (11)	0.5 (8)		
CO_2	1.7 ±0.2	1.2 ±0.09	1.1	1.8 ±0.3
	2.1 ±0.2 (11)			

[a]Attenuation of atomic resonance radiation (λ = 115.2 nm).
[b]Time-resolved emission (λ = 630 nm).
[c]Steady emission (λ = 630 nm).
[d]Recommended values from data compilation.

Table 1 shows the absolute values for k_Q derived from this investigation, together with those from previous measurements involving direct monitoring of $O(2^1D_2)$.

Regarding the consistency of the present measurements employing the logarithmic circuitry and those for $O(2^1D_2)$ absorption measurements made hitherto, whilst the present data for CO_2 and O_2 are marginally lower than those previously reported (11), the difference is small when the errors are included (Table 1). The absolute values of k_Q for NH_3, H_2O_2, C_2H_6, C_3H_8, and $C(CH_3)_4$ show these molecules to be highly efficient quenching species (Table 1). The only possible comparison with a direct measurement is that for k_{NH_3} which Schiff *et al.* (9) have found to be much smaller from their $O(2^1D_2)$ emission measurements and more in accord with the estimate given in the compilation of Cvetanović (2). It must be mentioned that Schiff and co-workers (9) did find anomalous emission profiles at 630 nm when using NH_3 (and also H_2, CH_4, and HCl). They believed this to be due to the (9–3) OH Meinel emission band in this region resulting from chemical reaction. In such cases, exponential decay profiles were subsequently restored by the addition of SF_6 which was presumed to relax the higher vibrational levels of OH. On the other hand, the majority of the data presented here (Table 1) is in reasonable accord with those from Cvetanović's 'recommended values' though it should be noted that these values (2) are strongly influenced by a standard for k_{CO_2} which is close to that given by Heidner *et al.* (11) (Table 1). However, within the context of the present method, attenuation of atomic resonance radiation on $O(2^1D_2)$ has yielded two independent measurements over the span of three years for CO_2 and O_2 which can be regarded as consistent.

Expressing the rate data relative to that for CO_2 for each set of measurements, the data for O_2 from both the absorption and emission investigations are in accord. The value obtained here for k_{NH_3} (relative to CO_2) still remains high relative to both that reported by Schiff and co-workers (9) and that derived from the rough estimate for the recommended value given by Cvetanović (2) (Table 2). It is clearly beyond the scope of this paper to discuss the various individual measurements leading to Cvetanović's recommended values and the related values derived therefrom. However, we would mention that recent measurements by Gauthier and Snelling (21) lead to relative quenching rates of $O(2^1D_2)$ for CO_2, O_2, C_3H_8, and $C(CH_3)_4$ which are, respectively, 1:0.37:4.0:5.2, in good agreement, when the quoted errors are included, with Cvetanović's relative data and that of the present work (Table 2).

Finally, this discussion cannot avoid a general comparison between data derived by the present method and those given by Schiff and co-workers (9). Table 3 lists the absolute rate data derived by the two methods where a comparison is possible. It is clear that the absorption technique has yielded higher values than the emission method; it is also clear that the two methods *cannot* be resolved by a constant factor. Phillips (22) has recently investigated the validity of eq. 1 in the present measurements by carrying out a calculation on the λ = 115.2 nm transition

Can. J. Chem. Downloaded from www.nrcresearchpress.com by 210.87.254.6 on 09/05/12
For personal use only.

TABLE 2. Relative rate data for the collisional removal of $O(2^1D_2)$ (relative to CO_2)

Q	Relative rate			
	This work	Schiff and co-workers (9)	Clark and Noxon (6)	Cvetanović (2)
NH_3	3.7	2.8		~2.2
H_2O_2	3.1			~2.8
C_2H_6	4.3			2.6
C_3H_8	5.6			4.4
$C(CH_3)_4$	7.2			6.8
O_2	0.31 0.33 (11)	0.34	0.5_5	0.41
CO_2	1	1	1	1

TABLE 3. Comparison of absolute rate data for the collisional quenching of $O(2^1D_2)$ from time-resolved absorption, $O(3^1D_2^0) \leftarrow O(2^1D_2)$, and time-resolved emission, $O(2^1D_2) \rightarrow O(2^3P_2)$

Method	$10^{10}\,k_Q$ (cm^3 molecule^{-1} s^{-1}, 300 K)				
	H_2	D_2	N_2	O_2	O_3
Time-resolved absorption ((10–14) + this work) ($\gamma = 0.41$)	2.7	1.8	0.69	0.53	2.7
Time-resolved absorption ((10–14) + this work) ($\gamma = 1$)	1.1	0.74	0.28	0.29	1.1
Time-resolved emission (9)	1.3	1.3	0.30	0.41	2.4

Method	$10^{10}\,k_Q$ (cm^3 molecule s^{-1}, 300 K)				
	CO_2	N_2O	H_2O	NH_3	CH_4
Absorption ($\gamma = 0.41$)	1.7	2.2	3.0	6.3	3.1
Absorption ($\gamma = 1$)	0.70	0.90	1.2	2.6	1.3
Emission	1.2	1.4	2.1	3.4	1.3

similar to that reported by Bemand and Clyne (23) for the $\lambda = 130$ nm resonance triplet of $O(2^3P_J)$. On the basis of various absolute estimates for the concentration of $O(2^1D_2)$ in the reaction vessel and a Lorentz broadening cross section of 3×10^{-15} cm^2 for helium together with various 'two layer' temperature profiles in the resonance source, Phillips has calculated that, for the range $L \equiv \ln(\ln(I_0/I_{tr})) = ca. -1.0$ to -3.5, γ is indistinguishable from unity. He proposes that a value of $\gamma = 0.90 \pm 0.10$ should be employed. It should be noted that the γ-value of 0.41 ± 0.03, which we have reconfirmed, was determined experimentally for the range $L = +0.3$ to -1.0 (10) and this is in reasonable accord with Phillips calculation in this range where $\gamma = ca.\ 0.5$ (22). Dividing the rate data from $O(2^1D_2)$ absorption measurements by the ratio $\gamma_{cal(22)}/\gamma_{obs(10)} = 0.90/0.41 = 2.2$ does not resolve the two sets of data as is clear from Table 3. Indeed, some of the data are in agreement.

Schiff and co-workers (9) have suggested that a value of $\gamma = 0.7$ might be employed to reconcile empirically the two sets of data. It seems to the authors that the analysis of the data derived from the attenuation technique could be considered from two viewpoints: either a γ-value of 0.41 as *measured* (10) be employed, or a value of unity, *i.e.*, adherence to the Beer–Lambert law, which is clearly seen from the appropriate plots in Phillips' line profile *calculations* (22), be adopted. Table 3 thus includes the data derived from the attenuation measurements in these two forms. One could clearly present all the data obtained from the line absorption measurements on this basis (10–14), including those for quenching by the noble gases (14). It can be seen that a γ-value of unity, or even 0.9, would result in a number of particularly low quenching rate constants for $O(2^1D_2)$ (Table 3). Certainly, the general trend between the two sets of data, *i.e.*, absorption and emission, appears to be significant and this aspect of the comparison, in our opinion, remains unresolved.

Apart from the absolute values of the quench-

Can. J. Chem. Downloaded from www.nrcresearchpress.com by 210.87.254.6 on 09/05/12
For personal use only.

ing rate constants, the comparison of the data for H_2 and D_2 perhaps merits separate comment. Sorbie and Murrell (24) have presented a detailed analytical potential function for the insertion of $O(2^1D_2)$ into H_2, and the reaction dynamics on the surface, unfortunately not including D_2, are in the course of preparation (25). One would expect some difference in dynamics between the two isotopes, if only on the basis of a mass effect. Certainly, a simplified r^{-6} long range potential of the type employed by Tully (26) and by Miller and co-workers (27) for $O(2^1D_2) + N_2$ leads to the ratio of $k_{H_2}/k_{D_2} = 2^{5/6} = ca.\ 1.8$, in reasonable accord with the observed ratio of 1.5 from the attenuation technique (Table 3) but not in agreement with the equality in the rates resulting from emission measurements (Table 3).[1] This is a further aspect of the absorption and emission data that requires resolution.

Acknowledgement

We are indebted to the Science Research Council of Great Britain for a Research Studentship to one of us (I.S.F.) during the tenure of which this work was carried out.

1. C. E. Moore (*Editor*). Atomic energy levels. Vols. I–III. Nat. Bur. Stand. Circular 467. U.S. Government Printing Office, Washington, D.C. 1958.
2. R. J. Cvetanović. Can. J. Chem. **52**, 1452 (1974).
3. R. J. Donovan and D. Husain. Chem. Rev. **70**, 489 (1970).
4. J. F. Noxon. Can. J. Chem. **47**, 1873 (1969).
5. J. F. Noxon. J. Chem. Phys. **52**, 1852 (1970).
6. I. D. Clark and J. F. Noxon. J. Chem. Phys. **57**, 1033 (1972).
7. R. H. Garstang. Mon. Not. Roy. Astronom. Soc. **111**, 115 (1951).
8. R. Gilpin, H. I. Schiff, and K. H. Welge. J. Chem. Phys. **55**, 1087 (1971).
9. J. A. Davidson, C. M. Sadowski, H. I. Schiff, G. E. Streit, C. J. Howard, D. A. Jennings, and A. L. Schmeltekopf. J. Chem. Phys. **64**, 45 (1976).
10. R. F. Heidner III, D. Husain, and J. R. Wiesenfeld. Chem. Phys. Lett. **16**, 530 (1972).
11. R. F. Heidner III, D. Husain, and J. R. Wiesenfeld. J. Chem. Soc. Faraday Trans. II, **69**, 927 (1973).
12. R. F. Heidner III and D. Husain. Nature, **241**, 10 (1973).
13. R. F. Heidner III and D. Husain. Int. J. Chem. Kinet. **V**, 819 (1973).
14. R. F. Heidner III and D. Husain. Int. J. Chem. Kinet. **VI**, 77 (1974).
15. W. H. Wing and T. M. Sanders, Jr. Rev. Sci. Instrum. **38**, 1341 (1967).
16. D. Husain, S. K. Mitra, and A. N. Young. J. Chem. Soc. Faraday Trans. II, **70**, 1721 (1974).
17. D. Husain and A. N. Young. J. Chem. Soc. Faraday Trans. II, **71**, 525 (1975).
18. A. Savitsky and M. J. E. Golay. Anal. Chem. **36**, 1627 (1964).
19. R. J. Donovan, D. Husain, and L. J. Kirsch. Trans. Faraday Soc. **66**, 2551 (1970).
20. W. C. Schumb, C. N. Salterfield, and R. L. Wentworth. Hydrogen peroxide. Reinhold, New York. 1955.
21. M. J. E. Gauthier and D. R. Snelling. J. Photochem. **4**, 27 (1975).
22. L. F. Phillips. Chem. Phys. Lett. **37**, 421 (1976).
23. P. P. Bemand and M. A. A. Clyne. J. Chem. Soc. Faraday Trans. II, **69**, 1643 (1973).
24. K. S. Sorbie and J. N. Murrell. Mol. Phys. **29**, 1387 (1975).
25. K. S. Sorbie. Private communication.
26. J. C. Tully. J. Chem. Phys. **61**, 61 (1974).
27. G. E. Zahr, R. K. Preston, and W. H. Miller. J. Chem. Phys. **62**, 1127 (1974).

[1]We are indebted to Dr. S. K. Sorbie for detailed discussion in this context.

Can. J. Chem. Downloaded from www.nrcresearchpress.com by 210.87.254.6 on 09/05/12
For personal use only.

The crystal and molecular structure of tribromo-*m*-carborane

ALICE ANN SAYLER AND HERBERT BEALL[1]

Department of Chemistry, Worcester Polytechnic Institute, Worcester, MA., U.S.A. 01609

Received January 26, 1976

ALICE ANN SAYLER and HERBERT BEALL. Can. J. Chem. **54**, 1771 (1976).

The sequence of electrophilic substitution for *o*- and *m*-carborane has been the subject of much experimental and theoretical work. The molecular structure of tribromo-*m*-carborane (m-$B_{10}Br_3H_7C_2H_2$) shows that the third bromine atom to be substituted is found bonded to boron atom 12 (or 5). The crystal data are: space group, *Pbcm*; a = 8.47(4), b = 12.19(8), and c = 12.25(8) Å; ρ_o = 1.98(2) and ρ_c = 2.00 g/cm³ for Z = 4. Data were collected using Weissenberg geometry and Ni-filtered CuK_α radiation. The visually estimated intensities of 920 reflections were used in the anisotropic block-diagonalized least-squares refinement of the 76 structural parameters. The final value of the conventional residual index was 0.087.

ALICE ANN SAYLER et HERBERT BEALL. Can. J. Chem. **54**, 1771 (1976).

La séquence de substitution électrophile des *o*- et *m*-carborane a fait l'objet de beaucoup de travaux expérimentaux et théoriques. La structure moléculaire du tribromo-*m*-carborane (m-$B_{10}Br_3H_7C_2H_2$) indique que le troisième atome de brome à se substituer se trouve lié à l'atome de bore en position 12 (ou 5). Les données cristallographiques sont: groupe d'espace, *Pbcm*; a = 8.47(4), b = 12.19(8) et c = 12.25(8) Å; ρ_o = 1.98(2) et ρ_c = 2.00 g/cm³ pour Z = 4. On a recueilli les données en faisant appel à la géométrie de Weissenberg et à une radiation CuK_α filtrée par le nickel. On a utilisé les intensités évaluées d'une façon visuelle pour 920 réflexions dans l'affinement anisotrope de la structure; pour y parvenir, les 76 paramètres structuraux ont été affinés par la méthode des moindres carrés (blocs diagonaux). La valeur finale de R est de 0.087.

[Traduit par le journal]

The stepwise electrophilic substitution of *o*-carborane (1,2-dicarba-*closo*-dodecaborane (12)) and its *C*-methyl derivatives with halogens in the presence of $AlCl_3$ has been extensively investigated (1–25). It has been found that the ground state charge distribution in *o*-carborane gives a reasonable account of the successive positions of electrophilic attack (10). It has been predicted that similar results can be expected for the electrophilic substitution in *m*-carborane (1,7-dicarba-*closo*-dodecaborane (12)) (26).

If the ground state charge distribution is not altered in the transition state and if steric and neighbor effects are not dominant, electrophilic halogenation should occur first at the borons where ground state charges are most negative. Since the carbon atoms in the carborane moiety withdraw electron density, a simple inductive rule gives the relative charges (27). Boron atoms 2 and 3, which are bonded to both carbon atoms, should be the most positive boron atoms while boron atoms 9 and 10, which are the farthest away from both carbon atoms, should be the most negative. The other boron atoms, which are bonded to only one carbon, should be intermediate in charge. A molecular orbital study of *m*-carborane predicted the charge distribution as −0.16 for B(9) and B(10), −0.03 for B(5) and B(12), −0.03 for B(4), B(6), B(8), and B(11), and +0.10 for B(2) and B(3) (28). A later study yielded charges of −0.25 for B(9) and B(10), −0.06 for B(5) and B(12), −0.03 for B(4), B(6), B(8), and B(11), and +0.13 for B(2) and B(3) (26). It has been shown that the electrophilic chlorination and bromination occurs first at the B(9) and B(10) in *m*-carborane and its C-methyl derivatives (2, 3, 7, 15, 16, 18, 22, 23, 26, 29–35). However, the third bromine substituent could occupy either the B(5 or 12) or B(4, 6, 8, or 11) since molecular orbital calculations and simple inductive rule give very similar framework charges.

The stepwise halogenation of 1-methyl-*m*-carborane has been investigated (34). It was found that the electrophilic bromination of 1-methyl-9,10-dibromo-*m*-carborane yields a mixture of the tribromo-*m*-carborane containing 73% of the 1-methyl-9,10,12-tribromo-*m*-carborane and 25% of the 1-methyl-4,9,10-tribromo-*m*-carborane. It appears that the third bromine preferentially substitutes at the B(12) position. However, the methyl group would be

Can. J. Chem. Downloaded from www.nrcresearchpress.com by 210.87.254.105 on 09/05/12
For personal use only.

Can. J. Chem. Downloaded from www.nrcresearchpress.com by 210.87.254.105 on 09/05/12
For personal use only.

expected to alter the charge distribution since it can donate electron density to the carborane moiety. In *o*-carborane, it was found that C-methyl substituents do not alter the position of electrophilic attack (11). In order to find whether the same holds true in *m*-carborane, we have determined the three-dimensional X-ray single crystal structure of tribromo-*m*-carborane. Substitution of third bromine was, in fact, found to occur at the B(12) (or B(5)) position.

Structure Determination

Photographically recorded X-ray patterns given by single crystals of tribromo-*m*-carborane, $B_{10}Br_3H_7C_2H_2$, showed reciprocal lattice symmetry of *mmm* and systematic absences of $0kl$ when k is odd and $h0l$ when l is odd. Two lozenge-shaped single crystals about 0.05 by 0.05 by 0.01 mm were mounted for rotation along the a and b axes for photographic collection of diffraction intensities by Weissenberg geometry. The pertinent crystal data are summarized below:

$B_{10}Br_3H_7C_2H_2$ fw = 380.9

Orthorhombic, $a = 8.47(4)$, $b = 12.19(8)$ and $c = 12.25(8)$ Å, $V = 1264.8$ Å^3, space group $Pbc2_1$ or $Pbcm$ (the latter being consistent with the proposed structure), $\rho_o = 1.98(2)$, $\rho_c = 2.00$ g/cm^3, $Z = 4$, $\mu = 127$ cm^{-1} for CuK_α, $\lambda = 1.542$ Å.

The unit cell dimensions were calibrated by Al powder diffraction lines and the observed density was measured by flotation in an aqueous $ZnCl_2$ solution.

Seventeen layers of equi-inclination Weissenberg intensity data, seven along a and ten along b, were recorded using multiple-film techniques and Ni-filtered CuK_α radiation. The intensity data were estimated visually and, because of the small size of the crystals, no absorption corrections were made. After the usual Lorenz-polarization corrections, the data were correlated and merged on a single scale by a method of least-squares which minimizes a sum of residuals linear in the logarithms of the scale factors for overlapping sets of intensity data (36). The overall reliability factor for the average intensities was 0.11. A total number of 920 independent reflections was thus obtained and all of these were considered observed in the structure analysis described below.

The positions of the three bromine atoms were determined by examination of the sharpened Patterson function, and the remaining non-hydrogen atoms appeared in a Fourier synthesis phased according to the bromine contributions to the structure factors.

The distinction between B and C atoms was based on consideration of electron density and atomic environment (see Table 2 *a propos* shorter interatomic distances where C atoms are involved). Block-diagonal least-squares refinement of positional and anisotropic temperature parameters for all non-hydrogen atoms was effected. The weighting scheme used in this refinement was $w = 1/(a + |F_o| + b|F_o|^2 + c|F_o|^3)$ where $a = 2F_{min}$, $b = 2/F_{max}$, and $c = 5/F_{max}^2$, *i.e.* $a = 88.0$, $b = 7.627 \times 10^{-4}$, $c = 7.272 \times 10^{-7}$. The scattering factors for all the atoms were taken from ref. 37. A correction for the anomalous scattering of the bromine atoms was included. The hydrogen atoms were not found in the Fourier difference synthesis. Therefore, the hydrogen atoms were fixed in theoretically calculated positions (extension of straight lines through opposite cage atoms 0.95 Å from the appropriate atoms) and the hydrogen contributions, with isotropic thermal values fixed at somewhat larger values than those of the atoms to which they were attached, were included in further block-diagonal least-squares refinement. The final $R = \sum||F_o| - |F_c||/\sum|F_o|$ was calculated to be 0.087 for the observed reflections. The R values for different classes of reflections are summarized in Table 1.

TABLE 1. Error summary for selected classes of reflections in tribromo-*m*-carborane

$\sin^2\theta$ ranges	*R*-index	Number of reflections
0.0–0.1	0.094	51
0.1–0.2	0.089	86
0.2–0.3	0.087	111
0.3–0.4	0.090	113
0.4–0.5	0.076	121
0.5–0.6	0.073	119
0.6–0.7	0.081	101
0.7–0.8	0.075	104
0.8–0.9	0.089	85
Ranges of *h*	***R*-index**	**Number of reflections**
$0kl$	0.094	81
$1kl$	0.080	132
$2kl$	0.082	139
$3kl$	0.081	136
$4kl$	0.087	103
$5kl$	0.109	117
$6kl$	0.106	85
$7kl$	0.081	48
$8kl$	0.071	38
$9kl$	0.072	33
$10kl$	0.068	8

Results and Discussion

The molecular structure is shown in Fig. 1; the crystal packing in Fig. 2. The final atomic parameters are listed in Table 2; the estimated hydrogen atom parameters, in Table 3; the bond distances and *meta* and *para* distances, in Table 4; the bond angles, in Table 5; and the structure factors, in Table 6.[1] No corrections of the bond distances for thermal motion have been made.

The position of electrophilic attack in the

[1]Photocopy of Table 6 is available, at a nominal charge, from the Depository of Unpubilshed Data, CISTI, National Research Council of Canada, Ottawa, Canada K1A 0S2.

Can. J. Chem. Downloaded from www.nrcresearchpress.com by 210.87.254.105 on 09/05/12
For personal use only.

Friedel–Crafts tribromination in m-$B_{10}H_{10}C_2H_2$ is B(9), B(10), and B(12 or 5). The order of substitution parallels that of the 1-methyl-m-carborane.

The average B—Br, C—B, and B—B distances of 1.99(1), 1.72(1), and 1.77(3) Å, respectively, are in agreement with those found in the other

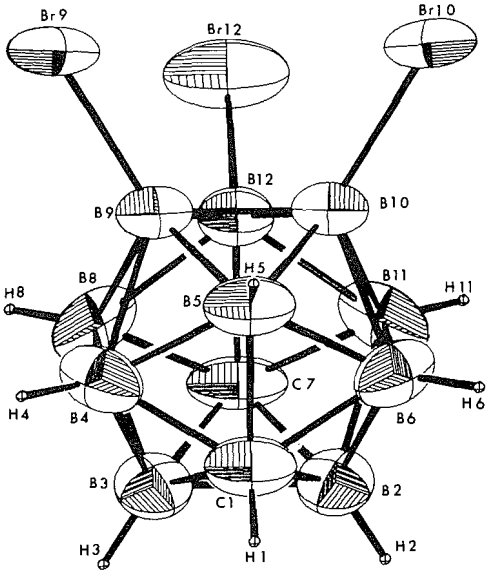

FIG. 1. The structure of tribromo-m-carborane.

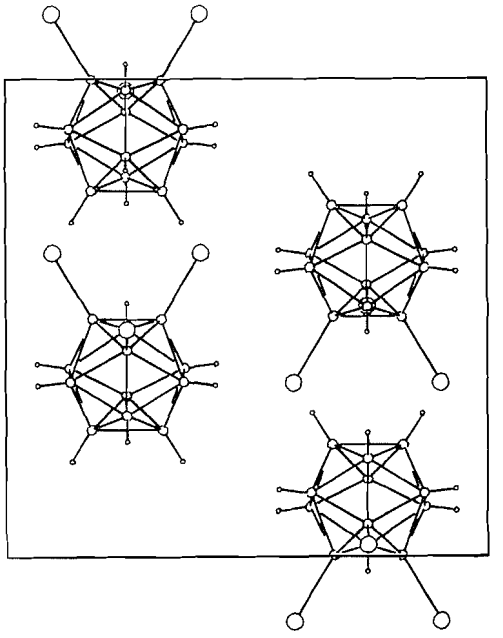

FIG. 2. Packing diagram for tribromo-m-carborane viewed with the c axis horizontal and the b axis vertical.

TABLE 2. Final atomic parameters $\times 10^4$ for tribromo-m-carborane*

Atom	x	y	z
Br(12)	−1239(2)	9754(2)	2500
C(1)	4514(18)	8374(12)	2500
C(7)	1494(19)	7949(11)	2500
B(5)	4246(20)	9772(13)	2500
B(12)	1024(20)	9322(13)	2500
Br(9)	2148(2)	11360(1)	964(2)
B(3)	3147(17)	7658(9)	1758(12)
B(4)	3853(17)	8956(10)	1308(13)
B(8)	1831(17)	8668(10)	1322(15)
B(9)	2512(14)	9974(9)	1785(11)

Atom	β_{11}	β_{22}	β_{33}	β_{23}	β_{13}	β_{12}
Br(12)	101(2)	71(1)	220(3)	—	—	28(1)
C(1)	111(22)	49(9)	117(16)	—	—	21(1)
C(7)	122(24)	32(8)	142(19)	—	—	28(1)
B(5)	83(20)	51(11)	117(19)	—	—	−31(4)
B(12)	114(24)	46(9)	81(14)	—	—	26(1)
Br(9)	264(3)	65(1)	119(1)	79(2)	14(3)	42(3)
B(3)	182(21)	44(7)	84(11)	−14(14)	7(24)	32(19)
B(4)	164(21)	56(7)	92(11)	−5(16)	61(26)	27(22)
B(8)	160(21)	55(8)	106(12)	−25(16)	−101(27)	−3(21)
B(9)	108(15)	42(6)	83(9)	10(13)	−6(21)	24(16)

*Numbers in parentheses are estimated standard deviations in the last significant figure. The anisotropic temperature factors are in the form $\exp[-(h^2\beta_{11} + k^2\beta_{22} + l^2\beta_{33} + 2hk\beta_{12} + 2hl\beta_{13} + 2kl\beta_{23})]$.

TABLE 3. Fractional coordinates × 10^4 and isotropic temperature factors (Å^2), assigned to hydrogen atoms

Hydrogen	x	y	z	B_{iso}
H(1)	5562	8087	2500	4.47
H(5)	5071	10308	2500	4.48
H(7)	676	7412	2500	7.27
H(3)	3331	7004	1353	4.68
H(4)	4413	9036	642	5.07
H(8)	1266	8587	656	4.27

crystal structure determinations of *m*-carborane derivatives (26, 34, 35, 38). In Table 7 selected cage atom distances for these structures are given for comparison. In *m*-$B_{10}Cl_{10}C_2H_2$ and *m*-$B_{10}Br_2H_8C_2H_2$, the B(2)—B(3) bond of 1.89(6) Å was found to be remarkably long while in 1-methyl-9,10,12-tribromo-*m*-carborane this distance was 1.74 Å. In our case, the B(2)—B(3) bond of 1.82(2) Å is midway between these values.

Examination of the other cage atom distances in tribromo-*m*-carborane reveals a slight distortion from true icosahedral symmetry in the cage. The C—B distances are somewhat shorter than the B—B distances. Similarly the C—B *meta* and *para* distances are shorter than those of the B—B. This is consistent with the general trends for the distances listed in Table 7 for compounds **1**, **2**, and **5**. However, it is in contrast to the undistorted icosahedral structure found in 1-methyl-9,10,12-tribromo-*m*-carborane although in this structure determination the standard deviations in bond lengths were not given (34). It is possible that the differences are the

TABLE 4. Bond distances and *meta* and *para* distances (Å) in tribromo-*m*-carborane*

Atom pairs		Distance	Atom pairs		Distance
Br-B Atoms			*B—B meta Atoms*		
Br(9)—B(9)		1.99(1)	B(3)—B(6)		2.91(2)
Br(12)—B(12)		1.99(2)	B(3)—B(11)		2.88(2)
	Ave.	1.99(0,0)	B(3)—B(5)		2.89(2)
			B(3)—B(9)		2.88(2)
C—B Atoms			B(3)—B(12)		2.86(2)
C(1)—B(3)		1.71(2)	B(4)—B(6)		2.92(2)
C(1)—B(4)		1.72(2)	B(4)—B(10)		2.88(2)
C(1)—B(5)		1.72(2)	B(4)—B(12)		2.84(2)
C(7)—B(3)		1.71(2)	B(5)—B(8)		2.84(2)
C(7)—B(8)		1.71(2)	B(5)—B(12)		2.78(2)
C(7)—B(12)		1.72(2)	B(8)—B(10)		2.87(2)
	Ave.	1.72(1,1)	B(8)—B(11)		2.89(2)
			B(9)—B(6)		2.88(2)
B—B Atoms				Ave.	2.87(3,9)
B(3)—B(2)		1.82(2)			
B(3)—B(4)		1.78(2)	*C—B meta Atoms*		
B(3)—B(8)		1.74(2)	C(1)—B(8)		2.72(2)
B(4)—B(5)		1.80(2)	C(1)—B(9)		2.73(2)
B(4)—B(8)		1.75(2)	C(7)—B(4)		2.76(2)
B(4)—B(9)		1.78(2)	C(7)—B(9)		2.76(2)
B(5)—B(9)		1.73(2)		Ave.	2.74(2,2)
B(8)—B(9)		1.79(2)			
B(8)—B(12)		1.79(2)	*C—C meta Atoms*		
B(9)—B(10)		1.75(2)	C(1)—C(7)		2.61(2)
B(9)—B(12)		1.73(2)			
	Ave.	1.77(3,5)	*C—B para Atoms*		
			C(1)—B(12)		3.18(2)
B—B para Atoms			C(7)—B(5)		3.22(2)
B(3)—B(10)		3.38(2)		Ave.	3.20(2,2)
B(4)—B(11)		3.39(2)			
	Ave.	3.39(1,1)			

*The numbers in parentheses are estimated standard deviations in the last significant figure. The numbers in parentheses following the average values are the mean and maximum deviation for the individual datum from the average value.

Can. J. Chem. Downloaded from www.nrcresearchpress.com by 210.87.254.105 on 09/05/12
For personal use only.

Can. J. Chem. Downloaded from www.nrcresearchpress.com by 210.87.254.105 on 09/05/12
For personal use only.

TABLE 5. Bond angles in tribromo-*m*-carborane*

Atoms	Angle (deg)	Atoms	Angle (deg)
B—C—B Angles		*B—B—B Angles*	
B(3)—C(1)—B(2)	64.3(8)	B(3)—B(4)—B(8)	59.3(8)
B(3)—C(1)—B(4)	62.5(8)	B(3)—B(8)—B(4)	61.3(8)
B(4)—C(1)—B(5)	63.1(8)	B(4)—B(3)—B(8)	59.5(8)
B(3)—C(7)—B(2)	64.3(8)	B(4)—B(5)—B(9)	60.7(8)
B(3)—C(7)—B(8)	61.4(8)	B(4)—B(8)—B(9)	60.5(8)
B(8)—C(7)—B(12)	62.7(8)	B(4)—B(9)—B(5)	61.6(8)
Ave.	63.1(9,1.7)	B(4)—B(9)—B(8)	58.7(8)
		B(5)—B(4)—B(9)	57.7(7)
C—B—B Angles		B(5)—B(9)—B(10)	59.6(8)
C(1)—B(3)—B(2)	57.9(8)	B(8)—B(4)—B(9)	60.8(8)
C(1)—B(3)—B(4)	58.9(8)	B(8)—B(9)—B(12)	61.0(8)
C(1)—B(4)—B(3)	58.6(7)	B(8)—B(12)—B(9)	61.1(8)
C(1)—B(4)—B(5)	58.5(7)	B(9)—B(5)—B(10)	60.8(8)
C(1)—B(5)—B(4)	58.4(7)	B(9)—B(8)—B(12)	57.9(7)
C(7)—B(3)—B(2)	57.9(8)	B(9)—B(12)—B(10)	60.8(8)
C(7)—B(3)—B(8)	59.5(8)	B(10)—B(9)—B(12)	59.6(8)
C(7)—B(8)—B(3)	59.2(8)	Ave.	60.1(1.0,2.4)
C(7)—B(8)—B(12)	58.9(8)		
C(7)—B(12)—B(8)	58.4(8)	*Br—B—B Angles*	
Ave.	58.6(4,9)	Br(9)—B(9)—B(4)	121.6(8)
		Br(9)—B(9)—B(5)	120.6(8)
Br—B—C Angle		Br(9)—B(9)—B(8)	123.1(8)
Br(12)—B(12)—C(7)	118.7(8)	Br(9)—B(9)—B(10)	120.1(8)
		Br(9)—B(9)—B(12)	122.3(8)
		Br(12)—B(12)—B(8)	119.2(8)
		Br(12)—B(12)—B(9)	125.6(8)
		Ave.	121.8(1.6,3.8)

*The numbers in parentheses are estimated standard deviations in the last significant figure. The numbers in parentheses following the average values are the mean and maximum deviation for the individual datum from the average value.

TABLE 7. Selected cage atom distances in *m*-carborane derivatives*

	Distance				
Atoms	**1**†	**2**‡	**3**§	**4**‖	**5**¶
C(1)—B(2)	—	1.64	1.73	1.71	1.72
C(1)—B(4)	—	1.68	1.73	1.72	1.73
C(1)—B(5)	—	1.74	1.73	1.72	1.72
C(7)—B(8)	—	1.72	1.74	1.71	1.73
Ave. C—B	1.70	1.69	1.73	1.72	1.72
B(2)—B(3)	1.89	1.89	1.74	1.82	1.81
B(3)—B(4)	—	1.72	1.74	1.78	1.74
B(4)—B(5)	—	1.83	1.73	1.80	1.79
B(4)—B(8)	—	1.81	1.73	1.75	1.79
B(4)—B(9)	—	1.80	1.73	1.78	1.81
B(5)—B(9)	—	1.70	1.74	1.73	1.76
B(9)—B(10)	—	1.77	1.74	1.75	1.84
Ave. B—B	1.75	1.78	1.73	1.77	1.79

*The compounds for which distances are cited are as follows: **1**, *m*-$B_{10}Cl_{10}C_2H_2$; **2**, *m*-$B_{10}Br_2H_8C_2H_2$; **3**, *m*-$B_{10}Br_3H_7C_2(CH_3)H$; **4**, *m*-$B_{10}Br_3H_7C_2H_2$; and **5**, *m*-$B_{10}Cl_2H_8C_2(CH_3)_2$.
†Reference 35.
‡Reference 26.
§Reference 34.
‖This work.
¶Reference 38.

result of the presence of the halogen atoms which interferes with the precise location of the cage atom positions.

Acknowledgments

The authors are grateful to Public Health Service Research Grant No. CA12025-01 from the National Cancer Institute for support of this work. A.A.S. is indebted to the National Defense Graduate Fellowship Program for a research fellowship. We acknowledge computer time donated by the Worcester Area College Computation Center and crystallographic programs made available to us by F. R. Ahmed of the National Research Council of Canada, C. K. Johnson of the Oak Ridge National Laboratory, and W. N. Lipscomb of Harvard University. Furthermore, we are grateful to a referee of an early version of this report for important constructive criticisms, particularly regarding space group assignments.

1. A. I. ECHEISTOVA, YU. T. SYRKIN, V. I. STANKO, and A. I. KLIMOVA. Zh. Strukt. Khim. **8**, 933 (1967).
2. V. I. STANKO, A. I. ECHEISTOVA, E. S. ASTAKHOVA, A. I. KLIMOVA, YU. T. STRUCHKOV, and Y. K. SYRKIN. Zh. Strukt. Khim. **8**, 928 (1967).
3. V. I. STANKO, YU. T. STRUCHKOV, and A. I. KLIMOVA. Zh. Strukt. Khim. **7**, 629 (1966).
4. E. V. BRYUKHOVA, V. I. STANKO, A. I. KLIMOVA, N. S. TITOVA, and G. K. SEMIN. Zh. Strukt. Khim. **9**, 39 (1968).
5. V. G. ANDRIANOV, V. I. STANKO, YU. T. STRUCHKOV, and A. I. KLIMOVA. Zh. Strukt. Khim. **8**, 707 (1967).
6. R. MARUCA, H. A. SCHROEDER, and A. W. LAUBENGAYER. Inorg. Chem. **6**, 572 (1967).
7. H. D. SMITH, T. A. KNOWLES, and H. SCHROEDER. Inorg. Chem. **4**, 107 (1965).
8. D. VOET and W. N. LIPSCOMB. Inorg. Chem. **3**, 1679 (1964).
9. J. A. POTENZA and W. N. LIPSCOMB. Inorg. Chem. **5**, 1471 (1966).
10. J. A. POTENZA and W. N. LIPSCOMB. Inorg. Chem. **5**, 1478 (1966).
11. J. A. POTENZA and W. N. LIPSCOMB. Inorg. Chem. **5**, 1483 (1966).
12. J. A. POTENZA and W. N. LIPSCOMB. Inorg. Chem. **3**, 1673 (1964).
13. J. A. POTENZA, W. N. LIPSCOMB, G. D. VICKERS, and H. A. SCHROEDER. J. Am. Chem. Soc. **88**, 628 (1966).
14. J. A. POTENZA and W. N. LIPSCOMB. J. Am. Chem. Soc. **86**, 1874 (1964).
15. V. I. STANKO, A. I. KLIMOVA, and T. P. KLIMOVA. Zh. Obshch. Khim. **37**, 2236 (1967).
16. V. I. STANKO, YU. T. STRUCHKOV, A. I. KLIMOVA, L. V. BRYUKHOVA, and G. K. SEMIN. Zh. Obshch. Khim. **36**, 1707 (1966).
17. V. I. STANKO and A. I. KLIMOVA. Zh. Obshch. Khim. **38**, 1194 (1968).
18. V. I. STANKO, V. A. BRATTSEV, T. N. VOSTRIKOVA, and G. N. DANILOVA. Zh. Obshch. Khim. **38**, 1348 (1968).
19. V. I. STANKO and YU T. STRUCHKOV. Zh. Obshch. Khim. **35**, 930 (1965).
20. L. I. ZAKHARKIN and V. N. KALININ. Dokl. Akad. Nauk. SSSR, **170**, 92 (1966).
21. L. I. ZAKHARKIN and V. N. KALININ. Izv. Akad. Nauk. SSSR, Ser. Khim. 1311 (1965).
22. L. I. ZAKHARKIN and V. N. KALININ. Izv. Akad. Nauk. SSSR, 575 (1966).
23. L. I. ZAKHARKIN, V. N. KALININ, and V. S. LOZOVSKAYA. Izv. Akad. Nauk. SSSR, 1780 (1968).
24. L. I. ZAKHARKIN, V. I. STANKO, and A. I. KLIMOVA. Izv. Akad. Nauk. SSSR, 1946 (1966).
25. L. H. HALL, A. PERLOFF, F. A. MAUES, and S. BLOCK. J. Chem. Phys. **43**, 3911 (1965).
26. H. BEALL and W. N. LIPSCOMB. Inorg. Chem. **6**, 874 (1967).
27. R. HOFFMANN and W. N. LIPSCOMB. J. Chem. Phys. **36**, 3489 (1962).
28. W. N. LIPSCOMB. Proc. Natl. Acad. Sci. U.S. **47**, 1791 (1961).
29. V. I. STANKO and A. I. KLIMOVA. Zh. Obshch. Khim. **36**, 432 (1966).
30. L. I. ZAKHARKIN and V. N. KALININ. Zh. Obshch. Khim. **37**, 964 (1967).
31. V. I. STANKO, A. I. KLIMOVA, and N. S. TITOVA. Zh. Obshch. Khim. **38**, 2817 (1968).
32. L. I. ZAKHARKIN and V. N. KALININ. Dokl. Akad. Nauk. SSSR, **169**, 590 (1966).
33. C. O. OBENLAND and S. PAPETTI. J. Org. Chem. **31**, 3868 (1966).
34. I. S. OSTAKHOVA, YU. T. STRUCHKOV, V. I. STANKO, and N. S. TITOVA. Zh. Struckt. Khim. **10**, 1063 (1969).
35. J. A. POTENZA and W. N. LIPSCOMB. Proc. Natl. Acad. Sci. U.S., **56**, 1917 (1966).
36. P. SIMPSON. Ph.D. Thesis. Harvard University, Cambridge, Mass. 1963.
37. International Tables for X-Ray Crystallography. Vol. III. 1962.
38. H. V. HART and W. N. LIPSCOMB. Inorg. Chem. **12**, 2644 (1973).

Can. J. Chem. Downloaded from www.nrcresearchpress.com by 210.87.254.105 on 09/05/12
For personal use only.

Les réactions de Friedel et Crafts d'acylation des hydrocarbures aromatiques polycycliques. IX. L'acétylation de l'anthracène et de ses homologues *méso*-méthylés[1]

FRANÇOIS PERIN, MARTINE CROISY-DELCEY ET PIERRE JACQUIGNON
Institut de Chimie des Substances Naturelles du C.N.R.S., 91190 – Gif sur Yvette, France

Reçu le 26 novembre 1975

FRANÇOIS PERIN, MARTINE CROISY-DELCEY et PIERRE JACQUIGNON. Can. J. Chem. **54**, 1777 (1976).

L'étude de l'influence de divers facteurs réactionnels (solvant, température, nature et quantité de catalyseur et d'agent acylant) sur le rendement et l'orientation de l'acétylation du méthyl-9 et du diméthyl-9,10 anthracène par rapport à l'anthracène lui-même, met en évidence l'importance du réarrangement de la *méso*-substitution vis à vis de la substitution des autres positions. L'analyse des conditions nécessaires à la réversibilité révèle que l'excès de catalyseur en est le principal responsable. Les résultats expérimentaux autorisent à proposer un mécanisme pour ce réarrangement et à formuler une hypothèse n'impliquant pas la dissociation préalable de l'agent acylant lors des acylations par les anhydrides d'acides.

FRANÇOIS PERIN, MARTINE CROISY-DELCEY, and PIERRE JACQUIGNON. Can. J. Chem. **54**, 1777 (1976).

A study of the influence of various reaction parameters (solvent, temperature, nature and quantity of the catalyst and of the acylating agent) on the yield and isomeric orientation of the acetylation of 9-methyl- and 9,10-dimethylanthracene relative to that of anthracene itself. reveals the importance of the rearrangement of the *meso*-substitution product vis à vis that of products substituted in other positions. Analysis of the conditions necessary for reversibility indicates that an excess of the catalyst is the main factor responsible. The experimental results allow one to propose a mechanism for this rearrangement which does not involve the prior dissociation of the acylating agent during acylations by acid anhydrides.

[Journal translation]

Dans une précédente étude expérimentale (1) nous avions montré qu'au cours de l'acétylation, le méthyl-9 anthracène **1** a un comportement comparable à celui de son homologue inférieur. C'est à dire qu'après une substitution rapide et massive sur la position *méso* libre, la labilité du substituant sur ce sommet se traduit par une désacétylation dépendant au moins, quant à sa vitesse, de la température et du solvant et dont découle l'acétylation lente des positions 2, 4 et 3. Le sommet 1, vraisemblablement trop encombré, n'étant pas impliqué dans la réaction, celle-ci conduit par conséquent à un mélange, variable selon les conditions expérimentales, des cétones **2**, **3**, **4** et **5**.

Cependant au vu des résultats expérimentaux divers aspects relatifs aux conditions, au rôle et à l'importance du réarrangement par rapport à une éventuelle substitution directe sur les positions α et β, nous ont incités à entreprendre une série d'essais se classant en trois catégories. (*i*) Comportement des principaux produits de l'acétylation du méthyl-9 anthracène **1** (cétones **2**, **3** et **4**) en présence de chlorure d'aluminium.

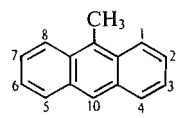

1

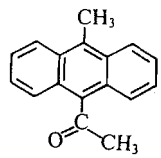

2

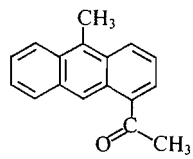

3

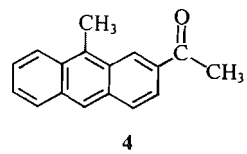

4

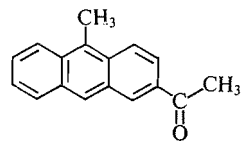

5

[1]Partie VIII, voir réf. 1.

Can. J. Chem. Downloaded from www.nrcresearchpress.com by 210.87.254.5 on 09/05/12
For personal use only.

TABLEAU 1. Essais de réarrangement d'acétyl méthyl-9 anthracènes

Cétone de départ	Produits formés (%)*					
	Anthracène	Methyl-9 anthracène	Isomère 10 **2**	Isomère 4 **3**	Isomère 2 **4**	Isomère 3 **5**
Isomère 10 **2**	Traces	38	Traces	19	30	9
Isomère 4 **3**	—	—	—	100	—	—
Isomère 2 **4**	—	—	—	—	100	—

*Pourcentages évalués, après correction de la réponse du détecteur, par intégration des pics de cpv.

(*ii*) Acétylation du diméthyl-9,10 anthracène. (*iii*) Comparaison avec l'acétylation de l'anthracène et interprétation des résultats.

Malgré les multiples travaux publiés sur l'acétylation de l'anthracène (réf. 3 et pour une revue des travaux antérieurs à 1964, réf. 2) ce dernier point nous a conduit à revoir expérimentalement cette réaction. Or ce sont ces essais qui se sont révélés les plus fructueux aussi bien en ce qui concerne les facteurs déterminant le rendement que du point de vue des conditions réactionnelles du réarrangement.

Action du chlorure d'aluminium sur les acétyl méthyl-9 anthracènes

En même temps que la réalité du réarrangement de l'isomère de *méso*-substitution, il paraissait nécessaire de vérifier la stabilité de la substitution sur les autres positions en replaçant les trois principaux produits de l'acétylation dans les conditions de la réaction.

Dans un premier temps, chacune des cétones (**2**, **3** et **4**) dissoute dans le chlorure de méthylène a été soumise, après passage durant 15 min de gaz chlorhydrique dans la solution, à l'action du chlorure d'aluminium (1.2 mol). Après 3 h de repos à température ambiante, le produit résultant du traitement habituel a été analysé par chromatographie en phase vapeur (cpv). Le résultat de ces trois essais, exprimé en proportion relatives, est donné dans le tableau 1.

Il ressort donc que seul l'acétyl-10 méthyl-9 anthracène **2** subit la transformation attendue et nous n'avons pas trouvé trace d'une quelconque isomérisation ou même desacétylation des deux autres cétones. La *méso*-desacétylation se révèle par contre totale en 3 h dans ces conditions, mais l'importante quantité d'hydrocarbure régénérée est révélatrice de la lenteur de la réacétylation.

Puisque la solvatation du complexe intermédiaire est au moins une condition nécessaire au réarrangement, c'est ensuite le rôle du solvant dans ce processus qui a été examiné, en omettant toutefois, pour juger de son influence, le passage, en début de réaction, d'acide chlorhydrique dans la solution.

Pour ces essais, le sulfure de carbone a naturellement été éliminé puisque l'insolubilité totale du complexe n'y autorise aucun réarrangement (2). Mais c'est pas contre en raison des importantes résinifications qui accompagnent son utilisation et qui fausseraient ici suffisamment le résultat pour le rendre sans valeur, que le nitrobenzène, pourtant souvent employé et reconnu comme très favorable au phénomène (4, 5), a également été rejeté. Les résultats obtenus dans les trois autres solvants les plus couramment utilisés sont consignés dans le tableau 2.

La relation entre la vitesse de desacétylation et la solubilité du complexe est nettement exprimée par la quantité décroissante de cétone **2** récupérée dans les trois solvants après le même temps de contact, puisque le complexe n'est que peu soluble dans le premier, moyennement dans le second et totalement dans le troisième. Cette même relation apparaît également dans la quantité d'hydrocarbure régénérée mais cette dernière valeur est surtout significative de la faible vitesse de la réacétylation, laquelle semble encore plus lente dans les solvants polaires où l'on s'attendrait, pourtant, à trouver une quantité plus importante de produits de réacétylation.

En même temps que la réacétylation préférentielle des positions β moins encombrées, cette dernière remarque est en faveur de la participation du solvant au complexe acylant. La même observation a d'ailleurs été faite par Hawkins (6)

Can. J. Chem. Downloaded from www.nrcresearchpress.com by 210.87.254.5 on 09/05/12
For personal use only.

TABLEAU 2. Rôle du solvant sur le réarrangement de l'acétyl-10 méthyl-9 anthracène

Solvant	Produits formés (%)					
	Anthracène	Méthyl-9 anthracène	Isomère 10 **2**	Isomère 4 **3**	Isomère 2 **4**	Isomère 3 **5**
Benzène	Traces	16	75		Mélange 10	
				≃3.5	≃5	≃1.5
Chlorure de méthylène	Traces	24	48	9	13	5
Nitro-méthane	9	48	—	7	21	14

qui, avec l'acétyl-9 anthracène et le chlorure d'aluminium dans le nitrobenzène, obtient avec un rendement médiocre, surtout l'acétyl-2 anthracène.

Une autre remarque, non dénuée d'intérêt, découle de la comparaison des deux essais effectués dans le chlorure de méthylène avec et sans acide chlorhydrique. Il apparaît en effet que l'enrichissement préalable du milieu en acide chlorhydrique se traduit par une accélération importante de la désacétylation. Il sera montré ultérieurement que cet aspect permet de mieux comprendre le mécanisme du réarrangement et d'expliquer certains résultats apparemment anormaux enregistrés lors de l'acétylation du méthyl anthracène (1).

Il ne semble pas par contre que l'on puisse attribuer à l'acide chlorhydrique, un rôle quelconque dans l'orientation de la réacétylation puisque dans les deux cas les proportions relatives des trois isomères sont sensiblement les mêmes.

Acétylation du diméthyl-9,10 anthracène

Malgré l'apport électronique supplémentaire d'un second groupement méthyle, le dérivé mésodiméthylé de l'anthracène pouvait, à priori, être considéré comme un modèle valable de la réactivité de la position β et de la substitution directe sur ce sommet au cours de l'acétylation.

En effet, à moins d'une déméthylation toujours possible et déjà observée avec l'homologue inférieur (1), l'accès aux positions α est, comme pour deux d'entre elles dans le dérivé monométhylé, stériquement empêché par l'encombrement des substituants.

Il était d'autre part possible ainsi que cela a été avancé pour l'*ortho* et le *para*-xylène (7), que l'augmentation globale de réactivité qui devrait résulter de l'introduction du second groupe électrodonneur soit, en raison même des positions relatives de ces deux groupements, compensée par la compétitivité dans la répartition des charges. Ceci se traduit théoriquement par le fait que pour une position β donnée, un seul d'entre eux peut être impliqué dans la stabilisation par hyperconjugaison du complexe σ intermédiaire (schéma 1).

N'ayant trouvé dans la littérature que trois exemples peu explicites d'acylation (tous trois des acétylations) de cet hydrocarbure (8) nous avons entrepris d'examiner l'influence des conditions réactionnelles sur la vitesse et le rendement de la réaction.

La principale constatation qui découle de la vingtaine d'essais effectués est que la (les) position(s) β se révèle(nt), malgré une certaine lenteur de la réaction, nettement plus réactive(s) que ne le laissaient supposer les remarques ci-dessus. Ainsi qu'attendu, par contre, aucune trace de substitution en α n'a pu être décelée. Ceci est en accord avec les observations d'Hewett (9) puis de Gore et Hoskins (10), à propos du diméthyl-1,4 et du tétraméthyl-1,2,3,4 naphtalène.

Mais nous nous proposons d'étendre ulté-

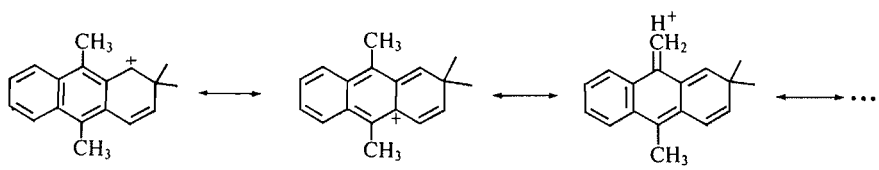

SCHÉMA 1

Can. J. Chem. Downloaded from www.nrcresearchpress.com by 210.87.254.5 on 09/05/12
For personal use only.

TABLEAU 3. Rôle du solvant sur l'acétylation du diméthyl-9,10 anthracène

Solvant*	Acétyl-2 diméthyl-9,10 anthracène (%)	Diméthyl-9,10 anthracène (%)	Déméthylation (%)
Sulfure de carbone	38	61	≃1
Benzène	70	28	1.5 à 2
Chlorure de méthylène	82	16	≃2

*150 ml pour 5 g d'hydrocarbure.

rieurement cet aspect stérique de l'acylation à divers diméthyl-anthracène tels que **6**, **7** et **8** qui présentent une ou deux positions *méso* libres mais encombrées.

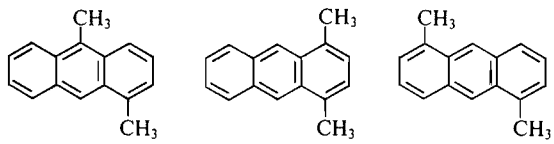

6 **7** **8**

En ce qui concerne le dérivé diméthyl-9,10, tous les essais ont été effectués à température ambiante selon la méthode d'Elbs (addition du catalyseur à la solution du mélange hydrocarbure, agent acylant) qui présente, sur les autres méthodes (Perrier, Bouveault) l'avantage de minimiser les réactions secondaires (desalkylation, diacylation, polymérisation . . .). Trois catégories de facteurs ayant une influence sur le rendement ont ainsi été mis en évidence.

Nature du solvant

Des divers solvants les plus couramment employés n'ont été retenus que le sulfure de carbone, le benzène et le chlorure de méthylène. De même que, pour les raisons déjà citées, le nitrobenzène, le nitrométhane a, en effet, été rejeté car il n'avait, malgré plusieurs tentatives, conduit qu'à un très faible rendement (22%) avec l'homologue inférieur (1). Les rendements déterminés par cpv après 5 h de contact sont donnés dans le tableau 3.

Il paraît raisonnable d'attribuer les écarts de rendement dans les trois solvants aux différences de solubilité du complexe acylant, ce qui, par conséquent, est significatif de la relative lenteur de la substitution. Sachant que quatre positions identiques sont simultanément offertes à la réaction, cette observation va dans le sens d'une réactivité tout compte fait, peu élevée de la position β.

Concentration

En effectuant l'acétylation dans les conditions préconisées par de Bruyn (8*b*), c'est-à-dire avec deux fois plus de benzène que dans l'essai précédent nous avions constaté que le rendement avoisinait 40% seulement. Ceci impliquait un effet de concentration habituellement inapparent dans la plupart des acylations d'hydrocarbures aromatiques dont les concentrations sont en général fort élevées.

Il est certain que la faible solubilité du diméthyl-9,10 anthracène, tout juste supérieure à celle de l'anthracène lui-même, ne permet pas les concentrations quatre à cinq fois plus fortes utilisées pour le dérivé monométhylé. C'est ainsi que la proportion de 1 g pour 30 ml utilisée dans les essais précédents constitue pour le benzène la limite de solubilité à température ambiante.

C'est donc le chlorure de méthylène qui a été choisi pour trois essais à concentration différente puisque tout en conduisant à de bons rendements il autorisait une concentration supérieure. L'évolution de la réaction représentée par les trois courbes de la fig. 1, a été suivie par cpv de prélèvements réguliers durant les six premières heures et par une dernière mesure après 20 h de contact.

En dépit de légères fluctuations liées aux erreurs expérimentales on constate d'une part, que dans les trois cas, le rendement est pratiquement acquis dans les 5 h et qu'après 3 h (et même moins) d'autre part, la progression du rendement demeure sensiblement la même dans les trois cas alors qu'on aurait pu s'attendre à une évolution, certes plus lente, mais plus durable pour les essais à concentration plus faible.

Puisque le rendement reste, même pour une durée de réaction de 24 h (donc relativement longue pour une acylation) fortement dépendant de la concentration, il est clair que l'obtention d'un rendement convenable nécessite beaucoup

Can. J. Chem. Downloaded from www.nrcresearchpress.com by 210.87.254.5 on 09/05/12
For personal use only.

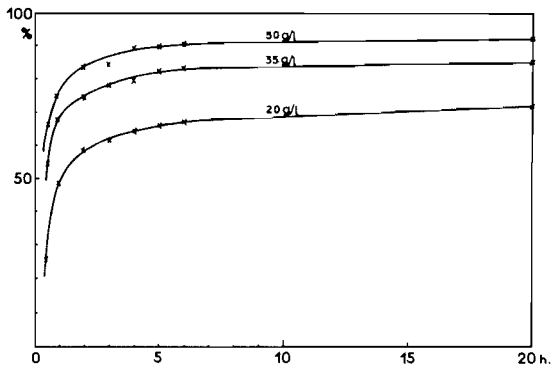

FIG. 1. Acétylation du diméthyl-9,10 anthracène. Influence de la concentration sur le rendement. Solvant: CH_2Cl_2; T = 20 °C.

plus l'emploi d'un bon solvant de l'hydrocarbure que la prolongation du temps de réaction.

Dans le même ordre d'idée, nous avons également constaté que des essais, effectués avec des quantités de solvant telles que l'hydrocarbure n'est que partiellement soluble, ne conduisent, en raison de la faible solubilisation ultérieure de l'hydrocarbure, qu'à des rendements médiocres souvent associés dans le cas de l'anthracène et de ses homologues, à des phénomènes secondaires (desalkylation diacylation, acylation du solvant lorsqu'il s'agit du benzène).

Nature du catalyseur et de l'agent acylant

Dans le tableau 4 figurent les rendements obtenus en 5 h dans le chlorure de méthylène à température ambiante en utilisant pour chacun des catalyseurs, chlorure d'aluminium et chlorure stannique, le chlorure d'acétyle ou l'anhydride acétique.

Apparemment surprenantes, les variations de rendement peuvent s'expliquer à notre point de vue, en tenant compte de la "force" du catalyseur donc de la nature et de la stabilité du complexe acylant.

Des résultats comparables ayant été enregistrés avec le méthyl-9 anthracène (1) et avec l'anthracène lui-même (*cf.* la partie suivante) une interprétation plus générale de l'acylation par les anhydrides d'acides sera développée en fin de ce mémoire.

TABLEAU 4. Les rendements obtenus avec des catalyseurs divers

Catalyseur (1.10 mol)	Agent acylant (1.05 mol)	Rendement* (%)
$AlCl_3$	CH_3COCl	82
$AlCl_3$	$(CH_3CO)_2O$	69
$SnCl_4$	CH_3COCl	35
$SnCl_4$	$(CH_3CO)_2O$	78

*Concentration en hydrocarbure: 35 g/l.

Comparaison avec l'anthracène

Réexamen de l'acétylation de l'anthracène

Alors que du point de vue qualitatif, les nombreux résultats signalés dans la littérature sur l'acétylation de l'anthracène, s'avèrent, grâce aux remarquables contributions de Gore et coll. (2–4, 11), relativement conciliables, sur le plan quantitatif (rendement global et proportions des isomères), leur diversité ne nous a pas permis de les confronter utilement à nos observations sur les homologues méthylés. C'est donc dans l'espoir d'obtenir quelques informations supplémentaires sur le rôle des conditions réactionnelles dans la détermination du rendement et l'apparition du processus de desacétylation–réacétylation que nous avons réexaminé quelques aspects de la réaction.

(a) Solvant—S'il n'est pas douteux que la solubilité du complexe intermédiaire (donc la nature du solvant) soit un facteur nécessaire au réarrangement et par conséquent responsable qualitativement du résultat final, il semble que peu d'auteurs aient accordé de l'importance, vis à vis du rendement, à la solubilité initiale de l'hydrocarbure et du complexe acylant.

C'est toutefois avec ce souci d'amélioration du rendement et de la reproductibilité que, pour obtenir préférentiellement l'isomère en *méso* ou l'isomère en 1, Bassilios *et al.* préconisent soit le chloroforme (13) soit le dichloréthane (12*b*). Il faut cependant remarquer que, pour améliorer la solubilisation de l'anthracène qui n'est encore que partielle, ces auteurs opèrent dans les deux cas, à 40 °C donc à une température qui favorise le réarrangement et les réactions secondaires (diacylations).

Pour notre part, il est apparu, après quelques essais peu satisfaisants, que seul un mélange de solvants pouvait permettre, à température ambiante, une concentration initiale convenable en hydrocarbure et la solvatation ultérieure du complexe.

C'est le mélange en parties égales de sulfure de carbone et de dichloréthane (à raison de 100 ml pour 5 g d'hydrocarbure) qui a donné les meilleurs résultats. Dans ces conditions, en effet,

Can. J. Chem. Downloaded from www.nrcresearchpress.com by 210.87.254.5 on 09/05/12
For personal use only.

TABLEAU 5. Les rendements obtenus après 2 h et 20 h de contact

Catalyseur (1.25 mol)	Agent acylant (1 mol)	R (%)	Acétyl-anthracène (%)		
			Acétyl-9	Acétyl-1	Acétyl-2
$AlCl_3$	CH_3COCl	97; 97	90; 39	10; 61	0; traces
$AlCl_3$	$(CH_3CO)_2O$	60; 63	$\geq$95; 62	$\leq$5; 30	0; 8
$SnCl_4$	CH_3COCl	18; 25	$\geq$97; 85	$\leq$3; 15	0; 0
$SnCl_4$	$(CH_3CO)_2O$	78; 85	>99; 92	Traces; 8	0; 0
$TiCl_4$	$(CH_3CO)_2O$	72; 81	100; 100	0; 0	0; 0

où la concentration malgré tout peu élevée autorise une addition rapide du catalyseur sans échauffement appréciable, le rendement en acétyl-9 anthracène pur dépasse 90% en 15 min.

Or ce rendement est atteint sans qu'il soit nécessaire de mettre en jeu plus de 1 mol de chlorure d'acétyle et plus de 1.2 mol de chlorure d'aluminium alors que bon nombre de techniques décrites (2) préconisent jusqu'à 6 mol du premier et 2 ou 3 mol du second.

Nous admettons que le souci de concision, trop souvent exigé des auteurs, ait fait omettre, dans bon nombre de cas, les raisons de l'utilisation d'excès aussi considérables de réactifs mais il n'en reste pas moins vrai qu'en dehors de leur intérêt pratique indéniable, les résultats ainsi obtenus n'apportent que peu d'informations sur le déroulement de la réaction.

Ceci constituant une raison supplémentaire à la poursuite de nos essais, tous ceux-ci ont été effectués dans le mélange précité selon le mode opératoire d'Elbs.

(b) Nature du catalyseur et de l'agent acylant—Le remplacement du chlorure d'acétyle par l'anhydride acétique et du chlorure d'aluminium par le chlorure stannique a conduit à des résultats tout à fait comparables, voire identiques, à ceux obtenus avec les homologues méthylés. Quoique la réaction ait été suivie tout au long de sa durée, seuls les rendements enregistrés après 2 h et 20 h de contact sont consignés dans le tableau 5 où figure également un essai réalisé avec le chlorure de titane et l'anhydride acétique.

Malgré leur apparente dispersion, mais en raison même de celle-ci, les valeurs obtenues se révèlent, tant du point de vue du rendement global que sous l'angle du réarrangement, parfaitement compatibles avec le classement habituellement admis de "force" des catalyseurs: $AlCl_3 > SnCl_4 > TiCl_4$ (2, 11*a*, 13). Les différences qui apparaîssent entre les cinq cas s'expliquent en effet, aisément pour peu que l'on considère cette notion d'efficacité du catalyseur par rapport à la nature de l'agent acylant utilisé.

C'est ainsi que les chutes de rendement des 2° et 3° cas découlent de phénomènes opposés: la "faiblesse" du chlorure stannique ne conduit, en présence de chlorure d'acétyle, qu'à une concentration réduite en ion acylium alors qu'au contraire, la "force" du chlorure d'aluminium lorsqu'il est associé à l'anhydride d'acide provoque la dissociation partielle de celui-ci avant sa fixation, ce qui entraîne la consommation (décomposition) d'une partie du catalyseur.

Ceci implique évidemment d'admettre la validité du processus d'acylation par les anhydrides proposé en fin de ce mémoire mais en constitue par ailleurs une preuve.

(c) Conditions du réarrangement—S'il est désormais acquis malgré les nombreuses controverses soulevées par le problème de la réversibilité de l'acylation en série aromatique, que la solubilité partielle ou totale du complexe en est une condition nécessaire et que des facteurs divers (température, concentration, efficacité du catalyseur) en déterminent la vitesse, il ne semble pas que les conditions de son déclenchement soient clairement établies ou aient fait l'objet d'études particulières.

Sans méconnaître les objections de Gore (2*b*), nos propres résultats nous incitaient à penser comme Baddeley (14) que le réarrangement n'intervient qu'en présence d'un excès de chlorure d'aluminium et met en jeu l'acide chlorhydrique nécessairement présent en plus ou moins grande quantité dans le milieu. Cette hypothèse apparaît d'autant plus fondée qu'il est logique d'envisager que, procédant de mécanismes analogues à ceux du réarrangement des groupements alkyles lors des alkylations selon Friedel et Crafts, la réversibilité de l'acylation doit nécessiter l'intervention de catalyseur libre, condition qui, contrairement aux alkylations, n'est remplie que par la présence d'un excès de celui-ci.

Can. J. Chem. Downloaded from www.nrcresearchpress.com by 210.87.254.5 on 09/05/12
For personal use only.

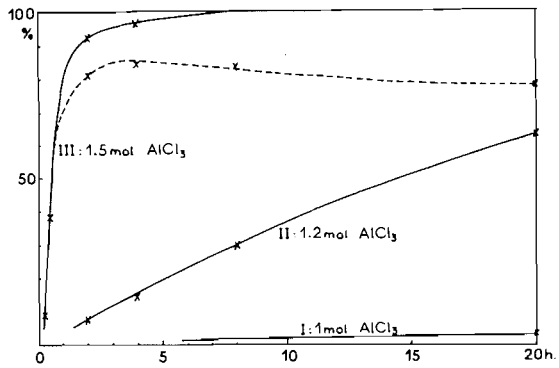

FIG. 2. Vitesse du réarrangement en fonction de l'excès de catalyseur, sans addition d'HCl.

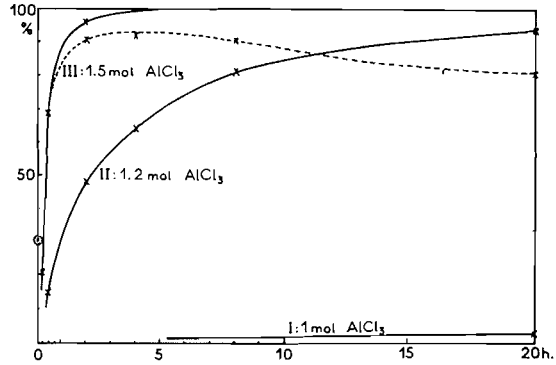

FIG. 3. Vitesse de réarrangement en fonction de l'excès de catalyseur, avec addition d'HCl.

Afin de vérifier cette assertion nous avons effectué trois acétylations de l'anthracène dans les conditions précitées, mais en utilisant, toujours pour 1 mol de chlorure d'acétyle, respectivement 1, 1.2 et 1.5 mol de chlorure d'aluminium. Dans les trois cas le rendement était supérieur à 95% après 15 min de réaction. L'évolution de celle-ci durant 20 h a ensuite été suivie par l'analyse en cpv de prises d'essais.

Etant donné que l'acétyl-2 anthracène n'apparaît qu'à l'état de traces en fin de réaction, le réarrangement est exprimé, dans les courbes de la fig. 2, par la variation dans le temps du pourcentage d'acétyl-1 par rapport à l'isomère en *méso*, seul produit initialement formé.

Le réarrangement étant pratiquement nul avec 1 mol de catalyseur, la courbe I représente plus une évaluation qu'une mesure réelle de la proportion d'acétyl-1 anthracène qui reste inférieure à 5% après 20 h de contact.

En ce qui concerne la courbe III, nous devons préciser qu'en raison de la grande rapidité du réarrangement, la partie en trait plein représente en réalité la disparition progressive et pratiquement totale en 8 h de l'isomère de *méso*-substitution. En effet la quantité réelle d'acétyl-1 anthracène (courbe pointillée) est sensiblement plus basse et diminue avec le temps. Cette diminution ne provient pas de sa dégradation ou de sa désacétylation mais résulte au contraire du fait que, par sa concentration rapidement élevée, il subit lui-même, parallèlement et concurremment à l'anthracène régénéré, une acétylation lente qui conduit, en fin de réaction, à 12% du mélange, déjà étudié par Gore (3), des diacétyl-1,5 et -1,8 anthracènes.

Le fait que le réarrangement n'intervienne pas avec la quantité juste nécessaire de catalyseur, implique que l'acide chlorhydrique, pourtant présent, ne suffit pas à lui seul, à déclencher le processus. D'ailleurs la saturation par un courant de gaz chlorhydrique d'une solution d'acétyl-9 anthracène dans le dichloréthane ne conduit, après 5 h de contact et malgré une forte coloration du milieu, à aucun réarrangement (ou désacétylation) perceptible.

Cependant, l'addition préalable d'acide chlorhydrique gazeux aux trois essais précédents conduit, en tenant compte des mêmes remarques que pour la fig. 2, aux courbes de la fig. 3 qui montrent sans ambiguité l'accélération du processus de réarrangement, celui-ci restant toujours négligeable en l'absence d'excès catalyseur (courbe I).

Enfin l'influence simultanée de la température et de l'acide chlorhydrique sur le réarrangement est exprimée dans le tableau 6 où figurent deux essais effectués dans le dichloréthane à 60 °C, en présence de 1.2 mol, de chlorure d'aluminium.

Quantitativement, la comparaison de ces résultats avec les courbes II des figs. 2 et 3, montre, dans les deux cas, la très nette, et d'ailleurs prévisible, augmentation par la température, de la vitesse de réarrangement.

Qualitativement par contre, il apparaît que si l'élévation de température favorise, dans le cas où la concentration en HCl est faible, la réacétylation en 5 ou 8 de l'acétyl-1 anthracène (préalablement formé) et non pas la formation d'acétyl-2 anthracène, c'est le contraire qui est observé dans le second essai où le rapport de répartition (4:1) des deux isomères est établi dès le début de la réaction.

Contrairement à Agranat *et al.* qui ont récemment étudié et démontré la réversibilité de la

Can. J. Chem. Downloaded from www.nrcresearchpress.com by 210.87.254.5 on 09/05/12
For personal use only.

TABLEAU 6. Réarrangement de l'acétyl-9 anthracène dans le dichloréthane à 60 °C. Durée de réaction 8 h

Conditions	Importance du réarrangement (%)	Produits presents (%)*			
		Acétyl-9	Acétyl-1	Acétyl-2	Diacétyls 1,5 et 1,8
Sans HCl	65	35	31	Traces	12
Avec HCl	100 (en 4 h)	0	65	16	Traces

*La différence entre la somme des produits formés et 100% correspond à de l'anthracène régénéré.

benzoylation du naphtalène à 140 °C dans l'A.P.P. (15), nous n'avons jamais constaté, dans les conditions à vrai dire moins sévères utilisées ici, de réarrangement de l'isomère α en isomère β thermodynamiquement plus stable. Il faut donc admettre que la formation de celui-ci, apparemment favorisée par la richesse du milieu en protons, s'effectue, grâce à l'élévation de température, à partir de l'ion protoné en *méso* sur lequel repose tout le processus du réarrangement (*cf.* interprétation des résultats).

Réactivité comparée de l'anthracène et de ses homologues

Dans l'ultime intention de corroborer l'ensemble de nos observations et d'évaluer, par leur compétitivité, la réactivité propre des différentes positions substituables des trois hydrocarbures, nous avons effectué d'une part le réarrangement de l'acétyl-9 anthracène et de l'acétyl-10 méthyl-9 anthracène en présence de diméthyl-9,10 anthracène, d'autre part l'acétylation du mélange équimoléculaire de méthyl-9 et de diméthyl-9,10 anthracène.

Ces trois expériences ont été menées à température ambiante dans le dichloréthane avec 1.2 mol de chlorure d'aluminium et ont été suivies durant 20 h par cpv. En raison de l'intervention simultanée d'une déméthylation non négligeable, la complexité du mélange (séparation incomplète de certains pics) n'a pas permis, malgré une identification (par addition d'échantillons authentiques dans le mélange) aisée des constituants, de mesurer correctement leurs proportions relatives.

L'examen des chromatogrammes confirme cependant entièrement les résultats obtenus avec chacun des hydrocarbures pris isolément et autorise quelques remarques supplémentaires.

(*i*) Pour l'anthracène et le méthyl anthracène, la substitution des positions α et β est, pour des conditions normales d'acétylation totalement dépendante du réarrangement. Contrairement à ce que nous avions suggéré (1) pour expliquer la forte proportion d'isomère en 4 dans certains cas d'acétylation du méthyl-9 anthracène, nous n'avons retrouvé aucune évidence expérimentale d'une quelconque substitution directe de ces positions.

(*ii*) En tenant compte de l'avantage statistique résultant du nombre de positions équivalentes, la vitesse de substitution sur le sommet 2 du diméthyl-9,10 anthracène apparaît encore supérieure à celle de la position 4 de l'homologue monométhylé. En conséquence, lors de l'acétylation du mélange le réarrangement de l'acétyl-10 méthyl-9 anthracène, d'abord formé en grande quantité, se fait en grande partie au profit du dérivé diméthylé avec régénération progressive du méthyl-9 anthracène.

(*iii*) De beaucoup plus lente pour des raisons à la fois stériques et électroniques que la *méso*-desacétylation, la réversibilité de la méthylation n'affecte que les seules positions *méso*, ce qui se traduit par l'absence dans tous les cas d'isomères méthylés autres que ceux normalement attendus. Cette particularité est surtout apparente lors du réarrangement de l'acétyl-9 anthracène au profit du diméthyl-9,10 où l'on constate en fin de réaction, la présence d'une quantité telle de méthyl-9 anthracène (et de ses dérivés acétylés) que sa formation implique nécessairement, en plus de la déméthylation partielle du dérivé diméthylé, la méthylation de l'anthracène régénéré par le départ du groupement acétyle.

Interprétation des résultats

Confirmant, si besoin était, la réalité de la réversibilité de l'acylation également constatée récemment à propos de la benzoylation du naphtalène (15) l'analyse des facteurs expérimentaux a surtout montré qu'en ce qui concerne

Can. J. Chem. Downloaded from www.nrcresearchpress.com by 210.87.254.5 on 09/05/12
For personal use only.

Can. J. Chem. Downloaded from www.nrcresearchpress.com by 210.87.254.5 on 09/05/12
For personal use only.

l'anthracène où elle se révèle particulièrement aisée, cette réversibilité n'est cependant pas un phénomène aléatoire. En conséquence, l'aspect complexe que revêt à priori l'acétylation de l'anthracène et de ses homologues alkylés résulte pour beaucoup de l'intervention, incontrôlée ou difficilement contrôlable dans certains modes opératoires, du réarrangement consécutif à la *méso*-désacétylation.

Selon Gore et Hoskins (11*a*), qui ont été les premiers à rechercher les raisons de l'exceptionnelle labilité du groupement acétyle sur cette position, celle-ci résulte de l'important volume du groupement méthyle qui, par la présence des hydrogènes en *péri*, s'oppose lors de la substitution, à la conjugaison du carbonyle donc à la stabilisation par délocalisation. Par contre cette contrainte stérique doit-être moindre avec le groupement benzoyle qui se révèle effectivement beaucoup plus stable. Bien qu'à notre connaissance aucune interprétation en termes réactionnels n'en ait été faite, cette explication était récemment reprise à propos de la dibenzoylation et de la dicinnamoylation de l'anthracène (16) qui peuvent s'effectuer par réarrangement du dérivé monosubstitué en présence d'un excès de chlorure d'aluminium et pour lesquelles les auteurs précisent cependant que la vitesse de réaction peut-être considérablement accrue par addition de gaz chlorhydrique.

Il découle par conséquent de cette observation et de nos propres résultats que le processus de desacylation ou de desacétylation peut se résumer par le schéma 2 où *A* représente le complexe intermédiaire, *B* le complexe final de la *méso*-substitution et *C* le complexe protoné plus stable que *A* pour les raisons précitées et dont la réalité n'est plus à démontrer (17).

Mais il apparaît alors que la formation de celui-ci à partir de *A* (ou de *B*) nécessite un apport de proton donc la présence d'un excès de catalyseur puisqu'une mole de celui-ci est utilisée soit par le complexe intermédiaire (ou final) soit par le complexe acylant initial ou régénéré. Les divers aspects que peut revêtir l'acétylation de l'anthracène sont donc contenus dans ce schéma et reposent sur les possibilités de formation de *C*. Sans excès de catalyseur, la réaction est effectivement limitée à la formation de *B* via *A*, alors que dans le cas contraire, la vitesse de desacétylation (donc du réarrangement) se révèle dépendante de la richesse du milieu en proton laquelle est déterminée par l'importance de l'excès et par la concentration en acide chlorhydrique.

Cette dernière condition qui fait intervenir la solubilité de l'acide chlorhydrique dans le milieu réactionnel pourrait expliquer que lors de l'acétylation du méthyl-9 anthracène à 40 °C nous ayons constaté (1) un réarrangement moindre qu'à température ambiante puisque l'élévation de température ne peut que favoriser l'élimination de l'acide chlorhydrique formé. Il n'est pas impossible que se soit cette même raison qui rende compte de la différence d'orientation de la substitution, signalée par Bassilios *et al.* (12), entre le chloroforme et le dichloréthane à 40 °C, ce dernier conduisant à une quantité prépondérante d'acétyl-1 anthracène. Il est difficile, en effet, de mettre en cause dans ce cas, la solubilité (apparemment totale dans les deux solvants) du complexe de *méso*-substitution dont le rôle est cependant prépondérant puisqu'elle conditionne tout le processus.

En ce qui concerne cette indispensable solvatation, il est vraisemblable que la plus ou moins grande participation du solvant au complexe est susceptible non seulement d'accroître la vitesse de desacétylation, mais de favoriser la réacétylation des positions β moins encombrées, ce qui est effectivement observé avec des solvants polaires comme le nitrométhane ou le nitrobenzene (1, 5, 18).

Que ce soit au vu de nos propres résultats sur les trois hydrocarbures ou de ceux de la littérature sur l'anthracène, il apparaît que ce sont ensuite les facteurs électroniques, stériques et thermodynamiques qui gouvernent l'orientation de la réacétylation (15). Il ne nous paraît pas

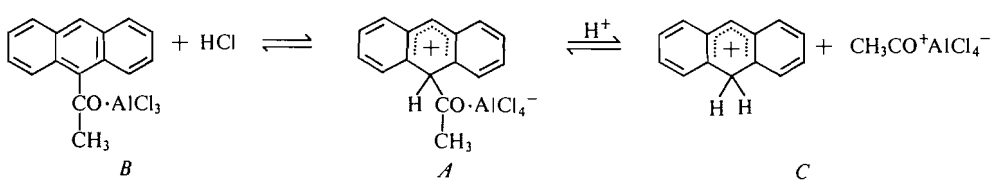

SCHÉMA 2

Can. J. Chem. Downloaded from www.nrcresearchpress.com by 210.87.254.5 on 09/05/12
For personal use only.

utile de détailler ici cette analyse qui découle en grande partie de l'examen des divers états de transition mais il est évident que la composition du produit final dépend avant tout de la vitesse de desacétylation par rapport à la durée de réaction et que se sont essentiellement le solvant et la température qui déterminent la prépondérance de l'un ou l'autre des isomères. Mais de ce fait, et en raison de la plus faible vitesse de réacétylation des positions α et β, le rendement global en produits acétylés risque, comme le montrent certains résultats de la littérature (2) d'être sérieusement réduit lorsque les conditions d'une désacétylation rapide sont remplies et que le temps de contact est trop court et (ou) la température trop basse. Dans le cas contraire le rendement n'est que légèrement affecté (pertes en ion acylium si l'agent acylant n'est pas en excès) par le réarrangement mais l'exceptionnelle rapidité de la *méso*-desacétylation dans certaines conditions pourrait conduire à conclure hâtivement à une substitution directe des positions α et β.

Ce n'est cependant pas à l'intervention du réarrangement qu'il faut imputer les variations de rendement enregistrées selon le catalyseur, lors de l'utilisation d'anhydride acétique, mais au processus même de ce type d'acylation qui, au moins dans certains cas, doit être considéré comme différent de celui qui met en jeu les chlorures d'acides.

En effet, que se soit avec les essais décrits ici ou à propos d'autres hydrocarbures (19) nous avons maintes fois constaté que, contrairement à ce qui est le plus souvent admis dans la littérature, l'emploi d'anhydride acétique, qui peut par ailleurs modifier l'orientation (18), n'exige pas nécessairement pour que le rendement soit élevé, la mise en oeuvre de deux, ou même trois moles et plus, de catalyseur.

Par conséquent, sans rechercher l'utilisation complète de l'anhydride en plus des eqs simplifiées habituelles 1 et 2, il faut admettre que la substitution sans dissociation préalable de l'anhydride selon l'éq. 3, doit intervenir d'une manière importante.

[1] $$(CH_3CO)_2O + 2MX_n \rightarrow CH_3COX\cdot MX_n + CH_3COOMX_{n-1}$$

[2] $$CH_3COX\cdot MX_n + ArH \rightarrow Ar^+(H)(C(CH_3)(X))O{-}MX_n \rightarrow Ar{-}CO(CH_3)\cdot MX_n + HX$$

[3] $$(CH_3CO)_2O\cdot MX_n + ArH \rightarrow Ar^+(H)(C(CH_3)(OCOCH_3))O{-}MX_n \rightarrow Ar{-}CO(CH_3)\cdot MX_n + CH_3CO_2H \leftrightharpoons$$

$$Ar{-}COCH_3 + H^+MX_nCH_3COO^- \rightarrow ArCOCH_3 + MX_{n-1}OCOCH_3 + HX$$

Déjà envisagée par Satchell (20) en tant qu'éventualité, cette voie d'acylation directe est nécessairement dépendante du mode opératoire, de la "force" du catalyseur et de la réactivité (pouvoir nucléophile et effets stériques) de l'hydrocarbure. Elle est en effet liée à la stabilité, donc à la vitesse de transformation en complexe acylant classique (éqs. 1 et 2), du complexe coordinatif D par rapport à la vitesse de formation du complexe de transition avec l'hydrocarbure.

$$CH_3{-}\overset{\delta^+}{C}O(OCOCH_3) \rightarrow \overset{\delta^-}{M}X_n$$

D

C'est pourquoi elle n'intervient probablement que peu ou pas lorsque le catalyseur (à fortiori s'il s'agit du chlorure d'aluminium) est préalablement mis en présence de l'anhydride selon un mode opératoire qui exige effectivement au moins 2 mol de catalyseur. Et c'est sans doute pour

Can. J. Chem. Downloaded from www.nrcresearchpress.com by 210.87.254.5 on 09/05/12
For personal use only.

cette raison que dans une étude de l'acétylation de divers substrats benzéniques, Olah *et al.* (21) considèrent, au vu des résultats sur le toluène et des spectres de rmn des complexes respectifs du chlorure d'acétyle et de l'anhydride acétique avec le chlorure d'aluminium, que l'entité réagissante est la même dans les deux cas.

Un avis un peu différent a été avancé précédemment par Burton et Parill (22) qui admettent qu'avec l'anhydride, l'entité réagissante est le complexe

$$CH_3CO^+MX_nOCOCH_3^-$$

mais qui constatant, ainsi que nous l'avons fait, que ce mode d'acylation en présence de catalyseurs faibles n'est pas accompagné de dégagement d'acide chlorhydrique, en déduisent que seuls les catalyseurs très efficaces comme le chlorure d'aluminium sont capables de provoquer la dissociation complète de l'acide acétique formé dans la réaction (dernière étape de l'éq. 3).

Ayant pour notre part, toujours opéré par addition finale du catalyseur (ce qui minimise les réactions secondaires) nous pensons pourtant que dans ces conditions, le complexe coordinatif, particulièrement avec le chlorure stannique, prédomine lors de l'acétylation avec l'anhydride et que c'est le complexe ionisé habituel qui intervient avec le chlorure d'acide.

Pour en revenir à l'anthracène et à ses homologues, il apparaît alors que la chute de rendement constatée avec le chlorure d'aluminium et l'anhydride acétique provient d'une consommation partielle de catalyseur par formation de complexe ionisé tandis que celle enregistrée avec le chlorure stannique et le chlorure d'acétyle résulte de l'ionisation insuffisante et de la faible réactivité du complexe coordinatif.

Le fait qu'au lieu d'être réduit ou empêché, lors de l'utilisation d'anhydride, par la desactivation de l'excès (toujours inférieur à 0.5 mol) de catalyseur, le réarrangement intervienne dans tous les cas, constitue un argument supplémentaire en faveur du processus.

Et comme enfin, l'encombrement vraisemblablement plus élevé du complexe coordinatif justifie simultanément la vitesse moins élevée de la *méso*-substitution et l'augmentation de proportion des produits d'acétylation en β, le seul jeu de ce processus et du réarrangement nous paraît suffisant pour rendre compte des divers résultats et montrer que l'acétylation de l'anthracène et de ses homologues n'est pas une réaction tout à fait dépourvue de reproductibilité.

Partie expérimentale

Les divers essais d'acétylation ont été effectués sur 0.03 mol d'hydrocarbure, à température ambiante dans les conditions précisées dans le texte, le catalyseur étant ajouté en dernier (procédé d'Elbs). Les essais de réarrangement direct ont été réalisés à température ambiante ou à chaud (voir texte) avec du chlorure d'aluminium préalablement repurifié par sublimation sous vide.

Le diméthyl-9,10 anthracène a été préparé par formylation, suivie d'une réduction du méthyl-9 anthracène selon la technique décrite pour celui-ci (1). Il est obtenu exempt de dérivé monométhylé par chromatographie sur colonne de silice au stade du dérivé formylé (élution cyclohexane puis benzène).

L'analyse des produits des diverses réactions a été effectuée par chromatographie en phase vapeur sur un appareil Girdel 75 FH équipé d'un détecteur à ionisation de flamme et d'une colonne de 2 m (ϕ $\frac{1}{8}$ po) chargée de Chromosorb W contenant 5% de SE 30. L'identification des divers constituants a été obtenue par addition dans le mélange d'échantillons purs. Dans la plupart des cas la température du four a été de 225 °C mais avec des mélanges complexes (acétylation simultanée des hydrocarbures, présence de dérivés diacétylés) une programmation de 210 à 250 °C à raison de 5 °C par minute, a été nécessaire.

La détermination des proportions des constituants a été effectuée par intégration des pics au moyen d'un intégrateur numérique L.T.T. 1103. Un facteur de correction propre à chaque composé a été appliqué aux valeurs obtenues, après évaluation de la réponse du détecteur au moyen de mélanges de proportions connues. Dans quelques cas un contrôle a été réalisé par séparation des produits de la réaction sur colonne de silice.

1. M. Croisy-Delcey, P. Jacquignon et N. P. Buu Hoi. Bull. Soc. Chim. 1084 (1972).
2. (*a*) P. H. Gore. Chem. Rev. **55**, 260 (1955). (*b*) P. H. Gore. *Dans* Friedel-Crafts and related reactions. Vol. 3. *Edité par* G. A. Olah. J. Wiley and Sons, N.Y. 1964. pp. 75, 266.
3. P. H. Gore and C. K. Thadani. J. Chem. Soc. 1729 (1966).
4. P. H. Gore. J. Org. Chem. **22**, 135 (1957).
5. I. G. Farbenindustrie A. G. Brevet français No. 633071 (1927).
6. E. G. E. Hawkins. J. Chem. Soc. 3856 (1957).
7. H. C. Brown et J. D. Brady. J. Am. Chem. Soc. **74**, 3570 (1952); H. C. Brown et L. M. Stock. J. Am. Chem. Soc. **79**, 1421 (1957).
8. (*a*) K. Shishido et G. Ishida. J. Am. Chem. Soc. **70**, 1289 (1948); (*b*) P. de Bruyn. C.R. Acad. Sci. **228**, 1809 (1949); (*c*) L. Van Hove. Bull. Soc. Chim. Belge **66**, 413 (1957).
9. C. L. Hewett. J. Chem. Soc. 293 (1940).
10. P. H. Gore et J. A. Hoskins. J. Chem. Soc. 3347 (1971).

11. P. H. GORE et J. A. HOSKINS. (*a*) J. Chem. Soc. 5666 (1964); (*b*) J. Chem. Soc. 5744 (1965).
12. H. F. BASSILIOS, M. SHAWKY et A. Y. SALEM. (*a*) Recl. Trav. Chim. **81**, 679 (1962); (*b*) Recl. Trav. Chim. **82**, 298 (1963).
13. N. O. CALLOWAY. Chem. Rev. **17**, 327 (1935); O. C. DERMER et R. A. BILLMEIER. J. Am. Chem. Soc. **64**, 464 (1942).
14. G. BADDELEY. Q. Rev. **8**, 372 (1954); Nature, **175**, 982 (1955).
15. I. AGRANAT, YU-SHAN SHIH et Y. BENTOR. J. Am. Chem. Soc. **96**, 1259 (1974).
16. A. T. BLAMINI, H. J. WILLIAMS et R. G. SHOTTER. Tetrahedron, **29**, 1327 (1973).
17. G. DALLINGA, E. L. MACKOR et A. A. BERRIJN-STUART. Mol. Phys. **1**, 123 (1958); C. MACLEAN et E. L. MACKOR. Mol. Phys. **4**, 241 (1961).
18. A. ETIENNE, G. ARDITTI et A. CHMELEVSKY. Bull. Soc. Chim. Fr. 669 (1965).
19. P. JACQUIGNON et F. PERIN. Bull. Soc. Chim. Fr. 1371 (1971).
20. D. P. N. SATCHELL. J. Chem. Soc. 1899 (1962); Q. Rev. **17**, 160 (1963).
21. G. A. OLAH, M. E. MOFFATT, S. J. KUHN et B. A. HARDIE. J. Am. Chem. Soc. **86**, 2198 (1964).
22. H. BURTON et P. F. G. PRAILL. J. Chem. Soc. 726 (1951).

Can. J. Chem. Downloaded from www.nrcresearchpress.com by 210.87.254.5 on 09/05/12
For personal use only.

On the extension of the Hückel rule to polycyclic non-alternant conjugated hydrocarbons

I. GUTMAN AND N. TRINAJSTIĆ
The Rugjer Bošković Institute, P.O.B. 1016, 41001 Zagreb, Croatia, Yugoslavia

Received September 16, 1975

I. GUTMAN and N. TRINAJSTIĆ. Can. J. Chem. **54**, 1789 (1976).

General rules for aromatic stability of non-alternant polycyclic conjugated hydrocarbons are obtained using graph–theoretical considerations. Every pair of odd-membered rings contained in the conjugated molecule has a stabilizing effect if one ring is of the size $4N + 1$ and the other of the size $4N + 3$. If both rings are of the size $4N + 1$ or $4N + 3$, a destabilizing effect occurs. This conclusion holds both for fused and disjointed rings. The π-electron system is said to be relatively more stable if the number of $(4N + 1)$-membered rings is equal to the number of $(4N + 3)$-rings.

I. GUTMAN et N. TRINAJSTIĆ. Can. J. Chem. **54**, 1789 (1976).

Faisant appel aux théories de graphes on déduit des règles générales permettant de déterminer la stabilité aromatique d'hydrocarbures conjugués polycycliques non alternants. Chaque paire de cycles contenant un nombre impair d'atomes dans la molécule conjuguée a un effet stabilisant sur l'ensemble si un cycle est de grandeur $4N + 1$ et l'autre de grandeur $4N + 3$. Si les deux cycles sont de grandeur $4N + 1$ ou $4N + 3$, il se produit un effet déstabilisant. Cette conclusion est valable autant pour les cycles condensés que pour les cycles disjoints. On dit que le système d'électron π est relativement plus stable si le nombre de cycle contenant $4N + 1$ chaînons est égale au nombre de cycle contenant $4N + 3$ chaînons.

[Traduit par le journal]

In the last couple of years a rapid development of the topological theory of conjugated molecules has produced a number of novel results (1–10). In spite of this advance, there has been rather limited work carried out on the elucidation of the structural factors determining the chemical behaviour of non-alternant hydrocarbons (2, 4, 11, 12). The recent work of Kruszewski and Krygowski (13) therefore presents an important break-through in this field.

The Hückel $4N + 2$ rule (14) is both theoretically and experimentally a well established fact for annulenes (15, 16). Although this rule was for a long time believed to hold for an arbitrary conjugated system (17), its general validity has been proved quite recently (18). The proof of that relatively complicated proposition was possible by applying graph spectral theory to the Coulson integral formula for π-electron energy (19, 20). In the present work we wish to use the same mathematical technique, discussed in detail in ref. 18, to obtain extensions of the Hückel rule of the same type as in ref. 13. However, it should be noted that while the results of Kruszewski and Krygowski are mainly based on numerical experience, our conclusions follow from a more formal graph–theoretical analysis. Hope can be expressed that these two approaches are complementary, that both are useful for predicting and rationalizing facts of current interest in the chemistry of conjugated compounds.

However, it should be noted that all our considerations are within the scope of the HMO approximation. Therefore, our conclusions are qualitative ones. Nevertheless, it has been recently demonstrated by Hess and Schaad (21) that the Hückel theory can also produce satisfactory quantitative agreements with experimental facts. In particular, the total π-electron energy of the HMO approximation was shown to be simply related to measurable thermodynamic constants of conjugated systems (22). Therefore, throughout this work the calculated π-electron energies are assumed to be equal to the actual stabilization or destabilization of molecules. The reader's attention is called to this limitation.

The Hückel Rule

The exact formulation of the Hückel $4N + 2$ rule is closely related to the understanding of the topological factors which determine the total

Can. J. Chem. Downloaded from www.nrcresearchpress.com by 210.87.254.5 on 09/05/12
For personal use only.

Can. J. Chem. Downloaded from www.nrcresearchpress.com by 210.87.254.5 on 09/05/12
For personal use only.

π-electron energy (E_π). In fact, it is necessary to establish the way in which a particular detail of the molecular structure contributes to the total value of E_π. If the contribution of a particular structural detail increases E_π, one says that it has a stabilizing effect. On the contrary, every structural detail which yields a negative contribution to E_π is said to destabilize the molecule. Unfortunately, an explicit expression for the dependence of E_π on the details of the molecular structure does not exist (23).

Suppose it is possible to determine the sign of the contribution to E_π of every ring contained in the conjugated molecule, then the Hückel $4N + 2$ rule reads: (*a*) Every $(4N + 2)$-membered ring contained in the conjugated molecule has an increasing contribution to E_π. (*b*) Every $(4N)$-membered ring contained in the conjugated molecule has a decreasing contribution to E_π. Thus, the presence of $(4N + 2)$-rings will in general stabilize and the presence of $(4N)$-rings destabilize the conjugated hydrocarbon. A rigorous proof of this proposition was given elsewhere (18).

In order to formulate statements of the analogous type for $(4N + 1)$- and $(4N + 3)$-membered rings let us introduce the following graph–theoretical concepts. The topology of a conjugated molecule will be presented by a graph (so-called molecular graph) in the usual way (10). The subgraphs of this graph, the components of which are rings (of the size 3, 4, 5, . . .) and complete graphs of degree two (these contain two vertices joined by an edge) are called Sachs graphs (1). Let the Sachs graph s contain $c_2(s)$ components which are complete graphs of degree two and $c_3(s)$, $c_4(s)$, $c_5(s)$, . . . components which are rings of the size 3, 4, 5, . . ., respectively. Then the total number of components $c(s)$ and the total number of rings $r(s)$ are

$$[1] \quad c(s) = c_2(s) + c_3(s) + c_4(s) + c_5(s) + \ldots$$

$$[2] \quad r(s) = c_3(s) + c_4(s) + c_5(s) + \ldots$$

The number $n(s)$ of vertices of the Sachs graph s is similarly

$$[3] \quad n(s) = 2c_2(s) + 3c_3(s) + 4c_4(s) + 5c_5(s) + \ldots$$

Finally, we introduce the quantities $R_0(s)$, $R_1(s)$, $R_2(s)$, and $R_3(s)$, the total number of $(4N)$-, $(4N + 1)$-, $(4N + 2)$-, and $(4N + 3)$-membered rings respectively, contained in the Sachs graph s.

$$[4] \quad \begin{aligned} R_0(s) &= c_4(s) + c_8(s) + \ldots \\ R_1(s) &= c_5(s) + c_9(s) + \ldots \\ R_2(s) &= c_6(s) + c_{10}(s) + \ldots \\ R_3(s) &= c_3(s) + c_7(s) + \ldots \end{aligned}$$

In ref. 18 the following variant of the Coulson integral formula 19 has been derived:

$$[5] \quad E_\pi = \frac{1}{2\pi}\int_{-\infty}^{\infty} \frac{dx}{x^2} \ln\left[\left(\sum_j (-1)^j a_{2j} x^{2j}\right)^2 + \left(\sum_j (-1)^j a_{2j+1} x^{2j+1}\right)^2\right]$$

where the term a_n (the nth coefficient of the characteristic polynomial (1)) is determined by

$$[6] \quad a_n = \sum (-1)^{c(s)} 2^{r(s)}$$

The summation in [6] goes over all Sachs graphs with n vertices.

Two properties of the coefficients a_n are important for the further discussion, namely

$$[7] \quad (-1)^j a_{2j} \geq 0$$

and

$$[8] \quad (-1)^j a_{2j+1} \begin{cases} \geq 0 & \text{if } \gamma = 4N + 3 \\ \leq 0 & \text{if } \gamma = 4N + 1 \end{cases}$$

with γ being the size of the smallest odd-membered ring in the molecule (18).

From eqs. 5 and 6 one sees easily that E_π depends solely on the structure of the Sachs graphs contained in the molecular graph. In fact, Sachs graphs represent exactly those structural details of the molecule, the contributions of which are known. Thus, the contribution from each Sachs graph either increases or decreases the value of E_π. Therefore, it seems reasonable to introduce a 'stability' function σ with the property

$$[9] \quad \sigma(s) = \begin{cases} +1 & \text{if } s \text{ increases } E_\pi \\ -1 & \text{if } s \text{ decreases } E_\pi \end{cases}$$

An inspection of [5]–[8] reveals that

$$[10] \quad \sigma = \begin{cases} (-1)^{c+n/2} & \text{for } n = \text{even} \\ (-1)^{c+(n-\gamma)/2} & \text{for } n = \text{odd} \end{cases}$$

In the case of alternant hydrocarbons (when R_1 and R_3 are zero for all Sachs graphs) one obtains (18):

$$[11] \quad \sigma(s) = (-1)^{R_0(s)}$$

Can. J. Chem. Downloaded from www.nrcresearchpress.com by 210.87.254.5 on 09/05/12
For personal use only.

which is an algebraic formulation of the Hückel rule. The meaning of [11] is that every Sachs graph containing an arbitrary number of $(4N + 2)$-rings but no $(4N)$-membered rings ($R_0 = 0$) has a positive contribution to E_π. Every Sachs graph containing a $(4N)$-ring ($R_0 = 1$) gives a negative contribution to E_π. The seeming contradiction that Sachs graphs with two $(4N)$-membered rings ($R_0 = 2$) stabilize the molecule is overcome by taking into account that the existence of such a Sachs graph necessarily implies the existence of additional four graphs with $R_0 = 1$. Details of these considerations are given elsewhere (18).

Hückel-type Rules for Odd-membered Rings

Equation 11 may be generalized for the case of presence of odd-membered rings in a conjugated molecule. An elementary, but tedious, calculation gives:

$$[12] \quad \sigma = \begin{cases} (-1)^{R_0+(R_1-R_3)/2} & \text{for } n = \text{even} \\ (-1)^{R_0+[\gamma-(R_1-R_3)]/2} & \text{for } n = \text{odd} \end{cases}$$

Without the loss of generality of the present discussion, one may take $R_0 = 0$, since the effect of the presence of $(4N)$-membered rings is discussed in the previous section.

Rules which follow are deduced from [12] using graph–theoretical considerations analogous to those of ref. 18. These elementary, but rather lengthy, derivations will be omitted. The reader should keep in mind that our rules are in fact mathematical theorems valid within the Hückel theory, which are not necessarily in agreement with chemical observations. However, we hope to be able to show that these rules indeed reflect relevant chemical facts.

From now on it is implied that two odd-membered rings are of the same type if their sizes are both $4N + 1$ or $4N + 3$; a $(4N + 1)$- and a $(4N + 3)$-membered ring will be said to be of the opposite type. Note, however, that in graphs representing chemically relevant non-alternant topologies, five- and seven-membered rings occur almost exclusively. Nevertheless, we will formulate our results in a more general 'modulo 4' (24) fashion.

Rule 1

If there is only one odd-membered ring present in the molecule, there will be a small stabilization effect arising from its presence.

Numerical calculations (25) confirm this conclusion, but show, however, that the quantitative effect in conjugated systems containing one odd-ring (*e.g.* fulvene) is rather small.

Rule 2

Similarly, in the polycyclic case there exist also positive contributions to E_π arising from all rings being of the same type as the smallest odd-ring in the molecule. Odd-rings of opposite type exhibit a destabilization effect.

However, these contributions are largely screened by some other topological phenomena (see Rules 3 and 4) and therefore seem not to be of chemical relevance.

Rule 3

A pair of *fused* odd-membered rings causes stabilization if the rings are of the opposite type, and destabilization if the rings are of the same type.

This rule applies directly to the relative stability of pentalene, **1**, azulene, **2**, and heptalene, **3** (see Table 1), but it can be used in a straightforward manner for all other polycyclic cases as well. In order to use the rule one has to count the number of pentalene-like, azulene-like, and heptalene-like subgraphs of the molecular graph and to take into account that every such subgraph will contribute to molecular stability according to Rule 3. Inspection of Table 1 shows a good agreement between our results, the calculated resonance energy per electron of Hess and Schaad (26), and the experimental findings. Thus, the parent compounds or methyl derivatives have been synthesized for all systems predicted to be stable (*e.g.*: **2**, **5**, **6**, **11**, **12**, **13**). All these molecules, except **2**, contain one pentalene or heptalene subgraph, the presence of which, perhaps, explains some anomalies in their chemistry (34).

Several molecules (*e.g.*: **3**, **9**, **10**, **14**, **15**) are predicted to be of low stability. Here experimental data are rather scarce, but those existing for heptalene, **3**, indicate this molecule to be too reactive to be isolated (28). An interesting prediction is that **10** should be less reactive (more stable) than **9**. Unfortunately, there are no experimental data, at present, available to test our prediction that **10** is a better candidate for synthesis than **9**. This, however, is confirmed in the case of **14** and **15**. Our prediction that **14** should be more stable than **15** because it con-

Can. J. Chem. Downloaded from www.nrcresearchpress.com by 210.87.254.5 on 09/05/12
For personal use only.

tains more azulene-like and less heptalene-like subgraphs is verified by experiment. The methyl derivative of **14** is known (30), whereas neither the parent compound nor the derivatives of **15** have been prepared.

Finally, all compounds (*e.g.*: **1**, **4**, **7**, **8**, **16**) predicted to be unstable are not yet known. However, it should be noted that hexaphenylpentalene, **17**, 1-methylpentalene, **18**, and dilithium hexachloroacepentylendiide, **19**, have been prepared (35–37). The reasons for stability of **17** have been discussed in refs. 2 and 38. These are related to the alternant part of the molecule. 1-Methylpentalene and dilithium hexachloroacepentylendiide are transient species obtained under severe experimental conditions at low temperatures; the former molecule is prepared at −196 °C while the latter at −70 °C.

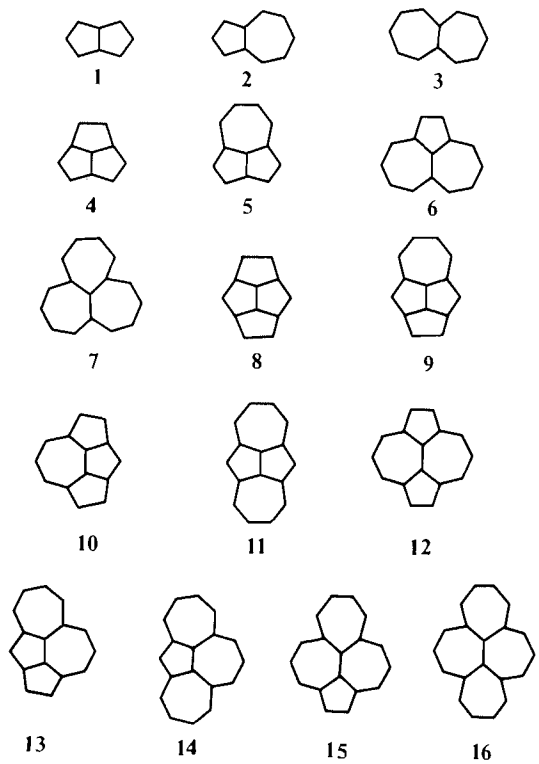

Consider compound **8**. This molecule, which contains pentalene-like subgraphs only and has a very low REPE value ($-0.036\,\beta$), is predicted to be a very unstable antiaromatic species, and has not been prepared yet. However, Garratt and Sargent (39) expressed an optimism about the possibility of its synthesis based on the $4N + 2$ π-electron perimeter of this molecule. Here we have, therefore, a very good example of the danger of applying the Hückel rule in its traditional form directly to the perimeter of polycyclic conjugated systems.

In more complicated molecular structures another effect is also playing an important role in determining stability. This is summarized in the subsequent rule.

Rule 4

A pair of *disjoint* odd-membered rings causes stabilization if the rings are of the opposite type, and destabilization if the rings are of the same type.

The analogy between Rules 3 and 4 is evident. Therefore it is worth mentioning that they have been derived using two relatively different proof techniques. The application of this rule to fulvalene and its homologues (13) is obvious.

Rules 3 and 4 together give the statement of Kruszewski and Krygowski (13):

Rule 5

A non-alternant system is relatively stable (aromatic) if the number F of $(4N + 1)$-membered rings is *equal* to the number S of $(4N + 3)$-membered rings.

However, if the difference $S - F$ is divisible by 4, but is not zero, such molecules are extremely reactive; no one compound to our knowledge with $S - F = \pm 4$ has been prepared yet. Examples of this case are the hypothetical structures **8** ($S - F = -4$) and **16** ($S - F = +4$).

As an additional improvement over the work (13) it is to be emphasized that all the obtained

TABLE 1. Fused non-alternant hydrocarbons containing five- and/or seven-membered rings*

Compound†	P	A	H	REPE (in β)	Status‡	Reference
1	1	0	0	−0.018	—	
2	0	1	0	0.023	i	27
3	0	0	1	−0.004	r	28
4	3	0	0	−0.062	—	
5	1	2	0	0.018	m	29
6	0	2	1	0.016	m	30
7	0	0	3	−0.019	—	
8	5	0	0	−0.036	—	
9	3	2	0	−0.002	—	
10	2	3	0	0.002	—	
11	1	4	0	0.021	i	31
12	0	4	1	0.022	i	32
13	1	3	1	0.016	m	33§
14	0	3	2	0.009	m	30
15	0	2	3	0.004	—	
16	0	0	5	−0.011	—	

*P, A, and H denote the number of pentalene, azulene, and heptalene subgraphs respectively, contained in the molecular graph. The REPE values are taken from (26).

†The list of the studied molecules is given in text.

‡i, isolated; r, existing in solution, but too reactive to be isolated; —, unknown; m, methyl derivatives known.

§In ref. 30 is mentioned the unpublished synthesis of unsubstituted **13** by K. Hafner and F. Bauer.

rules hold regardless whether the π-systems contain non-bonding orbitals or not.

Conclusions

Using graph–theoretical proof techniques, the rule proposed in ref. 13 has been proved and besides a number of additional results of similar form are obtained. The structural factors determining the aromatic stability of non-alternant conjugated hydrocarbons are, thus, to great extent understood.

1. A. GRAOVAC, I. GUTMAN, N. TRINAJSTIĆ, and T. ŽIVKOVIĆ. Theoret. Chim. Acta, **26**, 67 (1972).
2. I. GUTMAN, N. TRINAJSTIĆ, and T. ŽIVKOVIĆ. Tetrahedron, **29**, 3449 (1973).
3. G. G. HALL. Int. J. Math. Educ. Sci. Technol. **4**, 233 (1973).
4. I. GUTMAN and N. TRINAJSTIĆ. Croat. Chem. Acta, **46**, 243 (1974).
5. D. CVETKOVIĆ, I. GUTMAN, and N. TRINAJSTIĆ. J. Chem. Phys. **61**, 2700 (1974).
6. M. RANDIĆ. Tetrahedron, **30**, 2067 (1974).
7. W. C. HERNDON and M. L. ELLZEY, Jr. Tetrahedron, **31**, 99 (1975).
8. H. HOSOYA, K. HOSOI, and I. GUTMAN. Theoret. Chim. Acta, **38**, 37 (1975).
9. R. B. MALLION. Proc. Roy. Soc. (London) A**341**, 429 (1975).
10. I. GUTMAN and N. TRINAJSTIĆ. Topics Curr. Chem. **42**, 49 (1973).
11. C. F. WILCOX, Jr. J. Am. Chem. Soc. **91**, 2732 (1969).
12. W. C. HERNDON. Tetrahedron, **28**, 3675 (1972).
13. J. KRUSZEWSKI and T. M. KRYGOWSKI. Can. J. Chem. **53**, 945 (1975).
14. E. HÜCKEL. Z. Phys. **76**, 628 (1932).
15. F. SONDHEIMER. Pure Appl. Chem. **7**, 363 (1963); Proc. Roy. Soc. (London) A**297**, 173 (1967).
16. R. C. HADDON, V. R. HADDON, and L. M. JACKMAN. Topics Curr. Chem. **16**, 103 (1971).
17. M. J. S. DEWAR. Molecular orbital theory of organic chemistry. McGraw-Hill, New York. 1969. Chapt. 6.
18. I. GUTMAN and N. TRINAJSTIĆ. J. Chem. Phys. In press.
19. C. A. COULSON. Proc. Cambridge Phil. Soc. **36**, 201 (1940).
20. A. GRAOVAC, I. GUTMAN, and N. TRINAJSTIĆ. Chem. Phys. Lett. **35**, 555 (1975).
21. B. A. HESS, Jr. and L. J. SCHAAD. J. Am. Chem. Soc. **93**, 305 (1971); **93**, 2413 (1971).
22. L. J. SCHAAD and B. A. HESS, JR. J. Am. Chem. Soc. **95**, 3907 (1973).
23. I. GUTMAN. Theoret. Chim. Acta, **35**, 355 (1974).
24. M. J. GOLDSTEIN and R. HOFFMANN. J. Am. Chem. Soc. **93**, 6193 (1971).
25. I. GUTMAN, M. MILUN, and N. TRINAJSTIĆ. Unpublished results.
26. B. A. HESS, JR. and L. J. SCHAAD. J. Org. Chem. **36**, **3418** (1971).
27. W. HENTZSCHEL and J. WISLICENUS. Lieb. Ann. **275**, 312 (1893).
28. H. J. DAUBEN and D. J. BERTELLI. J. Am. Chem. Soc. **83**, 4659 (1961).
29. K. HAFNER and J. SCHNEIDER. Lieb. Ann. **624**, 37 (1959).

Can. J. Chem. Downloaded from www.nrcresearchpress.com by 210.87.254.5 on 09/05/12
For personal use only.

30. K. HAFNER, G. HAFNER-SCHNEIDER, and F. BAUER. Angew. Chem. **80**, 801 (1968).
31. H. REEL and E. VOGEL. Angew. Chem. **84**, 1064 (1972).
32. A. G. ANDERSON, JR., A. A. MACDONALD, and A. F. MONTANA. J. Am. Chem. Soc. **90**, 2993 (1968).
33. K. HAFNER, R. FLEISCHER, and K. FRITZ. Angew. Chem. **77**, 42 (1965).
34. K. HAFNER. Pure Appl. Chem. **28**, 153 (1972).
35. E. LEGOFF. J. Am. Chem. Soc. **84**, 3975 (1962).
36. R. BLOCH. R. A. MARTY, and P. de MAYO. J. Am. Chem. Soc. **93**, 3072 (1971).
37. I. T. JACOBSON. Chem. Scripta, **6**, 30 (1974).
38. W. C. HERNDON. Tetrahedron, **29**, 3 (1973).
39. P. J. GARRATT and M. V. SARGENT. Advan. Org. Chem. **6**, 1 (1969).

Can. J. Chem. Downloaded from www.nrcresearchpress.com by 210.87.254.5 on 09/05/12
For personal use only.

Nitration of the tetramethylbenzenes in acetic anhydride. Formation and rearomatization of adducts

ALFRED FISCHER AND DAVID R. A. LEONARD
Department of Chemistry, University of Victoria, Victoria, B.C., Canada V8W 2Y2

Received December 8, 1975

ALFRED FISCHER and DAVID R. A. LEONARD. Can. J. Chem. **54**, 1795 (1976).

Nitration of the tetramethylbenzenes in acetic anhydride at temperatures below −50 °C gives the 1-acetoxy-4-nitro and 5-acetoxy-2-nitro adducts from the 1,2,3,4 isomer, the 5-acetoxy-2-nitro adduct from the 1,2,3,5 isomer, and the 1-acetoxy-4-nitro adduct from the 1,2,4,5 isomer as well as the expected nitro derivatives. Corresponding nitritonitro adducts are also formed as well as side-chain (benzylic) derivatives: nitrates and phenylnitromethanes. Rearomatization of the tertiary acetate adducts leads to aryl acetates, benzylic derivatives, or nitroarenes, depending upon the acidity of the solvent. In the benzylic derivatives the methyl group substituted is that *ipso* to the acetate in the precursor adduct, that *para* to the most activated *ipso* position of the arene.

ALFRED FISCHER et DAVID R. A. LEONARD. Can. J. Chem. **54**, 1795 (1976).

On a réalisé la nitration des tétraméthylbenzènes dans l'anhydride acétique à des températures plus basses que −50 °C; l'isomère 1,2,3,4 conduit aux adduits acétoxy-1 nitro-4 et acétoxy-5 nitro-2 alors que les isomères 1,2,3,5 et 1,2,4,5 conduisent respectivement aux adduits acétoxy-5 nitro-2 et acétoxy-1 nitro-4; ces adduits sont formés en supplément des dérivés nitrés attendus. Il y a aussi formation des adduits correspondants nitritonitro de même que des dérivés sur la chaîne latérale (benzylique): nitrates et phénylnitrométhanes. La réaromatisation des adduits acétates tertiaires conduit, suivant l'acidité du solvant, aux acétates d'aryle, aux dérivés benzyliques ou aux nitroarènes. Dans les dérivés benzyliques, le groupe méthyle substitué est celui qui est *ipso* par rapport à l'acétate de l'adduit précurseur et qui est *para* par rapport à la position *ipso* la plus activée de l'arène.

[Traduit par le journal]

Electrophilic attack at a substituted (*ipso*) position often competes effectively with normal substitution in the course of aromatic nitration (1). In acetic anhydride solution *ipso*-nitration leads to the formation of 1,4-acetoxynitro adducts which, in favourable cases, may be isolated (2–4) but which are prone to undergo rearomatization leading to 'abnormal' nitration products (2–6). In an earlier study of the nitration of the tetramethylbenzenes in acetic anhydride substantial amounts of aryl acetates and side-chain nitro derivatives were found (7). In the cases of *p*-xylene and pseudocumene (1,2,4-trimethylbenzene) it was shown (2*b*, *i*, *k*) that such derivatives are secondary products obtained via the formation and rearomatization of adducts (Scheme 1) and it seemed clear that adducts must be formed in the cases of the tetramethylbenzenes although attempts to detect them were not successful (7). The high yields of 'abnormal' products obtained, reaching 75% in the case of prehnitene (1,2,3,4-tetramethylbenzene), and (Table 1) predictions based on partial rate factors for attack at *ipso*, *ortho*, *meta*, and *para* positions (8) indicated that potentially large amounts of adducts should be found with the tetramethylbenzene substrates. This paper reports the successful isolation of adducts from these systems and some rearomatization studies. Related studies include the nitration of dichloro-, dibromo-, and dinitrotetramethylbenzenes (9, 10), the nitration of the homologs of isodurene, ethylmesitylene, and propylmesitylene (11), and the chlorination of isodurene (6).

Results

Nitration of and Addition to Tetramethylbenzenes

Prehnitene (1,2,3,4-Tetramethylbenzene)

Careful reaction of prehnitene with nitric acid in acetic anhydride at −60 °C followed by quenching with ammonia at the same temperature, work-up, and chromatography at −50 °C gave as major products the diastereoisomeric

Can. J. Chem. Downloaded from www.nrcresearchpress.com by 210.87.254.6 on 09/05/12
For personal use only.

Can. J. Chem. Downloaded from www.nrcresearchpress.com by 210.87.254.6 on 09/05/12
For personal use only.

TABLE 1. Predicted relative extents of attack at the indicated positions in tetramethylbenzenes[a]

Tetramethylbenzene	Substitution or addition at position (%)					
	1	2	3	4	5	6
Prehnitene (1,2,3,4 isomer)	*22*	*18*	*18*	*22*	10	10
Isodurene (1,2,3,5 isomer)	*0.1*	*52*	*0.1*	24	*0.1*	24
Durene (1,2,4,5 isomer)	*21*	*21*	8	*21*	*21*	8

[a]Data for *ipso* positions in italics.

TABLE 2. Relative gradients (gradient 1-$OCOCH_3$ = 1.00) of proton chemical shifts for diene adducts from the addition of Eu([$^2H_9$]fod)$_3$[a]

Compound	1-CH_3	2-CH_3	3-X	4-CH_3	5-X	6-H
1*a*	0.55	0.35	0.18[b]	0.21	0.21[c]	0.85
1*b*	0.57	0.35	0.23[b]	0.19	0.27[c]	0.90
1*a*/**1***b* ratio	0.96	0.99	0.78[b]	1.11	0.78[c]	0.94
5*a*	0.53	0.34	0.33[c]	0.26	0.15[b]	0.87
5*b*	0.55	0.32	0.36[c]	0.21	0.17[b]	0.92
5*a*/**5***b* ratio	0.96	1.06	0.92[c]	1.24	0.86[b]	0.95

[a]Absolute gradients of 1-$OCOCH_3$: **1***a*, 15.1; **1***b*, 17.0; **5***a*, 15.1; **5***b*, 17.0 ppm mol of substrate per mol of shift reagent.
[b]X = CH_3.
[c]X = H.

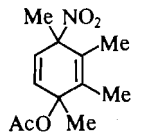

1

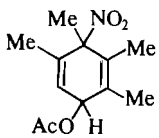

2

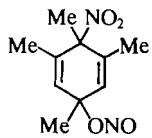

3

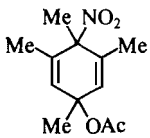

4

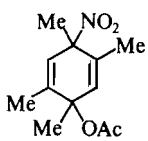

5

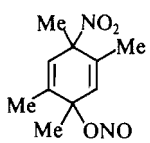

6

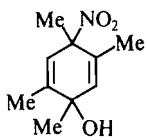

7

1-acetoxy-4-nitro adducts[1] **1***a* and **1***b*, the diastereoisomeric 5-acetoxy-2-nitro adducts **2***a* and **2***b* and 5-nitroprehnitene, together with smaller amounts of another 1,4 adduct, tentatively identified as 1,2,3,4-tetramethyl-4-nitro-1,4-dihydrophenyl nitrite, 2,3,4-trimethylphenylnitromethane, and 2,3,4-trimethylbenzyl nitrate. 2,3,4,5-Tetramethylphenyl acetate, although not isolated, was recognized in some column fractions.

The 1,4 adducts **1** were distinguished from the 2,5 adducts **2** and the structures assigned from the nuclear magnetic resonance spectra. The 1,4 adducts exhibited the typical AB quartet with J = 10 Hz, appropriate for the adjacent vinyl protons of **1**. When the methyl region was irradiated to remove longer range couplings, the 2,5 adducts revealed an AB quartet with a much smaller coupling, appropriate for the adjacent vinyl and allylic protons of **2** (2*c*, *f*, 12). The stereochemical assignment in the case of the 1,4 adduct **1** is based on the effect of the shift reagent *tris*-(1,1,1,2,2,3,3-heptafluoro-7,7-[$^2H_6$]-dimethyl-4,6-[$^2H_3$]octanedionato)europium(III) {Eu[$^2H_9$]fod_3} (Table 2). The relative shift ratio (**1***a*:**1***b*) for corresponding protons in **1***a* and **1***b* is 1.11 for the 4-methyl protons and less than or equal to unity for all other protons.[2] Hence, in

[1]Individual members of a pair of diastereoisomeric adducts are designated as *a* and *b*. In those cases (here **1** and **5**) for which the stereochemical assignment has been made the *a* designation is used for the *trans* NO_2,OAc isomer and *b* for the *cis*.

[2]Because of the normalization procedure the relative ratio for the acetate protons is exactly 1.00.

TABLE 3. Yields (%) of products of rearomatization of 1,2,3,4-tetramethyl-4-nitro-1,4-dihydrophenylacetate (**1**)[i]

Reagent	Nuclear (5-) substituted prehnitenes; substituent group			Side-chain (1-) substituted prehnitenes (2,3,4-trimethylbenzyl derivatives)		
	NO_2	OAc	Other	NO_2	OAc	Other
CH_3CO_2H		94			5	1[a]
$CH_3CH_2CO_2H$	1	45	45[b]	5[c]	5[d]	
50% HCO_2H in CH_2Cl_2	5	40	50[e]		5[f]	
CF_3CO_2H	100					
H_2SO_4 (100 μmol) in CH_3CO_2H		9		20	50	21[g]
H_2SO_4 (1 mmol) in $CH_3CH_2CO_2H$	2	3		15	70[h]	10[g]
H_2SO_4 (1 mmol) in HCO_2H	80	8				12[i]
H_2SO_4 (10 μmol) in $(CH_3CO_2)O$	10			40	50	
$BF_3 \cdot Et_2O$ (5 μmol) in CH_2Cl_2	8			52	40	
CH_3OH, reflux		70	30[j]			
H_2SO_4 (10 μmol) in CH_3OH	1	58	37[j]			4[k]
H_2SO_4 (1 mmol) in CH_3OH		49	45[j]			6[k]

[a]2,3,4-Trimethylbenzyl nitrate.
[b]2,3,4,5-Tetramethylphenyl propionate.
[c]Not distinguishable from the side-chain nitrate.
[d]And/or side-chain propionate.
[e]2,3,4,5-Tetramethylphenyl formate.
[f]And/or side-chain formate.
[g]2,3,4-Trimethylbenzaldehyde.
[h]2,3,4-Trimethylbenzyl propionate.
[i]2,3,4-Trimethylbenzyl formate.
[j]Methyl 2,3,4,5-tetramethylphenyl ether.
[k]Methyl 2,3,4-trimethylbenzyl ether.
[l]Reactions were carried out using **1***a* and **1***b* as substrates and similar results were obtained in both cases.

1*a* the acetate and 4-methyl groups are *cis*, *i.e.* **1***a* is the *trans* adduct and **1***b* the *cis* (2*f*). Because the relative shift ratio for the 4-methyl protons is only slightly greater than unity and because we are unable to account for the low (both are 0.78) relative shift ratios for the 3-methyl and the 5 protons, both of which should be unity, the structural assignment must be regarded as tentative. Similar problems have arisen in the cases of other tertiary acetate adducts (2*k*, *m*).[3]

Isodurene (1,2,3,5-Tetramethylbenzene)

Nitration at −65 °C gave 4-nitroisodurene, 3,4,5-trimethylbenzyl nitrate, the nitritonitro **3** and acetoxynitro **4** adduct diastereoisomers, and 3,4,5-trimethylphenylnitromethane. For the acetoxynitro adduct **4** the structure was assigned from the nmr spectra which indicate that there are two identical methyl groups and that the two ring protons are also identical. The 2,5 and 5,2 adducts would have similar nmr spectra but since the 2 position is 500 times as reactive as the 5 (Table 1) the nitro group must be attached to the 2 position and the acetate to the 5 position. Similarly, **3** must be the 2-nitro-5-nitrito adduct.

Durene (1,2,4,5-Tetramethylbenzene)

Nitration in acetic anhydride – methylene chloride solution at −55 °C gave after work-up the acetoxynitro adduct **5** as the major product together with some nitritonitro adduct **6** and hydroxynitro adduct **7**. 2,4,5-Trimethylbenzyl nitrate was the only aromatic product isolated. The relative shift for the 4-methyl protons of the first-eluted isomer of the acetoxynitro adducts is greater than that for the corresponding protons of the second isomer, the ratio being 1.24 (Table 2). On this basis the first-eluted isomer is assigned the *trans* adduct structure **5***a* and the second the *cis* structure **5***b* although, as in the case of the prehnitene adducts, the difference in shifts is not large and the assignments must be regarded with caution.

Rearomatization of Tetramethylbenzene Adducts

The acetoxynitro adducts of prehnitene and durene were rearomatized under a variety of conditions to give the products shown in Tables 3 and 4.

[3]In contrast, in the cases of secondary acetate adducts the relative shift of the 4-methyl protons in the *trans* isomer is much larger than that of the corresponding protons in the *cis* isomer, the ratio being 2 or larger (2*f*, *l*) and the stereochemical assignments in such cases can be accepted with confidence.

Can. J. Chem. Downloaded from www.nrcresearchpress.com by 210.87.254.6 on 09/05/12
For personal use only.

TABLE 4. Yields (%) of products of rearomatization of *trans*-1,2,4,5-tetramethyl-4-nitro-1,4-dihydrophenyl acetate (**5***a*)

Reagent	Nuclear (3-) substituted durene: substituent group			Side-chain (1-) substituted durene: substituent group		
	NO_2	OAc	Other	NO_2	OAc	Other
CH_3CO_2H		100				
CF_3CO_2H (10μmol) in CH_2Cl_2		40		36		24[a]
50% CF_3CO_2H in CH_2Cl_2	67			33[b]		
H_2SO_4 (100 μmol) in CH_3CO_2H		15		25	60	
CH_3OH, reflux		100				
$CH_3C_6H_4SO_3H$ in CH_3OH		44	14[c]			42[a]

[a]2,4,5-Trimethylbenzyl nitrate.
[b]Includes other unidentified side-chain products.
[c]Methyl 1,2,4,5-tetramethylphenyl ether.
[d]Methyl 2,4,5-trimethylbenzyl ether.

Discussion

Nitration Reactions

Nitration of the tetramethylbenzenes in acetic anhydride gave large amounts of adducts, in agreement with prediction (Table 1). In each case side-chain (benzylic) derivatives were also formed which evidently were derived through the intermediate formation of the adducts which subsequently underwent partial rearomatization during the reaction or in the course of the work-up.[4] The tetramethylbenzene adducts are exceedingly labile. When the nitration reactions were carried out at temperatures above -50 °C rearomatization was essentially complete and only the rearomatization products were obtained. Moreover, the adducts, when isolated, were prone to decomposition via rearomatization, particularly so when allowed to warm to room temperature, and this complicated the investigation of their physical properties and reactions. The failure of previous attempts (7) to detect the tetramethylbenzene adducts is easily understood. There are two different *ipso* positions (1 and 2) in prehnitene which are of comparable reactivity. Correspondingly both 1,4 and 2,5 adducts were isolated. Isodurene has three different *ipso* positions (1, 2, and 5). However, the 2 position is several hundred times more reactive than the others and thus only the 5-acetoxy-2-nitro adduct was formed. In durene all of the *ipso* positions are identical and accordingly structurally isomeric adducts are not possible. All of the acetoxynitro adducts were obtained as a mixture of diastereoisomers and the separate diastereoisomers were isolated.

Nitritonitro adducts were also formed in the course of the reactions. In principle, adducts containing a nitro group and the anion conjugate base of any acid (HX) present in the nitrating system can be formed according to a sequence analogous to **8** $\rightarrow$ **9** $\rightarrow$ **10** (Scheme 1). Acetic and nitric acids are obviously present although the latter is almost completely converted into acetyl nitrate in the presence of excess acetic anhydride (13). Stoichiometry requires that nitrous acid be formed in those rearomatization reactions of the adducts which lead to non nitro-containing products (2*a*, 14); *cf.* Scheme 1: **10** $\rightarrow$ **11** and **10** $\rightarrow$ **15** (Y $\neq$ NO_2). Moreover, mixtures of nitric acid in acetic anhydride are reported to develop nitrous acid spontaneously on standing. Since rearomatization reactions did occur in the course of the nitration these reactions and the reaction with the solvent could account for the nitrous acid required for the formation of the nitritonitro adducts. The hydroxynitro adduct **7** isolated from the nitration of durene was probably a solvolysis product of the nitritonitro adduct and formed on work-up. The formation of hydroxynitro adducts has been noted in the nitration of *p*-xylene (2*k*) and to a small extent in the nitration of *p*-cymene (2*m*). Solvolysis of the

[4]It is possible that the side-chain derivatives which are formed during the nitration are formed, wholly or in part, from the *ipso*-nitrocyclohexadienyl cation before the cation adds the nucleophile to form the conjugate acid of the adduct, or before the conjugate acid is deprotonated to the adduct. This would require closely similar rates of formation of side-chain product and of adduct from the cation. This is a more restrictive condition than that which follows from the assumption that the side-chain product is formed (via the cation (2*k*)) from the adduct. This would only require that the rate of formation of the side-chain product from the cation be slower than the rate of formation of the adduct.

Can. J. Chem. Downloaded from www.nrcresearchpress.com by 210.87.254.6 on 09/05/12
For personal use only.

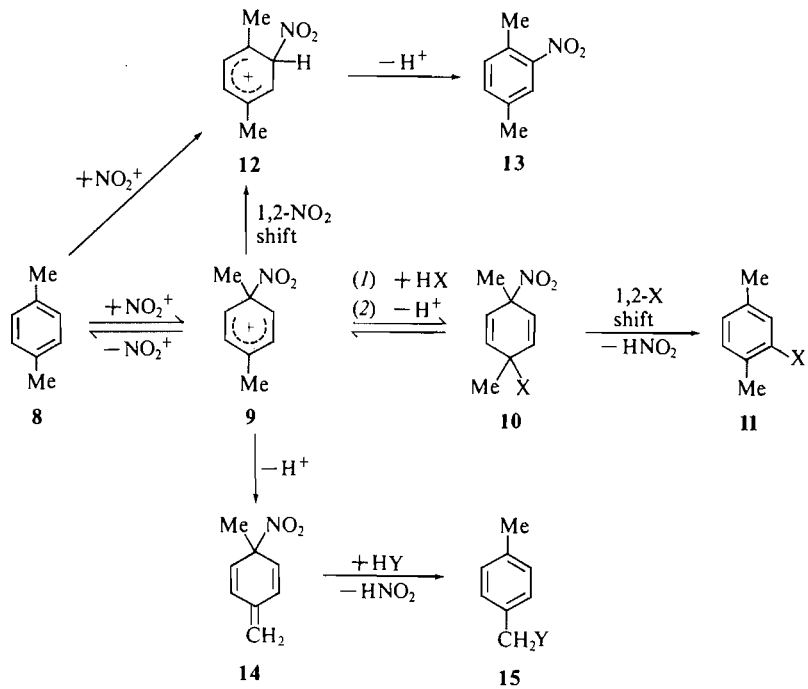

SCHEME 1. Formation and potential rearomatization reactions of 1,4-dimethylbenzene adducts.

nitritonitro adduct of isodurene in methanol resulted in isomerization to the dinitro adduct (**16**). Presumably the adduct ionized to form the

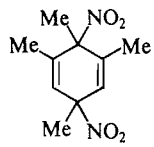

16

ipso-nitrocyclohexadienyl cation and nitrite anion (*cf.* **10** (X = ONO) → **9**) which recombined with the nitrogen of the ambident anion (15) behaving as the nucleophilic centre (*cf.* **9** → **10** (X = NO_2).

Nitration of the tetramethylbenzenes with methyl nitrate catalyzed by boron trifluoride gives the mononitro derivatives in yields of 97% or greater (16). Under conditions of low solvent nucleophilicity the *ipso*-cation (di-Me-**9**) rearranges before capture to form the non-*ipso* cation (di-Me-**12**), which is rapidly deprotonated to the nitro derivative (di-Me-**13**), the only observed product. The occurrence of this process in the nitration of *o*- and *p*-xylene and 1,2,3- and 1,2,4-trimethylbenzene in aqueous sulfuric acid has been demonstrated by Schofield and co-workers (17). At low acidity (high solvent nucleophilicity) the *ipso*-cation is captured by water and yields of the nitroarenes are low. As the acidity is increased and the solvent nucleophilicity decreased yields of the nitroarenes are increased because more of the *ipso*-cation rearranges before capture. Nitro group migration in the nitrohexamethylbenzenium cation has been directly observed by Olah *et al.* (18). Clearly, nitration of arenes should always be carried out in a strongly acidic medium (*e.g.* trifluoroacetic acid) if nitroarenes are the desired products. Under such conditions any *ipso* cation formed is encouraged to rearrange to the non-*ipso* cation and thus to form nitroarene rather than other products, such as benzylic derivatives.

Side-chain (benzylic) nitrate derivatives are formed when the dihalotetramethylbenzenes in methylene chloride are nitrated with nitric acid (9). Excellent yields of the side-chain nitrates are obtained when the dinitrotetramethylbenzenes are nitrated with mixed acid (10). Side-chain nitrates are also formed, together with nitroarenes and other products when ethylmesitylene and propylmesitylene, in methylene chloride, are nitrated with nitric acid (11). It is evident that

Can. J. Chem. Downloaded from www.nrcresearchpress.com by 210.87.254.6 on 09/05/12
For personal use only.

Can. J. Chem. Downloaded from www.nrcresearchpress.com by 210.87.254.6 on 09/05/12
For personal use only.

adduct intermediates are formed with these substrates.

Rearomatization Reactions

Rearomatization of the acetoxynitro adduct **1** was investigated in considerable detail and of **5** to a lesser extent. Rearomatization of **2** and **4** was not studied directly but some information is available from the rearomatization reactions which accompanied nitration. Adducts **1**, **4**, and **5** are tertiary acetates. In discussion of the rearomatization reactions of the parent tertiary acetate adduct, from *p*-xylene (2*k*), it has been noted that three types of rearomatization product are obtained: the (rearranged) nitroarene, side-chain (benzylic) derivatives, and the (rearranged) aryl acetate. The mechanisms of the first two reactions, which share the *ipso*-cyclohexadienyl cation **9** as a common intermediate, are depicted in Scheme 1: **10** (X = OAc) → **9** → **12** → **13** and **10** (X = OAc) → **9** → **14** → **15**. The third reaction involves an intramolecular 1,2-shift of the acetate, Scheme 1: **10** (X = OAc) → **11** (X = OAc), and **17** has been proposed as the transition state.

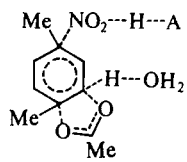

17

Rearomatization of 1

Substantial yields of 2,3,4,5-tetramethylphenyl acetate were obtained from the rearomatization reactions of **1** (Table 3) in acetic acid, propionic acid, 50% formic acid in methylene chloride, methanol, and acidified methanol. Comparable amounts of the corresponding propionate, formate, and methyl ether were obtained in the respective reactions. These other products are most likely formed by partial exchange of the acetate in **1** for propionate, formate, or methoxide (*cf.*, *e.g.* Scheme 1: **10** (X = OAc) → **9** → **10** (X = $OCOCH_2CH_3$)), followed by rearrangement–elimination (*cf.* **10** (X = $OCOCH_2CH_3$) → **11** (X = $OCOCH_2CH_3$)) involving a transition state analogous to **17**. Exchange reactions have been shown to occur in the case of the parent *p*-xylene adduct (2*k*). The extent of prior exchange before rearrangement is evidently greater in the case of **1** than for the *p*-xylene adduct under comparable conditions. Formation of the *ipso*-nitrotetramethylcyclohexadienyl cation di-Me-**9** should be much faster than formation of the *ipso*-nitrodimethylcyclohexadienyl cation **9**. The transition state for the rearrangement reaction (**17**) should be much less polar than that for cation formation and hence less affected by the additional methyl groups. Thus formation of the cation, and through it exchange, is able to compete more effectively with the acetate rearrangement in the case of the prehnitene adduct (and other tetramethylbenzene adducts) than in the case of the *p*-xylene adduct.[5] Small amounts of the side-chain products, 2,3,4-trimethylbenzyl acetate, propionate, formate, and methyl ether (di-Me-**15**) also accompanied the rearrangement–elimination products in the respective reactions. Under somewhat more acidic conditions, sulfuric acid in acetic acid, sulfuric acid in propionic acid, or a catalytic amount of boron trifluoride etherate in methylene chloride, the side-chain products predominated and, as well as the acetate or propionate, 2,3,4-trimethylphenylnitromethane was obtained. The greater amount of side-chain product formed in the reactions in acidified acetic and propionic acids is attributed to the removal of trace amounts of water from the system. In the cases of the *p*-xylene (2*k*) and *p*-cymene (2*m*) adducts it has been demonstrated that water has a striking catalytic effect on the rearrangement–elimination reaction leading to the aryl acetate. This is attributed to the requirement for water to act as a base in removing the proton, as depicted in transition state **17**. In the complete absence of water, *i.e.* by using anhydrous acetic acid, the rearrangement reaction of the *p*-xylene adduct is inhibited to such an extent that the reactions leading to side-chain products (**10** → **15**) compete effectively. In the reactions of **1** in acidified acetic and propionic acids the added strong acid should remove, through solvation, the trace (impurity) water present, thus producing the same result as the use of anhydrous acids. Support for this explanation is provided by the observation that in methanol added sulfuric acid had little effect in

[5]The lability of the tetramethylbenzene adducts noted earlier can likewise be explained in terms of the activating effect of the additional methyl groups on the formation of the cation, the intermediate for two rearomatization reactions, and on transition state **17**.

Can. J. Chem. Downloaded from www.nrcresearchpress.com by 210.87.254.6 on 09/05/12
For personal use only.

inhibiting the yield of the nuclear derivatives. Methanol would be expected to be sufficiently basic to be able to take the place of water in removing the proton in the transition-state of the rearrangement–elimination reaction. Addition of acid to methanol would not then significantly reduce the concentration of basic molecules present since these are present at the solvent concentration. In contrast, in acetic anhydride containing sulfuric acid, which must be completely anhydrous, no aryl acetate was formed. A base is also required to effect the conversion of the cation di-Me-**9** to the triene di-Me-**14**. Even a weak base, such as acetic acid, suffices to bring about this conversion; the stronger base water is not necessary. However, as the basicity (and nucleophilicity) of the solvent is reduced both this reaction (*cf.* **9** → **14**) and the cation capture reaction (*cf.* **9** → **10**) would be expected to become slower and the cation rearrangement reaction (**9** → **12**) is then able to compete, resulting in the formation of nitroarene. The onset of this change is apparent in formic acid solvent where 5% of the nitroarene was observed, compared with 1% in the less acidic propionic acid. In formic acid containing sulfuric acid the nitroarene was the major product and in the more acidic and less basic trifluoroacetic acid it was the only product.

Rearomatization of **5**

Results obtained from rearomatization of the durene adduct **5***a* support the conclusions reached from the study of rearomatization of the prehnitene adduct **1**. In acetic acid (presumably containing the catalytic base water), methanol and acidified methanol, where basic solvent molecules are present, the aryl acetate (and methyl ether) was obtained as the major product. In acetic acid containing sulfuric acid (in which the impurity water is not available to act as a base), a less basic solvent, the side-chain derivatives predominated, while in the very weakly basic solvent trifluoroacetic acid the nitroarene became the major product. Both aryl acetate and benzylic derivatives were formed when a catalytic amount of trifluoroacetic acid in methylene chloride was used. In this case as in the example of the reaction of **1** with catalytic boron trifluoride – etherate, the acidity or basicity of the system is affected to a major extent by the acetic and/or nitrous acid released in the rearomatization and is not dominated by the trace amount of catalyst added. The formation of side-chain products is consistent with this suggestion.

Side-chain Substitution

Formation of the particular side-chain derivatives obtained under the various reaction conditions can be explained in terms of a competition between the various nucleophiles (HY) present for the triene intermediate analog of **14** (2*k*). The 2,3,4-trimethylbenzaldehyde formed in some reactions of **1** is probably a secondary product derived from the corresponding nitrate (10*b*, 19) or nitrite (20).

As mentioned earlier side-chain (benzylic) derivatives were isolated from the nitration reactions on each substrate. Clearly, these rearomatization products were formed under anhydrous conditions (in acetic anhydride) in a moderately basic solvent. From the foregoing discussion these are just the conditions that favour the formation of side-chain products rather than aryl acetate or nitroarene. Some aryl acetate was detected in the column fractions from prehnitene nitration. However, this was likely formed from the 2,5 adduct, a secondary acetate, which by elimination of nitrous acid can form the aryl acetate without rearrangement. In the earlier work (7) on nitration of the tetramethylbenzenes aryl acetate was obtained from each substrate. Here rearomatization of the adducts occurred during the reaction and/or on work-up. Any rearomatization which did occur during the work-up, which involved quenching with water, would lead to formation of aryl acetate. 2,4,5-Trimethylbenzyl alcohol was isolated from nitration of durene (7). This likely arose from solvolysis of the corresponding nitrate.

It is to be noted that in formation of side-chain derivatives the methyl group substituted is that *para* to the position of *ipso* attack by the nitronium ion, *i.e.* that which is *ipso* to the acetate group in the adduct; consistent with the mechanism shown in Scheme 1. Thus the side-chain derivatives formed in the nitration of isodurene have the 5-methyl group of isodurene substituted. In the case of the derivatives from prehnitene symmetry prevents the distinction between the 1 and 4 groups of the original prehnitene but, significantly, it is the 4- (or 1-) methyl group which is substituted and not the 2-methyl. Because of the symmetry of durene it is not possible to say which methyl group of the adduct is the one substituted. By analogy, it would be

Can. J. Chem. Downloaded from www.nrcresearchpress.com by 210.87.254.6 on 09/05/12
For personal use only.

expected that the substituted methyl is that in a 1,4-relationship to the nitro group. Evidence that the methyl *ipso* to the acetate in the adduct is that substituted in the rearomatization to side-chain derivatives was first obtained for the structurally isomeric pseudocumene adducts (2*i*). An earlier observation (7), that it is the methyl group *para* to the most activated *ipso* position which is substituted, during nitration of arenes, is consistent with this. In the situation where structurally isomeric adducts, each containing 1- and 4-methyl groups, are possible (pseudocumene, isodurene), the predominant adduct and the major source of side-chain products is that with the nitro group at the most activated *ipso* position.

The side-chain products obtained in the nitration of substrates related to the tetramethylbenzenes are just those which have the substituted methyl group *para* to the most activated *ipso* site. Thus, it is the methyl *para* to the ethyl and propyl groups of ethyl and propylmesitylene which is attacked in the nitration of these substances (11). Nitration of 4,6-dinitroisodurene gives 2,6-dinitro-3,4,5-trimethylbenzyl nitrate (10). Here the 2-*ipso* position is both the most activated by the methyl groups (Table 1) and the least deactivated by the (*meta*) nitro groups. Nitration of the 4,6-dihaloisodurenes gives both 2,6-dihalo-3,4,5-trimethyl- and 3,5-dihalo-2,4,6-trimethylbenzyl nitrate (9). In this case the 4,6-halogens deactivate the (*meta*) 2-*ipso* position more strongly than the (*ortho*) 5-*ipso* position and act against the directing effect of the methyl groups. However, the methyl groups do just dominate the situation since the 2,6-dihalo nitrates are formed in greater amount than the 3,5-isomers. Because of symmetry the results of nitration of the dihalo- and dinitroprehnitenes and durenes are ambiguous. Yet it is to be noted that all of these compounds, which lead to side-chain products, contain the required *para* methyl groups and in the case of the prehnitenes, which have other methyl groups, it is only those (1-) methyl groups which have a *para* methyl which are substituted. Chlorination of isodurene in acetic acid gives 3,4,5-trimethylbenzyl chloride and 3,4,5-trimethylbenzyl acetate as well as the expected aryl chloride (6). Here again it is the methyl *para* to the most activated *ipso* position which is substituted, a conclusion which presumably may be generalized to all electrophilic substitution reactions.

Thermal Decomposition of 1

Thermolysis of **1** on injection into a gas chromatograph was also investigated. On PEGA the 5-NO_2 (4%), 5-OAc, and side-chain OAc (28%) derivatives of prehnitene and prehnitene itself (62%) were identified. On QF-1 the 5-NO_2 (9%), 5-OAc (22%), side-chain OAc (42%) aldehyde (7%) derivatives, and prehnitene (4%) were obtained. The different product distributions are unlikely to be related to the different column packings but rather to unperceived differences in the conditions in the injection chamber. Reversion of the adduct to the arene, which occurred on thermolysis, has not been observed in solution although the mechanism provides for this possibility (Scheme 1). Such reversion has been observed in solution for adducts from substituted arenes (2*h*, *j*, *l*).

Experimental

General experimental methods have been described previously (2). Alumina was deactivated with 3% of 10% aqueous acetic acid.

Nitration of Prehnitene (1,2,3,4-Tetramethylbenzene) in Acetic Anhydride

A solution of nitric acid (18.9 g, 0.3 mol) in acetic anhydride (200 cm^3) was added to a stirred solution of prehnitene (26.8 g, 0.2 mol) in acetic anhydride (200 cm^3) at −78 °C. The temperature was allowed to rise to −60 °C and maintained there for 4.5 h. The reaction mixture was then added to ether (1.5 dm^3) at −78 °C and quenched with ammonia, keeping the temperature below −60 °C. The nmr spectrum of the residue obtained after work-up indicated that 50% was dienes. Chromatography on alumina at −50 °C and elution with ether–pentane mixtures gave in the 0–20% ether fractions, in order: prehnitene, 2,3,4-trimethylphenylnitromethane; ir (film) 1550 and 1365 cm^{-1} (NO_2); nmr ($CDCl_3$) δ 2.18 (s, 3, ArCH_3), 2.24 (s, 3, ArCH_3), 2.27 (s, 3, ArCH_3), 5.39 (s, 2, CH_2), 7.02 ppm (s, 2, 5-*H* and 6-*H*); mass spectrum (70 eV) *m/e* (relative intensity) 179 (0.5, M), 133 (100, $M - NO_2$); 2,3,4-trimethylbenzyl nitrate; ir (film) 1630, 1280, 855 cm^{-1} (ONO_2); nmr ($CDCl_3$) δ 2.14 (s, 3, ArCH_3) 2.23 (s, 6, Ar$(CH_3)_2$), 5.35 (s, 2, CH_2), 6.99 ppm (s, 2, 5-*H* and 6-*H*); mass spectrum (70 eV) *m/e* (relative intensity) 195 (23, M), 149 ($M - NO_2$), 133 ($M - ONO_2$), 119 (100); a diene; ir (film) 1545 (NO_2), 680 cm^{-1} (ONO); nmr (CCl_4) δ 1.57 (s, 3, CH_3), 1.68 (s, 3, CH_3), 1.71 (s, 6, $(CH_3)_2$), 5.85 (nq, 1, J = 10 Hz, vinyl *H*), 6.02 (nq, 1, J = 10 Hz, vinyl *H*); 5-nitroprehnitene; mp 61 °C (lit. (21) mp 61 °C); ir (Nujol) 1520, 1350, 830 cm^{-1} (NO_2); nmr ($CDCl_3$) δ 2.23 (s, 6 Ar$(CH_3)_2$), 2.28 (s, 3, ArCH_3), 2.32 (s, 3, ArCH_3), 7.37 ppm (s, 1, 6-*H*).

Can. J. Chem. Downloaded from www.nrcresearchpress.com by 210.87.254.6 on 09/05/12
For personal use only.

The residues (12.3 g) from the 20 and 30% ether fractions were recrystallized (×5) from ether–pentane to give prisms of *trans*-1,2,3,4-tetramethyl-4-nitro-1,4-dihydrophenyl acetate (**1***a*) mp 64–65 °C (dec.); uv (CH_3OH) 198 nm (ϵ 4560 m^2 mol^{-1}); ir (Nujol) 1735, 1245 (OCO-CH_3), 1530 cm^{-1} (NO_2); nmr (CCl_4) δ 1.43 (s, 3, 1-CH_3), 1.70 (q, 3, J = 0.75 Hz, 3-CH_3), 1.72 (q, 3, J = 0.75 Hz, 2-CH_3), 1.73 (s, 3, 4-CH_3), 1.91 (s, 3, $OCOCH_3$), 5.76 (nq, 1, J = 10 Hz, 5-*H*), 5.84 ppm (nq, 1, J = 10 Hz, 6-*H*). *Mol. Wt.* calcd. for $C_{12}N_{17}NO_4$: 239; found: 241.

The diastereoisomer, *cis*-1,2,3,4-tetramethyl-4-nitro-1,4-dihydrophenyl acetate (**1***b*) was obtained by recrystallizing (×5) the residue (1.37 g) from the 80 and 90% ether fractions from ether–pentane, mp 53.0–54.3 °C (dec.); uv (CH_3OH) 198.5 nm (ϵ 3100 m^2 mol^{-1}); ir (Nujol) 1740, 1250 ($OCOCH_3$), 1540 cm^{-1} (NO_2); nmr (CCl_4) δ 1.41 (s, 3, 1-CH_3), 1.62 (s, 3, 4-CH_3), 1.68 (b, 3, 3-CH_3), 1.77 (b, 3, 2-CH_3), 5.77 (nq, 1, J = 10 Hz, 5-*H*), 6.24 ppm (nq, 1, J = 10 Hz, 6-*H*). *Mol. Wt.* calcd. for $C_{12}H_{17}NO_4$: 239; found: 242.

The residues (7 g) of the 50 and 60% ether fractions were rechromatographed. The new 50% ether fraction gave one diastereomer of 2,3,4,5-tetramethyl-4-nitro-1,4-dihydrophenyl acetate (**2***a*) after recrystallization (×5) from pentane, mp 33.5–34 °C (dec.); uv (CH_3OH) 196 nm (ϵ 5200 m^2 mol^{-1}); ir (Nujol) 1735, 1240 ($OCOCH_3$), 1540 cm^{-1} (NO_2); nmr (CCl_4) δ 1.68 (m, 3, 3-CH_3), 1.73 (s, 3, 4-CH_3), 1.74 (m, 3, 2-CH_3), 1.74 (m, 3, 5-CH_3), 2.00 (s, 3, $OCOCH_3$), 5.48 (m, 1, $J_{1,6}$ = 4.5 Hz, 1-*H*), 5.78 ppm (m, 1, $J_{1,6}$ = 4.5 Hz, $J_{5\text{-}CH_3,6}$ = 1.3 Hz, 6-*H*). *Mol. Wt.* calcd. for $C_{12}H_{17}NO_4$: 239; found: 241.

The 60% ether fraction of the second column afforded the other diastereomer of 2,3,4,5-tetramethyl-4-nitro-1,4-dihydrophenyl acetate (**2***b*, 80 mg), which was recrystallized from ether–pentane, mp 57.0–58.5 °C (dec.); uv (CH_3OH) 196 nm (ϵ 2840 m^2 mol^{-1}); ir (Nujol) 1730, 1240 ($OCOCH_3$), 1540 cm^{-1} (NO_2); nmr (CCl_4) δ 1.65 (s, 3, CH_3), 1.69 (3, 2-CH_3), 1.72 (6, 3-CH_3 and 5-CH_3), 5.48 (m, 1, 1-*H*), 5.67 (m, 1, $J_{1,6}$ = 3 Hz, $J_{5\text{-}CH_3,6}$ = 1.3 Hz, 6-*H*). *Mol. Wt.* calcd. for $C_{12}H_{17}NO_4$: 239; found: 241.

Nitration of Isodurene (1,2,3,5-Tetramethylbenzene)

A solution of nitric acid (9.5 g, 0.15 mol) in acetic anhydride (100 cm^3) was added slowly to a stirred solution of isodurene (13.4 g, 0.1 mol) in acetic anhydride (300 cm^3) at −65 °C and the resulting solution maintained at that temperature for 4 h. The reaction was worked-up as described for prehnitene to give a residue which contained (nmr) as main products 4-nitroisodurene and 3,4,5-tetramethylbenzyl nitrate together with 30% of diene adducts. Chromatography on alumina (400 g) and elution with pentane and ether–pentane mixtures gave isodurene (3.9 g) in the pentane fraction, a mixture (4.1 g) of 4-nitroisodurene (40%), 3,4,5-trimethylbenzyl nitrate (30%), and 1,3,4,5-tetramethyl-4-nitro-1,4-dihydrophenyl nitrite (**3**, 30%). Rechromatographing of this fraction gave 4-nitroisodurene which was recrystallized from pentane, mp 40–40.6 °C (lit. (22) mp 39 °C), ir (melt) 1525 and 1365 cm^{-1} (NO_2); nmr ($CDCl_3$) δ 2.14 (s, 6, Ar(CH_3)$_2$), 2.17 (s, 3, ArCH_3), 2.24 (s, 3, ArCH_3), 6.84 ppm (s, 1, 6-*H*). The trimethylbenzyl nitrate and the diene could not be separated but characteristic spectral peaks of each could be discerned in the mixed fractions. 3,4,5-Trimethylbenzyl nitrate had ir (film) 1620 and 1282 cm^{-1} (ONO_2); nmr ($CDCl_3$) δ 2.19 (s, 3, 4-CH_3), 2.30 (s, 6, 3-CH_3 and 5-CH_3), 5.32 (s, 2, CH_2), 6.07 ppm (s, 2, 2-*H* and 6-*H*); mass spectrum *m/e* 195 (M). Oxidation of the nitrate by heating under reflux for 30 min in sulfuric acid – water – acetic acid (1:10:20) gave 3,4,5-tetramethylbenzaldehyde which was recrystallized from pentane, mp 62.0–62.3 °C (lit. (23) mp 52 °C); ir (Nujol) 1675 cm^{-1} (CHO); nmr ($CDCl_3$) δ 2.23 (s, 3, 4-CH_3), 2.34 (s, 6, 3-CH_3 and 5-CH_3), 7.48 (s, 2, 2-*H* and 6-*H*), 9.87 ppm (s, 1, C*H*O); mass spectrum (70 eV) *m/e* (relative intensity) 148 (74, M), 147 (100), 119 (69). 3,4,5-Trimethylbenzaldoxime had mp 135.6–136.2 °C. The diastereoisomer of 1,3,4,5-tetramethyl-4-nitro-1,4-dihydrophenyl nitrite (**3***a*) had ir (film) 1635 and 753 (ONO), 1545 and 1365 cm^{-1} (NO_2); nmr ($CDCl_3$) δ 1.53 (s, 3, 1-CH_3), 1.61 (s, 3, 4-CH_3), 1.69 (d, 6, $J_{2,3\text{-}CH_3}$ = $J_{6,5\text{-}CH_3}$ = 0.7 Hz, 3-CH_3 and 5-CH_3), 5.84 ppm (br s, 2, 2-*H* and 6-*H*). On standing the mixture of diene and nitrate in methanol the diene isomerized to 1,3,4,5-tetramethyl-1,4-dinitro-1,4-dihydrobenzene (**16**), which was recrystallized from pentane, mp 76–77 °C; uv (C_6H_{12}) 195 nm (ϵ 1940 m^2 mol^{-1}); ir (Nujol) 1545 and 1378 cm^{-1} (NO_2); nmr ($CDCl_3$) δ 1.78 (s, 3, 4-CH_3), 1.80 (s, 3, 1-CH_3), 1.81 (d, 6, $J_{2,3\text{-}CH_3}$ = $J_{6,5\text{-}CH_3}$ = 0.7 Hz, 3-CH_3 and 5-CH_3), 5.94 ppm (br s, 2, 4-*H* and 6-*H*). *Mol. Wt.* calcd. for $C_{10}H_{14}N_2O_4$: 226; found: 224. The dinitrodiene **16** was also recognized in a column fraction of the nitration mixture.

The 15% ether fraction from the original reaction mixture contained a mixture of 3,4,5-trimethylphenylnitromethane and a second diastereomer of 1,3,4,5-tetramethyl-4-nitro-1,4-dihydrophenyl nitrite (**3***b*). 3,4,5-Trimethylphenylnitromethane, although the minor product, crystallized preferentially from pentane, mp 63–65 °C; ir (Nujol) 1545 and 1380 (NO_2); nmr ($CDCl_3$) δ 2.18 (s, 3, 4-CH_3), 2.29 (s, 6, 3-CH_3 and 5-CH_3), 5.30 (s, 2, CH_2NO_2), 7.05 ppm (s, 2, 2-*H* and 6-*H*); mass spectrum (70 eV) *m/e* (relative intensity) 179 (1.5, M), 133 (100, $M - NO_2$). The second crop of crystals was pale yellow leaflets of the second diastereoisomer of 1,3,4,5-tetramethyl-4-nitro-1,4-dihydrophenyl nitrite (**3***b*) which decomposed before melting; uv (C_6H_{12}) 198.5 nm (ϵ 5100 m^2 mol^{-1}); ir (Nujol) 1625 and 757 (ONO) 1540 cm^{-1} (NO_2); nmr ($CDCl_3$) δ 1.53 (s, 3, 1-CH_3), 1.77 (s, 3, 4-CH_3), 1.78 (d, 6, $J_{2,3\text{-}CH_3}$ = $J_{6,5\text{-}CH_3}$ = 0.7 Hz, 3-CH_3 and 5-CH_3), 5.97 ppm (br s, 2, 2-*H* and 6-*H*). *Mol. Wt.* calcd. for $C_{10}H_{14}N_2O_4$: 226; found: 225.

The residue (0.27 g) from the 40% ether fraction was one diastereomer of 1,3,4,5-tetramethyl-4-nitro-1,4-dihydrophenyl acetate (**4***a*), recrystallized from pentane, mp 59.5–60.5 °C; uv (CH_3OH) 199 nm (ϵ 1500 m^2 mol^{-1}); ir (Nujol) 1735 and 1249 cm^{-1} ($OCOCH_3$), 1540 cm^{-1} (NO_2); nmr ($CDCl_3$) δ 1.53 (s, 3, 1-CH_3), 1.75 (d, 6, $J_{2,3\text{-}CH_3}$ = $J_{6,5\text{-}CH_3}$ = 0.7 Hz, 3-CH_3 and 5-CH_3), 1.78 (s, 3, 4-CH_3), 1.96 (s, 3, $OCOCH_3$), 5.82 ppm (s, 2, J = 0.7 Hz, 2-*H* and 6-*H*). *Mol. Wt.* calcd. for $C_{12}H_{17}NO_4$: 239; found: 241.

Recrystallization of the residues (0.18 g) of the 80 and 90% ether fractions gave prisms of the other diastereomer of 1,3,4,5-tetramethyl-4-nitro-1,4-dihydrophenyl acetate (**4***b*), mp 84–85 °C; uv (CH_3OH), 199 nm (ϵ 1230 m^2 mol^{-1}); ir (Nujol) 1740 and 1246 ($OCOCH_3$), 1535 (NO_2);

Can. J. Chem. Downloaded from www.nrcresearchpress.com by 210.87.254.6 on 09/05/12
For personal use only.

nmr ($CDCl_3$) δ 1.35 (s, 3, 1-CH_3), 1.63 (s, 3, 4-CH_3), 1.80 (d, 6, $J_{2,3\text{-}CH_3} = J_{6,5\text{-}CH_3} = 0.7$ Hz, 3-CH_3 and 5-CH_3), 2.02 (s, 3, $OCOCH_3$), 5.89 ppm (br, 2, 2-*H* and 6-*H*). *Mol. Wt.* calcd. for $C_{12}H_{17}NO_4$: 239; found 242.

Nitration of Durene (1,2,4,5-Tetramethylbenzene)

A solution of nitric acid (9.5 g, 0.15 mol) in acetic anhydride (100 cm^3) was added slowly to a stirred solution of durene (13.4 g, 0.1 mol) in methylene chloride (200 cm^3) and acetic anhydride (100 cm^3) at −78 °C. The mixture was allowed to warm to −55 °C and maintained at that temperature for 3 h. The reaction solution was then added to ether (800 cm^3) at −78 °C and quenched with ammonia, keeping the temperature below −60 °C. The nmr spectrum of the residue obtained after work-up indicated that 65% was dienes. Chromatography on alumina (400 g) at −50 °C and elution with pentane and ether pentane mixtures gave a small amount of unchanged durene followed by 2,4,5-trimethylbenzyl nitrate; ir (film) 1635, 1280, and 860 cm^{-1} (ONO_2); nmr (CCl_4) δ 2.18 (s, 6, Ar(CH_3)$_2$), 2.26 (s, 3, ArCH_3), 5.26 (s, 2 ArCH_2ONO_2), 6.87 (s, 1, Ar*H*), 6.96 ppm (s, 1, Ar*H*), mass spectrum (70 eV) *m/e* (relative intensity) 195 (27, M), 133 (100, $M - ONO_2$), 119 (87). Confirmation of the structure of the nitrate was provided by its quantitative oxidation to 2,4,5-trimethylbenzaldehyde on heating under reflux for 30 min in sulfuric acid – water – acetic acid (1:5:10). The aldehyde after sublimation had mp 43.8–44 °C (lit. (24) mp 42 °C); ir (melt) 1690 cm^{-1} (CHO); nmr ($CDCl_3$) δ 2.25 (s, 6, 4-CH_3 and 5-CH_3), 2.54 (s, 3, 2-CH_3), 6.96 (s, 1, 3-*H*), 7.49 (s, 1, 6-*H*); mass spectrum (70 eV) *m/e* (relative intensity) 148 (76, M), 147 (100). The oxime had mp 106–107 °C after recrystallization from ligroin and 111–112 °C after recrystallization from aqueous ethanol (102 °C, from ligroin (24)).

The early column fractions (5–10% ether) which contained the benzyl nitrate also contained a small amount of diene which, on standing at −20 °C, crystallized as pale yellow rhombohedrons of 1,2,4,5-tetramethyl-4-nitro-1,4-dihydrophenyl nitrite (**6**), mp 75.5–76 °C; uv (CH_3OH) 199 nm (ϵ 1420 m^2 mol^{-1}); ir (Nujol) 1635 and 770 (ONO), 1540 and 1360 (NO_2); nmr (CCl_4) δ 1.63 (s, 3, 1-CH_3), 1.73 (s, 3, 4-CH_3), 1.82 (d, 6, $J_{3,2\text{-}CH_3} = J_{6,5\text{-}CH_3} = 2$ Hz, 2-CH_3 and 5-CH_3), 5.70 (q, 1, $J_{3,2\text{-}CH_3} = 2$ Hz, 3-*H*), 5.98 ppm (q, 1, $J_{6,5\text{-}CH_3} = 2$ Hz, 6-*H*). *Mol. Wt.* calcd. for $C_{10}H_{14}N_2O_4$: 226; found: 226.

The residue (5.7 g) from the 15–50% ether fractions afforded *trans*-1,2,4,5-tetramethyl-4-nitro-1,4-dihydrophenyl acetate (**5***a*) as colourless rhombohedrons after recrystallization from ether–pentane, mp 78–78.5 °C; uv (CH_3OH) 196 nm (ϵ 4000 m^2 mol^{-1}); ir (Nujol) 1745 and 1244 ($OCOCH_3$), 1530 and 1355 (NO_2); nmr (CCl_4) δ 1.43 (s, 3, 1-CH_3), 1.73 (d, 3, $J_{6,5\text{-}CH_3} = 1.0$ Hz, 5-CH_3), 1.75 (s, 3, 4-CH_3), 1.76 (d, 3, $J_{3,2\text{-}CH_3} = 1.0$ Hz, 2-CH_3), 1.91 (s, 3, $OCOCH_3$), 5.46 (q, 1, $J_{3,2\text{-}CH_3} = 1.0$ Hz, 3-H), 5.66 ppm (q, 1, $J_{6,5\text{-}CH_3} = 1.0$ Hz, 6-*H*). *Mol. Wt.* calcd. for $C_{12}H_{17}NO_4$: 239; found: 239.

The residue (0.73 g) from the 70 and 80% ether fractions gave *cis*-1,2,4,5-tetramethyl-4-nitro-1,4-dihydrophenyl acetate (**5***b*), colourless rhombohedrons mp 65–66 °C, after recrystallization from ether–pentane; uv 195 nm (ϵ 2230 m^2 mol^{-1}); ir (Nujol) 1745 and 1244 ($OCOCH_3$), 1540 and 1365 (NO_2); nmr (CCl_4) δ 1.46 (s, 3, 1-CH_3), 1.63 (s, 3, 4-CH_3), 1.78 (d, 3, $J_{6,5\text{-}CH_3} = 1.4$ Hz, 5-CH_3), 1.82 (d, 3, $J_{3,2\text{-}CH_3} = 1.4$ Hz, 2-CH_3), 1.96 (s, 3, $OCOCH_3$), 5.51 (q, 1, $J_{3,2\text{-}CH_3} = 1.4$ Hz, 3-*H*), 6.09 ppm (q, 1, $J_{6,5\text{-}CH_3}$, 6-*H*). *Mol. Wt.* calcd. for $C_{12}H_{17}NO_4$: 239; found: 239.

The residue (0.72 g) of the second and third 100% ether fractions afforded 1,2,4,5-tetramethyl-4-nitro-1,4-dihydrophenol (**7**), colourless needles mp 50.5–51.5 °C after recrystallization from carbon tetrachloride – pentane; uv 197 nm (ϵ 925 m^2 mol^{-1}); ir (Nujol) 3375 and 1080 (OH), 1535 and 1360 cm^{-1} (NO_2); nmr (CCl_4) δ 1.37 (s, 1, O*H*), 1.40 (s, 3, 1-CH_3), 1.74 (d, 3, $J_{6,5\text{-}CH_3} = 1.4$ Hz, 5-CH_3), 1.78 (s, 3, 4-CH_3), 1.90 (d, 3, $J_{3,2\text{-}CH_3} = 1.4$ Hz, 2-CH_3), 5.48 (q, 1, $J_{3,2\text{-}CH_3} = 1.4$ Hz, 3-*H*), 5.82 ppm (q, 1, $J_{6,5\text{-}CH_3} = 1.4$ Hz, 6-*H*). *Mol. Wt.* calcd. for $C_{10}H_{15}NO_3$: 197; found: 196.

Rearomatization Reactions

In the standard procedure the adduct (0.2 mmol, 48 mg) was dissolved in methylene chloride (1 cm^3), the solution cooled to −78 °C and treated with 9 cm^3 of a solution of the reagent. The solution was then allowed to warm to ambient temperature and stood for 2 h,[6] then added to distilled methylene chloride and washed with 2% ammonia solution.[7] After drying and removal of the solvent the residue was analyzed by nmr and glc.

Rearomatization of Adducts from Prehnitene

In addition to compounds isolated from the original nitration mixture and already described the following compounds were formed on rearomatization. 2,3,4-Trimethylbenzyl acetate was obtained as the major product when the *trans*-1,4-adduct **1***a* was decomposed in acetic acid in the presence of a catalytic amount of sulfuric acid. It was isolated by chromatography on silica gel; ir (film) 1735, 1230 cm^{-1} ($OCOCH_3$); nmr ($CDCl_3$) δ 2.06 (s, 3, $OCOCH_3$), 2.19 (s, 3, ArCH_3), 2.24 (s, 3, ArCH_3), 2.28 (s, 3, ArCH_3), 5.07 (s, 2, CH_2), 7.01 ppm (s, 2, 5-*H* and 6-*H*); mass spectrum (70 eV) *m/e* (relative intensity) 192 (6, M), 150 (12, $M - CH_2CO$), 135 (18), 133 (55, $M - CH_3CO_2$), 132 (100, $M - CH_3CO_2H$).

2,3,4,5-Tetramethylphenyl acetate was formed when the adducts were decomposed in acetic acid. It was purified by passage through alumina followed by recrystallization from pentane, affording needles mp 54–55 °C (lit. (21) mp 56–57 °C), ir (Nujol) 1755, 1205 cm^{-1} ($OCOCH_3$); nmr ($CDCl_3$) δ 2.05 (s, 3, ArCH_3), 2.15 (s, 3, ArCH_3), 2.19 (s, 3, ArCH_3), 2.23 (s, 3, ArCH_3), 2.28 (s, 3, $OCOCH_3$), 6.67 ppm (s, 1, 6-*H*); mass spectrum (70 eV) *m/e* (relative intensity) 192 (12, M), 150 (91, $M - CH_2CO$), 135 (100).

Methyl 2,3,4,5-tetramethylphenyl ether, formed in rearomatization reactions in methanol, was prepared by methylation of the corresponding phenol with methyl iodide – silver oxide (25) and purified by chromatography on silica gel; ir (film) 1122, 1098 cm^{-1}; nmr ($CDCl_3$) δ 2.15, 2.20, 2.26 (3s, 12, Ar(CH_3)$_4$), 3.75 (s, 3, OCH_3), 6.53

[6]Reactions in neat acetic acid were stood overnight.

[7]Reaction mixtures from reaction in methanol containing sulfuric acid were washed with brine in order to avoid loss of the phenol formed in the reaction.

Can. J. Chem. Downloaded from www.nrcresearchpress.com by 210.87.254.6 on 09/05/12
For personal use only.

ppm (s, 1, Ar*H*); mass spectrum (70 eV) *m/e* (relative intensity) 164 (66, M), 149 (100, $M - CH_3$). 2,3,4,5-Tetramethylphenol itself was obtained by methanolysis of the acetate with 5% sulfuric acid – methanol and was purified by chromatography on silica gel. After recrystallization from pentane it had mp 82.5–83.5 °C (lit. (26) mp 82.5–83.5 °C); (Nujol) 3280, 1070 cm^{-1}; nmr ($CDCl_3$) δ 2.09 (s, 3, ArCH_3), 2.16 (s, 9, Ar(CH_3)$_3$), 4.74 (s, 1, exchanged with D_2O, O*H*), 6.37 ppm (s, 1, 6-*H*); mass spectrum (70 eV) *m/e* (relative intensity) 150 (86, M), 149 (15, $M - H$), 135 (100, $M - CH_3$).

Methyl 2,3,4,-trimethylbenzyl ether, was prepared by heating the benzyl nitrate under reflux for 2 h in 5% sulfuric acid in methanol; ir (film) 1093 cm^{-1} (CH_2OCH_3); nmr ($CDCl_3$) δ 2.20 (s, 3, ArCH_3), 2.27 (s, 6, Ar(CH_3)$_2$), 3.35 (s, 3, OCH_3), 4.40 (s, 2, CH_2), 7.00 ppm (s, 2, 5-*H* and 6-*H*); mass spectrum (70 eV) *m/e* (relative intensity) 164 (21, M), 162 (15), 149 (36), 147 (24), 133 (66), 132 (100).

The position of side-chain substitution in the benzyl derivatives was confirmed by oxidation of each derivative (acetate, ether, and nitrate) to 2,3,4-trimethylbenzaldehyde by refluxing in sulfuric acid – water – acetic acid (1:10:20), to which was also added a 50% mol excess of nitric acid in the cases of the acetate and ether, ir (film) 1685 cm^{-1} (CHO); nmr ($CDCl_3$) δ 2.14 (s, 3, 3-CH_3), 2.28 (s, 3, 4-CH_3), 2.50 (s, 3, 2-CH_3), 7.06 (nq, 1, J = 8 Hz, 5-*H*), 7.43 (nq, 1, J = 8 Hz, 6-*H*), 10.14 ppm (C*H*O); mass spectrum (70 eV) *m/e* (relative intensity) 148 (89, M), 147 (100, $M - H$), 119 (56). Autoxidation of the aldehyde gave 2,3,4-trimethylbenzoic acid; mp 179–179.5 °C (lit. (27) mp 167–168 °C); ir (Nujol) 2700–2500, 1680, 1270 cm^{-1} (CO_2H); nmr ($CDCl_3$) δ 2.22 (s, 3, 3-CH_3), 2.32 (s, 3, 4-CH_3), 2.55 (s, 3, 2-CH_3), 7.00 (nq, 1, J = 9 Hz, 5-*H*), 7.68 (nq, 1, J = 9 Hz, 6-*H*), 11.64 ppm (b, 1, CO_2H); mass spectrum (70 eV) *m/e* (relative intensity) 164 (90, M) 147 (59, $M - OH$), 146 (92, $M - H_2O$), 119 (100).

Rearomatization of the Adduct from Durene

The following compounds were obtained on rearomatization of adduct **5**. 2,3,5,6-Tetramethylphenyl acetate; mp 78.5–79 °C (lit. (28) mp 79–80 °C); ir (Nujol) 1765, 1220 cm^{-1} ($OCOCH_3$); nmr ($CDCl_3$) δ 1.96 (s, 6, Ar-(CH_3)$_2$), 2.20 (s, 6, Ar(CH_3)$_2$), 2.23 (s, 3, O$COCH_3$), 6.73 ppm (s, 1, 4-*H*); mass spectrum (70 eV) *m/e* (relative intensity) 192 (18, M), 150 (100, $M - CH_2CO$). 2,4,5-Trimethylbenzylacetate, ir (film) 1745, 1230 cm^{-1} (OCO-CH_3); nmr ($CDCl_3$) δ 2.05 (s, 3, O$COCH_3$), 2.20 (s, 6, Ar(CH_3)$_2$), 2.26 (s, 3, ArCH_3), 5.02 (s, 2, CH_2), 6.93 (s, 1, Ar*H*), 7.04 ppm (s, 1, Ar*H*); mass spectrum (70 eV) *m/e* (relative intensity) 192 (10, M), 150 (39, $M - CH_2CO$), 135 (39), 133 (34, $M - CH_3CO_2$), 132 (100, $M - CH_3CO_2H$). 1,2,4,5-Tetramethyl-3-nitrobenzene; mp 113–114 °C (lit. (21) mp 112–113 °C); ir (Nujol) 1520 cm^{-1} (NO_2); nmr (CCl_4) δ 2.08 (s, 6, Ar(CH_3)$_2$), 2.23 (s, 6, Ar(CH_3)$_2$, 6.92 ppm (s, 1, 6-*H*); *m/e* 164 (M). 2,4,5-Trimethylphenylnitromethane; mp 52–53 °C (lit. (21) mp 52.5 °C); ir (film) 1550, 1365 cm^{-1} (NO_2); nmr ($CDCl_3$) δ 2.02 (s, 6, Ar(CH_3)$_2$), 2.30 (s, 3, ArCH_3), 5.39 (s, 2, CH_2), 7.01 (s, 1, Ar*H*), 7.08 (s, 1, Ar*H*); mass spectrum (70 eV) *m/e* (relative intensity) 179 (2, M) 133 (100, $M - NO_2$).

Acknowledgments

We thank the National Research Council of Canada and the University of Victoria for financial support.

1. S. R. Hartshorn. Chem. Soc. Rev. **3**, 167 (1974).
2. (*a*) D. J. Blackstock, A. Fischer, K. E. Richards, J. Vaughan, and G. J. Wright. Chem. Commun. 641 (1970); (*b*) D. J. Blackstock, J. Cretney, A. Fischer, M. P. Hartshorn, K. E. Richards, J. Vaughan, and G. J. Wright. Tetrahedron Lett. 2793 (1970); (*c*) A. Fischer, C. C. Greig, A. L. Wilkinson, and D. R. A. Leonard. Can. J. Chem. **50**, 2211 (1972); (*d*) A. Fischer and D. R. A. Leonard. Can. J. Chem. **50**, 3367 (1972); (*e*) A. Fischer and A. L. Wilkinson. Can. J. Chem. **50**, 3988 (1972); (*f*) A. Fischer and J. N. Ramsay. J. Chem. Soc. Perkin Trans. II, 237 (1973); (*g*) A. Fischer and D. R. A. Leonard. J. Chem. Soc. Chem. Commun. 300 (1973); (*h*) A. Fischer and C. C. Greig. J. Chem. Soc. Chem. Commun. 50 (1974); (*i*) A. Fischer and J. N. Ramsay. J. Am. Chem. Soc. **96**, 1614 (1974); (*j*) A. Fischer and C. C. Greig. Can. J. Chem. **52**, 1231 (1974); (*k*) A. Fischer and J. N. Ramsay. Can. J. Chem. **52**, 3960 (1974); (*l*) A. Fischer, C. C. Greig, and R. Röderer. Can. J. Chem. **53**, 1570 (1975); (*m*) A. Fischer and R. Röderer. Can. J. Chem. **54**, 423 (1976).
3. P. C. Myhre. J. Am. Chem. Soc. **94**, 7921 (1972).
4. (*a*) R. C. Hahn and M. B. Groen. J. Am. Chem. Soc. **95**, 6128 (1973); (*b*) R. C. Hahn and D. L. Strack. J. Am. Chem. Soc. **96**, 4335 (1974); (*c*) M. W. Galley and R. C. Hahn. J. Am. Chem. Soc. **96**, 4337 (1974).
5. H. Suzuki, H. Yaneda, and T. Hanafusa. Bull. Chem. Soc. Jpn. **48**, 2116 (1975); and references cited therein.
6. G. Illuminati, L. Mandolini, A. Patara, and E. Baciocchi. Tetrahedron Lett. 4161 (1972); and references cited therein.
7. D. J. Blackstock, A. Fischer, K. E. Richards, and G. J. Wright. Aust. J. Chem. **26**, 775 (1973); D. J. Blackstock. Ph.D. Thesis, University of Canterbury, Christchurch, New Zealand. 1970.
8. A. Fischer and G. J. Wright. Aust. J. Chem. **27**, 217 (1974).
9. H. Suzuki, K. Nakamura, and M. Takeshima. Bull. Chem. Soc. Jpn. **44**, 2248 (1971); H. Suzuki and K. Nakamura. Bull. Chem. Soc. Jpn. **45**, 1270 (1972).
10. (*a*) H. Suzuki and K. Nakamura. Bull. Chem. Soc. Jpn. **45**, 2534 (1972); (*b*) H. Suzuki and K. Nakamura. Synthesis, 606 (1972).
11. H. Suzuki, M. Sawaki, and R. Sakimoto. Bull. Chem. Soc. Jpn. **45**, 1515 (1972).
12. E. W. Garbisch, Jr. J. Am. Chem. Soc. **86**, 5561 (1964).
13. J. G. Hoggett, R. B. Moodie, J. R. Penton, and K. Schofield. Nitration and aromatic reactivity. Cambridge University Press, London. 1971. Chapt. 5.
14. A. Fischer, J. Packer, J. Vaughan, and G. J. Wright. J. Chem. Soc. 3687 (1964).
15. N. Kornblum, R. A. Smiley, R. K. Blackwood,

and D. C. IFFLAND. J. Am. Chem. Soc. **77**, 6269 (1955).
16. G. A. OLAH and H. C. LIN. Synthesis, 488 (1973).
17. J. W. BARNETT, R. B. MOODIE, K. SCHOFIELD, and J. B. WESTON. J. Chem. Soc. Perkin Trans. II, 648 (1975).
18. G. A. OLAH, H. C. LIN, and Y. K. MO. J. Am. Chem. Soc. **94**, 3667 (1972).
19. S. D. ROSS, F. R. COBURN, and M. FINKLESTEIN. J. Org. Chem. **33**, 585 (1968).
20. R. G. GILLIS. J. Org. Chem. **21**, 805 (1956).
21. R. BIEDERMANN and A. LEDOUX. Chem. Ber. **8**, 57 (1875).
22. L. I. SMITH and F. L. TAYLOR. J. Am. Chem. Soc. **57**, 2460 (1935).
23. H. KRÖMER. Chem. Ber. **24**, 2413 (1891).
24. L. GATTERMANN. Ann. Chem. **347**, 375 (1906).
25. H. G. WALKER, M. GEE and R. M. MCCREADY. J. Org. Chem. **27**, 2120 (1962).
26. E. BAMBERGER and L. BLANGEY. Ann. Chem. **384**, 307 (1911).
27. A. LAPWORTH and E. M. CHAPMAN. J. Chem. Soc. **77**, 316 (1900).
28. J. S. FITZGERALD. J. Appl. Chem. **5**, 289 (1955).

Can. J. Chem. Downloaded from www.nrcresearchpress.com by 210.87.254.6 on 09/05/12
For personal use only.

Defensive substances of *Coccinella transversoguttata* and *Hippodamia caseyi*, ladybugs indigenous to western Canada

WILLIAM A. AYER, MICHAEL J. BENNETT, LOIS M. BROWNE, AND JAMES T. PURDHAM

Department of Chemistry, University of Alberta, Edmonton, Alta., Canada T6G 2E2

Received January 5, 1976

WILLIAM A. AYER, MICHAEL J. BENNETT, LOIS M. BROWNE, and JAMES T. PURDHAM. Can. J. Chem. **54** 1807 (1976).

The defensive substances of two species of ladybug indigenous to western Canada have been isolated. The known compounds precoccinelline (**1**) and coccinelline (**2**) are present in *Coccinella transversoguttata*, and hippodamine (**3**) and convergine (**4**) in *Hippodamia caseyi*. From the latter insect we have also isolated two new alkaloids, a new base, *N*-oxide pair, which we have named hippocasine and hippocasine oxide. The structure of hippocasine oxide (**8**) was established by spectroscopic methods and confirmed by X-ray analysis of the hydrochloride (**9***d* and Fig. 1).

WILLIAM A. AYER, MICHAEL J. BENNETT, LOIS M. BROWNE et JAMES T. PURDHAM. Can. J. Chem. **54**, 1807 (1976).

On a isolé les substances défensives de deux espèces de coccinelles indigènes à l'ouest canadien. Les composés connus, précoccinelline (**1**) et coccinelline (**2**), sont présents dans la *Coccinella transversoguttata* et l'hippodamine (**3**) et la convergine (**4**) dans *l'Hippodamia caseyi*. On a isolé deux nouveaux alcaloïdes à partir de ce dernier insecte; il s'agit d'une nouvelle paire de base et d'oxyde d'azote correspondant que l'on a nommés respectivement hippocasine et oxyde d'hippocasine. On a établi la structure de l'oxyde d'hippocasine (**8**) par des méthodes spectroscopiques et on l'a confirmée par analyse de rayon-X du chlorhydrate (**9***d* et fig. 1).

[Traduit par le journal]

The polka-dotted beetles (ladybugs) because of their voracious appetite for aphids, mealy bugs, and scale insects have long been known as a friend of man (1). These colorful beetles, members of the family Coccinellidae, not only have potential economic impact in the biological control of plant pests on agricultural crops but also exhibit an interesting protective mechanism against their predators through secretion of defensive compounds associated with 'reflex bleeding' (2).

In recent years, Tursch and co-workers have investigated the defensive substances present in several species of Coccinellidae. They found that the defensive compounds are bitter-tasting alkaloids, many of which are related to 2-methylperhydro-9b-azaphenalene and the corresponding *N*-oxides. These include precoccinelline (**1**), coccinelline (**2**) (3), hippodamine (**3**), convergine (**4**) (4), myrrhine (**5**) (5), and propyleine (**6**) (6).

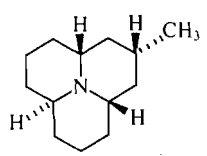

1

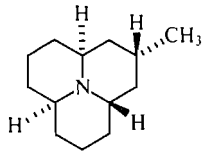

2 *N*-Oxide of **1**

3

4 *N*-Oxide of **3**

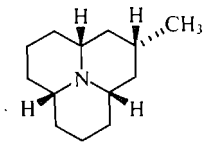

5

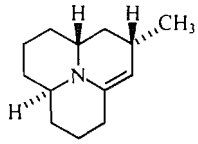

6

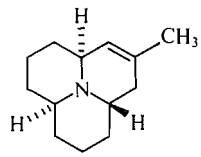

7

8 *N*-Oxide of **7**

We have examined the defensive substances present in two species of ladybugs indigenous to western Canada: *Coccinella transversoguttata* Faldermann and *Hippodamia caseyi* Johnson. At this time we wish to report the isolation and characterization of precoccinelline (**1**) and coccinelline (**2**) from *C. transversoguttata*;

Can. J. Chem. Downloaded from www.nrcresearchpress.com by 210.87.254.105 on 09/05/12
For personal use only.

TABLE 1. Alkaloids isolated from *H. caseyi*

Compound	R_f	M^+	Empirical formula
C	0.72	191	$C_{13}H_{20}N^*$ ($M^+ - 1$)
D	0.65	193	$C_{13}H_{23}N$
E	0.38	209	$C_{13}H_{23}NO^*$
F	0.31	207	$C_{13}H_{21}NO^*$

*Determined by high resolution mass measurement.

hippodamine (**3**), convergine (**4**), and two new alkaloids, hippocasine (**7**) and hippocasine oxide (**8**), from *H. caseyi*.

The beetles (~500 *Coccinella transversoguttata*) were blended with methanol and the supernatant was separated and partitioned between methanol–water (9:1) and pentane. Concentration of the aqueous methanol extract followed by chromatographic separation (alumina) led to the isolation of two alkaloids: compound *A* ($C_{13}H_{23}N$) and compound *B* ($C_{13}H_{23}NO$). That *B* was the *N*-oxide of *A* was shown as follows. Treatment of compound *A* with *m*-chloroperbenzoic acid followed by hydrochloric acid gave compound *B* hydrochloride (superimposable ir, co-tlc). Compound *B*, which crystallizes from acetone, shows a mass spectral fragmentation pattern similar to that reported for the 2-methyl-9b-azaphenalene *N*-oxides (3). Its nmr spectrum displays a methyl doublet (δ 1.03) and a three-proton low-field multiplet (δ 3.38). Its ^{13}C nmr spectrum shows eight signals. The evidence presented is consistent with that reported for coccinelline (3). Comparison of the spectra of compound *B* with that of an authentic sample of coccinelline revealed the two were identical. Thus compound *B* is coccinelline, **2**, and compound *A* is precoccinelline, **1**.

The extract from *Hippodamia caseyi* Johnson was obtained by the method described above. Chromatographic separation (alumina) of the crude extract led to the isolation of four alkaloids. The mass spectra of these compounds suggested the presence of two free base *N*-oxide pairs (see Table 1).

The relationship between compounds *C* and *F* and compounds *D* and *E* was shown in the following way. Treatment of compound *D* with *m*-chloroperbenzoic acid (8) followed by salt formation gave compound *E* hydrochloride (co-tlc, superimposable ir) while treatment of compound *C* with methanolic hydrogen peroxide (9), then salt formation, gave compound *F* hydrochloride (co-tlc, superimposable ir). As well, pyrolysis of compound *E* (150–155 °C) gave compound *D*, whereas pyrolysis of compound *F* gave compound *C*. Since the free bases, *C* and *D*, were isolated in small quantities and decomposed readily, they were characterized as their *N*-oxides.

Compound *E* ($C_{13}H_{23}NO$) was isolated as an oil. It was transformed to a crystalline hydrochloride by treatment with hydrochloric acid in acetone. The nmr spectrum shows a methyl doublet at δ 0.87, $J = 4$ Hz and low-field multiplets at δ 3.9 (1H) and δ 4.5 (2H). The mass spectrum shows a fragmentation pattern similar to that observed for the 2-methylperhydro-9b-azaphenalene *N*-oxide skeleton (3).

Comparison of the spectral data of compound *E* hydrochloride with that of a synthetic sample (10) of convergine hydrochloride, **4**, showed that they were identical in all respects. In addition, the ir spectrum of compound *E* hydrochloride was superimposable on that of convergine hydrochloride, **4**, isolated from *Hippodamia convergens* by Tursch and co-workers (4).

As mentioned previously compound *D* was transformed to compound *E* by treatment with *m*-chloroperbenzoic acid. Since compound *E* has been shown to be convergine, **4**, compound *D* must be hippodamine, **3**.

Compound *F* ($C_{13}H_{21}NO$, and for which we propose the name hippocasine oxide) is an optically active alkaloid which was isolated as an oil. It was characterized as its hydrochloride which decomposes without melting above 220 °C. The ir spectrum of hippocasine oxide hydrochloride shows salt (O—H) bands (2700–2500 cm^{-1}) and olefinic absorption (1675 cm^{-1}). The nmr spectrum shows a vinyl methyl (δ 1.78), a low-field, three-proton multiplet (δ 4.03–4.27, —CH—N—) and an olefinic proton (δ 5.42). Long range coupling between the olefinic proton and the vinyl methyl group as well as with an allylic methylene was established by double irradiation experiments. The mass spectral fragmentation pattern of hippocasine oxide hydrochloride is similar to that observed for the 2-methylperhydro-9b-azaphenalene *N*-oxide system except that each major fragment is two mass units less. Assuming the same carbon skeleton, this data is consistent with the structures **9***a*, **9***b*, **9***c*, **9***d*.

Can. J. Chem. Downloaded from www.nrcresearchpress.com by 210.87.254.105 on 09/05/12
For personal use only.

Can. J. Chem. Downloaded from www.nrcresearchpress.com by 210.87.254.105 on 09/05/12
For personal use only.

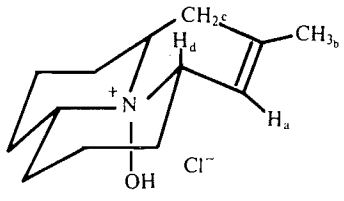

9*a*

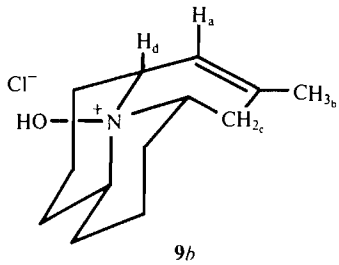

9*b*

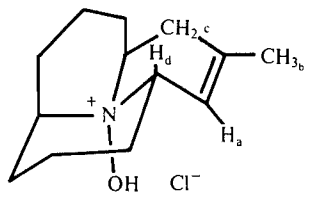

9*c*

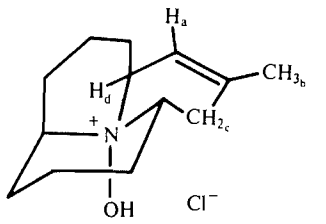

9*d*

Further analysis of the nmr spectrum of hippocasine oxide hydrochloride shows that the olefinic proton H_a, is a nine-line multiplet resulting from the overlapping of a doublet of sextets with coupling constants $J_{ab} = J_{ac} = 1.5$ Hz, $J_{ad} = 4.5$ Hz. Examination of molecular models of compounds, **9***a*, **9***b*, **9***c*, and **9***d* reveals that only in **9***d* is the dihedral angle between H_a and H_d small enough to account for the observed coupling (11). In the other three isomers (**9***a*, **9***b*, **9***c*) $\theta_{ad} \sim 90°$ and thus J_{ad} would be expected to be much smaller (11).

In order to verify that hippocasine oxide is **9***d* ≡ **8**, transformation of **8** to convergine **4**,

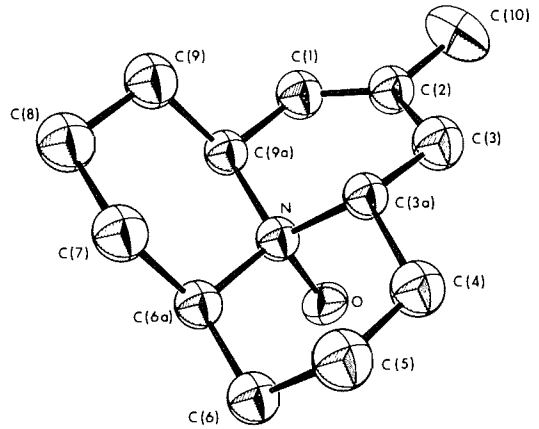

FIG. 1. The molecular structure of hippocasine oxide hydrochloride.

was attempted. Catalytic hydrogenation of **8** over palladium–charcoal led to the formation of a base $C_{13}H_{23}N$ which was transformed to the *N*-oxide hydrochloride in the usual manner. Comparison of the ir spectrum of this compound with that of convergine hydrochloride showed that the two compounds were not identical. Catalytic hydrogenation of hippocasine oxide may proceed from the α-face to give the compound with an axial methyl group. Attempted dissolving metal reduction of **8** was unsuccessful.

Since small quantities of hippocasine oxide remained, its structure was confirmed by X-ray analysis of the hydrochloride. The result is shown in Fig. 1. The average C—C bond length and the C=C distance are normal. The average C—N distance of 1.541 Å agrees well with that of 1.548 Å found in convergine hydrochloride (4). The N—O bond length of 1.430 Å is similar to that found in convergine hydrochloride and coccinelline hemihydrochloride (3*b*). Bond lengths and intramolecular angles are

TABLE 3. Interatomic distances with estimated standard deviations in parentheses

Bond	Distance (Å)	Bond	Distance (Å)
N—C9a	1.523(8)	C6—C6a	1.515(9)
N—C6a	1.541(8)	C7—C8	1.52(1)
N—C3a	1.560(8)	C8—C9	1.505(9)
N—O	1.430(7)	C9—C9a	1.511(9)
C3a—C4	1.504(9)	C9a—C1	1.488(9)
C3a—C3	1.514(9)	C1—C2	1.32(1)
C4—C5	1.50(1)	C2—C3	1.50(1)
C5—C6	1.56(1)	C2—C10	1.52(1)

Can. J. Chem. Downloaded from www.nrcresearchpress.com by 210.87.254.105 on 09/05/12
For personal use only.

TABLE 4. Intramolecular angles with estimated standard deviations in parentheses

Bonds	Angle (deg)	Bonds	Angle (deg)
O—N—C3a	105.3(4)	C7—C6a—N	111.3(6)
O—N—C6a	107.6(5)	C6a—C7—C8	109.8(6)
O—N—C9a	109.6(5)	C7—C8—C9	109.8(6)
C3a—N—C6a	112.3(5)	C8—C9—C9a	113.5(6)
C3a—N—C9a	110.8(5)	C9—C9a—C1	112.4(6)
C6a—N—C9a	111.0(5)	C9—C9a—N	112.5(6)
N—C3a—C4	109.6(6)	C1—C9a—N	110.2(5)
N—C3a—C3	108.9(6)	C9a—C1—C2	124.4(7)
C4—C3a—C3	108.9(6)	C1—C2—C10	122.8(8)
C3a—C4—C5	114.9(6)	C1—C2—C3	121.9(7)
C5—C6—C6a	111.0(6)	C10—C2—C3	115.4(7)
C6—C6a—C7	114.3(6)	C2—C3—C3a	116.1(6)
C6—C6a—N	110.3(5)		

TABLE 5. Atomic parameters

(*a*) Atom coordinates

Atom	*x*	*y*	*z*	*B*
Cl	0.6952(2)	0.2500	0.3116(3)	4.41
O	0.1710(5)	0.0605(6)	0.5808(6)	3.41
C10	−0.052(1)	0.256(2)	0.926(1)	5.86
N	0.2603(5)	0.1930(7)	0.6525(6)	2.74
C1	0.1864(7)	0.177(1)	0.9144(9)	3.56
C2	0.0686(6)	0.251(1)	0.8461(8)	3.40
C3	0.0462(7)	0.336(1)	0.6809(9)	3.93
C3a	0.1711(7)	0.3525(9)	0.6095(9)	2.85
C4	0.1323(7)	0.377(1)	0.4241(9)	3.88
C5	0.2510(8)	0.378(1)	0.3440(9)	4.41
C6	0.3355(7)	0.216(1)	0.3870(8)	3.52
C6a	0.3838(7)	0.1928(9)	0.5731(8)	3.13
C7	0.4931(7)	0.3141(9)	0.6586(9)	3.61
C8	0.5410(7)	0.285(1)	0.8435(9)	4.09
C9	0.4193(7)	0.287(1)	0.9199(8)	3.63
C9a	0.3063(7)	0.1692(9)	0.8388(8)	2.89

(*b*) Anisotropic parameters

Atom	U_{11}	U_{22}	U_{33}	U_{12}	U_{13}	U_{23}
C8	0.061(1)	0.0201(8)	0.080(1)	−0.003(1)	0.007(1)	0.002(1)
O	0.040(3)	0.019(3)	0.064(4)	−0.001(3)	0.001(3)	−0.010(3)
C10	0.079(7)	0.058(6)	0.087(7)	0.009(8)	0.044(6)	−0.006(8)

given in Tables 3 and 4 and atomic parameters are given in Table 5. Structure factor tables are available (Table 2).[1]

As discussed earlier compound *C* was transformed to compound *F* by treatment with methanolic hydrogen peroxide. Since compound *F*, hippocasine oxide, has been shown to be **8**, it follows that compound *C*, hippocasine, is represented by structure **7**.

[1]Table 2 is available, at a nominal charge, from the Depository of Unpublished Data, CISTI, National Research Council of Canada, Ottawa, Canada K1A 0S2.

Experimental

Optical rotatory dispersion (ord) spectra were measured in methanol using a Jasco Optical Rotatory Dispersion Recorder Model ORV/UV-5.

Infrared spectra (ir) were measured in KBr unless otherwise specified using a Perkin-Elmer 421 grating ir spectrophotometer or a Unicam SP 1000 grating ir spectrophotometer.

Can. J. Chem. Downloaded from www.nrcresearchpress.com by 210.87.254.105 on 09/05/12
For personal use only.

Proton magnetic resonance spectra were measured in $CDCl_3$ unless otherwise specified using a Varian Associates HA 100 spectrophotometer with TMS as internal standard. ^{13}C magnetic resonance spectra were measured in $CDCl_3$ using a Varian HA 100 15 in. system interfaced to a Digilab FTS/NMR 3 data system and pulse unit.

Mass spectra were recorded on an A.E.I. Model MS-9 mass spectrophotometer and are reported as *m/e* (relative intensity). Unless diagnostically significant, only peaks at least 20% as intense as the base peak are reported. For the hydrochloride of the *N*-oxides, the sample was allowed to stabilize at 155 °C, then recorded.

Optical density measurements were recorded in methanol using a Perkin-Elmer 141 Polarimeter.

Melting points were recorded on a hot-stage Fisher-Johns melting point apparatus and are uncorrected.

Insect Material

Coccinella transversoguttata were collected in the Edmonton area and identified by J. Belicek, Department of Entomology, University of Alberta, Edmonton, Alberta.

Hippodamia caseyi Johnson were collected from their over-winter site (7) in south-central British Columbia and identified by R. D. McMullen, Entomologist, Canada Department of Agriculture, Research Station, Summerland, British Columbia.

Extraction and Isolation of the Alkaloids of Coccinella transversoguttata

Approximately 500 ladybugs (*C. transversoguttata*) were extracted with methanol in a Waring blender. The extract was filtered, diluted with water (10% by volume), then washed several times with pentane. The aqueous methanol extract was concentrated *in vacuo* to give a crude extract. Thin layer chromatography (alumina, chloroform) of this material revealed the presence of two basic components as well as nonbasic material.

Elution chromatography of the extract (chloroform) over alumina led to fractions rich in compound *A* (150 mg). Further purification by acid–base extraction gave 90 mg compound *A*. Elution with chloroform–methanol (100:1) gave compound *B* (27 mg).

Precoccinelline, 1

Compound *A* was isolated as an oil: nmr δ 0.97 (d, 3H, J = 5 Hz, CH_3), 3.0 (m, 3H, N—C*H*); *Exact Mass* calcd. for $C_{13}H_{23}N$: 193.1830; found (ms): 193.1821; ms *m/e* 193.1821 (58), 192 (100), 178 (21), 164 (23), 151 (49), 150 (46), 137 (35), 136 (20), 41 (22).

Conversion of Precoccinelline, 1, to Coccinelline, 2

Compound *A* (40 mg) and *m*-chloroperbenzoic acid (40 mg) in chloroform were allowed to stand in the refrigerator overnight. The mixture was concentrated and the product isolated by preparative thin layer chromatography over alumina (chloroform–methanol, 20:1). Compound *A N*-oxide was converted to its hydrochloride salt in the usual manner. The ir spectrum of compound *A N*-oxide hydrochloride was superimposable on that of compound *B* hydrochloride.

Coccinelline, 2

Coccinelline was isolated as a solid which was recrystallized from acetone: mp >215 °C (chars); ir 3300, 2950, 2910, 2860, 2720, 2650, 1450, 1440, 1430, 1370, 1350, 1340, 1320, 1290, 1280, 1260, 1195, 1180, 1160, 1120, 1100, 1040, 990, 970, 940, 900, 870, 850, 840, 820, 800, 650, 600 cm^{-1}; nmr δ 1.03 (d, 3H, J = 5 Hz, C—C*H*$_3$), 3.38 (m, 3H, N—C*H*); ^{13}C nmr δ ($CDCl_3$), 73.9, 58.7, 36.0, 30.7, 27.6, 25.7, 21.5, 18.3; *Exact Mass* calcd. for $C_{13}H_{23}NO$: 209.1780; found (ms): 209.1785; ms *m/e* 209.1785 (9), 129 (100), 191 (64), 190 (75), 178 (22), 176 (95), 164 (30), 151 (49), 150 (62), 137 (41), 136 (41), 134 (20), 122 (24), 82 (23), 69 (23), 68 (23), 67 (30), 60 (22), 55 (67), 54 (26), 53 (26), 43 (57), 41 (100).

Coccinelline was converted to its hydrochloride salt in the usual way and recrystallized from methanol–ether: mp 220 °C (dec. without melting); ir (KBr) 3300, 2940, 2920, 2870, 2850, 2500, 1520, 1490, 1460, 1445, 1430, 1380, 1370, 1300, 1280, 1260, 1210, 1180, 1170, 1120, 1100, 1030, 990, 985, 970, 950, 910, 900, 880, 855, 770, 610 cm^{-1}.

Extraction and Isolation of the Alkaloids of Hippodamia caseyi Johnson

Approximately 5000 ladybugs (*H. caseyi* Johnson) were extracted with methanol in a Waring blender. The extract was filtered, diluted with water (10% by volume), then washed several times with pentane. The aqueous methanol extract (1.5 l) was stored in the refrigerator; further isolation work was carried out on portions of this extract.

In one experiment, the aqueous methanol extract (500 ml) was concentrated *in vacuo* to give an oil (2.9 g). Thin layer chromatography of this material (alumina, chloroform–methanol 50:1) showed the presence of four basic (Dragendorf positive) components (R_f: *C* 0.72, *D* 0.65, *E* 0.38, *F* 0.31) as well as nonbasic material.

Elution chromatography over alumina (BDH, 300 g) with chloroform led to isolation of fractions rich in base *C* (30 mg) and base *D* (47 mg). Each of these fractions was purified further by acid–base extraction to give base *C* (10 mg) and base *D* (12 mg). Elution with chloroform–methanol (50:1) led to isolation of base *E* (17 mg) and base *F* (47 mg).

The free bases appeared to decompose on standing and thus were converted to and stored as their hydrochloride salts.

General Method of Preparation of Hydrochlorides

The alkaloid was dissolved in acetone and a few drops of concentrated hydrochloric acid were added. The mixture was allowed to stand at room temperature for about 5 min, then concentrated *in vacuo*. If the residue was discolored it was dissolved in methanol and filtered through a small plug of charcoal (AU-4).

Hippodamine, 3

Compound *D* (R_f 0.65) was isolated as an oil: ir (neat) 2920, 2850, 1450 (sh), 1440, 1375, 1350, 1340, 1320, 1280, 1220, 1190, 1155 (sh), 1145, 1130, 1115, 1100, 1070, 1020, 885, 835, 830, 800, 710 cm^{-1}; ms *m/e* 193 (55), 192 (100), 178 (34), 165 (44), 152 (20), 151 (83), 150 (65), 149 (20), 137 (38), 136 (31), 111 (23), 109 (28), 97 (38), 96 (24), 95 (34), 85 (38), 83 (59), 81 (38), 71 (38), 68 (51), 66 (34), 57 (62), 55 (80), 43 (68), 41 (68); nmr δ 0.86, (d, J = 6 Hz), 1.5 (m), 1.9 (m), 2.2 (m), 3.0 (m).

Conversion of Hippodamine, 3, to Convergine Hydrochloride, 4

Compound *D* (12 mg) and *m*-chloroperbenzoic acid (15 mg) in chloroform were allowed to stand in the

Can. J. Chem. Downloaded from www.nrcresearchpress.com by 210.87.254.105 on 09/05/12
For personal use only.

refrigerator overnight. The reaction mixture was concentrated and the residue chromatographed over alumina (BDH). Elution with chloroform gave compound *D N*-oxide (6 mg).

Compound *D N*-oxide was converted to a hydrochloride in the usual manner. The ir spectrum of compound *D N*-oxide hydrochloride was superimposable on that of compound *E* hydrochloride.

Convergine, 4

Compound *E*, R_f 0.38, was isolated as an oil. It was converted to its *hydrochloride*; chars without melting >215 °C: ir 2940, 2880, 2550 (br), 1500, 1450, 1380, 1360, 1330, 1315, 1305, 1265, 1210, 1205, 1160, 1095, 1020, 1010, 1000, 970, 940, 930, 900, 890, 850, 820, 810, 740, 610 cm^{-1}; *Exact Mass* calcd. for $C_{13}H_{23}NO$: 209.1780; found (ms): 209.1794; ms *m/e* 209.1794 (20), 193 (34), 192 (100), 191 (24), 178 (20), 176 (36), 164 (28), 151 (32), 150 (32), 55 (22), 41 (28); nmr δ 0.87, (3H, d, J = 4 Hz), 3.9 (1H, m), 4.5 (2H, m).

The spectral data for compound *E* hydrochloride is identical with that obtained for a synthetic sample of convergine hydrochloride prepared in these laboratories (10). Additionally, the ir spectrum of the naturally occurring convergine hydrochloride is superimposable on the ir spectrum of convergine hydrochloride isolated by Tursch and co-workers (4).

Conversion of Convergine, 4, to Hippodamine, 3

Convergine (2 mg) was heated in a glass tube in a sublimation block at 150–155 °C for about 1 h. The portion of the glass tubing outside the block was cooled by a wick dipped in ice water. The oil obtained from this distillation has the same R_f (0.65) and ir spectrum as hippodamine, **3**.

Hippocasine, 7

Compound *C*, R_f 0.72 was isolated as an oil: ir (neat) 2880, 2820, 1625 (>C=C<), 1490, 1480, 1445, 1430, 1370, 1330, 1210, 1190, 1105, 1070, 1045, 1020, 955, 910, 880, 830, 820, 800, 735, 710 cm^{-1}; *Exact Mass* calcd. for $C_{13}H_{20}N$: 190.1596; found (ms): 190.1592; ms *m/e* 191 (60), 190.1592 (100), 176 (84), 162 (49), 148 (38), 147 (37), 120 (25), 107 (22), 94 (26), 93 (25), 91 (25), 81 (26), 70 (28), 66 (29), 55 (42), 43 (35), 41 (65).

Conversion of Hippocasine, 7, to Hippocasine Oxide, 8

Compound *C* (14 mg) and 30% hydrogen peroxide (1 drop) in methanol (2 ml) were allowed to stand at room temperature. Additional hydrogen peroxide (1 drop) was added after 2 h and 6 h. After 48 h, platinum black (few grains) was added. When oxygen evolution was complete the reaction mixture was filtered and concentrated. The residue was converted to the hydrochloride to give compound *C N*-oxide hydrochloride (13 mg). The ir spectrum of this compound was identical in all respects with that of hippocasine oxide hydrochloride.

Hippocasine Oxide, 8

Compound *F*, R_f 0.31, was isolated as an oil. It was converted to a *hydrochloride* which was crystallized from ethyl acetate containing a trace of methanol (dec. without melting above 220 °C), $[\alpha]_D^{25}$ +14.8 (*c*, 0.73, methanol): ir 2940, 2900, 2860, 2700, 2500, 1675, 1500, 1460, 1425, 1380, 1360, 1350, 1335, 1310, 1290, 1280, 1260, 1230, 1200, 1150, 1140, 1110, 1090, 1065, 1010, 970, 955, 925, 895, 870, 845, 835, 825, 800, 790, 730, 690, 650, 640, 620 cm^{-1}; *Exact Mass* calcd. for $C_{13}H_{21}NO$: 207.1623; found (ms): 207.1630; ms *m/e* 207.1630 (20), 191 (42), 190 (100), 188 (94), 176 (58), 174 (36), 162 (37), 160 (27), 148 (26), 94 (20) 55 (30), 43 (22), 41 (45); nmr (CD_3OD) δ 1.78, (br s, 3H, C=C—CH_3), 1.8 (m), 2.25 (m), 4.0–4.3, (m, 3H, —CH—N—); 5.42 (nine line m, 1H, J = 1.5, 4.5 Hz, C=C—H); irradiation at 5.42 sharpens 1.78 and 2.25; ord $[\alpha]_{400}$ +15.8, $[\alpha]_{300}$ +42.1, $[\alpha]_{250}$ +94.7 (*c* 1.9, methanol).

Conversion of Hippocasine Oxide, 8, to Hippocasine, 7

Hippocasine oxide (2 mg) was pyrolyzed as described for convergine. The oil obtained in the distillate had identical tlc behavior (R_f 0.72) and superimposable ir spectra with that of hippocasine, 7

Catalytic Hydrogenation of Hippocasine Oxide

A solution of hippocasine oxide hydrochloride (14 mg) in methanol containing palladium–charcoal (~10 mg) was hydrogenated under 48 psi hydrogen overnight. The solution was filtered and concentrated to give an oil (7 mg): *m/e* M^+ 193, 192 (base), 178, 164, 151, 150.

The hydrogenation product was dissolved in chloroform and treated with *m*-chloroperbenzoic acid (10 mg) for 12 h. The reaction mixture was concentrated and chromatographed over alumina (BDH). The *N*-oxide (5 mg) thus obtained was converted to a hydrochloride salt in the usual way: ir 3500, 2930, 2920, 2700 (br), 1600 (br, hydrate), 1450, 1430, 1390, 1355, 1340, 1310, 1270, 1220, 1160, 1130, 1100, 1065, 1030, 1020, 1000, 975, 940, 900, 870, 860, 830, 820, 810, 750, 670 cm^{-1}.

Crystal Structure Determination of Hippocasine Oxide Hydrochloride

Crystal data:

$C_{13}H_{22}NOCl$ f.w. = 243.5

Monoclinic, a = 10.011(2), b = 8.117(2), c = 8.312(2), β = 104.02(2), V = 655.3, ρ_o = 1.24(1), Z = 2, ρ_c = 1.234 (20 °C; CuK_α, λ = 1.54182 Å).

The molecule crystallizes in the space group $P2_1$. A total of 766 significantly above background reflections were measured on a Picker FACS I automatic diffractometer, using nickel filtered CuK_α radiation. The data were corrected for Lorentz and polarization effects and structure factor amplitudes and standard deviations calculated, using an uncertainty factor of 0.03 (12). Absorption and extinction corrections were not applied to the data.

The structure was solved by conventional Patterson and Fourier techniques and refined to a value for R = 0.057. In the refinement, each structure amplitude was given a weight which was the inverse of its standard deviation and the quantity minimized was $\Sigma\omega(|F_o| - |F_c|)$. The chlorine, oxygen, and methyl carbon atoms were refined anisotropically, all other atoms having isotropic temperature factors. The hydrogen atoms of the tricyclic system were included in calculated positions, with temperature factors 10% greater than the atom to which they were attached, and were not refined. The methyl hydrogens were located in a difference electron density map, and included in the refinement as a hindered rotor (13). No feature in the difference electron density map could be attributed to the hydrogen of the hydrochloride system and this atom was omitted from the calculations.

Scattering factors for all heavy atoms were those of Cromer (14), while for hydrogen those of Stewart, Davison, and Simpson were used (15). Anomalous dispersion factors were included for chlorine.

The statistically favoured configuration (16) is that shown in Fig. 1, but there was very little difference between the weighted R values for the two hands, and an unambiguous choice could not be made.

Acknowledgements

We wish to acknowledge with thanks the financial support provided by the National Research Council of Canada and the University of Alberta.

1. K. S. HAGEN. National Geographic, **137**, 543 (1970).
2. G. M. HAPP and T. EISNER. Science, **134**, 329 (1961).
3. (*a*) B. TURSCH, D. DALOZE, M. DUPONT, C. HOOTELE, M. KARAIN, J. M. PASTEELS, and D. ZIMMERMAN. Chimia. **25**, 307 (1971); (*b*) R. KARLSSON and D. LOSMAN. Chem. Commun. 626 (1972).
4. B. TURSCH, D. DALOZE, J. C. BRAEKMAN, C. HOOTELE, A. CRAVADOR, D. LOSMAN, and R. KARLSSON. Tetrahedron Lett. 409 (1974).
5. B. TURSCH, D. DALOZE, C. HOOTELE, J. C. BRAEKMAN, and J. M. PASTEELS. Tetrahedron, **31**, 1541 (1975).
6. B. TURSCH, D. DALOZE, and C. HOOTELE. Chimia, **26**, 74 (1972).
7. G. J. FIELDS and R. D. MCMULLEN. J. Entomol. Soc. B.C. **69**, 25 (1972).
8. J. C. CRAIG and K. K. PURUSHOTHAMAN. J. Org. Chem. **35**, 1721 (1970).
9. A. C. COPE and E. CIGANEK. Org. Syn. Coll. Vol. **4**, 399, 612 (1963).
10. W. A. AYER, R. DAWE, R. EISNER, and K. FURUICHI. Can. J. Chem. **54**, 473 (1976).
11. L. M. JACKMAN and S. STERNHELL. *In* Application of nuclear magnetic resonance spectroscopy in organic chemistry. 2nd ed. Pergamon Press, Toronto. 1969. pp. 294–298.
12. P. W. R. CORFIELD, R. J. DOEDENS, and J. A. IBERS. Inorg. Chem. **6**, 197 (1967).
13. M. J. BENNETT, W. L. HUTCHEON, and B. M. FOXMAN. Acta Crystallogr. Sect. A, **31**, 488 (1975).
14. D. T. CROMER. Acta Crystallogr. Sect. A, **24**, 321 (1968).
15. R. F. STEWART, E. R. DAVIDSON, and W. T. SIMPSON. J. Chem. Phys. **42**, 3175 (1965).
16. W. C. HAMILTON. Acta Crystallogr. **18**, 502 (1965).

Can. J. Chem. Downloaded from www.nrcresearchpress.com by 210.87.254.105 on 09/05/12
For personal use only.

Determination of $D[(C_2H_5)_3Sn—C_2H_5]$ by the toluene carrier method and studies of the reaction of C_2H_5 with toluene

MARY DALY AND S. JAMES W. PRICE[1]

Department of Chemistry, University of Windsor, Windsor, Ont., Canada N9B 3P4

Received February 9, 1976

MARY DALY and S. JAMES W. PRICE. Can. J. Chem. **54**, 1814 (1976).

The thermal decomposition of tetraethyltin in a toluene carrier flow system has been studied over the temperature range 725 to 833 K and decompositions of 3.4 to 98.0%. Total pressure in all runs were in the range 0.63 to 0.90 kPa and contact times of 0.59 to 4.2 s were used.

The progress of the reaction was followed by carrying out full analysis of all pyrolysis products involving the C_2H_5 radical, assuming that all four C_2H_5 groups are released. In selected runs analysis for unreacted alkyl was also performed. The agreement between the two methods indicates that reaction 1 is followed rapidly by reactions 2, 3, and 4,

[1] $$Sn(C_2H_5)_4 \rightarrow Sn(C_2H_5)_3 + C_2H_5$$

[2] $$Sn(C_2H_5)_3 \rightarrow Sn(C_2H_5)_2 + C_2H_5$$

[3] $$Sn(C_2H_5)_2 \rightarrow Sn(C_2H_5) + C_2H_5$$

[4] $$Sn(C_2H_5) \rightarrow Sn + C_2H_5$$

or alternate reactions that result in the release of all four C_2H_5 groups each time reaction 1 occurs.

The decomposition is essentially homogeneous and

$$\log k_1\ (s^{-1}) = 16.00 \pm 0.36 - \frac{248\,300 \pm 9\,000}{19.15\,T}$$

or $-59\,340/4.58T$ if the activation energy is expressed in cal rather than J.

Combination of present values of k_5 with data from previous studies

[5] $$C_2H_5 + C_6H_5CH_3 \rightarrow C_2H_6 + C_6H_5CH_2$$

where $Hg(C_2H_5)_2$ and $Zn(C_2H_5)_2$ were used as sources of ethyl radicals gives

$$\log k_5\ (cm^3\ mol^{-1}\ s^{-1}) = 11.28 - \frac{43\,100}{19.15T}$$

with an estimated uncertainty in E_5 of $\pm 4\,000$ J mol^{-1} (E_5 = 10 300 cal mol^{-1}).

MARY DALY et S. JAMES W. PRICE. Can. J. Chem. **54**, 1814 (1976).

On a étudié la décomposition thermique du tétraéthyl d'étain dans un système en mouvement utilisant du toluène comme gaz porteur; ces études ont été effectuées à des températures allant de 725 jusqu'à 833 K et des pourcentages de décomposition de 3.4% jusqu'à 98.0%. La pression totale dans tous les cas variaient de 0.63 à 0.90 kPa et on a utilisé des temps de contact de 0.59 jusqu'à 4.2 s.

On a suivi le progrès de la réaction en effectuant des analyses complètes de tous les produits de pyrolyse impliquant le radical C_2H_5 et en faisant l'hypothèse que les quatre groupes C_2H_5 sont éliminés. Dans des cas particuliers, on a aussi effectué l'analyse de l'alkyle qui n'a pas réagit. La concordance entre les deux méthodes indique que la réaction 1 est suivie rapidement par les réactions 2, 3 et 4,

[1] $$Sn(C_2H_5)_4 \rightarrow Sn(C_2H_5)_3 + C_2H_5$$

[2] $$Sn(C_2H_5)_3 \rightarrow Sn(C_2H_5)_2 + C_2H_5$$

[3] $$Sn(C_2H_5)_2 \rightarrow Sn(C_2H_5) + C_2H_5$$

[4] $$Sn(C_2H_5) \rightarrow Sn + C_2H_5$$

ou d'autres réactions qui conduisent à l'expulsion des quatre groupes C_2H_5 chaque fois que la réaction 1 se produit.

[1]To whom correspondence should be addressed.

Can. J. Chem. Downloaded from www.nrcresearchpress.com by 210.87.254.6 on 09/05/12
For personal use only.

La décomposition est essentiellement homogène et

$$\log k_1\ (s^{-1}) = 16.00 \pm 0.36 - \frac{248\ 300 \pm 9\ 000}{19.15\ T}$$

ou $-59\ 340/4.58T$ si l'énergie d'activation est exprimée en calories plutôt qu'en joules.

En combinant les valeurs que nous avons trouvées pour k_5 avec des données obtenues antérieurement pour

[5] $$C_2H_5 + C_6H_5CH_3 \rightarrow C_2H_6 + C_6H_5CH_2$$

où $Hg(C_2H_5)_2$ et $Zn(C_2H_5)_2$ avaient été utilisés comme sources de radicaux, on peut déterminer que

$$\log k_5\ (cm^3\ mol^{-1}\ s^{-1}) = 11.28 - \frac{43\ 100}{19.15T}$$

avec une incertitude que l'on estime à $\pm 4\ 000$ J mol^{-1} pour E_5 (E_5 = 10 300 cal mol^{-1}).

[Traduit par le journal]

Introduction

The present paper is the third in a series in the pyrolysis of ethyl metallic alkyls by the toluene carrier method and is related to previous studies on methyl metallic alkyls. The toluene carrier study of diethylmercury (1) gave log A (s^{-1}) = 15.4 and E = 191.2 kJ mol^{-1}, in excellent agreement with values proposed by Benson and O'Neal (2). Three previous studies of this compound (3–5) all gave slightly lower log A and E values but all four studies showed a reasonable degree of agreement when rate constants were compared. The toluene carrier work on diethylzinc (6) showed marked catalysis by zinc oxide. In the absence of zinc oxide log A (s^{-1}) = 14.3 and E = 205.0 kJ mol^{-1}. These are the only Arrhenius parameters available for this compound.

In both toluene carrier studies data was also obtained on the reaction of ethyl radicals with toluene. The present work extends this study.

Experimental

Materials

(i) Toluene

The toluene employed was toluene from sulfonic acid, number X325 as supplied by Eastman Organic Chemicals. It was dried by refluxing under vacuum at least 24 h over freshly pressed sodium ribbon and then degassed by bulb-to-bulb distillation.

(ii) Tetraethyltin

The tetraethyltin was obtained from Alfa Inorganics. It was carefully fractionated with head and tail fraction being discarded. Analysis by flame ionization gas chromatography showed no detectable impurities in the center cut used for the kinetic studies.

Apparatus and Procedure

The experiments were carried out in a system similar to that used in previous work (7). The reaction vessel had a volume of 205 cc. To test for surface effects a vessel was packed with small quartz tubes. This vessel had a volume of 101 cc and a surface-to-volume ratio twenty times that of the unpacked vessel. Both vessels were treated with hot concentrated nitric acid before use. The residual acid was baked out under vacuum after the vessels were installed in the reaction system.

The gaseous products were analyzed using a Perkin-Elmer model 154 gas chromatograph equipped with a 6 mm × 2 m silica gel column. The column was maintained at 80 °C, and a helium flow rate of 20 cm^3 per min was used. For hydrogen analysis nitrogen was used in place of helium.

The liquid products from selected runs were analyzed on either Perkin-Elmer model 800 or model 900 gas chromatographs equipped with flame ionization detectors. The model 800 employed a 0.5 mm i.d. by 46 m open tubular column coated with poly(propylene glycol) (Perkin-Elmer Column R). The column and injection port temperatures were set at 75 and 135 °C respectively. Nitrogen was used as the carrier gas. The analyses using the P.E. 900 were done on a 2 mm i.d. × 2 m column packed with 80–100 mesh *n*-octane/porasil C (chemically bonded Durapak). The column and injection port temperatures were 125 and 150 °C respectively.

The preparation of gas chromatographic standards and the method of analysis for butane dissolved in toluene have been previously described (6).

Analysis for residual tetraethyltin was performed concurrently with the gas chromatographic analyses of the liquid products. A digital integrator was used and all analyses and standardizations were based on peak areas.

Results and Discussion

Selected experimental results for the thermal decomposition of tetraethyltin in a toluene carrier flow system are given in Tables 1, 2,

Can. J. Chem. Downloaded from www.nrcresearchpress.com by 210.87.254.6 on 09/05/12
For personal use only.

TABLE 1. Experimental parameters and product distributions for selected runs

T (K)	P (kPa)	t_c (s)	[Toluene]/[Alkyl] (molar ratio)	Product (mol × 10^5) H_2	CH_4	C_2H_6	C_2H_4	*n*-Propyl benzene	C_4H_{10}
833	0.87	1.70	88	29.7	4.2	18.5	103.6	7.3	9.9
806	0.87	4.20	8	91.9	4.9	22.6	158.0	9.6	26.1
799	0.89	3.40	9	77.9	4.6	28.5	190.7	6.8	33.7
785	0.75	1.19	34	23.3	3.2	13.6	81.1	7.9	18.9
776	0.75	1.17	35	—	1 4	9.6	53.9	5.4	10.0
759	0.77	2.39	18	20.1	0.9	8.7	45.7	4.3	9.2
759	0.85	2.39	19	17.9	0.9	9.0	47.5	4.3	8.2
758	0.75	1.17	26	—	0.5	5.7	30.7	3.3	4.1
752	0.75	1.15	30	3.7	0.5	4.6	18.7	2.1	3.5
752	0.73	1.14	29	—	0.5	4.4	17.6	2.2	3.2

and 3. They may be discussed in terms of the following proposed mechanism.

[1] $Sn(C_2H_5)_4 \rightarrow Sn(C_2H_5)_3 + C_2H_5$

[2] $Sn(C_2H_5)_3 \rightarrow Sn(C_2H_5)_2 + C_2H_5$

[3] $Sn(C_2H_5)_2 \rightarrow Sn(C_2H_5) + C_2H_5$

[4] $Sn(C_2H_5) \rightarrow Sn + C_2H_5$

[5] $C_2H_5 + C_6H_5CH_3 \rightarrow C_2H_6 + C_6H_5CH_2$

[5a] $C_2H_5 + C_6H_5CH_2 \rightarrow C_6H_5C_3H_7$

[6] $2C_2H_5 \rightarrow C_4H_{10}$

[7] $2C_2H_5 \rightarrow C_2H_4 + C_2H_6$

[8] $C_2H_5 \rightarrow C_2H_4 + H$

[9] $H + C_6H_5CH_3 \rightarrow CH_3 + C_6H_6$

[10] $H + C_6H_5CH_3 \rightarrow H_2 + C_6H_5CH_2$

[11] $CH_3 + C_6H_5CH_3 \rightarrow CH_4 + C_6H_5CH_2$

[12] $CH_3 + C_2H_5 \rightarrow C_3H_8$

[13] $CH_3 + C_6H_5CH_2 \rightarrow C_6H_5C_2H_5$

[14] $H + C_6H_5CH_2 \rightarrow C_6H_5CH_3$

[15] $5H + C_6H_5CH_3 \rightarrow C_6H_{10}CH_3$

[16] $6H + C_6H_6 \rightarrow C_6H_{12}$

[17] $2H + M \rightarrow H_2 + M$

[18] $H + C_2H_5 \rightarrow C_2H_6$

In addition, based on recent studies on diethylzinc (6), reactions 19 and 20 were considered.

[19] $CH_3 + Sn(C_2H_5)_4 \rightarrow CH_3Sn(C_2H_5)_3 + C_2H_5$

[20] $H + Sn(C_2H_5)_4 \rightarrow HSn(C_2H_5)_3 + C_2H_5$

Even though the retention time for $CH_3Sn(C_2H_5)_3$ could be calculated from retention index values for $Sn(CH_3)_4$ and $Sn(C_2H_5)_4$, no trace of this compound was found when analysis by flame ionization gas chromatography was carried out. Similarly no $HSn(C_2H_5)_3$ could be detected. Based on these negative results reactions 19 and 20 were considered negligible under the conditions used in the present work.

Assuming all CH_4 observed is from reaction 11 and using previously published data (8) on reaction 21

[21] $2CH_3 + M \rightarrow C_2H_6 + M$

indicates that up to 10% of the C_2H_6 found may be from this reaction but in general this figure is well below 5%. Correction for reaction 21 is therefore significant in calculations of $k_5/k_6^{1/2}$ but is of limited importance in calculations of k_1 where, with one exception, it contributed to an overestimate of the percent decomposition of $Sn(C_2H_5)_4$ of less than (0.005 × percent decomposition).

Perhaps the major difference in the pyrolysis of $Sn(C_2H_5)_4$ compared to the previous studies on $Zn(C_2H_5)_2$ and $Hg(C_2H_5)_2$ from this laboratory is the much greater involvement of reaction 8 and therefore of secondary reactions involving hydrogen atoms.

Using values of k_{10} estimated from data on hydrogen abstraction from benzene by hydrogen atoms (9) in conjunction with the abstraction reactions of methyl radicals from benzene (10) and toluene (8) indicates that as the toluene to alkyl ratio changes from 200:1 to 8:1 the percent of the observed hydrogen formed by reaction 10 varies from 100% to approximately 50%. Similarly it may be estimated that based on the

Can. J. Chem. Downloaded from www.nrcresearchpress.com by 210.87.254.6 on 09/05/12
For personal use only.

Can. J. Chem. Downloaded from www.nrcresearchpress.com by 210.87.254.6 on 09/05/12
For personal use only.

TABLE 2. Comparison of percent decomposition of $Sn(C_2H_5)_4$* based on analysis for unreacted alkyl with the % decomposition based on product analysis

T (K)	% Decomposition (product analysis)*	% Decomposition (unreacted alkyl)
823	98	96
785	35	35
783	50	56
776	18	15
773	31	30
771	16	17
752	7.6	7.1
743	6.6	6.1

*Assuming four C_2H_5 radicals released for each $Sn(C_2H_5)_4$ undergoing reaction. That is, fraction decomposed = [2(mol C_4H_{10}) + mol (C_2H_6 + C_2H_4 + C_3H_8 + *n*-propylbenzene)]/4 (mol $Sn(C_2H_5)_4$ used).

TABLE 3. Effect of $Sn(C_2H_5)_4$ concentration on k_1

T (K)	Initial $Sn(C_2H_5)_4$ concentration (10^9 mol cm^{-3})	k_1 (s^{-1})
806	0.57	0.72
	8.2	0.67
	17.0	0.75
794	5.3	0.52
	16.0	0.49
758	3.3	0.074
	4.6	0.074
	4.7	0.080
	4.8	0.082
	6.9	0.085
	7.0	0.083
	9.7	0.079

literature value of reaction 18 (9) this reaction accounts for less than 1% of the total ethane and therefore involves only a minute fraction of the hydrogen atoms. To obtain a material balance in terms of hydrogen then still requires that as the toluene/alkyl ratio goes from 8:1 to 200:1 approximately 35% to 60% of the hydrogen atoms generated by reaction 8 must be removed by reactions 14, 15, and 16. The benzene concentrations are of the order of 10^{-3} of the toluene concentrations so that as expected no significant contribution from reaction 16 could be detected. However, particularly for runs with toluene to alkyl molar ratios of 20:1 or greater (the case in the majority of runs in this work), analysis for methyl cyclohexane indicates that reaction 15 accounts for 13–30% of the hydrogen. This still indicates however that reaction 14 or other similar process must be important.

In addition to the products shown in Table 1, small quantities of propane, benzene, and ethylbenzene were observed. The propane yields were about 0.5–1.0% of the ethylene while the ethylbenzene was 0.2–0.5% of the ethylene. The yields of benzene which ranged from 0.5×10^{-5} to 5.0×10^{-5} moles were in general agreement with the moles (methane + propane + ethylbenzene) as would be expected if CH_3 is removed primarily by reactions 11, 12, and 13.

Table 2 indicates that each time reaction 1 occurs it is rapidly followed by reactions 2, 3, and 4 or some equivalent processes. The values of k_1 in Table 3 and the 51 values of k_1 used to obtain Fig. 1 were calculated from the usual first order equation. The values in Table 3 indicate that the assumption of first order seems valid within the limits of experimental error. Of the 51 values of k_1 used in the figure 33 are based on product analysis and 18 on residual alkyl analysis. In 11 runs both methods were used. No significant heterogeneous contribution to k_1 was observed.

A linear least squares analysis of the points in Fig. 1 gives

$$\log k_1\,(s^{-1}) = 16.00 \pm 0.36 - \frac{248\,300 \pm 9\,000}{19.15T}$$

if the activation energy is expressed in J (E_1 = 59 340 cal mol^{-1}). The error limits are 90% confidence limits. With $\Delta H_{f298}^{0}(Sn(C_2H_5)_4,g)$ = −45.6 kJ mol^{-1} (11), $\Delta H_{f298}^{0}(C_2H_5,g)$ = 105 kJ mol^{-1} (11), and $\Delta H_{f298}^{0}(Sn,g)$ = 302 kJ mol^{-1} (11) the sum of the four metal–carbon bond dissociation energies in $Sn(C_2H_5)_4$ is 766 kJ mol^{-1}. Correcting E_1 to 298 K gives approximately $D_{298}^{0}[(C_2H_5)_3Sn—C_2H_5]$ = 239 kJ mol^{-1}. The average value for D_2 through D_4 is then 180 kJ mol^{-1}. With reasonable estimate of log A_2 = 9.5, log A_3 = 15, and log A_4 = 12 it is possible to satisfy the requirement $k_1 \ll k_2$, k_3, k_4 by assigning D_2, D_3, and D_4 in the ranges 125–150, 205–230, and 165–190 kJ mol^{-1} respectively. This certainly does not establish reactions 2, 3, and 4 as the steps subsequent to reaction 1 but at least indicates that this sequence is consistent with the thermochemistry of the system.

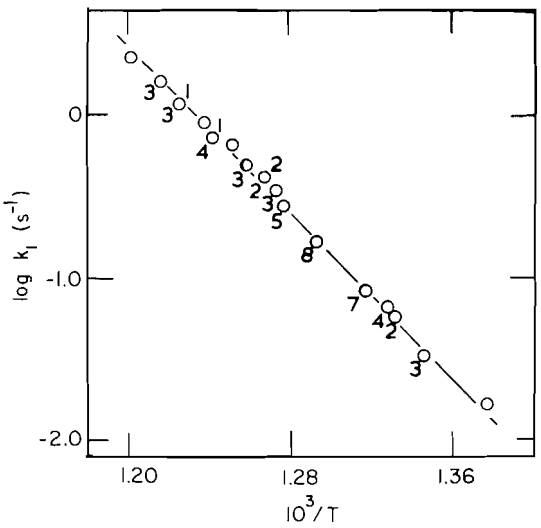

FIG. 1. Arrhenius plot for the decomposition of tetraethyltin. Subscripts indicate number of points averaged to obtain a given point. Superscripts indicate number of runs in packed vessel included in the point. The solid line shown is the linear least mean squares plot.

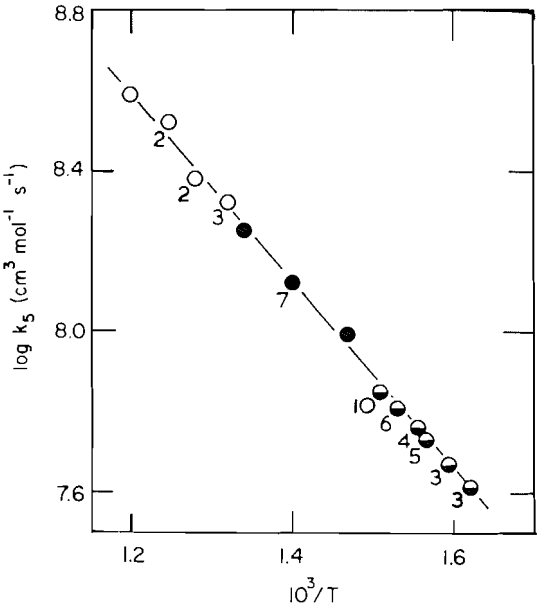

FIG. 2. Arrhenius plot for the abstraction of hydrogen from toluene by ethyl radicals: ○, radical source $Sn(C_2H_5)_4$ (present work); ●, radical source $Zn(C_2H_5)_2$ (6); ◒, radical source $Hg(C_2H_5)_2$ (1).

The low value for log A_2 is based on the assumption that the return of the tin 5*s* electron to its ground state occurs during reaction 2 and is a limiting factor. This is the most restrictive assumption that can be made. Relaxation of this assumption makes reactions 2 through 4 even more thermodynamically feasible.

Although no previous determinations of $D[(C_2H_5)_3Sn—C_2H_5]$ have been reported values of $D[(CH_3)_3Sn—C_2H_5] = 268 \pm 25$ kJ mol^{-1} and $D[(CH_3)_3Sn—CH_3] = 289 \pm 25$ kJ mol^{-1} have been calculated from self-consistent retarded potential difference (r.p.d.) appearance potential data (12). Previous toluene carrier studies (13) gave $D[(CH_3)_3Sn—CH_3] = 270 \pm 4$ kJ mol^{-1}. It might reasonably be expected that $D[(CH_3)_3Sn—C_2H_5]$ should differ little from $D[(C_2H_5)_3Sn—C_2H_5]$. If this is so then even though both r.p.d. values are above the kinetic values the difference $D[R_3Sn—CH_3] - D[R_3Sn—C_2H_5]$ of about 20 kJ mol^{-1} is very close to the difference observed in the kinetic results.

Values of k_5 obtained in the present study have been used along with the data from two previous studies (1, 6) to obtain the Arrhenius plot shown in Fig. 2. The values shown are relative to log $k_6 = 12.6$. The detailed method of calculation has been previously published (6).

The data may be represented by

$$\log k_5 \text{ (cm}^3 \text{ mol}^{-1} \text{ s}^{-1}) = 11.28 - \frac{43\,100 \pm 4\,000}{19.15T}$$

or alternately $-10\,300/4.58T$ if E_5 is expressed in cal mol^{-1}. The value of E_5 reported here is 1.5 kJ mol^{-1} higher than the previously reported value (6).

Acknowledgment

This work has been supported by a grant from the National Research Council of Canada.

1. A. C. LALONDE and S. J. W. PRICE. Can. J. Chem. **49**, 3367 (1971).
2. S. W. BENSON and H. E. O'NEAL. Kinetic data on gas phase unimolecular reactions. NSRDS-NBS21. 1970. p. 520.
3. H. V. CARTER, E. I. CHAPPELL, and E. WARHURST. J. Chem. Soc. 106 (1956).
4. W. PASTFIELD. Diss. Abstr. **15**, 1325 (1955).
5. C. HEITZ. J. Organomet. Chem. **8**, 401 (1967).
6. A. A. KOSKI, S. J. W. PRICE, and B. C. TRUDELL. Can. J. Chem. **54**, 482 (1976).
7. M. KRECH and S. J. PRICE. Can. J. Chem. **41**, 224 (1963).
8. A. N. DUNLOP, R. J. KOMINAR, and S. J. W. PRICE. Can. J. Chem. **48**, 1269 (1970).
9. J. A. KERR and E. RATAJCZAK. Second supplementary

Can. J. Chem. Downloaded from www.nrcresearchpress.com by 210.87.254.6 on 09/05/12
For personal use only.

tables of bimolecular gas reactions. Chemistry Department, University of Birmingham, U.K. 1973.
10. M. KRECH and S. J. PRICE. Can. J. Chem. **45**, 157 (1967).
11. Selected values of chemical thermodynamic properties. Natl. Bur. Std. U.S. Tech. Note 270-3. (1968).
12. M. R. LITZOW and J. R. SPALDING. Physical inorganic chemistry, monograph 2. Mass spectrometry of inorganic and organometallic compounds. *Edited by* M. F. Cappert. Elsevier, Amsterdam. 1973. p. 305.
13. R. P. JOHNSON and S. J. W. PRICE. Can. J. Chem. **50**, 50 (1972).

Can. J. Chem. Downloaded from www.nrcresearchpress.com by 210.87.254.6 on 09/05/12
For personal use only.

The kinetic activation volumes for the binding of chloride to iron(III), studied by means of a high pressure laser temperature jump apparatus[1]

BRIAN B. HASINOFF[2]

University Chemical Laboratory, University of Kent at Canterbury, Canterbury, Kent, England

Received January 19, 1976

BRIAN B. HASINOFF. Can. J. Chem. **54**, 1820 (1976).

The volumes of activation for the kinetics of the reaction of Cl^- with Fe^{3+} and $FeOH^{2+}$ have been determined by a laser temperature jump relaxation method at pressures up to 2.76 kbar. The results indicate that the two species, $FeOH^{2+}$ and Fe^{3+}, react with Cl^- by different mechanisms. The activation volume for the binding of Cl^- to $FeOH^{2+}$ is positive (7.8 ± 1.0 cm^3 mol^{-1}), which is consistent with a dissociative interchange mechanism. The activation volume for the binding of Cl^- to Fe^{3+} is negative (-4.5 ± 1.1 cm^3 mol^{-1}), which is consistent with an associative interchange mechanism.

BRIAN B. HASINOFF. Can. J. Chem. **54**, 1820 (1976).

On a déterminé, à des pressions allant jusqu'à 2.76 kbar et utilisant une méthode de relaxation par des sauts de température par laser, les volumes d'activation pour les cinétiques de réaction du Cl^- avec Fe^{3+} et $FeOH^{2+}$. Les résultats indiquent que les deux espèces $FeOH^{2+}$ et Fe^{3+} réagissent avec Cl^- par des mécanismes différents. Le volume d'activation pour la liaison du Cl^- avec le $FeOH^{2+}$ est positif (7.8 ± 1.0 cm^3 mol^{-1}) ce qui est en accord avec un mécanisme d'échange dissociatif. Le volume d'activation pour la liaison du Cl^- avec le Fe^{3+} est négatif (-4.5 ± 1.1 cm^3 mol^{-1}) ce qui est en accord avec un mécanisme d'échange associatif.

[Traduit par le journal]

A variety of ligands have been used to study the kinetics of ligand substitution on Fe(III) including chloride, azide, bromide, thiocyanate, and sulfate (1). In previous kinetic high pressure studies, the activation volumes ($\Delta V^{\neq}$) for substitution of several ligands on such metal ions as Co^{2+}, Ni^{2+}, Zn^{2+}, and Cu^{2+} (2–4) were found to be consistent with a dissociative interchange mechanism as suggested by Eigen and Wilkins (5, 6) in which in the activated complex a water molecule has begun to dissociate from the metal ion.

This work extends these studies of ligand substitution kinetics to another charged anionic ligand, Cl^-:

$$[1] \qquad Fe^{3+} + Cl^- \underset{k_d}{\overset{k_f}{\rightleftharpoons}} FeCl^{2+}$$

The weakly basic ligand Cl^- was chosen in order to eliminate the kinetic ambiguity that arises when the neutral acid formed from the ligand is also present in concentrations such that it can be a reactive species. Under the conditions of high acidity in which reaction 1 was carried out, HCl is present in only vanishingly small concentrations.

Brower (7) has measured the effect of pressure on the kinetics of thiocyanate substitution on Fe(III) at a single acid concentration but did not obtain the activation volumes for each term in the rate law.

Experimental

Reagents

All reagents used ($Fe(NO_3)_3$, NaCl, $NaClO_4$, $HClO_4$, and $Cu(NO_3)_2$) were of analytical reagent grade. Acid concentrations were determined by titration of stock solutions before known dilutions were made. All solutions were prepared with triply distilled water on a molar concentration scale. For the purposes of the pressure work, the rate and equilibrium constants are on a molality scale reduced to molarity at 1 bar; that is, no corrections to the rate and equilibrium constants were made for the compression of the solvent. The compression is less than 4% (8). The total ionic strength in all experiments was kept constant at 1.5 *M* by the addition of $NaClO_4$ to solutions containing NaCl and $HClO_4$.

Apparatus

The high pressure laser temperature jump apparatus used in previous studies has been described in some detail (2, 3, 9). It is sufficient to say that the kinetics of the reaction of Cl^- substitution were followed spectrophotometrically on a Tektronix 549 storage oscilloscope.

[1]This work has been supported by the Science Research Council by Research Grant B/SR/8667.

[2]Present address: Department of Chemistry and Faculty of Medicine, Memorial University of Newfoundland, St. John's, Newfoundland A1C 5S7.

Can. J. Chem. Downloaded from www.nrcresearchpress.com by 210.87.254.5 on 09/05/12
For personal use only.

Can. J. Chem. Downloaded from www.nrcresearchpress.com by 210.87.254.5 on 09/05/12
For personal use only.

The ruby laser pulse was 90% complete in 500 μs and was much faster than the observed chemical relaxations.

The temperature of the stainless steel pressure vessel was maintained constant to ±0.1 K through channels carrying circulating water from a thermostat bath.

All reaction solutions were 5×10^{-2} *M* in cupric nitrate which was used to absorb the light energy at 694 nm from the laser and convert it into heat; the temperature jump was 1.3 K. Since Cu(II) binds Cl^- to some extent a small correction of the order of 4 to 6% was made to the total $[Cl^-]$. Kinetic experiments conducted in the presence and absence of cupric nitrate on a joule heating temperature jump apparatus (Messanlaagen, Göttingen) indicated that there was no detectable chemical interaction between Cu(II) and the other reagents. The concentration of Fe(III) in all kinetic experiments was constant at 2.5×10^{-3} *M*. The sample solution was contained in a Pyrex spectrophotometric cell sealed by a KEL-F piston and rubber O-rings, which showed no deterioration after long exposure to the concentrated $HClO_4$ solutions.

The exponential traces obtained upon application of the temperature perturbation of the equilibrium of reaction 1 were measured by a trace matching method (9) to obtain τ^{-1}, the reciprocal relaxation time.

Results

Kinetic

The acid dependence of the kinetics of the binding of Cl^- to Fe(III) has been interpreted by a reaction scheme in which the species Fe^{3+} and $FeOH^{2+}$ react at different rates with Cl^- (10–12):

[2]
$$\begin{array}{ccccc} Fe^{3+} & + & Cl^- & \underset{k_{-1}}{\overset{k_1}{\rightleftharpoons}} & FeCl^{2+} \\ K_{OH}\uparrow\downarrow & & & & \uparrow\downarrow K_{OHCl} \\ FeOH^{2+} & + & Cl^- & \underset{k_{-2}}{\overset{k_2}{\rightleftharpoons}} & FeOHCl^+ \end{array}$$

where $K_{OH} = [FeOH^{2+}][H^+]/[Fe^{3+}]$ and $K_{OHCl} = [FeOHCl^+][H^+]/[FeCl^{2+}]$. The relaxation expression for reaction scheme 2 is

[3] $$\tau^{-1} = k_f(Fe(III)] + [Cl^-]) + k_d$$

where

[4] $$k_f = k_1 + k_2K_{OH}/[H^+]$$

and

[5] $$k_d = k_{-1} + k_{-2}K_{OHCl}/[H^+]$$

Combining eqs. 4 and 5 with eq. 3 gives

[6] $$\tau^{-1} = k_1([Fe(III)] + [Cl^-]) + k_2K_{OH}([Fe(III)] + [Cl^-])/[H^+] + k_{-1} + k_{-2}K_{OHCl}/[H^+]$$

The equilibrium constant for the binding of Cl^- according to reaction 1 is given by

[7] $$K_{Cl} = \frac{[FeCl^{2+}] + [FeOHCl^+]}{([Fe^{3+}] + [FeOH^{2+}])[Cl^-]}$$

However, under conditions of high acid concentration such as that used in this study, $[Fe^{3+}] \gg [FeOH^{2+}]$ and $[FeCl^{2+}] \gg [FeOHCl^+]$, so that eq. 7 reduces to

[8] $$K_{Cl} = [FeCl^{2+}]/[Fe^{3+}][Cl^-]$$

Hence

[9] $$K_{Cl} = k_1/k_{-1}$$

From the principle of detailed balance applied to reaction scheme 2 the rate and equilibrium constants are related by

[10] $$k_1k_{-2}K_{OHCl} = k_2K_{OH}k_{-1}$$

which has the effect of reducing the number of unknown parameters in eq. 6 from 4 to 3 at any given temperature and pressure.

The experimentally determined values of τ^{-1} as a function of $[H^+]$, $([Fe(III)] + [Cl^-])$ and *P* are given in Table 1. From transition state theory the change in rate constant with pressure is given by (8)

[11] $$(\partial \ln k/\partial P)_T = -\Delta V^*/RT$$

which is similar in form to the molar volume change in a reaction for which the equilibrium constant, *K*, varies with pressure.

[12] $$(\partial \ln K/\partial P)_T = -\Delta V^0/RT$$

The pressure dependence of ln *k* (or ln *K*) has usually been analyzed in terms of one of two equations: $\ln k = a + bP$ or $\ln k = a + bP + cP^2$. The latter is applied where the plot of ln *k* is curved with pressure. In cases where there is little or no curvature it is common to use the equation that is linear in *P*. A preliminary analysis of the relaxation data of Table 1 was carried out by putting eq. 6 in a form that could be analyzed by a series of linear plots whose slopes and intercepts were determined by a weighted linear least-squares analysis carried out by computer. In the first analysis k_f and k_d of eq. 3 were obtained from a least squares analysis of plots of τ^{-1} *vs.* $([Cl^-] + [Fe(III)])$ at each successive pressure. The logarithms of values of k_1 and k_2K_{OH} obtained from an

TABLE 1. Reciprocal relaxation times for the reaction of Fe(III) with Cl^- at various hydrogen ion concentrations and pressures at 25.0 °C and ionic strength 1.5 *M*

$[H^+]$ (*M*)	$[Fe(III)]+[Cl^-]$ (*M*)	$\tau^{-1}(s^{-1})$ at *P* (kbar)				
		0.001	0.69	1.38	2.07	2.76
0.812	0.049	10.9	11.2	11.9	12.2	12.7
0.812	0.097	11.5	12.1	13.4	14.5	16.3
0.812	0.192	13.4	13.5	14.0	15.5	16.7
0.812	0.282	14.2	14.2	14.6	15.9	17.5
0.812	0.385	15.8	17.0	16.5	17.7	19.8
0.812	0.483	17.4	16.8	16.8	18.7	22.1
0.612	0.049	13.6	13.4	14.5	16.1	19.2
0.612	0.097	14.1	14.2	15.1	16.4	17.9
0.612	0.192	16.7	16.1	19.0	17.6	19.3
0.612	0.282	18.6	17.6	18.4	19.1	20.5
0.612	0.385	19.7	19.3	19.0	19.5	20.8
0.612	0.483	21.5	21.1	21.0	22.1	23.1
0.412	0.049	18.0	17.5	18.9	20.0	21.5
0.412	0.097	18.8	18.3	18.6	19.3	20.9
0.412	0.192	21.5	20.8	20.8	21.9	22.4
0.412	0.282	24.7	23.2	23.9	23.7	24.9
0.412	0.385	25.6	24.7	24.8	25.4	26.5
0.412	0.483	28.6	26.9	26.2	26.3	27.9

analysis of eq. 4 and k_{-1} and $k_{-2}K_{OHCl}$ obtained from an analysis of eq. 5 were then plotted against *P*. In all cases it was found that the plots were linear within experimental error; the constants describing the curvature were insufficiently accurate to warrant analysis by this method. Hence for this preliminary analysis, values of ΔV^* were obtained from such plots for each term of eqs. 4 and 5.

The final analysis, the results of which are given in Table 2, was obtained by solving all of the data in Table 1 simultaneously by means of a non-linear least-squares computer program using the values obtained in the preceding linear least-squares analysis as the initial parameter estimates (IBM SHARE Library, Program SDA 3094, 1964). Also shown for comparison in Table 2 are rate constants determined by previous workers. When the pressure dependence is taken into account eq. 6 becomes

$$[13]\quad \tau^{-1} = k_1 e^{(-P\Delta V_1^*/RT)}([Fe(III)] + [Cl^-]) + k_2 K_{OH} e^{(-P\Delta V_{2OH}^*/RT)} \times ([Fe(III)] + [Cl^-])([H^+]^{-1}) + k_{-1} e^{(-P\Delta V_{-1}^*/RT)} + k_{-2} K_{OHCl} e^{(-P\Delta V_{-2OHCl}^*/RT)}([H^+]^{-1})$$

where the pre-exponential terms are the values of constants (rate and products of rate and equilibrium constants) at 0 bar which is effectively equal to 1 bar for this study. In eq. 13 there are three independent variables ($[H^+]$, $([Fe(III)] + [Cl^-])$, and *P*) and one dependent variable (τ^{-1}), along with 8 constant parameters. In the final analysis, the number of parameters in eq. 13 was reduced to 6 by means of eq. 10; $k_{-2}K_{OHCl}$ was replaced by $k_2K_{OH}k_{-1}/k_1$ and ΔV_{-2OHCl}^* by $(\Delta V_{2OH}^* + \Delta V_{-1}^* - \Delta V_1^*)$. These substitutions have the effect of reducing the number of unknown parameters and allowing all parameters to be determined with a greater degree of accuracy. The standard errors on the individual parameters were decreased by about half in going from the linear to the non-linear analysis.

All of the errors quoted are fitting errors of ± 1 standard deviation and are not equivalent to the estimated reliabilities of the parameters. The non-linear least-squares fit to the τ^{-1} data is shown in part in Figs. 1 and 2.

Equilibrium

The change in equilibrium constant with pressure for reaction 1 was measured spectrophotometrically by determining K_{Cl} at each successive pressure. A weighted linear least-squares analysis of a plot of $\Delta A/([Fe(III)] + [Cl^-])$ against ΔA gave K_{Cl} at each pressure (13).

Can. J. Chem. Downloaded from www.nrcresearchpress.com by 210.87.254.5 on 09/05/12
For personal use only.

TABLE 2. Volumes of activation and rate constants for the reaction of Fe(III) and Cl^- at 25.0 °C and ionic strength 1.5 M[a]

Reaction step	Rate constant at 0 bar[b]	ΔV^* ($cm^3\ mol^{-1}$)
$Fe^{3+} + Cl^- \xrightarrow{k_1}$	$4.8 \pm 0.4\ M^{-1}\ s^{-1}$	-4.5 ± 1.1
$FeOH^{2+} + Cl^- \xrightarrow{k_2}$	$(5.5 \pm 0.5) \times 10^3\ M^{-1}\ s^{-1}$	7.8 ± 1.0
$FeCl^{2+} \xrightarrow{k_{-1}}$	$3.2 \pm 0.2\ s^{-1}$	-9.2 ± 0.7
$FeOHCl^+ \xrightarrow{k_{-2}}$	$(4.7 \pm 1.0) \times 10^2\ s^{-1}$	—

Parameter	Value of Parameter at 0 bar	ΔV^* ($cm^3\ mol^{-1}$)
k_2K_{OH}	$8.2 \pm 0.4\ s^{-1}$	6.8 ± 0.8
$k_{-2}K_{OHCl}$	$5.6 \pm 0.7\ M\ s^{-1}$	2.2 ± 1.5

[a]Values of these parameters were determined by non-linear least squares analysis of eq. 13.

[b]Previous determinations for k_1 range from 9.4 to 19 $M^{-1}\ s^{-1}$ (10, 11, 26); for k_{-1} from 1.1 to 4.7 s^{-1} (10–12, 26); for k_2K_{OH} from 18 to 33 s^{-1} (10, 11, 26, 28) and for $k_{-2}K_{OHCl}$ from 3.4 to 10 $M\ s^{-1}$ (10–12, 26, 28). All these values at 25 °C but with the ionic strength variously from 0.6 to 2 M.

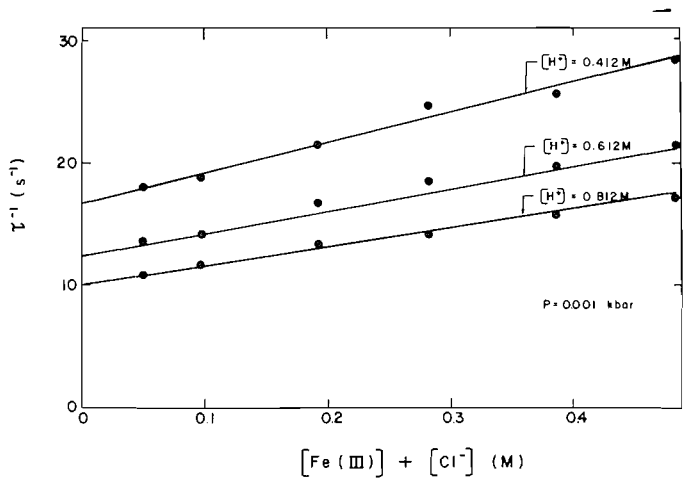

FIG. 1. The reciprocal relaxation time, τ^{-1}, observed for the reaction of Fe(III) with Cl^- plotted as a function of ([Fe(III)] + [Cl^-]) at 25.0 °C and an ionic strength of 1.5 M. The solid straight lines are those calculated from the overall non-linear least-squares analysis of all of the data in eq. 13. This function is linear when plotted against ([Fe(III)] + [Cl^-]) at a given constant pressure and [H^+].

A subsequent linear least-squares analysis of the data in terms of eq. 12 gave a value of $\Delta V^0 = 4.6 \pm 2.3\ cm^3\ mol^{-1}$, and a value of K_{Cl} at 1 bar of $5.5 \pm 1.4\ M^{-1}$. This compares well with a previous determination interpolated to an ionic strength of 1.5 M and at a pressure of 1 bar of $K_{Cl} = 4.5 \pm 0.2\ M^{-1}$ (13). The value of ΔV^0 determined spectrophotometrically agrees with the value calculated kinetically from the parameters of Table 2 and eq. 9, $\Delta V^0 = \Delta V_1^* - \Delta V_{-1}^* = 4.6 \pm 1.3\ cm^3\ mol^{-1}$. This is an independent check of the self consistency of mechanism 2. The magnitude and the sign of ΔV^0 is consistent with a reaction that involves charge neutralization resulting in a decrease in electrostriction of solvent water around the ions and a consequent increase in volume (8).

Knowing K_{OH} and K_{OHCl}, it is possible to calculate k_2 and k_{-2} from the value of k_2K_{OH} and $k_{-2}K_{OHCl}$ in Table 2. The value of K_{OH} at 1 bar

Can. J. Chem. Downloaded from www.nrcresearchpress.com by 210.87.254.5 on 09/05/12
For personal use only.

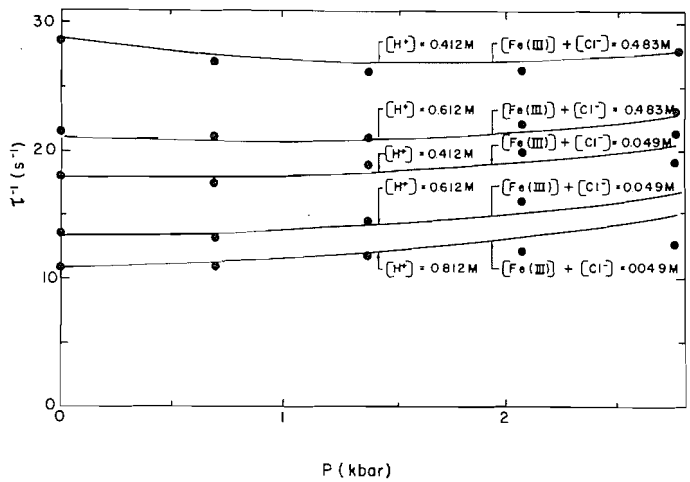

FIG. 2. The reciprocal relaxation time, τ^{-1}, observed for the reaction of Fe(III) with Cl^- plotted as a function of P at 25.0 °C and an ionic strength of 1.5 M. The solid curved lines are those calculated from the overall non-linear least-squares analysis of all of the data in eq. 13. Each of the data points that fall along the curved lines were determined at the indicated constant values of $[H^+]$ and ($[Fe(III) + [Cl^-]$). It is necessary to plot the data in this manner as eq. 13 contains 1 dependent and 3 independent variables.

and ionic strength 1.5 M has been determined as $K_{OH} = (1.5 \pm 0.1) \times 10^{-3}$ M (14) and $K_{OHCl} = (1.2 \pm 0.2) \times 10^{-2}$ M at 1 bar and ionic strength 0.4 M (12). Using these values gives $k_2 = (5.5 \pm 0.5) \times 10^3$ M^{-1} s^{-1} and $k_{-2} = (4.7 \pm 1.0) \times 10^2$ s^{-1} at 1 bar. Similarly, since $\Delta V_2^* = \Delta V_{2OH}^* - \Delta V_{OH}^0$, $\Delta V_2^* = 7.8 \pm 1.0$ cm^3 mol^{-1} taking $\Delta V_{2OH}^* = 6.8 \pm 0.8$ cm^3 mol^{-1} from Table 2 and $\Delta V_{OH}^0 = -1$ cm^3 mol^{-1}.[3]

Discussion

Reaction of $FeOH^{2+}$ with Cl^-

It would appear that a large number of ligand substitution reactions (15–18), particularly on divalent metals, follow Eigen's mechanism (5, 6) in which, after prior formation of an outer sphere complex, ligand water dissociates from the first coordination sphere of the metal ion. This mechanism predicts that for a reaction such as that of $FeOH^{2+}$ and Cl^-

$$[14] \qquad k_2 = K_{os} k_{H_2O}$$

where k_2 is the second order rate constant for ligand binding in reaction 2, K_{os} is the outer sphere formation equilibrium constant, and k_{H_2O} is the first order rate constant for dissociation of inner coordination sphere water from the metal ion – outer sphere complex. It follows from eq. 14 that the overall activation volume is given by

$$[15] \qquad \Delta V_2^* = \Delta V_{os}^0 + \Delta V_{H_2O}^*$$

Starting from a theoretical expression for K_{os} developed by Eigen (19) and Fuoss (20), Hemmes (21) showed that

$$[16] \qquad \Delta V_{os}^0 = RT[(|z_+ z_-| e^2/aDkT) \times (\partial \ln D/\partial P)_T - \beta]$$

where R is the gas constant; z_+ and z_- are the charges on the two ions; a is the distance of closest approach; D is the dielectric constant; k is Boltzmann's constant, and β is the solution compressibility. Using this formula, Hemmes (21) found reasonable agreement with experimentally determined values of ΔV_{os}^0. For the formation of an outer sphere complex between $FeOH^{2+}$ and Cl^- in water, following previous work (4, 21) and taking $z_+ z_-$ as -2, a as 0.5 nm, D as 78, $(\partial \ln D/\partial P)$ as 5.9×10^{-5} bar^{-1} in water at 25 °C and 1 bar (22), this gives $\Delta V_{H_2O}^0$ as about 3.2 cm^3 mol^{-1}. Hence the value of $\Delta V_{H_2O}^*$, calculated from eq. 15, is $\Delta V_{os}^0 = (7.8 - 3.2) = 4.6$ cm^3 mol^{-1}. This value is consistent with the results of previous work with some bivalent metal ions reacting with various ligands which

[3] D. R. Stranks, private communication to E. F. Caldin, 1973.

Can. J. Chem. Downloaded from www.nrcresearchpress.com by 210.87.254.5 on 09/05/12
For personal use only.

Can. J. Chem. Downloaded from www.nrcresearchpress.com by 210.87.254.5 on 09/05/12
For personal use only.

TABLE 3. Values of $\Delta V^{*}_{H_2O}$ calculated assuming a dissociative mechanism for ligand substitution

Metal ion	Ligand	$\Delta V^{*}_{H_2O}$ ($cm^3\ mol^{-1}$)
$FeOH^{2+}$	Cl^-	4.6 ± 1.0^a
Co^{2+}	PADA[d]	7.2 ± 0.2^b
	NH_3	4.8 ± 0.7^b
	Glycinate$^-$	5 ± 2^c
Ni^{2+}	PADA[d]	7.7 ± 0.3^b
	NH_3	6.0 ± 0.3^b
	Glycinate$^-$	7 ± 1^c
Cu^{2+}	Glycinate$^-$	9 ± 1^c
Zn^{2+}	Glycinate$^-$	4 ± 1^c

[a]This work.
[b]Reference 3.
[c]Reference 4.
[d]Pyridine-2-azo-*p*-dimethylaniline.

all give values in the range 4 to 9 $cm^3\ mol^{-1}$ (Table 3). It suggests that the activation volume is due to the stretching of the metal ion – water bond (3, 4, 8) in the activated complex in a dissociative process.

Reaction of Fe^{3+} with Cl^-

In contrast to the positive value of ΔV_2^{*} for the reaction of $FeOH^{2+}$, the value for the reaction of Fe^{3+} with Cl^- is negative; $\Delta V_1^{*} = -4.5 \pm 1.1\ cm^3\ mol^{-1}$. This result cannot be explained simply on the basis of the Eigen mechanism. Equation 16 would predict for reaction of a 3+ ion with a 1− ion, a value of ΔV_{os} of 5.4 $cm^3\ mol^{-1}$; hence, by eq. 15 $\Delta V_{H_2O}^{*} = (-4.5 - 5.4) = -9.9\ cm^3\ mol^{-1}$. This large negative value is not consistent with stretching of the metal ion – water bond in the activated complex in a dissociative mechanism.

The negative activation volume, ($\Delta V_1^{*} = -4.5 \pm 1.1\ cm^3\ mol^{-1}$), for the overall reaction is consistent with an associative mechanism (8) for ligand substitution in which in the activated complex the ligand is entering the inner coordination sphere of the metal ion. If it is further assumed that the mechanism is an associative interchange in which the ligand in the second coordination sphere (or outer sphere complex) enters the inner coordination sphere in the activated complex, the overall value of ΔV_1^{*} should consist of a bond-making component, ΔV_{bm}^{*}, and a contribution from outer sphere formation; thus $\Delta V_1^{*} = \Delta V_{bm}^{*} + \Delta V_{os}^{0}$. It may be calculated for this mechanism that the bond making component $\Delta V_{bm}^{*} = (-4.5 - 5.4) = -9.9\ cm^3\ mol^{-1}$. Such a value is typical of bond making processes (8).

The ligand dependence of the formation rate constant of reaction of Fe(III) given by the first term of eq. 6, with various ligands (1, 5, 23, 24, 25) has been well noted. Generally, dependence of a formation rate constant upon the nature of the ligand is taken as evidence for an associative type mechanism (15). But in the case of ligands that are weakly acidic (*e.g.*, azide, acetate, salicylate, etc.) (23, 24) there is a kinetic ambiguity as to which path or paths are kinetically significant. This ambiguity may give rise to a ligand dependence on the rate constant. This ambiguity has to do with the placement of the H^+ in the activated complex; as to whether it is on the metal ion or on the incoming ligand. This 'proton ambiguity' as it has also been called cannot be resolved from examining the $[H^+]$ dependence of k_f. Hence the following pathways are kinetically indistinguishable

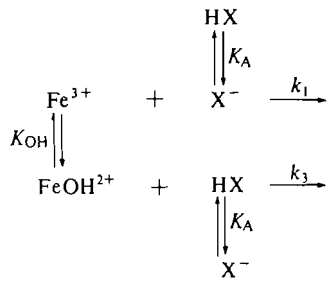

where K_A is the acid dissociation constant of an acidic ligand, HX. For the extended mechanism k_1 in eq. 6 may now be replaced by ($k_1 + k_3 K_{OH}/K_A$). For weakly acidic ligands it can be seen that the ligand dependence on the formation rate constant, k_f, can be explained by the presence of K_A in the above expression (23, 24). Values of k_{H_2O} calculated from eq. 14 in the expression above (assuming $k_1 = 0$) have been noted to 'cluster about' the value of $3 \times 10^4\ s^{-1}$ without any correlation with the acidity of the ligand. For the case of weakly acidic ligands this evidence would seem to indicate that this path could also be dissociative interchange.

However, in the case of ligands that are strong acids (Cl^-, Br^-, SCN^-) the k_3 term cannot be kinetically very significant due to the vanishingly small concentration of protonated ligand (HCl). For strongly acidic ligands the ratio K_{OH}/K_A will be small and the k_1 term will

predominate. Thus the observed 10-fold variation in k_1 with the acidity of the ligands Cl^-, Br^-, and SCN^- (23) is further evidence for the associative character of the k_1 reaction path.

A study (26, 27) of reaction 1 at high ionic strengths and acid concentrations, which had the effect of greatly reducing the activity of water showed that k_{-1}, $\Delta H_{-1}^{\ddagger}$ and $\Delta S_{-1}^{\ddagger}$ are essentially medium independent, indicating that the activated complex for the dissociation of $FeCl^{2+}$ closely resembles the reactants. Further it was concluded from the observed water activity dependence for the formation rate constant (k_1) that the most likely mechanism involves ion pair formation of Cl^- with Fe^{3+} followed by exchange of Cl^- for an inner sphere water molecule, rather than a mechanism involving loss of water followed by addition of Cl^-.

Swaddle (15) goes even further and suggests that there is a change in the general mechanism (except for cobalt) from dissociative interchange to associative interchange in going from divalent to trivalent transition metals.

Eigen (25) has proposed an 'internal hydrolysis' mechanism for ligand binding to Fe^{3+} that involves dissociation of water in the activated complex in order to explain the dependence of k_1 upon the acidity of the incoming ligand. This mechanism is not consistent with the measured negative activation volume of this reaction path as a dissociative mechanism would be expected to give a positive activation volume.

The reason for the change in mechanism (dissociative to associative) in going from $FeOH^{2+}$ to Fe^{3+} may well be that the higher charge density of Fe^{3+} raises the energy required to dissociate the metal cation – water bond. Hence the dissociative mechanism is energetically less favoured than the associative, in which the energy barrier is lowered because of the formation of the new Fe^{3+}—Cl^- bond.

The results of the investigation of the effect of pressure on the kinetics of the reaction of Cl^- with $FeOH^{2+}$ and Fe^{3+} indicate that these two species may undergo ligand substitution by different mechanisms. The reaction of the more labile $FeOH^{2+}$ has a positive activation volume consistent with a dissociative interchange type mechanism; the reaction of the more inert Fe^{3+} has a negative activation volume consistent with an associative interchange mechanism.

Acknowledgement

I would like to acknowledge the advice and encouragement of Professor E. F. Caldin in the course of this work.

1. D. J. Hewkin and R. H. Prince. Coord. Chem. Rev. **5**, 45 (1970).
2. E. F. Caldin, M. W. Grant, and B. B. Hasinoff. J. Chem. Soc. D., 1351 (1971).
3. E. F. Caldin, M. W. Grant, and B. B. Hasinoff. J. Chem. Soc. Faraday I, **68**, 2247 (1972).
4. M. W. Grant. J. Chem. Soc. Faraday I, **69**, 560 (1973).
5. M. Eigen and R. G. Wilkins. Adv. Chem. Ser. No. **49**, 55 (1965).
6. M. Eigen. Pure Appl. Chem. **6**, 97 (1963).
7. K. R. Brower. J. Am. Chem. Soc. **90**, 5401 (1968).
8. W. J. le Noble. Progr. Phys. Org. Chem. **5**, 207 (1965).
9. E. F. Caldin, M. W. Grant, B. B. Hasinoff, and P. A. Tregloan. J. Phys. E. **6**, 349 (1973).
10. R. E. Connick and C. P. Coppel. J. Am. Chem. Soc. **81**, 6389 (1959).
11. T. Yasunaga and S. Harada. Bull. Chem. Soc. Jpn. **42**, 2165 (1969).
12. R. Koren and B. Perlmutter-Hayman. Inorg. Chem. **11**, 3055 (1972).
13. E. Rabinowitch and W. H. Stockmayer. J. Am. Chem. Soc. **64**, 335 (1942).
14. R. M. Milburn and W. C. Vosburgh. J. Am. Chem. Soc. **77**, 1352 (1955).
15. T. W. Swaddle. Coord. Chem. Rev. **14**, 217 (1974).
16. R. G. Wilkins. The study of kinetics and mechanism of reactions of transition metal complexes. Allyn and Bacon, Boston. 1974. p. 181.
17. K. Kustin and S. Swinehart. Progr. Inorg. Chem. **13**, 107 (1970).
18. R. G. Wilkins. Acc. Chem. Res. **3**, 408 (1970).
19. M. Eigen. Z. Phys. Chem. N.F. **1**, 176 (1954).
20. R. Fuoss. J. Am. Chem. Soc. **80**, 5059 (1958).
21. P. Hemmes. J. Phys. Chem. **76**, 895 (1972).
22. B. B. Owen and S. R. Brinkley. Chem. Rev. **29**, 461 (1941).
23. S. Gouger and J. Stuehr. Inorg. Chem. **13**, 379 (1974).
24. P. G. T. Fogg and R. J. Hall. J. Chem. Soc. (A), 1365 (1971).
25. M. Eigen. Advances in the chemistry of coordination compounds. MacMillan, New York, N.Y. 1961. p. 371.
26. J. K. Rowley and N. Sutin. J. Phys. Chem. **74**, 2043 (1970).
27. T. C. King and J. K. Rowley. J. Phys. Chem. **75**, 1113 (1971).
28. H. Wendt and H. Strehlow. Z. Elektrochem. **66**, 228 (1962).

Can. J. Chem. Downloaded from www.nrcresearchpress.com by 210.87.254.5 on 09/05/12
For personal use only.

Effets de substituants en résonance magnétique nucléaire du ^{13}C. Etude des dérivés du phényl-2 furanne et du phényl-2 pyrrole

GILBERT DANA, ODILE CONVERT, JEAN-PIERRE GIRAULT ET ETIENNE MULLIEZ

Laboratoire de Chimie Organique Structurale, Université Pierre et Marie Curie, 4 place Jussieu, 75230 Paris Cedex 05, France

Reçu le 17 décembre 1975

GILBERT DANA, ODILE CONVERT, JEAN-PIERRE GIRAULT et ETIENNE MULLIEZ. Can. J. Chem. **54**, 1827 (1976).

On étudie les spectres rmn de ^{13}C dans des dérivés du phénylfuranne et du phénylpyrrole. Les carbones α et β de l'hétérocycle, conjugués au substituant X en *para* sur le benzène, présentent des variations de déplacement chimique en relation simple avec l'effet donneur de X. Ceci est interprété par le changement de densité électronique dû à cette conjugaison. Cette conjugaison apparaît plus importante dans la série du phényl-2 pyrrole que dans les séries du phényl-2 furanne notamment si on examine le comportement du pôle α.

GILBERT DANA, ODILE CONVERT, JEAN-PIERRE GIRAULT, and ETIENNE MULLIEZ. Can. J. Chem. **54**, 1827 (1976).

The ^{13}C nmr spectra of derivatives of phenylfuran and phenylpyrrole were studied. The α and β carbons of the heterocycle, conjugated to the substituent X in the *para* position of the benzene ring, show variations in chemical shifts which bear a simple relationship to the donor properties of X. This is interpreted by the change in electron density caused by this conjugation. This conjugation seems more important in the series of 2-phenylpyrroles than in the series of 2-phenylfurans especially if the behaviour of the α position is considered.

[Journal translation]

L'étude des substitutions électrophiles sur les hétérocycles pentagonaux (1) dans les substrats **1**, **2** et **3** a permis de mettre en évidence une différence importante dans les régles d'orientation suivant la nature de l'hétérocycle, en ce qui concerne la compétition entre les pôles β et β'.

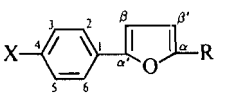

1 R = H
2 R = CH_3

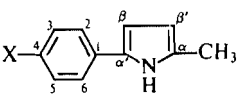

3

a X = NO_2 *d* X = Cl *g* X = OCH_3
b X = CO_2Et *e* X = H *h* X = NH_2
c X = CHO *f* X = CH_3

Ainsi, lorsque R = CH_3, l'orientation observée en série furannique **2** montre que le pôle β est activé par conjugaison avec un substituant benzénique X donneur (2*a*) alors que dans la série du pyrrole **3**, ce facteur électronique joue un rôle apparemment minime (2*b*).

Pour interpréter de façon précise l'ensemble des résultats observés, en tenant compte éventuellement du caractère π plus ou moins important des états de transition (3) dans ces réactions, nous avons été amenés à étudier ces molécules dans leur état fondamental. Ceci permettrait de préciser si le furanne n'est pas, d'une façon générale, plus sensible à la conjugaison du substituant X du noyau benzénique que le pyrrole.

En spectroscopie rmn du ^{13}C, une relation entre la distribution de densité électronique et le déplacement chimique du ^{13}C est souvent invoquée, aussi bien pour les cycles aromatiques benzéniques (4) que pour les hétérocycles du même type (5). Nous avons donc étudié l'influence du substituant X sur les δ ^{13}C des carbones des deux hétérocycles furanne et pyrrole dans les molécules **1** et **2** d'une part (séries du phénylfuranne) et **3** d'autre part (série du phénylpyrrole). Il est ainsi possible d'évaluer la différence de conjugaison de chacun des hétérocycles avec le noyau benzénique.

Résultats expérimentaux

Les spectres rmn ^{13}C ont été enregistrés à 25.15 MHz sur des solutions ($\sim$0.5 *M*) dans $CDCl_3$ (TMS en référence interne, δ positif vers les champs faibles) sur un spectrographe JEOL PS 100, équipé de transformée de Fourier. Les spectres sont normalement effectués avec découplage des protons par une bande de bruit

Can. J. Chem. Downloaded from www.nrcresearchpress.com by 210.87.254.6 on 09/05/12
For personal use only.

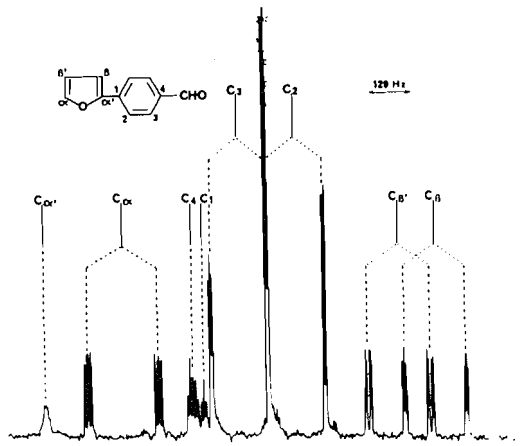

FIG. 1. Spectre non découplé (SD) des carbones aromatiques de **1***c*. On note l'existence d'un couplage supplémentaire du proton aldéhydique avec C_3 (^3J = 2 Hz) et C_4 (^2J = 5.5 Hz).

(DPB), sur une échelle de 5000 Hz en utilisant une mémoire de 8 K: la précision des mesures est donc de ± 0.04 ppm sur les déplacements chimiques. Toutefois, pour attribuer les différents signaux, nous avons également enregistré certains spectres avec découplage sélectif hors résonance (DSHR) ou sans découplage (SD) dans des conditions de relaxation quasi-totale (impulsions correspondant à un angle de 12° avec une répétition de 2.5 s (voir figs 1 et 2 par exemple)). Pour ces deux types de spectres, l'enregistrement a été effectué sur une échelle de 2500 Hz en utilisant une mémoire de 8 K: la précision des mesures est donc de ± 0.6 Hz sur les constantes de couplage. Certains de ces spectres ont été également enregistrés sur spectrographe Varian XL 100-12 à 25.20 MHz (voir par exemple fig. 1).

Phénylfurannes. Séries 1 et 2

Les spectres DPB des phénylfurannes **1** et **2** comportent huit signaux (tableau 1) attribués aux différents carbones aromatiques de la molécule grâce aux critères suivants.

(*a*) Pour la molécule de référence **1***e* (X = H), les carbones α et α' apparaissent à plus bas champ et les carbones β et β' à plus haut champ que les carbones du benzène(7). Les différents carbones du noyau benzénique, pour cette molécule **1***e*, sont attribués par les considérations suivantes. (*i*) Le carbone C_1 ne portant pas de proton donne lieu à un signal peu intense et ne présente pas de grand couplage dans le spectre SD (triplet simple, ^3J(*méta*) = 6.1 Hz). (*ii*) On distingue les pics correspondants à C_2, C_3, C_4 par leurs intensités dans le spectre DPB et par leurs structures fines dans le spectre SD. On sait, en effet, que dans un noyau benzénique, ^3JCH(*méta*) (5 à 7 Hz) est plus grand que ^2JCH(*ortho*) ou ^4JCH(*para*) (1 à 2 Hz) (8). On trouve dans ce cas pour C_3 deux doublets (^1J = 159.5 Hz et ^3J = 7.3 Hz), pour C_2 deux triplets (^1J = 159.9 Hz et ^3J = 6.7 Hz) et pour C_4 deux triplets (^1J = 161.7 Hz et ^3J = 7.4 Hz) d'intensité plus faible (spectre SD effectué dans des conditions de relaxation quasi totale).

Les différents carbones du noyau furannique de **1***e* sont discernables par leurs structures fines comparées à celle du méthyl-2 furanne (5*b*, 9). (*i*) C_α n'a pas de couplage ^1J (massif non résolu). (*ii*) C_α: deux quadruplets (^1J = 202 Hz, ^2J = 10.7 pour 10.4 Hz, et ^3J = 7.6 Hz pour 7.2 Hz (9)). (*iii*) C_β: deux quadruplets (^1J = 175.2 Hz, ^2J = 4.3 Hz pour 4.2 Hz et ^3J = 5.5 Hz pour 5.5 Hz). (*iv*) $C_{\beta'}$: deux quadruplets (^1J = 175.2 Hz, $^2J\mathrm{CH}_\alpha$ = 13.4 Hz pour 13.1 Hz et $^3J\mathrm{CH}_\beta$ = 3.6 Hz pour 4 Hz).

(*b*) Pour les autres termes de la série **1**, les attributions des carbones du noyau benzénique ont été établies sur la base des incréments de déplacements chimiques du substituant X observés pour les benzènes monosubstitués (10) (tableau 1). Celle des carbones α et α' du furanne est effectuée par simple examen du spectre SD de même que celle des carbones β et β' (fig. 1). Cette dernière est de plus confirmée par application de la méthode graphique de Feeney et coll. (11), utilisant des spectres DSHR. Cette méthode permet, en particulier, d'établir que celui des deux carbones C_β et $C_{\beta'}$ qui résonne à plus haut champ est lié, dans tous les cas examinés (y compris la référence **1***e*) au proton qui résonne à plus bas champ. Compte tenu des spectres ^{1}H (12), on vérifie l'attribution générale $\delta C_{\beta'} > \delta C_\beta$.

(*c*) L'interprétation des spectres de la deuxième série furannique **2** (R = CH_3) devient alors possible. On applique les mêmes méthodes que dans la série **1** (examen du spectre SD de **2***e* (X = H), méthode des incréments pour les carbones benzéniques, méthode graphique DSHR pour les carbones β et β'). De plus, cette série fournit deux confirmations de l'ensemble des attributions (séries **1** et **2**) pour les carbones du noyau furannique, d'une part en appliquant

Can. J. Chem. Downloaded from www.nrcresearchpress.com by 210.87.254.6 on 09/05/12
For personal use only.

Can. J. Chem. Downloaded from www.nrcresearchpress.com by 210.87.254.6 on 09/05/12
For personal use only.

TABLEAU 1. Déplacements chimiques $\delta^{13}C$ dans la série des phénylfurannes **1** (valeurs en ppm, par rapport au TMS en référence interne). Les valeurs indiquées entre parenthèses sont les déplacements chimiques calculés pour les carbones du cycle benzénique en utilisant les incréments de déplacement du substituant X dans le benzène (10) en prenant la molécule **1***e* (X = H) comme référence

Composé	X	σ_X	δC_α	$\delta C_{\beta'}$	δC_β	$\delta C_{\alpha'}$	δC_1	δC_2	δC_3	δC_4	δX
1*a*	NO_2	+0.78	143.98	112.30	108.87	151.53	136.26 (136.75)	124.11 (124.61)	123.76 (123.87)	146.23 (147.31)	
1*b*	CO_2Et	+0.45	142.87	111.86	107.06	152.79	134.49 (134.45)†	123.18 (123.31)†	129.87 (128.17)†	128.82 (128.61)†	165.89 60.77 14.30
1*c*	CHO	+0.45*	143.37	112.05	107.99	152.33	134.74 (136.45)	123.65 (124.41)	129.97 (129.97)	135.74 (135.91)	190.95
1*d*	Cl	+0.23	142.26	111.73	105.37	152.89	129.35 (129.05)	124.93 (125.11)	128.81 (129.07)	132.89 (133.51)	
1*e*	H	0	141.97	111.63	105.03	154.00	130.95	123.81	128.67	127.31	
1*f*	CH_3	−0.17	141.82	111.78	104.50	154.59	128.62 (128.05)	124.06 (123.71)	129.64 (129.37)	137.26 (136.21)	21.30
1*g*	OCH_3	−0.27	141.48	111.68	103.48	154.25	124.25 (123.25)	125.41 (124.81)	114.25 (114.27)	159.25 (158.71)	55.28
1*h*	NH_2	−0.66	140.68	111.27	102.24	154.37	121.83 (121.15)	125.05 (124.71)	114.99 (115.37)	145.64 (145.31)	

*Constante σ (CHO) (réf. 6*a*).
†Valeurs approchées, calculées avec l'incrément connu du groupe CO_2Me (6*b*).

Can. J. Chem. Downloaded from www.nrcresearchpress.com by 210.87.254.6 on 09/05/12
For personal use only.

TABLEAU 2. Déplacements chimiques δ ^{13}C dans la série des phénylméthylfurannes **2** (valeurs en ppm, par rapport au TMS en référence interne). Les valeurs indiquées entre parenthèses sont les déplacements chimiques calculés (*i*) pour les carbones du cycle benzénique en utilisant les incréments de déplacement du substituant X dans le benzène (10) et en prenant la molécule **2***e* (X = H) comme référence; (*ii*) pour les carbones du cycle furannique en utilisant les incréments de déplacement du groupe CH_3 dans le furanne (7) et en prenant la molécule **1** correspondante comme référence

Composé	X	σ_X	δC_α	$\delta C_{\beta'}$	δC_β	$\delta C_{\alpha'}$	δC_1	δC_2	δC_3	δC_4	δR	δX
2*a*	NO_2	+0.78	154.60 (153.16)	108.82 (108.16)	110.27 (109.61)	150.03 (149.70)	136.63 (136.99)	124.20 (124.13)	123.14 (123.77)	145.80 (146.68)		
2*d*	Cl	+0.23	152.21 (151.44)	107.84 (107.67)	106.34 (106.11)	151.19 (151.06)	129.35 (129.29)	124.44 (124.53)	128.71 (128.97)	132.21 (132.21)	13.63	
2*e*	H	0	151.82 (151.15)	107.30 (107.57)	105.81 (105.77)	152.26 (152.17)	131.19	123.23	128.57	126.68	13.59	
2*f*	CH_3	−0.17	151.43 (151.00)	107.65 (107.72)	105.13 (105.24)	152.60 (152.76)	128.67 (128.29)	123.33 (123.13)	129.30 (129.27)	136.43 (135.58)	13.63	21.16
2*g*	OCH_3	−0.27	151.04 (150.66)	107.55 (107.62)	104.20 (104.22)	152.35 (152.42)	124.40 (123.49)	124.73 (124.23)	114.06 (114.17)	158.66 (158.08)	13.59	55.08
2*h*	NH_2	−0.66	150.56 (149.86)	107.32 (107.21)	103.19 (102.98)	152.89 (152.54)	122.41 (121.39)	124.74 (124.13)	115.13 (115.27)	145.37 (144.68)		

Can. J. Chem. Downloaded from www.nrcresearchpress.com by 210.87.254.6 on 09/05/12
For personal use only.

TABLEAU 3. Déplacements chimiques δ ^{13}C dans la série des phénylméthylpyrroles **3** (valeurs en ppm, par rapport au TMS en référence interne). Les valeurs indiquées entre parenthèses sont les déplacements chimiques calculés pour les carbones du cycle benzénique en utilisant les incréments de déplacement du substituant X (10) et en prenant la molécule **3***e* (X = H) comme référence

Composé	X	σ_X	δC_α	$\delta C_{\beta'}$	δC_β	$\delta C_{\alpha'}$	δC_1	δC_2	δC_3	δC_4	δR	δX
3*a*	NO_2	+0.78	132.60	109.47	110.41	128.42	138.80 (138.59)	124.56 (124.08)	122.50 (123.87)	144.51 (145.41)	13.24	
3*d*	Cl	+0.23	129.59	108.14	106.68	129.59	130.95 (130.89)	124.44 (124.48)	128.91 (129.07)	131.43 (131.61)	13.10	
3*e*	H	0	129.01	107.80	106.00	130.61	132.79	123.18	128.67	125.41	12.91	
3*f*	CH_3	−0.17	128.52	107.70	105.51	130.90	130.27 (129.89)	123.23 (123.08)	129.44 (129.37)	135.12 (134.31)	13.05	21.01
3*g*	OCH_3	−0.27	128.43	107.80	105.13	130.95	126.39 (125.09)	124.93 (124.18)	114.40 (114.27)	157.98 (156.81)	13.15	55.33

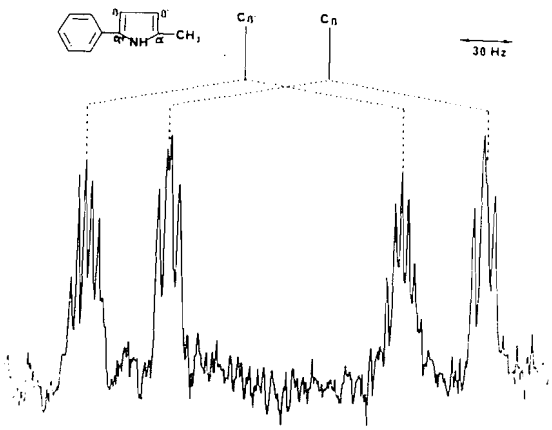

FIG. 2. Spectre non découplé (SD) des carbones β et β' du pyrrole dans **3***e* (voir tableau 2). On note les couplages caractéristiques suivants comparés à ceux observés dans le diméthyl-2,5 pyrrole (*5b*): C_β: ^1J = 169.1 Hz, $^2JC_\beta H_{\beta'}$ = 4.9 pour 4.6 Hz et $^3JC_\beta NH$ = 6.1 pour 7.1 Hz; $C_{\beta'}$: ^1J = 169.1 Hz, $^2J \simeq$ 3.7 pour 4.6 Hz, $^3JC_{\beta'}CH_3 \simeq$ 3.7 Hz et $^3JC_{\beta'}NH \simeq$ 7.3 pour 7.1 Hz.

une méthode d'incréments de déplacement chimique dû au méthyle en α (7) (tableau 2), et d'autre part grâce à l'existence d'un couplage des protons du méthyle avec le seul carbone β' (voir partie expérimentale).

Phénylpyrrole. Série 3

Bien que les carbones C_α et $C_{\alpha'}$ du pyrrole aient (contrairement au cas du furanne) des fréquences de résonance voisines de celles des carbones benzéniques (7, 13) l'analyse des spectres SD et DPB de **3***e* (X = H) est possible par simple examen, sauf pour les signaux de C_α et $C_{\alpha'}$. En particulier, les carbones C_β et $C_{\beta'}$ donnent deux signaux à haut champ attribués, dans chaque cas, par la méthode graphique de Feeney et coll. (11) (spectres DSHR). Ceci est d'ailleurs confirmé, comme dans la série **2**, par examen de la multiplicité des signaux dans le spectre SD (légende de la fig. 2). L'attribution des carbones benzéniques pour l'ensemble de la série est déduite de la référence **3***e* par la méthode des incréments et permet dans tous les cas d'identifier avec certitude les deux signaux de C_α et $C_{\alpha'}$ (tableau 3). L'attribution des pics correspondants à ces deux carbones C_α et $C_{\alpha'}$ a été effectuée par analogie avec les séries furanniques **1** et **2**. En effet, on a trouvé dans ces derniers que δC_α diminue lorsque l'effet donneur de X augmente, alors que $\delta C_{\alpha'}$ augmente. On remarque la coïncidence fortuite $\delta C_\alpha = \delta C_{\alpha'}$ pour **3***d* (X = Cl) (tableau 3); l'attribution des signaux pour les autres composés de la série en résulte sans ambiguité (fig. 3).

Interprétation des résultats

Nous avons cherché des corrélations entre le déplacement chimique de chaque carbone de l'hétérocycle et les constantes σ_p(X) de Hammett ou σ_p^+(X) de Brown (14). Le calcul montre que les meilleures corrélations (évaluées par la méthode des moindres carrés) sont obtenues avec les constantes σ(X) de Hammett (figs 3–5 et tableau 4). On voit que l'effet du substituant X sur le déplacement chimique des ^{13}C du noyau furannique ou pyrrole n'est pas lié de façon simple à son seul caractère donneur ou attracteur. En particulier, le sens des variations observées pour $\delta C_{\alpha'}$ est l'inverse (fig. 3 ou 5) de celui attendu en fonction du caractère donneur de X. De même, le déplacement chimique du

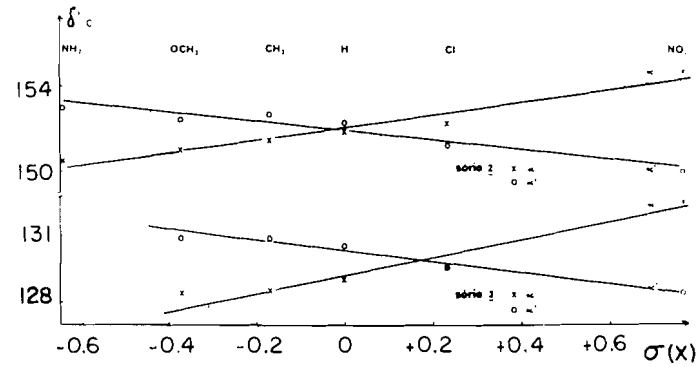

FIG. 3. Corrélation des déplacements chimiques des carbones C_α et $C_{\alpha'}$ dans les séries **2** et **3**, avec la constante de Hammett, σ(X).

Can. J. Chem. Downloaded from www.nrcresearchpress.com by 210.87.254.6 on 09/05/12
For personal use only.

TABLEAU 4. Corrélations des déplacements chimiques δ ^{13}C des carbones de l'hétérocycle dans les séries **1**, **2**, **3** et les constantes σ et σ^+ de Hammett et de Brown; r^2, coefficient de corrélation correspondant

	Série **1**		Série **2**		Série **3**	
δ		r^2		r^2		r^2
δC_α	$142.07 + 2.24\sigma_p$	0.963	$151.98 + 2.83\sigma_p$	0.94	$129.17 + 4.14\sigma_p$	0.96
	$142.35 + 1.39\sigma_p^+$	0.911	$152.38 + 1.80\sigma_p^+$	0.85	$129.74 + 2.75\sigma_p^+$	0.826
$\delta C_{\alpha'}$	$153.56 - 2.20\sigma_p$	0.852	$151.85 - 2.10\sigma_p$	0.91	$130.39 - 2.5\sigma_p$	0.972
δC_β	$105.08 + 4.76\sigma_p$	0.958	$105.90 + 4.92\sigma_p$	0.97	$106.18 + 5.03\sigma_p$	0.968
	$105.64 + 2.96\sigma_p^+$	0.938	$106.61 + 3.18\sigma_p^+$	0.896	$106.85 + 3.34\sigma_p^+$	0.852
$\delta C_{\beta'}$	$111.72 + 0.598\sigma_p$	0.843	$107.76 + 1.01\sigma_p$	0.77	$107.99 + 1.72\sigma_p$	0.91

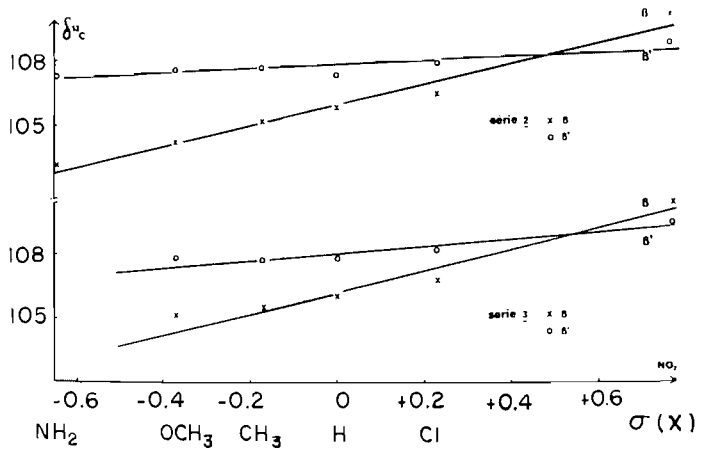

FIG. 4. Corrélation des déplacements chimiques des carbones C_β et $C_{\beta'}$ dans les séries **2** et **3**, avec la constante de Hammett, σ(X).

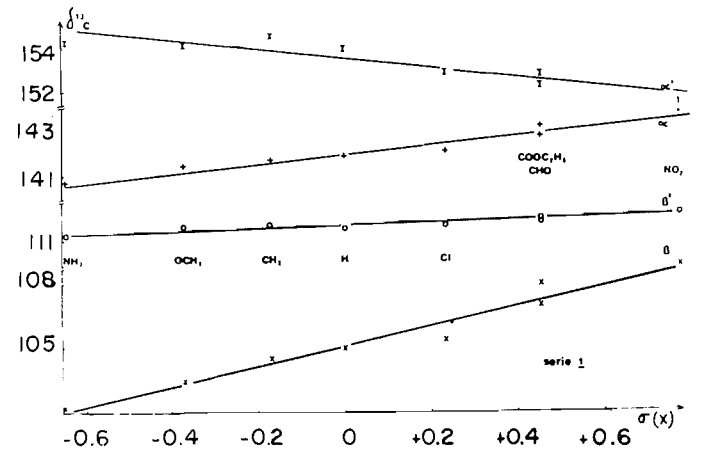

FIG. 5. Corrélation des déplacements chimiques des carbones du noyau furannique dans la série **1** avec la constante de Hammett, σ(X).

Can. J. Chem. Downloaded from www.nrcresearchpress.com by 210.87.254.6 on 09/05/12
For personal use only.

Can. J. Chem. Downloaded from www.nrcresearchpress.com by 210.87.254.6 on 09/05/12
For personal use only.

carbone $C_{\beta'}$ dépend faiblement de l'électronégativité de X (valeurs faibles des pentes ρ dans le tableau 4 et fig. 4). Ceci est à rapprocher du cas du benzène lui-même pour lequel les incréments de déplacements chimiques produits par un substituant X, surtout s'il est fortement mésomère donneur, peuvent présenter une alternance de signes. L'effet sur le carbone *méta* est souvent faible ou négligeable, mais l'effet sur le carbone *para* correspond généralement bien à un blindage supplémentaire pour les groupes donneurs et à un déblindage pour les groupes attracteurs (5*b*, 10). On note alors que les carbones $C_{\beta'}$, non conjugués à X, se comportent comme les carbones *méta* du benzène. Certains auteurs ont même tenté des corrélations pour des carbones dans la position analogue 3′ du biphényle **4** (15) avec les constantes σ_m et σ_m^+ relatives à la position *méta* de X. En fait, ils trouvent bien que la corrélation avec σ_p est de meilleure qualité, ce qui nous semble assez normal puisque le noyau B (dont on étudie une propriété) est bien un substituant en *para*, par rapport à X.

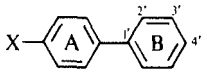

4

Nous nous sommes alors demandé si dans le cas des hétérocycles des séries **1**, **2** ou **3**, la situation est analogue au cas du biphényle. L'expérience montre que $\delta C_{\beta'}$ donne une meilleure corrélation avec $\sigma_p(X)$ qu'avec $\sigma_m(X)$ pour les séries **1** et **3**. En revanche, la corrélation est légèrement meilleure avec $\sigma_m(X)$ ($\rho = 1.60$, $r^2 = 0.855$) ou $\sigma_m^+(X)$ ($\rho = 1.61$, $r^2 = 0.837$) qu'avec $\sigma_p(X)$ pour la série **2**. En fait, pour ce carbone $C_{\beta'}$ les corrélations cherchées doivent rendre compte de variations minimes sur les déplacements chimiques, (tableaux 1–3). Sur ces petites variations, les incertitudes relatives sont grandes et nous pensons que les corrélations trouvées sont assez illusoires.

En ce qui concerne les carbones C_α et C_β, en position de conjugaison vis-à-vis de X, ils présentent des variations dans le sens attendu en fonction de l'électronégativité de X (pente ρ positive). Les coefficients de corrélation sont meilleurs avec les constantes σ_p que σ_p^+. Ceci est analogue au résultat observé dans la série du biphényle **4** pour le carbone 4′ ($\rho = +2.18$, $r^2 = 0.994$) (15) de même position que C_α dans

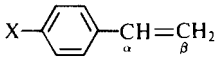

5

nos séries (tableau 4). Pour le carbone β, on peut trouver des analogies soit avec le carbone 2′ du biphényle **4** (15), soit avec le carbone β du styrène **5** (16).

Dans le premier cas, les auteurs trouvent une meilleure corrélation avec σ_p^+ ($\rho = +0.64$, $r^2 = 0.906$) alors que pour C_β du styrène **5**, σ_p convient mieux ($\rho = +6.28$, $r^2 = 0.955$) que σ_p^+ ($\rho = 3.87$, $r^2 = 0.925$) (valeurs calculées à partir des données de réf. 16). Il semblerait que notre cas rappelle davantage celui du styrène **5** que celui du biphényle **4**, aussi bien pour les valeurs de ρ observées (tableau 4) que pour la nature de la corrélation avec σ_p de Hammett plutôt que σ_p^+ de Brown.

Il reste alors le cas du comportement du carbone $C_{\alpha'}$ qui donne, dans nos séries **1**, **2**, **3** aussi bien que dans celles du biphényle **4** ($C_{1'}$) et du styrène **5** (C_α) une pente ρ négative. Il a été montré, notamment dans le cas des styrènes substitués (17), que ce comportement résulte de la plus grande importance, pour ce carbone, de l'effet de champ à travers l'espace par rapport à l'effet de résonance et à l'effet de polarisation des électrons π, qui se transmettent à travers le squelette. On peut d'ailleurs signaler que pour le biphényle **4**, les auteurs (15) préfèrent corréler δC_1, avec σ_m, ce qui constitue un autre point de vue sur la question mais ne change pas le problème du sens des variations observées. En fait dans notre cas, $\delta C_{\alpha'}$ donne la meilleure corrélation avec $\sigma_p(X)$ pour la série **3**, mais avec $\sigma_m^+(X)$ pour les séries **1** ($\rho = -3.60$, $r^2 = 0.956$) et **2** ($\rho = -3.35$, $r^2 = 0.989$). Dans la mesure où l'effet d'électronégativité de X n'est même pas directement responsable du sens des déplacements observés, il est probable que la plus ou moins bonne qualité des corrélations trouvées est plus ou moins fortuite.

Conclusion

A l'aide des résultats obtenus dans la présente étude, il est possible de comparer la transmission des effets électroniques de X dans chacun des hétérocycles pyrrole et furanne.

Le pôle le plus intéressant au point de vue des effets de conjugaison nous semble être le seul pôle α pour lequel on observe une sensi-

Can. J. Chem. Downloaded from www.nrcresearchpress.com by 210.87.254.6 on 09/05/12
For personal use only.

bilité aux variations de X nettement plus importante dans le cas des phénylpyrroles **3** ($\rho(\alpha) = +4.14$ pour **3** supérieur à $\rho(\alpha) = +2.83$ pour **2**, tableau 4).

Le pôle β, en position analogue au point de vue conjugaison avec X, mais plus proche du noyau benzénique donc éventuellement plus perturbé par des effets locaux, donne un résultat dans le même sens bien que nettement plus faible ($\rho(\beta) = +5.03$ pour **3** de même ordre que $\rho(\beta) = +4.92$ pour **2**).

Etant donnée la précision des déterminations actuelles (limitées par les difficultés de synthèse dans la série **3** du pyrrole), il semble donc que la plus grande sensibilité observée pour le pyrrole vis-à-vis des variations de X (comparée au furanne) révèle que la conjugaison de l'hétérocycle avec le benzène serait meilleure dans la série **3** du pyrrole que dans les séries **2** (ou **1**) du furanne. Ce résultat, inverse de celui observé pour les vitesses des substitutions électrophiles (1, 2) est important dans la mesure où il révèle, comme nous le montrerons dans un prochain mémoire, une différence de structure des états de transition pour chacune des deux séries hétérocycliques.

Partie expérimentale

Les spectres rmn de protons ont été effectués sur un spectrographe Varian A-60A (TMS en référence interne, échelle δ en ppm) en solution à 10% dans $CDCl_3$ ou CCl_4 (abréviations: s = singulet; d = doublet; q = quaruplet; m = multiplet).

Les points de fusion (pf) sont non corrigés.

Les formules brutes ont été déterminées par analyse des dérivés carbonylés obtenus lors de l'étude des substitutions électrophiles (résultats corrects à $\pm 0.2\%$ pour C, H et N et à $\pm 0.4\%$ pour Cl) et confirmées par les spectres de masse (sm) (spectrographe Hitachi-Perkin-Elmer RMU-6 EMS à 75 eV). Ces spectrographes, de même que ceux utilisés pour la rmn du ^{13}C, sont ceux du Groupement de Mesures Physiques de Paris Centre.

Préparation des aryl-2 furannes **1** *et des aryl-2 méthyl-5 furannes* **2**

Nous avons employé une synthèse de Gomberg: décomposition du sel de diazonium obtenu à partir d'une aniline *para* substituée, dans le furanne (12, 19) ou le méthylfuranne(2).

Pour le *para*-nitrophényl-2 méthyl-5 furanne, **2***a*, la réaction est réalisée avec le chlorobenzène comme solvant et le méthyl-2 furanne en léger excès ($\times 1.2$) par rapport au sel de diazonium. *p-Nitrophényl-2 méthyl-5 furanne* **2***a*: pf 115 °C (CCl_4) cristaux jaunes; mw $C_{11}H_9NO_3$ 203; sm $M^{+\cdot}$ 203; rmn $\delta CH_3 = 2.43$, $\delta H_\beta = 6.80$ (d), $\delta H_{\beta'} = 6.31$ (m) ppm; $JH_\beta H_{\beta'} = 3.2$ Hz, $JH_{\beta'}CH_3 = 1.1$ Hz.

L'amine **2***h* est obtenue par réduction du dérivé nitré précédent par la poudre d'étain dans HCl ou simplement par hydrogénation sur nickel (19). *p-Aminophényl-2 méthyl-5 furanne* **2***h*; liquide jaune clair, fragile à l'air; mw $C_{11}H_{11}ON$ 173; sm $M^{+\cdot}$ 173 (100%) et 130 (48%); rmn $\delta CH_3 = 2.27$ ppm, $\delta H_\beta = 6.25$ ppm, $\delta H_{\beta'} = 5.9$ ppm; $JH_{\beta'}CH_3 \simeq 1$ Hz, $JH_\beta H_{\beta'} = 2.4$ Hz, $\delta C_6H_4 = 6.6$ et 7.4 ppm (AA'BB'), NH_2 variable de 3.5 à 5 ppm; uv λ_{max}(EtOH) 295 nm.

Les composés de la série **1** ont été déjà décrits, sauf quelques fois en ce qui concerne leurs spectres rmn de ^1H. Nous avons trouvé dans ces cas les valeurs du Tableau 5, qui ont été utilisées pour les attributions des spectres de ^{13}C par la méthode graphique (DSHR).

Dans les spectres de ^{13}C, nous avons noté les couplages suivants avec les protons. (*i*) Série **1**: $JC_\alpha H_\alpha = 202 \pm 0.6$ Hz, $JC_\alpha H_{\beta'} = 7.5 \pm 0.2$ Hz, $JC_\alpha H_\beta = 10.7 \pm 0.3$ Hz, $JC_{\beta'}H_\alpha = 13.4$ Hz, $JC_{\beta'}H_{\beta'} = 174.9 \pm 0.4$ Hz, $JC_{\beta'}H_\beta = 3.6$ Hz, $JC_\beta H_\beta = 174.2 \pm 1$ Hz, $JC_\beta H_\alpha = 5.5$ Hz, $JC_\beta H_{\beta'} = 4.3$ Hz. (*ii*) Série **2**: $JC_{\beta'}H_{\beta'} = 171.5 \pm 1.2$ Hz, $JC_{\beta'}H_\beta = 3.3 \pm 0.3$ Hz, $JC_{\beta'}CH_3 = 3.3 \pm 0.3$ Hz, $JC_\beta H_\beta = 171.8 \pm 0.3$ Hz, et $JC_\beta H_{\beta'} = 4.0 \pm 0.3$ Hz.

Préparation des aryl-2 méthyl-5 pyrroles **3**

Ces composés ont été obtenus par cyclisation des aryl-1 pentanediones-1,4 correspondantes en présence d'ammoniaque: la préparation de ces γ-dicétones a été effectuée par les trois méthodes suivantes selon le substituant X.

Préparation des γ-dicétones X = Cl, H, CH_3

Nous avons suivi le mode opératoire décrit par Chiron et Graaf (20). Pour le cas non décrit par ces auteurs, X = Cl, le mode opératoire est identique sauf la température de la réaction qui est celle du reflux du chlorobenzène (p éb = 132 °C) utilisé comme solvant et comme réactif. On obtient ainsi après distillation et avec un rendement de 35%, la *para* chlorophényl-1 pentanedione-1,4.

Préparation de la γ dicétone X = CH_3O (p-anisyl-1 pentane dione-1,4)

La préparation de cette γ-dicétone s'effectue par hydrolyse acide de l'ester $\beta\gamma'$-dicétonique correspondant ob-

TABLEAU 5

X	δH_α	δH_β	$\delta H_{\beta'}$	$JH_\alpha H_{\beta'}$ (Hz)	$JH_\alpha H_\beta$ (Hz)	$JH_\beta H_{\beta'}$ (Hz)
NO_2	7.71	6.98	6.68	2	—	4
CO_2Et	7.52	6.78	6.51	1.5	—	3.6
CHO	7.53	6.78	6.65	1.8	0.8	3.6
NH_2	7.33	6.35	6.35	—	—	—

Can. J. Chem. Downloaded from www.nrcresearchpress.com by 210.87.254.6 on 09/05/12
For personal use only.

tenu par condensation acéto-acétique avec le chloro-2 méthoxy-4′ acétophénone (21).

Préparation de la γ-dicétone X = p-NO₂ (p-nitrophényl-1 pentanedione-1,4)

L'ester βγ′-dicétonique correspondant est purifié par chromatographie sur colonne de Florisil (éluant: benzène–éther) et est obtenu cristallisé pf 51 °C (éther).

L'hydrolyse et la décarboxylation de ce composé est très délicate, la saponification ou l'hydrolyse acide conduisent à la formation de polymères. Nous avons pu réaliser cette réaction par action de l'iodure de lithium en excès et à reflux 2 h dans le diméthylformamide (22); on obtient ainsi un rendement en produit pur de 35% (après chromatographie sur colonne de Florisil).

Cyclisation des γ-dicétones en pyrroles en présence d'ammoniaque

Les cinq termes de la série ont été synthétisés par cyclisation des γ-dicétones en solution diluée dans l'alcool éthylique: à 1 g de γ dicétone en solution dans 50 ml d'éthanol sont ajoutés 3 ml de NH_4OH à 28%. La solution est chauffée en autoclave avec agitation à 150 °C pendant 3 h. L'évaporation de l'alcool sous vide fournit un produit cristallisé que l'on purifie par chromatographie sur colonne de Florisil (éluant: benzène). Les pyrroles sont obtenus purs avec des rendements de l'ordre de 90%, ils sont peu colorés mais rougissent à la lumière.

Le pyrrole **3***a* (X = NO_2) est préparé avec un rendement de 27%. Le produit brut de la cyclisation est repris dans le benzène à reflux pour éliminer les résines puis chromatographié sur colonne de Florisil.

Les caractéristiques analytiques des pyrroles figurent ci-après.

Méthyl-5 phényl-2 pyrrole **3***e*: pf 94–95 °C (eau + méthanol, 1:1); Rendement 90%; rmn ($CDCl_3$), δMe_5 = 2.33, $\delta H_{\beta'}$ = 5.98(m), δH_β = 6.47(t), $\delta N\text{—}H$ = 8.2 (large); $JH_\beta\text{–}H_{\beta'} \simeq JH_\beta\text{–}NH$ = 2.8 Hz; uv (EtOH) λ_{max} 295 nm(ε 18 600).

p-Chlorophényl-2 méthyl-5 pyrrole, **3***d*: pf 121–123 °C (eau–méthanol); Rdt. 90%; rmn ($CDCl_3$) δMe = 2.34, $\delta H_{\beta'}$ = 6.01(m), δCH_β = 6.43(t), δNH = 8.7 (large), $JH_\beta\text{–}H_{\beta'} \simeq JH_\beta NH \simeq$ 2.8 Hz; uv (EtOH) λ_{max} 305 nm (ε 22 200).

Méthyl-5 p-tolyl-2 pyrrole **3***f*: pf 102–104 °C (eau–méthanol); Rdt. 90%; rmn ($CDCl_3$) δMe_5 et δMe-tolyl = 2.3, $\delta H_{\beta'}$ = 5.84(m), δH_β = 6.33(t), $JH_\beta\text{–}NH \simeq JH_\beta\text{–}H_{\beta'}$ = 2.8 Hz; uv (EtOH) λ_{max} 295 nm (ε 24 100).

p-Anisyl-2 méthyl-5 pyrrole **3***g*: pf 132–134 °C (eau–méthanol); Rdt. 90%; rmn ($CDCl_3$) δMe = 2.30(s), δMeO = 3.81(s); $\delta H_{\beta'}$ = 5.93(m), δH_β = 6.27(t), δNH = 8.01(large); $JH_\beta\text{–}NH = JH_\beta H_{\beta'}$ = 2.8 Hz; uv (EtOH) λ_{max} = 285 nm (ε 19 600).

p-Nitro-2 méthyl-5 pyrrole **3***a*: pf 124–125 °C (éther); Rdt. 27% cristaux rouges; rmn ($CDCl_3$) δMe_5 = 2.37(s), $\delta H_{\beta'}$ = 6.07(m), δH_β = 6.63(t), $JH_\beta\text{–}NH \simeq JH_\beta\text{–}H_{\beta'}$ = 3.2 Hz; sm $M^{+\cdot}$ = 202, $C_{11}H_{10}O_2N_2$.

1. G. Dana, P. Scribe et J. P. Girault. C. R. Acad. Sc. Sér. C, **275**, 49 (1972).
2. (*a*) J. P. Girault, P. Scribe et G. Dana. Bull. Soc. Chim. Fr. 1760 (1973); (*b*) E. Mulliez. Thèse de 3ème Cycle, Paris. 1975.
3. (*a*) G. A. Olah, S. Kobayashi et M. Tashiro. J. Am. Chem. Soc. **94**, 7448 (1972); (*b*) S. Clementi et G. Marino. J. Chem. Soc. Perkin Trans. II, 71 (1972).
4. (*a*) H. Spiesecke et W. G. Schneider. J. Chem. Phys. **35**, 731 (1961); (*b*) G. J. Martin, M. L. Martin et S. Odiot. Org. Magn. Reson. **7**, 2 (1975); (*c*) D. A. Dawson et W. F. Reynolds. Can. J. Chem. **53**, 373 (1975); (*d*) G. A. Olah, P. W. Westerman et D. A. Forsyth. J. Am. Chem. Soc. **97**, 3419 (1975).
5. (*a*) W. Adam, A. Grimison et G. Rodriguez. Tetrahedron, **23**, 2513 (1967); (*b*) F. J. Weigert et J. D. Roberts. J. Am. Chem. Soc. **90**, 3543 (1968).
6. (*a*) A. A. Humffray, J. J. Ryan, J. P. Warren et H. Y. Yung. J. Chem. Soc. Chem. Commun. 610 (1965); (*b*) K. S. Dhami et J. B. Stothers. Can. J. Chem. **45**, 233 (1967).
7. T. F. Page, Jr., T. Alger et D. M. Grant. J. Am. Chem. Soc. **87**, 5333 (1965).
8. F. J. Weigert et J. D. Roberts. J. Am. Chem. Soc. **89**, 2967 (1967).
9. J. Runsink, J. de Wit et W. D. Weringa. Tetrahedron Lett. 55 (1974).
10. G. L. Nelson, G. C. Levy et J. D. Cargioli. J. Am. Chem. Soc. **94**, 3089 (1972).
11. B. Birdsall, N. J. M. Birdsall et J. Feeney. J. Chem. Soc. Chem. Commun. 316 (1972).
12. D. C. Ayres et J. R. Smith. J. Chem. Soc. C, 2737 (1968).
13. R. J. Abraham, R. D. Lapper, K. M. Smith et J. F. Unsworth. J. Chem. Soc. Perkin Trans. II, 1004 (1974).
14. C. Laurence et B. Wojtkowiak. Ann. Chim. **5**, 163 (1970).
15. E. M. Schulman, K. A. Christensen, D. M. Grant et C. Walling. J. Org. Chem. **39**, 2686 (1974).
16. K. S. Dhami et J. B. Stothers. Can. J. Chem. **43**, 510 (1965).
17. G. K. Hamer, I. R. Peat et W. F. Reynolds. Can. J. Chem. **51**, 915 (1973).
18. S. Clementi et G. Marino. Tetrahedron, **25**, 4599 (1969).
19. A. W. Johnson. J. Chem. Soc. 895 (1946).
20. R. Chiron et Y. Graaf. C. R. Acad. Sc. Sér. C, **276**, 1207 (1973).
21. A. L. Wilds et T. L. Johnson. J. Am. Chem. Soc. **76**, 286 (1945).
22. P. D. G. Dean. J. Chem. Soc. 6655 (1965).

ERRATA-The authors wish to acknowledge Dr. G. P. Khare (York University) as a co-author of this paper.

COMMUNICATIONS

The reaction of catechol and derivatives with potassium superoxide

E. LEE-RUFF AND A. B. P. LEVER
Department of Chemistry, York University, Toronto, Ont., Canada M3J 1P3
AND
J. RIGAUDY
Laboratoire de Recherches Organiques de l'E.S.P.C.I., 10, rue Vauquelin, Paris, France
Received February 24, 1976

E. LEE-RUFF, A. B. P. LEVER, and J. RIGAUDY. Can. J. Chem. **54**, 1837 (1976).

Semiquinones are produced in the oxidation of *o*- and *p*-dihydroxyarenes with potassium superoxide. These radical anions in the case of *o*-dihydroxyarenes are further oxidized to dicarboxylic acids. The semiquinones were also obtained by reduction of the corresponding quinones with potassium superoxide.

E. LEE-RUFF, A. B. P. LEVER et J. RIGAUDY. Can. J. Chem. **54**, 1837 (1976).

On obtient des semiquinones par oxydation des *o*- et *p*-dihydroxyarènes par le superoxyde de potassium. Ces radicaux anions, dans le cas des *o*-dihydroxyarènes, sont transformés en acides dicarboxyliques. On peut aussi obtenir les mêmes semiquinones par réduction des quinones correspondantes par le superoxyde de potassium.

[Traduit par le journal]

The intervention of the superoxide anion radical in enzyme oxidation systems has recently been the subject of a number of investigations (1, 2). Its formation is the result of a one electron reduction of molecular oxygen and its presence can be tested by the use of superoxide dismutase, an enzyme which inhibits the oxidations by destruction of superoxide in these systems. For example, the presence of superoxide ion in the pyrocatechase–oxygen system has been suspected (3). With the recent report on the preparation of stable solutions of potassium superoxide in organic non-hydroxylic solvents by complexation with crown ethers (4), the organic chemistry of superoxide can be conveniently studied (5, 6). In order to gain insight as to the preliminary steps of the pyrocatechase catechol oxidations we decided to look at the reaction of catechol and other *o*-dihydroxy arenes with potassium superoxide with particular interest in the paramagnetic species involved by the use of esr spectroscopy.[1]

[1]During the course of this work we came across a preprint of Professor C. Foote's work on the oxidation of 2,5-di-*tert*-butylcatechol by superoxide in which a semiquinone radical ion is postulated.

The addition of diphenols **1–4** to THF solutions containing KO_2 and dicyclohexyl-18-crown-6 (DCC) produced strongly coloured radical species as evidenced from their esr spectra. In all cases the semiquinone radical anion was present and identified by comparison with the spectra obtained from the one electron reduction of the corresponding quinones under identical conditions (7). These were also compared with reported spectra (8, 9) and in all cases they were in good agreement. Table 1 summarizes the esr data for the semiquinones.

Careful quenching of these solutions with water and subsequent work-up with methylene chloride and isolation of the acidic material with bicarbonate resulted in the production of dicarboxylic acids **9–11** in yields ranging from 5% (in the case of **1**) to 60% (for **3**) (30% yield for **10**). These acids were identified by comparison to authentic samples obtained from the superoxide oxidation of the corresponding quinones under the conditions described by Le Berre and Berguer (10). Quenching of solutions of **8** with water resulted in isolation of unchanged **4** (80%) and *p*-quinone (20%).

These results suggest that if free superoxide

Can. J. Chem. Downloaded from www.nrcresearchpress.com by 210.87.254.105 on 09/05/12
For personal use only.

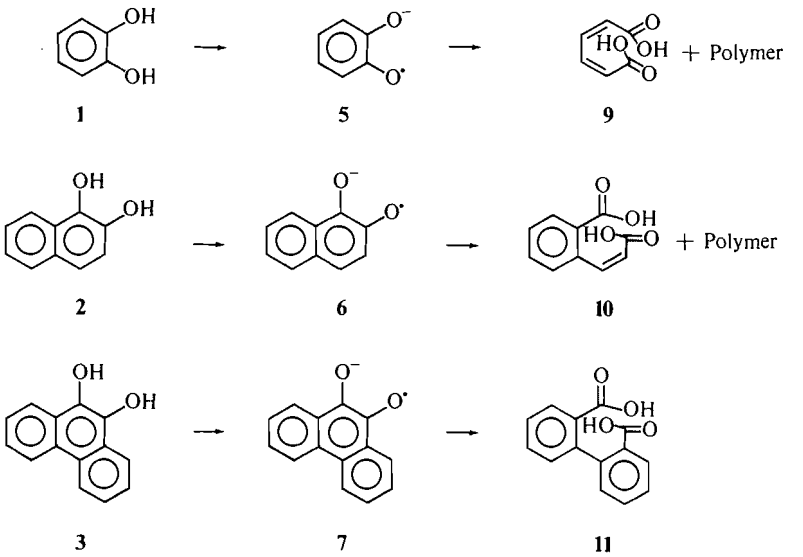

TABLE 1. Electron spin resonance data of semiquinones **5–8**

Semiquinone	g	Hyperfine splitting (G)†‡
5	2.0050±0.0002	a_0=3.60±0.01 (2H) a_m=1.40±0.01 (2H)
6*	2.0050±0.0002	a_1=4.00±0.01 a_2=1.47±0.01 a_3=1.14±0.01 a_4=0.34±0.01
7*	2.0049±0.0002	a_1=1.60±0.01 a_2=1.40±0.01
8	2.0060±0.0002	a_0=2.28±0.01 (4H)

*The hyperfine splittings in these cases were not assigned to specific protons.
†Slight differenees in a from literature values are probably due to changes in the electronegative behaviour of the oxygen atoms in different solvents and hence result in changes in the spin-density distribution of the odd electron within the molecule.
‡Solutions were prepared by dissolving 2 mg of quinone or dihydroxyarene in 250 ml of 0.01 M KO_2 and 0.05 M crown ether in tetrahydrofuran. All spectra were recorded at room temperature.

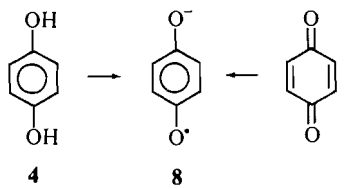

is involved in the enzyme system, then semiquinones would result as observable intermediates. Furthermore, the oxidation products appear to arise from semiquinones rather than the corresponding quinones since we, as well as Rao and Hayon (11), have observed that the one electron reduction by O_2^- of *o*- and *p*-quinones is a very efficient process ($k = 9.8 \times 10^8\ M^{-1}\ s^{-1}$). In fact, this may explain the quenching effect of 1,2-naphthoquinone on the activity of catechol 1,2-dioxygenase (12). If the first step involves hydrogen abstraction in the oxidation of catechol then it may not be expected to compete favourably with the one electron reduction of quinones (k hydrogen abstraction by O_2^- for *p*-hydroquinone $= 1.6 \times 10^7\ M^{-1}\ s^{-1}$) (11). Whether the semiquinones are produced by the sequence **1–2** or **3–4** is not clear. There is evidence from our esr studies of a transient radical prior to semiquinone formation in the case of **1** and the reaction is retarded by addition of KOH to the mixture, however, the latter observation does not necessarily negate the intervention of

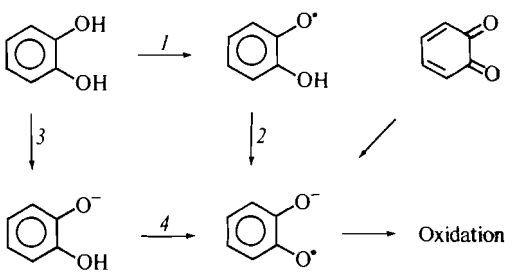

Can. J. Chem. Downloaded from www.nrcresearchpress.com by 210.87.254.105 on 09/05/12
For personal use only.

sequence **3–4** since in the presence of KOH the dianion may be formed. We are currently investigating the subsequent oxidation steps of the semiquinones as well as superoxide reactions with other organic substracts.

Acknowledgments

We would like to thank the National Research Council of Canada as well as the Centre National de Recherche Scientifique (France) for financial support.

1. I. FRIDOVICH. Acc. Chem. Res. **5**, 321 (1972).
2. J. W. CHU and T. KIMURA. J. Biol. Chem. **248**, 5183 (1973).
3. A. NISHINAGA, T. ITAHARA, and T. MATSUURA. Bull. Chem. Soc. Jpn. **47**, 1811 (1974).
4. J. S. VALENTINE and A. B. CURTIS. J. Am. Chem. Soc. **97**, 224 (1975).
5. J. SAN FILIPPO, C. I. CHERN, and J. S. VALENTINE. J. Org. Chem. **40**, 1678 (1975).
6. R. A. JOHNSON and E. G. NIDY. J. Org. Chem. **40**, 1681 (1975).
7. R. POUPKO and I. ROSENTHAL. J. Phys. Chem. **77**, 1722 (1973).
8. P. NETA and R. W. FESSENDEN. J. Phys. Chem. **78**, 523 (1974).
9. E. WARHURST and A. M. WILDE. Trans. Faraday Soc. **65**, 1413 (1969).
10. A. LE BERRE and Y. BERGUER. C. R. **260**, 1995 (1965).
11. P. S. RAO and E. HAYON. Biochem. Biophys. Res. Commun. **51**, 468 (1973).
12. J. M. VARGA and H. Y. NEUJAHR. Acta Chem. Scand. **26**, 509 (1972).

Can. J. Chem. Downloaded from www.nrcresearchpress.com by 210.87.254.105 on 09/05/12
For personal use only.

Gas phase nucleophilic reactions in 1,1-difluoroethylene

JOSÉ M. RIVEROS AND KEIKO TAKASHIMA
Instituto de Química, University of São Paulo, Caixa Postal 20.780, São Paulo, Brasil

Received January 12, 1976

JOSÉ M. RIVEROS and KEIKO TAKASHIMA. Can. J. Chem. **54**, 1839 (1976).

An ion cyclotron resonance study reveals that alkoxide ions react easily with 1,1-difluoroethylene in the gas phase to yield a species CH_2CFO^-. Rate parameters, thermochemical estimates and a rationalization for the mechanism are presented briefly.

JOSÉ M. RIVEROS et KEIKO TAKASHIMA. Can. J. Chem. **54**, 1839 (1976).

Une étude de résonance ionique par cyclotron révèle que les ions alcoolates réagissent facilement avec le difluoro-1,1 éthylène en phase gazeuse pour conduire à l'espèce CH_2CFO^-. On présente brièvement les paramètres de vitesse, les estimés thermochimiques et une rationalisation du mécanisme.

[Traduit par le journal]

The outcome of gaseous ion–molecule reactions reveals in many cases chemical processes which are attenuated in solution either by the bulk solvent or by the energetics of solvation phenomena. For the particular case of nucleophilic reactions in aromatic systems, it has been shown that reaction 1 is surprisingly the predominant reactive channel of fluorinated benzenes in the gas phase when the competing proton transfer is thermodynamically unfavorable (1).

[1] $RO^- + C_6H_4FX \rightarrow RF + C_6H_4O^-X$

$X = F, Cl, NO_2$

More recent studies have illustrated the usefulness of this type of reaction as an analytical tool (2), and as a guideline to new reactions in solution (3).

The formal similarities in the mechanism of nucleophilic substitution in aromatic and vinylic

sequence **3–4** since in the presence of KOH the dianion may be formed. We are currently investigating the subsequent oxidation steps of the semiquinones as well as superoxide reactions with other organic substracts.

Acknowledgments

We would like to thank the National Research Council of Canada as well as the Centre National de Recherche Scientifique (France) for financial support.

1. I. FRIDOVICH. Acc. Chem. Res. **5**, 321 (1972).
2. J. W. CHU and T. KIMURA. J. Biol. Chem. **248**, 5183 (1973).
3. A. NISHINAGA, T. ITAHARA, and T. MATSUURA. Bull. Chem. Soc. Jpn. **47**, 1811 (1974).
4. J. S. VALENTINE and A. B. CURTIS. J. Am. Chem. Soc. **97**, 224 (1975).
5. J. SAN FILIPPO, C. I. CHERN, and J. S. VALENTINE. J. Org. Chem. **40**, 1678 (1975).
6. R. A. JOHNSON and E. G. NIDY. J. Org. Chem. **40**, 1681 (1975).
7. R. POUPKO and I. ROSENTHAL. J. Phys. Chem. **77**, 1722 (1973).
8. P. NETA and R. W. FESSENDEN. J. Phys. Chem. **78**, 523 (1974).
9. E. WARHURST and A. M. WILDE. Trans. Faraday Soc. **65**, 1413 (1969).
10. A. LE BERRE and Y. BERGUER. C. R. **260**, 1995 (1965).
11. P. S. RAO and E. HAYON. Biochem. Biophys. Res. Commun. **51**, 468 (1973).
12. J. M. VARGA and H. Y. NEUJAHR. Acta Chem. Scand. **26**, 509 (1972).

Can. J. Chem. Downloaded from www.nrcresearchpress.com by 210.87.254.40 on 09/05/12
For personal use only.

Gas phase nucleophilic reactions in 1,1-difluoroethylene

JOSÉ M. RIVEROS AND KEIKO TAKASHIMA
Instituto de Química, University of São Paulo, Caixa Postal 20.780, São Paulo, Brasil

Received January 12, 1976

JOSÉ M. RIVEROS and KEIKO TAKASHIMA. Can. J. Chem. **54**, 1839 (1976).

An ion cyclotron resonance study reveals that alkoxide ions react easily with 1,1-difluoroethylene in the gas phase to yield a species CH_2CFO^-. Rate parameters, thermochemical estimates and a rationalization for the mechanism are presented briefly.

JOSÉ M. RIVEROS et KEIKO TAKASHIMA. Can. J. Chem. **54**, 1839 (1976).

Une étude de résonance ionique par cyclotron révèle que les ions alcoolates réagissent facilement avec le difluoro-1,1 éthylène en phase gazeuse pour conduire à l'espèce CH_2CFO^-. On présente brièvement les paramètres de vitesse, les estimés thermochimiques et une rationalisation du mécanisme.

[Traduit par le journal]

The outcome of gaseous ion–molecule reactions reveals in many cases chemical processes which are attenuated in solution either by the bulk solvent or by the energetics of solvation phenomena. For the particular case of nucleophilic reactions in aromatic systems, it has been shown that reaction 1 is surprisingly the predominant reactive channel of fluorinated benzenes in the gas phase when the competing proton transfer is thermodynamically unfavorable (1).

[1] $RO^- + C_6H_4FX \rightarrow RF + C_6H_4O^-X$

$X = F, Cl, NO_2$

More recent studies have illustrated the usefulness of this type of reaction as an analytical tool (2), and as a guideline to new reactions in solution (3).

The formal similarities in the mechanism of nucleophilic substitution in aromatic and vinylic

Can. J. Chem. Downloaded from www.nrcresearchpress.com by 210.87.254.40 on 09/05/12
For personal use only.

compounds in solution has led us to probe into the gas phase behavior of fluorinated olefins. The present communication reports that a remarkable similarity to reaction 1 is observed in the gas phase with 1,1-difluoroethylene suggesting a characteristic behavior for unsaturated systems.

Experiments were carried out in an ion cyclotron resonance spectrometer operating in the negative ion mode. Alkoxide ions were generated by electron impact of alkyl nitrites (1, 4) at pressures of 5×10^{-6} torr. Whereas vinyl fluoride, at a pressure of 5×10^{-5} torr, appears essentially unreactive with alkoxide ions in a drift cell with typical residence times varying between 1 and 4 ms, CH_2CF_2 gives rise to a product ion of *m/e* 61 under similar circumstances. Double resonance and pressure studies clearly identify this latter species as a reaction product, and not due to one of the components of the mixture.

The fact that CH_3O^-, CD_3O^-, $C_2H_5O^-$, $C_2D_5O^-$, and iso-$C_3H_7O^-$ give rise to the same product ion with CH_2CF_2 suggests by simple mass considerations the formation of a species $C_2H_2FO^-$. Such a product can be rationalized as a special case of the addition–elimination mechanism of vinylic compounds (5). Thus, nucleophilic attack at an activated carbon atom is followed by elimination of RF in a manner analogous to reaction 1.

[2] $$RO^- + CH_2CF_2 \longrightarrow \left[\begin{matrix} H \\ H \end{matrix}\!\!>\!C^- - C\!<\!\begin{matrix} F \\ OR \end{matrix}\right] \longrightarrow CH_2CFO^- + RF$$

m/e 61

A lower limit of 45 kcal/mol can be estimated for the exothermicity of reaction 2 based on observations of CH_2CFO^- as the major product of several ion–molecule reactions involving F^- and carbonyl derivatives (6).

Rate constants were measured at 296 K for several alkoxide ions, and are larger for all cases than those of the competing proton transfer reactions which give rise to CF_2CH^- (*m/e* 63):

Ion	k_2 (cm^3 molecule^{-1} s^{-1})	$k_2/k_{CF_2CH^-}$
CH_3O^-	$(1.00 \pm 0.27) \times 10^{-10}$	1.33
$C_2H_5O^-$	$(1.25 \pm 0.23) \times 10^{-10}$	~12
iso-$C_3H_7O^-$	$(0.85 \pm 0.13) \times 10^{-10}$	>27

These constants are believed to be better than 25% accurate based on estimates of the accuracy in pressure measurements and experimentally determined ion residence times.

The values of the rate constants indicate that reaction 2 is insensitive to the size of the alkyl group within the large experimental error. The significance of this fact with regard to a possible mechanism for the break-up of the intermediate can be assessed by comparison with well characterized gas phase processes. Elimination of RF from the intermediate can be accomplished by an internal nucleophilic displacement for which the alkyl dependence may be small if analogies can be made with gas phase S_N2 reactions. For the latter case, rate constants for the reactions of F^- with CH_3Cl and C_2H_5Cl differ by 5% (6). An alternate route possible for the larger alkyl groups involves an intramolecular elimination either to yield RF, or HF, and an olefin. Although the neutral product of reaction 2 could not be ascertained, this type of mechanism has been shown to lead to a dramatic enhancement in the rate constant of F^- with alkyl formates to yield $HCOO^-$ in going from the methyl to the ethyl and isopropyl derivative. Such a behavior makes this mechanism doubtful for the present case.

As in the case of aromatic systems, the ability of a second fluorine substituent in the olefin to promote reaction 2 is indeed remarkable.

Acknowledgements

The authors gratefully acknowledge the financial support of the Conselho Nacional de Desenvolvimento Científico e Tecnológico do Brasil and a FAPESP scholarship (K.T.).

1. S. M. J. Briscese and J. M. Riveros. J. Am. Chem. Soc. **97**, 230 (1975).
2. I. Dzidic, D. I. Carrol, R. N. Stilwell, and E. C. Horning. Anal. Chem. **47**, 1308 (1975).
3. P. F. Levonowich, H. P. Tannenbaum, and R. C. Dougherty. J. Chem. Soc. Chem. Commun. 597 (1975).
4. L. K. Blair, P. C. Isolani, and J. M. Riveros. J. Am. Chem. Soc. **95**, 1057 (1973).
5. Z. Rappoport. Adv. Phys. Org. Chem. **7**, 1 (1969).
6. S. M. J. Briscese and J. M. Riveros. 27th Meeting of the Sociedade Brasileira para o Progresso da Ciência, Belo Horizonte, July 1975, paper 5-F3.
7. J. F. G. Faigle, P. C. Isolani, and J. M. Riveros. J. Am. Chem. Soc. In press.

Can. J. Chem. Downloaded from www.nrcresearchpress.com by 210.87.254.105 on 09/05/12
For personal use only.

Canadian Journal of Chemistry

Published by
THE NATIONAL RESEARCH COUNCIL OF CANADA

Journal canadien de chimie

Publié par
LE CONSEIL NATIONAL DE RECHERCHES DU CANADA

Volume 54 Number 12 June 15, 1976

Volume 54 numéro 12 15 juin 1976

The charge storage and other electrical properties of a series of polyacene quinone radical polymers

R. N. O'BRIEN AND K. J. LUSHINGTON[1]

Department of Chemistry, University of Victoria, Victoria, B.C., Canada V8W 2Y2

Received December 29, 1975

R. N. O'BRIEN and K. J. LUSHINGTON. Can. J. Chem. **54**, 1841 (1976).

A series of polyacene quinone radical polymers were made. The chemical analysis showed that the severe reaction conditions favored the Scholl (elimination of H_2 and H_2O) over the Friedel–Crafts reaction. Electron paramagnetic resonance spectra confirmed the presence of a biradical. Conductivity measurements in the ohmic and space charge limited regions showed that large π systems existed and that carrier traps were shallow. The π system structure and absence of quinone structure was confirmed by ir spectrometry which also showed the optical absorption edge to be 0.8 eV. Charge was injected into the polymers forming electrets and thermally stimulated current emission spectra confirmed a shallow trap depth (~0.4 eV). It is postulated that thermal excitation to a triplet state produces the biradical and conduction is by hopping between adjacent π systems and charge storage is associated with the extensive π systems.

R. N. O'BRIEN et K. J. LUSHINGTON. Can. J. Chem. **54**, 1841 (1976).

On a préparé une série de polymères radicalaires de polyacène quinone. L'analyse chimique montre que les conditions expérimentales très drastiques utilisées favorisent la réaction de Scholl (avec l'élimination de H_2 et H_2O) par opposition à la réaction de Friedel–Crafts. Les spectres de rpe confirment la présence d'un biradical. Des mesures de conductivité dans la région ohmique et la région limitée d'espace chargé montrent que de grands systèmes π existent et que les pièges des vecteurs sont peu profonds. On a confirmé par spectroscopie infrarouge la structure du système π et l'absence d'une structure quinone; la spectroscopie infrarouge montre aussi que l'absorption optique est de 0.8 eV. On a injecté des charges dans les polymères de façon à former des électrets et des spectres de courant d'émission stimulés thermiquement confirment la présence de pièges faibles (~0.4 eV). On postule que l'excitation thermique vers un état triplet produit le biradical et que la conduction se produit par un saut entre des systèmes π adjacents et que l'emmagasinage de charge est associé avec les grands systèmes π.

[Traduit par le journal]

Introduction

Charge storage in dielectrics has, for many years, been associated with the electret phenomenon; that is, dielectrics which possess a permanent electric field. The proceedings of recent conferences on electrets provide a comprehensive review of charge storage and transport in dielectrics (1, 2).

The permanent electric field characteristic of the electret can be attributed to a number of internal charge storage mechanisms; permanent dipole alignment along some externally defined axes, microscopic distortions of ion species from their equilibrium lattice positions (again along some defined axes), ion formation or injection

[1]Present address: Department of Chemistry, McMaster University, Hamilton, Ontario.

Can. J. Chem. Downloaded from www.nrcresearchpress.com by 210.87.254.105 on 09/05/12
For personal use only.

during electret preparation, or electron-hole trapping. The first two mechanisms result in a dielectric sample with a well-defined electric field vector opposed to the external applied electric field used to create the electret. The final two mechanisms lead to complex charge distributions with no well-defined electric field vector; in fact the sample may no longer be electrically neutral.

The polyacene quinone radical (PAQR) polymer system was studied, as the polymers possess some interesting electronic properties which could influence charge storage. These polymers, first prepared and investigated by Pohl and coworkers (3–6) offer polymers whose conductivity (σ) ranges from 10^{-1} to 10^{-14} Ω^{-1} m^{-1}. Every polymer also contains a large, stable free radical population. In order to study charge storage effects, only polymers loosely classed as semi-insulators (10^{-9} Ω^{-1} $m^{-1} < \sigma < 10^{-14}$ Ω^{-1} m^{-1}) could be used.

The polymeric nature of the system made charge storage due to some polarisation mode unlikely, and thus, any charge storage observed could be ascribed to an electronic process. In low conductivity solids, however, the differences between electron or hole trapping and ion formation are slight, as an ion is simply an electron or hole trapped on a specific chemical entity. A study of several polymers should show the interrelations of such properties as electron mobility, free radical concentration, and chemical structure, with charge storage.

The polymers examined were first subjected to a series of standard chemical analysis techniques such as electron spin resonance, infrared–visible spectroscopy, elemental analysis, and X-ray powder photography, in order to determine as much as was possible about the chemical nature of the polymers (a problem still unclear after Pohl's extensive study of the semiconducting members of the series). The charge storage and conductivity behavior of the polymers were determined by first measuring the ohmic and space charge limited (scl) conductivities (7) of the untreated polymer, followed by measuring the thermally stimulated current (tsc) emission of the electret state (8). When dealing with a polymer in the electret state, the apparent surface charge was measured using the vibrating electrode method developed by Reedyk and Perlman (9).

A comparison of charge storage data with information from the conductivity and chemical analysis data lead to several interesting correlations.

Experimental

Four polymers from the PAQR series were prepared, following the procedure outlined by Pohl (3), using a Friedel–Crafts type, melt polymerisation at 529 K, with zinc chloride ($ZnCl_2$) as the catalyst. The specific precursors for each polymer are given in Table 1.

In all cases the resulting polymers were black, insoluble solids which were purified by exhaustive extraction (3).

The infrared spectrum of PAQR was obtained, over the region of 10 000 cm^{-1} to 350 cm^{-1}, using Beckman I.R.4 and Beckman I.R.20 spectrometers. The insoluble nature of the polymer required the use of mull and attenuated total reflection sampling techniques to obtain a reasonable spectrum. The spectrum of PAQR 2 was also obtained over the region from 30 000 cm^{-1} to 12 000 cm^{-1}, using a Cary 18 spectrometer, referenced against a magnesium carbonate standard.

In addition to these optical methods, a standard carbon, hydrogen, and oxygen analysis was performed for all four polymers.

The electron spin resonance spectrum was obtained, for all polymers prepared, using a Varian E-6s X band spectrometer with a dual cavity. The polymer sample was finely powdered and placed in an evacuated quartz tube. All spectra were calibrated against Fremy's salt (a_N = 13.09, g = 2.0055) which allowed the evaluation of g values to ± 0.0003.

An X-ray powder photograph of a PAQR 2 specimen was obtained using a Strauman's type powder camera with 0.5 mm collimating pinhole. Values of the dielectric constants were determined using a comparative capacitor bridge, one arm of which contained the unknown dielectric in a parallel plate capacitor. The bridge was calibrated against two known dielectrics, Teflon K = 2.05, and a polycarbonate K = 3.2. The PAQR polymer

TABLE 1. Precursors for preparation of PAQR polymers

Reference number	Acid anhydride	Aromatic hydrocarbon	Reactant ratio anhydride: hydrocarbon: catalyst
2	Phthalic($C_8H_4O_3$)	Triphenylmethane ($(C_6H_5)_3CH$)	1:1:2
5	Phthalic($C_8H_4O_3$)	p,p-Biphenol ($C_{12}H_8(OH)_2$)	1:1:2
6	Phthalic($C_8H_4O_3$)	Triphenylmethylchloride ($(C_6H_5)_3CCl$)	1:1:2
7	Phthalic($C_8H_4O_3$)	1,4-Diphenylpiperazine ($C_{16}H_{14}N_2$)	1:1:2

Can. J. Chem. Downloaded from www.nrcresearchpress.com by 210.87.254.105 on 09/05/12
For personal use only.

samples were in the form of compressed pellets, formed at 6.76×10^8 Pa, and were approximately 5×10^{-4} mm thick, by 25.4 mm diameter. The capacity of the parallel plate condenser was measured at frequencies from 100 to 1000 Hz for all polymers.

The conductivity measurements, both ohmic and space charge limited, were made using a plane, parallel electrode configuration. The problem of sample electrical contact was investigated and for this particular system no differences between a simple mechanical contact and a deposited electrode on the sample were measurable. The limited amount of polymer available made the mechanical contact more attractive, since if the sample cracked, recasting was possible. All measurements were made using silver mechanical contacts. The problem of surface currents was removed by the use of a guard ring.

The entire shielded electrode system was enclosed in a thermostated air bath capable of maintaining the temperature to within one degree, over the range from 298 to 363 K.

The steady-state d.c. conductivity was measured by impressing a constant voltage across the sample (using a Keithley 246 high voltage supply), and monitoring the resulting current, (with a Keithley 610B electrometer). The sample was always maintained at a constant temperature until an equilibrium current was established.

The only difference between the ohmic and space charge limited conductivity measurements was in the larger voltage required to initiate a space charge regime.

The thermally stimulated current (tsc) measurements were made on PAQR polymers in the electret state. The electrets were formed by one of two methods of sample charging; high field emission or corona discharge. Both methods used silver electrodes with a point-to-plane geometry.

The high field emission technique placed a high voltage (10 kV) point electrode in contact with the sample, such that the field at the tip of the probe was approximately 2×10^8 V m^{-1}. No current was allowed to flow through the sample as this inevitably lead to catastrophic breakdown. The alternate method placed the point electrode 5 mm from the sample in an atmosphere of nitrogen. The voltage on the point electrode was gradually increased until a corona discharge was initiated. The current through the sample was maintained at 3.5 mA. The samples were charged for 1 h using either technique.

The apparent surface charge on the PAQR polymers, in the electret state, was measured using the vibrating electrode method of Reedyk and Perlman (9).

The apparatus for tsc measurements must be able to measure low current levels (10^{-9} to 10^{-14} A), while the temperature is increased linearly with time. A block diagram of the apparatus is shown in Fig. 1.

The linear heating rate was obtained using a F and M 240 temperature programmer with the a.c. output passing through a full wave rectifier and filter. The rectification was needed to lower noise levels within the oven. The non-inductively wound heating coils were in the bottom section of the oven, electrically isolated from the oven body and surrounded by two layers of steel mesh.

The low signal levels required extensive shielding from the signal source (the sample) to the preamplifier of the Cary 401 vibrating capacitor electrometer, used to measure the current. The input lead was a low noise, 100% electrostatically shielded, high temperature (up to 450 K) coaxial cable, encased in a rigid steel pipe to limit cable movement. The oven contained three separate shields. The outside cylindrical case was made of 7 mm thick steel with a stainless steel cylinder coaxially mounted within. Both cylinders were grounded. The final shield was a complete copper electrostatic shield, grounded only to the electrometer to prevent ground loops.

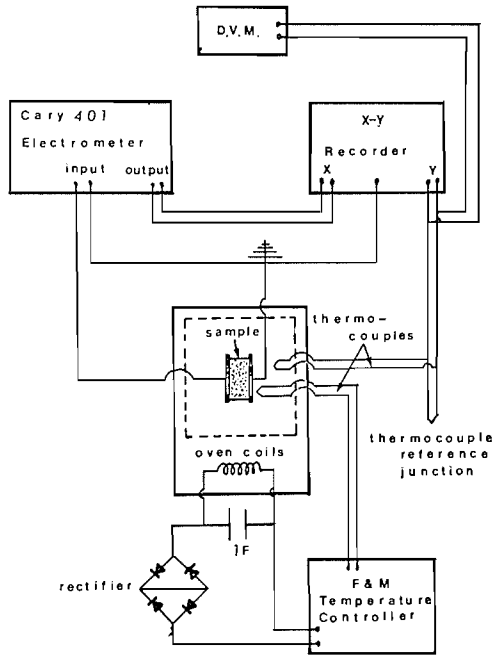

FIG. 1. Thermally stimulated current apparatus.

The sample, a compressed pellet of the PAQR polymer, was held between two springloaded silver electrodes with the input leads mechanically attached to the electrodes. A shielded thermocouple was in contact with the ground electrode.

The entire oven assembly and the electrometer preamplifier were mounted on anti-vibration pads to remove vibrationally induced electronic signals.

A tsc spectrum was obtained by feeding the output of the electrometer and a thermocouple into a X–Y recorder. This apparatus was capable of measuring currents as low as 10^{-15} A, while linearly sweeping the temperature from 273 to 423 K. An uncharged PAQR polymer sample gave a background noise level of approximately 3×10^{-15} A. The background noise appeared to be due mainly to Johnson thermal noise in the high impedance sample.

In most cases, the sample was recoverable after a tsc experiment and no loss in reproducibility was encountered upon the re-use of the sample material in other experiments.

Theory

Conduction Processes

In very low conductivity, intrinsic semicon-

Can. J. Chem. Downloaded from www.nrcresearchpress.com by 210.87.254.105 on 09/05/12
For personal use only.

ductors ($\sigma < 10^{-8}\,\Omega^{-1}\,m^{-1}$) d.c. conduction may be ohmic ($J \propto V$), or space charge limited (scl) ($J \propto V^n$ where $n \geq 2$). A comprehensive treatment of scl theory and techniques is given by Mark and Lampert (7).

Physical defects, such as dislocations, vacancies, and grain boundaries, and chemical structure irregularities in solids, can cause modifications to the band structure of the solid. Localised states within the band gap can be associated with such irregularities. These localised states can act as charge carrier traps and thus alter the conductivity behavior of the solid.

If a trap is situated in the band gap above the fermi level, with a depth ΔE below the bottom edge of the conduction band, then it is said to be shallow and a partition constant, θ, can be defined:

$$[1] \qquad \theta = \frac{n_0}{n_t} = \frac{N_c}{gN_t} \exp(-E/kT)$$

where n_0 = number of free charge carriers; n_t = number of trapped charge carriers; N_c = effective density of states in the conduction band; N_t = density of trapping states; and g = degeneracy factor (normally $g = 2$).

The partition constant defined by eq. 1 expresses the free carrier – trapped carrier ratio in terms of a discrete set of monoenergetic, shallow trapping levels. This is the simplest possible case.

In a shallow trapping regime, the apparent drift mobility, μ_e, is a product of the intrinsic mobility of the free carrier, μ_R, and the fraction of free carriers, θ, in the solid. Ohm's law can then be written:

$$[2] \qquad J = en_0(\theta\mu_R)E$$

where e = electronic charge; J = current density; and E = applied field.

In this equation two terms are temperature dependent, n_0, and θ. The intrinsic free carrier concentration, n_0, is formed by thermal promotion from the valence band and is given by:

$$[3] \qquad n_0 = N_c \exp[-(E_c - E_0)/kT]$$

where $-E_c$ is the energy at the bottom of the conduction band.

As the applied field is increased, charge is injected into the sample, but significant departures from Ohm's law cannot occur until the average injected carrier concentration is roughly equal to the intrinsic free charge concentration. The transition field E_x, is approximated by:

$$[4] \qquad E_x \approx en_0L/\epsilon$$

where L = sample thickness; ϵ = dielectric permittivity.

Once the injected carrier concentration exceeds the intrinsic concentration, injection becomes space charge limited and independent of n_0. The current density is given by the Mott–Gurney square law (10):

$$[5] \qquad J = \tfrac{9}{8}(\theta\mu_R)\epsilon\frac{E^2}{L}$$

The dependence of the current density on the square of the applied field is only true for the case where the charge trapping predominantly occurs in a set of monoenergetic shallow traps. Other trapping levels may be present but if their concentration is much lower or if they are deeper, they will have little effect on the form of the conductivity.

Equation 5 assumes that $\theta < 1$, for if $\theta \gg 1$, the trapped charge will exert a negligible effect on the conductivity, and the solid will behave as a trap-free conductor. The injection of current in the scl regime will shift the fermi level slightly, thus affecting relative trap depths and thermal promotion, but at the low current injection levels in those low conductivity semiconductors the shift could be expected to be small.

If the current density – field relationships are determined over a narrow temperature range (350–500 K) it is a good assumption that the temperature dependence of the intrinsic mobility, μ_R, is weak and can be neglected.

Thermally Stimulated Current Emission

Thermally stimulated current (tsc) analysis of charge and polarisation storage provides the best available means for studying these storage processes in dielectrics. In large polymers, such as the PAQR polymer system, charge storage strongly predominates over polarisation storage, as the latter requires a reorientation of all or part of the molecular framework.

Any form of charge storage is only kinetically stable, and the decay of such a charge state is prevented by a potential barrier impeding the progress of the charge through the dielectric. The tsc method measures the instantaneous charge decay rate, that is, the current flow, J, from the sample, while linearly increasing the

Can. J. Chem. Downloaded from www.nrcresearchpress.com by 210.87.254.105 on 09/05/12
For personal use only.

sample temperature with time. As the charges within potential wells gain thermal energy, the probability of escape will increase, and the externally measured current will register a corresponding increase. The location and form of such 'current peaks' yield information about the storage processes.

On a microscopic level, the charge decay process can be represented by first order kinetics, similar to nuclear decay, which lead to an exponential dependence of the charge decay rate on temperature. Unfortunately this simple relationship is complicated by the small number of charges in any given sample. In a tsc experiment, the induced charge decay causes a large decrease in the overall stored charge population, and thus, on a macroscopic scale, some measure of the instantaneous stored charge population must be included in the kinetics of decay.

Creswell and Perlman have developed an expression for charge storage release, assuming that all the charge is isolated in a thin layer at one face of the sample:

$$[6]\quad J(T) = A \exp\left[\left(\frac{-E_a}{kT}\right) - B\int_{T_0}^{T} \exp\frac{-E_a}{kT}\,dT\right]$$

where E_a is the potential barrier height, T, the temperature and T_0, the initial sample temperature at zero time (11). The constants A and B are model dependent, while the general form of the equation can be transformed into a more experimentally tractable form:

$$[7]\quad C \exp\left(\frac{E_a}{kT}\right) = \frac{\int_T^{\infty} J(T)dT}{J(T)}$$

The integral expresses the charge remaining in the sample at some temperature T, and it is therefore the population scaling factor necessary to describe the kinetics of charge decay. Using eq. 7 the entire peak in a tsc spectrum can be analyzed to obtain a value of the potential barrier height, E_a.

Results

Several standard chemical analysis techniques were performed on some of the polymers prepared. The outcome of these analyses was expected to indicate the nature of the chemical structure in this polymer system.

Elemental analysis of two polymers, PAQR 2 and PAQR 7, was used to assess the degree of polymerisation and possible reaction pathways. The results, accurate to within 0.5%, were used to calculate the best possible empirical formulae for each of the polymers, based on an assumption that the aromatic rings remained intact during the polymerisation. A further extension was made from the empirical formula and the average reacted monomer composition was calculated as an indication of the reaction pathway. In Table 2 these data are summarised, with the average reacted monomer composition expressed as the relative difference from the unreacted monomers.

The infrared spectrum of the polymers proved to be very difficult to obtain. For the polymer PAQR 2, however, a spectrum with several well resolved peaks was obtained. The strongest of these peaks were assigned to aromatic out-of-plane C—H bending (735 and 690 cm^{-1}), and to aromatic C—C skeletal vibration (1600 cm^{-1}). A weak peak at 3060 cm^{-1} was assigned to aromatic C—H stretch. Other peaks of low intensity were consistent with carbonyl stretch in aryl ketones or quinones (at 1660 cm^{-1}) and in aryl esters, anhydrides or five member lactone rings (at 1749 cm^{-1}).

A continuation of the optical spectrum of PAQR 2 through the near infrared to the visible region showed a sharp optical absorption edge, above which the sample absorbance appeared complete. The photon energy at the half maximum of the optical absorption was found to be 0.74 eV (1.19×10^{-19} J).

The X-ray powder pattern of PAQR 7 confirmed the suspicion based on the method and nature of the polymerisation, that these polymers are amorphous. The powder pattern had only a series of several very diffuse bands.

PAQR polymers have a large radical population and esr provides a useful probe into the chemical and electronic structure of the polymers. The esr spectrum was, for all polymers, a single broad lorentzian line for which the gyromagnetic ratio, g, and the peak width at the maximum slope, ΔH_{pp}, were measured.

The esr work by Pohl and Chartoff (4) established several interesting trends in the esr behavior of these polymers. The radical population has a weak exponential temperature dependence, suggesting that the radicals are created by thermal promotion to the first excited triplet

TABLE 2

(*a*) Results of analysis of PAQR 2 and PAQR 7

Polymer	Empirical formula	Empirical weight	Elemental analysis* C	H	N	O
PAQR 2	$C_{356}H_{202}O_{29}$	4938	86.6	4.1	0	9.3
PAQR 7	$C_{528}H_{354}O_{50}N_{38}$	8022	78.8	4.4	6.7	10.1

*Averaged over several analyses.

(*b*) Average reacted monomer composition

Polymer	Hydrocarbon Δ%C*	Δ%H	Δ%N	Acid anhydride Δ%C*	Δ%H	Δ%O
PAQR 2	0	26	—	0	0	31
PAQR 7	0	28	0	0	0	31

*Defined as zero by the assumptions used.

TABLE 3. Electron spin resonance results

PAQR	g	ΔH_{pp} (mT)
2	2.0028	0.617
5	2.0031	0.548
6	2.0028	0.650
7	2.0027	0.698

TABLE 4. Conductivity and dielectric constant for polymers of certain thickness

Polymer	σ_{298} (Ω^{-1} m^{-1})	κ	L (nm)
2	6×10^{-11}	2.85	70
6	8×10^{-13}	2.45	80
7	3×10^{-10}	2.20	70

state. The radical populations also varied with polymer conductivity, ranging from 10^{22} to 10^{26} spins m^{-3} on going from the lowest to highest conductivity polymers. An inverse relationship between the esr peak width and conductivity was also found by Pohl and Chartoff.

The temperature dependence of radical population for PAQR 2 was measured and an apparent activation energy of 0.002 eV was found. This implies that, at room temperature, almost every molecule is in an excited state.

The values for the gyromagnetic ratio shown in Table 3 indicated the radicals are hydrocarbon based, and not associated with semiquinone structures as first suggested by Pohl (3). The relatively narrow lorentzian peaks are strongly indicative of exchange narrowing, that is, radicals on neighbouring sites are rapidly exchanging, thus averaging out the assymmetries in the individual sites.

All the esr data suggest that PAQR polymers form stable biradicals by thermal promotion, within the aromatic system, of an electron from the singlet ground state to the excited triplet state. The low thermal excitation energy suggests that the π systems are very large.

The dielectric constant was measured (over the frequency range of 100–1000 Hz) and found to vary from 2.2 to 2.85 for the low conductivity polymers studied (see Table 4). No frequency dependence was found for these polymers.

The conductivity, σ, of each polymer was evaluated in the ohmic region, at 298 K, using as low an applied field as possible. The values are tabulated in Table 4. Most PAQR polymers have, superimposed on the ohmic current, a slight exponentially field-dependent current. Pohl and Rosen (5) had related this weak effect to the possibility that an electron in the aromatic π system could gain energy from the applied field, while suffering few collisions in the π systems. The net effect would be to lower the height of the potential barrier impeding conduction. Pohl correlated the current density increase with the average length of the π system, L, in the direction of the applied field. Measurements of the exponential field dependence of the current density in these low conductivity polymers used in this work allowed the estimation of the size of the aromatic systems, L, using Pohl and Rosen's model.

Can. J. Chem. Downloaded from www.nrcresearchpress.com by 210.87.254.105 on 09/05/12
For personal use only.

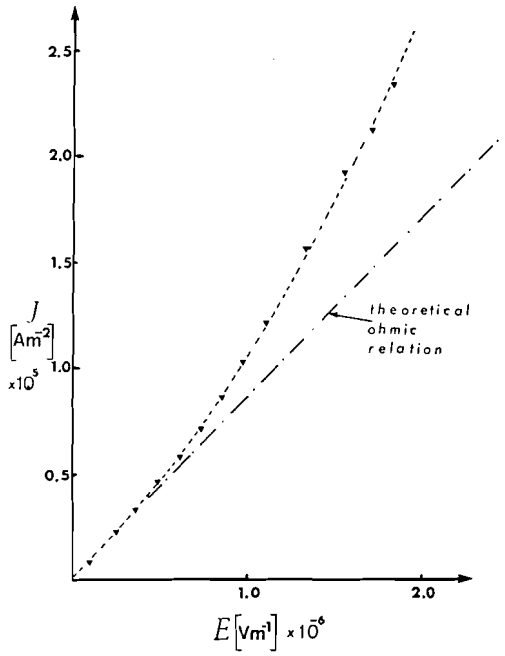

FIG. 2. Current density – field characteristic for PAQR 2.

The isothermal ohmic data allowed the magnitude of the free carrier density-effective mobility product, $n_0(\theta\mu_R)$, to be determined (using eq. 2), while the constant field temperature dependence of the ohmic current density allowed the determination of the trap depth in the solid. Once the ohmic region was investigated, the applied field was increased at constant temperature until an scl conduction region was entered.

The ohmic–scl transition fields E_x, were obtained from graphical analysis of the current density – field data. The transition was never found to be abrupt (see Fig. 2). and E_x could only be estimated. These estimated values for E_x were used to find the scaled free carrier density, n_0/θ (using eq. 3).

Above the transition field, E_x, the conduction was space charge limited, exhibiting the characteristic squared dependence on the applied field, and through eq. 4, a value for the effective mobility, $\theta\mu_R$, at 298 K was determined.

The temperature behavior of the conduction at constant field was examined in order to gain information about the partition constant, θ. The polymers were primarily investigated in the scl conduction region, as the higher current densities facilitated the measurements, but one polymer, PAQR 6, was extensively studied in the ohmic region. The trap depths found for each polymer are given in Table 5, along with the other basic quantities determined in the conduction experiments. For PAQR 6, the ohmic trap depth was found to be 0.05 eV deeper than for the equivalent depth determined in the scl region.

The temperature dependent conductivity also gave a value for the pre-exponential factor, $\theta_0\mu_R$, which is the high temperature limit of the effective mobility.

The values given in Table 5 are obtained directly from the conduction data, and are based only on the assumption that the functional forms chosen were correct. To break down these values to more useful parameters some approximations must be made. The nature of these approximations and the resulting quantities obtained will be given in the Discussion section.

The formation of the electret state in these polymers allowed the investigation of non-equilibrium charge trapping which could then be compared with the dynamic equilibrium case present in the conduction experiments.

The polymers were charged using both the negative corona discharge and the highly stressed electrode (positive and negative) methods. The measurement of the apparent surface charge gave little information of quantitative use, for the polymers all supported very large electrostatic charges. These static charges effectively masked all contributions from trapped charge. The polarity of the measured surface charge was in all cases the same as the charging polarity.

TABLE 5. Results of conduction experiments on polymers

Polymer	$N_0(\theta\mu_R)$ (at 298 K)	$\frac{N_0}{\theta}$	$\theta\mu_R$ (at 298 K)	$\theta_0\mu_R$	ΔE (eV)
2	4×10^{7}	3×10^{17}	1×10^{-10}	1×10^{-5}	0.31 (scl)
6	5×10^{6}	3×10^{17}	3×10^{-11}	5×10^{-4}	0.43 (scl) 0.48 (ohmic)
7	2×10^{9}	5×10^{17}	1×10^{-8}	1×10^{-3}	0.29 (scl)

Can. J. Chem. Downloaded from www.nrcresearchpress.com by 210.87.254.105 on 09/05/12
For personal use only.

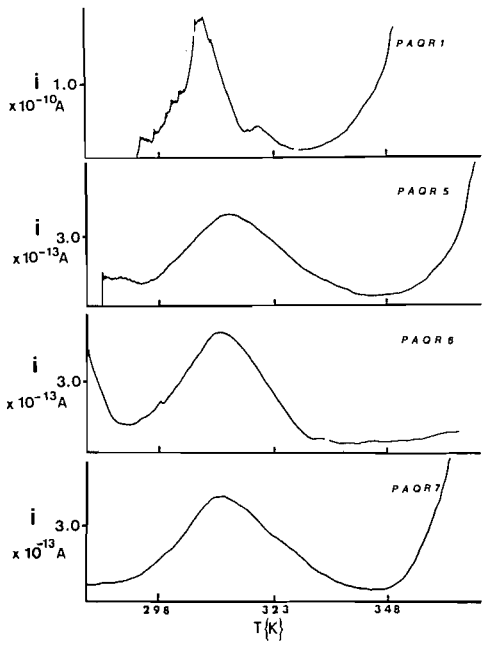

FIG. 3. Thermally stimulated current spectra from some PAQR polymers.

The electret state (*i.e.* charged state) was investigated using tsc techniques. All polymers examined had similar tsc spectra, a representative sample of which is shown in Fig. 3 with one broad peak occurring slightly above the temperature at which the samples were charged (298 K). This broad peak was assigned to the thermal release of trapped charge in the polymer.

These broad peaks, centered at approximately 315 K for all polymers studied, were fitted to an expression of the form of eq. 7, and in all cases a good fit was obtained by utilizing data from the entire peak.

The major result obtained from the curve fitting procedure was the magnitude of the trap depth, E_a. In addition, the total area under the tsc spectrum was measured and a value for the total trapped charge density, ρ_Q, was found. The pre-exponential factor, C, in eq. 7 was not a useful parameter, as it appears to depend on trapping lifetimes, retrapping probabilities, carrier mobilities, and even the exact nature of the charge distribution.

Quantitatively, the single peak indicated that only one type of trapping site predominated in the polymer. For some of the higher conductivity polymers, PAQR 7 and others, an anomalous effect was found above 380 K where the sample appeared to exhibit some form of thermoelectric effect entirely independent of trapped charge. Attempts to investigate the nature of the behavior did not lead to any definitive answers.

The information from tsc spectra of samples charged at different impressed voltages indicated that the charge was trapped in a layer near the surface being charged. As the potential was increased, however, there was evidence that appreciable charge density was present throughout the sample. In addition to this, the polymers appeared to be able to support excess positive and negative charge with equal ease.

Discussion and Conclusions

The integration of data from conduction and charge trapping experiments with some basic chemical knowledge of the PAQR polymer system allows a more complete understanding of the electronic processes occurring in these polymers. The examination of the chemical properties of a few polymers enabled the extraction of some of the more prominent chemical features of this polymer system.

The elemental analysis, of two different polymers, indicated that polymerisation had resulted in large losses of both oxygen and hydrogen. The Friedel–Crafts type of reaction originally intended to occur would cause elimination of water but the elemental analysis indicates that far more hydrogen has been lost than if this were the case. Other reactions are probably occurring. The harsh reaction conditions suggest many possible reactions. One favourable possibility is the Friedel–Crafts related Scholl reaction. The Scholl reaction leads to hydrogen elimination between two adjacent aromatic rings and a carbon–carbon bond is formed linking the two rings. Most possible reactions that can be devised have one factor in common; they all tend to increase the size of the conjugated system.

The optical data contain little conclusive information, but several interesting points can be deduced from the results. The very low energy optical absorption edge, above which the polymers exhibit almost total absorption, suggests that the polymers contain very large π systems, each of which have a large number of possible excited states. The infrared also has a few surprising details. All the major peaks are best assigned to aromatic and olefinic bond features,

Can. J. Chem. Downloaded from www.nrcresearchpress.com by 210.87.254.105 on 09/05/12
For personal use only.

Can. J. Chem. Downloaded from www.nrcresearchpress.com by 210.87.254.105 on 09/05/12
For personal use only.

such as C—H stretch and C—H out-of-plane bending, while there are no peaks corresponding to the normally strong carbonyl stretch, which would be present with quinone or ketone linkages in the polymer. This negative evidence suggests that the Friedel–Crafts reactions leading to quinones are not as important as was originally thought.

The data from the esr experiments are comparable to the results obtained in the earlier work by Pohl and Chartoff. Indeed the esr spectra were used as a partial check of polymerization techniques. The thermal creation of radicals in the PAQR polymer systems first reported by Pohl and Chartoff (4) and confirmed by this work, suggest that the triplet state, the first excited state in any aromatic system, has been lowered in energy to such an extent that significant mixing with the ground state occurs, thus destroying the validity of the spin selection rule.

The esr does not detect a triplet radical as the large size of the π system allows electron–electron interactions to be minimised, thus creating a biradical. Biradicals behave as singlets in an esr spectrum (12). In addition to spin birth energy information, the esr singlet, for all the polymers studied, has a gyromagnetic ratio, indicative of a hydrocarbon radical, rather than the g value of a semiquinone radical, thought previously to be present. This piece of esr data supports the conclusion drawn from the optical results which is that the aromatic ring systems are the dominant chemical feature of these polymers. Finally, the lorentzian line shape of the esr signal is indicative of electron exchange between adjacent radical sites. For radical exchange to occur, the electron orbital overlap must be significant, and if the radicals are confined in an extended π system, there is a strong implication that the adjacent radicals must be in π systems which are in close proximity to each other.

Finally, in connection with the polymer structure, Pohl and Rosen (5) found that the hyper electronic polarisability in the higher conductivity members of thin polymer series could best be described by an extended π system model.

All data obtained for these polymers indicates that polymerisation has resulted in the formation of large aromatic π systems which dominate the chemical and physical nature of these polymers. The conductivity and tsc data can be analysed in terms of this general picture to yield a self-consistent set of parameters for the electronic processes which occur in these polymers. No other model provides as good a framework for the analysis of the results.

The conductivity data allowed the determination of several useful parameters; the trap depth, the effective carrier mobility and the transition field for the ohmic–scl cross-over. The trap depths were found to be small for all polymers studied, which is consistent with the apparent shallow trapping regime observed in the scl region. If it is assumed that the traps lie close to the fermi level then the band gap in these polymers is approximately twice the trap depth (that is, about 0.8 eV). In normal semi-conducting materials, a band gap energy of this magnitude would imply high carrier concentrations in the conduction band and a reasonable conductivity. These polymers, however, exhibit a very low conductivity caused by an extremely low effective carrier mobility.

Using band formalism, a low effective mobility is the result of narrow bands (of the order of kT wide) which lead to extensive scattering of the carrier. Alternatively, a more physical interpretation of these results comes from the tight binding approximation. If the carrier source is an aromatic π system, then the magnitude of the carrier mobility will depend on the wave function overlap between adjacent π systems, and in the limit of the low overlap, the motion of the carrier can best be described by a hopping or tunneling mode between π systems. The carrier mobility then becomes a function of barrier height and width. The low values of the carrier mobility for the PAQR polymers suggest that the hopping model is the most applicable. The esr work by Pohl and Chartoff (4) displayed an inverse relationship between the conductivity and the esr line width and the lorentzian line shapes found in this work suggest the line width is, in turn, a function of electron exchange. Electron exchange, while different from carrier mobility, also depends on the wave function overlap between adjacent radical sites. The esr peak width serves as a measure of the probability of carrier hopping, provided the radicals and the carriers are associated with the same molecular feature.

The transition field, E_x, is important for it

Can. J. Chem. Downloaded from www.nrcresearchpress.com by 210.87.254.105 on 09/05/12
For personal use only.

allows the extraction of some fundamental parameters from the conduction data, but to accomplish this, some assumptions must be made. The effective mobility, $\theta\mu_R$, at 298 K was measured in the scl conduction region, while the free intrinsic carrier concentration – effective mobility product, $n_0(\theta\mu_R)$, was measured in the ohmic region. If we assume that the effective mobility is not strongly affected by the applied field, then an estimate of the magnitude of n_0 can be made. This assumption relies on two factors; the first is that the barrier impeding conduction is not altered significantly by the application of an electric field, while the second is that the fermi level does not radically shift when charge is injected into the solid. These assumptions are reasonable for molecular solids, but they could lead to some discrepancies. An examination of the activation energies for conduction in both the ohmic and scl regimes for PAQR 6 indicates that the trap depth appears to be slightly dependent on the applied field. The assumptions are, therefore, not strictly valid, but they do allow an order of magnitude estimate of n_0.

From E_x, the scaled free carrier density, n_0/θ, is known, and thus, by using the value for n_0, an estimate of the partition constant, θ, can be made. For all three polymers θ was found to be close to one. The effect of the partition constant, θ, can now be eliminated from the effective carrier mobility to obtain an estimate of the mean carrier mobility μ_R. All these values do, of course, rely on the initial assumptions and therefore should be used carefully.

The temperature dependence of the scl current allows the high temperature limit of the effective carrier mobility, $\theta_0\mu_R$, to be determined, and through this, θ_0 can be estimated. The constant θ_0 is the ratio of the density of states in the conduction band, N_c, to the density of the trapping states, gN_t. The free carrier density, n_0, is also related to N_c through eq. 3. By using the previously determined value of n_0, both N_c and gN_t can be evaluated. Finally, by using eq. 8, the trapped electron concentration, n_t, can be found (evaluated at 298 K with g assumed to be equal to 2) (13).

$$[8] \qquad n_t \approx \frac{N_t}{1 + \frac{1}{g}\frac{N_c \exp(-\Delta E/kT)}{n_0}}$$

The values for these conduction-related parameters are given for three of the PAQR polymers in Table 6.

The mean carrier mobilities, μ_R, finally obtained are very low and are highly characteristic of a hopping conduction mechanism. Furthermore, a comparison of the conductivity, the free carrier density, and the mean carrier mobility, all interrelated by eq. 2, suggests that the carrier mobility, not the free carrier density, is the dominant factor determining the polymer's conductivity.

The three polymers examined all have approximately the same free carrier density, but the carrier mobilities are spread over three orders of magnitude. The small changes in the chemical nature of the polymers appear to strongly affect the nature of the potential barriers between hopping sites. In terms of the extended π systems acting as hopping sites, the chemical structure of the non π system portion of the polymers plays a key role in determining the magnitude of the conductivity.

Pohl first recognised the interrelation between

TABLE 6. Values of conduction-related parameters of polymers

Polymer	n_0 (m^{-3})	θ (298 K)	μ_R ($m^2 s^{-1} V^{-1}$)	$\theta_0(T \rightarrow \infty)$
2	4×10^{17}	1.3	1×10^{-10}	1×10^{5}
6	2×10^{17}	0.6	5×10^{-11}	1×10^{7}
7	2×10^{17}	0.4	3×10^{-8}	3×10^{4}

Polymer	N_c (m^{-3})	gN_t (m^{-3})	n_t (m^{-3})
2	5×10^{22}	3×10^{17}	1×10^{17}
6	2×10^{25}	2×10^{18}	3×10^{17}
7	4×10^{22}	2×10^{18}	4×10^{17}

Can. J. Chem. Downloaded from www.nrcresearchpress.com by 210.87.254.105 on 09/05/12
For personal use only.

the radicals present in the polymer and the polymer's conductivity. He also noted, however, that the relationship must be indirect as the free carrier density, n_0, was much smaller than the radical density. The radical densities measured by Pohl ranged from 10^{22} to 10^{24} m^{-3}, on going from low conductivity polymers to the high conductivity polymers. The results obtained from the scl data provide a clue to the nature of the indirect relationship between the free carrier density and the free radical concentrations. The effective density of states in the conduction band N_c, is the maximum number of free carriers available as the temperature becomes very high. Thus N_c represents the number of potential free carriers present in the solid, and the magnitude of the density of carrier states is comparable to the magnitude of the radical densities measured by Pohl. It appears then that in the large aromatic π systems, the apparent source of free radicals in these polymers, are also the source of the charge carriers. The charge carriers must have, however, a much higher formation energy than the free radicals. The carriers are probably formed as ionic excitons, where an electron in a π system is transferred to a neighbouring π system, thus forming delocalised excitons which are split apart (or ionized) by an applied field. The resulting positive and negative ions could then migrate through the solid by an inter π system electron hopping mechanism. The extended π system model, first proposed by Pohl, thus allows a consistent physical interpretation of both the esr and the conductivity data.

The exact nature of the trapping sites still remains unclear. The reproducibility of conduction data for a given polymer, on going from one sample to another, suggests that defects in the solid are not a likely source of trapping sites. The other alternative is that some intrinsic chemical feature of the polymer can act as a trapping site. A possibility in this category is that the extended π systems could act as shallow traps, with the carrier localised in some intermediate level to facilitate carrier formation. The first step could involve the formation of an intra π system excitation, with an electron promoted to an intermediate level, followed by electron transfer to a neighbouring π system. Once the π system has been ionised the charge carriers could be trapped in the intermediate excitation level of any π system. The conduction data can thus be used to speculate about the nature of the trapping sites although nothing definite can be determined.

This work was originally initiated by a strong interest in charge storage phenomena and more specifically, the mechanism of charge storage. The investigation of charge storage aspects of the PAQR polymers gave some interesting results. These polymers were quite remarkable, compared to other materials which have been studied, as they appeared to be able to support excess positive and negative charge with equal facility. The extended π system model gives an adequate interpretation of this behavior. The polarisability of an extended π system would be very high (the PAQR polymers exhibit anomalous dielectric behavior attributable to very high polarisability) and a positive or negative excess charge residing in such a π system would tend to be effectively screened from its surroundings, thus reducing the intercharge repulsions. The stability of charge storage would then be greatly increased.

The PAQR polymers also exhibited extremely high surface charges which made surface charge measurements, as a means of assessing charge storage, completely erroneous. Information about the surface charge was obtained from the tsc experiments. It was found that if the sample was cooled below the charging temperature, then the tsc spectrum tended to have a large initial peak due to mobile static charge, followed by a small peak occurring at the charging temperature. The small peak results from a fraction of the static charge loosely bound in shallow traps on the polymer's surface. The loose binding of the surface charge would account for the exceptional stability of electrostatic charges on these polymers.

More importantly, the tsc spectrum also gave information about charge storage in the PAQR polymer system. The intense single peak, shown by all the polymers studied, was analysed to give an average trap depth energy and the magnitude of the trapped charge density. The single peak is characteristic of a single, dominant mode of charge storage, while the low temperature of the peak maximum suggested that the traps were shallow (relative to the system fermi level). The trap depths and charge densities, given in Table 7, were not exceptionally useful in determining the mechanism of the charge storage. An ap-

TABLE 7. Some properties of tsc spectra

Polymer	ρ_Q (C m^{-3})	E_a* (eV)	Peak maximum	C
2	1×10^{-2}	0.33 ± 0.02 (8)	310 ± 5	3×10^{-13}
6	2×10^{-2}	0.35 (1)	315	1×10^{-12}
7	2×10^{-2}	0.37 ± 0.03 (4)	320 ± 5	6×10^{-13}

*The number in parentheses is the number of tsc spectra averaged to obtain the data.

TABLE 8. Values of E_a, ρ_Q and n_t of polymers

Polymer	tsc E_a (eV)	scl E (eV)	tsc ρ_Q (m^{-3})	scl n_t (m^{-3})
2	0.33	0.31	6×10^{16}	1×10^{17}
6	0.35	0.43	1×10^{17}	3×10^{17}
7	0.37	0.29	1×10^{17}	4×10^{17}

proximate lifetime for the charge storage could, however, be calculated from the trap depth and the pre-exponential constant. The calculated lifetimes for the electrically isolated polymers were all found to be approximately 20 days.

The similarities between the tsc data and the conduction results do, however, allow some conclusion about the mechanism of charge storage.

The trap depth determined from the conduction experiments compares very well with the average trap depth, or activation energy for charge release, determined in the tsc experiment. This correspondence suggests that the trapping sites which impede conduction are also responsible for the charge storage. This conclusion is further supported by the close similarity between the magnitude of the stored charge density, ρ_Q, and the density of trapped charge, n_t, (from the scl measurements). These data are given for comparison in Table 8.

The activation energies given for polymers 2 and 7 are more significant as they are averaged over several experiments. The tsc activation energies are larger than the corresponding conduction trap depths probably due to field distortion of the potential barriers or an elevation of the fermi level caused by heavy charge injection during scl conduction. This is, of course, analogous to the similar trend found between the ohmic and scl conduction results.

1. L. M. BAXTER and M. M. PERLMAN (*Editors*). Electrets and related electrostatic charge storage phenomena. The Electro Chemical Society Inc., New Jersey. 1968.
2. M. M. PERLMAN (*Editor*). Electrets: charge storage and transport in dielectrics. The Electrochemical Society, Inc. New Jersey. 1973.
3. H. A. POHL and E. H. ENGLEHARDT. J. Phys. Chem. **66**, 2085 (1962).
4. H. A. POHL and R. P. CHARTOFF. J. Polymer Sci. PTA. **2**, 2787 (1964).
5. H. A. POHL and R. ROSEN. J. Polymer Sci. PTA-1, **4**, 135 (1966).
6. H. A. POHL. J. Polymer Sci. Pt. C. **17**, 13 (1967).
7. M. A. LAMPERT and P. MARK. Current injection in solids. Academic Press. New York. 1970.
8. C. BUCCI and R. FIESCHI. J. Phys. Rev. Lett. **12**, 16 (1964).
9. C. W. REEDYK and M. M. PERLMAN. J. Electrochem. Soc. **115**, 49 (1968).
10. N. F. MOH and R. W. GURNEY. Electronic processes in ionic crystals. 2nd ed. Dove Pub. New York. 1948. p. 172.
11. R. A. CRESWELL and M. M. PERLMAN. J. Appl. Phys. **41**, 2365 (1970).
12. R. S. ALGER. Electron paramagnetic resonance. Interscience Publication. New York. 1968. p. 475.
13. M. A. LAMPERT and P. MARK. Current injection in solids. Academic Press, New York. 1968. p. 19.

Can. J. Chem. Downloaded from www.nrcresearchpress.com by 210.87.254.105 on 09/05/12
For personal use only.

Chaleurs de dilution de solutions aqueuses d'acide polyméthacrylique et de ses sels de sodium et de rubidium

HUBERT DAOUST ET ALAIN LAJOIE

Département de Chimie, Université de Montréal, C.P. 6210, Succursale A, Montréal (Qué.) Canada H3C 3V1

Reçu le 20 août 1975[1]

HUBERT DAOUST et ALAIN LAJOIE. Can. J. Chem. **54**, 1853 (1976).

Des chaleurs de dilution de solutions aqueuses d'acide isobutyrique (AB) et de deux échantillons d'acide polyméthacrylique ayant des valeurs de masse moléculaire moyenne viscosimétrique de 5000 (APM-I) et 140 000 (APM-II) respectivement, ont été mesurées à l'aide d'un microcalorimètre Tian–Calvet à 25 °C. Les mêmes mesures ont été reprises en présence de HCl (0.2 *N*). Des solutions aqueuses de sels de sodium et de rubidium de APM-I et APM-II ont aussi été étudiées par la même méthode. La dilution de solutions de AB est endothermique à concentration élevée et devient exothermique lorsque la concentration décroit et la présence de HCl ne modifie en rien l'allure des résultats. La dilution de solutions de APM est exothermique sur toute la gamme des concentrations étudiée en accord avec les résultats d'Eliassaf et coll. L'échantillon APM-I donne des chaleurs de dilution plus exothermiques que APM-II dans le domaine des basses concentrations. La présence de HCl n'affecte pas beaucoup les résultats obtenus avec APM-II mais rend la dilution de solutions de APM-I moins exothermique. Les résultats sont discutés à la lumière du modèle suggéré par Liquori *et al.* pour la chaîne d'APM qui peut adopter une conformation globulaire ou celle d'une chaîne étendue selon les propriétés du milieu solvant. Les chaleurs de dilution des solutions aqueuses du sel de sodium des deux échantillons APM-I et APM-II sont endothermiques tandis que celles pour le sel de rubidium sont exothermiques.

HUBERT DAOUST and ALAIN LAJOIE. Can. J. Chem. **54**, 1853 (1976).

Heats of dilution of aqueous solutions of two polymethacrylic acid samples having a viscosity average molecular weight of 5000 (PMA-I) and 140 000 (PMA-II) respectively and of isobutyric acid (BA) have been measured at 25 °C using a Tian–Calvet microcalorimeter. The same measurements have been repeated in presence of HCl (0.2 *N*). Aqueous solutions of sodium and rubidium salts of PMA-I and II have also been investigated. Dilution of BA solutions is endothermic at high solute concentration and then becomes exothermic as concentration decreases and the presence of HCl does not affect the results. Dilution of PMA solutions is exothermic over the investigated concentration range in agreement with the results of Eliassaf and coworkers. PMA-I gives a more exothermic heat of dilution than PMA-II in the lower concentration range. The presence of HCl does not affect appreciably the results for PMA-II but it makes the dilution of PMA-I solutions less exothermic. The results are discussed in the light of Liquori *et al.*'s model for PMA chain which may adopt a globular or an extended solvated coil depending on solvent properties. Heats of dilution of aqueous solutions of sodium salts of both samples I and II are endothermic over the entire concentration range investigated whereas the heats of dilution of rubidium salts are exothermic.

Introduction

Les études sur le comportement de l'acide polyméthacrylique en solution sont réparties sur une période de plus de 20 années. Parmi les premiers travaux importants se trouve celui de Silberberg *et al.* (1) dans lequel ils montrent par l'étude du coefficient thermique de la diffusion de la lumière et de la viscosité intrinsèque que les chaleurs de dilution de solutions aqueuses d'acide polyacrylique (APA) sont endothermiques tandis que celle de l'acide polyméthacrylique (APM) sont exothermiques. Ils ont aussi trouvé que la conformation des chaînes d'APM dans l'eau et dans l'acide chlorhydrique dilué est celle d'une pelotte compacte. Afin d'expliquer le comportement d'APM, ils ont postulé l'existence de liens hydrogène intramoléculaires. Ils ont aussi souligné le fait que la présence d'un groupement méthyle et d'un groupement carboxyle sur le même carbone produit un effet de contraction important sur la chaîne. Plus tard, un changement de conformation de la chaîne d'APM a été mis en évidence par spectroscopie uv, potentiométrie et viscosimétrie (2–5). Il fut suggéré alors que des forces hydrophobes jouent un rôle important dans cette transition conformationnelle

[1]Revision reçue le 27 février 1976.

Can. J. Chem. Downloaded from www.nrcresearchpress.com by 210.87.254.5 on 09/05/12
For personal use only.

Can. J. Chem. Downloaded from www.nrcresearchpress.com by 210.87.254.5 on 09/05/12
For personal use only.

(5, 6), excluant les liens hydrogène intramoléculaires comme facteur important (3). Cependant, des études en spectroscopie Raman-laser (7) sur l'APM à l'état solide et en solution aqueuse ont montré que les groupements carboxyles d'APM sont presque tous impliqués dans des liens hydrogène à l'état solide et que cette situation persiste en solution aqueuse, ce qui est différent du cas d'APA; ces résultats sont confirmés par Michels et Zana (8).

Les liens hydrophobes chez l'APM viennent de l'existence des groupements latéraux méthyles et il appert, selon le modèle de Liquori *et al.* (5), qu'à faible degré d'ionisation des groupements carboxyles, les groupements méthyles se trouvent à l'intérieur de la molécule, de même qu'une fraction des groupements carboxyles, de façon à présenter une structure globulaire stabilisée par les intéractions hydrophobes. Au fur et à mesure que l'ionisation augmente, la structure va s'ouvrir de façon à donner une chaîne solvatée, *i.e.*, les groupements méthyles deviennent accessibles aux molécules d'eau. De toute évidence, cette ouverture de la structure est due à la répulsion entre les sites négatifs qui apparaissent le long de la chaîne. Des transitions conformationnelles semblables ont été observées dans le cas de protéines globulaires.

Les sels alcalins d'APM sont des polyélectrolytes forts et il est connu que la nature du cation joue un rôle important dans les résultats obtenus sur les chaleurs de dilution et sur les densités des solutions modérément concentrées de polyélectrolytes (8–11). L'association ionique de paire avec l'hydratation ionique sont spécifiques à chaque cation et la conformation de la chaîne peut alors être définie par la nature des cations. Les sels de sodium et de rubidium d'APM ont aussi été étudiés dans le présent travail de façon à comparer leur comportement à celui des sels d'autres polyacides.

TABLEAU 1. Chaleurs de dilution de l'acide isobutyrique à 25 °C

n_1	n_2	Δn_1	ΔE_d (J)
	Solvant: eau		
0.0467	0.2194	0.1821	157.215
0.0498	0.2339	0.1630	118.732
0.0481	0.2261	0.0505	206.628
1.1216	0.0359	0.3948	−24.968
1.1664	0.0276	0.4041	−16.050
1.2534	0.0220	0.3980	−9.345
1.2499	0.0167	0.3946	−5.009
1.1993	0.0121	0.4053	−1.098
1.2578	0.0094	0.3959	−0.381
1.2983	0.0072	0.3911	−0.265
1.4439	0.0061	0.4570	−0.156
1.2613	0.0041	0.4045	−0.069
1.2514	0.0011	0.3942	0
	Solvant: HCl 0.2 *N*		
0.0477	0.2261	0.1896	185.751
0.0486	0.2293	0.1437	167.821
0.0458	0.2170	0.1304	157.228
1.1066	0.0357	0.4047	−24.736
1.2242	0.0289	0.4007	−16.319
1.2400	0.0220	0.3957	−8.887
1.2260	0.0165	0.3958	−5.095
1.2295	0.0136	0.3967	−1.099
1.1757	0.0099	0.3819	−0.538
1.2100	0.0077	0.4220	−0.274
1.2019	0.0056	0.4001	−0.165
1.2640	0.0043	0.3886	−0.081
1.2397	0.0033	0.4227	−0.029
1.2413	0.0013	0.4186	0

Partie expérimentale

Produits utilisés

Deux échantillons d'acide polyméthacrylique furent utilisés dans ce travail. Le premier (APM-I), de masse moléculaire moyenne viscosimétrique ($\bar{M}_v$) égale à 5000 fut fourni gracieusement par la compagnie Rohm and Haas de Philadelphie, Pa. Le second (AMP-II) fut préparé selon un mode similaire à celui utilisé ailleurs (1, 12). La polymérisation de 100 ml d'acide méthacrylique (Eastman Kodak, Rochester, N.Y.), préalablement distillé à 60 °C sous une pression de 12 torr, fut initiée par 1.8 g d'azobisméthyl-2 proprionitrile-2,2′ (Eastman Kodak) en solution dans 300 ml de butanone-2 (J. F. Baker, Phillipsburg, N.J.). La réaction s'est faite à 48 °C pendant 15 h. Le taux de conversion était de 85%. Le polymère obtenu a été séché sous vide et purifié par dialyse durant une semaine. La solution aqueuse fut liophylisée et le polymère sec à 97% fut conservé sur P_2O_5. Sa valeur de $\bar{M}_v$ était de 140 000 en se basant sur les résultats de Silberberg *et al.* (1).

L'acide isobutyrique (Fisher Scientific Co., Fair Lawn, N.J.) fut distillé et la fraction passant entre 154.2 et 154.6 °C fut retenue.

Les sels de sodium et de rubidium furent préparés selon une méthode décrite ailleurs (13). L'hydroxyde de rubidium fut obtenu à partir du chlorure (Anachemia Chemicals, Montréal) en solution aqueuse passée dans une colonne de résine échangeuse d'ions Dowex 2X-8. Les solutions furent ensuite purifiées par dialyse pendant 12 h, puis liophylisées et les sels gardés à sec sur P_2O_5.

Calorimétrie

Les mesures de chaleurs de dilution furent réalisées à 25 °C à l'aide d'un microcalorimètre Tian–Calvet équipé de cellules de 25 et 35 mm de diamètre; les détails techniques sont décrits dans des travaux précédents (9, 14). Les concentrations initiales avant dilution variaient entre 0.5 et 15% en poids.

Can. J. Chem. Downloaded from www.nrcresearchpress.com by 210.87.254.5 on 09/05/12
For personal use only.

TABLEAU 2. Chaleurs de dilution de l'acide polyméthacrylique à 25 °C

n_1	n_2	Δn_1	ΔE_d (J)
	APM-I/H_2O		
1.1176	0.0344	0.3991	−0.624
1.2251	0.0278	0.4037	−0.298
1.2785	0.0218	0.4057	−0.200
1.3101	0.0170	0.4066	−0.112
1.2085	0.0145	0.4035	−0.093
1.3028	0.0129	0.3878	−0.071
1.3276	0.0668	0.4059	−0.024
1.3226	0.0033	0.3973	−0.005
1.2523	0.0013	0.3954	0
	APM-I/HCl 0.2 *N*		
1.2175	0.0450	0.4003	−0.515
1.1535	0.0395	0.4028	−0.440
1.1921	0.0302	0.3850	−0.206
1.2042	0.0231	0.4037	−0.096
1.2809	0.0184	0.3992	−0.028
1.2743	0.0139	0.4006	−0.009
1.3626	0.0056	0.3959	0.006
1.3105	0.0042	0.4045	0.007
1.2955	0.0019	0.4109	0.006
	APM-II/H_2O		
0.9557	0.0278	0.3589	−0.522
1.1000	0.0282	0.3928	−0.415
1.2108	0.0291	0.3974	−0.383
1.2477	0.0225	0.3999	−0.179
1.2568	0.0172	0.3932	−0.066
1.2555	0.0131	0.4036	−0.043
1.2705	0.0100	0.3871	−0.025
1.3216	0.0034	0.3964	0
1.2820	0.0017	0.3879	0
	APM-II/HCl 0.2 *N*		
1.0760	0.0345	0.3838	−0.553
0.0673	0.0253	0.4084	−0.304
0.1192	0.0241	0.4064	−0.288
1.2128	0.0208	0.3940	−0.110
1.2410	0.0161	0.4115	−0.072
1.2175	0.0118	0.4145	−0.046
1.2744	0.0100	0.4157	−0.025
1.2667	0.0049	0.3943	−0.008
1.2843	0.0018	0.3887	0

Résultats et discussion

Les résultats obtenus sont donnés dans les tableaux 1 à 3. La quantité n_1 représente le nombre de moles de solvant dans la solution avant la dilution, n_2, le nombre de moles de soluté ou de moles de motif de base (selon le cas) et Δn_1, le nombre de moles de solvant ajoutées lors de la dilution. Dans le cas de HCl 0.2 *N* utilisé comme solvant, n_1 et Δn_1 représentent le nombre de moles d'eau et de HCl globalement.

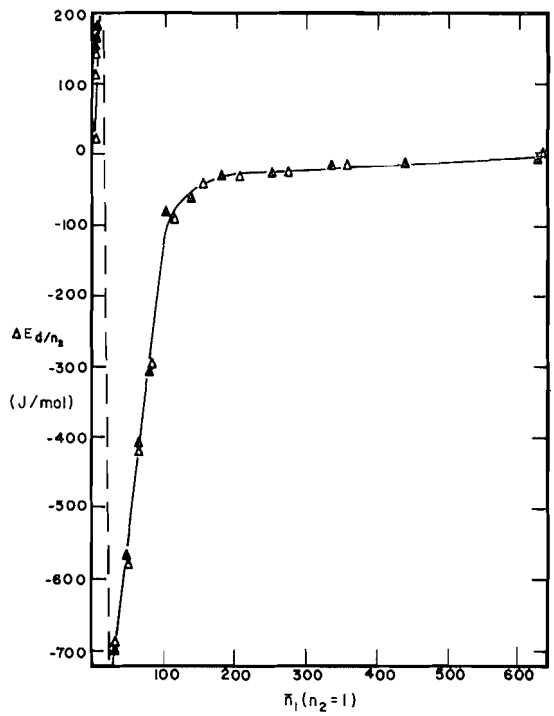

FIG. 1. Variation de l'énergie de dilution intermédiaire avec le nombre moyen de moles d'eau (pour une mole de soluté) pour l'acide isobutyrique à 25 °C: △ AIB/H_2O; ▲ AIB/HCl (0.2 *N*).

L'énergie de dilution intermédiaire, ΔE_d, est exprimée en joules. Les figs 1 à 3 représentent l'allure de la variation des chaleurs de dilution par mole de soluté ou mole de motif de base avec le nombre moyen de moles d'eau

$$\bar{n}_1 = \frac{2n_1 + \Delta n_1}{2n_2}$$

par mole de soluté.

Le système eau – acide isobutyrique étant partiellement miscible à 25 °C, les dilutions ont été faites au-dessus et au-dessous des deux concentrations conjugées. La fig. 1 montre qu'à concentration élevée, les chaleurs de dilution sont endothermiques car la rupture des ponts hydrogène persistants entre les molécules d'acide est un phénomène endothermique. Au-dessus de la concentration conjugée inférieure, les chaleurs de dilution sont fortement exothermiques et ceci a déjà été expliqué par la formation d'icebergs autour des groupements hydrophobes de l'acide organique (14). Au fur et à mesure que la dilution progresse, les molécules du soluté sont dispersées

Can. J. Chem. Downloaded from www.nrcresearchpress.com by 210.87.254.5 on 09/05/12
For personal use only.

TABLEAU 3. Chaleurs de dilution de sels de l'acide polyméthacrylique à 25 °C

n_1	n_2	Δn_1	ΔE_d (J)
		NaPM-I	
1.1764	0.0289	0.4008	1.234
1.2249	0.0225	0.4153	0.545
1.2483	0.0171	0.4043	0.210
1.2598	0.0130	0.4051	0.034
1.2843	0.0114	0.3964	0.015
1.2290	0.0096	0.3932	−0.002
1.2527	0.0085	0.4102	−0.005
1.2512	0.0064	0.4002	−0.011
1.3020	0.0050	0.4116	−0.015
1.2816	0.0031	0.4059	−0.019
1.2404	0.0014	0.4203	−0.005
1.2769	0.0009	0.3987	0
		NaPM-II	
1.1504	0.0291	0.4115	2.659
1.2055	0.0224	0.4068	1.244
1.2412	0.0172	0.3977	0.590
1.2558	0.0132	0.4019	0.272
1.2177	0.0097	0.3872	0.164
1.2510	0.0083	0.4063	0.063
1.2541	0.0063	0.3995	0.010
1.2716	0.0046	0.3932	0.005
1.2543	0.0036	0.4017	0.002
1.2985	0.0022	0.3987	0
1.2134	0.0014	0.4028	−0.002
		RbPM-I	
1.1495	0.0314	0.4124	0
1.2285	0.0180	0.4116	−0.257
1.2738	0.0139	0.3966	−0.212
1.2628	0.0105	0.4025	−0.181
1.2576	0.0079	0.4080	−0.135
1.3181	0.0076	0.3903	−0.091
1.3368	0.0054	0.4012	−0.056
1.3058	0.0045	0.4043	−0.041
1.2557	0.0033	0.3912	−0.029
1.2503	0.0025	0.3936	−0.018
1.2266	0.0018	0.3997	−0.011
1.2800	0.0007	0.4058	0
		RbPM-II	
1.1541	0.0289	0.3923	−0.217
1.1245	0.0272	0.4112	−0.284
1.0958	0.0205	0.3959	−0.267
1.1812	0.0209	0.4028	−0.264
1.1351	0.0156	0.3998	−0.240
1.2844	0.0130	0.3908	−0.218
1.2240	0.0095	0.3939	−0.168
1.2134	0.0082	0.4095	−0.104
1.3047	0.0074	0.3993	−0.053
1.3178	0.0057	0.4003	−0.043
1.3424	0.0034	0.4078	−0.025
1.2581	0.0024	0.4031	−0.015
1.3169	0.0019	0.4056	−0.010
1.4124	0.0016	0.4019	−0.005

uniformément dans le solvant et pratiquement seulement l'ionisation pourrait alors contribuer à la chaleur de dilution; l'ionisation en solution aqueuse est essentiellement un phénomène exothermique. De même que pour l'acide propionique (14), la présence de HCl, qui détruit la structure de l'eau, n'affecte pas le mécanisme de dilution de l'acide isobutyrique. Le fait que la présence de HCl ne modifie pas les valeurs de la chaleur de dilution montre que l'ionisation de l'acide propionique et de l'acide isobutyrique est négligeable dans le domaine de concentration où ces mesures ont été faites car évidemment la présence de HCl refoule toute ionisation possible de ces acides. Il faut donc supposer que l'hydratation exothermique des groupements hydrophobes se fait sentir même à dilution appréciable. Cependant, il est à noter que la chaleur de dilution augmente avec la dilution à concentration élevée, contrairement à l'acide propionique; cela pourrait s'expliquer par le fait que l'on s'approche de la démixtion.

L'allure des résultats obtenus pour les deux échantillons d'acide polyméthacrylique est représentée dans la fig. 2. L'ionisation de ce polyacide étant négligeable dans le domaine de concentration étudié ici, la chaleur de dilution serait due à la rupture de ponts hydrogène intramoléculaires entre les groupements carboxyles, phénomène endothermique, à l'hydratation des groupements méthyles venant en contact avec l'eau et qui est exothermique et probablement à la rupture de particules de gel qui peuvent être présentes dans des solutions concentrées d'APM à faible pH (15). Etant donné que les gels sont produits par la formation de liens hydrogène intermoléculaires (15), leur rupture devrait être endothermique. On peut également considérer l'effet de chaîne qui a déjà été mentionné pour expliquer les chaleurs de dilution endothermiques de solutions aqueuses d'acide polyacrylique (14); cet effet de chaîne aurait pour conséquence la rupture d'un certain nombre d'agrégats de molécules d'eau créant ainsi un effet endothermique d'autant plus important que la chaîne est longue. Afin de contrecarrer les trois effets endothermiques mentionnés ci-haut, l'hydratation des groupements méthyles doit être très importante. Contrairement à l'acide isobutyrique, le groupement méthyle d'APM n'est pas aussi accessible aux molécules d'eau. En effet,

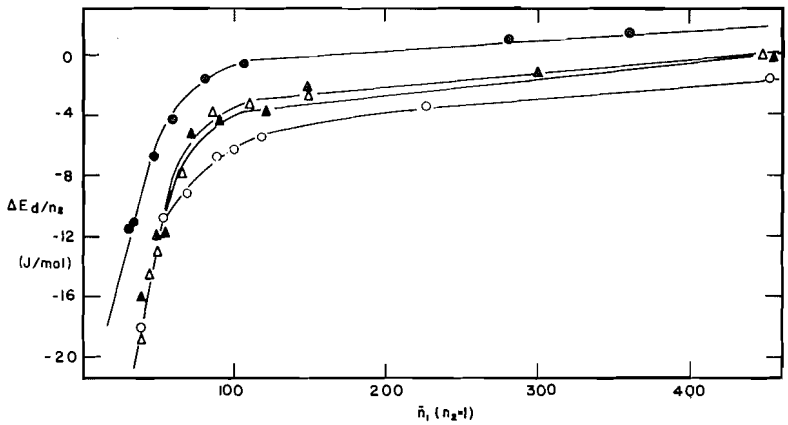

FIG. 2. Variation de l'énergie de dilution intermédiaire avec le nombre moyen de moles d'eau (pour une mole de motif de base) pour l'acide polyméthacrylique à 25 °C: ○ APM 5000/H_2O; ● APM 5000/HCl (0.2 *N*); △ APM 140 000/H_2O; ▲ APM 140 000/HCl (0.2 *N*).

d'après le modèle de Liquori *et al.*, à concentration élevée la majeure partie des groupements méthyles sont englobés à l'intérieur de la structure globulaire de même qu'un certain nombre de groupements carboxyles, ayant pour conséquence de diminuer l'effet de solvatation de ces groupements. Lors de la dilution de l'APM, il y aurait un phénomène coopératif qui comprendrait l'ouverture de la chaîne favorisant l'hydratation des groupes méthyles et carboxyles, un phénomène fortement exothermique. Les résultats indiquent que dans l'eau, l'accessibilité des groupes méthyle et carboxyle aux molécules de solvant est plus grande pour APM-I que pour APM-II ou peut être l'effet de chaîne est plus important pour une chaîne plus longue.

Lorsque HCl 0.2 *N* est utilisé comme solvant, les résultats ne changent guère appréciablement pour APM-II et ceci signifie que le nombre de liens intramoléculaires responsables de la structure globulaire postulée par Liquori *et al.*, et de liens intermoléculaires responsables de la formation de particules de gel ne change pratiquement pas lorsque le p*H* passe d'une valeur neutre à une valeur très acide pour une longue chaîne d'APM. Cependant, l'effet de HCl se fait sentir d'une façon non-négligeable pour APM-I, laissant supposer un effet plus grand du p*H* sur les chaînes plus courtes. Les changements de structure secondaire, tertiaire et même quaternaire seraient plus importants pour une courte chaîne, une situation que l'on rencontre dans le cas des polypeptides lorsque seules des courtes chaînes hélicoïdales tendent à donner la structure en feuillets, structure dite β, par agrégation (16).

Les résultats obtenus pour les chaleurs intermédiaires de dilution des solutions de sels de sodium et de rubidium sont illustrés à la fig. 3. Afin de comparer ces résultats avec d'autres semblables dans la littérature, la chaleur intégrale de dilution d'une solution de molalité moyenne $\bar{m}$ (correspondant à $\bar{n}_1$) à la molalité moyenne la plus faible $\bar{m}_0$, définie par

$$\sum_{\bar{m}_0}^{\bar{m}} \Delta E_d$$

a été calculée à partir des résultats de la fig. 3. Les résultats obtenus pour les sels de sodium sont représentés à la fig. 4 et ils sont comparés avec ceux calculés à partir de résultats déjà obtenus pour le NaPA (14) et le polystyrènesulfonate de sodium NaPSS (9). Il ressort que le comportement du NaPM-I et -II, du moins pour des concentrations diluées, diffère de celui des autres sels NaPA et NaPSS en ce qui concerne la chaleur intégrale de dilution. Ce n'est qu'à faible concentration que la dilution devient exothermique pour NaPM-II. En se basant sur le modèle de Liquori *et al.*, à haute valeur du p*H*, la chaîne polyméthacrylique serait dépliée et par conséquence, les groupements méthyles seraient déjà tous hydratés et la chaleur de dilution ne serait due qu'aux intéractions ioniques en solution concentrée. Le traitement utilisé par Eigen et Wicke (17) pour expliquer l'endothermicité de la

Can. J. Chem. Downloaded from www.nrcresearchpress.com by 210.87.254.5 on 09/05/12
For personal use only.

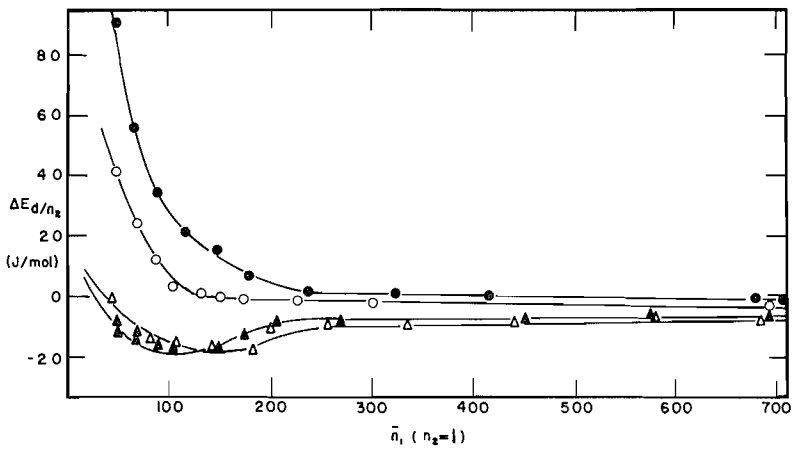

FIG. 3. Variation de l'énergie de dilution intermédiaire avec le nombre moyen de moles d'eau (pour une mole de motif de base) pour les sels de l'acide polyméthacrylique à 25 °C: ○ NaPM 5000/H_2O; ● NaPM 140 000/H_2O; △ RbPM 5000/H_2O; ▲ RbPM 140 000/H_2O.

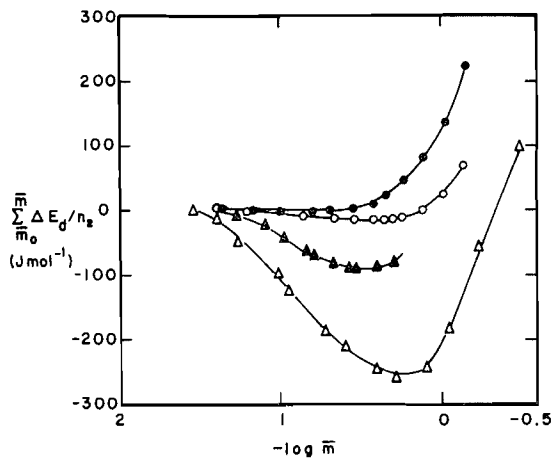

FIG. 4. Variation de l'énergie de dilution intégrale avec la molalité moyenne pour les sels de sodium à 25 °C: ○ NaPM-I; ◍ NaPM-II; △ NaPA (réf. 14); ▲ NaPSS (réf. 9).

dilution de solutions concentrées de certains électrolytes forts s'applique également aux solutions concentrées de polyélectrolytes forts (9). A concentration élevée, l'association entre les contre-ions et les sites chargés négativement le long de la chaîne est importante et ceci demande beaucoup d'énergie lors de la rupture. La dissociation s'accompagne de l'hydratation des espèces ioniques libérées, un phénomène fortement exothermique (9); l'allure des résultats pour NaPM-I et -II s'explique donc par la compétition entre ces deux effets de chaleur opposés. A la lumière des résultats, il faut conclure que l'ion sodium est plus fortement associé à la chaîne dans le cas présent que dans le cas du polyacrylate (14) et du polystyrènesulfonate (9). La différence des résultats entre les deux échantillons I et II serait due au nombre de sites chargés portés par la chaîne et ceci est conforme à une prédiction théorique (9) basée sur le modèle sphérique du macro-ion en solution concentrée.

L'association ionique devient plus importante lorsque la dimension du contre-ion augmente et ceci a été confirmé par les résultats sur les chaleurs de dilution de solutions aqueuses de polystyrènesulfonates d'alcalins (9, 10). Skerjanc *et al.* (10) ont obtenu une équation pour la chaleur intégrale de dilution à partir du modèle de polyions sous forme de bâtonnets orientés de Lifson et Katchalsky (18). Cependant, ils ont dû tenir compte de la dimension du cation afin d'expliquer l'allure des résultats expérimentaux. Par ailleurs, Mita et Okubo (19) ont aussi obtenu une relation pour la chaleur intégrale de dilution mais à partir de la loi limite de Manning (20). Cette dernière relation théorique prévoit que la chaleur intégrale de dilution varie linéairement avec ln m mais à la condition que la fraction des contre-ions "condensés" sur le polyion, supposément sous forme de bâtonnet, soit constante. Or, cette hypothèse n'est valable que pour les solutions suffisamment diluées afin de pouvoir traiter les contre-ions libres dans l'approximation de Debye-Hückel. Lorsque ξ, le paramètre de densité de charge, est plus petit que l'unité, la théorie prévoit que la chaleur intégrale de

Can. J. Chem. Downloaded from www.nrcresearchpress.com by 210.87.254.5 on 09/05/12
For personal use only.

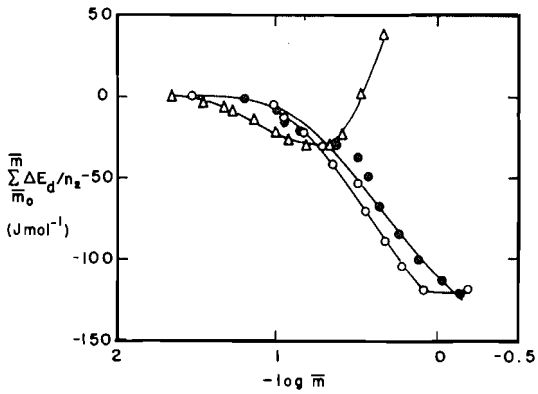

FIG. 5. Variation de l'énergie de dilution intégrale avec la molalité moyenne pour les sels de rubidium à 25 °C: ○ RbPM-I; ● RbPM-II; △ RbPSS (réf. 9).

dilution augmente avec ξ et passe par un maximum pour $\xi = 1$ pour ensuite décroître lorsque $\xi > 1$ à cause de la diminution des charges effectives due à la formation de paires d'ions. L'allure de la variation de la chaleur intégrale de dilution avec la molalité moyenne pour les sels de rubidium est représentée à la fig. 5. Par comparaison avec RbPSS, la dilution des solutions de RbPM-I et -II est exothermique sur toute la gamme des concentrations étudiées tandis que pour le RbPSS, la dilution devient endothermique à concentration relativement faible. La différence dans le comportement des sels RbPSS et RbPM peut s'expliquer comme suit. Dans le cas de RbPM, un nombre suffisant de sites négatifs le long de la chaîne sont neutralisés par association ionique afin de conférer à la chaîne une structure globulaire semblable à celle qu'elle possède à faible valeur de pH. Lorsque la dilution progresse, la dissociation ionique augmente et ceci est équivalent à augmenter le pH. Les groupements méthyles s'hydratent lorsque la chaîne passe d'une structure globulaire à une structure plus étendue. La dilution demeure exothermique car l'hydratation des groupements méthyles est beaucoup plus importante au point de vue chaleur de dilution que la dissociation ionique.

Pour conclure, il faut souligner l'importance de la nature de la chaîne dans le comportement des polyélectrolytes en solution. Les résultats pourraient laisser croire que les ions Na^+ sont plus fortement associés au polyion que les ions Rb^+ contrairement aux polystyrènesulfonates mais il faut maintenir que l'ordre relatif du degré d'association des cations ne change pas quand on passe d'un polyion à un autre. Il faut plutôt s'en remettre au caractère particulier de la chaîne polyméthacrylique qui subit une transition conformationnelle importante contrairement à la chaîne polystyrènesulfonique.

Remerciements

Ce travail a été rendu possible grâce à des octrois du Ministère de l'Education de la Province de Québec et du Conseil National de Recherche du Canada.

1. A. SILBERBERG, J. ELIASSAF et A. KATCHALSKY. J. Polym. Sci. **23**, 259 (1957).
2. J. C. LEYTE et M. MANDEL. J. Polym. Sci. Part A, **2**, 1879 (1964).
3. J. C. LEYTE. Polym. Lett. **4**, 245 (1966).
4. G. BARONE, N. CRESCENZI et F. GUADRIFOGLIO. Ric. Sci. **35**, 1069 (1965).
5. A. M. LIQUORI, G. BARONE, N. CRESCENZI, F. GUADRIFOGLIO et V. VITAGLIANO. J. Macromol. Chem. **1**, 291 (1966).
6. J. ELIASSAF. Polym. Lett. **3**, 767 (1965).
7. J. L. KOENIG, A. C. ANGOOD, J. SEMEN et J. B. LANDO. J. Am. Chem. Soc. **91**, 7520 (1969).
8. B. MICHELS et R. ZANA. Kolloid Z. Z. Polym. **234**, 1008 (1969).
9. H. DAOUST et A. HADE. Macromolecules, A paraître.
10. J. SKERJANC, D. DOLAR et D. LESKOVSEK. Z. Phys. Chem. Neue Folge, **56**, 207 (1967); **56**, 218 (1967); **70**, 31 (1970).
11. A. CAILLÉ ET H. DAOUST. J. Polym. Sci., Polym. Symp. **45**, 153 (1974).
12. S. NEWMAN, W. R. KRIGBAUM, C. LAUGIER et P. J. FLORY. J. Polym. Sci. **14**, 259 (1957).
13. A. PACKTER. J. Polym. Sci. Part A, **1**, 3021 (1963).
14. J.-P. CARTIER et H. DAOUST. Can. J. Chem. **49**, 3935 (1971).
15. J. ELIASSAF et A. SILBERBERG. Polymer, **3**, 555 (1962).
16. H. DAOUST et S. ST-PIERRE. Can. J. Chem. **53**, 1861 (1975).
17. M. EIGEN et E. WICKE. J. Phys. Chem. **58**, 702 (1954).
18. S. LIFSON et A. KATCHALSKY. J. Polym. Sci. **13**, 43 (1954).
19. K. MITA et T. OKUBO. J. Chem. Soc. Faraday Trans. I, **70**, 1546 (1974).
20. G. MANNING. J. Chem. Phys. **51**, 924 (1969).

Can. J. Chem. Downloaded from www.nrcresearchpress.com by 210.87.254.5 on 09/05/12
For personal use only.

Preparation and characterization of salts containing the triply bridged dimeric iridium(III) ion, $[H(Ar_3P)_2Ir(SAr')_2ClIr(PAr_3)_2H]^+$

TIMM L. KELLY[1] AND CAESAR V. SENOFF[2]

Department of Chemistry, University of Guelph, Guelph, Ont., Canada N1G 2W1

Received October 15, 1975

TIMM L. KELLY and CAESAR V. SENOFF. Can. J. Chem. **54**, 1860 (1976).

The dimeric iridium(III) hydride complexes $[IrHCl(SAr')(PAr_3)_2]_2$ where Ar = 4-$CH_3C_6H_4$ or C_6H_5 and Ar' = 4-$CH_3C_6H_4$, 4-$CH_3OC_6H_4$, 4-FC_6H_4, or C_6H_5 have been shown to react in halogenated solvents such as chloroform or 1,2-dichloroethane to form triply bridged dimeric hydrated complexes of the type, $[H(Ar_3P)_2Ir(SAr')_2ClIr(PAr_3)H]Cl\cdot 2H_2O$. When PAr_3 = (4-$FC_6H_4)_3P$, no triple bridge formation was observed. However, the dimeric complexes, $[IrHCl(SAr')(PAr_3)_2]_2$ including PAr_3 = (4-$FC_6H_4)_3P$ all react with $AgClO_4$ in acetone to form the complexes, $[H(Ar_3P)_2Ir(SAr')_2ClIr(PAr_3)_2H]ClO_4\cdot x(CH_3)_2CO$ (x = 0–3). The isolation and characterization of these triply bridged dimeric iridium(III) hydrides are discussed.

TIMM L. KELLY et CAESAR V. SENOFF. Can. J. Chem. **54**, 1860 (1976).

On a montré que les complexes dimères de l'hydrure d'iridium $[IrHCl(SAr')(PAr_3)_2]_2$, où Ar = 4-$CH_3C_6H_4$ ou C_6H_5 et Ar' = 4-$CH_3C_6H_4$, 4-$CH_3OC_6H_4$, 4-FC_6H_4, ou C_6H_5, peuvent réagir avec des solvants halogénés tels que le chloroforme ou le dichloro-1,2 éthane pour former des complexes hydratés dimères à triple pont qui sont du type $[H(Ar_3P)_2Ir(SAr')_2ClIr(PAr_3)H]Cl\cdot 2H_2O$. Quand PAr_3 = (4-$FC_6H_4)_3P$, on n'observe aucune formation d'espèce à triple pont. Toutefois les complexes dimères $[IrHCl(SAr')(PAr_3)_2]_2$, y compris PAr_3 = (4-$FC_6H_4)_3P$, réagissent tous avec $AgClO_4$ dans l'acétone pour donner des complexes $[H(Ar_3P)_2Ir(SAr')_2ClIr(PAr_3)_2H]ClO_4\cdot x(CH_3)_2CO$ (x = 0–3). On discute de l'isolement et de la caractérisation de ces hydrures d'iridium dimères à triple pont.

[Traduit par le journal]

Introduction

We have recently reported the preparation and characterization of some dimeric iridium(III) hydride complexes of the type, $[IrHCl(SAr)(PPh_3)_2]_2$ (1) where Ar = a *para*-substituted phenyl ring. During the course of investigating the reactivity of these complexes towards olefinic bonds, we have observed that these complexes will readily revert to novel triply bridged dimeric complexes having two arenethiolate and one chloride bridging ligands via (*a*) reaction in a halogenated solvent such as chloroform or 1,2-dichloroethane or (*b*) reaction with Ag^+ in acetone (2). Details of the preparation and characterization of these triply bridged species are herein reported.

Results and Discussion

The dimeric complexes, $[IrHCl(SAr)(PPh_3)_2]_2$ have been previously prepared by the reaction of $IrCl(PPh_3)_3$ (3) or $IrCl(C_2H_4)(PPh_3)_2$ (4) with the appropriate arenethiol in benzene at room temperature (1, 5). A more convenient synthetic route to complexes of the type, $[IrHCl(SAr')(PAr_3)_2]_2$ **1** where Ar' = 4-$CH_3OC_6H_4$, 4-$CH_3C_6H_4$, C_6H_5, or 4-FC_6H_4 and Ar = 4-$CH_3C_6H_4$, C_6H_5, or 4-FC_6H_4 was used in this investigation. This involves an initial reaction of the cyclooctene complex, $[IrCl(C_8H_{14})_2]_2$ (6) with PAr_3 in benzene followed by further reaction with the appropriate arenethiol, HSAr', according to [1]. Analytical

[1] $$[IrCl(C_8H_{14})_2]_2 + 4PAr_3 + 2HSAr' \rightarrow [IrHCl(SAr')(PAr_3)_2]_2 + 4C_8H_{14}$$

1

and pertinent infrared (ir) data for these complexes are given in Table 1. As expected, the presence of an electron-releasing substituent (CH_3) on the triarylphosphine causes a lowering of the ν_{Ir-H} frequency (*ca.* 20 cm^{-1}) relative to the analogous derivatives with PPh_3 (1) or $P(C_6H_4F)_3$.

The dimeric complexes, **1**, having Ar = C_6H_5 or 4-$CH_3C_6H_4$ will slowly dissolve in halogenated solvents such as $CHCl_3$, $CDCl_3$, or CH_2ClCH_2Cl at room temperature and undergo the reaction

[1]Present address: Amchem Products, Inc., Ambler, Pennsylvania, 19002, U.S.A.

[2]Author to whom all correspondence should be addressed.

Can. J. Chem. Downloaded from www.nrcresearchpress.com by 210.87.254.5 on 09/05/12
For personal use only.

TABLE 1. Analytical and infrared data for new complexes of the type $[IrHCl(SAr')(PAr_3)_2]_2$

Ar	Ar'	Analysis (%) Calcd.	Analysis (%) Found	Infrared ν_{Ir-H} (cm^{-1})	Infrared ν_{Ir-Cl} (cm^{-1})
4-$CH_3C_6H_4$	C_6H_5	C 60.90 H 5.08 Cl 3.75	C 60.98 H 5.21 Cl 4.09	2215	253
4-FC_6H_4	C_6H_5	C 51.97 H 3.09	C 52.25 H 3.20	2233	259

given by [2]. Complexes **2** contain the novel

[2] $[IrHCl(SAr')(PAr_3)_2]_2 \rightarrow [H(Ar_3P)_2Ir(SAr')_2ClIr(PAr_3)_2H]^+ + Cl^-$

2

triply bridging unit shown below which results

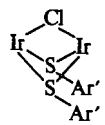

from the loss of one chloride ligand in **1** to the outer coordination sphere and bridge formation with the remaining chloride ligand in **1**. Once formed in solution, complexes **2** can be isolated from solution by the addition of petroleum ether as the *hydrates*, $[H(Ar_3P)_2Ir(SAr')_2ClIr(PAr_3)_2H]Cl\cdot 2H_2O$. Analytical data for these complexes are presented in Table 2. The presence of water of crystallization in these complexes has been confirmed by the presence of bands in their ir spectra at 1634, 3370, and 3320 cm^{-1} (7) as well as the presence of a sharp singlet at about 3 ppm in their ^1H nmr spectra recorded in acetone-d_6. The resonance of uncoordinated water in acetone-d_6 also occurs at about 3 ppm downfield from internal TMS as standard. The signal at 3 ppm also completely collapsed upon the addition of a small amount of DCl/D_2O to the acetone solutions containing **2**. The number of water molecules was determined by integration of the phenyl or CH_3 protons *vs.* the H_2O protons. Pertinent ir and ^1H nmr data are presented in Table 3. No absorption band was observed between 300–200 cm^{-1} which could be associated with the Ir—Cl—Ir moiety. The ν_{Ir-H} vibration occurs as a weak band at *ca.* 2280 cm^{-1}.

The electrical conductivity of **2** was measured at 25 °C in nitromethane and methanol. The conductivity data are given in Table 4. It may be

TABLE 2. Analytical data for the complexes $[H(Ar_3P)_2Ir(SAr')_2ClIr(PAr_3)_2H]Cl\cdot 2H_2O$ and $[H(Ar_3'P)_2Ir(SAr)_2ClIr(PAr_3')_2H]ClO_4\cdot x(CH_3)_2CO$

(*a*) $[H(Ar_3P)_2Ir(SAr')_2ClIr(PAr_3)_2H]Cl\cdot 2H_2O$

Ar	Ar'	Analysis (%) Calcd.	Analysis (%) Found
C_6H_5	C_6H_5	C 57.29 H 4.21 Cl 4.04 S 3.65 P 7.05	C 56.33 H 4.28 Cl 4.12 S 3.41 P 6.77
C_6H_5	4-$CH_3C_6H_4$	C 57.73 H 4.36 Cl 3.97	C 56.79 H 4.61 Cl 4.35
C_6H_5	4-$CH_3OC_6H_4$	C 56.72 H 4.40 Cl 3.90	C 56.05 H 4.20 Cl 4.71
C_6H_5	4-FC_6H_4	C 56.14 H 4.12 Cl 3.95	C 55.62 H 3.79 Cl 4.60
4-$CH_3C_6H_4$	C_6H_5	C 59.76 H 4.67 Cl 3.68	C 59.34 H 5.19 Cl 4.15

(*b*) $[H(Ar_3P)_2Ir(SAr')_2ClIr(PAr_3)_2H]ClO_4\cdot x(CH_3)_2CO$

Ar	Ar'	x	Analysis (%) Calcd.	Analysis (%) Found
C_6H_5	C_6H_5	3	C 56.89 H 4.59 Cl 3.62	C 56.82 H 4.51 Cl 4.07
C_6H_5	4-$CH_3C_6H_4$	1	C 57.00 H 4.38 Cl 3.79	C 56.69 H 4.40 Cl 4.21
4-$CH_3C_6H_4$	C_6H_5	0	C 58.90 H 4.91 Cl 3.63	C 58.06 H 5.17 Cl 4.43
4-FC_6H_4	C_6H_5	3	C 51.25 H 3.58 Cl 3.26	C 50.90 H 3.20 Cl 3.60

Can. J. Chem. Downloaded from www.nrcresearchpress.com by 210.87.254.5 on 09/05/12
For personal use only.

TABLE 3. Infrared and ^1H nmr data

(*a*) $[H(Ar_3P)_2Ir(SAr')_2ClIr(PAr_3)_2H]Cl \cdot 2H_2O$[a,b]

Ar	Ar′	ν_{Ir-H} (cm^{-1})[b]	δ_{H_2O} (ppm)[c]	δ_{Ir-H} (ppm)[d,e]	Other (ppm)[c]
C_6H_5	C_6H_5	2278	2.78	23.36	
C_6H_5	$4\text{-}CH_3C_6H_4$	2278	2.93	23.77	δ_{CH_3}, 2.16
C_6H_5	$4\text{-}CH_3OC_6H_4$	2277	2.88	23.42	δ_{CH_3O}, 3.21
C_6H_5	$4\text{-}FC_6H_4$	2277	2.15	23.45	
$4\text{-}CH_3C_6H_4$	C_6H_5	2265	2.63	23.77	δ_{CH_3}, 2.04

(*b*) $[H(Ar_3P)_2Ir(SAr')_2ClIr(PAr_3)_2H]ClO_4 \cdot x(CH_3)_2CO$[f]

Ar	Ar′	x	ν_{Ir-H} (cm^{-1})[b]	δ_{Ir-H} (ppm)[d,e]	Other[c]
C_6H_5	C_6H_5	3	2278	23.30	
C_6H_5	$4\text{-}CH_3C_6H_4$	1	2289	23.41	δ_{CH_3}, 2.13
$4\text{-}CH_3C_6H_4$	C_6H_5	0	2270	26.34	δ_{CH_3}, 2.21
$4\text{-}FC_6H_4$	C_6H_5	3	2073	22.77	

[a] ν_{OH} observed at 3370 and 3320 cm^{-1}; δ_{OH} observed at 1634 cm^{-1}.
[b] Recorded as Nujol mulls.
[c] Recorded in acetone-d_6.
[d] Recorded in $CDCl_3$.
[e] Observed as a poorly resolved triplet, upfield from TMS.
[f] ν_{CO} for free acetone observed at 1714 cm^{-1} (Nujol).

TABLE 4. Conductivity data[a]
$[H(Ar_3P)_2Ir(SAr')_2ClIr(PAr_3)_2H]Cl \cdot 2H_2O$

Ar	Ar′	Solvent[b]	Λ_M (ohm^{-1} mol^{-1} cm^2)
C_6H_5	C_6H_5	CH_3OH	69.4
		CH_3NO_2	53.2
C_6H_5	$4\text{-}CH_3C_6H_4$	CH_3OH	58.5
		CH_3NO_2	48.2
C_6H_5	$4\text{-}CH_3OC_6H_4$	CH_3OH	69.8
		CH_3NO_2	52.9
$4\text{-}CH_3C_6H_4$	C_6H_5	CH_3OH	66.5
		CH_3NO_2	48.3

[a] Conductivity of $[H(Ph_3P)_2Ir(SPh)_2ClIr(PPh_3)_2H]BPh_4$ determined in acetone at 25 °C was 96.8 ohm^{-1} mol^{-1} cm^2 (3.89×10^{-4} *M*).
[b] Concentrations used were $\sim 10^{-4}$ *M*.

noted that the observed molar conductivities are somewhat low for 1:1 electrolytes in this solvent (8). However, the ionic chloride in **2** can be readily displaced by tetraphenylborate ion and the conductivity of this derivative measured in acetone is reasonable for a 1:1 electrolyte (see Table 4). The low conductivities in methanol and nitromethane can be accounted for by the presence of the equilibrium shown in [3].

[3] $[H(Ar_3P)_2Ir(SAr')_2ClIr(PAr_3)_2H]Cl \rightleftharpoons [IrHCl(SAr')(PAr_3)_2]_2$

It may be noted that with $PAr_3 = (4\text{-}FC_6H_4)_3P$, reaction 2 does not proceed. The original dimer, **2**, may be recovered intact from either chloroform or 1,2-dichloroethane. Presumably, the iridium–chlorine bond in this particular dimer is quite strong and is not readily cleaved in these solvents. However, one of the Ir—Cl bonds is readily cleaved by Ag^+ ion (*vide infra*).

The source of the water of hydration in **2** is at present unknown. It may originate from the trace amounts of water present in the reagent grade solvents used or from the atmosphere since no precautions were taken to exclude air during the course of working-up the reaction mixtures.

In order to further establish the nature of the cation present in **2**, the dimeric hydrides, **1**, were reacted with $AgClO_4$ under reflux in acetone. This reaction proceeded smoothly according to

Can. J. Chem. Downloaded from www.nrcresearchpress.com by 210.87.254.5 on 09/05/12
For personal use only.

Can. J. Chem. Downloaded from www.nrcresearchpress.com by 210.87.254.5 on 09/05/12
For personal use only.

[4] and complexes of the type, $[H(Ar_3P)_2Ir(SAr')_2ClIr(PAr_3)H]ClO_4 \cdot x(CH_3)_2CO$ ($x = 0$–3) **3** were isolated. Analytical data for these complexes are

[4] $[IrHCl(SAr')(PAr_3)_2]_2 + AgClO_4 \rightarrow [H(Ar_3P)_2Ir(SAr')_2ClIr(PAr_3)_2H]ClO_4 + AgCl$

3

presented in Table 2.

Both the chloride, **2**, and perchlorate, **3**, salts exhibited a poorly resolved 'triplet' signal at about 23 ppm upfield from TMS in $CDCl_3$ for the hydrogen bonded to iridium (see Table 3). Resolution of this signal was not improved at −70 °C. This observation precluded a specific assignment of the stereochemistry of the phosphine ligands bonded to iridium and further ^1H nmr studies were not carried out.

However, single crystals of **3** having Ar = Ar′ = C_6H_5 were obtained and the structure of $[H(Ph_3P)_2Ir(SPh)_2ClIr(PPh_3)_2H]ClO_4 \cdot 3(CH_3)_2CO$ was determined (2) in the solid state confirming the presence of three bridging ligands as shown below where L = PPh_3. This result lends further

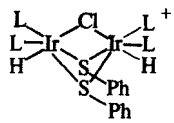

support to the structure originally proposed for **1** (1) having two arenethiolato bridging ligands.

The hydride ligands in **1** undergo a stereochemical rearrangement during the course of forming **2** or **3** ([2] and [4]). In **1** the hydride ligands are *trans* with respect to the two iridium atoms but are *cis* in **2** or **3**. This stereochemical change may involve cleavage of at least one of the iridium–sulfur bonds in **1** during the course of forming **2** or **3** accompanied by a rearrangement of one of the resulting five- or four-coordinate moieties (depending on whether or not a chloride ligand has been displaced from the appropriate iridium atom) according to Scheme 1.

An alternative route for the formation of the observed triply bridged product may be considered. This involves the presence of a '*cis* form' of **1** in solution which is in equilibrium with the '*trans* form'. The '*cis* form' can then dissociate a Cl^- ligand followed by bridge formation to yield the observed product according to Scheme 2.

However, this seems unlikely in view of the fact that [2] proceeds as indicated even in the presence of an excess of added triphenylphosphine and that the conversion from the '*trans* form' to the '*cis* form' of **1** must involve cleavage of at least one Ir—P bond.

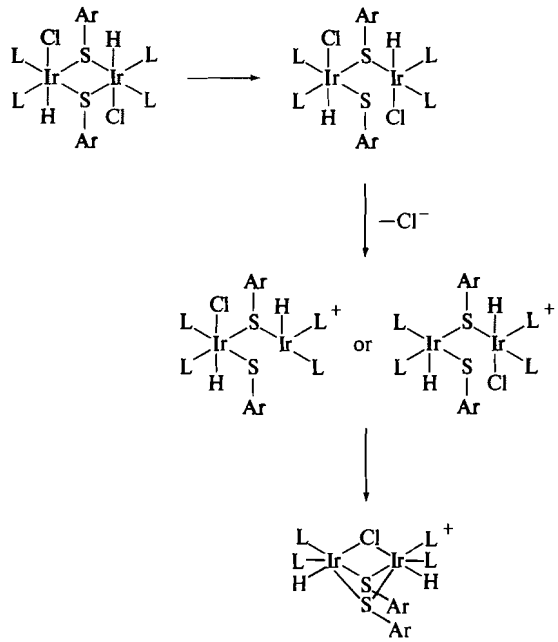

SCHEME 1

The reaction of **1** to form the triply bridged

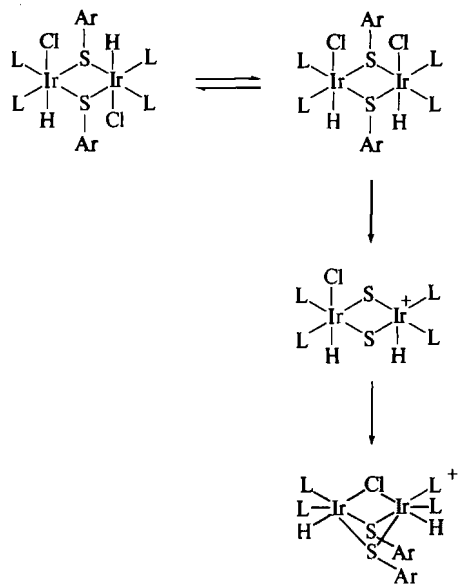

SCHEME 2

Can. J. Chem. Downloaded from www.nrcresearchpress.com by 210.87.254.5 on 09/05/12
For personal use only.

species **2** in a halogenated solvent is unexpected since transition metal hydride complexes normally undergo halogen exchange in halogenated solvents according to [5] (9).

[5] $$M{-}H + RX \rightarrow M{-}X + RH$$

It is also somewhat unusual to observe the conversion of a doubly bridged dimeric complex into a triply bridged dimeric complex ([2] and [4]). The propensity of iridium(III) to remain six-coordinate presumably is the driving force for this behaviour. It may also be noted that in the presence of excess Ag^+, **3** is also formed, indicating that once one chloride ligand is displaced by Ag^+; the rate of bridge formation with the remaining chloride is much faster than displacement by Ag^+ ion.

Experimental

Materials

Commercially available triphenylphosphine was recrystallized from ethanol prior to use. Iridium trichloride was purchased from Johnson–Matthey Co. Ltd. Solvents used were reagent grade. Other chemicals used were commercially available samples. Unless otherwise indicated all reactions were carried out under an atmosphere of N_2 or Ar.

Physical Measurements

Infrared Spectra and ^1H Nuclear Magnetic Resonance Spectra

These were recorded on a Beckman IR-12 spectrophotometer as Nujol mulls between KBr or CsI plates. ^1H nmr spectra were recorded on a Varian HA 100 spectrometer with tetramethylsilane as internal reference.

Conductivity Measurements

Electrical conductivities were recorded on a Beckman RC16BI conductivity meter at 1000 Hz using a standard conductivity cell with blackened platinum electrodes.

Preparation of Complexes

(1) $[IrCl(C_8H_{14})_2]_2$. This was prepared as described in the literature (6).

(2) $[IrHCl(SAr')(PAr_3)_2]_2$. The following general procedure was used to prepare these complexes. To a solution of $[IrCl(C_8H_{14})_2]_2$ (0.50 g; 0.56 mmol) in 15 ml of benzene (pre-saturated with dinitrogen or argon) was added 3.5 mmol of the appropriate triarylphosphine. The dark red solution was stirred for several minutes whereupon 0.30 g of the appropriate arenethiol was added and the solution immediately darkened. The reaction mixture was stirred under an N_2 atmosphere for 18 h during which time the product precipitated from solution. The solid was collected, washed with several portions of benzene, and dried *in vacuo* over boiling benzene.

(3) $[H(Ar_3P)_2Ir(SAr')_2ClIr(PAr_3)_2H]Cl \cdot 2H_2O$. The following general procedure was used to isolate these complexes. A sample (0.50 g) of the dimeric complex, $[IrH(SAr')(PAr_3)_2]_2$, was added to 100 ml of chloroform or 1,2-dichloroethane. After about 10–15 min a clear yellow solution resulted which was stirred for about 18 h. The volume of the solution was then reduced to about 5–10 ml on a rotoevaporator and the concentrated solution was filtered into 250 ml of petroleum ether (bp 63–75 °C). An off-white solid immediately formed which was filtered off, washed with petroleum ether, and dried *in vacuo* at 25 °C.

(4) $[H(Ph_3P)_2Ir(SPh)_2ClIr(PPh_3)_2H]BPh_4$. A sample of $[H(Ph_3P)_2Ir(SPh)_2ClIr(PPh_3)_2H]Cl \cdot 2H_2O$ (0.40 g) was dissolved in 50 ml of methanol and the resulting solution was filtered. Sodium tetraphenylborate (0.4 g) was dissolved in 5 ml of methanol and this solution filtered into the first solution to yield a white precipitate which was washed in succession with a small amount of acetone and methanol. The crude complex was recrystallized from acetone/methanol and dried *in vacuo* at 25 °C. *Anal.* calcd. for $[H(Ph_3P)_2Ir(SPh)_2ClIr(PPh_3)_2H]BPh_4$: C 64.58, H 4.58, Cl 1.77; found: C 64.00, H 4.87, Cl 1.40.

(5) $[H(PAr_3)_2Ir(SAr')_2ClIr(PAr_3)_2H]ClO_4 \cdot x(CH_3)_2CO$. Unless otherwise indicated, the following general procedure was used to prepare these complexes. The appropriate dimer, $[IrH(SAr')(PAr_3)_2]_2$ (0.50 g) was suspended in acetone (25 ml) and $AgClO_4$ (1.1 mol per iridium) was added. The resulting suspension was heated under reflux for 3 h, cooled to room temperature, and filtered twice through Whatman No. 5 filter paper to remove AgCl. The filtrate was stored overnight at −5 °C during which time pale yellow crystals of the perchlorate salt formed. If crystallization did not occur, *n*-hexane was added to the filtrate to promote crystallization. Identical products were obtained if the amount of $AgClO_4$ used were doubled.

Acknowledgements

The authors thank the National Research Council of Canada and Imperial Oil Limited for financial support.

1. J. L. HERDÉ and C. V. SENOFF. Can. J. Chem. **51**, 1016 (1973).
2. P. J. ROBERTS, G. FERGUSON, and C. V. SENOFF. J. Organomet. Chem. **94**, C26 (1975).
3. M. A. BENNETT and D. L. MILNER. J. Am. Chem. Soc. **91**, 6983 (1969).
4. A. VAN DER ENT and A. L. ONDERDELINDEN. Inorg. Chim. Acta, **7**, 203 (1973).
5. R. RESTIVO, G. FERGUSON, T. L. KELLY, and C. V. SENOFF. J. Organomet. Chem. **90**, 101 (1975).
6. J. L. HERDÉ, J. C. LAMBERT, and C. V. SENOFF. Inorg. Synth. **15**, 18 (1974).
7. K. NAKAMOTO. Infrared spectra of inorganic and coordination compounds. Wiley, New York, N.Y. 1963. p. 156.
8. W. J. GEARY. Coord. Chem. Rev. **7**, 81 (1971).
9. R. A. SCHUNN. Transition Metal Hydrides, **1**, 203 (1971).

An R.K.R.-like estimate of the effective non-adiabatic internuclear potential for the hydrogen molecule

MARY KURIYAN AND HUW O. PRITCHARD
Centre for Research in Experimental Space Science, York University, Downsview, Ont., Canada M3J 1P3

Received February 24, 1976

MARY KURIYAN and HUW O. PRITCHARD. Can. J. Chem. **54**, 1865 (1976).

An effective internuclear potential for the hydrogen molecule is deduced from the experimental energy levels; this potential is valid in the sense that it reproduces the rotation–vibration energy levels to an accuracy of the order of ± 0.1 cm^{-1}, and is unique in the sense that it is equally accurate for all observed values of the rotational quantum number J.

The implied corrections to the adiabatic relativistic internuclear potential are consistent with the estimated values for the non-adiabatic coupling correction over the whole range of internuclear separation.

MARY KURIYAN et HUW O. PRITCHARD. Can. J. Chem. **54**, 1865 (1976).

Utilisant les niveaux énergétiques expérimentaux, on en déduit un potentiel internucléaire effectif pour la molécule d'hydrogène; ce potentiel est valable puisqu'il permet de reproduire les niveaux d'énergies rotationnelles et vibrationnelles avec une précision de l'ordre de ± 0.1 cm^{-1} et de plus il est unique puisqu'il est aussi précis pour toutes les valeurs observées du nombre quantique rotationnel J.

Les corrections impliquées au potentiel internucléaire relativistique adiabatique sont en accord avec les valeurs estimées pour la correction de couplage nonadiabatique pour toutes les valeurs de séparation internucléaire.

[Traduit par le journal]

Since 1964 when Kołos and Wolniewicz published their accurate solution of the Schrödinger equation for the hydrogen molecule (1), considerable effort has been devoted to the achievement of an exact matching between the calculated and the observed rotation–vibration energy levels (2–6); the references cited here represent a very inexhaustive selection, and the flow of papers on this topic continues unabated (7–10). The following is a very brief historical sketch of the development of this problem. The original internuclear potential, corrected for adiabatic and relativistic effects (1, 2) yielded a set of rotation–vibration energy levels for the ground state of hydrogen which had two faults: one, that the calculated dissociation energy was too large by 4 cm^{-1}, and two, that the calculated vibrational spacings for low v were too large by the order of 0.8 cm^{-1} per spacing. In an analysis of these discrepancies, Wilkinson and Pritchard (5) concluded that the spectroscopic dissociation limits observed by Herzberg and Monfils (11) must be in error by about 4 cm^{-1}, and this was subsequently confirmed by Herzberg (12) although (8) some small uncertainties in the exact position of the limit may still remain; however, as far as the vibrational spacings were concerned, the origin of the discrepancy must be in the theoretical calculation. There are four possible reasons why the theoretical calculations might be inaccurate. (*i*) Simple lack of convergence of the variational calculations: this aspect has been examined recently by Kołos and Wolniewicz (7), and it is clear that the variational calculations are reasonably well converged in the important regions of internuclear separation (R). (*ii*) That the internuclear potential, although essentially correct, contains a 'noise' component because all points are not equally converged (or alternatively, that the interpolation scheme required in the Cooley method of solving for the energy levels could introduce that noise): this problem was examined extensively by LeRoy and Bernstein (3) and our own further examination shows that no difficulty of this kind could invalidate the results presented in this paper.[1] (*iii*) That there could be a logical

[1]One of the authors wishes to apologise for what he now realises was an unjust criticism of the work of LeRoy and Bernstein (3): we had argued (5) that it was improper to assume that the upper vibrational spacings of H_2 could be calculated correctly even though the lower ones were not; this would certainly have been true if an expansion method had been used to solve the Schrödinger equation

Can. J. Chem. Downloaded from www.nrcresearchpress.com by 210.87.254.5 on 09/05/12
For personal use only.

Can. J. Chem. Downloaded from www.nrcresearchpress.com by 210.87.254.5 on 09/05/12
For personal use only.

flaw in the original procedure for the solution of the Schrödinger equation for H_2 (14), but recent examination of this defect (10) reveals that the effect is at least an order of magnitude too small. (*iv*) Neglect of non-adiabatic coupling (3, 4, 6, 9), a conclusion which is supported, by and large, by the work reported below.

In view of the enormous complexity and costliness of these calculations on the hydrogen molecule, and of the extreme difficulty in making a rigorous calculation of the non-adiabatic effects, we decided to find out if it was possible to generate an acceptable internuclear potential function for H_2 by inverting the observed rotation–vibration energy-level scheme, with the expectation that it would then be rather clear what was the cause of the remaining discrepancies between theory and experiment!

An obvious way to approach this problem initially is to start with the R.K.R. potential for H_2 and improve it, either by including higher order corrections (15–17), or by using some other kind of iterative procedure (18, 19). The methods evolved so far are not easy to use, and are troubled by divergences, poor convergence or oscillatory behaviour, and although it is expected that many of these problems will be resolved in the near future (20), we meanwhile sought an alternative approach making use of the fact that in this particular case, we already have available an extremely good approximation to the required potential curve.

The following solution to the problem retains much of the flavour of the R.K.R. method (21), although it is a purely empirical approach. Curve I, Fig. 1, represents a good approximation to the rotationless internuclear potential, in this case the Kołos and Wolniewicz potential with adiabatic and relativistic corrections included, as tabulated by Bishop and Shih (9). The horizontal line which terminates at each end on I is the $v = 0$ energy level found using this approximate potential. The lower horizontal lines in each of the four diagrams represents the position of the observed $v = 0$ energy level, and the four curves labelled II represent possible forms of the potential which would give rise to the experimentally observed $v = 0$ level. These four sets of curves have one thing in common, that the cross-hatched areas equal the dotted areas and the problem is to find out how to calculate a unique curve II; the diagrams are, of course, very exaggerated and only schematic, the real discrepancies amounting only to 10^{-5} au or less.

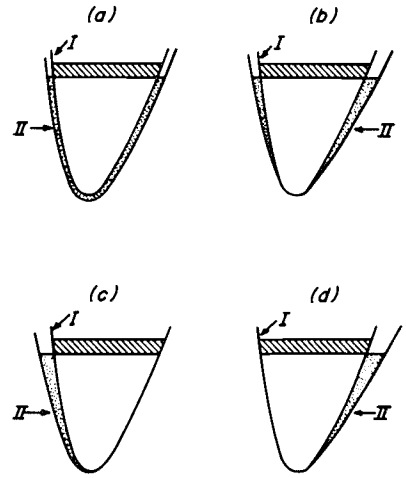

FIG. 1. Schematic representation of four possible model corrections to the approximate potential curve I to give an acceptable representation II of the true potential. In each diagram, the upper horizontal line is a vibrational level of potential curve I, and the lower one is the experimentally observed energy of that level. The construction of curve II from curve I proceeds by making the dotted area equal to the cross-hatched area.

First, one has the choice of making a correction which is generally of type (*a*) or generally of type (*b*): the major effect of the former is to shift the level down without altering the zero-point energy, whereas the latter reduces the zero-point energy. If we choose to measure energies with respect to the dissociation limit, then we are not precisely sure what is the energy of the $v = 0$ level (8), but this is immaterial if we measure our energies with respect to the $v = 0$ level itself, any required adjustment in the nature of a small change in dissociation energy can be accommodated later using a type (*a*) shift. However, to the extent that the potential curve itself has physical meaning, so does the zero-point energy, and there exists a discrepancy between the spectroscopically derived zero-point energy (11)

(13), but is not the case when the Cooley method is used. The essential result here is (ref. 3, Appendix I) that a small imperfection in the potential curve only affects the level whose turning point is close to that point, and therefore it follows that small imperfections in the potential in the region of the normal internuclear separation will not invalidate the computed energies of levels whose outer turning points are at large values of R (small imperfections at the inner turning points being much less important). We had not appreciated this sufficiently at the time (5).

Can. J. Chem. Downloaded from www.nrcresearchpress.com by 210.87.254.5 on 09/05/12
For personal use only.

and the calculated one (2) of about 0.5 cm^{-1}; thus, the shape of the curve has to be changed in the neighbourhood of the minimum, implying that the absolute correction may have a type (*a*) component, but must have a component resembling one of (*b*), (*c*), or (*d*).

Confining our attention now to the change in shape of the curve as opposed to any absolute shift, we have to choose between the three general types (*b*), (*c*), and (*d*). Assuming that the correction $\Delta V(R)$ to be added to the existing potential curve $V(R)$ is zero at the minimum, *i.e.* $R = 1.4a_0$, trial calculations were carried out for each of the three models: (*b*) increase in area equally disposed on either side of $R = 1.4a_0$; (*c*) increase in area all confined to the region $R < 1.4a_0$; (*d*) increase in area all confined to the region $R > 1.4a_0$. Moreover, it was assumed that since the correction term is very small, $\Delta V(R)$ could be taken as a first approximation to be proportional to $\rho = |R - R_e|$. Each of these three trial calculations was extended up to $v = 3$, using the Raman data of Stoicheff (22) to define the level spacings between $v = 0$, 1, 2, and 3, $J = 0$, and their estimated positions relative to the bottom of the potential curve; the constant of proportionality between $\Delta V(R)$ and ρ was of course different between each turning point. At this stage, we now have three different trial internuclear potentials, which are each the original smooth $V(R)$ curve (9) with small piecemeal linear correction patches $\Delta V(R)$ which are continuous, but have discontinuous $d\Delta V(R)/dR$ at each classical turning point. The Raman data of Stoicheff extends up to $J = 4$ for these four vibrational states, and of course, the same correction function $\Delta V(R)$ *must*, when the centrifugal term $J(J + 1)/2\mu R^2$ is included in the Schrödinger equation, yield simultaneously the correct level spacings for all v, J pairs. It turns out that the model (*c*) correction makes the rotational spacings much worse than for the original potential $V(R)$: likewise, the model (*b*) correction also makes the rotational spacings worse, whereas the model (*d*) correction yields the positions of all the twenty levels $0 \leq v \leq 3$, $0 \leq J \leq 4$ correct to within ± 0.1 cm^{-1}. This fortunate coincidence (because, as LeRoy and Bernstein (3) recognised, it is not possible in principle to obtain a unique solution to this problem this way) means that as far as the shape of the potential curve is concerned, we need only apply the correction $\Delta V(R)$ on the right-hand limb of the potential curve. One should add that the positions of the vibrational levels are much

TABLE 1. The effective potential as a function of internuclear separation R for the hydrogen molecule, in the region where it differs from the tabulation of Bishop and Shih[a]

R	$-10^5 \times \Delta V(R)$	$(V(R) + \Delta V(R))^*$
1.5	0	−1.17235555
1.6	0.40	−1.16809851
1.7	0.70	−1.16198591
1.8	1.10	−1.15460762
1.9	1.50	−1.14639957
2.0	1.80	−1.13768930
2.1	2.00	−1.12872530
2.2	2.35	−1.11969889
2.3	2.70	−1.11075262
2.4	2.90	−1.10199509
2.5	3.05	−1.09351099
2.6	3.10	−1.08536266
2.7	3.15	−1.07759760
2.8	3.25	−1.07024989
2.9	3.35	−1.06334176
3.0	3.38	−1.05688582
3.1	3.30	−1.05088745
3.2	3.25	−1.04534795
3.3	3.15	−1.04026047
3.4	3.00	−1.03561230
3.5	2.60	−1.03138738
3.6	2.60	−1.02757129
3.7	2.40	−1.02413714
3.8	2.30	−1.02106421
3.9	2.20	−1.01832616
4.0	2.00	−1.01589693
4.1	1.85	−1.01374875
4.2	1.65	−1.01185779
4.3	1.50	−1.01019903
4.4	1.40	−1.00874868
4.5	1.30	−1.00748346
4.6	1.20	−1.00638280
4.7	1.10	−1.00542740
4.8	0.80	−1.00459774
4.9	0.60	−1.00388100
5.0	0.50	−1.00326300
5.1	0.40	−1.00273012
5.2	0.40	−1.00227214
5.3	0.40	−1.00187819
5.4	0.40	−1.00154061
5.5	0.40	−1.00124883
5.6	0.40	−1.00099924
5.7	0.36	−1.00078471
5.8	0.34	−1.00060085
5.9	0.32	−1.00044318
6.0	0.30	−1.00030799
6.1	0.28	−1.00019207
6.2	0.25	−1.00009258
6.3	0.19	−1.00000690
6.4	0.10	−0.99993308
6.5	0.04	−0.99986988
6.6	0	−0.99981578

[a]All quantities in atomic units. The asterisk denotes that the potential listed in the final column has been smoothed.

Can. J. Chem. Downloaded from www.nrcresearchpress.com by 210.87.254.5 on 09/05/12
For personal use only.

TABLE 2. Comparison of vibrational energy levels for H_2, $J = 0$ calculated using the potential in Table 1, with the experimental values; units are cm^{-1}

	Vibrational energy levels (cm^{-1})		
v	Calculated	Observed	Source
$-\frac{1}{2}$	−2179.32	(−2179.27)	*a*
0	0.0	0.0	
1	4161.14	4161.14	*b*
2	8087.04	8087.11	*b*
3	11782.44	11782.35	*b*
4	15250.34	15250.36	*c*
5	18491.99	18492.10	*c*
6	21505.88	21505.84	*c*
7	24287.96	24288.15	*c*
8	26831.13	26831.11	*c*
9	29124.16	29124.39	*c*
10	31150.54	31150.55	*c*
11	32887.21	32887.22	*c*
12	34302.24	34302.33	*c*
13	35351.38	35351.54	*c*
14	35973.36	35973.48	*c*

[a]Herzberg and Monfils (11).
[b]Stoicheff (22).
[c]Herzberg and McKenzie, quoted by Bishop and Shih (9).

TABLE 3

(*a*) Calculated energy levels for H_2, $0 \leq v \leq 3$, $0 \leq J \leq 4$

	Energy level (cm^{-1})				
v	$J = 0$	$J = 1$	$J = 2$	$J = 3$	$J = 4$
0	0.0	118.49	354.38	705.52	1168.80
1	4161.14	4273.71	4497.79	4831.33	5271.30
2	8087.04	8193.82	8406.38	8722.70	9139.88
3	11782.44	12084.73	11883.53	12384.09	12778.79

(*b*) Comparison of the difference between theory and experiment for these states, as tabulated by Bishop and Shih, in italics, with the shift in these energy levels caused by adding $\Delta V(R)$ to $V(R)$ and smoothing, in Roman type

	Difference in energy (cm^{-1})				
v	$J = 0$	$J = 1$	$J = 2$	$J = 3$	$J = 4$
0	*0.0*	*0.01*	*0.02*	*0.05*	*0.10*
	0.0	0.0	0.02	0.05	0.08
1	*0.87*	*0.88*	*0.90*	*0.92*	*0.94*
	0.90	0.92	0.97	0.98	1.02
2	*1.66*	*1.67*	*1.68*	*1.70*	*1.75*
	1.62	1.64	1.66	1.70	1.75
3	*2.48*	*2.52*	*2.54*	*2.49*	*2.58*
	2.34	2.36	2.38	2.42	2.47

less sensitive to errors on the left-hand rather than on the right-hand side of the potential curve (3), so that there could be a small $\Delta V(R)$ term to be added for $R < 1.4a_0$, but it is certainly not large.

We then proceeded to extend the calculation from $v = 3, J = 0$ up to $v = 14, J = 0$ using the so far unpublished experimental data for these levels quoted by Bishop and Shih (9). We now have a corrected potential curve which has a small kink in $\Delta V(R)$ at each outer turning point, which as we have noted, could give rise to a spurious noise spectrum and shift the levels slightly. Thus, the potential function *i.e.* $(V(R) + \Delta V(R))$ was smoothed by taking first, second, and third differences of the interpolated potential (*i.e.* the function used in the Cooley program to solve for the energy levels), and making *small* adjustments to make these differences monotonic; these small smoothing corrections did alter the positions of the energy levels slightly (as can be judged from the fact that for $J = 0$, our final calculated energies are no longer identical with the experimental results whereas they were, before smoothing) but the changes were sufficiently small that it is not necessary to go back and repeat the whole procedure again. Table 1 shows the required correction $\Delta V(R)$, interpolated back to the tabular points of Kołos and Wolniewicz (1, 7), and which, when taken together with the adiabatic and relativistic corrections by Bishop and Shih (9) yields an effective potential $(V(R) + \Delta V(R))^*$, which is also tabulated. The potential $(V(R) + \Delta V(R))^*$, as opposed to $(V(R) + \Delta V(R))$, is smooth, and generates the rotationless vibrational energy levels shown in Table 2. It can be seen that the agreement is satisfactory. Table 3 demonstrates the essential uniqueness of our trial potential, because it shows that this potential automatically reproduces the correct energy-level spacings for all values of $0 \leq v \leq 3, 0 \leq J \leq 4$; in fact we have examined the differences between our computed energy-level spectrum and that quoted by Bishop and Shih (9) for all levels $0 \leq v \leq 14, 0 \leq J \leq 4$ and nowhere is there a discrepancy greater than 0.3 cm^{-1}. Figure 2(*a*) shows the form of the correction term $\Delta V(R)$ as a function of R, and it can be seen that it amounts to a little over 7 cm^{-1} at $R = 3a_0$. Figure 2(*b*) shows the lowering of the energy levels $\Delta E(v)$ brought about by the change in potential $\Delta V(R)$, compared with three semi-empirical estimates (3, 9) for the non-

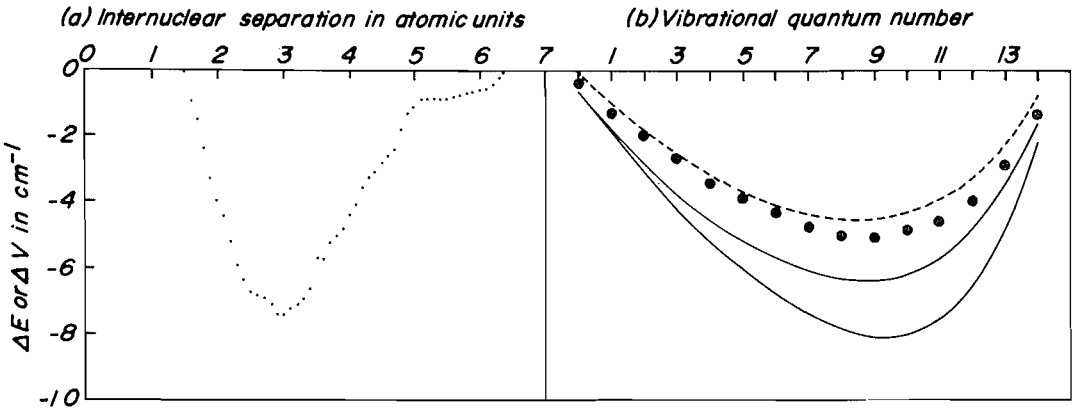

FIG. 2. The correction $\Delta V(R)$ required to force the Kołos and Wolniewicz potential (with adiabatic and relativistic corrections) to yield the observed rotation–vibration energy levels for H_2. (*a*) $\Delta V(R)$ plotted as a function of internuclear separation R. This correction has been adjusted (see text) so that the total potential is smooth, and so $\Delta V(R)$ itself is not smooth because the original potential $V(R)$ is not completely smooth, each individual point having been optimised differently. (*b*) $\Delta E(v)$ plotted as a function of vibrational quantum number v, denoted by the discrete points. The solid lines represent estimates of the non-adiabatic coupling correction made by LeRoy and Bernstein: the upper curve is their $\Delta E(v)$ and the lower one $\Delta E'(v)$; the dotted line is a semi-empirical estimate by Bishop and Shih.

adiabatic coupling corrections for the ground state of H_2.

We conclude two things. One, that it now appears virtually certain that, although non-adiabatic effects have been thought to be unimportant for H_2^+ (23), they are the main cause of the remaining discrepancies between theory and experiment for the ground state of H_2. Two, we believe that we have inverted the rotation–vibration energy-level scheme for H_2 in a satisfactory manner to yield an acceptable approximation to the effective internuclear potential, and in consequence, it appears that it is possible to represent these non-adiabatic effects as an effective correction to the potential, as we do in Fig. 2(*a*) and Table 2; whether this effective potential can usefully be used to describe properties of H_2 other than the rotation–vibration energy levels remains to be seen.

Acknowledgment

This work was supported by the National Research Council of Canada.

1. W. KOŁOS and L. WOLNIEWICZ. J. Chem. Phys. **41**, 3663 (1964).
2. W. KOŁOS and L. WOLNIEWICZ. J. Chem. Phys. **49**, 404 (1968).
3. R. L. LEROY and R. B. BERNSTEIN. J. Chem. Phys. **49**, 4312 (1968).
4. J. D. POLL and G. KARL. Can. J. Phys. **44**, 1467 (1966).
5. P. G. WILKINSON and H. O. PRITCHARD. Can. J. Phys. **47**, 2493 (1969).
6. P. R. BUNKER. J. Mol. Spectrosc. **42**, 478 (1972).
7. W. KOŁOS and L. WOLNIEWICZ. J. Mol. Spectrosc. **54**, 303 (1975).
8. R. J. LEROY and M. G. BARWELL. Can. J. Phys. **53**, 1983 (1975).
9. D. M. BISHOP and S.-K. SHIH. J. Chem. Phys. **64**, 162 (1976).
10. H. O. PRITCHARD and L. WOLNIEWICZ. Can. J. Chem. **54**, 651 (1976).
11. G. HERZBERG and A. MONFILS. J. Mol. Spectrosc. **5**, 482 (1960).
12. G. HERZBERG. J. Mol. Spectrosc. **33**, 147 (1970).
13. M. KURIYAN and H. O. PRITCHARD. Can. J. Chem. **54**, 1543 (1976).
14. R. E. KARI, A. C. H. CHAN, G. HUNTER, and H. O. PRITCHARD. Can. J. Chem. **51**, 2055 (1973).
15. J. T. VANDERSLICE, R. DAVIES, and S. WEISSMAN. J. Chem. Phys. **43**, 1075 (1965).
16. D. L. ALBRITTON, W. J. HARROP, A. L. SCHMELTEKOPF, and R. N. ZARE. J. Mol. Spectrosc. **46**, 25 (1973).
17. S. M. KIRSCHNER and J. K. G. WATSON. J. Mol. Spectrosc. **51**, 321 (1974).
18. F. Y. HAJJ. Phys. Rev. **A11**, 1138 (1975).
19. W. M. KOSMAN and J. HINZE. J. Mol. Spectrosc. **56**, 93 (1975).
20. H. G. KREEK and R. J. LEROY. Unpublished results.
21. J. T. VANDERSLICE, E. A. MASON, W. G. MAISCH, and E. LIPPINCOTT. J. Mol. Spectrosc. **3**, 17 (1959); **5**, 83 (1960).
22. B. P. STOICHEFF. Can. J. Phys. **35**, 750 (1957).
23. G. HUNTER, A. W. YAU, and H. O. PRITCHARD. Atomic Data and Nuclear Data Tables, **14**, 11 (1974).

Can. J. Chem. Downloaded from www.nrcresearchpress.com by 210.87.254.5 on 09/05/12
For personal use only.

Electronic absorption spectra and dipole moments of diazafluoren-9-ones studied by the MIM, PPP, and CNDO/2 methods

CONCETTA GANDOLFO, GIUSEPPE BUEMI, DOMENICO GRASSO, AND SALVATORE FASONE
Istituto di Chimica Fisica, Università di Catania, 95125 Catania, Italy

Received October 15, 1975

CONCETTA GANDOLFO, GIUSEPPE BUEMI, DOMENICO GRASSO, and SALVATORE FASONE. Can. J. Chem. **54**, 1870 (1976).

The electronic spectra of three diazafluoren-9-one isomers have been measured in cyclohexane solution and the results compared with those of 'molecules in molecules' (MIM) and PPP calculations. A satisfactory agreement between experimental and theoretical data has been found, and five $\pi \rightarrow \pi^*$ transitions can be assigned to their uv spectra. For two compounds dipole moments in benzene solution have been measured and results are compared with theoretical values obtained by MIM and CNDO/2 calculations.

CONCETTA GANDOLFO, GIUSEPPE BUEMI, DOMENICO GRASSO et SALVATORE FASONE. Can. J. Chem. **54**, 1870 (1976).

On a mesuré les spectres électroniques de trois isomères de la diazafluorénone-9. On a comparé ces mesures, effectuées en solution dans le cyclohexane, avec les résultats des calculs MIM ("molécule dans molécules") et PPP. On a trouvé une relation satisfaisante entre les données théoriques et expérimentales et on a pu attribuer cinq transitions $\pi \rightarrow \pi^*$ dans les spectres uv. Pour deux composés, on a mesuré les moments dipolaires en solution benzénique et comparé ces valeurs expérimentales avec les valeurs théoriques obtenues par des calculs MIM et CNDO/2.
[Traduit par le journal]

Introduction

In the last years the electronic absorption spectrum of fluorenone has been much discussed. After different interpretations on the nature of the lowest singlet–singlet transition, first believed to be an $n \rightarrow \pi^*$ transition (1) and successively assigned to a $\pi \rightarrow \pi^*$ transition (2–4), five $\pi \rightarrow \pi^*$ transitions have been definitely assigned in the near ultraviolet spectrum of fluorenone (5).

In this paper we have extended our study to the three diazafluoren-9-one isomers (Fig. 1) and carried out MIM, PPP, and CNDO/2 calculations to correlate their electronic spectra and dipole moments. For these molecules the relevant literature data provide only the preparation of compounds (6) and the uv spectrum of 4,5-diazafluoren-9-one in ethyl alcohol (7).

Experimental

Materials

4,5-Diazafluoren-9-one (**1**), 1,5-diazafluoren-9-one (**2**) and 1,8-diazafluoren-9-one (**3**) were prepared according to the procedure described in ref. 6.

Measurements

The ultraviolet absorption spectra of the compounds, dissolved in methanol and cyclohexane (spectrograde reagent), were recorded by a PYE-UNICAM SP 1800 spectrophotometer over the 210–370 nm range.

The electric dipole moments were determined in benzene solution at 25 ± 0.1 °C; for the dielectric

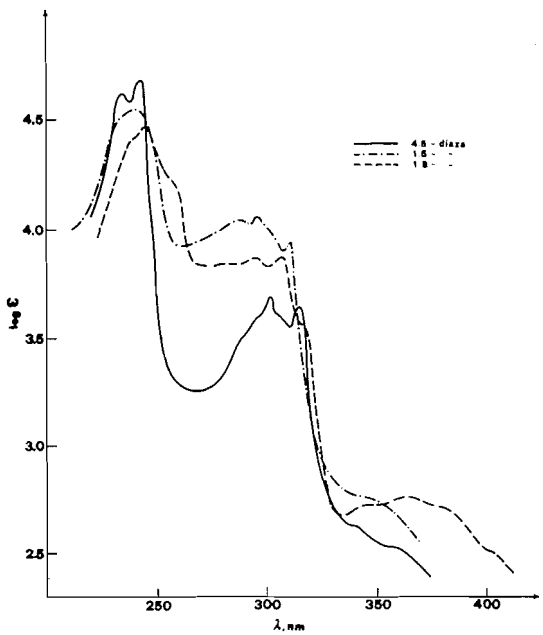

FIG. 1. Absorption spectra of diazafluoren-9-ones in cyclohexane.

Can. J. Chem. Downloaded from www.nrcresearchpress.com by 210.87.254.40 on 09/05/12
For personal use only.

Can. J. Chem. Downloaded from www.nrcresearchpress.com by 210.87.254.40 on 09/05/12
For personal use only.

constant measurements, a Dipolmeter WTW model 01 was used ($\Delta\epsilon/\epsilon = 10^{-5}$ at a frequency of 2 MHz).

The refractive indices were measured on a Bausch and Lomb refractometer with an accuracy of $\pm 3 \times 10^{-5}$.

The solute molar polarization, extrapolated to infinite dilution, was evaluated by the simplified Guggenheim method (8).

Theoretical Calculations and Results

The energies of the excited electronic states of the compounds have been calculated by the MIM and PPP methods and compared with experimental data.

The details of the MIM method are discussed in refs. 9 and 10. In this paper, the same two geometries adopted for the fluorenone (cases EG3 and EG4 in ref. 5) are used.

The fragments considered for the molecules studied are pyridine and formaldehyde. The SCF-MOs by Mataga and Nishimoto (11) and the activation energy and ionization potential values by Favini and Gamba (12) are used for pyridine, while the SCF-MOs and an activation energy of −1.78 eV by Edwards and Grinter (13) are used for the formaldehyde fragment. Also used are the same locally excited states of pyridine and formaldehyde as reported in refs. 13 and 14 respectively. For the EG4 symmetry the core resonance integrals were evaluated by Kon's relationship (15), while for the EG3 geometry the same values for fluorenone were used.

The two centre integrals were evaluated by the Pariser-Parr semiempirical formulas, using the parameter values reported in Table 1.

Dipole moment values were calculated by the MIM and CNDO/2 methods for both geometries.

In particular, in the MIM calculation, the experimental dipole moment of formaldehyde (2.29 D (16)), the σ moments reported in ref. 17, and the calculated mesomeric moments were considered.

TABLE 1. Two-centre electron repulsion integrals $(pp/qq) = a + br + cr^2$

p	q	a	b	c	r_{lim}(Å)*
C	C	11.130	−2.912	0.253	4.80
C	O	13.200	−4.205	0.452	3.95
C	N	11.735	−3.255	0.302	4.50
N	N	12.340	−3.779	0.414	3.25
N	O	13.805	−4.535	0.499	3.85

*For $r > r_{lim}$, the two-centre electron repulsion integrals were evaluated as e^2/r.

Conclusions

The absorption spectra of compounds in cyclohexane solutions are shown in Fig. 1; the experimental absorption ranges and oscillator strengths and the theoretical results are collected in Table 2.

The spectra show three different absorption ranges; for 1,8-diazafluoren-9-one the experimental band at longer wavelength is relatively well resolved and has very much the appearance of the band at longer wavelength of fluorenone (5).

Moreover, the red-shift of this band passing from cyclohexane to methanol ($\Delta\lambda = 9$ nm) is like that found for the fluorenone, characteristic of the $\pi \rightarrow \pi^*$ transitions.

The relatively small intensity for a $\pi \rightarrow \pi^*$ transition is substantiated by the theoretical results.

Possible $n \rightarrow \pi^*$ transition in the same range can be disguised from the superimposed $\pi \rightarrow \pi^*$ transition.

From an evaluation of these theoretical data, it appears that the calculations give a satisfactory interpretation of these spectra, and show five $\pi \rightarrow \pi^*$ transitions in the near ultraviolet region. A comparison between theoretical and experimental data suggests that the transition of lowest energy should correspond to the experimental band at the longest wavelength, while the two transitions at intermediate energy and the two energetically highest should be involved in the second and third absorption ranges respectively.

This assignment is similar to that proposed for fluorenone (5).

A careful analysis of the theoretical data shows that the results obtained assuming EG3 geometry as basis for the calculations are in every case energetically higher with respect to those obtained assuming the EG4 geometry. Similar results were obtained for fluorenone (5).

A comparison between the calculated energy values considering the same geometry shows that on going from the MIM to PPP method, the first and the last transitions for compounds **2** and **3** increase their energy, while the three intermediate transitions practically remain constant.

For compound **1** only the highest energy

Can. J. Chem. Downloaded from www.nrcresearchpress.com by 210.87.254.40 on 09/05/12
For personal use only.

TABLE 2. Electronic spectra of diazafluoren-9-ones

E_{exp} (eV) abs. range (cyclohexane)	f_{exp}	E (eV)				f				Polarization	Symmetry
		PPP EG3	PPP EG4	MIM EG3	MIM EG4	PPP EG3	PPP EG4	MIM EG3	MIM EG4		
4,5-Diazafluoren-9-one											
~3.60		3.98	3.64	3.99	3.61	0.35	0.26	~0	~0	x	$^1B_2 \leftarrow {}^1A_1$
4.00–4.20	0.09	4.23 4.43	4.07 4.17	4.49 4.20	4.30 4.01	~0 0.01	0.01 0.09	0.01 0.31	0.03 0.29	y x	$^1A_1 \leftarrow {}^1A_1$ $^1B_2 \leftarrow {}^1A_1$
4.73–5.08	0.33	4.97 5.52	4.84 5.17	4.91 4.98	4.74 4.69	0.01 0.06	0.06 0.01	0.88 0.91	0.26 0.96	y x	$^1A_1 \leftarrow {}^1A_1$ $^1B_2 \leftarrow {}^1A_1$
1,5-Diazafluoren-9-one											
~3.70		4.14	3.73	3.79	3.40	0.28	0.07	~0	0.07		
4.00–4.30	0.22	4.19 4.45	4.03 4.19	4.25 4.53	4.05 4.34	0.08 0.02	0.3 ~0	0.38 0.08	0.3 ~0		
5.14–5.25	0.74	4.99 5.51	4.81 5.20	4.81 5.06	4.59 4.80	0.03 0.26	0.10 0.06	0.34 0.66	0.10 0.06		
1,8-Diazafluoren-9-one											
3.28–3.59	0.02	4.07	3.63	3.57	3.16	0.13	~0	~0	~0	x	$^1B_2 \leftarrow {}^1A_1$
3.91–4.43	0.17	4.25 4.41	4.10 4.12	4.46 4.34	4.30 4.11	0.03 0.19	0.01 0.35	~0 0.59	~0 0.59	y x	$^1A_1 \leftarrow {}^1A_1$ $^1B_2 \leftarrow {}^1A_1$
4.84–5.12	0.67	4.97 5.46	4.78 5.17	4.88 5.00	4.68 4.71	0.02 0.54	0.06 0.38	0.22 0.56	0.25 0.66	y x	$^1A_1 \leftarrow {}^1A_1$ $^1B_2 \leftarrow {}^1A_1$

TABLE 3. Composition (%) of the excited electronic states of diazafluoren-9-ones*

Geometry	State (symmetry)	Combined configurations A_{py}	T^{py}_{py}	T^{CO}_{py}	A_{CO}	Dominating configurations
			4,5-Diazafluoren-9-one			
EG3	ψ_1 ($^1B_2$)	27.1	34.4	38.5		$A_2(17.8)$; $T^{4py}_{2py}(33.0)$; $T^{CO}_{2py}(38.4)$
	ψ_2 ($^1B_2$)	64.0	33.3	2.6		$A_1(58.0)$; $T^{3py}_{2py}(23.7)$
	ψ_3 ($^1A_1$)	67.7	23.7	8.0	0.2	$A_1(65.6)$; $T^{4py}_{2py}(16.3)$
	ψ_4 ($^1A_1$)	29.4	36.0	30.7	3.1	$A_1(18.6)$; $T^{4py}_{2py}(32.0)$; $T^{CO}_{2py}(28.7)$
	ψ_5 ($^1B_2$)	33.6	39.0	27.4		$A_4(25.6)$; $T^{4py}_{1py}(22.1)$; $T^{CO}_{1py}(22.1)$
			1,8-Diazafluoren-9-one			
EG3	ψ_1 ($^1B_2$)	34.5	30.4	35.1		$A_1(22.0)$; $T^{CO}_{2py}(29.4)$
	ψ_2 ($^1B_2$)	50.6	48.5	0.9		$A_1(27.2)$
	ψ_3 ($^1A_1$)	73.1	24.5	2.4		$A_1(72.0)$
	ψ_4 ($^1A_1$)	18.7	44.5	33.6	2.6	$T^{4py}_{2py}(39.8)$; $T^{CO}_{2py}(33.4)$
	ψ_5 ($^1B_2$)	36.0	38.0	26.0		$A_4(21.6)$; $T^{4py}_{1py}(23.0)$
			1,5-Diazafluoren-9-one			
EG3	ψ_1	33.3	30.6	36.0	—	$A_{1B}(15.0)$; $T^{4B}_2(13.6)$; $T^{CO}_{2A}(16.5)$; $T^{CO}_{2B}(16.8)$
	ψ_2	59.9	38.2	1.7	—	$A_{1A}(42.0)$; $T^{3A}_{2B}(13.3)$
	ψ_3	65.5	28.7	5.7	0.1	$A_{1A}(21.2)$; $A_{1B}(37.9)$; $T^{4A}_{2B}(18.3)$
	ψ_4	28.9	37.7	31.0	2.1	$A_{1B}(17.4)$; $T^{4B}_{2A}(12.2)$; $T^{CO}_{2A}(19.1)$
	ψ_5	30.9	39.6	28.5	0.8	$A_{4B}(12.5)$; $T^{CO}_{2B}(18.1)$

TABLE 4. Theoretical and experimental dipole moments (D)

Compound	μ_{exp}	μ_{MIM} EG3	μ_{MIM} EG4	$\mu_{CNDO/2}$ EG3	$\mu_{CNDO/2}$ EG4
1	1.16	0.14	0.34	1.05	1.37
2	3.75	3.75	3.93	3.23	2.91
3	(6.34)*	6.80	7.20	6.77	6.68

*Extrapolated value (see Conclusions).

transition increases strongly on passing from the MIM to PPP method.

The results obtained by this method for compounds **1** and **2**, adopting an EG4 geometry, seem to give a better interpretation of experimental absorption spectra than the MIM.

For compound **3**, the MIM method, using the EG3 geometry, gives the best results.

Table 3 reports the composition (%) of the excited electronic states for the compounds in the EG4 geometry, the values obtained for the EG3 geometry being very close. From our evaluation of these data it appears that both charge-transfers and locally excited states contribute remarkably at all transitions.

Experimental and theoretical dipole moment values are collected in Table 4. A value for the dipole moment of 1,8-diazafluoren-9-one can be extrapolated, by means of a qualitative argument, from the experimental values of the other two compounds. In fact, if one assumes that passing from 1,5-diazafluoren-9-one to 1,8-diazafluoren-9-one the dipole moment increases the same amount, then one has, passing from 4,5-diazafluoren-9-one to 1,5-diazafluoren-9-one, a value of 6.34 D. This result is very close to those obtained by the CNDO/2 and MIM calculations for both geometries.

For the other two compounds the MIM results reproduce satisfactorily the dipole moment of the compound **2** but not that of compound **1**, while the CNDO/2 ones give a fine agreement for both molecules.

1. J. PLOTT. J. Chem. Phys. **19**, 101 (1951).
2. A. KUBOYAMA. Bull. Chem. Soc. Jpn. **37**, 1540 (1964).
3. K. YOSHIHARA and D. R. KEARNS. J. Chem. Phys. **45**, 1991 (1966).
4. H. KUZODA and TOSIYASU L. KUNII. Theor. Chim. Acta, **9**, 51 (1967).
5. G. FAVINI, G. BUEMI, D. GRASSO, and G. CAPIETTI. J. Elect. Spectrosc. **2**, 239 (1973).
6. J. DRUEY and P. SCHMIDT. Helv. Chim. Acta, **XXXIII**, 1080 (1950).
7. G. E. INGLETT and G. F. SMITH. J. Am. Chem. Soc. **72**, 842 (1950).
8. J. W. SMITH. Electric dipole moments. Butterworths, London. 1959.

Can. J. Chem. Downloaded from www.nrcresearchpress.com by 210.87.254.40 on 09/05/12
For personal use only.

9. G. FAVINI, A. GAMBA, and M. SIMONETTA. Theor. Chim. Acta, **13**, 175 (1969).
10. K. H. GIOVANNELLI, G. HOHLNEICHER, and P. A. STRAUB. Ber. Bunsens, Phys. Chem. **75**, 857 (1971).
11. N. MATAGA and K. NISHIMOTO. Z. Phys. Chem. NF **13**, 140 (1957).
12. G. FAVINI and A. GAMBA. Gazz. Chim. Ital. **98**, 627 (1968).
13. T. G. EDWARDS and P. GRINTER. Theor. Chim. Acta, **12**, 387 (1968).
14. G. FAVINI, A. GAMBA, and I. R. BELLOBONO. Spectrochim. Acta, **23**A, 89 (1967).
15. H. KON. Bull. Chem. Soc. Jpn. **28**, 275 (1955).

Can. J. Chem. Downloaded from www.nrcresearchpress.com by 210.87.254.40 on 09/05/12
For personal use only.

Tertiary phosphine complexes of the cobalt(III) *NN'*-ethylenebis(salicylideneiminato) and bisdimethylglyoximato systems

C. W. SMITH, G. W. VAN LOON, AND M. C. BAIRD
Department of Chemistry, Queen's University, Kingston, Ont., Canada K7L 3N6

Received November 3, 1975

C. W. SMITH, G. W. VAN LOON, and M. C. BAIRD. Can. J. Chem. **54**, 1875 (1976).

Complexes of the types $[CosalenPR_3]X$, $[Cosalen(PR_3)_2]X$, $[Co(DH)_2PPh_3X]$, and $[Co(DH)_2(PR_3)_2]ClO_4$, many of them new, have been prepared and characterized with respect to ^1H nmr spectra, ligand field parameters, and equilibrium constants for the formation of the 2:1 salen complexes. ^1H chemical shifts appear to be dominated by anisotropic rather than inductive effects, while the relative tertiary phosphine ligand field strengths appear to correlate with the steric requirements of the phosphines as well as their expected σ donor strengths. Ease of formation of the 2:1 salen complexes is determined largely by steric effects, as are *trans* effects in the DH systems.

C. W. SMITH, G. W. VAN LOON et M. C. BAIRD. Can. J. Chem. **54**, 1875 (1976).

On a préparé et caractérisé, grâce à la spectroscopie rmn, aux paramètres de champ de ligand et aux constantes d'équilibre pour la formation de complexes 2:1, les complexes des types $[CosalenPR_3]X$, $[Cosalen(PR_3)_2]X$, $[Co(DH)_2PPh_3X]$ et $[Co(DH)_2(PR_3)_2]ClO_4$ parmi lesquels plusieurs étaient nouveaux. Il semble que les déplacements chimiques sont dominés par des effets anisotropiques plutôt qu'inductifs alors que les forces relatives de champ de ligand des phosphines tertiaires seraient corrélées avec les exigences stériques des phosphines de même qu'avec les forces que l'on peut attendre pour ces phosphines comme donneurs σ. La facilité de formation des complexes (salen) 2:1 est déterminée principalement par des effets stériques; il en est de même pour les effets *trans* dans les systèmes DH.

[Traduit par le journal]

Because of their anticipated similarity to the chemistry of vitamin B_{12}, a cobalt–corrin system, a number of octahedral and square pyramidal cobalt complexes containing essentially planar, tetradentate, strong-field chelate systems have been studied in recent years (1, 2). Pertinent to the work discussed here are investigations of the *NN'*-ethylenebis(salicylideneiminato)cobalt(III), $[CosalenL_2]^+$ (**1**) and bisdimethylglyoximatocobalt(III), $[Co(DH)_2L_2]^+$ (**2**) (L = neutral ligand), systems, which have been studied with a view to determining the effects of varying both the axial ligands (L) and the chelate group on the physical and chemical properties of the central cobalt ion.

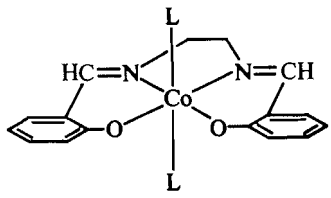

1

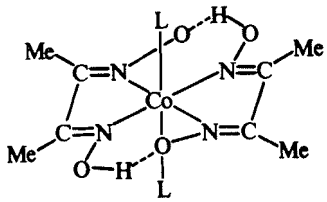

2

Measurements of ligand field parameters of the chelate systems are made difficult because of the low symmetry of the complexes (3) and because their electronic spectra are often dominated by intense charge transfer bands (4). Empirical crystal field calculations (5), however, suggest that the $(DH)_2$ grouping has a relatively high ligand field strength, above $(NH_3)_4$ and $(en)_2$, but below $(CN^-)_4$ (6) in the spectrochemical series. Generally there appears to be considerable covalency in the bonding to cobalt (5), and the metal ion in many cases exhibits unusual kinetic lability of the axial ligands (7, 8) and a preference for 'soft' axial ligands (9, 10).

A number of rather inconclusive attempts have been made to understand the mutual inductive influences of the axial and the in-plane ligands on the properties of each other. For instance, for the compounds $[Co(DH)_2LX]$ (L = neutral, X =

Can. J. Chem. Downloaded from www.nrcresearchpress.com by 210.87.254.105 on 09/05/12
For personal use only.

Can. J. Chem. Downloaded from www.nrcresearchpress.com by 210.87.254.105 on 09/05/12
For personal use only.

anionic ligands), it was reported that the DH methyl resonances become more shielded, the oxime proton resonances less shielded as the axial ligands become better donors (as measured by their Hammett σ_p values) (11). However some of the compounds have subsequently been shown to have been incorrectly formulated (12), and the chemical shift data may be better explained in terms of anisotropic shielding by paramagnetic currents on the cobalt rather than purely inductive effects (12). Also, for similar compounds, there is no apparent correlation between the pK_a of the oxime protons and the pK_a of HL^+ (13). Furthermore, the acidity of the coordinated water in the compounds $[Co(DH)_2(H_2O)L]^+$ decreases as the basicity of L increases when L is a tertiary phosphine, but does the opposite when L is a substituted aniline (7).

Although cobalt(III)(DH_2) complexes appear to be invariably six-coordinated, five-coordinated complexes of the type [CosalenX] are formed when X is a highly polarizable, strong σ donor such as an alkyl group or a tertiary phosphine (14, 15). Few axial ligand equilibrium studies are available, although the equilibrium constants for the reaction

[1] $[CosalenPR_3]^+ + NO_2^- \rightleftharpoons [CosalenPR_3NO_2]$

decrease in the order $PPh_3 < PEtPh_2 < PBu_3$ (15).

As much of the above work is concerned with complexes where L is a nitrogen donor, it seemed of interest to investigate a series of tertiary phosphine complexes. This paper extends the series of known tertiary phosphine cobalt complexes (15), and compares the relative influences of the four tertiary phosphines, PPh_3, $PMePh_2$, PMe_2Ph, and PBu_3, differing widely in electronic properties and steric requirements, on the physical and chemical properties of complexes of the types $[CosalenL_2]^+$ and $[Co(DH)_2L_2]^+$. Subsequent papers will consider the electrochemistry of the same complexes.

Experimental

The complexes $[CosalenPR_3]ClO_4 \cdot H_2O$ and $[Cosalen(PR_3)_2]ClO_4$ were prepared by methods described in literature (15–17), although product analysis and polarographic behaviour of the supposed $[Cosalen(H_2O)_2]ClO_4$ (17) suggested that the material was actually [Cosalen(H_2O)OH]. The desired diaquo complex was readily prepared *in situ* by suitable p*H* adjustment. It is not known whether the complexes $[CosalenPR_3]ClO_4 \cdot H_2O$ are five-coordinated or whether, in fact, the water molecules are coordinated. Their dark green colours, however, are very similar to the colours of their solutions in 95% ethanol, in which five-coordinated species are believed to be present (see below), and thus the solid materials are also probably five-coordinated. The nmr spectra of the bis-phosphine salen derivatives are consistent with the suggested formulations; however elemental analyses for these compounds were not obtained.

The complexes $[Co(DH)_2(PR_3)_2][ClO_4$ and $[Co(DH)_2(PR_3)_2]NO_3$ were prepared by the general methods of Costa *et al.* (18) using starting materials described in literature (19–21). Difficulties were encountered in attempts to isolate the mono-phosphine $(DH)_2$ complexes by treatment of the diaquo complex with slightly less than stoichiometric amounts of PR_3 (18). The materials isolated were found to be the bis-phosphine complexes for $PR_3 = PBu_3$ and PMe_2Ph, and mixtures of the bis- and mono-forms for $PMePH_2$, after recrystallization from methanol. Syntheses of the bis-phosphine complexes proceeded smoothly using the same route with excess tertiary phosphine. The compounds $[Co(DH)_2PPh_3X)$ were also prepared by standard procedures (11, 22).

Analyses were performed by A. B. Gygli Microanalysis Laboratory, Toronto, and Schwarzkopf Microanalytical

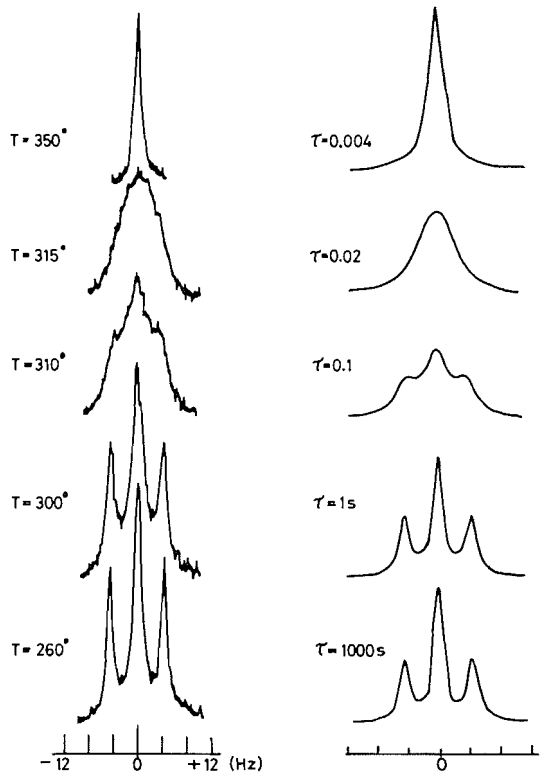

FIG. 1. Comparison of the temperature dependence of the nmr spectrum of $[Cosalen(PMePh_2)_2]^+$ with the computer generated spectra for triplet collapse due to phosphine exchange.

TABLE 1. Analytical data

Complex	Calculated			Found		
	C	H	N	C	H	N
$[Co(DH)_2(H_2O)_2]NO_3$	23.71	4.98	17.28	22.94	5.05	16.95
$[Co(DH)_2(PPh_3)_2ClO_4$	57.87	4.86	6.14	57.15	5.73	5.82
$[Co(DH)_2(PMe_2Ph)_2]NO_3$	45.94	5.78	11.16	45.87	6.15	11.21
$[Co(DH)_2(PBu_3)_2]ClO_4$	48.45	8.64	7.06	48.21	8.69	6.94
$[Cosalen(H_2O)OH]$	53.40	4.76	7.77	55.40	4.23	7.90
$[CosalenPPh_3]ClO_4 \cdot H_2O$	57.93	4.43	3.97	57.26	4.45	3.94
$[CosalenPMePh_2]ClO_4 \cdot H_2O$	54.18	4.55	4.36	54.96	4.36	4.59
$[CosalenPMe_2Ph]ClO_4 \cdot H_2O$	49.63	4.69	4.82	49.10	4.81	4.84
$[CosalenPBu_3]ClO_4$	53.64	6.59	4.47	53.88	6.72	4.58

TABLE 2. Nuclear magnetic resonance spectral parameters for $[CosalenL]ClO_4 \cdot H_2O$ and $[CosalenL_2]ClO_4$ in CD_3CN[a]

Complex	$\tau(C_2H_4)$	τ(CH)	τ(PMe)
$L = PBu_3$	6.02(br)	1.98 (d, J_{PH} = 3 Hz)	—
$L = PMe_2Ph$	6.12(br)	2.26 (d, J_{PH} = 3.5 Hz)	8.35 (d, J_{PH} = 13.5 Hz)
$L = PMePh_2$	6.04(br)	2.31 (d, J_{PH} = 3 Hz)	8.52 (d, J_{PH} = 14.5 Hz)
$L = PPh_3$	6.21(br)	[e]	—
$L_2 = (PBu_3)_2$[b]	6.25(br)[d]	2.12(br)[d]	—
$L_2 = (PMe_2Ph)_2$[b]	6.55(br)[d]	2.63(br)[d]	8.52 (t, $^2J_{PH} + {}^4J_{PH}$ = 8.8 Hz)
$L_2 = (PMePh_2)_2$[c]	6.43(br)	[e]	8.13 (t, $^2J_{PH} + {}^4J_{PH}$ = 9.0 Hz)

[a]d = doublet, t = triplet, br = broad.
[b]At 280 K.
[c]At 253 K.
[d]Resonance narrows on ^{31}P decoupling.
[e]Resonance obscured by aromatic multiplet.

Laboratory, Woodside, N.Y.; analytical data are presented in Table 1.

Ultraviolet–visible spectra were obtained using Unicam SP800 or Spectronic 505 spectrophotometers. When titrations with the air-sensitive phosphines were carried out, it was necessary to use anaerobic techniques. The titrations were done by adding aliquots of the phosphine with a Hamilton microlitre syringe to a solution of the cobalt(III) complex maintained under nitrogen. The photometric cell was fitted with a serum cap and was purged with nitrogen via two 22 gauge needles; after purging for 4 min, both needles were withdrawn, leaving a positive pressure. Aliquots of solution were transferred via a flushed 5 ml syringe and were injected through the serum cap into the cell.

Nuclear magnetic resonance experiments were carried out using a Bruker HX-60 instrument. Line-shape analysis for proton nmr triplet collapse reflecting chemical exchange in chemical systems is apparently unprecedented. A rate line-shape equation was therefore derived, following the analysis outlined by Meiboom and co-workers (23) for quartet collapse due to proton exchange from the methylammonium ion, using the Gutowsky, McCall, and Slichter model (24). A dissociative phosphine mechanism was assumed (8) and line shapes were computed for thirty values of the mean lifetime of the phosphine at the coordinated site between 10^3 and 10^{-3}. The input parameters T_2 (relaxation time in the absence of exchange) and δ_ω (coupling constant in radians per second) were obtained from the experimental spectra at low temperature; computed line shapes for $\tau = 10^3$ matched the low temperature spectra well with respect to coupling constants, bandwidths and normalized peak heights (see Fig. 1).

Results and Discussion

Proton Nuclear Magnetic Resonance Spectra

^1H nmr spectra data for the salen complexes are listed in Table 2. Assignments were based on integrations, phosphorus-decoupling experiments and data in the literature for similar compounds (25), and are reasonably straightforward. Although ^{31}P decoupling had no effect on the line widths of the ethylene and methine resonances of the 1:1 complexes, the corresponding resonances of the 2:1 complexes narrowed on ^{31}P decoupling in several cases, indicating long range phosphorus–hydrogen coupling in the latter cases. Interestingly, the methine chemical shifts of both the 1:1 and 2:1 complexes move to higher field in the order $PBu_3 < PMe_2Ph < PMePh_2 < PPh_3$, *i.e.* in the reverse direction to that expected on the basis of relative donor

Can. J. Chem. Downloaded from www.nrcresearchpress.com by 210.87.254.105 on 09/05/12
For personal use only.

TABLE 3. Activation parameters for dissociative phosphine exchange from the complexes $[Cosalen(PR_3)_2]ClO_4$

PR_3	E_a (kcal mol^{-1})	$\Delta G^{\ddagger}$ (kcal mol^{-1}) 298 K	$\Delta H^{\ddagger}$ (kcal/mol^{-1})	$\Delta S^{\ddagger}$ (eu)
PMe_2Ph	24.7	16.9	24.1	24
$PMePh_2$	14.9	13.4	14.3	2.9

TABLE 4. Nuclear magnetic resonance data for the complexes $Co(DH)_2PPh_3X$ and $Co(DH)_2(PR_3)_2(NO_3, ClO_4)$

X, PR_3	τDHMe (J_{PH})	$\tau_{\alpha\text{-CH}}$ (J_{PH})	$\tau_{\beta\text{-CH}}$ (J_{PH})	τ other resonances (excluding Ph)
Br[a]	8.02 (1.6 Hz)	—	—	—
I[a]	8.01 (1.9 Hz)	—	—	—
Me[a]	8.17 (3.1 Hz)	8.81 (3.9 Hz)	—	—
Et[b]	8.35 (3.0 Hz)	7.65 (3.8 Hz)	9.25 (7.8 Hz)	—
n-Pr[b]	8.38 (3.3 Hz)	7.66 (4.3 Hz)	Obscured by DH	9.05(PrMe)
iso-Pr[b]	8.19 (3.5 Hz)	Obscured by DH	9.58 (8.2 Hz)	—
o-anisyl[a]	8.30 (3.4 Hz)	—	—	6.37(OMe), 3–5(C_6H_4)
$PhCH_2$[a]	8.41 (3.0 Hz)	6.95 (6.5 Hz)	—	—
PPh_3[c]	8.38 (2.2 Hz)	—	—	—
$PMePh_2$[c]	8.53 (2.5 Hz)	—	—	8.11(PMe, $^2J_{PH} + {}^4J_{PH}$ = 10 Hz)
PMe_2Ph[c]	8.18 (2.5 Hz)	—	—	8.46(PMe, $^2J_{PH} + {}^4J_{PH}$ = 9.8 Hz)
PBu_3[c]	7.65 (2.5 Hz)	—	—	9–9.6(Bu)

[a]$CDCl_3$.
[b]C_6D_6.
[c]CD_3NO_2.

strengths. It is possible that through space anisotropic shielding by the phosphine phenyl rings could result in the order observed (11), particularly as the effect is greater for the 2:1 complexes. However, the correlation with the ethylene chemical shifts is less satisfactory, and more data are needed to explain this unusual *cis* influence.

The room temperature proton nmr spectrum of the complex *trans*-$[Cosalen(PMe_2Ph)_2]ClO_4$ in CD_3CN contains a 1:2:1 triplet at τ 1.48 which may be assigned to the phosphorus methyl groups. The triplet structure can be interpreted in terms of an $AA'X_6X_6'$ spin system in which $J_{AA'}$ (*i.e.* J_{PP}) $\gg J_{AX}$ (26). On raising the temperature, the triplet structure collapses to a singlet. In contrast, the phosphorus methyl resonance of *trans*-$[Cosalen(PMePh_2)_2]ClO_4$ is a singlet at τ 1.87 at room temperature, and can only be resolved into the triplet expected for an $AA'X_3X_3'$ spin system at lower temperatures.

Coalescence temperatures in both cases are independent of added free phosphine, suggesting a dissociative process and moderately fast exchange of phosphine between free and coordinated sites. The spectrum of $[Cosalen(PMe_2Ph)_2]ClO_4$ as a function of temperature is compared with computer-generated spectra for a range of τ (see Experimental section) in Fig. 1. The fit is reasonably satisfactory, suggesting that the process observed is indeed

[2] $[Cosalen(PMe_2Ph)_2]^+ \rightarrow [CosalenPMe_2Ph]^+ + PMe_2Ph$ (rate-determining)

[3] $[CosalenPMe_2Ph]^+ + PMe_2Ph \rightarrow [Cosalen(PMe_2Ph)_2]^+$ (fast)

The experimentally observed and calculated symmetrical collapse of the triplet is consistent with [2] being rate-determining, as unsymmetrical collapse would be expected if [3] were not rapid. The 1:1 and 2:1 species would probably exhibit different methyl chemical shifts, and collapse would be expected to a position intermediate to these two values if significant amounts of the 1:1 complex existed in solution.

Rate constants for the exchange process were determined over a range of approximately 100° for each complex, and the derived activation parameters are listed in Table 3. Unfortunately, similar information could not be obtained for the PPh_3 and PBu_3 complexes.

^1H data for the complexes $[Co(DH)_2(PR_3)_2]X$

Can. J. Chem. Downloaded from www.nrcresearchpress.com by 210.87.254.105 on 09/05/12
For personal use only.

Can. J. Chem. Downloaded from www.nrcresearchpress.com by 210.87.254.105 on 09/05/12
For personal use only.

($X = NO_3$, ClO_4) are listed in Table 4. In all cases, the DH methyl resonances are triplets because of spin–spin coupling to two equivalent phosphorus atoms in mutually *trans* positions. Triplets were also observed for the PMe resonances of the $PMePh_2$ and PMe_2Ph complexes for the same reasons as for the corresponding salen complexes, although the oxime resonances in all cases were broad, featureless bands. As with the salen complexes, there is no clear relationship between DH methyl chemical shifts and the electron donor properties of the tertiary phosphines. The ^1H nmr spectra for all four complexes retained the triplet structures up to the decomposition temperatures (>400 K); thus the complexes are much less labile than the corresponding salen complexes.

Room temperature proton nmr spectra of the complexes *trans*-$[Co(DH)_2PPh_3X]$ (X = Br, I, alkyl, aryl) in most cases contain a doublet for the methyl resonance of the DH ligands (J_{PH} = 1.6–3.0 Hz) (Table 4); the sole exception was that of the isopropyl complex, for which the DH methyl resonance was a singlet. In the cases of the bromo and iodo complexes, raising the temperature to the decomposition points (>360 K), had little effect on the spectra. On raising the temperature of most of the alkyl complexes, however, the DH methyl resonances broadened and coalesced into sharp singlets; in these cases, coupling of the phosphorus to the protons of the coordinated alkyl groups was also lost at higher temperatures. In the case of the isopropyl complex the situation was reversed, phosphorus coupling being observed only at lower temperatures.

Neither added phosphine nor change of solvent ($CDCl_3$, C_6D_6, CD_3CN, DMSO-d_6) affected the coalescence temperature of the methyl complex significantly, and thus a mechanism involving dissociation of the phosphine is again implied. Similar arguments have been applied previously to the complexes $[Co(DH)_2PR_3Me]$ (R = Ph, OMe) by Brown *et al.* (8), who carried out detailed line-shape analyses and obtained $\Delta H^{\ddagger}$ of approximately 20–22 kcal mol^{-1} and small, positive $\Delta S^{\ddagger}$, consistent with a dissociative process. For the compounds reported here, we have calculated only $\Delta G^{\ddagger}$ from the observed coalescence temperatures (T_c) (Table 5). The approach is justifiable because the $\Delta G^{\ddagger}$ values calculated this way can be expected to be very accurate (27). It is also expected that the values of $\Delta S^{\ddagger}$ should be small and approximately constant in all cases, and thus the derived values of $\Delta G^{\ddagger}$ should accurately reflect relative activation energies. Values of T_c and $\Delta G^{\ddagger}$ for the methyl complex agree very well with data obtained by Brown *et al.* (8).

TABLE 5. T_c and $\Delta G^{\ddagger}$ for the complexes $[Co(DH)_2PPh_3X]$

X	T_c (K)	$\Delta G^{\ddagger}$ (kcal/mol)
Br	>360	>20
I	>360	>20
PPh_3	>360	>20
Me	345	19.0±0.2
Et	323	17.7±0.2
n-Pr	318	17.4±0.2
iso-Pr	290	15.8±0.2
$PhCH_2$	330	18.1±0.2
p-$MeOC_6H_4$	342	18.7±0.2

Consideration of kinetic data obtained for both the salen and the DH systems leads to the conclusion that the complexes exhibit greater than normal lability for octahedral cobalt(III) systems (28). Similar observations have been noted previously (7–9, 29–31) and both *trans* effects of the axial ligands and *cis* effects of the in-plane chelating ligands appear to be important in labilizing the complexes. It has also been noted previously that salen complexes appear to be more labile than the corresponding DH complexes (7), as has been observed here.

The ordering of relative *trans* effects of the axial ligands agrees only partially with the orders expected for strongly σ bonding ligands (28) (taking pK_a values (32, 33) as a measure of the σ donor strengths of the tertiary phosphines). Thus while it is expected that alkyl ligands in the DH system should have higher *trans* effects than tertiary phosphines or halides, the order $PMePh_2 > PMe_2Ph$ is not expected in the salen system. Steric effects, however, appear to be very important. Tolman and co-workers (34, 35) have shown on the basis of tertiary phosphine exchange studies that steric effects are more important than electronic effects in determining complex stabilities for nickel(0) complexes of the type NiL_4 (L = phosphorus donor). As a quantitative criterion of ligand size, the 'cone angle' was defined as the apex angle of the cone, centred at the metal atom, which just

TABLE 6. Electronic spectra of the complexes $[CosalenL]ClO_4 \cdot H_2O$ and $[CosalenL_2]ClO_4$ in ethanol

Complex	E_{max} (kK) (log ϵ)		
$L = PPh_3$	14.0(2.88)	24.9(3.68)	
$L = PMePh_2$	~15.4(2.90)	25.3(3.69)	31.5(4.06)
$L = PMe_2Ph$	16.0(2.83)	25.3(3.70)	~33.3(4.13)
$L = PBu_3$	16.0(2.91)	25.1(3.72)	
$L_2 = (PPh_3)_2$	16.1(3.14)	~25.0(3.71)	~29.0(4.13)
$L_2 = (PMePh_2)_2$	20.2(3.84)	23.3(3.80)	30.2(4.20)
$L_2 = (PMe_2Ph)_2$	20.9(3.93)	23.3(3.92)	31.5(4.40)
$L_2 = (PBu_3)_2$	20.9(3.82)	22.5(3.89)	

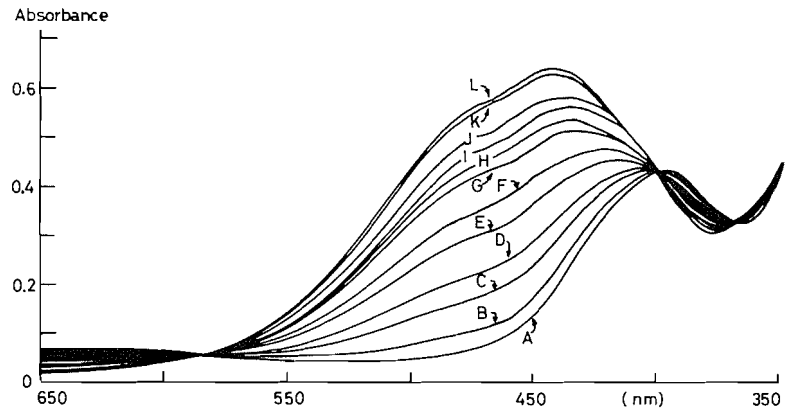

FIG. 2. Spectrophotometric titration of $[Cosalen(PBu_3)_2]ClO_4$ (0.0824 mM in 95% EtOH, 0.1 M $LiNO_3$, T = 24 °C). Ratio of PBu_3 to Co^{III}: *A*, 0; *B*, 0.39; *C*, 1.4; *D*, 2.3; *E*, 4.3; *F*, 6.3; *G*, 10.1; *H*, 14.0; *I*, 21.8; *J*, 60.9; *K*, 99.9; *L*, 198.

encloses the Van der Waals radii of the ligand atoms.

Phosphorus donor steric requirements, as exemplified by cone angles, appear to be important in octahedral complexes containing chelating ligands such as the dimethylglyoximate anion (DH). Thus the two chelate rings of *trans*-$[Rh(DH)_2PPh_3Cl]$ are tilted away from the PPh_3 such that the normals to the planes make an angle of 17.1° (36). Perhaps surprising, however, is the report (37) that phosphines with large cone angles decrease the rate of the reaction

[4] $2[Co(DH)_2L] + RX \rightarrow [Co(DH)_2LR] + [Co(DH)_2LX]$

L = phosphorus donor, RX = benzyl halide

The rate-determining step is believed to be the transfer of an electron from cobalt(II) to the organic substrate to form a benzyl radical. As this step should be enhanced by good electron-donating phosphines, it was suggested that sterically hindered ligands may have a lower 'effective basicity' than would be expected on the basis of substituent electronic effects.

It has also been reported that there is a good correlation between phosphine cone angles and the methanol methyl chemical shifts of the complexes $[Co(DH)_2(PR_3)MeOH]^+$ (38); although the nature of the relationship is not completely understood, electron donating properties of the phosphines appear to be less important than do the apparent steric requirements of the phosphines.

In the cases of the compounds studied here, the orders of lability ($PMePh_2 > PMe_2Ph$ for the complexes $[Cosalen(PR_3)_2]^+$ and iso-Pr > *n*-Pr > Et > Me, and benzyl, aryl > Me for the complexes $[Co(DH)_2PPh_3X]$) may well reflect the importance of steric effects.

Electronic Spectra, Ligand Field Parameters

Electronic spectral data for the salen complexes in ethanol are listed in Table 6; spectra in acetonitrile were very similar. The 1:1 complexes are green in colour, exhibiting low energy transitions in the visible region of the spectrum as noted previously (15). Spectra of this type

Can. J. Chem. Downloaded from www.nrcresearchpress.com by 210.87.254.105 on 09/05/12
For personal use only.

Can. J. Chem. Downloaded from www.nrcresearchpress.com by 210.87.254.105 on 09/05/12
For personal use only.

have been interpreted (15) as being characteristic of five-coordinated, square pyramidal complexes, analogous to complexes of the type [Cosalen-(alkyl)] (5, 14). Thus the tertiary phosphines appear to exhibit a thermodynamic *trans* influence comparable with those of alkyl groups.

Upon titration of $[CosalenPR_3]^+$ with PR_3, the solutions change to deep red, the low energy bands being replaced by more intense absorptions in the range 16 to 21 kK (see Fig. 2). The limiting spectra are essentially identical to those of $[Cosalen(PR_3)_2]ClO_4$ in the presence of excess PR_3, and are very similar to the reported spectra of $[CosalenPR_3NO_2]$ (15). Thus formation of the *trans* octahedral species is inferred.

Bands in the spectra of the complexes $[Co(DH)_2(PR_3)_2]X$ occur at somewhat higher energies than those of the corresponding salen complexes (Table 7). Except for possibly the PPh_3 complex, addition of up to 20:1 excess PR_3 does not cause significant changes in the spectra, and thus it is inferred that phosphine dissociation does not occur to an appreciable extent.

Busch and co-workers (5) have applied an empirical crystal field model of Wentworth and Piper (6) to cobalt(III) complexes similar to the salen and DH complexes considered here; the latter derived the ligand field parameters D_q^{xy} and D_q^z, felt to reflect the relative coordinating strengths of the in-plane and axial ligands, respectively. D_{4h} symmetry was assumed, and the two lowest energy bands in the spectra in 95% ethanol were used to obtain the parameters. Using an essentially identical approach, D_q^{xy} was estimated to be about 2560 cm^{-1} for the salen complexes discussed here, slightly lower than what has been found for [Cosalen(pyridine)-Me] (5).[1] Values of D_q, the ligand field parameter for the axial phosphine ligands, are shown in Table 8, compared with values reported for the methyl group (5). As can be seen, the apparent ligand field strengths decrease in the order $Me > PMe_2Ph \geq PBu_3 > PMePh_2 > PPh_3$. Similar calculations cannot be done with the $(DH)_2$ complexes because the relevant bands are shoulders on stronger absorptions and cannot be assigned with the necessary accuracy. Nevertheless, the positions of the peak maxima of the lower energy absorptions shift to lower energy in the order $PMe_2Ph > PBu_3 > PMePh_2 > PPh_3$, parallelling the order observed for the salen systems. There is no obvious trend of the low energy bands of the complexes $[Co(DH)_2PPh_3X]$, although the alkyl groups would appear to have higher ligand field strengths, as expected (ref. 39 and references therein).

Although the data may not be very significant for such a small number of phosphines, particularly when the limitations of applying a crystal field model to such highly covalent complexes are considered, the observed trends only partially parallel the expected σ donor or π acceptor properties of the ligands. Interestingly, however, the trends do correlate well with the apparent steric requirements of the tertiary phosphines in similar systems (38), as expressed by their cone angles. Thus steric and electronic factors may

TABLE 7. Electronic spectra of the complexes $[Co(DH)_2(PR_3)_2]X$ in 95% ethanol and $[Co(DH)_2PPh_3X]$ in $CHCl_3$

Complex		E_{max} (kK) (log ϵ)
PR_3 =	PPh_3	26.7(4.70)
	$PMePh_2$	29.4(4.56)
	PMe_2Ph	30.7(4.28)
	PBu_3	30.4(4.04)
X =	Br	29.9(4.22)
	I	22.2(3.57), 28.7(4.27)
	Me	23.2(2.59), 33.0(3.89)
	Et	23.6(2.85), 21.3(3.85)
	n-Pr	22.3(2.36), 31.3(3.80)
	iso-Pr	21.9(2.75), 31.2(3.77)
	$PhCH_2$	28.3(3.93)
	p-$MeOC_6H_4$	22.2(2.62), 32.9(4.00)

TABLE 8. Empirical crystal field parameters for the complexes $[CosalenL]^+$ and $[CosalenL_2]^+$

Complex	D_q^z (cm^{-1})
$L = PPh_3$	1680
$L = PMePh_2$	2240
$L = PMe_2Ph$	2480
$L = PBu_3$	2480
Me	2500
$L_2 = (Ph_3)_2$	1270
$L_2 = (PMePh_2)_2$	1890
$L_2 = (PMe_2Ph)_2$	2220
$L_2 = (PBu_3)_2$	2210
L_2 = Me, pyr	2350

[1]The electron mutual repulsion parameter C was arbitrarily estimated as 3 kK for purposes of calculation, as it is about 3.8 kK and is reasonably independent of X and Y for the complexes of the type $[Co(NH_3)_4XY]^{n+}$ (6).

TABLE 9. Formation constants for addition of PR_3 to $[CosalenPR_3]ClO_4$

PR_3	K_f (M^{-1}) 95% EtOH	MeCN
PPh_3	1.65×10	1.5×10^2
$PMePh_2$	1.10×10^3	4.4×10^3
PMe_2Ph	7.5×10^4	1.5×10^5
PBu_3	2.7×10^3	1.3×10^4

contribute to the strength of the cobalt–phosphorus interactions in these complexes.

Formation Constants of the Cobalt Salen Complexes

Formation constants, K_f, for the equilibrium

$$[5] \quad [CosalenPR_3]^+ + PR_3 \underset{}{\overset{K_f}{\rightleftharpoons}} [Cosalen(PR_3)_2]^+$$

were determined by spectrophotometric titrations of the monophosphine complexes. Formation of the 2:1 complex is indicated by a change from deep green to red, accompanied by two isobestic points; the spectrophotometric titration of $[CosalenPBu_3]ClO_4 \cdot H_2O$ in 95% ethanol, for example, is shown in Fig. 2. Values of K_f obtained from similar titrations for all phosphines studied in both 95% ethanol and acetonitrile are reported in Table 9.[2] There was no spectral evidence of dissociation of tertiary phosphine from the 1:1 complexes.

In both acetonitrile and 95% ethanol, there is an increasing tendency for the monophosphine form to be stabilized in the order $PMe_2Ph < PBu_3 < PMePh_2 < PPh_3$. An essentially opposite trend has been reported by Costa and co-workers for the addition of the relatively small nitrite to 1:1 complexes, *i.e.* $PBu_3 < PEtPh_2 < PPh_3$ (15). While the latter order is that expected for thermodynamic *trans* influence dominated by phosphine substituent inductive influences on the σ orbital donor strength of the phosphorus, the former correlates very well with the cone angles of the tertiary phosphines (38). Thus the extent of addition of a bulky second tertiary phosphine to the salen system appears to be largely determined by steric considerations.

[2] $K_f = (A - A_0)/(A_\infty - A)[PR_3]\ M^{-1}$ (40), where A_0 and A_∞ are absorbances at the frequency monitored with no added phosphine and with a large excess of added phosphine, respectively.

Acknowledgements

The National Research Council of Canada is thanked for financial support, including a scholarship to C.W.S. Thanks are also due to D. H. Groves for obtaining nmr spectra and for helpful discussions concerning these spectra.

1. G. N. SCHRAUZER. Acc. Chem. Res. **1**, 97 (1968).
2. A. BIGOTTO, G. COSTA, G. MESTRONI, G. PELLIZER, A. PUXEDDU, E. REISENHOFER, L. STEFANI, and G. TAUZHER. Inorg. Chim. Acta Rev. **4**, 41 (1970).
3. G. COSTA. Coord. Chem. Rev. **8**, 63 (1972).
4. G. DE ALTI, V. GALASSO, A. BIGOTTO, and G. COSTA. Inorg. Chim. Acta, **3**, 533 (1969).
5. E. OCHIAI, K. LONG, C. R. SPERATI, and D. H. BUSCH. J. Am. Chem. Soc. **91**, 3201 (1969).
6. R. A. D. WENTWORTH and T. S. PIPER. Inorg. Chem. **4**, 709 (1965).
7. G. COSTA, G. TAUZHER, and A. PUXEDDU. Inorg. Chim. Acta, **3**, 41 (1969).
8. T. L. BROWN, L. M. LUDWICK, and R. S. STEWART. J. Am. Chem. Soc. **94**, 384 (1972).
9. D. N. HAGUE and J. HALPERN. Inorg. Chem. **6**, 2059 (1967).
10. A. L. WILMARTH and H. C. TSIANG. Inorg. Chem. **7**, 2535 (1968).
11. H. A. O. HILL and K. G. MORALLEE. J. Chem. Soc. (A), 554 (1969).
12. W. C. TROGLER, R. C. STEWART, L. A. EPPS, and L. G. MARZILLI. Inorg. Chem. **13**, 1564 (1974).
13. A. V. ABLOV and M. FILIPPOV. Russ. J. Inorg. Chem. **7**, 525 (1962).
14. G. COSTA, G. MESTRONI, and L. STEFANI. J. Organomet. Chem. **7**, 493 (1967).
15. G. TAUZHER, G. MESTRONI, A. PUXEDDU, R. COSTANZO, and G. COSTA. J. Chem. Soc. (A), 2504 (1971).
16. S. YAMADA, H. NISHIKAWA, and E. YOSHIDA. Proc. Jpn. Acad. **40**, 211 (1964); Chem. Abstr. **61**, 7920 (1964).
17. G. COSTA, A. PUXEDDU, and G. TAUZHER. Inorg. Nucl. Chem. Lett. **4**, 319 (1968).
18. G. COSTA, G. TAUZHER, and A. PUXEDDU. Inorg. Chim. Acta, **3**, 45 (1969).
19. A. K. BABKO and M. V. KOROTUN. Zhur. Obsh. Khim. **24**, 597 (1954); Chem. Abstr. **49**, 2928*e* (1955).
20. A. V. ABLOV and N. M. SAMUS. Dokl. Acad. Nauk USSR, **133**, 1265 (1957); Chem. Abstr. **52**, 1919*c* (1958).
21. A. V. ABLOV, M. P. FILIPPOV, and N. M. SAMUS. Dokl. Acad. Nauk USSR, **133**, 575 (1960); Chem. Abstr. **54**, 24370*h* (1960).
22. G. N. SCHRAUZER and R. J. WINDGASSEN. J. Am. Chem. Soc. **89**, 1999 (1967).
23. E. GRUNWALD, A. LOEWENSTEIN, and S. MEIBOOM. J. Chem. Phys. **27**, 630 (1957).
24. H. GUTOWSKY, D. MCCALL, and C. SLICHTER. J. Chem. Phys. **21**, 279 (1953).
25. H. A. O. HILL, K. G. MORALLEE, G. PELLIZER, G. MESTRONI, and G. COSTA. J. Organomet. Chem. **11**, 167 (1968).
26. R. J. HARRIS. Can. J. Chem. **42**, 2275 (1964).

Can. J. Chem. Downloaded from www.nrcresearchpress.com by 210.87.254.105 on 09/05/12
For personal use only.

27. I. O. SUTHERLAND. Ann. Rep. NMR Spectrosc. **4**, 71 (1971).
28. F. BASOLO and R. G. PEARSON. Mechanisms of inorganic reactions. 2nd ed. Wiley and Sons, New York. 1967.
29. A. C. CRUMBLISS and W. K. WILMARTH. J. Am. Chem. Soc. **92**, 2593 (1970).
30. G. COSTA, G. MESTRONI, G. TAUZHER, M. GREEN, and H. A. O. HILL. Chem. Commun. **34** (1970).
31. T. SAKURAI, J. P. FOX, and L. L. INGRAHAM. Inorg. Chem. **10**, 1105 (1971).
32. C. A. STREULI. Anal. Chem. **32**, 985 (1960).
33. W. A. HENDERSON and C. A. STREULI. J. Am. Chem. Soc. **82**, 5791 (1960).
34. C. A. TOLMAN. J. Am. Chem. Soc. **92**, 2956 (1970).
35. C. A. TOLMAN, W. C. SEIDEL, and L. W. GOSSEN. J. Am. Chem. Soc. **96**, 53 (1974).
36. F. A. COTTON and J. G. NORMAN. J. Am. Chem. Soc. **93**, 80 (1971).
37. J. HALPERN and P. F. PHELAN. J. Am. Chem. Soc. **94**, 1881 (1972).
38. W. C. TROGLER and L. G. MARZILLI. Inorg. Chem. **14**, 2942 (1975).
39. J. THOMSON and M. C. BAIRD. Can. J. Chem. **51**, 1179 (1973).
40. L. G. MARZILLI, P. A. MARZILLI, and J. HALPERN. J. Am. Chem. Soc. **93**, 1374 (1971).

Can. J. Chem. Downloaded from www.nrcresearchpress.com by 210.87.254.105 on 09/05/12
For personal use only.

Solubilities in the system indium tribromide – sodium bromide – water at 25 °C

ELINOR M. KARTZMARK
Department of Chemistry, University of Manitoba, Winnipeg, Man., Canada R3T 2N2

Received February 9, 1976

ELINOR M. KARTZMARK. Can. J. Chem. **54**, 1884 (1976).

The system $InBr_3$–NaBr–H_2O shows the existence of the following solid phases at 25 °C: $InBr_3$(anhyd.), NaBr(anhyd.), and NaBr.$2H_2O$. A hydrated form of indium tribromide does not exist at 25 °C

ELINOR M. KARTZMARK. Can. J. Chem. **54**, 1884 (1976).

Dans le système $InBr_3$–NaBr–H_2O, on note l'existence des phases solides suivantes à 25 °C: $InBr_3$(anhydre), NaBr(anhydre) et NaBr.$2H_2O$. Il n'existe pas de forme hydratée du tribromure d'indium à 25 °C.

[Traduit par le journal]

Introduction

This work was undertaken in order to establish whether indium tribromide crystallises with water of hydration at 25 °C, analogous to indium trichloride which forms a trihydrate. A dihydrate of indium bromide was found by Ensslin *et al.* (1) to exist in equilibrium with solution between 22 and 34.5 °C, the work is reported in Linke and Seidell (2). The method of Ensslin *et al.* consisted in analysing the solid phase and reporting the water present as hydrate water. Like indium trichloride, indium tribromide is very hygroscopic, so this method seemed dubious.

Sodium bromide was chosen as third component, because the analogous chloride system did not form double salts (3); it was hoped that the ternary invariant solution might contain considerable indium tribromide and hence give tie-lines of sufficient slope to differentiate between possible hydrates. Several early authors (4–7) report on systems containing sodium bromide which crystallises at 25 °C as NaBr.$2H_2O$ and persists, according to Richards (6), until 50.674 °C. This readily obtainable system, NaBr.$2H_2O$ in equilibrium with NaBr and H_2O, was suggested by Richards as a fixed point for standardizing thermometers.

Experimental

Indium tribromide was prepared by the method described by Campbell (8) using metallic indium generously donated by Cominco, of Trail, B.C. (99.99% pure). Indium tribromide is very hygroscopic, analysis of the solid corresponded to $InBr_3.2H_2O$, a result which established the dihydrate as the maximum possible water content. Sodium bromide was the B.D.H. reagent grade, used without further treatment.

The systems were stirred in a thermostat at 25.00 °C for three to four days to ensure attainment of equilibrium. Solutions and solid phases were analyzed after separation and the formulae of the stable solids were determined by the well-known method of the 'wet rest'. Solutions high in indium bromide content were very viscous. They were filtered using suction for as short a time as possible. The solid phases were placed between two thick layers of filter paper and subjected to hydraulic pressure, so as to render them as free from mother liquor as possible. In this way, the error in extrapolating tie-lines is minimized.

Bromide was estimated by precipitation as silver bromide, with an accuracy of 0.05% and sodium bromide was estimated by flame spectrometry, using a Perkin–Elmer flame photometer, Model 146, with an accuracy of ±1%. Indium tribromide was obtained by difference.

Results

The compositions of equilibrium liquid and solid phases are plotted in Fig. 1 and summarized in Table 1; the data are to be found in the depository.[1]

Discussion

Little discussion is necessary, except to remark that indium tribromide, unlike indium trichloride, is anhydrous in the solid state at room temperature. This accounts for the fact that its heat of solution is much less negative than that

[1]The data may be obtained at a nominal charge from the Depository of Unpublished Data, CISTI, National Research Council of Canada, Ottawa, Canada K1A 0S2.

Can. J. Chem. Downloaded from www.nrcresearchpress.com by 210.87.254.40 on 09/05/12
For personal use only.

TABLE 1. Solubilities in the system $InBr_3$–NaBr–H_2O at 25 °C

Liquid phase				Nature of solid phase
Wt.% NaBr		Wt.% $InBr_2$		
0		83.97		$InBr_3$(anhyd.)
14		72		Invariant*: $InBr_3$(anhyd.) + NaBr(anhyd.)
23.00	23.85	50.07	49.14	Invariant: NaBr(anhyd.) + NaBr.$2H_2O$
24.55		47.77		
23.57		49.71		
24.28		49.01		
48.83		0		NaBr.$2H_2O$

*The invariant point involving $InBr_3$ and NaBr and solution was obtained by the intersection of the solubility curves, since it was very difficult to obtain this system experimentally.

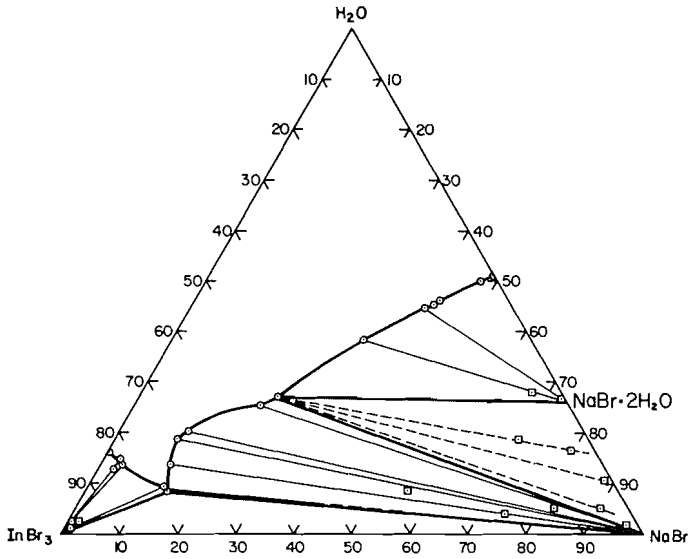

FIG. 1. System $InBr_3$–NaBr–H_2O at 25 °C. ○, composition of liquid phase (wt.%); □, composition of solid phase (wt.%).

for indium trichloride, which forms a trihydrate. The very high solubility, 84%, of indium tribromide explains the existence of anhydrous sodium bromide over a broad region of the ternary diagram. This dehydration of a hydrate by a highly soluble third component is a well known phenomenon. It occurs in this system even though the transition temperature of the binary system (50 °C) is well removed from the temperature of the ternary study.

1. F. ENSSLIN, B. ZIEMECK, and L. DE SCHAEPDRYVER. Z. Anorg. Chem. **254**, 293 (1947).
2. W. F. LINKE and A. SEIDELL. Solubilities of inorganic and metal organic compounds. Vol. 1. 4th ed. ACS Washington. 1958. p. 1292.
3. E. M. KARTZMARK. Can. J. Chem. **52**, 3460 (1974).
4. D. H. COCHERET. Dissertation Leiden 1911.
5. L. C. DE COPPET. Ann. Chim. Phys. [5] **30**, 417 (1883).
6. T. W. RICHARDS. Z. Phys. Chem. **28**, 314 (1899).
7. J. E. RICCI, J. BUDISH, and N. BORODULIA. J. Am. Chem. Soc. **59**, 868 (1937).
8. A. N. Campbell. In press.

Can. J. Chem. Downloaded from www.nrcresearchpress.com by 210.87.254.40 on 09/05/12
For personal use only.

The decomposition of dimethylbenzylanilinium chloride in alcoholic solvents

MUNAN KO, TSUNEYUKI SATO, AND TAKAYUKI OTSU[1]

Department of Applied Chemistry, Faculty of Engineering, Osaka City University, Sumiyoshi-ku, Osaka, Japan

Received November 13, 1974[2]

MUNAN KO, TSUNEYUKI SATO, and TAKAYUKI OTSU. Can. J. Chem. **54**, 1886 (1976).

The decomposition of dimethylbenzylanilinium chloride (DMBAC) was found to follow second-order kinetics in ethanol or aqueous ethanol solvents, but first-order kinetics in higher alcoholic solvents. From the activation parameters obtained at 80 °C, different isokinetic relationships were found for the ethanol series and the higher alcohol series. The dissociation constants of DMBAC in ethanol and isopropanol at 80 °C were calculated to be 7.34×10^{-3} and 2.10×10^{-4} mol/l, respectively, from conductivity measurements. Accordingly, it was concluded that in higher alcohols the major part of DMBAC exists as ion pairs, which are responsible for the decomposition reaction, but in ethanol the decomposition involves a bimolecular reaction between free ions.

MUNAN KO, TSUNEYUKI SATO et TAKAYUKI OTSU. Can. J. Chem. **54**, 1886 (1976).

On a trouvé que la cinétique de la décomposition du chlorure de diméthylbenzylanilinium (DMBAC) est du deuxième ordre dans l'éthanol ou dans des mélanges éthanol–eau; cette décomposition est toutefois du premier ordre dans des solvants alcooliques de poids moléculaires plus élevés. A l'aide des paramètres d'activation obtenus à 80 °C, on a trouvé différentes relations isocinétiques pour les séries éthanoliques et pour ses homologues supérieurs. On a calculé, à partir de mesures de conductivité à 80 °C, les constantes de dissociation du DMBAC dans l'éthanol et l'alcool isopropylique qui sont respectivement 7.34×10^{-3} et 2.10×10^{-4} mol/l. On en conclut donc que, dans les alcools de poids moléculaires plus élevés, la portion principale du DMBAC existe sous forme de paire d'ions qui sont responsables pour la réaction de décomposition; dans l'éthanol, la décomposition implique une réaction bimoléculaire entre ions libres.

[Traduit par le journal]

Introduction

In a previous paper (1), it was reported that the binary system of dimethylaniline and benzyl chloride or their quaternary salt, dimethylbenzylanilinium chloride (DMBAC), could serve as radical initiator of vinyl polymerization. From the results of kinetic and tracer studies on the polymerization of methyl methacrylate with DMBAC, the initiating radical was found to be a phenyl or methyl radical which might be formed via a redox reaction [2] between DMBAC and dimethylaniline, itself formed through a reverse Menshutkin reaction of DMBAC [1]:

[1] $R_1R_2N^+(R_3)_2X^- \rightarrow R_1N(R_3)_2 + R_2X$

$$R_1R_2N^+(R_3)_2X^- + R_1N(R_3)_2 \rightarrow \cdot C_6H_5 + R_2N(R_3)_2 + R_1\dot{N}^+(R_3)_2X^-$$

or

[2] $$\cdot CH_3 + R_1NR_2R_3 + R_1\dot{N}^+(R_3)_2X^-$$

where R_1, R_2, R_3, and X are C_6H_5, $C_6H_5CH_2$, CH_3, and Cl, respectively.

For the decomposition of ammonium and sulfonium salts in solution, the following two S_N2 mechanisms have been established kinetically (2–5):

S_N2 decomposition of the ion pair:

[3] $(R)_4N^+X^- \rightarrow (R)_3N + RX$

$$\text{Rate of decomposition} = k_1[(R)_4N^+X^-]$$

where k_1 is the first-order rate constant and $[(R)_4N^+X^-]$ is the concentration of the quaternary salt.

S_N2 decomposition of the free ions:

[4] $(R)_4N^+ + X^- \rightarrow (R)_3N + RX$

$$\text{Rate of decomposition} = k_2[(R)_4N^+X^-]^2$$

Ross *et al.* (3) investigated kinetically the decomposition of benzyldimethylanilinium thiocyanate in various solvents, and in the presence of various neutral salts, and pointed out that the

[1]Author to whom correspondence should be addressed.
[2]Revision received February 27, 1976.

Can. J. Chem. Downloaded from www.nrcresearchpress.com by 210.87.254.6 on 09/05/12
For personal use only.

Can. J. Chem. Downloaded from www.nrcresearchpress.com by 210.87.254.6 on 09/05/12
For personal use only.

kinetics changed with both the salt and solvent used, depending on the degree of association of the quaternary ammonium salt.

In the course of our earlier study on vinyl polymerization with DMBAC, the rate of decomposition of DMBAC was found to change widely with the solvents used.

The present paper will describe the results obtained kinetically on the decomposition of DMBAC in a series of alcoholic solvents.

Experimental

Materials

DMBAC was synthesized and purified according to the method described in the previous paper (1). Ethanol was refluxed with magnesium ethoxide, followed by distillation. Isopropanol, *n*-butanol, and *tert*-butanol were distilled. The other reagents were also purified by ordinary methods.

Determination of Rate of Decomposition of DMBAC

From the Determination of Dimethylaniline Produced

As reported previously (1), the main products from the decomposition of DMBAC in ethanol were confirmed to be dimethylaniline and benzyl chloride. Especially the former was produced in quantitative yield, as determined by gas chromatography. It was also confirmed that the rate of reaction of dimethylaniline with benzyl chloride was much slower than that of the decomposition of DMBAC under similar conditions. Therefore, the rates of decomposition of DMBAC in solution were determined by a spectroscopic measurement of dimethylaniline (λ_{max} 298 nm) produced, by using a Hitachi EPS-3T spectrometer.

The reactions were carried out in a sealed glass tube, which contained the required amounts of DMBAC and alcoholic solvent, in a thermostat maintained at a given temperature. After an appropriate reaction time, the tube was removed from the thermostat and cooled in a dry ice – methanol bath. Then a specific aliquot of the reaction mixture was transferred into a uv cell, and its spectrum measured. It was observed that there is a straight line relationship between the concentration of dimethylaniline and its absorbance.

From the Determination of Unreacted DMBAC

Since DMBAC reacts quantitatively with sodium tetraphenylborate ($(C_6H_5)_4BNa$) to give dimethylbenzylanilinium tetraphenylborate ($C_6H_5N^+(CH_3)_2CH_2C_6H_5$-$(C_6H_5)_4B^-$), the rate of decomposition was also determined by measuring the weight of tetraphenylborate salt obtained. The reactions were carried out in a sealed glass tube. After reaction for a given time, the contents of the tube were poured into a water solution containing excess sodium tetraphenylborate, and the resulting precipitate was filtered, washed with water, and then dried under vacuum. From the yield of this precipitate, the concentration of unreacted DMBAC was determined.

When the decomposition of DMBAC (0.1613 g) was performed in ethanol (10 ml) at 90 °C for 2 h, the extent of decomposition was 20.6% (from dimethylaniline) and 19.8% (from unreacted DMBAC). The fact that almost identical values were obtained by both methods, indicates that DMBAC decomposed into dimethylaniline and benzyl chloride quantitatively, within experimental error.

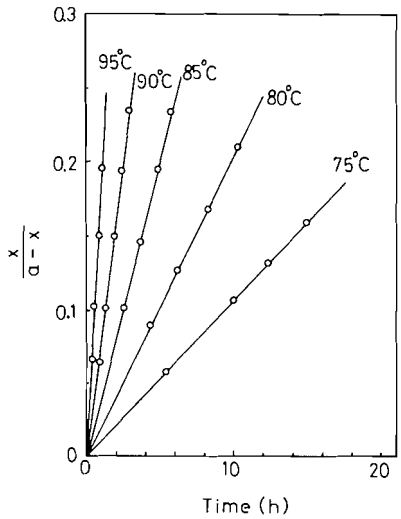

FIG. 1. Second-order plots for the decomposition of DMBAC in ethanol: [DMBAC] = 1.214×10^{-3} mol/l.

Results and Discussion

Decomposition Rates of DMBAC in Alcoholic Solvents

In order to investigate the effect of solvents on the decomposition reaction of DMBAC, the rates of decomposition were determined in various alcoholic solvents at temperatures between 60 and 95 °C. Figure 1 shows the second-order plot for the DMBAC decomposition in ethanol, determined from the dimethylaniline produced. When the plots were made for a first-order reaction, no straight line relationship was observed.

Similar second-order plots were also obtained for the reactions in 95%, 90%, and 80% aqueous ethanol solvents. From these results, the second-order rate constants (k_2) obtained at various temperatures are summarized in Table 1.

However, no second-order plot was observed for the decomposition in higher alcohols, *i.e.* isopropanol, *n*-butanol, and *tert*-butanol. In these cases, first-order plots were observed. Figure 2 shows the first-order plots for the decomposition of DMBAC in isopropanol. The first-order rate constants (k_1) thus obtained are also shown in Table 1.

Can. J. Chem. Downloaded from www.nrcresearchpress.com by 210.87.254.6 on 09/05/12
For personal use only.

TABLE 1. Rate constants for the decomposition reaction of DMBAC at various solvents and temperatures

Solvent	Temperature (°C)	$k_2 \times 10^3$ (l mol^{-1} s^{-1})	$k_1 \times 10^5$ (s^{-1})
Ethanol	70	1.89	—
	75	3.81	—
	80	4.65	—
	85	9.20	—
	90	18.0	—
	95	41.0	—
95% Ethanol	80	2.02	—
	85	3.78	—
	90	7.56	—
	95	14.6	—
90% Ethanol	80	0.967	—
	85	1.83	—
	90	3.52	—
	92.5	4.52	—
	95	6.38	—
80% Ethanol	80	2.52	—
	85	4.54	—
	90	8.65	—
	95	17.1	—
Isopropanol	65	—	1.01
	70	—	2.23
	75	—	4.61
	80	—	9.19
	85	—	18.4
n-Butanol	65	—	0.61
	70	—	1.32
	75	—	2.69
	80	—	5.70
tert-Butanol	60	—	4.10
	65	—	8.25
	70	—	17.3
	75	—	35.1
	80	—	69.2

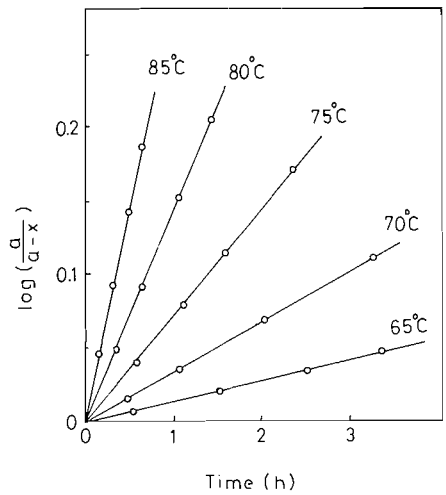

FIG. 2. First-order plots for the decomposition of DMBAC in isopropanol: [DMBAC] = 1.214×10^{-3} mol/l.

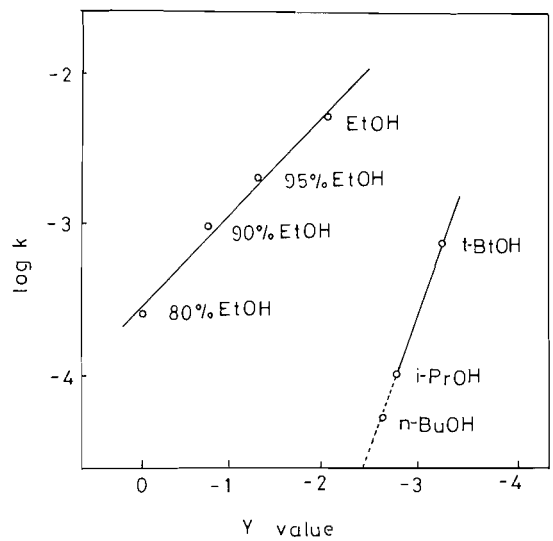

FIG. 3. Relationship between log k_1 or log k_2 and Y values in the Grunwald–Winstein equation (5).

To further clarify the solvent effect, the resulting rate constants were plotted against the Y values as a measure of ionization ability of the solvent in the Grunwald–Winstein equation [5] (6):

$$[5] \qquad \log k = mY$$

where m is a constant independent of the solvents used. The results are shown in Fig. 3, from which the straight line relationships were observed between log k_2 and Y ($m = -1.06$), and log k_1 and Y ($m = -2.75$).

Effect of Temperature

The effect of temperature on the decomposition of DMBAC in alcoholic solvents at temperatures ranging from 60° to 95 °C was investigated. From the data shown in Table 1, activation parameters were calculated and are summarized in Tables 2 and 3.

As can be seen from both tables, the activation entropies ($\Delta S^{\ddagger}$) in all solvents are large positive values, while the activation enthalpies ($\Delta H^{\ddagger}$) are about 30–35 kcal/mol. Such a result is expected from a reaction proceeding from a charged salt to two neutral molecules. Correspondingly, it

TABLE 2. Activation parameters for decomposition of DMBAC at 80 °C

Solvent	k_2 (l mol^{-1} s^{-1})	Relative rate	$\Delta H^{\ddagger}$ (kcal mol^{-1})	$\Delta S^{\ddagger}$ (cal deg^{-1} mol^{-1})	$\Delta G^{\ddagger}$ (kcal mol^{-1})
Ethanol	4.61×10^{-3}	10.2	34.0	26.7	24.6
95% Ethanol	2.02×10^{-3}	4.5	33.0	22.1	25.2
90% Ethanol	9.67×10^{-4}	2.1	32.2	18.3	25.7
80% Ethanol	4.54×10^{-4}	1	30.8	11.7	26.6
Methanol	4.04×10^{-4}	0.9	—	—	—

TABLE 3. Activation parameters for decomposition of DMBAC at 80 °C

Solvent	k_1 (s^{-1})	Relative rate	$\Delta H^{\ddagger}$ (kcal mol^{-1})	$\Delta S^{\ddagger}$ (cal deg^{-1} mol^{-1})	$\Delta G^{\ddagger}$ (kcal mol^{-1})
n-Butanol	5.70×10^{-5}	1	34.7	19.9	27.7
Isopropanol	9.19×10^{-5}	1.6	33.7	18.9	27.0
tert-Butanol	6.92×10^{-4}	12.2	32.3	18.2	25.9

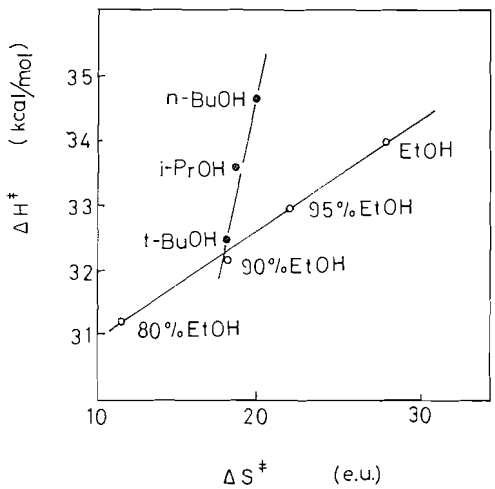

FIG. 4. Relationship between $\Delta H^{\ddagger}$ and $\Delta S^{\ddagger}$ in the decomposition of DMBAC in various solvents.

has been reported that in the Menshutkin reaction a large negative activation entropy is obtained (7).

The change in activation parameters with the solvents used is opposite in the two series of alcoholic solvents. In the higher alcohol series (Table 3), in which a first-order decomposition proceeds, the observed rates increase with a lowering of the polarity of the solvent, and this tendency corresponds to a decrease in activation enthalpy. In the ethanol or aqueous ethanol series (Table 2), in which a second-order reaction proceeds, the rates decrease with increasing of the solvent polarity, and this order relates to an increase in activation entropy. Accordingly, the reaction seems to be controlled by enthalpy in the former solvent series, but by entropy in the latter solvent series. Similar entropy-controlled reactions have been reported in some Menshutkin reactions (8).

From the data in Tables 2 and 3, the plots between $\Delta H^{\ddagger}$ and $\Delta S^{\ddagger}$ are shown in Fig. 4, from which isokinetic relationships are set up separately for the two solvent series. Both show straight line relationships, with isokinetic temperatures of 216 K in ethanol solvents and of 1396 K in the higher alcohol solvents.

Effect of Common Ions

The results of reactions in the presence or absence of lithium chloride and tetramethylammonium chloride are shown in Table 4. As can be seen from this table, the rate in ethanol is considerably accelerated by the presence of these salts, but in isopropanol it is only slightly accelerated. Such a difference is compatible with different reaction mechanisms, as is described later.

Conductivity Measurement

From the results shown in the preceding sections, it was assumed that the existing modes (free ion or ion pair) of DMBAC in these solvents largely determined the observed kinetic behavior. To further clarify the extent of dissociation of DMBAC in these solvents, conductivity measurements were undertaken. The

Can. J. Chem. Downloaded from www.nrcresearchpress.com by 210.87.254.6 on 09/05/12
For personal use only.

Can. J. Chem. Downloaded from www.nrcresearchpress.com by 210.87.254.6 on 09/05/12
For personal use only.

TABLE 4. Common ion effect of neutral salts on the decomposition of DMBAC in the solvent[a]

Neutral salt	Solvent	Temperature (°C)	Amount of DMA produced $\times 10^4$ (mol/l)	Relative rate
None	Ethanol	90	1.53	1
LiCl	Ethanol	90	2.38	1.56
$(CH_3)_4NCl$	Ethanol	90	2.31	1.51
None	Isopropanol	70	1.79	1
LiCl	Isopropanol	70	1.94	1.08
$(CH_3)_4NCl$	Isopropanol	70	2.09	1.17

[a]Reaction condition: [DMBAC] = [Neutral salt] = 1.214×10^{-3} mol/l, for 2 h.

TABLE 5. Dissociation of DMBAC in various alcohols from conductivity measurements

Solvent	Temperature (°C)	D	λ_∞ ($cm^2\ \Omega^{-1}\ mol^{-1}$)	$K \times 10^{-2}$ (mol/l)	r^a (%)
90% Ethanol	25	28.0	35.59	2.14	94.9
Ethanol	25	24.3	32.26	1.08	93.9
Ethanol	40	22.2	40.82	0.96	89.8
Isopropanol	25	17.4	16.39	0.098	58.1
Isopropanol	40	16.2	27.55	0.065	51.0
n-Butanol	25	17.1	13.95	0.113	60.3
tert-Butanol	30	12.2	1.72	0.012	26.7

[a]Degree of dissociation (r) was calculated from the equation: $K = cr^2/(1 - r)$ where $c = 1.214 \times 10^{-3}$ mol/l.

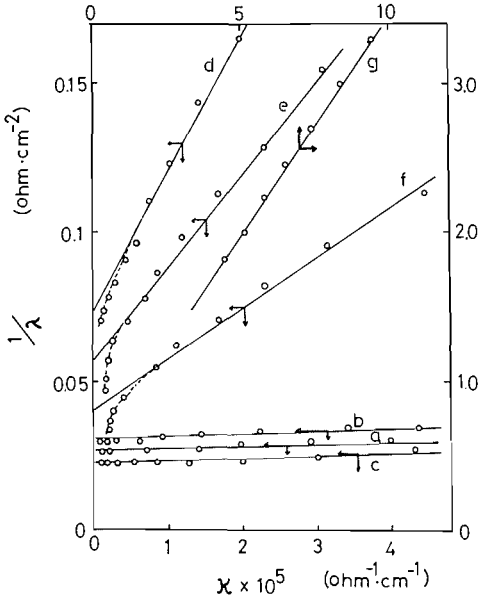

FIG. 5. Relationship between $1/\lambda$ and κ in various solvents: (*a*) ethanol (25 °C), (*b*) ethanol (40 °C), (*c*) 90% aqueous ethanol (25 °C), (*d*) isopropanol (25 °C), (*e*) isopropanol (40 °C), (*f*) *n*-butanol (25 °C), and (*g*) *tert*-butanol (25 °C).

results are shown in Fig. 5, in which λ is the equivalent conductivity and κ is the specific conductivity in the following equations [6], [7], and [8] (9):

$$[6] \qquad \frac{1}{\lambda} = \frac{1}{\lambda_\infty^2 K}\kappa + \frac{1}{\lambda_\infty}$$

$$[7] \qquad \kappa = \frac{k}{R}$$

$$[8] \qquad \lambda = \frac{\kappa}{c} \times 10^3$$

where k is the cell constant, R is the resistance, λ_∞ is the equivalent conductivity at infinite dilution, K is the dissociation constant, and c is the concentration of DMBAC.

From Fig. 5, the straight line relationships with an intercept of $1/\lambda_\infty$ and a slope of $1/\lambda_\infty^2 K$ are observed in plots of $1/\lambda$ *vs.* κ. The values of λ_∞ and K obtained in various solvents with their dielectric constants (D) are shown in Table 5.

In Table 5, the degree of the dissociation (r) calculated from the observed K value (see footnote in Table 5) for a given salt concentration is

Can. J. Chem. Downloaded from www.nrcresearchpress.com by 210.87.254.6 on 09/05/12
For personal use only.

also listed. The K values of DMBAC in alcohols coincided with those of other quaternary tetraalkylammonium salts in these alcohols, as reported by Fuoss *et al.* (10).

It is interesting to note from Table 5 that DMBAC dissociates more than 90% in ethanol and in 90% aqueous ethanol solvents, but it dissociates less than 60% in higher alcohols.

From Table 5, the enthalpies (ΔH^0) of the dissociation of DMBAC in ethanol and in isopropanol are calculated as -1.47 and -3.39 kcal/mol, by using the van't Hoff equation (11)

$$\Delta H^0 = -2.303\ Rd\ (\log K/d(1/T))$$

From these values, the dissociation constants and the degrees of the dissociation of DMBAC in ethanol and in isopropanol at 80 °C are calculated to be $K = 7.34 \times 10^{-3}$ mol/l, $r = 87.4\%$ and $K = 2.10 \times 10^{-4}$ mol/l, $r = 33.8$, respectively.

Mechanism of Reaction

The kinetic behavior of the decomposition of DMBAC was found to be different in ethanol or aqueous ethanol than in isopropanol or higher alcohols. By means of conductivity measurements of DMBAC in these solvents, it was concluded that in ethanol most of the DMBAC exists as free ions, while in isopropanol the major part exists as ion pairs. The difference in kinetic behavior is considered to originate from this fact.

In higher alcohol solvents, DMBAC exists largely as the ion pair, so that the rate of its decomposition is directly proportional to the concentration of DMBAC. This is in agreement with the observed first-order kinetics.

On the other hand, in ethanol and aqueous ethanol solvents, DMBAC dissociates into free ions. Since the concentration of the ion pairs is now presented as a product of both chloride and anilinium ions, the rate becomes second-order with respect to the DMBAC concentration. This result also agrees with the observed kinetic data and the common ion effect.

1. M. Ko, T. Sato, and T. Otsu. J. Polym. Sci. Part A, **7**, 3329 (1969).
2. Y. Pocker and A. J. Parker. J. Org. Chem. **31**, 1526 (1966).
3. S. D. Ross, M. Finkelstein, and R. C. Petersen. J. Am. Chem. Soc. **83**, 4853 (1961).
4. J. T. Burns and K. T. Leffek. Can. J. Chem. **47**, 3725 (1969).
5. K. T. Leffek and H-C. Tsuao. Can. J. Chem. **46**, 1215 (1968).
6. E. Grunwald and S. Winstein. J. Am. Chem. Soc. **70**, 846 (1948).
7. A. Von Hemptime and A. Bekaert. Z. Phys. Chem. **28**, 225 (1958).
8. E. A. Moelwyn-Hughes. Physical chemistry. Pergamon Press, London. 1957. p. 1232.
9. C. A. Kraus. J. Am. Chem. Soc. **35**, 1315 (1913).
10. R. M. Fuoss, L. Onsager, and J. F. Skinner. J. Phys. Chem. **69**, 2581 (1965).
11. K. J. Laidler. J. Phys. Colloid Chem. **54**, 519 (1950).

Studies on inorganic ion exchangers. I. Preparation, properties, and applications of ferric phosphate

J. P. RAWAT AND PRITAM SINGH THIND
Department of Chemistry Aligarh Muslim University, Aligarh, (U.P.) India

Received October 7, 1975

J. P. RAWAT and PRITAM SINGH THIND. Can. J. Chem. **54**, 1892 (1976).

Eight samples of ferric phosphates have been prepared at different p*H* values under different conditions. This material shows cation exchange properties. Ferric phosphate prepared by ferric nitrate and ammonium dihydrogen phosphate at p*H* 1 is the most stable and shows the maximum ion exchange capacity, hence, this sample is studied in detail. The mole ratio of Fe^{3+}:PO_4^{3-} is 1:2. The ion exchange capacity depends upon temperature and hydrated radii, and these relations are discussed. Certain important separations are achieved on the ferric phosphate column. Its oxidation properties are also qualitatively investigated with some reducing agents.

J. P. RAWAT et PRITAM SINGH THIND. Can. J. Chem. **54**, 1892 (1976).

On a préparé huit échantillons de phosphate ferrique à des valeurs différentes de p*H* sous diverses conditions. Ce matériel présente des propriétés d'échange cationique. Le phosphate ferrique préparé par réaction de nitrate ferrique et du phosphate diacide d'ammonium à un p*H* de 1 est le plus stable et présente la capacité maximale d'échange ionique; on a donc étudié cet échantillon en détail. Le rapport molaire de Fe^{3+}:PO_4^{3-} est de 1:2. La capacité d'échange ionique dépend de la température et des rayons hydratés. On discute de ces relations. On peut réussir certaines séparations importantes sur la colonne de phosphate ferrique. On a aussi étudié ses propriétés oxydantes par rapport à quelques agents réducteurs.
[Traduit par le journal]

Introduction

In the past ten years various inorganic ion exchangers have been prepared and used for several possible applications (1–5). Out of these, the phosphates are the most studied. Phosphates of zirconium (6), titanium (7), tin (8), cerium (9), chromium (10), tantalum (11), and antimony (12) have been synthesized and used for various separations in analytical chemistry. Few ion exchange studies on iron salts have been made. Iron phosphate was prepared by Kobayashi (13) by mixing ferric hydroxide and phosphoric acid. The phase equilibria was studied but this compound was slightly soluble in phosphoric acid.

We have prepared ferric phosphate by the combination of ferric nitrate and phosphoric acid or ammonium dihydrogen phosphate in different mole ratios and at various p*H* values. Of these, the sample prepared by mixing 0.1 *M* ferric nitrate and 0.1 *M* ammonium dihydrogen phosphate in the ratio of 1:2 at p*H* 1.0 seems stable and possesses the maximum ion exchange capacity. Therefore, the various studies, for example determination of K_d values, separations, p*H* titrations, stability etc., are performed on this sample. Chemical analysis and hydrolysis of a few other samples has also been performed. A relation of ion exchange capacity with hydrated radii of the metal ions is discussed. The electron transfer process of this compound by some reducing agents is also studied.

Experimental

Reagents

Ferric nitrate (BDH) and orthophosphoric acid or ammonium dihydrogen phosphate (BDH) were used. All other chemicals were of analytical grade.

Apparatus

An electric temperature controlled SICO shaker was used for shaking. A Bausch and Lomb spectronic 20 was used for spectrophotometric measurements. p*H* measurements were made with an Elico p*H*-meter model Li-10 (India). A Philips conductivity bridge p*H* 9500, Sargent Oscillometer type (V) was used for conductometric and high frequency titrations.

Synthesis

Ferric phosphate was precipitated by adding phosphoric acid or ammonium dihydrogen phosphate to the solution of ferric nitrate with constant stirring under the conditions given in Table 1. The required p*H* of the final product was adjusted by adding either hydrochloric acid or sodium hydroxide solution. On standing for 24 h, the precipitate settled. It was filtered, washed first with

Can. J. Chem. Downloaded from www.nrcresearchpress.com by 210.87.254.5 on 09/05/12
For personal use only.

TABLE 1. Conditions of preparation and properties of ferric phosphates

Sample	Conditions of synthesis: Molarity of reagents Fe	P	Mixing volume ratio (Fe:P)	p*H*	Properties: Colour in H^+ form	Ion exchange capacity (mequiv./g)	Composition (Moles of Fe:P)
1	0.1 FN*	0.1 ADP†	1:2	1.0	White	0.77	1:2
2	0.1 FN	0.1 PA‡	1:2	1.0	White	0.37	—
3	0.1 FN	0.1 PA	1:2	2.0	Light yellow	0.40	—
4	0.1 FN	0.1 PA	1:2	4.0	Light brown	0.40	1:2
5	0.1 FN	0.1 PA	1:2	6.0	Light brown	0.45	1:1.98
6	0.05 FN	0.05 PA	1:2	0.5	White	0.60	1:1.99
7	0.05 FN	0.05 ADP	1:4	0.5	White	0.32	—
8	0.05 FN	0.05 ADP	2:1	1.0	Brown	0.15	—

*FN, ferric nitrate.
†ADP, ammonium dihydrogen phosphate.
‡PA, phosphoric acid.

TABLE 2. Ion exchange capacity of ferric phosphate (sample 1) for different uni- and divalent metal ions

Metal ion	Salt solution used	p*H* of the solution	Hydrated radii (Å)	Ion Exchange capacity (mequiv./g)
Li^+	Lithium nitrate (2 *M*)*	5.9	3.40	0.69
Na^+	Sodium nitrate (2 *M*)	6.0	2.76	0.77
K^+	Potassium nitrate (2 *M*)	6.0	2.32	1.00
Mg^{2+}	Magnesium nitrate (1 *M*)	6.6	7.00	0.32
Ca^{2+}	Calcium nitrate (1 *M*)	6.7	6.30	0.35
Sr^{2+}	Strontium nitrate (1 *M*)	6.7	—	0.41
Ba^{2+}	Barium nitrate (1 *M*)	6.7	5.90	0.52
NH_4^+	Ammonium nitrate (2 *M*)	4.6	—	0.75

**M*, molarity.

water at the precipitation p*H*, then with demineralized water at p*H* 6, and dried in an oven at 40 °C. The material was converted into the H^+ form by treatment with 1.0 *M* nitric acid for 24 h with occasional shaking and intermittent changing of the acid. The product thus formed was dried at 40 °C in a temperature controlled oven.

Determination of Ion Exchange Capacity

The ion exchange capacity of the various samples of ferric phosphate was determined by column operation. The ion exchanger in the hydrogen form was placed in the column with a glass wool support. Sodium nitrate solution (1.0 *M*) was used as the eluent, and 400 ml of effluent was collected in every case. The hydrogen ions eluted from the column were titrimetrically determined with a standard solution of sodium hydroxide.

Determination of Optimum Mole Ratio

For the preparation of the ion exchanger the combining ratio was found by titrating $Fe(NO_3)_3$ with $NH_4H_2PO_4$ using high frequency and conventional conductometric methods. Breaks in the curves were obtained at the Fe^{3+}:PO_4^{3-} mole ratio of 1:2 in both cases. This ratio was obtained for the preparation of ferric phosphate for most of the samples.

Chemical Analysis

For this analysis 500 mg of the well powdered material was dissolved in 10 ml of hot concentrated hydrochloric acid. Ferric ion was estimated volumetrically by the usual iodometric titration and phosphorous pentoxide by ammonium phosphomolybdate precipitation, followed by neutralization titration.

Chemical Stability

To determine the solubility of the material, 0.5 g of the exchanger in H^+ form was shaken with 50 ml of the solution concerned at 30 ± 1 °C. After 6 h of equilibrium the supernatant liquid was removed and analysed for phosphate and iron. The phosphate analysis was per-

Can. J. Chem. Downloaded from www.nrcresearchpress.com by 210.87.254.5 on 09/05/12
For personal use only.

formed spectrophotometrically using the molybdovanado-phosphoric acid method (14) and the analysis of iron was also performed spectrophotometrically using the potassium cyanide – potassium ferrocyanide reagent method (15).

Ion Exchange Potentiometric Titrations

Potentiometric titrations on 0.5 g of ferric phosphate sample 1, having a total volume of 50 ml with 0.1 *M* solutions of lithium hydroxide, sodium hydroxide, potassium hydroxide, and ammonium hydroxide, were performed by the method of Topp and Pepper (16). In the case of added salt titrations, 0.1 *M* solutions of salts of the above mentioned alkalies were added. The p*H* of the solution after shaking with the reaction mixture for 4 h was noted.

Hydrolysis

Hydrolysis of samples 1, 4, 5, and 6 was studied by using 0.5 g of the ion exchanger in the hydrolysis apparatus (Visser's method) (17). For this purpose an apparatus was assembled in which the agitated sample was washed continuously with conductivity water (p*H* 7.0 to 6.5). The flow rate of the effluent was 6–8 drops per minute. The effluent was titrated with sodium hydroxide (0.01 *M*) in 10 ml fractions until the p*H* approached the value of pure water.

Distribution Coefficients

The distribution studies were carried out for 27 metal ions by a batch process in the usual manner (18) after attaining equilibrium by shaking the metal ion solution with exchanger beads for 6 h at room temperature (30 ± 1 °C. The K_d values for metal ions were calculated by using the following expression (for cases where the determination of the metal ion was feasible in the presence of PO_4^{3-}):

$$K_d = \frac{I - F}{F} \times \frac{50}{0.5}$$

where I is the volume of EDTA consumed by the original solution and F is the volume of EDTA consumed after equilibrium. The total volume of the solutions was 50 ml and the amount of exchanger used was 0.5 g. UO_2^{2+}, VO^{2+}, Ca^{2+}, and Co^{2+} could not be determined by EDTA titrations. The amounts of these metal ions present in solution initially and after equilibrium were determined by spectrophotometry. Uranium and vanadium were estimated by the peroxide method. Calcium was determined using murexide as the colour developing reagent. The estimation of Co^{2+} was performed by noting the absorbance of green colour developed in concentrated hydrochloric acid medium at 625 nm.

Separations

For separation studies, 2 g of ferric phosphate in the H^+ form was taken in a glass column 30 cm in height and 0.69 cm in diameter. It was regenerated with nitric acid (1.0 *M*) and washed with demineralized water until the effluent was neutral. The rate of flow in all separations was 0.5 ml/min. The separation of metal ions was tried for those for which the separation factor was greater than 6. The eluents were water, nitric acid, and acetic acid.

Oxidation Properties

To study the oxidation properties, a few granules of ferric phosphate sample 1 in H^+ form were treated with various lower oxidation state species and the colour change was noted.

Results and Discussion

Ferric phosphate possesses cation exchange capacity, reasonable stability, and differential selectivity for various metal ions and hence can be used for analytically important separations.

The results of the study of ion exchange capacity and composition of various samples of ferric phosphate are presented in Table 1. In order to determine the working capacity as an ion exchanger, the capacity of sample No. 1 was determined for some mono- and divalent cations, also. The results are given in Table 2. Ion exchange capacity depends upon the hydrated radii of the metal ions in the same group. We have used the equilibrium in the solution phase where hydrated radii play an important role. The plots of ion exchange capacity against hydrated radii of the metal ions of the alkali metal group and alkaline earth metal group are straight lines, which reveals that ion exchange capacity decreases as the hydrated radii increase in the same group. The results for NH_4^+ are not considered because the initial p*H* value of the NH_4NO_3 solution obtained as eluent was 4–5 which was considerably less than the p*H* value of the rest of the eluent solutions having initial p*H* value 6–7.

The studies on stability determinations revealed that Fe(III) is not dissolved in water and acetic acid while a slight dissolution (0.080 mg of Fe/50 ml) does occur in 0.1 *M* nitric acid. However, phosphate dissolved to a greater extent than iron. Phosphate dissolved was 0.412, 0.456, and 0.560 mg of P/50 ml in HNO_3 (p*H* 1), CH_3COOH (p*H* 3), and water (p*H* 6.8) respectively, which shows that as the p*H* of the solution increases the dissolution of phosphate also increases. These results are in agreement with those of Larsen and Vissers (17). Repeated ion exchange measurements for K^+ ion (1 *M* KNO_3) give ion exchange capacities of 1.28, 1.24, 1.20, 1.16, and 1.11 mequiv./g after 1, 2, 3, 4, and 5 cycles. These results reveal that a slight decrease in ion exchange capacity was observed after the fifth cycle and this loss of capacity is due to hydrolysis and dissolution of phosphate.

Can. J. Chem. Downloaded from www.nrcresearchpress.com by 210.87.254.5 on 09/05/12
For personal use only.

TABLE 3. Hydrolysis of ferric phosphate

Volume of effluent (ml)	Volume of NaOH (0.01 *M*) in ml				
	Sample 1 in H^+ form	Sample 4 in H^+ form	Sample 5 in H^+ form	Sample 6 in H^+ form	Sample 1 in Na^+ form
10	—	1.50	0.3	0.40	—
20	0.1	1.75	0.4	0.40	1.10
30	0.1	1.75	0.7	0.30	—
40	0.1	1.75	0.7	0.30	0.60
50	0.1	1.75	0.7	0.25	0.14
60	0.1	1.75	0.5	0.25	0.07
70	0.1	1.75	0.5	0.20	0.07
80	0.1	1.50	0.5	0.15	0.05
90	—	1.50	0.5	0.15	0.05
100	—	1.50	0.5	0.15	0.05

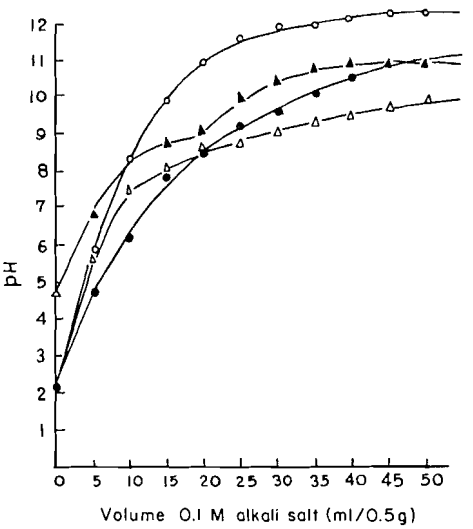

FIG. 1. p*H* titration of ferric phosphate (sample 1) with added salt method: ○ KCl; ▲ LiCl; ● NaCl; △ NH_4Cl.

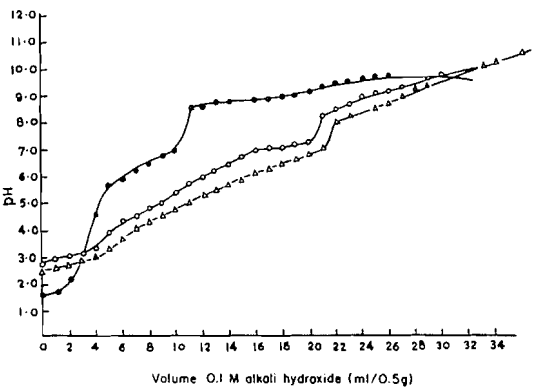

FIG. 2. p*H* titration of ferric phosphate (sample 1) with different alkali hydroxides: ● NaOH; ○ LiOH; △ KOH.

The potentiometric titration results plotted in Figs. 1 and 2 for different alkali salts and hydroxides indicate that ferric phosphate behaves as a weak acid. The shape of the curves is somewhat disturbed by the addition of salts.

The effect of heat on ferric phosphate was studied by drying sample 1 at different temperatures in a muffle furnace for 2 h and the ion exchange capacity for Na^+ (1 *M* $NaNO_3$) was determined. The capacities were 0.77, 0.60, 0.38, 0.22, 0.07, and 0.00 mequiv./g for the products dried at 45, 100, 200, 300, 400, and 600 °C respectively. These results indicate that the ion exchange capacity of this material decreases as the drying temperature is increased. A plot of ion exchange capacity against the square root of the temperature (°C) (Fig. 4) is a straight line. There seems no theoretical basis for this relation. The results of hydrolysis (Table 3) reveal that all the samples undergo hydrolysis when treated with water at p*H* 6.8. However, sample 1 undergoes the least hydrolysis. Hence sample 1 was studied in detail.

On the basis of the molar ratio of Fe^{3+}:PO_4^{3-} (1:2) determined by chemical analysis and predicted by high frequency and conductometric titration (keeping in mind the resemblance of ferric phosphate to phosphates of Zr^{4+} (6), Th^{4+} (19), Ce^{4+} (9), and Ti^{4+} (7) as $M(HPO_4)_2 \cdot nH_2O$ where M is the corresponding metal ion) a tentative formula of ferric phosphate can be proposed as $FeH(HPO_4)_2 \cdot nH_2O$.

The analytical importance of ferric phosphate

Can. J. Chem. Downloaded from www.nrcresearchpress.com by 210.87.254.5 on 09/05/12
For personal use only.

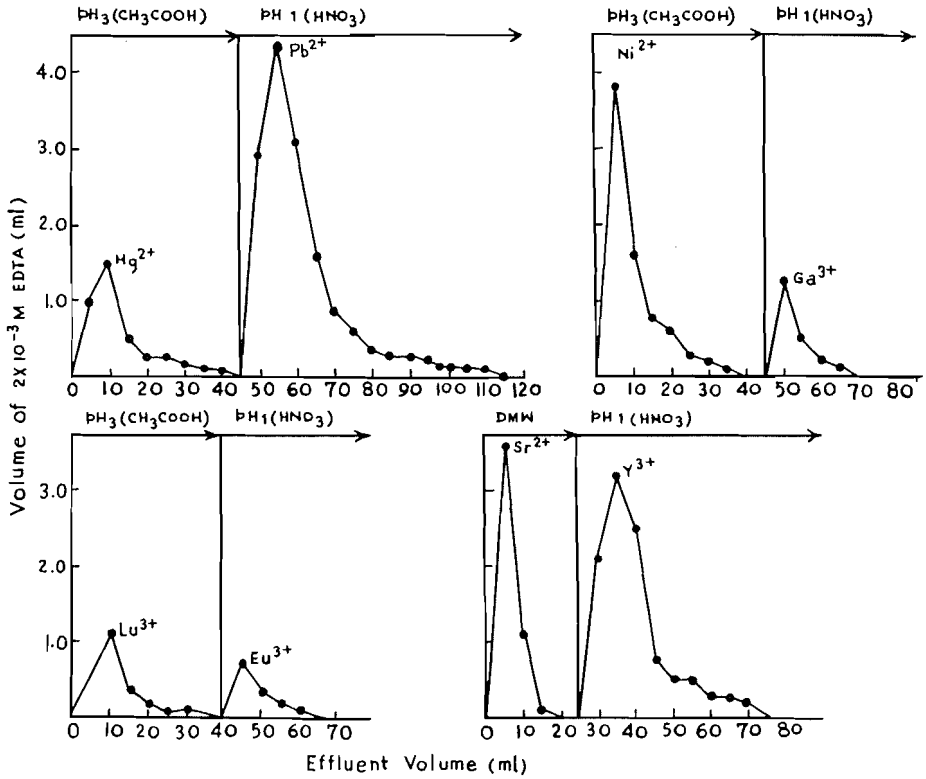

FIG. 3. Binary separations on a ferric phosphate column (sample 1).

can be deduced from the results of K_d values. On the basis of K_d values in nitric acid (pH 1) and acetic acid (pH 3), the selectivity sequence for some metal ions on ferric phosphate was found to be as follows.

At pH 1.0

$$Co^{2+} > Pr^{3+} > Eu^{3+} > Tm^{3+} > Ga^{3+} > Tb^{3+} > Gd^{3+} = Nd^{3+} > Ce^{4+} = Pb^{2+} > UO_2^{2+} > Sm^{3+} = Y^{3+} > Dy^{3+} > Er^{3+} = VO^{2+} > Ho^{3+} > Ni^{2+} > Al^{3+} > Zn^{2+} > Hg^{2+} = Cu^{2+} > Sr^{2+} > Ba^{2+} > Ca^{2+} > Mn^{2+} > Lu^{3+}$$

At pH 3.0

$$Pr^{3+} > Co^{2+} > Ga^{3+} > Tm^{3+} > Eu^{3+} > Tb^{3+} > Gd^{3+} = Nd^{3+} > Pb^{2+} > Dy^{3+} > Ce^{4+} > Y^{3+} > Sm^{3+} > Er^{3+} > Ho^{3+} > UO_2^{2+} > Ni^{2+} = VO^{2+} > Ba^{2+} > Al^{3+} > Cu^{2+} > Hg^{2+} > Sr^{2+} > Zn^{2+} > Ca^{2+} > Mn^{2+} > Lu^{3+}$$

These separation factors were defined as the ratio of K_d values. On the basis of the separation factor greater than 6, the anticipated separations were achieved (Fig. 3). These separations are quantitative as is clear from Table 5.

The separation of Hg(II) and Pb(II) is important because both are heavy metals and Pb(II) is often found as an impurity with Hg(II). The separation of Lu(III) and Eu(III) is of analytical importance because both are lanthanides and have similar properties.

Vissers (20) reported that Ce(IV) phosphate in contact with a manganese(II) solution, changed from bright yellow to nearly black. The assumption was made that the manganese exchanged with the protons on the solid, and then was oxidized to a state higher than two. The exact oxidation state was not determined because of analytical problems, but is assumed to be three.

The same behaviour of electron transfer was shown by Fe(III) phosphate sample No. 1 in H^+ form. It was observed that when the granules of Fe(III) phosphate were put into the solution of Ce(III) nitrate, first of all exchange of Ce(III) takes place for H^+ ions, then the Ce(III) is converted to Ce(IV) by giving an electron to Fe(III). This is confirmed by the change of colour of the solution and the granules from white to bright yellow. In this process the electrical neutrality is

Can. J. Chem. Downloaded from www.nrcresearchpress.com by 210.87.254.5 on 09/05/12
For personal use only.

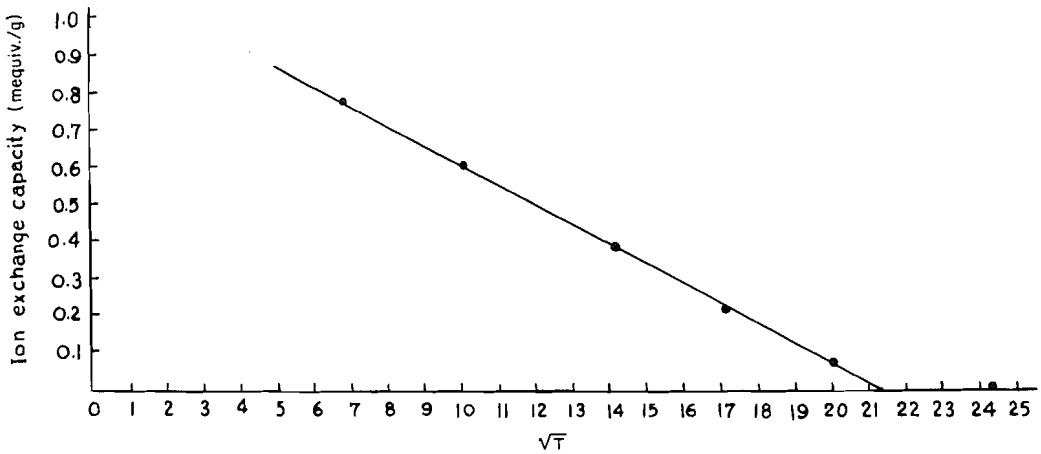

FIG. 4. Plot of ion exchange capacity as a function of the square root of temperature.

TABLE 4. Oxidation properties of ferric phosphate (sample 1)

Number	Substance added	Initial colour of solution	Colour of solution after the reaction	Probable colour change due to
1	Ce(III)	Colourless	Bright yellow	Ce(III)–Ce(IV)
2	Ti(III)	Violet	Colourless	Ti(III)–Ti(IV)
3	Cr(III)	Green	Yellow	Cr(III)–Cr(VI)
4	Cu(I)	Green	Blue	Cu(I)–Cu(II)
5	Mn(II)	Light pink	Black	Mn(II)–Mn(III)
6	I^-	Colourless	Dark brown	$3I^-$–I_3^-

internally maintained and the hydrogen ion release is only proportional to the moles of cerium exchanged. The process may be described by the following equation:

$$Fe(III)H(HPO_4)_2 + Ce(III) \xrightarrow[\text{step}]{\text{Ion exchange}}$$

$$Fe(III)Ce(III)(PO_4)_2 + 3H^+ \xrightarrow[\text{step}]{\text{Electron transfer}}$$

$$Fe(II)Ce(IV)(PO_4)_2$$
(Bright yellow colour)

This mechanism is confirmed by the electron transfer reactions observed (Table 4) with some metal ions (in the lower valency state). Thus Ti(III) changes to Ti(IV), and the violet colour of solution disappears. Similarly Cu(I) and Mn(II) convert to the Cu(II) and Mn(III) states. Cr(III) changes to chromate, in this case chromium(III) is first exchanged on the granules and then oxidized to the anionic species and released to the solution. In the case where the ferric phosphate granules are in contact with an iodide solution such as potassium iodide, an immediate release of hydrogen ion occurs, probably as the result of potassium exchange. There is also an immediate release of triiodide ion to the aqueous solution.

The change in the oxidation number of Fe(III) to Fe(II) in this reaction is confirmed by the experiment given below:

Granules of ferric phosphate $+ K_4(Fe(CN)_6) \rightarrow$ Granules become dark blue

Granules of ferric phosphate treated with lower oxidation state species $+ K_4(Fe(CN)_6) \rightarrow$ No colour

This indicates that the granules of ferric phosphate give a blue colour with $K_4Fe(CN)_6$ due to the presence of Fe(III) and if ferric phosphate is treated with any lower oxidation state species *viz.*, Mn(II) and then treated with $K_4Fe(CN)_6$ no

Can. J. Chem. Downloaded from www.nrcresearchpress.com by 210.87.254.5 on 09/05/12
For personal use only.

TABLE 5. Separations on ferric phosphate (sample 1) columns

Separation	Eluents	Vol. of effluent (ml)	Amount of cations		Amount of exchanger in the columns (g)	Error (%)
			Loaded (μg)	Recovered (μg)		
Hg^{2+}–Pb^{2+}	Hg^{2+}–p*H* 3 (CH_3COOH)	40	1604	1594	2.0	−0.62
	Pb^{2+}–p*H* 1 (HNO_3)	70	6008	6008	—	0.00
Ni^{2+}–Ga^{3+}	Ni^{2+}–p*H* 3 (CH_3COOH)	40	880	876	2.0	−0.45
	Ga^{3+}–p*H* 1 (HNO_3)	30	210	212	—	+0.95
Lu^{3+}–Eu^{3+}	Lu^{3+}–p*H* 3 (CH_3COOH)	30	656	658	2.0	+0.30
	Eu^{3+}–p*H* 1 (HNO_3)	30	378	378	—	0.00
Sr^{2+}–Y^{3+}	Sr^{2+}–DMW*	20	876	882	2.0	+0.67
	Y^{3+}–p*H* 1 (HNO_3)	30	1778	1792	—	+0.78

*DMW, demineralized water.

blue colour is observed due to the absence of Fe(III) which changes to Fe(II).

Acknowledgements

We thank Prof. W. Rahman for research facilities. Financial assistance to Pritam Singh by C.S.I.R. (India) is gratefully acknowledged.

1. C. B. AMPHLETT. Inorganic ion exchangers. Elsevier, Amsterdam. 1964.
2. J. INCZEDY. Analytical application of ion exchangers. Pergamon Press Ltd., Oxford. 1966.
3. H. F. WALTON. Anal. Chem. **42**, 86R (1970).
4. H. F. WALTON. Anal. Chem. **44**, 256R (1972).
5. H. F. WALTON. Anal. Chem. **46**, 398R (1974).
6. A. CLEARFIELD and G. D. SMITH. J. Inorg. Nucl. Chem. **30**, 327 (1968).
7. G. ALBERTI and E. TORRACCA. J. Inorg. Nucl. Chem. **30**, 317 (1968).
8. Y. INOUE. Bull. Chem. Soc. Jpn. **36**, 1316 (1963).
9. E. M. LARSEN and W. A. CILLEY. J. Inorg. Nucl. Chem. **30**, 287 (1968).
10. L. SZIRTES and L. SINHA, Izv. Khim. SSSR, **21**, 620 (1967).
11. M. NOMURA, M. ABE, and T. ITO. Nippon Kagaku Kaishi, 529 (1972).
12. R. CALETKA and C. KONECNY. Radiochem. Radioanal. Lett. **9**, 285 (1972).
13. E. KOBAYASHI. Kogyo Kagaku Zasshi, **73**, 1797 (1970).
14. N. H. FURMAN. Standard methods of chemical analysis. D. Van Nostrand Company. Inc. Princeton, New York, 1962. p. 819.
15. M. QURESHI and K. G. VARSHNEY. Anal. Chem. **39**, 1034 (1967).
16. N. E. TOPP and K. W. PEPPER. J. Chem. Soc. 3299 (1949).
17. E. M. LARSEN and D. R. VISSERS. J. Phys. Chem. **64**, 1732 (1960).
18. M. QURESHI, K. G. VARSHNEY, and A. H. ISRAILI. J. Chromatogr. **59**, 141 (1971).
19. G. ALBERTI and U. CONSTANTINO. J. Chromatogr. **50**, 482 (1970).
20. D. VISSERS. Ph.D. Thesis, University of Wisconsin, Madison. 1959; E. M. LARSEN and W. A. CILLEY. J. Inorg. Nucl. Chem. **30**, 287 (1968).

Can. J. Chem. Downloaded from www.nrcresearchpress.com by 210.87.254.5 on 09/05/12
For personal use only.

Influence du substituant tertiobutyl-4 sur les constantes d'acidité du cation cyclohexylammonium et de l'acide cyclohexane carboxylique dans les milieux mixtes eau–DMSO et méthanol–DMSO

JOHN T. EDWARD, PATRICK G. FARRELL ET JITKA KIRCHNEROVA
Department of Chemistry, McGill University, Montréal (Qué.), Canada H3C 3G1
ET
JEAN-CLAUDE HALLE ET ROBERT SCHAAL
Laboratoire de physicochimie des solutions, E.N.S.C.P., 11 rue Pierre et Marie Curie, 75231 Paris, Cedex 05, France

Reçu le 26 janvier 1976

JOHN T. EDWARD, PATRICK G. FARRELL, JITKA KIRCHNEROVA, JEAN-CLAUDE HALLE et ROBERT SCHAAL. Can. J. Chem. **54**, 1899 (1976).

Les constantes d'acidité des composés **1–6** ont été déterminées potentiométriquement dans divers milieux mixtes eau–DMSO et méthanol–DMSO. Quelque soit le mélange étudié, la position équatoriale est plus favorable à l'ionisation des fonctions amine et carboxylique que la position axiale. Les résultats obtenus dans les mélanges contenant suffisamment d'eau montrent que le substituant tertiobutyle influence l'ionisation des groupements ammonium et carboxylique. Une explication basée sur le déplacement des molécules de solvant au sein de la deuxième couche de solvatation est proposée.

JOHN T. EDWARD, PATRICK G. FARRELL, JITKA KIRCHNEROVA, JEAN-CLAUDE HALLE, and ROBERT SCHAAL. Can. J. Chem. **54**, 1899 (1976).

Acid dissociation constants for the compounds **1–6** in water–DMSO and methanol–DMSO of varying composition have been determined by a potentiometric method. In all solvents the equatorial group ionized more easily, by gain or loss of a proton, than the axial group, but in the more aqueous solvents the presence of a *tert*-butyl group across the cyclohexane ring inhibited this ionization slightly. An explanation based on displacement of solvent molecules from the outer solvation sphere is advanced.

Introduction

Depuis la mise en évidence de l'influence de la structure stéréochimique sur la dissociation d'acides divers (1), la détermination des constantes d'acidité est devenue une méthode de choix pour l'analyse conformationnelle (2, en particulier pp. 62–63 de la réf. 2*a* et les références citées à ce sujet). En effet, il a été montré qu'en général, les amines équatoriales sont des bases plus fortes que les amines axiales ($\Delta pK[\equiv pK_{NH_3^+}(\text{axial}) - pK_{NH_3^+}(\text{équatorial})] < 0$) (3) et que les acides carboxyliques équatoriaux sont plus forts que leurs épimères axiaux ($\Delta pK[\equiv pK_{COOH}(\text{axial}) - pK_{COOH}(\text{équatorial})] > 0$) (4–7). Ces résultats s'expliquent par une meilleure stabilisation des ions ammonium et carboxylate placés en position équatoriale en raison du moindre encombrement stérique, qui dans ce cas n'est pas de nature à gêner leur solvatation (2–7).

Quoique la généralisation concernant ces différences d'acidité ait été initialement retenue comme régle permettant de distinguer les groupements ionisants axiaux et équatoriaux, plusieurs exceptions sont apparues (3*a*, 3*b*, 8–11) avec des ΔpK quelquefois très petits (12). Ces exceptions ont amené Cremlyn et ses collaborateurs (9), à proposer un nouveau critère, qui consiste à ignorer le signe de ΔpK et à ne prendre en considération que la variation d'acidité qui résulte du changement de la composition du solvant mixte. L'acidité du groupement équatorial, plus sensible aux variations de solvatation que le groupement axial, doit en effet subir plus intensément l'influence du changement de solvant. Ces auteurs ont ainsi appliqué leur critère à la détermination des configurations de plusieurs paires épimériques d'acides α-aminés, obtenus par les réactions de Strecker et de Buchérer–Bergs, en se plaçant dans les mélanges eau–acétone contenant respectivement 25, 50 et 67% d'acétone en volume. Des travaux récents viennent cependant contredire les conclusions de Cremlyn (10, 11, 13) concernant les configurations de ces composés. Il est fort possible que ce résultat surprenant soit limité aux acides α-

Can. J. Chem. Downloaded from www.nrcresearchpress.com by 210.87.254.40 on 09/05/12
For personal use only.

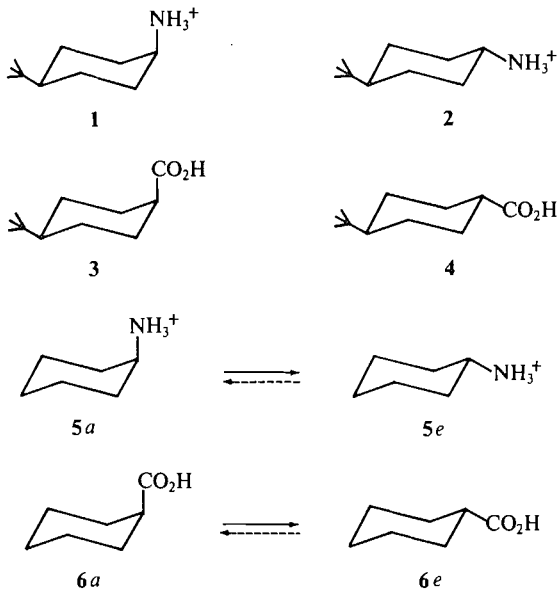

aminés puisque le critère de Cremlyn n'a jamais été testé avec des amines et des acides carboxyliques simples.

C'est donc un des buts de ce travail où nous avons effectué dans les milieux mixtes eau–diméthylsulfoxyde et méthanol–diméthylsulfoxyde de teneur en DMSO variable, les déterminations d'acidité relatives aux acides *cis* (**1**) et *trans* tertiobutyl-4 cyclohexyl ammoniums (**2**) ainsi que *cis* (**3**) et *trans* tertiobutyl-4 cyclohexane carboxyliques (**4**). Par ailleurs, nous avons examiné le comportement, dans ces mêmes solvants, des acides cyclohexylammonium (**5**) et cyclohexane carboxylique (**6**) en vue de tester l'hypothèse de Stolow (5) et Sicher et coll. (6) relative à l'étude des systèmes mobiles **5***a* ⇄ **5***e* et **6***a* ⇄ **6***e*.

Partie expérimentale

La purification des solvants et la préparation des mélanges eau–DMSO et MeOH–DMSO ont déjà été décrites (14, 15). L'acide cyclohexane carboxylique (produit Aldrich) a été purifié par cristallisations successives suivies d'un séchage sur P_2O_5. La cyclohexylamine (produit Merck) a été distillée sous vide et le coeur de la distillation transformé en chlorhydrate.

Les méthodes utilisées pour la préparation des acides *cis* et *trans* tertiobutyl-4 cyclohexane carboxyliques et des *cis* et *trans* tertiobutyl-4 cyclohexylamines sont celles de Stolow (5, 12); les deux amines ont également été transformées en chlorhydrates. Les points de fusion correspondent à ceux publiés par Sicher (6).

Les déterminations d'acidité ont été réalisées à 20 °C,

TABLEAU 1. pK à 20 °C des cations ammoniums **1**, **2**, **5** et des acides **3**, **4** et **6** dans les milieux mixtes eau–DMSO et méthanol–DMSO

(*a*) Milieux eau–DMSO*

	Fraction molaire en DMSO (%)											
Composé	0	5.9	9.6	13.5	19.5	26.6	35.6	48.7	59.3	69.7	83.1	100
5	10.70	10.53	10.42	10.33	10.25	10.13	10.13	10.25	10.46	10.72	11.02	11.70†
2	10.60†	10.43	10.34	10.24	10.19	10.10	10.08	10.20	10.42	10.74	11.06	11.75†
1	10.50†	10.35	10.24	10.14	10.08	10.04	10.01	10.14	10.34	10.64	10.91	11.60†
6	4.91	5.23	5.53	5.84	6.29	6.83	7.56	8.56	9.44	10.21	11.32	12.75†
4	5.10†	5.40	5.60	5.85	6.19	6.75	7.45	8.48	9.44	10.23	11.36	12.80†
3	5.55†	5.84	6.04	6.27	6.59	7.15	7.86	8.84	9.78	10.50	11.55	12.90†

(*b*) Milieux méthanol–DMSO

	Fraction molaire en DMSO (%)										
Composé	0	5.9	12.2	19.5	27.1	35.7	45.5	56.5	69.5	83.7	91.5
5	11.68	11.44	11.21	11.02	10.97	10.96	11.16	11.15	11.18	11.24	11.39
2	11.63	11.41	11.19	10.99	10.92	10.93	11.13	11.16	11.20	11.28	11.42
1	11.54	11.33	11.11	10.90	10.84	10.84	11.03	11.05	11.07	11.15	11.27
6	9.92	9.73	9.52	9.42	9.53	9.78	10.26	10.59	10.98	11.57	12.18
4	9.84	9.65	9.44	9.35	9.46	9.70	10.19	10.50	10.87	11.48	12.12
3	10.22	10.01	9.81	9.72	9.83	10.08	10.51	10.81	11.15	11.66	12.28

*Référence 16.
†Valeur extrapolée sur la fig. 1.

Can. J. Chem. Downloaded from www.nrcresearchpress.com by 210.87.254.40 on 09/05/12
For personal use only.

par potentiométrie (14, 15*b*), en mesurant à l'électrode d'hydrogène, indicatrice de l'activité du proton solvaté a_{S^+}, dans les milieux eau–DMSO (14) et méthanol–DMSO (15*b*), le pS^+ ($\equiv -\log a_{S^+}$) des solutions tamponnées préparées à partir des composés à étudier. Les forces électromotrices E_A et E_B des chaînes électrolytiques *A* et *B* suivantes:

$$(A)\quad \mathrm{Pt;\ H_2,\ \underset{\text{dans S } (\mu = C_a)}{\text{Solution tampon}}\ \Big|^{J'''}\ \underset{\text{dans S}}{\text{KCl saturé}}\ \Big|^{-J'}\ \underset{\text{dans S}}{\text{HCl } (C_a)^1}\ ,\ H_2;\ Pt}$$

$$(B)\quad \mathrm{Pt;\ H_2,\ \underset{\text{dans S } (\mu = C_b)}{\text{Solution tampon}}\ \Big|^{J'''}\ \underset{\text{dans S}}{\text{KCl saturé}}\ \Big|^{-J''}\ \underset{\text{dans S}}{\text{NaOH } (C_b)^1}\ ,\ H_2;\ Pt}$$

conduisent en effet indépendamment au pS^+ du tampon puisque pour chaque mélange, les activités $a_{S_a^+}$ et $a_{S_b^+}$ des solutions acides et basiques peuvent être calculées à partir des coefficients d'activité et du produit ionique du milieu (14–15*b*).

$$[1]\quad pS^+ = pS_a^+ + \frac{F}{2.3RT}E_A - \frac{F}{2.3RT}(E_{J'''} - E_{J'})$$

$$[2]\quad pS^+ = pS_b^+ + \frac{F}{2.3RT}E_B - \frac{F}{2.3RT}(E_{J'''} - E_{J''})$$

Rappelons que cette double détermination permet de s'assurer que, dans la mesure où les forces ioniques (μ) des compartiments de mesure des piles *A* et *B* sont les mêmes, l'incertitude sur la détermination des pS^+ due aux potentiels des jonctions liquides à écoulement (14), est très faible et inférieure aux autres incertitudes expérimentales ($E_{J'} \simeq E_{J''} \simeq E_{J'''}$) (14*b*).

Les constantes d'acidité sont ensuite calculées à partir des expressions [3], pour les acides carboxyliques, et [4] pour les cations ammoniums:

$$[3]\quad pK_a^S = pS^+ - \log r + \sqrt{\mu}.B$$

$$[4]\quad pK_a^S = pS^+ - \log r - \sqrt{\mu}.B$$

Dans ces expressions *r* représente le rapport entre les formes basique et acide du composé et *B* désigne le coefficient de la relation simplifiée de Debye–Hückel (14, 15*b*). Trois rapports d'ionisation *r* ont en général été utilisés: $\frac{1}{3}$, 1 et 3 et les solutions de mesure ont été préparées de telle sorte que la force ionique μ soit égale à 0.01. Cependant, dans les milieux eau–DMSO contenant moins de 30% de DMSO en masse ($\simeq$10% en fraction molaire), la faible solubilité de **3** et **4** d'une part, et des amines correspondant à **1** et **2** d'autre part, nous a contraints à travailler à force ionique plus faible ($0.001 < \mu < 0.01$) et à un seul rapport d'ionisation: 3 pour **3** et **4**, $\frac{1}{3}$ pour **1** et **2**. Dans ces conditions, la précision a été améliorée en répétant chaque mesure quatre ou cinq fois. Nous estimons que l'incertitude sur les p*K* est alors un peu plus grande ($\Delta pK \simeq 0.05$) que celle qui caractérise les autres déterminations ($\Delta pK \simeq 0.03$).

[1]Les solutions acides et basiques des mélanges méthanol–DMSO ont été respectivement préparées à partir d'acide benzènesulfonique anhydre et d'une solution méthanolique de méthylate de potassium (15*b*).

Résultats et discussion

Nos résultats, consignés dans le tableau 1, corrigent quelques erreurs parues dans un mémoire préliminaire (16). Il ressort de la fig. 1 où nous avons tracé les variations de p*K* en fonction de la fraction molaire en DMSO, que les deux courbes relatives au même composé se rejoignent dans les milieux les plus riches en solvant dipolaire aprotique. Tout en facilitant l'extrapolation au DMSO pur, cet excellent accord témoigne de la précision de notre méthode.

Influence du solvant sur l'acidité des groupements ammonium ou carboxylique, axiaux ou équatoriaux

Pour tester l'hypothèse de Cremlyn, nous avons rassemblé dans le tableau 2 les ΔpK qui séparent, dans les milieux eau–DMSO et méthanol–DMSO, les acidités des épimères axiaux et équatoriaux. En ce qui concerne les cations ammoniums, il apparaît, compte tenu des incertitudes expérimentales que l'influence du DMSO sur la ΔpK ($\equiv pK(\mathbf{1}) - pK(\mathbf{2})$) est négligeable jusqu'à 70% de DMSO en fraction molaire. Dans ces conditions, l'hypothèse de Cremlyn n'est pas satisfaite et les très faibles variations observées pour les teneurs supérieures à 70% en DMSO restent trop petites pour être significatives. On doit donc se demander si les plus grandes variations de ΔpK observées par Cremlyn dans les mélanges eau–acétone sont bien attribuables au comportement général des cations ammo-

Can. J. Chem. Downloaded from www.nrcresearchpress.com by 210.87.254.40 on 09/05/12
For personal use only.

TABLEAU 2. Influence du solvant sur les $\Delta pK = pK_{ax} - pK_{eq}$ des fonctions NH_3^+ et COOH situées sur le tertiobutyl-4 cyclohexane

Eau–DMSO			Méthanol–DMSO		
Fraction molaire en DMSO (%)	$pK(1) - pK(2)$	$pK(3) - pK(4)$	Fraction molaire en DMSO (%)	$pK(1) - pK(2)$	$pK(3) - pK(4)$
0	−0.10*	0.44*	0	−0.09	0.38
5.9	−0.08	0.44	5.9	−0.08	0.36
9.6	−0.10	0.44	12.2	−0.08	0.37
13.5	−0.10	0.42	19.5	−0.09	0.37
19.5	−0.11	0.40	27.1	−0.08	0.37
26.6	−0.06	0.40	35.7	−0.09	0.38
35.6	−0.07	0.41	45.5	−0.10	0.32
48.7	−0.06	0.36	56.5	−0.11	0.31
59.3	−0.08	0.34	69.5	−0.13	0.28
69.7	−0.10	0.27	83.7	−0.13	0.18
83.1	−0.15	0.19	91.5	−0.15	0.16
100.0	−0.16*	0.10*	100.0	−0.16*	0.10*

*Valeur calculée à partir des pK extrapolés.

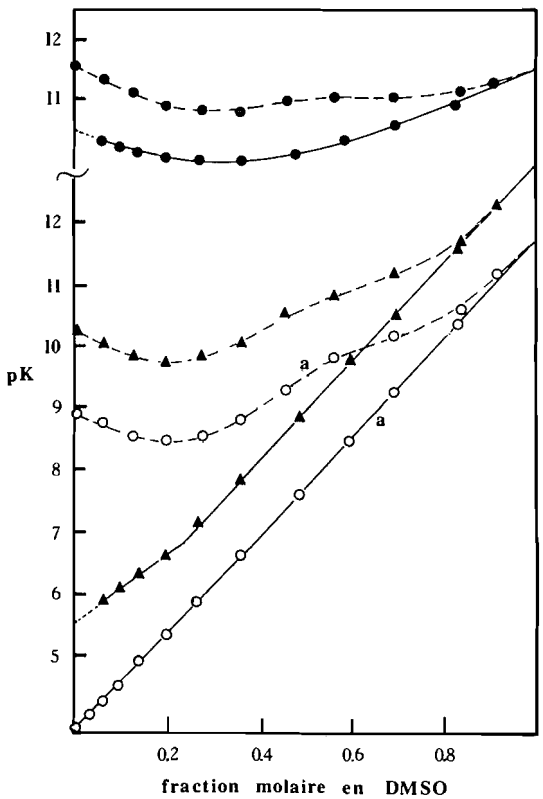

FIG. 1. Influence de la teneur en DMSO sur les pK du cation *cis* tertiobutyl-4 cyclohexylammonium (●) de l'acide *cis*-tertiobutyl-4 cyclohexane carboxylique (▲) et de l'acide cyclohexane carboxylique (○) dans les mélanges méthanol–DMSO (- - -) et eau–DMSO (—): (*a*) les courbes (○) sont décalées de −1 unité pK.

niums, auquel cas l'acétone serait responsable de l'effet observé, ou si elles ne seraient pas plutôt particulières aux acides α-aminés (seconde acidité) pour lesquels l'ionisation du groupement ammonium est fortement influencée par la désolvatation progressive de l'anion carboxylate, au fur et à mesure que la teneur en solvant dipolaire aprotique augmente (17). Par contre, les résultats relatifs aux acides cyclohexane carboxyliques sont conformes à la règle de Cremlyn dans les deux systèmes de solvants mixtes (voir réf. 16 ainsi que tableaux 1 et 2), bien que les variations de ΔpK observées sont encore inférieures à celles qui caractérisent la première ionisation des acides α-aminés dans les mélanges eau–acétone (9).

Le critère proposé par Cremlyn n'est donc pas d'application générale: quand il semble s'appliquer il est alors souhaitable de le contrôler en modifiant autant que possible le milieu et (ou) l'environnement de la fonction qui s'ionise.

Influence du substituant tertiobutyl-4 sur l'acidité du cation cyclohexylammonium

Pour fixer un groupement en configuration axiale ou équatoriale, Winstein et Holness (18) et Eliel et Lukach (19) ont introduit l'emploi du substituant *cis* ou *trans* tertiobutyl-4 qui "gèle" l'équilibre conformationnel cyclohexanique. Ces auteurs ont par ailleurs supposé que l'éloignement des sites -1 et -4 est suffisant pour que les effets polaires ou stériques du substituant tertiobutyl-4 n'affectent pas les propriétés du groupe-

Can. J. Chem. Downloaded from www.nrcresearchpress.com by 210.87.254.40 on 09/05/12
For personal use only.

Can. J. Chem. Downloaded from www.nrcresearchpress.com by 210.87.254.40 on 09/05/12
For personal use only.

ment -1. Ceci revient à admettre que les propriétés des dérivés axiaux ou équatoriaux du cyclohexane (*e.g.* **5***a* ou **5***e*) sont respectivement les mêmes que celles des composés *cis* (*e.g.* **1**) ou *trans* (*e.g.* **2**). Il résulte donc de cette approximation, que les propriétés du véritable cyclohexane substitué, qui est un mélange des deux conformères (*e.g.* **5***a* + **5***e*) en équilibre rapide, devraient être intermédiaires entre celles des composés modèles *cis* et *trans*. Par ailleurs, des calculs bien connus depuis 20 ans (5, 6, 18, 19) permettront d'estimer les proportions de ces conformères. Ainsi, la constante d'acidité apparente K(**5**) doit vérifier [6]:

$$[5] \qquad K(\mathbf{5}) = X_e K(\mathbf{5}e) + X_a K(\mathbf{5}a)$$

$$[6] \qquad \simeq X_e K(\mathbf{2}) + (1 - X_e) K(\mathbf{1})$$

où X_e et X_a désignent respectivement les fractions molaires des conformations équatoriale **5***e* et axiale **5***a* (5, 6). Même si l'approximation: $X_e \simeq 0.96$ (20) n'est pas tout à fait exacte, en raison de la petite influence du solvant sur la proportion des deux conformères (20), elle indique néanmoins, que le pK du cation **5** doit être très près du pK(**2**) tout en lui restant inférieur. Les valeurs de pK(**5**) sensiblement supérieures à celles de pK(**2**) surtout dans les milieux eau–DMSO contenant moins de 90% de DMSO en masse sont donc incompatibles avec [6]. De même dans les milieux riches en DMSO, l'utilisation de la relation 6 conduit, au fur et à mesure que l'on se rapproche du DMSO pur, à des pourcentages en forme axiale supérieurs à ce qui est habituellement admis (20). La valeur $X_a \simeq 0.5$ estimée pour le DMSO anhydre semble, en effet, peu probable.[2]

Ces anomalies, qui mettent en échec le postulat de Winstein et d'Eliel, ne peuvent s'expliquer que par une influence certaine du substituant tertiobutyl-4 sur l'ionisation du groupement ammonium. Dans la mesure où l'influence observée est, dans la plupart des milieux mixtes, contraire à ce que l'effet polaire du groupement tertiobutyle permettait d'attendre (augmentation de la basicité de la fonction amine), nous pensons pouvoir expliquer raisonnablement ce phénomène par une diminution de la solvatation du cation ammonium qui, moins stabilisé, sera donc plus acide. La fig. 2, construite d'après les distances et les angles connus pour les liaisons chimiques (21) et les rayons de van der Waals (21, 22), illustre dans l'eau la solvatation du cation **2**. Il y apparaît très nettement que le substituant tertiobutyle diminue le nombre de molécules d'eau de la deuxième couche de solvatation. Par ailleurs, cet effet permet d'expliquer les différentes acidités du groupement ammonium équatorial[3] porté par les carbones-2, -3, -6 et -7 du squelette cholestane (3*a*, 3*b*). Ce phénomène a été récemment reconnu par Arnett et coll. (24, 25) au cours de son analyse des enthalpies et des enthalpies libres de solvatation dans l'eau des cations ammoniums. Bien qu'en toute rigueur la solvatation de l'amine libre soit également à considérer (25) nous pensons que, dans le cas présent, la solvatation du cation ammonium est déterminante dans son processus d'ionisation.

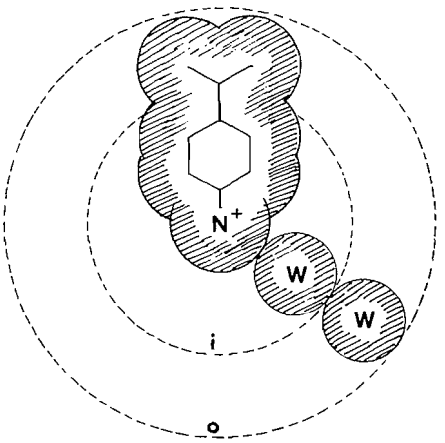

FIG. 2. Illustration à l'échelle des surfaces de van der Waals du *trans*-tertiobutyl-4 cyclohexylammonium avec deux molécules d'eau (W), une dans la couche intérieure (**i**) et l'autre dans la couche extérieure (**o**) de solvatation.

Influence du substituant tertiobutyl-4 sur l'acidité de l'acide cyclohexane carboxylique

La relation 8 sera justifiée si, quelle que soit la nature du solvant, la constante d'acidité apparente de l'acide cyclohexane carboxylique **6** est intermédiaire entre K(**3**) et K(**4**) avec $\Delta pK_{6,4}$ ($\equiv$ pK(**6**) − pK(**4**)) positif.

$$[7] \qquad K(\mathbf{6}) = X_e K(\mathbf{6}e) + X_a K(\mathbf{6}a)$$

[2]Un examinateur a soulevé la possibilité d'une proportion importante de conformations "bateaux-croisés" telle que proposée par Garbisch et Patterson (23). Cette possibilité peut aider à expliquer les résultats.

[3]J. T. Edward, résultats non publiés.

TABLEAU 3. Influence de la teneur en DMSO sur les ΔpK = pK(système mobile) − pK(conformation équatoriale fixée) relatifs aux fonctions NH_3^+ et COOH introduites respectivement sur le cyclohexane et le tertiobutyl-4 cyclohexane

Eau–DMSO			Méthanol–DMSO		
Fraction molaire en DMSO (%)	pK(**5**) − pK(**2**)	pK(**6**) − pK(**4**)	Fraction molaire en DMSO (%)	pK(**5**) − pK(**2**)	pK(**6**) − pK(**4**)
0	0.10	−0.20	0	0.05	0.08
5.9	0.10	−0.17	5.9	0.03	0.08
9.6	0.08	−0.07	12.2	0.02	0.08
13.5	0.09	−0.01	19.5	0.03	0.07
19.5	0.06	0.10	27.1	0.05	0.07
26.6	0.03	0.08	35.7	0.03	0.08
35.6	0.05	0.09	45.5	0.03	0.07
48.7	0.05	0.08	56.5	−0.01	0.09
59.3	0.04	0.00	69.5	−0.02	0.11
69.7	−0.02	−0.02	83.7	−0.04	0.09
83.1	−0.04	−0.04	91.5	−0.03	0.06
100.0	−0.05	−0.06	100.0	−0.05	−0.06

[8] $$\simeq X_e K(\mathbf{4}) + (1 - X_e)K(\mathbf{3})$$

En ce qui concerne la plupart des milieux méthanol–DMSO le tableau 3 fait apparaître que [8] semble assez bien vérifiée. En effet, les valeurs calculées pour X_e ($\simeq$0.70–0.74) d'une part, et l'enthalpie libre standard de l'équilibre: **6***a* $\rightleftarrows$ **6***e* ($\Delta G^0 \simeq$ 500–600 cal mol^{-1}) d'autre part, sont compatibles avec les données de la littérature (20). Il convient cependant de préciser que ces valeurs ne doivent pas être considérées comme absolues puisque les calculs ignorent complètement l'influence possible du groupement tertiobutyle sur la solvatation de **3** et de **4**. Les résultats obtenus dans les milieux eau–DMSO (tableau 3) riches en eau (contenant moins de 40% de DMSO en masse soit $\simeq$20% en fraction molaire) ou en DMSO (contenant plus de 85% de DMSO en masse soit $\simeq$60% en fraction molaire) apportent la preuve incontestable de cette influence. L'empêchement de solvatation[4] au niveau de la deuxième couche de l'anion *trans* tertiobutyl-4 cyclohexane carboxylate permet également d'expliquer l'affaiblissement notable de l'acidité, dû au substituant tertiobutyl-4, observé dans les mélanges riches en eau (dans l'eau $\Delta pK_{6,4} = -0.20$). Dans la mesure où le diméthylsulfoxyde est un mauvais solvant des anions à charge localisée (14*b*–17) la substitution tertiobutyl-4 perturbera moins la solvatation de l'anion cyclohexane carboxylate comme en témoignent les faibles valeurs de $\Delta pK_{6,4}$ négatives observées dans les milieux très riches en DMSO (tableau 3).

Il est fondamental de remarquer que les éqs 8 et 6 ont toujours été testées pour des milieux hydroorganiques dont la teneur en solvants organiques varie de 50 à 80% (5, 7). Il n'est donc pas surprenant que les valeurs positives de $\Delta pK_{6,4}$ et négatives de $\Delta pK_{5,2}$, aient conduites à retenir ces équations pour l'étude des équilibres conformationnels comme nous serions également tentés de le faire au seul regard des résultats concernant les milieux eau–DMSO de teneur en DMSO semblables (20 à 60% de DMSO en fraction molaire) pour lesquels $\Delta pK_{6,4}$ est positif (tableau 3). L'examen des résultats relatifs aux mélanges eau–DMSO de faibles ou fortes teneurs en DMSO montrent que l'approximation qui conduit à la relation 8 n'est pas justifiée ce qui rejoint notre conclusion concernant l'influence notable du substituant tertiobutyl-4 sur l'acidité du cation cyclohexylammonium.

Conclusion

La diminution de solvatation que le groupement tertiobutyl-4 apporte à un substituant introduit sur le site -1 du cyclohexane, doit également se manifester sur la cinétique de réactions affectant une fonction placée en -1, à

[4]Bien que les variations d'acidité qui accompagnent la substitution *trans* tertiobutyl-4 soient ici conformes à l'effet donneur de ce groupement, nous lui préférons l'explication évoqué précédemment; elle seule rend compte, en effet, de l'influence acidifiante du substituant *trans* tertiobutyl-4, sur l'ionisation du cation cyclohexylammonium.

Can. J. Chem. Downloaded from www.nrcresearchpress.com by 210.87.254.40 on 09/05/12
For personal use only.

Can. J. Chem. Downloaded from www.nrcresearchpress.com by 210.87.254.40 on 09/05/12
For personal use only.

condition que l'état de transition soit fortement solvaté. La saponification des esters en est un exemple. Cavell *et al.* (26) ont ainsi trouvé que la vitesse de saponification de l'ester méthylique de l'acide cyclohexane carboxylique est, dans le mélange eau–dioxanne contenant 50% de dioxanne en volume, 15% plus élevée que celle de l'homologue *trans* tertiobutylé en -4. Ce substituant tertiobutyl-4 exerce donc une influence sur cette réaction puisque s'il n'en était pas ainsi, la vitesse relative au composé non substitué serait un peu *moins* élevée en raison de la petite proportion du conformère axial. Le groupement tertiobutyl-4 perturbe donc bien la solvatation de l'état de transition de cette réaction. En revanche, la distance plus grande qui sépare le substituant tertiobutyl-4 de la charge négative de l'état de transition correspondant à la saponification dans l'eau du monophtalate de cyclohexyle, peut expliquer, dans ce cas, l'influence insignifiante du substituant tertiobutyl-4 sur la vitesse de saponification (18). Une telle influence, qui dépend du solvant, est évidemment prévisible pour d'autres réactions s'accompagnant du développement d'une charge (réaction de Menschutkin par exemple). Des travaux plus poussés dans cette voie s'avèrent donc souhaitables.

Remerciements

Nous remercions la Coopération France–Québec pour son soutien financier qui a permis les échanges entre les deux laboratoires et en particulier le stage de recherche de J.K. à Paris, où les déterminations d'acidité ont été faites. Nous remercions également le Dr. S. A. Samad pour la préparation des composés **1**, **2**, **3** et **4**.

1. (*a*) R. Kuhn et A. Wasserman. Helv. Chim. Acta, **11**, 50 (1928); (*b*) R. Gane et C. K. Ingold. J. Chem. Soc. 2153 (1931); (*c*) C. K. Ingold. J. Chem. Soc. 2179 (1931); (*d*) G. S. Hammond et D. A. Hogle. J. Am. Chem. Soc. **77**, 338 (1955).
2. (*a*) D. H. R. Barton et R. C. Cookson. Q. Rev. **10**, 44 (1956); (*b*) G. B. Barlin et D. D. Perrin. Techniques of chemistry. Vol. 4, Part II. *Edited by* A. Weissberger. Wiley–Interscience, New York. 1972. pp. 611–676.
3. (*a*) C. W. Bird et R. C. Cookson. Chem. Ind. (London), 1479 (1955); (*b*) C. W. Bird et R. C. Cookson. J. Chem. Soc. 2343 (1960); (*c*) J. Sicher, J. Jonas et M. Tichy. Tetrahedron Lett. 825 (1963).
4. J. F. Dippy, S. R. C. Hughes et J. W. Laxton. J. Chem. Soc. 4102 (1954).
5. R. D. Stolow. J. Am. Chem. Soc. **81**, 5806 (1959).
6. M. Tichy, J. Jonas et J. Sicher. Coll. Czech. Chem. Commun. **24**, 3434 (1953).
7. P. F. Sommer, V. P. Arya et W. Simon. Tetrahedron Lett. 18 (1960); P. F. Sommer, C. Pascual, V. P. Arya et W. Simon. Helv. Chim. Acta, **46**, 1734 (1963); C. Pascual et W. Simon. Helv. Chim. Acta, **47**, 683 (1964); W. Simon. Angew. Chem. **76**, 772 (1964); J. Sicher et M. Tichy. Tetrahedron Lett. 1393 (1966); E. van Bekkum, P. E. Verkade et B. M. Wepster. Tetrahedron Lett. 1401 (1966).
8. L. Munday. J. Chem. Soc. 4372 (1961).
9. R. J. W. Cremlyn, M. G. Chisholm et P. J. Taylor. Tetrahedron Lett. 1373 (1967); R. J. W. Cremlyn et M. G. Chisholm. J. Chem. Soc. 2269 (1967).
10. J. T. Edward et C. Jitrangsri. Can. J. Chem. **53**, 3339 (1975).
11. H. S. Tager et H. N. Christensen. J. Am. Chem. Soc. **94**, 968 (1972).
12. D. Y. Curtin, R. D. Stolow et W. Maya. J. Am. Chem. Soc. **81**, 3330 (1959).
13. Y. Maki et T. Masugi. Chem. Pharm. Bull. (Tokyo), **21**, 685 (1973).
14. (*a*) J. C. Halle, R. Gaboriaud et R. Schaal. Bull. Soc. Chim. Fr. 1851 (1969); (*b*) J. C. Halle. Thèse Paris. 1971; CNRS A.O. 5780.
15. (*a*) F. Terrier et F. Millot. Bull. Soc. Chim. Fr. 1743 (1970); (*b*) J. C. Halle, F. Terrier et R. Gaboriaud. Bull. Soc. Chim. Fr. 37 (1973).
16. J. Kirchnerova, J. C. Halle, P. G. Farrell, R. Schaal et J. T. Edward. C. R. Acad. Sci. Ser. C, **281**, 63 (1975).
17. (*a*) A. J. Parker. Chem. Rev. **69**, 1 (1969); (*b*) J. C. Halle. Bull. Soc. Chim. Fr. 1553 (1973).
18. S. Winstein et N. J. Holness. J. Am. Chem. Soc. **77**, 5562 (1955).
19. E. L. Eliel et C. A. Lukach. J. Am. Chem. Soc. **79**, 5986 (1957).
20. E. L. Eliel, N. L. Allinger, S. J. Angyal et G. A. Morrison. Conformational analysis. Interscience, New York. 1967, p. 44.
21. L. Pauling. The nature of the chemical bond. Cornell University Press, New York. 1942. p. 192.
22. J. T. Edward. J. Chem. Educ. **47**, 261 (1971).
23. E. W. Garbisch et D. B. Patterson. J. Am. Chem. Soc. **85**, 3228 (1963).
24. E. M. Arnett. *In* Proton-transfer reactions. *Edited by* E. F. Caldin and V. Gold. Chapman and Hall, London. 1975. p. 79.
25. F. M. Jones et E. M. Arnett. Prog. Phys. Org. Chem. **11**, 263 (1974).
26. E. A. S. Cavell, N. B. Chapman et M. D. Johnson. J. Chem. Soc. 1413 (1960).

The kinetics of the reactions of chlorodithioformate esters with azide ions in 70% aqueous acetone

ALAN QUEEN, DAVID M. MCKINNON, AND ALEXANDER W. BELL
Parker Chemical Laboratory, University of Manitoba, Winnipeg, Man., Canada R3T 2N2

Received January 7, 1976

ALAN QUEEN, DAVID M. MCKINNON, and ALEXANDER W. BELL. Can. J. Chem. **54**, 1906. (1976).

The rates of reaction of a series of chlorodithioformate esters with azide ions in 70% aqueous acetone decrease with increasing electron donation to the reaction site. This order is the reverse of that observed for S_N1 solvolysis. The entropies of activation are highly negative and the rapid rates of azide attack result from the low activation energies. These results indicate a bimolecular mechanism for azide attack and this is supported by the first-order dependence of the reaction rate on azide concentration.

ALAN QUEEN, DAVID M. MCKINNON et ALEXANDER W. BELL. Can. J. Chem. **54**, 1906. (1976).

Les vitesses de réaction d'une série d'esters de l'acide chlorodithioformique avec les ions azotures dans l'acétone aqueux à 70% diminuent avec une augmentation de la densité électronique au site de la réaction. Cet ordre est l'inverse de celui observé pour les réactions de solvolyse S_N1. Les entropies d'activation sont très négatives et les vitesses rapides de l'attaque par les ions azotures proviennent d'énergies d'activation faibles. Ces résultats indiquent que les ions azotures attaquent par un mécanisme bimoléculaire et cette conclusion est en accord avec la dépendance du premier ordre des vitesses de réaction sur la concentration des ions azotures.

[Traduit par le journal]

Introduction

Although esters of chlorodithioformic acid hydrolyse by the S_N1 mechanism in aqueous acetone (1), we have recently (2) presented evidence that the corresponding reaction of the methyl compound with azide ions in the same medium is largely a bimolecular process. However, although in this case substitutions by S_N1 pathways are swamped, within the limits of the experimental errors, by the rapid bimolecular reaction, it is reasonable to assume that a small amount of concurrent unimolecular azide attack also occurs. This conclusion is based on the fact that the rate of solvolysis is greatly decreased by the less nucleophilic chloride ion which, consequently, must capture a free acylium ion. We have used this evidence to exclude an ion-pair mechanism (3) for the nucleophilic substitution reactions of methyl chlorodithioformate and to support the concurrent operation of independent S_N1 and bimolecular processes.

In order to confirm the bimolecular natures of the azide reactions, we have now studied the reactions of phenyl, methyl, and ethyl chlorodithioformates with azide ions in 70% aqueous acetone. Activation parameters for the corresponding reactions of the phenyl and methyl compounds have also been measured.

Products

It would be expected that the reaction of chlorodithioformate esters (**1**) with azide ions would lead to the corresponding azides (**2**), but such compounds are unknown. Previous attempts to prepare them (4, 5) have led to 5-substituted thiatriazoles (**3**, R = alkyl), which can also be obtained (6) by treating the sodium salt of 5-mercaptothiatriazole (**3**, R = H) with alkyl iodides. The aryl analogues cannot be produced by this latter route and have not been previously prepared.

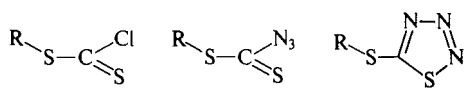

1 **2** **3**

Phenyl chlorodithioformate reacted with an excess of azide ions in 70% aqueous acetone to give an almost quantitative yield of a crystalline solid which analysed as $C_7H_5N_3S_2$, as required

Can. J. Chem. Downloaded from www.nrcresearchpress.com by 210.87.254.40 on 09/05/12
For personal use only.

TABLE 1. The effect of salts on the rates of hydrolysis of chlorodithioformate in 70% aqueous acetone

Compound	T (°C)	Salt	[Salt] (M)	$k \times 10^4$ (s^{-1})	$k^{0.05}/k^{0*}$
$CH_3S-C(=S)-Cl$	10.3	None		2.11 ± 0.03	
		$NaClO_4$	0.0496	2.93 ± 0.04	1.39
		NaCl	0.0608	0.273 ± 0.005	0.275
$C_6H_5S-C(=S)-Cl$	20.5	None		6.15 ± 0.05	
		$NaClO_4$	0.0515	8.32 ± 0.08	1.34
		NaCl	0.0478	1.72 ± 0.02	0.261

*Calculated for 0.05 molar salt, assuming a linear dependence on salt concentration.

TABLE 2. The rates of reaction of chlorodithioformate esters with azide ions in 70% aqueous acetone

		$C_6H_5S(CS)Cl$		$CH_3S(CS)Cl$		$C_2H_5S(CS)Cl$	
$[N_3^-]$ (M)	T (°C)	k_{obs} (s^{-1})	k_N ($s^{-1}\ M^{-1}$)	k_{obs} (s^{-1})	k_N ($s^{-1}\ M^{-1}$)	k_{obs} (s^{-1})	k_N ($s^{-1}\ M^{-1}$)
0.1922	3.88	3.84	20.0	0.415	2.16	0.203	1.06
0.1415	3.88	3.02	21.4	0.309	2.18	0.161	1.14
0.1107	3.88	2.46	22.2	0.256	2.31	0.143	1.29
0.05511	3.88	1.27	23.0	0.128	2.32	0.0916	1.66
0*	4.94	2.48×10^{-5}		12.6×10^{-5}		79.6×10^{-5}	

*See ref. 1.

by the structures **2** and **3** (R = C_6H_5). The compound did not absorb near 2140 cm^{-1}, the characteristic azide stretching frequency (7), but did have bands at 1600(w), 1310(s), 1240(s), and 1090(s) cm^{-1} which are consistent with the presence of the 1,2,3,4-thiatriazole ring (6).

The corresponding reaction of methyl chlorodithioformate yielded a pale yellow oil which crystallized on standing at 5°C but melted again on standing at room temperature. 5-Methylthio-1,2,3,4-thiatriazole (**3**, R = CH_3) has been prepared from methyl bromide and sodium thiatriazolinethionate and a melting point of 34 °C was reported (6). In our hands, this reaction gave an oil which crystallized on standing at 5 °C but which, like the earlier sample, turned to an oil when placed in the melting-point apparatus at room temperature. The two samples had identical infrared spectra lacking bands near 2140 cm^{-1} and identical ultraviolet spectra showing maxima at 278 nm. The phenyl compound also had a similar absorption band at 276 nm.

On the basis of these results, the products obtained by reacting chlorodithioformate esters with azide ions in aqueous acetone are considered to be the 5-substituted-1,2,3,4-thiatriazoles (**3**, R = aryl or alkyl).

Kinetic Results

Table 1 summarises the effects of sodium chloride and sodium perchlorate on the rates of solvolysis of methyl and phenyl chlorodithioformate. The large accelerating salt effects due to perchlorate and the massive common-ion rate depressions, which are far too large to be due to negative salt effects, are in accord with the S_N1 mechanism previously proposed (1) for these reactions.

In our earlier paper (2) we showed that the rate of reaction of methyl chlorodithioformate with azide ions is first order in azide ions, within experimental error. Table 2 lists additional results for the phenyl, methyl, and ethyl compounds at 3.88 °C, using a much wider range of nucleophilic concentrations than previously. In each case, it can be seen that the calculated second-order rate constants decrease with azide concentration. However, results obtained for the phenyl compound using a fixed azide concentration and varying amounts of sodium perchlorate show that these changes in k_N are due to negative salt effects (Table 3). Negative salt effects on bimolecular reactions involving neutral substrates and negatively charged nucleophiles have been previously reported (8).

Can. J. Chem. Downloaded from www.nrcresearchpress.com by 210.87.254.40 on 09/05/12
For personal use only.

Can. J. Chem. Downloaded from www.nrcresearchpress.com by 210.87.254.40 on 09/05/12
For personal use only.

TABLE 3. The effect of sodium perchlorate on the rate of attack of 0.09625 *M* sodium azide on phenyl chlorodithioformate in 70% aqueous acetone at 10.22 °C

$[NaClO_4]$ (*M*)	[Salts] (*M*)	k_{obs} (s^{-1})	k_N (s^{-1} M^{-1})
0.2016	0.2979	2.02±0.03	21.0
0.1428	0.2391	2.21±0.02	22.9
0.0925	0.1887	2.51±0.03	26.1
0.0504	0.1467	2.79±0.03	29.0
0	0.0963	3.08±0.03	32.0

Table 4 summarises data showing the effects of temperature on the rates of reaction of phenyl and methyl chlorodithioformate with 0.1 *M* sodium azide in 70% aqueous acetone.

Discussion

The different rate sequences for solvolysis and azide attack (Table 2) are in accord with the different mechanisms proposed (1, 2) for the two reactions; *i.e.* mechanism S_N1 for solvolysis being reflected in an increase of reactivity as electron donation to the reaction site increases due to increasing stabilization of the acylium ions while bimolecular azide attack decreases with increased electron donation due to repulsion of the negatively charged nucleophile. Bimolecular azide attack is also supported by the first-order dependence of the rates on nucleophile concentration. It is difficult to see how Sneen's ion-pair mechanism (3), Scheme 1, could readily account for these contrasting results.

The activation parameters for the azide reactions (Table 4) can be compared to those (1) for the solvolysis of methyl chlorodithioformate in 70% aqueous acetone; $\Delta H^{\ddagger} = 20.18$ kcal mol^{-1}, $\Delta S^{\ddagger} = -3.7$ cal mol^{-1} deg^{-1}. Clearly, the large effects of azide ions on the rates of reaction are due to the lower activation enthalpies, which more than compensate for the more negative entropies of activation. These differences provide further support for different paths for solvolysis and bimolecular azide attack. However, the results do not allow conclusions to be drawn concerning the mechanism of the bimolecular process. For solvolysis in 70% aqueous acetone, the entropies of activation for reaction by the S_N1 ($\Delta S^{\ddagger} \simeq -2$ to -5 cal mol^{-1} deg^{-1}), S_N2 ($\Delta S \simeq -15$ to -20 cal mol^{-1} deg^{-1}) and bimo-

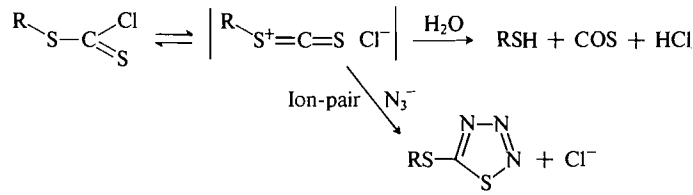

SCHEME 1

TABLE 4. The effects of temperature on the rates of reaction of methyl and phenyl chlorodithioformates with sodium azide in 70% aqueous acetone

Compound	*T* (°C)	k_{obs} (s^{-1})*	k_N (s^{-1} M^{-1})†	$\Delta H^{\ddagger}$ (kcal mol^{-1})	$\Delta S^{\ddagger}$ (cal mol^{-1} deg^{-1})
$CH_3S(CS)Cl$	−0.20	0.161	1.71	11.4	−15.5
	2.53	0.186	1.98		
	5.04	0.231	2.45		
	7.52	0.277	2.94		
	9.56	0.351	2.73		
$C_6H_5S(CS)Cl$	0.44	1.73	18.0	8.8	−20.2
	4.41	2.26	23.5		
	8.10	2.75	28.5		
	11.89	3.53	36.7		
	15.68	4.35	45.2		
	19.96	5.49	57.0		

*$[NaN_3]$ = 0.09412 *M*.
†$[NaN_3]$ = 0.09630 *M*.

Can. J. Chem. Downloaded from www.nrcresearchpress.com by 210.87.254.40 on 09/05/12
For personal use only.

lecular addition–elimination mechanisms ($\Delta S^{\ddagger} \simeq -30$ to -35 cal mol^{-1} deg^{-1}) are sufficiently different (9, 10) to enable a choice to be made. Unfortunately, the standard state to which the activation parameters for azide attack refer (Table 4) is not the same as for solvolysis. Data for bimolecular substitutions by azide ions in 70% aqueous acetone are not available. However, entropies of activation in the range -15 to -40 cal mol^{-1} deg^{-1} have been reported (11) for azide attack on vinyl halides by the addition–elimination mechanism. Unfortunately, the values depend markedly on the solvent system used and none of the results refer to 70% aqueous acetone, so that interpretations based on these figures must be accepted with caution.

Recent work by Guthrie (12) and Jencks (13) suggests that the specific rate constants for the expulsion of amine groups from negatively charged tetrahedral intermediates are about 10^8 s^{-1}. It has therefore been suggested that the lifetime for such species with chloride as the leaving groups would be less than a molecular vibration so that bond making and bond breaking are concerted, leading to the classical S_N2 mechanism for reactions involving an acid halide and a negatively charged nucleophile. In the absence of direct evidence, this conclusion must also be accepted with caution and our recent observation (14) that $k_F > k_{Cl}$ for the acetate catalysed hydrolysis of 4-methoxyphenyl haloformates indicates that it may not be always correct. These leaving group effects are most readily explained in terms of reaction via tetrahedral intermediates and a similar mechanism is likely to apply to the present reactions, although our results cannot confirm this.

We conclude that our results support an S_N1 mechanism for solvolysis and that the free acylium ion may also be captured by other nucleophiles. In the presence of a powerful nucleophile such as azide ions, the products mainly arise from the operation of an independent bimolecular pathway, the details of which cannot be decided at the present time.

Experimental

The preparation and purification of the chlorodithioformate esters and the preparation of the solvents have been previously described (1).

Salts were Analar reagents and were recrystallized and dried *in vacuo* at 100 °C over phosphorus pentoxide. Acetone (70%) was prepared by mixing 70 volumes of acetone and 30 volumes of water. All solvents were 'out-gassed' on the vacuum line before mixing.

Measurement of Rates

The slow reactions were followed at 325 nm using a Beckmann DK 1A spectrophotometer fitted with a thermostated cell holder. Temperatures were recorded in the reaction cell before and after each run and found to be constant to within ±0.02 °C. The fast rates were obtained with a 'Canterbury' stopped-flow apparatus (15) with on-line data processing (16). Temperatures were measured with a platinum resistance thermometer and were constant to better than 0.005 °C.

Products

In a typical experiment, phenyl chlorodithioformate (0.5 g) was added dropwise to a stirred solution of sodium azide (0.65 g) in 70% aqueous acetone (50 ml) at room temperature. After 10 min, the solvent was evaporated on the vacuum line, the residue shaken with water, and the organic material extracted with ether. After drying, the solvent was removed at room temperature and the solid residue recrystallized from methanol to yield 5-phenylthio-1,2,3,4-thiatriazole (**3**, R = C_6H_5), mp 61–62 °C, 0.49 g (94%). *Anal.* calcd. for $C_7H_5N_3S_2$: C 43.8, H 2.6, N 21.5, S 32.8; found: C 43.6, H 2.8, N 21.2, S 32.5.

Acknowledgments

The authors gratefully acknowledge grants by the National Research Council of Canada and the Research Board of the University of Manitoba.

1. D. M. McKinnon and A. Queen. Can. J. Chem. **50**, 1401 (1972).
2. A. Queen and T. C. Matts. Tetrahedron Lett. 1503 (1975).
3. R. A. Sneen and A. W. Larsen. J. Am. Chem. Soc. **91**, 6031 (1969).
4. L. F. Audrieth, J. R. Johnson, A. W. Brown, and C. W. Mason. J. Am. Chem. Soc. **52**, 1928 (1930).
5. E. Lieber, C. N. Pillai, J. Ramachandran, and R. D. Hites. J. Org. Chem. **22**, 1750 (1957).
6. E. Lieber, I. Oftendahl, and C. N. R. Rao. J. Org. Chem. **28**, 194 (1963).
7. E. Lieber, C. N. Rao, T. S. Chao, and C. W. W. Hoffman. Anal. Chem. **29**, 916 (1957).
8. R. A. Sneen and H. W. Robbins. J. Am. Chem. Soc. **91**, 3100 (1969).
9. G. Kohnstam. Adv. Phys. Org. Chem. **5**, 121 (1967).
10. A. Queen. Can. J. Chem. **45**, 1619 (1967).
11. Z. Rappoport. Adv. Phys. Org. Chem. **7**, 1 (1969).
12. J. P. Guthrie. J. Am. Chem. Soc. **96**, 3608 (1974).
13. W. P. Jencks. Chem. Rev. **72**, 705 (1972).
14. A. Queen and T. A. Nour. J. Chem. Soc., Perkin Trans. II. In press.
15. E. F. Caldin, J. E. Crooks, and A. Queen. J. Phys. E, **6**, 930 (1973).
16. A. Queen, J. L. Charlton, E. Dawson, and W. Buchannon. Chem. Instrum. **6**, 153 (1975).

A second species of polynuclear hydroxyaluminum cation, its formation and some of its properties[1]

ROBERT C. TURNER[2]

Saskatchewan Institute of Pedology, University of Saskatchewan, Saskatoon, Sask., Canada S7N 0W0

Received December 30, 1975

ROBERT C. TURNER. Can. J. Chem. **54**, 1910 (1976).

When a solution of $Al(ClO_4)_3$ or $AlCl_3$ with total Al concentration between 5×10^{-4} and 6×10^{-2} *M* is partially neutralized very slowly with a base, it is possible to produce a solution of polynuclear hydroxyaluminum cations with no solid phases present. When such a solution is aged, the polynuclear hydroxyaluminum cations, Al_{P1}, disappear very slowly at 25 °C and a second type of polynuclear hydroxyaluminum cations, Al_{P2}, is formed. The second type, Al_{P2}, has some properties that are the same as those of Al_{P1}, *e.g.* they both have an OH/Al mole ratio equal to or very nearly equal to 2.5, diffuse readily across a dialysis membrane, and are removed from solution by the clay mineral bentonite in an exchangeable form. Some of their properties, however, are entirely different, *e.g.* Al_{P1} reacts with 8-hydroxyquinoline about 250 times faster with a much lower energy of activation than does Al_{P2}, is much less resistant to attack by HCl, and is precipitated at a p*H* about 0.5 p*H* units lower than Al_{P2}. The transformation of Al_{P1} to Al_{P2} is a first order process with an energy of activation of 20.8 kcal per mol. The specific rate constant seems to be affected somewhat by the extraneous anion present and the degree of neutralization; experimental values varied from 0.57×10^{-3} to 3.5×10^{-3} day^{-1} at 25 °C.

ROBERT C. TURNER. Can. J. Chem. **54**, 1910 (1976).

Quand on neutralise partiellement et très lentement une solution de $Al(ClO_4)_3$ ou de $AlCl_3$ ayant des concentrations totales de Al entre 5×10^{-4} et 6×10^{-2} *M* par une base, il est possible de produire une solution de cations hydroxyaluminium polynucléaire dans laquelle il n'y a pas de phase solide. Quand on laisse vieillir une telle solution, le cation hydroxyaluminium polynucléaire Al_{P1} disparait très lentement à 25 °C et un second type de cation hydroxyaluminium polynucléaire Al_{P2} se forme. Les cations des types Al_{P1} et Al_{P2} ont quelques propriétés qui sont les mêmes; entre autre les deux ont un rapport molaire de OH/Al qui est égal ou presqu'égal à 2.5, ils diffusent tous les deux facilement à travers une membrane de dialyse et ils sont tous les deux enlevés d'une solution par l'argile minérale bentonite sous forme échangeable. Toutefois quelques unes de leurs propriétés sont complètement différentes; par exemple Al_{P1} réagit avec l'hydroxy-8 quinoléine environ 250 fois plus rapidement et avec une énergie d'activation beaucoup plus basse que ne le fait Al_{P2}; de plus Al_{P1} est beaucoup moins résistant à une attaque par HCl et par rapport à Al_{P2} on peut le précipité à un p*H*, environ 0.5 unité, plus bas que Al_{P2}. La transformation de Al_{P1} en Al_{P2} est un processus du premier ordre avec une énergie d'activation de 20.8 kcal par mole. La constante de vitesse spécifique semble être affectée jusqu'à un certain point par la présence d'anions extérieurs et par le degré de neutralisation; les valeurs expérimentales varient entre 0.57×10^{-3} jusqu'à 3.5×10^{-3} jours^{-1} à 25 °C.

[Traduit par le journal]

Introduction

It was shown in a previous paper (1) that it is possible to prepare polynuclear hydroxyaluminum cations without forming any solid phases. Methods for doing this were based on the assumption (2) that the principal reactions operating when a base is added to an aluminum perchlorate solution are:

$$[1]\quad Al{\cdot}6H_2O^{3+}{}_s + 3OH^- \rightleftharpoons Al(OH)_3{\cdot}XH_2O + (6 - X)H_2O$$

$$[2]\quad Al(OH)_3{\cdot}XH_2O \rightarrow Al(OH)_{3c} + XH_2O$$

$$[3]\quad mAl{\cdot}6H_2O^{3+}{}_s + nOH^- \rightleftharpoons Al_m(OH)_n{}^{(3m-n)+}{\cdot}YH_2O_s + (m6 - Y)H_2O$$

where s, c and italics denote solution, gibbsite, and amorphous solid, respectively. The extraneous ions are omitted, *X* and *Y* are not known and n/m is equal to or very nearly equal

[1]Publication No. R171.

[2]Present address: Department of Soil Science, University of Saskatchewan, Saskatoon, Sask., Canada S7N 0W0.

Can. J. Chem. Downloaded from www.nrcresearchpress.com by 210.87.254.40 on 09/05/12
For personal use only.

Can. J. Chem. Downloaded from www.nrcresearchpress.com by 210.87.254.40 on 09/05/12
For personal use only.

to 2.5. Reaction 1 is a very fast reaction but will not occur until the ion activity product $(Al)(OH)^3$ is increased to $10^{-31.7}$. Reaction 2 is a slow solid state reaction, or series of processes, whereby the initial solid phases (ISP) from reaction 1, through elimination of H_2O and rearrangement of the Al and OH ions, eventually becomes gibbsite. Reaction 3 is a competing reaction with respect to [1] and is slower than [1] but will occur with $(Al)(OH)^3$ less than $10^{-31.7}$. The products of the latter reaction are polynuclear hydroxyaluminum cations, which will be referred to as Al_{P1}, with an OH/Al mole ratio equal to or near 2.5. If $AlCl_3$ is used instead of $Al(ClO_4)_3$ the reactions are the same, providing the Cl^- concentration is not too high (3), except that the ISP contains appreciable amounts of Cl^- (3, 4) which retards the transformation of ISP to gibbsite.

In order to produce Al_{P1}, without forming any solid phases, the base was added at a very slow rate so that the formation of Al_{P1} maintained $(Al)(OH)^3$ below that at which reaction 1 could occur (1). The base was added as the gas NH_3 or as solid dolomite to eliminate the problem of nonhomogeneous distribution of added base solution (5). Although no solids were formed, the concentration of Al_{P1} decreased very slowly with length of time of aging. The decrease in concentration of Al_{P1} was not accompanied by any change in the specific rate constant of the pseudo first order reaction between Al_{P1} and 8-hydroxyquinoline by the standard method (1). A decrease of approximately 35% in the concentration of Al_{P1} during an aging period of 2 years at 25 °C was accompanied by a very small increase in the concentration of mononuclear Al cations and only a slight decrease in p*H*, which indicated that the Al_{P1} was not hydrolyzing to any extent to form a new product with an OH/Al mole ratio much different from that of Al_{P1}. From the foregoing and other observations it was concluded (1) that as Al_{P1} disappeared a new species of polynuclear hydroxyaluminum cation, Al_{P2}, was formed which had some properties that were entirely different from those of Al_{P1}.

The object of the work reported here was to gain experimental evidence in support of the existence of Al_{P2}, as a polynuclear hydroxyaluminum cation, by determining a number of its properties and to study the kinetics of the transformation from Al_{P1} to Al_{P2}. The properties studied were the kinetics of reaction between it and 8-hydroxyquinoline by the standard procedure for Al_{P1}, diffusion across a dialysis membrane, the p*H* of precipitation by a base and its cation exchange characteristics.

Experimental

The Al_{P1} was prepared as described in a previous paper (1) by Procedure A or B. With Procedure A finely ground dolomite was added to solutions of either $AlCl_3$ or $Al(ClO_4)_3$ and the suspensions were stirred vigorously with a magnetic stirrer. The Al concentrations used were 5×10^{-4} to 6×10^{-2} *M*. After 5 days the solutions were filtered through No. 42 Whatmann filter papers and CO_2-free air was bubbled through the filtrates for 4 h. With Procedure B a mixture of NH_3 and CO_2-free air was led into reaction vessels over 10^{-2} *M* Al salt solutions which were stirred vigorously with a magnetic stirrer. The concentration of NH_3 in the air was adjusted so that it required a month or more to reach 80% neutralization. The solutions from both procedures were then aged at 25 °C with gentle stirring for periods up to 2 years.

During the aging periods, reactions between aliquots of the solutions and 8-hydroxyquinoline – sodium acetate were followed until all of the Al in solution had reacted, using the standard procedure (6). The fraction that reacted with the usual first order specific rate constant of 0.16 min^{-1} was assumed to be Al_{P1}. The remainder, which reacted much more slowly but completely via a first order process, was assumed to be Al_{P2}.

The p*H*'s at which Al_{P1} and Al_{P2} were precipitated at 25 °C were determined by potentiometric titration of solutions containing different proportions of Al_{P1} to Al_{P2}. The base, 0.1 *N* NaOH, was added dropwise while the solutions were stirred with a magnetic stirrer. The p*H* was followed during titration by means of an expanded scale Beckman p*H* meter.

Cation exchange studies were done with Wyoming bentonite originally saturated with Na^+. One hundred mg of clay was mixed with 20 ml of solution containing known concentrations of Al in the form of Al_{P1} and Al_{P2}. The suspensions were then centrifuged at 15 000 rpm. The concentrations of Al in the form of Al_{P1} and Al_{P2} were determined in the supernatants by the procedure described above. The residues were extracted twice with 20 ml of 2 *N* NaCl and the two extracts combined. The concentrations of Al in the two forms were determined in the extracts.

The dialysis experiments were done by placing solutions containing known concentrations Al in the form of Al_{P1} and Al_{P2} in dialysis bags and placing the bags in redistilled H_2O. A continuous flow of H_2O was maintained outside the bag and the bag was agitated intermittently. The concentrations of Al in the form of Al_{P1} and Al_{P2} inside the bag were determined after dialysis.

Results

The results in Fig. 1(*b*), which show the con-

Can. J. Chem. Downloaded from www.nrcresearchpress.com by 210.87.254.40 on 09/05/12
For personal use only.

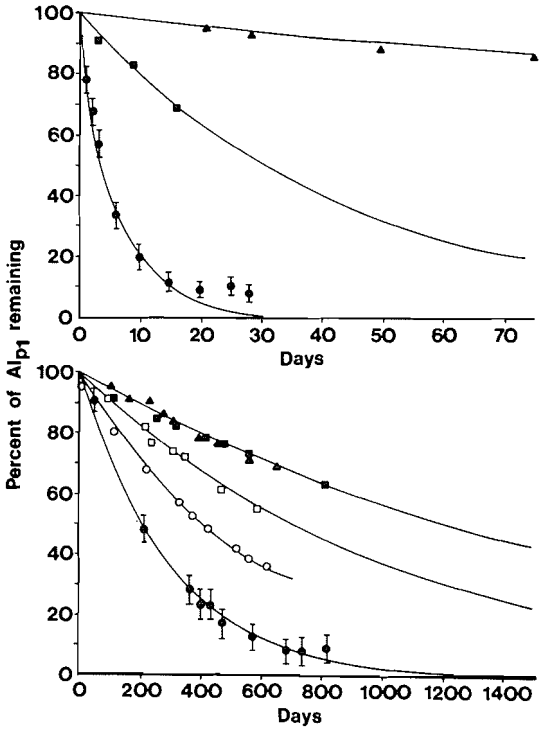

FIG. 1. (*a*) Effect of temperature on rate of decrease in concentration of Al_{P1} in 10^{-2} *M* $Al(ClO_4)_3$ 54% neutralized with NH_3. ▲, 26 °C, specific rate constant 0.0017 day^{-1}; ■, 50 °C, specific rate constant 0.023 day^{-1}; ●, 70 °C, specific rate constant 0.16 day^{-1}; and I, standard deviations. (*b*) Rate of decrease in concentration of Al_{P1} at 25 °C. ▲, 10^{-2} *M* $AlCl_3$, 81% neutralized with dolomite; specific rate constant 0.00057 day^{-1}; ■, 10^{-2} *M* $AlCl_3$, 81% neutralized with NH_3; specific rate constant 0.00057 day^{-1}; □, 10^{-2} *M* $AlCl_3$, 34% neutralized with NH_3; specific rate constant 0.0010 day^{-1}; ○, 6×10^{-2} *M* $Al(ClO_4)_3$, 70% neutralized with dolomite; specific rate constant 0.0017 day^{-1}; ●, 6×10^{-2} *M* $Al(ClO_4)_3$, 40% neutralized with dolomite; specific rate constant 0.0035 day^{-1}; I, standard deviations.

centrations of Al in the form of Al_{P1} as a function of length of time of aging at 25 °C, indicate that the reaction was a first order process. The results with 6×10^{-2} *M* $Al(ClO_4)_3$, which had been 40% neutralized with dolomite (Procedure A), show that the reaction appeared to be approaching equilibrium with 5 to 10% of the Al_{P1} remaining. The smooth curves were calculated with specific rate constants ranging from 5.7 to 10^{-4} to 3.5×10^{-3} day^{-1} (Fig. 1). The length of time of aging was calculated ignoring the time required for adding the base. Because the reactions were first order with equilibrium well over to the right and the results in the figure are expressed as percent of Al in the form of Al_{P1} remaining to react, ignoring the time required for adding the base should have no measurable effect on the calculated specific rate constants or on the results as shown in the figure. The effect of temperature on the rate of disappearance of Al_{P1} with a solution of 10^{-2} *M* $Al(ClO_4)_3$ 54% neutralized with NH_3 (Procedure B) is shown in Fig. 1(*a*). The solution was held at 26 °C for 75 days, raised to 50 °C for 15 days, and then raised to 70 °C for 38 days. The lengths of time of reaction at 26 and 50 °C were sufficient for calculation of specific rate constants assuming a first order process, an assumption supported by results in Fig. 1(*b*) and corroborated by the results at 70 °C shown in Fig. 1(*a*). At 70 °C the reaction appeared to be approaching equilibrium with 6 to 13% of the Al_{P1} remaining but, because the same solution was used at 26 and 50 °C, considerable reaction had occurred before the temperature was raised to 70 °C. Thus the percent of Al_{P1} originally present remaining at equilibrium would be considerably less than 6 to 13. The specific rate constants calculated from the experimental values were 1.7×10^{-3}, 2.3×10^{-2}, and 1.6×10^{-1} day^{-1}, respectively, at 26, 50, and 70 °C. The Arrhenius plot gave a straight line showing an activation energy of 20.8 kcal/mol.

The specific rate constant varied considerably at 26 °C from one experiment to another (Table 1). It can be seen that the rate constant increased with decrease in degree of neutralization at a given Al concentration except at the lowest concentration, 5×10^{-4} *M*, where the degree of neutralization seemed to have no effect. Besides this fairly consistent relationship with degree of neutralization, the rate constant appeared to be greater when perchlorate rather than chloride was the anion present, as can be seen by comparing rows 6, 7, and 8 with the last row in Table 1.

A number of experiments were made on the rate of reaction between Al_{P2} and 8-hydroxyquinoline using the standard method for reaction with Al_{P1} (6). During aging at 25 °C, discussed above, the reaction with 8-hydroxyquinoline was occasionally followed through to completion. In all cases all of the Al in the solution reacted in a matter of days. The procedure was to add an appropriate aliquot of the solution to the correct amount of the 8-hydroxyquinoline –

TABLE 1. Effect of degree of neutralization and extraneous anions in solution on the specific rate constant for the disappearance of Al_{P1} at 26 °C

[Al] $\times 10^3 M$	Salt	Base	Degree of neutralization	Length of time of reaction (days)	Specific rate constant (day^{-1})
60	$Al(ClO_4)_3$	Dolomite	0.70	773	0.0017
60	$Al(ClO_4)_3$	Dolomite	0.40	749	0.0035
10	$AlCl_3$	Dolomite	0.81	801	0.00057
10	$AlCl_3$	Dolomite	0.67	635	0.00077
10	$AlCl_3$	Dolomite	0.52	665	0.0010
10	$AlCl_3$	NH_3	0.81	707	0.00057
10	$AlCl_3$	NH_3	0.75	581	0.00083
10	$AlCl_3$	NH_3	0.34	589	0.0010
0.5	$AlCl_3$	Dolomite	0.72	519	0.0010
0.5	$AlCl_3$	Dolomite	0.52	645	0.0010
0.5	$AlCl_3$	Dolomite	0.34	699	0.0011
10	$Al(ClO_4)_3$	NH_3	0.54	114	0.0017

TABLE 2. Al_{P1} and Al_{P2} adsorbed by Wyoming bentonite and released again by 2 *N* NaCl

	Original solution $M \times 10^3$ Al as		Equilibrium solution $M \times 10^3$ Al as		Percent adsorbed[a]		Percent released[b]	
Expt	Al_{P1}	Al_{P2}	Al_{P1}	Al_{P2}	Al_{P1}	Al_{P2}	Al_{P1}	Al_{P2}
1	3.76	2.18	0.31	0.22	92	90	87	105
2	4.64	2.95	1.21	0.65	74	78	98	94
3*a*[c]	7.47	2.81	2.42	0.94	68	67	85	95
3*b*[c]	7.47	2.81	2.74	1.05	63	63	82	89
4[d]	3.76	2.18	0.17	0.26	98	88	77	108

[a]Percent of that in the original solution adsorbed by the clay.
[b]Percent of that adsorbed that was released to the NaCl solution.
[c]Duplicate experiments.
[d]Equilibration time 144 h. In the others the equilibration time was 5 min.

sodium acetate solution with sufficient H_2O added to give the correct volume in a separatory funnel. The separatory funnel was then placed in a constant temperature cabinet at 25 °C and allowed to react with gentle agitation for a given length of time. After each had reacted for the desired length of time, the procedure for extraction with chloroform and measurement of the Al concentration, the same as in the regular procedure (6), was used. The reaction after 30 min, *i.e.* after the time required for essentially all of the Al_{P1} to react, was a first order process and all of the Al in the system was extracted in the chloroform after one week of reaction. The mean value for the specific rate constant was 6×10^{-4} min^{-1} with a standard error of the mean of 0.2×10^{-4}. Knowing the specific rate constants for the two forms, the concentration of Al in the form of Al_{P1} and Al_{P2} could then be calculated from the rate curves. The effect of temperature on the specific rate constant was determined at 30, 50, 60, and 70 °C. The technique used at 30 °C was the same as that used at 25 °C but at 50, 60, and 70 °C the standard procedure (6) was used throughout, the reaction being continued until all of the Al in the solution had reacted as shown by the concentration of Al in the chloroform. The reactions with the Al_{P2} were first order at all temperatures with specific rate constants of 6.1×10^{-4}, 8.1×10^{-4}, 5.5×10^{-3}, 1.4×10^{-2}, and 3.3×10^{-2} min^{-1} at 25, 30, 50, 60, and 70 °C, respectively. The Arrhenius plot gave a straight line showing an energy of activation of 18.3 kcal/mol.

Results from the exchange experiments with Wyoming bentonite are shown in Table 2. The percent absorbed from the original solution was about the same for Al_{P2} as it was for Al_{P1}, the

Can. J. Chem. Downloaded from www.nrcresearchpress.com by 210.87.254.40 on 09/05/12
For personal use only.

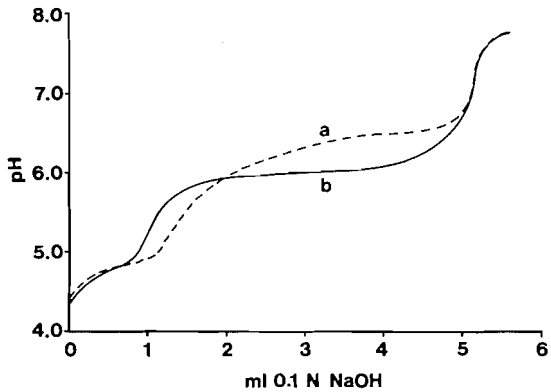

FIG. 2. Potentiometric titration of Al_{P1} and Al_{P2} with 0.1 *N* NaOH, (*a*) 6.3% mononuclear, 23.7% Al_{P1}, 70.0% Al_{P2}; (*b*) 4.3% mononuclear, 95.7% Al_{P1}.

means of the percent absorbed for the five experiments shown being 77.2 and 79.0, respectively. The percent of adsorbed material released to the 2 *N* NaCl was somewhat higher for Al_{P2} than it was for Al_{P1}, the means of the percents released for the four experiments in which the clay was in contact with the original solution for only 5 min being 96 and 88, respectively. When the original solution was in contact with the clay for 144 h the percent released to the NaCl solution was much greater for Al_{P2} than for Al_{P1} (last row of Table 2). Although the greater release of Al_{P2} than of Al_{P1} to the NaCl is probably significant, it would be dangerous to attempt an explanation of this with the few results available, especially because the duplicate experiments (3*a* and 3*b*) show that the experimental error in such work is appreciable. The object of these experiments was to show that both Al_{P1} and Al_{P2} are adsorbed in an exchangeable form by the clay mineral. The fact that the percent of each in the original solutions that was adsorbed by the clay was about the same is fairly strong evidence that the charges on Al_{P1} and Al_{P2} are not greatly different.

The potentiometric titration curves (Fig. 2) show that the buffer zone for Al_{P1}, where it is precipitated, is near p*H* 6.0 whereas the corresponding buffer zone for Al_{P2} is 0.40 to 0.50 p*H* units higher. Although this particular experiment was not done in duplicate, a number of such experiments were made with varying ratios of Al_{P1} to Al_{P2} and the buffer zone for Al_{P2} was always 0.40 to 0.50 p*H* units higher than that for Al_{P1}.

The dialysis experiments showed that both Al_{P1} and Al_{P2} diffused readily across a dialysis membrane. In one experiment, in which the concentrations of Al in the Al_{P1} and Al_{P2} forms were 8 and 42%, respectively, 59% of the Al_{P1} and 75% of the Al_{P2} diffused out of the dialysis bag in 1 h. In all other experiments, the length of time of dialysis was 24 h and all of the Al_{P1} and Al_{P2} diffused out of the bag regardless of the degree of neutralization, the ratio of the concentrations of Al_{P1} to Al_{P2}, or the temperature at which Al_{P2} was formed.

Discussion

The relatively rapid transformation of Al_{P1} to Al_{P2} at 70 °C indicates that the polynuclear hydroxyaluminum cations produced by Mesmer and Baes (7) and Macdonald *et al.* (8) were Al_{P2} type rather than Al_{P1}. The latter, being the first product, is very slowly transformed to the second type at 25 °C.

There is no way of deciding from the results to date whether Al_{P2} is formed very slowly from solution, which would make the solution unsaturated with respect to Al_{P1}, or from rearrangement of the ions in Al_{P1}, *i.e.* by the gradual transformation of Al_{P1} to Al_{P2}. The fact that the decrease in concentration of Al_{P1} followed a first order process (Fig. 1) supports the latter mechanism. This conclusion is based on the fact that the concentrations of Al^{3+} and OH^- in solution changed very little during aging (1) which would mean that the rate of formation of Al_{P2} should be very nearly a zero order process. The increase in concentration of Al_{P2}, however, corresponded quantitatively with the decrease in concentration of Al_{P1}, thus the formation of Al_{P2} was not a zero order process. On the other hand, the rate of decrease of Al_{P1}, and thus the rate of formation of Al_{P2}, was greater when ClO_4^- was the anion present rather than Cl^- (Table 1). This is difficult to explain if the formation of Al_{P2} is simply the rearrangement of ions in Al_{P1}, unless Al_{P1} contains some Cl^- replacing OH^- or that there is ion pairing between the polynuclear cations and Cl^-, either of which might slow down the transformation. There still remains the question of why this transformation would be faster at lower degrees of neutralization (Table 1). The final answer to this aspect of the problem will have to await further investigations.

Can. J. Chem. Downloaded from www.nrcresearchpress.com by 210.87.254.40 on 09/05/12
For personal use only.

There is no question concerning the relative resistance of the two forms Al_{P1} and Al_{P2} to attack from other chemicals. Al_{P1} is attacked much more readily by 8-hydroxyquinoline (specific rate constant 0.16 min^{-1} at 26 °C) (6) than is Al_{P2} where the specific rate constant is less by 260-fold. Al_{P2} also resists precipitation until the p*H*'s are well above that at which Al_{P1} is precipitated (Fig. 2). Although no formal experiments were made to determine the relative resistance of the two forms to attack by HCl, it was observed that in HCl solutions at p*H* 1.6 Al_{P1} was completely destroyed at 100 °C in less than $\frac{1}{2}$ h, whereas Al_{P2} was not completely destroyed until the length of time was extended to several hours. In some respects, however, the two forms are very similar. They are both removed from solution by bentonite in an exchangeable form and both diffuse readily across a dialysis membrane. The fact that they have about the same OH/Al mole ratio (1) and the same or nearly the same positive charge (Table 2) indicates that Al_{P2} is not the result of some form of polymerization or condensation of Al_{P1}.

Studies concerning the structure of both Al_{P1} and Al_{P2} may be necessary to explain why some of their properties are quite different while others are similar.

1. R. C. Turner. Can. J. Chem. **54**, 1528 (1976).
2. R. C. Turner and G. J. Ross. Can. J. Chem. **48**, 723 (1970).
3. G. J. Ross and R. C. Turner. Soil Sci. Soc. Am. Proc. **35**, 389 (1971).
4. R. C. Turner and G. J. Ross. Can. J. Soil Sci. **49**, 389 (1969).
5. A. V. Vermeulen, J. W. Geas, R. J. Stol, and P. L. de Bruyn. J. Colloid Interface Sci. **43**, 449 (1975).
6. R. C. Turner and W. Sulaiman. Can. J. Chem. **49**, 1683 (1971).
7. R. E. Mesmer and C. F. Baes, Jr. Inorg. Chem. **10**, 2290 (1971).
8. D. D. Macdonald, P. Butler, and D. Owen. J. Phys. Chem. **77**, 2474 (1973).

Can. J. Chem. Downloaded from www.nrcresearchpress.com by 210.87.254.40 on 09/05/12
For personal use only.

Thermodynamics of the dissociation of *trans*-cinnamic acid

REBATI CHARAN DAS
Department of Chemistry, University College of Engineering, Burla 768018 (Orissa) India
AND
UPENDRA NATH DASH AND KSHAMA NIDHI PANDA
Department of Chemistry, G. M. College, Sambalpur (Orissa) India

Received January 5, 1976

REBATI CHARAN DAS, UPENDRA NATH DASH, and KSHAMA NIDHI PANDA. Can. J. Chem. **54**, 1916 (1976).

The dissociation constant of *trans*-cinnamic acid in water has been determined at 15, 20, 25, 30, 35, 40, and 45 °C using a cell without liquid junction potential. From the temperature coefficient of the dissociation constant, the standard enthalpy, entropy, and free energy changes of the dissociation process have been calculated.

REBATI CHARAN DAS, UPENDRA NATH DASH et KSHAMA NIDHI PANDA. Can. J. Chem. **54**, 1916 (1976).

Utilisant une cellule sans potentiel de jonction liquide, on a déterminé les constantes de dissociation de l'acide cinnamique en solution dans l'eau à 15, 20, 25, 30, 35, 40 et 45 °C. A partir des coefficients de température sur les constantes de dissociation, on a calculé les changements standards d'enthalpie, d'entropie et d'énergie libre pour le processus de dissociation.
[Traduit par le journal]

Introduction

The present work has been undertaken as a part of our programme of the determination of dissociation constants and other thermodynamic parameters of organic acids in aqueous and mixed solvents. A survey of the literature shows that the dissociation constant of *trans*-cinnamic acid has been determined colorimetrically (1) at 25 °C, but data about other thermodynamic parameters (ΔH^0, ΔS^0 etc.) are lacking.

A cell without liquid junction,

$$\text{Pt} \mid \text{H}_2\text{Q-Q}, \text{HCi}(m_1), \text{NaCi}(m_2), \text{NaCl}(m_3) \mid \text{AgCl}_{(s)}, \text{Ag}$$

where Ci stands for cinnamate ion, was used.

Experimental

trans-Cinnamic acid (Bush, England) was crystallised three times from boiling conductivity water, dried at 60 °C for 2 h and kept in a vacuum desiccator over calcium chloride. Sodium cinnamate was prepared by adding calculated amount of sodium hydroxide (G.R.) solution to a known weight of pure cinnamic acid, evaporating the solution to dryness on a steam bath and recrystallising the product from 95% alcohol. The salt was dried at 110–120 °C and stored in vacuum desiccator over calcium chloride. Sodium chloride (BDH, AnalaR) was dried above 100 °C and stored in vacuo. The silver – silver chloride electrode was prepared by the latest method available (2). Electromotive force measurements were made with a Bajaj (India) potentiometer in conjunction with a d.c. galvanometer (OSAW) and a Weston standard cell (Muirhead and Co., England).

Results and Discussion

The dissociation constant of *trans*-cinnamic acid can be written as

$$[1] \quad K = \frac{m_{H^+} m_{Ci^-}}{m_{HCi}} \frac{\gamma_{H^+}\gamma_{Ci^-}}{\gamma_{HCi}} = \frac{m_{H^+} m_{Ci^-}}{m_{HCi}} \gamma_{\pm}^2$$

where m and γ are molality and activity coefficient, respectively (assuming $\gamma_{H^+} = \gamma_{Cl^-} = \gamma_{\pm}$ and $\gamma_{HCi} = 1$). The apparent hydrogen ion molality, m_{H^+}', is related to the emf of the cell by

$$[2] \quad -\log m_{H^+}' = \frac{F(E^0 - E)}{2.3026RT} + \log m_{Cl^-} + 2\log\gamma_{\pm} = \frac{F(E^0 - E)}{2.3026RT} + \log m_{Cl^-} - \frac{2A\sqrt{Id_0}}{1 + B\mathring{a}\sqrt{Id_0}}$$

where I and d_0 are the ionic strength of the solution and the density of the solvent, respectively. As a first approximation I was taken to be equal to $m_2 + m_3$ but subsequently an accurate value was obtained by successive approximation and refinement to a constant value of I. The apparent

Can. J. Chem. Downloaded from www.nrcresearchpress.com by 210.87.254.40 on 09/05/12
For personal use only.

dissociation constant, K', was calculated from the expression

$$[3]\quad \log K' = -\frac{2A\sqrt{Id_0}}{1 + B\mathring{a}\sqrt{Id_0}} + \log \frac{m_{H^+}'(m_2 + m_{H^+}')}{(m_1 - m_{H^+}')}$$

The true dissociation constant, K, was determined from the intercept of the log K' *vs.* I plot. At each temperature about 7 to 9 readings were taken with m_1 in the range of $0.3–0.9 \times 10^{-3}$ mol kg^{-1}, m_2 in the range $0.25–1.6 \times 10^{-3}$ mol kg^{-1}, and m_3 in the range $20–86 \times 10^{-3}$ mol kg^{-1}, and I between $3–9 \times 10^{-2}$. The final results[1] are tabulated in Table 1.

TABLE 1. Values of pK of *trans*-cinnamic acid in water at different temperatures

T(°C)	pK
15	4.59±0.03
20	4.53±0.02
25	4.50±0.01
30	4.49±0.02
35	4.48±0.01
40	4.46±0.02
45	4.42±0.02

In the calculation the standard electrode potentials of the silver – silver chloride and of the quinhydrone electrodes have been taken from literature (3). This calculation requires a suitable choice of the ion-size parameter, $\mathring{a}$, and it is well known that a wrong choice of the value of $\mathring{a}$ is often a source of considerable uncertainty in pK (4, 5). For example, the pK_1 of phosphoric acid shifted by 0.004 when the assumed $\mathring{a}$ value was changed from 4 to 6 Å. To ascertain the correct value of $\mathring{a}$, the pK at 25 °C was calculated for various values of $\mathring{a}$ (3 to 6 Å at intervals of 0.5 Å) from the data at that temperature and it was observed that its value had the least standard deviation for $\mathring{a}$ = 5 Å. Thus, following the principle adopted by Roy, Robinson, and Bates (6), $\mathring{a}$ was taken to be equal to 5 Å in our calculations.

The pK of *trans*-cinnamic acid has earlier been reported to be 4.44 at 25 °C by spectrophotometry. This is slightly different from our value of 4.50 ± 0.01 at the same temperature. Such differences exist even in very accurate determinations of equilibrium constants by different physical methods, examples are plentiful in literature (7).

The value of the ΔH^0 of the dissociation reaction has been calculated from the slope of the plot of pK against $1/T$, assuming it to be independent of temperature. The ΔG^0, ΔH^0, and ΔS^0 values of the dissociation process at 25 °C are 25.67 ± 0.07 kJ mol^{-1}, 2.87 ± 0.46 kJ mol^{-1}, and −76.5 ± 1.7 J deg^{-1} mol^{-1}, respectively.

[1]Detailed tables of experimental data are available, at nominal cost, from the Depository of Unpublished Data, CISTI, National Research Council of Canada, Ottawa, Canada K1A 0S2.

1. S. GLASSTONE. An introduction to electrochemistry. Van Nostrand Publishers. 1964. p. 330.
2. G. C. PAL and M. SENGUPTA. J. Indian Chem. Soc. **45**, 179 (1968).
3. (*a*) H. S. HARNED and B. B. OWEN. The physical chemistry of electrolytic solutions. Reinhold. 1967. p. 715. (*b*) R. G. BATES. Electrometric pH determination. Wiley, New York. 1954.
4. R. G. BATES. J. Res. Natl. Bur. Stand. **47**, 127 (1951).
5. E. J. KING and G. W. KING. J. Am. Chem. Soc. **74**, 1212 (1952).
6. R. N. ROY, R. A. ROBINSON, and R. G. BATES. J. Am. Chem. Soc. **95**, 8231 (1973).
7. L. G. SILLEN and A. E. MARTELL (*Editors*). Stability constants of metal ion complexes, 2nd ed. Chemical Society Publication, London. 1964.

Can. J. Chem. Downloaded from www.nrcresearchpress.com by 210.87.254.40 on 09/05/12
For personal use only.

The nuclear Overhauser effect between phosphorus and hydrogen in selected organo phosphorus compounds

H. BEIERBECK, R. MARTINO,[1] AND JOHN K. SAUNDERS
Département de chimie, Université de Sherbrooke, Sherbrooke (Qué.), Canada J1K 2R1

AND

CLAUDE BENEZRA
Département de chimie, Université d'Ottawa, Ottawa (Ont.), Canada K1N 6N5

Received August 15, 1975[2]

H. BEIERBECK, R. MARTINO, JOHN K. SAUNDERS, and CLAUDE BENEZRA. Can. J. Chem. **54**, 1918 (1976).

The nuclear Overhauser effect (nOe) observed between phosphorus and hydrogen together with carbon and phosphorus spin lattice relaxation time (T_1) data are presented for a number of phosphorus containing compounds. The dominant mechanism for phosphorus relaxation is shown to be the dipole–dipole interaction between phosphorus and hydrogen. From the nOe and T_1 data the determination of phosphorus–hydrogen internuclear distances is demonstrated.

H. BEIERBECK, R. MARTINO, JOHN K. SAUNDERS et CLAUDE BENEZRA. Can. J. Chem. **54**, 1918 (1976).

Nous avons mesuré, pour quelques composés phosphorés, l'effet nucléaire Overhauser (nOe) entre les atomes de phosphore et d'hydrogène ainsi que les temps de relaxation spin-réseau (T_1) des atomes de carbone et de phosphore. Les résultats obtenus montrent que le processus de relaxation dominant de l'atome de phosphore résulte des interactions dipole–dipole entre le phosphore et l'hydrogène. A partir des mesures de nOe et de T_1 nous avons pu déterminer les distances internucléaires entre le phosphore et l'hydrogène.

The nuclear Overhauser effect (nOe) arising from the interaction proton–proton has been used to advantage in structural and conformational studies (1–3). Also, the enhancement observed at carbon on saturation of protons has been of considerable use in spectral assignment and in relaxation mechanism studies (3, 4) as have the {H}–^{15}N (5) and {H}–Si nOes (6). However, to date, little mention has been made of the phosphorus–hydrogen interaction which is somewhat surprising as phosphorus occurs in a large number of molecules of biological interest and is reasonably easy to observe, having a natural abundance of 100% and a relatively high sensitivity. We wish to report the results of a study on a number of simple phosphorus containing molecules in order to demonstrate that the dipole interaction between phosphorus and hydrogen is significant and thus the phosphorus–proton nOe can be of use in structural and conformational analysis.

[1]Holder of a bourse post-doctorale France–Québec.
[2]Revision received March 4, 1976.

Theory

The nOe observed for the absorption of A when that of B is saturated is given by [1] (1)

$$[1] \qquad f_A(B) = \frac{\gamma_B}{2\gamma_A}\frac{\rho_{AB}}{R_A} - \sum_i \frac{\gamma_i}{2\gamma_A}\frac{\rho_{Ai}}{R_A} f_i(B)$$

with

$$\rho_{AB} = \frac{\hbar^2 \gamma_A{}^2 \gamma_B{}^2}{(r_{AB})^6}\,\tau_R$$

and

$$R_A = \rho_{AB} + \sum_i \rho_{Ai} + \rho^*$$

where i represents all other nuclei which are coupled in a time dependent manner to A, τ_R is the isotropic correlation time for molecular motion, r_{AB} is the internuclear distance between A and B and ρ^* is the contribution from all other relaxation mechanisms. Thus for a spin system consisting of one phosphorus and several hydrogen atoms, complete saturation of all hydrogen resonances would result in a maximum enhancement ($\rho^* = 0$) of $f_P(H) = \gamma_H/2\gamma_P = 1.24$.

For a three spin system consisting of two pro-

Can. J. Chem. Downloaded from www.nrcresearchpress.com by 210.87.254.105 on 09/05/12
For personal use only.

Can. J. Chem. Downloaded from www.nrcresearchpress.com by 210.87.254.105 on 09/05/12
For personal use only.

tons H_A and H_B and one phosphorus P, [1] can be solved to give equations such as [2] (1) from which the ratio of the relaxation rates can be calculated.

$$[2] \quad \frac{\rho_{PH_A}}{\rho_{PH_B}} = \frac{\gamma_H}{\gamma_H} \frac{[f_P(H_B) + f_P(H_A) f_{H_A}(H_B)]}{[f_P(H_A) + f_P(H_B) f_{H_B}(H_A)]}$$

Equation 2 can be simplified to give [3] provided $f_{H_A}(H_B) = f_{H_B}(H_A) = 0$ and the internuclear distances are independent of time. In [3], the

$$[3] \quad \frac{\rho_{PH_A}}{\rho_{PH_B}} = \frac{\tau_C(P\text{–}H_A)}{(r_{P\text{–}H_A})^6} \frac{(r_{P\text{–}H_B})^6}{\tau_C(P\text{–}H_B)} = \frac{f_P(H_A)}{f_P(H_B)}$$

correlation times represented by τ_C are the effective correlation times for the interactions P–H_A and P–H_B. Evidently, for a rigid molecule undergoing isotropic motion, the values of τ_C will be identical and the ratio of the internuclear distances can be obtained directly from the nOe data. However, if internal motion is present as is the case in the compounds studied here, then both correlation time and nOe data are required in order to determine internuclear distances.

In our examples, the values of τ_C can be determined using the ^{13}C relaxation time data. The overall correlation time can be obtained using [4] for carbons (α) whose C—H bond vectors are modulated only by the motion of the molecule itself.

$$[4] \quad \frac{1}{NT_1(\alpha)} = \frac{\hbar^2 \gamma_H^2 \gamma_C^2}{(r_{C\text{–}H})^6} \tau_R$$

The correlation time for carbons (β) whose C—H bond vectors are modulated by both overall molecular motion and internal rotation can then be calculated using [5] (7, 8).

$$[5] \quad \frac{NT_1(\alpha)}{NT_1(\beta)} = \left(A + B\frac{6}{6+\rho} + C\frac{3}{3+2\rho}\right)$$

and $\rho = R_\perp/R_{11}$ where $R_\perp$ and R_{11} are the diffusion rate constants relative to the axis of internal rotation and can be represented by $\rho = \tau_R/\tau_i$, where τ_i is the correlation time for internal motion. The values of A, B, and C depend on the angle ϕ between the C—H bond vector and the axis of rotation and are

$$A = \tfrac{1}{4}(1 - 3\cos^2\phi)^2$$

$$B = 3\sin^2\phi\cos^2\phi$$

$$C = \tfrac{3}{4}\sin^4\phi$$

The effective correlation times are then calculated from [5] where ϕ is now the angle that the P—H vector makes with the axis of internal rotation. Equation 3 gives the ratio of internuclear distances and the enhancement measured on saturation of all proton resonances gives the value of ρ^*. The internuclear distance is then calculated from a knowledge of the experimental phosphorus T_1 value. Thus in order to completely define the system we must obtain experimentally all nOe values as well as carbon and phosphorus T_1 values.

Experimental

The compounds in Table 1 were obtained commercially and were used without further purification in either CD_3COCD_3 or D_2O as solvent. The compounds in Table 2 were prepared as described previously (9) and were studied as $CDCl_3$ solutions. The D_2O solutions were degassed by passing nitrogen through the solution whereas the $CDCl_3$ or CD_3COCD_3 solutions were degassed by a freeze–thaw–freeze cycle. The T_1 and nOe data were obtained on a Bruker HX-90 equipped with a Nicolet 1083 computer operating in the Fourier transform mode.

The T_1 data were obtained under conditions of complete proton decoupling using $180°\text{–}\tau\text{–}90°\text{–}5T_1$ pulse sequences as described previously (10). The use of complete decoupling allows both spectrum simplification and also leads to a mono exponential solution of the Bloch equations (11) as shown below. The Bloch equation as modified by Solomon (12) is given in [6].

$$[6] \quad \frac{dM_Z^A}{dt} = R_A(M_Z^A - M_A^o) - \sum_i \rho_{Ai}(M_Z^i - M_o^i)$$

provided the only time dependent coupling is the dipole–dipole interaction. If A is phosphorus or carbon and the nuclei represented by i are all protons then saturation of all proton resonances causes M_Z^t to be zero for all values of t. If at time $t = 0$, we apply a 180° pulse then at time t the magnetization is given by (1, 3).

$$[7] \quad M_Z^A(t) = \left(M_0^A + M_o^A \frac{\gamma_i}{2\gamma_A} \sum \frac{\rho_{Ai}}{R_A}\right) \times (1 - 2e^{-t/T_1})$$

and at $t = \infty$

$$M_Z^A(\alpha) = M_o^A\left(1 + \frac{\gamma_i}{2\gamma_A}\frac{\rho_{Ai}}{R_A}\right)$$

The value of T_1 is obtained from the slope of a plot of $\ln (M_Z^A(\alpha) - M_Z^A(t))$ *vs.* t.

Experimentally the nOe is defined as

$$f_A(B) = \frac{M_Z^A(\alpha) - M_o^A}{M_o^A}$$

TABLE 1. Spin lattice relaxation time and nuclear Overhauser effect data[a]

Compound	Solvent	Concentration (M)	nOe
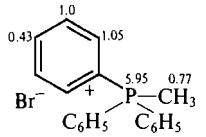	D_2O	0.55	f_P(all H) = 1.2±0.1 $f_P(CH_3)$ = 0.80±0.05 $f_P(C_6H_5)$ = 0.45±0.05
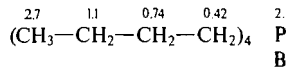	D_2O	0.8	f_P(all H) = 1.2±0.1
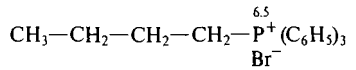	D_2O	0.1	f_P(all H) = 1.2±0.1 $f_P(C_6H_5)$ = 0.4±0.05
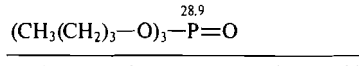	CD_3COCD_3	1.0	f_P(all H) = 0.9±0.1

[a] T_1 values written above respective nuclei in seconds; error limits for T_1 measurements ±5%.

with $M_Z^A(\alpha)$ being the equilibrium value of the magnetization of A with saturation of the B resonance and M_0^A the magnetization at equilibrium without saturation. The value of $M_Z^A(\alpha)$ is determined using $(-90°-5T_1-)$ pulse sequences with continuous saturation of the B resonance. The value of M_0^A is determined using the suppressed nOe technique in which the decoupler is turned on just during spectral accumulation and then the system is allowed to return to equilibrium after data acquisition with the decoupler off. This is shown in [8] which is the solution of [6] if at $t = 0$ the decoupler is turned on after having been off for $5T_1$ s.

$$[8] \quad M_Z^A = M_0^A + \frac{\gamma_i}{2\gamma_A} \frac{\sum_i \rho_{Ai}}{R_A} M_0^A(1 - e^{-R_A t})$$

Thus, if the system is sampled when $t = 0$, *i.e.* the decoupler is turned on as the pulse for data acquisition occurs, $M_Z^A = M_0^A$, and it is M_0^A that is measured. However, saturation of the second spin (s) requires a finite time during which undesired transients will affect the intensity of the observed signal (1). These transients will decay to zero with a time constant of T_2^*. Since under conditions of complete proton decoupling for ^{31}P or ^{13}C nmr, $T_2^* < T_1$ we could use values of t such that $t \approx 0.5T_1$. Experimentally we have found that if sampling is done at $t = 0$, the resulting resonances had unsatisfactory lineshapes and the intensities were irreproducible. For values of t such that $0.2T_1 < t < 0.5T_1$, the signals had normal lineshapes and gave reproducible results which were compatible with those obtained using CW methods. With values of $t > 0.5T_1$, the ratio of $M_Z^A(\alpha)$ to $M_Z^A(t)$ is such that the experimental error becomes significant. Thus various values of $M_Z(t)$ were measured with values of t such that $0.2T_1 < t < 0.5T_1$ in order to determine the value of M_0^A using [8].

The error limits for T_1 measurements are ±5%. For each carbon or phosphorus, $M_Z(\infty)$ was measured at least six times and $M_Z(t)$ values were obtained for at least 15 values of t. The standard deviation from the least-squares plot of log $(M_Z(\alpha) - M_Z(t))$ *vs.* t was always 1% or less. The use of the log $(M_Z(\infty) - M_Z(t)$ *vs.* t plot is very dependent on the value of $M_Z(\alpha)$ and any errors in this measurement will be reflected in the value of T_1 without changing the standard deviation. Thus the error limit will be greater than the 1% observed in the standard deviation. The error limit of ±5% was determined experimentally by repeating the T_1 determinations several times. In the compounds studied here, reasonably concentrated solutions were used and consequently good signal to noise ratios could be obtained relatively rapidly and also little or no resonance overlap occurred. For the nOe measurements, $M_Z(\alpha)$ was determined at least ten times and at least six measurements of $M_Z(t)$ at each value of t were made. The errors quoted were obtained experimentally and correspond in most cases to ±10%.

Results and Discussion

The relevant T_1 and nOe data for triphenylmethylphosphonium bromide are given in Table 1. The correlation time for the motion of the molecule was calculated using [4] and the T_1 values for the *para* carbon, since the C—H bond vector for this carbon is not modulated by internal rotation (13). The rotation rates about the respective P—C bonds were then calculated using [5] with values for the angle between the C—H bond vector and the axis of rotation of $\phi = 60°$ for the phenyl group and 109.7° for the rotation about the P—CH_3 bond. The ratios of the rotation rates, ρ, so calculated are 5.0 and 30.6 for rotation about the P—Ar and P—CH_3 bonds, respectively. Substitution of these values into [5] gave τ_C(P—Ar) = 0.48 τ_R and τ_C(P—CH_3) = 0.572 τ_R when angles between the P—H

Can. J. Chem. Downloaded from www.nrcresearchpress.com by 210.87.254.105 on 09/05/12
For personal use only.

TABLE 2. T_1 and nOe data for compounds **1–3**

Compound	T_1(P) (s)	f_P(all H)	f_P(OCH$_3$)
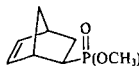 **1**	13.2	1.2±0.1	0.25±0.05
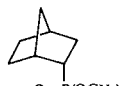 **2**	14.8	1.3±0.1	0.25±0.05
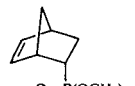 **3**	19.0	1.15±0.1	0.35±0.05

Error limits for T_1 measurements ±5%.

vector and the axis of rotation of 49.2° and 26.5°, respectively, are used. The ratio of internuclear P—H distances were then calculated from [3]

$$\frac{6\tau_C(\text{P–Ar})}{3\tau_C(\text{P–CH}_3)}\frac{(r_{\text{P–H}_{Me}})^6}{(r_{\text{P–H}_{Ar}})^6} = \frac{f_P(\text{H}_{Ar})}{f_P(\text{H}_{Me})} = \frac{0.45}{0.80}$$

where the factors 6 and 3 represent the number of equivalent hydrogens. The *meta* and *para* protons are too far removed from the phosphorus to give an enhancement. Substitution of this ratio together with the calculated τ_C's into

$$\left(\frac{1}{T_1}\right) = \hbar^2\gamma_H^2\gamma_P^2\left[\frac{6\tau_C(\text{P–Ar})}{(r_{\text{P–H}_{Ar}})^6} + \frac{3\tau_C(\text{P–CH}_3)}{(r_{\text{P–H}_{Me}})^6}\right]$$

gives values of $r_{\text{P–H}_{Me}} = 2.3 \pm 0.1$ Å and $r_{\text{P–H}_{Ar}} = 2.8 \pm 0.1$ Å which compare favourably with those calculated from molecular geometry (or measured from models) of 2.26 Å and 2.85 Å respectively.

As can be observed, the nOe is within experimental error of the maximum (1.24) and thus the phosphorus relaxation processes are dominated by the intramolecular dipole–dipole interaction. In Table 1, the nOe and T_1 data for several similar compounds are also given. The compounds where the phosphorus has geminal hydrogens all give nOe values close to the maximum. For the phosphate ester the nOe is 0.9 with a T_1 value of 28.9 s indicating that mechanisms other than dipole–dipole are significant, although the latter still dominates. From these, values of T_1(DD) = 40.4 s and T_1 (other mechanisms) = 101 s were calculated which demonstrate that relaxation processes other than the P—H dipole–dipole interaction are extremely inefficient.

The compounds **1–3** all gave nOe values approaching the maximum and thus in each compound the relaxation process is dominated by the dipole–dipole interaction (Table 2). In each case the nOe for the interaction between the two methoxyl groups and phosphorus could be measured. However, the resonances of the protons on the norbornane portion could not be saturated uniquely. The difference in T_1 between **2** and **3** is a consequence of the distance P–H$_3$ (*endo*) being significantly shorter in **2** than the distance P–H$_3$ in **3**.

For the triphenylphosphonium bromide, the rate constants for rotation about the P—Ar and P—CH$_3$ bonds are calculated to be 4.54×10^{10} rad/s and 2.81×10^{11} rad/s respectively. The corresponding barriers to rotation are then calculated using

$$k = \frac{N}{2}k_0e^{-\Delta E/RT}$$

where N = number of equivalent positions and $k_0 = (kT/I)^{1/2}$ (13). Thus $k_0 = 3.49 \times 10^{12}$ rad/s for the rotation about the P—Ar bond and 1.33×10^{13} rad/s for the rotation about the P—CH$_3$ bond. The barriers to rotation are then calculated to be 2.7 and 2.6 kcal/mol for rotation about the P—Ar and P—CH$_3$ bonds respectively.

It is apparent from the results presented here that the nOe, {H}–P, can be of significant use in the determination of structure and conformation since the phosphorus relaxation processes are dominated by the dipolar interaction. From an nOe standpoint, the advantage of phosphorus relative to carbon is that selective decoupling can be achieved since most compounds of interest do not have hydrogens directly bonded to phosphorus and hence the coupling constants J_{P-H} are significantly smaller than J_{C-H}.

Acknowledgements

We gratefully acknowledge generous financial assistance from the National Research Council of Canada and from the French and Quebec governments for a post-doctoral fellowship to one of us (RM).

Can. J. Chem. Downloaded from www.nrcresearchpress.com by 210.87.254.105 on 09/05/12
For personal use only.

1. J. H. NOGGLE and R. SCHIRMER. The nuclear Overhauser effect. Chemical applications. Academic Press. 1971.
2. R. A. BELL and J. K. SAUNDERS. Top. Stereochem. **7**, 1 (1972).
3. J. K. SAUNDERS and J. W. EASTON. *In* Organic structure determination by physical methods. Vol. 6. Academic Press, New York. Chapt. 5.
4. (*a*) A. J. JONES, D. M. GRANT, and K. F. KUHLMANN. J. Am. Chem. Soc. **85**, 1010 (1963); (*b*) J. R. LYERLA, D. M. GRANT, and R. D. BERTRAND. J. Phys. Chem. **75**, 3967 (1971); (*c*) K. H. KUHLMANN and D. M. GRANT. J. Chem. Phys. **55**, 2998 (1971); and references therein; (*d*) D. DODDRELL, V. GLUSHKO, and A. ALLERHAND. J. Chem. Phys. **56**, 3683 (1972).
5. (*a*) R. L. LICHTER and J. D. ROBERTS. J. Am. Chem. Soc. **94**, 2495 (1972); (*b*) P. A. COOPER, R. L. LICHTER, and J. D. ROBERTS. J. Am. Chem. Soc. **95**, 3724 (1973).
6. (*a*) R. L. SCHOLL, G. E. MACIEL, and W. K. MUSHER. J. Am. Chem. Soc. **94**, 6376 (1972); (*b*) G. C. LEVY. J. Am. Chem. Soc. **94**, 4793 (1972); G. C. LEVY, J. D. CARGIOLI, P. C. JULIANO, and T. D. MITCHELL. J. Am. Chem. Soc. **95**, 3445 (1973).
7. D. E. WOESSNER. J. Chem. Phys. **37**, 647 (1962).
8. A. ALLERHAND, D. DODDRELL, and R. KOMOROSKI. J. Chem. Phys. **55**, 189 (1971).
9. H. J. CALLOT and C. BENEZRA. Can. J. Chem. **50**, 1078 (1972).
10. J. W. APSIMON, H. BEIERBECK, and J. K. SAUNDERS. Can. J. Chem. **53**, 338 (1975).
11. (*a*) F. BLOCH. Phys. Rev. 460 (1946); (*b*) F. BLOCH and R. K. WANGNESS. Phys. Rev. **99**, 729 (1955).
12. I. SOLOMON. Phys. Rev. **99**, 559 (1955).
13. G. C. LEVY, J. D. CARGIOLI, and F. A. L. ANET. J. Am. Chem. Soc. **95**, 1527 (1973).
14. T. D. ALGER, D. M. GRANT, and R. K. HARRIS. J. Chem. Phys. **76**, 281 (1972).

Can. J. Chem. Downloaded from www.nrcresearchpress.com by 210.87.254.105 on 09/05/12
For personal use only.

A simple synthesis of alkylated and acylated dihydrothiopyrans

JOHN M. MCINTOSH AND HAMDY KHALIL[1]
Department of Chemistry, University of Windsor, Windsor, Ont., Canada N9B 3P4

Received January 19, 1976

JOHN M. MCINTOSH and HAMDY KHALIL. Can. J. Chem. **54**, 1923 (1976).

The reaction of β-mercaptoaldehydes and ketones with vinylphosphonium salts results in the ready formation of 3,6-dihydro-(2*H*)thiopyrans. The presence of an α-substituent on the salt blocks this reaction. It has also been shown that both α- and β-mercaptoaldehydes can be condensed with conjugated aldehydes to give 5,6-dihydro-(2*H*)thiopyran-3-carboxaldehydes (**13–15**) or 2,5-dihydrothiophene-3-carboxyaldehydes (**16**, **17**). The potential synthetic application of these reactions to stereospecific olefin synthesis is indicated.

JOHN M. MCINTOSH et HAMDY KHALIL. Can. J. Chem. **54**, 1923 (1976).

La réaction des β-mercaptoaldéhydes et cétones avec les sels de vinylphosphonium conduit à la formation facile de dihydro-3,6 (2*H*)thiopyrannes. La présence d'un substituant en α sur le sel empêche la réaction. On a aussi montré que les α et les β mercaptoaldéhydes peuvent se condenser avec des aldéhydes conjugués pour donner les dihydro-5,6 (2*H*)thiopyrannecarboxaldéhydes-3 (**13–15**) ou des dihydro-2,5 thiophènecarboxyaldéhydes-3 (**16**, **17**). On indique les possibilités d'application de ces réactions pour effectuer la synthèse stéréospécifique d'oléfines.
[Traduit par le journal]

The synthesis of organic molecules containing an isolated double bond of specific position and configuration is a challenging problem and is of considerable interest in connection with such problems as insect pheromone synthesis (I). The two general approaches that have been used center either on means of increasing the stereoselectivity of known reactions (*e.g.* the Wittig reaction (2)) or on methods which afford the product in a necessarily stereospecific manner. One of the classical methods which falls into the second group involves forming the olefin as part of a ring which is subsequently cleaved.

Recently, Biellmann and Ducep have shown (3) that reductive desulfurization of allylic sulfides can be achieved without apparent isomerization of the double bond either in position or stereochemistry using lithium in ethyl amine. Others have improved this procedure (4) and applied the technique to the synthesis of *Cecropia* Juvenile hormone utilizing the 3,6-dihydro-(2*H*)thiopyran system (**1**) (4,5). This allows the exclusive formation of the thermodynamically less stable *Z*-olefin isomer.

The usual method for the synthesis of **1** involves the Claisen condensation of appropriately substituted thiodipropionic esters, decarboxylation (6), and subsequent reduction and elimination. It seems clear that, even if the formidable synthetic obstacles to the preparation of unsymmetrically substituted **2** could be overcome, eliminations of water in such a system would not lead to a single isomer of **1**. A partial solution to this problem exists in the regioselective alkylation of **1** which introduces substituents at the allylic position adjacent to sulfur (3–5), but an alternate synthesis which would allow substitution at other positions would greatly expand the scope of the method. Our interest in the reactions of vinylphosphonium salts (7) with mercaptocarbonyl compounds (8) led us to consider the possibility of a regiospecific synthesis of **1**.

1

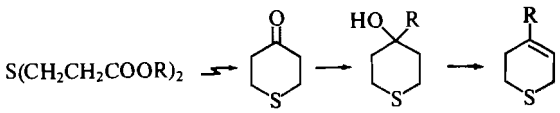

2 **1**

The advantages to this method are clear. The flexibility of substitution available in the vinyl salts and the ease of their formation has already

[1]National Research Council of Canada predoctoral fellow, 1974–present.

Can. J. Chem. Downloaded from www.nrcresearchpress.com by 210.87.254.42 on 09/05/12
For personal use only.

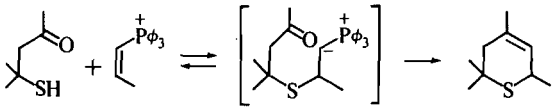

3 4

been established (8*a*) and in theory the use of appropriately substituted mercaptans, derived by addition of hydrogen sulfide to the olefinic aldehydes or ketones, would allow the introduction of substituents at any or all positions of **1**. Most important, the position of the double bond relative to the substituents would be known with certainty.

Results and Discussion

The mercaptans **3** are extremely viscous oils which possess strongly objectionable odors.[2] Unlike the α-mercaptocarbonyl compounds which exist as dimeric hemithioacetals (8*a*, 9), **3** appear to be polymeric in nature. Distillation is very difficult and is attended by severe decomposition, the products of which make the purification of **1** tedious. Fortunately, many of the mercaptans **3** are obtained relatively pure and we have found it advantageous to use them without further purification. In other cases, notably those of **3***b* and **3***c* the product was obviously highly impure. However, attempts at purification were both malodorous and unproductive and the crude material was best used directly.

The results of the investigation are shown in Tables 1 and 3. From these it can be seen that the reaction did proceed as expected and that the yields obtained make the method a synthetically viable one. It should be noted that the quoted yields are based on pure **3** and thus, especially in the cases of impure mercaptans (**3***b* and **3***c*), the actual yields of **8** and **9** are probably significantly higher than indicated.

When vinyl salts which bore an alkyl substituent on the α-carbon atom (**11**) were used, a completely different reaction ensued, leading to the formation of **13**. Schlosser (2) has noted that the presence of an α-alkyl group in a phosphorus ylide results in a tenfold decrease in the rate of betaine decomposition in the Wittig reaction. We have already observed and commented on

[2]Compound **3** is one of the principal odiferous components of cats' urine (10).

TABLE 1. Products and yields of dihydrothiopyrans from phosphonium salts

Mercaptan	Salt	Product	Time (h)	Yield (%)
3*a*[a]	**4***a*	**5**	20	85
3*a*	**4***b*	**6**	20	81
3*a*	**4***c*	**7**	20	65
3*b*	**4***b*	**8**	24	45
3*c*	**4***a*	**9**[b]	20	25
3*d*	**4***a*	**10**	20	51

[a]Reference 13.
[b]Reference 6.

(11) the fact that retardation of the normal Wittig cyclization in this type of system appears to allow time for competing reactions to intervene. Apparently in this case, the elimination of hydrogen sulfide from **3** is the most favourable competing reaction and subsequent condensation of **3** with the elimination product leads to **13** (Scheme 1). It is interesting to note that no sign of hydrogen sulfide elimination could be detected using the unsubstituted salts **4**, which

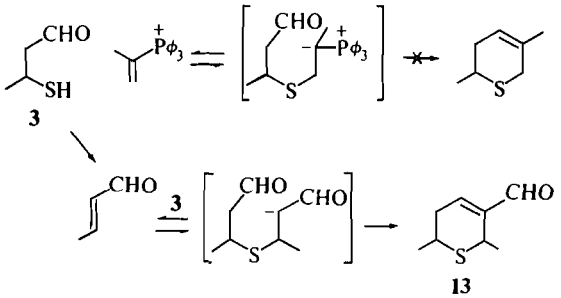

SCHEME 1

Can. J. Chem. Downloaded from www.nrcresearchpress.com by 210.87.254.42 on 09/05/12
For personal use only.

Can. J. Chem. Downloaded from www.nrcresearchpress.com by 210.87.254.42 on 09/05/12
For personal use only.

TABLE 2. Products and yields of formyldihydrothiopyrans

Mercaptan	Acceptor	Product	Time (h)	Yield (%)[a]
3*a*			18	94
	12*a*	**13**		
3*a*		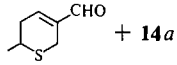 + **14***a*	18	85
	12*b*	**14**		
3*a*		+ **13**	18	65
	12*c*[b]	**15**		
	12*a*	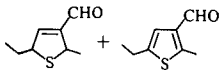	18	63
3*e*		**16** **16***a*		
3*e*	**12***b*	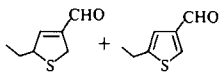	18	65
		17 **17***a*		

[a]Based on unrecovered mercaptan.
[b]Two equiv. used.

suggests a relatively rapid rate of ring closure in these cases.

The implication that vinyl salt **11** was not involved in the reaction was verified by carrying out the condensation between **3** and a variety of conjugated carbonyl compounds **12** and isolating the products in good yields (Table 2). Furthermore α-mercaptoaldehydes (*e.g.* **3***e*) could be used and the expected dihydrothiophenes **16** and **17** were formed. Products of this type are not available from the previously reported reactions of vinylphosphonium salts.[3] Compounds **13–17** as collected from glc were uniformly clear oils which rapidly turned yellow. Consequently, although we were able to obtain good spectral data, attempts at elemental analysis were fruitless. However, high resolution mass spectrometry gave parent peaks whose composition supported the assigned structures.

As is indicated in Table 2, **16** and **17** were contaminated with varying amounts of the corresponding thiophenes **16***a* and **17***a*. It was easily shown that simple contact with air caused a significant and rapid increase in the amounts of these oxidation products. When precautions were taken to exclude air during the reaction, the amounts of these products were minimized. The ease with which dihydrothiophenes carrying electron-withdrawing substituents at the 3-position are oxidized, and the fact they produce thiophenes rather than 3-sulfolenes, has been previously noted (12).

Support for the concept that elimination of hydrogen sulfide can compete when the rate of ring closure is reduced is found in the reaction of **3***a* and **12***c*. A 65% yield of product which consisted of 65:35 mixture of **15** and **13** was obtained. The rate of ring closure of a ketone would be expected to be slower than that of an aldehyde and thus it is consistent that products derived from the elimination reaction would be found in this case. Furthermore, when the reaction of **12***a* with the mercaptan derived from mesityl oxide (**3***d*) was attempted, mass spectral analysis showed that the mixture of products contained a component with a molecular weight of 202. This is highly suggestive of the presence of the simple addition product **18** and other intense peaks at *m/e* 43 and 99 are also explicable in these terms. The occurrence of an intense peak at *m/e* 156 suggests the presence of significant amounts of **13** which can be derived from **18** in a straightforward manner. In this case, cyclization of **18** appears to have been almost completely sup-

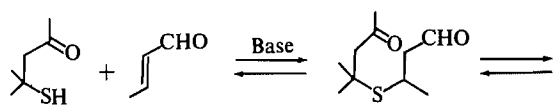

18

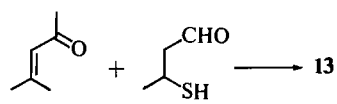

pressed as judged by the very low intensity of the peak at *m/e* 184.[4] Unfortunately, separation of the mixture into its components could not be achieved.

An important result was obtained from the

[3]Formation of this type of product would require the use of the unknown α-formylvinylphosphonium salts or a 3-mercapto-2-ketoaldehyde.

[4]Previous experience has shown that compounds of type **13** have the molecular ion as the base peak.

Can. J. Chem. Downloaded from www.nrcresearchpress.com by 210.87.254.42 on 09/05/12
For personal use only.

TABLE 3. Spectral and analytical data for products

Compound	n_D^{25}	Infrared[a]	Nuclear magnetic resonance[b,c]	Analysis (%) Calculated C	Calculated H	Found C	Found H
5	1.5238	[d]	5.88(m,2), 3.20(m,2), 2.83(m,1), 2.25(m,2), 1.33(d,3,J=7.5 Hz)	63.14	8.83	63.16	8.74
6	1.4892	[d]	5.78(m,2), 3.70(m,1), 3.00(m,1), 2.20(m,2), 1.30(d,6,J=7.5 Hz)	65.60	9.44	65.94	9.75
7	1.5231	[d]	5.73(m,2), 3.63(m,1), 3.08(m,1), 2.21(m,2), 1.6(q,2,J=7.5 Hz), 1.30(d,3,J=6 Hz), 1.03(t,3,J=7.5 Hz)	67.57	9.92	67.86	9.73
8	1.5275	[d]	7.33(s,5), 5.83(m,2), 4.00(m,2), 2.48(m,2), 1.35(d,3,J=7.5 Hz)	75.74	7.41	75.43	7.29
9[e]	1.5228[e]	[d]	5.53(m,1), 3.18(m,2), 2.08(m,2)				
10	1.5107	[d]	5.57(m,1), 3.18(m,2), 2.08(m,2), 1.72(m,3), 1.33(s,6)	67.57	9.92	67.71	9.56
13	1.5265	2700(w), 1690(s), 1645(m)	9.66(s,1), 6.83(m,1), 3.70(m,1), 2.95(m,1), 2.55(m,2), 1.45, 1.43(2d,3,J=6 Hz), 1.33, 1.30(2d,3,J=6 Hz)				
14	[f]	[f]	9.2(s,1), 6.83(m,1), 3.33(d,2,J=3 Hz), 3.1–2.3(m,3), 1.35(d,3,J=6 Hz)[g]	59.10	7.09	59.12	7.47
14*a*	[f]	[f]	9.1(s,1), 6.83(m,1), 3.65(q,1,J=6 Hz), 3.1–2.3(m,4), 1.45(d,3,J=6 Hz)[g]				
15	1.5651	1692(vs), 1658(m), 1635(s)	6.83(m,1), 3.71(m,1), 2.98(m,3), 2.63–1.53(m,6), 1.33, 1.23(2d,3,J=6 Hz)	[h]		[h]	
16	1.3428	2710(w), 1690(vs), 1635(w)	10.02(s,1), 6.72(m,1), 4.42(m,2), 1.77(m,2), 1.50(d,3,J=6.5 Hz), 1.05(t,3,J=7 Hz)	61.47	7.75	60.73	7.78
16*a*	1.4126	2715(w), 1685(vs), 1555(w), 1490(w)	10.20(s,1), 7.05(s,1), 2.77(q,2,J=7 Hz), 1.75(s,3), 1.30(t,3,J=7 Hz)	62.28	6.78	62.17	6.78
17	[f]	[f]	9.40(s), 6.80(m), 3.90(m), 3.30(m), 1.95(m), 1.13(t)[g]				
17*a*	1.3140	2715(w), 1688(vs), 1525(w)	9.03(s,1), 7.90(m,1), 7.23(m,1), 2.80(q,2,J=7 Hz), 1.30(t,3,J=7 Hz)	[i]		[i]	

[a]Run in chloroform solution.
[b]Run in $CDCl_3$ solution.
[c]Tabulation follows the order: chemical shift (δ), multiplicity, number of protons, coupling constant.
[d]Featureless.
[e]Reference 6 (n_D = 1.5239).
[f]Pure sample not available.
[g]Obtained by subtraction.
[h]m/e (M^+) calcd.: 182.0766; found 182.0681.
[i]m/e (M^+) calcd.: 140.0296; found 140.0290.

reaction of **3***a* with acrolein (**12***b*). Although the glc showed only one product on several columns, and the elemental analysis was in good agreement with the expected product **14**, the nmr spectrum quickly showed that two isomeric materials, **14** and **14***a*, were present in a ratio of 7:3. The presence of the latter was indicated by a quartet (δ = 3.65) due to the allylic methine proton adjacent to sulfur which was coupled to a doublet at δ = 1.45. In comparison, the methyl doublet of **14** appears at δ = 1.35 and the allylic methylene adjacent to sulfur occurs at δ = 3.33. The occurrence of both **14** and **14***a* suggests that, in addition to the elimination of hydrogen sulfide, proton transfer leading to equilibration of the reaction intermediates can also occur (Scheme 2).

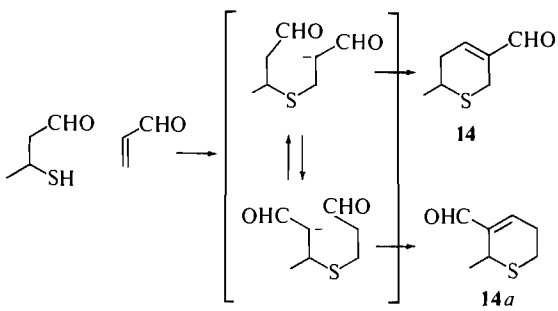

SCHEME 2

The factors which determine the relative rates of the various reactions, a point of some synthetic interest, are not clear and further work in this area is required.

The potential for synthetic use of compounds like **13** and **17** is apparent and forms the basis for future work.

Experimental

Nuclear magnetic resonance spectra were recorded on Varian EM360 or JEOLCO C60 HL instruments and are reported in parts per million downfield from TMS as internal standard. Gas chromatography was performed on an F and M Model 720 instrument utilizing an 8 ft × 0.375 in. column packed with 20% SE30 on Chromosorb W. The flow rate of the helium carrier gas was 60 ml/min. Mass spectra were obtained using a Varian MAT CH5-DF spectrometer controlled by an INCOS computer system. Microanalyses were performed by A. B. Gygli, Microanalysis Laboratory, Toronto, Ontario.

Mercaptans **3***a* (13) and **3***d* (14) were prepared according to literature procedures.

3-Mercapto-3-phenylpropanal (3b)

Cinnamaldehyde (33 g, 0.25 mol) was added in the presence of 10 ml of triethylamine to a saturated solution of hydrogen sulfide in 250 ml of chloroform at −10 °C and stored at this temperature for 14 h. Hydrochloric acid (150 ml, 2 *N*) was added and the mixture was stirred for 30 min. The organic layer was separated and washed with 2 *N* acid, with water and was dried over sodium sulfate. Evaporation of the solvent gave 39 g of very thick oil which was used directly.

4-Mercapto-2-butanone (3c)

Using the procedure of Kollonitsch (15) 10.5 g (0.15 mol) of methyl vinyl ketone afforded 14 g of product which was used without further purification. The compound was previously obtained in very low yield by Murata and Arai (14).

*Preparations of Dihydrothiopyrans **5–10***

The allylic triphenylphosphonium salt was first isomerized to the vinyl isomer by heating in pyridine solution containing a catalytic amount of triethylamine (**7***a*).

To a well-stirred solution of the vinyl salt **4** (0.01 mol) in 50 ml of pyridine containing triethylamine (0.012 mol) was added a pyridine solution of the appropriate **3** (0.01 mol). The reaction mixture was refluxed for the time indicated in Table 1, cooled, diluted with water (500 ml), and extracted with ether (4 × 150 ml). The combined extracts were washed with 10% hydrochloric acid, water, dried, and evaporated. The residue was chromatographed on alumina using pentane–ether (1:2 v/v) to afford essentially pure thiopyran. Analytical samples were collected from glc. Yields and spectral data are incorporated in Tables 1 and 3.

*Synthesis of 5,6-Dihydro-(2H)thiopyran-3-aldehydes **13–15***

In a typical experiment, a solution of **3***a* (1.04 g, 0.01 mol) in 50 ml of pyridine which contained 2.02 g (0.02 mol) triethylamine was stirred under nitrogen for 20 min at room temperature. To this yellow solution was added 0.7 g (0.01 mol) of crotonaldehyde (**12***a*) in 15 ml of pyridine and stirring was continued for 20 min at ambient temperature. The solution was refluxed for 14 h, cooled, added to 300 ml of water, and extracted with three 100 ml portions of ether. The organic phase was washed with 10% hydrochloric acid (2 × 100 ml) and with water until the washings were neutral. After drying and evaporation of the solvent, 1.47 g (94%) of **13** was obtained; which was pure to glc analysis; (2,4-DNP mp 237 °C (lit. (13) mp 234–236 °C).

*Synthesis of 2,5-Dihydrothiophene-3-aldehydes **16** and **17***

The following procedure is representative. A mixture of α-mercaptobutyraldehyde (**3***e*) (1.04 g, 0.01 mol), triethylamine (2.02 g, 0.02 mol) and 60 ml of pyridine was stirred under nitrogen for 15 min at room temperature. A solution of 0.7 g (0.01 mol) of crotonaldehyde (**12***a*) in 15 ml of pyridine was added dropwise with stirring. After stirring for 20 min, the solution was refluxed for 11 h, cooled, poured into 400 ml of water, and extracted with ether (4 × 100 ml). The combined organic layer was washed with 10% hydrochloric acid (2 × 100 ml) and water. The dried solution was evaporated, leaving 1.31 g of thick yellow oil which was shown by glc to be a mixture

Can. J. Chem. Downloaded from www.nrcresearchpress.com by 210.87.254.42 on 09/05/12
For personal use only.

of unreacted mercaptan **3***e* (24%), dihydrothiophene **17**, and thiophene **17***a*. This corresponds to a combined yield of 64% based on unrecovered **3***e* of which 63% is **17** and 37% is **17***a*.

Further exposure to air caused conversion of **17** to **17***a*.

Acknowledgments

Financial support for this project came from the Hoffman-LaRoche Co. (Nutley, N.J.) and the National Research Council of Canada. Mass spectra were run by Mr. R. Charlton. For all of this assistance we are deeply grateful.

1. D. A. Evans and C. L. Green. Chem. Soc. Rev. **2**, 75 (1973).
2. M. Schlosser. Top. Stereochem. **5**, 1 (1970).
3. J. F. Biellmann and J. B. Ducep. Tetrahedron, **27**, 5861 (1971).
4. P. L. Stotter and R. E. Hornish. J. Am. Chem. Soc. **95**, 4444 (1973).
5. K. Kondo, A. Negishi, K. Matsui, D. Tunemoto, and S. Masamune. Chem. Commun. 1311 (1972).
6. R. F. Naylor. J. Chem. Soc. 2749 (1949).
7. E. E. Schweizer, A. T. Wehman, and D. M. Nycz. J. Org. Chem. **38**, 1583 (1973), and earlier paper in the series; E. Zbiral. Synthesis, 775 (1974).
8. (*a*) J. M. McIntosh, H. B. Goodbrand, and G. M. Masse. J. Org. Chem. **39**, 202 (1974); (*b*) J. M. McIntosh and R. S. Steevensz. Can. J. Chem. **52**, 1934 (1974); (*c*) J. M. McIntosh and G. M. Masse. J. Org. Chem. **40**, 1294 (1975).
9. F. Asinger, M. Thiel, and H. Kaltwasser. Justus Liebig's Ann. Chem. **606**, 67 (1957).
10. R. L. S. Patterson. Chem. Ind. 548 (1968).
11. J. M. McIntosh and F. P. Seguin. Can. J. Chem. **53**, 3526 (1975).
12. T. Takaya, S. Kosaka, Y. Otsuji, and E. Imoto. Bull. Chem. Soc. Jpn. **41**, 2086 (1968).
13. F. Asinger and M. Fischer. J. Prakt. Chem. **35**, 81 (1967).
14. N. Murata and H. Arai. J. Chem. Soc. Jpn. **59**, 129 (1956).
15. Z. Foeldi and J. Kollonitsch. J. Chem. Soc. 1683 (1948).

Can. J. Chem. Downloaded from www.nrcresearchpress.com by 210.87.254.42 on 09/05/12
For personal use only.

Application of photoelectron spectroscopy to intramolecularly hydrogen-bonded systems. Part III. The photoelectron spectra of *cis* and *trans* 2-substituted cyclopentanols and *cis* and *trans* 2-substituted cyclohexanols

R. S. BROWN

Department of Chemistry, The University of Alberta, Edmonton, Alta., Canada T6G 2G2

Received January 27, 1976

R. S. BROWN. Can. J. Chem. **54**, 1929 (1976).

The photoelectron spectra of several well defined molecules exhibiting intramolecular hydrogen bonding has been determined and the analysis of the spectra is in accord with recent molecular orbital calculations of related systems. The experimentally determined enthalpies of the hydrogen bonds in *cis*-2-aminocyclopentanol and *cis*- and *trans*-2-aminocyclohexanol do not correlate in any simple fashion with the shifts in the ionization energies of the n_O and n_N orbitals compared to a model which precludes hydrogen bonding. The spectral differences attributed to hydrogen bonding in the *cis* and *trans* 2-substituted cyclanols cannot be attributed to differences in the through-bond interaction of the n orbitals on either atom since the *cis* and *trans* isomers of 1,2-dimethoxycyclopentane and 1,2-dimethoxycyclohexane show virtually identical pe spectra. A discussion of the applicability of Koopmans' theorem and the effect of the hydrogen bond in both the ion and ground states is presented.

R. S. BROWN. Can. J. Chem. **54**, 1929 (1976).

On a déterminé les spectres photoélectroniques de plusieurs molécules bien définies montrant des ponts hydrogène intramoléculaires; l'analyse de ces spectres est en accord avec les calculs récents d'orbitale moléculaire de systèmes qui leur sont reliés. Les enthalpies déterminées expérimentalement pour les ponts hydrogène dans l'amino-2 cyclopentanol-*cis* et les amino-2 cyclohexanols *cis* et *trans* ne peuvent pas être reliés d'une façon simple avec les déplacements dans les énergies d'ionisation des orbitales n_O et n_N comparés avec un modèle qui empêche les ponts hydrogène. Les différences spectrales attribuées aux ponts hydrogène dans des cyclanols substitués en position 2 (*cis* et *trans*) ne peuvent pas être attribuées à des différences dans les interactions à travers les liens des orbitales n de chacun des atomes puisque les isomères *cis* et *trans* des diméthoxy-1,2 cyclopentane et diméthoxy-1,2 cyclohexane présentent des spectres photoélectriques pratiquement identiques. On présente une discussion sur la possibilité d'appliquer le théorème de Koopman et sur l'effet des ponts hydrogène dans l'ion et les états fondamentaux.

[Traduit par le journal]

The fundamental importance of hydrogen-bonding is best realized when one considers the large quantity of research expended toward its understanding (for a compendium of leading references see ref. 1). Recently several sophisticated molecular orbital calculations concerning this phenomenon have elucidated the subtle electronic redistributions which occur within molecules during hydrogen-bonding (H-bonding) (2). The majority of calculations reach similar conclusions in that charge cloud repulsion and electrostatic and charge redistributions contribute significantly to the H-bonding interaction, and that while the H involved in the interaction loses electrons, the electronegative atoms at the termini of the H-bond gain electrons upon bond formation (2*c*).

Our previous investigations concerning intramolecular H-bonding reported changes in the photoelectron spectra (pes) of isomeric α-amino-alcohols (3*a*) and α-hydroxy ketones (3*b*). The general observation for those compounds which exhibited an intramolecular H-bond was that the electron pair involved in the formation of the H-bond exhibited a higher ionization energy (IP), and the electron pair residing on the hydrogen donor atom exhibited a lower IP than those in a geometrical isomer in which H-bonding was precluded. Two other investigations of temperature induced variations in the pe spectra of flexible aminoalcohols (4*a*) and carboxylic acid dimers (4*b*), although reporting similar observations to ours (3), were not without ambiguity since such spectral variations may have resulted

Can. J. Chem. Downloaded from www.nrcresearchpress.com by 210.87.254.42 on 09/05/12
For personal use only.

Can. J. Chem. Downloaded from www.nrcresearchpress.com by 210.87.254.42 on 09/05/12
For personal use only.

from conformational changes as a function of temperature.

Several questions which seemed of importance were raised as a result of these investigations. Firstly, since the differences in the pe spectra were consistent with the formation of an intramolecular H-bond in one of the geometric isomers, it was not without reason that such shifts might reflect the extent of the perturbation of the orbitals by the H-bond, and therefore perhaps a quantitative measure of the enthalpy of H-bond formation could be derived from the pe spectra. Secondly, it has been theoretically predicted by Hoffman (5) and experimentally demonstrated by Heilbronner and co-workers (6) that lone pairs within a molecule can interact by either a direct through-space mechanism or a through-bond mechanism. Such an interaction generally increases the splitting between the orbitals in contrast to those observations already presented and attributed to H-bonding (3), however, one does not know to what extent these interactions may be significant in the above cases. Therefore it is important to show that the spectral differences between the geometric isomers that we attribute to H-bonding do not arise from unrelated orbital interactions. Thirdly, it is desirable to demonstrate that this technique can be used to detect the consequences of intramolecular H-bonding in related systems in which other groups serve as the electron donor. To this end we have synthesized and determined the pe spectra of *cis*- and *trans*-2-methoxycyclopentanol and *cis*- and *trans*-2-methoxycyclohexanol. The following represents the findings concerning these questions.

Experimental

The *cis*- and *trans*-2-aminocyclohexanols were prepared by the method of Bannard *et al.* (7). Methylation of the *cis* isomer by the Eschweiller–Clarke procedure (8) afforded *cis*-2-(*N*,*N*-dimethylamino)cyclohexanol while the corresponding *trans* isomer was produced by opening of cyclohexene oxide with dimethylamine (9). *trans*-2-Methoxycyclohexanol, and *trans*-2-methoxycyclopentanol were quantitatively prepared by the sulfuric acid catalysed opening of the corresponding epoxides in anhydrous methanol and gave physical properties which compared well with those published (10, 11). The *trans* isomers were converted into the corresponding *cis* isomers by the method of Buck *et al.* (11).

trans-1,2-Dimethoxycyclohexane and *trans*-1,2-dimethoxycyclopentane were prepared from the corresponding *trans*-2-methoxycyclanols by the methylation procedure of Diner *et al.* (12), while the *cis*-1,2-dimethoxycylanes were prepared by complete methylation (12) of the *cis*-1,2-diols (13). Each of these diethers had spectral and physical properties consistent with the assigned structures (14).

Photoelectron spectra and ir spectral measurements were determined under conditions described previously (3*a*).

Results and Discussion

Aminocyclanols

The observed vertical ionization energies (VIP) for the aminocyclohexanols (**1–4**) and aminocyclopentanols (**5–8**) are presented in Table 1.

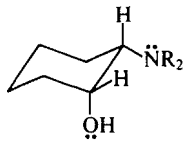

1 R = H
3 R = CH_3

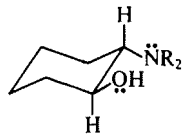

2 R = H
4 R = CH_3

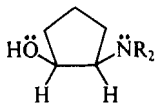

5 R = H
7 R = CH_3

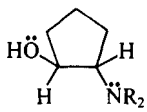

6 R = H
8 R = CH_3

Since the gross trends and general appearance of the pe spectra of the cyclohexane series resembles that of the cyclopentane series, they need not be reproduced here. It was hoped that the pe spectra of the more flexible aminocyclohexanols compared with the relatively rigid aminocyclopentanols, might reveal differences in the spectra which might be related to differences in the H-bond strength. For that reason, it might be reasonable to compare the differences in the VIP values of the easily identifiable lone pairs on nitrogen (n_N) and oxygen (n_O).[1] Hence, if *trans*-2-aminocyclopentanol (**6**) in which intramolecular H-bonding is absent (3*a*) can be taken as a

[1]The term 'lone pair' used to describe the electron pair associated with the oxygen or nitrogen atoms is somewhat misleading since this molecular orbital is probably extensively delocalized and contains significant components of atomic orbitals centered on adjacent atoms. Nevertheless, we shall use this terminology throughout for the sake of simplicity to refer to that pair of electrons associated with the nitrogen and oxygen atoms.

TABLE 1. Vertical ionization energies (VIP) in electron volts (eV) and assignments for the 2-aminocyclohexanols (**1**–**4**)[a] and 2-aminocyclopentanols (**5**–**9**)[b]

Compound	VIP n_N	VIP n_O	$\Delta IP(n_N - n_O)$
cis-2-Aminocyclohexanol (**1**)	9.59	10.09	0.50
trans-2-Aminocyclohexanol (**2**)	9.49	10.19	0.70
cis-2-Aminocyclopentanol (**5**)	9.70	10.11	0.41
trans-2-Aminocyclopentanol (**6**)	9.25	10.24	0.99
cis-2-(*N*,*N*-Dimethylamino)cyclohexanol (**3**)	8.64	9.70	1.06
trans-2-(*N*,*N*-Dimethylamino)cyclohexanol (**4**)	8.36	9.86	1.50
cis-2-(*N*,*N*-Dimethylamino)cyclopentanol (**7**)	8.69	9.89	1.20
trans-2-(*N*,*N*-Dimethylamino)cyclopentanol (**8**)	8.30	10.02	1.72

[a]This work.
[b]Reference 3*a*.

model compound, then the pe spectra of *cis*-2-aminocyclopentanol (**5**) and *cis*- and *trans*-2-aminocyclohexanol (**1** and **2** respectively) which clearly demonstrate H-bonding may be compared with that of (**6**). Differences in the spectra may arise from H-bond induced perturbations of the orbitals. A similar sort of comparison may be attempted in the *N*,*N*-dimethylamino series.

We have previously determined the enthalpy of the intramolecular H-bond in *cis*-2-aminocyclopentanol (**5**) to be -1.92 kcal mol^{-1} (3*a*). Utilizing similar techniques and solvents (15) we have now determined the ΔH values for the H-bonds of *cis*- and *trans*-2-aminocyclohexanol (**1** and **2**) to be -2.5 kcal mol^{-1} and -2.8 kcal mol^{-1} respectively. Hence it seems clear that the magnitude of the spectral shifts obtained for these compounds from Table 1 correlates in no simple way with the enthalpies of H-bonding. Apparently it is a gross oversimplification to expect that the magnitude of the shifts in the n_N and n_O orbitals on H-bonding will reflect quantitatively the enthalpy of the interaction. What we have neglected due to the uncertainty of measurement, are the changes in the energy of several of the σ-bonds and in particular the O—H σ-bond which should be perturbed by H-bond formation. Thus, while it appears that pe spectral shifts of geometric isomers can be qualitatively ascribed to H-bonding, it is not likely that the simple shifts of the two non-bonded pairs of electrons (n_N and n_O) will quantitatively lead to H-bond enthalpy in these systems.

Orbital Interactions

In order to assess the importance of orbital interactions in the observed pe shifts attributed to H-bonding, we decided to look at isomers in which no H-bonding is possible. If there were no interaction between the n_O orbitals in *cis*- and *trans*-1,2-dimethoxycyclopentane then these orbitals would be degenerate. However the pe spectra of these compounds presented in Fig. 1 indicates that some interaction has removed their degeneracy. It is significant to notice that the pe spectra of the *cis* and *trans* isomers in both the cyclopentane and cyclohexane series are virtually superimposable and that the orbital splitting obtained from Table 2 is the same for both isomers. The dihedral angle between the two C—OCH_3 bonds in **9** is shown from

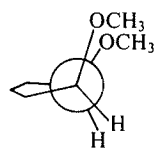

9

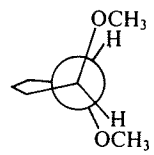

10

models to be nearly 0° (even if some torsional strain is allowed) while that exhibited in **10** is roughly 120°. Assuming that through-space interaction depends upon the overlap and hence distance between the interacting orbitals one would expect that this interaction would be far less for **10** than **9** since the distance between the oxygens increases appreciably in the former. Since the splitting observed in the pe spectra is constant, one can rule out this direct type of interaction. On the other hand, through-bond interactions of the type elaborated by Hoffman *et al.* (16) and later experimentally verified for 1,4-diazabicyclooctane by Heilbronner and Muszkat (6*d*) are not expected to be markedly

Can. J. Chem. Downloaded from www.nrcresearchpress.com by 210.87.254.42 on 09/05/12
For personal use only.

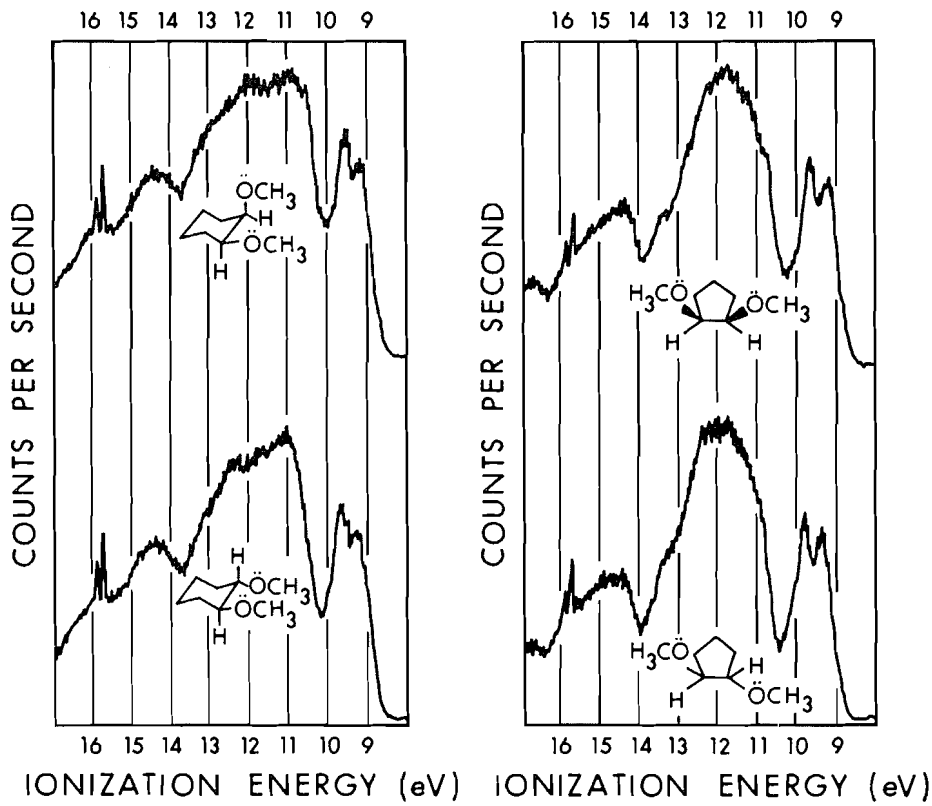

FIG. 1. The pe spectra of *cis*- and *trans*-1,2-dimethoxycyclopentane (**9** and **10**) and *cis*- and *trans*-1,2-dimethoxycyclohexane using argon as an internal calibration.

TABLE 2. Vertical ionization energies (VIP) in electron volts (eV) and assignments[a] of the two highest orbitals in *cis*- and *trans*-1,2-dimethoxycyclopentane and *cis*- and *trans*-1,2-dimethoxycyclohexane

Compound	VIP n_+	VIP n_-	$\Delta IP(n_- - n_+)$
cis-1,2-Dimethoxycyclopentane	9.29	9.75	0.46
trans-1,2-Dimethoxycyclopentane	9.39	9.84	0.45
cis-1,2-Dimethoxycyclohexane	9.24	9.64	0.40
trans-1,2-Dimethoxycyclohexane	9.31	9.69	0.38

[a]See text for the origin of assignment.

dependent upon rotational variations about the central C—C axis as long as the overlap between each n_O orbital and the central C—C bond is constant. That the experimentally observed splitting in **9** and **10** remains equivalent seems to dictate that this must be the case. Unless there are anomalous cancellations and an exactly compensatory reordering of n_- and n_+ in passing from the *trans* isomer to the *cis* isomer, we would follow the predictions of Hoffman *et al.* (16) in assigning n_+ as the highest occupied molecular orbital (homo), in these *cis*- and *trans*-1,2-dimethoxycyclanes.

Regardless of the ordering, the important point of the experiment is that because there exists no change in the splitting of the n_+ and n_- orbitals in passing from the *trans* to *cis* isomer, the importance of such orbital interactions in the pe spectral differences attributed to the presence of the H-bond is minimal.

Can. J. Chem. Downloaded from www.nrcresearchpress.com by 210.87.254.42 on 09/05/12
For personal use only.

TABLE 3. Vertical ionization energies (VIP) in electron volts (eV) and assignments for *cis*- and *trans*-2-methoxycyclopentanol (**11** and **12**) and *cis*- and *trans*-2-methoxycyclohexanol (**13** and **14**)

Compound	VIP($n_{\ddot{O}CH_3}$)	VIP($n_{\ddot{O}H}$)	$\Delta IP(n_{\ddot{O}H} - n_{\ddot{O}CH_3})$
cis-2-Methoxycyclopentanol (**11**)	9.80	10.19	0.39
trans-2-Methoxycyclopentanol (**12**)	9.60	10.36	0.76
cis-2-Methoxycyclohexanol (**13**)	9.68	10.11	0.45
trans-2-Methoxycyclohexanol (**14**)	9.69	10.14	0.43

Methoxycyclanols

In our hopes to establish that such pe spectral changes could result from intramolecular H-bonding in other systems, we decided to investigate the 2-methoxycyclopentanols and 2-methoxycyclohexanols (compounds **11**–**14**). The VIP values and assignments for the ionizations are given in Table 3.

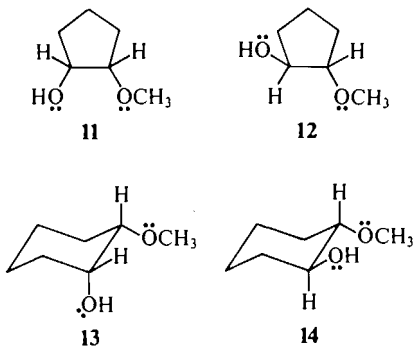

The assignments of the lone pair ionizations are based on the accepted lowering of ionization potential with increasing alkyl substitution (VIP $CH_3\ddot{O}H$, 10.96 eV (17); VIP $CH_3\ddot{O}CH_3$, 10.04 eV (18)). A comparison of *cis*- and *trans*-2-methoxycyclopentanol shows that the ionization of the methoxyl lone pair ($n_{\ddot{O}CH_3}$) is more difficult by 0.2 eV and hydroxyl lone pair ($n_{\ddot{O}H}$) less difficult by 0.17 eV in the former. Therefore, as a result of H-bonding present in the *cis* isomer (**11**) the ionization of the oxygen lone pairs tend to approach each other in terms of energy. This is undoubtedly a consequence of the electronic reorganization initiated by the presence of the H-bond and is totally consistent with the observations made on the amino alcohols (3*a*). One might rationalize these observations by considering that the H-bond involves both electrostatic and charge-transfer interactions between the electron donor and proton donor termini of the H-bond (2). As a result of the interaction with the proton, the electron pair now becomes somewhat more bonding and moves to lower energy than in the absence of the H-bond. Concomitantly, charge transfer from the electron donor concentrates more electron density on the proton donor, facilitating the ionization of its lone pair. The *cis* and *trans* isomers of 2-methoxycyclohexanol exhibit the same ionization energies for the $\ddot{O}CH_3$ and $\ddot{O}H$ lone pairs suggesting similar interactions in both isomers.

Solution phase ir data are presented in Table 4 and indicate that all the 2-methoxycyclanols show marked intramolecular H-bonding except *trans*-2-methoxycyclopentanol (**12**). We have not attempted to see if a correlation exists between the enthalpy of the H-bond and the induced pe spectral shifts in comparison to **12** since none of those compounds in which an intramolecularly-bonded OH stretching frequency is observed exhibit a free —OH stretch, thus precluding enthalpy measurements (15). As in the case of the 2-aminocyclanols however, it is not likely that such a correlation will exist since the spectral shifts in the σ-bonding region, which undoubtedly represent major electronic changes in the C—C, C—Ö—, and C—H skeleton, defy analysis.

It is apparent that intramolecular H-bonding can cause appreciable changes in the pe spectra of 2-aminocyclanols (3*a*), α-hydroxy ketones (3*b*), and 2-methoxycyclanols, in comparison with model compounds which possess similar substituent effects but in which the molecular geometry precludes H-bonding. While pe spectroscopy has been used previously to probe H-bonding in flexible aminoalcohols (4*a*) and carboxylic acid dimers (4*b*) such determinations relied upon temperature induced differences in

Can. J. Chem. Downloaded from www.nrcresearchpress.com by 210.87.254.42 on 09/05/12
For personal use only.

TABLE 4. Infrared O—H stretching frequencies of *cis* and *trans* 2-substituted cyclanols determined in $Cl_2C{=}CCl_2$ solution at room temperature

Compound	νOH (cm^{-1})		
	Free	Intramolecular	Intermolecular[a]
cis-2-Methoxycyclopentanol (**11**)	—	3560[c]	3475
trans-2-Methoxycyclopentanol (**12**)	3625	—	3450[b]
cis-2-Methoxycyclohexanol (**13**)	—	3570[c]	3461
trans-2-Methoxycyclohexanol (**14**)	—	3595[c]	3478
cis-2-Aminocyclohexanol (**1**)	3625[d]	3490	3250
trans-2-Aminocyclohexanol (**2**)	3625[d]	3520	3250
cis-2-(*N*,*N*-Dimethylamino)-cyclohexanol (**3**)	—	3470	—
trans-2-(*N*,*N*-Dimethylamino)-cyclohexanol (**4**)	—	3468	—

[a]Exhibits diminishing intensity as dilution increases.
[b]Position of this intermolecular band shifts to higher frequency (but lower intensity) as dilution increases.
[c]Previous values reported in CCl_4: **11**, 3570; **13**, 3586; **14**, 3594 cm^{-1} (ref. 11).
[d]Exhibits free N—H stretch at 3390 cm^{-1}.

the pe spectra to infer the presence of the H-bond. That such shifts are exclusively attributable to such bonding is ambiguous since Ames and Turner (19) have shown that the pe spectrum of 1-bromo-2-chloroethane, which obviously cannot intramolecularly H-bond, is subject to temperature dependence, presumably due to different molecular conformations.

In our studies we have attempted to verify the consequence of H-bonding on the pe spectra of some well-defined systems at ambient temperature in order to minimize the effects of conformational heterogeneity. In all cases in which intramolecular H-bonding could be demonstrated by conventional techniques (ir) the pe spectra showed large shifts when compared to a non H-bonding model.

By a consideration of only two of the pairs of electrons perturbed during H-bond formation we could see no well-defined correlation which would allow quantitative assessment of the H-bond strength as determined by standard techniques (15). The H-bond energy reflects the net change in energy of the entire molecule upon bond formation which cannot be meaningfully approximated by determining changes occurring in the ionization energies of only two of the occupied orbitals.

Another important factor which is perhaps more to the point when assessing the applicability of pes to such subtle phenomena as H-bonding concerns the validity of applying Koopmans' theorem (20) to such systems. If we were to simply assume that Koopmans' theorem holds for the ionization, then the increase in the ionization energy of the electron-donor orbital in passing from *trans*- to *cis*-2-methoxycyclopentanol (**12** to **11** respectively) might be attributed to the stabilization of that orbital upon H-bond formation. At the same time, H-bond formation *raises* the energy level of the n_O orbital on the proton donor if one assumes that the $-IP$ value corresponds to the orbital energy level. Of course this analysis does not actually conform to reality in that it assumes that electronic reorganization is negligible during ionization.

However, as pointed out by Eland (21), the experimental ionization energies can be exactly defined as the energy difference between the neutral molecule and the molecular ion in a particular state. Thus one must ask what influence the presence of the H-bond has on the ground state energy *and* the energy of an ion state created by instantaneous removal of an electron from a particular orbital. The ideas of Pimentel (22) are particularly relevant to this question. When a carbonyl-containing molecule is placed in an H-bonding solvent, a decided $n{-}\pi^*$ blue shift occurs. While this phenomenon was originally attributed to H-bond induced lowering of the n-orbital (23), Pimentel discussed it in terms of solvation of the ground state and first excited singlet state, and the Franck–Condon principle. He suggested (22) that while H-bond formation might stabilize the ground

Can. J. Chem. Downloaded from www.nrcresearchpress.com by 210.87.254.42 on 09/05/12
For personal use only.

Can. J. Chem. Downloaded from www.nrcresearchpress.com by 210.87.254.42 on 09/05/12
For personal use only.

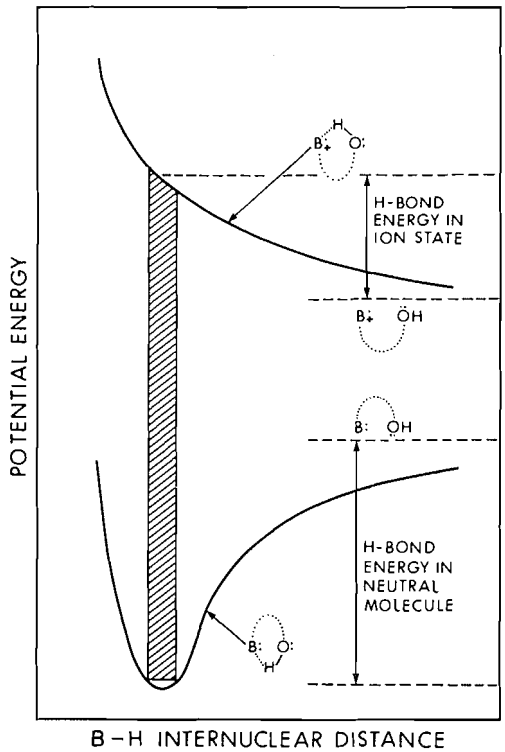

FIG. 2. A potential energy diagram for an intramolecularly H-bonded molecule as a function of internuclear distance for both the ground and ion state created by removal of a non-bonding electron localized on the B: residue. It is projected that the ground state of the molecule is stabilized by H-bond formation, while the vertically produced ion state of the same molecular dimensions may be destabilized by the H-bond. See footnote 2.

state of a molecule (by lowering the energy of the electron-donor orbital), it might possibly destabilize the first excited singlet state. An extension of these ideas to ionization processes such as that illustrated in [1] can be envisioned.

[1] 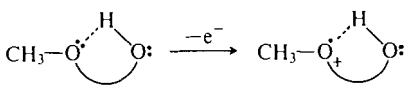

Since removal of that electron is an instantaneous process (within the Franck–Condon principle (for a discussion of the application of the Franck–Condon principle to pe spectroscopy see ref. 24)) and no nuclear reorganization is permitted, the ion may well be destabilized by the presence of the hydrogen of the formerly stabilizing H-bond. Hence what we are experimentally determining is not simply a consequence of the ground state stabilization, but rather the change in energy between two states which may be differentially influenced by the presence of the H-bond.

In accord with these beliefs, Del Bene has calculated the potential curve for the first excited singlet state of the formaldehyde–water dimer as a function of internuclear separation and found it to be repulsive (25). Her calculations suggest that removal of an electron from the carbonyl oxygen n_O orbital and transferring it to the orthogonal π^* orbital promotes the formerly neutral, stabilized H-bonded dimer into an excited state of the same molecular dimensions, but no longer stabilized by the presence of the H-bond.

If we can extrapolate these calculations to our intramolecularly H-bonded system, then a potential energy diagram of the ground state and excited state like that shown in Fig. 2 may be envisioned.

Figure 2 illustrates that the potential curve for the ion-state created by removal of an electron from base B may be repulsive, and the vertical ionization energy is simply the vertical line connecting the two states of equal molecular dimensions.[2] One might qualitatively explain the upper curve by recalling that if the H-bonded species in the ground state can be represented by the polarized structure **15**, then instantaneous removal of the localized non-bonding electron from B converts the molecule into ion **16** which

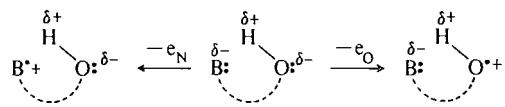

16 **15** **17**

[2]The calculations dealing with the acetone–water and formaldehydewater dimers (25) show that the first excited singlet state produced by excitation is no longer stabilized (but not necessarily destabilized) by the presence of the hydrogen-bond. It is entirely probable, however, that the ion state produced by electron removal may be somewhat more sensitive to the neighboring hydrogen and show such destabilization. Unfortunately we have no theoretical data which bears directly on this point. (See Acknowledgement.)

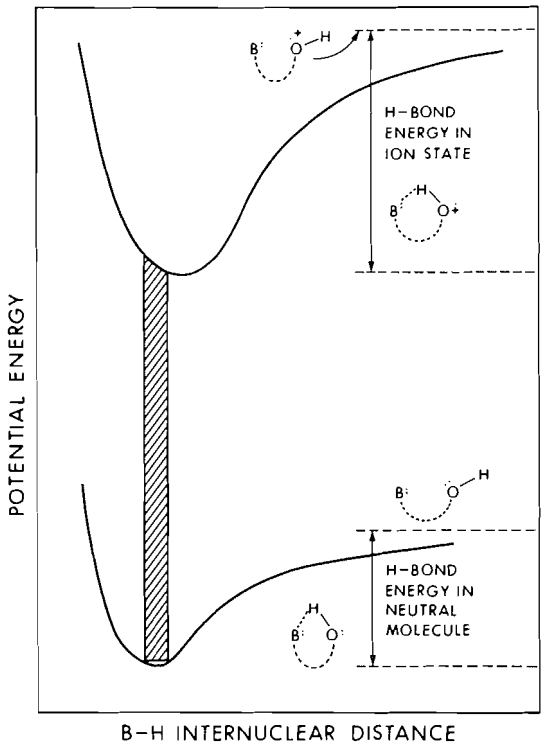

FIG. 3. A potential energy diagram for an intramolecularly H-bonded molecule as a function of internuclear distance in both the ground state and ion state created by removal of a non-bonding electron localized on the Ö—H moiety. It is speculated that this ion-state may well possess a stronger H-bond than the ground state due to increased polarity of the O—H σ-bond in the latter. The exact positioning of the well of the potential curve for the ion state is uncertain at this time.

experiences strong dipole repulsion. On the other hand removal of the oxygen non-bonded electron creates an ion (**17**) in which the effective electronegativity of the oxygen is markedly increased leading to even larger polarization of the O—H σ-bond than in the ground state. Hence the H-bond in ion **17** may well be stronger than in the neutral ground state. This situation is qualitatively represented in Fig. 3. Once again the experimental ionization energy is defined as the energy required to interconvert the two states.

The important projection of the above discussion is that if the potential curve for the ion state is vastly different than that of the ground state, then the experimental ionization energies cannot be treated under the assumption of Koopmans' theorem. It would be of great benefit to determine these curves before any pe data can be used to infer orbital energies for H-bonded systems.

Acknowledgments

The author gratefully acknowledges the general financial support of The University of Alberta and the National Research Council of Canada. He is also grateful to Prof. Janet E. Del Bene for her enlightening comments concerning the manuscript and to Dr. R. A. B. Bannard for providing comparison samples of *cis*- and *trans*-2-aminocyclohexanol.

1. (*a*) M. D. JOESTEN and L. J. SCHAAD. Hydrogen bonding. Marcel Dekker Inc., New York. 1974; (*b*) S. N. VINOGRADOV and R. H. LINNELL. Hydrogen bonding. Van Nostrand Reinhold Co., New York. 1971; (*c*) G. C. PIMENTEL and A. L. MCCLELLAN. The hydrogen bond. W. H. Freeman and Co., San Francisco. 1960.
2. (*a*) S-I YAMABE and K. MOROKUMA. J. Am. Chem. Soc. **97**, 4458 (1975); (*b*) J. E. DEL BENE. J. Am. Chem. Soc. **95**, 5460 (1973), and references therein; (*c*) P. A. KOLLMAN and L. C. ALLEN. Chem. Rev. **72**, 283 (1972).
3. (*a*) R. S. BROWN. Can. J. Chem. **54**, 642 (1976); (*b*) R. S. BROWN. Submitted for publication.
4. (*a*) S. LEAVELL, J. STEECHEN, and J. L. FRANKLIN. J. Chem. Phys. **59**, 4343 (1973); (*b*) R. K. THOMAS. Proc. R. Soc. London Ser. A, **331**, 249 (1972).
5. R. HOFFMAN. Acc. Chem. Res. **4**, 1 (1971), and references therein.
6. (*a*) P. BISCHOFF, J. A. HASHMALL, E. HEILBRONNER, and V. HORNUNG. Helv. Chim. Acta, **52**, 1745 (1969); (*b*) R. HOFFMANN, E. HEILBRONNER, and R. GLEITER. J. Am. Chem. Soc. **92**, 706 (1970); (*c*) P. BISCHOF, R. GLEITER, and E. HEILBRONNER. Helv. Chim. Acta, **53**, 1425 (1970); (*d*) E. HEILBRONNER and K. A. MUSZKAT. J. Am. Chem. Soc. **92**, 3818 (1970).
7. R. A. B. BANNARD, N. C. C. GIBSON, and J. H. PARKKARI. Can. J. Chem. **49**, 2064 (1970).
8. H. T. CLARKE, H. B. GILLESPIE, and S. Z. WEISSHAUSE. J. Am. Chem. Soc. **55**, 4571 (1933).
9. S. L. FRIESS and H. D. BALDRIDGE. J. Am. Chem. Soc. **78**, 2482 (1956).
10. R. A. B. BANNARD, A. A. CASSELMAN, E. J. LANGSTAFF, and R. Y. MOIR. Can. J. Chem. **45**, 2605 (1968).
11. K. W. BUCK, A. B. FOSTER, A. LABIB, and J. M. WEBBER. J. Chem. Soc. 2846 (1964).
12. U. E. DINER, F. SWEET, and R. K. BROWN. Can. J. Chem. **44**, 1591 (1966).
13. M. F. CLARKE and L. N. OWEN. J. Chem. Soc. 315 (1949).
14. J. WINKLER and H. F. GRÜTZMACHER. Org. Mass. Spectrom. **3**, 1117 (1970).
15. P. J. KRUEGER and H. D. METTEE. Can. J. Chem. **43**, 2970 (1965).

Can. J. Chem. Downloaded from www.nrcresearchpress.com by 210.87.254.42 on 09/05/12
For personal use only.

16. R. HOFFMANN, A. IMAMURA, and W. J. HEHRE. J. Am. Chem. Soc. **90**, 1499 (1968).
17. A. D. BAKER, D. BETTERIDGE, N. R. KEMP, and R. E. KIRBY. Anal. Chem. **43**, 375 (1971).
18. S. CRADOCK and R. A. WHITEFORD. J. Chem. Soc. Faraday Trans. II, **68**, 281 (1972).
19. D. L. AMES and D. W. TURNER. J. Chem. Soc. Chem. Commun. 179 (1975).
20. T. KOOPMANS. Physica, **1**, 104 (1934).
21. J. H. D. ELAND. Photoelectron spectroscopy. Butterworths, London. 1974. p. 83.
22. G. C. PIMENTEL. J. Am. Chem. Soc. **79**, 3323 (1957).
23. G. J. BREALEY and M. KASHA. J. Am. Chem. Soc. **77**, 4462 (1955).
24. D. W. TURNER, C. BAKER, A. D. BAKER, and C. R. BRUNDLE. Molecular photoelectron spectroscopy. Wiley–Interscience, London. 1970. p. 7.
25. J. E. DEL BENE. J. Am. Chem. Soc. **96**, 5643 (1974); **95**, 6517 (1973).

Can. J. Chem. Downloaded from www.nrcresearchpress.com by 210.87.254.42 on 09/05/12
For personal use only.

Product yields and mechanism of penicillamine radiolysis at p*H* 5

GREESH CHAND GOYAL[1] AND DAVID ANTHONY ARMSTRONG
Department of Chemistry, University of Calgary, Calgary, Alta., Canada T2N 1N4

Received November 14, 1975

GREESH CHAND GOYAL and DAVID ANTHONY ARMSTRONG. Can. J. Chem. **54**, 1938 (1976).

The major products from the radiolysis of penicillamine in N_2O-saturated solutions at p*H* 5 are penicillamine disulfide, penicillamine trisulfide, and valine with yields of 2.0, 1.2, and 1.5 molecules per 100 eV in 10^{-2} *M* solutions and 1.8, 0.94, and 0.60 molecules per 100 eV in 10^{-3} *M* solutions respectively. These yields remain essentially the same when the major attacking radical is changed from ·OH to $\cdot CH_2OH$, $\cdot Br_2^-$ or $\cdot(CNS)_2^-$, and it is concluded that all four species produce predominantly penS· radicals on attacking penicillamine. The formation of trisulfide and an equivalent amount of valine is attributed to secondary reactions of penS· radicals and discussed in the light of recent pulse radiolysis experiments and other work.

In deaerated solutions hydrogen and H_2S were observed in significant yields and the valine yield increased. These observations can be accounted for quantitatively by the reactions:

[7*a*] $\cdot H + penSH \rightarrow penS\cdot + H_2$

[7] $\cdot H + penSH \rightarrow pen\cdot + H_2S$

[13] $e_{aq}^- + penSH \rightarrow pen\cdot + SH^-$

[25] $pen\cdot + penSH \rightarrow penH + penS\cdot$

The yields of minor ($G < 0.5$ molecules per 100 eV) products like NH_3 and $CH_2{=}C(CH_3)$-$CH(NH_3^+)COO^-$ indicated that fragmentation of pen· and other secondary radicals from penSH was more important than for cys· and other radicals from cysSH.

GREESH CHAND GOYAL et DAVID ANTHONY ARMSTRONG. Can. J. Chem. **54**, 1938 (1976).

Les produits majeurs de la radiolyse de la pénicillamine dans des solutions saturées de N_2O à un p*H* de 5 sont le disulfure de pénicillamine, le trisulfure de pénicillamine et la valine avec des rendements respectifs de 2.0, 1.2 et 1.5 molécules par 100 eV pour des solutions à 10^{-2} *M* et de 1.8, 0.94 et 0.60 molécules par 100 eV pour des solutions à 10^{-3} *M*. Ces rendements ne changent pratiquement pas quand le radical provoquant l'attaque majeure change de ·OH à $\cdot CH_2OH$, $\cdot Br_2^-$ ou $\cdot(CNS)_2^-$ et on en conclut que les quatre espèces produisent principalement des radicaux penS· par attaque sur la pénicillamine. On attribue la formation du trisulfure et une quantité équivalent de valine à des réactions secondaires des radicaux penS· et on discute de cette formation en fonction d'expériences récentes de radiolyse pulsée et d'autres travaux.

Dans des solutions ne contenant pas d'air, on a observé la formation d'hydrogène et de H_2S avec des rendements importants et le rendement de valine augmente. On peut expliquer ces observations par les réactions:

[7*a*] $\cdot H + penSH \rightarrow penS\cdot + H_2$

[7] $\cdot H + penSH \rightarrow pen\cdot + H_2S$

[13] $e_{aq}^- + penSH \rightarrow pen\cdot + SH^-$

[25] $pen\cdot + penSH \rightarrow penH + penS\cdot$

Les rendements des produits formés en quantités mineures, ($G < 0.5$ molécules par 100 eV) comme NH_3 et $CH_2{=}C(CH_3)CH(NH_3^+)COO^-$, indiquent que la fragmentation du pen· et des autres radicaux secondaires à partir du penSH est plus importante que pour cys· et d'autres radicaux provenant de cysSH.

[Traduit par le journal]

Introduction

The sulfhydryl amino acid cysteine ($HS{-}CH_2CH(NH_3^+)CO_2^-$) and the 1,2-amino thiols related to it are generally among the most efficient *in vivo* radiation protectors (1). However penicillamine, which differs from cysteine in possessing two methyl groups adjacent to the sulfhydryl (*viz.* $HS{-}C(CH_3)_2CH(NH_3^+)CO_2^-$), is an exception to this rule and in some situations may even act as a radiation sensitizer (2, 3). The explanation for the lack of protective ability in penicillamine is clearly of fundamental impor-

[1]Present address: Biophysics Laboratory, Department of Physics, Illinois Institute of Technology, Chicago, Illinois.

tance to an understanding of the mechanism of sulfhydryl protection. For this reason and also because of the significant role played by molecules related to penicillamine in medicinal chemistry, the present investigation of the products of degradation of penicillamine by free radicals was undertaken. For convenience the formula of the molecule is henceforth abbreviated to penSH.

Earlier esr studies (4) in flow systems have led to the conclusion that the radicals formed by OH attack are predominantly thiyl radicals:

[1] $\cdot OH + penSH \rightarrow H_2O + penS\cdot$

More recent research on the pulse radiolysis of nitrous oxide-saturated solutions is in agreement with this (5–8) and has shown (6) that $\cdot CH_2OH$ radicals also produce penS· radicals:

[2] $\cdot CH_2OH + penSH \rightarrow CH_3OH + penS\cdot$

At pH's where the $penS^-$ concentration is significant ($pH \geq 7$; $pK_{penSH} = 7.9$ (6)) penS· radicals form $penS\dot{S}^-pen$ radical anions, which possess a strong optical absorption with λ_{max} at 450 nm (5–8). The absorption attributed to

[3] $penS\cdot + penS^- \rightleftarrows penS\dot{S}^-pen$

penS· radicals is much weaker and has a maximum at 330 nm (5–8). The kinetics of the decays of the optical absorptions were consistent with the following radical–radical reactions:

[4] $penS\cdot + penS\cdot \rightarrow penSSpen$

and

[5] $penS\cdot + penS\dot{S}^-pen \rightarrow penS^- + penSSpen$

However, there was also evidence for a first order decay of $penS\dot{S}^-pen$ at low doses per pulse (6), which was tentatively attributed to reaction 6.

[6] $penS\dot{S}^-pen\ (+ H_2O) \rightarrow penSS\cdot + penH + OH^-$

Purdie, Gillis, and Klassen (6) have reported yields of penSSpen, penSSSpen, penH, and H_2S from the pulse and ^{60}Co γ radiolysis of nitrous oxide-saturated solutions at pH 5 and 8. The hydrogen sulfide ($G(H_2S) = 0.5$ to 0.7) was attributed primarily to reaction 7

[7] $\cdot H + penSH \rightarrow H_2S + pen\cdot$

which had previously been observed at $pH = 1$ by Peterson (9) and investigated by competition kinetics by Tung and Kuntz (10). The formation of trisulfide was attributed to reactions 6, 8, and 9:

[8] $penS\cdot + penSS\cdot \rightarrow penSSSpen$

[9] $penSS\cdot + penSS\cdot \rightarrow penSSSSpen$

with the tetrasulfide reacting with penSH probably in reaction 10:

[10] $penSSSSpen + penSH \rightarrow penSSSpen + penSSH$

The rate of this reaction was such that any tetrasulfide produced would have disappeared in the time which elapsed between radiolysis and analysis (approximately 1 h) in the experiments of ref. 6. The penSSH from reaction 10 may reasonably be expected to form further trisulfide in reaction 11:

[11] $penSSH + penSSpen \rightarrow penSSSpen + penSH$

Purdie *et al.* (6) found that the yield of trisulfide increased with increasing pH, and this supports the involvement of $penS\dot{S}^-pen$ ions in the formation of trisulfide. The yield also increased at lower dose rates which is consistent with the longer time available for reaction 6. However, the increase was not as great as expected for quantitative agreement with the rates of reactions 3 to 6 at pH 8.

Apart from the above studies and the hydrogen yield determinations of Tung and Kuntz (10) no systematic investigations of product yields from penicillamine radiolysis have been reported. The present study was undertaken to obtain a more complete picture of the products resulting from the reactions of e_{aq}^-, $\cdot H$, and $\cdot OH$ at pH 5 where the $penS^-$ concentration is small. Experiments were also performed with $\cdot CH_2OH$, $\cdot(Br)_2^-$, and $\cdot(CNS)_2^-$, since it seemed important to determine whether the production of trisulfide occurred only with $\cdot H$ and $\cdot OH$.

Experimental

Reagents

D-Penicillamine and L-norleucine from the Sigma Chemical Co., D-valine from Mann Research Laboratories, grade 'A' β-hydroxyvaline from Calbiochem, and D-penicillamine disulfide and 5,5'-dithiobis-(2-nitrobenzoic acid) from the Aldrich Chemical Co. were used without further purification. The penicillamine trisulfide was kindly supplied by J. W. Purdie of the Defence Research Board in Ottawa. Only the free base forms of amino acids were used in this work to avoid possible formation of $\cdot Cl_2^-$ from the hydrochloride salts.

The sources of potassium bromide, sodium thiocyanate,

perchloric acid, and methanol were as given in ref. 11, which also states the source and method of purification of the nitrous oxide. All other chemicals were of analar or reagent grade.

Procedures and Analyses

Penicillamine solutions were prepared in fresh triply distilled nitrogen-purged water which contained the solutes needed for the production of the radicals being investigated. The use of buffers was avoided, the solutions being allowed to assume their natural p*H*'s which lay in the range 4.8 to 5.4. Aliquots of 5 ml were transferred to the carefully cleaned Pyrex cells and attached to the vacuum line. After thorough degassing (12) the samples were equilibrated with N_2O at 760 torr and sealed. One served as an unirradiated standard and was injected immediately into the Technicon amino acid analyser. The remaining samples were stored in a refrigerator prior to irradiation. Immediately after the irradiation a small accurately measured volume (usually 1 ml) was taken and the analysis for amino-containing products was performed on the amino acid analyser. Norleucine was used as an internal standard and elution buffers of p*H* 3.18, 3.80, and 5.00 were employed in succession for periods of 130, 90, and 80 min respectively. These were first passed through a Hi-Rez Type DC-3 resin (Pierce Chemical Co.) to remove ammonia impurities. Standardisation procedures and other details of the amino acid analyses may be found in refs. 12 and 13. As the vinyl compound (CH_2=$CH(CH_3)CH(NH_3^+)CO_2^-$) has been carefully identified as a product of the radiolysis of penSSpen (14) and since no standard sample of it was available, it was prepared by irradiating a solution of the disulfide. This solution was injected into the analyser and used to determine the elution time for the vinyl compound, which is also produced from penSH but in a relatively small yield.

Hydrogen sulfide yields were determined with the molybdate reagent (15) using previously described calibration procedures (12), and hydrogen yields by the technique outlined in ref. 12.

The loss of penSH was normally calculated from the reduction in the height of the penSH peak on the amino acid chromatogram for the irradiated solution. However, in some cases the loss of penSH was confirmed with Ellman's reagent (5,5'-dithiobis-(2-nitrobenzoic acid)) after purging the irradiated solution with purified nitrogen to remove H_2S. The procedure has already been described (16, 17).

In preliminary experiments the number of amino- and sulfur-containing products was established by high voltage ionophoresis. Small aliquots of the irradiated solutions were applied to Whatmann 3 MM paper as a band and crystal violet dye marker was applied as a spot. Amino acid markers (R and T) were applied as 5μl aliquots to a 1 cm band. After vertical ionophoresis at p*H* 2 and 4 kV for 30 min the dye had migrated 18 cm and the paper was dried and cut into strips. Amino acids were detected by treating one of the penSH strips with collidine–ninhydrin reagent (18). The presence of sulfur-containing products was established by treating a second strip with freshly prepared platinic iodide reagent (19).

Irradiations

All irradiations were performed at 23 °C in a 'Gamma Cell 220' purchased from Atomic Energy of Canada. The dose rate was determined several times during the course of the study using ferrous sulfate dosimetry and assuming $G(Fe^{3+}) = 15.6$ (p. 217 of ref. 20). The mean value over the duration of the investigation was 5×10^{16} eV ml^{-1} min^{-1}.

Results

Identification of Amino Products

In addition to the peaks for residual penicillamine and the internal standard norleucine, the amino acid chromatograms of irradiated solutions exhibited six other peaks. Comparison of their elution times with those of standards led to the following identifications, which are given in the order of appearance: β-hydroxyvaline (a very small peak), vinyl compound (CH_2=$CH(CH_3)$-$CH(NH_3^+)CO_2^-$, a small peak), penSH, penH, penSSpen, norleucine, penSSSpen, and ammonia (a small peak). There are therefore two major amino products containing sulfur (penSSpen and penSSSpen) and one without it (penH). The formation of the two sulfur-containing amino products agreed with the results of the ionophoresis experiments. These also gave evidence for the vinyl compound and penH, but did not detect the very small yield of β-hydroxyvaline or the ammonia.

Particular care was taken to substantiate the identification of the trisulfide peak since it was not expected as a product in the radiolysis of a monosulfhydryl. In one experiment an aliquot of an irradiated penicillamine solution was analysed to obtain the area of the peak assigned to penSSSpen. A second aliquot was then mixed with a standard solution of penSSSpen and also chromatographed. Only one uniform peak attributable to penSSSpen was observed and its area had increased to that expected for the combined penSSSpen concentrations. In a second experiment which was kindly performed for us by P. J. Krueger and G. Lee the Raman spectrum of an irradiated solution was taken on a Cary model 82 laser Raman spectrometer and analysed. This solution exhibited a band at 510 cm^{-1}, which has been assigned to trisulfide vibrations (21). Other bands at 590 and 560 cm^{-1} due to the C—S and S—S stretching modes were also observed. These occur in both di- and trisulfides.

Product Yields

For every system the number of radicals of

TABLE 1. G values for radicals reacting with penicillamine and radical balances for deaerated and N_2O saturated 10^{-2} M penicillamine solutions at pH 4.8 to 5.4

Solute system	Solute radicals	G(Radicals attacking penSH) Primary H_2O radical species g_{OH}	$g_{e_{aq}^-}$	g_H	Total of all radicals	$2[G(RSSR)+G(RSSSR)]$ for 10^{-2} M penSH
Deaerated solutions						
10^{-2} M penSH only	—	2.8_5[a]	2.7_5[a]	0.6_0[b]	6.2	6.0(97%)[i]
N_2O saturated solutions						
(i) 10^{-2} M penSH only	—	5.4_5[c]	0.5_2[c]	0.6_0[b]	6.6	6.5(98%) (6.0)[d]
(ii) 10^{-2} M penSH with 1 M CH_3OH	$g_{CH_2OH}=5.9_1$[e]	0.2_9[e]	0.5_2[c]	0.3_3[e]	7.0	6.3(90%)
(iii) 10^{-2} M penSH with 0.15 M KBr	$g_{(Br)_2^-}=4.4_7$[f]	1.0_9[f]	0.5_2[c]	0.5_0[g]	6.6	6.3(95%)
(iv) 10^{-2} M penSH with 0.10 M NaCNS	$g_{(CNS)_2^-}=5.7_4$[h]	0.2_4[h]	0.5_2[c]	0.5_0[g]	7.0	6.5(93%)

[a] From yield–reactivity curves (25) using $k_{e_{aq}^-+penSH} \times (penSH) = 5.1 \times 10^7\ s^{-1}$ and $k_{OH+penSH} \times (penSH) = 4.5 \times 10^7\ s^{-1}$. $k_{e_{aq}^-+penSH} = 5.1 \times 10^9\ M^{-1}\ s^{-1}$ was taken from refs. 23 and 24 and $k_{OH+penSH} = 4.5 \times 10^9\ M^{-1}\ s^{-1}$ from refs. 4 and 6; average of $4.7 \times 10^9\ M^{-1}\ s^{-1}$ and $4.3 \times 10^9\ M^{-1}\ s^{-1}$.

[b] From ref. 20, p. 140.

[c] Calculated from the yields $g_e = 3.05$ and $g_{OH} = 2.90$ based on the data of ref. 26, using $k_{e_{aq}^-+penSH}$ from footnote a and $k_{e_{aq}^-+N_2O} = 9.0 \pm 0.3 \times 10^9\ M^{-1}\ s^{-1}$ from ref. 22.

[d] From data of ref. 6.

[e] g_{OH} was increased from 2.90 (see footnote c) to 3.40 based on yield reactivity curves (25), to take account of the increased reactivity to OH due to $k_{OH+CH_3OH} \times (CH_3OH) = 8.4 \times 10^8\ s^{-1}$. We took $k_{OH+CH_3OH} = 8.4 \times 10^8\ M^{-1}\ s^{-1}$ in neutral solutions from ref. 27. The proportion of OH reacting with CH_3OH to form $\cdot CH_2OH$ was calculated using this rate constant and that in [a]. k_{H+CH_3OH} was taken as $1.6 \times 10^6\ M^{-1}\ s^{-1}$ (28) and $k_{H+penSH}$ as $1.9 \times 10^9\ M^{-1}\ s^{-1}$ (10).

[f] g_{OH} was increased from 2.90 to 3.00 to take account of reactivity (25) due to 0.15 M Br^-. $k_{OH+Br^-} \times (Br^-) = 1.8 \times 10^8\ s^{-1}$ based on $k_{OH+Br^-} = 1.2 \times 10^9\ M^{-1}\ s^{-1}$ (27).

[g] g_H in Br^- and CNS^- solutions was reduced by 0.1 to allow for scavenging of H (29).

[h] g_{OH} was increased by 0.5 to take account of reactivity (25) due to 0.1 M CNS^-. $k_{OH+CNS^-} \times (CNS^-) = 1.10 \times 10^9\ s^{-1}$ based on $k_{OH+CNS^-} = 1.1 \times 10^{10}\ M^{-1}\ s^{-1}$ (27).

[i] Numbers in parentheses in right hand column are percentage radical balances equal to: $100 \times 2[G(RSSR) + G(RSSSR)]/G$(Total of all radicals).

each type expected to react with penicillamine was calculated from the known rate constants for the competing reactions. For the nitrous oxide-saturated solutions reaction 12 competes with reaction 13,

[12] $e_{aq}^- + N_2O\ (+H_2O) \rightarrow N_2 + \cdot OH^- + \cdot OH$

[13] $e_{aq}^- + penSH \rightarrow pen\cdot + SH^-$

the rate of which has been measured (8, 22, 23). Also in the presence of added methanol (see Table 1) reactions 14 and 15 are in competition with [1] and [7] plus [7a] respectively,

[14] $\cdot OH + CH_3OH \rightarrow H_2O + \cdot CH_2OH$

[15] $\cdot H + CH_3OH \rightarrow H_2 + \cdot CH_2OH$

[7a] $\cdot H + penSH \rightarrow H_2 + penS\cdot$

while reactions 16 to 19

[16] $\cdot OH + Br^- \rightarrow OH^- + \cdot Br$

[17] $\cdot Br + Br^- \rightarrow \cdot Br_2^-$

[18] $\cdot OH + CNS^- \rightarrow OH^- + CNS\cdot$

[19] $CNS\cdot + CNS^- \rightarrow \cdot(CNS)_2^-$

occur when KBr and NaCNS are present along with N_2O. The numbers of radicals reacting with penSH in each solute system have been calculated assuming straightforward competitions between the solutes and penSH. They are listed in Table 1 along with the rate constants employed in the calculations. Initial experiments showed that at p$H \sim 5$ reaction with hydrogen peroxide occurred as was observed for cysteine.

[20] $2penSH + H_2O_2 \rightarrow penSSpen + 2H_2O$

However, its rate was slow enough (*cf.* ref. 13) that any contribution from it could be neglected since the samples were injected into the analyser directly after radiolysis.

G values were calculated from the slopes of product concentration – dose plots. Examples of such plots are shown in Fig. 1a for H_2 and H_2S from 10^{-3} M deaerated solutions, and in Fig. 1b for penSSpen and penSSSpen from 10^{-3} and 10^{-2} M solutions and NH_3, penH, and vinyl

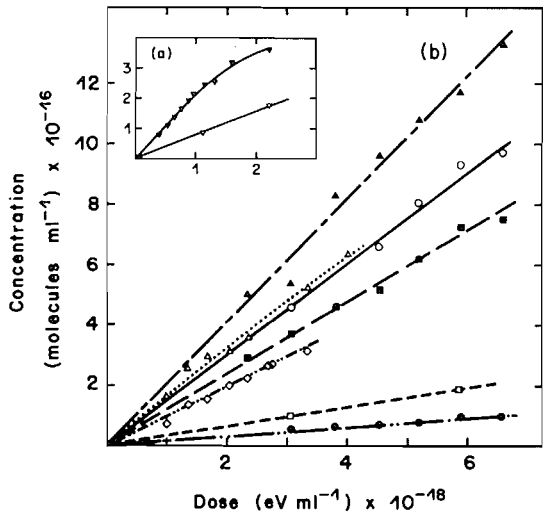

FIG. 1. Plots of product concentration *vs.* dose: (*a*) deaerated solutions; 10^{-3} *M* penSH: ▼ H_2S, ▽ H_2; (*b*) N_2O saturated solutions; 10^{-3} *M* penSH: △ penSSpen, ◇ penSSSpen; 10^{-2} *M* penSH: ▲ penSSpen, ○ penH, ■ penSSSpen, □ NH_3, ● $CH_2{=}C(CH_3)CH(NH_3^+)CO_2^-$.

compound from 10^{-2} *M* solutions, all of which were N_2O-saturated. As illustrated in Fig. 1*b*, for 10^{-2} *M* solutions these plots were linear up to at least 6×10^{18} eV ml^{-1} and the *G* values calculated from them are expected to be within experimental error equal to the initial *G* values for this concentration. This is borne out by arguments presented in the Discussion.

Detection of most amino products was not feasible below 0.4×10^{18} eV ml^{-1} and for the 10^{-3} *M* penSH solutions *G* values were derived from the slopes in the 0 to 2×10^{18} eV ml^{-1} range. Since 10^{18} eV ml^{-1} corresponds to 10 mol% consumption of the penSH,[2] these *G* values will be lower than initial *G* values and must be interpreted with caution. Thus our conclusions regarding the mechanism are based primarily on the yields for 10^{-2} *M* solutions. However, the results for 10^{-3} *M* solutions are useful for purposes of comparison for certain products and a few yields for this concentration are therefore reported also.

It is worth noting that the plots for the penSSSpen concentrations do not curve upward with dose in either the 10^{-2} or 10^{-3} *M* penSH solutions. Such curvature would be expected if disulfide were an intermediate in the formation of penSSSpen. Further evidence against this possibility was derived from experiments in which 5–10 mol% of penSSpen was added to 10^{-3} *M* penSH solutions before irradiation. While this tended to depress product yields it caused no marked rise in *G*(penSSSpen).

[2]In 10^{-3} *M* penSH. For 10^{-2} *M* penSH the mol% consumption at this dose is <2.

TABLE 2. Product yields from reactions of OH, e_{aq}^-, and H with penicillamine in deaerated solutions

Parameter	Value: pH = 5.0±0.1 [penSH] = 10^{-2} *M*	Value: pH = 5.4±0.1 [penSH] = 10^{-3} *M*
G(penSSpen)	$1.8_5 \pm 0.1_4$	$1.4_0 \pm 0.2_0$
G(penSSSpen)	$1.1_6 \pm 0.0_5$	$0.9_6 \pm 0.0_6$
G(penH)	$3.5_1 \pm 0.2_0$	$2.7_7 \pm 0.2_0$
G(vinyl)	$0.1_7 \pm 0.0_3$	$0.1_3 \pm 0.0_3$
G(NH_3)	$0.1_9 \pm 0.0_3$	$0.2_5 \pm 0.0_4$
G(H_2)	$0.6_4 \pm 0.0_3$	$0.7_9 \pm 0.0_6$
G(H_2S)	$3.0_0 \pm 0.3_0$	$2.1_7 \pm 0.2_0$
Total *G*(—N)[a]	9.9±0.6	7.9±0.8
Total *G*(—S)[b]	10.2±0.7	7.9±0.6
G(—penSH)	10.5±1.0	8.0±0.5

[a]*G*(—N) = Sum of (*G* value) × (number of N atoms per molecule) for all N-containing products.
[b]*G*(—S) = Sum of (*G* value) × (number of S atoms per molecule) for all S-containing products.

G values for the products obtained in deaerated and nitrous oxide solutions are listed in Tables 2 and 3 respectively. Stoichiometry requires that the number of molecules of penSH destroyed per 100 eV, *G*(—penSH), be equal to the total yield of nitrogen, *G*(—N), appearing in products and also to the total yield of sulfur, *G*(—S), appearing in products. The degree of agreement between these three quantities provides a test of the completeness of product identification. As seen from Table 2, for the deaerated solutions *G*(—N), *G*(—S), and *G*(—penSH) agreed within 6%. For the nitrous oxide-saturated solutions (see Table 3) *G*(—N) agreed with *G*(—penSH) to within 5% except for the $\cdot(Br)_2^-$ solutions. Here the difference was 10% but it is still within the combined standard deviations. Hydrogen sulfide was not determined by us in nitrous oxide-saturated solutions. However, if one uses $G(H_2S) = 0.7$ per 100 eV as reported for 10^{-2} *M* solutions in ref. 6 *G*(—S) is 8.4, in an excellent agreement with *G*(—N) and *G*(—penSH) in column two of Table 3. In view of the highly satisfactory agreement between *G*(—penSH), *G*(—N), and *G*(—S) for our conditions the con-

TABLE 3. Product yields from reactions of oxidising radicals with penicillamine in N_2O saturated solutions

Parameter	Value					
	(*a*)	(*b*)	(*c*)	(*d*)	(*e*)	(*f*)
G(penSSpen)	$2.0_4 \pm 0.1_6$	$2.0_0 \pm 0.2_0$	$1.9_4 \pm 0.1_7$	$2.0_8 \pm 0.1_3$	$1.8_1 \pm 0.1_5$	$2.0_1 \pm 0.1_5$
G(penSSSpen)	$1.1_9 \pm 0.0_4$	$1.1_6 \pm 0.0_4$	$1.1_9 \pm 0.0_4$	$1.1_9 \pm 0.0_4$	$0.9_4 \pm 0.0_5$	$0.9_0 \pm 0.0_4$
G(penH)	$1.5_0 \pm 0.1_0$	$1.5_8 \pm 0.1_0$	$1.4_5 \pm 0.1_0$	$1.3_3 \pm 0.0_5$	$0.6_0 \pm 0.0_4$	$0.6_8 \pm 0.0_4$
G(vinyl)	$0.1_5 \pm 0.0_2$	$0.6_3 \pm 0.0_7$	$0.0_8 \pm 0.0_4$	$0.0_5 \pm 0.0_3$	$0.1_2 \pm 0.0_5$	$0.4_3 \pm 0.0_4$
G(NH_3)	$0.3_1 \pm 0.0_3$	$0.1_4 \pm 0.0_3$	$0.4_7 \pm 0.0_5$	$0.1_6 \pm 0.0_5$	$0.3_8 \pm 0.0_5$	—
Total *G*(—N)	8.4 ± 0.6	8.7 ± 0.7	8.3 ± 0.6	8.1 ± 0.7	6.6 ± 0.5	7.0 ± 0.5
G(—penSH)	8.8 ± 0.8	9.0 ± 0.8	9.4 ± 1.0	8.5 ± 1.0	6.7 ± 0.5	7.1 ± 0.5

[a] No added solute; p*H* = 5.0 ± 0.1; major attacking radical = ·OH; [penSH] = 10^{-2} *M*.
[b] Added solute = 1 *M* CH_3OH; p*H* = 5.0 ± 0.1; major attacking radical = ·CH_2OH; [penSH] = 10^{-2} *M*.
[c] Added solute = 0.15 *M* KBr; p*H* = 4.8 ± 0.1; major attacking radical = ·$(Br_2)^-$; [penSH] = 10^{-2} *M*.
[d] Added solute = 0.1 *M* NaCNS; p*H* = 5.2 ± 0.1; major attacking radical = ·$(CNS)_2^-$; [penSH] = 10^{-2} *M*.
[e] No added solute; p*H* = 5.4 ± 0.1; major attacking radical = ·OH; [penSH] = 10^{-3} *M*.
[f] Added solute = 1 *M* CH_3OH; p*H* = 5.4 ± 0.1; major attacking radical = ·CH_2OH; [penSH] = 10^{-3} *M*.

clusion that the total yield of as yet unidentified products is less than 1 per 100 eV appears to be reasonably well justified.

Discussion

Free radical reactions with the penicillamine molecule may conveniently be classified in terms of the sites at which chemical damage initially occurs. These are shown in the following diagram,

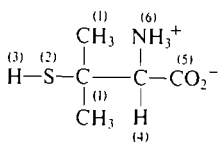

and Scheme 1 gives sequences of reactions which lead to the formation of the vinyl compound, penH, ammonia, and H_2S after attack by a radical ·X at sites (*1*), (*2*), and (*4*). The rapid elimination of ·SH assumed to occur in reactions 22 and 29 is consistent with the low C—S bond dissociation energy in free radicals (~10 kcal mol^{-1} (30, 31)). Reactions of oxidising radicals at sites (*5*) and (*6*) could also lead to ·SH elimination and ammonia formation. However, we found less literature evidence for such processes and have not discussed them here. Non-amino products from the fragmentation of the molecule (for example $CH(CH_3)_2COCO_2^-$ formed in the multistep reaction 27) are not detected by our techniques, but the extent of their formation inferred from the ammonia yields is <0.4 per 100 eV, except for the solutions with ·$(Br)_2^-$ as

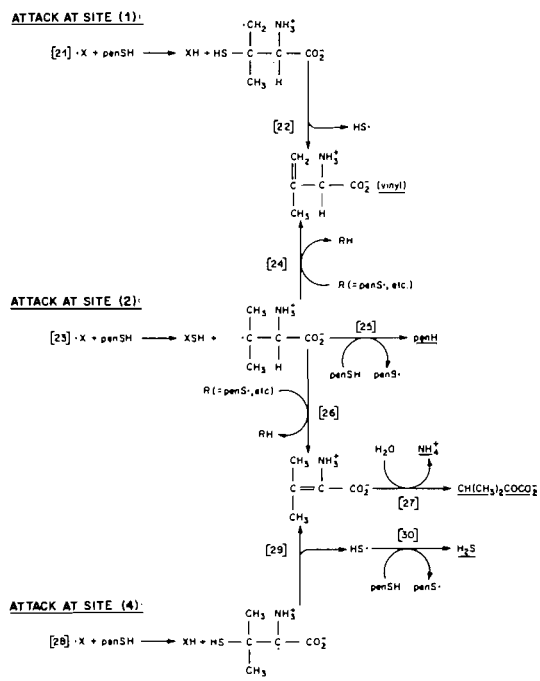

SCHEME 1

major reactant (see Table 3). Abstraction of the H atom at site (3) produces penS·.

The magnitudes of *G*(penSSpen) and *G*(penSSSpen) for the 10^{-2} *M* solutions in Tables 2 and 3 are constant and independent of the nature of the attacking radicals. Except for *G*(penSSpen) in the deaerated solutions this feature also applies to the 10^{-3} *M* solutions. It is best explained if ·OH, ·CH_2OH, ·$(Br)_2^-$, ·$(CNS)_2^-$,

and pen· each produce predominantly penS· radicals, which form the di- and trisulfide in subsequent reactions. Stoichiometry requires that these reactions also contribute to the penH yield and we assume these contributions to be equal to the mean values of G(penSSSpen) for the 10^{-2} and 10^{-3} M solutions, 1.18 and 0.93 per 100 eV respectively. The nature of the secondary reactions of penS· will be discussed later. The reactions of $\cdot H$ and e_{aq}^- and processes producing the vinyl compound and ammonia are considered first.

Reactions of $\cdot H$ and e_{aq}^-

Analogy with other low molecular weight sulfhydryl molecules suggests that initial attack by e_{aq}^- will occur at site (*2*) and by $\cdot H$ at sites (*2*) or (*3*). If reactions 7, 7*a*, and 13 are the only reactions producing significant yields of hydrogen and hydrogen sulfide then the relation $G(H_2) + G(H_2S) = g_{e_{aq}^-} + g_H + G_{H_2}{}^M$ should hold for the deaerated solutions. The results in Table 2 give $G(H_2) + G(H_2S) = 3.6$ per 100 eV for the 10^{-2} M solutions and 3.0 per 100 eV for the 10^{-3} M solutions. These values are very similar to 3.6 and 3.1 per 100 eV for 10^{-2} and 10^{-3} M cysteine solutions at pH 5.6 (13). The lower magnitude of $G(H_2) + G(H_2S)$ in the 10^{-3} M solutions is attributed to the fact that the radical yields are smaller at the lower concentration and to the greater proportion of primary and secondary radicals reacting with products.

Allowing for the effect of intra-spur scavenging (25, 13) we estimate $G_{H_2}{}^M = 0.3_0$ per 100 eV for the 10^{-2} M solutions. Hence, $g_{e_{aq}^-} + g_H = G(H_2) + G(H_2S) - 0.3_0 = 3.3$, which is in agreement with 3.3_5 per 100 for $g_{e_{aq}^-} + g_H$ from Table 1. The observed hydrogen yield is 0.64 per 100 eV which leaves $0.6_4 - 0.3_0 = 0.3_4$ molecules per 100 eV to be attributed to reaction 7*a*. On this basis $g_H k_{7a}/(k_{7a} + k_7)$ is 0.34, whence we calculate $k_{7a}/k_7 = 1.3$.

For the deaerated solutions $G(H_2S)$ should be equal to $[g_{e_{aq}^-} + g_H k_7/(k_{7a} + k_7)]$. Using $g_{e_{aq}^-} = 2.7_5$ and $g_H = 0.6_0$ per 100 eV from Table 1, and the above value of k_{7a}/k_7 one obtains 3.0 per 100 eV, which is again in good agreement with the experimental result in Table 2 for the deaerated 10^{-2} M penSH solutions. The significantly smaller value of $G(H_2S)$ for the 10^{-3} M solutions (2.1_7) is believed to be caused to a large extent by secondary reactions of this product with pen· and other radicals, since the H_2S concentration – dose plots for these solutions exhibited curvature. For the 10^{-2} M nitrous oxide-saturated solutions the number of electrons reacting directly with penSH is 0.5_2 (see Table 1) and the total H_2S yield from [7] and [13] should be 0.7_8 molecules per 100 eV. This is close to 0.7 molecules per 100 eV reported in ref. 6 for these conditions. Therefore the hydrogen and hydrogen sulfide yields at pH = 5 can be satisfactorily explained by reactions 7*a*, 7, and 13 with $k_{7a}/k_7 = 1.3$. This value of k_{7a}/k_7 is about three times larger than 0.44 and 0.50 observed at pH = 1 (10) and pH = 0 (32) respectively, suggesting that k_{7a}/k_7 is pH dependent.

If all pen· radicals from reactions 7 and 13 were converted to penH in reaction 25, then for the 10^{-2} M deaerated solutions the combined yield from this reaction and the secondary reactions of penS· radicals (1.18 per 100 eV see above) would be 4.18 per 100 eV ($= G(H_2S) + 1.18$). The observed magnitude of G(penH) was 3.5, implying that about 0.7 pen· radicals per 100 eV are lost in reactions other than [25]. Like [13] this is a counterpart of a reaction occurring in the cysteine system, where there is no significant deficit of the corresponding product, CysH (13). The lower bond dissociation energy for the tertiary C—H bond of penH ($D_{\text{tertiary C—H}} \simeq 91$ kcal mol^{-1} as opposed to $D_{\text{primary C—H}} \simeq 95$–100 kcal mol^{-1} (33)) formed in the penSH case will decrease the exothermicity of reaction 25. This together with the steric hindrance of the methyl radicals will tend to slow the rate of H atom transfer, permitting a greater proportion of alternative reactions of the pen· radical. Those shown in Scheme 1 ([24] and [26]) yield ammonia and the vinyl compound. Some pen· radicals may combine with penS· to form penSpen. However, the absence of significant peaks attributable to penSpen indicates that G(penSpen) < 0.2 per 100 eV.

Reactions of $\cdot OH$, $\cdot CH_2OH$, $\cdot(Br)_2^-$, and $\cdot(CNS)_2^-$

Minor Products

The yield of pen· radicals will be drastically reduced in nitrous oxide saturated solutions where most e_{aq}^- react with N_2O. Thus the increase in $G(NH_3)$ to 0.31 in the 10^{-2} M nitrous oxide-saturated solutions from 0.19 ± 0.03 in

deaerated solutions of the same concentration means that there are sources of NH_3 other than the reactions of pen· radicals. A similar behaviour occurs in the 10^{-3} *M* solutions (Tables 2 and 3). Reactions 28, 29, and 27 are probable additional sources of ammonia and their analogues in the cysteine system have been proposed previously (11). Rather interestingly for the 10^{-2} *M* solutions $G(NH_3)$ is greatest for $\cdot(Br)_2^-$, for which the negative charge and strong oxidising power would enhance the rate of reaction at site (*4*) relative to site (*2*) or (*3*). It is next highest for ·OH and comparatively small for $\cdot CH_2OH$ and $\cdot(CNS)_2^-$. However, for each radical species $G(NH_3)$ is larger than was observed with cysteine, and this must be due to steric or inductive effects of the methyl groups, which reduce the likelihood of attack on the SH group of penSH.

From Table 3 vinyl production is most efficient for $\cdot CH_2OH$, suggesting an enhanced contribution from reactions 21 and 22 or some other process in this system.

penSSpen and penSSSpen

Although the yields of ammonia and vinyl compound in Table 3 show that radical attacks at sites other than the sulfhydryl H atom are more frequent with penicillamine than with cysteine (*cf.* the smaller ammonia yields in ref. 11), they are still small relative to the yields of the major products. This is consistent with the previously mentioned conclusion that ·OH, $\cdot CH_2OH$, $\cdot(Br)_2^-$, $\cdot(CNS)_2^-$, and pen· produce predominantly penS· radicals upon reacting with penSH in reactions 1, 2, 31, 32, and 25. In the cysteine system the corresponding radical

[31] $\cdot(Br)_2^- + penSH \rightarrow 2Br^- + H^+ + penS\cdot$

[32] $\cdot(CNS)_2^- + penSH \rightarrow 2CNS^- + H^+ + penS\cdot$

[25] $pen\cdot + penSH \rightarrow penH + penS\cdot$

cysS· disappears primarily by combination to form cysSScys and for any set of conditions the relation $2G(cysSScys) = G(\text{total radicals})$ holds. If reactions 4–6 and 8–11 are responsible for the production of penSSpen and penSSSpen in the present system, the corresponding relation would be $2[G(penSSpen) + G(penSSSpen)] = G(\text{total radicals})$. The values of $2[G(penSSpen) + G(penSSSpen)]$ for 10^{-2} *M* solutions in the penultimate column of Table 1 have been expressed as a percentage of the calculated total radical yields and are given in the last column. These percentages lie in the range 92 to 98%, showing that the relationship holds to a good approximation. The small deficiencies in the yields are expected in view of the probable occurrence of radical disproportion reactions such as [24] and [26] (see Scheme 1), which do not produce penSSpen or penSSSpen.

For the 10^{-3} *M* nitrous oxide-saturated solutions $2[G(penSSpen) + G(penSSSpen)] = 5.8_2$ with 1 *M* CH_3OH and 5.5_0 with no solute (*i.e.* for ·OH as the major attacking radical). These quantities are significantly smaller than the estimated total radical yields in Table 1, reflecting the enhanced importance of product–radical reactions at this concentration. Similarly $2[G(penSSpen) + (penSSSpen)] = 4.7$ for the deaerated 10^{-3} *M* solutions is much smaller than 6.0 per 100 eV calculated for the total radical yield using $g_H = 0.6$, $g_{e_{aq}^-} = 2.6_5$ and g_{OH} and 2.7_0 from yield–reactivity curves in ref. 25. It is also less than $2G(cysSScys) = 6.0$ for 10^{-3} *M* cysteine, which indicates a higher proportion of radical–product and radical–radical reactions (other than [4] and [5]) in the penSH system.

Taking $K_{33} = 10^{-8}$ *M* (6) and $K_3 = 300\ M^{-1}$

[33] $penSH \rightleftharpoons pens^- + H^+$

(6) one finds $[penSS^-pen] = 3 \times 10^{-3} \times [penS\cdot]$ in 10^{-2} *M* penSH at p*H* = 5, which means that reaction 5 can be neglected. Applying the steady state approximation to the concentrations of penS·, penSS· and penSS$^-$pen one then obtains

$$\rho - 2k_4[penS\cdot]^2 - 2\frac{d[penSSSpen]}{dt} = 0$$

where ρ is the total rate of production of penS· radicals. From this relationship it follows that

$$[penS\cdot] = \left\{\left(\rho - 2\frac{d[penSSSpen]}{dt}\right)\Big/2k_4\right\}^{1/2}.$$

Also

$$\frac{d[penSSSpen]}{dt} = k_6[penSS^-pen]$$

Assuming reaction 3 maintains an equilibrium and writing $d[penSSSpen]/dt = r$, one can derive the expression

[34] $$\{(2r/\rho)/(1 - 2r/\rho)^{1/2}\}\rho^{1/2} = \sqrt{2}k_6k_4^{-1/2}K_3K_{33}[penSH][H^+]^{-1}$$

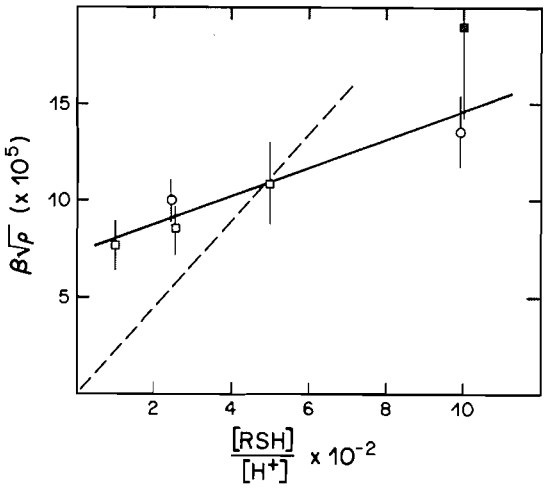

FIG. 2. Dependence of normalised trisulfide yields on penicillamine concentration and pH: O, data of this study at pH 5.4 for 10^{-3} M penSH and pH 5.0 for 10^{-2} M penSH and 5×10^{16} eV ml^{-1} min^{-1}; ■, from ref. 6 and □ from Purdie[2] at pH 5.0, varying [penSH] and 4.9×10^{17} eV ml^{-1} min^{-1}. For definitions of β and ρ see Discussion. The estimated errors in β are larger at 4.9×10^{17} eV ml^{-1} min^{-1} because of the much smaller values of G(penSSSpen). Dashed line shows value expected for reaction 6 in 10^{-2} M penSH at pH 5.

The quantity r/ρ is equal to G(penSSSpen) divided by G(total penS· radicals formed), which can be assumed to be 6.6 per 100 eV. In Fig. 2 we test expression 34 for pH in the range 5 to 5.4, using the present data and other values of G(penSSSpen) observed at a tenfold higher dose rate. One of these was given in ref. 6 and the remainder have been obtained by Purdie.[3] The left hand side of expression 34 is denoted as $\beta\sqrt{\rho}$. The dashed line passing through the origin shows quantitatively the behaviour expected, assuming the rate constants for reactions 4 and 6 and the equilibrium constant for reaction 3 are pH independent.

The fact that the high and low dose rate results in Fig. 2 are brought into coincidence on multiplying β by $\sqrt{\rho}$ confirms the dependence of G(penSSSpen) on this parameter and supports the view that a first order reaction of a radical intermediate competes with radical combination. On the other hand the solid line in Fig. 2 does not pass through the origin,[4] showing that a mechanism based only on reactions 3 to 6 and 8 is inadequate to explain the trisulfide formation at pH = 5. Hence it would appear that species other than penSS$^-$pen may be involved, and in this regard the possible intermediacy of the sulfenium radical (penSS(H)pen) cannot be ignored. Although this radical is currently believed to be much less stable than penSS$^-$pen (7, 8) it may conceivably exist in a high enough concentration at pH = 5 for reactions 35 to 38

[35] $\text{penS}\cdot + \text{penSH} \rightleftharpoons \text{penS}\dot{\text{S}}\text{(H)pen}$

[36] $\text{penS}\dot{\text{S}}\text{(H)pen} \rightarrow \text{penSS}\cdot + \text{penH}$

[37] $2\text{penS}\dot{\text{S}}\text{(H)pen} \rightarrow \text{penSSpen} + 2\text{penSH}$

[38] $\text{penSS(H)pen} + \text{penS}\cdot \rightarrow \text{penSSpen} + \text{penSH}$

to provide a significant pathway to penSS· formation.

Since the number of penSS· radicals is small relative to penS·, reaction 9 was neglected in deriving expression 34. However, the situation is still complicated by the possibility that penSSSSpen produced in a significant yield from reaction 9 may react with penS· radicals.

[39] $\text{penS}\cdot + \text{penSSSSpen} \rightarrow \text{penSSSpen} + \text{penSS}\cdot$

Reactions of this type have been postulated to occur with sulfanes (34) and methyl polysulfides (35). They will tend to decrease the penSSSpen yield, since they reduce the lifetime of penS·. This could contribute to the fact that for experiments all done at pH close to 5 (as in Fig. 2) β is not directly proportional to [penSH]. Likewise it may be a reason why G(penSSSpen) from the γ radiolysis at pH 8 is less than predicted from the rate constants determined from pulse radiolysis at that pH, which indicated that reaction 6 should be the dominant mode of penSS$^-$pen decay (6).

More work on the dependence of G(penSSSpen) on [H$^+$] and [penSH] in the pH range 0 to 6 will be required before the mechanism of trisulfide formation in acid solutions can be settled, and further pulse radiolysis studies of the intermediates in the pH = 0 to 6 region would also be of great value.

[3]We are indebted to Dr. J. W. Purdie for making these data available to us.

[4]The dependence of $\beta\sqrt{\rho}$ on [penSH]/[H$^+$] may if anything be slightly less than indicated by the solid line in Fig. 2, since the values of β for low [penSH]/[H$^+$] are calculated from G(penSSSpen) for 10^{-3} M penSH. As seen above from a comparison with radical yields, the product yields in these solutions tend to be smaller than expected.

Acknowledgments

The authors wish to express their thanks to Drs. M. H. Benn, J. W. Purdie, H. Gillis, and N. V. Klassen for helpful discussions, and to Dr. Purdie for other assistance. They are grateful to Drs. P. J. Krueger and G. Lee for the Raman spectral analysis.

Financial support for this work came from Defence Research Board of Canada grant number 957004 and from National Research Council of Canada grant number A 3571.

1. L. ELDJARN and A. PIHL. *In* Mechanisms in radiobiology. *Edited by* M. Errera and A. Forssberg. Academic Press, London. 1960. p. 231.
2. C. NOFRE and A. CIER. *In* Electronic aspects of biochemistry. *Edited by* B. Pullman. Academic Press, London. 1964. p. 397.
3. H. LANGENDORFF, M. LANGENDORFF, and P. KOCH. Strahlentherapie, **107**, 121 (1958).
4. W. A. ARMSTRONG and W. G. HUMPHREYS. Can. J. Chem. **45**, 2589 (1967).
5. J. W. PURDIE, H. A. GILLIS, and N. V. KLASSEN. Chem. Soc. Chem. Commun. 1163 (1971).
6. J. W. PURDIE, H. A. GILLIS, and N. V. KLASSEN. Can. J. Chem. **51**, 3132 (1973).
7. M. Z. HOFFMAN and E. HAYON. J. Am. Chem. Soc. **94**, 7950 (1972).
8. M. Z. HOFFMAN and E. HAYON. J. Phys. Chem. **77**, 990 (1973).
9. R. M. PETERSON. Ph.D. Thesis, University of Delaware, Newark, Delaware, 1968.
10. TZU-LIN TUNG and R. R. KUNTZ. Radiat. Res. **55**, 10 (1973).
11. G. C. GOYAL and D. A. ARMSTRONG. Can. J. Chem. **53**, 1475 (1975).
12. V. G. WILKENING, MANOHAR LAL, M. ARENDS, and D. A. ARMSTRONG. Can. J. Chem. **45**, 1209 (1967).
13. V. G. WILKENING, MANOHAR LAL, M. ARENDS, and D. A. ARMSTRONG. J. Phys. Chem. **72**, 185 (1968).
14. J. W. PURDIE. Can. J. Chem. **47**, 1029 (1969).
15. W. ANDO, K. SUGIMOTO, and S. OAE. Bull. Chem. Soc. Jpn. **36**, 893 (1963).
16. G. L. ELLMAN. Arch. Biochim. Biophys. **82**, 70 (1959).
17. E. BEUTLER, O. DURON, and B. M. KELLY. J. Lab. Clin. Med. **61**, 882 (1963).
18. J. L. BAILEY. Techniques in protein chemistry, 2nd ed. Elsevier, Amsterdam and New York. 1967. p. 17.
19. C. W. EASLEY. Biochim. Biophys. Acta, **107**, 386 (1965).
20. I. G. DRAGANIĆ and Z. D. DRAGANIĆ. The radiation chemistry of water. Academic Press, New York. 1971.
21. P. J. KRUEGER and G. LEE. To be published.
22. M. Anbar, M. Bambenek, and A. B. Ross. Selected specific rates of reactions of transients from water in aqueous solution. 1. Hydrated electron. U.S. Dept. of Commerce, National Bureau of Standards, Washington, D.C. 1973.
23. R. BRAAMS. Radiat. Res. **27**, 319 (1966).
24. TZU-LIN TUNG and R. R. KUNTZ. Radiat. Res. **55**, 256 (1973).
25. Z. D. DRAGANIĆ and I. G. DRAGANIĆ. J. Phys. Chem. **77**, 765 (1973).
26. G. E. ADAMS, J. W. BOAG, J. CURRANT, and B. D. MICHAEL. *In* Pulse radiolysis. *Edited by* M. Ebert, J. P. Keene, A. J. Swallow, and J. H. Baxendale. Academic Press, London. 1965. p. 117.
27. L. M. DORFMAN and G. E. ADAMS. Reactivity of hydroxyl radicals in aqueous solutions. U.S. Department of Commerce, Natl. Bur. Stand. No. 46, Washington, D.C. 1973.
28. P. NETA, R. W. FESSENDEN, and R. H. SCHULER. J. Phys. Chem. **75**, 1654 (1971).
29. Z. D. DRAGANIĆ and I. G. DRAGANIĆ. J. Phys. Chem. **76**, 2733 (1972).
30. D. M. GRAHAM, R. L. MELVILLE, and C. SIVERTZ. Can. J. Chem. **42**, 2250 (1964).
31. D. M. GRAHAM and J. F. SOLTYS. Can. J. Chem. **47**, 2529 (1969).
32. G. C. GOYAL and D. A. ARMSTRONG. To be published.
33. J. A. KERR. Chem. Rev. **66**, 465 (1966).
34. E. MULLER and J. B. HYNE. J. Am. Chem. Soc. **91**, 1907 (1969).
35. T. L. PICKERING, K. J. SAUNDERS, and A. V. TOBOLSKY. *In* The chemistry of sulfides. *Edited by* A. V. Tobolsky. Interscience, New York. 1968.

A self-consistent field wavefunction suited for calculation of the electric field gradient in HCl[1]

J. E. GRABENSTETTER[2] AND M. A. WHITEHEAD
Chemistry Department, McGill University, Montreal, P.Q., Canada H3C 3G1

Received August 22, 1975[3]

J. E. GRABENSTETTER and M. A. WHITEHEAD. Can. J. Chem. **54**, 1948 (1976).

A single-centre basis set on Cl is developed for an SCF calculation on HCl to give an accurate expectation value for the electric field gradient at the Cl nucleus. The SCF energy, orbital eigenvalues, dipole moment, molecular electric quadrupole moment, Hellmann–Feynman force on Cl and virial ratio are also reported, and the variation of the electric field gradient at Cl with changes in internuclear distance is examined.

J. E. GRABENSTETTER et M. A. WHITEHEAD. Can. J. Chem. **54**, 1948 (1976).

On a développé un ensemble de fonction de base à centre unique orientée sur le chlore permettant d'effectuer un calcul SCF du HCl de façon à obtenir une valeur moyenne dans la sens de mecanique ondulatoine qui soit précise pour le gradient de champ électrique au niveau de l'atome de chlore. On rapporte aussi les énergies SCF, les valeurs propre des orbitales, les moments dipolaires, les moments quadrupolaires électriques moléculaires, les forces Hellman-Feyman sur le chlore et les rapports viriels; on examine aussi la variation du gradient de champ électrique au niveau du chlore avec un variationement de la distance internucléaire.
[Traduit par le journal]

Introduction

One-centre expansion (OCE) basis sets are no longer appropriate for general calculations of electronic wavefunctions and molecular properties, results of greater accuracy usually being attainable in comparable computing times with multicentre bases. However, an OCE approach may be the most efficient way to generate a wavefunction accurate for those one-electron properties whose operators are strongly dependent upon the electron density near the heavy nucleus in a hydride.

The electric field gradient (EFG) at the Cl nucleus in HCl, given by the operator

$$[1] \qquad \hat{q} = (3\cos^2\theta - 1)/r^3$$

with θ measured from the principal axis of the EFG tensor and r measured from the Cl nucleus, is strongly dependent on the electron distribution near the Cl nucleus (1). This suggests that an SCF wavefunction for HCl with an OCE basis on the Cl would give a relatively accurate expectation value of $\hat{q}$ with a moderately sized basis set and little computational expense.

Moccia (2) reported an OCE-SCF wavefunction for HCl in a basis consisting of 71 Slater-type orbitals (STO's) centred on Cl (31 σ orbitals, 20 π pairs), and calculated an SCF energy (E_{SCF}) of -460.05810 hartrees (at $R = 2.424$ bohrs) and an expectation value for $\frac{1}{2}\hat{q}$ over the electronic and nuclear charges of 5.95×10^{15} esu (at $R = 2.4085$ bohrs in the same basis), which corresponds to an expectation value for $\hat{q}$ over the electronic wavefunction (q_{elec}) of 3.53 atomic units (au, an au of EFG is $1\ ea_0^{-3}$). This calculated result was in excellent agreement with the experimental quadrupole coupling constant of $^2H^{35}Cl$, at 2.4085 bohrs, of 67.3 Mc/s (2). However, these wavefunctions were calculated with electron repulsion integrals stored to only six significant figures (3); the calculations were here repeated with integrals stored to full double-precision length and giving $E_{SCF} = -460.05261$ hartrees and $q_{elec} = 3.73$ au. These are to be compared with the near-Hartree–Fock values obtained in a large two-centre basis by McLean and Yoshimine (4), $E_{SCF} = -460.1119$ hartrees and $q_{elec} = 3.42$ au. The difference in E_{SCF} between Moccia and the present result, caused by integral storage length, is numerically significant but not qualitatively important; q_{elec}, however,

[1]This paper is dedicated to Professor C. A. Winkler of McGill University on the occasion of his sixty-fifth birthday by one of his colleagues (M.A.W.).

[2]Present address: Chemistry Department, University of Waterloo, Waterloo, Ontario, Canada.

[3]Revision received March 8, 1976.

Can. J. Chem. Downloaded from www.nrcresearchpress.com by 210.87.254.5 on 09/05/12
For personal use only.

TABLE 1. OCE basis for HCl, σ orbitals 1 through 10 and all π orbitals are taken from Gilbert and Wahl (5), all orbitals centred on Cl

Orbitals	n	l	m	ζ	r_{max} (bohrs)
σ-orbital					
1	1	0	0	18.424	0.0
2	2	0	0	16.187	0.062
3	2	0	0	6.092	0.164
4	3	0	0	2.608	0.767
5	3	0	0	1.597	1.252
6	2	1	0	10.267	0.097
7	2	1	0	5.608	0.178
8	3	1	0	2.608	0.767
9	3	1	0	1.463	1.367
10	3	2	0	1.943	1.029
11	9	0	0	3.32129	2.4087
12	9	1	0	3.32129	2.4087
13	9	2	0	3.32129	2.4087
14	9	3	0	3.32129	2.4087
15	9	4	0	3.32129	2.4087
16	9	5	0	3.32129	2.4087
17	9	6	0	3.32129	2.4087
18	9	7	0	3.32129	2.4087
19	9	8	0	3.32129	2.4087
π-pairs					
1	2	1	± 1	10.267	0.097
2	2	1	± 1	5.608	0.178
3	3	1	± 1	2.608	0.767
4	3	1	± 1	1.463	1.367
5	3	2	± 1	1.943	1.029

which involves near cancellation of contributions from σ and π MO's, goes from a reasonably accurate prediction by Moccia to a rather poor value with the present calculation.

Thus Moccia's large OCE basis does not yield q_{elec} to a near-Hartree–Fock accuracy when the integrals are accurately calculated. However, since Moccia chose the orbital exponents to minimize E_{SCF} (2), an OCE basis chosen on other grounds might yield q_{elec} nearer the Hartree–Fock limit.

Choice of Basis

It would be expected that an OCE basis accurate for q_{elec} in HCl could be developed starting with a good basis for the Cl atom or ion, and adding orbitals to describe the wavefunction at the proton. Consequently the double-ζ plus polarization basis of STO's optimized for Cl_2 by Gilbert and Wahl (5) was the starting basis. To this were added σ orbitals with principal quantum number $n = 9$ and all allowed orbital angular momentum numbers ($l = 0$ to 8). The choice of $n = 9$ was made arbitrarily. The quantum number n determines the sharpness of peaking of the radial factor of the orbital (6); for $n > 9$ the change in width of the radial factor (measured between points of maximum derivative) becomes small with a change in n or l for the exponents used in this work. Thus it is assumed that the choice of $n = 9$ is not critical in that choosing $n = 10$ and adding 10 orbitals should change the result little; this point has not, however, been established by calculations.

The exponents ζ of the $n = 9$ orbitals were chosen to place the maximum of the radial factor, $r_{max} = (n - 1)/\zeta$, at the internuclear distance to allow the wavefunction to peak as sharply as possible at the proton. However, the electron density due to a radial function $\phi(r)$ in an infinitesimally thin, hollow spherical shell of radius r is proportional to $r^2\phi^2(r)$; for an STO this reaches a maximum at $r = n/\zeta$. Thus the present basis, with $\zeta = (n - 1)/R$, where R is the internuclear distance, ensures peaking of the wavefunction, rather than the electron density, at the proton. The resulting 29 STO basis (19σ orbitals, 5π pairs) is given in Table 1.

Can. J. Chem. Downloaded from www.nrcresearchpress.com by 210.87.254.5 on 09/05/12
For personal use only.

TABLE 2. Selected properties of HCl, from present OCE-SCF calculation, near Hartree–Fock SCF calculation of McLean and Yoshimine (4), and experiment, all calculations at R_e = 2.4087 bohrs

Parameter	Value		
	OCE-SCF	Reference 4	Expt (or exact) wavefunction
Energy (hartrees)	−460.06894	−460.1119	−462.184[a]
q_{elec} (e/a_0^3)	3.49	3.42	3.49[b]
$q_{total} = q_{elec} + q_{nucl}$	3.64[d]	3.56	3.63[b]
Dipole moment (D)	1.362	1.215	1.1085
Molecular quadrupole moment (10^{-26} esu cm^2)	3.80	3.74	3.74[c]
Virial theorem ratio	−2.00013	−2.00003	2.0
Hellman–Feynman force on Cl nucleus (e^2/a_0^2)	−0.2761	−0.0682	0.0
Orbital eigenvalues (hartrees)			
1σ	−104.8466	−104.8479	
2σ	−10.5716	−10.5732	
3σ	−8.0332	−8.0405	
4σ	−1.1113	−1.1164	
5σ	−0.6159	−0.6254	
1π	−8.0376	−8.0387	
2π	−0.4762	−0.4763	

[a]Estimated in ref. 9.
[b]Reference 8.
[c]Reference 12.
[d]$q_{nucl} = 2/(2.4087)^3 = 0.14311$ au.

Results

The SCF q_{elec} in this basis is 3.49 au at the experimental bond length (2.4087 bohrs),[4] compared to McLean and Yoshimine's near-Hartree–Fock value of 3.42 au and the experimental value of 3.49 au (8). The three-figure agreement with experiment is fortuitous, but it indicates that q_{elec} in this basis is accurate enough for detailed analysis (1).

E_{SCF} in the basis of Table 1 is −460.06894 hartrees at R = 2.4087 bohrs. A lower E_{SCF} can be obtained in a similar basis by varying the exponent of the n = 9 orbitals to minimize the energy; calculations at R = 2.4087 bohrs for several ζ and interpolation to the energy minimum gave E_{SCF} = −460.076579 hartrees at $\zeta(n = 9) = 3.59397$. This exponent is close to $(n - \frac{1}{2})/R$, midway between the wavefunction-peaking value $\zeta = (n - 1)/R$ chosen for this work and the density-peaking value $\zeta = n/R$. However q_{elec} in the $\zeta(n = 9) = 3.359397$ basis is interpolated to be 3.35 au, a rather poor value. This illustrates that a moderately sized basis, optimal for the energy, may be poor for one-electron properties. The interpolated E_{SCF} given above is the lowest yet reported for HCl with an OCE-SCF wavefunction, even though the basis is much smaller than that employed by Moccia. It still lies significantly above McLean and Yoshimine's value, −460.1119 hartrees.

The energy, orbital eigenvalues, q_{elec}, electric dipole and quadrupole moments, virial theorem ratio, and Hellman–Feynman force on the Cl nucleus are compared in Table 2 as calculated in the OCE basis of Table 1, and as reported by McLean and Yoshimine (4). Experimental values are given where applicable. All calculations refer to the $X^1\Sigma^+$ state of HCl at the equilibrium internuclear distance, 2.4087 bohrs. It is to be noted that all properties in Table 2 which depend strongly on electron density at moderate or large distances from the Cl nucleus (*i.e.* all properties except q_{elec}) are given more accurately by the two-centre wave function of McLean and Yoshimine than by the OCE-SCF wavefunction, as expected.

It is of interest to examine the variation of q as the internuclear distance is changed, by determining the coefficients q_i in

$$[2] \qquad q(\xi) = q_0 + q_1\xi + q_2\xi^2 + \ldots$$

where $\xi = (R - R_e)/R_e$, R_e = 2.4087 bohrs. The

[4]Reference 7(*a*) gives R_e = 1.27460 ± 0.00005 Å; the 1965 conversion factor 1 bohr = 0.529167 Å (7(*b*)) gives R_e = 2.4087 bohrs.

Can. J. Chem. Downloaded from www.nrcresearchpress.com by 210.87.254.5 on 09/05/12
For personal use only.

Can. J. Chem. Downloaded from www.nrcresearchpress.com by 210.87.254.5 on 09/05/12
For personal use only.

value of q in [2] now includes the nuclear contribution to the EFG of 0.143114 due to the proton. Accurate experimental values are known, Kaiser (8) found $q_0 = 3.6339 \pm 0.0003$, $q_1 = 5.32 \pm 0.22$, and $q_2 = -6.00 \pm 0.85$ au, all with the same dimension as q. Near-Hartree–Fock theoretical values are also available, Cade and Huo found (reported in ref. 8), using the Cade–Huo wavefunctions (9), $q_0 = 3.569$, $q_1 = 5.31$, and $q_2 = -5.50$ au, all very close to the experimental values.

OCE-SCF calculations were performed at $R = 2.3887$, 2.3987, 2.4087, 2.4187, and 2.4287 bohrs in the basis of Table 1, except with $\zeta(n = 9) = (n - 1)/R$ at each R. Polynomial fitting of the calculated q from the wavefunctions gave $q_0 = 3.6373$, $q_1 = 5.651$, and $q_2 = -9.96$ au. The numbers of significant figures quoted in the q_i reflect the 95% confidence limits calculated by a least-squares fitting routine. These values of q include the nuclear contribution q_{nucl} and consequently 0.143114 has to be added to the q_{elec} of Table 2. These agree well with experiment except for q_2, which is of the correct sign but 50% bigger than the experimentally determined coefficient. For sufficiently large ξ any SCF calculation, whether one- or two-centre, must give $q(\xi)$ significantly less than the experimental values, because the SCF wavefunction dissociates to a bare proton and a Cl^- ion, with $q = 0$; the $X^1\Sigma^+$ state of HCl, however, dissociates to Cl and H atoms in the ground states, q for the Cl atom in the ground state being 5.6 au (10). The OCE-SCF wavefunction tends to the Cl^- wavefunction more quickly with increasing R than does the two-centre wavefunction because of the absence of basis orbitals on the proton; this is reflected in the more negative q_2.

Conclusions

The closeness of the OCE q_{elec} to the experimental and near Hartree–Fock values shows that an OCE calculation may still be worthwhile for an operator like $\hat{q}$, whose expectation value in HCl is strongly dependent on the electron distribution near the Cl nucleus. The simplicity of the prescription for choosing the basis suggests that a basis suitable for the analysis of properties strongly dependent on the electron density near the heavy nucleus in a hydride may be chosen without an expensive optimization procedure for the orbital exponents. The addition of a relatively large number, 9, of basis orbitals centred on Cl is preferable, for calculating the EFG at Cl, to the addition of a smaller number of orbitals on the proton, even though the integral calculating times might be comparable and the electronic energy lower, because, as shown in detail elsewhere (1), the net EFG at Cl is almost entirely due to the electron density in bonding orbitals *within* 0.3 bohrs of the Cl nucleus (11).

Acknowledgment

This work was supported by the National Research Council of Canada.

1. J. E. Grabenstetter and M. A. Whitehead. Chem. Phys. Lett. **37**, 547 (1976).
2. R. Moccia. Theor. Chim. Acta, **8**, 8 (1967).
3. R. Moccia. Private communication.
4. A. D. McLean and M. Yoshimine. J. Chem. Phys. **47**, 3256 (1967).
5. T. L. Gilbert and A. C. Wahl. J. Chem. Phys. **55**, 5247 (1971).
6. D. M. Bishop. Adv. Quant. Chem. **3**, 25 (1967).
7. (*a*) P. R. Bunker. J. Mol. Spectrosc. **39**, 90 (1971). (*b*) E. R. Cohen and J. W. M. Du Mond. Rev. Mod. Phys. **37**, 537 (1965).
8. E. W. Kaiser. J. Chem. Phys. **53**, 1686 (1970).
9. P. E. Cade and W. M. Huo. J. Chem. Phys. **47**, 649 (1967).
10. V. Jaccarino and J. G. King. Phys. Rev. **83**, 471 (1951).
11. M. A. Whitehead. Proceedings of the Second International Symposium on NQR Spectroscopy. *Edited by* A. Vallerini. Pisa, Italy. 1975. p. 27.
12. F. H. De Leeuw and A. Dymanus. J. Mol. Spectrosc. **48**, 427 (1973).

Enthalpies de mélange du tétrachlorure de carbone avec des hydrocarbures à l'aide d'un microcalorimètre Picker à écoulement continu, équipé de séparateurs

JEAN-PIERRE E. GROLIER ET AMERICO INGLESE[1]

Centre de Recherches de Microcalorimétrie et de Thermochimie du CNRS, 26, rue du 141e RIA 13003 Marseille, France

Reçu le 8 décembre 1975

JEAN-PIERRE E. GROLIER et AMERICO INGLESE. Can. J. Chem. **54**, 1952 (1976).

Les enthalpies de mélange pour les systèmes tétrachlorure de carbone + heptane *n*, + nonane *n*, + décane *n*, et + dodécane *n* ont été mesurées à 298.15 K à l'aide du microcalorimètre Picker à écoulement continu équipé de séparateurs qui empêchent les liquides réactifs d'être en contact avec les pompes d'injection. L'appareil a été testé à 298.15 K avec deux mélanges binaires, tétrachlorure de carbone + benzène et dichlorométhane + benzène; on a montré que son exactitude n'est pas affectée par l'utilisation de ces séparateurs.

JEAN-PIERRE E. GROLIER and AMERICO INGLESE. Can. J. Chem. **54**, 1952 (1976).

Molar enthalpies of mixing for carbon tetrachloride + *n*-heptane, + *n*-nonane, + *n*-decane, and + *n*-dodecane have been measured at 298.15 K using the Picker dynamic flow microcalorimeter equipped with separators which prevent the direct contact of the reacting liquids with the injection pumps. The apparatus was checked at 298.15 K with two binary mixtures, carbon tetrachloride + benzene and dichloromethane + benzene; and it was shown that its accuracy is not affected by the use of the separators.

Ce travail est la suite d'une étude systématique des possibilités d'utilisation du microcalorimètre Picker à écoulement continu. Dans les travaux précédents (1, 2) nous avons montré que l'appareil permet de tracer en continu la courbe d'enthalpie de mélange de non électrolytes en fonction de la composition avec une précision de l'ordre de 1% et une reproductibilité de l'ordre de 0.5%.

Cependant les petits joints toriques en viton situés dans les micropompes d'injection des liquides "réactifs" ne sont pas toujours inertes chimiquement. Leurs caractéristiques ou leurs propriétés mécaniques peuvent être altérées, parfois de façon considérable, par suite d'un contact prolongé avec certaines substances organiques (produits chlorés, cétones, etc.). Ces modifications se traduisent directement par des variations de débit qui affectent la mesure des enthalpies de mélange.

Afin d'éviter cet inconvénient, nous avons introduit des séparateurs dans le système d'injection, entre les micropompes et le calorimètre. Dans ces séparateurs, une fine membrane de téflon sépare le liquide "pousseur", provenant des micropompes, du liquide "réactif" injecté dans le calorimètre. Le débit du liquide "réactif" est ainsi identique au débit du liquide "pousseur", inerte vis-à-vis des joints en viton et dont le débit est lui-même contrôlé par les micropompes.

D'autre part, l'utilisation de ces séparateurs se justifie entièrement si l'on veut étudier des molécules dont la taille ou la fragilité empêche qu'elles soient pompées directement par les micropompes. Ces séparateurs sont donc indispensables pour l'étude de substances d'intérêt biochimique (protéines) ou d'autres grosses molécules (polymères).

Nous avons vérifié le microcalorimètre équipé de ces séparateurs avec le système test endothermique tétrachlorure de carbone – benzène et avec le système légèrement exothermique dichlorométhane – benzène. Puis nous avons déterminé les enthalpies de mélange des systèmes tétrachlorure de carbone + heptane *n*, nonane *n*, décane *n* et dodécane *n* pour lesquels les valeurs dans la littérature sont assez dispersées.

Partie expérimentale

Appareillage

Nous avons utilisé la version commerciale fabriquée par Setaram (Lyon, France), du microcalorimètre Picker. Par rapport au prototype que nous avions utilisé (1), cet appareil présente les deux modifications indiquées précédemment (2): une chambre de mélange, qui assure une

[1]En stage post-doctoral; Institut de Chimie Physique de l'Université de Bari, Italie.

Can. J. Chem. Downloaded from www.nrcresearchpress.com by 210.87.254.105 on 09/05/12
For personal use only.

Can. J. Chem. Downloaded from www.nrcresearchpress.com by 210.87.254.105 on 09/05/12
For personal use only.

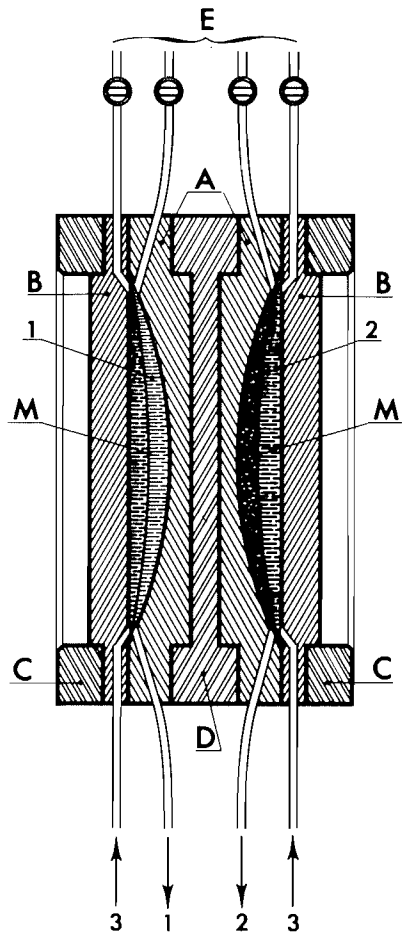

FIG. 1. Schéma des séparateurs. A: téflon; B: plexiglass; C: cerclages métalliques servant à l'assemblage; D: cerclage métallique assurant la rigidité générale et servant de support à l'ensemble; E: petites vannes; M: membranes en téflon; 1 et 2: liquides "réactifs"; 3: liquide "pousseur".

meilleure mise en contact des liquides, et une programmation des débits des micropompes d'injection plus fiable.

Au cours des travaux antérieurs (1, 2), nous avions utilisé cet appareil pour tracer en continu la courbe d'enthalpie de mélange, en fonction de la composition. Dans le cas présent, nous avons également travaillé en programmant les débits des liquides "réactifs"; mais la programmation a été obtenue, par l'intermédiaire des membranes des séparateurs, grâce au liquide "pousseur" circulant dans les micropompes d'injection.

Le schéma des séparateurs[2] est indiqué sur la fig. 1. Les compartiments qui servent de réservoir aux liquides "réactifs" 1 et 2 sont usinés dans un rondin de téflon (diamètre extérieur 12 cm). Chaque compartiment a un volume maximum d'environ 32 cm^3. Une membrane M, en téflon, très souple (épaisseur 0.05 mm) sépare le liquide "pousseur" 3 des liquides "réactifs". Ce dispositif permet de transmettre très fidèlement aux liquides "réactifs" la pression du liquide "pousseur", de l'eau dans ce cas, qui provient des micropompes contrôlant son débit. Nous estimons que le déplacement, sans déformation irréversible, de la membrane de téflon permet de disposer d'un volume utile de 25 cm^3 environ. Nous avons en effet vérifié que, pour un tel volume de liquide délivré par les séparateurs, le débit des liquides "réactifs" reste identique, à mieux que 1%, à celui du liquide "pousseur".

Chaque compartiment est pourvu d'une sortie haute, munie d'un petit robinet, qui permet d'éliminer les bulles lors du remplissage. Les faces externes des deux séparateurs, en contact seulement avec le liquide "pousseur", sont en plexiglass et permettent ainsi de voir si ce remplissage se fait correctement.

Ces séparateurs présentent plusieurs avantages. (*i*) Les liquides "réactifs" ne sont en contact qu'avec un seul matériau en général inerte (téflon). (*ii*) On peut distiller directement dans ces compartiments des produits particulièrement délicats à manipuler. (*iii*) Un seul liquide inerte vis-à-vis des joints circule dans les micropompes; d'autre part ce liquide peut être choisi avec une tension de vapeur relativement faible, permettant ainsi d'éviter la formation de bulles dans les micropompes comme on le constate avec des produits volatils.

Produits utilisés

Les substances organiques choisies parmi les plus pures disponibles dans le commerce ont été utilisées sans purification supplémentaire. Les spécifications indiquées dans le tableau suivant sont celles données par le fabricant.

Produits	Analyse	Pureté (mole %)
Benzène, Fluka puriss sans thiophène	175098 25	⩾99.5
Tétrachlorure de carbone, Fluka puriss	21297 114	⩾99.5
Dichlorométhane, pour spectro uv avec garantie Fluka	171642 44	
Heptane *n*, pour spectro uv avec garantie Fluka	18083 11	
Heptane *n*, Phillips research grade reagent	lot 1405	⩾99.92
Nonane *n*, Phillips research grade reagent	lot 1378	⩾99.72
Décane *n*, Fluka purum sans oléfine	171548 74	⩾99
Dodécane *n*, Phillips pure grade reagent		⩾99.3

Tous les solvants ont été partiellement dégazés sous pression réduite avant d'être introduits, à l'aide d'une seringue, dans les compartiments correspondants des séparateurs. L'eau bidistillée servant de liquide "pousseur"

[2]Le principe de ces séparateurs est dû à Picker. L'un de nous (J.-P. E. G.) les a utilisés lors d'une étude des enthalpies de mélange de systèmes contenant des cétones (3). Les séparateurs utilisés au cours de la présente étude ont été réalisés au C.R.M.T. à Marseille.

TABLEAU 1. Valeurs des coefficients A_i (J mol^{-1}), éq. 1, et écarts standards σ, éq. 2

Mélanges	A_0	A_1	A_2	A_3	σ
$CCl_4(1) + C_6H_6(2)$	458.6±0.2	30.6±0.8	80.3±2.3		0.19
$CCl_2H_2(1) + C_6H_6(2)$	−328.2±0.3	142.9±0.9	123.4±2.3		0.18
$CCl_4(1) + C_7H_{16}(2)$*†	1391.5±0.7	253.4±2.6	154.4±6.4		0.60
$CCl_4(1) + C_9H_{20}(2)$	1595.7±1.6	376.8±7.0	306±21	272±37	1.10
$CCl_4(1) + C_{10}H_{22}(2)$	1660.0±1.0	462.6±3.9	253±13	390±21	0.62
$CCl_4(1) + C_{12}H_{26}(2)$	1836.2±3.1	393±12	294±49	764±69	1.77

*Heptane *n*, Phillips research grade.
†Avec heptane *n* Fluka les valeurs des coefficients sont respectivement: 1399.1 ± 0.9; 260.9 ± 3.3; 198.5 ± 8.2.

a été également partiellement dégazée sous pression réduite, directement dans les flacons réservoirs des micropompes (2).

Résultats et discussions

Toutes les mesures ont été effectuées à 298.15 K. La technique opératoire et le traitement des données ont été identiques à ceux décrits précédemment (2).

Les valeurs de l'enthalpie molaire d'excès H^E, en fonction de la fraction molaire x_1 du produit chloré, ont été lissées avec une équation de la forme

$$[1] \qquad H^E = x_1(1 - x_1)\sum_{i=0}^{n-1} A_i(2x_1 - 1)^i$$

Les erreurs sur les coefficients A_i, consécutives au lissage et à la pondération utilisée, ont été également calculées, de même que l'écart standard défini par

$$[2] \qquad \sigma = \left(\frac{\sum_{j=1}^{N} w_j(H^E_{j,\text{exp}} - H^E_{j,\text{calc}})^2}{N - n}\right)^{1/2}$$

où w_j est le poids statistique du point j. Nous donnons dans le tableau 1 les valeurs des coefficients A_i de l'éq. 1 calculées à partir des valeurs H_j^E.

Sur les figs 2 à 6 les courbes représentent les valeurs de H^E lissées à l'aide de l'éq. 1. La partie de ces courbes tracée en trait plein correspond au domaine de concentration où la précision est la meilleure et de l'ordre de 1%.

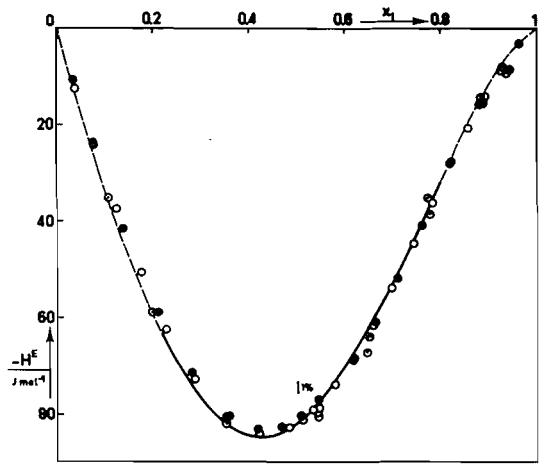

FIG. 2. Enthalpie d'excès H^E, à 298.15 K, pour le mélange $CCl_2H_2(1) + C_6H_6(2)$ en fonction de la fraction molaire x_1. La courbe en trait plein et en tirés (voir texte) représente nos valeurs lissées à l'aide de l'éq. 1 et en utilisant les coefficients du tableau 1: ○, Otterstedt et Missen (6); ○, Benson (7); ●, Tanaka *et al.* (8).

Système tétrachlorure de carbone(1) + benzène(2)

Ce système a été choisi pour vérifier la concordance des enthalpies de mélange obtenues avec et sans l'intermédiaire de séparateurs. Nous avons constaté que l'accord est en général à mieux que 1% (tableau 2); les séparateurs n'altèrent donc pas le débit des liquides "poussés" dans le calorimètre. Rappelons (2) par ailleurs que la vérification d'un calorimètre, surtout à écoulement, avec ce système test, est plus sévère, par suite des différences assez grandes de densité et de viscosité des deux liquides, que la vérification avec le système cyclohexane – hexane *n*.

Système dichlorométhane(1) + benzène(2)

Ce système est le premier mélange exothermique de non électrolytes, étudié avec le microcalorimètre Picker à écoulement continu, pour lequel il existe d'excellentes valeurs de comparaison dans la littérature (6, 7, 8). Les viscosités et les densités des produits étant assez différentes et la courbe $\mathscr{H}^E(\varphi_1)$ de l'enthalpie volu-

Can. J. Chem. Downloaded from www.nrcresearchpress.com by 210.87.254.105 on 09/05/12
For personal use only.

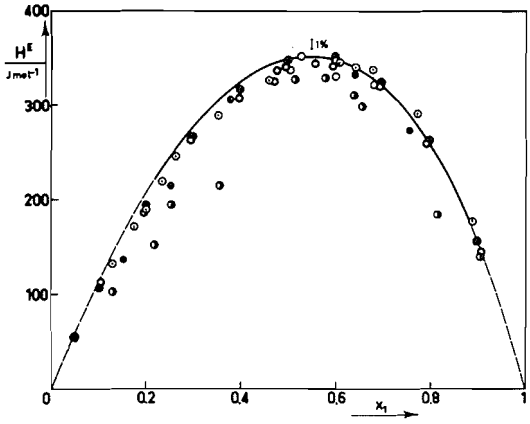

FIG. 3. Enthalpie d'excès H^E, à 298.15 K, pour le mélange $CCl_4(1)$ + heptane $n(2)$ en fonction de la fraction molaire x_1. La signification de la courbe est identique à celle indiquée fig. 2: ○, nos mesures avec le calorimètre Calvet–CRMT; ⊙, Moon (13); ●, Berryman et Heric (12); O, Bissel *et al.* (11); ⊗, Harsted et Thomsen (17) (valeurs interpolées); ◑, Jain *et al.* (10) à 300.05 K.

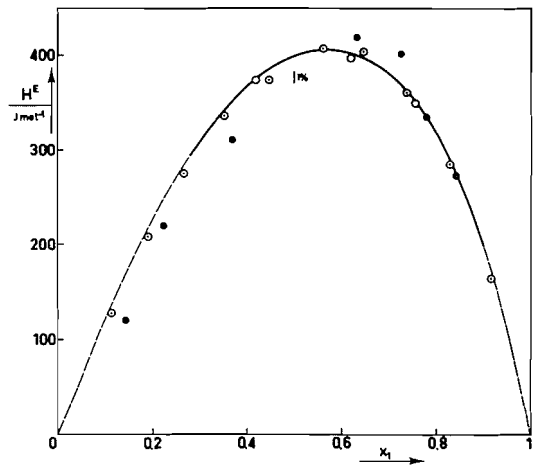

FIG. 4. Enthalpie d'excès H^E, à 298.15 K, pour le mélange $CCl_4(1)$ + nonane $n(2)$ en fonction de la fraction molaire x_1. La signification de la courbe est identique à celle indiquée fig. 2: ○, nos mesures avec le calorimètre Calvet–CRMT; ⊙, Moon (13), ●, Berryman et Heric (12).

mique d'excès $\mathscr{H}^E$ enregistrée en fonction de la fraction volumique φ_1 très asymétrique, l'étude de ce système constitue un test encore plus sévère du calorimètre à écoulement. La fig. 2 montre que l'accord est en général bon. Seulement dans le domaine où la dérivée $d\mathscr{H}^E/d\varphi_1$ est très grande ($x_1 < 0.5$), nos valeurs sont légèrement ($\sim 3\%$) plus élevées en valeur absolue (tableau 3).

TABLEAU 2. Comparaison des enthalpies molaires d'excès H^E, à 298.15 K, obtenues pour le système tétrachlorure de carbone(1) + benzène(2) avec et sans (2) séparateurs

	H^E (J mol^{-1})		
x_1	Réf. 2	Ce travail	Marsh (5)
0.300	99.77	101.57	99.59
0.350	106.92	108.06	106.95
0.400	111.84	112.30	112.01
0.450	114.61	114.46	114.86
0.500	115.29	114.65	115.54
0.550	113.89	112.95	114.07
0.600	110.41	109.37	110.46
0.650	104.82	103.89	104.69
0.700	97.05	96.44	96.74
0.750	87.04	86.89	86.57
0.800	74.70	75.07	74.11
0.850	59.94	60.76	59.30

TABLEAU 3. Résultats expérimentaux de l'enthalpie molaire d'excès, à 298.15 K, pour le système dichlorométhane(1) + benzène(2)

x_1	H^E (J mol^{-1})	x_1	H^E (J mol^{-1})
0.2195	−63.8	0.5536	−77.2
0.2601	−71.2	0.5866	−72.8
0.2999	−76.8	0.6190	−67.9
0.3387	−81.1	0.6507	−62.0
0.3766	−83.3	0.6817	−56.5
0.4136	−84.5	0.7121	−50.2
0.4498	−84.3	0.7418	−44.2
0.4852	−82.9	0.7709	−37.8
0.5197	−80.5	0.7994	−31.8

Systèmes tétrachlorure de carbone(1) + alcanes normaux(2)

Les valeurs expérimentales directes H_j^E choisies sur la courbe $H^E(x_1)$, pour ces systèmes, sont publiées par ailleurs sous la forme de tables 'DATA' (4).

L'étude de ces mélanges est d'un grand intérêt, à la fois expérimental et théorique (9). Les différences de taille et de forme entre les molécules d'alcanes et de CCl_4 se traduisent par des courbes $H^E(x_1)$ de plus en plus asymétriques quand la longueur de l'alcane croît.

Les différences de densité et de viscosité, associées aux différences de taille et de forme des molécules, rendent la mesure des enthalpies de mélange délicate. Ce qui explique le désaccord entre les différents auteurs.

Les résultats de Jain *et al.* (10) à 300.05 K obtenus à l'aide d'un calorimètre isotherme à

Can. J. Chem. Downloaded from www.nrcresearchpress.com by 210.87.254.105 on 09/05/12
For personal use only.

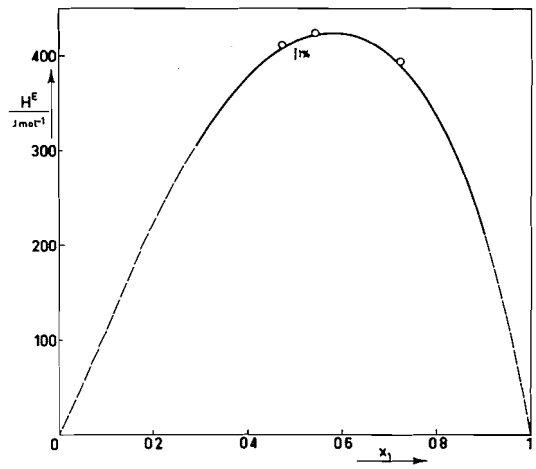

FIG. 5. Enthalpie d'excès H^E, à 298.15 K, pour le mélange $CCl_4(1)$ + décane $n(2)$ en fonction de la fraction molaire x_1. La signification de la courbe est identique à celle indiquée fig. 2: ○, nos mesures avec le calorimètre Calvet–CRMT.

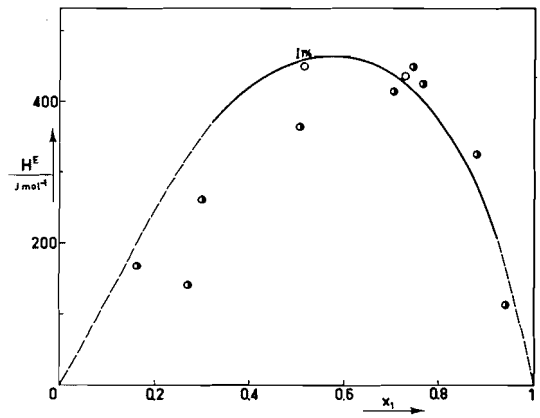

FIG. 6. Enthalpie d'excès H^E, à 298.15 K, pour le mélange $CCl_4(1)$ + dodécane $n(2)$ en fonction de la fraction molaire x_1. La signification de la courbe est identique à celle indiquée fig. 2: ○, nos mesures avec le calorimètre Calvet–CRMT; ◑ Jain *et al.* (10) à 300.05 K.

changement de phase, présentent une très grande dispersion. Berryman et Heric (12), Bissel *et al.* (11) ainsi que Moon (13), ont déterminé récemment les enthalpies de mélange, à 298.15 K, du CCl_4 avec différents alcanes. Bien qu'ils aient utilisé des calorimètres d'un même type (McGlashan et coll. (14, 15)) leurs résultats diffèrent notablement. Nous pensons que ces écarts sont consécutifs à des processus de mélange incomplets. Il était donc intéressant de comparer nos résultats à ces différentes séries de mesures. Pour compléter cette comparaison, nous avons mesuré les H^E à quelques concentrations avec un calorimètre du type Calvet–CRMT (16).

Les figs 3 à 6 montrent que les valeurs déterminées avec le calorimètre Calvet–CRMT sont en bon accord avec nos valeurs déterminées avec le calorimètre à écoulement. D'autre part, ces dernières sont légèrement plus élevées (2–3%) que celles des autres auteurs (figs 3 et 4). Ceci indique, nous pensons, que le processus de mélange s'effectue bien sinon mieux dans notre calorimètre à écoulement.

La comparaison de nos valeurs avec celles, interpolées à 298.15 K, que Harstedt et Thomsen (17) ont déterminées avec un calorimètre à écoulement du type Wadsö (18) (LKB 10700-1) montre (fig. 3) que nos valeurs ne sont que très légèrement supérieures ($\sim 1\%$).

Il n'est pas possible d'expliquer ces déviations faibles mais systématiques seulement par la pureté des produits. En effet, et plus particulièrement dans le cas du mélange CCl_4 + heptane n, où l'écart de nos valeurs avec celles des autres auteurs est plus grand, nous avons utilisé de l'heptane de deux origines différentes (Fluka et Phillips, sans purification supplémentaire). On constate que les courbes d'enthalpies de mélange obtenues dans les deux cas sont en très bon accord ($< 1\%$) entre elles. On rappelle, d'autre part, que l'accord de nos valeurs avec celles de la littérature pour le système test cyclohexane + hexane n, est excellent (2).

Le désaccord que nous constatons entre nos valeurs et celles de la littérature pour les systèmes CCl_4 + alcanes normaux nous amène à suggérer qu'une étude de ces systèmes soit entreprise avec des produits de même origine et en utilisant différents types de calorimètres. Tout particulièrement des mesures qui, à notre connaissance, n'existent pas, réalisées avec un calorimètre à dilution de type Van Ness (19) devraient permettre d'élucider ce point.

1. J.-P. E. GROLIER, G. C. BENSON et P. PICKER. J. Chem. Thermodyn. **7**, 89 (1975).
2. J.-P. E. GROLIER. Thermochim. Acta. Sous presse.
3. J.-P. E. GROLIER, G. C. BENSON et P. PICKER. Résultats non encore publiés.
4. J.-P. E. GROLIER et A. INGLESE. Int. DATA Ser. A, 71 (1975).
5. K. N. MARSH. Int. DATA Ser. A, 3 (1973); R. H. STOKES, K. N. MARSH et R. P. TOMLINS. J. Chem. Thermodyn. **1**, 211 (1969).

Can. J. Chem. Downloaded from www.nrcresearchpress.com by 210.87.254.105 on 09/05/12
For personal use only.

6. J.-E. A. OTTERSTEDT et R. W. MISSEN. J. Chem. Eng. Data, **11**, 360 (1966).
7. G. C. BENSON. Int. DATA Ser. A, 20 (1974); S. MURAKAMI et G. C. BENSON. J. Chem. Thermodyn. **1**, 559 (1969).
8. R. TANAKA, S. MURAKAMI et R. FUJISHIRO. Bull. Chem. Soc. Jpn. **45**, 2107 (1972).
9. D. PATTERSON. Communication personnelle.
10. D. V. S. JAIN, O. P. YADAV et S. S. GILL. Indian J. Chem. **9**, 339 (1971).
11. T. G. BISSEL, G. E. OKAFOR et A. G. WILLIAMSON. J. Chem. Thermodyn. **3**, 393 (1971).
12. J. M. BERRYMAN et H. L. HERIC. Can. J. Chem. **50**, 3799 (1972).
13. A. MOON. Ph.D. Thesis, University of Georgia, Ga., U.S.A. 1972.
14. D. S. A. ADCOCK et M. L. MCGLASHAN. Proc. Roy. Soc. Ser. A, **226**, 266 (1954).
15. J. A. LARKIN et M. L. MCGLASHAN. J. Chem. Soc. 3425 (1961).
16. D. BARES, M. SOULIE et J. METZGER. J. Chim. Phys. Physiochim. Biol. **70**, 1531 (1973).
17. B. S. HARSTEDT et E. S. THOMSEN. J. Chem. Thermodyn. **6**, 557 (1974).
18. P. MONK et I. WADSÖ. Acta Chem. Scand. **22**, 1842 (1968).
19. R. V. MRAZEK et H. C. VAN NESS. Am. Inst. Chem. Eng. J. **7**, 190 (1961).

Can. J. Chem. Downloaded from www.nrcresearchpress.com by 210.87.254.105 on 09/05/12
For personal use only.

Chemistry of proximal π-bond systems. Part IV.[1] The structure of 5,6-dimethylenebicyclo[2,2,1]hept-2-ene molybdenum tricarbonyl

BRYAN F. ANDERSON AND GLEN B. ROBERTSON

Research School of Chemistry, Australian National University, Canberra, Australian Capital Territory

AND

DOUGLAS N. BUTLER

Chemistry Department, York University, Downsview, Ont., Canada M3J 1P3

Received August 18, 1975[2]

BRYAN F. ANDERSON, GLEN B. ROBERTSON, and DOUGLAS N. BUTLER. Can. J. Chem. **54**, 1958 (1976).

Crystals of 5,6-dimethylenebicyclo[2,2,1]hept-2-ene molybdenum tricarbonyl **1** (M = Mo) are monoclinic, $a = 7.4451(3)$ Å, $b = 13.5783(7)$ Å, $c = 11.2691(4)$ Å, $\beta = 92.593(3)°$, $Z = 4$, space group $P2_1/c$. The structure was solved by the 'heavy atom' method and was refined by full-matrix least square procedures to a final $R = 0.031$. The weighted R factor was 0.051. Experimental bond lengths and angles are close to other reported values for bicyclo[2,2,1]hept-2-ene systems except for three major distortions in the triene ligand namely: the closing of the angles C(2)—C(1)—C(6) and C(3)—C(4)—C(5) by about 5.3°, the bending of the butadiene fragment plane C(8)—C(5)—C(6)—C(9) toward the metal atom by about 20° and the twisting of the terminal methylene hydrogens H(8i) and H(9i) out of the butadiene fragment plane (0.44 and 0.53 Å respectively) away from the molybdenum atom.

BRYAN F. ANDERSON, GLEN B. ROBERSTON et DOUGLAS N. BUTLER. Can. J. Chem. **54**, 1958 (1976).

Les cristaux du diméthylene-5,6 bicyclo[2,2,1] heptène-2 tricarbonyle de molybdène **1** (M = Mo) sont monocliniques, $a = 7.4451(3)$ Å, $b = 13.5783(7)$ Å, $c = 11.2691(4)$ Å, $\beta = 92.593(3)°$, $Z = 4$, groupe d'espace $P2_1/c$. On a résolu la structure par la méthode des atomes lourds et on l'a affinée par la méthode des moindres carrés (matrice complète) jusqu'à une valeur finale de $R = 0.031$. Le facteur R_w est égal à 0.051. Les valeurs expérimentales pour les angles et les longueurs de liaisons se rapprochent de celles rapportées pour des systèmes bicyclo[2,2,1] heptène-2 à l'exception de trois distorsions importantes dans le ligand triénique soit: le rapetissement des angles C(2)—C(1)—C(6) et C(3)—C(4)—C(5) par environ 5.3°, le plissement du plan du fragment butadiénique C(8)—C(5)—C(6)—C(9) vers l'atome métallique par environ 20°, et le déplacement des hydrogènes méthyléniques terminaux H(8i) et H(9i) hors du plan du fragment butadiénique (respectivement 0.44 et 0.53 Å) et loin de l'atome de molybdène.

[Traduit par le journal]

Introduction

In 1961, King and Stone (1) described the preparation of three metal tricarbonyl complexes of 5,6-dimethylenebicyclo[2,2,1]hept-2-ene (2) of the type $C_9H_{10}.M(CO)_3$ **1** (M = Mo, Cr, or W) and compared some of their physical and chemical properties with certain related polyene metal carbonyls, notably those of bicyclo[2,2,1]hepta-2,5-diene **2** and cycloheptatriene **3**. The geometric differences between the trienes **2** and **3** as well as our difficulty in interpreting the reported pmr data, provoked us to re-examine the molybdenum tricarbonyl adduct **1**.

The X-ray crystallographic structure of cycloheptatriene molybdenum tricarbonyl **4** (3) shows that the three double bonds are nearly planar (Mo—C = 2.31–2.46 Å) and alternate with C—C single bonds. The methylene —CH_2— is bent upwards out of this plane by 0.67 Å, implying a torsional twist at the termini of the triene system. The three carbonyl groups adopt a staggered conformation with respect to the C=C bonds. A planar geometry of the triene **2**

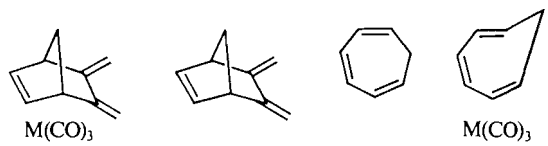

1 **2** **3** **4**

[1]For Part III see ref. 24.

[2]Revision received March 11, 1976.

Can. J. Chem. Downloaded from www.nrcresearchpress.com by 210.87.254.42 on 09/05/12
For personal use only.

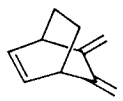

5

6

is obviously unavailable in compounds of type **1** and the distances from the incyclic double bond and the co-ordination site of the butadiene fragment appear too large unless considerable distortion of the triene takes place in forming the complexes. Hence a structure determination was made on the complex **1** (M = Mo) to help clarify the nature of the bonding of the unusual tridentate π-ligand. Two triene hydrocarbons, related to **2** (2) were also shown to readily form similar complexes **5** and **6** when reacted with molybdenum hexacarbonyl.

Experimental

All melting points are uncorrected. The ir spectra were determined on a Perkin-Elmer 257 spectrophotometer. The pmr spectra were recorded on a Jeol Minimar instrument using tetramethylsilane as the internal reference. Mass spectra were taken at 70 eV using an A.E.I. MS9 instrument. The uv spectra were recorded on a Unicam SP800 spectrophotometer.

5,6-Dimethylenebicyclo[2,2,1]hept-2-ene Molybdenum Tricarbonyl **1** *(M = Mo)*

5,6-Dimethylenebicyclo[2,2,1]hept-2-ene **2** was obtained as described (2). The molybdenum tricarbonyl adduct **1** (M = Mo) was prepared using *n*-octane as solvent rather than ethylcyclohexane and purified as described (1).

Crystals were grown by slow evaporation of a methylene chloride/pentane solution of the sublimed complex, mp 108.5–109 °C (lit. (2) 105–107 °C); pmr δ ($CDCl_3$) 3.70 (m, 2H), 3.57 (m, 2H), 3.15 (m, 2H), 2.29 (d, J = 9 Hz, 1H), 1.89 (d, J = 9 Hz, 1 H), 1.75 (s, 2H); *m/e* M^+ 294 (Mo = 92, the other parent ions appeared approximately in proportion to their respective isotopic abundances).

5,6-Dimethylenebicyclo[2,2,2]oct-2-ene Molybdenum Tricarbonyl **5**

5,6-Dimethylenebicyclo[2,2,2]oct-2-ene (2) (0.53 g) and molybdenum hexacarbonyl (0.82 g) were heated to reflux under N_2 in *n*-octane (7 ml) for 3 h. The solvent was evaporated under vacuum and the residue sublimed twice at 110°/0.05 mm to afford the pure adduct **5** as orange crystals (0.74 g), mp 127–128 °C; pmr δ ($CDCl_3$) 3.64 (m, 2H), 3.39 (s, 2H), 2.79 (m, 2H), 1.74 (A_2B_2q, 4H), and 1.52 (s, 2H); ir (cyclohexane) 1994, 1932, and 1903 cm^{-1}; uv (cyclohexane) λ_{max}218 (29 700) and 334 (11 500) nm; *m/e* M^+ 308 (Mo = 92, the other parent ions appeared approximately in proportion to their respective isotopic abundances).

8,9-Dimethylenetricyclo[3,2,2,0^{2,4}]non-6-ene Molybdenum Tricarbonyl **6**

Prepared as described for **5** from 8,9-dimethylenetricyclo[3,2,2,0^{2,4}]non-6-ene (2) (0.58 g) to afford the pure adduct **6** as orange crystals (0.88 g) mp 157–158 °C; pmr δ ($CDCl_3$) 3.43 (s, 2H), 3.17 (m, 2H), 3.01 (m, 2H), 1.66 (s, 2H), 1.40 (m, 2H), 0.91 (m, 1H), and 0.44 (dd, 1H); ir (cyclohexane) 1995, 1934, and 1904 cm^{-1}; uv (cyclohexane) λ_{max}218 (31 000) and 331 (11 500) nm; *m/e* M^+ 320 (Mo = 92, the other parent ions appeared approximately in proportion to their respective isotopic abundances).

X-Ray Data Collection and Structure Analysis of **1** *(M = Mo)*[3]

The complex **1** (M = Mo) crystallised from methylene chloride/pentane as red hexagonal shaped prisms exhibiting point group symmetry 2/*m*. Oscillation and Weissenberg photographs confirmed the crystal class as monoclinic, space group $P2_1/c$ and afforded preliminary estimates of the unit cell dimensions. Precise dimensions were subsequently determined in the usual way from least-squares analysis of the setting angles for twelve carefully centered high-angle reflections using a Picker FACS-1 four-circle diffractometer (4).

Crystal data for 5,6-dimethylenebicyclo[2,2,1]hept-2-ene molybdenum tricarbonyl are as follows

$MoC_{12}H_{10}O_3$ f.w. = 297.9 daltons

Monoclinic, a = 7.4451(3) Å, b = 13.5783(7) Å, c = 11.2691(4) Å, β = 92.593(3)°. Space group $P2_1/c$, ρ_m(by flotation) = 1.73 g cm^{-3}, ρ_c = 1.739 g cm^{-3}, Z = 4, λ(CuKα_1) = 1.54051 Å, μ(CuK$\bar{\alpha}$) = 86.3 cm^{-1}, F(000) = 592.

A typical crystal with approximate dimensions of 0.030 × 0.015 × 0.020 mm was mounted with the a axis parallel to the goniometer ϕ direction and used for all data collection. A total of 2218 unique reflections (reflection forms $hk \pm l$) were collected within the limits $2° \leqslant 2\theta \leqslant 126°$ on an automated four circle diffractometer using graphite monochromated CuKα radiation. The take off angle was set at 3.5° and the room temperature was maintained at a constant 20 ± 1°. Each reflection was measured from 0.8° below the calculated position of the α_1 maximum to 0.8° above the α_2 peak using the θ–2θ scan mode and a 2°/min scanning rate. Backgrounds were measured for 10 s at either end of the scan range. Three standard reflections were remeasured every 50 data and a small decline (*ca.* 5%) in intensity noted over the period of the collection. Data were subsequently corrected for this effect according to the procedure suggested by Churchill and Kalra (5).

Data were also corrected[4] in the usual manner for Lorentz and polarization effects and for the effects of specimen absorption (6). Reflections for which individual background measurements differed significantly (*i.e.* if $\Delta B/\sigma(\Delta B) \geqslant 3$) were discarded as were those reflections with $I/\sigma(I) \leqslant 3$. After sorting and averaging

[3]All computations were carried out on the UNIVAC 1108 computer at the Australian National University. The programs used were those of the A.N.U. System for the Crystal Structure Analysis developed by Drs. P. O. Whimp and D. M. Taylor.

[4]The Lorentz-polarization correction was assumed to have the form $Lp = (\cos^2 2\theta + \cos^2 2\theta_m)/[\sin 2\theta\ (1 + \cos^2 2\theta_m)]$. θ and θ_m (= 13.25°) are the reflection and monochromator Bragg angles respectively.

Can. J. Chem. Downloaded from www.nrcresearchpress.com by 210.87.254.42 on 09/05/12
For personal use only.

Can. J. Chem. Downloaded from www.nrcresearchpress.com by 210.87.254.42 on 09/05/12
For personal use only.

of equivalent reflection forms the final data set contained 1754 unique reflections to each of which was assigned an individual weight $w = 1/[\sigma^2(F_o)]^2$ with $\sigma^2(F_o) = \{[\sigma(I)/Lp]^2 + (\rho|F_o|^2)^2]^{1/2}/2|F_o|$ and ρ, the 'instrumental uncertainty factor' (7), being assigned the value 0.001.

The heavy atom coordinates were obtained from the unsharpened Patterson synthesis and all the light atoms were found from the first heavy atom Fourier calculation. Refinement by full-matrix least-squares of a model including nonhydrogen atoms only, first with isotropic and then with anisotropic temperature factors, resulted in weighted $(R_w = \{\sum w(|F_o| - |F_c|)^2/\sum w|F_o|^2\}^{1/2}$; $w = (\sigma^2)^{-1})$ and unweighted reliability factors $(R = \sum||F_o| - |F_c||/\sum|F_o|)$ of 0.080 and 0.039 respectively.

The nonhydrogen atomic formfactors used were those of Cromer and Waber (8) while the molybdenum anomalous dispersion contributions were calculated from Cromer's tables (9).

A difference synthesis calculated at this stage revealed all 10 hydrogen atoms and these were included in the least squares calculations with the scattering factor given in ref. 10 and isotropic temperature factors set initially at 5.0 Å^2. The refinement converged with all parameter shifts less than 0.1 times the appropriate esd. Terminal values of R_w and of R were 0.051 and 0.031 respectively, while the estimated standard error of an observation of unit weight $[\sum w(|F_o| - |F_c|)^2/(n - s)]^{1/2}$ was 1.5. The terminal difference Fourier contains only two residual peaks of height greater than 0.4 ē Å^{-3} (0.44 and 0.44 ē Å^{-3} *cf.* 0.51 ē Å^{-3} av. for hydrogen atoms), neither of which can be associated with the hydrogen containing coordinated triene moiety.

Results and Discussion

Figure 1 shows the atom numbering system adopted for the molecule and the final atom parameters together with their esd's are given in Table 1. Table 2 lists the relevant interatomic separations and interbond angles while Table 3 gives details of various least squares planes calculated through the 5,6-dimethylenebicyclo-[2,2,1]hept-2-ene moiety. Tables of observed and calculated structure factors are available from the Depository of Unpublished Data.[5]

Most bond lengths and angles in the hydrocarbon moiety agree well with values found for various uncomplexed bicyclo[2,2,1]hept-2-ene derivatives (11–14). Bond lengths are not significantly different ($\leqslant 3\sigma$) from standard values (15) and like the other X-ray structure determinations of such molecules (11–14), the bonds C(1)—C(7) (1.531(5) Å) and C(4)—C(7) (1.531(5) Å) are within experimental error of the values observed for the adjacent C(1)—C(2),

[5]The structure factor table is available, at a nominal charge, from the Depository of Unpublished Data, CISTI, National Research Council of Canada, Ottawa, Canada K1A 0S2.

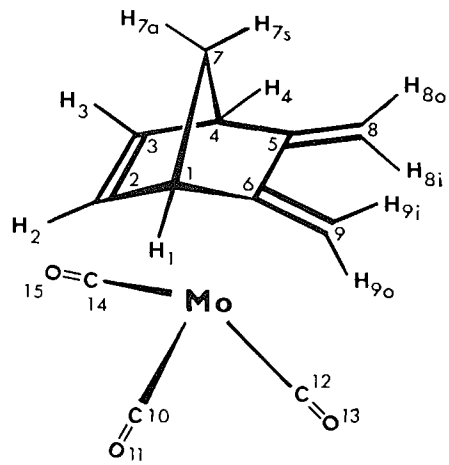

FIG. 1. Atom numbering scheme of 5,6-dimethylenebicyclo[2,2,1]hept-2-ene molybdenum tricarbonyl.

C(1)—C(6), C(4)—C(3), and C(4)—C(5) bonds (average = 1.522 Å). Baenziger and co-workers have reported a similar result from their low temperature analysis of the structure of bicyclo-[2,2,1]hepta-2,5-diene palladium dichloride (16). For a strain free system standard Csp^3—Csp^3 and Csp^3—Csp^2 bond distances are about 1.54 and 1.51 Å respectively. The present observations (Csp^3—Csp^3, average = 1.531(4) Å; Csp^3—Csp^2, average = 1.522(6) Å do not differ significantly from these values. However, in bicyclo[2,2,1]hepta-2,5-diene palladium dichloride the Csp^3—Csp^2 distances (average = 1.553(4) Å) are each significantly longer than the standard value, whereas the Csp^3—Csp^3 distances (average = 1.547(6) Å) appear to be relatively unaffected by strain. For the uncomplexed bicyclo[2,2,1]hepta-2,5-diene ligand, gas phase electron diffraction studies give Csp^3—Csp^2 and Csp^3—Csp^3 distances of 1.535 ± 0.007 Å and 1.57 ± 0.01 Å respectively (18), suggesting that both types are strain affected to a similar degree. Within the quoted error limits the X-ray result for the complexed ligand is not inconsistent with the electron diffraction observation.

In the present complex **1** (M = Mo) the interbond angles within the ring system are appreciably distorted vis-à-vis unstrained tetrahedral and trigonal values, but except for the angles C(2)—C(1)—C(6) and C(3)—C(4)—C(5), differ only in detail from those in related uncomplexed molecules (11–14). The C=C distances (average 1.363(7) Å) are likewise relatively

Can. J. Chem. Downloaded from www.nrcresearchpress.com by 210.87.254.42 on 09/05/12
For personal use only.

TABLE 1. Fractional atomic positional and thermal parameters for **1** (M = Mo)

(*a*) Refined positional and anisotropic thermal parameters*

Atom	*X/A*	*Y/B*	*Z/C*	β_{11}	β_{22}	β_{33}	β_{12}	β_{13}	β_{23}
Mo	0.2118(1)	0.0841(1)	0.2181(1)	0.0139(1)	0.0038(1)	0.0068(1)	−0.0002(1)	−0.0003(1)	0.0005(1)
C(1)	0.3980(5)	0.2449(2)	0.3572(3)	0.0246(7)	0.0064(2)	0.0108(3)	0.0027(3)	−0.0036(4)	−0.0041(2)
C(2)	0.3707(4)	0.2395(2)	0.2227(3)	0.0187(6)	0.0038(1)	0.0101(2)	−0.0007(2)	−0.0027(3)	0.0001(1)
C(3)	0.4892(4)	0.1719(2)	0.1853(2)	0.0150(5)	0.0054(1)	0.0076(2)	−0.0016(2)	0.0001(3)	−0.0001(1)
C(4)	0.5922(4)	0.1338(2)	0.2952(3)	0.0140(5)	0.0061(2)	0.0102(3)	0.0011(2)	−0.0024(3)	−0.0011(2)
C(5)	0.4482(5)	0.0739(2)	0.3535(3)	0.0189(7)	0.0067(2)	0.0078(2)	0.0018(2)	−0.0031(3)	0.0012(1)
C(6)	0.3208(4)	0.1459(2)	0.3951(2)	0.0234(7)	0.0092(2)	0.0050(2)	0.0013(3)	0.0002(3)	−0.0011(2)
C(7)	0.6003(5)	0.2260(3)	0.3735(3)	0.0231(7)	0.0072(2)	0.0116(3)	0.0000(3)	−0.0059(4)	−0.0021(2)
C(8)	0.4152(6)	−0.0241(3)	0.3345(4)	0.0289(9)	0.0059(2)	0.0149(4)	0.0018(4)	−0.0055(5)	0.0031(2)
C(9)	0.1470(6)	0.1278(5)	0.4219(3)	0.0296(10)	0.0145(5)	0.0084(3)	0.0015(6)	0.0045(4)	−0.0007(3)
C(10)	0.0181(4)	0.1659(2)	0.1424(2)	0.0147(5)	0.0058(1)	0.0096(2)	−0.0018(2)	−0.0009(3)	0.0014(2)
O(11)	−0.0937(3)	0.2151(2)	0.1030(3)	0.0186(5)	0.0089(2)	0.0179(3)	0.0004(2)	−0.0048(3)	0.0050(2)
C(12)	0.0371(5)	−0.0231(3)	0.2434(3)	0.0229(7)	0.0067(2)	0.0154(4)	−0.0022(3)	−0.0020(4)	0.0038(2)
O(13)	−0.0642(6)	−0.0847(2)	0.2583(4)	0.0348(9)	0.0104(3)	0.0293(6)	−0.0101(4)	−0.0038(6)	0.0081(3)
C(14)	0.2569(4)	0.0261(2)	0.0617(3)	0.0197(6)	0.0060(2)	0.0101(3)	−0.0009(3)	−0.0022(3)	−0.0022(2)
O(15)	0.2850(4)	−0.0071(2)	−0.0292(2)	0.0341(7)	0.0124(2)	0.0131(3)	−0.0009(3)	−0.0007(3)	−0.0075(2)

*Anisotropic thermal parameters are of the form $\exp[-(\beta_{11}h^2 + \beta_{22}k^2 + \beta_{33}l^2 + 2\beta_{12}hk + 2\beta_{13}hl + 2\beta_{23}kl)]$.

(*b*) Final hydrogen atom coordinates and isotropic thermal parameters

Atom	*X/A*	*Y/B*	*Z/C*	*B*(Å^2)	Atom	*X/A*	*Y/B*	*Z/C*	*B*(Å^2)
H(1)	0.347(6)	0.296(3)	0.406(3)	6.9(9)	H(7s)	0.633(6)	0.212(3)	0.460(3)	8.3(11)
H(2)	0.310(5)	0.282(2)	0.170(3)	5.3(7)	H(8i)	0.324(6)	−0.053(3)	0.385(3)	6.5(9)
H(3)	0.522(5)	0.154(3)	0.111(3)	5.9(8)	H(8o)	0.520(8)	−0.067(3)	0.287(4)	8.3(12)
H(4)	0.708(6)	0.102(2)	0.277(3)	5.7(8)	H(9o)	0.057(6)	0.184(3)	0.427(3)	7.9(11)
H(7a)	0.665(5)	0.276(3)	0.337(3)	6.0(8)	H(9i)	0.135(8)	0.069(4)	0.459(5)	9.9(16)

Can. J. Chem. Downloaded from www.nrcresearchpress.com by 210.87.254.42 on 09/05/12
For personal use only.

TABLE 2. Structural parameters for 5,6-dimethylenebicyclo[2,2,1]hept-2-ene molybdenum tricarbonyl*

(*a*) Bond lengths

Bond	Length (Å)	Bond	Length (Å)
Mo—C(1)	2.992(3)	Mo—C(4)	3.001(3)
Mo—C(2)	2.419(3)	Mo—C(3)	2.427(3)
Mo—C(6)	2.280(3)	Mo—C(5)	2.281(3)
Mo—C(9)	2.441(4)	Mo—C(8)	2.448(4)
Mo—H(9o)	2.99(4)	Mo—H(8o)	3.15(5)
Mo—H(9i)	2.81(5)	Mo—H(8i)	2.75(4)
C(1)—C(2)	1.522(4)	C(4)—C(3)	1.518(4)
C(1)—C(6)	1.530(5)	C(4)—C(5)	1.519(4)
C(1)—C(7)	1.531(5)	C(4)—C(7)	1.531(5)
C(1)—C(4)	2.224(4)		
C(1)—H(1)	0.97(4)	C(4)—H(4)	0.99(4)
C(2)—C(3)	1.355(4)		
C(2)—H(2)	0.93(3)	C(3)—H(3)	0.91(4)
C(6)—C(5)	1.456(5)		
C(6)—C(9)	1.364(6)	C(5)—C(8)	1.368(5)
C(7)—H(7a)	0.94(4)		
C(7)—H(7s)	1.01(4)		
C(8)—H(8i)	0.99(4)	C(9)—H(9i)	0.91(5)
C(8)—H(8o)	1.13(6)	C(9)—H(9o)	1.02(5)
C(8)—C(9)	3.064(7)		
Mo—C(10)	1.983(3)	C(10)—O(11)	1.142(4)
Mo—C(12)	1.981(4)	C(12)—O(13)	1.145(5)
Mo—C(14)	1.974(3)	C(14)—O(15)	1.146(4)

(*b*) Bond angles

Bonds	Angle (deg)	Bonds	Angle (deg)
C(10)—Mo—C(12)	90.2(1)		
C(10)—Mo—C(14)	89.4(1)		
C(12)—Mo—C(14)	88.6(1)		
C(2)—C(1)—C(6)	101.6(2)	C(3)—C(4)—C(5)	101.3(2)
C(2)—C(1)—C(7)	101.4(3)	C(3)—C(4)—C(7)	101.4(2)
C(2)—C(1)—H(1)	124(2)	C(3)—C(4)—H(4)	113(2)
C(6)—C(1)—C(7)	101.5(3)	C(5)—C(4)—C(7)	101.5(3)
C(6)—C(1)—H(1)	108(2)	C(5)—C(4)—H(4)	120(2)
C(7)—C(1)—H(1)	117(2)	C(7)—C(4)—H(4)	117(2)
C(1)—C(2)—C(3)	106.5(2)	C(4)—C(3)—C(2)	106.8(2)
C(1)—C(2)—H(2)	130(2)	C(4)—C(3)—H(3)	121(2)
C(3)—C(2)—H(2)	122(2)	C(2)—C(3)—H(3)	132(2)
C(1)—C(6)—C(5)	104.0(3)	C(4)—C(5)—C(6)	105.2(2)
C(1)—C(6)—C(9)	126.3(4)	C(4)—C(5)—C(8)	125.3(3)
C(5)—C(6)—C(9)	126.1(4)	C(6)—C(5)—C(8)	126.1(3)
C(6)—C(9)—H(9o)	121(3)	C(5)—C(8)—H(8o)	117(3)
C(6)—C(9)—H(9i)	112(4)	C(8)—C(8)—H(8i)	115(2)
H(9o)—C(9)—H(9i)	124(5)	H(8i)—C(8)—H(8o)	125(3)
C(1)—C(7)—C(4)	93.2(3)		
C(1)—C(7)—H(7a)	110(2)		
C(1)—C(7)—H(7s)	110(3)		
C(4)—C(7)—H(7a)	111(2)		
C(4)—C(7)—H(7s)	114(3)		
H(7a)—C(7)—H(7s)	117(3)		
Mo—C(10)—O(11)	177.3(3)		
Mo—C(12)—O(13)	179.7(4)		
Mo—C(14)—O(15)	179.2(3)		

*The figures in parentheses are the esd's in the last significant figures shown.

Can. J. Chem. Downloaded from www.nrcresearchpress.com by 210.87.254.42 on 09/05/12
For personal use only.

TABLE 3.

(*a*) Equations of various planes* within the 5,6-dimethylenebicyclo[2,2,1]hept-2-ene moiety of **1** (M = Mo)

Plane	Atoms in plane	Equation of plane*	Deviation of atoms from plane			
			Atom	Deviation (Å)	Atom	Deviation (Å)
A	C(1), C(2), C(3), C(4)	$0.6887X + 0.7188Y - 0.0955Z - 3.9210 = 0$	C(1) C(3)	0.0002(33) 0.0002(27)	C(2) C(4)	−0.0003(27) −0.0002(29)
B	C(1), C(4), C(5), C(6)	$-0.4797X - 0.0624Y - 0.8752Z + 5.0632 = 0$	C(1) C(5)	0.0021(34) 0.0030(32)	C(4) C(6)	−0.0016(29) −0.0027(27)
C	C(1), C(7), C(4)	$0.1947X + 0.5624Y - 0.8036Z + 0.8205 = 0$				
D	C(9), C(6) C(5), C(8)	$-0.2558X + 0.1986Y - 0.9461Z + 4.3742 = 0$	C(9) C(5)	0.0004(39) 0.0004(31)	C(6) C(8)	−0.0003(26) −0.0003(44)

*The orthoganalised coordinates X, Y, Z are given by $X = 7.4450x - 0.5098z$, $Y = 13.5780y$, $Z = 11.2575z$.

(*b*) Dihedral angles between planes

Planes	Dihedral angle (deg)
AB	106.95
AC	127.95
BC	125.09
BD	159.78

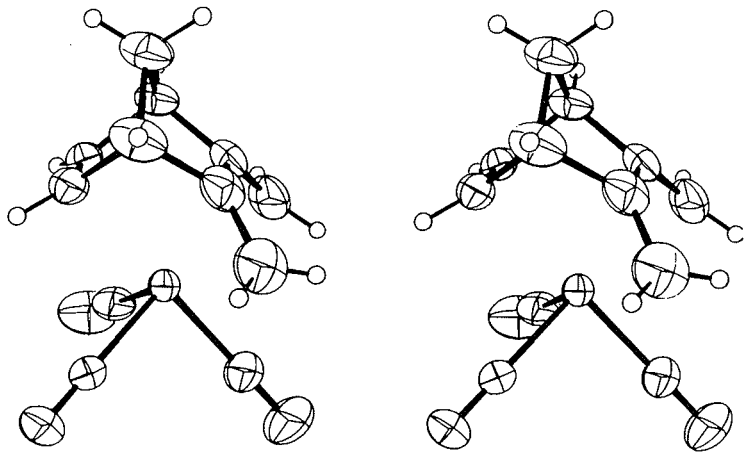

FIG. 2. Stereoscopic view of 5,6-dimethylenebicyclo[2,2,1]hept-2-ene molybdenum tricarbonyl showing the 41% probability thermal ellipsoids for the nonhydrogen atoms.

unperturbed by complexation and do not differ significantly from those in but-2-ene (1.339(5) Å) or propene (1.353(5) Å) (17). Indeed the main perturbation of the free ligand configuration due to complex formation is the decrease in the interbond angles C(2)—C(1)—C(6) and C(3)—C(4)—C(5) from about 107° in analogous uncomplexed molecules to about 101° in the present complex. This decrease results from an increased bend of the ligand about the line C(1) → C(4) which appears in turn, to result from the requirement that all three carbon–carbon double bonds be brought simultaneously within bonding distance of the metal atom. Thus in the complex, the dihedral angle between the planes C(1)—C(2)—C(3)—C(4) and C(1)—C(6)—C(5)—C(4) becomes 106.9° (compare 111° in bicyclo[2,2,1]hept-2-ene *p*-bromobenzoate (13), 112.4° in dicyclopentadienol *p*-bromobenzoate (12), and 113° in 5,6-*endo*-bicyclo-[2,2,1]hept-2-ene dicarboxylic acid anhydride (11). In the present complex, the steric requirement (*vide supra*) is further facilitated by a second bend along the line of the bond C(5)—C(6) such that the interplanar angle between the planes C(8)—C(5)—C(6)—C(9) and C(1)—C(6)—C(5)—C(4) is reduced to 159.8°, the terminal methylene carbons being bent *towards* the metal atom. Despite these distortions, the metal–diene fragment bonding is still slightly asymmetric with terminal methylene carbon – metal distances (Mo—C(8) = 2.448(3) Å, Mo—C(9) = 2.441(3) Å) averaging 2.445 Å while the incyclic methylene carbon – metal distances (Mo—C(5) = 2.281(3) Å, Mo—C(6) = 2.280(3) Å) average only 2.281 Å. In contrast, the incyclic double bond is symmetrically bound (Mo—C(2) = 2.419(3) Å, Mo—C(3) = 2.427(3) Å) but is positioned marginally further from the metal atom than either of the exocyclic methylene groups.

The terminal methylene hydrogens are displaced significantly from the plane of the conjugated diene moiety. Within experimental error, these displacements are symmetric with the inner hydrogens H(8i) and H(9i) lying 0.44 and 0.53 Å *above* the plane (*i.e.* away from the molybdenum(+)) and the outer hydrogens H(8o) and H(9o) displaced 0.19 and 0.27 Å *below* the plane(−). Similar displacements of the methylene hydrogen atoms from the coordinated ligand plane have also been observed in the *cis*-1,3-butadiene complexes $(C_4H_6)(C_8H_8)FeCO$ (H(i) = 0.56 Å(+), H(o) = 0.21 Å(−)) (19) and $(C_4H_6)_2MnCO$ (H(i) = 0.72 Å(+), H(o) = 0.00 Å(−)) (20). All three complexes exhibit inequivalence of the methylene hydrogen – metal distances with the H(i)–metal distance uniformly less than the H(o)–metal distance. In the present complex the inequivalences observed at each of the crystallographically independent methylene groups are each apparently significant in a statistical sense (Δ(8) = 0.30(5) Å; Δ(9) = 0.18(5) Å). The relevance of this result to the pmr data is discussed below.

The three carbonyl ligands all appear normal and are disposed in a staggered configuration with respect to the three π bonds so that the

Can. J. Chem. Downloaded from www.nrcresearchpress.com by 210.87.254.42 on 09/05/12
For personal use only.

Can. J. Chem. Downloaded from www.nrcresearchpress.com by 210.87.254.42 on 09/05/12
For personal use only.

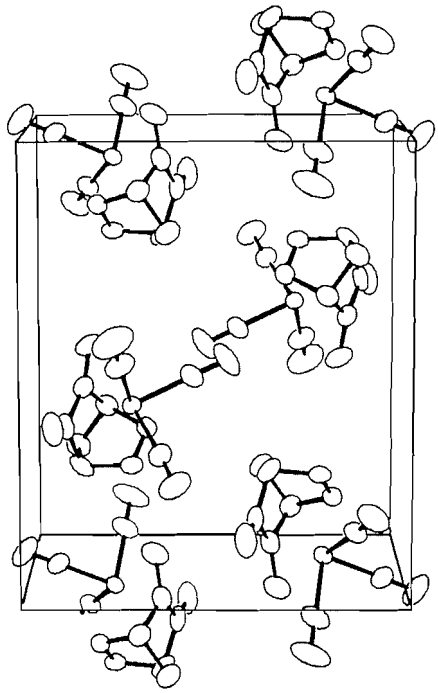

FIG. 3. Packing diagram for 5,6-dimethylenebicyclo-[2,2,1]hept-2-ene molybdenum tricarbonyl.

molybdenum maintains a distorted octahedral bonding arrangement. As shown in Fig. 2 the molecule has near C_s symmetry in the solid state.

Figure 3 shows the packing of the molecules into the unit cell and Table 4 gives those intermolecular contacts less than 3.5 Å. The closest contact is between the carbonyl oxygen O(15) and its centrically related equivalent (3.25 Å).

The usual distortions of the triene ligand, particularly in the butadiene fragment, as revealed by this X-ray study, led us to attempt to prepare similar adducts from less strained bicyclic trienes with structures related to **2** and to try to rationalize their pmr spectra.

The analogous triene molybdenum tricarbonyl complexes **5** and **6** were also isolated as orange-red crystals and their pmr spectra are shown in Fig. 4 together with our assignments. As mentioned earlier, it is difficult to rationalize the published pmr data (1, 19) obtained in CS_2 solvent. In all three compounds the ineyclic vinyl proton absorptions are about 2.6 ppm downfield from their corresponding positions in the respective parent hydrocarbons (2) (compare bicyclo[2,2,1]hepta-2,5-diene vinyl CH(δ

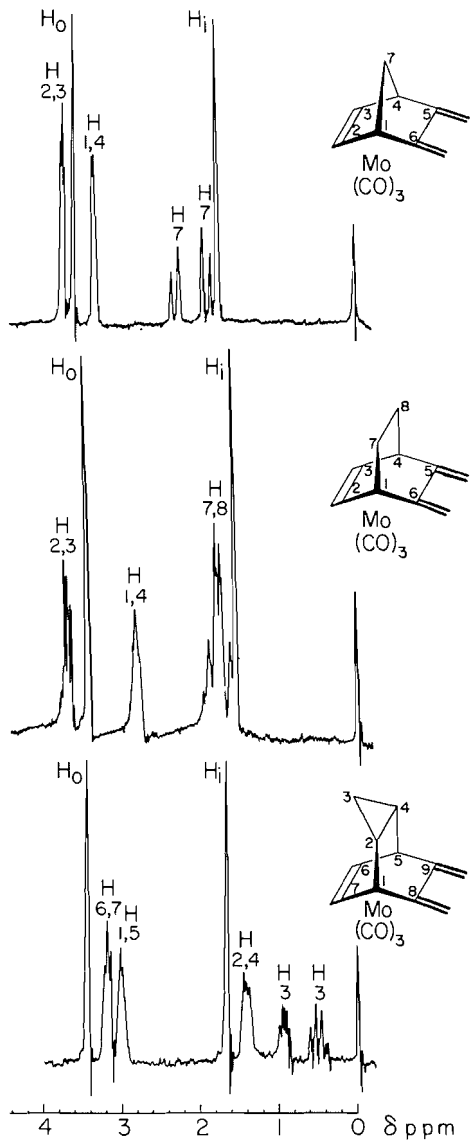

FIG. 4. Proton magnetic resonance spectra in $CDCl_3$ of the complexes **1**, **5**, and **6**.

TABLE 4. Intermolecular distances less than 3.5 Å

Atoms	D (Å)	Symmetry operation		
C(3)–O(11)	3.33	$1+x$	y	z
C(3)–O(15)	3.35	$1-x$	$\bar{y}$	$\bar{z}$
C(4)–O(11)	3.44	$1+x$	y	z
C(7)–O(11)	3.46	$1+x$	$\frac{1}{2}-y$	$\frac{1}{2}+z$
O(13)–C(2)	3.32	$\bar{x}$	$y-1$	$\frac{1}{2}-z$
O(13)–O(11)	3.32	$\bar{x}$	$y-1$	$\frac{1}{2}-z$
C(14)–O(15)	3.46	$1-x$	$\bar{y}$	$\bar{z}$
O(15)–O(15)	3.25	$1-x$	$\bar{y}$	$\bar{z}$

6.62) and bicyclo[2,2,1]hepta-2,5-diene molybdenum tetracarbonyl vinyl CH(δ 4.97) (1)). The bridgehead protons however appear little affected by the presence of the metal atom, absorbing only about 0.1 ppm upfield from their respective positions in the parent trienes. Most striking are the 'inside' and 'outside' methylene absorptions. For the parent hydrocarbons, the 'inside' proton absorptions are downfield from the 'outside' signals (20). By analogy with the accepted designations of the corresponding 'inside' and 'outside' proton absorptions of iron tricarbonyl complexes of 1,3-butadiene (21), we assign the sharp singlet absorptions of **1** (M = Mo), **5** and **6** nearest TMS as the 'inside' methylene protons. It should be noted that in the structure of **1** (M = Mo), the 'inside' methylene protons are slightly nearer to the Mo atom than those 'outside' in spite of the twisting of the methylene groups out of planarity as already discussed. Unfortunately these compounds proved to be too unstable in solution to allow a nuclear Overhauser effect study to be made and thus allow a definite assignment.

The mass spectra of these three compounds all show the successive loss of the three CO ligands from their respective parent ions as their most significant feature with the natural abundances of the seven molybdenum isotopes being repeated at each successive decarbonylation. The infrared spectra of **5** and **6** (cyclohexane) showed three carbonyl bonds between 1900 and 2000 cm^{-1} as expected (2).

1. R. B. KING and F. G. A. STONE. J. Am. Chem. Soc. **83**, 3590 (1961).
2. D. N. BUTLER and R. A. SNOW. Can. J. Chem. **50**, 795 (1972).
3. J. D. DUNITZ and P. PAULING. Helv. Chim. Acta, **43**, 2188 (1960).
4. W. R. BUSING and H. A. LEVY. Acta Crystallogr. **22**, 457 (1967).
5. M. R. CHURCHILL and K. L. KALRA. Inorg. Chem. **13**, 1427 (1974).
6. J. DE MEULENAER and H. TOMPA. Acta Crystallogr. **19**, 1014 (1965).
7. (*a*) W. R. BUSING and H. A. LEVY. J. Chem. Phys. **26**, 563 (1957). (*b*) P. W. R. CORFIELD, R. J. DOEDENS, and J. A. IBERS. Inorg. Chem. **6**, 197 (1967).
8. D. T. CROMER and J. T. WABER. Acta Crystallogr. **18**, 104 (1965).
9. D. T. CROMER. Acta Crystallogr. **18**, 17 (1965).
10. R. F. STEWART, E. R. DAVIDSON, and W. T. SIMPSON. J. Chem. Phys. **42**, 3175 (1965).
11. R. DESTRO, G. FILLIPPINI, C. M. GRAMACCIOLI, and M. SIMONETTA. Acta Crystallogr. **B25**, 2465 (1969).
12. I. R. BELLOBONO, R. DESTRO, C. M. GRAMACCIOLI, and M. SIMONETTA. J. Chem. Soc. (B), 710 (1969).
13. A. C. MACDONALD and J. TROTTER. Acta Crystallogr. **19**, 456 (1965).
14. A. C. MACDONALD and J. TROTTER. Acta Crystallogr. **18**, 243 (1965).
15. L. E. SUTTON (*Editor*). Tables of interatomic distances and configuration in molecules and ions, Supplement 1956–1959, The Chemical Society, Special Publication No. 18. S14s–S16s.
16. N. C. BAENZIGER, G. F. RICHARDS, and J. R. DOYLE. Acta Crystallogr. **18**, 924 (1965).
17. A. YOKOZEKI and K. KUCHITSU. Bull. Chem. Soc. Jpn. **44**, 2356 (1971).
18. G. DALLINGA and L. H. TONEMAN. Rec. Trav. Chim. **87**, 805 (1968).
19. I. W. BASSI and R. SCORDAMAGLIA. J. Organomet. Chem. **37**, 353 (1972).
20. G. HUTTNER, D. NEUGEBAUER, and A. RAZAVI. Angew. Chem. Internat. Edit., **14**, 352 (1975).
21. M. L. MADDOX, S. L. STAFFORD, and H. D. KAESZ. Adv. Organomet. Chem. **3**, 64 (1965).
22. D. N. BUTLER and R. A. SNOW. Unpublished results.
23. (*a*) G. F. EMERSON, J. E. MAHLER, R. KOCHHAR, and R. PETTIT. J. Org. Chem. **29**, 3620 (1964). (*b*) H. C. PRESTON and J. C. DAVIS. J. Am. Chem. Soc. **88**, 1585 (1966).
24. D. N. BUTLER and R. A. SNOW. Can. J. Chem. **53**, 256 (1975).

Can. J. Chem. Downloaded from www.nrcresearchpress.com by 210.87.254.42 on 09/05/12
For personal use only.

Equilibria in the liquid system V_2O_5–V_2O_4 at temperatures up to 1130 K

ANDREW BLOCK-BOLTEN[1]

Department of Metallurgy and Materials Science, University of Toronto, Toronto, Ont., Canada

Received March 22, 1976

ANDREW BLOCK-BOLTEN. Can. J. Chem. **54**, 1967 (1976).

The equilibrium oxygen pressure in the V_2O–V_2O_4 system from temperatures near melting, up to 1130 K has been measured. A closed system solid electrolyte cell with a Ni/NiO reference electrode was used. The results of the present investigation for liquid solutions consistently extend those reported for solid solutions.

ANDREW BLOCK-BOLTEN. Can. J. Chem. **54**, 1967 (1976).

On a mesuré la tension d'équilibre de l'oxygène dans le système V_2O_5–V_2O_4 à partir de températures proches de la fusion et jusqu'à 1130 K. Une cellule électrolytique fermée avec électrode de référence en Ni/NiO a été utilisée. Les résultats présentés ici pour les solutions liquides constituent une extension des données expérimentales communiquées par d'autres chercheurs pour les solutions solides.

Can. J. Chem. Downloaded from www.nrcresearchpress.com by 210.87.254.5 on 09/05/12
For personal use only.

Recently Endo *et al.* (1) have studied the phase equilibria of solid V_2O_5–V_2O_4 solutions. Oxygen pressures were measured and phases were identified after quenching by both the X-ray diffraction method and the gravimetric method. Also, a new paper by Fotiev *et al.* (2) and an older paper by Flood and Kleppa (3) give reliable data on the solid region and are used here for comparison.

The P_{O_2} values obtained here for liquid solutions meet the results obtained for solid solutions by refs. 1–3, forming an extension of their curves into the liquid region. The results of Suito and Gaskell (4) extrapolated to 1100 K give $\log P_{O_2} = -3.86$ while the present measurements give an average value of -3.94, which is in excellent agreement with the former. Data presented in ref. 5 could not be compared for two reasons. First, the experiments by Katsura and Hasegawa were conducted isothermally at 1600 °C, and secondly the vanadium pentoxide equilibrium was not quoted. The old paper by Milan (6) gave, at 1130 K, results one order of magnitude higher than the present work. The results of Allen, Kubaschewski, and Goldbeck (7) suffer from an arithmetic arror in the combination of enthalpy of fusion of V_2O_5 (4). The results for P_{O_2} of MacChesney *et al.* (8) are approximately 12 orders of magnitude lower than those quoted in refs. 1 to 4 and in the present study. In ref. 8 gas mixtures of CO/CO_2 were equilibrated with the vanadium oxides. Assuming that MacChesney *et al.* employed correct data for the oxidation of CO to CO_2, it must then be concluded the values of oxidation of V_2O_4 to liquid V_2O_5 compiled by Couglin (9) must be in error. Perhaps some side reactions also take place under the experimental conditions of ref. 8. Hughes and Hill (10) describe the formation of the species VOCO when CO is contacted with lower vanadium oxides. The excellent calorimetric data of Mah and Kelley (11) are affected by the same error as ref. 7 in the estimation of the free energy of oxidation of V_2O_4 to liquid V_2O_5. Two other papers (12, 13) having an entirely different character are noted. Here the oxygen partial pressures were imposed and the response read. If Kachi and Roy's (14) phase diagram is used, the results of ref. 13 are 2 to 3 orders of magnitude lower than ours at the liquidus line at 1130 K; however, the use of activities in place of mole fractions in eq. 4 of ref. 13 could correct the situation. On the other hand, it must be stated that nitrogen has not been found to be inert in the presence of melts containing V_2O_5 (15), and that its use (13) to establish oxygen partial pressures in this system, may in part account for the discrepancy.

The purpose of this work was to measure the partial pressure of oxygen for the reaction

$$[1] \qquad V_2O_{5,liq} = \tfrac{1}{2}O_2 + V_2O_{4\,dissolved}$$

over the temperature range extending 200 K above the V_2O_5–V_2O_4 eutectic point, and to close the gap in existing data.

[1]Present address: Department of Chemical Engineering, University of Toronto, Toronto, Ont., Canada.

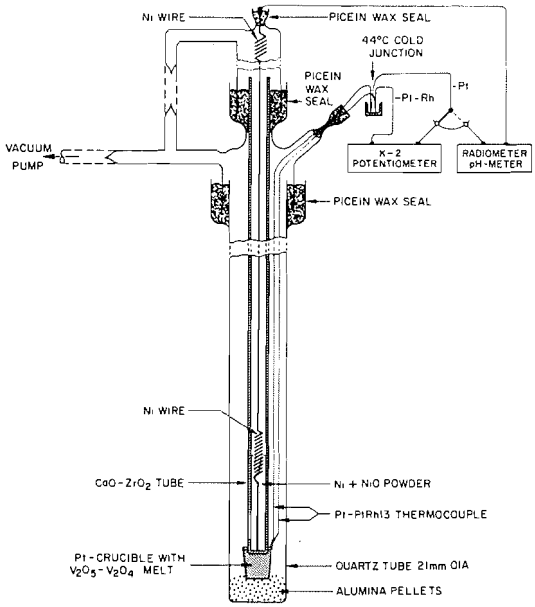

FIG. 1. Solid electrolyte cell.

The heart of the apparatus was a sealed solid electrolyte cell. The advantage of such a design is that thermodynamic data may be calculated from measured emf's directly with the aid of only one extra equation: namely, the well established free energy of formation of NiO. The disadvantage of this arrangement is that for the purpose of identification of the solid phases present it was not possible either to withdraw samples for X-ray analysis or to perform X-ray analysis (of the melts) *in situ*.

Experimental

The cell $Ni/NiO-CaO/ZrO_2-V_2O_5/V_2O_4-Pt$ (Fig. 1) was built in the following way: a closed-end calcia-stabilized zirconia tube (Zirconium Corporation of America) was filled with a mixture of Ni and NiO powders (Fisher Scientific Co.) and connected with the top of the apparatus by means of a pure nickel wire (Electronic Space Products Inc., Los Angeles). The $CaO-ZrO_2$ tube was placed inside a quartz tube, 21 mm i.d. A Pt/Pt – 13% Rh thermocouple was connected to the platinum crucible. After simultaneous evacuation of both sides of the cell, the glass connections to both compartments were sealed by flame. A volt-potentiometer (Leeds and Northrup K2) served to measure the temperature, and a p*H*-meter (Radiometer model 22) was used to measure the emf of the cell. After agglomeration of the Ni/NiO mixture, which typically occurred at approximately 800 °C, stable, reversible cell emf's were observed. In contrast to the behaviour of an earlier cell which employed an open gas reference electrode (air or oxygen) the present cell showed no signs of drifting emf's, and responded quickly to temperature changes. About 130 measurements of oxygen pressure were made in three independent cells of this type. The results are shown in Fig. 2 and have been corrected for the thermal emf produced by the Pt and Ni leads. The magnitude of the correction determined herein was about −9.5 mV at 1130 K and −7.7 mV at 950 K. This compares well with that reported in ref. 16.

Theoretical

On one side of the calcia–zirconia solid electrolyte the Ni/NiO solid mixture characterized by low P_{O_2} is present; on the other the $V_2O_5-V_2O_4$ liquid solution with high P_{O_2}. The free energy change of the overall cell reaction is given by

$$[2]\quad \Delta G = \frac{RT}{2}\ln P_{O_2,\text{low}} - \frac{RT}{2}\ln P_{O_2,\text{high}}$$

and

$$[3]\quad E_{\text{cell}}(V) = -\Delta G/2zF \qquad \text{where } z = 2$$

this means that

$$[4]\quad E_{\text{cell}}(V) = -\frac{\Delta_f G_{NiO}{}^0}{2F} + \frac{RT}{4F}\ln P_{O_2,\text{high}}$$

and finally

$$[5]\quad \log P_{O_2,\text{high}} = (E_{\text{cell}}(\text{V}) - E_{NiO}(\text{V}))/0.0000496T$$

The E_{NiO} values are those reported by Charette and Flengas (17).

$$[6]\quad E_{NiO}(\text{V}) = 1.21083 - 0.00043993T$$

Results

The results of the three independent experiments are very consistent. Only a part of the experimental points is visible in Fig. 2, as most of them cover each other exactly. Series I is different from series II and III by the different initial concentration of V_2O_4 in V_2O_5. This is seen in Fig. 2 where the P_{O_2} line splits in the solid region. In the liquid region, however, which was the principal area of study, there is no detectable difference. It is noteworthy that the results of the present work meet all three curves measured by Endo *et al.* (1), Fotiev and Volkov (2), and by Flood and Kleppa (3) at the eutectic temperature. The local maximum in the curve at about 700 °C, which is really a minimum as far as oxygen pressure is concerned, can be explained by the presence of the oxygen-

Can. J. Chem. Downloaded from www.nrcresearchpress.com by 210.87.254.5 on 09/05/12
For personal use only.

Can. J. Chem. Downloaded from www.nrcresearchpress.com by 210.87.254.5 on 09/05/12
For personal use only.

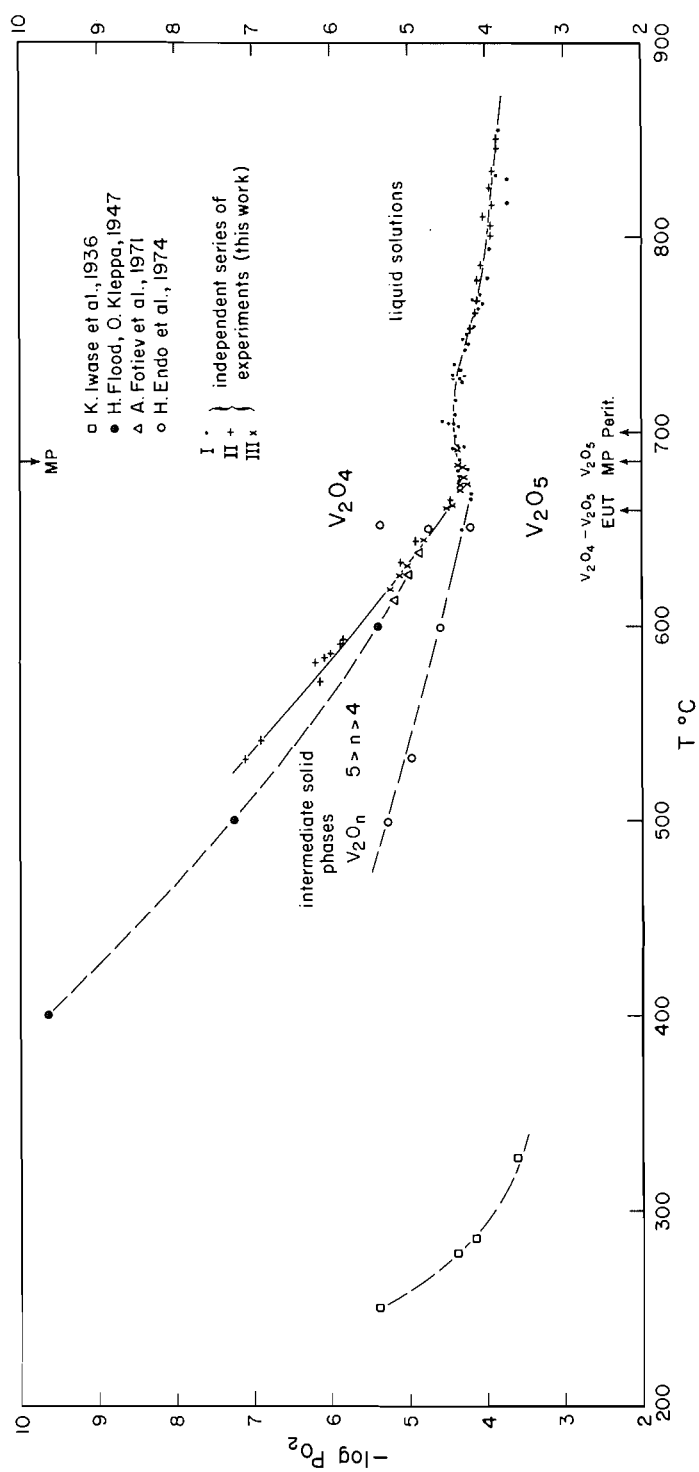

FIG. 2. Temperature dependence of oxygen pressure.

consuming peritectic reaction at this temperature.

Acknowledgments

The author acknowledges Professor S. N. Flengas for his helpful discussions.

The construction of the glassware of the apparatus by Mr. R. H. Chappell is appreciated.

1. H. ENDO, M. WAKIHARA, and M. TANIGUCHI. Chem. Lett. Jpn. 905 (1974).
2. A. A. FOTIEV and V. L. VOLKOV. Russ. J. Phys. Chem. **45**, 1516 (1971). (English translation of Zh. Fiz. Khim. **45**, 2671 (1971)).
3. H. FLOOD and O. J. KLEPPA. J. Am. Chem. Soc. **69**, 998 (1947).
4. H. SUITO and D. R. GASKELL. Met. Trans. **2**, 3299 (1971).
5. T. KATSURA and M. HASEGAWA. Bull. Chem. Soc. Jpn. **40**, 561 (1967).
6. E. F. MILAN. J. Phys. Chem. **33**, 498 (1929).
7. N. P. ALLEN, O. KUBASCHEWSKI, and O. VON GOLDBECK. J. Electrochem. Soc. **98**, 417 (1951).
8. J. B. MACCHESNEY, J. F. POTTER, and H. J. GUGGENHEIM. J. Electrochem. Soc. **115**, 52 (1968).
9. J. P. COUGLIN. U. S. Bureau of Mines Bull. No. 542 (1954).
10. M. F. HUGHES and G. R. HILL. J. Phys. Chem. **59**, 388 (1955).
11. A. D. MAH and K. K. KELLEY. Bureau of Mines Report No. 5858 (1961).
12. A. RAHMEL. Corrosion Sci. **12**, 307 (1972).
13. D. A. PANTONY and K. I. VASU. J. Inorg. Nucl. Chem. **30**, 423 (1968).
14. S. KACHI and R. ROY. Second Quarterly Report (1966), Materials Research Laboratory, The Pennsylvania State University, Contract DA-28-043-AMC-01304E.
15. A. BLOCK-BOLTEN, B. J. M. BERTRAND, and S. N. FLENGAS. Can. J. Chem. **52**, 2068 (1974).
16. American Institute of Physics, Handbook (1963), pp. 4–8.
17. G. G. CHARETTE and S. N. FLENGAS. J. Electrochem. Soc. **115**, 796 (1968).

Can. J. Chem. Downloaded from www.nrcresearchpress.com by 210.87.254.5 on 09/05/12
For personal use only.

Structure of radicals produced by γ-radiolysis. Part 4. Adamantane matrices doped with various 5-membered heterocyclic molecules

D. L. WINTERS

Department of Chemistry, West Virginia University, Morgantown, WV, 26506 U.S.A.

AND

A. CAMPBELL LING[1]

Nuclear Science Facility, San José State University, San José, CA, 95192 U.S.A.

Received September 26, 1974[2]

D. L. WINTERS and A. CAMPBELL LING. Can. J. Chem. **54**, 1971 (1976).

The effects of γ-radiolysis at room temperature on adamantane and adamantane-d_{16} matrices doped with 5-membered heterocyclic molecules has been examined by X-band electron spin resonance (esr) spectrometry. Radical structures formed from heterocyclic solute molecules are discussed and tentative assignments made for 2-methyl-, 3-methyl-, and 2,5-dimethylthiophene, 2-methyl-, and 2,5-dimethylfuran. Discussion of possible radical structures derived from furan, tetrahydrofuran, 2-methyl- and 3-methyltetrahydrofuran, 2,5-dihydrofuran, and 4,5-dihydro-2-methylfuran, is included, but unambiguous assignments of structure cannot be made for these compounds from the esr data obtained. Other molecules examined included thiophene, pyrrole, and 1-methyl- and 1,2,5-trimethylpyrrole. For these latter molecules, experimentally obtained first derivative X-band esr spectra were too poorly resolved to allow rational discussion of possible structures. It was noted that perdeuterated adamantane matrices provided superior resolution for esr spectra derived from radicals with a delocalized spin center such as allyl or allenyl species.

D. L. WINTERS et A. CAMPBELL LING. Can. J. Chem. **54**, 1971 (1976).

On a examiné par la spectrométrie rpe de la bande X les effets de la radiolyse γ, à la température de la pièce, sur des matrices d'adamantane et d'adamantane-d_{16} dopées avec des molécules hétérocycliques à cinq membres. On discute des structures radicalaires formées à partir des molécules de solutés hétérocycliques et on fait des attributions non-définitives pour le méthyl-2, le méthyl-3 et le diméthyl-2,5 thiophène et le méthyl-2 et le diméthyl-2,5 furanne. On inclut aussi une discussion des structures radicalaires possibles pouvant dérivées du furanne, du tétrahydrofuranne, des méthyl-2 et -3 tétrahydrofuranne, du dihydro-2,5 furanne et du dihydro-4,5 méthyl-2 furanne; toutefois on ne peut faire d'attributions non-ambiques pour ces composés à partir des données rpe obtenues. Parmi les autres molécules qui ont été examinées, on note le thiophène, le pyrrole et les méthyl-1 et triméthyl-1,2,5 pyrroles. Pour ces dernières molécules, les premières dérivés obtenues expérimentalement à partir des spectres rpe de la bande X ne sont pas assez bien résolus pour permettre une discussion rationnelle des structures possibles. On a noté que les matrices de perdeutéroadamantane fournissent une meilleure résolution pour les spectres rpe dérivés des radicaux avec un centre de spin délocalisé, tels que les espèces allyle et allényle.

[Traduit par le journal]

Introduction

In conjunction with a study of 5-membered alicyclic molecules (1) and to provide supporting data concerning radiolyses of furanose sugars and pyrimidine bases (2), we have used adamantane isolation techniques to examine the effects of γ-radiolysis on adamantane doped with selected 5-membered heterocyclic molecules. In view of their structure and relative resonance energies, furan, thiophene, and pyrrole are of intrinsic interest to radiation chemistry, since they may display both H-atom loss and H-atom addition, together with the possibility of stabilized electron attachment modes of reaction. This latter mode has been reported by Kasai and co-workers (3) to occur for furan and other small heterocyclic compounds trapped in inert gas matrices at 4 K, but has not been seen in other studies. Trofimov *et al.* (4) report the results of a study of radiolysed pure-phase polycrystalline furan and thiophene compounds, and indicate that at 113–143 K H-atom addition predominates following an initial primary event of H-atom abstraction. Wood and co-workers (5) have shown that for adamantane matrices

[1]To whom correspondence should be addressed.

[2]Revision received March 18, 1976.

Can. J. Chem. Downloaded from www.nrcresearchpress.com by 210.87.254.5 on 09/05/12
For personal use only.

Can. J. Chem. Downloaded from www.nrcresearchpress.com by 210.87.254.5 on 09/05/12
For personal use only.

containing aromatic solutes, the ratio of H-atom addition to H-atom loss can be markedly altered by conducting radiolyses under an O_2 (or air) atmosphere relative to *in vacuo* studies. We were unable to produce similar results in aliphatic alkenes (6) or pyrimidine bases (2), but did note H-atom addition reactions in cyclopentadiene (1), as did Wan and co-workers in cyclooctatetraene held in adamantane matrices (7). This may merely reflect the relative size of the π-cloud in each molecular system.

Radiolysis studies of aqueous liquid phase furan solutions by Schuler *et al.* (8), radiolysis studies of pyrrole in aqueous solutions by Samuni and Neta (9), studies involving ·OH radical generation from Fenton's reagent and other metal ion/hydrogen peroxide radical generators in the presence of various selected heterocyclic substrates (10), and pulse radiolysis studies of nitrofuran compounds in aqueous solution (11), all indicate that addition reactions (of ·OH radicals) predominate. Further, single crystal studies by Whiffen and co-workers (12) with carboxylic acid derivatives of furan and thiophene show that H·-atom addition reactions are the preferred mode.

Of particular interest to radiation chemists is the structure of the radical formed from 2-methyltetrahydrofuran (2-MTHF), and much controversy has been evident as to the nature of this radical, and the reactions leading to its formation (13). The structure of this radical is also pertinent to studies recently initiated by Kevan and co-workers (14) concerning the environment of the trapped electron in MTHF glasses at various temperatures. Both 2-MTHF and propylene carbonate (15) are structurally similar, form stable glasses at 77 K, and would be expected to yield tertiary radicals, as was seen previously for aliphatic alkane systems (16). The exact mechanism of radical formation in the pure phase glassy state is still speculative, but could involve H^+-transfer from neighbouring parent ions. However, solid state interactions in the glass have precluded direct and unambiguous assignments of radical structures in these systems, and others, from esr spectral data.

Experimental

Radiolyses were performed initially with a 150 Ci ^{60}Co water well source, dose rate (Fricke dosimetry) of *ca.* 3×10^{16} eV g^{-1} min^{-1}, and total doses of *ca.* 10^{18} eV g^{-1}. Radiolyses performed in revising this manuscript were done through the agency of a newly installed 850 Ci ^{60}Co dry cavity source,[3] dose rate maximum (Fricke dosimetry) of *ca.* 6×10^{17} eV g^{-1} min^{-1},[4] total doses were usually in the range 10^{18} eV g^{-1}, but some exposures were made up to 10^{20} eV g^{-1}. The esr monitoring was via a Varian Associates Model E3 spectrometer, typically at 9.45 GHz, 100 KHz modulation, and 0.1 to 2.0 G amplitude, 16 min to 4 h scan at 3375 ± 50 G. Radical lifetimes were in excess of 10^2 min at room temperature, and it was usual to monitor esr spectra for any one sample at regular intervals over 5–10 days. Computer simulations were performed via an IBM-360/75 computer with Cal-Comp plotter accessory using a program written by one of us (17). Adamantane ($C_{10}H_{16}$), perdeuterated adamantane ($C_{10}D_{16}$), and all solutes were obtained from commercial sources; adamantane was purified by multiple vacuum sublimations (6–10 successive sublimations), and perdeuterated adamantane via one sublimation; solutes were usually distilled once prior to use. 2-MTHF, 3-MTHF, and tetrahydrofuran (THF), were distilled, passed through a 10% w/w $AgNO_3$ – silica gel column 5–8 times, refluxed over Cu(II) chloride for 2–3 h, distilled from over KOH pellets into a receiver containing $LiAlH_4$ under a N_2 atmosphere, refluxed for 2–3 h, and then transferred to a vacuum line and stored in a thoroughly degassed state over an Na mirror until required. Samples were then made up under vacuum in the manner used to prepare cyclopentadiene samples described previously (1). All spectra displayed in this report have the magnetic field increasing from left to right.

Results and Discussion

Line widths for esr spectra of radicals held in adamantane isolation matrices are usually far narrower than those found in other solid state matrices. We have found values at room temperature of *ca.* 0.7–1.5 G (FWHM, Lorentzian absorption lines, corresponding to *ca.* 0.9–2.0 G for peak-to-peak separation of first derivative representations), with an apparently lower limit of 0.7 G found for the N,N,N′,N′-tetramethyl-*p*-phenylenediamine cation at room temperature. A further increase in esr line resolution *may* be (but apparently not always) achieved by the use of perdeuterated adamantane ($C_{10}D_{16}$) matrices, with values of *ca.* 0.3 to 0.4 G found for the toluenyl radical (2), and for some radicals formed from thiophene derivatives herein. Unfortunately, even with $C_{10}D_{16}$ matrices, esr resolution for some species was inadequate and precluded rational discussion of possible structures. The situation was

[3]A dry cavity ^{60}Co source installed at West Virginia University Department of Chemistry as of January 1975.

[4]We thank Mr. James J. Carni, B.S. undergraduate research participant from W.V.U., for making these measurements.

Can. J. Chem. Downloaded from www.nrcresearchpress.com by 210.87.254.5 on 09/05/12
For personal use only.

often further complicated by the appearance of signals from the matrix molecule itself. However, the use of $C_{10}D_{16}$ minimizes this factor, since the resulting spectrum from γ-irradiated $C_{10}D_{16}$ is considerably narrower than that from $C_{10}H_{16}$ under the same conditions (18, 19)[5] and thus does not obscure such a large proportion of the solute esr spectrum.

Apart from the actual question of whether H-atom loss or H-atom addition predominates and under what conditions, the source of H-atoms that add to unsaturated centers is of interest. It is therefore pertinent to point out that from *prima facie* evidence, the H-atoms appear to originate from the solute molecules and not the matrix. This is unusual. For solutes that are postulated to exhibit both H-atom loss and H-atom addition to give two radicals simultaneously, there is no evidence at all to show that D-atom addition occurs in $C_{10}D_{16}$, although H-atom addition is seen in $C_{10}D_{16}$ matrices for the same solute. Further work is in progress to determine relative yields of H_2, D_2, and HD, in various selected systems. Peripheral support for this hypothesis is found from other experimentally noted points. The lifetime of solute radicals in $C_{10}D_{16}$ matrices is significantly longer (qualitatively) than for the same solute radical species held in $C_{10}H_{16}$. This type of 'secondary isotope effect' involving deuterated matrices is not unusual, and one example is the tenfold increase in lifetime seen for the methyl radical held in 3-methylpentane (3-MP) compared to the methyl radical in perdeuterated 3-MP, where initial half-lives of *ca.* 16 and 150 min were noted for 3-MP and 3-MP-d_{14}, respectively (20). More pertinently, little or no evidence is found for H-atom addition in $C_{10}H_{16}$ matrices, whereas this mode of reaction is thought to contribute to the observed spectrum in $C_{10}D_{16}$ matrices (*e.g.* 2,5-dimethylthiophene (2,5-DMT), see discussion below). On this basis, it may be tentatively hypothesized that H-atoms are more easily lost from the system in $C_{10}H_{16}$ matrices and that perhaps this loss is partly attributable to

[5]A more complete description of the complex changes seen when adamantane itself is radiolysed at low temperatures and then monitored by X-band and Q-band esr spectrometry, together with the changes seen when 2-methyltetrahydrofuran is radiolysed in adamantane and adamantane-d_{16} matrices under similar conditions, has been published, ref. 21.

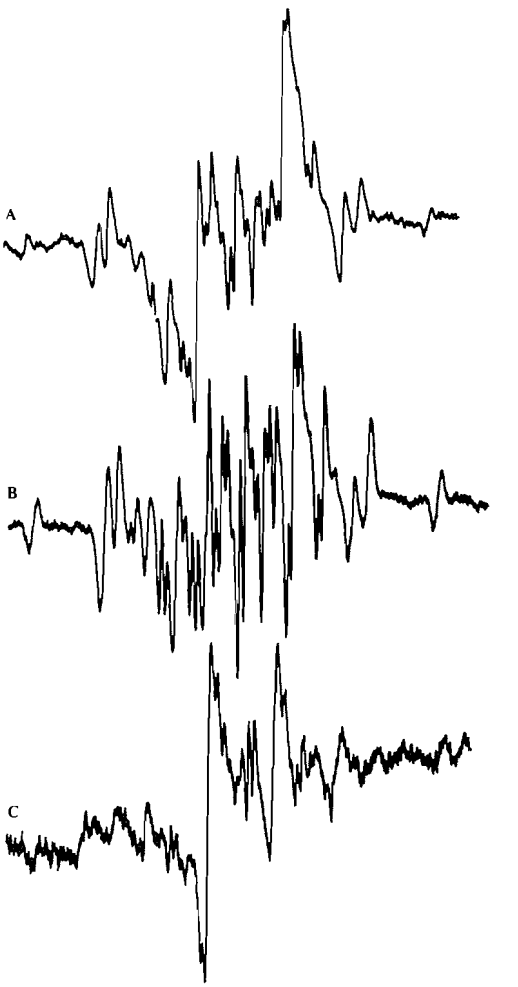

FIG. 1. First derivative esr spectra taken at room temperature and obtained from γ-radiolysis of 2,5-dimethylthiophene held in adamantane-d_{16} at room temperature; taken (*A*) *ca.* 7 mins, (*B*) 3 h, (*C*) 117 h, after termination of γ-irradiation.

H_2 (or correspondingly HD) formation by abstraction from the matrix, since there is no apparent reason why O_2-scavenging of H-atoms should differ markedly in efficiency in $C_{10}H_{16}$ relative to $C_{10}D_{16}$. Mass spectrometric measurements of relative H_2:HD:D_2 ratios are not available at this time to allow further support or denial of these qualitative speculations.

Two other experimentally noted points deserve comment prior to a discussion of radical structures derived from individual molecules. Firstly, the esr spectrum from any particular solute develops positively with time from the

Can. J. Chem. Downloaded from www.nrcresearchpress.com by 210.87.254.5 on 09/05/12
For personal use only.

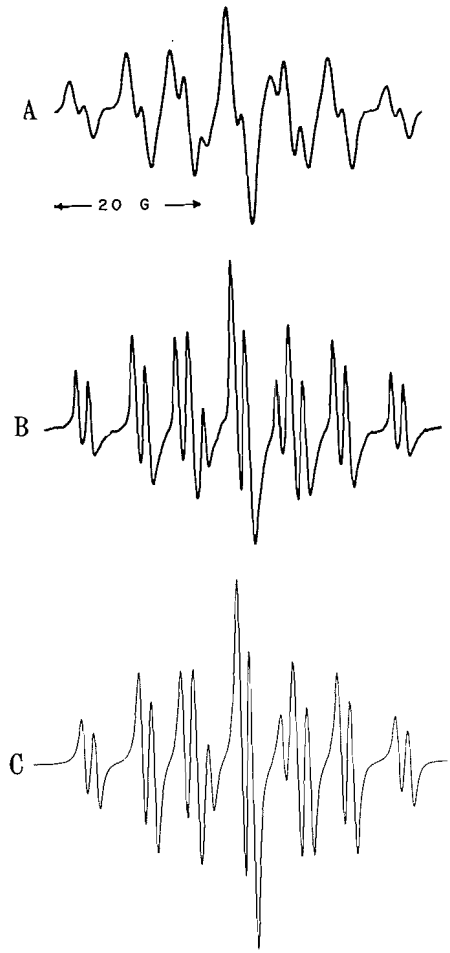

FIG. 2. First derivative esr spectra for the radical derived from 2-methylthiophene by γ-radiolysis at room temperature in adamantane and adamantane-d_{16} matrices; (*A*) in adamantane, (*B*) in adamantane-d_{16}, (*C*) computer simulation of the experimental spectrum.

termination of γ-irradiation and while monitoring the sample. This is illustrated for 2,5-DMT and exhibited in Fig. 1. The signal intensity, and particularly the spectrum resolution, grows and/or alters over a period of several hours, and the observed spectrum does not develop fully until approximately 2–4 h after the irradiation process has ended. The spectrum then continues to change with time, but now involving a degradation process as one, or more, radical decays. In cases where two radicals are seen, this decay process is different for each, as evidenced by different half-lives for decay. It is tempting to ascribe this observed effect to solute radical formation via an abstraction process initiated by a radical derived from the matrix, but there is no definitive evidence for a concommittant loss of esr signal attributable to adamantyl radicals as the solute radical signal develops. Equally, we do not have data from optical spectral analysis to speculate whether an ion, or some species that does not exhibit an esr signal, is initiating the radical growth. A second experimental observation is that the solute radical decay process is faster when the γ-dose is increased. This is partly attributable to the fact that radical decay follows second-order kinetics (2), and thus the initial half-life is concentration dependent. It may also be due to a radical-site interaction, *i.e.* recombination of solute radicals with radicals or other species formed directly from the matrix (21).

2-Methylthiophene (2-MT) and 2-Methylfuran (2-MF)

The esr spectra for the radicals derived from 2-MT and 2-MF following γ-radiolysis in adamantane matrices at room temperature are shown in Figs. 2 and 3, respectively. The spectra labelled *A* in each of Figs. 2 and 3 are those from radicals held in $C_{10}H_{16}$, those labelled *B* are from $C_{10}D_{16}$ matrices, and those labelled *C* are computer simulations of esr spectra based on parameters shown in structures **1** and **2**

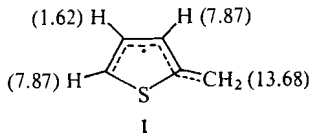

1

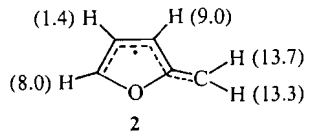

2

(coupling constants given in gauss). The only point of controversy concerns structure **2**, as to whether the proton at C-3 or C-5 in the furan derivative yields an 8.0 or 9.0 G coupling, and we do not have data from deuterium labelling experiments to distinguish this point specifically. However, by analogy with the cyclopentanonyl radical discussed by Pratt and co-workers (22), it is probable that the 5-position proton will have a smaller coupling constant than the 3-position proton due to the influence of the adjacent oxygen atom. Moreover, Schuler *et al.* (8) describe

Can. J. Chem. Downloaded from www.nrcresearchpress.com by 210.87.254.5 on 09/05/12
For personal use only.

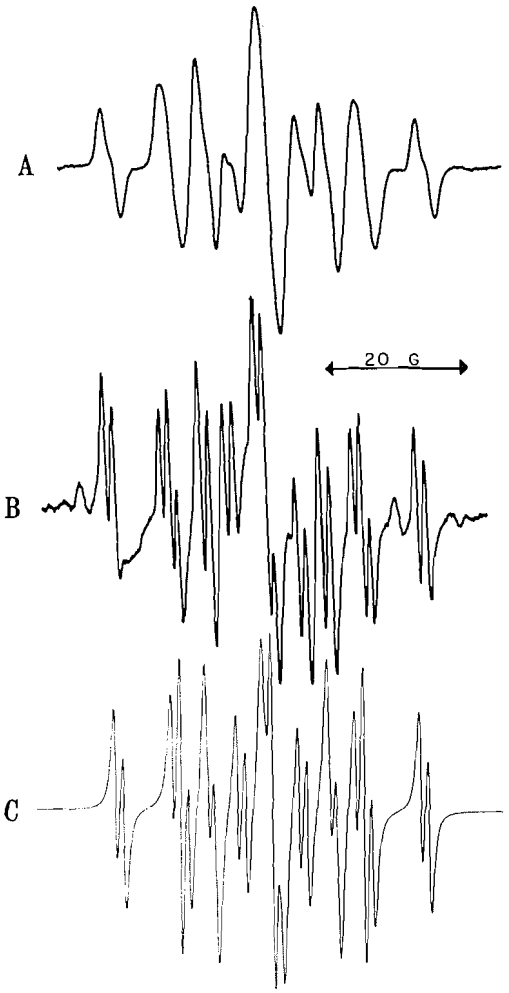

FIG. 3. First derivative esr spectra for the radical derived from 2-methylfuran (2-MF) by γ-radiolysis at room temperature in adamantane and adamantane-d_{16} matrices; (*A*) in adamantane, (*B*) in adamantane-d_{16}, (*C*) computer simulation of the experimental spectrum.

several allylic and allenylic systems involving a terminal oxygen atom, and show that the terminal proton for such systems is often characterized by an 8 G coupling. Finally, it is pertinent to this discussion that the 3-position proton in 2,5-dimethylfuran (2,5-DMF) has a coupling constant of 9.2 G (see below) as a tentative assignment. All of these inferential points support the assignment made in structure **2**. It is interesting to note the inequivalency of the $=CH_2$ group protons in the furan derivative, but apparently equivalent protons in the thiophene derivative. Resolution of the experimental

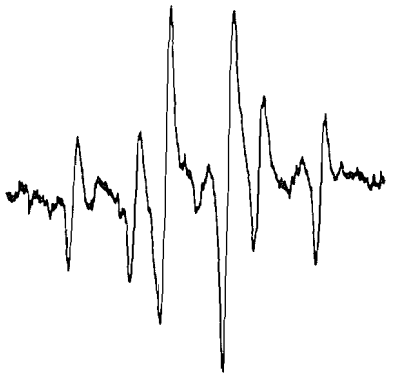

FIG. 4. First derivative esr spectrum for the radical derived from 2,5-dimethylthiophene by γ-radiolysis at room temperature in an adamantane matrix.

spectrum from $C_{10}D_{16}$ matrices is sufficient to distinguish this clearly, and computer simulations emphasize their differences unambiguously. It is apparent from the agreement between experimental spectra and simulated spectra in Figs. 2 and 3, that only H-atom loss is occurring; there is no evidence for H-atom addition, or for D-atom addition derived from the matrix itself. We conclude that either addition is not favored for this system, or that H-atoms are being scavenged by a mechanism involving other than O_2 or O-atoms.

2,5-Dimethylthiophene (2,5-DMT) and 2,5-Dimethylfuran (2,5-DMF)

The esr spectra from γ-radiolysis of 2,5-DMT in $C_{10}D_{16}$ matrices are shown in Fig. 1 and for 2,5-DMT in $C_{10}H_{16}$ in Fig. 4; equivalent esr spectra for 2,5-DMF are shown in Fig. 5. The spectrum obtained from γ-radiolyses of 2,5-DMF in $C_{10}D_{16}$ (Fig. 5*B*) is poorly resolved when compared to those obtained from 2-MF and 2-MT under similar experimental conditions, but can be assigned on a reasonably unambiguous basis to radical **3** via computer simulation studies, and by analogy with the data obtained from other structural analogues. The resolution, however, is too poor to allow distinction between the two protons of the $=CH_2$ group as was seen in 2-MF, and which is

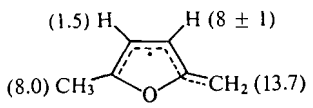

3

Can. J. Chem. Downloaded from www.nrcresearchpress.com by 210.87.254.5 on 09/05/12
For personal use only.

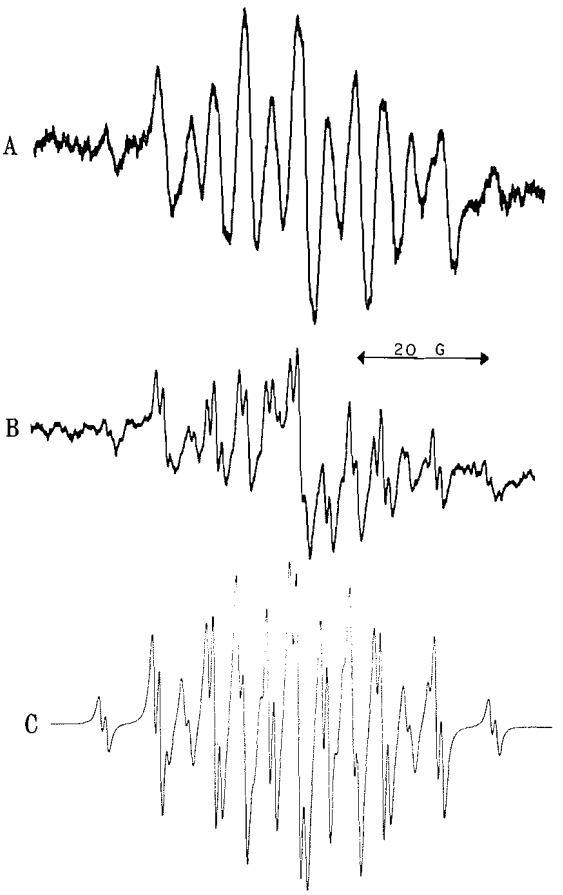

FIG. 5. First derivative esr spectra for the radical derived from 2,5-dimethylfuran by γ-radiolysis at room temperature in adamantane and adamantane-d_{16} matrices; (*A*) in adamantane (*B*) in adamantane-d_{16}, (*C*) computer simulation of experimental spectrum.

characteristic of furan derivatives but not thiophene derivatives.

The data obtained from 2,5-DMT is more complex. Firstly, the esr spectrum obtained from room temperature radiolyses of 2,5-DMT in $C_{10}H_{16}$ is quite different to that obtained from 2,5-DMT in $C_{10}D_{16}$ matrices (compare Fig. 4 with Fig. 1*B*, respectively), although it should be noted that the spectral pattern shown in Fig. 4 makes a significant contribution to the spectrum displayed in Fig. 1*B*. Secondly, the spectrum obtained from 2,5-DMT in $C_{10}D_{16}$ changes markedly with time, and shows a growth pattern involving both enhancement of spectral resolution and development of new spectral features for a time period of >3 h after termination of γ-irradiation. Thirdly, the spectrum exhibits a differential rate of decay over a further period of more than 100 h, indicating the presence of at least two radicals whose rates of decay differ significantly from each other. Fourthly, the spectrum is clearly asymmetric and exhibits two distinct line widths, a further indication that at least two species are contributing to the observed esr spectrum displayed in Fig. 1. From both computer simulation techniques and methods involving spectral subtraction of observed lines and their postulated symmetry partners, analysis unambiguously indicates that *three* species contribute to Fig. 1*B*.

One species produces a contribution to the observed esr spectrum with a line width[6] of *ca.* 0.65 G, a characteristic value for radicals with an allylic or allenylic delocalized spin center. The spectrum appears to display four hyperfine constants, and by analogy with other data and via a detailed computer simulation study, we assign a structure shown by radical **4**.

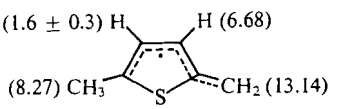

4

The computer simulations are not sensitive to small changes in one coupling constant assigned to the 4-position, but small variations in the remaining three coupling constants lead to significant changes in terms of overall spectral width, and line overlap.

A second species exhibits a quartet (a^H = 19.5 G) of triplets (a^H = 25.8 G) and a FWHM line width in both $C_{10}H_{16}$ and $C_{10}D_{16}$ of *ca.* 2 G, characteristic of a saturated radical center (1, 2, 16, 19). Since H-atom addition to molecules containing extensive delocalized electron systems has been observed by several investigators (1, 5, 7) and since tertiary radicals are generally more stable than secondary radicals, we assign this spectrum to radical **5**, produced by H-atom addition at the 3-position. Note that H-atom addition to the electrophilically

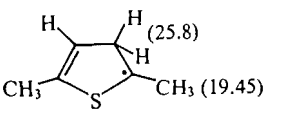

5

[6]FWHM width corresponding to *ca.* 1 G peak-to-peak in the first derivative.

Can. J. Chem. Downloaded from www.nrcresearchpress.com by 210.87.254.5 on 09/05/12
For personal use only.

favoured 2-position will produce the allylic species **6**, and this should exhibit line widths similar to those seen for radical **4**, and radicals derived from 2-MF and 2-MT. Further support for this assignment comes from a recent study of the γ-radiolysis of 2-methyltetrahydrofuran (2-MTHF) in $C_{10}H_{16}$ and $C_{10}D_{16}$ via Q-band esr spectrometry (21). One radical, identified as **7**, formed by H-atom loss[7] from the 2-position tertiary carbon of 2-MTHF, has been assigned the structure shown. The slightly reduced value for $a_{CH_3}^{H}$ in 2-MTHF compared to 2,5-DMT is consistent with a greater degree of spin density loss to the more electrophilic oxygen of the furan system compared to the sulfur atom in thiophene derivatives.

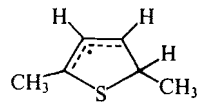

6

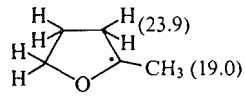

7

It is interesting to comment on the spectral growth observed in Fig. 1, which manifests itself primarily in the appearance of lines attributable to radical **5**. This growth at room temperature is relatively slow (2–3 h), and denies support for a mechanism involving prompt addition of H-atoms directly following γ-initiated H-atom formation elsewhere in the system. Since there is neither indication of a concommittant decrease of any spectral feature as **5** grows in, nor indication of H-atom trapping in adamantane matrices at room temperature, we must conclude that a slow intermolecular transfer of H-atoms is occurring from a species that does not itself exhibit any esr signal.[8] This latter species could be one of the many ionic species necessarily present in any γ-irradiated solid system. Moreover, little or no sign of **5** can be seen in the spectrum obtained in $C_{10}H_{16}$ matrices, see Fig. 4, a matrix effect that is quite striking. This appears to indicate that a competing reaction exists to scavenge H-atoms initially, or one that interferes with the slower intermolecular transfer postulated, or both. This can be accounted for in part by an increased incidence of H-atom abstraction from the matrix by H-atoms produced initially by the γ-induced abstraction process. This predominantly 'hot' process is curtailed in perdeuterated matrices, and leads to appreciable populations of H-atoms migrating freely in $C_{10}D_{16}$. Since no signs of D-atom addition can be discerned, the H-atoms that are postulated to add to 2,5-DMT must originate from other 2,5-DMT solute molecules. It is probable that this process still obtains in $C_{10}H_{16}$ matrices also.

A third species contributes to the observed spectrum in Fig. 1*B*, and produces the spectrum shown in Fig. 4. The yield of this species is considerably enhanced in $C_{10}H_{16}$ and/or depressed in $C_{10}D_{16}$ matrices, in direct contrast to the behaviour of radical **5**, which is enhanced in $C_{10}D_{16}$ matrices. The observed line width of this species, *ca.* 2.5 G, characterizes a radical with a saturated spin center, and thus indicates a radical derived from 2,5-DMT solute by a radical addition process, or a radical derived from $C_{10}H_{16}$ or $C_{10}D_{16}$ by H-atom or D-atom abstraction, respectively. The observed hyperfine structure of 1:2:1 triplets (24.1 G) split into 1:1 doublets (16.3 G) could be assigned, *prima facie*, to the 2-adamantyl radical (one α-proton and two β-protons at the adjacent bridgehead positions). In support of this assignment, it should be noted that secondary radicals derived from bicyclo[2.2.2]octane show a_{α}^{H} = 21.5 G and a_{β}^{H} = 37 G, whereas bridgehead

[7]As pointed out by a referee, it is possible that tertiary radical **7** is formed from MTHF in adamantane (Ad) by a proton transfer mechanism analogous to that already proposed for glassy matrices (13*h*), but involving charge transfer from adamantyl cations. If the reasonable assumption is made that the ionization potential of adamantane is greater than that for the solute MTHF, a scheme can be envisaged involving:

$$Ad \rightsquigarrow Ad^+$$

$$Ad^+ + MTHF \rightarrow MTHF^+ + Ad$$

$$MTHF^+ \rightarrow MTHF^{\cdot} + H^+$$

where $MTHF^{\cdot}$ represents **7**. It would be expected that H^+ could escape from the trapping cage, a process seen for H-atoms in adamantane.

[8]The nature of this slow intermolecular process is not known, but it could involve self-diffusion and/or solute diffusion (translational/rotational) in the solid adamantane matrix at these temperatures (*ca.* 25 °C), and thus effectively 'encounter controlled kinetics'.

Can. J. Chem. Downloaded from www.nrcresearchpress.com by 210.87.254.5 on 09/05/12
For personal use only.

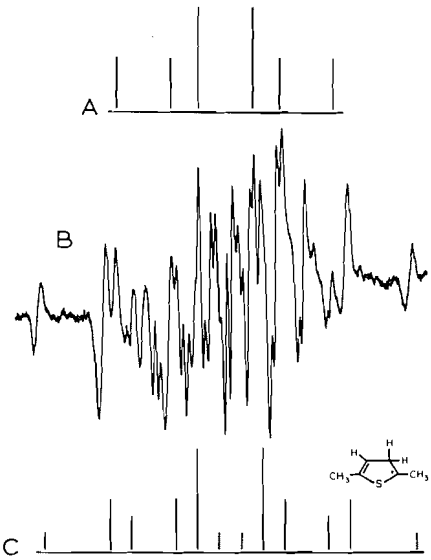

FIG. 6. First derivative esr spectrum taken at room temperature and derived from γ-radiolysis at room temperature of 2,5-dimethylthiophene held in perdeuterated adamantane; (*A*) stick spectrum for 'triplet of doublets' spectrum observed from 2,5-dimethylthiophene in adamantane (see Fig. 4), (*B*) experimentally observed spectrum in $C_{10}D_{16}$ 6 h after γ-radiolysis ended, (*C*) stick spectrum for radical **5**.

radicals in this system, and in norbornane derivatives (23, 24),[9] and the bridgehead radical from adamantane itself (1-adamantyl) reported by Krusic *et al.* (25), exhibit considerably smaller a^H values than those for the 2-radicals of each molecule. Data for authentic 2-adamantyl radicals are presently unavailable. However, this assignment is difficult to reconcile with the following two points. Firstly, 3-dimensional cage type molecules exhibit substantial coupling to the γ-protons,[9] and even to the δ-protons (Krusic *et al.* (25) report $a_\delta^H = 2.67$ G for the bridgehead radical derived from the bicyclo [2.2.2]octane molecule), and values of *ca.* 4–6 G for a_γ^H values. This magnitude of coupling ought to be resolved in our system. Secondly, if this species is assigned to 2-adamantyl, it is difficult to explain why it should be observed from experiments involving $C_{10}D_{16}$; although it *is* observed to be considerably enhanced in $C_{10}H_{16}$. Thus, it is necessary to postulate substantial contamination of $C_{10}D_{16}$ samples by $C_{10}H_{16}$, together with the proviso that preferential energy transfer takes place to the $C_{10}H_{16}$ minority population from the major mole fraction content of $C_{10}D_{16}$. This latter proviso is observed in many systems, and in the absence of specific deuterium assays of the commercially supplied $C_{10}D_{16}$, this second factor cannot be discounted entirely.

A second alternative is that this radical species is derived from the solute by radical addition following a mechanism that is favored in $C_{10}H_{16}$ but suppressed in $C_{10}D_{16}$. There are data that deny the possibility of free migration by species larger than H-atoms in adamantane matrices at room temperature (2). Thus an acceptable alternative is that this spectrum results from addition of H-atoms to 2,5-DMT and a subsequent or consequent rearrangement of the molecule formed. Simple addition to the 3- or 4-position of 2,5-DMT would lead to a spectrum assigned to radical **6**, and simple addition to the 2- or 5-position should lead to an allylic species. Addition at the S-atom and subsequent rearrangements, including ring opening, and bond rearrangements have been considered, but we are unable at this time to assign this triplet of doublets to any radical structure derived from 2,5-DMT. A stick spectrum for radical **5**, and a stick spectrum for this unknown triplet of doublets spectrum, are shown appended to an experimental spectrum taken 6 h after the end of room temperature γ-irradiation of 2,5-DMT in $C_{10}D_{16}$, see Fig. 6.

3-Methylthiophene (3-MT)

First derivative esr spectra obtained from room temperature γ-radiolysis of 3-MT in adamantane matrices are shown in Fig. 7. The data from 3-MT in $C_{10}H_{16}$, shown in Fig. 7*A*, appear to exhibit the basic 'triplet of doublets' seen from 2,5-DMT in $C_{10}H_{16}$, but with a superimposed further doublet splitting. The spectrum obtained from 3-MT in $C_{10}D_{16}$ clearly mimics this basic pattern, but now exhibits a well resolved doublet of doublets pattern. The increased resolution obtained in $C_{10}D_{16}$ already noted for radicals with delocalized spin centers (3), serves to emphasize the asymmetry seen in Fig. 7*B*; this is particularly obvious when the

[9]Bonnazola and Marx (23), and Lemaire and co-workers (24), report substantial coupling to the γ-protons in 3-dimensional cage type molecules, *ca.* 4–6 G in bridgehead radicals (tertiary spin center) and secondary radicals derived from bicyclo[2.2.2]octane and norbornane derivatives, and Krusic *et al.* (25) report $a_\gamma^H = 4.7$ G for 1-adamantyl radicals.

Can. J. Chem. Downloaded from www.nrcresearchpress.com by 210.87.254.5 on 09/05/12
For personal use only.

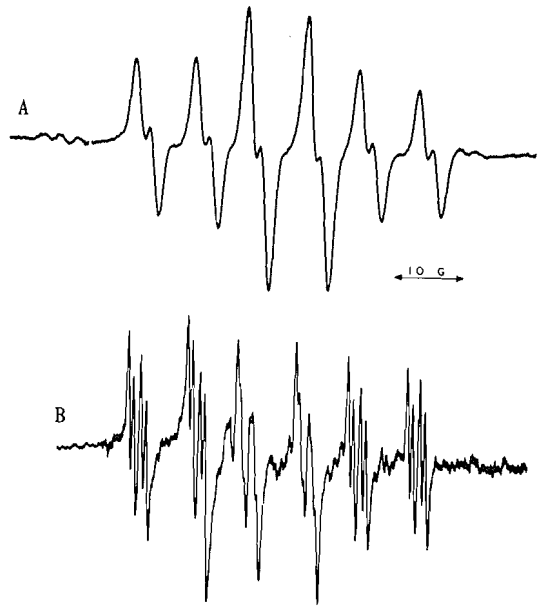

FIG. 7. First derivative esr spectra for the radical derived from 3-methylthiophene by γ-radiolysis at room temperature in adamantane and adamantane-d_{16} matrices; (*A*) in adamantane, (*B*) in adamantane-d_{16}.

center high-field set is compared to the center low field set of lines. The basically $3 \times 2 \times 2 \times 2$ line format with a^H values of 16.25, 8.7, 1.5, and 0.75 G, respectively, together with an observed line width characteristic of delocalized spin centers, precludes any possibility of H-atom or D-atom addition to 3-MT. Thus by analogy with previous data for 2-MT, 2,5-DMT, and equivalent furan derivatives (together with data from toluene in ref. 3), we assume that H-atom abstraction has occurred at the methyl group. An assignment that is consistent with these data is radical **8**; where the asymmetry noted could be due either to a contribution from a second species, or to a slight non-equivalence of the protons of the $=CH_2$ group.[10] We are unable

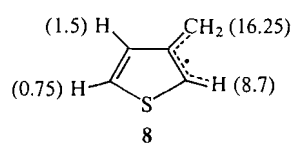

8

to reproduce this asymmetry by computer simulations involving different a^H values for the two protons of the $=CH_2$ group, and we are inclined to believe that a second species is contributing to the observed spectrum. One point can be made concerning this possible second radical, the esr spectrum derived from it has to have a very narrow overall width, *ca.* 16–20 G, since line overlap is seen to affect the inner pair of line groups to only a small extent. Such narrow spectra are characteristic of π-radicals derived from such species as benzene, cyclooctatetraene anions, and C_5H_5 radicals from cyclopentadiene, perhaps suggesting that we are observing e^--attachment to the 3-MT molecule. Further experiments involving spin trapping with 2-methyl-2-nitrosopropane did not yield any additional data.

Furan and Hydrogenated Furan Derivatives

Adamantane samples containing either furan, tetrahydrofuran (THF), 2-methyltetrahydrofuran (2-MTHF), 3-methyltetrahydrofuran (3-MTHF), 2,5-dihydrofuran (DHF), or 4,5-dihydro-2-methylfuran (DHMF), were γ-irradiated at room temperature exposed to air, and monitored via an esr spectrometer at room temperature. Experimental first derivative esr spectra for furan, THF, 2-MTHF, and 3-MTHF, are shown in Fig. 8. All of these spectra are characterized by relatively poor resolution (not improved by use of perdeuterated matrices) and a prominent central line probably attributable to the signal generated by the matrix radical (1-adamantyl radical). It has not proven possible to assign unambiguous structures to the radicals observed, but some specific points deserve comment. Foremost among these is the narrow overall width of the spectrum from THF (*ca.* 35–45 G), together with the relatively simple hyperfine pattern. This small overall width seems to preclude the possibility of H-atom loss from either the 2- or the 3-position, since the resultant alkyl type radical would resemble the cyclopentyl radical (from 3-position loss), or for 2-position loss might be expected to exhibit hyperfine coupling constants similar to those seen by Pratt and coworkers (22) in cyclobutanone and cyclopentanone radical systems (a_α^H values *ca.* 18.5 G, a_β^H values *ca.* 35 G). Equally, neither H-atom addition nor electron capture reactions are viable alternatives for these saturated heterocyclic molecules. Tertiary H-atom abstraction in 2-MTHF and 3-MTHF would be expected

[10]We thank one of the referees for assistance in this assignment.

Can. J. Chem. Downloaded from www.nrcresearchpress.com by 210.87.254.5 on 09/05/12
For personal use only.

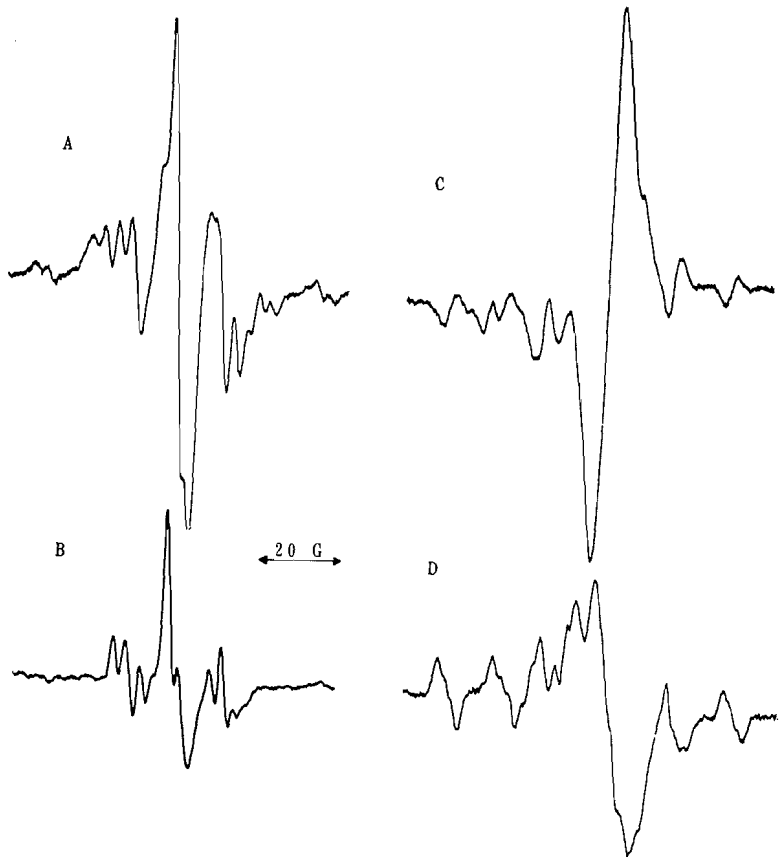

FIG. 8. First derivative esr spectra for the radicals derived from furan derivatives by γ-radiolysis at room temperature in an adamantane matrix: (*A*) furan, (*B*) tetrahydrofuran, (*C*) 2-methyltetrahydrofuran, (*D*) 3-methyltetrahydrofuran.

to produce a basic quartet pattern, and H-atom abstraction from the methyl group would lead to a triplet pattern. This latter reaction mode would be most unusual, and the preferred method of radiation attack is expected to be H-atom abstraction from the heterocyclic ring. If this loss were from the 5-position in 2-MTHF or 3-MTHF, then it is possible that an overall doublet pattern would be observed if the two protons at carbon-4 are nonequivalent (21); this pattern of equal intensity single lines forming a doublet pattern overall (with large superimposed singlet envelope in the center) can be distinguished throughout Fig. 8.

Since previous reports have described both H-atom addition reactions and H-atom loss from furan and due to the disappointing results obtained from adamantane isolation studies reported here, a different approach to this problem was utilized. It seems to be well established that radiolyses of alkenes will lead to allylic radical formation at room temperatures via H-atom loss adjacent to the double bond (2). Thus, radiolysis of 2,5-dihydrofuran (DHF) could lead to a radical identical to that obtained by H-atom addition to the 2-position in furan itself (*i.e.* structure **9** in Scheme 1) the expected position for the fundamentally electrophilic attack by H-atoms if this mechanism obtains. Accordingly, samples of DHF in $C_{10}D_{16}$ were subjected to γ-radiolysis at room temperature, and the experimental spectrum is shown in Fig. 9*B*. The resulting spectrum does not contain sufficient matching points to warrant identification with that from furan itself. The observed spectrum from DHF (Fig. 9*B*) is asymmetrical, and probably consists of contributions from two or more species. Power

Can. J. Chem. Downloaded from www.nrcresearchpress.com by 210.87.254.5 on 09/05/12
For personal use only.

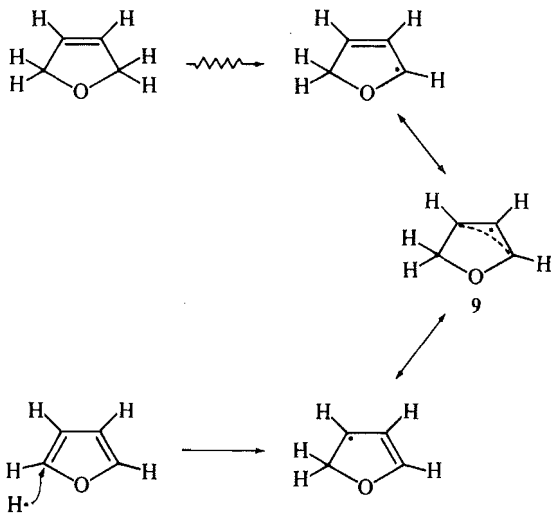

SCHEME 1

saturation experiments have not added any additional information. There appear to be two possible reaction mechanisms in the light of the above data, and by comparison with reports from other investigators; H-atom addition to DHF can only lead to one species, **10**, and allylic H-atom loss can only lead to structure **11**.

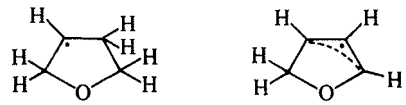

Structure **10** can be discounted as the predominant contributor to the observed spectrum since this radical would exhibit a spectrum that is structurally related to the cyclopentyl or cyclohexyl radical, albeit that one pair of the β-protons might be expected to be different from the other pair. The expected esr spectrum would be >100 G wide, rather than the 60 G width observed, and we have been unable to simulate the observed spectrum using coupling constants considered representative of such alkyl radicals. The allylic radical, structure **11**, should yield a narrower overall esr pattern consistent with the observed spectrum, but we have failed to obtain satisfactory computer simulations based on this structure and matching the spectrum shown in Fig. 9*B*.

Radiolysis of 4,5-dihydro-2-methylfuran (DHMF) in adamantane matrices at room temperatures leads to the esr spectrum shown in

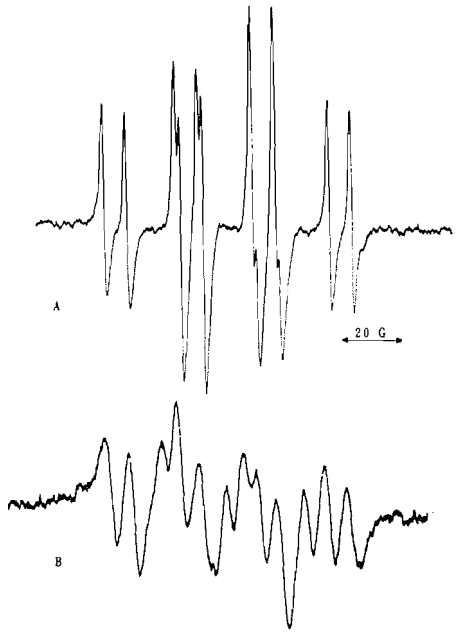

FIG. 9. First derivative esr spectra of radicals derived from: (*A*) 4,5-dihydro-2-methylfuran and (*B*) 2,5-dihydrofuran by γ-radiolysis at room temperature in an adamantane matrix.

Fig. 9*A*. The spectrum from DHMF is very much better resolved compared to that from DHF, and consists of a triplet (a^H = 12.8 G) of doublets (a^H = 12.0 G) split into a further set of doublets (a^H = 3.8 G). This pattern can be reproduced by computer simulation techniques, but does not account satisfactorily for the more probable structures that might result from radiolysis of DHMF. For example, allylic H-atom loss from DHMF leads to either **12** or **13**. For structure **12**, the 12.8 G triplet is assignable to the terminal $=CH_2$ of the allyl system, although previous data indicate that the protons of such a group in furan derivatives are usually inequivalent (*cf.* 2-methylfuran dis-

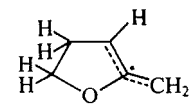

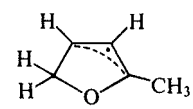

Can. J. Chem. Downloaded from www.nrcresearchpress.com by 210.87.254.5 on 09/05/12
For personal use only.

cussed above). Equally, the 12.8 G triplet could be assigned to the β-protons at the 4-position carbon. Whichever assignment is made, there are now only two remaining coupling constants to be assigned to three apparently inequivalent protons. Structure **13** presents equal difficulties. The 12.0 and 3.8 G doublet couplings are typical of allyl systems, and allowing for a considerable reduction in spin density adjacent to the oxygen of the heterocycle, the 12.8 G triplet could be assigned to the two β-protons at the 5-position. However, there is no discernible quartet pattern expected from the allylic terminal methyl group. Among the remaining possibilities are H-atom loss from the 5-position, to produce radical **14**,

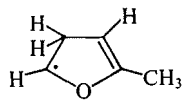

14

and radicals formed by H-atom addition to the double bond in DHMF. Radical **14**[11] would require assignment of one of the doublet a^H values to the lone proton at carbon-3, and thus an a_γ^H value approaching 4 G. This is improbable in these systems. H-atom addition to the 3-position should yield a predominating quartet pattern, which is not observed. H-atom addition to the 2-position would produce radical **15**, which would be expected to have a

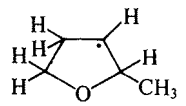

15

$3 \times 2 \times 2$ pattern as observed, but necessitates assigning an a_β^H value of *ca.* 12 G to apparently standard alkyl β-protons, and then retaining the other 12–13 G a^H value for an apparently conventional alkyl α-proton. This leaves the lone tertiary β-proton at carbon-2 with an assigned value of $a_\beta^H = 3.8$ G, a possible value if the electrophilic nature of oxygen and factors associated with the β-dihedral angle combine to reduce a_β^H by a considerable margin. However, the α-proton and 4-position β-proton a^H values if assigned in this manner are sufficiently unusual with respect to other alkyl radicals, that in the absence of supporting data at the present, we discount **15** as a possible contributor to the observed spectrum in Fig. 9*A*. A final possibility, that of ring opening by the furan system following H-atom addition to the oxygen (a well known reaction of furans when initiated by H^+), or ring opening following e^--attachment, has been investigated, but we are unable to assign the observed esr spectrum to any open chain radical species at this time.[12] Spin-trapping experiments with 2-methyl-2-nitrosopropane did not produce any further data to help in this assignment.

Other Experimental Systems

Adamantane samples containing thiophene, 2-chloro, 2-iodo, and 2-cyano derivatives of thiophene, 2-carboxaldehyde derivatives of thiophene and furan, 2-amino derivatives of furan and tetrahydrofuran, dioxane, pyrrole, *N*-methylpyrrole, and 1,2,5-trimethylpyrrole, were prepared and γ-irradiated at room temperature. All data from these compounds, except the latter, were poorly resolved and very disappointing; the spectrum from 1,2,5-trimethylpyrrole was resolved adequately, but is presently unassigned.

Summary

These data presented indicate clearly that H-atom abstraction from subsidiary methyl groups attached to the delocalized heterocyclic ring predominates, and the resulting $-\dot{C}H_2$ group exhibits nonequivalent protons in furan derivatives, but not in thiophene derivatives. Reactions involving H-atom addition to the unsaturated heterocyclic ring occur for selected systems, but they constitute a minor reaction pathway under these conditions, and are suppressed in $C_{10}H_{16}$ matrices; this indicates that some of the initially produced H-atoms are being scavenged by a mechanism probably involving H-atom abstraction from $C_{10}H_{16}$ by the H-atoms produced and which is energetically

[11]This radical **14** has a spin center similar to one already identified (21) from 2-MTHF, which has the structure

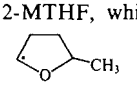

and has assigned values of $a_\alpha^H = 13$–14 G, and $a_\beta^H = 22$–24 G and $a_\beta^H = 30$–33 G. However, the β-protons of **14** are expected to be equivalent, and have an a_β^H value intermediate between these values. No trace of any δ-coupling was observed for the radical derived from 2-MTHF.

[12]Data for possible open chain radicals derived from furan can be found in a report by Simic *et al.* (26).

TABLE 1. Structures of radicals formed by γ-radiolysis of some 5-membered heterocyclic molecules held in adamantane*

Molecule	Abbreviation in text	Radical structures† (a^H values are given in gauss)	Structure number in text
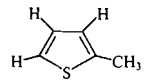	2-MT	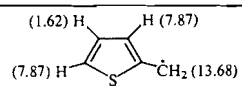	1
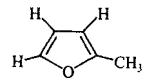	2-MF	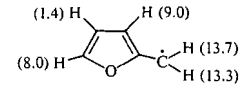	2
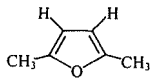	2,5-DMF	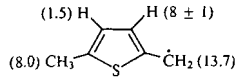	3
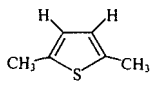	2,5-DMT	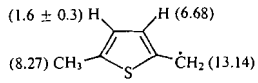	4
		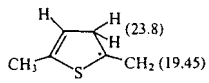	5
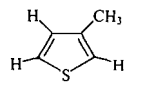	3-MT	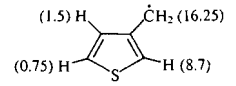	8

*γ-Radiolyses performed at room temperature, samples exposed to air, esr monitoring performed at room temperature.
†All except **5** are delocalized spin centers with allylic or allenylic structures.

unfavourable in $C_{10}D_{16}$ for comparable D-atom abstraction (27). Where H-atom addition is seen, it seems certain that the H-atoms originated from other solute molecules, since no evidence can be found for D-atom addition in $C_{10}D_{16}$ under the conditions of our experiments (room temperature γ-irradiations, samples exposed to atmosphere, room temperature esr monitoring). Systems containing 2,5-DMT as a solute exhibit anomalous growth behaviour with respect to their time development of observed esr spectra. A third species, in addition to the two radicals derived from 2,5-DMT by H-addition and H-abstraction, is presently unidentified. It has been seen in both $C_{10}H_{16}$ and $C_{10}D_{16}$ matrices; and could be identified as the 2-adamantyl radical, but it is not clear why 2,5-DMT should be the only solute system to exhibit this behaviour. A possible mechanism of radical formation has been tentatively identified as involving a relatively slow transfer of H-atoms, this is analogous to the mechanism already proposed by Filby and Gunther for radical production in $C_{10}H_{16}$ (28). An increased resolution of esr spectra from radicals with a delocalized spin center is seen when $C_{10}D_{16}$ matrices are used instead of $C_{10}H_{16}$ (with line widths at FWHM that can be as small as *ca.* 0.4 G in X-band first derivative presentations), but saturated alkyl radicals do not appear to undergo a similar enhancement following this experimental change. It has not proven possible to assign unambiguous structures to many of the radicals observed, or in some cases even, to obtain resolved spectra that will allow any form of rational interpretation. This latter is particularly true for furan derivatives, where the change from a sulphur containing heterocyclic to an oxygen containing heterocyclic molecule introduced severe problems of spectral resolution and/or spectral overlap by several contributing radical species. This probably reflects the lower resonance energy and general instability of furan derivatives relative to thiophene. However, it should be noted that

Can. J. Chem. Downloaded from www.nrcresearchpress.com by 210.87.254.5 on 09/05/12
For personal use only.

preliminary experiments with pyrrole derivatives were equally unrewarding also. A summary of the radicals observed, and structures assigned, is given in Table 1.

Acknowledgments

Material presented herein was taken from work submitted by D. L. Winters to the Graduate School of West Virginia University in partial fulfillment of the requirements of an M.S. degree, January 1974. We wish to thank the Research Corporation, the American Cancer Society, and the Dreyfus Foundation for partial support of this project.

1. R. E. Linder and A. C. Ling. Can. J. Chem. **50**, 3982 (1972).
2. M. E. Manzuk, D. L. Winters, G. J. Hyfantis, and A. C. Ling. Int. J. Radiat. Biol. **26**, 51 (1974).
3. (*a*) P. H. Kasai. Acc. Chem. Res. **4**, 329 (1971); (*b*) P. H. Kasai and D. McLeod. J. Am. Chem. Soc. **95**, 4801 (1973).
4. V. I. Trofimov, I. I. Chkeidze, L. I. Belen'kii, and N. Ya. Buben. Khim. Geterotsikl. Soedin. **3**, 488 (1967).
5. S. Di Gregorio, M. B. Yim, and D. E. Wood. J. Am. Chem. Soc. **95**, 8455 (1973).
6. R. E. Linder, D. L. Winters, and A. C. Ling. Can. J. Chem. **54**, 1405 (1976).
7. A. R. McIntosh, D. R. Gee, and J. K. S. Wan. Spectrosc. Lett. **4**, 217 (1971).
8. R. H. Schuler, G. P. Laroff, and R. W. Fessenden. J. Phys. Chem. **77**, 456 (1973).
9. A. Samuni and P. Neta. J. Phys. Chem. **77**, 1629 (1973).
10. C. Corvaja, M. Brustolon, and G. Giacometti. Z. Physik. Chem. Neue Folge, **66**, 279 (1969); **82**, 272 (1972).
11. (*a*) C. L. Greenstock, I. Dunlop, and P. Neta. J. Phys. Chem. **77**, 1187 (1973); (*b*) C. L. Greenstock and I. Dunlop. J. Phys. Chem. **77**, 1834 (1973).
12. (*a*) B. Eda, R. J. Cook, and D. H. Whiffen. Trans. Faraday Soc. **60**, 1497 (1964); (*b*) R. J. Cook, J. R. Rowlands, and D. H. Whiffen. Mol. Phys. **7**, 57 (1963).
13. (*a*) P. S. Rao, J. R. Nash, J. P. Guarino, M. R. Ronayne, and W. H. Hamill. J. Am. Chem. Soc. **84**, 500 (1962); (*b*) M. R. Ronayne, J. P. Guarino, and W. H. Hamill. J. Am. Chem. Soc. **84**, 4230 (1962); (*c*) G. A. Salmon. Discuss. Faraday Soc. **36**, 284 (1963); (*d*) F. S. Dainton and G. A. Salmon. Proc. Roy. Soc. Ser. A, **285**, 319 (1965); (*e*) M. Shiron and J. E. Willard. J. Phys. Chem. **72**, 1702 (1968); (*f*) K. V. S. R. Rao and A. V. Sapra. Radiat. Eff. **3**, 183 (1970); (*g*) F. P. Sargent. Can. J. Chem. **48**, 3453 (1970); (*h*) D. R. Smith and J. J. Pieroni. Can. J. Chem. **43**, 876 (1965).
14. (*a*) L. Kevan. Trapped electrons in organic glasses. *In* Adv. Radiat. Chem. **4**, 181 (1974); (*b*) K. Fueki, D. F. Feng, and L. Kevan. J. Chem. Phys. **56**, 5351 (1972); (*c*) R. N. Schwartz, M. K. Bowman, and L. Kevan. J. Chem. Phys. **60**, 1690 (1974).
15. E. A. Shaede. Can. J. Chem. **50**, 782 (1972).
16. S. W. Kanick, R. E. Linder, and A. C. Ling. J. Chem. Soc. A, 2971 (1971).
17. A. C. Ling. J. Chem. Educ. **51**, 174 (1974).
18. G. J. Hyfantis and A. C. Ling. Chem. Phys. Lett. **24**, 335 (1974).
19. G. J. Hyfantis and A. C. Ling. Can. J. Chem. **52**, 1206 (1974).
20. W. G. French and J. E. Willard. J. Phys. Chem. **72**, 4604 (1968).
21. A. C. Ling and L. Kevan. J. Phys. Chem. **80**, 592 (1976).
22. D. M. Camaioni, H. F. Walter, J. E. Jordan, and D. W. Pratt. J. Am. Chem. Soc. **95**, 7978 (1973).
23. L. Bonnazola and L. Marx. Mol. Phys. **19**, 405 (1970); **19**, 899 (1970).
24. J. Gloux, M. Guglielmi, and H. Lemaire. Mol. Phys. **17**, 425 (1969).
25. P. J. Krusic, T. A. Rettig, and P. von R. Schleyer. J. Am. Chem. Soc. **94**, 995 (1972).
26. M. Simic, P. Neta, and E. Hayon. J. Phys. Chem. **77**, 2662 (1973).
27. J. E. Willard. Int. J. Radiat. Phys. Chem. **6**, 325 (1974).
28. W. G. Filby and K. Gunther. Z. Natursforsch. **27**, 1289 (1972).

Can. J. Chem. Downloaded from www.nrcresearchpress.com by 210.87.254.5 on 09/05/12
For personal use only.

A study of molecular motion in tetramethylphosphonium halides by proton magnetic resonance

T. T. ANG[1] and B. A. DUNELL

Department of Chemistry, University of British Columbia, Vancouver, B.C., Canada V6T 1W5

Received January 12, 1976

T. T. ANG and B. A. DUNELL. Can. J. Chem. **54**, 1985 (1976).

Spin–lattice relaxation times of tetramethylphosphonium chloride, bromide, and iodide were measured between 100 and 500 K and the two minima in T_1 found for each compound have been assigned to methyl group reorientation and whole cation tumbling. The second moments also indicate that the cations are tumbling isotropically at nmr frequencies in the upper half of this temperature range, and suggest that librational oscillation of the whole cation occurs at frequencies at least of the order of 10^5 s^{-1} near 150 K. The energy barriers for both methyl group reorientation and isotropic tumbling decrease from chloride to bromide but increase when one goes from bromide to iodide. Powder photograph X-ray diffraction analysis indicates that the chloride and bromide have hexagonal crystal structures (*a* and *c* measured), but that the iodide has lower, undetermined symmetry.

T. T. ANG et B. A. DUNELL. Can. J. Chem. **54**, 1985 (1976).

On a mésure, entre 100 et 500 K, les temps de relaxation spin–réseau des chlorures, bromures et iodures de tétraméthylphosphonium et on a attribué les deux minima dans T_1, trouvés pour chacun des composés, à la réorientation du groupe méthyle et à un renversement complet du cation. Les moments seconds indiquent aussi que les cations se renversent d'une façon isotrope aux fréquences rmn dans la partie supérieure de l'intervalle de température et ces résultats suggèrent que l'oscillation librationnelle du cation complet se produit à des fréquences au moins de l'ordre de 10^5 s^{-1} près de 150 K. Les barrières énergétiques, pour la réorientation du groupe méthyle ainsi que celle pour le renversement isotrope, tous les deux, diminuent lorsque l'on passe du chlorure au bromure mais augmentent quand on passe du bromure à l'iodure. Les analyses de diffraction de rayon-X en poudre indiquent que le chlorure et le bromure ont des structures cristallines et hexagonales (on a mesuré *a* et *c*); toutefois l'iodure a une symétrie plus basse et non déterminée.

[Traduit par le journal]

Motional properties of compounds of the type $(CH_3)_4Z$, where Z = C, Si, Ge, Sn, and Pb, have been studied extensively by both broadline nmr and nmr spin–lattice relaxation times (1–5). There has also been considerable interest recently in the motional properties of the tetramethylammonium ion (5–10). In this paper we report a spin–lattice relaxation study of polycrystalline samples of the compounds $(CH_3)_4P^+X^-$, where X = Cl, Br, and I. Infrared and Raman spectroscopy have shown that the tetramethylphosphonium ion in $(CH_3)_4PCl$ has the same tetrahedral configuration as the tetramethylammonium ion (11).

Experimental

The tetramethylphosphonium halides were prepared (11) by mixing $(CH_3)_3P$ (Pfaltz and Bauer, New York) in dry ether with the appropriate methyl halide (Matheson) and refluxing for 2 days under nitrogen. The precipitated product was filtered off, washed with dry ether, dried under vacuum at room temperature for 2 days, and finally sealed off under vacuum in sample tubes. Proton spin–lattice relaxation times were measured at 30 MHz using a π–t–$\pi/2$ pulse sequence from a Bruker BKR-322s pulse spectrometer and a Bruker box-car integrator. Following van Putte (12), a correction was made to the relaxation time to allow for the inhomogeneity of the rf field H_1. The relaxation time T_1 was given by the slope of a least squares fit of log $(M_0 - M_z(t))/2M_0$ *vs.* t, where $M_z(t)$ is the magnetization in the direction of the external field at a time t after the π pulse, and M_0 is the equlibrium magnetization.

Because the variation of relaxation times with temperature led to values of activation energies of molecular motions which did not change monotonically in the sequence chloride, bromide, iodide, a fresh set of samples was prepared and the experiments repeated on the new samples. Particular care was taken to be sure the samples were thoroughly dry by heating them under vacuum at 110 °C for at least 2 days. Since the correction for inhomogeneity of H_1 was very small in the first set of results, it was not applied in the second set. Microanalyses for C and H were run on the new samples of the bromide and

[1]Visiting Scientist. Permanent address: School of Chemical Sciences, Universiti Sains Malaysia, Penang, Malaysia.

Can. J. Chem. Downloaded from www.nrcresearchpress.com by 210.87.254.6 on 09/05/12
For personal use only.

Can. J. Chem. Downloaded from www.nrcresearchpress.com by 210.87.254.6 on 09/05/12
For personal use only.

iodide and showed good agreement with theoretical values. *Anal.* Calcd. for $(CH_3)_4PBr$: C 28.07, H 7.07; found: C 28.07, H 7.20. *Anal.* Calcd. for $(CH_3)_4PI$: C 22.02, H 5.55; found: C 22.07, H 5.43. The chloride was so hygroscopic that it was impossible to obtain a microanalysis without elaborate techniques. Instead, a high resolution nmr spectrum of the sample in D_2O was run on a Varian T-60 spectrometer. The spectrum showed no indication of any organic impurity and we believe that drying the sample for 4 days at 110–120 °C under a vacuum of about 0.01 mm of Hg removed all water. The results for the two iodide samples were sufficiently alike to be described by a single curve, as were the results for the two bromide samples. The curves for the two chloride samples could not be combined into a single curve, but the new activation energies obtained from the second sample differed from the first by only 12% and 6% and produced no new sequence in the series chloride, bromide, iodide.

The relaxation function $(M_0 - M_z(t))/2M_0$ decreased exponentially with time over the whole temperature range for all three compounds. This statement should perhaps be qualified by noting that non-exponential behaviour was observed in the first prepared sample of chloride below about 210 K.

Continuous wave spectra were obtained at 8 MHz for the bromide and the iodide and second moments calculated from the spectra. Our chloride sample was so small that we were unable to obtain a satisfactory CW spectrum for it at most temperatures, and second moments were obtained above 250 K by fitting the solid echo following a $90\text{-}\tau\text{-}90_{90}$ pulse sequence to the expression (13, 14)

$$f(t) = 1 - (M_2/2!)t^2 + (M_4/4!)t^4 - \cdots$$

where $f(t)$ is the height of the solid echo, normalized to $f(0) = 1$ at the maximum point of the echo, and M_n is is the nth moment of the line shape.

Debye–Scherrer X-ray powder photographs were taken of each of the salts, using the second set of samples. A Philips X-ray set was used and the radiation was CuKα (λ taken to be 1.425 Å). The d_{hkl} spacings were calculated and attempts were made, using Hull and Davey charts (15), to index the arcs to cubic, tetragonal, or hexagonal symmetries.

Results and Interpretation

X-Ray Powder Photographs

Since the lattices of the tetramethylammonium halides are tetragonal at room temperature (6, 16–19) and tetramethylarsonium bromide is hexagonal (20), it was expected that the tetramethylphosphonium halides might be tetragonal or hexagonal. The arcs of the Debye–Scherrer photographs of the tetramethylphosphonium chloride and bromide could be indexed in the hexagonal system and the cell parameters were found to be $a = 6.90 \pm 0.01$ Å, $c = 9.72 \pm 0.05$ Å for the chloride and $a = 7.03 \pm 0.01$ Å, $c = 9.98 \pm 0.05$ Å for the bromide. For 16 arcs indexed on the chloride photograph, the average deviation $|(d_{hkl})_{calc} - (d_{hkl})_{obs}|$ was 0.0045 Å and for 14 arcs indexed on the bromide photograph, the average deviation was 0.012 Å. The powder photograph of the iodide could not be indexed to either a tetragonal or a hexagonal lattice. A single crystal study of tetramethylarsonium bromide (20) has shown its space group to be $P6_3mc$. No systematic absence demanded by that space group appears in the indexed lines of the tetramethylphosphonium chloride or bromide, so there is a good possibility that these two phosphonium salts are isostructural with $(CH_3)_4AsBr$. The tetramethylphosphonium iodide crystal must have lower symmetry.

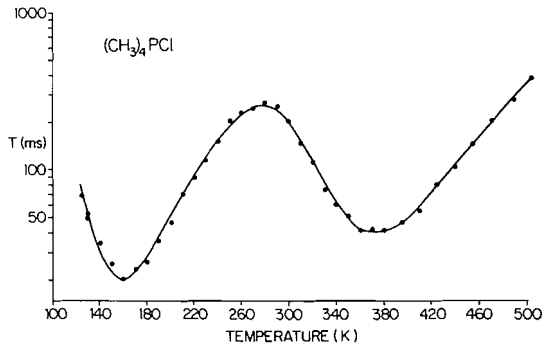

FIG. 1. The variation of T_1 with temperature for tetramethylphosphonium chloride. The line through the points is calculated from [1] and [4] and the best fit parameters.

Spin–Lattice Relaxation Times

The variation with temperature of the spin–lattice relaxation times of tetramethylphosphonium chloride, bromide, and iodide is shown in Figs. 1, 2, and 3. In the case of the bromide and iodide the points for both the independently prepared samples are shown and are distinguished by open circles for the first prepared samples and filled circles for the second preparations. In the case of the chloride only the points for the second sample are shown. In all cases, the lower temperature minimum in T_1 has a depth of about 20 ms and can be identified with relaxation by reorientation of all four methyl groups about their C_3 axes. The higher temperature minimum in T_1 has a depth of about 40 ms in each case, which, as discussed below, agrees quite well with the theoretical value for isotropic reorientation of the whole

Can. J. Chem. Downloaded from www.nrcresearchpress.com by 210.87.254.6 on 09/05/12
For personal use only.

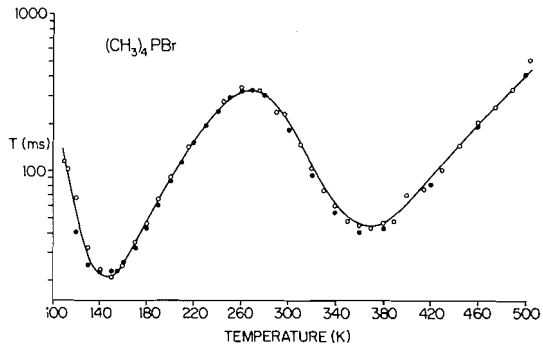

FIG. 2. The variation of T_1 with temperature for tetramethylphosphonium bromide. The open circles are for the first sample that was prepared and the filled circles are for the new sample. The solid line is calculated from [1] and [4] and the best fit parameters.

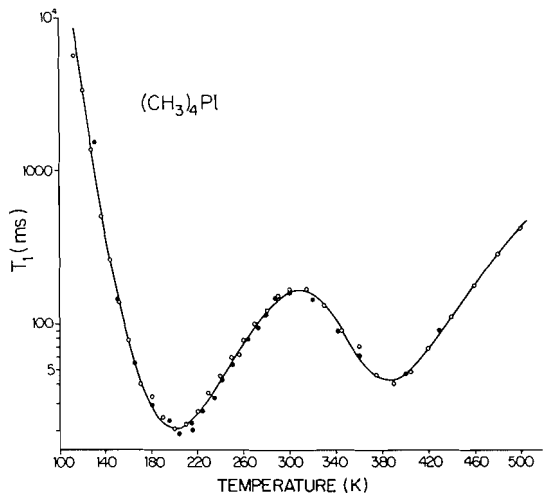

FIG. 3. The variation of T_1 with temperature for tetramethylphosphonium iodide. The open circles are for the first sample that was prepared and the filled circles are for the new sample. The solid line is calculated from [1] and [4] and the best fit parameters.

cation superimposed on methyl group reorientation.

If we assume that the lattice motions which give proton spin-lattice relaxation in these compounds are the same as those which relax the tetramethylammonium halides (9), namely, reorientation of the methyl groups about their C_3 axes with a correlation time τ_c, and isotropic tumbling of the cation with a correlation time τ_{c1}, we can use the relation of Albert, Gutowsky, and Ripmeester (9) for the relaxation rate

$$[1] \qquad T_1^{-1} = Ag(\omega_0\tau_{c2}) + Bg(\omega_0\tau_{c1})$$

where

$$\tau_{c2}^{-1} = \tau_c^{-1} + \tau_{c1}^{-1}$$

$$g(\omega_0\tau) = \frac{\omega_0\tau}{1 + \omega_0^2\tau^2} + \frac{4\omega_0\tau}{1 + 4\omega_0^2\tau^2}$$

$$[2] \qquad A = (9/20)(\gamma^4\hbar^2/\omega_0 r^6)$$

and

$$[3] \qquad B = (3/20)(\gamma^4\hbar^2/\omega_0 r^6) + (27/10)(\gamma^4\hbar^2/\omega_0 r_\star^6)$$

In [3], r is the interproton distance in a methyl group and $r_\star$ is the distance between centres of the equilateral triangles formed by each methyl group. The second term of [3] estimates the contribution to the relaxation rate made by interactions between protons in different methyl groups when $\tau_c \ll \tau_{c1}$.

With the assumption that the correlation times have an Arrhenius dependence on temperature

$$[4] \qquad \tau = \tau^0 \exp(E/RT)$$

the experimental curves of Figs. 1–3 were fitted to [1] by a non-linear least-squares computer program (21). The best fit parameters A and B, $\omega_0\tau_c$ and E for C_3 motion of the methyl groups, and $\omega_0\tau_{c1}$ and E_1 for isotropic tumbling of the cations are listed in Table 1, and the best fit curves are the solid lines in Figs. 1–3. The uncertainties shown in the experimental parameters represent the asymptotic standard deviations for the parameters given by the iterative fitting procedure. Theoretical values of A and B, as well as theoretical values of the depths of the minima in T_1 are also shown in Table 1. They have been calculated on the assumption that the bond angles are tetrahedral and the bond distances C—H = 1.10 Å and C—P = 1.84 Å, so that r = 1.80 Å and $r_\star$ = 3.60 Å. Since the agreement between experimental and theoretical values is quite good, the assignment of relaxation mechanisms to the two minima is consistent with the observations. This conclusion is supported for the higher temperature mechanism by consideration of the second moments of the CW spectra. These second moments are 0.7 ± 0.1 G^2 above 260 K for the chloride and bromide and above 300 K for the iodide. The theoretical second moment for the hexagonal structure of $(CH_3)_4PBr$, with presumed space group $P6_3mc$,

Can. J. Chem. Downloaded from www.nrcresearchpress.com by 210.87.254.6 on 09/05/12
For personal use only.

TABLE 1. Spin–lattice relaxation parameters for tetramethylphosphonium chloride, bromide, and iodide*

Motion	Activation energy (kcal/mol)	τ_0 (s^{-1})	$(T_1)_{min}$ (ms)		A or B (s^{-1})	
			Expt.	Theory	Expt.	Theory
$(CH_3)_4PCl$						
C_3 rotation of CH_3	2.58±0.05	$(8.9\pm1.4)\times10^{-13}$	20.3±0.7	17.4	34.6±1.2	40.4
Isotropic rotation of cation	8.9±0.2	$(2.1\pm0.5)\times10^{-14}$	40.9±1.4	40.8	17.2±0.6	17.2
$(CH_3)_4PBr$						
C_3 rotation of CH_3	2.39±0.06	$(8.5\pm1.6)\times10^{-13}$	20.5±0.9	17.4	34.2±1.6	40.4
Isotropic rotation of cation	8.5±0.3	$(3.1\pm1.1)\times10^{-14}$	46.4±2.3	40.8	15.1±0.8	17.2
$(CH_3)_4PI$						
C_3 rotation of CH_3	3.52±0.04	$(4.7\pm0.5)\times10^{-13}$	20.1±0.6	17.4	34.9±1.1	40.4
Isotropic rotation of cation	10.8±0.4	$(2.6\pm1.2)\times10^{-15}$	44.8±2.1	40.8	15.7±0.8	17.2

*The uncertainties are the standard deviations of the best fit parameters.

Can. J. Chem. Downloaded from www.nrcresearchpress.com by 210.87.254.6 on 09/05/12
For personal use only.

two molecules per unit cell, and isotropic tumbling of the cations, is 0.66 G^2 according to Smith's calculation in which all the protons of a given molecule are located at the centre of the isotropic motion (3). With decreasing temperature, the second moments of these halides increase to about 6 $\pm$ 1 G^2 in the range 120–190 K and increase again as the temperature goes to 77 K, where the second moment is about 10 G^2. With C_3 motion of the methyl groups the theoretical second moment of these compounds would be 6.8 G^2 plus the interion contribution of at least 1 G^2. It appears, therefore, that the step in the second moment of some 6 G^2 in the general region of 150 K corresponds to reorientation of all the methyl groups at a rate much in excess of that required to influence the second moment, plus additional motion with a correlation frequency greater than about 6×10^4 s^{-1} (*i.e.*, $\gamma\sqrt{M_2}$, where M_2 is the second moment of 6 G^2). The additional motion is probably librational oscillation of relatively small amplitude of the $(CH_3)_4P^+$ ion about one or more symmetry axes.

Neither the activation energy of methyl group reorientation nor that of cation tumbling changes monotonically in the sequence chloride, bromide, iodide. Our value of 3.52 kcal/mol for the activation energy of methyl group reorientation in the iodide agrees well with the value 3.20 $\pm$ 0.5 found by Rager and Weiss (22). If we consider separately the best fit parameters for the experimental points for the two samples we prepared, the two values for the methyl rotation barrier are 3.42 $\pm$ 0.03 for the first sample and 3.71 $\pm$ 0.07 for the second. Again the uncertainties are standard deviations. For the two samples together it would probably be appropriate to indicate the energy barrier height as 3.5 $\pm$ 0.2 kcal/mol, and our value is the same as that of Rager and Weiss within the probable errors. Our observed decrease in activation energy for both methyl reorientation and isotropic tumbling as one goes from chloride to bromide conforms with the behaviour observed for the tetramethylammonium halides (6, 9) and rationalized theoretically for cation tumbling in terms of the energy barriers calculated from simple electrostatic interactions within the ionic lattice (9, 23). The increase we observe in the two barriers in going from bromide to iodide is probably accounted for by the change in crystal structure which occurs between iodide and the other two halides. One should note, however, that in the case of the simple phosphonium halides, PH_4X, there is a small increase in the barrier to cation tumbling as one goes from the bromide to the iodide, even though they both have a tetragonal unit cell (24). This might be related to increasing importance of Lennard–Jones potential terms in the interionic interactions in the phosphonium iodide (25). Further elucidation and rationalization of the nature of the barriers in the tetramethylphosphonium halides would be aided by a single crystal X-ray diffraction analysis of the compounds.

Acknowledgments

The authors wish to express their gratitude to the National Research Council of Canada for a grant-in-aid to support this research.

1. J. G. Powles and H. S. Gutowsky. J. Chem. Phys. **21**, 1695 (1953).
2. E. O. Stejskal, D. E. Woessner, T. C. Farrar, and H. S. Gutowsky. J. Chem. Phys. **31**, 55 (1959).
3. G. W. Smith. J. Chem. Phys. **42**, 4229 (1965).
4. S. Albert and J. A. Ripmeester. J. Chem. Phys. **57**, 2642 (1972).
5. S. B. W. Roeder and D. C. Douglass. J. Chem. Phys. **52**, 5525 (1970).
6. J. Dufourcq and B. Lemanceau. J. Chim. Phys. **67**, 9 (1970).
7. D. J. Blears, S. S. Danyluk, and E. Bock. J. Phys. Chem. **72**, 2269 (1968).
8. A. A. V. Gibson and R. E. Raab. J. Chem. Phys. **57**, 4688 (1972).
9. S. Albert, H. S. Gutowsky, and J. A. Ripmeester. J. Chem. Phys. **56**, 3672 (1972).
10. E. R. Andrew and P. C. Canepa. J. Magn. Reson. **7**, 429 (1972).
11. R. Baumgärtner, W. Sawodny, and J. Goubeau. Z. Anorg. Allgem. Chem. **333**, 171 (1964).
12. K. Van Putte. J. Magn. Reson. **2**, 174 (1970).
13. A. Abragam. The principles of nuclear magnetism. Clarendon Press, Oxford, 1961. p. 119.
14. J. G. Powles and J. H. Strange. Proc. Phys. Soc. **82**, 6 (1963).
15. C. W. Bunn. Chemical crystallography. Clarendon Press, Oxford, 1954. p. 132.
16. M. Stammler. J. Inorg. Nucl. Chem. **29**, 2203 (1967).
17. G. L. Bottger and A. L. Geddes. Spectrochim. Acta, **21**, 1701 (1965).
18. R. G. Wyckoff. Z. Krist. **67**, 61 (1928).
19. L. Vegard and K. Sollesnes. Phil. Mag. **24**, 985 (1927).

20. E. COLLINS, D. J. SUTOR, and F. G. MANN. J. Chem. Soc. 4051 (1963).
21. BMD X85, originally written by P. Sampson, Health Sciences Computing Facility, University of California at Los Angeles.
22. H. RAGER and A. WEISS. Z. Phys. Chem. (Frankfurt), **93**, 299 (1974).
23. H. S. GUTOWSKY, G. E. PAKE, and R. BERSOHN. J. Chem. Phys. **22**, 643 (1954).
24. T. TSANG, T. C. FARRAR, and J. J. RUSH. J. Chem. Phys. **49**, 4403 (1968).
25. A. SEQUEIRA and W. C. HAMILTON. J. Chem. Phys. **47**, 1818 (1967).

Can. J. Chem. Downloaded from www.nrcresearchpress.com by 210.87.254.6 on 09/05/12
For personal use only.

A total synthesis of (±)-cedrol and (±)-cedrene via an intramolecular Diels–Alder reaction

EDWARD G. BREITHOLLE AND ALEX G. FALLIS

Department of Chemistry, Memorial University of Newfoundland, St. John's, Nfld., Canada A1C 5S7

Received March 8, 1976

EDWARD G. BREITHOLLE and ALEX G. FALLIS. Can. J. Chem. **54**, 1991 (1976).

A total synthesis of racemic cedrol and cedrene is described in which a key step is the intramolecular Diels–Alder reaction of alkyl cyclopentadiene **3** to give the tricyclic olefin **4**. Oxidation of this material followed by ring expansion gives cedrone (**6**) which is converted to the sesquiterpenes. Modification of the functionality of the starting materials will permit the application of this general route to diverse tricyclic systems.

EDWARD G. BREITHOLLE et ALEX G. FALLIS. Can. J. Chem. **54**, 1991 (1976)

On décrit une synthèse totale du cédrol et du cédrène racémique; l'étape clé de cette séquence est la réaction de Diels–Alder intramoléculaire de l'alkylcyclopentadiène **3** conduisant à l'oléfine tricyclique **4**. L'oxydation de ce composé, suivi d'une extension de cycle, conduit à la cédrone (**6**) qui est ensuite transformée en sesquiterpènes. En modifiant les fonctions présentes dans les produits de départ, il sera possible d'appliquer cette méthode générale à la préparation de systèmes tricycliques divers.

[Traduit par le journal]

Interest in the tricyclic cedrenoid sesquiterpenes is widespread and a number of diverse syntheses of these natural products continue to be reported (see ref. 1*a* for first total synthesis and ref. 1*b* for biogenic-type syntheses). In view of both the steric and electronic requirements of the Diels–Alder reaction intramolecular applications of this useful cyclization to different natural product systems are increasing (2). When the diene component is cyclic the opportunity to prepare stereoselectively a variety of tricyclic sesquiterpenes is apparent and we report herein a total synthesis of (±)-cedrol (**1**) and (±)-cedrene (**2**) via an intramolecular Diels–Alder reaction of an alkyl cyclopentadiene. The stereoselective route is direct and should be suitable for construction of related compounds.

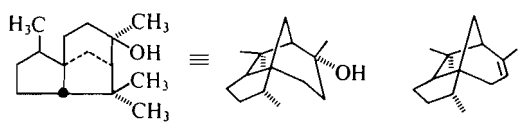

1 **2**

The approach is based on the generation of a suitable tricyclo[5.2.1.$0^{1,5}$]dec-8-ene intermediate (*i.e.*, **4**) by internal cycloaddition of the alkyl cyclopentadiene **3**. It was anticipated, due to the stereochemical constraints of the system, that the cyclopentane side chain would have the correct *exo* orientation (*cf.* ref. 3) and that hydroboration would give the desired ketone **5** for ring expansion to cedrone (**6**).

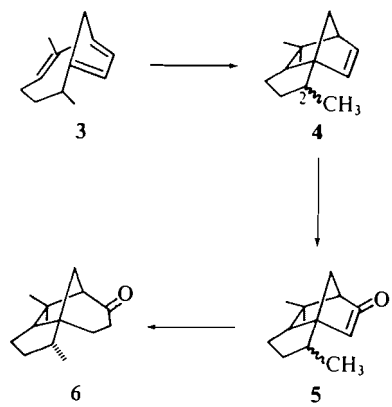

3 **4** **6** **5**

Alkylation of sodium cyclopentadiene with tosylate **7**[1] (from 6-methyl-5-hepten-2-ol (4)) in

[1]Elemental analysis, proton magnetic resonance, and infrared spectra were in accord with the assigned structure.

Can. J. Chem. Downloaded from www.nrcresearchpress.com by 210.87.254.40 on 09/05/12
For personal use only.

Can. J. Chem. Downloaded from www.nrcresearchpress.com by 210.87.254.40 on 09/05/12
For personal use only.

THF (0 °C 0.5 h, 23 °C 4 h) afforded, after work up, the isomer **3***b*. The pmr spectrum, which displayed a multiplet at δ 2.80 due to the two allylic cyclopentyl hydrogens and a complex signal from δ 5.8–6.5 representing the three vinyl ring hydrogens, was consistent with this structure.

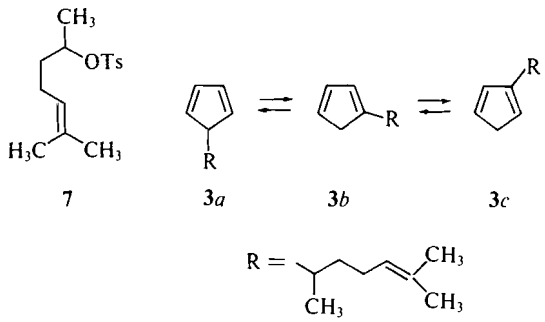

7 **3***a* **3***b* **3***c*

Cyclization of **3** was effected by heating in hexamethylphosphoramide at 205 ± 5 °C for 7 hours to give the tricyclic olefin **4** (36%).[1] The isomeric internal Diels–Alder structures (see *i* and *ii*)[2] are excluded by the pmr spectrum. The olefinic signals appeared as an unsymmetrical multiplet δ 6.01 representing the AB portion of an ABX system while the single allylic bridgehead proton (X) gave rise to a broad resonance at δ 2.27 ($W_{1/2}$ = 6 Hz). The methyl signals appeared as singlets at δ 0.80 and δ 1.05 due to the *endo* and *exo* geminal group and as a doublet at δ 0.91 (J = 6.5 Hz) representing the secondary methyl function. From models it appeared that the preferred orientation of this group during cyclization might be that found in the natural product but unfortunately, although **4** was homogeneous by both glc and tlc, the proton noise decoupled cmr spectrum[3] indicated it was an epimeric mixture at C_2 (~1:1). This spectrum confirmed the single mode of attachment of the cyclopentane side chain and the success of the synthesis indicated this was *exo*.

Hydroboration of **4** in dimethoxyethane gave, after oxidative workup with Jones' reagent, the desired ketone **5** (ir 1735 cm^{-1}). Since **5** was inert to diazomethane (even with Lewis acid catalysis) and conventional cyanohydrin formation failed, the trimethylsilyl cyanohydrin derivative was prepared (Me_3SiCN, ZnI_2, 5 h 23 °C) (5). The primary amine obtained upon lithium aluminum hydride reduction was treated with nitrous acid (9 h, 5–25 °C) to give the ring expanded ketones in 73% overall yield from **5**. The resulting epimeric cedrone mixture **6** was converted, after tlc separation of ~20% of the positional ketone isomer, to a 1:1 mixture of (±)-cedrol (**1**) and (±)-*epi*-cedrol by stereoselective addition of methyl lithium (1). The alcohols were separated by glc and the spectral (pmr, ir, ms) and chromatographic properties (glc, tlc) of the synthetic cedrol were indistinguishable from an authentic sample of the natural material. Dehydration (pyridine, $SOCl_2$, 5 °C) afforded (±)-α-cedrene (**2**) and (±)-β-cedrene in quantitative yield (ratio 80:20) to complete the synthesis.[4]

Several related more highly oxygenated sesquiterpenes possessing the tricyclo[5.3.1.$0^{1,5}$]-undecane skeleton, such as shellolic acid (7) and other vetiver oil and lac resin components (8), are known. Extension of this route using modified side chains should provide access to these compounds as well as the related tricyclo-[6.2.1.$0^{1,6}$]undecane ring system possessed by isolongifolene.

Acknowledgment

We are grateful to Memorial University of Newfoundland for financial support of this research.

1. (*a*) G. Stork and F. H. Clark, Jr. J. Am. Chem. Soc. **77**, 1073 (1955); **83**, 3114 (1961); (*b*) E. J. Corey, N. N. Girotra, and C. T. Mathew. J. Am. Chem. Soc. **91**, 1557 (1967); T. G. Crandall and R. G. Lawton. J. Am. Chem. Soc. **91**, 2127 (1969); E.

[2]Although *3a*, if present (it was not detected), would cyclize to the wrong product *i*, **3***c*, (also not detected) was not expected to give monomeric tricyclic material since the product *ii* violates Bredt's rule. Other 'twistane' type products are precluded due to the inefficient overlap of the reacting centres allowed by the geometry of the system.

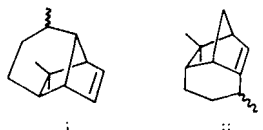

i ii

[3]We are grateful to A. W. McCulloch and J. A. Walter, National Research Council of Canada, Halifax, N.S. for obtaining this spectrum.

[4]Similar dehydration of natural cedrol gave α- and β-cedrene in a ratio of 83:17 compared to the literature value of 5:3 (6).

DEMOLE, P. ENGGIST, and C. BORER. Helv. Chim. Acta, **54**, 1845 (1971); N. H. ANDERSON and D. D. SYRDAL. Tetrahedron Lett. 2455 (1972); E. J. COREY and R. D. BALANSON. Tetrahedron Lett. 3135 (1973); P. T. LANSBURY, V. R. HADDON, and R. C. STEWART. J. Am. Chem. Soc. **96**, 896 (1974).
2. R. G. CARLSON. Ann. Reports Med. Chem. **9**, 270 (1974).
3. E. J. COREY and R. S. GLASS. J. Am. Chem. Soc. **89**, 2600 (1967); A. KRANTZ and C. Y. LIN. J. Am. Chem. Soc. **95**, 5662 (1973).
4. O. WALLACH. Ann. Chem. **275**, 171 (1893); J. MORI. Tetrahedron, **31**, 3011 (1975).
5. D. A. EVANS, G. L. CARROLL, and L. K. TRUESDALE. J. Org. Chem. **39**, 914 (1974).
6. E. V. RUDLOFF. Can. J. Chem. **39**, 1860 (1961).
7. P. YATES and G. F. FIELD. J. Am. Chem. Soc. **82**, 5764 (1960).
8. R. KAISER and P. NAEGELI. Tetrahedron Lett. 2009 (1972); A. N. SINGH, A. B. UPADHYE, V. V. MHASKER, S. DEV, A. V. POL, and V. G. NAIK. Tetrahedron, **30**, 3689 (1974).

Can. J. Chem. Downloaded from www.nrcresearchpress.com by 210.87.254.40 on 09/05/12
For personal use only.

Canadian Journal of Chemistry

Published by
THE NATIONAL RESEARCH COUNCIL OF CANADA

Journal canadien de chimie

Publié par
LE CONSEIL NATIONAL DE RECHERCHES DU CANADA

Volume 54 Number 13 July 1, 1976

Volume 54 numéro 13 1 juillet 1976

Can. J. Chem. Downloaded from www.nrcresearchpress.com by 210.87.254.5 on 09/05/12
For personal use only.

On the entropy production in chemically reacting systems

EDUARDO LISSI
Departamento de Química, Universidad Técnica del Estado, Santiago, Chile

Received January 6, 1976

EDUARDO LISSI. Can. J. Chem. **54**, 1995 (1976).

The concept of monotonicity of entropy production is discussed regarding its application to chemically reacting systems. It is concluded that the concept cannot be generally applied even to elementary reactions in ideal homogeneous systems.

EDUARDO LISSI. Can. J. Chem. **54**, 1995 (1976).

On discute du concept de la monotonicité de la production d'entropie par rapport à son application à des systèmes chimiques en réaction. On en conclut que ce concept ne peut pas être appliqué d'une façon générale même pour des réactions élémentaires dans des systèmes homogènes idéaux.

[Traduit par le journal]

In 1966, McKean introduced the idea of monotonicity of entropy production (1). This monotonicity implies that the derivatives of the total entropy production have the following property

$$[1] \qquad (-1)^n \mathrm{d}^n S/\mathrm{d}t^n \leq 0$$

In a most interesting paper on the entropy production in chemically reacting systems, Pritchard, Labib, and McElwain have extended this concept to chemically reacting systems (2). In a second paper on the entropy production in simple chemical reactions taking place isothermally and in closed systems, Pritchard concluded that entropy production appears to be a completely monotonic function of time for several chemical reactions or reaction sequences, including elementary processes and consecutive reactions (3). On the other hand, it was shown that the monotonicity principle does not extend to autocatalytic or oscillatory processes (3). In the present paper, we show that this concept cannot be generally applied to a series of simple reactions: (*a*) exothermic reactions which take place under adiabatic conditions; (*b*) successive reactions for which the entropy production in the second step is larger than in the initial step; and (*c*) reactions whose rate law is zero-order with respect to one or more reactants.

Exothermic Reactions Carried out under Adiabatic Conditions at Constant Volume

Let us consider with some detail the first mentioned example. This is a particularly relevant one since it involves a simple chemical reaction:

$$[2] \qquad \mathrm{B} \rightleftharpoons \mathrm{C}$$

where B and C can be considered ideal gases. Under adiabatic conditions, and if the reaction is slow enough to assure thermal equilibrium, the first derivative of the entropy is given by

$$[3] \qquad \mathrm{d}S/\mathrm{d}t = (A/T)v$$

where A is the affinity of the reaction considered, and v is the reaction rate (4). For the system considered

Can. J. Chem. Downloaded from www.nrcresearchpress.com by 210.87.254.5 on 09/05/12
For personal use only.

[4] $A = T(\bar{S}_C^0 - \bar{S}_B^0) - RT \ln (N_C/N_B) - \Delta H$

and

[5] $v = fkN_B$

where k is the specific rate constant for the forward reaction, and f is defined by

[6] $f = 1 - N_C/(KN_B)$

In eq. 6, K is the equilibrium constant.

Considering eqs. 3 and 5 we obtain

[7] $dS/dt = (AfN_B)\, k/T$

Since chemical reactions which are far from the equilibrium cannot be treated generally by the methods of the thermodynamics of irreversible processes (4), this equation has to be analyzed rather empirically (3). In eq. 7, A, f, N_B, T, and k will be determined by the initial conditions and the conversion. The factor (AfN_B/T) will usually decrease when the time increases but, if the reaction is exothermic, the value of k will increase rapidly due to the increase in temperature. For reactions which have a high activation energy, this factor dominates and the value of dS/dt increases with time. This result is then contrary to that required by eq. 1. Let us demonstrate this with the aid of a simplified example which employs reasonable kinetic and thermodynamic parameters. If

$(N_B)_{t=0} = 1$

$(N_C)_{t=0} = 0$

$(C_V)_B = (C_V)_C = 20$ cal deg^{-1} mol^{-1} at 400 K

$(\bar{S}_B^0 = \bar{S}_C^0)$

$\Delta H = -10$ kcal mol^{-1} at 400 K

$k = 10^{14} \exp(-23000/T)$

$(T)_{t=0} = 400$ K

the values of dS/dt can be obtained as a function of N_B if we know the change in the specific heat of the mixture with temperature. If we assume that

[8] $C_V = aT$

which overestimates the increase in C_V with temperature (5), we obtain the values shown in Table 1. From this table we can see that the rate of entropy change increases by more than a factor of 10^7, due to the increase in reaction rate.

TABLE 1. Evaluation of dS/dt as a function of the conversion

N_C (mole)	Temperature (K)	k (s^{-1})	dS/dt (cal K^{-1} s^{-1})
10^{-6}	400	10^{-11}	5.3×10^{-10}
10^{-5}	400	10^{-11}	4.8×10^{-10}
10^{-4}	400	10^{-11}	4.3×10^{-10}
10^{-3}	400.5	10^{-11}	3.9×10^{-10}
10^{-2}	405	2×10^{-11}	6.7×10^{-10}
5×10^{-2}	423	2×10^{-10}	7×10^{-9}
10^{-1}	445	3×10^{-9}	8×10^{-8}
2×10^{-1}	490	4×10^{-7}	7×10^{-6}
5×10^{-1}	600	2×10^{-3}	2×10^{-2}

This conclusion is quite general and almost independent of the parameters assumed for the reaction considered, provided that the reaction is exothermic, the heat capacity of the system is small, and the reaction has a high activation energy (*i.e.* for the thermal isomerization of cyclopropane to propylene (6)). A similar increase in dS/dt with time was obtained by Pritchard in an analysis of the methyl isocyanate isomerization under similar conditions to those considered in the present work (7).

Consecutive Reactions at Constant T and V

Let us consider the simplest set of consecutive reactions:

[9] $A \xrightarrow{v_1} B \xrightarrow{v_2} C$

which is a simplification of scheme 11 of Pritchard's work (3). For this system

[10] $dS/dt = A_1 v_1 + A_2 v_2$

If the reactions considered are highly exothermic and the concentrations are not extremely low, eq. 10 reduces to

[11] $dS/dt = -(k_1 N_A \Delta H_1 + k_2 N_B \Delta H_2)/T$

If

$$|\Delta H_2| \gg |\Delta H_1|$$

dS/dt will increase when N_B increases. This conclusion is contrary to that reached by Pritchard for simple consecutive first order reactions (3).

Zero Order Reactions

Let us consider the following reaction

[12] $A + 2C \rightarrow 2D$

which takes place with a rate law given by

[13] $$v = kN_A$$

If

$$(N_D)_{t=0} = 0$$

and

$$N_A \gg N_C$$

the first derivative of the entropy will be given by

$$dS/dt = b + R \ln (N_C/2vt)$$

where b and v can be considered as constants. It can be easily shown that under these conditions d^2S/dt^2 goes through a maximum at $N_C = 0.5(N_C)_{t=0}$, and that d^3S/dt^3 becomes negative beyond this point. It can be mentioned that a situation like that represented by eqs. 12 and 13 will hold for several homolyses in the presence of scavengers (*i.e.* in the photolysis of azomethane in the presence of a small amount of nitric oxide and a large excess of nitrogen).

From the preceding examples we can conclude that, even for simple chemical reactions, the concept of monotonicity of entropy production cannot be generally applied.

1. H. McKean. Arch. Ratl. Mech. Anal. **21**, 343 (1966).
2. H. O. Pritchard, N. I. Labib, and L. L. S. McElwain. Can. J. Chem. **52**, 2618 (1974).
3. H. O. Pritchard. Can. J. Chem. **53**, 1756 (1975).
4. I. Prigogini. Thermodynamics of irreversible processes. Interscience Publishers, New York. 1967.
5. S. W. Benson. Thermochemical kinetics. J. Wiley and Sons, New York. 1968.
6. H. O. Pritchard, R. G. Sowden, and A. F. Trotman-Dickenson. Proc. Roy. Soc., A, **217**, 563 (1953).
7. H. O. Pritchard. Personal communication.

Can. J. Chem. Downloaded from www.nrcresearchpress.com by 210.87.254.5 on 09/05/12
For personal use only.

Alkaline methanolysis of 1,1,1-trichloro-2-hydroxy-4-alkanones

EBERHARD KIEHLMANN AND J. I. WELLS
Department of Chemistry, Simon Fraser University, Burnaby, B.C., Canada V5A 1S6
AND
WILKINS REEVE
Department of Chemistry, University of Maryland, College Park, MD, U.S.A.

Received October 9, 1975

EBERHARD KIEHLMANN, J. I. WELLS, and WILKINS REEVE. Can. J. Chem. **54**, 1998 (1976).

Derivatives of the carboxylic acids $RCOCH_2CH(OCH_3)COOH$ and $RCOCH{=}CHCOOH$ (R = Me, *i*-Bu, or *tert*-Bu) have been identified among the major methanolysis products of three 1,1,1-trichloro-2-hydroxy-4-alkanones, $RCOCH_2CH(OH)CCl_3$. In addition, β-methoxy esters $RCOCH(OCH_3)CH_2COOCH_3$ are obtained if hydrogen atoms are present at the alkyl carbon directly attached to the carbonyl group (R = Me or *i*-Bu). 1,1,1-Trichloro-2-hydroxy-4-pentanone (**1**) yields the known methyl 5-chloro-2,4-pentadienoate (**9**) as a minor by-product. An α,α-dichloro epoxide (**15**) is postulated as the key intermediate in the methanolysis mechanism leading to the β-methoxy esters.

EBERHARD KIEHLMANN, J. I. WELLS et WILKINS REEVE. Can. J. Chem. **54**, 1998 (1976).

On a identifié les dérivés d'acides carboxyliques $RCOCH_2CH(OCH_3)COOH$ et $RCOCH{=}CHCOOH$ (R = Me, *i*-Bu ou *tert*-Bu) parmi les produits majeurs formés lors de la méthanolyse de trois trichloro-1,1,1 hydroxy-2 alkanones-4 $RCOCH_2CH(OH)CCl_3$. Si des atomes d'hydrogène sont présents sur le carbone de l'alkyle attaché directement au groupe carbonyle (R = Me ou *i*-Bu) on obtient en plus les β-méthoxy esters $RCOCH(OCH_3)CH_2COOCH_3$. La trichloro-1,1,1 hydroxy-2 pentanone-4 (**1**) conduit, comme sous produit mineur, au chloro-5 pentadiène-2,4 oate de méthyle (**9**) qui est connu. On fait l'hypothèse qu'un α,α-dichloroépoxyde (**15**) est l'intermédiaire clé dans le mécanisme de méthanolyse conduisant aux β-méthoxy esters.
[Traduit par le journal]

Introduction

Phenyl(trichloromethyl)carbinol and its ring-substituted derivatives are known to react with methanolic potassium hydroxide to form α-methoxyarylacetates in high yield (1, 2) [1].

[1] $ArCHOH{-}CCl_3 + KOH/CH_3OH \rightarrow ArCHOCH_3{-}COO^-$

α-Methoxyphenylacetic acid, obtained from the parent compound (Ar = C_6H_5) by this method, may be used as an analytical reagent for the detection of sodium ions (3), and several of its chlorinated derivatives are effective plant growth regulators (4). These observations suggested the synthesis of aliphatic trichloromethylcarbinols and a study of their behavior toward base in methanolic solution.

Caujolle *et al.* (5) found that certain 1,1,1-trichloro-2-hydroxy-4-alkanones react with 4 equiv. of sodium hydroxide per mole of starting material to form 3 mol of sodium chloride, and β-ketoaldehydes and sodium formates were postulated as the major organic reaction products. However, they were not successful in isolating and identifying these compounds. Breusch and Keskin (6) obtained α,β-unsaturated γ-keto acids on treatment of 1,1,1-trichloro-2-hydroxy-4-alkanones with aqueous potassium hydroxide or potassium carbonate solution at elevated temperature [2]. The product structures

[2] $RCOCH_2CHOH{-}CCl_3 + KOH$ or $K_2CO_3/H_2O \rightarrow RCOCH{=}CHCOO^-$

were proven by hydrogenation of the double bond and independent synthesis of authentic product samples. Under similar reaction conditions, 1,1,1-trichloro-2-hydroxy-4-pentanone (**1**) has been shown to give 5-chloro-2,4-pentadienoic acid (**2**) in low yield (7–9) [3]. Since 1,1,1-tri-

[3] $\underset{\mathbf{1}}{CH_3COCH_2CHOH{-}CCl_3} + KOH/H_2O$, then $HCl \rightarrow \underset{\mathbf{2}}{ClCH{=}CHCH{=}CHCOOH}$

chloro-2-methoxy-4-pentanone yields the methyl ester of the same acid on treatment with methanolic sodium carbonate, the latter reaction is

Can. J. Chem. Downloaded from www.nrcresearchpress.com by 210.87.254.6 on 09/05/12
For personal use only.

Can. J. Chem. Downloaded from www.nrcresearchpress.com by 210.87.254.6 on 09/05/12
For personal use only.

likely to proceed via 4,5-dichloro-2-cyclopentenone as intermediate (10), although dehydration of **1** followed by a Favorski-type rearrangement of the resulting alkenone (9) cannot be entirely ruled out as an alternative mechanistic pathway. The remarkable dependence of the composition and structure of the products formed during the alkaline methanolysis of three homologous 1,1,1-trichloro-2-hydroxy-4-alkanones $RCOCH_2CH(OH)CCl_3$ (R = Me, *i*-Bu, and *tert*-Bu) on the nature of R, as reported below, indicates intramolecular interactions between the (trichloromethyl)carbinyl group and the α'-carbon (C-5) and thus provides further indirect support for the former rearrangement mechanism.

Results

1,1,1-Trichloro-2-hydroxy-4-pentanone (**1**), 1,1,1-trichloro-2-hydroxy-6-methyl-4-heptanone (**3**), and 1,1,1-trichloro-2-hydroxy-5,5-dimethyl-4-hexanone (**4**) were chosen as starting materials for this investigation since they are readily synthesized in pure form (*i.e.*, free of structural and stereoisomers) by the crossed aldol condensation of chloral with the corresponding methyl ketones ($RCOCH_3$; R = Me, *i*-Bu and *tert*-Bu, respectively) (5, 6, 11). Their reaction with 5 mol equiv. of methanolic potassium hydroxide at 50 °C under conditions exactly identical to those reported for the methanolysis of phenyl(trichloromethyl)carbinol [1] yielded potassium chloride (93–98%) and mixtures of various carboxylic acids and esters, with the number of components formed depending strongly on the structure of the starting material.

Thus, ketol **3** gave three methyl esters (**5**, **6**, and **7**) in the ratio 7:8:24 after acidification of the crude product mixture and methylation of the acid fraction with excess methyl iodide and silver oxide [4]. They were separated by preparative

[4] $(CH_3)_2CHCH_2COCH_2CHOH—CCl_3$ (**3**) $\xrightarrow[(2)\ HCl]{(1)\ KOH/CH_3OH}$ $(CH_3)_2CHCH_2COCH{=}CHCOOCH_3$ (**5**)

$+ (CH_3)_2CHCH_2CO—CHOCH_3—CH_2COOCH_3$ (**6**) $+ (CH_3)_2CHCH_2COCH_2CHOCH_3—COOCH_3$ (**7**)

[5] *i*-$BuCOCH_3$ + *n*-$BuOCOCHO$ $\xrightarrow[76\%]{110\ °C/24\ h}$ *i*-$BuCOCH_2CHOH—COOC_4H_9$ $\xrightarrow[Ag_2O]{CH_3I}$ *i*-$BuCOCH_2CHOCH_3—COOC_4H_9$ (**8**)

i-$BuCOCH_2CHOH—COOC_4H_9$ $\xrightarrow{HOAc/HCl,\ 110\ °C/2\ h}$ *i*-$BuCOCH{=}CHCOOH$ $\xrightarrow{CH_3I/Ag_2O}$ *i*-$BuCOCH{=}CHCOOCH_3$ (**5**)

vpc (elution order **5**–**6**–**7**), and their structures were determined by spectroscopic and quantitative elemental analysis. The ester of lowest retention time was identified as methyl β-isovalerylacrylate (**5**) by its typical olefinic double doublet (τ 2.93 and 3.40) in the nmr spectrum, its C=C stretching vibration (1635 cm^{-1}) in the infrared (ir) spectrum, and by independent synthesis [5]. Furthermore, the corresponding carboxylic acid, a small quantity of which was isolated in crystalline form from the crude acid fraction, had the correct melting point (6) and mixture melting point with an authentic sample. Quantitative methoxyl determination, CH analysis, and nmr revealed the two major products clearly as methyl α- and β-methoxyisovalerylpropionate. However, because of the close similarity in the nmr chemical shifts and splitting patterns (*vide infra*), unambiguous structure assignments were possible only by mass spectrometry and independent synthesis of one of the two isomers. The strong *m/e* 143 and 117 peaks in the mass spectra of **7** and **6**, respectively, are attributed to the resonance-stabilized oxonium ions *i*-$BuCOCH_2CHOCH_3^+$ and $^+CH(OCH_3)CH_2COOCH_3$ formed by α-cleavage. A sample of pure *n*-butyl α-methoxy-β-isovalerylpropionate synthesized by an entirely different route (12, 13) from *n*-butyl glyoxylate and methyl isobutyl ketone [5] had a vpc retention time identical to that of the least volatile of the *n*-butyl analogs of **5**, **6**, and **7** prepared by alkaline methanolysis of **3**, acidification, and esterification with *n*-butyl iodide and silver oxide.

To verify the above structural assignments, we investigated the methanolysis of the homologous ketols **1** and **4** which, as expected, revealed

[6] $CH_3COCH_2CHOH—CCl_3$ (**1**) $\xrightarrow[(3)\ CH_3I/Ag_2O]{(1)\ KOH/CH_3OH}$ $ClCH{=}CHCH{=}CHCOOCH_3$ (**9**) $+ CH_3COCH{=}CHCOOCH_3$ (**10**)

$+ CH_3COCH_2CHOCH_3—COOCH_3$ (**11**) $+ CH_3CO—CHOCH_3—CH_2COOCH_3$ (**12**)

[7] 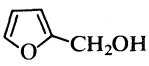 $\xrightarrow[H^+]{CH_3OH}$ $CH_3COCH_2CHOCH_3—CH(OCH_3)_2$

$\xrightarrow[(2)\ Ag_2O]{(1)\ H^+/H_2O}$ $CH_3COCH_2CHOCH_3—COOH$ $\xrightarrow{CH_2N_2}$ **11**

similar reaction patterns. In the case of ketol **1**, four products (ratio 2:3:4:10, [6]) were isolated from the esterified crude acid fraction and identified as methyl 5-chloro-2,4-pentadienoate (**9**), methyl β-acetylacrylate (**10**), and methyl α- and β-methoxy-β-acetylpropionate (**11** and **12**). The dienoate **9** gave the same nmr spectrum and vpc retention time as an authentic sample prepared from 1,1,1-trichloro-2-penten-4-one (9, 10), and the acrylate **10** was identical in its physical and spectral properties to a sample obtained from methyl levulinate by bromination and subsequent dehydrobromination (14). The α-methoxy ester **11** was synthesized from furfuryl alcohol by the four-step procedure [7] reported in the literature (15) and it was found to be identical (nmr and vpc) to the third component of the ester mixture. The completely analogous nmr chemical shifts and splitting patterns found for **11** and **7**, on one hand, and **12** and **6**, on the other hand, not only revealed the structure of the fourth and major product of reaction 6 but also confirmed the assignments for the two major methanolysis products (**6** and **7**) of ketol **3**. Thus both **11** and **7** give, surprisingly, a sharp doublet at τ 7.17 and 7.20, respectively, for the two diastereotopic methylene protons, and a sharp triplet at τ 5.77 for the methine proton, while these patterns are less symmetrical and additional fine-splitting is observed for the corresponding protons of **12** (CH_2 at τ 7.32, CH at τ 6.03) and **6** (CH_2 at τ 7.32, CH at τ 6.02). The prominent oxonium ion fragments at *m/e* 101 ($CH_3COCH_2CHOCH_3^+$) and 117 ($^+CHOCH_3$-CH_2COOCH_3) found in the mass spectra of **11** and **12**, respectively, further support the assigned structures.

In sharp contrast to ketols **1** and **3**, 1,1,1-trichloro-2-hydroxy-5,5-dimethyl-4-hexanone (**4**) yielded only two products (**13** and **14**, ratio 1:15) on treatment with methanolic potassium hydroxide followed by esterification. Separation and purification by preparative vpc and nmr spectroscopic analysis led to the structural assignments shown in [8]. The expected β-methoxy

[8] $(CH_3)_3CCOCH_2CHOH—CCl_3$ (**4**) $\xrightarrow[(3)\ CH_3I/Ag_2O]{(1)\ KOH/CH_3OH}$

$(CH_3)_3CCOCH{=}CHCOOCH_3$ (**13**)

$+ (CH_3)_3CCOCH_2CHOCH_3—COOCH_3$ (**14**)

isomer of **14** was detected neither in the nmr spectrum of the crude product mixture nor by vpc on three different columns (30% QF-1 at 215 °C, 10% Carbowax at 140 °C, and 5% DEGS at 150 °C). We conclude from this result that the α-hydrogen, absent at the fully methylated α'-carbon of **4**, may participate in the mechanism leading to the formation of the analogous esters **6** and **12** from ketols **1** and **3**, respectively.

Contrary to our expectations, the reaction of the title compounds with sodium methoxide in dry methanol, followed by a simple extraction–distillation work-up, gave less satisfactory results than the three-step methanolysis–acidification–esterification sequence described above, yielding mainly unidentifiable nonvolatile products. In the case of ketol **3**, application of this alternative procedure led to the formation (18% yield) of an ester mixture containing 28% **5**, 25% **6**, 35% **7** (identified by vpc, ir, and nmr), and three minor components of lower vpc retention times.

Discussion

Reeve and co-workers (1, 2) have proposed that the alkaline methanolysis of aryl(trichloromethyl)carbinols [9] proceeds via an α,α-dichloro epoxide which undergoes ring-opening either by nucleophilic attack of methoxide at the aryl-

Can. J. Chem. Downloaded from www.nrcresearchpress.com by 210.87.254.6 on 09/05/12
For personal use only.

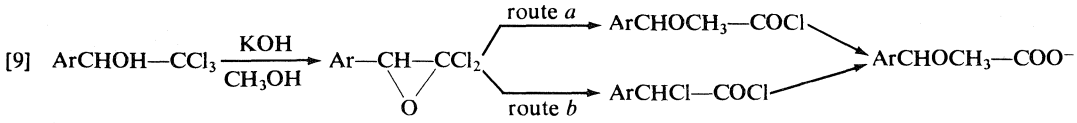

substituted carbon, followed by acyl chloride hydrolysis (route *a*), or by an α-chloro expoxide-α-chloro carbonyl rearrangement (16) followed by methanolysis of the intermediate α-chloroacyl chloride (route *b*). Mechanistic studies on optically active phenyl(trichloromethyl)carbinol (17) have shown that at least 75% of the reaction proceeds by route *a*, *i.e.*, with inversion of configuration at the α-carbon. The failure of 1,1,1-trichloro-2-methoxy-4-pentanone, the methylated derivative of ketol **1** which is incapable of epoxide ring closure, to give compounds **10**, **11**, and **12** on treatment with methanolic potassium hydroxide (10) strongly suggests that the transformation of ketols **1**, **3**, and **4** to the α-methoxy esters **7**, **11**, and **12**, respectively, occurs by an analogous mechanism. The other esters may arise from the postulated epoxide intermediate **15** via one or more of several pathways, one of which involves abstraction of an α-methylene proton and subsequent ring opening to yield the olefinic products **5**, **10**, and **13** [10]. Dehydration

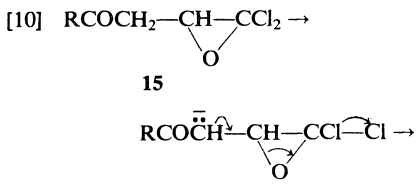

RCOCH=CHCOCl → **5**, **10**, and **13**

of the 1,1,1-trichloro-2-hydroxy-4-alkanone as an initial reaction step, followed by hydrolysis of the trichloromethyl group and methanol addition to the double bond is considered unlikely because, due to the C—O bond strengthening effect of the electron-withdrawing chlorine atoms (19), all known attempts (10, 11) to synthesize 1,1,1-trichloro-2-alken-4-ones by this route, without prior conversion of the hydroxyl group to a better leaving group (20), have failed. Conversion of the originally formed α-methoxy compounds to their respective α,β-unsaturated derivatives by E2 elimination followed by partial readdition of methanol to give the β-methoxy esters **6** and **12** represents another mechanistic possibility. The conjugate addition of methanol to methyl β-acetylacrylate is indeed a known reaction (18), which, under our ketol methanolysis conditions, led to the formation of methyl α- and β-methoxy-β-acetylpropionate (**11** and **12**) in the approximate ratio 1:5, and the saponification of *n*-butyl α-methoxy-β-isovalerylpropionate (**8**) followed by reesterification with methyl iodide and silver oxide yielded small amounts of **5**, **6**, and **7**. However, this reaction sequence, when applied to ketol **4**, would be expected to give not only the observed esters **13** and **14** but also the β-methoxy isomer of **14** which was not detected experimentally. We, therefore, conclude that the β-methoxy esters **6** and **12** arise, at least in part, via a 1,4-cyclopentadione intermediate (**16** or **17**)

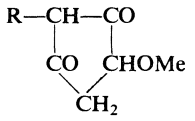

16

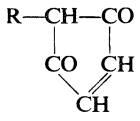

17

formed by abstraction of an α′-hydrogen from epoxide **15** (or from the initially produced esters **5**, **7**, **10**, or **11**) and subsequent internal Claisen-type condensation. Since all attempts to isolate the postulated cyclic structures **16** or **17** have failed, the experimental evidence to date does not permit a clear distinction among the proposed reaction pathways.

Experimental

Elemental analyses were performed by A. Bernhardt Microanalytical Laboratory, Elbach, Germany, and methoxyl determinations by Dr. Franz Kasler. The nmr spectra were recorded on a Varian A 56/60 spectrometer using TMS as internal standard and $CDCl_3$ as solvent, and ir spectra on a Beckman IR-12 spectrometer using a thin film of neat liquid (or melt) between sodium chloride plates. Vapor phase chromatographic (vpc) analyses were performed on a Varian Aerograph 1200-1 HY-FI III and an FM 300 gas chromatograph using 10% Carbowax 20M on Aeropak 30 (12 ft × ⅛ in.), 10% Carbowax 20M on silanized diatomaceous earth (7 ft × ¼ in.), or 20% decyl phthalate on acid-washed Chromosorb P (7 ft × ¼ in.) at 140 to 160 °C. All quantitative estimates of the composition of product mixtures by vpc are based on a comparison of integrated peak areas obtained for the individual components with those obtained for standard mixtures prepared from the pure components. The peak areas were measured planimetrically. For the purpose of identification and characterization, small samples of all esters were isolated in >95% purity by preparative vpc

Can. J. Chem. Downloaded from www.nrcresearchpress.com by 210.87.254.6 on 09/05/12
For personal use only.

Can. J. Chem. Downloaded from www.nrcresearchpress.com by 210.87.254.6 on 09/05/12
For personal use only.

on a Varian Aerograph A90-P3 chromatograph using a 30% QF-1 column (20 ft × ⅜ in.) at 150 to 200 °C. Mass spectra were run on a double-focusing RMU-6E Hitachi–Perkin-Elmer instrument.

1,1,1-Trichloro-2-hydroxy-4-alkanones ***1***, ***3***, *and* ***4*** *($RCOCH_2CHOHCCl_3$; R = CH_3, i-Bu and tert-Bu)*

The title compounds were prepared from acetone, methyl isobutyl ketone, and pinacolone, respectively, with chloral, glacial acetic acid as solvent and sodium acetate as catalyst as described in the literature (11). They were obtained in 44, 46, and 40% yield after recrystallization from cyclohexane.

Methanolysis of 1,1,1-Trichloro-2-hydroxy-6-methyl-4-heptanone ***(3)***

A solution of 49.6 g (0.2 mol) of **3** in 60 ml methanol was heated to 50 °C in a 500-ml flask equipped with thermometer, stirrer, dropping funnel, and reflux condenser. Then, a solution of 56.0 g (1.0 mol) of potassium hydroxide pellets in 240 ml of methanol was added dropwise (45 min), the temperature of the reaction mixture being maintained constant between 49 and 51 °C by occasional cooling. Stirring was continued for an additional 2 h with the reaction temperature being kept between 42 and 58 °C by immersing the flask in a hot water bath. The mixture was allowed to cool, filtered, and the filter cake was washed with 60 ml methanol and dried in a dessicator to give a 98% yield (43.8 g, 0.588 mol) of potassium chloride. The filtrate was concentrated to a volume of 140 ml by distillation under reduced pressure at a bath temperature <55 °C. After the addition of 200 ml water, the mixture was extracted with three 120-ml portions of ether, the combined organic layers were dried over anhydrous $MgSO_4$, and the solvent was evaporated to give 2.7 g of a neutral fraction which was not further investigated. The alkaline aqueous layer (p*H* 10) was acidified with 6 *N* hydrochloric acid (46 ml) to Congo red, extracted twice with ether, and dried ($MgSO_4$) to give 29.5 g of a brown, oily crude acid fraction. Upon standing in the refrigerator for several days, a small amount (1.5 g) of crystals were formed. They were isolated by suction filtration and recrystallized from cyclohexane and carbon tetrachloride, successively, to give isovalerylacrylic acid, mp 91.5–92.5 °C (lit. (6) mp 91–92 °C).

Esterification of Carboxylic Acid Mixture

The crude acid (29.5 g) obtained in the preceding experiment was dissolved in 192 ml (3.2 mol) of methyl iodide, and 86 g (0.404 mol) of silver oxide, freshly prepared from sodium hydroxide and silver nitrate according to Hudson and co-workers (21), were added slowly with cooling. The mixture was magnetically stirred for 4 h in a 500-ml Erlenmeyer flask equipped with reflux condenser and calcium chloride tube, subsequently diluted with ether, and filtered. The solvent and excess methyl iodide were removed from the filtrate on a steam bath, and the reaction product (32.5 g) was distilled *in vacuo* to give 19.6 g (50% yield) of a clear yellow ester mixture boiling at 79–89 °C/0.7 torr. The *n*-butyl esters were prepared analogously from the crude acid fraction of a second run, using *n*-butyl iodide instead of methyl iodide as the alkylating agent.

The methyl ester mixture containing 17.5% methyl β-isovalerylacrylate (**5**), 20% methyl β-methoxy-β-isovalerylpropionate (**6**), and 60% methyl α-methoxy-β-isovalerylpropionate (**7**) was separated by preparative vpc to give pure samples of the individual components. Oxidation of a small aliquot with 5% cold aqueous permanganate solution in acetic acid removed **5** selectively from the ester mixture.

Characterization of **5**: *Anal.* calcd. for $C_9H_{14}O_3$: C 63.51, H 8.29, CH_3O 18.23; found: C 63.66, H 8.20, CH_3O 18.40; ir 1635 (C=C), 1703 and 1736 (C=O) cm^{-1}; nmr τ 2.93 (d, —COCH=), 3.40 (d, =CHCOOR, *J* = 16 Hz), 6.20 (s, $COOCH_3$), 7.48 (d, CH_2), 7.80 (m, CH), and 9.05 (d, $2CH_3$, *J* = 6 Hz).

Characterization of **6**: *Anal.* calcd. for $C_{10}H_{18}O_4$: C 59.39, H 8.97, CH_3O 30.69; found: C 59.30, H 9.06, CH_3O 29.14; mass spectrum (17 eV) *m/e* 75 (96%) and 117 (100%); nmr τ 6.02 (t, CHOR), 6.33 (s, $COOCH_3$), 6.60 (s, $ROCH_3$), 7.32 (d, CH_2COOR), 7.58 (m, >CH-CH_2), and 9.07 (d, $2CH_3$).

Characterization of **7**: *Anal.* calcd. for $C_{10}H_{18}O_4$: see **6**; found: C 59.20, H 8.69, CH_3O 29.08; mass spectrum (80 eV) *m/e* 75 (72%), 85 (100%), and 143 (62%); nmr τ 5.77 (t, CHOR), 6.27 (s, $COOCH_3$), 6.60 (s, $ROCH_3$), 7.20 (d, CH_2COOR), 7.70 (m, >$CHCH_2$), and 9.08 (d, $2CH_3$).

n-Butyl α-Methoxy-β-isovalerylpropionate ***(8)***

n-Butyl glyoxylate was prepared by the oxidation of *n*-butyl tartrate with lead tetraacetate (22). Following the procedure given by Arbuzov and Klimova (13), a mixture of 92.4 g (0.71 mol) of *n*-butyl glyoxylate (bp 63–79 °C/18 torr) and 213 g (2.13 mol) of methyl isobutyl ketone was heated at 110 °C for 24 h. Excess ketone was removed by distillation at reduced pressure (18 torr). High vacuum distillation of the residue gave 106 g of 80% pure *n*-butyl α-hydroxy-β-isovalerylpropionate (75% yield), bp 139–146 °C/3–5 torr. Methylation with methyl iodide and silver oxide yielded the title compound with a vpc retention time (Carbowax 20M, 160 °C) identical to that of the least volatile component of the *n*-butyl ester mixture prepared by methanolysis of ketol **3** and subsequent butylation of the crude acid fraction (as described above).

β-Isovalerylacrylic Acid and Methyl Ester ***(5)***

A mixture of 23.0 g (0.10 mol) of *n*-butyl α-hydroxy-β-isovalerylpropionate, 100 ml glacial acetic acid and 10 ml 2 *N* hydrochloric acid was placed in a 250-ml flask equipped with a reflux condenser, and heated on a steam bath for 2 h. After removal of the solvent and hydrochloric acid by distillation under reduced pressure, 18.2 g of a yellow liquid was obtained which solidified to a white paste upon cooling and yielded the title compound, mp 91–91.5 °C (lit. (6) 91–92 °C), after recrystallization from aqueous ethanol (50:50 v/v). A mixture melting point test and nmr spectroscopy showed this compound to be identical to the unsaturated carboxylic acid isolated from the methanolysis products of ketol **3** after acidification of the reaction mixture. Methylation with silver oxide and methyl iodide (see above) gave the corresponding ester (**5**) with a vpc retention time (decyl phthalate, 160 °C) and an nmr spectrum identical to that of the most volatile component of the ester mixture obtained from ketol **3** [4].

Methanolysis of 1,1,1-Trichloro-2-hydroxy-4-pentanone (1)

Following the procedure described above for the methanolysis of **3**, 16.0 g (59% yield) of a crude acid fraction was obtained from the title compound which yielded methyl 5-chloro-2,4-pentadienoate (**9**), methyl β-acetylacrylate (**10**), methyl α-methoxy-β-acetylpropionate (**11**), and methyl β-methoxy-β-acetylpropionate (**12**) in the approximate ratio 2:3:4:10 after esterification (with CH_3I and Ag_2O, as before) and vacuum distillation (bp 60–70 °C/1.0 torr). The individual components were separated by preparative vpc and identified by nmr analysis. The spectra and gas chromatograms of **9**, **10**, and **11** were found to be superimposable on those of independently prepared authentic samples.

Characterization of **9**: *Anal.* calcd. for $C_6H_7ClO_2$: C 49.17, H 4.81, Cl 24.19; found: C 49.29, H 4.61, Cl 23.95. Independent synthesis from 1,1,1-trichloro-2-penten-4-one (10).

Characterization of **10**: nmr τ 3.00 (d, —COCH═), 3.37 (d, ═CHCOOR, J = 16 Hz), 6.20 (s, $COOCH_3$), and 7.65 (s, CH_3CO). Independent synthesis from methyl levulinate (14).

Characterization of **11**: nmr τ 5.78 (t, CH), 6.25 (s, $COOCH_3$), 6.60 (s, $ROCH_3$), 7.17 (d, CH_2), and 7.83 (s, CH_3CO); mass spectrum (80 eV) *m/e* 43 (100%) and 101 (60%). Independent synthesis from furfuryl alcohol (15).

Characterization of **12**: nmr τ 6.03 (t, CH), 6.33 (s, $COOCH_3$), 6.58 (s, $ROCH_3$), 7.32 (d, CH_2), and 7.78 (s, CH_3CO); mass spectrum (20 eV) *m/e* 75 (100%) and 117 (90%).

Reaction of Methyl β-Acetylacrylate (10) with Methanolic KOH

A mixture of 3.84 g (0.03 mol) of **10**, 41 ml methanol and 8.4 g potassium hydroxide was subjected to the same reaction conditions and work-up procedure as described for the methanolysis of ketol **3**. Esterification of the crude acid fraction (1.0 g, 21% yield) with diazomethane and distillation (bp 45 °C/0.25 torr) yielded a clear liquid containing the methoxy esters **11** and **12** in the approximate ratio 1:5 (by vpc on XF-1150 at 150 °C) and a trace of unreacted starting material.

Methanolysis of 1,1,1-Trichloro-2-hydroxy-5,5-dimethyl-4-hexanone (4)

Application of the standard methanolysis procedure (see ketol **3**) to ketol **4** gave a crude acid fraction in 75% yield which was esterified with diazomethane, distilled (75–80 °C/0.05 torr), and analyzed by vpc (10% Carbowax 20M at 140 °C). The two products formed in the approximate ratio 1:15 were separated by preparative vpc and identified as methyl β-pivaloylacrylate (**13**) and methyl α-methoxy-β-pivaloylpropionate (**14**), respectively. The nmr of **13**: τ 2.53 (d, —COCH═), 3.27 (d, ═CHCOOR), 6.22 (s, $COOCH_3$) and 8.82 (s, $3CH_3$), nmr of **14**: τ 5.73 (unsym. q, CH), 6.27 (s, $COOCH_3$), 6.60 (s, $ROCH_3$), 7.12 (1:1:1:1 q, CH_2), and 8.87 (s, $3CH_3$).

Acknowledgements

The financial support of these investigations by the Celanese Corporation and the National Research Council of Canada, and the technical assistance of Miss Rosemary Wald are gratefully acknowledged.

1. W. Reeve and E. L. Compere, Jr. J. Am. Chem. Soc. **83**, 2755 (1961).
2. W. Reeve and C. W. Woods. J. Am. Chem. Soc. **82**, 4062 (1960).
3. W. Reeve. Anal. Chem. **31**, 1066 (1959).
4. J. W. Mitchell, B. C. Smale, and W. H. Preston, Jr. J. Agric. Food Chem. **7**, 841 (1959).
5. F. Caujolle, P. Couturier, and C. Dulaurans. Bull. Soc. Chim. Fr. 19 (1950).
6. F. L. Breusch and H. Keskin. Arch. Biochem. Biophys. **18**, 305 (1948).
7. P. Uschakov. Zh. Russ. Fiz.-Khim. Ova. **29**, 113 (1897).
8. J. Salkind. Zh. Russ. Fiz.-Khim. Ova. **30**, 906 (1898).
9. A. Takeda and S. Tsuboi. J. Org. Chem. **38**, 1709 (1973).
10. E. Kiehlmann, B. C. Menon, and J. I. Wells. Can. J. Chem. **50**, 2561 (1972).
11. E. Kiehlmann and P. W. Loo. Can. J. Chem. **49**, 1588 (1971).
12. A. W. Noltes and F. Kogl. Recl. Trav. Chim. **80**, 1334 (1961).
13. Y. A. Arbuzov and E. I. Klimova. J. Gen. Chem. U.S.S.R. (Eng. Transl.) **32**, 3606 (1962).
14. W. G. Overend, L. M. Turton, and L. F. Wiggins. J. Chem. Soc. 3500 (1950).
15. L. Birkofer and R. Dutz. Justus Liebigs Ann. Chem. **608**, 7 (1957).
16. R. C. Cousins. Ph.D. Thesis. Kansas State University, Manhattan, Kansas. 1974.
17. W. Reeve, R. J. Bianchi, and J. R. McKee. J. Org. Chem. **40**, 339 (1975).
18. R. Luft, S. Delattre, and J. Basso. C.R. Acad. Sci. Ser. C, **271**, 1623 (1970).
19. S. Mamedov and F. Gadshisade. Zh. Obshch. Khim. **32**, 799 (1962).
20. E. Kiehlmann, P. W. Loo, B. C. Menon, and N. McGillivray. Can. J. Chem. **49**, 2964 (1971).
21. W. Reeve, R. S. Hudson, and C. W. Woods. Tetrahedron **19**, 1243 (1963).
22. F. L. Wolf and J. Weijlard. Org. Synth. Coll. Vol. IV, 124 (1963).

Can. J. Chem. Downloaded from www.nrcresearchpress.com by 210.87.254.6 on 09/05/12
For personal use only.

The metal-ligand oxidations of dibenzobicyclo[2.2.2]octatriene by lead tetraacetate – hydrogen fluoride, lead tetraacetate, thallium(III) acetate, and mercuric acetate

DENNIS D. TANNER, PETER B. VAN BOSTELEN,[1] AND MATHEW LAI
Department of Chemistry, University of Alberta, Edmonton, Alta., Canada T6G 2G2

Received December 17, 1975

DENNIS D. TANNER, PETER B. VAN BOSTELEN, and MATHEW LAI. Can. J. Chem. **54**, 2004 (1976).

The isoelectronic series lead tetraacetate – hydrogen fluoride, lead tetraacetate, thallium(III) acetate, and mercuric acetate were used to oxidize the bicyclic olefin dibenzobicyclo[2.2.2]-octatriene. The stereochemistry of the products formed from these reactions substantiates the proposal that the first formed intermediate in these oxidations is the *cis*-molecular addition product of the metal and its ligand to the bicyclic olefin. Subsequent stereospecific rearrangement of the adducts in the case of the lead and thallium reagents verified the absence of the involvement of homolytic processes in the formation or decomposition of the adducts.

DENNIS D. TANNER, PETER B. VAN BOSTELEN et MATHEW LAI. Can. J. Chem. **54**, 2004 (1976).

On a utilisé les séries isoélectroniques tétraacétate de plomb – fluorure d'hydrogène, tétraacétate de plomb, acétate de thallium(III) et acétate mercurique pour oxyder l'oléfine bicyclique dibenzobicyclo[2.2.2.]octatriène. La stéréochimie des produits formés à partir de ces réactions supporte la proposition que la premier intermédiaire formé dans ces oxydations est le produit d'addition moléculaire *cis* du métal et de son ligand à l'oléfine bicyclique. Un réarrangement stéréospécifique ultérieur des adduits dans le cas des réactifs du plomb et du thallium a permis de vérifier l'absence d'une implication des processus homolytiques dans la formation ou la décomposition des adduits.

[Traduit par le journal]

Introduction

Recently a mechanism was proposed for the reaction of the lead tetraacetate – hydrogen fluoride reagent (LTA–HF) with several unsaturated hydrocarbons (1). It was suggested that in the case of the reactions with norbornene, a *cis*-molecular addition of the reagent to the bicyclic olefin led to an unstable intermediate organolead compound which yielded stable products by the backside displacement of the metal from the carbon to which it was bonded (paths *a*, *b*, *c*).

The intermediacy of a lead ligand addition product was also utilized to rationalize the products formed upon the treatment of 1,1-diphenylethylene with the LTA–HF reagent. Since the publication of the proposal that an organolead intermediate was involved as an intermediate in the LTA–HF reaction with olefins (1, 2) an organolead addition intermediate has been isolated from the reaction of pregnenolone and the reagent (3).

[1]Taken in part from the Ph.D. dissertation of Peter Van Bostelen, University of Alberta, 1972.

The mechanism for the LTA–HF reaction with norbornene was proposed by analogy to other metal-ligand oxidations of that olefin by mercuric acetate (4) and thallium(III) acetate (5), where the intermediate organometalic addition products were stable, and could be isolated and characterized. In analogous reactions of lead tetraacetate with other olefins, however, both

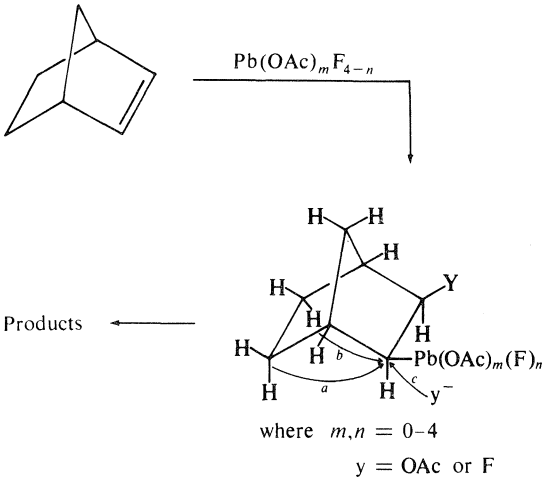

where $m,n = 0$–4
y = OAc or F

Can. J. Chem. Downloaded from www.nrcresearchpress.com by 210.87.254.6 on 09/05/12
For personal use only.

Can. J. Chem. Downloaded from www.nrcresearchpress.com by 210.87.254.6 on 09/05/12
For personal use only.

homolytic and heterolytic pathways, as well as oxidation of the intermediate radicals (in the homolytic path) to the corresponding carbonium ions by Pb^{IV}, have been invoked to rationalize the reaction products (6*a*–*f*).

$$Pb^{IV} + R\cdot \rightarrow R^+ + Pb^{III}$$
$$2Pb^{III} \rightarrow Pb^{II} + Pb^{IV}$$

The possibility existed that processes of this type were, likewise, involved in the oxidation of norbornene with the LTA–HF reagent, since a homolytic process had first been suggested to explain the products obtained from the reaction of 1,1-diphenylethylene with this reagent (7). The stereochemical consequence of the oxidation of another bicyclic olefin, dibenzobicyclo[2.2.2]-octatriene **1** has been used as a probe to investigate the possible involvement of the oxidation–reduction process previously proposed. The stereochemistry of the products of the oxidation of **1** with LTA–HF was compared (in a manner similar to that used for norbornene) to that of the products obtained from its reaction with mercuric acetate, thallium(III) acetate, and lead tetraacetate to substantiate the conclusion, previously reached, that these isoelectronic metal-ligand oxidations followed analogous methanistic pathways.

Results

The reaction of dibenzobicyclo[2.2.2]octatriene, **1**, with LTA–HF gave five detectable products, **2**–**6**, obtained and characterized in a 98% isolated yield.

Compound **4**, dibenzobicyclo[3.2.1]octadien-*exo*-2-*syn*-8-diol diacetate, was identified by comparing its melting point, mixture melting point, and nmr spectrum with those of the authentic material. Admixed with **4**, traces ~1.4%, of the epimeric diacetate, dibenzobicyclo[3.2.1]octadien-*endo*-2-*syn*-8-diol diacetate (**6**) could be detected in the nmr spectrum of isolated **4**. The structures of compounds **2**, *syn*-8-*exo*-4-difluorodibenzobicyclo[3.2.1]octadiene, and **3**, *syn*-8-fluorodibenzobicyclo[3.2.1]octadien-*exo*-2-ol acetate were assigned on the basis of their microanalysis and nmr spectrum and from the observation that **2** underwent solvolysis in glacial acetic acid, under mild conditions, to yield a mixture of **3** and **7** (its epimeric isomer), *syn*-8-fluorodibenzobicyclo[3.2.1]octadien-*endo*-2-ol acetate.

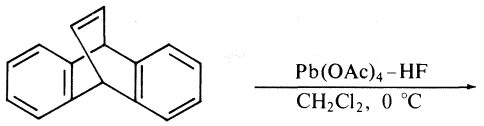

1

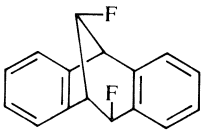

2
23.9%

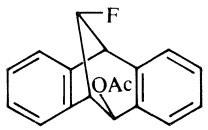

3
37.5%

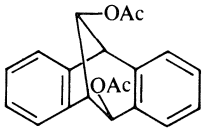

4
23.6%

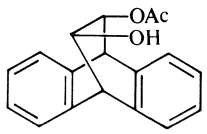

5
12.3%

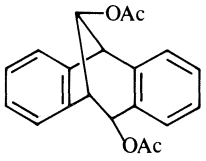

6
1.4%

The structure of **5**, *cis*-dibenzobicyclo[2.2.2]-octadiene-2,3-diol monoacetate was assigned on the basis of its microanalysis and nmr and mass spectra, and from the observation that when **4**

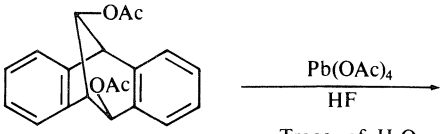

4

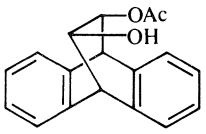

5

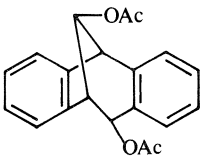

6

Can. J. Chem. Downloaded from www.nrcresearchpress.com by 210.87.254.6 on 09/05/12
For personal use only.

was subjected to the reaction conditions two products were obtained, **5** and **6** (dibenzobicyclo-[3.2.1]octadien-*endo*-2-*syn*-8-diol diacetate). The structural assignment of the *cis*-diol monoacetate, **5**, was further confirmed since its melting point and infrared (ir) spectrum were the same as a compound given that structure by Cristol *et al.* (8) which was obtained after aqueous work-up, from the reaction of **4** with sulphuric acid in acetic acid solution.

When **1** was allowed to react with lead tetraacetate in glacial acetic acid (80 °C) a 92% yield of two products was isolated, in a ratio of 99.5:0.5. The major isomer, was shown to be **4** and the minor one is presumed, on the basis of its nmr spectrum, to be its *endo* epimer **6**.

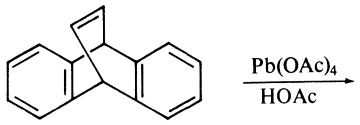

1

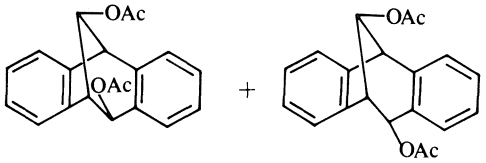

4 6

Treatment of **1** with mercuric acetate in glacial acetic acid followed by sodium chloride gave a quantitative yield of the oxymercuration compound, *cis*-dibenzobicyclo[2.2.2]octadienzyl-3-acetoxy-2-mercuric chloride (**8**).

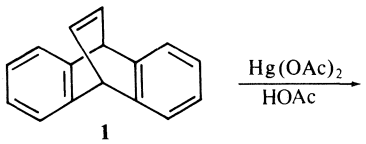

1

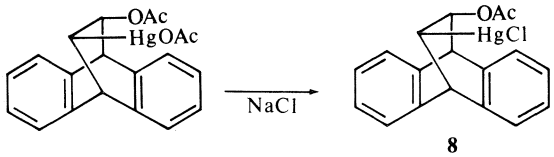

8

The structure of **8** was assigned on the basis of its nmr and mass spectra and by the observation that upon reduction with basic sodium borohydride it was transformed to the known compound, dibenzobicyclo[2.2.2]octadien-2-ol acetate (**9**).

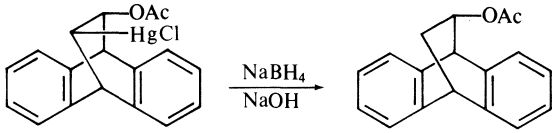

8 9

The treatment of **1** with thallium(III) acetate in acetic acid led to the near quantitative (97%) production of **4**.

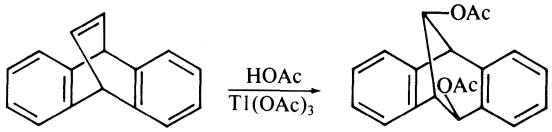

1 4

Discussion

The *cis-exo*-metal-ligand additions of mercuric acetate (4) and thallium(III) acetate (5) to norbornene have been mechanistically rationalized by Traylor (9) by his suggestion that the electrophilic metal bonds simultaneously the ligand and the strained olefin, and *cis*-addition will be preferred over *trans*-addition due to the twist strain introduced into the transition state for *trans*-addition:

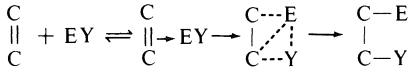

This proposal has been adopted by analogy to rationalize the products obtained from the treatment of norbornene with LTA–HF (1); however, it was necessary to extend the analogy by comparing the reactions of ethenoanthracene **1**, with mercuric acetate, thallium(III) acetate, and lead tetraacetate in order to use the reaction of **1** as a probe for the mechanism of decomposition into products of the organometallic intermediates formed from the LTA–HF reactions with bicyclic olefins.

Reactions with Mercuric Acetate

The reaction of mercuric acetate (followed by sodium chloride) with **1** gave only one product, **8**, which on reduction with sodium borohydride yielded unrearranged acetate, **9**. Since **9** has the [2.2.2] ring skeleton, and since borohydride

Can. J. Chem. Downloaded from www.nrcresearchpress.com by 210.87.254.6 on 09/05/12
For personal use only.

reduction products of bicyclic organomercurials are formed without rearrangement (10, 4), the organomercurial resulting from the reaction of mercuric acetate with **1** was assigned the unrearranged [2.2.2] skeleton. An examination of the nmr spectrum of **8** confirms this assignment and further allows the assignment of the stereochemistry of the substituents. The nmr spectra of a large number of 2,3-disubstituted ethanoanthracenes, of known structure, have been analyzed (11). The average values of the spin–spin coupling constants for the 2,3-protons of the *cis*-2,3-disubstituted dibenzobicyclo[2.2.2]octadienes were reported as $J_{2,3} = 8.8 \pm 0.8$ while those for the *trans*-protons were $J_{2,3} = 3.5 \pm 1.1$. The coupling constant recorded for **8**, $J_{2,3} = 8.5$, confirms the proposal that the metal-ligand addition of mercuric acetate to **1** proceeded by a concerted *cis*-addition. Nonconcerted ionic additions to this system under nonequilibrium conditions lead exclusively to rearranged products (12).

Reaction with Thallium(III) Acetate

Since the organometallic intermediate from the oxidation of **1** by thallium acetate was not stable under the reaction conditions, the stereochemistry of the organothallium intermediate must be deduced from the stereochemistry of the products of its solvolysis. By analogy to the addition products formed from the oxidation of norbornene a *cis*-molecular addition to **1** would lead to intermediate **10**.

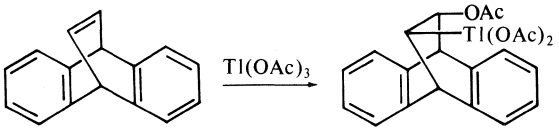

1 **10**

The heterolysis reactions of 2,3-disubstituted dibenzobicyclo[2.2.2]octadienes under conditions leading to kinetic control of products show only clean backside rearrangement with no loss of stereochemical identity (*i.e.*, no [2.2.2] cation is involved) (12*a*, 8).[2,3] Capture of the rearranged

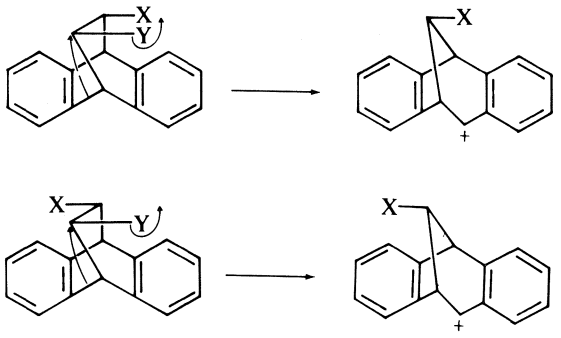

[3.2.1] cation by most nucleophiles favours *exo* substitution.

By analogy, the production of **4** from the heterolysis of **10** is consistent with the structure proposed.

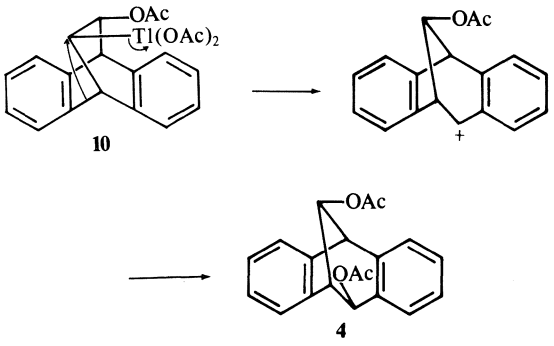

Reactions with Lead(IV) Reagents

The stereochemistry of the three rearranged, previously unknown, compounds **2**, **3**, and **6** obtained from the reaction of **1** with LTA–HF could be assigned on the basis of their nmr spectra, as could the stereochemistry of the previously reported unrearranged addition product **5**. Upon inspection of the spectra of compounds **2**, **3**, and **6** it is evident that one is dealing with the rearranged [3.2.1] skeletal ring system (13) rather than that of the [2.2.2] structure (11). Spin decoupling experiments (^{1}H and ^{19}F) verified that each spectrum showed in addition to the aromatic protons, and in the case of **3** and **6** the acetate methyl protons, four unique proton signals (1-H each) each having the first order coupling expected for the rearranged [3.2.1] system, which in the case of **2** and **3**, is further split by fluorine substituents. Once it was established that one was dealing with the rearranged [3.2.1] ring system for compounds **2**, **3**, and **6**, the steric

[2]A high energy intermediate [2.2.2] cation has been recognised in the mechanism leading to products formed reversibly; however, if this were the case in the organometallic oxidations in question the stereochemical integrity of the system would not be maintained, see ref. 21.

[3]The possible intervention of the cyclic acetoxonium ion, **11**, formed from the solvolysis of a *trans* adduct can be ruled out since the intermediacy of **11** and other cyclic onium ions have been shown to yield unrearranged [2.2.2] reaction products (8).

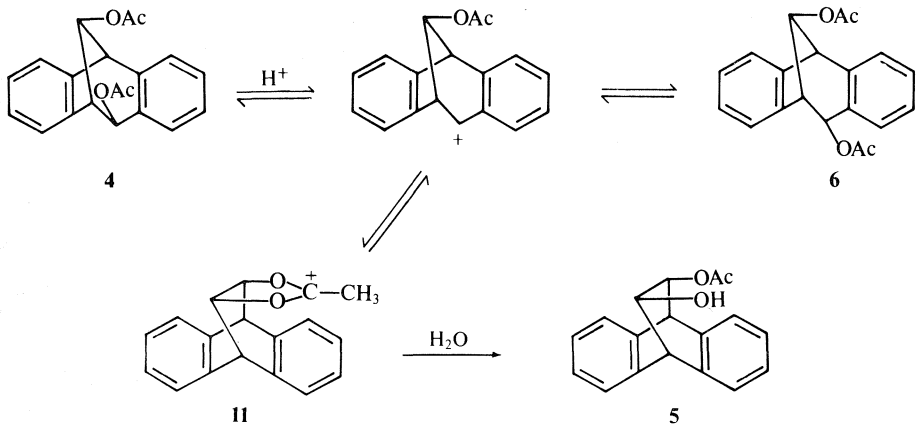

arrangement at the C-8 and C-2 positions could be established by a comparison of the proton coupling constants observed with those assigned previously for a large number of 2,8-disubstituted dibenzobicyclo[3.2.1]octadienes (13).

The nmr spectrum of **3** compares well with those of the other *syn*-8-halodibenzobicyclo-[3.2.1]octadien-*exo*-2-ol-acetates previously reported (13).

Solvolysis of **2** in dry acetic acid at 115 °C for 576 h resulted in the displacement of the C-4 fluorine and the formation of two compounds, **3**, and *syn*-8-fluorodibenzobicyclo[3.2.1]octadien-*endo*-2-ol acetate, **7**, in a 1:2 ratio (nmr integration). The nmr spectra of the solvolysis mixture were in good agreement with those of the chloro and bromo analogs of compounds **3** and **7** previously reported (13). The results of the solvolysis reaction confirm that one is dealing with the rearranged dibenzobicyclo[3.2.1]octadiene system. Had **2** been an unrearranged dibenzobicyclo[2.2.2]octadiene it would not have solvolysed unless more forcing conditions had been used (12*a*).

In the nmr spectrum of **4**, isolated from the reaction of **1** with LTA–HF, was also seen a small amount (~1.4%) of another product tentatively assigned the structure of **6** on the basis of its nmr absorption and coupling constants (12*d*, 13).

The amount of compounds **5** and **6** initially formed in the reaction of **1** with LTA–HF appeared, by a rough visual estimation of the amounts separated by tlc, to be variable depending upon the length of time that the reaction mixture was allowed to stand before the products were isolated. From this observation it was assumed that both **5** and **6** were secondary reaction products formed from the reaction of **4** with the reagent. This assumption was confirmed when **4** was subjected to the reaction conditions and found by tlc to yield a mixture of two products, **5** and **6**, besides starting material, **4**. The mole ratio (nmr integration) of **4**:**5**:**6** was 2:2:1. The mixture of products could be separated into two fractions by tlc, one fraction a mixture of **4** and **6** and the other containing **5**. The hydroxy acetate, **5**, was identical (ir, nmr, mp) with that isolated from the reaction of **1** with LTA–HF. The mixture of **4** and **6** gave the same nmr absorption pattern as that obtained from the mixture isolated from the reaction of **1** with LTA–HF, except the amount of **6** relative to **4** (1:2) was greater.

The observation that **4** could be converted stereospecifically into **5**, under acidic conditions followed by aqueous work-up, had been reported previously by Cristol *et al.* (8). The mechanism proposed for this conversion leads to a stabilized cation, **11**, which upon reaction with water yields **5**. Presumably, the intermediate epimeric *syn-endo*-diacetate, **6**, was formed, in the LTA–HF reaction, from the [3.2.1] cation by reaction with an acetate anion at an early stage of the reaction.

Mechanistic Conclusions

The reaction of **1** with both $Pb(OAc)_4$ and $Pb(OAc)_4$–HF, likewise, follows the same stereochemical course as the $Tl(OAc)_3$ oxidations.

Can. J. Chem. Downloaded from www.nrcresearchpress.com by 210.87.254.6 on 09/05/12
For personal use only.

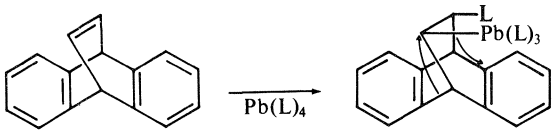

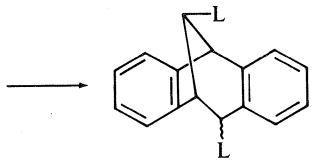

L = OAc or F

A different scheme has previously been proposed by Alder *et al.* to rationalize the oxidation of norbornene with LTA (14). The production of

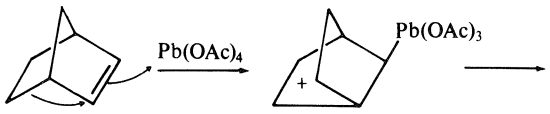

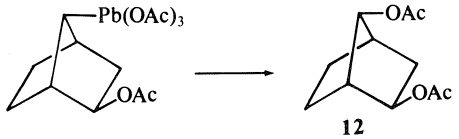

12

12, via this scheme necessitates, however, an unprecedented stereospecific front side displacement of lead by the acetoxy group in order to produce the *syn*-7-*exo*-2-diacetoxynorbornane. The products of the reaction can more readily be explained, by analogy to the metal-ligand oxidation of thallium(III) acetate, mercuric acetate, and LTA–HF, by a *cis*-molecular addition process followed by the displacement of lead to yield an acetoxy norbornyl cation and ultimately

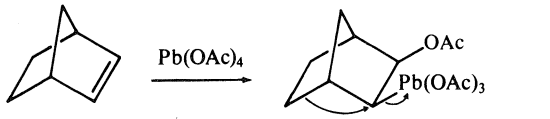

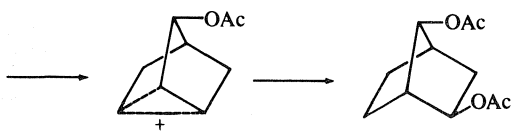

diacetate. Norman and co-workers have likewise, recently suggested that the reaction of lead(IV) (15, 16), thallium(III) (16), and mercury(II) acetate (16) with several acyclic olefins yields oxidation products by a mechanism which involves cationic species at two stages of the reaction (*i.e.*, at the addition and the homolysis). It is not necessary, however, that the first stage of these reactions must involve cationic intermediates, since under the reaction conditions it is not unlikely that the initial 1,2-addition products would be unstable and by an analogy to the mechanisms proposed for the bicyclic systems yield the products observed. However, lead-ligand oxidations of olefins less strained than the bicyclic systems studied may not proceed via the concerted *cis*-addition process proposed, since the analogous additions of mercuric acetate follow a *cis*-addition process during the oxymercuration of strained olefins, but yield *trans*-addition products from the reactions of monocyclic olefins and open chained alkenes. The stereochemistry of the latter additions are stereospecific and *trans*, although it is reported that they do not proceed through free cationic intermediates (17).

Since the reaction of **1** with either LTA or LTA–HF leads to completely rearranged products in a stereospecific manner (if one omits the stereospecific secondary reaction of **4** leading to **5**), and since both reactions cleanly maintain the *syn-exo* (or *endo*) stereochemistry, then the mechanism established for norbornene, *cis*-molecular addition, satisfactorily rationalizes the products and stereochemistry observed, while the reactions proceeding via the alternative routes, *a* and *b*, are much less attractive (see Scheme 1). Reaction proceeding through path *a* requires, as in the case of norbornene, a stereospecific front side displacement of lead from the bridge position and although this process has been proposed (14, 15) there seems to be no evidence to support its occurrence. A homolytic reaction proceeding via path *b* to form a radical center at the 3-position could conceivably lead to rearrangement, followed by oxidation of the rearranged radical to give the benzylic cation or oxidation of the unrearranged radical to give directly the rearranged cation. Rearrangement of 3-position radicals in this system have been observed: however, they proceed non-stereospecifically to

Can. J. Chem. Downloaded from www.nrcresearchpress.com by 210.87.254.6 on 09/05/12
For personal use only.

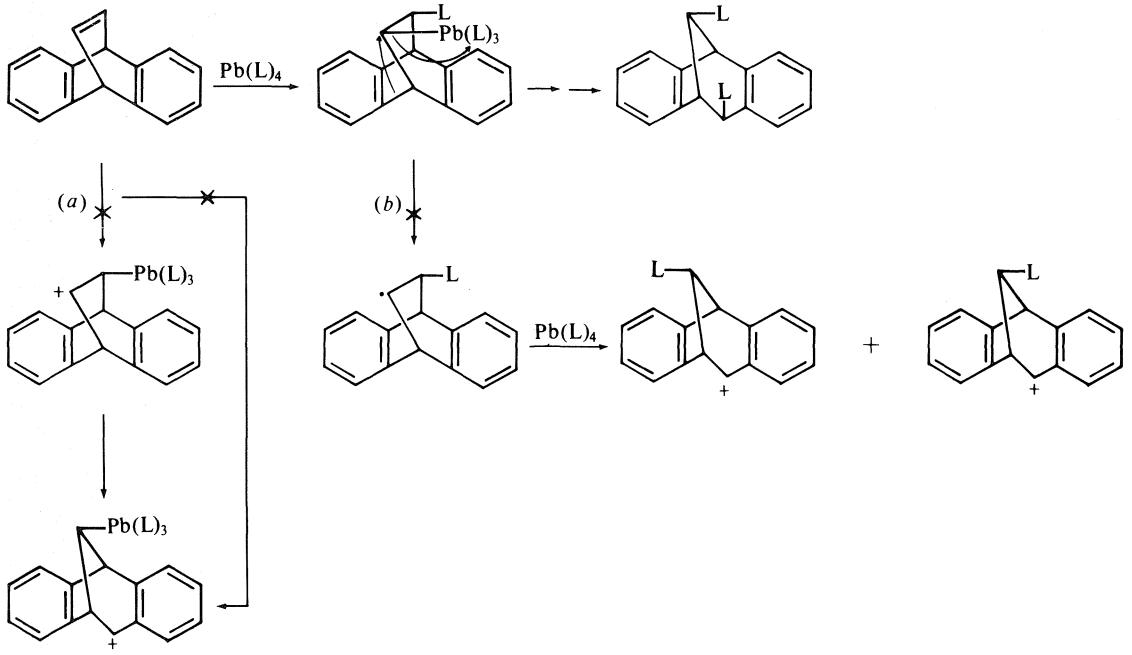

SCHEME 1

give products having both *syn* and *anti* stereochemistry (18). The unrearranged radicals upon atom transfer prior to rearrangement yield both *cis*- and *trans*-2,3-addition products (18). On the basis of the above, it is unlikely that a homolytic process would, upon oxidation to a cationic intermediate, yield products stereospecifically.

The production of rearranged products in a stereospecific manner from the entire isoelectronic series studied, Hg^{II}, Tl^{III}, Pb^{IV}, strongly supports the suggestion that for the reaction of strained bicyclic olefins these oxidations all proceed via a similar mechanism having as its first step a *cis*-molecular addition process.

Experimental

Material

Lead tetraacetate (Matheson reagent grade) was recrystallized several times from acetic acid containing 4% of acetic anhydride and the white crystals were washed with acetic acid, and filtered. The lead tetraacetate used in each reaction was determined by titration.

Anhydrous hydrogen fluoride (Matheson) was distilled and condensed into an open polyethylene flask cooled to −80 °C, and was used without further purification. When used in this manner it could no longer be considered anhydrous.

Methylene chloride was distilled from phosphorus pentoxide prior to use.

Dibenzobicyclo[2.2.2]octatriene was prepared by the method of Cristol *et al.*, mp 121–122 °C (lit. (12*a*) mp 119.5–120 °C). The purity of the compound was confirmed by its nmr spectrum and by the observation that it behaved as a homogeneous compound when subjected to tlc (silica gel, $CHCl_3$).

Mercury(II) acetate (Fisher, reagent grade) was dried under vacuum over phosphorus pentoxide.

Glacial acetic acid was dried by distillation of glacial acetic acid containing 4% acetic anhydride and a drop of concentrated sulfuric acid.

Dibenzobicyclo[2.2.2]octadien-2-ol acetate was prepared by the method of Alder and Rickert, mp 99–100 °C (lit. (19) mp 100–101 °C). The nmr spectrum was identical to that reported (11).

Dibenzobicyclo[3.2.1]octadien-*exo*-2-*syn*-8-diol diacetate was prepared by the method of Cristol *et al.*, mp 169–171 °C (lit. (12*a*) mp 168–169 °C). The nmr spectrum was identical to that reported (13).

Reaction of Dibenzobicyclo[2.2.2]octatriene with Lead Tetraacetate–Hydrogen Fluoride (LTA–HF)

To a precooled, 0 °C, solution of LTA (43.2 g, 0.0974 mol) in 300 ml of methylene chloride was added liquid hydrogen fluoride (3.8 g, 0.19 mol). The mixture, in a polyethylene flask, protected from additional atmospheric moisture by a calcium chloride drying tube, was stirred at 0 °C for 1 h to preform the reagent. To the stirred mixture was added 30 ml of a precooled, 0 °C, solution of **1** (9.95 g, 0.0488 mol), and the reaction was stirred for an additional 30 min at 0 °C. The reaction mixture was poured into a cold, 0 °C, saturated potassium carbonate solution and the organic and inorganic layers were separated. The organic layer was filtered through Celite

Can. J. Chem. Downloaded from www.nrcresearchpress.com by 210.87.254.6 on 09/05/12
For personal use only.

Can. J. Chem. Downloaded from www.nrcresearchpress.com by 210.87.254.6 on 09/05/12
For personal use only.

Filter Aid. The aqueous layer was extracted with methylene chloride, and the combined organic phase was washed with water, a solution of saturated sodium bicarbonate, again with water, and dried over anhydrous magnesium sulfate. Evaporation of the solvent left a residue of 13.10 g which showed five distinct bands on tlc (silica gel GF, $CHCl_3$). The residue was subjected to preparative tlc. Each of the five bands was isolated and the silica gel containing the compound from each fraction was extracted with chloroform. The chloroform was evaporated leaving a combined total residue weight of 13.02 g (*i.e.*, 98% recovery). The first fraction (nearest the solvent front) contained unreacted starting olefin (1.952 g, 0.0095 mol), mp, mixture mp, and ir and nmr spectra, were identical to those of the authentic material.

The second compound isolated, 23.9% of the olefin reacted, (2.271 g, 0.00938 mol) was *syn*-8-*exo*-4-difluorodibenzobicyclo[3.2.1]octadiene **2**, mp 152–153 °C; nmr ($CDCl_3$) τ 4.58 (H-8, 1H, d of t, $J_{8H,8F}$ = 54 Hz, J_t = 5 Hz), 4.51 (H-4, 1H, br d, J_d = 50 Hz, $W_{1/2}$ = 3 Hz), 5.87 (H-1, 1H, d, $J_{1,4}$ = 5 Hz), 6.10 (H-5, 1H, d of m, $J_{4F,5H}$ = 11 Hz). Spin decoupling experiments verified the assignments. When the signal at τ 5.87 was irradiated the signal at τ 4.58 collapsed to a d of d. Irradiation of the absorption at τ 6.10 affected the signals at τ 4.58 and 4.51. *Anal.* calcd. for $C_{16}H_{12}F_2$: C 79.32, H 4.99; found: C 79.47, H 5.12.

The third compound isolated, *syn*-8-fluorodibenzobicyclo[3.2.1]octadien-*exo*-2-ol acetate **3**, after recrystallization from Skelly B yielded 4.144 g, 0.0147 mol (37.5% based on olefin reacted), mp 136.5–137 °C; nmr ($CDCl_3$) τ 4.32 (H-2, 1H, d, $J_{1,2}$ = 1.5 Hz), 4.69 (H-8, 1H, d of t, J_d = 52 Hz, J_t = 5 Hz), 6.03 (H-5, 1H, d, $J_{5,8}$ = 5 Hz), 6.42 (H-1, 1H, d of d, J = 5 Hz, $J_{1,2}$ = 1.5 Hz), 7.91 (CH_3-H, 3H, s); ir (CCl_4), 1740, 1238 cm^{-1}; *m/e* 282.1054 (calcd. for $C_{18}H_{15}FO_2$: 282.1056). *Anal* calcd. for $C_{18}H_{15}FO_2$: C 76.58, H 5.36; found: C 76.53, H 5.33.

The fourth compound isolated, dibenzobicyclo[3.2.1]-octadien-*exo*-2-*syn*-8-diol diacetate **4**, after recrystallization from Skelly B, yielded 3.396 g (0.0102 mol, 26.0% based on olefin reacted); mp 169–171 °C (lit. (12*a*) mp 168–170 °C). The ir spectrum was identical to that of the authentic material. The nmr spectrum before recrystallization showed the presence of another minor compound, **6**, representing 5.5% of the mixture; the nmr ($CDCl_3$) was identical to that previously reported (13). The nmr of the minor component **6** showed absorption at τ 3.72 (H-2, 1H, d, $J_{1,2}$ = 5.0 Hz), 4.48 (H-8, 1H, t, $J_{5,8}$ = 5.0 Hz) 7.91 (CH_3, 3H, s), 8.15 (CH_3, 3H, s), 5.85 (H-5, 1H, d). The absorption for the C-1 hydrogen was coincident with the C-1H absorption at τ 6.10 in compound **4**.

The fifth compound isolated, *cis*-dibenzobicyclo[2.2.2]-octadiene-2,3-diol monoacetate (**5**) was isolated in 12.3% yield (1.357 g, 0.00481 mol), mp 169–171 °C (lit. (8) mp 169–170 °C). *Anal.* calcd for $C_{18}H_{16}O_3$: C 77.12, H 5.75; found: C 76.95, H 5.88. The ir was identical to that reported (8). The nmr ($CDCl_3$), τ 5.59 (H-1 and H-4, 2H), 4.99 (H-2, 1H, d of d), 5.81 (H-3, 1H, m), 8.37 (OH, 1H, d), 8.07 (CH_3, 3H, s).

When the nmr sample was shaken with D_2O the absorption at τ 8.37 disappeared and the absorption at τ 5.81 became a quartet. Spin decoupling experiments confirmed the *cis* assignment of the stereochemistry at carbons 2 and 3. $J_{3,OH}$ = 9.0, $J_{2,3}$ = 7.5, $J_{3,4}$ = 3.0 = $J_{1,2}$. The large coupling constant $J_{2,3}$ = 7.5 was consistent, as in the case of **8**, with the assignment of a *cis*-stereochemistry (11).

Solvolysis of syn-8-exo-4-Difluorodibenzobicyclo[3.2.1]-octadiene ***2***

Compound **2** (51 mg, 0.21 mmol) was dissolved in 6 ml of dry glacial acetic acid sealed in a Pyrex ampoule, and heated at 115 °C for 576 h. The reaction mixture was poured into 20 ml of water and extracted with chloroform. The organic layer was washed with water, saturated sodium bicarbonate solution, and dried over anhydrous sodium sulfate. The solvent was removed by rotary evaporation and the residue was studied by nmr (see Results and Discussion).

Reaction of ***4*** *with LTA–HF*

To a cold solution, 0 °C, of LTA (800 mg, 1.8 mmol) in 10 ml of methylene chloride was added 0.5 ml (20 mmol) of liquid hydrogen fluoride. The mixture was stirred for 1 h at 0 °C. To the preformed reagent was added a 10 ml methylene chloride solution of **4** (162 mg, 0.487 mmol) together with a drop of distilled water. The mixture was stirred for 30 min at 0 °C and the products were isolated, as were those from the reaction of **1** with the reagent, yielding 154 mg of a waxy solid. Nuclear magnetic resonance analysis of the residue showed three compounds, **6**, **4**, and **5** in the ratio of 1:2:2. The mixture could be separated into two fractions by preparative tlc (silica gel GF, $CHCl_3$). Extraction of the two fractions from the silica gel yielded 39 mg (0.138 mmol) of **5** and 115 mg (0.325 mmol) of a 2:1 mixture (nmr integration) of **4** and **6**.

The mp, 169–171 °C, and nmr and ir spectra of **5** were identical with those for the sample of **5** isolated from the reaction of **1** with LTA–HF.

The nmr and ir spectra of the mixture of **4** and **6** were identical (except for absorption intensities) with the mixture of these compounds obtained from the reaction of **1** with LTA–HF.

Reaction of ***1*** *with Lead Tetraacetate*

A solution of **1** (347 mg, 1.70 mmol) and LTA (1631 mg, 3.68 mmol) in 15 ml of dry glacial acetic acid was stirred for 21 h at 80 °C. The reaction mixture was extracted with ether, washed with sodium carbonate solution, then water, dried over anhydrous magnesium sulfate, filtered, and the solvent evaporated. A light yellow solid (0.527 g) was obtained. Thin layer chromatography (silica gel GF, $CHCl_3$) showed a trace of a yellow compound and one major component. The nmr (CCl_4) of the crude product showed the presence of two compounds in the ratio of 99.5:0.5. The major product had the spectrum of **4** while the minor compound was assigned the structure of **6**. Recrystallization of the crude product from Skelly B gave 0.511 g (0.00159 mol) of a white compound **4**, mp 169–171 °C.

Reaction of Mercury(II) Acetate – Sodium Chloride with ***1***

A solution of mercuric acetate (2.120 g, 0.0665 mol) and **1** (0.595 g, 0.00292 mol) in 16 ml of dry glacial acetic acid was stirred at room temperature for 1 h. The reaction mixture was then poured into 75 ml of ice water containing sodium chloride (0.93 g, 0.016 mol). The heterogeneous mixture which now contained a white precipitate was stirred for another 2 h. The white solid

Can. J. Chem. Downloaded from www.nrcresearchpress.com by 210.87.254.6 on 09/05/12
For personal use only.

was filtered, washed with ice water, and dried *in vacuo* over phosphorus pentoxide. The yield of the product, *cis*-dibenzobicyclo[2.2.2]octadienyl-3-acetoxy-2-mercuric chloride (**8**), was 1.458 g (0.00292 mol), 100%; mp 187–190 °C; mass spectrum M^+ *m/e* 500.0456 (calcd. for $C_{18}H_{15}O_2{}^{202}Hg^{35}Cl$: 500.0467), base peak $(M - C_4H_5ClHgO_2)^+$ *m/e* 178.0788 (calcd. for $C_{14}H_{10}$: 178.0783); nmr ($CDCl_3$) τ 5.33 (H-4, 1H, d, $J_{3,4}$ = 3.0 Hz), 5.42 (H-1, 1H, d, $J_{1,2}$ = 2.5 Hz), 4.67 (H-3, 1H, q, $J_{3,4}$ = 3.0 Hz, $J_{2,3}$ = 8.5 Hz), 6.76 (H-2, 1H, q, $J_{2,3}$ = 8.5 Hz, $J_{1,2}$ = 2.5 Hz); ir ($CHCl_3$), 1745 cm^{-1}. *Anal.* calcd. for $C_{18}H_{15}O_2HgCl$: C 43.29, H 3.03; found: C 42.76, H 3.01.

*Reduction of **8** with Sodium Borohydride*

The oxymercuration product, **8**, (186 mg, 0.374 mmol) was dissolved in 10 ml of tetrahydrofuran. A solution (12 ml of 3:1 THF–H_2O) of sodium borohydride (0.25 *M*) and sodium hydroxide (3 *M*) was then added. The mixture was stirred for 1 min. The THF layer was separated, filtered, washed twice with water, and dried over anhydrous magnesium sulfate. The resulting bright yellow solution was decolorized with activated charcoal and filtered. The filtrate was evaporated to dryness leaving a white solid which was then recrystallized from water – ethyl alcohol to yield 97.8 mg (0.370 mmol) of **9**; mp 99–100 °C (lit. (19) mp 100–101 °C); ir and nmr spectra were identical with those of an authentic sample.

*Reaction of **1** with Thallium(III) Acetate*

To a mixture of thallium(III) oxide (2.741 g, 0.00600 mol), acetic anhydride (2.04 g, 0.02 mol), and 40 ml of dry glacial acetic acid (*i.e.*, the *in situ* preparation of thallium(III) acetate) (20) was added **1** (0.816 g, 0.00400 mol), and the heterogeneous mixture was stirred for 24 h at 80 °C. The thallium oxide dissolved after 12 h to form a clear yellow solution. The reaction mixture was poured into 40 ml of water and the product was extracted with ether. The ethereal solution was washed with water, sodium bicarbonate, and again with water, dried over anhydrous magnesium sulfate and filtered. A white solid, **4** (1.220 g, 0.0038 mol) was obtained after the ether was evaporated, mp 169–171 °C (lit. (13) mp 168–169 °C). The ir and nmr spectra were identical with those of an authentic sample of **4**.

Acknowledgements

The authors wish to thank the National Research Council of Canada and the University of Alberta for their generous support of this work. One of the authors (D.D.T.) is also grateful to the administration and faculty of the Department of Chemistry at the University of St. Andrews, St. Andrews, Scotland, for their hospitality during the period in which this manuscript was prepared.

1. D. D. Tanner and P. Van Bostelen. J. Am. Chem. Soc. **94**, 3187 (1972).
2. J. Levisalles and J. Molimard. Bull. Soc. Chim. 2037 (1971).
3. M. Ephritikhine and J. Levisalles. Chem. Commun. 429 (1974).
4. T. G. Traylor and A. E. Baker. J. Am. Chem. Soc. **85**, 2746 (1963).
5. K. C. Pande and S. Winstein. Tetrahedron Lett. 3393 (1964).
6. (*a*) R. Criegee. *In* Oxidation in organic chemistry. Part A. *Edited by* K. B. Wiberg. Academic Press, New York. 1965. Chapt. 5; (*b*) C. D. Hurd and O. E. Edwards. J. Org. Chem. **19**, 1319 (1954); (*c*) E. Detilleux and J. Jadot. Bull. Soc. R. Sci. Liege, **29**, 208 (1960); (*d*) T. Aratani. J. Chem. Soc. Jpn. **78**, 1534 (1957); (*e*) B. Cross and G. H. Whitham. J. Chem. Soc. 3895 (1960); (*f*) R. O. C. Norman and C. B. Thomas. J. Chem. Soc. (B), 771 (1967).
7. J. Bornstein, M. R. Borden, F. Nunes, and H. I. Tarlin. J. Am. Chem. Soc. **85**, 1609 (1963).
8. S. J. Cristol, F. P. Parungo, D. E. Plorde, and K. Schwarzenbach. J. Am. Chem. Soc. **87**, 2879 (1965).
9. T. G. Traylor. Acc. Chem. Res. **2**, 152 (1969).
10. G. M. Whitesides and J. S. Filippo, Jr. J. Am. Chem. Soc. **92**, 6611 (1970).
11. S. J. Cristol, T. W. Russell, J. R. Mohrig, and D. E. Plorde. J. Org. Chem. **31**, 581 (1966).
12. (*a*) S. J. Cristol, F. P. Parungo, and D. E. Plorde. J. Am. Chem. Soc. **87**, 2870 (1965); (*b*) S. J. Cristol and R. K. Bly. J. Am. Chem. Soc. **82**, 6155 (1960); (*c*) S. J. Cristol, R. P. Arganbright, and D. D. Tanner. J. Org. Chem. **28**, 1374 (1963); (*d*) D. D. Tanner and B. G. Brownlee. J. Am. Chem. Soc. **88**, 771 (1966).
13. S. J. Cristol, J. R. Mohrig, and D. E. Plorde. J. Org. Chem. **30**, 1956 (1965).
14. K. Alder, F. H. Flock, and H. Wirtz. Chem. Ber. **91**, 609 (1958).
15. R. O. C. Norman and C. B. Thomas. J. Chem. Soc. (B), 604 (1967).
16. A. Lethbridge, R. O. C. Norman, C. B. Thomas, and W. J. E. Parr. J. Chem. Soc. (B), 231 (1975).
17. R. C. Fahey. Topics in stereochemistry. Vol. 3. Interscience Inc., New York, N.Y. 1968.
18. B. B. Jarvis, J. P. Govoni, and P. J. Zeil. J. Am. Chem. Soc. **93**, 313 (1971).
19. K. Alder and H. Rickert. Ann. **573**, 1 (1939).
20. R. J. Ouellette, G. Kordosky, C. Levin, and S. Williams. J. Org. Chem. **34**, 4104 (1969).
21. S. J. Cristol and R. J. Bopp. J. Org. Chem. **39**, 1336 (1974).

Addition of iodine to dimethyl norbornadiene-2,3-dicarboxylate: nuclear magnetic resonance (^{1}H and ^{13}C) spectra and stereochemistry of nortricyclenes[1]

A. W. McCulloch, A. G. McInnes, D. G. Smith, and J. A. Walter

Atlantic Regional Laboratory, National Research Council of Canada, Halifax, N.S., Canada B3H 3Z1

Received January 16, 1976

A. W. McCulloch, A. G. McInnes, D. G. Smith, and J. A. Walter. Can. J. Chem. **54**, 2013 (1976).

The free radical addition of iodine to dimethyl bicyclo[2.2.1]hepta-2,5-diene-2,3-dicarboxylate (**3***a*) yields three stereoisomeric dimethyl 3,5-diiodotricyclo[2.2.1.0^{2,6}]heptane-2,3-dicarboxylates (nortricyclenes **4**–**6**), as well as dimethyl 5,6-diiodobicyclo[2.2.1]hept-2-ene-2,3-dicarboxylate (**9**). By-products are two dimethyl 3-hydroxy-5-iodotricyclo[2.2.1.0^{2,6}]heptane-2,3-dicarboxylates (nortricyclenes **7**, **8**). Compounds **4** and **5** are also obtained as major products of addition of iodine to dimethyl tetracyclo[2.2.1.0^{2,6}0^{3,5}]heptane-2,3-dicarboxylate (quadricyclane **10***a*). The structures of these various products were elucidated with the aid of ^{1}H and ^{13}C nmr and high-resolution mass spectroscopy.

A. W. McCulloch, A. G. McInnes, D. G. Smith et J. A. Walter. Can. J. Chem. **54**, 2013 (1976).

L'addition radicalaire d'iode au bicyclo[2.2.1]heptadiène-2,5 dicarboxylates-2,3 de diméthyle (**3***a*) conduit aux trois diiodo-3,5 tricyclo[2.2.1.0^{2,6}]heptanedicarboxylates-2,3 de diméthyle (nortricyclènes **4**–**6**) de même qu'au diiodo-5,6 bicyclo[2.2.1]heptène-2 dicarboxylate-2,3 de diméthyle (**9**). On retrouve comme sous-produits les deux hydroxy-3 iodo-5 tricyclo[2.2.1.0^{2,6}]-heptanedicarboxylate-2,3 de diméthyle (nortricyclènes **7** et **8**). On obtient aussi les composés **4** et **5** comme produits majeurs de l'addition de l'iode au tétracyclo[2.2.1.0^{2,6}0^{3,5}]heptanedicarboxylates-2,3 de diméthyle (quadricyclane **10***a*). On a établie les structures de ces divers produits à l'aide de la rmn du ^{1}H et du ^{13}C et de la spectroscopie de masse à haute résolution.

[Traduit par le journal]

Introduction

We have recently reported the iodine-promoted isomerization of 7-oxanorbornadienes **1** to 6-hydroxyfulvenes **2** (1). In the course of investigating the mechanism of this rearrangement we studied the reaction of iodine with the structurally analogous norbornadiene diester **3***a*. The

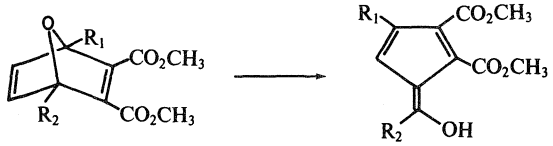

1 **2**

reaction product contained five 3,5-disubstituted nortricyclenes **4**–**8**, as well as the norbornene **9**.

A survey of the literature showed that although a considerable amount of work has been carried out on the ^{1}H nmr spectra of various substituted nortricyclenes, many of the data are incomplete. In only a few cases has a detailed analysis of the spectra been undertaken, and here the compounds involved have either been symmetrically

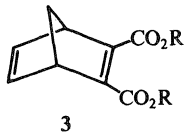

3

a) R = CH_3
b) R = H

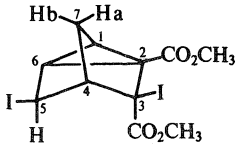

4

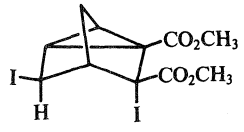

5

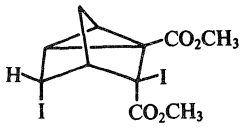

6

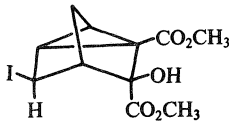

7

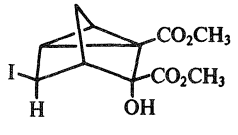

8

[1]Issued as NRCC No. 15269.

Can. J. Chem. Downloaded from www.nrcresearchpress.com by 210.87.254.40 on 09/05/12
For personal use only.

Can. J. Chem. Downloaded from www.nrcresearchpress.com by 210.87.254.40 on 09/05/12
For personal use only.

substituted (2) or have lacked protons at C-7 (3). In addition, apart from some work on nortricyclene itself (4), the only significant ^{13}C data reported appear in a study of the chemical shifts of some substituted nortricyclenes by Lippmaa *et al.* (5). [2] The isolation of a series of similarly substituted nortricyclenes thus presented an excellent opportunity to carry out an nmr study (^1H and ^{13}C).

Results and Discussion

Homoconjugate addition to the norbornadiene system is well known and may proceed under ionic or free-radical conditions. The major products formed by addition of bromine (7) or chlorine (8) to norbornadiene, for example, are isomeric 3,5-dihalonortricyclenes; addition of iodine is reported to give a mixture (not separated) of 3,5-diiodonortricyclenes (9). While it has been reported that the quadricyclane diacid **10***b* forms a moderately stable diiodide (structure not investigated), the corresponding norbornadiene diacid **3***b* was found to be unreactive (10).

We have found that reaction of **3***a* with iodine (in daylight) gave *three* isomeric 3,5-diiodonortricyclenes **4** (46%), **5** (20%), and **6** (1%), together with a pair of isomeric 3-hydroxy-

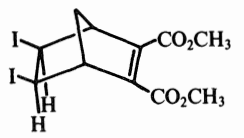

9

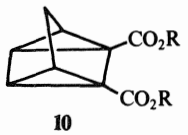

10

a) R = CH_3
b) R = H

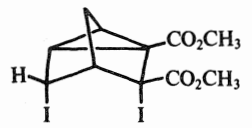

11

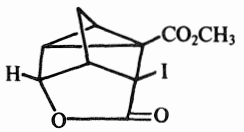

12

5-iodonortricyclenes **7** and **8** (total 2%) and the *exo-cis* 5,6-diiodonorbornene **9** (5%).

In accord with a free-radical mechanism for the reaction (Scheme 1), iodination of **3***a* in the dark was significantly slower (by a factor of *ca.* 8). Supplementary evidence for the intermediacy of radicals **a** and **b** (Scheme 1) in the formation of **4** and **5** was provided by the isolation of the two corresponding nortricyclyl alcohols formed by *exo* or *endo* attack by ·OH[3] on radical **b**. The isolation of **9** was also consistent with a radical pathway; products of *exo-cis* addition have been observed previously in free-radical additions to norbornadienes (11).

Iodination of the corresponding quadricyclane **10***a* under identical conditions gave the two nortricyclenes **4** and **5** in a *ca.* 2:1 ratio. In view of the similarity of the product ratio it seems highly probable that the intermediates involved are the same as those involved in the radical addition to **3***a* (Scheme 1) (*cf.* 12). Similar additions to other quadricyclane 2,3-dicarboxylic acid derivatives have also been reported to give a pair of C-3 epimers (3, 13, 14).

Isolation of the third isomer **6** from addition to **3***a* was unexpected. This minor product most likely arose via the less favored *endo* attack by iodine at C-5 in **3***a* (to give **c**), followed by preferred *exo* attack at C-3 in the rearranged radical **d** (Scheme 1). We were unable to detect any product having the spectral characteristics expected of the fourth possible isomer **11**, theoretically also derivable from radical **d**.

The pathways outlined in Scheme 1 also explain the partial isomerization of **4** to **5** on standing or on irradiation at 3000 Å, as well as the conversions of both **4** and **5** to **12** on pyrolysis (see Experimental). These pyrolytic conversions must both have proceeded via intramolecular lactonization of **4** (*cf.* 3, 13). As expected, the rearrangement of **5** to **12** occurred more slowly than that of **4**, and both **4** and **5** could be detected in each crude pyrolysis product.

Structures

Compounds 4, 5, and 6

The overall 2,3-dicarbomethoxy-3,5-diiodonortricyclene structure of products **4**, **5**, and **6** was confirmed by their ^1H and ^{13}C nmr spectra. All three compounds in addition gave mass and ir spectra in accord with their structures (see Experimental).

The ^{13}C nmr data (Table 2) for each compound indicated two cyclopropyl methine carbons (with characteristic high-field chemical

[2]We have recently reported ^{13}C nmr data for two 7-oxanortricyclene derivatives (6).

[3]No special precautions were taken to ensure anhydrous experimental conditions. The alcohols are apparently not formed via hydrolysis of **4** and/or **5**: attempted hydrolyses of **4** and **5** (moist ether) at room temperature were unsuccessful. Increased amounts of **7** and **8** were, moreover, obtained after irradiation of **4** (see Experimental).

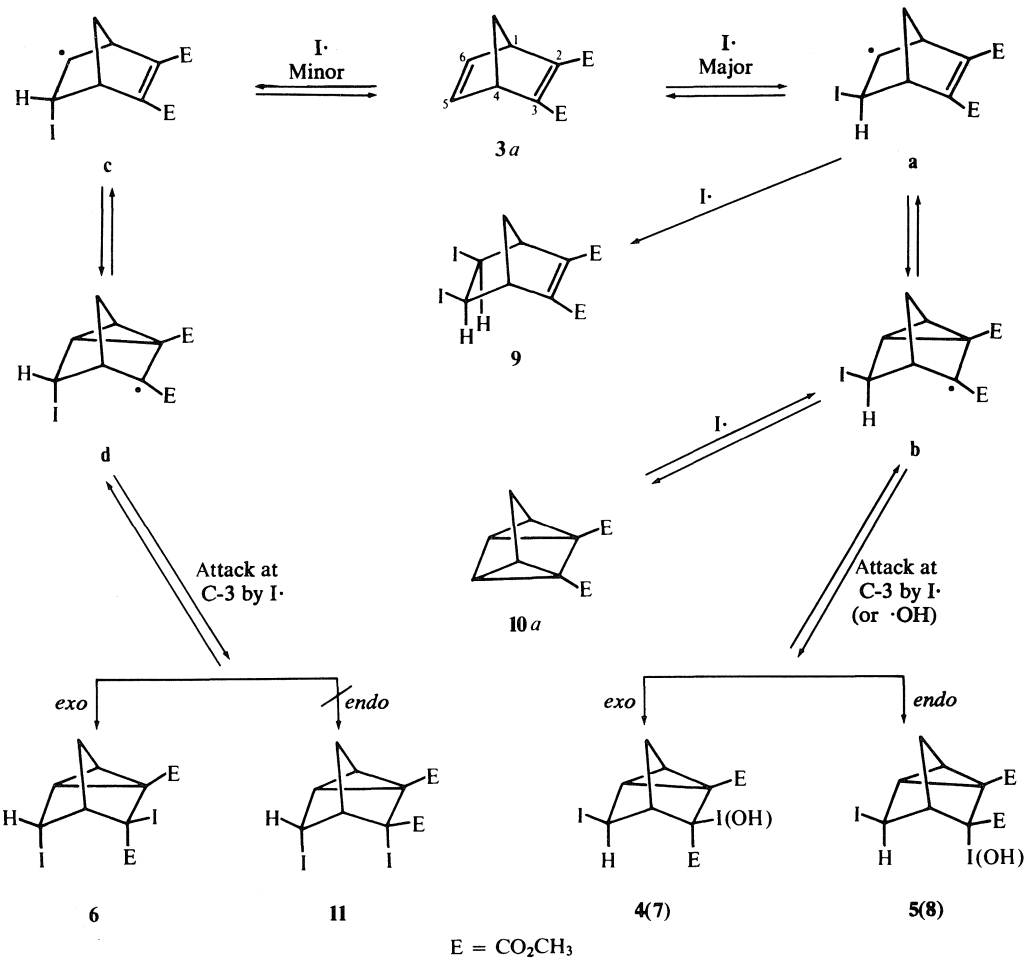

SCHEME 1

shifts (15*a*, 16) and high $^1J_{^{13}C-H}$ values (15*b*)), and two other high-field quaternary carbons consistent with cyclopropyl (15*a*, 16) or iodine-substituted (15*a*) centers. The remaining carbon resonances (methine, bridge, and carbomethoxyl carbons) could be readily identified on the basis of their chemical shifts and multiplicities.

The ^{1}H nmr spectra (Table 1) also exhibited shifts and coupling constants in accord with literature values for other nortricyclenes (17–19). With the exception of $J_{7a,7b}$ and $J_{1,6}$, all coupling constants were in the range 0–2 Hz.

Additions to both the norbornadiene (7, 8, 19–21) and to the quadricyclane (3, 13, 14) systems have consistently afforded a pair of C-3 epimeric 3,5-disubstituted nortricyclenes. Analogous addition to **3***a* would thus be expected to yield **4** and **5** as predominant products. The facility with which **4** is converted to **12** indicates that in **4** the carbomethoxyl substituent at C-3 must be oriented *endo*, and the iodine at C-5 *exo*, to the bridged ring (*cf.* 3, 13).[4]

It is well known that chemical shifts (^{1}H and ^{13}C) in norbornyl and nortricyclyl compounds are extremely sensitive to changes in molecular geometry (2, 5, 22). The most important long range effects in the nortricyclene system are steric interactions of the type shown in Fig. 1. Interactions of substituent X lead to changes (usually diamagnetic) in the chemical shifts of

[4]The formation of **12** involves elimination of methyl iodide from **4**, and indeed a singlet resonance in the ^{1}H nmr spectrum of the crude pyrolysis product at 2.17 δ can be attributed to this compound.

Can. J. Chem. Downloaded from www.nrcresearchpress.com by 210.87.254.40 on 09/05/12
For personal use only.

TABLE 1. 100 MHz ^{1}H nmr parameters for **4**–**9** and **12** (C_6D_6)

Parameter	4	5	6	7	8	12	9*
Chemical shifts (δ)							
H-1	1.77	1.89	1.39	2.01	2.06	2.15	3.62
H-4	2.44	2.38	2.42	2.03	1.99	2.07	
H-5	3.79	4.66	3.13	4.54	4.69	3.97	4.27
H-6	2.27	2.03	2.28	2.45	2.22	1.82	
H-7a	2.37	1.31	2.20	2.48	1.80	1.57	2.09
H-7b	2.16	1.81	0.89	2.15	1.91	1.01	2.48
$-CO_2CH_3$	3.14	3.20	3.40	3.18	3.20	3.30	3.78
	3.34	3.33	3.43	3.24	3.30	—	
—OH	—	—	—	3.68	3.60	—	—
Coupling constants (Hz)							
1,4	1.2	1.2	1.2	1.2	1.2	1.3	†
1,5	<0.3	<0.3	0.3	<0.3	<0.3	< 0.3	<0.3
1,6	5.0	5.1	5.7	5.2	5.1	5.1	<0.3
1,7a	1.4	1.4	1.6	1.4	1.4	1.6	1.8
1,7b	1.4	1.4	1.4	1.4	1.4	1.4	1.4
4,5	1.4	1.4	1.3	1.4	1.4	2.8	<0.3
4,6	1.4	1.4	1.1	1.4	1.2	1.0	<0.3
4,7a	1.4	1.4	1.8	1.4	1.4	1.6	1.8
4,7b	1.4	1.5	1.4	1.4	1.4	1.4	1.4
5,6	1.4	1.4	1.1	1.4	1.2	2.2	†
5,7a	0.9	0.6	<0.3	0.9	0.8	−0.4	2.2
5,7b	−0.4	−0.4	<0.3	−0.4	−0.4	<0.3	<0.3
6,7a	<0.3	<0.3	0.3	<0.3	<0.3	<0.3	2.2
6,7b	<0.3	<0.3	<0.3	<0.3	<0.3	<0.3	<0.3
7a,7b	−12.4	−12.4	−11.8	−11.2	−12.2	−12.4	−10.0

*Spectrum in $CDCl_3$: in C_6D_6 signal for H-1/H-4 is obscured by the OCH_3 resonance.
†Value cannot be obtained directly from the spectrum or from simulation (spectrum is independent of this parameter).

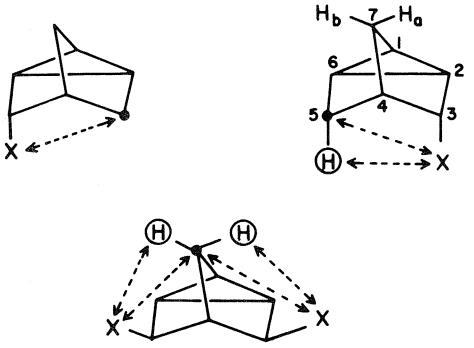

FIG. 1. (C/X) and δ(H/X) steric interactions in nortricyclenes.

C-3, C-5, or C-7 (5), while interactions of H-5, H-7a, or H-7b with substituent X result in shifts (usually paramagnetic) of these hydrogens (2). The differences observed in the nmr spectra of **4** and **5**, in the chemical shifts of H-5, H-7a, C-5, and C-7 (Tables 1, 2) thus confirm that these compounds are epimeric at C-3.

There are two possible structures for the third isomer, *viz.* **6** and **11**. Confirmation that the iodine at C-5 is *endo* is provided by (*a*) the significant downfield change in the chemical shift of C-3 (relative to that in **4** and **5**), reflecting the new characteristic steric interaction with the C-5 halogen; (*b*) the separation in the pmr spectrum of the bridge methylene hydrogens, H-7b appearing as expected at much higher field (19), while H-7a remains deshielded by the C-3 iodine, and (*c*) the small value of $J_{H\text{-}5,H\text{-}7a}$. This coupling constant is larger when H-5 is *endo* (**4** and **5**) and in a 'W' configuration relative to H-7a, and smaller when *exo* (**6**) and in a 'sickle' arrangement with H-7a (23).

Additional evidence of the stereochemistry at C-5 was provided by the observation that H-5 (*exo*) in **6** was shifted upfield by 0.8 ppm when the solvent was changed from $CDCl_3$ to C_6D_6, while the chemical shift of H-5 (*endo*) in **4** and **5** was found to be virtually independent of this solvent change (Table 3). The dramatic shielding effect is due to solvation with benzene which will be sterically favored when H-5 is *exo*.

Assignment of the stereochemistry at C-3 in **6**

Can. J. Chem. Downloaded from www.nrcresearchpress.com by 210.87.254.40 on 09/05/12
For personal use only.

TABLE 2. ^{13}C nmr (25.16 MHz) parameters for **4**–**9** and **12** (C_6D_6)

	4		**5**		**6**		**7**		**8**		**12**		**9**	
Carbon	δ and mult.*	*J*(Hz)†	δ and mult.	*J*(Hz)	δ and mult.	*J*(Hz)	δ and mult.	*J*(Hz)	δ and mult.	*J*(Hz)‡	δ and mult.	*J*(Hz)	δ and mult.	*J*(Hz)
C-1	26.6 dm	182.7	23.7 dm	184.3	27.7 dd	186.3 6.2	25.2 dm	182.5	26.7 d	182.5	31.6 dm	182.0	58.2 dd	157.1 9.0
C-2	35.4 s	—	35.5 s	—	35.1 s	—	36.8 s	—	35.6 s	—	36.7 or 37.9	—	143.1	
C-3	38.1 d	8.0	39.5 d	9.4	45.0 d	~7	80.8 d	5.6	82.2 s	—	36.7 or 37.9	—	s	
C-4	51.0 dm	161.8	50.9 dm	163.0	49.6 bd	161.2	49.4 bd	157.5	49.1 d	156.6	55.5 bd	155.1	58.2 dd	157.1 9.0
C-5	20.5 dm	162.0 9.0, 2	29.4 dd	163.6 8.6	17.9 dd	161.3 11.3	26.0 dm	165.5 9.4, 2	29.1 d	159.8	82.5 dd	170.1 7.6	32.2	162.7
C-6	31.0 dt	188.9 6.2	32.9 dt	187.4 7.0	30.5 dt	190.0 6.2	34.8 dt	185.7 7.0	32.1 d	188.0	33.2 bd	186.3	d	
C-7	35.0 tm	138.0	29.4 tm	137.9	35.8 tm	138.8	33.6 tm	138.2	30.0 t	135.3	29.1 t	136.3	43.9 t	140.0
OCH_3	51.3 q	146.8	51.3 q	147.0	51.5 q	147.0	51.4 q	147.2	51.3	147.5	51.8 q	147.5	51.8 q	147.6
	52.7 q	147.7	52.6 q	147.8	52.2 q	147.5	52.6 q	148.0	52.3	147.5				
C=O	167.2 168.6	—	167.1 167.6	—	168.4 169.0	—	169.3 172.9	—	169.6 171.5	—	168.5 170.3	—	163.5	—

*s = singlet, d = doublet, t = triplet, q = quartet, m = multiplet, b = broad.
†Multiplicities and coupling constants were derived from high-resolution spectra.
‡Coupling constants were calculated from the residual couplings in the off-resonance decoupled spectrum, on the basis of a coupling in the methoxyl resonances of 147.5 Hz.

TABLE 3. Effect of solvent on δ(H-5) in nortricyclenes

Compound	Orientation of H-5	δ(H-5) in C_6D_6	δ(H-5) in $CDCl_3$
4	*endo*	3.79	3.93
5	*endo*	4.66	4.78
6	*exo*	3.13	3.93
7	*endo*	4.54	4.50
8	*endo*	4.69	4.76
12	*exo*	3.97	4.94

is based on the fact that the shift (17.9 ppm) of C-5, which is susceptible to changes in substituent orientation at C-3, corresponds closely to that (20.5 ppm) of C-5 in **4**. For the alternative structure **11** the shift of C-5 would be expected to be similar to that (29.4 ppm) observed in **5** (identical stereochemistry at C-3).

Compounds 7 and 8

It was possible to achieve only partial separation of these isomers and only **7** was obtained in a pure state. However, examination of the ^1H and ^{13}C (proton noise decoupled and off-resonance decoupled) nmr spectra of a mixture rich in the minor isomer **8**, and comparison with the spectra of pure **7**, allowed complete data to be determined for **8**. The ^{13}C parameters of both compounds were quite similar to those of **4** and **5** except that one carbon was significantly deshielded. The fact that this resonance, obviously due to the carbon carrying the hydroxyl group, is for a quaternary carbon, confirms the substitution pattern.

The relatively low-field chemical shift of H-7b and large value of $J_{H\text{-}5,H\text{-}7a}$ in **7** and **8** strongly indicate that H-5 in both isomers is *endo* to the bridged ring, confirming that these two compounds are also epimeric at C-3. The assignment of the stereochemistry is based on their mode of formation (the major isomer should correspond to **4**), and comparison of their chemical shifts with those of the corresponding centers in **4** and **5**.

Can. J. Chem. Downloaded from www.nrcresearchpress.com by 210.87.254.40 on 09/05/12
For personal use only.

Can. J. Chem. Downloaded from www.nrcresearchpress.com by 210.87.254.40 on 09/05/12
For personal use only.

Compound 12

The structure of **12** follows from its mass (M^+ 320), ir (lactone C=O at 1779 cm^{-1}, ester C=O at 1720 cm^{-1}), ^1H, and ^{13}C nmr spectra (Tables 1, 2). The chemical shift of C-5 indicated lactonization at this center, and the *exo* orientation of H-5 was confirmed by (*a*) the high field chemical shift of H-7b (*cf.* 19); (*b*) the small value of $J_{H\text{-}5,H\text{-}7a}$ resulting from the 'sickle' orientation of these two protons (23); and (*c*) the upfield shift (0.97 ppm) of H-5 when $CDCl_3$ was replaced by C_6D_6 as solvent (see above and Table 3).

Compound 9

The symmetry of the unsaturated product was readily revealed by the limited number of resonances in its ^{13}C and ^1H nmr spectra. In addition to signals for a methylene and for pairs of equivalent carbonyl, methoxyl, and quaternary olefinic carbons, the ^{13}C spectrum of **9** shows resonances with chemical shifts indicative of pairs of equivalent bridgehead and iodine-substituted carbons (Table 2).

The absence of significant coupling between the bridgehead protons H-1,H-4 and the adjacent methine hydrogens H-5,H-6 in the ^1H nmr spectrum (Table 1) indicates that the latter are both *endo* to the bridged ring (*cf.* 24). The relatively large coupling (J = 2.2 Hz) between H-5,H-6 and the bridge proton H-7a is also consistent (characteristic 'W' arrangement (*cf.* 23)), with H-5,H-6 being oriented *endo*.

Experimental

Proton magnetic resonance (pmr) spectra were recorded in benzene-d_6 (unless otherwise stated) on a Varian HA-100 spectrometer, the tetramethylsilane or benzene-H resonance being used to provide the field-frequency lock. Initial simplification of the spectrum of **5** was achieved by addition of the shift reagent Eu(fod)$_3$ which permitted resolution of the cyclopropyl, bridge, and bridgehead hydrogens. The analysis was completed with the aid of spin-decoupling experiments and spectral simulation using a Varian VT-100 data system associated with a Varian XL-100 nmr spectrometer. With the parameters of **5** available it became much simpler to analyze the corresponding ^1H spectra of **4**, **7**, and **8**, using multiple-irradiation experiments and spectral simulations to confirm assignments. Analysis of the pmr spectrum of **6** was simplified on account of the much wider separations of H-7a and H-7b and of H-1 and H-6.

^{13}C nmr spectra at 25.16 MHz were obtained on a Varian XL-100-15 spectrometer. Samples (50–100 mg/0.5 ml) in benzene-d_6 were contained in 5 mm tubes. The deuterium resonance from the solvent was used for the field-frequency lock. Spectral width was 5120 Hz, with an acquisition time of 0.8–3.2 s, using 8–32K transforms and yielding a resolution of $\pm$0.6 to $\pm$0.15 Hz. Coupling constants ($J_{^{13}C\text{-}^1H}$) were measured from high resolution spectra enhanced by applying the noise modulated decoupling field between data acquisition periods to retain the nuclear Overhauser enhancement. In the case of compound **8** signal assignments were made with the assistance of the off-resonance, single-frequency decoupled spectrum.

High-resolution mass spectra were recorded using a Dupont-C.E.C. 21-110B instrument, with electrical detection being used for mass measurements. Infrared absorptions were measured in a Perkin-Elmer 521 spectrometer. Column chromatographic separations were carried out on Mallinckrodt silicic acid (100 mesh) and preparative thin-layer chromatography (plc) on 2.0 mm Merck silica gel F-254 precoated plates.

Preparation of 3a

Freshly-distilled cyclopentadiene (5.62 g, 0.085 mol) and dimethyl acetylenedicarboxylate (11.97 g, 0.085 mol) were mixed in CH_2Cl_2 (100 ml) at 0 °C, and the mixture then allowed to stand overnight at room temperature. Removal of CH_2Cl_2 under reduced pressure afforded dimethyl bicyclo[2.2.1]hepta-2,5-diene-2,3-dicarboxylate **3***a* as a pale yellow oil in almost quantitative yield.

Reaction of 3a with Iodine

A solution of **3***a* (7.16 g, 0.034 mol) in Et_2O (220 ml) was treated with a solution of iodine (10.13 g, 0.040 mol) in Et_2O (200 ml). The mixture was allowed to stand in daylight for 4 h at ambient temperature, and after washing with sodium bisulfite solution and H_2O, was finally dried (Na_2SO_4). Evaporation of Et_2O under reduced pressure afforded a paste. Trituration of this with methanol gave dimethyl 3-*exo*, 5-*exo*-diiodotricyclo-[2.2.1.0^{2,6}]heptane-2,3-*endo* dicarboxylate **4** as a cream-colored solid (7.01 g, 44%). Crystallization from methanol gave prisms, mp 117–118 °C. Molecular ion (≪1%) at m/e 462 ($C_{11}H_{12}O_4I_2$ requires 462); base peak at m/e 334.9788 ($C_{11}H_{12}O_4I$ requires 334.9783); ions at m/e 430.8621 (3%) ($C_{10}H_9O_3I_2$ requires 430.8645), 403 (2%), 303 (27%), 275 (7%), 254 (21%), 208 (15%), 207 (12%), 177 (15%), 176 (23%), 149 (35%), 148 (14%), 128 (17%), and 127 (15%). ν_{max} (KBr) 1728, 1714 cm^{-1}.

The methanol-soluble portion of the product was a viscous oil (6.62 g) which was submitted to column chromatography (25% ethyl acetate – petroleum ether). The products eluted in the following order: **4** (2%), **5** (20%), **9** (5%), **6** (1%), and **7** and **8** (combined 2%). (Total yields were estimated from the pmr spectra of the various column fractions; no unreacted **3***a* was detected.)

(*i*) Repeated plc (25% ethyl acetate – petroleum ether) of one fraction (0.32 g) afforded pure dimethyl 5-*exo*, 6-*exo*-diiodobicyclo[2.2.1]hept-2-ene-2,3-dicarboxylate **9** as a pale yellow oil (0.21 g, 1.3%). Molecular ion (3%) at m/e 461.8815 ($C_{11}H_{12}O_4I_2$ requires 461.8829); base peak at m/e 128 (HI^+); ions at m/e 431 (8%), 403 (<1%), 335 (79%), 303 (46%), 275 (8%), 254 (47%), 208 (41%), 207 (21%), 193 (16%), 177 (43%), 176 (54%), 161 (11%), 149 (97%), and 127 (55%). ν_{max} (liquid film) 1720, 1620 cm^{-1}.

(*ii*) Repeated plc ($CHCl_3$) of another fraction (0.33 g)

Can. J. Chem. Downloaded from www.nrcresearchpress.com by 210.87.254.40 on 09/05/12
For personal use only.

afforded dimethyl 3-*exo*, 5-*endo*-diiodotricyclo[2.2.1.0^{2,6}]-heptane-2,3-*endo*-dicarboxylate **6** as a colorless solid. Crystallization from ethyl acetate – petroleum ether gave pure **6** as colorless rosettes (73 mg, 0.5%), mp 131.5–133.5 °C. Molecular ion (≪1%) at *m/e* 461.8806 ($C_{11}H_{12}O_4I_2$ requires 461.8829); base peak at *m/e* 334.9781 ($C_{11}H_{12}O_4I$ requires 334.9783); ions at *m/e* 430.8643 (2%) ($C_{10}H_9O_3I_2$ requires 430.8645), 402.8690 (1.5%) ($C_9H_9O_2I_2$ requires 402.8696), 303 (10%), 275 (5%), 254 (38%), 208 (19%), 207 (15%), 193 (7%), 177 (19%), 176 (26%), 161 (5%), 149 (40%), 148 (9%), 128 (23%), and 127 (19%). ν_{max} (KBr) 1720, 1696 cm^{-1}.

(*iii*) The major fraction (3.39 g) was rechromatographed under the same conditions. From this column was obtained a pure sample of dimethyl 3-*endo*, 5-*exo*-diiodotricyclo[2.2.1.0^{2,6}]heptane-2,3-*exo*-dicarboxylate **5** as a cream-colored solid (1.29 g, 8%), mp 65–67 °C. Molecular ion (≪1%) at *m/e* 461.8815 ($C_{11}H_{12}O_4I_2$ requires 461.8829); base peak at *m/e* 334.9785 ($C_{11}H_{12}O_4I$ requires 334.9783); ions at *m/e* 430.8625 (2%) ($C_{10}H_9O_3I_2$ requires 430.8645), 403 (2%), 303 (32%), 275 (7%), 254 (19%), 208 (18%), 207 (17%), 193 (7%), 177 (17%), 176 (27%), 161 (6%), 149 (42%), 148 (11%), 128 (25%), and 127 (21%). ν_{max} (KBr) 1724, 1716 cm^{-1}.

(*iv*) The slowest running fractions (177 mg) contained the two alcohols **7** and **8** (see below) in a ratio of *ca.* 2.5:1.

Effect of Illumination

The above reaction was repeated, the reactants being mixed and allowed to stand in the dark. Work-up as above after 4 h gave an oil containing approximately 40% **3***a* (from pmr). Time studies of the light reaction showed that reaction of **3***a* was 60% complete after only 30 min (complete after 1 h), indicating that it is approximately eight times faster than the dark reaction.

*Irradiation of **4***

A solution of **4** (5.00 g) in Et_2O (450 ml) was irradiated at 3000 Å for 4 h at 30 °C. The residue obtained on evaporation of the solvent was chromatographed (25% ethyl acetate – petroleum ether). In order of their elution from the column, were obtained **4** (37%), **5** (26%), and a mixture of **7** and **8** (combined 11%), the yields being estimated from the pmr spectra of the various fractions.

A small amount (93 mg, 2.4%) of pure dimethyl 3-*exo*-hydroxy-5-*exo*-iodo tricyclo[2.2.1.0^{2,6}]heptane-2,3-*endo*-dicarboxylate **7** was obtained directly from the column as a colorless solid, mp 98–100 °C. Molecular ion (≪1%) at *m/e* 352 ($C_{11}H_{13}O_5I$ requires 352); base peak at *m/e* 165; ions at *m/e* 335 (<1%), 320.9633 (2%) ($C_{10}H_{10}O_4I$ requires 320.9626), 293 (10%), 261 (8%), 225 (48%), 197 (68%), 193 (19%), 137 (9%), 133 (22%), 128 (15%), 127 (9%), and 105 (22%). ν_{max} (KBr) 3458, 1728, 1688 cm^{-1}.

Repeated plc ($CHCl_3$) of fractions containing mixtures of **7** and **8** afforded a fraction (50 mg) containing 80% dimethyl 3-*endo*-hydroxy-5-*exo*-iodotricyclo[2.2.1.0^{2,6}]-heptane-2,3-*exo*-dicarboxylate **8**. ^{1}H and ^{13}C data (Table 1 and 2) were obtained by comparison of the spectra of this fraction with those of pure **7**.

*Preparation of Quadricyclane **10***a *(cf. ref. 10)*

A solution of freshly-prepared norbornadiene **3***a* (4.0 g) in Et_2O (400 ml) was irradiated at 3000 Å for 4½ h at 30 °C. Evaporation of the solvent gave dimethyl tetracyclo[2.2.1.0^{2,6}0^{3,5}]heptane-2,3-dicarboxylate **10***a* as a viscous pale yellow oil (3.99 g). $\delta(C_6D_6)$ 1.88 and 2.08 (m, each 1H, H-7a and H-7b, $J_{7a,7b}$ = 12.0 Hz), 2.17 and 2.32 (m, each 2H, H-1/H-4 and H-5/H-6, $J_{1,6} = J_{4,5}$ = 5.0 Hz), 3.55 (s, 6H, OCH_3).

*Reaction of **10***a *with Iodine*

A mixture of freshly-prepared **10***a* (2.95 g, 0.014 mol) and iodine (3.61 g, 0.014 mol) in Et_2O (150 ml) was allowed to stand at room temperature in daylight for 4 h. The mixture was washed with sodium bisulfite then H_2O, and dried (Na_2SO_4). Concentration gave a viscous pale yellow oil which partially crystallized on standing. Trituration with methanol afforded **4** (2.66 g, 41%). The methanol-soluble portion of the residue was chromatographed (25% ethyl acetate – petroleum ether) to give pure **5** (0.712 g, 11%) together with a mixture (1.077 g, 16.5%) of **4** and **5** (ratio 1:2.2).

*Isomerization of **4** to **5***

After one month at room temperature a solution (0.4 *M*) of **4** in benzene-d_6 showed 40% conversion to **5** (pmr). When a solution (0.07 *M*) of **4** in benzene was refluxed for 24 h, approximately 25% isomerization to **5** was observed. After 120 h reflux pmr indicated a ratio of **4**:**5** = 9:4.

*Pyrolysis of **4***

(*a*) Pure **4** (3.33 g) was heated under reflux at 130–135 °C (oil bath) for 2 h, during which time some iodine crystals sublimed from the melt. After cooling the dark red residue was submitted to column chromatography ($CHCl_3$). The initial fractions (1.60 g) contained a mixture of **4** and **5** (in an approximate ratio of 5:7). Later fractions afforded 2-carbomethoxy-3-*exo*-iodotricyclo[2.2.1.0^{2,6}]-heptane-5-*endo*-hydroxy-3-*endo*-carboxylic acid lactone **12** as a colorless solid (1.10 g, 48%), mp 129–129.5 °C. Molecular ion (81%) at *m/e* 319.9556 ($C_{10}H_9O_4I$ requires 319.9548); base peak at *m/e* 149; ions at *m/e* 289 (15%), 276 (18%), 246 (14%), 245 (15%), 208 (16%), 163 (11%), 128 (76%), and 127 (38%). ν_{max} (KBr) 1779, 1720 cm^{-1}.

(*b*) Progress of separate experiments was monitored by pmr, aliquots being withdrawn at various times. During the early stages of the pyrolysis a sharp singlet was observed ($CDCl_3$) at 2.17 δ, probably due to methyl iodide.

Very high conversion to **12** could be achieved by increasing the reaction time or temperature (to 150–160 °C). The conversion was almost complete after 10 min at 180 °C.

*Pyrolysis of **5***

(*a*) Compound **5** (200 mg) was heated at 140–150 °C (oil-bath) for 60 min. After cooling, the dark purple residue was submitted to plc ($CHCl_3$). This afforded one band containing **5**, together with a small amount of **4** (total weight 0.077 g), and a second band yielding pure **12** (89 mg, 64%).

(*b*) Heating **5** (168 mg) at 120–130 °C for 60 min caused partial isomerization to **4** (ratio **5**:**4** ≈ 3:1), but only low conversion to **12**.

Acknowledgments

We wish to thank Mrs. M. G. Flack for her

excellent technical assistance, Mr. P. F. Seto for infrared measurements, and Mr. D. J. Embree for the high-resolution mass spectra.

1. R. K. BANSAL, A. W. MCCULLOCH, P. W. RASMUSSEN, and A. G. MCINNES. Can. J. Chem. **53**, 138 (1975).
2. B. FRANZUS, S. WU, W. C. BAIRD, and M. L. SCHEINBAUM. J. Org. Chem. **37**, 2759 (1972).
3. S. F. NELSEN, J. P. GILLESPIE, and P. J. HINTZ. Tetrahedron Lett. 2361 (1971); S. F. NELSEN and J. C. CALABRESE. J. Am. Chem. Soc. **95**, 8385 (1973).
4. J. B. GRUTZNER, M. JAUTELAT, J. B. DENCE, R. A. SMITH, and J. D. ROBERTS. J. Am. Chem. Soc. **92**, 7107 (1970); N. H. WERSTIUK, R. TAILLEFER, R. A. BELL, and B. SAYER. Can. J. Chem. **51**, 3010 (1973).
5. E. LIPPMAA, T. PEHK, and J. PAASIVIRTA. Org. Magn. Reson. **5**, 277 (1973).
6. A. W. MCCULLOCH, D. G. SMITH, and A. G. MCINNES. Can. J. Chem. **52**, 1013 (1974).
7. S. WINSTEIN, and M. SHATAVSKY. Chem. Ind. 56 (1956); S. WINSTEIN. J. Am. Chem. Soc. **83**, 1516 (1961).
8. S. MASSON and A. THUILLIER. Bull. Soc. Chim. Fr. 4368 (1969).
9. H. W. JOHNSON, and P. N. LANDERMAN. J. Org. Chem. **27**, 303 (1962); *cf.* Brit. Patent 717 010; Chem. Abstr. **49**, 15 970 (1955).
10. S. J. CRISTOL and R. L. SNELL. J. Am. Chem. Soc. **80**, 1950 (1958).
11. S. J. CRISTOL, G. D. BRINDELL, and J. A. REEDER. J. Am. Chem. Soc. **80**, 635 (1958); A. A. OSWALD, K. GRIESBAUM, and B. E. HUDSON. J. Org. Chem. **28**, 1262 (1963); D. J. TRECKER and J. P. HENRY. J. Am. Chem. Soc. **85**, 3204 (1963).
12. T. C. MORRILL and B. E. GREENWALD. J. Org. Chem. **36**, 2769 (1971).
13. S. J. CRISTOL, J. K. HARRINGTON, T. C. MORRILL, and B. E. GREENWALD. J. Org. Chem. **36**, 2773 (1971).
14. G. F. KOSER, P. R. PAPPAS, and S.-M. YU. Tetrahedron Lett. 4943 (1973); G. F. KOSER and S.-M. YU. J. Org. Chem. **38**, 1755 (1973).
15. J. B. STOTHERS. Carbon-13 NMR spectroscopy. Academic Press, New York. 1972. (*a*) Chapt. 5, (*b*) Chapt. 10.
16. G. C. LEVY and G. L. NELSON. Carbon-13 nuclear magnetic resonance for organic chemists. Wiley-Interscience, New York. 1972 Chapt. 3.
17. G. M. WHITESIDES and J. SAN FILIPPO. J. Am. Chem. Soc. **92**, 6611 (1970).
18. S. MASSON and A. THUILLIER. Bull. Soc. Chim. Fr. 3508 (1971).
19. R. S. NEALE and E. B. WHIPPLE. J. Am. Chem. Soc. **86**, 3130 (1964).
20. N. O. BRACE. J. Org. Chem. **27**, 3027 (1962).
21. S. J. CRISTOL, J. K. HARRINGTON, and M. S. SINGER. J. Am. Chem. Soc. **88**, 1529 (1966).
22. E. LIPPMAA, T. PEHK, J. PAASIVIRTA, N. BELIKOVA, and A. PLATE. Org. Magn. Reson. **2**, 581 (1970).
23. V. MARK. Tetrahedron Lett. 299 (1974).
24. F. A. L. ANET. Can. J. Chem. **39**, 789 (1961).

Can. J. Chem. Downloaded from www.nrcresearchpress.com by 210.87.254.40 on 09/05/12
For personal use only.

Influence des substituants sur la basicité de pyridines en milieu apolaire

C. LAURENCE ET M. LUÇON

Laboratoire de Spectrochimie Moléculaire, U.E.R. de Chimie, B.P. 1044, 44037 Nantes Cedex, France

Reçu le 21 janvier 1976

C. LAURENCE et M. LUÇON. Can. J. Chem. **54**, 2021 (1976).

La fréquence ν(OH. . .N) des complexes méthanol – pyridines substituées semble un détecteur sensible des effets de substituant sur la basicité des pyridines en milieu apolaire. Les coefficients ρ_I et ρ_R de sensibilité aux effets I et R obtenus à partir de l'équation de Taft–Ehrenson concordent pour les trois positions de substitution avec ceux trouvés pour les pK_a des ions pyridinium. Les divergences observées s'expliquent par le pouvoir électroattracteur très supérieur du groupe azonium par rapport au groupe aza.

C. LAURENCE and M. LUÇON. Can. J. Chem. **54**, 2021 (1976).

The frequency ν(OH. . .N) of methanol complexes with substituted pyridines appears to be a sensitive detector of substituent effects on the basicity of pyridines in an apolar medium. The coefficients ρ_I and ρ_R, which respond to I and R effects and which are obtained from the Taft–Ehrenson equation, agree with those found for the pK_a of pyridinium ions for the three substitution positions. Those values which are observed to diverge are explained by the much greater electron attracting power of the azonium group compared to that of the aza group.

[Journal translation]

Can. J. Chem. Downloaded from www.nrcresearchpress.com by 210.87.254.40 on 09/05/12
For personal use only.

De nombreuses corrélations ont été établies (1, 2) entre la fréquence de groupe d'un vibrateur porté par un noyau benzénique différemment substitué et les facteurs de Hammett (3). Leur intérêt naît de la facilité d'obtention de la grandeur physique considérée et de mesures généralement effectuées dans un solvant apolaire sans interaction avec le substituant. La précision de ces corrélations est souvent limitée cependant par des effets non électroniques tels que couplage de vibrations (4), isomérie de rotation (5) ou résonance de Fermi (6). Aussi avions-nous étudié les effets électroniques dans les molécules XC_6H_5 à l'aide d'un observateur extérieur, le vibrateur ν(OH) de phénols complexés par liaison d'hydrogène sur leur nuage π (7). Cette méthode est ici étendue à une nouvelle série, les pyridines XC_6H_4N, en mesurant en solvant apolaire la fréquence ν(OH. . .N) du méthanol complexé sur le doublet libre de l'azote. Cette fréquence constitue une mesure de la basicité des pyridines puisqu'elle est proportionnelle à $\Delta\nu = \nu(OH) - \nu(OH. . .N)$, grandeur qui, dans une série structuralement homogène, traduit la force de la liaison d'hydrogène (8, 9) c'est-à-dire le pouvoir accepteur de proton de la base engagée dans le complexe.

Résultats

Une quarantaine de pyridines *o*-, *m*- ou *p*-substituées par des groupes appartenant à toutes les classes selon les critères dictés par Ehrenson *et al.* (10) ont été étudiées. Le manque de solubilité dans CCl_4 des *o*-, *m*-, *p*-amino, *m*-hydroxy et *p*-nitropyridines ainsi que la transformation des pyridine-aldéhydes en acétals par le méthanol ont contraint à abandonner leur étude. Le tableau 1 rassemble les fréquences ν(OH. . .N). Pour les substituants X = *o*-OPh, *o*-OMe, *o*-, *m*- ou *p*-CN et *o*-, *m*- ou *p*-COR, on observe une deuxième bande associée correspondant à un deuxième complexe 1–1 du type OH. . .X (l'observation d'un complexe 2–1 est rendue improbable par les concentrations de méthanol et de pyridine choisies; voir partie expérimentale). La bande correspondant au complexe OH. . .N se situe aux fréquences les plus basses; elle est la plus intense, sauf pour les substituants *m*-$CON(Me)_2$ et *o*-COR, ce qui traduit une basicité des amines plus grande que celle des éthers, nitriles et dérivés carbonylés.

Les corrélations ont été établies par la méthode des moindres carrés sous la forme

$$[1]^1 \qquad \nu - \nu^0 = \rho_I\sigma_I + \rho_R\sigma_R + h$$

ν et ν^0 sont les fréquences respectives des pyridines substituées et non substituée, ρ_I, ρ_R et h les coefficients de la régression; σ_I mesure les effets inductifs et σ_R les effets de délocalisation des

[1]Cette forme est utilisée par Charton (11) et Swain et Lupton (12). Ehrenson *et al.* (10) préfèrent fixer $h = 0$.

Can. J. Chem. Downloaded from www.nrcresearchpress.com by 210.87.254.40 on 09/05/12
For personal use only.

TABLEAU 1. Fréquences ν(OH. . .N) des complexes méthanol–pyridines

Substituant *para*	ν(cm^{-1})	Substituant *méta*	ν(cm^{-1})	Substituant *ortho*	ν(cm^{-1})
$N(Me)_2$	3283.8	H	3364	Et	3333.7
Me	3343.5	Et	3344.5	Me	3335.6
Et	3346	Me	3347.6	$CH{=}CH_2$	3360.3
Ph	3359	COPh	3390.2	OMe	3416.2
$CH{=}CH_2$	3359.4	COOEt	3393.3	Pyridazine	3417
SH	3385	COOMe	3394.2	COMe	~3443
COPh	3389.3	COMe	3394.3	OPh	3451
COMe	3391.4	I	3401.5	Br	3451.3
COOMe	3393.6	Br	3406.1	Cl	3452
COOEt	3393.7	Cl	3406.1	COPh	~3455
Cl	3395.2	Pyrimidine	3435.9	F	3477
Br	3398.8	CN	3442.7	CN	3481.2
CN	3428.5				
Pyrazine	3444.9				

électrons π (10). Le rapport $\lambda = \rho_R/\rho_I$ des coefficients de sensibilité aux effets R et I mesure leur importance relative. Selon les critères établis par Ehrenson *et al.* (10) les effets de résonance peuvent être du type σ^+, σ, σ^0 ou σ^- et s'expriment alors par quatre échelles σ_R^+, σ_R, σ_R^0 ou σ_R^-. La quantité f = écart-type de l'estimation/écart-type des données permet de comparer les précisions des corrélations obtenues avec ces différentes échelles. L'expérience montre (10) que les corrélations très précises correspondent à $f \leq 0.1$. Le tableau 2 rassemble les valeurs de ρ_I, ρ_R, h, λ et f, obtenues pour les corrélations établies à partir d'un nombre n de données et rappelle, à des fins comparatives, les résultats de Ehrenson *et al.* (10) pour la dissociation des ions pyridinium dans l'eau.

Discussion

Dans le cadre de la méthodologie de Hammett–Taft, dont la cohérence est parfois discutée (13), l'effet de substituant sur la basicité de pyridines est traduit de manière similaire par la fréquence ν(OH. . .N) des complexes méthanol – pyridines substituées et le pK_a des ions pyridinium correspondants, ceci pour deux solvants aussi différents que l'eau et le CCl_4.

En effet, on observe pour ces deux propriétés: (i) que les effets de résonance des substituants

TABLEAU 2. Basicité des pyridines substituées: corrélations avec σ_I et σ_R

Position de substitution	Meilleure corrélation	h	ρ_I	ρ_R	λ	n	f
			(*a*) ν(OH. . .N) des complexes méthanol–pyridines, CCl_4, 33 °C				
ortho	$E^a(\sigma_R^+)$	−11	230	−4	−0.02	8	0.168 (0.172[b]–0.163[c]–0.170[d])
méta	$E^a(\sigma_R^0)$	−7	129	37	0.28	8	0.220 (0.209[e]–0.220[c]–0.249[b])
para	σ_R^+	−5	111	46	0.41	9	0.108 (0.550[b]–0.202[c]–0.342[d])
			(*b*) pK_a des ions pyridinium, H_2O, 25 °C				
ortho	σ_R^+	—	10.60	1.39	0.13	11	0.142
méta	$E^a(\sigma_R^0)$	—	6.02	2.63	0.43	14	0.076
para	σ_R^+	—	5.15	2.69	0.52	13	0.060

[a]Corrélations équivalentes pour toutes les échelles σ_R; les résultats sont donnés pour l'échelle σ_R indiquée entre parenthèses.
[b]Pour σ_R^-.
[c]Pour σ_R.
[d]Pour σ_R^0.
[e]Pour σ_R^+.

para sont du type σ^+. En effet le groupe aza est fortement demandeur d'électrons π aux substituants +R selon la structure limite **1**.

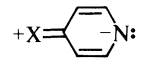

1

(ii) qu'en *méta* les différences observées entre les échelles ne sont pas significatives.

(iii) que le coefficient λ de pondération des effets I et R suit l'ordre

[2] $$\lambda^p > \lambda^m \gg \lambda^o$$

La première inégalité traduit la plus forte transmission bien connue des effets R à partir de la position *para*. Pour la position *ortho*, on observe plutôt

[3] $$\lambda^p > \lambda^o > \lambda^m$$

lorsque le groupe fonctionnel est exocyclique. Sa position endocyclique conduirait donc à l'inversion. Cet effet électrique *ortho* 'anormal' a déjà été noté par Charton (14) pour plusieurs hétérocycles. La valeur λ^p, faible pour un effet du type σ^+ doit être attribuée au fait que la forme **1** est moins stabilisée que la forme quinonique habituelle **2**

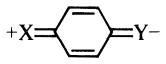

2

(iv) que si l'on définit finalement les nombres $K_I^o = \rho_I^o/\rho_I^p$, $K_I^m = \rho_I^m/\rho_I^p$ et K_I^p, on confirme la séquence classique

[4] $$K_I^p < K_I^m < K_I^o$$

L'influence nulle du solvant sur ces valeurs K

[5] $$K_I^m(H_2O) = K_I^m(CCl_4) = 1.16$$

et

$$K_I^o(H_2O) = K_I^o(CCl_4) = 2.06$$

s'explique probablement par une transmission du champ électrique uniquement à travers la cavité moléculaire: les lignes de force ne passant pas à travers le solvant, la constante diélectrique de ce dernier n'influe pas notablement sur ρ_I.

Par ailleurs, il convient de remarquer:

(i) que les valeurs de f sont plus grandes pour ν(OH. . .N), CCl_4 que pour pK_a, H_2O. Cette imprécision supérieure peut correspondre à une inadaptation de certaines valeurs de σ_I et σ_R en passant de l'eau, leur solvant de définition, à CCl_4 et (ou) à la détermination moins précise d'une fréquence ν(OH. . .N) que d'un pK_a (voir partie expérimentale).

(ii) que le coefficient $\lambda^p(CCl_4)$ est significativement inférieur à $\lambda^p(H_2O)$. Plutôt qu'à l'influence du solvant, qui ne semble jouer un rôle sur λ que lorsque des formes quinoniques **2** contribuent aux effets de résonance (10), nous attribuons cette différence aux effets électromères +R (forme limite **1**) plus grands dans l'ion pyridinium que dans la molécule neutre, puisque le groupe azonium ($\sigma_p \simeq 2.34$ à 2.63 selon réf. 3, p. 101) est beaucoup plus électroattracteur que le groupe aza ($\sigma_p \simeq 0.76$ à 0.96 selon réf. 3, p. 101).

(iii) On peut expliquer de même l'inégalité $\lambda^o(H_2O) \gg \lambda^o(CCl_4)$. En fait, en *ortho* $\rho_R(CCl_4)$ n'est pas significativement différent de zéro (le t de Student indique qu'il y a 65% de chances que la différence $\rho_R - 0$ soit due au hasard). A l'instar du déplacement chimique du ^{19}F dans les fluorobenzènes *méta*-substitués (15), la fréquence ν(OH. . .N) des complexes méthanol–pyridines *ortho*-substituées ne dépend que du facteur inductif σ_I et pourrait servir à sa définition.

Partie expérimentale

Les pyridines utilisées sont des produits commerciaux purifiés. Le méthanol et CCl_4 de qualité spectroscopique ont été séchés sur tamis moléculaire. Les complexes méthanol–pyridines sont formés en solution ternaire dans CCl_4:$C_{methanol} \simeq 0.01$ M et $C_{pyridines} \simeq 0.2$ à 0.4 M. L'épaisseur des cellules est fixée à 8 mm. Les solutions sont préparées sous atmosphère sèche.

Les bandes ν(OH. . .N) sont enregistrées à l'aide d'un spectrophotomètre Beckman IR 9. Le $d\nu/dt$ non négligeable de la bande ν(OH. . .N) oblige à maintenir les solutions à température constante (33 °C).

Entre 0 et 1.5 M de pyridine on observe de plus une variation $d\nu/dC$ voisine de 13 cm^{-1}/M. En toute rigueur la fréquences ν(OH. . .N) en l'absence de tout effet d'environnement serait celle extrapolée à dilution infinie de pyridine (16). L'imprécision de l'extrapolation, due aux difficultés inhérentes à la détermination du maximum d'une bande large (l'écart-type de trois mesures varie de 0.2 à 1.5 cm^{-1}), et l'observation que les gradients $d\nu/dC$ ne sont pas trop différents pour les diverses pyridines (fig. 1), nous ont conduits à considérer comme satisfaisantes les valeurs obtenues avec une faible concentration de pyridine.

Pour la 4-picoline par exemple, on estime l'erreur commise sur $\nu - \nu^0$ à 1.5 cm^{-1} (fig. 1) soit une précision d'environ 7%, alors que la reproductibilité de 0.05 unité pK obtenue généralement pour la détermination du pK_a

Can. J. Chem. Downloaded from www.nrcresearchpress.com by 210.87.254.40 on 09/05/12
For personal use only.

des ions pyridinium (17) correspond à une précision de 6% sur ΔpK_a.

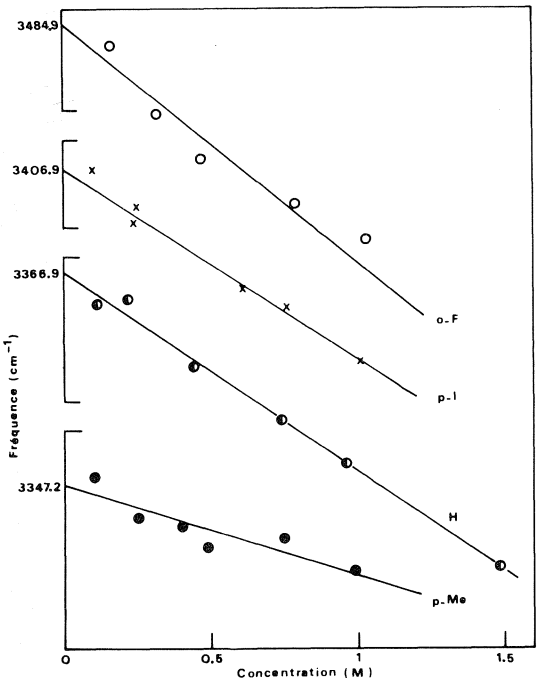

FIG. 1. Variation de la fréquence ν(OH. . .N) en fonction de la concentration en pyridine. Droites des moindres carrés: 4-picoline $\nu = -6.3C + 3347.2$; pyridine $\nu = -13.8C + 3366.9$; *p*-I-pyridine $\nu = -13.2C + 3406.9$; *o*-F-pyridine $\nu = -16.7C + 3484.9$.

1. R. T. C. BROWNLEE, J. DI STEFANO et R. D. TOPSOM. Spectrochim. Acta, Part A, **31**, 1685 (1975).
2. C. LAURENCE et B. WOJTKOWIAK. Bull. Soc. Chim. Fr. 3124, 3833, 3870, 3874 (1971).
3. C. D. JOHNSON. The Hammett equation. Cambridge University Press, London, England. 1973.
4. O. EXNER, S. KOVAK et E. SOLCANIOVA. Collect. Czech. Chem. Commun. **38**, 50 (1973).
5. M. BERTHELOT et C. LAURENCE. C. R. Acad. Sci. Ser. C, **276**, 979 (1973).
6. M. BERTHELOT, M. CHABANEL et C. LAURENCE. Spectrochim. Acta, à paraitre.
7. M. BERTHELOT, C. LAURENCE et B. WOJTKOWIAK. J. Mol. Struct. **18**, 435 (1973).
8. M. D. JOENSTEN et L. J. SCHAAD. Hydrogen bonding. Dekker, New York. 1974.
9. S. N. VINOGRADOV et R. H. LINNELL. Hydrogen bonding. Van Nostrand, New York. 1971.
10. S. EHRENSON, R. T. C. BROWNLEE et R. W. TAFT. *Dans* Progress in physical organic chemistry. Vol. 10. *Rédigé par* Interscience, New York. 1973. p. 1.
11. M. CHARTON. *Dans* Progress in physical organic chemistry. Vol. 10. *Rédigé par* Interscience, New York. 1973. p. 81.
12. C. G. SWAIN et E. C. LUPTON. J. Am. Chem. Soc. **90**, 4328 (1968).
13. M. J. S. DEWAR. The molecular orbital theory of organic chemistry. McGraw-Hill, New York. 1969. p. 421.
14. M. CHARTON. J. Org. Chem. **30**, 3346 (1965).
15. R. W. TAFT, E. PRICE, I. R. FOX, I. C. LEWIS, K. K. ANDERSEN et G. T. DAVIS. J. Am. Chem. Soc. **85**, 709 (1963).
16. A. ALLERHAND et P. V. R. SCHLEYER. J. Am. Chem. Soc. **85**, 371 (1963).
17. H. H. JAFFE et G. O. DOAK. J. Am. Chem. Soc. **77**, 4441 (1955).

Can. J. Chem. Downloaded from www.nrcresearchpress.com by 210.87.254.40 on 09/05/12
For personal use only.

Crystal structure of tetraammonium diphosphate, $(NH_4)_4P_2O_7$ at 22 °C

NORA MIDDLEMISS AND CRISPIN CALVO
Department of Chemistry, McMaster University, Hamilton, Ont., Canada L8S 4M1

Received January 28, 1976

NORA MIDDLEMISS and CRISPIN CALVO. Can. J. Chem. **54**, 2025 (1976).

Crystals of tetraammonium diphosphate, $(NH_4)_4P_2O_7$, crystallize in the monoclinic system with space group $C2/c$, $Z = 4$ and lattice parameters $a = 11.758(3)$, $b = 6.486(2)$, $c = 13.659(2)$ Å and $\beta = 104.81(1)°$. The structure was refined using full-matrix least-squares methods with 810 reflections to an R value of 0.092. The diphosphate anion contains a crystallographic two-fold axis, and has a configuration intermediate between staggered and eclipsed. The bridging P—O bond length is 1.624(2) Å and the terminal P—O bonds average 1.507 Å. The diphosphate groups lie in sheets defined by $(20\bar{2})$ and are bridged by NH_4^+ groups which hydrogen bond to only the terminal oxygen atoms. Each hydrogen is bonded to one oxygen atom but each of the terminal oxygen atoms interacts with either two or three hydrogen atoms.

NORA MIDDLEMISS et CRISPIN CALVO. Can. J. Chem. **54**, 2025 (1976).

Les cristaux du diphosphate de tétraammonium, $(NH_4)_4P_2O_7$ cristallisent dans le système monoclinique avec un groupe d'espace $C2/c$, $Z = 4$ et les paramètres de réseaux sont $a = 11.758(3)$, $b = 6.486(2)$, $c = 13.659(2)$ Å et $\beta = 104.81(1)°$. On a affiné la structure par la méthode des moindres carrés (matrice complète) avec 810 réflexions jusqu'à une valeur de R de 0.092. L'anion diphosphate contient un axe cristallographique binaire et a une configuration intermédiaire entre décalé et éclipsé. La longueur du lien faisant le pont entre le P—O est de 1.624(2) Å et les liens terminaux P—O ont une longueur moyenne de 1.507 Å. Les groupes diphosphates se trouvent en feuillets définis par $(20\bar{2})$ et sont liés par des groupes NH_4^+ qui forment des ponts hydrogènes uniquement avec les atomes d'oxygène terminaux. Chaque hydrogène est lié à un atome d'oxygène mais chaque atome d'oxygène terminal interagit soit avec deux ou trois atomes d'hydrogène.

[Traduit par le journal]

Can. J. Chem. Downloaded from www.nrcresearchpress.com by 210.87.254.5 on 09/05/12
For personal use only.

Introduction

Ammonium polyphosphates are well known fertilizers consisting of mixtures of the ammonium salts of ortho and condensed polyphosphates of various orders (1). Frazier, Smith, and Lehr (2) showed that of the fourteen crystalline components obtained upon reacting ammonia with phosphoric acid, six were diphosphates with various degrees of substitution of ammonium for hydrogen and with various degrees of hydration. The present study concerns the structure of a non-hydrated fully ammoniated member of the series. It has been undertaken as a member of the series of compounds with the general formula $M_4X_2O_7$ where X = P, As, or V. $Na_4P_2O_7$ shows a variety of phase transformations basically consisting of a series of first order phase transitions in one direction superimposed upon a continuous disorder in the orthogonal plane (3). $Na_4As_2O_7$ also has a solid–solid phase transformation (4) but based upon a different structure type compared with $Na_4P_2O_7$. It would appear that the variety of structure types might provide an interesting field of investigation.

Experimental

Crystals of tetraammonium diphosphate were prepared as suggested by Coates and Woodard (5). A saturated sodium diphosphate solution was passed through an ammoniated amberlite IR-120(H form) ion exchange resin. Tetraammonium diphosphate crystals were grown from the resulting aqueous solution made saturated by the slow addition of ethanol. Crystals, which decomposed slowly in air, were clear, colourless and rod-shaped up to 0.8 mm in length. Precession photographs showed extinctions consistent with the space groups $C2/c$ (as suggested by Frazier, Smith, and Lehr (2)) or Cc. A crystal approximately $0.25 \times 0.25 \times 0.45$ mm was selected for data collection and mounted in a sealed capillary tube to prevent decomposition.

Accurate parameters were obtained by least squares refinement of the lattice parameters using 15 moderately high 2θ values measured with a Syntex $P\bar{1}$ automatic diffractometer. The crystal data are:
$(NH_4)_4P_2O_7$ fw = 246.10
Monoclinic $a = 11.758(3)$, $b = 6.486(2)$, $c = 13.659(2)$ Å, $\beta = 104.81(1)°$ at 22 °C, $V = 1006.97$ Å^3, $Z = 4$, $\rho_{calc} = 1.623$ g/cm^3.

Intensities were collected on a $P\bar{1}$ automatic diffractometer using graphite monochromatized MoKα radia-

TABLE 1. Positional and thermal parameters for $(NH_4)_4P_2O_7$ with estimated standard deviations in parentheses (all values except for fractions are multiplied by 10^4)

Atom	x	y	z	U_{11}*	U_{22}	U_{33}	U_{12}	U_{13}	U_{23}
P	4069(1)	1444(2)	1529(1)	243(8)	151(7)	41(7)	−36(7)	28(5)	12(7)
O1	½	444(8)	¼	299(28)	147(27)	64(26)	0	−38(21)	0
O2	4720(4)	2986(6)	1053(3)	468(25)	279(24)	152(22)	−119(20)	38(19)	53(18)
O3	3684(4)	9577(6)	868(3)	513(26)	221(22)	132(20)	−113(21)	−5(18)	−13(19)
O4	3103(3)	2397(7)	1922(3)	330(22)	456(28)	189(23)	104(22)	70(18)	48(21)
N1	2305(4)	6332(8)	1179(3)	398(26)	226(25)	158(24)	−38(25)	102(20)	−11(23)
N2	5715(4)	6767(8)	1045(4)	393(27)	222(27)	202(26)	−3(22)	82(22)	12(22)
H1	2786	7394	1144	600†					
H2	1829	6684	1573	600†					
H3	2737	5227	1445	600†					
H4	1868	6024	553	600†					
H5	6428	7012	1464	600†					
H6	5459	5518	1182	600†					
H7	5766	6798	400	600†					
H8	5205	7740	1136	600†					

*U_{ij}'s in Å² are computed from $\beta_{ij} = 2\pi^2 b_i b_j U_{ij}$ where $T = \exp -(\beta_{11}h^2 + \ldots + 2\beta_{12}hk + \ldots)$ appear in the structure factor expression and b_j's are reciprocal lattice vectors.

†These are the fixed isotropic thermal parameters.

tion ($\lambda = 0.71069$ Å). A θ–2θ scanning mode, with variable scanning rates of 4–24° per min depending on the peak intensities, was used. Background intensities were measured 1° from either side of the peak. All the intensities of positive measure were used. The resulting intensities were corrected for background, Lorentz, and polarization effects. Absorption corrections were deemed negligible and were not made ($\mu = 4.57$ cm^{-1}). The standard deviation, σ, for each reflection was obtained from counting statistics. A total of 810 symmetry independent reflections were obtained within a sphere defined by a maximum 2θ value of 50°. A statistical analysis of the E-values distribution suggested that the space group is centrosymmetric. This requires the bridging oxygen to lie on an element of symmetry if the structure is not disordered. The phosphorous atom position was found from a Patterson map. The P—P vector generated by the two-fold axis was short enough to suggest that the bridging oxygen must lie on this symmetry element. The remaining oxygen and nitrogen atom positions were located using a difference Fourier synthesis. This model was refined initially with isotropic thermal parameters, and when the shift/error ceased to be significant, individual components of the anisotropic thermal parameters were varied. Hydrogen atom positions determined from a difference Fourier map at this state, yielded unrealistic N—H bond lengths and NH_4^+ geometries upon refinement. The two ammonium groups were then taken as rigid tetrahedral groups with N—H bond lengths fixed at 0.90 Å (and $U = 0.06$ Å²). The orientation and centre of these groups, initially placed as suggested by a ΔF map, were varied. A full-matrix least-squares program written by Stephens was used. Scattering curves for P, O^-, and N were taken from Cromer and Mann (6) and for H from the International Tables for X-ray Crystallography (7). A weighting scheme ($\omega = (1.0 - 0.05F + 0.004F^2 + 800(\sigma/F)^2)^{-1}$) was used with the coefficients chosen so that $\omega|F_o - F_c|^2 \simeq 1$. The refinement was terminated when the maximum shift per error was less than 0.014. This gave final reliability values of $R\omega = ((\sum\omega|F_o - F_c|^2)/\sum\omega|F_o|^2)^{1/2} = 0.080$ and $R = (\sum||F_o| - |F_c||)/\sum|F_o| = 0.092$.

The peaks in the final ΔF map did not exceed 1/20 of an oxygen atom. The atomic parameters are in Table 1 and a table of observed and calculated structure factors is available.[1]

Description of the Structure

The structure of $(NH_4)_4P_2O_7$ consists of corner sharing PO_4^{3-} groups forming diphosphate anions which lie in sheets defined by $(20\bar{2})$ planes (Fig. 1). The anion lies on a crystallographic two-fold axis and has a configuration 23° from being eclipsed as based on the Neumann projection along *PP* of the two P—O3 bonds. These anions are arranged in a diamond configuration within the sheets with two neighbours, those along b, having the same orientation, and the remaining four with the direction of the P—O—P moiety inverted because of the centers of inversion. The ammonium ions lie between the sheets of these diphosphates and bridge neighbouring anions forming zig-zag rows along b separated by nearly 1/2 b. Both NH_4^+ groups are hydrogen bonded to only terminal oxygen atoms. The $N(2)H_4^+$ group hydrogen bonds by sharing an edge with one PO_4 member end of an anion and corner sharing with two $P_2O_7^{4-}$ groups in the next adjacent sheet. $N(1)H_4^+$ in contrast shares three apices with anions in one sheet and a fourth with the next adjacent sheet (Fig. 1).

A pair of $N(1)H_4^+$ and a pair of O(3) atoms on separate anions join to form hydrogen bonded rings about the centers of symmetry at 1/4 1/4 1/2 and 3/4 3/4 1/2. A similar ring is formed about the center of symmetry between $N(2)H_4^+$ at 1/2 1/2 1/2 and two O(2) atoms

[1]Photocopies of Table 2 are available, at a nominal charge, from the Depository of Unpublished Data, CISTI, National Research Council of Canada, Ottawa, Canada K1A 0S2.

Can. J. Chem. Downloaded from www.nrcresearchpress.com by 210.87.254.5 on 09/05/12
For personal use only.

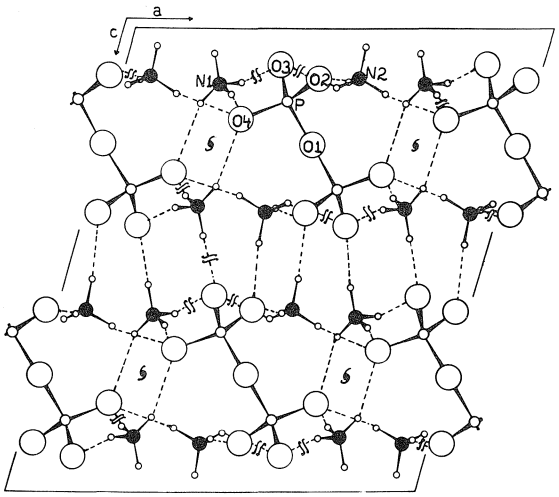

FIG. 1. The structure of $(NH_4)_4P_2O_7$ projected onto the *ac* plane. The proposed hydrogen bonding is indicated by the dashed lines.

from separate diphosphates. This hydrogen bonding network runs along the *a* direction while that along *c* involves the $N(1)H_4^+$ and O(3) rings alternating with helices composed of $N(1)H_4$ and O(4).

The phosphate groups of the anion are distorted in characteristic manner. The bridging P—O bond is larger (1.624 Å) than the average terminal P—O bond length (1.507 Å) (Table 3). The terminal P—O bonds do not differ significantly although O(2) is involved in only two hydrogen bonds while O(3) and O(4) each participates in three. The O—P—O bond angles involving the bridging atom are all less than ideal and those involving only terminal oxygen atoms are greater, suggesting that the phosphorus atom is displaced primarily along the pseudo three-fold axis away from the bridging oxygen atom.

TABLE 3. Bond lengths and angles for $(NH_4)_4P_2O_7$*

(*a*) P_2O_7 group

Bond	Length (Å)	Bonds	Angle (deg)
P—O1	1.624(2)	O1—P—O2	107.9(2)
P—O2	1.504(5)	O1—P—O3	101.8(2)
P—O3	1.509(4)	O1—P—O4	106.6(2)
P—O4	1.507(5)	O2—P—O3	112.5(3)
P—P	2.977(2)	O2—P—O4	113.2(3)
		O3—P—O4	113.9(3)
		P—O—P	132.9(3)

(*b*) Hydrogen bonding†

Bond	Length (Å)	Bonds	Angle (deg)
H1—O3*a*	1.861(4)	O3—H1—N1	171.6(3)
H2—O4*f*	2.089(4)	O4—H2—N1	140.5(3)
H3—O4*a*	1.958(5)	O4—H3—N1	159.1(4)
H4—O3*g*	1.923(4)	O3—H4—N1	165.3(4)
H5—O4*e*	1.924(4)	O4—H5—N2	159.9(4)
H6—O2*a*	1.846(4)	O2—H6—N2	162.8(3)
H7—O2*c*	1.924(4)	O2—H7—N2	159.3(4)
H8—O3*a*	2.101(4)	O3—H8—N2	160.1(3)

*Symmetry transformations are: $a = x,y,z$; $b = -x,y,\frac{1}{2},-z$; $c = -x,-y,-z$; $d = x,-y,\frac{1}{2}+z$; $e = \frac{1}{2}+x,\frac{1}{2}+y,z$; $f = \frac{1}{2}-x,\frac{1}{2}+y,\frac{1}{2}-z$; $g = \frac{1}{2}-x,\frac{1}{2}-y,-z$; $h = \frac{1}{2}+x,\frac{1}{2}-y,\frac{1}{2}+z$.

†The e.s.d.'s do not include the uncertainty in the positions of the hydrogen atoms.

Discussion

The structure of $(NH_4)_4P_2O_7$ is unlike that of any previously reported compound with the same stoichiometry. This is not unexpected because of the specificity of the hydrogen bonding of the cation. On the other hand, the geometry of the diphosphate group is very much in keeping with that found in other diphosphate structures. P—O—P angles at the bridging oxygen range from 123 to 157° for structures with nearly staggered anion configurations (8). The nearly eclipsed anion configuration shows a narrower range of 127 to 138° (8). It is gratifying that the P—O—P angle, at 139.2°, is intermediate since the anion configuration lies most nearly halfway between the extreme configuration. Generally, the smaller bridging angle occurs with some additional cationic bonding to the central oxygen. The terminal P—O bond lengths seem to be limited by intra-ionic oxygen–oxygen repulsion to values no lower than about 1.50 Å whereas the bridging P—O bonds show considerable variability and inequality, where permitted by the symmetry, within a given anion. As has been indicated, some correlation between the difference between the average bridging and average terminal P—O bond and the P—O—P exists (8), particularly so, if the highly disordered linear P—O—P groups are disregarded. The P—O(—P) bond is the largest reported for a diphosphate but comparable with that found for the inner P—O(—P) bond in $Na_5P_3O_{10}$ (9) and $Zn_5(P_3O_{10})_2 \cdot 17H_2O$ (10).

The systematics of the anion configuration upon replacing successive NH_4^+ by protons and for various degrees of hydration should prove interesting.

Acknowledgements

The authors wish to thank the National Research Council of Canada for support of this research. One of us (N.M.) is grateful to the Ontario Government for a research fellowship.

Can. J. Chem. Downloaded from www.nrcresearchpress.com by 210.87.254.5 on 09/05/12
For personal use only.

1. M. M. STRIPLIN, JR. Chem. Eng. **68**, 160 (1961).
2. A. W. FRAZIER, J. P. SMITH, and J. R. LEHR. J. Agr. Food Chem. 316 (1965).
3. K. Y. LEUNG and C. CALVO. Can. J. Chem. **50**, 2519 (1970).
4. K. Y. LEUNG and C. CALVO. Can. J. Chem. **51**, 2082 (1973).
5. R. V. COATES and G. D. WOODARD. J. Chem. Soc. 1780 (1964).
6. D. T. CROMER and J. B. MANN. Acta Crystallogr. A**24**, 321 (1968).
7. International Tables for X-ray Crystallography. Vol. III. Kynoch Press, Birmingham, 1963.
8. H. N. NG and C. CALVO. Can. J. Chem. **51**, 2613 (1973).
9. D. R. DAVIES and D. E. C. CORBRIDGE. Acta Crystallogr. **11**, 315 (1958).
10. M. T. AVERBUCH-POUCHOT, A. DURIF, and J. C. GUITEL. Acta Crystallogr. B**31**, 2482 (1975).

Can. J. Chem. Downloaded from www.nrcresearchpress.com by 210.87.254.5 on 09/05/12
For personal use only.

The hydrogen and methane chemical ionization mass spectra of some formate esters

ALEX. G. HARRISON AND CHUN WAI TSANG[1]

Department of Chemistry, University of Toronto, Toronto, Ont., Canada M5S 1A1

Received January 28, 1976

ALEX G. HARRISON and CHUN WAI TSANG. Can. J. Chem. **54**, 2029 (1976).

The H_2 and CH_4 chemical ionization mass spectra of formate esters up to the butyl formates have been determined. Deuterium labelling of the ester and deuterated reagent gases have been used to establish reaction mechanisms. The major fragmentation reactions of the protonated molecular ion are

(*a*) $HCO_2R.H^+ \rightarrow ROH_2^+ + CO$

(*b*) $\rightarrow HCO_2H_2^+ + (R—H)$

(*c*) $\rightarrow R^+ + HCO_2H$

Reaction (*a*) is the dominant fragmentation for methyl formate, (*b*) is the dominant fragmentation for ethyl formate, while (*c*) is the dominant fragmentation for higher formate esters. The results show that the relative importance of the fragmentation routes cannot be predicted from the enthalpy of reaction of ground state $HCO_2R.H^+$ but are determined by the fragmentation rate coefficients averaged over the appropriate internal energy distribution of the excited $HCO_2R.H^+$ ions.

ALEX G. HARRISON et CHUN WAI TSANG. Can. J. Chem. **54**, 2029 (1976).

On a déterminé les spectres de masse par ionisation chimique à l'aide du H_2 et du CH_4 des esters de l'acide formique jusqu'au formate de butyle. On a utilisé des gaz réactifs deutérés et le marquage au deutérium des esters pour établir les mécanismes réactionnels. Les réactions principales de fragmentation de l'ion moléculaire protoné sont

(*a*) $HCO_2R.H^+ \rightarrow ROH_2^+ + CO$

(*b*) $\rightarrow HCO_2H_2^+ + (R—H)$

(*c*) $\rightarrow R^+ + HCO_2H$

La réaction (*a*) est la réaction principale de fragmentation du formate de méthyle, (*b*) est la réaction principale de fragmentation du formate d'éthyle alors que (*c*) est la réaction principale de fragmentation des esters de l'acide formique de poids moléculaires plus élevés. Les résultats montrent que l'on ne peut pas prédire l'importance relative des chemins de fragmentation à partir de l'enthalpie de la réaction de l'état fondamental $HCO_2R.H^+$; ces importances relatives sont plutôt déterminées par les coefficients de vitesse de fragmentation moyennés sur la distribution appropriée de l'énergie interne des ions excités $HCO_2R.H^+$.

[Traduit par le journal]

Introduction

As part of the initial survey of the potential usefulness of chemical ionization (CI) mass spectrometry as an analytical technique, Munson and Field (1) reported the CH_4 CI mass spectra of a series of propionate esters as well as the spectra of a representative selection of other esters. More recently, the CH_4 CI mass spectra of a few formate, acetate, and propionate esters have been reported (2). Additional studies have been concerned with the CI of mono-enoic and mono-epoxy fatty acid methyl esters (3) and with the H_2 and CH_4 CI mass spectra of methyl *n*-alkanoates up to methyl stearate (4). However, apart from a study, using deuterium labelling, of the origin of $CH_3CO_2H_2^+$ in the CH_4 CI of ethyl acetate (5) and a more general study (2), using deuterium labelling and icr techniques, of the CH_4 CI of ethyl acetate, there have been no detailed mechanistic studies of the chemical ionization of simple esters.

The present work reports a detailed study of the H_2 and CH_4 chemical ionization of the lower alkyl formates. Deuterium labelling of the esters and the use of deuterated reagent gases (both D_2 and CD_4) have permitted the elucidation of the major ionization and fragmentation processes

[1]Present address: Department of Mathematics and Sciences, Hong Kong Polytechnic, Kowloon, Hong Kong.

Can. J. Chem. Downloaded from www.nrcresearchpress.com by 210.87.254.42 on 09/05/12
For personal use only.

occurring and their dependence on molecular structure. It has been shown (6, 7) that H_2 CI mass spectra depend strongly on the internal excitation of the H_3^+ reactant ion. This excitation is controlled by the total H_2 pressure which determines the extent of collisional deactivation of the H_3^+* ions formed initially. The dependence of the H_2 CI mass spectra of the formate esters on the internal energy of the H_3^+ reactant has been investigated qualitatively in the present work by varying the H_2 pressure by a factor of 4.5, the limits being determined by the instrumentation available.

Experimental

The chemical ionization mass spectra were obtained using a Dupont 21-490 mass spectrometer equipped with a high pressure chemical ionization source. With this instrument source pressures cannot be measured directly; however, approximate measurements, using a thermocouple gauge probe inserted in place of the solid sample probe, indicated that the instrument could be operated over the range from 0.2 to 0.9 mm pressure. The accompanying figures for the variation of product yields with H_2 pressure cover this approximate pressure range. The CH_4 CI mass spectra were obtained with a source pressure of methane of approximately 0.4 mm. Other operating conditions were a source temperature of ~150 °C and a heated inlet system temperature of ~130 °C. Spectra obtained using 70 and 400 eV ionizing electrons were identical. The repeller plates were held at cage potential.

All samples were admitted through the heated inlet system. The unlabelled esters and alcohols were commercial samples of high purity. Methyl formate-*d*, ethyl formate-*d*, isopropyl formate-*d*, ethyl-d_5 formate, and CD_4 were obtained from Merck, Sharp and Dohme, Montreal. Methane, hydrogen, and deuterium, all research grade, were obtained from Matheson and Co. The deuterium was purified before use by passing it through a heated palladium thimble to remove a low-level impurity of mass 28, which gave a prominent ion at m/q 30 under CI conditions.

Results and Discussion

Chemical Ionization of Methyl Formate

Figure 1 shows the variation of product yields (% of total additive ionization) with pressure of reactant gas for the HCO_2CH_3–H_2, DCO_2CH_3–H_2, and HCO_2CH_3–D_2 systems. In the H_2 CI of methyl formate the protonated molecule, MH^+ (m/q 61) is ~10% of the total ionization and, as expected, shifts quantitatively to m/q 62 in the other two systems investigated. The major fragment ion is m/q 33 which accounts for ~75% of the total ionization at higher H_2 pressures. This

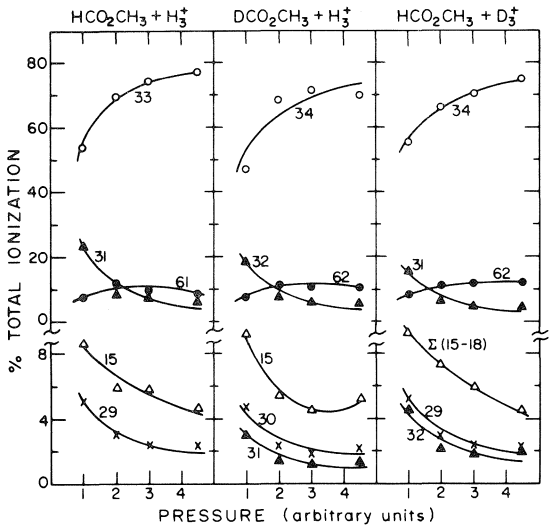

FIG. 1. H_2 and D_2 CI mass spectra of methyl formates as function of reagent gas pressure.

product shifts to m/q 34 in both the DCO_2CH_3–H_2 and HCO_2CH_3–D_2 systems indicating incorporation of the formyl hydrogen and one hydrogen from the reactant H_3^+ ion and, thus, fragmentation reaction 1, probably originating from the ether-oxygen protonated form of MH^+.

[1] 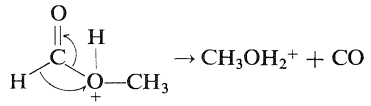 $\rightarrow CH_3OH_2^+ + CO$

In the electron impact mass spectrum of methyl formate an analogous rearrangement of the formyl hydrogen in the molecular ion leads to the $CH_3OH^{+\cdot}$ fragment ion (8).

The m/q 31 fragment shifts almost completely to m/q 32 in the DCO_2CH_3–H_2 system but largely remains at m/q 31 in the HCO_2CH_3–D_2 system, indicating incorporation of the formyl hydrogen in the fragment but very little incorporation of the proton from the H_3^+ reactant ion. Huntress and Bowers (6) have shown that reaction 2 in the CI of methanol yields equal

[2] $$CH_3OHD^+ \begin{cases} \rightarrow CH_2OH^+ + HD \\ \rightarrow CH_2OD^+ + H_2 \end{cases}$$

amounts of CH_2OH^+ and CH_2OD^+. If the m/q 31 observed in our system originated by further fragmentation of the $CH_3OH_2^+$ ion formed in reaction 1 one would expect equal yields of

Can. J. Chem. Downloaded from www.nrcresearchpress.com by 210.87.254.42 on 09/05/12
For personal use only.

Can. J. Chem. Downloaded from www.nrcresearchpress.com by 210.87.254.42 on 09/05/12
For personal use only.

CH_2OH^+ (m/q 31) and CH_2OD^+ (m/q 32) in the DCO_2CH_3–H_2 and HCO_2CH_3–D_2 systems. The failure to observe equal yields must mean that the major reaction sequence forming CH_2OH^+ (m/q 31) is hydride abstraction followed by fragmentation (reaction 3)

$$[3]\quad H_3^+ + HCO_2CH_3 \rightarrow 2H_2 + H{-}\overset{\overset{O}{\|}}{C}{-}OCH_2^+ \rightarrow CH_2OH^+ + CO$$

A similar rearrangement of the $HCO_2CH_2^+$ ion in the electron impact mass spectrum of methyl formate leads to m/q 31 as the base peak in the 70 eV mass spectrum (8). The low yields of m/q 31 and m/q 32 in the DCO_2CH_3–H_2 and HCO_2CH_3–D_2 systems, respectively, probably indicate that a small fraction of the CH_2OH^+ product originates by loss of H_2 from $CH_3OH_2^+$. The decrease in the yield of the m/q 31 product with increasing H_2 pressure is consistent with the observations by Huntress and Bowers (6) that hydride abstraction by H_3^+ decreases in importance with increasing collisional deactivation of excited H_3^+ ions.

The minor products at m/q 29 and m/q 15 undoubtedly arise by reactions 4 and 5,

$$[4]\quad H{-}\overset{\overset{O}{\|}}{C}{-}\overset{\overset{H}{|}}{\underset{+}{O}}{-}CH_3 \rightarrow H{-}\overset{\overset{O}{\|}}{C}^+ + HOCH_3$$

$$[5]\quad H{-}\overset{\overset{{}^+OH}{\|}}{C}{-}O{-}CH_3 \rightarrow H{-}\overset{\overset{O}{\|}}{C}{-}OH + CH_3^+$$

although for formation of CH_3^+ an entirely analogous reaction can be written involving initial protonation at the ether oxygen rather than the carbonyl oxygen. In the HCO_2CH_3–D_2 system the methyl ion product is distributed from m/q 15 (CH_3^+) to m/q 18 (CD_3^+) due to the exchange reaction of CH_3^+ with D_2 (9).

In the CH_4 CI mass spectrum of methyl formate the protonated molecule (m/q 61) accounted for ~95% of the total additive ionization, with only minor fragmentation to yield $CH_3OH_2^+$ (~3% of total ionization). A small (~2% of total ionization) ion signal at m/q 101 results from the collisionally-stabilized addition of $C_3H_5^+$ to the ester. Interestingly, the analogous peak corresponding to $C_2H_5^+$ addition to the ester was not observed, and $C_2H_5^+$ must react entirely by proton transfer.

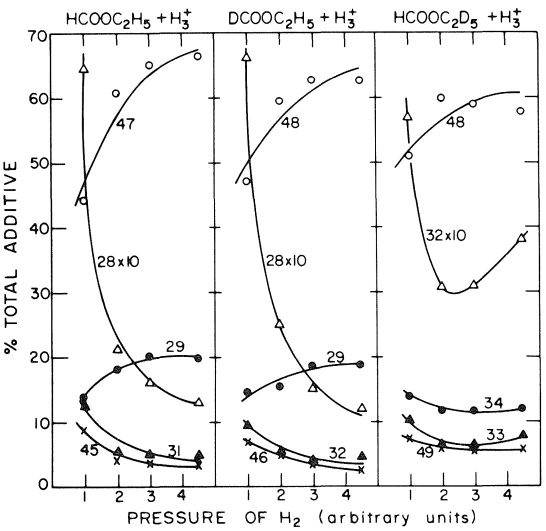

FIG. 2. H_2 CI mass spectra of ethyl formates as function of reagent gas pressure.

Chemical Ionization of Ethyl Formate

Figure 2 shows the variation with H_2 pressure of the product yields in the H_2 CI of $HCO_2C_2H_5$, $DCO_2C_2H_5$, and $HCO_2C_2D_5$. The protonated molecule, MH^+, accounted for ~2% of the total ionization over the whole pressure range and is not shown in Fig. 2. The dominant product ion observed in the CI mass spectrum of $HCO_2C_2H_5$ is m/q 47. This product shifts to m/q 48 in the H_2 CI of both $DCO_2C_2H_5$ and $HCO_2C_2D_5$, and in the D_2 CI of $HCO_2C_2H_5$, indicating that the ion is $HCO_2H_2^+$ rather than $C_2H_5OH_2^+$, analogous to the $CH_3OH_2^+$ product observed in the H_2 CI of methyl formate. In the H_2 CI of $HCO_2C_2D_5$ no ion signal was observed at m/q 52 corresponding to $C_2D_5OH_2^+$. The m/q 47 product contains the formyl hydrogen, one proton from the H_3^+ reactant ion, and one hydrogen from the ethyl group, as indicated in reaction 6, although a similar hydrogen transfer in the ether protonated form cannot be excluded.

$$[6]\quad H{-}\overset{\overset{{}^+OH}{\|}}{C}{-}OC_2H_5 \rightarrow HCO_2H_2^+ + C_2H_4$$

The second most abundant fragment ion is observed at m/q 29. From the shifts on deuterium labelling this product obviously corresponds entirely to the ethyl cation, formed by the reaction analogous to [5], with no contribution from HCO^+. The increase with H_2 pressure of

Can. J. Chem. Downloaded from www.nrcresearchpress.com by 210.87.254.42 on 09/05/12
For personal use only.

m/q 33 and, at higher pressures, m/q 32 in the H_2 CI of $HCO_2C_2D_5$ suggests that there is a slow exchange of the $C_2D_5^+$ ion with H_2, similar to the known exchange reaction of CH_3^+ with D_2 (9). The m/q 28 product ($C_2H_4^+$) is ~6–8% of the total ionization at low H_2 pressures and decreases rapidly in importance with increasing H_2 pressure. The mechanism of formation is not clear; however this product may arise by charge transfer from highly excited H_3^+ ions. The abundance of such highly excited ions is strongly dependent on H_2 pressure (10, 11).

The labelling results indicate that the m/q 45 and m/q 31 products result from further fragmentation of the ions produced by hydride ion abstraction (reaction 7) and CH_3^- abstraction (reaction 8), respectively.

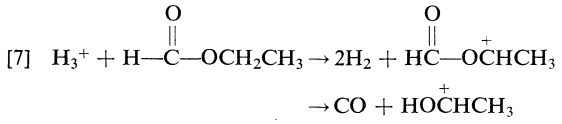

[7] $H_3^+ + H{-}C(=O){-}OCH_2CH_3 \rightarrow 2H_2 + HC(=O)^+{-}OCHCH_3 \rightarrow CO + HO^+CHCH_3$

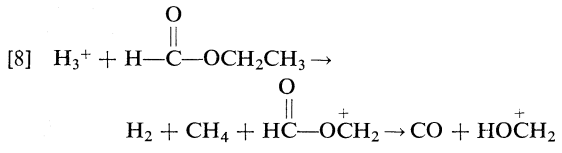

[8] $H_3^+ + H{-}C(=O){-}OCH_2CH_3 \rightarrow H_2 + CH_4 + HC(=O)^+{-}OCH_2 \rightarrow CO + HO^+CH_2$

To avoid overlap of product species at the same nominal mass, the CH_4 CI mass spectrum of $HCO_2C_2D_5$ was determined. The spectrum is shown in bar graph form in Fig. 3*a*. As expected, the less exothermic proton transfer from $CH_5^+/C_2H_5^+$ results in a much-increased abundance of the protonated molecule, MH^+, and decreased abundance of ions resulting from fragmentation of MH^+. The $C_2D_5^+$ fragment ion is almost completely absent and protonated formic acid has become the major fragmentation product. Of particular interest is the low-abundance ion at m/q 52 corresponding to $C_2D_5OH_2^+$ produced by the reaction

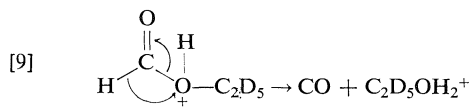

[9] $H{-}C(=O){-}O{-}C_2D_5 \rightarrow CO + C_2D_5OH_2^+$

which was not observed in the H_2 CI. The ion signal observed at m/q 120 corresponds to $C_3H_5^+$ addition to the ester. No adduct of $C_2H_5^+$ was observed but rather the product (m/q 76)

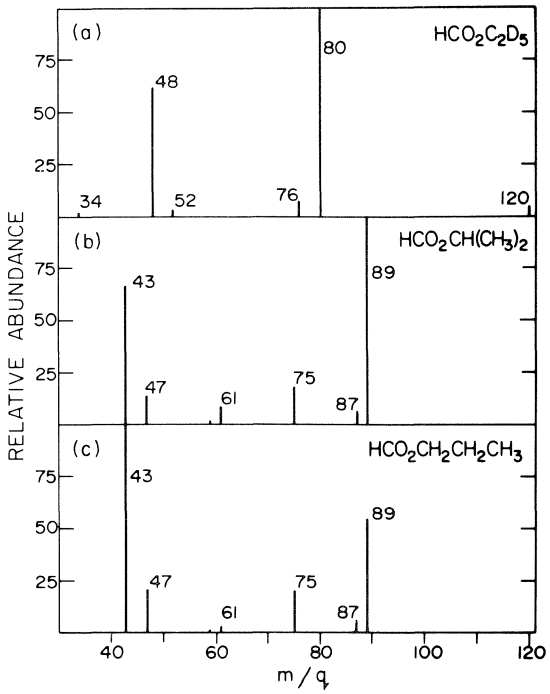

FIG. 3. CH_4 CI mass spectra of (*a*) ethyl-d_5 formate, (*b*) isopropyl formate, (*c*) *n*-propyl formate.

resulting from $C_2H_5^+$ addition followed by C_2D_4 elimination (reaction 10)

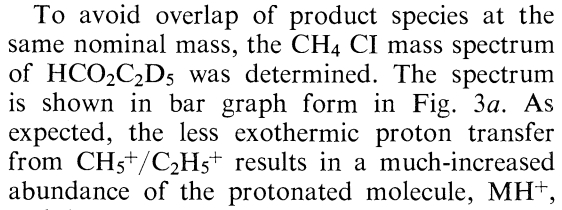

[10] $C_2H_5^+ + H{-}C(=O){-}OC_2D_5 \rightarrow HC(OC_2D_5)^+{-}OC_2D_5 \rightarrow H{-}C(=O^+D){-}OC_2H_5 + C_2D_4$

Chemical Ionization of Isopropyl Formate

Figure 4 shows the variation of product yields with reagent gas pressure in the $HCO_2CH(CH_3)_2$–H_2, $DCO_2CH(CH_3)_2$–H_2, and $HCO_2CH(CH_3)_2$–D_2 systems. The protonated ester accounted for ~1.5% of the total ionization over the pressure range studied and is not included in Fig. 4. In contrast to methyl formate and ethyl formate, the alkyl ion $C_3H_7^+$ (m/q 43) is the major product of fragmentation of the protonated molecule (reaction 11).

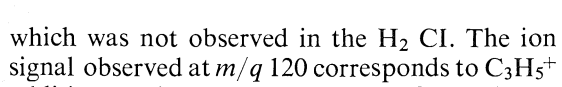

[11] $H{-}C(=O^+H){-}OCH(CH_3)_2 \rightarrow C_3H_7^+ + H{-}C(=O){-}OH$

No protonated alcohol is observed and protonated formic acid (m/q 47 or m/q 48), which

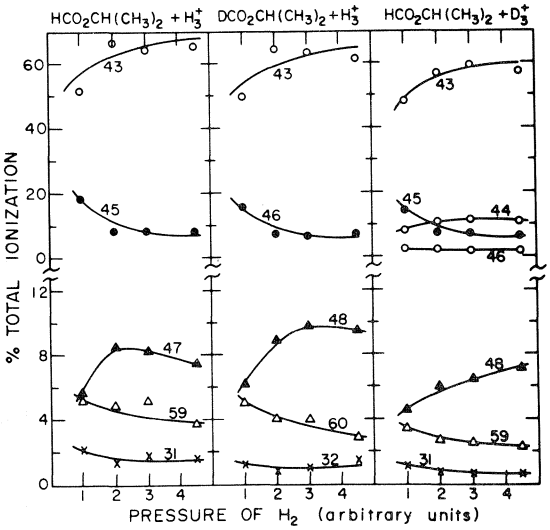

FIG. 4. H_2 and D_2 CI mass spectra of isopropyl formates as function of reagent gas pressure.

was the most abundant ion in the CI of ethyl formate, accounts for only 8–10% of the total ionization.

The other minor fragment ions observed are m/q 45, m/q 59, and m/q 31, presumably arising by hydride or CH_3^- abstraction with subsequent decomposition (reactions 12 and 13).

[12]
$$H_3^+ + HCO_2CH(CH_3)_2 \rightarrow H_2 + CH_4 + HC(=O)-\overset{+}{O}CHCH_3$$
$$\rightarrow CO + \overset{+}{H}OCHCH_3 \quad (m/q\ 45)$$

[13]
$$H_3^+ + HCO_2CH(CH_3)_2 \rightarrow 2H_2 + HC(=O)-\overset{+}{O}C(CH_3)_2$$
$$\rightarrow CO + \overset{+}{H}OC(CH_3)_2 \quad (m/q\ 59)$$
$$\downarrow$$
$$C_2H_4 + \overset{+}{H}OCH_2 \quad (m/q\ 31)$$

These fragmentation sequences are identical to reactions occurring in the electron impact induced fragmentation of isopropyl formate (8). A moderately abundant (~6%) m/q 42 ($C_3H_6^+$) product is observed at low H_2 pressures presumably arising by charge transfer from excited H_3^+.

The CH_4 CI mass spectrum of isopropyl formate is shown in Fig. 3*b*. The much higher abundance of the protonated molecule, compared to the H_2 CI, again reflects the lower exothermicity of the protonation reaction. The major product ions resulting from fragmentation of MH^+ are $C_3H_7^+$ (m/q 43) and $HCO_2H_2^+$ (m/q 47) as observed in the H_2 CI. In addition, the low-intensity signal at m/q 61 (shifting to m/q 62 in $DCO_2CH(CH_3)_2$) must correspond to protonated isopropyl alcohol formed by reaction 14, a reaction not observed in the H_2 ci.

[14]
$$H-\overset{O}{\overset{\|}{C}}-\overset{+}{O}CH(CH_3)_2 \rightarrow CO + (CH_3)_2CHOH_2^+$$
(H bonded to C)

Also of interest are the ion signals at m/q 75 and m/q 87 corresponding, respectively, to the addition of $C_2H_5^+$ and $C_3H_5^+$ to the ester, followed in each case by elimination of C_3H_6 (reaction 15).

[15]
$$R^+ + H-\overset{O}{\overset{\|}{C}}-OCH(CH_3)_2 \rightarrow H-\overset{OR}{\overset{|}{\underset{+}{C}}}-OCH(CH_3)_2$$
$$\rightarrow HC(=\overset{+}{O}H)-OR + C_3H_6$$

Although $C_3H_5^+$ addition to ethyl formate is observed (m/q 120, Fig. 3*a*), the subsequent olefin elimination step is not observed.

Chemical Ionization of n-Propyl Formate

Figure 5 shows the variation with pressure of the product yields in the H_2 and D_2 CI of *n*-propyl formate. As for the isopropyl formate system the yield of MH^+ was small (~1%), the major fragmentation reaction yielding $C_3H_7^+$ (m/q 43) with a smaller yield of $HCO_2H_2^+$ (m/q 47). The low yield of m/q 44 in the $HCO_2C_3H_7$–D_2 system suggests a slow exchange reaction of $C_3H_7^+$ with D_2. The other major fragment ions observed are m/q 31, m/q 59, and m/q 45, presumably arising from H^- or alkide ion abstraction reaction with subsequent fragmentation of the ions so formed. The major distinction between the two propyl formates lies in the relative intensities of the m/q 31 and m/q 45 ions which in each case reflect the dominant alkide ion abstraction reaction, *i.e.*, CH_3^- abstraction from isopropyl formate and $C_2H_5^-$ abstraction from *n*-propyl formate. As was observed for the isopropyl formate, the *n*-propyl ester showed an abundant (~11%) $C_3H_6^+$ (m/q 42) fragment at low H_2 pressures, with the yield decreasing rapidly with increasing H_2 pressure, consistent with a charge transfer reaction from highly excited H_3^+.

Can. J. Chem. Downloaded from www.nrcresearchpress.com by 210.87.254.42 on 09/05/12
For personal use only.

Can. J. Chem. Downloaded from www.nrcresearchpress.com by 210.87.254.42 on 09/05/12
For personal use only.

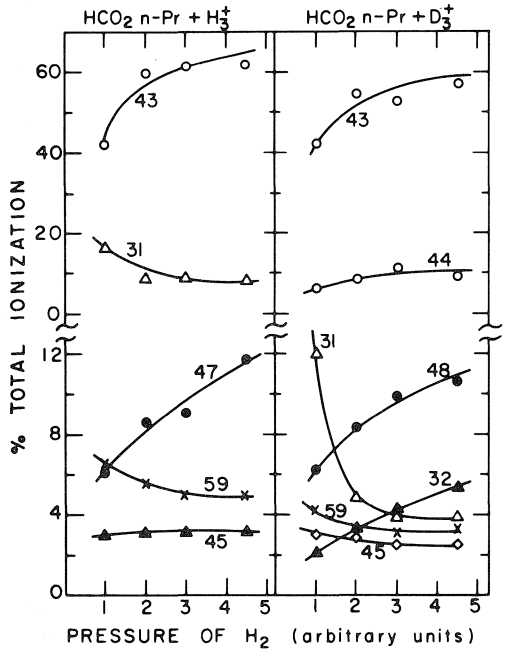

FIG. 5. H_2 and D_2 CI mass spectra of *n*-propyl formate as function of reagent gas pressure.

The CH_4 CI mass spectrum of *n*-propyl formate is shown in Fig. 3*c*. The spectrum is very similar to that observed for isopropyl formate and the origin of the ions is as discussed above for the latter ester. The major difference between the two spectra lies in the $C_3H_7^+/MH^+$ (m/q 89) ratio which was always significantly larger for the *n*-propyl ester, indicating a more facile fragmentation of MH^+ in this case. Using the thermochemical data summarized in the Appendix we calculate for the two fragmentation reactions

$$[16] \quad \overset{+OH}{\overset{\|}{HC}}\text{—O—}i\text{-}C_3H_7 \rightarrow i\text{-}C_3H_7^+ + HCOOH$$

$$[17] \quad \overset{+OH}{\overset{\|}{HC}}\text{—O—}n\text{-}C_3H_7 \rightarrow n\text{-}C_3H_7^+ + HCOOH$$

$\Delta H_{16} = 28$ kcal mol^{-1} and $\Delta H_{17} = 38$ kcal mol^{-1}. Both reaction endothermicities are much less than the ~70 kcal mol^{-1} exothermicity of proton transfer from CH_5^+ to the esters, indicating that fragmentation of MH^+ would be anticipated. However, contrary to observations, the relative values predict that the fragmentation should be more extensive for the isopropyl ester. On the other hand, if we assume that the $C_3H_7^+$ ion formed in reaction 17 has the isopropyl rather than the *n*-propyl structure ΔH_{17} becomes 22 kcal mol^{-1} and reaction 17 becomes energetically favoured compared to reaction 16. Electron impact induced fragmentation of *n*-propyl derivatives leads to formation of the isopropyl cation, at least at threshold energies (12), and the above observations may imply that the same is true for fragmentation reactions induced by chemical ionization.

Chemical Ionization of Higher Alkyl Formates

Figure 6 compares the H_2 CI mass spectra of methyl, ethyl, and the propyl formates with the H_2 CI mass spectra of the corresponding alcohols. For the methyl and ethyl compounds there are significant differences in the CI spectra, particularly in view of the fact that m/q 47 is $C_2H_5OH_2^+$ for ethyl alcohol but $HCO_2H_2^+$ for ethyl formate. However the H_2 CI mass spectra of the propyl formates are very similar to the spectra of the alcohols from which they are derived. The only significant differences are the observation of ion signals at m/q 47 ($HCO_2H_2^+$) for the esters with an intensity 12–15% of the $C_3H_7^+$ base peak; the very low intensity MH^+ peaks for the esters could easily be missed if the background was high.

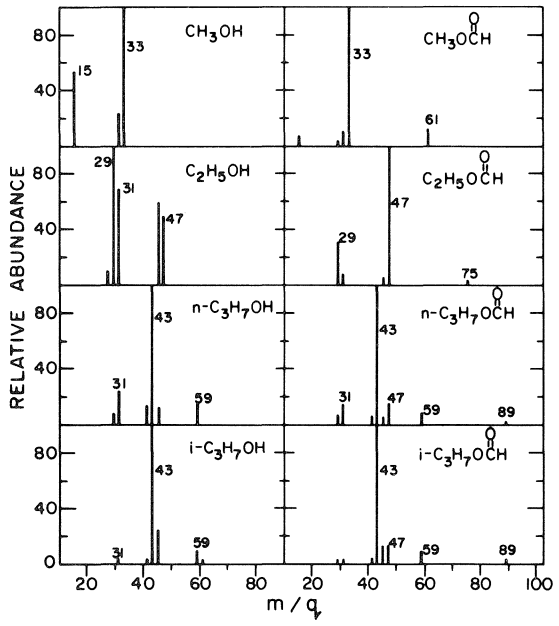

FIG. 6. Comparison of H_2 CI mass spectra of ROH and RO_2CH.

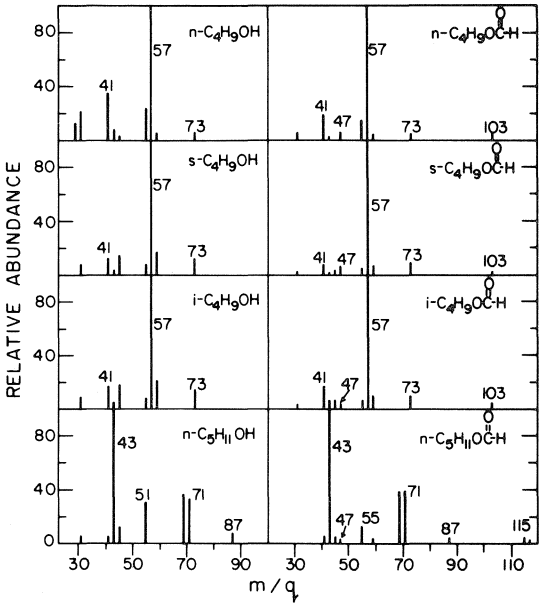

FIG. 7. Comparison of H_2 CI mass spectra of ROH and RO_2CH.

This similarity of the spectra of the formate esters to the spectra of the corresponding alcohol appears to extend to all higher alkyl formates. Figure 7 shows the comparison for three butyl compounds and the *n*-pentyl compound. As was the case for the propyl compounds the only notable differences are the low intensity m/q 47 ($HCO_2H_2^+$) peaks for the formate esters which are missing from the spectra of the alcohols. For identification purposes the presence of the m/q 47 peak is sufficient to distinguish the formate ester from the free alcohol; however, the CH_4 CI mass spectra (Fig. 8) of the higher formates are much more informative since they show abundant MH^+ ions as well as moderately abundant peaks corresponding to $C_2H_5^+$ and $C_3H_5^+$ addition to HCO_2R with loss of (R—H). In addition the CH_4 CI spectra show the characteristic alkyl ions which dominate the H_2 CI spectra.

Role of Energetics in the Fragmentation of MH^+

The three major fragmentation reactions of the protonated molecular ion observed in the H_2 CI of formate esters are

[18] $HCO_2R.H^+ \rightarrow ROH_2^+ + CO$

[19] $\rightarrow HCO_2H_2^+ + (R—H)$

[20] $\rightarrow R^+ + HCO_2H$

Table 1 summarizes the fractional abundances of these product ions for the esters studied and also presents the reaction endothermicities calculated for decomposition of ground state HCO_2RH^+ using the thermochemical data summarized in the Appendix.

For protonated methyl formate reaction 18 is strongly favoured energetically and is the major fragmentation reaction observed. However, for ethyl formate, although reaction 18 is energetically favoured no $C_2H_5OH_2^+$ is observed and $HCO_2H_2^+$, the product of reaction 19, is the major fragment ion. In addition, $C_2H_5^+$, the product of reaction 20 accounts for ~20% of the total ionization even though ΔH_{20} is considerably greater than ΔH_{19}. The failure to observe $C_2H_5OH_2^+$ cannot be due to decomposition of this ion to $C_2H_5^+ + H_2O$ since, as shown in Fig. 6, the reaction of H_3^+ directly with ethyl alcohol leads to formation of $C_2H_5OH_2^+$ ions which have a lifetime sufficient to be detected. We must conclude that for ethyl formate reaction 18 does not occur in the H_2 CI even though it is the most favoured reaction energetically.

Similar conclusions apply to the propyl and butyl formates where no protonated alcohol is observed even though reaction 18 has the lowest

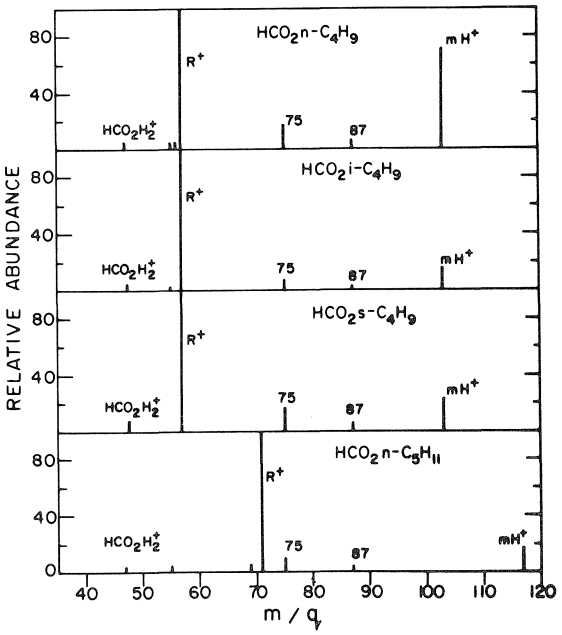

FIG. 8. CH_4 CI mass spectra of butyl formates and *n*-pentyl formate.

Can. J. Chem. Downloaded from www.nrcresearchpress.com by 210.87.254.42 on 09/05/12
For personal use only.

TABLE 1. Fractional yields and reaction endothermicities[a] in H_2 CI of formates

	Product ion					
	ROH_2^+		$HCO_2H_2^+$		R^+	
Ester	ΔH	Yield	ΔH	Yield	ΔH	Yield
HCO_2CH_3	15	0.78	—	0	50	0.05
$HCO_2C_2H_5$	12	0	25	0.68	44	0.20
HCO_2n-C_3H_7	10	0	23	0.12	38	0.65
HCO_2i-C_3H_7	10	0	28	0.09	27	0.67
HCO_2n-C_4H_9	10	0	25	0.03	38	0.61
HCO_2i-C_4H_9	13	0	25	0.02	40	0.60
HCO_2s-C_4H_9	11	0	26	0.03	24	0.73

[a]Reaction endothermicity (kcal mol^{-1}) for fragmentation of ground state protonated ester.

endothermicity for ground state protonated ester molecules. For these esters the dominant fragmentation reaction is [20] in all cases, even though in most cases reaction 19 is more favoured energetically. These observations indicate that one cannot readily predict the relative abundances of fragment ions in chemical ionization processes from calculated reaction endothermicities for ground state species, particularly if one is comparing simple bond cleavage reactions (reaction 20) with rearrangement reactions (reactions 18 and 19).

The reaction of H_3^+ with the formate esters is approximately 90 kcal mol^{-1} exothermic. Although it is not known what fraction of the reaction exothermicity is retained as internal energy in the protonated ester the observations that essentially no MH^+ ions are observed and that $C_2H_5^+$ ions are observed in the H_2 CI of ethyl formate indicates that the internal excitation of the protonated esters must be at least 40 kcal mol^{-1} and that little deactivation by collision with H_2 occurs. To predict relative fragment ion abundances one must compare not relative activation energies for fragmentation of ground state species but relative rate coefficients for the possible fragmentation reactions suitably averaged over the internal energy distribution of the fragmenting ion. For the protonated esters formed by H_2 CI this internal energy distribution may extend from 40 to 90 kcal mol^{-1}. While simple bond cleavage reactions (reaction 20) may have substantially higher activation energies than rearrangement reactions (reaction 18 and/or 19) the energy independent term in the rate coefficient expression (*i.e.*, the frequency factor or entropy of activation) also will be larger with the result that at high internal energies the reaction of higher activation energy may be the dominant fragmentation route. This appears to be the situation in the H_2 CI of the formate esters.

In terms of the above description one would anticipate that when MH^+ is formed by a less exothermic route, thus decreasing the average excitation of MH^+, the relative contribution of ions arising by rearrangement fragmentation of the protonated molecule should increase in importance compared to those ions formed by simple bond cleavage reactions of high activation energy. This is borne out in the present work by the observation of ROH_2^+ fragment ions in the CH_4 CI of ethyl and propyl formates; these products are not observed in the H_2 CI. In addition the ion current ratios HCO_2H^+/R^+ which are 3.4, 0.16, and 0.14 in the H_2 CI of ethyl formate, *n*-propyl formate, and isopropyl formate, respectively, increase to 70, 0.22, and 0.21 in the CH_4 ci indicating that the rearrangement reaction 19 has become more competitive with the simple bond cleavage reaction 20 as the average excitation of the MH^+ ions decrease. Thus we conclude that to predict relative fragment ion abundances from chemical ionization reactions one must compare relative fragmentation rate coefficients over the appropriate internal energy region, rather than simply comparing activation energies (2).

Acknowledgments

The authors are indebted to the National Research Council of Canada for financial support and to Professor P. Kebarle for communication of results prior to publication.

1. M. S. B. MUNSON and F. H. FIELD. J. Am. Chem. Soc. **88**, 4337 (1966).

Can. J. Chem. Downloaded from www.nrcresearchpress.com by 210.87.254.42 on 09/05/12
For personal use only.

2. C. V. PESCHEK and S. E. BUTTRILL. J. Am. Chem. Soc. **96**, 6027 (1974).
3. R. J. WEINKAM. J. Am. Chem. Soc. **96**, 1032 (1974).
4. C. W. TSANG and A. G. HARRISON. J. Chem. Soc. Perkin Trans. II, 1718 (1975).
5. B. L. JELUS, B. MICHNOWICZ, and B. MUNSON. J. Org. Chem. **39**, 2130 (1974).
6. W. T. HUNTRESS and M. T. BOWERS. Int. J. Mass Spectrom. Ion Phys. **12**, 1 (1973).
7. M. T. BOWERS, W. J. CHESNAVICH, and W. T. HUNTRESS. Int. J. Mass Spectrom. Ion Phys. **12**, 357 (1973).
8. D. VAN RAALTE and A. G. HARRISON. Can. J. Chem. **41**, 2054 (1963).
9. A. G. HARRISON and B. G. KEYES. Can. J. Chem. **51**, 1265 (1973).
10. J. J. LEVENTHAL and L. FRIEDMAN. J. Chem. Phys. **49**, 1974 (1968).
11. M. T. BOWERS and D. D. ELLEMAN. J. Am. Chem. Soc. **92**, 7258 (1970).
12. F. P. LOSSING and G. P. SEMELUK. Can. J. Chem. **48**, 955 (1970).
13. Ionization Potentials, Appearance Potentials, and Heats of Formation of Gaseous Positive Ions. NSRDS-NBS 26, Washington. D.C. 1969.
14. R. YAMDAGNI and P. KEBARLE. J. Am. Chem. Soc. **98**, 1320 (1976).
15. A. G. HARRISON, P.-H. LIN, and C. W. TSANG. Int. J. Mass Spectrom. Ion Phys. **19**, 23 (1976).

Appendix

Thermochemical data: The heats of formation used for the neutral esters, the protonated esters, the protonated alcohols, and alkyl ions are summarized in Table 2. Data for all neutral species as well as $\Delta H_f(H^+) = 366$ kcal mol^{-1} were taken from ref. 13. The heats of formation of the alkyl ions have been reported by Lossing and Semeluk (12). The $\Delta H_f(HCO_2R.H^+)$ were derived from the proton affinities of the esters using the average of the values reported by Yamdagni and Kebarle (14) and Harrison *et al.* (15),[2] *i.e.* $PA(HCO_2CH_3) = 187$ kcal mol^{-1}, $PA(HCO_2C_2H_5) = 192$ kcal mol^{-1}, $PA(HCO_2n\text{-Pr}) = 192$ kcal mol^{-1}, and $PA(HCO_2i\text{-Pr}) = 194$ kcal mol^{-1}). For the butyl formates a proton affinity of 195 kcal mol^{-1} was assumed in all cases. The $\Delta H_f(ROH_2^+)$ were derived from $PA(CH_3OH) = 182$ kcal mol^{-1} (14), $PA(C_2H_5OH) = 186.5$ kcal mol^{-1} (14, 15) and assumed values of 189 for the propyl and butyl alcohols since no reliable values for the latter have been reported. From $PA(HCO_2H) = 178$ kcal mol^{-1} (14) we derive $\Delta H_f(HCO_2H_2^+) = 98$ kcal mol^{-1}.

[2]Some of the proton affinities reported in ref. 15 are relative to an assumed value of 202 kcal mol^{-1} for acetone. These have been recalculated relative to the value of 195 kcal mol^{-1} measured by Yamdagni and Kebarle (14).

TABLE 2. Standard heats of formation (kcal mol^{-1})

R	$\Delta H_f(HCO_2R)$	$\Delta H_f(HCO_2R.H^+)$	$\Delta H_f(ROH_2^+)$	$\Delta H_f(R^+)$
CH_3	−83.7	95	136	260
C_2H_5	−89	85	123	219
$n\text{-}C_3H_7$	−94	80	~116	208
$i\text{-}C_3H_7$	−97	75	~111	192
$n\text{-}C_4H_9$	−98	73	~109	201
$s\text{-}C_4H_9$	−102	69	~106	183
$i\text{-}C_4H_9$	−102	69	~108	199

Can. J. Chem. Downloaded from www.nrcresearchpress.com by 210.87.254.42 on 09/05/12
For personal use only.

A study of non-bonded interactions of nitro and nitronate substituents in inositols[1]

HANS H. BAER AND JAN KOVÁŘ
Department of Chemistry, University of Ottawa, Ottawa, Ont., Canada K1N 6N5

HANS H. BAER and JAN KOVÁŘ. Can. J. Chem. **54**, 2038 (1976).

In the family of mutually interconvertible δ-*O*-methyl-deoxynitroinositols having the *myo*-5 (**1**), *neo*-2 (**2**), *allo*-5 (**3**), *epi*-1 (**4**), *epi*-6 (**5**), and *cis* (**6**) configurations the relative thermodynamic stabilities of the individual members and of the three corresponding sodium nitronates **1′**, **3′**, and **5′** were assessed by determining equilibria of epimerization at p*H* 8.2 and p*H* > 12. The orders of stability are **1** ≫ **4** ≈ **5** > **3** > **2** ≫ **6** and **1′** > **3′** > **5′**. The equilibrium data, together with those previously obtained for the stereoisomeric series comprising the corresponding *scyllo* (**7**), *myo*-1 (**8**), *epi*-3 (**9**), and *muco*-3 (**10**) epimers and their nitronates **7′**, **8′**, and **9′**, were compared with theoretical values that were obtained from calculated conformational energies. The non-bonded interactions of the nitro and the nitronate group were evaluated and variable energy parameters were devised on the basis of differing *gauche* arrangements.

HANS H. BAER et JAN KOVÁŘ. Can. J. Chem. **54**, 2038 (1976).

Dans la famille des δ-*O*-méthyl-désoxynitroinositols qui peuvent être interconvertis mutuellement et qui ont les configurations *myo*-5 (**1**), *neo*-2 (**2**), *allo*-5 (**3**), *épi*-1 (**4**), *épi*-6 (**5**) et *cis* (**6**), on a évalué les stabilités thermodynamiques relatives des membres individuels et des trois nitronates de sodium correspondants (**1′**, **3′** et **5′**) en déterminant les équilibres d'épimérisation à p*H* 8.2 et p*H* > 12. Les ordres de stabilité sont **1** ≫ **4** ≈ **5** > **3** > **2** ≫ **6** et **1′** > **3′** > **5′**. Les mesures d'équilibre ainsi que celles obtenues auparavant pour la série stéréoisomérique comprenant les épimères correspondants *scyllo* (**7**), *myo*-1 (**8**), *epi*-3 (**9**) et *muco*-3 (**10**) ainsi que leurs nitronates (**7′**, **8′** et **9′**) ont été comparées aux valeurs théoriques qui ont été obtenues à partir des énergies conformationnelles calculées. Les interactions non-liées des groupes nitro et nitronate ont été évaluées, et des paramètres variables d'énergie ont été établis sur la base de differents arrangements *gauches*.

Introduction

In a detailed recent study (2), base-catalyzed cyclizations of 6-deoxy-3-*O*-methyl-6-nitro-D-allose and -L-talose have been shown to furnish δ-*O*-methylated deoxynitroinositols having the *myo*-5 (**1**), *neo*-2 (**2**), D-*allo*-5 (D-**3**), L-*allo*-5 (L-**3**), D-*epi*-1 (D-**4**), L-*epi*-1 (L-**4**), and *epi*-6 (**5**) configurations. These are seven out of a possible eight members of the configurational family of epimers which is characterized by an identical *cis,cis* arrangement of the methoxyl and its two flanking hydroxyl groups. The eighth member, the *cis* epimer (**6**), has not been detected among the products. The distribution of stereoisomers in the cyclization mixtures was found to depend on reaction conditions as these may favor kinetic control or allow for thermodynamic equilibrations of epimers (2), according to principles previously discussed in respect of another configurational family of stereoisomeric deoxynitroinositols (3–5). The present article is to show that the relative thermodynamic stabilities of **1**–**6** (and also those of their sodium nitronates), which are reflected in their equilibria of epimerization, correlate well with calculations of conformational free energies based on non-bonded substituent interactions. The data on hand permit, as will be seen, an analysis of steric requirements of the nitro and nitronate groups in variable environments.

The proportions of individual epimers obtainable by alkaline equilibration are p*H* dependent since the free-energy differences of the undissociated nitro compounds are not proportional to the free-energy differences of their corresponding conjugate bases, the nitronates. The equilibrium constants for the free nitro compounds can be obtained in close approximation by measuring product ratios after equilibration in a *weakly* alkaline medium (p*H* 8–9) where nitronate concentrations are negligible yet epimerization proceeds, if slowly, at a tolerable rate. The constants for the nitronates can be determined similarly at a *higher* alkalinity (p*H*

[1]Part XXXVI in a series on reactions of nitro sugars. For part XXXV (erroneously numbered XXXIV) and part XXXIV, see refs. 1*a* and 1*b*, respectively.

Can. J. Chem. Downloaded from www.nrcresearchpress.com by 210.87.254.40 on 09/05/12
For personal use only.

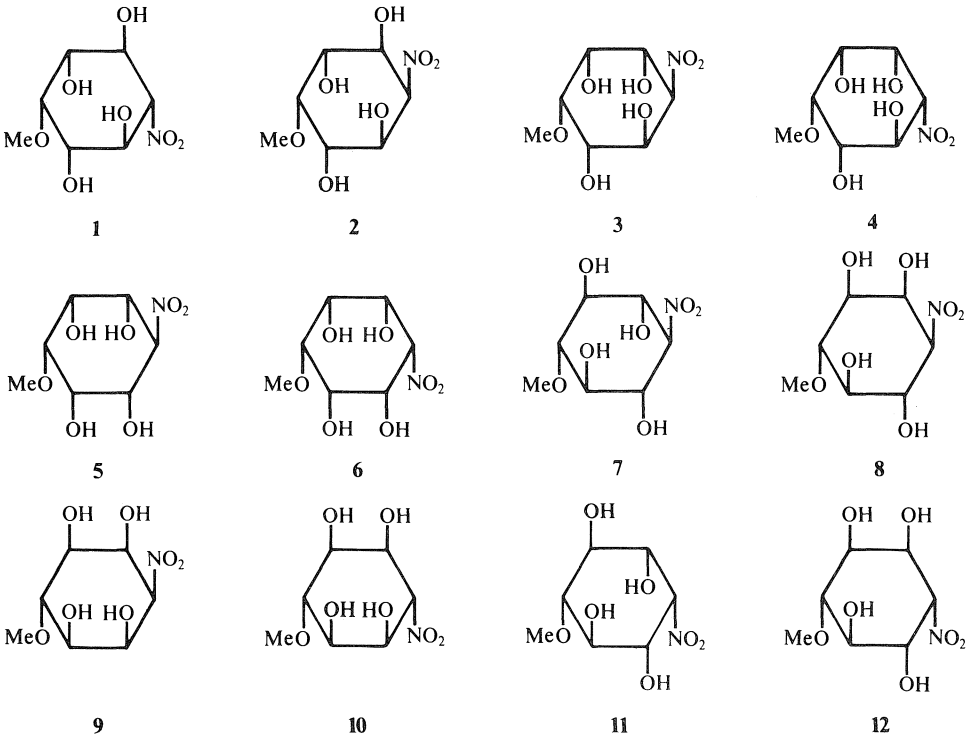

11–12) which assures the concentration of conjugate acid to be insignificant. At whatever p*H* the equilibrium of epimers is established, any chiral components (D-**3**, L-**3**, D-**4**, L-**4**, or the corresponding nitronates) will eventually exist as racemates, and it is to these that the formula numbers **3** and **4** will refer.

Results and Discussion

Equilibrium of Free Nitro Compounds

As already reported (2), the *myo*-5 and *neo*-2 derivatives **1** and **2**, which are epimeric at the nitromethine carbon atom, undergo mutual interconversion in 1% aqueous sodium bicarbonate solution at p*H* 8.2 and 25 °C, reaching equilibrium between themselves in the course of one day. Very slowly, epimerization then progresses to involve neighboring carbinol centers, giving rise to *allo*-5 (**3**) as well as *epi*-1 and *epi*-6 epimers (**4** and **5**, which were not separated from each other by our method of glc analysis). This slow process was incomplete after 8 days. A similar if somewhat more complicated sequence of processes, likewise incomplete after 8 days, was found to take place with D-**3** (2). We have now determined the final equilibrium compositions, which were reached after 7 weeks and, as expected, proved virtually independent of the starting compound. The proportions were 79–82% of **1**, 2–3% of **2**, 4–5% of **3**, and 11–13% of **4** + **5**. Conformational considerations outlined below suggest that **4** and **5** are quite similar in energy so that they were probably present in comparable amounts, and since the *cis* isomer **6** was not detected we may surmise that its proportion was less than 1%. Therefore, we provisionally write for the equilibrium composition **1**:**2**:**3**:**4**:**5**:**6** ≈ 81:2.5:4.5:6:6:< 1.

In order to see if the relative thermodynamic stabilities revealed by this result accord with conformational theory, we calculated the relative conformational enthalpy for each of the two chair conformers of **1**–**6** (Table 1) and obtained from these data the conformational free energies ΔG^0, taking into account where applicable the entropy changes due to mixing of conformers and (or) enantiomers. Therefrom were derived the energy differences $\Delta\Delta G^0$ and equilibrium constants K relative to the most stable isomer **1**. It may be seen that the percentage proportions correspondingly calculated agree well with the experimentally obtained ratio, and it is also

Can. J. Chem. Downloaded from www.nrcresearchpress.com by 210.87.254.40 on 09/05/12
For personal use only.

TABLE 1. Conformational energy calculations for free deoxynitroinositols

Compound (configuration)	ΔH^0 (kcal/mol) *eq* MeO	ΔH^0 (kcal/mol) *ax* MeO	ΔG^0 (kcal/mol)	$\Delta\Delta G^0$ (kcal/mol)	K	% in equilibrium Calcd.	% in equilibrium Found
1 (*myo*-5)	9.00	3.30	3.30	0.00	1.0	79.0	79–82
2 (*neo*-2)	6.60	5.50	5.40	2.10	35.5	2.2	2–3
3 (DL-*allo*-5)	5.45	6.30	4.93	1.63	15.8	5.0	5
4 (DL-*epi*-1)	8.55	5.20	4.79	1.49	12.5	6.35	11–13
5 (*epi*-6)	4.70	7.90	4.70	1.40	10.7	7.38	
6 (*cis*)	8.90	7.50	7.45	4.15	1100	0.07	—
7 (*scyllo*)	2.10	10.80	2.10	0.00	1.0	70.9	71.5
8 (DL-*myo*-1)	3.20	8.75	2.79	0.69	3.2	22.0	22
9 (*epi*-3)	4.70	9.10	4.70	2.60	81.5	0.9	~1.2
10 (*muco*-3)	5.10	4.90	4.60	2.50	69.0	1.0	~1.8
11 (*myo*-2)	4.30	8.40	4.30	2.20	42.0	1.7	
12 (DL-*chiro*-1)	4.30	6.45	3.89	1.79	21.0	3.5	

obvious that one could not expect to observe the isomer **6**. Of course this agreement is predicated on the choice of reasonable, empirical energy parameters for the various types of non-bonded interactions present, and although accepted parameters were used as far as possible, some additional values had to be introduced which require detailed justification. (See the next section.) An important check for the validity of the chosen parameters is found in the fact that the calculations are consistent with *independent* experimental data. Thus, the thermodynamic equilibrium of the deoxynitroinositol δ-methyl ethers having the *scyllo* (**7**), DL-*myo*-1 (**8**), *epi*-3 (**9**), and *muco*-3 (**10**) configurations, which are *not* interconvertible with their stereoisomers **1–6** by spontaneous epimerization, has been found (4) to be 71.5:22:1.2:1.8. Table 1 shows that the revised mode of calculation gives excellent agreement with this finding. Also included with this second set of isomers in Table 1 are calculated energy data for the unknown *myo*-2 (**11**) and DL-chiro-1 (**12**) compounds. These epimers have not been identified in our studies (3, 4) although the calculations now made do suggest that they should be present at equilibrium in detectable proportions which, in fact, should slightly exceed those of **9** and **10**. It seems possible that unidentified products amounting to 3–4%, which have been observed (4), partly represented the missing epimers.[2]

Non-bonded Interaction Energies in the Free Nitro Compounds

The parameters used for the computation of conformational enthalpies (Table 1) were, as far as interactions of hydroxyl or methoxyl groups with each other and with ring hydrogen atoms are concerned, essentially those proposed by Angyal (6) and widely employed in conformational analysis of inositol and pyranose systems in aqueous solution. Thus, we assigned 0.45 kcal/mol to 1,3-diaxial OH—H and OMe—H, and 1.7 kcal/mol to 1,3-diaxial OH—OH and

[2]Furthermore, in glc of epimerization mixtures the peak of **8** invariably was accompanied by a minor peak that was unexplained (4). Since this minor peak arose also from pure, crystalline **8** it was integrated together with the main peak in the evaluation of product analyses. However, it may well have belonged to **12** and its appearance in pure **8** could be due to epimerization during the process of trimethylsilylation.

Can. J. Chem. Downloaded from www.nrcresearchpress.com by 210.87.254.40 on 09/05/12
For personal use only.

Can. J. Chem. Downloaded from www.nrcresearchpress.com by 210.87.254.40 on 09/05/12
For personal use only.

OMe—OH interactions.[3] To *gauche* OH—OH and OH—OMe interactions we applied 0.35 kcal/mol. However, some recent observations (7) appear to indicate that an additional strain exists when an axial OMe group has two equatorial substituents as neighbors, and we took this into account by adding 0.3 kcal/mol for any such OH_{eq}—OMe_{ax}—OH_{eq} moiety.[4]

A more detailed discussion is needed with respect to the interactions involving the nitro group. For the unknown energy of a 1,3-diaxial NO_2—OH interaction we have chosen for the purpose of this exercise an arbitrary figure of 2.0 kcal/mol, assuming that it should be somewhat greater than that of a 1,3-diaxial OH—OH grouping. Precise knowledge of it is not a critical factor at this juncture since the arrangement occurs only in unstable conformers whose enthalpies are so high that variations within reason would scarcely affect the calculated free energies of the compounds in question. Of greater significance, on the other hand, is the choice of parameters for interaction of an axial nitro group with opposing ring hydrogen atoms, and for *gauche* nitro–hydroxyl arrangements. As regards the former, the study of nitro carbohydrates had hitherto furnished no value. In a previous conformational evaluation we adopted (4) an *A*-value of 1.05 kcal/mol for an axial nitro group interacting with *two syn*-axial hydrogen atoms, which is an average value obtained (9) in studies of the nitrocyclohexane system, but in another context (10) we found indirect evidence that a considerably larger energy may be associated with an axial nitro group in certain circumstances. The data now available lead us to retain the previous value (but rounded off to 1.1 kcal/mol) and to ascribe special energy contributions to the interaction of the axial nitro group with neighboring equatorial hydroxyl groups as will be explained in the following paragraph.

The *gauche* NO_2—OH interaction had previously been treated under the simplistic assumption that the energies associated with equatorial–equatorial and axial–equatorial situations are not significantly different. On this premise a numerical value was normally not required in the computation of free-energy differences since molecules to be compared would in most cases have an equal number of such *gauche* interactions so that the unknown parameter would cancel. When a numerical value was needed in one special case, 0.35 ± 0.05 kcal/mol was tentatively used as it appeared that the energy was similar to that in a *gauche* OH—OH grouping (4, 10, 11). Although application of the same procedure to the present set of experimental data gave reasonable agreement on the whole, there occurred one striking discrepancy: the energy so calculated for **2** was too low by 1 kcal/mol to account for the small equilibrium concentration of this compound which was actually found, and this could not be put down to experimental error. Now compound **2** is peculiar in that its prevalent conformation is the NO_2-axial one (2), and in order to eliminate the discrepancy one might have contemplated doubling the energy value of its *syn*-axial NO_2—H interactions. However, such trivial expedient would cause incongruities elsewhere and could not readily be justified. It rather appeared that the problem must be approached by a more refined consideration of nitro group interactions which includes a differentiation between the various kinds of *gauche* arrangements. The following concept is proposed. Let us first consider compound **1**, which is the most stable of the epimers **1**–**6** and almost exclusively exists in the NO_2-equatorial conformation, and let us retain for each of its two NO_2—OH interactions the arbitrary (though reasonable) value of 0.35 kcal/mol, that is, 0.7 kcal/mol for the whole triequatorial (*e*,*e*,*e*) nitrodiol grouping. Now one may postulate that certain other steric arrangements in nitrodiols

[3]The latter value gives the most satisfactory agreement with our experimental data; previously, 1.9 and 1.5 kcal/mol had been used in inositols and pyranoses, respectively (6).

[4]This interaction appears to result from the inability of the Me—O bond to adopt a conformation which is not encumbered by either a 1,3-parallel C—O bond or two *syn*-diaxial ring hydrogens, or by eclipsing with the vicinal C—H bond. A numerical value for this condition has not been recorded. Limited data pertaining to 3-*O*-methyl-D-allose (7*a*) and 3-*O*-methyl-D-psicose (7*b*) suggest that it could amount to more than 0.6 kcal/mol but our results are better in line with a lower value. A similar strain should actually occur in systems having an equatorial OMe group flanked by equatorial substituents, and the conformational equilibrium of methyl 2,3,4,6-tetra-*O*-methyl-α-D-idopyranoside in water (8) seems to bear this out. However, we refrained from adding any increment in such instances since, in our particular case, the effect on $\Delta\Delta G^0$ values would have happened to be negligible. We thank Professor S. J. Angyal for discussions on this subject.

with *gauche* relationships will differ in energy because of the conformational requirements of the nitro group in respect of torsion about the C—N bond. Inspection of a molecular model shows that in **1** the preferred torsion angle is 0° (in the notation of Klyne and Prelog (12)), which

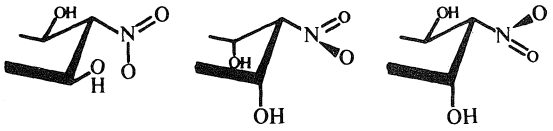

e,e,e *a,e,a* *e,e,a*

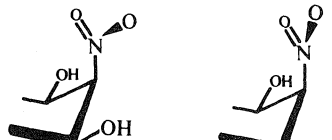

e,a,e *e,a,a*

means that the plane of the nitro group is perpendicular to the plane of the carbon ring. This permits maximum separation of oxygen atoms although there is eclipsing between one N—O bond and the nitromethine hydrogen atom. In an *a,e,a* arrangement as for instance in the equatorial-nitro conformer of **2**, the same torsion angle of 0° would cause severe interaction of the *syn*-triaxial type between nearly parallel N—O and C—O bonds, and the preferred angle will be 90°, with the plane of the nitro group lying parallel to the plane of the carbon ring. This shortens the distance between nitro and hydroxyl oxygen atoms by about 12% and accordingly should increase the enthalpy but, at the same time, the aforementioned eclipsing is removed and the torsion angle is that which is favored in unhindered nitrocyclohexane systems (13), so that there will probably result little net change in enthalpy. The value of 0.7 kcal/mol is therefore applied to this arrangement also. In the unsymmetrical *e,e,a* arrangement, on the other hand, the nitro group is forced to seek a torsion angle of energic compromise between 0 and 90°. An angle near 30° would provide equidistance between the two hydroxyl oxygens and the nearest nitro oxygen; the distance would then be the same as in the *a,e,a* case but there would be greater bond eclipsing and it therefore appears justified to assume a moderately increased enthalpy (0.9 kcal/mol). A rather strong increase in *gauche* interaction is likely associated with an axial nitro group in the *e,a,e* case, as for example in the preferred conformer of **2**. The torsion angle will be 90°, *i.e.*, the plane of the nitro group will be parallel to the line connecting the two adjacent carbinol carbon atoms. The nitro to hydroxyl oxygen distance in this arrangement is about 25% shorter than in the *e,e,e* case, and since repulsion increases exponentially with approach a value of 0.9 kcal/mol for *each* of the two *gauche* interactions may appear reasonable.[5] Finally, for the *e,a,a* arrangement with only one *gauche* relationship, we also apply the value of 0.9 kcal/mol to the latter, assuming that possible steric relief by a limited change in torsion angle would be cancelled by enhanced eclipsing of N—O with C—O bonds. In support of the ideas presented in this paragraph it is to be mentioned that Angyal and Luttrell (14) have on similar grounds invoked different *gauche* interactions of the nitro group in *cis* and *trans* 1-nitro-2-phenylcyclohexane.

Equilibrium of Nitronates

We designate the nitronate that corresponds to the *myo*-5 and *neo*-2 inositols as **1′**; that of the DL-*allo*-5 and DL-*epi*-1 isomers, as **3′**; and that of the *epi*-6 and *cis* isomers, as **5′**. Table 2 shows the results of the thermodynamic equilibrations of these nitronates in 0.1 *N* NaOH solution at 25 °C. As expected, the reactions were much faster than those at low p*H*. Especially the equilibrium between **3′** and **5′** was established within a few minutes, and over-all equilibrium was almost reached after 5 h. The final product ratios remained constant for at least two days. The reaction mixtures were analyzed by glc after

[5]Even in this preferred rotameric form, interaction of the nitro group with the two *syn*-axial hydrogen atoms is more than 1 kcal/mol. A torsion angle of 0° would place one of the nitro oxygen atoms in the *endo* position with respect to the carbon ring and therefore much closer to the opposing hydrogens, and the N—O bond would be nearly parallel to two C—O bonds like in a highly unfavorable *syn*-triaxial situation.

We have contended (10) that a conformational energy of an axial nitro group equal to only 1 kcal/mol would be unable to account for the behavior of methyl 3-deoxy-3-nitro-β-D-ribopyranoside which exists predominantly in the $^1C_4$ form (*e* NO_2). An explicit proviso was equivalence of the *gauche* interactions in both chair forms. The concept that these are not in fact equivalent but are particularly large in the *e,a,e* arrangement of the nonfavored $^4C_1$ form (*a* NO_2) of this glycoside readily explains the observed conformational preference.

Can. J. Chem. Downloaded from www.nrcresearchpress.com by 210.87.254.40 on 09/05/12
For personal use only.

Can. J. Chem. Downloaded from www.nrcresearchpress.com by 210.87.254.40 on 09/05/12
For personal use only.

TABLE 2. Epimeric equilibration of deoxynitroinositols in excess 0.1 *N* NaOH at 25 °C

Time (h)	Starting compound	Products (%)*			
		1	**2**	**3**	**4 + 5**
0.05	**1**	65	20	13	2
0.05	**3**	6	3	78	13
0.05	**5**	7	3	73	17
1	**1**	61	17	17	3
1	**3**	37	3	45	11
1	**5**	37	3	45	11
5	**1**	67	9	19	5
5	**3**	67	5	20	8
5	**5**	64	7	23	6
48	**1**	64	6	18	7
48	**3**	65	5	19	7
48	**5**	68	4	18	6
48	Mean:	65.7	5.0	18.3	6.7

*Where the sum of percentages is less than 100, small peaks of unidentified substances other than deoxynitroinositols were present.

acidification. Consequently, the amount of **1′** present in a given nitronate mixture is defined by the sum of the amounts of **1** and **2** found in glc.[6] Unfortunately it was not possible to determine in a similarly definitive manner the proportions of **3′** and **5′**. This was so because **4** and **5** could not be separated by glc and it was therefore not determinable what part, if any, of the corresponding peak was attributable to **4** (*i.e.*, was contributed by **3′**) and what part was due to **5** (*i.e.*, represented **5′**). Nevertheless, one can deduce from the data of Table 2 certain limits for **3′** and **5′**. Thus, the proportion of **3** that was found represents the *minimum* value for **3′**, and addition thereto of the entire **4 + 5** peak gives the *maximum* (which would apply only for the unlikely case of **5** = 0%). Conversely, the **4 + 5** peak indicates the possible *maximum* proportion of **5′** (which would apply for the case of **4** = 0%). Hence, the equilibrium ratio **1′:3′:5′** can be approximated as 70.7:18.3–25.0:≤6.7. Therefrom, $K_{1'/3'}$ = 3.85–2.83 ($\Delta\Delta G^0$ = 0.80–0.61 kcal/mol) and $K_{1'/5'} = \geq 10.6$ ($\Delta\Delta G^0 \geq$ 1.39 kcal/mol). In the independent series of nitronates derived from **7**, **8**, and **9** (or **10**), the equilibrium ratio **7′:8′:9′** had been determined (4) to be 6.5:30.1:63.4,

[6]The ratio of **1**:**2** produced on acidification is irrelevant in this connection. The ratio seems quite sensitive to conditions of acidification (see also ref. 14), and in our preceding paper (2) we have described experiments yielding a greater proportion of **2** than **1**. The reason for the observed time dependence of the ratio is not clear.

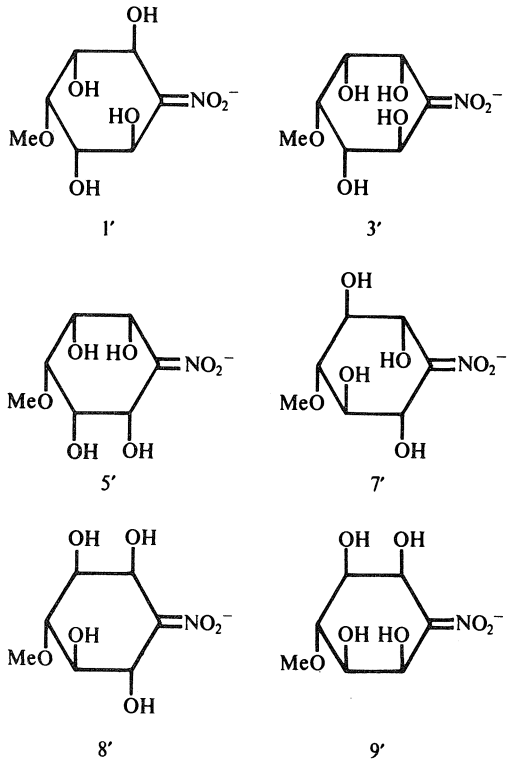

corresponding to $K_{9'/8'}$ = 2.1 ($\Delta\Delta G^0$ = 0.44 kcal/mol) and $K_{9'/7'}$ = 9,75 ($\Delta\Delta G^0$ = 1.34 kcal/mol).

Interaction Energy of the Nitronate Group

Table 3 contains calculated conformational energies for the two groups of nitronates, and good agreement with the experimental results just mentioned is noted. The parameters used for hydroxyl and methoxyl group interactions are those listed in a preceding section. As regards the $A^{(1,3)}$ effect, the non-bonded interaction between nitronate oxygen and a vicinal, equatorial hydroxyl group, which previous work had revealed (10, 11) to be of the order of 2 kcal/mol, the following refined treatment was devised. A single $A^{(1,3)}$ condition was credited with an energy of 2.5 kcal/mol. If a second $A^{(1,3)}$ condition existed in the molecule due to flanking of the nitronate group by two equatorial hydroxyls, an increment of only 1.5 was allowed, for a total of 4.0 kcal/mol. Such unequal increments appear justified because one may assume that a first, and rather severe, steric interaction will tend to cause a ring distortion by which the ring is flattened and concomitantly, the unfavorably

TABLE 3. Conformational energy calculations for nitronates

Compound	ΔH^0 (kcal/mol) Conformation *eq* MeO	ΔH^0 (kcal/mol) Conformation *ax* MeO	ΔG^0 (kcal/mol)	$\Delta\Delta G^0$ (kcal/mol)	K Calcd.	K Found
1′	5.00	6.60	4.95	0.00	1.0	
3′	6.15	6.80	5.61	0.66	3.05	2.83–3.85
5′	7.10	6.80	6.53	1.58	14.5	>10.6
7′	5.40	6.80	5.36	1.36	10.0	9.75
8′	4.80	7.15	4.39	0.39	1.95	2.1
9′	4.00	7.30	4.00	0.00	1.0	

small dihedral angles between the C=N bond and neighboring equatorial bonds are widened so that introduction of a second equatorial hydroxyl group in β' position should entail less additional strain. It is recognized that such ring distortion may also alter some of the remaining substituent interactions whereby slight increases as well as decreases may occur. Often these secondary effects will tend to cancel and it does not seem profitable or necessary to consider them for a first-order analysis based on the data presently available.

Experimental

The compounds, processing of reaction mixtures, and glc method of analysis used in this study were described earlier (2). The epimerization experiments at p*H* 8.2 (in 1% sodium hydrogen carbonate solution) were identical with those recorded (2) except that attainment of final equilibrium was awaited (7 weeks). The epimerizations at p$H > 12$ were performed in exactly the same way with equal volumes of 0.1 *N* sodium hydroxide solution substituted for the sodium hydrogen carbonate solution.

Acknowledgment

The authors gratefully acknowledge financial support from the National Research Council of Canada.

1. (*a*) H. H. BAER and C. B. MADUMELU. Carbohydr. Res. **39**, C8 (1975); (*b*) H. H. BAER, J. M. J. FRÉCHET, and U. WILLIAMS. Can. J. Chem. **52**, 3337 (1974).
2. J. KOVÁŘ and H. H. BAER. Carbohydr. Res. **45**, 161 (1975).
3. J. KOVÁŘ and H. H. BAER. Can. J. Chem. **51**, 2836 (1973).
4. J. KOVÁŘ and H. H. BAER. Can. J. Chem. **51**, 3373 (1973).
5. J. KOVÁŘ and H. H. BAER. Carbohydr. Res. **39**, 19 (1975).
6. S. J. ANGYAL. Aust. J. Chem. **21**, 2737 (1968); S. J. ANGYAL and V. A. PICKLES. Aust. J. Chem. **25**, 1695 (1972).
7. (*a*) S. J. ANGYAL. Aust. J. Chem. **25**, 1957 (1972); (*b*) S. J. ANGYAL and G. S. BETHELL. Aust. J. Chem. In press.
8. H. PAULSEN and M. FRIEDMANN. Chem. Ber. **105**, 705 (1972).
9. F. R. JENSEN, C. H. BUSHWELLER, and B. H. BECK. J. Am. Chem. Soc. **91**, 344 (1969); H. FELTKAMP and N. C. FRANKLIN. J. Am. Chem. Soc. **87**, 1616 (1965); N. C. FRANKLIN and H. FELTKAMP. Tetrahedron, **22**, 2801 (1966); R. J. OUELLETTE and G. E. BOOTH. J. Org. Chem. **31**, 587 (1966).
10. H. H. BAER and J. KOVÁŘ. Can. J. Chem. **49**, 1940 (1971).
11. J. KOVÁŘ, K. ČAPEK, and H. H. BAER. Can. J. Chem. **49**, 3960 (1971).
12. W. KLYNE and V. PRELOG. Experientia, **16**, 521 (1960).
13. G. SNATZKE. J. Chem. Soc. 5002 (1965).
14. S. J. ANGYAL and B. M. LUTTRELL. Aust. J. Chem. **23**, 1485 (1970).

Can. J. Chem. Downloaded from www.nrcresearchpress.com by 210.87.254.40 on 09/05/12
For personal use only.

Effet de solvant en résonance magnétique nucléaire du ^{13}C. I. Cas d'un soluté apolaire: *n*-pentane[1]

BERNARD TIFFON ET JEAN-PIERRE DOUCET

Laboratoire de Chimie Organique Physique de l'Université de Paris VII, associé au C.N.R.S., 1, rue Guy de la Brosse, 75005, Paris, France

Reçu le 24 juillet 1975[2]

BERNARD TIFFON et JEAN-PIERRE DOUCET. Can. J. Chem. **54**, 2045 (1976).

L'importance quantitative (plusieurs ppm) des interactions de van der Waals soluté-solvant sur le déplacement chimique du ^{13}C est mise en évidence sur un soluté non polaire, le *n*-pentane, étudié en solution dans 17 solvants ainsi qu'en phase gazeuse. Le terme de constante d'écran de van der Waals est discuté par rapport aux différentes expressions théoriques fonctions de l'indice de réfraction du solvant. L'extension au cas du ^{13}C de l'échelle de paramètre de solvant caractérisant en rmn du ^{19}F les interactions de van der Waals rend compte quantitativement du phénomène et permet de séparer le terme d'anisotropie dans le cas de C_6H_6. Cette échelle de paramètres est étendue au cas de plusieurs solvants. La variation linéaire en fonction de la fraction volumique de l'effet de van der Waals sur le déplacement chimique est interprétée, conduisant à une relation permettant de calculer le paramètre d'un mélange de solvants. La variation de sensibilité à cet effet des différents sites magnétiques suivant leur position dans la chaîne carbonée est discutée. L'expression théorique de l'effet de site ne rend compte que qualitativement de cette variation.

BERNARD TIFFON and JEAN-PIERRE DOUCET. Can. J. Chem. **54**, 2045 (1976).

The quantitative importance (several ppm) of the effect of solute–solvent van der Waals' interactions on the ^{13}C chemical shift is shown for a non polar solute, *n*-pentane, in solution in 17 solvents and in the gas phase. The van der Waals screening constant term is discussed in respect to several theoretical functions of the solvent refractive index. The extension to the case of ^{13}C of the solvent parameter scale which characterises the van der Waals interactions in ^{19}F nmr explains quantitatively this phenomenon and allows the separation of the anisotropic term in the case of C_6H_6. This parameter scale is extended to several solvents. The linear variation of this van der Waals effect on the chemical shift in terms of the volume fraction is interpreted leading to a relationship which allows calculation of this parameter for a solvent mixture. The variation of the sensitivity to this effect of the different magnetic sites depending on their position in the carbon chain is discussed. The theoretical expression of the site factor leads only to a qualitative explanation of this variation.

Introduction

La plupart des travaux consacrés aux effets de solvant sur le déplacement chimique du carbone en rmn portent sur des effets de grande amplitude dus à des interactions intermoléculaires fortes (effets polaires, liaisons hydrogène) (1–8). Les variations de déplacement chimique dues à des interactions intermoléculaires faibles (forces de dispersion de van der Waals) ont été presque totalement négligées. Seuls Bergmann et Dahm (9) ont étudié l'effet de quelques méthanes halogénés sur certains alcanes linéaires. Une forte variation de la sensibilité à l'effet de ces solvants suivant la position du carbone dans la chaîne a été mise en évidence. Toutefois, ces résultats restent limités à un seul type de solvant.

Nous nous proposons d'étudier l'importance de l'effet de van der Waals sur le déplacement chimique des carbones d'un soluté modèle apolaire (*n*-pentane), ceci pour une large gamme de solvants associants et non-associants, les résultats acquis ici devant servir à évaluer l'effet de van der Waals afin de pouvoir en tenir compte dans le cas d'un soluté polaire où les interactions fortes prédominent.

La constante d'écran d'un site magnétique est la somme d'un terme intramoléculaire correspondant à la molécule isolée (en pratique la phase gazeuse) et de termes intermoléculaires correspondant à l'influence du milieu où se trouve la molécule considérée:

$$[1] \qquad \sigma = \sigma_{gaz} + \sigma_b + \sigma_{milieu}$$

σ_b, terme de susceptibilité magnétique volumique du milieu; σ_{milieu} peut s'exprimer sous la forme

[1]Cet article fait partie de la thèse de doctorat de Bernard Tiffon à soutenir devant l'Université Paris VII.

[2]Revision reçue le 18 mars 1976.

Can. J. Chem. Downloaded from www.nrcresearchpress.com by 210.87.254.6 on 09/05/12
For personal use only.

Can. J. Chem. Downloaded from www.nrcresearchpress.com by 210.87.254.6 on 09/05/12
For personal use only.

d'une somme de plusieurs termes correspondant à des phénomènes différents (10, 11):

$$[2] \qquad \sigma_{\text{milieu}} = \sigma_a + \sigma_w + \sigma_E + \sigma_H$$

σ_a, terme d'anisotropie magnétique des molécules environnantes; σ_w, terme dû aux interactions faibles de van der Waals; σ_E, terme dû aux effets polaires; σ_H, terme global correspondant aux interactions fortes (liaisons hydrogène par exemple).

Le choix du soluté modèle répond au double souci, d'une part, d'éliminer les termes σ_H et σ_E en utilisant une molécule aussi inerte que possible vis-à-vis de tous les solvants utilisés (alcane) et apolaire,[3] et d'avoir, d'autre part, un soluté de volume moléculaire proche de celui de l'acétone, modèle étudié en parallèle.[4] Le terme de susceptibilité magnétique volumique σ_b est calculé. Les seules contributions à σ_{milieu} sont σ_w et, dans le cas de solvants magnétiquement anisotropes, le terme d'anisotropie σ_a.

En rmn du proton, de nombreux auteurs ont étudié les effets de van der Waals sur le déplacement chimique, notamment du méthane ou de composés $X(CH_3)_4$ et d'alcanes linéaires (11–18). Abraham et coll. (19, 20) ont montré l'importance de σ_w en rmn du ^{19}F et défini statistiquement un paramètre de solvant S_v et un paramètre de soluté S_u tels que:

$$[3] \qquad \sigma_w = S_u S_v$$

quel que soit le couple solvant-soluté.[5]

Dans cette étude l'ensemble des 17 solvants choisis, apolaires, polaires, et anisotropes nous a permis de séparer et d'évaluer les termes σ_w et σ_a. La phase gazeuse a également fait l'objet d'une mesure. Pour préciser l'interaction soluté–solvant nous avons effectué quelques mesures sur le perfluoro-*n*-hexane afin de comparer la solvatation des groupes méthyle et fluorométhyle.

Partie expérimentale

L'appareil utilisé est un spectromètre rmn par transformation de Fourier JEOL PS 100/PFT 100 fonctionnant à 25 MHz. Tous les spectres ont été obtenus en découplage complet des protons (soluté *n*-pentane) ou partiel du fluor (soluté n-C_6F_{14}). L'incertitude expérimentale est de ± 0.04 ppm (résolution digitale 1 Hz environ: 4096 points dans le domaine de fréquence pour 4 kHz de largeur spectrale). Toutes les mesures ont été faites à une température de 22 °C.

Pour une telle étude des interactions faibles soluté–solvant, il est impératif que le composé chargé de fournir une raie rmn de référence ne soit pas soumis à ces interactions. Par conséquent, les déplacements chimiques ont été mesurés en référence externe (benzène). Celle-ci, ainsi que le composé deutéré (DMSO-d_6) nécessaire au verrouillage hétéronucléaire du champ magnétique sur le signal rmn du deutérium, est contenue dans un tube coaxial au tube porte échantillon. Ce tube coaxial d'un diamètre extérieur de 3.5 mm est positionné par des entretoises en téflon dans le tube porte-échantillon de diamètre extérieur et intérieur 8 et 7 mm respectivement. Le même tube référence a été utilisé pour toutes les mesures en phase liquide. Les tubes porte-échantillon sont scellés.

Nous avons tenu compte du terme σ_b de [1] de la façon suivante: les déplacements chimiques sont corrigés du terme de susceptibilité magnétique volumique (qui pour un échantillon cylindrique est $\sigma_b = 2\pi/3\ \chi_V$) en ramenant arbitrairement les valeurs numériques des déplacements chimiques à celles qui auraient été mesurées dans un milieu de susceptibilité magnétique volumique constante (ici χ_v du soluté; *n*-pentane ou perfluoro-*n*-hexane):

$$[4] \qquad \Delta\sigma_b = \frac{2\pi}{3}\left[\chi_v\ (\text{solution}) - \chi_v\ (n\text{-pent. liquide})\right]$$

Les valeurs de χ_v proviennent de la réf. 22 sauf pour n-C_6F_{14} (19) et le DMSO (20). Pour les solutions χ_v a été évalué par interpolation linéaire en fonction de la fraction volumique (23). χ_v de la phase gazeuse a été prise égale à 0 (11) (χ_v (solution) = 0 dans [4]).

Les déplacements chimiques sont comptés positivement champ faible par rapport au benzène (il n'a pas été tenu compte de la correction, constante pour tous les déplacements chimiques, due à la différence de χ_v entre le *n*-pentane pur et le benzène à 10% dans le DMSO-d_6). Les mesures ont été effectuées pour chaque solvant à un minimum de six concentrations différentes, la plus faible (1% en volume) correspondant à la sensibilité de l'appareil pour un temps de mesure d'une nuit. Dans le cas du DMSO non totalement miscible au *n*-pentane, seules les plus faibles concentrations ont été mesurées. La mesure en phase gazeuse a été effectuée sur la vapeur saturante du *n*-pentane à 22 °C (pression 0.6 atm soit 0.03 mol/l environ). L'échantillon a été dégazé et le tube porte-échantillon (porte-capillaire Wilmad 520 contenant du benzène à 10% dans du DMSO-d_6, dans un tube 513 A) scellé sous vide dans l'azote liquide. Un temps de mesure de 3 jours (350 000 accumulations) n'a permis de mesurer que les déplacements chimiques des deux sites magnétiques doubles (méthyles 1 et méthylènes 2) de la molécule de *n*-pentane, le signal du méthylène central ne se distinguant pas du bruit de fond (fig. 1), avec une incertitude de ± 0.08 ppm (résolution digitale deux fois plus faible que pour les mesures en phase liquide pour gagner un facteur 2 en sensibilité).

[3]Nous vérifions à posteriori que σ_E est nul dans le cas d'un soluté apolaire dans des solvants polaires.

[4]B. Tiffon et J. E. Dubois, à paraître.

[5]Pendant que ce travail était soumis au journal, une revue critique due à Rummens a été publiée (21) concernant le problème du terme de constante d'écran de van der Waals.

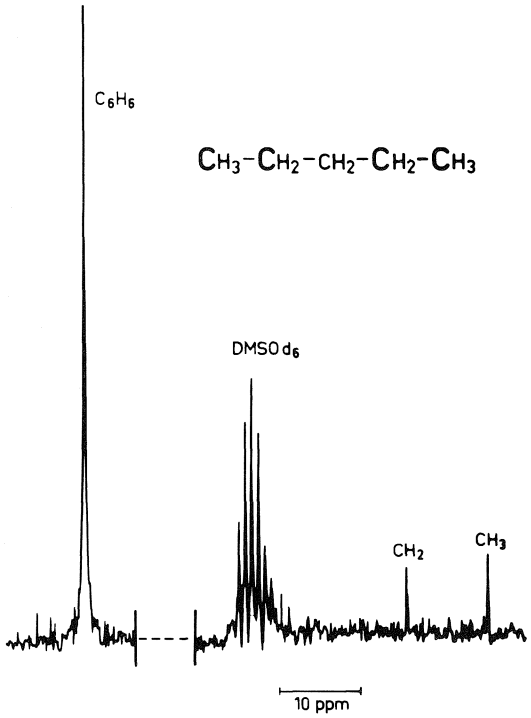

FIG. 1. Spectre ^{13}C du *n*-pentane en phase gazeuse (temps de mesure: 72 h).

Quelques mesures ont été effectuées sur le perfluoro-*n*-hexane en tant que soluté. L'importance des constantes de couplage ^{13}C, ^{19}F ($^1J \simeq 300$ Hz, $^2J \simeq 30$ Hz) oblige à un découplage cohérent séparément sur chacun des trois sites magnétiques en ^{19}F pour avoir une puissance suffisante. Dans ces conditions, seuls les déplacements chimiques des carbones 1 et 3 ont pu être mesurés.

$$\underset{1}{CF_3}\text{—}\underset{2}{CF_2}\text{—}\underset{3}{CF_2}\text{—}\underset{3}{CF_2}\text{—}\underset{2}{CF_2}\text{—}\underset{1}{CF_3}$$

Les carbones (2) sont couplés en ^2J à deux types de fluors de déplacements chimiques très différents (40 ppm); le couplage ^1J étant éliminé par irradiation des fluors (2), les couplages ^2J ne le sont pas et la multiplicité des raies est trop grande pour que le signal soit visible. Par contre, les CF_3 découplés en ^1J donnent un triplet (^2J) qui est mesurable. Les CF_2 (3) sont pratiquement totalement découplés.

Les solvants utilisés sont donnés dans le tableau 1. Ils sont, ainsi que le *n*-pentane, de qualité spectroscopique et utilisés sans autre purification. Les indices de réfraction des solvants proviennent de la réf. 22.

Résultats et discussion

Nous avons d'abord déterminé le déplacement chimique du *n*-pentane à dilution infinie dans chacun des solvants. Nous avons ensuite corrélé ces résultats avec, d'une part les fonctions de l'indice de réfraction du solvant auxquelles devrait être proportionnel le terme σ_w selon les différentes théories proposées dans la littérature (24–26) et d'autre part, avec le paramètre de solvant empirique S_v d'Abraham et Wileman (19, 20).

Détermination des déplacements chimiques à dilution infinie

La variation du déplacement chimique des trois sites magnétiques du *n*-pentane est linéaire en fonction de la fraction volumique ou de la concentration du soluté (mais non en fonction de la fraction molaire) quel que soit le solvant utilisé. Une telle variation linéaire a déjà été relevée par Lumbroso-Bader et coll. (17) en rmn du proton (*n*-C_6H_{14} et *n*-C_7H_{16} dans CCl_4). La fig. 2 illustre ce résultat dans le cas des méthyles pour quelques solvants, dont ceux donnant les déplacements maximaux champ fort (perfluoro-*n*-hexane) et champ faible (bromoforme) ainsi que pour le sulfure de carbone. Les variations sont les plus importantes dans le cas des méthyles (environ 4 ppm du perfluoro-*n*-hexane au bromoforme).

Moyennant les hypothèses suivantes: (*i*) l'effet de van der Waals dû à un solvant est proportionnel au nombre de molécules de ce solvant entourant le soluté (en accord avec la théorie de la cage proposée par Rummens *et al.* (13*a*)), (*ii*) les contributions à σ_w dues à chacun de deux solvants mélangés sont additives, (*iii*) le volume de mélange des deux solvants est négligeable, un raisonnement simple montre que la linéarité de la variation du déplacement chimique avec la fraction volumique implique simplement que la répartition des molécules des deux solvants autour d'une molécule de soluté est la répartition statistique des solvants dans le mélange, en d'autres termes qu'il n'y a pas d'accumulation préférentielle de l'un ou de l'autre des solvants autour d'une molécule de soluté.

Dans le cas des solvants anisotropes, la linéarité en fonction de la fraction volumique est également vérifiée. Ceci implique que le terme d'anisotropie σ_a est proportionnel à la fraction volumique, ce qui a déjà été montré par Schug (23) en rmn du proton. Un raisonnement similaire démontre la proportionnalité de σ_a au nombre de molécules de solvant anisotrope entourant le soluté. Une telle proportionnalité est d'ailleurs une des hypothèses conduisant à

Can. J. Chem. Downloaded from www.nrcresearchpress.com by 210.87.254.6 on 09/05/12
For personal use only.

Can. J. Chem. Downloaded from www.nrcresearchpress.com by 210.87.254.6 on 09/05/12
For personal use only.

TABLEAU 1. Déplacements chimiques extrapolés à dilution infinie des carbones du *n*-pentane et du perfluoro-*n*-hexane*

$$\underset{1}{CH_3}-\underset{2}{CH_2}-\underset{3}{CH_2}-\underset{2}{CH_2}-\underset{1}{CH_3}$$

$$\underset{1}{CF_3}-\underset{2}{CF_2}-\underset{3}{CF_2}-\underset{3}{CF_2}-\underset{2}{CF_2}-\underset{1}{CF_3}$$

Soluté	Solvant	C_1	C_2	C_3
n-C_5H_{12}	Gaz	−118.60	−107.95	(−95.80)†
	n-C_6F_{14}	−117.43	−107.72	−95.58
	n-C_5H_{12}	−115.80	−106.86	−94.93
	n-C_6H_{14}	−115.61	−106.80	−94.90
	n-C_7H_{16}	−115.50	−106.77	−94.89
	C_6H_{12}	−115.60	−106.80	−94.94
	n-$C_{16}H_{34}$	−115.10	−106.62	−94.75
	CCl_4	−114.71	−106.55	−94.77
	$CBrCl_3$	−114.35	−106.39	−95.65
	$CHCl_3$	−114.89	−106.60	−94.80
	CH_2Cl_2	−115.20	−106.65	−94.87
	$CHBr_3$	−113.63	−106.04	−94.37
	C_6H_6	−115.48	−107.03	−95.29
	CS_2	−114.03	−105.62	−94.09
	DMSO	−114.46	−106.63	−94.89
	CH_3COCH_3	−115.71	−107.01	−95.15
	Cyclopentanone	−115.41	−106.82	−95.02
	1,4-Dioxanne	−115.44	−106.87	−95.00
	CH_3OH	−116.08	−107.06	−95.09
n-C_6F_{14}	*n*-C_6F_{14}	−31.87	—	−38.83
	n-C_5H_{12}	−31.30	—	−38.75
	CCl_4	−30.80	—	−38.60

*En ppm, positivement champ faible à partir du benzène à 10% dans le DMSO-d_6 (*n*-pentane); ou d'une référence arbitraire, la fréquence porteuse RF, pour le perfluoro-*n*-hexane.
†Voir note 6.

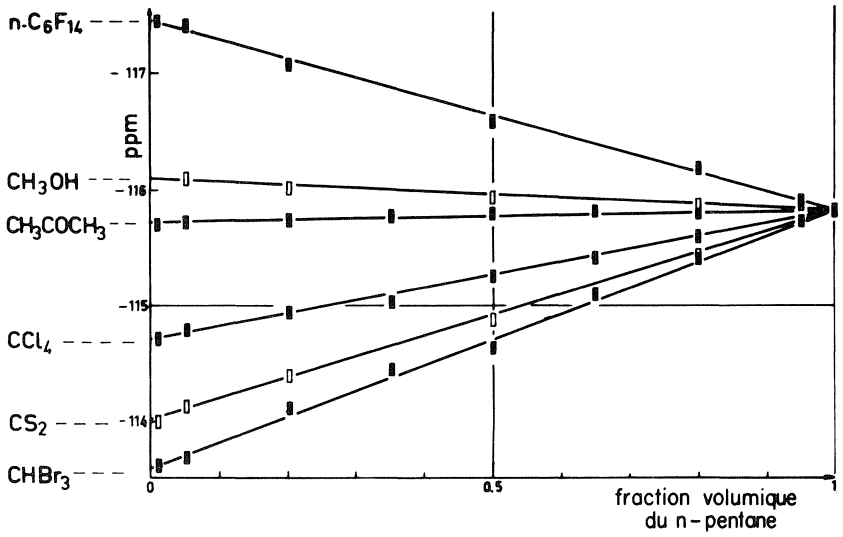

FIG. 2. Déplacement chimique des méthyles du *n*-pentane en fonction de la fraction volumique dans quelques solvants.

Can. J. Chem. Downloaded from www.nrcresearchpress.com by 210.87.254.6 on 09/05/12
For personal use only.

l'expression théorique du terme d'anisotropie proposée par Rummens (27), cette hypothèse ayant également été reprise par Homer et Redhead (28).

Les déplacements chimiques extrapolés linéairement à dilution infinie par une méthode de moindres carrés sont donnés dans le tableau 1. Les résultats sont en accord pour les solvants communs (CCl_4 et CH_2Cl_2) avec ceux de Bergmann et Dahm (9).

Corrélations avec les fonctions de l'indice de réfraction du solvant

Le terme de constante d'écran σ_w dû aux interactions de van der Waals est selon Stephen (29) théoriquement proportionnel à la moyenne du carré du champ électrique dû aux dipoles induits dans les molécules de solvant par les fluctuations électroniques du soluté. La valeur moyenne de ce champ électrique est nulle mais celle de son carré ne l'est pas.

Utilisant le principe du champ de réaction, plusieurs expressions quantitatives de σ_w ont été proposées (24–26) décrivant ce phénomène de façon macroscopique en caractérisant le solvant par son indice de réfraction.[6]

Howard et coll. (24) font intervenir la fonction de l'indice de réfraction du solvant:

$$[5] \qquad g = \frac{n^2 - 1}{2n^2 + 1}$$

alors que Montgolfier (25) propose une expression de σ_w proportionnelle à

$$[6] \qquad f = \left(\frac{n^2 - 1}{2n^2 + 1}\right)^4 \left(\frac{2n^2 + 1}{n^2 + 2}\right)^2$$

Récemment Rummens (26) a reconsidéré le problème et proposé une nouvelle expression de σ_w où le solvant (indice 2) intervient par le carré de la fonction g:

$$[7] \qquad \sigma_w = -\frac{6KBh\nu_1}{\alpha_1}\left(\frac{n_1^2 - 1}{n_1^2 + 2}\right)\left(\frac{n_2^2 - 1}{2n_2^2 + 1}\right)^2$$

ν_1, fréquence caractéristique du soluté ($h\nu_1$ est assimilable à l'énergie de transition entre l'état fondamental et le premier état excité); α_1, polarisabilité du soluté; n_1, indice de réfraction du soluté; n_2, indice de réfraction du solvant. Remarquons que σ_w est le produit de deux termes respectivement fonction du soluté et du solvant.

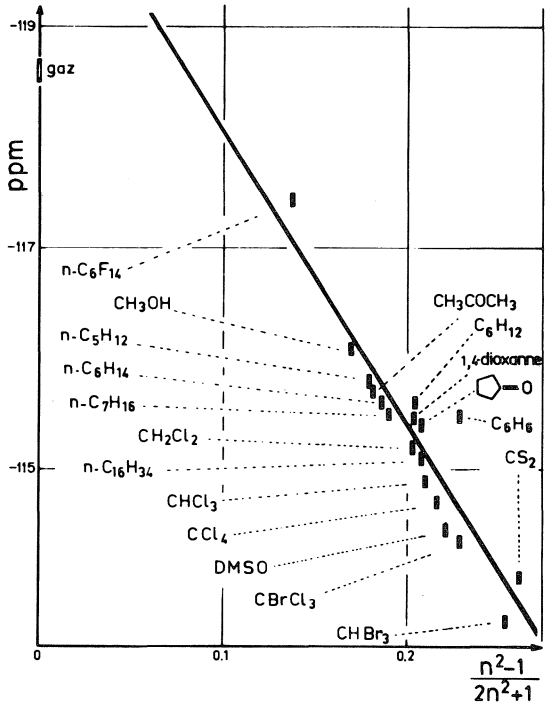

FIG. 3. Déplacement chimique des méthyles du *n*-pentane en fonction de $(n^2 - 1)/2n^2 + 1)$: pente = 26.9, écart-type 0.3 ppm (gaz exclu).

Nous avons corrélé les déplacements chimiques δ extrapolés à dilution infinie avec les fonctions g et g^2 de l'indice de réfraction du solvant (la fonction de Montgolfier n'étant valable selon Rummens (26*a*) que dans le cas des liquides purs).

Avec la fonction g les corrélations sont linéaires pour la plupart des solvants mais la phase gazeuse en est exclue ainsi que le montre la fig. 3 relative aux groupes méthyles, comme c'est le cas en rmn du proton (12, 17), du ^{19}F (19) et du ^{31}P (30).

Par contre les corrélations avec g^2 de même qu'en rmn du proton (26) incluent la phase gazeuse mais l'écart-type est très largement supérieur à l'incertitude expérimentale (figs. 4 et 5).

L'exclusion des deux solvants s'écartant le plus des corrélations (C_6H_6 et CS_2) améliore considérablement la représentation. Pour tous les

[6]Rummens *et al.* (13*a*) ont proposé une théorie basée sur un modèle de collisions binaires établie dans le cas des gaz par Raynes *et al.* (13*b*). Toutefois la nécessité de connaître les paramètres des potentiels de Lennard-Jones qui interviennent dans l'expression de σ_w rend difficile son application.

Can. J. Chem. Downloaded from www.nrcresearchpress.com by 210.87.254.6 on 09/05/12
For personal use only.

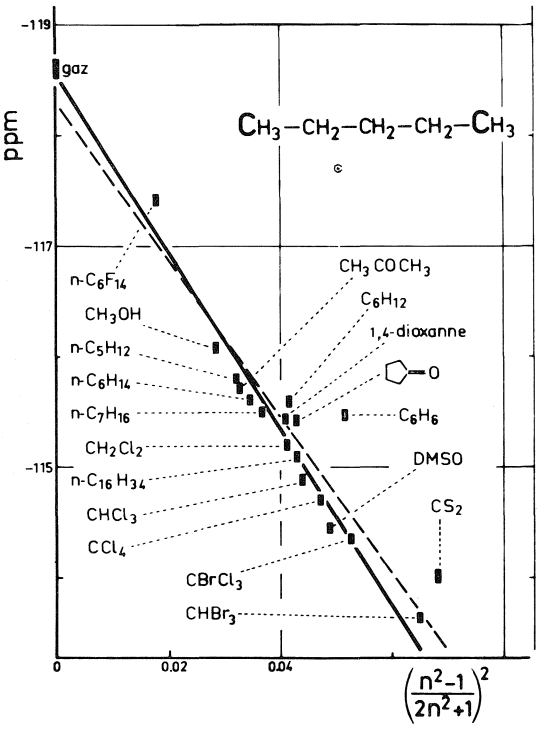

FIG. 4. Déplacement chimique des méthyles du *n*-pentane en fonction de $[(n^2 - 1)/(2n^2 + 1)]^2$: - - - ■+□, pente = 70.5, écart-type 0.34 ppm, intercept −118.28 ppm; —■ pente = 79.4, écart-type 0.20 ppm, intercept −118.54.

autres solvants, la proportionnalité de σ_w à la fonction g^2 suivant [7] est sensiblement vérifiée pour les trois sites magnétiques du *n*-pentane et pour les deux sites mesurables du perfluoro-*n*-hexane (les pentes des corrélations figurent dans le tableau 2), justifiant ainsi la validité de la fonction g^2. Mais [7] ne rend pas compte de la variation du facteur de soluté pour des sites magnétiques différents appartenant à une même molécule. Ce point sera discuté ci-dessous.

Parmi les deux solvants exclus des corrélations, l'un au moins (C_6H_6) est magnétiquement anisotrope (11, 23, 27, 28, 31–36), le terme d'anisotropie (champ fort) variant en rmn du proton de 0.2 à 0.6 ppm. L'anisotropie de CS_2 (d'un point de vue macroscopique) par contre est discutée (14, 26*a*, 26*c*) bien que certains auteurs (11, 23, 28, 31, 34–36) aient avancé en rmn du proton un terme d'anisotropie champ faible, jusqu'à −0.42 ppm (11).

Les écarts verticaux aux droites de corrélation des points correspondants à C_6H_6 et CS_2 sont donnés dans le tableau 3. Dans le cas de C_6H_6 ces écarts ont le sens théorique du terme d'anisotropie (la valeur obtenue pour les méthyles paraît toutefois trop grande), mais dans le cas de CS_2 la déviation des méthyles de près de 1 ppm champ fort est incompatible avec le terme d'anisotropie théorique (champ faible).

Les écarts aux corrélations δ/g^2 n'étant pas interprétables en terme d'anisotropie, nous avons cherché à appliquer une procédure due à Abraham et Wileman (20) établie en rmn du ^{19}F et ayant permis de séparer du terme de van der Waals un terme d'anisotropie dans le cas de C_6H_6 et CS_2 (tableau 3).

Corrélations avec le paramètre de solvant S_v

Abraham et coll. (19) ont défini une échelle de paramètres de solvant S_v et une échelle de paramètres de soluté S_u, telles que pour tout couple soluté non polaire, solvant le terme de van der Waals en rmn du ^{19}F s'écrive:

$$[8] \qquad \sigma_w = S_u S_v$$

ceci pour des solvants aussi bien non polaires (19) que polaires (20).

Ces deux échelles de paramètres sont définies

TABLEAU 2. Pentes des corrélations δ/g^2 et paramètre de solutés S_u (obtenues en excluant les points correspondant à C_6H_6 et CS_2)

	n-Pentane			Perfluoro-*n*-hexane		
	C_1	C_2	C_3	C_1	C_2	C_3
Pente δ/g^2	79.4	30.4	21.8	37.6	—	18.1
Facteur de site*	3.64	1.39	1	—	—	—
S_u (^{13}C)	−0.70	−0.26	−0.21	−0.32	—	−0.07
Facteur de site*	3.33	1.24	1	—	—	—
S_u (^{19}F)†	—	—	—	−1.00	−0.79	−0.69
Pente $(\delta/g^2)/-S_u$ (^{13}C)	113.4	116.9	103.8	117.5	—	115.7

*Rapporté à C3.
†Référence 19.

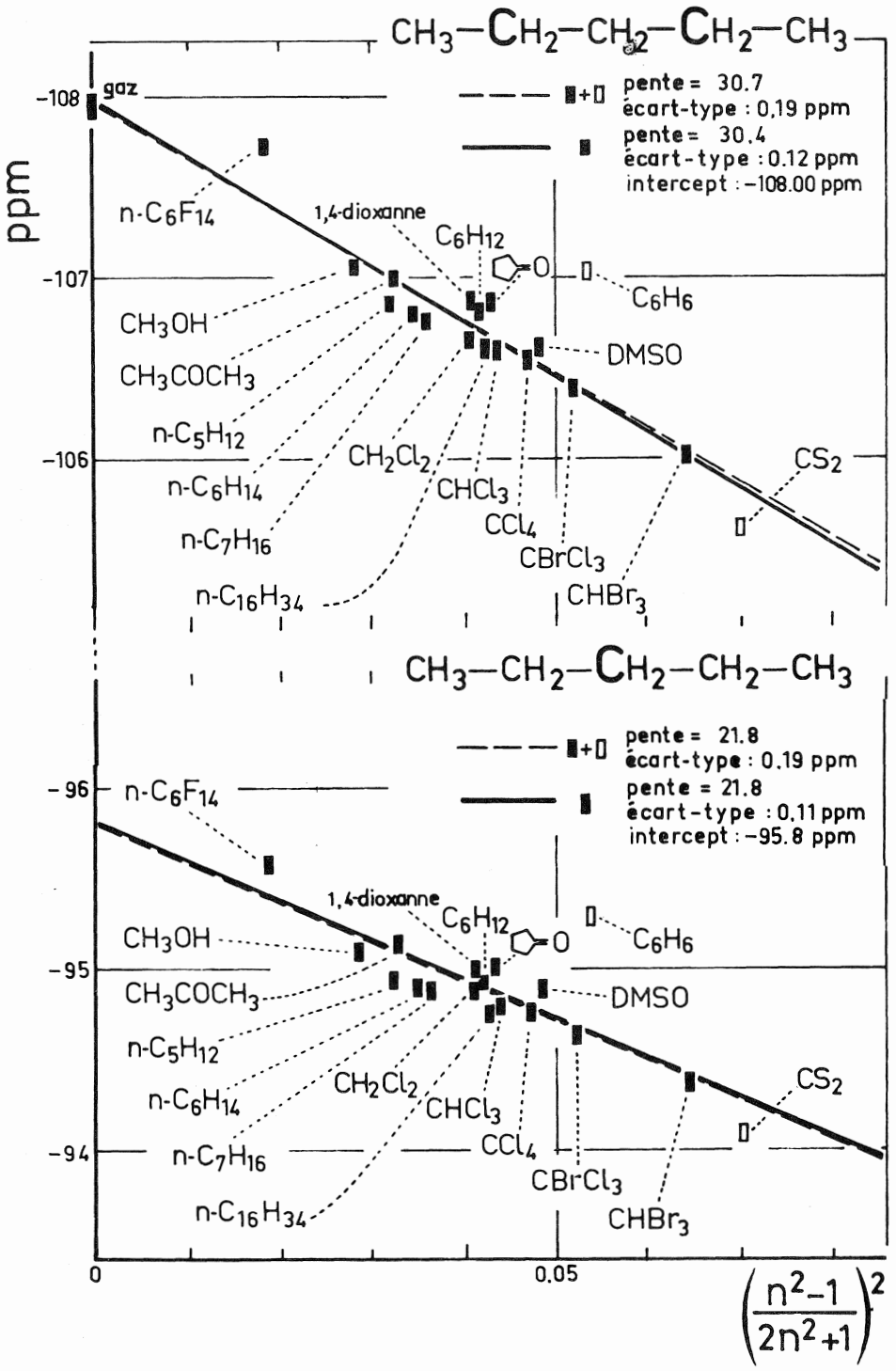

FIG. 5. Déplacement chimique des méthylènes du *n*-pentane en fonction de $[(n^2 - 1)/(2n^2 + 1)]^2$.

Can. J. Chem. Downloaded from www.nrcresearchpress.com by 210.87.254.6 on 09/05/12
For personal use only.

TABLEAU 3. Ecarts verticaux aux droites de corrélation et paramètres S_v (les écarts sont comptés en ppm positivement champ fort selon l'échelle des σ)

Solvant	Ecarts/(δ/g^2)			Ecarts/(δ/S_v)			σ_{suppl} (moyen)*	σ_a (^{19}F)†	S_v (^{13}C)‡	S_v (^{19}F)
	C_1	C_2	C_3	C_1	C_2	C_3				
C_6H_6	1.05	0.61	0.62	0.31	0.33	0.42	0.52 ± 0.11	0.25	5.56	5.60
CS_2	0.91	−0.31	−0.22	−0.78	−0.98	−0.70	-0.69 ± 0.27	−0.50	5.21	5.22
Cyclo-pentanone							0.19 ± 0.08		4.83	
1,4-Dioxanne							0.17 ± 0.02		4.70	
CH_2Cl_2							0.06 ± 0.09		4.94	
CH_3OH							0.08 ± 0.02		3.70	

*Ordonnée à l'origine de la corrélation δ/S_u.
†Référence 20.
‡Pente de la corrélation δ/S_u.

à un facteur constant arbitraire près (par définition $S_v = 0$ pour la phase gazeuse et arbitrairement $S_u = 1$ pour le soluté CF_3CCl_3). Pour des solvants anisotropes il est possible également de déterminer un paramètre de solvant ainsi que le terme d'anisotropie à condition de faire l'hypothèse que celui-ci est constant quelque soit le soluté:

$$[9] \qquad \sigma_{milieu} = \sigma_w + \sigma_a = S_u S_v + \sigma_a$$

En portant σ_{milieu} en fonction de S_v pour un certain nombre de solvants, on détermine le facteur du soluté considéré et, éventuellement, le terme d'anisotropie. Inversement les paramètres S_u ayant été déterminés au préalable pour un certain nombre de solutés, si la corrélation entre σ_{milieu} et les paramètres S_u est linéaire, la pente de la droite définit le paramètre S_v du solvant anisotrope et l'ordonnée à l'origine est le terme d'anisotropie supposé constant pour tous les solutés.

Nous avons corrélé avec S_v les déplacements chimiques des trois sites du *n*-pentane infiniment dilué dans les solvants de paramètre connu (19, 20). Les corrélations sont sensiblement linéaires. De nouveau l'exclusion de C_6H_6 et de CS_2 améliore considérablement les représentations: l'écart-type diminue de moitié (figs. 6 et 7).

Ceci nous a amené à considérer séparément le cas de la phase gazeuse et des solvants satisfaisants aux relations linéaires δ/S_v (solvants I) et d'autre part celui de C_6H_6 et de CS_2 (solvants II).

Pour les solvants I, compte tenu de la linéarité des relations δ/S_v nous posons:

$$[10] \qquad \sigma_{solv} - \sigma_{gaz} = \sigma_{milieu} = S_u S_v$$

Les valeurs de S_u, paramètre de soluté en ^{13}C sont données pour les trois sites du *n*-pentane ainsi que pour les deux sites mesurables du perfluoro-*n*-hexane dans le tableau 2 (les constantes d'écran étant comptées positivement champ fort, les paramètres S_u sont négatifs).

Les solvants polaires ($CHCl_3$, $CHBr_3$, CH_2Cl_2,

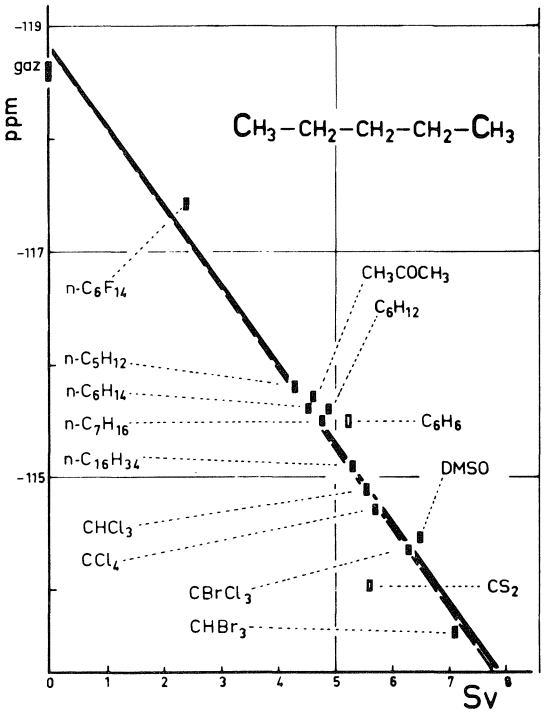

FIG. 6. Déplacement chimique des méthyles du *n*-pentane en fonction du paramètre de solvant S_v: - - - ■+□, pente = 0.71, écart-type 0.27 ppm, intercept −118.85 ppm; —■, pente = 0.70, écart-type 0.14 ppm, intercept −118.83 ppm.

Can. J. Chem. Downloaded from www.nrcresearchpress.com by 210.87.254.6 on 09/05/12
For personal use only.

Can. J. Chem. Downloaded from www.nrcresearchpress.com by 210.87.254.6 on 09/05/12
For personal use only.

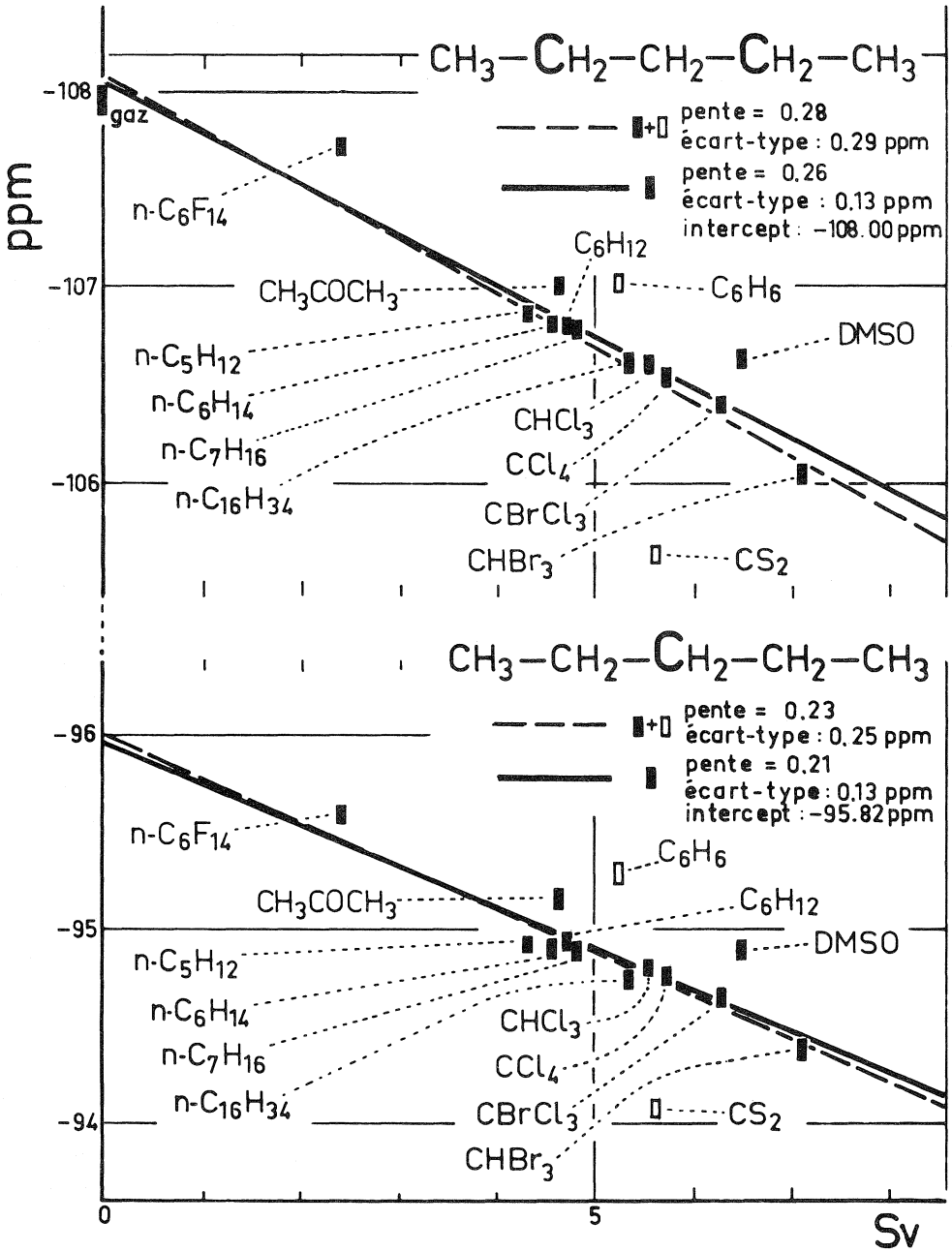

FIG. 7. Déplacement chimique des méthylènes du *n*-pentane en fonction du paramètre de solvant S_v.

CH_3OH, CH_3COCH_3, DMSO) ne se distinguent pas des solvants apolaires. Il en résulte que le terme σ_E est bien nul pour un soluté non polaire. Il en résulte également que le terme σ_{E^2} traduisant un effet moyen du carré du champ électrique dû aux fluctuations des dipôles permanents du solvant polaire et dont l'expression théorique [7] fondée sur le principe du champ de réaction ne tient pas compte est négligeable pour ces solvants. (La même conclusion peut être tirée du fait que ces solvants polaires ne se distinguent pas des autres solvants I dans les corrélations δ/g^2.)

Can. J. Chem. Downloaded from www.nrcresearchpress.com by 210.87.254.6 on 09/05/12
For personal use only.

Rummens (26*c*) aboutit à une conclusion identique dans le cas du proton du méthane.

Récemment, de Haan et coll. (37) ont étudié les variations de déplacement chimique de mélanges d'alcanes linéaires, dont le *n*-pentane dans le *n*-heptane et le *n*-hexadécane et interprètent ces variations comme résultant en partie de changements conformationnels dans les alcanes considérés. Nos résultats montrent que de telles variations peuvent être plus simplement interprétées par la prise en compte de la seule variation de l'effet de van der Waals liée au passage d'un solvant à un autre. Il n'est donc pas utile de faire appel aux modifications conformationnelles pour expliquer les variations de déplacement chimique du carbone constatées lors de la dilution d'un alcane par un autre.

Dans le cas de C_6H_6 et de CS_2, il est nécessaire d'ajouter un terme supplémentaire de constante d'écran:

$$[11] \quad \sigma_{solv} - \sigma_{gaz} = \sigma_{milieu} = S_u S_v + \sigma_{suppl}$$

Pour déterminer ce terme supplémentaire, nous avons à ce stade deux possibilités: (*1*) Les paramètres S_v de ces solvants (déterminés à partir des résultats en ^{19}F (20)) étant connus, écrire simplement comme il a été déjà fait ci-dessus à partir des corrélations δ/g^2 que les écarts verticaux aux droites de corrélation représentent les termes supplémentaires σ_{suppl} cherchés. On ne fait alors aucune hypothèse sur la constante de ce terme quel que soit le carbone considéré. Les résultats figurent dans le tableau 3. Remarquons que ces écarts sont, pour tous les sites, dans le même sens que le terme théorique d'anisotropie champ faible (σ_a négatif) pour CS_2 et champ fort (σ_a positif) pour C_6H_6. (*2*) Utiliser le traitement exposé ci-dessus impliquant l'hypothèse de constante de σ_{suppl} quel que soit le site magnétique:[7] nous trouvons (tableau 3) des valeurs du paramètre de solvant S_v en très bon accord avec celles d'Abraham et Wileman (20) pour le benzène et le sulfure de carbone. Les valeurs de σ_{suppl} sont comparables avec celles déterminées ci-dessus, compte-tenu des écarts-types des corrélations δ/S_v et δ/S_u. Les deux méthodes permettent de déterminer des valeurs comparables entre elles d'un terme de constante d'écran. Toutefois l'incertitude importante sur les valeurs de ce terme ne permet pas de décider si l'hypothèse de son invariabilité suivant le site magnétique est justifiée ou non.

Dans le cas de C_6H_6, le terme σ_{suppl} peut être attribué à l'anisotropie, les valeurs obtenues sont raisonables (alors que l'écart des méthyles par rapport à la droite δ/g^2 est nettement plus grand que les valeurs de σ_a en proton ou en ^{19}F).

Il n'est toutefois pas possible étant donnés les écarts-types des corrélations de déterminer si le terme d'anisotropie est constant quel que soit le site ou bien s'il varie comme l'a prévu théoriquement Beconsall (33) et comme l'ont montré expérimentalement Rummens et Louman (38) dans le cas de molécules de soluté non sphériques.

Dans le cas de CS_2, on obtient maintenant des écarts dans le sens du terme d'anisotropie théorique, mais l'ordre de grandeur, s'il est compatible avec celui obtenu par la même méthode en ^{19}F (20), est incompatible avec les valeurs obtenues en rmn du proton (11, 23, 28, 34–36) (0 à -0.15 ppm).

Si on admet comme Rummens (26*c*) que le comportement macroscopique de CS_2 est isotrope, l'écart champ fort relevé par rapport au terme en g^2 pour les méthyles, reste inexplicable même en adjoignant à [7] le facteur de site de Rummens (26*c*) (voir ci-dessous).

La méthode de détermination du paramètre de solvant S_v a été appliquée aux quatre solvants de S_v inconnu: pour le méthanol et le chlorure de méthylène, l'ordonnée à l'origine est pratiquement nulle, ces deux solvants s'intègrent aux solvants I. Pour la cyclopentanone et le 1,4-dioxanne, les ordonnées à l'origine sont respectivement de 0.19 et 0.17 ppm champ fort mais restent de l'ordre de grandeur des écarts-types des corrélations δ/S_v et ne permettent donc pas de conclure à l'existence d'un terme d'anisotropie. Les paramètres S_v de ces quatre solvants figurent dans le tableau 3.

Il résulte de la linéarité de la variation de σ_w avec la fraction volumique v que, le paramètre S_u de soluté étant constant,

$$[12] \quad S_v(\text{mélange}) = v(n\text{-pent.})\, S_v(n\text{-pent.}) + v(\text{solv.})\, S_v(\text{solv.})$$

et plus généralement le facteur de solvant d'un

[7]Pour le méthylène central de n-C_5H_{12}, δ_{gaz} n'ayant pas pu être déterminé expérimentalement nous avons utilisé l'ordonnée à l'origine de la corrélation δ/g^2, soit 95.80 ppm, plutôt que celle de la corrélation δ/S_v (95.97 ppm) car cette dernière est établie avec un nombre de solvants plus faible (12) que la précédente (16) et que d'autre part la représentation δ/g^2 intègre mieux la phase vapeur que δ/S_v dans le cas des deux autres sites.

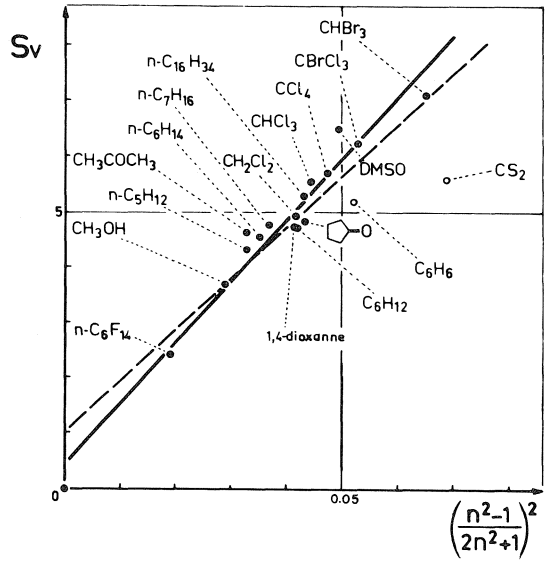

FIG. 8. Paramètre de solvant S_v en fonction de $[(n^2-1)/(2n^2+1)]^2$: - - - ● + ○, pente = 93.1, écart-type 0.60 unité S_v; — ●, pente = 112.2, écart-type 0.34 unité S_v.

mélange de deux solvants I est:

$$[13] \qquad S_v = v_1 S_{v1} + v_2 S_{v2}$$

Les résultats précédents montrent que l'échelle de paramètres de solvant S_v est extensible au cas du ^{13}C.

Nous avons corrélé S_v avec g^2: comme on pouvait s'y attendre étant donné la linéarité des corrélations δ/g^2 et δ/S_v, la corrélation est linéaire sauf pour C_6H_6 et CS_2 (fig. 8). Pour les solvants non anisotropes le paramètre S_v est sensiblement proportionnel à la fonction g^2. Bien que la corrélation δ/S_v soit meilleure que la corrélation δ/g^2 pour les méthyles du *n*-pentane (et comparable pour les deux types de méthylènes) l'intérêt de l'échelle S_v paraît limité pour ces solvants (un paramètre de soluté relatif au paramètre de solvant g^2 peut être défini par une relation analogue à la relation 10). Dans le cas de CS_2 l'utilisation de S_v aboutit à un résultat en contradiction avec l'anisotropie de ce solvant en rmn du proton. Par contre pour C_6H_6 l'utilisation du paramètre S_v permet de déterminer des termes d'anisotropie plus cohérents que ceux obtenus avec la fonction g^2. Il semble donc que pour ces solvants dont l'indice de réfraction est très élevé compte tenu de leur masse moléculaire le terme de van der Waals ne soit pas proportionnel à la fonction d'indice g^2.

Paramètres de soluté. Effet de site

Les valeurs relatives du paramètre de soluté S_u ou des pentes des corrélations δ/g^2 qui leur sont sensiblement proportionnelles (tableau 2) traduisent la sensibilité d'un site magnétique donné aux interactions de van der Waals (facteur de site).

Les valeurs du paramètre S_u pour les trois sites magnétiques du *n*-pentane montrent que le méthyle est nettement plus sensible aux interactions de van der Waals que les deux méthylènes. Abraham et coll. (19) ont montré une décroissance empirique approximativement linéaire des paramètres de soluté avec la fonction de l'environnement électronique dû aux atomes voisins du site considéré:

$$[14] \qquad \sum_i \frac{z_i}{r_i^2}$$

z_i numéro atomique de l'atome, r_i distance de cet atome au site magnétique.

Cette fonction a pour valeur (sommée sur des atomes distants jusqu'à deux liaisons du carbone considéré):

$$\underset{7.2}{CH_3}—\underset{9.2}{CH_2}—\underset{10.0}{CH_2}$$

Nous trouvons une décroissance linéaire de S_u avec une pente de -0.2, trois fois plus faible en valeur absolue qu'en ^{19}F (19). Le paramètre soluté décroît beaucoup plus vite le long de la chaîne carbonée que ne le laissent prévoir les résultats en ^{19}F. Cette fonction de l'écran électronique n'est pas le seul facteur gouvernant la sensibilité d'un atome aux interactions de van der Waals.

En effet, les fluors de tous les solutés (19) sont toujours situés à la périphérie de la molécule et offrent donc une possibilité d'approche comparable aux solvants. Par contre, il n'en est pas de même dans une chaîne carbonée. Le méthyle est entourable d'un plus grand nombre de molécule de solvant que les méthylènes d'où une plus grande sensibilité aux interactions de van der Waals étant donné la proportionnalité de cet effet au nombre de molécules de solvant en interaction avec le soluté (voir ci-dessus).

De même, en comparant (tableau 2) les valeurs du paramètre de soluté des carbones du *n*-pentane d'une part et du perfluoro-*n*-hexane d'autre part, il apparaît que le CF_3 de ce dernier est beaucoup moins sensible que le CH_3 du *n*-pentane. De même, la sensibilité du CF_2 (3) est beaucoup plus faible que celle du CH_2 (3) du

Can. J. Chem. Downloaded from www.nrcresearchpress.com by 210.87.254.6 on 09/05/12
For personal use only.

Can. J. Chem. Downloaded from www.nrcresearchpress.com by 210.87.254.6 on 09/05/12
For personal use only.

n-pentane. Ceci peut s'interpréter comme résultant des deux mêmes causes que précédemment, tendant toutes deux à diminuer S_u dans le cas de l'alcane fluoré: (*1*) Une moindre accessibilité des carbones liés à des fluors (longueur C—F + rayon van der Waals F = 1.41 + 1.35 = 2.76 Å, et longueur C—H + rayon van der Waals H = 1.09 + 0.9 = 1.99 Å) d'où une distance moyenne solvant–site magnétique nettement plus grande dans le cas de CF_3. (*2*) Une valeur de la fonction d'écran électronique $\sum_i \frac{z_i}{r_i^2}$ plus grande pour le groupe fluorométhyle CF_3 (20.2) que pour le groupe méthyle CH_3 (7.2). Cette interprétation reste qualitative et la variation avec la fonction de l'écran électronique ne repose sur aucune base théorique.

Ce problème de facteur de site dans les effets de solvant en rmn a été abordé théoriquement par Rummens et Bernstein (39) et Rummens (40) d'abord dans le cas d'interaction entre deux molécules de symétrie sphérique. Dans le cas des interactions de van der Waals, pour une molécule de soluté complètement entourée de molécules de solvant, ce dernier auteur a proposé (*26c*):

$$[15] \qquad S = \frac{1}{(1-q^2)^3}$$

avec

$$[16] \qquad q = \frac{d}{r_1 + r_2} = \frac{d}{r}$$

d, distance du site au centre de la molécule de soluté; r_1 et r_2 rayons moléculaires respectivement du soluté et du solvant. Ce facteur de site n'est pas séparable en un produit de deux facteurs, l'un caractéristique du soluté, l'autre du solvant. Nous avons néanmoins cherché si pour un site donné (d et r_1 étant constants) il existe une correlation $\delta/(S.g^2)$.

Les r_1 et r_2 ont été évalués pour chaque solvant en les assimilant au rayon calculé à partir du volume molaire à 20 °C (21) (lequel varie de 300 environ pour *n*-$C_{16}H_{34}$ à 40 pour le méthanol, S variant alors de 1.31 à 1.75 dans le cas des méthyles du *n*-pentane pour lesquels d = 2.51 Å). Les corrélations $\delta/(S.g^2)$ sont moins bonnes que les corrélations δ/g^2 que l'on exclue ou non C_6H_6 et CS_2 pour les méthyles et les méthylènes (2) (pour les méthylènes (3), on a évidemment S = 1 quel que soit le solvant puisque d = 0).

D'autre part si on calcule S avec r_1 et r_2 constants (ici $r_1 = r_2$ = 3.58 Å pour le *n*-pentane pur), on obtient:

S = 1.48 pour les méthyles (d = 2.51 Å)
= 1.15 pour les méthylènes (2) (d = 1.54 Å)
= 1.0 pour les méthylènes (3) (d = 0)

alors que les sensibilités relatives expérimentales de ces trois carbones sont respectivement: 3.64–1.39–1 (corrélations en fonction de g^2), ou 3.33–1.24–1 (corrélations en fonction de S_v). La variation réelle de l'effet de site est donc beaucoup plus importante que celle prévue par l'expression 15.

Remarquons que [15] s'écrit, si $d^2/r^2 \ll 1$ ce qui est généralement vérifié ici:

$$[17] \qquad S \simeq \left(1 + \frac{d^2}{r^2}\right)^3 = 1 + 3\frac{d^2}{r^2} + \ldots$$

expression peu différente du rapport des σ_w pour les deux types de protons de $Si(C_2H_5)_4$ proposé par Rummens et coll. (*13a*):

$$[18] \qquad \frac{\sigma_w(d_2)}{\sigma_w(d_1)} = 1 + 3.5\frac{d_2^2 - d_1^2}{r^2} + \ldots$$

(modèle du gaz)

$$[19] \qquad \frac{\sigma_w(d_2)}{\sigma_w(d_1)} = 1 + 5\frac{d_2^2 - d_1^2}{r^2} + \ldots$$

(modèle du cage)

Aucune de ces deux expressions ne rend compte du rapport

$$\frac{\sigma_w(CH_3)}{\sigma_w(CH_2(3))} \sim 3.5$$

obtenu expérimentalement dans le cas du *n*-pentane ($0.09 < d^2(CH_3)/r^2 < 0.17$ suivant les solvants).

Dans le cas de CS_2, r_2 étant petit (2.88 Å), toutes choses égales par ailleurs (d et r_1), le facteur de site devrait être plus grand que pour un solvant ayant un r_2 plus grand. Ceci ne peut donc pas expliquer la déviation champ fort des méthyles (σ_w plus petit que ne le prévoit l'expression 7 à cause de la valeur élevée de l'indice de réfraction de CS_2).

Enfin, si l'effet de site variait aussi considérablement avec le solvant, il ne devrait y avoir aucune corrélation entre d'une part σ_{milieu} du carbone C3 du *n*-pentane (pour lequel, du fait de la position de ce carbone au centre de la molécule, S est égal à 1 quel que soit le solvant) et d'autre part σ_{milieu} des deux carbones C1 et

Can. J. Chem. Downloaded from www.nrcresearchpress.com by 210.87.254.6 on 09/05/12
For personal use only.

C2 pour lesquels S varie avec le solvant. Or, sauf pour C_6H_6 et CS_2 les corrélations sont sensiblement linéaires.

L'effet de site semble donc moins dépendant du solvant (r_2) et beaucoup plus du soluté (d et r_1) que ne l'indique l'expression de S. Cela est une justification supplémentaire de la validité au moins en première approximation, de la décomposition de σ_w en un produit facteur de soluté $\times$ facteur de solvant, l'effet de site étant inclus dans le facteur de soluté. Toutefois, la molécule de *n*-pentane est très éloignée du modèle à symmétrie sphérique inhérent à l'expression 15, et dans notre cas, le problème de l'interprétation théorique de l'effet de site reste entier. Il est possible qu'une théorie de σ_w plus raffinée comme la théorie statistique de Raynes *et al.* (13*b*) puisse rendre compte avec une plus grande précision des résultats expérimentaux et expliquer le comportement de CS_2, bien que, pour ce même solvant en rmn du proton, cette théorie (avec un facteur de site empirique) conduise également à un σ_w calculé trop grand (38).

Remarquons pour terminer que, du fait de la forte variation de sensibilité aux interactions de van der Waals suivant le site magnétique considéré, il résulte qu'on ne peut pas s'affranchir du terme σ_w en utilisant une référence interne pour la mesure des déplacements chimiques: le paramètre de soluté du carbone de référence ne pouvant être simultanément le même que ceux des différents carbones de la molécule étudiée. Par conséquent, on doit tenir compte du terme σ_w lors de l'analyse des effets de milieu et ne pas attribuer la totalité des variations de déplacement chimique aux autres composantes de σ_{milieu} (σ_E et σ_H). La variation du terme de van der Waals en passant d'un solvant à un autre peut être évaluée avec une bonne approximation à partir, soit de la fonction de l'indice de réfraction du solvant g^2, soit de l'échelle de paramètre S_v, le ou les paramètres de soluté correspondants pouvant être déterminés à partir de l'effet de solvants non anisotropes ($\sigma_a = 0$), apolaires ($\sigma_E = 0$) et parfaitement inertes vis-à-vis du soluté ($\sigma_H = 0$).

Remerciements

Nous remercions vivement le Professeur J. E. Dubois pour de fructueuses discussions et l'intérêt qu'il a toujours porté à ce travail, ainsi que le Docteur F. H. A. Rummens pour nous avoir communiqué avant publication certains de ses résultats.

1. (*a*) G. E. Maciel et G. C. Ruben. J. Am. Chem. Soc. **85**, 3903 (1963); (*b*) G. E. Maciel et D. D. Traficante. J. Am. Chem. Soc. **88**, 220 (1966); (*c*) G. E. Maciel et R. V. James. J. Am. Chem. Soc. **86**, 3893 (1964); (*d*) G. E. Maciel et D. D. Traficante. J. Phys. Chem. **69**, 1030 (1965); (*e*) G. E. Maciel et J. J. Natterstad. J. Chem. Phys. **42**, 2752 (1965); (*f*) T. T. Nakashima, D. D. Traficante et G. E. Maciel. J. Phys. Chem. **78**, 124 (1974).
2. W. H. de Jeu. Mol. Phys. **18**, 31 (1970).
3. H. Spiesecke et W. G. Schneider. J. Chem. Phys. **35**, 722 (1961).
4. J. E. Beconsall et P. Hampson. Mol. Phys. **10**, 21 (1965).
5. A. Marker, D. Dodrell et N. V. Riggs. J. Chem. Soc. Chem. Commun. **12**, 724 (1972).
6. R. L. Lichter et J. D. Roberts. J. Phys. Chem. **74**, 912 (1970).
7. G. L. Nelson, G. C. Levy et J. D. Cargioli. J. Am. Chem. Soc. **94**, 3089 (1972).
8. H. Saito, Y. Tanaka, S. Nagata et K. Nukada. Can. J. Chem. **51**, 2118 (1973).
9. G. Bergmann et J. Dahm. Angew. Chem. Int. Ed. Engl. **11**, 1032 (1972).
10. J. W. Emsley, J. Feeney et L. H. Sutcliffe. High Resolution NMR spectroscopy. Pergamon Press, Oxford. 1965. p. 841.
11. A. D. Buckingham, T. Schaefer et W. G. Schneider. J. Phys. Chem. **32**, 1227 (1960).
12. P. Lazlo, A. Speert et W. T. Raynes. J. Chem. Phys. **51**, 1969 (1967).
13. (*a*) F. H. A. Rummens, W. T. Raynes et H. J. Bernstein. J. Phys. Chem. **72**, 2111 (1968); (*b*) W. T. Raynes, A. D. Buckingham et H. J. Bernstein. J. Chem. Phys. **36**, 3481 (1962).
14. W. T. Raynes et M. A. Raza. Mol. Phys. **17**, 157 (1969).
15. M. A. Raza et W. T. Raynes. Mol. Phys. **19**, 199 (1970).
16. F. H. A. Rummens. Mol. Phys. **21**, 535 (1971).
17. M. T. Chenon, J. Bouquant et N. Lumbroso-Bader J. Chim. Phys. **67**, 1252 (1970).
18. P. H. Weiner et E. R. Malinowski. J. Phys. Chem. **75**, 3160 (1971).
19. R. J. Abraham, D. F. Wileman et G. R. Bedford. J. Chem. Soc. Perkin Trans. II, **7**, 1027 (1973).
20. R. J. Abraham et D. F. Wileman. J. Chem. Soc. Perkin Trans. II, **7**, 1521 (1973).
21. F. H. A. Rummens. Van der Waals Forces in NMR intermolecular shielding. *In* NMR, basic principles and progress. Vol. 10. *Edited by* P. Diehl, E. Fluck, and R. Kosfeld. Springer Verlag, Heidelberg. 1976.
22. R. C. Weast (*Editor*). Handbook of chemistry and physics. 49th ed. Chemical Rubber Co., Cleveland, Ohio, U.S.A. 1968.
23. J. C. Schug. J. Phys. Chem. **70**, 1816 (1966).
24. B. B. Howard, B. Linder et M. J. Emerson. J. Chem. Phys. **36**, 485 (1962).

25. P. DE MONTGOLFIER. J. Chim. Phys. (*a*) **64**, 639 (1967); (*b*) **66**, 685 (1969).
26. (*a*) F. H. A. RUMMENS. J. Chim. Phys. **72**, 448 (1975); (*b*) F. H. A. RUMMENS. Chem. Phys. Lett. **31**, 596 1975; (*c*) F. H. A. RUMMENS. Can. J. Chem. **54**, 254 (1976).
27. F. H. A. RUMMENS. J. Am. Chem. Soc. **92**, 3124 (1970).
28. J. HOMER et O. L. REDHEAD. Trans. Faraday Soc. 793 (1972).
29. M. J. STEPHEN. Mol. Phys. **21**, 223 (1958).
30. G. HECKMANN et E. FLUCK. Mol. Phys. **23**, 175 (1972).
31. R. J. ABRAHAM. Mol. Phys. **4**, 369 (1961).
32. J. K. BECONSALL. Mol. Phys. **15**, 129 (1968).
33. J. K. BECONSALL. Mol. Phys. **18**, 337 (1970).
34. P. H. WEINER et E. R. MALINOWSKI. J. Phys. Chem. **75**, 1207 (1971).
35. E. R. MALINOWSKI et P. H. WEINER. J. Am. Chem. Soc. **92**, 4193 (1970).
36. J. HOMER. Tetrahedron, **23**, 4065 (1967).
37. A. R. N. WILSON, L. J. M. VAN DE VEN et J. W. DE HAAN. Org. Magn. Reson. **6**, 601 (1974).
38. F. H. A. RUMMENS et F. J. A. LOUMAN. J. Magn. Reson. **8**, 332 (1972).
39. F. H. A. RUMMENS et H. J. BERNSTEIN. J. Chem. Phys. **43**, 2971 (1965).
40. F. H. A. RUMMENS. Mol. Phys. **19**, 423 (1970).

Can. J. Chem. Downloaded from www.nrcresearchpress.com by 210.87.254.6 on 09/05/12
For personal use only.

^{13}C Fourier transform nuclear magnetic resonance. XII. Structure of the phytol–lecithin bilayer. Application of electric field effects

ROBERT J. CUSHLEY AND BRUCE J. FORREST
Department of Chemistry, Simon Fraser University, Burnaby, B.C., Canada V5A 1S6

Received November 17, 1975

ROBERT J. CUSHLEY and BRUCE J. FORREST. Can. J. Chem. **54**, 2059 (1976).

Phytol has been incorporated into lecithin bilayers. ^{13}C spin–lattice relaxation times, which have been measured for both components of the model membrane, indicate a marked destabilization of the bilayer due to intercalated phytol. The disruption of normal phospholipid packing is due to the highly branched nature of the phytyl hydrocarbon chain. In addition, the position of phytol in the bilayer has been determined by means of a linear electric field effect of the polar lipid head group upon the ^{13}C chemical shifts of the phytol olefinic carbons.

ROBERT J. CUSHLEY et BRUCE J. FORREST. Can. J. Chem. **54**, 2059 (1976).

On a incorporé du phytol dans des doubles couches de lécithine. Les temps de relaxation spin–réseaux du ^{13}C, qui ont été mesurés pour les deux composés de la membrane modèle, indiquent une déstabilisation marquée des doubles couches due à l'introduction du phytol. On attribue la destruction de l'organisation normale du phospholipide à la nature très ramifiée de la chaîne hydrocarbonée du phytol. De plus la position du phytol dans la double couche a été déterminée au moyen d'un effet de champ électrique linéaire du groupe de tête du lipide polaire sur les déplacements chimiques du ^{13}C des carbones oléfiniques du phytol.
[Traduit par le journal]

Can. J. Chem. Downloaded from www.nrcresearchpress.com by 210.87.254.40 on 09/05/12
For personal use only.

Introduction

As an initial study on the factors affecting membrane stability we wish to report the effect of added phytol (**1**) on the conformation and fluidity of lecithin bilayers.

A number of reports have appeared indicating the isoprenoid phytyl moiety is effective in the treatment of several disorders. For example, phytol and phytanic acid (**2**) were found to be as effective as vitamin E (D-α-tocopherol, **3**) in alleviating symptoms of nutritional muscular dystrophy in chicks (1). Vitamin E is ineffective in the treatment of progressive muscular dystrophy in mammals.

Another disorder, methylmalonic aciduria, results in the excretion of large amounts of methylmalonic acid in the urine of children. It has been proposed that the buildup of methylmalonyl CoA, which occurs when a deficiency of B_{12} coenzyme exists, may lead to the biosynthesis of branched chain fatty acids which are not usually produced, and possibly cause the harmful neurological effects (2).

Patients with Refsum's disease cannot α-oxidize and decarboxylate phytanic acid and, as a consequence, this fatty acid accumulates (3). The result is a degeneration (severe demyelina-

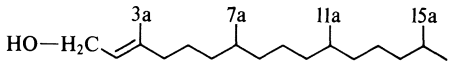

1 Phytol
3,7,11,15-Tetramethylhexadec-*trans*-2-en-1-ol

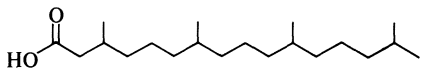

2 Phytanic acid
3,7,11,15-Tetramethylhexadecanoic acid

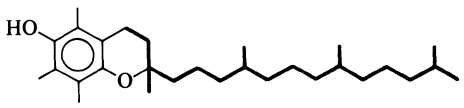

3 α-Tocopherol
D-2,5,7,8-Tetramethyl-2-(4,8,12-trimethyltridecyl)-6-chromanol

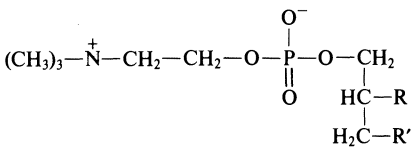

Egg lecithin

R = Oleic (18:1) or linoleic acid (18:2)
R′ = Palmitic (16:0) or stearic acid (18:0)

Can. J. Chem. Downloaded from www.nrcresearchpress.com by 210.87.254.40 on 09/05/12
For personal use only.

tion)[1] of the nervous system, neurological defects, and eventual death.

Other studies point to the isoprenoid moiety as being the physiologically active component. Thus, Lucy and Dingle (4) found that the rapid hemolysis of rabbit erythrocytes *in vitro* by addition of retinol is inhibited by α-tocopherol, as well as other branched chain compounds such as 6-*O*-acetyl-α-tocopherol, squalene, ubiquinone-30, vitamin K_1, and phytol, while *N*,*N*′-diphenyl-*p*-phenylenediamine and hydroquinone were completely without effect. Weber *et al.* (5) have shown that cytochrome-c reductase, which has been inactivated by its extraction from pig liver, can be reactivated not only by D-α-tocopherol, but also by 6-*O*-acetyl-α-tocopherol, phytanic acid, phytol, and isophytol. Both groups concluded that the redox system of α-tocopherol is not responsible for the physiological activity but it is due to the *isoprenoid side chain*.

It is well known that added cholesterol incorporates into phospholipid bilayers by interlacing the hydrophobic fatty acid chains (6). This addition places the bilayer in an 'intermediate fluid condition' due to the necessary deviation from normal lipid packing. The fatty acid carbons near the head group become sterically hindered due to the bulky steroid nucleus while the fatty acid carbons near the terminal end and paralleling the D-ring side-chain experience a lessened effect. It is clear that any change in the packing of the lipid molecules severely alters the properties of the membrane (7).

Phytol, like cholesterol, intercalates between the fatty acid chains of a lecithin bilayer, but the resultant effect on the lipid packing is completely different. Because of the disruptive effect of the phytol branched chain, a general destabilization of the membrane occurs. This is evidenced by the ^{13}C T_1 measurements reported herein. Resonances were resolved not only for lecithin, but also for the interjacent phytol.

On a molecular level, intercalation of compounds **1–3** tends to disrupt the packing of the hydrocarbon region of the myelin and of other lipid bilayers because of the highly branched nature of the phytyl chain. Since the London attractive forces between the hydrocarbon chains of lipid bilayers are highly distance dependent, even a small expansion of the bilayer would lead to a large decrease in the interaction of adjacent lipid molecules.

Additionally, we have been able to determine the position of phytol in the lipid bilayer by means of a ^{13}C *intermolecular* electric field effect.

[1]Myelin has a lipid composition which results in an unusually stable bilayer.

Experimental

Lecithin was extracted from fresh egg yolks by the method of Singleton *et al.* (8). Thin layer chromatographic (tlc) analysis ($CHCl_3$–MeOH–H_2O 65:25:4) showed a single spot when sprayed with 50% H_2SO_4 and heated. Phytol was obtained from Nutritional Biochemical Corporation. Synthetic dipalmitoyl lecithin (DPL), grade 1, 99% pure, was obtained from Sigma Chemical Co. Lecithin dispersions (20% by weight) were prepared by adding D_2O to the dry lipid and mechanical shaking. The dispersions were then sonicated under nitrogen on a Biosonik III probe type sonicator until translucence (20 min – 2 h). The vesicle preparations were centrifuged and/or passed through a 0.22 μ Millipore filter to remove titanium fragments and subsequently transferred, under nitrogen, to a 12 mm nmr tube. The ^{13}C spectra were taken immediately.

Mixed vesicle preparations (20% egg lecithin by weight, 1:1 mole ratio lecithin–phytol; 20% DPL, 2:1 mole ratio lecithin–phytol) were prepared in a similar manner.

Phytol was dispersed in D_2O 10–20% w/v by the addition of 2–20 mol % sodium dodecyl sulphate (SDS) and shaking. The mixture was then sonicated in the manner described above. Chemical shifts of the phytol resonances, measured relative to external TMS, were determined to be independent of the SDS concentration in the range used to within ±0.05 ppm.

All ^{13}C spectra were taken on a Varian XL-100 spectrometer operating at 25.2 MHz in the pulse Fourier transform mode using an internal deuterium field-frequency lock with an 8K data-set. Thus, chemical shifts are accurate to ±0.05 ppm. The ^{13}C T_1 relaxation times were measured using the inversion-recovery technique of Vold *et al.* (9) which employs a $(\pi-\tau-\pi/2-T)$ pulse sequence where τ is the delay time between π and $\pi/2$ pulses. The pulse sequence was repeated after a delay time, T, of at least five times the largest T_1 value to be measured. The percentage error for each measurement is included in parentheses and averages ±7%; occasionally duplicate runs showed variance in the two runs up to 10%. Thus, our confidence limit is set at ±10%. If the variance exceeds the percentage error, we report the variance in Tables 3–5.

Although the time required for a set of inversion-recovery spectra is up to 48 h, the sample remained homogeneous and subsequent tlc analysis showed little decomposition of the lipid. In addition, there were no major differences in proton noise-decoupled ^{13}C spectra obtained before and after the inversion-recovery experiments.

Results and Discussion

The chemical shifts of the lecithin carbons at 52 and 11 °C are given in Table 1 for bilayers

TABLE 1. Lecithin ^{13}C chemical shifts for sonicated dispersions of lecithin and lecithin–phytol 1:1 mixtures in D_2O

Carbon		Chemical shift* at 52 °C		Chemical shift at 11 °C	
		Lecithin	Lecithin + phytol	Lecithin	Lecithin + phytol
Choline	$N^+(CH_3)_3$	54.87	54.78	54.30	54.24
	N^+CH_2	66.96	66.80	66.36	65.98
	CH_2OP	60.08	60.00	59.79	59.79
Chain	C1	174.04	173.87	173.90	173.50
	C2	34.73	34.66	34.33	34.40
	C3	25.62	‡	25.46	‡
	$(CH_2)_n$	30.39	29.91 30.39	30.27	30.03 30.30
	CH_3	14.47	14.46	14.36	14.33
	CH_2CH_3	23.24	23.15†	23.16	22.90†
	$CH_2CH_2CH_3$	32.57	32.49	32.45	32.42
	C11 linoleic	26.25	26.22	25.91	25.83
	C8 and 11 oleic C8 and 14 linoleic	27.85	27.75	27.57	27.46
	C9 oleic	129.95	129.91	129.75	129.47
	C10 oleic C9 linoleic	130.19	130.18	130.01	129.81
	C10 linoleic	128.90	128.76	128.38	128.41
	C12 linoleic	128.49	128.37	128.14	128.11

*Chemical shift (ppm) relative to external TMS.
†Resonance coincident with phytol carbons 15*a* and 16.
‡Resonance coincident with phytol carbons 9 and 13.

TABLE 2. ^{13}C chemical shifts* for phytol

Carbon number	Chemical shift at 52 °C			Chemical shift at 11 °C		
	Neat	D_2O dispersion (20% + 2% SDS)	1:1 phytol–lecithin vesicles (20% in D_2O)	Neat	D_2O dispersion (20% + 2% SDS)	1:1 phytol–lecithin vesicles (20% in D_2O)
1	58.73	58.91	58.78	58.31	58.34	58.08
2	124.80	124.91	124.45	124.54	124.60	—
3	137.35	137.90	138.41	136.83	137.17	137.91
4	40.27	40.54	40.25	40.15	40.31	39.63
14	39.80	40.06	40.05	39.40	39.75	
15	28.28	28.53	28.56	28.15	28.29	28.35
6	37.19	37.48	37.51	37.05	37.27	37.78
8, 10, 12	37.84	38.11	37.95	37.67	37.79	
7, 11	33.12	33.38	33.35	32.98	33.15	32.99
9	24.87	25.13		24.83	24.91	
5	25.64	25.92	25.33	25.42	26.03	25.65
13	25.15	25.38		25.09	25.24	
3a	16.32	16.55	16.41	16.12	16.27	16.09
7a, 11a	20.10	20.34	20.19	19.91	20.05	19.80
15a, 16	23.01	23.23	23.15†	22.93	23.06	22.90

*Chemical shift (ppm) from external TMS.
†Resonance coincident with penultimate carbon of lecithin chain.

with and without incorporated phytol. Assignments were taken from those made by Batchelor *et al.* (10) and by comparison with ^{13}C chemical shifts of a series of fatty acids and their methyl esters (11). Chemical shifts of phytol carbons at 52 and 11 °C are given in Table 2 for neat phytol, phytol dispersed in D_2O by sonication with the addition of 2 mol% SDS, and for phytol incorporated into the bilayer. The phytol ^{13}C assignments are taken from Goodman *et al.* (12).

The high field portion of the proton noise-decoupled ^{13}C nmr spectrum of a 1:1 mole ratio

Can. J. Chem. Downloaded from www.nrcresearchpress.com by 210.87.254.40 on 09/05/12
For personal use only.

Can. J. Chem. Downloaded from www.nrcresearchpress.com by 210.87.254.40 on 09/05/12
For personal use only.

of lecithin–phytol vesicles at 52 °C is shown in Fig. 1. At 52 °C the resonance signals of both lecithin and phytol are strikingly sharp. In light of recent work by Finer (13) and Bloom *et al.* (14), such high resolution linewidths must be attributed to increased rotational tumbling of the vesicle and/or rapid lateral diffusion of lecithin molecules above the phase transition (15).

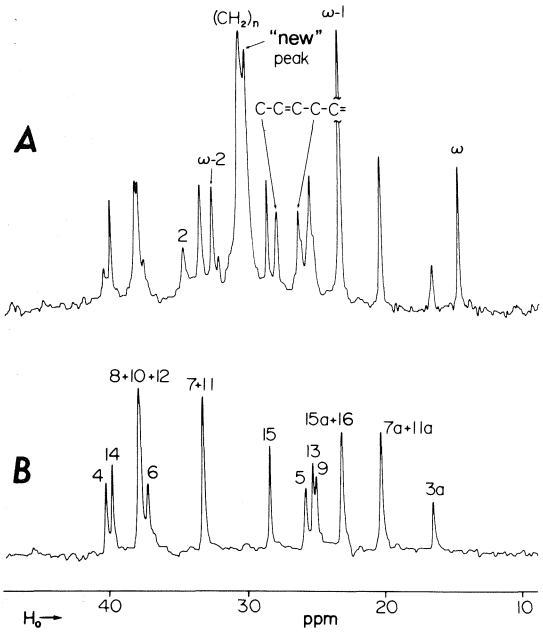

FIG. 1. Proton noise decoupled ^{13}C nmr spectra for the region 5 ppm to 45 ppm in D_2O at 52 °C. (*A*) 20% w/v lecithin vesicles with the incorporation of an equal mole ratio of phytol. (*B*) sonicated dispersion of 20% w/v phytol with the addition of 2 mol % SDS.

A noteworthy feature of the ^{13}C spectrum of the lecithin–phytol mixture is the splitting of the main methylene envelope of lecithin into two distinct peaks by the addition of phytol. In addition to the $(CH_2)_n$ resonance at 30.39 ppm observed with egg lecithin alone, a 'new' peak of nearly equal intensity is observed approximately 0.5 ppm upfield in the lecithin–phytol admixture.

^{13}C T_1 relaxation times for the lecithin carbons generally reflect segmental motion along the acyl chains provided the correlation time, τ_c, is faster than other aggregate motions. Thus, the T_1 values in Table 3 provide carbon by carbon analysis of motional freedom along the acyl chain. In keeping with previous studies (16), segmental motion increases upon increased distance from the head group culminating with a large increase for the last few carbons in the chain (*cf.* column 2, Table 3).

An *increase* in ~75% of the lecithin T_1 values

TABLE 3. Lecithin ^{13}C relaxation times for sonicated dispersions of lecithin and lecithin–phytol 1:1 mixtures in D_2O

Carbon		T_1 (s) at 52 °C		T_1 (s) at 11 °C	
		Lecithin	Lecithin + phytol	Lecithin	Lecithin + phytol
Choline	$N^+(CH_3)_3$	0.88(±0.07)	1.16(±0.08)	0.24(±0.02)	0.38(±0.03)
	N^+CH_2	0.51(±0.04)	0.52(±0.05)	0.24(±0.02)	0.17(±0.01)
	CH_2OP	0.50(±0.04)	0.53(±0.04)	0.21(±0.01)	<0.07
Chain	C1	2.80(±0.21)	2.22(±0.24)	1.81(±0.14)	0.80(±0.06)
	C2	0.28(±0.02)	0.87(±0.06)	0.09(±0.01)	0.10(±0.01)
	C3	0.32(±0.03)	†	†	†
	$(CH_2)_n$	0.59(±0.05)	1.03(upfield)(±0.07) 0.76(downfield)(±0.05)	0.23(±0.02)	0.25(upfield) (±0.02) 0.18(downfield)(±0.01)
	CH_3	4.12(±0.29)	4.00(±0.32)	1.58(±0.11)	1.72(±0.12)
	CH_2CH_3	2.25(±0.18)	2.44*(±0.17)	0.73(±0.05)	0.76*(±0.05)
	$CH_2CH_2CH_3$	1.11(±0.08)	1.64(±0.11)	0.50(±0.04)	0.41(±0.03)
	C11 linoleic	1.22(±0.11)	1.15(±0.08)	0.35(±0.02)	0.25(±0.02)
	C8 and 11 oleic C8 and 14 linoleic	0.76(±0.07)	1.11(±0.08)	0.28(±0.03)	0.25(±0.02)
	C9 oleic	0.90(±0.06)	1.20(±0.08)	0.30(±0.02)	0.55(±0.05)
	C10 oleic C9 linoleic	1.05(±0.10)	1.33(±0.12)	0.26(±0.02)	0.51(±0.04)
	C10 linoleic	0.90(±0.06)	1.36(±0.10)	0.33(±0.02)	0.41(±0.04)
	C12 linoleic	1.39(±0.12)	1.56(±0.11)	0.53(±0.04)	0.42(±0.03)

*Resonance coincident with phytol carbons 15*a* and 16.
†Resonance coincident with phytol carbons 9 and 13.

TABLE 4. ^{13}C relaxation times for phytol

Carbon number	T_1 (s) at 52 °C			T_1 (s) at 11 °C		
	Neat	D_2O dispersion	1:1 phytol–lecithin vesicles	Neat	D_2O dispersion	1:1 phytol–lecithin vesicles
1	0.42(±0.03)	0.34(±0.02)	0.81(±0.06)	0.10(±0.01)	0.15(±0.01)	0.15(±0.01)
2	0.48(±0.03)	0.43(±0.03)	0.58(±0.05)	0.19(±0.01)	0.18(±0.01)	—
3	3.06(±0.21)	3.52(±0.25)	2.85(±0.22)	1.18(±0.09)	0.95(±0.07)	1.18(±0.08)
4	0.33(±0.03)	0.28(±0.02)	0.54(±0.04)	0.10(±0.01)	0.13(±0.01)	0.17(±0.02)
14	0.72(±0.05)	0.85(±0.08)	1.05(±0.07)	0.20(±0.01)	0.31(±0.03)	0.19(±0.01)
15	1.51(±0.11)	1.40(±0.15)	1.54(±0.12)	0.32(±0.02)	0.34(±0.03)	0.22(±0.02)
6	0.29(±0.02)	0.20(±0.01)	0.49(±0.04)	0.07(±0.01)	0.12(±0.01)	0.21(±0.01)
8, 10, 12	0.40(±0.03)	0.29(±0.03)		0.07(±0.01)		
7 and 11	0.50(±0.04)	0.42(±0.03)	0.75(±0.05)	0.10(±0.01)	0.20(±0.01)	0.45(±0.03)
9	0.31(±0.02)	0.22(±0.02)	0.79(±0.05)	0.09(±0.01)	0.13(±0.01)	0.54(±0.05)
5	0.32(±0.02)	0.31(±0.02)		0.13(±0.01)		
13	0.60(±0.05)	0.44(±0.03)		0.12(±0.01)		
3a	2.22(±0.16)	1.73(±0.15)	1.92(±0.13)	0.85(±0.06)	0.63(±0.05)	0.81(±0.07)
7a and 11a	0.95(±0.07)	1.04(±0.07)	1.27(±0.09)	0.32(±0.03)	0.55(±0.04)	0.46(±0.03)
15a and 16	2.00(±0.19)	1.69(±0.13)	2.44*(±0.17)	0.63(±0.07)	0.47(±0.04)	0.76*(±0.05)

*Resonance coincident with penultimate carbon of lecithin chain.

upon addition of phytol at 52 °C (column 3) reflects the increased internal motion due to the disruptive influence of the intercalated phytol. In contrast, at the same temperature, cholesterol increases the packing of dioleoyl lecithin molecules with a concommitant *decrease* in T_1's (17).

The increase in the fluidity of the bilayer at 52 °C is especially evidenced by the increase in the relaxation times of the main methylene envelope. As the terminal carbon is approached (*i.e.* $\omega - 2$ to ω), the effect of the interjacent phytol is lessened, since at this temperature, even in the absence of phytol, there is significant freedom of motion of the chain termini. The increased rate of motion in the bilayer is also evidenced by substantial increases in the relaxation times for phytol backbone carbons (Table 4, compare columns 3 and 4) and by lesser increases in the T_1 values for the phytol methyl groups which we propose are in the closest proximity to the lecithin fatty acid chains. The phytol methyls are likely to show smaller increases in T_1 in the mixed bilayer as their motions will already be quite large in dispersion.

Since the phytol hydroxyl extends into the hydrophilic region, the effect of phytol would be to create a larger volume of relatively free movement for the terminal lecithin carbons. Thus, at 52 °C, we observe T_1 for $\omega - 2$ of lecithin increases 48% upon addition of phytol (Table 3).

While the ^{13}C relaxation time of the choline CH_2OP in the absence of phytol is reduced approximately twofold on going from 52 to 11 °C, the reduction in motional freedom is much greater in the presence of phytol (Table 3). It should also be noted that this differential decrease as the temperature is lowered is smaller for the adjacent CH_2N^+, while the $N^+(CH_3)_3$ relaxation time is increased in the phytol admixture, even at 11 °C. Such a trend in head group correlations indicates that the phytol hydroxyl must extend into the hydrophilic region of the bilayer.

As the temperature is lowered, and the transition temperature, T_m, approached, the bilayer packing becomes more ordered as reflected by decreased T_1 values (compare columns 2 and 4, Table 3). Upon addition of phytol at the lower temperature, the T_1 value for CH_2OP shows a much accelerated decrease from 0.21 s to <0.07 s. Such a marked decrease in CH_2OP motional freedom is consistent with H-bonding of the phytol hydroxyl to the negatively charged phosphate. The T_1 of the $N^+(CH_3)_3$ carbons would then increase, as is observed, due to decreased ionic interaction with the negatively charged phosphate of adjacent, but now more distant, lecithin molecules.

As one approaches the head group, the effect of phytol at 11 °C is varied. The relaxation times of the 9,10-unsaturated carbons (oleic) increase, while for the 12-unsaturated carbon (linoleic),

Can. J. Chem. Downloaded from www.nrcresearchpress.com by 210.87.254.40 on 09/05/12
For personal use only.

Can. J. Chem. Downloaded from www.nrcresearchpress.com by 210.87.254.40 on 09/05/12
For personal use only.

TABLE 5. ^{13}C T_1 measurements for sonicated dispersions of DPL and DPL–phytol (s) at 52 °C

DPL carbon	20% w/v DPL	20% w/v DPL containing 33 mol % phytol
C16	3.11(±0.22)	3.32(±0.28)
C15	1.59(±0.11)	2.07*(±0.14)
C14	0.80(±0.06)	1.23(±0.11)
C4-C13	0.42(±0.03)	0.77(±0.08)
C3	0.38(±0.03)	0.38(±0.03)
C2	0.25(±0.02)	0.23(±0.02)
C1	2.17(±0.15)	2.35(±0.16)
$N^+(Me)_3$	0.81(±0.16)	0.86(±0.06)
CH_2OP (choline)	0.64(±0.04)	0.44(±0.03)
CH_2N^+	0.54(±0.04)	0.40(±0.03)

*Peak coincident with phytol carbons 15a and 16.

T_1 decreases. Similarly, the resonance of the main methylene envelope which is considerably broadened at 11 °C, experiences a differential effect. The 'new' peak at high field (30.03 ppm) has approximately the same T_1 as $(CH_2)_n$ in the absence of phytol, while the relaxation time of the peak at low field is reduced by approximately 22%. Of course, the T_1 value for this peak envelope is the average of a number of methylene carbons.

The phytol backbone, up to C14, displays more internal mobility in the lecithin vesicle than when dispersed in D_2O, as evidenced by the T_1 values in Table 4. Methyl carbons 7a and 11a, on the other hand, are more hindered since they are proximate to the fatty acid chains of lecithin, and the T_1 values drop from 0.55 to 0.46 s (16.4%) at 11 °C (*i.e.*, when packing requirements become more stringent as the transition temperature, T_m is approached).

Dipalmitoyl Lecithin

Relaxation times determined for synthetic dipalmitoyl lecithin vesicles, and for dipalmitoyl lecithin with 33 mol% incorporated phytol are presented in Table 5. DPL assignments were taken from Levine *et al.* (16). Several phytol resonances were also resolved, but, due to the lesser amount incorporated, these resonances were not generally of sufficient intensity to allow an accurate determination of their relaxation times.

An examination of the T_1 values obtained (Table 5, columns 2 and 3) reveals trends similar to those observed for phytol incorporation into egg lecithin bilayers at 52 °C. Increases in the majority of the hydrocarbon chain relaxation times again indicate greater motional freedom in the hydrophobic region of the model membrane. The T_1 of the main methylene envelope resonance (C4–C13) increases by 83% upon the incorporation of 33 mol% phytol. Increases of 56% and 30% are observed for carbons 14 ($\omega - 2$) and 15 ($\omega - 1$) respectively. Relaxation times for carbons 2 and 3 however are relatively unchanged.

The trend in the T_1's for the head group carbon atoms is also similar to that observed with egg lecithin. The relaxation time for the choline CH_2OP resonance is decreased by 38% in the presence of incorporated phytol, consistent with hydrogen bonding of the phytol hydroxyl function to the negatively charged lecithin phosphate moiety.

Intermolecular Field Effects

The incorporation of phytol into the bilayer is characterized by a relatively large effect on the chemical shifts of the unsaturated phytol carbons 2 and 3. At 52 °C, C2 is shifted upfield by 0.46 ppm, while C3 is shifted downfield by 0.51 ppm from their positions in D_2O dispersions (Table 2). These shifts cannot be attributed simply to a change in the solvent system, but must be a result of the proximity of the unsaturated carbons of phytol to the polar surface of the lecithin bilayer.

The characteristic upfield–downfield chemical shift for an olefinic pair can be interpreted in terms of an intermolecular linear electric field effect (11, 18). The electric field polarizes the double bond causing an equal and opposite electron density change at the two carbons, with the olefinic carbon near the head group bearing the increased charge. Changes in the electron density, δq, at a carbon atom as a result of the polarization of the bond by an electric field can be estimated by

$$\delta q = \sum \frac{b_{11} E_1}{el} \quad [1]$$

where the sum is over all the bonds of an atom, E_1 is the field resolved parallel to the bond, l is the length of the bond, b_{11} is the longitudinal bond polarizability and e is the electronic charge.

The resulting chemical shift is then given by

$$\delta_{el} = (\delta/e)\delta q \quad [2]$$

where δ/e is the shift/electron value obtained

Can. J. Chem. Downloaded from www.nrcresearchpress.com by 210.87.254.40 on 09/05/12
For personal use only.

from the literature (19, 20). Due to the large polarizability of a C=C bond relative to a C—C or C—H bond, the sum in [1] may be approximated by a single term.

Electrostatic and electrokinetic studies carried out on bilayers suggest that the phosphatidyl choline head group of lecithin is oriented in a plane perpendicular to the fatty acid chains (21). This is in agreement with surface dipole moment measurements of lecithin in monolayers.

The value of the electric field resolved parallel to the phytol double bond may be estimated from the formalism of Zürcher (22) by using the surface dipole moment. Since the surface dipole moment is the normal component of the dipole averaged over the whole surface, it will be assumed in this treatment that the field experienced by the unsaturated phytol carbons arises from a point directly above the phytol hydroxyl moiety, and in the plane of the lecithin head group. It is further assumed that the intercalated phytol chain will parallel the lecithin fatty acid chains.

In this approximation, the field resolved parallel to the phytol double bond is given by

$$[3] \qquad E_1 = 2\mu_\perp / r^3$$

where $\mu_\perp$ is the surface dipole moment and r is the distance from the surface dipole to the midpoint of the C=C bond.

While it would not be expected that the phytol hydroxyl would penetrate into the highly charged plane of the choline head group, it is most probable that phytol is engaged in hydrogen bonding with the phosphate $O^{1/2-}$. Using a hydrogen bond length of 1.75 Å, this would place the phytol hydroxyl approximately 0.88 Å below the dipole surface. This would be at the point of closest possible approach of the branched phytol molecule to the lecithin chains.

Using bond lengths and angles for structurally similar molecules, we calculate that the distance from the dipole to the midpoint of the phytol C2 double bond is 4.72 Å. For a surface dipole moment of 0.6 D (23), the value of the field is found to be 1.14×10^4 esu-cm/cm^3. Therefore using [1] and [2], the calculated theoretical chemical shift difference for the phytol unsaturated carbons due to the linear electric field effect is 0.90 ppm (observed = 0.97 ppm).

It should also be noted that the observed field effect shift for C3 increases from 0.51 to 0.74 ppm as the temperature of the mixed bilayer is lowered from 52 to 11 °C. Such an increase is most likely a consequence of increased molecular packing at the lower temperature.

In the case of DPL a smaller linear electric field effect is observed (0.70 ppm for DPL) *vs.* 0.97 ppm for egg lecithin). A decreased chemical shift nonequivalence for DPL compared with egg lecithin is due to a difference in the magnitude of the surface dipole moment.

From monolayer surface potential measurements, the surface dipole moment per molecule may be calculated by

$$[4] \qquad \Delta V = Kn\mu_\perp$$

where ΔV is the observed surface potential, n is the number of molecules per square centimetre of film, $\mu_\perp$ is the surface dipole moment, and K is a constant (24). Using the surface potential measurements of Shah and Schulman (25), it is found at both low and high surface pressures that the surface dipole moment per molecule egg lecithin is approximately 25% greater than that of DPL. Since the magnitude of the surface dipole is increased in egg lecithin, the observed field effect should also increase, as is observed.

The observed chemical shift nonequivalence of phytol C2 and C3 is consistent with the known direction of the lecithin dipole moment. The total surface dipole moment of a lecithin molecule may be thought of as being the sum of four components. These are the carbonyls of the fatty acid chains which produce a negligible vertical component since they are oriented in an approximately horizontal plane, the glycerol carbons and the oxygens of the ester linkage, the phosphate group, and the trimethylammonium group. The resultant surface dipole moment is oriented such that the negative pole is pointing outwards into the aqueous phase (25, 26). This orientation of the resultant dipole has been confirmed by surface dipole moment measurements of plasmalogen (25).

It has been shown that the addition of sodium ions to the subphase of the lecithin monolayers increases the surface dipole moment, $\mu_\perp$, by approximately 40% (23). Such an increase, probably due to increased ion–dipole interactions, would be expected to increase the linear electric field effect on the phytol C=C in the mixed bilayer. When we added 150 m*M* NaCl to the DPL–phytol bilayer, the olefinic chemical

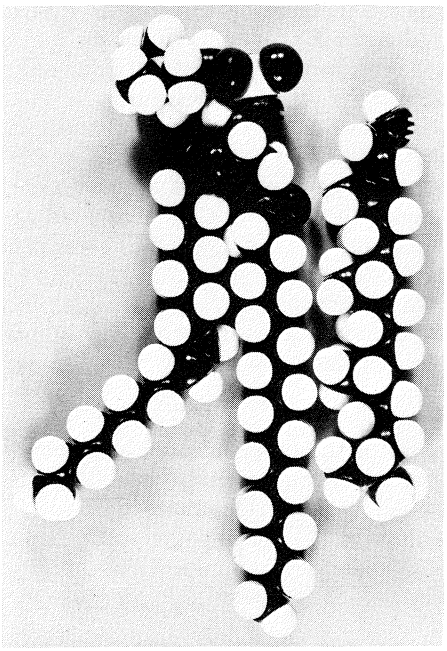

FIG. 2. Space filling molecular models illustrating the proposed structure of the lecithin–phytol bilayer.

shift nonequivalence increased to 0.94 ppm (*i.e.* by 34%) exactly as predicted by [1].

Although subject to a considerable amount of error due to the necessary assumptions, the above field effect values are in qualitative agreement with the structure we propose for the lecithin–phytol bilayer, as shown in Fig. 2, since it places the phytol hydroxyl close enough for H-bonding to the head group.

Conclusion

Based on ^{13}C T_1 relaxation measurements and on ^{13}C chemical shifts we have shown that incorporation of phytol into a model membrane system greatly increases the fluidity of the bilayer above the transition temperature. Only as the transition temperature is approached, and the packing requirements of the bilayer become much more stringent, does the fluidity of the mixed bilayer approach that of the pure phospholipid. The phytol–lecithin system serves as a model for branched chain compounds such as phytanic acid or α-tocopherol incorporated into lipid bilayers. The demonstrated effects of added phytol may prove of fundamental importance in explaining the progression of degenerative (nerve) membrane diseases or diseases wherein branched chain compounds accumulate.

Acknowledgment

We wish to thank the National Research Council of Canada for their financial support of this work.

1. J. BARAUD, P. COURBIN, and A. MAURICE. Arch. Sci. Physiol. **23**, 437 (1969).
2. G. J. CARDINALE, T. J. CARTY, and R. H. ABELES. J. Biol. Chem. **245**, 3771 (1970).
3. M. C. MACBRINN and J. S. O'BRIEN. J. Lipid Res. **9**, 552 (1968).
4. J. A. LUCY and J. T. DINGLE. Nature, **204**, 156 (1964).
5. F. WEBER, U. GLOOR, and O. WISS. Helv. Chim. Acta, **41**, 1038 (1958).
6. K. M. KEOUGH, E. OLDFIELD, and D. CHAPMAN. Chem. Phys. Lipids, **10**, 37 (1973).
7. L. L. M. VAN DEENEN. *In* The molecular basis of membrane function. *Edited by* D. C. Tosteson. Prentice Hall, Englewood Cliffs, N.J. 1969. p. 47.
8. W. S. SINGLETON, M. S. GRAY, M. L. BROWN, and J. L. WHITE. J. Am. Oil Chem. Soc. **42**, 53 (1965).
9. R. L. VOLD, J. S. WAUGH, M. P. KLEIN, and D. E. PHELPS. J. Chem. Phys. **48**, 3381 (1968).
10. J. G. BATCHELOR, J. H. PRESTEGARD, R. J. CUSHLEY, and S. R. LIPSKY. Biochem. Biophys. Res. Commun. **46**, 1488 (1972).
11. J. G. BATCHELOR, R. J. CUSHLEY, and J. H. PRESTEGARD. J. Org. Chem. **39**, 1698 (1974).
12. R. A. GOODMAN, E. OLDFIELD, and A. ALLERHAND. J. Am. Chem. Soc. **95**, 7553 (1973).
13. E. G. FINER. J. Magn. Reson. **13**, 76 (1974).
14. M. BLOOM, E. E. BURNELL, M. I. VALIC, and G. WEEKS. Chem. Phys. Lipids, **14**, 107 (1975).
15. P. DEVAUX and H. M. MCCONNELL, J. Am. Chem. Soc. **94**, 4475 (1972).
16. Y. K. LEVINE, N. J. M. BIRDSALL, A. G. LEE, and J. C. METCALFE. Biochemistry, **11**, 1416 (1972).
17. J. C. METCALFE, N. J. M. BIRDSALL, and A. G. LEE. *In* Proceedings of the 8th meeting of the Federation of European Biochemistry Societies. Vol. 28. Mitochondria and biomembranes. North Holland, Amsterdam. 1972. pp. 197–217.
18. J. G. BATCHELOR, J. H. PRESTEGARD, R. J. CUSHLEY, and S. R. LIPSKY. J. Am. Chem. Soc. **95**, 6358 (1973).
19. G. L. NELSON, G. C. LEVY, and J. D. CARGIOLI. J. Am. Chem. Soc. **94**, 3089 (1972).
20. H. SPEISECKE and W. G. SCHNEIDER. Tetrahedron Lett. 468 (1961).
21. T. HANAI, D. A. HAYDON, and J. TAYLOR. J. Theor. Biol. **9**, 278 (1965).
22. R. F. ZÜRCHER, Prog. NMR Spectrom. **2**, 205 (1967).
23. M. CEREIJIDO, F. VILALLONGA, M. FERNANDEZ, and C. A. ROTUNNO. *In* The molecular basis of membrane function. *Edited by* D. C. Tosteson. Prentice Hall, Englewood Cliffs, N.J. 1969. p. 161.

Can. J. Chem. Downloaded from www.nrcresearchpress.com by 210.87.254.40 on 09/05/12
For personal use only.

24. D. O. SHAH and J. H. SCHULMAN. *In* Molecular association in biological and related systems. Advances in chemistry series. Vol. 84. *Edited by* R. F. Gould. American Chemical Society Publications, Washington, D.C. 1968. p. 195.
25. D. O. SHAH and J. H. SCHULMAN. J. Lipid Res. **6**, 341 (1965).
26. G. L. GAINES, JR. *In* Insoluble monolayers at liquid–gas interfaces. Interscience monographs on physical chemistry. Vol. 1. *Edited by* I. Prigogine. Interscience, New York, N.Y. 1966. p. 191.

Can. J. Chem. Downloaded from www.nrcresearchpress.com by 210.87.254.40 on 09/05/12
For personal use only.

Synthesis and reactions of some cyclopentadienyl complexes of platinum

H. C. Clark and Alan Shaver[1]

Department of Chemistry, University of Western Ontario, London, Ont., Canada N6A 5B7

Received December 30, 1975

H. C. Clark and Alan Shaver. Can. J. Chem. **54**, 2068 (1976).

Reaction of PtCl(X)(COD), COD = 1,5-cyclooctadiene (X = CH_3, Cl) with TlC_5H_5 gives η^1-C_5H_5 complexes Pt(η^1-C_5H_5)(Y)(COD) (Y = CH_3, Cl, η^1-C_5H_5). Pt(η^1-C_5H_5)(CH_3)(COD) is converted to Pt(η^5-C_5H_5)(CH_3)L by treatment with L = CO, $P(OCH_3)_3$, $P(OC_6H_5)_3$, $P(OCH_3)(C_6H_5)_2$; treatment with $CF_3C{\equiv}CCF_3$ or maleic anhydride results in a Diels–Alder addition to the diene residue of the η^1-C_5H_5 ring from the side of the ring opposite the Pt atom. Diels–Alder addition occurs between $CF_3C{\equiv}CCF_3$ and one η^1-C_5H_5 ring of Pt(η^1-C_5H_5)$_2$COD; the other η^1-C_5H_5 converts to η^5 displacing the COD, and the norbornadiene is bidentate. ^1H and ^{13}C nmr data are presented for some η^1 and η^5-C_5H_5 complexes.

H. C. Clark et Alan Shaver. Can. J. Chem. **54**, 2068 (1976).

La réaction du PtCl(X)(COD), COD = cyclooctadiène-1,5 (X = CH_3, Cl) avec le TiC_5H_5 conduit aux complexes η^1-C_5H_5 Pt(η^1-C_5H_5)(Y)(COD), (Y = CH_3, Cl, η^1-C_5H_5). On peut transformer le Pt(η^1-C_5H_5)(CH_3)(COD) en Pt(η^5-C_5H_5)(CH_3)L par traitement avec L = CO, $P(OCH_3)_3$, $P(OC_6H_5)_3$, $P(OCH_3)(C_6H_6)_2$; le traitement par le $CF_3C{\equiv}CCF_3$ ou l'anhydride maléique conduit à un produit d'addition de Diels–Alder au résidu diénique du cycle η^1-C_5H_5 provenant du côté du cycle opposé à l'atome de Pt. Une réaction d'addition de Diels–Alder se produit entre $CF_3C{\equiv}CCF_3$ et un cycle η^1-C_5H_5 du Pt(η^1-C_5H_5)$_2$COD; l'autre η^1-C_5H_5 est transformé en η^5 déplacant le COD et le norbornadiène est bidentate. On présente des données rmn du ^1H et ^{13}C pour quelques complexes η^1 et η^5-C_5H_5.

[Traduit par le journal]

Recent work shows that tridentate polypyrazolylborate ligands can stabilize five coordinate 18 electron complexes of platinum such as in **1** (1). Such complexes are very stable and will not undergo insertion reactions of the acetylene

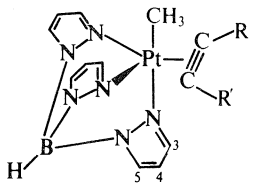

1

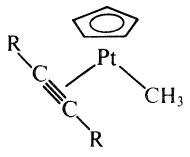

2

into the platinum–carbon bond. An analogy is often drawn between the tridentate polypyrazolylborate and cyclopentadienide ligands since both occupy three coordination sites and are 6 electron donor anions (2). Thus, attempts to synthesize **2** have been undertaken leading to the characterization of a number of new η^1-C_5H_5 complexes. These undergo a number of interesting reactions which include η^1 to η^5 rearrangements of the C_5H_5 ring, and Diels–Alder cycloadditions (for a preliminary account, see ref. 3).

Experimental

Inert atmosphere techniques were used for all preparations and recrystallizations. THF was distilled from sodium benzophenone just before use. PtCl(CH_3)(COD), where COD = 1,5-cyclooctadiene, was prepared by reported procedures (4). TlC_5H_5, obtained commercially or prepared as described (5), was purified by sublimation (0.01 torr, 80–90 °C) and stored under nitrogen in the dark.

^1H nmr spectra were run on a Varian Associates HA-100 spectrometer at 100 MHz with TMS as an internal reference/lock signal. ^{13}C nmr spectra were obtained using a Varian XL-100-15 spectrometer.[2] Chemical shifts are reported in ppm downfield (positive) from TMS. The mass spectra were obtained on a Varian M-66 mass spectrometer. Melting points were obtained using a Thomas Hoover 'unimelt' capillary melting point apparatus and are uncorrected. Analyses were performed by Spang Microanalytical Laboratory, Ann Arbor, Michigan or Midwest Microlab, Ltd., Indianapolis, Indiana.

[1]Present address: Department of Chemistry, McGill University, P.O. Box 6070, Station 'A', Montreal, Quebec H3C 3G1.

[2]We thank Dr. J. B. Stothers of this Department for assistance.

Can. J. Chem. Downloaded from www.nrcresearchpress.com by 210.87.254.6 on 09/05/12
For personal use only.

Can. J. Chem. Downloaded from www.nrcresearchpress.com by 210.87.254.6 on 09/05/12
For personal use only.

Preparation of Pt(η^1-C_5H_5)(CH_3)(COD), 3

To a solution of PtCl(CH_3)(COD) (1.02 g, 2.89 mmol) in 30 ml THF was added TlC_5H_5 (0.78 g, 2.89 mmol) in one portion.

The flask was wrapped in aluminum foil to keep light out, and was stirred vigorously. After 2 h the reaction mixture was filtered (under a nitrogen atmosphere). The yellow filtrate was stripped to dryness and the yellow residue pumped on for 1 h (10^{-2} torr). The residue was extracted with 20 ml ether (deoxygenated by a nitrogen purge) and the extract filtered (under a nitrogen atmosphere) through a short (10 mm wide by 20 mm long) column of florisil. The filtrate was concentrated to about 8 ml by passage of a stream of N_2. Crystallization was initiated by scratching and the solution cooled, first to −20 °C overnight, and finally to −40 °C. The mother liquors were removed by means of a syringe, the crystals washed with cold (−78 °C) ether and dried *in vacuo*; yield = 0.89 g. Mass spectrum: *m/e* 383(M^+), 368(M^+ − CH_3), 318(M^+ − C_5H_5).

Preparation of Pt(η^1-C_5H_5)$_2$(COD), 4

In a similar manner $PtCl_2$(COD) (0.99 g, 2.65 mmol) in 50 ml THF was treated with TlC_5H_5 (1.47 g, 5.50 mmol). Because the product is quite insoluble in ether, 75 ml of acetone was used for the extraction. The filtered extract was cooled to −20 °C and then to −78 °C overnight. The crystals were isolated as before, yield 0.87 g. Mass spectrum: *m/e* 433(M^+), 368(M^+ − C_5H_5), 325(M^+ − C_8H_{12}).

Preparation of PtCl(η^1-C_5H_5)(COD), 5

$PtCl_2$(COD) (1.00 g, 2.68 mmol) was treated with one equivalent of TlC_5H_5 (0.72 g, 2.68 mmol). The acetone extract was cooled to −20 °C, yield 0.43 g. The mass spectrum gave only peaks corresponding to the mass ion of **4** and fragments thereof.

Preparation of Pt(η^5-C_5H_5)COD.Cl, 6 and Pt(η^5-C_5H_5)COD.PF_6, 7

If the mother liquors from the crystallization of **5** are concentrated, then **6** is isolated, yield 0.21 g. Alternatively, if **5** is dissolved in acetone and warmed to 60 °C for 1 h, then **6** is obtained in quantitative yield.

Treatment of **5** (0.10 g, 0.25 mmol) in 8 ml CH_2Cl_2 with $AgPF_6$ (0.07 g, 0.26 mmol) in 2 ml CH_2Cl_2 plus 4 ml acetone gave a white precipitate which was compacted by centrifugation. The supernatant liquid was poured off and stripped to a colourless residue. This was recrystallized from CH_2Cl_2/hexane to give **7**, yield = 0.08 g.

Preparation of Pt(η^5-C_5H_5)(CH_3)(CO), 8

Pt(η^1-C_5H_5)(CH_3)(COD) (0.30 g, 0.78 mmol) was dissolved in 15 ml acetone in a 100 ml two-necked flask equipped with a nitrogen inlet and a stopper. The yellow solution was stirred and treated with CO for 10 min during which time it turned green. The nitrogen inlet was replaced with a short adapter tube which was connected to a vacuum distillation collector and 5 ml flask. The reaction solution was cooled to about −50 °C with dry ice. The collector was connected to a trap which was cooled by liquid nitrogen and which was connected to the vacuum line. The apparatus was carefully evacuated and the 5 ml flask cooled to −20 °C with an acetone bath. The reaction mixture was fractionated by allowing it to warm without stirring. The acetone and displaced COD were collected in the −198 °C trap and the yellow Pt(η^5-C_5H_5)(CH_3)(CO) was collected in the flask at −20 °C; yield >0.20 g. Mass spectrum: *m/e* 303(M^+), 288(M^+ − CH_3), 275(M^+ − CO), 260(M^+ − CO—CH_3). ν(CO) = 2036 (in cyclohexane).

Preparation of Pt(η^5-C_5H_5)(CH_3)[$P(OCH_3)_3$], 9

Pt(η^1-C_5H_5)(CH_3)(COD) (0.21 g, 0.55 mmol) in 30 ml acetone was treated with $P(OCH_3)_3$ (0.063 ml in a microsyringe, 0.55 mmol). The solution was stirred for 1 h then stripped to a yellow oil. This was transferred to a microdistillation apparatus and distilled (10^{-2} torr, 60 °C) yield >0.12 g. Mass spectrum: *m/e* 398(M^+ − 2H) plus a fragmentation pattern expected due to the loss of C_5H_5 and CH_3.

Preparation of Pt(η^5-C_5H_5)(CH_3)[$P(OC_6H_5)_3$] and Pt(η^5-C_5H_5)(CH_3)[$P(OCH_3)(C_6H_5)_2$]

These complexes were prepared in a manner identical to that for **9** except that they could not be isolated in high purity due to their tendency to decompose before they distilled. These complexes were identified by nmr only. Yields were high in each case.

Preparation of Pt(η^1(7)-$C_9F_6H_5$)(CH_3)(COD), 10

Pt(η^1-C_5H_5)(CH_3)(COD) (0.32 g, 0.84 mmol) in 10 ml acetone was cooled to −198 °C (liquid nitrogen) and 1.1 equivalents of $CF_3C{\equiv}CCF_3$ were condensed on to the frozen solution. The system was sealed and allowed to warm over a period of 1.5 h with stirring. The original bright yellow solution became paler. The solution was stripped to a yellow oil which was dissolved in pentane and passed through a short (2 in.) florisil column and again stripped. The pale yellow solid was recrystallized from hexane at −20 °C, yield = 0.28 g. Mass spectrum: *m/e* 545(M^+).

Preparation of Pt(η^1(7)-$C_9H_7O_3$)(CH_3)(COD), 11

Pt(η-C_5H_5)(CH_3)(COD) (0.11 g, 0.29 mmol) in 0.4 ml acetone-d_6 was treated with maleic anhydride (0.028 g, 0.28 mmol), and the reaction followed by observing the ^1H nmr spectrum. After 15 min, the reaction was complete as signified by the disappearance of the peak due to the η^1-Cp. The solution was stripped and the oil taken up in CH_2Cl_2 and passed through a short column of florisil. The solution was concentrated with a stream of N_2 and hexane was added until the solution was just cloudy. After cooling to −20 °C, clear, colourless needles, 0.060 g, were collected, washed, and dried. Mass spectrum: no parent peak was observed; a peak at *m/e* 445 and a spectrum due to **3** were observed.

Preparation of Pt(η^3(7,2,3)-$C_9F_6H_5$)(η^5-C_5H_5), 12

Pt(η^1-C_5H_5)$_2$(COD) (0.22 g, 0.50 mmol) was treated with 4 equivalents of $CF_3C{\equiv}CCF_3$ in the same manner used to prepare **11**. The bright yellow product was too soluble to recrystallize from pentane so it was sublimed (10^{-2} torr, room temperature), yield 0.15 g. Mass spectrum: *m/e* 487(M^+), 325(M^+ − C_4F_6).

Preparation of Pt(CH_3)(POF_2)(COD), 13

Pt(η^1-C_5H_5)(CH_3)(COD) (0.21 g, 0.55 mmol) was treated with PF_3 as in the preparation of **8**. There was an

TABLE 1. Analytical and physical data

Compound	Number	Yield (%)	Melting point (°C)	% Carbon		% Hydrogen		% Other	
				Calcd.	Found	Calcd.	Found	Calcd.	Found
$Pt(\eta^1\text{-}C_5H_5)(CH_3)(COD)$	**3**	80	74–75	43.86	44.12	5.22	5.39		
$Pt(\eta^1\text{-}C_5H_5)_2(COD)$	**4**	76	110–120[a]	49.88	49.94	5.08	5.41		
$PtCl(\eta^1\text{-}C_5H_5)(COD)$	**5**	46	100[a]	38.66	38.72	4.21	4.30		
$Pt(\eta^5\text{-}C_5H_5)(COD)\cdot Cl$	**6**	[b]	171	38.66	38.24	4.21	4.32		
$Pt(\eta^5\text{-}C_5H_5)(COD)\cdot PF_6$	**7**	[b]	152	31.27	30.95	3.78	3.22		
$Pt(\eta^5\text{-}C_5H_5)(CH_3)(CO)$	**8**	84	Liquid	27.72	27.80	2.64	3.02	64.36	63.96 (Pt)
$Pt(\eta^5\text{-}C_5H_5)(CH_3)(P(OCH_3)_3)$	**9**	55	Liquid	27.00	27.99	4.25	4.24	49.00	48.20 (Pt)
$Pt(\eta^1(7)\text{-}C_9F_6H_5)(CH_3)(COD)$	**10**	84	93	39.63	39.64	3.67	3.67	20.92	21.00 (F)
$Pt(\eta^1(7)\text{-}C_9H_7O_3)(CH_3)(COD)$	**11**	45	119	44.91	45.08	4.57	4.20		
$Pt(\eta^3(7,2,3)\text{-}C_9F_6H_5)(\eta^5\text{-}C_5H_5)$	**12**	61	66	34.50	34.36	2.05	2.27	23.41	23.27 (F)
$Pt(CH_3)(POF_2)(COD)$	**13**	29	133	26.80	26.99	3.72	4.00	9.42	13.9 (F)

[a]Decomposes.
[b]See Experimental section.

immediate lightening of the colour which then became brown. After 5 min the solution was stripped to a black solid. This was dissolved in CH_2Cl_2, passed through a florisil column, concentrated, and treated with hexane to give grey crystals (0.065 g). These were recrystallized from CH_2Cl_2/hexane. Molecular weight: calcd. = 403; found = 395 (in $CHCl_3$).

Analytical and physical data are given in Table 1.

Results and Discussion

When $PtCl(CH_3)(COD)$ is allowed to react with $KHBPz_3$ and $AgPF_6$ the COD ligand is displaced (1) but in reactions with TlCp the COD ligand is retained leading to the preparation of three new η^1-Cp compounds. Cyclopentadienyl–platinum complexes of any kind, η^1 or η^5, are not plentiful (6), probably due to a lack of suitable synthetic pathways rather than to inherent instability. It is noteworthy that with few exceptions successful syntheses of such compounds have involved the cleavage of chloro-bridged platinum dimers. One exception is the compound $PtCl_2[C_6H_4(AsEt_2)_2]$ which reacts smoothly with one equivalent of TlCp to give $PtCl(\eta^1\text{-}C_5H_5)[C_6H_4(AsEt_2)_2]$ (6). This result, taken together with our observations, indicates that the use of monomeric platinum complexes with chelating ligands of the type PtCl(X)(A—A) might be a general route to cyclopentadienyl–platinum complexes.[3] The preparation of **3** is depicted in reaction 1.

[1] 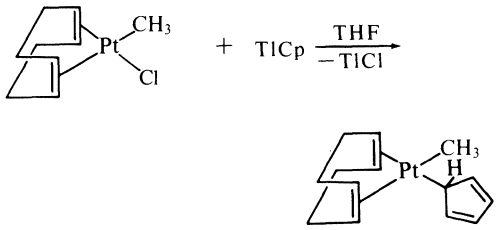

Compounds **4** and **5** were prepared by similar reactions. These are highly crystalline yellow solids, which are stable to air, but the compounds decompose steadily in solution. Compound **3** is unstable in hexane solution decomposing completely even under a nitrogen atmosphere to a brown precipitate within a few minutes. However, in solvents such as THF, acetone and ether, **3** is quite stable.

The Cp protons in **3**, **4**, and **5** appear as sharp peaks in the nmr between τ 3.7 and τ 4.0 accompanied by ^{195}Pt satellites $J(Pt—H) \approx 40$ HZ (Table 2). Observation of ^{195}Pt—H coupling to the protons of the vinyl groups establishes that the COD is bidentate in all cases. The proposed structure of **3** has been confirmed by an X-ray analysis (8). Cooling an nmr sample of **3** to −90 °C does not cause any broadening of the Cp resonance which is consistent with rapid ring 'whizzing' (9) at this temperature and above.

Two peaks in the nmr spectrum for each of **3** and **5** are observed for the olefinic protons. Unlike **4** where both olefinic groups are equivalent, these positions in **3** and **4** are different due to the presence of different *trans* ligands. The assignment of these peaks is possible by compar-

[3]After the completion of our work, a report appeared (7) describing the preparation of some $\eta^1\text{-}C_5H_5$ complexes of Pt, by the same route with A—A = cyclooctatetraene, COD, and dicyclopentadiene.

Can. J. Chem. Downloaded from www.nrcresearchpress.com by 210.87.254.6 on 09/05/12
For personal use only.

Can. J. Chem. Downloaded from www.nrcresearchpress.com by 210.87.254.6 on 09/05/12
For personal use only.

TABLE 2. ^1H and ^{19}F nmr data for Cp–Pt complexes and derivatives

Compound	Solvent	CH_3		C_5H_5		COD			Other resonances and couplings
		τ	J(Pt—H)[a]	τ	J(Pt—H)[a]	$\tau(CH_2)$	τ(CH)	J(Pt—H)[a]	
$Pt(\eta^1\text{-}C_5H_5)(CH_3)(COD)$	$CDCl_3$	9.24	75.8	3.97	43.5	7.81	5.46[b] 5.81[c]	53.6 36.2	
$Pt(\eta^1\text{-}C_5H_5)_2(COD)$	$CDCl_3$			3.95	37.8	7.84	5.89	49.0	
$PtCl(\eta^1\text{-}C_5H_5)(COD)$	Acetone-d_6			3.76	35.0	7.60	6.09[d] 4.46[b]	72.5 47.5	
$Pt(\eta^5\text{-}C_5H_5)(COD)\cdot PF_6$	CD_2Cl_2			3.88	16.6	7.49	4.44	83.0	
$Pt(\eta^5\text{-}C_5H_5)(CH_3)(CO)$	Acetone-d_6	8.83	92.2	4.18	12.2				
$Pt(\eta^5\text{-}C_5H_5)(CH_3)[P(OCH_3)_3]$	Acetone-d_6	9.21	93.2	4.36	10.5				$\tau(OCH_3)$6.51,J(Pt—H) = 3.2, J(P—H) = 13.6,J(P—C_5H_5) = 2.7, J(P—CH_3) = 2.2
$Pt(\eta^5\text{-}C_5H_5)(CH_3)[P(OC_6H_5)_3]$	Acetone-d_6	9.05	92.3	4.85	11.6				$\tau(OC_6H_5)$2.78,J(P—C_5H_5) = 2.8, J(P—CH_3) = 3.2
$Pt(\eta^5\text{-}C_5H_5)(CH_3)[P(OCH_3)(C_6H_5)_2]$	Acetone-d_6	9.33	93.2	4.33	10.7				$\tau(OCH_3)$6.41,J(Pt—H) = 2.5, J(P—H) = 14.6 $\tau(C_6H_5)$2.88–3.00;J(P—C_5H_5) = 1.9,J(P—CH_3) = 3.5
$Pt(\eta^1(7)\text{-}C_9F_6H_5)(CH_3)(COD)$[e]	$CDCl_3$	9.40	84.0			7.73	5.22[f]	41.7	$\tau(CH)_{1,4}$5.92,J(Pt—H) = 15.0, $\tau(CH)_{5,6}$3.14,J(H—H) = 2.0
							5.14[f]	39.0	$\tau(CH)_7$6.67,J(Pt—H) = 64.2, $\delta(CF_3)$58.8,J(Pt—F) = 11.2
$Pt(\eta^1(7)\text{-}C_9H_7O_3)(CH_3)(COD)$	$CDCl_3$	9.36	81.2			7.73	5.24[f]	37.6	$\tau(CH)_{1,2,3,4}$6.32–6.50,$\tau(CH)_{5,6}$3.79, J(H—H) = 1.8
							5.06[f]	42.0	$\tau(CH)_7$7.90,J(Pt—H) = 78.0
$Pt(\eta^3(7,2,3)\text{-}C_9F_6H_5)(\eta^5\text{-}C_5H_5)$	$CDCl_3$			4.36	15.3				$\tau(CH)_{1,4}$5.97,J(Pt—H) = 24.0; $\tau(CH)_{2,3}$5.69,J(Pt—H) = 80.8, $\tau(CH)_7$8.15,J(Pt—H) = 97.5, $\delta(CF_3)$61.3,J(Pt—F) = 14.2, J(F—H) = 0.5
$Pt(CH_3)(POF_2)(COD)$	Acetone-d_6	8.98	73.0			7.42	4.50[c] 4.17[g]	38.0 48.0	J(P—CH_3) = 2.5,J(P—CH)[g] = 5.5, $\delta(POF_2)$26.52,J(Pt—F) = 1150, J(P—F) = 1225

[a] J values in Hz.
[b] *trans* to *Cp*.
[c] *trans* to CH_3.
[d] *trans* to Cl.
[e] All ^{19}F chemical shifts in ppm upfield from $CFCl_3$.
[f] No assignment with respect to being *cis* or *trans* to the CH_3 has been made.
[g] *trans* to POF_2.

TABLE 3. J(Pt—H) to olefin *trans* to group (Hz)

Group	J(Pt—H)
Cl	72.5
Cp	53.6, 49.0, 47.5; average = 50.0
CH_3	36.2

ing the J(Pt—H) values to those previously determined for a series of COD compounds (4). Thus the peak in the spectrum of **3** with J(Pt—H) = 36.2 Hz is assigned to the olefinic group *trans* to methyl while in the spectrum of **5** the peak with J(Pt—H) = 72.5 is assigned to the olefin *trans* to chloride. Olefinic groups with J(Pt—H) $\approx$ 50 are *trans* to Cp ligands. This establishes an nmr *trans* influence (10) for Cp. From Table 3, it is perhaps surprising that the *trans* influence for Cp should be so much weaker than CH_3 especially since both are bonded to Pt by sp^3 hybridized carbon atoms.[4]

The nmr spectrum of **5** was observed to change with time. New peaks grew in while the original ones decreased in intensity and finally disappeared. This occurred much faster in $CDCl_3$ than in acetone-d_6, to the extent that it was impossible to record the spectrum of **5** in CDCl without the presence of these peaks.

Analysis of these peaks, particularly a sharp peak in the Cp region with J(Pt—H) $\approx$ 17 Hz, leads to the conclusion that they were due to the compound Pt(η^5-C_5H_5)(COD).Cl, **6** (reaction 2).

[2] 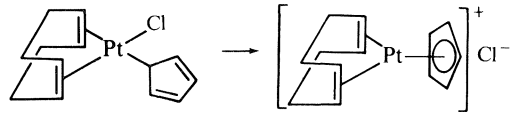

4

This was confirmed by the synthesis of the compound Pt(η^5-C_5H_5)(COD).PF_6, **7**, by reacting **5** with $AgPF_6$. Compound **7** is an analogue of a previously reported complex Pt(η^5-C_5H_5)(COD).-BF_4 (11).

The COD in **3** can be displaced by CO and $P(OR)_3$, where R = alkyl or aryl, to give η^5-Cp compounds (reaction 3).

[3] 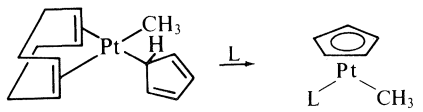

3

L = CO, $P(OCH_3)_3$, $P(OC_6H_5)_3$, $P(OCH_3)(C_6H_5)_2$

In contrast to the η^1-Cp compounds which are highly crystalline these are yellow liquids. Compound **8**, with L = CO, is particularly volatile and has a strong characteristic mushroom-like odour. It is also somewhat thermally unstable and must be stored at -20 °C. The complex with L = $P(OCH_3)_3$ is much less volatile but could be distilled with difficulty. The other complexes of this type could not be distilled without extensive decomposition contaminating the distillate. It is reasonable to assume that the formation of these η^5-Cp complexes involves initial attack on **3** to form a 5-coordinate intermediate. The diene residue of the Cp ring then displaces the COD, resulting in an interesting η^1-Cp to η^5-Cp transformation.

It will be noted that **8** is an analogue of **2**, the initial goal of the project. Attempts to prepare **2** by treating **8** with $CF_3C{\equiv}CCF_3$ gave no reaction. Treatment of **8** with $P(C_6H_5)_3$ led to evolution of gas, probably CO, and formation of an intractable tan precipitate.

The nmr data for the compounds discussed so far, contained in Tables 2 and 4, show that η^1-Cp rings are more highly coupled to Pt than η^5-Cp rings. This has been noted before for the protons on the Cp ring by Cross and Wardle (6). The three compounds reported here that contain η^1-Cp rings have J(Pt—H) > 35 Hz while the five η^5-Cp rings have J(Pt—H) < 17 Hz. A similar trend is observed for carbon where for **3** and **4** J(Pt—C) > 87 Hz while for **8** and **9** J(Pt—C) < 10 Hz. These data form the basis for a useful diagnostic test whereby the bonding mode of a Cp–Pt complex can be determined easily from data readily obtainable from an nmr spectrum. Since the protons on the η^5-Cp rings of Pt(η^5-C_5H_5)$(CH_3)_3$ (12) and Pt(η^5-C_5H_5)-$(CH_3)_2$(C(O)CH_3) (13) have J(Pt—H) < 6 Hz one can also distinguish between Cp–Pt(II) and CP–Pt(IV) compounds.

The relative nmr *trans* influences of Cp and CH_3 in **3** are again revealed by the much larger J(Pt—C) values for groups *trans* to Cp as compared to identical groups *trans* to CH_3. This is

[4]The Pt—Cp bond is significantly longer than the Pt—CH_3 bond and the Pt—olefin bond is longer for the olefinic group *trans* to CH_3 than for that *trans* to Cp (8). In order to explain the nmr and structural results, the existence of hyperconjugation between the Pt—Cp bond and the 4π system of the Cp ring has been proposed (8).

Can. J. Chem. Downloaded from www.nrcresearchpress.com by 210.87.254.6 on 09/05/12
For personal use only.

Can. J. Chem. Downloaded from www.nrcresearchpress.com by 210.87.254.6 on 09/05/12
For personal use only.

consistent with the ^1H nmr data discussed earlier.

The spectroscopic properties of the CO and CH_3 groups in **8** are of interest when compared to those of square planar complexes (14, 15). The carbonyl stretching frequency (ν(CO) = 2036 cm^{-1}) is just beyond the range observed for a series of other carbonyl complexes (2041–2149 cm^{-1}). The chemical shift for the CO in **8** (δ(CO) = 163 ppm) is within the range observed for the square planar complexes but J(Pt—C) = 2.459 Hz which is 50% greater than that previously observed (14). The chemical shift of the methyl (δ(CH) = 44.1 ppm) is abnormally high but the coupling constant is normal (15). The unusual values are probably related to great differences in structure between **8** (an 18 electron complex) and the square planar (16 electron) complexes studied.

When **3** was treated with $CF_3C{\equiv}CCF_3$ in an attempt to prepare **2**, it was soon apparent from the nmr spectrum of the reaction solution that a quite new product, **10**, had been formed. The presence of a norbornadiene residue in **10** was easily detected by means of its characteristic nmr spectrum (17). Diels–Alder reactions between C_5H_5 rings bonded to metals and acetylenes (see, for example, refs. 16–18) are of interest particularly with respect to the stereochemistry of addition. For **3**, a ($2\pi + 4\pi$) reaction of the η^1-Cp metal species and an acetylene could give rise to four possible products depending on the stereochemistry of addition, **10***a–d*.

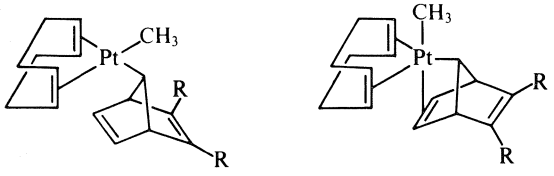

10*a*

10*b*

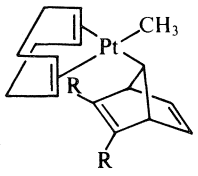

10*c*

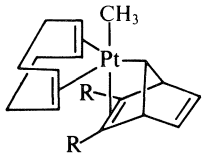

10*d*

R = CF_3

Compounds **10***a* and **10***b* result from acetylene attack on the η^1-Cp ring from the side opposite the metal, while **10***c* and **10***d* result from attack on the ring from the same side as the metal. Interconversion of **10***a* with **10***c* or **10***b* with **10***d* requires inversion at the apical carbon which is σ-bonded to the metal, a high energy process which is unlikely.

In **10***b* and **10***d* an olefin residue is bonded to the platinum to give a 5-coordinate structure. Precoordination of the acetylene to the metal would probably be necessary to achieve the formation of **10***c* and **10***d* by attack on the most hindered side. Such pre-coordination has been postulated in the reaction of Ni(η^5-C_5H_5)$_2$ with $CF_3C{\equiv}CCF_3$ since addition occurs from the same side of the ring as the nickel atom such that the double bond formed from the acetylene is bonded to the metal.

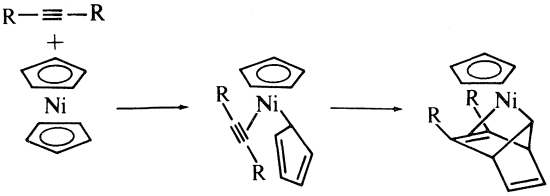

R = CF_3, $COOCH_3$

It was not possible to choose between **10***a–d* on the basis of spectroscopic data. The observed coupling for **10** between the ^{195}Pt and ^{19}F atoms was 11.2 Hz. This seems rather small to arise from a direct bonding interaction such as **10***d* yet too large to arise from anything other than some type of bonding interaction. A direct bonding interaction **10***d*, a long range five bond coupling, **10***a* or **10***b*, or perhaps a through-space coupling in **10***c*, might each constitute an adequate description. The question has been resolved by means of an X-ray structure which shows that **10***a* is the correct structure (3).

This result is important with respect to other similar reactions (17, 18) where the stereochemistry for the addition of the dieneophile has been assigned by comparison of the spectroscopic data (nmr) with that reported for the product obtained from Ni(η^5-C_5H_5)$_2$ and $CF_3C{\equiv}CCF_3$ (16). A similar comparison of the nmr data for **10** would have led to the wrong conclusion. Assignments of geometry on this basis must be regarded as highly tentative.

The result is also important to the more general topic of the role of metals in cycloaddition reactions between cyclic polyolefins coordin-

TABLE 4. ^{13}C nmr data[a]

Compound	CH_3		C_5H_5		COD			
	δ	J(Pt—C)	δ	J(Pt—C)	$\delta(CH_2)$	J(Pt—C)	δ(CH)	J(Pt—C)
Pt(η^1-C_5H_5)(CH_3)(COD)	6.2	724	115.2	87.8	31.1[b] 29.0[c]	11.1 [d]	92.3[b] 106.5[c]	104.3 55.0
Pt(η^1-C_5H_5)$_2$(COD)			116.5	96.8	30.1	[d]	101.3	110.5
					Other resonances and couplings			
Pt(η^5-C_5H_5)(CH_3)(CO)	−44.1	691	94.1	8.4	δ(CO)163.4,J(Pt—C) = 2459			
Pt(η^5-C_5H_5)(CH_3)[$P(OCH_3)_3$]	−47.8	795	93.2	3.8	J(P—CH_3) = 15.0,δ(OCH_3)52.3,J(Pt—C) = 21.0			

[a] ^{13}C chemical shifts are reported in ppm (positive) downfield from TMS; couplings are in hertz; perdeuterodioxane was the solvent.
[b] *Trans* to Cp.
[c] *Trans* to CH_3.
[d] Not observed.

ated to transition metals and electrophilic acetylenes. Of particular interest are reactions where the metal is thought to lift symmetry constraints of otherwise 'symmetry forbidden' thermal cycloadditions (19). The exact manner in which this is achieved is not known but metals might cause normally forbidden concerted reactions to proceed in a stepwise manner (20). The ability of metals to overcome large negative entropy factors by binding both reactants in close proximity and in the proper orientation must also be important. In the case of the reaction of **3** with $CF_3C{\equiv}CCF_3$ there is no participation by platinum in the mechanism of addition. The presence of the platinum atom as a substituent on the Cp ring may affect the rate of reaction, just as any other substituent might, by electronic or steric effects. The fact that only one isomer of **10** is isolated in high yield implies a high steric effect for the Pt(CH_3)(COD) residue.

Compound **3** reacts with maleic anhydride to give another Diels–Alder product **11**. We assume that this reaction proceeds via the same mechanism as that with $CF_3C{\equiv}CCF_3$, so that structure **11** is assigned which results from attack of the olefin on the η^1-Cp ring from the side opposite the metal. A normal *endo* addition is assumed.

When Pt(η^1-C_5H_5)$_2$COD was treated with $CF_3C{\equiv}CCF_3$ a Diels–Alder reaction occurs to form a norbornadiene unit. However, a major rearrangement occurs: the unreacted η^1-Cp displaces the COD and changes from η^1 to η^5, and the norbornadiene is bonded as shown.

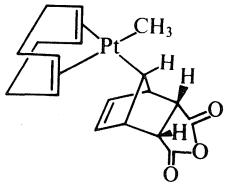

11

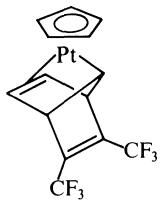

12

The presence of the η^5-C_5H_5 is easily confirmed by the J(Pt—H) coupling constant of 15.3 Hz. The vinyl protons of the norbornadiene unit in **12** are shifted upfield to τ 5.69 and coupled to platinum, J(Pt—H) = 80.8 Hz, while in **10** these protons appear at 3.14 τ and are not coupled to platinum. The large upfield shift and large coupling constant are characteristic of olefins bonded to platinum, consistent with the above structure for **12**. Significantly, a coupling constant between the platinum atom and the fluorine atoms of 14.2 Hz was observed to be very similar to the value found for **10**. These long range coupling constants (5 bonds) are probably due to the rigid cage structure of the norbornadiene units. It can very certainly be concluded that cycloaddition has occurred on the Cp ring on the opposite side to platinum.

It is notable that **12** has a η^3-norbornadiene ligand similar to the one in the product obtained from Ni(η^5-C_5H_5)$_2$ and $CF_3C{\equiv}CCF_3$ except that in **12** the bonded olefin residue originates in the Cp ring, not the acetylene. Formally at least,

Can. J. Chem. Downloaded from www.nrcresearchpress.com by 210.87.254.6 on 09/05/12
For personal use only.

Can. J. Chem. Downloaded from www.nrcresearchpress.com by 210.87.254.6 on 09/05/12
For personal use only.

12 can be considered to result from the Diels–Alder addition of $CF_3C{\equiv}CCF_3$ to $Pt(\eta^5\text{-}C_5H_5)_2$. The ease with which the COD is displaced in this system suggests that **4** might be a precursor to $Pt(\eta^5\text{-}C_5H_5)_2$. A peak in the mass spectrum of **4** appears at *m/e* 325 corresponding to $PtCp_2$ but attempts to observe this compound by following the changes in the nmr spectrum of a sample heated to 85 °C for 1 h were not successful; **4** has considerable thermal stability. In another experiment an nmr sample of **4** was irradiated with uv light. Compound **4** showed surprising stability but eventually decomposed to form a dark red solution. A very weak peak at τ 4.35 J(Pt—H) 13.6 was observed. The coupling constant and chemical shift values fall in the range for η^5-Cp rings bonded to platinum but nothing more can be said. Efforts along these lines will be continued.

Compound **3** reacts with PF_3 to give **8** in relatively low yield. It seems probable that the structure of **8** is that shown resulting from the

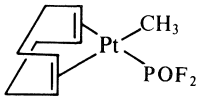

13

partial hydrolysis of PF_3 to POF_2^-.[5] The H nmr spectrum and analytical data indicate that no C_5H_5 ring or residue is present. The ^{1}H nmr spectrum is quite similar to that of $PtCl(CH_3)$-(COD) consisting of two peaks for the olefinic protons at τ 4.5 and τ 4.17, a broad peak for the methylene region and a sharp doublet with ^{195}Pt satellites for the Pt—CH_3 group in the ratio 2:2:8:3 respectively. The peak at τ 4.5 has J(Pt—H) = 38.0 Hz consistent with the olefin being *trans* to CH_3. The other peak has J(Pt—H) = 48.0 Hz and additional coupling to phosphorus J(P—H) = 5.5 Hz which was resolved when the sample was double irradiated at the methylene peak τ 7.42. The Pt—CH_3 group also shows phosphorus coupling J(P—H) = 2.5 Hz in addition to platinum coupling J(Pt—H) = 73.0 Hz. The ^{19}F nmr spectrum consists of a widely spaced doublet of triplets centered at 26.52 ppm with J(Pt—F) = 1150 Hz and J(P—F) = 1225 Hz. In the infrared spectrum (Nujol) there was in addition to strong P—F peaks at 790 and 535 cm^{-1} a strong band at 1240 cm^{-1} which we assign to νP=O.

The ^{19}F nmr and infrared data are very similar to those obtained for other Pt–POF_2 complexes (21). If it were a PF_3 complex **8** would necessarily contain paramagnetic Pt(I). This is not consistent with nmr data. These facts taken together strongly support the assigned structure.

Compound **3** also reacts with phosphines PR_3, where R = alkyl or aryl, to form apparently, a homologous series of products differing only in the phosphine present. The ^{1}H nmr spectroscopic parameters of these products are consistent with the presence of both a methyl group and a phosphine bonded to platinum, and analytical data indicated that the Cp and COD moieties are also retained in the product.

Complete characterization is difficult but it seems likely that some intramolecular rearrangement involving the Cp ring and the COD has occurred. Our results do not preclude the possibility of a simple transfer of the Cp to a vinyl carbon of COD as has been postulated (7) for some similar systems. Work is continuing on this problem.

[5]We are indebted to Professor Reinhard Schmutzler for pointing out the possibility of hydrolysis of PF_3.

Acknowledgements

The financial support of the National Research Council of Canada and the award of an NRCC Post-doctorate Fellowship (to A.S.) are gratefully acknowledged.

1. H. C. Clark and L. E. Manzer. Inorg. Chem. **13**, 1291 (1974).
2. S. Trofimenko. Acc. Chem. Res. **4**, 17 (1971).
3. H. C. Clark, D. G. Ibbot, N. C. Payne, and A. Shaver. J. Am. Chem. Soc. **97**, 3555 (1975).
4. H. C. Clark and L. E. Manzer. J. Organomet. Chem. **59**, 411 (1973).
5. F. A. Cotton and L. T. Reynolds. J. Am. Chem. Soc. **80**, 269 (1958).
6. R. J. Cross and R. Wardle. J. Chem. Soc. (A), 2000 (1971).
7. M. N. S. Hill, B. F. G. Johnson, T. Keating, and J. Lewis. J. Chem. Soc. Dalton Trans. 1197 (1975).
8. V. W. Day, H. C. Clark, and A. Shaver. In preparation.
9. F. A. Cotton. Acc. Chem. Res. **1**, 257 (1968).
10. T. G. Appleton, H. C. Clark, and L. E. Manzer. Coord. Chem. Rev. **10**, 335 (1973).
11. B. F. G. Johnson, J. Lewis, and D. A. White. J. Chem. Soc. (A), 1738 (1970).
12. S. D. Robinson and B. L. Shaw. Z. Naturforsch. Part B, **18**, 507 (1963).

13. H. C. CLARK and A. SHAVER. Unpublished results.
14. W. J. CHERWINSKI, B. F. G. JOHNSON, J. LEWIS, and J. R. NORTON. J. Chem. Soc. Dalton Trans. 1155 (1975).
15. M. H. CHISHOLM, H. C. CLARK, L. E. MANZER, J. B. STOTHERS, and J. E. H. WARD. J. Am. Chem. Soc. **97**, 721 (1975); **95**, 8574 (1973). H. C. CLARK and J. E. H. WARD. J. Am. Chem. Soc. **96**, 1741 (1974), Can. J. Chem. **52**, 570 (1974). H. C. CLARK, L. E. MANZER, and J. E. H. WARD. Can. J. Chem. **52**, 1165 (1974), **52**, 1973 (1974).
16. D. W. MCBRIDE, E. DUKEK, and F. G. A. STONE. J. Chem. Soc. 1752 (1964). L. F. DAHL and C. H. WEI. Inorg. Chem. **2**, 714 (1963).
17. W. P. GIERING, S. RAGHU, M. ROSENBLUM, A. CUTLER, D. EHNTHOLT, and R. W. FISH. J. Am. Chem. Soc. **94**, 8251 (1972).
18. J. L. DAVIDSON, M. GREEN, F. G. A. STONE, and A. J. WELCH. J. Chem. Soc. Chem. Commun. 286 (1975).
19. R. E. DAVIS, T. A. DODDS, T.-H. HSEU, J. C. WAGNON, T. DEVON, J. TANCREDE, J. S. MCKENNIS, and R. PETTIT. J. Am. Chem. Soc. **96**, 7562 (1974).
20. R. DAVIS, M. GREEN, and R. P. HUGHES. J. Chem. Soc. Chem. Commun. 405 (1975).
21. J. GROSSE, R. SCHMUTZLER, and W. S. SHELDRICK. Acta Crystallogr. B**30**, 1623 (1974). J. GROSSE and R. SCHMULTZLER. J. Chem. Soc. Dalton Trans. In press.

Can. J. Chem. Downloaded from www.nrcresearchpress.com by 210.87.254.6 on 09/05/12
For personal use only.

Perfluoroalkyl- and fluoroalkyl- complexes of rhodium(III)

HOWARD C. CLARK AND KENNETH J. REIMER
Department of Chemistry, University of Western Ontario, London, Ont., Canada N6A 5B7

Received February 17, 1976

HOWARD C. CLARK and KENNETH J. REIMER. Can. J. Chem. **54**, 2077 (1976).

A series of perfluoroalkyl (R_f—) and fluoroalkyl (R_fCH_2—) complexes of rhodium(III) have been prepared by oxidative addition reactions of R_fI and R_fCH_2I (R_f = CF_3, C_2F_5 and C_3F_7) with *trans*-$RhClCO(PMe_2Ph)_2$. The reaction of CF_3I with *trans*-$RhClCO(PMePH_2)_2$ gave $RhClI(CF_3)CO(PMePh_2)_2$ but no reaction was observed with CF_3CH_2I. The *trans* stereochemistry of addition has been assigned to all complexes by nuclear magnetic resonance measurements and the comparison of the far-infrared spectra to those of some bromo compounds: $RhBrI(CF_3)CO(PMe_2Ph)_2$ and $RhBrI(C_3F_7CH_2)CO(PMe_2Ph)_2$. Both ^1H and ^{19}F nmr data are presented and discussed.

HOWARD C. CLARK et KENNETH J. REIMER. Can. J. Chem. **54**, 2077 (1976).

On a préparé une série de complexes perfluoroalkyle (R_f—) et fluoroalkyle (R_fCH_2—) du rhodium(III) par des réactions d'addition oxydative de R_fI et R_fCH_2I (R_f = CF_3, C_2F_5 et C_3F_7) au $RhClCO(PMe_2Ph)_2$ *trans*. La réaction du CF_3I avec le $RhClCO(PMeOh_2)_2$ *trans* conduit au $RhClI(CF_3)CO(PMePh_2)_2$ mais on n'observe aucune réaction avec le CF_3CH_2I. On a attribué la stéréochimie *trans* pour l'addition à tous les complexes à l'aide de mesures de résonance magnétique nucléaire et par comparaison des spectres infrarouges lointains de ces composés avec ceux de quelques dérivés bromés; $RhBrI(CF_3)CO(PMe_2Ph)_2$ et $RhBrI(C_3F_7CH_2)CO(PMe_2PH)_2$. On présente et on discute des données rmn du ^1H et du ^{19}F.

[Traduit par le journal]

Introduction

Oxidative addition reactions comprise a particularly important aspect of the chemistry of organometallic compounds (1–4). Besides their significance in catalytic processes, they can often provide convenient synthetic routes to new compounds such as perfluoroalkyl complexes (5). Thus, there has been considerable interest in the characterization and structures of the products of oxidative addition as well as in the kinetics and mechanisms of such reactions (6–10).

Although oxidative addition reactions of complexes of the type $IrXCOL_2$ (X = halide; L = tertiary phosphine or arsine) have been extensively studied (1–3, 6–9, 11–13), those of the corresponding rhodium compounds have received less attention (14, 15). For example, the perfluoroalkyliridium compounds, $IrClI(R_f)COL_2$ (R = CF_3, C_2F_5, C_3F_7; L = PPh_3 and $PMePh_2$), were prepared by Collman and coworkers (3, 16) but analogous rhodium complexes have not been reported. Because of the significance of both oxidative addition reactions and fluorocarbon derivatives; and previous studies by this group of some fluorocarbon-platinum compounds (17) the following study was undertaken. In addition to perfluoroalkyliodides, R_fI, comparative reactions of fluoroalkyliodides, R_fCH_2I (R_f = CF_3, C_2F_5, C_3F_7), with some rhodium complexes were also examined.

Results and Discussion

Preparation and Stereochemistry

The complex *trans*-$RhClCO(PMe_2Ph)_2$, **1**, reacts in acetone at room temperature with CF_3I, C_2F_5I, C_3F_7I, CF_3CH_2I, $CF_3CF_2CH_2I$, and $CF_3(CF_2)_2CH_2I$ to give air-stable, yellow, or orange crystalline compounds (Table 1).

Although all reactions were allowed to proceed for 24 h, there were some notable differences in the apparent rates of the reactions depending on the fluorinated alkyl iodide used. For example, crystals of the trifluoromethyl derivative separated from the reaction mixture within 2 h. In all reactions with the perfluoroalkyl iodides, R_fI, the solutions changed from the yellow colour characteristic of acetone solutions of **1** to an orange colouration (denoting formation of the rhodium(III) product) within a few minutes of mixing the reactants. This contrasts with the several hours required for any discernible colour change in reactions involving the fluoroalkyl iodides, R_fCH_2I.

When the compound *trans*-$RhClCO(PMePh_2)_2$, **2**, was allowed to react with trifluoro-

Can. J. Chem. Downloaded from www.nrcresearchpress.com by 210.87.254.105 on 09/05/12
For personal use only.

TABLE 1. Analytical and physical data for perfluoroalkyl- and fluoroalkyl-rhodium(III) complexes

Compound[a]	Colour	Melting point[b] (°C)	Analysis %C Found	%C Calculated	%H Found	%H Calculated	Method of preparation	Yield %
$RhClI(CF_3)COL_2$	Orange	170–175	33.54	33.86	3.53	3.47	A	73
$RhBrI(CF_3)COL_2$	Dark orange	162–164	31.60	31.65	3.18	3.25	A	70
$RhCl_2(CF_3)COL_2$	Yellow	159–160	39.42	39.52	3.79	4.05	D	85
$RhClI(C_2F_5)COL_2$	Yellow	160–162	33.15	33.14	3.32	3.22	A	63
$RhClI(C_3F_7)COL_2$	Orange	152–153	32.79	32.52	3.29	3.00	B	48
$RhClI(CF_3CH_2)COL_2$	Pale orange	164–165	34.73	34.97	3.72	3.71	B	82
$RhClI(C_2F_5CH_2)COL_2$	Yellow	165–166	34.49	34.20	3.55	3.44	B	75
$RhClI(C_3F_7CH_2)COL_2$	Orange	139–140	33.64	33.51	3.47	3.21	B	70
$RhBrI(C_3F_7CH_2)COL_2$[c]	Orange	>125	32.25	30.60	3.53	3.08	B	25
$RhClI(CF_3)COL_2'$	Orange	165–167	43.83	44.09	3.77	3.44	C	72

[a]L = PMe_2Ph, L′ = $PMePh_2$.
[b]All compounds melt with decomposition.
[c]Samples were always contaminated with acetone; see Experimental section.

methyl iodide for 24 h under conditions identical to those used in the analogous reaction with **1**, a mixture of the desired product and the starting material was isolated. However, after shaking a solution of **2** with a ten-fold excess of CF_3I for 7 days, $RhClI(CF_3)CO(PMePh_2)_2$ was obtained. No reaction was observed between **2** and a large excess of CF_3CH_2I even after several days.

The propensity for d^8 metals to undergo oxidative addition reactions generally increases upon descending a triad or passing from right to left within Group VIII (2, 3). This is consistent with the above greater sensitivity of rhodium to ligand changes relative to iridium, and also with the fact that Collman and Sears (16) obtained the perfluoroalkyliridium derivatives, $IrClI(R_f)COL_2$, where L = PPh_3, $PMePh_2$, the reactions requiring only 3 min.

All compounds obtained from the reactions of *trans*-$RhClCOL_2$ (L = PMe_2Ph or $PMePh_2$) are tentatively assigned configuration **3** resulting from *trans* addition of the fluorinated alkyl iodide.

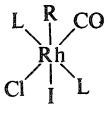

3

L = PMe_2Ph and for R = CF_3 only, $PMePh_2$

Alternative configurations such as those resulting from *cis* additions, or with *cis*-phosphine ligands seem unlikely in view of the following evidence:

(*i*) For all complexes where L = PMe_2Ph the methyl groups bonded to phosphorus show two main resonances in the ^1H nmr spectra indicating that their time-averaged magnetic environments are different. This is a consequence of the absence of a plane of symmetry along the P—Rh—P axis making the two methyl groups attached to a given phosphorus atom magnetically nonequivalent (14, 18, 19). Moreover, except for R = C_2F_5 and C_3F_7 (which will be discussed in greater detail later), the phosphine–methyl resonances appear as 1:2:1 triplets due to strong phosphorus–phosphorus coupling characteristic of mutually *trans* phosphines (20). For $RhClI(CF_3)CO(PMePh_2)_2$, only the one expected phosphine–methyl resonance is observed but it is a 1:2:1 triplet verifying the *trans* disposition of the phosphine ligands.

(*ii*) It has been suggested that the relative intensity of two weak infrared bands at *ca.* 1570 and 1585 cm^{-1} is dependent on the relative position of phenyl substituted phosphine ligands. In *trans* complexes the lower energy band is more intense (11, 21, 22). In all the complexes prepared in this study the low energy band is the more intense of the two, consistent with *trans* phosphine ligands.

(*iii*) For iridium complexes, extensive studies (23) have indicated a marked dependence of ν(Ir—Cl) on the *trans* ligand, and similar effects have been found for a variety of other metal complexes. Although fewer correlations have been made for rhodium compounds, sufficient data are available to establish stereochemistry.

Can. J. Chem. Downloaded from www.nrcresearchpress.com by 210.87.254.105 on 09/05/12
For personal use only.

TABLE 2. Infrared spectra (cm^{-1}) of perfluoroalkyl- and fluoroalkyl-rhodium compounds

Compound[a]	ν(CO)[b]	ν(Rh—Cl)[c]	Carbon–fluorine vibrations[c]	Other[c]
$RhClI(CF_3)COL_2$	2091	328	1095sbr, 1025vs, 1015sh	280m,br
$RhCl_2(CF_3)COL_2$	2100	328[d]	1090sbr, 1029vs, 1013sh	295m,br
$RhBrI(CF_3)COL_2$	2090		1096vsbr, 1022vs, 1018sh	280s,br
$RhClI(CF_3)COL_2'$	2092	325	1095vsbr, 1036sh, 1022vs	280m,br
$RhClI(C_2F_5)COL_2$	2090	328	1285sbr, 1216vs, 1186m, 1174s, 1025sbr, 1003vs	286sh, 268m,br
$RhClI(C_3F_7)COL_2$	2083	328	1315mbr, 1243sh, 1225s, 1195vsbr, 1159w, 1049m, 1024w, 1006w	295sh, 275m,br
$RhClI(CF_3CH_2)COL_2$	2069	312	1262vs, 1222s, 1166m, 1080vs, 995s, 536m	
$RhClI(C_2F_5CH_2)COL_2$	2066	312	1345—, 1264vw, 1228vsbr, 1184m,[e] 1093m, 1003m	
$RhClI(C_3F_7CH_2)COL_2$	2071	312	[f]	
$RhBrI(C_3F_7CH_2)COL_2$	2068		[f]	

[a]L = PMe_2Ph, L′ = $PMePh_2$.
[b]Measured in benzene solution.
[c]Nujol mulls.
[d]Cl^- *trans* to CO, ν(Rh—Cl) for Cl^- *trans* to CF_3 could not be located with certainty.
[e]Not assigned with certainty, coincident with some ligand vibrations.
[f]Spectrum identical to that of $RhClI(C_2F_5CH_2)COL_2$ in region 1400–300 cm^{-1}.

For the perfluoroalkyl compounds prepared in this study ν(Rh—Cl) occurs at 328 cm^{-1} (L = PMe_2Ph) and 325 cm^{-1} (L = $PMePh_2$) and at 312 cm^{-1} for the fluoroalkyl derivatives, consistent with a chlorine atom *trans* to carbon monoxide (23).

The assignment of the rhodium chloride stretching frequencies was accomplished by comparison with the spectra of corresponding bromo complexes. As the spectra of all of the compounds within each class in the region 500–200 cm^{-1} were essentially identical, only two bromo derivatives, $RhBrI(CF_3)CO(PMe_2Ph)_2$ and $RhBrI(C_3F_7CH_2)CO(PMe_2Ph)_2$, were prepared. They were obtained by the oxidative addition of the appropriate fluorinated alkyl iodide to *trans*-$RhBrCO(PMe_2Ph)_2$.

(*iv*) Further support for these conclusions is provided by the formation of a yellow precipitate of silver iodide when silver hexafluorophosphate is added to acetone solutions of the complexes. If the higher *trans* influence of alkyl or perfluoroalkyl groups relative to carbon monoxide found for other systems may be extended to these rhodium(III) complexes, the halide ligand (*trans* to R_f or R_fCH_2 groups) would be expected to be labile (23). This property may be exploited synthetically. If lithium chloride is added to a filtered solution of the cation obtained after the reaction of $AgPF_6$ with $RhClI(CF_3)CO(PMe_2Ph)_2$, the dichloro complex, $RhCl_2(CF_3)CO(PMe_2Ph)_2$ is obtained in high yield. Spectroscopic data confirm the assignment of configuration **3** with the iodide replaced by chloride.

Infrared Spectra

In addition to the far-infrared spectroscopic absorptions referred to above, all compounds show characteristic bands due to the phosphine ligands as well as carbonyl stretching bands. The latter are in the range 2050–2100 cm^{-1} (Table 2) characteristic of rhodium(III) complexes (14). Notably, the values of ν(CO) for the perfluoroalkyl compounds are 12–29 cm^{-1} higher than the fluoroalkyl derivatives suggestive of greater removal of electron density from the metal in the former case. There are also strong absorptions in the region 1350 to 900 cm^{-1} indicative of carbon–fluorine vibrations (24–31).

The spectra of the trifluoromethyl – transition metal compounds usually exhibit two bands in the region 1100–1000 cm^{-1}. The higher frequency band is attributed to the symmetric C—F stretching vibration and the lower frequency band to the degenerate stretching mode. For some complexes, the lower (degenerate) band is split, presumably as a result of low molecular symmetry (26–31). Consistent with these observations, all of the trifluoromethylrhodium complexes exhibit a strong broad band at *ca.* 1095 cm^{-1} and a very strong band near 1000 cm^{-1} which is split into two components. Although there are some weak bands in this region which may be attributed to other ligand vibrations, the carbon–fluorine modes are readily identified because of their much greater intensity. Assignments of the C—F infrared bands of the other perfluoroalkyl groups are less definitive, but those reported here are similar to previously

Can. J. Chem. Downloaded from www.nrcresearchpress.com by 210.87.254.105 on 09/05/12
For personal use only.

TABLE 3. ^{1}H nmr data[a] for perfluoroalkyl- and fluoroalkyl-rhodium compounds

Compound[b]	Phosphine methyls $\delta(CH_3)$[c]	J^*[d] (Hz)	$\delta(CH_2)$[c]	R_fCH_2 Coupling constants (Hz)
$RhClI(CF_3)COL_2$	2.37	8.5		
	2.06	8.0		
$RhCl_2(CF_3)COL_2$	2.08	9.0		
	2.00	8.0		
$RhBrI(CF_3)COL_2$	2.44	8.0		
	2.10	6.5		
$RhClI(CF_3)COL_2'$	2.54	8.5		
$RhClI(C_2F_5)COL_2$	2.37	8.5		
	1.95	[e]		
$RhClI(C_3F_7)COL_2$	2.35	8.5		
	1.97	[e]		
$RhClI(CF_3CH_2)COL_2$	2.25	7.0	1.69	J(H—F) = 15, J(P—H) = 6.5, J(Rh—H) = 3.0
	2.19	8.5		
$RhClI(C_2F_5CH_2)COL_2$	2.28	7.3	1.63	Triplet J(H—F) = 26
	2.21	8.0		
$RhClI(C_3F_7CH_2)COL_2$	2.26	6.0	1.72	Triplet J(H—F) = 28
	2.14	9.0		

[a]Measured at 100 MHz in dichloromethane.
[b]L = PMe_2Ph, L′ = $PMePh_2$.
[c]Chemical shifts are reported in ppm downfield (positive) from TMS.
[d]$J^* = {}^2J$(P—H) + ^4J(P—H) (ref. 20).
[e]See text and Fig. 1.

published data (30). There have been very few reports of infrared spectra of fluoroalkyl complexes and vibrational assignments must await the accumulation of a sufficient body of data.

Additional bands (300–250 cm^{-1}), found in the spectra of some CF_3–Ir complexes, have been tentatively assigned to vibrations involving some ν(M—C) character (13). For the CF_3–Rh compounds reported here, similar spectral characteristics have been observed, *i.e.* bands at 280 cm^{-1} for CF_3 *trans* to I^-, and 295 cm^{-1} for CF_3 *trans* to Cl^-. These bands are shifted to lower energy in the spectra of the perfluoroethyl and perfluoropropyl derivatives. The suggested assignments (13) for these bands are further supported by the absence of any bands below 300 cm^{-1} in the infrared spectra of the fluoroalkyl complexes.

^{1}H Nuclear Magnetic Resonance Data

Nuclear magnetic resonance data for the compounds are presented in Table 3 (^{1}H nmr) and Table 4 (^{19}F nmr).

Perfluoroalkyl Compounds

As described earlier, the phosphine–methyl resonances for $RhClI(CF_3)CO(PMe_2Ph)_2$ appear as two well-defined 1:2:1 triplets. For the compounds $RhClI(R_f)CO(PMe_2Ph)_2$ ($R_f = C_2F_5$, C_3F_7), although two resonances are observed, only one of these is a well-defined triplet. The other band appears as a broad multiplet. These features are illustrated in Fig. 1. Moreover, this pattern is unchanged in a variety of solvents, and (in benzene containing $CFCl_3$) over the range −20 to 100 °C. Close examination of an expanded spectrum of this multiplet suggests that it could be a triplet of triplets, presumably due to coupling with the α-CF_2 group, with $J^* = {}^2J$(P—H) + ^4J(P—H) = *ca.* 8.4 Hz, and J(H—F) = *ca.* 1.5 Hz. For purposes of this discussion, groups are labelled according to the scheme:

$$\underset{\alpha\ \ \beta\ \ \gamma}{Rh—CF_2CF_2CF_3} \qquad \underset{\alpha\ \ \beta}{Rh—CH_2CF_2CF_3}$$

Broadening of the higher field resonance has also been observed for some fluorocarbon–platinum complexes.

Fluoroalkyl Compounds

For the R_fCH_2-derivatives the phosphine–methyl resonances are also triplets but the differences in chemical shift are not as great and the signals are overlapping. The difference in chemical shift between the magnetically nonequivalent methyl groups increases with increasing length of the fluoroalkyl group.

For all of the fluoroalkyl compounds the resonance due to the CH_2 protons appears at

Can. J. Chem. Downloaded from www.nrcresearchpress.com by 210.87.254.105 on 09/05/12
For personal use only.

TABLE 4. ^{19}F nmr data for perfluoroalkyl- and fluoroalkyl-rhodium compounds

Compound[a]	δF[b]	J(P—F)[c]	J(Rh—F)	J(H—F)	Description	Assignment	Other coupling constants
$RhClI(CF_3)COL_2$	3.63	18.0	14.5		Triplet of doublets	α-CF_3	
$RhCl_2(CF_3)COL_2$	1.75	17.6	14.0		Triplet of doublets	α-CF_3	
$RhBrI(CF_3)COL_2$	1.28	17.8	14.5		Triplet of doublets	α-CF_3	
$RhClI(CF_3)COL_2'$	1.2	18.3	13.8		Triplet of doublets	α-CF_3	
$RhClI(C_2F_5)COL_2$	62.3	26		[d]	Broad triplet	α-CF_2	
	79.2				Singlet	β-CF_3	
$RhClI(C_3F_7)COL_2$	65.6			[d]	Multiplet	α-CF_2	
	115.3				Singlet	β-CF_2	
	79.1				Triplet	γ-CF_3	$J(F_\alpha—F_\gamma) = 12$
$RhClI(CF_3CH_2)COL_2$	56.05		3.8	15.0	Triplet of doublets	α-CF_3	
$RhClI(C_2F_5CH_2)COL_2$	101.3			26.0	Triplet	α-CF_2	
	85.1				Singlet	β-CF_3	
$RhClI(C_3F_7CH_2)COL_2$	97.5			28.0[e]	Multiplet	α-CF_2	
	126.4				Singlet	β-CF_2	
	80.9				Triplet	γ-CF_3	$J(F_\alpha—F_\gamma) = 10$
$RhBrI(C_3F_7CH_2)COL_2$	97.7			28.0[e]	Multiplet	α-CF_2	
	126.2				Singlet	β-CF_2	
	80.8				Triplet	γ-CF_3	$J(F_\alpha—F_\gamma) = 10$

[a] L = PMe_2Ph, L' = $PMePh_2$.
[b] δ in ppm upfield relative to internal $CFCl_3$; measured at 94.1 MHz; in dichloromethane.
[c] Coupling constants are given in Hertz.
[d] See text.
[e] Resolved by homonuclear decoupling.
[f] Rh—$\underset{\alpha\ \beta\ \gamma}{CF_2CF_2CF_3}$, Rh—$\underset{\alpha\ \beta}{CH_2CF_2CF_3}$ etc.

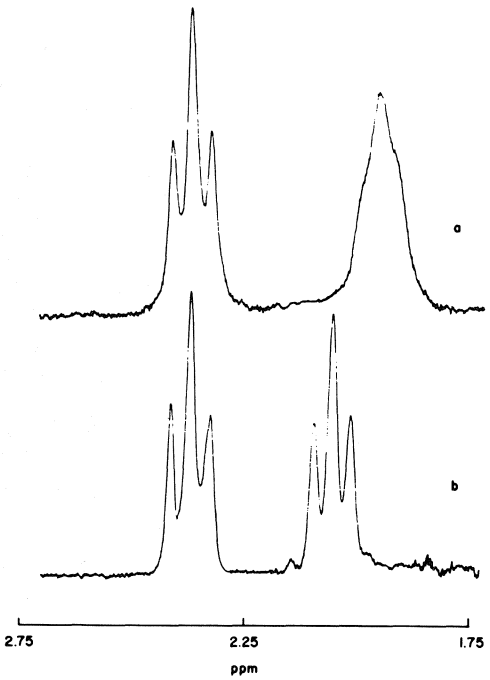

FIG. 1. ^1H nmr spectra of $RhClI(R_f)CO(PMe_2Ph)_2$ complexes (*a*, $R_f = C_3F_7$, *b*, $R_f = CF_3$) showing phosphine–methyl resonances. Measured at 100 MHz in dichloromethane using a 250 Hz sweep width.

higher field ($\delta \approx 1.7$ ppm) than that of the phosphine-methyl protons. This contrasts to a position to lower field ($\delta \approx 3.1$ ppm) for $PtI(Me)_2(CF_3CH_2)(AsMe_2Ph)_2$ (17). For the rhodium–CH_2CF_3 derivative, the ^1H nmr spectrum of the CH_2 protons exhibits a complex pattern (Fig. 2) which is rarely observed. There is a large coupling with the CF_3 group ($J = 15$ Hz), confirmed by inspection of the ^{19}F spectrum. Each peak of the quartet is split further into triplets due to coupling with ^{31}P ($J = 6.5$ Hz) and the resulting quartet of triplets is additionally doubled by coupling with rhodium ($I = 1/2$, 100% abundance). The rhodium–proton coupling constant of 3.0 Hz compares with the value of J(Rh—Me) = 2.2 Hz observed in $RhBr_2(Me)CO(PMe_2Ph)_2$ (14).

For the $CF_3CF_2CH_2$— and $CF_3(CF_2)_2CH_2$— compounds the CH_2 resonances appear essentially as 1:2:1 triplets due to very large coupling with the α-CF_2 groups (J(H—F) = 26 and 28 Hz respectively). This increase in the magnitude of H—F coupling to the α-CF_2 groups with increasing length of the fluoroalkyl chain has also been noted for $PtI(Me)_2(R_fCH_2)(PMe_2Ph)_2$ ($R_f = CF_3$ and CF_3CF_2: $J = 15$ and 25 Hz respectively (17)). For the present compounds,

Can. J. Chem. Downloaded from www.nrcresearchpress.com by 210.87.254.105 on 09/05/12
For personal use only.

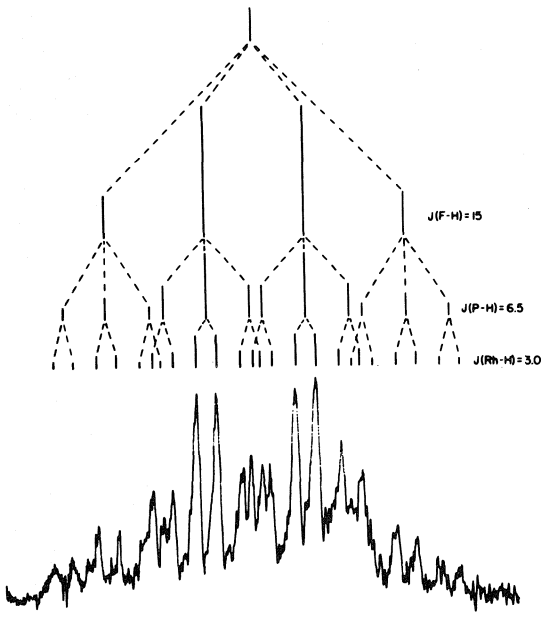

FIG. 2. ^1H nmr spectrum of $RhClI(CF_3CH_2)CO(PMe_2Ph)_2$ showing coupling to CH_2 resonance. Measured at 100 MHz in dichloromethane using a 250 Hz sweep width.

each part of the triplets shows additional fine structure but we are unable to resolve them sufficiently to assign accurate values to the phosphorus and rhodium coupling constants. They do, however, appear to be similar to those calculated for the CF_3CH_2 compound.

^{19}F *Nuclear Magnetic Resonance Data (32)*

Perfluoroalkyl Complexes

The ^{19}F resonance of the CF_3 group (Table 4) is found at very low field, much lower than for the α-CF_2 groups in the other compounds. The coupling constants to phosphorus and rhodium are very similar (J(P—F) = *ca.* 18 Hz, J(Rh—F) = *ca.* 14 Hz) in all of the complexes.

For both the perfluoroethyl and perfluoropropyl complexes the α-CF_2 resonance consisted of a very broad signal in the expected region. Only in the former case could phosphorus–fluorine coupling be resolved (J = 26 Hz) but each part of the triplet was complex due to small rhodium coupling as well as the H–F coupling considered earlier. A change in rhodium–fluorine coupling is not unexpected as such coupling appears to decrease with increasing length of the fluorocarbon chain. Thus for $RhI(CF_3)(\eta^5\text{-}C_5H_5)(CO)$, J(Rh—F) = 11.7 Hz whereas the coupling (to the α-CF_2) in the perfluoropropyl analogue falls to 4 Hz (33). Moreover, no metal–fluorine coupling was observed in the spectrum of $RhI(C_3F_7)(\eta^5\text{-}C_5H_5)(C_2H_4)$ (34). Similar trends have been noted in a series of platinum compounds $PtI(Me)_2(R_f)(PMe_2Ph)_2$ where J(Pt—F) (to adjacent CF_3 or CF_2 groups) is 517, 273, and 260 Hz for R_f = CF_3, C_2F_5, and C_3F_7 respectively (17).

For the $RhClI(C_3F_7)CO(PMe_2Ph)_2$ complex, the α-CF_2 resonance could not be resolved, presumably because it consists of a large number of lines. Unfortunately, homonuclear decoupling of the triplet due to the CF_3 group did not improve the resolution of the α-CF_2 band. For both the perfluoroethyl and perfluoropropyl compounds the resonances due to the β groups appeared as the expected (for discussions of ^{19}F nmr see ref. 32), although slightly broadened, singlets. They were unaffected by homonuclear decoupling experiments and the slight broadening is probably due to very small contributions from rhodium and possibly, phosphorus coupling.

Fluoroalkyl Compounds

The most significant features of the ^{19}F nmr spectra of the R_fCH_2 compounds are the decreased rhodium–fluorine and increased hydrogen–fluorine coupling constants with increasing length of the fluoroalkyl chain.

Consequently the spectrum of $RhClI(CF_3CH_2)CO(PMe_2Ph)_2$ showed a triplet of doublets: each peak of the triplet being further split by small coupling to rhodium (J = 3.8 Hz). Only a triplet was observed for the α-CF_2 resonance in the $CF_3CF_2CH_2$ compound. The CF_3 band showed an expected, although slightly broadened, singlet. The α-CF_2 resonance of $RhClI(C_3F_7CH_2)CO(PMe_2Ph)_2$ appeared as a complex multiplet. Irradiation of the triplet $J(F\alpha F\gamma)$ = 10 Hz due to the CF_3 group allowed resolution of the triplet attributed to J(H—F) = 28 Hz but no rhodium coupling was observed.

Experimental

Reactions were conducted under nitrogen or under an atmosphere of the perfluoroalkyl iodide (for R_fI = CF_3I or C_2F_5I). However, work-up (recrystallization, handling and storage) was performed without special precautions as none of the compounds exhibited instability with respect to air or moisture. All solvents, although of 'spectroquality', were dried over molecular sieves (BDH,

Can. J. Chem. Downloaded from www.nrcresearchpress.com by 210.87.254.105 on 09/05/12
For personal use only.

Can. J. Chem. Downloaded from www.nrcresearchpress.com by 210.87.254.105 on 09/05/12
For personal use only.

Type 5A) and were vacuum degassed or purged with nitrogen before use.

Infrared spectra were recorded on a Perkin-Elmer Model 621 Grating Spectrophotometer. Solid state spectra (4000–450 cm^{-1}) were obtained as Nujol mulls between KBr plates or as KBr pellets. For examination of the region 500–200 cm^{-1} Nujol mulls were smeared on polyethylene strips and the instrument was purged with dry air to remove water vapor. The reproducibility of all solid state spectra suggests an accuracy of *ca.* ± 2 cm^{-1}. Solution spectra were obtained using benzene as a solvent and the carbonyl absorptions are somewhat broad. Accuracy is therefore probably no greater than ± 5 cm^{-1}.

^1H and ^{19}F nmr spectra were run on a Varian Associates HA-100 spectrometer at 100 MHz and 94.1 MHz with tetramethylsilane and "Freon-11" ($CFCl_3$) as the internal reference-lock signals respectively.

Analyses were obtained from Midwest Microlab Ltd., Indianapolis, Indiana. Melting points were determined in air using a Thomas Hoover 'unimelt' capillary melting point apparatus and are uncorrected.

Perfluoro- and fluoro-alkyl iodides were purchased from Peninsular Chemresearch Inc., except trifluoromethyl iodide and heptafluoropropyl iodide which were obtained from Columbia Organic Chemical Co. Inc. Free iodine was removed from C_2F_7I by shaking it with mercury. The other chemicals were used without further purification, as were $RhCl_3.3H_2O$ (Alfa Inorganics and Johnson, Matthey and Mallory) and dimethylphenylphosphine (Maybridge Chemical Co.).

Preparation of Complexes

The syntheses of *trans*-$RhXCO(PMe_2Ph)_2$ (X = Cl, Br) and *trans*-$RhClCO(PMePh_2)_2$ have been previously described (35).

Procedure A: Two equivalents of the perfluoroalkyl iodide were condensed on to an acetone solution (5 ml) of the appropriate rhodium complex, *trans*-$RhClCO(PMe_2Ph)_2$ (0.4 g, 0.91 mmol) or $RhBrCO(PMe_2Ph)_2$ (0.15 g, 0.31 mmol), in a 20 ml Carius tube. The tube was sealed under vacuum, allowed to warm to room temperature and agitated on a mechanical shaker for 24 h. The tube was then opened, the contents transferred to a 25 ml round-bottomed flask and evaporated to dryness under reduced pressure. The residue was recrystallized from dichloromethane–hexane.

Procedure B: The appropriate fluorinated alkyl iodide (1 ml) was added to an acetone solution (10 ml) of *trans*-$RhXCO(PMe_2Ph)_2$, X = Cl or Br (0.15 g) in a nitrogen filled Schlenk tube and the mixture stirred at room temperature for 24 h. The solution was evaporated to dryness under reduced pressure and the residue recrystallized from dichloromethane–hexane. In the case of $RhBrI(C_3F_7CH_2)CO(PMe_2Ph)_2$ the compound could not be recrystallized. Samples evaporated to dryness always contained traces of acetone. However, ^{19}F nmr and infrared spectra indicated that reaction had occurred.

Procedure C: Trifluoromethyl iodide (2.6 mmol) was condensed on to an acetone solution (5 ml) of *trans*-$RhClCO(PMePh_2)_2$ (0.15 g, 0.26 mmol) in a 20 ml Carius tube. The tube was sealed and allowed to warm to room temperature. After it had been shaken for 7 days, the tube was opened, the orange solution was transferred to a 25 ml round-bottomed flask and evaporated to dryness. The residue was recrystallized from dichloromethane–hexane to give orange crystals of carbonylchlorobis(methyldiphenylphosphine)iodotrifluoromethylrhodium.

Procedure D: To a solution of $RhClI(CF_3)CO(PMe_2Ph)_2$ (0.22 g, 0.34 mmol) in acetone (10 ml) was added $AgPF_6$ (0.087 g, 0.34 mmol). Yellow silver iodide was precipitated immediately. After stirring for 15 min the solution was filtered into a nitrogen filled Schlenk tube containing lithium chloride (0.04 g, 0.94 mmol). The yellow solution was stirred for 20 min and evaporated to dryness. The residue was extracted with benzene, filtered, and freeze-dried. Recrystallization from dichloromethane–hexane gave carbonyldichlorobis(dimethylphenylphosphine)trifluoromethylrhodium (0.159 g, 85% yield).

Acknowledgements

The continued financial support of the National Research Council of Canada is gratefully acknowledged and also the award of a NRCC postgraduate scholarship (1971–1973) and a Province of Ontario graduate fellowship (1973–1974) to K.J.R. We thank Heather Schroeder for her perseverance and skill in obtaining the nmr data.

1. L. Vaska. Acc. Chem. Res. **1**, 335 (1968).
2. J. Halpern. Acc. Chem. Res. **3**, 386 (1970).
3. J. P. Collman and W. R. Roper. Adv. Organomet. Chem. **7**, 53 (1968).
4. C. A. Tolman. Chem. Soc. Rev. **1**, 337 (1972).
5. R. B. King and W. C. Zipperer. Inorg. Chem. **11**, 2119 (1972) and references therein.
6. M. Kubota, G. W. Kiefer, R. M. Ishikawa, and K. E. Bencala. Inorg. Chim. Acta, **7**, 195 (1973).
7. P. B. Chock and J. Halpern. J. Am. Chem. Soc. **88**, 3511 (1966).
8. J. S. Bradley, D. E. Connor, D. Dolphin, J. A. Labinger, and J. A. Osborn. J. Am. Chem. Soc. **94**, 4043 (1972).
9. R. G. Pearson and W. R. Muir. J. Am. Chem. Soc. **92**, 5519 (1970).
10. A. V. Kramer and J. A. Osborn. J. Am. Chem. Soc. **96**, 7832 (1974).
11. D. M. Blake, S. Shields, and L. Wyman. Inorg. Chem. **13**, 1595 (1974).
12. E. M. Miller and B. L. Shaw. J. Chem. Soc. Dalton, 480 (1974).
13. D. M. Blake, A. Winkelman, and Y. L. Chung. Inorg. Chem. **14**, 1326 (1975).
14. A. J. Deeming and B. L. Shaw. J. Chem. Soc. A, 597 (1969).
15. R. F. Heck. J. Am. Chem. Soc. **86**, 2796 (1964).
16. J. P. Collman and C. T. Sears Jr. Inorg. Chem. **7**, 27 (1968).
17. H. C. Clark and J. D. Ruddick. Inorg. Chem. **9**, 2556 (1970).
18. B. L. Shaw and A. C. Smithies. J. Chem. Soc. A, 2784 (1968).
19. P. R. Brookes and B. L. Shaw. J. Chem. Soc. A, 1079 (1967).

20. R. K. HARRIS. Can. J. Chem. **42**, 2275 (1964).
21. M. KUBOTA and B. M. LOEFFLER. Inorg. Chem. **11**, 469 (1972).
22. W. J. BLAND and R. D. W. KEMMITT. J. Chem. Soc. A, 2062 (1969).
23. T. G. APPLETON, H. C. CLARK, and L. E. MANZER. Coord. Chem. Rev. **10**, 335 (1973) and references therein.
24. P. M. TREICHEL and F. G. A. STONE. Adv. Organomet. Chem. **1**, 143 (1964).
25. F. A. COTTON and J. A. MCCLEVERTY. J. Organomet. Chem. **4**, 490 (1965).
26. F. A. COTTON and R. M. WING. J. Organomet. Chem. **9**, 511 (1967).
27. R. B. KING and M. B. BISNETTE. J. Organomet. Chem. **2**, 15 (1964).
28. R. B. KING and A. EFRATY. J. Organomet. Chem. **27**, 409 (1971).
29. D. T. ROSEVEAR and F. G. A. STONE. J. Chem. Soc. A, 164 (1968).
30. E. PITCHER and F. G. A. STONE. Spectrochem. Acta, **18**, 585 (1962).
31. M. P. JOHNSON. Inorg. Chim. Acta, **3**, 232 (1969).
32. (*a*) E. PITCHER, A. D. BUCKINGHAM, and F. G. A. STONE. J. Chem. Phys. **36**, 124 (1961); (*b*) M. L. MADDOX, S. L. STAFFORD, and H. D. KAESZ. Adv. Organomet. Chem. **3**, 1 (1965); (*c*) R. G. KIDD. Characterization of organometallic compounds. Part II. *Edited by* M. Tsutsui. Interscience. 1971. p. 374; (*d*) J. W. EMSLEY, J. FEENEY, and L. H. SUTCLIFFE. High resolution nuclear magnetic resonance spectroscopy. Vol. 2. Pergamon. 1966.
33. J. A. MCCLEVERTY and G. WILKINSON. J. Chem. Soc. 4200 (1964).
34. A. J. MUKHEDKAR, V. A. MUKHEDKAR, M. GREEN, and F. G. A. STONE. J. Chem. Soc. A, 3158 (1970).

Can. J. Chem. Downloaded from www.nrcresearchpress.com by 210.87.254.105 on 09/05/12
For personal use only.

Charge distributions and chemical effects. X. Enthalpies of formation of alkanes, a calculation from ^{13}C nuclear magnetic resonance shifts[1]

HERVÉ HENRY AND SÁNDOR FLISZÁR[2]
Département de Chimie, Université de Montréal, Montréal (P.Q.), Canada H3C 3V1

AND

ANDRÉ JULG
Laboratoire de Chimie Théorique, Université de Provence, Centre de St-Charles, Marseille, France

Received January 7, 1975[3]

HERVÉ HENRY, SÁNDOR FLISZÁR, and ANDRÉ JULG. Can. J. Chem. **54**, 2085 (1976).

An analysis of the molecular energy in terms of bond contributions indicates that the latter (ϵ_{ij}) can be approximated by a linear combination of the changes in net charges q_i and q_j. From the equation ΔH(atomization) = $\sum\epsilon_{ij}$, and the relationship between ^{13}C chemical nmr shifts and C net charges, it is then possible to derive a two-parameter equation, $\Delta H_f^0 = \Delta H_f^0(C_2H_6) + \nu(N-2) + \lambda\sum(N_{cc}+1)\delta^{eth}$, which enables the calculation of enthalpies of formation of alkanes C_NH_{2N+2} from ^{13}C nmr shifts (δ^{eth} = shift relative to ethane, N_{cc} = number of CC bonds formed by the C atom whose shift is δ^{eth}).

HERVÉ HENRY, SÁNDOR FLISZÁR et ANDRÉ JULG. Can. J. Chem. **54**, 2085 (1976).

L'analyse de l'énergie moléculaire en termes de contributions de liaisons (ϵ_{ij}) indique que celles-ci sont bien représentées par une combinaison linéaire des variations des charges nettes q_i et q_j. L'équation ΔH(atomisation) = $\sum\epsilon_{ij}$ et la relation entre les déplacements chimiques du ^{13}C et les charges nettes des atomes de C conduisent ainsi à une équation à deux paramètres, $\Delta H_f^0 = \Delta H_f^0(C_2H_6) + \nu(N-2) + \lambda\sum(N_{cc}+1)\delta^{eth}$, permettant le calcul des enthalpies de formation des alcanes C_NH_{2N+2} à partir de leurs spectres rmn pour le ^{13}C (δ^{eth} = déplacement relatif à l'éthane, N_{cc} = nombre d'atomes C reliés à celui auquel δ^{eth} se réfère).

In a first approximation, the heat of formation of saturated molecules can be estimated by additive rules, assuming that the contribution of each bond is the same as for any other molecule containing the same bond. In practice, the situation is somewhat different from this simple additivity scheme. Indeed, various corrections accounting for steric effects were brought in (1), involving extensive empirical parametrizations. The present approach is different, in that steric effects are neglected altogether. Here, changes in bond properties are studied in terms of inductive effects. While each bond is still regarded as a separate unit, the present treatment recognizes that, because of some charge transfer from neighboring bonds, a given bond is not exactly the same in the various environments. Ultimately, the changes in bond properties are evaluated in terms of charges allocated to the bond-forming atoms.

[1]Work extracted from the Ph.D. thesis of H.H.
[2]To whom correspondence to be addressed.
[3]Revision received March 24, 1976.

Molecular Energy in terms of Bond Contributions

Apparently at variance with the classical chemical concept of binding pairs, quantum mechanics yields electron densities which are delocalized over the whole molecule. It is well known, however, that it is possible, by means of an appropriate unitary transformation, to replace the above orbitals by new functions which would largely localize the various electron pairs according to classic schemes (2): core electrons, binding pairs, and lone pairs. The total energy and the electronic charges remain unchanged in this transformation if all the levels are doubly occupied. Such a description, which is that of the classical chemical concepts, is closely related to the concept of hybridization (3). Indeed, since the hybrid atomic orbitals are constructed to point toward each other, they represent an effective basis for constructing localized molecular functions.

In the present approach we postulate (*i*) that the total energy of a molecule can be regarded as the sum of the energies, ϵ_{ij}, assigned to the

Can. J. Chem. Downloaded from www.nrcresearchpress.com by 210.87.254.5 on 09/05/12
For personal use only.

Can. J. Chem. Downloaded from www.nrcresearchpress.com by 210.87.254.5 on 09/05/12
For personal use only.

individual bonds ij, *i.e.*,

$$[1] \qquad E = \sum_{[ij]} \epsilon_{ij}$$

and (*ii*) that the ϵ_{ij} term can be expressed by some function, ϵ_{ij} (Q_i,Q_j), of the total populations Q_i and Q_j of atoms i and j.

Provided that for a given bond the variations in Q_i and Q_j due to changes in molecular environment are small, we obtain from a Taylor series limited to the first order that

$$[2a] \qquad \epsilon_{ij} = \epsilon_{ij}^{0} + \Delta Q_i\left(\frac{\partial \epsilon_{ij}}{\partial Q_i}\right)_{Q_i^0,Q_j^0} + \Delta Q_j\left(\frac{\partial \epsilon_{ij}}{\partial Q_j}\right)_{Q_i^0,Q_j^0}$$

i.e., in terms of net charges q_i and q_j, where $\Delta q = -\Delta Q$,

$$[2b] \qquad \epsilon_{ij} = \epsilon_{ij}^{0} - \Delta q_i\left(\frac{\partial \epsilon_{ij}}{\partial Q_i}\right)_0 - \Delta q_j\left(\frac{\partial \epsilon_{ij}}{\partial Q_j}\right)_0$$

Following this argument, we write for the C—C bonds

$$[3] \qquad \epsilon_{CC} = \epsilon_{CC}^{0} + a(\Delta q_{C_i} + \Delta q_{C_j})$$

where, if the C—C bond of ethane is chosen as a reference (ϵ_{CC}^{0}), the Δq_C's are simply $q_C - 1$, because of the choice made earlier (4) for defining charges on a scale of relative units with respect to $q_C^{0} = q_C(\text{ethane}) = 1$. Similarly, with reference to ϵ_{CH}^{0} for the ethane C—H bond, our approximation yields

$$[4] \qquad \epsilon_{CH} = \epsilon_{CH}^{0} + b\Delta q_C + c\Delta q_H$$

remembering that $q_H^{0} = q_H(\text{ethane}) = -1/3$ (relative units) (4).

Net Atomic Charges q

The charge distributions which shall be used are those derived from the theory (4) which is explicitly based on the inductive effects of the alkyl groups. These 'inductive' net charges were shown to be in good agreement with quantum mechanical results from semi-empirical and partially or non-optimized *ab initio* methods and are virtually identical to fully optimized *ab initio* (STO-3G) charges. On a scale of relative units defined by $q_C(\text{ethane}) = 1$ (arbitrary unit), the various C and H charges are functions of a parameter, n, whose value is critical in any comparison of a property with C net charges (4, 5). The charge distributions in alkanes reflecting the 'most even electron distribution', *i.e.*, a situation where the various C charges are as similar as possible among themselves, correspond to $n \simeq -4.4$ (5). 'Experimental' determinations of the inductive parameter n indicated $n = -4.4083$ from adiabatic ionisation potentials (6), and $n = -4.4122$ from ^{13}C chemical shifts (5, 7).[4] The latter are correlated to the C net charges, in relative units, by eq. 5.

$$[5] \qquad \delta_C = -237.1q_C + 242.64 \text{ (from TMS)}$$

Whenever the 'inductive' charges were known from the 'inductive theory' and/or from optimized *ab initio* calculations, eq. 5 appeared to be in excellent agreement with experimental δ_C results. Indeed, the standard deviation (0.3 ppm) is small in comparison with the error (~2.4 ppm) in δ_C, which would correspond to a 1% error in the estimate of q_C. On these grounds, eq. 5 can now be used to calculate C net charges (relative to $q_C = 1$ for ethane) when these are not known from previous work. In fact, it turns out to be more practical to rewrite eq. 5 as follows:

$$[6] \qquad \delta_C(\text{ppm from ethane}) = -237.1(q_C - 1)$$

Expressions for ΔH(atomization) and ΔH(formation)

Adopting the simplest possible scheme, we can write, conforming to common use,[5]

$$[7] \qquad \Delta H(\text{atomization}) = \Delta H_a = \sum \epsilon_{ij}$$

Such a bond energy scheme has been studied earlier by Laidler and co-worker (9) who considered that the energy terms of primary, secondary, and tertiary C—H bonds are not identical, whereas the C—C terms were presumed constant. Tatevskii's modification (10) is based on the assumption that not only should the C—H bonds in paraffins be classified according to their immediate environment, but that the C—C bonds should be similarly classified. In the present work, the fine-tuning of the individual ϵ_{ij} contributions is provided by their charge-dependence

[4]These results support the hypothesis made in writing eq. 2*a* and 2*b*, *i.e.*, that the charges experience only small variations due to changes in molecular environment.

[5]For a detailed discussion, see review article ref. 8.

Can. J. Chem. Downloaded from www.nrcresearchpress.com by 210.87.254.5 on 09/05/12
For personal use only.

(eqs. 3 and 4). Their summation[6] (eq. 7) for paraffins C_NH_{2N+2} gives eq. 8, where N_{CC} = the number of C—C bonds formed by the C atom to which Δq_C refers.

$$[8]\quad \Delta H_a = 2\epsilon_{CH}^0 - \epsilon_{CC}^0 + 2c/3 + (\epsilon_{CC}^0 + 2\epsilon_{CH}^0 - c/3)N + (a-b)\sum N_{CC}\Delta q_C + (4b-c)\sum \Delta q_C$$

By means of the relation $\Delta H_f^0 = N\Delta H_f^0(C) + (2N + 2)\Delta H_f^0(H) - \Delta H_a$, and of eq. 6, it is now easy to derive an expression for the enthalpies of formation, ΔH_f^0, in terms of C chemical shifts.

$$[9]\quad \Delta H_f^0 = \epsilon' + \nu N + \lambda_1\sum N_{CC}\delta^{eth} + \lambda_2\sum\delta^{eth}$$

where $\epsilon' = 2\Delta H_f^0(H) - 2\epsilon_{CH}^0 + \epsilon_{CC}^0 - 2c/3$, $\nu = 2\Delta H_f^0(H) + \Delta H_f^0(C) - \epsilon_{CC}^0 - 2\epsilon_{CH}^0 + c/3$, $\lambda_1 = (a - b)/237.1$, and $\lambda_2 = (4b - c)/237.1$. Inserting $\delta^{eth} = 0$ in eq. 9 it is seen that $\epsilon' + 2\nu = \Delta H_f^0(C_2H_6)$, *i.e.*

$$[10]\quad \Delta H_f^0 = \Delta H_f^0(C_2H_6) + \nu(N - 2) + \lambda_1\sum N_{CC}\delta^{eth} + \lambda_2\sum\delta^{eth}$$

A comparison of eq. 10 with experimental enthalpies of formation (Table 1) indicated that $\lambda_1 \simeq \lambda_2$. Equation 10 can, therefore, be written as follows, without any significant loss in precision

$$[11]\quad \Delta H_f^0 = \Delta H_f^0(C_2H_6) + \nu(N - 2) + \lambda\sum(N_{CC} + 1)\delta^{eth}$$

The results presented in Table 1 were calculated using[7] $\Delta H_f^0(C_2H_6) = -20.14$, $\nu = -1.651$, and $\lambda = -0.04657$ (kcal/mol). The chemical shifts relative to ethane, δ^{eth}, were calculated from the nmr results extracted from refs. 13 and 14.

[6]For paraffins C_NH_{2N+2}, in which the number of C—C bonds is $N - 1$, their contribution is $\sum\epsilon_{CC} = (N - 1)\epsilon_{CC}^0 + a\sum N_{CC}\Delta q_C$. Similarly, remembering that the number of C—H bonds is $2N + 2$, their contribution is $\sum\epsilon_{CH} = (2N + 2)\epsilon_{CH}^0 + b\sum N_H\Delta q_C + c\sum\Delta q_H$, where N_H = the number of H atoms bonded to the C atom of which Δq_C is computed, *i.e.*, $N_H = 4 - N_{CC}$. Finally, observing that $\sum\Delta q_H = \sum q_H - (2N + 2)q_H^0 = -\sum q_C + (2N + 2)/3$, the summation over all the ϵ_{ij} terms yields eq. 8.

[7]This value was selected considering the experimental ones -20.04 ± 0.07 (11) and -20.24 ± 0.12 (12) kcal/mol (gas, at 25 °C).

TABLE 1. Comparison of experimental and calculated heats of formation (kcal/mol), using eq. 11*

Compound	$-\Delta H_f^0$ (exp) (25 °C)	Deviation ΔH_f^0(calc) − ΔH_f^0(exp)
C_1	17.89	−0.22
C_2	20.14	0.00
C_3	24.82	−0.20
C_4	30.15	0.01
2-MeC_3	32.15	−0.05
C_5	35.00	−0.20
2-MeC_4	36.92	0.22
2,2-Me_2C_3	40.27	0.52
C_6	39.96	−0.31
2-MeC_5	41.66	−0.13
3-MeC_5	41.02	−0.19
2,3-Me_2C_4	42.49	0.25
C_7	44.89	−0.14
2-MeC_6	46.60	−0.04
3-MeC_6	45.96	−0.05
3-EtC_5	45.34	0.77
2,2-Me_2C_5	49.29	0.21
2,3-Me_2C_5	46.65	0.29
2,4-Me_2C_5	48.30	0.25
2,2,3-Me_3C_4	48.96	0.27
C_8	49.82	−0.24
2-MeC_7	51.50	−0.19
3-MeC_7	50.82	−0.46
4-MeC_7	50.69	−0.43
3-EtC_6	50.40	0.66
2,2-Me_2C_6	53.71	0.01
2,3-Me_2C_6	51.13	−0.40
2,4-Me_2C_6	52.44	0.02
2,5-Me_2C_6	53.21	−0.02
3,3-Me_2C_6	52.61	0.51
3,4-Me_2C_6	50.91	−0.03
2-Me-3-EtC_5	50.48	0.14
2,2,3-Me_3C_5	52.61	−0.96
2,3,3-Me_3C_5	51.73	0.25
2,3,4-Me_3C_5	51.97	0.10
2,2,3,3-Me_4C	53.99	−0.61
C_9	54.74	−0.29
4-MeC_8	56.19	0.14
2,2-Me_2C_7	58.83	0.12
2,2,5-Me_3C_6	60.53	0.33
2,3,3-Me_3C_6	57.31	0.32
2,3,5-Me_3C_6	57.97	0.27
2,2,3,3-Me_4C_5	57.07	−0.67
2,3,3,4-Me_4C_5	56.68	0.28

*Except as noted below, experimental data are from ref. 17. The value selected for ethane is discussed in footnote 7. For neopentane, the value is that of ref. 15. For 2,3-Me_2C_5, the value given in API Table 3p is based on the work of Prosen and Rossini (18). According to these authors the sample of 2,3-Me_2C_5 available to them was impure. Following Somayajulu and Zwolinski (1*d*), we chose Jessup's value quoted by Prosen and Rossini. The values for the C-9 alkanes are extracted from ref. 1*d*.

Discussion

The multiple correlation coefficient (0.99937) and the mean deviation (± 0.27 kcal/mol) are satisfactory considering the simplicity of eq. 11

Can. J. Chem. Downloaded from www.nrcresearchpress.com by 210.87.254.5 on 09/05/12
For personal use only.

which, admittedly, represents the crudest possible approach in terms of charges. There are, however, several compounds (not listed in Table 1) for which the disagreement between calculated and experimental enthalpies of formation is quite marked: $EtCMe_3$ (exp. −44.35, deviation = 0.91), Et_2CMe_2 (−48.17, 1.94), Et_3CMe (−51.38, 2.20), and 2,2,4-Me_3C_5 (−53.57, −2.74). Interestingly, these molecules, as well as 2,2,3-Me_3C_5, also give unusually large deviations in Allen's calculations (1*b*) and both Allen's and our calculated deviations are in the same direction. While it is possible that these deviations point at the necessity for a more sophisticated treatment, it should also be considered that any attempt directed toward better numerical fits should be preceded by an examination of the experimental data.[8] In addition, possible errors in calibration of the nmr results should also be examined.[9]

Considering the results given in Table 1, we may thus regard that, at this stage, any further numerical improvement is illusory. Indeed, if quadratic terms of charges in the ϵ_{ij} contributions (or specific steric effects) which were hitherto neglected, were to be taken into consideration, the accompanying proliferation of parameters would certainly help in reducing the deviations without adding, however, anything substantial to the understanding of the basic phenomena involved. Present results support (despite its crudeness) our analysis of the molecular energy in terms of bond contributions, and the view that the latter can be adequately approximated by a linear combination of the variations in net charges, Δq_i and Δq_j, of the bond-forming atoms.

Acknowledgment

The financial aid given by the National Research Council of Canada is gratefully acknowledged.

[8]For example, combustion calorimetry has recently led to a revised value for the heat of formation of neopentane (15), *i.e.*, −40.27 kcal/mol, formerly −39.67 kcal/mol (16).

[9]An error in calibration, $\Delta\delta$, leads to an error of $\lambda(3N - 2)\Delta\delta$ in ΔH_f^0, *i.e.*, ~0.2 kcal/mol for $\Delta\delta = 0.2$ ppm for a C_8 alkane.

1. (*a*) T. L. Allen. J. Chem. Phys. **31**, 1039 (1959); (*b*) A. J. Kalb, A. L. H. Chung, and T. L. Allen. J. Am. Chem. Soc. **88**, 2938 (1966); (*c*) G. R. Somayajulu and B. J. Zwolinski. Trans. Faraday Soc. **62**, 2327 (1966); (*d*) G. R. Somayajulu and B. J. Zwolinski. J. Chem. Soc. Faraday II, **68**, 1971 (1972); **70**, 967 (1974); (*e*) J. B. Greenshields and F. D. Rossini. J. Phys. Chem. **62**, 271 (1958).
2. K. Rüdenberg. *In* Modern quantum chemistry (Istambul lectures), Part I. *Edited by* O. Sinanoğlu. Academic Press, N.Y. 1965.
3. J. H. Van Vleck and A. Sherman. Rev. Modern Phys. **7**, 174 (1935).
4. S. Fliszár, G. Kean, and R. Macaulay. J. Am. Chem. Soc. **96**, 4353 (1974).
5. S. Fliszár, A. Goursot, and H. Dugas. J. Am. Chem. Soc. **96**, 4358 (1974).
6. H. Henry and S. Fliszár. Can. J. Chem. **52**, 3799 (1974).
7. R. Roberge and S. Fliszár. Can. J. Chem. **53**, 2400 (1975).
8. H. A. Skinner and G. Pilcher. Quart. Rev. **17**, 264 (1963).
9. K. J. Laidler. Can. J. Chem. **34**, 626 (1956); E. G. Lovering and K. J. Laidler. Can. J. Chem. **38**, 2367 (1960).
10. V. M. Tatevskii, V. A. Benderskii, and S. S. Yarovoi. Rules and methods for calculating the physico-chemical properties of paraffinic hydrocarbons. *Translation editor* B. P. Mullins. Pergamon Press, Oxford. 1961.
11. D. A. Pittam and G. Pilcher. J. Chem. Soc. Faraday I, **68**, 2224 (1972).
12. E. J. Prosen, F. W. Maron, and F. D. Rossini. J. Res. Nat. Bur. Stand. **46**, 106 (1951).
13. D. M. Grant and E. G. Paul. J. Am. Chem. Soc. **86**, 2984 (1964).
14. L. P. Lindeman and J. A. Adams. Anal. Chem. **43**, 1245 (1971).
15. G. Pilcher and J. D. M. Chadwick. Trans. Faraday Soc. **63**, 2357 (1967).
16. Selected Values of Properties of Hydrocarbons and Related Compounds, American Petroleum Institute Research Project **44**, Thermodynamics Research Centre, Department of Chemistry, Texas A and M University, College Station, Texas.
17. F. D. Rossini, K. S. Pitzer, R. L. Arnett, R. M Braun, and G. C. Pimentel. Selected values of physical and thermodynamic Properties of Hydrocarbons and related compounds. Carnegie Press, Pittsburgh, Pa., 1952.
18. E. J. R. Prosen and F. D. Rossini. J. Res. Nat. Bur. Stand. **27**, 519 (1941).

Reactions of oxygen and sulphur anions with oxazolidine and thiazolidine derivatives of 2-mesyloxymethylglyceraldehyde acetonide

GEORGE JUST, BONG YOUNG CHUNG,[1] SUNGGAK KIM,[2] GERALD ROSEBERY,[3] AND PHILLIP ROSSY
Department of Chemistry, McGill University, Montreal, Que., Canada H3C 3G1

Received February 9, 1976

GEORGE JUST, BONG YOUNG CHUNG, SUNGGAK KIM, GERALD ROSEBERY, and PHILLIP ROSSY. Can. J. Chem. **54**, 2089 (1976).

Reactions of the oxazolidine (**2**) and thiazolidine (**3**) derivatives of 2-mesyloxymethylglyceraldehyde acetonide with oxygen and sulphur anions are described. Whereas oxazolidine formation does not protect the aldehyde function against nucleophilic attack, the thiazolidine group is completely inert to these nucleophiles.

GEORGE JUST, BONG YOUNG CHUNG, SUNGGAK KIM, GERALD ROSEBERY et PHILLIP ROSSY. Can. J. Chem. **54**, 2089 (1976).

La réaction des derivés oxazolidine (**2**) et thiazolidine (**3**) de l'acétonide du mésyloxyméthyle-2 glycéraldéhyde avec des anions oxygène et soufre est descrite. Tandis que la formation d'un dérivé oxazolidine ne protège pas la fonction aldéhyde contre une attaque nucléophile, le groupe thiazolidine est inerte à ces nucléophiles.

Can. J. Chem. Downloaded from www.nrcresearchpress.com by 210.87.254.5 on 09/05/12
For personal use only.

In connection with a synthesis of cephalosporin and oxacephalosporin derivatives, we studied the condensation of aldehyde **1** or of a suitably blocked derivative **2** or **3** (1, 2) with sulphur and oxygen anions **6***a*, **9***a*, and **12***a* in the hope of obtaining the product of displacement of the mesylate by these anions.

Direct displacement of the mesylate function in aldehyde **1** by thiolate **9***a* did not proceed in the desired manner. Since conventional protecting groups such as the methyl acetals could not be removed without the destruction of the molecule formed, we studied the potential usefulness of the oxazolidine and thiazolidine protecting groups.

The formation of the latter has been described by Bergmann and Kaluszyner (3), and it has been used as an aldehyde producing group by Meyers *et al.* (4), but to our knowledge it has never been used as an aldehyde protecting group.

The reaction of oxazolidine mesylate **2** with potassium thioacetate in acetone gave the anticipated displacement product **4** in 96% yield (1).

We next set out to apply this reaction to mesylate **2** and thiomethyleneoxazolone (**6**).

Thiomethyleneoxazolone **9** was prepared in 10% yield by treating a pyridine solution of ethoxymethyleneoxazolone **5** (5*b*) with hydrogen sulfide for 24 h. It was then discovered that if the ethoxymethyleneoxazolone **5** was treated with 1 equiv. of sodium hydrosulfide in methanol for 3 min at 0 °C and the reaction mixture poured into hot dioxane, the sodium thiolate **6***a* separated as yellow starlike crystals on cooling in 85% yield. The free thiol **6**, prepared from **6***a* by precipitation from an aqueous solution with acetic acid, proved to be different from **9**. The structures of **6** and **9** were assigned, based mainly on their infrared (ir) spectra, which showed for **6** the anhydride doublet at 1805 and 1795 cm^{-1}, and a hydrogen-bonded C=N band at 1660 cm^{-1}, whereas **9** showed the hydrogen-bonded anhydride doublet at 1760 and 1710 cm^{-1} and the C=N band as a shoulder at 1690 cm^{-1}.

Condensation of **6***a* with mesylate **2** in butanone, followed by filtration through alumina, gave **7**, mp 127 °C, in 50–55% yield. The relatively low yield may be attributed to a competing reaction of the thiolate anion on the labile oxazolidine group. Hydrolysis of **7** with 50% aqueous acetic acid gave **8**, mp 80–81 °C, in 80% yield. Analogous results were obtained when thiolate **9***a* was reacted with mesylate **2**, giving, after hydrolysis, **9**, mp 83–85 °C.

We next turned to the study of the reaction of mesylate **2** with the sodium and thallium salts of the readily available methyl 2-phthalimido-3-hydroxyacrylate **12** (6).

[1]Holder of a National Research Council of Canada Scholarship, 1974–1975.

[2]Holder of a McConnell Fellowship, 1974–1976.

[3]Holder of a National Research Council of Canada Scholarship, 1970–1973.

Can. J. Chem. Downloaded from www.nrcresearchpress.com by 210.87.254.5 on 09/05/12
For personal use only.

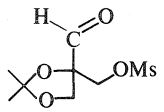

1

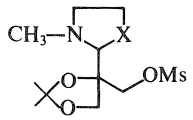

2 X = O
3 X = S

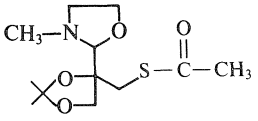

4

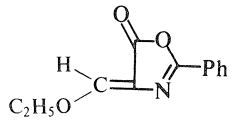

5

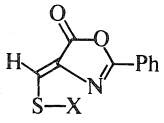

6 X = H
6*a* X = Na

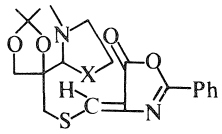

7 X = O
7*a* X = S

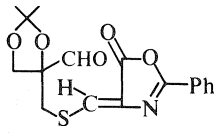

8

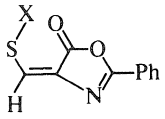

9 X = H
9*a* X = Na

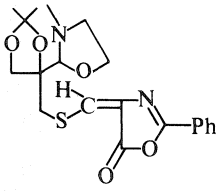

10

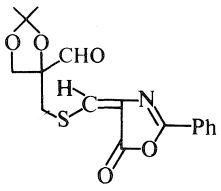

11

Condensation of the sodium or thallium salt of **12** with oxazolidine mesylate **2** gave a mixture of the crystalline perhydrooxazepine derivative **14** and of the desired product **13**.

There are two possible structures, **14** and **15**, for the perhydrooxazepine derivative. Since it is known (7) that oxazolidines containing a secondary amine function exist in part as the tautomeric Schiff base, it could be assumed that oxazolidine mesylate **2** may exist to a small extent as the immonium ion. Reaction of the immonium ion with the nucleophile **12***a* may then give an intermediate, which may be expected to cyclize to give **15**. However, the nmr data of the isomeric product did not fit this structure, but that of the perhydrooxazepine derivative **14**. One would also anticipate that **15** would not be stable to 50% aqueous acetic acid, but the product was stable to these reaction conditions. The product was perhaps formed by attack of the tertiary amine on the mesylate, followed by ring opening by the anion, although other reaction paths cannot be excluded.

Since the oxazolidine protecting group was not stable to nucleophilic attack, it was decided to use a thiazolidine protecting group.

Treatment of the thiazolidine mesylate **3** (2) with 1.3 equiv. of the thallium salt of the methyl ester **12** in refluxing butanone gave a quantitative yield of the thiazolidine methyl ester **16** as an amorphous solid.

Hydrolysis of the thiazolidine function of the thiazolidine methyl ester **16** to the corresponding aldehyde methyl ester **17** was carried out by treatment of **16** with mercuric chloride (4) in a mixture of tetrahydrofuran and water (5:1), giving a crystalline aldehyde methyl ester **17** in 95% yield. Hydrolysis of the oxazolidine methyl ester **13** with 50% aqueous acetic acid also gave a quantitative yield of the aldehyde **17** as a crystalline compound. Similar condensation re-

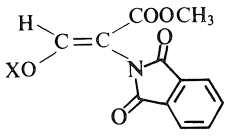

12 X = H
12*a* X = Tl

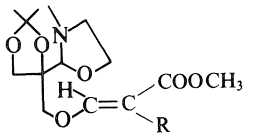

13

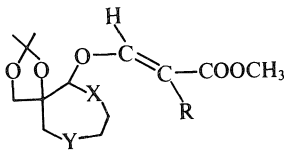

14 X = O, Y = N—CH$_3$
15 X = NCH$_3$, Y = O

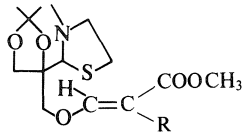

16

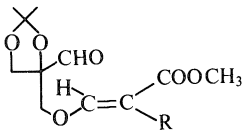

17

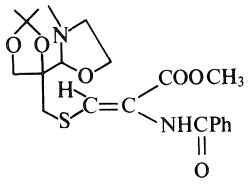

18

R = phthalimido

Can. J. Chem. Downloaded from www.nrcresearchpress.com by 210.87.254.5 on 09/05/12
For personal use only.

actions could be carried out with salts of the analogous benzyl and trichloroethyl esters.

The chemical shift of the vinyl proton in **17** and **18** (8) ranges from 7.3 to 7.6 ppm, and opening of the oxazolidine ring deshields the vinyl proton slightly. In its geometric isomers **10**, the corresponding vinyl proton is found at 8.3 ppm. Since substitution of the sulphur atom on the vinyl group by oxygen should deshield the vinyl proton, and since that vinyl proton appears in **13** at 7.8 ppm., we think that the geometry of **13** is as depicted.

The yield of formation of thiomethylene-oxazolone **8** could be considerably improved when the thiazolidine protecting group was used. Condensation of thiazolidine mesylate **3** with thiolate anion **6***a* gave **7***a* as a mixture of epimers at C-1 in over 85% yield. Hydrolysis of the thiazolidine group at room temperature for 1–2 h with mercuric chloride in aqueous acetonitrile gave aldehyde **8** in 85% yield.

Experimental

Melting points were determined on a Gallenkamp block and are uncorrected. Mass spectra were obtained on an AEI-MS-902 mass spectrometer at 70 eV using a direct insertion probe. Nuclear magnetic resonance spectra were recorded on a Varian T-60 spectrometer using tetramethylsilane as an internal standard. Infrared spectra were obtained on a Unicam SP-1000 ir spectrophotometer. Ultraviolet spectra were recorded using a Unicam SP-800 spectrophotometer. Microanalyses were carried out by C. Daessle, Montreal.

2-Phenyl-4-thiomethylene-5-oxazolone Sodium Salt (6a)

To a stirred ice-cooled suspension of 5 g of 2-phenyl-4-ethoxymethylene-5-oxazolone (**5**) in 10 ml of methanol was added 1.3 g (1 equiv.) of sodium hydrosulfide. The solution was stirred for 3 min at 0 °C and then poured into 80 ml of dioxane heated to 70 °C. The clear red solution was cooled in an ice bath until precipitation of the bright yellow sodium thiol was complete (about 1 h). The product was removed by filtration, washed with ether, and dried *in vacuo*, giving 4.9 g (95%) of **6***a*, mp 245 ~ 247 °C (dec.); δ (D_2O) 7.35–8.1 (m, 5H, aromatic), 9.14 ppm (s, 1H, C═CH). *Anal.* calcd. for $C_{10}H_6NO_2SNa$: C 52.86, H 2.64, N 6.16; found: C 52.41, H 2.83, N 6.32.

2-Phenyl-4-thiomethylene-5-oxazolone (6) from 6a

Sodium thiolate **6***a* (1.0 g) was dissolved in 10 ml of water and 2 ml of glacial acetic acid was added. The product precipitated and was removed by filtration, washed well with water, and dried *in vacuo*, giving 0.9 g of **6**, mp 180–181 °C; λ_{max} (EtOH) 405 nm (ϵ 22 300); *m/e* 205 (M^+); ir ($CHCl_3$) 2460 (SH), 1805/1795 (C═O), 1660 cm^{-1} (C═N); δ ($CDCl_3$) 7.3 (s, 1H, C═CH), 7.3 ~ 8.2 (m, 5H, aromatic), 11.8 ppm (br s, 1H, SH).

2-Phenyl-4-thiomethylene-5-oxazolone 9

Hydrogen sulfide was passed for 10 min through a solution of 5 g of **5** in 25 ml of dry pyridine at 0 °C in a pressure bottle, which was then sealed and kept at room temperature for 24 h. The mixture was poured with vigorous stirring into ice-cold dilute hydrochloric acid and filtered immediately; giving 0.47 g (10%) of **9**, mp 176 °C (lit. (5*a*) mp 175–176 °C); ir ($CHCl_3$), 2480 (SH), 1760/1710 (C═O), 1690 cm^{-1} (C═N); δ ($CDCl_3$) 7.3–8.2 (m, 5H, phenyl), 8.25 (s, 1H, C═CH), 11.9 ppm (br s, 1H, SH).

2-Phenyl-4-thiomethylene-5-oxazolone Sodium Salt (9a)

To a solution of 200 mg of the thiol **9** in 2 ml of absolute ethanol was added a solution of 22.5 mg (1 equiv.) of sodium in 2 ml of absolute ethanol. The mixture was dripped slowly into 50 ml of ice-cold vigorously stirred ether. The sodium salt precipitated, was removed by vacuum filtration, washed with ether, and dried *in vacuo*, giving 190 mg (80%) of **9***a*; δ (D_2O) 7.4–8.2 (m, 5H, aromatic), 9.30 ppm (s, 1H, C═CH).

Oxazolidine Oxazolone 7

A solution of 1.2 g of oxazolidine mesylate **2** in 30 ml of dry 2-butanone and 1.2 g (1.3 equiv.) of sodium thiolate **6***a* was refluxed for 1.5 h. After filtration and evaporation, the residue was filtered on 10 g of neutral alumina (Woelm, activity I). Elution with 50 ml of chloroform–ether (1:1) gave a pale orange residue which was taken up in 4 ml of ether and cooled at −20 °C until crystallization was complete. Filtration and washing with 5 ml of cold ether gave 0.82 g (50%) of **7**, mp 127 °C, λ_{max} (MeOH) 361 nm (ϵ 45 600); *m/e* 404 (M^+); ir (KBr) 1780 (C═O), 1633 cm^{-1} (C═N); δ ($CDCl_3$) 1.4 (s, 6H), 2.5 (s, 3H, N—CH_3), 2.4–2.8 (m, 1H), 3.0–4.0 (m, 7H), 4.1 (s, 1H, N—CH—O), 7.3–8.3 ppm (m, 6, C═CH and phenyl). *Anal.* calcd. for $C_{20}H_{24}N_2O_5S$: C 59.41, H 5.94, N 6.93, S 7.92; found: C 59.21, H 5.88, N 7.18, S 7.89.

Aldehyde 8 from Oxazolidine 7

A solution of 0.9 g of oxazolidine **7** in 10 ml of 50% aqueous acetic acid was allowed to stand at room temperature for 1 h and diluted with 40 ml of water. Chloroform extraction and crystallization from 5 ml of ethyl ether gave 0.62 g (80%) of aldehyde **8**, mp 80–81 °C; λ_{max} (MeOH) 361 nm (ϵ 42 800); *m/e* 347 (M^+); ir (KBr) 1780 (C═O), 1740 (H—C═O), 1630 cm^{-1} (C═N); δ ($CDCl_3$) 1.5 (2s, 3H each), 3.5 (s, 2H, CH_2—S), 4.2 (ABq, 2H, J = 10 Hz, —O—CH_2—C—O), 7.2–8.2 (m, 6, phenyl and C═CH), 8.9 ppm (s, 1H, H—C═O). *Anal.* calcd. for $C_{17}H_{17}NO_5S$: C 58.79, H 4.93, N 4.03, S 9.23; found: C 57.03, H 4.82, N 4.23, S 9.25.

Aldehyde-oxazolone 11

This compound was prepared in 35% yield, based on **2**, in the same way as **8**, but using **9***a* instead of **6***a* (see preparation of **7** and **8**); mp 83–85 °C; ir (KBr) 1765/1760 (C═O), 1730 (H—C═O), 1640 cm^{-1} (C═N); δ ($CDCl_3$) 1.55 (2s, 3H each), 4.25 (ABq, 2H, J = 10 Hz, —O—CH_2—C), 4.65 (s, 2H, H_2C—S), 7.3–8.2 (m, 5H, phenyl) 8.25 (s, 1H, C═CH), 9.9 ppm (s, 1H, H—C═O).

Methyl 2-Phthalimido-3-hydroxyacrylate Thallium Salt 7a

Methyl 2-phthalimido-3-hydroxyacrylate **12** (6) (2.47 g) was dissolved in hot benzene (50 ml) and thallium

ethoxide (2.74 g, Aldrich, 98%) was added. The pale yellow powder which settled down immediately was collected by filtration and recrystallized from ethanol, giving a quantitative yield of **12***a*, mp 245–247 °C (dec.); ir (KBr) 3600–3300 (salt), 1800/1730 (phthalimido), 1720 (ester), 1670 cm^{-1} (C═C); δ (DMSO-d_6) 3.6 (s, 3H, CH_3), 7.9 (s, 4H, phthalimido), 8.98 ppm (s, 1H, C═CH). *Anal.* calcd. for $C_{12}H_8NO_5Tl$: C 32.03, H 2.04, N 3.11; found: C 31.76, H 2.01, N 3.23.

Oxazolidine Methyl Ester ***13***

The thallium salt **12***a* (3.375 g) was suspended in a solution of the oxazolidine mesylate **2** (1.475 g) in dry 2-butanone (50 ml). The mixture was refluxed for 6 h, allowed to cool, and filtered. The yellow filtrate was concentrated under reduced pressure. The resulting foamy solid showed two spots in tlc. This crude product was passed through an alumina column using methylene chloride – ethyl ether (5:1) as eluent. A total of 100 ml of the eluent was collected and evaporated *in vacuo*. The white foamy solid was dissolved in ethyl ether (5 ml) and kept overnight in the refrigerator. The crystalline compound **14** was filtered off and the filtrate was evaporated, giving 1.0 g (45%) of **13**, mp 43–45 °C; ir ($CHCl_3$) 1800/1740 (phthalimido), 1735 (ester), 1670 cm^{-1} (C═C), *m/e* 446 (M^+); δ ($CDCl_3$) 1.27, 1.38 (3H each, s, acetonide), 2.45, 2.50 (2 s, 3H, N—CH_3), 2.4–2.7 and 3.0–3.3 (m, 2H, N—CH_2—CH_2—O), 3.72 (s, 3H, O—CH_3), 3.6–4.02 (m, 2H, N—CH_2—CH_2—O), 3.91 (s, 1H, N—CH—O), 4.0 (s, 2H, O—CH_2), 4.22 (q, 2H, OCH_2), 7.68–8.0 ppm (m, 5H, phthalimido and C═CH). *Anal.* calcd. for $C_{22}H_{26}N_2O_8$: C 59.18, H 5.87, N 6.28; found: C 58.93, H 6.04, N 6.42.

Perhydrooxazepine Derivative ***14***

This crystalline compound was separated by the method mentioned above, giving a 46% yield of **14**, mp 173–174 °C; ir (KBr) 1800/1740 (phthalimido), 1725 (ester), 1670 cm^{-1} (C═C); *m/e* 446 (M^+); δ ($CDCl_3$) 1.15, 1.25 (each s, 6H, acetonide), 2.34 (s, 3H, N—CH_3), 2.4–2.7 (m, 4H, CH_2—N—CH_2), 3.73 (s, 3H, OCH_3), 3.7–4.14 (m, 4H, OCH_2), 5.13 (s, 1H, O—CH—O), 7.63–7.94 (m, 4H, phthalimido) 7.92 ppm (s, 1H, C═CH). *Anal.* calcd. for $C_{22}H_{26}N_2O_8$: C 59.18, H 5.87, N 6.28; found: C 58.89, H 6.01, N 6.54.

Thiazolidine Methyl Ester ***16***

The thallium salt **12***a* (10 g) was suspended in a solution of the thiazolidine mesylate **3** (6.22 g) in dry 2-butanone (100 ml). The mixture was refluxed for 6 h, cooled, and filtered. Evaporation of the solvent gave a foam, which was passed through a silica gel column using methylene chloride – ethyl ether (1:1) as an eluent. Evaporation of the solvent gave 9.2 g (100%) of the white foamy **16**, ir ($CHCl_3$) 1800/1735 (phthalimido), 1720 (ester), 1667 cm^{-1} (C═C); *m/e* 462 (M^+); δ ($CDCl_3$) 1.27, 1.37 (each s, 6H, acetonide), 2.28, 2.35 (each s, 3H, N—CH_3), 2.78–3.23 (m, 4H, N—CH_2—CH_2—S), 3.73 (s, 3H, OCH_3), 3.8–4.02 (m, 2H, OCH_2), 4.14–4.33 (m, 3H, OCH_2 and N—CH—S), 7.7–8.02 ppm (m, 5H, phthalimido and C═CH). *Anal.* calcd. for $C_{22}H_{26}N_2O_7S$: C 57.14, H 5.67, N 6.04, S 6.92; found: C 57.38, H 6.02, N 5.89, S 6.62.

Aldehyde Methyl Ester ***17*** *from* ***16***

The thiazolidine methyl ester **16** (4.62 g) was dissolved in tetrahydrofuran–water (4:1) (50 ml) and mercuric chloride (3.0 g = 1.1 equiv.) was added. The immediately formed milky suspension was refluxed for 1 h, cooled, and filtered. The filtrate was concentrated under reduced pressure and the residue extracted three times with benzene. The combined extracts were washed with dilute hydrochloric acid and water, dried over anhydrous sodium sulfate, and filtered. Evaporation of the solvent gave 3.89 g (100%) of the white foamy **17**; ir (KBr) 3500 (hydrate form of aldehyde), 1800/1735 (phthalimido), 1735 (ester), 1720 (aldehyde), 1670 cm^{-1} (C═C); *m/e* 389 (M^+); δ ($CDCl_3$) 1.43 (s, 6H, acetonide), 3.72 (s, 3H, $COOCH_3$), 3.9–4.12 (m, 2H, OCH_2), 4.33 (s, 2H, OCH_2), 7.68–8.0 (m, 4H, phthalimido), 7.9 (s, 1H, C═CH), 9.8 ppm (s, 1H, aldehyde). *Anal.* calcd. for $C_{19}H_{19}NO_8H_2O$: C 56.02, H 5.20, N 3.44; found: C 56.29, H 5.21, N 3.89.

Aldehyde Methyl Ester ***17*** *from* ***13***

The oxazolidine methyl ester **13** (446 mg) was dissolved in 50% aqueous acetic acid (10 ml) and the mixture stirred for 2 h at room temperature. Water (20 ml) was added and the mixture extracted three times with chloroform. The extracts were back-washed twice with water, combined, and dried over anhydrous sodium sulfate. Evaporation of the solvent gave 380 mg (99%) of a white foamy **17**. The nmr, ir, and mass spectral data were the same as those of the product from the thiazolidine ester **17**.

Thiazolidine Oxazolone ***7a***

To a solution of 520 mg of thiazolidine mesylate **3** in 20 ml of dry 2-butanone was added 500 mg (1.3 equiv.) of sodium thiol **6***a*. The mixture was refluxed under nitrogen for 4 h and allowed to cool. After filtration and evaporation, the residue was passed through a column of silica gel (6 g, Woelm Activity III). Elution with 60 ml of chloroform–ether (1:1) gave 620 mg (88%) of **7***a*, λ_{max} (EtOH) 361 nm (ε 44 200); *m/e* 420 (M^+); ir ($CHCl_3$) 1780 (C═O), 1635 (C═N), 1600 cm^{-1}; δ($CDCl_3$) 1.5 (s, 6H) 2.4–2.6 (d, 3H, N—CH_3) 3.0–3.4 (m, 4H, —SCH_2CH_2N), 3.5 ∼ 3.9 (m, 2H, —S—CH_2), 4.0–4.4 (m, 2H, —O—CH_2—C—O), 4.5 ∼ 4.8 (m, 1H, N—CH—S), 7.4 ∼ 8.4 (m, 6H, C═CH and phenyl). *Anal.* calcd. for $C_{20}H_{24}N_2O_4S_2$: C 57.14, H 5.71, N 6.67, S 15.24; found: C 57.20, H 5.63, N 6.46, S 14.78.

Aldehyde ***8*** *from Thiazolidine* ***7a***

A solution of 120 mg of thiazolidine oxazolone **7***a* in 12 ml of acetonitrile–water (5:1) containing 100 mg (1.2 equiv.) of mercuric chloride was stirred at room temperature for 2 h and filtered. Evaporation, ether extraction, and crystallization gave 85 mg of **8** (85%), identical in all respects with **8** prepared from **7**.

Acknowledgement

We wish to thank the National Research Council of Canada for financial support.

Can. J. Chem. Downloaded from www.nrcresearchpress.com by 210.87.254.5 on 09/05/12
For personal use only.

1. G. JUST and P. ROSSY. J. Org. Chem. **38**, 1534 (1973).
2. G. JUST, B. Y. CHUNG, G. ROSEBERY, and M. DUPRÉ. Can. J. Chem. **54**, 1260 (1976).
3. E. D. BERHMANN and A. KALUSZYNER. Recl. Trav. Chim. **28**, 289 (1959).
4. A. I. MEYERS, R. MUNAVU, and J. DURANDETTA. Tetrahedron Lett. 3929 (1972).
5. H. T. CLARKE, J. R. JOHNSON, and R. ROBINSON (*Editors*). The chemistry of penicillin. Princeton University Press. 1949. (*a*) p. 820, (*b*) p. 803.
6. J. C. SHEEHAN and D. A. JOHNSON. J. Am. Chem. Soc. **76**, 158 (1954).
7. E. D. BERGMANN. Chem. Rev. **53**, 309 (1953).
8. G. D. ROSEBERY. Ph.D. Thesis, McGill University, Montreal, Que. 1973.

Can. J. Chem. Downloaded from www.nrcresearchpress.com by 210.87.254.5 on 09/05/12
For personal use only.

Stereoselective epimerization of pilocarpine in aqueous solution as determined by ^{13}C nuclear magnetic resonance spectroscopy

GEORGE A. NEVILLE

Drug Research Laboratories, Health Protection Branch, Health and Welfare Canada, Ottawa, Ont., Canada K1A 0L2

AND

FARIZA B. HASAN AND IAN C. P. SMITH

Division of Biological Sciences, National Research Council of Canada, Ottawa, Ont., Canada K1A 0R6

Received December 22, 1975

GEORGE A. NEVILLE, FARIZA B. HASAN, and IAN C. P. SMITH. Can. J. Chem. **54**, 2094 (1976).

Cleavage and recyclization of the lactone ring of pilocarpine (**1**) and of isopilocarpine (**2**) in D_2O with varying p*D* have been studied by ^{13}C nmr spectroscopy. Alkaline treatment (p*D* 10–13) results in rapid epimerization of pilocarpine to form isopilocarpine (28 ± 3% at 30 °C) and hydrolysis of the parent compound(s) to form the open chain pilocarpinate (isopilocarpinate). By contrast, isopilocarpine does not epimerize to pilocarpine under similar treatment. A mechanism is discussed for the epimerization of pilocarpine and the nonepimerization of the isopilocarpine is rationalized. pK_a values of 5.7 and 8.5, respectively, have been determined for pilocarpinic acid and for the dissociation of the protonated quaternary nitrogen of the imidazole ring of pilocarpine. A basis for assay of degradation products in aqueous pilocarpine solutions utilizing differences in ^{13}C chemical shift for C-8 is discussed.

GEORGE A. NEVILLE, FARIZA B. HASAN et IAN C. P. SMITH. Can. J. Chem. **54**, 2094 (1976).

On a étudié, par spectroscopie rmn du ^{13}C, la coupure et la recyclisation du cycle lactonique de la pilocarpine (**1**) et de l'isopilocarpine (**2**) dans la D_2O à des p*D* variables. Le traitement alcalin (p*D* 10–13) conduit à une épimérisation rapide de la pilocarpine pour former l'isopilocarpine (28 ± 3% à 30 °C) et à l'hydrolyse des composés parents pour former les composés en chaîne ouverte pilocarpinate et isopilocarpinate. Par opposition, l'isopilocarpine ne s'épimérise pas en pilocarpine par un traitement similaire. On discute d'un mécanisme pour l'épimérisation de la pilocarpine; la non-épirémisation de l'isopilocarpine est rationalisée. On a déterminé des valeurs respectives de pK_a de 5.7 et de 8.5 pour l'acide pilocarpinique et pour la dissociation de l'azote quaternaire protoné du cycle imidazole de la pilocarpine. On discute d'une base pour déterminer le pourcentage des produits de dégradation dans des solutions aqueuses de pilocarpine utilisant les différences dans les déplacements chimiques du ^{13}C pour le carbone C-8.

[Traduit par le journal]

Pilocarpine as an ophthalmic solution is valued as a topical miotic in the treatment of glaucoma because it is less irritating than physostigmine salicylate and can be used for extended periods without producing undesirable side effects (1). While acidic aqueous preparations of pilocarpine are relatively stable (2–4), the stability of pilocarpine decreases progressively with increasing p*H* especially at elevated temperatures (2, 3, 5–7) and is affected by phosphate and carbonate buffers (6, 8). The hydrolysis of pilocarpine in aqueous solution has been studied at various p*H* values and temperatures (2, 3, 5–7, 9–11) including a recent kinetic study of the hydrolysis and epimerization of pilocarpine to isopilocarpine (11). The absolute configuration of the two asymmetric centers in the lactone moiety of these two stereoisomers has been established as 2*S*:3*R* for the *cis*-isomer, pilocarpine (**1**) and as 2*R*:3*R* for the *trans*-isomer, isopilocarpine **2** (12).

Degradation of aqueous pilocarpine solutions can occur by hydrolysis to pilocarpinic acid and by epimerization to isopilocarpine. As either degradative pathway results in loss of pharmacological activity, it is important to be able to monitor, physically or chemically, pilocarpine ophthalmic solutions for evidence of such degradation. Unfortunately there has been no simple or adequate method for separating the two diastereoisomers. No method of quantitating either epimer in the presence of the other was available until Nunes and Brochmann-Hanssen (11) showed recently by proton nmr spectroscopy that the methyl proton chemical shifts of the ethyl substituents differed by 0.1 ppm for the two epimers and provided a means of quantitating epimerization by integration of the scale-

Can. J. Chem. Downloaded from www.nrcresearchpress.com by 210.87.254.42 on 09/05/12
For personal use only.

TABLE 1. ^{13}C chemical shifts for pilocarpine and isopilocarpine*

	Pilocarpine			Isopilocarpine		
C†	D_2O	Base	Acid	D_2O	Base	Acid
2	136.38	139.42	136.76	136.54	139.69	136.39
4	117.88	126.80	118.23	118.05	126.73	118.03
5	133.59	132.39	133.86 133.56	133.41	132.69	133.27
6	21.76	24.33	22.14 27.12	26.88	24.17	26.84
7	37.15	42.82 42.57	37.47 38.75	38.63	42.74	38.56
8	72.22	61.33 62.80	72.73 73.51	73.23	63.05	73.21
10	183.06	185.01	183.47	184.50	185.13	183.74
11	45.50	52.95	45.85 47.62	47.49	53.48	47.43
12	18.90	23.46 23.87	19.29 23.01	22.77	23.89	22.72
13	12.46	13.09	12.87 11.61	11.21	13.16	11.29
14	34.37	32.20	34.83	34.32	32.30	34.45

*δ_c, ppm from external TMS.
†See 1 of Fig. 3 for numbering of carbon atoms.

expanded triplet patterns. In spite of this recent work, little is still known concerning the epimerization reaction of pilocarpine, it being considered that epimerization does not occur after the lactone ring has been opened, whether in the anion or in the free acid form (11, 13, 14). As ^{13}C Fourier transform nmr spectroscopy is admirably suitable for providing detailed insight into the molecular nature of species formed upon degradation of pilocarpine, the purposes of this investigation were to develop an unambiguous method for quantitating epimerization and to characterize the products of hydrolysis more specifically, in order to provide a fuller interpretation of the epimerization reaction.

Experimental

Pilocarpine hydrochloride, mp 204–205 °C, and isopilocarpine nitrate, mp 157 °C were used as obtained from the Aldrich Chemical Company. Pilocarpine reference standard was obtained from U.S.P.–N.F. Reference Standards, 12601 Twinbrook Parkway, Rockville, Maryland, U.S.A. 20852.

^{13}C nmr spectra were recorded in D_2O using 10-mm tubes at 30 °C on a Varian CFT-20 spectrometer. A Varian XL-100-15 spectrometer utilizing 12 mm tubes was used for temperature studies ranging between 9.5 and 65 °C. Both instruments were operated in the pulsed Fourier transform mode to provide spectra with and without proton coupling. Chemical shifts are reported in parts per million (ppm) downfield from external tetramethylsilane (TMS) contained in a concentric 5 mm tube.

The spectra used for the calculations were obtained by using 4K data points over a spectral width of 4 kHz, an acquisition time of 0.5 s, a pulse angle of 45°, and no pulse delay. In order to check the accuracy of the observed intensities (peak height), spectra of a sample of U.S.P. Standard pilocarpine nitrate in D_2O at p*D* 13.1 were obtained using 8K data points within a 2 kHz spectral width, and acquisition time of 2 s, and no pulse delay (same pulse angle). These conditions eliminated any error due to insufficient data points and error due to differences in relaxation times in the spectra. The integrated peak areas from these spectra were in good agreement (±8% of measured values) with the results obtained by the more rapid method.

The p*D* was adjusted with NaOD or DCl, and p*D* values were measured by meter (p*D*, p*H* meter reading + 0.4) (15). The pK_a values were determined from corrected p*H* meter readings in D_2O, and they do not necessarily represent the pK_a values in H_2O because of a possible isotope effect (16). Solutions were allowed to equilibrate for at least ½ h at each p*D* and temperature before scanning was commenced.

Results

The ^{13}C chemical shifts for pilocarpine and isopilocarpine under different conditions, are given in Table 1, comparative spectra with changing p*D* are shown in Fig. 1, and the varia-

Can. J. Chem. Downloaded from www.nrcresearchpress.com by 210.87.254.42 on 09/05/12
For personal use only.

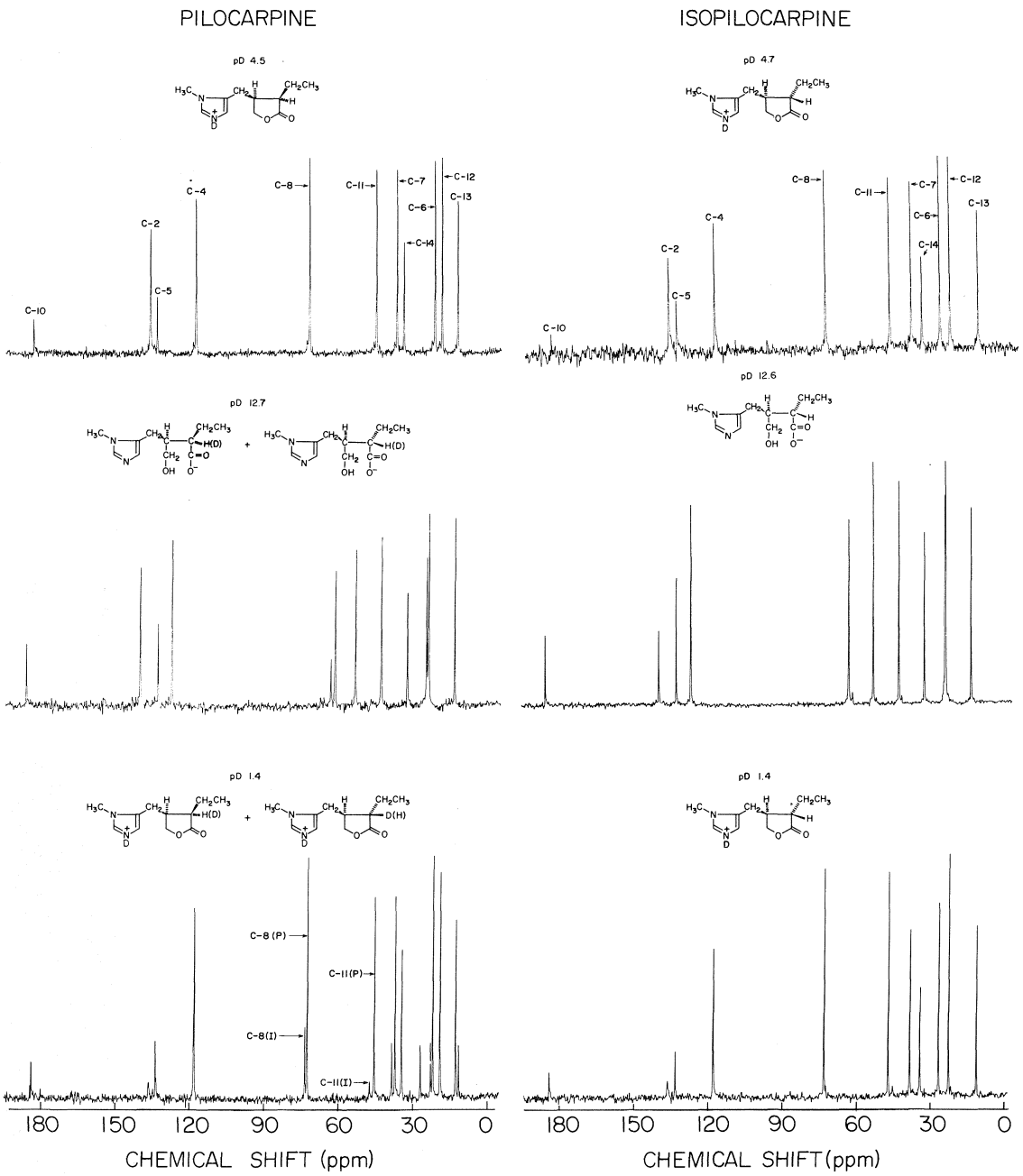

FIG. 1. Comparative ^{13}C nmr spectra of pilocarpine and of isopilocarpine in D_2O with changing p*D*.

tion in ^{13}C chemical shift for various carbon nuclei with changing p*D* is plotted in Fig. 2. The assignment of carbon frequencies was based on a comparison of proton coupled and decoupled spectra and knowledge of shielding effects (17). The ^{13}C nmr spectra of pilocarpine solutions in D_2O at p*D* 10–14 at room temperature (30 °C) show the presence of $28 \pm 3\%$ of the ring-opened form of isopilocarpine (isopilocarpinate) admixed with that of pilocarpine

Can. J. Chem. Downloaded from www.nrcresearchpress.com by 210.87.254.42 on 09/05/12
For personal use only.

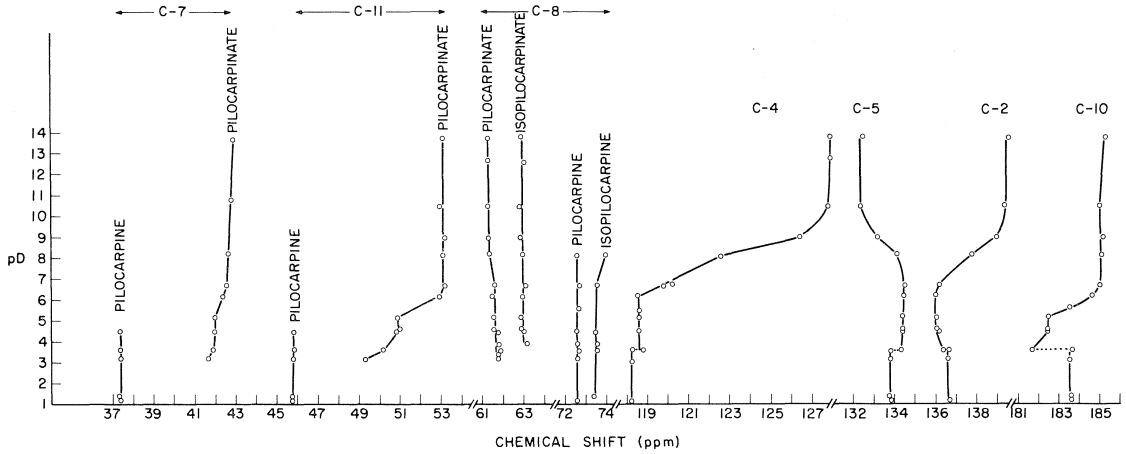

FIG. 2. Variation of ^{13}C chemical shift for various carbon nuclei of pilocarpine with changing pD (for numbering, see **1** of Fig. 3).

(pilocarpinate). When D_2O solutions of isopilocarpine were similarly treated with base, no evidence of pilocarpinate could be found admixed with isopilocarpinate. Upon acidification of the pilocarpinate and isopilocarpinate solutions to pD 1 to recyclize the lactone structure, the pilocarpinate mixture yielded spectra indicating the presence of 28 ± 3% isopilocarpine whereas the isopilocarpinate solutions provided spectra identical with that of isopilocarpine nitrate in D_2O.

At lower temperature (9.5 °C) at pD 12.5 the ^{13}C spectra show only 38 ± 3% of the pilocarpine is delactonized, of which 25 ± 3% is converted to the isopilocarpinate form. At higher temperature (65 °C) at the same pD, pilocarpine was completely delactonized and the proportion of isopilocarpinate was 27 ± 3%. Under any of these conditions the C-11 hydrogen undergoes exchange in D_2O which causes considerable diminution of the C-11 carbon resonance. This effect is readily seen in the lower left spectrum of Fig. 1. The weak remaining resonance at 47.6 ppm is due to residual protonated C-11 of isopilocarpine. The resonance of the deuterated C-11, which might be expected to undergo a slight isotope shift with respect to the resonance of the C—H moiety and to manifest a triplet structure due to spin–spin coupling with deuterium, is not visible in the spectrum. This low signal-to-noise ratio is due to: (*i*) a decrease to 0.3 of the intensity of the resonance of the protonated analog due to splitting into three components, (*ii*) considerable saturation of the resonance resulting from rapid acquisition of data relative to the spin–lattice relaxation time (T_1) of the deuterated carbon which is approximately 45 times longer than that of the protonated analog.

By plotting variation in ^{13}C chemical shift for various carbon nuclei of pilocarpine with changing pD (Fig. 2), one obtains values of pK_a = 5.7 ± 0.1 (from C-10 and C-11) for dissociation of the open chain hydroxy acid form (pilocarpinate) and pK_a = 8.5 ± 0.1 (from C-2, C-4, and C-5) for dissociation of the protonated quaternary nitrogen of the imidazole ring of pilocarpine.

Discussion

On treating pilocarpine (**1**) with base, the lactone is cleaved by hydrolysis (see Fig. 3) to yield an epimeric mixture of γ-hydroxy carboxylates, pilocarpinate (major), and isopilocarpinate (minor). The kinetics of the hydrolysis of pilocarpine have received some study (7, 11). Comparison of ^{13}C spectra of base treated pilocarpine and isopilocarpine (Fig. 1) reveals the presence of three resonances for isopilocarpinate carbons differing in frequency from those of the corresponding pilocarpinate carbon sites. The C-8 methylene carbon of isopilocarpinate at 62.80 ppm is well resolved from the C-8 pilocarpinate carbon at 61.33 ppm and as such the C-8 carbon resonances constitute the best indicators for monitoring pilocarpine solu-

Can. J. Chem. Downloaded from www.nrcresearchpress.com by 210.87.254.42 on 09/05/12
For personal use only.

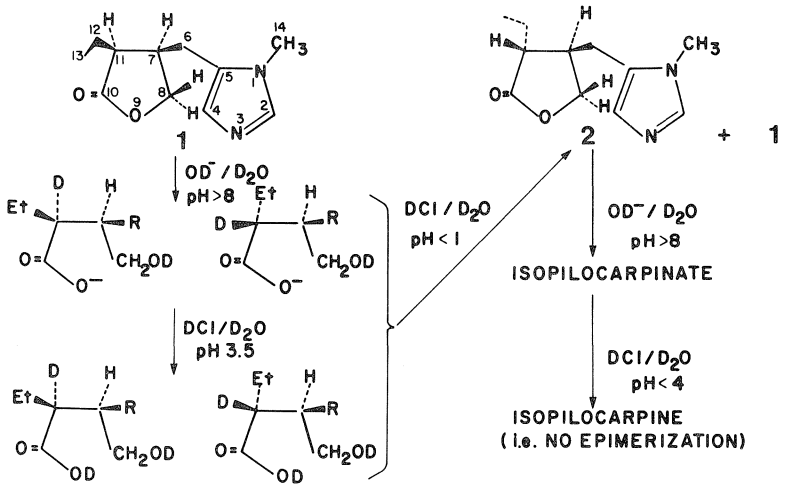

FIG. 3. Epimerization of pilocarpine (1) to isopilocarpine (2) by base–acid cyclization.

tions for epimerization. A shoulder at 42.82 ppm for the tertiary C-7 of isopilocarpinate is seen on the 42.57 ppm resonance for the pilocarpine C-7. Similarly a shoulder at 23.87 ppm for the C-12 methylene carbon of isopilocarpinate is seen on the 23.46 ppm resonance for C-12 of pilocarpinate. Pilocarpinate and isopilocarpinate appear to have all other ^{13}C resonances in common, a feature which is consistent with the remoteness of these carbon atoms from the diastereoisomeric centres. The isopilocarpinate reference spectrum affords an ideal comparison because no evidence of epimerization of isopilocarpine is seen either on treatment with base or upon strong acidification of the isopilocarpinate to effect lactone closure.

The lability of the lactone ring of pilocarpine is illustrated graphically in Fig. 2 where the ^{13}C chemical shift is plotted against changing p*D*. Under alkaline conditions extending to approximately p*D* 8, the stable molecular species is the lactone cleaved, hydroxy carboxylate (pilocarpinate). As the p*D* is decreased, lactone formation occurs resulting in the formation of pilocarpine whose C-8 resonance affords the best resolved and most sensitive indicator of its generation. From p*D* 7 to 5 proton association of pilocarpinate occurs to form the free hydroxy acid (pilocarpinic acid, $pK_a = 5.7 \pm 0.1$) as indicated by the inflections of the titration curves for the C-10 and C-11 resonances. By p*D* 4.5, proton association by pilocarpinate is virtually complete and the titration curves for resonances C-11, C-10, C-8, and C-7, formerly representing pilocarpinate, now essentially reflect pilocarpinic acid in equilibrium with pilocarpine from p*D* 4.5 to 3.6. By p*D* 3.6, the C-10, C-2, C-4, and C-5 resonances indicate appreciable formation of pilocarpine in equilibrium with the open-chain pilocarpinic acid; however, at lower p*D* values, pilocarpine resonances are seen exclusively.

It has been reported that if solutions of pilocarpinate and isopilocarpinate are carefully acidified with deuterochloride to about p*H* 3.5 (*i.e.* p*D* 3.9), the deuterochloride salts of the corresponding free acids, pilocarpinic acid and isopilocarpinic acid can be obtained (7, 11). This p*H* was used by Nunes and Brochmann-Hanssen (11) for the preparation of reference solutions of pilocarpinic and isopilocarpinic acids for their kinetic studies. At this p*H*, the rate of lactone formation, as inferred from kinetic modelling, was assumed to be slow (7). The carbonyl ^{13}C resonances provide a means to identify the free acid forms of both compounds. From our ^{13}C nmr spectral examination of the progressive acidification of pilocarpine and isopilocarpine solutions (Fig. 2), it is seen that pilocarpinic acid does not exist alone in solution except in equilibrium with pilocarpinate (p*D* 5–7) and with pilocarpine (p*D* 3.6–8). The proton nmr spectral data reported by Nunes and Brochmann-Hanssen (11) for pilocarpinic acid and isopilocarpinic acid, allegedly obtained by neutralizing alkaline solutions with deuterochloride to

Can. J. Chem. Downloaded from www.nrcresearchpress.com by 210.87.254.42 on 09/05/12
For personal use only.

Can. J. Chem. Downloaded from www.nrcresearchpress.com by 210.87.254.42 on 09/05/12
For personal use only.

p*H* 3.5 (p*D* 3.9), therefore represent equilibrium mixtures of parent compounds and their respective open chain forms. At p*D* 3.6 following acidification of alkaline pilocarpine solution, we find from analysis of the three ^{13}C nmr resonances for C-8 that the solution contains 42 ± 3% pilocarpine, 31 ± 3% isopilocarpine, and 27 ± 3% pilocarpinic acid.

The cyclization of pilocarpinate solutions was further checked by acidifying solutions to p*H* 1 (p*D* 1.4) to effect lactonization followed by an adjustment of the solution p*D*, *i.e.* same p*D* as the reference solution of pilocarpine HCl dissolved in D_2O. Comparison of the ^{13}C spectrum from the base acidified mixture with the reference pilocarpine spectrum revealed the presence of isopilocarpine (28 ± 3%). This was verified by matching of chemical shifts with a reference solution of isopilocarpine nitrate at the same p*H*. When isopilocarpine was similarly hydrolyzed completely by base and recycled in acid media, the ^{13}C nmr spectrum of the product was identical with that of the isopilocarpine reference solution before hydrolysis. Isopilocarpine, therefore, does not epimerize under these conditions, at least to an extent that could be detected by ^{13}C nmr spectroscopy ($\geq 3\%$), in agreement with the conclusion reached by Nunes and Brochmann-Hanssen (11) from proton nmr spectroscopy at 100 MHz.

Rationalization of the Epimerization Reaction

From kinetic studies of the base hydrolysis of aqueous pilocarpine solutions, Chung *et al.* (7) considered hydrolysis to pilocarpinic acid and epimerization to isopilocarpine to be independent pathways of degradation. They considered opening of the lactone ring to be the most important of these pathways, and considered that as long as the lactone ring was intact, the alkaloid would maintain its stereochemical configuration. Nunes and Brochmann-Hanssen (11) extended this kinetic modelling by assuming that the overall effect of aqueous base on pilocarpine could be considered to be the result of three principal reactions: hydrolysis to pilocarpinate, epimerization to isopilocarpine, and hydrolysis to isopilocarpinate. From the advantage afforded us by the specificity of ^{13}C nmr spectroscopy to reveal the integral molecular nature of reaction constituents, we can now offer a rationalization of the epimerization reaction.

It is known that α-protons of γ-lactones are more acidic than those of open esters (18), and Döpke and d'Heureuse (14) have shown that epimerization of pilocarpine to isopilocarpine with sodium methoxide under anhydrous conditions occurs exclusively at the α-carbon of the lactone ring. Under alkaline aqueous conditions, therefore, it is not unreasonable to assume, as in kinetic analysis (11), formation of the enolate of pilocarpine. This is confirmed by our observed exchange in D_2O of the C-11 hydrogen with concomitant broadening of the C-11 carbon resonance, and it constitutes evidence for epimerization of pilocarpine and for the absence of epimerization by isopilocarpine. Once formed, however, the enolate would be readily attacked by water resulting in uptake of a proton and generation of a 50:50 mixture of isopilocarpinate and pilocarpinate (Fig. 4). The enolate should contribute a different set of resonances in ^{13}C nmr spectra for the ethyl carbon atoms from either pilocarpinate and isopilocarpinate. The absence of resonances attributable to the enolate form in ^{13}C spectra suggests that the equilibrium concentration of the enolate is very low or that its lifetime is very short. The epimerization of pilocarpine (28 ± 3%) at room temperature indicates rapid attack of the enolate by water. Since 28% of the pilocarpinate in solution would be generated from the enolate, the remaining 44% pilocarpinate in solution would have to arise by direct hydrolysis of pilocarpine (Fig. 4). This evidence and line of reasoning suggests that enolization does provide a significant pathway for epimerization of pilocarpine. The observations of others that once the lactone is hydrolyzed and the hydroxy acid is in the anionic form, no further epimerization takes place (7, 11, 13, 14) are verified by our ^{13}C nmr spectral findings that the pilocarpine/isopilocarpine ratio following acidification is the same as the pilocarpinate/isopilocarpinate ratio under alkaline conditions.

The question naturally arises as to why isopilocarpine in basic aqueous media does not suffer epimerization to pilocarpine. Isopilocarpine is regarded as the thermodynamically more stable *trans*-epimer (11–14) but examination of Dreiding stereomodels provides a clue to differing enolization behaviour. In pilocarpine, the severe steric interaction of the *cis* ethyl and imidazole substituents can be relieved through

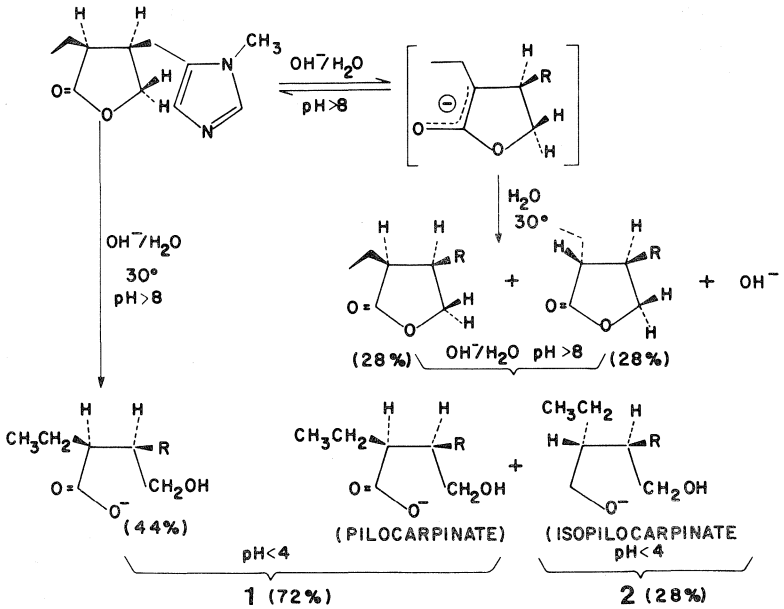

FIG. 4. Mechanism for epimerization of pilocarpine via enolization.

dissociation of the α-proton to give the enolate with a nearly planar sp^2 α-carbon. In isopilocarpine, there is little, if any, steric interaction between the ethyl and imidazole substituents; thus, the α-proton is probably less acidic and not prone to enolization under aqueous conditions. This interpretation is supported by the observed absence of deuterium exchange at C-11 with isopilocarpine.

Finally, our temperature studies indicate that basic hydrolysis of the lactone of pilocarpine is strikingly impaired with decreasing temperature with little concomitant impairment to the enolization process which affords the pathway to epimerization. This finding based on ^{13}C nmr spectral studies is contradictory to the finding based on kinetic studies (11) with assumed solution composition to the effect that the rate of hydroxide ion catalyzed epimerization increases more rapidly with temperature than does the rate of hydrolysis.

1. I. H. LEOPOLD and E. KEATES. Clin. Pharmacol. Ther. **6**, 262 (1965).
2. S. RIEGELMAN and D. G. VAUGHAN. J. Am. Pharm. Assoc. Pract. Pharm. Ed. **19**, 474 (1958).
3. C. J. BLOK. Pharm. J. **155**, 282 (1945).
4. R. FAGERSTROM. J. Pharm. Pharmacol. **15**, 479 (1963).
5. W. H. MORRISON and S. M. TRUHLSEN. Am. J. Ophthalmol. **33**, 357 (1950).
6. R. A. ANDERSON and S. D. FITZGERALD. Aust. J. Pharm. Sci. **48**, 108 (1967).
7. P.-H. CHUNG, T.-F. CHIN, and J. L. LACH. J. Pharm. Sci. **59**, 1300 (1970).
8. R. A. ANDERSON. Can. J. Pharm. Sci. **2**, 25 (1967).
9. K. BAESCHLIN, J. C. ETTER, and H. MOLL. Pharm. Acta Helv. **44**, 301 (1969).
10. K. BAESCHLIN and J. C. ETTER. Pharm. Acta Helv. **44**, 339 (1969).
11. M. A. NUNES and E. BROCHMANN-HANSSEN. J. Pharm. Sci. **63**, 716 (1974).
12. R. K. HILL and S. BARCZA. Tetrahedron, **22**, 2889 (1966).
13. M. POLONOVSKI and M. POLONOVSKI. Bull. Soc. Chem. **31**, 1314 (1922).
14. W. DÖPKE and G. d-HEUREUSE. Tetrahedron Lett. 1807 (1968).
15. P. K. GLASCOE and F. A. LONG. J. Phys. Chem. **64**, 188 (1960).
16. D. H. SACHS, A. N. SCHECHGER, and J. S. COHEN. J. Biol. Chem. **246**, 6576 (1971).
17. J. B. STOTHERS. *In* Carbon-13 NMR spectroscopy. Academic Press, New York. 1972.
18. J. DALE and S. MORGENLIE. Acta Chem. Scand. **24**, 2408 (1970).

Can. J. Chem. Downloaded from www.nrcresearchpress.com by 210.87.254.42 on 09/05/12
For personal use only.

Basicité de solvants dipolaires aprotoniques

ROBERT DOMAIN, MARCEL RINFRET ET ROBERT L. BENOIT
Département de Chimie, Université de Montréal, C.P. 6210, Montréal (Qué.), Canada H3C 3V1

Reçu le 23 février 1976

ROBERT DOMAIN, MARCEL RINFRET et ROBERT L. BENOIT. Can. J. Chem. **54**, 2101 (1976).

Les basicités des cinq solvants dipolaires aprotoniques, sulfolane, carbonate de propylène, acétonitrile, diméthylformamide, diméthylsulfoxyde, et de l'eau, ont été caractérisées en utilisant comme paramètre l'enthalpie de solvatation du proton gazeux. Les valeurs correspondantes de $\Delta H(g \rightarrow s)(H^+)$ sont déduites de données calorimétriques expérimentales sur la réaction $HCl(g) \rightarrow H^+(s) + Cl^-(s)$ et des changements d'enthalpie connus correspondant à $H^+(g) \rightarrow H^+(aq)$ et à $Cl^-(aq) \rightarrow Cl^-(s)$. Les enthalpies de transfert de Cl^-, de l'eau au solvant sont évaluées sur la base d'une hypothèse extrathermodynamique. Les valeurs de $\Delta H(g \rightarrow s)(H^+)$ obtenues (kcal mol^{-1}) sont: TMS(−252.6), AN(−256.6), CP(−259.5), H_2O(−270.0), DMF(−276.7), DMSO(−276.1). On compare ces valeurs aux autres paramètres couramment utilisés pour caractériser la basicité de ces solvants soit à l'état moléculaire soit en tant que milieux. Ainsi, les affinités protoniques sont telles, qu'en phase gazeuse, l'acétonitrile est de 17 kcal mol^{-1} plus basique que l'eau, alors qu'en phase liquide, nos résultats indiquent que l'acétonitrile est cette fois de 13 kcal mol^{-1}, moins basique que l'eau. Cette variation de 30 kcal mol^{-1} est attribuée aux différences dans la nature du proton solvaté $H^+(s)$ dans les deux solvants: divers indices suggèrent que $H^+(s)$ est sous la forme $H^+(AN)_2$ dans l'AN, solvant aprotonique, alors qu'il est stabilisé sous la forme $H^+(H_2O)_n$ dans l'eau, solvant protonique, par suite de la formation de liaisons hydrogène de type coopératif. On montre que les ordres de basicité des solvants correspondant à $\Delta H(g \rightarrow s)(H^+)$ et $\Delta H(g \rightarrow s)(HA)$ diffèrent et on en examine les conséquences quant à l'effet de solvant sur la dissociation des acides HA. Par ailleurs, une relation sensiblement linéaire est obtenue pour les cinq solvants dipolaires aprotoniques entre les valeurs de $\Delta H(g \rightarrow s)(H^+)$ et l'enthalpie de protonation dans l'acide fluorosulfonique.

ROBERT DOMAIN, MARCEL RINFRET, and ROBERT L. BENOIT. Can. J. Chem. **54**, 2101 (1976).

The basicities of five dipolar aprotic solvents, sulfolane, propylene carbonate, acetonitrile, dimethylformamide, dimethyl sulfoxide, and of water have been characterized by using as parameter the solvation enthalpy of the gaseous proton. The corresponding values of $\Delta H(g \rightarrow s)(H^+)$ are deduced from experimental calorimetric data on the reaction $HCl(g) \rightarrow H^+(s) + Cl^-(s)$ and the known enthalpy changes for $H^+(g) \rightarrow H^+(aq)$ and $Cl^-(aq) \rightarrow Cl^-(s)$. The transfer enthalpies of Cl^- from water to solvent are estimated on the basis of an extrathermodynamic assumption. The values obtained for $\Delta H(g \rightarrow s)(H^+)$ are (kcal mol^{-1}): TMS(−252.6), AN(−256.6), PC(−259.5), H_2O(−270.0), DMF(−276.7), DMSO(−276.1). These values are compared to other parameters currently used to define the basicity of these solvents whether as molecules or as media. Thus, proton affinities are such that in the gas phase, acetonitrile is more basic than water by 17 kcal mol^{-1}, while in the liquid phase our results indicate that acetonitrile is less basic than water by 13 kcal mol^{-1}. This variation of 30 kcal mol^{-1} is attributed to differences in the nature of the solvated proton $H^+(s)$ in both solvents: several indications suggest that $H^+(s)$ is present as $H^+(AN)_2$ in AN, an aprotic solvent, while it is stabilized as $H^+(H_2O)_n$ in water, a protic solvent because of the formation of hydrogen bonds of a cooperative nature. Solvent basicity orders as defined with respect to $\Delta H(g \rightarrow s)(H^+)$ and $\Delta H(g \rightarrow s)(HA)$ are shown to differ and the consequences as to the solvent effect on the dissociation of acids HA are considered. Further, there is a nearly linear relationship for the five dipolar aprotic solvents between the values of $\Delta H(g \rightarrow s)(H^+)$ and the enthalpy of protonation in fluorosulfonic acid.

Introduction

Parmi les propriétés qui caractérisent la réactivité d'un solvant, la basicité occupe une place importante puisque tout effet de solvant sur un processus comporte une composante due à la basicité du solvant, chaque fois, et le cas est fréquent, que les espèces chimiques impliquées ont des propriétés acides. Ainsi la basicité du solvant influence des processus physicochimiques tels que la dissociation des acides, les réactions acides–bases. . . . Les propriétés spectroscopiques de solutés acides, soit moléculaires, soit cationiques, sont aussi affectées par la basicité du solvant.

Can. J. Chem. Downloaded from www.nrcresearchpress.com by 210.87.254.105 on 09/05/12
For personal use only.

Can. J. Chem. Downloaded from www.nrcresearchpress.com by 210.87.254.105 on 09/05/12
For personal use only.

La plupart des solvants moléculaires possèdent des propriétés basiques en ce sens que les molécules de solvants, de par la disponibilité des électrons sur certains des atomes, peuvent généralement être considérées comme des bases de Lewis. La basicité serait ainsi une propriété moléculaire intrinsèque. Cependant, bien que l'on ait, dans cette optique, proposé d'utiliser les décalages en énergie de liaison d'électrons de coeur comme mesure opérationelle de la basicité de Lewis (1), les basicités sont généralement comparées à partir des paramètres thermodynamiques (ΔG ou ΔH) de réactions impliquant les différentes bases avec un acide de référence commun (2). Cette approche conduit malheureusement à des résultats qui dépendent, dans une certaine mesure, du choix de l'acide de référence, du milieu réactionnel, et aussi du type de réaction acide–base impliquée (3).

Etant donné le rôle capital joué par le proton dans les réactions chimiques (3) nous avons choisi, dans ce travail, de prendre H^+ comme acide de référence. Nous avons déterminé comme paramètre réactionnel l'enthalpie, plutôt que l'énergie libre (4), vu la simplicité relative des mesures calorimétriques. Nous avons aussi utilisé comme milieu réactionnel le solvant lui-même. Nous avons donc caractérisé la basicité des solvants sur la base de l'enthalpie de solvatation du proton gazeux c'est-à-dire à partir du changement d'enthalpie, $\Delta H(g \rightarrow s)(H^+)$,[1] associé à la réaction 1. Les solvants étudiés sont l'eau et

[1] $$H^+(g) \rightarrow H^+(s)$$

une série de solvants dipolaires aprotoniques (dpa). Nous comparons ensuite les valeurs de $\Delta H(g \rightarrow s)(H^+)$ ainsi obtenues avec les principaux paramètres généralement utilisés pour caractériser la basicité des solvants (2).

Notre méthode d'obtention de $\Delta H(g \rightarrow s)(H^+)$ implique la détermination expérimentale des changements d'enthalpie,[2] $\Delta H(d, g \rightarrow s)$, associés aux réactions 2.

[2] $$HCl(g) \rightarrow H^+(s) + Cl^-(s) \quad \Delta H(d, g \rightarrow s)$$

On combine ensuite ces valeurs avec les variations d'enthalpie connues correspondant aux réactions 3, 4 et 5.

[3] $$H^+(aq) + Cl^-(aq) \rightarrow HCl(g)$$
$$-\Delta H(d, g \rightarrow aq) = 17.9 \text{ kcal mol}^{-1}$$

[4] $$Cl^-(s) \rightarrow Cl^-(aq) \quad \Delta H(s \rightarrow aq)(Cl^-)$$

[5] $$H^+(g) \rightarrow H^+(aq)$$
$$\Delta H(g \rightarrow aq)(H^+) = -270.0 \text{ kcal mol}^{-1}$$

Les changements d'enthalpie associés aux réactions 4, c'est-à-dire les enthalpies de transfert de Cl^-, sont obtenues en utilisant l'hypothèse extrathermodynamique tétraphénylarsonium-tétraphénylborate (tatb) (5). Le cycle thermodynamique décrit par les réactions 2, 3, 4 et 5 conduit alors aux valeurs cherchées de $\Delta H(g \rightarrow s)(H^+)$ correspondant à la réaction 1.

Partie expérimentale

Réactifs

Le sulfolane, fourni gracieusement par Shell Canada a été purifié (5). Avant chaque utilisation le produit distillé est soumis à chaud, pendant plusieurs heures à un vide de 10^{-1} torr, de manière à réduire la concentration en eau à moins de 5×10^{-3} *M*. L'acétonitrile (Eastman Kodak X-488) a été agité pendant 24 h avec du tamis moléculaire 4 Å, la concentration en eau est alors inférieure à 2×10^{-3} *M*. Le carbonate de propylène (Eastman Kodak 7050) a été purifié par distillation sous pression réduite (10^{-1} torr). On conserve la fraction centrale du distillat (température de passage 63 °C), soit environ 60%. Le produit est transparent dès 320 nm, la conductivité spécifique 6×10^{-8} Ω^{-1} cm^{-1} à 25 °C et la concentration en eau voisine de 4×10^{-3} *M*. Le diméthylformamide (Fisher D-133) est agité en présence de CaH_2 puis distillé sous pression réduite (1 torr). La concentration en eau est de l'ordre de 5×10^{-3} *M*. Le diméthylsulfoxyde (Fisher D-136) est distillé sous pression réduite (1 torr), sa concentration en eau après distillation et séchage est voisine de 7×10^{-3} *M*. Les solutions de chlorure d'hydrogène ont été obtenues par barbotage de HCl anhydre (Matheson). Le chlorure de tétraéthylammonium, un produit Eastman Kodak, est recristallisé deux fois dans un mélange éthanol 5% – acétate d'éthyle 95% puis séché sous vide à 40 °C. Les solutions de chlorure sont préparées par pesée. Le pentachlorure d'antimoine, produit "Reagent" de Fisher, et l'acide trifluorométhanesulfonique (3M Chemical) ont été utilisés sans purification ultérieure.

Mesures

Pressions de vapeur

Les mesures de pression de vapeur ont été effectuées à l'aide d'une jauge de Bourdon (modèle 145-01 Texas Instruments) antérieurement décrite (6).

Calorimétrie

Les chaleurs de solution de $SbCl_5(l)$ dans les solvants,

[1] Les symboles s et (s) ont été choisis de préférence à (solv) afin de ne pas alourdir les notations.

[2] Toutes nos valeurs des ΔH peuvent être confondues avec les changements d'enthalpie standard compte-tenu des faibles concentrations utilisées et de la précision des mesures calorimétriques. La présence d'eau résiduelle dans les solvants rendrait d'ailleurs difficile une extrapolation des ΔH à concentration nulle d'acide.

Can. J. Chem. Downloaded from www.nrcresearchpress.com by 210.87.254.105 on 09/05/12
For personal use only.

les chaleurs de réaction de $SbCl_5$(l) avec les solutions de chlorures d'ammonium substitués ou de HCl, et celle de NEt_4Cl avec une solution d'acide fort, ont été mesurées en utilisant la même cellule et le même calorimètre isopéribolique (L.K.B. modèle 8725-2) que lors d'une étude précédente (6). Le calcul des quantités de chaleur dégagées a été fait comme précédemment (6). Les chaleurs de solution de HCl(g) dans les solvants ont été mesurées à l'aide d'un calorimètre à gaz que nous avons mis au point (7). Ce calorimètre simple, du type isopéribolique, comprend une rampe de purification du gaz, une fiole de stockage du gaz et la cellule calorimétrique proprement dite toutes deux immergées dans un bain thermostaté (± 0.01 °C), ainsi qu'un circuit électrique de calibration. Le chlorure d'hydrogène est purifié par passage successif dans l'acide sulfurique concentré puis dans un piège acétone – glace sèche. Il est ensuite conservé dans une fiole conique de 500 ml immergée dans le bain. La vidange de ce réservoir et par suite l'écoulement du gaz dans la cellule calorimétrique contenant le solvant, se fait grâce à la pression exercée par du mercure contenu dans un réservoir supérieur. Dépendant du but poursuivi un deuxième montage a aussi été utilisé. On substitue aux deux fioles de 500 ml un serpentin de verre immergé dans le bain entre la rampe et la cellule. Ce second montage nous permet d'atteindre des concentrations en HCl dissous supérieures à 0.2 *M*. L'entrée du gaz dans la cellule calorimétrique se fait par un tube capillaire immergé et terminé à son extrémité par une cloche de verre de 1 cm^3 afin d'augmenter la surface de contact gaz–solvant. La cellule, qui peut recevoir 200 ml de solvant est constituée d'un vase Dewar dont la partie supérieure, en dehors du bain, est fermée par un bouchon de téflon. Trois orifices permettent d'introduire le tube d'entrée du gaz, un thermomètre et un agitateur flexible actionné manuellement. Un quatrième orifice est destiné à l'évacuation du trop plein de gaz lors du barbotage. Le circuit électrique de calibration est alimenté par une source de tension stabilisée (potentiostat PRT 2000 Tacussel). La résistance chauffante de calibration (~15 ohms), un fil de chromel recouvert d'une gaine d'amiante, est placée en série avec une résistance étalon constituée de deux résistances de 10 ohms (± 0.00001 ohm) en parallèle. Le calorimètre est calibré électriquement avant et après chaque barbotage de gaz. La quantité de chaleur dissipée par la résistance chauffante est déterminée en mesurant le voltage à ses bornes, le voltage aux bornes de la résistance étalon et le temps de chauffage. L'élevation de température observée au cours de ces calibrations (ou pendant le barbotage du gaz) est repérée à l'aide d'un thermomètre gradué au 1/100 de degré. On suit alors la température en fonction du temps. La méthode graphique d'extrapolation de Dickinson est utilisée pour trouver les quantités de chaleur dégagées. Les qualités de l'appareillage ont été testées en déterminant la chaleur de solution de HCl(g) dans l'eau. Les valeurs obtenues correspondent aux valeurs de la littérature à mieux de 1.0% (8). Cette précision, bien que modérée, est suffisante pour le type d'étude entrepris ici.

Résultats

La détermination expérimentale des changements d'enthalpie $\Delta H(\mathrm{d, g \rightarrow s})$ associés aux réactions 2

$$[2] \qquad HCl(g) \rightarrow H^+(s) + Cl^-(s)$$

est effectuée en deux étapes. Dans un premier temps, on mesure $\Delta H(\mathrm{g \rightarrow s})$ l'enthalpie de solution de HCl(g) dans les différents solvants:

$$[6] \qquad HCl(g) \rightarrow HCl(s)$$

La dissociation de HCl dans les solvants TMS, AN et CP est négligeable de telle sorte que $\Delta H(\mathrm{g \rightarrow s})(HCl)$ est obtenu directement suivant [6]. Des corrections sont apportées dans le cas du DMF et du DMSO. Dans un deuxième temps, on détermine indirectement l'enthalpie de dissociation $\Delta H(\mathrm{d})$ de HCl(s):

$$[7] \qquad HCl(s) \rightarrow H^+(s) + Cl^-(s)$$

Les réactions 6 et 7 combinées conduisent à la réaction 2 et $\Delta H(\mathrm{d, g \rightarrow s})$.

Enthalpies de solution de HCl gazeux

La présence d'eau résiduelle (2×10^{-3} *M* – 1×10^{-2} *M*) dans les solvants nous a imposé l'utilisation de deux méthodes différentes pour déterminer l'enthalpie de solution de HCl(g). Avec les solvants les plus basiques, DMF et DMSO, l'eau résiduelle n'a pas d'influence notable (9) sur la réaction 2, les ions H^+ et Cl^- restant peu hydratés (10). En conséquence, les valeurs de $\Delta H(\mathrm{g \rightarrow s})(HCl)$ ont été déterminées par calorimétrie directe en dissolvant des quantités d'HCl correspondant à des concentrations comprises entre 0.07 *M* et 0.25 *M*. Les quantités de chaleur expérimentales sont corrigées, la correction étant inférieure à 2%, pour tenir compte de la faible dissociation de HCl. On a utilisé pour le DMSO, $K(\mathrm{d}) = 10^{-2.0}$ (9) et $\Delta H(\mathrm{d}) = -1.2$ kcal mol^{-1} et pour le DMF, $K(\mathrm{d}) = 10^{-3.6}$ (11) et $\Delta H(\mathrm{d}) = -1.7$ kcal mol^{-1}, les deux valeurs de $\Delta H(\mathrm{d})$ étant celles déterminées par après (tableau 2). Les valeurs de $\Delta H(\mathrm{g \rightarrow s})(HCl)$ rapportées dans le tableau 1

TABLEAU 1. Enthalpies de solution de HCl(g) $\Delta H(\mathrm{g \rightarrow s})$ (kcal mol^{-1}) dans les solvants

Solvant	$-\Delta H(\mathrm{g \rightarrow s})(HCl)$	Température (°C)
TMS*	5.8 ± 0.1†	28–45
AN	5.7 ± 0.1†	13–31
CP	6.3 ± 0.2†	19–36
DMF	17.8 ± 0.1‡	25
DMSO	18.3 ± 0.1‡	24

*Référence 6, 30 °C.
†Mesures de pressions de vapeur.
‡Mesures calorimétriques.

sont des moyennes de trois déterminations pour chaque solvant.

Dans le cas des solvants moins basiques TMS, AN et CP, l'eau résiduelle influence la réaction 2, deux équilibres accessoires (7) venant s'ajouter, soit

[8] $$2HCl + H_2O = H_3O^+ + HCl_2^-$$

[9] $$HCl + H_2O = H_2O\cdots HCl$$

Ces deux réactions étant exothermiques, les valeurs de $\Delta H(g \rightarrow s)(HCl)$ déterminées par calorimétrie directe sont trop élevées. Ainsi, dans le cas de l'AN, on a trouvé une valeur de -6.1 kcal mol^{-1} (HCl 0.20 *M* et H_2O 1.3×10^{-2} *M*) c'est-à-dire d'environ 8% supérieure à la valeur adoptée -5.7 kcal mol^{-1} (tableau 1). On a donc utilisé pour la détermination de $\Delta H(g \rightarrow s)(HCl)$ dans les solvants AN et CP, la méthode indirecte impliquant la mesure de pressions de vapeur à différentes températures et l'application de l'équation de Van't Hoff. De cette façon, on peut minimiser l'influence des réactions 8 et 9 en opérant avec des concentrations d'HCl plus élevées et d'eau plus faibles qu'en calorimétrie directe (la manipulation des solutions étant plus simple). Les mesures ont été effectuées pour chaque solvant à quatre températures entre 13 et 37 °C sur deux solutions d'HCl de concentrations différentes comprises entre 0.25 et 0.9 *M*. Dans le cas de l'AN, la pression d'HCl a été obtenue en retranchant de la pression totale, la pression partielle du solvant calculée à partir de la pression du solvant pur en supposant que la solution se comporte idéalement aux faibles fractions molaires utilisées ($x \leq 0.03$). Les moyennes des valeurs des enthalpies de solution d'HCl ainsi obtenues sont dans le Tableau 1. Les résultats pour le sulfolane ont été donnés précédemment (6). Il ne nous a pas été possible de faire de mesures valables des pressions partielles trop faibles, d'HCl au-dessus de solutions dans le DMF et le DMSO même en utilisant des solutions aussi concentrées que 5 *M*. Avec le DMSO les très faibles pressions mesurées étaient vraisemblablement dues à des traces de diméthylsulfure provenant d'une légère décomposition du solvant.

Enthalpies de dissociation de HCl

L'enthalpie de dissociation de HCl dissous, [2], est obtenue pour les solvants TMS, AN, CP et DMF en combinant les valeurs expérimentales des enthalpies associées aux deux réactions 10 et 11:

[10] $$SbCl_5(l) + Cl^-(s) \rightarrow SbCl_6^-(s)$$

[11] $$SbCl_5(l) + HCl(s) \rightarrow SbCl_6^-(s) + H^+(s)$$

On opère dans chaque cas en faisant réagir $SbCl_5(l)$ avec un excès de Cl^- et HCl (0.05–1 *M*) en solution. La formation complète de $SbCl_6^-$ et $HSbCl_6$ est indiquée par la proportionalité, aux erreurs d'expérience près, entre la chaleur dégagée et la quantité de $SbCl_5$ ajoutée. On a de plus montré précédemment, par conductivité, que $HSbCl_6$ était complètement dissocié dans le TMS (12), le solvant le moins basique de la série TMS, AN, CP. Les quantités de chaleur mesurées pour la réaction 11 sont corrigées afin de prendre en considération la réaction de protonation de l'eau résiduelle (10), qui, compte-tenu des faibles quantités d'eau présentes, s'écrit

[12] $$H^+(s) + H_2O(s) \rightarrow H_3O^+(s)$$

La valeur du changement d'enthalpie de cette réaction, -11.4 kcal mol^{-1} (10) déterminée dans le TMS, a aussi été utilisée pour estimer la correction pour l'AN et CP, solvants de basicité voisine.

Une deuxième méthode a permis de vérifier les valeurs ainsi obtenues pour l'enthalpie de dissociation de HCl dans les solvants TMS et DMF et de déterminer une valeur pour le DMSO. On combine cette fois les valeurs expérimentales des enthalpies correspondant aux deux réactions 13 et 14:

[13] $$NEt_4Cl(c) + H^+(s) \rightarrow NEt_4^+(s) + HCl(s)$$

[14] $$NEt_4^+(s) + Cl^-(s) \rightarrow NEt_4Cl(c)$$

On a pris comme acide fort dans la réaction 13, HCF_3SO_3 pour le DMSO (9) et le DMF (13), et $HSbCl_6$ pour le TMS (12). Les valeurs de l'enthalpie de solution de NEt_4Cl [14] dans les trois solvants ont été tirées de la littérature et sont respectivement 2.42 kcal mol^{-1} dans le DMSO (14), 1.66 kcal mol^{-1} dans le DMF (15) et 3.94 kcal mol^{-1} dans le TMS (5). Des corrections ont été apportées dans le cas du DMSO et du DMF pour tenir compte de la dissociation incomplète de HCl dans ces deux solvants $K(d) = 10^{-2.0}$ dans le DMSO (9) et $K(d) = 10^{-3.6}$ dans le DMF (11). Les valeurs finales des enthalpies de dissociation de HCl, $\Delta H(d)$ obtenues par les deux méthodes sont rassemblées dans le tableau 2.

Can. J. Chem. Downloaded from www.nrcresearchpress.com by 210.87.254.103 on 05/05/12
For personal use only.

TABLEAU 2. Enthalpie de dissociation de HCl(s) ΔH(d) (kcal mol^{-1}) dans les solvants à 25 °C

Solvant	$-\Delta H$(réaction 10) $SbCl_5(l) + Cl^-(s)$	$-\Delta H$(réaction 11) $SbCl_5(l) + HCl(s)$	ΔH(d)	ΔH(réaction 13) $NEt_4Cl(c) + H^+(s)$	ΔH(réaction 14) $NEt_4^+(s) + Cl^-(s)$	ΔH(d)
TMS*	36.6±0.6	24.3±0.4	+11.7	−7.5±0.2	−3.9	+11.4
AN	33.2±0.3	26.4±0.3	+6.8			
CP	36.2±0.5	30.6±0.2	+5.6			
DMF	36.7±0.1	38.2±0.1	−1.5	3.6±0.1	−1.7	−1.9
DMSO				3.6±0.2	−2.4	−1.2

*30 °C.

TABLEAU 3. Données enthalpimétriques ΔH (kcal mol^{-1})

Solvant	$-\Delta H$(g → s) (HCl)	ΔH(d) (HCl)	ΔH(d, g → s) (HCl)	ΔH(aq → s) (H^+,Cl^-)	ΔH(aq → s) (Cl^-)	ΔH(aq → s) (H^+)
TMS*	5.8	11.5†	5.7	23.6	6.2	17.4
AN	5.7	6.8	1.1	19.0	5.6	13.4
CP	6.3	5.6	−0.7	17.2	6.7	10.5
DMF	17.8	−1.7†	−19.5	−1.6	5.1	−6.7
DMSO	18.3	−1.2	−19.5	−1.6	4.5	−6.1
H_2O	∼15§	∼ −3	−17.9‡	0	0	0

*à 30 °C.
†Valeurs déduites du tableau 2.
‡Référence 8.
§Cette valeur (réf. 7), en désaccord avec la valeur (4.3) de McCoubrey, est voisine de celle (12.5) estimée récemment par Myers (réf. 31).

Enthalpies de transfert

Le calcul de ΔH(g → s)(H^+) est fait comme suit. L'addition des changements d'enthalpie des réactions 6 et 7 donne ΔH(d, g → s)(HCl) = ΔH(g → s)(HCl) + ΔH(d)(HCl); puis en combinant [2] et [3], on déduit l'enthalpie de transfert du couple (H^+, Cl^-) suivant: ΔH(aq → s)(H^+, Cl^-) = ΔH(d, g → s) − ΔH(d, g → aq). On calcule ensuite (réactions 2, 3 et 4) ΔH(aq → s)(H^+) = ΔH(aq → s)(H^+, Cl^-) − ΔH(aq → s)(Cl^-), les enthalpies de transfert de l'ion Cl^-, ΔH(aq → s)(Cl^-), étant obtenues à partir de l'hypothèse extrathermodynamique tatb. Les valeurs récentes de Parker et coll. (16) sont utilisées pour les enthalpies de transfert de l'eau vers les solvants TMS, CP, DMF et DMSO. Pour le transfert eau → AN, on a combiné ΔH(aq → AN)(Br^-) = 2.00 kcal mol^{-1} (16) avec les enthalpies de transfert eau → AN des électrolytes Me_4NBr et Me_4NCl données par Abraham (17), soit respectivement −1.71 et +1.90 kcal mol^{-1}. Finalement, on obtient ΔH(g → s)(H^+) = ΔH(aq → s)(H^+) + ΔH(g → aq)(H^+) avec ΔH(g → aq)(H^+) = −270.0 kcal mol^{-1} (18).[3] Toutes les valeurs des enthalpies utilisées sont résumées dans le tableau 3.

[3]Cette valeur a été adoptée ici de préférence à la valeur −260.7 kcal mol^{-1} utilisée dans notre précédent article (10).

Discussion

L'ordre de basicité des solvants, tel que déduit de nos valeurs (kcal mol^{-1}) de ΔH(g → s)(H^+) (ou de ΔH(aq → s)(H^+)) est TMS (−252.6) < AN (−256.6) < CP (−259.5) < H_2O (−270.0) < DMSO (−276.1) ∼ DMF (−276.7). La faible différence, 0.6 kcal mol^{-1}, entre les valeurs correspondant aux deux solvants DMSO et DMF n'est en effet pas significative, l'erreur sur ΔH(aq → s)(H^+) étant la somme d'une erreur estimée, pour ces deux solvants, à ±0.5 kcal mol^{-1} sur ΔH(aq → s)(H^+, Cl^-) et d'une erreur, difficile à évaluer, sur ΔH(aq → s)(Cl^-). Les valeurs obtenues pour ΔH(aq → s)(H^+) reposent évidemment sur les valeurs des enthalpies de transfert de Cl^-, ΔH(aq → s)(Cl^-), évaluées à partir de l'hypothèse extrathermodynamique tatb. Bien que l'on ne puisse que spéculer sur la validité des valeurs de ΔH(aq → s)(Cl^-), on remarque qu'elles sont sensiblement constantes pour les cinq solvants dpa (tableau 3). Cette observation, que les enthalpies de transfert d'un anion varient peu entre solvants dpa, semble bien confirmée par les faibles variations (tableau 2) dans les changements d'enthalpies de la réaction 10 pour les cinq solvants dpa. Des résultats

[10] $SbCl_5(l) + Cl^-(s) = SbCl_6^-(s)$

analogues ont aussi été obtenus pour d'autres

Can. J. Chem. Downloaded from www.nrcresearchpress.com by 210.87.254.105 on 09/05/12
For personal use only.

TABLEAU 4. Paramètres enthalpimétriques de basicité ΔH (kcal mol^{-1})

Solvant	$-\Delta H$(g → s) (H^+)	$-\Delta H$(r → s) (PFP)*	$-\Delta H$(g → s) (H···OH)†	$-\Delta H$(g → s) (H_2O)‡	$-\Delta H$ ($SbCl_5$ + B)§	$-\Delta H_i$ (B)‖
TMS	252.6	4.94, 4.25	6.15	8.9	14.8	11.8
AN	256.6		6.13	8.5	14.1	14.6
CP	259.5	4.99, 4.53	6.20	8.6	15.1	17.8
DMF	276.7	8.13, 6.97	7.85	11.4	26.6	29.5
DMSO	276.1	7.66, 7.21	8.13	11.8	29.8	28.6
H_2O	270.0		7.68	10.5	18.0	16.5

*Enthalpie de solution du *p*-fluorophénol (en solution dans r = CCl_4) dans le solvant (réf. 3); la seconde valeur est corrigée pour tenir compte d'interactions non-spécifiques (réf. 3).
†Enthalpie de solvatation de l'espèce hypothétique H···OH (réf. 22).
‡Enthalpie de solution de H_2O(g) calculée à partir de l'enthalpie de vaporisation de l'eau +10.5 kcal mol^{-1} et de la chaleur de solution de H_2O(l) (réf. 10 et 7).
§Changement d'enthalpie associé à la réaction entre le solvant B et $SbCl_5$ dans $C_2H_4Cl_2$ (réf. 27).
‖Enthalpie de protonation du solvant B dans HSO_3F (réf. 3).

réactions anions–molécules (19).

Nos valeurs de ΔH(aq → s)(H^+) lorsque comparées à celles de ΔG(aq → s)(H^+) obtenues par Kolthoff et Chantooni (4) pour trois des solvants déjà étudiés ici, AN (11.1), DMF (−3.4) et DMSO (−4.5 kcal mol^{-1}) indiquent que les variations d'entropie de transfert ΔS(aq → s)(H^+) jouent un rôle non négligeable comme le laissaient entrevoir les quelques valeurs de ΔS(aq → s) données pour des cations autres que H^+ (17, 20, 21).

Nous pouvons effectuer des comparaisons intéressantes entre nos valeurs de ΔH(g → s)(H^+) et d'autres paramètres caractérisant la basicité des solvants étudiés (tableau 4), soit en tant que milieux, soit en tant que molécules isolées dans une phase inerte ou un milieu de référence acide. Examinons tout d'abord les paramètres caractérisant la basicité des solvants en tant que milieux S. On peut ainsi comparer nos valeurs de ΔH(g → s)(H^+) avec les changements d'enthalpie ΔH(g → s) donnés aux tableaux 1 et 4 pour les acides de Brønsted, HCl, *p*-fluorophénol (g est remplacé par CCl_4), H_2O et l'espèce hypothétique H···OH telle que définie par Krishnan et Friedman (22). L'ordre de basicité par rapport à ces acides est TMS ∼ AN ∼ CP ≤ DMF ∼ DMSO, il diffère de l'ordre correspondant à H^+. La basicité des solvants varie ainsi suivant que l'on considère pour la caractériser, soit la réaction de protonation S + H^+ = SH^+, soit une réaction conduisant à la formation d'une liaison hydrogène S + HA = S···HA. Arnett *et al.* (3) ont déjà noté cette différence au niveau de la basicité des molécules B et l'ont attribuée à la nature différente des deux réactions.

Que le solvant se comporte différemment vis-à-vis des acides H^+ et HA met bien en évidence les difficultés qui existent pour rendre compte ou prévoir l'effet du solvant (s) sur la dissociation (pK(d)) d'un acide HA (9) suivant:

[11] $$HA(s) \rightleftarrows H^+(s) + A^-(s)$$

Ainsi d'après le tableau 3, pour HCl = HA, on note qu'en passant du solvant TMS à AN, la variation de ΔH(d) (4.7 kcal mol^{-1}), soit ΔpK(d) = 3.5, provient presqu'uniquement d'un effet de solvant sur H^+(s); par contre, en passant du TMS au DMSO la différence des ΔH(d) (12.7 kcal mol^{-1}), ΔpK(d) = 9.3, résulte principalement de l'effet de solvant sur H^+(s), ΔpK(d) = 17.3, compensé par un effet important et contraire d'environ 8 unités sur HCl(s). Si l'on considère de plus que pour une série d'acides HA les interactions entre HA et les deux solvants pourront ne pas varier régulièrement, on comprend pourquoi les ΔpK(d) pour deux solvants sont difficiles à rationaliser (9), même pour les solvants dpa où l'effet du solvant sur l'anion A^-(s) est faible et n'apporte ainsi pas de complications supplémentaires.

Considérons maintenant les relations entre nos valeurs de ΔH(g → s)(H^+) et les paramètres caractérisant la basicité des molécules de solvant isolées B, soit en phase gazeuse, soit dans un milieu inerte. Arnett *et al.* (3) ont suggéré que le paramètre le plus simple pour caractériser la basicité d'une molécule B est son affinité protonique AP, c'est-à-dire l'enthalpie de la réaction de protonation de B en phase gazeuse suivant:

[12] $$B(g) + H^+(g) \rightarrow BH^+(g)$$

Can. J. Chem. Downloaded from www.nrcresearchpress.com by 210.87.254.105 on 09/05/12
For personal use only.

Can. J. Chem. Downloaded from www.nrcresearchpress.com by 210.87.254.105 on 09/05/12
For personal use only.

Les valeurs retenues[4] de l'AP pour les solvants considérés ici (kcal mol^{-1}), -171 (H_2O), -188 (AN) et -209 (DMF) (2) sont à comparer aux valeurs de $\Delta H(g \rightarrow s)(H^+)$, -270 (H_2O), -257 (AN) et -277 (DMF). Considérons d'abord les cas de l'AN et H_2O. Les résultats indiquent que si l'AN est plus basique que H_2O en phase vapeur, la situation est inversée quand on considère l'AN et H_2O en tant que solvants. Cette inversion de la basicité est due aux caractères aprotonique et protonique respectifs des deux solvants. Les résultats de Grimsrud et Kebarle (23) laissent prévoir qu'en phase gazeuse, lorsque B est un donneur de liaison hydrogène comme H_2O, la réaction avec H^+ conduit à une série d'ions H^+B_n de stabilités graduellement décroissantes. Par contre, lorsque B n'est pas un donneur de liaison hydrogène comme l'AN, la stabilité des ions H^+B_n où $n > 2$ diminue brusquement par suite de l'absence de stabilisation possible par liaison hydrogène. De la même façon, en milieu solvant, les ions $H^+(s)$ seraient stabilisés sous forme de H^+S_n dans les solvants protoniques par formation de liaisons hydrogène de type coopératif, alors que dans les solvants dipolaires aprotoniques, l'absence de liaisons hydrogène de ce type ne permettrait pas d'aller au delà de H^+S_2. Ce point de vue se trouve confirmé par des résultats de rmn. Olofsson et coll. (24, 25) ont étudié les réactions entre le DMSO, le diméthylacétamide (DMA), très voisin du DMF, et HCl–$SbCl_5$ dans $C_2H_4Cl_2$. Ces auteurs ont mis en évidence le complexe protoné $[H^+B]SbCl_6^-$ et en présence d'un excès de B, $[H^+B_2]SbCl_6^-$. Les déplacements chimiques δ des protons acides du complexe H^+B_2 se trouvent à 8–9 ppm au delà de ceux du complexe H^+B, les $\delta(H^+B)$ étant d'ailleurs en bon accord avec les valeurs observées pour les bases B protonées dans HSO_3F ou HSO_3F–SbF_5. Les valeurs de $\delta(H^+B_2)$ (ppm) obtenues par Olofsson, 14.63 (DMSO) et 18.67 (DMA) sont très voisines de celles que nous avons déterminées pour des solutions d'acides forts dans les deux solvants DMSO et DMF, 14.5 (DMSO) (9), 18.8 (DMF) (7). On pourrait donc conclure sur la base de cette comparaison que le proton est bien solvaté sous la forme H^+S_2 dans ces solvants dpa. On comprend aussi pourquoi les valeurs de $\delta(H^+H_2O)$ extrapolées à partir de mesures sur des solutions d'acides forts dans l'eau sont par contre variables (réf. 26 et références citées) les espèces H^+S_n étant mal définies quand S est un solvant protonique. Nous avons aussi essayé de comparer les résultats calorimétriques d'Olofsson et coll. (24) sur la protonation du DMSO et du DMA, par HCl–$SbCl_5$ dans $C_2H_4Cl_2$, avec nos résultats sur la protonation des solvants DMSO et DMF. Les changements d'enthalpie (kcal mol^{-1}) calculés d'après les valeurs d'Olofsson sont pour la réaction

[13] $2B + HCl(g) + SbCl_5(l) \rightarrow [H^+B_2][SbCl_6^-](C_2H_4Cl_2)$

-51 (B = DMSO) et -57 (B = DMA), et respectivement ~ -36 et -46 pour les réactions analogues donnant $[H^+B][SbCl_6^-]$. Nos valeurs pour

[14] $HCl(g) + SbCl_5(l) \rightarrow H^+(s) + SbCl_6^-(s)$

sont ~ -55 (S = DMSO) et -56 (S = DMF). Bien que les effets de solvatation sur $[H^+B_2][SbCl_6^-]$ ne puissent être évalués, les faibles écarts observés pour les enthalpies des deux réactions 13 et 14 sont en faveur de notre interprétation quant à la présence de la même espèce soit H^+S_2 dans $C_2H_4Cl_2$, et le DMSO et le DMF. D'autres auteurs ont aussi conclu, à partir de résultats de spectroscopie ir, à la présence de l'ion $H^+(DMSO)_2$ dans des solutions d'acides dans le DMSO (27, 28, 29) et l'ion lui-même a été isolé dans le complexe $[H^+(DMSO)_2][AuCl_4^-]$ (29).

Revenons à la comparaison des valeurs (kcal mol^{-1}) de l'AP cette fois pour l'AN (-188) et le DMF (-209) avec celles de $\Delta H(g \rightarrow s)(H^+)$, -257 (AN) et -277 (DMF). On note, à l'encontre de ce qui a été vu pour l'AN et H_2O, qu'il y a pour ces deux solvants aprotoniques une excellente correspondance ($\Delta \sim 20$ kcal mol^{-1}) entre les basicités en phases vapeur et liquide. La différence entre $\Delta H(g \rightarrow s)(H^+)$ et l'AP augmentée de la chaleur de vaporisation du solvant, soit globalement -77 (AN) et -79 (DMF) correspond à l'enthalpie de solvatation de H^+S dans S. Ces deux valeurs sont évidemment nettement plus faibles que dans le cas de H_2O (-109), solvant protonique, où le proton se trouve stabilisé. Des comparaisons plus complètes entre l'AN et DMF pourraient être faites si l'on disposait, comme pour le diméthyléther aprotonique (23), des valeurs de l'enthalpie de la réaction

[4]Ces valeurs récentes nous ont été aimablement communiquées par le Professeur J. L. Beauchamp.

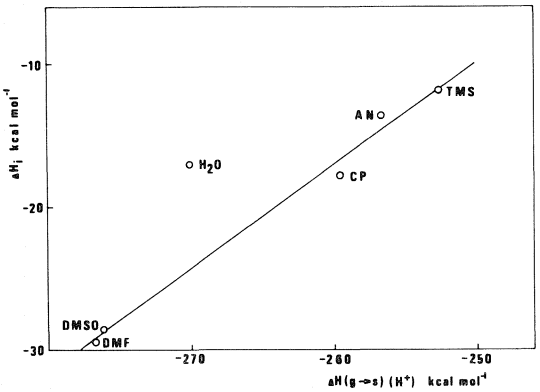

FIG. 1. Relation entre ΔH_i, l'enthalpie de protonation du sulfolane, de l'acétonitrile, du carbonate de propylène, du diméthylformamide, du diméthylsulfoxyde et de l'eau dans HSO_3F, et $\Delta H(g \rightarrow s)(H^+)$, l'enthalpie de solvatation de $H^+(g)$ dans ces solvants.

[15] $$H^+S(g) + S(g) \rightarrow H^+S_2(g)$$

puisque l'on pourrait alors évaluer l'enthalpie de solvatation de l'espèce définie H^+S_2 dans S.

Considérons maintenant les relations entre $\Delta H(g \rightarrow s)(H^+)$ et les paramètres caractérisant la basicité de B dans un milieu inerte. Les valeurs du changement d'enthalpie de la réaction dans $C_2H_4Cl_2$ des solvants dpa avec l'acide de Lewis $SbCl_5$, couramment utilisé comme paramètre de basicité ("nombre donneur" de Gutmann et Schmid (30)), sont données dans le tableau 4. L'absence de corrélation que l'on note entre ces valeurs et celles de $\Delta H(g \rightarrow s)(H^+)$ peut, là encore, être attribuée à la nature différente des deux réactions considérées.

Finalement, nous avons comparé les valeurs de $\Delta H(g \rightarrow s)(H^+)$ avec celles des enthalpies de protonation ΔH_i des molécules de solvants dans le milieu de référence acide HSO_3F. Ces enthalpies telles que déterminées par Arnett *et al.* (3) sont données dans le tableau 4. On note une relation sensiblement linéaire entre les deux séries de valeurs pour les cinq solvants dpa (fig. 1). Des mesures sont en cours pour déterminer si cette relation intéressante s'étend à d'autres solvants dpa. Il n'est pas surprenant d'observer que l'eau, un solvant protonique, échappe à la corrélation: la valeur pour H_2O $\Delta H(g \rightarrow s)(H^+)$, -260 kcal mol^{-1} qui correspondrait sur la droite de la fig. 1, à $\Delta H_i = -16.5$ kcal mol^{-1} est inférieure à la valeur réelle -270 puisque cette dernière correspond à la basicité, plus forte, de l'eau en tant que milieu alors que la valeur -260 serait liée à la basicité de la molécule d'eau isolée. Les raisons de la corrélation entre $\Delta H(g \rightarrow s)(H^+)$ et ΔH_i sont vraisemblablement complexes puisque $\Delta H(g \rightarrow s)(H^+)$ se réfère au proton sous la forme H^+S_2 dans le solvant S, alors que ΔH_i caractérise le proton sous la forme H^+B dans HSO_3F. Afin d'essayer d'expliquer la corrélation, on a cherché s'il y avait une relation entre $\Delta G(g \rightarrow s)(H^+)$, ces dernières valeurs étant plus nombreuses que celles de ΔH, et l'affinité protonique AP, pour d'autres solvants dpa que ceux étudiés ici, mais la corrélation observée entre $\Delta G(g \rightarrow s)(H^+)$ et l'AP n'est qu'approximative (2). Par ailleurs, Arnett (3) ayant établi pour une série de bases, une relation linéaire entre ΔH_i et les pK, déterminés dans l'eau et les mélanges H_2O–H_2SO_4, on peut prévoir sur la base de nos résultats, une relation linéaire entre les pK des solvants dpa et les valeurs de $\Delta H(g \rightarrow s)(H^+)$.

Remerciements

Nous remercions le Conseil National des Recherches du Canada pour son aide financière et le Conseil des Arts pour l'octroi d'une bourse à l'un de nous (R.D.). Nos remerciements vont aussi à J. Charbonneau et S. Y. Lam pour leur collaboration.

1. R. L. MARTIN et D. A. SHIRLEY. J. Am. Chem. Soc. **96**, 5299 (1974).
2. R. L. BENOIT et C. LOUIS. *Dans* The chemistry of non-aqueous solvents. Vol. V. *Edité par* J. J. Lagowski. Academic Press, New York. Sous presse.
3. E. M. ARNETT, E. J. MITCHELL et T. S. S. R. MURTY. J. Am. Chem. Soc. **96**, 3875 (1974).
4. I. M. KOLTHOFF et M. K. CHANTOONI, JR. J. Phys. Chem. **76**, 2024 (1972).
5. G. CHOUX et R. L. BENOIT. J. Am. Chem. Soc. **91**, 6221 (1969).
6. R. L. BENOIT, M. RINFRET et R. DOMAIN. Inorg. Chem. **11**, 2603 (1972).
7. R. DOMAIN. Thèse de Doctorat, Université de Montréal, Montréal, Qué. 1975.
8. C. E. VANDERZEE et J. D. NUTTER. J. Phys. Chem. **67**, 2521 (1963).
9. R. L. BENOIT et C. BUISSON. Electrochim. Acta, **18**, 105 (1973).
10. R. L. BENOIT et S. Y. LAM. J. Am. Chem. Soc. **96**, 7385 (1974).
11. P. G. SEARS, R. K. WOLFORD et L. R. DAWSON. J. Electrochem. Soc. **103**, 633 (1956); L. F. SILVESTER et P. A. ROCK. J. Electrochem. Soc. **121**, 518 (1974).
12. R. L. BENOIT, C. BUISSON et G. CHOUX. Can. J. Chem. **48**, 2353 (1970).
13. C. LOUIS. Thèse de Doctorat, Université de Montréal, Montréal, Qué. 1975.

Can. J. Chem. Downloaded from www.nrcresearchpress.com by 210.87.254.105 on 09/05/12
For personal use only.

14. E. M. ARNETT et D. R. MCKELVEY. J. Am. Chem. Soc. **88**, 2598 (1966).
15. C. V. KRISHNAN et H. L. FRIEDMAN. J. Phys. Chem. **75**, 3606 (1971).
16. B. G. COX, G. R. HEDWIG, A. J. PARKER et D. W. WATTS. Aust. J. Chem. **27**, 477 (1974).
17. M. H. ABRAHAM. J. Chem. Soc. Faraday Trans. 1, **69**, 1375 (1973).
18. J. E. DESNOYERS et C. JOLICOEUR. *Dans* Modern aspects of electrochemistry. Vol. 5. *Edité par* B. E. Conway et J. O. M. Bockris. Plenum Press, New York. 1969; H. L. FRIEDMAN et C. V. KRISHNAN. *Dans* Water, a comprehensive treatise. Vol. 3. *Edité par* F. Franks. Plenum Press, New York. 1973; L. G. HEPLER et E. M. WOOLEY. *Dans* Water, a comprehensive treatise. Vol. 3. *Edité par* F. Franks. Plenum Press, New York. 1973.
19. S. Y. LAM, C. LOUIS et R. L. BENOIT. J. Am. Chem. Soc. **98**, 1156 (1976).
20. B. G. COX et A. J. PARKER. J. Am. Chem. Soc. **95**, 408 (1973).
21. C. M. CRISS. J. Phys. Chem. **78**, 1000 (1974).
22. C. V. KRISHNAN et H. L. FRIEDMAN. J. Phys. Chem. **75**, 3598 (1971).
23. E. P. GRIMSRUD et P. KEBARLE. J. Am. Chem. Soc. **95**, 7939 (1973).
24. Q. APPLETON, L. BERNANDER et G. OLOFSSON. Tetrahedron, **27**, 5921 (1971).
25. L. BERNANDER et G. OLOFSSON. Tetrahedron, **28**, 3251 (1972).
26. R. J. GILLESPIE. *Dans* Physicochemical processes in mixed aqueous solvents. *Edité par* F. Franks. American Elsevier Publishing Co. Inc., New York. 1967.
27. J. M. WILLIAMS et M. KREEVOY. J. Am. Chem. Soc. **89**, 5499 (1967).
28. I. KAMPSCHULTE-SCHEUING et G. ZUNDEL. J. Phys. Chem. **74**, 2363 (1970).
29. R. A. POTTS. Inorg. Chem. **9**, 1284 (1970).
30. V. GUTMANN et R. SCHMID. Coord. Chem. Rev. **12**, 263 (1974).
31. R. T. MYERS. J. Chem. Educ. **53**, 17 (1976).

Can. J. Chem. Downloaded from www.nrcresearchpress.com by 210.87.254.105 on 09/05/12
For personal use only.

Metals intercalated in graphite. III. The reactions of aromatic, olefinic, and acetylenic hydrocarbons with potassium–graphite intercalates

JEAN MARC LALANCETTE AND ROGER ROUSSEL
Département de chimie, Université de Sherbrooke, Sherbrooke (Qué.), Canada J1K 2R1

Received February 10, 1976

JEAN MARC LALANCETTE and ROGER ROUSSEL. Can. J. Chem. **54**, 2110 (1976).

Potassium–graphite intercalates ($C_{24}K$) can act as a catalyst for the reduction of olefins and alkynes. $C_{24}K$ is a very efficient catalyst for the isomerization of *cis*-stilbene to *trans*-stilbene. $C_{24}K$ can promote deuterium exchange with hydrogens carried by hydrocarbons having an acidity equal to or higher than that of benzene. $C_{24}K$ can condense benzene to biphenyl and can isomerize 2-alkynes to 1-alkynes at low temperature.

JEAN MARC LALANCETTE et ROGER ROUSSEL. Can. J. Chem. **54**, 2110 (1976).

Les composés d'insertion du potassium dans le graphite ($C_{24}K$) présentent des propriétés catalytiques pour la réduction des alcènes et des alcynes. $C_{24}K$ s'avère un agent très efficace pour la convertion du *cis*-stilbene en *trans*-stilbene. $C_{24}K$ permet l'échange de deuterium avec des hydrocarbures portant des hydrogènes d'acidité comparable ou plus grande que celle du benzène. $C_{24}K$ permet la condensation du benzène en biphényle et donne l'isomerisation des alcynes-2 en alcynes-1 à de basses températures.

Can. J. Chem. Downloaded from www.nrcresearchpress.com by 210.87.254.42 on 09/05/12
For personal use only.

The reaction of hydrocarbons in the presence of potassium–graphite intercalates has been reported by several authors. For example, Ichikawa *et al.* (1) have described exchange reactions of methane and other hydrocarbons with deuterium at 300 °C, in the presence of graphite–potassium lamellar compounds. Potassium intercalates in graphite have also been reported as catalysts for polymerization of olefins (2). An excellent review of the catalytic properties of alkali metals – graphite intercalation compounds has appeared recently and summarizes well the state of the literature on this subject (3). In our work, we have used the preparative techniques described by earlier authors without difficulties (3). The physical and chemical properties of our intercalates were consistent with those reported in the literature and no structural determinations have been done by us on these intercalates.

As part of a study of the chemistry of metals intercalated in graphite (4) we have examined the reactions of hydrocarbons with intercalated potassium. This has led to a better understanding of the system hydrogen – potassium–graphite intercalates – hydrocarbons. Also, we have noted several new reactions typical of this system. Three areas have been examined as described below.

(1) The State of Hydrogen or Deuterium in the Presence of Potassium Intercalated in Graphite

A very basic question that must be solved in order to understand the behavior of hydrocarbons in the presence of potassium intercalated in graphite is to know the state of hydrogen or deuterium in equilibrium with this solid phase. It has been reported that potassium–graphite intercalates can adsorb (5) or absorb (6) hydrogen, even at atmospheric pressure. *A priori*, the hydrogen held up by potassium intercalates can exist, in part or entirely, under one of the following states: (*a*) as a hydride ion, chemically bonded to potassium, (*b*) dissociated as a $H^{\cdot}$ radical, or (*c*) as a molecule H_2 physically adsorbed on the surface of the solid phase or held within the lattice of the intercalate. The presence of available hydride ions in the intercalated potassium treated by hydrogen is unlikely if the report of Saehr and Herold (7) on this matter is taken into account.

The other alternatives have been examined in order to understand the ability of hydrogen to dissociate when held on C_8K. It has been reported that C_8K is inactive for promoting hydrogen–deuterium exchange reactions but that the potassium intercalate, when it already holds

TABLE 1. Reduction of olefins with H_2 in the presence of $C_{24}K$

System	Solvent	P (psi)	T (°C)	Duration (h)	Results: Hydrocarbon	Results: % yield[a]	Results: Ratio
1-Octene	Nil				Octane	28	14
1-Methyl-1-cyclohexene		1000	100	20	1-Methylcyclohexane	2.0	
1-Octene	Nil	1000	100	20	Octane	28	1
1-Dodecene					Dodecane	28	
cis-2-Octene	Nil				Octane	12	12
1-Methyl-1-cyclohexene		1000	100	24	Methylcyclohexane	1	
trans-Stilbene	C_6H_6	1000	100	60	1,2-Diphenylethane	92	—
cis-Stilbene	C_6H_6	1000	100	20	1,2-Diphenylethane	90	—
trans-Stilbene					*cis*-Stilbene	0	
					trans-Stilbene	10	
cis-Stilbene	C_6H_6	200	100	20	1,2-Diphenylethane	91	—
trans-Stilbene					*cis*-Stilbene	0	
					trans-Stilbene	9	
cis-Stilbene	C_6H_6	200	25	20	1,2-Diphenylethane	4	—
trans-Stilbene					*cis*-Stilbene	0	
					trans-Stilbene	96	
cis-Stilbene	C_6H_6	0[b]	25	48	1,2-Diphenylethane	7[c]	—
					cis-Stilbene	0	
					trans-Stilbene	93	

[a]The % yield represents the product distribution in the recovered material. The total yield of recovered material was in the range of 90–95% of the weight of the starting hydrocarbons.
[b]Hydrogen was replaced by 1 atm of nitrogen.
[c]Main product, plus other minor aromatic products.

either hydrogen or deuterium, can promote the exchange (8). We have performed two different experiments to verify the capacity of exchange of deuterium held on potassium–graphite intercalates. In a first experiment, methanol was added to C_8K saturated with a measured volume of deuterium. The gas evolved from the attack of methanol on C_8KD_x had exchanged to the amount of 18%. In a second experiment a measured volume of deuterium was adsorbed over C_8K. The system was then filled with hydrogen. The amount of exchange noted after 36 h was 30%, the system being kept at room temperature and atmospheric pressure. From these results, in good agreement with the reports of Watanabe *et al.* (9) and Colin and Herold (10), we believe that deuterium is physically adsorbed either on the surface or within the lattice of C_8K and that in this state, deuterium (or hydrogen) is partly dissociated or at least activated to an extent that allows exchange at a measurable rate at 25 °C with either nascent or molecular hydrogen.

(2) Reduction and Isomerization of Olefinic Hydrocarbons with $C_{24}K$

We have found that $C_{24}K$ behaves as a moderately active catalyst for the hydrogenation of olefins. Typical results are reported in Table 1. It can be seen that even at high pressure, and after a long contact time, the reduction of aliphatic olefins remains incomplete. Also, it is apparent that the steric environment around the double bond markedly influences the speed of the reduction. With the aromatic olefins studied, the *cis* and *trans*-stilbenes, it appears that the reduction proceeds more readily to the saturation stage. By adjustment of the conditions of reactions, it has been possible to show that prior to reduction, the *cis* isomer is transformed into the *trans* isomer. In fact, $C_{24}K$ alone at room temperature, in the absence of H_2, can achieve the isomerization of *cis*-stilbene to *trans*-stilbene, a reaction that cannot be performed by potassium alone. The reduction then appears as a process subsequent to the rearrangement of the double bond. The reduction of *trans*-stilbene by hydrogen in the presence of $C_{24}K$ is a relatively rapid reaction in comparison with the reduction of less sterically hindered aliphatic olefins. However, the speed of isomerization of *cis*-stilbene is faster than the speed of reduction. Consequently the 'sites' of $C_{24}K$, active for the

Can. J. Chem. Downloaded from www.nrcresearchpress.com by 210.87.254.42 on 09/05/12
For personal use only.

Can. J. Chem. Downloaded from www.nrcresearchpress.com by 210.87.254.42 on 09/05/12
For personal use only.

isomerization, are either more numerous or more active (or both) than the 'sites' for reduction. If the same 'sites' are used for isomerization and reduction, then, these 'sites' have a better ability for isomerization than for reduction, at least for the system we have studied. The nature of these 'sites' remains an open question.

We have noted that when *cis*-stilbene was isomerized to *trans*-stilbene, in the absence of hydrogen, a small percentage of secondary products was formed. This secondary fraction was mainly 1,2-diphenylethane. Partial reduction of the *trans*-stilbene, to explain the small amount of 1,2-diphenylethane, called for a source of hydrogen from within the reaction mixture, since there was no external source of this agent. This led us to examine the stability of benzene, used as a solvent in this experiment, towards $C_{24}K$. To our surprise, we found that benzene, at reflux temperature in cyclohexane, will react in the presence of $C_{24}K$ to give biphenyl. After a reflux of 48 h, up to 20% of the starting benzene had been transformed into biphenyl. Consequently, we believe that the small amount of 1,2-diphenylethane formed when *cis*-stilbene is isomerized to *trans*-stilbene may come from dehydrogenation of a portion of the material present in the system.

These interesting reactions with benzene and *cis*/*trans*-stilbenes establish the remarkable reactivity of $C_{24}K$ in the system hydrogen–olefin. We believe that with hydrocarbons of acidity equal to or higher than that of benzene (pK_a 37) $C_{24}K$ will be able, at moderate temperature, to promote reactions such as deuterium exchanges, involving the rupture of the C—H bonds of the hydrocarbon. This opinion is supported by the fact that 1,2-diphenylethane, toluene (pK_a 35), and triphenylmethane (pK_a 31.5) do exchange deuterium for hydrogen, in an atmosphere of deuterium at temperatures of the order of 100 °C, as we have shown. The rate of exchange is faster for protons in the α position of an aromatic ring than on the aromatic ring itself, as shown by our analysis of the reaction mixture obtained for the exchange reaction with 1,2-diphenylethane. It is certain that $C_{24}K$ is responsible for this effect. We have noted that neither potassium nor graphite will give the isomerization or reduction reactions with *cis*-stilbene or the formation of biphenyl under the very mild conditions used. The different reactions of stilbenes with $C_{24}K$ and hydrogen are presented in eq. 1.

[1] 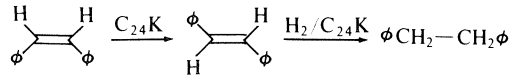

$$2\phi\text{—H} + C_{24}K \longrightarrow \phi\text{—}\phi + [C_{24}KH_x] \longrightarrow C_{24}K + H_2$$

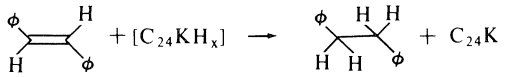

(3) The Reduction and Isomerization of Alkynes with $C_{24}K$

Alkynes can be reduced by hydrogen in the presence of $C_{24}K$. This has been illustrated by the reduction of 1-phenyl-1-butyne, the main reaction product being 1-butylbenzene, obtained with a yield of 75%. This main product was accompanied by secondary products showing olefinic protons in the nmr.

The main interest of $C_{24}K$ as a reagent in the chemistry of alkyne appears to be the activity of this intercalate as an agent for isomerization of the triple bond. Under mild experimental conditions, 86% of 2-octyne can be converted to 1-octyne. This represents a relatively simple method of isomerization of a triple bond to the 1,2-position in an aliphatic chain allowing the reaction to proceed at much lower temperature than other methods (11*a*). We have noted the presence of the corresponding allene in the course of the isomerization. The formation of allene has already been postulated as an intermediate in the process of isomerization of 2-alkyne to 1-alkynes (11*b*). The use of potassium alone in C_6H_6 at 25 °C does not isomerize 2-decyne. When potassium is intercalated to give $C_{24}K$, a yield of 20% of 1-decyne and 9% of 1,2-decadiene is noted (see Table 2). When the reaction is performed in the presence of an aliphatic hydrocarbon, there are no secondary products such as biphenyl. Although alkali metals, such as potassium or sodium are reported to isomerize 2-alkynes to 1-alkynes above 100 °C (12) the results reported here indicate that the intercalation of the alkali metal greatly facilitates the isomerization and lowers the temperature at which this conversion takes place.

TABLE 2. Isomerization of alcynes in the presence of $C_{24}K$

System	T (°C)	Duration (h)	Solvent	Products	
				Hydrocarbon	% yield[a]
2-Decyne	25	48	C_6H_6	1-Decyne	20
				1,2-Decadiene	9
				2-Decyne	71
2-Decyne	80	60	C_6H_6	1-Decyne	65
				1,2-Decadiene	4
				2-Decyne	15
				Biphenyl[b]	16
2-Octyne	80	100	C_6H_6	1-Octyne	26
				1,2-Octadiene	2
				2-Octyne	5
				Biphenyl	52
				Unidentified product	14
2-Decyne	80	40	Cyclohexane	1-Decyne	86
				1,2-Decadiene	7
				2-Decyne	7

[a]Same as footnote *a* of Table 1.
[b]Formed from the benzene used as solvent.

Conclusion

The examination of the behavior of $C_{24}K$ with the systems olefins–hydrogen and alkynes–hydrogen has led to new results in terms of intermediates and reaction products. This study should emphasize the much modified reactivity induced by intercalation of an entity such as potassium in the lattice of graphite. The observed properties of $C_{24}K$ should be common, at least as a trend, to homologous intercalates in graphite.

Experimental

(1) Preparation of Potassium Intercalates

Potassium intercalates were prepared by mild heating of a mixture of graphite and potassium, in measured amounts at 100–120 °C. The intercalation was rapid and gave colored products, as reported (3). Potassium was handled under petroleum ether and the graphite (spectroscopic grade, 20 mesh) was dried at 150 °C, under 1.0 torr for 24 h. All manipulations of intercalates were done under inert atmosphere.

(2) Exchange Reaction of Deuterium with Hydrogen Generated in situ from C_8K

In a well-dried 50 ml three-necked flask were placed 1.0 g of graphite and 0.40 g of potassium. The intercalate was formed and after cooling to 25 °C, a volume of 147 ml (STP) of deuterium (99.5% D_2) was adsorbed over this weight of C_8K at atmospheric pressure. To this product, at 25 °C, was added first 10 ml of dry ethyl ether and then 5 ml of methanol, in one portion. The evolved gas was collected and analyzed by mass spectrometry (Hitachi RMU-6); *m/e*: 2, relative intensity (ri) 78 (69.6%); 3, ri 20 (17.9%); 4, ri 14 (12.5%).

(3) Exchange Reaction of Hydrogen with Deuterium Adsorbed over C_8K

The intercalate was prepared as in section 2. After cooling to 25 °C a volume of 122 ml (STP) of deuterium was adsorbed over C_8K. The system was flushed rapidly with H_2 and kept in an atmosphere of hydrogen, at atmospheric pressure for 36 h. After this contact time, at 25 °C, the gas in contact with the intercalate was analyzed by mass spectrometry; *m/e*: 2, ri 320 (66.9%); 3, ri 144 (30.0%); 4, ri 15 (3.1%). The experiment was repeated under identical conditions, except that the duration of contact was 24 h. The analysis of the gas gave 76.7% H_2, 21.5% HD, and 1.8% D_2.

(4) Hydrogenation of a Mixture of 1-Octene and 1-Methyl-1-cyclohexene in the Presence of $C_{24}K$

The hydrogenation was performed in a Parr hydrogenation bomb, of 500 ml capacity. The intercalate was obtained as described above, from 10.0 g of graphite and 1.45 g of potassium. At room temperature and in an inert atmosphere 1-octene (7.15 g, 0.064 mol) and 1-methyl-1-cyclohexene (8.13 g, 0.085 mol) were added to the intercalate and the system heated at 100 °C for 20 h, under a pressure of 1000 psi of hydrogen (large excess of hydrogen). After cooling, the $C_{24}K$ which was still very reactive was destroyed by careful addition of methanol. After extraction of the organic phase with ether, in the presence of water, the reaction mixture was isolated by distillation of the solvent. The reaction products were identified by analytical vpc with a SE30 10% 5 ft column, the position of the peaks being identified by reference products. Results are reported in Table 1 which includes reactions performed on several olefins and olefin mixtures. With aromatic olefins, identification of the reaction products was completed, beside

Can. J. Chem. Downloaded from www.nrcresearchpress.com by 210.87.254.42 on 09/05/12
For personal use only.

Can. J. Chem. Downloaded from www.nrcresearchpress.com by 210.87.254.42 on 09/05/12
For personal use only.

using vpc analysis; by nmr analysis: found for *trans*-stilbene: δ 7.25 (s, 2H), 7.55 (m, 10H); found for *cis*-stilbene: δ 6.78 (s, 2H), 7.35 (d, J = 1.5 Hz, 10H).

(5) Treatment of cis-Stilbene with $C_{24}K$

An intercalate of potassium was prepared in a 125 ml erlenmeyer flask from 5.0 g of graphite and 0.75 g of potassium. After cooling to 25 °C, a solution of 0.50 g (0.0028 mol) of *cis*-stilbene in 10 ml of dry benzene was added. The reaction mixture was kept at room temperature for 48 h, the suspension being stirred from time to time. After this contact, the reaction mixture was diluted to 100 ml with benzene, stirred for 5 min, and filtered. By evaporation of the solvent, a white solid was obtained. The material recovered (0.450 g) was a mixture of 1,2-diphenylethane (7% of the recovered products; nmr δ 2.9 (s), 7.30 (s)) and *trans*-stilbene (93% of the recovered products; nmr δ 7.2 (s), 7.5 (m)). The relative proportion of these two products was established by vpc analysis. The absence of *cis*-stilbene and the presence of *trans*-stilbene was confirmed by comparison of nmr and vpc with measurements made on authentic samples of the two isomers.

The presence of 1,2-diphenylethane was positively established in a similar fashion but there is a possibility that other products might be present, along with 1,2-diphenylethane. The small amount of this fraction prevented a more exhaustive analysis.

The experiment was repeated twice, following the identical procedure, and gave the same results. Also, the experiment was carried out as above but with potassium alone. The starting *cis*-stilbene was then recovered quantitatively (94%) and unaltered.

(6) Reaction of Benzene with $C_{24}K$

In a 100 ml three-necked flask an intercalate of potassium was prepared from 5.0 g of graphite and 0.80 g of potassium. A solution of 2.0 g of benzene (Spectro grade) in 50 ml of dry cyclohexane (Reagent grade) was then added to the intercalate. After a reflux of 42 h, the suspension was cooled, treated with an excess of methanol and water, filtered, dried, and the organic solvent evaporated. These operations gave 0.40 g of biphenyl, mp 67–69 °C (lit. (00) 70 °C), a yield of 20% from the starting benzene. The reaction was repeated several times giving typical yields such as 23.5% of biphenyl after a contact time of 4 days. Mass spectrometry of biphenyl: m/e 154 (C_6H_5—C_6H_5), 77 (C_6H_5); nmr δ 7.6 (m); identical with nmr of an authentic sample of biphenyl.

It has been noted that potassium alone (0.80 g), under reflux conditions similar as above, with a solution of 2.0 g of benzene in cyclohexane gave no biphenyl. Graphite alone (5.0 g) was also inert toward benzene under experimental conditions as described.

(7) Exchange Reaction of Hydrocarbons with Deuterium in the Presence of $C_{24}K$

In order to proceed with these exchange reactions, we used a steel bomb of 2 ml capacity. The intercalate was prepared as above with 0.40 g of graphite and 0.10 g of potassium. The intercalate, prepared in a glass capsule, was covered with a solution of 0.45 g of 1,2-diphenylethane in 0.75 ml of benzene. The reactor, under a pressure of 200 psi of deuterium, was kept at 110 °C for 48 h. After the usual operations, the organic phase was taken up with pentane and fractionated with an efficient column. The recovered diphenylethane (0.38 g, 85%) was identified by its nmr: δ 2.9 (s), 7.35 (s), ratio of intensity at 7.35 over 2.9: 3.72. This ratio for the fully protonated starting 1,2-diphenylethane was measured as 2.29.

Using identical solutions of protonated and partly deuterated 1,2-diphenylethane we found differences in intensities at 7.35 δ and 2.9 δ indicating 56% of exchange of the aliphatic protons and 29% of exchange of the aromatic protons. The ms m/e: 182, ($C_{14}H_{14}$) ri 100; 183, ($C_{14}H_{13}D$) ri 43; 184, ($C_{14}H_{12}D_2$) ri 38; 185, ($C_{14}H_{11}D_3$) ri 40; 186, ($C_{14}H_{10}D_4$) ri 41; 187, ($C_{14}H_9D_5$) ri 29; 91, (C_7H_7) ri 100; 92, (C_7H_6D) ri 49; 93, ($C_7H_5D_2$) ri 46; 94, ($C_7H_4D_3$) ri 28.

Similar experiments were performed with toluene and triphenylmethane. Deuterated triphenylmethane: nmr δ 5.7 (s), 7.3 (d, J = 1.5 Hz). Ratio 7.3 over 5.7 for the deuterated sample 46. The measured ratio for the starting triphenylmethane was 17. With toluene the following peaks are observed from ms: m/e: 92, (C_7H_8) ri 68; 93, (C_7H_7D) ri 100; 94, ($C_7H_6D_2$) ri 90; 95, ($C_7H_5D_3$) ri 59; 96, ($C_7H_4D_4$) ri 24.

(8) Reduction of 1-Phenyl-1-butyne with Hydrogen in the Presence of $C_{24}K$

The experimental procedure was similar to section 4, 10.0 g of graphite and 1.5 g of potassium being used to form the intercalate and 4.57 g (0.035 mol) 1-phenyl-1-butyne being reduced. After a contact of 20 h at 100 °C and under a pressure of 1000 psi of hydrogen, the reaction mixture was treated to extract the organic phase (3.75 g, 82% by weight) which was analyzed by vpc, the main fraction being separated by preparative vpc. The main product, 75% of the recovered material, was *n*-butyl benzene: nmr δ 0.95 (t, 3H), 1.6 (m, 4H), 2.70 (t, 2H), 7.35 (s, 5H). The residual material was olefinic in nature as suggested by its peak at 5.8 and 6.5 δ in the nmr. The problem of separating and isolating these minor fractions prevented a full identification.

(9) Isomerization of Alkynes

In a three-necked 100 ml flask, 5.0 g of graphite and 0.80 g of potassium were transformed into an intercalate. A solution of 1.0 g (0.0072 mol) of 2-decyne in 50 ml of C_6H_6 was added and refluxed for 60 h. After hydrolysis with methanol and water, the organic phase was extracted with benzene, dried, and the solvent distilled. A weight of 0.96 g was recovered, containing a small amount of biphenyl, thus leaving a yield of the order of 80% of the C_{10} material from the starting 2-decyne. The reaction mixture was analyzed by vpc, ir, and nmr; yields are reported in Table 2. In the case of the reaction done in cyclohexane, the yield was 0.90 g from 1.00 g of starting 2-decyne. Infrared of the reaction mixture: band at 3300 (H—C≡C), 1960 cm^{-1} (C=C=C); nmr δ 1.8 (m, CH_3—C≡C—, H—C≡C—CH_2), 5.5 (m), and 5.9 (m, CH_2=C=CH—). In order to identify the presence of the allene, 1,2-decadiene was prepared according to the method of Meisters and Swan (13). The ir and nmr of this synthetic material were identical to the reported values in the literature: nmr δ 0.91 (t, 3H), 1.32 (br s, 10H), 2.0 (m, 2H), 4.72 (m, 2H), 5.16 (m, 1H). Infrared: band at 1960 cm^{-1} (medium). Identical retention times with vpc; the presence of the typical band at 1960 cm^{-1} and nmr

indicated the presence of allene in the reaction mixture.

The experiment has been repeated with 2-octyne and results are shown in Table 2. The reaction with 2-decyne at room temperature gave 9% allene and 20% 1-alkyne. Under similar conditions at room temperature potassium alone had no effect on the starting 2-alkyne, this substance being recovered unaltered with a yield of 92%.

Acknowledgment

This project has been supported by the National Research Council of Canada.

1. M. ICHIKAWA, K. KAWASE, and K. TAMARU. Chem. Commun. 177 (1972).
2. (*a*) L. FORMI. U.S. Patent No. 3 758 416 (1972); (*b*) M. ICHIKAWA, M. SOMA, T. ONISHI, and K. TAMARU. J. Catal. **9**, 418 (1967); (*c*) D. M. OTTMERS and H. F. RASE. J. Ind. Eng. Chem. Fundamentals, **5**, 302 (1966); (*d*) J. PARROD and G. BEINERT. J. Polym. Sci. **53**, 99 (1961).
3. M. A. M. BOERSMA, Catal. Rev. Sci. Eng. **10**, 243 (1974).
4. J. M. LALANCETTE, M. J. FOURNIER-BREAULT, and R. THIFFAULT. Can. J. Chem. **52**, 589 (1974).
5. P. LAGRANGE, A. MÉTROT, and A. HEROLD. C.R. Acad. Sci. Paris, **275**, 765 (1972).
6. A. HEROLD and D. SAEHR. C. R. Acad. Sci. Paris, **250**, 545 (1960).
7. D. SAEHR and A. HEROLD. Bull. Soc. Chim. Fr. 3130 (1965).
8. K. WATANABE, T. KONDOW, M. SOMA, T. ONISHI, and K. TAMARU. Chem. Commun. 39 (1972).
9. K. WATANABE, T. KONDOW, M. SOMA, T. ONISHI, and K. TAMARU. Proc. R. Soc. London, Ser. A, **333**, 51 (1973).
10. M. COLIN and A. HEROLD. Bull. Soc. Chim. Fr. 1982 (1971).
11. (*a*) B. WOJTKOWIAK and R. ROMANET. Bull. Soc. Chim. Fr. 805 (1962); (*b*) J. BAINVEL, B. WOJKOWIAK, and R. ROMANET. Bull. Soc. Chim. Fr. 978 (1963).
12. B. J. BARRY, W. J. BEALE, M. D. CARR, S. K. HEI, and I. REID. Chem. Commun. 177 (1973).
13. A. MEISTERS and J. M. SWAN. Aust. J. Chem. **18**, 155 (1965).

Can. J. Chem. Downloaded from www.nrcresearchpress.com by 210.87.254.42 on 09/05/12
For personal use only.

Radiolysis of ferric hexafluoroacetylacetonate – toluene solutions

K. W. CHAMBERS[1] AND E. A. CHERNIAK[2]
Department of Chemistry, Carleton University, Ottawa, Ont., Canada K1S 5B6

AND

G. TAYLOR AND J. YU
Department of Chemistry, Brock University, St. Catharines, Ont., Canada L2S 3A1

Received October 31, 1975

K. W. CHAMBERS, E. A. CHERNIAK, G. TAYLOR, and J. YU. Can. J. Chem. **54**, 2116 (1976).

In the 120 krad/h, ^{60}Co-γ radiolysis of air-free, anhydrous solutions of ferric hexafluoroacetylacetonate ($Fe(HFA)_3$) in toluene at 27 °C, $G(-Fe(HFA)_3) = G(Fe(HFA)_2) = 1.05 \pm 0.03$ molecules/100 eV and $G(HHFA) = 0$ where $Fe(HFA)_2$ is radiolytically inert ferrous hexafluoroacetylacetonate and HHFA is hexafluoroacetylacetone. $G(H_2) = 0.13 \pm 0.03$ is not affected by $Fe(HFA)_3$ while $G(CH_4)$ is reduced from 0.0088 ± 0.0020 to 0.0052 ± 0.0020 and $G(\phi CH_2CH_2\phi)$ is increased from 0.102 ± 0.019 to 0.307 ± 0.026 by $Fe(HFA)_3$. Activation energies for the radiolytic formation of $Fe(HFA)_2$, H_2, CH_4, and $\phi CH_2CH_2\phi$, in the temperature range −95 to 27 °C, are 670 ± 130, 0, 1200 ± 900, and 1280 ± 25 cal mol^{-1}, respectively.

$G(-Fe(HFA)_3) = 1.05$ represents the total yield of radicals scavenged since at the concentrations of solute used in the radiolyses the quantum yield for the disappearance of $Fe(HFA)_3$ by reaction with solvent S_1 and/or T_1 states, generated by flash photolysis, is negligible ($\simeq 10^{-3}$). Radicals trapped by $Fe(HFA)_3$ are $\cdot CH_3$ ($G \approx 0.004$) and unknown radicals ($G \approx 0.4$) which are capable of combining with $\phi\dot{C}H_2$. $Fe(HFA)_3$ does not scavenge $\phi\dot{C}H_2$ radicals ($G \approx 0.6$). The formation of H_2 in scavenger inaccessible spurs and CH_4 and $\phi CH_2CH_2\phi$ outside spurs has been confirmed.

K. W. CHAMBERS, E. A. CHERNIAK, G. TAYLOR et J. YU. Can. J. Chem. **54**, 2116 (1976).

A des taux de dose de 120 krad/h, la radiolyse par ^{60}Co-γ de solutions sans air et anhydre d'hexafluoroacétylacétonate ferrique ($Fe(HFA)_3$) dans le toluène à 27 °C, $G(-Fe(HFA)_3) = G(Fe(HFA)_2 = 1.05 \pm 0.03$ molécules/100 eV et $G(HHFA) = 0$; $Fe(HFA)_2$ correspond à l'hexafluoroacétylacétonate ferreux inerte du point de vue radiolyse et HHFA est l'hexafluoroacétylacétone. $G(H_2) = 0.13 \pm 0.03$ n'est pas affecté par $Fe(HFA)_3$ alors que l'addition de $Fe(HFA)_3$ réduit $G(CH_4)$ de 0.0088 ± 0.0020 à 0.0052 ± 0.0020 et augmente $G(\phi CH_2CH_2\phi)$ de 0.120 ± 0.019 à 0.307 ± 0.026. Les énergies d'activation pour la formation radiolytique de $Fe(HFA)_2$, H_2, CH_4 et $\phi CH_2CH_2\phi$ à des températures allant de −95 à 27 °C sont respectivement de 670 ± 130, 0, 1200 ± 900 et 1280 ± 25 cal mol^{-1}.

$G(-Fe(HFA)_3) = 1.05$ représente le rendement total des radicaux piégés; en effet aux concentrations de solutés utilisés dans la radiolyse, les rendements quantiques pour la disparition de $Fe(HFA)_3$ par réaction avec les états S_1 et/ou T_1 du solvant, générés par photolyse éclair, sont négligeables ($\simeq 10^{-3}$). Les radicaux piégés par $Fe(HFA)_3$ sont $\cdot CH_3$ ($G \approx 0.004$) et des radicaux inconnus ($G \approx 0.4$) qui sont capables de se combinés avec $\phi\dot{C}H_2$. Le $Fe(HFA)_3$ ne piège pas les radicaux $\phi\dot{C}H_2$ ($G \approx 0.6$). On a confirmé la formation de H_2 dans des cavités inaccessibles aux pièges et CH_4 et $\phi CH_2CH_2\phi$ dans les cavités extérieures.

[Traduit par le journal]

Introduction

In the radiolysis of liquid toluene very rapid ion recombinations (1) result in the formation of excited singlet and triplet states (ϕCH_3*) with $G(\phi CH_3^*) \approx 4$–5 molecules/100 eV (2, 3). A small percentage of these states are converted to radicals as the yield of radicals captured by the scavengers DPPH, aroxyl and styrene monomer is 0.9 or 1.23, 1.5, and 1.1, respectively (4). The primary radicals are considered to be ϕCH_2, tolyls, $\phi\cdot$, $\cdot CH_3$ and H· which readily abstract H atoms from and add to toluene to produce secondary $\phi\dot{C}H_2$, tolyls, cyclohexadienyl and various substituted cyclohexadienyl radicals (4–6). Many final products of radiolysis have been characterized (4). Of these H_2, CH_4, and $\phi CH_2CH_2\phi$ are relevant to this investigation. H_2 is mainly formed in spurs by processes

[1]Present address: Analytical Chemistry Branch, Whiteshell Nuclear Research Establishment, Pinawa, Manitoba.

[2]Present address: Department of Chemistry, Brock University, St. Catharines, Ontario.

Can. J. Chem. Downloaded from www.nrcresearchpress.com by 210.87.254.40 on 09/05/12
For personal use only.

Can. J. Chem. Downloaded from www.nrcresearchpress.com by 210.87.254.40 on 09/05/12
For personal use only.

involving ϕCH_3* (7, 8) and CH_4 and $\phi CH_2CH_2\phi$ are mainly formed outside of spurs by reactions 1 (4, 7, 8) and 2 (4, 9), respectively.

[1] $$\cdot CH_3 + \phi CH_3 \rightarrow CH_4 + \phi\dot{C}H_2$$

[2] $$2\phi\dot{C}H_2 \rightarrow \phi CH_2CH_2\phi$$

In this study the paramagnetic, quasi-aromatic chelate ferric hexafluoroacetylacetonate, Fe(HFA)$_3$ (HFA = $CF_3COCHCOCF_3$), has been used (*a*) to determine the yield of radicals captured in the ^{60}Co-γ radiolysis of air-free, anhydrous toluene at 27 °C, (*b*) to show that the reaction of Fe(HFA)$_3$ with radicals (R·) is [3] where Fe(HFA)$_2$ is ferrous hexafluoroacetylacetonate and RHFA is a derivative of HHFA (hexafluoroacetylacetone, $CF_3COCH_2COCF_3$),

[3] $$R\cdot + Fe(HFA)_3 \rightarrow Fe(HFA)_2 + RHFA$$

(*c*) to ascertain whether or not the chemical quenching of ϕCH_3* by Fe(HFA)$_3$ occurs and (*d*) to determine, through the study of the influence of Fe(HFA)$_3$ on $G(H_2)$, $G(CH_4)$, and $G(\phi CH_2CH_2\phi)$, the validity of hypotheses regarding the origins of H_2, CH_4, and $\phi CH_2CH_2\phi$, the reactivity of Fe(HFA)$_3$ towards $\cdot CH_3$ and $\phi\dot{C}H_2$ and *G*-values for $\cdot CH_3$ and $\phi\dot{C}H_2$ scavenged by this solute. Activation energies for the radiolytic formation of H_2, CH_4, and $\phi CH_2CH_2\phi$ (in the presence and absence of Fe(HFA)$_3$) and the radiolytic disappearance of Fe(HFA)$_3$ have also been determined in the temperature range −95 to 27 °C.

There is some evidence, in various studies reported on systems analogous to Fe(HFA)$_3$, that [3] is important. For example, while *tert*-butoxy radicals abstract H from the 3-position of HHFA they do not abstract H from the ligand 3-positions in ferric acetylacetonate, Fe(acac)$_3$ (acac = $CH_3COCHCOCH_3$) (10). Some reduction of Co(acac)$_3$ to Co(acac)$_2$ occurs during the ^{60}Co-γ radiolysis of toluene solutions containing Co(acac)$_3$ (11) and Bamford and Ferrar (12) have shown that manganic trifluoroacetylacetonate, Mn(TFA)$_3$ (TFA = $CF_3COCHCOCH_3$), reacts with polymethylmethacrylate and polystyryl radicals to retard the polymerizations of methyl methacrylate and styrene monomers, respectively. These authors presume that these reactions 'result in reduction of the oxidation state of the metal'.

In view of the large yields of excited states produced in the radiolysis of liquid toluene, the known similarities in the radiation physics (1) and chemistry (4) of toluene and benzene, the importance of paramagnetic and heavy atom quenching of electronically excited states (13*a*) and the fact that at very low doses the paramagnetic radical scavenger $FeCl_3$ is observed to chemically quench excited benzene in the liquid state (14) and in low temperature crystalline benzene (15) it was anticipated that similar indirect evidence for the chemical quenching of ϕCH_3* by Fe(HFA)$_3$ might be obtained in this work.

Direct photochemical evidence for this quenching has also been sought. Lintvedt and Kernitsky (16) have assigned the 284 nm (log ϵ = 4.4), 383 nm (log ϵ = 3.6) and 446 nm (log ϵ = 3.6) absorption bands of Fe(HFA)$_3$ in $CHCl_3$ to intraligand ($\pi^* \leftarrow \pi$), metal-to-ligand ($\pi \leftarrow t_{2g}$) and ligand-to-metal ($e_g \leftarrow \pi$) transitions, respectively. Gafney, Lintvedt, and Jaworiwsky (17) have shown that direct excitation of the ligand-to-metal (345 nm) transition of Fe(HFA)$_3$ in ethanol leads to photoreduction of the chelate [4] and oxidation of the ethanol [5].

[4] $$Fe(HFA)_3 + h\nu \rightarrow Fe(HFA)_2HFA \xrightarrow{C_2H_5OH} Fe(HFA)_2.2C_2H_5OH + \cdot HFA$$

[5] $$\cdot HFA + C_2H_5OH \rightarrow HHFA + \text{oxidized ethanol}$$

A very intense flash photolysis source has been used, in conjunction with suitable optical filters, to selectively excite intraligand and charge transfer transitions in Fe(HFA)$_3$ as well as $S_1 \leftarrow S_0$ transitions in ϕCH_3 to determine quantum yields for direct and ϕCH_3* sensitized photolyses of Fe(HFA)$_3$.

Experimental

Reagent grade toluene was treated with concentrated H_2SO_4 followed by 10% (w/v) aqueous Na_2CO_3. The acid-free toluene was filtered through Na_2SO_4, dried over P_2O_5, and then fractionally distilled over sodium in a Todd Precise Fractionator. Reagent grade toluene was also purified by preparative glc (Aerograph 'Autoprep') on a 10 ft, $\frac{3}{8}$ in. (i.d.) aluminum column packed with 20% (w/w) DC-710 silicone oil on 60–80 mesh Celite. The purified toluene was dearated by the freeze–pump–thaw method and dried *in vacuo* over reactivated Linde molecular sieve 4A. The results reported here were independent of the method of solvent purification used.

Fe(HFA)$_3$ was prepared *in vacuo* by reacting excess anhydrous HHFA with vacuum sublimed $FeCl_3$ in anhydrous ether at room temperature. (Anhydrous HHFA was obtained by treating an ethereal solution of HHFA.2H_2O with P_2O_5. The dihydrate was prepared by

Can. J. Chem. Downloaded from www.nrcresearchpress.com by 210.87.254.40 on 09/05/12
For personal use only.

the method of Henne *et al.* (18).) After removal of ether and unreacted HHFA the product was sublimed at 35 °C into Pyrex vials filled with break seals. The ruby red, triply vacuum sublimed crystals melted at 51.8 ± 0.8 °C. *Anal.* Calcd. for $C_{15}H_3F_{18}O_6Fe$: C 26.62, H 0.45, F 50.50, Fe 8.25. Found: C 26.46, H 0.66, F 50.37, Fe 8.02. The principal ir absorption frequencies for this compound were 1642, 1618, 1440, 1251, and 1110 cm^{-1} (Nujol mull) which agreed well with those reported for $Fe(HFA)_3$ by Morris *et al.* (19).

$Fe(HFA)_2{\cdot}2H_2O$ was prepared by reacting an aqueous solution of Mohr's salt with a methanolic solution of $HHFA.2H_2O$. An aqueous solution of NaOAc was added to the mixture which was then stirred and allowed to stand overnight at 0 °C. The fine brown crystals which deposited were filtered, washed with ice-cold water and recrystallized from aqueous CH_3OH overnight at 0 °C to yield violet black crystals which melted at 193 ± 1 °C. *Anal.* Calcd. for $C_{10}H_6F_{12}O_6Fe$: C 23.7, H 1.2, F 45.1, Fe 11.0. Found (after recrystallization from hot, aqueous CH_3OH): C 23.9, H 1.4, F 45.2, Fe 11.0. The principal ir frequencies for this compound were 3475, 1347, 1268, 1148, and 805 cm^{-1} (Nujol mull) which agreed well with those reported for $Fe(HFA)_2.2H_2O$ by Morris *et al.* (19).

Two views of the apparatus used for irradiations and analysis are shown in Fig. 1. The Pyrex radiolysis bulb (R) and the quartz spectrophotometric cell (S) were cleaned with chromic acid solution and baked at 400 °C for 1 h before incorporation in the apparatus shown. (A) was used to introduce weighed amounts of $Fe(HFA)_3$ or known volumes of $Fe(HFA)_2{\cdot}2H_2O$ in methanol into (R). After sealing off at (A) and evacuating the apparatus, crystals of $Fe(HFA)_3$ could be sublimed into (R), through the glasswool plug (P), while crystals of $Fe(HFA)_2.2H_2O$ were left behind in (R) following evaporation of the solvent. After evacuation of the apparatus, with the chelate in (R) immersed in liquid nitrogen, the apparatus was sealed off below (P) and at (Y). (B) was then fused to the high vacuum system. A quantity of air-free anhydrous toluene was distilled through the broken seal near (E) and, with the solid chelate–toluene mixture in (R) under liquid nitrogen, the apparatus was sealed off at (X).

Irradiations of samples in (R) were performed in a 2400 Ci Gammacell 220 irradiator. During irradiation (S) was surrounded by a lead shield to minimize radiation induced discoloration of quartz. For irradiation of samples at temperatures less than 25 °C the radiolysis bulbs were immersed in various low temperature baths in a Dewar within the irradiator cavity and the temperatures of these baths were measured with a thermocouple.

Electron density corrected Fricke dosimetry was used to obtain rates of energy deposition in toluene–chelate solutions and in pure toluene. The dose rates determined for the dosimetry solution were in the range (6.77–9.08) × 10^{18} eV ml^{-1} h^{-1}.

Chelate concentrations were determined spectrophotometrically with either a Beckman DU or Bausch and Lomb 505 spectrophotometer. The path lengths of the (S) cells were determined by measuring the absorbances of standard alkaline potassium chromate solutions in these cells and by comparing these values with those obtained for standard (Beckman) 1 cm cells. The absorbances of the irradiated toluene–chelate solutions were corrected for the radiation induced coloration of the (S) cells.

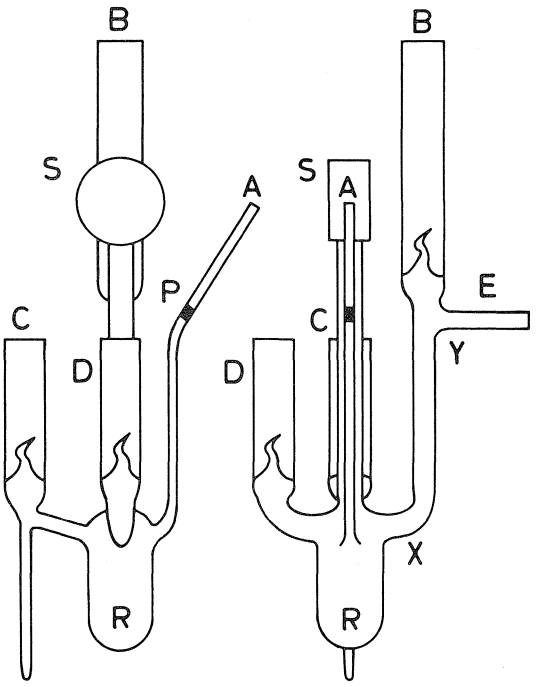

FIG. 1. Two views of apparatus used for irradiations and analysis. (R), pyrex radiolysis bulb; (S), cyclindrical quartz spectrophotometric cell; tubes for (A), introduction of solute; (B), introduction of toluene *in vacuo*; (C), glc analysis of liquid products; (D), analysis of gaseous products; (E), to high vacuum system; (P), glass wool plug; (X), (Y), seal-off points.

Absorption spectra of $Fe(HFA)_3$ in toluene were obtained for each of the (S) cells at chelate concentrations in the range 50 to 1000 μM from which calibration curves for the analysis of $Fe(HFA)_3$ at λ = 455 nm were constructed. The absorption spectra of $Fe(HFA)_3$ and $Fe(HFA)_2$, as determined with the Beckman DU spectrophotometer, are shown in Fig. 2. The absorption spectrum of $Fe(HFA)_2$ is that of the anhydrous chelate. It was found that $Fe(HFA)_2{\cdot}2H_2O$ could be readily dehydrated by evacuating at room temperature overnight.

A Töpler-McLeod system was used to remove gases produced in radiolysis, to determine the total number of moles of gas collected, and to collect gaseous products in gas sample bulbs for mass spectrometric analysis.

Analyses of liquid samples were performed with the Beckman GC-2A chromatograph with either hydrogen flame or thermal conductivity detector. Pyrex glass ampoules, containing the liquid samples *in vacuo*, were crushed directly in the He carrier gas stream. DC-710 silicone oil (20% w/w) on 60–80 mesh Celite 545 was used at 84 °C for HHFA calibrations and analyses while 23% (w/w) α-bis(α-)α-phenoxyphenoxy)-phenoxybenzene (Monsanto 7P6E) on 60–80 mesh, nonacid washed, Chromasorb W was used at 154 °C for $\phi CH_2CH_2\phi$ calibrations and analyses.

Can. J. Chem. Downloaded from www.nrcresearchpress.com by 210.87.254.40 on 09/05/12
For personal use only.

A solution containing 24.2 mg $Fe(HFA)_3$ in 25 ml air-free anhydrous toluene was irradiated for 20 h in the Gammacell 220 irradiator. The irradiated liquid was evaporated to dryness in a stream of moist N_2 and the residue was extracted with methanol. The extract was evaporated to 1 ml and heated to 60 °C. On addition of 0.7 ml of hot water a flocculent, brownish yellow precipitate was formed which was immediately removed by filtration. A further 0.3 ml of hot water was added to the heated filtrate and the solution was allowed to stand overnight at 0 °C. The black needle-like crystals which formed were removed by centrifugation, redissolved in 1.5 ml of hot 50% (v/v) aqueous methanol and recrystallized by cooling the solution slowly to 0 °C. The melting point of the crystals was 191.5 ± 1.5 °C. Elementary analysis of this compound gave C 25.4, H 1.53, F 44.12, Fe 11.66. The ir, near uv, and visible absorption spectra of this product were identical to the spectra obtained for synthetic $Fe(HFA)_2 \cdot 2H_2O$.

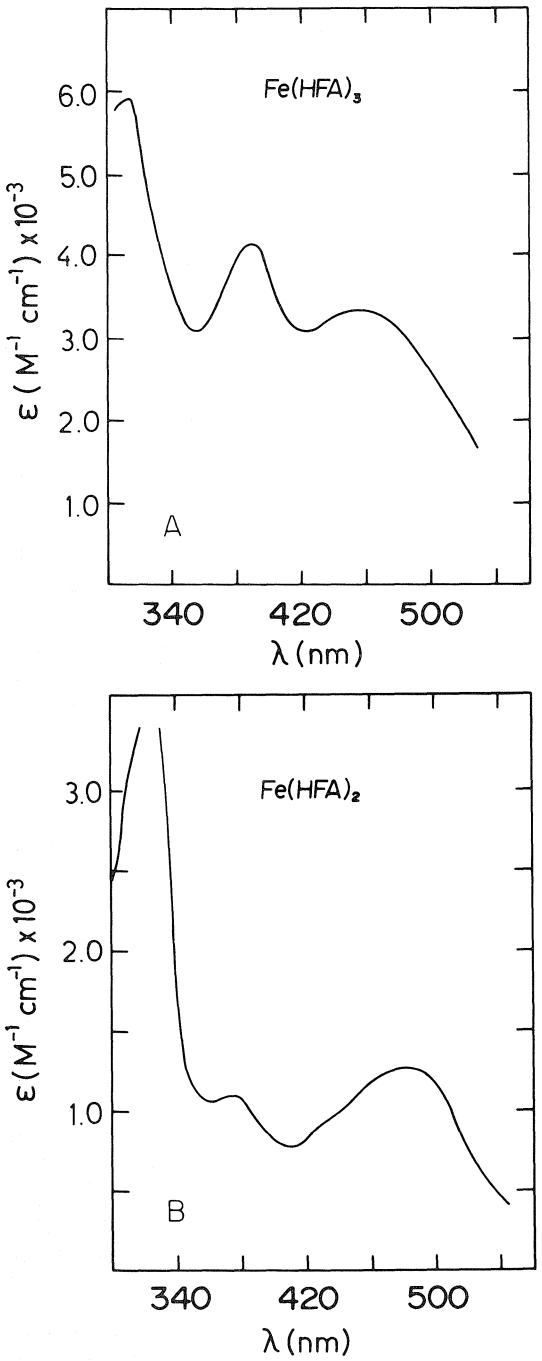

FIG. 2. (*A*) Absorption spectra of $Fe(HFA)_3$ and $Fe(HFA)_2$ in toluene. (*B*) ϵ-decadic molar absorption coefficient.

Two solutions of $Fe(HFA)_2$ in toluene, with concentrations of 673 and 1240 μM were irradiated and absorbance measurements were made at $\lambda = 455$ nm at various irradiation times. No change in absorbance was noted even after irradiating for a period of 11 h.

Air-free and dry oxygen saturated solutions of $Fe(HFA)_3$ in anhydrous toluene, with concentrations in the range 300 to 650 μM, were photolyzed in 4 cm × 1 cm × 1 cm Hellma Suprasil quartz fluorescence cells which were sealed to Young greaseless valves. Irradiations took place between a parallel pair of series coupled, 1900J, Xe-filled (P = 5 torr) flash lamps with 30 μs duration at half pulse maximum (measured at 410 nm). Preliminary kinetic spectrophotometric studies at λ = 410 nm (unfiltered flash output) and a sweep rate of 20 μs/cm provided no evidence for the rapid disappearance of $Fe(HFA)_3$. Accordingly, absorption spectra were recorded before and after repeated flashing and changes in the concentration of $Fe(HFA)_3$ per flash were determined spectrophotometrically at any one of three wavelengths; 390, 410, and 455 nm. Potassium ferrioxalate (6 mM) actinometry (20) was used to determine flash intensities and average quantum yields for the disappearance of $Fe(HFA)_3$ ($\Phi_{-Fe(HFA)_3}$) for various spectral ranges isolated by Schott (GG420 and GG375) as well as soft glass and Pyrex transmission filters with cut-offs at 400, 350, 300, and 280 nm, respectively. Average outputs per flash were 1.8×10^{17} quanta (in the range 200–300 nm) and 3.9×10^{17} quanta (in the range 300–490 nm). For each spectral range average values of the actinometer quantum yield and fractions of radiation absorbed by the actinometer and toluene solutions were used to calculate $\Phi_{-Fe(HFA)_3}$ values (20).

Results and Discussion

Typical observed dependences of $[Fe(HFA)_3]_a$ on the irradiation time are shown in Fig. 3 where $[Fe(HFA)_3]_a$ is the apparent concentration of $Fe(HFA)_3$. Initial apparent G-values for the radiation induced disappearance of $Fe(HFA)_3$, $G(-Fe(HFA)_3)_a$, were independent of the initial concentrations of $Fe(HFA)_3$, $[Fe(HFA)_3]_0$, in the range 50 to 1400 μM at 27 °C (Fig. 4) and

Can. J. Chem. Downloaded from www.nrcresearchpress.com by 210.87.254.40 on 09/05/12
For personal use only.

dependent on temperature in the range −95 to 27 °C (Fig. 4). At 27 °C, $G(\text{—Fe(HFA)}_3)_a$ = 0.54 ± 0.05 and the activation energy for the radiation induced disappearance of $(Fe(HFA)_3$, in the above temperature range, was 670 ± 130 cal mol^{-1}.

Figure 3 shows that $[Fe(HFA)_3]_a$ attains a constant, nonzero value after a sufficiently long, $[Fe(HFA)_3]_0$-dependent period of irradiation. This effect arises because $Fe(HFA)_3$ is radiolytically reduced to $Fe(HFA)_2$, which is not subject to radiolysis. At any time (t) the absorbance (A_t) of the irradiated solution is given by [6]

$$[6] \quad A_t = \epsilon_F([Fe(HFA)_3]_0 - X_t)L + \epsilon_f X_t L$$

where ϵ_F and ϵ_f are the decadic molar extinction coefficients of $Fe(HFA)_3$ and $Fe(HFA)_2$, respectively, L is the path length of the irradiation cell used and X_t is the change in the $Fe(HFA)_3$ concentration at time t. If $Fe(HFA)_2$ is not radiolyzed then after a certain time τ, X_τ becomes $[Fe(HFA)_3]_0$ and A_τ becomes $\epsilon_f[Fe(HFA)_3]_0L$, *i.e.* a constant. For the four curves shown in Fig. 3 the values of $A_\tau/[Fe(HFA)_3]_0L$ at λ =

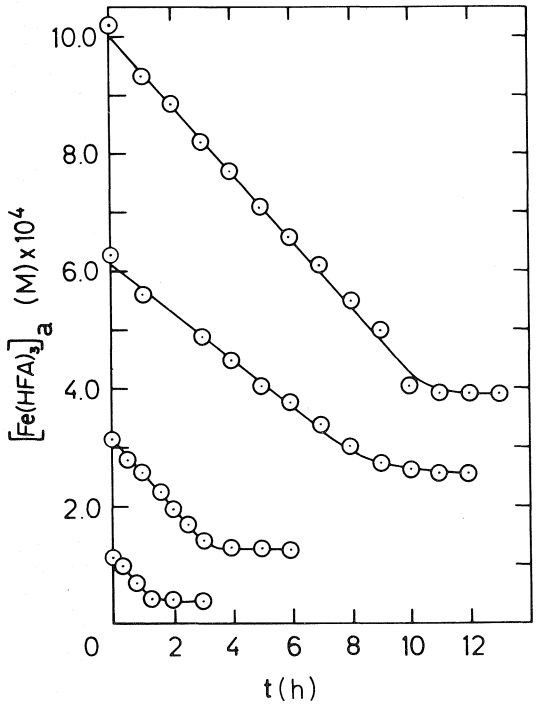

FIG. 3. Dependence of apparent $Fe(HFA)_3$ concentrations ($[Fe(HFA)_3]_a$) on irradiation time (t).

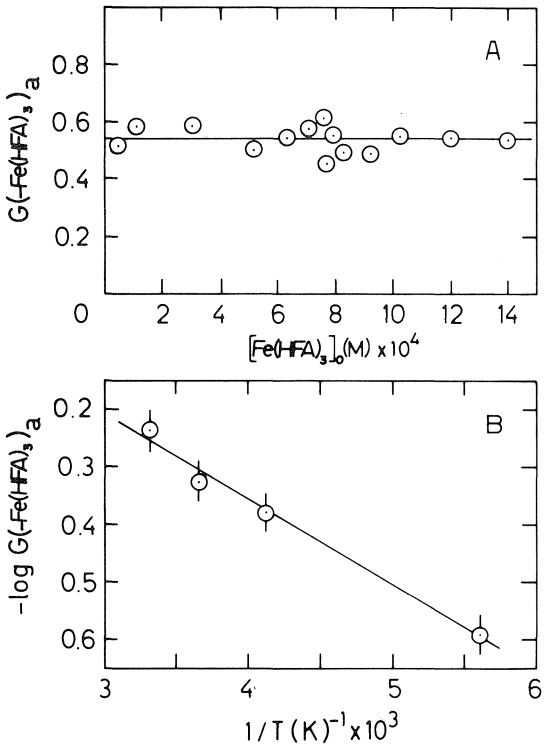

FIG. 4. (A) Dependence of $G(\text{—Fe(HFA)}_3)_a$ on $[Fe(HFA)_3]_0$ (mol l^{-1}) at 27 °C. (B), Arrhenius temperature dependence of $G(\text{—Fe(HFA)}_3)_a$ in the range −95 to 27 °C.

455 nm should then be (1.25 ± 0.05) × 10^3 M^{-1} cm^{-1}, the value of ϵ_f at 455 nm. This is found to be the case for the average value calculated is (1.39 ± 0.07) × 10^3 M^{-1} cm^{-1}.[3]

Equation 6 was used to obtain the true concentrations of $Fe(HFA)_3$ at different irradiation times and to determine the true G-values for the radiation induced disappearance of $Fe(HFA)_3$. At 27 °C, $G(\text{—Fe(HFA)}_3) = G(Fe(HFA)_2)$ = 1.05 ± 0.03. This value is in very good agreement with G(—DPPH) = 0.9 or 1.23, G(—aroxyl) = 1.5 and $G(R\cdot)$ = 1.1 (polymerization of styrene) reported for toluene (4). There is no evidence in our work that at low doses (≤60 krad, which correspond to irradiation times ≤0.5 h) the initial value of $G(\text{—Fe(HFA)}_3)$ is significantly greater than 1.05 ± 0.03 and is

[3]Further proof that $Fe(HFA)_3$ is radiolytically reduced to $Fe(HFA)_2$ and that $Fe(HFA)_2$ is radiolytically inert was obtained by performing the radiolytic synthesis of $Fe(HFA)_2$ and by showing that $G(\text{—Fe(HFA)}_2) = 0$ at 27 °C (see Experimental).

Can. J. Chem. Downloaded from www.nrcresearchpress.com by 210.87.254.40 on 09/05/12
For personal use only.

strongly dependent on $[Fe(HFA)_3]_0$. Effects of this kind were observed in the β-radiolysis of solutions of $FeCl_3$ in benzene at low doses ($\leq$30 krad) and were taken as evidence for the chemical quenching of electronically excited benzene molecules by $FeCl_3$ (14). Thus in solutions for which $[Fe(HFA)_3]_0 \leq 1400\ \mu M$ chemical quenching of ϕCH_3* by $Fe(HFA)_3$ is not observed and G(—$Fe(HFA)_3$) = 1.05 represents the yield of radicals intercepted by $Fe(HFA)_3$ and other reactive scavengers in the radiolysis of liquid toluene.

The insignificance of chemical quenching of ϕCH_3* was confirmed by the results of the flash photochemical studies. When air-free solutions were flashed at wavelengths $\geq$400, $\geq$350, $\geq$300, and $\geq$280 nm, $\Phi_{-Fe(HFA)_3} = 0$, *in each case*. This behaviour is similar to that reported for $Fe(HFA)_3$ in ϕH by Gafney *et al.* (17). No photoreduction of $Fe(HFA)_3$ was observed in this solvent on continuous irradiation of solutions by a much less intense Hg source at wavelengths $\geq$290 nm. Thus direct photolysis of $Fe(HFA)_3$, through excitation of ligand-to-metal, metal-to-ligand, and intraligand transitions, which for $Fe(HFA)_3$ in ϕCH_3 are located at 455 nm ($\log \epsilon = 3.5$), 390 nm ($\log \epsilon = 3.6$) and 290–310 nm ($\log \epsilon = 3.8$), respectively (by analogy with assignments made for $Fe(HFA)_3$ in $CHCl_3$ (16)), either does not take place or does so with extremely small quantum yields ($\ll 10^{-3}$).[4]

When air-free solutions were irradiated at wavelengths $\geq$200 nm (the Suprasil quartz cutoff) $\Phi_{-Fe(HFA)_3}$ was found to be $(1.3 \pm 0.9) \times 10^{-3}$ for $232\ \mu M < [Fe(HFA)_3]_0 < 634\ \mu M$ and when the same O_2 saturated solutions were irradiated at wavelengths $\geq$200 nm, $\Phi_{-Fe(HFA)_3}$ was reduced to zero. $\Phi_{-Fe(HFA)_3} = (1.3 \pm 0.9) \times 10^{-3}$ thus represents the quantum yield for the decomposition of $Fe(HFA)_3$ for wavelengths in the range $200 < \lambda < 280$ nm. Since the $S_1(^1L_b) \leftarrow S_0$ absorption band of ϕCH_3 is located in this wavelength range (13*b*) and ϕCH_3 is the principal absorber of radiation in this range, sensitized decomposition of $Fe(HFA)_3$ must be taking place. In view of the strong quenching of this decomposition by O_2 and the known ability of O_2 to quench singlet and triplet states at very low concentrations (22) $\Phi_{-Fe(HFA)_3} = (1.3 \pm 0.9) \times 10^{-3}$ represents the quantum yield for the decomposition of $Fe(HFA)_3$ sensitized by the S_1 state of ϕCH_3, or more probably, because of efficient intersystem ($T_1 \leftarrow S_1$) crossing in toluene (23), the T_1 state of ϕCH_3. While chemical quenching of ϕCH_3* by $Fe(HFA)_3$ appears to occur it is very unimportant in view of the very low value measured for $\Phi_{-Fe(HFA)_3}$. Photophysical processes, including the physical quenching of ϕCH_3* by $Fe(HFA)_3$, appear to compete strongly with chemical quenching. Preliminary calculations indicate that physical quenching of S_1 and T_1 states of ϕCH_3 by $Fe(HFA)_3$ may be 2 to 20 times faster than chemical quenching of these states depending on the nature of the excitations induced in $Fe(HFA)_3$ by ϕCH_3*.[5]

No HHFA was found in the radiolyses of $Fe(HFA)_3$–toluene solutions, *i.e.* G(HHFA) = 0. It is probable that H· atoms, which survive reactions in spurs, readily add to ϕCH_3 and are thereby prevented from reacting with the chelate. Also this result may indicate that ·HFA radicals cannot be produced in [3]. If they were formed they would probably abstract H from ϕCH_3 to form HHFA. Analogous H atom abstraction from ϕH by ·acac and ·TFA radicals has been reported by Bamford and Ferrar (12).

$G(H_2) = 0.13 \pm 0.03$, which agrees with $G(H_2)$ values reported by others (7, 24), was independent of irradiation time (dose), $[Fe(HFA)_3]_0$ (in the range 110 to 1400 μM at 27 °C) (Fig. 5) and temperature, in the range −95 to 27 °C, within the limits of experimental error (Fig. 6). These observations provide further evidence for the view that H_2 formation occurs in spurs by unimolecular and bimolecular reactions involving ϕCH_3* (7).

In the radiolysis of toluene at 27 °C, $G(CH_4) = 0.0088 \pm 0.0020$ and in the radiolysis of toluene–$Fe(HFA)_3$ solutions at 27 °C, $G(CH_4) = 0.0052 \pm 0.0020$ (Fig. 7). The temperature dependence of $G(CH_4)$ in the radiolysis of toluene–$Fe(HFA)_3$ solutions ($[Fe(HFA)_3]_0 = 570 \pm 30\ \mu M$), in the range −95 to 27 °C, is shown in Fig. 6 from which the activation energy for CH_4 formation (1200 ± 900 cal mol^{-1}) has been obtained. In the radiolysis of toluene at 40 °C $G(CH_4)$ is estimated to be 0.0094 ± 0.0020 which is in good agreement with $G(CH_4) = 0.012$ re-

[4]By contrast, direct photoreduction of $FeCl_3$ through excitation of ~350 nm solvent-to-complex charge transfer transitions in ϕH and ϕCH_3 occurs with quantum yields of 0.061 and 0.14, respectively (21).

[5]E. A. Cherniak, unpublished results.

Can. J. Chem. Downloaded from www.nrcresearchpress.com by 210.87.254.40 on 09/05/12
For personal use only.

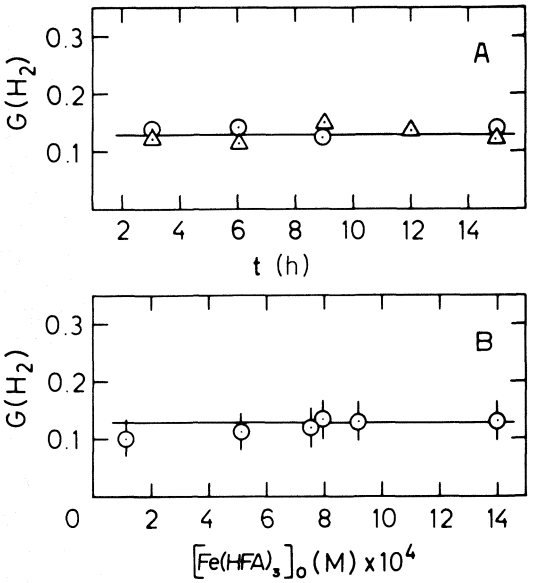

FIG. 5. Dependence of $G(H_2)$ on (A), irradiation time (t). △, toluene; ○, toluene + $Fe(HFA)_3$ (1250 μM) and (B), $[Fe(HFA)_3]_0$ (mol l^{-1}) at 27 °C.

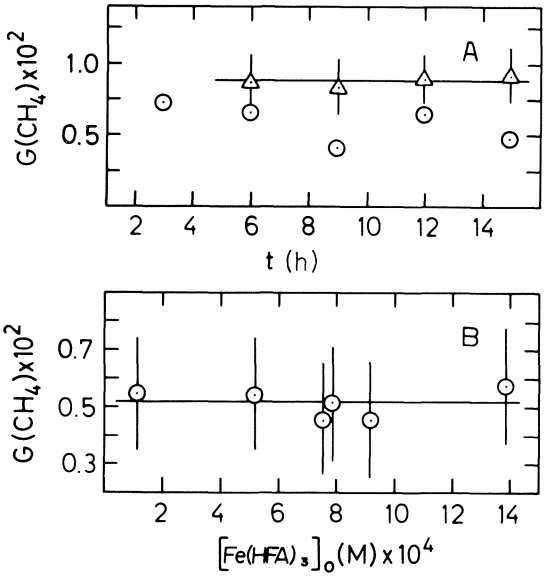

FIG. 7. Dependence of $G(CH_4)$ on (A), irradiation time (t), △, toluene; ○, toluene + $Fe(HFA)_3$ (1250 μM) and (B), $[Fe(HFA)_3]_0$ (mol l^{-1}) at 27 °C.

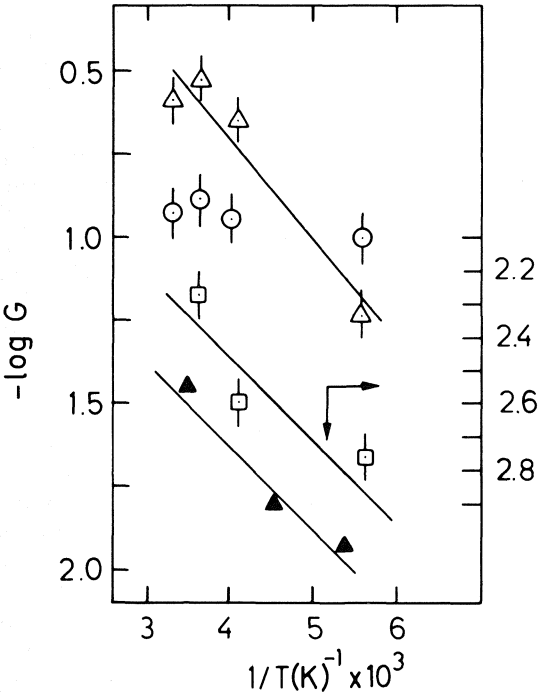

FIG. 6. Arrhenius temperature dependences of $G(H_2)$ (○), $G(CH_4)$ (□), $G(\phi CH_2CH_2\phi)$ (△) (this work) and $G(\phi CH_2CH_2\phi)$ (▲) Ingalls *et al.* (24), in the range −95 to 27 °C. G-values are obtained for pure toluene except $G(CH_4)$ which was obtained for toluene–$Fe(HFA)_3$ where $[Fe(HFA)_3]_0 = (570 \pm 30)\ \mu M$.

ported by Weiss and Collins (7). If the difference between $G(CH_4) = 0.0088$ and $G(CH_4) = 0.0052$ is significant it may be concluded that $\cdot CH_3$ radicals, which escape from spurs (4, 7), are in part responsible for the radiation induced conversion of $Fe(HFA)_3$ to $Fe(HFA)_2$ and that the G-value for trapped $\cdot CH_3$ radicals (~0.004 at 27 °C) is a very small fraction of the total trapped radical yield ($G \approx 1$).

Figure 8 shows that in the radiolysis of toluene at 27 °C $G(\phi CH_2CH_2\phi)$ decreases as dose increases. A similar observation has been made by Hoigné and Gäumann (6) whose data also show that at the doses used in this study (0.4–2) Mrad $G(\phi CH_2CH_2\phi)$ may be as large as 0.09 or 0.1 which compares favorably with our $G(\phi CH_2CH_2\phi) = 0.102 \pm 0.019$ (Fig. 8). While our activation energy (1280 ± 250 cal mol^{-1}) for the formation of $\phi CH_2CH_2\phi$ in the radiolysis of toluene in the range −95 to 27 °C is in good agreement with 1220 cal mol^{-1}, obtained from the data of Ingalls *et al.* (24) (Fig. 6), our $G(\phi CH_2CH_2\phi)$ values are significantly greater, due to the different doses used.

Figure 8 also shows that, in the presence of $Fe(HFA)_3$, $G(\phi CH_2CH_2\phi)$ increases as dose and $[Fe(HFA)_3]_0$ increase and at $[Fe(HFA)_3]_0 = 1250\ \mu M$, has a value of 0.307 ± 0.026 which is

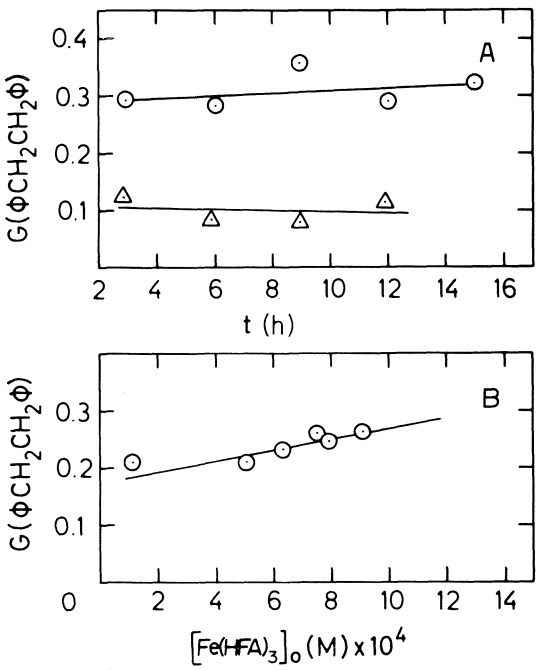

FIG. 8. Dependence of $G(\phi CH_2CH_2\phi)$ on (*A*) irradiation time (*t*). △, toluene; ○, toluene + $Fe(HFA)_3$ (1250 μM) and (*B*) $[Fe(HFA)_3]_0$ (mol l^{-1}) at 27 °C.

three times greater than $G(\phi CH_2CH_2\phi)$ obtained in the absence of $Fe(HFA)_3$.

The above observations suggest that $\phi\dot{C}H_2$ radicals may be scavenged by unknown radical radiolysis products which may contribute to the formation of 'polymer' which also may act as a scavenger of $\phi\dot{C}H_2$ (6). $Fe(HFA)_3$, however, does not react with $\phi\dot{C}H_2$ but does scavenge these unknown radical radiolysis products. If [2] is the only source of $\phi CH_2\dot{C}H_2\phi$ then the yield of primary and secondary $\phi\dot{C}H_2$ may be as large as 0.6 and the yield of the unknown radicals, which are trapped by $Fe(HFA)_3$, is ~0.4.

Acknowledgements

We thank the Ontario Research Foundation and the National Research Council of Canada for financial support. One of us (K.W.C.) thanks the Ontario Research Foundation for providing financial support and the Province of Ontario for providing a Graduate Fellowship. We also thank Dr. F. P. Lossing and Mr. R. Pilon for assistance with the mass spectrometric analyses, Mr. J. Ross for technical assistance, and Dr. J. Betts for helpful suggestions.

1. R. COOPER and J. K. THOMAS. J. Chem. Phys. **48** 5097 (1968).
2. J. H. BAXENDALE and E. J. RASBURN. J. Chem. Soc. Faraday Trans. I, **69**, 771 (1973).
3. E. FISCHER, G. FISCHER, and G. STEIN. Chem. Phys. Lett. **2**, 405 (1968).
4. J. HOIGNÉ. *In* Aspects of hydrocarbon radiolysis. *Edited by* T. Gäumann and J. Hoigné. Academic Press, London. 1968. Chapt. 3.
5. J. HOIGNÉ and T. GÄUMANN. Helv. Chim. Acta, **46**, 365 (1963).
6. J. HOIGNÉ and T. GÄUMANN. Helv. Chim. Acta, **44**, 2141 (1961).
7. J. WEISS and C. H. COLLINS. Rad. Res. **33**, 274 (1968).
8. J. WEISS and C. H. COLLINS. Rad. Res. **28**, 1 (1966).
9. Y. YAMAMOTO, S. TAKAMUKU, and H. SAKURAI. J. Phys. Chem. **74**, 3325 (1970).
10. R. J. GRITTER and E. L. PATMORE. Proc. Chem. Soc. 328 (1962).
11. J. KIVEL. Organometallic Radiation Dosimetry Systems, NYO-2979-34, USAEC Division of Technical Information, Oak Ridge, Tennessee. 1965. p. 37.
12. C. H. BAMFORD and A. N. FERRAR. J. Chem. Soc. Faraday Trans. I, **68**, 1243 (1972).
13. J. B. BIRKS. Photophysics of aromatic molecules. Wiley-Interscience, London. 1970. (*a*) Chapt. 9. (*b*) p. 70.
14. E. A. CHERNIAK, E. COLLINSON, and F. S. DAINTON. Trans. Faraday Soc. **60**, 1408 (1964).
15. E. COLLINSON, J. J. CONLAY, and F. S. DAINTON. Discuss. Faraday Soc. **36**, 153 (1963).
16. R. L. LINTVEDT and L. S. KERNITSKY. Inorg. Chem. **9**, 491 (1970).
17. H. D. GAFNEY, R. L. LINTVEDT, and I. S. JAWORIWSKY. Inorg. Chem. **9**, 1728 (1970).
18. A. HENNE, H. NEWMAN, L. QUILL, and R. STANIFORTH. J. Am. Chem. Soc. **72**, 2948 (1950).
19. M. L. MORRIS, H. W. MOSHIER, and E. E. SIEVERS. Inorg. Chem. **2**, 411 (1963).
20. J. G. CALVERT and J. N. PITTS, JR. Photochemistry. J. Wiley, New York. 1966. Chapt. 7.
21. V. BALZANI and V. CARASSITI. Photochemistry of coordination compounds. Academic Press, London. 1970. p. 182.
22. S. P. MCGLYNN, T. AZUMI, and M. KINOSHITA. Molecular spectroscopy of the triplet state. Prentice-Hall, Englewood Cliffs, N.J. 1969. Chapt. 8.
23. R. B. CUNDALL, L. C. PEREIRA, and D. A. ROBINSON. J. Chem. Soc. Faraday Trans. II, **69**, 701 (1973).
24. R. B. INGALLS, P. SPIEGLER, and A. NORMAN. J. Chem. Phys. **41**, 837 (1964).

Can. J. Chem. Downloaded from www.nrcresearchpress.com by 210.87.254.40 on 09/05/12
For personal use only.

The oxidation of cyclobutanol by ruthenium tetroxide and sodium ruthenate

DONALD G. LEE, UDO A. SPITZER, JAMES CLELAND, AND MERLE E. OLSON
Department of Chemistry, The University of Regina, Regina, Sask., Canada S4S 0A2

Received January 16, 1976

DONALD G. LEE, UDO A. SPITZER, JAMES CLELAND, and MERLE E. OLSON. Can. J. Chem. **54**, 2124 (1976).

The only detectable product obtained from the oxidation of cyclobutanol by ruthenium tetroxide or sodium ruthenate is cyclobutanone. This indicates that both of these reagents act as two-electron transfer oxidants and that the oxidation of alcohols by ruthenium tetroxide likely proceeds via a mechanism that involves a pair of successive two-electron transfer steps.

DONALD G. LEE, UDO A. SPITZER, JAMES CLELAND et MERLE E. OLSON. Can. J. Chem. **54** 2124 (1976).

Le seul produit que l'on peut détecter lors de l'oxydation du cyclobutanol par le tétroxyde de ruthénium ou le ruthénate de sodium est la cyclobutanone. Ce résultat indique que ces deux réactifs agissent comme oxydant transferant deux électrons et que l'oxydation des alcools par le tétroxyde de ruthénium se produit vraisemblablement par un mécanisme impliquant une paire d'étapes successives transférant deux électrons.

[Traduit par le journal]

Can. J. Chem. Downloaded from www.nrcresearchpress.com by 210.87.254.40 on 09/05/12
For personal use only.

Ruthenium tetroxide is a highly effective oxidant for the conversion of secondary alcohols into ketones (1). Its use has found particular application in the oxidation of hydroxy compounds that are unreactive toward other common oxidants (2).

The stoichiometry of the reaction indicates that 1 mol of ruthenium tetroxide is capable of oxidizing 2 mol of alcohol with a total transfer of four electrons (3). However, it is likely that the reaction actually involves a number of successive one- and/or two-electron transfer steps and that ruthenium oxides of intermediate oxidation states are involved. In fact, previous mechanism studies have suggested that the reaction proceeds via hydride abstraction with formation of an intermediate ruthenium(VI) oxide (4).

Since the completion of the mechanism studies Roček and his co-workers have shown that the oxidation of cyclobutanol can be used to determine if an oxidant acts as a one-electron or a two-electron oxidant (5–8). With two-electron transfer oxidants such as chromium(VI) and (V), cyclobutanone is obtained as the sole product, but with one-electron transfer oxidants such as chromium(IV), cerium(IV), manganese (III), and vanadium(V) the products are acyclic four-carbon compounds which appear to be derived from the primary free radical found in [2].

Consequently, in order to test the previously proposed mechanism, we have now examined the products obtained from the oxidation of cyclobutanol by ruthenium tetroxide (RuO_4) and ruthenate ion (RuO_4^{2-}).

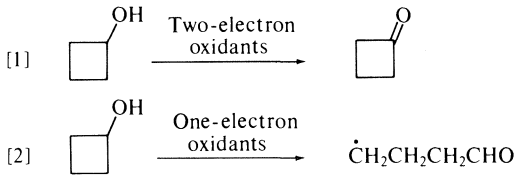

Experimental

The Preparation of Cyclobutanol

Cyclobutanol was prepared by refluxing 12 g of cyclopropyl carbinol and 12 ml of concentrated HCl in 100 ml of water for 100 min (9). The resulting solution was treated with 5 g of NaOH followed by sufficient potassium carbonate to neutralize all of the acid and then continuously extracted with ether for 48 h. The ether solution was dried over anhydrous magnesium sulfate and evaporated to give 8.2 g (68%) of crude product which was first distilled (100–110 °C/760 torr) and then purified by use of gas–liquid chromatography. The nmr and ir spectra corresponded exactly with those given in the literature (8, 10).

The Preparation of Ruthenium Tetroxide Solution

Ruthenium tetroxide was prepared by stirring a suspension of ruthenium dioxide dihydrate (Engelhard Industries) in an aqueous solution of sodium metaperiodate (11) or sodium hypochlorite (12). It was then extracted into carbon tetrachloride and stored over an aqueous periodate solution. The uv spectrum agreed well

Can. J. Chem. Downloaded from www.nrcresearchpress.com by 210.87.254.40 on 09/05/12
For personal use only.

with published spectra and the concentrations were determined using known extinction coefficients for the maxima at 385 nm and 310 nm (13, 14).

The Preparation of Sodium Ruthenate

A solution of sodium ruthenate was prepared by stirring an aqueous sodium hydroxide ($\sim$1 *M*) solution over a solution of ruthenium tetroxide in carbon tetrachloride for 2 days (15). The tetroxide was first reduced to perruthenate ion and then to ruthenate ion. The ultraviolet–visible spectrum was identical to published spectra and the concentrations were determined using absorption maxima at 465 and 383 nm (13, 16).

Oxidation of Cyclobutanol by Ruthenium Tetroxide

In a typical experiment ruthenium tetroxide (3.25 mmol) in about 20 ml of carbon tetrachloride was added to 6.9 mmol of cyclobutanol in 30 ml of carbon tetrachloride with stirring. The mixture was allowed to stand for 1 h, gravity filtered, and concentrated on a rotary evaporator. The residue was analyzed by gas chromatography and found to contain only two compounds with retention times corresponding to those for cyclobutanol and cyclobutanone. The identity of cyclobutanone was confirmed by preparing a 2,4-dinitrophenylhydrazone derivative (17), mp 144–145 °C (lit. (18) mp 147 °C). No evidence could be found for aldehydic C—H bands in the ir spectrum of the crude derivative. The yield of cyclobutanone, as obtained from an analysis of the gas chromatograms, was 80 to 90%.

In other experiments where a large excess of ruthenium tetroxide was used, a mass of intractable products was produced.

Oxidation of Cyclobutanol by Sodium Ruthenate

In a typical experiment cyclobutanol (0.50 g, 6.9 mmol) was dissolved in 50 ml of 1.0 *M* NaOH and 100 ml of 0.0413 *M* Na_2RuO_4 (4.13 mmol) was added slowly. After stirring for 1 h the solution was continuously extracted with diethyl ether for 20 h. The ether solution was concentrated and, on analysis by gas–liquid chromatography, found to contain 0.23 g (3.3 mmol, 80%) cyclobutanone and 0.15 g of unreacted cyclobutanol. No acyclic products were detected despite the fact that known mixtures of cyclobutanone, butyraldehyde, and crotonaldehyde were well separated under the conditions used. The identity of the product was confirmed to be cyclobutanone by preparation of a 2,4-dinitrophenylhydrazone derivative (17), mp 144–146 °C (lit. (18) mp 147 °C). No evidence could be found for aldehydic C—H bands in the ir spectrum of the crude derivative. In an attempt to achieve a mass balance the aqueous solution was neutralized by addition of sulfuric acid and continuously extracted for an additional 20 h. However, no additional products were found when the ether extract was concentrated and analyzed by gas–liquid chromatography. In a number of other experiments yields of 50 to 90% cyclobutanone were obtained, but no acyclic products were ever detected.

Discussion

The observation that cyclobutanone is the only detectable product obtained from the oxidation of cyclobutanol by either ruthenium tetroxide or ruthenate ion indicates that both of these reagents are two-electron transfer oxidants and it strongly suggests that ruthenium tetroxide must oxidize alcohols by a pair of successive two-electron transfer steps. This is consistent with the previously proposed mechanism (4) in which it was suggested that the reaction between ruthenium tetroxide and an alcohol involves, initially, the transfer of a hydride ion as in [3] and [4].

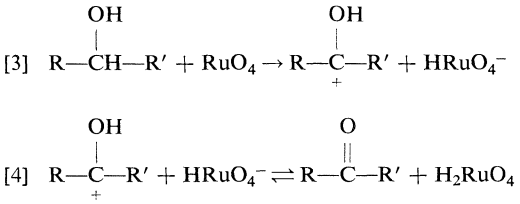

$$[3]\quad R-\overset{\overset{\displaystyle OH}{|}}{C}H-R' + RuO_4 \rightarrow R-\underset{\underset{\displaystyle +}{|}}{\overset{\overset{\displaystyle OH}{|}}{C}}-R' + HRuO_4^-$$

$$[4]\quad R-\underset{\underset{\displaystyle +}{|}}{\overset{\overset{\displaystyle OH}{|}}{C}}-R' + HRuO_4^- \rightleftharpoons R-\overset{\overset{\displaystyle O}{\|}}{C}-R' + H_2RuO_4$$

Since the final product of this reaction is ruthenium dioxide, the ruthenium(VI) oxide formed in this reaction must be further reduced by reaction with a second molecule of alcohol, presumably in another two-electron transfer step. This supposition is consistent with the fact that cyclobutanone is the major product obtained from the oxidation of cyclobutanol by ruthenate ion. The reactivity of H_2RuO_4 in carbon tetrachloride is likely to be much greater than RuO_4^{2-} in aqueous solutions (19), thus explaining why it is not detected as an intermediate in these reactions despite the fact that ruthenium tetroxide and ruthenate have different spectral properties (1). Unfortunately, because ruthenate ion is stable only under very basic conditions, it was not possible to make this study entirely consistent by also using a nonpolar solvent when the oxidation of cyclobutanol by ruthenium(VI) was studied.

Acknowledgements

The authors are pleased to acknowledge the financial assistance of the National Research Council of Canada.

1. D. G. Lee and M. van den Engh. *In* Oxidation in organic chemistry. Part B. *Edited by* W. S. Trahanovsky. Academic Press, Inc., New York. 1973. pp. 177–227.
2. K. C. Ramey, D. C. Lini, R. M. Moriarty, H. Gopal, and H. G. Welsh. J. Am. Chem. Soc. **89**, 2401 (1967).

3. P. J. BEYNON, P. M. COLLINS, D. GARDINER, and W. G. OVEREND. Carbohydr. Res. **6**, 431 (1968).
4. D. G. LEE and M. VAN DEN ENGH. Can. J. Chem. **50**, 2000 (1972).
5. J. ROČEK and A. E. RADKOWSKY. J. Am. Chem. Soc. **95**, 7123 (1973).
6. J. ROČEK and D. E. AYLWARD. J. Am. Chem. Soc. **97**, 5452 (1975).
7. K. MEYER and J. ROČEK. J. Am. Chem. Soc. **94**, 1209 (1972).
8. J. ROČEK and A. E. RADKOWSKY. J. Org. Chem. **38**, 89 (1973).
9. M. C. CASERIO, W. H. GRAHAM, and J. D. ROBERTS. Tetrahedron, **11**, 171 (1960).
10. K. L. SERVIS and J. D. ROBERTS. J. Am. Chem. Soc. **86**, 3773 (1964).
11. P. J. BEYNON, P. M. COLLINS, P. T. DOGANGES, and W. G. OVEREND. J. Chem. Soc. C, 1131 (1966).
12. S. WOLFE, S. K. HASAN, and J. R. CAMPBELL. J. Chem. Soc. D, 1420 (1970).
13. R. E. CONNICK and C. R. HURLEY. J. Am. Chem. Soc. **74**, 5012 (1952).
14. J. L. WOODHEAD and J. M. FLETCHER. J. Chem. Soc. 5039 (1961).
15. D. G. LEE, D. T. HALL, and J. H. CLELAND. Can. J. Chem. **50**, 3741 (1972).
16. G. NOWOGROCKI and G. TRIDOT. Bull. Soc. Chim. Fr. 684 (1965).
17. A. I. VOGEL. Elementary practical organic chemistry. 3rd ed. Longmans, London. 1956.
18. Dictionary of organic compounds. Eyre and Spottiswoode Ltd., London. 1965.
19. J. C. SHEPPARD and A. C. WAHL. J. Am. Chem. Soc. **79**, 1020 (1957).

Can. J. Chem. Downloaded from www.nrcresearchpress.com by 210.87.254.40 on 09/05/12
For personal use only.

Comportement photochimique de cétones α,β-insaturées sous excitation directe

ANDRÉ DEFLANDRE, ANDRÉ LHEUREUX, ARMEL RIOUAL ET JACQUES LEMAIRE
Laboratoire de Photochimie, U.E.R. Sciences Exactes et Naturelles, Université de Clermont-Ferrand, Clermont-Ferrand, France

Reçu le 16 décembre 1975

ANDRÉ DEFLANDRE, ANDRÉ LHEUREUX, ARMEL RIOUAL et JACQUES LEMAIRE. Can. J. Chem. **54**, 2127 (1976).

Les rendements quantiques initiaux des processus primaires photochimiques qui interviennent dans cinq cétones α,β-insaturées sont mesurés dans des conditions d'excitation monochromatique. Les rendements quantiques d'isomérisation *EZ* et éventuellement de transposition (déconjugaison) permettent d'interpréter quantitativement la désactivation non radiative des états excités S_1 ($n\pi$) et S_2 ($\pi\pi$) de ces cétones. Ces substances présentent une photostabilité interessante, même en présence d'oxygène dissous.

ANDRÉ DEFLANDRE, ANDRÉ LHEUREUX, ARMEL RIOUAL, and JACQUES LEMAIRE. Can. J. Chem. **54**, 2127 (1976).

The initial quantum yields of the primary photochemical processes which occur with five α,β-unsaturated ketones were measured under conditions of monochromatic excitation. The quantum yields of *EZ* isomerization and possibly of transposition (deconjugation) lead to a quantitative interpretation of the nonradiative deactivation of the S_1 ($n\pi$) and S_2 ($\pi\pi$) excited states of these ketones. These substances show a remarkable photostability even in the presence of dissolved oxygen.

[Journal translation]

Introduction

Les cétones α,β-insaturées ont été l'objet de nombreuses études photochimiques, car elles sont essentiellement le siège de processus non radiatifs intramoléculaires. Dans les cétones où il n'existe pas d'atome d'hydrogène sur un carbone en δ du carbonyle pouvant être impliqué dans un processus de Norrish type II, l'isomérisation *cis–trans* (ou *Z–E*) et la transposition ont été tout particulièrement étudiées (*cf.* par exemple réf. 1).

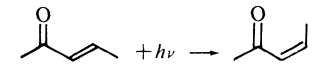

Forme *Z* ou forme *trans* — Forme *E* ou forme *cis*

Isomérisation *cis–trans* ou *Z–E*

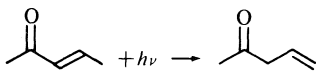

Transposition ou déconjugaison

Ces cétones donnent également lieu à des photoadditions (2).

Le comportement photochimique des cétones α,β-insaturées et des aldéhydes correspondants a été examiné sur le plan théorique (3, 4), et des études expérimentales ont été conduites pour élucider les mécanismes des processus intervenant sous irradiation lumineuse (*cf.* par exemple réfs 4 et 5). Il est à noter que ces études de mécanismes, souvent qualitatives, ont été limitées aux cétones α,β-insaturées cycliques ou polycycliques; ces cétones ont, en effet, l'avantage de présenter des fluorescences ou des phosphorescences de faible intensité, mais observables (6–9). Par exemple, la nature du plus bas niveau triplet de telles cétones est déduite de mesures de durée de vie et de polarisation de phosphorescence (1, 6).

Les études rapportées dans ce mémoire s'inscrivent dans un cadre général de recherches sur le comportement photochimique de cétones insaturées "photostables" menées au laboratoire de Photochimie de l'Université de Clermont-Ferrand. Bonnet a en effet, engagé en 1970 une étude quantitative de la désactivation des états excités S_1 ($n\pi^*$) et S_2 ($\pi\pi^*$) de l'oxyde de mésityle (10). L'oxyde de mésityle ou méthyl-4 pentène-3 one-2 est une cétone insaturée réputée pour sa grande photostabilité (11, 12) et elle s'est avérée être un bon modèle pour l'étude des états

excités singulets. Le seul processus photochimique observable en solution aqueuse est une transposition en oxyde d'isomésityle:

$$CH_3C(CH_3)=CH-COCH_3 + h\nu \rightarrow CH_2=C(CH_3)-CH_2-CO-CH_3$$

Le rendement quantique initial de transposition varie de 0.007 à 0.10 quand le p*H* croit de 2.5 à 13. En milieu basique un processus de retour thermique de l'oxyde d'isomésityle vers la cétone initiale se superpose à la réaction photochimique.

La transposition est le résultat d'une photo-énolisation primaire issue des niveaux singulets; une valeur minimale du rendement quantique de photo-énolisation serait respectivement égale à 0.10 et à 0.035 quand l'oxyde de mésityle est excité à l'état $S_2(\pi\pi^*)$ et à l'état $S_1(n\pi^*)$.

L'oxyde de mésityle ne manifeste pas de processus photochimiques attribuables aux niveaux triplets inférieurs. C'est la raison pour laquelle nous étudions depuis 1972 les cétones isomérisables suivantes: (*i*) la pentène-3 one-2 sous forme *trans* ou *cis* (I) et (II), (*ii*) l'hexène-4 one-3 *trans* (III), (*iii*) la diméthyl-4,5 hexène-4 one-3 *trans* (IV), et (*iv*) la phényl-5 pentène-4 one-3 *trans* (V). Nous avons eu le souci particulier de mesurer les rendements quantiques des processus photochimiques intervenant en excitation directe. Ce n'est qu'en 1975 qu'est parue une autre étude quantitative de la photo-isomérisation d'une cétone α,β-éthylénique non transposable, la méthyl-3 pentène-3 one-2; les résultats de cette étude relatifs à l'isomérisation sont très semblables aux nôtres (13).

Techniques expérimentales

Préparation et purification des substances de départ

La pentène-3 one-2 *trans* est extraite d'un produit commercial Aldrich, qualité technique, mélange contenant essentiellement les deux isomères de la pentène-3 one-2, l'oxyde de mésityle et l'oxyde d'isomésityle. Une première distillation sur colonne Nester-Faust permet d'éliminer l'oxyde de mésityle et d'obtenir une phase riche en pentène-3 one-2 *trans*; cette phase est ensuite traitée par chromatographie préparative (sur un appareil Hupe et Busch APG 402 équipé d'une colonne à 5% de Carbowax 20M). Cette technique fournit la forme *trans* sans impuretés notables. La pentène-3 one-2 *cis* a été préparée par irradiation sous une lampe à vapeur de mercure "haute pression" non filtrée. Ce composé *cis* est très volatil et doit être conservé au réfrigérateur en ampoules scellées.

L'addition de chlorure de propionyle (2 mol) à un mélange de méthyl butènes (3 mol) obtenus par déshydratation d'alcool amylique tertiaire par l'acide orthophosphorique, conduit en particulier à la cétone β-chlorée correspondante (14, 15). Il s'agit d'une réaction d'acylation analogue à celle de Friedel et Craft, catalysée par le chlorure stannique anhydre. La cétone β-chlorée est ensuite déchlorhydratée par la potasse alcoolique en diméthyl-4,5 hexène-4 one-3*.[1]

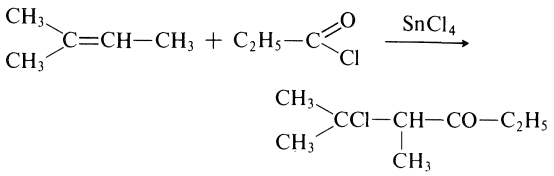

Rendement 45%; p éb 57–60 °C/10 torr; ir $\bar{\nu}$(CO) 1695 cm^{-1}, $\bar{\nu}$(C=C) 1626 cm^{-1}; rmn 1.75 (s, $H_{a,b}$), 1.79 (s, H_c), 2.46 (q, H_d) et 1.02 ppm (t, H_e). La cétone a été purifiée par chromatographie en phase gazeuse préparative.

L'hexène-4 one-3 *trans** a été préparée par réaction d'un organocadmien C_2H_5CdCl (0.5 mol) avec le chlorure de crotonyle (0.25 mol) (15–17)

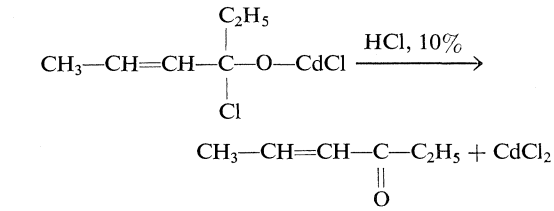

L'hydrolyse du mélange fournit en particulier la cétone cherchée:

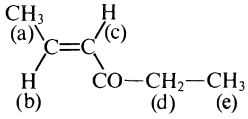

Rendement 35%; p éb 40–41 °C/10 torr; ir $\bar{\nu}$(CO) 1684 cm^{-1}, $\bar{\nu}$(C=C) 1642 cm^{-1}; rmn 1.86 (dd, H_a), 6.81 (m, H_b), 6.03 (m, H_c), 2.51 (q, H_d) et 1.02 ppm (t, H_e). Cette cétone a été également purifiée par chromatographie en phase gazeuse préparative.

La phényl-5 pentène-4 one-3 *trans** peut être obtenue par condensation de la butanone-2 (0.4 mol) et du benzaldéhyde distillé (0.4 mol) par catalyse basique (15, 18, 19)

[1]La synthèse des substances marquées du signe * a été réalisée au sein du Groupe de Chimie Organique II, U.E.R. de Sciences Exactes et Naturelles de l'Université de Clermont (Professeur R. Vessiere).

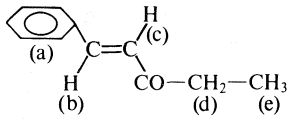

Rendement 65%; p éb 131–133.5 °C/10 torr; ir $\bar{\nu}$(CO) 1674 cm^{-1}, $\bar{\nu}$(C=C) 1612 cm^{-1}; rmn 7.32 (m, H_a), 7.47 (d, H_b), 6.63 (d, H_c), 2.57 (q, H_d) et 1.09 ppm (t, H_e).

Dispositifs d'étude des processus photochimiques et photophysiques

Nous utilisons deux types de sources, une lampe à vapeur de mercure type "résonance" (Philips TUV 15 W) et une lampe à vapeur de mercure "forte pression" (Osram HBO 200 W) associée à un monochromateur Bausch et Lomb Modèle "haute intensité". Les réacteurs sont en quartz Suprasil, ils sont munis de réservoirs latéraux en pyrex où s'effectuent les cycles de dégazages. L'intensité lumineuse est mesurée par une actinométrie basée soit sur la photolyse du complexe acide oxalique-nitrate d'uranyle, soit sur l'isomérisation *trans* → *cis* de l'azobenzène (20).

L'étude analytique du mélange irradié est effectuée soit par spectrophotométrie d'absorption électronique (Optica CF4, Jobin et Yvon Monospac), soit par chromatographie en phase vapeur (Aerograph Varian série 1400 équipé d'une colonne à 10% de Carbowax 20M de 10 pieds de longueur ou d'une colonne Chromosorb T avec phase stationnaire 4% Ethofat et 2% d'acide isophtalique). Les techniques spectrophotométriques peuvent être effectuées *in situ*. Nous présentons à titre d'exemple d'analyse, les chromatogrammes obtenus lors de photolyse mixte d'oxyde de mésityle et de pentène-3 one-2 (*cf.* fig. 1).

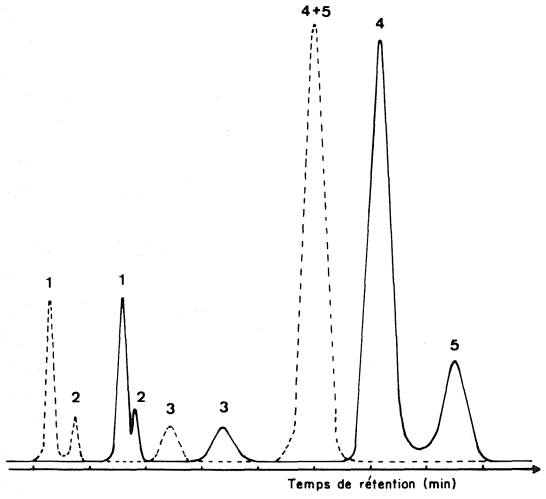

FIG. 1. Chromatogramme d'un mélange obtenu par photolyse mixte d'oxyde de mésityle et de pentène-3 one-2: trait continu—analyse sur colonne Ethofat; trait pointillé --- analyse sur colonne Carbowax 20M: (*1*) pentène-3 one-2 *cis*, (*2*) pentène-4 one-2 (transposé), (*3*) oxyde d'isomésityle (méthyl-4 pentène-4 one-2), (*4*) pentène-3 one-2 *trans*, (*5*) oxyde de mésityle (méthyl-4 pentène-3 one-2).

Les spectres d'émission et d'excitation sont mesurés à l'aide d'un spectrofluorimètre Perkin-Elmer–Hitachi modèle MPF3.

Résultats experimentaux

Propriétés absorbantes et émettrices des cétones étudiées

Les différentes caractéristiques des spectres d'absorption des cétones étudiées sont rassemblées dans le tableau 1 où λ_{max} représente les longueurs d'onde des maximums et ϵ_{max} les coefficients d'extinction molaires correspondants).

Les cétones α,β-insaturées aliphatiques ne présentent pas de fluorescence notable. Si on enregistre, à l'aide du spectrofluorimètre très sensible employé, les spectres d'émission et d'excitation des solutions diluées de ces cétones dans du *n*-heptane, on peut observer une émission diffuse d'intensité très inférieure à celle de l'émission Raman du solvant. Si on utilise un étalon fluorescent comme le benzène, le rendement quantique d'une telle émission apparait être inférieur à 0.0003. Le spectre d'excitation correspondant aux trois cétones aliphatiques étudiées a un maximum vers 290 nm; on pourrait donc attribuer l'émission très faible observée à des cétones saturées présentes à l'état de traces dans les solutions.

Transposition photochimique

La transposition photochimique intervient primairement dans les formes où le groupement carbonyle est au voisinage immédiat d'un groupement méthyle, donc dans les formes *cis*. L'étude d'un tel processus est plus facile dans le cas de la diméthyl-4,5 hexène-4 one-3 ou quand la forme *cis* de la cétone étudiée a pu être préparée; elle peut aussi être effectuée en étudiant l'évolution sous irradiation d'une solution contenant initialement la forme *trans*. En solution aqueuse, dégazée ou non, le rendement quantique de transposition est fonction du p*H*, comme nous l'avons montré dans le cas de l'oxyde de mésityle.

Ainsi l'étude de l'apparition de diméthyl-4,5 hexène-5 one-3 par irradiation à 253.7 nm d'une solution 10^{-4} *M* de diméthyl-4,5 hexène-4 one-3 conduit aux résultats illustrés par la fig. 2. La quantité de transposé formé a été évaluée directement par chromatographie; dans une solution aussi diluée, les mesures sont entachées d'erreurs importantes. Néanmoins, on note une

TABLEAU 1. Caractéristiques des spectres d'absorption des cétones étudiées

Cétone	Eau		Cyclohexane *n*-heptane	
	λ_{max} (nm)	ϵ_{max} (l mol^{-1} cm^{-1})	λ_{max} (nm)	ϵ_{max} (l mol^{-1} cm^{-1})
		Transition $n\pi^*$		
Pentène-3 one-2				
trans	300	62	325	29
cis	303	60	330	27
Diméthyl-4,5 hexène-4 one-3				
trans			314	61
Hexène-4 one-3				
trans	297	56	320	25
Phényl-5 pentène-4 one-3	Insoluble dans l'eau		Pas de maximum apparent	
trans			(ϵ = 90 à 365 nm)	
		Transition $\pi\pi^*$		
Pentène-3 one-2				
trans	226	14 500	215	11 500
cis	231	9 650	222.5	8 700
Diméthyl-4,5 hexène-4 one-3				
trans	250–251	4 490	239	5 850
Hexène-4 one-3				
trans	227	11 390	217	9 830
Phényl-5 pentène-4 one-3				
trans			279	23 950

nette variation du rendement quantique initial de transposition.

$$\Phi_T^0 = 0.003 \pm 0.003 \text{ à } pH < 9$$

$$\Phi_T^0 = 0.075 \pm 0.003 \text{ à } pH > 10$$

Sur la figure on remarque aussi que, bien que le degré d'avancement de la réaction de transposition soit faible après 10 min d'irradiation à

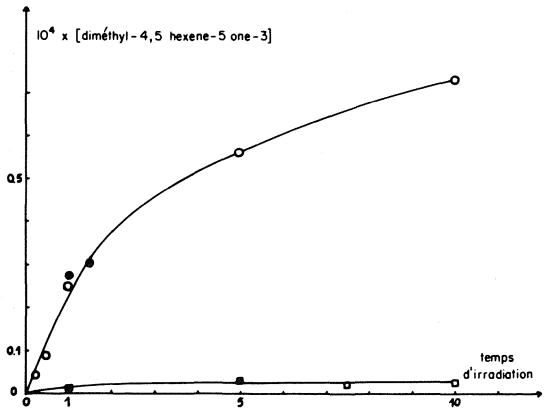

FIG. 2. Transposition de la diméthyl-4,5 hexène-4 one-3 en diméthyl-4,5 hexène-5 one-3 en solution aqueuse: □ pH = 4.5; ■ pH = 9; ○ pH = 10; ● pH = 11.

pH égal à 11, la vitesse de cette réaction décroit quand la concentration de transposé augmente. En milieu basique, le transposé se transforme en effet en la cétone initiale selon un processus thermique catalysé par les bases. On peut aussi vérifier que la transposition est le seul processus de disparition d'importance notable de la diméthyl-4,5 hexène-4 one-3 en solution aqueuse. Enfin, en solution dans le *n*-heptane, cette cétone ne se transpose pas.

Une étude détaillée de la transposition de la pentène-3 one-2 *cis* a été effectuée en solution aqueuse 10^{-3} M à différents pH. La désoxygénation de la solution ne modifie pas la vitesse des processus de transposition et d'isomérisation. En irradiant une solution contenant initialement la pentène-3 one-2 *trans*, à 253.7 nm ou à 313 nm, en déterminant à chaque instant la composition du mélange par chromatographie ou par spectrophotométrie, et en calculant le nombre de photons absorbés par chaque constituant, on peut déterminer les rendements quantiques de transposition rassemblés dans le tableau 2.

A pH égal à 5, la valeur de Φ_T^0 a été vérifiée en irradiant une solution 10^{-3} M de pentène-3 one-2

TABLEAU 2. Variations du rendement quantique de transposition de la pentène-3 one-2 *cis* avec le p*H*

Excitation à 253.7 nm		Excitation à 313 nm (mesures par chromatographie)		Excitation à 313 nm (mesures par spectrophotométrie)	
p*H*	Φ_T	p*H*	Φ_T	p*H*	Φ_T
2.1	0.03	2	0.035		
5.5	0.055	3	0.05	5.3	0.05
10.8	0.09	5	0.06	9.5	0.055
12	0.045	9.5	0.075	10.35	0.095
		10.8	0.035	10.7	0.015

cis à 313 nm ($\Phi_T^0 = 0.06$). Ce rendement Φ_T^0 passe par un maximum car il y a, en passant des milieux acides aux basiques, d'une part une augmentation de la vitesse du processus photochimique de transposition et d'autre part une augmentation de la vitesse du processus thermique de retour du transposé vers la cétone initiale. Cette valeur maximale (0.075 à 0.09) est atteinte pour un p*H* qui dépend en particulier du flux de photons incidents; (p*H* = 10.8 sous 253.7 nm où $I_0 = 3 \times 10^{15}$ photon cm^{-3} s^{-1}; p*H* = 9.5 sous 313 nm où $I_0 = 1.2 \times 10^{15}$ photon cm^{-3} s^{-1}). Le rendement quantique de la photo-énolisation ne semble donc pas dépendre de la nature de l'état excité singulet produit. L'effet de longueur d'onde observé pour l'oxyde de mésityle pourrait s'interpréter dans les mêmes termes.

La transposition de la diméthyl-4,5 hexène-4 one-3 et de la pentène-3 one-2 s'effectue selon un mécanisme analogue à celui proposé pour l'oxyde de mésityle (10). Les p*K* des énols des transposés correspondants peuvent être estimés à: (*i*) p*K* (énol de la diméthyl-4,5 hexène-5 one-3) = 9.5; (*ii*) p*K* (énol de la pentène-4 one-2) = 9.5; (*iii*) p*K* (énol de la méthyl-4 pentène-4 one-2) = 8.5. Les rendements quantiques maximaux de transposition indiquent qu'au moins 10% des états singulets S_2 ($\pi\pi^*$) ou S_1 ($n\pi^*$) participent au processus primaire de photoénolisation.

On peut remarquer aussi que le transposé de la pentène-3 one-2 *cis* est beaucoup plus instable en milieu basique que les transposés des deux autres cétones α,β-insaturées. La présence d'un groupement électrophobe CH_3 rend les hydrogènes de ces derniers transposés moins labiles que ceux de

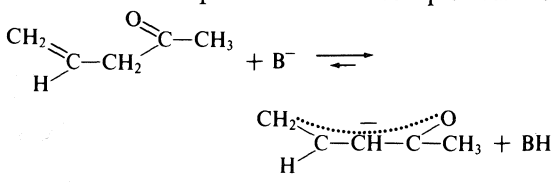

la pentène-4 one-2. En milieu basique la pentène-4 one-2 existera donc essentiellement sous forme énolate alors qu'une telle réaction est plus difficile avec les cétones méthylées. L'anion énolate de la pentène-4 one-2 peut être reprotoné et l'expérience montre que cette reprotonation conduit uniquement à l'isomère *trans*.

Isomérisation photochimique E-Z ou cis ⇄ trans

Nous avons examiné l'influence de la concentration et (ou) de la longueur d'onde d'excitation sur l'isomérisation des cétones α,β-insaturées en solution dans l'eau, le *n*-heptane et dans le tétrachlorure de carbone. L'étude la plus détaillée a été faite dans le cas de la pentène-3 one-2 *trans* et *cis* où nous avons vérifié, en outre, que cette cétone ne disparaissait pas par dissociation ou par photoréduction, quels que soient le solvant utilisé et la longueur d'onde d'excitation (entre 313 et 253.7 nm).

L'ensemble des résultats acquis en solution aqueuse est présenté dans le tableau 3. $\Phi^0_{t\to c}$ et $\Phi^0_{c\to t}$ sont les rendements quantiques initiaux d'isomérisation. Nous avons indiqué également les rendements initiaux de transposition Φ_T^0 déterminés à différentes concentrations. Nous n'observons pas d'effet notable de la longueur d'onde d'irradiation et de la concentration sur les rendements quantiques des processus issus des deux formes de la pentène-3 one-2.

Le tableau 4 rassemble les résultats acquis dans différents solvants, à deux longueurs d'onde d'excitation en l'absence d'oxygène. On remarque simplement que les rendements quantiques d'isomérisation ne dépendent pas des conditions expérimentales choisies. On remarquera aussi que l'excitation à 313 nm dans le tétrachlorure de carbone ne conduit pas à une chloration de la cétone insaturée. En solution aérée, ces rendements quantiques restent voisins de ceux mesurés en solution dégazée.

TABLEAU 3. Rendements quantiques d'isomérisation des pentène-3 ones-2 en solution aqueuse

Longueur d'onde d'excitation (nm)	Concentration (mol l^{-1})	Forme *trans*	Forme *cis*	
		$\Phi^0_{t\to c}$	$\Phi^0_{c\to t}$	$\Phi_T{}^0$
253.7	10^{-3}	0.42 ± 0.04	—	—
	2.5×10^{-3}	0.45 ± 0.04	0.35	0.05
297	10^{-4}	0.38 ± 0.04	—	—
	10^{-3}	0.40 ± 0.04	0.38	0.05
313	10^{-4}	0.40 ± 0.04	0.40	0.05
	10^{-3}	0.40 ± 0.04	0.40	0.06
	2.5×10^{-3}	0.40 ± 0.04	0.40	0.08

TABLEAU 4. Influence de la nature des solvants sur les rendements quantiques des processus photochimiques des pentène-3 ones-2 en solution dégazée

Solvants	Longueur d'onde d'excitation (nm)	Forme *trans*	Forme *cis*	
		$\Phi^0_{t\to c}$	$\Phi^0_{c\to t}$	$\Phi_T{}^0$
H_2O (pH = 5.3)	253.7	0.42 ± 0.04	0.35 ± 0.04	0.06
	313	0.40 ± 0.04	0.40 ± 0.04	0.06
n-C_7H_{16}	253.7	0.55 ± 0.05	0.43 ± 0.04	0.00
	313	0.40 ± 0.04	0.40 ± 0.04	0.00
CCl_4	313	0.45 ± 0.04		—

TABLEAU 5. Rendement quantique d'isomérisation de l'hexène-4 one-3 *trans*

Solvants	Excitation (nm)	Milieu	$\Phi^0_{t\to c}$
Eau (pH = 5.4)	253.7	Dégazé ou aéré	0.37 ± 0.04
	313	Dégazé ou aéré	0.44 ± 0.04
n-Heptane	253.7	Aéré ou dégazé	0.37 ± 0.07
	313	Aéré ou dégazé	0.42 ± 0.04

TABLEAU 6. Rendement quantique d'isomérisation de la phényl-5 pentène-4 one-3 *trans*

Solvants et concentrations utilisés	Excitation (nm)	Milieu	$\Phi^0_{t\to c}$
Cyclohexane (10^{-3} M)	365	Dégazé	0.40 ± 0.04
Cyclohexane (10^{-2} M)	253.7	Dégazé	0.33 ± 0.05

Nous avons également étudié les rendements quantiques d'isomérisation de l'hexène-4 one-3 et de la phényl-5 pentène-4 one-3 sous forme *trans*. Nous avons vérifié expérimentalement que ces formes ne participent à aucun autre processus photochimique que l'isomérisation (Tableaux 5 et 6).

L'isomérisation *cis–trans* peut être sensibilisée en particulier par l'acétone, l'acétophénone, la benzophénone.[2] Nous ne citerons dans le présent article que les résultats relatifs à l'emploi de benzophénone en solution dans le tétrachlorure de carbone et excitée à 313 nm. Pour une concentration de pentène-3 one-2 *trans* voisine de 10^{-2} M, le processus d'autodésactivation du niveau triplet de la benzophénone devient négligeable devant le transfert triplet–triplet exothermique (le rapport des vitesses est estimé à 67 (21)).

La phosphorescence de la benzophénone peut être observée à température ambiante dans le tétrachlorure de carbone; sous excitation à 385 nm, cette phosphorescence dont le maximum est situé à 450 nm, est éteinte par la pentène-3 one-2 *trans* en concentration voisine de 10^{-2} M; le transfert d'énergie triplet–triplet est alors quantitatif. Les rendements quantiques d'isomérisation sensibilisée sont rassemblés dans le tableau 7.

Le rendement quantique limite d'isomérisation sensibilisée extrapolé à partir de la droite de

[2]A. Rioual, résultats à publier.

TABLEAU 7. Rendements quantiques d'isomérisation de la pentène-3 one-2 *trans* sensibilisée par la benzophénone (2×10^{-2} *M*) dans CCl_4

Concentration de pentène-3 one-2 *trans* (*M*)	$\Phi^0_{t\to c}$
2×10^{-4}	0.015
1.35×10^{-3}	0.07
2×10^{-3}	0.10
3.4×10^{-3}	0.15
5.4×10^{-3}	0.18
1.08×10^{-2}	0.31

Stern-Volmer illustrant les variations de $1/\Phi_{t\to c}{}^{S}$ en fonction de $1/(trans)$ est égal à:

$$(\Phi_{t\to c}{}^{S})_{lim} = 0.50 \pm 0.05$$

Par ailleurs les analyses effectuées par chromatographie en phase gazeuse n'ont mis en évidence aucune disparition sensibilisée de la pentène-3 one-2 par une autre voie que l'isomérisation.

Des mesures analogues ont été effectuées avec l'hexène-4 one-3 en concentration égale à 10^{-2} *M* dans le tétrachlorure de carbone, la benzophénone étant excitée à 365 nm. Le rendement quantique d'isomérisation sensibilisée peut être évalué à:

$$\Phi_{t\to c}{}^{S} = 0.55 \pm 0.05$$

On atteint un régime photostationnaire caractérisé par le rapport des concentrations:

$$(cis)_\infty/(trans)_\infty = 0.39$$

Conclusions

La désactivation des états excités S_1 ($n\pi^*$) et S_2 ($\pi\pi^*$) des cétones étudiées est de nature non radiative; ces substances sont en effet essentiellement non fluorescentes. La conversion interne S_2 ($\pi\pi^*$) $\rightarrow S_1$ ($n\pi^*$) apparait être totale puisqu'aucun effet de longueur d'onde ne se manifeste sur les rendements quantiques étudiés.

La désactivation de l'état excité S_1 ($n\pi^*$) des formes *cis* intervient par photo-énolisation avec un rendement quantique qui serait égal au moins à 0.10 ± 0.01. Cette photo-énolisation primaire peut conduire à la transposition de la cétone ou elle peut fournir à cette cétone une voie de désactivation non radiative.

Les résultats obtenus en sensibilisation par la benzophénone dans le tétrachlorure de carbone montrent qu'une population totale des niveaux triplets inférieurs des cétones α,β-insaturées par transfert d'énergie conduit à une isomérisation de la moitié des molécules excitées; on peut donc penser qu'un niveau triplet d'un isomère se désactive avec une égale probabilité vers les deux formes *cis* et *trans*. Les rendements quantiques d'isomérisation directe montrent alors que par excitation dans les états S_1 ($n\pi^*$) et S_2 ($\pi\pi^*$) des formes *trans* ou *cis*, le niveau triplet isomérisable est peuplé avec un rendement:

$$\varphi_{TIS} = 0.80 \pm 0.10$$

Ainsi la désactivation des états singulets des formes *cis* était justifiée par la complémentarité à l'unité des deux rendements:

$$\varphi_T = 0.10 \pm 0.01$$

$$\varphi_{TIS} = 0.80 \pm 0.10$$

On peut noter toutefois que dans les formes *trans* où la photo-énolisation primaire ne peut intervenir, le rendement quantique d'isomérisation n'est pas supérieur à celui mesuré pour les formes *cis*, sauf dans la pentène-3 one-2. Un déficit apparait donc dans le bilan photonique de la plupart des composés. Ce même déficit apparait dans la cétone non transposable étudiée par Rodriguez et Morrison (13).

Toutes les cétones étudiées dans cet article présentent une photostabilité interessante; le seul processus de transformation irréversible, c'est-à-dire la transposition, peut même dans certains cas être rendu réversible (en milieu basique). Il est également interessant de remarquer que cette photostabilité est conservée en milieu aéré.

1. J. KOSSANYI et B. FURTH. L'Actual. Chim. N° 3, mars 1974.
2. P. DE MAYO, A. A. NICHOLSON et M. F. TCHIR. Can. J. Chem. **48**, 225 (1970).
3. A. DEVAQUET et L. SALEM. Can. J. Chem. **49**, 977 (1971); A. DEVAQUET. J. Am. Chem. Soc. **94**, 5160 (1972).
4. R. R. BIRGE et P. A. LEERMAKERS. J. Am. Chem. Soc. **94**, 8105 (1972).
5. J. GLOOR, G. BERNARDINELLI, R. GERDIL et K. SCHAFFNER. Helv. Chim. Acta, **56**, 2520 (1973).
6. G. MARSH, D. R. KEARNS et K. SCHAFFNER. Helv. Chim. Acta, **51**, 1890 (1968).
7. R. JONES, D. R. KEARNS et R. M. WING. J. Chem. Phys. **58**, 1370 (1972).
8. R. O. LOUFTY et J. M. MORRIS. Chem. Phys. Lett. **19**, 377 (1973).
9. W. AMREIN, I. M. LARSSON et K. SCHAFFNER. Helv. Chim. Acta, **57**, 2519 (1974).

10. F. BONNET et J. LEMAIRE. Bull Soc. Chim. 1185 (1973); F. BONNET. Thèse de 3° cycle, Université de Clermont. 1972.
11. N. C. YANG et M. JORGENSON. Tetrahedron Lett. 1203 (1964); J. Am. Chem. Soc. **85**, 1698 (1963).
12. N. C. YANG et DO MINH THAP. J. Org. Chem. **32**, 2462 (1967).
13. H. MORRISON et O. RODRIGUEZ. J. Photochem. **3**, 471 (1974/75).
14. D. D. FAULK et A. FRY. J. Org. Chem. **35**, 369 (1970).
15. L. NYFFENEGGER. Thèse d'Ingénieur C.N.A.M., Clermont-Ferrand. 1973.
16. W. COLE et P. L. JULIAN. J. Am. Chem. Soc. **67**, 1369 (1945); R. PINSON et S. L. FRIESS. J. Am. Chem. Soc. **72**, 5333 (1950); D. A. SHIRLEY. Org. React. **8**, 31, (1954); E. O. FISCHER et W. HAFNER. Z. Naturforsch. Teil B, **9**, 503 (1954).
17. J. CASON. Chem. Rev. **40**, 15 (1947); J. Am. Chem. Soc. **68**, 2078 (1946).
18. U. E. MATTER, G. PASCUAL, E. PRETSCH, A. PROSS, W. SIMON et S. STERNHELL. Tetrahedron, **25**, 691 (1969).
19. G. N. BANNELL et N. SHEPPARD. Discuss. Faraday Soc., **34**, 115, (1962).
20. J. RONAYETTE, R. ARNAUD et J. LEMAIRE. Can. J. Chem. **52**, 1848 (1974).
21. A. DEFLANDRE. Thèse de 3° cycle, Université de Clermont. 1974.

Préparation et étude des isothiocyanatoboranes halogénés

J. DAZORD, H. MONGEOT ET H. ATCHEKZAI

Laboratoire de Physico-Chimie Minérale, Associé au C.N.R.S. N° 116, Service du Pr. Cueilleron, 43, Boulevard du 11 Novembre 1918, 69621 Villeurbanne, France

ET

J. P. TUCHAGUES,

Laboratoire de Chimie de Coordination, 205, Route de Narbonne, B.P. 4142, 31030 Toulouse, France

Reçu le 2 juillet 1975[1]

J. DAZORD, H. MONGEOT, H. ATCHEKZAI et J. P. TUCHAGUES. Can. J. Chem. **54**, 2135 (1976).

Nous avons obtenu au cours de cette étude les dérivés mixtes halogénés et pseudohalogénés du bore $BX_n(NCS)_{3-n}$, (X = Cl, Br, I; n = 1, 2). Ces composés on été préparés par deux méthodes différentes en faisant réagir les halogénures de bore soit sur les isothiocyanates métalliques, soit sur le triisothiocyanatoborane $B(NCS)_3$. Nous avons caractérisé ces composés par spectrométrie de masse, spectrométrie infrarouge et Raman et par résonance magnétique du noyau ^{11}B; cependant, il n'est pas possible d'isoler ces espèces par suite de réactions de redistribution rapides. Les spectres de vibration montrent que dans ces composés le bore est lié à l'azote du groupement NCS et pas à l'atome de soufre.

J. DAZORD, H. MONGEOT, H. ATCHEKZAI, and J. P. TUCHAGUES. Can. J. Chem. **54**, 2135 (1976).

The mixed halide–pseudohalides $BX_n(NCS)_{3-n}$ (n = 1 or 2) have been obtained except for X = F. Mixtures of these compounds with boron trihalide and boron triisothiocyanate are prepared by the reaction of BX_3 either with metal isothiocyanates or with boron triisothiocyanate. Mass spectrometry, infrared, Raman, and ^{11}B nmr data are reported. Rapid redistribution reactions prevent the isolation of the mixed species. Vibration spectrometry shows that boron is bonded to the nitrogen of the NCS group and not to the sulfur.

Introduction

La chimie des dérivés pseudohalogénés du bore s'est développée considérablement depuis une quinzaine d'années, essentiellement grâce aux nombreux travaux de Lappert et collaborateurs (1–6). Signalons en particulier les combinaisons $(RO)_2B(NCS)$, $(R_2N)_2B(NCS)$ et $Ph_2B(NCS)$ (2) qui ont été obtenues par action du dérivé monohalogéné correspondant sur un isothiocyanate métallique. Ces dérivés, quelques-uns de leurs composés d'addition et $[B(NCS)NH]_3$ ont été étudiés par rmn du proton, calorimétrie, spectrométrie infrarouge et ultraviolet (4, 5). Les propriétés optiques, magnéto-optiques et de résonance magnétique du noyau ^{11}B des composés $(Et_2N)_2B(NCS)$ et $[N(R)B(NCS)]_3$ ont été également étudiées (7). Récemment, Kendall et Lipscomb (8) ont préparé les composés $NH_3BH_2(NCS)$ et $B_{10}H_{13}(NCS)$ et en ont déterminé la structure cristalline et moléculaire. D'autre part, des réactions d'échange des groupements NCS et alcoyl ont été observées par Costes (9) à propos des systèmes $BR_3/B(NCS)_3$.

Les halogénures de bore mixtes sont connus pour tous les halogènes (sous forme libre et complexée). Au contraire, parmi les dérivés mixtes halogénés et pseudohalogénés, seules les espèces $BBr(NCS)_2$ (2, 6) et $BBr_2(NCS)$ (6) ont déjà été décrites. Bien que ces deux composés aient été préparés selon des méthodes analogues à celles que nous avons utilisées, les observations des auteurs concernant leurs spectres infrarouge et de rmn du noyau ^{11}B, ainsi que celles concernant leur stabilité sont très différentes des nôtres. Après avoir préparé les dérivés $BX_n(NCS)_{3-n}$ (X = Cl, Br ou I, n = 1, 2) par deux méthodes différentes, nous avons étudié quelques-unes de leurs propriétés chimiques et physico-chimiques.

Résultats

La réaction des halogénures de bore sur l'isothiocyanate de sodium, de potassium ou d'argent solide conduit en présence ou non de solvant (CS_2, CCl_4, CH_2Cl_2, C_2Cl_4, n-heptane),

[1]Revision reçue le 25 mars 1976.

Can. J. Chem. Downloaded from www.nrcresearchpress.com by 210.87.254.105 on 09/05/12
For personal use only.

Can. J. Chem. Downloaded from www.nrcresearchpress.com by 210.87.254.105 on 09/05/12
For personal use only.

à des mélanges de produits plus ou moins substitués.

Il est possible d'obtenir des mélanges $BX_3/BX_2(NCS)$ en faisant réagir l'isothiocyanate d'argent sur un excès de BX_3. L'addition de nouvelles quantités d'isothiocyanate entraîne la formation de $BX(NCS)_2$ puis celle de $B(NCS)_3$ alors que BX_3 et $BX_2(NCS)$ disparaissent progressivement. En présence d'un excès de AgNCS, on obtient le dérivé trisubstitué $B(NCS)_3$ pur, ceci très rapidement avec BBr_3, et très lentement avec BI_3; l'action de BCl_3 ne conduit cependant qu'à des mélanges de $B(NCS)_3$ et de $BCl(NCS)_2$.

Les isothiocyanates de potassium ou de sodium réagissent beaucoup plus lentement que le sel d'argent sur le triiodure ou le tribromure de bore. Ils ne réagissent pas sur BCl_3 dans nos conditions opératoires.

L'obtention simultanée de plusieurs composés au cours des réactions précédentes aussi bien que la formation connue de $BBr_2(NCS)$ (6) à partir de BBr_3 et $BBr(NCS)_2$ sont dues à l'existence d'équilibres réactionnels entre les divers composés tricoordinés envisagés. En effet, la mise en présence des composés BX_3 et $B(NCS)_3$ conduit instantanément aux mêmes mélanges que ceux obtenus par action des thiocyanates métalliques sur BX_3. Ceci constitue d'ailleurs une méthode simple de préparation des dérivés mixtes:

[1] $$2BX_3 + B(NCS)_3 \rightleftharpoons 3BX_2(NCS)$$

[2] $$BX_3 + 2B(NCS)_3 \rightleftharpoons 3BX(NCS)_2$$

On peut déplacer les équilibres précédents soit par addition ultérieure de trihalogénure de bore ou de triisothiocyanate de bore, soit par élimination du trihalogénure de bore; cette dernière opération n'étant possible qu'avec les produits chlorés ou bromés. Ces phénomènes de redistribution empêchent d'isoler les espèces intermédiaires $BX_2(NCS)$ et $BX(NCS)_2$. Il est possible cependant d'obtenir des mélanges à l'équilibre renfermant une proportion importante d'un des composés. C'est le cas notamment de $BCl(NCS)_2$.

Les solutions de ces mélanges dans les solvants précédents évoluent de manière lente et irréversible du fait de la polymérisation de $B(NCS)_3$ qui conduit à un solide totalement insoluble dans les solvants utilisés.

Notons enfin que BF_3 possède un comportement différent de celui des autres halogénures de bore vis-à-vis des réactions précédentes puisqu'il ne réagit pas sur les isothiocyanates métalliques ou sur $B(NCS)_3$. Lorsqu'il est mis en présence d'un mélange contenant des produits mixtes bromés ou chlorés, son action se limite à la formation d'halogénures de bore mixtes.

Tous les dérivés mixtes que nous avons obtenus au cours de ce travail ont été caractérisés par différentes méthodes spectrométriques.

TABLEAU 1. Spectrométrie de masse

Composé	Masse	Intensité Calculée	Intensité Mesurée
$BCl(NCS)^+$	103	3	3.9
	104	12	12
	105	1	1.6
	106	4	4
$BCl_2(NCS)^+$	138	9	9.5
	139	36	36
	140	6	6.8
	141	24	24
	142	1	3
	143	4	6.5
$BCl(NCS)_2^+$	161	3	2.7
	162	12	12
	163	1	1.5
	164	4	4.2
$BBr(NCS)^+$	147	1	1
	148	4	4
	149	1	1
	150	4	4
$BBr_2(NCS)^+$	226	1	1
	227	3	5
	228	2	2.2
	229	6	8.5
	230	1	1
	231	3	5
$BBr(NCS)_2^+$	205	9	10
	206	36	45
	207	10	10
	208	39	48
	209	1	1
	210	4	4
$BI(NCS)^+$	195	1	1
	196	4	3.5
$BI_2(NCS)^+$	322	1	1
	323	4	3.9
$B(NCS)_2^+$	126	18.6	18.6
	127	74.5	71
	128	1.8	
	129	7.2	7.1
$B(NCS)_3^+$	184	17	17
	185	68	68
	186	2.6	6.8
	187	10.4	9.5

Can. J. Chem. Downloaded from www.nrcresearchpress.com by 210.87.254.105 on 09/05/12
For personal use only.

Spectrométrie de masse

Chacun des composés attendus $BX_2(NCS)$, $BX(NCS)_2$ et $B(NCS)_3$ donne lieu à un ensemble de pics dont les hauteurs correspondent à celles calculées à partir de la répartition isotopique de chacun des éléments (voir tableau 1). On note une certaine fragmentation des composés avec apparition de $BX(NCS)^+$ et $B(NCS)_2^+$. Il apparaît de plus le massif moléculaire de BX_3, ainsi que BX_2^+, BX_2^{2+}, BX^+, X^+, X^{2+}, X_2^+, HX^+, $HNCS^+$ et $HNCS^{2+}$, la présence de ces trois derniers ions ne pouvant s'expliquer que par une légère hydrolyse.

Spectrométrie de résonance magnétique du noyau ^{11}B

Le noyau ^{11}B ne donnant pas de couplage appréciable avec l'azote, chacun des composés est donc caractérisé par un seul pic de résonance. Le fait que ce noyau soit par ailleurs lié à des noyaux présentant un moment quadripolaire favorise l'élargissement des raies de résonance. Cette circonstance ne constitue par un obstacle à la mise en évidence des composés mixtes $BCl_2(NCS)$, $BCl(NCS)_2$, $BBr_2(NCS)$ et $BBr(NCS)_2$ étant donné les fortes différences de déplacement $\delta^{11}B$ qui caractérisent ces composés. Pour ce qui est des composés $BI_2(NCS)$ et $BI(NCS)_2$, cet élargissement des pics, conjugué à une plus grande proximité des fréquences de résonance: $\delta^{11}B$ -5.5 pour BI_3 et $+5$ pour $B(NCS)_3$, ne permet pas de caractériser leur présence avec certitude en rmn du noyau ^{11}B. (Voir tableau 2.)

Spectrométrie de vibration

Les spectres de chacune des espèces mixtes $BX_2(NCS)$ et $BX(NCS)_2$ ont été déduits de la comparaison des spectres de divers mélanges. Les spectres du triisothiocyanate de bore sont obtenus à partir de solutions du produit pur. Les bandes observées et leur attribution sont reportées sur les tableaux 3, 4 et 5. A l'exception des mélanges $BCl_3/BCl_2(NCS)$ et dans une certaine mesure $BBr_3/BBr_2(NCS)$, les produits étudiés sont très sensibles au rayonnement laser.

TABLEAU 2. Déplacements chimiques du noyau ^{11}B (en ppm)

Composés chlorés		Composés bromés		Composés iodés	
Composé	$\delta^{11}B$	Composé	$\delta^{11}B$	Composé	$\delta^{11}B$
BCl_3	$+47.5$	BBr_3	$+40$	BI_3	-5.5
BCl_2NCS	$+30.5$	BBr_2NCS	$+26$		
$BCl(NCS)_2$	$+15.5$	$BBr(NCS)_2$	$+16$		
$B(NCS)_3$	$+5$	$B(NCS)_3$	$+5$	$B(NCS)_3$	$+5$

TABLEAU 3. Fréquence en cm^{-1} et attribution des bandes observées en spectrométrie ir et Raman pour les composés BX_2NCS (f, faible; m, moyenne; F, forte; P, polarisée)

BCl_2NCS		BBr_2NCS		BI_2NCS		
ir	Raman	ir	Raman	ir	Raman	Attribution
2835f		2805		2780		$\nu CN+\nu CS$
		2580f		2560f		$2\nu^{10}BN$
		2525m		2510m		$2\nu^{11}BN$
2045F		2050F		2040F		νCN
1290m	1295mP	1292m	1293mP	1284f		$\nu^{10}BN$
1260F	1265FP	1265F	1265FP	1259m		$\nu^{11}BN$
	945fP	990m	992f	980f		$2\delta NCS$
		850m		742F		$\nu a^{10}BX_2$
		812F		712F		$\nu a^{11}BX_2$
800m	800mP	766F	762mP	753m		νCS
504m						$\Gamma^{11}BX_2N$
468m		495m				δNCS
	434FP	325f	325FP			νsBX_2
330m	330f					$\delta^{11}BX_2$

Can. J. Chem. Downloaded from www.nrcresearchpress.com by 210.87.254.105 on 09/05/12
For personal use only.

TABLEAU 4. Fréquence en cm^{-1} et attribution des bandes observées en spectrométrie ir et Raman pour les composés $BX(NCS)_2$ (f, faible; m, moyenne; F, forte, P, polarisée)

$BCl(NCS)_2$		$BBr(NCS)_2$		$BI(NCS)_2$		
ir	Raman	ir	Raman	ir	Raman	Attribution
2010F		2000F		2000F		νCN
1337m		1358m		1360f		$\nu a^{10}BN_2$
1315m		1325F		1325m		$\nu a^{11}BN_2$
1195f	1195fP	1190m	1190mP	1165f		$\nu s^{10}BN_2$
1175m	1175mP	1170F	1170FP	1152fm		$\nu s^{11}BN_2$
1015f		965f		972f		2δNCS
762m				758m		νCS
598f		530f				$\Gamma^{10}BXN_2$
576f		520m				$\Gamma^{11}BXN_2$

TABLEAU 5. Fréquence en cm^{-1} et attribution des bandes observées en spectrométrie ir et Raman pour $B(NCS)_3$ (f, faible; m, moyenne; F, forte; P, polarisée)

ir	Raman	Attribution
2780F		νCN+νCS
2660m		$2\nu^{10}$BN
2592F		$2\nu^{11}$BN
2495m		νCN+δNCS
2010F	2010m	νCN
1338F		$\nu a^{10}BN_3$
1303F		$\nu a^{11}BN_3$
1073f	1067FP	νsBN_3
969F	970fP	2δNCS
768m		νCS
598F		$\Gamma^{10}BN_3$
577F		$\Gamma^{11}BN_3$
483f	485m	δNCS

Dans ces conditions, l'observation des raies Raman est très difficile pour certains composés.

L'analyse des différents spectres nous a permis de caractériser les vibrations de valence BN et de montrer par là que le bore était lié à l'azote du groupe NCS et non au soufre. En effet les masses respectives des atomes d'azote et de soufre sont telles que les vibrations de valence BS apparaîtraient à des fréquences nettement inférieures à celles observées. C'est ainsi que dans les composés BX_2SH (10) et $BX(SH)_2$ (11), celles-ci sont inférieures à 1000 cm^{-1}. Les fréquences des vibrations de valence pseudo-antisymétriques du groupement NCS peuvent, elles aussi, être considérées comme caractéristiques d'une structure iso (5, 12, 13, 14, 15). L'attribution des autres bandes a été effectuée à partir de travaux concernant certains dérivés halogénés du bore (16, 17, 18) et de dérivés contenant le groupement NCS (14, 19, 20, 21).

Discussion

Les réactions de redistribution observées entre BX_3 et $B(NCS)_3$ sont tout à fait semblables à celles, bien connues, qui se produisent par simple mélange de deux halogénures de bore. Ce type de réaction ne se limite d'ailleurs pas aux dérivés tricoordinés du bore contenant un halogène. Il a été également très étudié dans le cas des organoboranes (22). Il est admis que l'échange entre deux molécules s'effectue par formation transitoire d'un dimère dans lequel l'atome de bore est tétracoordiné et joue le rôle d'accepteur. Ces échanges sont favorisés quand l'un au moins des réactifs contient des groupes d'atomes pouvant jouer le rôle de donneur (22). Il n'est donc pas surprenant que les échanges entre halogènes et groupes NCS soient rapides puisque ces derniers possèdent un atome d'azote et un atome de soufre susceptibles de se coordiner avec le bore. Notre échec dans l'obtention des dérivés mixtes fluorés est probablement dû au fait que BF_3 donne lieu beaucoup plus difficilement que les autres halogénures de bore à des réactions de redistribution. C'est ainsi que par exemple l'énergie d'activation de réactions d'échange entre BF_3 et BCl_3 (23) est élevée alors qu'elle est pratiquement nulle dans le cas de BCl_3 et BBr_3 (24). Le comportement particulier de BF_3 s'explique par l'existence de liaisons de rétrocoordination du fluor au bore qui affaiblissent le pouvoir accepteur du bore (22).

Notre désaccord avec les résultats de Lappert et collaborateurs (2, 6) concernant $BBr(NCS)_2$ et

Can. J. Chem. Downloaded from www.nrcresearchpress.com by 210.87.254.105 on 09/05/12
For personal use only.

$BBr_2(NCS)$ a pour origine le fait que les auteurs considèrent les deux dérivés bromés précédents comme suffisamment stables pour être isolés. C'est ainsi que les bandes d'absorption infrarouge reportées pour $BBr(NCS)_2$ (2) nous indiquent que l'échantillon analysé contenait essentiellement $B(NCS)_3$ dont le spectre est voisin de celui du dérivé monobromé. On note par exemple qu'aucune bande n'est signalée vers 1170 cm^{-1}, région dans laquelle $BBr(NCS)_2$ possède une bande caractéristique, alors qu'une bande faible est signalée vers 1064 cm^{-1}. Cette dernière correspond probablement à la bande faible mais caractéristique que nous avons observée avec une solution diluée de $B(NCS)_3$ à 1073 cm^{-1}.

La comparaison des résultats de résonance magnétique du noyau ^{11}B fournis par Jefferson et Lappert (6) à ceux que nous avons obtenus, confirme, à notre avis, que les composés décrits par ces auteurs comme étant $BBr_2(NCS)$ et $BBr(NCS)_2$ sont en réalité respectivement $BBr(NCS)_2$ et $B(NCS)_3$. Dans cet ordre d'idée, nous noterons que: (*i*) La valeur $\delta^{11}B = +5$ ppm que nous reportons pour $B(NCS)_3$ est confirmée par d'autres travaux (9); (*ii*) Il n'est pas raisonnable de penser que le signal de résonance du noyau ^{11}B pour le composé mixte $BBr(NCS)_2$ puisse se trouver en dehors de l'intervalle compris entre BBr_3 ($\delta^{11}B = +40$ ppm) et $B(NCS)_3$ ($\delta^{11}B = +5$ ppm); et (*iii*) Par contre, il est légitime de penser que la valeur $\delta^{11}B = +3.5$ ppm obtenue par Jefferson et Lappert est, à la précision des mesures près, la même que celle que nous avons obtenue pour $B(NCS)_3$ ($\delta^{11}B = +5$ ppm). Dans cette hypothèse, la valeur que ces auteurs attribuent à $BBr_2(NCS)$ ($\delta^{11}B = 12$ ppm) serait comparable à celle que nous avons obtenue pour $BBr(NCS)_2$ ($\delta = +16$ ppm). Remarquons enfin que les composés que nous avons étudiés possèdent comme tous les dérivés thiocyanatés connus du bore, une structure iso.

Partie expérimentale

Obtention des composés

Les produits préparés étant aussi hydrolysables que les halogénures de bore, toutes les manipulations sont effectuées en atmosphère d'azote sec.

Les réactivités des halogénures de bore vis-à-vis de AgNCS sont très différentes: BCl_3 réagit rapidement au-dessous de 0 °C, BBr_3 ne réagit que très lentement dans les mêmes conditions mais son action est très violente à la température ambiante; avec BI_3, il convient d'opérer en solution et à chaud pour avoir une cinétique assez rapide.

Pour obtenir des mélanges $BX_3/BX_2(NCS)$ (X = Cl, Br), on condense 100 mmol de BX_3 à la température de l'air liquide dans un ballon de 2 l contenant 30 mmol de AgNCS et éventuellement un solvant (CS_2, CCl_4, CH_2Cl_2, C_2Cl_4, *n*-heptane). On laisse ensuite réchauffer lentement le mélange en l'agitant. Avec les produits chlorés, la réaction est terminée dès le retour à la température ambiante. Avec les produits bromés, on doit en revanche laisser réagir pendant 1 h à 0 °C. L'utilisation de quantités croissantes de AgNCS conduit à des mélanges de produits de plus en plus substitués. Pour obtenir $B(NCS)_3$ pur, on fait réagir dans les mêmes conditions 430 mmol de AgNCS sur 100 mmol de BBr_3. L'utilisation d'un solvant tel que CCl_4 (60 ml) est nécessaire pour éviter une réaction violente.

Pour obtenir des mélanges $BI_3/BI_2(NCS)$, on chauffe la solution à reflux pendant environ 3 h en présence d'un excès de AgNCS. Dans ces conditions, $BI(NCS)_2$ n'apparait en concentration importante qu'après 40 h. Il se transforme complètement en $B(NCS)_3$ après environ 60 h.

NaNCS et KNCS utilisés en excès permettent de préparer des mélanges $BBr_3/BBr_2(NCS)$. On opère alors avec BBr_3 pur et on chauffe à reflux pendant plusieurs heures. Des mélanges $BI_3/BI_2(NCS)$ sont obtenus dans des conditions identiques à partir d'une solution de BI_3. Cette réaction peut être accélérée en opérant à 120–130 °C en l'absence de solvant dans une ampoule scellée et agitée.

On peut mettre aisément à profit la volatilité de BCl_3 ou de BBr_3 pour les éliminer d'un mélange de façon à déplacer les équilibres réactionnels. La distillation sous pression réduite (ou encore l'entraînement par un courant d'azote sec) permet d'éliminer les trihalogénures BCl_3 ou BBr_3. Ainsi, partant d'un mélange $BX_3/BX_2(NCS)$ on aboutit à $B(NCS)_3$ dans le cas des dérivés bromés, et à un mélange $BCl(NCS)_2/B(NCS)_3$ dans le cas des dérivés chlorés. Les quantités de $BX_2(NCS)$ entraînées avec BX_3 sont alors très faibles.

$B(NCS)_3$ a été également préparé selon la méthode de Sowerby (25) à partir de BCl_3 et NaNCS ou KNCS en solution dans SO_2 liquide. Il est alors nécessaire de distiller soigneusement le produit final pour éviter la présence de $BCl_2(NCS)$ et $BCl(NCS)_2$ dont nous avons noté la présence en fin de réaction. Cette méthode n'est pas transposable à la préparation des dérivés $BI_2(NCS)$ et $BI(NCS)_2$ car BI_3 est détruit par SO_2 liquide.

Spectrométrie de masse

Les spectres de masse ont été enregistrés à l'aide d'un appareil Varian CH7 avec un potentiel d'ionisation de 70 eV.

Partant de mélanges $BCl_3/BCl_2(NCS)$ ou $BBr_3/BBr_2(NCS)$ préparés en l'absence de solvant, on fait évoluer progressivement la composition par élimination des composés volatils. On met ainsi en évidence successivement BCl_3, $BCl_2(NCS)$ et $BCl(NCS)_2$ dans le cas des dérivés chlorés et BBr_3, $BBr_2(NCS)$, $BBr(NCS)_2$ et $B(NCS)_3$ dans le cas des dérivés bromés.

Les produits iodés sont introduits (après élimination du solvant éventuellement présent) à l'aide d'un petit creuset en verre pyrex maintenu à la température ambiante.

Spectrométrie infrarouge

Les spectres sont enregistrés entre 4000 et 250 cm^{-1} sur

un appareil Perkin-Elmer 457 à l'aide d'une cellule à liquide munie de fenêtres en CsI.

Spectrométrie Raman

Les spectres Raman sont enregistrés avec un spectromètre Coderg PHO couplé à un laser Spectra-Physic à argon, modèle 160-00, la fréquence généralement utilisée étant 20492 cm^{-1}. Afin d'éviter une coloration de la solution et la formation rapide de solide sous l'effet du rayonnement laser, les échantillons analysés sont placés dans une cellule tournante.

Résonance magnétique nucléaire

Les spectres ont été obtenus à l'aide d'un spectrographe Perkin-Elmer R-10, en opérant à 19.25 MHz (^{11}B). Les composés ont été examinés en solution dans CS_2, CCl_4 ou CH_2Cl_2.

Les déplacements chimiques reportés sont exprimés en ppm par rapport à un étalon externe d'éthérate de trifluorure de bore (Et_2OBF_3). Les déplacements se situant à champ fort par rapport à l'étalon sont comptés négativement.

Remerciements

Nous tenons à remercier Monsieur J. Carré, du Laboratoire de Physico-Chimie Minérale associé au C.N.R.S. No 116, d'avoir bien voulu enregistrer les spectres de masse des échantillons.

1. M. F. Lappert et H. Pyszora. Proc. Chem. Soc. 350 (1960).
2. M. F. Lappert, H. Pyszora et M. Rieber. J. Chem. Soc. 4256 (1965).
3. M. F. Lappert et H. Pyszora. Adv. Inorg. Chem. Radiochem. **9**, 133 (1966).
4. M. F. Lappert et H. Pyszora. J. Chem. Soc. A, 854 (1967).
5. M. F. Lappert et H. Pyszora. J. Chem. Soc. A, 1024 (1968).
6. R. Jefferson et M. F. Lappert. Intra-Sci. Chem. Rep. **7**, 123 (1973).
7. A. François. Thèse, Université Paul Sabatier, Toulouse, 1971.
8. D. S. Kendall et W. N. Lipscomb. Inorg. Chem. **12**, 2915 (1973).
9. J. P. Costes. Thèse, Université Paul Sabatier, Toulouse, 1975.
10. J. Bouix, M. Fouassier et M. T. Forel. J. Mol. Struct. **15**, 103 (1973).
11. M. Fouassier, M. T. Forel, J. Bouix et R. Hillel. J. Chim. Phys. Physicochim. Biol. **70**, 1518 (1973).
12. N. S. Ham et J. B. Wallis. Spectrochim. Acta, **16**, 279 (1960).
13. G. L. Caldow et H. W. Thompson. Spectrochim. Acta, **13**, 212 (1958).
14. K. Oba, F. Watari et K. Aida. Spectrochim. Acta, Part A, **23**, 1515 (1967).
15. J. Goubeau et J. Reyhing. Z. Anorg. Allg. Chem. **96**, 294 (1958).
16. A. J. Banister, N. N. Greenwood, B. P. Straughan et J. Walker. J. Chem. Soc. 995 (1964).
17. R. J. H. Clark et P. D. Mitchell. J. Chem. Phys. **56**, 2225 (1972).
18. L. P. Lindeman et M. K. Wilson. J. Chem. Phys. **24**, 244 (1956).
19. J. R. Durig et D. W. Wertz, J. Chem. Phys. **46**, 3069 (1967).
20. A. Sabatini et I. Bertini. Inorg. Chem. **4**, 1959 (1965).
21. K. Nakamoto. Infrared spectra of inorganic and coordination compounds. Second ed. Wiley Interscience, New York. 1970. p. 188.
22. T. Onak. Organoborane chemistry. Academic Press, New York. 1975. p. 25.
23. R. E. Nightingale et B. L. Crawford, Jr. J. Chem. Phys. **22**, 1468 (1954).
24. L. H. Long et D. Dollimore. J. Chem. Soc. 4457 (1954).
25. D. B. Sowerby. J. Am. Chem. Soc. **84**, 1862 (1962)

Can. J. Chem. Downloaded from www.nrcresearchpress.com by 210.87.254.105 on 09/05/12
For personal use only.

A potentiometric study of the effects of molecular complexing on acid–base equilibria[1]

A. K. COLTER[2] AND D. BUBEN[3]

Department of Chemistry, Carnegie–Mellon University, Pittsburgh, PA, U.S.A. 15213, and Guelph–Waterloo Centre for Graduate Work in Chemistry, University of Guelph, Guelph, Ont., Canada N1G 2W1

Received February 14, 1976

A. K. COLTER and D. BUBEN. Can. J. Chem. **54**, 2141 (1976).

The effect of molecular complexing on several acid–base equilibria involving organic π donor acids has been studied by a potentiometric method. The method leads to complexation constants for the acceptor with the donor acid and its conjugate base. In several cases the two association constants can be determined with sufficient precision to obtain an estimate of the acidity constant for the 1:1 acceptor – donor acid complex. In all situations where charge-transfer and electrostatic interactions are expected to have opposing effects on the acidity, electrostatic effects dominate. The range of the validity and usefulness of the potentiometric method in studies of molecular complexation equilibria is discussed, together with the results obtained in this work.

A. K. COLTER et D. BUBEN. Can. J. Chem. **54**, 2141 (1976).

On a étudié, par méthode potentiométrique, l'effet de la complexation moléculaire sur plusieurs équilibres d'acide–base impliquant des acides pouvant donner des électrons π. La méthode conduit aux constantes de complexation pour l'accepteur avec l'acide donneur et sa base conjuguée. Dans plusieurs cas on a pu déterminer les deux constantes d'association avec une précision telle qu'il a été possible d'estimer la constante d'acidité du complexe 1:1 accepteur – acide donneur. Dans tous les cas où on peut s'attendre à ce que les transferts de charge et les interactions électrostatiques aient des effets opposés sur l'acidité, les effets électrostatiques prédominent. On discute de l'étendue de la validité et de l'utilité de la méthode potentiométrique pour des études d'équilibre de complexation moléculaire; on en discute aussi en relation avec les résultats obtenus dans ce travail.

[Traduit par le journal]

Can. J. Chem. Downloaded from www.nrcresearchpress.com by 210.87.254.42 on 09/05/12
For personal use only.

Introduction

Acid–base reactions occupy a position of unique importance in the study of structural, solvent, and other environmental influences on the chemical properties of organic compounds. Our interest in the influence of molecular complexing on chemical properties (1) has therefore led us to investigate the effects of molecular complexing in acid–base equilibria.

Several early studies possibly having some bearing on the modification of acid–base properties by molecular complexing have been reported. In 1928, Brønsted (2), measuring the relative acidities of a series of organic acids in benzene solution using an indicator method, found picric acid (pK_a in water at 25 °C $\simeq -0.33$ (3) to 0.71 (4)) to fall between dichloroacetic acid ($pK_a \simeq$ 1.25) and chloroacetic acid ($pK_a \simeq 2.9$) in acidity. Complexation of picric acid with benzene could account qualitatively for the apparent decrease in relative acidity. We have argued elsewhere (5), however, that such complexing cannot account for a decrease of more than about 0.8 pK units.

In the 1930's Brønsted, Bell, and Caldin (6–8) carried out a series of investigations designed to test the applicability of the Brønsted catalysis law in aprotic solvents. For the rearrangement of *N*-bromoacetanilide in chlorobenzene (7) the catalytic constants at infinite dilution for ten carboxylic acids and phenols were well correlated with their pK_a values in aqueous solution by means of a Brønsted catalysis law expression, while that of picric acid was less than $\frac{1}{20}$ of the value predicted. Similar results were obtained for the acid-catalyzed mutarotation of *l*-menthone in chlorobenzene (8) and the acid-catalyzed reaction of phenol with ethyl diazoacetate in benzene (6). In all of these studies it seems reasonable to attribute at least part of the un-

[1]Abstracted in part from the Ph.D. thesis of D. Buben, Carnegie–Mellon University, 1968.

[2]Present address: Department of Chemistry, University of Guelph, Guelph, Ontario.

[3]U.S. Public Health Service Predoctoral Fellow, June 15, 1966 to June 14, 1967.

Can. J. Chem. Downloaded from www.nrcresearchpress.com by 210.87.254.42 on 09/05/12
For personal use only.

expectedly low catalytic effectiveness of picric acid to charge-transfer interaction with the π donor solvent and/or steric hindrance resulting from complexing, though such an explanation was apparently not considered at the time.

An example of enhanced acidity which may be a result of intramolecular complexing has been reported by Shifrin (9). The pK_a of *N*-(β-4-imidazolylethyl)-3-carbamoylpyridinium chloride (**1**) was found to be 5.5, compared to 6.0 for the model compound histamine hydrochloride

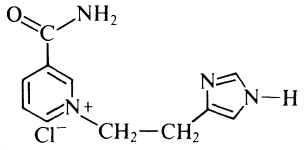

1

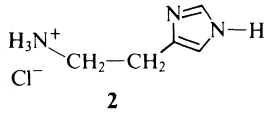

2

(**2**). Intramolecular charge-transfer interaction in (**1**) was also indicated by parallel spectrophotometric measurements (9).

Of several possible approaches to an investigation of the effects of molecular complexing on acid–base properties, that chosen for the present study is based on potentiometric measurements in aqueous solution. The method which has been developed leads to 1:1 complexation constants for an acid and its conjugate base with a complexing agent (donor or acceptor). As used in the present study the method is limited to complexing agents having negligible acidity or basicity under the conditions of the measurements. The choice of water further limits the method to donors or acceptors of high water solubility, since the complexing agent must be in large excess over the acid and its conjugate base. In the present study we have investigated the influence of complexation of cationic and uncharged donor acids by cationic and anionic acceptors. Of the four charge type combinations possible within this group we were able to obtain quantitative results only for systems involving a cationic donor acid plus a cationic acceptor, and an uncharged donor acid plus an anionic acceptor.

Theory

The problem of the influence of molecular complexing on acid–base equilibria can be more sharply defined by considering the relevant equilibria in a solution of a donor acid, HD, its conjugate base, D^-, and an acceptor, A, which forms a 1:1 complex with both HD and D^- [1].

[1]

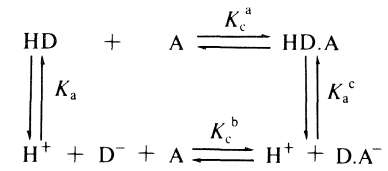

The quantities K_a and K_a^c are acid dissociation constants for uncomplexed and complexed acid, respectively; K_c^a and K_c^b are association constants for the acid and its conjugate base. The quantity of most direct interest is K_a^c, the acid dissociation constant of the 1:1 complex, which is related to the other equilibrium constants by

$$[2] \qquad K_a^c = K_a K_c^b / K_c^a$$

[2]. Thus, the effect of complexation on K_a can be determined by independent determination of K_c^b and K_c^a. However, separate determination of K_c^b and K_c^a will not be possible for most acids of interest since secondary reactions of most of the common π acceptors occur at p*H*'s necessary to maintain $>99\%$ of HD as D^-. It will often be the case that one of the complexation constants will be very small and will therefore have a very large relative uncertainty. In such circumstances the relative uncertainty in the ratio K_c^b/K_c^a, and consequently K_a^c, will also be very large.

In a solution containing HD, D^-, and A, we can define an *apparent* acidity constant, K_a^{app}, according to [3].

$$[3] \qquad K_a^{app} = \frac{[H^+]\{[D^-] + [D.A^-]\}}{\{[HD] + [HD.A]\}}$$

For simplicity, this equation and those developed below are expressed in terms of concentrations rather than activities. The consequences of activity coefficient corrections are considered separately. Making the substitutions

$$[HD.A] = K_c^a[HD][A]$$

and

$$[D.A^-] = K_c^b[D^-][A]$$

[3] is converted to [4].

$$[4] \qquad K_a^{app} = \frac{K_a\{1 + K_c^b[A]\}}{\{1 + K_c^a[A]\}}$$

Can. J. Chem. Downloaded from www.nrcresearchpress.com by 210.87.254.42 on 09/05/12
For personal use only.

Under conditions where the acceptor concentration is much greater than the concentrations of the components of the buffer solution, the concentration of uncomplexed acceptor, [A], can be replaced by the stoichiometric acceptor concentration, c_A. Making this substitution and rearranging, [5] is obtained.

$$[5] \quad \frac{K_a}{K_a^{app} - K_a} = \frac{K_c^a}{K_c^b - K_c^a} + \frac{1}{(K_c^b - K_c^a)c_A}$$

This equation has a form similar to those used for spectrophotometric and kinetic determinations of complexation constants (10) and predicts that a plot of $K_a/(K_a^{app} - K_a)$ *vs.* $1/c_A$ should yield a straight line of slope $1/(K_c^b - K_c^a)$ and intercept $K_c^a/(K_c^b - K_c^a)$. The two complexation constants are then given by: K_c^a = intercept/slope, and $K_c^b = (1 + \text{intercept})/\text{slope}$.

Application of [5] now depends on experimental determination of K_a^{app} at different stoichiometric acceptor concentrations. Taking an uncharged donor acid HD plus anionic acceptor A^- as an example, equations based on buffer mass balance, acceptor mass balance, and total charge balance lead to the expressions:

$$\{[D^-] + [D.A^{2-}]\} = c_{D^-} - [OH^-] + [H^+]$$

and

$$\{[HD] + [HD.A^-]\} = c_{HD} - [H^+] + [OH^-]$$

where c_{HD} and c_{D^-} are the stoichiometric concentrations of the donor acid and its conjugate base. Substitution into [3] leads to [6]. Exactly

$$[6] \quad K_a^{app} = \frac{[H^+]\{c_{D^-} - [OH^-] + [H^+]\}}{\{c_{HD} - [H^+] + [OH^-]\}}$$

analogous expressions are obtained for the other charge type combinations. All of the quantities in [6] are experimentally accessible provided that the relationships between the measured pH, $[H^+]$, and $[OH^-]$ are known for the conditions of the measurements.

Results

In the experiments, a known volume of buffer solution (generally 1.00×10^{-3} M in each component) of the acid – conjugate base pair under study, plus a sufficient amount of an inert (*i.e.*, non-acceptor) salt to bring the ionic strength to some specified level (generally 0.1) was placed in a thermostatted cell compartment under nitrogen atmosphere. In a water-jacketed buret thermostatted to the same temperature, was placed a solution identical to that in the cell except that the inert, or model, salt was replaced by an acceptor salt (*e.g.*, *N*-methylquinolinium chloride). The pH was then measured before addition of the buret solution and after addition of measured volumes of buret solution. In this way, a series of pH readings at constant stoichiometric acid plus conjugate base concentration and ionic strength was obtained for a series of acceptor concentrations.[4] Values of K_a^{app} were then calculated for each set of measurements using [6] and the relationships $[H^+]$ = antilog $(-pH)$ and $[OH^-] = K_w/[H^+]$. The initial pH reading obtained before addition of any acceptor provides a value of K_a. The data were then treated according to [5] to obtain K_c^a and K_c^b.

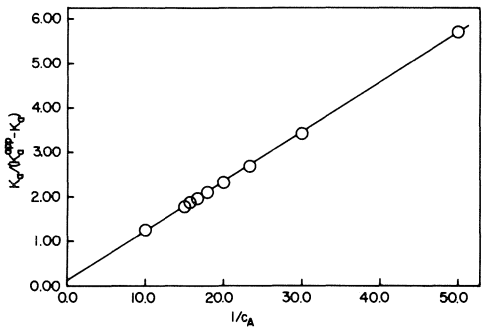

FIG. 1. Plot of $K_a/(K_a^{app} - K_a)$ *vs.* $c_A^{-1}(M^{-1})$ for run 34.

The results of these analyses are summarized in Table 1. Plots of $K_a/(K_a^{app} - K_a)$ *vs.* $1/c_A$ for the systems included in Table 1 showed no systematic deviations from linearity and generally very little scatter from the best fit straight line. The plots shown in Figs. 1 and 2 are typical.

Values of K_a and K_a^{app} calculated as described above are 'mixed' constants (ref. 11, p. 57), that is, they are calculated from a mixture of concentrations and activities. In theory, therefore, values of K_a determined at different buffer component concentrations should differ slightly where $[H^+]$ or $[OH^-]$ is a significant fraction of c_{D^-} or c_{HD}. In fact, the expected variation of K_a ('mixed') with changes in buffer component concentrations used in this work are smaller than the experimental error in K_a in all cases (Ex-

[4]We thank Professor R. H. Stokes for suggesting this experimental modification.

Can. J. Chem. Downloaded from www.nrcresearchpress.com by 210.87.254.42 on 09/05/12
For personal use only.

TABLE 1. Summary of potentiometric results[a]

Runs	Acid[b]	Acceptor[c]	Model salt[d]	$10^3 c_{HD}$ (M)	$10^3 c_D$ (M)	Ionic strength	K_a	K_e^a (M^{-1})	K_e^b (M^{-1})	Average sd[e]
1–8	NA^+Cl^-	NMQ^+Cl^-	K^+Cl^-	1.0	1.0	0.10	$1.06\pm0.08\times10^{-4}$	$-1.3\ \pm0.7$	9.2 ± 1.0	0.21
9–14				0.50	0.50	0.10	$0.97\pm0.11\times10^{-4}$	$-2.0\ \pm0.6$	7.7 ± 0.9	0.08
15–17			TMA^+Cl^-	0.50	0.50	0.10	$1.11\pm0.11\times10^{-4}$	$-1.4\ \pm0.3$	7.6 ± 0.9	0.17
18–21	2-MeO-NA^+Cl^-	NMQ^+Cl^-	TEA^+Cl^-	0.50	0.50	0.10	$1.38\pm0.02\times10^{-4}$	-0.30 ± 0.10	8.4 ± 0.1	0.14
22–25	5-MeO-NA^+Cl^-	NMQ^+Cl^-	TMA^+Cl^-	1.0	1.0	0.10	$1.23\pm0.01\times10^{-4}$	0.36 ± 0.29	12.3 ± 0.4	0.22
26–30				0.50	0.50	0.10	$1.13\pm0.05\times10^{-4}$	0.59 ± 0.40	11.4 ± 0.8	0.51
31–36			TEA^+Cl^-	1.0	1.0	0.10	$1.44\pm0.02\times10^{-4}$	0.83 ± 0.26	10.0 ± 0.3	0.21
37–41			TMA^+Cl^-	1.0	1.0	0.20	$1.13\pm0.05\times10^{-4}$	0.86 ± 0.37	10.9 ± 0.2	0.03
42–49	I-3-CA	K^+DNB^-	K^+Cl^-	0.50	1.5	0.10	$3.93\pm0.13\times10^{-6}$	$20.1\ \pm0.3$	2.5 ± 0.3	0.30
50–54		Na^+DNBS^-	Na^+Cl^-	0.50	1.0	0.10	$3.96\pm0.29\times10^{-6}$	$8.3\ \pm0.8$	2.1 ± 0.0	0.14
55–57				0.50	1.5	0.10	$4.28\pm0.19\times10^{-6}$	$9.0\ \pm0.7$	2.8 ± 0.3	0.34
58						0.12	4.65×10^{-6}	8.2	2.1	0.15
59						0.16	4.57×10^{-6}	7.7	1.9	0.09
60	I-3-CA	Na^+DNBS^-	Na^+Cl^-	0.50	1.5	0.20	4.75×10^{-6}	8.3	2.1	0.05
61			$Na^+NO_3^-$			0.10	3.73×10^{-6}	8.4	2.1	0.18
62			$K^+NO_3^-$			0.10	3.48×10^{-6}	8.4	3.0	0.17
63			$2K^+SO_4^{2-}$			0.10	3.52×10^{-6}	8.9	3.2	0.37
64–67	1-N	K^+DNB^-	K^+Cl^-	1.5	0.5	0.10	$7.27\pm0.04\times10^{-10}$	$17.0\ \pm0.3$	1.6 ± 0.1	0.15
68–71				1.0	1.0	0.10	$7.77\pm0.07\times10^{-10}$	$16.4\ \pm0.4$	1.8 ± 0.1	0.14

[a]Temperature = 30.00 ± 0.05 °C. K_a, K_e^a, and K_e^b listed as averages of indicated runs, together with average deviation.
[b]Abbreviations: NA^+Cl^-, 1-naphthylammonium chloride; 2-MeO-NA^+Cl^-, 2-methoxy-1-naphthylammonium chloride; 5-MeO-NA^+Cl^-, 5-methoxy-1-naphthylammonium chloride; I-3-CA, indole-3-carboxylic acid; 1-N, 1-naphthol.
[c]Abbreviations: NMQ^+Cl^-, N-methylquinolinium chloride; K^+DNB^-, potassium 3,5-dinitrobenzoate; Na^+DNBS^-, sodium 2,4-dinitrobenzenesulfonate.
[d]Abbreviations: TMA^+Cl^-, tetramethylammonium chloride; TEA^+Cl^-, tetraethylammonium chloride.
[e]Average standard deviation in K_e^a and K_e^b, obtained from standard deviations in slopes and intercepts of individual plots.

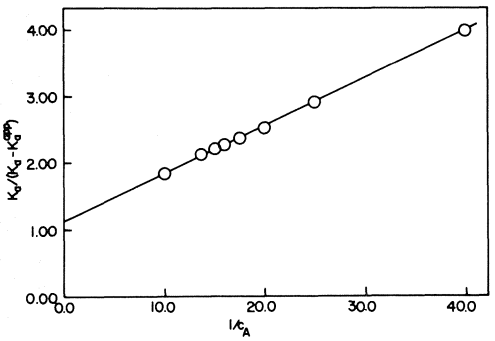

FIG. 2. Plot of $K_a/(K_a - K_a^{app})$ *vs.* $c_A^{-1}(M^{-1})$ for run 68.

perimental). Since the K_a values listed in Table 1 are averages of values based on single p*H* measurements on buffer solutions with very low stoichiometric acid and base concentrations (0.5×10^{-3} to 1.5×10^{-3} *M*) their experimental errors are quite large (probably around $\pm 10\%$). Since they were measured at ionic strengths of 0.1 or higher, accurate calculation of thermodynamic K_a's is not possible, nor are K_a's measured in the presence of different salts directly comparable. Approximate thermodynamic pK_a's (30 °C), calculated by applying a Debye–Hückel correction as described in the Experimental are: 1-naphthylammonium chloride (NA^+Cl^-), 3.86; 2-methoxy-1-naphthylammonium chloride (2-MeO-NA^+Cl^-), 3.72; 5-methoxy-1-naphthylammonium chloride (5-MeO-NA^+Cl^-), 3.80; indole-3-carboxylic acid (I-3-CA), 5.51; 1-naphthol (1-N), 9.23. Making approximate temperature corrections based on the usual temperature variations of K_a for anilinium and phenol acids (ref. 11, p. 14; ref. 12) we obtain for the approximate thermodynamic pK_a's at 25 °C: NA^+Cl^-, 3.92; 1-N, 9.29. Literature values for these two acids are 3.93 (13) and 9.39 (14) respectively. To our knowledge, no acidity constant measurements have been reported for the other three acids studied in this work.

Systems Involving a Cationic Donor Acid Plus Cationic Acceptor

Three systems of this charge type were investigated: NA^+Cl^-, 2-MeO-NA^+Cl^-, and 5-MeO-NA^+Cl^-, all with the acceptor *N*-methylquinolinium chloride (NMQ^+Cl^-). The pK_a of NMQ^+Cl^- was independently determined to be 12.60 ± 0.01 at 30 °C (K_a 'mixed', ionic strength 0.1) too weakly acidic to have a measurable effect on the p*H* with these systems. Cation–cation repulsion is expected to make K_c^a very small in these systems, hence electrostatic and charge-transfer interactions should both operate to increase the acidity of the buffer. In agreement with expectations, addition of acceptor was accompanied by a decrease in p*H* with all three systems.

Mixtures of 1-naphthylamine with NMQ^+Cl^- were yellow-orange in colour due to a broad absorption band around 380–400 nm, absent in solutions of the amine, buffer, or acceptor alone, and indicating charge-transfer interaction between the acceptor and amine donor. Replacement of model salt by acceptor (to 0.1 *M*) was accompanied by a decrease in p*H* of 0.282 ± 0.017 units in runs 1–8, 0.345 ± 0.047 units in runs 9–14, and 0.234 ± 0.018 units in runs 15–17. As a control, in the second set of runs (9–14) the stock solutions of acceptor and model salt were adjusted to the same neutral p*H* by addition of a few drops of dilute NaOH. Although this adjustment had no significant effect on the results, the precision appears to be somewhat poorer at the lower buffer concentration. The intercepts of the plots according to [5] are negative, leading to apparent negative values of K_c^a. If the true value of $K_c^a \simeq 0$, experimental scatter would lead to some negative and some positive values in this analysis. However, the intercepts appear to be less than zero by an amount which exceeds the experimental scatter. Possible reasons for this anomalous result are considered below. Overall average values for the complexation constants are: $K_c^a = -1.6 \pm 0.7\ l\ mol^{-1}$ and $K_c^b = 8.5 \pm 1.1\ l\ mol^{-1}$. Concerning the ratio of K_c^b to K_c^a (or K_a^c/K_a), we can only say that it is large (certainly greater than 10).

Mixtures of 2-MeO-NA^+Cl^- buffer and NMQ^+Cl^- were yellow, again indicating charge-transfer absorption. Replacement of model salt by acceptor (to 0.1 *M*) was accompanied by a decrease in p*H* of 0.183 ± 0.005 for runs 18–21. The apparent average K_c^a value is probably within experimental error of zero in this system and again we can only say that the enhancement in acidity constant by complexation (K_c^b/K_c^a) is at least 10.

Mixtures of 5-MeO-NA^+Cl^- buffer and NMQ^+Cl^- were yellow due to a broad charge-

Can. J. Chem. Downloaded from www.nrcresearchpress.com by 210.87.254.42 on 09/05/12
For personal use only.

Can. J. Chem. Downloaded from www.nrcresearchpress.com by 210.87.254.42 on 09/05/12
For personal use only.

transfer absorption around 400–420 nm. Replacement of model salt by acceptor (to 0.1 *M*) was accompanied by a decrease in p*H* of 0.254 ± 0.003 in runs 22–25, 0.190 ± 0.017 in runs 26–30, and 0.197 ± 0.004 in runs 31–36. Replacement of model salt by acceptor to 0.2 *M* produced a decrease in p*H* of 0.335 ± 0.020 in runs 37–41. The stock acceptor and model salt solutions were adjusted to an identical neutral p*H* in runs 22–25 and 37–41, again with no significant effect on the results. In this system, K_c^a appears to be significantly greater than zero. Average complexation constants at ionic strength 0.1 are $K_c^a = 0.62 \pm 0.35$ l mol^{-1}, $K_c^b = 11.0 \pm 1.0$ l mol^{-1}. The enhancement in acidity by complexation (K_c^b/K_c^a) is therefore around 20.

Systems Involving an Uncharged Donor Acid Plus Anionic Acceptor

Three systems of this charge type were investigated: I-3-CA with the acceptors potassium 3,5-dinitrobenzoate (K^+DNB^-), and sodium 2,4-dinitrobenzenesulfonate (Na^+DNBS^-), and 1-N with K^+DNB^-. The benzenesulfonate acceptor is too weakly basic to have a measurable effect on the p*H* of the I-3-CA buffers. The K_a of 3,5-dinitrobenzoic acid is 1.5×10^{-3} (15). The basicity of 3,5-dinitrobenzoate is not significant provided buffer p*H*'s are above about 5.8, as was the case with the 1-N and 1:3 I-3-CA-indole-3-carboxylate buffers, however, at lower p*H*'s its basicity cannot be ignored. In systems of this charge type the ratio K_c^b/K_c^a should be increased by charge-transfer interaction, which should be greater in the conjugate base complex, but decreased by electrostatic anion–anion repulsion. In the three systems studied, replacement of model salt by acceptor was accompanied by an increase in p*H*, suggesting that electrostatic forces are of dominant importance here.

Mixtures of I-3-CA buffers and K^+DNB^- were orange, indicating charge-transfer complexing. Replacement of model salt by acceptor (to 0.1 *M*) was accompanied by a p*H* increase of 0.391 ± 0.004 units in runs 42–49. K_c^b values are clearly greater than zero and $K_c^a/K_c^b = 8.0 \pm 1.1$, *i.e.*, complexation by 3,5-dinitrobenzoate results in an 8-fold decrease in the acidity constant of I-3-CA.

Mixtures of I-3-CA buffers and K^+DNBS^- were orange. Replacement of model salt by acceptor (to 0.1 *M*) was accompanied by a p*H* increase of 0.180 ± 0.015 units in runs 50–54 and 0.177 ± 0.003 units in runs 55–57, while p*H* changes in runs 58, 59, and 60 were, respectively, 0.211 (0.12 *M* acceptor), 0.240 (0.16 *M* acceptor), and 0.279 (0.20 *M* acceptor). In runs 61–63 p*H* changes were 0.198, 0.168, and 0.166, respectively. Although the p*H* change varied somewhat with changes in model salt, K_c^a and K_c^b values are independent of model salt, ionic strength, and buffer ratio within experimental error. For the 11 runs at ionic strength of 0.1, average complexation constants are $K_c^a = 8.5 \pm 0.6$ and $K_c^b = 2.4 \pm 0.6$. Again, K_c^a values are significantly greater than zero and the decrease in acidity due to complexation, $K_c^a/K_c^b = 3.6 \pm 1.2$.

Mixtures of 1-N buffers and K^+DNB^- were orange. Replacement of model salts by acceptor (to 0.1 *M*) was accompanied by a p*H* increase of 0.360 ± 0.004 units in runs 64–67 and 0.340 ± 0.005 units in runs 68–71. Stock solutions of acceptor and model salt were adjusted to the same neutral p*H* in all runs. Average complexation constants are $K_c^a = 16.7 \pm 0.4$ l mol^{-1} and $K_c^b = 1.7 \pm 0.2$ l mol^{-1}, and the decrease in acidity due to complexation, $K_c^a/K_c^b = 9.8 \pm 1.2$.

Systems Involving an Uncharged Donor Acid Plus Cationic Acceptor

In complexation of an uncharged donor acid with a cationic acceptor, both electrostatic and charge-transfer interactions should contribute to making K_c^b/K_c^a greater than one, yet with appropriate choice of acid and acceptor, both complexation constants should be of reasonable size. Though this prediction was confirmed qualitatively with one system, all attempts to obtain quantitative information for charge combinations of this type were unsuccessful. Two such systems investigated were 3,4,5-trimethoxybenzoic acid (TMBA) and I-3-CA plus NMQ^+Cl^-.

Solutions of TMBA buffer and NMQ^+Cl^- showed no visible evidence for charge-transfer absorption but spectra of mixtures show some enhancement of absorption between 365 and 400 nm, over the long wavelength tail of the NMQ^+Cl^- absorption. Replacement of model salt (0.1 *M* KCl) by NMQ^+Cl^- in 1:1 1.0×10^{-3} *M* TMBA buffer led to decreases in p*H* of around 0.060 units. The very small p*H* changes

Can. J. Chem. Downloaded from www.nrcresearchpress.com by 210.87.254.42 on 09/05/12
For personal use only.

lead to enormous uncertainties in the two complexation constants. For example, average results for three runs were $K_c^a = 30 \pm 13$ l mol^{-1} and $K_c^b = 34 \pm 13$ l mol^{-1}. Although we cannot obtain any reasonable measure of the complexation constants for this system, the ratio K_c^b/K_c^a calculated from the results of individual runs is much more nearly constant (1.24, 1.13, 1.06) indicating qualitatively that complexation has a slight acidifying influence. For reasons discussed later, however, we believe that these results are highly suspect (Discussion).

Mixtures of I-3-CA buffer and NMQ^+Cl^- were yellow. Replacement of model salt (0.1 *M* KCl) by NMQ^+Cl^- led initially to decreases in p*H* which slowly drifted upward, eventually returning to the original p*H*. We have no reasonable explanation for this behaviour.

Systems Involving a Cationic Donor Acid Plus Anionic Acceptor

With this type of system, appropriate choice of donor and acceptor should lead to substantial values for both K_c^a and K_c^b with either constant larger, depending on whether charge-transfer or electrostatic interaction is the more important. Two such systems were investigated: NA^+Cl^- plus Na^+DNBS^- and benzimidazolium chloride (BI^+Cl^-) plus K^+DNB^-.

Mixtures of NA^+Cl^- buffers and Na^+DNBS^- were orange. Replacement of model salt (0.1 *M* NaCl) by Na^+DNBS^- in a 1:1 1.0×10^{-3} *M* buffer led to increases in p*H* (approx. 0.035 units) which were too small to yield any quantitative information.

Mixtures of BI^+Cl^- buffers and K^+DNB^- gave no visible evidence for charge-transfer complexing. Replacement of model salt (0.1 *M* KCl) in a buffer solution 0.5×10^{-3} *M* in BI^+Cl^- and 1.5×10^{-3} *M* in benzimidazole by K^+DNB^- produced small (approximately 0.10 units) p*H* increases leading to small and widely divergent values of K_c^a and K_c^b. If these results have qualitative significance, electrostatic interaction is again more important than charge-transfer interaction (see Discussion, however).

Control Experiments

Several control experiments were carried out in order to test the validity of our analysis. Already mentioned are variation of buffer ratios and concentrations (compare runs 1–8 with 9–14, 22–25 with 26–30, 50–54 with 55–57, and 64–67 with 68–71) and variation of model salt (compare runs 9–14 with 15–17, runs 22–25 with 31–36, and runs 55–57 with 61, 62, and 63). In no case do the calculated complexation constants depend significantly on the buffer concentration or buffer ratio. In none of the above comparisons did K_c^a or K_c^b depend significantly on the model salt, even where the initial p*H*'s (and hence K_a values) are significantly different. In contrast, an experiment identical to runs 55–57, 61, 62, and 63 using $MgSO_4$ as the model salt gave a p*H* change of +0.132 units, $K_c^a = 5.9$ l mol^{-1}, and $K_c^b = 0.45$ l mol^{-1} indicating that $Mg^{2+}SO_4^{2-}$ is not a suitable model for Na^+DNBS^-. The model salt assumption is considered in more detail below. A limited investigation of the influence of ionic strength (runs 55–57 and 58–60) reveals no significant changes in the complexation constants for I-3-CA and its conjugate base with $DNBS^-$. Since stock solutions of acceptor and model salt (see Experimental) are unbuffered, their p*H*'s were characteristically more variable. These solutions were in some cases (runs 9–14, 22–25, 37–41, and 64–71) adjusted to neutrality by addition of minute amounts of acid or base. Again, where comparisons can be made (runs 9–13 with 1–8 and runs 22–25 with 26–30) such adjustments had no significant effect on the results, supporting the assumption that any intrinsic acidity or basicity of the acceptor is negligible in these experiments.

Perhaps the most convincing support for our interpretation of the p*H* changes accompanying addition of acceptor salts is provided by two control experiments showing that the p*H* change accompanying addition of acceptor to non-donor buffers is very small. The p*H* of a 1.0×10^{-3} *M* potassium hydrogen phthalate buffer 0.1 *M* in KCl was 4.150. An identical buffer in which the KCl was replaced by NMQ^+Cl^- had a p*H* of 4.145. Titration of a buffer solution which was 0.25×10^{-3} *M* in acetic acid, 0.75×10^{-3} *M* in sodium acetate, and 0.1 *M* in NaCl with an identical buffer containing 0.1 *M* Na^+DNBS^- in place of the model salt again gave essentially no change in p*H*. The initial p*H* (5.317) was similar to that (~5.7) in runs 50–54 where p*H* changes of 0.18 units were observed. An attempt to run a control using 6-*tert*-butylindole-3-carboxylic acid as a model for I-3-CA in which complexing should be hindered by the *tert*-butyl group was unsuccessful because this acid proved to have

Can. J. Chem. Downloaded from www.nrcresearchpress.com by 210.87.254.42 on 09/05/12
For personal use only.

insufficient water solubility to study potentiometrically.

Acceptor Salts Discarded as Unsuitable

N-methylacridinium, *N*-methylphenanthridinium, and *N*-methyl-6-nitroquinolinium salts proved to be too acidic to use with any of the donor buffers studied in this work. Potassium 2,4,6-trinitrobenzenesulfonate had insufficient water solubility.

Discussion

Precision of Results

The precision as indicated by standard deviations in K_c^a and K_c^b for individual determinations, is in nearly every case much better than that indicated by average deviations in K_c^a and K_c^b for duplicate runs (Table 1). That is, although individual plots often show negligible scatter, agreement between duplicate runs is usually much poorer. This is a consequence of the extreme sensitivity of the derived complexation constants to the experimental p*H* readings, particularly when the total p*H* change is small. For example, in runs 51 and 52 changes in p*H* at identical volumes of added acceptor solution agreed to within ± 0.003 p*H* units (total p*H* change 0.180 units), yet K_c^a and K_c^b were, respectively, 8.21 *vs.* 7.37 and 1.77 *vs.* 1.23 l mol^{-1}. It is possible, nevertheless, for two titrations with substantially different total p*H* changes to give nearly identical complexation constants. In general the total p*H* change in duplicate runs was highly reproducible. An exception was the NA^+Cl^-–NMQ^+Cl^- system. The precision increases with increasing range of acceptor concentration (compare runs 37–41 with runs 22–30, and run 60 with runs 55–57) but the model salt assumption (below) becomes increasingly difficult to justify with increasing ionic strength.

As a consequence of the mathematics of the analysis the two complexation constants obtained from a single determination have the same absolute standard deviation. Therefore, if either constant is small its relative uncertainty and that of the ratio of the two constants will be very large.

Accuracy and Validity of the Results

We now consider each of the approximations and assumptions made in the analysis as it affects the accuracy of the derived complexation constants.

Errors resulting from replacement of [A] by c_A in [5] are largest for runs 42–49, where the concentrations of complexed species are largest. Such errors can be estimated by using the initially determined complexation constants to calculate [A] for each point in the titration and to then replot $K_a/(K_a^{app} - K_a)$ *vs.* $[A]^{-1}$ to obtain new values of K_c^a and K_c^b. This procedure can then be repeated until the K_c values converge (16). When carried through for run 42, K_c^a increased from 10.5 to 10.8 l mol^{-1} and K_c^b from 3.1 to 3.2 l mol^{-1}. These corrections are of marginal significance in runs 42–49, hence errors due to replacement of [A] by c_A are negligible in all other runs.

Calculation of K_a^{app} (eq. 6) was based on the relation $[H^+] = \text{antilog}(-pH)$, which amounts to approximation of $[H^+]$ by a_{H^+} (conventional) (17). Exact calculation of K_a^{app} (as defined by [6]) would require independent determination of the relationship between $[H^+]$ and p*H* for each of the acceptor-model salt mixtures studied (using, say, standard HCl solutions). Such a procedure, if necessary, would be sufficiently tedious to severely limit the usefulness of the method. A theoretical estimate of the validity of replacing $[H^+]$ by antilog$(-pH)$ was made as follows. The activity coefficient of H^+ on the molarity scale, y_{H^+}, was assumed to be related to the ionic strength, *I*, by [7] (ref. 17 p. 449, ref. 18)

$$[7] \qquad \log y_{H^+} = \frac{-AI^{1/2}}{1 + B\alpha I^{1/2}}$$

where $A = 0.5161\ l^{1/2}\ mol^{1/2}$, $B = 0.3301\ l^{1/2}\ mol^{-1/2}$, $\alpha = 9$ Å. At $I = 0.1$, [7] leads to [8].

$$[8] \qquad [H^+] = \text{antilog}\,(0.08417 - pH)$$

This correction was incorporated into the computer program for K_c^a and K_c^b for runs 46–49. The resulting changes in K_c^a varied from -0.005 to 0.023 l mol^{-1} and changes in K_c^b from -0.011 to 0.007 l mol^{-1}, all much smaller than the experimental uncertainty. Though individual K_a^{app} values are significantly changed by using [8], the derived complexation constants depend on the manner in which K_a^{app} varies with c_A and this variation is essentially unaffected by using a_{H^+}(conventional) in place of $[H^+]$.

Initial p*H* readings for duplicate titrations sometimes differed as widely as 0.1 p*H* units,

Can. J. Chem. Downloaded from www.nrcresearchpress.com by 210.87.254.42 on 09/05/12
For personal use only.

while the change in pH accompanying addition of acceptor was essentially constant. It is particularly difficult to reproduce the initial pH when buffer components are as dilute as 5×10^{-4} M. It was shown, however, that if all of the pH readings are adjusted by a constant increment, even as large as 0.1 unit, there is no significant change in the calculated values of K_c^a and K_c^b. Replacement of $[H^+]$ by a_{H^+}(conventional) (above) is really equivalent to changing all pH readings by about 0.08 units.

The analysis described in this work is based on the assumption that the ionic atmosphere effect of the acceptor salt is exactly matched by the model salt, *i.e.*, that in the absence of complexing no pH change would be observed (model salt assumption). Direct evidence that the pH changes are due to π complexing is provided by the results of control experiments with non-donor buffers (above). The model salt assumption will never be exactly true, of course; our concern here, however, is the extent to which its breakdown influences the calculated complexation constants. Indirect support for the validity of our analysis is provided by experiments in which the model salt is varied (Table 1). In none of the cases reported in Table 1 did changing the model salt result in a significant change in the complexation constants, even in the rather extreme case (run 63) where K_2SO_4 was used as a model for Na^+DNBS^-.

In order to examine the model salt assumption in more detail it is instructive to develop an expression for the change in pH resulting from addition of salt. From the definition of K_a (thermodynamic) for an acid HD we can write

$$[9] \quad -\log a_{H^+} = -\log K_a + \log \frac{[D^-]}{[DH]} + \log \frac{y_{D^-}}{y_{DH}}$$

where the y's are activity coefficients on the molarity scale. The result of addition of an inert salt to a 1:1 HD–D^- buffer (ref. 17 pp. 118–122) will be a substantial decrease in log y_{D^-}/y_{DH} and a very small opposing increase in log $[D^-]/[DH]$, leading to a net decrease in $-\log a_{H^+}$. If $[D^-]$ and [DH] are much larger than $[H^+]$, log $[D^-]/[DH]$ will be essentially constant. The decrease in log y_{D^-}/y_{DH} therefore represents the maximum decrease in pH which can be observed.

$$[10] \quad \Delta(-\log a_{H^+})_{max} = \Delta pH_{max} = \Delta \log y_{D^-} - \Delta \log y_{HD} \simeq \Delta \log y_{D^-}$$

Since $\Delta \log y_{HD}$ (which may be either positive or negative) (19) will generally be much smaller than $\Delta \log y_{D^-}$, we can take the first term in [10] as a good approximation for the maximum pH change accompanying addition of salt.

According to Brønsted's principle of specific ion interaction (20) expressed in quantitative form in the Guggenheim extension of the Debye–Hückel limiting law (21), in considering salt effects on y_{D^-} we need only (up to I of at least 0.1) to match the ion in the acceptor salt which is opposite in charge to the charged buffer component. Thus, with the cationic acids plus NMQ^+Cl^-, any salt of the type M^+Cl^- is a perfect match, to the limit of the Guggenheim equation. Similarly, for the uncharged acids I-3-CA and 1-NA plus the acceptors K^+DNB^- and Na^+DNBS^- it is necessary to match only the cation. With systems of charge type $HD + A^+X^-$ and $HD^+ + M^+A^-$ a perfect match is no longer possible and this could account in part for our lack of success with all such systems.

As the ratio of acid to conjugate base in the buffer increases, the increase in log $[D^-]/[DH]$ (eq. 9) accompanying addition of salt also increases, until in a solution of the acid by itself the change in $-\log a_{H^+}$ accompanying addition of salt to $I = 0.1$ is almost zero (ref. 17 pp. 118–122). Hence in a solution of HD (or HD^+) alone the model salt assumption becomes inconsequential. It can be shown, however, that the pH change arising from addition of acceptor will also be smaller in such solutions. Nevertheless, it may be possible to extend the application of the potentiometric method to the other charge combinations using solutions of HD or HD^+ alone. This possibility was not investigated in the present work.

As a final test of the validity of the potentiometric method, three complexation constants were independently determined by other methods. Spectrophotometric determination of the 1-naphthylamine–NMQ^+Cl^- association constant (I = 0.06–2.20) gave K_c^b 8.0 ± 0.7 l mol^{-1}, in good agreement with the potentiometric value (8.5 ± 1.1 l mol^-). Spectrophotometric determination of the 5-methoxyl-1-naphthylamine–NMQ^+Cl^- association constant (I = 0.06–0.20)

Can. J. Chem. Downloaded from www.nrcresearchpress.com by 210.87.254.42 on 09/05/12
For personal use only.

gave $K_c^b = 9.1 \pm 1.1$ l mol^{-1}, in fair agreement with the potentiometric value (11.0 ± 1.0 l mol^{-1}). K_c^b for the 1-N + K$^+$DNB$^-$ system, determined by differential refractometry (16) is 15 ± 3 l mol^{-1} (25 °C), again in reasonable agreement with the results of this work (16.7 ± 0.3 l mol^{-1}). Our value of K_c^a for I-3-CA + K$^+$DNB$^-$ (20.1 ± 0.3 l mol^{-1}) can also be compared with complexation constants for *N*-(indoleacryloyl)imidazole + K$^+$DNB$^-$ in 0.83% acetonitrile–H_2O (25 °C, $I = 0.50$) determined kinetically (21.5 l mol^{-1}) and spectrophotometrically (23.6 l mol^{-1}) (22).

Interpretation of the Results

Values of K_c^a for 1-NA$^+$Cl$^-$ with NMQ$^+$Cl$^-$ are less than zero by an amount greater than the average deviation. This result is not without precedent; Hanna and Ashbaugh (23) obtained a negative complexation constant for tetracyanoethylene with benzene in dioxane, from nmr measurements. A possible explanation for negative K_c's is provided by the solvation theory of Carter *et al.* (24). The theory, which is based on the assumption that each solute species has associated with it a well-defined solvent shell containing a constant and integral number of solvent molecules, leads to the prediction that with weak complexes the usual spectrophotometric method will lead to negative complexation constants when the solute in large excess is heavily solvated and a large number of solvent molecules are excluded when the complex is formed. Making the further assumptions that the two ionizations (*i.e.*, those of HD and HD.A) proceed with the same net change in solvation and that the two associations (*i.e.*, HD and D with A) proceed with the same change in solvation we have carried out a derivation paralleling that of Carter *et al.* (24, 25). The relationship between the true and observed complexation constants (either K_c^a or K_c^b) is given by [11],

$$[11] \qquad (K_c)_{true} \simeq (K_c)_{observed} - \frac{d(i-j)}{55.5}$$

where d is the number of solvent molecules displaced by complexation, i is the total number of solvent molecules associated with the model salt (*e.g.*, K$^+$Cl$^-$), and j is the total number of solvent molecules associated with the acceptor salt (*e.g.*, NMQ$^+$Cl$^-$). If $i = 8$, $j = 20$, and $d = 5$, the correction term is about 1 litre mol^{-1}. The correction should be similar for the three naphthylammonium systems and the fact that K_c^a for complexation with NMQ$^+$Cl$^-$ increases in the order NA$^+$Cl$^-$ < 2-MeO-NA$^+$Cl$^-$ < 5-MeO-NA$^+$Cl$^-$, as expected, strongly suggests that for 5-MeO-NA$^+$Cl$^-$ + NMQ$^+$Cl$^-$, at least, K_c^a is greater than zero.

Of several possible reasons why all attempts to apply the method to systems of charge types HA + A$^+$ and HD$^+$ + A$^-$ were unsuccessful, we have already considered the possible breakdown of the model salt assumption in these cases. Another possibility is that in associations involving ion pairing (D$^-$ + A$^+$ or DH$^+$ + A$^-$) clusters containing more than one donor and acceptor species are formed so that such systems are not adequately described by the equilibria in [1].

With the cationic acid – cationic acceptor combinations both electrostatic and charge-transfer interaction should contribute to the enhancement in acidity resulting from complexation. For the 5-MeO-NA$^+$-NMQ$^+$ complex this enhancement is of the order of 20-fold. For the other naphthylammonium–NMQ$^+$ complexes the ratio is likely very similar. In the absence of other information we cannot say what proportion of the enhancement is due to a direct electrostatic field effect and what proportion to charge-transfer interaction. Results of the studies with uncharged acid – anionic acceptor combinations, as well as independent studies with uncharged acceptors (26) indicate that the major part of the enhancement is a direct electrostatic field effect. With the uncharged acid – anionic acceptor combinations, electrostatic and charge-transfer interactions should have opposing effects on the acidity of the complex. We find that electrostatic effects dominate in all systems studied, the 1:1 complex being a weaker acid than the uncomplexed acid by a factor of 8.0 ± 1.0 with the I-3-CA-DNB$^-$ complex, a factor of 3.6 ± 1.2 with the I-3-CA-DNBS$^-$ complex and a factor of 9.8 ± 1.2 with the 1-N-DNB$^-$ complex. The smaller reduction of the acidity of I-3-CA by complexation with the sulfonate anion than with the carboxylate anion may be due to a smaller field effect by the more delocalized charge on the sulfonate group, to greater electron withdrawal by charge-transfer with the sulfonate acceptor, or both. In relation to catalysis by charge-transfer complexing (1, 5)

Can. J. Chem. Downloaded from www.nrcresearchpress.com by 210.87.254.42 on 09/05/12
For personal use only.

the domination of electrostatic field effects in this work suggests the possibility of catalysis by anionic acceptors in reactions of donors with electron-deficient transition states (*e.g.*, solvolysis or other carbonium ion reactions of aromatic donors) or catalysis by cationic donors in reactions of acceptors with electron-rich transition states (*e.g.*, nucleophilic substitution reactions of aromatic acceptors).

Scope of the Potentiometric Method

There are several practical limitations of the potentiometric method developed in the present study. In theory, the acid may be either a donor or an acceptor but the ionic acceptor or donor added in large excess is limited to species having negligible acidity or basicity. The complexation constants K_c^a and K_c^b must be significantly different, otherwise there will be no change in p*H*. Only in very favourable cases where the two complexation constants are significantly different and both significantly greater than zero, can a quantitative estimate of the effect of complexation on acidity be obtained. Finally, as discussed above, it may be very difficult to find an adequate model salt for combinations of charge type $HD + A^+$ and $HD^+ + A^-$.

Experimental

Melting points were measured on a Thomas–Hoover apparatus and are uncorrected. Microanalyses were performed by Galbraith Laboratories, Knoxville, Tennessee. Nuclear magnetic resonance spectra were obtained with a Varian A-60 spectrometer; spectra of salts were determined in D_2O solvent and chemical shifts are reported relative to the HDO peak (δ 4.80) as internal standard.

Reagents

1-Naphthylamine (Fisher, highest purity) was purified by steam distillation and crystallization from 30–60 °C petroleum ether, mp 49.0–50.5 °C (lit. (27) mp 50 °C).

2-Methoxy-1-naphthylamine (K and K) was purified by steam distillation and crystallization from 65–110 °C petroleum ether, mp 53–54 °C (lit. (28) mp 54 °C).

5-Methoxy-1-naphthylamine was prepared from 5-amino-1-naphthol (Eastman, practical) by the method of Teuber and Lindner (29). Repeated crystallization from 65–110 °C petroleum ether gave a 60% yield of white crystalline material, mp 79–80.5 °C (lit. (29) mp 80 °C).

1-Naphthylammonium chloride (Eastman, white label) was recrystallized from absolute ethanol and dried under vacuum.

2-Methoxy-1-naphthylammonium chloride was obtained in quantitative yield by bubbling dry hydrogen chloride through an ether solution of 2-methoxy-1-naphthylamine until precipitation ceased. Crystallization from absolute ethanol gave white crystalline product; nmr (D_2O) δ 4.23 (s, 3H), 7.4–8.4 (m, 6H). 5-Methoxy-1-naphthylammonium chloride was prepared in an identical manner from the corresponding amine to give off-white crystals, nmr (D_2O) δ 4.21 (s, 3H), 8.2–8.6 (m, 6H).

Indole-3-carboxylic acid was synthesized from indole (Fisher, highest purity) using the procedure of Doyle *et al.* (30). Recrystallization of the crude product from ethanol–water gave a 36% yield of light tan plates, mp 234–235 °C (dec.) (lit. (30) mp 220–224 °C).

Potassium indole-3-carboxylate was prepared by dissolving, with warming, equivalent amounts of indole-3-carboxylic acid and potassium carbonate in water, filtration, evaporation, and slow crystallization. The white product was isolated as a stable monohydrate, mp 218 °C (foaming). *Anal.* calcd. for $C_9H_6NO_2K \cdot H_2O$: C 49.75, H 3.71, N 6.44; found: C 50.57, H 3.81, N 6.11.

1-Naphthol (Fisher, highest purity) was purified by steam distillation followed by repeated crystallization from 65–110 °C petroleum ether giving fine white needles, mp 95–96.5 °C (lit. (31) mp 95.8–96.0 °C).

3,4,5-Trimethoxybenzoic acid (Eastman, white label) was recrystallized from water, mp 171–172 °C (lit. (32) mp 172 °C).

Potassium 3,4,5-trimethoxybenzoic acid was prepared by dropwise addition of dilute aqueous KOH to a suspension of the carboxylic acid in water until all of the acid had dissolved and the solution was neutral to litmus. The filtered solution was evaporated to dryness under reduced pressure and the salt recrystallized from 2-propanol to give a white crystalline product, mp 252 °C (dec.).

Benzimidazole was prepared by the method of Wagner and Millett (33), mp 170.5–172.0 °C (lit. (33) mp 170–172 °C). Benzimidazolium chloride was prepared as described above for the methoxynaphthylammonium chlorides.

N-Methylquinolinium chloride (Eastman, white label) was purified by repeated slow crystallization from acetonitrile to yield light green crystals, mp 128–129 °C (dec.) (lit. (34) mp 126 °C); nmr (D_2O) δ 4.72 (s, 3H), 7.8–8.4 (m, 5H), 9.1 (d, 1H), 9.4 (d, 1H).

Potassium 3,5-dinitrobenzoate was prepared as described for potassium indole-3-carboxylate.

Sodium 2,4-dinitrobenzenesulfonate was Eastman, white label, used without further purification.

Distilled water was redistilled over potassium permanganate and redistilled a second time in an apparatus protected from atmospheric carbon dioxide before use as a solvent for buffer, salt, or acceptor solutions.

Potentiometric Measurements

A Beckman Research Model p*H* meter powered through a constant voltage transformer and equipped with a Sargent model S-30072-15 combination glass–thallium amalgam electrode was used for all p*H* measurements. Readings were reproducible to ± 0.002 p*H* units. The titrations were carried out as described under Results with the cell and buret solutions maintained to $30.00 \pm < 0.05$ °C by circulation of thermostatted water. The buret solution was injected directly into the cell and both solutions were kept under a nitrogen atmosphere. The cell solution was stirred magnetically between readings.

Donor buffer stock solutions were freshly prepared

Can. J. Chem. Downloaded from www.nrcresearchpress.com by 210.87.254.42 on 09/05/12
For personal use only.

from either weighed amounts of donor acid and conjugate base, or from a weighed amount of donor acid or donor base alone plus a measured volume of standard aqueous KOH or HCl, by dilution to a known volume of solution with distilled water. Stock solutions of donor buffer, acceptor salt, and model salt were generally prepared at exactly twice the concentration desired for the titration. The cell solution was then prepared by mixing equal volumes of donor buffer and model salt solutions and the buret solution in a similar way from buffer and acceptor salt solutions. Occasionally (see Results) the model salt and acceptor salt stock solutions were adjusted to neutrality by addition of minute amounts of dilute acid or base.

The pH meter was calibrated internally and standardized before each run using a 0.0500 M solution of U.S. National Bureau of Standards potassium hydrogen phthalate, the pH of which is defined to ± 0.001 unit at several temperatures. A small volume (usually 15.00 ml) of cell solution was pipetted into the cell and the pH measured. Measured volumes (at increments of about 5 ml) of buret solution were then added and the pH measured after each addition. After addition of 40–50 ml of buret solution the cell was cleaned out and the pH of the pure buret solution measured. Finally, the pH meter was checked with the standard buffer to ensure that the calibration had been stable during the titration.

Calculations

Calculations were done by computer. The program uses solute concentrations, volume of titrant, pH readings (including that of the pure buret solution, which corresponds to an infinite volume of titrant), eq. 6, and the relation $[H^+]$ = antilog $(-pH)$ to calculate K_a^{app} for each point in the titration. The initial pH reading on the cell solution gives K_a. The program then draws a plot of $K_a/(K_a^{app} - K_a)$ *vs.* c_A^{-1} and calculates the least squares slope (m) and intercept (b) and their standard deviations (s_m and s_b). The first point used in the least squares analysis corresponded to $c_A = 2.0 \times 10^{-2}$ M or greater. K_c^a, K_c^b, and their standard deviation (s_K) were then calculated using the following relations:

$$K_c^a = b/m$$

$$K_c^b = (1 + b)/m$$

$$s_K = \left[\frac{s_b^2}{m^2} + \left(\frac{b^2}{m^4}\right)s_m^2\right]^{1/2}$$

The estimates of K_a (thermodynamic) listed in the text were obtained from the initial pH readings and stoichiometric concentrations of buffer components making the assumption that $pH = -\log a_{H^+}$ and that all ionic activity coefficients are given by [7] using $\alpha = 6$ Å. Making the same assumptions it can be shown that K_a (mixed) will vary by up to 4.4% with the differences in buffer concentrations and ratios used.

Spectrophotometric Association Constants

Spectrophotometric measurements utilized a Guilford model 200 uv–visible spectrophotometer equipped with a thermostatted cell compartment. For each determination, freshly prepared stock solutions of acceptor (NMQ^+Cl^-) and donor (1-naphthylamine or 5-methoxy-1-naphthylamine) were used to prepare a series of five to nine solutions containing variable concentrations of acceptor and a smaller concentration of donor. At the same time, a second series of solutions identical to the first except containing no donor were prepared. Optical densities of the solutions were measured separately. For the 1-naphthylamine system, c_D was 8×10^{-4} M, c_A varied from 1.25×10^{-2} to 5×10^{-1} M, and optical densities were measured at 10 nm intervals between 390 and 410 nm. For the 5-methoxynaphthalene system c_D was $2.5\text{–}9.0 \times 10^{-4}$ M, c_A varied from 5×10^{-2} to 3.75×10^{-1} M, and optical densities were measured at 10 nm intervals from 390 to 450 nm. Data were treated according to [12] (10)

$$[12] \quad \frac{c_D}{OD - \varepsilon_A c_A} = \frac{1}{K(\varepsilon_{DA} - \varepsilon_A)c_A} + \frac{1}{(\varepsilon_{DA} - \varepsilon_A)}$$

where OD is the optical density at a particular c_A, c_D, and wavelength, and the ε's are molar extinction coefficients. The two spectrophotometric complexation constants in the text are averages of two and four separate determinations, respectively (each determination leading to a K for each of three or seven wavelengths) listed with their average deviations.

Acknowledgments

We wish to thank D. Kubiak, D. Krezenski and R. K. Boeckman, Jr. for technical assistance with the spectrophotometric measurements. This research was supported by the U.S. Department of Health, Education and Welfare (Grant GM 11967-03).

1. A. K. Colter, A. L. McKenna III, and M. A. Kasem. Can. J. Chem. **52**, 3748 (1974), and earlier papers in this series.
2. J. N. Brønsted. Chem. Ber. **61**, 2049 (1928).
3. D. J. G. Ives and P. G. N. Mosley. J. Chem. Soc. B, 757 (1966).
4. J. F. J. Dippy, S. R. C. Hughes, and J. W. Laxton. J. Chem. Soc. 2995 (1956).
5. A. K. Colter and M. R. J. Dack. *In* Molecular complexes. Vol. 1. *Edited by* R. Foster. Elek Science, London. 1973. p. 306.
6. J. N. Brønsted and R. P. Bell. J. Am. Chem. Soc. **53**, 2478 (1931).
7. R. P. Bell. Proc. Roy. Soc. Ser. A, **143**, 377 (1934).
8. R. P. Bell and E. F. Caldin. J. Chem. Soc. 382 (1938).
9. S. Shifrin. Biochemistry, **3**, 829 (1964).
10. R. Foster. Organic charge-transfer complexes. Academic Press, New York. 1969. Chapt. 6.
11. A. Albert and E. P. Serjeant. Ionization constants of acids and bases. Methuen, London. 1962.
12. E. J. King. Acid–base equilibria. The MacMillan Company, New York. 1965. Chapt. 8.
13. A. Fischer, G. J. Sutherland, R. G. Topsom, and

J. VAUGHAN. J. Chem. Soc. 5948 (1965).
14. L. K. CREAMER, A. FISCHER, B. R. MANN, J. PACKER, R. B. RICHARDS, and J. VAUGHAN. J. Org. Chem. **26**, 3148 (1961).
15. D. A. MACINNES. J. Am. Chem. Soc. **48**, 2068 (1926).
16. A. K. COLTER and E. GRUNWALD. J. Phys. Chem. **74**, 3637 (1970).
17. R. G. BATES. Determination of p*H*, theory and practice. John Wiley and Sons, Inc., New York. 1973. Chapt. 4.
18. G. N. LEWIS and M. RANDALL. Thermodynamics. 2nd ed. Revised by K. S. Pitzer and L. Brewer. McGraw-Hill, Inc. New York. 1961. p. 344.
19. F. A. LONG and W. F. MCDEVIT. Chem. Rev. **51**, 119 (1952).
20. J. N. BRØNSTED. J. Am. Chem. Soc. **44**, 877 (1922); **45**, 2898 (1923).
21. E. A. GUGGENHEIM. Philos. Mag. **19**, 588 (1935).
22. F. M. MENGER and M. L. BENDER. J. Am. Chem. Soc. **88**, 131 (1966).
23. M. W. HANNA and A. L. ASHBAUGH. J. Phys. Chem. **68**, 811 (1964).
24. S. CARTER, J. N. MURRELL, and E. J. ROSCH. J. Chem. Soc. 2048 (1965).
25. D. BUBEN. Ph.D. Thesis, Carnegie–Mellon University, Pittsburgh, Pennsylvania. 1968.
26. R. J. KERSTING. Ph.D. Thesis, Carnegie–Mellon University, Pittsburgh, Pennsylvania. 1969.
27. K. BECK and K. EBBINGHAUS. Ber. **39**, 3872 (1906).
28. H. SCHROETER. Ann. **426**, 137 (1922).
29. H. J. TEUBER and H. LINDNER. Ber. **92**, 921 (1959).
30. F. P. DOYLE, W. FERRIER, D. O. HOLLAND, M. D. MEHTA, and J. H. C. NAYLER. J. Chem. Soc. 2853 (1956).
31. O. E. MAY, J. F. T. BERLINER, and D. F. J. LYNCH. J. Am. Chem. Soc. **49**, 1012 (1927).
32. L. SCHMID and F. TADROS. Ber. **65**, 1689 (1932).
33. E. C. WAGNER and W. H. MILLETT. Org. Synth. **19**, 12 (1939).
34. E. OSTERMAYER. Ber. **18**, 591 (1885).

Can. J. Chem. Downloaded from www.nrcresearchpress.com by 210.87.254.42 on 09/05/12
For personal use only.

Theoretical study of the ν_3 and ν_4 Raman bands of methane in rare gas matrices

KOJI KOBASHI, YOSUKE KATAOKA, AND TSUNENOBU YAMAMOTO

Department of Chemistry, Faculty of Science, Kyoto University, Kyoto, 606 Japan

Received December 8, 1975

KOJI KOBASHI, YOSUKE KATAOKA, and TSUNENOBU YAMAMOTO. Can. J. Chem. **54**, 2154 (1976).

Theoretical study has been carried out on the Raman spectra of the ν_3 and ν_4 vibration bands of methane in Ar, Kr, and Xe matrices at low temperatures. The present study is a continuation of a theoretical work by Nishiyama and Yamamoto on the infrared spectra of the same systems. We consider the symmetry of the system under the group $\bar{O}_h O_h$, introducing the inversion functions to generalize Wigner's rotational functions. As a result, dual assignments are given to each vibration–rotation state. The allowed transitions of the Raman scattering are compared with those of the infrared absorption, and it is found that a kind of 'rule of mutual exclusion' holds. The relative intensities and spacings of the Raman spectra are calculated and successfully compared with experiment.

KOJI KOBASHI, YOSUKE KATAOKA et TSUNENOBU YAMAMOTO. Can. J. Chem. **54**, 2154 (1976).

On effectué des études théoriques des bandes de vibration ν_3 et ν_4 des spectres Raman du méthane dans des matrices de Ar, Kr et Xe à basse température. Le travail actuel est une continuation des travaux théoriques de Nishiyama et Yamamoto sur les spectres infrarouges de ces mêmes systèmes. On considère la symétrie du système sous le groupe $\bar{O}_h O_h$ introduisant l'inversion des fonctions pour généraliser les fonctions rotationnelles de Wigner. Il en résulte que des attributions doubles sont faites pour chaque état de vibration–rotation. On compare les transitions permises du spectre Raman avec celles de l'absorption infrarouge et on trouve qu'une sorte de "règle d'exclusion mutuelle" est plausible. Les intensités relatives et les distances du spectre Raman ont été calculés et comparés avec succès avec ceux trouvés expérimentalement.

[Traduit par le journal]

Introduction

A methane molecule embedded in a rare gas matrix is a pertinent object for a quantitative study of the rotational motion of a polyatomic molecule in the solid state. Experimental studies of the infrared absorption (1–3) and Raman scattering (4) have been carried out on such systems. The observed spectra provide reliable information on the molecular rotation under the influence of the surrounding host molecules. In particular, the rotational structures of the intramolecular vibrational bands reflect directly the crystalline field which the molecule feels in the matrix. Theoretically, Nishiyama and Yamamoto (N.Y.) (5) studied the pure rotational states and the low-lying vibration–rotation states of the ν_3 and ν_4 modes of methane in the crystalline field which Yasuda (6) had derived from the assumption of additivity of pairwise interatomic potentials, and successfully analyzed the observed infrared spectra in Ar, Kr, and Xe matrices.

The main aim of the present article is to calculate the Raman spectra employing the same model as N.Y. and analyze the experimental spectrum in a Kr matrix which was observed by Cabana *et al.* (4). In order to derive the selection rule for the Raman scattering, we have to utilize the full symmetry of the Hamiltonian. For this purpose we introduce a set of inversion functions to generalize Wigner's rotational functions (WRF's) (7) so that we can deal with improper rotations as well as proper rotations. Then we rewrite the Hamiltonian and the wavefunctions of N.Y. in terms of the generalized rotational functions (GRF's). Consideration of the symmetry properties of the rotational and vibrational–rotation states obtained in this manner enables us to derive the allowed transitions for the Raman scattering. Comparing them with those of the infrared absorption, we find that a kind of 'mutual exclusion' holds between the infrared and Raman spectra with respect to their rotational structures of the ν_3 and ν_4 vibration bands at low temperatures.

Making use of the numerical results of the level schemes and the corresponding wave-

Can. J. Chem. Downloaded from www.nrcresearchpress.com by 210.87.254.40 on 09/05/12
For personal use only.

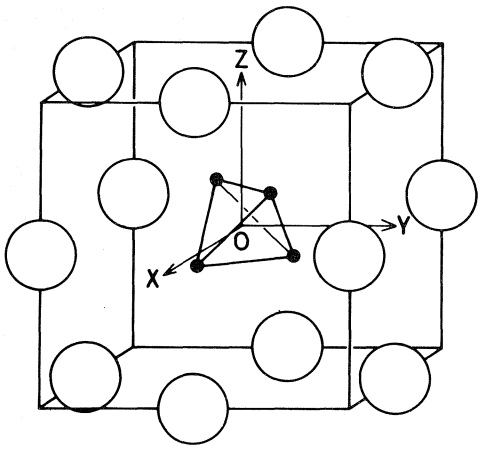

FIG. 1. A methane molecule substituted in a rare gas matrix.

functions of N.Y., we calculate the relative spacings and intensities of the Raman spectra of a CH_4 molecule in an Ar, Kr, or Xe matrix. The calculated spectra of methane in a Kr matrix is as a whole compatible with the observed band shape obtained by Cabana *et al.*

Inversion Functions

We assume that a CH_4 molecule is substitutionally put in a rare gas matrix (Fig. 1). We can separately perform symmetry operations with respect to the molecule-fixed frame (MFF) and those with respect to the crystal-fixed frame (CFF). To distinguish the two kinds of operations from each other, we use barred symbols for the symmetry groups and their irreducible representations with respect to MFF. Thus we will use the symbol $\bar{\Gamma}\Gamma/\bar{G}G$ to represent an irreducible representation $\bar{\Gamma}\Gamma$ of a direct-product group $\bar{G}G$.

The Hamiltonian of the present problem has the symmetry $\bar{O}_h O_h$, as will be shown in the next section. Therefore, in order to utilize the full symmetry of our Hamiltonian, we have to take into account improper rotations in addition to proper rotations. To this end we generalize Fox and Ozier's idea (8) in the following way. Let us introduce a set of inversion functions such that

$$[1]\qquad \begin{aligned} \bar{i}\,\bar{\mathcal{I}}_g &= \bar{\mathcal{I}}_g, & \bar{i}\,\bar{\mathcal{I}}_u &= (-)\bar{\mathcal{I}}_u \\ i\,\mathcal{I}_g &= \mathcal{I}_g, & i\,\mathcal{I}_u &= (-)\mathcal{I}_u \end{aligned}$$

where $\bar{i}$ and i denote the inversion operation of MFF and CFF, respectively. We then define the following four kinds of the GRF's:

$$[2]\qquad \begin{aligned} &\bar{\mathcal{I}}_g\mathcal{I}_g\mathfrak{D}^{(J)}_{KM}(\omega), \qquad \bar{\mathcal{I}}_g\mathcal{I}_u\mathfrak{D}^{(J)}_{KM}(\omega) \\ &\bar{\mathcal{I}}_u\mathcal{I}_g\mathfrak{D}^{(J)}_{KM}(\omega), \qquad \bar{\mathcal{I}}_u\mathcal{I}_u\mathfrak{D}^{(J)}_{KM}(\omega) \end{aligned}$$

where $\mathfrak{D}^{(J)}_{KM}(\omega)$ are the WRF's. Since $\bar{O}_h O_h = (\bar{O} \times \bar{i})\ (O \times i)$, we multiply the symmetry-adapted functions (SAF's) of $\bar{O}O$ (5, 9, 10) by $\bar{\mathcal{I}}_g\mathcal{I}_g$, $\bar{\mathcal{I}}_g\mathcal{I}_u$, $\bar{\mathcal{I}}_u\mathcal{I}_g$ or $\bar{\mathcal{I}}_u\mathcal{I}_u$ to obtain the SAF's of $\bar{O}_h O_h$. These new SAF's help us to derive unambiguously the allowed transitions both for the infrared absorption and Raman scattering, as will be shown below.

Vibration–Rotation States

Let us assume that the center of mass of the methane molecule under consideration is fixed at a site of the rare gas matrix, *i.e.*, the methane molecule rotates and vibrates in the crystalline field. We use the same Hamiltonian as N.Y. in which the vibrational motion is described as a three-dimensional isotropic harmonic oscillation, since the consideration is confined to the three-fold degenerate ν_3 and ν_4 vibrations only. The Coriolis coupling between the vibration and rotation is included in the Hamiltonian. Here we introduce the inversion functions $\bar{\mathcal{I}}_g\mathcal{I}_g$ into the expression for the crystalline field so that it reflects the full symmetry of the real system. Thus, we have

$$[3]\qquad H = H_r + H_v + H_C$$

$$[4]\qquad H_r = B\mathbf{J}^2 + \bar{\mathcal{I}}_g\mathcal{I}_g V(\omega)$$

$$[5]\qquad H_v = \tfrac{1}{2}(P_x^2 + P_y^2 + P_z^2) + \tfrac{1}{2}\Omega^2(Q_x^2 + Q_y^2 + Q_z^2)$$

$$[6]\qquad H_C = -2B\zeta\mathbf{p}\cdot\mathbf{J}$$

where B ($=7.558$ K, 1 K $= 1.38 \times 10^{-23}$ J) is the rotational constant of a free CH_4 molecule, $\mathbf{J}$ the total angular momentum operator, (Q_x, Q_y, Q_z) and (P_x, P_y, P_z) are the normal mode coordinates and the conjugate momenta, respectively, of the ν_3 or ν_4 mode with frequency Ω, $\mathbf{p} = \mathbf{Q} \times \mathbf{P}$ the vibrational angular momentum and ζ the Coriolis coupling constant the value of which is assumed equal to that in the gaseous state (0.04 for ν_3 and 0.46 for ν_4 (11)). The crystalline field is specifically expressed as

$$[7]\qquad V(\omega) = \beta_4 BV_4(\omega) + \beta_6 BV_6(\omega)$$

Can. J. Chem. Downloaded from www.nrcresearchpress.com by 210.87.254.40 on 09/05/12
For personal use only.

Can. J. Chem. Downloaded from www.nrcresearchpress.com by 210.87.254.40 on 09/05/12
For personal use only.

TABLE 1. Numerical values of the parameters β_4 and β_6 of the crystalline fields (5, 6)

Gas	β_4	β_6
Ar	13.2	−16.1
Kr	7.16	−8.29
Xe	4.64	−4.81

where ω collectively denotes the Euler angles of the MFF with respect to the CFF, β_4 and β_6 are dimensionless constants, the numerical value of which are shown in Table 1, and $V_4(\omega)$ and $V_6(\omega)$ are the linear combinations of WRF's of the fourth and the sixth order, respectively. As regards the details of the crystalline field, see refs. 5 and 6.

Nishiyama and Yamamoto (5), assuming $\bar{O}O$ for the symmetry of the total Hamiltonian [3], elaborated the rotational and the low-lying vibration–rotation states in the truncated rotational space $J \leq 10$, using the WRF's as the basis functions. Now we construct the wavefunctions of the rotational and vibration–rotation eigenstates utilizing the GRF's given in the preceding section, and thus make the assignment for each state under the group $\bar{O}_h O_h$ instead of $\bar{O}O$. In spite of the fact that the real system has the symmetry $\bar{T}_d O_h$, we deal with it under the larger group $\bar{O}_h O_h$. The reason for this is as follows: the crystalline field in [4] has the symmetry $\bar{O}_h O_h$. The three-fold degenerate ν_3 and ν_4 mode has been replaced by a three-dimensional isotropic harmonic oscillation as in [5]. Therefore, the total Hamiltonian [3] has the symmetry $\bar{O}_h O_h$. One should note that $\bar{O}_h O_h$ is more directly correlated to $\bar{T}_d O_h$ than $\bar{O}O$. However, we have to bear in mind the following two points: First, the total wavefunctions including nuclear-spin part must have the symmetry $\bar{A}_{1u}/\bar{O}_h$ or $\bar{A}_{2g}/\bar{O}_h$ to reflect the fact that they must have $\bar{A}_2/\bar{T}_d$ symmetry by the Pauli principle. Second, the normal coordinates of the molecular vibration must be assumed to have the symmetry either $\bar{T}_{1u}/\bar{O}_h$ or $\bar{T}_{2g}/\bar{O}_h$, because each of them belongs to $\bar{T}_2/\bar{T}_d$. As a result, we make dual assignments to each vibration–rotation state. Since the $\bar{T}_{1u}/\bar{O}_h$ component of the vibration yields the electric dipole, it is responsible for the infrared absorption. The $\bar{T}_{2g}/\bar{O}_h$ component causes distortion in the polarizability and is responsible for the Raman scattering. Thus we will make use of either assignment alternatively according to the purpose.

TABLE 2. Correspondence of the symmetry representations of the pure rotational states under various symmetry groups

$\|0;\bar{\Gamma}\Gamma/\bar{O}O\rangle$*	$\|0;\bar{\Gamma}\Gamma/\bar{O}_h O\rangle$	$\|0;\bar{\Gamma}\Gamma/\bar{T}_d O\rangle$
$\bar{E}E$	$\bar{E}_g E$, $\bar{E}_u E$	$\bar{E}E$
$\bar{T}_2 T_2$	$\bar{T}_{2u} T_2$	$\bar{T}_1 T_2$
$\bar{E}T_2$	$\bar{E}_g T_2$, $\bar{E}_u T_2$	$\bar{E}T_2$
$\bar{T}_2 E$	$\bar{T}_{2u} E$	$\bar{T}_1 E$
$\bar{T}_1 T_1$	$\bar{T}_{1g} T_1$	$\bar{T}_1 T_1$
$\bar{A}_1 A_1$	$\bar{A}_{1u} A_1$	$\bar{A}_2 A_1$

*Nishiyama and Yamamoto (5). As regards the energy level scheme, see Fig. 2 of ref. 5.

We summarize the results of the assignment in Tables 2 and 3. Table 2 shows the representations of low-lying pure-rotational states in the crystalline field. The first column gives the assignment by N.Y. (5). The second column lists the corresponding new assignments under $\bar{O}_h O$. Here it is unnecessary to refer to $\bar{O}_h O_h$, because the parity simply doubles each rotational state. We give the result due to $\bar{T}_d O$ in the third column for completeness. Table 3 shows the representation of low-lying vibration–rotation states. First column is just what N.Y. reported, where the first-excited vibrational state is assigned as $\bar{T}_1/\bar{O}$. Second and third columns give the representations under $\bar{O}_h O$, the vibrational state being assigned as $\bar{T}_{1u}/\bar{O}_h$ and $\bar{T}_{2g}/\bar{O}_h$, respectively. Finally, the last column gives the representations under $\bar{T}_d O$ for illustration.

Selection Rules and Intensities

The intensity of the infrared absorption which corresponds to the transition from an initial state $|0;\bar{\Gamma}_i\Gamma_i\rangle$ to a final state $|1;\bar{\Gamma}_f\Gamma_f\rangle$ is written as

$$[8] \qquad I_\sigma \propto |\langle 1;\bar{\Gamma}_f\Gamma_f|\boldsymbol{\varepsilon}_\sigma \cdot \boldsymbol{d}\,|0;\bar{\Gamma}_i\Gamma_i\rangle|^2 \rho_i(T)$$

where $\boldsymbol{d}$ is a dipole moment vector, $\boldsymbol{\varepsilon}_\sigma$ the polarization vector of the incident light along the σ-axis ($\sigma = X$, Y, or Z) of CFF, $\rho_i(T)$ the statistical weight of the initial state which depends on the spin equilibration temperature T and on the nuclear spin state. The intensity of the Raman scattering is analogously written as

$$[9] \qquad I_{\sigma\rho} \propto |\langle 1;\bar{\Gamma}_f\Gamma_f|\boldsymbol{\varepsilon}_\sigma \cdot \boldsymbol{\alpha} \cdot \boldsymbol{\varepsilon}_\rho|0;\bar{\Gamma}_i\Gamma_i\rangle|^2 \rho_i(T)$$

TABLE 3. Correspondence of the symmetry representations of the Coriolis-coupled vibration–rotation states under various symmetry groups*

$\|1;\bar{\Gamma}\Gamma/OO\rangle$†	$\|1;\bar{\Gamma}\Gamma/\bar{O}_hO\rangle$‡	$\|1;\bar{\Gamma}\Gamma/\bar{O}_hO\rangle$‡	$\|1;\bar{\Gamma}\Gamma/\bar{T}_dO\rangle$‡
$^{\dagger}\bar{T}_1E$	$^{\dagger}\bar{T}_{1g}E$	$\bar{T}_{2u}E$	$^{\dagger}\bar{T}_1E^{\dagger}$
$\bar{T}_2E$	$\bar{T}_{2u}E$	$\bar{T}_{1g}E^{\dagger}$	$^{\dagger}\bar{T}_1E^{\dagger}$
$^{\dagger}\bar{T}_1T_2$	$^{\dagger}\bar{T}_{1g}T_2$	$\bar{T}_{2u}T_2$	$^{\dagger}\bar{T}_1T_2^{\dagger}$
$\bar{T}_2T_2$	$\bar{T}_{2u}T_2$	$\bar{T}_{1g}T_2^{\dagger}$	$\bar{T}_1T_2^{\dagger}$
$\bar{A}_2T_2$	$\bar{A}_{2g}T_2$	$\bar{A}_{1u}T_2^0$	$\bar{A}_2T_2^0$
$\bar{A}_2E$	$\bar{A}_{2g}E$	$\bar{A}_{1u}E^0$	$\bar{A}_2E^0$
$\bar{E}T_2$	$\bar{E}_gE$, $\bar{E}_uE$	$\bar{E}_uE$, $\bar{E}_gE$	$\bar{E}E$
$\bar{T}_2E$	$\bar{T}_{2u}E$	$\bar{T}_{1g}E^{\dagger}$	$^{\dagger}\bar{T}_1E^{\dagger}$
$\bar{T}_2T_2$	$\bar{T}_{2u}T_2$	$\bar{T}_{1g}T_2^{\dagger}$	$^{\dagger}\bar{T}_1T_2^{\dagger}$
$\bar{E}E$	$\bar{E}_gE$, $\bar{E}_uE$	$\bar{E}_uE$, $\bar{E}_gE$	$\bar{E}E$
$^{\dagger}\bar{T}_1T_2$	$^{\dagger}\bar{T}_{1g}T_2$	$\bar{T}_{2u}T_2$	$^{\dagger}\bar{T}_1T_2^{\dagger}$
$^{\dagger}\bar{T}_1E$	$^{\dagger}\bar{T}_{1g}E$	$\bar{T}_{2u}E$	$^{\dagger}\bar{T}_1E^{\dagger}$
$\bar{T}_2T_1$	$\bar{T}_{2u}T_1$	$\bar{T}_{1g}T_1^{\dagger}$	$\bar{T}_1T_1^{\dagger}$
$\bar{E}T_1$	$\bar{E}_gT_1$, $\bar{E}_uT_1$	$\bar{E}_uT_1$, $\bar{E}_gT_1$	$\bar{E}T_1$
$^{\dagger}\bar{T}_1T_1$	$^{\dagger}\bar{T}_{1g}T_1$	$\bar{T}_{2u}T_1$	$^{\dagger}\bar{T}_1T_1^{\dagger}$
$^{0}\bar{A}_1T_1$	$^{0}\bar{A}_{1u}T_1$	$\bar{A}_{2g}T_1$	$^{0}\bar{A}_2T_1$
$^{\dagger}\bar{T}_1A_1$	$^{\dagger}\bar{T}_{1g}A_1$	$\bar{T}_{2u}A_1$	$^{\dagger}\bar{T}_1A_1^{\dagger}$

*The symbols, † and 0, on the left side of the first, second, and fourth columns stand for the allowed transitions from $|0;\bar{A}_{1u}A_1/\bar{O}_hO\rangle$ and $|0;\bar{T}_{1g}T_1/\bar{O}_hO\rangle$, respectively, in the case of the infrared absorption, and those on the right side of the third and fourth columns have the same meanings for the Raman scattering. As regards the energy level scheme, see Fig. 3 of ref. 5.

†Nishiyama and Yamamoto (5). $\bar{T}_1/\bar{O}$ is assigned to the first-excited vibrational states.

‡Present results. $\bar{T}_{1u}/\bar{O}_h$, $\bar{T}_{2g}/\bar{O}_h$ and $\bar{T}_2/\bar{T}_d$ are assigned to the vibrational states, respectively.

where $\boldsymbol{\alpha}$ is the polarizability tensor and $\boldsymbol{\varepsilon}_\sigma$ and $\boldsymbol{\varepsilon}_\rho$ are the polarization vectors of the incident and scattered lights, respectively. As regards the initial states of the transitions relevant in the low temperature region, it suffices to confine ourselves to the lowest two levels, $|0;\bar{A}_{1u}A_1/\bar{O}_hO\rangle$ and $|0;\bar{T}_{1g}T_1/\bar{O}_hO\rangle$.

The operators $\boldsymbol{\varepsilon}_\sigma\cdot\boldsymbol{d}$ and $\boldsymbol{\varepsilon}_\sigma\cdot\boldsymbol{\alpha}\cdot\boldsymbol{\varepsilon}_\sigma$ are invariant under any symmetry operations of the group $\bar{O}_h$. Therefore the symmetry of the operators with respect to MFF should be $\bar{A}_{1g}/\bar{O}_h$. Consequently, $\boldsymbol{\varepsilon}_\sigma\cdot\boldsymbol{d}$ has $\bar{A}_{1g}T_1/\bar{O}_hO$ and $\boldsymbol{\varepsilon}_\sigma\cdot\boldsymbol{\alpha}\cdot\boldsymbol{\varepsilon}_\rho$ has $\bar{A}_{1g}A_1$, $\bar{A}_{1g}E$, and $\bar{A}_{1g}T_2/\bar{O}_hO$ symmetry representations, respectively. In the case of the infrared absorption, we have to find the final states among those in the second column of Table 3. The results are also shown in the table, which coincide with the results already obtained by N.Y. (5). The symbols † and 0 indicate the final states of the allowed transitions from $|0;\bar{A}_{1u}A_1/\bar{O}_hO\rangle$ and $|0;\bar{T}_{1g}T_1/\bar{O}_hO\rangle$, respectively. On the other hand, in the case of the Raman scattering, the final states should be found among those in the third column of Table 3 and the results are also shown there. The last column of Table 3 shows the allowed transitions under the group $\bar{T}_dO$. The symbols † and 0 on the left and right sides correspond to the infrared and the Raman spectra respectively. The transitions to still higher levels are omitted, for simplicity.

We may notice two features of the allowed transitions shown in Table 3. First, the selection rule considered under the group $\bar{O}_hO$ forbids some transitions that are allowed under $\bar{T}_dO$. We checked it by numerical calculations. Second, comparing the second and third columns of Table 3 with each other, we find that the allowed transitions in the Raman spectra are forbidden in the infrared spectra and vice versa. A kind of 'rule of mutual exclusion' holds between the infrared and the Raman spectra. The reason for this can be understood as follows: If a methane molecule is rotating freely, or if it were rotating in the crystalline field without the Coriolis interaction, the allowed transitions for both spectra would not necessarily be mutually exclusive because of the degeneracy of the vibration–rotation levels. However, in the present case, the crystalline field and the Coriolis inter-

Can. J. Chem. Downloaded from www.nrcresearchpress.com by 210.87.254.40 on 09/05/12
For personal use only.

Can. J. Chem. Downloaded from www.nrcresearchpress.com by 210.87.254.40 on 09/05/12
For personal use only.

action collaborate to lift the degeneracies of the vibration–rotation states. Furthermore the initial states are confined to the lowest two levels because of the low temperatures. These two facts bring about the 'rule of mutual exclusion'. Thus the rotational fine structures of the infrared and Raman spectra of the ν_3 (and ν_4) vibrational band are entirely different from each other and give complementary information about the vibration–rotation states.

For intensity calculation, we rewrite the Cartesian components $\alpha_{\sigma\rho}$ of the polarizability tensor which refers to CFF by spherical components $\alpha_{l,\mu}$ (12):

$$\begin{aligned}
\alpha_{0,0} &= \frac{1}{\sqrt{3}}\{\alpha_{XX} + \alpha_{YY} + \alpha_{ZZ}\} \\
\alpha_{2,0} &= \frac{1}{\sqrt{6}}\{2\alpha_{ZZ} - \alpha_{XX} - \alpha_{YY}\} \\
\alpha_{2,\pm1} &= \mp\{\alpha_{ZX} \pm i\alpha_{ZY}\} \\
\alpha_{2,\pm2} &= \frac{1}{2}\{\alpha_{XX} - \alpha_{YY} \pm 2i\alpha_{XY}\}
\end{aligned} \qquad [10]$$

The tensor components $\bar{\alpha}_{\sigma\rho}$ which refer to MFF are also rewritten by $\bar{\alpha}_{l,\mu}$ in the same manner. These two sets of tensors are related through the GRF's such that (5, 7, 13)

$$\alpha_{l,\mu} = \sum_{\nu} \bar{\alpha}_{l,\nu} \bar{\mathscr{F}}_g \mathscr{J}_g \mathfrak{D}^{(l)}_{\nu\mu}(\omega) \qquad [11]$$

where the inversion functions are introduced so that inversion symmetry of both sides of [11] is consistent. Each component of the polarizability $\bar{\alpha}_{\sigma\rho}$ is expanded with respect to the normal coordinates Q_η of the ν_3 or ν_4 vibration.

$$\bar{\alpha}_{\sigma\rho}{}^{0} = \bar{\alpha}_{\sigma\rho}{}^{-0} + \sum_{\eta=x,y,z} \left(\frac{\partial\bar{\alpha}_{\sigma\rho}}{\partial Q_\eta}\right)_0 Q_\eta + \cdots\cdots \qquad [12]$$

The nonvanishing components of $(\partial\bar{\alpha}_{\sigma\rho}/\partial Q_\eta)_0$ have a common value, as shown by Loudon (ref. 14, p. 441):

$$\begin{aligned}
(\partial\bar{\alpha}_{xy}/\partial Q_z)_0 &= (\partial\bar{\alpha}_{yz}/\partial Q_x)_0 \\
&= (\partial\bar{\alpha}_{zx}/\partial Q_y)_0 \\
&= (\partial\bar{\alpha}_{yx}/\partial Q_z)_0 \\
&= (\partial\bar{\alpha}_{zy}/\partial Q_x)_0 \\
&= (\partial\bar{\alpha}_{xz}/\partial Q_y)_0
\end{aligned} \qquad [13]$$

Using [9] to [13], we can calculate the Raman intensities for the seven allowed transitions from $|0;\bar{A}_{1u}A_1\rangle$ and $|0;\bar{T}_{1g}T_1\rangle$ to $|1;\bar{\Gamma}\Gamma\rangle$ of the third column of Table 3.

Results and Discussion

We assume that the incident light is directed along the Y axis of the CFF and the scattered light is observed in the X direction. Since the system has cubic symmetry, we calculate only I_{ZX} and I_{ZZ} given in [9] without loss of generality. For the unpolarized light, we should have the intensity, I_u, such that

$$I_u = 3I_{ZX} + I_{ZZ} \qquad [14]$$

If the crystal axes are randomly orientated, we have to take the average over all possible orientations of the crystal axes. The intensities, $\langle I_{ZX}\rangle$, $\langle I_{ZZ}\rangle$ and $\langle I_u\rangle$, are related to I_{ZX} and I_{ZZ} as follows (15, 16):

$$\begin{aligned}
\langle I_{ZX}\rangle &= \frac{3}{5}I_{ZX} \\
\langle I_{ZZ}\rangle &= I_{ZZ} + \frac{4}{5}I_{ZX} \\
\langle I_u\rangle &= I_{ZZ} + \frac{13}{5}I_{ZX}
\end{aligned} \qquad [15]$$

The relative intensities and relative spacings of the Raman lines of the ν_3 and ν_4 fundamentals were numerically calculated. The calculated spectra in Ar, Kr, and Xe matrices are shown in Tables 4 and 5. In addition to the spectra in rare gas matrices, we also calculated the Raman spectra of a free CH_4 molecule, and the result is shown in Table 6. The spacings are measured from $Q(1)$ in cm^{-1}. The intensities I_{ZX} and I_{ZZ} are normalized such that I_{ZX} of $Q(1)$ has unit intensity, and $\langle I_u\rangle$ are also normalized in the same way. Then the relative intensities of $R(1)$ lines become temperature independent. On the other hand, the relative intensities of $S(0)$ lines, which correspond to the transitions from $|0;\bar{A}_{1u}A_1/\bar{O}_hO\rangle$, depend on the spin equilibration temperature. In Tables 4, 5, and 6, the intensities of $S(0)$ with superscripts a and b correspond to the spin temperature 20 and 10 K, respectively. As the spin temperature is lowered, the T-nuclear spin species converts into the A-spin species, and, therefore, the relative intensities of the two $S(0)$ lines increase.

Can. J. Chem. Downloaded from www.nrcresearchpress.com by 210.87.254.40 on 09/05/12
For personal use only.

TABLE 4. Calculated spectra of the ν_3 mode in rare gas matrices*

Line	Ar intensity			Kr intensity			Xe intensity		
	Spacing (cm^{-1})	I_{zx}	I_{zz}	$\langle I_u \rangle$	Spacing (cm^{-1})	I_{zx}	I_{zz}	$\langle I_u \rangle$	Spacing (cm^{-1})	I_{zx}	I_{zz}	$\langle I_u \rangle$
$Q(1)$	0.0	1.00	5.57	1.00	0.0	1.00	4.53	1.00	0.0	1.00	3.26	1.00
$R(1)$	8.34	1.16	3.58	0.81	11.03	0.95	2.88	0.77	13.47	0.74	2.27	0.72
	8.63	1.07	—	0.34	11.39	0.87	—	0.33	13.86	0.68	—	0.30
	15.11	0.39	4.96	0.73	18.85	0.19	3.89	0.63	21.26	0.04	2.92	0.52
	40.10	0.67	—	0.21	40.25	0.80	—	0.30	34.93	0.84	—	0.37
$S(0)$	15.35	—	16.65^a	2.04^a	20.00	—	15.07^a	2.17^a	23.64	—	12.97^a	2.21^a
		—	26.85^b	3.29^b		—	27.30^b	3.93^b		—	24.23^b	4.13^b
	21.60	6.15^a	—	1.96^a	27.24	6.34^a	—	2.37^a	30.86	6.47^a	—	2.87^a
		9.91^b	—	3.15^b		11.49^b	—	4.30^b		12.08^b	—	5.36^b

*Superscripts a and b denote spin temperatures equal to 20 and 10 K, respectively.

TABLE 5. Calculated spectra of the ν_4 mode in rare gas matrices*

Line	Ar intensity			Kr intensity			Xe intensity		
	Spacing (cm^{-1})	I_{zx}	I_{zz}	$\langle I_u \rangle$	Spacing (cm^{-1})	I_{zx}	I_{zz}	$\langle I_u \rangle$	Spacing (cm^{-1})	I_{zx}	I_{zz}	$\langle I_u \rangle$
$Q(1)$	0.0	1.00	5.57	1.00	0.0	1.00	4.35	1.00	0.0	1.00	3.26	1.00
$R(1)$	4.14	1.51	1.02	0.61	5.69	1.13	0.86	0.55	7.19	0.77	0.69	0.46
	8.19	0.81	—	0.26	10.23	0.53	—	0.20	11.71	0.26	—	0.12
	14.94	0.05	7.51	0.94	19.12	0.01	5.91	0.85	22.41	0.01	4.52	0.78
	38.32	0.93	—	0.30	38.33	1.14	—	0.43	33.36	1.26	—	0.56
$S(0)$	18.66	—	16.66^a	2.04^a	23.85	—	15.07^a	2.17^a	27.72	—	12.97^a	2.21^a
		—	26.85^b	3.29^b		—	27.30^b	3.93^b		—	24.23^b	4.13^b
	20.60	6.15^a	—	1.96^a	27.09	6.34^a	—	2.37^a	32.14	6.47^a	—	2.87^a
		9.91^b	—	3.15^b		11.49^b	—	4.30^b		12.08^b	—	5.36^b

*Superscripts a and b denote spin temperatures equal to 20 and 10 K, respectively.

Can. J. Chem. Downloaded from www.nrcresearchpress.com by 210.87.254.40 on 09/05/12
For personal use only.

TABLE 6. Calculated spectra of the ν_3 and ν_4 modes of a free CH_4 molecule*

Line	ν_3 spacing (cm^{-1})	ν_4 spacing (cm^{-1})	Intensity I_{zx}	Intensity I_{zz}	Intensity I_u
$Q(1)$	0.0	0.0	1.00	1.33	1.00
$R(1)$	20.17	11.35	0.18	0.24	0.18
	21.43	25.85	1.48	1.98	1.48
$S(0)$	31.94	36.35	5.91[a]	7.89[a]	5.91[a]
			12.59[b]	16.79[b]	12.59[b]

*Superscripts *a* and *b* denote spin temperatures equal to 20 and 10 K respectively.

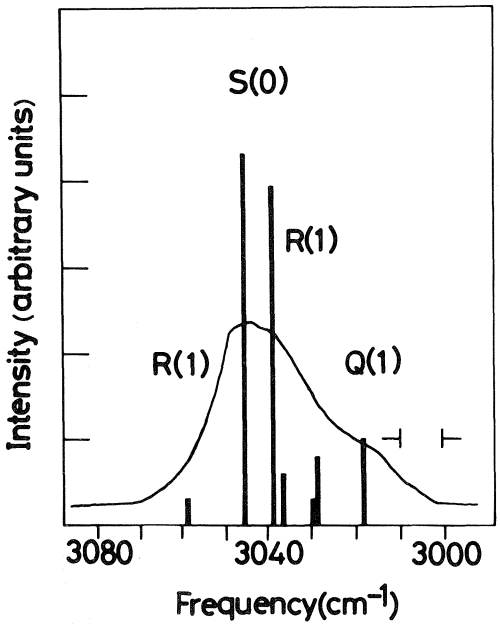

FIG. 2. Raman spectrum of the ν_3 vibrational mode of a CH_4 molecule in a Kr matrix. The intensities are averaged over all orientations of the crystal axes. The spin temperature is equal to 10 K. The curve is the experimental result by Cabana *et al.* (4).

By comparing the spectra of a free molecule with those in rare gas matrices, we observe that the rotational fine structures of the Raman spectra are substantially influenced by the crystalline field.

Figure 2 shows the intensities $\langle I_u \rangle$ of the ν_3 spectrum in a Kr matrix at the spin temperature 10 K, together with the experimental result by Cabana *et al.* (4). We set the position of $Q(1)$ equal to 3018 cm^{-1}, referring to the observed infrared spectrum (3). The calculated result is compatible with the observed spectrum. The main peak and the shoulder of the experimental spectrum correspond to the two $S(0)$'s and $Q(1)$, respectively. It is found that such lines as $P(1)$ and $R(0)$ are forbidden by the selection rule, contrary to the speculation given by Cabana *et al.* (4). Experiments with higher resolution are expected to reveal the rotational fine structures of the ν_3 and ν_4 Raman bands, their temperature dependences and the behaviour for polarized light.

Acknowledgments

The authors would like to thank Dr. K. Nishiyama of Kyushu University for valuable discussions and for allowing them to use some outputs of his computation. They also thank Dr. K. Okada and Dr. H. Yasuda for kind discussions. They also acknowledge Kyoto University Data Processing Center for services.

1. A. CABANA, G. B. SAVITSKY, and D. F. HORNIG. J. Chem. Phys. **39**, 2942 (1963).
2. F. H. FRAYER and G. E. EWING. J. Chem. Phys. **46**, 1994 (1967); **48**, 781 (1968).
3. A. CHAMBERLAND, R. BERZILE, and A. CABANA. Can. J. Chem. **48**, 1129 (1970).
4. A. CABANA, A. ANDERSON, and R. SAVOIE. J. Chem. Phys. **42**, 1122 (1965).
5. K. NISHIYAMA and T. YAMAMOTO. J. Chem. Phys. **58**, 1001 (1973).
6. H. YASUDA. Progr. Theoret. Phys. **45**, 1361 (1971).
7. E. P. WIGNER. Group theory and its application to the quantum mechanics of atomic spectra. Academic Press, New York. 1955.
8. K. FOX and I. OZIER. J. Chem. Phys. **52**, 1416 (1970).
9. S. L. ALTMANN and A. P. CRACKNELL. Rev. Mod. Phys. **37**, 19 (1965).
10. K. FOX and I. OZIER. J. Chem. Phys. **52**, 5044 (1970).
11. G. HERZBERG. Molecular spectra and molecular structure. II. Infrared and Raman spectra of polyatomic molecules. D. Van Nostrand, New York. 1945.

12. R. RASMUSSEN and S. BRODERSEN. J. Mol. Spectrosc. **25**, 166 (1968).
13. M. E. ROSE. Elementary theory of angular momentum. John-Wiley and Sons, New York. 1957.
14. R. LOUDON. Adv. Phys. **13**, 423 (1964).
15. E. B. WILSON, J. C. DECIUS, and P. C. CROSS. Molecular vibrations; the theory of infrared and Raman vibrational spectra. McGraw-Hill, New York. 1955.
16. S. J. CYVIN, J. E. RAUCH, and J. C. DECIUS. J. Chem. Phys. **43**, 4083 (1965).

Can. J. Chem. Downloaded from www.nrcresearchpress.com by 210.87.254.40 on 09/05/12
For personal use only.

Can. J. Chem. Downloaded from www.nrcresearchpress.com by 210.87.254.42 on 09/05/12
For personal use only.

Canadian Journal of Chemistry

Published by
THE NATIONAL RESEARCH COUNCIL OF CANADA

Journal canadien de chimie

Publié par
LE CONSEIL NATIONAL DE RECHERCHES DU CANADA

Volume 54 Number 14 July 15, 1976

Volume 54 numéro 14 15 juillet 1976

Thermodynamic properties of tetraalkylammonium halides: volumes, heat capacities, and expansibilities in H_2O, D_2O and urea–water mixtures from 278 to 328 K[1]

GÉRALD PERRON, NICOLE DESROSIERS, AND JACQUES E. DESNOYERS[2]
Department of Chemistry, Université de Sherbrooke, Sherbrooke, P.Q., Canada J1K 2R1

Received February 4, 1976

GÉRALD PERRON, NICOLE DESROSIERS, and JACQUES E. DESNOYERS. Can. J. Chem. **54**, 2163 (1976).

The densities and heat capacities per unit volume of the symmetrical tetraalkylammonium bromides (R_4NBr) were measured in H_2O, D_2O, and 3 *m* aqueous urea from 0.01 to 1 mol kg^{-1} and from 5 to 55 °C with a flow digital densimeter and a flow microcalorimeter. Expansibilities were also measured at 25 °C for the same electrolytes in H_2O and urea–water mixtures with a dilatometer. Apparent molal volumes (ϕ_V), heat capacities (ϕ_C), and expansibilities (ϕ_E) were derived. The ϕ_C of R_4NCl and R_4NI were also measured in H_2O at 25 °C. The effect of urea concentration was investigated at 25 °C in the case of Bu_4NBr.

Once allowance is made for the anion, the properties of the larger R_4N^+ behave essentially as hydrophobic nonelectrolytes in water. The transfer functions from H_2O to D_2O have the same sign as the hydration functions and the transfer functions from H_2O to urea–water mixtures the opposite sign. Whatever is the origin of the interactions giving rise to the peculiar behavior of hydrophobic R_4N^+ in water, these interactions are larger in D_2O and smaller in the presence of urea.

The excess volumes, heat capacities, and expansibilities of Bu_4NBr and Pen_4NBr, once corrected for the long-range Debye–Hückel interactions, all have the same sign as the hydration functions at infinite dilution, in contrast with excess free energies and enthalpies. This suggests some kind of cooperative effect as two hydrophobic solutes interact with each other without the formation of a hydrophobic bond. No conclusions can be drawn from the difference in excess functions in the various aqueous solvents.

GÉRALD PERRON, NICOLE DESROSIERS et JACQUES E. DESNOYERS. Can. J. Chem. **54**, 2163 (1976).

Les masses volumiques et les capacités calorifiques par unité volumique des bromures des tétraalkylammoniums symétriques (R_4NBr) ont été mesurées dans H_2O, D_2O et un mélange 3 *m* d'urée dans l'eau de 0.01 à 1 mol kg^{-1} et de 5 à 55 °C au moyen d'un densimètre digital et d'un microcalorimètre à écoulement continu. Les expansibilités ont aussi été mesurées par dilatométrie à 25 °C pour les mêmes électrolytes dans l'eau et les mélanges eau–urée. Les volumes (ϕ_V), capacités calorifiques (ϕ_C) et expansibilités (ϕ_E) molaires apparentes ont été déduites. Les ϕ_C des R_4NCl et R_4NI ont aussi été mesurées dans H_2O à 25 °C. L'influence de la concentration d'urée a été étudiée dans le cas du Bu_4NBr.

Une fois que nous avons tenu compte de la contribution des anions, les propriétés des gros R_4N^+ sont essentiellement celles des nonélectrolytes hydrophobes dans l'eau. Aussi les fonctions

[1]Presented at the International Conference on Participation énergétique de l'eau solvant dans des systèmes biologiques, Roscoff, France, June 1975.

[2]To whom correspondence should be addressed.

de transfert de H_2O à D_2O sont du même signe que les fonctions d'hydratation et les fonctions de transfert de H_2O aux mélanges eau–urée de signe contraire. Quelque soit l'origine des interactions causant le comportement particulier des ions hydrophobes dans H_2O, ces interactions sont plus fortes dans D_2O et moins prononcées en présence d'urée.

Les volumes, capacités calorifiques et expansibilités d'excès, une fois corrigées pour les interactions coulombiennes de longue portée, sont du même signe que les fonctions d'hydratation à dilution infinie, ce qui contraste avec les enthalpies et les enthalpies libres. Ceci suggère qu'il existe un effet coopératif quelconque lorsqu'il y a interaction entre deux solutés hydrophobes dans l'eau sans formation de liaison hydrophobe. Aucune conclusion ne peut être tirée des différences entre les fonctions d'excès dans les divers solvants aqueux.

Can. J. Chem. Downloaded from www.nrcresearchpress.com by 210.87.254.42 on 09/05/12
For personal use only.

Introduction

Hydrophobic interactions play an important role in the specificity of reactions and on the stability of biological systems in water. Since hydrogen bonding and electrostatic interactions are also involved in biological systems, most of the information on hydrophobic interactions comes from systematic studies of model compounds. In this respect, the symmetrical tetraalkylammonium halides (R_4NX) have been widely used, since the more ideal solutes, such as the rare gases and hydrocarbons, are practically insoluble in water. Frank and Wen (1) were among the first to draw attention to the anomalies of these electrolytes in water. Since then, an enormous quantity of data has been accumulated, and the most important data up to about 1972 have been well reviewed by Wen (2, 3) and Sarma and Ahluwalia (4). Essentially, it is found that the higher members of these homologous cations behave more or less like nonpolar nonelectrolytes in water, and as such, the properties related to solute–solvent interactions are significantly different in water than in nonaqueous solvents. The origin of this effect, known as hydrophobic hydration, is still far from being fully understood. While some thermodynamic, transport, and spectroscopic data suggest that hydrophobic solutes can promote the structure of water, the scaled-particle theory, which does not specifically assume any change in the structure of water due to the presence of the solute, can account for the sign and the magnitude of many hydration functions of such solutes (5, 6).

The interactions between two or more hydrophobic solutes are also important. Irrespective of the origin of hydrophobic hydration, contact pairing or association, usually called hydrophobic bonding, leads to a negative free energy change and is thus favorable (7). A well-known example of this is the micellization of surfactants. What is less understood is the origin of the interactions between two hydrophobic solutes when they do not form contact pairs. With some excess properties (activity data, excess enthalpies), this interaction seems to have the opposite sign as the hydrophobic hydration contribution, and this has led to the destructive cosphere overlap models (8, 9). However, there are some exceptions to this rule, notably with heat capacities (10, 11).

Thermodynamic properties have been used extensively for the characterization of hydrophobic hydration and interactions. While it is fully recognized that thermodynamics in itself cannot give direct information on the molecular nature of the interaction between the various species in solution, these data are essential to test the proposed models and theories. Of particular interest is the heat capacity. Even though this property was used as one of the first evidence for the existence of structural effects in water (12), it is not easy to interpret it unambiguously (13, 14). The high heat capacity of water is usually attributed to some form of equilibrium between hydrogen-bonded species and less-bonded ones (1, 12); as the temperature is increased the shift in equilibrium acts as a heat reservoir. The high partial molal heat capacity of hydrophobic solutes is obviously related to the structure of liquid water, but the exact way in which this is accomplished is still puzzling. Nevertheless, heat capacity is the property which gives the temperature dependence of enthalpies and free energies, and models or theories must be able to explain all thermodynamic data over a wide range of temperatures.

Compressibilities and expansibilities are parent properties, being related to the pressure and temperature dependences of volumes. They are, like heat capacities, related to the shift in equilibrium of the water species during a change in temperature or pressure. In addition, expansibilities and heat capacities are required to calculate iso-

Can. J. Chem. Downloaded from www.nrcresearchpress.com by 210.87.254.42 on 09/05/12
For personal use only.

thermal compressibilities from adiabatic ones (15). Expansibilities and compressibilities are also used to calculate heat capacities at constant volume from heat capacities at constant pressure (16).

Recently, much data has been accumulated on the partial molal heat capacities of R_4NX in water. Ahluwalia and co-workers (17–19), de Visser and Somsen (20, 21), Mastroianni and Criss (22), and Arnett and Campion (23) have measured the standard enthalpies of solution at various temperatures and derived the change in heat capacity of R_4NX from the pure solid state to infinite dilution. The standard partial molal heat capacities $\overline{C}_p^0$ can then be calculated if the specific heat capacities of the solid electrolytes are known. Burns and Verrall (24) have measured these for some R_4NX. While this integral heat method gives the general trends in heat capacities, it has some inherent limitations. The difference in heat capacities can seldom be measured to better than 2% and the heat capacities of the solids to 1% (24). Therefore, under the best conditions, $\overline{C}_p^0$ is obtained to 3%. Also this technique is usually limited to infinite dilution and gives no information on excess properties.

Direct specific heat capacity measurements have been made for R_4NBr by Ackermann and co-workers (25) and Philip and Desnoyers (26). The data of Ackermann were limited to rather high concentrations while those of Philip and Desnoyers were at 25 °C only. We therefore felt it would be useful to measure the heat capacities of R_4NCl and R_4NI over a wide range of concentration and extend the data of R_4NBr to high and low temperatures. At the same time, the densities of each of those systems were determined since they are required to calculate the apparent molal heat capacities ϕ_C from heat capacities per unit volume. A comparison of the apparent molal volumes ϕ_V with previously published data at 298 K (27) will serve as a check of the purity and concentration of the electrolytes.

Reliable apparent molal adiabatic compressibilities ϕ_{Ks} of some R_4NX are available (28). On the other hand, the apparent molal expansibilities were usually obtained indirectly from the temperature dependence of apparent molal volumes (2), and we were afraid that they were not sufficiently reliable. They were therefore directly measured at 25 °C with a dilatometer and compared with those derived from densities.

Transfer functions have been used extensively for the study of structural interactions since they eliminate the need of an inconvenient reference state (gas phase or intrinsic value). Also, if the reference solvent is well chosen, much of the electrostatic type of interactions can be largely eliminated. For this purpose, the transfer functions from H_2O to D_2O and from H_2O to urea–water mixtures have been widely used. D_2O has about the same dipole moment as H_2O (29) but is usually considered more structured; then, any charge–dipole type of interaction should be approximately the same in both solvents, but interactions related to the three-dimensional structure of water should be accentuated in D_2O (30). The urea–water systems are also interesting for similar reasons. The dielectric constant of those mixtures does not change too much from that of pure water over a certain concentration range (31); for example, at 3 *m* urea, the dielectric constant is only about 8% higher than that of water. It seems that the solute–urea interactions are such that the transfer functions from water to urea–water mixtures are usually in the direction of a decrease in the structural hydration of the solute (32, 33).

The heat capacities of transfer of R_4NBr from H_2O to D_2O (26) and from H_2O to urea–water mixtures (33) have previously been determined at 25 °C. These measurements were now extended to cover the temperature range 5 to 55 °C. The volumes of transfer were also measured in the same temperature range. The expansibilities of transfer from water to urea–water mixtures were obtained directly at 25 °C only. The actual technique of measuring expansibilities (32) did not allow us to study the transfer from H_2O to D_2O in view of the large quantity of solution required.

Experimental Section

Purification Technique and Procedure

The general purification procedure of most R_4NX and urea have been given elsewhere (34, 35); Me_4NBr, Et_4NBr, and urea were from Baker Chemicals while the other R_4NX were from Eastman Kodak. The heavy water (99.8%, Stohler Isotope Chemicals) was used as such.

All aqueous solutions were prepared by weight with deionized (Continental Deionized Water System) distilled water. Concentrations are often expressed in aquamolalities (number of moles of solute per 55.51 mol of solvent or mixed solvent) with D_2O and mixed solvents. However, the apparent molal quantities are independent of the units in which concentrations are expressed, and we

Can. J. Chem. Downloaded from www.nrcresearchpress.com by 210.87.254.42 on 09/05/12
For personal use only.

have verified that, with D_2O and urea–water mixtures, the trends in the concentration dependence of the apparent molal quantities and of the transfer functions are qualitatively the same if the concentrations are expressed in molalities or aquamolalities. For simplicity, molalities were therefore used in all cases as the concentration scale. These can readily be converted to aquamolalities if desired.

Differences in heat capacities per unit volume ($\sigma - \sigma_0$) are obtained with a flow microcalorimeter (36, 37) to 7×10^{-5} J K^{-1} cm^{-3}. Densities of similar accuracy are required to calculate the apparent molal heat capacities, ϕ_C. Differences in densities ($d - d_0$), measured with a flow digital densimeter (38), are obtained to 3×10^{-6} g cm^{-3}.

The densimeter at 25 °C was calibrated by the method described by Picker *et al.* (38). At other temperatures it was necessary to find the variation with temperature of the parameter K of the equation

$$d - d_0 = K(\tau^2 - \tau_0^2)$$

where τ is the oscillation period of the cell containing the fluid. For this purpose, the oscillation period of pure water and dry nitrogen was measured at various temperatures. The water sample was partially degassed especially for high temperature measurements (65 °C), and the flow rate in the instrument was approximately 0.5 cm^3 min^{-1}. The density of water was taken as that of Kell (39). The cells were flushed with acetone and dry nitrogen to remove all adsorbed water from the walls before measuring the oscillation period of dry nitrogen at a flow rate equal to that of water. The density of nitrogen was calculated from the ideal gas law since the difference between these densities and those recommended by the National Bureau of Standards is less than 1 ppm at various temperatures. The calibration was also checked by evacuating the cell with a mechanical pump. The agreement between the two methods of calibration was $\pm 0.00005 \times 10^{-7}$ for a value of K at 25 °C of 5.98440×10^{-7}. This value is the same as the one calculated from solutions of NaCl in water at 25 °C. At low (1 °C) and high (65 °C) temperatures the uncertainty of K is $\pm 0.0001 \times 10^{-7}$. As a final test the apparent molal volumes of NaCl were also measured at various temperatures and are in excellent agreement with those of the literature (67).

The coefficients of thermal expansion, α, were measured with a dilatometer (32) to 1×10^{-6} K^{-1}. Under the best conditions (above 0.1 m), apparent molal volumes ϕ_V can be determined to 0.02 cm^3 mol^{-1}, heat capacities ϕ_C to 0.5 J K^{-1} mol^{-1}, and expansibilities ϕ_E to 0.002 cm^3 K^{-1} mol^{-1}. In the case of heat capacities in D_2O and urea–water mixtures, the precision is further limited by the error in the determination of the absolute specific heat of the solvent or mixed solvent. This increases the minimum uncertainty on ϕ_C to 1 J K^{-1} mol^{-1}. The temperature of the flow cells can be controlled to ± 0.001 K near 25 °C, but at high and low temperature this uncertainty increases to about 0.005 K. At high temperatures, further complications occur due to the presence of dissolved gases. At 5 and 55 °C, the uncertainty of ϕ_C is of the order of 5 J K^{-1} mol^{-1}. At concentrations lower than 0.1 m, the uncertainties of ϕ_V, ϕ_C, and ϕ_E all increase since we are now limited by the precision at which $d - d_0$, $\sigma - \sigma_0$, and $\alpha - \alpha_0$ can be measured. With the present systems, 0.02 m is the lower limit at which reliable data can be obtained.[3]

The same solutions were used for all the measurements as a function of temperature. In order to verify that the solutions were not contaminated during the process, the densities at 25 °C were remeasured at the end. The differences never exceeded 8 ppm for solutions in H_2O and 15 ppm in D_2O. Since the solvent and solutions were handled in exactly the same way, any absorption of H_2O which could be responsible for the 15 ppm would essentially cancel for the measurements in D_2O.

In the calculation of ϕ_V, ϕ_C, and ϕ_E, absolute values of d_0, c_{p0} and α_0 are required at various temperatures. In water, reliable data exist for d_0 (39), c_{p0} (40), and α_0 (39). In D_2O, literature values exist for d_0 but there are significant differences between the c_{p0} of various authors at temperatures other than 25 °C (41). The volumetric specific heats and densities of D_2O relative to H_2O were therefore remeasured carefully in the temperature range 5 to 65 °C, and these results will be reported elsewhere (42). The parameters for the urea–water mixtures were determined experimentally.

In all these studies, the absolute temperatures were determined to 0.01 K with a Hewlett-Packard quartz thermometer, calibrated at the factory.

Results

Apparent molal quantities can be fitted, in general, with an equation of the type

$$[1] \qquad \phi_Y = \phi_Y^0 + A_Y(d_0 m)^{1/2} + B_Y m$$

ϕ_Y^0 being equal to the standard partial molal quantity $\bar{Y}^0$, A_Y is the Debye–Hückel limiting slope and B_Y an adjustable parameter depending on all solute–solute interactions other than those originating from the limiting long-range cou-

[3]A systematic error in the measurement of the relative change $\Delta\sigma/\sigma_0$ by the flow technique was found after this project was terminated (36*b*). This error depends on the way the instrument was calibrated and probably results from some dissymmetry in the electronic design. Fortunately it was relatively easy to correct the results by multiplying $\Delta\sigma/\sigma_0$ by the factor f. When $\sigma - \sigma_0$ is negative (usual case) $f = 1.020$ and when $\sigma - \sigma_0$ is positive $f = 0.987$. It is also possible to correct the derived ϕ_C directly from the relation $\phi_C(\text{corrected}) = f\phi_C + (1 - f)\phi_V\sigma_0$. All the ϕ_C data in this paper have been corrected accordingly. With the larger R_4NBr the differences between the corrected and uncorrected ϕ_C differ by 1 to 2 J K^{-1} mol^{-1}, which is comparable with the experimental uncertainty, but with the smaller homologs the difference becomes of the order of 6 J K^{-1} mol^{-1}. This error has little effect on the transfer functions and on the concentration dependence of ϕ_C. With the exception of Fig. 4, the figures were therefore not redrawn. Most data on ϕ_C obtained in our laboratory prior to 1976 have been corrected in a similar fashion (36*b*).

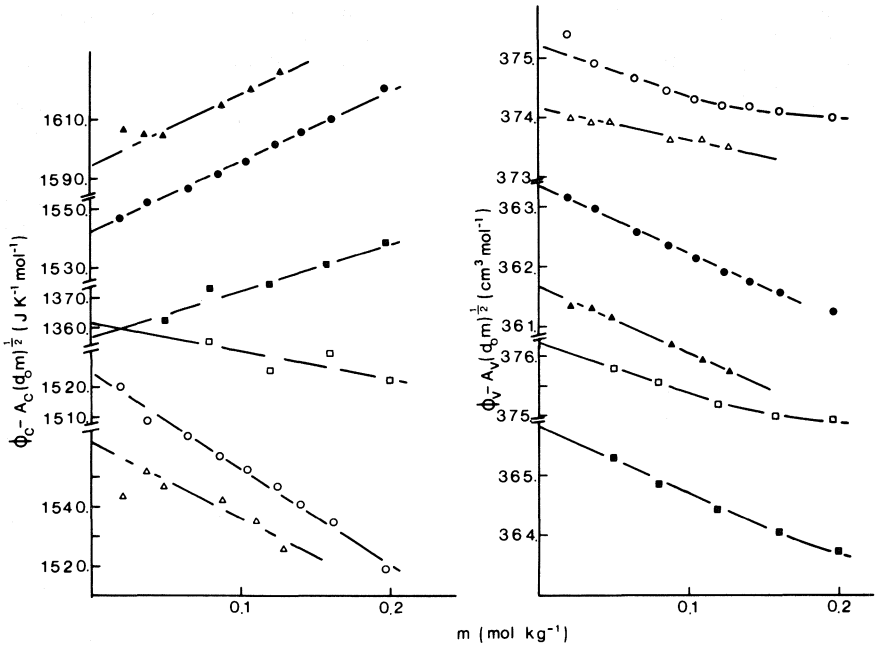

FIG. 1. Apparent molal heat capacities and volumes of tetrapentylammonium bromide. At 25 °C: ● in H_2O, ▲ in D_2O, ■ in 3 *m* urea; at 55 °C: ○ in H_2O, △ in D_2O, □ in 3 *m* urea.

TABLE 1. Debye-Hückel limiting law parameters for 1:1 electrolytes in H_2O and D_2O for ϕ_V in cm^3 mol^{-1} and ϕ_C in J K^{-1} mol^{-1}

	H_2O		D_2O	
T (°C)	$A_V d_0^{1/2}$	$A_C d_0^{1/2}$	$A_C d_0^{1/2}$	$A_V d_0^{1/2}$
5	1.529	22.522	23.020	1.608
10	1.612	24.229	25.180	1.695
15	1.696	25.835	27.113	1.784
20	1.780	27.395	28.906	1.871
25	1.865	28.945	30.616	1.960
30	1.952	30.516	32.284	2.050
35	2.040	32.129	33.944	2.141
40	2.131	33.805	35.619	2.235
45	2.223	35.561	37.332	2.329
50	2.319	37.417	39.102	2.427
55	2.418	39.390	40.947	2.528
60	2.522	41.499	42.886	2.634

lombic forces. In general, with the lower members of the homologous series R_4NX, eq. 1 can fit the data up to about 1 *m*, but for the higher ones deviations occur at much lower concentrations ($\sim$0.5 *m* for Bu_4NBr and $\sim$0.2 *m* for Pen_4NBr).

The parameters A_V and A_C have been calculated for 1:1 electrolytes in H_2O at various temperatures (10, 43). The parameters A_C for D_2O solutions at 25 °C have also been reported (26). These parameters were calculated at other temperatures for D_2O solutions and are given here, in Table 1, with the corresponding values for H_2O. For urea–water mixtures, the temperature and pressure dependences of the dielectric constant are not known, and A_V and A_C had to be assumed equal to those for H_2O (33). Finally, at 25 °C, the value of A_E for 1:1 electrolytes in H_2O is 0.017 cm^3 K^{-1} l$^{1/2}$ mol$^{-3/2}$ (32), and again this value was assumed to be the same in urea–water mixtures.

The original data and derived ϕ_V, ϕ_C, and ϕ_E of the R_4NX in H_2O, D_2O, and urea–water mixtures are given elsewhere.[4] Examples of plots of $\phi_V - A_V(d_0m)^{1/2}$ and $\phi_C - A_C(d_0m)^{1/2}$ against m are shown in Fig. 1 for Pen_4NBr in H_2O, D_2O, and urea–water mixtures at some temperatures. Despite the low solubility of this salt in water, reasonably good linear plots can be obtained with the flow techniques.

The parameters ϕ_V^0, B_V, ϕ_C^0, and B_C of the R_4NX in H_2O at 25 °C are given in Table 2.

[4]Complete set of tabular data is available, at a nominal charge, from the Depository of Unpublished Data, CISTI, National Research Council of Canada, Ottawa, Canada K1A 0S2.

Can. J. Chem. Downloaded from www.nrcresearchpress.com by 210.87.254.42 on 09/05/12
For personal use only.

TABLE 2. Apparent molal volumes and heat capacities of tetraalkylammonium halides in water at 25 °C; parameters of eq. 1

	ϕ_V^0/(cm^3 mol^{-1})			ϕ_C^0/(J K^{-1} mol^{-1})				
	Cl^-	Br^-	I^-	Cl^-	Δ	Br^-	Δ	I^-
Me_4N^+	107.27	114.35	125.74	107.7	−1.4	106.3	10.9	117.2
Et_4N^+	166.52	173.65	185.18	388.6	−7.2	381.4	10.4	391.8
Pr_4N^+	232.22	239.32	250.76	795.8	−6.8	789.0	14.5	803.5
Bu_4N^+	293.43	300.40	311.97[a]	1208.7	−0.7	1208.0	10.3	1218.3
Pen_4N^+		363.40				1542.6		

	B_V/(cm^3 mol^{-2} kg)			B_C/(J K^{-1} mol^{-1} kg)		
	Cl^-	Br^-	I^-	Cl^-	Br^-	I^-
Me_4N^+	−1.33	−0.97	0.24	−5.0	−4.1	−18.3
Et_4N^+	−4.07	−3.42	−2.22	−26.5	−12.4	−23.8
Pr_4N^+	−8.54	−7.83	−5.57	−53.4	−53.3	−89.1
Bu_4N^+	−11.33	−10.60	−7.2	−19.3	−31.9	−120
Pen_4N^+		−12.20			+241.6	

[a]Value estimated from additivity.

The densities of the R_4NX had been measured previously with a sinker method at 25 °C (27). The new data were combined with the older values and new parameters ϕ_V^0 and B_V were derived by a least-squares method. With most systems equivalent fits were obtained if weight factors were used or not in the least-squares analyses. Usually weight factors were used, but when it appeared obvious that the scattering of points from different sources were larger than the expected error, some points were rejected and the analysis made on the remaining points without a weight factor. The slight differences between the ϕ_V^0 given in Table 2 and those previously published (27) mostly result from the different concentration scale used to fit ϕ_V; molalities are used in the present case while molarities were used previously. The only new data which seem somewhat in error are those of Pr_4NCl and Bu_4NCl. The variations of $\phi_V - A_V(d_0m)^{1/2}$ were systematically lower than the previous results but with identical slopes. Further recrystallization did not improve the agreement. A chlorine analysis of these two salts gave a percentage of Cl of 99.4 and 98.5 for Pr_4NCl and Bu_4NCl. This therefore confirms that there are some impurities which recrystallize with the salts and which cause a shift in ϕ_V of 0.42 and 1.21 cm^3 mol^{-1} respectively. With all the other electrolytes the deviations between the new ϕ_V and the previous ones were in agreement within 0.3 cm^3 mol^{-1}. An error of 0.3 cm^3 mol^{-1} in ϕ_V would cause a corresponding one of about 1 J K^{-1} mol^{-1} in ϕ_C. Since the uncertainty in $\sigma - \sigma_0$ could cause an uncertainty as large as 3 J K^{-1} mol^{-1}, the uncertainty in ϕ_V is negligible in all cases except Bu_4NCl.

The values of ϕ_C of R_4NBr at 25 °C, given in Table 2, are essentially those previously published (26) in the case of Et_4NBr and Pr_4NBr. A few extra data points at higher concentrations were added to get a better value of ϕ_C^0 of Bu_4NBr. Some problem arose with Me_4NBr since the original parameter B_C seemed out of line with the other halides. The measurements were therefore repeated and, as seen from Fig. 2, the concentration dependence of $\phi_C - A_C(d_0m)^{1/2}$ is now slightly negative as expected from a comparison with the other halides. On the other hand, the additivity of ϕ_C^0 was not very good. Recently, de Visser *et al.* (44) repeated the measurements of Me_4NBr. These new data, also shown in Fig. 2, have essentially the same concentration dependence as the previous data but the extrapolated ϕ_C^0 is now additive with the other electrolytes.

The additivity rule can also be used as a check of the reproducibility of the data. At 25 °C, the average differences between ϕ_C^0 of Br^- and Cl^- and between I^- and Br^- for alkali halides (37) are −4 and 10 J K^{-1} mol^{-1}. An examination of Table 2 shows that most of the observed differences are the same as those of the alkali halides to ±3 J K^{-1} mol^{-1}. The value of ϕ_C^0 of Bu_4NCl

Can. J. Chem. Downloaded from www.nrcresearchpress.com by 210.87.254.42 on 09/05/12
For personal use only.

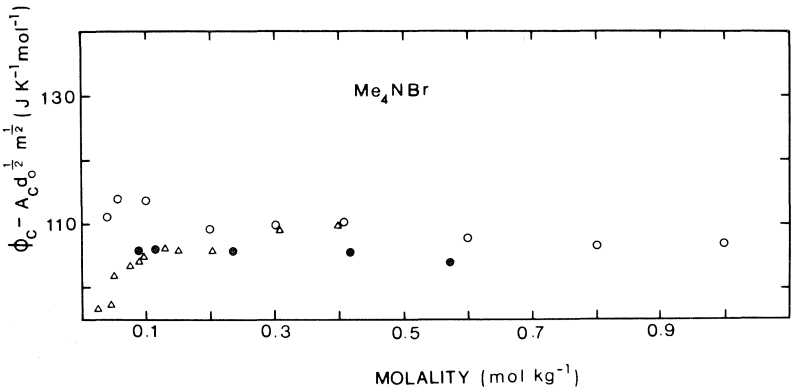

FIG. 2. Apparent molal heat capacities of Me_4NBr in water at 25 °C: △ Philip and Desnoyers (26), ○ present results, ● de Visser *et al.* (44).

is about 5 J K^{-1} mol^{-1} too low as expected from the discussion on ϕ_V. The best conventional $\overline{C}_p^0$ of ions, based on $\overline{C}_p^0(H^+) = 0$, are given elsewhere (36*b*).

The parameters ϕ_V^0, B_V, ϕ_C^0, and B_C of R_4NBr in H_2O, D_2O, and 3 *m* urea at various temperatures are given in Table 3. A comparison of the present ϕ_V results at various temperatures with the few literature values available confirm in general the accuracy of the present measurements. Wen and Saito (45) measured the densities of Bu_4NBr at 15 and 35 °C and their ϕ_V agree with ours within 0.1 cm^3 mol^{-1}. Franks and Smith (46) also studied the R_4NBr at 5 °C and agreement is observed to 0.2 cm^3 mol^{-1} for Me_4NBr, 0.6 for Et_4NBr, 0.1 for Pr_4NBr, and 0.3 for Bu_4NBr. Finally the ϕ_V we can calculate from the densities of Schiavo *et al.* (47) are generally in excellent agreement with ours.

The ϕ_V values of R_4NBr in D_2O at 25 °C used in a previous study (26) to calculate ϕ_C were the ones given by Conway and Laliberté (48). However, when we measured the analogous ϕ_V at other temperatures, it was realized that there were discrepancies between their results and ours. We therefore repeated the measurements at 25 °C and again found significant disagreement with their values, especially with the larger R_4NBr. Our differences $\phi_V^0(D_2O) - \phi_V^0(H_2O)$ remain negative for all the R_4NBr while Conway and Laliberté had observed positive ones for Et_4NBr, Pr_4NBr, and Bu_4NBr. The disagreement between $d - d_0$ of Conway and Laliberté and the present measurements is well beyond the uncertainty of either technique. Some systems were repeated in our laboratory with new samples of D_2O and the same results were obtained. What is more surprising is that at 25 °C, ϕ_V^0 of NaCl in D_2O (37, 48) and ϕ_V of Pen_4NBr in H_2O (35) obtained in both laboratories are in excellent agreement. It seems that the difference between both sets of data mostly occurs when $d - d_0$ becomes negative. Some independent measurements in another laboratory would be required to solve this dilemma. However, since the volumes of transfer from H_2O to D_2O of bolaform electrolytes (49) and of unsymmetrical tetraalkylammonium halides (50) are also negative, we feel confident that our ϕ_V data in D_2O are most probably the correct ones.

The temperature dependences of $\overline{V}^0$ and $\overline{C}_p^0$ of R_4NBr are shown in Figs. 3 and 4; NaCl (51) is also included for comparison. Literature $\overline{C}_p^0$ are also given in the case of Me_4NBr. The data of de Visser and Somsen (21) and of Mastroianni and Criss (22) are generally in good agreement with the present data but as expected from the less precise integral heat method the scatter is larger. Data also exists in the literature for $\overline{C}_p^0$ of Bu_4NBr and Pen_4NBr (19–23, 52). These values (not shown) are of the same order of magnitude as the present one but again the scatter is much larger; for example the maximum cannot be seen.

The standard transfer functions of the electrolyte E from H_2O (W) to D_2O (D) and from water to 3 *m* urea (3 *m* U) are defined by

$$[2]\quad \Delta Y_E^0(W \rightarrow D) = \overline{Y}_E^0(D_2O) - \overline{Y}_E^0(H_2O)$$

and

Can. J. Chem. Downloaded from www.nrcresearchpress.com by 210.87.254.42 on 09/05/12
For personal use only.

Can. J. Chem. Downloaded from www.nrcresearchpress.com by 210.87.254.42 on 09/05/12
For personal use only.

TABLE 3. Apparent molal volumes and heat capacities of tetraalkylammonium halides in H_2O, D_2O, and 3 *m* urea at various temperatures

		H_2O		D_2O		3 *m* U		H_2O		D_2O		3 *m* U	
T (°C)	Electrolyte	ϕ_V^{0a}	B_V^b	ϕ_V^{0a}	B_V^b	ϕ_V^{0a}	B_V^b	ϕ_C^{0c}	B_C^d	ϕ_C^{0c}	B_C^d	ϕ_C^{0c}	B_C^d
5.00	Me_4NBr	112.05	−0.42					55.7	+11.2				
	Et_4NBr	170.39	−3.16					346.6	−31.7				
	Pr_4NBr	235.98	−8.82					778.7	−85.7				
	Bu_4NBr	295.15	−12.58					1198.0	−15.0				
	Pen_4NBr	355.17	−11.40	353.13	−17.87			1507.1	326.1	1509.3	303.1		
10.00	Me_4NBr			111.88	−0.19	113.85	−1.20			31.3	25.4	110.1	14.1
	Et_4NBr					170.87[e]						346.1[e]	
	Pr_4NBr					235.20[e]						691.5[e]	
	Bu_4NBr			294.87	−13.28	297.73	−7.55			1222.7	−24.2	1035.1	76.0
	Pen_4NBr	357.67	−13.56	355.50	−16.31	360.33	−9.80	1527.1	309.3	1545.4	358.0	1320.0	304.8
15.00	Me_4NBr	113.37	−0.74					90.1	1.10				
	Me_4NCl	106.45	−1.19					89.7	+0.04				
	Et_4NBr	172.33	−3.47					369.9	−32.4				
	Pr_4NBr	237.44	−7.94					791.3	−73.7				
	Bu_4NBr	297.60	−10.49					1211.2	−20.9				
	Bu_4NCl	289.49	−11.28					1208.9	−8.5				
25.00	Me_4NBr	114.35	−0.97	113.91	−1.00	115.40	-2.5_4	106.3	−4.1	83.6	0.6	137.7	−26.2
	Et_4NBr	173.65	−3.42	173.19	−4.11	173.16[e]		381.4	−12.4	371.4	−9.9	379.1[e]	
	Pr_4NBr	239.32	−7.83	238.86	−9.32	238.28[e]		789.0	−53.3	809.4	−76.0	715.4[e]	
	Bu_4NBr	300.40	−10.60	299.50	−11.91	301.32	-6.6_4	1208.0	−31.9	1237.3	−35.6	1054.5	+11.2
	Pen_4NBr	363.40	−12.20	361.66	−11.17	365.78	-10.5_7	1542.6	241.6	1593.1	240.8	1355.4	166.2

Can. J. Chem. Downloaded from www.nrcresearchpress.com by 210.87.254.42 on 09/05/12
For personal use only.

TABLE 3 *(Concluded)*

		H_2O		D_2O		3 *m* U		H_2O		D_2O		3 *m* U	
T (°C)	Electrolyte	ϕ_V^{0a}	B_V^b	ϕ_V^{0a}	B_V^b	ϕ_V^{0a}	B_V^b	ϕ_C^{0c}	B_C^d	ϕ_C^{0c}	B_C^d	ϕ_C^{0c}	B_C^d
30.00	Me_4NBr			114.46	−1.37					92.0	0.1		
35.00	Me_4NBr	115.17	−1.20					119.4	−5.2				
	Me_4NCl	107.93	−1.45					120.5	−5.9				
	Et_4NBr	174.66	−3.60					396.6	−22.9				
	Pr_4NBr	240.77	−7.59					795.2	−51.4				
	Bu_4NBr	303.02	−8.69					1201.0	−52.9				
	Bu_4NCl	294.30	−7.84					1198.6	−41.6				
40.00	Me_4NBr			115.00	−0.78[f]	115.62	-1.5_3			104.3	−4.6[f]	163.9	−20.6
	Et_4NBr					174.42[e]						386.3[e]	
	Pr_4NBr					240.78[e]						739.1[e]	
	Bu_4NBr			303.50	−8.61[f]	305.36	-8.2_2			1234.1	−94.8[f]	1075.4	−41.8
	Pen_4NBr	368.84	−8.58[f]	367.56	−7.48[f]	371.20	-10.7_6	1540.3	2.0[f]	1585.2	42.4[f]	1365.5	26.3
45.00	Me_4NBr	115.79	−1.30					129.5	−8.4				
	Et_4NBr	175.22	−3.60					404.1	−23.6				
	Pr_4NBr	242.31	−6.80					799.2	−56.4				
	Bu_4NBr	305.91	−8.36					1191.6	−84.3				
55.00	Me_4NBr			116.18	−1.43	116.66	-2.2_3			134.2	−57.2	173.5	−28.4
	Et_4NBr					176.11[e]						438.2[e]	
	Pr_4NBr					243.49[e]						754.0[e]	
	Bu_4NBr			308.08	−8.18	309.23	-8.3_6			1214.5	−153.3	1073.3	−52.8
	Pen_4NBr	375.23	−8.72	374.11	−4.83	376.23	-8.8_7	1524.7	−328.3	1551.2	−189.1	1358.5	−90.4

[a] In $cm^3\ mol^{-1}$.
[b] In $cm^3\ mol^{-2}\ kg$.
[c] In $J\ K^{-1}\ mol^{-1}$.
[d] In $J\ K^{-1}\ mol^{-2}\ kg$.
[e] Value at 0.1 *m*.
[f] *T* = 3.40 °C.

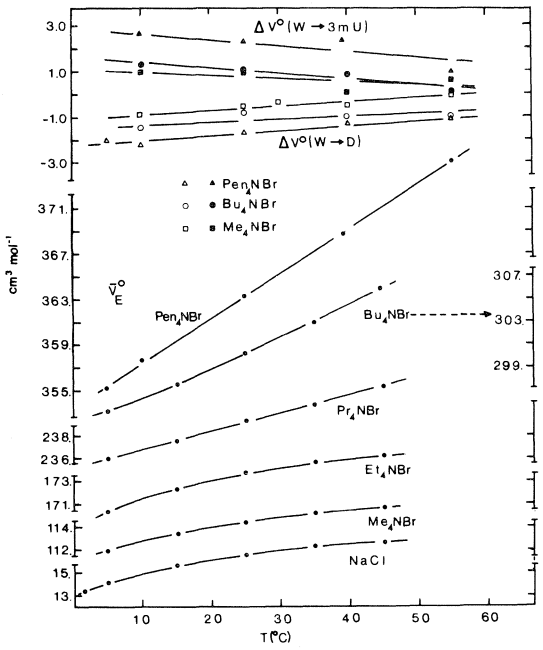

FIG. 3. Standard partial molal volumes in water and volumes of transfer from H_2O to D_2O and from H_2O to 3 *m* urea of tetraalkylammonium bromides at various temperatures.

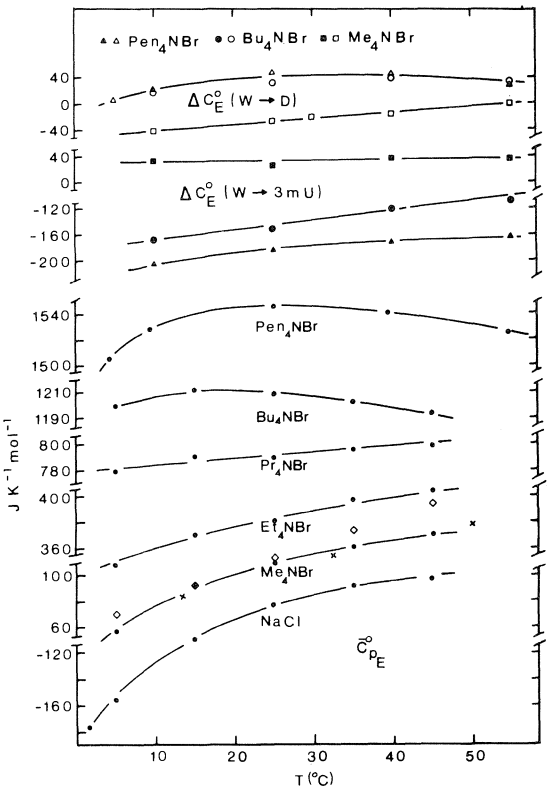

FIG. 4. Standard partial molal heat capacities in water and heat capacities of transfer from H_2O to D_2O to 3 *m* urea of tetraalkylammonium bromides at various temperatures: ● present results, ◇ de Visser and Somsen (21), × Mastroianni and Criss (22).

[3] $$\Delta Y_E^0(W \rightarrow 3\ m\ U) = \bar{Y}_E^0(3\ m\ U) - \bar{Y}_E^0(H_2O)$$

These functions are also plotted in Figs. 3 and 4 as a function of temperature.

The values of $\phi_E - A_E(d_0m)^{1/2}$ of the R_4NBr in H_2O and 3 *m* U at 25 °C are plotted against the molality in Fig. 5. The parameters ϕ_E^0 and B_E obtained from a least-squares fit are reported in Table 4.

These results are compared with the analogous ones derived from the temperature derivatives of ϕ_V^0 and of the excess parameter B_V. We have also added for completeness $\partial\phi_V^0/\partial T$ in D_2O and $\partial\phi_C^0/\partial T$ in H_2O, D_2O, and 3 *m* U, all at 25 °C. This value of ϕ_E^0 of Bu_4NBr can be compared with $\partial\phi_V^0/\partial T$ of Wen and Saito (45), 0.24 cm^3 K^{-1} mol^{-1}, which agrees with the present values within the experimental uncertainty.

Most of the studies in urea–water mixtures were limited to 3 *m* U since the transfer functions usually vary in a smooth way as a function of U concentration and 3 *m* was found a convenient concentration from the experimental point of view (32, 33). We felt, however, that it would be useful in the case of Bu_4NBr to measure the

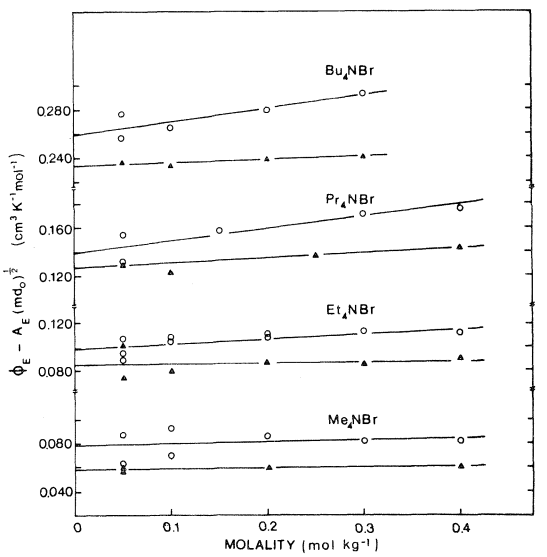

FIG. 5. Apparent molal expansibilities of tetraalkylammonium bromides at 25 °C: ○ in H_2O, ▲ in 3 *m* urea.

Can. J. Chem. Downloaded from www.nrcresearchpress.com by 210.87.254.42 on 09/05/12
For personal use only.

TABLE 4. Apparent molal expansibilities of tetraalkylammonium bromides in H_2O, D_2O, and 3 *m* urea at 25 °C; temperature dependence of apparent molal heat capacities in H_2O

Electrolyte	Solvent	ϕ_E^{0a}	B_E^b	$\partial\phi_V^0/\partial T^a$	$\partial B_V/\partial T^b$	$\partial\phi_C^0/\partial T^c$	$\partial B_C/\partial T^d$
Me_4NBr	H_2O	0.077	0.01_4	0.090	−0.02	1.44	−0.3
	D_2O			0.104	−0.02	2.39	−1.0
	3 *m* U	0.058	0.00_6	0.059	−0.01		
Et_4NBr	H_2O	0.098	0.04_2	0.117	−0.01	1.31	0.4
	D_2O						
	3 *m* U	0.085	0.00_9	0.118		1.32	
Pr_4NBr	H_2O	0.139	0.10_0	0.166	0.02	0.19	1.1
	D_2O						
	3 *m* U	0.127	0.04_0	0.186		1.57	
Bu_4NBr	H_2O	0.259	0.10_7	0.271	0.09	−0.49	−1.6
	D_2O			0.288	0.16	0.37	−2.2
	3 *m* U	0.233	0.02_3	0.254	−0.02	1.34	−3.9
Pen_4NBr	H_2O			0.372	0.17	−0.49	−1.6
	D_2O			0.402	0.29	1.31	−10.3
	3 *m* U			0.362	−0.03	1.52	−9.1

[a] In $cm^3\ K^{-1}\ mol^{-1}$.
[b] In $cm^3\ K^{-1}\ mol^{-1}\ kg$.
[c] In $J\ K^{-2}\ mol^{-1}$.
[d] In $J\ K^{-2}\ mol^{-2}\ kg$.

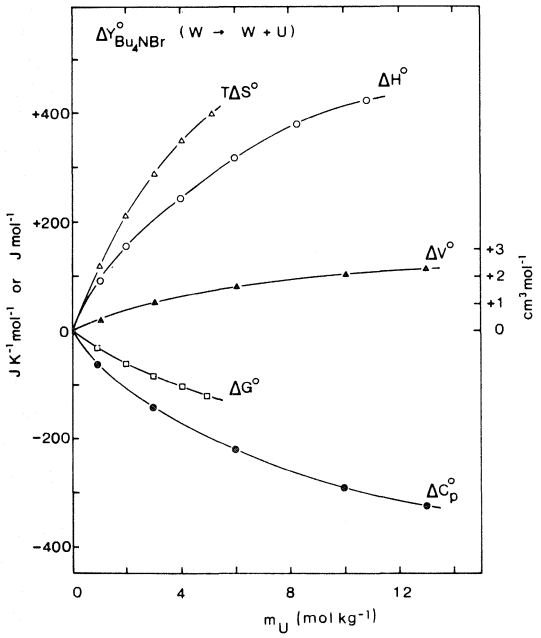

FIG. 6. Thermodynamic functions of transfer of Bu_4NBr in urea–water mixtures at 25 °C.

functions ϕ_Y up to 13 *m* U since in the case of NaCl (32), ϕ_Y seemed to be tending to the intrinsic values. As with NaCl, the electrolyte concentration was kept at 0.1 mol kg^{-1} of mixed solvent for these measurements. These data for the transfer function are shown in Fig. 6. The corresponding standard free energies of transfer of Wen and Chen (53) and standard enthalpies and entropies of transfer of Cassel and Wen (54) are also included for completeness.

Discussion

The apparent molal quantities at infinite dilution, equal to the standard partial molal quantities $\bar{Y}_E^0$ of an electrolyte E, are, by definition, independent of any solute–solute interactions. They are therefore given by

[4] $\bar{Y}_E^0 =$

$$Y_E(\text{in}) + \sum \text{solute–solvent interactions}$$

where the intrinsic property Y_E(in) can be taken as the molar property of the pure 'liquid' solute or as the partial molal property of the solute in an ideal nonpolarizable solvent. The solute–solvent interactions can be of various types: charge–dipole, polarization, cavity effects, structural changes, etc.

The intrinsic properties can sometimes be estimated reasonably well, or else they may be eliminated through transfer functions.

The apparent molal excess functions of the electrolyte E are given by the concentration dependence of the apparent molal quantities,

[5] $$Y_E^{EX} = \phi_Y - \phi_Y^0$$

This function measures all solute–solute inter-

Can. J. Chem. Downloaded from www.nrcresearchpress.com by 210.87.254.42 on 09/05/12
For personal use only.

Can. J. Chem. Downloaded from www.nrcresearchpress.com by 210.87.254.42 on 09/05/12
For personal use only.

actions and modification of the solute–solvent ones. However, since we are interested in the interactions other than those resulting from long-range coulombic forces, the parameter B_Y of [1] can be examined for this purpose; the term $B_Y m$ of [1] gives a measure of all deviations from the limiting Debye–Hückel law.

Effect of Urea

A solution of an electrolyte in an urea–water mixture should be treated as a ternary system. Consequently, following the approach of Friedman and Krishnan (55) the transfer functions from water to urea–water mixtures should be given in terms of pair and triplet interaction parameters and molalities m (number of moles of solute per kilogram of water):

$$[6]\quad \Delta Y_E^0(W \rightarrow W + U) = 2y_{EU}m_U + 3y_{EUU}m_U^2 + \ldots$$

At low m_U, where only pair interactions should be significant, it therefore follows that

$$[7]\quad \partial \Delta Y_E^0(W \rightarrow W + U)/\partial m_U \equiv \partial \Delta Y_U^0(W \rightarrow W + E)/\partial m_E$$

This identity which can be derived from the reciprocity theorem (56) can be shown to hold for urea–electrolyte–water systems (57, 58). The pair interaction parameter y_{EU} is not only a measure of the new interactions between the pair of ions and urea but also includes all modification of the electrolyte–water and urea–water interactions brought about by the presence of the third component. The observation that $\Delta Y_E^0(W \rightarrow W + U)$ seems to be opposite in sign to the hydration function of the electrolyte (32) suggests that the decrease in electrolyte–water interactions is the leading term of y_{EU}.

If this argument could be pushed further, we were hoping that at high m_U all structural interactions of the electrolyte would have been eliminated and $\Delta Y_E^0(W \rightarrow W + U)$ would tend to $Y_E(\text{in}) - \overline{Y}_E^0$. The transfer functions in Fig. 6 do in fact tend to level off at high urea concentration but, contrary to NaCl, $\Delta C^0_{Bu_4NBr}(W \rightarrow 13\ m\ U)$ does not seem to be tending to $C_p(\text{in}) - \overline{C}_p^0$ which is more of the order of -600 than -300 J K^{-1} mol^{-1}. Despite this failure, it is probably correct to expect that a large contribution to $\Delta Y_E^0(W \rightarrow 3\ m\ U)$ would be the reduction of the electrolyte–water structural interactions.

Standard Heat Capacities

The various solute–solvent interactions should be discussed in terms of the difference $\overline{C}_p^0 - C_p(\text{in})$. The evaluation of $C_p(\text{in})$ presents no serious problem with monatomic ions. It can be taken as the ideal gas contribution ($5R/2$ per ion or 42 J K^{-1} mol^{-1} per ion pair) or the molar heat capacities of crystalline alkali halides which are all around 50 J K^{-1} mol^{-1} (59). Further evidence that this order of magnitude is correct for $C_p(\text{in})$ comes from the $\overline{C}_p^0$ of alkali halides in non-aqueous solvents. If we assume that heat capacities are not too sensitive to coulombic-type interactions (charge–dipole, charge–quadrupole, etc.) then in solvent systems where there are no structural interactions $\overline{C}_p^0$ should be approximately equal to $C_p(\text{in})$. For example, $\overline{C}_p^0$ of CsBr in formamide varies from 50 J K^{-1} mol^{-1} at 25 °C to 32 J K^{-1} mol^{-1} at 55 °C (21). It therefore seems probable that $C_p(\text{in})$ of monatomic ions is somewhere between 20 and 25 J K^{-1} mol^{-1}.

The evaluation of $C_p(\text{in})$ of polyatomic ions is more complicated since internal vibrations and rotations also contribute to the heat capacity, and usually indirect methods have to be used to estimate $C_p(\text{in})$. Mogul (60) has estimated the molar heat capacities of liquid tetraalkylgermanes from vapor pressure measurements and the values obtained at 25 °C are:

Me_4Ge 108 J K^{-1} mol^{-1}; Bu_4Ge 531 J K^{-1} mol^{-1}

Et_4Ge 352 J K^{-1} mol^{-1}; Pen_4Ge 632 J K^{-1} mol^{-1}

Pr_4Ge 381 J K^{-1} mol^{-1}

An estimate of $C_p(\text{in})$ can also be obtained from $\overline{C}_p^0$ of the R_4NBr in nonassociated solvents, if we accept that $\overline{C}_p^0$ is primarily measuring structural interactions in the solution. Combining the differential heat capacities of de Visser and Somsen (21) in dimethylformamide with the heat capacity of the solid electrolytes of Burns and Verrall (24), the $\overline{C}_p^0$ of Me_4NBr and Bu_4NBr are found to be 185 and 600 J K^{-1} mol^{-1} at 25 °C. Subtracting from these values the contribution of Br^- (21 J K^{-1} mol^{-1}) approximate values for $C_p(\text{in})$ are obtained for Me_4N^+ and Bu_4N^+ which are about 50 J K^{-1} mol^{-1} higher than those estimated from the germanes, which probably reflects some solute–solvent interaction in dimethylformamide. The agreement between these two estimates being satisfactory, it therefore

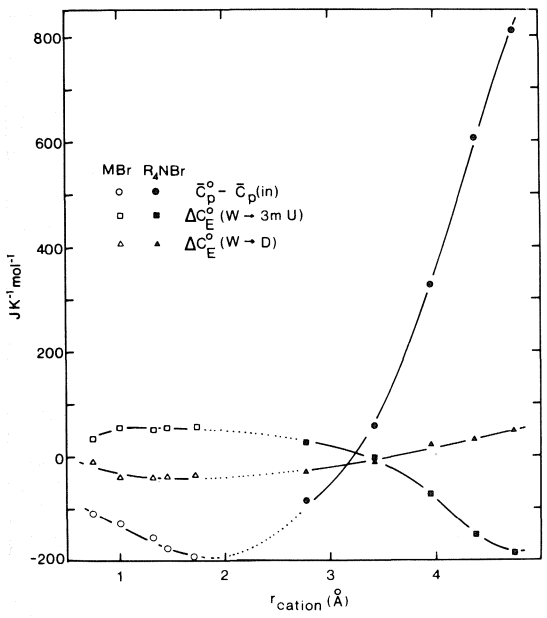

FIG. 7. Dependence of heat capacities of alkali and tetraalkylammonium bromides on cationic size at 25 °C: ○, ●, $\overline{C}_p^0 - C_p$(in) in H_2O; □, ■ heat capacities of transfer from H_2O to 3 *m* urea; △, ▲ heat capacities of transfer from H_2O to D_2O.

seems that the molar heat capacities of the germanes can be taken as approximately equal to the C_p(in) of the R_4N^+.

The dependences of $\overline{C}_p^0 - C_p$(in), ΔC_E^0(W → D) and ΔC_E^0(W → 3 *m* U) of alkali and tetraalkylammonium bromides on cation molecular weight are compared in Fig. 7. In such a plot the choice of the scale of ionic radii is not critical and we have used Waddington's scale (61) for alkali ions M^+ and that derived by Desrosiers and Desnoyers (62) for R_4N^+.

For all electrolytes smaller than Et_4NBr, $\overline{C}_p^0 - C_p$(in) are negative and for the higher members of the series R_4NBr they are significantly positive. The signs of ΔC_E^0(W → D) are the same as $\overline{C}_p^0 - C_p$(in) while those of ΔC_E^0(W → 3 *m* U) are opposite. It therefore seems that whatever is the origin of the interactions leading to $\overline{C}_p^0 - C_p$(in), these interactions are larger in D_2O and less so in urea–water mixtures. Even if we would correct for the structural contribution due to the anion, Br^-, taken for example as one-half the hydration or transfer function of NaBr, it would attenuate the magnitude of the functions for the alkali halides and Me_4NBr, but would simply accentuate them for the higher R_4N^+.

The signs of these functions are often taken as evidence for structural hydration (1, 4, 32): all electrolytes up to Et_4NBr are considered overall structure breakers and the higher homologous hydrophobic salts structure makers. The magnitude of $\overline{C}_p^0 - C_p$(in) in water compared with that in other solvents and the similarity in the size dependence of the hydration and transfer functions strongly suggest that the overall structure of water plays an important role in determining the sign and magnitude of these functions.

The temperature dependences of $\overline{C}_p^0$ and of the transfer functions are shown in Fig. 4. The trends are simple with the lower R_4NBr. As with NaCl, whatever is causing the negative contribution to $\overline{C}_p^0$ is decreasing in absolute value as the temperature is increased. Similarly, $\Delta C^0_{Me_4NBr}$(W → D) and $\Delta C^0_{Me_4NBr}$(W → 3 *m* U) are also decreasing in magnitude as the temperature is increased. Recently, Fortier *et al.* (63) and Desrosiers *et al.* (32) have applied the Frank and Wen model (1) to hydration and transfer functions of alkali halides. For example, with heat capacities, the leading term for the solvent isotope effect would be

$$[8] \quad \Delta C_E^0(W \rightarrow D) = (n_h + n_{sb})(C_p^W - C_p^D)$$

where n_h is the number of water molecules strongly held by the ion, n_{sb} is the number of water molecules in the structure-broken region, and C_p^W and C_p^D are the molar heat capacities of pure H_2O and D_2O. Since C_p^D is more positive than C_p^W, ΔC_E^0(W → D) of structure breakers is negative. Since $C_p^W - C_p^D$ decreases only slightly in magnitude as a function of temperature, the decrease in the magnitude of $\Delta C^0_{Me_4NBr}$(W → D) could be interpreted as a decrease in the overall structure-breaking effect of the pair of ions. The same kind of conclusion can be reached from an analysis of $\Delta C^0_{Me_4NBr}$(W → 3 *m* U).

However, this model should not be pushed too far since it is known that $\overline{C}_p^0$ of many inorganic and some organic salts never reach C_p(in) at high temperatures but rather reach a maximum at around 80 °C (25). The value of $\Delta C^0_{Me_4NBr}$(W → D) is equal to zero at about 55 °C; at higher temperatures it might well change signs. It would be important to measure accurately $\overline{C}_p^0$ and

Can. J. Chem. Downloaded from www.nrcresearchpress.com by 210.87.254.42 on 09/05/12
For personal use only.

Can. J. Chem. Downloaded from www.nrcresearchpress.com by 210.87.254.42 on 09/05/12
For personal use only.

transfer functions of structure breakers at high temperatures but this was not possible with the present experimental set-up.

Very recently, Owicki *et al.* (64) have applied their statistical model to liquid D_2O and they concluded that the evidence that D_2O is more structured than H_2O is not as obvious as was earlier believed. This conclusion does not affect the applicability of the Frank and Wen model. The implication of [8] is that a transfer function will be measurable for a structure-breaking solute if the properties of pure D_2O and H_2O are different, and this is independent of the origin of the difference between the two solvents.

The trends in the temperature dependence of the heat capacities, shown in Fig. 4, are more complicated with the hydrophobic R_4NBr. There is definitely a positive $\bar{C}_p^0 - C_p(\text{in})$ in water starting with Pr_4NBr and this extra heat capacity is reflected in the transfer functions (Fig. 7). However, $\bar{C}_p^0$ and the transfer functions go through maxima or minima near room temperature. Such a behavior is not observed with hydrophobic nonelectrolytes like *tert*-butanol (42) in water where $\bar{C}_p^0 - C_p(\text{in})$ is largest at low temperatures. It is therefore probable that the maximum or minimum in $\bar{C}_p^0$ and in the transfer functions is due to the effect of Br^-. As seen from Fig. 4, $\bar{C}_p^0$ of Me_4NBr and NaCl increase markedly with temperature in the temperature range investigated. As a first approximation, an estimate of $\bar{C}_p^0(Br^-)$ at various temperatures can probably be taken as $\frac{1}{2}\bar{C}_p^0$-(NaCl) since the temperature dependence of $\bar{C}_p^0$ is essentially constant for various alkali halides (32). Correcting the data of R_4NBr salts for the Br^- in such a way, approximate values for R_4N^+ are obtained and their $\bar{C}_p^0$ are plotted in Fig. 8. The temperature dependence of $\bar{C}_p^0(R_4N^+)$ is now as expected; $\bar{C}_p^0(Me_4N^+)$ still increases with temperature, $\bar{C}_p^0(Et_4N^+)$ hardly changes, and those of Pr_4N^+ and Bu_4N^+ decrease in a way similar to *tert*-butanol (42). Essentially the same trends are observed between 15 and 55 °C if the Br^- contribution is estimated by taking $\frac{1}{2}\bar{C}_p^0$-(CsBr) derived from the data of de Visser and Somsen (20). It is not possible to establish at present if the remaining slight maximum with Pen_4NBr is real or if it results from the experimental uncertainty in ϕ_C^0 at 5 °C. However, if ϕ_C^0 does not vary much with temperature, $\phi_C^0 - C_p(\text{in})$ will decrease appreciably since the heat capacity of pure R_4NBr increases significantly with temperature (49).

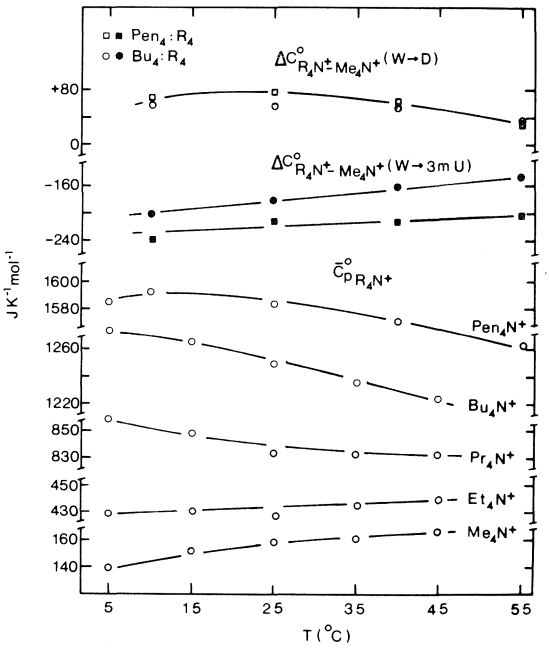

FIG. 8. Temperature dependence of the standard gram ionic heat capacities in water and of the transfer heat capacities from H_2O to D_2O and from H_2O to 3 *m* urea of tetraalkylammonium ions.

The decrease in the transfer heat capacities of the hydrophobic salts, at low temperatures, also seems to be due to Br^-. Corresponding transfer heat capacities for alkali halides were not measured as a function of temperature. However, the difference between the transfer functions of Bu_4NBr or Pen_4NBr and those of Me_4NBr seems to decrease continuously in absolute value (see Fig. 8) as in the case of $\Delta C^0_{t\text{-BuOH}}(W \rightarrow 3\ m\ U)$ (42). Evidently, by subtracting the properties of Me_4NBr we are left with a structural effect reflecting the difference between Bu_4N^+ and Me_4N^+ or Pen_4N^+ and Me_4N^+. However, the opposite effect due to the slight structure breaker, Me_4N^+, is probably relatively smaller in magnitude than the hydrophobic effect of the larger R_4N^+.

The values of $\bar{C}_p^0$ of hydrophobic R_4NBr are not tending rapidly to $C_p(\text{in})$ at high temperatures (55 °C) nor are $\Delta C_E^0(W \rightarrow D)$ and $\Delta C_E^0(W \rightarrow 3\ m\ U)$ tending to zero even when allowance is made for the anion, Br^-. It is not simple to use the Frank and Wen model for hydrophobic

Can. J. Chem. Downloaded from www.nrcresearchpress.com by 210.87.254.42 on 09/05/12
For personal use only.

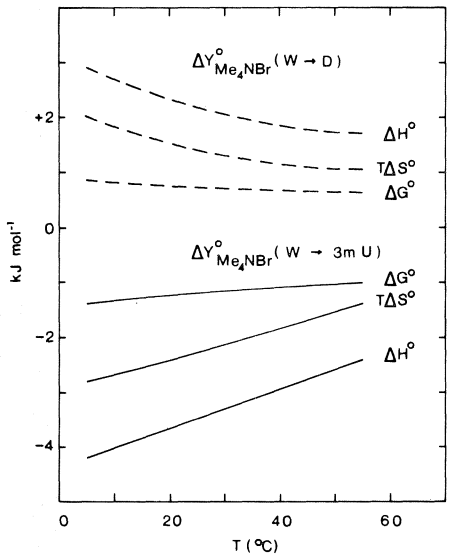

FIG. 9. Temperature dependence of the thermodynamic functions of transfer of Me_4NBr from H_2O to D_2O and from H_2O to 3 *m* urea.

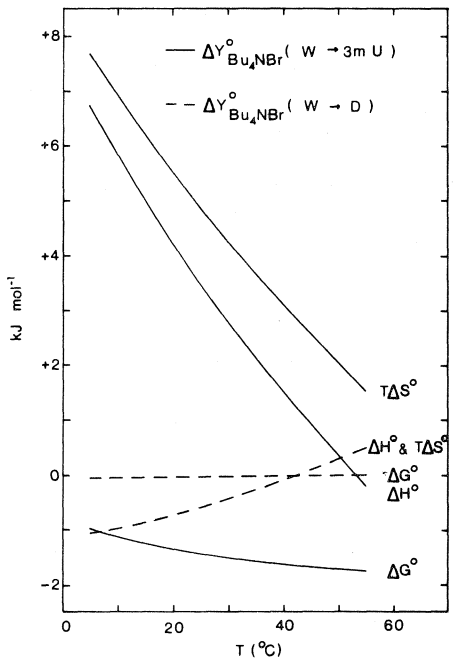

FIG. 10. Temperature dependence of the thermodynamic functions of transfer of Bu_4NBr from H_2O to D_2O and from H_2O to 3 *m* urea.

solutes. It was relatively easy to make reasonable assumptions on the properties of water in the structure-broken region (32, 63) near hydrophilic ions, but what are the properties of water in the hydrophobic co-sphere? Is it different in D_2O? Therefore, until we have a reasonable model for hydrophobic hydration, it will be difficult to interpret semi-quantitatively the transfer functions of hydrophobic solutes. Two-state water models (26, 65) can account for the sign of the transfer function $\Delta C_E^0(W \rightarrow D)$ but rapidly become ambiguous if the temperature dependence is considered.

Free Energies, Enthalpies, and Entropies of Transfer

The temperature dependence of the standard free energies, enthalpies, and entropies of transfer can readily be calculated from the literature values at 25 °C and the $\Delta C_E^0(W \rightarrow D)$ and $\Delta C_E^0(W \rightarrow 3\,m\,U)$ at various temperatures. These functions were calculated for Me_4NBr (Fig. 9) and Bu_4NBr (Fig. 10). All the transfer functions of Me_4NBr decrease in magnitude as the temperature is increased as we would expect from a decrease in the structure-breaking effect. The situation is more complicated with Bu_4NBr. While $\Delta C^0_{Bu_4NBr}(W \rightarrow D)$ and $\Delta C^0_{Bu_4NBr}(W \rightarrow 3\,m\,U)$ change only slightly in magnitude with temperature, $\Delta H^0_{Bu_4NBr}(W \rightarrow D)$ and $\Delta H^0_{Bu_4NBr}(W \rightarrow 3\,m\,U)$ vary significantly and even change signs in the region 45 to 50 °C. There are at least two possible explanations for the apparent contradiction between the enthalpies and heat capacities of transfer. For hydrophilic ions, the Frank and Wen model suggests that the heat capacity of transfer should be a linear function of the difference in the molar heat capacities of the two solvents. It is also possible that a relation similar to [8] holds for hydrophobic solutes. Since $C_p^D - C_p^W$ decreases only slowly in the temperature range 0 to 100 °C, it is not surprising that $\Delta C^0_{Bu_4NBr}(W \rightarrow D)$ is relatively constant. On the other hand, it is quite possible that $H^D - H^W$ varies significantly with temperature and even changes sign at some temperature, thus accounting for the change in sign of $\Delta H^0_{Bu_4NBr}(W \rightarrow D)$. An alternative explanation could be that Bu_4NBr is becoming a structure breaker at high temperatures (66). If this structure-breaking effect is increasing with temperature, then the sign of the heat capacities of transfer can be explained; the heat capacity being a measure of the change in the energy distribution with temperature, a positive $\overline{C}_p^0 - C_p(\text{in})$ could

Can. J. Chem. Downloaded from www.nrcresearchpress.com by 210.87.254.42 on 09/05/12
For personal use only.

mean that an ice-like co-sphere is melting or that the structure-breaking effect near a hydrophobic co-sphere is increasing with temperature. Both cases would be typical of hydrophobic solutes. However, at very high temperatures, structural effects must disappear. Therefore, eventually, all structural hydration contributions should tend to zero at high enough temperatures. Again this shows the need for accurate data at high temperatures if we wish to understand the nature of structural interaction in water.

The absolute values of $\Delta G^0_{Bu_4NBr}(W \rightarrow 3\,m\,U)$ seem to be inconsistent with those of $\Delta G^0_{Bu_4NBr}(W \rightarrow D)$. The former are significantly negative while the latter are close to zero. Free energies of transfer are difficult to interpret in terms of structural changes. Therefore, the observed effects might be real or one of the transfer functions taken at 25 °C might be in error. It would therefore be useful to remeasure these free energies of transfer before attempting to interpret these trends.

Standard Volumetric Properties

With simple electrolytes like alkali halides there are various ways of calculating V(in) which all give similar values (67). Thus, for simplicity, we will adopt the equation of Conway *et al.* (68)

$$[9] \qquad V(\text{in}) = 2.52r^3 + 3.15r^2$$

where the second term is a correction for the free volume near the ions. The radii used with alkali halides are those of Waddington (61) but other scales would give approximately the same V(in).

The evaluation of V(in) of R_4N^+ is more difficult. With such large ions, the calculation of the volume from ionic radii becomes very sensitive to the choice of the radii and of the equation. It has been shown (69) that the ionic radii of alkali halides derived from the scaled-particle theory are in good agreement with crystallographic data. There are therefore hopes that the radii of R_4N^+ derived from this approach should also be reasonably reliable. Two sets of radii of R_4N^+ in water have been obtained from this scaled-particle theory. Masterton *et al.* (70) have derived a set from a fit of salting coefficients and Desrosiers and Desnoyers (62) from isothermal compressibilities.

While the radii calculated from salting coefficients agree reasonably well with those estimated from conductance data (68), those from compressibilities agree closely with those estimated from $\overline{V}^0$ (35). The values of V(in) calculated with the compressibility set of radii using the equation of Conway *et al.* (68) are compared in Table 5 with the ionic volumes of R_4N^+ in methanol and in dimethylformamide given by Kawaizumi and Zana (71) using the method of Zana and Yeager (72).

TABLE 5. Intrinsic and partial gram ionic volumes ($cm^3\ mol^{-1}$) of R_4N^+ and Br^- at 25 °C

Ion	$\overline{V}_0(H_2O)$	$\overline{V}_0(MeOH)^a$	$\overline{V}_0(DMF)^a$	$V(in)^b$
Me_4N^+	84.2	70		78
Et_4N^+	143.7	129	126	138
Pr_4N^+	209.0	202	198	206
Bu_4N^+	270.3	268	266	269
Pen_4N^+	333.3		337	341
Br^-	30.1	18	23	32

[a]From ref. 74.
[b]From scaled-particle theory using compressibility data (62).

The values of $\overline{V}^0$ in nonaqueous solvents are more negative than V(in) for the Br^- and the lower R_4N^+, as expected from some electrostriction of these ions. On the other hand, $\overline{V}^0 \simeq V$(in) for the higher homologs, again as expected if these large ions are not very solvated in nonaqueous solvents. Therefore the values of V(in) of R_4N^+ are probably fairly close to the true ones. The hydration function $\overline{V}^0 - V$(in) of the alkali bromides and R_4NBr is shown in Fig. 11. With the exception of Pen_4NBr, these values for the R_4NBr are all less than 5 $cm^3\ mol^{-1}$ which is the magnitude of the uncertainty on V(in). Therefore the best we can say is that $\overline{V}^0 - V$(in) of R_4NBr is decreasing with cationic size and is probably negative for Pen_4NBr.

The standard volumes of transfer of R_4NBr are also compared with those of alkali bromides in Fig. 11. As with heat capacities, $\Delta V_E^0(W \rightarrow 3\,m\,U)$ qualitatively varies with the cationic size in the same way as $\Delta V_E^0(W \rightarrow D)$ and the signs are in general opposite. Allowing for the uncertainty in the determination of V(in), it seems that $\Delta V_E^0(W \rightarrow D)$ varies in a way analogous to $\overline{V}^0 - V$(in) and $\Delta V_E^0(W \rightarrow 3\,m\,U)$ in an opposite way. As in the case of heat capacities, it seems that a good part of the interactions giving rise to $\overline{V}^0 - V$(in) are accentuated in D_2O and attenuated in urea–water mixtures. The signs of $\overline{V}^0 - V$(in) and of the transfer functions are probably the same for MBr and R_4NBr. Negative

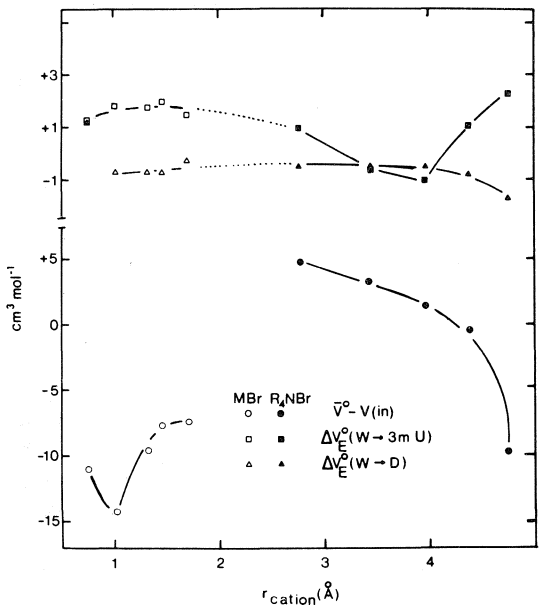

FIG. 11. Dependence of volumes of alkali and tetraalkylammonium bromides on cationic size at 25 °C: ○, ●, $\bar{V}_0 - V$(in) in H_2O; □, ■ volumes of transfer from H_2O to 3 *m* urea; △, ▲ volumes of transfer from H_2O to D_2O.

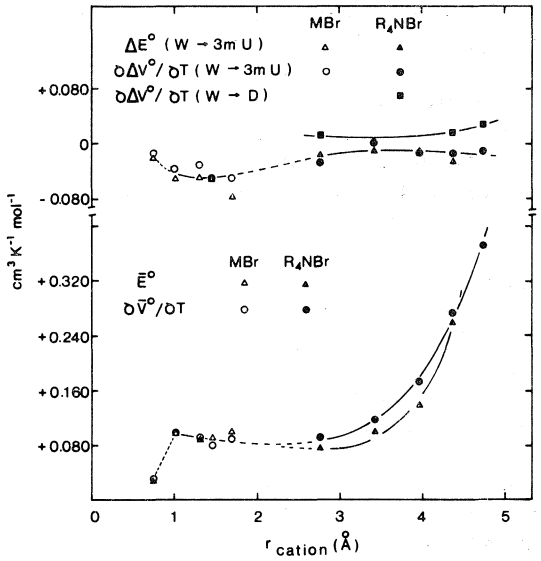

FIG. 12. Dependence of expansibilities in water and expansibilities of transfer from H_2O to D_2O and from H_2O to 3 *m* urea of alkali and tetraalkylammonium bromides on cationic size in water at 25 °C.

$\Delta V_E^0(W \rightarrow D)$ are also observed with bolaform electrolytes (49) and with asymmetrical R_4NX (50). The effect therefore seems general. The $\Delta V_E^0(W \rightarrow D)$ of alkali halides are nearly twice as negative as those of the three first members of the R_4NBr series. If we correct for the presence of Br^- assuming that large alkali metal and halide ions have about equal contributions to the transfer functions, it then appears that much of the transfer volumes of the R_4NBr are due to the anion contribution; it is therefore only with Pen_4N^+ that there seems to be some evidence for a solvent isotope effect above the experimental uncertainty on the transfer functions. Similarly, with $\Delta V_E^0(W \rightarrow 3\,m\,U)$, a correction for the presence of Br^- would make the transfer volumes slightly negative for Et_4N^+ and Pr_4N^+ and positive for the higher homologs. In addition, it was observed that $\Delta V_{t\text{-BuOH}}(W \rightarrow 3\,m\,U)$ is slightly negative (42). Therefore, contrary to previous suggestions (26, 48), it seems that the sign alone of $\Delta V_E^0(W \rightarrow D)$ and of $\Delta V_E^0(W \rightarrow 3\,m\,U)$ cannot give much information on hydrophobic hydration.

The temperature dependence of $\bar{V}^0$ and of the transfer functions are shown in Fig. 3. These functions all vary in a fairly regular way. From these slopes we can derive the standard partial molal expansibilities $\bar{E}^0$ and the corresponding expansibilities of transfer, $\Delta E_E^0(W \rightarrow D)$ and $\Delta E_E^0(W \rightarrow 3\,m\,U)$. These functions obtained indirectly are compared with the directly measured ones in Fig. 12. In the case of $\Delta E_E^0(W \rightarrow D)$ only the indirect values are available. The $\bar{E}^0$ and $\Delta E_E^0(W \rightarrow 3\,m\,U)$ obtained directly and indirectly are approximately the same. While in principle direct measurements should yield better values, in actual fact it is not possible to decide which set of data is the best.

The values of $\bar{E}^0$ reflect directly the hydration function since V(in) can usually be taken as temperature independent. The positive $\bar{E}^0$ of alkali halides tells us that the ion–solvent interactions giving rise to the negative $\bar{V}^0 - V$(in) are decreasing with temperature. The negative value of $\Delta E_{MX}^0(W \rightarrow 3\,m\,U)$ suggests that a good part of $V^0 - V$(in) is structural in origin (32). If there is a shift in equilibrium of a bulky phase of water to a more close-packed one as the temperature is increased, then the model of Frank and Wen (1) as extended by Desrosiers *et al.* (32) explains a positive contribution to $\bar{E}^0$ of the structure-breaking effect.

Can. J. Chem. Downloaded from www.nrcresearchpress.com by 210.87.254.42 on 09/05/12
For personal use only.

With hydrophobic solutes, $\bar{E}^0$ is also positive; as expected $\Delta E^0_{R_4NBr}(W \rightarrow D)$ is also positive for the higher members and $\Delta E^0_{R_4NBr}(W \rightarrow 3\ m\ U)$ negative. It therefore seems from the large positive $\bar{E}^0$ of the hydrophobic solutes and the signs of the corresponding transfer functions that the structural contribution to $\bar{V}^0 - V(\text{in})$ is also negative.

Apparent Molal Excess Functions

Any solute–solute interactions in addition to the long-range Debye–Hückel ones will be reflected in the parameter B_Y of [1]. It would of course be preferable to use a better theoretical basis to interpret the various interactions between ions, such as the Friedman approach (73). However, while the HNC equation has helped to elucidate the nature of solute–solute interactions with excess free energies and enthalpies, it is at present not too successful with higher free energy derivatives like $\bar{C}_p$ and $\bar{E}$ (74).

A model (8) has been proposed previously to interpret the excess functions of electrolytes in terms of co-sphere overlap. With hydrophobic electrolytes there are three possible structural interactions: hydrophobic–hydrophobic, hydrophobic–hydrophilic, and hydrophilic–hydrophilic. In general, the interactions involving hydrophobic ions are larger than the hydrophilic–hydrophilic ones, and these latter can be neglected. This model had been applied to free energies but it now seems that many of the anomalies observed with activity data of aqueous electrolyte solutions are not entirely structural in origin since they also occur in *N*-methylacetamide (75). With excess enthalpies and volumes it appears that the hydrophobic–hydrophobic and hydrophobic–hydrophilic interactions have the same sign: $B_H(+)$ and $B_V(-)$. It was concluded from this that the co-sphere overlap was destructive for hydrophobic electrolytes; whatever happens at infinite dilution is reduced when two solutes approach each other. Philip and Desnoyers (26) measured B_C of R_4NBr at 25 °C and found them to be negative, which seemed to be consistent with a destructive overlap model: $\bar{C}_p^0 - C_p(\text{in})$ is positive at infinite dilution and should become less positive as the concentration increases. However, Leduc and Desnoyers (76) found that B_C of tetrabutylammonium octanoate was very positive in contradiction with the destructive overlap model. Also, all very hydrophobic nonelectrolytes such as *t*-butanol (11) and piperidine (77) have positive B_C. It therefore seems that the hydrophobic–hydrophobic interaction led to a positive B_C, in contradiction to the destructive overlap approach.

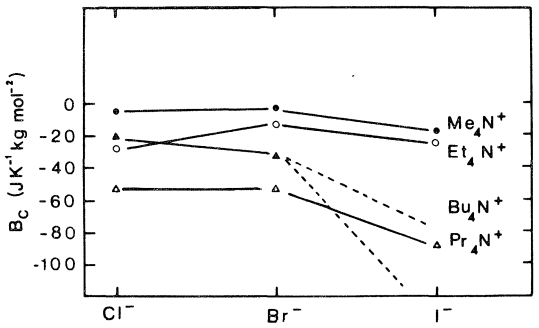

FIG. 13. B_C parameter of tetraalkylammonium halides in H_2O at 25 °C.

On the other hand, the interaction between a hydrophobic solute and a hydrophilic ion seems to result in a negative B_C. For example $\Delta C^0_{t\text{-BuOH}}(W \rightarrow W + MX)$ (78) and $\Delta C^0_{Bu_4NBr}(W \rightarrow W + MX)$ (79), where W stands for water and MX for an alkali halide, are both negative.

The parameters B_C of [1] are shown for the tetraalkylammonium chlorides, bromides, and iodides in Fig. 13. This parameter has a value close to zero for Me_4NX and becomes increasingly negative when going from Et_4NX to Pr_4NX. For Bu_4NX, B_C is less negative than for Pr_4NX and Pen_4NBr (not shown) has a large positive B_C. It therefore appears that with the lower members of these series it is the hydrophobic–hydrophilic interaction which predominates but with the higher members the hydrophobic–hydrophobic ones take over. The nature of the anion does not seem to have a marked effect on B_C as seen from Fig. 13.

The temperature dependence of B_C for R_4NBr is shown in Fig. 14. With Me_4NBr, B_C is close to zero and varies only slightly with temperature, with Et_4NBr it is negative but becomes less so as the temperature increases. With the two most hydrophobic electrolytes there is an inversion between the order of B_C at low and high temperatures. At high temperatures B_C decreases in the order Me_4NBr to Pen_4NBr suggesting a predominance of hydrophobic–hydrophilic interactions. At low temperatures B_C goes through a minimum with Pr_4NBr. The same kind of inversion of B_C with temperature was observed

Can. J. Chem. Downloaded from www.nrcresearchpress.com by 210.87.254.42 on 09/05/12
For personal use only.

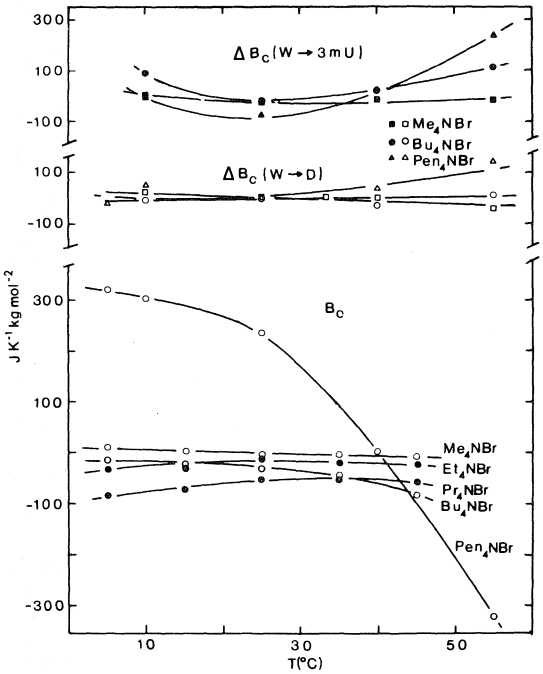

FIG. 14. Temperature dependence of the B_C parameter in H_2O and of the difference in H_2O and in 3 *m* urea and H_2O of tetraalkylammonium bromides.

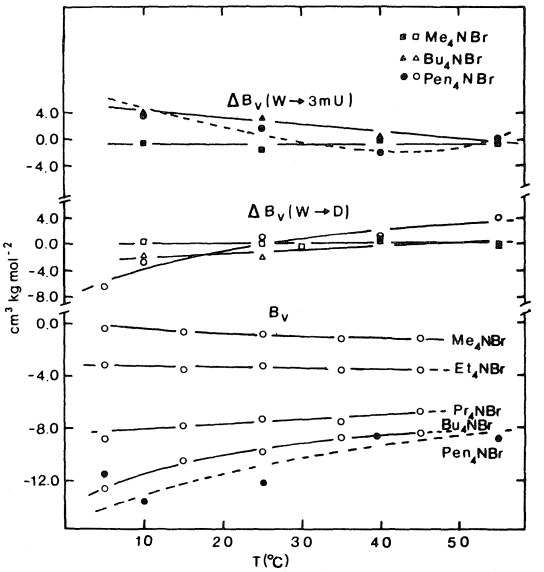

FIG. 15. Temperature dependence of the B_V parameter in H_2O and of the difference in D_2O and H_2O and in 3 *m* urea and H_2O of tetraalkylammonium bromides.

with ionic surfactants (80). It therefore appears that with hydrophobic interactions, the excess heat capacities suggest a cooperative effect. Whatever happens at infinite dilution happens even more so when two hydrophobic solutes approach each other without associating. When they do associate (contact pairs) then there is a large decrease in heat capacity.

The difference in B_C between H_2O, D_2O, and urea–water mixtures is also shown in Fig. 14. Surprisingly enough these ΔB_C are all very small and possibly with the exception of Pen_4NBr are, within the experimental uncertainty, approximately equal to zero. This had also been noted by Philip and Desnoyers (26) for Et_4NBr and Pr_4NBr. They had seen a solvent isotope effect with Bu_4NBr because the ϕ_C data in D_2O was based on erroneous ϕ_V data. With the new ϕ_V data, there is hardly any solvent isotope effect on B_C. The signs of $\Delta B_C(W \rightarrow 3\,m\,U)$ and $\Delta B_C(W \rightarrow D)$ are both the same for Pen_4NBr and the sign of $\Delta B_C(W \rightarrow D)$ is opposite that of $B_C(W)$, which seems to contradict the trends in the properties at infinite dilution. The possibility that the sign of ΔB_C could be due to an experimental error cannot be excluded since in view of the low solubility of Pen_4NBr (0.2 mol kg^{-1}) the uncertainty on B_C at low and high temperatures can be relatively high. It therefore seems that even though B_C of Pen_4NBr is very large, it hardly changes from one aqueous solvent to another.

An explanation for the consistency of B_C can be offered for the urea–water mixtures. At low R_4NBr and urea concentrations where only pair interactions occur, the R_4N^+–R_4N^+ interactions would be independent of urea. The effect of urea would show only when triplet interactions of the type E–E–U would become important. However, this explanation does not hold for the solvent isotope effect.

Apparent Molal Excess Volumetric Properties

The parameters B_V and changes $\Delta B_V(W \rightarrow D)$ and $\Delta B_V(W \rightarrow 3\,m\,U)$ are shown in Fig. 15. All B_V are negative and for the hydrophobic solutes they are more negative at low temperatures. This is consistent with the hydrophobic–hydrophobic and hydrophilic–hydrophilic interactions being both negative. These data are not inconsistent with a cooperative overlap model. The change in volume $\bar{V}^0 - V(\text{in})$ is probably slightly negative and becomes more negative as two solutes approach each other. When they associate (con-

Can. J. Chem. Downloaded from www.nrcresearchpress.com by 210.87.254.42 on 09/05/12
For personal use only.

tact pair) there is then a destructive overlap effect and a large increase in volume occurs as in micelle formation (80). Again it is not easy to see definite trends in $\Delta B_V(W \rightarrow D)$ and $\Delta B_V(W \rightarrow 3\ m\ U)$. It seems, at low temperatures, that ΔB_V are in the direction expected (B_V is more negative in D_2O and less so in 3 *m* urea), but the trends are comparable to the experimental uncertainty.

The slopes of $\phi_E - A_E(d_0 m)^{1/2}$ versus m for the R_4NBr in Fig. 5 are also consistent with a cooperative overlap effect. At infinite dilution ϕ_E^0 is positive and ϕ_E becomes more so as the concentration increases (B_E is positive) with the higher members of the series.

It therefore seems that when two hydrophobic solutes approach each other there is first of all some stabilization of the co-spheres. This could occur for example at a separation of one or two water molecules as is usually observed with solid clathrates. At shorter distances there is some collapse of the water structure: two solutes together will perturb the water structure less than two isolated solutes. Both phenomena would be favorable, *i.e.* lead to a negative excess free energy. The only exception to this rule seems to be excess enthalpies. While it seems that the hydrophobic hydration contribution to ΔH_h^0 is negative, the experimental excess enthalpies are positive whether the solutes are in contact or not. We can offer no explanation for this at the present time.

Acknowledgments

We would like to thank Dr. C. de Visser for his useful comments on this manuscript and for his collaboration in repeating the heat capacity measurements of Me_4NBr in water. We are also grateful to the National Research Council of Canada for financial assistance and for the award of a scholarship to one of us (N.D.).

1. H. S. Frank and W.-Y. Wen. Discuss. Faraday Soc. **24**, 133 (1957).
2. W.-Y. Wen. *In* Water and aqueous solutions. *Edited by* R. A. Horne. Wiley, N.Y. 1972. Chapt. 15.
3. W.-Y. Wen. J. Solution Chem. **2**, 253 (1973).
4. T. S. Sarma and J. C. Ahluwalia. Chem. Soc. Rev. **2**, 203 (1973).
5. M. Lucas and A. Feillolay. J. Phys. Chem. **75**, 2330 (1971).
6. P. R. Philip and C. Jolicoeur. J. Solution Chem. **4**, 105 (1975).
7. A. Ben-Naim. Water and aqueous solutions. Plenum, N.Y. 1974.
8. J. E. Desnoyers, M. Arel, G. Perron, and C. Jolicoeur. J. Phys. Chem. **73**, 3346 (1969).
9. P. S. Ramanathan, C. V. Krishnan, and H. L. Friedman. J. Solution Chem. **1**, 237 (1972).
10. P.-A. Leduc, J. L. Fortier, and J. E. Desnoyers. J. Phys. Chem. **78**, 1217 (1974).
11. L. Avédikian, G. Perron, and J. E. Desnoyers. J. Solution Chem. **4**, 331 (1975).
12. G. N. Lewis and M. Randall. Thermodynamics. McGraw-Hill, N.Y. 1923. Chapt. 7.
13. A. Ben-Naim. Trans. Faraday Soc. **66**, 2749 (1970).
14. M. Lucas. J. Phys. Chem. **77**, 2479 (1973).
15. J. E. Desnoyers and P. R. Philip. Can. J. Chem. **50**, 1094 (1972).
16. H. S. Harned and B. B. Owen. The physical chemistry of electrolytic solutions. Reinhold Publications, N.Y. 1958. Chapt. 8.
17. T. S. Sarma, R. K. Mohanty, and J. C. Ahluwalia. Trans. Faraday Soc. **65**, 2333 (1969).
18. T. S. Sarma and J. C. Ahluwalia. Trans. Faraday Soc. **67**, 2528 (1971).
19. R. K. Mohanty and J. C. Ahluwalia. J. Chem. Thermodyn. **4**, 53 (1972).
20. C. de Visser and G. Somsen. J. Chem. Thermodyn. **5**, 147 (1973).
21. C. de Visser and G. Somsen. J. Chem. Soc. Faraday Trans. I, **69**, 1440 (1973).
22. M. J. Mastroianni and C. M. Criss. J. Chem. Thermodyn. **4**, 321 (1972).
23. E. M. Arnett and J. J. Campion. J. Am. Chem. Soc. **92**, 7097 (1970).
24. J. A. Burns and R. E. Verrall. Thermochim. Acta, **9**, 277 (1974).
25. H. Rüterjans, F. Schreiner, U. Sage, and T. Ackermann. J. Phys. Chem. **73**, 986 (1969).
26. P. R. Philip and J. E. Desnoyers. J. Solution Chem. **1**, 353 (1972).
27. G. Perron and J. E. Desnoyers. J. Chem. Eng. Data, **17**, 136 (1972).
28. J. G. Mathieson and B. E. Conway. J. Solution Chem. **3**, 455 (1974).
29. C. G. Malmberg and A. A. Maryot. J. Res. Natl. Bur. Stand. **56**, 1 (1956). C. G. Malmberg. J. Res. Natl. Bur. Stand. **60**, 609 (1958).
30. G. Nemethy and H. A. Scheraga. J. Chem. Phys. **41**, 680 (1964).
31. J. Wyman. J. Am. Chem. Soc. **55**, 4116 (1933).
32. N. Desrosiers, G. Perron, J. G. Mathieson, B. E. Conway, and J. E. Desnoyers. J. Solution Chem. **3**, 789 (1974).
33. P. R. Philip, J. E. Desnoyers, and A. Hade. Can. J. Chem. **51**, 187 (1973).
34. D. D. Perrin, W. L. E. Armarego, and D. R. Perrin. Purification of laboratory chemicals. Pergamon Press, New York. 1961.
35. B. E. Conway, R. E. Verrall, and J. E. Desnoyers. Trans. Faraday Soc. **62**, 2738 (1966).
36. (*a*) P. Picker, P.-A. Leduc, P. R. Philip, and J. E. Desnoyers. J. Chem. Thermodyn. **3**, 631 (1971). (*b*) J. E. Desnoyers, C. de Visser, G. Perron, and P. Picker. J. Solution Chem. In press.
37. J.-L. Fortier, P.-A. Leduc, and J. E. Desnoyers. J. Solution Chem. **3**, 523 (1974).

Can. J. Chem. Downloaded from www.nrcresearchpress.com by 210.87.254.42 on 09/05/12
For personal use only.

38. P. PICKER, E. TREMBLAY, and C. JOLICOEUR. J. Solution Chem. **3**, 377 (1974).
39. G. S. KELL. J. Chem. Eng. Data, **12**, 66 (1967).
40. H. F. STIMSON. Am. J. Phys. **23**, 614 (1955).
41. P. Z. ROSTA. Specific heat and enthalpy of liquid heavy water. Atomic Energy of Canada Ltd., TOAI-43 (AECL-3689, 1971).
42. G. PERRON and J. E. DESNOYERS. In preparation.
43. L. A. DUNN. Trans. Faraday Soc. **64**, 2951 (1968).
44. C. DE VISSER, G. PERRON, and J. E. DESNOYERS. Unpublished results.
45. W.-Y. WEN and S. SAITO. J. Phys. Chem. **68**, 2639 (1964).
46. F. FRANKS and H. T. SMITH. J. Phys. Chem. **68**, 3581 (1964).
47. S. SCHIAVO, B. SCROSATI, and A. TOMMASINI. Ric. Sci. **37**, 211 (1967); **37**, 219 (1967).
48. B. E. CONWAY and L. H. LALIBERTÉ. Trans. Faraday Soc. **66**, 3032 (1970).
49. J. A. BURNS and R. E. VERRALL. J. Solution Chem. **3**, 289 (1974).
50. J. G. MATHIESON and B. E. CONWAY. J. Chem. Soc. Faraday Trans. I, **70**, 752 (1974).
51. G. PERRON, J.-L. FORTIER, and J. J. DESNOYERS. J. Chem. Thermodyn. **7**, 4922 (1975).
52. J. M. STURTEVANT. J. Phys. Chem. **79**, 2737 (1975).
53. W.-Y. WEN and C. L. CHEN. J. Phys. Chem. **73**, 2895 (1969).
54. R. B. CASSEL and W.-Y. WEN. J. Phys. Chem. 1369 (1972).
55. H. L. FRIEDMAN and C. V. KRISHNAN. J. Solution Chem. **2**, 119 (1973).
56. J. H. STERN, J. LAZARTIC, and D. FROST. J. Phys. Chem. **72**, 3053 (1968).
57. M. Y. SCHRIER, P. J. TURNER, and E. E. SCHRIER. J. Phys. Chem. **79**, 1391 (1975).
58. J. E. DESNOYERS, O. KIYOHARA, G. PERRON, and L. AVÉDIKIAN. Adv. Chem. Ser. In press.
59. F. D. ROSSINI. Selected values of chemical thermodynamic properties. Natl. Bur. Stand. (U.S.) Circ. 500. 1972.
60. P. H. MOGUL. Unpublished results, private communication.
61. T. C. WADDINGTON. Trans. Faraday Soc. **62**, 1482 (1966).
62. N. DESROSIERS and J. E. DESNOYERS. Can. J. Chem. In preparation.
63. J.-L. FORTIER, P. R. PHILIP, and J. E. DESNOYERS. J. Solution Chem. **3**, 523 (1974).
64. J. C. OWICKI, B. R. LENTZ, A. T. HAGLER, and H. A. SCHERAGA. J. Phys. Chem. **79**, 2352 (1975).
65. P. R. PHILIP and C. JOLICOEUR. J. Solution Chem. **4**, 3 (1975).
66. M. M. MARCIAQ-ROUSSELOT, A. DE TROBRIAND, and M. LUCAS. J. Phys. Chem. **76**, 1455 (1972).
67. F. J. MILLERO. Water and aqueous solutions. *Edited by* R. A. Horne. Wiley, N.Y. 1972. Chapt. 13.
68. B. E. CONWAY, R. E. VERRALL, and J. E. DESNOYERS. Z. Phys. Chem. Leipzig, **230**, 157 (1965).
69. N. DESROSIERS and M. LUCAS. J. Phys. Chem. **78**, 2367 (1974).
70. W. L. MASTERTON, D. BOLOCFSKY, and T. P. LEE. J. Phys. Chem. **75**, 2809 (1971).
71. F. KAWAIZUMI and R. ZANA. J. Phys. Chem. **78**, 627 (1974); **78**, 1099 (1974).
72. R. ZANA and E. YEAGER. J. Phys. Chem. **70**, 954 (1966); **71**, 521 (1967).
73. H. L. FRIEDMAN. *In* Modern aspects of electrochemistry. Vol. 6. *Edited by* J. O'M. Bockris and B. E. Conway. 1971. p. 1.
74. W. H. STRENG and W.-Y. WEN. J. Solution Chem. **3**, 865 (1974).
75. R. H. WOOD, R. A. ROONEY, and J. N. BRADDOCK. J. Phys. Chem. **73**, 1673 (1969).
76. P.-A. LEDUC and J. E. DESNOYERS. Can. J. Chem. **51**, 2993 (1973).
77. O. KIYOHARA, G. PERRON, and J. E. DESNOYERS. Can. J. Chem. **53**, 2591 (1975).
78. J. E. DESNOYERS, G. PERRON, J.-P. MOREL, and L. AVÉDIKIAN. *In* Chemistry and physics of aqueous gas solutions. *Edited by* W. A. Adams. The Electrochemical Society, Princeton. 1975. p. 172.
79. N. DESROSIERS and J. E. DESNOYERS. Can. J. Chem. **53**, 3206 (1975).
80. G. M. MUSBALLY, G. PERRON, and J. E. DESNOYERS. J. Colloid Interface Sci. **54**, 80 (1976).

Can. J. Chem. Downloaded from www.nrcresearchpress.com by 210.87.254.42 on 09/05/12
For personal use only.

The synthesis, Mössbauer and vibrational spectra of some triorganotin derivatives of phosphorus oxyacids

T. CHIVERS AND J. H. G. VAN ROODE

Department of Chemistry, The University of Calgary, Calgary, Alta., Canada T2N 1N4

AND

J. N. RUDDICK AND J. R. SAMS

Department of Chemistry, Tne University of British Columbia, Vancouver, B.C., Canada V6T 1W5

Received February 5, 1976

T. CHIVERS, J. H. G. VAN ROODE, J. N. RUDDICK, and J. R. SAMS. Can. J. Chem. **54**, 2184 (1976).

Trimethyltin hypophosphite, $Me_3SnPO_2H_2$, bis(trimethyltin) phosphite dihydrate, $(Me_3Sn)_2PO_3H.2H_2O$, and bis(triphenyltin) phosphite, $(Ph_3Sn)_2PO_3H$, have been obtained from the organotin chloride and aqueous solutions of the sodium salt of the corresponding phosphorus oxy-acid. $(Me_3Sn)_2PO_3H.2H_2O$ can be dehydrated under vacuum at 25 °C, but disproportionation occurs on heating. Tris(trimethyltin) orthophosphate, $(Me_3Sn)_3PO_4$, was prepared from trimethyltin chloride and silver phosphate in methanol and gave an adduct formulated as $(Me_3Sn)_3PO_4.\frac{3}{8}$dioxane after recrystallization from 1,4-dioxane. Vibrational spectra and Mössbauer data for $Me_3SnPO_2H_2$ are consistent with a trigonal bipyramidal structure in which planar Me_3Sn groups are bridged symmetrically by PO_2H_2 groups. The Mössbauer spectra of $(Me_3Sn)_2PO_3H$, $(Ph_3Sn)_2PO_3H$, and $(Me_3Sn)_2PO_3H.2H_2O$ suggest that the two tin atoms are in similar (probably pentacoordinate) environments, implying at least one three coordinate oxygen per formula unit. For $(Me_3Sn)_3PO_4$, the vibrational spectra, Mössbauer data, and physical properties are consistent with a weakly associated structure in which all three tin atoms are in similar environments. It is suggested that association is achieved via the phosphoryl (P=O) oxygen atom, which is weakly coordinated to three tin atoms leading to a distortion of the tetrahedral arrangement around tin towards trigonal bipyramidal.

T. CHIVERS, J. H. G. VAN ROODE, J. N. RUDDICK et J. R. SAMS. Can. J. Chem. **54**, 2184 (1976).

On a obtenu l'hypophosphite de triméthylétain, $Me_3SnPO_2H_2$, le dihydrate du phosphite du bis(triméthylétain) $(Me_3Sn)_2PO_3H.2H_2O$ et le phosphite du bis(triphénylétain), $(Ph_3Sn)_2PO_3H$. en faisant réagir du chlorure d'organoétain avec des solutions aqueuses du sel de sodium de l'oxy-acide phosphoreux correspondant. On peut déshydraté le $(Me_3Sn)_2PO_3H.2H_2O$ sous vide à 25 °C mais une disproportionnation se produit par chauffage. L'orthophosphate du tris(triméthylétain), $(Me_3Sn)_3PO_4$, peut être préparé par réaction du chlorure de triméthylétain avec le phosphate d'argent dans le méthanol; par recristallisation dans le dioxanne-1,4, on obtient un adduit qui possède la formule $(Me_3Sn)_3PO_4.\frac{3}{8}$ de dioxanne. Les spectres vibrationnels et les données de Mossbauer pour le $Me_3SnPO_2H_2$ sont en accord avec une structure trigonale bipyramidale dans laquelle des groupes Me_3Sn sont liés d'une façon symétrique par des groupes PO_2H_2. Les spectres Mossbauer du $(Me_3Sn)_2PO_3H$, $(Ph_3Sn)_2PO_3H$ et $(Me_3Sn)_2PO_3H.2H_2O$ suggèrent que les deux atomes d'étain sont dans des environnements similaires (probablement pentacoordonnée) ce qui implique qu'au moins un atome d'oxygène par unité de formule est tricoordonné. Pour le $(Me_3Sn)_3PO_4$, les spectres vibrationnels, les donnés de Mossbauer et les propriétés physiques sont en accord avec une structure faiblement associée dans laquelle les trois atomes d'étain sont dans des environnements semblables. On suggère que l'association se fait par l'intermédiaire de l'atome d'oxygène du groupe phosphoryle (P=O), qui est coordonnée faiblement avec trois atome d'étain, conduisant à une distorsion de l'arrangement tétraédrique autour de l'étain en faveur d'un arrangement trigonal bipyramidal.

[Traduit par le journal]

Introduction

Although organotin(IV) derivatives of inorganic acids are widespread and a number have been structurally characterized (1), information concerning derivatives of phosphorus oxy-acids is scant. In view of the biological activity of organotin(IV) compounds (2) and their use as pesticides and fungicides (2, 3), the products of reactions between organotin(IV) derivatives and the anions of phosphorus oxy-acids appeared

Can. J. Chem. Downloaded from www.nrcresearchpress.com by 210.87.254.5 on 09/05/12
For personal use only.

TABLE 1. Analytical data for $Me_3SnO_2PH_2$, $(Me_3Sn)_2PO_3H.2H_2O$, $(Me_3Sn)_2PO_3H$, $(Ph_3Sn)_3PO_3H$, $(Me_3Sn)_3PO_4$, and $(Me_3Sn)_3PO_4.\frac{3}{8}$dioxane

Compound	Yield (%)	Melting point (°C)	Analysis (%) C Calcd.	C Found	H Calcd.	H Found
$Me_3SnO_2PH_2$	61	92	15.75	15.45	4.85	4.84
$(Me_3Sn)_2PO_3H.2H_2O$	82	88	16.25	16.27	5.23	5.08
$(Me_3Sn)_2PO_3H$	—	90	17.68	17.69	4.69	4.67
$(Ph_3Sn)_2PO_3H$	92	210	55.43	54.61	4.01	3.81
$(Me_3Sn)_3PO_4$	73	180	18.44	18.99	4.64	4.87
$(Me_3Sn)_3PO_4.\frac{3}{8}$dioxane*	—	178	20.35	20.63	4.88	4.87

*This formula is derived from preliminary X-ray data (K. A. Kerr and J. H. G. van Roode, unpublished observations).

worthy of more detailed investigation. We have reported earlier the synthesis, infrared and Mössbauer spectra of a number of diorganotin(IV) derivatives of phosphorus oxyacids (4) and an X-ray structural investigation of $(Me_2Sn)_3(PO_4)_2.8H_2O$ (5), and we now describe the synthesis and structural studies of some corresponding triorganotin(IV) compounds.

The synthesis of anhydrous triorganotin(IV) orthophosphates $(R_3Sn)_3PO_4$ has been reported (R = Et (6), *n*-Bu (7), Ph (8)) but structural information is lacking. $(n\text{-}Bu_3Sn)_3PO_4$ has been mentioned as a stabilizer for organic halogen-containing compounds (7). Phytotoxicity and fungicidal activity have been reported for $(Me_3Sn)_2PO_3H$ (9). In this investigation the reactions of triorganotin chlorides with aqueous solutions of salts of the following phosphorus oxy-anions: $PO_2H_2^-$, PO_3H^{2-}, $H_2PO_4^-$, HPO_4^{2-}, and PO_4^{3-} have been studied. Various structural types may be expected depending on the charge on the anion and we have studied the vibrational and ^{119}Sn Mössbauer spectra of $Me_3SnPO_2H_2$, $(Me_3Sn)_2PO_3H.2H_2O$, $(Me_3Sn)_2PO_3H$, $(PH_3Sn)_2PO_3H$, and $(Me_3Sn)_3PO_4$ in an attempt to characterize structurally these compounds.

Experimental

Chemicals

The sources of chemicals are indicated: $NaH_2PO_2.H_2O$, $Na_2HPO_3.5H_2O$, and $NaH_2PO_4.H_2O$ (Fisher), $Na_2HPO_4.2H_2O$ (Baker), $Na_3PO_4.12H_2O$ (BDH), Ag_3PO_4 (Research Organic/Inorganic Chemical Corp.). Trimethyltin chloride and triphenyltin chloride were generous gifts from M and T Chemicals Inc. These were reagent grade chemicals used without further purification.

Instrumentation

The following instruments were used to obtain spectroscopic data: infrared spectra, Perkin Elmer 337; far infrared spectra, Digilab FTS 16; Mössbauer spectra, spectrometer described previously in ref. 10*a*; ^1H nmr spectra, Varian A60. Raman spectra were obtained using a He/Ne laser operating at 6328 Å, collinear excitation and viewing with a Cary 81 spectrophotometer.

Preparations

(a) In Aqueous Solution

Aqueous solutions (*ca.* 0.5 *M*) of trimethyltin chloride were added to aqueous solutions of the sodium or potassium salts of the phosphorus oxy-acid in a stoichiometric ratio appropriate for the quantitative formation of the trimethyltin(IV) derivative of the phosphorus oxyacid. $Me_3SnPO_2H_2$ and anhydrous $(Me_3Sn)_2PO_3H$ were obtained by drying the corresponding hydrates for 72 h in an Aberhalden pistol at 25 °C/0.01 mm.

In the preparation of $(Ph_3Sn)_2PO_3H$, a solution of Ph_3SnCl in benzene was slowly added to an aqueous solution of Na_2HPO_3. The mixture was stirred vigorously for several hours. The benzene layer was separated, washed with water and solvent was removed to give a glassy residue of $(Ph_3Sn)_2PO_3H$.

(b) Anhydrous $(Me_3Sn)_3PO_4$

Trimethyltin chloride (5.98 g, 0.03 mol) and silver phosphate (4.19 g, 0.01 mol) were refluxed for 3 h in reagent grade dry methanol (100 ml). The grey precipitate was filtered off, and solvent was removed from the filtrate under vacuum to give a pale yellow solid which was recrystallized from carbon tetrachloride to give tris(trimethyltin) orthophosphate as white needles. Recrystallization from 1,4-dioxane gave white triangular-shaped platelets of an adduct formulated as $(Me_3Sn)_3PO_4.\frac{3}{8}$dioxane on the basis of preliminary X-ray data.

The yields, melting points and analytical data for trimethyltin derivatives of phosphorus oxyacids are shown in Table 1.

Analytical Data

All compounds were identified by C and H microanalysis, performed by Chemalytics Inc., Arizona, U.S.A. and the Environmental Science Laboratory, of the Department of Chemical Engineering of the University of Calgary. Molecular weight determinations were carried out by Alfred Bernhardt Microanalytical Laboratory, Elbach, W. Germany.

Thermal Decomposition of $(Me_3Sn)_2PO_3H.2H_2O$

$(Me_3Sn)_2PO_3H.2H_2O$ was heated under vacuum at 140 °C for 17 h. The volatile products were identified as

Can. J. Chem. Downloaded from www.nrcresearchpress.com by 210.87.254.5 on 09/05/12
For personal use only.

Can. J. Chem. Downloaded from www.nrcresearchpress.com by 210.87.254.5 on 09/05/12
For personal use only.

water and tetramethyltin by their infrared spectra. The white solid residue had an infrared spectrum similar to that of Me_2SnPO_3H. *Anal.* Calcd. for $(Me_3Sn)_2PO_3H$: C 17.68, H 4.69. *Anal.* Calcd. for Me_2SnPO_3H: C 10.50, H 3.08. Found: C 11.58, H 3.45.

Results and Discussion

Synthesis

The compounds $Me_3SnPO_2H_2$ and $(Me_3Sn)_2PO_3H.2H_2O$ were obtained in high yields when aqueous solutions of Me_3SnCl and the sodium salt of the appropriate phosphorus oxy-acid were mixed at room temperature. In general, however, the reactions of trimethyltin chloride with aqueous solutions of sodium salts of phosphorus oxyacids were more complicated than the corresponding reactions of dimethyltin dichloride. For example, when aqueous solutions of Me_3SnCl and K_2PO_3F were mixed and heated a white precipitate, identified as Me_2SnPO_3F by its infrared and Mössbauer spectra (4), was formed. In contrast, the reaction of Me_3SnCl with K_2PO_3F in aqueous solution without heating gave a product whose elemental analysis was close to that expected for $(Me_3Sn)_2PO_3F.H_2O$. The infrared spectrum, however, showed a sharp strong band at 3650 cm^{-1} (in addition to broad bands at 3400 and 3170 cm^{-1} due to water of crystallization) indicating a non-hydrogen-bonded O—H group bonded to tin (*cf.* Me_3SnOH (10*b*)). The Mössbauer spectrum gave no indication of more than one tin site, $\Delta = 3.88$ mm s^{-1}, average line-width 1.13 mm s^{-1}, and a complex polymeric structure involving Me_3SnOH units in addition to $(Me_3Sn)_2PO_3F$ units is indicated. The attempted preparation of $Me_3SnPO_4H_2$ (from Me_3SnCl and $NaPO_4H_2$ in hot aqueous solution) gave $(Me_2Sn)_3(PO_4)_2.8H_2O$ identified by its infrared spectrum (4, 5).[1]

The disproportionation reaction was investigated in detail for $(Me_3Sn)_2PO_3H.2H_2O$. Anhydrous $(Me_3Sn)_2PO_3H$ is obtained by heating the hydrate below 80 °C in air, or at 25 °C under vacuum. When the hydrate is heated at 140 °C under vacuum, however, both water and tetramethyltin were identified in the volatile products, suggesting that disproportionation had occurred.

[1]It should be emphasized that no attempt was made to control p*H* in these syntheses. The products obtained will undoubtedly depend on the p*H*, since the nature of the tin species formed from Me_3SnCl (or Me_2SnCl_2) in aqueous solution is p*H*-dependent (11).

TABLE 2. Infrared and Raman spectra of $Me_3SnO_2PH_2$ and the infrared spectrum of $NaH_2PO_2.H_2O$ (cm^{-1})*

		$Me_3SnO_2PH_2$	
$NaH_2PO_2.H_2O$	Assignment	Infrared	Raman
2360s	$\nu_s PH_2$ (A_1)	2360s	
2295s	$\nu_{as} PH_2$ (B_1)	2300w,sh	
1230s	$\nu_{as} PO_2$ (B_2)	1173vs,b	1180w
1160s	PH_2 bend (A_1)	1152vs	
1090s	PH_2 wagging (B_2)	1084s	
1060s	$\nu_s PO_2$ (A_1)	1067s	1062mw
	PH_2 twist (A_2)		927w
820s	PH_2 rocking (B_2)	810s	
	Sn—C rocking	780s	
	ν_{as}Sn—C	550s	552m
	ν_sSn—C		519s
472s	PO_2 bend	469m	

*vs = very strong, s = strong, m = medium, mw = medium weak, w = weak.

$$(Me_3Sn)_2PO_3H.2H_2O \rightarrow Me_2SnPO_3H + Me_4Sn + 2H_2O$$

Although the infrared and Mössbauer spectra of the white residue were indistinguishable from the corresponding spectra of Me_2SnPO_3H, the Raman spectrum showed a band for $\nu_{as}SnC_3$ at 550 cm^{-1} in addition to $\nu_{as}SnC_2$ at 582 cm^{-1}. Furthermore, the C and H analyses were slightly higher than expected for Me_2SnPO_3H suggesting that the disproportionation reaction did not go to completion, and that the product contains some Me_3Sn groups, *e.g.*, $(Me_2SnPO_3H)_5(Me_3Sn)_2PO_3H$. Disproportionation of $Ph_3SnNO_3 \rightarrow Ph_4Sn + Ph_2Sn(NO_3)_2$ has previously been observed (12).

Trimethyltin(IV) Hypophosphite

Table 2 shows infrared and Raman data for $Me_3SnO_2PH_2$ and the infrared spectrum of $NaH_2PO_2.H_2O$. As for $R_2Sn(O_2PH_2)_2$ (4), the eight infrared active vibrations of the H_2PO_2 group, assuming C_{2v} symmetry, are observed in the infrared spectrum of $Me_3SnO_2PH_2$. The PH_2 twisting mode is not observed in the infrared spectrum but is present as a weak band in the Raman spectrum at 927 cm^{-1}. The preservation of C_{2v} symmetry suggests a bridging or chelating H_2PO_2 group with coordination to tin through oxygens. The frequency of $\Delta_{as}PO_2$ is lowered by about 55 cm^{-1} in $Me_3SnO_2PH_2$, compared to $H_2PO_2^-$, although there is little change in $\nu_s PO_2$ or in the PH_2 stretching frequencies. The former

TABLE 3. ^{119}Sn Mössbauer parameters of triorganotin(IV) derivatives of phosphorus oxyacids

Compound	δ*†	Δ*	Γ_1*		Γ_2*	T (K)
$Me_3SnO_2PH_2$	1.30	3.65	1.07		1.07	80
	No effect					298
$(Me_3Sn)_2PO_3H.2H_2O$	1.36	3.79	1.08		1.11	80
	Weak effect					298
$(Me_3Sn)_2PO_3H$	1.33	3.71	1.11		1.06	80
	1.31	3.66	1.13		1.10	298
$(Ph_3Sn)_2PO_3H$	1.22	3.05		0.98‡		80
$(Me_3Sn)_3PO_4$	1.29	3.23	1.22		1.26	80
	1.24	3.32				298
$(Me_3Sn)_3PO_4.\frac{3}{8}$dioxane	1.25	2.97		1.06‡		80

*In mm s^{-1}.
†Relative to $BaSnO_3$.
‡Average of Γ_1 and Γ_2.

TABLE 4. Observed and calculated values of Δ for $R_3SnO_2PX_2$ compounds (X = H, Cl, alkyl) in three different tin environments

R_2Sn	Δ_{obs}*
$Me_2Sn(O_2PH_2)_2$†	4.36
$Me_2Sn(O_2PCl_2)_2$‡	4.66
n-$Bu_2Sn[OP(O)(C_6H_{13})_2]_2$‡	4.00

		Δ_{calcd}*		
R_3Sn	Δ_{obs}*	*cis*-R_3SnO_2	*eq*-R_3SnO_2	*mer*-R_3SnO_2
$Me_3SnO_2PH_2$	3.65	2.23	3.53	3.95
$Me_3SnO_2PCl_2$‡	4.01	2.38	3.77	4.20
n-$Bu_3SnOP(O)(C_6H_{13})_2$§	3.72	2.05	3.20	3.68

*In mm s^{-1}.
†Reference 4.
‡Reference 14.
§Reference 13.

suggests some charge withdrawal from P—O into the Sn—O bond region. Further structural information is obtained from the Sn—C stretching modes for $Me_3SnO_2PH_2$. In the infrared spectrum only $\nu_{as}SnC_3$ and not ν_sSnC_3 is observed. The symmetric stretching mode is, however, observed as a strong band in the Raman spectrum. This is strong evidence for a planar Me_3Sn group and thus a chelating H_2PO_2 group is unlikely. The structural model that is most consistent with the vibrational spectra is a linear polymer involving pentacoordinate tin with planar Me_3Sn groups bridged by H_2PO_2 groups (see Fig. 1) (*cf.* trialkyltin phosphinates (13)). The far-infrared spectrum of $Me_3SnO_2PH_2$ shows only one band in the Sn—O stretching region at 250 cm^{-1} consistent with a linear O—Sn—O arrangement with symmetrical H_2PO_2 bridges. This structural assignment for $Me_3SnO_2PH_2$ is supported by the ^{119m}Sn Mössbauer data given in Tables 3 and 4. The observed values of Δ for $Me_3SnO_2PH_2$, $Me_3SnO_2PCl_2$, and n-$Bu_3SnO_2P(C_6H_{13})_2$ are compared (in Table 4) with the calculated values for three different trigonal bipyramidal configurations of tin in these compounds on the basis of the values of Δ

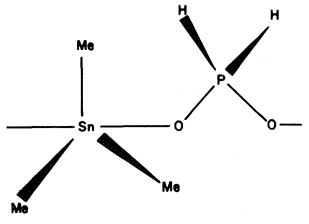

FIG. 1. Suggested structure for $Me_3SnO_2PH_2$.

Can. J. Chem. Downloaded from www.nrcresearchpress.com by 210.87.254.5 on 09/05/12
For personal use only.

TABLE 5. Infrared and Raman spectra of $(Me_3Sn)_2PO_3H.2H_2O$, $(Me_3Sn)_2PO_3H$, and $(Ph_3Sn)_2PO_3H$, and the infrared spectrum of K_2PO_3H(aq) (cm^{-1})

		$(Me_3Sn)_2PO_3H.2H_2O$		$(Me_3Sn)_2PO_3H$		$(Ph_3Sn)_2PO_3H$†	
K_2PO_3H*	Assignment	Infrared	Raman	Infrared	Raman	Infrared	Raman
	νO—H (water)	3500–3200 3100					
						2600w,b	
				2390w,sh			
2315m,sh	νP—H (A_1)	2365m		2360m		2390w	
	δP—O—H	1645m					
		1130vs	1131mw	1130s,b	1130w	1115s	
1085vs,b	$\nu_{as}PO_3$ (E)	1052vs		1062s,b		1065s	
1027vs,v	PHdef (E)	1038s,sh	1046mw	1022m,sh	1037mw	1032mm	1027m
979m,sh	$\nu_s PO_3$ (A_1)	980m,sh	987mw	984ms	987mw	990mm	990m
	Sn—C rocking	785s		770s,b			
567m	$\delta_s PO_3$ (A_1)	584m		590m		565w,b	
	ν_{as}Sn—C			574m	564m,sh		
	ν_{as}Sn—C	557m	558m	550m	554m	276s	
	ν_sSn—C	520vw,b	525s		526s	216w	216s
				510w			
465m,b	$\delta_{as}PO_3$ (E)	480w,b		480w,sh 440w		442m	

*Reference 15.
†Internal modes of the phenyl groups have been omitted.

for the corresponding dialkyltin(IV) derivatives using the empirical relationship derived by Bancroft and co-workers (14). Evidently the assignment of a planar Me_3Sn group is correct for $Me_3SnO_2PH_2$ while the intermediate value of Δ for $Me_3SnO_2PCl_2$ suggests that this compound is distorted from the ideal geometry, *i.e.*, trigonal bipyramidal with *equatorial*-Me_3Sn. For *n*-$Bu_3SnO_2P(C_6H_{13})_2$ the *mer*- configuration seems likely on the basis of the calculated and observed Δ values.

Bis(trimethyltin(IV)) Phosphite and Bis(triphenyltin) Phosphite

Infrared and Raman data for $(Me_3Sn)_2PO_3H.2H_2O$, $(Me_3Sn)_2PO_3H$, $(Ph_3Sn)_2PO_3H$, and K_2PO_3H are shown in Table 5. The C_{3v} symmetry of the PO_3H^{2-} group is lowered to C_s or C_1 in the triorganotin derivatives since three distinct bands due to PO_3 stretching modes are observed. In the Sn—C stretching region, $\nu_s SnC_3$ is observed as a very weak band in the infrared spectrum and as a strong band at 525 cm^{-1} in the Raman spectrum for both $(Me_3Sn)_2PO_3H$ and its dihydrate, suggesting that the deviation from planarity of the Me_3Sn groups is slight. In the infrared and Raman spectrum of $(Me_3Sn)_2PO_3H$ the band due to $\nu_{as}SnC_3$ at *ca.* 550 cm^{-1} is accompanied by a shoulder at *ca.* 560 cm^{-1} which is not observed in the infrared or Raman spectra of the dihydrate. The appearance of three Sn—C stretching frequencies could indicate a T-shaped arrangement of the Me_3Sn groups (local C_{2v} symmetry), in which case the double degeneracy of the asymmetric stretching mode is removed. It should be noted, however, that in the anion $Me_3SnCl_3^{3-}$, for which a T-shaped Me_3Sn unit is proposed on the basis of Mössbauer data, only one $\nu_{as}SnC_3$ frequency was observed in the infrared and Raman spectra, possibly due to accidental degeneracy (16). Alternatively, the two $\nu_{as}SnC_3$ bands in $(Me_3Sn)_2PO_3H$ could be due to two Me_3Sn groups in slightly different environments due to asymmetric bridging by PO_3H moieties. A double $\nu_{as}SnC_3$ mode is also observed for the adduct $Me_3SnOH.Me_3SnNCS$, but not for $Me_3SnOH.Me_3SnNCO$ (17).

The Mössbauer spectrum of $(Me_3Sn)_2PO_3H$ (Table 3), however, shows normal line widths and gives no indication of significantly different tin environments. Furthermore, removal of water of crystallization from $(Me_3Sn)_2PO_3H.2H_2O$ has little effect on the Mössbauer parameters, which tends to suggest that the water molecules are co-

Can. J. Chem. Downloaded from www.nrcresearchpress.com by 210.87.254.5 on 09/05/12
For personal use only.

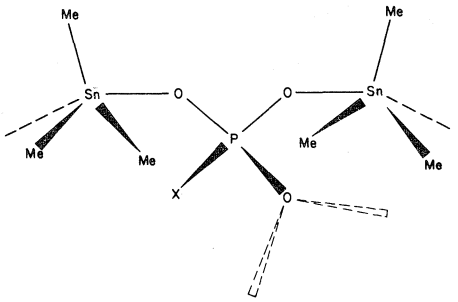

FIG. 2. Suggested structure for $(Me_3Sn)_2PO_3H$.

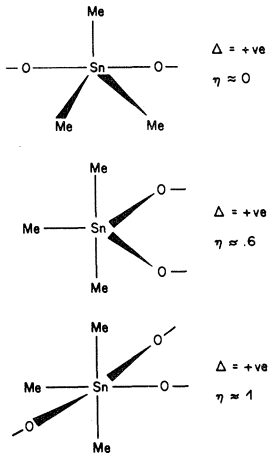

FIG. 3. Possible geometries around tin in $(Me_3Sn)_2PO_3H$.

ordinated to PO_3H groups via hydrogen bonding *cf.* $(Me_2Sn)_3(PO_4)_2.8H_2O$ (5) and are not involved in the immediate coordination sphere of the tin atoms. It should be noted, however, that in $Me_3SnNO_3.H_2O$ the water molecule is bonded to tin (18) and that the Mössbauer parameters of adducts $Me_3SnNO_3.L$ are remarkably similar to those of Me_3SnNO_3 in which five coordinate tin atoms are bridged by nitrate groups (19). Also adducts of $(Me_3Sn)_2XO_4$ (X = S, Se) with water, DMF, methanol, or pyridine show only slight changes in the Mössbauer spectra compared with the parent compounds (20). The magnitude of Δ for $(Me_3Sn)_2PO_3H$ and its dihydrate leave little doubt that the tin atoms are in a penta- (or hexa-) coordinate environment, although hexacoordinated triorganotin derivatives are unusual (17). The observed linewidths give no indication of more than one tin environment in contrast to the formally similar compound $(Bu_3Sn)_2PO_3CH_3$, which shows two doublets, Δ = 2.63 and 3.65 mm s^{-1}, corresponding to one tetrahedral and one trigonal bipyramidal tin atom per formula unit (13). In $(Me_3Sn)_2PO_3H$, pentacoordination for each tin implies at least four tin–oxygen contacts per formula unit (six for hexacoordination) and hence at least one three coordinate oxygen must be invoked (Fig. 2). The possible geometries around tin in $(Me_3Sn)_2PO_3H$ are shown in Fig. 3. These possible structures cannot be distinguished in the absence of a determination of the asymmetry parameter, η, from the magnetic hyperfine Mössbauer spectrum.

In triphenyltin compounds, the Sn—Ph vibrations fall within the 300–200 cm^{-1} range (21). In $(Ph_3Sn)_2PO_3H$, ν_{as}Sn—Ph is assigned to a strong band at 276 cm^{-1} in the infrared spectrum, and ν_sSn—Ph is attributed to a band at 216 cm^{-1} which is weak in the infrared and strong in the Raman spectrum. There is no indication of more than one ν_{as}Sn—Ph mode in $(Ph_3Sn)_2PO_3H$. The Mössbauer spectrum of $(Ph_3Sn)_2PO_3H$ shows a well-resolved doublet, Δ = 3.05 mm s^{-1}, indicative of similar environments for the two tin atoms. The value of Δ is significantly lower than that of the methyl derivative, but similar differences in Δ values are observed for the methyl and phenyl anions $(R_3SnX_2)^-$ (X = Cl, Br) and they probably result from the greater polarity of the tin–phenyl bond (22). Wedd and Sams measured quadrupole splittings for a number of adducts of Ph_3SnCl with oxygen-donating Lewis bases and found values in the range 2.84–3.25 mm s^{-1} (23) compared to 2.54 mm s^{-1} for Ph_3SnCl (22), which is tetrahedral (24). The adducts were therefore assigned a pentacoordinate structure and a similar structure for $(Ph_3Sn)_2PO_3H$ in which the Ph_3Sn groups are significantly nonplanar seems likely. The relatively high melting point and absence of νP═O in the infrared spectrum is also consistent with the structure indicated in Fig. 2.

Tris(trimethyltin) Orthophosphate

Infrared and Raman data for $(Me_3Sn)_3PO_4$ and $(Me_3Sn)_3PO_4.\frac{3}{8}$dioxane are shown in Table 6. For the free PO_4^{3-} ion (T_d symmetry) there are four normal modes of vibration, all of which are Raman active whereas only ν_3 and ν_4 are infrared active (25). These two bands are observed at 1017 and 567 cm^{-1}, respectively, in PO_4^{3-} (26). In the infrared spectrum of $(Me_3Sn)_3PO_4$ three strong bands are observed in the PO_4 stretching region

Can. J. Chem. Downloaded from www.nrcresearchpress.com by 210.87.254.5 on 09/05/12
For personal use only.

TABLE 6. Infrared and Raman data for $(Me_3Sn)_3PO_4$ and $(Me_3Sn)_3PO_4.\frac{3}{8}$dioxane ($cm^{-1}$)*

$(Me_3Sn)_3PO_4$		$(Me_3Sn)_3PO_4.\frac{3}{8}$dioxane		
Infrared	Raman†	Infrared	Raman†	Assignment
1115s		1113s		$\nu_{as}PO_4$
1058s		1050s		
990s		987s		ν_sPO_4
780s		778s		Sn—C rocking
730sh				
624m		634m		$\delta_{as}PO_4$
590m		613m		
552s	547m	549s	550m	ν_{as}Sn—C
522m	520s		529s	ν_sSn—C
		516m	517vs	ν_sSn—C
470mw				δ_sPO_4

*Internal modes of 1,4-dioxane have been omitted for clarity.
†Only recorded in Sn—C stretching region.

Can. J. Chem. Downloaded from www.nrcresearchpress.com by 210.87.254.5 on 09/05/12
For personal use only.

(950–1200 cm^{-1}) and a further three bands due to PO_4 bending modes appear at 624, 590, and 470 cm^{-1}, consistent with a lowering of symmetry of the PO_4 group from T_d to C_{3v}. $\nu_{as}SnC_3$ and ν_sSnC_3 are present in both the infrared and the Raman spectra of $(Me_3Sn)_3PO_4$ showing that the Me_3Sn groups are non-planar. There is no band attributable to a P═O group expected for an unassociated structure. Since there is only one phosphoryl group per three tin atoms in the formula unit of $(Me_3Sn)_3PO_4$, association might lead to two different environments for tin, *e.g.*, two tetracoordinate and one pentacoordinate tin atoms. The Mössbauer spectrum, however, shows a doublet ($\Delta = 3.23$ mm s^{-1}) with linewidths which suggest that all three tin atoms are in similar, if not identical, environments. The value of Δ for $(Me_3Sn)_3PO_4$ is somewhat lower than that for $Me_3SnO_2PH_2$ for which a pentacoordinate structure was assigned but higher than expected for tin in a tetrahedral environment. For R_3SnX compounds, quadrupole splitting values can be calculated from the values of the partial quadrupole splitting parameters of the individual ligands, $(pqs)_L = \frac{1}{2}e^2|Q|[L]$, where $|Q|$ = the absolute value of the nuclear quadrupole moment and [L] = the partial field gradient of the ligand L. Assuming ideal tetrahedral geometry, the Z-component of the electric field gradient is $V_{zz} = \{2[X] - 2[R]\}e$ and hence Δ can be calculated from the difference between [X] and [R]. For alkyl groups a value of $[R]^{tet} = -1.37$ mm s^{-1} was obtained (22, 27). The value of $[PO_4]^{tet}$ is unknown but values of related ligands suggest that it is likely to be less than the value of 0 arbitrarily assigned to Cl (22, 27). The observed value of Δ for $(Me_3Sn)_3PO_4$ is thus unlikely to be due entirely to the difference between [X] and [R]. Clark and co-workers (27*a*) have calculated the variation of Δ with a change in the tetrahedral angle RSnX. As this angle approaches 90°, *i.e.*, a planar Me_3Sn group, an increase in Δ is predicted. Thus the structure most consistent with the Mössbauer data and vibrational spectra for $(Me_3Sn)_3PO_4$ is one in which three of the four phosphate oxygens are bonded each to one tin atom with the fourth oxygen weakly coordinated to three other tin atoms giving three pentacoordinate tin atoms per formula unit in which the tetrahedral environment of tin has been distorted towards trigonal bipyramidal (Fig. 4). In the far-infrared spectrum

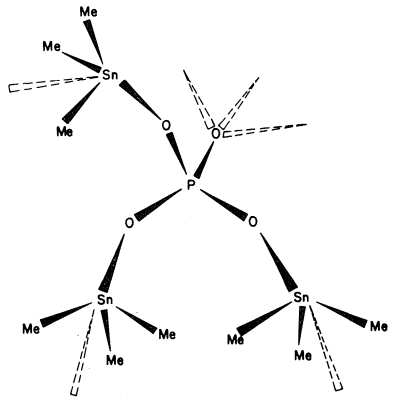

FIG. 4. Suggested structure for $(Me_3Sn)_3PO_4$.

Can. J. Chem. Downloaded from www.nrcresearchpress.com by 210.87.254.5 on 09/05/12
For personal use only.

of $(Me_3Sn)_3PO_4$ only one Sn—O stretching frequency is observed at 236 cm^{-1}. This is consistent with the proposed structure, since it has been observed that long, and therefore weak, Sn—O bonds do not give rise to an infrared band above 200 cm^{-1} in methyltin nitrate (19). Resonant γ-ray absorption at room temperature is observed for $(Me_3Sn)_3PO_4$, but this cannot by itself be taken as strong evidence for a polymeric structure (28). The solubility of $(Me_3Sn)_3PO_4$ in solvents such as carbon tetrachloride and benzene suggest that the structure is only weakly associated, and the molecular weight determined by osmometry in benzene was ~4500–4900 suggesting that the average polymeric species in solution consists of ~8 monomeric units. The ^1H nmr spectrum of $(Me_3Sn)_3PO_4$ in methylene chloride shows a single sharp peak at τ9.54 with $J_{^{117}Sn-C-H} = 61.6$ Hz and $J_{^{119}Sn-C-H} = 64.4$ Hz. In methanol solution, a single sharp peak is observed at τ9.55 with $J_{^{117}Sn-C-H} = 64.0$ Hz and $J_{^{119}Sn-C-H} = 65.6$ Hz.

The infrared spectrum of $(Me_3Sn)_3PO_4.\frac{3}{8}$dioxane shows the same bands as $(Me_3Sn)_3PO_4$ in the 950–1200 cm^{-1} region. PO_4 bending frequencies are observed at 634 and 613 cm^{-1}, but the 470 cm^{-1} band is absent in the spectrum of the dioxane adduct. $\nu_{as}SnC_3$ is observed at 549 cm^{-1} in the infrared spectrum and at 550 cm^{-1} in the Raman spectrum. ν_sSnC_3 appears at 516 cm^{-1} in the infrared spectrum. In the Raman spectrum two bands attributable to ν_sSnC_3 at 529 and 517 cm^{-1} are observed, suggesting that two Me_3Sn environments are present. However, the narrow linewidths observed for the dioxane adduct in the Mössbauer spectrum are incompatible with two distinct tin environments. The lower value of the quadrupole splitting for $(Me_3Sn)_3PO_4.\frac{3}{8}$dioxane ($\Delta = 2.97$ mm s^{-1}) compared to $(Me_3Sn)_3PO_4$ ($\Delta = 3.23$ mm s^{-1}) indicates that the tin environment is closer to tetrahedral in the dioxane adduct. It is likely that the dioxane molecules are weakly coordinated to Me_3Sn groups instead of or in addition to the postulated weak coordination by the P=O oxygen in $(Me_3Sn)_3PO_4$.

Conclusion

Vibrational spectra and Mössbauer data for $Me_3SnO_2PH_2$, $(R_3Sn)_2PO_3H$ (R = Me, Ph), and $(Me_3Sn)_3PO_4$ indicate that these compounds have polymeric structures with five coordinate tin. For $(R_3Sn)_2PO_3H$ and $(Me_3Sn)_3PO_4$ this necessarily invokes the presence of three and four coordinate oxygen, respectively. That the association in these triorganotin derivatives of phosphorus oxyacids is weaker than in the corresponding dimethyltin compounds is evidenced by their relatively low melting points and their solubility in organic solvents.

Acknowledgments

We gratefully acknowledge the National Research Council of Canada for financial support in the form of operating grants (T. Chivers and J. R. Sams), a postgraduate scholarship (J. H. G. Van Roode) and a capital equipment grant for the purchase of the far-infrared spectrometer.

1. B. Y. K. Ho and J. J. Zuckerman. J. Organomet. Chem. **49**, 1 (1973).
2. W. P. Neumann. The organic chemistry of tin. (Engl. Transl.) John Wiley, New York, 1970. pp. 230–246.
3. R. C. Poller. The chemistry of organotin compounds. Logos, London, 1970. pp. 271–282.
4. T. Chivers, J. H. G. Van Roode, J. N. R. Ruddick, and J. R. Sams. Can. J. Chem. **51**, 3702 (1973).
5. J. P. Ashmore, T. Chivers, K. A. Kerr, and J. H. G. Van Roode. J. Chem. Soc. Chem. Commun. 653 (1974).
6. H. H. Anderson. J. Org. Chem. **19**, 1766 (1954).
7. J. M. Church. Chem. Abstr. **48**, 1420e (1954). Metal and Thermit Corp. U.S. 2,630,436, March 3 (1953).
8. T. N. Srivastava and S. K. Tandon. Indian J. Appl. Chem. **26**, 171 (1963).
9. Ethyl Co. and Esso R. and E. Co., Brit. 806, 535, Dec. 31 (1958); Chem. Abstr. **53**, 13496 (1959).
10. (*a*) P. A. Yeats, B. L. Poh, B. F. E. Ford, J. R. Sams, and F. Aubke. J. Chem. Soc. A, 2188 (1970). (*b*) R. Okawara and K. Yasuda. J. Organomet. Chem. **1**, 356 (1963).
11. R. S. Tobias. Organomet. Chem. Rev. **1**, 93 (1966).
12. T. T. Tsai, A. Cutler, and W. L. Lehn. J. Org. Chem. **30**, 3049 (1965).
13. R. E. Ridenour and E. E. Flagg. J. Organomet. Chem. **16**, 393 (1969).
14. G. M. Bancroft, V. G. Kumar Das, T. K. Sham, and M. G. Clark. J. Chem. Soc. Chem. Commun 236 (1974).
15. M. Tsuboi. J. Am. Chem. Soc. **79**, 1351 (1957).
16. R. Barbieri and G. C. Stocco. Gazz. Chim. Ital. **104**, 149 (1974).
17. N. Bertazzi, G. Alonzo, F. Di Bianca, and G. C. Stocco. Inorg. Chim. Acta, **12**, 123 (1975).
18. R. E. Drew and F. W. B. Einstein. Acta Crystallogr. Sect. B, **28**, 345 (1972).
19. D. Potts, H. D. Sharma, A. J. Carty, and A. Walker. Inorg. Chem. **13**, 1205 (1974).

20. B. F. E. FORD, J. R. SAMS, R. G. GOEL, and D. R. RIDLEY. J. Inorg. Nucl. Chem. **33**, 23 (1971).
21. R. C. POLLER. Spectrochim. Acta, **22**, 935 (1966).
22. G. M. BANCROFT and R. H. PLATT. *In* Advances in inorganic chemistry and radiochemistry. Vol. 15. *Edited by* H. J. Emeleus and A. G. Sharpe, Academic Press, New York. 1972. pp 111–115.
23. R. W. J. WEDD and J. R. SAMS. Can. J. Chem. **48**, 71 (1970).
24. N. G. BOKII, G. N. ZAKHAROVA, and YU. T. STRUCHKOV. J. Struct. Chem. USSR, **11**, 828 (1970).
25. K. NAKAMOTO. Infrared spectra of inorganic and coordination compounds. 2nd ed. Wiley-Interscience. New York. 1970. p. 106.
26. E. STEGER and K. HERZOG. Z. Anorg. Chem. **331**, 169 (1964).
27. (*a*) M. G. CLARK, A. G. MADDOCK, and R. H. PLATT. J. Chem. Soc. Dalton, 281 (1972); (*b*) G. M. BANCROFT. *In* Mössbauer spectroscopy, McGraw Hill, London. 1973. pp. 137–138.
28. G. M. BANCROFT, K. D. BUTLER, and T. K. SHAM. J. Chem. Soc. Dalton, 1483 (1975).

Can. J. Chem. Downloaded from www.nrcresearchpress.com by 210.87.254.5 on 09/05/12
For personal use only.

The influence of neutral salts on the easily polarizable hydrogen bond of $H_5O_2^+$ groupings in acid solutions

DAG SCHIÖBERG[1] AND GEORG ZUNDEL

Physikalisch-Chemisches Institut der Universität München, Theresienstraße 41, D-8000 München 2, West Germany

Received August 5, 1975

DAG SCHIÖBERG and GEORG ZUNDEL. Can. J. Chem. **54**, 2193 (1976).

The influence of neutral salts on the easily polarizable hydrogen bond of $H_5O_2^+$ groupings in aqueous acid solutions is studied, using ir spectroscopy. The absorbance of the ir continuum, caused by the polarizable hydrogen bond in the $H_5O_2^+$ groupings, usually decreases with increasing neutral salt concentration. This is explained by the polarization of the hydrogen bonds caused by local fields due to the neutral salt ions. The H^+ becomes more or less trapped at one of the H_2O of the $H_5O_2^+$. The prominence of this effect increases with increasing cation field, *i.e.*, from Cs^+ to Li^+, and is more pronounced with bivalent than with monovalent cations. The opposite effect is observed with tetraethylammonium chloride. The symmetry of $H_5O_2^+$ groups is less strongly disturbed in the presence of neutral salts with ions with very large radii, *i.e.*, small electrical fields, than in pure acid solutions. Considering the torsional vibration of the water molecules, it is finally shown that the hydrate structure network around the $H_5O_2^+$ becomes disintegrated due to the presence of neutral salts.

It is known from electrochemical investigations that the activity coefficient of the excess proton usually increases strongly due to the addition of neutral salts to acid solutions. The opposite is true with the addition of tetraethylammonium salt. Furthermore, the addition of neutral salt decreases the excess proton conductivity. All these observations are discussed on the basis of the ir spectroscopic results.

DAG SCHIÖBERG et GEORG ZUNDEL. Can. J. Chem. **54**, 2193 (1976).

On étudie, grâce à la spectroscopie infrarouge, l'influence des sels neutres sur les liaisons hydrogène facilement polarisables des groupe $H_5O_2^+$ dans des solutions aqueuses d'acide. L'absorption du continuum ir, causée par les liaisons hydrogène polarisables dans les groupes $H_5O_2^+$, diminue généralement avec une augmentation dans la concentration d'un sel neutre. On explique ce résultat par une polarisation des liaisons hydrogène causée par les champs locaux dus aux sels d'ions neutres. Les ions H^+ deviennent plus ou moins coincés par une des molécules d'eau du $H_5O_2^+$. L'importance de cet effet augmente avec une augmentation du champ du cation, *i.e.* à partir de Cs^+ jusqu'à Li^+, et est plus prononcé avec les cations biqu'avec les cations monovalents. On observe l'effet inverse avec le chlorure de tétraéthylammonium. La symétrie des groupes $H_5O_2^+$ est moins fortement influencée en présence de sels neutres d'ions de rayons très larges, *i.e.* des petits effets électriques, que dans des solutions d'acides purs. Considérant la vibration torsionnelle des molécules d'eau, on montre finalement que le réseau structural de l'hydrate autour du $H_5O_2^+$ se désintègre en présence de sels neutres.

Il est connu, à partir d'études électrochimiques, que le coefficient d'activité du proton en excès augmente généralement d'une façon importante par l'addition de sels neutres à des solutions acides. L'inverse est vrai pour l'addition du sel de tétraéthylammonium. De plus, l'addition de sels neutres diminue la conductivité de l'excès de proton. On discute de toutes ces observations sur la base des résultats spectroscopiques en ir.

[Traduit par le journal]

Introduction

The p*H* value of aqueous acid solutions may shift considerably due to the addition of neutral salts, as has been known for a long time (1). Schwabe and co-workers studied such ternary systems (water + acid or base + neutral salt) in more detail (2, 3) and obtained the following results: The p*H* value of aqueous acid solutions decreases in proportion to the addition of neutral salts, *i.e.*, $\log f_\pm$ increases in proportion to the neutral salt concentration. The activity coefficient of the excess proton f_{H^+} may change more than two orders of magnitude, whereas the activity coefficient of the anion f_{A^-} remains constant. The decrease of the p*H* value is all the more pronounced the smaller the radius of the neutral salt cations. In contrast to these results, the p*H* increases on the addition of tetraethyl-

[1]Present address: Fachbereich Physikalische Chemie, Universität Marburg, Biegenstraße 12, D-3550 Marburg/Lahn, West Germany.

Can. J. Chem. Downloaded from www.nrcresearchpress.com by 210.87.254.105 on 09/05/12
For personal use only.

Can. J. Chem. Downloaded from www.nrcresearchpress.com by 210.87.254.105 on 09/05/12
For personal use only.

ammonium salt, *i.e.*, cations with very large radii.

As regards the catalytical activity of excess protons analogous effects are found (4, 5). Trautmann and Ambard (4), for instance, studied the H^+ catalyzed hydrolysis of sacharose. They found that the catalytical activity of the excess protons increases on neutral salt addition. This effect becomes more pronounced in the series KCl, NaCl, LiCl.

The effect on the specific conductivities $\mathscr{H}$, which is due to the addition of neutral salts to aqueous acid solutions, was first studied by Suhrmann and Wiedersich (6) and later in detail by Kálmán (7–9) with the following results (for summary see ref. 3): $\mathscr{H}_{acid} + \mathscr{H}_{salt}$ is considerably different from $\mathscr{H}_{(acid + salt)}$, *i.e.*, in ternary systems the specific conductivities are not additive. In ternary systems containing acid, $\mathscr{H}$ usually increases with salt addition, but to a smaller extent as one should expect when considering $\mathscr{H}_{acid} + \mathscr{H}_{salt}$. Hence the addition of neutral salt reduces excess proton conductivity (3).

Infrared spectroscopic investigations provide a better understanding of the molecular processes in acid and base solutions. The following is already known from extensive experimental and theoretical investigations (10–15*a*): $H_5O_2^+$ groupings are of special importance within the solvate structure network around the excess proton, since the hydrogen bond of this grouping is extremely easily polarizable.

The excess proton in $H_5O_2^+$ may usually fluctuate between the two water molecules. Therefore, this grouping is to be illustrated by two proton boundary structures. This was first demonstrated by ir investigations with strongly acidic polyelectrolytes (ref. 10, p. 165*ff*) and later with aqueous solutions of strong acids (15*b*). Neutron diffraction studies by Williams and co-workers (15*c*) confirmed this result. With regard to the hydrated excess proton, these authors write: "The correct formulation is believed to be ($H_2O \cdot H^+ \cdot H_2O$) and *not* $H_3O^+ \cdot H_2O$, although intermediate cases may exist".

The polarizability of the $H_5O_2^+$ grouping is the reason for strong interaction effects of these hydrogen bonds with their environment, as, for instance, for induced dipole interactions of the hydrogen bond in $H_5O_2^+$ groupings with ion fields and dipole fields of solvate molecules. With systems containing easily polarizable hydrogen bonds continuous absorption is observed in the ir spectra. Hence such ir continua may provide information on the nature of hydrated excess protons.

Results and Discussion

Neutral Salt Effects

Figure 1 shows ir spectra of 5 *M* aqueous HCl solutions containing 0, 2, 6, and 10 *M* LiCl. With 1 and 5 *M* aqueous HCl solutions (see Experimental section) the absorbance of the continuum is plotted in Fig. 2 for various neutral salts, dependent on neutral salt concentration. The following results are obtained: (*1*) The absorbance of the continuum decreases in proportion to the addition of neutral salts in the cases of alkali and earth alkali salts (Fig. 2 *a* and *b*). (*2*) The decrease of the absorbance of the continuum caused by the neutral salt cations is largely proportional to the HCl concentration. (*3*) Comparison of cations with equal valency shows that this decrease of the absorbance is all the more pronounced the smaller the radius of the neutral salt cations, *i.e.*, the stronger the fields in their environment are. (*4*) Comparison of monovalent with bivalent cations with similar radii, for instance, Li^+ with Mg^{2+} in Fig. 2*b*, shows that the decrease of the absorbance is twice as large with bivalent Mg^{2+} ions as with monovalent Li^+ ions. (*5*) On addition of tetraethylammonium chloride the absorbance of the continuum increases with increasing salt concentration (Fig. 2*c*), which is in contrast to the observations with alkali and earth alkali salts. (*6*) On addition of neutral salt the band of the torsional vibration of the water molecules observed as a very broad band (maximum in the region 750–550 cm^{-1}) shifts strongly toward smaller wave numbers (Fig. 1).

With all these experiments the anions of the neutral salts are Cl^- ions, *i.e.*, the same type of anions are present. We considered the influence of neutral salt cations, since these were also preferentially considered by the electrochemical investigations (2–9). As reported elsewhere (ref. 10, p. 66*ff*, ref. 15 *d*, *e*, *f*), the attachment of water molecules to anions causes, however, significant changes of bands in ir spectra.

Hayd (16*a*) calculated the continuous absorption of $H_5O_2^+$ using the transition moments

Can. J. Chem. Downloaded from www.nrcresearchpress.com by 210.87.254.105 on 09/05/12
For personal use only.

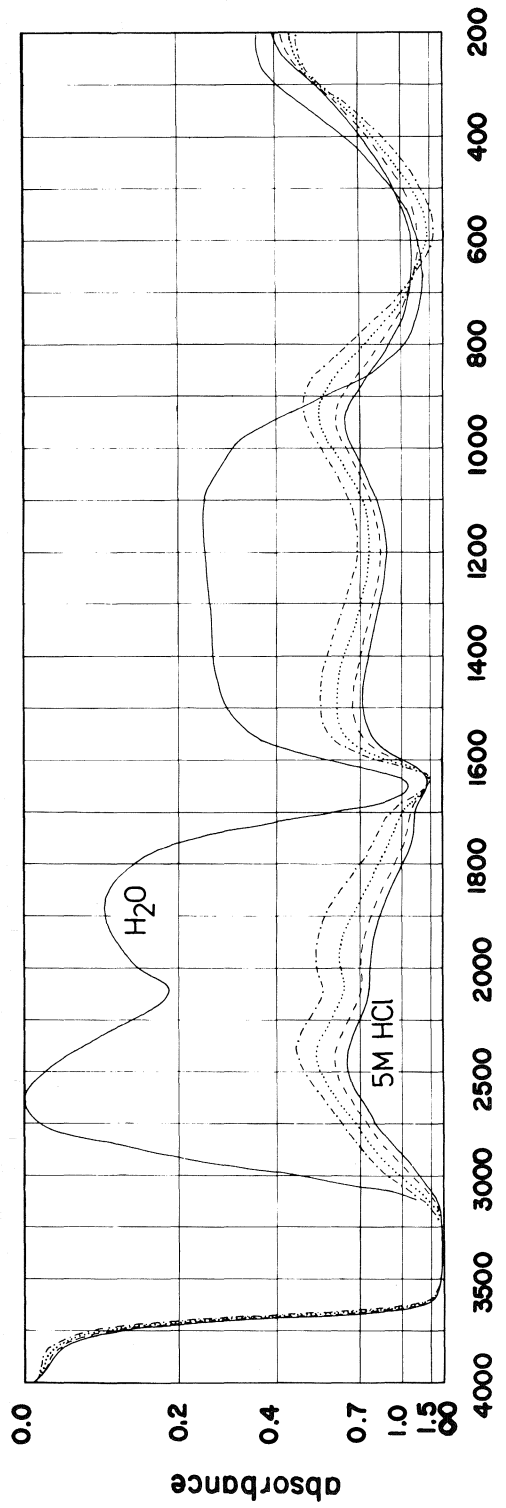

FIG. 1. Infrared spectra of 5 *M* aqueous HCl solutions containing 0, —; 2, - - -; 6, · · ·; and 10, ·-·-·-·- mole LiCl/l (layer thickness 13.6 μ; 25 °C) (see Experimental section). Spectrum of H_2O for comparison.

Can. J. Chem. Downloaded from www.nrcresearchpress.com by 210.87.254.105 on 09/05/12
For personal use only.

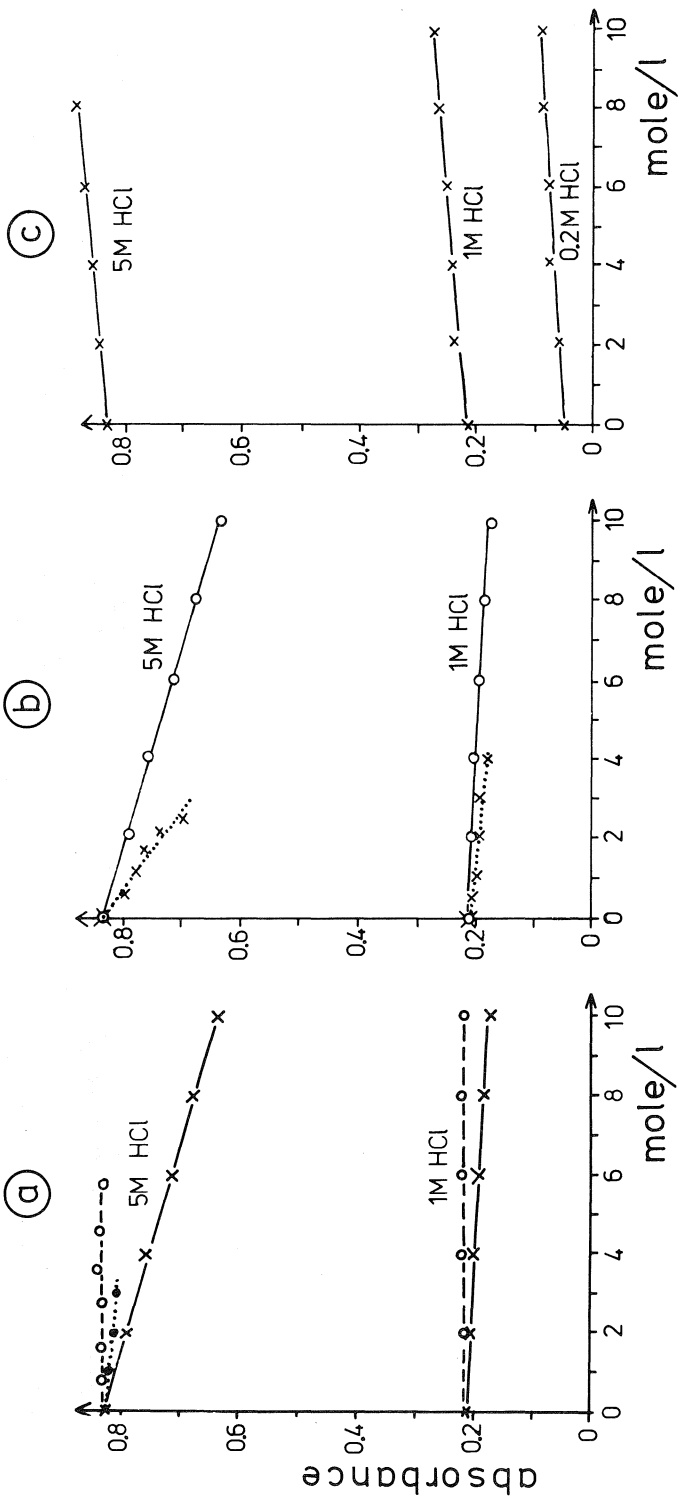

FIG. 2. Absorbance of ir continua of aqueous HCl solutions, concentration 1 mol/l and 5 mol/l, dependent on moles neutral salt/l (layer thickness 13.6 μ; 25 °C) (see Experimental section). (*a*) Neutral salts: LiCl, RbCl, and CsCl; (*b*) comparison of LiCl and $MgCl_2$; (*c*) neutral salt: tetraethylammonium chloride.

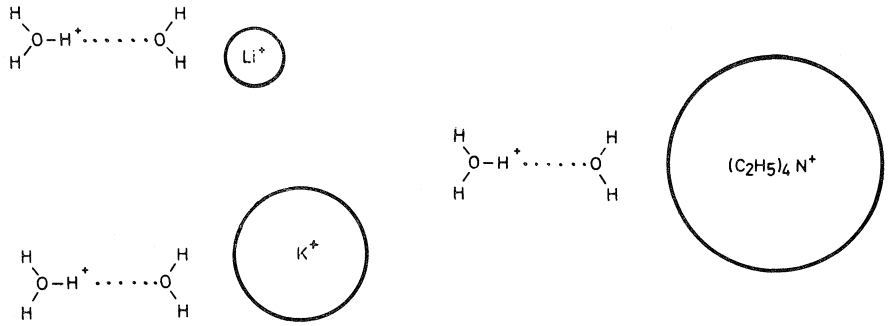

FIG. 3. Schematic representation of addition of cations to $H_5O_2^+$ groups.

obtained by the SCF calculations given in ref. 14. With these calculations a mean distribution of electrical fields at the hydrogen bonds was taken into account. It was shown that with increasing mean field strength the absorbance of the continuum decreases in the whole wave number range in which the continuum is observed.

On the basis of this result the observed changes of the absorbance of the continuum due to neutral salt are easily understandable: The decrease of the absorbance of the continuum with increasing alkali or earth alkali salt concentrations (result (*1*)) indicates that the local electrical fields at the $H_5O_2^+$ groupings in the solution become stronger due to the presence of neutral salt ions. The polarizable hydrogen bonds of the $H_5O_2^+$ groups become polarized more strongly by the local fields in the solutions. The local fields cause a rise of the lingering time of the excess charge at one side of the $H_5O_2^+$ grouping, *i.e.*, in the position opposite to the cation. Thus these local fields favor the trapping of the excess charge.

The question arises how the local fields are increased by the presence of the neutral salt ions. These ions may increase the local fields directly or indirectly; indirectly, since they disturb the hydrate structure around $H_5O_2^+$ and, in this way, decrease the symmetry of the environment of $H_5O_2^+$. The latter effect is probably shown by the shift of the torsional vibration (result (*6*)) which indicates a disintegration of the hydrate structure network around $H_5O_2^+$. Whether it is the direct or the indirect effect that causes changes of the local fields more strongly cannot, however, be decided from the presented experiments (see also ref. 16*b*).

With the change of the absorbance of the continuum, cations with small radii are more effective (result (*3*)). Hence the local fields at the $H_5O_2^+$ groupings become stronger the smaller the radii of the cations. In the case of extremely concentrated solutions this is immediately understandable, since cations with small radii can approach the $H_5O_2^+$ groupings more closely (Fig. 3), and hence their electrical fields at the $H_5O_2^+$ groups are stronger. In the case of less concentrated solutions one would at first suppose that the cation fields do not sufficiently influence the $H_5O_2^+$ grouping. However, the influence of cations in less concentrated solutions can be understood on the basis of the same considerations by which Schwabe and co-workers (17, 18) explain the change of the activity coefficient due to neutral salt. They consider the local dielectric constant in the neighborhood of ions and conclude that with cations with smaller radii the fields are more easily transferred into their environment, since in the first hydration shell these cations bind the water molecules so strongly that local dielectric saturation occurs. Thus smaller cations can also polarize the grouping $H_5O_2^+$ more strongly in more diluted solutions. Hence the fact that the decrease of the absorbance in the series of the alkali salts becomes stronger from CsCl to LiCl (result (*3*)) is immediately understandable.

The radii of Li^+ and Mg^{2+} are similar, but with regard to valency the electrical field in the neighborhood of the Mg^{2+} ions is twice as large. This explains result (*4*): $MgCl_2$ compared to LiCl induces a twice as large decrease of absorbance. With addition of tetraethylammonium chloride an increase of the absorbance instead of a decrease is observed (result (*5*)). Before neutral salt is added the hydrogen bond in the $H_5O_2^+$ groupings is more or less strongly polarized by the dipole fields of H_2O molecules and by the

Can. J. Chem. Downloaded from www.nrcresearchpress.com by 210.87.254.105 on 09/05/12
For personal use only.

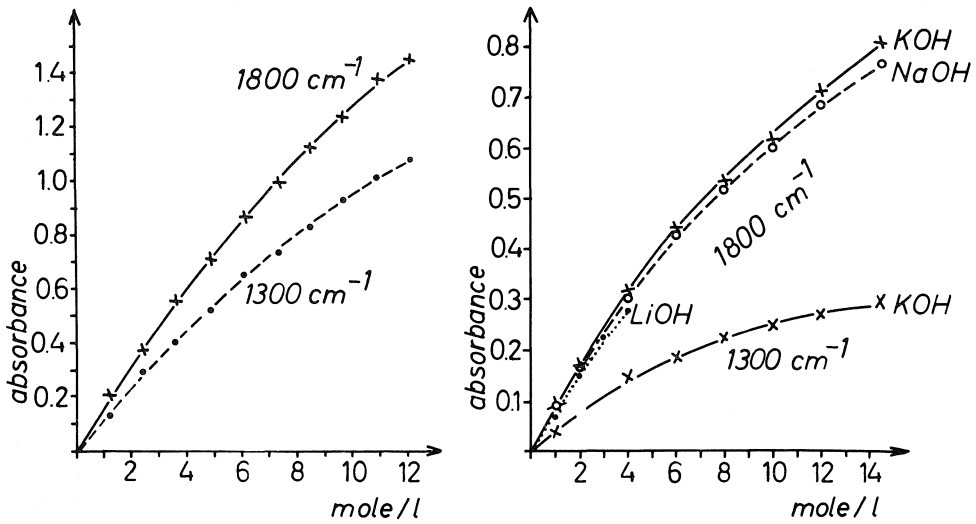

FIG. 4. Absorbance of ir continua, dependent on concentration. (*a*) Aqueous HCl solutions dependent on mole HCl/l (layer thickness 13.6 μ; 25 °C). (*b*) Aqueous base solutions dependent on mole base/l (layer thickness 10 μ; 28 °C).

fields of the Cl^- ions in their environment. When tetraethylammonium chloride is added, tetraethylammonium ions, which have a very large radius (2.2 Å) and additional Cl^- ions (radius 1.81 Å) are present in the environment of the $H_5O_2^+$ groupings. Hence, when neutral salt ions with very large radii are present the increase of the absorbance of the continuum indicates that the local electrical fields at the hydrogen bond in the $H_5O_2^+$ become smaller. The hydrogen bond in the $H_5O_2^+$ groupings becomes less strongly polarized.

Recently, Roberts (16*b*) studied diffusion and activity of excess protons in similar systems by tracer experiments. His results, obtained by a completely different method, are in very good agreement with the results obtained by our spectroscopic investigations.

Besides the polarization of the hydrogen bond in the $H_5O_2^+$ groupings due to neutral salt the ir spectra also indicate effects of the neutral salt ions on the hydrate structure network.

The shift of the torsional vibration of the water molecules toward smaller wave numbers (result (*6*)) demonstrates the following: The hydrogen bonds in the hydrate structure network become less strong due to the influence of the neutral salt ions, *i.e.*, the hydrate structure network becomes disintegrated.

Dependence of the Absorbance of the Continuum on Acid or Base Concentration

In Fig. 4 the absorbance of the continuum plotted is dependent on the acid or base concentration, respectively. The following result is obtained: with aqueous HCl and aqueous base solutions at low concentrations the absorbance of the continuum increases in proportion to the concentration. However, with increasing concentration the slope of the curves decreases. Thus the absorbance per polarizable hydrogen bond decreases with increasing concentration of $H_5O_2^+$ or $H_3O_2^-$ groupings,[2] respectively.

This decrease of the absorptivity coefficient of the polarizable hydrogen bonds with increasing concentration cannot be caused by a change of the dissociation equilibrium, since with these strong acids and bases at the concentrations investigated by us H^+ or OH^- is always present in $H_5O_2^+$ or $H_3O_2^-$ groupings, respectively.

The decrease of the absorptivity coefficient can, however, be understood in a fashion similar to that of the neutral salt effects, *i.e.*, as follows. With increasing concentration the local environ-

[2]The fact that the absorbance of the continuum/polarizable hydrogen bond is half as strong with $H_3O_2^-$ as compared to $H_5O_2^+$ is in very good agreement with the continua calculated, using the transition moments obtained by SCF calculations (16*a*).

Can. J. Chem. Downloaded from www.nrcresearchpress.com by 210.87.254.105 on 09/05/12
For personal use only.

Can. J. Chem. Downloaded from www.nrcresearchpress.com by 210.87.254.105 on 09/05/12
For personal use only.

ments of the polarizable hydrogen bonds become more and more asymmetrical, *i.e.*, the local fields at the hydrogen bonds become stronger. Hence, as discussed above, the absorbance per hydrogen bond decreases. Thus the absorbance of the continuum should increase with increasing concentration less than in proportion to the concentration, which is in agreement with our observations.

Finally, the following result is obtained from Fig. 4*b*. The slope of the curves, *i.e.*, the absorbance of the continuum, decreases with the base solutions in the series KOH, NaOH, LiOH. Hence the absorptivity of the easily polarizable hydrogen bonds decreases with decreasing radius of the cations of the base. This becomes immediately understandable. The explanation is the same as in the case of the neutral salt effects.

Comparison with Electrochemical Results

We mentioned in the Introduction that the pH decreases strongly due to addition of alkali and earth alkali salts, *i.e.*, log f_{H^+} increases. In contrast to this result the pH increases with addition of tetraethylammonium salts, *i.e.*, log f_{H^+} decreases.

Schwabe (2, 3), who reported on all these results, states the following (18): the concentration of hydrated ions relative to water available for hydration increases, since water is used for the hydration of the neutral salt. This may explain the increase of $f_{\pm}$ but not the different behavior of f_+ and f_-, since the increase in concentration becomes perceptible to both ions.

Schwabe and co-workers (17, 18), moreover, showed that the increase of f_{H^+} in the case of alkali and earth alkali salts is mainly due to the interaction of the excess proton with the alkali and earth alakli cations. The smaller the local dielectric constant in the neighborhood of these cations due to local dielectric saturation, the stronger the interaction effects of these cations with the excess protons.

These excess protons are, however, present in the easily polarizable hydrogen bond of the $H_5O_2^+$ groupings. Hence, on account of the large polarizability, very strong ion induced dipole interaction of these hydrogen bonds occurs due to the local fields of their environment (15*a*).

Hence the ir results suggest that the stronger polarization of the hydrogen bond in the $H_5O_2^+$ groupings due to the alkali and earth alkali salts is of importance to the increase of log f_{H^+}. With stronger polarization of the $H_5O_2^+$ the positive charge becomes localized to a larger degree at one side of the $H_5O_2^+$. The entropy decreases. The OH groups of the water molecule at which the positive charge is present become stronger hydrogen bond donors and more acidic than the OH groups in a largely symmetrical $H_5O_2^+$ with fluctuating proton. This may explain the increase of the activity coefficient f_{H^+} due to neutral salts. The opposite is true with the tetraethylammonium ions, since the $H_5O_2^+$ groupings become less strongly polarized due to the presence of tetraethylammonium and additional chloride ions. This decrease of the localization of the excess proton and the change of the hydrogen bond donor property of the OH groups of the water molecules of the $H_5O_2^+$ connected with it may (together with the screening of the excess proton by additional Cl^- ions (18)) be responsible for the pH increase due to tetraethylammonium chloride.

As regards conductivity, $\mathscr{H}_{(acid + salt)}$ is smaller than $\mathscr{H}_{acid} + \mathscr{H}_{salt}$. Hence the addition of neutral salt reduces the excess proton conductivity (3, 6–9). This is not only true in the case of alkali and earth alkali salts, but especially with tetraethylammonium salts.

This conductivity decrease may have the following reasons. The hydrate structure network around the excess proton becomes disintegrated due to neutral salt addition (result (*6*)). In such a disintegrated network Grotthus conductivity cannot proceed as easily, since the structure diffusion is more or less disturbed.

Besides this reason for the excess proton conductivity decrease due to neutral salt, in the case of alkali and earth alkali salts, the polarization of the hydrogen bonds in the $H_5O_2^+$ groupings may also decrease the excess proton conductivity. The field sensitive mechanism of the Grotthus conductivity is the polarization of the hydrogen bond in $H_5O_2^+$ due to the external electrical field. This polarization gives the structure diffusion of the $H_5O_2^+$ a preferred direction, and this is observed as anomalous excess proton conductivity (see refs. 11, 12, 15*a*). The polarizability of a hydrogen bond decreases with increasing polarization of the hydrogen bond (13, 14). Thus, if the hydrogen bond of the $H_5O_2^+$ groupings is already more or less polarized due

Can. J. Chem. Downloaded from www.nrcresearchpress.com by 210.87.254.105 on 09/05/12
For personal use only.

to the local electrical fields in the solution, the external field can no longer polarize the hydrogen bond and induce a preferred direction of the $H_5O_2^+$ structure diffusion. This effect may also be of importance for the decrease of excess proton conductivity due to neutral salt.

Experimental Procedure

For the described investigations cells with Ge and Si windows, respectively, were used. Because of the high reflectivity of these windows considerable interference superposes the spectrum when the windows are arranged parallel. Therefore wedge-shaped layers were used (19). The mean layer thickness was calculated from the absorbance of the benzene bands at 1950 and 1815 cm^{-1}. The dependence of the absorbance of these bands on the layer thickness was determined with the help of a cell with varying layer thicknesses. The reproducibility of the mean layer thickness of the cell with wedge-shaped windows was $\pm 0.1\ \mu$.

The absorbance taken from the spectra (*e.g.*, Fig. 1) had to be corrected, taking into account the following points of view:

(*1*) In the case of a wedge-shaped layer Lambert–Beer's law is no longer valid. The necessary corrections dependent on the absorbance were determined by studying mixtures of paraffin oil and CCl_4. The absorbance of these substances is almost completely independent of their interaction.

(*2*) Figure 4 shows the continuous absorbance at some representative wave numbers, dependent on the acid or base concentration, respectively. Acid or base solutions do, of course, contain less water molecules than pure water. Thus with these solutions less water molecules are in the beam at equal layer thicknesses. When taking this into account, the absorbance change due to the presence of H^+ or OH^- can be calculated from the spectra as follows:

$$A_c = A_{HCl} - \frac{M_{H_2O}}{55.3} A_{H_2O}$$

where A_c is absorbance of the continuum; A_{HCl}, absorbance of the background of the HCl solutions; A_{H_2O}, absorbance of the background in the spectrum of pure water; and M_{H_2O}, mole water per litre of solution.

(*3*) Figure 2 shows the continuous absorbance spectra of aqueous HCl solutions containing neutral salts. Due to the addition of neutral salt the number of acid molecules per volume is changed. For a correct evaluation of salt effects on the absorbance of the acid, the absorbance taken from the spectra of aqueous HCl solutions containing neutral salt (*e.g.*, taken from Fig. 1) has to be corrected by referring to the same mole number of acid molecules. Thus the absorbance of the continuum A_c is obtained as follows:

$$A_c = \frac{M_1}{M_2} A_{HCl+s} - \frac{M_{H_2O}}{55.3} A_{H_2O}$$

where A_c is absorbance of the continuum; A_{HCl+s}, absorbance of the background of the HCl solutions with neutral salt; A_{H_2O}, absorbance of the background in the spectrum of pure water; M_1, mole HCl per litre of the aqueous HCl solution; M_2, mole HCl per litre of the aqueous HCl neutral salt solution; and M_{H_2O}, mole water per litre of the aqueous HCl – neutral salt solution.

Acknowledgements

Our thanks are due to the Deutsche Forschungsgemeinschaft and to the Fonds der Chemischen Industrie for providing the facilities for this work. We should like to express our thanks to Professor E. G. Weidemann of the Sektion Physik, University of Munich, for many valuable discussions.

1. B. F. Reiff. Z. anorg. allgem. Chem. **208**, 321 (1932).
2. K. Schwabe. Electrochim. Acta, **12**, 67 (1967).
3. K. Schwabe. Sitzungsberichte der Sächsischen Akademie der Wissenschaften zu Leipzig, Math. naturwiss. Klasse, vol. 109, no. 6 (1972).
4. S. Trautmann and L. Ambard. J. Chim. Phys. **53**, 389 (1956).
5. P. T. McTigue and A. R. Watkins. Aust. J. Chem. **18**, 1943 (1965).
6. R. Suhrmann and I. Wiedersich. Z. anorg. allgem. Chem. **272**, 167 (1953).
7. E. Kálmán. Z. Phys. Chem. Leipzig, **246**, 141 (1971).
8. E. Kálmán. Z. Phys. Chem. Leipzig, **248**, 123 (1971).
9. E. Kálmán. Acta Chim. Acad. Sci. Hung. **72**, 407 (1972).
10. G. Zundel. Hydration and intermolecular interaction. Academic Press, New York. 1969. and Mir, Moscow. 1972.
11. G. Zundel. Allgem. Prakt. Chem. Wien, **21**, 329 (1970).
12. E. G. Weidemann and G. Zundel. Z. Naturforschg. **25a**, 627 (1970).
13. R. Janoschek, E. G. Weidemann, H. Pfeiffer, and G. Zundel. J. Am. Chem. Soc. **94**, 2387 (1972).
14. R. Janoschek, E. G. Weidemann, and G. Zundel. J. Chem. Soc. Faraday II, **69**, 505 (1973).
15. (*a*) G. Zundel. *In* The hydrogen bond – recent developments in theory and experiments, Vol. II. *Edited by* P. Schuster, G. Zundel, and C. Sandorfy. North Holland Publ. Co. 1976. Chapt. 15, p. 683ff. (*b*) D. Schiöberg and G. Zundel. Z. Phys. Chem. Frankfurt. In press. (*c*) J. M. Williams and S. W. Peterson. *In* Spectroscopy in inorganic chemistry. Vol. 2, Academic Press, New York. 1971. (*d*) T. Ackermann, G. Zundel, and K. Zwernemann. Ber. Bunsenges. Phys. Chem. **73**, 446 (1969). (*e*) P. Rhine, D. Williams, G. M. Hale, and M. R. Querry. J. Phys. Chem. **78**, 238 (1974). (*f*) D. Schiöberg, K. P. Hofmann, and G. Zundel. Z. Phys. Chem. Frankfurt, **90**, 189 (1974).
16. (*a*) A. Hayd. Ph.D. Thesis, University of Munich, Munich, West Germany. 1975. (*b*) N. K. Roberts. J. Phys. Chem. In press.
17. H. Kelm and K. Schwabe. Z. Phys. Chem. Leipzig, **255**, 475 (1974).
18. K. Schwabe, H. Kelm, and Chr. Queck. Z. Phys. Chem. Leipzig, **255**, 1149 (1974).
19. K. P. Hofmann and G. Zundel. Z. Naturforschg. **29c**, 29 (1974).

Reaction of organic compounds under high temperature – dilute acid (HTDA) conditions. II. The hydration–exchange of norbornadiene and benzonorbornadiene in aqueous acetic acid at 250 °C[1]

NICK HENRY WERSTIUK AND TONU KADAI

Department of Chemistry, McMaster University, Hamilton, Ont., Canada L8S 4M1

Received November 14, 1975

NICK HENRY WERSTIUK and TONU KADAI. Can. J. Chem. **54**, 2201 (1976).

The hydration of norbornadiene (**1**) under the HTDA conditions of aqueous acetic acid at 250 °C gives via norbornanediols and norbornenols as intermediates, the sink-product aldehydes **3**, **4**, **5**, and norcamphor (**6**). When the reaction is carried out in deuterated medium on the average, 2.5 atoms of deuterium are incorporated into each of the products. Hydration of benzonorbornadiene (**2**) at 250 °C gives the alcohols **40** and **41** and the acetates **42***a* and **42***b* as products. When the hydration is carried out in deuterated medium, while only one atom of deuterium is incorporated into the [2.2.1]-framework, exchange of the aromatic moiety proceeds to completion.

NICK HENRY WERSTIUK et TONU KADAI. Can. J. Chem. **54**, 2201 (1976).

L'hydratation du norbornadiène (**1**), dans des conditions HTDA de l'acide acétique aqueux à 250 °C, conduit, par l'intermédiaire des norbornanediols et des norbornénols comme intermédiaire, aux aldéhydes **3**, **4**, **5** et au norcamphre (**6**) comme produits finaux. Quand on effectue la réaction dans un milieu deutéré, il y a incorporation, dans chacun des produits, d'une moyenne de 2.5 atomes de deutérium. L'hydratation du benzonorbornadiène (**2**) à 250 °C conduit aux alcools **40** et **41** et aux acétates **42***a* et **42***b*. Quand on effectue l'hydratation dans un milieu deutéré, il n'y a qu'un atome de deutérium qui s'incorpore dans le système bicyclo [2.2.1]; toutefois la partie aromatique s'échange complètement.

[Traduit par le journal]

Introduction

The acid-catalyzed additions of methanol, acetic acid, deuterated acetic acid, and deuterium chloride to norbornadiene (**1**), at temperatures less than 200 °C, have been studied extensively (2–6). Likewise, the acid-catalyzed additions of acetic acid and hydrochloric acid and their deuterated derivatives, to benzonorbornadiene (**2**) have also been examined (7, 8).

Reaction of **1** with electrophilic reagents such as D_2SO_4–DOAc yields norbornenyl and nortricyclyl products (Scheme 1). The incoming atom of deuterium ($E^+ = D^+$) is scrambled between C-3 and C-7 in the norbornenyl systems. Morrill and Greenwald (6) have established recently that deuterium is located in the nortricyclyl product as described in Scheme 1. Multiple deuteration of the products is not observed under the conditions utilized in the studies reported thus far.

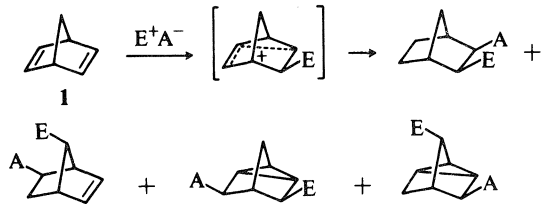

SCHEME 1

The addition of deuterated acid ($E^+ = D^+$) to **2** (Scheme 2) results in the scrambling of the incoming atom of deuterium between C-3 and C-7 (7, 8) in the benzonorbornenyl products. Here also, there is no evidence for multiple deuteration.

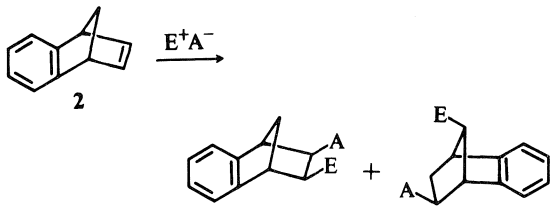

SCHEME 2

As a continuation of our studies on the

[1]For a preliminary account see ref. 1. For the first full paper in this series see ref. 9.

Can. J. Chem. Downloaded from www.nrcresearchpress.com by 210.87.254.6 on 09/05/12
For personal use only.

TABLE 1. Data for the hydration of norbornadiene at 250 °C

Entry[a] (run)	Time (h)	Medium	Relative % yield[b] 3 + 4	5	6	Diols	Other[c]	% yield[d] 3 + 4	5	6	Excess D/molecule[e] 3 + 4	5	6
1	0.5	H^+	4	3	8	55	30						
2	3	H^+	17	19	45	15	4						
3	5	H^+	14[f]	17	52	14	3						
4	9.5	D^+	14	17	54	14	1	8	13	33	2.5	2.6	2.4
5	10	H_2O only	Norbornadiene + polymer										

[a]Typically, a solution of **1** in 10% v/v HOAc–H_2O or 10% v/v DOAc–D_2O was degassed and heated in a sealed tube at 250 °C in a Carius oven. For glpc analyses of runs 1 and 2 see Figs. 1 and 2, respectively.
[b]The relative percent yields were determined gas chromatographically on $\frac{1}{8}$ in. × 10 ft 10% SE-30 and 10% Carbowax on Chromosorb W columns.
[c]The norbornenols and nortricyclanol are included here.
[d]The yields were determined by preparative glpc. Each is corrected for collection losses as described in the Experimental.
[e]The enolizable deuterium in **3**, **4**, and **5** was washed out by three injections through a $\frac{3}{8}$ in. × 10 ft 5% KOH + 20% Carbowax column maintained at 170 °C. Deuterated **6** was treated three times with a KOH–MeOH–H_2O solution.
[f]A composite of *ca.* 15% **3** and 85% **4** as determined by ir fingerprint region assay (9).

solvolysis and hydration of organic molecules in dilute aqueous acid (1, 9) at moderately high temperatures (≥250 °C), we have studied the reaction of norbornadiene and benzonorbornadiene in deuterated and non-deuterated media under high temperature – dilute acid (HTDA) conditions.

Results and Discussion

Norbornadiene

The results of the hydration of **1** under high temperature – dilute acid (HTDA) conditions are listed in Table 1. The data in entry 1, Table 1, and Fig. 1 establish that the hydration of **1** proceeds through nortricyclanol (**7**), the norbornenols **8**, **9** and perhaps **10**, and norbornanediols as intermediates. The intermediates are gradually converted (Fig. 1 and Fig. 2) into the sink-compounds, the cyclopentenylacetaldehydes **3** and **4**, 3-formylcyclohexene (**5**), and norcamphor (**6**) (Scheme 3). That **3**, **4**, **5**, and **6** are the sink-compounds was established by isolating each and comparing their remittant spectroscopic data with that of authentic samples. The hydration of norbornadiene under HTDA conditions thus proceeds via the reaction sequence followed by norbornenols and 3-substituted-nortricyclanes as has been communicated previously (9). Certainly the same hydroxy cations **11**, **12**, **13**, and **14** (Scheme 3) are key intermediates.

That the reaction is acid-catalyzed is established by the experiment described in entry 5, Table 1. That is, when **1** is heated in water only, **3**, **4**, **5**, and **6** are not formed.

That the hydroxy cation **11** can be considered the precursor to **5**, and indeed fits into the generally observed cleavage of 3-hydroxy cations, is supported by reports in the literature. Cristol and Bly (10) have shown that the diol **15**, in the presence of toluenesulfonic acid, ring-opens to

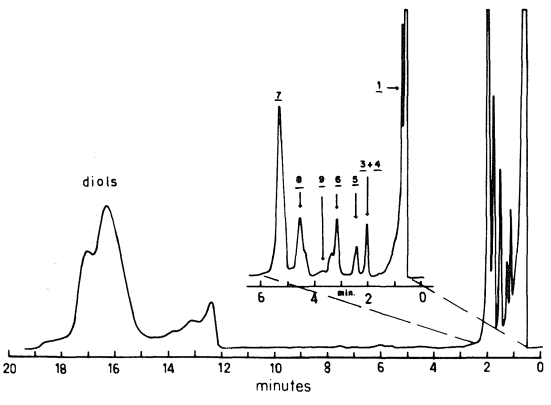

FIG. 1. Products of the hydration–exchange of norbornadiene; reaction time 0.5 h. Insert is the expansion of the short retention time region at a lower column temperature.

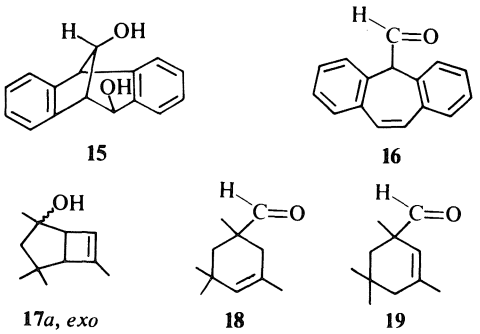

Can. J. Chem. Downloaded from www.nrcresearchpress.com by 210.87.254.6 on 09/05/12
For personal use only.

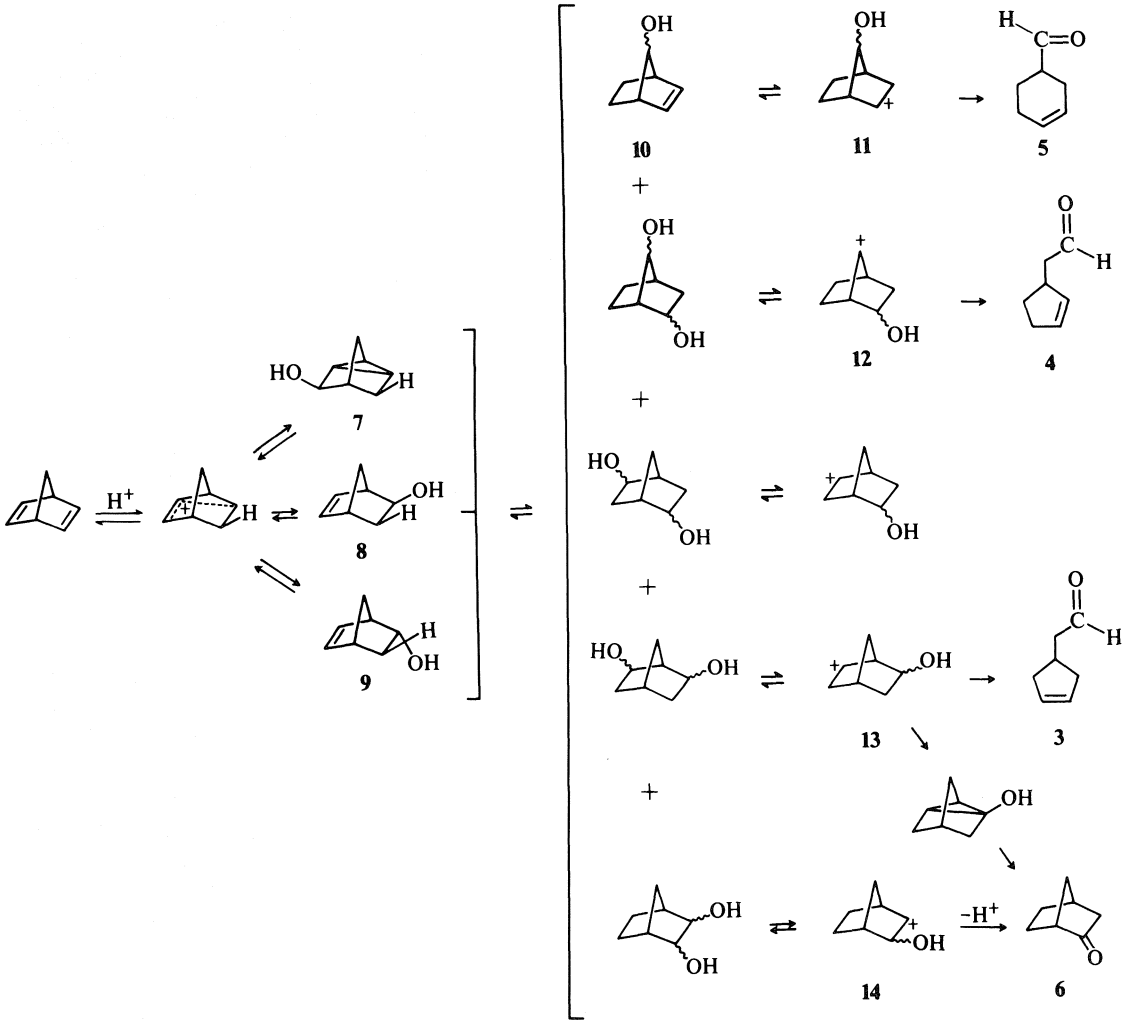

SCHEME 3

give aldehyde **16**. Jones and Jones (11) have shown that the reaction of *exo*- or *endo*-2,4,4,6-tetramethyl[3.2.0]hept-6-en-2-ols **17***a* and **17***b* in aqueous sulfuric acid gives, through *anti*-2,2,4,6-tetramethylbicyclo[2.2.1]hept-5-en-7-ol as the intermediate, the formylcyclohexenes **18** and **19**. Cox *et al.* (12) have shown that the acid-catalyzed ring opening of epoxide **20** gives the aldehyde **21**, and the ketones **22** and **23** as the major products. Rickborn and Gerkin (13) have established that norbornene oxide (**24**) in the presence of $LiClO_4$ in benzene rearranges to **5** and **6**.

We established previously (9), that isomerization (<5%) of **5** → 2-formylcyclohexene, under HTDA conditions, is not important. This is again supported by the fact that, within experimental error, **3**, **4**, **5**, and **6** contain essentially identical amounts of deuterium (Table 1). Thus, although the strained double bond in **1**, **8**, and **9** is protonated in dilute aqueous acetic acid at 250 °C, the cyclopentenyl and cyclohexenyl moieties in **3**, **4**, and **5** remain unreactive.

The premise that **4** is formed from **12** under solvolytic conditions is supported by the work of Gassman *et al.* (14) who established that the tosylate **25**, under high temperature solvolysis, yields the cyclopenten-2-yl isobutyric acid **26**. The authors suggested that the cleavage occurred

Can. J. Chem. Downloaded from www.nrcresearchpress.com by 210.87.254.6 on 09/05/12
For personal use only.

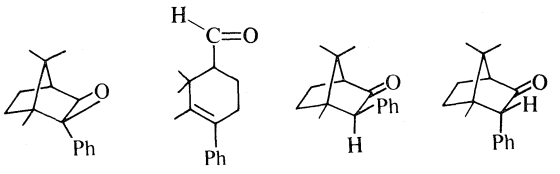

20 **21** **22** **23**

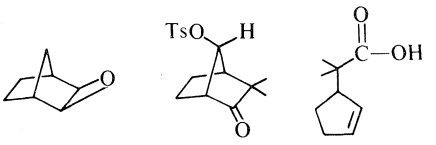

24 **25** **26**

via the adduct formed from the addition of acetic acid to the carbonyl group.

To establish the ease of the cleavage of the C-1, C-2 bond in the process **12** → **4** we prepared the hydroxy tosylates **27***a* and **27***b*, a 78:22 *anti–syn* mixture, and carried out the solvolysis in 10% v/v HOAc–H_2O at 95 °C. That **4** is the major product (>95%) establishes the facility with which C-1, C-2 cleavage occurs and implies major communication between the C-1, C-2 and C-1, C-6 bonds and the cationic center at C-7. The facile ring opening of **27***a* and **27***b* establishes that the cleavage may be a useful synthetic route to substituted cyclopenten-2-yl acetaldehydes not readily available by other routes. As we established previously (*vide supra*) (9) isomerization of **4** to isomeric cyclopentenyl acetaldehydes is not a competitive process. Again this is supported by the fact that **3** + **4** contain, within experimental error, the same amount of deuterium as **5** and **6**.

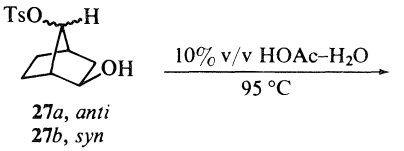

27*a*, *anti*
27*b*, *syn*

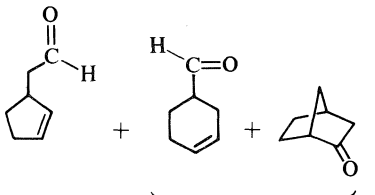

4 (>95%) Trace

That **3** is formed via **13** also has some precedent in the literature. Abrusov (15) established that pinene oxide (**28**) in the presence of $ZnBr_2$ is converted to campholenic aldehyde (**29**). Gwynn and Skillern (16) have shown that treatment of *endo*-6-bromomethyl-*exo*-norbornanol in collidine at 170 °C gave through protonation of the alcohol **30** the cleavage product 3-methylcyclopenten-3-yl acetaldehyde (**31**). Also, Cha-

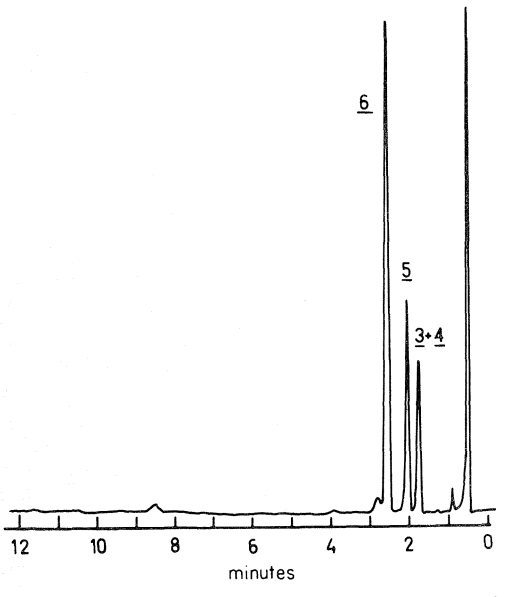

FIG. 2. The glpc trace of products from hydration–exchange of norbornadiene; reaction time 3 h.

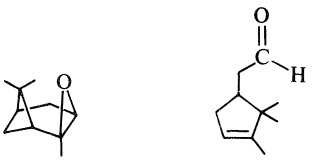

28 **29**

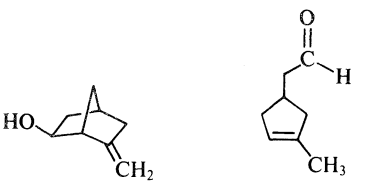

30 **31**

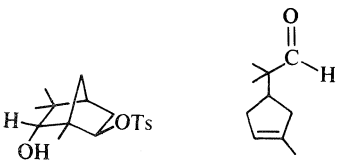

32 **33**

Can. J. Chem. Downloaded from www.nrcresearchpress.com by 210.87.254.6 on 09/05/12
For personal use only.

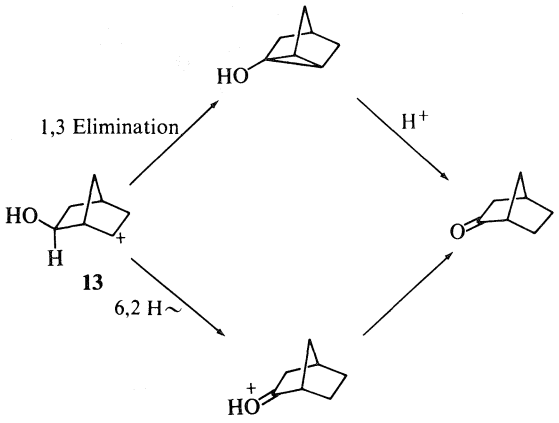

SCHEME 4

budzinski *et al.* (17) have shown that under solvolytic conditions *exo*-2-tosyloxy-*endo*-6-hydroxyfenchone (**32**) gives the aldehyde **33** as the sole product.

We also attempted to establish the facility of the cleavage **13** → **3** and whether or not **13** is converted to norcamphor through 1-hydroxynortricyclene that could be formed from **13** via 1,3 elimination of H^+, or by a direct 6,2 hydride shift (Scheme 4). Our plan of attack was to

34*a*, X = OBs
34*b*, X = OTs

prepare 6-hydroxy systems of the type **34** and carry out solvolysis studies under moderate temperatures. The synthetic sequence described in Scheme 5 was used to prepare *exo*-6-hydroxy-*endo*-2-norbornyl brosylate (**38**).[2]

[2]We first attempted to prepare 2,6-disubstituted norbornanes via the reaction of nortricyclane with CF_3COOOH (18) known to be a source of electrophilic oxygen (formally ^+OH). Although the addition of CF_3COOOH to the double bond in norbornene proceeded normally to give a mixture of *syn*- and *anti*-7-hydroxy-*exo*-2-norbornyl trifluoroacetates, preliminary studies on the reaction of nortricyclane in our hands gave predominantly *exo*-2-norbornyl trifluoroacetate, the product of the acid-catalyzed addition of CF_3COOH. Therefore, either ^+OH is indeed not the electrophilic species as has been suggested (18) or there is a substantial preference for reaction of ^+OH with olefins over cyclopropanes unlike the proton which attacks both species with equal facility (19). We are currently examining the reaction of nortricyclane with CF_3COOOH in greater detail.

Solvolysis of **38** gave **3** as the major product with <1% norcamphor and established the facility with which the hydroxy cation **13** undergoes 6,1 cleavage and that norcamphor is not

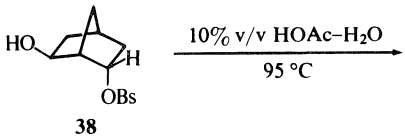

38

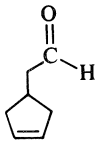

3 (95%) + Other products (5%)

formed from **13** via the pathways described in Scheme 4.

Therefore, norcamphor is formed via a 3,2 hydride shift and/or proton loss from the hydroxy cations **14**. It is expected that **14**-*endo*

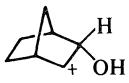

14-*endo*

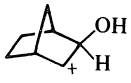

14-*exo*

is converted to norcamphor more readily than **14**-*exo* in the [2.2.1]-system since an *exo* → *exo*-3,2 hydride shift is more facile than an *endo* → *endo* shift (20). However, the large preference for an *exo* → *exo* shift over the *endo* → *endo* shift may not be maintained at 250 °C.

Thus the novel conversion of norbornadiene (**1**) to norcamphor (**6**) in the presence of aqueous acid that involves the net addition of a molecule

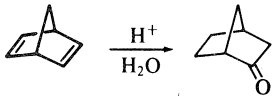

of H_2O to the diene system may find utility in the preparation of substituted bicyclic ketones. Certainly norbornadiene can be converted to norcamphor on a preparative scale. Attempts to hydrate 7-phenylnorbornadiene (**39**) at 250 °C

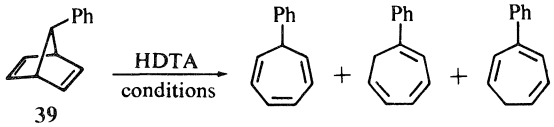

39

gave a mixture of products >80% of which did not contain a carbonyl or a hydroxyl group as determined by ir analysis. Likely this is due to

Can. J. Chem. Downloaded from www.nrcresearchpress.com by 210.87.254.6 on 09/05/12
For personal use only.

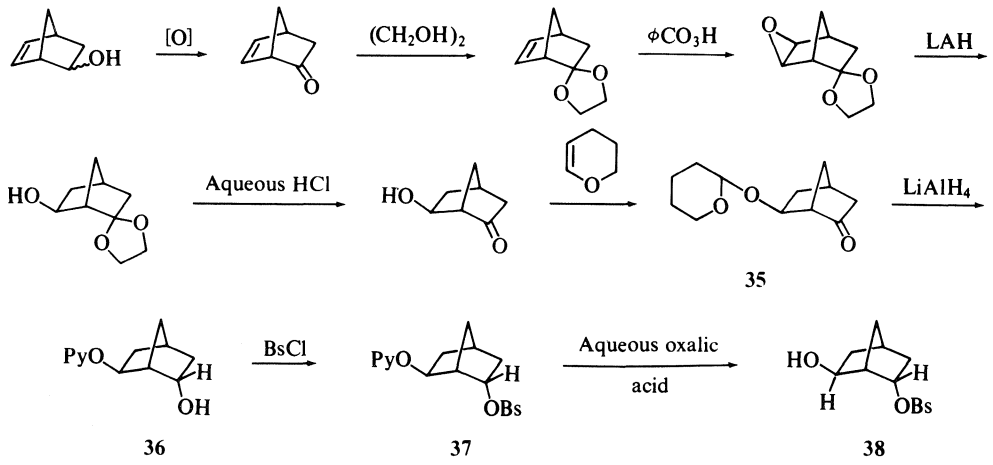

SCHEME 5

the fact that **39** undergoes a 1,3 sigmatropic rearrangement at 170 °C to a mixture of phenylcycloheptatrienes (21). Interestingly, since the major products isolated from the reaction of **39** were not alcohols or ketones the phenylcycloheptatrienyl moiety appears to be stable under the conditions of 10% v/v HOAc–H_2O at 250 °C.

That deuterium is incorporated into the sink-compounds **3**, **4**, **5**, and **6** when **1** is treated in deuterated medium is a consequence of an elimination–protonation (deuteration) sequence which involves the formation of nortricyclanol and norbornenols from the hydroxy cations and diols. Previous studies (9) on the hydration of nortricyclanes and norbornenols established that the deuterium was distributed over all the sites in norcamphor and the aldehydes and that deuterium is not incorporated into norcamphor by acid-catalyzed homoenolization. That the deuterium content in **3** + **4**, **5**, and **6**, in each case, is identical within experimental error establishes that protonation (deuteration) and hence isomerization of the cyclopentenyl and cyclohexenyl moieties is minimal under the conditions of 10% v/v HOAc–H_2O at 250 °C.

Benzonorbornadiene

The results of the hydration of benzonorbornadiene (**2**) in non-deuterated and deuterated medium are given in Table 2. The results are

TABLE 2. Hydration of benzonorbornadiene at 250 °C

Entry[a]	Time (h)	Relative % yield[b]					% yield[c]		Excess D/molecule[e]	Position of D (by pmr)
		2	**40**	**41**	**42***a* + **42***b*	Other	**40**	**41**	**40**	
1[f]	3	3.0	85.4	3.2	7.7	0.7	39	[d]	—	—
2	3	6.9	74.6	11.7	6.1	0.7	35	[d]	1.2	—
3[g]	12	0.1	64.2	34.2	0.8	0.7	—	[d]	2.9	2.0 aromatic 1.0 norbornyl
4	114	1.8	72.2	22.4	1.9	1.7	42	28	4.3	2.9 aromatic 1.2 norbornyl
5[h]	48	—	36.2	3.8	—	60	7	[d]	[d]	

[a]Typically, a solution of substrate in 10% v/v CH_3COOD–D_2O was degassed and heated in a sealed tube.
[b]Determined by glpc on a 10 ft × ⅛ in. 10% Carbowax on Chromosorb W column.
[c]Determined by preparative glpc and uncorrected for collection losses.
[d]Not determined.
[e]Determined by mass spectrometry at low voltage.
[f]Run in 10% v/v CH_3COOH–H_2O. See Fig. 3 for glpc of products.
[g]The benzonorbornenol from entry 2 containing 1.20 D/molecule was used in this run.
[h]Run in 10% v/v CH_3COOD – 1% v/v concentrated HCl–D_2O.

Can. J. Chem. Downloaded from www.nrcresearchpress.com by 210.87.254.6 on 09/05/12
For personal use only.

Can. J. Chem. Downloaded from www.nrcresearchpress.com by 210.87.254.6 on 09/05/12
For personal use only.

accountable on the basis of initial protonation of the double bond in **2** followed by collapse of the cation with a nucleophile to give **40**, **41**, and **42***a*, and **42***b* (Scheme 6).

Based on the experiment described in entry 4 the combined yield of the alcohols is in the order of 50–70%. Prolonged heating results in the equilibration of the alcohols. When a trace of strong acid (1% v/v concentrated HCl) is used, decomposition of the materials occurs at 250 °C with a resultant reduction in yields.

Interestingly, when **2** is reacted in deuterated medium (entries 2, 3, 4) deuterium exchange in the phenyl group exceeds that in the norbornyl skeleton in which the deuterium is scrambled between C-3 and C-7 as was established by nmr analysis. Although we have established (22) that the dialkyl benzene *meta*-xylene, exchanges 24% of the hydrogen on the aromatic nucleus after 48 h at 250 °C in 10% v/v CH_3COOD–D_2O, the increased ease of exchange of the aromatic nucleus in **2** is likely a consequence of strain. It is interesting to note that, while exchange proceeds to totality in the aromatic moiety, essentially only one atom of deuterium is incorporated into the norbornyl moiety. This establishes that the reversal of the **40**, **41**, and **42** to **2** via elimination is slow after initial hydration and that the alcohols once formed exchange predominantly in the aromatic nucleus (Scheme 7).

We predict therefore that the *exo*-2- and *endo*-2-benzonorbornenols would undergo exchange predominately in the aromatic nucleus. Furthermore, it is expected the benzonorbornadienes and benzonorbornenes with electron-donating substituents on the aromatic ring would exhibit facile exchange in the benzene ring under

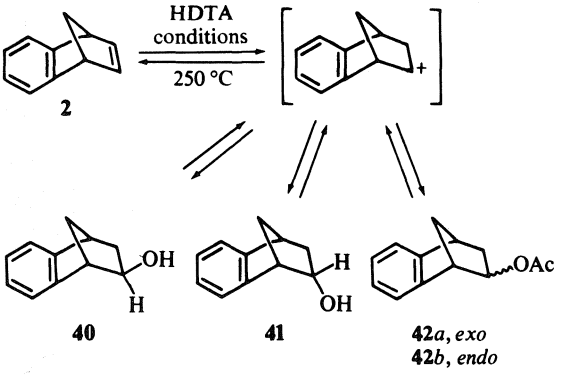

SCHEME 6

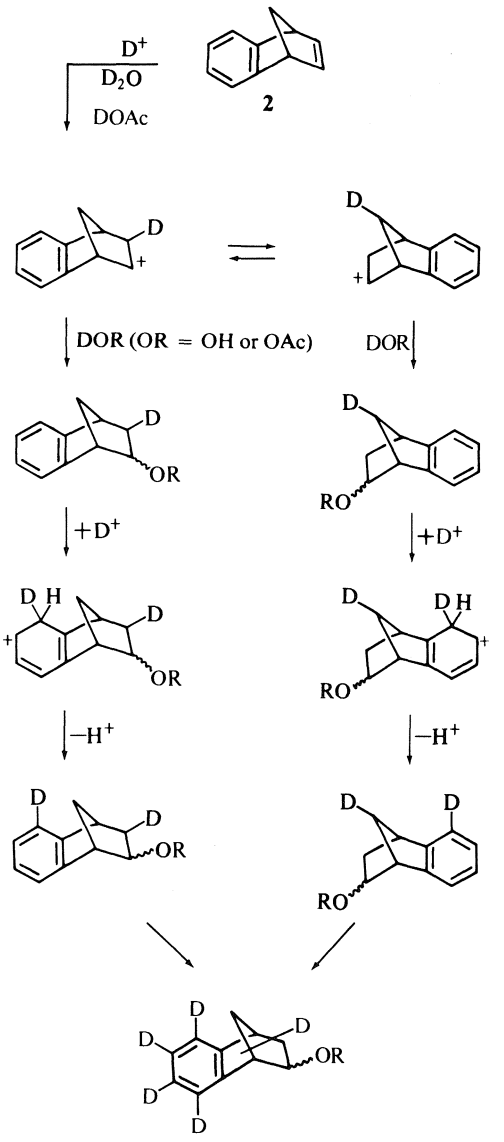

SCHEME 7

the conditions of 10% v/v CD_3COOD–D_2O at 250 °C.

Experimental

Determination of Collection Losses

To establish the collection losses which occur during preparative glpc, aliquots of known concentration (similar to that expected in the solution to be analyzed) were injected and collected and a comparison of quantities was made.

Can. J. Chem. Downloaded from www.nrcresearchpress.com by 210.87.254.6 on 09/05/12
For personal use only.

Hydration of Norbornadiene in 10% v/v CH_3COOH–H_2O at 250 °C

In a typical run, norbornadiene (Aldrich Chem. Co., 0.50 g, 5.4×10^{-3} mol) and 10% v/v HOAc–H_2O (8 ml) were placed in a glass tube (12 in. × 0.5 in.) degassed three times by the freeze–pump–thaw method, and the tube was sealed under vacuum. The reaction mixture was heated at 250 °C for 5 h in a Carius oven. The tube was opened and the contents were diluted with water (4 ml), neutralized with solid sodium bicarbonate, saturated with sodium chloride, and extracted with ether (4 × 10 ml). The combined ether extracts were dried and concentrated by distillation of the solvent through a 12 in. Vigreux column. Analytical glpc (Fig. 2) on 10 ft × $\frac{1}{8}$ in. 10% Carbowax on Chromosorb W column (the temperature was maintained at 155 °C for 5 min then rapidly stepped up to 220 °C) showed that the mixture was composed of a mixture of the cyclopenten-2- and -3-yl acetaldehydes (14%), 3-formylcyclohexene (17%), norcamphor (52%), norbornanediols (14%), and 3% of other products. The aldehydes and norcamphor were isolated by preparative glpc on a 15 ft × $\frac{3}{8}$ in. 15% Carbowax on Chromosorb W column (150 °C): cyclopenten-2- and -3-yl acetaldehydes: ir (CS_2) 3052 ($^{H}\!>\!C\!=\!C\!<^{H}$), 2710 (H—C$\lesssim^{O}$), 1730 (>C=O), 910, 718, and 666 cm^{-1} ($^{H}\!>\!C\!=\!C\!<^{H}$); nmr (CCl_4) δ 9.74 (m, 1H, H—C$\lesssim^{O}$), 5.67 (m, 2H, $^{H}\!>\!C\!=\!C\!<^{H}$), 2.8–1.8 (m, 7H). Infrared fingerprint region assay analysis (9) established that the mixture of cyclopentenyl acetaldehydes was a composite of approximately 15% **3** and 85% **4**. 3-Formylcyclohexene: ir (CS_2), 3024 ($^{H}\!>\!C\!=\!C\!<$), 2700 (H—C$\lesssim^{O}$), 1730 (>C=O) 1655 (>C=C<), 660 cm^{-1} ($^{H}\!>\!C\!=\!C\!<^{H}$); nmr (CCl_4), δ 9.55 (s, 1H, H—C$\lesssim^{O}$), 5.68 (m, 2H, $^{H}\!>\!C\!=\!C\!<^{H}$), 2.2–1.8 (m, 7H). The ir and nmr spectra were identical to those obtained from an authentic sample of 3-formylcyclohexene. Norcamphor: mp 88–90 °C (lit. (23) mp 90–91 °C); ir (CS_2) 1735 (>C=O), 1170, 1064, 938, 909, 849 and 755 cm^{-1}; nmr (CCl_4) δ 2.70 (m, 1H, C-1 bridgehead), 2.50 (m, 1H, C-4 bridgehead), 2.1–1.5 (m, 8H). The ir and nmr spectra were identical to those from an authentic sample of norcamphor. Two identical runs were carried out with reaction times of 0.5 and 3 h respectively. See Table 1, entries 1 and 2 and Fig. 1 for the product analysis for run 1.

Hydration in Deuterated Medium

Norbornadiene (13.5 g, 0.146 mol) and 10% v/v-CH_3COOD–D_2O (35 ml) were introduced into a thick, walled glass tube. The solution was degassed three times, sealed under vacuum, and heated for 9.5 h at 250 °C in a Carius oven. The dark brown reaction mixture was neutralized with solid sodium bicarbonate, saturated with sodium chloride, and extracted with ether (5 × 20 ml). The combined ether extracts were decolorized with Norit, dried with anhydrous $MgSO_4$, and concentrated by distillation through a 12 in. Vigreux column. Analytical glpc on a 10 ft × $\frac{1}{8}$ in. 10% Carbowax on Chromosorb W column (temperature maintained at 170 °C for 5 min and stepped up to 230 °C) showed cyclopenten-2- and -3-yl acetaldehydes 14%, 3-formylcyclohexene 17%, norcamphor 54%, norbornanediols 14%, and 1% of other products. The concentrated ether extract was quantitatively transferred into a 25 ml volumetric flask and made up to volume. Preparative glpc established the yields of the acetaldehydes, 3-formylcyclohexene and norcamphor as 0.6 g (4%), 0.9 g (7%), and 3.5 g (26%), respectively. Correction for collection losses established the actual yields as 1.0 g (8%) of cyclopentenyl acetaldehydes, 1.8 g (13%) of 3-formylcyclohexene, and 4.4 g (33%) of norcamphor.

The enolizable deuterium in the aldehydes was washed out by three injections of each material through a 5% KOH column (170 °C) as described previously (9). The deuterated norcamphor was washed three times with a MeOH–H_2O–KOH solution as described previously (9).

A mass spectrometric deuterium assay at 11 eV, on the samples from which the enolizable deuterium was washed out, established that (*a*) the mixture of cyclopentenyl acetaldehydes was composed of 4.2% d_5, 13.8% d_4, 30.4% d_3, 36.3% d_2, and 14.3% d_1 species (2.5 excess atoms of deuterium); (*b*) 3-formylcyclohexene was composed of 1.7% d_6, 5.2% d_5, 13.8% d_4, 28.0% d_3, 38.7% d_2, 8.7% d_1, and 3.9% d_0 species (2.6 excess atoms of deuterium); and (*c*) norcamphor was composed of 1.5% d_6, 3.8% d_5, 10.1% d_4, 23.7% d_3, 44.1% d_2, 13.4% d_1, and 3.4% d_0 species (2.4 excess atoms of deuterium).

Preparative Scale Hydration of Norbornadiene

A mixture of norbornadiene (125 g, 1.35 mol) and 10% v/v HOAc–H_2O (500 ml) was heated for 18 h at 250 °C in a 2 litre Parr Monel bomb. The resultant mixture consisted of a black organic layer and a yellow aqueous layer. This mixture was neutralized with solid sodium bicarbonate, saturated with sodium chloride, and extracted with ether (5 × 200 ml). The combined ether extracts were washed with a saturated sodium bisulfite solution (5 × 150 ml) (to remove the aldehydes). The ether extract was then dried with anhydrous Na_2SO_4 and concentrated by distillation through a 12 in. Vigreux column. Analytical glpc analysis showed 1% of cyclopentenyl acetaldehydes, 6% of 3-formylcyclohexene, 92% of norcamphor, and 1% of another product. The concentrated ether extract was vacuum distilled through a 15 in. vacuum jacketed Vigreux column to yield norcamphor (34 g, 23%, bp 40–50 °C/4 torr). Analytical glpc analysis showed 87% of norcamphor and 13% of 12 other products. Infrared and nmr spectra of a sample isolated by preparative glpc were identical to an authentic sample of norcamphor: mp 88–90 °C (lit. (23) mp 88–91 °C).

Treatment of Norbornadiene with H_2O at 250 °C

Norbornadiene (0.82 g, 8.8×10^{-3} mol) and water (6 ml) were placed in a glass tube, degassed three times by the freeze–pump–thaw method, and the tube was sealed under vacuum. After the tube was heated at 250 °C for 10 h in a Carius oven, the reaction mixture which contained some white solid material, was extracted with ether (5 × 8 ml). The combined ether extracts were dried and concentrated by distillation through a 12 in. Vigreux column. The white solid was only slightly soluble in ether and precipitated out in the concentrated ether extract. Analytical glpc on a 5 ft × $\frac{1}{8}$ in. 5% SE-30 on Carbowax column at 115 °C showed that only norbornadiene was present.

Can. J. Chem. Downloaded from www.nrcresearchpress.com by 210.87.254.6 on 09/05/12
For personal use only.

exo-2-syn-7-Ditosyloxynorbornane

exo-2-*syn*-7-Dihydroxynorbornane (6.46 g, 5.1×10^{-2} mol, 95–90% *syn*, 5–10% *anti*, mp 180–186 °C; prepared by the solvolysis of nortricyclanol and norbornenols as described previously (9)) and freshly recrystallized tosyl chloride (21.2 g, 0.11 mol, mp 67–68 °C) were dissolved in dry pyridine (120 ml). The mixture was kept in the refrigerator for 6 days then was poured into a separatory funnel containing ice water (500 ml) and extracted with chloroform (4×80 ml). The combined extracts were washed with dilute HCl (3×60 ml), saturated sodium bicarbonate (2×60 ml), water (1×60 ml), and dried. The dried extract was concentrated on the rotatory evaporator and pumped to dryness on the vacuum pump to yield a slightly coloured solid. This solid was recrystallized twice from hot methanol to yield *exo*-2-*syn*-7-ditosyloxynorbornane containing 6–10% of the *anti*-isomer; 11.2 g, 51%, mp 114–115 °C (lit. (24) mp of pure *syn*-isomer 121.5–121.6 °C); nmr ($CDCl_3$) δ 7.9–7.3 (m, 8H, aromatic protons), 4.80 (m, 2H, C-2-*exo* and C-7-*syn* with 6–10% C-7-*anti*), 2.48 (s, 6H, $-CH_3$), 2.40–1.0 (norbornyl envelope); ir ($CDCl_3$) 2950 ($\geqslant$C—H), 1600 (aryl C=C), 1190 ($-SO_2-O-$), and 865 cm^{-1} (aryl C—H).

Preparation of a Mixture of syn- and anti-7-Tosyloxy-exo-2-hydroxynorbornanes

The solvolysis of *exo*-2-*syn*-7-ditosyloxynorbornane (8.93 g, 0.020 mol, mp 114–115 °C) was carried out in refluxing 75% v/v aqueous acetone (200 ml) containing an excess of powdered calcium carbonate (2.2 g, 0.02 mol) (14). After a 2 week reflux, the reaction was diluted with water (50 ml) and extracted with carbon tetrachloride (5×40 ml). The combined extracts were dried over anhydrous magnesium sulphate and concentrated on the rotatory evaporator. The remaining residue which was pumped on overnight yielded a viscous oil (5.17 g, 89%). Initial attempts to recrystallize the oil from ether–petroleum ether failed. After the oil remained in the refrigerator for 2 weeks, a white oily solid was formed. This oily solid was washed with petroleum ether (30–60°) and after four recrystallizations from pentane–ether yielded white plates (mp 79.5–81 °C); nmr (CCl_4) δ 7.6 (quartet with fine structure, 4H, aromatic protons), 4.78 (s, 0.22H, C-7-*syn*-H), 4.50 (s, 0.78H, C-7-*anti*-H), 3.80 (bm, 1H, C-1-H), 2.48 (s, 3H, $-CH_3$), 2.3–1.0 (norbornyl envelope); ir (CCl_4) 3600 (—O—H), 2955 ($\geqslant$C—H), 1600 (aryl C=C), 1190 (doublet, $-SO_2-O-$), 1095 (C—O), and 865 cm^{-1} (aryl C—H). Nuclear magnetic resonance integration analysis showed that the *syn*- and *anti*-7-tosyloxy-*exo*-2-hydroxynorbornanes were present in a ratio of 78:22. *Anal.* calcd. for $C_{14}H_{18}SO_4$: C 59.55, H 6.43; found: C 59.67, H 6.57.

Solvolysis of a 78:22 Mixture of syn- and anti-7-Tosyloxy-exo-2-hydroxynorbornanes in Buffered 10% v/v $HOAc-H_2O$ at 95 °C

The mixture of *syn*- and *anti*-hydroxytosylates (0.11 g, 0.40×10^{-3} mol, mp 79.5–81 °C) was introduced into a glass ampoule (3 in. $\times$ 0.15 in.) containing 10% v/v $HOAc-H_2O$ (2 ml) buffered with 0.1 *M* NaOAc. The mixture was degassed three times by the freeze–pump–thaw method and the tube was sealed under vacuum. When the sample reached room temperature, it was placed into a constant temperature oil bath at 95 $\pm$ 1 °C. After 7 days, a yellowish globule was observed in the bottom of the ampoule. The cooled solvolysis mixture was poured into ice water (4 ml), neutralized with solid sodium bicarbonate, and then extracted with petroleum ether (3×10 ml) respectively. Both extracts were separately dried and concentrated by distilling the solvent through a glass helicies column (12 in.). Both extracts were quantitatively transferred onto separate watch glasses and allowed to evaporate to dryness. The petroleum ether extract yielded cyclopenten-2-yl acetaldehyde (0.036 g, 90%) while the ether extract yielded a semisolid (0.003 g). The glpc analysis on a 10 ft $\times$ $\frac{1}{8}$ in. 10% Carbowax on Chromosorb W column at 110 °C of the petroleum ether extract showed only cyclopenten-2-yl acetaldehyde (>99%) while the ether extract indicated more than 95% of 2-(cyclopentene)acetaldehyde and less than 5% of 3-formylcyclohexene, norcamphor, and two other unidentified products.

The 3-formylcyclohexene, norcamphor, and two other products in the ether extract may have arisen from traces of unreacted hydroxy tosylate which reacted on the glpc injector block and/or column as described in the following section. Comparison of the ir fingerprint region of the aldehyde, isolated from the petroleum ether extract by preparative glpc, with that of an authentic sample showed that the product was pure cyclopent-2-yl acetaldehyde with characteristic absorptions at 912 and 718 cm^{-1} (9).

Stability of the Hydroxytosylates 27a and 27b in the Gas Chromatograph

The mixture of hydroxytosylates ***27a*** and ***27b*** was dissolved in acetone and injected in the glpc on a 10 ft $\times$ $\frac{1}{8}$ in. 10% Carbowax on Chromosorb W column at 110 °C with the injector temperature at 235 °C. The gas chromatogram showed that the pyrolysis products were predominantly the aldehydes **3** + **4**, **5**, and norcamphor. In addition to the sink compounds, five other products were present. Although the relative percentages of products varied from one injection to another, the sink compounds were always the major products.

Norbornen-2-one

Norbornen-2-one was prepared from 20 g of norbornenol according to the procedure of Cristol (25). After work-up the norbornenone was distilled through a vacuum jacketed Vigreux column using biphenyl (3 g) as a chaser, to yield 13.8 g (70%) of norbornen-2-one: bp 97–98 °C/91 torr.

Norbornen-2-one Ethylene Ketal

The ketal was prepared from norbornenone (13 g) according to the procedure of Meinwald and Cadoff (26).

5-Ethylenedioxy-exo-2,3-epoxynorbornane

The epoxide was prepared from 17.0 g of the ketal and perbenzoic acid as described by Meinwald and Cadoff (26) to give 17.6 g (93%) of product bp 103–107 °C/8 torr (lit. (26) bp 53 °C/0.23 torr).

exo-6-Hydroxy-2-ethylenedioxynorbornane

The previously obtained epoxy ketal (17.6 g, 0.105 mol) was added to a slurry of lithium aluminum hydride (4.0 g, 0.10 mol) in *N*-ethylmorpholine (150 ml, freshly distilled from LAH) and converted to the hydroxy ketal

Can. J. Chem. Downloaded from www.nrcresearchpress.com by 210.87.254.6 on 09/05/12
For personal use only.

as described by Meinwald and Cadoff (26). Vacuum distillation through a 4 in. vacuum jacketed Vigreux column gave the desired alcohol (8.17 g, 46%, bp 70–72 °C/0.1 torr (lit. (26) bp 70–72 °C/0.1 torr)); nmr (CCl_4) δ 4.22 (doublet with fine structure, 1H, C-2-*endo*), 3.80 (s, 4H, ketal), 2.38–1.22 (norbornyl envelope); ir (CS_2), 3600–3500 (O—H), 1190, 1078, 1042, and 955 cm^{-1}.

exo-6-Pyranyloxy-norbornan-2-one ***(35)***

A mixture of hydroxy ketone (1.02 g, 8.1 $\times$ 10^{-3} mol), prepared from the hydroxy ketal as described by Meinwald and Cadoff (26), dihydropyran (1.03, 12.2 $\times$ 10^{-3} mol), and concentrated hydrochloric acid (1 drop) was stirred for 4 h at room temperature. The resultant mixture was taken up in ether, washed with 10% NaOH (3 $\times$ 15 ml), water (1 $\times$ 15 ml), and dried. Removal of the solvent on the rotatory evaporator and pumping on the vacuum line yielded crude product (1.55 g, 91%); nmr (CCl_4) δ 4.62 (m, 1H), 3.81 (m, 2H), 2.8 (m, 1H), 2.2–1.5 (norbornyl envelope and pyranyl ether protons); ir (neat) 1750 (C=O), 1125 cm^{-1} (C—O).

exo-6-Pyranyloxy-endo-2-hydroxynorbornane ***(36)***

The previously prepared *exo*-6-pyranyloxy-norbornan-2-one (1.54 g, 7.3 $\times$ 10^{-3} mol) was reacted with $LiAlH_4$ (0.152 g, 4 $\times$ 10^{-3} mol) in refluxing ether (50 ml) for 5 h. The usual work-up gave 1.24 g (80%) of crude product; nmr (CCl_4) δ 5.0–3.3 (m, 5H), 2.2–1.5 (norbornyl envelope and pyranyl ether protons); ir (neat) 3400 (O—H), 1025 cm^{-1} (C—O).

exo-6-Pyranyloxy-endo-2-brosyloxynorbornane ***(37)***

The hydroxypyranyl ether (1.20 g, 5.68 $\times$ 10^{-3} mol) and recrystallized brosyl chloride (1.48 g, 5.8 $\times$ 10^{-3} mol, mp 76–78 °C) in dry pyridine (40 ml) were stored in the refrigerator at 0 °C for 6 days. The resultant reaction mixture was quenched with ice water (60 ml) and extracted with ether (3 $\times$ 25 ml). The combined ether extracts were washed with dilute HCl (4 $\times$ 15 ml), saturated sodium bicarbonate (1 $\times$ 15 ml), and dried. The ether was removed on the rotatory evaporator and the residue was pumped to dryness on the vacuum line to yield crude pyranylether brosylate (1.63 g, 67%); nmr (CCl_4) δ 7.6 (bm, 4H, aryl), 4.2–3.4 (m, 4HP), 2.3–1.4 (norbornyl envelope and pyranyl ether protons); ir (CCl_4) 1586 (aryl C=C), 1185 cm^{-1} (doublet, —SO_2—O—). Attempts to recrystallize the ether brosylate from methanol and ether – petroleum ether failed, and consequently the crude product was used in the following hydrolysis.

exo-6-Hydroxy-endo-2-brosyloxynorbornane ***(38)***

The pyranyl ether brosylate (1.42 g, 3.30 $\times$ 10^{-3} mol) was dissolved in 2% wt/v oxalic acid – 70% v/v aqueous methanol (50 ml) and stirred at room temperature. After 2.5 h, addition of water (20 ml) turned the clear reaction mixture milky. This solution was extracted with ether (3 $\times$ 20 ml). The combined ether extracts were washed with saturated sodium bicarbonate (1 $\times$ 10 ml), water (2 $\times$ 10 ml), saturated sodium chloride (1 $\times$ 10 ml), and dried over anhydrous magnesium sulphate. The ether was removed on the rotatory evaporator to yield an oil. On adding carbon disulfide (2 ml) to this oil, white crystals slowly appeared. These crystals were rinsed twice more with carbon disulfide, pumped on the vacuum line for 20 min, and finally recrystallized thrice from ether–pentane to afford an analytical sample of white fluffy crystals (0.36 g, 31%, mp 113–115 °C); nmr ($CDCl_3$) δ 7.60 (s, 4H, aryl), 4.78 (m, 1H, C-6-*exo*), 4.38 (d, C-2-*endo*), 2.51–1.1 (norbornyl envelope); ir ($CDCl_3$) 3600 (O—H), 3085 (aryl C—H), 1586 (aryl C=C), 1185 (d, —SO_2—O—), 1090 (—C—O), and 960 cm^{-1} (aryl C—H). *Anal.* calcd. for $C_{13}H_{15}SO_4Br$: C 44.97, H 4.35; found: C 45.08, H 4.39.

Solvolysis of exo-6-Hydroxy-endo-2-brosyloxynorbornane in Buffered 10% v/v HOAc–H_2O at 95 °C

The hydroxy brosylate (0.12 g, 0.343 $\times$ 10^{-3} mol, mp 113–115 °C) was introduced into a glass ampoule (3 in. $\times$ 1.5 in.) containing 10% v/v HOAc–H_2O (2 ml) buffered with 0.1 *M* NaOAc. The mixture was degassed three times, sealed under vacuum, and placed in a constant temperature oil bath at 95 $\pm$ 1 °C. After 13 days, the cooled brownish solvolysis mixture was poured into ice water (2 ml), neutralized with solid sodium bicarbonate, and extracted with pentane (6 $\times$ 10 ml) and then with ether (4 $\times$ 10 ml). Both extracts were dried separately and concentrated by distillation through a glass helicies column (12 in.). Both extracts were quantitatively transferred onto tared watch glasses and allowed to evaporate to dryness. The pentane extract yielded a pungent smelling liquid, cyclopenten-3-yl acetaldehyde (**3**) (0.028 g, 74%) whereas the ether extract yielded a CS_2 insoluble white solid (0.016 g). The glpc analysis of the pentane extract on a 10 ft $\times$ $\frac{1}{8}$ in. 10% Carbowax on Chromosorb W column at 115 °C showed cyclopenten-3-yl acetaldehyde (94%), 3-formylcyclohexene (3%), and one unidentified product (3%) while the ether extract indicated 51% of cyclopenten-3-yl acetaldehyde and 49% of nine other unidentified products whose retention times were shorter than the norbornanediols. An ir, (CS_2), of the pentane extract showed that the product was in fact **3** with characteristic absorptions at 3052 ($^{H}>C=C<^{H}$), 2710 ($H—C\lesssim^{O}$), 1730 (>C=O), 666 cm^{-1} ($^{H}>C=C<^{H}$).

Stability of the Hydroxybrosylate on the Gas–Liquid Partition Chromatography Injector Block and/or Column

Pure *exo*-6-hydroxy-*endo*-2-brosyloxynorbornane was dissolved in acetone and injected in the glpc on a 10 ft. $\times$ $\frac{1}{8}$ in. 10% Carbowax on Chromosorb W column at 115 °C with the injector and detector temperatures at 225 °C. The gas chromatogram showed that the pyrolysis product had the same retention time as **3** and **4**. No **5** or **6** could be detected.

Benzonorbornadiene ***(2)***

Benzonorbornadiene was prepared from 13 g of 2-bromofluorobenzene and 4.1 g of cyclopentadiene by the method of Wittig and Knauss (27). Distillation of the reaction mixture through a Vigreux column gave 7 g of benzonorbornadiene (66%, bp 82–83 °C/12 torr, >99% pure as established by gas chromatographic analysis); nmr (CCl_4) δ 6.62–7.18 (m, 6H, 4 aromatic and 2 olefinic), 3.78 (m, 2H, bridgehead C—H), 2.22 (m, 2H, C-7).

Typical Hydration of ***2*** *in 10% v/v HOAc–H_2O at 250 °C*

Benzonorbornadiene (0.50 g, 3.5 $\times$ 10^{-3} mol, bp 82–83 °C/12 torr) and 10% v/v CH_3COOH–H_2O (3 ml) were introduced into a glass tube (11 in. $\times$ 0.5 in. i.d.).

Can. J. Chem. Downloaded from www.nrcresearchpress.com by 210.87.254.6 on 09/05/12
For personal use only.

The sample was degassed three times by the freeze–pump–thaw method, sealed under vacuum, and heated at 250 °C for 3 h in a 2 litre Parr bomb containing water to equalize pressure. The slightly yellowish reaction mixture was diluted with water (3 ml), neutralized with solid sodium bicarbonate, saturated with NaCl, and extracted with ether (4 × 20 ml). The ether extract was dried, concentrated on the rotatory evaporator, and quantitatively transferred into a 2 ml volumetric flask. Analytical glpc on a 10 ft × ⅛ in. 5% SE-30 on Chromosorb W column at 125 °C showed that the mixture was composed of benzonorbornadiene (3.0%), *endo*-benzonorbornenol (3.2%), *exo*-benzonorbornenol (85.4%), benzonorbornenyl acetate (7.7%), and an unknown (0.7%). (See entry 1, Table 2 and Fig. 3.) The products were isolated by preparative glpc on a 5 ft × ¼ in. 5% SE-30 on Chromosorb W column at 195 °C. *exo*-Benzonorbornenol: mp 72–74 °C (lit. (28) mp 74–75 °C); ir (CCl_4) 3620 (O—H), 3030 (aryl-H), 1070 and 1050 (C—O), 862 (C—H), and 730 cm^{-1} (aryl-H); nmr (CCl_4) δ 6.96 (m, 4H, aryl), 3.86 (bd, 1H, C-2 proton), 3.17 (d, 2H, bridgehead C—H), and 2.1–1.56 (norbornyl envelope, 4H); ms (80 eV); M^+ at *m/e* 160 corresponds to $C_{11}H_{12}O$. The ir and nmr spectra were identical to an authentic sample of *exo*-benzonorbornenol obtained from the hydroboration of benzonorbornadiene. *endo*-Benzonorbornenol: mp 69–74 °C (lit. (28) mp 74 °C); ir (CCl_4) 3580 (O—H), 3030 (aryl-H), 1155, 1140, 1130, 1115 (C—H), 1072 and 1050 (C—O), and 728 cm^{-1} (aryl-H); ms (80 eV); M^+ at *m/e* 160 corresponds to $C_{11}H_{12}O$. The ir was identical to an authentic sample of *endo*-benzonorbornenol obtained as the minor product in the hydroboration of benzonorbornadiene. The ir fingerprint region was used to distinguish between the *exo*- and *endo*-benzonorbornenol, since an unsymmetrical quartet present at 1155, 1140, 1130, and 1115 cm^{-1} in the *endo*-alcohol is absent in the *exo*-alcohol while a band at 862 cm^{-1} in the latter is absent in the *endo*-alcohol. Benzonorbornenyl acetate: ir (CCl_4) 3030 (aryl-H), 1742 (>C=O), 1244 and 1029 (≥C—OAc), and 728 cm^{-1} (aryl-H); ms (80 eV) M^+ at *m/e* 202 corresponds to $C_{13}H_{14}O_2$ while *m/e* 159 corresponds to $M^+ - O{-}\overset{\overset{O}{\|}}{C}{-}CH_3$.

Injection of several aliquots (0.08 ml) of the ether extract through the 5% SE-30 column established the recovered yield (not corrected for collection losses) of *exo*-benzonorbornenol as 0.22 g (39%).

Hydration in 10% v/v CH_3COOD–D_2O at 250 °C

Benzonorbornadiene (0.43 g, 3.1 × 10^{-3} mol, bp 82–83 °C/12 torr and 10% v/v CH_3COOD–D_2O (3 ml) were introduced into a glass tube (11 × 0.5 in. i.d.). The sample was degassed three times by the freeze–pump–thaw method, sealed, and heated at 250 °C for 3 h in the Parr bomb. The slightly yellowish reaction mixture was diluted with water (3 ml), neutralized with solid sodium bicarbonate, saturated with NaCl, and extracted with ether (4 × 20 ml). The ether extract was washed with water (4 × 25 ml) to remove the exchangeable O—D, dried, concentrated on the rotatory evaporator, and quantitatively transferred into a 1 ml volumetric flask. Analytical glpc on a 10 ft × ⅛ in. 15% Carbowax on Chromosorb W column at 140 °C showed that the mixture was composed of 6.9% benzonorbornadiene, 11.7% *endo*-benzonorbornenol, 74.6% *exo*-benzonorbornenol, 6.1% benzonorbornenyl acetate, and 0.7% of an unknown. Injection of several aliquots (0.05 ml) of the ether extract through the preparative 5% SE-30 column established the yield (not corrected for collection losses) of pure *exo*-benzonorbornenol as 0.17 g (35%).

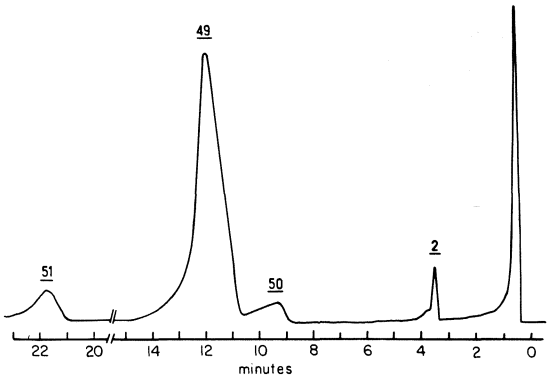

FIG. 3. The glpc trace of products from the hydration–exchange of benzonorbornadiene.

A mass spectrometric deuterium assay (15 eV) established that *exo*-benzonorbornenol was composed of 3.4% d_3, 18.0% d_2, 73.2% d_1, and 5.4% d_0 species (1.2 excess atoms of deuterium per molecule).

The *exo*- and *endo*-benzonorbornenol from the above experiment containing 1.20 excess atoms of deuterium was treated with a fresh batch of 10% v/v CH_3COOD–D_2O for 12 h at 250 °C. Work-up in the usual manner gave an 85% yield which analyzed for 0.1% benzonorbornadiene, 34.2% *endo*-benzonorbornenol, 64.2% *exo*-benzonorbornenol, 0.8% benzonorbornenyl acetate, and 0.7% of an unknown.

A mass spectrometric deuterium assay (15 eV) established that *exo*-benzonorbornenol was composed of 1.2% d_6, 6.3% d_5, 22.5% d_4, 36.2% d_3, 24.2% d_2, 7.7% d_1, and 1.9% d_0 species (2.9 excess atoms of deuterium): nmr (CCl_4) area integral analysis using the O—H as an internal standard established the following deuterium distribution; 2.0 ± 0.1 D in aromatic ring and 1.0 ± 0.1 D at C-3 and C-7 (a total of 3.0 excess atoms of deuterium).

Hydration of Benzonorbornadiene. Reaction Time 114 h

Benzonorbornadiene (0.47 g, 3.31 × 10^{-3} mol) was heated at 250 °C with 3 ml of 10% v/v DOAc–D_2O in a 8 × ½ in. medium-walled tube in the usual manner for 114 h. Usual work-up gave 0.43 g of crude product (80%). Preparative glpc in the usual manner established the recoverable yield (not corrected for collection losses) of *exo*- and *endo*-benzonorbornenols as 0.22 g (42%) and 0.15 g (28%) respectively. Mass spectral analysis at 15 eV of the *exo*-alcohol established that it was a composite of 12.9% d_6, 34.3% d_5, 31.9% d_4, 14.8% d_3, 4.5% d_2, and 1.8% d_0 species (4.3 excess atoms of deuterium per molecule). An nmr integration analysis established that the deuterium distribution was as follows: aromatic ring 2.95 ± 0.1, C-3, C-7 of the norbornyl system, 1.05 ± 0.1, and C-2 0.15 ± 0.05.

Acknowledgment

Financial support of the National Research Council of Canada is gratefully acknowledged.

1. N. H. WERSTIUK and T. KADAI. Chem. Commun. 1613 (1970).
2. S. J. CRISTOL, W. K. SEIFERT, D. W. JOHNSON, and J. B. JURALE. J. Am. Chem. Soc. **84**, 3918 (1962).
3. S. J. CRISTOL, T. C. MORRILL, and R. A. SANCHEZ. J. Org. Chem. **31**, 2719 (1966).
4. S. J. CRISTOL, T. C. MORRILL, and R. A. SANCHEZ. J. Org. Chem. **31**, 2726 (1966).
5. S. J. CRISTOL, T. C. MORRILL, and R. A. SANCHEZ. J. Org. Chem. **31**, 2733 (1966).
6. T. C. MORRILL and B. E. GREENWALD. J. Org. Chem. **38**, 616 (1973).
7. S. J. CRISTOL and R. CAPLE. J. Org. Chem. **31**, 2741 (1966).
8. S. J. CRISTOL and J. M. SULLIVAN. J. Am. Chem. Soc. **93**, 1967 (1971).
9. N. H. WERSTIUK and T. KADAI. Can. J. Chem. **50**, 3350 (1972).
10. S. J. CRISTOL and R. K. BLY. J. Am. Chem. Soc. **82**, 6155 (1960).
11. L. B. JONES and V. K. JONES. J. Org. Chem. **36**, 1017 (1971).
12. J. M. COX, M. P. HARTSHAM, and A. J. LEWIS. Aust. J. Chem. **24**, 1009 (1971).
13. B. RICKBORN and R. M. GERKIN. J. Am. Chem. Soc. **93**, 1693 (1971).
14. P. G. GASSMAN, J. L. MARSHALL, and J. M. HORNBACK. J. Am. Chem. Soc. **91**, 5811 (1969).
15. B. ARBUSOV. Ber. **68**, 1430 (1935).
16. D. E. GWYNN and L. SKILLERN. Chem. Commun. 490 (1968).
17. Z. CHABUDZINSKI, U. LIPNICKA, and Z. RYKOWSKI. Rocz. Chem. **44**, 2181 (1970).
18. H. HART. Acc. Chem. Res. **4**, 337 (1971).
19. F. P. CAPPELLI, G. TIMMINS, and N. H. WERSTIUK. Can. J. Chem. **50**, 2163 (1972), and references therein.
20. A. J. JONES, E. HUANG, R. HASELTINE, and T. S. SORENSEN. J. Am. Chem. Soc. **97**, 1133 (1975).
21. R. K. LUSTGARTEN and H. C. RICHEY, JR. J. Am. Chem. Soc. **96**, 6393 (1974).
22. N. H. WERSTIUK and T. KADAI. Can. J. Chem. **51**, 1485 (1973).
23. J. K. CRANDALL. J. Org. Chem. **29**, 2830 (1964).
24. P. G. GASSMAN, J. L. MARSHALL, and J. M. HORNBACK. J. Am. Chem. Soc. **91**, 5811 (1969).
25. S. J. CRISTOL and P. K. FREEMAN. J. Am. Chem. Soc. **83**, 4427 (1961).
26. J. MEINWALD and B. C. CADOFF. J. Org. Chem. **27**, 1539 (1962).
27. G. WITTIG and E. KNAUSS. Chem. Ber. **91**, 895 (1958).
28. P. D. BARTLETT and W. P. GIDDINGS. J. Am. Chem. Soc. **82**, 1240 (1960).

Can. J. Chem. Downloaded from www.nrcresearchpress.com by 210.87.254.6 on 09/05/12
For personal use only.

Reaction of organic compounds under high temperature – dilute acid (HTDA) conditions. III. The perdeuteration of bicyclo[2.2.1]heptanes[1]

NICK HENRY WERSTIUK AND TONU KADAI

Department of Chemistry, McMaster University, Hamilton, Ont., Canada L8S 4M1

Received November 14, 1975

NICK HENRY WERSTIUK and TONU KADAI. Can. J. Chem. **54**, 2213 (1976).

The hydration of norbornene (**1**) and nortricyclane (**2**) under the high temperature and dilute acid (HTDA) conditions of aqueous acetic acid at 250 °C gives as products *exo*-2-norborneol, *endo*-2-norborneol, *exo*-2- and *endo*-2-norbornyl acetate, and a mixture of stereoisomeric dinorbornyl ethers **4**. When the reactions are carried out in deuterated medium perdeuteration (>90% in one cycle) of the [2.2.1]-products is accomplished. Respectable overall yields (50–70%) of the products are obtained. Solvolysis of the products *exo*-norborneol, and *endo*-norbornyl acetate under HTDA(D) conditions also leads to perdeuterated **3***a*, **3***b*, **3***c*, **3***d*, and **4**.

NICK HENRY WERSTIUK et TONU KADAI. Can. J. Chem. **54**, 2213 (1976).

L'hydratation du norbornène (**1**) et du nortricyclane (**2**) à haute température et dans des conditions diluées d'acide acétique (HTDA) à 250 °C conduit aux produits suivants: le norbornéol-2 *exo*, le norbornéol-2 *endo* et les acétates de norbornyles-2 *endo* et -2 *exo* et un mélange d'éthers dinorbornyles stéréoisomères **4**. Quand les réactions sont effectuées dans un milieu deutéré, on produit une perdeutération (>90% dans un cycle) des produits [2.2.1]. On obtient des rendements globaux de produits qui sont respectables (50–70%). La solvolyse du norbornéol *exo* et de l'acétate de norbornyle *endo* dans les mêmes conditions (HTDA deutéré) conduit aussi aux produits perdeutérés **3***a*, **3***b*, **3***c*, **3***d* et **4**.

[Traduit par le journal]

Introduction

The acid-catalyzed addition of reagents HX to norbornene (**1**) yields only *exo*-substituted bicyclo[2.2.1]heptyl products (2–7, 12). Mechanistic studies directed to establish the nature of the intermediate norbornyl cation in these reactions, have involved the addition of deuterated acids DX to norbornene (8–11). In all the mechanistic studies described thus far, the solitary incoming atom of deuterium is scrambled predominately between C-3 and C-7.

There has been but one report on the multiple deuteration of the bicyclo[2.2.1]heptyl system (13). Complete deuteration (99%) of norbornyl bromide was accomplished in four cycles, beginning with the reaction of norbornene in refluxing 44% DBr in D_2O. The deuterated bromide, at an average yield of 15% per cycle, was isolated and recycled.

Studies (9, 14) on the addition of deuterated acids to nortricyclane (2), have established that multiple deuteration of the product occurs only when DCl is added to **2** in pentane (14). The product *exo*-norbornyl chloride was a composite of 21.5% d_0, 52% d_1, 22.5% d_2, and 4% d_3 species.

[1]For a preliminary account see ref. 1.

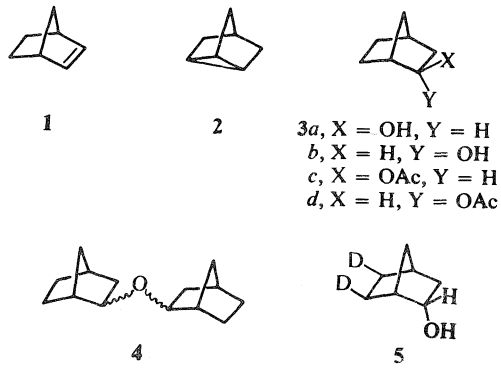

1 2 **3***a*, X = OH, Y = H; *b*, X = H, Y = OH; *c*, X = OAc, Y = H; *d*, X = H, Y = OAc

4 5

Through a continuation of our studies (1, 15–19) on the hydration–exchange of organic compounds under high temperature – dilute acid conditions, to establish the scope and limitations of the reaction as a general labelling method, we have reacted norbornene (**1**), nortricyclane (**2**), *exo*-2-norborneol (**3***a*), and *endo*-2-norbornyl acetate (**3***d*) under HTDA conditions in deuterated medium.

Results and Discussion

The results of the study are given in Table 1. The products (Fig. 1), of the hydration–exchange of **1** and **2** are *exo*- and *endo*-2-norborneol (**3***a*, **3***b*), *exo*- and *endo*-2-norbornyl acetate (**3***c*, **3***d*)

Can. J. Chem. Downloaded from www.nrcresearchpress.com by 210.87.254.6 on 09/05/12
For personal use only.

Can. J. Chem. Downloaded from www.nrcresearchpress.com by 210.87.254.6 on 09/05/12
For personal use only.

TABLE 1. Data for hydration–exchange of norbornene (**1**), nortricyclane (**2**), *exo*-norborneol (**3***a*), and *endo*-norbornyl acetate (**3***d*)

Entry[a]	Substrate	Time (h)	Relative % yield[b]							% yield[c] **3***a* + **3***b*	Excess D/molecule[d] in **3***a* + **3***b*	% exchange[h] in **3***a* + **3***b*
			1	**2**	**3***a*	**3***b*	**3***c* + **3***d*	**4**	Other			
1	**1**	1.5	63.2		22.9	5.7	7.2	—	1.0	21	2.2	20
2	**1**	3	25.0	7.0	48.5		8.0	6.0	5.5	41	5.9	54
3	**1**	4	8.1	9.2	42.8	19.3	9.1	6.8	4.7	36	9.8	89
4	**1**	15	2.8	3.1	57.4	26.0	7.2	1.3	2.2	69	9.6	87
5[e]	**1**	15	15.4	—	23.8	10.8	—	2.6	27.4	29	9.9	90
6[f]	**1**	60	99.0	—	—	—	—	—	1.0			
7[g]	**1**	120	1.2	—	56.2	20.9	9.2	7.4	5.1	80	10.1	91
8	**1**	528	0.7	0.6	23.1	10.2	7.8	4.7	53.0	10	9.9	90
9	**2**	15	—	—	93.5		5.0	—	1.5	42	9.8	89
10	**3***a*	15	0.7	1.3	61.0	28.2	8.0	0.4	0.4	79	9.8	89
11	**3***d*	15	0.8	0.5	37.3	16.7	39.2	—	5.5	51	10.3	93

[a]Typically a solution of substrate in 10% v/v CH_3COOD–D_2O was degassed and heated in a sealed tube.
[b]Determined by glpc on 10 ft × ⅛ in. 10% SE-30 and 10% Carbowax on Chromosorb W columns. In several of the cases a small amount of norcamphor was formed.
[c]Determined by preparative glpc and corrected for collection losses as described in the preceding paper (19).
[d]Determined mass spectrometrically on the acetates at low voltage. The estimated error in these values is ±2–3%.
[e]Run in 1% v/v HCl–D_2O.
[f]Run in D_2O only.
[g]Run in 10% v/v CD_3COOD–D_2O. See Fig. 1 for glpc trace.
[h]Other than O—H.

Can. J. Chem. Downloaded from www.nrcresearchpress.com by 210.87.254.6 on 09/05/12
For personal use only.

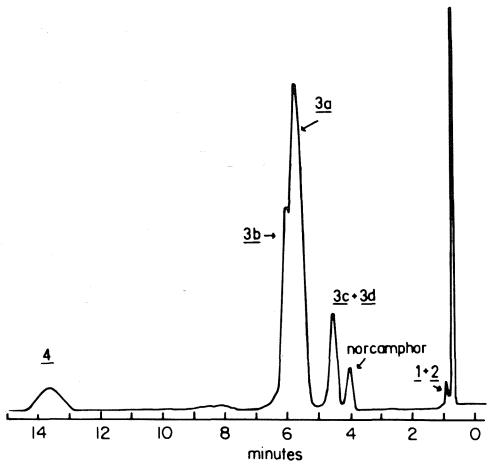

FIG. 1. The glpc trace of the products of the hydration–exchange of norbornene in DOAc–D_2O at 250 °C (120 h).

and the dinorbornyl ether (**4**). In some cases under extended reaction periods very minor amounts of norcamphor <5% and other minor products were also formed. The norborneols and norbornyl acetates are the products expected from the acid-catalyzed addition of solvent to **1** and **2**. The dinorbornyl ether (**4**), an unexpected product, is formed via total equilibration of the products and solvent under the HTDA conditions. That equilibration occurs is established by the fact that the composition of the norborneol mixture, 80% *exo* – 20% *endo*, corresponds to the equilibrium composition for these alcohols (20). Also, the dinorbornyl ether **4** contains 70 ± 5% *exo* and 30 ± 5% *endo* ether linkages as was established by nmr integration. The perdeuteration of the bicyclo[2.2.1]heptyl system in one cycle, with a good product yield, under the conditions of dilute acid is remarkable and is unprecedented in the literature.

Deuterium incorporation certainly occurs via recycled norbornene and nortricyclane that are formed via 3,2 (1,2) and 6,2 (1,3) elimination processes (deprotonation, dehydration, deacetylation). When the norbornene–nortricyclane cycle is coupled with 1,2 Wagner–Meerwein rearrangements, 6,2 and 3,2 hydride shifts, all the protons in the [2.2.1]-system face exchange (Scheme 1). That the hydration–exchange is acid-catalyzed is established by the experiment described in entry 6. That is, **1** is stable or at least does not give **3***a*, **3***b*, or **4** in H_2O only at 250 °C. The hydration–exchange of **1**, **2**, and **3***a* is best carried out in a dilute solution of a weak acid since the inclusion of strong acid (entry 5) produces pronounced decomposition and a lowered yield of the alcohols. As described in entries 1, 2, 3, 4, 7, 9,

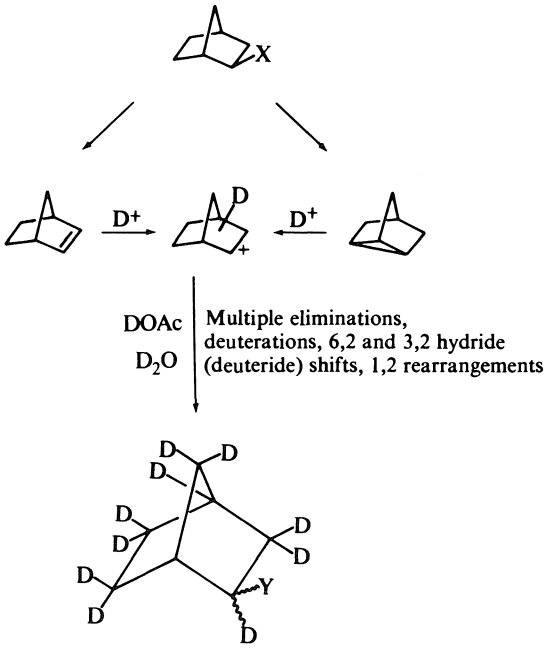

SCHEME 1

10, and 11 a reaction time in the order of 4–15 h only is required to accomplish complete hydration–exchange of **1** and **2** and complete equilibra-

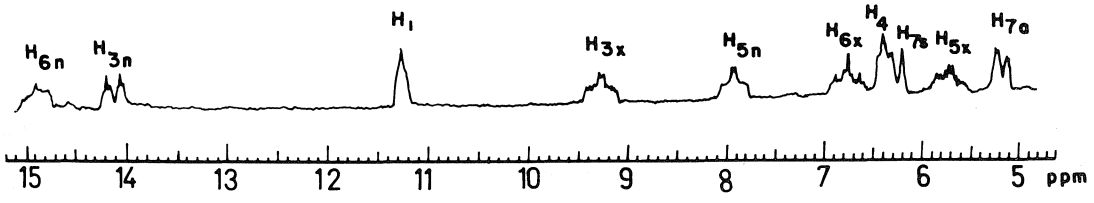

FIG. 2. The nmr spectrum (100 MHz) of *endo*-2-norborneol in CCl_4 in the presence of $Eu(DPM)_3$ at an $Eu(DPM)_3$–alcohol ratio of 0.63. H_{2x} is not shown and appears at 23.6 ppm.

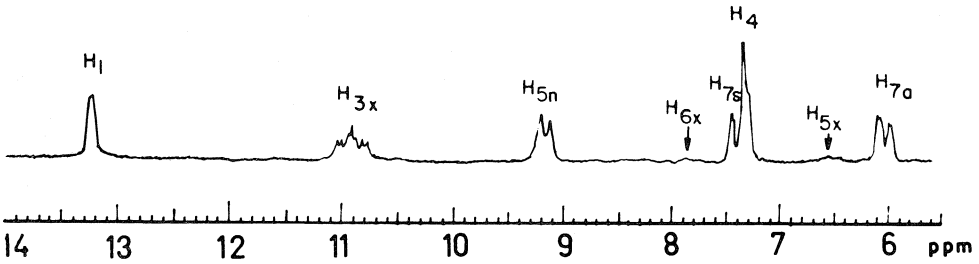

FIG. 3. The nmr spectrum of *endo*-2-norborneol-*exo*-5-*exo*-6-d_2 in the presence of Eu(DPM)$_3$ at an Eu(DPM)$_3$–alcohol ratio of 0.83. H_{3n}, H_{6n} and H_{2x} protons are not shown and appear at 10.4, 11.3, and 17.4 ppm, respectively.

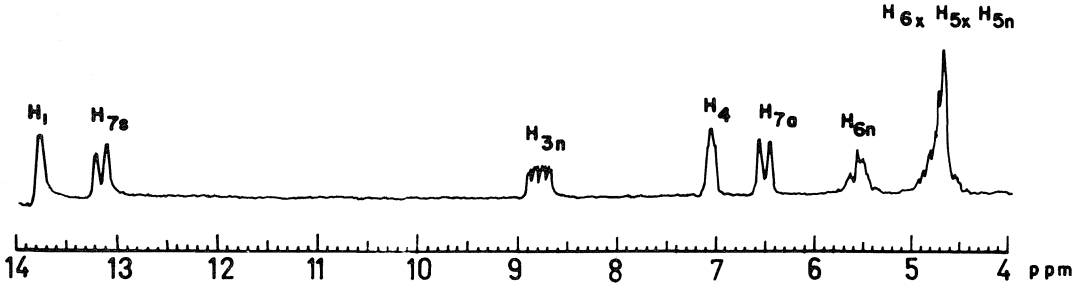

FIG. 4. The nmr spectrum (100 MHz) of *exo*-2-norborneol in CCl_4 in the presence of Eu(DPM)$_3$ at an Eu(DPM)$_3$–alcohol ratio of 0.66. H_{3x} and H_{2n} are not included.

tion of **3***a*, **3***b*, **3***c*, **3***d*, and **4** with the deuterium pool. Prolonged heating, as described in entry 8, leads to a lowered yield of the alcohols. To establish the deuterium distribution after only partial hydration of **1** (entry 2), the reaction was interrupted after 3 h and the norborneol mixture was converted to norcamphor that was reduced to *endo*-2-norborneol. The conversion of the norborneol mixture to *endo*-norborneol was accomplished to facilitate Eu(DPM)$_3$ shift analysis of the system. The nmr spectrum of *endo*-norborneol in the presence of Eu(DPM)$_3$ is shown in Fig. 2. The assignments were made by consideration that the protons nearest the complexing site would be shifted farthest downfield, by double resonance experiments and by the consideration of the nmr spectrum (Fig. 3) of *endo*-2-norborneol-*exo*-5-*exo*-6-d_2 (5), obtained in the presence of Eu(DPM)$_3$. This allowed for the definite assignment of the resonances of the *exo*-5 and *exo*-6-hydrogens in *endo*-2-norborneol. The shifted spectrum (Fig. 4) of *exo*-2-norborneol is included for comparison purposes to show that only shift analysis of the *endo* alcohol provides a view of all the protons.

The *endo*-2-norborneol, obtained from the norborneol mixture from the experiment described in entry 2, was subjected to shift analysis (Fig. 5). The following deuterium distribution was established when H-2 was used as the standard: 0.60 ± 0.05 C-1, 0.5 ± 0.05 at C-3-*exo*, 0.5 ± 0.05 at C-3-*endo*, 0.5 ± 0.05 at C-4, 0.5 ± 0.05 at C-5-*exo*, 0.5 ± 0.05 at C-5-*endo*, 0.6 ± 0.05 at C-6-*exo*, 0.6 ± 0.05 at C-6-*endo*, and 0.5 ± 0.05 at C-7-*syn* and 0.5 ± 0.05 at C-7-*anti*, respectively, a total of 5.3 ± 0.5 atoms of deuterium. Since the deuterium situated at C-2 was lost during oxidation of the norborneol mixture to norcamphor, an approximate value (0.6) was obtained for that site by difference since the *exo*-norborneol isolated from the hydration–exchange of **2** contained 5.9 ± 0.15 atoms of deuterium as was determined by mass spectrometric analysis. These results indicate that all sites are equally accessible at 250 °C, although there is some indication that the *exo*-6- and *endo*-6-positions carry a slight excess of deuterium over the other sites.

The temperature (250 °C) is an especially critical factor in the perdeuteration sequence since the addition of deuterio protic acids to norbornene at −78 → 100 °C yields only *exo*-norbornyl derivatives in which its lone deuterium atom is incorporated and distributed primarily

Can. J. Chem. Downloaded from www.nrcresearchpress.com by 210.87.254.6 on 09/05/12
For personal use only.

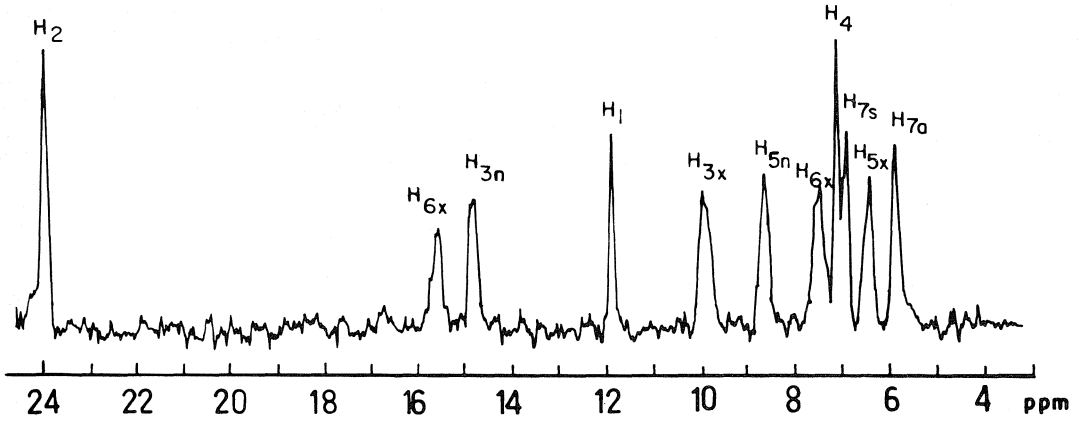

FIG. 5. The nmr spectrum (100 MHz) of *endo*-2-norborneol-$d_{5,2}$ in CCl_4 in the presence of $Eu(DPM)_3$ at an $Eu(DPM)_3$–alcohol ratio of 0.68.

between the C-3-*exo* and C-7-*syn*-positions (9, 10, 11). In order to force the equilibration of the products, temperatures of >200 °C are required (17). Interestingly, even at 250 °C we did not observe any cyclopentenyl products derivable from cleavage of the C1—C6 bond.

This study establishes therefore that any system that generates a 2-norbornyl cation under the conditions specified would undergo perdeuteration. Whether or not the HDTA conditions can be used to perdeuterate other cyclic systems, as for example, cyclohexenes and cyclopentenes, will be established by additional studies.

Experimental

Nuclear Magnetic Resonance Analysis of exo- and endo-Norborneol in the Presence of the Chemical Shift Reagent, Eu(DPM)$_3$

Weighed quantities of tris(dipivalomethanato)europium ($Eu(DPM)_3$) and norborneol were placed in a 2 dram sample vial containing CCl_4 (0.5 ml), the mixture was shaken vigorously for 5 min, and filtered through glass wool. Spectra were run on a Varian HA-100 instrument with tetramethylsilane as the internal standard.

The *endo*-norborneol proton resonances were assigned by a combination of first order analysis of the splitting patterns, double resonance experiments, and by using *endo*-2-norborneol-*exo*-5-*exo*-6-d_2 (Fig. 3). Nuclear magnetic resonance integral analysis (Fig. 5) of partially deuterated *endo*-2-norborneol, obtained from the partial exchange experiment, was carried out with the *exo*-2-proton as the internal standard.

Hydration of Norbornene in 10% v/v CH_3COOH–H_2O at 250 °C; Reaction Time 60 h

Norbornene (5.14 g, 5.46×10^{-2} mol, mp 45–47 °C) and 10% v/v HOAc–H_2O (25 ml) were introduced into a thick-walled glass tube, the mixture was degassed three times by the freeze–pump–thaw method and sealed under vacuum. After solution was heated at 250 °C for 60 h in a Carius oven, the resultant two phase reaction mixture was diluted with water (30 ml), neutralized with solid sodium bicarbonate, saturated with sodium chloride, and extracted with ether (4 × 40 ml). The combined ether extracts were dried over anhydrous $MgSO_4$ and concentrated by a slow distillation through a 15 in. glass helicies column. Analytical glpc on a 10 ft × $\frac{1}{8}$ in. 10% Carbowax on Chromosorb W column (temperature maintained at 110 °C for 3 min then rapidly increased to 185 °C) showed that the reaction mixture consisted of 2% norbornene, 4% nortricyclane, 8% *exo*- and *endo*-norbornyl acetate, 28% *exo*-norborneol, 11% *endo*-norborneol, and 47% dinorbornyl ether. The concentrated ether extract was quantitatively transferred into a 10 ml volumetric and made up to volume. Preparative glpc on a 10 ft × $\frac{3}{8}$ in. 15% Carbowax Chromosorb W column at 175 °C established the yields of *exo*- and *endo*-norbornyl acetate, *exo*- and *endo*-norborneol, and dinorbornyl ether as 0.36 g (4%), 1.76 g (29%), and 2.0 g (18%), respectively. Correction for collection losses established the yield of the norborneol mixture as 2.05 g (33%). *exo*- and *endo*-Norbornyl acetate: ir (neat) 1738 (C=O), 1018 and 1072 cm^{-1} (C—O stretch); nmr 60 MHz (CCl_4) δ 4.72 (m, 0.13H, C-2-*exo*-H), 4.50 (bd, 0.87H, C-2-*endo*-H), 2.24 (bs, 2H, bridgehead C—H), 1.92 (s, 3H, —O—C(=O)—CH_3), 1.74–1.05 (norbornyl envelope, 8H); ms (15 eV) M^+, *m/e* 154, $C_9H_{14}O_2$. An nmr integration analysis of the C-2-*exo*- and *endo*-protons showed that the *exo*:*endo* ratio of norbornyl acetates was 87:13. *exo*- and *endo*-Norborneol: mp 127–130 °C (lit. (21) mp *exo*-isomer 127–128 °C); ir (CS_2) 3600 (free —OH), 3350 (H bonded —OH), 1118, 1110 (C—H), 1082 (C—O stretch), 1032, 1022 (C—H), 1000 (C—O stretch),

Can. J. Chem. Downloaded from www.nrcresearchpress.com by 210.87.254.6 on 09/05/12
For personal use only.

Can. J. Chem. Downloaded from www.nrcresearchpress.com by 210.87.254.6 on 09/05/12
For personal use only.

916, 832, 806 cm^{-1} (C—H); nmr 60 MHz ($CDCl_3$) δ 4.05 (m, 0.25H, C-2-*exo*-H), 3.74 (bd, 0.75H, C-2-*endo*-H), 2.18 (m, 2H, bridgehead C—H), 1.7–0.9 (8H, norbornyl envelope); ms (15 eV) M^+, *m/e* 112, $C_7H_{12}O$; M^+ of the acetylated alcohol at *m/e* 154 corresponded to $C_9H_{14}O_2$. An nmr integration analysis established that the alcohol was a mixture of 80 ± 5% *exo*-norborneol and 20 ± 5% *endo*-norborneol. Dinorbornyl ether (a glassy solid): mp 51–53 °C; ir (CCl_4) 1095 (C—O), 1248, 1176, 1152, 1026, 862, and 693 cm^{-1} (C—H); nmr 60 MHz (CCl_4) δ 3.76 (bm, 0.55H, C-2-*exo*-H), 3.32 (m, 1.45H, C-2-*endo*-H), 2.22 (bs, 4H, bridgehead C—H) and 1.76–0.94 (norbornyl envelope, 16H); ms (15 eV) M^+, *m/e* 206, $C_{14}H_{22}O$. *Anal.* calcd. for $C_{14}H_{22}O$: C 81.50, H 10.75; found: C 81.79, H 10.86.

An nmr area integration of the C-2-*exo*- and *endo*-H of dinorbornyl ether showed that the stereoisomeric mixture was composed of 70 ± 5% *exo* and 30 ± 5% *endo* linkages.

Hydration in Deuterated Medium at 250 °C

Norbornene (0.52 g, 5.56×10^{-3} mol) and 10% v/v CD_3COOD–D_2O (8 ml) were sealed in a thick-walled glass tube (7 in. × ½ in.) as described previously. After the mixture was heated at 250 °C for 120 h, a milky aqueous layer and a pale yellow organic layer were formed. After the usual work-up, analytical glpc (Fig. 1) showed that the reaction mixture consisted of 1.0% norbornene and nortricyclane, 6.0% *exo*- and *endo*-norbornyl acetate, 56.0% *exo*-norborneol, 21.0% *endo*-norborneol, 8.0% dinorbornyl ether, and 8.0% of three other products. The concentrated ether extract was quantitatively transferred into a 1 ml volumetric flask and made up to volume. Preparative glpc on a 15 ft × ⅜ in. 15% Carbowax on Chromosorb W column at 155 °C established the yield of *exo*- and *endo*-norborneol as 0.40 g (69%); correction for collection losses (19) established a yield of 0.46 g (80%).

Since mass spectrometric deuterium assay on the norbornyl acetate is more accurate than analysis on the norborneol, due to the large $M^+ - 1$ and $M^+ - 2$ peaks associated with the latter, the norborneol was converted to the acetate by the following procedure. The norborneol (0.23 g, 2.05×10^{-3} mol) isolated by preparative glpc was dissolved in pyridine (8 ml) and acetic anhydride (6 ml) and stirred at room temperature for 24 h. The mixture was added to crushed ice (15 ml). After the ice had melted, the solution was diluted with water (80 ml) and extracted with ether (3 × 20 ml). The ether extract was washed with dilute HCl (3 × 10 ml) and water (2 × 20 ml), dried, and concentrated on the rotatory evaporator. Mass spectrometric deuterium assay on the *exo*- and *endo*-norbornyl acetate mixture showed that it was a composite of 44.0% d_{11}, 36.5% d_{10}, 14.2% d_9, and 3.5% d_8 species, that corresponded to a total of 10.1 excess atoms of deuterium per molecule.

Incomplete Exchange in Deuterated Medium

Norbornene (1.26 g, 1.34×10^{-2} mol) and 10% v/v CH_3COOD–D_2O (20 ml) in a degassed sealed tube were heated at 250 °C for 3 h in a Parr 2 litre bomb containing water to equalize pressure. After the usual work-up, analytical glpc on a 10 ft × ⅛ in. 10% Carbowax on Chromosorb W column with temperature programming from 85–125 °C showed 25% norbornene, 7% nortricyclane, 8% *exo*- and *endo*-norbornyl acetate, 48.5% *exo*- and *endo*-norborneol, 6% dinorbornyl ether, and 5.5% of four other products. The concentrated ether extract was quantitatively transferred into a volumetric flask (2 ml). Preparative glpc (125 °C) as described previously established the yield of norborneol as 0.53 g (35%), corrected for collection losses 0.61 g (41%). Some of the alcohol mixture collected by preparative glpc was converted to the acetates with pyridine and acetic anhydride as described previously. Mass spectrometric deuterium assay on the *exo*- and *endo*-norbornyl acetate mixture showed 4.3% d_{11}, 11.7% d_{10}, 13.3% d_9, 11.1% d_8, 8.7% d_7, 8.0% d_6, 6.1% d_5, 5.9% d_4, 7.1% d_3, 9.2% d_2, 12.7% d_1, and 2.0% d_0 species corresponding to a total of 5.9 excess atoms of deuterium per molecule.

The remainder of the alcohol isolated by preparative glpc was oxidized by Jones reagent according to the following procedure. *exo*- and *endo*-Norborneol (0.31 g, 2.76×10^{-3} mol), ether (10 ml), and a chromic acid solution (3 ml, prepared from 5 g $Na_2Cr_2O_7 \cdot 2H_2O$ and 3.75 ml concentrated H_2SO_4 which is then diluted to 25 ml) were mixed and stirred overnight. The ether layer was separated and the aqueous phase was extracted with ether (2 × 5 ml). The combined ether extracts were washed with saturated sodium bicarbonate (3 × 5 ml), water (1 × 5 ml), dried, and the ether was removed slowly by distillation through a 12 in. glass helicies packed column to yield norcamphor (0.22 g, 2.0×10^{-3} mol, 72%). To determine the location of the deuterium, the deuterated *endo*-norborneol (0.024 g, 2.0×10^{-4} mol) obtained from the lithium aluminum hydride in ether reduction of norcamphor, was subjected to nmr area integral analysis in the presence of $Eu(DPM)_3$ (0.098 g, 1.39×10^{-4} mol) in CCl_4 as described in Fig. 5. The analysis established the following deuterium distribution: 0.6 ± 0.05 at C-1, 0.5 at C-3-*exo*, 0.5 at C-3-*endo*, 0.5 at C-4, 0.5 at C-5-*exo*, 0.5 at C-5-*endo*, 0.6 at C-6-*exo*, 0.6 at C-6-*endo*, 0.5 at C-7-*syn* and 0.5 at C-7-*anti* (5.3 excess atoms of deuterium). Since the original *exo*- and *endo*-norborneol contained 5.9 atoms of deuterium and the *endo*-norborneol obtained from the oxidation and reduction sequence contained 5.3 atoms of deuterium, the original *exo*- and *endo*-norborneol before oxidation contained approximately 0.6 D at C-2.

Preparation of Nortricyclane

Norcamphor tosylhydrazone (18.7 g, 6.73×10^{-2} mol, mp 205–208 °C) prepared from norcamphor was added to purified diglyme (250 ml) in a three-neck flask equipped with a stoppered condenser and a nitrogen inlet and outlet. Freshly prepared sodium methoxide (30.2 g, 0.56 mol) was added and the reaction mixture was heated to reflux (140–150 °C). As nitrogen was vented through the solution, the product (4.5 g, 72%) was carried through a water wash, a KOH pellet drying system, and collected in a small flask and 'U' tube cooled in dry ice. Analytical glpc on a 10 ft × ⅛ in. 5% SE-30 on Chromosorb W column at 105 °C established that the product was composed of 99% nortricyclane and 1% norbornene.

Hydration of Nortricyclane in Deuterated Medium at 250 °C

Nortricyclane (0.15 g, 160×10^{-3} mol) and 10% v/v

Can. J. Chem. Downloaded from www.nrcresearchpress.com by 210.87.254.6 on 09/05/12
For personal use only.

DOAc–D_2O (8 ml) were introduced into a thick-walled glass tube (8 in. × ½ in. i.d.), degassed three times by the freeze–pump–thaw method, and sealed under vacuum. After the mixture was heated at 250 °C for 15 h in a Carius oven, the two phase reaction mixture was diluted with water (8 ml), neutralized with solid sodium bicarbonate, saturated with sodium chloride, and extracted with ether (4 × 15 ml). The combined ether extracts were dried and concentrated by a slow distillation through a 15 in. glass helicies packed column. Analytical glpc on a 10 ft × ⅛ in. 10% Carbowax on Chromosorb W column with temperature programming from 85–155 °C showed 5% *exo*- and *endo*-norbornyl acetate and 93.5% *exo*- and *endo*-norborneol. The concentrated ether extract was quantitatively transferred into a 1 ml volumetric flask and made up to volume. Preparative glpc as described previously established the yield of norborneol as 0.064 g (36%); yield, corrected for collection losses, 0.075 g (42%). As described previously, the alcohol was converted to the norbornyl acetate which was subjected to mass spectrometric deuterium assay: (15 eV), 37.1% d_{11}, 35.5% d_{10}, 14.8% d_9, 4.3% d_8, 1.3% d_7, and 7.0% d_6 species (9.8 excess atoms of deuterium per molecule).

Solvolysis of exo-Norborneol in Deuterated Medium at 250 °C

As described in the hydration of nortricyclane experiment, *exo*-norborneol (0.71 g, 6.28×10^{-3} mol) and 10% v/v DOAc–D_2O were heated at 250 °C for 15 h. Analytical glpc on a 10 ft × ⅛ in. 10% Carbowax on Chromosorb W column with temperature programming from 85–155 °C showed 0.7% norbornene, 1.3% nortricyclane, 8.0% *exo*- and *endo*-norbornyl acetate, 61.0% *exo*-norborneol, 28.0% *endo*-norborneol, 0.5% dinorbornyl ether, and <1% of another product. The concentrated ether extract was quantitatively transferred into a 2 ml volumetric flask and made up to volume. Preparative glpc established the yield of norborneol as 0.48 g (67%); yield, corrected for collection losses, 0.56 g (79%). Mass spectrometric deuterium assay (15 eV), on the acetylated alcohol showed 27.4% d_{11}, 38.7% d_{10}, 23.2% d_9, 8.5% d_8, and 2.2% d_7 species, corresponding to a total of 9.8 excess atoms of deuterium per molecule.

Solvolysis of endo-Norbornyl Acetate in Deuterated Medium at 250 °C

As described previously, norcamphor was reduced with lithium aluminum hydride in ether predominantly to *endo*-norborneol. The *endo* alcohol was then converted to *endo*-norbornyl acetate with pyridine and acetic anhydride.

As described in the hydration of nortricyclane experiment, *endo*-norbornyl acetate (0.55 g, 3.59×10^{-3} mol) was heated at 250 °C for 15 h. Analytical glpc on a 10 ft × ⅛ in. 10% Carbowax on Chromosorb W column at 95 °C showed 0.8% norbornene, 0.5% nortricyclane, 39.2% *exo*- and *endo*-norbornyl acetate, 37.3% *exo*-norborneol, 16.7% *endo*-norborneol, and 5.5% of two other products. The concentrated ether extract was quantitatively transferred into a 1 ml volumetric flask and made up to volume. Preparative glpc established the yield of norborneol as 0.18 g (45%); yield, corrected for collection losses, 0.20 g (51%). Mass spectrometric deuterium assay (15 eV) of the norbornyl acetate isolated from the reaction mixture by preparative glpc, established the presence of d_{14}, d_{13}, and d_{12} species, indicating that the acetate methyl group was also being exchanged under the reaction conditions. To obtain an accurate analysis of the deuterium incorporated into the norborneols, mass spectrometric deuterium assay was carried out on the acetylated alcohols. As before, the *exo*- and *endo*-norborneol mixture was converted to the norbornyl acetates and mass spectrometric deuterium assay at 15 eV, showed that the alcohol was a composite of 39.6% d_{11}, 38.5% d_{10}, 17.2% d_9, and 4.7% d_8 species, corresponding to a total of 10.3 excess atoms of deuterium per molecule.

Acknowledgment

Financial support of the National Research Council of Canada is gratefully acknowledged.

1. N. H. Werstiuk and T. Kadai. Chem. Commun. 1349 (1971).
2. H. A. Bruson and T. N. Riener. J. Am. Chem. Soc. **67**, 723 (1945).
3. L. Schmerling. J. Am. Chem. Soc. **68**, 195 (1946).
4. J. D. Roberts, E. R. Turnbull, Jr., W. Bennett, and R. Armstrong. J. Am. Chem. Soc. **72**, 3116 (1950).
5. L. Schmerling, J. P. Luvisi, and R. W. Welch. J. Am. Chem. Soc. **78**, 2819 (1956).
6. T. G. Traylor and A. W. Baker. Tetrahedron Lett. 14 (1959).
7. J. K. Stille and R. D. Hughes. J. Org. Chem. **36**, 340 (1971).
8. H. C. Brown and K.-T. Liu. J. Am. Chem. Soc. **89**, 3900 (1967).
9. J. M. Brown and M. C. McIvor. Chem. Commun. 238 (1969).
10. H. C. Brown and K.-T. Ling. J. Am. Chem. Soc. **97**, 600 (1975).
11. H. C. Brown and K.-T. Ling. J. Am. Chem. Soc. **97**, 2469 (1975).
12. J. Passivirta. Acta Chem. Scand. **27**, 374 (1973).
13. C. E. Frosst and Co. German Patent 2 122 254 (1971); Chem. Abstr. **76**, 33419 (1972).
14. A. Nickon and J. H. Hammons. J. Am. Chem. Soc. **86**, 3322 (1964).
15. N. H. Werstiuk and T. Kadai. Chem. Commun. 1613 (1970).
16. N. H. Werstiuk and T. Kadai. Can. J. Chem. **50**, 3350 (1972).
17. N. H. Werstiuk and T. Kadai. Can. J. Chem. **52**, 1485 (1974).
18. N. H. Werstiuk and T. Kadai. Can. J. Chem. **52**, 2169 (1974).
19. N. H. Werstiuk and T. Kadai. Can. J. Chem. This issue.
20. C. F. Wilcox, Jr., M. Sexton, and M. F. Wilcox. J. Org. Chem. **28**, 1079 (1963).
21. S. Winstein, B. K. Morse, E. D. Trifan, and H. Marshall. J. Am. Chem. Soc. **74**, 1127 (1952).

The infrared and Raman spectra of 1,2-dibromotetrafluoroethane

H. F. SHURVELL, F. CAHILL, AND V. DEVARAJAN
Department of Chemistry, Queen's University, Kingston, Ont., Canada K7L 3N6

AND

D. W. JAMES
Department of Chemistry, University of Queensland, St. Lucia, Brisbane, Australia 4067

Received February 6, 1976

H. F. SHURVELL, F. CAHILL, V. DEVARAJAN, and D. W. JAMES. Can. J. Chem. **54**, 2220 (1976).

Infrared and Raman spectra of 1,2-dibromotetrafluoroethane have been recorded in vapour, liquid, and polycrystalline solid states. Assignments have been made to *trans* and *gauche* isomers. A force field has been obtained for the *trans* isomer and used to predict the frequencies of the *gauche* form.

H. F. SHURVELL, F. CAHILL, V. DEVARAJAN et D. W. JAMES. Can. J. Chem. **54**, 2220 (1976).

On a déterminé les spectres infrarouges et Raman du dibromo-1,2 tétrafluoroéthane à l'état de vapeur, de liquide et de solide polycristallin. On a fait des attributions pour les isomères *trans* et *gauche*. On a obtenu une force de champ pour l'isomère *trans* et on l'a utilisée pour prédire les fréquences de la forme *gauche*.

[Traduit par le journal]

Introduction

The infrared and Raman spectra of 1,2-dibromotetrafluoroethane (DBTFE), CF_2Br-CF_2Br, have been reported previously (1). The infrared spectra were studied at various temperatures and it was concluded that the *trans* (*anti*) form of the compound was the more stable isomer. However, no assignment of the observed frequencies was given.

Our interest in DBTFE arose from the possibility of using this compound in conjunction with other materials as matrices for matrix isolation studies. Sandorfy (2) has reported that a 1:1 mixture of DBTFE and CCl_3F forms a transparent glass suitable for both infrared and visible spectroscopy at liquid nitrogen temperature. Before using DBTFE in matrix isolation work it is desirable to have a knowledge of the spectrum of the solid.

In the present work we have recorded infrared and Raman spectra of both solid and liquid DBTFE at various temperatures as well as infrared and Raman spectra of the vapour. We have assigned the observed frequencies to *trans* and *gauche* forms and have carried out normal coordinate analyses on both isomers. These calculations have been helpful in locating the A_u and B_u fundamentals of the *trans* form and predicting the frequencies of the *gauche* isomer.

Experimental

Dibromotetrafluoroethane bp 47.3 °C was obtained from PCR Inc., and Pfalz and Bauer. Solid samples were prepared for infrared studies by condensation of the vapour onto a CsI window mounted in a copper block cooled by liquid nitrogen in an evacuated Dewar. Annealing was carried out by warming the deposits and recooling to 77 K.

Liquid phase spectra were recorded from films held between CsI plates or using polyethylene cells. Vapour phase spectra were obtained using a heated cell described previously (3). All infrared spectra were recorded on a Perkin-Elmer model 180 spectrometer. The instrument was calibrated using various gases (4).

Raman spectra of solid DBTFE were recorded on a Cary 82 spectrometer at the University of Queensland. The 5145 Å line of a C.R.L. model 52 Argon laser was used to excite the spectra. The cryostat used was an Oxford Instruments CF100 liquid transfer crystat. Liquid phase spectra were obtained using sealed glass capillary tubes. Raman spectra of DBTFE vapour were obtained using a Cary multiple reflection attachment and a heated gas cell with brewster angle windows. Calibration was made using laser lines. The Raman and infrared wavenumbers reported in Table 1 are believed to be correct to within ± 1 cm^{-1}.

Results and Discussion

The infrared spectra of DBTFE in liquid and solid phases are shown in Fig. 1. Raman survey spectra of liquid and solid DBTFE are shown in Fig. 2. Observed frequencies in liquid and solid states are listed in Table 1 together with assignments to *trans* or *gauche* isomers.

TABLE 1. Observed wavenumbers (cm^{-1}) of the fundamentals of dibromotetrafluoroethane[a]

Raman		Infrared		
Solid 77 K	Liquid 300 K	Solid 77 K	Liquid 300 K	Assignment
49s	—	—	—	Lattice mode
—	60sh,dp	—	—	*gauche* (*B*)
—	118w,dp	—	—	*gauche* (*B*)
—	—	—	177vw	*gauche* (*B*)
181, 184s	180vs,p	—	—	*trans* (A_g)
—	—	227w	227vw	*trans* (A_u)
—	275wsh,dp	—	275vw	*gauche* (*B*)
286m	282w,p	—	—	*trans* (B_g)
—	309w,p	—	308w	*gauche* (*A*)
322vs	322s,p	—	—	*trans* (A_g)
—	—	345w	345w	*trans* (A_u)
—	345m,dp	—	~350sh	*gauche* (*B*)
—	—	—	360w	*gauche* (*A*)
367s	369s,p	—	—	*trans* (A_g)
—	466vw,p	—	462w	*gauche* (*A*)
526m	525vw,dp	—	—	*trans* (B_g)
—	—	585s	585m	*trans* (B_u)
—	—	—	596m	*gauche* (*B*)
649vw	650s,p	—	650m	*gauche* (*A*)
682s	680m,p	—	—	*trans* (A_g)
—	—	767vs	766vs	*trans* (B_u)
—	872vw,dp	—	874s	*gauche* (*B*)
1008w	1008w,p	—	1008vs	*gauche* (*A*)
1022vs	1025s,p	—	—	*trans* (A_g)
—	—	1120vs	1128vs	*trans* (B_u)
1156w	—	—	—	*trans* (A_g)
—	1164w,dp	—	~1170sh	*gauche* (*B*)
—	—	1172vs	1180vs	*trans* (A_u)
—	—	—	1247s	*gauche* (*A*)
1254w	1252vw,dp	—	—	*trans* (B_g)

[a]Intensities are denoted by v = very, s = strong, m = medium, w = weak, sh = shoulder, p = polarized, dp = depolarized.

Assignments to *trans* and *gauche* isomers were based on the assumption that the solid state spectra contain only bands due to *trans* isomer. Also since the *trans* isomer has a centre of symmetry, a mutual exclusion between infrared and Raman wavenumbers should be observed for this isomer. On the other hand, vibrations of the *gauche* isomer should be observed at the same wavenumber in both infrared and Raman spectra of the liquid, but should be absent in the spectra of the solid.

The *trans* isomer is assumed to belong to the point group C_{2h} and the 18 fundamentals comprise $6A_g + 3B_g + 4A_u + 5B_u$ modes. The A_g and B_g modes are active in the Raman spectrum, while the A_u and B_u species are infrared active. Measurement of depolarization ratios of Raman lines leads to a distinction between the A_g and B_g modes. However, distinction between the A_u and B_u modes is not so straightforward and the normal coordinate calculations described below have been helpful in this regard.

The *gauche* isomer is assumed to belong to the point group C_2. The $10A + 8B$ fundamentals are both infrared and Raman active. The *A* modes should give rise to polarized Raman lines. Frequencies due to the *gauche* isomer should be observed in both spectra, but should disappear at low temperatures. However, many bands assigned to the *gauche* form are very weak and again, the normal coordinate calculation described below was helpful in making assignments to this isomer.

Infrared and Raman spectra of the vapour at various temperatures were also recorded. The bands were generally broader than those of the liquid due to unresolved rotational structure. However, the wavenumbers observed were very

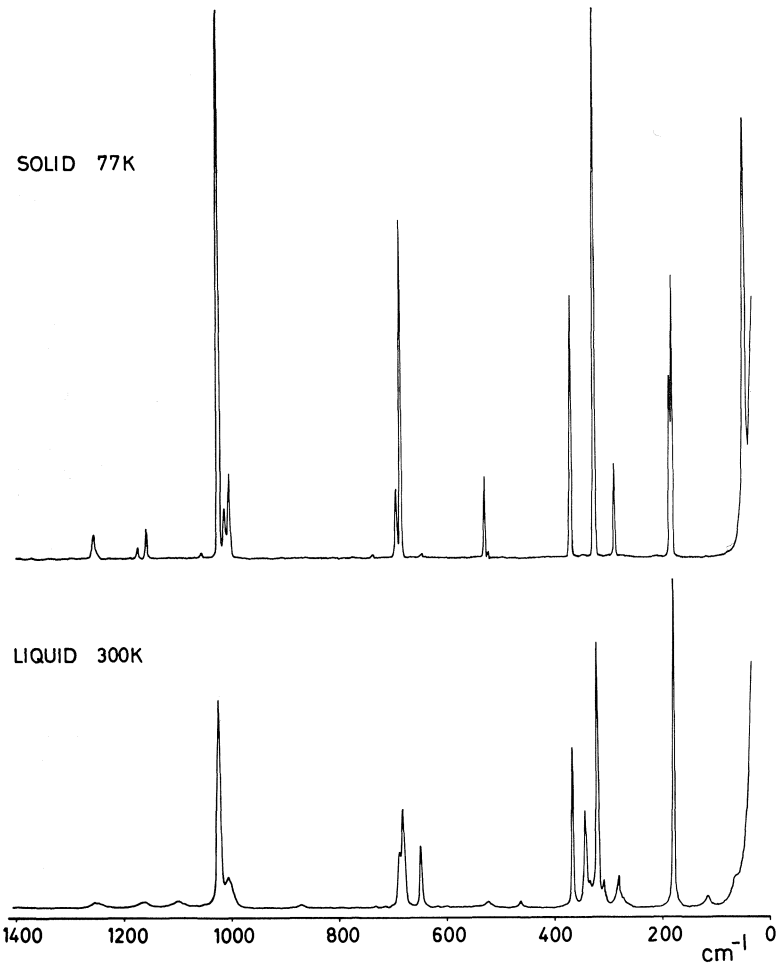

FIG. 1. Raman survey spectra of DBTFE. Upper trace: a polycrystalline film at 77 K, slits 2 cm^{-1}, sensitivity 5000 counts/s. Lower trace: the liquid at room temperature, slits 1.3 cm^{-1}, sensitivity 50 000 counts/s.

close to those of the liquid phase spectrum and no new features were found. The discussion here refers to liquid and solid phase infrared and Raman spectra only.

Assignments

The trans Isomer

Strong polarized Raman lines of the liquid at 180, 322, 369, 1025 and a line of medium intensity at 680 cm^{-1} are assigned to A_g species vibrations of *trans*-DBTFE. These lines are also present in the solid state spectrum and no infrared absorption was observed at any of these wavenumbers. Group theory predicts six A_g modes and the normal coordinate analysis suggests an A_g frequency near 1150 cm^{-1}. We have therefore assigned the weak Raman line at 1156 cm^{-1} in the spectrum of the solid to this mode.

Depolarized Raman lines at 282, 525, and 1252 cm^{-1} are assigned to the B_g species vibrations. Again, these wavenumbers are only observed in the Raman spectrum and again they are present in the solid state spectrum.

Of the nine infrared active A_u and B_u modes, calculations indicate that two are expected at frequencies below the range of our instrument. Very strong infrared absorptions are observed at 1180, 1128, 766 cm^{-1}. These, together with a band of medium intensity at 585 cm^{-1} and two

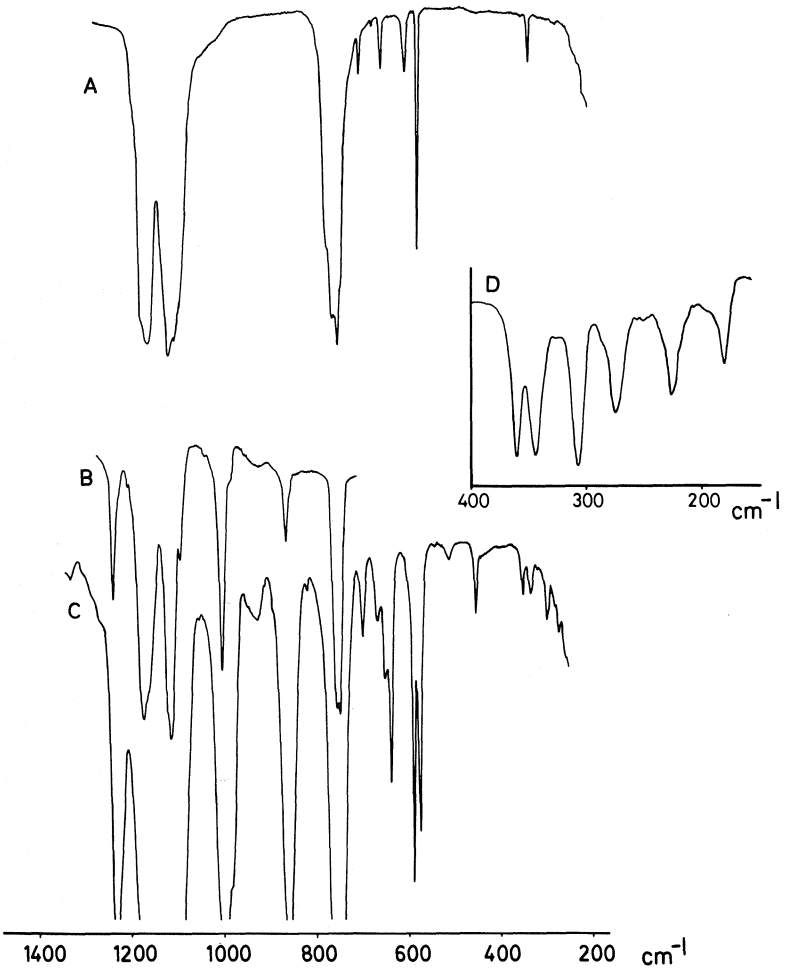

FIG. 2. Infrared survey spectra of DBTFE. *A*, a very thin polycrystalline film at 77 K. *B*, a very thin liquid film. *C*, a thick liquid film. *D*, the liquid in a 0.5 mm polyethylene cell.

weak absorptions at 345 and 227 cm^{-1}, are assigned to A_u and B_u modes. In every case these wavenumbers are observed in both liquid and solid phase spectra and are absent in the Raman spectrum. The normal coordinate calculation suggests that a B_u mode should be found near 370 cm^{-1}. However, no infrared band is observed in the solid near this wavenumber. The other two unobserved infrared active fundamentals are calculated at 132 and 114 cm^{-1}.

The gauche Isomer

As was found for the *trans* isomer, it has not been possible to locate all 18 fundamentals and some assignments given in Table 1 are uncertain. Infrared absorptions at 1247, 1008, 874, 650, 462, 308, and 275 cm^{-1} all coincide in wavenumber with Raman lines and in nearly every case both infrared and Raman bands are absent in the spectrum of the solid at 77 K.

Infrared absorptions at 596, 360, and 177 cm^{-1} disappear at low temperatures and are therefore assigned to the *gauche* form. These bands have no Raman counterparts. Depolarized Raman lines at 1164 and 345 cm^{-1} may correspond to shoulders at approximately 1170 and 350 cm^{-1} in the infrared spectrum of liquid DBTFE. These lines also are absent at low temperatures and are therefore assigned to the *gauche* isomer. The low frequency Raman spectrum of the liquid has a band at 118 cm^{-1} and a shoulder at approximately 60 cm^{-1}. These lines both disappear at low temperatures and are

also assigned to the *gauche* isomer. This leaves four fundamentals unaccounted for. The normal coordinate analysis has suggested wavenumbers for the unobserved vibrations and these may be seen in Table 4.

Unassigned Bands

A few weak features of the spectra of Figs. 1 and 2 have not been included in Table 1, since it is felt that they are due to overtones or combinations, or in the case of the solid state spectra, to crystal splittings.

In Fig. 1 the Raman lines in question are seen at 690 cm^{-1} (*trans*) and 1102 cm^{-1} (*gauche*) in the liquid and 690, 1002, and 1177 cm^{-1} in the solid. The line at 690 cm^{-1} could be the combination 369 + 322 ($A_g \times A_g = A_g$) in Fermi resonance with the strong A_g fundamental at 680 cm^{-1}. The 1102 cm^{-1} feature could be 462 + 650 ($A \times A = A$). The lines appearing in the solid are almost certainly due to the *trans* isomer. The sharp doublet at 181 and 184 cm^{-1} may be correlation field components of the 180 cm^{-1} line of the liquid phase spectrum. The sharp line of medium intensity at 1002 cm^{-1} could be 682 + 322 ($A_g \times A_g = A_g$), in Fermi resonance with the very strong A_g fundamental at 1022 cm^{-1}.

In the infrared spectrum of the liquid (Fig. 2*C*), a weak absorption at 524 cm^{-1}, two shoulders on the 650 cm^{-1} band, a sharp band at 710 and a weak broad feature between the 874 and 1008 cm^{-1} bands are all unassigned. In the solid state spectrum (Fig. 2*A*), three sharp peaks are seen between the 585 and 767 cm^{-1} absorptions. These features cannot be assigned as fundamentals and are therefore attributed to overtones or combinations of the *trans* isomer.

Normal Coordinate Analysis

A normal coordinate analysis was carried out for both *trans* and *gauche* isomers of DBTFE using the Wilson **FG** matrix method (5). The internal coordinates for *trans* $CF_2Br—CF_2Br$ are defined in Fig. 3. A torsional coordinate was defined around the C—C bond. Bond lengths and angles were obtained from the literature (6). A total of 20 internal coordinates including two redundancies were used to calculate the **G** matrix using the computer programs of Schachtschneider (7). A valence force field containing 25 force constants was used to construct an **F** matrix. As there are only 18 normal modes for DBTFE it is obviously not possible to determine

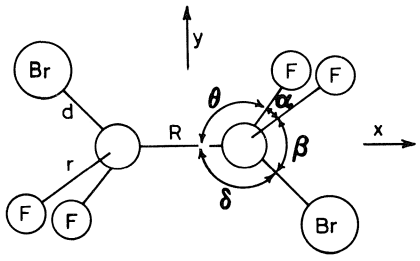

FIG. 3. The internal coordinates of *trans*-DBTFE.

25 force constants uniquely. However, we were able to fit the observed frequencies by adjusting the force constants by a trial and error procedure and making use of the elements of the Jacobian matrix $\partial\nu_i/\partial f_j$.

Initial values of stretching, bending and some interaction force constants were obtained from the results of calculations of C_2F_6 and C_2Br_6 (8) and CF_3CH_3 and CBr_3CH_3 (9). The adjustment of force constants was started by fitting observed and calculated wavenumbers of the A_g and B_g modes of *trans*- DBTFE, because the assignments of these modes were most reliable. Symmetry coordinates were not used, because of the redundancy problem in the A_g and B_u species. The redundant symmetry coordinates can be recognized as the + and − combinations of the angle bends around the two carbon atoms. However, these linear combinations cannot be made orthogonal to the other 18 symmetry coordinates. The calculation could be carried out with a non-redundant set of internal coordinates and Cyvin (10) has made such a calculation. However, we wish to use the valence force constants obtained for *trans*-DBTFE to predict the frequencies of the *gauche* isomer, so we prefer to work with the redundant unsymmetrized problem. It was not difficult to identify the species of each calculated eigenvalue, since a print-out of the eigenvectors was available.

Once the observed and calculated wavenumbers for the A_g and B_g species were sufficiently close, the calculated frequencies for the A_u and B_u species were compared with the observed infrared frequencies in Table 1 and assignments to $4A_u$ and $5B_u$ species were then made. This somewhat arbitrary procedure is justified by further consideration of the vibrations. The CF stretches are calculated at 1179 cm^{-1} (A_u) and 1133 cm^{-1} (B_u). These can be correlated with observed infrared bands at 1184

TABLE 2. Observed and calculated wavenumbers (cm^{-1}) for *trans*-dibromotetrafluorethane

Species	Observed	Calculated	Description[a]	Important force constants[b]
A_g	1156	1150	C—F stretch, CBr stretch, BrCC bend	$f_r, f_d, f_\alpha, f_\beta, f_\delta, f_{\beta\beta}, f_{\beta\delta}$
	1025	1022	C—C stretch	$f_R, f_r, f_{Rr}, f_{R\theta}$
	680	691	C—F stretch, FCF bend + BrCC bend	$f_r, f_\alpha, f_\delta, f_{r\alpha}$
	369	376	FCF bend, CBr stretch	$f_d, f_\alpha, f_\beta, f_\delta, f_{d\beta}, f_{\beta\delta}$
	322	330	FCC bend, CBr stretch, C—C stretch	$f_R, f_d, f_\alpha, f_\beta, f_\theta, f_{R\theta}, f_{d\beta}$
	180	175	BrCC bend, CBr stretch	$f_d, f_\beta, f_\delta, f_{d\beta}, f_{d\delta}$
B_g	1252	1237	C—F stretch	$f_r, f_\beta, f_\theta, f_{rr}$
	525	505	FCC bend, CF stretch	$f_r, f_\beta, f_\theta, f_{r\theta}$
	282	272	BrCF bend, FCC bend	$f_\beta, f_\theta, f_{\beta\beta}, f_{\beta\theta}$
A_u	1180	1179	C—F stretch	f_r, f_β, f_{rr}
	345	356	BrCF bend, torsion	$f_\beta, f_{\beta\beta}, f_\tau'$
	227	233	FCC bend	$f_\theta, f_{r\theta}, f_{\beta\theta}$
	—	114	Torsion	f_τ
B_u	1128	1133	C—F stretch, FCF bend	$f_r, f_\alpha, f_{r\alpha}$
	766	763	C—Br stretch, BrCF bend	$f_d, f_\beta, f_\theta, f_{d\beta}, f_{\beta\beta}$
	585	568	FCF bend	$f_r, f_\alpha, f_\theta, f_{r\alpha}$
	—	371	CBr stretch, FCF bend, BrCF bend	$f_d, f_\alpha, f_\beta, f_{d\beta}$
	—	132	BrCC bend, FCC bend	$f_\delta, f_\theta, f_{\beta\delta}, f_{\delta\theta}$

[a]Taken from the P.E.D. in internal coordinates.
[b]Force constants contributing more than 10% to P.E.D. in force constants.

and 1128 cm^{-1}. The BrCF bend is calculated at 356 cm^{-1} for the A_u species and, mixed with C—Br stretching, at 371 cm^{-1} for the B_u species. These calculated frequencies correlate with infrared bands at 345 and 360 cm^{-1}. Two frequencies are calculated for the B_u species at 763 and 568 cm^{-1} which have no counterparts in the A_u species. These can be correlated with bands at 766 and 585 cm^{-1} in the infrared spectrum. The assignment of the infrared band at 227 cm^{-1} to an FCC bend of species A_u calculated at 233 cm^{-1} is reasonable. The remaining fundamentals are a BrCC bend (B_u) and the torsion (A_u). The calculation indicates that these modes occur at low frequencies and they have not been observed in the present work.

TABLE 3. Final values of force constants calculated for *trans* $CF_2Br—CF_2Br$

Force constant	Value[a]	Force constant	Value[a]
f_R	4.25	$f_{R\theta}$	0.50
f_r	5.50	$f_{d\beta}$	0.65
f_d	2.97	$f_{d\delta}$	0.40
f_α	1.40	$f_{r\alpha}$	0.39
f_β	1.80	$f_{r\beta}$	0.15
f_δ	1.80	$f_{r\theta}$	0.65
f_θ	1.12	$f_{\alpha\beta}$	0.20
f_τ	0.10	$f_{\beta\beta}$	0.56
f_{Rr}	0.90	$f_{\beta\delta}$	0.47
f_{Rd}	0.09	$f_{\beta\theta}$	0.24
f_{rd}	0.40	$f_{\delta\theta}$	0.25
f_{rr}	0.70	$f_{\theta\theta}$	0.02
$f_{R\delta}$	0.50		

[a]Units for stretching and stretch–stretch interaction constants are mdyn/Å, for bending and bend–bend interaction constants units are mdyn Å, and stretch–bend interaction constants have units of mdyn.

After making the assignments to the various symmetry species an improvement in the overall fit was made manually using the Jacobian elements as a guide. Attempts to improve the fit by the least-squares procedure were abandoned when a study of the Jacobian matrix indicated that the problem would not converge. Potential energy distributions in both force constants and internal coordinates were calculated using standard expressions (11). The Schachtschneider (RVIB) (7) and Shimanouchi (LSMB) (11) programs were used for the calculations. The results for *trans*-DBTFE are shown in Table 2 and the final set of force constants is listed in Table 3.

The force field obtained for *trans*-DBTFE was used to predict the wavenumbers of the *gauche* isomer. The internal coordinates are defined in Fig. 4. The calculation was carried out using Schachtschneider's program (RVIB) (7) and the predicted wavenumbers are compared with observed values in Table 4. In most cases an infrared band or a Raman line, assigned to *gauche* isomer, was observed close to a predicted wavenumber. The frequencies assigned to the *A* and *B*

TABLE 4. Observed and calculated wavenumbers (cm^{-1}) for *gauche* $CF_2Br—CF_2Br$

Species	Observed	Calculated	Description[a]
A	1247	1235	C—F stretch
	—	1040	C—F stretch, C—C stretch, FCF bend
	1008	1013	C—C stretch
	650	644	FCF bend, C—F stretch
	462	459	FCBr bend, FCC bend, FCF bend
	360	367	C—Br stretch
	308	315	FCBr bend, FCC bend, CC stretch
	—	276	FCBr bend, FCC bend
	118	132	BrCC bend
	60	97	Torsion
B	—	1221	C—F stretch
	1164	1155	C—F stretch
	874	882	C—Br stretch, FCBr bend, FCC bend
	596	582	FCF bend, C—F stretch
	—	386	FCBr bend, FCF bend
	345	355	C—Br stretch, FCBr bend
	275	260	FCC bend, FCBr bend
	177	188	BrCC bend, FCC bend

[a]Taken from the P.E.D. in internal coordinates.

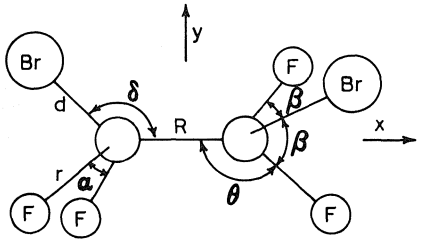

FIG. 4. The internal coordinates of *gauche*-DBTFE.

species vibrations were usually of infrared bands chosen on the basis of closeness to calculated frequencies. However, when Raman depolarization ratios were available, the polarized lines of the *gauche* form were assigned to *A* species vibrations.

Conclusions

An assignment of the infrared and Raman spectra of dibromotetrafluoroethane has been made. It is concluded that the *trans* isomer is more stable than the *gauche* and is the predominant form at low temperatures. Using the temperature dependence of bands in the spectra and the mutual exclusion of vibrations of the *trans* isomer in infrared and Raman spectra, it was possible to assign bands to *trans* and *gauche* forms.

The results of a normal coordinate analysis given in Tables 2 and 4 support the assignments to *trans* and *gauche* isomers and from the potential energy distributions, descriptions of the normal modes can be given. The force constants given in Table 3 are not unique but they appear to be reasonable and reproduce the observed frequencies of both *trans* and *gauche* isomers quite well. This indicates that any differences in frequencies between the two isomers are due to the geometrical differences.

The Raman spectrum of solid DBTFE is fairly simple and there are large clear regions. The compound would appear to be suitable as a matrix material for Raman matrix isolation studies. The infrared spectrum of the solid on the other hand has two broad regions of absorption below 1300 cm^{-1} and many overtones and combinations occur in the region between 2000 and 1300 cm^{-1}.

Acknowledgements

This work was supported by the National Research Council of Canada and the Australian Research Grants Commission. Helpful discussions with Dr. S. J. Cyvin are gratefully acknowledged.

1. R. E. KAGARISE and L. W. DAASCH. J. Chem. Phys. **23**, 130 (1955).
2. C. SANDORFY. Can. Spectrosc. **10**, 85 (1965); also private communication.
3. H. F. SHURVELL and J. A. FANIRAN. Can. Spectrosc. **13**, 109 (1968).
4. I.U.P.A.C. Tables of wavenumbers for calibration of

infrared spectrometers. Butterworths, London. 1961.
5. E. B. WILSON, JR., J. C. DECIUS, and P. C. CROSS. Molecular vibrations. McGraw-Hill, New York. 1955.
6. L. E. Sutton (*Editor*). Interatomic distances. Special Publications Nos. 11 and 18, The Chemical Society, London. 1958, 1965.
7. J. H. SCHACHTSCHNEIDER. Technical Reports Nos. 231-64 and 57-65, Shell Development Co., 1965.
8. R. S. CARNEY, E. A. PIOTROWSKY, A. G. MEISTER, J. H. BRAUN, and F. F. CLEVELAND. J. Mol. Spectrosc. **7**, 209 (1961).
9. D. R. STENGLE and R. C. TAYLOR. J. Mol. Spectrosc. **34**, 33 (1970).
10. S. J. CYVIN. Private communication.
11. T. SHIMANOUCHI. Computer programs for normal coordinate treatment of polyatomic molecules. University of Tokyo, Tokyo, Japan. 1968.

Proton spin–spin coupling constants and intramolecular hydrogen bonding in bromine derivatives of 1,3-dihydroxybenzene

TED SCHAEFER AND J. BRIAN ROWBOTHAM
Department of Chemistry, University of Manitoba, Winnipeg, Man., Canada R3T 2N2

Received February 4, 1976

TED SCHAEFER and J. BRIAN ROWBOTHAM. Can. J. Chem. **54**, 2228 (1976).

The conformational preferences in CCl_4 solution at 32 °C of the hydroxyl groups in bromine derivatives of 1,3-dihydroxybenzene are deduced from the long-range spin–spin coupling constants between hydroxyl protons and ring protons over five bonds. Two hydroxyl groups hydrogen bond to the same bromine substituent in 2-bromo-1,3-dihydroxybenzene but prefer to hydrogen bond to different bromine substituents when available, as in 2,4-dibromo-1,3-dihydroxybenzene. When the OH groups can each choose between two *ortho* bromine atoms, as in 2,4,6-tribromoresorcinol, they apparently do so in a very nearly statistical manner except that they avoid hydrogen bonding to the common bromine atom.

TED SCHAEFER et J. BRIAN ROWBOTHAM. Can. J. Chem. **54**, 2228 (1976).

Les préférences conformationnelles, en solution dans le CCl_4 à 32 °C, des groupes hydroxyles dans les dérivés bromés du dihydroxy-1,3 benzène sont déduites à partir des constantes de couplage spin–spin à longue distance à travers cinq liaisons entre les protons hydroxyliques et les protons du cycle. Deux groupes hydroxyles sont unis par des ponts hydrogènes au même atome de brome dans le bromo-2 dihydroxy-1,3 benzène; toutefois les hydroxyles préfèrent former des ponts hydrogènes avec différents atomes de brome lorsque ceux-ci sont disponibles, comme dans le dibromo-2,4 dihydroxy-1,3 benzène. Quand chaque groupe OH peut choisir entre deux atomes de brome *ortho*, comme dans le tribromo-2,4,6 résorcinol, ils le font apparemment d'une façon presque statistique; ils essaient toutefois d'éviter la formation de ponts hydrogènes vers un atome de brome commun.

(Traduit par le journal)

Introduction

Previous measurements (1, 2) of stereospecific long-range spin–spin coupling constants between hydroxyl protons and ring protons or fluorine nuclei in halophenols yielded the relative stability of **A** and **B** in carbon tetrachloride solution at 32 °C.

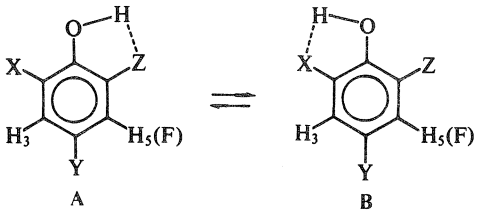

A B

It was deduced that the intramolecular hydrogen bond strength to fluorine is greater than that to iodine by 75 ± 20 cal/mol, that the strengths to chlorine and bromine are 460 ± 60 cal/mol greater than to iodine; and that, if a distinction can be made, chlorine hydrogen bonds more strongly than bromine by only a few tens of calories per mole. These conclusions agree qualitatively with deductions based on hydroxyl stretching band intensities (3).

Recent measurements (4) of the hydroxyl torsion bands of the *o*-halophenols in cyclohexane solution gave the enthalpies of formation of the intramolecular hydrogen bonds as −1.62, −1.57, −1.45, −1.44 kcal/mol (all with an error of 0.12 kcal/mol) for Cl, Br, I and F, respectively. On the other hand, chemical shift data for the hydroxyl protons (5) indicated enthalpies of −2.36, −2.14, −1.65 kcal/mol for Cl, Br, I, respectively, in carbon disulfide solution and implied the absence of an intramolecular hydrogen bond in *o*-fluorophenol.

In this paper the conformational preferences of the two hydroxyl groups in bromine derivatives of 1,3-dihydroxybenzene (resorcinol) are investigated via the long-range spin–spin coupling constants over five bonds, ${}^5J_m^{H,OH}$, between hydroxyl and ring protons. It is of interest under what substituent conditions the two hydroxyl groups will hydrogen bond to the same bromine atom.

Experimental

The 2,4,6-tribromo-, and 2,4,6-triiodo-1,3-dihydroxybenzenes were commercial materials. Treatment of the former with bisulfite (6) yielded the 2-bromo-, the 2,4-dibromo-, and 4,6-dibromoresorcinols. Samples for nmr measurements were about 3% by weight in CCl_4 ($CDCl_3$

Can. J. Chem. Downloaded from www.nrcresearchpress.com by 210.87.254.6 on 09/05/12
For personal use only.

Can. J. Chem. Downloaded from www.nrcresearchpress.com by 210.87.254.6 on 09/05/12
For personal use only.

for tribromoresorcinol) and contained a small amount of tetramethylsilane, TMS. They were degassed and dried as described previously (1, 2). Proton magnetic resonance spectra were calibrated at 32 °C in the frequency-sweep mode on an HA-100 spectrometer. Sweep rates were 0.01 Hz/s.

Results and Discussion

Spectral Analyses

The spectral analyses were straightforward. The couplings to the hydroxyl protons are of interest and are given in the text at appropriate points. They are accurate to 0.02 Hz and sometimes to 0.01 Hz. In Fig. 1 the hydroxyl proton resonance peaks of 2,4,6-tribromoresorcinol are displayed. The doublet splitting is 0.19 Hz and the linewidth at half-height is about 0.11 Hz.

Conformational Deductions

As discussed in some detail previously (1, 2) there is no reason why nonplanar conformations of halophenol derivatives should be preferred over planar conformations. Furthermore, no evidence for intermolecular hydrogen bonds was found (1) at concentrations similar to those (less than 3 mol%) used in the present study. Therefore the present discussion will assume the existence of planar, monomeric, conformations.

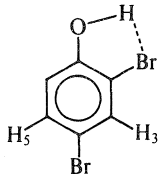

1

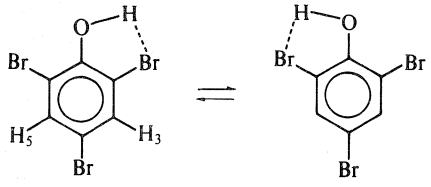

2a **2b**

A 1.6 mol% solution in CCl_4 of 2,4-dibromophenol, **1**, displays $J_3 = J_{cis} = {}^5J_m^{H_3,OH} = 0.00$ Hz and $J_5 = J_{trans} = {}^5J_m^{H_5,OH} = 0.48$ Hz (1). In **2**, rapid conversion between **2***a* and **2***b* ensures $J_3 = J_5 = 0.29$ Hz. It is assumed that ${}^5J_{cis} = 0.00$ Hz and that therefore ${}^5J_{trans} = 0.58$ Hz. No evidence exists for ${}^5J_{cis} \neq 0$. Note, however, that a substituent effect is present, in that ^5J increases with the degree of ring substitution by halogen atoms.

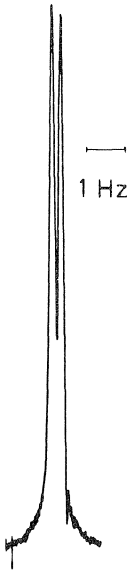

FIG. 1. The proton magnetic resonance spectrum at 100 MHz of the hydroxyl protons in 2,4,6-tribromoresorcinol dissolved as a 3% by weight solution in $CDCl_3$. The splitting is 0.19 ± 0.01 Hz and the linewidth at half height is about 0.12 Hz.

In 4,6-dibromoresorcinol ^5J is unobservably small, so that **3** is the only conformation significantly populated under the present experimental conditions.

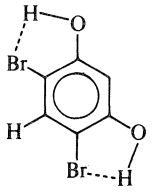

3

This result is entirely expected if the hydrogen bond energy at each site in **3** is comparable to that in *o*-bromophenol (see Introduction).

In 2,4-dibromoresorcinol, **4**, ${}^5J_m^{H_5,OH_1}$ is 0.42 Hz, while ${}^5J_m^{H_5,OH_3}$ is zero (the O—H_1 resonance is easily identified on the basis of its chemical shift). Consequently **4***d* and **4***c* are not important contributors to the equilibrium. The simplest and, in our view, the most probable interpretation of the data is then that **4***b* is not significantly populated and that *meta* substitution by a hydroxyl group reduces ${}^5J_{trans}$ in **1** by 0.06 Hz.

In 2-bromoresorcinol, **5**, *both* hydroxyl protons are coupled to H_5 by 0.42 Hz. Again, the simplest conclusion is that only **5***a* is appreciably popu-

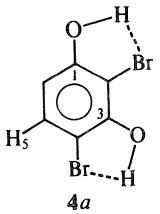
4a

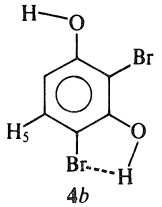
4b

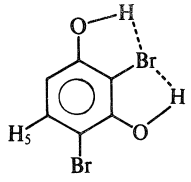
4c

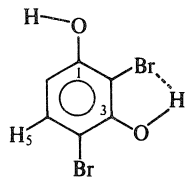
4d

lated in dilute CCl_4 solution at 32 °C, so that bromine is forming two hydrogen bonds.

Of the possible conformers of 2,4,6-tribromoresorcinol, **6**, **6***b* is favoured by a statistical factor of 2. Now, **4***c* is negligibly populated and, by analogy, **6***a* is assumed to be of negligible importance. Furthermore, **6***c* has $^5J^{H,OH} = 0$, so that the observed ^5J of 0.19 Hz can be interpreted as arising from a rapidly equilibriating mixture of **6***b* and **6***c*. In tribromophenol, $^5J_{trans}$ is 0.58 Hz and if substitution by a hydroxyl group reduces $^5J_{trans}$ by 0.06 Hz (as in 2,4-dibromophenol and 2-bromoresorcinol) then the population of **6***b*, P_b, is given by $0.5P_b \times (0.52 + 0.00) + (1 - P_b)(0.00 + 0.00) = 0.19$, so that $P_b = 0.73$. Hence **6***b* is more stable than **6***c* by $-RT$ ln $0.27/0.365 = 180$ cal/mol. Of course, if $^5J_{trans}$ were 0.57 Hz, *i.e.*, the same as in tribromophenol, **6***b* and **6***c* would be of equal stability. Equal stability of **6***b* and **6***c* demands that ^5J in tribromophenol does not change on substitution by a second hydroxyl group. In any event, it seems very likely that the difference in stability between **6***b* and **6***c* is small.

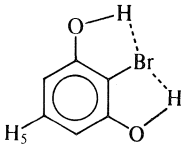
5a

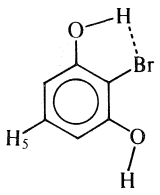
5b

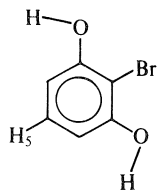
5c

Solvent Effects on ^5J_m

In dilute benzene-d_6 solution, ^5J_m is the same in 2,4,6-tribromoresorcinol and 2,4,6-triiodoresorcinol, to within the experimental error of 0.01 Hz. Furthermore, it is equal to that for ^5J_m in 2,4,6-tribromoresorcinol in $CDCl_3$ solution, 0.19 Hz. Many of the compounds were insufficiently soluble in C_6H_{12}, clearly a more inert solvent. As before (1), changes of a few % in concentration did not alter the measured ^5J values.

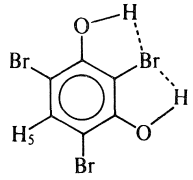
6a

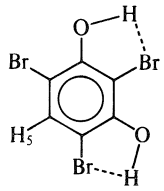
6b

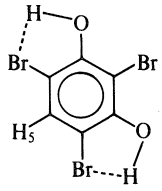
6c

Conclusions

In solution in nonpolar solvents, the hydroxyl groups in bromine derivatives of resorcinol apparently will hydrogen bond to the same bromine atom, as in 2-bromoresorcinol; but when given a choice prefer to hydrogen bond to different bromine atoms, as in 2,4-dibromoresorcinol or in 2,4,6-tribromoresorcinol.

Acknowledgment

We are grateful to the National Research Council of Canada for financial assistance.

1. J. B. Rowbotham and T. Schaefer. Can. J. Chem. **52**, 3037 (1974).
2. J. B. Rowbotham, M. Smith, and T. Schaefer. Can. J. Chem. **53**, 986 (1975).
3. A. W. Baker and W. F. Kaeding. J. Am. Chem. Soc. **81**, 5904 (1959).
4. G. L. Carlson, W. G. Fateley, A. S. Manocha, and F. F. Bentley. J. Phys. Chem. **76**, 1553 (1972).
5. E. A. Allan and L. W. Reeves. J. Phys. Chem. **66**, 613 (1962); **67**, 591 (1963).
6. T. L. Davis and V. F. Harrington. J. Am. Chem. Soc. **56**, 129 (1934).

Can. J. Chem. Downloaded from www.nrcresearchpress.com by 210.87.254.6 on 09/05/12
For personal use only.

Spin–spin coupling between proximate protons on neighbouring aromatic rings and between hydroxyl protons in 2,2′-dihydroxy-4-methoxybenzophenone. Coupling through the hydrogen bond

TED SCHAEFER AND KALVIN CHUM

Department of Chemistry, University of Manitoba, Winnipeg, Man., Canada R3T 2N2

Received February 5, 1976

TED SCHAEFER and KALVIN CHUM. Can. J. Chem. **54**, 2231 (1976).

The doubly hydrogen bonded conformation of 2,2′-dihydroxy-4-methoxybenzophenone ensures substantial nonbonded interactions between C—H bonds on neighbouring aromatic rings and gives rise to spin–spin coupling between the protons in those bonds. Because of the relative orientation of the C—H bonds containing the coupled protons, the coupling represents a direct mechanism which probably does not depend on the orbitals of the carbon atom. The observed coupling between the hydroxyl protons, formally over eight bonds, is small and indicative of an inappreciable covalent character of the hydrogen bond, in agreement with recent conclusions that a weak hydrogen bond is best represented by electrostatic and non-bonded forces only.

TED SCHAEFER et KALVIN CHUM. Can. J. Chem. **54**, 2231 (1976).

La conformation doublement pontée par les hydrogènes de la dihydroxy-2,2′ méthoxy-4 benzophénone assure l'existence d'interactions non liées importantes entre les liens C—H des cycles aromatiques voisins et conduit à une augmentation des constantes de couplage spin–spin entre les protons dans ces liens. A cause de l'orientation relative des liens C—H contenant les protons couplés, le couplage représente un mécanisme direct qui ne dépend probablement pas des orbitales de l'atome de carbone. Le couplage observé entre les protons hydroxyliques, formellement à travers huit liaisons, est petit et indique probablement un caractère covalent non appréciable pour le pont hydrogène; ceci est en accord avec les conclusions récentes à l'effet qu'un pont hydrogène peut être mieux représenté uniquement par des forces électrostatiques et non-liées.

[Traduit par le journal]

Introduction

Nuclear spin–spin coupling between proximate nuclei in nonbonded but mutually crowded atoms occurs via through-space or direct (1) interactions and is extensively documented (2–6) for ^{19}F, ^{19}F and ^{1}H, ^{19}F nuclear pairs. The magnitude of the coupling apparently depends not only on the internuclear distance but also on the relative orientation of the bonds containing the relevant atoms (2, 5).

Relatively few examples of ^{1}H, ^{1}H coupling constants, $^{n}J(H,H)$, where n is the formal number of intervening bonds, have been attributed to the proximity between the coupled protons. Examples include the couplings between protons in italics in **1** to **4**. In **1**, $^{5}J(H,H)$ is -0.15 Hz (7, 8); in **2**, $^{5}J(H,CH_3)$ is -0.33 Hz (9); in **3** a broadening of the resonance peaks is attributed (10) to a small $^{6}J(H,H)$; and, in **4**, $^{8}J(H,H)$ has a magnitude of 0.3 Hz (11).

In this paper, a careful analysis of the 12 spin proton magnetic resonance spectrum of 2,2′-dihydroxy-4-methoxybenzophenone, **5**, is reported. Two kinds of proximate coupling constants are observed, that between the hydroxyl protons, $^{8}J(OH,OH)$, and that between H_6 and H_6', $^{6}J(H_6,H_6')$.

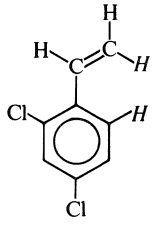

1

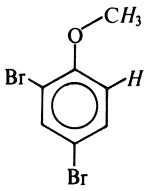

2

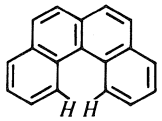

3

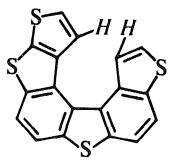

4

Can. J. Chem. Downloaded from www.nrcresearchpress.com by 210.87.254.5 on 09/05/12
For personal use only.

TABLE 1. Proton chemical shifts and coupling constants for 2,2′-dihydroxy-4-methoxybenzophenone[a]

Chemical shift	Value	Coupling constant	Value
ν_2[b]	1142.99	$^6J_{6,6'}$	±0.15
ν_3	640.343	$^8J_{2,2'}$	±0.1
ν_5	635.693	$^3J_{5,6}$[c,d]	9.083(17)
ν_6	749.891	$^3J_{3',4'}$	8.400(6)
ν_{OCH_3}	382.0	$^3J_{4',5'}$	7.255(6)
$\nu_{2'}$	1018.0	$^3J_{5',6}$	7.945(6)
$\nu_{3'}$	696.778	$^4J_{3,5}$	2.553(5)
$\nu_{4'}$	737.298	$^4J_{4',6'}$	1.700(7)
$\nu_{5'}$	681.951	$^4J_{3',5'}$	1.194(6)
$\nu_{6'}$	748.714	$^4J_{2,3}$	(−)0.1
		$^5J_{3,6}$	0.174(17)
		$^5J_{3',6'}$	0.432(7)
		$^5J_{2',4'}$	0.475(9)
		$^5J_{3,OCH_3}$	(−)0.18

[a]As a 5 mol% solution in CCl_4.
[b]In Hz to low field of TMS at 100 MHz.
[c]In Hz, numbers in parentheses giving the standard deviations in the last place, see **5**.
[d]The rms deviations between calculated and observed transition frequencies were 0.014 and 0.017 Hz for the primed and unprimed protons, respectively. The largest deviations between calculated and observed frequencies were 0.029 and 0.042 Hz for primed and unprimed protons, respectively.

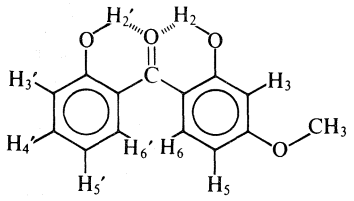

5

Experimental

A 5 mol% solution of **5** in CCl_4, containing a small amount of tetramethylsilane (TMS), was degassed by a freeze–pump–thaw technique. The proton magnetic resonance spectrum was calibrated in the frequency sweep mode on an HA-100 spectrometer at sweep rates of 0.02 and 0.01 Hz/s. For some measurements the manual oscillator was replaced by an HP-4204A audio oscillator.

A second such oscillator was used in decoupling experiments in which H_2', H_2, OCH_3 were irradiated, as well as in which selected multiplets from the resonance of H_3', H_4', H_5', and H_3 were decoupled from the spin system.

Results and Discussion

Spectral Analysis

The five and seven spin systems, representing the protons associated with the two aromatic groups, were separately analyzed by means of the computer program LAME (12, 13). Coupling between H_6 and H_6', and between OH_2 and OH_2', was then introduced. The composite spectra were plotted for various magnitudes of these two couplings so as to arrive at a best fit between calculated and observed spectra. The presence of small couplings could be ascertained by the appropriate multiple irradiation experiments, *e.g.*, irradiation of OH_2 removed small splittings in the peaks from OH_2'.

The final spectral parameters are given in Table 1, the data indicating that most coupling constants are known to an accuracy of 0.03 Hz or better. In Fig. 1 the observed spectra for

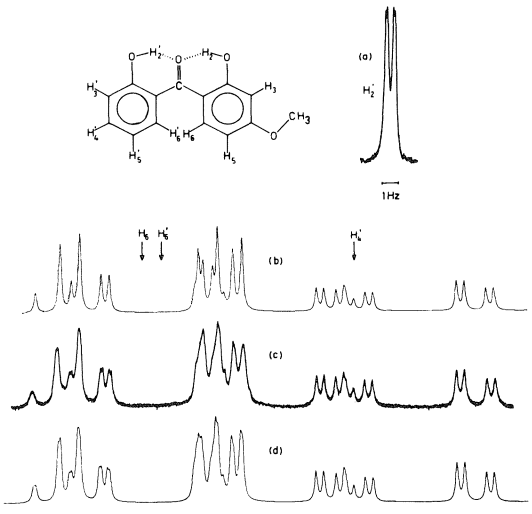

FIG. 1. The magnetic resonance spectrum of H_6, H_6', H_4', and of H_2' at 100 MHz is displayed in (*c*) and (*a*), and in (*b*) the H_6, H_6', H_4' spectrum calculated with the parameters in Table 1, but with zero coupling between H_6 and H_6', is shown. In (*d*) the calculated spectrum assumes the latter coupling as ±0.15 Hz.

Can. J. Chem. Downloaded from www.nrcresearchpress.com by 210.87.254.5 on 09/05/12
For personal use only.

Can. J. Chem. Downloaded from www.nrcresearchpress.com by 210.87.254.5 on 09/05/12
For personal use only.

H_4', H_6', H_6, and OH_2' are displayed. The calculated spectra for these three ring protons are presented in the presence and in the absence of coupling between H_6 and H_6'. Clearly, this coupling exists and has a magnitude of 0.15 $\pm$ 0.02 Hz. The smaller splitting in the spectrum of OH_2' arises from coupling to OH_2.

Conformation of **5**

The presence of the stereospecific (14, 15) coupling $^5J(H_4',OH_2')$, equalling 0.47 Hz, and the absence of an observable magnitude for $^5J(H_6',OH_2')$ and for $^5J(H_6,OH_2)$ implies that **5** exists mainly in the doubly hydrogen bonded conformation. This implication is corroborated by the chemical shifts of the hydroxyl protons, whose resonances lie at over 11 ppm to low field of TMS (Table 1). Estimates (16, 17) of the enthalpy of formation of the OH...O=C hydrogen bond for aromatic systems suggest a lower limit of -7 kcal/mol. Hence, even if the total hydrogen bond energy in **5** is rather less than twice this magnitude, the molecule exists predominantly in the doubly bonded conformation at 32 °C, the temperature at which the measurements were made.

From nmr measurements on salicylaldehyde in a nematic solvent (18), the inference has been drawn that the hydroxyl and aldehyde groups are twisted out of the benzene plane by up to 15°. Larger deviations from planarity in **5** are probable because of strong steric interactions of the H_6 and H_6' atoms, an internuclear distance of less than 1 Å being present in a planar conformation of **5**. It appears reasonable, therefore, that in the actual conformation of **5** the H_6 and H_6' atoms undergo appreciable nonbonded interactions.

Proximate Coupling, $^6J(H_6,H_6')$

The sign of $^6J(H_6,H_6')$ could not be determined because these protons are not coupled to the same third proton. In view of the data for **1** and **2**, it is probable that the sign is negative. Furthermore, the coupling most likely arises via an interaction between the electrons in the C—H_6 and C—H_6' bonds, *i.e.*, by a direct coupling mechanism (1), and not via interactions involving the four intervening C—C bonds. In terms of the theoretical formulations recently summarized by Barfield *et al.* (19), $^6J(H_6,H_6')$ is very likely an example of a through-space mechanism associated with the proximity of the hydrogen atoms in the two C—H bonds. Direct interactions associated with the orbitals on the carbon atoms to which the coupled protons are attached are potentially of larger magnitude but are presumably small in **5** because of the relative orientation of the C—H_6 and C—H_6' bonds.

Perhaps the best example of a direct mechanism similar to the latter is still the coupling of $\pm$1.1 Hz between H_b and H_o in **6** (20), where a strong nonbonded (repulsive) interaction occurs between the C—H_b and O—H_o bonds. Most probably the direct mechanism involves the lone pair orbitals on the oxygen atom.

The molecular orbital formulation of Hirao *et al.* (21) does not allow through-space coupling between protons. However, because these coupling mechanisms are apparently an order of magnitude smaller than for ^1H, ^{19}F and ^{19}F, ^{19}F coupling, the observed ^1H, ^1H through-space couplings do not constitute a very serious criticism of theoretical formulations.

Proximate Coupling, $^8J(OH_2,OH_2')$

This coupling, of magnitude 0.1 $\pm$ 0.02 Hz, must come about via interactions with the electrons on the oxygen atom to which both hydroxyl groups are hydrogen bonded. The hydrogen bonds are strong (see above) and the small coupling magnitude is consistent with a small covalent character of the hydrogen bond, in the sense that covalency introduces spin correlation and must facilitate the transmission of spin state information. However, very small geminal coupling constants are known, so that the small magnitude of the present coupling constant does not constitute a proof of noncovalency. In this connection it is of interest that recent force field calculations on amides (22) demonstrate that the N—H...O=C hydrogen bond is best represented by electrostatic and nonbonded interactions only, in partial agreement with a number of quantum mechanical calculations.

A test of these conclusions, based on coupling constants, would involve the measurement of

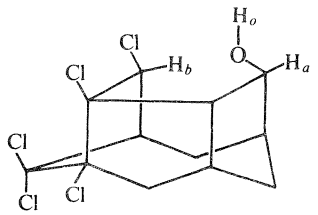

6

^{17}O, ^{1}H couplings in the X—H. . .O=C hydrogen bond. It may be noted that the OH, ^{19}F coupling in the intramolecularly hydrogen bonded form of 2-fluorophenol is -4.4 Hz (4); again very small in magnitude compared, say, to the ^{1}H, ^{19}F coupling of 530 Hz in hydrogen fluoride (23, 24).

Acknowledgments

We are grateful to the National Research Council of Canada for financial assistance and thank a referee for a valuable comment concerning the hydrogen bond.

1. M. Barfield and M. Karplus. J. Am. Chem. Soc. **91**, 1 (1969).
2. F. B. Mallory, C. W. Mallory, and W. M. Ricker. J. Am. Chem. Soc. **97**, 4770 (1975), and references therein; later references are given in 3 to 6.
3. T. Schaefer, W. Niemczura, and K. Marat. J. Chem. Soc. Faraday II, **71**, 1526 (1974).
4. J. B. Rowbotham, M. Smith, and T. Schaefer. Can. J. Chem. **53**, 986 (1975).
5. R. E. Wasylishen and M. Barfield. J. Am. Chem. Soc. **97**, 4545 (1975).
6. C. W. Haigh, J. Hilton, L. H. Sutcliffe, and G. J. T. Tiddy. J. Magn. Res. **18**, 241 (1975); C. Schumann and F. Cavagna. J. Magn. Reson. **18**, 172 (1975).
7. M. Barfield, C. J. Macdonald, I. R. Peat, and W. F. Reynolds. J. Am. Chem. Soc. **93**, 4195 (1971).
8. M. Barfield and S. Sternhell. J. Am. Chem. Soc. **94**, 1905 (1972).
9. H. A. Gaur, J. Vriend, and W. G. B. Huysmans. Tetrahedron Lett. 1999 (1969).
10. K. D. Bartle and D. W. Jones. J. Chem. Soc. A, 437 (1969).
11. J. H. Dopper, D. Oudman, and H. Wynberg. J. Am. Chem. Soc. **95**, 3692 (1973).
12. S. Castellano and A. A. Bothner-By. J. Chem. Phys. **41**, 3863 (1964).
13. C. W. Haigh and J. M. Williams. J. Mol. Spectrosc. **32**, 398 (1969).
14. S. Forsén and B. Åkermark. Acta Chem. Scand. **17**, 1712 (1963).
15. J. B. Rowbotham and T. Schaefer. Can. J. Chem. **52**, 3037 (1974).
16. U. Koelle and S. Forsén. Acta Chem. Scand. **A28**, 531 (1974).
17. T. Schaefer. J. Phys. Chem. **79**, 1888 (1975).
18. P. Diehl and P. M. Henrichs. J. Magn. Reson. **5**, 134 (1971).
19. M. Barfield, A. M. Dean, C. J. Fallick, R. J. Spear, S. Sternhell, and P. W. Westerman. J. Am. Chem. Soc. **97**, 1482 (1975).
20. F. A. L. Anet, A. J. R. Bourn, P. Carter, and S. Winstein. J. Am. Chem. Soc. **87**, 5249 (1965).
21. K. Hirao, H. Nakatsuji, and H. Kato. J. Am. Chem. Soc. **95**, 31 (1973).
22. A. T. Hagler, E. Huler, and S. Lifson. J. Am. Chem. Soc. **95**, 5319 (1974).
23. J. S. Muenter and W. Klemperer. J. Chem. Phys. **52**, 6033 (1970).
24. J. S. Martin and F. Y. Fujiwara. J. Am. Chem. Soc. **96**, 7632 (1974).

Can. J. Chem. Downloaded from www.nrcresearchpress.com by 210.87.254.5 on 09/05/12
For personal use only.

Unexpected signs of five-bond and six-bond proton spin–spin coupling constants in some acyclic conjugated systems. Through-space couplings.

TED SCHAEFER, HYMAN D. GESSER, AND J. BRIAN ROWBOTHAM
Department of Chemistry, University of Manitoba, Winnipeg, Man., Canada R3T 2N2

Received February 5, 1976

TED SCHAEFER, HYMAN D. GESSER, and J. BRIAN ROWBOTHAM. Can. J. Chem. **54**, 2235 (1976).

The signs and magnitudes of spin–spin coupling constants over five and/or six bonds in some *N*-methyl and *N,N*-dimethyl hydrazones, in methyl vinyl ether, 4-methoxy-3-butene-2-one, 1-methoxy-1,3-butadiene, 1-butene, and in anisole are discussed in terms of coupling mechanisms. In the hydrazones the five-bond couplings between methyl and olefinic protons are negative, while six-bond couplings between protons in methyl groups are positive, a reversal of the expected sign sequence. INDO-MO-FPT calculations are not in agreement with observation, but the disagreement may be a consequence of faulty structural assumptions. The sizeable six-bond couplings imply a negative σ–π contribution to the five-bond constants. The calculated and observed negative couplings over five bonds in methyl vinyl ether and the other molecules above emphasize their dependence on the proximity of the bonds containing the coupled nuclei and are reliable indicators of bond arrangements in these molecules.

TED SCHAEFER, HYMAN D. GESSER et J. BRIAN ROWBOTHAM. Can. J. Chem. **54**, 2235 (1976).

On discute, en termes de mécanisme de couplage, des signes et des amplitudes des constantes de couplage spin–spin à travers cinq ou six liens dans quelques *N*-méthyles et *N,N*-diméthylhydrazones, dans le méthylvinyléther, dans la méthoxy-4 butène-3 one-2, dans le méthoxy-1 butadiène-1,3, dans le butène-1 et dans l'anisole. Dans les hydrazones, les couplages à travers cinq liens entre les protons du méthyle et les protons oléfiniques sont négatifs alors que les couplages à travers six liens entre les protons des groupes méthyles sont positifs; ces résultats sont à l'opposée de la séquence attendue pour les signes. Des calculs INDO-MO-FPT ne sont pas en accord avec ces observations mais les divergences peuvent être une conséquence d'hypothèses structurales fausses. Les couplages importants à travers six liens impliquent une contribution σ–π négative pour les constantes à travers cinq liaisons. Les couplages négatifs calculés et observés à travers cinq liaisons dans le méthylvinyléther et les autres molécules mentionnées ci-dessus mettent en relief leur dépendance sur la proximité des liens contenant les noyaux couplés et sont des indicateurs fiables de l'arrangement des liens dans ces molécules.
[Traduit par le journal]

Can. J. Chem. Downloaded from www.nrcresearchpress.com by 210.87.254.40 on 09/05/12
For personal use only.

Introduction

Exceptions to the rule, that spin–spin coupling constants between protons separated by five formal bonds are positive, include **1** and **2**,

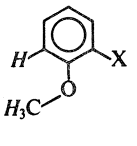

1

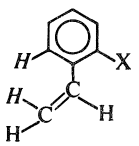

2

the bulky groups X ensuring a relatively close approach to the hydrogen atoms (in italics) containing the coupled protons. The couplings are small in magnitude, being −0.33 Hz in 2,4-dibromoanisole (1) and −0.15 Hz in 2,5-dichlorostyrene (2).

Both couplings can be loosely described as examples of a 'through-space' interaction (3, 4) and, more precisely, as arising from direct mechanisms (3, 4) involving the overlap of orbitals centered on the proximate nuclei and on the carbon atoms to which the protons are bonded. INDO-MO-FPT computations predict negative five-bond coupling constants for the bond arrangement in **2** (2) and also for those exemplified by **3** (4) and **4** (5),

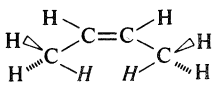

3

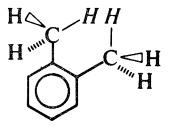

4

but are not measured in **3** and **4** because the observed values are averages over the protons in a methyl group and the positive apparently outweigh the negative contributions.[1]

[1]Calculations for anisole are described below.

TABLE 1. Proton chemical shifts* and spin–spin coupling constants† of some methyl hydrazones

Molecule	ν_1	ν_2	ν_3	$^2J_{H_1,H_2}$	$^3J_{H_1,CH_3}$	$^5J_{H,CH_3}$	$^6J_{CH_3,CH_3}$
(3) 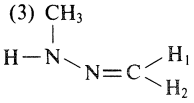	609.9‡	598.6	245.6	11.8	—	−0.6 −0.6	—
(3) 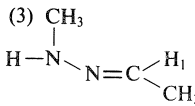 (2)	674.1§	181.1	269.4	—	5.24	-0.5_0	0.3_2
(3) 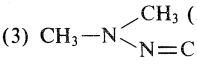 (3)	607.3_5‡	595.1	272.6	11.4_5	—	−0.45 −0.45	—
(3) 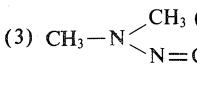 (3) (2)	651.1§	182.5	262.5	—	5.2	−0.45	0.3_0

*In Hz at 100 MHz to low field of internal tetramethylsilane.
†In Hz.
‡20 mol% in benzene-d_6.
§20 mol% in CCl_4.

In this paper five-bond, ^5J, and/or six-bond, ^6J, proton–proton couplings are reported for **5** to **10** and are discussed in terms of coupling mechanisms. Ambiguities remain in the description of these mechanisms.

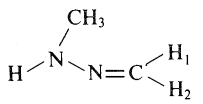

5

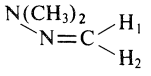

6

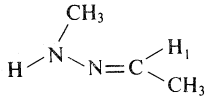

7

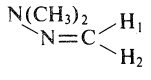

8

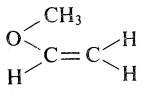

9

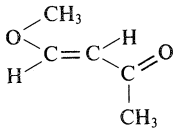

10

Experimental

Compounds **5** to **8** were prepared by known methods (6, 7) and their proton magnetic resonance spectra were calibrated on degassed solutions in the frequency-sweep mode on an HA-100 spectrometer. The relative signs of the coupling constants were determined by standard partial decoupling (8) and weak irradiation (9) experiments. Similar statements hold for the other compounds, which were of commercial origin.

Results and Discussion

Spectral Analyses

The Hydrazones

These were inherently simple but were complicated by incompletely relaxed spin–spin coupling to the ^{14}N quadrupolar nuclei. The two-bond coupling, $^2J^{H_2,N}$, is much larger in magnitude (10) than is $^2J^{H_1,N}$ in **5** to **8**; so that the H_2 resonance peaks are relatively broad in all solvents employed, including CCl_4 and C_6D_6 in Table 1. Furthermore, the N—H proton resonance is broad and, in **7**, the proton was also undergoing rapid intermolecular exchange. For these reasons only the signs of the coupling parameters given in Table 1 could be determined and are assigned on the basis of $^2J^{H_1,H_2} > 0$, as is certain (10), and of $^3J^{H,CH_3} > 0$. The *cis* isomer of **7** was present to the extent of about 28%, in agreement[2] with previous work (7), but attempts at sign determinations were unsuccessful; primarily because of the broadening of the olefinic proton peaks caused by $^2J^{H,N}$. Again, the *cis* isomer of **8** was not detected, also in agreement with former measurements (7). Rapid

[2]The extensive work on the conformational behaviour of hydrazones by Karabatsos and co-workers can be found in ref. 7.

Can. J. Chem. Downloaded from www.nrcresearchpress.com by 210.87.254.40 on 09/05/12
For personal use only.

TABLE 2. Long-range proton coupling constants in Hz for some ethylene derivatives

Molecule	$^4J^{H,CH_3}$	$^5J_t{}^{H,CH_3}$	$^5J_c{}^{H,CH_3}$
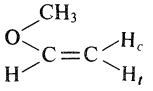	−0.40*	−0.20	−0.32
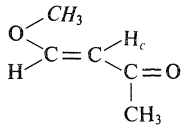	−0.47†	—	−0.27
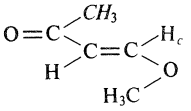	+0.27†	—	−0.12
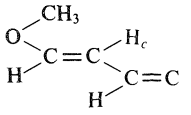	−0.34‡	—	−0.29
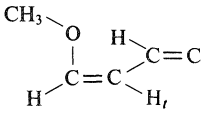	<0.1‡	<0.1	—
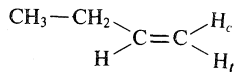	(−)0.20*	≤0.02	≤0.02

*20 mol% solutions in CCl_4.
†10 mol% in CS_2.
‡In tetramethylsilane, ref. 16. Signs determined in that work.

rotation about the N—N bond occurs (11) for each molecule.

Other Molecules, 9 to 11

These were also analyzed by means of the program LAME (12, 13) and the signs of the long-range couplings are given in Table 2, previous work (14–16) having ascertained chemical shifts and other coupling constants. For **11**,

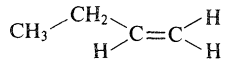

11

repeated simulations of the spectrum showed that the five-bond couplings between the methyl and olefinic protons were ≤0.02 Hz. All signs in Table 2 are relative to those of vicinal proton coupling constants, taken as positive. Precision of measurement is 0.02 Hz for these couplings.

The Signs of $^5J^{H,CH_3}$ and $^6J^{CH_3,CH_3}$ in 5 to 8

Comparison with other Couplings over the C=N Bond

The striking aspect of these couplings (Table 1) is their signs, $^5J < 0$ and $^6J > 0$; all the more so because $^4J^{H,CH_3}$ is reported as −1.6 Hz in **12** and $^5J^{CH_3,CH_3}$ as +1.4 Hz in **13** (17).

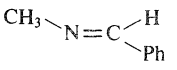

12

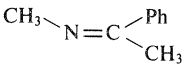

13

These couplings approximate to the cisoid allylic coupling, $^4J_c{}^{H,CH_3}$, of −1.75 Hz in propene (15) and the transoid homoallylic coupling, $^5J^{CH_3,CH_3}$, of +1.59 Hz in *trans*-2-butene (18). Such coupling constants contain large contributions from a σ–π electron mechanism (4, 19) and INDO-MO-FPT calculations (20), among others (4, 19, 21–23), are fairly successful in the reproduction of their observed signs and magnitudes.

Assuming conjugation between the C=N double bond and the lone-pair on the N—CH_3 group also emphasizes the exceptional signs of $^5J^{H,CH_3}$ in **5** to **8**. In other conjugated systems, *e.g.*, toluene and *m*-xylene (24), both σ and σ–π electron contributions to $^5J_m{}^{H,CH_3}$ are positive, totalling about 0.35 Hz; and to $^6J_m{}^{CH_3,CH_3}$ are negative, amounting to −0.2 Hz. Again, INDO-

Can. J. Chem. Downloaded from www.nrcresearchpress.com by 210.87.254.40 on 09/05/12
For personal use only.

TABLE 3. INDO-MO-FPT coupling constants over five bonds between methyl and olefinic protons in **5***

	Coupling constant for θ (deg) =					
ϕ (deg)	0	60	120	180	240	300
0	−5.32(−0.92)*	−1.38(0.20)	−0.09(0.12)	−0.01(1.12)	−0.02(0.50)	−1.02(0.61)
45	−0.76(0.77)	−0.64(0.21)	0.19(0.47)	0.50(1.43)	0.04(0.81)	0.08(0.29)
90	0.57(1.61)	0.13(0.78)	0.00(0.13)	0.82(2.28)	0.53(1.61)	0.07(0.25)
135	0.52(1.46)	0.26(0.60)	−0.11(0.13)	0.79(2.61)	0.75(1.83)	0.07(0.17)
180	0.45(1.19)	0.19(0.19)	0.09(0.61)	0.70(2.54)	0.57(1.21)	0.16(0.20)
225	0.62(1.18)	0.27(0.10)	0.16(0.82)	0.73(2.30)	0.50(0.71)	0.22(0.26)
270	0.77(1.27)	0.46(0.29)	0.01(0.38)	0.13(2.07)	0.82(0.92)	0.95(0.17)
315	−0.71(0.59)	0.18(0.40)	−0.15(0.09)	−0.37(1.41)	0.71(1.35)	0.60(0.17)

θ	$\langle\theta\rangle$	$\langle 0° + 120° + 240° \rangle$	$\langle 60° + 180° + 300° \rangle$
0°	−1.31(0.27)Hz	−1.81(−0.10)	−0.80(0.64)
45°	−0.10(0.66)	−0.18(0.68)	−0.02(0.64)
90°	0.35(1.11)	0.37(1.11)	0.34(1.10)
135°	0.38(1.13)	0.38(1.14)	0.37(1.13)
180°	0.36(0.99)	0.37(1.00)	0.35(0.98)
225°	0.42(0.90)	0.43(0.90)	0.41(0.88)
270°	0.52(0.85)	0.53(0.86)	0.51(0.84)
315°	0.04(0.67)	−0.05(0.68)	0.14(0.66)

*Parentheses refer to the olefinic proton *trans* to N—CH_3.

MO-FPT calculations (5) reproduce the signs of these couplings.

Quantitative Calculations of $^5J^{H,CH_3}$

INDO-MO-FPT calculations (25) were performed for **5** using a geometry, **14**, based on microwave (26) and molecular orbital (27) data.

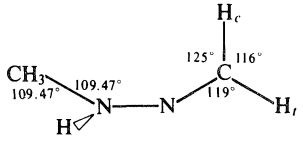

14*a*

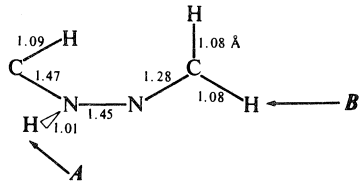

14*b*

The original parameterization (28) was employed, together with a convergence criterion of 0.01 Hz in the computed coupling constants. Two dihedral angles, θ and ϕ, are defined in **15** and **16**, describing rotation about the CH_3—N and N—N bonds, respectively.

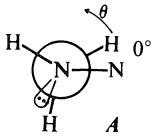

15

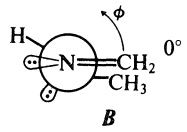

16

Vectors ***A*** and ***B*** in **14***b* define the lines of sight in **15** and **16**, respectively. In Table 3 the computed values of $^5J^{H,CH_3}$ are presented as a function of θ and ϕ. Included are average values over θ and for arrangements in which a methyl C—H bond eclipses or 'staggers' the N=C bond.

The data in Table 3 suggest sizeable negative $^5J_c^{H,CH_3}$ and $^5J_t^{H,CH_3}$ values only when a C—H bond of the methyl group lies very near an olefinic C—H bond, *e.g.*, $\theta = \phi = 0°$ in **15** and **16**. Then both ^5J_c and ^5J_t are negative (compare structures **14**, **15**, and **16**). Of course, this conformation is energetically unfavourable. In fact, the INDO energies are lower by at least 2.0 kcal/mol for $\theta = 60°$, $\phi = 135°$ than for any other pair of angles in Table 3. The computations did not optimize the geometry for a given conformation and also ignore solvation energies. Nevertheless, it appears unlikely that the calculations can approximate to the observed negative signs and nearly equal magnitudes of $^5J_c^{H,CH_3}$

Can. J. Chem. Downloaded from www.nrcresearchpress.com by 210.87.254.40 on 09/05/12
For personal use only.

Can. J. Chem. Downloaded from www.nrcresearchpress.com by 210.87.254.40 on 09/05/12
For personal use only.

and $^5J_t^{H,CH_3}$ in **5**. Further computations, being costly and unpromising, were not carried out on the hydrazones, **5** to **8**.

Qualitative Considerations in Terms of Mechanisms

The equality of ^5J_c and ^5J_t in **5** and **7**, respectively, suggests a σ–π mechanism insofar as the spin state information would be transferred via a p_π orbital on the olefinic carbon atom to the two olefinic C—H bonds; perhaps via the resonance structure **17**.

$$H_3C-\overset{+}{N}=N=\overset{-}{C}H_2$$

17

Unless the hyperfine interaction between the methyl protons and an electron in the lone pair of the amino nitrogen atom is negative, however, this mechanism preducts equal but *positive* couplings, ^5J_c and ^5J_t; similar to $^5J_m^{H,CH_3}$ in toluene (5, 24).

Another mechanism invokes a preferred *trans* arrangement of the lone pairs on the two nitrogen atoms and, in the language of esr, a positive γ interaction between the p_π orbital on the imino nitrogen atom and the C—H bonds of the methyl group. This interaction would be a maximum at $\theta = 0°$, $\phi = 90°$ and 270° and would yield a negative ^5J, just as a σ–π mechanism produces negative allylic couplings in propene. The INDO-MO-FPT calculations do not yield negative ^5J values for these conformations (Table 3).

A third tentative mechanism is schematically indicated in **18**,

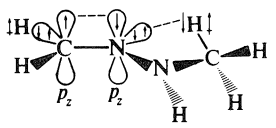

18

in which negative σ–π interactions occur at the olefinic carbon and at the imino nitrogen atom, the lone pair on the latter atom being invoked. The data in Table 3 do not support this mechanism, but it must be remembered that they depend on somewhat artificial geometries and that the INDO method neglects a large number of two-center integrals. Perhaps the latter cannot be neglected in these molecules.

In any event, the existence of a σ–π contribution to ^5J is hardly in doubt, as shown by the signs and magnitudes of $^6J^{CH_3,CH_3}$ for **6** and **8** in Table 1. The magnitudes of ^5J are larger than those of ^6J, so that the equality of ^5J_c and ^5J_t in a given molecule is apparently accidental. However, it is unlikely that ^6J contains a σ electron contribution. Its sign firmly indicates a negative σ–π contribution to ^5J in **5** to **8** and indicates one of the very few failures of INDO-MO-FPT calculations for long-range coupling constants between protons in conjugated systems.

Comparison with Ethylene Derivatives

*Methyl Vinyl Ether, **9***

Again, the two $^5J^{H,CH_3}$ values are negative (Table 2) but $^5J_c^{H,CH_3}$ is 0.1 Hz larger in magnitude, suggesting a contribution from a through-space or proximate interaction to the latter coupling.

In view of infrared (29), microwave (30), electron diffraction (31), Kerr constant (32) and *ab initio* SCF (33) studies, it appears that near room temperature, at least in the gas phase, methyl vinyl ether exists about 66% in the (heavy atom) *cis* planar form, **19**, and about 34% in a *gauche* form; the latter corresponding to rotation about the =C—O bond by 90 ± 10°.

For INDO-MO-FPT calculations the geometry of the planar C—O—C=C fragment was taken from electron diffraction data (31) and the hydrogen atom positions were taken from the microwave work (30). These data are summarized in **19** and **20**. The angles θ and ϕ are defined in **21** and **22**

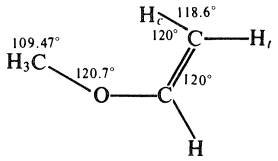

19 *cis*

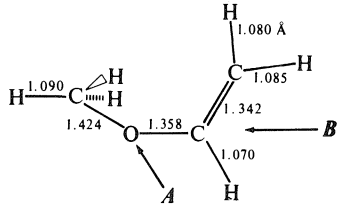

20

TABLE 4. INDO-MO-FPT coupling constants over five bonds between methyl and olefinic protons in methyl vinyl ether*

	Coupling constant for θ (deg) =					
ϕ	0	60	120	180	240	300
0	−0.68(−0.37)*	−0.31(−0.15)	−0.10(0.04)	−0.09(0.37)	−0.10(0.04)	−0.31(−0.15)
45	−0.15(−0.01)	−0.13(−0.19)	0.16(0.24)	0.11(0.52)	−0.18(0.07)	−0.06(−0.09)
90	0.17(0.27)	0.03(−0.09)	0.13(0.09)	0.30(0.90)	0.07(0.49)	0.04(0.03)
135	0.11(0.17)	0.00(−0.15)	−0.05(−0.05)	0.25(0.98)	0.19(0.66)	−0.02(−0.07)
180	0.03(0.05)	0.06(−0.20)	0.03(0.24)	0.20(0.93)	0.03(0.24)	0.06(−0.20)

ϕ	$\langle\theta\rangle$	$\langle 0° + 120° + 240°\rangle$	$\langle 60° + 180° + 300°\rangle$†
0	−0.26(−0.03)	−0.29(−0.10)	−0.23(0.03)
45	−0.04(0.10)	−0.06(0.10)	−0.02(0.10)
90	0.12(0.28)	0.12(0.28)	0.12(0.28)
135	0.08(0.25)	0.08(0.26)	0.08(0.25)
180	0.07(0.18)	0.03(0.18)	0.11(0.18)

*Parentheses refer to coupling to the olefinic proton *trans* to the methyl group.
†For the *cis* form in which the methyl group is staggered about the O—C bond, the conformation identified from microwave transitions.

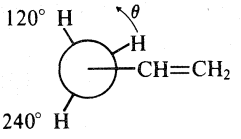

21

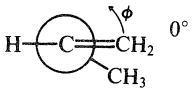

22

and give the angles of rotation about the H_3C—O bond and about the =C—O bond and about the =C—O bond, respectively, viewing along ***A*** in **21** and ***B*** in **22**. The computed couplings are tabulated in Table 4.

The stable form is **20** in which the methyl group is staggered about the O—C bond (30), having $\theta = 60°, 180°$, and $300°$; $\phi = 0°$. $^5J_c^{H,CH_3}$ is calculated as −0.23 Hz by averaging over the three values of θ, a reasonable procedure in that the barrier to rotation about the O—CH_3 bond is 3.8 kcal/mol (30). $^5J_t^{H,CH_3}$ is calculated as 0.03 Hz for this conformation (Table 4). The *gauche* form has $\phi \approx 90°$ but θ is not known, nor are the other structural parameters, so that the numbers in Table 4 cannot be properly weighted for this form.

However, it is interesting to note that both ^5J_c and ^5J_t are calculated as negative for a number of values of θ in the planar *cis* form in which $\phi = 0°$. A shift of −0.1 Hz in ^5J_c and ^5J_t would yield numbers rather close to those observed in Table 2.

The dipole moment of the *cis* form is calculated as 0.98 D, the observed value being 0.96 D (30). However, the planar *trans* form is calculated as 0.6 kcal/mol more stable than the *cis* form. The *ab initio* calculations give the *cis* form as more stable than the *trans* form by about 2 kcal/mol; the *gauche* form having a calculated energy maximum of about 5.5 kcal/mol at $\phi = 85°$.

$^4J^{H,CH_3}$ for the planar *cis* form was calculated as −0.24 Hz, as compared to the observed value of −0.40 Hz. For observed couplings it must be remembered that they represent averages over torsional oscillations and over bond vibrations in the actual molecule. It appears that the present INDO-MO-FPT calculations for the idealized rigid structures yield long-range couplings in reasonable agreement with experiment for methyl vinyl ether.

Other Conjugated Molecules in Table 2

$^5J_c^{H,CH_3}$ is −0.27 Hz for *trans*-4-methoxy-3-butene-2-one, **10**, suggesting that the O—CH_3 group is *cis* planar with respect to the C=C bond (compare $^5J_c^{H,CH_3} = -0.32$ Hz in methyl vinyl ether). On the other hand, the five-bond coupling to the keto methyl group is only −0.12 Hz; yet its negative value can likely be interpreted as evidence for the *s-trans* arrangement of the double bonds in **10**.

In the *cis* form of 1-methoxy-1, 3-butadiene, $^5J_c^{H,CH_3}$ is −0.29 Hz, but is <0.1 Hz in the *trans* form; providing strong evidence for the conformations indicated in Table 2 (16). Furthermore $^5J_t^{H,CH_3}$ is <0.1 Hz in the *trans* form; implying the necessity for a *cis* arrangement of

Can. J. Chem. Downloaded from www.nrcresearchpress.com by 210.87.254.40 on 09/05/12
For personal use only.

Can. J. Chem. Downloaded from www.nrcresearchpress.com by 210.87.254.40 on 09/05/12
For personal use only.

the O—CH_3 and the adjacent C=C bonds if ^5J_c and ^5J_t are to be observable.

1-Butene

The magnitudes of $^5J_c^{H,CH_3}$ and $^5J_t^{H,CH_3}$ are both ≤ 0.02 Hz (Table 2), and it is therefore probable that in the conformation **23** the methyl

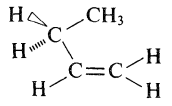

23

protons do not approach the olefinic protons as closely as in methyl vinyl ether. This suggestion is supported by the gas phase structure (35).

Anisole

A bulky *ortho* group apparently yields a conformation, **1**, in which the O—CH_3 bond lies *cis* to a C—H bond of the aromatic nucleus. INDO-MO-FPT calculations on **24**, employing

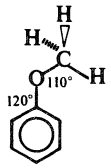

24

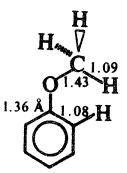

$\theta = 0°$

25

a standard geometry (34) for the phenyl group and other parameters as indicated in **24** and **25**, gave $^5J_c^{H,CH_3}$ as -4.66, -0.73, -0.14, -0.15, -0.12 and -0.80 Hz for $\theta = 0$, 60, 120, 180, 240, and 300°, respectively.[3] Assuming a staggered arrangement with respect to the C—H bond of the phenyl group, the average calculated value ($\theta = 60$, 180, 300°) is -0.53 Hz. This is somewhat larger in magnitude than the observed value of -0.33 Hz in 2,4-dibromoanisole. However, note that the C—O—C angle is taken as 110°, no doubt somewhat too small. Comparison with the calculated and observed data for methyl vinyl ether, where this angle is taken as 120.7°, emphasizes the sensitivity of these five-bond couplings to internuclear distances.

[3]Convergence was not obtained for a heavy atom coplanar form. Therefore the C—C—O—C dihedral angle was taken as 1°, accounting for the small asymmetry in the calculated values.

Conclusions

The relatively satisfactory agreement between calculated and observed negative coupling constants over five bonds in the molecules other than the hydrazones suggests that either the structural assumptions or the calculations are at fault for the hydrazones. Structural work on the latter molecules would help to resolve the conundrum.

Acknowledgments

We are grateful to Mr. Kalvin Chum for some of the measurements and to the National Research Council of Canada for financial assistance.

1. H. A. Gaur, J. Vriend, and W. G. B. Huysmans. Tetrahedron Lett. 1999 (1969).
2. M. Barfield, C. J. Macdonald, I. R. Peat, and W. F. Reynolds. J. Am. Chem. Soc. **93**, 4195 (1971).
3. M. Barfield and M. Karplus. J. Am. Chem. Soc. **91**, 1 (1969).
4. M. Barfield and S. Sternhell. J. Am. Chem. Soc. **94**, 1905 (1972).
5. R. Wasylishen and T. Schaefer. Can. J. Chem. **50**, 1852 (1972).
6. J. B. Class, J. G. Aston, and T. S. Oakwood. J. Am. Chem. Soc. **75**, 2937 (1953).
7. G. J. Karabatsos, B. L. Shapiro, F. M. Vane, J. S. Fleming, and J. S. Ratka. J. Am. Chem. Soc. **85**, 2784 (1963); G. J. Karabatsos, R. A. Taller, and F. M. Vane. Tetrahedron Lett. 1081 (1964); G. J. Karabatsos and K. L. Krumel. Tetrahedron, **23**, 1097 (1967); G. J. Karabatsos and C. E. Osborne. Tetrahedron, **24**, 3361 (1968); G. J. Karabatsos and R. A. Taller. Tetrahedron, **24**, 3361 (1968); **24**, 3923 (1968).
8. J. P. Maher and D. F. Evans. Proc. Chem. Soc. 208 (1961).
9. R. Freeman and W. A. Anderson. J. Chem. Phys. **37**, 2053 (1962).
10. D. Crépaux, J. M. Lehn, and R. R. Dean. Mol. Phys. **16**, 225 (1969).
11. H. Kessler. Angew. Chem. Internat. Edit. **9**, 219 (1970).
12. S. Castellano and A. A. Bothner-By. Mellon Institute Publication, Pittsburgh, Pa. 1967.
13. C. W. Haigh and J. M. Williams. J. Mol. Spectrosc. **32**, 398 (1969).
14. J. Feeney and L. H. Sutcliffe. Spectrochim. Acta, **24A**, 1135 (1968).
15. A. A. Bothner-By and C. Naar-Colin. J. Am. Chem. Soc. **83**, 231 (1961).
16. E. Diez and M. Rico. J. Mol. Spectrosc. **37**, 131 (1971).
17. K. Tori, M. Ohtsuri, and T. Kubota. Bull. Chem. Soc. Jpn. **39**, 1089 (1966).
18. F. H. A. Rummens and L. W. Kaslander. Can. J. Spectrosc. **17**, 99 (1972).

19. M. BARFIELD, A. M. DEAN, C. J. FALLICK, R. J. SPEAR, S. STERNHELL, and P. W. WESTERMAN. J. Am. Chem. Soc. **97**, 1482 (1975).
20. J. A. POPLE, J. W. MCIVER, JR., and N. S. OSTLUND. J. Chem. Phys. **49**, 2960 (1968); **49**, 2965 (1968).
21. M. BARFIELD. J. Chem. Phys. **46**, 811 (1967); **48**, 4458 (1968).
22. M. KARPLUS. J. Chem. Phys. **33**, 1842 (1960).
23. A. V. CUNLIFFE, R. GRINTER, and R. K. HARRIS. J. Mag. Reson. **3**, 299 (1970).
24. C. J. MACDONALD and W. F. REYNOLDS. Can. J. Chem. **48**, 1002 (1970).
25. P. A. DOBOSH. Program 141, QCPE, University of Indiana, Bloomington, Indiana.
26. K. V. L. SASTRY and R. F. CURL, JR. J. Chem. Phys. **41**, 77 (1964).
27. P. BOTSCHWINA. Chem. Phys. Lett. **29**, 580 (1974).
28. J. A. POPLE and D. L. BEVERIDGE. Approximate molecular orbital theory. McGraw-Hill Book Company, New York, N.Y. 1970.
29. N. L. OWEN and N. SHEPPARD. Trans. Faraday Soc. **60**, 634 (1964).
30. P. CAHILL, L. P. GOLD, and N. L. OWEN. J. Chem. Phys. **48**, 1620 (1968).
31. N. L. OWEN and H. M. SEIP. Chem. Phys. Lett. **5**, 162 (1970).
32. M. J. ARONEY, R. J. W. LEFÉVRE, G. L. D. RITCHIE, and J. D. SAXBY. Aust. J. Chem. **22**, 1539 (1969).
33. B. CADIOLI and U. PINCELLI. J. Chem. Soc. Faraday II, **68**, 991 (1972).
34. J. A. POPLE and M. S. GORDON. J. Am. Chem. Soc. **89**, 4253 (1967).
35. S. KONDO, E. HIROTA, and Y. MORINO. J. Mol. Spectrosc. **28**, 471 (1968).

Can. J. Chem. Downloaded from www.nrcresearchpress.com by 210.87.254.40 on 09/05/12
For personal use only.

A proton magnetic resonance estimate of the extent of intramolecular hydrogen bonding in derivatives of 2-trifluoromethyl phenol. Solvent effects

TED SCHAEFER AND J. BRIAN ROWBOTHAM[1]

Department of Chemistry, University of Manitoba, Winnipeg, Man., Canada R3T 2N2

Received March 1, 1976

TED SCHAEFER and J. BRIAN ROWBOTHAM. Can. J. Chem. **54**, 2243 (1976).

The long-range spin–spin coupling constants between hydroxyl protons and ring protons or fluorine nuclei are used to establish the conformer populations in iodine and bromine derivatives of 2-trifluoromethylphenol in C_6H_{12}, CCl_4, and C_6D_6 solutions. The sequence Cl, Br > F > I ≫ CF_3 is established for the so-called hydrogen bonding preferences of the hydroxyl group in 2,4,6-trisubstituted phenols, the corresponding free energy sequence being $-\Delta G$ = 1690, 1690 > 1300 > 1230 > 0 ± 200 cal/mol at 32 °C in CCl_4 solution. An indirect estimate of the free energy differences in the vapor phase suggests the sequence $-\Delta G$ = 2800, 2800 > 2400 > 2300 > 1100 ± 300 cal/mol; the latter value meaning that the hydroxyl group in 4-bromo-2-trifluoromethylphenol prefers the CF_3 group by this amount in the vapor phase. Benzene interacts preferentially with the OH group in this compound to the extent of 1300 cal/mol (ΔG), referenced to the vapor phase.

TED SCHAEFER et J. BRIAN ROWBOTHAM. Can. J. Chem. **54**, 2243 (1976).

On a utilisé les constantes de couplage spin–spin à longue distance entre les protons hydroxyles et les protons ou les noyaux de fluor du cycle pour déterminer les populations de conformères dans les dérivés iodés et bromés du trifluorométhyl-2 phénol en solution dans C_6H_{12}, CCl_4 et C_6D_6. On a établi la séquence Cl, Br > F > I ≫ CF_3 pour ce qui est appelé la préférence dans les formations de pont hydrogène par le groupe hydroxyle dans des phénols trisubstitués en 2,4,6; en solution dans CCl_4 à 32 °C, la séquence correspondante d'énergie libre est $-\Delta G$ = 1690, 1690 > 1300 > 1230 > 0 ± 200 cal/mol. Un estimé indirect des différences d'énergie libre en phase vaporeuse suggère la séquence $-\Delta G$ = 2800, 2800 > 2400 > 2300 > 1100 ± 300 cal/mol; cette dernière valeur signifierait en phase vapeur que le groupe hydroxyle du bromo-4 trifluorométhyl-2 phénol préfère le groupe CF_3 par cette quantité. Le benzène interagit préférentiellement avec le groupe OH dans ce composé jusqu'à concurence d'environ 1300 cal/mol (ΔG) par rapport à la phase vaporeuse.

[Traduit par le journal]

Introduction

In previous work (1, 2) conditions were found under which long-range spin–spin coupling constants over five bonds between hydroxyl protons and ring protons could be measured in 2,4-dihalo- and 2,4,6-trihalophenols. A comparison of $^5J_m^{OH,H_5} \equiv {}^5J_{cis} \equiv {}^5J_c$ and of $^5J_m^{OH,H_3} \equiv {}^5J_{trans} \equiv {}^5J_t$, as defined by **1***a*, yielded the free energy differences between **1***a* and **1***b* for pairs of halogens X, Y. The difference was largest for the pair Cl, I and the order of preference for halogen–hydroxyl interaction was Cl ≥ Br > F > I, in qualitative agreement with enthalpy data based on the intensities of the hydroxyl stretching bands for 2,6-dihalophenols (3).

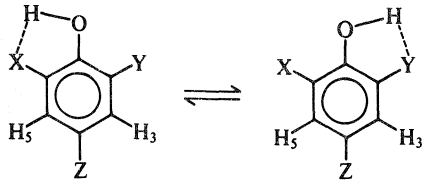

1*a* **1***b*

There exists infrared (4) and ^{19}F chemical shift (5) evidence that, when X = Z = H, Y = CF_3, **1***b* is preferred to **1***a*; suggesting a preferred hydroxyl–trifluoromethyl interaction, *i.e.*, that the free energy of **1***b* is lower than that of **1***a*. However, contrary to the observed low-frequency shift of the infrared band for the halophenols in CCl_4, the stretching frequency increases when Y = CF_3 in **1***b*. This phenomenon has been described as a 'preferred repulsive interaction' (4), probably because the frequency

[1]Research Associate, summer 1975.

Can. J. Chem. Downloaded from www.nrcresearchpress.com by 210.87.254.105 on 09/05/12
For personal use only.

shift was not referred to the vapor phase value for phenol.

In this paper an approach based on long-range coupling constants in derivatives of 2-hydroxybenzotrifluoride is used in an attempt to estimate the free energy of formation of the conformer having the $CF_3\cdots H—O$ interaction.

Experimental

The *o*-hydroxybenzotrifluoride derivatives were prepared by standard methods. Samples for nmr measurements were prepared in the previous (1, 2) manner and were carefully degassed prior to repeated calibration of the pmr spectra at sweep rates of 0.01 and 0.02 Hz/s. Signs of long-range coupling constants were found in the prescribed way (6, 7) and small couplings were determined by carefully decoupling the relevant protons from the spin system; followed by matching of simulated and observed line widths, which were as small as 0.11 Hz. See ref. 1 for the quality of a typical hydroxyl proton resonance spectrum in dry solutions of phenols.

Results and Discussion

Spectral Analysis

The spectra were analyzed with the computer program LAME (8, 9) in the presence and in the absence of intermolecular hydroxyl proton exchange. This procedure ensured reliable values for all the parameters. The standard deviations in the final values were 0.005 Hz or less, all transitions of relative intensity greater than 0.01 having been assigned. The very small couplings (less than 0.1 Hz) between the hydroxyl proton and H_5 in 4,6-diiodo- and 4,6-dibromo-2-trifluoromethylphenol were ascertained by a procedure involving the decoupling of the hydroxyl proton, followed by computer simulations of the spectrum of H_5 under conditions of coupling and decoupling of the hydroxyl proton. No coupling was ascertainable in the latter compound.

The final parameters are given in Table 1, together with solvent conditions. The spectrum of 2-hydroxybenzotrifluoride itself was too complex for a reliable analysis, in our opinion, at least under the conditions of signal to noise dictated by the low concentrations used in the present work.

Paucity of Intermolecular Hydrogen Bonding for 4-Bromo-2-trifluoromethylphenol, 2, in CCl_4

It is known (10, 11) that 2-halophenols form intermolecularly hydrogen bonded dimers, as opposed to *n*-mers for phenol and 3- and 4-halophenols (11, 12), and that the enthalpy of formation is -5.5 ± 0.5 kcal/mol, insensitive to the particular halogen substituent. For 2-fluorophenol in CCl_4 solution the dimerization constant is 0.15 M^{-1} at 20 °C (11), the chemical shift of the intermolecularly hydrogen bonded hydroxyl proton being 7.2 ppm. The correspond-

TABLE 1. Proton chemical shifts* and coupling constants†‡ in derivatives of 2-trifluoromethyl phenol at 32 °C

	4-Bromo§			4,6-Dibromo§		4,6-Diiodo§
Parameter	C_6H_{12} (1.5)	CCl_4 (3.3)	C_6D_6 (3.2)	CCl_4 (2.6)	C_6D_6 (2.4)	CCl_4 (2.2)
ν_{OH}	527.3	537.2 (531.5)‖	427.0	583.1	531.5	568.0
ν_3	754.2	758.8	743.5	762.7	732.4	777.4
ν_5	740.6	748.6	691.5	775.7	711.3	808.4
ν_6	675.1	683.7	575.0	—	—	—
$^3J_o^{H,H}$	8.758	8.765	8.717	—	—	—
$^4J_m^{H,H}$	2.434	2.444	2.457	2.338	2.346	2.064
$^5J_p^{H,H}$	0.361	0.344	0.337	—	—	—
$^4J_o^{H,CF_3}$	−0.609	−0.648	−0.636	−0.641	−0.619	−0.680
$^5J_m^{H,CF_3}$	0.699	0.718	0.728	—	—	—
$^6J_p^{H,CF_3}$	−0.680	−0.683	−0.660	−0.578	−0.593	−0.600
$^5J_m^{H_3,OH}$	0.144	0.176	0.401	0.576	0.601	0.570
$^5J_m^{H_5,OH}$	0.396	0.398	0.284	0.00	0.00	0.075±0.02
$^5J_o^{OH,CF_3}$	−3.478	−3.069	−0.959	0.271	0.378	±0.10 ±0.01

*Relative to internal tetramethylsilane at 100 MHz.
†Root mean square deviation between calculated and observed transitions was 0.015 Hz or less in all cases.
‡Standard deviations of the parameters were 0.005 Hz or less.
§Mole percent of solvent in parentheses.
‖CCl_4 1.3 mol %.

Can. J. Chem. Downloaded from www.nrcresearchpress.com by 210.87.254.105 on 09/05/12
For personal use only.

Can. J. Chem. Downloaded from www.nrcresearchpress.com by 210.87.254.105 on 09/05/12
For personal use only.

ing low-field shift for **2** will hardly be smaller than that.

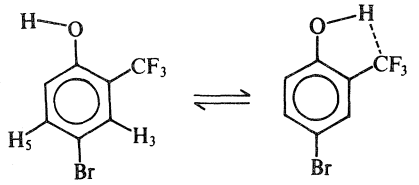

2a **2b**

The 3.3 mol% solution of **2** in CCl_4 has ν_{OH} = 5.37 ppm while a 1.27 mol% solution has ν_{OH} = 5.31_5 ppm (Table 1). Extrapolation to zero concentration yields the monomer shift as 5.28_5 ppm at 32 °C. Clearly, not more than about 2% of **2** exists as a dimer at 3.2 mol% (0.4 *M*) in CCl_4 at 32 °C (this estimate implies that the dimerization constant is near 0.15 and that ν_{OH} in the dimer is near 7.5 ppm). Similar remarks follow for the 1.5 mol% solution of **2** in C_6H_{12} (reliable analysis of spectra characterized by so many small coupling constants as in **2** is improbable at lower concentrations).

Intramolecular Equilibrium in 2

In previous work on halophenols (1, 2) it was shown that $^5J_m^{OH,H_3} \equiv J_3$ and $^5J_m^{OH,H_5} \equiv J_5$ (compare **2a** and **2b**) provide a reliable measure of the intramolecular equilibrium. For example, in 2,4-dihalophenols, **3**, in CCl_4 solution J_3 is too small to observe, indicating the predominance of **3b**. On the other hand, a series of trihalo-

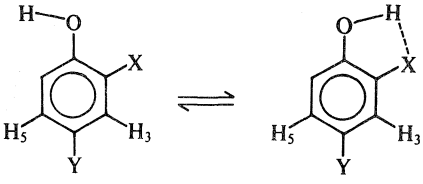

3a **3b**

phenols gave observable J_3 and J_5 values, from which a reasonably consistent set of populations of **1a** and **1b** could be derived on the assumption that $J_3 = 0$ in **1b** and $J_5 = 0$ in **1a**.

Now, from the J_3 and J_5 values for **2** in Table 1, it then follows that 0.398/(0.176 + 0.398) or 69% of **2** exists as **2b** in CCl_4 solution at 32 °C. If, as appears likely (10), the dimer is formed between **2a** and **2b**, 29% of **2** exists as the monomer **2a**. Then the free energy difference between monomers **2b** and **2a** is $-RT \ln K$ = −606 ln 29/67 or −510 cal/mol. The errors in measurement of J_3 and J_5 and the possible errors in the estimate of the extent of dimerization suggest to us that **2b** has a lower free energy than **2a** of 510 ± 50 cal/mol at 32 °C in CCl_4 solution.

A similar treatment of the data for the C_6H_{12} solution gives $\Delta G = -630 \pm 50$ cal/mol for the equilibrium **2a** ⇌ **2b**, while ΔG is +210 ± 50 cal/mol for the benzene solution.

For the latter solution the ASIS (13) numbers for **2** in Table 1 indicate a specific interaction of the benzene molecules with the hydroxyl group. Thus, the numbers for OH and H_6 are both 1.00 ppm (C_6H_{12} as reference solution) and are dramatically smaller for H_3 and H_5. Because only 29% of **2** exists as **2a**, the ASIS number for OH in **2a** must be actually larger than 1 ppm. In other words, a specific interaction of the hydroxyl group with the π cloud of the benzene ring, estimated to involve a free energy decrease of 0.6 ± 0.2 kcal/mol (14), could account for the specific ASIS numbers.

Note that such specific shifts for the OH proton resonance are of much smaller magnitude in the 4,6-dibromo compound (Table 1), *i.e.*, in the presence of two *ortho* substituents.

$^5J_o^{OH,F}$ as an Indicator of the Intramolecular Equilibrium

In Fig. 1, $^5J_o^{OH,F}$ is plotted *vs.* the population of the conformer having the hydroxyl group oriented *cis* to the CF_3 group. The population of this conformer is deduced from the J_3 and J_5 values. Apart from point 3 for the C_6D_6 solution of the 4-bromo compound, a (dashed) straight line can be drawn through the other points. Extrapolation yields −4.7 ± 0.2 Hz as the value of $^5J_o^{OH,F}$ for a 100% *cis* conformer.

The magnitude of $^5J_o^{OH,F}$ for the benzene solution of the 4-bromo compound is 0.7 Hz smaller in magnitude than expected on the basis of J_3 and J_5. This deviation cannot be a result of a solvent effect on the latter couplings (compare data in Table 1). Rather, it is a consequence of the specific interaction of the benzene solvent with the solute molecules. $^5J_o^{OH,F}$ is dominated by a through-space mechanism which is exceedingly sensitive to the distance between the proton and the fluorine nucleus (15) and an average increase of 0.02 Å between the hydroxyl hydrogen atom and the fluorine atoms in the benzene solution is sufficient to account for the deviation (15). Competition between the benzene

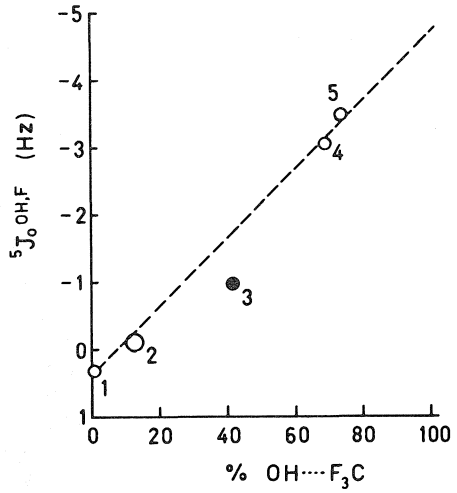

FIG. 1. The spin–spin coupling constant, formally over five bonds, between the hydroxyl proton and the fluorine nucleus, $^5J_o^{OH,F}$, in derivatives of 2-trifluoromethylphenol is plotted *vs.* the population of the *cis* conformer as deduced from the hydroxyl proton, ring proton coupling constants in Table 1. Point 1 refers to the 2,4-dibromo compound, point 2 to the 2,4-diiodo compound. Points 3, 4, and 5 refer to the 4-bromo compound in C_6D_6, CCl_4, and C_6H_{12} solutions, respectively.

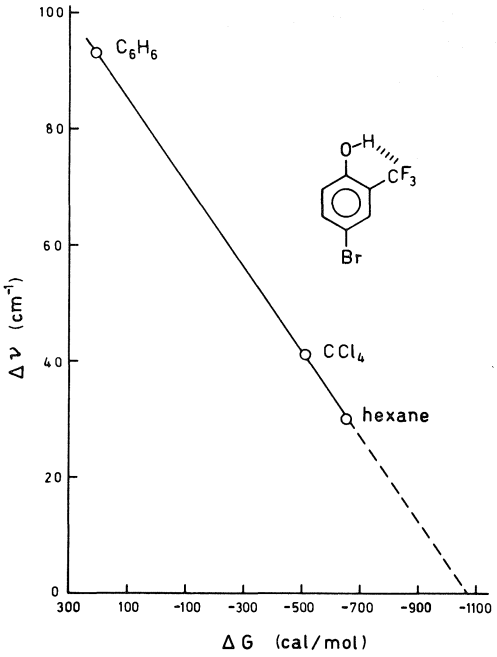

FIG. 2. The shifts to low frequency in solution relative to the vapour phase, $\Delta\nu$, of the hydroxyl fundamental stretching frequency of phenol is plotted *vs.* the free energy difference between the *cis* conformer (sketched) and the *trans* conformer of 4-bromo-2-trifluoromethylphenol in solution. The free energy differences are deduced in the text from the data in Table 1 and the $\Delta\nu$ values are taken from ref. 19.

molecules and the CF_3 group for the hydroxyl group in the *cis* conformation **1***b* could reasonably lead to such an increase in interatomic distances.

Solvent Effect on the Intramolecular Equilibrium

Infrared data on the 2-halophenols in the vapor phase (16) and in CCl_4 and other solutions (4, 17) demonstrate that in CCl_4 the hydrogen bonded conformer is destabilized by up to 2 kcal/mol relative to the other conformer. A general non-specific effect arising from the solvent considered as a dielectric continuum (18) would stabilize the more polar form, as observed. On the other hand, the frequency shifts observed for phenol in various solvents (19) suggest a specific interaction of the hydroxyl group with the solvent molecules. The dielectric constants of CCl_4, C_6H_{12}, and C_6H_6 lie within 0.2 units of one another and for purposes of the following discussion a specific solvent interaction model is assumed.

Compared to the vapor phase, the hydroxyl stretching frequency of phenol is shifted to lower values by 30, 41, and 93 cm^{-1} in *n*-hexane, CCl_4, and C_6H_6, respectively (19). The value for cyclohexane is assumed equal to that in *n*-hexane. In Fig. 2, these frequency shifts are plotted *vs.* ΔG in the **2***a* $\rightleftharpoons$ **2***b* equilibrium. Extrapolation to zero frequency shift yields ΔG as -1070 ± 50 cal/mol for the equilibrium of 4-bromo-2-trifluoromethyl phenol in the vapor phase.

The empirical relationship in Fig. 2 implies that the interaction OH$\cdots$CF$_3$ is considerably weaker than the OH$\cdots$I interaction. If ΔG can be equated with ΔH, *i.e.*, the entropy of **2***b* is the same as that of **2***a*, a direct comparison is possible. Thus ΔH is -2.75 ± 0.07 kcal/mol for 2-iodophenol in the vapor phase, indicating an enthalpy difference of 1680 ± 120 cal/mol between the OH$\cdots$CF$_3$ and OH$\cdots$I interactions.

Now, in *sym*-trisubstituted phenols, specific OH–solvent interactions are presumably preempted by the *ortho* substituents. Therefore measurements on the 2,4-diiodo- and the 2,4-dibromo compounds in Table 1 become of interest.

Can. J. Chem. Downloaded from www.nrcresearchpress.com by 210.87.254.105 on 09/05/12
For personal use only.

Can. J. Chem. Downloaded from www.nrcresearchpress.com by 210.87.254.105 on 09/05/12
For personal use only.

Competitive Hydroxyl Interaction with CF_3 and I, Br Substituents

In the iodine derivative, X = Z = I, Y = CF_3 in **1**, the J_3 and J_5 values in Table 1 show **1***a* as more stable than **1***b* by a free energy of 1230 ± 200 cal/mol. Previous J_3 and J_5 values for the trihalophenols (1) gave a difference of 460 ± 60 cal/mol for the Br, I pair, so that the Br, CF_3 pair has ΔG = 1700 ± 250 cal/mol. The larger value of 1950 cal/mol implies J_5 = 0.02 Hz in the 2,4-dibromo compound, a value we evidently could not detect (Table 1).

If the vapor phase estimate of ΔG for **2** is correct and specific solvent interactions for compounds of type **1** can be neglected, it follows that in the vapor phase ΔG is −2300 ± 250 cal/mol for the equilibrium **4***a* ⇌ **4***b* and is −2760 ± 310 cal/mol for the equilibrium **5***a* ⇌ **5***b*.

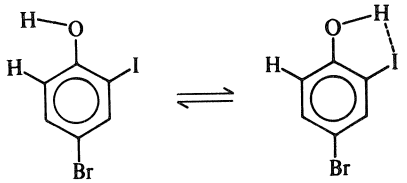

4*a* **4***b*

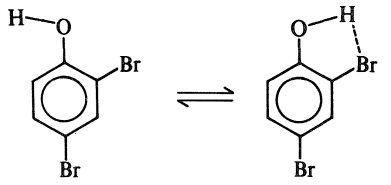

5*a* **5***b*

In this connection it is of interest that the enthalpies for the corresponding equilibria in the vapor phase for 2-iodophenol and 2-bromophenol are −2750 ± 70 and −3130 ± 350 cal/mol, respectively (16). The small discrepancies between the ΔG values for **4** and **5** and these ΔH values could be caused by the polarization of the O—H bond by the electric field of the C—Br bond in **4** and **5**, or by small entropy differences between the conformers in the equilibria or, perhaps, by unrecognized classical solvation energies (18).

Conclusions

In any event, the sequence X = Cl, Br > F > I ≫ CF_3 is safely established for the hydroxyl–X interaction in trisubstituted phenols in CCl_4 solution. The free energy sequence is $-\Delta G(X)$ = 1690, 1690 > 1300 > 1230 ≫ 0 ± 200 cal/mol, the error of 200 cal/mol lying in the last number. In the vapor phase an indirect estimate suggests the sequence X = Cl, Br > F > I ≫ CF_3 ≫ H for 2,4-disubstituted phenols, the corresponding free energy sequence being $-\Delta G(X)$ = 2800, 2800 > 2400 > 2300 ≫ 1000 ± 300 ≫ 0 cal/mol; the large error again occurs for the I, CF_3 pair.

It is interesting that the sequence Cl, Br > F > I has the same order as the group dipole moment sequence for the carbon–halogen bonds in aromatic systems (20). On the other hand, the CF_3 group dipole moment is substantially larger than that for the halogens. Of course, the formation of the weak hydrogen bond in the halophenols completes a five-membered ring while the weak hydrogen bond in 2-trifluoromethyl phenol completes a six-membered ring, so that a direct comparison of the sequences is probably invalid. One may note that the closest distance of approach between the hydroxyl proton and a fluorine nucleus in the CF_3 group in **2** is less than 1.5 Å, implying a strong Pauli repulsion which opposes electrostatic attractions between the OH and CF_3 dipoles.

It is also noteworthy that in 2-fluorophenol derivatives $^4J_{cis}^{OH,F}$ has a magnitude of only 4.5 Hz (2). If the hydrogen bond in these molecules had a large covalent character, electron correlation effects could well produce a coupling larger by an order of magnitude (21, 22); particularly as $^4J_{cis}^{OH,F}$ arises from a proximity mechanism (15) and not via the intervening C—C and C—O bonds.

Acknowledgment

We are grateful to the National Research Council of Canada for financial support.

1. J. B. Rowbotham and T. Schaefer. Can. J. Chem. **52**, 3037 (1974).
2. J. B. Rowbotham, M. Smith, and T. Schaefer. Can. J. Chem. **53**, 986 (1975).
3. A. W. Baker and A. T. Shulgin. Can. J. Chem. **43**, 650 (1965).
4. A. W. Baker and A. T. Shulgin. Nature, **206**, 712 (1965).
5. D. Doddrell, E. Wenkert, and P. V. Demarco. J. Mol. Spectrosc. **34**, 162 (1969).
6. J. P. Maher and D. F. Evans. Proc. Chem. Soc. 208 (1961).

7. R. FREEMAN and W. A. ANDERSON. J. Chem. Phys. **37**, 2053 (1962).
8. S. CASTELLANO and A. A. BOTHNER-BY. J. Chem. Phys. **41**, 3863 (1964).
9. C. W. HAIGH and J. M. WILLIAMS. J. Mol. Spectrosc. **32**, 398 (1969).
10. E. A. ALLEN and L. W. REEVES. J. Phys. Chem. **66**, 613 (1962).
11. A. J. DALE and T. GRAMSTAD. Spectrochim. Acta, Part A, **28**, 639 (1972).
12. M. SAUNDERS and J. B. HYNE. J. Chem. Phys. **29**, 253 (1958); **31**, 270 (1959).
13. P. LASZLO. Prog. N.M.R. Spectrosc. **3**, 231 (1967).
14. Z. YOSHIDA and E. OSAWA. J. Am. Chem. Soc. **87**, 1467 (1965).
15. T. SCHAEFER and J. B. ROWBOTHAM. Chem. Phys. Lett. **29**, 633 (1974).
16. T-S. LIN and E. FISHMAN. Spectrochim. Acta, Part A, **23**, 491 (1967).
17. A. W. BAKER and A. T. SHULGIN. Spectrochim. Acta, **22**, 95 (1966).
18. R. J. ABRAHAM and E. BRETSCHNEIDER. *In* Internal rotation in molecules. *Edited by* W. J. Orville-Thomas. J. Wiley and Sons, New York. 1974. Chapt. 13.
19. K. SZCZEPIANAK and W. J. ORVILLE-THOMAS. J. Chem. Soc. Faraday Trans. II, **70**, 1175 (1974).
20. J. W. SMITH. Electric dipole moments. Butterworths Publications, London. 1955. pp. 92, 96.
21. J. S. MUENTER and W. KLEMPERER. J. Chem. Phys. **52**, 6033 (1970).
22. J. S. MARTIN and F. Y. FUJIWARA. J. Am. Chem. Soc. **96**, 7632 (1974).

Can. J. Chem. Downloaded from www.nrcresearchpress.com by 210.87.254.105 on 09/05/12
For personal use only.

Isothermal compressibility of water–glycerol mixtures at 60.0 °C measured relative to water[1]

E. WHALLEY AND J. B. R. HEATH
Division of Chemistry, National Research Council of Canada, Ottawa, Ont., Canada K1A 0R9

Received March 15, 1976

E. WHALLEY and J. B. R. HEATH. Can. J. Chem. **54**, 2249 (1976).

The compression of aqueous glycerol relative to pure water has been measured up to ~250 bar at 60 °C, and the measurements analyzed to yield the compressibilities at zero pressure to an accuracy of ~0.02–0.1 $Mbar^{-1}$ depending on the concentration. The method used is a simplified version of a more elaborate method (by Kell and Whalley) and is particularly suitable for measuring accurately and quickly the compression of one liquid relative to another.

E. WHALLEY et J. B. R. HEATH. Can. J. Chem. **54**, 2249 (1976).

On a mesuré à 60 °C à des pressions allant jusqu'à 250 bar la compression du glycérol aqueux par rapport à celle de l'eau pure et on a analysé les mesures pour obtenir les compressibilités à une pression de zéro avec une précision de ~0.02–0.1 $Mbar^{-1}$ dépendant de la concentration. La méthode est une version simplifiée d'une méthode plus élaborée (Kell et Whalley) et s'applique plus particulièrement pour mesurer avec précision et rapidité la compression d'un liquide par rapport à un autre.

[Traduit par le journal]

Introduction

The compressibility of glycerol–water mixtures at 60 °C and zero pressure was required in connection with some kinetic measurements (1). The compressibilities have, however, a wider significance in that few isothermal compressibilities of aqueous organic solutions have been measured, although a few *compression* measurements have been reported.

Since only the compressibility at zero pressure was required for this work, only a small pressure range was required. The actual range chosen was a compromise between the greater relative accuracy of the compressions when they are large, and the greater curvature of the curve of the compressions against pressure at higher pressures. A high curvature will of course limit the accuracy of the zero-pressure compressibility. A range of 250 bar was chosen as a suitable compromise.

It is not easy to measure the compressibility of liquids accurately. Fortunately, relative compressions can be measured fairly easily and the compression of one component of the mixture, water (2–4), is known accurately and can be used as a reference. Compressions relative to water have therefore been measured.

[1]NRCC No. 15302.

Experimental Methods and Results

The apparatus is based on the same principles as the apparatus described by Kell and Whalley (2), but is simpler because the required accuracy is less, and only the compressions of mixtures relative to that of one component is required. It consists of a 304 stainless steel vessel of about 250 cm^3 capacity connected to a screw injector and to a 250-bar Heise bourdon gauge which was calibrated by ourselves against a pressure balance. The vessel and the injector were immersed in a thermostat bath controlled to 0.01 °C. To prevent wear on the O-ring seal of the injector shaft, the seal was kept just above the bath surface and was cooled by circulating water through a copper coil wrapped around the injector near the seal.

The apparatus was evacuated and filled with the degassed experimental fluid. Usually some vapor space was left, and this was filled by screwing in the injector to give 250 bar and leaving overnight to allow any dissolved air to diffuse or be convected from the place where it dissolved. The pressure was then reduced to 2 bar by backing off the injector, and the injector shaft was set to a predetermined position by bleeding off solution. Thus, the same volume of all mixtures was present in the apparatus. This volume was measured by weighing both the mixture put into the vessel and the amount bled off. One measurement with a 0.05 volume fraction glycerol–water mixture and two with pure water gave a mean volume of 282.2 cm^3 with a standard deviation of 0.4 cm^3.

The pressure was increased in about 13 increments to about 250 bar, and the travel of the injector shaft was measured with an Ames catalogue No. 14224 dial gauge with a 4-in. travel graduated at intervals of 0.001 in. The dial was calibrated with gauge blocks and was accurate to 0.0005 in.; no corrections were needed. Thermal

Can. J. Chem. Downloaded from www.nrcresearchpress.com by 210.87.254.40 on 09/05/12
For personal use only.

Can. J. Chem. Downloaded from www.nrcresearchpress.com by 210.87.254.40 on 09/05/12
For personal use only.

equilibrium occurred with a half-life of about 4 min and about 1 h was usually allowed. In the earlier runs the measurements were repeated with pressure decreasing; because the up and down run always agreed, in the later runs only two or three points were taken in the downward direction, finishing at 2 bar, to verify that the system was stable.

The volumetric displacement of the injector, aR, where a is the cross-sectional area of the piston and R is the linear displacement from the starting position, is the sum of the volume changes of the vessel (including injector, tubing, bourdon gauge, etc.) ΔV_V and of the liquid ΔV_L

$$aR = \Delta V_V + \Delta V_L$$

The compression of water is accurately known and can be used as a reference to eliminate the expansion of the vessel, etc. Thus, if R_W and R_L are the displacements at the same pressure for pure water and the experimental liquid, then

$$a(R_W - R_L) = \Delta V_W - \Delta V_L$$

The slope at 2 bars of a curve of $R_W - R_L$ against the pressure is related to the difference of compressibility of water and the liquid.

$$\frac{\partial(R_W - R_L)}{\partial p} = \frac{V}{a}(\kappa_W - \kappa_L)$$

where V is the volume of the vessel.

Values of R_L at predetermined pressures were obtained by interpolating graphically the measured values of R_L using a difference equation to increase the accuracy. A typical curve of $R_W - R_L$ against pressure, for a 0.05 volume fraction glycerol–water mixture, is shown in Fig. 1. The compressibility of water was taken as 44.50 $Mbar^{-1}$ (2–5) without significant error for present purposes, and the compressibilities at 1 bar of the mixtures so obtained are given in Table 1 and shown graphically in Fig. 2. The uncertainty of the difference of compressibilities is about 1%, which is 0.1 $Mbar^{-1}$ for 0.75 volume fraction glycerol–water and correspondingly less in more aqueous solutions.

The compression of glycerol has been measured by Bridgman (6) at pressure up to 12 000 kgf cm^{-2} at 0, 50, and 95 °C. The measurements at lower pressures (0, 500, 1000, 2000, 3000, and 4000 kgf cm^{-2}) were analyzed by plotting the reciprocal compression $p/\Delta V$, where ΔV is the change of volume between zero pressure and pressure

TABLE 1. Isothermal compressibilities of glycerol–water mixtures at 60.0 °C

Volume fraction glycerol	κ/$Mbar^{-1}$
0.00	(44.50)[a]
0.05	43.12
0.125	41.16
0.25	38.26
0.50	33.95
0.75	29.93

[a]Reference value.

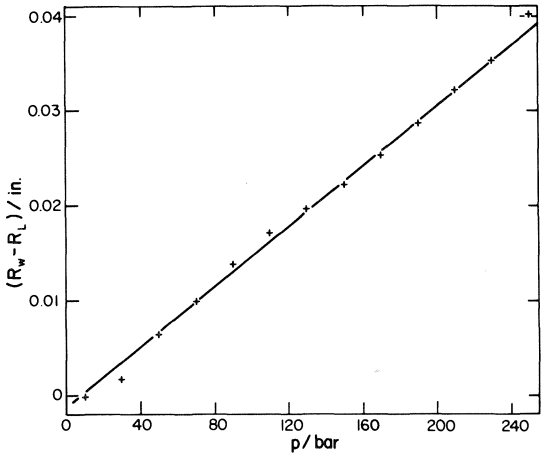

FIG. 1. A typical curve of $R_W - R_L$ against the pressure. The mixture was 0.05 volume fraction glycerol in water. The slope of the line corresponds to a difference of compressibility between water and solution of 1.38 $Mbar^{-1}$.

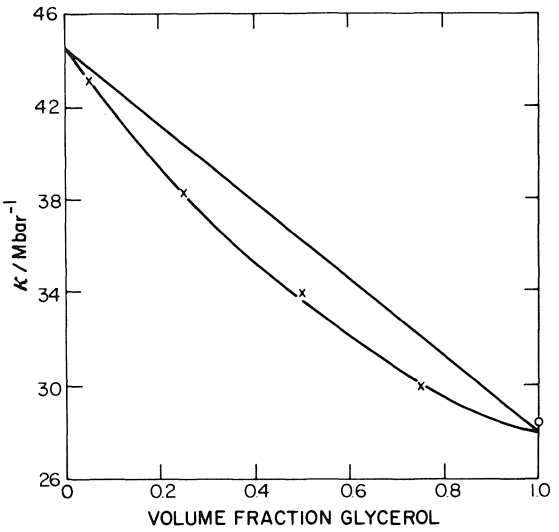

FIG. 2. Compressibility of glycerol–water mixtures at 60 °C and zero pressure. The crosses represent the present measurements and the circle the value interpolated from ref. 6.

p, against the pressure and extrapolating to zero pressure. The zero-pressure compressibility can be obtained from the intercept, and the values obtained at 0 and 50 °C are 20.9 and 27.3 $Mbar^{-1}$ with an apparent accuracy of about 0.4 $Mbar^{-1}$. At 95 °C, compressions were measured starting from 1000 kgf cm^{-2}, and so $\Delta p/\Delta V$, where Δp and ΔV are the differences in pressure and volume between adjacent points, was plotted against the mean pressure of the points. The zero-pressure compressibility obtained by a rather long extrapolation of this plot was

32 $Mbar^{-1}$, with an accuracy of perhaps 1 or 2 $Mbar^{-1}$. By interpolating between the three compressibilities, the compressibility at 60 °C and 1 bar is 28.4 ± ~0.5 $Mbar^{-1}$. This value is plotted as a circle in Fig. 2. If the correct value is 27.9 $Mbar^{-1}$, then the excess compressibility κ^e, which is the difference between the actual compressibility and the compressibility that would occur if the mixture were ideal, is symmetrical in the volume fraction. This is illustrated in Fig. 2, where the straight line for the ideal mixture and the curved line for a mixture governed by the equation

$$[1] \qquad \kappa^e = -9.5\phi_1\phi_2 \text{ Mbar}^{-1}$$

where ϕ_1 and ϕ_2 are the volume fractions of the components, are plotted. Equation 1 is the first non-zero term in an expansion of the excess compressibility as a Taylor series in the volume fractions, and, although the first term need not be the dominant one, there appears to be no significant deviation from it. This provides some support for the assumed compressibility of pure glycerol.

Discussion

The maximum deviation of the compressibility from the ideal is about −2.3 $Mbar^{-1}$, which is much smaller than that of many aqueous organic mixtures. For example, the compressibility of an 0.5 volume fraction ethanol–water mixture at 25 °C as calculated (7) from Moesveld's (8) data is 47.5 $Mbar^{-1}$, whereas the ideal compressibility is 71.5 $Mbar^{-1}$, about 50% greater. The compression, or fractional change of volume, of acetone–water mixtures at 1000 atm and 25 °C (9) is 0.042 at 0.5 volume fraction, compared with the ideal value of 0.060. The ideal value is 43% greater than the real.

The compression of water is due to two main changes, the decrease in the distance of nearest neighbors and the deviation of the intermolecular angles from tetrahedral. The decrease in the nearest-neighbor distance with increasing pressure in water is much less than in ice, and probably contributes only about 3 or 4 $Mbar^{-1}$ to the compressibility (10). Consequently, nearly all the volume change is caused by the bending of intermolecular angles. Acetone, alcohol, and similar solvents, therefore, greatly stiffen the intermolecular angles, but gycerol stiffens them only slightly. No doubt acetone and alcohol stiffen them because their non-polar parts occupy space that would otherwise be empty. Glycerol presumably cannot do this because all its parts can hydrogen bond with the water in a fully three-dimensional manner, and so it does not greatly stiffen the intermolecular angles.

The volume of mixing of glycerol–water mixtures at 60 °C and a volume fraction of 0.5 is about −0.007 $cm^3\ g^{-1}$ according to the data of Gerlach (1881) as reported by Timmermans (11). If the excess compressibility were independent of the pressure, water and glycerol would mix without change of volume at a pressure of about 3.5 kbar, and at higher pressures would presumably expand on mixing.

1. D. L. Gay and E. Whalley. Can. J. Chem. **48**, 2021 (1970).
2. G. S. Kell and E. Whalley. Phil. Trans. Roy. Soc. **A258**, 565 (1965).
3. R. A. Fine and F. J. Millero. J. Chem. Phys. **59**, 5529 (1973).
4. G. S. Kell and E. Whalley. J. Chem. Phys. **62**, 3496 (1975).
5. G. S. Kell. J. Chem. Eng. Data, **20**, 97 (1975).
6. P. W. Bridgman. Proc. Am. Acad. Arts Sci. **67**, 1 (1937).
7. B. T. Baliga and E. Whalley. Can. J. Chem. **42**, 1835 (1964).
8. A. L. Th. Moesveld. Z. Physik. Chem. **105**, 450 (1923).
9. D. M. Newitt and K. E. Weale. J. Chem. Soc. 3092 (1951).
10. E. Whalley. J. Chem. Phys. **63**, 5205 (1975).
11. J. Timmermans. Physiochemical constants of binary systems, Vol. 4. Interscience Publishers, New York. 1960.

Can. J. Chem. Downloaded from www.nrcresearchpress.com by 210.87.254.40 on 09/05/12
For personal use only.

^{13}C magnetic resonance spectra of some isoquinoline alkaloids and related model compounds

DONALD W. HUGHES, HERBERT L. HOLLAND,[1] AND DAVID B. MACLEAN
Department of Chemistry, McMaster University, Hamilton, Ont., Canada L8S 4M1

Received November 12, 1975

DONALD W. HUGHES, HERBERT L. HOLLAND, and DAVID B. MACLEAN. Can. J. Chem. **54**, 2252 (1976).

The natural abundance ^{13}C nuclear magnetic resonance spectra of a number of isoquinoline alkaloids and related model compounds have been recorded. In almost all cases comparison of the spectra of the alkaloids with those of the model compounds has permitted unambiguous assignment of the alkaloid carbon resonances. The ability of ^{13}C nmr spectroscopy to distinguish between diastereomeric pairs of both protoberberine and phthalideisoquinoline alkaloids has been demonstrated.

DONALD W. HUGHES, HERBERT L. HOLLAND et DAVID B. MACLEAN. Can. J. Chem. **54**, 2252 (1976).

On a déterminé les spectres rmn du ^{13}C en abondance naturelle d'un certain nombre d'alcaloïdes de l'isoquinoléine et de composés modèles qui leur sont reliés. Dans presque tous les cas, la comparaison des spectres des alcaloïdes avec ceux des composés modèles a permis d'attribuer sans ambiguité les positions des résonances des atomes de carbone des alcaloïdes. On a démontré la possibilité qui existe, avec la spectroscopie rmn du ^{13}C, de distinguer entre des paires de diastéréoisomères des alcaloïdes de la protoberbérine et du phthalideisoquinoléine.
[Traduit par le journal]

In recent years ^{13}C nuclear magnetic resonance spectroscopy has been used extensively in the study of natural products. In the case of the alkaloids, Wenkert *et al.* have made thorough studies in the piperidine and indole series (1). More recently this technique has been applied to the lupin alkaloids (2), the *Nuphar* alkaloids (3), and the *Lycopodium* alkaloids (4). Despite the variety of ring systems found in the isoquinoline series, only a few reports have been published on their ^{13}C spectra. Some early investigations were made on the *Amaryllidaceae* (5) and the protopine (6) alkaloids, and more recently a report on the tetrahydroprotoberberines (7) has appeared. Aside from these studies there has not been, to our knowledge, any systematic examination of the isoquinoline alkaloids. Here we report on our investigation of the protoberberines and phthalideisoquinolines. We have also examined a number of simple isoquinolines as models for the alkaloids.

We have made use of what are now standard techniques in ^{13}C magnetic resonance spectroscopy. The spectra of all compounds were recorded using broad band decoupling, and where applicable the off-resonance technique was used to determine the substitution at carbon. In some cases the alternately-pulsed or gated decoupling method (8–10) was employed. Deuterium labelling and selective proton decoupling have also been used to make unequivocal assignments of several carbon resonances. Reference is frequently made to model systems in which the assignments are already secure, while in other cases calculated chemical shifts of model systems have been used as reference.

This work was begun with an examination of the 6,7-dimethoxy-1,2,3,4-tetrahydroisoquinolines, **1** and **2**, and the 6,7-dimethoxy-3,4-dihydroisoquinolines **3** and **4** (Fig. 1), since this substitution pattern is frequently found in the isoquinoline rings of the alkaloids. The assignment of the aliphatic carbons of **1** follows readily by comparison with the reported spectra of piperidine (**5**) and tetralin (**6**). Of the two carbons adjacent to nitrogen, C-1 is at lower field because of the α phenyl group. The specific assignment of C-5 and C-8 was achieved by selective proton decoupling. Although the proton chemical shifts are separated by only 8 Hz, C-5 and C-8 were differentiated by running a series of spectra in which the proton decoupling frequency was progressively increased over the relevant frequency range. Carbons 6 and 7 were

[1]Present address: Department of Chemistry, Brock University, St. Catharines, Ontario.

Can. J. Chem. Downloaded from www.nrcresearchpress.com by 210.87.254.40 on 09/05/12
For personal use only.

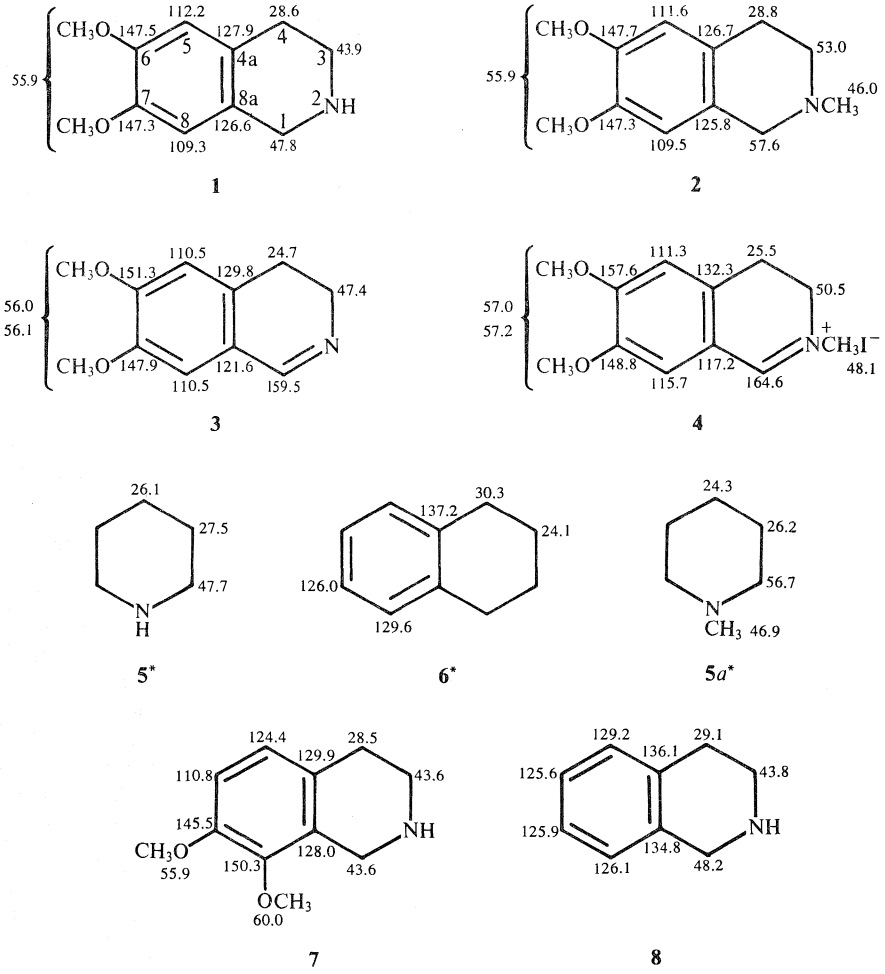

FIG. 1. ^{13}C chemical shifts of simple isoquinolines and other model compounds. *Reference 11.

readily differentiated from C-4a and C-8a (11), but because of the nearly identical chemical shifts of C-4a and C-8a, and C-6 and C-7, unambiguous assignments of the signals could not be made.

Examination of **2** revealed that the aromatic carbons undergo very little change in chemical shifts from those of **1**, whereas C-1 and C-3 are shifted downfield by 9.8 and 9.1 ppm, respectively, because of the β-*N*-methyl group (12). Similar results have been observed for piperidine (**5**) and *N*-methylpiperidine (**5***a*).

The assignments of the C-3 and C-4 resonances of **3** and **4** are apparent from the previous discussion, and those of C-1 by virtue of its unsaturated character. Again C-5 and C-8 are readily differentiated from substituted aromatic carbons. Because of charge delocalization through resonance in **4**, carbons 4a, 6, and 8 should appear at lower field than their counterparts, 8a, 7, and 5, respectively. It is for these reasons that the assignments shown in Fig. 1 have been made. Although **3** does not bear a formal positive charge the same resonance arguments may be applied in assigning the aromatic signals.

In Fig. 2, the spectrum of 6,7-dimethoxyisoquinoline, calculated by applying the shift parameters for two *ortho*-methoxy groups to the reported spectrum of isoquinoline, (11) is listed. The calculated values for the chemical shifts of the aromatic carbons of the benzenoid ring of 6,7-dimethoxyisoquinoline are very similar to

Can. J. Chem. Downloaded from www.nrcresearchpress.com by 210.87.254.40 on 09/05/12
For personal use only.

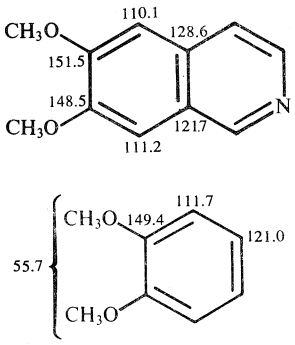

FIG. 2. ^{13}C chemical shifts of 6,7-dimethoxyisoquinoline and veratrole.

those observed for **3**. In this and other appropriate calculated spectra, shift parameters calculated by comparison of the spectra of benzene and veratrole (C-1, +20.8; C-2, −16.9; C-3, −7.6 ppm) (Fig. 3) were applied for the *ortho*-dimethoxy substituents. In almost all cases examined, these figures expressing the combined effect of two *ortho*-methoxy groups gave a closer fit with the observed spectra than those calculated from comparison of the spectra of anisole and benzene.

In many isoquinoline alkaloids, notably the protoberberines, the 7,8-disubstituted 1,2,3,4-tetrahydroisoquinoline unit is present. For this reason we examined 7,8-dimethoxy-1,2,3,4-tetrahydroisoquinoline, **7**. The assignments of the aromatic carbons of **7** are in harmony with those calculated by applying the shift parameters for *ortho*-dimethoxy groups to the observed spectrum of tetrahydroisoquinoline **8**. The assignments in **8** were made by comparison with **5** and **6** and have not been verified by other methods. Regardless of the assignments made in **8** the differences in shift parameters are sufficiently large that the calculated spectrum always leads to the same order of chemical shifts for C-5, C-6, C-4a, and C-8a. The assignments at C-7 and C-8 agree with those made for analogous centres in ring D of the protoberberine series (*vide infra*). It is noteworthy that C-1 of **7** is shielded relative to **8** (−4.6 ppm) as a result of steric perturbation at C-1 by the C-8 methoxy group. Assignment of the signal at 60.0 ppm to the C-8 methoxy group was based on analogous results obtained by Dhami and Stothers on *ortho*-disubstituted anisoles (13). Experimental verification of this assignment is provided in an analogous system, canadine, below.

The phthalideisoquinolines were the first group of alkaloids to be considered by us. Naturally occurring β-hydrastine (**9**) and its diastereomer, α-hydrastine (**10**), and the pair of natural diastereomeric bases, corlumine (**11**) and adlumine (**12**) were examined (see Fig. 3).

The carbon resonances of rings A and B of **9** and **10** were tentatively assigned by comparison with the previous data (compounds **1** and **2** of Fig. 1) and with the spectrum of methylenedioxybenzene, **13**. Meconin (**14**) and phthalide (**15**) were used as models in the assignment of the resonances in ring D. The spectrum of phthalide itself was interpreted as follows. By comparison with the calculated spectrum of 2-carbomethoxybenzyl alcohol (C-1, 143.4; C-2, 130.2; C-3, 130.4; C-4, 128.0; C-5, 134.3; C-6, 127.8) it was possible to assign C-3a and C-7a with some certainty and C-5 and C-7 tentatively. The apparent absence of resonance at 128.5 in the spectrum 6-deuteriophthalide (**15***c*) confirmed the assignment shown for C-6. By selective proton decoupling, carried out on **15***c*, C-7 was assigned unequivocally; the proton at C-7 is well downfield from other protons in the ^1H spectrum so that there was no ambiguity in the selective decoupling experiment. The observed spectrum of 6-nitrophthalide (**15***a*) and 6-aminophthalide (**15***b*) agreed closely with those calculated by applying appropriate shift parameters to the spectrum of phthalide, and so strengthened the assignments made for the phthalide resonances.

The aromatic carbon resonances of meconin were tentatively assigned by comparison of the observed spectrum with the calculated spectrum and verified by selective proton decoupling. The calculated spectrum was obtained by using the shift parameters for *ortho*-methoxy groups (*vide supra*) on the already assigned spectrum of phthalide. The assignments at C-4 and C-5 were verified by selective proton decoupling. The protons at C-4 and C-5 form an AB quartet with signals centred at 6.97 δ and 7.13 δ, respectively. The proton at C-4 was identified because of long-range coupling to the benzylic protons at C-3.

In the alkaloids **9** and **10** the pattern observed for meconin is preserved. C-1′ in both alkaloids is downfield, as expected, relative to the corresponding carbon of meconin, while C-6′ and C-7′ have become more nearly equal in chemical shift than the corresponding carbons of meconin.

Can. J. Chem. Downloaded from www.nrcresearchpress.com by 210.87.254.40 on 09/05/12
For personal use only.

Can. J. Chem. Downloaded from www.nrcresearchpress.com by 210.87.254.40 on 09/05/12
For personal use only.

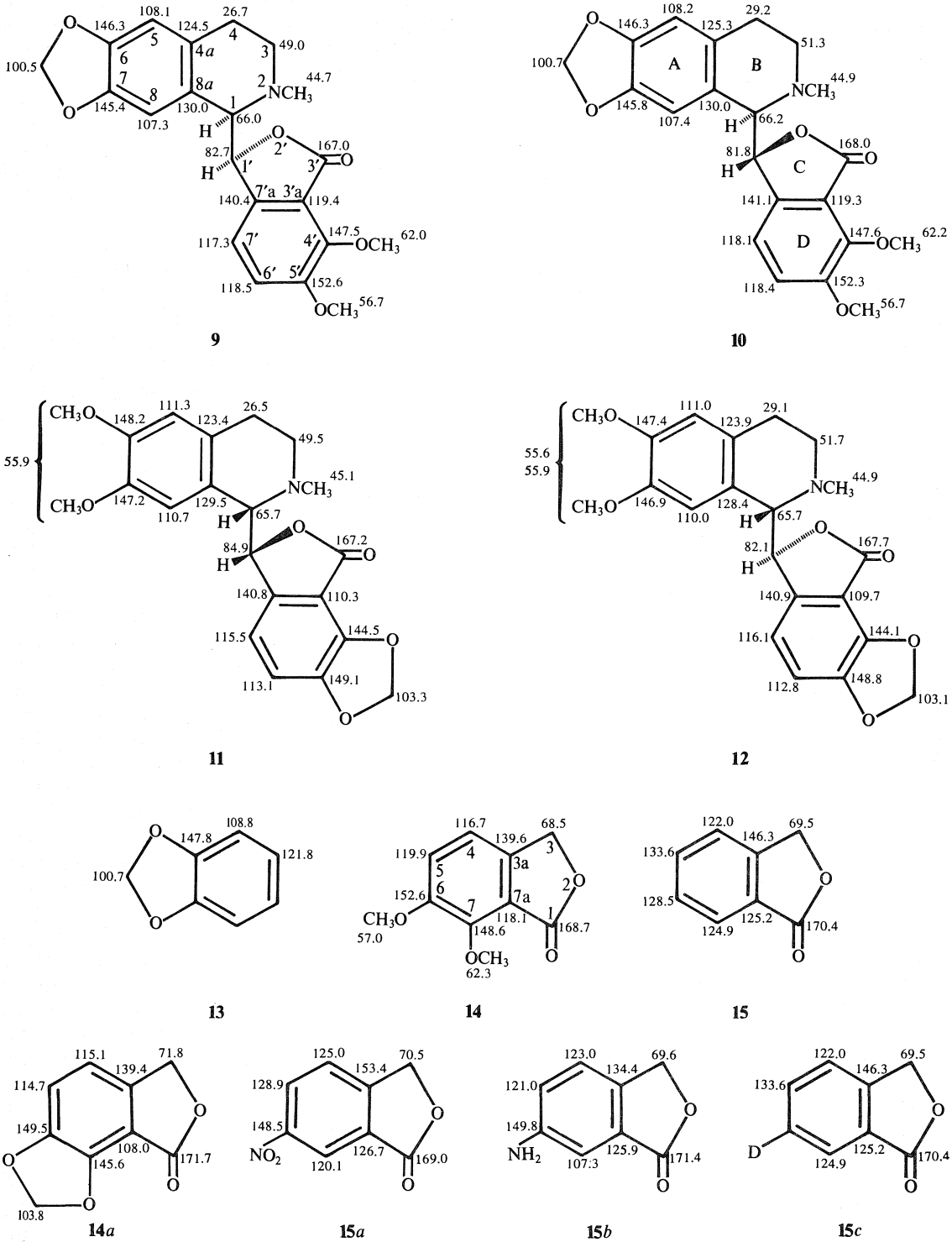

FIG. 3. ^{13}C chemical shifts of phthalideisoquinoline alkaloids and model compounds.

Can. J. Chem. Downloaded from www.nrcresearchpress.com by 210.87.254.40 on 09/05/12
For personal use only.

The signals of the methoxy groups of **9**, **10**, and **14** were assigned in analogy with those made for model compound **7**, the more hindered methoxy group being placed at lower field.

Similar reasoning was used in assigning the signals in the spectra of **11** and **12**. For the phthalide part of the molecule, however, the model chosen was 6,7-methylenedioxyphthalide **14***a*, for which the calculated spectrum is as follows: C-3a, 139.5; C-4, 115.2; C-5, 113.8; C-6, 147.7; C-7, 144.1, C-7a, 105.4. This calculation was made by applying the shift parameters for a methylenedioxy group, obtained from a comparison of the spectra of benzene and methylenedioxybenzene (Fig. 3), C-1, 19.2; C-2, −19.8; C-3, −6.8) to the already established spectrum of phthalide. The validity of this approach was confirmed by the spectrum of **14***a* (Fig. 3). The resonances at C-4 and C-5 were assigned by selective proton decoupling. The C-4 and C-5 hydrogens appear as an AB quartet (J = 8 Hz) at 7.27 δ and 7.0 δ, and the C-4 hydrogen was assigned by virtue of its long-range coupling to the C-3 hydrogens.

Selective proton decoupling experiments were also carried out on **9**, **11**, and **12** and verified the assignment shown for the unsubstituted aromatic carbons in these alkaloids. In the case of **9** the protons at C-5 and C-7′ were differentiated from C-8 and C-6′, respectively, by virtue of their long-range coupling to benzylic protons. Selective proton decoupling then enabled us to assign the ^{13}C resonances. The assignments in **10** were made by analogy with **9**. In **11** the protons at C-6′ and C-7′ form an AB quartet centred at 6.90 δ and 6.14 δ, respectively. The proton at 6.14 δ is long-range coupled to the benzylic proton at C-1′. In the case of **12** there is again an AB quartet centred at 6.84 δ and 7.13 δ corresponding to the protons at C-6′ and C-7′, respectively. Again the proton at C-7′ is long-range coupled to the benzylic hydrogen and was differentiated in this manner. The hydrogen resonances at C-5 and C-8 in both alkaloids were established similarly. The carbon resonances were then established by selective proton decoupling.

A closer examination of the diastereomeric pairs **9** and **10**, and **11** and **12** shows that the isomers may be differentiated by ^{13}C magnetic resonance spectroscopy. In **10** and **12** both C-3 and C-4 are deshielded relative to the corresponding carbons in **9** and **11** whereas the opposite effect is observed at C-1′. Chemical shifts at C-3 and C-4 are therefore diagnostic of the relative stereochemistry of these systems and ^{13}C magnetic resonance spectroscopy may thus be used to assign the relative configuration to a pair of diastereomeric phthalideisoquinolines. It should be pointed out that similar stereochemical assignments have been made from analysis of proton spectra (14) and that the cmr results are in agreement.

The C–H coupling constants at C-1, C-3, C-4, and C-1′ were also measured for the diastereomers **11** and **12**. The values of $^1J^{13}C^1H$ for the respective carbons were as follows: for **11**, 133.8, 133.5, 128.3, and 155.2 Hz and for **12**, 132.3, 136.0, 127.9, and 155.2 Hz. Although differences are observed between **11** and **12**, especially in the coupling constants at C-3, their significance with respect to structure is still obscure.

That the structural assignment of phthalideisoquinoline alkaloids is facilitated by ^{13}C magnetic resonance data is apparent from a comparison of the spectrum of **9** or **10** with that of **11** or **12**. In particular, the chemical shift of C-3a′ is characteristic of the presence of either methylenedioxy or *ortho*-dimethoxy substitution at C-4′ and C-5′. In **9** or **10**, the presence of the C-3a′ resonance at a chemical shift *ca.* 10 ppm lower field than the corresponding carbon of **11** or **12** may be attributed to steric perturbation caused by the C-4′ and C-5′ methoxy substituents. Such steric crowding is absent where the substituent at C-4′ and C-5′ is methylenedioxy. This effect is discussed in greater detail below.

The protoberberines are tetracyclic alkaloids that are derivatives of the dibenzo(*a*,*g*)quinolizidine system. The majority of this group carry oxygen substituents on the aromatic rings but are otherwise unsubstituted. There is however a small group of compounds with a methyl group at C-13. The compounds of this group exist in two diastereomeric forms and several examples were examined to determine if their stereochemistry could be assigned by ^{13}C magnetic resonance spectroscopy.

The assignments shown for canadine (**16**) in Fig. 4 were made by comparison with the model systems of Fig. 1 and Fig. 3 and with the phthalideisoquinolines, and also through study of several deuterated derivatives. The reduction of berberine chloride with $NaBD_4$ yielded (±)-canadine labelled with deuterium at C-8 and C-14. The spectrum of the labelled compound is

Can. J. Chem. Downloaded from www.nrcresearchpress.com by 210.87.254.40 on 09/05/12
For personal use only.

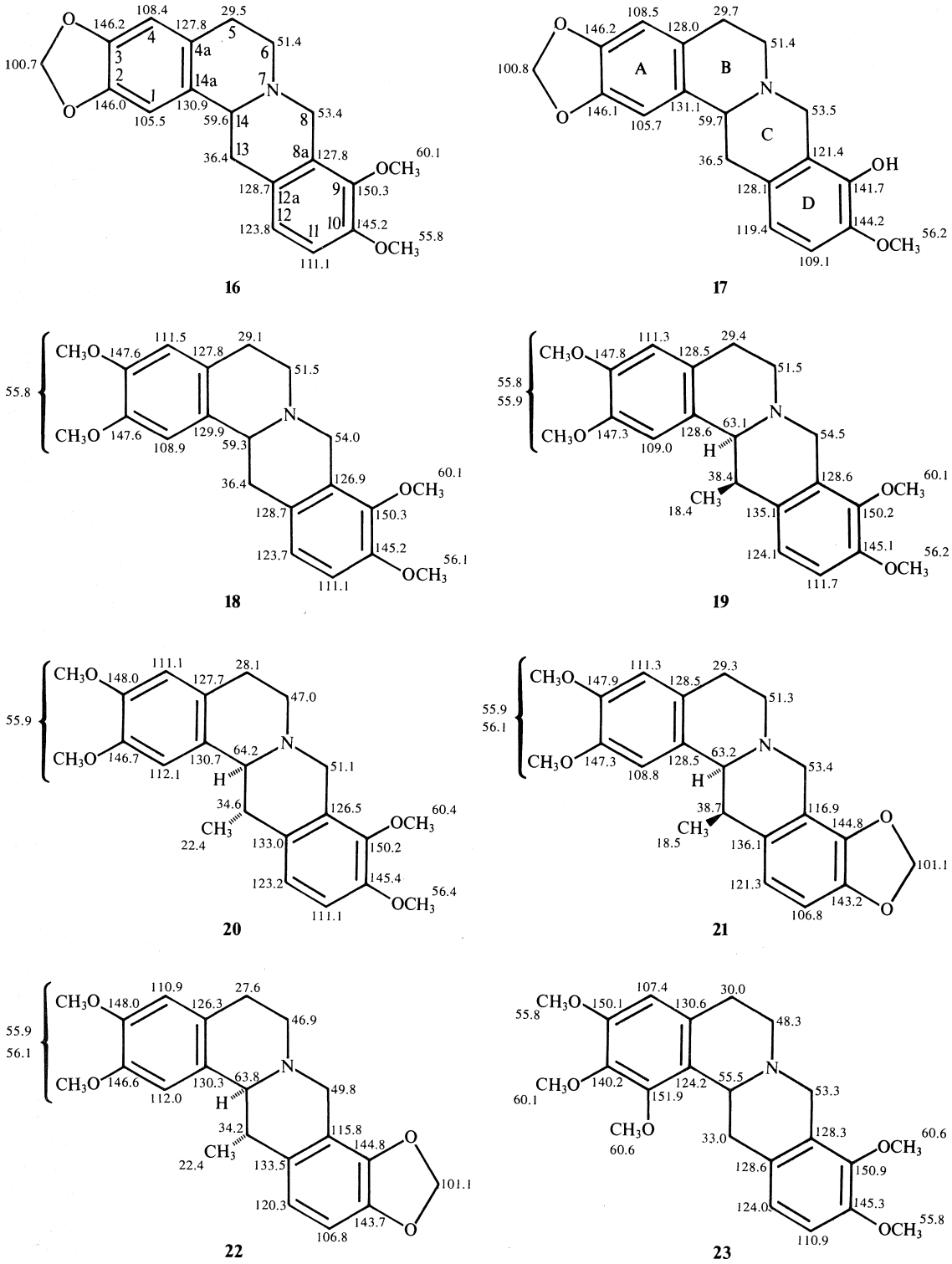

FIG. 4. ^{13}C chemical shifts of protoberberine alkaloids.

Can. J. Chem. Downloaded from www.nrcresearchpress.com by 210.87.254.40 on 09/05/12
For personal use only.

identical with that of canadine except that the signals at 59.6 and 53.4 ppm are virtually absent. Accordingly, these signals are assigned to C-14 and C-8, respectively. Canadine, bearing deuterium in the 9-methoxy group, was prepared by treatment of nandinine (**17**) with diazomethane and D_2O. The labelled compound did not have a signal at 60.1 ppm in its spectrum and therefore this signal in canadine must be assigned to the methoxy carbon at C-9. There was not sufficient information to differentiate C-4a from C-14a, C-2 from C-3, or C-8a from C-12a but the other assignments seem secure. The spectrum of nandinine differs appreciably from that of canadine only in the aromatic signals of ring D, particularly those of C-8a and C-9. It is noteworthy that the signal of C-8 remains unaffected despite removal of the methyl group from the methoxyl of C-9. The shift of C-8a to higher field may be attributed in part to a release from the steric crowding, discussed above, caused by the C-9 methoxy group of **16**. The spectrum of tetrahydropalmatine (**18**) was recorded to serve as a model for the corydalines discussed below. The assignments of **18** are in accord with those of canadine and need no further comment.

Corydaline (**19**) and mesocorydaline (**20**) (Fig. 4) are diastereomeric 13-methyltetrahydroprotoberberines. It is known from pmr studies (15) that corydaline is a *trans*-quinolizidine and mesocorydaline a *cis*-quinolizidine, in which the methyl groups are axial and equatorial, respectively, in ring C. The change from a *trans* to a *cis* configuration in going from **19** to **20** is evident in the upfield shift of carbons, 5, 6, 8, and 13 and is attributed to γ-gauche interactions (12, 16, 17) in the *cis* compound. On the other hand C-14 moves slightly downfield, a trend also observed in the quinolizidine systems of the *Nuphar* and *Lycopodium* alkaloids (3, 4). The methyl group also moves downfield as it changes from an axial to an equatorial position, and a similar shift is observed at C-1. It is of interest that the same downfield shift is observed in the proton spectrum at these two positions (15). Both steric and anisotropic effects may play a role in causing the observed changes.

The analogous diastereomeric pair, cavidine (**21**) and thalictrifoline (**22**) were also examined and gave similar results. It is apparent then that ^{13}C magnetic resonance spectroscopy may be used to assign the relative configuration to the 13-methylprotoberberines.

Kametani *et al.* (7) have used ^{13}C magnetic resonance spectroscopy as a probe to study the effect of substituents at C-1 on the stereochemistry of the quinolizidine system of alkaloids of the protoberberine family. When a methoxy group was present at C-1 they concluded that the quinolizidine system was preferentially in the *cis* form. This conclusion was based on the upfield shift of the signal at C-6. Comparison of the published (7) spectrum of **23** with those of **19**, **20**, and **21** reveals some interesting differences. Whereas in our *cis* compounds C-5, C-6, C-8, and C-13 all undergo upfield shifts relative to the *trans* compounds, only C-6 and C-13 are appreciably affected in **23**. C-14 in **23** is shifted upfield relative to **18** in a manner analogous to that discussed previously for C-1 in compound **8** and this effect probably outweighs any change associated with a *cis–trans* interconversion. Surprisingly, C-5 and C-8 of **23** do not undergo an upfield shift as they do in the 13-methyl compounds. Thus the conformations of the *cis* compounds resulting from methoxy substitution at C-1 must differ appreciably from those of the *cis* compounds resulting from methyl substitution at C-13. The nature of this difference is not apparent from the data available and further work is necessary to resolve the problem.

Throughout this work use has been made of calculations based on the shift parameters for *ortho*-dimethoxy or methylenedioxy substituents. Chemical shifts calculated from these figures (*q.v.*) are generally in good agreement with observed values, with the exception of the value calculated for a substituted carbon *ortho* to two adjacent methoxy groups. Examples are C-8a of **7**, C-3a′ of **9** and **10**, C-7a of **14**, and C-8a of **16–20**, where the values calculated as described above are *ca.* 10 ppm lower than those observed. A similar discrepancy has been noted by Dhami and Stothers in the case of *ortho*-disubstituted anisoles (13) and attributed to steric perturbation. Our observation that the less bulky methylenedioxy substituent gives shift parameters which are in close agreement with observed values at a substituted *ortho* carbon, such as C-7a of **14**a, and C-8a of **21** and **22**, supports this. As noted above, however, this difference between *ortho*-dimethoxy and methylenedioxy substituents may be of diagnostic value in structural assignment.

The relationships established in this study are therefore potentially useful in structural and in biosynthetic studies in this family of alkaloids.

Experimental

Apparatus, Methods, and Materials

Natural abundance ^{13}C nuclear magnetic resonance spectra were recorded in the pulse Fourier transform mode of a Brucker WH-90 spectrometer at 22.62 MHz and a temperature of +35.0 °C. Samples were 0.25 to 0.45 *M* in $CDCl_3$. Tetramethylsilane was used as internal reference. The deuterium signal of $CDCl_3$ provided the field/frequency lock.

Broad band proton decoupled spectra were obtained with the decoupler frequency at 4 ppm downfield from TMS with approximately 8 W of decoupler power and with a bandwidth of 2 kHz. The off-resonance spectra were recorded using a single frequency 15 ppm upfield from TMS and a decoupler power of 2 W. Selective proton decoupling experiments were run using a low decoupling power of approximately 0.3 W and irradiation at the specific proton resonance frequency. Gated decoupling was achieved by using a 5 s delay after switching off the decoupling power and the application of a 90° rf pulse.

Proton magnetic resonance spectra were recorded on a Varian HA 100 spectrometer in the frequency sweep mode. Chloroform-*d* was used as solvent and TMS as internal reference.

Mass spectra were determined on a C.E.C. 21-110B mass spectrometer at an ionizing voltage of 80 eV and a source temperature of 200–250 °C. Deuterium content was estimated by repeated scanning of the molecular ion and application of the appropriate corrections for the natural abundance of ^{13}C and the presence of $M-1$ and $M-2$ fragment ions.

Melting points were determined on a Kofler hot stage and are uncorrected. Infrared spectra were recorded on a Perkin-Elmer 337 spectrometer. Thin layer chromatography was performed on silica gel F_{254}.

The following compounds were obtained from commercial sources: tetrahydroisoquinoline (**8**), β-hydrastine (**9**), methylenedioxybenzene (**13**), and phthalide (**15**). We are indebted to Dr. R. H. F. Manske of the University of Waterloo, Waterloo, Ontario, for providing generous samples of the following alkaloids: (+)-corlumine (**11**), (+)-adlumine (**12**), (±)-canadine (**16**), (±)-tetrahydropalmatine (**18**), (+)-corydaline (**19**), (±)-mesocorydaline (**20**), (±)-cavidine (**21**), and (+)-thalictrifolin (**22**).

The following compounds were prepared by standard procedures and gave satisfactory spectral and physical data: *6,7-dimethoxy-1,2,3,4-tetrahydroisoquinoline* (**1**) (21, 22), *6,7-dimethoxy-2-methyl-1,2,3,4-tetrahydroisoquinoline* (**2**) (23), *6,7-dimethoxy-3,4-dihydroisoquinoline* (**3**) (21), *6,7-dimethoxy-2-methyl-3,4-dihydroisoquinolinium iodide* (**4**) (21), *7,8-dimethoxy-1,2,3,4-tetrahydroisoquinoline* (**7**) (24), *(±)-(α)-hydrastine* (**10**) (25), *6,7-dimethoxyphthalide* (**14**) (26), *6,7-methylenedioxyphthalide* (**14***a*) (27), *6-nitrophthalide* (**15***a*) (28), *6-aminophthalide* (**15***b*) (28, 29), and *(±)-nandinine* (**17**) (30).

(±)-Canadine-8,14-d_2 (18, 31)

To a stirred suspension of berberine chloride (0.89 g) in methanol (13.5 ml) and water (4 ml) was added in portions 0.11 g of sodium borodeuteride. The reaction mixture was then refluxed for ½ h, cooled, and the product (0.53 g, 64%), filtered and recrystallized from absolute alcohol. Mass spectral analysis indicated the following isotopic composition in the molecular ion region: d_2, 88.5%, d_1, 8.3%, d_0, 3.2%.

(±)-Canadine-9-OCD_2H

A mixture of (±)-nandinine (0.20 g in 15 ml of dioxane), diazomethane (approximately 1 g in 50 ml of ether) and deuterium oxide (2 ml) was allowed to stand at room temperature for 24 h (19). The product was recovered by evaporation of the solvent and recrystallized from absolute alcohol giving 0.169 g (80%). Mass spectral analysis indicated the following isotopic composition in the molecular ion region: d_3, 4%; d_2, 22%, d_1, 34%, d_0, 40%.

Phthalide-6-d (15c)

A solution of 6-phthalidediazonium fluoborate (20) (248 mg) in DMF-d_7 (1 ml) at −5 °C was added dropwise to refluxing DMF-d_7 (1 ml). After addition was complete, the solution was poured onto water and the mixture extracted with chloroform. The extract was washed, dried, and evaporated, and the residue purified by passage through a column of alumina in ether solution, to give phthalide-6-*d* (53 mg, 39%). Mass spectral analysis showed the isotopic composition to be >95% d_1.

Acknowledgments

We are grateful to Dr. R. H. F. Manske for providing samples as detailed in the Experimental. Thanks are also due to Mr. B. Sayer for recording many of the ^{13}C spectra, and to Dr. R. A. Bell for many helpful discussions both on the execution of the work and the interpretation of the results.

We thank the National Research Council of Canada for financial support.

1. E. Wenkert, J. S. Bindra, C. Chang, D. W. Cochran, and F. M. Schell. Acc. Chem. Res. **7**, 46 (1974), and references therein.
2. F. Bohlmann and R. Zeisberg. Chem. Ber. **108**, 1043 (1975).
3. R. T. LaLonde, T. N. Donvito, and A. I-M. Tsai. Can. J. Chem. **53**, 1714 (1975).
4. T. T. Nakashima, P. P. Singer, L. M. Browne, and W. A. Ayer. Can. J. Chem. **53**, 1936 (1975).
5. W. O. Crain, Jr., W. C. Wildman, and J. D. Roberts. J. Am. Chem. Soc. **93**, 990 (1971).
6. T. T. Nakashima and G. E. Maciel. Org. Magn. Reson. **5**, 9 (1973).
7. T. Kametani, K. Fukumoto, M. Ihara, A. Ujiie, and H. Koizumi. J. Org. Chem. **40**, 3280 (1975).
8. O. A. Gansow and W. Schittenhelm. J. Am. Chem. Soc. **93**, 4294 (1971).
9. R. Freeman and H. D. W. Hill. J. Magn. Reson. **5**, 278 (1971).

Can. J. Chem. Downloaded from www.nrcresearchpress.com by 210.87.254.40 on 09/05/12
For personal use only.

10. J. FEENEY, D. SHAW, and P. J. S. PAUWELS. Chem. Commun. 554 (1970).
11. J. B. STOTHERS. Carbon-13 NMR spectroscopy. Academic Press, New York. 1972.
12. D. K. DALLING and D. M. GRANT. J. Am. Chem. Soc. **89**, 6612 (1967).
13. K. S. DHAMI and J. B. STOTHERS. Can. J. Chem. **44**, 2855 (1966).
14. S. SAFE and R. Y. MOIR. Can. J. Chem. **42**, 160 (1964).
15. C. K. YU, D. B. MACLEAN, R. G. A. RODRIGO, and R. H. F. MANSKE. Can. J. Chem. **48**, 3673 (1970).
16. D. K. DALLING and D. M. GRANT. J. Am. Chem. Soc. **96**, 1827 (1974).
17. D. K. DALLING, D. M. GRANT, and E. G. PAUL. J. Am. Chem. Soc. **95**, 3718 (1973).
18. I. SALLAY and R. H. AYERS. Tetrahedron, **19**, 1397 (1963).
19. A. F. THOMAS. Deuterium labeling in organic chemistry. Appleton-Century-Crofts, New York. 1972. p. 64.
20. D. T. FLOOD. Org. Synth. Coll. Vol. **2**, 295 (1943).
21. W. M. WHALEY and M. MEADOW. J. Chem. Soc. 1067 (1953).
22. F. D. POPP and W. E. MCEWEN. J. Am. Chem. Soc. **79**, 3773 (1957).
23. K. KNABE. Arch. Pharm. **292**, 652 (1959).
24. G. GRETHE, H. L. LEE, M. USKOKOVIC, and A. BROSSI. J. Org. Chem. **33**, 494 (1968).
25. M. A. MARSHALL, P. L. PYMAN, and R. ROBINSON. J. Chem. Soc. 1315 (1934).
26. J. W. WILSON, C. L. ZIRKLE, E. L. ANDERSON, J. J. STEHLE, and G. E. ULLGOT. J. Org. Chem. **16**, 792 (1951).
27. S. N. CHAKRAVARTI. J. Ind. Chem. Soc. **20**, 382 (1943).
28. J. TIROUFLET. Bull. Soc. Sci. Bretagne, **26**, 7 (1951); Chem. Abstr. **47**, 8692g (1953).
29. C. W. FERRY, J. S. BUCK, and R. BALTZLY. Org. Synth. Coll. Vol. **2**, 239 (1955).
30. R. H. F. MANSKE, R. RODRIGO, D. B. MACLEAN, and L. BACZYNSKYJ. An. Quim. **68**, 689 (1972), and references therein.
31. R. MIRZA. J. Chem. Soc. 4400 (1957).

Can. J. Chem. Downloaded from www.nrcresearchpress.com by 210.87.254.40 on 09/05/12
For personal use only.

The dehydrogenation of 1,4-dihydronaphthalene by tetrachloro-*p*-benzoquinone

Z. M. HASHISH[1] AND I. M. HOODLESS[2]
Chemistry Department, The University, Glasgow, Scotland

Received January 23, 1975[3]

Z. M. HASHISH and I. M. HOODLESS. Can. J. Chem. **54**, 2261 (1976).

The dehydrogenation of 1,4-dihydronaphthalene by tetrachloro-*p*-benzoquinone in phenetole solution has been investigated. The present work does not fully confirm earlier studies which report that the reaction follows second-order kinetics and that the hydride ion transfer is rate determining. In the investigations described in this paper second-order kinetics are only observed in the later stages of the reaction and a 1:1 stoichiometry of the reactants in the process is not obtained. Substitution of tritium in the 1,4-positions of the hydrocarbon appears to not significantly affect the reaction rate. The present results indicate that charge-transfer complexes are formed in the reaction and it is suggested that electron transfer within these complexes could be the rate-determining step in the dehydrogenation.

Z. M. HASHISH and I. M. HOODLESS. Can. J. Chem. **54**, 2261 (1976).

On a étudié la déshydrogénation du dihydro-1,4 naphtalène par la tétrachloro-*p*-benzoquinone en solution dans le phénétole. Les résultats obtenus dans le présent travail ne confirment pas complètement les études antérieures qui rapportaient que la réaction suit une cinétique du deuxième ordre et qu'un transfert d'hydrure se produit dans l'étape déterminante. Dans les travaux décrits dans le présent travail, on observe des cinétiques du second ordre uniquement dans la dernière partie de la réaction et on n'obtient pas une stoechiométrie 1:1 des réactifs dans le processus. Il ne semble pas que l'introduction du tritium dans les positions 1 et 4 de l'hydrocarbure affecte d'une façon importante la vitesse de la réaction. Les résultats actuels indiquent que des complexes de transfert de charge sont formés dans les réactions et on suggère que le transfert d'électron à l'intérieur de ces complexes pourrait être l'étape déterminante de la déshydrogénation.

[Traduit par le journal]

Although quinones have been extensively used as agents for the dehydrogenation of hydroaromatic compounds in solution (1), relatively few detailed studies have been made concerning the mechanism of these reactions. The majority of experimental evidence indicates that the reaction involves heterolytic (2) rather than homolytic (3) rupture of the carbon–hydrogen bond in the hydrocarbon. Braude and co-workers (2, 4), who have studied the reaction kinetics with a number of quinones of differing redox potentials, propose a two-step mechanism in which hydride abstraction by the quinone is rate determining. Measurements of the isotope effect in dehydrogenation of acenaphthene by 2,3-dichloro-5,6-dicyano-*p*-benzoquinone and by tetrachloro-*o*-benzoquinone (5) add support to this proposal.

The present paper reports on an investigation of the dehydrogenation of 1,4-dihydronaphthalene (DHN) with tetrachloro-*p*-benzoquinone (TCQ) in phenetole solution. Some results of a 'competitive' reaction with non-tritiated DHN and DHN, partially tritiated in the 1,4-positions, are shown in Table 1. Since all the reactive positions in the tritiated DHN do not contain the heavier isotope, the isotopic effect results are qualitative but the lack of an increase in the specific activity of the reactant, particularly at low reactant conversions, is indicative of the absence of a significant primary isotope effect. While weak isotope effects have been observed (6) in some other reactions involving hydride ion transfer it appears that, in the present system, the results could be explained either by a concerted process involving rupture of both carbon–hydrogen bonds (2) or that an equilibrium complex is formed in the rate-determining step (7).

The ability of quinones to form charge-transfer complexes is well established (8) and it has been suggested that the dehydrogenation of hydroaromatics proceeds via their formation (1).

---

[1]Present address: Chemistry Department, University College for Girls, Ain Shams University, Cairo, Egypt.

[2]Present address: Chemistry Department, Lakehead University, Thunder Bay, Ont., Canada P7B 5E1.

[3]Revision received March 2, 1976.

Can. J. Chem. Downloaded from www.nrcresearchpress.com by 210.87.254.40 on 09/05/12
For personal use only.

Can. J. Chem. Downloaded from www.nrcresearchpress.com by 210.87.254.40 on 09/05/12
For personal use only.

TABLE 1. Comparison of the extent of reaction of DHN and tritiated DHN as a function of reaction time (reaction temperature 80 °C)

Reaction time (min)	Fraction of DHN unreacted ($[DHN]/[DHN]_0$)	Fraction of tritiated DHN unreacted (cpm/cpm_0)	Specific activity of DHN (cpm/g) $\times 10^{-4}$
0	1.00	1.00	3.53
15	0.89	0.87	3.45
30	0.78	0.76	3.41
45	0.72	0.63	3.07
60	0.67	0.67	3.49
90	0.65	0.56	3.05
120	0.58	0.67	4.03

Charge-transfer complex formation was therefore investigated in mixtures of DHN–TCQ, naphthalene–TCQ, and phenetole–TCQ using chloroform as a solvent. A range of donor concentrations was used with a constant concentration of acceptor, the spectra being compared with that of TCQ in chloroform. Naphthalene–TCQ and phenetole–TCQ mixtures gave characteristic broad absorption bands with peak maxima at 470 nm and 450 nm respectively. The equilibrium constant, K, for complex formation was calculated using the Benesi–Hildebrand (9) relationship

$$[1] \qquad \frac{Qb}{A} = \frac{1}{K\varepsilon_C}\cdot\frac{1}{D} + \frac{1}{\varepsilon_C}$$

where Q and D are the molar concentrations of the acceptor and donor respectively, A is the absorption at λ_{max} of the charge-transfer band, b the path length and ε_C is the molar extinction coefficient of the complex. Plots of Qb/A against $1/D$ are shown in Fig. 1. The values of K at 22 °C, so determined, are 0.15 M^{-1} for TCQ–phenetole and 0.68 M^{-1} for the TCQ–naphthalene complex. The latter value is in reasonable agreement with that previously reported in the literature (10). In the case of the TCQ–DHN mixtures there was a marked increase in absorption at the longer wavelengths, *i.e.* 400–550 nm, but no peak maximum was observable. The solution exhibited a characteristic deep red colour and it is probable that the peak maximum was obscured due to overlap with the main TCQ band.

Previous studies (2–4) of these dehydrogenation reactions have indicated that the kinetics are of the second-order type and, on the basis of preparative experiments, a 1:1 stoichiometry of the reactants was assumed. The kinetics can then be investigated by measurement of the concentration changes in one component of the reaction mixture. In the present study, concentration changes in either DHN or the hydroquinone have been determined as a function of the reaction time; some typical reaction plots are shown in Fig. 2. A comparison of the amounts of DHN consumed and hydroquinone formed in the reaction is given in Table 2. The overall stoichiometry suggests that two molecules of DHN are used for every molecule of hydroquinone formed. Spectra of the reaction mixture

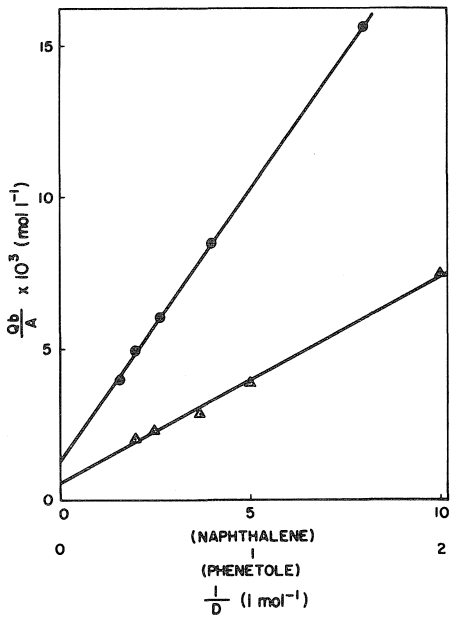

FIG. 1. Benesi–Hildebrand plot for charge-transfer complexes of TCQ-naphthalene (●) and TCQ–phenetole (△).

TABLE 2. Concentration changes in DHN and hydroquinone during reaction at 80 °C

Experiment number	Initial concentrations (*M*) DHN/TCQ	DHN consumed in 120 min (*M*)	Hydroquinone formed in 120 min (*M*)
1	0.263/0.104	0.085	—
2*	0.268/0.104	0.106	0.048
3	0.282/0.104	0.089	—
4	0.250/0.098	0.096	—
5†	0.110/0.100	0.064	0.029
6	0.301/0.104	—	0.042
7	0.301/0.104	—	0.042
8‡	0.100/0.099	n.d.	0.064

*Naphthalene added to reaction mixture.
†Reaction time of 240 min.
‡Sealed tube experiment, reaction time approximately 90 h; n.d., no DHN detected.

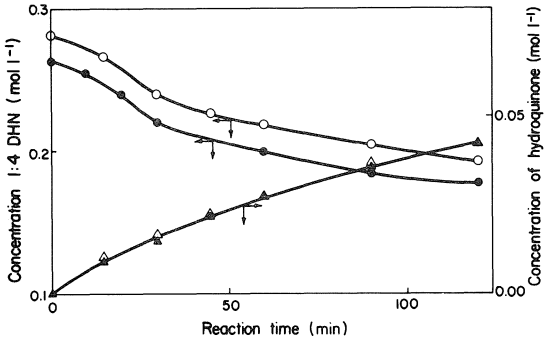

FIG. 2. Change in concentration of DHN and hydroquinone as a function of reaction time. Initial DHN/TCQ concentrations (*M*) are given in parentheses. ○, DHN (0.282/0.104); ●, DHN (0.263/0.104); ▲, hydroquinone (0.301/0.104); △, hydroquinone (0.301/0.104).

taken after various periods of the reaction exhibit peaks which can be associated mainly with phenetole, TCQ, and the charge-transfer complexes. A spectroscopic estimation of the decrease in TCQ concentration has been made at a wavelength of 500 nm, a region in which the absorption is mainly due to the TCQ–phenetole complex. A decrease of 0.036 *M* in TCQ concentration during the 120 min reaction period is obtained, which, considering the uncertainties in this measurement, is in reasonable agreement with the amount of hydroquinone formed in this period (Table 2, experiments 6 and 7).

It has been suggested (2) that non-oxidizable quinol ethers may be products of side reactions in these types of system and these ethers have been isolated in the reaction of hexamethylbenzene with 2,3-dichloro-5,6-dicyano-*p*-benzoquinone (11). In the present system it appears that the formation of naphthyl-substituted quinones by displacement of chloride could be a major side reaction since hydrogen chloride has been detected as a product in the DHN–TCQ reaction. Quantitative estimation of the amounts of hydrogen chloride has not been possible because of its solubility in phenetole but the amounts detected in the vapour phase correspond to approximately 0.006 *M*. The hydrogen chloride originates from a TCQ–DHN reaction since it has not been detected in TCQ–phenetole, DHN–hydroquinone–phenetole, naphthalene–TCQ–phenetole, or TCQ–hydroquinone–phenetole mixtures under the typical conditions and concentrations of the TCQ–DHN reaction. It should be noted that the naphthyl-substituted quinone would be expected to have the quinone spectrum so that no decrease in the effective quinone concentration, as measured spectrophotometrically, would be anticipated. Similar replacement of chlorine in TCQ has been reported in its reaction with amines (12) and amino acids (13).

The later stages of the reaction, *i.e.* beyond 30 min, can be fitted to second-order kinetics, Fig. 3, although the significance of this observation in such a complex system is dubious. Braude *et al.* (2) have reported that the reaction is catalysed by the presence of acid and the observed change in concentration of DHN with reaction time, Fig. 2, is not inconsistent with this behaviour due to the presence of hydrogen chloride. It is interesting to note that if a 1:1 stoichiometry of the reactants is assumed, *i.e.* the DHN and TCQ concentrations are estimated from the amount of hydroquinone formed, then, for the later stages of the reaction, good second-order plots are also obtained. For example, in the reactions in which the initial concentrations

Can. J. Chem. Downloaded from www.nrcresearchpress.com by 210.87.254.40 on 09/05/12
For personal use only.

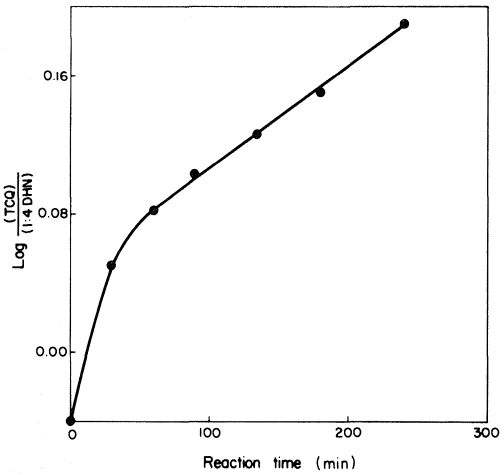

FIG. 3. Second-order kinetic plot DHN–TCQ reaction, initial concentrations (M) of DHN/TCQ are 0.110/0.100.

of TCQ and DHN are approximately decimolar, a second-order rate constant of $2.60 \times 10^{-4}\ M^{-1}\ s^{-1}$ is obtained; this compares favourably with the value of $2.88 \times 10^{-4}\ M^{-1}\ s^{-1}$ previously reported (2).

One possible interpretation of the absence of a significant primary isotope effect is that the rate-determining step is associated with electron transfer in the charge-transfer complex. Following the proposal of Buckley *et al.* (12) (modified by the assumption of equilibrium), the reaction between the hydroaromatic compound (RH_2) and the quinone (Q) may be represented by

$$[2]\quad RH_2 + Q \overset{1}{\rightleftharpoons} [RH_2 \cdot Q] \overset{2}{\rightleftharpoons} [RH_2^+ \cdot Q^-] \overset{3}{\rightarrow} RH^+ + QH^- \rightarrow R + QH_2$$

The ground state of the charge–transfer complex, *i.e.* step *1*, involves very little transfer of charge. If step *2* is rate determining no primary isotope effect would be observed. In comparing the DHN–TCQ reaction with those investigated by Trost (5) it may be noted that in the latter, the quinones have higher redox potentials (2) and that acenaphthene would have a lower ionization potential than DHN. Step *2* would be more easily accomplished and hence the net effect would be that hydride ion transfer was rate determining. It is significant that structures of charge-transfer complexes in the solid state indicate that both overlap of filled and unfilled orbitals and dipole-induced dipole effects between the donor and acceptor are important in determining the final structure (14). In considering the DHN–TCQ complex, the aromatic rings in the donor and acceptor will be off-set which could facilitate the hydrogen chloride elimination reaction. Additionally the observations (15) that bromo-substituted quinones appear to be less effective dehydrogenating agents than chloro-substituted quinones of similar redox potentials may be due to increased steric restrictions in the formation of the charge-transfer complexes.

Experimental

Materials

DHN was prepared by the reduction of naphthalene with sodium in alcohol solution following the procedure described by Cook and Hill (16). The product was purified by reduced pressure distillation. DHN partially tritiated in the 1,4-positions was prepared by a similar method using tritiated benzoic acid and sodium in ethereal solution (17). The product was purified immediately before use by quantitative gas chromatography and had a final specific activity of 0.13 μCi g^{-1}.

TCQ was obtained from B.D.H. Ltd. and was purified by recrystallization from benzene solution. The solvent phenetole was purified by heating under reflux over sodium, the fraction boiling between 168–170 °C being collected.

Kinetic Studies

The reaction system was similar to that used by Braude *et al.* (2). A weighed amount of DHN, usually sufficient to give approximately either a 0.3 or a 0.1 M solution, was dissolved in phenetole and the system allowed to stabilize at the reaction temperature over a period of 2 h. At this point a weighed amount of the quinone was introduced into the reaction vessel and the mixture vigorously shaken to facilitate dissolution of the quinone. An inert atmosphere was maintained in the system by bubbling pure, dry nitrogen through the reaction vessel, and, at appropriate intervals, 1 ml samples of the mixture were withdrawn for analysis. The reaction vessel was thermostatted to maintain the system temperature at 80 ± 0.5 °C, the temperature employed for all kinetic studies.

Analytical Methods

Quantitative analysis for DHN was carried out by gas chromatography, the analytical column being 20% carbowax coated on a 44/85 mesh graded brick dust support. The column was maintained at a temperature of 120 °C. The system was frequently calibrated by injection of known amounts of DHN; comparison of the peak areas for several samples of the same weight of DHN indicates that the reproducibility of the analytical technique is better than ±2%. In the measurements with tritiated DHN, the samples were passed through the analytical column in duplicate; one sample was used to estimate the amount of DHN, while with the second sample a trapping system was incorporated in the apparatus to enable quantitative recovery of the DHN. The tritium content of the DHN was determined by

Can. J. Chem. Downloaded from www.nrcresearchpress.com by 210.87.254.40 on 09/05/12
For personal use only.

liquid scintillation counting using an E.M.I. 6097B photomultiplier. Counting efficiency was measured with reference to a standardized *n*-hexadecane-1-2-*t* source provided by the Radiochemical Centre, Amersham, U.K.

The hydroquinone formed in the reaction was determined by titration of an aliquot of the mixture with standardized cerium(IV) sulphate using sodium diphenylamine sulphonate as the indicator.

Spectroscopic Measurements

Absorption spectra were measured in a Unicam SP800 spectrophotometer. Purified chloroform was used as the solvent and the spectra of each of the main components of the reaction mixture, *i.e.* DHN, naphthalene, TCQ, 2,3,5,6-tetrachloro-*p*-benzohydroquinone, and phenetole, were in very good agreement with those previously reported (18–21). All measurements were made at a temperature of 22 °C.

Acknowledgement

Appreciation is expressed to the Egyptian Ministry of Higher Education for the award of a research studentship to one of us (Z.M.H.).

1. L. M. JACKMAN. Advances in organic chemistry. Vol. II. *Edited by* R. A. Raphael, E. C. Taylor, and H. Wynberg. Interscience Publishers Inc., New York. 1960.
2. E. A. BRAUDE, L. M. JACKMAN, and R. P. LINSTEAD. J. Chem. Soc. 3548, (1954); 3564, (1954).
3. N. DOST and K. VAN NES. Recl. Trav. Chim. **70**, 403 (1951).
4. E. A. BRAUDE, L. M. JACKMAN, R. P. LINSTEAD, and J. S. SHANNON. J. Chem. Soc. 3116 (1960).
5. B. M. TROST. J. Am. Chem. Soc. **89**, 1847 (1967).
6. W. H. SAUNDERS, JR. Technique of organic chemistry. Vol. II, Part I. *Edited by* S. L. Friess, E. S. Lewis, and A. Weissberger. Interscience Publishers Inc., New York. 1961.
7. L. MELANDER. Isotope effects on reaction rates. Ronald Press, New York. 1960.
8. R. FOSTER. Organic charge-transfer complexes. Academic Press, New York. 1969.
9. H. A. BENESI and J. H. HILDEBRAND. J. Am. Chem. Soc. **71**, 2703 (1949).
10. S. K. CHAKRABARTI and S. BASU. Trans. Faraday Soc. **60**, 465 (1964).
11. R. FOSTER and I. HORMAN. J. Chem. Soc. (B), 1049 (1966).
12. D. BUCKLEY, S. DUNSTAN, and H. B. HENBEST. J. Chem. Soc. 4880 (1957).
13. R. FOSTER, N. KULEVSKY, and D. S. WANIGASEKERA. J. Chem. Soc. Perkin Trans. I, 1318 (1974).
14. C. K. PROUT and J. D. WRIGHT. Agnew. Chem. **80**, 688 (1968).
15. E. A. BRAUDE, A. G. BROOK, and R. P. LINSTEAD. J. Chem. Soc. 3569 (1954).
16. E. S. COOK and A. J. HILL. J. Am. Chem. Soc. **62**, 1995 (1940).
17. W. HÜCKEL and H. SCHLEE. Chem. Ber. **88**, 349 (1955).
18. R. A. MORTON and A. J. A. DE GOUVEIA. J. Chem. Soc. 916 (1934).
19. K. BOWDEN and E. A. BRAUDE. J. Chem. Soc. 1068 (1962).
20. M. MARTYNOFF. Bull. Soc. Chim. Fr. **16**, 258 (1949).
21. R. PLUMMER, G. SCHMIDUTZ, and H. SEIFERT. Chem. Ber. **85**, 535 (1952).

Can. J. Chem. Downloaded from www.nrcresearchpress.com by 210.87.254.40 on 09/05/12
For personal use only.

Nuclear quadrupole resonance and intermolecular interactions: temperature and pressure effects in Group V trichlorides

GRANT CALLUM GILLIES AND RICHARD JULIAN CHALLIS BROWN
Department of Chemistry, Queen's University, Kingston, Ont., Canada K7L 3N6

Received February 23, 1976

GRANT CALLUM GILLIES and RICHARD JULIAN CHALLIS BROWN. Can. J. Chem. **54**, 2266 (1976).

Nuclear quadrupole resonance frequencies for the metal and chlorine atoms in $AsCl_3$ and $SbCl_3$ have been measured as functions of temperature and pressure. These data are analysed to obtain the isothermal volume dependences and the isochoric temperature dependences of the field gradient parameters. Existing knowledge of the Group V trichlorides shows that the strength of intermolecular bonding increases in the order $AsCl_3 < SbCl_3 < BiCl_3$, and this trend is reflected in the relative importance of volume effects in determining the nqr frequencies in these solids. A simple theory of the pressure dependences of nqr frequencies in molecular crystals is proposed, which accounts for all data presently available. The pressure coefficient contains static and dynamic contributions which are of opposite signs; the static contribution is negative and becomes numerically larger as the strength of intermolecular bonding increases.

GRANT CALLUM GILLIES et RICHARD JULIAN CHALLIS BROWN. Can. J. Chem. **54**, 2266 (1976).

On a mesuré les fréquences de résonance nucléaire quadrupolaire des atomes métalliques et des chlores dans le $AsCl_3$ et le $SbCl_3$ en fonction de la température et de la pression. On a analysé ces données pour obtenir des dépendances volumiques isothermes et les dépendances isochore de température pour les paramètres de gradient de champ. Les connaissances existantes des trichlorures du groupe V montrent que la force des liaisons intermoléculaires augmente dans l'ordre $AsCl_3 < SbCl_3 < BiCl_3$; cette tendance se reflète dans l'importance relative des effets volumiques lors de la détermination des fréquences rnq de ces solides. On propose une théorie simple pour expliquer la dépendance entre la pression et les fréquences rnq des cristaux moléculaires; cette théorie tient compte de toutes les données qui existent présentement. Les coefficients de pression contiennent des contributions statiques et dynamiques qui sont de signes opposés. La contribution statique est négative et devient numériquement plus grande à mesure que la force de liaison intermoléculaire augmente.

[Traduit par le journal]

1. Introduction

Nuclear quadrupole resonance (nqr) as a source of chemical information about molecules is limited in a number of ways, despite being superficially attractive. In principle, the nuclear quadrupole coupling tensor in a molecule is a source of information against which bonding theories may be tested, and a good deal of work on the interpretation of experimental data has been done. However, much data is derived from nqr of molecules in the solid phase, and there is some uncertainty about the difference between the field gradient tensors in the crystal and in the isolated molecules, except that the coupling constant is usually reduced in magnitude by about 10%. Nuclear quadrupole resonance frequencies are temperature dependent, and in order to make comparisons between compounds it is necessary to measure spectra at a standard temperature. However, temperature dependences also differ between compounds, and this procedure is not wholly satisfactory.

In attempting to understand the effect of the crystal lattice on nqr parameters, the experimenter can readily change the temperature and pressure of the sample. However, variations of these thermodynamic parameters influence the quadrupole frequency through two mechanisms: firstly by changes in the average lattice geometry (*i.e.* thermal expansion and hydrostatic compression), and secondly by changes in the thermal averaging of the field gradient tensor by lattice vibrations. The separation of lattice and vibrational effects is facilitated by the approach developed by Kushida, Benedek, and Bloembergen (1) (referred to hereafter as KBB). A further complication is that complex effects of lattice distortion may occur in addition to the effects of a simple volume change; these effects are difficult to treat quantitatively at present, and can only be considered by examining a series of compounds with related chemical properties and similar crystal structures.

The present measurements are a continuation

Can. J. Chem. Downloaded from www.nrcresearchpress.com by 210.87.254.105 on 09/05/12
For personal use only.

TABLE 1. Temperature dependence of ^{35}Cl nqr frequencies

Resonance	a_0 (kHz)	a_1 (kHz K^{-1})	a_2 (Hz K^{-2})	T_0 (K)	Range (K)
$AsCl_3$					
(1)	24 756.7±0.3	−5.09 ±0.05	—	250.3	238–254
(2)	24 493.3±0.2	−4.45 ±0.04	—	250.3	238–254
(3)	24 426.2±0.2	−4.34 ±0.04	—	250.3	238–254
$SbCl_3$					
(1)	20 407.0±0.5	−2.898±0.009	−3.2±0.3	298.6	240–345
(2)	19 175.5±0.2	−1.119±0.005	−3.1±0.2	298.6	240–345

TABLE 2. Pressure dependence of ^{35}Cl nqr frequencies

Resonance	b_0 (kHz)	b_1 (kHz MPa^{-1})	b_2 (Hz MPa^{-2})	T (K)	P_{max} (MPa)
$AsCl_3$					
(1)	24 746.4±0.8	+0.66 ±0.15	−0.71±0.05	250.3	276
(2)	24 483.8±0.7	+0.37 ±0.01	−0.51±0.05	250.3	276
(3)	24 417.4±0.6	+0.30 ±0.01	−0.48±0.04	250.3	276
$SbCl_3$					
(1)	20 538.3±0.5	−0.043±0.003	—	250.2	250
	20 476.3±0.2	+0.008±0.004	−0.09±0.01	273.3	288
	20 408.5±0.5	+0.048±0.006	−0.09±0.01	298.1	401
	20 319.2±0.4	+0.142±0.005	−0.23±0.02	327.6	296
(2)	19 220.9±0.2	−0.616±0.001	—	250.2	254
	19 200.2±0.2	−0.601±0.001	—	273.3	331
	19 175.4±0.4	−0.578±0.001	—	298.1	411
	19 140.1±0.3	−0.514±0.004	−0.11±0.01	327.6	297

of work on $BiCl_3$, which has already been reported (2, 3). The Group V trihalides are a useful series of compounds for study by nqr since every nucleus (except phosphorus) has quadrupole resonances in a convenient range, the compounds show well-defined periodic trends, and in two cases the metal nuclei have high spins and the coupling constant and asymmetry parameter data can be separately evaluated. The nqr spectra have been previously reported in detail (4–6).

2. Experimental

Spectra were recorded using either a Dean oscillator (7) or a Williams oscillator (8); both oscillators were self-quenched and sideband suppression (9) was used occasionally to assist in determination of the central component of the signal. Frequency modulation or Zeeman modulation was used for recording resonances; a stepping motor with gearbox was used to sweep the detector oscillator. Frequencies were generally determined by zero beat with an external signal generator.

Pressures were generated in a hydraulic pressure system using Stannolax oil or hexane as the pressure transmitting fluid. Pressure was measured using a Heise bourdon pressure gauge. Two different stainless steel pressure vessels were used, depending upon which oscillator was used (2, 10). Temperatures were controlled by a heater with proportional controller, or by immersion in a suitable liquid bath. Temperatures were measured by a copper–constantan thermocouple, taped to the outside of the pressure vessel. Temperature dependences were determined using samples sealed in glass ampoules. For pressure dependences, samples were held in Teflon containers and the oscillator coil was immersed in the sample. The samples were loaded into the containers in dry bags and, in the case of $AsCl_3$, required freezing in dry ice before transferring to the pre-cooled pressure vessel. Bismuth trichloride was dried *in vacuo* over P_2O_5 before use; $SbCl_3$ and $AsCl_3$ were purified by sublimation and distillation respectively.

3. Results

The temperature and pressure dependences of the nqr frequencies in $AsCl_3$ and $SbCl_3$ are summarised in Tables 1 to 4. Each set of data was fitted to a least squares polynomial by means of Chebyshev polynomials (11); a quadratic polynomial was sufficient to describe the data in cases where curvature was significant. Each series of measurements was checked for hystere-

Can. J. Chem. Downloaded from www.nrcresearchpress.com by 210.87.254.105 on 09/05/12
For personal use only.

TABLE 3. Temperature dependence of Group V nqr frequencies

Resonance	a_0 (kHz)	a_1 (kHz K^{-1})	a_2 (Hz K^{-2})	T_0 (K)	Range (K)
$AsCl_3$					
^{75}As	76 044 ±2	−22.04±0.09	—	250.3	238–255
$SbCl_3$					
^{121}Sb (1/2–3/2)	58 074.6±1.0	−9.77±0.02	−7.0±0.7	304.2	240–345
^{123}Sb (1/2–3/2)	37 331.5±0.6	−9.99±0.01	−8.7±0.4	304.2	240–345
^{123}Sb (3/2–5/2)	67 718.9±0.4	−7.11±0.03	−13.3±0.4	304.2	240–310

TABLE 4. Pressure dependence of Group V nqr frequencies

Resonance	b_0 (kHz)	b_1 (kHz MPa^{-1})	b_2 (Hz MPa^{-2})	T (K)	P_{max} (MPa)
$AsCl_3$					
^{75}As	76 043.5±1.6	+2.16 ±0.4	−3.2 ±0.2	250.3	185
$SbCl_3$					
^{121}Sb (1/2–3/2)	58 597.7±0.9	−1.328±0.009	—	250.2	172
	58 376.0±0.4	−1.195±0.009	−0.19±0.04	273.3	208
	58 138.2±0.9	−1.104±0.010	—	298.1	175
	57 832.0±0.4	−0.742±0.011	−0.68±0.05	327.7	208
^{123}Sb (1/2–3/2)	37 839.9±0.6	+0.580±0.007	—	250.2	164
	37 634.3±0.5	+0.685±0.007	−0.26±0.02	273.3	369
	37 393.2±1.6	+0.92 ±0.03	−0.59±0.1	298.1	298
	37 083.7±0.6	+1.091±0.007	−0.61±0.02	327.7	405

TABLE 5. Temperature dependence of Sb field gradient parameters in $SbCl_3$

Parameter	Source	a_0 (kHz)	a_1 (kHz K^{-1})	a_2 (Hz K^{-2})	T_0
e^2qQ^{121}	*	376 864±10	−41.1±0.2	−24±7	304.2
e^2qQ^{123}	†	480 412± 2	−61.3±0.2	−97±3	304.2

Parameter	Source	a_0 (kHz)	a_1 (K^{-1})	a_2 (K^{-2})	T_0
η^{121}	*	(15 931±3)×10^{-5}	−(1560±6)×10^{-7}	−(25±2)×10^{-8}	304.2
η^{123}	†	(15 929±1)×10^{-5}	−(1443±4)×10^{-7}	−(9±1)×10^{-8}	304.2

*From (1/2–3/2) transitions of ^{121}Sb and ^{123}Sb.
†From (1/2–3/2) and (3/2–5/2) transitions of ^{123}Sb.

sis by plotting data for increasing and decreasing temperature (or pressure) separately. The functional dependences of the data are described by polynomial equations such as

$$\nu = a_0 + a_1 t + a_2 t^2$$

$$\nu = b_0 + b_1 P + b_2 P^2$$

where $t = T - T_0$, T_0 is a suitable reference temperature, and P is the pressure. The coefficients a_i and b_i are given in the tables, together with the ranges of temperature and pressure covered; the errors given are the statistical standard errors of the coefficients. The discrepancy of approximately 10 kHz between the a_0 and b_0 values for ^{35}Cl and $AsCl_3$ corresponds to the quench frequency used in the high pressure measurements, suggesting that a sideband was measured rather than the central resonance; the quench frequency did not vary significantly during the experiment.

The extraction of the coupling constant and asymmetry parameter for the antimony site in $SbCl_3$ was carried out in two ways. The use of two resonances of the same isotope (^{123}Sb) was

Can. J. Chem. Downloaded from www.nrcresearchpress.com by 210.87.254.105 on 09/05/12
For personal use only.

TABLE 6. Pressure dependence of ^{121}Sb field gradient parameters in $SbCl_3$*

Parameter	b_0	b_1 (kHz MPa^{-1})	b_2 (Hz MPa^{-2})	T (K)
e^2qQ^{121}	379 354±5	−16.12±0.05	—	250.2
	378 252±3	−15.47±0.03	—	273.3
	377 162±12	−15.13±0.13	—	298.1
	375 770±4	−13.14±0.11	−2.9±0.5	327.7

Parameter	b_0	b_1 (MPa^{-1})	b_2 (MPa^{-2})	T (K)
η^{121}	(16 639±4)×10^{-5}	+(571±3)×10^{-7}	—	250.2
	(16 381±3)×10^{-5}	+(597±7)×10^{-7}	−(1.1±0.3)×10^{-8}	273.3
	(16 027±7)×10^{-5}	+(624±8)×10^{-7}	—	298.1
	(15 539±2)×10^{-5}	+(685±5)×10^{-5}	−(2.2±0.2)×10^{-8}	327.7

*Source: (1/2–3/2) transitions of ^{121}Sb and ^{123}Sb.

TABLE 7. Logarithmic temperature and pressure coefficients

Resonance	T (K)	$\left(\frac{\partial \ln e^2qQ}{\partial T}\right)_P$ (10^{-4} K^{-1})	$\left(\frac{\partial \ln e^2qQ}{\partial P}\right)_T$ (10^{-4} MPa^{-1})	$\left(\frac{\partial \ln e^2qQ}{\partial T}\right)_V$ (10^{-4} MPa^{-1})	$\left(\frac{\partial \eta}{\partial T}\right)_V$ (10^{-4})
$AsCl_3$					
^{75}As	250.2	−2.90	+0.284	−2.16	
$^{35}Cl(1)$	250.2	−2.06	+0.265	−1.37	
$^{35}Cl(2)$	250.2	−1.82	+0.153	−1.42	
$^{35}Cl(3)$	250.2	−1.77	+0.123	−1.45	
$SbCl_3$					
^{121}Sb	250.2	−1.09	−0.425	−2.11	+0.08
	273.3	−1.13	−0.409	−2.15	+0.09
	298.1	−1.16	−0.401	−2.18	+0.06
	327.7	−1.20	−0.350	−2.11	+0.10
$^{35}Cl(1)$	250.2	−1.26	−0.021	−1.31	
	273.3	−1.33	+0.004	−1.32	
	298.1	−1.42	+0.024	−1.36	
	327.7	−1.52	+0.070	−1.34	
$^{35}Cl(2)$	250.2	−0.424	−0.320	−1.19	
	273.3	−0.500	−0.313	−1.28	
	298.1	−0.582	−0.301	−1.35	
	327.7	−0.680	−0.269	1.38	
$BiCl_3$*					
^{209}Bi	298.1	−1.27	−1.05	−4.42	+1.91
$^{35}Cl(1)$	298.1	−1.01	−0.20	−1.61	
$^{35}Cl(2)$	298.1	+0.24	−0.763	−2.05	

*Data from refs. 2 and 3.

used in a conventional way to obtain the temperature dependence of the field gradient parameters. However, to avoid the measurement of unnecessarily high frequencies in the pressure vessel, the lowest frequency resonances of ^{121}Sb and ^{123}Sb were combined to obtain the field gradient parameters; this can be done since these two isotopes have different spins and the ratio of nuclear quadrupole moments is accurately known (4). This procedure was checked by determination of the temperature dependence, and comparison with the results of the conventional procedure; the results are shown in polynomial form in Table 5 and indicate satisfactory agreement over the range of temperatures for which both methods were applied.

The pressure dependence of the ^{121}Sb field gradient parameters is given in Table 6. Table 7

Can. J. Chem. Downloaded from www.nrcresearchpress.com by 210.87.254.105 on 09/05/12
For personal use only.

Can. J. Chem. Downloaded from www.nrcresearchpress.com by 210.87.254.105 on 09/05/12
For personal use only.

summarises the logarithmic temperature coefficients, and pressure coefficients at zero pressure, for $AsCl_3$ and $SbCl_3$; data for $BiCl_3$ is included for purposes of comparison. For the spin 3/2 nuclei (^{75}As and ^{35}Cl), derivatives of the resonance frequencies are assumed to reflect only changes in the coupling constants.

The pressure dependences of the resonances in $SbCl_3$ were determined at four different temperatures, which allowed a volume dependence study using the data (1), and allowed comparison with the $AsCl_3$ data, taken at low temperature since that substance is liquid at room temperature. Several phase transitions have been reported in $SbCl_3$, one at a pressure of 350 MPa (12), and others near the melting point at atmospheric pressure (13). No evidence of any of these transitions was found in these measurements; other investigations of the high temperature phase transitions have been reported elsewhere (14).

4. Isochoric Temperature Dependences

The isochoric (constant volume) temperature dependences of the nqr parameters can be calculated from the measured temperature and pressure coefficients, provided that the ratio of bulk thermal expansion coefficient (α) to bulk compressibility (κ) is known, using equations such as

$$[1] \qquad \left(\frac{\partial \nu}{\partial T}\right)_V = \left(\frac{\partial \nu}{\partial T}\right)_P + \frac{\alpha}{\kappa}\left(\frac{\partial \nu}{\partial P}\right)_T$$

While this equation does not explicitly allow for changes in the shape of the unit cell, it does provide some measure of the relative importance of static and dynamic contributions to the variation of the nqr parameters with temperature.

The ratio α/κ may be estimated from the Gruneisen–Mie equation of state for solids, which leads to the relation $\alpha/\kappa = \gamma C_v/V$ where γ is the Gruneisen constant; this equation is a good approximation in simple solids (15), and will be used since compressibilities have not been measured for $SbCl_3$ and $AsCl_3$. The value of the Gruneisen constant will be assumed to be 2. The value of C_v is not generally measured, but if α and C_p are known, self-consistent values of C_v and α/κ can be determined by iteration using the Gruneisen–Mie relation and the thermodynamic equation

$$C_p = C_v + \alpha^2 VT/\kappa$$

TABLE 8. Thermal expansion and compressibility coefficients

Crystal	T (K)	α (10^{-5} K^{-1})	α/κ (MPa K^{-1})
$AsCl_3$	250	28	2.6
$SbCl_3$	250	21	2.4
	273	23	2.5
	298	24	2.55
	328	26	2.6
$BiCl_3$	298	17	3.0

The heat capacity of $AsCl_3$ is 107 J K^{-1} mol^{-1} (16); the molar volume has been measured at several temperatures (17), leading to the values $\alpha = 28 \times 10^{-5}$ K^{-1} and $V = 71.8 \times 10^{-6}$ m^3 mol^{-1} at 250 K. The heat capacity of $SbCl_3$ has been reported as

$$C_p = 43.1 + 0.214T \text{ J K}^{-1} \text{ mol}^{-1}$$

for the range 273 K $< T <$ 346 K (18). Measurements of the molar volume of $SbCl_3$ (17, 19–21) can be fitted by the equation

$$V(T) = 73.5 \times 10^{-6}[1 + 24 \times 10^{-5}(T - 298) + 0.06 \times 10^{-5}(T - 298)^2] \text{ m}^3 \text{ mol}^{-1}$$

from which the molar volume and thermal expansion coefficients can be obtained at the four temperatures of the pressure dependence measurements in $SbCl_3$. Table 8 contains the values of α and α/κ used, and the resulting isochoric temperature coefficients are given in Table 7.

It has been shown previously (3) that the large difference between the isobaric temperature dependences of the chlorine resonances in $BiCl_3$ is due to volume effects; the isochoric temperature dependences are almost equal. The same behaviour is shown by the chlorine resonances in the other two compounds. The isobaric temperature derivatives are more negative for the higher frequency resonances in each compound, but the isochoric derivatives are almost equal for the two resonances in $SbCl_3$ and for the three resonances in $AsCl_3$. In comparing different compounds, the magnitude of the volume effects increase in the order $AsCl_3 < SbCl_3 < BiCl_3$. Volume effects in $AsCl_3$ are so weak that their presence may be doubted; however, the small differences shown in the isobaric temperature derivatives are consistent with the more marked differences shown in the pressure derivatives (Table 2), and with the trends within Group V of the periodic table.

TABLE 9. Volume dependences in $SbCl_3$

nqr parameter		Range of V/V_0	n	n'
^{121}Sb	e^2q_0Q	1.056–1.063	$+0.65\pm0.05$	+0.45
	η_0	1.056–1.063	$-3.6\ \pm0.3$	−4.15
	V_{xx0}	1.056–1.063	$+1.37\pm0.04$	—
	V_{yy0}	1.056–1.063	$+0.14\pm0.07$	—
^{35}Cl	$\nu_0(1)$	1.040–1.063	$+0.13\pm0.06$	−0.01
	$\nu_0(2)$	1.040–1.063	$+0.49\pm0.03$	+0.35

Volume effects also affect the temperature dependence of field gradient parameters at the Group V sites in these crystals; the isochoric temperature derivatives of the coupling constants are more negative than the isobaric temperature derivatives, and the volume effects become more marked in the order $AsCl_3 < SbCl_3 < BiCl_3$. The isobaric temperature dependence of the Sb asymmetry parameter in $SbCl_3$ is due almost entirely to volume effects, since the isochoric temperature dependence is essentially zero.

5. Volume Dependences of Field Gradient Parameters In $SbCl_3$

The pressure dependence of the antimony and chlorine nqr parameters were determined at four temperatures, so that a more detailed study of the volume dependences could be carried out, following the procedures of Kushida *et al.* (1). It is as well to recall at the outset that there are not sufficient data available to describe any anisotropies in the thermal expansion coefficient and in the compressibility, or any changes in atomic positions within the unit cell; despite this, the analysis should allow qualitative interpretation of the trends shown by the experimental data.

The variation of sample volume with temperature and pressure was calculated using the values of α and κ from Table 7. In addition the dependence of compressibility on pressure was estimated by assuming that $(\partial(1/\kappa)/\partial P)_T = 5$; for most solids this coefficient lies between 4 and 6 (15, 22, 23). This leads to a reduction of about 20% in the value of the compressibility at the highest pressures used. The pressure dependences of the ^{121}Sb coupling constant and asymmetry parameter, and of the two ^{35}Cl resonance frequencies, were used to calculate the volume dependence of these quantities at the four temperatures quoted in Table 6. The isochoric temperature dependences of these four quantities were then obtained for a number of different volumes; the temperature dependences obtained in this were essentially linear, with slopes consistent with the isochoric coefficients given in Table 7. Values of the quantities at absolute zero, e^2q_0Q, η_0, $\nu_0(1)$, and $\nu_0(2)$, were then obtained for several different volumes, by linear extrapolation of the isochoric temperature dependences. Following KBB (1), volume dependences at absolute zero are written as

$$\frac{q_0(V)}{q_0(V_0)} = \left(\frac{V}{V_0}\right)^{n(V)} \quad \text{or} \quad \frac{\mathrm{d}\ln q_0}{\mathrm{d}\ln V} = n(V)$$

where V_0 is the volume at zero pressure and zero Kelvin. The above extrapolated results were used to determine the value of the exponent n, with the results tabulated in Table 9. Since the coupling constant and asymmetry parameter are known for ^{121}Sb, the volume dependences of V_{xx} and V_{yy} at zero Kelvin were also calculated, and are included. Errors quoted reflect the range of values of $n(V)$ obtained in each case, and do not include systematic errors introduced in the extrapolation over the temperature range 250 K to 0 K.

For a molecular crystal in which the nuclear electric field gradient is entirely intramolecular in origin, one would expect that the static field gradient parameters would be independent of volume, and the corresponding values of n would be zero. This is found to be the case for *p*-dichlorobenzene (1), *p*-dibromobenzene (24), stannic iodide (24), and hexamethylenetetramine (25) in which the frequencies of the halogen nuclei have values of n ranging from +0.05 to −0.05. For a purely ionic crystal, q_0 should depend upon interionic distance as $1/r_0^3$, and so n should be −1; cuprous oxide fits this model with $n = -0.96$ (1). Positive values of n as large as +3.5, for ^{23}Na in rhombohedral $NaNO_3$ (26),

Can. J. Chem. Downloaded from www.nrcresearchpress.com by 210.87.254.105 on 09/05/12
For personal use only.

Can. J. Chem. Downloaded from www.nrcresearchpress.com by 210.87.254.105 on 09/05/12
For personal use only.

have also been reported, resulting from negative pressure coefficients.

The values of n for e^2q_0Q for ^{121}Sb and for the ^{35}Cl frequencies $\nu_0(1)$ and $\nu_0(2)$ are all positive, indicating that these parameters are decreased when the lattice dimensions become smaller. The n value for $\nu_0(1)$, the resonance frequency near 20 MHz, is less than that for $\nu_0(2)$, indicating that $\nu(1)$ is less affected by the static lattice dimensions than is $\nu(2)$. The asymmetry parameter shows a very strong volume dependence, and becomes larger where the lattice dimensions become smaller; the majority of the variation of η_0 with volume is due to variation of V_{xx0} rather than V_{yy0}.

The volume dependence of the quadrupole parameters at ordinary temperatures is due primarily to static effects, except in the case of the higher ^{35}Cl frequency, $\nu(1)$. This is shown by comparing $n' = (\partial \ln q/\partial \ln V)_T$ at room temperature with the value of $n = \mathrm{d} \ln q_0/\mathrm{d} \ln V$, since the following relation holds within the approximations of the KBB method (1):

$$\left(\frac{\partial \ln q}{\partial \ln V}\right)_T = \frac{\mathrm{d} \ln q_0}{\mathrm{d} \ln V} + \left(\frac{\partial \ln q}{\partial \ln \langle\theta^2\rangle}\right)\left(\frac{\partial \ln \langle\theta^2\rangle}{\partial \ln V}\right)_T$$

Values for n' are given in Table 9. In the case of $\nu(1)$, the contributions of q_0 and $\langle\theta^2\rangle$ have almost exactly opposite volume dependences so that $\nu(1)$ is almost independent of volume at room temperature; in other cases, the values of n and n' are approximately equal, indicating that the volume dependence at room temperature is dominated by the static field gradient rather than by the amplitude of lattice vibrations.

6. Quasiharmonic Analysis of Temperature Dependences

Since the isobaric temperature dependences of the low frequency Raman lines in $SbCl_3$ have been reported (13, 27) and the curvatures of the isobaric temperature dependences of the nqr parameters in $SbCl_3$ have been measured over the temperature range 240–346 K, it is possible to test the quasiharmonic theory of temperature dependences (28) as a description of the resonances in this compound.

All Raman frequencies (ν_l) below 100 cm^{-1} vary with temperature according to the equation

$$[2] \qquad \nu_l(t) = \nu_l{}^0(1 - g_l t)$$

TABLE 10. Quasiharmonic analysis for $SbCl_3$

nqr parameter	$\langle g\rangle$ (K^{-1})	b^0 (K^{-1})
^{121}Sb e^2qQ	2.9×10^{-4}	-0.99×10^{-4}
^{123}Sb e^2qQ	8.6×10^{-4}	-0.83×10^{-4}
^{35}Cl(1)	5.9×10^{-4}	-1.05×10^{-4}
^{35}Cl(2)	16×10^{-4}	-0.30×10^{-4}

where $t = T - T_0$ and the coefficient g_l lies between $3.5 \times 10^{-4}\,K^{-1}$ and $9.8 \times 10^{-4}\,K^{-1}$. This provides experimental justification for one of the assumptions of the quasiharmonic theory, that curvature in the isobaric temperature dependence is due to temperature dependent torsional lattice modes; the other assumption, that there is no appreciable volume dependent contribution to the quadrupole coupling constant may therefore be tested with the quadrupole data.

Assuming that one lattice mode is dominant in averaging the electric field gradient, the approximation $\langle g^2\rangle = \langle g\rangle^2$ can be made (28), and then the values of the first derivatives of the quadrupole frequency (or coupling constant) at $t = 0$ can be written

$$\frac{1}{\nu_0}\left(\frac{\partial \nu}{\partial T}\right)_{P,t=0} = (1 + 2T_0\langle g\rangle)b^0$$

$$\frac{1}{\nu_0}\left(\frac{\partial^2 \nu}{\partial T^2}\right)_{P,t=0} = (4\langle g\rangle + 6T_0\langle g\rangle^2)b^0$$

where b^0 is the value of $(\partial\nu/\partial T)$ with the lattice frequencies held constant, and under the assumptions of the theory should be equal to $(\partial\nu/\partial T)_V$ at temperature T_0, given in Table 7. The values of $\langle g\rangle$ and b^0 derived in this way from the polynomial coefficients of Tables 1 and 5 are summarised in Table 10. Of the four temperature dependences the best fit is obtained for the ^{35}Cl(1) resonance; the other ^{35}Cl resonance and the two sets of data on the Sb site give qualitatively sensible results, but the $\langle g\rangle$ and b^0 values do not agree with the independent estimates from the Raman spectra and the isochoric temperature coefficients in Table 7. These results are consistent with the discussions of the two preceding sections, in which it was shown that volume effects are larger for the ^{35}Cl(2) resonance than for the ^{35}Cl(1) resonance. The quasiharmonic theory does not provide a meaningful description of the isobaric temperature dependence in cases where volume effects are significant, as might be

Can. J. Chem. Downloaded from www.nrcresearchpress.com by 210.87.254.105 on 09/05/12
For personal use only.

TABLE 11. M—Cl interatomic distances (nm) in Group V trichlorides

	$BiCl_3$	$SbCl_3$	$AsCl_3$
	Gas phase		
	0.248	0.2333	0.2162
	Crystal phase		
Intramolecular	0.2468	0.230	—
	0.2518	0.236	
	0.2513	0.236	
Intermolecular	0.3224	0.357	—
	0.3216	0.371	
	0.3398	0.341	
	0.3450	0.341	
	0.3256	0.371	

expected from a study of the assumptions. However, in some cases, the theory appears to provide a useful description (25, 28).

The range of temperatures covered for $AsCl_3$ in this work was too small to allow determination of curvature of the isobaric temperature dependences. Yusupov *et al.* (29) applied the quasiharmonic theory to the ^{75}As resonance in $AsCl_3$; the temperature dependences of the low frequency Raman lines were used in applying the theory, and good agreement was obtained. This is consistent with the conclusion that volume dependent effects in $AsCl_3$ are smaller than in $SbCl_3$. It is clearly pointless to attempt to treat the case of $BiCl_3$, where volume effects are so large that the isobaric temperature coefficient of the lower ^{35}Cl frequency is positive.

7. Crystal Structures and Zeeman Analysis

Electron diffraction studies indicate that gaseous arsenic, antimony, and bismuth trichlorides all have a pyramidal structure with C_{3v} symmetry (30–32). The bond lengths and angles of the gas phase molecules are listed in Table 11.

Lindquist and Niggli (21) reported that antimony trichloride crystallizes with an orthorhombic unit cell, having space group *Pnma*, with four discrete $SbCl_3$ molecules per unit cell; it was concluded that molecules in the solid phase of $SbCl_3$ had the same structure as those in the gas phase. This is inconsistent with the nqr spectrum for $SbCl_3$ which indicates that there are two nonequivalent chlorine sites and that the field gradient at antimony sites has a substantial asymmetry parameter. Peterson (20) reinvestigated the crystal structure by X-ray analysis and an nqr Zeeman study. His X-ray results indicate that the $SbCl_3$ molecule is distorted, and that there are some short intermolecular distances. The space group and unit cell obtained were in agreement with those of Lindquist and Niggli. Interatomic distances in crystalline $SbCl_3$ as determined by Peterson are given in Table 11. There are two nonequivalent chlorine sites, one Sb—Cl bond length being significantly shorter than the other two. The *Pnma* space group requires that the antimony atom and the unique chlorine atom lie on a mirror plane; the two long Sb—Cl intramolecular bonds are related by reflection in the mirror plane. Thus, the ^{35}Cl nqr spectrum of $SbCl_3$ should show two resonances and the electric field gradient at antimony sites should be asymmetric due to distortion of the molecule from C_{3v} symmetry. This is consistent with the nqr spectrum.

The crystal structure of bismuth trichloride, as determined by Nyburg *et al.* (33), is very similar to that of antimony trichloride. The structure consists of four discrete bismuth trichloride molecules in an orthorhombic unit cell belonging either to the centrosymmetric space group *Pnma* or the noncentrosymmetric $Pn2_1a$. The authors concluded that the latter space group was slightly favoured on the basis of a statistical test. The molecules have a distorted trigonal shape and the interatomic distances are given in Table 11. The mirror plane of the *Pnma* space group is a pseudomirror plane for space group $Pn2_1a$.

The choice of $Pn2_1a$ as the space group for the bismuth trichloride crystal is inconsistent with the ^{35}Cl nqr spectrum of $BiCl_3$. Such a structure indicates three nonequivalent chlorine sites which ought to give rise to three ^{35}Cl nuclear resonances of nearly equal intensity. Only two ^{35}Cl nqr signals have been observed; one is significantly stronger than the other. Furthermore, the Zeeman patterns observed by Furukawa (34) for the ^{35}Cl nqr spectra of a single crystal of $BiCl_3$ are inconsistent with there being three nonequivalent chlorines, and indicate that there is a mirror plane in $BiCl_3$.

Both Nyburg *et al.* (33) and Peterson (20) remark on the proximity of extramolecular chlorine atoms to the metal atom. Van der Waals radii for antimony, bismuth, and chlorine are 0.205 nm, 0.215 nm and 0.175 nm respectively

Can. J. Chem. Downloaded from www.nrcresearchpress.com by 210.87.254.105 on 09/05/12
For personal use only.

(35). From the data given in Table 11, it is evident that there are five intermolecular metal–chlorine distances of less than the sum of the van der Waals radii from the metal atom, for both $SbCl_3$ and $BiCl_3$ solids. The resulting eightfold coordination of the metal atoms forms a right trigonal prism with two chlorine atoms in face-bridging positions (33); the face-bridging chlorine atoms are those which lie off the mirror plane. Peterson refers to the five relatively short intermolecular Sb---Cl distances as 'intermolecular bonds' and Nyburg *et al.* refer to the five relatively short intermolecular Bi---Cl distances as 'bridges'. In the $SbCl_3$ and $BiCl_3$ crystals, the two face-bridging chlorine atoms participate in two intermolecular bonds, and the mirror plane chlorine atoms participate in only one. The intramolecular bonds to the face-bridging chlorine atoms are longer than the gas phase bond length, while the other intramolecular bond is shortened upon crystallization. From the intermolecular distances given in Table 11 for both solids, it may be concluded that intermolecular interaction is greater for $BiCl_3$ than for $SbCl_3$ (33).

Zeeman studies of the nqr spectra of single crystals of antimony trichloride (20) and bismuth trichloride (34) have been carried out. These studies yield the asymmetry parameters of the electric field gradients at the ^{35}Cl sites and the directions of the principal axes of the field gradients at both the metal and chlorine sites, and allow unambiguous assignment of the ^{35}Cl resonance frequencies to the particular chlorine sites in the crystal. For both $BiCl_3$ and $SbCl_3$, the Zeeman analysis indicates that the low frequency ^{35}Cl resonance Cl(2) can be assigned to the two face-bridging chlorine atoms which participate in two intermolecular bonds; the high frequency ^{35}Cl resonance Cl(1) is assigned to the mirror plane chlorine, which participates in one intermolecular bond. In both trichlorides, the principal z axes of the electric field gradients at the two chlorine sites lie along the metal–chlorine bond, consistent with the metal–chlorine bonds having substantial covalent character in the solid. The principal z axis of the electric field gradient tensor at Bi in $BiCl_3$ lies in the mirror plane at an angle of 47.9 deg to the Bi—Cl(1) direction; the corresponding angle in $SbCl_3$ is 52.5 deg. These values are close to the angles between the threefold axis and the metal–chlorine bonds in the gaseous molecules. For $SbCl_3$, the principal x axis lies in the mirror plane and the principal y axis is perpendicular to the mirror plane indicating that the face-bridging chlorine atoms make a substantial contribution to the electric field gradient at the antimony site. The directions of the minor axes of the principal axis system for the field gradient at bismuth sites in $BiCl_3$ cannot be extracted from Furukawa's data (34), as he performed the Zeeman analysis on the ^{209}Bi $(5/2 \leftrightarrow 7/2)$ transition. However, with regard to the similarity of the two trichlorides in all other respects, it is not unreasonable to speculate that these axes are similar in orientation to those of the field gradient at antimony sites in $SbCl_3$.

The crystal structure of arsenic trichloride would be expected to be quite similar to that of the other two Group V trichlorides. The nqr spectrum indicates that it cannot belong to space group *Pnma*, since there are three ^{35}Cl resonances to one ^{75}As resonance. Its structure possibly belongs to space groups $Pn2_1a$ or $P2_12_12_1$, to which crystalline $AsBr_3$ belongs (36), both of which can account for the observed nqr spectrum as well as allowing structures which would be very similar to those of $SbCl_3$ and $BiCl_3$. It is assumed that intermolecular bonding is weaker in this crystal than in $SbCl_3$ and $BiCl_3$.

Support for the assumed relative strengths of intermolecular interaction is lent by a comparison of the heats of sublimation for the three solids, and from Raman spectra. The heats of sublimation are related to the degree of intermolecular interaction in molecular crystals and should be a good indication of the strength of such interactions. The heats of sublimation of $AsCl_3$, $SbCl_3$, and $BiCl_3$ are 46 kJ mol^{-1} (37), 66 kJ mol^{-1} (37), and 114 kJ mol^{-1} (38) respectively. These are consistent with the above ordering of the three compounds with regard to intermolecular interaction. Fung *et al.* (39) and Denchik *et al.* (40) both comment that intermolecular bonding is weaker in solid $SbCl_3$ than in solid $BiCl_3$ on the basis of Raman spectra.

8. Qualitative Trends in the Results: A Simple Model for Pressure Dependences

The original theory proposed by Bayer (41) has been the main foundation for understanding the temperature dependence of nqr frequencies.

Can. J. Chem. Downloaded from www.nrcresearchpress.com by 210.87.254.105 on 09/05/12
For personal use only.

The majority of resonances fit the theory qualitatively, and minor modifications of the theory often lead to quantitative agreement. Close examination of the assumptions involved, using the methods of lattice dynamics (42), throws some doubt on the meaning of the moments of inertia and lattice frequencies of any given resonance, but the original simple theory remains of value in understanding resonances in substances too complex for the methods of lattice dynamics. In essence, the resonance frequency drops as the crystal is heated because of increased amplitudes of the torsional oscillations of molecules; cases which do not fit this picture can be accounted for if the static field gradient tensor depends strongly on the size or shape of the unit cell of the crystal.

There is no corresponding simple picture of pressure dependences of nqr frequencies, despite the gradual accumulation of experimental data in this area. In this section, an attempt is made to develop an elementary understanding of pressure coefficients in molecular crystals, which may serve as a basis for developing a proper theory. In principle, nqr at high pressures can be used to study changes in molecular wave functions as the molecules are forced together in the crystal; such a project is very ambitious, even for the simplest of crystals, but a start may be made along semi-empirical lines. The development is based primarily on the separation of static and dynamic effects, first carried out by KBB (1).

The effect of lattice vibrations on the average value of the electric field gradient (43) can be expressed as

$$[3] \qquad q = q_0(1 - \tfrac{3}{2}\langle\theta^2\rangle)$$

where $\langle\theta^2\rangle$ is the effective mean square amplitude of torsional vibration of the axes of the electric field gradient tensor; the field gradient in the absence of all lattice vibrations, q_0, is a function of the unit cell dimensions and atomic position parameters only. Taking the logarithms of both sides of [3] and differentiating with respect to pressure,

$$\left(\frac{\partial \ln q}{\partial P}\right)_T = \left(\frac{\partial \ln q_0}{\partial P}\right)_T + \frac{\partial}{\partial P}\ln(1 - \tfrac{3}{2}\langle\theta^2\rangle)$$

$$\simeq \left(\frac{\partial \ln q_0}{\partial P}\right)_T - \tfrac{3}{2}\left(\frac{\partial\langle\theta^2\rangle}{\partial P}\right)_T$$

where quadratic and higher terms in $\langle\theta^2\rangle$ have been neglected. If simple torsional oscillations of the molecule are assumed, $\langle\theta^2\rangle = kT/4\pi^2\nu_1^2 I$ in the high temperature limit, where ν_1 is the frequency of the torsional oscillation and I is the moment of inertia. The value of $\langle\theta^2\rangle$ is affected by pressure through the pressure dependence of the lattice frequency, while the moment of inertia is assumed to be determined by molecular geometry, and so is independent of pressure. Let γ_1 be the appropriate Gruneisen constant to describe the volume dependence of the lattice frequency ν_1; then

$$\left(\frac{\partial\langle\theta^2\rangle}{\partial P}\right)_T = -\frac{kT}{2\pi^2\nu_1^3 I}\left(\frac{\partial\nu_1}{\partial P}\right)_T$$

$$= -\frac{k\,T\,\kappa\gamma_1}{2\pi^2\nu_1^2 I}$$

$$= -2kT\,\kappa\gamma_1/k_1$$

where k_1 is the force constant for the torsional oscillation. Combining the last two equations we find

$$[4] \qquad \left(\frac{\partial \ln q}{\partial P}\right)_T = \left(\frac{\partial \ln q_0}{\partial P}\right)_T + \frac{3kT\kappa\gamma_1}{k_1}$$

The first term in [4], the 'static' term, represents the effect of pressure on the field gradient at the nuclear site in the static lattice, in which the amplitudes of thermal oscillations have been reduced to zero. The second term, the 'dynamic' term, represents the effect of pressure on the amplitude of the torsional oscillation which is affecting the field gradient, and is inherently positive.

8.1 Field Gradients at Halogen Sites

The pressure dependences of the ^{35}Cl resonances in Group V trichlorides can be understood by making the hypothesis that the effect of intermolecular bonding is to lower the value of q_0; as the crystal is compressed the effect of intermolecular bonding becomes stronger, q_0 is lowered further, and so the static term $(\partial \ln q_0/\partial P)_T$ is negative for initial changes in pressure. For a crystal in which the intermolecular bonding is very weak, q_0 is determined primarily by intramolecular interactions and so the static term is approximately zero; for such a crystal, the pressure coefficient of the nqr frequencies is positive. In a series of compounds in which the strength of intermolecular bonding increases, the static term becomes more negative; the measured pressure coefficient of the nqr fre-

Can. J. Chem. Downloaded from www.nrcresearchpress.com by 210.87.254.105 on 09/05/12
For personal use only.

quency becomes less positive, becoming zero when the two terms are equal, and then increasingly negative as the static term becomes dominant.

In the discussion of the crystal structures of the Group V trichlorides, it was shown that the strength of intermolecular bonding increases in the order $AsCl_3 < SbCl_3 < BiCl_3$; reference to Table 7 shows that the initial pressure coefficients become more negative in the order indicated. Note that comparisons between compounds should be made at equal temperatures. Furthermore, the crystal structures show that the face-bridging chlorine atoms are more involved in intermolecular bonding than the mirror-plane chlorine atoms; this is reflected in the corresponding resonance as a lower frequency and a more negative pressure coefficient, compared with the other resonance in the same compound at the same temperature.

The pressure coefficient at higher pressures may be altered by two effects, both of which tend to make the pressure coefficient more negative. Firstly, the dynamic term is reduced by a smaller value of the compressibility (15), and a larger torsional frequency (43). Secondly, the static term may become more negative as the effects of intermolecular bonding are enhanced by smaller intermolecular distances. Table 2 shows that all the measured quadratic coefficients b_2 are negative, in agreement with these predictions. Generally, pressure dependences are found to be nearly linear when there is an appreciable initial slope, but when the pressure coefficient is small, the static and dynamic terms are approximately equal numerically, and nonlinear effects become measurable. This effect is particularly well demonstrated by the $^{35}Cl(1)$ resonance in $SbCl_3$ at room temperature; the resonance frequency passes through a maximum at aproximately 270 MPa, and at higher pressures the pressure coefficient is negative.

The temperature dependence of the pressure coefficient has two possible contributing factors. Thermal expansion reduces the magnitude of the static term, and the explicit temperature dependence increases the magnitude of the dynamic term, as the temperature is increased. These two effects work together to make the measured pressure coefficient more positive as the temperature is increased. This trend is demonstrated by both ^{35}Cl resonances in $SbCl_3$ (Table 7).

Pressure dependences of halogen nqr frequencies have been measured at several temperatures in *p*-dichlorobenzene (1), *p*-dibromobenzene (24), and stannic iodide (24). These are molecular crystals, and the volume dependence of q_0 as determined by the KBB method (1) is small in all cases, with values of $n(V)$ which are positive or only very slightly negative. The observed behaviour is consistent with the above hypothesis in all cases; the pressure coefficients are positive at high temperatures and low pressures, and become negative when the temperature is lowered, and when the pressure is increased to high values. The behaviour of these resonances is very similar to that of Cl(1) in $SbCl_3$, and suggests that the strength of the intermolecular interactions are comparable in these crystals.

In mercuric chloride (44), there are two resonances, and the pressure coefficient of the low frequency resonance is more negative than that of the high frequency resonance, as in the cases of the Group V trichlorides.[1]

Recently, pressure dependence studies at room temperature on ^{35}Cl resonances in two chlorocyclodiphosphazanes $(Cl_3PNR)_2$, R = CH_3 and C_6H_5, have been reported (45); in each compound there are three resonances, corresponding to one axial and two equatorial positions which are slightly nonequivalent crystallographically (46, 47). In the compound with R = CH_3, the equatorial chlorine atoms interact with equatorial chlorine atoms in adjacent molecules, whereas the axial chlorine atoms do not take part in any close intermolecular contacts (46). The nqr results do not correspond with this crystallographic data, for the axial resonance has a negative $(\partial\nu/\partial P)_T$ and the equatorial resonances have positive $(\partial\nu/\partial P)_T$ values in both compounds. This discrepancy requires further investigation. Otherwise these data are consistent with the hypothesis; all pressure dependences show curvature of the predicted sign, and the lower frequency equatorial resonance has a less positive $(\partial\nu/\partial P)_T$ and a less negative $(\partial\nu/\partial T)_P$ than the other equatorial resonance, in both compounds.

[1]NOTE ADDED IN PROOF: The pressure dependences of the ^{35}Cl resonances in $HgCl_2$ have been measured at three temperatures by Balashov and Ikhenov (59). For the lower frequency resonance $(\partial\nu/\partial P)_T$ increases with temperature, while for the higher frequency resonance $(\partial\nu/\partial P)_T$ is almost independent of temperature.

Can. J. Chem. Downloaded from www.nrcresearchpress.com by 210.87.254.105 on 09/05/12
For personal use only.

In the chlorocyclophosphazatriene $N_3P_3Cl_6$, there are four closely spaced resonances (48), resulting from a slight distortion of the ring from planarity by intermolecular interactions (49). The pressure dependences of the resonances have been measured (50) and exhibit a good correlation between $(\partial\nu/\partial T)_P$ and $(\partial\nu/\partial P)_T$. However, the resonance with the smallest value of $(\partial\nu/\partial P)_T$ is not the lowest frequency resonance, but the second lowest. The reason for this lies in the hypothesis itself; examination of the temperature dependences of the resonances (48) shows that the lowest two resonances cross at a temperature of about 100 K, since the resonance which lies lowest at absolute zero has the less negative value of $(\partial\nu/\partial T)_P$. Crossings of resonances of this sort are not unusual, and this possibility must be considered when examining the correlation of $(\partial\nu/\partial P)_T$ with ν for closely spaced resonances; the proper correlation is with the resonance frequency at absolute zero.

8.2. Field Gradients at Other Sites

The trends in the logarithmic pressure coefficients of the Group V metal atom coupling constants shown in Table 7 are the same as those of the ^{35}Cl frequencies. The coefficients become more negative, progressing from $AsCl_3$ to $BiCl_3$, as intermolecular bonding becomes stronger; for $SbCl_3$, the coefficient becomes more negative as the temperature is lowered. These trends suggest that the hypothesis made in section 8.1 also applies to the metal atom coupling constants in this series of compounds. Azheganov *et al.* (51) have measured the pressure coefficients of the ^{121}Sb quadrupole parameters in $SbCl_3$, with results in agreement with the present work; they suggest that the observed coupling constant contains molecular and intermolecular contributions,

$$q = q_m + q_{im}$$

and deduce that q_{im} is about 3% of q_m and is of the opposite sign. However, no account is taken of the dynamic contribution to the pressure coefficient.

The pressure dependences of the ^{121}Sb quadrupole parameters in two complexes of $SbCl_3$ have been reported (52). In the complex with naphthalene, $2SbCl_3.C_{10}H_8$, $(\partial \ln q/\partial P)_T = -0.184 \times 10^{-4}$ MPa^{-1}, which is substantially less negative than in $SbCl_3$ itself. The crystal structure of the complex (53) shows that layers of $SbCl_3$ molecules alternate with layers of naphthalene molecules, and that the main interaction of the Sb atom is with the naphthalene molecule. The effect of the interaction with the naphthalene molecule on the Sb coupling constant is not so sensitive to pressure as the intermolecular interaction in $SbCl_3$ itself.

Pressure dependence studies on nuclei other than halogens in molecular crystals are few in number, and it is not possible to determine how widely the hypothesis applies. The ^{14}N resonance in hexamethylenetetramine (25) suggests that this crystal is a good example of a 'pure' molecular crystal, for $(\partial\nu/\partial P)_T$ is positive at room temperature, and becomes essentially zero at liquid nitrogen temperature. Data for other crystals are needed in order to show whether intermolecular interactions lead to a negative static contribution to the pressure coefficient, in general.

9. Mechanisms for the Effects of Intermolecular Bonding

The hypothesis adopted in the last section apparently applies in a variety of different crystals, and it is necessary to consider why a quadrupole coupling constant is made smaller by the proximity of another molecule. There is perhaps no single reason, and only a full scale quantum mechanical analysis will demonstrate the most important effect. In this section some possible effects are considered briefly.

Furukawa proposed that the electric field gradient (q) at the chlorine sites in $BiCl_3$ is affected by transfer of electrons from filled $p\pi$ orbitals on the chlorine atoms to empty $6d$ orbitals on the bismuth atoms (34). This would lower the value of q, and could increase the asymmetry parameter, in a way which would be pressure dependent, and which would be more important as the strength of intermolecular bonding increased.

Brill and co-workers have suggested that the lowering of ^{35}Cl resonance frequencies in crystals is strongly correlated with the intermolecular repulsive energy (54, 55); the mechanism proposed for this effect is a quenching of the Sternheimer antishielding factor. This mechanism would also lead to a negative value of the static contribution to the pressure coefficient. It is reasonable to expect repulsive interactions to be important in crystals where halogen–halogen dis-

tances are the shortest intermolecular distances. However, it is difficult to accept for the Group V trichlorides, since the heat of sublimation increases in the order $AsCl_3 < SbCl_3 < BiCl_3$. This theory requires further theoretical study.

Bersohn suggested that dipolar electric fields in crystals act so as to change the ionic character of the bonds to halogen atoms (56). This theory does not require $(\partial \ln q_0/\partial P)_T$ to be negative in general.

Haas and Marram proposed that intramolecular $p\pi$–$d\pi$ bonding is responsible for the positive isobaric temperature dependences of ^{35}Cl frequencies in hexachloro complexes of some transition metals (57). Such multiple bonding should be reflected as bond shortening, whereas in $SbCl_3$ and $BiCl_3$, the chlorine resonances with the more positive values of $(\partial\nu/\partial T)_P$ are those corresponding to chlorine atoms having the longest intramolecular bonds. Furthermore, the photoelectron spectrum of $SbCl_3$ suggests that such π back-bonding is not important (58). This mechanism is apparently not responsible for the effects observed in the Group V trichlorides.

Acknowledgements

This work was supported in part by the National Research Council of Canada, by the Advisory Research Committee of Queen's University, and by our colleagues. The support of an NRCC Scholarship (G.C.G.) is acknowledged.

1. T. KUSHIDA, G. B. BENEDEK, and N. BLOEMBERGEN. Phys. Rev. **104**, 1364 (1956).
2. G. C. GILLIES and R. J. C. BROWN. Can. J. Chem. **50**, 2586 (1972).
3. G. C. GILLIES and R. J. C. BROWN. Can. J. Chem. **51**, 2290 (1973).
4. T. C. WANG. Phys. Rev. **99**, 566 (1955).
5. T. OKUDA, A. NAKAO, M. SHIROYAMA, and H. NEGITA. Bull. Chem. Soc. Jpn. **41**, 61 (1968).
6. S. OGAWA. J. Phys. Soc. Jpn. **13**, 618 (1958).
7. C. DEAN. Rev. Sci. Instrum. **29**, 1047 (1958).
8. D. WILLIAMS. Physica, **17**, 456 (1951).
9. C. DEAN and M. POLLAK. Rev. Sci. Instrum. **29**, 630 (1958).
10. R. J. C. BROWN and S. SEGEL. J. Phys. F, **5**, 1073 (1975).
11. C. W. CLENSHAW. Comput. J. **2**, 170 (1960).
12. B. F. BOWLES, G. J. SCOTT, and S. E. BABB. J. Chem. Phys. **39**, 831 (1963).
13. W. M. C. JULIEN and H. GERDING. Rec. Trav. Chim. Pays-Bas, **91**, 743 (1972).
14. R. J. C. BROWN, G. C. GILLIES, R. E. HALLIWELL, and S. SEGEL. J. Magn. Reson. **20**, 286 (1975).
15. C. A. SWENSON and M. S. ANDERSON. J. Phys. Chem. Solids, **36**, 145 (1975).
16. V. KURBATOV. J. Gen. Chem. USSR, **20**, 997 (1950).
17. W. BILTZ and A. SAPPER. Z. Anorg. Chem. **203**, 277 (1932).
18. K. K. KELLEY. U.S. Bur. of Mines No. 584 (1960).
19. W. KLEMM. Z. Anorg. Chem. **176**, 11 (1928).
20. G. E. PETERSON. Ph.D. Thesis. University of Pittsburgh, Pittsburgh, Pa. 1962.
21. I. Lindquist and A. Niggli. J. Inorg. Nucl. Chem. **2**, 345 (1956).
22. O. L. ANDERSON. J. Phys. Chem. Solids, **27**, 547 (1965).
23. C. A. SWENSON. J. Phys. Chem. Solids, **29**, 1337 (1968).
24. T. FUKE. J. Phys. Soc. Jpn. **16**, 266 (1961).
25. G. A. MATZKANIN, T. N. O'NEAL, T. A. SCOTT, and P. J. HAIGH. J. Chem. Phys. **44**, 4171 (1966).
26. T. A. SCOTT and G. J. D'ALESSIO. J. Magn. Reson. **5**, 416 (1971).
27. A. T. KOZULIN. Opt. Spectrosc. USA, **32**, 374 (1972).
28. R. J. C. BROWN. J. Chem. Phys. **32**, 116 (1960).
29. M. Z. YUSUPOV, V. S. GRECHISHKIN, A. T. KOSULIN, V. P. ANFEROV, and V. S. VERSILOV. Org. Magn. Reson. **3**, 515 (1971).
30. S. KONAKA and M. KIMURA. Bull. Chem. Soc. Jpn. **43**, 1693 (1970).
31. S. KONAKA and M. KIMURA. Bull. Chem. Soc. Jpn. **46**, 404 (1973).
32. H. A. SKINNER and L. E. SUTTON. Trans. Faraday Soc. **36**, 681 (1940).
33. S. C. NYBURG, G. A. OZIN, and J. T. SZYMANSKI. Acta Crystallogr. Sect. B, **27**, 2298 (1971); **28**, 2885 (1972).
34. Y. FURUKAWA. J. SCI. HIROSHIMA Univ. Ser. A, **37**, 357 (1973).
35. N. W. ALCOCK. Adv. Inorg. Chem. Radiochem. **15**, 1 (1972).
36. J. TROTTER. Z. Kristallogr. **122**, 230 (1965).
37. O. KUBASCHEWSKI, E. L. L. EVANS, and C. B. ALCOCK. Metallurgical thermochemistry. Pergamon Press, London. 1967.
38. D. CUBBICIOTTI. J. Phys. Chem. **70**, 2410 (1966).
39. K. W. FUNG, G. M. BEGUN, and G. MAMANTOV. Inorg. Chem. **12**, 53 (1973).
40. E. DENCHIK, S. C. NYBERG, G. A. OZIN, and J. T. SZYMANSKI. J. Chem. Soc. A, 3157 (1971).
41. H. BAYER. Z. Physik. **130**, 227 (1951).
42. H. M. VAN DRIEL, M. M. MCENNAN, and R. L. ARMSTRONG. J. Magn. Reson. **18**, 485 (1975).
43. D. S. PERCY, G. A. SAMARA, and B. MOROSIN. J. Phys. Chem. Solids, **36**, 1123 (1975).
44. D. DAUTREPPE and B. DREYFUS. C.R. Acad. Sci. **242**, 766 (1956).
45. W. H. DALGLEISH and A. L. PORTE. J. Magn. Reson. **20**, 359 (1975).
46. L. G. HOARD and R. A. JACOBSON. J. Chem. Soc. A, 1203 (1966).
47. D. HESS and H. FORST. Z. Anorg. Chem. **342**, 240 (1966).
48. M. KAPLANSKY and M. A. WHITEHEAD. Can. J. Chem. **45**, 1669 (1967).

Can. J. Chem. Downloaded from www.nrcresearchpress.com by 210.87.254.105 on 09/05/12
For personal use only.

49. A. WILSON and D. F. CARROLL. J. Chem. Soc. 2548 (1950).
50. W. H. DALGLEISH, R. KEAT, A. L. PORTE, and R. A. SHAW. J. Magn. Reson. **20**, 351 (1975).
51. A. S. AZHEGANOV, N. E. AINBINDER, and YU. I. MANZHURA. Sov. Phys. Solid State, **17**, 1013 (1975).
52. N. E. AINBINDER, YU. I. MANZHURA, and I. A. KYUNTSEL. Sov. Phys. Solid State, **16**, 2288 (1975).
53. R. HULME and J. T. SZYMANSKI. Acta Crystallogr. Sect. B, **25**, 753 (1969).
54. T. B. BRILL, R. C. GEARHART, and W. A. WELSH. J. Magn. Reson. **13**, 27 (1974).
55. T. B. BRILL. J. Chem. Phys. **61**, 424 (1974).
56. R. BERSOHN. J. Appl. Phys. Suppl. 1, **33**, 286 (1962).
57. T. E. HAAS and E. P. MARRAM. J. Chem. Phys. **43**, 3985 (1954).
58. D. G. NICHOLSON and P. RADEMACHER. Acta. Chem. Scand. Ser. A, **28**, 1136 (1974).
59. D. B. BALASHOV and D. A. IKHENOV. Sov. Phys. Solid State, **17**, 1788 (1975).

Downloaded from www.nrcresearchpress.com by 210.87.254.105 on 09/05/12
For personal use only.

Thermodynamic properties of binary liquid mixtures

MURARI VENKATA PRABHAKARA RAO AND PULIGUNDLA RAMACHANDRA NAIDU
Sri Venkateswara University, Chemical Laboratory, Tirupati, 517502, A.P.

Received October 14, 1975

MURARI VENKATA PRABHAKARA RAO and PULIGUNDLA RAMACHANDRA NAIDU. Can. J. Chem. **54**, 2280 (1976).

Excess volumes of the three binary mixtures: (*1*) cyclohexane – diethyl ketone, (*2*) cyclohexane–benzonitrile, and (*3*) toluene–benzonitrile have been measured at 303.15 K using a dilatometer. Excess volumes of the first two systems are positive over the whole range of composition and are negative for the third system. The measured excess volumes and the excess heats of mixing reported in the literature for the three binary systems have been analysed in the light of the statistical theory of liquid mixtures developed by Flory. The analysis has shown that the theory in its modified form is approximately applicable to the mixtures cyclohexane–diethylketone and cyclohexane–benzonitrile.

MURARI VENKATA PRABHAKARA RAO et PULIGUNDLA RAMACHANDRA NAIDU. Can. J. Chem. **54**, 2280 (1976).

A l'aide d'un dilatomètre, on a mesuré, à 303.15 K, les volumes d'excès de trois mélanges binaires: (*1*) cyclohexane–diéthylcétone, (*2*) cyclohexane–benzonitrile et (*3*) toluène-benzonitrile. Les excès volumiques des deux premiers systèmes sont positifs sur toute l'étendue des compositions des mélanges; les valeurs de V^E sont négatives pour le troisième système. Les volumes d'excès mesurés et les chaleur de mélanges d'excès rapportées dans la littérature pour les trois systèmes binaires ont été analysés à la lumière de la théorie statistique des mélanges liquides développée par Flory. L'analyse a montré que la théorie sous sa forme modifiée peut être appliquée pour les mélanges cyclohexane diéthylcétone et cyclohexane benzonitrile.

[Traduit par le journal]

Can. J. Chem. Downloaded from www.nrcresearchpress.com by 210.87.254.6 on 09/05/12
For personal use only.

Introduction

The excess thermodynamic functions of binary liquid mixtures can reasonably be predicted on the basis of the statistical theory developed by Flory and co-worker (1, 2). This theory has been extended to mixtures containing one polar component by Nigam and Singh (3) and Raman and Naidu (4). These workers treated the single interaction parameter defined by Flory as an adjustable quantity in their analyses. In this paper, the measured excess volumes of the three binary mixtures cyclohexane – diethyl ketone, cyclohexane–benzonitrile, and toluene–benzonitrile and the excess enthalpies of the mixtures reported by Amaya (5) have been analysed in the light of the Flory theory both in its original form and also the modified form.

Experimental

Measurement of Excess Volumes

The excess volumes have been determined at 303.15 K using a single composition per loading type dilatometer described by Rao and Naidu (6). The values are accurate to ± 0.003 cm^3 mol^{-1}.

Purification of Liquid

Cyclohexane (BDH) and toluene (BDH) were purified by the methods reported earlier (7, 8). Diethylketone (Fluka) was dried over anhydrous sodium sulphate for two days then fractionally distilled ($\rho^{303.15\ K} = 0.80455$ g/ml). Benzonitrile (Riedel) was dried over freshly fused calcium chloride for two days and distilled at atmospheric pressure in an all glass apparatus ($\rho^{303.15\ K} = 0.99621$ g/ml).

The purity of the samples has been verified from densities and boiling points reported in literature (9).

Results and Calculations

The excess volumes for the three binary liquid mixtures are included in Table 1, in which x refers to the mole fraction of the first component.

The experimental values of V^E may be represented by an empirical equation of the form

$$[1] \qquad V^E = x_1 x_2 \sum_{K=1}^{p} a_K (x_1 - x_2)^{K-1}$$

where p is the number of fitting parameters which are determined by a least-squares method. Equation 1 with three parameters fits the data included here satisfactorily. The values of the three parameters obtained by least-squares analysis and the standard deviation are presented in Table 2.

The interaction parameter, X_{12}, defined by

Can. J. Chem. Downloaded from www.nrcresearchpress.com by 210.87.254.6 on 09/05/12
For personal use only.

Flory has been evaluated by two different methods. In the first method X_{12} was calculated from the characteristic properties of the pure components presented in Table 3. This value of X_{12} was in turn used to predict the theoretical values of V^E and h^E at 303.15 K (*cf.* Table 4; *F*). In the second method, the values of X_{12} which fit the experimental values of V^E and h^E were evaluated separately. The derived values of X_{12} were in turn used to predict the values of h^E at 303.15 K and V^E at 298.15 K respectively (*cf.* Table 4, $F(V^E)$ and $F(h^E)$. The equations which have been described by Flory and Abe were used in these calculations.

TABLE 1. Experimental values of excess volumes at 303.15 K

x	V^E (cm^3 mol^{-1})
Cyclohexane+diethyl ketone	
0.1141	0.272
0.1787	0.402
0.2538	0.541
0.3359	0.667
0.4851	0.778
0.6607	0.764
0.7462	0.696
0.8200	0.577
0.8872	0.402
Toluene+benzonitrile	
0.1089	−0.089
0.1700	−0.125
0.2469	−0.166
0.3367	−0.208
0.4881	−0.257
0.6415	−0.270
0.7408	−0.264
0.8093	−0.226
0.8774	−0.181
Cyclohexane+benzonitrile	
0.1049	0.044
0.1687	0.075
0.2391	0.114
0.3316	0.150
0.4835	0.248
0.6384	0.291
0.7390	0.290
0.8179	0.259
0.8835	0.205

Discussion

A comparison of observed and calculated values of V^E included in Table 4 shows that the values predicted by the theory, in its original form, differ in sign in all three mixtures. However, the Flory theory correctly predicts the sign of the excess function when X_{12} is treated as an adjustable quantity in respect of cyclohexane–diethylketone system (I) and cyclohexane–benzonitrile system (II) mixtures. Similarly an examination of predicted and observed values of h^E (*cf.* Table 4) shows that Flory theory correctly predicts the sign of the excess function both in the original form and in the modified form in the case of cyclohexane–diethylketone and cyclohexane–benzonitrile mixtures. Further, the values predicted by the modified theory for these two systems are closer to the observed values than those predicted by the original theory. Hence, it is concluded that Flory theory in its modified form is approximately applicable to the first two systems.

TABLE 2. Values of parameters (and standard deviations) of eq. 1[a]

System	a_1	a_2	a_3	σ
Cyclohexane – diethyl ketone	3.1687	0.8529	0.3365	0.010
Cyclohexane–benzonitrile	0.9898	0.9752	0.4028	0.007
Toluene–benzonitrile	−1.0245	0.4900	0.4524	0.004

[a]In cm^3 mol^{-1}.

TABLE 3. Parameters of pure components at 303.15 K

Component	$\alpha \times 10^3$ (deg^{-1})	V (cm^3 mol^{-1})	$\tilde{v}$	V^* (cm^3 mol^{-1})	P^* cal cm^{-3}	$\bar{T}$
Cyclohexane	1.229	109.46	1.297	84.41	126.0	0.06431
Toluene	1.078	107.44	1.267	84.82	131.6	0.05981
Benzonitrile	0.891	103.51	1.228	84.29	151.5	0.05399
Diethyl ketone	1.200	107.07	1.291	82.94	131.1	0.06330

TABLE 4. Comparison of experiment with theories for equimolar compositions

Method	System I	System II	System III
		V^E (cm^3 mol^{-1})	
Experiment	0.778	0.248	−0.257
Theory: F^a	−0.006	−0.339	0.085
$F(h^E)^b$	0.921	0.506	0.011
		h^E (cal mol^{-1})	
Experiment	250.4	323.8	0.1
Theory: F^a	1.9	22.7	30.9
$F(V^E)^c$	212.3	203.8	−101.6

[a] X_{12} evaluated theoretically.
[b] X_{12} determined from experimental h^E.
[c] X_{12} determined from experimental V^E.

Acknowledgement

One of the authors (M.V.P.R.) is thankful to the Council of Scientific and Industrial Research, New Delhi for the award of a senior research fellowship.

1. P. J. FLORY. J. Am. Chem. Soc. **87**, 1833 (1965).
2. A. ABE and P. J. FLORY. J. Am. Chem. **87**, 1838 (1965).
3. R. K. NIGAM and P. P. SINGH. Ind. J. Chem. **7**, 156 (1969).
4. G. K. RAMAN and P. R. NAIDU. Proc. Indian Acad. Sci. **A77**, 263 (1973).
5. KAZUO AMAYA. Bull. Chem. Soc. Jpn. **34**, 1271 (1961).
6. M. V. P. RAO and P. R. NAIDU. Can. J. Chem. **52**, 788 (1974).
7. P. R. NAIDU and V. R. KRISHNAN. Trans. Faraday Soc. **61**, 1347 (1965).
8. P. R. NAIDU and V. R. KRISHNAN. J. Phys. Soc. Jpn. **29**, 1554 (1965).
9. J. TIMMERMANS. Physico-chemical constants of pure organic compounds. Elsevier Publishing Co., Amsterdam. 1950.

Can. J. Chem. Downloaded from www.nrcresearchpress.com by 210.87.254.6 on 09/05/12
For personal use only.

A deuterium magnetic resonance study of a lamellar lyotropic liquid crystalline phase

ALAN S. TRACEY AND PETER DIEHL
Department of Physics, University of Basel, CH-4056 Basel, Switzerland

Received July 4, 1975[1]

ALAN S. TRACEY and PETER DIEHL. Can. J. Chem. **54**, 2283 (1976).

Deuterium magnetic resonance spectra have been obtained from the specifically deuterium labelled hydrocarbon chains of a lyotropic lamellar mesophase which spontaneously aligns in a magnetic field. It was found that the behaviour of both the decanol and decylsulphate chains was similar to other lamellar and to nematic phases except that the degrees of order of the chain segment axes were abnormally small, being a factor of four to six less than that observed for other phases. Since the chain behaviour seemed normal it was suggested that the small alignment arose because the preferential orientation of the hydrocarbon chains was not perpendicular to the superstructure of the phase but rather at an angle of about 45° to the normal.

ALAN S. TRACEY et PETER DIEHL. Can. J. Chem. **54**, 2283 (1976).

On a obtenu des spectres de résonance magnétique du deutérium pour une mésophase lamellaire lyotrope qui s'aligne spontanément dans le champ magnétique et qui avait été marqué d'une façon spécifique dans les chaînes hydrocarbonées. On a trouvé que les comportements des chaînes du décanol et du décylsulphate sont tous les deux semblables à ceux d'autres phases lamellaires et nématiques; toutefois les degrés d'ordre des axes du segment de la chaîne sont anormalement plus bas soit de quatre à six fois moins élevés que les valeurs observées pour d'autres phases. Puisque le comportement de la chaîne semble normal, on suggère que le petit alignement provient d'une orientation préférentielle des chaînes hydrocarbonées qui n'est pas perpendiculaire à la superstructure de la phase mais plutôt à un angle de 45° par rapport à la normale.

[Traduit par le journal]

Introduction

Lyotropic liquid crystalline soap solutions are increasingly important as media for the determination of the structure of molecular and ionic species. The value of these materials as an anisotropic solvent has been greatly enhanced by recent observations which showed that the more commonly used thermotropic nematic liquid crystals do not always provide unambiguous results, particularly when relatively small molecules are investigated (1–3). This does not seem to be the case with lyotropic phases and they are therefore becoming solvents of necessity if not of choice.

Because of the wide occurrence of lyotropic liquid crystalline materials in living systems much work has been invested in many attempts to gain information about the properties of these materials (4). Little of this effort has been directed towards lyotropic mesophases which can be aligned by a magnetic field. Two phases which are capable of being aligned by the magnetic fields of nmr spectrometers are commonly encountered. One phase (Type I) has its optic axis parallel to the magnetic field and when in a conventional iron core spectrometer cannot be rotated without destruction of its order although spinning of the sample tube is possible in a cryogenic system (5, 6). The second phase (Type II) is the one most commonly used as an nmr solvent (4) and can undergo rotation in either type of spectrometer.

The association of the alkyl chains of the surfactant molecules leads to the formation of a hydrocarbon 'superstructure' and thus to the development of long range order in those materials. As a consequence information concerning the hydrocarbon chains is of particular value. Deuterium magnetic resonance investigations of the specifically labelled chains have been shown to be of value for investigations into both lyotropic lamellar (7, 8) and nematic (9, 10) materials. The deuterium studies of nematic phases have been concerned only with the Type II phase. A Type I phase, prepared from sodium decylsulphate, was used for an investigation of the

[1]Revision received March 8, 1976.

Can. J. Chem. Downloaded from www.nrcresearchpress.com by 210.87.254.42 on 09/05/12
For personal use only.

Can. J. Chem. Downloaded from www.nrcresearchpress.com by 210.87.254.42 on 09/05/12
For personal use only.

anilinium ion. It was found that the ion had become a constituent of the superstructure with the aromatic ring protruding into its interior while leaving the $—NH_3^+$ substituent sitting in the highly polar superstructure/water interface region. It was shown that if a lamellar arrangement, as opposed to the cylindrical structure of the Type II phase, was assumed for the superstructure then degrees of order for the long axis of the hydrocarbon chains were about 0.15 at positions 1 and 2 (6). The degree of order at similar positions of the Type II phase has been found to be about 0.5 to 0.6 (9, 10). Lamellar phases, aligned between glass plates, have been investigated and order parameters of about 0.6 also obtained for these materials (7, 8, 11). Dipalmitoyllecithin bilayers have an order parameter of 0.45 for the fatty acid chains (12). Clearly the value of 0.15 which was found for the Type I phase is an unusually small value.

In an effort to find an explanation for the small order parameter we have examined several specifically deuterated decylsulphates and decanols in the lyotropic Type I phase by deuterium magnetic resonance.

Experimental

Deuterium magnetic resonance spectra were obtained at 27 °C from a Bruker HX-90 Fourier Transform spectrometer. Spectral widths were 25 or 50 kHz. Proton decoupling was employed to obtain better resolved spectra.

The partially deuterated alcohols and decylsulphates were prepared as described in the literature (10). The lyotropic phase was prepared according to the composition given below with the appropriate deuterated species, one or more, to replace the standard component.

Compound	% by weight
Sodium decylsulphate	37.5
9,9;10,10,10-Pentadeuterodecanol	3.6
Decanol	3.6
H_2O	55.3

Results and Discussion

Nuclei with spin greater than 1/2 give rise to quadrupole splittings when they are in an anisotropic medium. Since deuterium has a spin of 1 and is readily substituted for hydrogen it is becoming increasingly important as a probe into the properties of liquid crystalline phases. This results from the fact that proton spectra from species containing large numbers of protons are extremely complex and not readily interpretable. The deuterium quadrupole splitting, on the other hand, is obtained directly from the spectrum, and is much more easily understood.

The general relationship between the quadrupole splitting $\Delta\nu$ and degree of order is given by eq. 1

$$[1] \qquad \Delta\nu = \tfrac{3}{2}Q[S_{zz}' + \tfrac{\eta}{3}(S_{xx}' - S_{yy}')]$$

where η is the asymmetry parameter and Q is the quadrupole coupling constant. S_{zz}', S_{xx}', and S_{yy}' are the degrees of order of the quadrupole fixed coordinate system and S_{zz}' is directed along the major quadrupolar axis. For deuterium in saturated hydrocarbons η is very small, 0.03 or less (13), and the major quadrupole axis deviates only slightly from the C—D bond direction. As a consequence eq. 1 is considerably simplified and the expression, [2], is obtained.

$$[2] \qquad \Delta\nu = \tfrac{3}{2}Q_{\mathrm{D}}S_{\mathrm{CD}}$$

Thus for the case of hydrocarbons the deuterium quadrupole splitting is of particular interest since it gives the degree of order of the individual carbon–deuterium bonds. The deuterium quadrupole coupling constant, Q_{D}, has been determined for many saturated hydrocarbon systems and is about 170 kHz (13, 14), the value used here.

In principle we are more interested in the degrees of order along the major hydrocarbon chain axis. Each C—D bond of the individual methylene segments is perpendicular to this axis. Since the hydrocarbon chains are flexible there is no reason to expect all chain segments to show the same degree of order. The degree of order of each chain segment axis, S_{Ch}, may be obtained from the degrees of order of the respective methylene C—D bonds if it is assumed that the hydrocarbon chains behave as an axially symmetric system, that is, only one S value is required to describe the order at any particular segment. This assumption has been supported by studies of macroscopically aligned lamellar systems (15). For axial symmetry it follows that

$$S_{\mathrm{CD}} = \tfrac{1}{2}(3\cos^2 90° - 1)S_{\mathrm{Ch}} = -\tfrac{1}{2}S_{\mathrm{Ch}}$$

from which eq. 3 is obtained.

$$[3] \qquad \Delta\nu = -\tfrac{3}{4}Q_{\mathrm{D}}S_{\mathrm{Ch}}$$

TABLE 1. The deuterium quadrupole splittings, in kHz, observed from the various lyotropic phases are given. Order parameters corresponding to positions 1 to 4 of the decyl chains are also shown*

Ternary phase	$\Delta\nu_1$	$\Delta\nu_2$	$\Delta\nu_3$	$\Delta\nu_4$	$\Delta\nu_8$	$\Delta\nu_9$	$\Delta\nu_{10}$	S_1	S_2	S_3	S_4
Decylsulphate Splittings											
1	13.52	—	—	—	—	—	—	0.106	—	—	—
2	—	14.63	—	—	—	—	—	—	0.115	—	—
3	—	12.2†	11.5†	—	—	—	—	—	0.095	0.090	—
4	—	—	13.54	12.56	—	—	—	—	—	0.106	0.099
5	12.35	—	—	—	8.96	7.02	2.244	0.097	—	—	—
Decanol Splittings											
1	—	—	—	—	—	8.79	2.125	—	—	—	—
2	—	—	—	—	—	9.17	2.225	—	—	—	—
3	—	—	—	—	—	8.78	2.113	—	—	—	—
4	—	—	—	—	—	8.04	1.921	—	—	—	—
6	14.17	—	—	—	11.17	8.57	2.067	0.111	—	—	—
7	—	14.08	15.11	—	—	8.55	2.058	—	0.110	0.119	—
8	—	—	15.4	15.4	—	8.61	2.054	—	—	0.121	0.121

*Estimated errors in $\Delta\nu_1$, $\Delta\nu_2$, $\Delta\nu_3$, $\Delta\nu_4$, and $\Delta\nu_8$ are ~0.1 kHz; $\Delta\nu_9$, ~0.04 kHz, and $\Delta\nu_{10}$, ~0.015 kHz, unless otherwise stated.
†Estimated errors in these values are ~0.3 kHz.

For lamellar phases in which the optic axis is parallel to the magnetic field, S_{Ch} gives the micro degree of order of the chain axis, *i.e.* the order of the chain segment when resolved parallel to the magnetic field. For phases having a cylindrical superstructure with the optic axis perpendicular to H_0 the micro degree of order is slightly more complex (9) and is given by

$$S_{CD} = -(1/8)S_{Ch}$$

It is the micro degree of order which is of major interest since this value allows one to easily draw comparisons between different systems.

We have investigated both specifically labelled decanol and sodium decylsulphate in pure ternary phases prepared from sodium decylsulphate and have obtained the deuterium spectra. These decylsulphate phases are of Type I since they give rotationally dependent dipole splittings according to $(3\cos^2\theta - 1)$ where θ is the angle of rotation from the equilibrium angle of 0°. The optic axis is thus parallel to the magnetic field, H_0. This behaviour is the same as was observed previously (5, 6, 16).

Interestingly if the sample is rotated and not returned to the equilibrium angle the process of destruction of the original order and formation of a new orientation with the optic axis again parallel to H_0 can be observed directly on the oscilloscope of the spectrometer.

That the Type I phase has a superstructure different from the Type II phase is quite clear from previous work (5, 6, 16). The behaviour of a Type II phase is that expected for a hydrocarbon superstructure composed of indefinitely long cylinders with the hydrocarbon chains filling the interior of the cylinders and separated from the interstitial water by the ionic headgroups of the chains. The cylinders then order perpendicular to H_0. The behaviour of the Type I phase is consistent with a superstructure composed of bilayers of indefinite extent which order so that the planes of the bilayers are perpendicular to H_0. Unfortunately for neither the Type I nor Type II phases has an X-ray determination been reported.

Table 1 gives the deuterium quadrupole splittings observed from the various samples studied. In order to make comparison easier Fig. 1 shows a plot of the various positions along the decyl chains versus the quadrupole splitting at the respective position divided by the quadrupole splitting from position 10 of decanol. The division is performed since decanol acts as an internal reference so that effects resulting from slightly different phase composition are accounted for.

The region of quite constant order followed by a rapid decrease near the terminal positions is characteristic of lyotropic systems and has been investigated in considerable detail (8, 10–12, 17). Of some note is the fact that decanol behaves quite differently from decylsulphate at all positions along the hydrocarbon chain. Individual

Can. J. Chem. Downloaded from www.nrcresearchpress.com by 210.87.254.42 on 09/05/12
For personal use only.

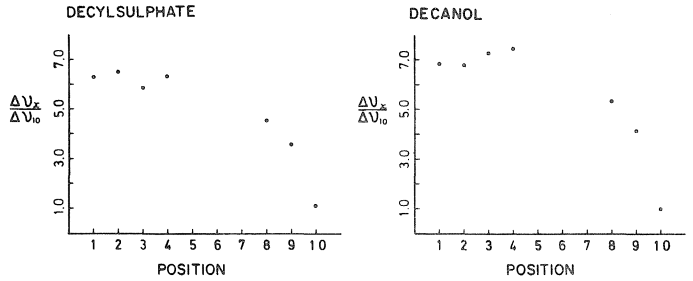

FIG. 1. Ratios of deuterium quadrupole splittings ($\Delta\nu_x/\Delta\nu_{10}$) for decylsulphate and decanol, where $\Delta\nu_{10}$ is the splitting from the 10 position of decanol, are given. The position of labelling, x, is plotted along the horizontal axis. The absolute magnitudes of the splittings correspond to much smaller order parameters than have previously been observed for lyotropic phases.

methylene groups of decanol are significantly more highly ordered than the corresponding ones in decylsulphate. This behaviour has also been observed in the Type II phase (10) and indicates that decanol is more tightly bound than the decylsulphate. This is also borne out by the ratio $\Delta\nu_9/\Delta\nu_{10}$. The value obtained from 9,9;10,10,10-pentadeuterodecylsulphate is 4.2 while for 9,9;-10,10,10-pentadeuterodecanol it is 3.1. These ratios show that the formation of *gauche* rotamers at the C_8—C_9 bond is much easier in decylsulphate than in decanol as has been discussed for the Type II phase (10). This result is consistent with decanol being more tightly bound thus limiting its freedom of motion. This occurs probably because decanol has no charge and has hydrogen bonding capability. It is therefore capable of relieving some of the repulsive interactions between charged decylsulphate ions.

Of considerable interest in these phases is the magnitude of the degrees of order of the chain segment axes. These values, as seen in Table 1, are about 0.11 for the decyl chains (positions 1 to 4) of the ternary phase and have been found to be about 0.15 for the same phase but containing anilinium ion (6). Slight deviations in alignment from sample to sample for the same positions arise because all phase compositions are not identical. Order parameters have been obtained for corresponding positions in Type II (9, 10) and macroscopically aligned lamellar phases (8, 11, 15) and are usually about 0.6. In one study of a Type II phase (9) the deuterium quadrupole splitting was determined as a function of temperature. It was found that the phase, prepared from decylammonium chloride, began to go isotropic when S_{Ch} had decreased to about 0.35 from an initial value of 0.55. This may indicate that with S values of this magnitude the hydrophobic interactions are no longer strong enough to stabilize the large units necessary for the formation of an anisotropic phase. At 82 °C lamellar potassium dodecanoate had an S_{Ch} of $\sim$0.5 (7). The order parameters observed for the Type I phase are thus seen to be remarkably small. The explanation for the small order probably lies in the packing of the hydrocarbon chains.

It has previously been suggested that the value, S_{Ch}, of 0.6 indicated an average 30° deviation of the chain axis from the normal to the lamellar superstructure which was taken to have an order of near unity (11). In view of other work (8, 12) such a 'tilt' angle seems unlikely but rather the order parameter of 0.6 arises from the normal *trans/gauche* isomerization and other motions of the hydrocarbon chains.

Since, except for the order, the hydrocarbon chains of Phase I seem to behave normally, it may well be that this small order does derive from a collective tilt of the chain axes. If it is assumed that an S_{Ch} of 0.6 represents the 'normal' degree of order then we may estimate the required tilt angle, γ, from

$$S_{Ch} = \tfrac{1}{2}(3\cos^2\gamma - 1) \times 0.6$$

From this, γ is about 45°. As this phase gives a rotation diagram according to $\frac{1}{2}(3\cos^2\theta - 1)$ then the chain motion, individual or collective, must be sufficiently rapid to average such a tilt over a cone, failure of this would result in a biaxial phase. The angle, 45°, seems very large but it is difficult to think of an alternate explanation for the stability of the phase, particularly since warming it does not produce the isotropic phase which might be expected if the S_{Ch} simply

Can. J. Chem. Downloaded from www.nrcresearchpress.com by 210.87.254.42 on 09/05/12
For personal use only.

reflected a low order for the phase superstructure. It should also be mentioned that addition of about 2 to 3 wt.% of a salt such as sodium sulphate to this ternary phase causes a phase transition to a Type II phase with its corresponding large order (5, 16) while the anilinium ion containing phase is stable with the addition of sodium sulphate (6).

The spectra from anilinium ion and methanol in Type I phases are essentially independent of field strength, *i.e.* of 60, 90, 100 or 220 Mhz spectrometers. This shows that the magnetic field is saturating and that the low order does not result from an incompletely aligned material.

Acknowledgement

We are grateful to the Swiss National Foundation for the Advancement of Science for its financial support of this work.

1. P. DIEHL, S. SÝKORA, W. NIEDERBERGER, and E. E. BURNELL. J. Mag. Res. **14**, 260 (1974).
2. E. E. BURNELL, J. R. COUNCIL, and S. E. ULRICH. Chem. Phys. Lett. **31**, 395 (1975).
3. P. DIEHL, M. REINHOLD, A. S. TRACEY, and E. WULLSCHLEGER. Mol. Phys. **30**, 1781 (1975).
4. C. L. KHETRAPAL, A. C. KUNWAR, A. S. TRACEY, and P. DIEHL. *In* NMR-basic principles and progress. Vol. 9. *Edited by* P. Diehl, E. Fluck, and R. Kosfeld. Springer Verlag, Berlin. 1975.
5. K. RADLEY, L. W. REEVES, and A. S. TRACEY. J. Phys. Chem. **80**, 174 (1976).
6. P. DIEHL and A. S. TRACEY. Can. J. Chem. **53**, 2755 (1975).
7. J. CHARVOLIN, P. MANNEVILLE, and B. DELOCHE. Chem. Phys. Lett. **23**, 345 (1973).
8. J. SEELIG and W. NIEDERBERGER. Biochem. **13**, 1585 (1974).
9. D. M. CHEN, L. W. REEVES, A. S. TRACEY, and M. M. TRACEY. J. Am. Chem. Soc. **96**, 5349 (1974).
10. L. W. REEVES and A. S. TRACEY. J. Am. Chem. Soc. **97**, 5729 (1975).
11. C. DIJKEMA and H. J. C. BERENDSEN. J. Mag. Res. **14**, 251 (1974).
12. A. SEELIG and J. SEELIG. Biochem. **13**, 4839 (1974).
13. F. S. MILLETT and B. P. DAILEY. J. Chem. Phys. **56**, 3249 (1972).
14. L. J. BURNETT and B. M. MÜLLER. J. Chem. Phys. **55**, 5829 (1971).
15. P. DIEHL and W. NIEDERBERGER. J. Mag. Res. **15**, 391 (1974).
16. D. M. CHEN, K. RADLEY, and L. W. REEVES. J. Am. Chem. Soc. **96**, 5251 (1974).
17. S. MARČELJA. Biochim. Biophys. Acta, **367**, 165 (1974).

Can. J. Chem. Downloaded from www.nrcresearchpress.com by 210.87.254.42 on 09/05/12
For personal use only.

Mécanisme d'inhibition par des alcools de la photo-oxydation de l'heptanal en phase liquide

J. C. ANDRÉ

Laboratoire de Chimie Générale, E.R.A. n° 136 du C.N.R.S., 1, rue Grandville, 54042 Nancy Cedex

ET

J. LEMAIRE

Laboratoire de Photochimie, U.E.R. de Sciences Exactes et Naturelles, Université de Clermont-Ferrand, Ensemble Scientifique des Cézeaux, B.P. 45 63170 Aubière

Reçu le 16 décembre 1975

J. C. ANDRÉ et J. LEMAIRE. Can. J. Chem. **54**, 2288 (1976).

L'inhibition de la photo-oxydation de l'heptanal par des alcools primaires et secondaires est due à la réaction des radicaux peroxy de l'aldéhyde avec l'alcool, conduisant à la formation d'espèces moins réactives qui disparaissent essentiellement du milieu dans des processus de recombinaison des chaînes. Un schéma cinétique est proposé, rendant compte des résultats expérimentaux. Par ailleurs, on montre que les alcools sont susceptibles de solvater les radicaux présents dans le milieu, modifiant ainsi leur réactivité.

J. C. ANDRÉ and J. LEMAIRE. Can. J. Chem. **54**, 2288 (1976).

The photooxidation of heptaldehyde *n*-$C_6H_{13}CHO$ can be inhibited by primary and secondary alcohols; this inhibition occurs through reaction between the peroxy radical $C_6H_{13}CO_3\cdot$ and the alcohol, leading to less reactive species disappearing by recombination processes. Moreover, the reactivity of free radicals is modified by alcohols which solvate these radicals by hydrogen bonding. A kinetic scheme is proposed which accounts for the experimental results.

Les alcools primaires et secondaires sont des inhibiteurs de l'oxydation de certaines substances organiques, comme le cumène (1) et l'éthanal (2). Le mécanisme de l'inhibition, par les alcools, de l'oxydation thermique ou photochimique des aldéhydes, n'a jamais été examiné en détail; il nous a semblé intéressant, dans le cadre plus général d'études de "co-oxydation", d'examiner la photo-oxydation de l'heptanal en phase liquide, en présence d'alcools primaires ou secondaires. Les premiers résultats de cette étude ont déjà été publiés (3).

Etude analytique de l'oxydation de l'heptanal en présence d'alcools

En l'absence d'alcools Lemaire et coll. (4) ont montré au laboratoire que: (*i*) l'acide perheptanoïque, produit primaire de l'oxydation de l'heptanal, réagit secondairement avec l'aldéhyde en excès pour former un peroxyde d'addition appelé peroxyde X; (*ii*) la décomposition thermique de ce peroxyde est responsable de la formation de deux molécules d'acide heptanoïque; (*iii*) le peroxyde X a la structure suivante (4, 5): C_6H_{13}—CO—O—O—CH(OH)—C_6H_{13}.

La présence d'un alcool pouvant être responsable d'une modification de la stoechiométrie d'oxydation de l'aldéhyde, nous avons entrepris, préalablement à l'étude cinétique, une étude analytique de l'oxydation de l'heptanal en présence d'alcools.

Mode opératoire

L'heptanal en présence d'alcools, irradié à 313 nm, (amorçage photochimique), est oxydé en phase liquide. L'oxygène à la pression atmosphérique barbote dans la solution. Au cours de l'oxydation on prélève des échantillons qui sont examinés immédiatement par spectrophotométrie infrarouge à l'aide d'un spectrophotomètre Perkin-Elmer modèle 221. On enregistre ainsi l'évolution du mélange réactionnel en fonction du degré d'avancement de la réaction. De plus, à la fin de l'oxydation, la cellule contenant la solution du dernier échantillon est maintenue dans le faisceau infrarouge; on enregistre ainsi l'évolution thermique du mélange réactionnel.

Résultats expérimentaux

Les résultats obtenus par Lemaire et coll. (4) concernant l'oxydation de l'heptanal seul et nos résultats concernant l'oxydation de ce même

Can. J. Chem. Downloaded from www.nrcresearchpress.com by 210.87.254.6 on 09/05/12
For personal use only.

Can. J. Chem. Downloaded from www.nrcresearchpress.com by 210.87.254.6 on 09/05/12
For personal use only.

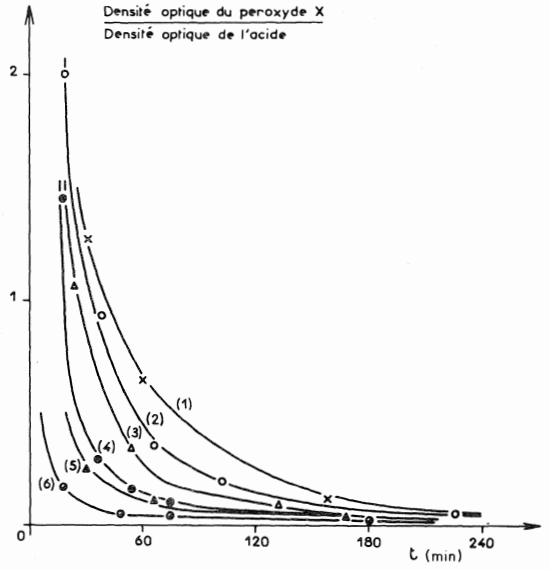

FIG. 1. Variations du rapport de la densité optique du peroxyde X (mesurée à 1778 cm^{-1}) à celle de l'acide heptanoïque (mesurée à 1710 cm^{-1}) en fonction du temps de photo-oxydation: température de la phase liquide 3 °C, spectres de solutions à 10% dans CCl_4: (*1*) heptanal pur, (*2*) mélange heptanal (6.7 mol l^{-1}) – 1-hexanol (0.7 mol l^{-1}), (*3*) mélange heptanal (6.7 mol l^{-1}) – 3-méthyl 3-pentanol (0.7 mol l^{-1}), (*4*) mélange heptanal (6.7 mol l^{-1}) – cyclohexanol (0.6 mol l^{-1}), (*5*) mélange heptanal (3.7 mol l^{-1}) – 3-méthyl 3-pentanol (4 mol l^{-1}), (*6*) mélange heptanal (4.8 mol l^{-1}) – cyclohexanol (2.3 mol l^{-1}) cellule infrarouge: épaisseur 0.052 mm.

aldéhyde en présence de 2-pentanol (des résultats identiques ont été obtenus avec d'autres alcools: 1-hexanol, cyclohexanol, etc. . . .), montrent que: (*i*) l'acide perheptanoïque est présent en quantité stationnaire très faible en présence de 2-pentanol; (*ii*) la décomposition thermique du peroxyde X, formé dans la réaction d'une molécule d'acide perheptanoïque avec une molécule d'heptanal, en présence d'alcools, conduit à la formation de deux molécules d'acide heptanoïque, produit final de l'oxydation. Par ailleurs, la fig. 1 montre que les variations du rapport de la densité optique du peroxyde X à celle de l'acide heptanoïque est une fonction décroissante du temps de photo-oxydation; ce rapport est d'autant plus petit, pour un même temps d'irradiation, que la concentration d'alcool primaire ou secondaire est plus grande.

Ainsi, en présence d'alcools, l'acide heptanoïque n'est jamais le produit primaire de l'oxydation. Il apparaît donc que la réaction globale d'oxydation de l'heptanal n'est pas modifiée chimiquement par la présence d'alcools: (*i*) le produit primaire de l'oxydation est l'acide perheptanoïque; (*ii*) le peracide donne ensuite, par une réaction d'addition avec l'aldéhyde, et non avec l'alcool, le peroxyde X:

$$C_6H_{13}CO_3H + C_6H_{13}CHO \rightleftharpoons$$

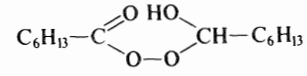

(*iii*) la décomposition du peroxyde X, conduit à deux molécules d'acide heptanoïque, produit final de la réaction:

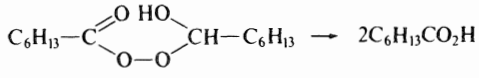

Etude cinétique de l'influence d'alcools primaires et secondaires sur l'oxydation de l'heptanal amorcée photochimiquement a l'instant initial

Pour réaliser les expériences d'inhibition de la photo-oxydation de l'heptanal par les alcools avec une précision suffisante, nous nous sommes placés dans le cas où la vitesse d'amorçage des chaînes est la plus grande possible, c'est-à-dire en présence de fortes concentrations d'aldéhyde (6). On étudie alors l'inhibition de l'oxydation de l'aldéhyde en présence d'alcools dans le cas où la concentration stationnaire des radicaux C_6H_{13}-CO· (R·) est supérieure à celle des radicaux peroxy $C_6H_{13}CO_3$· (RO_2·).

Nous avons utilisé la nomenclature employée dans un article théorique et général de co-oxydation (7), c'est-à-dire que RH représente l'heptanal, R′H l'inhibiteur, V_{O_2} la vitesse à l'instant initial d'oxydation globale du mélange de co-oxydation, représentée par $(d[O_2]/dt)_{t=0}$, V_{RH} la vitesse initiale d'oxydation de RH en l'absence de R′H, toutes autres choses égales par ailleurs.

Conditions expérimentales

Les expériences ont été effectuées entre 3 et 30 °C, à des pressions d'oxygène P_{O_2} surmontant la phase liquide, comprises entre 50 et 450 torr, avec de l'heptanal pur ou en solution dans le décane, en présence ou non d'alcool. Au cours d'une série de manipulations de photo-oxydation, on fait varier [R′H] en maintenant [RH] sensiblement constante pour éviter une variation importante de la vitesse d'amorçage des chaînes (*cf.* réf. 6 par exemple).

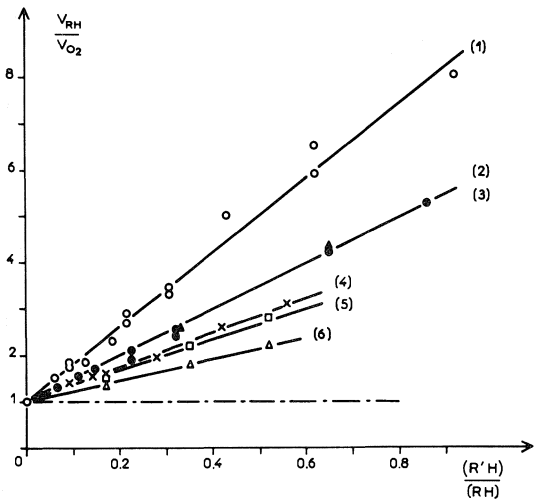

FIG. 2. Variations de V_{RH}/V_{O_2} avec [R'H]/[RH]. Inhibition de la photo-oxydation de l'heptanal par des alcools: température de la phase liquide $\theta = 5$ °C, [RH] = 5 mol l^{-1}, $P_{O_2} = 450$ torr, irradiation 313 nm: ○ 2-pentanol, ▲ 2-propanol, ● cyclohexanol, × 3-octanol, □ 2,2,4-triméthyl 3-pentanol, △ 2,4-diméthyl 3-hexanol.

Efficacités relatives des alcools et de l'hydroquinone dans l'inhibition de la photo-oxydation de l'heptanal

Nous avons comparé préalablement l'efficacité des alcools primaire (1-hexanol), secondaires (2-pentanol, 2-propanol, cyclohexanol, 3-octanol, 2,2,4-triméthyl 3-pentanol, 2,4-diméthyl 3-hexanol) et de l'hydroquinone pour l'inhibition de la photo-oxydation de l'heptanal à l'instant initial. Comme le montrent les résultats expérimentaux présentés sur la fig. 2, V_{RH}/V_{O_2} varie linéairement avec [R'H]/[RH] selon la loi:

$$\frac{V_{RH}}{V_{O_2}} = 1 + E_I \frac{[R'H]}{[RH]}$$

où E_I est l'efficacité d'inhibition que l'on peut définir plus généralement comme la pente à l'origine de la courbe représentative des variations de V_{RH}/V_{O_2} en fonction de [R'H]/[RH].

Le tableau 1 montre que les efficacités d'inhibition des alcools primaires et secondaires sont voisines et très inférieures à celle de l'hydroquinone (qui est un inhibiteur classique d'oxydations radicalaires en chaîne).

L'efficacité d'inhibition dépend essentiellement de l'encombrement stérique qui existe au voisinage de l'atome d'hydrogène mobile de l'alcool et non de l'effet inductif créé par les atomes de carbone au voisinage de cet atome d'hydrogène (conduisant à un effet opposé en diminuant l'énergie d'arrachement de l'atome d'hydrogène mobile).

TABLEAU 1. Efficacité d'inhibition (E_I) des alcools et de l'hydroquinone*

R'H	E_I
Décane	0
Hydroquinone	20 000
1-Hexanol†	7.5
2-Pentanol†	8
2-Propanol†	5
Cyclohexanol†	5
3-Octanol†	3.7
2,2,4-Triméthyl 3-pentanol	3.3
2,4-Diméthyl 3-hexanol	2.4

*Conditions expérimentales: [RH] = 5 mol l^{-1}, $\theta = 5$ °C, $P_{O_2} = 450$, amorçage photochimique (irradiation 313 nm).

†Les résultats relatifs aux inhibiteurs marqués ont déjà été rapportés dans une note préliminaire (3).

Nous ne considérerons, dans la suite de ce travail, que les inhibitions par le 2-pentanol et le cyclohexanol.

Influence de l'intensité lumineuse absorbée

Par interposition de grilles optiques entre la lampe et le réacteur, on modifie l'intensité lumineuse absorbée I_a (et donc la vitesse d'amorçage, proportionnelle à I_a) dans le mélange réactionnel. Dans une note préliminaire (3) nous avons déjà rapporté l'étude de *l'ordre n* par rapport à l'intensité lumineuse absorbée I_a; cet ordre n peut être défini par:

$$V_{O_2} = \alpha I_a^n$$

où α est un coefficient indépendant de I_a. Dans les inhibitions par le cyclohexanol et le 2-pentanol, nous avons alors montré que l'ordre n croît de 0.5 à pratiquement 1 quand [R'H]/[RH] augmente de 0 à environ 1.3.

Influence de la pression d'oxygène

Quand la pression d'oxygène surmontant la phase liquide décroît de 450 à 50 torr, l'efficacité d'inhibition (E_I) du cyclohexanol décroît. Ce résultat est illustré sur la fig. 3 et par le tableau 2.

Influence de la température

A intensité absorbée constante, nous avons étudié l'influence de la température sur V_{O_2}/V_{RH} pour différentes valeurs du rapport [R'H]/[RH], R'H étant le 2-pentanol. Il apparaît que l'effi-

Can. J. Chem. Downloaded from www.nrcresearchpress.com by 210.87.254.6 on 09/05/12
For personal use only.

Can. J. Chem. Downloaded from www.nrcresearchpress.com by 210.87.254.6 on 09/05/12
For personal use only.

TABLEAU 2. Variation de l'efficacité d'inhibition E_I du cyclohexanol avec la pression d'oxygène*

P_{O_2} (torr)	E_I
50	0.5
150	1.5
450	5

*Conditions expérimentales: [RH] = 4.5 mol l^{-1}, θ = 4.5 °C, amorçage photochimique (irradiation 313 nm).

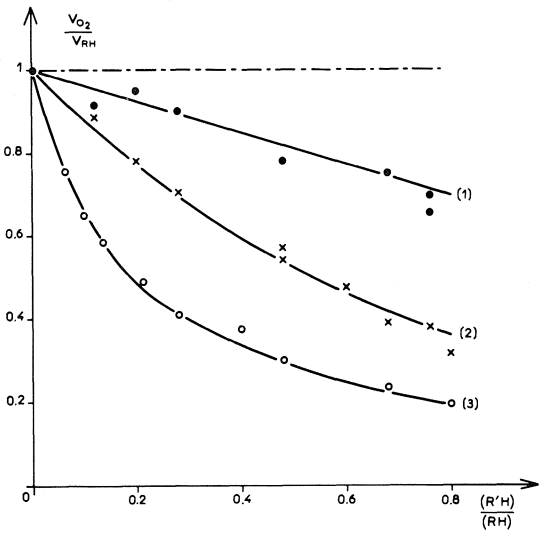

FIG. 3. Influence de la pression d'oxygène P_{O_2} sur les variations de V_{O_2}/V_{RH} avec [R'H]/[RH] dans le cas de la photo-oxydation de l'heptanal en présence de cyclohexanol: température de la phase liquide θ = 4.5 °C, [RH] = 4.5 mol l^{-1}, irradiation 313 nm: (*1*) P_{O_2} = 50 torr, (*2*) P_{O_2} = 150 torr, (*3*) P_{O_2} = 450 torr.

cacité d'inhibition (E_I) diminue quand la température augmente.

Nous avons représenté la variation du logarithme de la pente de (V_{RH}/V_{O_2}) en fonction de l'inverse de la température $1/T$ (K^{-1}) sur la fig. 4.

La valeur de la pente de la droite obtenue conduit à une "énergie d'activation" égale à −8.5 kcal/mol, quand on emploie le 2-pentanol comme inhibiteur; [RH] = 4.5 mol l^{-1}, P_{O_2} = 445 torr, amorçage photochimique (irradiation 313 nm).

Interpretation des résultats obtenus

Il est possible, à priori, d'interpréter l'inhibition de l'oxydation de l'heptanal par des alcools

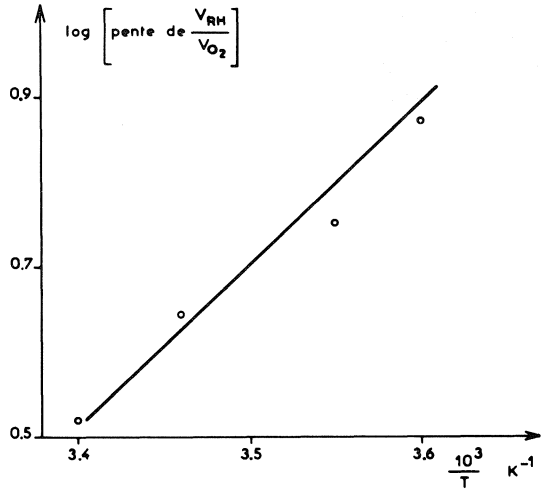

FIG. 4. Influence de la température sur la photo-oxydation de l'heptanal en présence de 2-pentanol. Variations de log (pente de V_{RH}/V_{O_2}) avec $10^3/T$ (K^{-1}): [RH] = 4.5 mol l^{-1}, P_{O_2} = 445 torr, irradiation 313 nm.

à partir du mécanisme général de cooxydation, que nous avons proposé (7):

Amorçage

Production de radicaux libres R· avec une vitesse $2v$

Propagation (I)

[2] $$R\cdot + O_2 \xrightarrow{k_2} RO_2\cdot$$

[3] $$RO_2\cdot + RH \xrightarrow{k_3} RO_2H + R\cdot$$

Propagation (II)

[2'] $$R'\cdot + O_2 \xrightarrow{k_{2'}} R'O_2$$

[3'] $$R'O_2\cdot + R'H \xrightarrow{k_{3'}} R'O_2H + R'\cdot$$

Croisements

[4 & 4'] $$R\cdot + R'H \underset{k_{4'}}{\overset{k_4}{\rightleftarrows}} RH + R'\cdot$$

[5] $$RO_2\cdot + R'H \xrightarrow{k_5} RO_2H + R'\cdot$$

[5'] $$R'O_2\cdot + RH \xrightarrow{k_{5'}} R'O_2H + R\cdot$$

Terminaison

Destructions, deux à deux, des radicaux R·, R'·, $RO_2\cdot$ et $R'O_2\cdot$.

Dans le cas de la co-oxydation heptanal-alcools, ce schéma cinétique appelle les remarques suivantes:

(*a*) Le schéma cinétique proposé admet une

Can. J. Chem. Downloaded from www.nrcresearchpress.com by 210.87.254.6 on 09/05/12
For personal use only.

certaine stabilité des radicaux $R'O_2\cdot$. Or, nous avons montré que (8, 9) dès 3 °C, les radicaux $R'O_2\cdot$ impliqués dans l'oxydation du cyclohexanol participent à deux processus compétitifs, l'un étant la décomposition thermique de ces radicaux en cyclohexanone et $HO_2\cdot$, l'autre étant une extraction d'un atome d'hydrogène mobile du cyclohexanol pour conduire à l'α-hydroxyhydroperoxyde et à un radical α-hydroxy.

Par ailleurs, dans le cas du 2-pentanol, on n'observe pratiquement pas d'α-hydroxyhydroperoxyde primaire, les radicaux $R'O_2\cdot$ du 2-pentanol étant certainement plus instables (9).

Si l'on tient compte de l'instabilité des radicaux $R'O_2\cdot$, les processus [2′], [3′] et [5′] sont remplacés par les processus suivants:

$$R'\cdot + O_2 \rightarrow \text{Cétone ou aldéhyde} + HO_2\cdot$$

$$HO_2\cdot + R'H \rightarrow H_2O_2 + R'\cdot$$

$$HO_2\cdot + RH \rightarrow H_2O_2 + R\cdot$$

Il apparaît alors que $HO_2\cdot$ joue le rôle du radical $R'O_2\cdot$ et donc que les conséquences cinétiques de ce mécanisme ne sont pas modifiées notablement quand on tient compte de l'instabilité des radicaux $R'O_2\cdot$.

(*b*) Le processus [4′], possible énergétiquement, a une importance négligeable, car la concentration quasi-stationnaire des radicaux $R'O_2\cdot$ (ou $HO_2\cdot$) est très supérieure à celle des radicaux $R'\cdot$. En effet, les radicaux $R'O_2\cdot$ (ou $HO_2\cdot$) s'accumulent dans le milieu réactionnel, car la réaction de ces radicaux avec R′H ou RH (comme nous le verrons ultérieurement) est un processus difficile. Les processus de croisement dont nous tiendrons compte sont donc les processus [4], [5] et [5′]. On ne peut éliminer à priori le processus [4] qui est légèrement endothermique, si la concentration des radicaux $R\cdot$ est très supérieure à celle des radicaux $RO_2\cdot$.

Dans le cas où, au contraire, $[R\cdot]/[RO_2\cdot] \ll 1$, les seuls processus de croisement qui doivent intervenir dans la co-oxydation sont les processus [5] et [5′].

(*c*) La solubilité de l'oxygène peut varier quand on ajoute de l'alcool. En fait, il apparaît que la solubilité de l'oxygène varie peu dans les mélanges hydrocarbures–alcools–aldéhydes ($\pm 20\%$ environ) (10, 11), ce qui ne modifie pas sensiblement les résultats cinétiques de l'inhibition par des alcools de l'oxydation de l'heptanal.

(*d*) En faisant varier la quantité $[RH]/P_{O_2}$, il est possible de se placer, de façon approchée, dans des cas limites simples, où le processus de terminaison prépondérant, pour l'oxydation de l'heptanal seul, est soit la destruction de deux radicaux $R\cdot$, soit la destruction de deux radicaux $RO_2\cdot$.

(*A*) *Etude du mécanisme de l'inhibition de la photo-oxydation de l'heptanal par les alcools dans les conditions où* $[R\cdot]/[RO_2\cdot] > 1$ *et* $[R'\cdot]/[R'O_2\cdot] \ll 1$

Remarque préliminaire: stabilité de la vitesse d'amorçage photochimique de l'heptanal en milieu alcoolique

Zeldes et Livingston (12) ont montré, par résonance paramagnétique, l'existence de radicaux $CH_3—\dot{C}(OH)—CH_3$ et $CH_3—\dot{C}H(OH)$ provenant de la désactivation chimique de l'acétaldéhyde excité électroniquement, par le 2-propanol. Un phénomène d'inhibition primaire dû à un processus de ce type peut apparaître. Néanmoins, son importance peut être réduite car il y a compétition entre trois processus de désactivation des états excités de l'aldéhyde, à savoir, par l'aldéhyde lui-même (auto-désactivation), l'oxygène et l'alcool. Par ailleurs, les alcools sont des inhibiteurs de l'oxydation thermique de l'heptanal (8); il existe donc aussi une inhibition secondaire, les alcools réagissant avec les radicaux porteurs de chaînes.

Pour évaluer l'importance de ces deux types d'inhibition, on peut faire les remarques suivantes:

(*a*) La compétitivité entre les processus d'auto-désactivation de l'état triplet du benzaldéhyde:

$$[1]\quad C_6H_5—CHO\,(T_1) + C_6H_5—CHO \xrightarrow{k_1} C_6H_5—\dot{C}H(OH) + C_6H_5CO\cdot$$

et de désactivation de cet état par un alcool R′H:

$$[1']\quad C_6H_5—CHO\,(T_1) + R'H \xrightarrow{k_{1'}} C_6H_5—\dot{C}H(OH) + R'\cdot$$

a été déterminée par Bäckström et Åquist (13) qui ont utilisé, comme substances R′H, le 2-propanol ou l'alcool benzylique.

Le rapport des constantes $k_1/k_{4'}$ a été évalué à 15 dans le cas du 2-propanol et à 4.6 dans le cas de l'alcool benzylique. L'heptanal se comportant, du point de vue amorçage, de façon voisine du

Can. J. Chem. Downloaded from www.nrcresearchpress.com by 210.87.254.6 on 09/05/12
For personal use only.

benzaldéhyde, on peut admettre un rapport des constantes $k_1/k_{4'}$ du même ordre que celui calculé quand on utilise le 2-pentanol comme désactivant. Dans ce cas, la vitesse d'amorçage n'est modifiée que de 7% quand les concentrations en aldéhyde et en alcool sont égales.

(*b*) Les alcools sont transparents à 313 nm; ils ne modifient donc pas l'intensité lumineuse absorbée par l'heptanal.

(*c*) Lorsque l'on induit l'oxydation de l'heptanal en présence d'alcools par le biacétyle B excité dans son premier état singulet, les résultats cinétiques obtenus sont en tout point comparables aux résultats cinétiques de l'étude de l'inhibition de la photo-oxydation de l'heptanal par les alcools. Or, dans ce cas, les alcools ne peuvent pas modifier la vitesse d'induction, car la vitesse du processus:

$$T_1{}^B + R'H \rightarrow CH_3{-}CO{-}\dot{C}(OH){-}CH_3 + R'\cdot \quad (14)$$

représente moins de 1% de la vitesse de formation des radicaux libres par le processus:

$$T_1{}^B + O_2 \rightarrow \text{Radicaux libres}^1$$

quand $P_{O_2} = 450$ torr et $[R'H] = 4$ mol l^{-1}.

En conséquence, on pourra considérer que la vitesse d'amorçage photochimique v dans l'oxydation de l'heptanal en présence d'alcools est sensiblement égale à v_0, vitesse d'amorçage photochimique dans l'oxydation de l'heptanal seul, toutes choses égales par ailleurs.

Mécanisme de l'inhibition de la photo-oxydation de l'heptanal par les alcools $[R\cdot]/[RO_2\cdot] > 1$ *et* $[R'\cdot]/[R'O_2\cdot] \ll 1$

Dans le cas limite où la concentration des radicaux R· est supérieure à celle des radicaux $RO_2\cdot$, les processus de terminaison prépondérants sont:

Terminaison

$$[6] \quad R\cdot + R\cdot \xrightarrow{k_6}$$
$$[9] \quad R\cdot + R'O_2\cdot \xrightarrow{k_9} \quad \text{Produits stables}$$
$$[8''] \quad R'O_2\cdot + R'O_2\cdot \xrightarrow{k_{8''}}$$

[1]En solution dans le décane, nous avons déterminé la valeur de la constante d'inhibition par l'oxygène du premier état singulet du biacétyle; elle vaut à 20 °C, 1.8×10^9 l mol^{-1} s^{-1}. Compte tenu de la valeur de la durée de vie de cet état (10^{-8} s (15, 16)) et de la solubilité de l'oxygène dans le solvant, pour une pression de 450 torr, la désactivation de cet état par O_2 est de l'ordre de 7%. Dans ces conditions, pratiquement tous les radicaux libres proviennent de $T_1{}^B$.

Ce cas limite est sensiblement atteint aux fortes valeurs de $[RH]/P_{O_2}$ ($[RH]/P_{O_2} > 10^{-2}$ mol l^{-1} torr^{-1}) et alors:

$$[II] \quad \frac{[R\cdot]}{[RO_2\cdot]} = \frac{k_3[RH] + k_5[R'H]}{k_2[O_2] + k_4[R'H]}$$

Si l'on admet tout d'abord que le processus [4] est négligeable devant le processus [5], $[R\cdot]/[RO_2\cdot]$ étant alors une fonction croissante de R'H, il n'y a pas de modifications, quand [R'H]/[RH] augmente, des processus de terminaison prépondérants.

$$[III] \quad \frac{V_{RH}}{V_{O_2}} \simeq 1 + \frac{V_{RH}}{2v}\frac{k_5[R'H]}{k_3[RH]}$$

Expérimentalement, V_{RH}/V_{O_2} varie linéairement avec [R'H]/[RH] (*cf.* fig. 2) selon:

$$[I] \quad \frac{V_{RH}}{V_{O_2}} = 1 + E_I\frac{[R'H]}{[RH]}$$

$R'O_2\cdot$ doit donc être un radical sensiblement inactif vis-à-vis de RH et de R'H; $R'O_2\cdot$ disparaît alors essentiellement par les processus de terminaison [9] et [8'']. *Si maintenant on admet que le processus [5] est négligeable devant le processus [4]* et si $R'O_2\cdot$ est pratiquement inactif, on obtient la relation suivante:

$$[IV] \quad \frac{V_{RH}}{V_{O_2}} \simeq 1 + \frac{V_{RH}}{2v}\frac{k_4[R'H]}{k_2[O_2]}$$

On ne peut différencier ces deux possibilités qu'en examinant l'influence de la pression d'oxygène sur V_{RH}/V_{O_2}: V_{RH} étant proportionnelle à $[O_2]$ ($V_{RH} = v^{1/2}(k_2[O_2]/k_6{}^{1/2})$ dans nos conditions expérimentales et si le processus [5] est prépondérant devant le processus [4], V_{RH}/V_{O_2} doit être une fonction croissante de $[O_2]$.

Par contre, si le processus [4] est prépondérant devant le processus [5], V_{RH}/V_{O_2} doit être indépendant de $[O_2]$.

Or le tableau 3 et la fig. 3 montrent que V_{RH}/V_{O_2} est une fonction croissante de $[O_2]$: ce résultat implique que, malgré un rapport $[R\cdot]/[RO_2\cdot] > 1$, le processus [4] est un processus d'importance négligeable par rapport à celle du processus [5] et donc que V_{RH}/V_{O_2} peut s'écrire sous la forme III.

(*i*) *Influence de l'intensité lumineuse absorbée* I_a—L'ordre n par rapport à la vitesse d'amorçage

Can. J. Chem. Downloaded from www.nrcresearchpress.com by 210.87.254.6 on 09/05/12
For personal use only.

photochimique (proportionnelle à I_a)[2] a été calculé (3, 8):

$$[V] \quad n = \frac{1}{2}\left[1 + \left(1 + \frac{2v}{V_{RH}}\frac{k_3}{k_5}\frac{[RH]}{[R'H]}\right)^{-1}\right]$$

On s'attend donc à ce que n soit une fonction croissante de [R'H]/[RH]: n est égal à 0.5 pour [R'H]/[RH] = 0 et tend vers 1 quand [R'H]/[RH] augmente indéfiniment. Les résultats expérimentaux rapportés dans la référence 3 montrent qu'il en est bien ainsi. Ce résultat confirme à nouveau le fait que le processus [5'] est un processus d'importance négligeable par rapport aux processus de terminaison des chaînes.

(*ii*) *Estimation de* k_5/k_3—Sachant que, à θ = 5 °C et P_{O_2} = 450 torr, E_I = 8 quand R'H est le 2-pentanol, $v \simeq 25 \times 10^{-8}$ mol l^{-1} s^{-1}, $V_{RH} \simeq 10^{-3}$ mol l^{-1} s^{-1}; alors:

$$k_5/k_3 \simeq 4 \times 10^{-3} \quad \text{à} \quad \theta = 5\ °C$$

Il apparaît donc que la réactivité de RO_2· vis-à-vis de R'H est 250 fois plus faible que la réactivité de ce même radical vis-à-vis de RH.

Remarque: Si l'on tient compte de tous les processus impliqués dans la co-oxydation, l'expression de V_{O_2}/V_{RH} est la suivante (7):

$$[VI] \quad \frac{V_{O_2}}{V_{RH}} = \frac{1 + \dfrac{2k_5}{k_3}\dfrac{[R'H]}{[RH]} + \dfrac{k_5}{k_3}\dfrac{k_{3'}}{2v^{1/2}k_{8''}^{1/2}}\dfrac{[R'H]^2}{[RH]}}{1 + \dfrac{k_5}{k_3}\dfrac{V}{2v}\dfrac{[R'H]}{[RH]}}$$

Dans les expériences d'inhibition que nous avons réalisées, les mesures ont été effectuées dans le cas où [R'H]/[RH] < 1. Le terme $2k_5[R'H]/k_3[RH]$ est donc inférieur à 8×10^{-3}.

Par ailleurs, sachant que:

$$k_{3'}[R'H] \simeq v^{1/2}k_{8''}^{1/2} \quad (8, 9)$$

$$\frac{k_5}{k_3}\frac{k_{3'}[R'H]^2}{2v^{1/2}k_{8''}^{1/2}[RH]} \simeq \frac{k_5}{2k_3}\frac{[R'H]}{[RH]} < 2 \times 10^{-3}$$

ainsi, on fait une erreur inférieure à 1% quand on remplace l'inverse de l'expression générale écrite plus haut par III.

(*iii*) *Influence de la température*—Nous avons montré sur la fig. 4 que l'efficacité d'inhibition E_I est d'autant plus grande que la température θ est plus faible. Or:

$$[VII] \quad E_I \simeq \frac{V_{RH}}{2v}\frac{k_5}{k_3} \simeq \frac{k_2[O_2]}{2v^{1/2}k_6^{1/2}}\frac{k_5}{k_3}$$

Compte tenu de:

$$E_2 - \tfrac{1}{2}E_6 - Q \simeq 0.5 \pm 1 \text{ kcal/mole}^3 \quad (4,7)$$

$$E_3 \simeq 4.5 \pm 0.5 \text{ kcal/mole}$$

$$E(E_I) \simeq -8.5 \pm 1 \text{ kcal/mole}$$

$$E_v \simeq 8 \pm 2 \text{ kcal/mole}$$

(E_v représente l'énergie d'activation de la vitesse d'amorçage (8, 17, 18)) alors:

$$E_5 \simeq -0.5 \pm 3.5 \text{ kcal/mole}$$

Malgré l'imprécision sur la détermination de E_5, il apparaît que l'énergie d'activation correspondant à la réaction [5] est légèrement négative et inférieure à E_3, résultat qu'on ne peut expliquer si l'on considère que [5] est un processus élémentaire car, compte tenu des énergies de dissociation de R—H et R'—H (19), on devrait obtenir $E_5 > E_3$.

Si maintenant, on considère que [5] n'est plus un processus élémentaire, mais un ensemble de processus faisant intervenir un complexe par liaison hydrogène entre les radicaux libres issus de l'aldéhyde et l'alcool[4] l'interprétation des résultats obtenus devient possible.

Pour valider cette hypothèse, nous avons entrepris une étude annexe (8, 20) de l'inhibition de la photo-oxydation de l'heptanal par l'eau qui met en évidence uniquement le rôle des liaisons hydrogène qui peuvent s'établir entre les groupements hydroxyle et les radicaux libres porteurs de chaînes de l'aldéhyde. On montre alors que la solvatation des radicaux libres porteurs de chaînes par l'eau entraîne une diminution de la reactivité de ceux-ci vis-à-vis, soit de l'aldéhyde, soit de l'oxygène, et favorise les processus de rupture.

Le processus [5] n'est donc pas un processus élémentaire et l'on peut interpréter ce résultat expérimental en considérant que le radical RO_2·

[2] I_a est l'intensité lumineuse absorbée par l'heptanal (irradiation 313 nm), proportionnelle à la vitesse d'amorçage.

[3] Q représente alors la chaleur de dissolution de l'oxygène dans la solution.

[4] Cette hypothèse a déjà été formulée par Durup (1) pour interpréter l'inhibition par des alcools de l'oxydation du cumène.

forme avec l'alcool un complexe par liaison hydrogène:

$$RO_2\cdot + R'H \overset{K}{\rightleftarrows} (RO_2\cdot \ldots R'H)$$

et en supposant que le complexe se transforme chimiquement en donnant un radical R'· et une molécule de peracide RO_2H

$$[5''] \qquad (RO_2\cdot \ldots R'H) \xrightarrow{k_{5''}} RO_2H + R'\cdot$$

Si l'on admet, en première approximation, que $RO_2\cdot$ et $(RO_2\cdot \ldots R'H)$ sont deux formes en équilibre, alors:

$$[IX] \qquad k_5 \simeq Kk_{5''}$$

Or, une élévation de température défavorise la formation du complexe par liaison hydrogène entre alcool et $RO_2\cdot$, ce qui explique une valeur de E_5 légèrement négative.

Par ailleurs, si l'association entre radicaux libres porteurs de chaînes de l'oxydation de l'heptanal et l'eau entraîne une diminution de l'efficacité des processus de propagation des chaînes et (ou) favorise les processus de rupture des chaînes, en présence d'alcools, on peut assister à: (*i*) une diminution de k_5 (les radicaux $R'O_2\cdot$ étant eux aussi solvatés par l'alcool, leur réactivité vis-à-vis de RH doit diminuer); (*ii*) une augmentation de $k_{8''}$. L'attaque de RH par un radical $R'O_2\cdot$ ou $HO_2\cdot$ qui est, en l'absence d'association, un processus difficile (60 fois plus faible au moins que l'attaque de RH par $RO_2\cdot$ (21)) est donc encore plus difficile quand interviennent des liaisons hydrogène entre alcool et radicaux porteurs de chaînes.

De plus, les radicaux $RO_2\cdot$ et R· étant solvatés par l'alcool, leur réactivité vis-à-vis respectivement de RH (qui peut aussi former un complexe par liaison hydrogène avec l'alcool) et de O_2 doit également diminuer.

1. M. Durup. J. Chim. Phys. **63**, 476 (1966).
2. J. B. Farmer et C. A. McDowell. Trans. Faraday Soc. **47**, 624 (1951).
3. J. C. André et J. Lemaire. C. R. Acad. Sci. Ser. C, **272**, 1396 (1971).
4. J. Lemaire. Thèse de Doctorat ès Sciences, Université de Nancy, Nancy. 1964.
5. J. C. André, J. F. Large, X. Deglise, J. Lemaire, et M. Niclause. Rev. Inst. Fr. Pét. **23**, 219 (1968).
6. J. C. André, F. Baronnet, J. Lemaire, et M. Niclause. J. Chim. Phys. **68**, 1177 (1971).
7. J. C. André, F. Baronnet et J. Lemaire. Rev. Inst. Fr. Pét. **29**, 813 (1974).
8. J. C. André. Thèse de Doctorat ès Sciences, Université de Nancy, Nancy. 1971.
9. J. C. André et J. Lemaire. Bull. Soc. Chim. Fr. 4231 (1969).
10. J. Landolt et L. Börnstein. Zahlenwerte und Funktionen aus Physik-Chemie-Astronomie-Geophysik und Technik. Sechste Auflage, **2** (2ième partie). Springer Verlag, Heidelberg. 1962. pp. 1–164.
11. H. Stephen et T. Stephen. Solubilities of inorganic and organic compounds. Pergamon Press, London. 1963. p. 569.
12. H. Zeldes et R. Livingston. J. Chem. Phys. **47**, 1465 (1967).
13. H. L. J. Bäckström et C. F. Åquist. Acta Chem. Scand. **24**, 1431 (1970).
14. H. L. J. Bäckström et K. Sandros. Acta Chem. Scand. **12**, 823 (1958); **14**, 48 (1960).
15. L. C. Anderson et C. S. Parmenter. J. Chem. Phys. **52**, 466 (1970).
16. P. G. Turro et R. Engel. J. Am. Chem. Soc. **91**, 7113 (1969).
17. J. C. André, M. Bouchy, J. Lemaire et M. Niclause. C. R. Acad. Sci. Ser. C, **272**, 1192 (1971).
18. J. C. André, M. Bouchy et M. Niclause. J. Photochem. **5**, 1 (1976).
19. J. A. Kerr. Chem. Rev. **66**, 465 (1966).
20. J. C. André, M. Bouchy et J. Lemaire. C. R. Acad. Sci. **280**, 1065 (1975).
21. G. E. Zaikov, J. A. Howard et K. U. Ingold. Can. J. Chem. **47**, 3017 (1969).

Can. J. Chem. Downloaded from www.nrcresearchpress.com by 210.87.254.6 on 09/05/12
For personal use only.

Isomérisation du *cis*-butène-2 photosensibilisée par le soufre hexafluoré dans l'ultraviolet à vide[1]

HÉLÈNE GAGNON-DESLAURIERS ET GUY J. COLLIN

Département des Sciences Pures, Université du Québec à Chicoutimi, Chicoutimi (Qué.), Canada G7H 4L9

Reçu le 27 février 1976

HÉLÈNE GAGNON-DESLAURIERS et GUY J. COLLIN. Can. J. Chem. **54**, 2296 (1976).

Le *cis*-butène-2 a été photolysé à 8.44, 8.44–9.56 et 10.03 eV en présence de SF_6 et de divers additifs. Une importante isomérisation est observée à 10.03 eV: Φ(*trans*-butène-2) est de l'ordre de 500. A 8.44 eV, ce rendement est de l'ordre de l'unité. Un mécanisme en chaîne amorçé par des atomes d'hydrogène excité est proposé pour rendre compte de la majorité des effets observés. Bien que nous n'ayons pas pu identifier définitivement le porteur de chaîne, ni écarter la possibilité d'un amorçage partiel ionique à 10.03 eV, le porteur de chaîne est un dérivé du SF_6, possiblement le radical SF_5.

HÉLÈNE GAGNON-DESLAURIERS and GUY J. COLLIN. Can. J. Chem. **54**, 2296 (1976).

cis-2-Butene has been photolysed at 8.44, 8.44–9.56, and 10.03 eV in the presence of SF_6 and of several other additives. A major isomerization process is observed at 10.03 eV: Φ(*trans*-butene-2) $\simeq$ 500. At 8.44 eV this yield is of the order of unity. A chain mechanism initiated by kinetically excited hydrogen atoms is proposed to explain the observed effects. Although we were unable either to identify the chain carrier with certainty or to eliminate the possibility of an ionic initiation at 10.03 eV, the chain carrier is a derivative of SF_6, possibly the SF_5 radical.

Introduction

Le soufre hexafluoré est un additif couramment utilisé en radiolyse comme intercepteur d'électrons (1, 2). Son usage est d'autant plus aisé qu'il est pratiquement inerte envers les autres réactifs chimiques et ses effets secondaires sont ainsi très limités. Cependant, il induit l'isomérisation *cis–trans* du butène-2 (3, 4), isomérisation également observée en photoionisation (4, 5). Nous avons repris cette étude en photochimie de l'ultraviolet à vide afin de mieux préciser la nature du mécanisme réactionnel conduisant à l'isomérisation observée.

Procédure expérimentale

Les techniques photolytiques et analytiques ont déjà été décrites ainsi que la préparation des échantillons (6). Les produits chimiques utilisés ont une pureté supérieure à 99.8% excepté pour le pentadiène-1,3 (97%, Aldrich Chemical Co., Inc.). Le *cis*-butène-2 (CB2) contient moins de 10 ppm de butadiène-1,3 et 110 $\pm$ 10 ppm de *trans*-butène-2. Les réactifs sont dégasés à la température de l'azote liquide avant usage dans un système à vide (10^{-6} torr) muni de robinets sans graisse sauf l'oxygène, les gaz rares et le méthane qui sont utilisés tels que reçus (99.99%, Matheson of Canada). Les lampes utilisées ont aussi été décrites dans la littérature (7). La lampe au xénon est équipée d'une fenêtre en LiF (1 mm) et émet deux raies efficaces: 129.6 nm, 9.56 eV (2%) et 147.0 nm, 8.44 eV (98%). La lampe au krypton est munie d'une fenêtre en CaF_2 et n'émet comme raie efficace que la raie à 123.6 nm, 10.03 eV. Toutes les irradiations ont été faites à la température de la chambre (23 $\pm$ 2 °C). Les rendements obtenus ont été comparés à ceux de l'acétylène et de l'allène afin d'en connaître les rendements quantiques (8). Dans certaines expériences on a mesuré les courants ioniques libérés dans la cellule à l'aide de plaques en nickel reliées à une source de tension continue et variable (9). La cellule d'irradiation a un volume de 1050 $\pm$ 50 cm^3 sauf la cellule utilisée pour mesurer les courants de saturation: 360 $\pm$ 20 cm^3.

[1]Travail subventionné par le Conseil National de Recherches du Canada.

Résultats

A 10.0 eV

Le rendement quantique de l'isomérisation du CB2 en présence de SF_6 est de l'ordre de 100 à 500 dépendant des conditions expérimentales. L'addition progressive d'oxygène tend à faire décroître ce rendement (tableau 1). L'isoméri-

TABLEAU 1. Photolyse du système *cis*-butène-2–SF_6–O_2 (266:10.0:*y* Nm^{-2}) à 123.6 nm[a]

Oxygène (*y*)	Φ(*trans*-C_4H_8-2)
—	440
6.65	390
27	310
54	240
80	200

[a]Temps d'irradiation: 60 min; intensité de la lampe de l'ordre de 10^{12} photon s^{-1}.

Can. J. Chem. Downloaded from www.nrcresearchpress.com by 210.87.254.42 on 09/05/12
For personal use only.

Can. J. Chem. Downloaded from www.nrcresearchpress.com by 210.87.254.42 on 09/05/12
For personal use only.

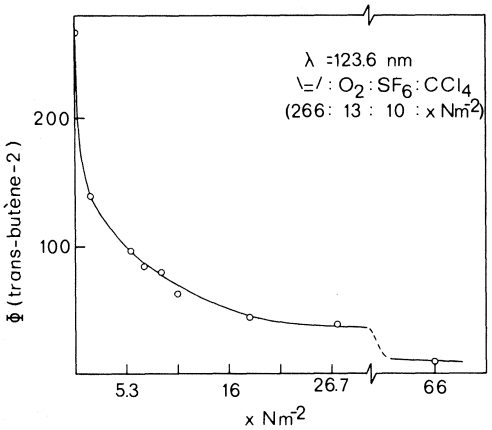

FIG. 1. Rendement quantique du *trans*-butène-2 en présence de CCl_4: $I = 8 \pm 0.8\ 10^{11}$ photon s^{-1}.

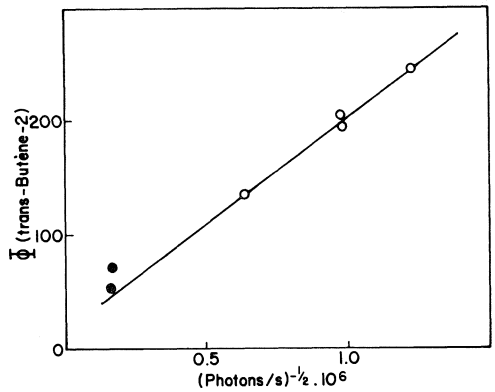

FIG. 2. Rendement quantique du *trans*-butène-2 en fonction de l'inverse de la racine carrée de l'intensité. λ = 123.6 nm; mélange irradié: CB2–SF_6–O_2 (266:10:13 Nm^{-2}).

sation est beaucoup plus sensible à la présence de CCl_4 (fig. 1). L'addition d'amine a un effet négatif de même le pentadiène-1,3 tandis que l'ammoniac et l'oxyde nitreux sont pratiquement sans effet (tableau 2). La quantité de *trans*-butène-2 formé croît linéairement avec le temps d'exposition. Par contre, il décroît lorsque l'intensité de la lampe croît: $\Phi(trans\text{-butène-2}) \simeq \alpha(I)^{-1/2}$ (fig. 2). Enfin, l'addition d'hélium au mélange CB2–O_2–SF_6 (266:13.3:9.3 Nm^{-2}) fait rapidement décroître le rendement de l'isomérisation (fig. 3).

A 8.44–9.56 eV

Les rendements de l'isomérisation sont ici beaucoup plus faibles que ceux mesurés à 10.0 eV (tableau 3). Puisque les deux raies de la lampe peuvent avoir un effet différent, on a éliminé la raie située à 9.56 eV en utilisant le méthane comme filtre gazeux (à 8.44 eV: $\epsilon < 1\ atm^{-1}\ cm^{-1}$ et à 9.56 eV: $\epsilon \simeq 470\ atm^{-1}cm^{-1}$) (10) en

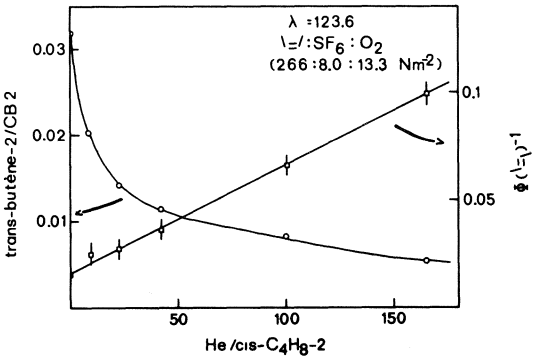

FIG. 3. Rapport final *trans*-butène-2/CB2 et inverse du rendement quantique en *trans*-butène-2 en présence d'hélium. λ = 123.6 nm.

TABLEAU 2. Photolyse du système *cis*-butène-2–O_2–SF_6–additif (266:13.3:10.0:*x* Nm^{-2}) à 123.6 nm[a]

Additif (*x*)	$\Phi(trans\text{-}C_4H_8\text{-}2)$
—	270
N_2O(8.0)	220
NH_3(8.0)	320
CH_3NH_2 (10)	85
$(CH_3)_2NH_2$ (13)	1.5
$(CH_3)_3N$ (10)	1.3
C_5H_8-1,3(4.0)	0.5

[a]Conditions expérimentales identiques à celles du tableau 1.

TABLEAU 3. Photolyse du *cis*-butène-2 (133 Nm^{-2}) en présence d'additifs avec la lampe au xénon[a]

Additifs (Nm^{-2})	Intensité de la lampe	$\Phi(trans\text{-}C_4H_8\text{-}2)$
—	4.5[b]	0.10±0.02
O_2(13.3)	4.0	0.05±0.01
SF_6(13.3)	6.0	0.81±0.06
SF_6(133)	3.0	0.89±0.06
SF_6(13.3) + NH_3(13.3)	4.0	0.84±0.06
O_2(13.3)	2.5	0.21±0.03
CH_4(13300)	4.5	0.08±0.02
Ar(2000)	6.2	0.36±0.04
Ar(13300)	5.0	0.35±0.04
Ar(20000) + O_2(20)	3.3	0.05±0.02

[a]Temps d'irradiation 5 min.
[b]× 10^{14} photon s^{-1}.

Can. J. Chem. Downloaded from www.nrcresearchpress.com by 210.87.254.42 on 09/05/12
For personal use only.

remplissant la première cellule ($P \simeq 500\ Nm^{-2}$) d'une double cellule (11). La seconde cellule contient le mélange CB2–SF_6–O_2 (160:20:20 Nm^{-2}). Lorsque la première cellule est vide il y a possibilité d'ionisation partielle du CB2 puisque son potentiel d'ionisation est de 9.13 eV (12). On a mesuré dans ce cas un courant ionique de l'ordre de 3×10^{-10} A et Φ(*trans*-butène-2) = 0.23 ± 0.02. Lorsque la première cellule contient le méthane, le courant ionique libéré dans la deuxième cellule a décru d'au moins un facteur 20 (limite de détection) et le rendement de l'isomérisation est inchangé. Dans les deux cas, le nombre de photons entrant dans la deuxième cellule est de l'ordre de 2.5×10^{12} photon s^{-1}.

Discussion

A 10.0 eV

La première remarque concerne les rendements élevés de la formation de l'isomère. Comme cela a déjà été observé en radiolyse, l'isomérisation se produit dans un mécanisme en chaîne (3). A 10.0 eV l'énergie incidente est absorbée par le CB2 puisque son coefficient d'absorption est environ cinquante fois plus élevé que celui du SF_6 (9). L'absorption d'un photon conduit soit à la formation de l'ion parent, dont l'énergie interne est insuffisante pour le décomposer, soit à la formation d'une molécule surexcitée qui se fragmente pour donner des produits moléculaires stables (M) et des radicaux et des atomes d'hydrogène (8):

[1] $CB2 + h\nu \rightarrow C_4H_8^+ + e^- \quad \Phi = 0.207$ (9)

[2] $CB2 + h\nu \rightarrow (C_4H_8)^{**} \quad \Phi = 0.793$

[3] $(C_4H_8)^{**} \rightarrow M + R + H\cdot$

L'influence de l'oxygène et du pentadiène-1,3 montre un caractère radicalaire du mécanisme de l'isomérisation. De plus, l'influence des dérivés azotés montre un caractère ionique de cette isomérisation. Ajouté en faibles proportions au CB2, l'oxygène intercepte tous les radicaux thermiques formés dans la fragmentation du CB2 (8). Par contre, on sait qu'il n'empêche pas les réactions des atomes d'hydrogène, en particulier lorsque ceux-ci sont cinétiquement excités. On a déjà montré (voir tableau 3, ref. 8) que de tels atomes d'hydrogène existent à 10.0 eV bien qu'on n'en connaisse ni la quantité, ni la quantité moyenne d'énergie qu'ils transportent (encore moins la distribution de cette énergie). Une réaction d'amorçage de la chaîne cinétique de l'isomérisation en présence de SF_6 serait la suivante, réaction proposée dans la photochimie du méthanol pour expliquer l'effet du SF_6 (13):

[4] $H^* + SF_6 \rightarrow HF + SF_5$

Cette réaction requiert une énergie élevée d'activation: $E_a = 30$ kcal mol^{-1} (14) mais n'est pas impossible dans ce système. L'effet de l'hélium (fig. 3) est intéressant car il est explicable sur la base du ralentissement des atomes d'hydrogène chauds par collision. Il faut quand même retenir que le rendement en atomes d'hydrogène qui véhiculent 30 kcal mol^{-1} d'énergie est probablement bas.

L'alternative à cet amorçage pourrait être une, ou plusieurs, réactions ioniques. Les amines sont relativement insensibles envers les radicaux. Par contre, elles réagissent rapidement avec les ions positifs (15, 16).

[5] $CB2^+ + (CH_3)_2NH \rightarrow C_4H_8 + (CH_3)_2NH^+$

Le remplacement des ions parents $CB2^+$ par des ions amines empêcherait l'isomérisation. Par contre l'ammoniac n'a pas l'effet négatif des amines. Dans ce cas, l'ion parent réagit par transfert de proton (17):

[6] $CB2^+ + NH_3 \rightarrow NH_4^+ + C_4H_7$

[7] $NH_4^+ + nNH_3 \rightarrow NH_4^+(NH_3)_n$

Dans ce cas, le remplacement des ions parents par des ions de type ammonium ne gênerait pas l'isomérisation. L'effet de CCl_4 est aussi intéressant car il peut mettre en cause la présence d'ions négatifs. L'affinité électronique du CCl_4 est plus grande que celle de SF_6 (1) et il intercepte les électrons thermalisés plus rapidement que SF_6: $k(e^- + CCl_4) = 4.0 \times 10^{-7}$ et $k(e^- + SF_6) = 2.2 \times 10^{-7}$ cm^3 $molécule^{-1}$ s^{-1} (18). En négligeant tout autre effet que celui de la capture électronique et en admettant que CCl_4 ne perturbe pas la chaîne cinétique une fois celle-ci amorçée, on obtient la relation

$$\frac{k(e^- + CCl_4)}{k(e^- + SF_6)} = \frac{[SF_6]}{[CCl_4]} \frac{\Phi_0(trans) - \Phi(trans)}{\Phi_0(trans)}$$

où Φ_0(*trans*) et Φ(*trans*) représentent les rendements en *trans*-butène-2 en absence et en présence de CCl_4. Appliquée aux six derniers points de la fig. 1, cette relation donne $k(e^- + CCl_4)/k(e^- + SF_6) = 2.25 \pm 0.30$. Cette valeur est en

Can. J. Chem. Downloaded from www.nrcresearchpress.com by 210.87.254.42 on 09/05/12
For personal use only.

bon accord avec le rapport des deux valeurs précédemment indiquées. Cet accord peut cependant être fortuit. De son côté l'oxyde nitreux ne présente pas d'effet majeur en accord avec le fait que sa vitesse de capture électronique est au moins 10 fois plus faible que celle de SF_6 (1, 18).

Hummel a suggéré que l'interaction entre l'ion SF_6^- et les orbitales π du butène-2 est responsable de l'isomérisation (3):

[8] $\quad CB2 + SF_6^- \rightarrow trans\text{-}C_4H_8\text{-}2 + SF_6^-$

Ce mécanisme est insuffisant car il n'explique pas l'effet observé des amines, du pentadiène, de l'oxygène et de l'hélium bien que la chimie des ions SF_6^- soit loin d'être bien connue. Niedzielski et Gawlowski (4) ont proposé un mécanisme faisant intervenir des ions positifs et négatifs:

[9] $\quad RH^+ + SF_6^- \rightarrow R + HF + SF_5$

[10] $\quad SF_5 + CB2 \rightleftarrows SF_5C_4H_8$

[11] $\quad SF_5C_4H_8 \rightleftarrows SF_5 + trans\text{-}C_4H_8\text{-}2$

La réaction 9 a été proposée en phase liquide (19); quant aux réactions 10 et 11 elles ont été proposées par Sidebottom *et al.* (20) pour expliquer l'addition du chloropentafluorure de soufre sur l'éthylène. Ce mécanisme est intéressant car il met en évidence le rôle des ions positifs et négatifs, et des radicaux dans la période d'initiation et de propagation respectivement. Récemment, Gawlowski et Herman ont montré que la réaction de neutralisation entre l'ion NH_4^+ solvaté et l'ion SF_6^- ne produit des radicaux SF_5 qu'avec de faibles rendements (21):

[12] $\quad NH_4^+(NH_3)_n + SF_6^- \rightarrow SF_5 + \text{produits}$

[13] $\quad C_4H_8^+ + SF_5^- \rightarrow R + HF + SF_5$

Comme il est peu probable que les réactions 12 et 13 aient des rendements similaires en radicaux SF_5, il s'ensuit qu'on devrait s'attendre à une perturbation non négligeable du rendement de l'isomérisation sur addition d'ammoniac. De plus, l'effet de l'hélium ne s'explique pas facilement sur la base des réactions 9–13.

Afin de réconcilier l'effet de l'hélium avec un mécanisme d'amorçage lui-même initié par voie ionique, on peut penser que la réaction de neutralisation produit des atomes d'hydrogène excités. La réaction 9 a été proposé en phase liquide. Etant donné la fréquence de collision beaucoup plus petite en phase gazeuse, il n'est pas impossible d'obtenir des atomes d'hydrogène suffisamment excités:

[14] $\quad C_4H_8^+ + SF_6^- \rightarrow H^* + \text{produits}$

L'isomérisation serait alors entretenue soit directement par les atomes d'hydrogène excités, soit par les radicaux SF_5 produits dans la réaction 4, soit par une autre espèce.

[15] $\quad H^* + CB2 \rightarrow trans\text{-}C_4H_8\text{-}2 + H^*$
$\Delta H = -1.1$ kcal mol^{-1}

Si tel est le cas, et pourvu que le rendement en atome d'hydrogène excité produit dans la réaction 14 soit non-négligeable, on devrait observer un accroissement des rendements en propène et en éthylène (8):

[16] $\quad H + C_4H_8 \rightarrow (s\text{-}C_4H_9)^*$

[17] $\quad (s\text{-}C_4H_9)^* \rightarrow (n\text{-}C_4H_9)^*$

[18] $\quad (C_4H_9)^* + M \rightarrow C_4H_9 + M\ (S_i)$

[19] $\quad (s\text{-}C_4H_9)^* \rightarrow CH_3 + C_3H_6\ (D_s)$

[20] $\quad (n\text{-}C_4H_9)^* \rightarrow C_2H_4 + C_2H_5\ (D_n)$

En photolysant les mélanges *cis*-C_4H_8-2–O_2–He (2.0:0.1:0–300 torr) et *cis*-C_4H_8-2–O_2–SF_6–He (2.0:0.1:0.07:0–300 torr) on obtient les mêmes rendements en éthylène et en propène. Il faut cependant dire qu'à 2.0 torr, on n'est pas dans les meilleures conditions et compte tenu des rapports S_s/D_s et S_n/D_n à cette pression et à cette longueur d'onde, (8) et de l'incertitude expérimentale, le rendement de la réaction 14 peut-être égal au rendement quantique d'ionisation.

A 8.44 eV

Les rendements observés ici sont au moins de deux ordres de grandeur plus faibles que ceux rapportés à 10.0 eV. L'explication des résultats du tableau 3 est compliquée par le fait de la présence de la raie située à 9.56 eV. Les expériences faites avec la double cellule explicitent en particulier le rôle du méthane (voir section Résultats). La suppression de la raie à 9.56 eV, donc l'élimination de l'ionisation du milieu réactionnel, ne diminue pas le rendement de l'isomérisation. Par conséquent, le rôle du méthane, en plus d'absorber la raie la plus énergétique, agit comme déactivant, rôle similaire à celui de l'hélium dans les irradiations à 10.0 eV, bien qu'avec une efficacité moindre. L'efficacité de l'argon, efficacité elle-même moindre que celle du méthane, milite aussi en faveur d'un méca-

nisme où les atomes d'hydrogène excités ont un rôle important. Enfin, la double cellule montre que l'ionisation du milieu réactionnel n'est pas nécessaire à l'isomérisation. Cette isomérisation à 8.44 eV a été observée par Niedzielski et Gawlowski (4*b*). Cependant, étant donné les coefficients d'absorption respectifs des deux composés (9), et le mélange irradié, le SF_6 pouvait absorber jusqu'à 80% des photons incidents et former ainsi directement, par décomposition de la molécule $(SF_6)^{**}$ photoexcitée, le radical SF_5 ou tout autre porteur de chaîne.

1. G. R. Freeman. Radiat. Res. Rev. **1**, 1 (1974).
2. Y. Hatano et H. Shimamori. J. Phys. Chem. **78**, 954 (1974).
3. R. W. Hummel. Nature, **218**, 1050 (1968).
4. (*a*) J. Niedzielski et J. G. Gawlowski. Int. J. Radiat. Phys. Chem. **5**, 239 (1973); (*b*) J. Phys. Chem. **77**, 2853 (1973).
5. P. Ausloos, L. Hellner, S. G. Lias et L. W. Sieck. J. Res. Natl. Bur. Stand. Sect. A, **76**, 115 (1972).
6. G. J. Collin, P. M. Perrin et C. M. Gaucher. Can. J. Chem. **50**, 2391 (1972).
7. R. Gorden, Jr., R. E. Rebbert et P. Ausloos. Natl. Stand. Ref. Data Ser. Natl. Bur. Stand. Note Tech. 496 (1969).
8. G. J. Collin et P. M. Perrin. Can. J. Chem. **50**, 2823 (1972).
9. C. Bertrand, G. J. Collin et H. Gagnon. J. Chim. Phys. 719 (1975).
10. H. Okabe et D. A. Becker. J. Chem. Phys. **39**, 2549 (1963).
11. R. Gorden, Jr., R. Doepker et P. Ausloos. J. Chem. Phys. **44**, 373 (1966).
12. K. Watanabe, T. Nakayama et J. Mottl. J. Quant. Spectrosc. Radiat. Transfer, **2**, 369 (1962).
13. J. Hagège, P. C. Roberge et C. Vermeil. Ber. Bunsenges. Phys. Chem. **72**, 138 (1968); Trans. Faraday Soc. **64**, 3288 (1968).
14. N. Fenimore et C. Jones. Combust. Flame, **8**, 231 (1964).
15. L. W. Sieck, S. K. Searles et P. Ausloos. J. Am. Chem. Soc. **91**, 7627 (1969); S. G. Lias et P. Ausloos. J. Am. Chem. Soc. **92**, 1840 (1970).
16. P. S. Gill, Y. Inel et G. G. Meisels. J. Chem. Phys. **54**, 2811 (1971).
17. L. W. Sieck, R. Gorden, Jr. et P. Ausloos. J. Am. Chem. Soc. **94**, 7157 (1972).
18. K. Mori, K. Ito et Y. Hatano. J. Phys. Chem. **79**, 2093 (1975).
19. J. W. F. Van Ingen et W. A. Cramer. J. Phys. Chem. **74**, 1134 (1970).
20. H. W. Sidebottom, J. M. Tedder et J. C. Walton. Trans. Faraday Soc. 2103 (1970).
21. J. Gawlowski et J. A. Herman. Can. J. Chem. **52**, 3631 (1974).

Can. J. Chem. Downloaded from www.nrcresearchpress.com by 210.87.254.42 on 09/05/12
For personal use only.

Configurational effects on ^{13}C chemical shifts of 1,6-anhydrohexopyranoses and related compounds. Utility of $^{13}C-^{1}H$ coupling patterns for signal assignments[1]

R. GEORGE S. RITCHIE, NATSUKO CYR, AND ARTHUR S. PERLIN
Department of Chemistry, McGill University, Montreal, P.Q., Canada H3C 3G1

Received February 9, 1976

R. GEORGE S. RITCHIE, NATSUKO CYR, and ARTHUR S. PERLIN. Can. J. Chem. **54**, 2301 (1976).

An analysis of configurational effects on the ^{13}C chemical shifts of bicyclic compounds of the 1,6-anhydrohexopyranose and 2,7-anhydroheptulopyranose type is presented. As with other saturated ring systems, strong upfield shifts are found in association with an axial orientation of the substituents, although in this respect ^{13}C nuclei of the anhydro ring appear to exhibit atypical behaviour. Deshielding changes characterize a *syn*-diaxial orientation of hydroxyl groups, and also of a hydroxyl group with respect to the bridgehead bonds. No appreciable effects of *antiperiplanar* hydroxyl groups on ^{13}C chemical shifts have been detected. Possible interrelationships between ^{13}C or ^{1}H chemical shifts and steric interactions are discussed with reference to the relative stability of isomeric anhydrosugars and C—H bond polarization. Some characteristics of one-, two-, and three-bond $^{13}C-^{1}H$ coupling are described, and are shown to be of value in several instances for the assignment of ^{13}C signals. The ^{1}H-coupled signal for methylenic C-6 of 1,6-anhydrides is commonly non-first order, in contrast to the simpler pattern exhibited by methylenic C-1 of 2,7-anhydrides.

R. GEORGE S. RITCHIE, NATSUKO CYR et ARTHUR S. PERLIN. Can. J. Chem. **54**, 2301 (1976).

On présente une analyse des effets configurationnels sur les déplacements chimiques du ^{13}C de composés bicycliques du type anhydro-1,6 hexopyrannose et anhydro-2,7 heptulopyrannose. Comme on l'avait observé avec d'autres systèmes cycliques saturés, on observe qu'il y a une association entre de forts déplacements vers les hauts champs et l'orientation axiale des substituants; toutefois dans ce domaine les noyaux ^{13}C du cycle anhydro ne présentent pas de comportement typique. Les changements des blindages caractérisent une orientation *syn*-diaxiale des groupes hydroxyles ainsi que d'un groupe hydroxyle par rapport aux liens se trouvant en tête de pont. On n'a pu détecter aucun effet appréciable des groupes hydroxyles antipériplanaires sur les déplacements chimiques du ^{13}C. On discute des interrelations possibles entre les déplacements chimiques du ^{13}C ou du ^{1}H et les interactions stériques; cette discussion se fait par rapport à la stabilité relative des sucres anhydro isomères et de la polarisation du lien C—H. On décrit quelques caractéristiques des couplages $^{13}C-^{1}H$ sur un, deux ou trois liens et on montre qu'il peuvent s'avérer utiles dans plusieurs cas pour attribuer des signaux ^{13}C. D'une façon générale le signal couplé avec des protons ^{1}H pour le groupe méthylène en C-6 des anhydrides-1,6 n'est pas du premier ordre et ceci est en opposition avec les patrons plus simples présentés par le groupe méthylène en C-1 des anhydrides-2,7.

[Traduit par le journal]

Introduction

Several studies have been made of configurational and conformational effects on ^{13}C chemical shifts of aldopyranoses (1–4), ketopyranoses (5, 6), and aldofuranoses (7). This study deals with some anhydrides[2] of these sugars which, by furnishing a bicyclic type of ring system (as in 1,6-anhydro-β-D-idopyranose (**1***a*)), have permitted an examination of the orientational influences of substituents with geometries more rigidly defined than those of their monocyclic counterparts. In addition, since all eight diastereoisomeric 1,6-anhydro-β-D-aldohexopyranoses (and most of the 2,7-anhydro-β-D-heptulopyranoses (*e.g.*, the *ido* isomer, **1***b*)) are considered here, the current analysis is more complete than that carried out with their parent sugars, and the numerical evaluation of shielding terms is more precise.

Some characteristics of $^{13}C-^{1}H$ coupling in

[1]Presented to the 58th Canadian Chemical Conference of the Chemical Institute of Canada, Toronto, Ont., May 1975.

[2]The generosity of N. K. Richtmyer, who provided most of the compounds described here, made this study possible. To the regret of the authors, Dr. Richtmyer declined to share in the authorship of this article; he pointed out that he has already specifically announced (8) that he plans no further publications.

Can. J. Chem. Downloaded from www.nrcresearchpress.com by 210.87.254.40 on 09/05/12
For personal use only.

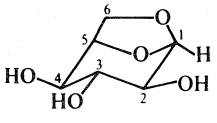

1*a*

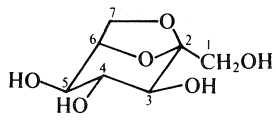

1*b*

these bicyclic compounds are described, and examples are given of how coupling across two or three bonds ($^2J_{C-H}$ or $^3J_{C-H}$) has been utilized in the identification of ^{13}C resonance signals.

Results and Discussion

Analysis of the ^{13}C Nuclear Magnetic Resonance Spectra

^{13}C chemical shift data for the various anhydro sugars studied are summarized in Table 1. Assignments for individual resonances are based on a number of considerations, which are discussed below mainly for the 1,6-anhydro-β-hexopyranoses (series A). However, many of the same considerations apply for their triacetates (series C), as well as for corresponding carbons of 2,7-anhydro-β-heptulopyranoses (series B).

Carbons 1, 5, and 6 (1, 2, 6, and 7, Series B)

For certain ^{13}C nuclei, the signal assignments are relatively straightforward. Carbon-1 of 1,6-anhydrides always produces the signal at lowest field because of its bonding to two oxygen atoms. The analogous nucleus in the 2,7-anhydrides, carbon-2, resonates at even lower field (by ~6 ppm) due to the additional deshielding effect of the primary carbinol group.

A triplet structure in off-resonance ^1H-de-

TABLE 1. Experimental ^{13}C nmr chemical shifts (ppm) for (*a*) 1,6-anhydro-β-hexopyranoses, (*b*) 2,7-anhydro-β-heptulopyranoses, (*c*) 1,6-anhydro-2,3,4-tri-*O*-acetyl-β-hexopyranoses, and (*d*) *O*-isopropylidene derivatives[a]

		C-1[c]	C-1[b] C-2[c]	C2-[b] C-3[c]	C-3[b] C-4[c]	C-4[b] C-5[c]	C-5[b] C-6[c]	C-6[b] C-7[c]
	1*a*		101.9	74.7	74.7	71.4	75.8	65.4
ido	**1***b*	60.5	108.1	74.8	75.4	71.7	76.6	66.5
(*e,e,e*)	**1***c*[e]		98.7	72.3	70.1[d]	70.0[d]	73.5	65.2
	2*a*		101.9	72.9	70.3[d]	69.9[d]	77.6	66.0
altro	**2***b*	60.4	107.9	72.8	70.7	70.7	78.3	67.0
(*e,e,a*)	**2***c*		99.2	71.8	67.0	69.2	74.7	65.6
	3*a*		102.1	70.9	73.3	71.6	76.9	65.8
gluco	**3***b*	61.4	107.2	71.0[d]	74.4	70.6[d]	78.3	66.7
(*a,a,a*)	**3***c*		99.5	70.1[d]	69.9[d]	71.0	74.0	65.5
	4*a*		101.9	66.6	70.9	72.2	76.4	65.3
	4*b*	60.9	107.7	66.5	71.3	72.7	78.6	66.5
manno	**4***c*		99.2	67.0	67.6	71.8	73.8	65.2
(*e,a,a*)	**4***d*[f]		99.2	72.1	75.8[d]	69.4	76.1[d]	64.4
	5*a*		101.7	70.5	70.5[d]	69.9[d]	74.9	63.8
gulo	**5***b*	60.8	107.9	70.4	70.2[d]	69.9[d]	76.1	65.1
(*a,e,e*)	**5***c*		98.9	68.9	66.7	68.6	71.8	63.9
allo	**6***a*		101.5	70.2[d]	63.5[h]	70.1[d]	76.8	65.4
(*a,e,a*)	**6***c*		99.0	68.0	62.4	67.7	74.0	64.8
	7*a*		101.3	71.9	70.8	64.9	74.9	64.1
galacto	**7***b*	61.1	107.1	71.7	71.7	64.9	76.3	65.2
(*a,a,e*)	**7***c*		98.7	70.9	67.3	64.6	71.9	64.3
	7*d*[g]		100.9	70.0	72.2	68.9	76.1	63.3
talo	**8***a*		101.2	69.1[h]	69.2[h]	67.1[h]	74.8	65.1
(*e,a,e*)	**8***c*		99.0	68.6[h]	66.4[h]	66.0	72.1	65.6

[a]Expected orientations of the 2-, 3-, and 4-hydroxyl groups are in parentheses.
[b]1,6-Anhydride.
[c]2,7-Anhydride.
[d]Assignments may be reversed.
[e]*O*-Acetyl methyl shifts for this and other *c* compounds: equatorial 20.3 ppm; axial 20.7 ppm.
[f]*O*-Isopropylidene signals at 110.0, 26.0, 25.9 ppm.
[g]*O*-Isopropylidene signals at 108.6, 25.7, 24.3 ppm.
[h]Assignments confirmed by deuterium labelling.

Can. J. Chem. Downloaded from www.nrcresearchpress.com by 210.87.254.40 on 09/05/12
For personal use only.

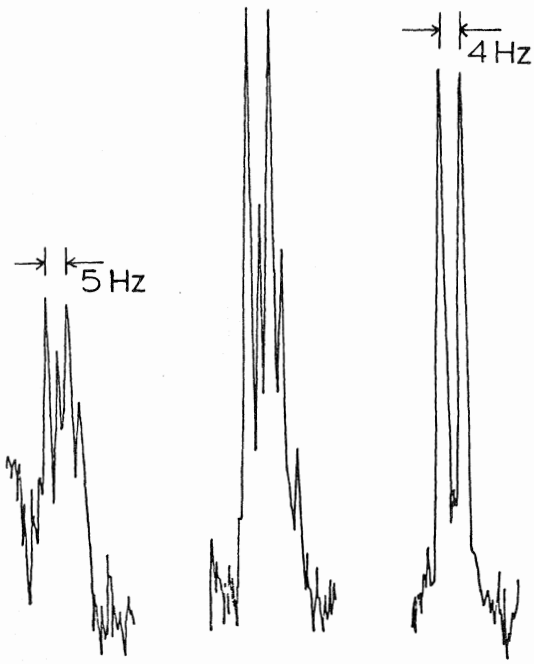

FIG. 1. The three components of the proton-coupled ^{13}C-6 signal of 1,6-anhydro-β-D-mannopyranose (**4***a*), showing non-first order effects.

coupled spectra served to locate the signal of carbon-6 (or of C-1 and -7 in series B) which usually[3] is the most strongly shielded of the ^{13}C ring nuclei. The appearance of these primary carbon signals in *fully coupled* spectra is itself noteworthy. That is, very often the C-6 signal (at 22.63 MHz) is considerably more complex than a simple triplet, or even a doublet of doublets ($^1J_{\text{C-6,H-6}_{endo}} \neq {}^1J_{\text{C-6,H-6}'_{exo}}$). Line separations are unequal and combination transition lines are observed, such as those shown in Fig. 1 for 1,6-anhydro-β-D-mannopyranose (**4***a*). This complexity is due to the fact that the chemical shift difference between H-5 and H-6′ (at 90 MHz) is nearly equal to $\frac{1}{2}(^1J_{\text{C-6,H-6}'} - {}^2J_{\text{C-6,H-5}})$, and that protons H-5 and H-6′ are fairly strongly coupled (~5 Hz) (9). By contrast, the signal for C-1 in series B is always a simple triplet ($J_{\text{C-1,H-1}}$ = 143.5–144.5 Hz, $J_{\text{C-1,H-3}} < 1$ Hz). This difference helped, therefore, to differentiate between C-1 and C-7 in the spectra of the 2,7-anhydrides.

[3]Notable exceptions are C-3 of 1,6-anhydro-β-D-allopyranose (**6***a*) and C-5 of 2,7-anhydro-β-D-galactoheptulopyranose (**7***b*).

The signal for C-5 is readily identified in series A downfield of all except the C-1 signal, its position being attributed to the effect of the C-5, O-5,C-1 bridge and also to the fact that it is located within a five-membered ring (7) (as well as a pyranose ring). Another distinguishing characteristic of this nucleus is that it exhibits a larger value of $^1J_{\text{C-H}}$ (155–160 Hz) than do the other ^{13}C nuclei that bear one oxygen atom ($^1J_{\text{C-H}}$ = 143–152 Hz). Again, this feature may be associated with the fact that ^{13}C nuclei in five-membered rings have larger one-bond coupling constants (^1J) than those of six-membered rings, or of side chains (unpublished results).

Carbons 2, 3, and 4 (3, 4, and 5, Series B)

Assignments for C-2, -3, and -4 have been derived extensively from two- and three-bond ^{13}C–^{1}H coupling data. This approach utilized the fact that (*a*) $^3J_{\text{C-H}}$ in sugars is ~5 Hz when the nuclei are *anti*, and usually <2 Hz when they are *gauche* (1, 10*a*), and (*b*) $^2J_{\text{C-H}}$ is ~5 Hz when the ^{13}C—O and C—^{1}H bonds are *gauche*, and <1 Hz when they are *anti* (1, 10*a*, *b*, *c*). Also, it was assumed that corresponding carbons in homologous pairs (A and B series) or their acetates (C series) can be interrelated by their chemical shift and splitting patterns.

For C-3 assignments, it was useful to compare the ^{1}H-coupled spectrum of a 1,6-anhydride (A) with that of its analog in the 2,7-anhydro (B) series. In A, C-3 should exhibit an extra coupling (vicinally with *anti* H-1) in comparison with the corresponding C-4 of B. As seen in Fig. 2 for the *manno* isomers (**4***a* and **4***b*), the respective C-3 and C-4 assignments for these two compounds may be deduced from the fact that the latter signal is only a triplet (J = 5 Hz) whereas the former is a quartet.

A choice between C-2 and C-4 of a 1,6-anhydride took account of the following: C-2 may exhibit coupling with H-3 and H-4 (occasionally with H-1 (10*c*)), whereas C-4 may couple with H-3, H-5 (^2J) and with H-2, -6, and -6′ (^3J). In general, therefore, the C-4 signal should appear as a doublet of complex multiplets, whereas C-2 should reflect less coupling.

Examples of these splitting characteristics are cited in the following outline of assignment procedures; for simplicity, the large $^1J_{\text{C-H}}$ couplings are disregarded and only one half of each signal is described (as in Fig. 2).

Can. J. Chem. Downloaded from www.nrcresearchpress.com by 210.87.254.40 on 09/05/12
For personal use only.

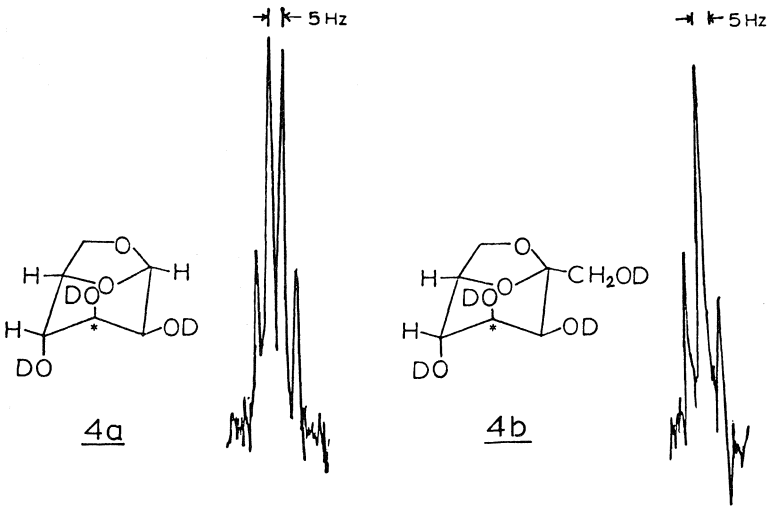

FIG. 2. Proton-coupled ^{13}C signals (upfield half) for C-3 of 1,6-anhydro-β-D-mannopyranose (**4***a*) and C-4 of 2,7-anhydro-β-D-mannoheptulopyranose (**4***b*).

1. Isomers of the manno, allo, galacto, and talo Configurations

Selective deuteration established assignments for the 2-, 3-, and 4-carbons of the *allo* (**6**) and *talo* (**8**) isomers (Table 1). The preparation of *O*-isopropylidene compounds proved to be helpful with *cis*-diols **4***a* and **7***a*. Thus a comparison of the spectrum of the derivative (**4***d* or **7***d*) with that of its parent gave the following results: the ^{13}C nuclei involved in formation of the isopropylidene ring experienced a substantial deshielding change (~5 ppm)[4] and *also* an increase in ^1J of 5–10 Hz, whereas the other ^{13}C nuclei exhibited relatively minor effects. Such changes are illustrated in Fig. 3 for 1,6-anhydro-β-D-mannopyranose (**4***a*) and its 2,3-*O*-isopropylidene derivative (**4***d*). Together with the data of Fig. 2, this accounts for the assignments in the *manno* series. Similarly, for the *galacto* isomer (**7***a*), the spectrum of **7***d* (Table 1) served to designate C-3 and C-4; in turn, the latter were distinguished by the fact that the signal at 64.9 ppm was a broad multiplet, as expected for C-4, whereas the signal at 70.8 ppm was only a quartet and thus more consistent with C-3.

2. Isomers of the ido, altro, gluco, and gulo Configurations

In the spectrum of *ido* isomer **1***b*, the resonances of which were better separated than those of **1***a*, the signals at 74.8, 75.4, and 71.7 ppm constituted a quartet, doublet, and broad multiplet. Accordingly, they were ascribed to C-4, -3, and -5 respectively. By analogy, a broad multiplet at 71.4 ppm in the spectrum of **1***a* was attributed to C-4; the remaining signals (C-2 and -3) are coincident in chemical shift.

Signals of **2***a* and **2***b* at 72.9 and 72.8 ppm were triplets of virtually identical structure. This eliminated from consideration a C-3, C-4 relationship of the type illustrated in Fig. 2, and also was inconsistent with the greater multiplicity expected for the C-4 (**2***a*) and C-5 (**2***b*) signals.

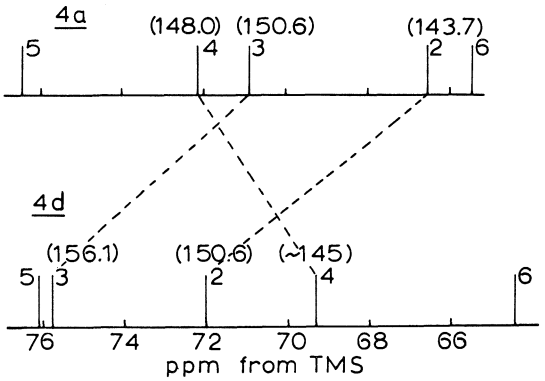

FIG. 3. A comparison of the ^{13}C chemical shifts of 1,6-anhydro-β-D-mannopyranose (**4***a*) and its 2,3-*O*-isopropylidene derivative (**4***d*). Bracketed numbers are the observed $^1J_{C-H}$ values in Hz.

[4]By contrast, some examples have been reported (11) in which the *O*-isopropylidene group appears to have a negligible effect on ^{13}C chemical shifts.

Can. J. Chem. Downloaded from www.nrcresearchpress.com by 210.87.254.40 on 09/05/12
For personal use only.

TABLE 2. Calculated ^{13}C shielding terms (X) associated with *cis vs. trans* configurations of substituents in 1,6-anhydro-β-hexopyranoses (A) and their 2,3,4-triacetates (C)

^{13}C nuclei		X(*cis* minus *trans*)[a]						
		2,3	2,4	3,4	2,$\overline{15}$[b]	3,$\overline{15}$[b]	4,$\overline{15}$[b]	Error[c]
C-1	A	−0.2	0.0	−0.4	0.1	−0.1	−0.3	±0.1
	C	0.0	0.0	−0.4	0.0	0.1	−0.4	±0.3
C-2	A	−3.5	0.8	0.3	−0.1	−2.5	1.4	±0.0
	C	−3.1	0.0	0.3	0.5	−1.1	1.0	±0.3
C-3	A	−3.9	−0.3	−3.8	1.9	1.5	1.7	±0.7
	C	−2.9	0.1	−2.9	1.1	1.3	0.9	±0.7
C-4	A	0.3	0.9	−3.2	1.1	−1.3	−2.7	±0.1
	C	−0.2	0.1	−3.5	1.3	−0.5	−2.6	±0.2
C-5	A	−0.6	0.1	0.0	0.3	−0.5	−1.8	±0.1
	C	−0.6	0.3	−0.1	0.6	−0.6	−1.8	±0.2
C-6	A	−0.4	0.6	0.1	0.7	−0.1	−1.0	±0.1
	C	−0.3	0.5	0.1	0.8	0.3	−0.5	±0.3

[a]Numerical values (in ppm) which are negative imply upfield shifts.
[b]Terms involving the bridgehead.
[c]Calculated shift minus experimental value.

As for the remainder, the chemical shift difference between C-3 and -4 of **2***a* is trivial, and the signals for C-4 and -5 of **2***b* coincide.

A C-3 assignment for the resonance of the D-*gluco* compound, **3***a*, at 73.3 ppm was warranted by the fact that this signal was a quintet, whereas the corresponding signal of **3***b* at 74.4 ppm was only a quartet (C-4). Of the **3***a* signals at 70.9 and 71.6 ppm, the former was a narrow quasi-triplet whereas the latter was a broad multiplet, indicating that they were due to C-2 and C-4, respectively.

Only very small differences are found in the chemical shifts of the 2-, 3-, and 4-carbons of the *gulo* isomers (**5***a* and **5***b*), and these signals virtually coincided in the ^1H-coupled spectra. Nevertheless, one of the **5***a* signals at 70.5 ppm was clearly evident as essentially a singlet superimposed on the other, broader, signals. Accordingly one signal at 70.5 ppm is ascribed to C-2.

Data also are given in Table 1 for the 2,3,4-tri-*O*-acetyl derivatives of the 1,6-anhydropyranoses (series C). The assignments are based on comparisons of the chemical shift and (particularly) ^1H–^{13}C coupling patterns for the individual compounds with the corresponding data for the unsubstituted (series A) compounds. Relative to the A spectra, two changes are generally discernable: (*i*) the ^{13}C nuclei resonate slightly upfield (aside from C-6, which is essentially unaffected) (Table 1), and (*ii*) values for ^1J are usually increased by several Hz; possibly, both of these effects are associated with the change in solvent.

Configurational Effects on ^{13}C Chemical Shifts

A numerical analysis, such as applied earlier to furanoses (7), has been performed (Table 2) in order to interrelate configurational changes among the 1,6-anhydro sugars with the observed differences in their ^{13}C chemical shifts. This involved the assumption that shielding changes may be expressed in terms of all possible arrangements of the pyranose ring substituents, by considering the relative orientations of two substituents at a time (while maintaining a chair conformation for the pyranose ring[5]). Thus, the ^{13}C shielding terms listed in Table 2 are associated with differences between *cis* and *trans* arrangements; *e.g.*, X(2,3) represents the term for the 2- and 3-hydroxyl groups (or acetoxyl in series C), and X(4,$\overline{15}$) for a 4-substituent and the bridgehead bonds.

The following three generalizations summarize the data of Table 2; they are expected to apply, at least qualitatively, to ^{13}C nuclei in other six-membered ring systems:

[5]Proton magnetic resonance spectra (12) indicate that most, if not all, of these compounds possess a chair conformation.

Can. J. Chem. Downloaded from www.nrcresearchpress.com by 210.87.254.40 on 09/05/12
For personal use only.

Can. J. Chem. Downloaded from www.nrcresearchpress.com by 210.87.254.40 on 09/05/12
For personal use only.

(*i*) Vicinal *cis* arrangements are associated with upfield shifts of 3–4 ppm.

(*ii*) A ^{13}C nucleus experiences greater shielding by ~1.5 ppm when the adjacent C—O bond is axial rather than equatorial. This reflects differences between *trans-e,e* and *a,a* values, and also between *cis-a,e* and *e,a*.

(*iii*) A ^{13}C nucleus experiences greater shielding (by 2.2 ppm) when there is an axial C—O bond (**2**) rather than an equatorial one (**3**) at the γ position, although the effect is noticeably smaller (~1.4 ppm) when the α and γ bonds are *syn*-axial (**4**).

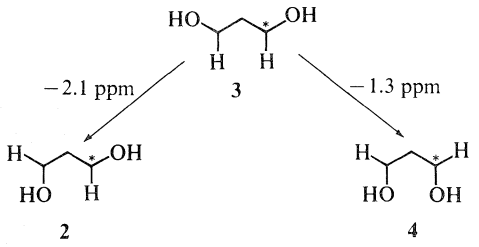

2 **4**

These generalizations may now be considered more specifically in relation to individual ^{13}C nuclei. Although the discussion deals with compounds of series A, the same reasoning applies to series C and, probably as well, to series B compounds.

(*a*) None of the carbon-1 terms demonstrate a significant shielding influence, including the vicinal *cis* arrangement [$X(2,\overline{15})$]. Considering projections **5** (equatorial O-2) and **6** (axial O-2) along with the C-1,C-2 bond, it is seen that both involve one *gauche* and one *anti* relationship of C—O bonds, and hence overall similar environments for C-1. Presumably for this reason, C-1 remains unaffected by a configurational change at C-2.[6]

5 R = H
7 R = CH_2OH

6 R = H
8 R = CH_2OH

(*b*) The effect of the *cis*-1,2 arrangement [$X(2,\overline{15})$] is similarly small for C-2 (probably for the same reasons). A large shielding influence is attributable to the *cis*-2,3 arrangement [$X(2,3)$] and a substantial additional one when the C-3, O-3 bond is axial [$X(3,\overline{15})$]. An axial C-4, O-4 bond is associated with an upfield change in shielding of −2.2 ppm when O-2 is equatorial and *trans* to O-4 (that is, $-X(4,\overline{15}) - X(2,4) = -1.4 - 0.8$ ppm) and a smaller one of −1.4 ppm (*i.e.*, $-X(4,\overline{15}) = -1.4$ ppm) when O-2 is *syn*-diaxial with respect to O-4, in accord with item *iii*.

(*c*) Carbon-3 experiences an upfield shift when there is a *cis*-2,3 or *cis*-3,4 arrangement (~4 ppm each), and when O-2 or O-4 is axial (~2 ppm each). Thus, a remarkably large upfield shift (>10 ppm) is found when several of these arrangements apply simultaneously: as for C-3 of 1,6-anhydro-β-D-allopyranose (**6***a*) as compared with C-3 of 1,6-anhydro-β-D-idopyranose (**1***a*). Deshielding is observed when O-3 is axial, and hence *syn*-diaxial with respect to the bridgehead ($X(3,\overline{15}) = 1.5$ ppm).

(*d*) Both the *cis*-3,4 and *cis*-4,5 arrangements are associated with strong increases in the shielding of carbon-4. There are lesser upfield shifts when O-3 is axial (−1.3 ppm), O-2 is axial [$-X(2,\overline{15}) = -1.1$ ppm], or both O-2 and O-4 are axial [$-X(2,4) = -0.9$ ppm].

(*e*) The *cis*-4,5 arrangement gives rise to an upfield shift (−1.8 ppm) for carbon-5 but otherwise, as found with carbon-1, orientational changes produce no appreciable effects. This difference between the $4,\overline{15}$ term (for C-5) and $2,\overline{15}$ term (for C-1) may be related to the fact that a *cis* → *trans* (equatorial → axial) change at C-4 involves differing arrays of nuclei close to C-5, (**9**) and (**10**), which is in contrast to the essentially equivalent arrays seen in **5** and **6**.

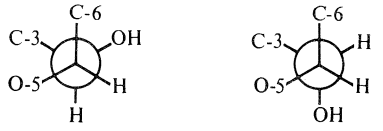

9 **10**

(*f*) Carbon-6 appears to be remarkably impervious to configurational change, although a small upfield shift (−1.0 ppm) is associated with a *gauche* relationship between this carbon and equatorial O-4[$X(4,\overline{15})$].

Shielding Changes Related to syn-Diaxial Substituents

The current results provide information about

[6]Analogous considerations apply for the relatively constant chemical shift of C-2 in 3-epimeric 2,7-anhydrides (**7** and **8**).

Can. J. Chem. Downloaded from www.nrcresearchpress.com by 210.87.254.40 on 09/05/12
For personal use only.

shielding changes associated with *syn*-diaxial hydroxyl groups (**4**). Earlier observations (1, 3, 13) on monocyclic compounds had suggested that such an arrangement involves a downfield shift (by 0.5–1.5 ppm) for the 1- and 3-carbons, relative to these carbons in an axial, equatorial arrangement (**2**). This type of effect is seen also with the more rigidly defined geometry of the anhydro sugars: as shown above, the difference observed between **2** and **4** amounts to 0.8 ppm.

A more pronounced deshielding effect has been found for *syn*-diaxial structures such as **11** in appropriate norbornane (14) and decalin derivatives (15), the methyl carbon being less shielded than that of its equatorial isomer. This has been referred to as a 'δ effect' (14), in contrast to the well known 'γ-*gauche* effect' (represented in **2**) and its attendant upfield shifts (16). Since the OH,OH relationship in **4** is spatially similar to the OH,CH relationship in **11**, the deshielding change associated with the *syn*-diaxial diol may be regarded as another manifestation of the δ effect (although, strictly speaking, this term has been introduced to describe the effect on a δ carbon atom).

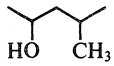

11

Features of both **4** and **11** appear to be involved when there is a *syn*-diaxial relationship between OH-3 and the bridgehead. In fact, from an overall comparison of the equatorial and axial OH-3 epimers (**12**) it is found (from Table 2) that the axial isomer is associated with downfield, as well as upfield, shifts: *i.e.*, although C-2 and C-4 of the latter resonate upfield, C-3 is downfield, and the position of C-6 is unchanged. Hence, examples of a deshielding type of effect are seen here also, although the δ carbon (C-6)[7]

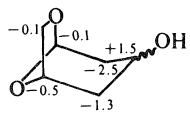

12

($\Delta\delta$, axial–equatorial)

does not itself exhibit a net change in chemical shift, in contrast to the δ carbon (CH_3) of **11**.

[7]Strictly speaking, however, the C-5,C-6 bond in these compounds is not axial (17).

TABLE 3. A comparison of the ^{13}C (and ^{1}H) chemical shifts of 1,6-anhydrohexopyranoses with their stabilities

Isomer	Relative stability[a]	^{13}C chemical shift (ppm)[b]	^{1}H chemical shift (ppm)[b]
ido	76	77.3	3.98
altro	63	76.4	4.05
gulo	59	75.2	4.10
allo	37	74.6	4.12
talo	7	74.4	4.15
manno	3	75.6	4.12
galacto	3	74.7	4.12
gluco	1	76.8	4.02

[a]Data from ref. 19.
[b]Average of chemical shift for all 6 carbons, or 7 protons; relative to tetramethylsilane.

^{13}C *Chemical Shifts and Steric Interactions*

Upfield shifts attributable to the γ-*gauche* effect have been rationalized in terms of steric compression between the *gauche* substituents (16). In agreement with this, it has been found within several series of isomeric compounds that those species incorporating a progressively greater number of *gauche* interactions are characterized by more pronounced upfield ^{13}C chemical shifts; *i.e.*, the least stable isomers contain the most strongly shielded carbons (18).

The anhydro sugars afford a more complex pattern. Calculated values[8] for the relative stabilities of the 1,6-anhydrohexopyranoses are compared in Table 3 with ^{13}C chemical shifts; the latter have been averaged for all six nuclei of each isomer, so as to facilitate comparisons between individual compounds. The compounds are listed in two groups: in the sequence *ido* to *allo* there is a progressive upfield shift as stability decreases. Of the remaining four, only the *talo* isomer falls into this sequence. However, these latter compounds incorporate the axial O-3, bridgehead (3,$\overline{15}$) arrangement which, as noted above, is characterized by downfield (and reduced upfield) shifts. Furthermore, the *gluco* isomer is most strikingly out of sequence, possibly because it also incorporates *syn*-diaxial O-2 and O-4, which should contribute further to the downfield position of its ^{13}C signals.[9]

[8]These are based on free energies calculated with reference to the parent hexoses, and agree fairly well with experimental data for hexose-anhydride equilibria (19).

[9]It is noteworthy that the corresponding average values for compounds of the B and C series follow virtually the same overall sequence as for the A compounds:
(A) $1 > 3 > 2 > 4 > 5 > 7 > 6 > 8$,
(B) $1 > 3 > 2 > 4 > 5 > 7$,
(C) $1 = 3 > 2 > 4 > 5 > 7 = 8 \simeq 6$.

Can. J. Chem. Downloaded from www.nrcresearchpress.com by 210.87.254.40 on 09/05/12
For personal use only.

TABLE 4. Changes in ^{13}C chemical shifts associated with *antiperiplanar* and *gauche* orientations of oxygen

	$\Delta\delta^a$ (ppm)
Carbon 2	
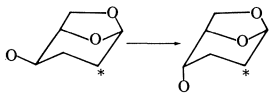	
ido ⟶ *altro*	1.8
gulo ⟶ *allo*	0.3[b]
talo ⟶ *manno*	3.0
galacto ⟶ *gluco*	1.0[b]
Carbon 4	
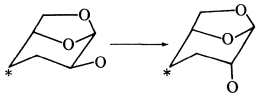	
ido ⟶ *gulo*	1.5
altro ⟶ *allo*	−0.2[b]
talo ⟶ *galacto*	2.2
manno ⟶ *gluco*	0.6[b]

[a]Chemical shift of C-2 or C-4 of isomer in the left column *minus* that in the right column; data from Table 1.
[b]Involves *syn*-diaxial O-2,O-4 relationship.

Therefore, although *γ-gauche* interactions are consistently associated with an increased shielding of ^{13}C, the determining factor may not be steric compression *per se*. Otherwise, strongly destabilizing *syn*-diaxial interactions should lead to upfield shifts as well (or *γ-gauche* interactions to downfield shifts). Perhaps a more important consideration is the fact that the spatial relationship of the nuclei involved in these two types of interactions is different, and hence need not be expected to lead to analogous chemical shift patterns.

Proton chemical shifts of the 1,6-anhydrohexoses (12) merit comment in this context. The values given in Table 3, like the ^{13}C data, are averages of all ^{1}H chemical shifts for each of the compounds. These numbers follow a progression that is the inverse of the ^{13}C values (*i.e.*, *on the average*, the more shielded a ^{13}C nucleus, the less shielded is a proton appended to it). This type of interrelationship, referred to as a 'bond polarization' (16), is an integral feature of the model for the *γ-gauche* effect. According to the data of Table 3, bond polarization appears to be a more general characteristic since it applies not only for the compounds (column 1) whose ^{13}C chemical shifts are dominated by *γ-gauche* effects, but also those incorporating *syn*-diaxial interactions.

^{13}C Shielding Changes Associated with Antiperiplanar Oxygen Atoms

It has been found recently (20) that an *antiperiplanar* heteroatom, as in **13**, may promote an upfield ^{13}C shift comparable to that associated with the related *gauche* arrangement (**14**). Consequently, the observed shifts for the δ carbons in isomeric species represented by **13** and **14** may be about the same. Because the anhydro sugars provide many instances of arrays resembling **13** and **14**, the current ^{13}C data have been examined for possible effects of this kind.

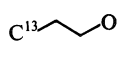

13

14

Table 4 summarizes the changes in chemical shift of C-2 associated with *antiperiplanar* or *gauche* O-4 and of C-4 with analogous orientations of O-2.[10] Half of the examples involve upfield shifts of 1.5–3.0 ppm, which is in the range normally expected for *γ-gauche* effects. Although the chemical shift differences for the other examples are small, in each of these instances the *gauche* arrangement brings O-2 and O-4 into a *syn*-diaxial relationship and, therefore, it should involve less of an upfield shift (by ~0.8 ppm) than the other four *gauche* arrangements. A similar examination of the possible effect of O-3 on C-1 or C-5 should likewise lead to ambiguous results, because in these instances allowance would have to be made for the 3,$\overline{15}$ *syn*-diaxial arrangement. Consequently, there is no clear indication that ^{13}C nuclei of the 1,6-anhydrohexopyranoses experience upfield shifts due to the presence of antiperiplanar O atoms.

Experimental

1,6-Anhydro-β-D-talopyranose-2*d*, -3*d*, and -4*d* were prepared as reported by Horton and Jewell (21). 1,6-Anhydro-β-D-allopyranose-3*d* (12) was prepared from the known D-allose-3*d* (22) by the method of Zissis and Richtmyer (23). 1,6-Anhydro-3,4-*O*-isopropylidene-β-D-

[10]Since the '*antiperiplanar* effect' probably involves a back-donation of charge from the lone pairs (20), the rotamer populations of the hydroxyl groups would have to be determined in order to permit a fuller evaluation of possible contributions by these oxygen atoms.

galactopyranose (**7***d*) and 1,6-anhydro-2,3-*O*-isopropylidene-β-D-mannopyranose (**4***d*) were prepared by standard procedures.

The numerical analysis of the ^{13}C chemical shifts utilized the same approach as described previously (7). ^{13}C magnetic resonance spectra were measured at a frequency of 22.63 MHz with a Bruker WH-90 FT spectrometer, employing a ^{2}H-lock. Deuterium oxide was used as a solvent for water-soluble sugars, and methanol was used as the internal standard (MeOH 49.6 ppm downfield from TMS). Chloroform-*d* was used both as the solvent and as the internal standard ($CDCl_3$ 76.9 ppm downfield from TMS) for the remaining compounds.

Acknowledgments

The authors gratefully acknowledge the generous support given by the National Research Council of Canada and the Pulp and Paper Research Institute of Canada.

1. A. S. PERLIN and B. CASU. Tetrahedron Lett. 292 (1969); A. S. PERLIN, B. CASU, and H. J. KOCH. Can. J. Chem. **48**, 2596 (1970).
2. L. D. HALL and L. F. JOHNSON. Chem. Commun. 509 (1969).
3. D. E. DORMAN and J. D. ROBERTS. J. Am. Chem. Soc. **92**, 1355 (1970).
4. W. VOELTER, E. BREITMAIER, and G. JUNG. Angew. Chem. Int. Ed. Engl. **10**, 935 (1971).
5. D. DODDRELL and A. ALLERHAND. J. Am. Chem. Soc. **93**, 2779 (1971).
6. A. S. PERLIN, P. C. M. HERVE DU PENHOAT, and H. S. ISBELL. Adv. Chem. Ser. **117**, 39 (1973); P. C. M. HERVE DU PENHOAT and A. S. PERLIN. Carbohydr. Res. **36**, 111 (1974); L. QUE, JR. and G. A. GRAY. Biochemistry, **13**, 146 (1974).
7. R. G. S. RITCHIE, N. CYR, B. KORSCH, H. J. KOCH, and A. S. PERLIN. Can. J. Chem. **53**, 1424 (1975); A. S. PERLIN, N. CYR, H. J. KOCH, and B. KORSCH. Ann. N.Y. Acad. Sci. **222**, 935 (1973).
8. N. K. RICHTMYER. Carbohydr. Res. **23**, 319 (1972).
9. N. CYR, R. G. S. RITCHIE, T. M. SPOTSWOOD, and A. S. PERLIN. Can. J. Spectrosc. **19**, 190 (1974).
10. (*a*) J. A. SCHWARCZ and A. S. PERLIN. Can. J. Chem. **50**, 3667 (1972). (*b*) J. A. SCHWARCZ, N. CYR, and A. S. PERLIN. **53**, 1872 (1975). (*c*) N. CYR and A. S. PERLIN. Unpublished results.
11. D. M. VYAS, H. C. JARRELL, and W. A. SZAREK. Can. J. Chem. **53**, 2748 (1975).
12. K. HEYNS and J. WEYER. Ann. **718**, 224 (1968).
13. D. E. DORMAN, S. J. ANGYAL, and J. D. ROBERTS. J. Am. Chem. Soc. **92**, 1351 (1970).
14. S. H. GROVER, J. P. GUTHRIE, J. B. STOTHERS, and C. T. YAN. J. Magn. Reson. **10**, 227 (1973).
15. S. H. GROVER and J. B. STOTHERS. Can. J. Chem. **52**, 870 (1974).
16. D. M. GRANT and E. G. PAUL. J. Am. Chem. Soc. **86**, 2984 (1964); D. K. DALLING and D. M. GRANT. J. Am. Chem. Soc. **86**, 5315 (1964); D. M. GRANT and B. V. CHENEY. J. Am. Chem. Soc. **89**, 5315 (1967).
17. Y. J. PARK, H. S. KIM, and G. A. JEFFREY. Acta Crystallogr. Sect. B, **27**, 220 (1971).
18. A. S. PERLIN and H. J. KOCH. Can. J. Chem. **48**, 2639 (1970).
19. S. J. ANGYAL and K. DAWES. Aust. J. Chem. **21**, 2747 (1968).
20. E. L. ELIEL, W. F. BAILEY, L. D. KOPP, R. L. WILLER, D. M. GRANT, R. BERTRAND, K. A. CHRISTENSEN, D. K. DALLING, M. W. DUCH, E. WENKERT, F. M. SCHELL, and D. W. COCHRAN. J. Am. Chem. Soc. **97**, 322 (1975).
21. D. HORTON and J. S. JEWELL. Carbohydr. Res. **2**, 251 (1966); **3**, 255 (1966); **5**, 149 (1967).
22. H. J. KOCH and A. S. PERLIN. Carbohydr. Res. **15**, 403 (1970).
23. E. ZISSIS and N. K. RICHTMYER. J. Org. Chem. **36**, 5244 (1961).

Can. J. Chem. Downloaded from www.nrcresearchpress.com by 210.87.254.40 on 09/05/12
For personal use only.

A synthesis of homosafranic acid and related compounds

CIRILL SCHMIDT

Department of Chemistry, University of Prince Edward Island, Charlottetown, P.E.I., Canada C1A 4P3

Received February 26, 1976

CIRILL SCHMIDT. Can. J. Chem. **54**, 2310 (1976).

A four step sequence was found to convert 2,2,6-trimethylcyclohexanone, **1**, to 1-(2-hydroxyethyl)-2,6,6-trimethyl-1,3-cyclohexadiene, **2***a* (overall yield 76%). An efficient route to homosafranic acid **3** is also described (overall yield 80% from ketone **1**).

CIRILL SCHMIDT. Can. J. Chem. **54**, 2310 (1976).

On a trouvé une séquence en quatre étapes pour transformer la triméthyl-2,2,6 cyclohexanone **1** en (hydroxy-2 éthyl)-1 triméthyl-2,6,6 cyclohexanediène-1,3 (**2***a*) avec un rendement global de 76%. On décrit aussi une méthode efficace pour arriver à l'acide homosafranique (**3**) avec un rendement global de 80% à partir de la cétone **1**.

[Traduit par le journal]

In the course of other synthetic work we were faced with the conversion of 2,2,6-trimethylcyclohexanone **1** to the alcohol **2***a*. The latter could be obtained by the reduction of the known homosafranic acid **3** with $LiAlH_4$. This acid was previously prepared in three steps from β-cyclocitral in a 15% overall yield (1). In our hands this procedure gave even lower yields. We were therefore prompted to consider other synthetic routes. A further incentive towards an improved synthesis of homosafranic acid **3** was that a series of natural products such as loliolide and actiniolide were synthesized from it (1).

We first investigated whether the method of Saucy *et al.* (2) (silver catalyzed rearrangement of acetate **4** through enolacetate **5** to aldehyde **6**) could be extended vinylogously, via acetate **9***b* (R = CH_3CO) and compound **10**. This could then lead to homosafranic acid **3** via **11** followed by oxidation and a prototropic change.

Reaction of ketone **7**[1] with a large excess of lithium acetylide in liquid ammonia gave only low yields, but use of the complex $LiC{\equiv}CH\cdot\cdot H_2NCH_2CH_2NH_2$ (4) resulted in a 90% yield of **8**. The unique efficiency of this complex has also been demonstrated by Huffmann and Arapakos (5).

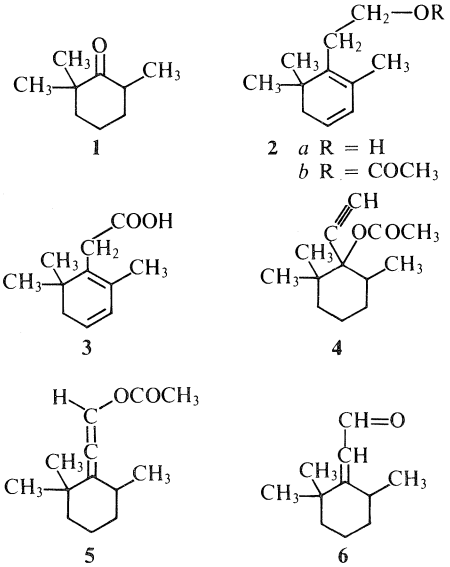

1

2 *a* R = H
b R = $COCH_3$

3

4

5

6

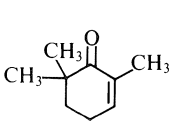

7

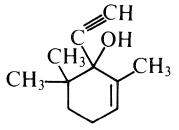

8

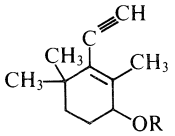

9 *a* R = H
b R = $COCH_3$

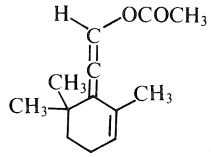

10

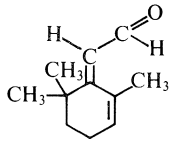

11

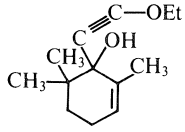

12

The acetylenic alcohol **8** could readily be rearranged to **9***a* (R = H) as demonstrated by a

[1]Prepared from ketone **1** in 90% overall yield (3).

Can. J. Chem. Downloaded from www.nrcresearchpress.com by 210.87.254.6 on 09/05/12
For personal use only.

Can. J. Chem. Downloaded from www.nrcresearchpress.com by 210.87.254.6 on 09/05/12
For personal use only.

one proton triplet at τ 5.93, and also by the fact that it could be acetylated to **9***b* (R = CH_3O) under the usual conditions pertinent to secondary alcohols.

When, however, the acetate **9***b* was subjected to silver catalyzed rearrangement only polymerization occurred.

In the second approach, ketone **7** was reacted with ethoxyacetylene magnesium bromide in tetrahydrofuran leading to a virtually quantitative yield of alcohol **12**. The same compound was previously prepared in liquid ammonia using lithium ethoxyacetylide in an unspecified yield (6). Hydration of **12** led to a mixture of

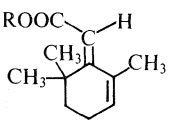

13 *a* R = Et
b R = H

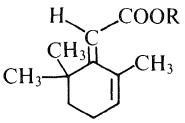

14 *a* R = Et
b R = H

esters **13***a* and **14***a* as expected (7). In the nmr of ester **13***a* the olefinic proton α to the carbethoxy group resonates at τ 4.20 as compared to 4.3 for the same proton in **14***a*. This deshielding effect is assigned to the closer proximity of the $\Delta^{2,3}$ double bond to the same proton in **13***a* than in ester **14***a* (8).

When the mixture of **13***a* and **14***a* was heated in diethylene glycol with KOH at 180 °C for 20 h the double bond system isomerized completely to homosafranic acid **3** (91% yield), spectroscopically identical with the compound prepared from citral (1). Use of sodium ethylate in refluxing ethanol for the isomerization led only to the crystalline acid **13***b*, without formation of homosafranic acid. Higher basic strength with lower temperature (liquid ammonia and tetrahydrofuran containing a large excess of sodium amide) gave a mixture containing about 50% homosafranic acid **3**, as estimated from the nmr spectrum by the clear singlet at τ 6.85 (due to CH_2COOH). Thus for the completion of this prototropic change a high temperature as well as a strong base are required.

The fact that during the prototropic change the unconjugated homosafranic acid **3** rather than **13***b* or **14***b* is preferred can be attributed to an $A^{1,3}$ steric repulsion (9) existing between the COOH and the 2 or 6 methyl groups in both of the conjugated acids **13***b* and **14***b*. After deconjugation the carboxyl group can freely rotate.

The reduction of homosafranic acid to homosafranyl alcohol **2** was accomplished by $LiAlH_4$ (96%). Thus the conversion of 2,2,6-trimethylcyclohexanone to alcohol **2** could be achieved in a 76% overall yield.

Experimental

All melting points were taken on a Fisher–Johns melting point apparatus and are uncorrected. The elemental analyses were carried out by Pascher Mikroanalytical Laboratorium, Bonn, West Germany, and Schwarzkopf Mikroanalytical Laboratory, Woodside, N.Y. The ir spectra were recorded on a Perkin-Elmer Model 137B infracord spectrophotometer. The uv spectra were taken on a Coleman–Hitachi Model 124 double beam grating spectrophotometer. The nmr spectra were recorded on a Varian Associates T60 spectrophotometer. The mass spectra were obtained with a Hitachi–Perkin-Elmer Model RMS-4 spectrometer, using electrons of 70 eV energy.

1-Ethynyl-2,6,6-trimethyl-2-cyclohexan-1-ol, **8**

A solution of 2,6,6-trimethyl-2-cyclohexen-1-one (3) (1.38 g) in dry tetrahydrofuran (150 ml) was stirred magnetically with $LiC{\equiv}CH \cdot NH_2CH_2CH_2NH_2$ (6 g) for 18 h under an atmosphere of dry nitrogen at room temperature. The reaction mixture was then poured on crushed ice and extracted with ether (4 × 70 ml). The combined ether extracts were washed with 5% sulfuric acid (100 ml) in the presence of crushed ice, then with 5% $NaHCO_3$ solution (100 ml), dried ($MgSO_4$), and concentrated *in vacuo*. The tlc homogeneous oil (1.48 g, yield 90%) was distilled at 112 °C/0.3 torr for analysis (1.1 g). Mass spectrum *m/e* (relative intensity) 164 (50, $M^{+\cdot}$), 149(55), 131(100); ir ($CHCl_3$) 3600, 3300, 2920, 1450, 1300, 970, 860, 820 cm^{-1}; uv end absorption; nmr ($CDCl_3$) τ 8.9 (s, 3, angular methyl), 8.87 (s, 3, angular methyl), 8.10 (s, 3, $=C-CH_3$), 7.50 (s, 1, $\equiv$C—H), 4.44 (m, 1, olefinic proton). *Anal.* calcd. for $C_{11}H_{16}O$: C 80.44, H 9.83; found: C 80.59, H 9.77.

3-Ethynyl-2,4,4-trimethyl-2-cyclohexen-1-ol, **9***a*

A solution of acetylenic alcohol **8** (820 mg) in ether (20 ml) was magnetically stirred for 18 h under nitrogen at room temperature with 3% sulfuric acid (10 ml). The water layer was extracted with ether (3 × 30 ml) and the combined ethereal phase was washed with sodium bicarbonate solution and dried ($MgSO_4$). Concentration *in vacuo* gave a homogeneous oil (tlc) (710 mg, 86.5%) with the following spectroscopic properties. Mass spectrum *m/e* (relative intensity) 164 (100, $M^{+\cdot}$), 149(70), 136(65); ir ($CHCl_3$) 3650, 3300, 2920, 1660, 1450, 1350, 1000, 900 cm^{-1}; uv_{max} (96% C_2H_5OH) 234 nm (ϵ 10 000); nmr at 60 MHz ($CDCl_3$) τ 8.97 (s, 3, angular methyl), 8.9 (s, 3, methyl), 8 (s, 3, $=C-CH_3$), 6.87 (s, 1, $\equiv$C—H), 5.93 (t, J = 6 Hz, 1, *CH*OH). This compound polymerizes in two weeks. Since the corresponding acetate **9***b* is stable, alcohol **9***a* was characterized in terms of its acetate **9***b*, which was prepared with acetic anhydride in pyridine; from 1.64 g of **9***a*, 1.5 g of acetate **9***b* (73%) was obtained after distillation, bp 111 °C/0.1 torr. Mass spectrum *m/e* (relative intensity) 206 (30 $M^{+\cdot}$), 191(15), 164(30),

Can. J. Chem. Downloaded from www.nrcresearchpress.com by 210.87.254.6 on 09/05/12
For personal use only.

146(100); ir ($CHCl_3$) 3300, 2950, 1725, 1450, 1360, 1240, 1060, 950, 960, 905, 870 cm^{-1}; uv_{max} (96% C_2H_5OH) 231 nm (ϵ 11 500); nmr ($CDCl_3$) 8.9 (s, 3, angular methyl), 8.8 (s, 3, angular methyl), 8.13 (s, 3, =C—CH_3), 7.9 (s, 3, $OCOCH_3$), 6.80 (s, 1, ≡C—H), 4.67 (t, J = 6 Hz, 1, C*H*OCOCH$_3$). *Anal.* calcd. for $C_{13}H_{18}O_2$: C 75.69, H 8.80; found: C 75.51, H 8.89.

1-Ethoxyethynyl-2,6,6-trimethyl-2-cyclohexen-1-ol, ***12***

Ethoxyacetylene (10) (14.10 g) in THF (25 ml) was added dropwise over 15 min to ethyl magnesium bromide (24.64 g) in dry THF (500 ml) at room temperature under dry nitrogen. After the cessation of gas evolution (1 h) a solution of the ketone **7** (13.8 g) in dry THF (30 ml) was added dropwise over 20 min, then the mixture was allowed to stand for 18 h at room temperature.

The reaction mixture was then poured on ice and extracted with ether (4 × 500 ml) and the emulsion was filtered through celite. The filtrate was extracted with ether, and the combined extracts were dried and concentrated. The solvent free residue (20.1 g, 96.5%) was practically pure adduct **12** (tlc, silica gel, 10% ether – 90% benzene); ir, ($CHCl_3$) 3660, 3500, 2950, 2270, 1450, 1280, 1230, 1170, 1140, 1120, 1080, 1050, 1000, 950, 900, 850, 820 cm^{-1}; nmr ($CDCl_3$) 9.00 (s, 6, *gem*-dimethyl), 8.62 (t, J = 6 Hz, 3, OCH_2CH_3) 8.13 (s, 3, 2 methyl), 5.9 (q, J = 6 Hz, 2, O—CH_2—CH_3), 4.6 (t, l, olefinic proton); uv end absorption.

Hydration of Acetylenic Alcohol ***12***

To a solution of acetylenic alcohol **12** (2.08 g) in ethanol (15 ml) at 5 °C 5% H_2SO_4 (2 ml) was added. After 18 h, the mixture was diluted with water (50 ml) and extracted with ether (4 × 50 ml). The combined ether extracts were washed, dried ($MgSO_4$), and concentrated to yield 2.1 g of oil exhibiting two spots on tlc (silica gel, 10% ether – 90% benzene). The two components were separated on silica gel preparatory plates into 0.95 g (42%) of the less polar ester **13***a* and 1.05 g (46%) of the more polar ester **14***a*. Ester **13***a* had the following spectra: ir ($CHCl_3$) 2950, 1715, 1650, 1600, 1450, 1380, 1360, 1320, 1240, 1160, 1120, 1090, 1020, 950, 910, 870, 830 cm^{-1}; uv_{max} (96% C_2H_5OH) 257 nm (ϵ 8400); nmr at 60 MHz ($CDCl_3$) 8.70 (s, 6, *gem*-dimethyl), 8.16 (s, 3, =C—CH_3) 5.8 (q, J = 6 Hz, 2, OCH_2, CH_3) 4.20 (s, 1, =CH—COOEt), 4.00 (m, 1, proton at C3).

Ester **14***a* exhibited the same peaks in its ir spectrum with minor intensity changes; nmr ($CDCl_3$) 8.80 (s, 6, *gem*-dimethyl), 8.2 (s, 3, =C—CH_3), 5.8 (q, J = 6 Hz, 2, OCH_2CH_3) 4.3 (br s, 2, olefinic protons); uv_{max} (96% C_2H_5OH) 257 nm (ϵ 7100).

Homosafranic Acid, ***3***

(a) Saponification and Isomerization at High Temperature

A solution of crude esters **13***a* and **14***a* (22.6 g) in diethylene glycol (110 ml) was heated (oil bath at 180 °C) under nitrogen while stirring with potassium hydroxide (20 g) for 20 h. After cooling, the dark reaction mixture was poured on ice (200 g) and extracted with ether (2 × 500 ml) in the presence of ice. More ice was added to the water phase and after acidification with 10% sulfuric acid, it was extracted with ether (4 × 70 ml). The combined ether extracts were washed, dried ($MgSO_4$), and concentrated. The residue was dissolved in benzene (100 ml) and refluxed while stirring with charcoal (0.5 g). Filtration and evaporation yielded 16.5 g (91%) of crystals, mp 73–75 °C. The product was recrystallized from 10 ml of hexane (10 g, 55%, mp 78 °C). From the filtrate a second crop was obtained (5.1 g, 28%, mp 74 °C). All spectroscopic properties were identical with those of a sample prepared from β-cyclocitral according to the procedure of Demole and Enggist (1).

(b) Saponification of Ester ***13a*** *to Acid* ***13b*** *with Attempted Isomerization to Homosafranic Acid,* ***3***

A solution of ester **13***a* (250 mg) in absolute ethanol was refluxed for 10 h in the presence of sodium ethylate (175 mg) under N_2. The solution was then poured on a mixture of ice and 10% sulfuric acid (5 ml) and extracted with chloroform (4 × 50 ml). The combined chloroform extracts were washed with water, dried ($MgSO_4$), and evaporated. The residue was recrystallized from hexane (150 mg, 61%, mp 121 °C). From the mother liquour a second crop was collected (71 mg, 36%). Mass spectrum *m/e* (relative intensity) 180(40, $M^{+\cdot}$) 165(100), 152(70); ir ($CHCl_3$) 3500, 2950, 1700, 1600, 1450, 1400, 1280, 1180, 1120, 920 cm^{-1}; uv_{max} (96% C_2H_5OH) 256 nm (ϵ 10 020); nmr ($CDCl_3$) τ 8.74 (s, 6, *gem*-dimethyl), 8.2 (s, 3, =C—CH_3), 4.2 (s, 1, CH—COOH), 4.00 (m, 1, proton at C3), −1.95 (s, COOH). *Anal.* calcd. for $C_{11}H_{16}O_2$: C 73.30, H 8.95; found: C 73.41, H 9.17.

(c) Partial Isomerization of Acid ***13b*** *to Homosafranic Acid,* ***3***

A solution of acid **13***b* (210 mg) in tetrahydrofuran (5 ml) was added over 5 min to 250 ml of liquid ammonia containing sodium amide (11) (180 mg). The solution was stirred for 6 h, then the ammonia was allowed to evaporate. After addition of ice and acidification with 10% sulfuric acid the solution was extracted with chloroform (4 × 50 ml). The combined extracts were washed, dried ($MgSO_4$), and evaporated. The nmr of the semicrystalline residue (190 mg) contained all the peaks of homosafranic acid as well as **13***b*: nmr ($CDCl_3$) τ 9.00, 8.74, 8.2, 6.85, 4.25, 4.00. The intensity of the singlet at τ 6.85 (CH_2—COOH) was only about half of that in homosafranic acid.

1-(2-Hydroxyethyl)-2,6,6-trimethyl-1,3-cyclohexadiene, ***2a*** *(R=H)*

To a solution of homosafranic acid (500 mg) in anhydrous tetrahydrofuran (40 ml), $LiAlH_4$ (110 mg) was added over 10 min while stirring magnetically and cooling with ice water. The reaction mixture was stirred at room temperature for 18 h. The mixture was poured into 10% sulfuric acid (10 ml) containing crushed ice (20 g) and the product extracted with chloroform (4 × 50 ml). The extracts were combined, washed with water, and dried ($MgSO_4$). After the removal of the solvent a tlc homogeneous oil was obtained (350 mg, 96%). Mass spectrum *m/e* (relative intensity) 166 (25, $M^{+\cdot}$), 151(20), 133(100), 122(40); ir, ($CHCl_3$) 3500, 2950, 1440, 1370, 1250, 1120, 1050, 900 cm^{-1}; uv_{max} (96% C_2H_5OH) 265 nm (ϵ 4050); nmr at 60 MHz ($CDCl_3$ + D_2O) 9.00 (s, 6, *gem*-dimethyl), 8.23 (s, 3, =C—CH_3), 8.00 (d, J = 3 Hz, 2, on C_5) 7.58 (t, J = 6 Hz, 2, CH_2—OH), 6.37 (t, J = 6 Hz, 2, CH_2—OH), 4.4 (m, 2, olefinic). Alcohol **2***a* was characterized in terms of its acetate **2***b*.

1-(2-Acetoxyethyl)-2,6-trimethyl-1,3-cyclohexadiene, **2***b*

The alcohol (510 mg) was acetylated in pyridine (5 ml) with acetic anhydride (5 ml) to give 602 mg of pure acetate **2***b* (94%). Mass spectrum *m/e* (relative intensity) 208(20), 180(10), 148(70), 133(100); ir, ($CHCl_3$) 2950, 1740, 1360, 1250, 1040 cm^{-1}; uv_{max} (96% C_2H_5OH) 265 nm (ϵ 4250); nmr ($CDCl_3$) 9.03 (s, 6, *gem*-dimethyl), 8.26 (s, 3, $=C-CH_3$), 8.00 (s, 3, $OCOCH_3$), 7.57 (t, J = 6 Hz, 3, $-CH_2-CH_2-OAc$), 5.93 (t, J = 6 Hz, 3, CH_2-CH_2-OAc), 4.4 (m, 2, olefinic). For microanalysis, the acetate was distilled, bp 123 °C/0.7 torr. *Anal.* calcd. for $C_{13}H_{20}O_2$: C 74.96, H 9.68; found: C 74.85, H 9.61.

Acknowledgements

The financial assistance of the National Research Council of Canada and the Senate Research Committee of University of Prince Edward Island is gratefully acknowledged. Mrs. E. Schmidt is thanked for technical assistance. Drs. J. Rigney and R. Duffy are thanked for encouraging and promoting this work. Mrs. S. MacQuarrie is thanked for secretarial work.

1. E. Demole and P. Enggist. Helv. Chim. Acta, **51**, 481 (1968).
2. G. Saucy, R. Marbet, H. Lindlar, and O. Isler. Helv. Chim. Acta, **42**, 1945 (1959).
3. Z. Horii, T. Yagami, M. Ito, and M. Hanaoka. Chem. Pharm. Bull. (Tokyo) **16**, 848 (1968).
4. O. F. Beumel, Jr. and R. F. Harris. J. Org. Chem. **28**, 2775 (1963); **29**, 1872 (1964).
5. J. W. Huffmann and P. G. Arapakos. J. Org. Chem. **30**, 1604 (1965).
6. O. Isler, M. Montavon, R. Rüegg, and P. Zeller. Helv. Chim. Acta, **39**, 259, (1959).
7. H. G. Viehe. Chemistry of acetylenes. Marcel Dekker, New York. 1969.
8. L. M. Jackmann and S. Sternhell. Applications of nuclear magnetic resonance spectroscopy in organic chemistry. 2nd ed. Pergamon Press, New York. 1969.
9. F. Johnson. Chem. Rev. **68**, 375 (1968).
10. G. Stork and M. Tomasz. J. Am. Chem. Soc. **86**, 471 (1964).
11. T. H. Vaughn, R. R. Vogt, and J. A. Nieuwland. J. Am. Chem. Soc. **56**, 2120 (1934).

Can. J. Chem. Downloaded from www.nrcresearchpress.com by 210.87.254.6 on 09/05/12
For personal use only.

Dehydration of 1,1′-ethylenedicyclopentanol

DENNIS G. M. DIAPER

Chemistry Department, Royal Military College of Canada, Kingston, Ont., Canada K7L 2W3

Received March 12, 1976

DENNIS G. M. DIAPER. Can. J. Chem. **54**, 2314 (1976).

The major product from the dehydration of 1,1′-ethylenedicyclopentanol is the tetrahydrofuran, 6-oxadispiro[4.1.4.2]tridecane, parent of a previously unknown ring system. The olefinic products are the conjugated diene, dicyclopentylideneethane, and the endocyclic diene, 1,2-di(1-cyclopentenyl)ethane in a ratio of about 1:2.

DENNIS G. M. DIAPER. Can. J. Chem. **54**, 2314 (1976).

Le produit le plus important obtenu par la déshydratation de l'éthylène-1,1′ dicyclopentanol est le tétrahydrofuranne, oxa-6 dispiro[4.1.4.2]tridécane, système cyclique de base qui était inconnu antérieurement. Les produits oléfiniques sont le diène conjugué, le dicyclopentylidène éthane, et le diène endocyclique di(cyclopentène-1 yl)-1,2 éthane; ces deux oléfines sont présentes dans un rapport d'environ 1:2.

Introduction

Our general synthesis of ketoacids through 1-alkylcycloalkanols (1, 2) was extended to diketodiacids (3, 4) with some success in all cases except those in which bis(1-hydroxycycloalkyl)ethanes were intermediates. It has been reported (5) that the major product obtained by the dehydration of 1,1′-ethylenedicyclopentanol (**1**) under acid conditions is the endocyclic diene,

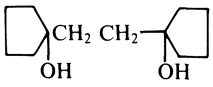

1

1,2-di(1-cyclopentenyl)ethane (**2**) but this result is difficult to reconcile with our low yields of the diketodiacid (4); moreover, the study identifying (**2**) as the major product of dehydration of **1** was based on the assumption that the only other possible product was the conjugated diene dicyclopentylideneethane (**3**). As we wished to consider also the possibility of the presence of the tetrahydrofuran, 6-oxadispiro[4.1.4.2]tridecane (**4**), the diene (**5**), and 1-cyclopentylidene-2-(1′-hydroxycyclopentyl)ethane (**6**) we have now used methods not available at the time of the earlier study of the dehydration of **1** to reexamine the products.

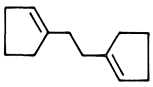

2

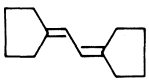

3

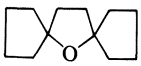

4

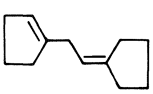

5

Under all dehydration conditions used, the liquid product was found to be a mixture containing about 70% of **4** and 30% of a mixture of dienes, unseparable by gas chromatography under the conditions used. Only 10% was the conjugated diene, **3**.

Experimental

1,1′-Ethylenedicyclopentanol (1)

This diol (prisms, mp 134 °C) was made by known procedures (5, 6). An intermediate in the hydrogenation of 1,1′-ethynylenedicyclopentanol was identified as the *cis* isomer (cf. ref. 7) of 1,1′-vinylenedicyclopentanol (silky fibrous crystals, ir peak at 13.90 μm, nmr peak at δ 5.42 ppm). Its dipole moment in dioxane at 20 °C was 2.90 $\pm$ 0.15 D, and the intensity of its OH peak in the ir spectrum was unaffected by dilution.

Dehydration of 1

Five procedures were employed: (*a*) heating at 130 °C for 1 h with a trace (about 0.1%) of iodine, (*b*) heating the diol (10 g) for 30 min with 0.2 ml of a 25% aqueous solution of sulphuric acid, (*c*) distillation under reduced pressure in the presence of a trace of *p*-toluenesulphonic acid, (*d*) distillation under reduced pressure over phos-

Can. J. Chem. Downloaded from www.nrcresearchpress.com by 210.87.254.6 on 09/05/12
For personal use only.

phorus pentoxide (10 mg for 10 g of diol), and (*e*) 1 h at 130 °C over 2% by weight of aluminium sulphate hydrate. In all cases a liquid product was obtained in yields of about 90%.

Gas chromatography in all cases showed two peaks, almost completely resolved, having retention times of 4.5 (smaller) and 5.5 min. The smaller peak had the same retention time as **3** and disappeared on ozonolysis. In all cases the ratio of peak areas indicated about 30% of diene mixture and 70% of the tetrahydrofuran **4**. Overheating the diol gave evidence of at least two other products in the chromatogram.

In support of the above conclusion, quantitative microhydrogenation (8) agreed with a yield of 30% of mixed dienes, the Deniges reagent (9) confirmed the presence of an ether, and the ir spectrum of the dehydration product, like authentic **3**, had a peak at 6.1 μm.

The ultraviolet spectrum had only the three-peak absorption of **3**. In all cases the apparent extinction coefficient at 249 nm indicated the presence of about 10% of **3**. The nmr spectrum of the dehydration product mixture had a sharp singlet at δ 1.84 (tetrahydrofuran), broad absorption centred about δ 1.7 and 2.3 (alicyclic CH_2—CH_2CH_2C=, and CH_2C—O), and an unstructured vinyl peak, δ 5.48 ppm. Integral values agreed with 25–30% mixed dienes and 70–75% **4**. There was no spectral evidence of **6**.

By ozonolysis of the dehydration product, followed by reduction by LAH, and treatment with trifluoroacetic anhydride in excess, cyclopentyl trifluoroacetate was identified gas chromatographically using methyl hexanoate as an internal standard, in yields corresponding to 10% of the conjugated diene **3**. The method should, in principle, give the content of **3** and **5** but in practice was not sufficiently accurate. From the ozonized dehydration product, **4** was isolated by chromatography on silica as a liquid, bp 112 °C/11 torr, n_D^{25} 1.5482. *Anal.* calcd for $C_{12}H_{20}O$: C 79.94, H 11.18; found: C 79.8, H 11.0. This compound is a member of a hitherto unreported ring system, 6-oxadispiro[4.1.4.2]tridecane.

Dicyclopentylidene Ethane (3)

This diene was made by the Wittig reaction in two steps from ethylene dibromide and cyclopentanone in a sequence analogous to that used for dicyclohexylidene ethane (10), as a pale yellow, waxy solid, mp 35 °C. The nmr spectrum showed a sharp vinyl singlet at δ 5.38 ppm. There were three uv maxima at 241, 249 (the largest), and 260 nm and a shoulder at 269 nm.

1. D. G. M. Diaper. Can. J. Chem. **33**, 1720 (1955).
2. D. G. M. Diaper. Can. J. Chem. **44**, 2819 (1966).
3. D. G. M. Diaper and A. Kuksis. Chem. Rev. **59**, 89 (1959).
4. A. S. Bailey, D. G. M. Diaper, and M. V. H. Schwemin. Can. J. Chem. **39**, 1147 (1961).
5. C. D. Nenitzescu and I. Necsoiu. J. Am. Chem. Soc. **72**, 3483 (1950).
6. Yu. S. Zal'kind and I. M. Gverdstsiteli. J. Gen. Chem. USSR, **9**, 855 (1939); Chem. Abstr. **34**, 387^6 (1940).
7. J. D. Chanley. J. Am. Chem. Soc. **71**, 829 (1949).
8. C. L. Ogg and F. J. Cooper. Anal. Chem. **21**, 1400 (1949).
9. E. M. Marks and D. Lipkin. J. Org. Chem. **3**, 598 (1939).
10. I. T. Harrison, B. Lythgoe, and S. Trippett. J. Chem. Soc. 4016 (1955).

Can. J. Chem. Downloaded from www.nrcresearchpress.com by 210.87.254.6 on 09/05/12
For personal use only.

Pyrochlores. X. Madelung energies of pyrochlores and defect fluorites[1]

WILLIAM W. BARKER,[2] PETER S. WHITE,[3] AND OSVALD KNOP
Department of Chemistry, Dalhousie University, Halifax, N.S., Canada B3H 4J3

Received January 13, 1976

WILLIAM W. BARKER, PETER S. WHITE, and OSVALD KNOP. Can. J. Chem. **54**, 2316 (1976).

Electrostatic (Madelung) lattice energies have been calculated for a wide range of compounds $A_2B_2X_6Y$ with the pyrochlore-type structure. The cases of disorder and partial disorder on the non-metal sites have been examined, as well as the inverse case, where Y is a positive ion. The results of the calculations are compared with those for defect fluorite structure and an attempt is made to relate them to the conditions under which the pyrochlore phase is found. The effect of the site potential in restricting the existence boundaries of the pyrochlore phase is examined, as the potential must have the correct sign relative to the charge occupying the site. Alternative pyrochlore arrangements in which the 8(*b*) or 32(*e*) equipoints are occupied have also been explored.

WILLIAM W. BARKER, PETER S. WHITE et OSVALD KNOP. Can. J. Chem. **54**, 2316 (1976).

Les énergies électrostatiques de réseau (énergies de Madelung) ont été calculées pour une variété de structures $A_2B_2X_6Y$ de type pyrochlore. On a examiné des structures à désordre complet ou partiel sur les sites anioniques ainsi que des structures "inverses" ou Y représente une charge cationique. Nous comparons les résultats de ces calculs à ceux obtenus pour les structures fluorine déficitaires, en cherchant à établir un rapport entre l'énergie de réseau et les conditions d'existence de la phase pyrochlore. On a aussi examiné l'effet du potentiel de site sur le domaine de stabilité de la pyrochlore, étant donné que le signe du potentiel d'un site et celui de la charge ionique placée en ce site ne doivent pas être pareils. Les arrangements pyrochlore dans lesquels les sites 8(*b*) ou 32(*e*) sont occupés, ont été également étudiés.

Recent interest in synthetic pyrochlore (*P*) phases in which oxygen is partially replaced by fluorine (2–10) prompts us to report briefly the results of our Madelung energy calculations for such compounds as well as for purely oxidic and purely fluoride pyrochlores.[4]

In the idealized crystal structure of a 'classical' pyrochlore $A_2B_2X_6Y$ (space group $Fd3m$, origin at centre in 16(*c*); Sleight's (12) case A_0) the metal atoms are in 16(*c*) (0, 0, 0; etc.) and 16(*d*) ($\frac{1}{2}$, $\frac{1}{2}$, $\frac{1}{2}$; etc.) and the nonmetal atoms in 8(*a*) ($\frac{1}{8}$, $\frac{1}{8}$, $\frac{1}{8}$; etc.) and 48(*f*) (x, $\frac{1}{8}$, $\frac{1}{8}$; etc.) sites (13). When each atomic species is segregated in an equipoint of its own (arrangement *I*) the structure is completely ordered. Normally the A and B atoms are of different effective sizes and do not form mixed populations on a sublattice. However, the X and Y can occur randomly distributed over 48(*f*). Depending on the occupancy of 8(*a*) arrangement *II* or arrangement *III* results. Structure *II* is ordered on 8(*a*) and disordered on 48(*f*), while *III* is disordered on both nonmetal equipoints. To indicate the type of ordering the occupancies of the four equipoints will be written in the order 16(*c*)|16(*d*)|48(*f*)|8(*a*), soth at the formula $A_2B_2(X_6)Y$ will refer to arrangement *I*, $A_2B_2(X_5Y)X$ to arrangement *II*, while $A_2B_2(X_6Y)$ will represent a statistical distribution of X and Y over 48(*f*) + 8(*a*), type *III*. This symbolism is easily extended to compositions $A_2B_2X_{7-\epsilon}Y_\epsilon$, $0 \leq \epsilon \leq 7$.

In 'inverse' pyrochlore compositions of the type $RbNiCrF_6 = B^{2+}B^{3+}X_6M^{1+}$ reported by Babel *et al.* (14) (but actually discussed as early as 1943 by Schrewelius (15) in his extensive

[1]For Part IX, see ref. 1.

[2]Killam Postdoctoral Fellow, 1968–1970. Present address: Minerals Research Laboratories, Division of Mineralogy, C.S.I.R.O., Wembley, W.A. 6014, Australia.

[3]Holder of an N.R.C.C. postgraduate scholarship, 1971–1972. Present address: Department of Chemistry, The University of New Brunswick, Fredericton, N.B., Canada E3B 5A3.

[4]Madelung energies for the pyrochlores $A_2^{a+}B_2^{b+}O_6Y^{h-}$ ($a|b|h$ = 1|6|2, 2|5|2, 1.5|5|1, 3|4|2) have been presented, in dependence on x(O), in ref. 11.

Can. J. Chem. Downloaded from www.nrcresearchpress.com by 210.87.254.40 on 09/05/12
For personal use only.

Can. J. Chem. Downloaded from www.nrcresearchpress.com by 210.87.254.40 on 09/05/12
For personal use only.

investigation of thallium antimonates[5]) a large cation M = K, Rb, Cs is located in 8(*a*) while the 16(*c*) sites are vacant: $\square_2B_2(F_6)M$; a variety of *P* phases of this type have been investigated since (9, 17–22). This formulation is the consequence of the requirement that there be no direct cation–cation contact between atoms in 8(*a*) and 16(*c*), M(*a*)—A(*c*) = $a_0\sqrt{(\frac{3}{8})}$ (7, 15). This requirement would be satisfied if only half the M atoms were present, *i.e.* for compositions $B_2(X_6)M_{1/2} = \square_{16}|B_{16}|X_{48}|M_4\square_4$, provided the vacancies in 8(*a*) were ordered. The splitting of the 8(*a*) equipoint into two subsets of cubic symmetry can be realized in $F\bar{4}3m$–T_d^2 and $F23$–T^2. In either case the four M would be in 4(*a*) (0, 0, 0; etc.) and the four vacancies in 4(*c*) ($\frac{1}{4}$, $\frac{1}{4}$, $\frac{1}{4}$; etc.) or *vice versa*, with the attendant splitting of 48(*f*) of *Fd*3*m* into 24(*f*) + 24(*g*) of the tetrahedral space groups. Distributions of this type (arrangement *IV*) do not seem to have been reported as yet. The existence of non-stoichiometric statistical distributions A_ϵ^{3+}-$Sb_2^{5+}O_6M_{2-3\epsilon}^{1+}$ (A = Tl, Sb; M = Tl, Cs?; $\frac{1}{3} \leq \epsilon \leq \frac{2}{3}$) was discussed by Schrewelius (15).[5] From his results it would appear that in such *P* phases simultaneous occupancy of 8(*a*) and 16(*c*) is possible for $\epsilon < \frac{2}{3}$. Partial substitution of A^{3+} by A^{2+} would introduce flexibility in manipulating the occupancy of 8(*a*) relative to that of 16(*c*).

Refinements, from X-ray powder intensities, of the structures of B_2X_6M pyrochlores with M placed in 8(*a*) have been reported (23–26) to lead to abnormally large isotropic temperature factors *B*(M) and unsatisfactory values of the discrepancy index $R = \sum|I_c - kI_o|/\sum I_c$, $k = \sum I_c/\sum I_o$. A significant improvement in *R* and *B*(M) resulted when each of the eight M atoms was displaced from 8(*a*) to one of the four 32(*e*) (*y*, *y*, *y*; etc.) positions associated with each 8(*a*) position. Two minima in R_{final} *vs.* *y* plots were obtained, the two $y(R_{min})$ values being almost symmetric with respect to $y = \frac{1}{8}$, *i.e.* the positions corresponding to 8(*a*). Subsidiary arguments were used to rule out one of the $y(R_{min})$ values.

To obtain an idea of the overall, primary electrostatic stability of the various atomic distributions in the cubic pyrochlores, we have computed Madelung energies U_M from point-charge models as functions of *x*(48*f*) and formal ionic charges. The distributions $A_2^{a+}B_2^{b+}$-$X_6^{g-}Y^{h-}$ and $A_2^{a+}B_2^{b+}X_6^{g-}Y^{h+}$ for which U_M values have been obtained, and presented graphically in this paper, are listed in Table 1. Distributions involving 32(*e*) sites have also been examined, and U_M values have been obtained for defect fluorite (*F*) structures in which occupancy of the 8(*b*) equipoint of *Fd*3*m* is involved in addition to that of the standard *P* sites.

Our U_M calculations differ from those recently published by Pannetier (27) in that they cover a much larger variety of *P* compositions and charge combinations; where overlap occurs the two sets appear to be in complete agreement. In many cases our range of *x*(48*f*) extends from 0.35 to 0.50 (for the fluorites from 0.25 to 0.50) compared with Pannetier's range 0.37 to 0.45. This greater *x*(48*f*) range will be found useful for predictive purposes and for comparing relative U_M stabilities of alternative structures, even though the values of *x*(48*f*) so far observed in *P* phases fall within a fairly narrow interval of *ca.* 0.40 to 0.44. Results for ordered fluorites, for pyrochlores with ordered vacancies on 8(*a*), and for inverse pyrochlores with cation occupancy of 32(*e*) are being reported here for the first time.

Method of Calculation

All calculations in this work are based on the unmodified point-charge model. The Madelung energies were evaluated by the Ewald method for triclinic potential as described and modified by Slater and Decicco (28).

Use was made of the fact that the U_M sums can be split into two parts, one purely geometric and the other, charge dependent. The geometric part need only be calculated once. The energy gained by inserting, in the *i*th type of site of potential $P_i = (1/a_0)\sum_j G_{ij}z_j$ (esu/Å), an ion of charge z_i is $E_i = P_iz_i$ (esu²/Å), where $j = 1, 2, \ldots, t$ re-

[5]Schrewelius stated that cations larger than Rb^{1+} cannot be accommodated in 16(*c*). His suggestion that such cations (Tl^{1+}, Cs^{1+}) are located in 8(*a*) was supported by X-ray diffraction intensities and other experimental evidence. He considered the atomic distributions in the large variety of his Tl antimonate preparations to be essentially of three types: $Tl_y^{3+}|Sb_{16}^{5+}|O_{48}|Tl_x^{1+}$; $Tl_y^{3+}|Sb_{16}^{5+}|(O, OH)_{48}|Tl_x^{1+}$; or $Tl_y^{3+}Sb_z^{3+}|Sb_{16}^{5+}|O_{48}|$-$Tl_x^{1+}$, $\frac{8}{3} \leq y + z \leq \frac{16}{3}$, $x = 16 - 3(y + z)$. His formulation utilizing the 8(*a*) sites for large cations remained largely unnoticed. It was proposed again, independently, for *P* phases of other compositions only in 1967 (14). Unfortunately only a small portion of Schrewelius's results has been published (16). The bulk of the thesis has yet to receive the attention it deserves.

TABLE 1. Pyrochlore compositions for which Madelung energies U_M are presented in Figs. 4–9

Negative charges per formula	Composition	Type of anion distribution and Figure number		
		I	*II*	*III*
14	$A_2B_2O_7$	$(O_6)O$ 4	—	—
13	$A_2B_2O_6F$	$(O_6)F$ 4, 8	$(O_5F)O$ 6, 8	$(O_6F)^a$
12	$A_2B_2O_6$	$(O_6)\square$ 4, 8	—	$(O_6\square)$ 8
	$A_2B_2O_5F_2$		$(O_5F)F$ 7 $(O_4F_2)O$ 6	$(O_5F_2) = (O_6\square)$
	$A_2B_2MO_6$	$(O_6)M$ 4	—	—
11	$A_2B_2O_4F_3$		$(O_4F_2)F$ 7 $(O_3F_3)O$ 6	$(O_4F_3)^b$
	$A_2B_2O_5F$		$(O_5F)\square$ 9	$(O_5F\square) = (O_4F_3)$
	$A_2B_2MO_5F$		$(O_5F)M$ 6, 7	—
10	$A_2B_2O_3F_4$		$(O_3F_3)F$ 7 $(O_2F_4)O$ 6	$(O_3F_4)^b$
	$A_2B_2O_4F_2$		$(O_4F_2)\square^c$	$(O_4F_2\square) = (O_3F_4)$
	$A_2B_2MO_5F$		$(O_4F_2)M$ 6, 7	—
9	$A_2B_2O_2F_5$		$(O_2F_4)F$ 7 $(OF_5)O$ 6	$(O_2F_5)^b$
	$A_2B_2O_3F_3$		$(O_3F_3)\square$ 9	$(O_3F_3\square) = (O_2F_5)$
	$A_2B_2MO_3F_3$		$(O_3F_3)M$ 6, 7	—
8	$A_2B_2OF_6$	$(F_6)O$ 5, 8	$(OF_5)F$ 7, 8	$(OF_6)^a$
	$A_2B_2O_2F_4$		$(O_2F_4)\square^c$	$(O_2F_4\square) = (OF_6)$
	$A_2B_2MO_2F_4$		$(O_2F_4)M$ 6, 7	—
7	$A_2B_2OF_5$		$(OF_5)\square$ 9	$(OF_5\square) = (F_6)F$
	$A_2B_2MOF_5$		$(OF_5)M$ 6, 7	—
	$A_2B_2F_7$	$(F_6)F$ 5, 9	—	—
6	$A_2B_2F_6$	$(F_6)\square$ 5, 8	—	$(F_6\square)$ 8
	$A_2B_2MF_6$	$(F_6)M$ 5	—	—

[a]Interpolate in Fig. 8 between $(O_6)F$ and $(O_5F)F$; $(F_6)O$ and $(OF_5)F$.
[b]Interpolate in Figs. 6 and 7 between $(O_4F_2)F$ and $(O_3F_3)O$; $(O_3F_3)F$ and $(O_2F_4)O$; $(O_2F_4)F$ and $(OF_5)O$.
[c]Interpolate in Fig. 9.

TABLE 2. The geometric lattice sums G_{ij}

i \ j	16(*c*)	16(*d*)	48(*f*)	8(*a*)	8(*b*)
16(*c*)	−0.633240	−0.283726	$G_{cf}(x)$	0.086582	−0.166772
16(*d*)	G_{cd}	G_{cc}	$G_{df}(x)$	G_{cb}	G_{ca}
48(*f*)	$\frac{1}{3}G_{cf}(x)$	$\frac{1}{3}G_{df}(x)$	$G_{ff}(x)$	$\frac{1}{6}G_{af}(x)$	$\frac{1}{6}G_{bf}(x)$
8(*a*)	$2G_{ca}$	$2G_{da}$	$G_{af}(x)$	−0.538678	−0.189167
8(*b*)	$2G_{da}$	$2G_{ca}$	$G_{bf}(x)$	G_{ab}	G_{aa}
$x(48f)$	$G_{cf}(x)$	$G_{df}(x)$	$G_{af}(x)$	$G_{bf}(x)$	$G_{ff}(x)$
0.3500	−0.071859	−0.397106	−0.195951	−0.572966	−0.982445
0.3750	−0.240567	−0.240567	−0.407072	−0.407072	−0.999217
0.4000	−0.397106	−0.071859	−0.572966	−0.195951	−0.982432
0.4100	−0.454912	−0.003003	−0.629599	−0.094854	−0.965452
0.4200	−0.509663	0.065431	−0.681623	0.018062	−0.941492
0.4300	−0.561228	0.132523	−0.729513	0.144761	−0.909426
0.4375	−0.597776	0.181361	−0.762968	0.250245	−0.879206
0.4400	−0.609553	0.197274	−0.773678	0.287626	−0.867820
0.4500	−0.654629	0.258655	−0.814453	0.449565	−0.814917
0.4600	−0.696492	0.315656	−0.852122	0.634171	−0.748560
0.4700	−0.735217	0.367340	−0.886927	0.845936	−0.666105
0.5000	−0.833305	0.483792	−0.975780	1.710023	−0.283997

Can. J. Chem. Downloaded from www.nrcresearchpress.com by 210.87.254.40 on 09/05/12
For personal use only.

Can. J. Chem. Downloaded from www.nrcresearchpress.com by 210.87.254.40 on 09/05/12
For personal use only.

fers to the different types of sites (equipoints) in the model structure. G_{ij} is the geometric factor involved in the interaction of the ions in the jth sites with the ions in the ith sites. The total Madelung energy is then $U_M = C \sum_1^t E_i p_i$, where p_i is the number of sites of type i in the unit cell. The lattice sums G_{ij} are tabulated in the calculation as functions of $x(48f)$ (Table 2) or $y(32e)$ or both; using these G_{ij} values and $C = 1661.1$ gives U_M in kcal/g-formula. All calculations were made for a cubic unit cell of $a_0 = 10$ Å.

A statistical distribution of unlike charges of equal sign over an equipoint gives the same U_M value as a homogeneous population of the averaged charges in that equipoint. Thus the U_M *vs.* $x(48f)$ curve for $A_2^{1.5+}B_2^{4+}(O_4F_2)F$ is the same as that for $(A^{1+}A^{2+})(B^{3+}B^{5+})(O_4F_2)F$, $(A_{1.5}^{1+}A_{0.5}^{3+})B_2^{4+}(O_5\square)F$ etc.

As pointed out by Pannetier, the Madelung energies of arrangements in which a cation is displaced from equipoint 8(*a*) to equipoint 32(*e*) cannot be obtained by direct summation. Each 8(*a*) site is coordinated by four 32(*e*) sites at the corners of a regular tetrahedron, but only one of these four sites is occupied by a cation; placement of the cation in the tetrahedron is at random. Although the result is a one-quarter populated 32(*e*) equipoint, this distribution of p cations over $4p$ 32(*e*) sites is not equivalent to an *unconstrained* statistical distribution of p cations over $4p$ 32(*e*) sites of the idealized structure, in which coordination tetrahedra may occur containing more than one or no cation. The following method was therefore devised to evaluate the G_{ee} sums. The potential at the 32(*e*) site $A(y, y, y)$ due to the other 32(*e*) sites, excepting the other three 32(*e*) sites associated with 8(*a*) ($\frac{1}{8}, \frac{1}{8}, \frac{1}{8}$), $B(y, \frac{1}{4} - y, \frac{1}{4} - y)$, $C(\frac{1}{4} - y, y, \frac{1}{4} - y)$, and $D(\frac{1}{4} - y, \frac{1}{4} - y, y)$, was obtained by direct summation in real space up to a radial distance of $a_0 S_{max} = 10a_0$, $S = (n_1^2 + n_2^2 + n_3^2)^{1/2}$, n_1, n_2 and n_3 being the lattice translation vectors. The contributions from charges at sites $(y \pm n_1, \frac{1}{4} - y \pm n_2, \frac{1}{4} - y \pm n_3)$ etc. were approximated by the contribution from $(y \pm n_1, y \pm n_2, y \pm n_3)$. The summation was repeated for B, C, and D. The differences between the sums calculated for A, B, C, and D rapidly became constant with increasing S and gave the required correction factor. The error in the computed G_{ee} potentials was $\pm 3 \times 10^{-6}$.

It should be noted that the $G_{ee}(y)$ values obtained in this manner are not for one particular distribution of '8(*a*)' cations over the 32(*e*) sites but are *mean values* applicable to a system of charges where a sufficiently large sample has been used, and similarly for $G_{ec}(y)$, $G_{ed}(y)$, $G_{ef}(x, y)$. Thus, for a given y, the potentials at *all* the 32(*e*) sites due to charges in the 16(*c*) sites have the same value, and likewise for the effect of charges in the 16(*d*) and the 48(*f*) sites. Conversely, the potential at any 16(*c*) site due to the 32(*e*) charges is one-quarter the value obtained by assuming that all the 32(*e*) sites are occupied etc.

Results and Discussion

The main results of our calculations are described below. The volume of the computations is large and only the most obvious trends can be described here.[6]

The conclusions drawn from the U_M calculations are subject to all the inherent restrictions and limitations of the unmodified point-charge model, *i.e.* the idealized structures are strictly ionic and no allowance is made for displacements of the point charges from their ideal lattice sites when dealing with disordered structures containing mixed-charge populations. Stabilization by possible crystal-field effects is not considered. Changes in polarizability, *e.g.* on replacing oxygen by sulfur to form $A_2B_2O_6S$ and $A_2B_2F_6S$ pyrochlores (29–31), clearly are a factor, but they too will not be considered.

The contribution made to the total lattice energy U of the pyrochlores by the Born repulsion term U_B is not known. If, for a particular stoichiometry and for homogeneous populations on all the sublattices, U_B was the same fraction of U_M for the different possible arrangements, say *I* to *III*, the relative stabilities of these arrangements could be predicted simply by comparing the U_M values. However, it is not known how far this can be assumed even for alternative distributions possible for a cubic P phase of a given composition. For competing structural *types* (*e.g.* P *vs.* defect F or cubic perovskite $A_2B_2X_6$) the validity of such an assumption is even less clear.

The U_M values apply to long-range ordering, or to 'averaged' distributions of point charges. Hence in incompletely disordered structures the stabilizing effect of short-range order is also a factor, especially when differences in the U_M of alternative arrangements are small, such as might be the case for nonstoichiometric compositions. While U_M can be obtained for particular computer-generated samples of disordered P structures subject to predetermined short-range constraints, little can be said about this effect in general.

The value of U_M, adjusted to the observed a_0, is not the sole criterion of the electrostatic stability of a P arrangement. The sign of the *site potential* (SP) must be the opposite of that of the charge to be accommodated at the site. Sign inversion of SP with changes of $x(48f)$ and a/b thus determines whether or not an ion can in fact reside at that site (Fig. 1). Even if SP has the correct sign relative to a particular ion, its

[6]Enquiries about results available but not presented in this paper may be directed to the last-named author.

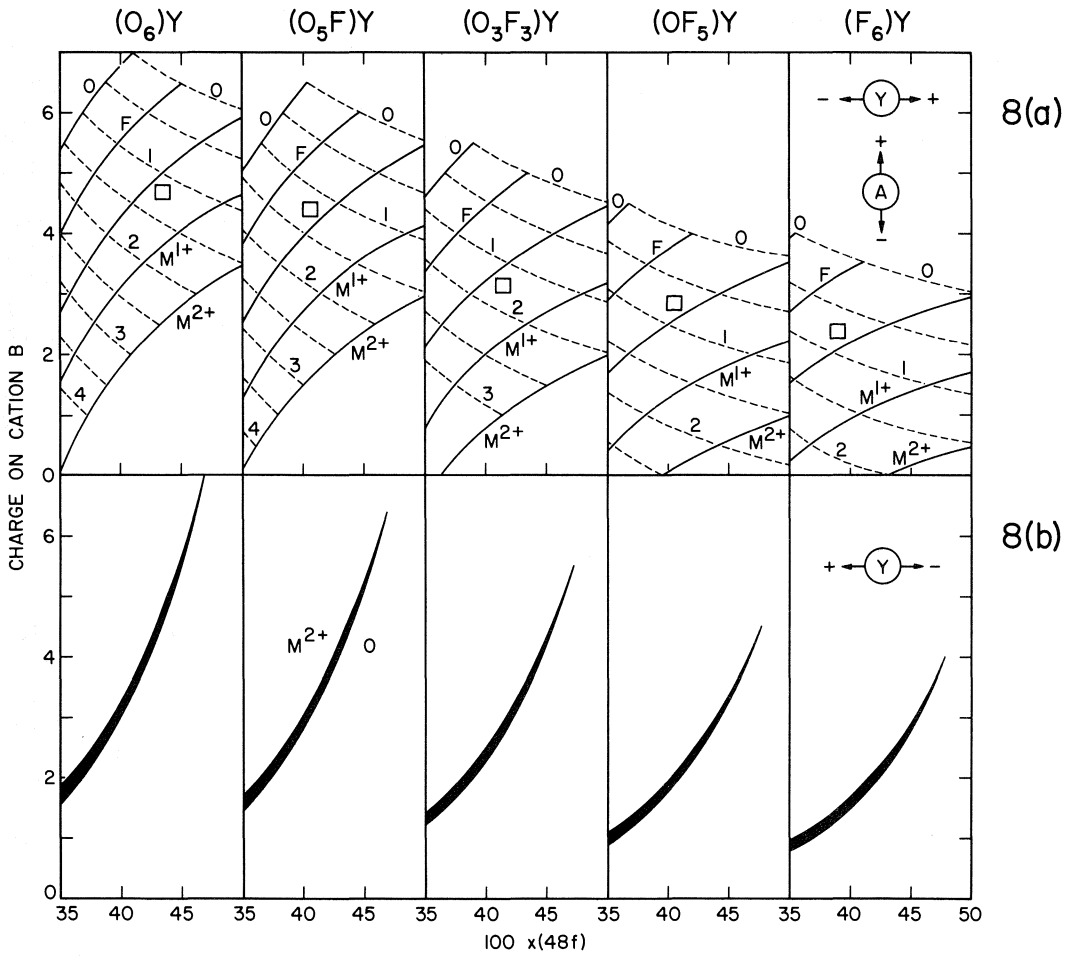

FIG. 1. Sign inversion of site potentials at 8(*a*) and 8(*b*) in $A_2B_2(X_6)Y$ pyrochlores. Contours of equal charge on A are in broken lines. Contours referring to Y are shown as solid lines. The total range of variation of the sign-inversion locus for 8(*b*) with Y is indicated by the width of the line.

absolute value is also important. The anion must 'see' a minimum stabilizing potential in order to stay in the site. For O^{2-} in ionic oxides the energy required to stabilize the ion has been estimated to be at least 10 eV (32). For the defect fluorites $A_2B_2(O_7\square)$, for example, this requirement restricts the range of $x(48f)$ much more severely than the sign inversion of SP at the anion sites (Fig. 2).

The regions of instability owing to sign inversion of SP are shown in the various plots (Figs. 9–11, 16, 17; see text below) as broken lines, as are the 10 eV contours (Fig. 12); both the 0 and 10 eV limits are indicated for a variety of P compositions in Fig. 3.

The SP values can also be used to judge the incipient tendency to formation of nonstoichiometric P phases that are more U_M-stable than the corresponding stoichiometric parent pyrochlores. It is, for example, unlikely that a doping ion would enter a vacant site of the incorrect SP. Similarly, a site of zero SP would be indifferent to the charge of the species occupying it and a species of no net charge would not be held strongly (*cf.* the proposed location of water molecules in the 8(*a*) sites of hydrated pyrochlores, refs. 14, 20, 21, 33, and Fig. 3). Sites of the incorrect SP sign would not be included in ionic diffusion paths except at high kT values and at SP $\approx$ 0.

Can. J. Chem. Downloaded from www.nrcresearchpress.com by 210.87.254.40 on 09/05/12
For personal use only.

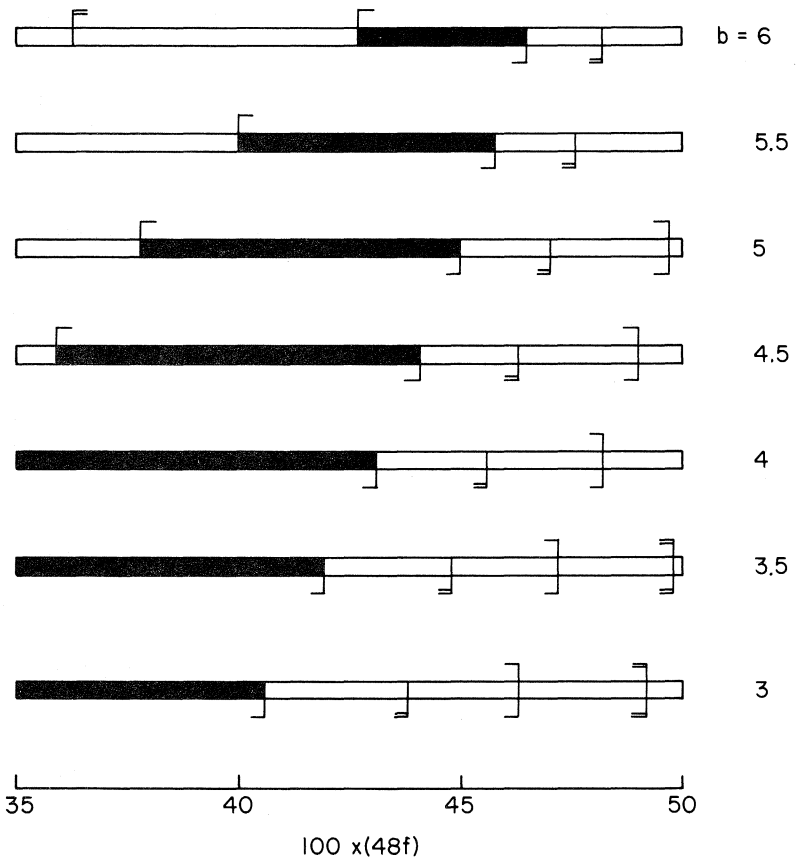

FIG. 2. Sign of SP(8*a*), SP(8*b*), and SP(48*f*) in the fluorites $A_2^{a+}B_2^{b+}(O_7\square)$ with ordered cations. Flag at top, SP(8*a*) = 0; flag at bottom, SP(8*b*) = 0; at top and bottom, SP(48*f*) = 0. Double flag, SP = 0; single flag, positive SP corresponding to O^{2-} site energy SE of 10 eV. SP increases in the direction of the flag. The region of SE > 10 eV in all three anion sites is shown in black.

The effect of a_0 on the normalized U_M values is not great. In most cases the total range of variation for a particular charge arrangement would be well within 10% of the U_M. In series of compositions corresponding to a given formula the effect of a_0 can be readily allowed for if the change of a_0 with r(A) or r(B) is known or can be estimated.

The description of results that follows and their discussion concern exclusively the normalized U_M and SP. No account has been taken of geometric factors (absolute and relative ionic sizes, excluded volume etc., *cf.* ref. 34)[7] which, when unfavourable, will prevent an electrostatically favourable arrangement from being adopted.

The U_M-stability of *P* arrangements relative to the corresponding perovskite arrangements is not considered in the present work. A discussion of this aspect will be found in ref. 27 (*cf.* also ref. 36).

Classical Pyrochlores $A_2B_2X_6Y$

The largest normalized U_M values within the range $0.375 \leq x(48f) \leq 0.46$ are obtained for $A_2^{a+}B_2^{b+}O_7$ (Fig. 4). This of course is the consequence of the formal double charge on the oxygen atom. For small a/b charge ratios the variation of U_M with $x(48f)$ is steep. As the a/b ratio increases and approaches unity, the sensitivity of U_M to changes in $x(48f)$ decreases markedly, even though a maximum of $|U_M|$ may

[7]For a discussion of the stability of the *P* structure based on electrostatic valency considerations, see Pyatenko (35).

Can. J. Chem. Downloaded from www.nrcresearchpress.com by 210.87.254.40 on 09/05/12
For personal use only.

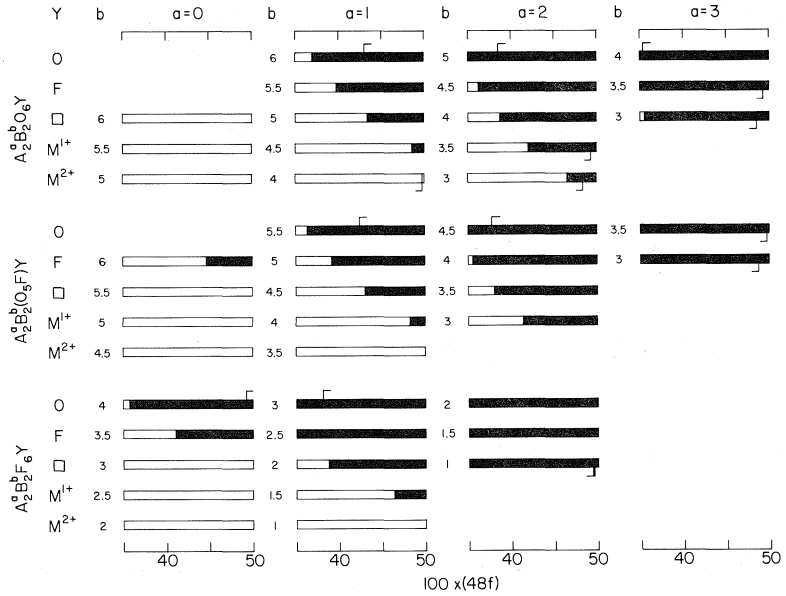

FIG. 3. Sign of SP(8*a*) and SP(48*f*) in the ordered pyrochlores $A_2B_2(X_6)Y$. Open, SP(8*a*) < 0; filled, SP(8*a*) > 0. Flag at top, SE(8*a*) = 10 eV (*cf.* caption of Fig. 2), increasing in the direction of the flag. Flag at bottom, SE(48*f*) = 10 eV; thick flag at bottom, SP(48*f*) = 0. The 10 eV boundaries are shown only where the atom occupying the site is, or can be, oxygen.

still fall within the $x(48f)$ range shown. For Y = O, F, or □ the curves begin to cross once the a/b ratio has attained or exceeds unity, while for Y = M there exists a clear separation of the curves for all the a/b ratios illustrated. This is important for compositions where size factors permit charge inversion, $a/b \rightarrow b/a$, as exemplified by $Pb_2^{4+}M_2^{3+}O_7$, M = Rh or Os (37). The curves for $a/b = 1$ are all below the dotted lines referring to the random defect fluorite distributions (the exception is $A_2B_2(O_6)M^{2+}$), and the difference in U_M for the two arrangements increases with the negative charge at 8(*a*). Consequently the U_M-stability of the *P* arrangements is almost always greater than that of the completely statistical distributions over the *F*-type lattice at constant a_0.

Similar results are obtained for the fluoride pyrochlores (Fig. 5). The stoichiometry $A_2^{1+}B_2^{2.5+}F_7$ corresponds to that of the orthorhombic[8] mineral *weberite*, Na_2MgAlF_7, whose structure type (*W*) is an alternative to *P* for compositions $A_2B_2X_7$ (38). While the *P* and *W* structures compete, the factors (relative and absolute atomic size, electronic) determining whether an $A_2B_2X_7$ phase will have the *P* or the *W* structure are not known at present. The relative stabilities of the two structures cannot be discussed in terms of U_M, for the U_M values for the *W* structure are not available. However, the *W* phases appear to occur much more rarely than the *P* phases (38), so that the decisive factors involved may be of a specialized nature.[9]

In mixed oxide–fluoride pyrochlores (Figs. 6 and 7) the problem of ordering in 8(*a*) is of interest. Comparing the U_M values for the different arrangements in *P* phases of identical stoichiometry (Figs. 8 and 9) shows that for $A_2B_2O_6$ the difference in U_M due to ordering can amount to as much as 10% of $U_M(III)$ in the $x(48f)$ range shown, and to somewhat more for $A_2B_2F_6$ and the oxide–fluoride phases. The differences between $U_M(I)$ and $U_M(II)$ are

[8]The true symmetry of natural weberite may in fact be lower than orthorhombic (personal communication from Dr. J. B. Faught).

[9]In addition to $A_2Sb_2O_7$ (A = Ca, Sr, Cd; *cf.* ref. 38), $Sr_2Bi_2O_7$ (39) and weberite itself, $Na_2MgB^{3+}F_7$ (B = Sc, V, Cr, Fe, Ga, In) (40), $Na_2B^{2+}CrF_7$ (B = Co, Ni, Zn) (41), $Na_2B^{2+}FeF_7$ (B = Mn, Fe, Co, Ni) (41–43), $Na_2Ni^{2+}Co^{3+}F_7$ (42), $Na_2TiWO_5F_2$ (25), and $Ag_2NiB^{3+}F_7$ (B = Cr, Fe, Al, In) (44) are also of the *W* type.

Can. J. Chem. Downloaded from www.nrcresearchpress.com by 210.87.254.40 on 09/05/12
For personal use only.

Can. J. Chem. Downloaded from www.nrcresearchpress.com by 210.87.254.40 on 09/05/12
For personal use only.

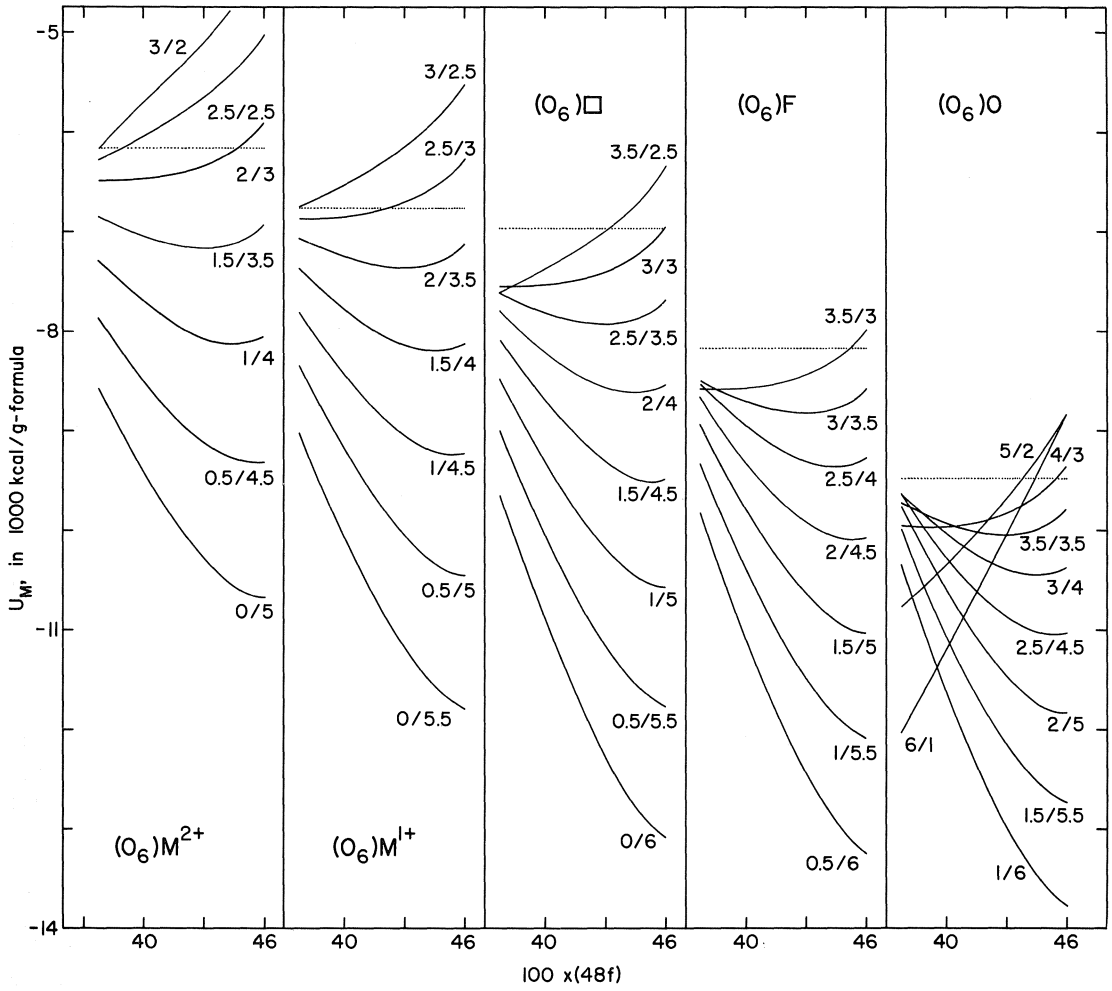

FIG. 4. Variation of the Madelung energy U_M (normalized to a_0 = 10 Å) with x(O) in $A_2^{a+}B_2^{b+}$-$(O_6)Y$ = $A_2|B_2|O_6|Y|\square$ pyrochlores. The horizontal dotted lines refer to random defect fluorite arrangements 8A + 8B|8A + 8B|36O + 8Y + 8□|6O + Y + □|6O + Y + □, x(O) = $\frac{3}{8}$ (see text). The a and b charge values are shown as a/b.

smaller but far from negligible, up to *ca.* 4% for $A_2B_2O_6F$ and $A_2B_2F_6$. There is a general decrease in these differences as a/b decreases; eventually the curves for $U_M(I)$ and $U_M(III)$, or $U_M(I)$ and $U_M(II)$, cross and the order of relative U_M-stability changes. However, for all the cases with $a/b \leq 1$ shown in Fig. 8 the U_M curves lie below the dotted horizontal lines indicating the U_M values for the random defect fluorite arrangements. Thus if the normalized U_M alone determined the relative stabilities of competing P and defect F arrangements (see below), the structures of $A_2B_2X_6$ and $A_2B_2X_6Y$ phases of a/b ratios known actually to occur should all be of type I This is in fact observed in all $A_2B_2O_6$ pyrochlores with the radius ratio r(A);r(B) below a certain limiting value which depends on a/b (11).

The positions of zero SP(8a) and SP(48f) relative to x(48f) in $A_2B_2O_6Y$, $A_2B_2(O_5F)Y$ and $A_2B_2F_6Y$ arrangements are shown in Fig. 3. The sign of SP(8a) changes *outside* the x(48f) interval of 0.4 to 0.45 in most of the cases. The exceptions are the charge combinations $a|b|g|h$ = 1|5.5|−2|0, 2|3.5|−2|1, 1|4.5|−1.833|0, 2|3|−−1.833|1, and 0|3.5|−1|−1. In the range of

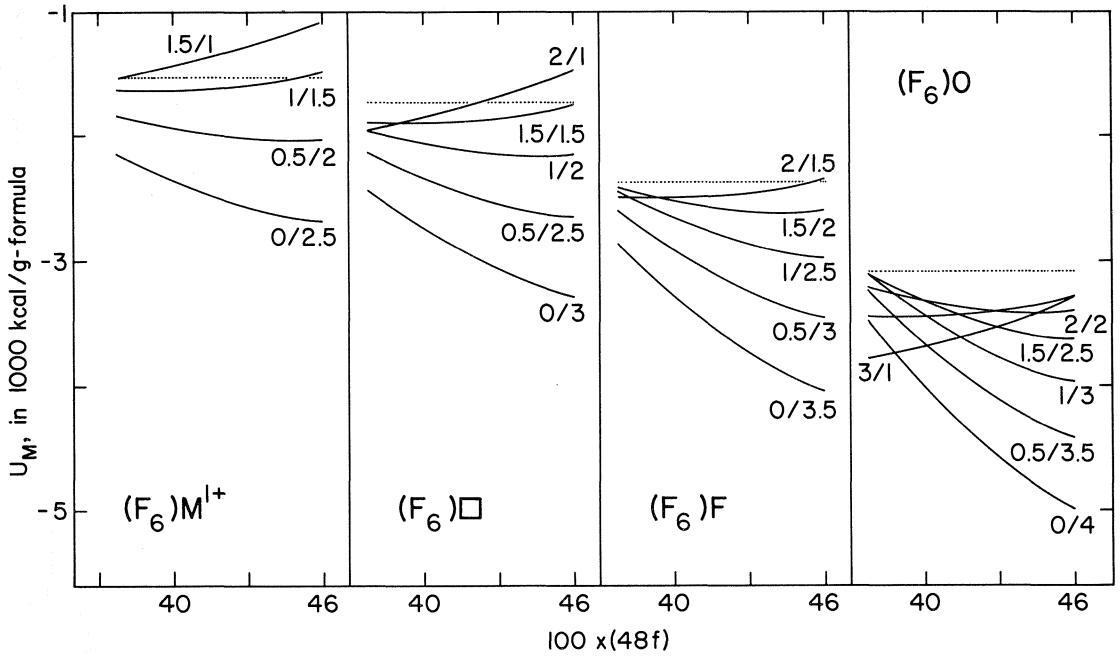

FIG. 5. U_M *vs.* x(F) for $A_2B_2(F_6)Y$ pyrochlores (see Fig. 4).

$x(48f)$ and for the charge combinations presented in Fig. 3, SP(48*f*) is always positive except for $2|1|-1|0$, and then only close to $x(48f) = 0.5$.

Inverse Pyrochlores $\square_2B_2X_6M$

The pure inverse pyrochlores have compositions $A_2{}^0B_2{}^{b+}X_6{}^{g-}M^{m+}$ (Figs. 4–7). Of these, $\square_2B_2{}^{5.5+}(O_6)M^{1+}$ has the largest $|U_M|$ value because of the high formal charges, and the steepest variation of U_M with $x(48f)$. Otherwise the U_M *vs.* $x(48f)$ curves show no unusual features.

The $|U_M|$ of $\square_2B_2{}^{5.5+}O_6M^{1+}$ is about 0.15–0.2% higher than that of $A_2{}^{0.5+}B_2{}^{5.5+}O_6\square$ for the entire 0.375 to 0.46 $x(48f)$ range, $SP(48f)_{max}$ being in both cases at $x(48f) = 0.4443$, and about 0.8 to 1% higher for $\square_2B_2{}^{2.5+}F_6M^{1+}$ compared with $A_2{}^{0.5+}B_2{}^{2.5+}F_6\square$.

For the inverse *P* phases with $a > 0$ discussed by Schrewelius (15), *i.e.* those with partial simultaneous occupancy of 16(*c*), the limiting composition at $\epsilon = \frac{1}{3}$ corresponds to $A_2B_2(O_6)M^{1+}$ with $a/b = 0.5/5$ (Fig. 4), while for $\frac{1}{3} < \epsilon \leq \frac{2}{3}$, U_M curves intermediate between $A_2{}^{0.5+}B_2{}^{5+}(O_6)M^{1+}$ and $A_2{}^{1+}B_2{}^{5+}(O_6)\square$ are appropriate.

In inverse *P* arrangements of type *IV*, $\square_2B_2{}^{b+}X_6{}^{g-}M_{1/2}{}^{m+}$, the ordering energy $U_M(\text{ord}) - U_M(\text{rand})$ is negative for the charge combinations $b|g|m = 2.5|-1|2$, $2.75|-1|1$, and $5.5|-2|2$ (curves *A* and *B*, Fig. 10), and for $5.75|-2|1$ (curve *C*) up to $x(48f)$ of about 0.465. The vacancies at 8(*a*) in the pyrochlores $\square_2B_2{}^{2.5+}F_6M_{1/2}{}^{2+}$, $\square_2B_2{}^{2.75+}F_6M_{1/2}{}^{1+}$, $\square_2B_2{}^{5.5+}O_6M_{1/2}{}^{2+}$, and $\square_2B_2{}^{5.75+}O_6M_{1/2}{}^{1+}$ might thus be expected to be ordered, provided of course that the ordering Madelung energies, which do not exceed about 4% of U_M(rand), and are much smaller for $\square_2B_2{}^{5.75+}O_6M_{1/2}{}^{1+}$, are by themselves sufficient to stabilize the ordered arrangement. Compositions in which the 8(*a*) equipoint is half-occupied by an anion Y^{h-} instead of M^{m+} (curves *E*, *F*, *G*) would, on the U_M criterion, also favour ordering, but SP(8*a*) changes sign, thereby significantly restricting the admissible $x(48f)$ range. In addition, the charge on B would have to be high and the structure could no longer be considered 'ionic' even in the first approximation. For $\square_2B_2{}^{6.5+}O_6O_{1/2}$, SP(8*a*) is less than what would correspond to 10 eV over the entire $x(48f)$ range shown in Fig. 10 (curve *F*), hence the *P* structure should not exist for this composition.

Can. J. Chem. Downloaded from www.nrcresearchpress.com by 210.87.254.40 on 09/05/12
For personal use only.

Can. J. Chem. Downloaded from www.nrcresearchpress.com by 210.87.254.40 on 09/05/12
For personal use only.

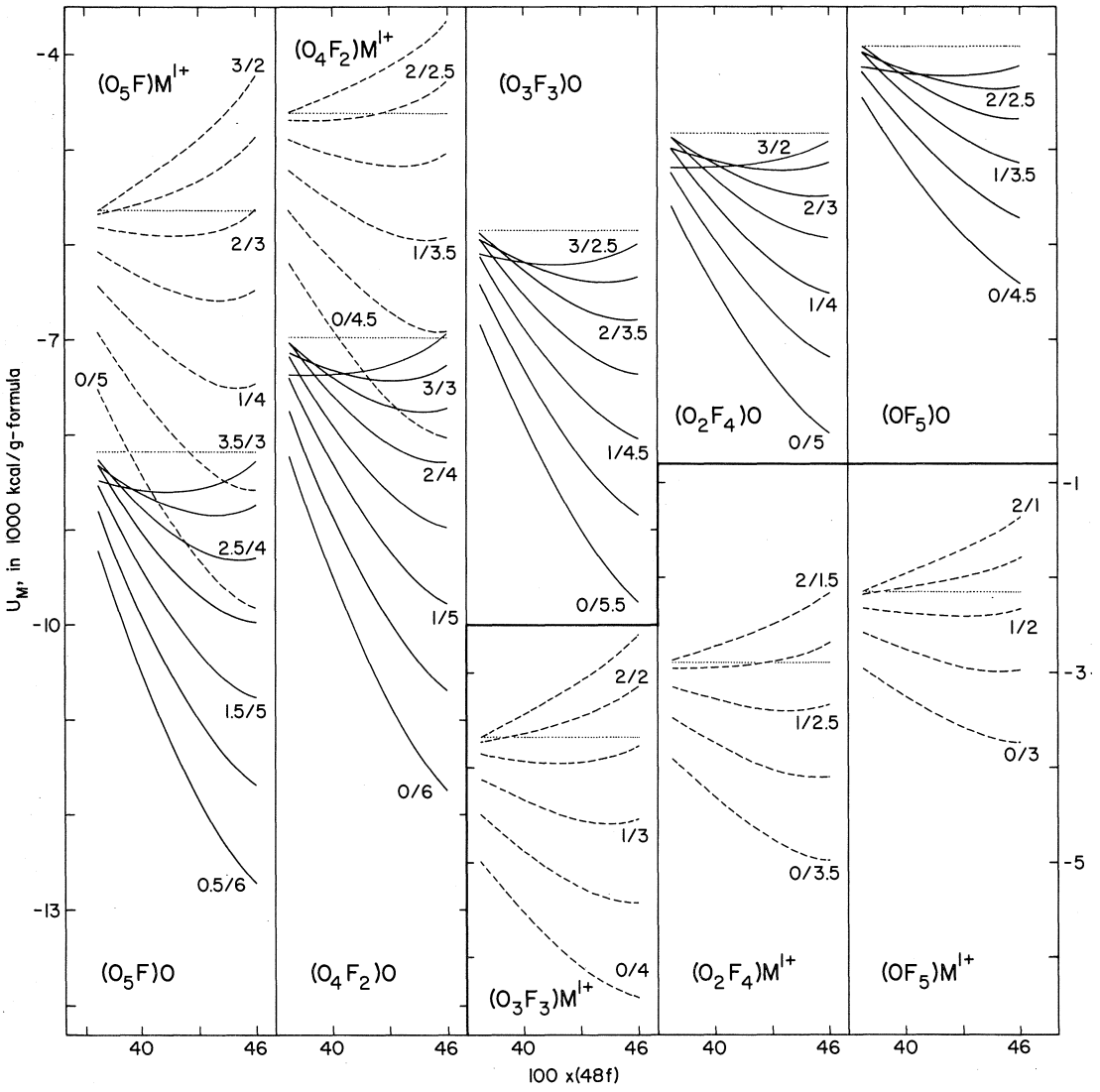

FIG. 6. U_M *vs.* $x(48f)$ for cubic pyrochlores of compositions $A_2B_2(O_{6-n}F_n)O$ (solid lines) and $A_2B_2(O_{6-n}F_n)M^{1+}$ (dashed lines), $n = 1, 2, \ldots, 5$ (see Fig. 4).

Defect Fluorites

In classical pyrochlores sites of the 8(*b*) ($\frac{3}{8}$, $\frac{3}{8}$, $\frac{3}{8}$; etc.) equipoint of *Fd*3*m* are vacant. However, distributions of the type 16(*c*)|16(*d*)|48(*f*)|8(*a*)|8(*b*) must be considered when it is desired to compare, for a given composition, the U_M values for the *P* structures with the U_M values of the competing 'defect fluorite' structures. In the intuitively most plausible distribution for $A_2B_2X_6Y$ (Y = O or F or both), the cations would populate the 16(*c*) + 16(*d*) sites at random, and the anions and anion vacancies would be distributed statistically over 48(*f*) + 8(*a*) + 8(*b*), with $x(48f) = \frac{3}{8}$. The resulting distribution, 8A+8B|-8A+8B|36X+6Y+6□|6X+Y+□|6X+Y+□, would correspond to the *random defect fluorite* arrangement, which could of course be described on the simple *Fm*3*m* unit cell.

The U_M values for such distributions are shown in Figs. 4–8 by horizontal dotted straight lines; the corresponding lines for $A_2B_2X_6M$ are also shown. The variation of U_M with $x(48f)$ for

Can. J. Chem. Downloaded from www.nrcresearchpress.com by 210.87.254.40 on 09/05/12
For personal use only.

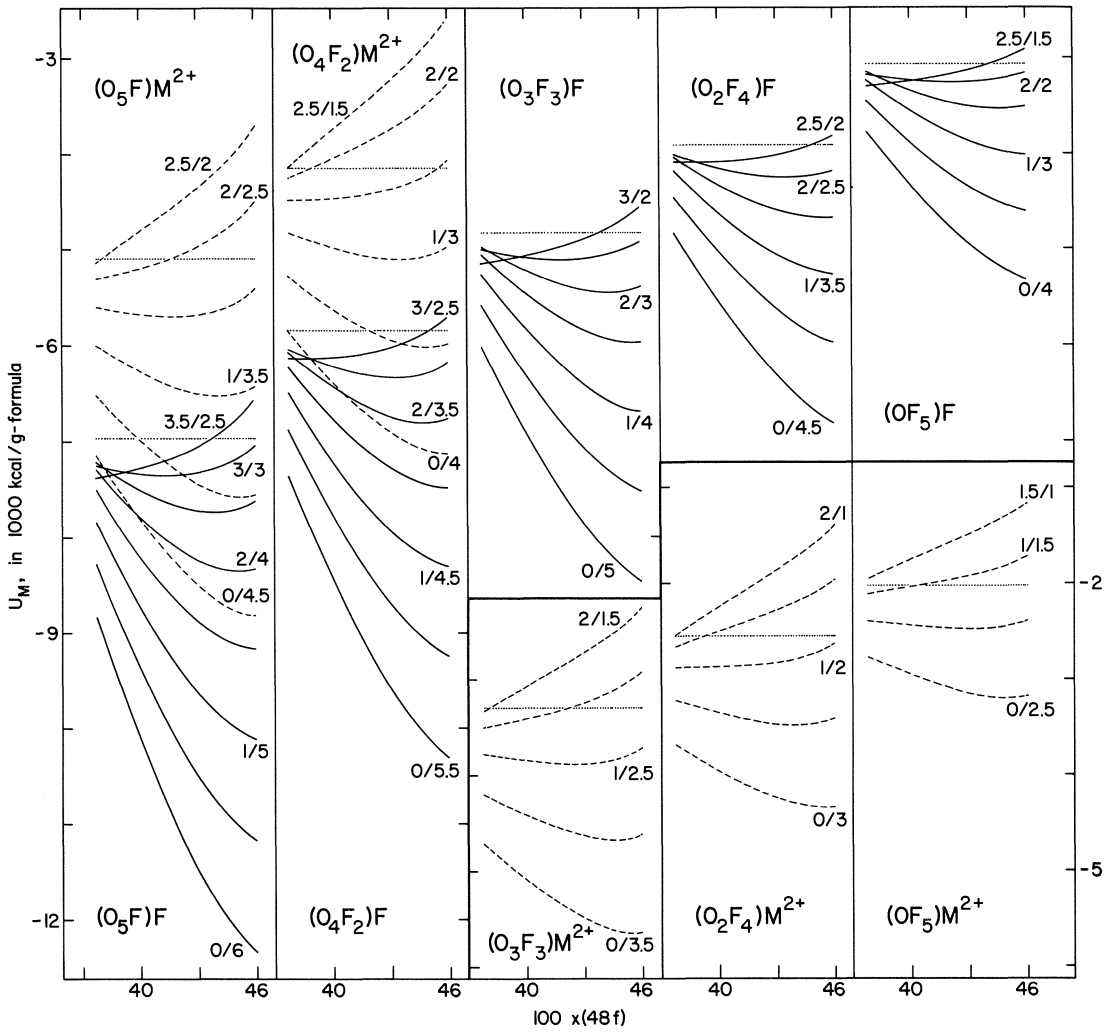

FIG. 7. U_M *vs.* $x(48f)$ for cubic pyrochlores of compositions $A_2B_2(O_{6-n}F_n)F$ (solid lines) and $A_2B_2(O_{6-n}F_n)M^{2+}$ (dashed lines), $n = 1, 2, \ldots, 5$ (see Fig. 4).

Can. J. Chem. Downloaded from www.nrcresearchpress.com by 210.87.254.40 on 09/05/12
For personal use only.

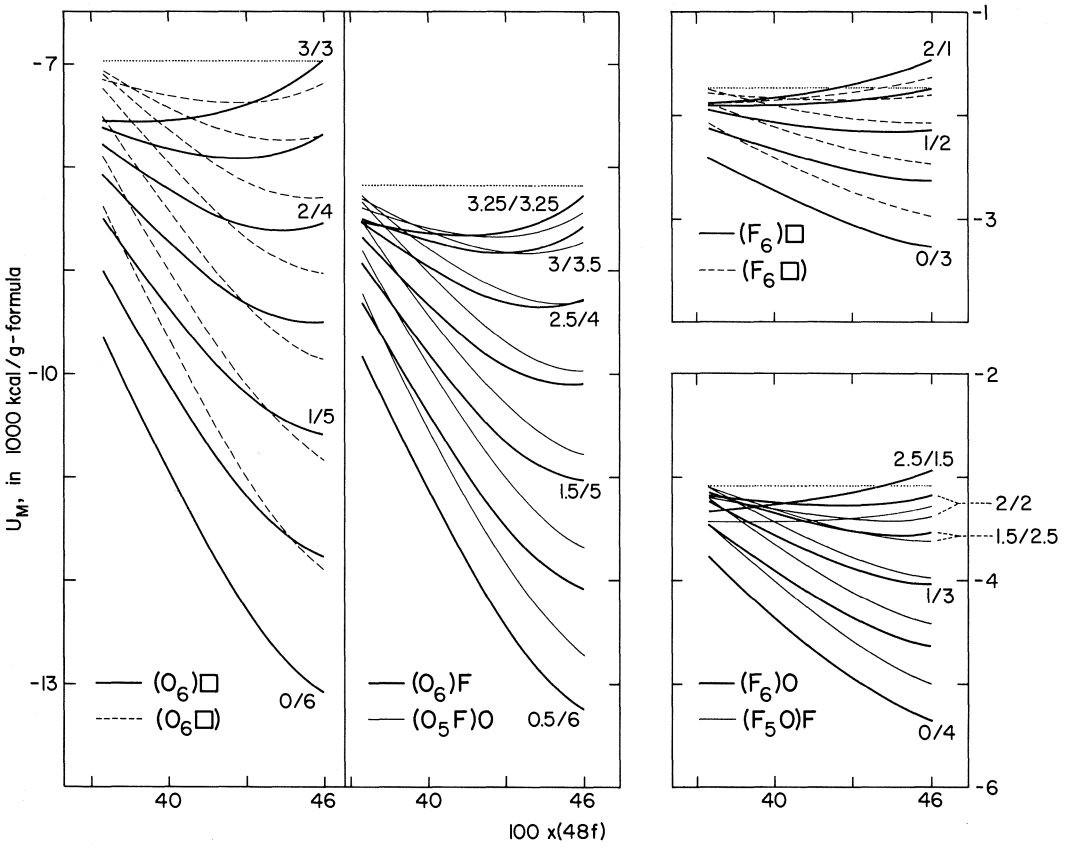

FIG. 8. Dependence of U_M on the occupancy of 8(*a*) for the cubic pyrochlores $A_2B_2O_6$, $A_2B_2O_6F$, $A_2B_2F_6O$, and $A_2B_2F_6$. $(F_6)\square$ refers to arrangement *I* etc. (see text). The curves for $A_2B_2(O_6F)$ would be close to those for $A_2B_2(O_5F)O$; the curves for $A_2B_2(F_6O)$ would be close to those for $A_2B_2(F_5O)F$.

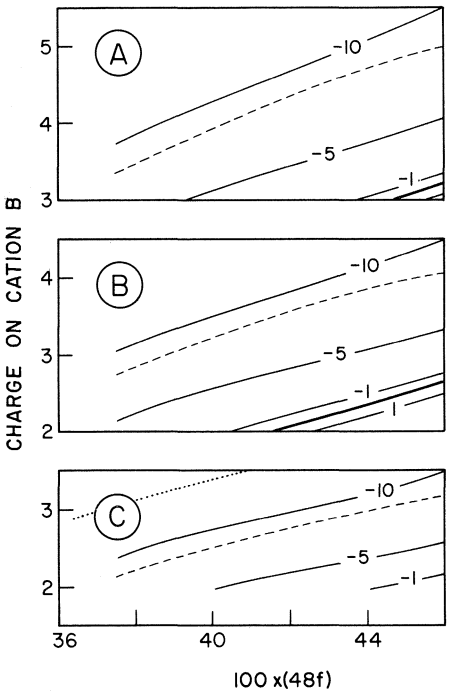

FIG. 9. Variation, with $x(48f)$, of $100[U_M(2) - U_M,(1)]/|U_M|$ for the pyrochlore pairs (*A*) $A_2B_2(O_5F\square) = A_2B_2(O_4F_3)$ (1) $- A_2B_2(O_5F)\square$ (2); (*B*) $A_2B_2(O_3F_3\square) = A_2B_2(O_2F_5)$ (1) $- A_2B_2(O_3F_3)\square$ (2); (*C*) $A_2B_2(OF_5\square) = A_2B_2F_6F$ (1) $- A_2B_2(OF_5)\square$ (2). The loci of zero SP at 8(*a*) are indicated by broken lines: component 1 (*III*), dotted; component 2 (*II*), dashed. Regions of positive SP are to the right.

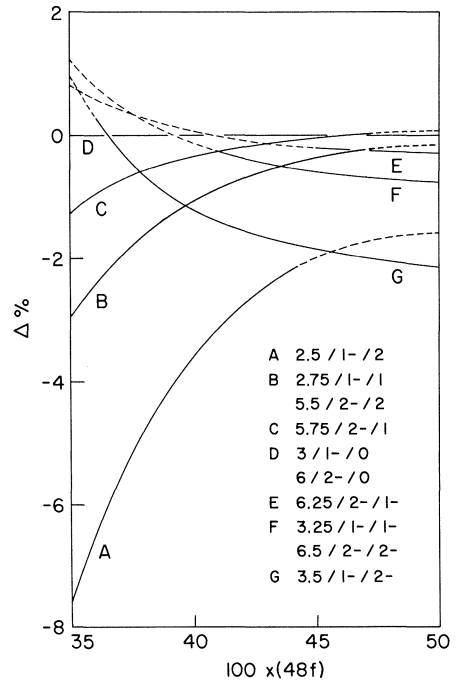

FIG. 10. The Madelung energy of ordering Δ of atoms in 8(*a*) sites for pyrochlores of composition $\square_2B_2^{b+}X_6^{g-}Y_{1/2}^{h\pm} = 16\square|16B|48X|4Y + 4\square|8\square$ (arrangement *IV*). $\Delta\% = 100[U_M(\text{ord}) - U_M(\text{rand})]/|U_M(\text{rand})|$. The charge combinations $b|g|h$ are shown. The dashed sections of the curves indicate regions of $x(48f)$ where the sign of SP is opposite to that required for stabilization (positive in 16(*c*), curves *A*, *B*, *C*; negative in 8(*a*), curves *E*, *F*, *G*).

$A_2B_2X_6Y$ arrangements with A and B ordered, *i.e.* $16A|16B|36X+6Y+6\square|6X+Y+\square|6X+Y+\square$, is shown in Fig. 11. To simplify presentation, only U_M values normalized to the average ionic charge of -1.5 appear in the drawing; multiplication by $(\text{charge}/1.5)^2$ will generate the corresponding U_M curves for other values of anionic charge. U_M of the random fluorites $(A_2B_2)(X_6Y\square)$ (curve $3|3|-1.5$ in Fig. 11) varies little with $x(48f)$ in the immediate vicinity of the minimum at $x(48f) = \frac{3}{8}$.

The relative Madelung stabilities of alternative arrangements for $A_2B_2O_6O$, as measured by $100(U_M - U_M')/|U_M'|$, are shown in Fig. 12. If the zero value of this difference is taken as the minimum criterion of relative stability, then other things being equal, (*i*) *P*(ord) is always more stable than *P*(rand), *F*(ord), *F*(rand), and (*ii*) *P*(rand) and *F*(ord) are always more stable than *F*(rand), for the observed range of b and $x(48f)$. On the other hand, *P*(rand) is more stable than *F*(ord) only for $b < 4.5$. Consideration of a minimum stabilizing potential at *any* oxygen site (Figs. 2 and 12) narrows down some of the relative stability regions, but, while the extent of these regions is consistent with the observed facts, no useful restriction on the b or $x(48f)$ ranges results for *P*(ord) *vs.* *F*(rand), where a criterion of predictive value would be desired most (*cf.* the tendency of $A_2^{3+}Zr_2O_7$ and $A_2^{3+}Hf_2O_7$ toward formation of disordered arrangements).[10] Thus U_M cannot by itself be used to predict the stability of the *P*(ord) phase relative to the corresponding random defect fluorite, nor is such stabilization predictable on the assumption of an O^{2-} site energy of 10 eV.

[10]For a recent demonstration of this tendency using Eu^{3+} as a spectroscopic probe of site symmetry, see ref. 45.

Can. J. Chem. Downloaded from www.nrcresearchpress.com by 210.87.254.40 on 09/05/12
For personal use only.

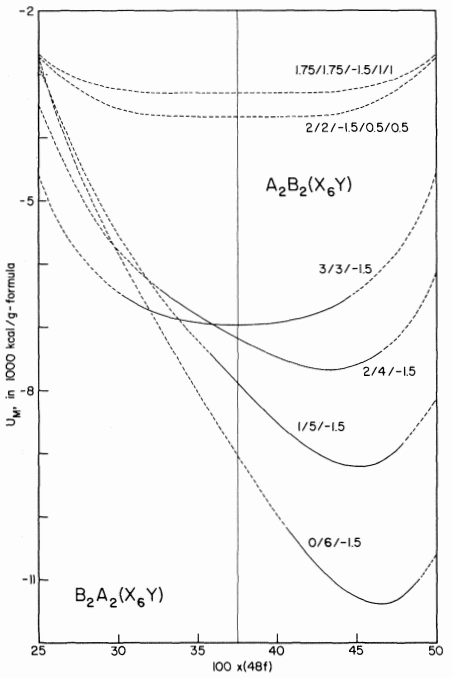

FIG. 11. Variation of U_M with $x(48f)$ for random defect fluorites $A_2B_2X_6Y = 8A|8B|36X + 8Y + 8\square|6X + Y + \square|6X + Y + \square$ having an average ionic charge of -1.5. To convert to charge s, multiply the U_M values by $(s/1.5)^2$. The broken lines indicate that the SP at 8(a) or 8(b) or both (and also at 48(f) at and near $x(48f) = \frac{1}{4}$ for $a/b = 0/6, 1/5, 2/4, 3/3$, and at and near $x(48f) = \frac{1}{2}$ for $a/b = 3/3$) are negative, hence these sites cannot contain anions. The top two curves refer to distributions specified in the drawing.

Variation of the Maximum of the Site Potential at 48(f)

As pointed out by Pannetier (27), the variation of SP(48f) with $x(48f)$ in the pyrochlores goes through a maximum. The position of this maximum in compositions $A_2B_2X_6Y$ varies little, for a particular X, with Y, but there is considerable variation with the charge on B (Fig. 13). Pannetier noticed that the value of SP$(48f)_{max}$ coincides with the observed $x(48f)$ in the 2–5 and 3–4 $A_2B_2O_7$ pyrochlores. The more extensive range of computation presented in Fig. 13 shows this to hold also for the inverse pyrochlores for which $x(48f)$ have been determined.

It is unlikely that the upper limit of the $x(48f)$ range, for a particular a/b and X, is determined by the course of SP(48f). While the width of the SP(48f) *vs.* $x(48f)$ curve decreases with increasing b, even for $a/b = 1/6$ the width is appreciable compared with the observed range of $x(48f)$ in $A_2B_2O_6Y$ at SP(48f) values corresponding to site energies of O^{2-} much in excess of 10 eV (Fig. 14).

The relation of $SP(48)_{max}$ to $|U_M|_{max}$ for $A_2B_2(O_7\square)$ fluorites and the corresponding $A_2B_2O_6O$ pyrochlores is displayed in Fig. 15. The two quantities coincide only at $x(48f) = \frac{3}{8}$: for $b = 3.5$ for the F arrangement (random distribution of A + B and O + □), and for $b \approx 2.9$ for the P arrangement.

Arrangements Involving 32(e) Sites

Displacing M in inverse pyrochlores from 8(a) to 32(e) has a relatively small effect on U_M unless the displacement is considerable and at the same time $x(48)f$ is well outside the range of 0.4 to 0.45 (Figs. 16 and 17). In all the eight cases considered the relative U_M difference, $\Delta = 100[U_M(32e) - U_M(8a)]/|U_M(8a)|$, is zero not only, trivially, for $y(32e) = \frac{1}{8}$, but along a well-established curved locus with $y > \frac{1}{8}$ as well. In one case, $\square_2B_2^{5.5+}O_6M^{1+}$, there is also a $\Delta = 0$ locus for $y < \frac{1}{8}$ (Fig. 17).[11] Thus there would be no difference in U_M, for a given $x(48f)$, between $y = \frac{1}{8}$ and the $y \neq \frac{1}{8}$ value defined by the curved $\Delta = 0$ contour. For $\square_2B_2^{2.5+}F_6M^{1+}$, $\square_2B_2^{5.5+}O_6M^{1+}$ and $\square_2B_2^{5+}O_6M^{2+}$ this possibility exists within the range of $x(48f)$ actually observed. For $\square_2B_2^{5.5+}O_6M^{1+}$, *three* $y(\Delta = 0)$ values could correspond to a value of $x(48f)$.

It would be difficult to say to what extent values of Δ as small as 0.05% stabilize actual arrangements with M displaced from 8(a) to 32(e), for the anion–anion repulsive forces can become critical for the stability of the pyrochlore arrangement itself (*cf.* ref. 11) and contributions from this source to the lattice energy may easily outweigh any contribution to U_M arising from a displacement of M.[12] There are strong indications that in structure refinements $y(32e)$ and the

[11]A corresponding $\Delta = 0$ locus may exist for $\square_2B_2^{5+}O_6M^{2+}$ but cannot be demonstrated: owing to the finite precision the computed Δ values for y in the vicinity of $\frac{1}{8}$ are indeterminate and the shape and position of the Δ contours close to $y = \frac{1}{8}$ are often uncertain.

[12]Since the ionic radius of O^{2-} appears to be very structure-dependent, polarization forces also become important. Furthermore, it is not known whether the repulsive forces follow an inverse power or an exponential law. The calculation of the repulsive parameter of the O^{2-} ion is then not only a major enterprise but one the outcome of which is uncertain.

Can. J. Chem. Downloaded from www.nrcresearchpress.com by 210.87.254.40 on 09/05/12
For personal use only.

Can. J. Chem. Downloaded from www.nrcresearchpress.com by 210.87.254.40 on 09/05/12
For personal use only.

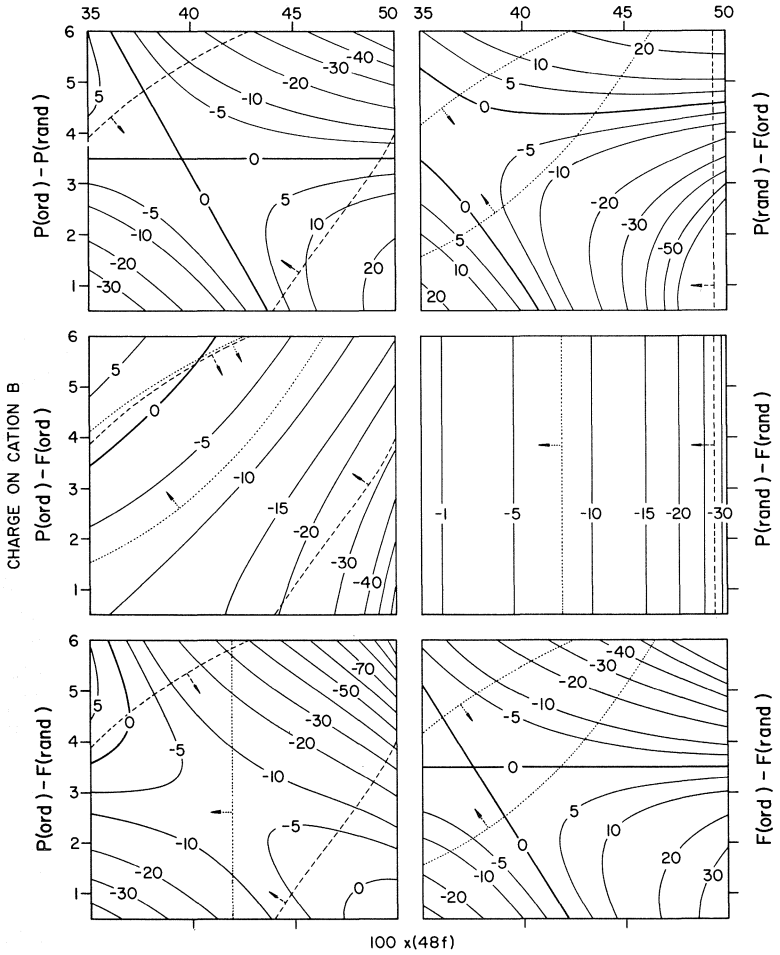

FIG. 12. The minimum regions of stability of oxide pyrochlores relative to the corresponding defect fluorites (ordered and random arrangements) expected from differences in U_M (normalized to a_0 = 10 Å) and from SP criteria. *P*(ord), $A_2B_2O_6O\square$; *P*(rand), $(A_2B_2)O_6O\square$; *F*(ord), $A_2B_2(O_7\square)$; *F*(rand), $(A_2B_2)(O_7\square)$. Solid lines, contours of $100(U_M - U_M')/|U_M'|$; dashed lines, SE = 10 eV contours (*cf.* caption of Fig. 2) at *any* anion site of the *P* structure; dotted lines, ditto for the *F* structure. Regions of SE > 10 eV are indicated by arrows. For the first-named arrangement in each pair to be stable, on these criteria, relative to the last-named, $x(48f)$ and the charge on B must fall within a region of negative U_M difference and within the high-side of the 10 eV contour.

Can. J. Chem. Downloaded from www.nrcresearchpress.com by 210.87.254.40 on 09/05/12
For personal use only.

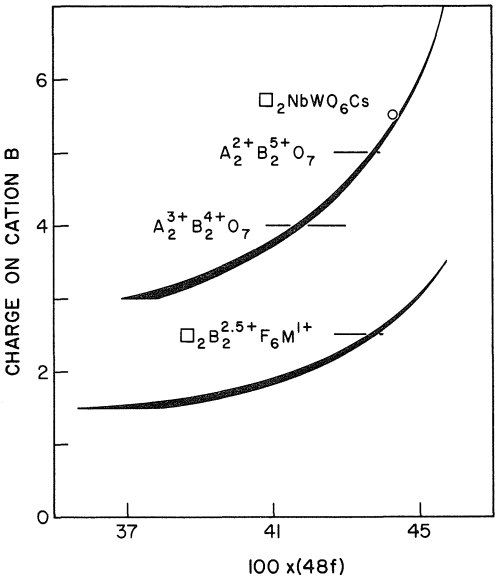

FIG. 13. Position of the maximum of SP(48*f*) for cubic $A_2B_2O_6Y$ (top curve) and $A_2B_2F_6Y$ (bottom curve) pyrochlores (Y = O, F, □, M^{1+}, M^{2+}). The line width indicates the range of variation of $SP(48f)_{max}$ with Y. The observed ranges of $x(48f)$ are shown as horizontal bars ($A_2B_2O_7$, ref. 38; inverse pyrochlores, refs. 14 and 24).

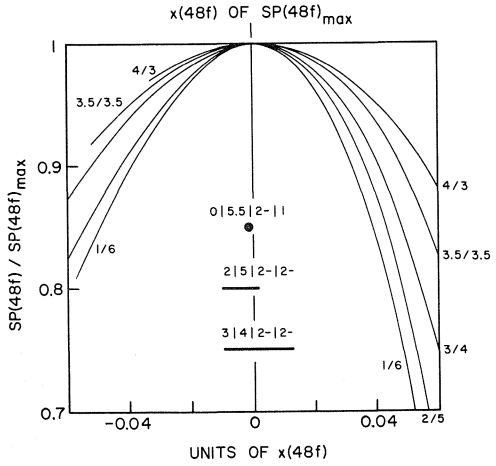

FIG. 14. Variation of SP(48*f*) relative to $SP(48f)_{max}$ in the pyrochlores $A_2^{a+}B_2^{b+}O_6Y$ with different a/b ratios. The observed ranges of $x(48f)$ are shown for comparison.

thermal parameters of the M atom are highly correlated (22, 23, 33). An accurate refinement from a generous number of reflections from a single crystal of an inverse pyrochlore, preferably from a neutron-diffraction experiment,

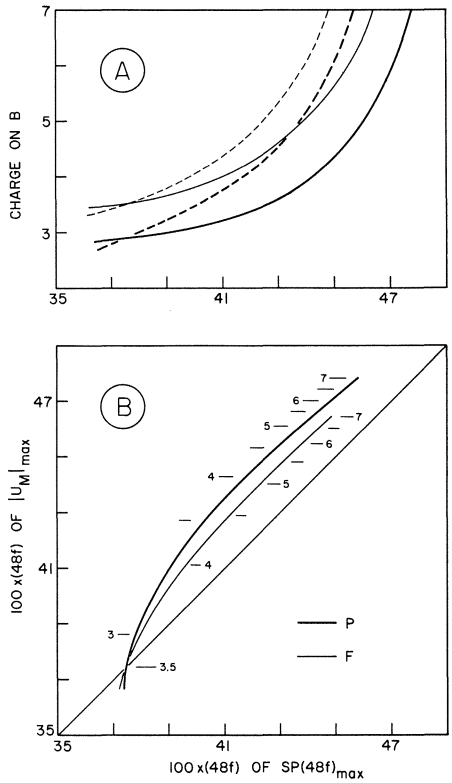

FIG. 15. (*A*) Variation of $|U_M|_{max}$ (solid lines) and $SP(48f)_{max}$ (dashed) with $x(48f)$ and the charge on B for the pyrochlores $A_2B_2O_6O$ and fluorites $A_2B_2(O_7\square)$. (*B*) Same as *A* in a different presentation. The charges on B are indicated by horizontal bars.

might well reveal that the 32(*e*) hypothesis is a description equivalent to one with M in 8(*a*) and with the thermal motions of the atoms in 16(*d*) and 48(*f*) anisotropic.[13,14] However, such y values as have been reported (23–26, 46–48) fall within permissible regions of Δ in Figs. 16 and 17. Where decision between two $y(R_{min})$ values symmetric about $y = \frac{1}{8}$ was made from geometric or other subsidiary considerations ($\square_2Nb_2(O_5F)$-Tl, $\square_2TiW(O_5F)Tl$, $\square_2TiNb(O_4F_2)Tl$, refs. 23,

[13]In Figs. 16 and 17, a displacement ∂y of |0.01| from 8(*a*), regarded as a thermal root-mean-square amplitude, would correspond to an isotropic temperature factor *B* of about 2.3 Å^2.

[14]However, Gasperin (49) has recently reported the occurrence of the 442 reflection in single-crystal photographs of a pyrochlore formulated as $Tl_{0.77}H_{0.63}(H_2O)_y(Nb_{1.40}W_{0.60})O_6$. This reflection would appear if the 32(*e*) site were occupied. The diffraction data were interpreted on the assumption that three sets of 32(*e*) sites are partially occupied by the Tl atoms.

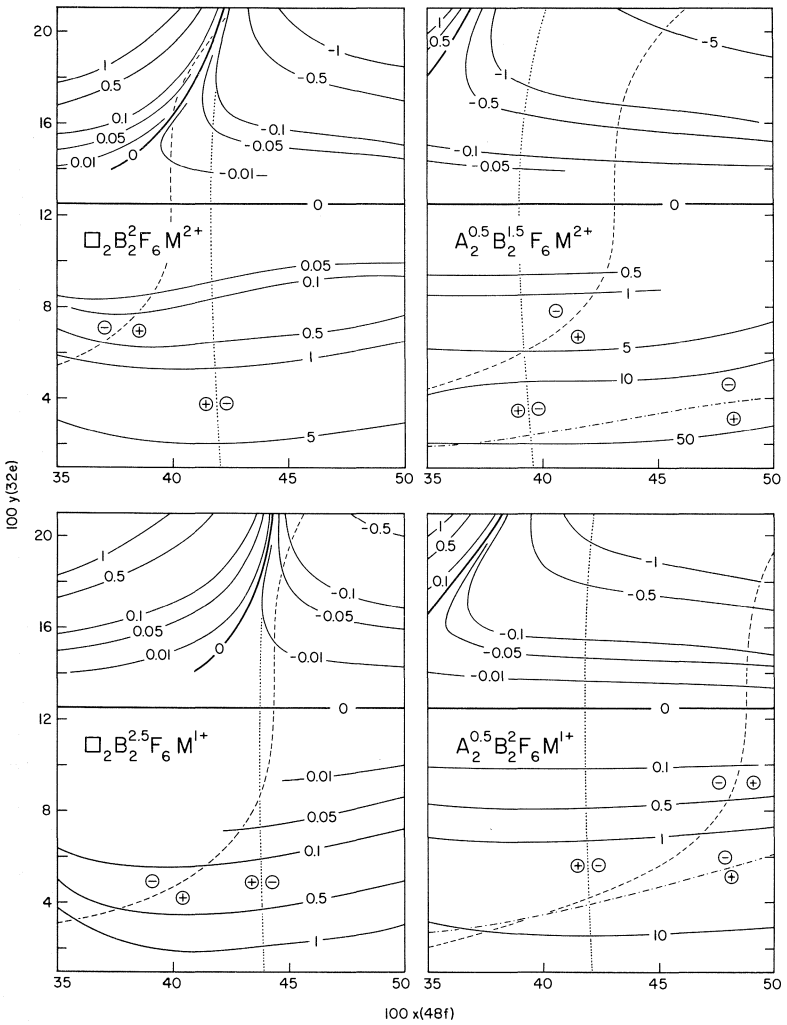

FIG. 16. $\Delta\% = 100[U_M(32e) - U_M(8a)]/|U_M(8a)|$ as a function of $x(48f)$ and $y(32e)$ for inverse pyrochlores $\square_2B_2F_6M$ and $A_2^{0.5+}B_2F_6M$. The loci of SP = 0 are indicated by broken lines: 16(*c*), dashed; 8(*b*), dotted; 32(*e*), dot–dash.

25, 26; $\square_2M^{5+}WO_6M^{1+}.H_2O$, M^{5+} = Nb, Ta, Sb, M^{1+} = Li, Na, K, ref. 47), the value chosen falls in a region of $\Delta < 0$ (allowing for the substitution of O by F), while the other value falls in a region of $\Delta > 0$. Analogy would favour $y(R_{min}) < \frac{1}{8}$ also for $\square_2SbWO_6(H_3O)$ and $\square_2SbWO_6(NH_4)$ (46) and for $\square_2Nb_2(O_5F)Rb$ and $\square_2Nb_2(O_5F)Cs$ (23). For $\square_2Li_{0.5}Cr_{1.5}F_6Rb$ (24), on the other hand, the Δ plot (Fig. 16) seems to favour $y(R_{min}) > \frac{1}{8}$.

Finally the occurrence of cubic pyrochlores of reduced space-group symmetry cannot be ruled out. The weak extra reflections which were recently reported (47) in the X-ray powder diffraction pattern of the hydrated pyrochlore $NaNbWO_6.H_2O$, could be indexed on a unit cell of $F23$ symmetry. Since the proposed atomic distributions in $F23$ are derived from those in $Fd3m$, the above general conclusions concerning U_M-stability are likely to apply also to pyrochlores of this type.

Acknowledgments

We wish to thank Dr. J. S. Carlow for assistance with the computations. Financial support

Can. J. Chem. Downloaded from www.nrcresearchpress.com by 210.87.254.40 on 09/05/12
For personal use only.

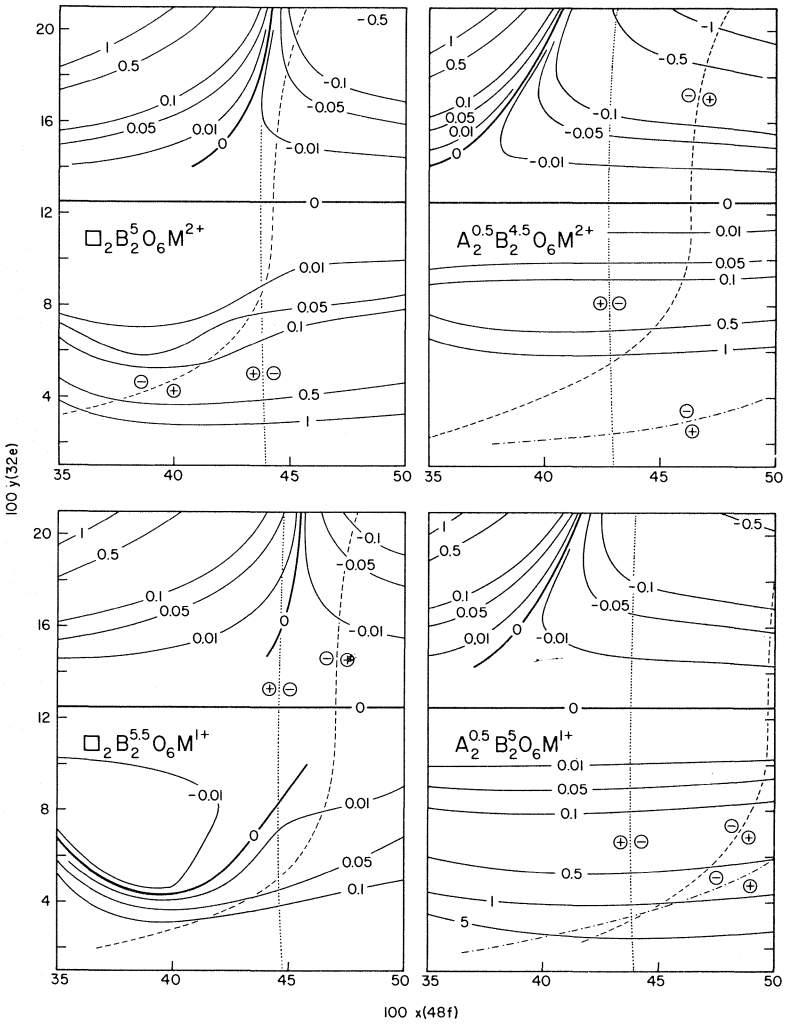

FIG. 17. Same as Fig. 16 but for $\square_2B_2O_6M$ and $A_2^{0.5+}B_2O_6M$.

by the National Research Council of Canada and by IBM Canada Ltd. is hereby acknowledged.

1. D. J. STEWART, O. KNOP, R. E. MEADS, and W. G. PARKER. Can. J. Chem. **51**, 1041 (1973).
2. F. N. BRADLEY. J. Am. Ceram. Soc. **52**, 114 (1969).
3. D. LAGUITTON and J. LUCAS. C.R. **269C**, 105 (1969).
4. D. LAGUITTON and J. LUCAS. C.R. **269C**, 228 (1969).
5. J. PANNETIER and J. LUCAS. C.R. **270C**, 1013 (1970).
6. Y. CALAGE, J. PANNETIER, and J. LUCAS. J. Solid State Chem. **3**, 425 (1971).
7. J.-L. FOURQUET, G. ORY, G. GAUTHIER, and R. DE PAPE. C.R. **271C**, 773 (1970).
8. A. G. TUTOV, V. I. BADER, and I. E. MYL'NIKOVA. Kristallografiya, **17**, 406 (1972); Sov. Phys. Crystallogr. **17**, 345 (1972).
9. J.-C. BEYS, A. VÉDRINE, and J.-P. BESSE. C.R. **274C**, 857 (1972).
10. I. N. BELYAEV and E. N. EVSTIFEEV. Zh. Neorg. Khim. **19**, 3187 (1974); Russ. J. Inorg. Chem. **19**, 1745 (1974).
11. W. W. BARKER, J. GRAHAM, O. KNOP, and F. BRISSE. Crystal chemistry of oxide pyrochlores. *In* The chemistry of extended defects in non-metallic solids. *Edited by* L. Eyring and M. O'Keeffe. North-Holland Publ. Co., Amsterdam-London, 1970. pp. 198–206.
12. A. W. SLEIGHT. Inorg. Chem. **7**, 1704 (1968).
13. O. KNOP, F. BRISSE, L. CASTELLIZ, and SUTARNO. Can. J. Chem. **43**, 2812 (1965).
14. D. BABEL, G. PAUSEWANG, and W. VIEBAHN. Z. Naturforsch. **22b**, 1219 (1967).
15. N. SCHREWELIUS. Doctoral thesis. University of Stockholm, Stockholm, Sweden. 1943. (In Swedish.)

Can. J. Chem. Downloaded from www.nrcresearchpress.com by 210.87.254.40 on 09/05/12
For personal use only.

16. N. SCHREWELIUS. Z. Anorg. Allg. Chem. **238**, 241 (1938).
17. C. JACOBONI, G. COURBION, J.-L. FOURQUET, G. GAUTHIER, and R. DE PAPE. C.R. **270C**, 1455 (1970).
18. G. LE FLEM and R. SALMON. C.R. **271C**, 1182 (1970).
19. E. BANKS, O. BERKOOZ, and J. A. DE LUCA. Mat. Res. Bull. **6**, 659 (1971).
20. M. HERVIEU, C. MICHEL, and B. RAVEAU. Bull. Soc. Chim. Fr. 3939 (1971).
21. B. DARRIET, M. RAT, J. GALY, and P. HAGENMULLER. Mat. Res. Bull. **6**, 1305 (1971).
22. G. ALLAIS, C. MICHEL, and B. RAVEAU. C.R. **274C**, 1625 (1972).
23. G. ORY, J.-L. FOURQUET, C. JACOBONI, J.-P. MIRANDAY, and R. DE PAPE. C.R. **273C**, 747 (1971).
24. G. COURBION, C. JACOBONI, and R. DE PAPE. C.R. **273C**, 809 (1971).
25. J.-P. MIRANDAY, G. GAUTHIER, and R. DE PAPE. C.R. **273C**, 970 (1971).
26. G. ORY. Thèse de doctorat. Université de Bordeaux I. Bordeaux. 1972.
27. J. PANNETIER. J. Phys. Chem. Solids, **34**, 583 (1973).
28. J. C. SLATER and P. DECICCO. M.I.T. Solid State Mol. Theory Group, Quart. Progr. Rept. No. 50. October 1963. p. 46.
29. J. PANNETIER and J. LUCAS. Mat. Res. Bull. **7**, 57 (1972).
30. F. CHAMPLON, D. BERNARD, and J. PANNETIER. C.R. **278C**, 1185 (1974).
31. D. BERNARD, J. PANNETIER, J. Y. MOISAN, and J. LUCAS. J. Solid State Chem. **8**, 31 (1973). D. BERNARD, J. PANNETIER, and J. LUCAS. J. Solid State Chem. **14**, 328 (1975).
32. D. ADLER. J. Chem. Phys. **52**, 4908 (1970).
33. D. GROULT, C. MICHEL, and B. RAVEAU. C.R. **274C**, 374 (1972).
34. L. G. NIKIFOROV. Kristallografiya, **17**, 408 (1972); Sov. Phys. Crystallogr. **17**, 347 (1972). V. A. ISUPOV. Sov. Phys. Crystallogr. **3**, 96 (1958).
35. YU. A. PYATENKO. Zh. Strukt. Khim. **2**, 591 (1961); **11**, 1131 (1970).
36. R. D. ROSENSTEIN and R. SCHOR. J. Chem. Phys. **38**, 1789 (1963).
37. A. W. SLEIGHT. Mat. Res. Bull. **6**, 775 (1971).
38. F. BRISSE, D. J. STEWART, V. SEIDL, and O. KNOP. Can. J. Chem. **50**, 3648 (1972). G. DESGARDIN, G. JEANNE, and B. RAVEAU. C.R. **279C**, 565 (1974).
39. G. DEMAZEAU and O. KNOP. Unpublished results.
40. J. CHASSAING. C.R. **268**, 2188 (1969).
41. R. HÄNSLER and W. RÜDORFF. Z. Naturforsch. **25b**, 1306 (1970).
42. R. COSIER, A. WISE, A. TRESSAUD, J. GRANNEC, R. OLAZCUAGA, and J. PORTIER. C.R. **271C**, 142 (1970).
43. G. HEGER and R. VIEBAHN-HÄNSLER. Solid State Commun. **11**, 1119 (1972).
44. J.-M. DANCE, J. GRANNEC, C. JACOBONI, and A. TRESSAUD. C.R. **279C**, 601 (1974).
45. M. FAUCHER and P. CARO. J. Solid State Chem. **12**, 1 (1975).
46. D. GROULT, C. MICHEL, and B. RAVEAU. J. Inorg. Nucl. Chem. **35**, 3095 (1973).
47. C. MICHEL, D. GROULT, and B. RAVEAU. J. Inorg. Nucl. Chem. **37**, 247 (1975).
48. C. MICHEL. Thèse de doctorat. Université de Caen. Caen, 1974.
49. M. GASPERIN. Mat. Res. Bull. **9**, 1053 (1975).

Can. J. Chem. Downloaded from www.nrcresearchpress.com by 210.87.254.40 on 09/05/12
For personal use only.

Photochemistry of *trans*-$[Cr(en)_2Br_2]^+$ and *trans*-$[Cr(en)_2Cl_2]^+$

W. J. ROSEBUSH AND A. D. KIRK
Department of Chemistry, University of Victoria, Victoria, B.C., Canada V8W 2Y2

Received February 23, 1976

W. J. ROSEBUSH and A. D. KIRK. Can. J. Chem. **54**, 2335 (1976).

trans-$[Cr(en)_2Br_2]^+$ has been found to photoaquate mainly with bromide loss ($\phi_{578} = 0.36$, $\phi_{436} = 0.27$, $\phi_{406} = 0.27$) but accompanied by a small, also wavelength dependent, proton uptake ($\phi_{578} = 0.003$, $\phi_{436} = 0.075$, $\phi_{406} = 0.042$). The main photoproduct of *trans*-$[Cr(en)_2Br_2]^+$ and *trans*-$[Cr(en)_2Cl_2]^+$ has been shown to be predominantly *cis* in configuration (95 ± 5% for the dibromo and 99.2% for the dichloro system). The results are discussed in the context of current models of chromium(III) photochemistry. The observed wavelength dependence requires participation of more than one excited state in reaction. The high degree of stereochemical change requires entry of solvent in a manner concerted with halide loss.

W. J. ROSEBUSH et A. D. KIRK. Can. J. Chem. **54**, 2335 (1976).

On a trouvé que le $[Cr(en)_2Br_2]^+$ *trans* subit une réaction de photoaquation conduisant principalement à la perte de brome ($\phi_{578} = 0.36$, $\phi_{436} = 0.27$, $\phi_{406} = 0.27$); cette réaction est toutefois accompagnée par une petite réaction, qui est aussi dépendante de la longueur d'onde, provoquant une absorption de proton ($\phi_{578} = 0.003$, $\phi_{436} = 0.075$, $\phi_{406} = 0.042$). On a démontré que les photoproduits principaux du $[Cr(en)_2Br_2]^+$ *trans* et $[Cr(en)_2Cl_2]^+$ *trans* possèdent principalement la configuration *cis* (95 ± 5% pour le dibromé et 99.2% pour le système dichloré). On discute des résultats en terme des modèles courants pour la photochimie du chrome(III). Le fait que les réactions dépendent de la longueur d'onde implique une participation de plus d'un état excité dans la réaction. Par ailleurs la stéréospécificité des changements stéréochimiques implique une entrée du solvant d'une façon concertée avec la perte de l'halogénure.

[Traduit par le journal]

Introduction

Knowledge of chromium(III) photochemistry has continued to expand on several fronts: for a number of complexes reaction from quartet states has been established (1–4) while definite evidence for doublet reaction still appears to be lacking. Models based upon properties of quartet (and doublet) states have been proposed (5–8), tested (6, 9–13), and extended (11, 14, 15). Consequently, some degree of unanimity exists regarding the principles enabling qualitative prediction of reaction modes and approximate relative quantum yields in aqueous solutions. The main existing problems, which may persist for a while, relate to the detailed mechanism of photoreaction and also to the quantitative aspects; for example the prediction of the effects of wavelength; temperature (10), and medium (16–19) on yields and yield ratios. The consideration of the latter effects requires more data on the photophysical processes involved and promises to be difficult to obtain.

One of the aspects which remains in dispute is the exact nature of the stereochemistry of photoreactions of D_{4h} or C_{4v} complexes. One of the writers suggested (15) that stereochemical change might be general and supportive therefore of an associative mode of reaction. This was questioned (13) on the basis that several complexes which photoreact by loss of an in-plane ethylenediamine ligand appear to give a stereoretentive product. Also the degree to which stereochemical change has been demonstrated for other systems was questioned.

This study of the photochemistry of *trans*-$[Cren_2Br_2]^+$ was undertaken to see if the compound fitted appropriately into the framework of present theory. Secondly, the purpose was to examine the *cis*/*trans* nature of the photoproduct for this compound, and for *trans*-$[Cren_2Cl_2]^+$, based upon the implementation in our laboratory of a system (20) for quantitative ion-exchange chromatography capable of resolving completely isomer pairs such as *cis*- and *trans*-$[Cr(en)_2H_2OX]^{2+}$.

Results and Discussion

Photolysis of *trans*-$[Cr(en)_2Br_2]^+$ in acidic aqueous solution was observed to lead to bromide loss as the predominant reaction mode,

Can. J. Chem. Downloaded from www.nrcresearchpress.com by 210.87.254.105 on 09/05/12
For personal use only.

Can. J. Chem. Downloaded from www.nrcresearchpress.com by 210.87.254.105 on 09/05/12
For personal use only.

TABLE 1. Photolysis quantum yields for *trans*-$[Cr(en)_2Br_2]^+$

λ_{exc} (nm)	T (°C)	Conversion (%)	ϕ_{Br^-}	ϕ_{H^+}
578	1	3.6	0.333	
	1	5.7	0.380	
			Ave. 0.36 ± 0.02	
	5	10		0.003 ± 0.002[a]
436	1	3.7	0.257	
	1	3.8	0.290	
			Ave. 0.27 ± 0.02	
	5	6.3		0.075 ± 0.002[a]
406	1	<1	0.267	
	1	<1	0.279	
			Ave. 0.27 ± 0.01[b]	
	5	6.2		0.042 ± 0.002[a]

[a]This uncertainty estimated from electrode characteristics, which is the main source of statistical error in this measurement. Uncorrected for secondary photolysis, see text.

[b]These runs carried out when only low intensity available at 406 nm. Consequently the conversion was low, and the thermal correction large so that these results may be less certain despite the consistency of the values found.

while a small, wavelength-dependent pH change was also observed. The latter was a very minor reaction mode, so it was not possible to identify the product complex directly. Nevertheless, experience with photolysis of other ethylenediamine containing chromium(III) complexes gives one some confidence in believing the process to be reaction 2 below. The product of Br^- loss was $[Cr(en)_2H_2OBr]^{2+}$. The reaction modes were therefore:

$$[1] \quad \textit{trans}\text{-}[Cr(en)_2Br_2]^+ \xrightarrow[\phi_{Br^-}]{H_2O} [Cr(en)_2H_2OBr]^{2+} + Br^-$$

$$[2] \quad \xrightarrow[\phi_{H^+}]{H_3O^+} [Cr(en)enHH_2OBr_2]^{2+}$$

Reaction 1 also occurs thermally, to yield the *trans* aquobromo product. We observed a rate constant of about 8×10^{-6} s^{-1} for thermal bromide loss at 1 °C, consistent with literature data (21).

Because of the relatively rapid thermal reaction 1, quantum yield data, Table 1, were obtained only at the lowest possible temperatures of 1 °C for bromide determination and 5 °C for pH determination. Since apparent activation energies for photochemical quantum yields are quite small this small temperature difference does not preclude comparison of quantum yields to obtain an overall picture of behaviour.

The data show that at all wavelengths studied the photoreaction mode is mainly bromide loss, and only a small, wavelength-dependent quantum yield of proton uptake is observed. Since information is not available to make exact corrections the data of Table 1 has been left uncorrected for secondary photolysis. As will be established later, the primary photoproduct is *cis*-$[Cr(en)_2H_2OBr]^{2+}$. This complex, by analogy to similar *cis* complexes, would be expected to photolyse (ligand field irradiation) with a proton uptake quantum yield no greater than around 0.2, while bromide release should be very small. Consequently no correction to the bromide quantum yields is necessary. The maximum correction to the proton uptake quantum yields is calculated to be (using literature spectral data (21) for *cis*-$[Cr(en)_2H_2OBr]^{2+}$ and published theory (11, 20) for the corrections) -0.015 (578 nm), -0.006 (436 nm), and -0.008 (406 nm). The fact that the correction is larger than the observed quantum yield at 578 nm suggests that these values are overestimates, due to an overestimate of ϕ_{H^+} for *cis*-$[Cr(en)_2H_2OBr]^{2+}$ but they do enable one to estimate the possible ranges of values for ϕ_{H^+} at various wavelengths. The photochemistry of *trans*-$[Cr(en)_2Br_2]^+$ follows therefore, the pattern typical of compounds (22) showing 'axial labilization', namely loss of the strong σ donor ligand on the axis of weakest overall σ donor strength (except where strong π donors are involved (7, 8)).

The significance of the actual quantum yield values, and their wavelength dependence, is more difficult to assess, particularly in relation to other compounds such as the spectroscopically similar dichloro compound. The problem resides in the composite nature of a quantum yield. Even were only the lowest quartet state of the compound reactive, which is denied by the observation of the wavelength dependence of proton uptake, one would have to consider the structural variations of the rate constants for reaction, intersystem crossing, and non-radiative conversion to the ground state. Moreover it has been shown for a number of compounds that the photoreaction quantum yield often consists of a 'prompt' and 'delayed' (by thermal repopulation of the quartet from the doublet state) component; the magnitudes of these could alter

Table 2. Chromatographic peak areas in photolysis of *trans*-$[Cr(en)_2Br_2]^+$ and *trans*-$[Cr(en)_2Cl_2]^+$

Complex	Run	Time (s)	T (°C)	Conversion (%)	Product[a] *cis*	Product[a] *trans*	Photolytic[c] *trans* (%)
$[Cr(en)_2Br_2]^+$	1 photo	1500	1	10	42.65	27.53	~4
	dark	1500	1	4	3.88	25.98[b]	
	2 photo	1500	1	8	42.42	9.03	<0
	dark	1500	1	2	0.00	13.73	
$[Cr(en)_2Cl_2]^+$	1 photo	2000	1	10	70.2	1.98	0.8
	dark	2000	1	~0.2	0.0	1.43	

[a]These values are relative chromatographic peak areas. While comparable for a given photo/dark pair, they are not comparable from run to run.
[b]Because of lability of *trans*-$[Cr(en)_2Br_2]^+$ and the appreciable activation energy for its thermal aquation, detail of handling of individual samples leads to significant scatter in the data for the moles of *trans* product. This leads in turn to uncertainty in the final % photolytic *trans* product for this compound.
[c]After subtraction of the contribution from thermal aquation.

together or in opposition upon structural changes. Add to this the fact that more than one state must react, and it becomes impossible to make a detailed analysis given only presently available information.

It is, however, noticeable that the halide quantum yields for the dibromo and dichloro (9) compounds are very similar (and very similar to a whole range of other compounds (22) of approximately the same overall ligand field strength). Since the corresponding thermal reactions differ in rate by more than an order of magnitude it is reasonable to conclude that the quantum yields are primarily determined by photophysical processes. One possible explanation of this constancy of overall quantum yield would be similar photophysical rate constants, with a similar rate determining step for reaction. This could be the rate of dissociation of the leaving ligand to form a five coordinate species, or, and in our opinion a likely possibility, the bonding of entering solvent, probably at a rate close to the diffusion limit to form a seven coordinate species. Certainly an extremely fast process is required by recent attempts (23) to study quartet state lifetimes.

For irradiation into the ^4E_g state (578 nm) the reaction mode corresponds almost exclusively to axial labilization. At shorter wavelengths corresponding to the $^4B_{2g}$ and higher states a small yield corresponding to equatorial (in-plane) reaction appears. This behaviour has now become well established for a number of these compounds and is consistent with participation of the $^4B_{2g}$ (thexi?) state reaction in the manner earlier suggested (10, 20, 24, 25).

The results obtained on the isomeric nature of the photoproducts are shown in Table 2. For *trans*-$[Cr(en)_2Br_2]^+$ the thermal lability (and its large activation energy which led to irreproducibilities due to warming during handling) caused a large thermal reaction correction, leading to greater uncertainties. The data show that at most $5 \pm 5\%$ of the product could be in the *trans* configuration. The results for *trans*-$[Cr(en)_2Cl_2]^+$ where the thermal reaction was less troublesome, were more definite and a figure of 0.8% *trans* compound was established after correction for thermal reaction. In view of the importance of this result the chromatographic data on which it is based are reproduced in Fig. 1. It will be seen that the amount of *trans* compound found is of the order of the uncertainty of the data and it may be that none at all is produced photolytically. The result shows that the photolysis of *trans*-$[Cr(en)_2Cl_2]^+$ occurs with stereochemical change. Where reactions are thought to occur by dissociative mechanisms stereochemical preferences due to thermodynamic or kinetic factors are not of this magnitude except for certain strained systems (26). It seems inescapable therefore that the above photoreaction occurs by a mechanism in which the entry of the solvent is concerted with halide loss.

Experimental

trans-$[Cr(en)_2Br_2]Br$ and *trans*-$[Cr(en)_2Cl_2]Cl.H_2O$ were prepared by literature methods (27).

Quantum yield determinations and ion-exchange analysis were carried out using techniques recently described (20).

Can. J. Chem. Downloaded from www.nrcresearchpress.com by 210.87.254.105 on 09/05/12
For personal use only.

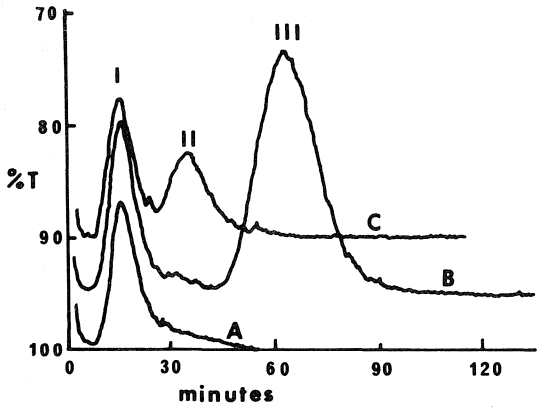

FIG. 1. These chromatograms were obtained under the following conditions: Column; 10 cm × 1.0 cm Baker Analysed CGC-241 (200–400 mesh) cation exchange resin at 2 °C; eluant; 200 ml volume ammonium sulphate solution with concentration gradient of 0.5–0.9 *M* at 100 ml h^{-1} (*i.e.* 0.2 *M* h^{-1}) followed by required volume of 0.9 *M*. In all cases, before chromatography *trans*-$[Cr(en)_2Cl_2]^+$ was precipitated with $NaClO_4$ to reduce interference; trials showed that added *cis*- and *trans*-$[Cr(en)_2H_2OCl]^{2+}$ did not co-precipitate significantly. The curves above are for 10^{-2} *M* *trans*-$[Cr(en)_2Cl_2]^+$ solution 10^{-3} *M* in HNO_3 (*A*) kept dark at 1 °C for 2000 s, (*B*) photolysed (578 nm) at 1 °C for 2000 s, (*C*) unphotolysed but with added *trans*-$[Cr(en)_2H_2OCl]^{2+}$. For clarity *B* and *C* have been scale shifted −5% and −10% respectively. Peak *I* is unprecipitated starting complex and peak *II* and *III* respectively *trans*- and *cis*-$[Cr(en)_2H_2OCl]^{2+}$.

Acknowledgements

The authors wish to thank the National Research Council of Canada, the University of Victoria Faculty Research Fund, and the British Columbia Department of Labour for financial support. We also wish to thank C. F. C. Wong for his assistance with some of the measurements. A.D.K. is most grateful to the School of Molecular Sciences, University of Sussex for use of their facilities while on leave.

1. S. N. CHEN and G. B. PORTER. Chem. Phys. Lett. **6**, 41 (1970).
2. H. F. WASGESTIAN. J. Phys. Chem. **76**, 1947 (1972).
3. N. A. P. KANE-MAGUIRE and C. H. LANGFORD. J. Am. Chem. Soc. **94**, 2125 (1972).
4. R. BALLARDINI, G. VARANI, H. F. WASGESTIAN, L. MOGGI, and V. BALZANI. J. Phys. Chem. **77**, 2947 (1973).
5. A. W. ADAMSON. J. Phys. Chem. **71**, 798 (1967).
6. S. C. PYKE and R. G. LINCK. J. Am. Chem. Soc. **93**, 5281 (1971).
7. J. I. ZINK. J. Am. Chem. Soc. **94**, 8039 (1972).
8. M. WRIGHTON, H. B. GRAY, and G. S. HAMMOND. Mol. Photochem. **5**, 165 (1973).
9. A. D. KIRK, K. C. MOSS, and J. G. VALENTIN. Can. J. Chem. **49**, 1524 (1971).
10. M. T. GANDOLFI, M. F. MANFRIN, A. JURIS, L. MOGGI, and V. BALZANI. Inorg. Chem. **13**, 1342 (1974).
11. G. WIRTH and R. G. LINCK. J. Am. Chem. Soc. **95**, 5913 (1973).
12. A. D. KIRK and T. L. KELLY. Inorg. Chem. **13**, 1613 (1974).
13. C. BIFANO and R. G. LINCK. Inorg. Chem. **13**, 609 (1974).
14. J. I. ZINK. Inorg. Chem. **12**, 1957 (1973).
15. A. D. KIRK. Mol. Photochem. **5**, 127 (1973).
16. H. F. WASGESTIAN. J. Phys. Chem. **76**, 1947 (1972).
17. C. H. LANGFORD and L. TIPPING. Can. J. Chem. **50**, 887 (1972).
18. F. SCANDOLA, M. A. SCANDOLA, and G. BARTOCCI. J. Am. Chem. Soc. **97**, 4747 (1975).
19. C. F. C. WONG and A. D. KIRK. Can. J. Chem. **53**, 419 (1975).
20. C. F. C. WONG and A. D. KIRK. Inorg. Chem. In press.
21. D. A. HOUSE and C. S. GARNER. *In* Transition metal chemistry. Vol. 6. *Edited by* R. L. Carlin. Marcel Dekker, New York. 1970.
22. E. ZINATO. *In* Concepts of inorganic photochemistry. *Edited by* A. W. Adamson and P. D. Fleischauer. John Wiley, New York. 1975.
23. A. D. KIRK, P. E. HOGGARD, G. B. PORTER, M. C. ROCKLEY, and M. W. WINDSOR. Chem. Phys. Lett. **37**, 199 (1976).
24. P. RICCIERI and E. ZINATO. J. Am. Chem. Soc. **97**, 6071 (1975).
25. W. COLEMAN and W. SCHAAP. J. Chem. Soc. Chem. Commun. **6**, 226 (1975).
26. R. D. ARCHER. Coord. Chem. Rev. **4**, 243 (1969).
27. W. W. FEE, J. N. MAC. B. HARROWFIELD, and W. G. JACKSON. J. Chem. Soc. A, 2620 (1970).

Can. J. Chem. Downloaded from www.nrcresearchpress.com by 210.87.254.105 on 09/05/12
For personal use only.

Can. J. Chem. Downloaded from www.nrcresearchpress.com by 210.87.254.6 on 09/05/12
For personal use only.

The effect of steric crowding on an E2 transition state

GEORGE STANLEY DYSON AND PETER JAMES SMITH
Department of Chemistry and Chemical Engineering, University of Saskatchewan, Saskatoon, Sask., Canada S7N 0W0

Received April 23, 1976

GEORGE STANLEY DYSON and PETER JAMES SMITH. Can. J. Chem. **54**, 2339 (1976).

The mechanism of the reaction of 9-(4-substituted benzyl)fluorene-9-trimethylammonium ions with ethoxide is a normal E2 process. The magnitude of the primary hydrogen–deuterium isotope effect at 60 °C increased with increasing electron-donating ability of the 4-substituent, *i.e.*, 4.15, 5.10, 5.34, 5.65, 5.75, and 5.91 for the 4-CF_3, 4-Br, 4-Cl, 4-H, 4-CH_3, and 4-OCH_3 substituents, respectively. The magnitude of the nitrogen isotope effect at 70 °C decreased with increased electron-donating power of the 4-substituent, *i.e.*, $[(k^{14}/k^{15}) - 1]100 = 1.24$, 0.95, 0.92, 0.91, and 0.80 for the 4-CF_3, 4-F, 4-H, 4-CH_3, and 4-OCH_3 substituents, respectively. A small Hammett ρ value of +1.33 was observed for the reaction. It is concluded that the reaction proceeds via a transition state where the proton is more than one-half transferred to base. It is further concluded that for a reaction in which the 4-substituents decrease the rate, both carbon–hydrogen and carbon–nitrogen bond rupture is more advanced in the transition state. This variance with Hammond's postulate is discussed in the light of steric crowding at the transition state.

GEORGE STANLEY DYSON et PETER JAMES SMITH. Can. J. Chem. **54**, 2339 (1976).

Le mécanisme de la réaction des ions (*p*-substitué benzyl)-9 fluorènyl-9 triméthylammonium avec l'éthanolate est un processus E2 normal. L'importance de l'effet isotopique, hydrogène–deutérium primaire à 60 °C augmente avec l'augmentation de l'effet donneur d'électrons du substituant en position 4, c'est-à-dire: 4.15, 5.10, 5.34, 5.65, 5.75 et 5.91 respectivement pour les substituants: -CF_3, -Br, -Cl, -H, -CH_3 et -OCH_3 en position 4. L'importance de l'effet isotopique de l'azote à 70 °C diminue avec l'augmentation de l'effet donneur d'électrons du substituant en position 4, c'est-à-dire: $[(k^{14}/k^{15}) - 1]100 = 1.24$, 0.95, 0.92, 0.91 et 0.80 respectivement pour les substituants: -CF_3, -F, -H, -CH_3 et -OCH_3. Pour la réaction on a observé une petite valeur ρ de Hammett de +1.33. On en conclue que la réaction procède selon un état de transition où le proton est plus qu'à demi transferé à la base. De plus, dans les cas où la substitution en position -4 cause une diminution de la vitesse, on arrive à la conclusion additionnelle que la rupture des liens carbone–hydrogène et carbone–azote est plus avancée à l'état de transition. Ce désaccord avec le postulat de Hammond est discuté à l'aide de l'encombrement stérique à l'état de transition.

[Traduit par le journal]

Recent studies on the E2 reaction of 2-arylethyl- and 1-arylethyltrimethylammonium salts (1–3) with base have shown that electron-withdrawing substituents on the phenyl ring increase the rate of reaction with the corresponding transition state becoming more reactant-like, having decreased C—H and C—$\overset{+}{N}$ bond weakening. The effect of the substituent on the transition state geometry is in accord with Hammond's postulate (4) and also with Thornton's theory (5) where it is considered that the effect of a substituent is usually felt more strongly on the reaction coordinate motion.

It has been established that the transition state for reaction of the 2-arylethyl- and 1-arylethyltrimethylammonium ions with base is carbanionic with relatively more C—H bond rupture than C—$\overset{+}{N}$ bond rupture. A change to better leaving groups, 4-substituted dimethylanilines, for the 2-arylethyl system leads to a more reactant-like transition state (6) but one in which the proton is more than one-half transferred to base at the transition state.

In a search for a system which might react via a transition state where C—H bond rupture has not progressed to the half-way point, a series of 9-(4-substituted benzyl)fluorene-9-trimethylammonium ions (1) was synthesized (7). The

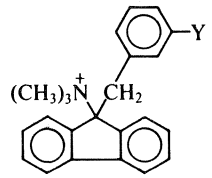

1

hydrogen–deuterium and nitrogen isotope effects were measured for various 4-substituted benzyl substrates by procedures previously described (1) and the results are shown in Table 1. The Hammett ρ value for reaction promoted by ethoxide ion in ethanol at 60 °C was found to be +1.33.

It is seen that the magnitude of the hydrogen–deuterium isotope effects *decrease* with increased electron-withdrawing power of the 4-substituent, *i.e.*, k^H/k^D = 5.91 and 4.15 for Y = OCH_3 and CF_3, respectively. As well, the nitrogen isotope effects *increase* when the 4-substituent becomes an electron-withdrawer, *i.e.*, $[(k^{14}/k^{15}) - 1]100$ = 0.80 and 1.24 for Y = OCH_3 and CF_3, respectively. The trends in the magnitude of both isotope effects with substituents are opposite to those observed in both the 1-arylethyl- and 2-arylethyl systems.

The rate of reaction of compound **1**, Y = H, with ethoxide is surprisingly slower than the corresponding reaction of 9-methylfluorene-9-trimethylammonium ion (7) and the 2-phenylethyl salt. Dreiding stereomodels indicate considerable steric interaction of the phenyl ring with the fluorene nucleus when they are in the same plane as required for a dihedral angle of 180°. Hence, the phenyl ring is probably twisted out of the plane of the fluorenyl ring and the forming *p*-orbital at the benzylic carbon as C—H bond rupture advances will not, therefore, be able to effectively overlap with the π-system of the phenyl ring. This is consistent with the observation of a small ρ of +1.33 for the reaction of **1** and may be compared with ρ = +3.77 (8) for reaction of the 2-arylethyl salts.

Consequently, assuming that ρ does not provide a measure of the degree of C—H bond rupture for the present system, it is possible to interpret the hydrogen–deuterium results in the light that the proton is more than one-half transferred to base.[1] The decrease in k^H/k^D and increase in the nitrogen effect, when the 4-substituent is made electron-withdrawing and the rate of reaction increases, means that there is *increased* both C—H and C—$\overset{+}{N}$ bond rupture.[2]

TABLE 1. Isotope effects for the reaction of 9-(4-substituted benzyl)fluorene-9-trimethylammonium salts with ethoxide in ethanol

4-Substituent	k^H/k^D (60 °C)*	$[(k^{14}/k^{15}) - 1]100$ (70 °C)†
CH_3O	5.91 ± 0.08	0.80 ± 0.03
CH_3	5.75 ± 0.10	0.91 ± 0.09
H	5.61 ± 0.07	0.92 ± 0.04
F	—	0.95 ± 0.03
Cl	5.34 ± 0.08	—
Br	5.10 ± 0.07	—
CF_3	4.15 ± 0.12	1.24 ± 0.07

*Ratio of rates of elimination; deviation = $\pm k^H/k^D[(r^H/k^H)^2 + (r^D/k^D)^2]^{1/2}$, where r is the standard deviation in k.
†The limits shown are the standard deviation.

The effect of substituents on the nature of the transition state for the reaction under discussion is contrary to both Hammond's postulate and Thornton's predictions. The most reactive substrate has a transition state where both C—H and C—$\overset{+}{N}$ bond rupture processes have advanced to the greatest degree.

A tentative explanation is that initially the electron-withdrawing substituent makes it more favourable for C—H rupture. As electron density builds up at the benzylic carbon, however, the stabilization of the developing charge by the phenyl ring becomes less important for steric reasons. Eventually there is sufficient electron density to 'push off' the leaving group and reaction occurs. Alternatively, it is more difficult to break the C—H bond for the 4-OCH_3 substrate but there will be sufficient electron density to promote reaction earlier along the reaction coordinate.

Acknowledgment

The authors acknowledge the financial support of the National Research Council of Canada.

1. P. J. SMITH and A. N. BOURNS. Can. J. Chem. **52**, 749 (1974).
2. P. J. SMITH and S. K. TSUI. Tetrahedron Lett. **10**, 917 (1972).

[1]This is consistent with the conclusions for reactions of all other quaternary salts studied.

[2]Electron withdrawers in the 2-arylethyl system lead to a transition state with *decreased* C—H and C—N bond weakening.

Can. J. Chem. Downloaded from www.nrcresearchpress.com by 210.87.254.6 on 09/05/12
For personal use only.

3. P. J. SMITH and S. K. TSUI. Tetrahedron Lett. **1**, 61 (1973).
4. G. S. HAMMOND. J. Am. Chem. Soc. **77**, 334 (1955).
5. E. R. THORNTON. J. Am. Chem. Soc. **89**, 2915 (1967).
6. P. SCHMID and A. N. BOURNS. Can. J. Chem. **53**, 3513 (1975).
7. P. J. SMITH and S. K. TSUI. J. Am. Chem. Soc. **95**, 4760 (1973).
8. W. H. SAUNDERS, JR., D. G. BUSHMAN, and A. F. COCKERILL. J. Am. Chem. Soc. **90**, 1775 (1968).

Can. J. Chem. Downloaded from www.nrcresearchpress.com by 210.87.254.6 on 09/05/12
For personal use only.

High power TEA-CO_2 laser induced polymerization of ethylene[1]

S. L. CHIN

Laboratoire de Recherches en Optique et Laser, Département de Physique, Université Laval, Québec, P.Q., Canada G1K 7P4

Received April 23, 1976

S. L. CHIN. Can. J. Chem. **54**, 2341 (1976).

A 100-MW double-discharged TEA-CO_2 laser was used to induce the polymerization of ethylene gas at pressures ranging from 250 to 900 psi at room temperature. The polymerization product was mainly tetradecane ($CH_3(CH_2)_{12}CH_3$) (~80%) and octadecane ($CH_3(CH_2)_{16}CH_3$) (~20%).

S. L. CHIN. Can. J. Chem. **54**, 2341 (1976).

Un laser CO_2-TEA double-décharges de puissance 100 MW sut utilisé pour initier la polymérisation du gaz d'éthylène à des pressions allant de 250 à 900 psi à la température ambiante de la pièce. Le produit de la polymérisation était principalement le tétradécane ($CH_3(CH_2)_{12}CH_3$) (~80%) et l'octadécane ($CH_3(CH_2)_{16}CH_3$) (~20%).

It has recently been predicted theoretically that high power infrared lasers can be used to initiate radical polymerization even though the photon energy of the laser is much less than the dissociation of the monomer molecule (1, 2). We present in this work some experimental results showing that polymerization can indeed be initiated in ethylene at room temperature by a high power TEA-CO_2 laser. A multimode double-discharged TEA-CO_2 laser (3) operating at the P(18) line (10.57 μ) and capable of producing ~70 ns (FWHM) pulses with an average peak power of ~150 MW was used. Commercial ethylene (purity: 99.5%) was used in a high pressure cell fitted with 2.54 cm-thick NaCl or Ge windows. The interior dimension of the cell was 5.1 cm diameter × 7.6 cm. The cell was pumped down by a mechanical pump, then flushed several times with the pure ethylene before maintaining the gas at a fixed pressure. The 6 cm-diameter laser beam was focused down to ~2 cm diameter by a 1 m focal length salt lens before entering the 2 cm window of the cell. After every 50 shots with the laser power and ethylene pressure kept constant, the high pressure cell was opened for inspection. When the laser was below a threshold intensity of ~10^7 W/cm^2, nothing was seen for any pressure up to 900 psi. When the laser was raised above the threshold intensity, a fluffy black powder was formed all over the interior wall of the cell. Most of the black material was formed right next to the entrance window. Whenever this occurred, we observed that during the laser bombardment, a 'white' spark was created right near the entrance window, and downstream in the ethylene along

[1]This work was supported in part by a grant from the Imperial Oil Limited, Canada. The kind permission to use the CO_2 laser by Professor R. Tremblay and Dr. P. A. Bélanger of LROL is appreciated. The chemical analysis of the extracted polymer was carried out with the aid and advice of Dr. V. S. Salvi and Mr. D. Mukarjee of the Chemistry Department and Professor L.-P. Blanchard and Dr. S. L. Malhotra of the Chemical Engineering Department.

3. P. J. SMITH and S. K. TSUI. Tetrahedron Lett. **1**, 61 (1973).
4. G. S. HAMMOND. J. Am. Chem. Soc. **77**, 334 (1955).
5. E. R. THORNTON. J. Am. Chem. Soc. **89**, 2915 (1967).
6. P. SCHMID and A. N. BOURNS. Can. J. Chem. **53**, 3513 (1975).
7. P. J. SMITH and S. K. TSUI. J. Am. Chem. Soc. **95**, 4760 (1973).
8. W. H. SAUNDERS, JR., D. G. BUSHMAN, and A. F. COCKERILL. J. Am. Chem. Soc. **90**, 1775 (1968).

Can. J. Chem. Downloaded from www.nrcresearchpress.com by 210.87.254.5 on 09/05/12
For personal use only.

High power TEA-CO_2 laser induced polymerization of ethylene[1]

S. L. CHIN

Laboratoire de Recherches en Optique et Laser, Département de Physique, Université Laval, Québec, P.Q., Canada G1K 7P4

Received April 23, 1976

S. L. CHIN. Can. J. Chem. **54**, 2341 (1976).

A 100-MW double-discharged TEA-CO_2 laser was used to induce the polymerization of ethylene gas at pressures ranging from 250 to 900 psi at room temperature. The polymerization product was mainly tetradecane ($CH_3(CH_2)_{12}CH_3$) (~80%) and octadecane ($CH_3(CH_2)_{16}CH_3$) (~20%).

S. L. CHIN. Can. J. Chem. **54**, 2341 (1976).

Un laser CO_2-TEA double-décharges de puissance 100 MW sut utilisé pour initier la polymérisation du gaz d'éthylène à des pressions allant de 250 à 900 psi à la température ambiante de la pièce. Le produit de la polymérisation était principalement le tétradécane ($CH_3(CH_2)_{12}CH_3$) (~80%) et l'octadécane ($CH_3(CH_2)_{16}CH_3$) (~20%).

It has recently been predicted theoretically that high power infrared lasers can be used to initiate radical polymerization even though the photon energy of the laser is much less than the dissociation of the monomer molecule (1, 2). We present in this work some experimental results showing that polymerization can indeed be initiated in ethylene at room temperature by a high power TEA-CO_2 laser. A multimode double-discharged TEA-CO_2 laser (3) operating at the P(18) line (10.57 μ) and capable of producing ~70 ns (FWHM) pulses with an average peak power of ~150 MW was used. Commercial ethylene (purity: 99.5%) was used in a high pressure cell fitted with 2.54 cm-thick NaCl or Ge windows. The interior dimension of the cell was 5.1 cm diameter × 7.6 cm. The cell was pumped down by a mechanical pump, then flushed several times with the pure ethylene before maintaining the gas at a fixed pressure. The 6 cm-diameter laser beam was focused down to ~2 cm diameter by a 1 m focal length salt lens before entering the 2 cm window of the cell. After every 50 shots with the laser power and ethylene pressure kept constant, the high pressure cell was opened for inspection. When the laser was below a threshold intensity of ~10^7 W/cm^2, nothing was seen for any pressure up to 900 psi. When the laser was raised above the threshold intensity, a fluffy black powder was formed all over the interior wall of the cell. Most of the black material was formed right next to the entrance window. Whenever this occurred, we observed that during the laser bombardment, a 'white' spark was created right near the entrance window, and downstream in the ethylene along

[1]This work was supported in part by a grant from the Imperial Oil Limited, Canada. The kind permission to use the CO_2 laser by Professor R. Tremblay and Dr. P. A. Bélanger of LROL is appreciated. The chemical analysis of the extracted polymer was carried out with the aid and advice of Dr. V. S. Salvi and Mr. D. Mukarjee of the Chemistry Department and Professor L.-P. Blanchard and Dr. S. L. Malhotra of the Chemical Engineering Department.

Can. J. Chem. Downloaded from www.nrcresearchpress.com by 210.87.254.5 on 09/05/12
For personal use only.

the laser axis, a pencil of yellowish-red glow was formed simultaneously. (This 'white' spark has been imaged through the exit window into a prism spectrograph. The spectrum showed two continuous bands, a strong one between 5600–6200 Å and a weak one between 4300–4800 Å.) Soon after the cessation of the 'white' spark near the entrance window, a dark cloud was observed which diffused away with a rather strong turbulence. Similar results were obtained with the ethylene pressures ranging from 250 to 900 psi. The following is a typical result corresponding to a pressure of 600 psi. About 20 mg of the black material was collected after 500 shots of the laser, each having an average peak intensity $\sim 3 \times 10^7$ W/cm^2 and an energy of ~ 7 J at the entrance window. Using CCl_4 as a solvent, about 5 mg of a brown waxy material was extracted from the black material. The remaining insoluble fine black powder was presumably carbon. The brown material was analysed by taking its ir, nmr, and gpc (gel permeation chromatography) spectra. The ir spectrum showed the CH_2 and CH_3 bands as well as a characteristic band of a long $(CH_2)_n$ chain. The 90 MHz nmr spectrum showed only a major CH_2 peak and a minor CH_3 peak, indicating that the brown material is a hydrocarbon most probably with CH_3 endings. The gpc spectrum gave a major and a side band peaked at positions corresponding to the molecular weights of 200 and 254 respectively. The observation led us to conclude that the brown products were most probably tetradecane ($CH_3(CH_2)_{12}CH_3$) ($\sim 80\%$) and octadecane ($CH_3(CH_2)_{16}CH_3$) ($\sim 20\%$).

The polymers were probably formed via free radical polymerization (4). The free radicals might be produced via resonant multiphoton absorption and subsequent dissociation of the ethylene molecules, similar to the case of CO_2 laser isotope enrichment of SF_6 in ^{34}S (5) where a similar high level of laser intensity had to be used. Although we may add that the evidence of the dissociation is given by the occurrence of luminescence in accordance with the recent observation by Bagratashvili *et al.* (6), the physical mechanism involved still is subject to debate (7). Our results indicated that during the dissociation, the ethylene molecules had been shattered into many different fragments consisting of mostly carbon, and a substantial number of free radicals such as $CH_2\cdot$, $CH_3\cdot$, etc., which participated in the free radical polymerization. Since many free radicals were created within a small region, the polymerization would not propagate too far before encountering a free radical that terminated the reaction. This might be a reason for the observed low molecular weight product. However, other explanations might exist. For instance, because of the high collision rate of the ethylene molecules ($\sim 10^{11}$ s^{-1}) high molecular weight product might have been produced before the laser irradiation was over. The remaining laser irradiation, being still very intense, might have caused an ablation of this product thus giving rise to low molecular weight polymers.

It should be noted that whenever polymerization occurred, the inner surface of the entrance window was damaged after about 10 shots. It was also covered by the black fluffy material. Thus, the real efficiency of the polymerization reaction could be higher than that indicated by the above data.

1. A. N. Oraevskii, V. P. Pimenov, A. A. Stepanov, and V. A. Shcheglov. Sov. J. Quant. Electron. **4**, 711 (1974).
2. A. N. Oraevskii, V. P. Pimenov, and V. A. Shcheglov. Sov. J. Quant. Electron. **4**, 1018 (1975).
3. J. L. Lachambre, J. Gilbert, F. Rheault, R. Fortin, and M. Blanchard. IEEE J. Quant. Electron. QE-**9**, 459 (1973).
4. R. A. W. Raff and J. B. Allison. Polyethylene. Interscience Publisher Inc., New York. 1956.
5. John L. Lyman, R. J. Jensen, J. Rink, C. Paul Robinson, and S. D. Rockwood. Appl. Phys. Lett. **27**, 87 (1975). R. V. Ambartsumyan, Yu. A. Gorokhov, V. S. Letokhov, and G. N. Makarov. Sov. Phys. JETP Lett. **21**, 171 (1975).
6. V. N. Bagratashvili, I. N. Knyazez, V. S. Letokhov, and V. V. Lobko. Opt. Commun. **14**, 426 (1975).
7. (*a*) 'Photochemistry: theory is catching up'. Laser focus. April 1976, pp. 12–16. (*b*) N. Bloembergen. Opt. Commun. **15**, 416 (1975).

Can. J. Chem. Downloaded from www.nrcresearchpress.com by 210.87.254.5 on 09/05/12
For personal use only.

Canadian Journal of Chemistry

Published by
THE NATIONAL RESEARCH COUNCIL OF CANADA

Journal canadien de chimie

Publié par
LE CONSEIL NATIONAL DE RECHERCHES DU CANADA

Volume 54 Number 15 August 1, 1976

Volume 54 numéro 15 1 août 1976

Lewis base complexes of tungsten and molybdenum hexafluorides[1]

S. BROWNSTEIN, BEVERLEY H. CHRISTIAN, G. LATREMOUILLE, AND ALOIS STEIGEL[2]

Division of Chemistry, National Research Council of Canada, Ottawa, Canada K1A 0R9

Received January 12, 1976

S. BROWNSTEIN, BEVERLEY H. CHRISTIAN, G. LATREMOUILLE, and ALOIS STEIGEL. Can. J. Chem. **54**, 2343 (1976).

Fluorine resonance spectroscopy has been used to calculate stoichiometry and equilibrium constants for formation of 1:1 and 2:1 complexes between dimethyl sulfide and tungsten hexafluoride at several temperatures. The 2:1 complex has fine structure from spin–spin coupling at very low temperature, but the simplicity of the spectra prevent detailed mechanistic studies. Many other Lewis base complexes of tungsten and molybdenum hexafluorides have been prepared.

S. BROWNSTEIN, BEVERLEY H. CHRISTIAN, G. LATREMOUILLE et ALOIS STEIGEL. Can. J. Chem. **54**, 2343 (1976).

On a utilisé la spectroscopie de résonance du fluor pour calculer la stoechiométrie et les constantes d'équilibre pour la formation des complexes 1:1 et 2:1 entre le sulfure de diméthyle et l'hexafluorure de tungsten à plusieurs températures. Le complexe 2:1 a une structure fine pour le couplage spin–spin à très basse température mais la simplicité du spectre empêche de faire des études mécanistiques plus détaillées. On a aussi préparé plusieurs autres complexes avec les bases de Lewis, hexafluorure, tungsten et de molybdène.

[Traduit par le journal]

Introduction

Tungsten hexafluoride is reported to form complexes with Lewis bases (1–4) and also charge-transfer complexes (5). Only charge-transfer complexes have been reported for molybdenum hexafluoride (5). Except for a preliminary communication there has been no study of the equilibria between free tungsten hexafluoride and its complexes of different stoichiometry, nor of the kinetics of these reactions (4). It has been reported that molybdenum hexafluoride is a stronger oxidizing agent than tungsten hexafluoride but there is no data concerning the relative electron accepting ability of the two fluorides in formation of Lewis acid–base complexes (6, 7). The present study is an attempt to fill in some of these gaps in our knowledge of the chemistry of these fluorides.

Experimental

Molybdenum and tungsten hexafluorides were used directly as supplied by Ozark Mahoning Ltd. They were manipulated in a stainless steel vacuum system equipped with bellows valves and the system was baked before use. Samples for fluorine magnetic resonance were prepared using glass-to-metal seals to ensure a grease free system. Solvents and other reagents were purified in the usual manner (8, 9). There was no evidence of impurities in the fluorine resonance spectra of the hexafluorides and the satellite lines from spin–spin coupling with less abundant magnetic isotopes were sharp, indicating the absence of rapid exchange with any unobservable impurities. The 2:1 complex of dimethyl sulfide with tungsten hexafluoride was prepared, using an excess of dimethyl sulfide, by precipitation from sulfuryl chlorofluoride as white crystals

[1]NRCC No. 15328.

[2]Present address: Institute of Organic Chemistry, University of Dusseldorf, D-4 Dusseldorf, Universitatsstrasse 1, West Germany.

Can. J. Chem. Downloaded from www.nrcresearchpress.com by 210.87.254.5 on 09/05/12
For personal use only.

stable for a few days at room temperature. It was readily brought into solution by adding a small quantity of sulfur dioxide to the sulfuryl chlorofluoride. The 1:1 complex was also precipitated from sulfuryl chlorofluoride with stoichiometric quantities of dimethyl sulfide and tungsten hexafluoride. These white crystals were only stable for a few hours at room temperature. They were less soluble than the 2:1 complex and required approximately an equal volume of sulfur dioxide to bring them into solution.

Samples for study by fluorine resonance spectroscopy were prepared by addition of the appropriate quantities of reagents, using known volumes and pressures, to an nmr tube on the vacuum line. Solvent would normally be added between the active reagents. After sealing the samples would be thawed and mixed at Dry Ice temperature and stored at Dry Ice temperature until their spectra were gathered.

Fluorine resonance spectra were obtained on a Varian Associates HA100D spectrometer at 94.1 MHz. Chemical shifts are reported in ppm relative to $CFCl_3$ as zero. Low field is considered positive to agree with newly established standards (10), which is opposite to the convention previously used by this laboratory. Data analysis was by least-squares procedures and errors are listed as one standard deviation except for chemical shifts, which are estimated.

Results and Discussion

A listing of complexes with tungsten hexafluoride, along with some examples where complexing is not observed, is given in Table 1. The chemical shifts are those of fluorine in the complexed tungsten hexafluoride. Slow exchange is used to indicate that magnetic averaging of the peaks from free and complexed tungsten hexafluoride did not occur at temperatures below -20 °C. In this temperature range the complexes were stable with respect to decomposition.

For the trimethylamine system signals from free tungsten hexafluoride, the 1:1 complex and the complex with two amine molecules were all present at appropriate concentration ratios in SO_2, methylene chloride, and vinyl chloride as solvents. The relative intensities of these peaks varied with the ratio of amine to fluoride in the correct manner for the peak assignments. Sufficiently accurate intensities could not be obtained for the calculation of reliable equilibrium constants. The chemical shift of the 1:1 complex agrees with that previously reported (2).

There was no evidence for a 2:1 complex with triethyl phosphine in sulfur dioxide solution. An insoluble complex was formed with methylene chloride as solvent. There was no evidence for phosphorus–fluorine nor tungsten–fluorine spin coupling although they have been observed for the trimethyl phosphine complex (2). The trimethyl arsine tungsten hexafluoride complex was only sparingly soluble in sulfur dioxide but dissolved readily in acetonitrile. In the latter solvent exchange between free and complexed tungsten hexafluoride is rapid at room temperature.

In a preliminary communication it was reported that although the resonances of free and complexed tungsten hexafluoride could be distinguished in the system with dimethyl sulfide, the exchange between 1:1 and 2:1 complexes could not be slowed sufficiently to determine their individual chemical shifts (4). At low temperature and with an excess of dimethyl sulfide the 2:1 complex is essentially the only tungsten fluoride species present so its chemical shift may be measured directly. The chemical shift of the 1:1 complex was used as an adjustable parameter in calculation of the equilibrium constants for formation of the 1:1 and 2:1 complexes. Con-

TABLE 1. Fluorine chemical shifts for some tungsten hexafluoride complexes

Ligand	Shift (ppm) δ1:1	Shift (ppm) δ2:1	Exchange rate
$(CH_3)_3N$	148.0	178.6	Slow
$(CH_3CH_2)_3P$	148.5	—	Slow
$(CH_3)_3As$	148.7		Rapid
$(CH_3)_2O$	Decomposition(11)		
$(CH_3)_2S$	160 ± 2	90 ± 1	Rapid
$(CH_3)_2Se$	148.6		Moderate
Cl^-[a]	148.7		Moderate
Br^-[a]	144.0		Moderate
NH_3	144.2	Insoluble	
CH_3CN	No complex formation		
No ligand	167.0		

[a]As the tetrabutylammonium salt.

Can. J. Chem. Downloaded from www.nrcresearchpress.com by 210.87.254.5 on 09/05/12
For personal use only.

sistent values for the equilibrium constants over a 58 degree temperature range and a twofold variation in concentration for five samples were obtained only for a chemical shift of 160 ppm for the fluorines of the 1:1 complex. The calculations were quite sensitive to slight changes in this value.

The observable quantities are: R, the ratio of intensities of signals from free and complexed tungsten hexafluoride; δ, the chemical shift of the averaged signal from the complex species; $\delta 2{:}1$, the chemical shift of the 2:1 complex; $\delta 1{:}1$, the chemical shift of the 1:1 complex (adjustable and assumed to be an observable); [total WF_6], the concentration of all WF_6 containing species in the solution; [total sulfide], the concentration of all dimethyl sulfide containing species in the solution. From these the following quantities may be calculated according to eqs. 1 through 7.

We define

[2:1]/[1:1]
= The ratio of concentrations of 2:1 and 1:1 complexes

[Free WF_6]
= The concentration of uncomplexed WF_6

[Free sulfide]
= The concentration of uncomplexed dimethyl sulfide

$$[1] \qquad \frac{[2{:}1]}{[1{:}1]} = \frac{\delta 1{:}1 - \delta}{\delta - \delta 2{:}1}$$

$$[2] \qquad [\text{Free } WF_6] = \frac{R[\text{total } WF_6]}{R+1}$$

$$[3] \qquad [1{:}1] = \frac{[\text{Total } WF_6] - [\text{free } WF_6]}{1 + [2{:}1]/[1{:}1]}$$

$$[4] \qquad [2{:}1] = [1{:}1] \times \frac{[2{:}1]}{[1{:}1]}$$

$$[5] \qquad [\text{Free sulfide}] = [\text{Total sulfide}] - [1{:}1] - 2[2{:}1]$$

$$[6] \qquad K_1 = \frac{[1{:}1]}{[\text{Free } WF_6][\text{free sulfide}]}$$

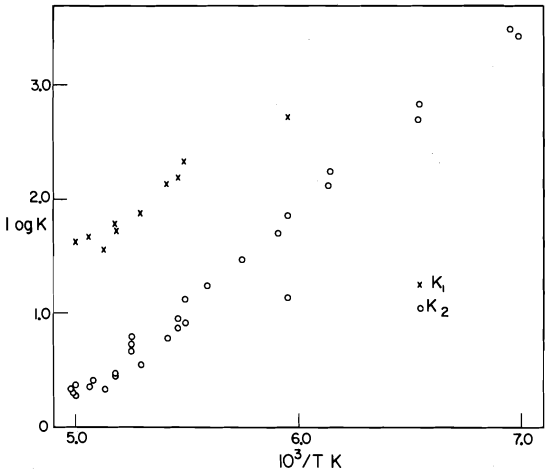

FIG. 1. The temperature dependence of the equilibrium constants for formation of complexes between dimethyl sulfide and tungsten hexafluoride.

$$[7] \qquad K_2 = \frac{[2{:}1]}{[1{:}1][\text{free sulfide}]}$$

A plot of the results is shown in Fig. 1. A least-squares analysis of these results yields -5.9 ± 0.5 kcal/mol for the heat of formation of the 1:1 complex and -7.4 ± 0.2 kcal/mol for the 2:1 complex.

The WF_6 complexes with dimethyl sulfide are quite unusual since the heat of formation of the 2:1 complex is greater than that for the 1:1 complex and the chemical shifts of the complexed WF_6 are rather different than those found for other complexes. The 2:1 dimethyl sulfide complex is the only one in which intramolecular fluorine exchange could be slowed sufficiently to observe individual fluorine resonance signals.

Theoretical spectra were calculated by a stochastic method (12) for one pair intramolecular exchange between the two and four nonequivalent fluorines observed for the 2:1 dimethyl sulfide – tungsten hexafluoride complex. The probability matrix employed is

	1	2	3	4	5	6	7	8
1	−1	0.376	0	0.078	0.234	0.234	0.078	0
2	0.188	−1	0.188	0.039	0.156	0.234	0.156	0.039
3	0	0.376	−1	0	0.078	0.234	0.234	0.078
4	0.375	0.375	0	−1	0.250	0	0	0
5	0.187	0.376	0.187	0.125	−1	0.125	0	0
6	0.187	0.376	0.187	0	0.125	−1	0.125	0
7	0.187	0.376	0.187	0	0	0.125	−1	0.125
8	0	0.375	0.375	0	0	0	0.250	−1

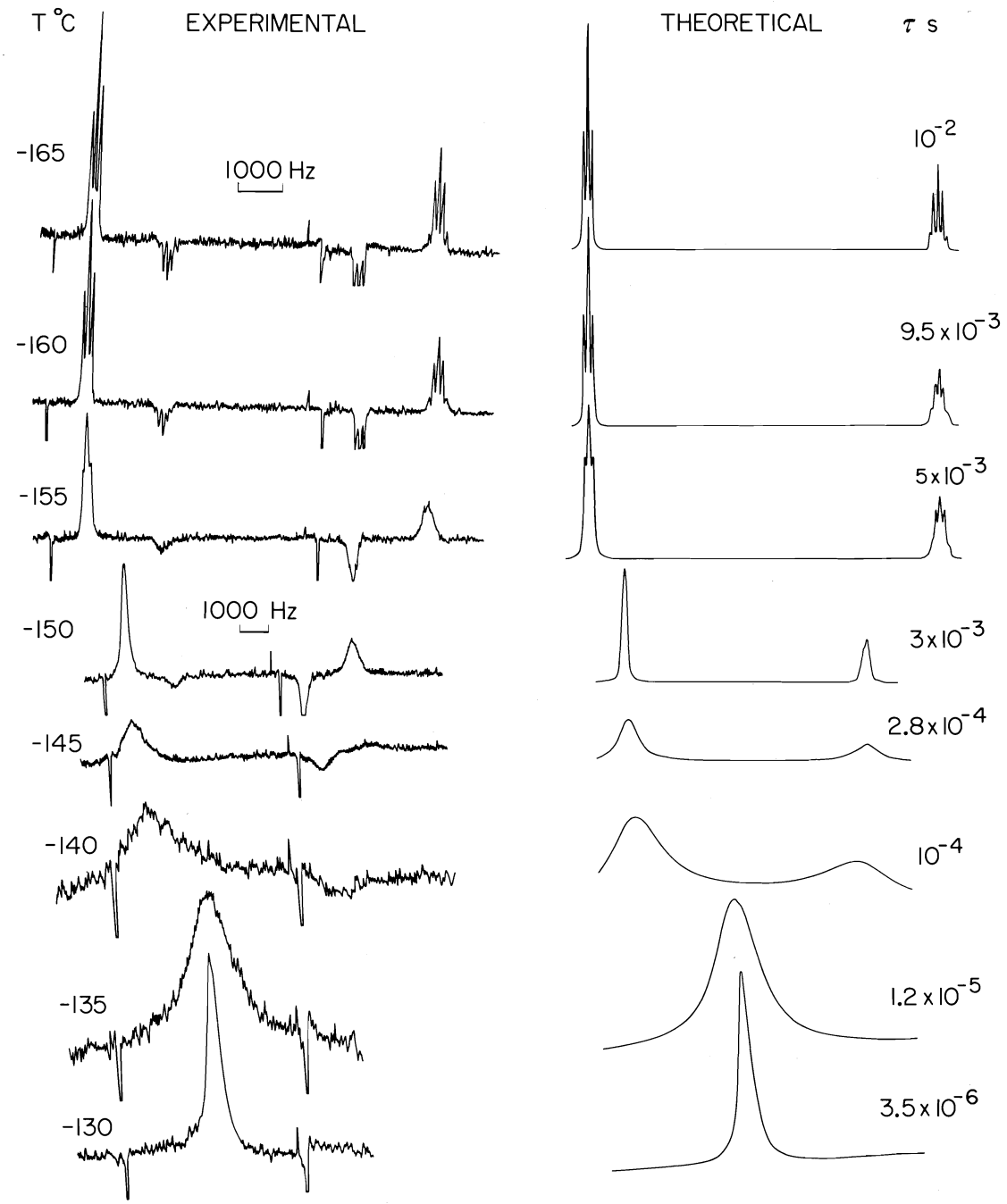

FIG. 2. A comparison of theoretical and experimental spectra for a 3:1 sample of dimethyl sulfide and tungsten hexafluoride in vinyl chloride solution.

where the lines are those of the triplet and quintet from low to high field respectively. From a comparison of theoretical and experimental spectra as a function of exchange rate and temperature, as illustrated in Fig. 2, the exchange rates in Fig. 3 were obtained. Although the postulated exchange mechanism need not be correct, the calculated exchange rates will still

Can. J. Chem. Downloaded from www.nrcresearchpress.com by 210.87.254.5 on 09/05/12
For personal use only.

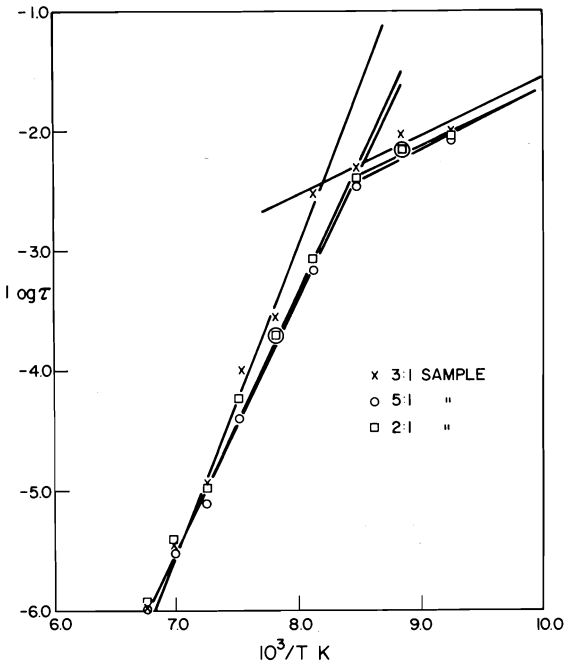

FIG. 3. Exchange rates as a function of temperature and concentration for dimethyl sulfide tungsten hexafluoride samples.

correspond reasonably closely to those of other mechanisms. It is therefore possible to state that the fluorine exchange mechanism at the lowest temperatures does not involve free dimethyl sulfide in the rate limiting step. It is probable that a second exchange mechanism predominates at temperatures above −150 °C, and also does not involve free dimethyl sulfide. The simplicity of the spectra do not allow a more detailed interpretation, however some general geometric conclusions can be stated.

Eight co-ordinate structures are the dodecahedron, cube, square antiprism, undecahedron, and hexagonal bipyramid (13, 14). Only for the hexagonal bipyramid is it possible to have a rigid structure with two and four equivalent fluorine atoms. This geometry has been observed for neptunyl acetate (15) and uranyl nitrate and acetate (16). The observed fluorine resonance results could be explained by this structure with two fluorines in the axial positions and the two ligands in *para* positions in the hexagonal girdle. In such a case exchange of fluorines could occur by the intramolecular one pair exchange between an axial and an equatorial fluorine.

If the actual structure of the complex is a cube or a square antiprism the low temperature fluorine resonance results may be explained by a *trans* position of the two dimethyl sulfide groups on one face and a rapid rotation of the four groups on this face with respect to the four fluorine atoms on the opposite face. Intramolecular averaging of the two and four equivalent fluorines may arise from the one pair exchange between a fluorine on each face.

The regular dodecahedron may be considered as two interpenetrating tetrahedra, one flattened and one elongated (14). The least low temperature motion is required if the four equivalent fluorine atoms are located at the corners of the elongated tetrahedron. The two equivalent fluorines are located on opposite corners of the flattened tetrahedron with rapid rotation of this tetrahedron, relative to the other. Intramolecular averaging of the two and four equivalent fluorines would occur by a one pair exchange between a fluorine of the flattened tetrahedron and a fluorine of the elongated tetrahedron.

For an undecahedral structure to yield the observed fluorine resonance results there must be a dimethyl sulfide group on each triangular face and the two fluorine atoms normal to these faces must be exchanging rapidly. This appears to be a rather unlikely possibility (13). Considerable low temperature motion is required for all the possible structures except the hexagonal bipyramid so it is the most favored arrangement even though it has not been observed very frequently.

The complex between dimethyl selenide and tungsten hexafluoride is only stable at low temperature and tends to slowly react with sulfur dioxide as solvent to give WOF_4 even at −70 °C. Complexes with tetrabutylammonium chloride and bromide are unexceptional. Tungsten hexafluoride has been reported to react with an excess of ammonia to yield a solid complex containing four equivalents of ammonia (1). In acetonitrile as solvent a soluble 1:1 complex with ammonia was observed. With two equivalents of ammonia only insoluble material was obtained and no signal remained from the 1:1 complex, suggesting that a 2:1 complex is also formed. No other satisfactory solvents were found for the 1:1 or 2:1 complexes.

No complex formation is found with acetonitrile, carbon disulfide, carbon oxysulfide,

Can. J. Chem. Downloaded from www.nrcresearchpress.com by 210.87.254.5 on 09/05/12
For personal use only.

TABLE 2. Fluorine chemical shifts for some molybdenum hexafluoride complexes

Ligand	Shift δ1:1	Exchange rate
$(CH_3)_3N$	Decomposition	
$(CH_3)_2O$	δ1:2 = 315.9	Fast
$(CH_3)_2S$	Decomposition	
Cl^{-a}	274.0	Moderate
Br^{-a}	Decomposition	
NH_3	Insoluble	
CH_3CN	No complex formation	
No ligand	282.1	

[a]As the tetramethylammonium salt.

thiophene, hexafluoroacetone, and trifluoromethyl ether. Decomposition of the organic moiety occurs rapidly with acetone and furan.

A few complexes with molybdenum hexafluoride along with an example of no complex formation and cases of other reactions are listed in Table 2. With three equivalents of MoF_6 for each dimethyl ether separate lines from uncomplexed MoF_6 and the 1:2 complex are found at −135 °C, although they merge by −125 °C. With two equivalents of MoF_6 only the line from the 1:2 complex is observed. As one increases the relative concentration of dimethyl ether to three equivalents for each MoF_6 only a single line is observed in both the fluorine and proton resonance spectra even at −135 °C. The fluorine resonance line moves steadily upfield with varying ether concentration to 297.8 ppm with three equivalents of ether. One can conclude that there is at least partial formation of an ether-rich complex but its stoichiometry and extent of formation cannot be determined.

The only complex formed by both tungsten and molybdenum hexafluorides is with chloride ion. It is not possible to compare the relative complexing strength of the two fluorides for this ligand since there is essentially complete formation of the 1:1 complex and no further complex formation.

1. H. C. CLARK and H. J. EMELEUS. J. Chem. Soc. 4778 (1957).
2. F. N. TEBBE and E. L. MUETTERTIES. Inorg. Chem. **7**, 172 (1968).
3. A. M. NOBLE and J. M. WINFIELD. Inorg. Nucl. Chem. Lett. **4**, 339 (1968).
4. A. STEIGEL and S. BROWNSTEIN. J. Am. Chem. Soc. **96**, 6227 (1974).
5. R. R. MCLEAN, D. W. A. SHARP, and J. M. WINFIELD. Chem. Commun. 452 (1970).
6. T. A. O'DONNELL and D. F. STEWART. Inorg. Chem. **5**, 1434 (1966).
7. A. PRESCOTT, D. W. A. SHARP, and J. M. WINFIELD. Chem. Commun. 667 (1973).
8. S. BROWNSTEIN. Can. J. Chem. **47**, 605 (1969).
9. S. BROWNSTEIN. Inorg. Chem. **12**, 584 (1973).
10. American Society for Testing and Materials. Standard E386.
11. A. M. NOBLE and J. M. WINFIELD. J. Chem. Soc. (A), 2574 (1970).
12. C. S. JOHNSON and C. G. MORELAND. J. Chem. Educ. **50**, 477 (1973).
13. J. L. HOARD and J. V. SILVERTON. Inorg. Chem. **2**, 235 (1963).
14. R. J. H. CLARK, D. L. KEPERT, R. S. NYHOLM, and J. LEWIS. Nature, 559 (1963).
15. W H. ZACHARIASEN. Acta Crystallogr. **2**, 388 (1949).
16. W. H. ZACHARIASEN and H. A. PLETTINGER. Acta Crystallogr. **12**, 526 (1959).

Can. J. Chem. Downloaded from www.nrcresearchpress.com by 210.87.254.5 on 09/05/12
For personal use only.

Nuclear charge distribution in the region of symmetric fission of ^{238}U by protons of energy 20–85 MeV[1]

S. SARKAR[2] AND L. YAFFE
Department of Chemistry, McGill University, Montreal, Que., Canada H3C 3G1

Received January 21, 1976

S. SARKAR and L. YAFFE. Can. J. Chem. **54**, 2349 (1976).

Independent formation cross sections in the fission of ^{238}U by protons of energy 20–85 MeV were obtained for the nuclides ^{111}Ag, ^{112}Ag, ^{117}In, ^{115}In, ^{111}Pd, and ^{115}Cd. The last three mentioned were estimated on the basis of measurements and isomeric yield data. Charge dispersion curves were constructed and Z_p, the most probable charge, determined. The values for $(Z_A - Z_p)$ lie intermediate between those measured for fission products of higher and lower mass. The number of neutrons emitted was estimated and found to be higher than in asymmetric fission, leading to the conclusion that the former are events arising from higher deposition energies.

S. SARKAR et L. YAFFE. Can. J. Chem. **54**, 2349 (1976).

Les sections efficaces de formation indépendantes des nucléides suivants: ^{111}Ag, ^{112}Ag, ^{117}In, ^{115}In, ^{111}Pd et ^{115}Cd, issus de la fission de ^{238}U par protons d'énergies comprises entre 20 et 85 MeV, ont été obtenues. Les trois dernières ont été estimées à partir des mesures et de données sur les rendements isomériques. Les courbes de distribution de charge ont été construites et Z_p, la charge la plus probable, a été determinée. Les valeurs de $(Z_A - Z_p)$ se situent entre celles mesurées dans le cas de produits de fission de masse supérieure et inférieure. Une estimation du nombre de neutrons émis a conduit à des valeurs supérieures à celles déduites dans le cas de fissions asymetriques. Nous en avons conclu que ceux-ci sont le résultat d'évènements consécutifs à des dépots d'énergie plus élevés.

Introduction

The variation of yields of primary fission fragments can be used to determine the nuclear charge distribution in fission. This can be done by determining the fractional yield in a mass chain or by the determination of independent yields in a narrow mass region when the variation of the yield with mass is minimal.

If the probability of formation of fractional independent yield of a product with atomic number, Z, within a particular mass chain is $P(Z)$, and each chain is characterized by a single most probable (not necessarily integral) atomic number, Z_p, then $P(Z)$ has been shown by many investigators to be given adequately by the Gaussian equation

$$[1] \qquad P(Z) = A \exp - (Z - Z_p)^2/c$$

The constant c, reflects the relative width of the Gaussian function. The maximum amplitude is given by A, which is related to c:

$$[2] \qquad A = (\pi c)^{-1/2}$$

Available data regarding nuclear charge distribution in medium-energy fission are relatively limited compared with those done at thermal energies. Nevertheless, a variety of fissile systems (1–14) has been studied at medium energies.

The conclusions drawn from these studies can be summarized as follows:

(*a*) All the data can be effectively correlated by the assumption of a Gaussian charge dispersion.

(*b*) The equal charge displacement (ECD) hypothesis (15) which can be used to describe nuclear charge distribution at thermal energies is not an adequate, unambiguous description at higher energies. The unchanged charge distribution (UCD) (16), while valid for some systems at medium energies, does not uniformly describe all the data either.

(*c*) A study of charge distribution curves as a function of incident proton energy shows that the peak of the curve, corresponding to Z_p, the most probable nuclear charge, moves towards Z_A, the most stable nuclear charge for mass A, as the proton energy, E_p, increases.

(*d*) In the most probable split, A_H = 130–140

[1]With financial assistance from the National Research Council of Canada.

[2]Present address: Chemicals Department, Gulf Oil of Canada Limited, 2020 University Street, Montreal, Quebec.

Can. J. Chem. Downloaded from www.nrcresearchpress.com by 210.87.254.6 on 09/05/12
For personal use only.

Can. J. Chem. Downloaded from www.nrcresearchpress.com by 210.87.254.6 on 09/05/12
For personal use only.

and A_L = 90–100 (where A_H and A_L are the mass numbers of the heavy and light fission products, respectively), the relationship of $(Z_A - Z_p)$ as a function of proton energy, E, is virtually independent of the target for the light fragment for a variety of fissile systems, *e.g.* ^{233}U, ^{235}U, and ^{238}U and are found to carry virtually identical excitation energy. With the heavier fragments the above function shows a steeper gradient, depends on the original neutron-to-proton (N/Z) ratio of the target, and most of the increase in incident proton energy reflects itself in increased excitation energy of the heavy fragment.

(*e*) As the proton bombardment energy is increased, the Gaussian charge dispersion curves widen. This is explained by the variety of fissile systems which is a result of direct interaction cascades and neutron evaporation as the bombardment energy is increased.

The present study was undertaken to determine the behaviour, not in the region of the most probable fission split, but in the symmetric and near-symmetric mass regions. Very little data have been gathered in this region. The production cross section is low at medium energies, the decay schemes are complex, and isomerism is abundant. This paper attempts to measure independent formation cross sections in this area as accurately as possible and to provide an estimate for those nuclides where only partial data are available from isomers. Charge distribution curves obtained have been compared with the systematics quoted above.

Experimental

Targets and Irradiation

(a) Target Arrangement

The uranium foil target was of natural isotopic composition. The foil superficial density varied between 170 and 230 mg cm^{-2} depending on the nature of the experiment. The degradation in proton bombardment energy introduced by the target thickness was computed at each energy from the data of Williamson *et al.* (17) and was found to lie within the ±2 MeV spread in the energy of the internal circulating beam of the McGill synchrocyclotron. The target assembly consisted of the following, (*i*) uranium foil, cleaned with dilute HNO_3 to remove the oxide coating, subsequently washed with water, acetone, and dried, (*ii*) high-purity Al catcher foils (front and back) approximately 10 mg cm^{-2} superficial density, sufficient to stop the recoil of the fission fragments (18, 19) and (*iii*) a Cu monitor coil (99.99% pure) of superficial density 44 mg cm^{-2} upstream of the target. Estimates (20, 21) of the range of the copper recoil atoms indicate a maximum loss due to recoil of less than 0.003% and thus no catcher foils were used with the monitor foil.

The assembly was carefully trimmed to ensure that identical surfaces of all foils were exposed to the beam, then wrapped in Al foil of identical purity to that of the catcher foils and attached to a target holder which was fastened to the cyclotron probe.

(b) Irradiation

Irradiations were performed in the internal circulating beam of the McGill proton synchrocyclotron at radial distances corresponding (22) to energies of 20, 35, 40, 55, 70, and 85 MeV. For extremely short irradiations the procedure was further modified by (*i*) ensuring that the target was placed in the holder to ensure maximum utilization of the vertical oscillation of the beam (23, 24), (*ii*) reducing the target thickness to allow for more rapid dissolution, and (*iii*) tilting the target assembly to obtain greater effective thickness presented to the beam.

The duration of the irradiation, a direct function of the formation cross section of the nuclide of interest, nature of the fission yield, and beam intensity, varied between 2 and 25 min.

(c) Monitoring of the Intensity of the Beam

The beam was monitored by the reaction $^{65}Cu(p,pn)^{64}Cu$. The absolute cross sections have been obtained by a Faraday cup measurement in the external beam facility and have been previously described (25). The values, for ready reference, determined to within a standard error of ±5.9%, are given in Table 1.

TABLE 1. Cross sections for the reaction $^{65}Cu(p,pn)^{64}Cu$ (25)

Mean bombardment energy (MeV)	Cross section (mb)
102.1	128
97.3	121
89.8	141
83.0	141
78.0	157
73.0	154
67.3	156
62.2	170
56.6	162
51.3	187
45.1	194
40.1	245
35.8	250
29.5	408
23.2	429

Chemical Separations and Preparation of Samples for Activity Measurements

After irradiation a leading edge of the target assembly was sheared off for chemical processing and radiochemical assay. The U foil was dissolved in a minimum of HNO_3 to which was added the Al catcher and Al sheath portions which had been dissolved in a minimum volume of concentrated NaOH. The Cu foil was treated as described in the Appendix.

In the present work only a single element was isolated

TABLE 2. Summary of the decay properties of observed nuclides

Isotope	Mode of decay	Half-life	Radiation detected	Emitted radiation per disintegration (26)
^{117m}In	46% I.T; 54% β^-	1.94 h	158.6-keV γ from daughter	0.87
^{117g}In	β^-(100%)	44 min	158.6-keV γ from daughter	0.87
$^{117m+g}$Cd	β^-(100%)	3.4 and 2.4 h respectively	Daughter	0.87
^{115}Ag	β^-(100%)	21 min	229.7-keV γ	1.00
^{115m}Cd	β^-(100%)	43 days	336.3-keV γ (daughter)	0.45
^{115g}Cd	β^-(100%)	2.3 days	527.9-keV γ	0.275
^{115m}In	95% I.T; 5% β^-	4.5 h	336.3-keV γ	1.00
^{113}Ag	β^-(100%)	5.37 h	298.6-keV γ	1.00
^{112}Pd	β^-(100%)	21.0 h	Daughter	
^{112}Ag	β^-(100%)	3.2 h	β^-	1.00
^{111m}Pd	71% I.T; 29% β^-	5.3 h	Daughter	
^{111g}Pd	100% β^-	22 min	Daughter	
^{111}Ag	100% β^-	7.5 days	β^-	1.00

from each aliquot of the mixed fission product solution. Operations were performed in 40-ml centrifuge tubes in which all precipitations and dissolutions were made. Several extractions were made at different times to evaluate the contribution from the β^--decay chain, as well as that formed directly in the fission act.

The sample was finally prepared for activity measurements by filtration of the precipitate on to a millipore filter assembly consisting of a glass fibre 25-mm filter (previously weighed) placed in a filter holder on a fritted glass base. The final precipitate was washed finally with acetone, dried, and weighed to determine the chemical yield. The filter was mounted in the centre of a pre-cut standard mounting card and the entire assembly covered by a Mylar film (1.75 mg cm^{-2}). The activity of the copper monitor was assayed as a liquid in a 'counting vial'. The preparation of this sample, as well as the specific separation methods are given in the Appendix.

Activity Measurements

The pertinent decay characteristics of the various nuclides of interest and their methods of detection are summarized in Table 2.

(a) β^--Measurements

The formation cross sections of ^{111}Ag and ^{112}Ag are so small at the bombardment energies studied in this work that the resolution of γ-decay curves would have been a formidable task. A low-background β-counter Beckman 'Widebeta II' was used with a counter gas mixture of 90% Ar – 10% CH_4. The background varied between 1.8 to 2.0 counts per min and the resolving time of the system was 0.5 μs at a counting rate of 10^6 per min. The detector was calibrated using standard techniques (27, 28). The nuclide ^{111}Ag has E_{max} = 1.06 MeV for the β^--particle resulting from the 'allowed' transition to its daughter. A calibrated sample of ^{210}Pb (E_{max} = 1.1 MeV, 'normal' first-forbidden), prepared under identical measurement conditions to those used with ^{111}Ag, was used to determine the overall efficiency for ^{111}Ag. The absolute efficiency for the 'hard' β's of ^{112}Ag (E_{max} = 4.0 MeV) was obtained by cross-calibration on the 40-cm^3 Ge(Li) detector described below. For this purpose the sample was covered by an Al foil, 800 mg cm^{-2}, sufficient to absorb the β^--particles.

(b) γ-Measurements

(*i*) Scintillation detector. The 511-keV annihilation radiation from the β^+ rays of ^{64}Cu were detected and measured by a 3 in. × 3 in. NaI(Tl) crystal coupled to a 400-channel pulse-height detector. Sufficient material surrounded the counting vial to ensure efficient absorption of the positrons. The 'live-timer' of the analyser was found to give results accurate to ±1.5% when the indicated dead-time was below 8%. All data using this detector were gathered at or below an 8% indicated dead-time. The system was calibrated using a ^{22}Na standard, prepared for measurement under conditions identical to those for ^{64}Cu. (The positron energies are not very different.)

(*ii*) Solid-state detectors. Two systems were used. The first was a 30-cm^3 Ge(Li) detector coupled to a 4096-channel pulse-height analyzer. The counting data were recorded on magnetic tape and analyzed using the McGill IBM 360-75 computer. All samples to be measured were placed at such a distance from the detector that the dead-time was less than 10%. Under these conditions the 'live-time' mode of this system accurately self-corrected for dead-time losses. The resolution of the set-up was 3.1 keV (full-width at half-maximum) at the 1333-keV ^{60}Co line. The second system was a 40-cm^3 Ge(Li) detector coupled to a 1600-channel pulse-height analyzer. The resolution was 0.4% (full-width at half-maximum) in the region of interest. All measurements were made with a plastic absorber, sufficiently thick to absorb any β^--particles, placed in between the sample and the detector to avoid β^-–γ summing effects. The measurement of all activity was carried out at a distance of 106.5 mm (source-to-detector) to minimize errors due to source-geometry effects.

Treatment of Data

Data which were obtained using gas-flow β^--counters were resolved into the various components by the CLSQ programme (29) modified for use on the IBM-360 (30). For γ-decay analyses two least-squares programmes were used, ORGLS (31) modified for use on the IBM-360 (30) and that of von Holdt (32), adapted to the IBM-360-75 (33).

The evaluation of areas under the photopeaks which

Can. J. Chem. Downloaded from www.nrcresearchpress.com by 210.87.254.6 on 09/05/12
For personal use only.

TABLE 3. Fission product decay chains*

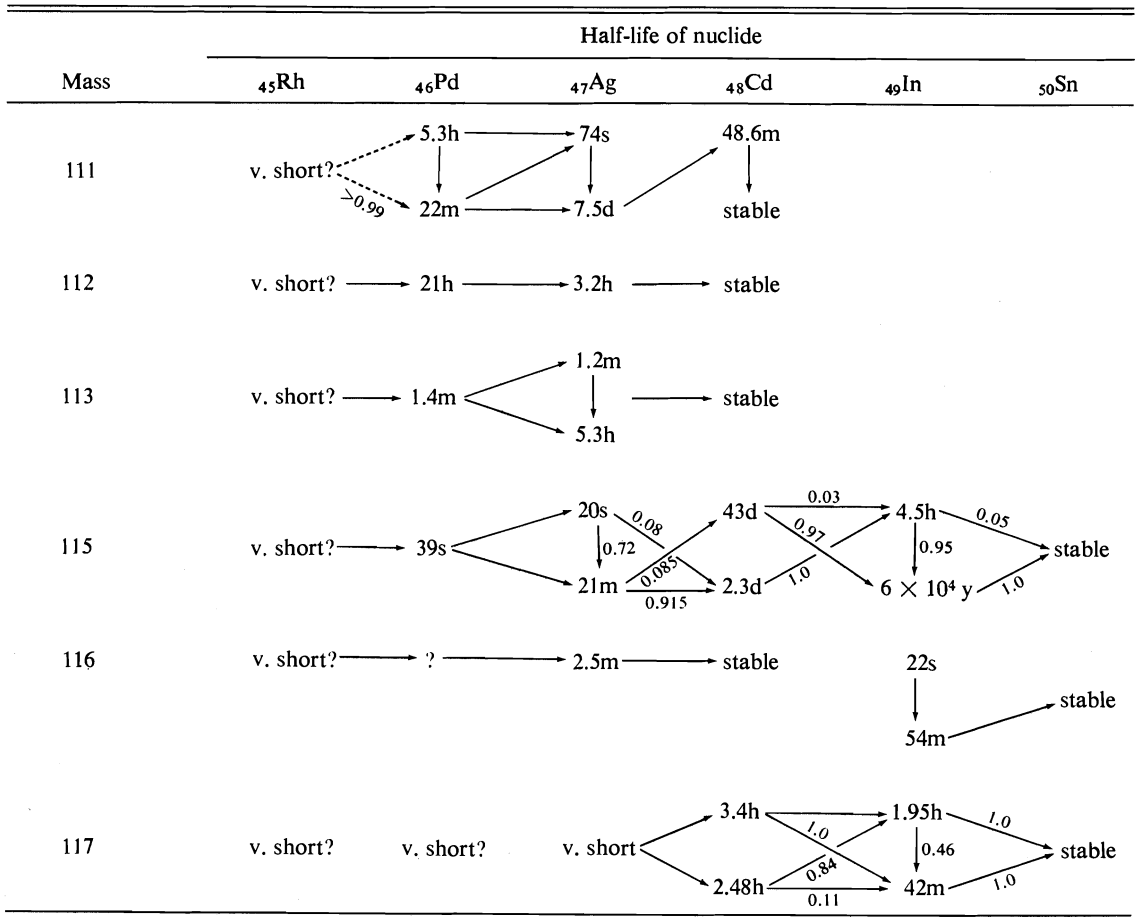

*v = very, y = years, d = days, h = hours, m = minutes, s = seconds.

are representative of the counting rate was done either manually or by a computer code (34, 35). The counting rates at the end of bombardment or separation time (whichever was applicable) were converted to absolute disintegration rates by correcting for the chemical yields, detector efficiencies, dilution factors, and branching ratios.

The fission product decay chains investigated are shown in Table 3. The numbers shown over the arrows give the isomeric branching ratios.

The measured activities of ^{117}In and ^{111}Pd were increased by 4% and 3% respectively in order to take into account scavenge losses as determined from tracer work.

No self-absorption corrections were made since the superficial densities of all samples were within ± 1 mg cm^{-2} of the superficial density of the standard calibration samples. The total self-absorption correction if made would only have been of the order of 1%.

Corrections for growth and decay were made by using the standard Bateman equations, greatly complicated by the occurrence of isomerism. The equations and treatment of each individual chain are given in detail in ref. 36.

Errors were divided into 'systematic' and 'random' according to the scheme suggested by Bevington (37).

The systematic errors are associated with monitor cross sections, detector efficiencies, branching ratios, and half-life values. Errors involved in cross sections used in beam monitoring have already been quoted as $\pm 5.9\%$ (25). Errors in decay scheme uncertainties varied between 1 and 12% while isomer branching ratio uncertainties were 2–3%. Errors in the actual sample measurements, because of the use of different detectors, were 1–3%. The energy spread in the internal circulating beam is on the average ± 2 MeV. Errors in efficiency calibration of detectors are 2% for the γ-ray detectors and 7% for the cross calibration used for ^{112}Ag. An error of $\pm 3\%$ was allowed for sample reproducibility.

The random errors are connected with β^-- and γ-activity measurements, chemical yields, foil thickness, and alignments. The main source of error lies in the determination of photopeak areas (5–15%) depending on

Can. J. Chem. Downloaded from www.nrcresearchpress.com by 210.87.254.6 on 09/05/12
For personal use only.

TABLE 4. Independent formation cross sections of products from the fission of ^{238}U by 20–85 MeV protons

E_p (MeV)	σ (mb) ^{117}In (N/Z = 1.387)	^{115}In* (N/Z = 1.346)	^{115}Cd* (N/Z = 1.395)	^{111}Pd* (N/Z = 1.413)	^{112}Ag (N/Z = 1.382)	^{111}Ag (N/Z = 1.361)
20	0.16±0.04	0.01±0.003	0.5±0.1	1.8±0.3	0.18±0.03	0.05±0.008
30	0.55±0.07	0.03±0.005	1.2±0.3	2.0±0.3	0.4 ±0.06	0.08±0.01
40	1.2 ±0.2	0.05±0.01	1.9±0.3	3.9±0.6	0.8 ±0.1	0.2 ±0.03
55	2.6 ±0.5	0.2 ±0.03	2.8±0.4	4.8±0.7	1.8 ±0.3	0.8 ±0.1
70	5.3 ±0.8	0.9 ±0.2	4.5±0.7	9.0±1.4	3.8 ±0.5	1.5 ±0.2
85	7.0 ±1.0	2.0 ±0.4	10.6±1.6	12.3±2.0	7.0 ±1.0	3.3 ±0.4

*Estimated cross sections based on independent isomer ratio values explained in text.

the complexity of the γ-ray spectra. The error in obtaining the initial disintegration rate varied from 2% (extrapolation of ^{64}Cu decay curve) to 10% for specific nuclides. Weighing and pipetting contributed 1.5–2%, 1–3% was contributed by timing in separations. Chemical yields were determined in duplicate or triplicate. They agreed within 3–5%. The error in foil area determination was assessed at 1%.

The total error was assessed for each nuclide by taking the square root of the sum of the squares of individual errors connected with both the nuclide and the monitor. The error varied between ±11% and ±25%.

Results

The independent formation cross sections for the nuclides ^{117}In, ^{112}Ag, and ^{111}Ag were computed directly at each energy (1, 13) and are shown in Table 4. The independent cross section of ^{115}Cd was computed from the measured independent yield of ^{115m}Cd and the ratio of the isomeric products $^{115m}Cd/^{115g}Cd$ given by Tilbury and Yaffe (38) in this energy range. In addition, from the experimentally-determined values of the ^{115m}In independent formation cross sections a total cross section value for ^{115}In was determined by assuming, at each value of the bombardment energy, an isomer ratio (high-to-low spin) equal to that of ^{117}In determined in this work. The isomer spins of ^{115}In and ^{117}In are identical. The isomer ratios found for ^{117}In agree well with those of Hagebø (39) as is shown in Table 5.

Schmitt and Zumwalt (40) have pointed out that the cross section of ^{111m}Pd could be considered independent since the decay of the ^{111}Rh parent is greater than 99% to the ground state. Panontin and Porile (41) have reported the isomer ratio of (σ (^{111m}Pd) independent/σ(^{111g}Pd) independent) to be 2.5 ± 0.6 and to be virtually identical in low- and high-energy fission and

TABLE 5. Independent isomeric yield ratio $^{117g}In/^{117m}In$

Irradiation energy (MeV)	Yield ratio Present work	Hagebø (39)
15	0.8±0.5	0.6±0.4
29	1.6±0.4	1.2±0.2
43	2.5±0.5	2.7±0.7
57	4.8±0.8	4.2±0.8
70	8.5±0.8	
85	9.8±0.9	9.0±1.0
110		12.0±1.0

TABLE 6. Cumulative formation cross sections of products from the fission of ^{238}U by 20–85 MeV protons

E_p (MeV)	σ (mb) ^{112}Pd	^{111}Ag	^{115}Ag	^{113}Ag*
20	11±2	11±2	8±1	11±2
30	14±2	16±2	16±2	18±3
40	23±3	22±3	21±3	23±3
55	30±4	26±5	30±5	32±5
70	36±5	28±4	32±5	39±6
85	44±7	47±6	38±6	48±6

*A partial cumulative yield, since there is a partial loss from the decay of ^{113m}Ag to ^{113}Cd.

thus the total cross section could be computed for this nuclide.

The cumulative yield recorded for ^{113}Ag is considered 'partial' to allow for a partial 'loss' by direct decay of ^{113m}Ag to ^{113}Cd.

The cumulative formation cross sections measured in this work are listed in Table 6. Excitation functions are not shown, except for that of ^{115g}Ag in Fig. 1 in order to compare with the data of Hicks and Gilbert (41).

Discussion

The independent yield data shown in Table 4 were converted into fractional chain yields using

Can. J. Chem. Downloaded from www.nrcresearchpress.com by 210.87.254.6 on 09/05/12
For personal use only.

TABLE 7. Fractional chain yields used in construction of charge-dispersion curves

E_p (MeV)	Fractional chain yield ^{117}In (N/Z = 1.387)	^{115}In* (N/Z = 1.346)	^{115}Cd* (N/Z = 1.395)	^{111}Pd* (N/Z = 1.413)	^{112}Ag (N/Z = 1.382)	^{111}Ag (N/Z = 1.361)
20	0.003 ±0.0006	0.00015 ±0.00003	0.009 ±0.001	0.025 ±0.005	0.0029 ±0.0004	0.00025 ±0.00005
30	0.01 ±0.002	0.0008 ±0.00002	0.03 ±0.005	0.05 ±0.008	0.009 ±0.001	0.002 ±0.0003
40	0.03 ±0.004	0.003 ±0.0006	0.04 ±0.006	0.08 ±0.01	0.02 ±0.003	0.004 ±0.0007
55	0.04 ±0.008	0.003 ±0.0007	0.06 ±0.008	0.08 ±0.02	0.03 ±0.004	0.02 ±0.002
70	0.07 ±0.01	0.01 ±0.002	0.06 ±0.009	0.10 ±0.02	0.05 ±0.005	0.02 ±0.003
85	0.09 ±0.01	0.03 ±0.004	0.10 ±0.02	0.14 ±0.02	0.08 ±0.01	0.03 ±0.004

*Best estimated value (see text).

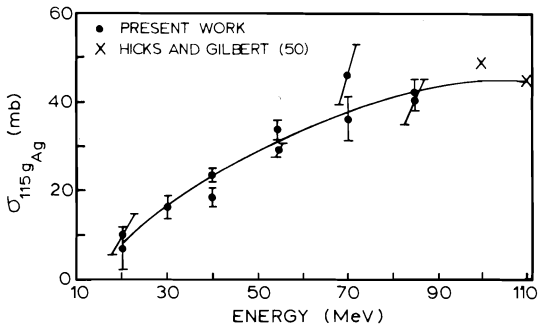

FIG. 1. Cumulative formation cross section of ^{115g}Ag.

the cumulative yield data shown in Table 6 and data reported by Baba, Umezawa and Baba (42), Miller (43), Hicks and Gilbert (41), Stevenson *et al.* (44), and Lindner and Osborne (45). The fractional chain yield data shown in Table 7 were used to construct charge dispersion curves. The yields were plotted against N/Z (neutron-to-proton ratio of the nuclide) using the convention initiated by Friedlander *et al.* (46). Two constraints were used. The data were assumed to accord with a Gaussian fit (eq. 1) and were computer-fitted to this format. In addition the curve was so drawn that all independent isobaric yields read from the curve had to sum to the measured cumulative chain yield for these isobars. This has been shown to be an exceedingly sensitive constraint (46). Typical curves at 30, 55, and 85 MeV bombarding energy are shown in Figs. 2–4.

The values of N/Z at the peak of the charge dispersion curves and the mass number of the silver isotope, (A_p), having the neutron-to-proton nearest the peak value were used to obtain the most probable charge, Z_p, for this mass. The values of N/Z at half-maximum were similarly obtained from the charge dispersion curves and were converted to Z values for the same mass to obtain the full-width at half-maximum in Z units. The parameters thus obtained are shown in Table 8.

The general features of the charge dispersion curves conform with those found by others working in this energy region, but in a different region of the fission product mass distribution. The most probable charge, Z_p, shifts to less neutron-rich nuclides with increasing bombard-

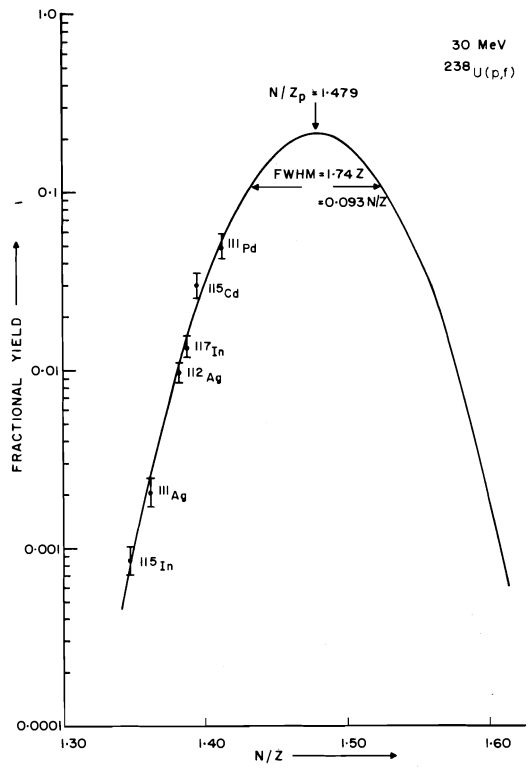

FIG. 2. Charge distribution in the symmetric mass region, 30 MeV protons.

Can. J. Chem. Downloaded from www.nrcresearchpress.com by 210.87.254.6 on 09/05/12
For personal use only.

TABLE 8. Parameters of charge dispersion curves for ^{238}U

Proton energy (MeV)	Full-width at half-maximum		Peak position		
	N/Z	Z	N/Z	Z_p	$Z_A - Z_p$
20	0.088	1.28	1.480	46.36	2.94
30	0.093	1.74	1.479	46.39	2.91
40	0.098	1.92	1.475	46.46	2.84
55	0.101	1.96	1.468	46.59	2.70
70	0.111	2.16	1.463	46.69	2.61
85	0.115	2.36	1.455	46.84	2.46

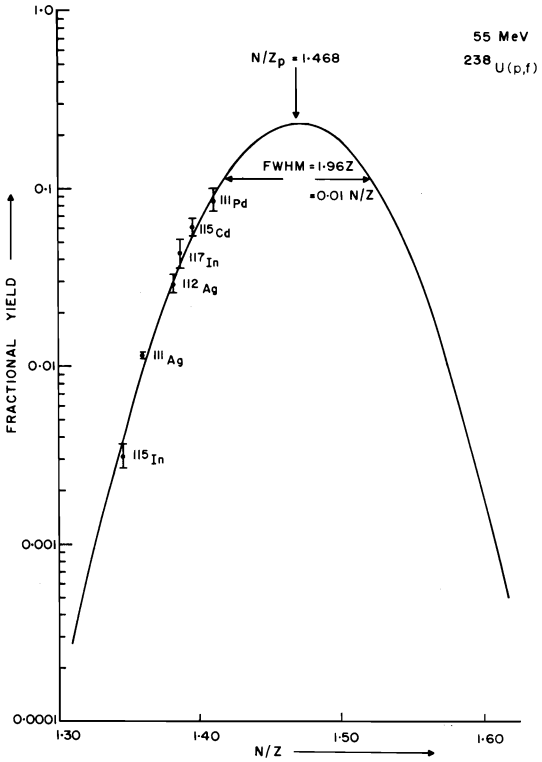

FIG. 3. Charge distribution in the symmetric mass region, 55 MeV protons.

ment energy. The shift, however, is less drastic than those found in the regions of mass asymmetry, *cf.* Fig. 5. Values of Z_A, the most stable charge for A (= 115 in this case), were obtained from Coryell (47). The values for $(Z_A - Z_p)$ were found to lie in between those obtained from light and heavy fragments from ^{238}U.

The variation of the magnitude of the FWHM curves has proved very difficult to interpret. Pate *et al.* (1) have attributed the broadening to the competition between neutron evaporation and fission competing at each successive step and the effect of post-fission neutron evaporation. Results available (40, 48–50) in the bombarding energy interval 170–720 MeV show that in the symmetric fission product mass region the width of the charge dispersion curves remains relatively constant (2.8–2.9 Z units). This can be explained by a very slow variation of E^*, the average deposition energy in this mass region. The studies of Panontin and Porile (51) at 11.5-GeV proton bombardment of natural

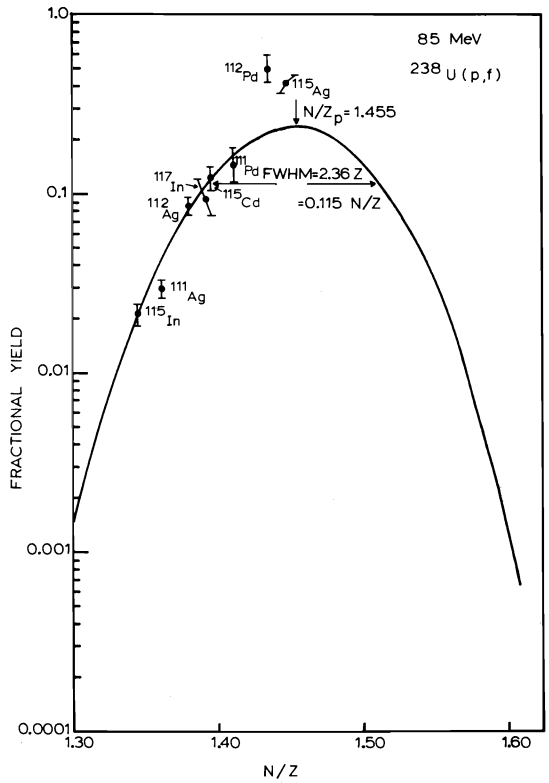

FIG. 4. Charge distribution in the symmetric mass region, 85 MeV protons.

Can. J. Chem. Downloaded from www.nrcresearchpress.com by 210.87.254.6 on 09/05/12
For personal use only.

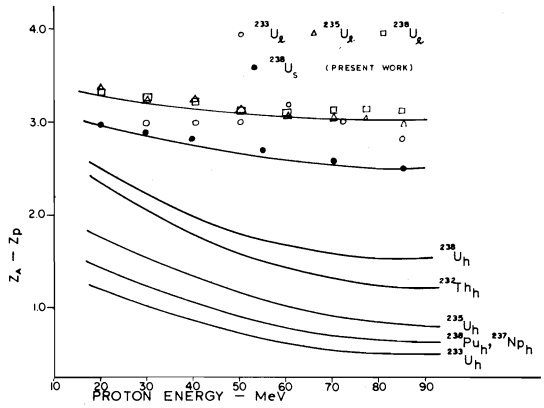

FIG. 5. Variation of $(Z_p - Z_A)$ with bombarding energy: $^{238}U_l$, A = 90–100; $^{235}U_l$, A = 90–100; ^{233}U, A = 90–100; $^{238}U_h$, A = 130–140; ^{232}Th, A = 130–140; ^{235}U, A = 130–140; $^{239}Pu_h$ and $^{237}Np_h$, A = 130–140; $^{233}U_a$, A = 130–140; ^{238}U, A = 111–117.

uranium showed that E^*, leading to products in the symmetric mass region, is not very different than at an energy of 450 MeV. However, in the present energy range, the work of Ramamoorthy *et al.* (18) shows a significant variation in E^* of primary fragments in the symmetric mass region as the bombardment energy is increased.

McHugh and Michel (5) have developed an equation describing the rate of change of neutron emission to the rate of change of Z_p with excitation energy.

$$[3] \qquad (\partial\nu/\partial E)_{Z_p} = (\partial Z_p/\partial E)_A/(\partial Z_p/\partial A)_E$$

These have been used in this work to estimate the number of post-fission neutrons emitted at different incident proton bombardment energies. At a given excitation energy the variation of Z_p with mass number can be approximated by the variation of Z_A with mass number, *i.e.*

$$[4] \qquad (\partial Z_p/\partial A)_E = (\partial Z_A/\partial A)_E$$

Coryell (47) has determined $(\partial Z_A/\partial A) = 0.38$. In addition, Dikšić *et al.* (14) have recently determined $(\partial Z_p/\partial A)_{E_p} = 0.38 \pm 0.02$ for isobaric studies along various mass chains, showing the above approximation to be very good indeed. Thus

$$[5] \qquad \partial\nu_T/\partial E = (\partial Z_p/\partial E)/0.38$$

where ν_T refers to the addition of the contribution from the heavy and the light fragments, ν_h and ν_l respectively. In the case of symmetric fission $\nu_h = \nu_l$. For the present system, from the above, and from the experimentally-determined value of $\partial Z_p/\partial E = 0.018$ MeV^{-1}, and $\partial\nu_T/\partial E = 0.096$ MeV^{-1}, the total number of post-fission neutrons has been evaluated.

TABLE 9. Total number of neutrons in the $^{238}U(p,f)$ reaction from a study of products in the symmetric and near symmetric mass region

E_p (MeV)	$\langle E \rangle$	Total number of neutrons ν_t	Prefission cascade neutrons ν_c	Prefission evaporated neutrons ν_E
20	25.2	3.1	—	0.72
30	26.7	3.9	0.29	1.12
40	32.09	5.1	0.45	1.63
55	39.62	6.7	0.60	2.38
70	45.44	8.2	0.74	3.09
85	53.93	9.6	0.81	3.63

The number of pre-fission neutrons has been calculated at different excitation energies using both the VEGAS Stepno code (52) and a Monte Carlo evaporation code by Dikšić *et al.* (14) for the same fissioning system at the identical bombardment energies. At 20 MeV the calculation assumed a pure compound nucleus mechanism. The data are shown in Table 9. The data show a higher neutron emission than in the mass range A = 130–135 as reported by Dikšić *et al.* (14). This supports the conclusion that symmetric fission is a result of fission events leading to fragments with higher than average excitation energy.

Acknowledgments

The authors acknowledge with pleasure the ready cooperation of Dr. S. K. T. Mark, Director of the Foster Radiation Laboratory. Special thanks are due to Professor R. B. Moore, Dr. M. Dikšić, and Dr. M. Fowler for help and discussions during various phases of this work.

1. B. D. PATE, J. S. FOSTER, and L. YAFFE. Can. J. Chem. **36**, 1691 (1958).
2. J. H. DAVIES and L. YAFFE. Can. J. Phys. **41**, 762 (1963).
3. N. A. WAGMAN, J. A. POWERS, and J. W. COBBLE. Phys. Rev. **152**, 3167 (1966).
4. S. H. FRIED, J. L. ANDERSON, and G. R. CHOPPIN. J. Inorg. Nucl. Chem. **30**, 3155 (1968).
5. J. A. MCHUGH and M. C. MICHEL. Phys. Rev. **172**, 1160 (1968).
6. P. P. BENJAMIN, D. A. MARSDEN, N. T. PORILE, and L. YAFFE. Can. J. Chem. **47**, 301 (1969).

Can. J. Chem. Downloaded from www.nrcresearchpress.com by 210.87.254.6 on 09/05/12
For personal use only.

Can. J. Chem. Downloaded from www.nrcresearchpress.com by 210.87.254.6 on 09/05/12
For personal use only.

7. L. YAFFE, Proc. Symp. on Physics and Chemistry of Fission, paper SM-122/3, Intl. At. Energy Agency, Vienna (1969).
8. A. H. KHAN, G. B. SAHA, and L. YAFFE. Can. J. Chem. **48**, 1924 (1970).
9. G. B. SAHA and L. YAFFE. J. Inorg. Nucl. Chem. **32**, 745 (1970).
10. T. MCGEE, C. L. RAO, and L. YAFFE. J. Inorg. Nucl. Chem. **34**, 3323 (1972).
11. HEATHER MARSHALL and L. YAFFE. J. Inorg. Nucl. Chem. **35**, 1797 (1973).
12. L. YAFFE and R. HOLUB. J. Inorg. Nucl. Chem. **35**, 3391 (1973).
13. L. D. MILLER and L. YAFFE. J. Inorg. Nucl. Chem. **35**, 1805 (1973).
14. M. DIKŠIĆ, D. K. MCMILLAN, and L. YAFFE. J. Inorg. Nucl. Chem. **36**, 7 (1974).
15. L. E. GLENDENIN, C. D. CORYELL, and R. R. EDWARDS. *In* Radiochemical studies: the fission products. Vol. 9. *Edited by* C. D. Coryell and N. Sugarman, National Nuclear Energy Series, Division IV – Plutonium Project Record. McGraw–Hill Book Co., New York. 1951. Paper 52.
16. R. H. GOECKERMANN and I. PERLMAN. Phys. Rev. **76**, 628 (1949).
17. C. F. WILLIAMSON, J. P. BOUJOT, and J. PICARD. Centre d'Etudes Nucleaires de Saclay, Rapport CEA-R3042. 1966.
18. A. N. RAMAMOORTHY, G. B. SAHA, and L. YAFFE. Nucl. Phys. **A150**, 545 (1970).
19. N. SUGARMAN, H. MUNZEL, J. A. PANONTIN, K. WIELGOZ, M. V. RAMANIAH, G. LANGE, and E. L. MENCHERO. Phys. Rev. **143**, 952 (1966).
20. L. C. NORTHCLIFFE and R. F. SCHILLING. Nucl. Data Tables, **7**, 233 (1970).
21. M. K. DEWANJEE, G. B. SAHA, and L. YAFFE. Can. J. Chem. **46**, 3157 (1968).
22. P. M. PORTNER. Foster Radiation Lab. report, McGill University, Montreal, Quebec, Canada (Jan. 15, 1964).
23. H. M. SKARSGARD. Ph.D. Thesis, McGill University, Montreal, Quebec. 1961.
24. M. A. WHITEHEAD. Ph.D. Thesis, McGill University, Montreal, Quebec. 1961.
25. D. NEWTON, S. SARKAR, L. YAFFE, and R. B. MOORE. J. Inorg. Nucl. Chem. **35**, 361 (1973).
26. M. A. WAKAT. Nucl. Data Tables, **8**, 445 (1971).
27. B. P. BAYHURST and R. J. PRESTWOOD. Nucleonics, **17**, No. 3, 82 (1959).
28. E. M. CORN, M. D. DEVONS, B. R. ERDAL, D. D. RITTERSKAMP, and A. C. WAHL. Detection efficiency of beta proportional counters. Washington University Report No. coo-1162-42, St. Louis, Mo. (USA) June 1971.
29. J. B. CUMMING. U.S. National Academy of Science-National Research Council Nuclear Science Series, No. NAS-NS-3107, 25. 1962.
30. B. R. ERDAL. Ph.D. Thesis, Washington University, St. Louis, Missouri. 1966.
31. L. A. BUSING and H. A. LEVY. Oak Ridge National Laboratory Report No. ORNL-TM-271. 1962.
32. J. VON HOLDT. Proceedings of the Western Computer Conference. 1959. p. 256, quoted in NAS-NS-3109 National Academy of Sciences, National Research Council, Washington, D.C. 1966.
33. D. NEWTON. Private communication.
34. W. W. BOWMAN. Texas A and M report No. ORO-3921-5. 1972, Vol. 2, 1964.
35. H. P. YULE. Anal. Chem. **44**, 1245 (1972).
36. S. SARKAR. Ph.D. Thesis, McGill University, Montreal, Quebec. 1974.
37. P. R. BEVINGTON. Data reduction and error analysis for the physical sciences. McGraw–Hill, New York. 1969.
38. R. S. TILBURY and L. YAFFE. Can. J. Chem. **41**, 1956 (1963).
39. E. HAGEBØ. J. Inorg. Nucl. Chem. **27**, 927 (1965).
40. R. A. SCHMITT and S. R. ZUMWALT. American Institute of Physics Handbook. McGraw-Hill, New York. 1963.
41. J. A. PANONTIN and N. T. PORILE. J. Inorg. Nucl. Chem. **30**, 2017 (1968).
42. S. BABA, H. UMEZAWA, and H. BABA. Nucl. Phys. **A175**, 177 (1971).
43. L. MILLER. Ph.D. Thesis, McGill University, Montreal, Quebec. 1970. pp. 105, 106.
44. P. C. STEVENSON, H. G. HICKS, W. E. NERVIK, and D. R. NETHAWAY. Phys. Rev., **111**, 886 (1958).
45. M. LINDNER and R. N. OSBORNE. Phys. Rev. **94**, 1323 (1954).
46. G. FRIEDLANDER, L. FRIEDMAN, B. GORDON, and L. YAFFE. Phys. Rev. **129**, 1809 (1963).
47. C. D. CORYELL. Ann. Rev. Nucl. Sci. **2**, 305 (1953).
48. E. HAGEBØ and A. C. PAPPAS. J. Inorg. Nucl. Chem. **28**, 1769 (1966).
49. E. HAGEBØ. CERN Lab. Report, July 1969.
50. J. M. ALEXANDER, C. BALTZINGER, and M. F. GAZDIK. Phys. Rev. **129**, 1826 (1963).
51. J. A. PANONTIN and N. T. PORILE. J. Inorg. Nucl. Chem. **32**, 1775 (1970).
52. K. CHEN, Z. FRANKEL, G. FRIEDLANDER, J. R. GROVER, J. M. MILLER, and Y. SHIMAMOTO. Phys. Rev. **166**, 949 (1968).
53. J. E. HUDGENS and L. C. NELSON. Anal. Chem. **24**, 1472 (1952).
54. B. R. ERDAL and A. C. WAHL. J. Inorg. Nucl. Chem. **33**, 2763 (1971).
55. G. A. COWAN. Collected radiochemical procedures. Los Alamos Report LA-1721. January 1958.
56. H. L. HAMESTER and MILTON KHAN. The absorptive and radiocolloidal properties of carrier-free silver. Sandia Corporation Monograph, No. SCR-593. 1963.
57. L. GLENDENIN. Collected radiochemical procedures. Los Alamos Report, LA-1721. 1954
58. A. KJELBERG, H. TANIGUCHI, and L. YAFFE. Can. J. Chem. **39**, 635 (1961).
59. G. G. J. BOSWELL and T. MCGEE. Analyst, **92**, 769 (1967).
60. K. A. KRAUS, and G. E. MOORE. J. Am. Chem. Soc. **75**, 1460 (1953).
61. W. W. MEINKE. U.S. Atomic Energy Comm. Report UCRL 432 (1949).

Can. J. Chem. Downloaded from www.nrcresearchpress.com by 210.87.254.6 on 09/05/12
For personal use only.

Appendix

Full details of the chemical procedures used are given in ref. 36. Abbreviated procedures are given below:

(*a*) Indium. The separation involved removing indium without entrainment or loss of the parent cadmium, and purification of the indium from contaminants.

The primary separation step was the extraction of $InBr_3$, in the presence of Cd^{2+} hold-back carrier, from 4.5 *N* HBr into isopropyl ether (53). However, tracer experiments with ^{115m}Cd showed that if this extraction were carried out, about 9% of the Cd is lost from the mother solution thus, in addition to not contributing to the formation of In in subsequent extractions, will complicate each yield determination. Similar data for extraction into ethyl ether were found by Hagebø (39). Thus, before the extraction, In was quantitatively removed from cadmium by the precipitation of $In(OH)_3$ with concentrated NH_4OH.

Special precautions had to be taken to remove Sn and Sb isotopes, since the half-lives and radiations emitted are in many cases similar to those of In. Recently, Erdal and Wahl (54) have reported the use of a CdS-cellulose filter bed to absorb preferentially Sn–Sb fission products. Tracer experiments with ^{114m}In and ^{115}Cd were used to extend this work.

A funnel with a coarse sintered-glass filter was used as the filtration assembly. The stem of the funnel led into a beaker placed inside a bell-jar with suction outlet and ground-glass bottom. The filter bed was formed by suspending CdS-cellulose (8% CdS) in 5 ml 0.6 *N* HCl, and the suspension saturated with H_2S for 30 s.

The In was finally precipitated as the 8-hydroxyquinoline derivative (55).

The timed extractions involved two separations of In from the Cd parent. The first typically took place 6–8 min after the end of an irradiation not exceeding 10 min. The second took place approximately 6–8 h later.

(*b*) Silver. An aliquot of the master solution was made 1 *N* in HNO_3 and AgCl precipitated with 0.1 *N* HCl (56). The precipitate was dissolved in concentrated NH_4OH and scavenged with $Fe(OH)_3$ precipitations alternating with precipitations of Ag_2S with $(NH_4)_2S$ (57). The purified AgCl, however, was found to be contaminated with 1–5% ^{131}I. An additional step was incorporated involving the addition of I^- holdback carrier and boiling with $Na_2S_2O_3$ to remove I_2. This removed any measurable contamination.

In the timed-extraction procedure, for the separation of Ag from its Pd parent, the separation time was taken to be that of centrifugation, 2 min after precipitation. This takes care of the exchange between AgCl and active silver after precipitation (58).

(*c*) Palladium. The procedure used followed that of Boswell and McGee (59) whereby one takes advantage of the action of acetylacetone as a chelating agent and the solvent extraction into benzene where the p*H* used acts as a discriminator.

The specific scheduling of timed extractions and intervals depended on the Pd isotope under observation.

(*d*) The copper foils were weighed, dissolved in 3 *M* HCl with a little H_2O_2, the solution was evaporated to dryness and redissolved in 2 drops 4.5 *N* HCl, to which was added 5 mg Co carrier as cobaltous chloride. The solution was loaded on to a 20×0.7 cm ion-exchange column of purified Dowex-1×8 anion-exchange resin (100–200 mesh size) which had been pretreated with 4.5 *N* HCl. The cobalt was eluted by further addition of 4.5 *N* HCl, the elution then continued with 2 *N* HCl and the copper fraction was collected after the first 10% of the fraction was discarded (60).

The copper was precipitated with a slight excess of 6 *N* NaOH, washed, redissolved in a minimum of 0.2 *N* H_2SO_4, reduced to Cu^+ by a two-fold excess of 0.1 *M* ferrous ammonium sulphate in 0.1 *N* H_2SO_4 and CuCNS precipitated by the drop-wise addition of 10% NH_4CNS until a slight excess of thiocyanate was present. The mixture was heated to 90 °C for 2 h, centrifuged, and washed with dilute ferrous ammonium sulphate, 95% ethanol, acetone, and ether (61).

A glass scintillation 'counting vial' was heated at 100 °C for 2 h, cooled, and weighed to ± 0.00001 g. A slurry of the CuCNS in ether was added and the ether evaporated by gentle warming until there was no further weight loss. The vial was then re-weighed and the precipitate (70 mg) was dissolved by the addition of 10.0 ml of NH_4OH to the vial which was sealed after dissolution was complete.

Hydrogen abstraction by perfluoroethyl radicals from methylfluorosilanes

THOMAS N. BELL, TOSHITSUGU YOKOTA, AND ALDEN G. SHERWOOD
Department of Chemistry, Simon Fraser University, Burnaby, B.C., Canada V5A 1S6

Received October 14, 1975

THOMAS N. BELL, TOSHITSUGU YOKOTA, and ALDEN G. SHERWOOD. Can. J. Chem. **54**, 2359 (1976).

Arrhenius parameters have been measured for hydrogen abstraction by C_2F_5 radicals (produced from the photolysis of perfluoropropionic anhydride) from methylfluorosilanes and tetramethylsilane.

Compound	log A (ml mol^{-1} s^{-1})	E (kcal mol^{-1})
$(CH_3)_4Si$	11.33 ± 0.03	7.00 ± 0.05
$(CH_3)_3SiF$	11.56 ± 0.04	8.64 ± 0.08
$(CH_3)_2SiF_2$	11.57 ± 0.07	10.05 ± 0.15
$(CH_3)SiF_3$	11.28 ± 0.12	11.32 ± 0.27

The results are discussed in relation to those of similar reactions involving the CF_3 and the CH_3 radical, and interpreted in terms of polar effects.

THOMAS N. BELL, TOSHITSUGU YOKOTA et ALDEN G. SHERWOOD. Can. J. Chem. **54**, 2359 (1976).

On a mesuré les paramètres d'Arrhenius pour l'enlèvement, par les radicaux C_2F_5 (produit par photolyse de l'anhydride perfluoropropionique), d'hydrogène des méthylfluorosilanes et tétraméthylsilane.

Composé	log A (ml mol^{-1} s^{-1})	E (kcal mol^{-1})
$(CH_3)_4Si$	11.33 ± 0.03	7.00 ± 0.05
$(CH_3)_3SiF$	11.56 ± 0.04	8.64 ± 0.08
$(CH_3)_2SiF_2$	11.57 ± 0.07	10.05 ± 0.15
$(CH_3)SiF_3$	11.28 ± 0.12	11.32 ± 0.27

On discute des résultats par rapport à ceux obtenus pour des réactions semblables impliquant des radicaux CF_3 et CH_3 et on les interprète en termes d'effets polaires.

[Traduit par le journal]

Introduction

There is now a considerable body of information on the reactions of free radicals with alkyl and hydro silanes. A review of the literature to date is in press (1). We have previously studied (2, 3) the reactions of the CF_3 and CH_3 radical with compounds having the formula $(CH_3)_x$-SiF_{4-x}. These systematic studies showed a reactivity for each radical varying along the compound series, and a different relative radical reactivity with each compound. The results were interpreted in terms of both enthalpy and polar effects. From these results it appears that the methyl fluorosilane system is an ideal model system for examining the effect of structural changes in the substrate molecule with regard to radical and molecule reactivity. The idea of attractive and repulsive polar effects is of intrinsic interest, and the present work involving the perfluoroethyl radical was designed to shed further light on this effect.

Experimental

Materials

The sources of compounds used in this work were perfluoropropionic anhydride and methylfluorosilanes (Penninsular Chemicals Inc.), tetramethylsilane (Mallincrodt), pentafluoroethane (Chemical Procurement Laboratories), and perfluorobutane (Columbia Organic Chemical Co.). Each was fractionated in the usual manner through various slush baths, middle cuts being retained and stored in blackened bulbs. No impurities were detectable by gas chromatography.

Can. J. Chem. Downloaded from www.nrcresearchpress.com by 210.87.254.42 on 09/05/12
For personal use only.

Can. J. Chem. Downloaded from www.nrcresearchpress.com by 210.87.254.42 on 09/05/12
For personal use only.

Apparatus

A typical glass vacuum line was used, with photolyses being carried out in an Ultrasil cell (illuminated volume 126 ml). The cell was enclosed in a tubular aluminium block furnace, whose temperature was controlled to $\pm 0.5°$ with an RFL platinum resistance controller.

The light source (PEK 200 W mercury arc) was filtered (Interference filter A2 Baird Atomic Inc.) to yield a band between 2400 and 2550 Å with a maximum at 2470 Å.

Pressure measurements were made using a Ruska Instrument Co. precision quartz spiral gauge.

Procedures

After reaction, CO was separated from the condensables and measured using gas chromatography and a gas burette. $(C_2F_5CO)_2O$ was separated from the condensables at $-90\,°C$, and the material volatile at that temperature passed through an initial separation column of Porapak Q (60/80 mesh). The volatiles of interest (CO_2, C_2F_5H, C_4F_{10}) were condensed and separated from the bulk of the fluorosilane in the column effluent. Alumina (60/80 mesh) was used in place of Porapak Q for the CH_3SiF_3 system. In this case CO_2 was lost by absorption on the column.

The volatiles of interest were then subject to quantitative analysis by gas chromatography using either Porapak Q or alumina columns.

Results

Photolysis of Perfluoropropionic Anhydride

Chamberlain and Whittle (4, 5) have shown that the photolysis of perfluoropropionic anhydride is a useful source of C_2F_5 radicals, its decomposition being described by the overall reaction

$$[1] \qquad (C_2F_5CO)_2O \xrightarrow{h\nu} CO + CO_2 + 2C_2F_5$$

Our results on the photolysis agree with those of Chamberlain and Whittle, with product ratios agreeing with those expected from the above equation. The results for experiments carried out at 102 and 204 °C with or without added third body (CO_2) are given in Table 1, and show the reproducibility of the results as a test of the analytical procedure.

Hydrogen Abstraction

In the presence of hydrogen containing compounds, C_2F_5 radicals should abstract hydrogen, and with the silanes,

$$[2] \quad C_2F_5 + (CH_3)_{4-x}SiF_x \rightarrow C_2F_5H + CH_2(CH_3)_{3-x}SiF_x$$

The recombination of C_2F_5 radicals should lead to C_4F_{10} via

$$[3] \qquad 2C_2F_5 \rightarrow C_4F_{10}$$

Thus the ratio $k_2/k_3^{1/2}$ can be determined from

$$[4] \qquad R_{C_2F_5H}/R^{1/2}{}_{C_4F_{10}}[\text{silane}] = k_2/k_3^{1/2}$$

Given our previous experience (2, 3) with these silanes, which show well behaved characteristics, it was felt only necessary to test the validity of this equation over a temperature range for one case, namely $(CH_3)_3SiF$. The results are shown graphically in Fig. 1, and a linear dependence on the pressure of the silane is seen, as predicted by eq. 4.

Our system appears better behaved than the methane and cyclohexane systems studied by Chamberlain and Whittle (5), where there was some indication of a variation in $k_2/k_3^{1/2}$ with concentration of substrate.

TABLE 1. Photolysis of $(C_2F_5CO)_2O$

Temperature (°C)	Time (min)	Perfluoro propionic anhydride $\times 10^7$ mol ml^{-1}	$\frac{R_{CO_2}+R_{C_4F_{10}}}{2R_{CO}}$	$\frac{R_{CO}}{R_{CO_2}}$	$\frac{R_{C_4F_{10}}}{R_{CO}}$
102	64	5.33	*1.04	*1.02	*0.991
101	90	5.43	1.02	1.00	0.995
102	90	5.32	1.02	0.991	1.02
102†	90	5.37	—	0.975	0.987
102	120	5.34	0.974	1.00	0.995
102	120	5.40	0.975	0.991	1.02
101	120	5.40	1.01	1.04	0.983
204	90	5.58	—	—	1.03
204‡	90	5.64	—	—	1.04
204§	90	5.56	—	—	1.06

*Yields of CO, CO_2 and C_4F_{10} were greater than 9×10^{-7} moles in these experiments.
†Mixed with Me_3SiF after reaction, for testing separation of the components by chromatography.
‡With excess CO_2 added, $[CO_2] = 47 \times 10^{-7}$ mol ml^{-1}.
§With excess CO_2 added, $[CO_2] = 77 \times 10^{-7}$ mol ml^{-1}

Can. J. Chem. Downloaded from www.nrcresearchpress.com by 210.87.254.42 on 09/05/12
For personal use only.

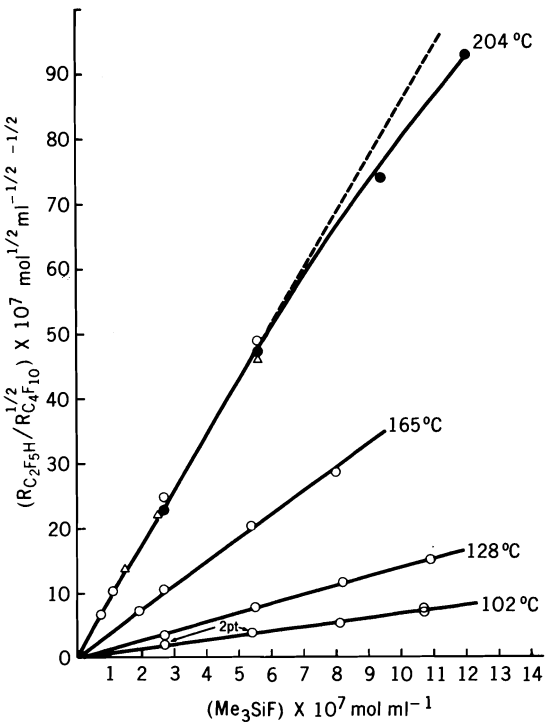

FIG. 1. First order plots $C_2F_5 + (CH_3)_3SiF$. △, third body added CF_4 (46×10^{-7} mol ml^{-1}); ●, perfluoropropionic anhydride approximately doubled.

Additional data points are shown in Fig. 1 for the effect of added third body, (CF_4), and of doubling the anhydride concentration. Over our experimental range for the measurement of rate constants, little or no effect is observed. However, at relatively high concentrations of silane and anhydride some curvature results.

Over the limits of concentration of anhydride and substrate used for obtaining the Arrhenius parameters, the rate constant ratios are well behaved and show insignificant variation. The data from which figures in this paper are derived are available.[1]

Relative Product Quantum Yields

It is to be expected that there will be some missing C_2F_5 radicals in the presence of substrates as a result of secondary reactions involving free radicals, for example,

[5] $C_2F_5 + CH_2Si\leqslant \rightarrow (C_2F_5CH_2Si\leqslant)^*$

Asterisk denotes vibrationally hot molecule.

A typical relative quantum yield plot is shown in Fig. 2 which confirms the above expectation.

It might be expected that the radical combination product $(C_2F_5CH_2Si\leqslant)^*$ would lead to a β-fluoro transfer elimination reaction and the formation of CF_3CFCH_2.

[6] $(CF_3CF_2CH_2Si\leqslant)^* \rightarrow CF_3CFCH_2 + FSi\leqslant$

While there was a stray peak in the chromatographic analysis of the volatile products, the amount of material was insufficient to identify and confirm the above reaction.

This is in contradistinction to the facile reaction occurring with CF_3 radicals as the radical source

[7] $(CF_3CH_2Si\leqslant)^* \rightarrow CF_2CH_2 + FSi\leqslant$

Rate Experiments

A series of experiments were carried out for each of the compounds over a temperature range,

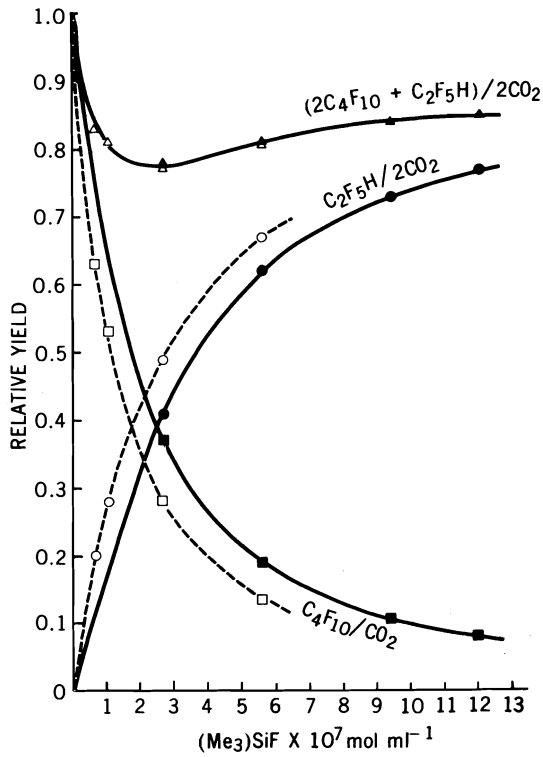

FIG. 2. Relative quantum yields $C_2F_5 + (CH_3)_3SiF$ at 204 °C. Concentration of perfluoropropionic anhydride in mol ml^{-1}: open symbols, 5.6×10^{-7}; solid symbols, 11.7×10^{-7}.

[1]A complete set of tabular data, upon which Figs. 1, 2 and 3 are based, is available, at a nominal charge, from the Depository of Unpublished Data, CISTI, National Research Council of Canada, Ottawa, Ontario, Canada K1A 0S2.

Can. J. Chem. Downloaded from www.nrcresearchpress.com by 210.87.254.42 on 09/05/12
For personal use only.

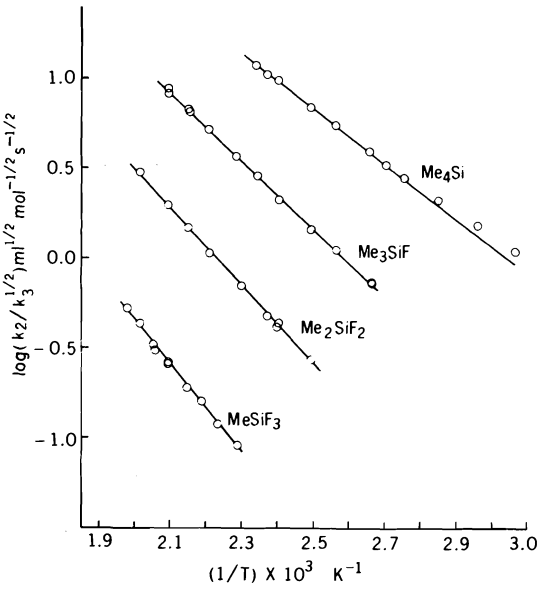

FIG. 3. Arrhenius plot log $(k_{abst}/k_{recomb}{}^{1/2})$ *vs.* $1/T$ $C_2F_5 + (CH_3)_xSiF_{4-x}$.

to determine the ratio $k_2/k_3{}^{1/2}$. Arrhenius plots of log $k_2/k_3{}^{1/2}$ *vs.* $1/T$ are shown in Fig. 3. Distinct curvature occurs with $(CH_3)_4Si$ at temperatures less than ~85 °C, and the Arrhenius parameters are derived from the results obtained at 90 °C and above. From a least-squares analysis of the data, and assuming a value of $k_3 = 2.3 \times 10^{13}$ ml mol^{-1} s^{-1} with $E_3 = 0$, (the same as for CF_3 recombination), for the rate constant for the recombination of C_2F_5 radicals, Arrhenius parameters for hydrogen abstraction were obtained. These are given in the abstract.

In the Discussion, comparisons are made with the corresponding CD_3 and CF_3 reactions, and the rate constant results quoted (3) previously for the CD_3 system are slightly in need of correction. This arises because of, (*1*) a wrongly evaluated k value in one case (for $(CH_3)_4Si$ at 150 °C $k_{abs}/k_{comb} = 0.498$), and (*2*) a re-evaluation of the least-squares calculation. These corrections are as follows:

Reactants	log k (ml mol^{-1} s^{-1})
$CD_3 + (CH_3)_4Si$	$11.91 - 10.74/2.3RT$
$CD_3 + (CH_3)_3SiF$	$11.98 - 11.62/2.3RT$
$CD_3 + (CH_3)_2SiF_2$	$11.99 - 12.00/2.3RT$
$CD_3 + (CH_3)SiF_3$	$12.24 - 12.79/2.3RT$

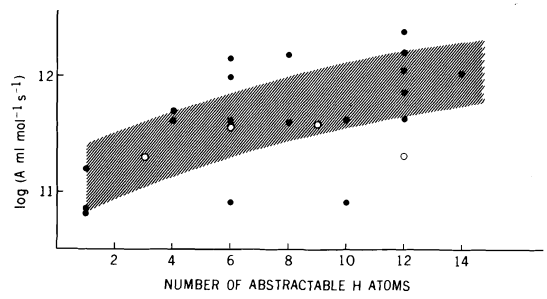

FIG. 4. log A *vs.* number abstractable H atoms for C_2F_5 radical attack: ○, present work $(CH_3)_xSiF_{4-x}$; ●, mainly hydrocarbon data.

Discussion

The A factors for the reactions of C_2F_5 obtained in this study (11.45 ± 0.15) are a little less than those obtained for similar studies involving CF_3 and CD_3 (~12.0). This may be expected given the larger size of the C_2F_5 radical. As yet there is not a significant body of data involving abstraction by C_2F_5 radicals with which to compare our values for the A factors. Such values as are available are shown in Fig. 4 as a function of the number of abstractable hydrogen atoms of the same sort being abstracted. This comparison would suggest consistency in the values obtained in the present work, except that the value for $Si(CH_3)_4$ would appear to be a little low.

As with abstraction by CF_3 radicals the main factor leading to the difference in reactivity from compound to compound lies in the activation energy for abstraction. The reactivity differences between the radicals CF_3, CD_3, and C_2F_5 and the trends in reactivity along the series of com-

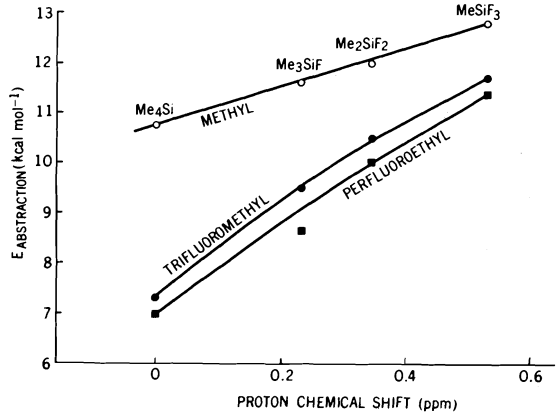

FIG. 5. E_{abst} *vs.* proton chemical shift $R + (CH_3)_xSiF_{4-x}$ (R = CF_3, CD_3, and C_2F_5).

Can. J. Chem. Downloaded from www.nrcresearchpress.com by 210.87.254.42 on 09/05/12
For personal use only.

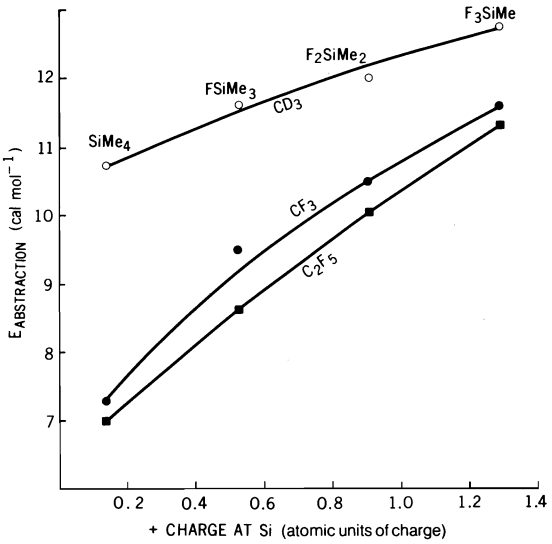

FIG. 6. E_{abst} *vs.* charge on Si, R + $(CH_3)_xSiF_{4-x}$ (R = CF_3, CD_3 and C_2F_5).

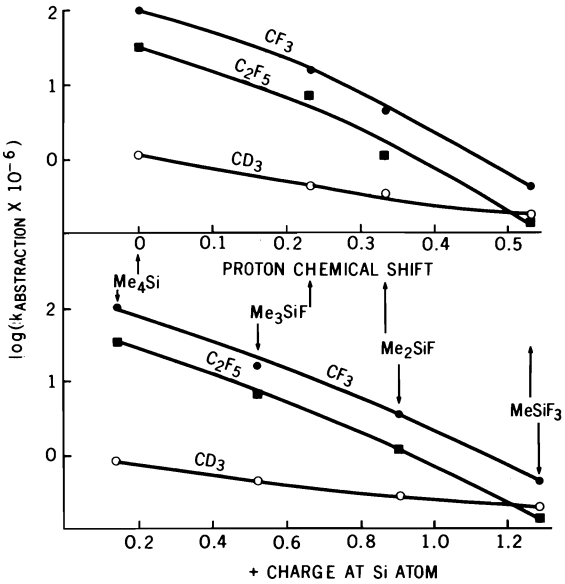

FIG. 7. log k_{abst} *vs.* proton chemical shift and charge on silicon at 400 K, R + $(CH_3)_xSiF_{4-x}$ (R = CF_3, CD_3, and C_2F_5).

pounds are shown graphically in Figs. 5, 6, and 7 as functions of activation energy and rate constant against certain parameters of the compounds under discussion. The parameters selected are the proton chemical shift (a function of the charge density on the H atom), and the positive charge on the silicon atom, a function of the polar nature of the molecule. The values of charge density were determined by Perkins and were reported in a previous paper (6). Numerical values of the relative reactivities of the three radicals with regard to abstraction from the silane substrates are compared below at 400 K.

	$(k_{abst\ 400\ K}) \times 10^{-6}$			
Compound	CD_3	CF_3	C_2F_5	$R_{CF_3}/R_{C_2F_5}$
$(CH_3)_4Si$	1.1	100	32	3.1
$(CH_3)_3SiF$	0.43	16	6.9	2.3
$(CH_3)_2SiF_2$	0.28	3.7	1.2	3.1
$(CH_3)SiF_3$	0.18	0.41	0.13	3.1

It is clear that the reactivities of all three radicals towards hydrogen abstraction decreases with increasing fluorine substitution on the silane substrate, with very marked effects with the fluororadicals. Further, the relative magnitude $R_{CF_3}/R_{C_2F_5}$ is approximately constant with the reactivity of CF_3 being three times that of C_2F_5.

Polar Effects

In the CF_3 and CD_3 + methylfluorosilane systems (2, 3) we ascribed part of the activation energy difference $E_{CD_3} - E_{CF_3}$ to enthalpy effects $\Delta(\Delta H) = D_{CF_3-H} - D_{CH_3-H}$ (~2 kcal). A further component of the activation energy difference was ascribed to polar effects δ, attractive or repulsive in nature, thus,

$$\Delta E \propto (\text{constant} - \Delta(\Delta H)) - \delta$$

In the case of C_2F_5 radicals, $D_{C_2F_5-H}$ has been determined by Bassett and Whittle (7) as 103 ± 1 kcal which when combined with D_{CH_3-H} = 104 leads to an enthalpy difference in H abstraction by CD_3 and C_2F_5 of essentially 0 or slightly negative. Thus enthalpy effects cannot be invoked to account for the differences $E_{CD_3} - E_{C_2F_5}$ which are even slightly larger than those for $E_{CD_3} - E_{CF_3}$. A comparison is given below using the corrected values for E_{CD_3} given above.

Compound	$E_{CD_3} - E_{CF_3}$	$E_{CD_3} - E_{C_2F_5}$
$(CH_3)_4Si$	3.4	3.7
$(CH_3)_3SiF$	2.1	3.0
$(CH_3)_2SiF_2$	1.5	2.0
$(CH_3)SiF_3$	1.1	1.5

The activation energies from which these differences are derived were determined relative to the corresponding radical combination processes, the activation energies of which were assumed to be zero. If these are non-zero for perfluoro radicals (Pimental and co-workers (9) have suggested that E for CF_3 combination is non-zero), all activation energies for abstraction by CF_3 and C_2F_5 would have to be reduced by $\frac{1}{2}E_{comb}$.

The correlations observed, Figs. 5, 6 and 7, which strikingly relate the activation energies for abstraction with the polar properties of the molecules, lead us to the conclusion that strong polar effects are operative with both the CF_3 and C_2F_5 radicals.

The differences are such that we suggest the polar effects become successively less attractive as the hydrogen atom becomes less hydridic, due to the increasing inductive effect of fluorine substitution on the silicon atom, from compound to compound.

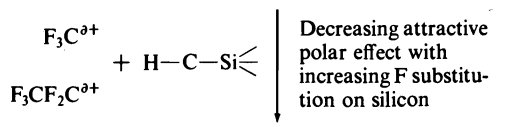

Acknowledgement

We are grateful to the National Research Council of Canada for financial support.

1. T. N. Bell and N. L. Arthur. Unpublished data.
2. T. N. Bell and U. F. Zucker. J. Phys. Chem. **74**, 979 (1970).
3. T. N. Bell and A. E. Platt. J. Phys. Chem. **75**, 603 (1971).
4. E. A. Chamberlain and E. Whittle. Chem. Commun. 396 (1971).
5. G. A. Chamberlain and E. Whittle. J. Chem. Soc. Faraday Trans. I, **68**, 96 (1972).
6. T. N. Bell, R. Berkley, A. E. Platt, and A. G. Sherwood. Can. J. Chem. **52**, 3158 (1974).
7. J. E. Bassett and E. Whittle. J. Chem. Soc. Faraday Trans. I, **68**, 492 (1972).
8. J. C. Amphlett and E. Whittle. Trans. Faraday Soc. **62**, 1662 (1966).
9. T. Ogawa, G. A. Carlson, and G. C. Pimentel. J. Phys. Chem. **74**, 2090 (1970).

Can. J. Chem. Downloaded from www.nrcresearchpress.com by 210.87.254.42 on 09/05/12
For personal use only.

Juvabione and its analogues. II.[1,2] Isolation, identification, and occurrence of juvabiol and its epimer isojuvabiol from the whole wood of *Abies balsamea*

JOHN FIEVE MANVILLE

Environment Canada, Forestry Directorate, Western Forest Products Laboratory, 6620 N.W. Marine Drive, Vancouver, B.C., Canada V6T 1X2

Received February 10, 1976

JOHN FIEVE MANVILLE. Can. J. Chem. **54**, 2365 (1976).

Epimeric mixtures of juvabiol (**3***a*) and isojuvabiol (**4***a*) have been detected in six North American *Abies balsamea* (L.) Mill. trees and isolated from the whole-wood extract of three. These juvabione related alcohols are insect juvenile hormone analogues with selective action typical of juvabione (**1**) and $\Delta^{4'}$-dehydrojuvabione (**2**). The widespread occurrence of these alcohols indicates that the original 'paper factor' *was not* due to **1** alone, nor was it due to a mixture of **1** and **2**. In addition a fifth IJHA with selective action, $\Delta^{3'}$-dehydrojuvabi-5'-ol (**5**), was detected in the hot ethanol extract of four trees and isolated from one tree. It is shown that **5** is an allylic rearrangement product of the $\Delta^{4'}$-dehydrojuvabiols **6***a* and **7***a*. Mixtures of campesterol and sitosterol are the major crystalline components present in all the petroleum ether soluble extracts.

JOHN FIEVE MANVILLE. Can. J. Chem. **54**, 2365 (1976).

Des mélanges épimères de juvabiol (**3***a*) et d'isojuvabiol (**4***a*) ont été décelés dans six sapins baumiers (*Abies balsamea* (L.) Mill.), et isolés de l'extrait du bois entier de trois d'entre eux. Ces alcools apparentés à la juvabione sont analogues aux hormones juvéniles d'insectes ayant une action sélectrive typique de la juvabione (**1**) et de la $\Delta^{4'}$-déhydrojuvabione (**2**). La présence de ces alcools sur une grande étendue démontre que le 'facteur papier' original *n'était pas* uniquement dû à **1**, ni au mélange de **1** et **2**. De plus, un cinquième IJHA à action sélective, le $\Delta^{3'}$-déhydrojuvabiol-5' (**5**), a été décelé dans des extraits de quatre arbres et isolé de l'un de ces arbres. On peut voir que **5** est un produit à réarrangement allylique des $\Delta^{4'}$-déhydrojuvabiols **6***a* et **7***a*. Des mélanges de campestérol et de sitostérol sont les principales composantes cristallines retrouvées dans tous les extraits solubles d'éther de pétrole.

Introduction

While it has been known for some time that the wood of balsam fir (*Abies balsamea* (L.) Mill.) contains factors exhibiting juvenile hormone activity on the bug *Pyrrhocoris apterus* L. (1, 2), to date only two active insect juvenile hormone analogue (IJHA) components have been isolated and identified (3, 4).[3] They are (+)-juvabione (**1**) (3) and (+)-$\Delta^{4'}$-dehydrojuvabione (**2**) (4).[3,4] In 1966, Bowers *et al.* (3) isolated (**1**) from the wood of *A. balsamea*. They claimed it to be *the* compound responsible for the failure of the hemipteran bugs to metamorphose into adults following contact by the larvae with certain paper products. Thus arose the term 'the paper factor'.[5]

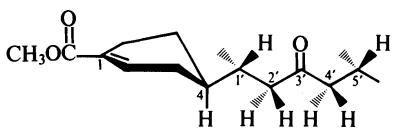

1

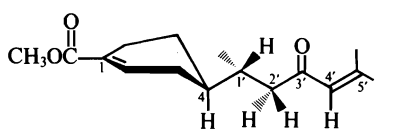

2

The recent isolation of **2** as a second IJHA from the wood of *A. balsamea* indicates that the origin of 'paper factor' activity is more complex than first believed (3, 6–8).

This paper reports the isolation and identification of three additional IJHA. They are juvabiol

[1]Presented, in part, at the 167th National Meeting of the American Chemical Society, Los Angeles, California, April 1974.

[2]For part I of this series see ref. 4.

[3]K. Sláma, private communication.

[4]Cerny *et al.* (6) isolated the *R,S*-diastereoisomers of **1** and **2** from a Slovak fir (see ref. 4). Both are active IJHA.

[5]For a more detailed explanation of 'the paper factor' see ref. 7 or 8.

Can. J. Chem. Downloaded from www.nrcresearchpress.com by 210.87.254.40 on 09/05/12
For personal use only.

(**3***a*), isojuvabiol (**4***a*), and $\Delta^{3'}$-dehydrojuvabi-5′-ol (**5**). Compounds **3***a* and **4***a* occur naturally in the wood of *A. balsamea*, whereas **5** is an artifact of the isolation procedure.

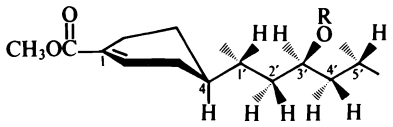

3

a R = H
b R = $COCH_3$

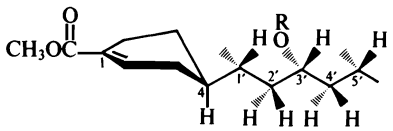

4

a R = H
b R = $COCH_3$

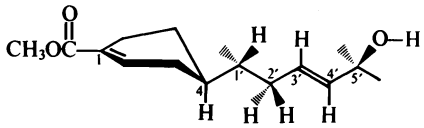

5

Isolation

Details of the isolation procedure and tree locations have been given in part I (4). This study concerns the identification of some of the compounds present in the more polar components, which were previously obtained from the extracts of each of three trees (numbers 1–3). These polar components gave rise to peak V (4) when analyzed by gas–liquid chromatography (glc, column A).

Trees 4 to 6 were only examined by tlc and glc. However, the room temperature petroleum ether (PE) extracts, as well as the petroleum ether solubles of the hot ethanol (PE sol.) extracts, were examined prior to and after acetylating accessible hydroxyl groups.

Results and Discussion

Portions of the above polar components isolated from trees 1 and 2 crystallized on standing. This crystalline material was identified by the method of Rozanski (9) as being composed of a mixture of campesterol and sitosterol[6] in a ratio of approximately 1:2. Further amounts of these sterols could be induced to crystallize from an aqueous ethanol solution kept at 0 °C for several days. The removal of the sterols left syrups (*A*) which upon examination by glc gave rise to peak V, but were impure by tlc (low R_f streaks). Purification of these syrups was achieved by rechromatographing them on silicic acid columns (a separate column for each tree), collecting only those fractions (see Experimental) that were pure by glc, tlc, and proton magnetic resonance (pmr) analyses. In this manner, homogeneous (glc and tlc) colourless syrups (*A*) were obtained.

Syrup *A* from tree 1 (similar results were obtained from tree 2) had $[\alpha]_D^{23}$ +67.8° and an empirical formula of $C_{16}H_{28}O_3$ as determined by high resolution mass spectrometry (ms). The infrared (ir) spectrum clearly demonstrated the presence of a hydroxyl (3450 cm^{-1}), and an α,β-unsaturated carboxylic acid methyl ester (bands at 1430, 1650, and 1705 cm^{-1}). The pmr spectrum was indicative of the juvabione skeleton with resonances at δ 6.92 (H_2), 3.68 (methyl ester), and 0.91 (three methyls doublet); an additional resonance was noted at δ 3.73 (1H) which was tentatively assigned to the proton geminal to the hydroxyl substituent. Confirmation was obtained by observing that this resonance shifted to lower field (by 1.3 ppm) for the derived acetate(s), and the appearance of a single acetoxy methyl resonance at δ 2.00. This syrup (*A*) and its acetate also appeared (pmr) to be homogeneous in acetone-d_6 and benzene-d_6 solutions.

A more complete characterization of this alcohol was obtained following the oxidation of a portion of syrup *A*. The product of this reaction was (+)-juvabione (**1**) (3, 4), thus locating the hydroxyl function at C-3′ and establishing the *R*-stereoconfigurations at both C-4 and C-1′.

However, this oxidation sequence did not establish the configuration of the hydroxyl substituent at C-3′, nor was it established

[6]These sterols did not chromatograph (glc) under the conditions used previously (column A) and therefore did not contribute to the areas of peak V (shown in a previous publication, ref. 4), nor is their presence accounted for in the percentage figures (glc) of the petroleum ether soluble neutrals. Identified by mp as sitosterol, but glc (column B) showed them to be mixtures of campesterol and sitosterol in a ratio of 1:2 (9).

Can. J. Chem. Downloaded from www.nrcresearchpress.com by 210.87.254.40 on 09/05/12
For personal use only.

TABLE 1. Composition of peak V (r_t 1.35)

Tree no.	PE sol. extract			PE extract		
		Area due to‡			Area due to‡	
	%*	3*a* and 4*a*	5	%†	3*a* and 4*a*	5
1	14.1	14.1	0	n.d.		
2	24.3	24.3	0	n.d.		
3	8.2	1.0	7.2	13.2	12.1	1.1
4	5.1	0.6	4.5	7.3	4.9	2.4
5	2.7	0.5	2.2	4.7	3.5	1.2
6	11.2	3.7	7.5	8.5	7.4	1.1

*See part I (ref. 4) for relative amounts of other, previously identified components from the PE sol. extracts.

†Absolute, as well as relative, amounts differ due to method of extraction.

‡Compositions of peak V were determined by glc analyses of the acetylated extracts. Amounts of **5** were indicated by residual areas of peak V whereas 3*a* and 4*a* were represented by a new peak (r_t 0.88, $V_{acetate}$, 3*b* and 4*b*).

spectroscopically. This configuration was eventually determined by following the sodium borohydride reduction of **1** to an epimeric mixture of juvabiol (**3***a*) and isojuvabiol (**4***a*).[7]

The above reduced mixture of **3***a* and **4***a* appeared homogeneous and identical with the isolated syrups (*A*) from trees 1 and 2. However, high field pmr spectra and high performance liquid chromatography (hplc) of these syrups revealed (see Experimental section) the epimeric nature of *both* the isolated and synthesized juvabiols.

Thus, the major polar fractions from the PE sol. of trees number 1 and 2, contain mixtures of campesterol and sitosterol, mixtures of (+)-4(*R*)-[1′(*R*)-5′-dimethyl-3′(*S*)-hydroxyhexyl]-1-cyclohexene-1-carboxylic acid methyl ester, (juvabiol(**3***a*)),(+)-4(*R*)-[1′(*R*)-5′-dimethyl-3′(*R*)-hydroxyhexyl]-1-cyclohexene-1-carboxylic acid methyl ester, (isojuvabiol (**4***a*)), together with complex mixtures of still more polar material.

The mixtures of **3***a* and **4***a* accounted, fully, for the areas of peak V (3) (see Table 1) observed for the PE sol. from trees number 1 and 2.

The major polar fraction of tree number 3 contained, in addition to the mixtures of sterols and juvabiols (**3***a* and **4***a*), another alcohol (**5**) which was not found in the PE sol. extract of either tree number 1 or 2. The presence of **5** was noted by tlc and glc following acetylation of a portion of the major polar fraction of tree number 3. The sterols and the juvabiols were isolated as their acetates. Neither the r_t (glc) nor R_f (tlc) (which were identical with those found for **3***a* and **4***a*) of this material (**5**) was altered by further attempts to acetylate it with acetyl chloride and pyridine. This meant that the area of peak V for the PE sol. portion of tree 3 was not due to **3***a* and **4***a* alone, but was also due, in part, to this new alcohol (**5**).

The structural elucidation of this new alcohol (**5**) was straightforward. The hydroxyl function was clearly evident in the ir spectrum. Mass spectrometry indicated the empirical formula $C_{16}H_{26}O_3$, which meant that **5** had one more degree of unsaturation than the juvabiols (**3***a* and **4***a*). The pmr spectrum of **5** revealed the presence of three olefinic protons; the lowest field resonance was typical for H_2 of the juvabiols, the other two were strongly coupled and indicated a *trans*-disubstituted double bond. Chemical shifts of the methyl ester (δ 3.58) and the C-1′ methyl (δ 0.86) groups were again typical of the juvabione skeleton. The shift (δ 1.30) and multiplicity (singlet) observed for the C-5′ methyls were significant and pointed to the hydroxyl function being located at C-5′. The *trans*-disubstituted double bond was most likely $\Delta^{3'}$. On the basis of these physical parameters, **5** appeared to be (+)-4(*R*)-[1′(*R*)-5′-dimethyl-5′-hydroxy-3′-hexenyl]-1-cyclohexene-1-carboxylic acid methyl ester, $\Delta^{3'}$-dehydrojuvabi-5′-ol.

This structure and the *R*,*R*-stereoconfigurations were proven by synthesizing **5** from $\Delta^{4'}$-

[7]Chemical reductions of the ketone at C-3′ to the epimeric juvabiols resulted in unequal product ratios (4:3). The major alcohol was tentatively assigned the *R*-(*cis*)-configuration (**4***a*), since the determinant factor would necessarily be the assymmetric centre at C-1′ (Cram's rule (10)). The *trans* alcohol **3***a* (minor isomer) would thus have the *S*-configuration.

Can. J. Chem. Downloaded from www.nrcresearchpress.com by 210.87.254.40 on 09/05/12
For personal use only.

Can. J. Chem. Downloaded from www.nrcresearchpress.com by 210.87.254.40 on 09/05/12
For personal use only.

dehydrojuvabione (**2**) in two steps. Sodium borohydride reduction of **2** gave an epimeric mixture (as shown by pmr) of $\Delta^{4'}$-dehydrojuvabiol (**6***a*) and $\Delta^{4'}$-dehydroisojuvabiol (**7***a*) in essentially quantitative yield.[8] This syrupy mixture (**6***a* and **7***a*) was chromatographed on a silicic acid column using petroleum ether – diethyl ether (3:1) as eluent. An alcohol fraction was obtained in approximately 50% yield and

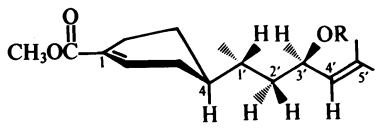

6

a R = H
b R = $COCH_3$

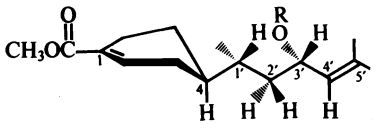

7

a R = H
b R = $COCH_3$

was shown (pmr and hplc) to contain nearly equal amounts of $\Delta^{3'}$-dehydrojuvabi-5′-ol (**5**) and the $\Delta^{4'}$-dehydrojuvabiols **6***a* and **7***a*.

It appears that chromatographing the $\Delta^{4'}$-dehydrojuvabiols **6***a* and **7***a* on a neutral silicic acid column resulted in the formation of an intermediate carbonium ion (**8**) which either was quenched by attack of hydroxyl anion at C-5′ or C-3′, resulting in formation of **5** and recovery of epimerized starting material, or lost a proton forming a mixture of dienes. These dienes then

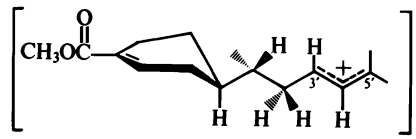

8

polymerized and were adsorbed onto the silicic acid column.

This mixture of **5**, **6***a*, and **7***a* was reacted with acetic anhydride in pyridine solution and the resulting syrup was chromatographed. The $\Delta^{4'}$-dehydrojuvabiol acetates (**6***b* and **7***b*) were eluted first, followed by pure **5**.

It is this author's belief that **5** is not a natural product, but an artifact of the isolation procedure. This means that the original conditions used in isolating the PE sol. extracts were too harsh, causing some precursor(s) (presumably **6***a* and/or **7***a*) to rearrange into **5**, which was isolated and/or observed.

Corroboration of this belief was obtained by examining (glc and tlc) the acetylated PE sol. and the PE extracts of trees number 3–6. The relative areas[9] of peaks V (**5**) and $V_{acetate}$ (**3***b* and **4***b*) are listed in Table 1. Thus, for trees number 3, 4, and 6 the amount of **5** (area peak V) relative to **3***b* and **4***b* (area peak $V_{acetate}$) decreased markedly for the acetylated PE extracts from those observed for the acetylated PE sol. extracts. The fact that there appears to be some **5** in the PE extracts (especially in tree 5) might well reflect the *in situ* degradation of some precursor(s) (such as **6***a* and/or **7***a*) caused by Wiley milling the wood prior to extraction.[10] Nevertheless, the relative amount of **5** in the PE extracts is appreciably reduced compared with the PE sol. extracts, thus supporting the assumption that **5** is an artifact.

These observations of **5** in the extracts of several *A. balsamea* can be best explained by postulating that the $\Delta^{4'}$-dehydrojuvabiols **6***a* and **7***a* occur naturally and undergo an allylic rearrangement to form **5** which is demonstrably more stable.

Results (5) of the bioassays performed on juvabione (**1**), $\Delta^{4'}$-juvabione (**2**), the juvabiols (**3***a* and **4***a*), the $\Delta^{4'}$-dehydrojuvabiols (**6***a* and **7***a*), and $\Delta^{3'}$-dehydrojuvabi-5′-ol (**5**) are listed in

[8]Note that the work-up procedure is most important. Use of a strong mineral acid to destroy excess sodium borohydride will result in dehydration of these dehydrojuvabiols (**6***a* and **7***a*) if the p*H* drops much below 7, resulting in a mixture of dienes which will further react to form a polymeric mixture. Therefore the use of acetic acid to destroy excess sodium borohydride is recommended. A mixture of **6***a* and **7***a* is stable in a solution of ethanol–water–acetic acid (75:10:15) heated under reflux for several hours.

[9]For the purpose of these analyses, it is assumed that, for the acetylated extracts, all of the residual area of peak V (r_t 1.35) is due to **5** alone and not due to other material with the same r_t. Therefore, these analyses (Table 1) represent an upper limit to the amount of **5** present in the PE and PE sol. extracts. The juvabiol acetates **3***b* and **4***b* give rise to peak $V_{acetate}$ (r_t 0.88).

[10]A recent publication (11) by Zinkel has outlined several improved ways of maintaining the integrity of the sample. These improvements in procedure will be incorporated in future studies.

Can. J. Chem. Downloaded from www.nrcresearchpress.com by 210.87.254.40 on 09/05/12
For personal use only.

TABLE 2. Insect juvenile hormone activities

Compound	Insect bioassay*†			
	P_5E	D_5E	G_5E	T_pE
Juvabione (**1**)	1.7	2.3	‡	‡
$\Delta^{4'}$-Dehydrojuvabione (**2**)	5.0	2.0	‡	‡
Juvabiols (**3***a* and **4***a*)	5.6	4.7	‡	‡
$\Delta^{4'}$-Dehydrojuvabiols (**6***a* and **7***a*)	6.0	0.7	‡	‡
$\Delta^{3'}$-Dehydrojuvabi-5′-ol (**5**)	2.1	2.1	‡	‡

*P_5E = *Pyrrhocoris apterus* L. last instar larvae; D_5E = *Dysdercus cingulatus* F. last instar larvae; G_5E = *Graphosoma italicum* Müll. last instar larvae; T_pE = *Tenebrio molitor* L. pupae.

†ID-50 (Morphological) units. The values indicate amount of the compound in micrograms per specimen which cause just the standard 50% effect.

‡Compound does not show any activity at 500 μg/specimen in topical application.

Table 2. They all show typical juvabione-type IJH activity. Details of these and other bioassays on compounds of this sesquiterpenoid (juvabione) series will be published elsewhere as they are concluded.

In view of the demonstrated IJH activity of the newly isolated **3***a*, **4***a*, and **5**, it is important to note that neither Bowers *et al.* (3) nor Cerny *et al.* (6) observed IJH activity for any compounds more polar than juvabione (**1**) or $\Delta^{4'}$-dehydro-*epi*-juvabione in the whole wood of balsam fir or a Slovak fir, respectively. However, Cerny *et al.* (6) did note the occurrence of a polar component that accounted for most of the IJH activity from a sample of paper of North American origin. It could be that they had actually isolated a mixture of juvabiols and/or the $\Delta^{4'}$-dehydrojuvabiols. Possibly the considerable tree-to-tree variation (4), both qualitative and quantitative, in the occurrence of the individual juvabione type components, might account for the failure of their investigations to find **3***a* and **4***a*, **6***a* and **7***a*, **5**, or their *R,S*-diastereomers.

Nevertheless, the wide occurrence (4) of **3***a* and **4***a* which are IJHA in the wood of balsam fir trees means that the original 'paper factor' (1) is not due to juvabione (**1**) alone, as originally thought (3).

The 'paper factor' would appear to result from the combined action of **1**, **2**, **3***a*, **4***a*, and possibly **6***a* and **7***a* which are all closely related juvabione type compounds.

The results of this and a previous publication (4) on the petroleum ether soluble fraction of the whole wood extract of *A. balsamea* indicate that the juvabione type sesquiterpenoids are an important class of extractives whose wide occurrence has not been noted.[11] A survey of other *Abies* species is currently being carried out to ascertain how widespread is the occurrence of this important class of compounds.

Experimental

Most pmr spectra were determined on samples dissolved in deuteriochloroform containing tetramethylsilane as internal standard using a Varian HA-100 spectrometer. Several pmr spectra were also obtained at the Canadian 220 MHz Centre, Ontario Research Foundation, Sheridan Park, Ont. Mass spectra were recorded in the molecular spectroscopy laboratory of the Fisheries and Marine Service, Vancouver Laboratory, Department of the Environment, Vancouver, using a Nuclide 12-90-G spectrometer. High resolution mass spectra were recorded in the Department of Chemistry, University of British Columbia, using an AEI-MS-9 spectrometer. Accurate mass measurements were made by reference to appropriate ions of the perfluorokerosene spectrum. Infrared spectra were recorded with a Perkin-Elmer 521 spectrophotometer. Samples were placed as liquid films on the surface of KBr discs. Optical rotations were recorded on a Perkin-Elmer 141 Polarimeter made available by the Department of Chemistry, University of British Columbia. Gas–liquid chromatographic analyses were performed on a Hewlett Packard Model 7620A equipped with flame ionization detector. The columns used were 6 ft × $\frac{1}{8}$ in. o.d. stainless steel packed with either (A) 10% EGSS-X on 100–120 mesh Gas Chrom. P. or (B) 3% SE 30 on Gas Chrom. Q, purchased from Applied Science Laboratories, Inc. Column A was held isothermally at 190 °C, Column B was at 250 °C. The nitrogen carrier gas flow rate was 25 ml/min. The injector port was maintained at 270 °C. All retention times (glc r_t) are relative to internal (+)-juvabione (**1**).

The hplc analyses were performed on a Spectra-Physics 3500 B liquid chromatograph equipped with their Chromatronix model 230 U.V. (280/254 nm) detector. The column used was 3 × 250 mm spherisorb ODS (10 μm). The solvent system was water–acetonitrile; gradient elution was used (40–55% acetonitrile at 0.5% per min); the flow rate was 1 ml/min at approximately 600 psi. Thin-layer chromatograms were performed on E. Merck, silica gel 60 F-259 (0.25 mm) plates using petroleum ether – diethyl ether (3:1) as developer. The ord curves were measured on a JASCO-ORD-UV-5 spectrophotometer, on loan to the Western Forest Products Laboratory from the Department of Biochemistry, Faculty of Medicine, University of British Columbia, Vancouver.

[11]Leach and Thakore reported (12) the isolation, from mechanical pulping effluent, of several juvabione related compounds. The relationships between their isolations, tentative structures, the extractives of *A. lasiocarpa* (referred to as 'balsam fir') and the stereoconfigurational implications of these in relation to a previous study (4) will be dealt with, in detail, in a forthcoming publication.

Can. J. Chem. Downloaded from www.nrcresearchpress.com by 210.87.254.40 on 09/05/12
For personal use only.

The initial isolation procedure, site locations, and chemical constituents for each individual tree have been recorded previously (4).

Bioassays

All of the insect bioassays reported have been performed in the laboratories of Professor Karel Sláma, Institute of Entomology, Department of Insect Physiology, Praha, C.S.S.R. Material: P_5E = *Pyrrhocoris apterus* L. last instar larvae; D_5E = *Dysdercus cingulatus* F. last instar larvae; G_5E = *Graphosoma italicum* Müll. last instar larvae; T_pE = *Tenebrio molitor* L. pupae. Application: topical in 1 μl of acetone to freshly ecdysed (0–20 h old) last instar larvae or to freshly ecdysed pupae (Tenebrio). Evaluation of activity: according to the degree of morphological inhibition of metamorphosis. Expression of the activity: in ID-50 (Morphological) units. The values indicate amount of the compound in μg per specimen which cause just the standard 50% effect (7).

*Compounds **3a** and **4a** (Juvabiol (R,R,S) and Isojuvabiol (R,R,R))*

Compounds **3a** and **4a**, isolated together as a colourless oil and characterized as an epimeric mixture, had tlc R_f 0.08–0.2 (concentration dependent) hplc r_t 18.2 (minor, *trans*, **3a**) and 19.1 min (major, *cis*, **4a**), glc r_t 1.35 and $[\alpha]_D^{23}$ +67.8° (*c* 0.99, CH_3OH). The pmr δ 6.92 (1H, m, H_2), 3.73 (1H, m, $H_{3'}$), 3.68 (3H, s, methyl ester), 0.91 (9H, d, J = 6.8 Hz, C-1′ and 2(C-5′) methyls), 2.6–1.0 (14H); (C_6D_6) δ 0.94, 0.92, and 0.78 (9H, d, J = 6.8 Hz, C-5′, C-1′ methyls); (220 MHz, C_6D_6) δ 7.04 (1H, m, H_2), 3.64 (1H, m, $H_{3'}$), 3.49 (3H, s, methyl ester), 2.59 (1H, m), 2.19 (1H, m), 0.93_9 (3H, d, J = 6.8 Hz, C-5′ methyl), 0.92_5 *and* 0.91_8 (3H, d, J = 6.8 Hz, C-5′ methyls of **3a** and **4a**), 0.78_4 *and* 0.77_7 (3H, d, J = 6.8 Hz, C-1′ methyls of **3a** and **4a**). Mass spectrum (*m/e*): 268(1%) (M), 251(3), 250(18) ($M - H_2O$), 193(15), 179(22), 165(15), 150(18), 139(49), *138(100)*, 137(72), 134(17), 133(21), 107(55), 105(22), 95(22), 93(30), 91(23), 82(15), 81(32), 79(61), 77(21), 69(46), 67(19), 59(21), 57(25), 55(33), 53(18), 45(18), 43(44), and 41(48). Infrared (cm^{-1}): 3450 s, 2950 vs, 2925 vs, 2870 s, 1705 vs, 1650 m, 1460 m, 1430 s, 1380 m, 1365 mw, 1310 w, 1250 vs, 1210 mw, 1190 w, 1080 s, 920 mw, 830 w, 800 w, 740 m, and 710 m. *Mol. Wt.* calcd. for $C_{16}H_{28}O_3$: 268.2038; found (high resolution mass spectrometry): 268.2040.

*Oxidation of **3a** and **4a** by CrO_3·(pyridine)$_2$*

A solution of a mixture of juvabiols (**3a** *and* **4a**) (1 mmol) in CH_2Cl_2 (5 ml) was oxidized with CrO_3·(pyridine)$_2$ according to the procedure of Ratcliff and Rodehorst (5). The crude, syrupy product, on purification by passage through a silicic acid column in petroleum ether – diethyl ether (3:1), afforded an oil (0.85 mmol), identical in all respects glc r_t, tlc R_f, nmr, ir, ms, $[\alpha]_D$ and ord with (**1**) (3).

*Reduction of Juvabione (**1**) by Sodium Borohydride*

A solution of juvabione (**1**) (1 mmol) in methanol (10 ml) was reacted with sodium borohydride (1 mmol) at room temperature for 2 h. The solution was neutralized with aqueous acid (2 *N* HCl), poured into water (50 ml), and extracted with $CHCl_3$ (3 × 10 ml). The extract was washed and then dried and evaporated to give a colourless syrup (0.95 mmol) which was homogeneous by tlc and glc. The pmr (100 MHz) appeared identical with the natural, isolated juvabiols (**3a** and **4a**), as did an acetylated sample with **3b** and **4b**. High performance liquid chromatography analytically separated the minor *trans* isomer (**3a**) with r_t of 18.2 min from the major *cis* isomer (**4a**) with r_t of 19.1 min.

*Compounds **3b** and **4b** (Juvabiol Acetate (R,R,S) and Isojuvabiol Acetate (R,R,R))*

Compounds **3a** and **4a** were acetylated in the usual manner (Ac_2O/py, etc.) to give compounds **3b** and **4b** as colourless oils, with tlc R_f 0.33, hplc r_t 22.7 min, glc r_t 0.88 and $[\alpha]_D^{23}$ +54.3° (*c* 0.69, CH_3OH). The pmr, δ 6.90 (1H, m, H_2), 5.03 (1H, m, $H_{3'}$), 3.69 (3H, s, methyl ester), 2.00 (3H, s, acetate methyl, found as s in $(CD_3)_2CO$ at 1.97 and (220 MHz) in C_6D_6 at 1.76_8), 0.90 (9H, d, $J \simeq 6$ Hz, C-1′ and 2(C-5′) methyls), 2.6–1.0 (13H). Mass spectrum (*m/e*): 310(0.3%) (M), 250(33) ($M -$ HOAc), 193(21), 179(16), 165(23), 150(21), 139(48), *138(100)*, 137(81), 134(32), 133(23), 121(10), 107(48), 105(25), 94(29), 92(35), 90(23), 82(22), 81(29), 79(55), 77(21), 69(44), 67(19), 59(21), 57(25), 55(39), 53(16), 43(90), 41(35). Infrared (cm^{-1}): 2960 s, 2940 s, 2880 ms, 1735 vs, 1716 vs, 1650 w, 1460 w, 1440 m, 1380 m, 1250 vs, 1210 m, 1085 ms, 1020 m, 950 w, 925 w, 805 w, 745 w, and 710 mw. *Mol. Wt.* calcd. for $C_{18}H_{30}O_4$: 310.2143; found (high resolution mass spectrometry): 310.2156.

*Compounds **6a** and **7a** (Δ$^{4'}$-Dehydrojuvabiol (R,R,R) and Δ$^{4'}$-Dehydroisojuvabiol (R,R,S))*

A mixture of compounds **6a** and **7a** was obtained in 98% yield by $NaBH_4$ reduction of **2** in methanol at room temperature. Excess $NaBH_4$ was destroyed with acetic acid, diluted with water, and the product extracted with $CHCl_3$ (3 × 10 ml). The $CHCl_3$ layer was washed with aqueous $NaHCO_3$, H_2O, and dried (Na_2SO_4). The solvent was evaporated under reduced pressure to yield a colourless syrup (**6a** and **7a**).

The colourless syrup (**6a** and **7a**) was homogeneous tlc R_f 0.08–0.2 (concentration dependent), hplc r_t 19.2 min, and $[\alpha]_D^{23}$ +72.7° (*c* 0.286, CH_3OH). The pmr δ 6.97 (1H, m, H_2), 5.20 and 5.12 (1H (total), m (appears as a tripleted septet), $H_{4'}$), 4.42 (1H, m, $H_{3'}$), 3.71 (3H, s, methyl ester), 1.72 (6H, m, 2(C-5′) methyls), 0.93 (3H, d, $J \simeq 6$ Hz, C-1′ methyl), 2.6–1.0 (11H). Mass spectrum (*m/e*): 266(2%) (M), 250(3) ($M - 16$), 248(7) ($M - 18$), 234(5) ($M - 32$), 182(22), 139(59), 134(44), 109(40), 107(42), 105(19), 93(19), 91(18), *85(100)*, 83(25), 81(22), 79(41), 77(18), 69(18), 67(28), 59(16), 57(15), 55(30), 53(15), 43(22), 41(43). Infrared (cm^{-1}): 3420 s, 2940 ms, 2930 s, 2870 m, 2850 m, 1705 vs, 1650 m, 1430 m, 1380 w, 1250 vs, 1210 w, 1080 m, 1050 w, 1025 w, 920 vw, 840 vw, 800 vw, 740 w, 710 mw. *Mol. Wt.* calcd. for $C_{16}H_{26}O_3$: 266.1881; found (high resolution mass spectrometry): 266.1895.

*Compounds **6b** and **7b** (Δ$^{4'}$-Dehydrojuvabiol Acetate (R,R,R) and Δ$^{4'}$-Dehydroisojuvabiol Acetate (R,R,S))*

Compounds **6a** and **7a** were acetylated as before to give **6b** and **7b** as a homogeneous colourless oil, with tlc R_f 0.28, hplc r_t 20.4 min, and $[\alpha]_D^{27}$ +58.2° (*c* 0.226, CH_3OH). The pmr δ 6.95 (1H, m, H_2), 5.57 (1H, m, $H_{3'}$), 5.11 (0.6H, doubleted septet, $J_{4',3'}$ = 5 Hz, $J_{4'}$ methyls = 1.5 Hz, $H_{4'}$ (**7b**)), 5.03 (0.4H, doubleted septet, $J_{4',3}$ = 5.4 Hz, $J_{4'}$ methyls = 1.5 Hz, $H_{4'}$ (**6b**)), 3.72 (3H, s, methyl

ester), 2.01 (3H, s, acetate methyl) 1.74 (6H, m, 2(C-5′) methyls), 0.90 (3H, d, $J \simeq 6$ Hz, C-1′ methyl), 2.6–1.0 (10H). Mass spectrum (*m/e*): 308(8%) (M), 248(22), 205(15), 192(27), 189(26), 188(21), 163(31), 139(27), 138(24), 137(39), 134(16), 133(25), 109(80), 107(59), 105(38), 95(24), 93(38), 91(29), 85(79), 83(32), 82(37), 81(39), 79(72), 77(28), 69(37), 67(40), 55(46), *43(100)*, 41(52). Infrared (cm^{-1}): 2940 s, 2880 m, 2865 m, 1730 vs, 1720 vs, 1655 m, 1440 ms, 1380 ms, 1245 vs, 1090 ms, 1020 m, 945 w, 930 w, 840 vw, 810 vw, 750 w, 715 w, 600 vw. *Mol. Wt.* calcd. for $C_{18}H_{28}O_4$: 308.1986; found (high resolution mass spectrometry): 308.1982.

Compound 5 ($\Delta^{3'}$-Dehydrojuvabi-5′-ol)

Compound **5** was isolated as a colourless oil with tlc R_f 0.06–0.18 (concentration dependent), hplc r_t 16.0 min, glc r_t 1.39 (some decomposition), $[\alpha]_D^{27}$ +54.0° (*c* 0.25, CH_3OH). The pmr δ 6.92 (1H, m, H_2), 5.62 (1H, m, $\sum J$'s $\simeq$ 20 Hz, $H_{3'}$), 5.48 (1H, m, $\sum J$'s $\simeq$ 20 Hz, $H_{4'}$), 3.58 (3H, s, methyl ester), 130 (6H, s, C-5′ methyls), 0.86 (3H, d, $J = 6.4$ Hz, C-1′ methyl), 2.6–1.0 (11H). Mass spectrum (*m/e*): 266(0.5%) (M), 248(4) ($M - 18$), 149(13), 139(10), 109(17), 107(21), 105(9), 93(11), 91(8), 85(11), 82(10), 81(10), 79(18), 69(11), 67(13), 59(13), 58(26), 55(14), *43(100)*, 41(18). Infrared (cm^{-1}) 3450 ms, 2960 s, 2930 s, 2885 s, 1705 vs, 1645 ms, 1435 s, 1380 ms, 1255 vs, 1150 m, 1085 ms, 1030 w, 970 m, 920 mw, 800 w, 740 m, 710 m. *Mol. Wt.* calcd. for $C_{16}H_{26}O_3$: 266.1881; found (high resolution mass spectrometry): 266.1908.

Acknowledgments

The author is indebted to Dr. Karel Sláma, Institute of Entomology, Prague, C.S.S.R., for performing the insect bioassays. Mr. C. R. Daniels obtained the hplc results. Excellent technical assistance was provided throughout this study by Mrs. C. D. Kriz (née Freeman).

1. K. Sláma and C. M. Williams. Proc. Natl. Acad. Sci. U.S. **54**, 411 (1965).
2. A. Mansingh, T. S. Sahota, and D. A. Shaw. Can. Entomol. **102**, 49 (1970).
3. W. S. Bowers, H. M. Fales, M. J. Thompson, and E. C. Uebel. Science, **154**, 1020 (1966).
4. J. F. Manville. Can. J. Chem. **53**, 1579 (1975).
5. R. Ratcliffe and R. Rodehorst. J. Org. Chem. **35**, 4000 (1970).
6. V. Cerny, L. Dolejs, L. Labler, F. Sorm, and K. Sláma. Coll. Czech. Chem. Commun. **32**, 3926 (1967).
7. K. Sláma, M. Romanuk, and F. Sorm (*Editors*). *In* Insect hormones and bioanalogues. Springer-Verlag, New York. 1974. pp. 170–177.
8. C. M. Williams. *In* Chemical Ecology. *Edited by* E. Sondheimer and J. B. Simeone. Academic Press, New York. 1970. pp. 103–132.
9. A. Rozanski. Anal. Chem. **38**, 36 (1966).
10. D. J. Cram and F. A. A. Elhafez. J. Am. Chem. Soc. **74**, 5828 (1952).
11. D. F. Zinkel. Tappi, **58**, 109 (1975).
12. J. M. Leach and A. N. Thakore. CPAR Report 149-2, Canadian Forestry Service, Ottawa, Ontario. 1974.

Can. J. Chem. Downloaded from www.nrcresearchpress.com by 210.87.254.40 on 09/05/12
For personal use only.

On the interpretation of measured rotational and vibrational relaxation times. II. Sudden change experiments

HUW OWEN PRITCHARD

Centre for Research in Experimental Space Science, York University, Downsview, Ont., Canada M3J 1P3

Received February 18, 1976

HUW OWEN PRITCHARD. Can. J. Chem. **54**, 2372 (1976).

This paper examines, in terms of the normal-mode analysis developed earlier (Part I), the nature of relaxations in which a diatomic gas, highly diluted in a heat bath of inert gas atoms, is subjected to a sudden change as in shock-wave excitation or laser schlieren experiments.

It is shown in detail how the observed relaxation time in a shock-wave excitation *to a fixed final temperature* depends on the initial temperature. At the same time, it is confirmed that the characterisation as 'mainly rotational' of the measured relaxation time in H_2 when it is heated from room temperature to 1500 K in a shock wave is perfectly plausible.

On the other hand, the calculations show that in laser schlieren experiments in which the $v = 1, J = 1$ level of H_2 is overpopulated, the vibrational relaxation time of H_2 at the temperature in question is recovered, although interesting effects should appear if other J levels were populated initially, or if the experiments were carried out at much higher ambient temperatures.

The calculations also demonstrate that it is not generally possible to derive relaxation times by following the variation in population of any particular level of the molecule: multiple overshoots sometimes occur, and apparent relaxation times both longer or shorter than the true relaxation times could often result from attempts to follow level populations as a function of time.

HUW OWEN PRITCHARD. Can. J. Chem. **54**, 2372 (1976).

Dans ce travail on examine, en terme de l'analyse de mode normal développé antérieurement (partie I), la nature des relaxations qui se produisent dans un gaz diatomique à haute dilution dans un milieu d'atomes de gaz inertes quand le mélange soumis à un changement subit comme il s'en produit dans des expériences d'excitations par onde de choc ou par "laser schlieren."

On montre en détail la relation qui existe entre la température initiale et le temps de relaxation observé lors d'une excitation par onde de choc vers une température finale fixe déterminée. On confirme en même temps qu'il est parfaitement plausible de caractériser comme "principalement rotationnel" le temps de relaxation mesuré dans H_2 quand celui-ci est chauffé de la température de la pièce à 1500 K dans une onde de choc.

Par ailleurs des calculs montrent que dans des expériences de "laser schlieren," dans lesquelles le niveau $v = 1, J = 1$ de H_2 est surpeuplé, le temps de relaxation vibrationnel de H_2 à la température en question est récupéré; des effets intéressants devraient toutefois apparaître si les autres niveaux J étaient initialement remplis ou si les expériences avaient lieu à des températures ambiantes beaucoup plus élevées.

Les calculs démontrent aussi qu'il n'est généralement pas possible de dériver les temps de relaxation en suivant la variation de la population d'un niveau particulier de la molécule. En effet il se produit quelquefois des "dépassements" multiples et si l'on essaye de suivre les populations des niveaux en fonction du temps on observe souvent des temps de relaxation apparents soit plus longs soit plus courts que les temps réels de relaxation.

[Traduit par le journal]

Introduction

In an earlier paper bearing a similar title (1),[1] it was shown that the total energy of a system of diatomic molecules immersed in a heat bath of inert atoms, and having a non-equilibrium rotation–vibration population distribution, decays according to eq. I[11] *viz.*:

$$[1]\quad E(t) - E_{\text{initial}} = \xi_{N-1} + \xi_{N-2}e^{\lambda_{N-2}t} + \xi_{N-3}e^{\lambda_{N-3}t} + \ldots$$

or, using eq. I[12]

$$[2]\quad E(t) - E_{\text{Boltzmann}} = \xi_{N-2}e^{\lambda_{N-2}t} + \xi_{N-3}e^{\lambda_{N-3}t} + \ldots$$

The nomenclature is such that the molecule has N rotation–vibration levels numbered 0 to $(N - 1)$, and there are therefore $(N - 1)$ normal

[1]Henceforth denoted by I: equations taken from I will be denoted by their equation number in that paper with a prefix I; likewise Figures and Tables.

Can. J. Chem. Downloaded from www.nrcresearchpress.com by 210.87.254.6 on 09/05/12
For personal use only.

Can. J. Chem. Downloaded from www.nrcresearchpress.com by 210.87.254.6 on 09/05/12
For personal use only.

modes of relaxation, each with a characteristic time constant $\lambda_j, j = 0, 1, \ldots, (N-2)$; there is also a zero eigenvalue λ_{N-1} which ensures conservation of particles. The quantity ξ_j, defined by eq. I[10], represents the amount of energy which decays via mode j during the relaxation process, and this quantity is a function of the initial distribution; finally (eq. I[12]), ξ_{N-1} is (minus) the total energy difference between the initial distribution and the Boltzmann distribution and is therefore also (minus) the sum of all the other ξ_j.

The forms of the normal modes of relaxation were shown in detail in I, and another example is shown in Fig. 3 below. As was noted previously, the modes appear to be very complicated, but at low temperatures, relatively few of them are required to describe any relaxation (*cf.* eq. 3), and under favourable circumstances, only one, the slowest one having a relaxation time of $-\lambda_{N-2}^{-1}$, may be sufficient to describe the principal features adequately.

Shock-wave Excitation

A series of calculations to simulate a shock-wave excitation experiment was performed using the standard set of transition probabilities (Table I(1)) and the corresponding normal modes (Fig. I(1)). The final temperature was chosen as 500 K and a series of initial temperatures ranging from 300 to 499.5 K was examined. In the relaxation from 499.5 to 500 K, our earlier calculations had shown that (for *ortho*-H_2) two normal modes of relaxation were dominant in the sense that 92% of the total energy change relaxed through these two modes. The nature of the processes involved (Table I(2) and Fig. I(1)) is for mode M_3

$$[v = 0, J = 1\ (94\%) \text{ and } J = 5\ (6\%)] \leftrightarrow [v = 0, J = 3]$$

and for mode M_6

$$[v = 0, J = 1] \leftrightarrow [v = 0, J = 3\ (22\%) \text{ and } J = 5\ (78\%)]$$

These two modes differ in relaxation time by a little more than a factor of two, M_6 being slower than M_3 since M_6 is predominantly $(J = 1) \leftrightarrow (J = 5)$ whereas M_3 is predominantly $(J = 1) \leftrightarrow (J = 3)$. The remaining 8% of the energy relaxes through a third and still slower mode M_9 which connects levels $J = 1$, 3, 5, and 7, and in this particular calculation λ_3, λ_6, and λ_9 are -4.7×10^7, -2.0×10^7, and $-1.0 \times 10^7\ s^{-1}$ respectively.

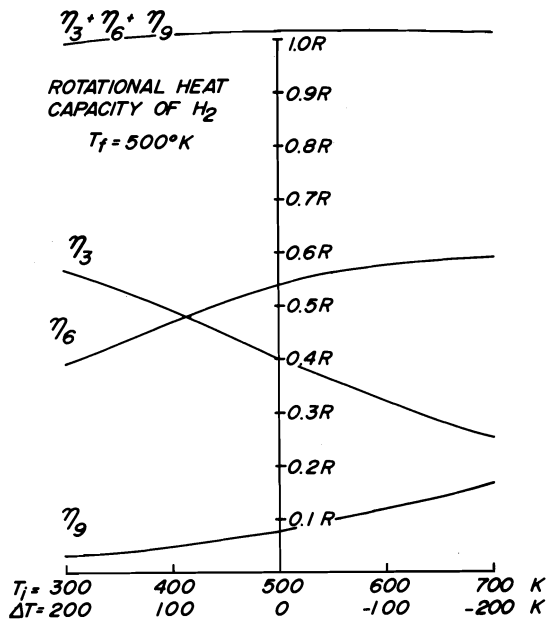

FIG. 1. Contributions from three normal modes to the rotational relaxation behaviour of *ortho*-H_2 when the temperature of the gas is changed suddenly from T_i to 500 K.

The left-hand side of Fig. 1 summarises the results of these calculations: since vibrational excitation is very slight in H_2 at 500 K, the relaxation of the total energy may be represented very accurately by the formula

$$[3] \quad E(t) - E_{\text{Boltzmann}} = \xi_3 e^{\lambda_3 t} + \xi_6 e^{\lambda_6 t} + \xi_9 e^{\lambda_9 t}$$

Figure 1 plots the quantities $\eta_i = \xi_i/\Delta T$ where ΔT is the change in temperature in the shock-wave experiment (always *terminating* at 500 K): thus, η_i is the apparent heat capacity of mode M_i, *from the starting temperature in question*; the modes used, and the corresponding eigenvalues, are the same throughout since the heat-bath temperature is always 500 K. Also plotted at the top of the diagram is $(\eta_3 + \eta_6 + \eta_9)$ which is the average rotational heat capacity of *ortho*-H_2 over the temperature jump in question.[2] It is seen that

[2]Notice that above 400 K this rotational heat capacity is greater than R, the classical value for a rigid rotor: this is because the rotational energy levels used in this calculation are affected by centrifugal distortion, etc., and are slightly closer together than the levels of a rigid rotor; hence, the heat capacity is greater.

Can. J. Chem. Downloaded from www.nrcresearchpress.com by 210.87.254.6 on 09/05/12
For personal use only.

if the starting temperature is low (300 K), about 56% of the energy relaxes with a time constant of $-4.7 \times 10^7\ s^{-1}$ and 39% with a time constant of $-2.0 \times 10^7\ s^{-1}$. If the starting temperature is about 410 K, equal amounts of energy (about 48%) relax with each time constant, and very close to 500 K, say 499.5 K as we found previously (1), only 39% relaxes via the fastest mode M_3, about 53% via the slower one M_6, and a third mode M_9 is becoming important (now accounting for about 8% of the energy relaxed). The right-hand side of Fig. 1 shows the extension of these calculations to include hypothetical sudden cooling experiments, with starting temperatures ranging up to 700 K, and with the same final temperature, 500 K. The increasing importance of M_9 (involving $J = 7$) becomes apparent for $T_i = 700$ K, and in fact another mode M_{10} (involving $J = 9$) would just be perceptible at the bottom of the graph, but is not included for simplicity.[3] It is very clear, therefore, that if eq. 3 represents the functional form of the energy relaxation with $\lambda_3 \simeq 2\lambda_6 \simeq 4\lambda_9$, and since ξ_3, ξ_6, and ξ_9, which always add up to $\sim R\Delta T$ (*i.e.* the total rotational energy change for the process) are differently weighted for each initial temperature, any attempt to approximate eq. 3 to a single exponential is bound to lead to the conclusion that the derived 'relaxation time' is different for every starting temperature. Clearly, as discussed at length in I, the detailed form of the computed results is somewhat dependent on the chosen set of transition probabilities, but the general conclusion is inescapable.

The Shock-heating of Hydrogen to 1500 K

Dove, Jones and Teitelbaum (2) found that when hydrogen was heated to temperatures above 1300 K, the thickness of the shock front was inconsistent with a simple vibrational relaxation (preceded by a very fast rotational relaxation) and one had to assume that the slowest relaxation being observed had a considerable amount of rotational character. The essential plausibility of this conclusion was given some support by our calculations on the speed of sound in our model gas using the standard set of transition probabilities (Table I(1)) and the resulting normal modes (Fig. I(4)), which showed that most of the heat capacity for an infinitesimal temperature change at 1500 K arose from rotational processes which were slower than the vibrational relaxation. Four rotational modes of relaxation appear to be the slowest processes at this temperature with this set of transition probabilities, they all involve very high J states (up to $J = 15$), and the transition rates for equilibration of large quanta of rotational energy were assumed to be rather slow (1).

If we repeat the calculation described in the preceding section, using a starting temperature of 300 K, and a final temperature of 1500 K, we find that seven normal modes make a significant contribution to the apparent mean heat capacity ($1.129R$) over this temperature jump, and between them account for 99.5% of the total energy uptake. The relative importance of these seven modes is shown in Fig. 2(*b*) where the vertical sticks denote the η_i, *i.e.* the mean heat capacity per degree of the change, for each mode M_i: the horizontal axis in this diagram is the relaxation time, displayed logarithmically. The point made in Fig. 1 is emphasised by comparing Fig. 2 (*b*) with (*a*) which shows the relative importance of the same seven modes (plus an eighth involving $J = 15$) when the gas is heated by only 0.5° from 1499.5 to 1500 K (the approximate simulation of a sound wave used in I); modes involving low J are less important, the vibrational component is more in evidence, and transitions of high J are dominant in the latter case. Rewriting eq. 3 in the form

$$[4] \qquad E(t) - E_{\text{Boltzmann}} = \Delta T \sum_i \eta_i e^{\lambda_i t}$$

where the η_i and λ_i are as displayed in Fig. 2 (*a*) and (*b*), the dependence of the *mean* or *apparent* 'relaxation time' on the starting distribution is quite evident.

Returning to the experiment of Dove *et al.*, Fig. 2(*b*) shows that if, as we have argued before, our standard set of transition probabilities (Table I(1)) is reasonably acceptable for H_2, then (for *ortho*-H_2) we can expect about seven modes to be important in this sudden heating process (and since T_f is high, the behaviour of *para*-H_2 and therefore *n*-H_2 will be qualitatively similar). Since the scale of these seven relaxation times spans only a factor of 20, it is unlikely (1) that they would ever be resolved into their individual components, the smallest of which ($\eta_{15} = 0.078R$), the one which is essentially

[3] Omission of η_{10} is the cause of the apparent decline at high temperatures in the total rotational heat capacity ($\eta_3 + \eta_6 + \eta_9$) in Fig. 1.

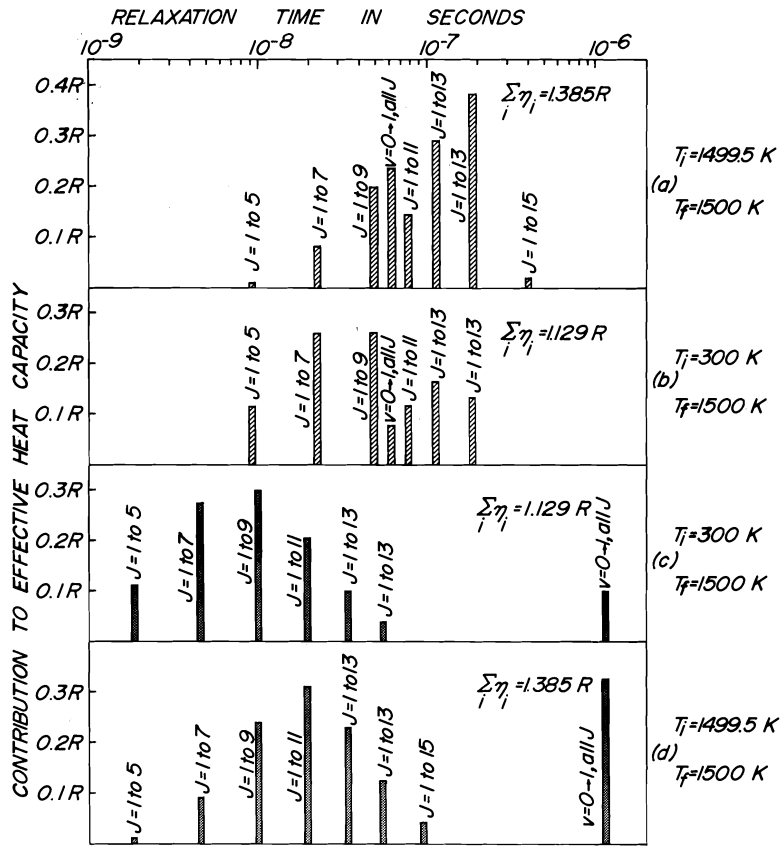

FIG. 2. Normal-mode analysis of the apparent relaxation time for two model molecules at 1500 K. (*a*) and (*b*): model molecule is *ortho*-H_2 with standard set of transition probabilities, Table I(1); the normal modes are as depicted in Fig. I(4) and the contributing modes in (*a*), from left to right, are M_4, M_{11}, and M_{14}–M_{19} inclusive. (*c*) and (*d*): model molecule is *ortho*-H_2 with modified set of transition probabilities (see text); the normal modes are as depicted in Fig. 3 and the contributing modes in (*d*), from left to right, are M_4, M_7, M_{10}, M_{12}, M_{14}, M_{15}, M_{16}, M_{19}. (*a*) and (*d*) represent the contributions of each mode to the total heat capacity in a sound dispersion experiment, and (*b*) and (*c*) a shock-heating experiment. The label attached to each contribution *e.g.* '$J = 1$ to 11' represents a rough description of the nature of the mode, and is to be interpreted to mean that in such a mode, there are significant changes in population of *all J levels from* $v = 0, J = 1$ to $v = 0, J = 11$ *inclusive.*

vibrational in character, being sandwiched in the middle of the six mathematically distinct rotational relaxations. Thus, we conclude from these model calculations that the original interpretation of these shock-wave relaxation experiments (2) was entirely plausible.

As we noted previously (1), H_2 is a rather poor model to use for the purposes of elucidating the behaviour of ordinary diatomic molecules, because it has too large a rotational spacing in comparison with its vibrational spacing, and there is therefore not enough disparity between the rotational and the vibrational transition rates. We attempted to examine this problem previously, not by increasing the number of rotational levels within each vibrational gap (which would have made the calculations much more costly), but, using the same set of energy levels, mimicking the real behaviour by multiplying the probabilities of all rotational transitions by a factor of 10, and dividing the probabilities of all transitions in which v changed (whether J changed or not) by a factor of 10. This has the effect of decoupling to a much larger extent[4] the rotational and the vibrational modes, as described before, and as shown diagrammatically in Fig. 3, although the details of this uncoupling

[4]Remembering we have already argued in I that even using our standard set of transition probabilities, the coupling is still weak.

Can. J. Chem. Downloaded from www.nrcresearchpress.com by 210.87.254.6 on 09/05/12
For personal use only.

Can. J. Chem. Downloaded from www.nrcresearchpress.com by 210.87.254.6 on 09/05/12
For personal use only.

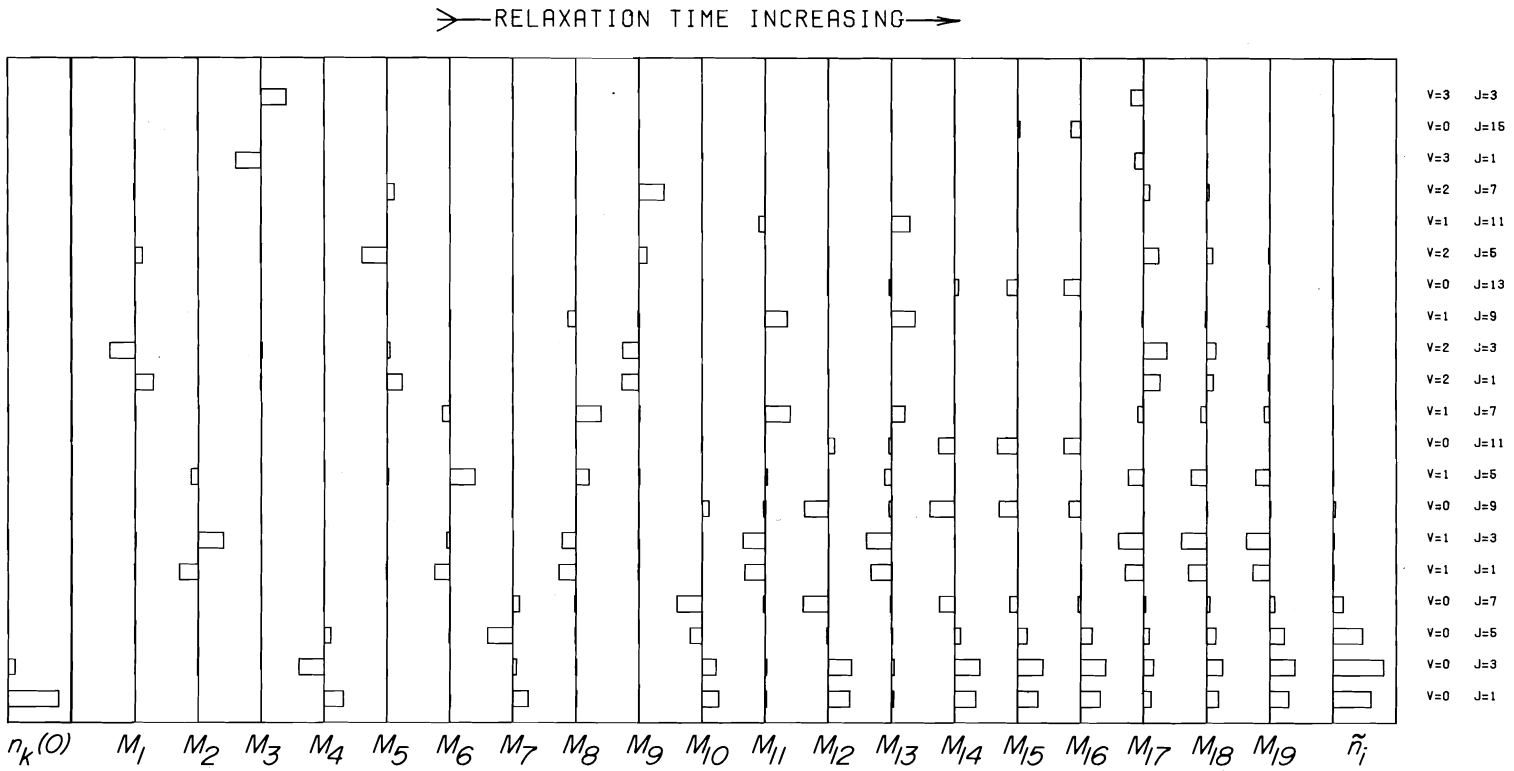

FIG. 3. Normal modes of relaxation: modified set of assumed transition probabilities; $N = 20$, $T = 1500$ K. (modification: rotational rates 10 times faster, vibrational rates 10 times slower). The left-most box depicts an initial distribution for $T_i = 300$ K.

Can. J. Chem. Downloaded from www.nrcresearchpress.com by 210.87.254.6 on 09/05/12
For personal use only.

are a little more revealing than that described in I for lower temperatures. Figure 2(*c*) shows the contributing heat capacities for the shock-wave heating of this model molecule from 300 to 1500 K using these scaled transition probabilities. One interesting fact emerges immediately: the relaxation times of all six modes which are rotational in character are reduced by a factor of about *five*, and the relaxation time of the mode which is predominantly vibrational is increased by a factor of *twenty*! This is a result of increasing rotational transition probabilities by a factor of 10 and decreasing vibrational transition probabilities by the same factor, which is further evidence of the subtle nature of rotation–vibration coupling in these processes. Figure 2(*c*) depicts more nearly our traditional picture of rotational relaxation followed by vibrational relaxation: the left-most six modes add up nearly to the rotational heat capacity, and the right-most mode is almost equal to the mean vibrational heat capacity for the jump in question; this is not surprising since the 'rotational' modes now precede the 'vibrational' modes by a significant time interval. A somewhat larger disparity still between the assumed rotational and vibrational transition probabilities would effect a virtually complete separation of the two processes (in the sense that the modes in Fig. 3 would become either more purely rotational or more purely vibrational in character, with corresponding division of the η_i into two groups) thus yielding the typical behaviour of heavy diatomic molecules in relaxation processes.

Figure 2(*d*), the analogue of Fig. 2(*a*), shows the results for these scaled probabilities for a small temperature jump (1499.5 to 1500 K). Notice again the reduction in contribution from modes involving low values of J and the corresponding increase in importance of those involving higher values of J. Notice also the relatively large contribution to the heat capacity by the ($v = 0$, all $J \leftrightarrow v = 1$, all J) transition, much larger than the analogous process in Fig. 2(*a*); again reflecting the influence of rotation–vibration coupling in that case, in the sense that some molecules achieve vibrational excitation using normal modes which are essentially rotational in character, but with a small vibrational component. One other point of interest in Fig. 2 is that for those rotational modes having little vibrational component, *i.e.* the left-most three in each case, it hardly matters which set of probabilities is used, the same amount of energy is accumulated through similar modes *cf.* Fig. 2 (*b*) and (*c*), (*a*) and (*d*).

Laser Schlieren Experiments

Ducuing and co-workers (3, 4) have carried out a series of experiments in which hydrogen, diluted in an inert gas, is excited to the $v = 1$, $J = 1$ state, and the decay of the excitation is then followed by a schlieren technique which measures the rate of creation of translational energy in the gas. Depending upon the strength of the excitation, the population of the $v = 1$, $J = 1$ state can be raised to between 0.1% and 10% of the total hydrogen molecule concentration.

Imitating these experiments with the present computational scheme reveals simply that at low temperatures ($T < 500$ K), after some initial transients have died out, the total energy of the H_2 molecules present relaxes in a true exponential manner, and with a relaxation time which is exactly $-\lambda_{N-2}^{-1}$. This is true for *either type* of transition probability discussed above, and this is because in both instances the rotation–vibration coupling is either weak (standard set) or very weak (scaled set); consequently, these experiments appear to be a true measurement of the vibrational relaxation time, at least under the experimental conditions so far explored. Nevertheless, there are some interesting features which may be amenable to further experimental observation, and we will discuss three here.

The first is that immediately after the initial excitation, the internal energy of the molecules *rises* before beginning to fall. What is happening is that $v = 1$, $J = 1$ is highly overpopulated with respect to $v = 1$, $J = 3, 5, 7, \ldots$ at the ambient temperature in question: consequently, the populations of these higher J states of $v = 1$ rise in an attempt to establish thermal equilibrium with the heat-bath temperature, given the very high population of $v = 1$, $J = 1$. The dominant modes used in this process are not ones we have discussed before, but M_2, M_5, and M_7 (*cf.* Fig. I(1)), which in fact represent nothing more than the rotational relaxation of $v = 1$; these relaxation modes are slightly faster than the corresponding rotational relaxations M_3, M_6, and M_9 of $v = 0$. This energy increase shows

Can. J. Chem. Downloaded from www.nrcresearchpress.com by 210.87.254.6 on 09/05/12
For personal use only.

itself in the numerical scheme by the fact that ξ_2, ξ_5, and ξ_7 have the opposite sign from that of the dominant relaxation strength ξ_{14}, and of course the effect is rather small, ξ_2, ξ_5, and ξ_7 together being about 0.05 of $-\xi_{14}$ for the case where the initial $v = 1, J = 1$ population is 10% of the total H_2 molecules present. For H_2, according to our standard set of transition probabilities, the total energy would only rise by about 2%, however, because of other competing decay modes, but for other molecules imitated by our scaled set of transition probabilities, the full 5% initial rise in rotational energy would be realised before the vibrational decay commenced. (A similar effect is apparent in some exploratory calculations, termed 'box calculations' by Rabitz and Lam (5), their Fig. 5, curve I where the total internal energy of the molecules rises initially before decaying to the equilibrium value).

Second, it is interesting to see what one might expect to find if these experiments could be repeated at much higher temperatures, for example, $T = 1500$ K. For most molecules, one would expect the situation to be as just described, but for H_2, in view of the experiments of Dove *et al.* (2) and our qualified support for them, we might expect the results to be more complicated. Our calculations predict two overshoots in the energy. The first is the initial increase in the rotational energy of $v = 1$ as described in the preceding paragraph. Then follows a period during which the major portion of the energy relaxes by the vibrational mode M_{15} (*cf.* Fig. I(4), also Fig. 2 (*a*) and (*b*)), from which, under favourable conditions, it might be possible to deduce the vibrational relaxation time. However, this relaxation overshoots the final energy according to our calculations, and this, if it occurred in the experiment, could render the interpretation of the results a little difficult depending upon the severity of the overshoot. The reason this second overshoot occurs is because the rotational relaxation of $v = 1$ to very high J levels is slow, and the vibrational deactivation is taking place before $v = 1$ is properly equilibrated rotationally. Hence, the result of the vibrational relaxation M_{15} (which is essentially $v = 1$, all $J \leftrightarrow v = 0$, all J) leaves the high rotational states of $v = 0$ underpopulated; examination of the changes in population with time shows that the last equilibrations to occur are those of $v = 0$, $J = 11$, 13, and 15 whose populations *rise* towards their equilibrium values. The prediction of this second overshoot is obviously sensitive to the chosen set of transition probabilities, and may or may not be readily observable.

Thirdly, we can ask what we might observe if we were to populate another excited state, rather than $v = 1, J = 1$. If one looks at eq. I[10] which is the one which determines whether a particular mode will be heavily used during the relaxation under consideration, one can see that it can be represented pictorially by the normal modes as we have plotted them in I and in Fig. 3. A mode will be heavily used if there is a strong overlap between the initial distribution (left-most box), the mode, and the final distribution (right-most box). Examination of Fig. I(1) shows that if we choose to populate $v = 1, J = 5$ at low ambient temperature, there is no mode that connects it directly to the final distribution, and we must therefore get two consecutive decays: first a rotational relaxation (in the normal sense) of $v = 1$, dominated by mode M_5 (with a small contribution from M_2) followed by the vibrational relaxation M_{14}. This conclusion is virtually independent of our choice of transition probabilities for reasons explained in I. However, if the temperature is high, the modes are too complicated even in a well-decoupled case like Fig. 3 for this simple pictorial approach to work, and numerical analysis is necessary.

Measuring Relaxation Times by Following Population Changes

Alongside all of the calculations reported in this paper, the population distribution as a function of time was derived using eq. I[3]. It appears that the situation is very complicated indeed, and only a few highlights will be documented. What is true, of course, is that all populations approach the final distribution with a relaxation time which is $-\lambda_{N-2}^{-1}$, but in many cases, if a dominant relaxation precedes this process (as for example in the hypothetical laser schlieren experiment described above), these terminal rates of change may be too small to be resolved experimentally. There are, as we have seen, overshoots in energy which are, of course, associated with complicated population changes. Populations themselves overshoot in all kinds of circumstances (*cf.* also ref. 5, Fig. 4 and ref. 6, Fig. 1): for example, if H_2 is heated from 499.5 to 500 K, the populations of the states $v = 1$,

Can. J. Chem. Downloaded from www.nrcresearchpress.com by 210.87.254.6 on 09/05/12
For personal use only.

$J = 1$ and $v = 2$, $J = 1$ set off in the wrong direction before turning around to approach the new equilibrium distribution! This is because these two states are depleted by rotational relaxation of their respective vibrational manifolds before they can be repopulated by the slower vibrational relaxations from $v = 0$: this kind of behaviour will occur in all molecules. When more extreme changes in temperature than 0.5 K are imposed, depending upon the conditions, several states may overshoot in this way or more often if they do not overshoot, they may show incipient signs of so doing. This effect manifests itself sometimes as the apparent existence of a very slow relaxation persisting over a considerable time period. In other words, the level in question is in a steady state, or almost so, and in our calculations we have many examples of levels exhibiting apparent time constants of the order of $-10^5\ s^{-1}$ over a decade or more in time, when the smallest eigenvalue in the system is near $-10^6\ s^{-1}$, or of levels exhibiting apparent time constants intermediate between but not coinciding with any real time constant of the system. If we alter the probabilities so as to increase the disparity in rate between rotational and vibrational processes, this latter difficulty is somewhat mitigated, but is not removed altogether. Thus, it would appear that in general (but not for H_2) it may often be possible to derive relaxation times by following population decays, but the technique need not necessarily work and needs to be applied with considerable caution.

Conclusions

These calculations show very clearly that if one attempts to characterise a rotational relaxation, or a mixed rotation–vibration relaxation by a single relaxation time, then that 'relaxation time' must depend on the disparity between the initial and the final distributions in the relaxation and therefore, must depend on the method used. In general, we have argued that rotation–vibration coupling (in the present sense) is unimportant for most diatomic molecules except hydrogen, its isotopes and possibly some light hydrides. Thus, the common behaviour is expected to be rotational relaxation followed by vibrational relaxation, as we have always believed, but hydrogen at temperatures above 1300 K is apparently an exception, as we have discussed at length. Rotational relaxation times, however, *must always be subject to this qualification*, that they will be method-dependent, or will be sensitive to the initial population distribution. Here again, except in the case of hydrogen and perhaps some light hydrides, rotational relaxation times are usually very fast indeed, and it may not always be possible to resolve these effects in a decisive fashion. Hydrogen is a special case among all the diatomic molecules, and in one sense it is unfortunate that so much effort is being devoted to attempts to calculate the rotation–vibration energy-transfer properties of H_2 and its isotopes, because that will not reveal for us the general behaviour of diatomic molecules. On the other hand, the calculation of these properties for H_2 is a challenge in which we can hope to succeed, and in the near future obtain good matching between theoretically calculated and experimentally observed behaviour from a wide range of techniques including sound dispersion, shock-wave, and laser schlieren experiments. Furthermore, the relaxation behaviour of polyatomic molecules having small moments of inertia about one or more axis probably has much in common with the hydrogen molecule; consequently, a good understanding of the 'vibrational' relaxation behaviour of hydrogen and light hydrides should lead to a much better insight into the Lambert–Salter relationships, somewhat along the lines we suggested previously (7).

An analysis of the results presented here (and in I) in terms of the information-theory approach will be presented at a later date (8).

Acknowledgements

This work was supported by the National Research Council of Canada, and was greatly helped by computational assistance from Dr. N. I. Labib.

1. H. O. Pritchard and N. I. Labib. Can. J. Chem. **54**, 329 (1976).
2. J. E. Dove, D. G. Jones, and H. Teitelbaum. Fourteenth Symposium (International) on Combustion. The Combustion Institute, Pittsburgh, Pa. 1973. p. 177.
3. F. DeMartini and J. Ducuing. Phys. Rev. Lett. **17**, 117 (1966).
4. M.-M. Audibert, C. Joffrin, and J. Ducuing. Chem. Phys. Lett. **19**, 26 (1973); J. Chem. Phys. **61**, 4357 (1974).
5. H. Rabitz and S.-H. Lam. J. Chem. Phys. **63**, 3532 (1975).
6. I. Procaccia, Y. Shimoni, and R. D. Levine. J. Chem. Phys. **63**, 318 (1975).
7. E. Kamaratos and H. O. Pritchard. Can. J. Chem. **51**, 1923 (1973).
8. A. W. Yau and H. O. Pritchard. In preparation.

The thermal isomerisation of methyl isocyanide in the temperature range 120–320 °C

JOHN LEWIS COLLISTER AND HUW OWEN PRITCHARD
Chemistry Department, York University, Downsview, Ont., Canada M3J 1P3

Received March 23, 1976

JOHN LEWIS COLLISTER and HUW OWEN PRITCHARD. Can. J. Chem. **54**, 2380 (1976).

The thermal isomerisation of methyl isocyanide has been measured in the rigorous absence of self-heating over a temperature range from 120–320 °C and at pressures from 2–100 torr. Expressions are given for the rate constant as functions of both temperature and pressure in these ranges of the two variables. The infinite-pressure rate constant is accurately represented by an Arrhenius line with no curvature having $E_\infty = 38.2 \pm 0.2$ kcal mol^{-1} and $\log_{10} A_\infty$ (s^{-1}) = 13.35 ± 0.11, although at all other pressures, E is a function of temperature.

A number of tests on the cleanliness of the reaction were made, and some previously expressed concerns about side reactions are alleviated considerably.

JOHN LEWIS COLLISTER et HUW OWEN PRITCHARD. Can. J. Chem. **54**, 2380 (1976).

On a mesuré l'isomérisation thermique de l'isocyanure de méthyle à des températures allant de 120–320 °C et à des pressions de 2–100 torr en s'assurant d'une façon rigoureuse qu'il n'y avait pas d'autochauffage. On donne les équations exprimant les constantes de vitesse en fonction de la température et de la pression dans les limites de ces deux variables. La constante de vitesse à pression infinie est représentée d'une façon précise par une droite d'Arrhénius ne présentant pas de courbure et dans laquelle $E_\infty = 38.2 \pm 0.2$ kcal mol^{-1} et $\log_{10} A_\infty$ (s^{-1}) = 13.35 ± 0.11; toutefois à toutes les autres pressions, E est une fonction de la température.

On a effectué un certain nombre d'essais pour vérifier la propreté de la réaction; on considère que quelques unes des inquiétudes exprimées antérieurement concernant les réactions secondaires avaient été grossièrement surestimées.

[Traduit par le journal]

Introduction

It has been suggested recently that the explosive isomerisation of methyl isocyanide may prove to be a sensitive and reliable standard against which to test theories of gaseous thermal explosions (1); the required kinetic and thermodynamic data on methyl isocyanide and its isomerisation are, however, incomplete for this purpose. As far as the kinetics of the isomerisation are concerned, the rate of the reaction has been studied extensively as a function of pressure at three temperatures only, 200, 230, and 260 °C (2), and extrapolation of these rates into the explosion region (310–360 °C) is very sensitive to small imperfections in the data. The uncertainty of this extrapolation is aggravated by the fact that in some experiments a correction had to be made for self-heating in the reaction, and this correction although small, is itself rather uncertain, giving rise to possible errors in the required extrapolated data. In the work described in this paper, self-heating was eliminated by the appropriate choice of reaction-vessel size for the temperature and pressure in question, and the temperature range was made as wide as possible in order to reduce both the length of the required extrapolation and, therefore, its uncertainty. We found that it was possible to cover the range 120–240 °C in conventional static experiments, and 240–320 °C in relatively conventional flow experiments.

Experimental

Materials, etc.

Methyl isocyanide was prepared from *N*-methyl formamide by reaction, in the presence of an amine, either with phosgene (3) or toluene-*p*-sulphonyl chloride (4). The product was purified by vapour-phase chromatography, and was stored in brown glass, both on and off the vacuum system.

Propane and propylene were Phillips Research Grade, and gas-chromatographic and mass-spectrometric analysis showed that they conformed to specifications.

Analysis of the extent of the reaction was performed using a gas chromatograph with hot-wire thermal conductivity detectors and a 6 ft × 0.125 in. glass column with a Pennwalt 223/Chromosorb R packing at 70 °C. The effluent from the column was analysed with a mass spectrometer as required.

Self-heating and the Choice of Vessel Size

If we are interested in only small temperature rises

Can. J. Chem. Downloaded from www.nrcresearchpress.com by 210.87.254.105 on 09/05/12
For personal use only.

Can. J. Chem. Downloaded from www.nrcresearchpress.com by 210.87.254.105 on 09/05/12
For personal use only.

TABLE 1. Comparison, as a function of reactant pressure, of the radii of the spherical reaction vessels used in these experiments with the maximum allowable radii required to keep ΔT below 0.1 °C at T = 220 °C

Reactant pressure (torr)	Vessel radius (cm)	Maximum radius (cm)
2	7.9	37
5	5.0	17
10	4.2	9.5
20	3.1	5.7
50	2.3	2.9
100	1.3	1.8

caused by self-heating, we can use the approximate formulae

$$[1] \qquad \Delta T = -R\Delta H r^2/n\lambda_0$$

with $n = 6$ for a sphere, $n = 4$ for an infinite cylinder, and where ΔT is the *maximum* temperature rise at the centre of the vessel. ΔH is the enthalpy change per mole of reaction, r is the radius of the vessel in cm, λ_0 is the thermal conductivity in cal (cm °C s)$^{-1}$ and R is the rate of reaction in mol cc^{-1} s^{-1} (5, 6). Neither ΔH nor λ_0 is too well known (1), but they are sufficiently accurate for use in this expression.

For static experiments, it is convenient to analyse the total content of the reaction vessel, thus avoiding sampling problems. Table 1 shows, in column 2, the most convenient size of spherical reaction vessel as a function of reactant pressure, column 1; application of eq. 1 with ΔT set at 0.1 °C and R calculated for 220 °C (2) gives the maximum allowable size of reaction vessel, column 3. In all cases, the chosen vessel size in column 2 is less than the allowable vessel size in column 3, so that in every static experiment carried out at 220 °C and below, the maximum temperature rise at the centre of the vessel was less than 0.1 °C. Consequently, rate constants were determined at all the (nominal) pressures listed in Table 1, at 20° intervals from 120–220 °C: at 120 °C, reaction times were of the order of 1–4 × 10^6 s, depending on pressure, for 1% reaction, and 300–1000 s at 220 °C. Because of the limitations imposed by constraining the self-heating temperature rise ΔT to be less than 0.1 °C, only two pressures were accessible at 240 °C, *viz.* 2 and 5 torr, where the vessel radii have to be less than 19 and 8 cm respectively. The static experiments need no further description, and full details are available elsewhere (7); in total, 148 experiments were carried out at seven temperatures, and our agreement with the results of Schneider and Rabinovitch (2) at 200 °C is excellent at all pressures.

Since the region of interest for explosion studies is above 300 °C, it is obviously necessary to use a flow technique to make measurements nearer to, and possibly up into this range. The static experiments serve only as a consistency check on the flow results, and provide a 'handle' which is useful in extrapolating the flow results to even higher temperature. Given the constraints that we could not use a non-condensable carrier gas because that would change the rate constant in the fall-off region, that the measured pressure drop along the reaction vessel (8, 9) should not exceed 10% of the mean pressure, so that the pressure itself would be fairly well-defined, that the collection time has to be sufficiently long to be measured accurately, etc., and that ΔT should not exceed 0.1 °C, we chose to use a 1 m length of 2 mm-bore glass tubing at the higher end of the temperature range (280–320 °C) and a 10 m length of the same tubing at the lower end of the range (240–300 °C). These tubes were made into coils of about 10 cm diameter, and at the two temperatures where both columns were used, the results were indistinguishable. Contact times ranged from 0.08 to 0.5 s, depending upon pressure, in the 1 m tube at 320 °C, and from 130–760 s in the 10 m tube at 240 °C. We note, also, that at 320 °C and 100 torr pressure, application of eq. 1 (for an infinite cylinder) yields a maximum temperature rise of 0.19 °C at the centre of the tube, which is just outside our design specifications, but nevertheless still negligible. A total of 43 flow experiments were carried out at five temperatures and again, full details of the conditions used and of the raw experimental data are available (7).

Tests for Side Reactions

Since the thermal isomerisation of methyl isocyanide is now the principal test case in unimolecular reaction theory, it is important to define the limits of existence of any side reactions. On the other hand, from the point of view of explosion studies, it is a knowledge of the rate that is of primary importance, and the means by which the reaction achieves that rate are of somewhat lesser concern. It has been reported (10) that the rate of isomerisation of methyl isocyanide at 200 °C is reduced by about 30% in the presence of 100 amagats of propane, whereas the rate remains unchanged in the presence of similar amounts of carbon dioxide. It was conjectured, therefore, that there could be a hitherto undetected free-radical chain component to this reaction, involving the well-characterised (11) reaction

$$[2] \qquad CH_3 + CH_3NC \rightarrow CH_3CN + CH_3$$

This suggestion was disputed by Rabinovitch and coworkers (12), and the situation has never been satisfactorily resolved: consequently, we carried out a number of auxiliary experiments designed to test for the presence of side reactions.

First, two relatively conventional tests were performed. At 320 °C, the reaction was carried out in the presence of propylene (1%), but there was no change in the rate of isomerisation, nor were there any spurious products detected by GC/MS analysis of the products. Then, a second 1 m column of wider diameter was constructed so that when packed with glass beads, it had the same mean cross-section as the 2 mm-bore open tube but a surface-to-volume ratio of 91 cm^{-1} instead of 14 cm^{-1}. Rates measured in this tube at 300 and 320 °C were identical with the original results, confirming not only the absence of a significant heterogeneous component, but also eliminating the existence of errors in the calculated contact times for the flow experiments due to streaming or other defects in the assumed gas flow.

Subsequently, a thermal explosion apparatus similar to that used previously (1) was constructed, and evidence for side reactions was sought by investigation of the behaviour of the reaction just above and just below criti-

Can. J. Chem. Downloaded from www.nrcresearchpress.com by 210.87.254.105 on 09/05/12
For personal use only.

cality, in the belief that this might provide a more sensitive test for side reactions. In two parallel sets of experiments, the explosion limits were measured in the presence of 1% propane and 1% propylene: it is difficult to find an efficient methyl-radical trap which does not react with methyl isocyanide, but the rates of reaction of methyl radicals with propane and with propylene are sufficiently different that if reaction 2 made a significant contribution to the overall rate of isomerisation, the explosion limits should be differently affected in the two cases. We found that the explosion limits were the same in both cases which, assuming that propane and propylene have similar collision efficiencies (13) and thermal conductivities (14), suggests that radical chains like [2] are not important. Again, we looked for spurious reaction products by GC/MS in the subcritical experiments, but found none apart from ethyl cyanide which we reported previously.

The persistent occurrence of ethyl cyanide in these subcritical explosions was puzzling, but the cause was eventually located. Newly purified methyl isocyanide does not yield any ethyl cyanide. However, on storage in glass on a vacuum line for a few days, traces of ethyl cyanide ($\sim$1 part in 10^5) are formed, and these of course persist through the reaction and appear in the reaction products. It is of interest to note, however, that although ethyl cyanide is not produced in subcritical experiments using newly purified methyl isocyanide, it is formed in small quantities if an explosion actually occurs.

We conclude that all the conventional tests carried out here, and previously (12), together with our use of explosion limit behaviour, suggest that there are no side reactions to the thermal isomerisation of methyl isocyanide which are of concern from the point of view of testing either explosion or unimolecular-reaction theory. This leaves the interpretation of our own high-pressure work (10) in an unsatisfactory state, and it would seem that an independent investigation of that problem should be undertaken.

Data Reduction

The ideal experiment would involve the measurement of the rate constant for isomerisation at 30 or more values of the pressure for each temperature, rather as was done by Schneider and Rabinovitch (2) for three temperatures; it would then be possible to extrapolate each set of data to a unique value of k_∞ at each temperature, and so characterise the reaction rate completely. Clearly, the number of temperatures and the range of temperatures excludes such a comprehensive attack on this problem, and we decided to be satisfied with the range of experiments described in the preceding section, and to be guided by the current very successful theories of unimolecular reactions in reducing the data to useable form.

The raw experimental data, consisting usually of groups of two or three rate constants $k_p(T)$ at some or all of the six nominal pressures were fitted to a simple quadratic function by least squares, and the best value of $k_{100}(T)$, *i.e.* the rate constant for 100 torr pressure at the temperature under consideration, was obtained. Since we have far too few data with which to derive reliable values of $k_\infty(T)$ for each temperature, the infinite-pressure rate constant was determined by a theoretical extrapolation. Using the RRKM computer program written by Holbrook and Robinson (15) and the theoretical model of the isomerisation due to Rabinovitch and coworkers (2, 16), theoretical fall-off curves were calculated for each temperature, and the theoretical value of $k_\infty(T)/k_{100}(T)$ was used to derive an extrapolated 'experimental' value for $k_\infty(T)$. These extrapolated rate constants, using all the data from 120–320 °C, when plotted in Arrhenius form, fall on an exceptionally good straight line having $E_\infty = 38.2 \pm 0.2$ kcal mol^{-1} and $A_\infty = 10^{13.35\pm0.11}$ s^{-1}, in excellent agreement with the more limited data of Schneider and Rabinovitch ($E_\infty = 38.4$ kcal mol^{-1} and $A_\infty = 10^{13.6}$ s^{-1}).

The theoretically calculated fall-off curves were then superimposed on the experimental plots, and visual inspection showed that the theoretical fall-off curve was equally as good a representation of the data as the original 2–100 torr segment of quadratic (the two curves, of course, coincide at 100 torr by definition). Again, we note that we do not have the volume of raw data that would be required to assign a statistical significance to this assertion. Accepting this, however, we are now in a position to generate empirical interpolation formulae for the rate constant as a function of both temperature and pressure, in the range $2 < p < 100$ torr, $120 < T < 320$ °C and with the confidence, because of the extremely good Arrhenius behaviour of $k_\infty(T)$, that these formulae can be used to extrapolate rate constants at these pressures up into the top end of the explosion temperature range, *i.e.* $T \simeq 360$ °C. These interpolation formulae are shown in Tables 2 and 3. Table 2 presents the behaviour of $k_p(T)$ at constant pressure in the form of a quadratic in the absolute temperature T, *viz.*

$$[3] \quad \ln [k_\infty(T)/k_p(T)] = a + bT^{-1} + cT^{-2}$$

for a series of values of the pressure p, and Table 3 presents the behaviour of $k_p(T)$ in the form of a quadratic in $\ln p$, *viz.*

Can. J. Chem. Downloaded from www.nrcresearchpress.com by 210.87.254.105 on 09/05/12
For personal use only.

TABLE 2. Coefficients a, b, and c in the equation $\ln [k_\infty(T)/k_p(T)] = a + bT^{-1} + cT^{-2}$ as a function of the reactant pressure in the temperature range $393 < T < 593$ K

Reactant pressure (torr)	a	b	c
2	5.91263	−2851.90	468030
5	4.90310	−2606.31	436115
10	4.13008	−2341.62	398264
20	3.37536	−2026.00	350715
50	2.43622	−1556.59	275742
100	1.79968	−1193.90	214946

TABLE 3. Coefficients A, B, and C in the equation $\ln k_p(T) = A + B \ln p + C (\ln p)^2$ as a function of temperature, with the reactant pressure p in torr

Temperature (K)	A	B	C
373	−23.1655	0.803245	−0.080710
423	−17.1929	0.839287	−0.080913
473	−12.5208	0.863600	−0.079702
523	−8.78284	0.891258	−0.078651
573	−5.71522	0.913855	−0.076708
623	−3.17576	0.932429	−0.074444

$$[4] \qquad \ln k_p(T) = A + B \ln p + C(\ln p)^2$$

Figure 1 shows eq. 3 plotted in Arrhenius form: the slopes of these lines represent the differences between E_∞ and $E_p(T)$, showing how the 'activation energy' varies with both p and T in the fall-off region: numerical values can easily be generated from

$$[5] \qquad E_\infty - E_p(T) = -R(b + 2cT^{-1})$$

using the values of b and c listed in Table 2 for the pressure in question.

Conclusion

The aim of this work was to enhance the reliability of the extrapolation of the data of Schneider and Rabinovitch (2) into the range of temperatures required for thermal explosion studies (1). This has been done by extending the temperature range in both directions and conducting a limited number of experiments at a few key values of the pressure. The final data reduction uses the well-established theoretical model of this reaction in lieu of the aquisition of perhaps four or five times as much raw experimental data; in our view, an acceptable expedient in this

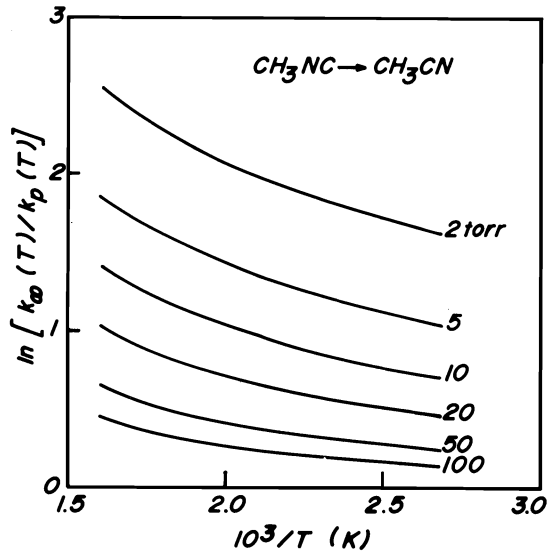

FIG. 1. Arrhenius plot of the rate constant for the thermal isomerisation of CH_3NC to CH_3CN, as a function of pressure. $k_\infty(T) = 10^{13.35}$ exp $(-38\,200/RT)$ s^{-1}.

case. Our experiments have also included a determined attempt to find unwanted side reactions, and doubts about the cleanliness of the reaction have been reduced considerably.

Comparison with previous work of Schneider and Rabinovitch (2) is excellent both in the sense of detailed agreement at 200 °C and also in the derived Arrhenius parameters for the infinite-pressure rate constant. Extrapolation of our results, however, to the temperature range covered in the shock-wave experiments of Lifshitz, Carroll, and Bauer (17), does not yield good agreement with their results. Selecting two of their runs (Nos. 11 and 14) at 828 K, we calculated their experimental conditions to be $p(CH_3NC) = 31$ torr and $p(Ar) = 1400$ torr: using the value for the relative efficiency (13) of argon on a pressure basis $\beta_p = 0.136$, the equivalent pressure of argon is 190 torr, and so the equivalent total pressure is about 220 torr. Extrapolating $k_\infty(T)$ to 828 K and reducing it to 220 torr via the standard model RRKM calculation for this temperature suggests that the rate constant ought to be about $1.3–1.5 \times 10^3$ s^{-1}, compared with the actual values obtained of 332 and 359 s^{-1}. Part of this discrepancy could be removed if argon were to be a much less efficient collider at higher temperatures, but not all of it. In fact, excellent agreement with our

estimates could only be obtained if the equivalent total pressures were to be approximately the figures given by Lifshitz *et al.* for $\rho_5 p_1(CH_3NC)/\rho_1$ in Table II of their paper (17), which is of course even less than $p(CH_3NC)$ itself by a factor of 828/298.

Acknowledgements

This work was supported by the National Research Council of Canada, and we are indebted to Peggy R. Hill for computational assistance in the data reduction.

1. H. O. Pritchard and B. J. Tyler. Can. J. Chem. **51**, 4001 (1973).
2. F. W. Schneider and B. S. Rabinovitch. J. Am. Chem. Soc. **84**, 4215 (1962).
3. I. Ugi, U. Fetzer, U. Eholzer, H. Knupter, and K. Offermann. Angew. Chem. intern. Ed. Engl. **4**, 472 (1965).
4. J. Casanova, R. E. Schuster, and N. D. Werner. J. Chem. Soc. 4280 (1963).
5. S. W. Benson. J. Chem. Phys. **22**, 46 (1954).
6. D. J. Wilson. J. Phys. Chem. **62**, 653 (1958).
7. J. L. Collister. Ph.D. Thesis, York University, Downsview, Ontario. 1976.
8. H. W. Melville and B. G. Gowenlock. Experimental methods in gas reactions. Macmillan, London. 1964.
9. M. F. R. Mulcahy and M. R. Pethard. Aust. J. Chem. **16**, 527 (1963).
10. C. K. Yip and H. O. Pritchard. Can. J. Chem. **48**, 2942 (1970).
11. D. H. Shaw and H. O. Pritchard. Can. J. Chem. **45**, 2749 (1967).
12. T. Fujimoto, F. M. Wang, and B. S. Rabinovitch. Can. J. Chem. **50**, 3251 (1972).
13. S. C. Chan, B. S. Rabinovitch, J. T. Bryant, L. D. Spicer, T. Fujimoto, Y. N. Lin, and S. P. Pavlou. J. Phys. Chem. **74**, 3160 (1970).
14. Y. S. Touloukian, P. E. Liley, and S. C. Saxena. Thermal properties of matter, Vol. 3. Thermal conductivity. Plenum Press, New York. 1970.
15. K. Holbrook and P. J. Robinson. Unimolecular reactions. Wiley Interscience, New York. 1972.
16. F. J. Fletcher, B. S. Rabinovitch, K. W. Watkins, and D. J. Locker. J. Phys. Chem. **70**, 2823 (1966).
17. A. Lifshitz, H. F. Carroll, and S. H. Bauer. J. Am. Chem. Soc. **86**, 1488 (1964).

Can. J. Chem. Downloaded from www.nrcresearchpress.com by 210.87.254.105 on 09/05/12
For personal use only.

Synthesis of azacyclic compounds by an aminium radical route:[1] orbital overlap requirements

RICHARD A. PERRY, SHI C. CHEN, B. C. MENON, KAORU HANAYA, AND YUAN L. CHOW
Department of Chemistry, Simon Fraser University, Burnaby, B.C., Canada V5A 1S6

Received December 9, 1975

RICHARD A. PERRY, SHI C. CHEN, B. C. MENON, KAORU HANAYA, and YUAN L. CHOW. Can. J. Chem. **54**, 2385 (1976).

Model compounds of $\Delta^{4,5}$-, $\Delta^{5,6}$-, and $\Delta^{6,7}$-alkenylnitrosamines were synthesized and photolyzed to generate the corresponding alkenylaminium radicals. The $\Delta^{5,6}$-alkenylaminium radicals underwent efficient intramolecular addition leading to the exclusive formation of pyrrolidine derivatives, the yield of which was lower if the steric strain and hindrance were severe in the cyclization transition state. The $\Delta^{6,7}$-alkenylaminium radical cyclized inefficiently to piperidine derivatives and the $\Delta^{4,5}$-alkenylaminium radicals did not appear to cyclize; in both cases other pathways having lower activation energies, such as elimination and hydrogen abstraction, predominated. Evidence that the direction of cyclization is controlled by the degree of *p*-orbital overlap, but not by stability of the developing products, in the transition state is presented. The stereochemical factors associated with the overlap determined the yields of the cyclization products. This is in excellent agreement with the fact that the transition state of cyclization is reached at an early stage in the reaction coordinate. Metal ion catalyzed or radical initiated decomposition of some alkenyl chloramines were found either to cyclize to a mixture of pyrrolidine and piperidine derivatives or to undergo no cyclization.

RICHARD A. PERRY, SHI C. CHEN, B. C. MENON, KAORU HANAYA et YUAN L. CHOW. Can. J. Chem. **54**, 2385 (1976).

On a synthétisé et photolysé des composés modèles de $\Delta^{4,5}$-, $\Delta^{5,6}$- et $\Delta^{6,7}$-alkenylnitrosamines qui ont conduit aux radicaux alkènylaminium correspondants. Les radicaux $\Delta^{5,6}$-alkènylaminium subissent des réactions d'addition intramoléculaires efficaces conduisant à la formation exclusive de dérivés de la pyrolidine; le rendement de ce composé est diminué si l'empêchement et la contrainte stérique sont importants dans l'état de transition menant à la cyclisation. Le radical $\Delta^{6,7}$-alkènylaminium se cyclise d'une façon inefficace pour conduire à des dérivés de la piperidine et les radicaux $\Delta^{4,5}$-alkènylaminium ne semblent pas se cycliser; dans les deux cas d'autres chemins réactionels ayant des énergies d'activation plus basses, tels que les éliminations et les enlèvements d'hydrogène, prédominent. On présente des données indiquant que la direction de la cyclisation est contrôlée par le degré de recouvrement des orbitales *p* dans l'état de transition; il ne semble pas que cette direction soit influencée par la stabilité des produits qui se forment. Les facteurs stéréochimiques associés avec le recouvrement déterminent les rendements des produits de cyclisation. Ceci est en excellent accord avec le fait que, dans les coordonnées de la réaction, l'état de transition de la cyclisation est atteint tôt. On a trouvé que les décompositions catalysées par les ions métalliques ou initiées par les radicaux de quelques chloramines d'alkènyles conduisent soit à une cyclisation fournissant un mélange de dérivés de la pyrolidine et de la pipéridine soit qu'ils ne conduisent pas à des cyclisations.

[Traduit par le journal]

Introduction

Radical reactions are frequently avoided in synthetic chemistry owing to a general belief that a reaction involving highly reactive radical species must necessarily be unselective. This may be true in intermolecular processes in which the polar effects of a radical reaction as measured by Hammett ρ constants are generally small (2); a literature survey reveals that the largest ρ values are -1.34 for the piperidinium radical addition to styrenes (3) and -1.5 for the benzylic hydrogen abstraction by trichloromethyl radical (4). However, in intramolecular radical reactions, the presence of stereochemical controls may facilitate one process and retard others. Such cases have been observed in a number of stereospecific intramolecular radical reactions, *e.g.*, hydrogen abstraction in the Barton (alkoxy radical) reaction (5) and the Hofmann–Löffler (aminium radical) reaction (6), and intramolecu-

[1]Part of the results have been published as a preliminary communication; see ref. 1.

Can. J. Chem. Downloaded from www.nrcresearchpress.com by 210.87.254.40 on 09/05/12
For personal use only.

TABLE 1. Radical cyclization

$CH_2{=}CH_2(CH_2)_nX\cdot$	Yield of cyclic products (%)						Reference
	$n = 2$		$n = 3$		$n = 4$		
	4-membered	5-membered	5-membered	6-membered	6-membered	7-membered	
$X = CH_2\cdot$	0	0	90	0	0	0	14
$= \dot{C}(CO_2Et)(CN)$	0	30	80 9	20[a] 49[b]	34	0	13
$= O\cdot$	0	0	68	0	0	0	7, 8, 9
$= \dot{N}R$	0	0	56	0	10	3.5	23, 24, 58
$= {}^{+}\dot{N}(R)X$, $X = H$	0	0	82	0	0	0	23, 24, 58
$X = Ti^{3+}$	0	13	66	0	72	0	
$= S\cdot$	0	39	16	42	31 54	14[c] 6[b]	12
$= \dot{P}R_2$	0	38	0	64	0	41	21

[a]At 70 °C.
[b]At 80 °C.
[c]At 5 °C.

lar addition of alkoxy (7–9), amido (10, 11), and mercapto (12) radicals.

Intramolecular radical[2] addition has been more extensively investigated with alkenyl carbon radicals (13–17), although other radical cyclizations (7–12) have begun to attract attention in recent years. As summarized in Table 1, the efficiency and stereospecificity of alkenyl radical cyclizations are fairly distinctive except for two cases, *i.e.* the cyclizations of carbon radicals substituted with electron-withdrawing groups (13) and thiyl radicals (12). Significantly, reversibility of addition has been demonstrated in these two cases, from which one may conclude that the thermodynamically more stable product is not necessarily the kinetically controlled product. For the more extensively investigated system ($n = 3$), a number of rationales have been advanced to explain the preferential formation of the kinetically controlled products with five-membered rings as opposed to the thermodynamically more stable six-membered rings (8, 13, 18–20).

Certain aspects of the intramolecular radical additions shown in Table 1 are worthy of comment. Phosphoranyl radical cyclization (21, 22) is unique in that the larger-membered rings are always formed exclusively. Amine radical cyclization (23–26) is in marked contrast to the failure of intermolecular amine radical addition which has been suggested to result from a high activation energy (27). In these cases (23–26), however, the possibility has to be considered that aminium radical might be the reactive intermediate since hydrogen chloride is generated by side reactions of chloramines. An amine radical coordinated with titanous ion (or metal ion in general) has been proposed as the reactive intermediate in the titanous chloride catalysed chloramine decomposition (23, 24). Such an intermediate behaves very similarly to an aminium radical.

The tendency of aminium radicals to undergo obviously irreversible addition to a carbon–carbon double bond has been well established (28, 29). In view of their ready generation from nitrosamine photolysis under mild conditions (29), we have extended our research to study the patterns of aminium radical cyclization, aiming to establish a synthetic route for azapolycyclic compounds. For comparison, decompositions of some of the corresponding alkenyl chloramines catalysed either by a radical initiator (30) or ferrous ion (31) and catalysed by silver nitrate (25, 26, 32, 33) have been investigated. The last method has been claimed to involve either a nitrenium ion (32) or, alternatively, an amine radical (25, 26) as the reactive intermediate. While it is much simpler to use a nitrenium ion to visualize the chloramine decomposition, the

[2]Throughout this discussion the radical center will be designated as position 1.

Can. J. Chem. Downloaded from www.nrcresearchpress.com by 210.87.254.40 on 09/05/12
For personal use only.

Can. J. Chem. Downloaded from www.nrcresearchpress.com by 210.87.254.40 on 09/05/12
For personal use only.

reaction is obviously very complex owing to the simultaneous Ag^+/Ag^0 redox process (26).

Results

The necessary alkenylamines were prepared in yields better than 50% by straightforward reactions involving key steps such as nucleophilic substitution of alkenyl bromide with methylamine (34), metal hydride reduction of amides or isocyanates (26, 33), and acetate pyrolysis. The details of the syntheses are described later. The alkenylamines were not rigorously purified but their structures were ascertained by the presence of appropriate absorption peaks for the olefin and the secondary amine groups in their nmr and ir spectra (Bohlmann bands at 2800–2650 cm^{-1}) (35). The alkenyl nitrosamines were prepared either from sodium nitrite (36) or a modified procedure using nitrogen tetraoxide (N_2O_4) (37). As these reagents are known to attack olefinic bonds to produce nitrate, nitro, and nitrite derivatives (38), control of nitrosation conditions was essential to obtain a clean product. In two cases, the products (**29** and **33**) were badly contaminated by these side products as shown by the ir absorptions at 1650 (nitrate) and 1550 cm^{-1} (nitro) and the proportionally lower olefinic proton intensities in their nmr spectra.

As with the dialkylnitrosamines, most of these alkenylnitrosamines could be purified by distillation or chromatography except in two cases (**29** and **33**) where extensive decomposition occurred on attempted purification. The ir absorptions at 1335–1325 cm^{-1}, and the uv n–π^* transition bands at 340–345 nm (ϵ 90 ~ 100) exhibited by these alkenyl nitrosamines are common to all nitrosamines (39). In analogy to dialkylnitrosamines, these compounds exist as mixtures of *E*-isomers (78–91%) and *Z*-isomers[3] in solution as shown by their nmr spectra (see Experimental) (40, 41). The nmr signals for the olefinic protons were slightly displaced downfield (0.1 ~ 0.2 ppm) relative to the parent alkenylamines, likely resulting from a long range anisotropic effect of the nitrosamino group.

The alkenyl chloramines were prepared by published methods (26, 33) and, due to their instability, were reacted immediately without further purification. Their ir and nmr spectra indicated that the olefinic group remained intact after hypochlorite treatment. The chloramine contents before and during the experiments were analysed by thiosulfate titration (26).

The photolyses of the alkenylnitrosamines in acidified methanol (29) were carried out under purified nitrogen to avoid the photooxidation processes (43) and with a Nonex filter (transparent >330 nm) which allowed irradiation of the n → π^* transition band. The formation of *C*-nitroso dimers during the photolysis was indicated by the uv absorption at *ca.* 290 nm (44) in the photolysate. No effort was made to isolate the dimers and the photolysates were worked up to give 'neutral' (5 ~ 10%, usually unreacted nitrosamines) and 'basic' fractions.

Metal ion catalysed and radical initiated decompositions of alkenyl chloramines were carried out according to published procedures (26, 30–33). In all experiments the yields were calculated based upon the amount of reacted starting nitrosamines or chloramines. The following description of results will be arranged according to the position of the olefinic group.

$\Delta^{5,6}$-*Alkenyl Derivatives*

Photolysis of *N*-nitroso-*N*-methyl-4-pentenylamine (2) gave 83% of the basic fraction containing two 2-formylpyrrolidine oximes *E*-**3** and *Z*-**3** in a 4:1 ratio. While the major oxime *E*-**3** was obtained as a crystalline compound showing the typical aldoxime doublet at τ 2.75 and the N—CH_3 singlet at τ 7.67, oxime *Z*-**3** (the corresponding doublet at τ 3.25 and the singlet at τ 7.40) was always contaminated with some *E*-**3**. As oxime *Z*-**3** was shown to isomerize gradually to the more stable oxime *E*-**3** on storage, it was assumed that the contamination was derived from the isomerization process. Further confirmation of the pyrrolidine ring was obtained by dehydration of a crude oxime mixture, via the tosylates, to give the common nitrile **4** which is a known compound (45).

Decomposition of the corresponding chloramine **5** in methanol containing silver nitrate gave a 5:1 mixture of *N*-methyl-3-methoxypiperidine (**6**) and *N*-methyl-2-methoxymethylpyrrolidine (**7**) in addition to 35% of the parent amine. Separation of these two compounds was hampered by their volatility and a small difference

[3]The *E* and *Z* nomenclature (40) is used to describe geometric isomers of oximes and nitrosamines and the *syn–anti* to describe the position of protons in these isomers (42).

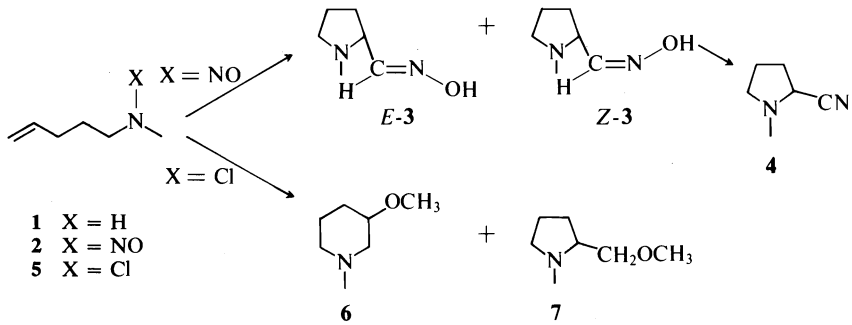

SCHEME 1

in chromatographic mobility. Only a small amount of piperidine **6** was isolated in the pure state; it exhibited a nmr spectrum containing a poorly resolved triplet at τ 6.72 characteristic of the C-3 methine proton and singlets at τ 7.60 (N—CH_3) and τ 6.68 (OCH_3). The presence of pyrrolidine **7** in a chromatographic fraction was indicated by the tlc and vpc analysis and by the nmr multiplet (the AB portion of an ABX system) in τ 6.6 region for the —CH_2O— moiety and the N—CH_3 singlet at τ 7.84. Decomposition of chloramine **5** in the presence of the radical initiator, azobisisobutyronitrile (30), gave no cyclization product; only ionic addition products to the double bond were isolated.

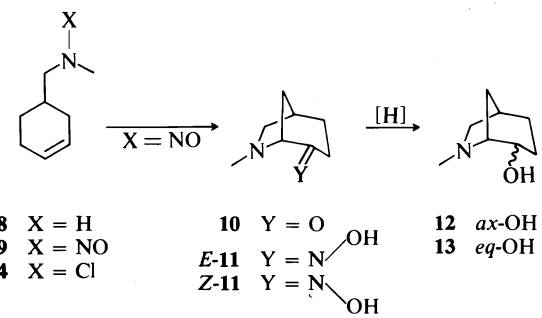

SCHEME 2

The need for acidic conditions in nitrosamine photolysis (28) was reconfirmed by the failure of nitrosamine **9** to disappear when irradiated in neutral solution. Under the usual photolysis conditions carrying 1 equiv. of hydrochloric acid (29), nitrosamine **9** disappeared quickly and afforded, after chromatography, *N*-methyl-7-azabicyclo[3.2.1]octan-2-one (**10**, 11%) and its oximes *E*-**11** (37%) and *Z*-**11** (13%). A mixture of oximes *E*-**11** and *Z*-**11** was hydrolysed with sodium bisulfite (46) to ketone **10** and was also reductively hydrolysed with sodium borohydride – sodium hydroxide (47) to a mixture of the corresponding alcohols **12** and **13**. These alcohols had high volatilities and co-distilled readily with organic solvents, resulting in low yields. Ketone **10** showed identical ir and nmr spectra to those obtained from the sample prepared by a different route by Professor Waegell's group (48).[4]

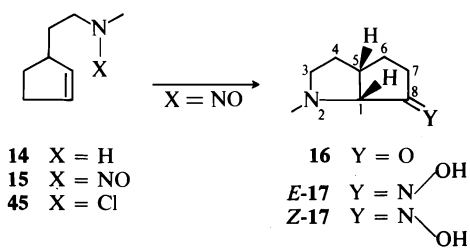

SCHEME 3

A similar photolysis of nitrosamine **15** followed by alumina chromatography of the basic fraction gave *cis*-*N*-methyl-2-azabicyclo[3.3.0]-octan-8-one (**16**, 9%), and its oximes *E*-**17** and *Z*-**17** (77%, ratio 1.4:1). The basic fraction was also directly hydrolysed to afford ketone **16** in up to a 50% yield by a dilute hydrochloric acid or sodium bisulfite solution. Ketone **16** possessed a typical cyclopentanone ir absorption (49) at 1745 cm^{-1} with a shoulder at 1737 cm^{-1}; the latter was presumably due to Fermi interaction (50). The mass spectrum of **16** exhibited intense peaks at *m/e* 139 (M^+, 35%), 111 (**18**, 35%), and 83 (**19**, 100%) in addition to the $M + 1$ peak which is about $\frac{1}{3}$ intensity of M^+.

[4]We are grateful to Professor B. Waegell and Dr. R. Furstoss who have communicated to us the synthesis of the compound and have kindly supplied us with these spectra and specimens for comparisons.

Can. J. Chem. Downloaded from www.nrcresearchpress.com by 210.87.254.40 on 09/05/12
For personal use only.

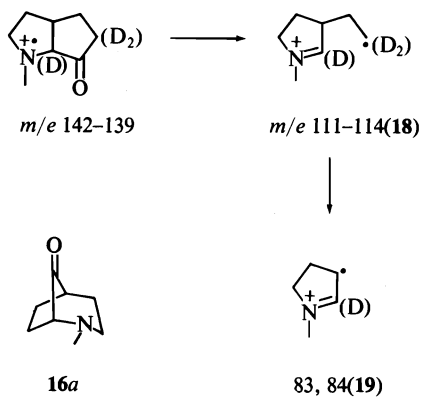

SCHEME 4

The fragments corresponding to these peaks were proposed as in Scheme 4. Under mild D_2O–pyridine exchange conditions (51), an average of 1.7 deuterium atoms was incorporated into ketone **16** as shown by the nmr integration curve. The mass spectrum of deuterated **16** displayed the molecular ion peaks at *m/e* 139(10%), 140(32%), 141(47%) and 142(12%).[5] The peak intensities at 111 ~ 114 mass units showed the same ratios as above and the peaks at *m/e* 84 mass units were 11% of that at 83. These data showed that at least 11 ~12% of ketone **16** had incorporated three deuterium atoms and eliminated structure **16***a* derived from the alternating cyclization pathway.

Oximes *E*-**17** and *Z*-**17** could be separated by silicic acid chromatography but *Z*-**17** isomerized slowly to *E*-**17** on storage as shown by nmr spectral examinations. Both compounds exhibited appropriate ir absorptions for the oxime group and Bohlmann bands. The nmr spectra showed a one proton doublet at τ 6.12 (J = 8 Hz) and a singlet at τ 7.32 (N—CH_3) for *Z*-**17**, and a one proton doublet at τ 6.90 (J = 8 Hz), superimposed on a diffused multiplet, and a singlet at τ 7.59 (N—CH_3) for *E*-**17**. Since the doublets were undoubtedly due to the C-1 protons in both isomers, the chemical shifts indicated the geometric isomerism (42) as assigned and the coupling constant suggested the *cis*-ring fusion.

Irradiation of *N*-nitroso-4-vinylpiperidine (**21**) built up a considerable amount of the *C*-nitroso dimer intermediate as indicated by the emergence of an intense peak at 290 nm. When photolysis was carried to completion, *i.e.* complete disappearance of the nitrosamine absorption, it gave *N*-nitrosohydroxylamino-(1-azabicyclo[2.2.1]heptane-7-yl)methane (**22**, 13%),[6] 7-formyl-1-azabicyclo[2.2.1]heptane oxime (**23**, 18%), *N*-(4-vinylpiperidino)formamide (**24**, 4%), and 4-vinylpiperidone oxime (**25**, 9%). In addition, a considerable amount of the basic material containing a vinyl group was found to be strongly adsorbed on the alumina column. This material appeared to be a mixture of polymers formed from the 1,2-dehydropiperidine which was derived from HNO elimination (52). The yield of oxime **23** was much increased at the cost of **22** when the photolysis was stopped before completion, indicating that the *C*-nitroso dimer was photolytically decomposed to **22**. In spite of careful searches, 3-quinuclidone oxime **26** was not found among the photolysis products as indicated by the absence of the characteristic singlet at τ 6.42 for the C-2 protons.

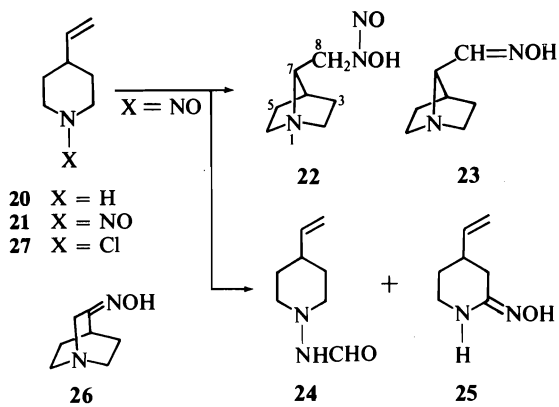

SCHEME 5

Formamide **24** and amidoxime **25** were formed by photoreduction and photoelimination processes similar to those observed with *N*-nitrosopiperidine and other nitrosamines, and the presence of a formamido group in the former and an amidoxime group in the latter were readily detected from their spectra by analogy to similar types of compounds (52). If there is no

[5]As the undeuterated **16** has the $M^+ + 1$ peak with $\frac{1}{3}$ the intensity of the M^+ peak, the observed percentages of the molecular ion peaks of the deuterated **16** were corrected with this factor to give the actual percentages of the molecular ions shown in parentheses. The details of the experiment and calculation are given in ref. 53.

[6]The percentage was calculated on the basis of 1 mol of **21** giving 1 mol of **22** though it was obvious that stoichiometrically 2 mol of **21** were required.

Can. J. Chem. Downloaded from www.nrcresearchpress.com by 210.87.254.40 on 09/05/12
For personal use only.

Can. J. Chem. Downloaded from www.nrcresearchpress.com by 210.87.254.40 on 09/05/12
For personal use only.

other facile reaction path, these two processes prevail in nitrosamine photolysis. Formation of amides such as **24** has been established (52) in the presence of a hydrogen donating solvent (methanol or ethanol). The presence of the vinyl group, as indicated by the appropriate absorption peaks in ir and nmr spectra, confirmed them as uncyclized products.

Hydroxylamine **22** was obtained by continuous liquid–liquid extraction of the aqueous basic solution. The compound exhibited ir absorptions at 2570, 1510, 1240, 945 and intense mass spectral peaks corresponding to elimination of OH (154), NO (141), H_2NO_2 (123), N_2O_2 (111), HN_2O_2 (110), and $CH_2N_2O_2H$ (96); these spectral patterns were similar to those found in the analogous compounds and typical of a *N*-nitrosohydroxylamino group (53, 54). In the nmr spectra of **22**, the two-proton multiplet at τ 5.70 and the one proton multiplet at τ 5.90 were assigned respectively to the C-8 and the C-7 protons that formed an ABX system; the patterns were complex, owing to the similar chemical shifts. The next lower signal centered at τ 6.57, equivalent in intensity to four protons, could be assigned to the C-2 and C-6 protons. The unusually low τ-values for protons geminal to an amine group had been observed in another hydroxylamine derivative (54), and suggested that **22** might be a zwitterion in which the amine group was protonated by the nearby weakly acidic *N*-nitrosohydroxylamino group.

Oxime **23** had the *E*-configuration as shown by the chemical shift of the aldoxime proton at τ 2.18 (doublet) (29) which was coupled with the C-7 bridge proton at 6.70 (J = 5 Hz). The latter signal was a doublet and each peak was slightly broadened by coupling (<0.5 Hz) with the triplet of the C-4 proton, as shown by decoupling experiments. The ir and nmr spectral patterns of oxime **23** were distinctly different from those of the alternative cyclization product **26** which was synthesized from 3-quinuclidone. The mass spectrum of **23** exhibited intense peaks at 123 (M − OH) and 69 (C_4H_7N). Observation of a metastable peak at 38.7 allowed us to formulate a straightforward fragmentation pattern as shown in Scheme 6.

In contrast to the above results, when *N*-chloro-4-vinylpiperidine (**27**) was treated with methanolic silver nitrate solution, no cyclization product was obtained and only the parent amine **20** was recovered.

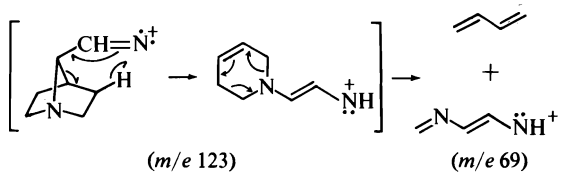

(*m/e* 123) (*m/e* 69)

SCHEME 6

Δ^{6,7}-Alkenyl Derivatives

For unknown reasons, nitrosation of *N*-methyl-2-(3′-cyclohexenyl)ethylamine (**28**) and *N*-methylcyclohex-3-enylamine (**33**, *vide infra*), under various conditions, always resulted in addition of the reagents across the double bond. Since neither chromatography nor distillation was effective for purification, the crude *N*-nitroso-*N*-methyl-2-(3′-cyclohexenyl)ethylamine (**29**, 78% purity) was photolysed under the usual conditions.

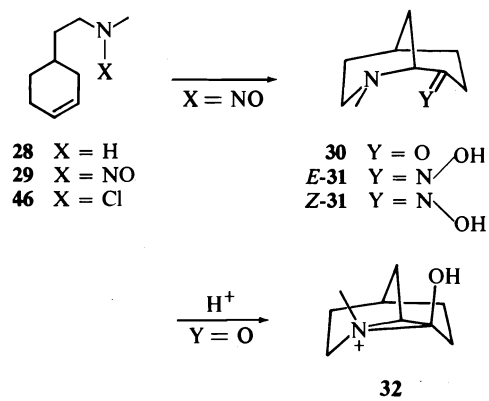

SCHEME 7

On chromatography, the photolysate yielded *N*-methyl-2-azabicyclo[3.3.1]nona-8-one (**30**, 6%) and its oximes *E*-**31** (16%) and *Z*-**31** (9%). Both our ketone **30** and that prepared by a different procedure by Waegell[4] exhibited the same nmr and ir (1710 cm^{-1}) spectra (48). The nmr spectrum showed few distinctive features in support of the assigned structure, other than a triplet at τ 7.13 (J = 4 Hz) which might be due to the C-1 proton. The picrate prepared from our ketone **30**, however, revealed OH absorptions at 3615 and 3345 cm^{-1} but no carbonyl absorption in its ir spectrum. As the elemental analysis agreed with the original molecular formula, it was suspected that protonation occurred at the carbonyl oxygen but not at the amine group as in **32**.

Can. J. Chem. Downloaded from www.nrcresearchpress.com by 210.87.254.40 on 09/05/12
For personal use only.

The assignment of the stereochemistry to the oxime pair was based on the chemical shifts of the multiplets due to the C-1 and the C-7 equatorial protons and the N—CH_3 singlet; the τ-values were 7.2, 6.75, and 7.75 for *E*-**31** and 6.4, 7.10, and 7.40 for *Z*-**31**. The assignments followed analogies to those 2-aminocyclohexanone oximes discussed previously (29). The occurrence of the strong mass-spectral peak at 96 in both oximes as well as ketone **30** could be interpreted as the presence of a piperidine moiety (as opposed to azepine) (33) in these compounds on the basis of fragmentation patterns suggested in Scheme 8. This evidence must be accepted with caution since examples of a skeletal rearrangement of azapolycyclic compounds on electron impact has been reported (26).

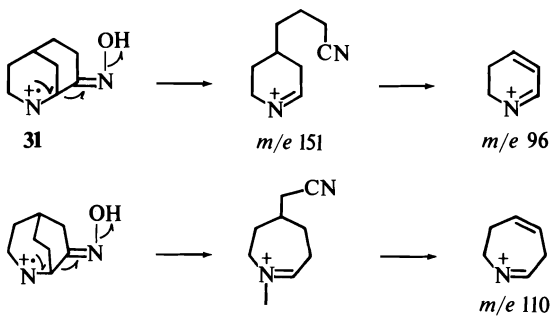

SCHEME 8

$\Delta^{4,5}$-*Alkenyl Derivatives*

Photolysis of *N*-nitroso-*N*-methylcyclohex-3-enylamine (**34**, *ca.* 75% of the olefinic bond remaining intact) and *N*-nitroso-*N*-methyl-(2-cyclopentenyl)methylamine (**42**) in either acidic methanol or in acetic acid containing hydrochloric acid gave complex mixtures of basic fractions from which no cyclized product could be isolated on chromatography. In the latter case, chromatography was complicated by high polarity and volatility of the products causing a low recovery of the material. Since most of the chromatographic fractions exhibited nmr olefinic signals and/or no N—CH_3 singlet, detailed investigations were not carried out except that the parent amines **33** (30%) and **41** (16%) were identified. In the neutral fractions of the photolysates, the presence of 3-cyclohexenone (1720 cm^{-1}) in the former case and that of 2-cyclopentenone oxime (τ 3.85 and 4.20) in the latter case were indicated by their ir and nmr spectra. The former were isolated as a mixture of 2,4-DNPH derivatives of cyclohexenones.

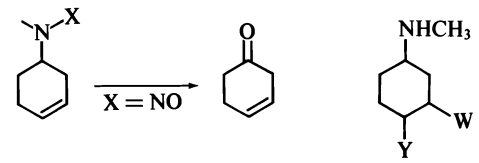

33 X = H
34 X = NO
36 X = Cl

35

37 Y = W = Cl
38 Y = OAc, W = Cl
39 Y = Cl, W = OAc
40 Y = OH, W = Cl

SCHEME 9

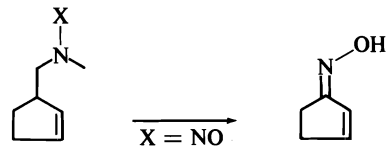

41 X = H
42 X = NO

43

SCHEME 10

Treatment of the corresponding chloramine **36** with ferrous/ferric ion couple in aqueous acetic acid (23, 31) gave a complex mixture which contained the parent amine **33** (30%), dichloramine **37** (23%), chloracetoxylamines **38** and **39** (39% total), and a hydroxychloramine **40** (5%) as indicated by gc–ms analysis. The analysis also indicated that there were more than 10 minor products (each <3%) in the mixture. Chromatography of the mixture gave **37**, **38**, and **39** in a semi-pure state and their structures were deduced from the spectral data as described later. The structures of **38** and **39** were tentatively assigned by noting that the *N*-methyl group will cause a greater downfield chemical shift of the C-3 than the C-4 methine proton (55). The low field multiplets of **37**, **38**, and **39** all exhibited large coupling constants (~10 Hz) suggesting a *trans*-configuration of the addition products.

Discussion

Intramolecular addition of an aminium radical to a suitably located olefinic bond within the molecular framework is, as described above, very much dependent on the position of the olefin. The photolytically initiated ring closures of $\Delta^{5,6}$-alkenylnitrosamines **2**, **9**, **15**, and **21** are no doubt the most efficient cases, followed by $\Delta^{6,7}$-**29** and $\Delta^{4,5}$-alkenylnitrosamines (**34** and **42**) in that order. Although product recovery in the photolysis of nitrosamine **42** was too low to be

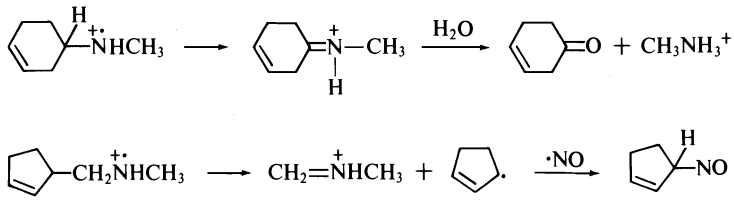

SCHEME 11

very decisive, the complexity of the products in this case as well as in that of **34**, appears to indicate that the corresponding aminium radicals have undergone different pathways, *e.g.*, β-scission of a C—H or C—C bond (elimination pathway) and hydrogen abstraction (52). Isolation of cyclohexenone and 2-cyclopentenone oxime in the present cases and also the isolation of benzaldehyde oxime in the photolysis of *N*-nitroso-*N*-methylphenethylamine (52) suggest the occurrence of the elimination pathway (Scheme 11).

The efficiency of ring closure for the $\Delta^{5,6}$-alkenylaminium radical, in contrast to those for its immediate homologues, is in good agreement with the behaviour of other radicals (see Table 1). For the $\Delta^{5,6}$-alkenylnitrosamines cyclization is regiospecific, giving pyrrolidine derivatives exclusively, though the yields vary depending on other factors such as steric strain and steric hindrance in the transition state of cyclization. Kinetically controlled radical cyclization implies that the transition state is reached at an early stage in the reaction coordinate, *i.e.* the structure of the transition state must be very similar to that of the starting material (56). This means that the bond formation step is controlled by the incipient conformation associated with overlap between *p*-orbitals of the aminium radical and the olefinic bond. In a $\Delta^{5,6}$-alkenylaminium radical the five-membered ring closure would be easier than the six-membered ring closure since molecular models suggest that the maximum overlap in the former requires less conformational energy and entropy loss in the transition state than in the latter. The aminium radical derived from **15**, having fewer degrees of freedom, falls into the cyclization pattern more readily than those from **2** and **9**. The aminium radicals from **9** require a certain amount of conformational energy to assume the axial orientation of the radical side chain; this leads to a lesser degree of cyclization.

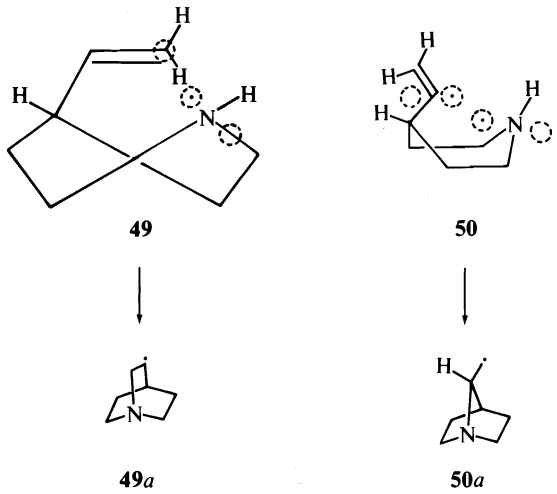

SCHEME 12

That *p*-orbital overlap influences these radical cyclizations can be seen clearly in the formation of five-membered cyclization products **22** and **23** in the photolysis of nitrosamine **21**. If it is assumed that the transition states of these radical cyclizations resemble the products more than the starting aminium radicals (*i.e.*, the C—N bond formation has progressed considerably at the transition state), product stability will be the dominant factor determining the mode of cyclization. That is, the six-membered ring closure is clearly much more favored than the five-membered one, since secondary C-radical **49***a* from the former pathway is more stable than primary C-radical **50***a* from the latter; also, while the six-membered process can twist the bicyclo[2.2.2] system **49***a* to avoid the nonbonded interactions, the five-membered [2.2.1] system **50***a* demands higher strain and eclipsing energies. Inspection of stereomodels clearly shows that the constraints of molecular geometry permit the required *p*-orbital overlap to occur in the five-membered ring closure as in **50** whereas in the alternative six-membered ring

Can. J. Chem. Downloaded from www.nrcresearchpress.com by 210.87.254.40 on 09/05/12
For personal use only.

Can. J. Chem. Downloaded from www.nrcresearchpress.com by 210.87.254.40 on 09/05/12
For personal use only.

closure the corresponding *p*-orbitals are in a nearly orthogonal arrangement (see **49**). The failure to isolate quinuclidone oxime **26** indicates that the *p*-orbital overlap requirements, but not the product stability requirements, control the transition state that allows the exclusive formation of bicyclo[2.2.1] derivatives **22** and **23**. The yields are, however, necessarily lower because of the higher conformational energy requirements; as a result, some competitive photoreduction and photoelimination (52) occur as the side reactions. The six-membered cyclization to form chloroazatwistane **52** in the photolysis of the corresponding $\Delta^{5,6}$-alkenyl chloramine **51** (57) is the only reported exception at present; this case provides further insight to the *p*-orbital overlap theory discussed above. As indicated by model examinations, *p*-orbital overlap in the five-membered cyclization of the corresponding $\Delta^{5,6}$-alkenylaminium radical entails several major non-bonded interactions in the transition state, *e.g.* those of the eclipsing, bowsprit-flagpole, and 1,3-diaxial types. When the ring system of the aminium radical is twisted, these non-bonded interactions are eliminated by staggering of the C—H bonds and the *p*-orbitals for six-membered cyclization are aligned in closer proximity than in the case of five-membered cyclization. It is clear that *p*-orbital overlap controls the reaction path which results in the formation of azatwistane **52** instead of giving a five-membered ring compound.

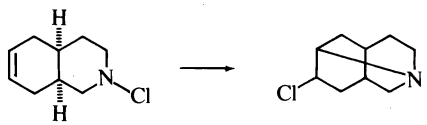

51 **52**

On the basis of similar arguments, in the cyclization of $\Delta^{6,7}$-alkenylnitrosamine **29**, the entropy gains associated with the six-membered ring closure might be higher than with the seven-membered ring closure though obviously such gains are not high enough to make the cyclization pathway overwhelmingly facile. Examinations of molecular models also show that cyclizations in the $\Delta^{4,5}$-alkenyl aminium radical derived from **34** and **42** require much higher conformational energies for *p*-orbital overlap. Consequently, other lower energy pathways, such as β-scission and hydrogen abstraction, dominate the photolysis of nitrosamines **29**, **34**, and **42**.

Finally, it is noteworthy that the alkenylaminium radicals derived from nitrosamines **9** and **15** exclusively undergo intramolecular addition to give bicyclic products **10**, **11**, **16**, and **17**, without any trace of the products arising from the intramolecular δ-hydrogen abstraction (the Hofmann–Löffler reaction pathway). In these cases, the stereochemical requirements for hydrogen abstraction are probably about the same as those for the addition process. In particular, hydrogen abstraction is expected to be relatively facile in the alkenylaminium radical derived from **9**, since it involves the allylic hydrogen of the 5′-position. The absence of such processes is in good agreement with the tendency of aminium radicals to add to an olefin in preference to abstracting an allylic hydrogen in intermolecular reactions (28).

Azapolycyclic syntheses utilizing chloramine cyclization are found to be generally less satisfactory than those utilizing nitrosamine cyclization. Free radical initiated reaction of alkenyl chloramine **5** or ferrous–ferric ion catalysed decomposition of **36**, both in acidic conditions, undergo ionic addition pathways and fail to give any cyclization product. Obviously these alkenylchloramines, instead of generating an aminium radical or a metal coordinated amine radical, decompose more readily to give a chlorinating agent. Titanium ion catalysed decomposition of $\Delta^{5,6}$-alkenyl chloramines, such as the *N*-isopropyl analogues of **5** and **44**, have been shown by Surzur's group to give satisfactory yields of cyclization products (23, 24). These authors have suggested that such a process involves a metal ion complexing with both the amine radical as well as with the olefinic bond as the reactive intermediate facilitating ring formation. This may well be the case since *N*-chloro-*N*-methylbut-3-enylamine is decomposed by titanous chloride to give 13% of *N*-methyl-3-chloropyrrolidine (58) whereas cyclizations of $\Delta^{4,5}$-alkenylaminium radical from **34** and **42** have not been successful. Minisci *et al.* have also suggested a similar ferric ion complex to explain the *cis*-addition of *N*-chloropiperidine to cyclohexene (31).

The reactive intermediate of silver ion catalysed alkenyl chloramine decomposition is more likely to involve an amine radical (25, 26) rather than a nitrenium ion (32), and the yields of hetero-

Can. J. Chem. Downloaded from www.nrcresearchpress.com by 210.87.254.40 on 09/05/12
For personal use only.

cycles from $\Delta^{5,6}$-alkenyl chloramines such as **44** and **45** have been reported to be good (26, 32). However, the method suffers from the disadvantage of producing a mixture of pyrrolidine and piperidine derivatives, as have also been observed in the cyclization of **5**. The failure of chloramine **27** to cyclize by silver ion catalysis may reflect the inability of the reactive intermediate to surmount the conformational energy requirements (*vide supra*). A similar treatment of $\Delta^{4,5}$-alkenyl chloramine **36** results in recovery of the parent amine, but solvolysis of $\Delta^{6,7}$-alkenyl chloramine **46** has been reported to result in cyclization to the corresponding piperidine derivative (32).

In conclusion, aminium radicals are useful reactive intermediates for the synthesis of azapolycyclic compounds, and they can be easily generated under mild conditions. Their addition reactions to internal olefinic bonds are highly regiospecific, as in the Hofmann–Löffler reaction.

Experimental

Unless stated otherwise, the following procedures were used. Melting points (mp) were determined on a Fisher–Johns or a Gallenkamp apparatus and were uncorrected. The ir spectra were recorded with a Perkin-Elmer 457 spectrophotometer as liquid films or Nujol mulls, uv spectra with a Unicam SP 800 spectrophotometer, mass spectra (ms) and high resolution mass spectra (hrms) with a Hitachi–Perkin-Elmer RMU-6E instrument at 80 eV (intensity was given as a percentage of the most intense peak), and nmr spectra with a Varian A56/60 or XL-100 spectrophotometer in $CDCl_3$ using TMS as an internal standard. Decouplings were done on the XL-100. Elemental analyses were obtained on a Perkin-Elmer 240 Microanalyzer by M. K. Yang, gas chromatography on a Varian 1200 (flame ionization detector, Disc Chart Integrator 244, uncorrected for individual response factors) with a 20% SE-30 (10 ft × $\frac{1}{8}$ in.) column. The gas chromatographic – mass spectra (gc–ms) used the same column in a Varian 1400 which was directly coupled to the mass spectrometer.

Materials

The starting materials commercially available from Aldrich Chemical Co., Milwaukee, were 4-pentenol, cyclohex-3-ene carboxylic acid, cyclopent-2-ene acetic acid, 2-(4′-piperidinyl)ethanol, and 4-vinylcyclohexene. Column chromatography was performed on Brockmann alumina or Mallinckrodt silicic acid unless specified otherwise, and thin layer chromatography (tlc) on alumina or silica gel plates. Organic solvents were distilled and stored over molecular sieves or sodium. For extraction, unpurified organic solvents were used. The combined organic layers were dried over anhydrous magnesium sulfate, filtered, and the solvent evaporated under reduced pressure using a rotary evaporator.

Nitrosation and Chlorination of Amines

N-Nitrosamines were prepared following standard procedures using sodium nitrite (36) or N_2O_4 (37). Better results were obtained using only a minimal excess of nitrosating agent and by adding the solution of N_2O_4 to the amine solution (rather than inverse procedure) in the latter cases (36). *N*-Chloramine was prepared using NaOCl (Purex bleach) as in the published procedures (26, 33). The crude samples of *N*-chloramines were analysed with iodimetry (26) which was also used to follow the decomposition of chloramines.

Photolyses

Generally the procedures previously described (nitrogen atmosphere, 200 W Hanovia lamp, Nonex filter) were utilized (29). The photolysate was worked-up in the usual manner to yield neutral and basic material (42). The percentage yields were normally estimated from column chromatography and based on reacted nitrosamine.

Preparation of Alkenylamines

N-Methylpent-4-enylamine (1)

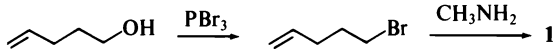

A mixture of 4-pentenol (10 g) and pyridine (2.5 g) was added to phosphorus tribromide (12.5 g) in 15 min at −5 °C. This mixture was distilled after 1 h to give a crude oil which was redistilled to afford 4-pentenyl bromide (9.19 g): bp 29–32 °C/12 torr; ir 3100, 1650, 1000, and 925 cm^{-1}.

A solution of the bromide (26 g) and methylamine (27 g) in ether (100 ml) was placed in a sealed glass tube and was heated for 40 h in a water bath. The basic fraction (16.3 g) was nearly pure *N*-methyl-4-pentenylamine (**1**); ir 3250, 3025, 1630, 1120, 1000, and 920 cm^{-1}; nmr τ 4.25 (m, 1H), 5.05 (m, 2H), 7.40 (t, J = 6.5 Hz, 2H), 7.55 (s, 3H).

N-Methyl-(3-cyclohexenyl)methylamine (8)

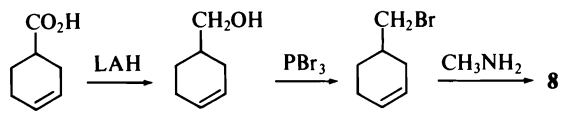

3-Cyclohexene-1-carboxylic acid (20 g) was reduced with lithium aluminum hydride (13 g) in refluxing ether for 5 h to give cyclohexen-3-ylmethyl alcohol (15.3 g); bp 90.5 °C/10 torr.

A mixture of the alcohol (15.3 g), phosphorus bromide (14.6 g), and pyridine (2.85 g) was heated under 15 torr vacuum to distill until the white fumes appeared. The collected oil was redistilled to give cyclohex-3-enylmethyl bromide (13.9 g): bp 79.5–82.5 °C/12 torr.

The bromide (10.9 g), methylamine (15.0 g), and ether (100 ml) were placed in a steel bomb. The mixture was heated at 80 °C for 72 h and was worked-up in the usual manner to give a basic fraction which was distilled to give amine **8** (8.2 g): bp 60 °C/8 torr; 3300, 3025, 1650, 1135, and 655 cm^{-1}; nmr τ 4.34 (m, $W_{1/2}$ = 4 Hz, 2H), 7.5 (d, J = 6 Hz, 2H), 7.57 (s, 3H), 7.6–8.7 (m, 7H), 8.66 (s, D_2O exchangeable, 1H).

Can. J. Chem. Downloaded from www.nrcresearchpress.com by 210.87.254.40 on 09/05/12
For personal use only.

N-Methyl-2 (cyclopent-2'-enyl)ethylamine ***(14)***

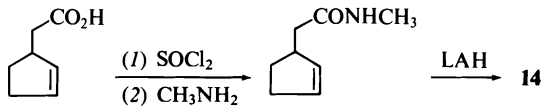

14

2-Cyclopentene-1-acetic acid (10 g, 0.079 mol) dissolved in freshly distilled thionyl chloride (25 ml) and pyridine (1 ml) was left at room temperature for 12 h. The excess thionyl chloride was distilled. The residue was taken up in benzene (150 ml) and methylamine gas was bubbled through the solution until basic to litmus (*ca.* 2–3 h). The solution was filtered and evaporated to give a residue which was distilled under reduced pressure to give *N*-methyl-1-(cyclopent-2'-enyl)acetamide (6.0 g, 54%): bp 125–126 °C/0.8 torr; ir 3300, 3050, 2940, 2850, 1640, 1555, 720 cm^{-1}; nmr τ 3.3 (D_2O exchangeable, 1H), 4.31 (s, $W_{1/2}$ = 3 Hz, 2H), 6.9 (m, 1H), 7.22 (s, $W_{1/2}$ = 4 Hz, 3H, sharpened on D_2O exchange), 7.45–8.9 (m, 6H); ms (%) 139(M^+, 24), 138(11), 107(11), 81(35), 79(20), 73(100), 67(54), 58(49), 41(22).

The amide (10.65 g, 0.077 mol) in ether (150 ml) was added to LAH (4.8 g, 0.12 mol) in ether (150 ml) and was stirred at 25 °C for 28 h. After decomposition of the reaction mixture with 3 *N* sodium hydroxide, the ether was decanted. The solid was washed several times with ether. The combined ether solutions were used for the subsequent experiments.

4-Vinylpiperidine ***(20)***

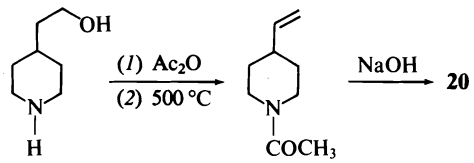

20

2-(Piperidin-4'-yl)ethyl alcohol (10 g, 77.5 mmol) was acetylated overnight in pyridine (10 ml) and excess acetic anhydride (30 ml) at room temperature to give 4-(2'-acetoxyethyl)-*N*-acetylpiperidine: bp 151–152 °C/1 torr); ir 1733, 1640, and 1240 cm^{-1}; nmr τ 5.52 (d, J = 13 Hz, 1H), 5.96 (t, J = 6 Hz, 2H), 6.17 (d, J = 12 Hz, 1H), 6.94 (t, J = 12 Hz, 1H), 7.50 (t, J = 12 Hz, 1H), 7.90 (s, 6H).

The above diacetyl compound was introduced dropwise to a fractional distillation apparatus equipped with a heated Vigreaux column (25 cm). The flask was heated with a Woods metal bath to 500 °C and the column maintained at 450 °C. Nitrogen was used to purge the system as well as to sweep the product out of the apparatus. The dark brown distillate was taken up in methylene chloride solution (100 ml), washed with saturated sodium bicarbonate solution, and then water. The organic layer was separated, dried, and evaporated to give a light brown liquid, which was distilled at 125–135 °C/125 torr to give crude 4-vinyl-*N*-acetylpiperidine: bp 133 °C/13.5 torr; ir 3010, 1640, 1225, 990, and 910 cm^{-1}; nmr τ 4.2–5.2 (m, 2H), 5.50 (br d, 1H), 7.65 (br t, J = 12 Hz, 1H), 7.25 (m, 1H). The residual liquid was recycled to give more of the vinyl compound. The combined yield was 5.61 g corresponding to 47% yield from the starting alcohol.

The *N*-acetyl compound obtained above was hydrolyzed with hot 10% sodium hydroxide solution (25 ml) under a nitrogen atmosphere for 24 h. The hydrolysate was worked-up in the usual manner to afford 4-vinylpiperidine (3.3 g); bp 134–135 °C/14.5 torr; ir 2960, 2800, 1642, 995, and 915 cm^{-1}; nmr τ 4.2–5.2 (m, 3H), 6.70–7.40 (m, 4H), 6.56 (br, 1H, D_2O exchangeable).

N-Methyl-2-(cyclohex-3'-enyl)ethylamine ***(28)***

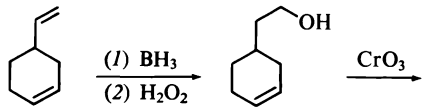

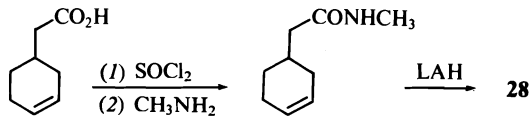

28

Hydroboration and oxidation of 4-vinylcyclohexene (60) resulted in a 63% yield of 2-(cyclohex-3'-enyl)-ethanol. To the primary alcohol (5 g, 0.04 mol) in acetone (100 ml) was added Jones reagent (15 ml, CrO_3 2.65 *M*) dropwise and it was stirred for 0.5 h at 0 °C. After filtration and evaporation, the residue was stirred with sodium hydroxide solution (*ca.* 100 ml) for 1 h. The solution was acidified with hydrochloric acid and extracted with methylene chloride to yield 3-cyclohexene-1-acetic acid (2.82 g, 51%): ir 3200, 3025, 2920, 2860, 1705, 1650 (sh), 655 (m) cm^{-1}; nmr τ 0.28 (D_2O exchangeable, 1H), 4.82 (s, $W_{1/2}$ = 4.5 Hz, 2H), 7.5–8.8 (9H, m); ms (%), 140(M^+, 9), 122(13), 80(100), 41(25), 39(33). An Arndt–Eistert sequence (61), starting from cyclohexene-1-carboxylic acid, gave the above acid in 15% yield.

3-Cyclohexene-1-acetic acid (15.07 g) was reacted with thionyl chloride, then with methylamine gas as above for **14**, and the product chromatographed through neutral alumina to yield *N*-methyl-3-cyclohexene-1-acetamide (7.75 g, 47%): mp 46–50 °C; ir 3300 (b), 3080, 3020 (m), 2920, 2850, 1640, 1550, 650 (m) cm^{-1}; nmr τ 2.8 (D_2O exchangeable, 1H), 4.37 (s, $W_{1/2}$ = 4.5 Hz, 2H), 7.25 (d, J = 5 Hz, collapses to s on D_2O exchange, 3H), 7.6–9.1 (9H, m); ms (%) 153(M^+, 9), 74(14), 73(100), 58(21), 45(9).

The methylamide (3.3 g, 0.022 mol) was stirred for 40 h with LAH (4 g, 0.1 mol) in ether (200 ml) and worked-up as described previously to yield *N*-methyl-2-(cyclohex-3'-enyl)ethylamine (**28**, 2.5 g, 83%): ir 3300, 3020 (m), 2920, 2850, 2790, 1650 (w), 1450, 655 (m) cm^{-1}; nmr τ 4.37 (s, $W_{1/2}$ = 4 Hz, 2H), 7.4 (t of d, J = 7 and 2 Hz, 2H), 7.58 (s, 3H), 7.94 (D_2O exchangeable, 1H), 7.7–9.2 (9H, m).

N-Methylcyclohex-3-enylamine ***(33)***

The acylchloride of 3-cyclohexene-1-carboxylic acid (15.0 g, 0.12 mol) was prepared as usual and dissolved in benzene (200 ml). The benzene solution was slowly added to an aqueous solution (40 ml) containing sodium azide (16 g, 0.2 mol), keeping the temperature lower than 5 °C. After 4 h stirring at 0 °C, the layers were separated and the aqueous solution extracted with benzene. The combined benzene solutions were dried (0 °C, $MgSO_4$), then refluxed for 40 h. A solution of sodium bis(2-methoxyethoxy)aluminium hydride (Red-Al®, 60 ml, 60 g, 0.2

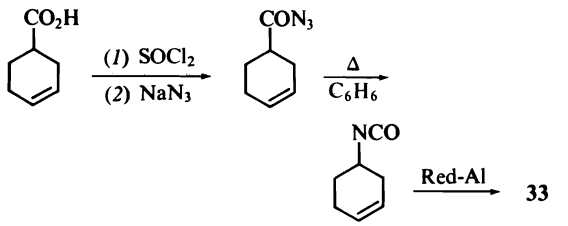

mol)[7] in benzene (60 ml) was added to the above benzene solution. After 12 h refluxing, the excess hydride was decomposed with water. The benzene solution was extracted several times with dilute hydrochloric acid solution, then the acidic solutions were basified and re-extracted with ether. The ether extracts were dried and evaporated using a Vigreaux column to yield methylamine **33** (7.36 g, 55% overall): ir 3300, 3030 (m), 2920, 2840, 2790, 1650 (w), 1440, 655 (m) cm^{-1}; nmr τ 4.34 (2H, s, $W_{1/2}$ = 5 Hz), 7.1–7.4 (m, 1H), 7.3 (s, D_2O exchangeable, 1H), 7.53 (s, 3H), 7.55–8.9 (m, 6H); ms (%), 111(M^+, 23), 85(25), 83(35), 70(20), 57(100).

N-Methylcyclopent-2-enylmethylamine (41)

The Curtius rearrangement sequence starting from 2-cyclopentene-1-acetic acid (5.0 g) was carried out as described above and the resulting isocyanate was reduced with Red-Al® to yield methylamine **41** (3.0 g, 65%): ir 3300, 3050 (m), 2930, 2850, 1640 (w), 720 (m) cm^{-1}, nmr τ 4.43 (s, $W_{1/2}$ = 4 Hz, 2H), 6.7 (D_2O exchangeable, 1H), 7.77 (s, 3H), 7.4–8.7 (m, 7H).

Preparation and Photolysis of Nitrosamines

N-Nitroso-N-methylpent-4-enylamine (2)

To a cold solution of amine (8.0 g) in 3 *N* hydrochloric acid (34 ml), a sodium nitrite (11 g) solution in water (15 ml) was added dropwise. The mixture was left in a refrigerator overnight. The basified solution was extracted with methylene chloride and the methylene chloride solution was washed with water, dried, and evaporated. The residue was distilled to afford nitrosamine **2** (7.2 g); bp 104–108 °C/9 torr; ir 3080, 1635, 1430, 1035, 990, and 910 cm^{-1}; nmr τ 4.3 (m, 1H), 5.00 (m, 2H), 5.85 (t, J = 7 Hz), 6.40 (J = 7 Hz), 6.25 (s) and 6.95 (s). The ratio of the last two methyl signals was *ca.* 1:3.

The nitrosamine (1.01 g) and concentrated hydrochloric acid (0.71 ml) in methanol (200 ml) were photolysed as described before (29) and were worked-up to give neutral (88 mg) and basic (825 mg) fractions. The neutral fraction was the starting nitrosamine as shown by the identical ir spectrum. The basic fraction showed nmr signals at τ 2.75 (d, J = 7.5 Hz) and 7.67 (s) for the major *anti*-aldoxime and at 3.25 (d, J = 6 Hz) and 7.53 (s) for the minor *syn*-aldoxime. This was recrystallized from petroleum ether many times to afford the *anti*-aldoxime of 2-formyl-1-methylpyrrolidine (*E*-**3**); mp 63–64 °C; ir 3175, 1680, 1500, 1200, 955, 925, and 850; nmr τ 2.75 (d, J = 7.5 Hz, 1H), 7.0 (m, 3H), 7.65 (s, 3H), 8.1 (m); ms 128.0944 (M^+ calcd. for $C_{16}H_{12}N_2O$: 128.0950), 91, and 85.

By recrystallization or silicic acid chromatography, the *syn*-aldoxime *Z*-**3** was obtained as impure fractions contaminated by *E*-**3**. This sample showed strong nmr signals at 3.25 (d) and 7.53 (s) and weak signals at 2.75 (d) and 7.67 (s). The intensity of the latter set increased at the cost of the former set when the spectra were retaken after each 24 h interval. A mixture of *E*-**3** and *Z*-**3** (380 mg) and *p*-toluenesulfonyl chloride (590 mg) were dissolved in pyridine (1 ml). The mixture was diluted with water (10 ml) and was made basic. The crude oil (307 mg) obtained from ether extractions was refluxed in triethylamine (2 ml). Evaporation of triethylamine and extraction with methylene chloride followed by the usual work-up afforded a crude oil (198 mg): ir 2240 and 1220 cm^{-1}. Treatment of this oil with picric acid in benzene gave the picrate of 1-methyl-2-cyanopyrrolidine; mp 137–141 °C (lit. (45) mp 135–140 °C).

N-Nitroso-N-methylcyclohex-3-enylmethylamine (9)

Amine **8** (5.0 g) was nitrosated with sodium nitrite (15 g) and the crude product was chromatographed through alumina to give nitrosamine **9** (4.9 g, 88%): ir 3025 (m), 2920, 2840, 1630 (w), 1430, 1345, 1325, 1155, 1030, 650 (m), nmr τ 4.25 (s, $W_{1/2}$ = 4.5 Hz, 2H), 5.89 (d, J = 8 Hz, 1.36H), 6.16 (s, 0.66H), 6.40 (d, J = 8 Hz, 0.44H), 6.91 (s, 2.34H), 7.7–8.9 (m, 7H); ms (%), 154(M^+, 1), 137(51), 94(28), 81(81), 79(72), 74(64), 53(34), 44(100), 42(57); uv (in MeOH–HCl) 345 nm (ϵ, 105). Nitrosamine **9** exists as 78% *E*-isomer.

Nitrosamine **9** (0.75 g, 5 mmol) in methanol (220 ml) was photolyzed for 3.5 h without any acid; the uv absorption at 340 nm showed no decrease. Addition of concentrated hydrochloric acid (0.08 ml, 1 mmol), followed by irradiation for an additional 2 h caused *ca.* 10% decrease in uv absorption. Following a normal work-up procedure, nitrosamine **9** (0.66 g, 89%) was recovered.

Photolysis of nitrosamine **9** (2.0 g) in methanol (200 ml) containing hydrochloric acid (20 mmol) for 75 min gave a neutral fraction (0.1 g, nitrosamine **9**) and a basic fraction (1.61 g). The basic material was chromatographed on silicic acid to give, as the first eluted compound, *N*-methyl-2-keto-7-azabicyclo[3.2.1]octane (**10**, 0.19 g, 11%): ir 2940, 2870, 2770, 1710, 1450, 1200 cm^{-1}; nmr τ 6.69 (dd, J = 9.5 and 6 Hz, 1H), 6.76 (dd, J = 5.5 and 1 Hz, 1H), 7.4 (m, 1H), 7.55 (s, 3H), 7.6–8.6 (m, 7H); ms (%) 139(M^+, 25), 111(23), 83(23), 82(100), 67(7), 55(7), 42(39). The spectra were identical to those of an authentic sample provided by Professor B. Waegell (48).[4]

Further elution with 10% methanol in chloroform gave a solid which was recrystallized from petroleum ether to give oxime *E*-**11** (752 mg): mp 95–97 °C; ir 3200, 3050, 2780, 1640, 1440, 1200, 950, and 900 cm^{-1}; nmr τ 6.48 (br d, J = 5.5 Hz, 1H), 6.8 (m, 1H), 7.64 (s, 3H); ms (%) 154 (M^+) and 137: the HCl salt mp 205 °C (dec.). Elution with 15% MeOH–$CHCl_3$ gave an oil (158 mg) containing a higher proportion of oxime *Z*-**11**; the nmr spectra showed the signals at τ 5.44 (d, J = 5.5 Hz) and 7.59 (s) in addition to the corresponding signals of *E*-**11**. The ratio of the oximes was estimated by the *N*-methyl nmr signals, which gave the yields of 37% and 13% for *E*-**11** and *Z*-**11** respectively.

A mixture of *E*-**11** and *Z*-**11** (0.17 g) and sodium bisulfite (0.4 g) in 50% aqueous ethanol (5 ml) was heated for 5 h (46), evaporated, and the aqueous residue acidified with 1 *N* hydrochloric acid to p*H* 2. The solution, after being made basic, was extracted with chloroform

[7]Supplied by Aldrich Chemical Co. Inc., as 70% solution in benzene.

Can. J. Chem. Downloaded from www.nrcresearchpress.com by 210.87.254.40 on 09/05/12
For personal use only.

Can. J. Chem. Downloaded from www.nrcresearchpress.com by 210.87.254.40 on 09/05/12
For personal use only.

which was evaporated to afford a residue (80 mg). The oil was chromatographed on silicic acid from which amino ketone **10** was obtained with 2% methanol in chloroform.

A mixture of oximes *E*-**11** and *Z*-**11** (0.14 g, *ca.* 1:1 ratio) were refluxed for 3 h in 2 *N* NaOH (10 ml) with $NaBH_4$ (0.4 g) (47). Extraction with methylene chloride and evaporation gave a mixture of epimeric alcohols **12** and **13** (0.02 g, 15%, *ca.* 1:1 ratio): ir 3400, 2940, 2860, 1455, 1080, 1010 cm^{-1}; nmr τ 6.1 (m), 6.55 (m), 7.52 (s). These alcohols had a high vapor pressure and co-distilled with solvents, and were identified by tlc and vpc comparisons with alcohols **12** and **13** obtained by another method (10, 56).

*N-Nitroso-N-methyl-2-(cyclopent-2-enyl)ethylamine (**15**)*

The combined ether solutions containing amine **14** were stirred with 2 *N* hydrochloric acid solution at 0 °C. To this sodium nitrite (12 g, 0.16 mol) was added portionwise over 1 h and the mixture stirred for 5 h. The ether layer was evaporated to give an oil which was chromatographed through silicic acid to yield nitrosamine **15** (4.52 g, 38% yield based on the amide): ir 3040, 2920, 2840, 1620 (w), 1430, 1330, 1280, 1030, 720 cm^{-1}; nmr τ 4.40 (s, $W_{1/2}$ = 3.5 Hz, 2H), 5.90 (t, J = 7 Hz, 1.56H), 6.34 (s, 0.66H), 6.45 (t, J = 7 Hz, 0.44H), 7.08 (s, 2.44H), 7.2–8.8 (m, 7H); uv (in HCl–MeOH) 345 nm (ϵ, 95). Nitrosamine **15** exists 75% in the *E*-isomer.

In a typical photolysis, nitrosamine **15** (2.31 g, 0.015 mol) in methanol (200 ml) containing hydrochloric acid (1.5 ml, 0.018 mol) was irradiated for 3.5 h under the conditions previously described. The normal work-up gave neutral material (0.2 g, identical ir and nmr spectra to **15**) and basic material (1.96 g).

A portion of the crude basic material (0.87 g) was refluxed for 2 h with 5 *N* hydrochloric acid (20 ml), then the solution was basified and extracted with methylene chloride to yield amino ketone **16** (0.39 g, 50%): ir 2930, 2840, 2780, 1745, 1737 (sh), 1450 cm^{-1}; nmr τ 6.7–7.1 (m, 2H), 7.45 (d, J = 7 Hz, 1H), 7.53 (s, 3H), 7.5–8.7 (m, 7H); ms 140(M + 1, 12), 139(M^+, 35), 111(35), 83(100), 82(75), 42(45); picrate mp 132–135 °C (unstable in hot EtOH). Other methods of converting oximes to ketones using reagents such as cerium salts (62), sodium nitrite (63), and zinc metal (64) were found to be less successful. Hydrolysis by the sodium bisulfite method (46) gave a 45% yield when reacted with a mixture of *E*-**17** and *Z*-**17** oximes (1:1). Amino ketone **16** (0.21 g) was hydrogenated in dilute aqueous hydrochloric acid with PtO_2 catalyst and gave a mixture of epimeric alcohols (0.13 g): ir 3300, 2945, 2860, 1020 cm^{-1}; nmr τ 7.63 and 7.69 (singlets of equal intensity). Jones oxidation of the alcohol mixture gave back ketone **16**.

A crude basic fraction (1.60 g) was chromatographed on silicic acid (60 g) to elute first with 0–10% MeOH–CH_2Cl_2 amino ketone **16** (3%). Elution with 20% MeOH–CH_2Cl_2 gave an oil which was distilled to afford oxime *E*-**17** (0.46 g): ir 3350, 3100, 2940, 2870, 2830, 2780, 1660 (w), 1450, 1050, 950, 875; nmr τ 1.5 (1H, D_2O exchangeable), 6.9 (br d, J = 8 Hz, 2H), 7.59 (s, 3H), 7.2–8.6 (m, 8H); ms (%) 154(M^+, 7), 137(100), 96(91), 94(20), 83(48), 82(38), 67(11), 42(45), 41(22). *Anal.* calcd. for $C_8H_{14}N_2O$: C 62.30, H 9.15, N 18.17; found: C 62.18, H 9.23, N 18.35.

Following the elution of a 1:1 mixture of oximes (0.12 g), elution with 20–50% MeOH–CH_2Cl_2 gave oxime *Z*-**17** (0.26 g): ir 2250, 3100, 2940, 2870, 2830, 2780, 1650 (w), 1450, 1050, 945, 930 cm^{-1}; nmr τ 1.7 (D_2O exchangeable, 1H), 6.12 (br d, J = 8 Hz, 1H), 7.0 (m, 2H), 7.32 (s, 3H), 7.2–8.7 (m, 7H). When stored at room temperature or upon attempted distillation, oxime *Z*-**17** isomerized to *E*-**17** as observed by the changes in the nmr patterns. An additional mixture of oximes (0.2 g) was obtained with MeOH elution, and the overall yields after chromatography were ketone **16** (3%), oxime *E*-**17** (36%), and oxime *Z*-**17** (25%).

Amino ketone **16** in a solution of 20% D_2O–pyridine (51) was heated at 50 °C for 1 h and the nmr spectrum of the mixture recorded. The total proton count decreased by 1.7H and the DHO signal (τ 5.2) increased by the same amount. Injection of the solution directly in the gc–ms (to separate D_2O and pyridine) showed mass peaks at m/e 139(6%), 140(22%), 141(38%), 142(17%) which, when corrected for the M + 1 peak having $\frac{1}{3}$ the intensity of the M^+ peak, gave a relative ratio of the deuterated species of d_0 (10%), d_1 (32%), d_2 (47%), and d_3 (12%) with a maximum error of ±3%. The m/e 84 peak was 11% the intensity of m/e 83.

*N-Nitroso-4-vinylpiperidine (**21**)*

4-Vinylpiperidine obtained above was nitrosated with sodium nitrite (3.1 g, 1.5 equiv.) in 1 *N* aqueous hydrochloric acid solution (40 ml). The product was distilled to give *N*-nitroso-4-vinylpiperidine (**21**, 4.15 g), bp 104–106 °C/4.5 torr. The overall yield in the four step synthesis from the 2-(4′-piperidinyl)ethanol was 38%. Nitrosamine **21** has ir 3040, 1435, 1280, 990, and 935 cm^{-1}; nmr τ 4.2–5.2 (m, 3H), 5.34 (t, J = 7 Hz, 2H), 6.33 (dt, J = 4 and 12 Hz, 1H), 7.45 (dt, J = 4 and 12 Hz, 1H). *Anal.* calcd. for $C_7H_{12}N_2O$: C 59.98, H 8.63, N 19.98; found: C 59.73, H 8.85, N 19.81.

A solution of nitrosoamine **21** (1.4 g, 10 mmol) and concentrated hydrochloric acid (1 ml, 12 mmol) in methanol (250 ml) was irradiated for 1 h as described previously. The photolysate was evaporated under vacuum and treated with ether (10 ml). Extraction under acidic conditions gave a liquid (30 mg) which was shown to be **21** by ir and nmr spectroscopy. The aqueous layer was basified with sodium carbonate and extracted with benzene (30 ml × 3) to give a mixture (350 mg). Upon treatment of this mixture with cold benzene, crystals (90 mg) were obtained and shown by tlc to be nearly a 1:1 mixture of **23** and **25**. The residue was chromatographed on an alumina column (Woelm, 8 g) to afford the following eluates:

(*i*) The first eluate from benzene was further chromatographed on a silicic acid column and eluted with 0.5% methanol in chloroform to afford a solid (62 mg) which was sublimed to give 4-vinylpiperidinylformamide (**24**): mp 76–77 °C; ir 3250, 3150, 1730, 1645, 983, and 910 cm^{-1}; nmr τ 1.70 (d, J = 11 Hz, 1H), 2.7 (br, 1H), 4.2–5.2 (m, 3H), 7.00 (m, 2H), 7.50 (dt, J = 3.5 and 10 Hz); ms (%) 154, 109(100), 81(60) and 55(67). On D_2O exchange, the signal at τ 2.7 disappeared and that at τ 1.70 collapsed to a singlet.

(*ii*) A 2% solution of methanol in methylene chloride eluted a solid (81 mg) which was recrystallized from benzene to give 7-formyl-1-azabicyclo[2.2.1]heptane oxime (**23**): mp 171–172 °C, ir 3200, 3100, 1650, 1530,

Can. J. Chem. Downloaded from www.nrcresearchpress.com by 210.87.254.40 on 09/05/12
For personal use only.

and 960 cm^{-1}; nmr τ 2.18 (d, J = 5 Hz, 1H), 6.70 (bd, J = 5 Hz, 1H), 7.10 (m, 2H), 7.60 (m, 3H), 8.45 (m, 2H), and 9.05 (m, 2H); ms (%) 140(17), 123(78), 82(19), 69(100), 54(9) and a metastable peak at 38.71. *Anal.* calcd. for $C_7H_{12}N_2O$: C 59.98, H 8.63, N 19.98; found: C 60.12, H 8.74, N 19.88.

(*iii*) Further elution with 5% methanol in methylene chloride gave crystals (80 mg) which were recrystallized from methanol to give 4-vinyl-2-piperidone oxime (**25**): mp 135–136 °C; ir 3430, 1650, 1345, 975, and 920 cm^{-1}; nmr τ 2.15 (br, 1H, D_2O exchangeable), 4.2–5.2 (m, 3H); 6.65–7.00 (m, 2H) and 7.50–7.90 (m, 2H); ms (%) 140.0947 (M^+, calcd. for $C_7H_{12}N_2O$: 140.0950, 94%), 123(100), 69(50), 55(100).

The basic aqueous solution was continuously extracted with benzene to afford a residue (400 mg), from which a further amount of **23** (122 mg) was obtained by a similar chromatographic separation. The fraction, which was eluted after **23**, could not be purified but showed a vinyl absorption in the ir and nmr spectra. The total isolated yield of **23** was 239 mg (17%).

The remaining aqueous solution, after benzene extraction, was evaporated to dryness leaving a solid residue. This solid was leached with hot isopropyl alcohol (100 ml × 2). The residue from this alcohol extract was recrystallized from ether to give *N*-nitrosohydroxylamino-(1-azabicyclo[2.2.1]hepta-7-yl)methane (**22**) (223 mg, 13%) mp 200–201 °C; ir 3380, 2570, 1510, 1240, 945, and 730 cm^{-1}; nmr (D_2O) τ 5.70 (m, 2H), 6.57 (m, 4H), 7.05 (m, 1H), 7.7 (m, 2H), 8.1 (m, 2H); ms (%) 171(7), 111(19), 110(34), 96(43), 82(42), 69(49), and 55(100). *Anal.* calcd. for $C_7H_{13}N_3O_2$: C 49.11, H 7.65, N 24.54; found: C 49.35, H 7.86, N 24.21.

An ethanol (20 ml) solution of 3-quinuclidone hydrochloride (1.22 g), hydroxylamine hydrochloride (550 mg), and 10% NaOH (10 ml) was heated on a water bath for 2 h. The excess sodium hydroxide was neutralized with acetic acid and the mixture was continuously extracted with ethyl acetate. The extract was worked-up in the usual manner, and the residue (784 mg) was recrystallized from a mixture of ethanol and methylene chloride to give 3-quinuclidone oxime: mp 205–210 °C; ir 2750, 1660, 985, 930, and 800 cm^{-1}; nmr (D_2O) τ 6.42 (s, 2H), 7.16 (m, 4H), 7.43 (quintet, $J \simeq 3$ Hz), 8.20 (m, 4H).

*N-Nitroso-N-methyl-2-(cyclohex-3′-enyl)ethylamine (**29**)*

Ethylamine **28** (2.5 g) was nitrosated by the N_2O_4 nitrosation procedure to afford a crude yellow oil (2.3 g). The oil dissolved in benzene was filtered through neutral alumina (15 g) to give an impure nitrosamine **29** (1.3 g, 43%): ir 3025 (m), 2930, 1855, 1430, 1335, 1040, 655 (m) cm^{-1}; nmr τ 4.31 (s, $W_{1/2}$ = 4 Hz, 1.5H), 5.80 (t of d, J = 7 and 2 Hz, 1.54H), 6.25 (s, 0.65H), 6.35 (m, 0.46H), 6.95 (s, 2.35H), 7.8–9.2 (m, 10H); ms (%) 168(M^+, 0), 153(25), 151(41), 137(44), 109(19), 97(22), 74(50), 55(62), 44(100); uv (in HCl–MeOH) 343 nm (ϵ 97). The nmr spectrum indicated that nitrosamine **29** existed 78% in the *E*-isomer, and that there is 75% of the olefine still unreacted. Since impure nitrosamine **29** decomposed on attempted distillation, it was used in the crude form.

A mixture of nitrosamine **29** (0.7 g, 4 mmol), concentrated hydrochloric acid (0.6 ml), and methanol (220 ml) was photolyzed as above for 2.5 h. The usual separation procedure gave a basic fraction (0.48 g) and a neutral fraction (0.125 g): the latter containing nitrosamine **29** and two minor products which had the same tlc retention times as the impurities in the starting sample.

The basic material was chromatographed on basic alumina (50 g). Eluted with 1% MeOH–CH_2Cl_2 was an amino ketone assigned as **30** (0.03 g, 6%, *vide infra*). With 3–5% MeOH–CH_2Cl_2 as eluent, an oil was obtained and was distilled to give oxime *E*-**31** (0.09 g, 16%): sublimed 65–70 °C/0.5 torr; ir 3300(b), 2920, 2850, 2800, 1650 (m), 1450, 1270, 1145, 930 cm^{-1}; nmr τ 0.8 (D_2O exchangeable, 1H), 6.75 (m, 1H), 7.2 (m, 1H), 7.67 (m, 2H), 7.75 (s, 3H), 7.8–9.1 (m, 9H); ms (%) 168.1325 (calcd. for $C_9H_{16}N_2O$: 168.1263), 151(100), 110(6), 96(56), 82(11), 70(39), 60(22), 59(25), 55(22), 42(31). Further elution with up to 100% ethanol gave a compound assigned as oxime *Z*-**31** (0.05 g, 9%): ir 3300(b), 2920, 2850, 2800, 1650 (m), 1450, 1270, 1145, 930 cm^{-1}; nmr τ 2.2 (D_2O exchangeable, 1H), 6.4 (m, 1H), 6.9–7.3 (m, 2H), 7.40 (s, 3H), 7.4–9.3 (m, 10H); ms (%) 168 (M^+, 4), 151(20), 141(20), 96(11), 82(7), 57(26), 44(100).

A basic fraction (0.27 g) from another photolysis was heated with sodium bisulfite (1.0 g) in 50% aqueous methanol (10 ml) for 4 h (47). Concentrated hydrochloric acid (1 ml) was added and the bulk of the solvent evaporated. The basified solution was extracted with methylene chloride to give crude amino ketone **30**; 0.06 g; ir 2920, 2855, 1710, 1450 cm^{-1}; nmr τ 7.2–7.7 (m), 7.13 (br d), 7.73 (s); ms (%) 153(M^+, 15), 125(20), 117(33), 96(100), 83(61), and 41(35). This fraction was contaminated with a small amount of the *E*-oxime as shown by the ir absorption at 3300 cm^{-1} and the nmr signal at τ 7.75 (s). Continuous extraction of the aqueous phase with $CHCl_3$ yielded a mixture of oximes *E*-**31** and *Z*-**31** (0.09 g, *vide supra*).

Amino ketone **30** turned to a tar on an attempted distillation at 70 ~ 80 °C/0.5 torr. The nmr, ir, and mass spectra of a chromatographic sample of **30** were identical to those of the amino ketone **30** prepared by R. Furstoss, Université D'Aix-Marseille.[4] The picrate of amino ketone **30** was taken up in ethyl acetate and was chromatographed on silicic acid to afford crystals; mp 205–210 °C (dec.); ir (Nujol) 3615, 3550, 3090, 1630, 1615, 1570, 1430, 1340, 1280, 1165, 910, 790, and 760 cm^{-1}. *Anal.* calcd. for $C_{15}H_{18}N_4O_8$: C 47.12, H 4.75, N 14.65; found: C 47.05, H 5.02, N 14.51.

*N-Nitroso-N-methylcyclohex-3-enylamine (**34**)*

Amine **33** (7.0 g, 0.063 mol) was treated with sodium nitrite (15.0 g, 0.22 mol) to yield impure nitrosamine **34** (3.8 g, *ca.* 43%); ir 3030(m), 2940, 2850, 1650 (m), 1440, 1365, 1330 cm^{-1}; nmr τ 4.25 (s, $W_{1/2}$ = 4 Hz, 1.5H), 5.5 (m, 1H), 6.29 (s, 0.3H), 6.91 (s, 2.7H); uv (HCl–MeOH) 340 nm (ϵ 95). The nmr spectrum indicated the presence of 91% *E*-isomer of **34**, and of *ca.* 75% of the unreacted olefin linkage.

Photolysis in methanol—Crude nitrosamine **34** (1.5 g) was photolyzed for 1.5 h in methanol (320 ml) containing concentrated hydrochloric acid (1.7 ml). The uv spectra of the photolysate showed a peak appearing below 308 nm which tailed into the nitrosamine absorption region. The normal work-up gave a basic fraction (0.5 g), of which the major portion was parent amine **33** (the identical nmr spectrum) and neutral material (0.65 g) consisting largely of unreacted nitrosamine **34** as shown by tlc and

Can. J. Chem. Downloaded from www.nrcresearchpress.com by 210.87.254.40 on 09/05/12
For personal use only.

nmr comparison. The latter fraction showed a medium peak at 1720 cm^{-1} in the ir spectrum and gave a precipitate with 2,4-dinitrophenylhydrazine (DNPH).

The combined basic fractions (0.91 g) from several photolyses were chromatographed on basic alumina (50 g). The material (0.2 g) eluted with 1% MeOH–CH_2Cl_2 was a mixture showing signals for olefinic protons (τ 4.34, s, $W_{1/2}$ = 4.5 Hz) but no *N*-methyl singlets in the nmr spectrum. A sample distilled (85–95 °C/2 torr) showed polymeric peaks in the ms and an olefinic ir absorption at 3030 (m) cm^{-1}. The remaining material (0.45 g) eluted with 3–50% MeOH–CH_2Cl_2 contained a small amount of free amine **33** (τ 7.5 s) but the major component was the HCl salt of **33**; ir 3350, 3030 (m), 2930, 2840, 2720, 2450, 1440, 660 (m) cm^{-1}; nmr τ 2.85 (D_2O exchangeable, 2H), 4.30 (s, $W_{1/2}$ = 5 Hz, 2H), 7.0 (m, 1H), 7.36 (s, 3H), 7.4–8.4 (m, 6H).

Photolysis in acetic acid—Nitrosamine **34** (1.1 g) and concentrated hydrochloric acid (1.0 ml) in glacial acetic acid (600 ml) were photolyzed for 5.5 h under the above conditions. The zero hour uv spectrum showed only a shoulder at 330 nm for the n → π^* transition, and during photolysis a strong absorption appeared which tailed above 300 nm. After photolysis, water (500 ml) was added and the solution basified with solid potassium hydroxide, then extracted with methylene chloride. The methylene chloride extracts were washed with dilute hydrochloric acid, and evaporated to yield a liquid (0.34 g) containing nitrosamine **34** as the major component. The distilled solvent was treated with DNPH and the precipitate recrystallized from 95% EtOH. The solid (0.02 g) was assigned as a mixture of 2- and 3-cyclohexenone dinitrophenylhydrazones; mp 128–132 °C; ms (180 °C) 276(M^+, 100), 241(7), 183(4), 153(4), 122(7), 97(79), 79(71), 77(64), 67(82), 41(46); uv 372 nm.

The acid washes mentioned above were basified and extracted with methylene chloride. Evaporation gave mixture (0.2 g) exhibiting six spots in tlc. The nmr of this mixture was very similar to that of amine **33** showing signals at τ 3.3 (b, D_2O exchangeable), 4.35 (s, $W_{1/2}$ = 5 Hz), 7.55 (s) and 6.7–8.8 (m)

N-Nitroso-N-methylcyclopent-2-enylmethylamine (42)

Amine **41** (3 g) was nitrosated with N_2O_4 as above and purified by filtration of a benzene solution through neutral alumina to give nitrosamine **42** (1.56 g, 28% overall yield from the acid): ir 3050 (m), 2930, 2855, 1450, 1430, 1330, 680 (m) cm^{-1}; nmr τ 4.3 (m, $W_{1/2}$ = 18 Hz, 2H), 5.96 (d, J = 7 Hz, 1.6H), 6.25 (s, 0.6H), 6.48 (d, J = 7 Hz, 0.4H), 6.99 (s, 2.4H), 7.4–8.8 (m, 5H); ms (%) 140(M^+, 5), 80(66), 73(41), 67(100), 44(98); uv (in HCl–MeOH) 345 nm (ϵ 89). The ratio of the *N*-methyl singlets indicated 80% *E*-isomer.

Nitrosamine **42** (0.74 g, 5 mmol) and concentrated hydrochloric acid (0.6 ml) in methanol (220 ml) were photolyzed as above for 3.5 h. No peak appeared in the 390 nm region during the photolysis. Normal work-up gave neutral material (0.6 g) which was largely a phthalate plasticizer and a small amount of what appeared to be 2-cyclopentenone oxime; ir 3300, 1030, 950 cm^{-1}; nmr τ 3.85 (m), 4.2 (m), 7.2–8.2 (m). The basic fraction (0.4 g) showed at least 15 component peaks in gc (80 °C). The major peaks were parent amine **41** (16%, retention time 7.8 min; ms 102(2), 89(45), 87(9), 58(72), 50(100)) and an unknown compound (18%, retention time 10.4 min; ms 154(4), 97(93), 96(100), 80(56), 75(26), 54(37), 53(81), 52(37), 36(41)). The basic material was lost during attempted distillation at 30 °C/20 torr. In a separate experiment, the basic fraction was chromatographed on a silicic acid column from which the products could not be obtained in a pure state and the recovery was low. The spectra of the chromatographic fractions indicated the presence of an olefinic bond and/or absence of a N—CH_3 group.

Preparation and Reaction of N-Chloramine

N-Chloro-N-methylpent-4-enylamine (5)

To a cold aqueous dispersion of amine **1** (0.5 g) 1.0 *N* hydrochloric acid (0.5 ml) solution was added to make p*H* 6–7. This cold solution was added drop by drop to a mixture of 5% sodium hypochloride solution (20 ml) and ether (20 ml) during which the reaction was stirred and cooled in an ice bath. The ether layer was separated. The aqueous layer was washed with additional amounts of ether (10 ml × 2). The total ether solution was washed with water, dried, and was evaporated to leave an oil (0.42 g); ir 3070, 1640, 1175, 990, 910 cm^{-1}; nmr τ 4.25 (m, 1H), 5.05 (m, 2H), 7.15 (s, 3H).

The chloramine (1.2 g) and azobisisobutyronitrile (50 mg) were added to a 4 *M* sulfuric acid solution in acetic acid (25 ml) while the reaction mixture was purged with nitrogen. This solution was kept in the dark at 30 °C for 24 h and was poured into ice. During the reaction, aliquots were removed for titration with a standard thiosulfate solution. The decrease of the chloramine was rapid for the first few hours and became slower afterward. The aqueous solution, after being washed with ether, was brought to p*H* 9 by addition of sodium carbonate and was extracted with methylene chloride. The methylene chloride solution was worked-up in the usual manner to afford an oil (1.24 g); ir 3400, 1735, 1370, 1240, and 1035 cm^{-1}. This oil showed at least five spots on tlc analysis and was chromatographed on a silicic acid column. The middle four fractions afforded an oil (610 mg); ir 3350, 1730, 1630, 1370, 1240, and 1040 cm^{-1}. The nmr spectrum of the oil exhibited two major sets of signals, *i.e.*, τ 8.8 (d, J = 6 Hz), 5.1 (m), 7.73 (s), 7.85 (s) for one and 6.4 (d, J = 7), 5.1 (m), 7.73 (s), 7.95 (s) for the other. The former was presumably due to *N*-methyl-4-acetoxypentylamine and the latter due to *N*-methyl-4-acetoxy-5-chloropentylamine with a ratio of about 4:5.

The chloramine (1.4 g) and silver nitrate (2.8 g) in methanol (50 ml) were refluxed for 3.5 h. The methanol solution was filtered and was concentrated by distillation. The residue was diluted with 10% sodium hydroxide solution and was extracted with methylene chloride. The basic material was extracted with 1 *N* hydrochloric acid solution which was made basic and reextracted with methylene chloride. The methylene chloride solution was worked-up in the usual manner to give an oil (1.46 g). The oil was distilled under vacuum (12 torr) and the distillate chromatographed on a silicic acid column. The fraction eluted with 2% methanol in methylene chloride gave, after evaporation, the starting amine **1** (367 mg, 35%) as shown by the identical ir and nmr spectra. The oil obtained (760 mg) from methylene chloride eluent containing 5 ~ 10% methanol gave a mixture of *N*-methyl-3-methoxypiperidine (**6**) and *N*-methyl-2-methoxy-

Can. J. Chem. Downloaded from www.nrcresearchpress.com by 210.87.254.40 on 09/05/12
For personal use only.

methylpyrrolidine (**7**): ir 2900, 2750, 1460, 1360, 1100, 1005, and 905 cm^{-1}; nmr (benzene) τ 6.2–7.0 (m) 6.79 (s, 3H), 7.63 and 7.84 (both s, ratio 5:1); ms 129, 114, and 99. On both vpc and tlc this mixture showed unresolved peaks or spots indicating the two compounds had similar mobility. Silicic acid chromatography of this mixture afforded a fraction containing **6** as the major compound showing the signal at τ 6.75 (t of t) 6.65 (s) and 7.65 (s) and another fraction containing about 65% of **7** showing the signal at τ 6.4–6.8 (the AB portion of a ABX system), 6.70 (s) and 7.84 (s). Repeated chromatography of the former fraction on silicic acid gave an oil (260 mg), eluted with 2% MeOH–CH_2Cl_2, which was distilled to afford **6**: nmr τ 7.68 (s, 3H), 6.68 (s, 3H), 6.72 (t of t, J = 8 and 3 Hz, 1H), 7.25 (m), ir 2900, 2750, 1100, 1005, and 905 cm^{-1}. *Anal.* calcd. for $C_7H_{15}NO$: C 65.07, H 11.70, N 10.84; found: C 65.10, H 11.95, N 10.62.

N-Chloro-4-vinylpiperidine (27)

The amine **20** (1.5 g) was chlorinated to the chloramine **27** as described above; ir 3050, 1640, 1000, and 930 cm^{-1}; nmr τ 4.2 (m, 1H), 5.00 (m, 2H). Chloramine **27** (2 g) and silver nitrate (3.5 g) in methanol (7.5 ml) were refluxed for 4 h. The reaction mixture was worked-up as described above to give crude oil which exhibited virtually the same ir and nmr spectra of the starting amine **20**. It showed two faint spots in addition to a prominent spot corresponding to **20** on tlc.

N-Chloro-N-methylcyclohex-3-enylamine (36)

Amine **33** (1.0 g, 9 mmol) in ether (50 ml) was reacted with a sodium hypochlorite solution (50 ml, Purex bleach) at 0 °C for 1 h (20). Separation of the ether layer and evaporation gave chloramine **36** (0.88 g, 67%): ir 3025 (m), 2920, 2845, 1640 (w), 1440, 1365, 660 (m) cm^{-1}; nmr τ 4.34 (s, $W_{1/2}$ = 4.5 Hz, 2H), 7.07 (s, 3H), 6.9–7.3 (m, 1H), 7.5–8.5 (m, 6H).

Chloramine **36** (0.88 g) and ferric chloride (0.75 g) in 50% aqueous acetic acid (20 ml) were stirred under N_2 at 0 °C and a solution of hydrated ferrous sulfate (0.5 g) in the same solvent (15 ml) was added (16). The stirred mixture was allowed to warm to room temperature over 11 h, and was filtered. The filtrate was extracted with methylene chloride, and the extracts washed with dilute sodium carbonate solution before being evaporated to yield a residue. The major products were identified with gc–ms (130 °C) as parent amine **33** (20%, retention time 2.75 min), **40** (5.5%, retention time 4.8 min; ms 164(6), 125(11), 83(100), 82(67), 42(50)) the dichloro adduct **37** (23%, retention time 13.3 min, ms 183(6), 181(M^+, 9), 148(37), 146(100), 118(12), 110(29), 104(26), 70(35), 57(44)), and the chloroacetoxy adducts **38** and **39** (48%, retention time 24.2 min, ms 207(2), 205(M^+, 5), 170(40), 148(8), 146(25), 128(30), 110(50), 86(65), 70(80), 57(100), 43(70)). The other ten gc peaks were each less than 3%.

Chromatography of a portion of the residue (0.5 g) on the basic alumina (35 g) resulted in fractions primarily composed of one product. The spectral characteristics of these fractions were for dichloramine **37** (nmr τ 5.71 (m), 7.57 (s)), for chloroacetoxy **38** (ir 1740 cm^{-1}; nmr τ 5.1 (m), 5.9 (m), 7.84 (s)) and chloroacetoxy **39** (ir 1740 cm^{-1}; nmr τ 4.9 (m), 5.95 (m), 7.92 (s)). The low field multiplets all had large couplings (J = *ca.* 10 Hz). The ratio of **38** to **39** was estimated to be 3:2 from nmr spectral analysis.

Acknowledgement

The authors are grateful to the National Research Council of Canada for operating grants.

1. Y. L. Chow, R. A. Perry, B. C. Menon, and S. C. Chen. Tetrahedron Lett. 1545 (1971); 1549 (1971).
2. G. A. Russell. *In* Free radicals. Vol. 1. *Edited by* J. K. Kochi. John Wiley and Sons, New York, N.Y. 1973. p. 275.
3. T. Mojelsky and Y. L. Chow. J. Am. Chem. Soc. **96**, 4549 (1974).
4. E. S. Huyser. J. Am. Chem. Soc. **82**, 391 (1960); **82**, 394 (1960).
5. M. Akhtar. *In* Advances in photochemistry. Vol. 2. Interscience Publishers, Inc., New York. 1964. pp. 263–303.
6. G. Sosnovsky and D. J. Rawlinson. *In* Advances in free radical chemistry. Vol. 4. *Edited by* G. H. Williams. Academic Press, New York, N.Y. 1972. p. 203.
7. J. M. Surzur, P. Cozzone, and M. P. Bertrand. C. R. Acad. Sci. Ser. C, 267 (1968); 908 (1968).
8. R. D. Rieke and N. A. Moore. J. Org. Chem. **37**, 413 (1972).
9. R. Nougier and J. M. Surzur. Bull. Soc. Chim. Fr. 2399 (1973).
10. Y. L. Chow and R. A. Perry. Tetrahedron Lett. 531 (1972).
11. E. Flesia, A. Croatto, P. Tordo, and J. M. Surzur. Tetrahedron Lett. 535 (1972).
12. J. M. Surzur, R. Nougier, and C. Dupuy. Tetrahedron Lett. 2035 (1971).
13. M. Julia. Acc. Chem. Res. **4**, 386 (1971).
14. (*a*) C. Walling and A. Cioffari. J. Am. Chem. Soc. **94**, 6059 (1972); (*b*) A. L. J. Beckwith. *In* Essays on free-radical chemistry. Chem. Soc. Spec. Publ. No. 24, London. 1970. Chapt. 9.
15. J. K. Crandall and D. J. Keyton. Tetrahedron Lett. 1653 (1969).
16. Z. Cekovic. Tetrahedron Lett. 749 (1972).
17. E. Van Bruggen. Recl. Trav. Chim. **87**, 1134 (1968).
18. B. Capon and C. W. Rees. Ann. Rep. Chem. Soc. **61**, 221 (1964).
19. A. L. J. Beckwith and G. Moad. J. Chem. Soc. Chem. Commun. 472 (1974); A. L. J. Beckwith, G. E. Gream, and D. L. Struble. Aust. J. Chem. **25**, 1081 (1972).
20. A. L. J. Beckwith, I. Blair, and G. Phillipou. J. Am. Chem. Soc. **96**, 1613 (1974).
21. J. H. Davis, J. D. Downer, and P. Kirby. J. Chem. Soc. 245 (1966).
22. A. G. Davis, M. J. Parrot, and B. P. Roberts. J. Chem. Soc. Chem. Commun. 27 (1974).
23. J. M. Surzur, L. Stella, and P. Tordo. Bull. Soc. Chim. Fr. 115 (1970).
24. J. M. Surzur, L. Stella, and R. Nougier. Tetrahedron Lett. 903 (1971); 3107 (1971).
25. J. W. Bastable, J. D. Hobson, and W. D. Riddell. J. Chem. Soc. Perkin Trans. I, 2205 (1972).
26. O. E. Edwards, G. Bernath, J. Dixon. J. M. Paton, and D. Vocello. Can. J. Chem. **52**, 2123 (1974);

O. E. EDWARDS, D. VOCELLO, and J. W. APSIMON. Can. J. Chem. **50**, 1167 (1972).
27. S. SHIH, R. J. BUENKER, S. D. PEYERIMHOFF, and C. J. MICHEJDA. J. Am. Chem. Soc. **94**, 7620 (1972).
28. Y. L. CHOW. Acc. Chem. Res. **6**, 354 (1973).
29. (*a*) Y. L. CHOW, S. C. CHEN, K. S. PILLAY, and R. A. PERRY. Can. J. Chem. **50**, 1051 (1972); (*b*) Y. L. CHOW, C. J. COLON, H. H. QUON, and T. MOJELSKY. Can. J. Chem. **50**, 1065 (1972).
30. J. SPANSWICK and K. U. INGOLD. Can. J. Chem. **48**, 546 (1970); **48**, 554 (1970).
31. F. MINISCI, R. GALLI, and M. CECERE. Tetrahedron Lett. 3136 (1963); Chim. Ind. (Milan), **48**, 132 (1966); **48**, 347 (1966).
32. P. G. GASSMAN and J. H. DYGOS. Tetrahedron Lett. 4745 (1970); 4749 (1970); P. G. GASSMAN, F. HOYDA, and J. DYGOS. J. Am. Chem. Soc. **90**, 2716 (1968).
33. M. MOKOTOFF and R. F. SPRECHER. Tetrahedron, **30**, 2623 (1974).
34. P. GAUBERT, R. P. LINSTEAD, and H. N. RYDON. J. Chem. Soc. 1971 (1937).
35. S. WOLFE, H. B. SCHLEGEL, M. H. WHANGBO, and F. BERNARDI. Can. J. Chem. **52**, 3738 (1974).
36. S. R. SANDLER and W. KARO. Organic functional group preparations. Vol. 12. Part II. Org. Chem. Monographs. Academic Press, New York. 1971. Chapt. 17.
37. E. H. WHITE. J. Am. Chem. Soc. **77**, 6008 (1955).
38. F. W. STACEY and J. F. HARRIS. Org. React. **13**, 225 (1963).
39. P. A. S. SMITH. Open chain nitrogen compounds. Vol. 2. W. A. Benjamin, New York. 1966. Chapt. 15.
40. R. A. PERRY and Y. L. CHOW. Can. J. Chem. **52**, 315 (1974); E. L. ELIEL. J. Chem. Educ. **48**, 163 (1971).
41. J. W. APSIMON and J. D. COONEY. Can. J. Chem. **49**, 2377 (1971); J. D. COONEY, S. K. BROWNSTEIN, and J. W. APSIMON. Can. J. Chem. **52**, 3028 (1974).
42. Y. L. CHOW and C. J. COLON. J. Org. Chem. **33**, 2598 (1968).
43. Y. L. CHOW, J. N. S. TAM, C. J. COLON, and K. S. PILLAY. Can. J. Chem. **51**, 2469 (1973).
44. Y. L. CHOW, J. N. S. TAM, and K. S. PILLAY. Can. J. Chem. **51**, 2477 (1973).
45. C. A. GROB and A. SIEBER. Helv. Chim. Acta, **50**, 2520 (1967).
46. S. H. PINES, J. M. CHEMERDA, and M. A. KOSLOWSKI. J. Org. Chem. **31**, 3446 (1966).
47. K. H. BELL. Aust. J. Chem. **24**, 1089 (1971).
48. G. ESPOSITO, R. FURSTOSS, and B. WAEGELL. Tetrahedron Lett. 899 (1971); R. FURSTOSS, P. TEISSIER and B. WAEGELL. J. Chem. Soc. Chem. Commun. 384 (1970); R. TADAYONI, A. HEUMANN, R. FURSTOSS, and B. WAEGELL. Tetrahedron Lett. 2879 (1973).
49. C. L. ANGELL, P. J. KRUGER, R. LAUZON, L. C. LECTON, K. NOACK, R. J. D. SMITH, and R. N. JONES. Spectrochim. Acta, **11**, 926 (1959).
50. H. O. HOUSE and H. C. MILLER. J. Org. Chem. **27**, 4436 (1962).
51. G. M. CREE and A. S. PERLIN. Can. J. Biochem. **46**, 765 (1968).
52. (*a*) Y. L. CHOW, M. P. LAU, R. A. PERRY, and J. N. S. TAM. Can. J. Chem. **50**, 1044 (1972); (*b*) S. C. CHEN. Ph.D. Thesis. Simon Fraser University, Burnaby, British Columbia, 1970.
53. (*a*) Y. L. CHOW, S. C. CHEN, and D. W. L. CHANG. Can. J. Chem. **48**, 157 (1970); (*b*) R. A. PERRY. Ph.D. Thesis. Simon Fraser University, Burnaby, British Columbia, 1974.
54. K. S. PILLAY, S. C. CHEN, T. MOJELSKY, and Y. L. CHOW. Can. J. Chem. **53**, 3014 (1975).
55. H. BOOTH. *In* Progress in NMR spectroscopy. Vol. 5. Pergamon Press, Oxford. 1969. Chapt. 3.
56. G. S. HAMMOND. J. Am. Chem. Soc. **77**, 334 (1955).
57. K. HEUSLER. Tetrahedron Lett. 97 (1970).
58. L. STELLA. Thesis Doctor D'Etat. Universite de Provence, Marseille. 1972.
59. R. F. GARWOOD, C. J. SCOTT, and B. C. L. WEEDON. J. Chem. Soc. Chem. Commun. 14 (1965).
60. (*a*) H. C. BROWN and G. ZWEIFEL. J. Am. Chem. Soc. **82**, 3223 (1960); (*b*) R. MONSON. Advanced organic synthesis. Academic Press, New York. 1971.
61. W. R. BOEHME. J. Org. Chem. **26**, 2107 (1961).
62. J. W. BIRD and D. G. M. DIAPER. Can. J. Chem. **47**, 145 (1969).
63. M. L. WOLFROM, L. W. GEORGES, and S. SOLTZBERG. J. Am. Chem. Soc. **56**, 1794 (1934).
64. M. S. AHMAD and A. H. SIDDIQUI. J. Ind. Chem. Soc. **46**, 44 (1969).

Can. J. Chem. Downloaded from www.nrcresearchpress.com by 210.87.254.40 on 09/05/12
For personal use only.

Synthèse de nouveaux phospholènes et phospholes avec substituants fonctionnels sur le phosphore

FRANÇOIS MATHEY, JEAN-PIERRE LAMPIN ET DANIEL THAVARD
Institut National de Recherche Chimique Appliquée, 91710, Vert le Petit, France

Reçu le 30 décembre 1975

FRANÇOIS MATHEY, JEAN-PIERRE LAMPIN et DANIEL THAVARD. Can. J. Chem. **54**, 2402 (1976).

Le bromo-1 diméthyl-3,4 phospholène-3 est facilement quaternarisé par les halogénures organiques fonctionnels $Z—(CH_2)_n—X$ quand Z = OR, SR, C(O)R, $CH(OR)_2$, COOR, $CONR_2$, CN, n = 1 ou 2 et X = Cl ou Br. Les composés d'addition ainsi obtenus ont la même structure que les composés d'addition diène-dihalogénophosphine décrits par McCormack. Ils réagissent avec H_2O ou H_2S pour fournir les oxydes ou sulfures de phospholènes correspondants qui sont fonctionnalisés sur le phosphore. Par réaction avec le DBU ils donnent les phospholes si n = 1 et Z = OR, SR ou si n = 2 et Z = CN. Quelques propriétés chimiques de nouveaux composés ainsi préparés sont décrites. Les données de rmn du proton sont fournies.

FRANÇOIS MATHEY, JEAN-PIERRE LAMPIN, and DANIEL THAVARD. Can. J. Chem. **54**, 2402 (1976).

1-Bromo-3,4-dimethyl-3-phospholene quaternizes readily with functional organic halides $Z—(CH_2)_n—X$ with Z = OR, SR, C(O)R, $CH(OR)_2$, COOR, $CONR_2$, CN, n = 1 or 2, and X = Cl or Br. The adducts thus obtained are formally related to the diene-dihalophosphine McCormack cycloadducts. When reacting with H_2O or H_2S they yield the corresponding P-functional phospholene oxides or sulfides. Phospholes are also obtained by reaction with DBU when n = 1 and Z = OR, SR, or when n = 2 and Z = CN. Some chemical properties of these new compounds are described and pmr data are given.

La synthèse des phospholènes repose sur la cycloaddition d'une dihalogénophosphine avec un diène conjugué suivant le procédé de McCormack (1*a*). L'halogénure d'halogénophospholénium ainsi obtenu réagit avec l'eau pour donner des oxydes de phospholènes (1*b*), avec H_2S pour fournir des sulfures de phospholènes (1*c*), avec le magnésium (2) ou $LiAlH_4$ (3) pour fournir des phospholènes trivalents et avec le diazabicycloundécène (DBU) (4) pour fournir des phospholes. L'obtention de cet intermédiaire clef suppose que la dihalogénophosphine est connue et qu'elle réagit convenablement avec le diène, ce qui est loin d'être toujours le cas.

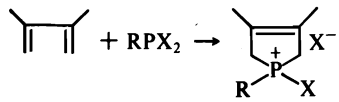

La préparation suivant ce procédé des phospholènes et phospholes comportant un substituant fonctionnel sur le phosphore du type $Z—(CH_2)_n—$ avec n = 1 ou 2 et Z = OR, SR, C—R, $CH(OR)_2$, C—OR, $C—NR_2$ (R = alkyle), CN, C—Ar (Ar = aryle) présuppose donc l'existence de $Z(CH_2)_nPX_2$, sa réaction avec le diène et la stabilité de l'halogénure d'halogénophospholénium ainsi obtenu. Or, d'une part, les dihalogénophosphines de ce type ne sont généralement pas connues et, d'autre part, la plupart des fonctions considérées peuvent réagir avec les composés du type $R_3\overset{+}{P}—X \cdot X^-$. Par exemple, les cétones sont converties en *gem*-dihalogénures (5), les éthers sont coupés en fournissant deux halogénures d'alkyle ou d'aryle (6), etc.

Les phospholènes et phospholes de structure **I** et **II** étaient donc, jusqu'à présent, inconnus, leur

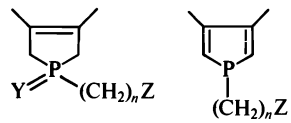

I **II**

Y = O, S ou rien

préparation suivant la voie classique posant des problèmes probablement insurmontables. Leur obtention par une méthode simple présentait pourtant un gros intérêt pour les raisons suivantes. (*a*) La présence d'une fonction Z réactive doit permettre le greffage des noyaux phospholes et phospholènes sur presque toute structure organique préformée. (*b*) La réactivité de **I** et **II** doit être modifiée par la présence de la fonction

Can. J. Chem. Downloaded from www.nrcresearchpress.com by 210.87.254.42 on 09/05/12
For personal use only.

Can. J. Chem. Downloaded from www.nrcresearchpress.com by 210.87.254.42 on 09/05/12
For personal use only.

Z. Ainsi, pour Y = O, Z = CN et $n = 1$, **I** se métalle sur le CH_2 exocyclique et non sur les CH_2 endocycliques comme dans le cas général, d'où une utilisation possible pour des synthèses d'oléfines du type Horner-Emmons avec effet de cycle (travail à paraître). (*c*) **I** et **II** sont des coordinats bidentés originaux et ont, par conséquent, des applications possibles pour l'extraction liquide–liquide des cations métalliques (**I**, Y = O) et pour l'obtention de nouveaux complexes des métaux de transition.

Nous avons donc cherché à préparer **I** et **II** par une voie détournée. Pour ce faire, nous avons étudié la quaternarisation par $Z(CH_2)_nX$ des *P*-halogénophospholènes trivalents récemment préparés (7, 8) par réduction des composés d'addition diènes-trihalogénures de phosphore (9). La réaction espérée s'écrit:

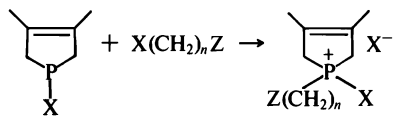

Nous avons été encouragés dans cette voie par les essais de Quin (10) qui a montré que le bromo-1 diméthyl-3,4 phospholène-3 était facilement quaternarisé par le bromure de benzyle mais réagissait mal avec le bromure de butyle. Nous étions donc assurés du succès pourvu que l'halogène de $X(CH_2)_nZ$ soit suffisamment mobile et que la fonction Z ne réagisse pas avec le motif $\overset{+}{P}$—X X^- formé au cours de la quaternarisation.

(I) Synthèse des phospholènes dérivés du P^V

Les résultats de nos essais sont consignés dans le tableau 1 et les données de rmn du proton des produits ainsi préparés réunies dans le tableau 2. Les points suivants méritent d'être notés.

(*a*) Parmi les *P*-halogénophospholènes trivalents, seul le bromo-1 diméthyl-3,4 phospholène-3 se quaternarise dans de bonnes conditions. Cette réactivité généralement réduite est probablement liée à un effet de contrainte cyclique (16). Dans le cas présent, cette contrainte est, en effet, assez forte: $\angle CPC \simeq 94°$ (17) contre $\simeq 100°$ dans les phosphines acycliques et $\simeq 112°$ dans les sels de phosphoniums correspondants.

(*b*) Très logiquement la quaternarisation réussit mieux pour $n = 1$ que pour $n = 2$; seules les fonctions très électroattractrices (COCl, CN) rendent l'halogène X suffisamment mobile pour permettre l'obtention des dérivés avec $n = 2$.

(*c*) D'une façon générale, les monohalogénophosphines R_2PX se quaternarisent beaucoup plus difficilement que les phosphines R_3P. Cependant, un certain nombre d'exemples de quaternarisation de monohalogénophosphines (en général Me_2PCl, Et_2PCl et Ph_2PCl) par des halogénures fonctionnels, sans altération de la fonction, ont été décrits dans la littérature avant ce travail. On a relevé les exemples suivants: $n = 1$, Z = OR (18, 19); $n = 1$, Z = SR (20); $n = 1$, Z = COOEt (21); $n = 1$, Z = COMe (21). En revanche, les exemples de quaternarisation avec: $n = 1$, Z = COPh; $n = 1$, Z = $CONMe_2$; $n = 1$, Z = CN; $n = 1$, Z = $CH(OEt)_2$; $n = 2$, Z = CN; $n = 2$, Z = COCl sont décrits ici pour la première fois à notre connaissance et sont très vraisemblablement transposables pour obtenir des oxydes ou des sulfures de phosphines fonctionnelles acycliques.

Outre ces remarques générales, nous avons relevé quelques cas particuliers que nous discutons ci-après.

Quaternarisation par $ClCH_2CH(OC_2H_5)_2$

Le produit brut résultant de la quaternarisation est un liquide ne réagissant pas avec H_2O ou H_2S à froid et ne comprenant, par conséquent, pas de liaison covalente P—Br ou P—Cl. D'après l'analyse élémentaire (C, H, halogènes) sa formule brute correspondrait pourtant sensiblement à celle du sel de phosphonium attendu. La rmn du proton indique d'ailleurs la présence des $2(CH_3)$ et $2(CH_2P)$ caractéristiques du cycle diméthyl-3,4 phospholène-3 ainsi que des $2(OC_2H_5)$, du CH_2P et du CH caractéristiques du groupement fonctionnel. Cependant, on note que les deux groupements OC_2H_5 sont fortement inéquivalents et que le CH est anormalement déblindé (5.83 ppm); les données de la littérature pour les composés du type $R_2P—CH_2—\underset{\underset{O}{\|}}{CH}-(OC_2H_5)$ sont en effet les suivantes: R = OEt $\delta = 4.88$ (CH, réf. 22); R = Ph $\delta = 5.02$ (CH, réf. 23).

Pour tenir compte de ces données, nous suggérons donc la transposition suivante:

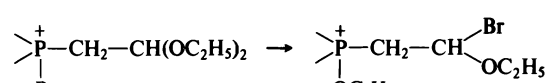

19

(Échange partiel possible entre Cl et Br)

TABLEAU 1. Synthèse des phospholènes fonctionnels par quaternization de 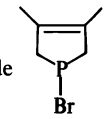

Halogénure utilisé	Oxyde obtenu	Rdt (%)	Propriétés physiques	Sulfure obtenu	Rdt (%)	Propriétés physiques
$ClCH_2OCH_3$	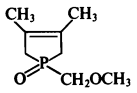 **1**	75	p éb = 100 °C/0.2 torr pf = 64 °C	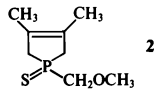 **2**	45	p éb = 123 °C/0.6 torr
$ClCH_2OC_8H_{17}$	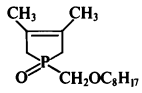 **3**	60	p éb = 116 °C/5 × 10^{-5} torr	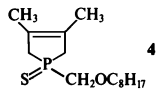 **4**	40	p éb = 146 °C/0.1 torr
$ClCH_2OC_{12}H_{25}$	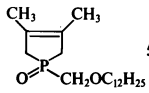 **5**	50	p éb = 145 °C/10^{-5} torr	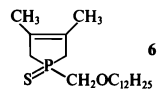 **6**	40	p éb = 120 °C/10^{-4} torr
$ClCH_2OCH_2CH_2Cl$	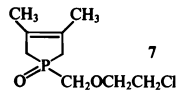 **7**	87	p éb = 148 °C/0.4 torr			
$ClCH_2SCH_2$	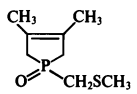 **8**	70	Isolé par chromato (acétate éthyle)	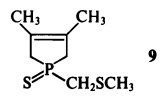 **9**	65	p éb = 127 °C/0.2 torr
$ClCH_2C(=O)CH_3$	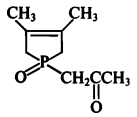 **10**	12	Isolé par chromato (acétate 90:MeOH 10)			
$ClCH_2C(=O)-C_6H_5$	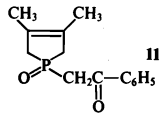 **11**	42	p éb = 145 °C/10^{-5} torr pf = 96 °C			
$ClCH_2C(=O)-OC_2H_5$	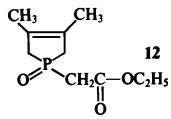 **12**	67	p éb = 125 °C/0.05 torr	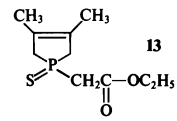 **13**	60	p éb = 140 °C/0.4 torr
$ClCH_2C(=O)-N(CH_3)_2$	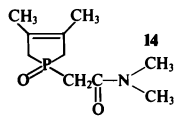 **14**	62	p éb = 160 °C/0.2 torr	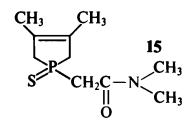 **15**	40	p éb = 172 °C/0.3 torr
$ClCH_2CN$	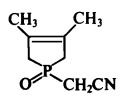 **16**	35	Isolé par chromato (acétate 90:MeOH 10) pf = 96 °C p éb = 115 °C/10^{-5} torr			
$ClCH_2CH_2CN$ $BrCH_2CH_2CN$	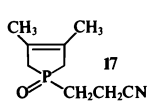 **17**	10 36	Isolé par chromato (acétate 90:MeOH 10) pf = 110 °C p éb = 148 °C/10^{-5} torr			
$BrCH_2CH_2C(=O)-Cl$	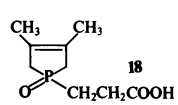 **18**	20	pf = 190 °C Précipité à l'acidification de la phase aqueuse			

Can. J. Chem. Downloaded from www.nrcresearchpress.com by 210.87.254.42 on 09/05/12
For personal use only.

19 est très instable et, par traitement à la soude ou par simple distillation, il fournit l'éther d'énol **20** qui est caractérisé sans ambiguïté par son spectre de masse comprenant le pic moléculaire de m/e 200 (I = 100%) et par son spectre

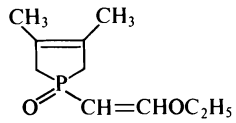

20

p éb = 128 °C/1 torr
rdt = 75%

TABLEAU 2. Données de rmn du proton* des oxydes et sulfures de phospholènes fonctionnels

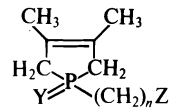

Produit		Cycle				$(CH_2)_n$	
Y	Z	n	N°	CH_3	$CH_2(J_{H-P})$	(J_{H-P})	Z
O	OCH_3	1	**1**	1.74	2.56(11.1)	3.84(5.9)	OCH_3: 3.47
S	OCH_3	1	**2**	1.74	2.70 multiplet complexe	3.91(4.4)	OCH_3: 3.48
O	$O_nC_8H_{17}$	1	**3**	1.73	2.55(12)	3.88(6.6)	OCH_2: 3.55 multiplet CH_3: 0.89(CH_2)$_6$ 1.29
S	$O_nC_8H_{17}$	1	**4**	1.72	2.71 multiplet complexe	3.93(4.7)	OCH_2: 3.57 multiplet CH_3: 0.88(CH_2)$_6$ 1.28
O	$O_nC_{12}H_{25}$	1	**5**	1.73	2.53(10.6)	3.86(6.1)	OCH_2: 3.55 multiplet CH_3: 0.89(CH_2)$_{10}$ 1.28
S	$O_nC_{12}H_{25}$	1	**6**	1.73	2.64 multiplet complexe	3.92(4.7)	OCH_2: 3.57 multiplet CH_3: 0.89(CH_2)$_{10}$ 1.28
O	OCH_2CH_2Cl	1	**7**	1.75	2.61(11.3)	Forme un système complexe avec le OCH_2CH_2Cl	
O	SCH_3	1	**8**	1.74	2.61(11.3)	2.84(8.3)	SCH_3: 2.33
S	SCH_3	1	**9**	1.72	2.76 multiplet complexe	3.05(8.1)	SCH_3: 2.34
O	CCH_3 ‖ O	1	**10**	1.73	2.63(11.7)	3.22(14.4)	C—CH_3: 2.34 ‖ O
O	C—C_6H_5 ‖ O	1	**11**	1.48	2.62(14)	3.82(16.3)	C_6H_5: *m,p* 7.48 *o*, 8.03
O	COC_2H_5 ‖ O	1	**12**	1.72	2.68(12.2)	3.07(16)	C_2H_5: CH_3 1.27 CH_2 4.15
S	COC_2H_5 ‖ O	1	**13**	1.71	2.87 multiplet complexe	3.13(14.7)	C_2H_5: CH_3 1.28 CH_2 4.13
O	$CN(CH_3)_2$ ‖ O	1	**14**	1.73	2.68(10.7)	3.12(14.4)	$N(CH_3)_2$: CH_3 2.97 et 3.17
S	$CN(CH_3)_2$ ‖ O	1	**15**	1.73	Multiplet complexe	3.24(13.9)	$N(CH_3)_2$: CH_3 2.98 et 3.29
O	CN	1	**16**	1.77	2.72(11.8)	3.08(14.3)	
O	CN	2	**17**	1.75	2.60(9.3)	Multiplet centré à 2.49	
O	COOH	2	**18**	1.74	Forme un système complexe avec le CH_2CH_2COOH		

*δ en ppm, J en Hz, TMS interne; produits en solution dans $CDCl_3$.

Can. J. Chem. Downloaded from www.nrcresearchpress.com by 210.87.254.42 on 09/05/12
For personal use only.

TABLEAU 3. Préparation des phospholes fonctionnels et leurs dérivés

Halogénure utilisé	Phosphole obtenu	Rdt (%)	Propriétés physiques	Dérivés
$ClCH_2OCH_3$	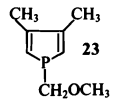 **23**	36	p éb = 58 °C/0.1 torr	Oxyde dimère: pf = 122 °C **24** Sulfure monomère: pf = 106 °C **25** Sel de phosphonium avec IMe: pf = 158 °C monomère **26**
$ClCH_2SCH_3$	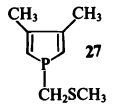 **27**	32	p éb = 69 °C/0.1 torr	Sel de phosphonium avec IMe: pf = 114 °C monomère **28**
$BrCH_2CH_2CN$	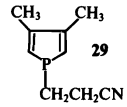 **29**	15	p éb = 80 °C/0.1 torr	Sulfure monomère pf = 96 °C **30**

de rmn du proton: OC_2H_5: δ 1.33 (t, CH_3) et 3.90 (q, OCH_2); CH=CH système complexe à 5.32–5.16–4.69. Les CH_3 du cycle sont à 1.78 et les CH_2 forment un doublet dissymétrique centré à 2.56 J_{H-P} = 15.9 Hz.

En outre, le spectre ir comprend une bande forte de double liaison à 1602 cm^{-1}, dont la position est caractéristique des éthers d'énol et qui est absente dans les oxydes de diméthyl-3,4 phospholènes-3 usuels.

Quaternarisation par $ClCH_2C(=O)Cl$ *ou* $BrCH_2C(=O)Br$

Au lieu d'obtenir l'acide attendu nous avons obtenu le dioxyde de pontage **21** par une réaction

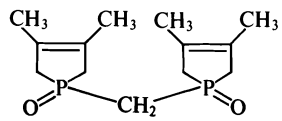

pf = 207 °C
rdt = 25%

21

de décarbonylation dont le mécanisme précis nous échappe pour le moment. Ce produit a été caractérisé sans équivoque par son spectre de masse qui comprend le pic moléculaire de *m/e* 272, le pic de base se situant à *m/e* 126 et par son spectre RMN: CH_3 à 1.73; —P—CH_2 à 2.74 (J_{H-P} = 9.4 Hz), P—CH_2—P, triplet centré à 2.47 (J_{H-P} = 12.7 Hz). En outre le spectre ir confirme sans ambiguïté l'absence du groupement carbonylé.

Quaternarisation par $ClCH_2OCH_2Cl$

Lors de la réaction on constate un clivage partiel du pont éther conduisant à l'alcool **22**.

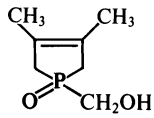

pf = 137 °C
rdt = 25%

22

Il est caractérisé par son spectre rmn: 1.72 (CH_3) 2.50 (CH_2 cycliques, J_{H-P} = 9.3), 3.97 (CH_2—OH, J_{H-P} = 3.2) et 5.56 (OH mobile, $CDCl_3$) et par son spectre ir: ν OH = 3240 cm^{-1} (KBr). Ce clivage partiel correspond, en fait, à la réaction que nous craignions dans le cas général.

(II) Synthèse des phospholes

Lorsqu'on cherche à préparer le phosphole **II** (n = 1) par déshydrohalogénation de l'halogénure d'halogénophosphonium correspondant, on enregistre un échec si Z est trop fortement électroattracteur (CN, COOEt) sans doute parce que les protons du groupement CH_2Z deviennent plus acides que les protons en α du phosphore dans le cycle et que la déshydrohalogénation fournit alors initialement l'ylure exocyclique:

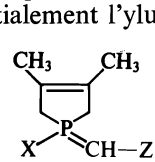

qui, à l'hydrolyse, donne l'oxyde de phospholène correspondant. Par contre, si Z n'est pas trop

Can. J. Chem. Downloaded from www.nrcresearchpress.com by 210.87.254.42 on 09/05/12
For personal use only.

TABLEAU 4. Données de rmn du proton* des phospholes fonctionnels et de leurs dérivés monomères

Produit	Protons du cycle (J_{H-P}) CH_3	Protons du cycle (J_{H-P}) CH	$(CH_2)_n$ (J_{H-P})	Z (J_{H-P})
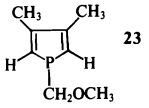 **23**	2.07(2.45)	6.34(38.2)	3.93(5.8)	OCH_3 3.32
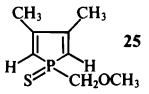 **25**	2.11(2.1)	6.03(31.4)	4.01(2.77)	OCH_3 3.44
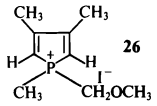 **26**	2.31(1.8)	6.88(32.3)	5.06(3.55)	OCH_3 3.57 CH_3P^+ 2.46(12.2)
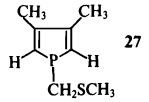 **27**	1.99(2.9)	6.29(38)	2.68(3.8)	SCH_3 2.09
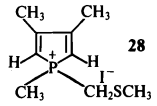 **28**	2.31(2.2)	6.85(33.5)	4.21(8.4)	SCH_3 2.38 CH_3P^+ 2.49(14.4)
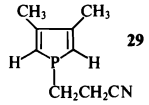 **29**	2.11(~3)	6.29(39.3)	Système complexe	
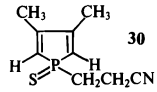 **30**	2.09	6.10(32)	Système complexe	

*δ en ppm, J en Hz, TMS interne; produits en solution dans $CDCl_3$.

fortement électroattracteur (OR, SR) la réaction se déroule normalement et fournit les phospholes correspondants avec un bon rendement (tableau 3). Le risque de déshydrohalogénation exocyclique disparaît avec les halogénures d'halogénophospholénium pour lesquels $n = 2$.

Comme, toutefois, il n'est pas possible de préparer ces composés si Z n'est pas puissamment électroattracteur (voir 1ère partie), nous n'avons pu tenter la synthèse des phospholes correspondants que dans le cas particulier Z = CN. La réaction fournit bien le phosphole attendu (tableau 3) qui présente un intérêt particulier puisqu'il est le résultat de l'addition théorique de l'acrylonitrile sur le phosphole P—H et qu'il peut éventuellement le remplacer dans certains types de réactions.

A partir de ces phospholes nous avons synthétisé quelques dérivés classiques: oxydes, sulfures, iodures de méthylphospholium. Tous ces dérivés sont décrits dans le tableau 3. Les données de rmn du proton de ces composés sont résumées dans le tableau 4, sauf celles de l'oxyde dimère **24** dérivé de **23**. Sur le phosphole **23** nous avons étudié deux types de réactions: l'hydrolyse du sel de méthylphospholium et l'extension de cycle par réaction avec le chlorure de benzoyle.

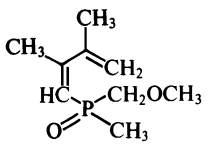
31

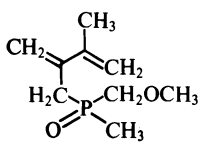
32

Can. J. Chem. Downloaded from www.nrcresearchpress.com by 210.87.254.42 on 09/05/12
For personal use only.

Can. J. Chem. Downloaded from www.nrcresearchpress.com by 210.87.254.42 on 09/05/12
For personal use only.

TABLEAU 5. Données de rmn du proton pour les composés **31** et **32**

	Composé	δ	J_{H-P} (Hz)
31	CH_3—P	1.60	13
	CH_2—P	3.75	7
	OCH_3	3.44	
	C*H*=P	5.68	23.5
	CH_3—C=CH	2.34	2
	CH_3—C=CH_2	1.95	
	=CH_2	multiplet complexe de 5.14 à 5.36	
32	CH_3—P	1.47	12.7
	OCH_2—P	3.67	7
	OCH_3	3.42	
	CH_2—P	2.92	15
	CH_3—C	1.95	
	CH_2=C	multiplet complexe de 5.14 à 5.36	

L'hydrolyse basique de **26** fournit les deux oxydes non cycliques **31** et **32** en mélange équimoléculaire (cpv, rmn), pour lesquels les données de rmn du proton sont consignées dans le tableau 5.

L'ouverture du cycle observée n'est pas surprenante puisque dans l'hydroxyphosphorane intermédiaire

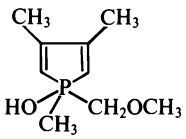

le phosphole est certainement en position apicale équatoriale ($\angle CPC \simeq 90°$ (11)) et que ce sont les liaisons P—C apicales qui se rompent préférentiellement dans l'hydrolyse des sels de phosphonium. Une telle ouverture des sels de phospholium a d'ailleurs été décrite auparavant par Bergesen (12).

Nous avons décrit par ailleurs (13) la réaction des phospholes avec le chlorure de benzoyle en présence d'eau basique qui fournit les oxydes de phényl-2 hydroxy-2 dihydro-1,2 phosphorine. Nous avons voulu vérifier, sur l'exemple de **23**, si la présence d'un substituant fonctionnel n'altérait pas le cours de cette réaction. Nous avons constaté qu'il n'en était rien et nous avons pu préparer avec un bon rendement la phosphorine **33** dont les données rmn du proton sont les suivantes: $\delta(CDCl_3)$ 1.94 et 2.05 (CH_3), 5.90 et 5.93 (C*H*, J_{H-P} = 16.2 et 12.9) 7.38 (C_6H_5), 4.31 (OH mobile), 4.10 (A) et 3.90 (B)

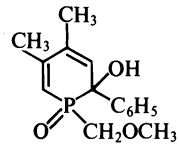

pf = 180 °C
rdt = 75%

33

(P—CH_2, système ABX, J_{A-B} = 13.1 Hz), 3.43 (OCH_3).

(III) Essais de reduction des phospholènes dérivés du P^V

Nous avons étudié l'action de $LiAlH_4$, de $HSiCl_3$ et de Bu_3P sur quelques uns des composés décrits dans la première partie. L'action de $LiAlH_4$ sur les sels de phospholénium (3) s'est traduite par un échec pour Z = OCH_3 et Z = OC_8H_{17}: nous n'avons pu récupérer que les oxydes correspondants **1** et **3**. Un essai de réduction de **1** a également échoué. Par contre, la réaction de $LiAlH_4$ sur le sel avec Z = $CN—CH_3$ nous a fourni un mélange de la

phosphine **34** et de son oxyde **35** avec un rendement global de l'ordre de 20%. L'action de $LiAlH_4$ sur l'oxyde de phospholène **14** fournit le même mélange, mais avec un rendement plus faible.

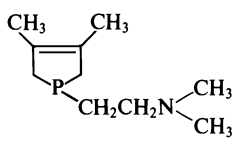

34

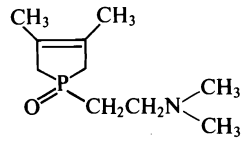

35

Nous avons également effectué une série d'essais de réduction des oxydes de phospholène par $HSiCl_3$ (14). Nous avons enregistré des échecs avec **1** et **12** mais le mélange de **34** et **35** est, par contre, transformé en phosphine pure **34** avec un rendement convenable de l'ordre de 60%; ce dernier résultat doit s'expliquer par la présence de la fonction amine tertiaire favorisant ce type de réduction (14).

Enfin, nous avons étudié l'action de la tributylphosphine sur le sulfure de phospholène **2** (15). En chauffant ce mélange jusqu'à 165 °C, on peut récupérer par distillation un mélange de Bu_3P et de phosphine **36**. Le rendement en **36** est de 45 à 50%, mais il est impossible d'éliminer le Bu_3P du mélange obtenu.

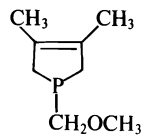

36

Partie expérimentale

Les spectres de rmn du proton ont été réalisés à 60 MHz sur un appareil Perkin-Elmer R 12. Les résultats analytiques des analyses C, H, N sont dans tous les cas corrects.

Quaternarisation par $Z(CH_2)_nX$

On ajoute, sous argon, 0.12 mol de $Z(CH_2)_nX$ à 0.1 mol de bromo-1 diméthyl-3,4 phospholène-3. On bouche le ballon et on laisse le mélange au repos pendant 3 à 4 jours.

Oxydes de phospholène

L'halogénure d'halogénophospholénium est hydrolysé. Le mélange réactionnel est neutralisé au bicarbonate de sodium et extrait au chloroforme. Les extraits chloroformiques sont séchés sur sulfate de magnésium et concentrés. L'oxyde de phospholène est alors isolé soit par distillation, soit par précipitation soit par chromatographie sur colonne de gel de silice.

Dérivé caractéristique pour **11**. Oxime **37** pf = 168 °C,

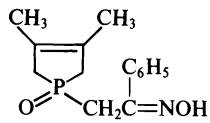

37

rdt = 80%; rmn δ 1.47 (CH_3), 2.55 (CH_2 cycliques, J_{H-P} = 11.8 Hz), 3.69 (CH_2 exocyclique, J_{H-P} = 18.2 Hz), élargi vers 11.2 (OH), 7.35 (*m*- et *p*-C_6H_5), 7.65 (*o*-C_6H_5).

Sulfures de phospholène

On recouvre l'halogénure d'halogénophospholénium par du benzène sec et on fait passer un courant d'H_2S anhydre jusqu'à dissolution complète. On traite alors le mélange réactionnel comme pour les oxydes.

Synthèse des phospholes

L'halogénure d'halogénophospholénium est broyé en boîte à gants, lavé avec un peu de benzène puis avec de l'heptane. Il est mis alors en suspension dans le benzène et traité par la quantité théorique de DBU en solution dans un mélange de benzène et de chlorure de méthylène. On laisse réagir pendant 4 h puis on hydrolyse. On décante la phase organique, on la sèche, on la concentre puis on distille le phosphole cherché.

Essais de réduction des phospholènes dérivés du P^V

Par $LiAlH_4$

Le sel de phospholénium (ou l'oxyde) est mis en suspension dans l'éther et traité, avec précautions, par un excès de $LiAlH_4$. On termine la réaction en chauffant le mélange réactionnel pendant 4 h. On hydrolyse alors par de la soude et on extrait à l'éther.

Par $HSiCl_3$

L'oxyde de phospholène en solution dans le benzène est traité par un large excès de $HSiCl_3$. Le mélange réactionnel est chauffé à reflux pendant 2 h (réfrigérant acétone–carboglace). On hydrolyse alors à la soude et extrait la phase aqueuse à l'éther. Après concentration, l'extrait organique est distillé.

Données pour **34** et **36**. **34**: p éb = 68 °C/0.5 torr; rmn du proton δ 1.69 (CH_3—C=), 2.19 (CH_3—N), massif complexe entre 2.29 et 2.85 (CH_2). **36**: p éb = 63 °C/0.8 torr (en mélange avec Bu_3P); rmn du proton δ 1.65 (CH_3—C=), système complexe centré à 2.48 (PCH_2), 3.44 (PCH_2—O, J_{H-P} = 5.8 Hz), 3.28 (OCH_3).

1. (*a*) W. B. McCormack. E. I. Dupont de Nemours. Brevet U.S. 2 663 736 (décembre 1953), Chem. Abstr. **49**, 7602c (1955); (*b*) Brevet U.S. 2 663 737 (décembre 1953), Chem. Abstr. **49**, 7601a (1955); (*c*) Brevet U.S. 2 663 738 (décembre 1953), Chem. Abstr. **49**, 7602d (1955).
2. L. D. Quin et D. A. Mathewes. J. Org. Chem. **29**, 836 (1964).
3. W. J. Balon. E. I. Dupont de Nemours. Brevet U.S. 2 853 518 (septembre 1958), Chem. Abstr. **53**, 5202b (1959).
4. F. Mathey et R. Mankowski-Favelier. Bull. Soc. Chim. Fr. 4433 (1970).
5. L. Horner, H. Oediger et H. Hoffmann. Ann. **626**, 26 (1959).
6. A. G. Anderson, Jr. et F. J. Freenor. J. Am. Chem. Soc. **86**, 5037 (1964); A. P. Marchand et W. R. Weimar, Jr. Chem. Ind. **7**, 200 (1969).
7. D. K. Myers et L. D. Quin. J. Org. Chem. **9**, 1285 (1971).
8. C. P. Smith et H. Ulrich. Upjohn. Brevets U.S. 3 723 520 et 3 723 521 (mars 1973), Chem. Abstr. **78**, 159 860n et 159 861p (1973); Brevet U.S. 3 714 246 (janvier 1973), Chem. Abstr. **78**, 136 411c (1973); Brevet U.S. 3 803 225 (avril 1974), Chem. Abstr. **80**, 146 296z (1974); Brevet U.S. 3 737 456 (juin 1973), Chem. Abstr. **79**, 78 959v (1973).
9. U. Hasserodt, K. Hunger et F. Korte. Tetrahedron, **19**, 1563 (1963); Shell Internationale. Brevet belge. 631 416 (novembre 1963), Chem. Abstr. **61**, 688h (1964).
10. L. D. Quin, S. G. Borleske et J. F. Engel. J. Org. Chem. **38**, 1858 (1973).
11. P. Coggon et A. T. McPhail. J. Chem. Soc. Dalton Trans. 1888 (1973).
12. K. Bergesen. Acta Chem. Scand. **20**, 899 (1966).
13. F. Mathey. Tetrahedron, **29**, 707 (1973).
14. H. Fritzsche, U. Hasserodt et F. Korte. Chem. Ber. **97**, 1988 (1964); Shell Internationale. Brevet allemand. 1 203 773 (octobre 1965); Chem. Abstr. **64**, 3601f (1966).
15. L. Maier. Helv. Chim. Acta, **47**, 2137 (1964); G. W. Parshall. Inorg. Nucl. Chem. **14**, 291 (1960).
16. R. F. Hudson et C. Brown. Acc. Chem. Res. **5**, 204 (1972).
17. A. T. McPhail, R. C. Komson, J. F. Engel et L. D. Quin. J. Chem. Soc. Dalton Trans. 874 (1972).
18. V. S. Tsivunin, Gil'm. Kamai et R. Sh. Khisamutdinova. Zh. Obshch. Khim. **35**, 1815 (1965); Chem. Abstr. **64**, 2122f (1966).
19. V. S. Tsivunin, Gil'm. Kamai, R. R. Shagidullin et R. Sh. Khisamutdinova. Zh. Obshch. Khim. **35**,

Can. J. Chem. Downloaded from www.nrcresearchpress.com by 210.87.254.42 on 09/05/12
For personal use only.

1811 (1965); Chem. Abstr. **64**, 3588g (1966).
20. V. S. TSIVUNIN, G. KH. KAMAI et V. V. KORMACHEV. Zh. Obshch. Khim. **36**, 271 (1966); Chem. Abstr. **64**, 15 917g (1966).
21. B. M. GLADSHTEIN et V. M. ZIMIN. Zh. Obshch. Khim. **37**, 2055 (1967); Chem. Abstr. **68**, 49 687x (1968).
22. L. MAIER. Z. Anorg. Allg. Chem. **394**, 111 (1972).
23. A. M. AGUIAR, C. J. MORROW, R. M. TURKEL et N. S. BHACCA. J. Org. Chem. **35**, 2820 (1970).

Can. J. Chem. Downloaded from www.nrcresearchpress.com by 210.87.254.42 on 09/05/12
For personal use only.

Some synthetic routes to 2,3,6-trideoxy-hex-2-enopyranosides and -hex-2-enopyranosid-4-uloses[1,2]

MARK BERNARD YUNKER,[3] STEVE YIK-KAI TAM,[4] D. R. HICKS,[5] AND B. FRASER-REID

Department of Chemistry, Guelph–Waterloo Centre for Graduate Work in Chemistry, University of Waterloo, Waterloo, Ont., Canada N2L 3G1

Received December 17, 1975

MARK BERNARD YUNKER, STEVE YIK-KAI TAM, D. R. HICKS, and B. FRASER-REID. Can. J. Chem. **54**, 2411 (1976).

Routes to 6-deoxy-hex-2-enopyranosides and the corresponding 4-ulo derivatives have been investigated. The route (Scheme 2) beginning with the readily prepared ethyl 2,3-dideoxy-α-D-*erythro*-hex-2-enopyranoside is preferred, and the steps involve selective tosylation, iodinolysis, and reduction with Raney nickel. During the iodinolysis step a rearrangement occurs leading to furan derivatives. However, this is suppressed completely by the addition of pyridine to the iodinolysis medium. If the 4-ulo derivative is the desired substance, the most direct route (Scheme 3) utilises the well-known 2,3-dideoxy-hex-2-enopyranosid-4-ulose, the primary hydroxyl group being removed in two simple steps.

MARK BERNARD YUNKER, STEVE YIK-KAI TAM, D. R. HICKS et B. FRASER-REID. Can. J. Chem. **54**, 2411 (1976).

On a étudié les voies pouvant conduire aux 6-déoxy-hex-2-ènopyrannosides et aux dérivés ulo-4 correspondants. On préfère le chemin (schéma 2) commençant avec le 2,3-didéoxy-α-D-*erythro*-hex-2-ènopyrannoside d'éthyle qui est préparé facilement; les étapes impliquent une tosylation sélective, une iodonolyse et une réduction par le nickel de Raney. Durant l'étape de l'iodonolyse, un réarrangement se produit conduisant à des dérivés furanniques. Toutefois on peut supprimer complètement cette réaction par addition de pyridine au milieu conduisant à l'iodonolyse. Si le dérivé ulo-4 est la substance désirée, le chemin le plus direct (schéma 3) utilise le 2,3-didéoxy-hex-2-ènopyrannosid-4-ulose bien connu; le groupe hydroxyle primaire est alors éliminé en deux étapes simples.

[Traduit par le journal]

For projects underway in our laboratory, we require ready routes to the 6-deoxy sugars **1** and **2**. The L-enantiomer of **1** has been synthesized from L-rhamnose in good yield (1, 2), and both **1** and **2** have been synthesized in racemic form from furan precursors (3). Although the published routes are excellent, we wished to use accessible and inexpensive starting materials. In view of the interest in 6-deoxyhexoses as a result of their frequent occurrence in biologically important substances (4), we report herein the results of our experiments.

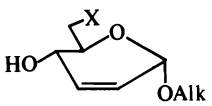

1*a* X = H, Alk = Me
1*b* X = H, Alk = Et

3 X = I, Alk = Et

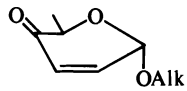

2*a* Alk = Me
2*b* Alk = Et

The most widely used method for creating a 6-deoxy functionality in carbohydrates involves hydrogenolysis of the corresponding sulfonate ester or halide. However, lithium aluminium hydride cannot be used with substrates such as **3** because the double bond is prone to reductive rearrangement (5). Our options were therefore either to create the 6-deoxy functionality first and then introduce the 2,3-double bond, or to use a method of hydrogenolysis that does not affect 2,3-double bonds. Synthetic routes based on these options are outlined in Schemes 1 and 2, respectively.

The conversion of methyl 4,6-*O*-benzylidene-2,3-di-*O*-methanesulfonyl-α-D-glucopyranoside

[1]Pyranosiduloses. Part XI. For part X see ref. 19.

[2]Taken in part from the Ph.D. Theses of M.B.Y. (1975) and S.Y-K.Y. (1974).

[3]Holder of NRCC studentships 1972–1975. Present address: Chemistry Department, University of Hawaii, Honolulu, Hawaii.

[4]Present address: Sloan–Kettering Institute for Cancer Research, 145 Boston Post Road, Rye, New York.

[5]Present address: Ayerst Laboratories, P.O. Box 6115, Montreal, P.Q.

Can. J. Chem. Downloaded from www.nrcresearchpress.com by 210.87.254.5 on 09/05/12
For personal use only.

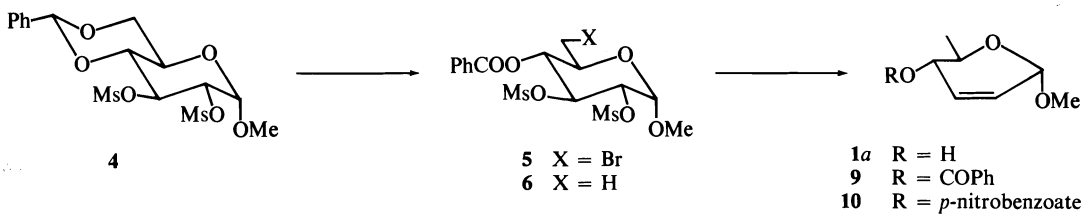

4 5 X = Br 6 X = H 1*a* R = H 9 R = COPh 10 R = *p*-nitrobenzoate

SCHEME 1

4, (6) to methyl 4-*O*-benzoyl-6-bromo-6-deoxy-2,3-di-*O*-methanesulfonyl-α-D-glucopyranoside (**5**) was accomplished in good yield as described (7); however, for the hydrogenolysis of **5**, the published procedure was uneconomical for large scale work, since the weight ratio of substrate to catalyst (Pd/C) was 4:1. Zinc–copper couple in boiling ethanol was effective, but slow, and a number of side products were formed. However, with boiling acetic acid as solvent, the hydrolysis could be carried out on 80 g quantities of **5** in 4–8 h, affording the crystalline 6-deoxy compound **6** in 74% yield.

It is of some interest that the process expressed by the arrows in **7** did not occur as we had feared. Had it occurred, the product **8** would have undoubtedly undergone further reaction and decomposition would have ensued. How-

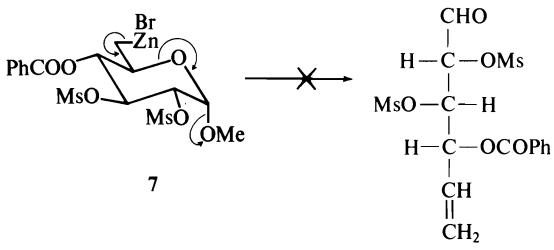

7 8

ever, thin layer chromatograms gave no evidence of such decomposition.

The reductive elimination of the dimesylate **6** was performed in the previously described manner (8, 9), the primary product **9** undergoing deesterification, as normally observed (9, 10), thereby giving compound **1***a* directly. Compound **1***a* tended to co-distill with the solvent (dimethylformamide) upon concentration of the reaction solution, and this lowered the yield. However, the overall yield for the conversion **6** → **9** → **1***a* was 30–40%.

An alternative, shorter route involving the iodide **3** was devised, but the preparation of **3** from the diol **11** proved to be more difficult than anticipated. When the tosylate **12** was treated with sodium iodide in acetone (sealed tube) or methyl ethyl ketone, the desired iodide **3** was formed. However, it was rapidly converted to the furan **13**, the structure of which was suggested by (*i*) a positive qualitative test for iodine, (*ii*) a mass spectral molecular ion *m/e* 238, and (*iii*) an infrared (ir) absorption at 875 cm^{-1} for furan (11). The nmr spectrum showed a triplet for one proton at 4.81 ppm, which was shifted down to 5.96 ppm in the acetylated derivative (14), thereby confirming the positions of the functionalities on the side chain. Supportive mass spectral fragmentation was obtained (see Experimental), but **13** was so unstable that satisfactory elemental analysis could not be obtained. Chemical correlation with the known diol **15** (12) was achieved through selective tosylation to **16**, which upon iodinolysis gave a single product having the same nmr spectrum and R_f values as **13**.

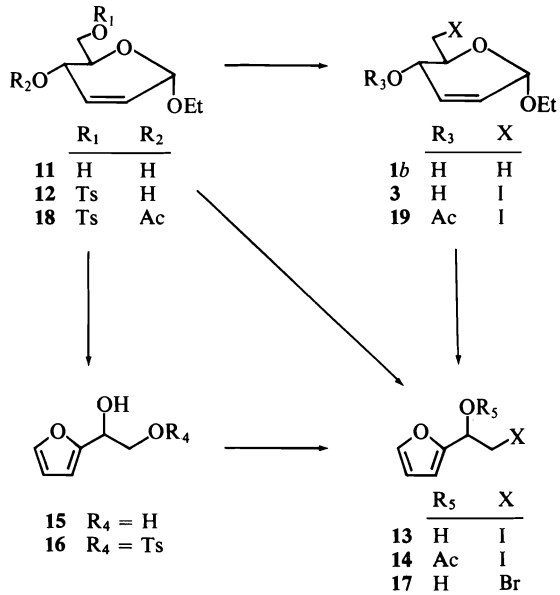

	R_1	R_2
11	H	H
12	Ts	H
18	Ts	Ac

	R_3	X
1*b*	H	H
3	H	I
19	Ac	I

15 R_4 = H
16 R_4 = Ts

	R_5	X
13	H	I
14	Ac	I
17	H	Br

SCHEME 2

Can. J. Chem. Downloaded from www.nrcresearchpress.com by 210.87.254.5 on 09/05/12
For personal use only.

Can. J. Chem. Downloaded from www.nrcresearchpress.com by 210.87.254.5 on 09/05/12
For personal use only.

In an effort to prevent the reaction of **12** → **13**, brominolysis of **11** using triphenylphosphine and *N*-bromosuccinimide according to the procedure of Hanessian *et al.* (13) was attempted. However, the furan bromide **17** was produced in good yield.

The conversion of hex-2-enopyranosides (*e.g.* **11**) to furans (*e.g.* **15**) is a well-known acid-catalyzed process (12), a mechanism for which has been proposed by Zamojski *et al.* (14). In view of this, it was decided to examine the reaction in the presence of pyridine. Accordingly, addition of pyridine completely suppressed the rearrangement giving **3** as the only product of the iodinolysis. The effect of the added pyridine is difficult to rationalize since acids should not be formed in the reaction medium.

It was also found that the acetate **18** derived from **12** was converted cleanly to the acetylated iodide **19**. This is in keeping with Zamojski's mechanism which requires a free carbon-4 hydroxyl group for rearrangement to furan. However, this route was less favourable, for our eventual objective, than that in the preceding paragraph since it required the extra acetylation step.

With the iodide **3** thereby available, it was found that deactivated W-2 Raney nickel (15) would hydrogenolyse the iodide without hydrogenating the double bond. The yield in this step was 90% while the overall yield for the sequence **11** → **12** → **3** → **1***b* was 70%.

The oxidation of **1** to **2** was readily accomplished by either manganese dioxide or chromium trioxide in the usual way.

When the enone **2***b* was the product of interest, a much shorter route from **11** was developed which avoids the chromatographic isolation of **12** (Scheme 3). Thus the readily prepared enone **20** (16) upon treatment with triphenoxyphosphonium methiodide (17) gave the iodide **21** which was hydrogenolysed with deactivated W-2 Raney nickel (15) to **2***b*. The last step could also be done with tri-*n*-butyl tin hydridide (18); however, it proved impossible to isolate the product from the inorganic material.

In summary, the route outlined in Scheme 1 can be carried out on a large scale, however, the final step is problematic in that the high boiling solvent and the product tend to co-distill. The alternative route in Scheme 2 beginning with the well-known compound **11** is preferable, particularly since inclusion of pyridine prevents rearrangement to **13**. When the enone is the compound of interest, the route in Scheme 3 is preferred.

Experimental

General

Melting points were determined on a Fischer–Johns heating stage or a Mel-Temp apparatus, and are uncorrected. The pmr spectra were determined, unless otherwise stated, in deuteriochloroform containing 1% tetramethylsilane as internal standard with either a Varian T-60 or a Varian HA 100. Coupling constants were obtained by measuring spacings of spectra judged to be first order.

Thin layer chromatography (tlc) was performed on glass plates coated with silica gel (HF-254, E. Merck) to a thickness of 0.3 mm. The chromatograms were first viewed under ultraviolet light, then exposed to iodine vapor, and finally sprayed with concentrated sulfuric acid. Heating in an oven is required for complete visualisation. For column chromatography, E. Merck silica gel (0.05–0.20 mm, 70–325 mesh A.S.T.M.) was used.

Methyl 4-O-Benzoyl-6-bromo-6-deoxy-2,3-di-O-methanesulfonyl-α-D-glucopyranoside, 5

This procedure is a modified form of that described by Hanessian and Plessas (7) suitable for large scale preparation. Methyl 4,6-*O*-benzylidene-2,3-di-*O*-methanesulfonyl-α-D-glucopyranoside, (**4**) (100 g, 0.226 mol), was dissolved in a mixture of tetrachloroethylene (300 ml) and carbon tetrachloride (3400 ml), and then barium carbonate (100 g, 0.500 mol) and *N*-bromosuccinimide (48 g, 0.270 mol) were added to the efficiently stirred solution. After gentle refluxing for 2½ h, the reaction mixture was filtered through celite and the filtrate was evaporated to dryness. The residue was then extracted with chloroform, and the extract was washed with sodium bicarbonate and water. The dried (Na_2SO_4) chloroform solutions on evaporation afforded a syrup which easily crystallized on trituration with ether, to give **5** (86 g, 71%) mp 134–135 °C; $[\alpha]_D^{23}$ +60° (*c* 2, $CHCl_3$) (lit. (7) mp 134–135 °C, $[\alpha]_D^{23}$ +53.5° (*c* 1.01, $CHCl_3$)). Normally the extraction step could be omitted and the crude **5** obtained was used directly in the next step of reaction without any purification.

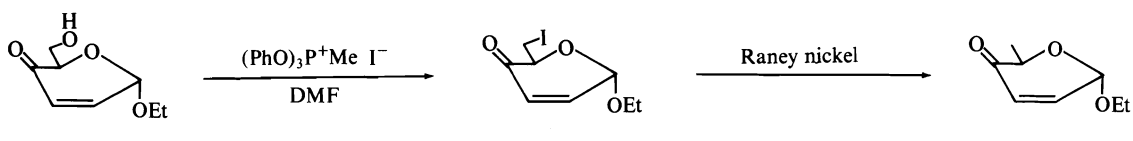

20 **21** **2***b*

SCHEME 3

Can. J. Chem. Downloaded from www.nrcresearchpress.com by 210.87.254.5 on 09/05/12
For personal use only.

Methyl 4-O-Benzoyl-6-deoxy-2,3-di-O-methanesulfonyl-α-D-glucopyranoside, ***6***

Zinc–copper couple (102 g, 1.56 mol) was added to a solution of the 6-bromo compound **5** (80 g, 0.156 mol) in glacial acetic acid (800 ml), and the mixture was refluxed with efficient stirring. After 5 h, the hot reaction mixture was filtered through a sintered-glass funnel and the filtrate was poured slowly into a mechanically stirred ice–water mixture. Compound **6** precipitated, was removed by filtration, and was washed with water until neutral. The dried product weighed 50 g (74%). After recrystallization from methanol: mp 127–128.5 °C, $[\alpha]_D^{23}$ +53.4° (*c* 2, $CHCl_3$) (lit. (7) mp 129–130 °C, $[\alpha]_D$ +54.4° (*c* 0.25, $CHCl_3$).

Methyl 2,3,6-Trideoxy-α-D-erythro-hex-2-enopyranoside, ***1a***

The dimesylate **6** (50 g, 0.127 mol) was added to a mixture of potassium iodide (210 g, 1.27 mol) and zinc–copper couple (9) (92 g, 1.4 mol) in dry dimethylformamide (550 ml). After refluxing for 4½ h, the cooled solution was diluted with ether and the mixture was stirred for 15 min. The insoluble material was removed by filtration and the filter cake was stirred with ether and filtered again. The combined filtrates were evaporated to a thick syrup, which was extracted with ethyl acetate and washed with half of its volume of water. After decolorization with charcoal, the ether solution was evaporated to an oily residue which was purified on a silica column with 50% EtOAc – petroleum ether as eluant (R_f 0.33). The product **1***a* obtained was a mobile oil (7.0 g, 40%). The nmr spectrum of **1***a* was identical to that of the authentic racemic mixture (3).[6] It was further characterized as its *p*-nitrobenzoate, **10**. After recrystallization from methanol: mp 136–137 °C. *Anal.* calcd. for $C_{14}H_{15}O_6N$: C 57.34, H 5.16, N 4.78; found: C 57.33, H 5.17, N 4.70.

Methyl 4-O-Benzoyl-2,3,6-trideoxy-α-D-erythro-hex-2-enopyranoside, ***9***

The alcohol **1***a* (4.9 g, 34 mmol) was dissolved in dry pyridine (20 ml) and benzoyl chloride (5.6 g, 40 mmol) was added. After stirring at room temperature for 1 h, the reaction mixture was poured into sodium bicarbonate solution and then extracted with chloroform and washed with water. The dried (Na_2SO_4) chloroform solution on evaporation afforded compound **9** as a thick syrup (7 g, 82%) which crystallized slowly on standing (1 month). After recrystallization from methanol: mp 47–48 °C, $[\alpha]_D^{23}$ +104.8° (*c* 0.5, $CHCl_3$). For the L-enantiomer (3): mp 43–45 °C, $[\alpha]_D^{23}$ −215 °C. *Anal.* calcd. for $C_{14}H_{16}O_4$: C 67.73, H 6.50; found: C 67.72, H 6.59.

Methyl 2,3,6-Trideoxy-α-D-glycero-hex-2-enopyranosid-4-ulose, ***2a***

A mixture of chromium trioxide (1.74 g, 17.4 mmol) and calcium sulfate (3.4 g, 28 mmol) in dry methylene chloride (100 ml) was stirred at 0 °C for 20 min before the addition of dry pyridine (2.4 ml, 34.8 mmol). After stirring at 0 °C for another 20 min, a solution of compound **1***a* (420 mg, 2.9 mmol) in dry methylene chloride (12 ml) was added. The mixture was then allowed to warm up to room temperature and the stirring was continued for 7 h. Dilution of the reaction mixture with ether, filtration, and evaporation of the filtrate afforded a light brown syrup which was redissolved in ether and decolorized with carbon at room temperature. Removal of the carbon and ether gave a light-yellow residue which weighed 240 mg (crude yield 60%). The nmr spectrum of **2***a* was identical to that for the racemic mixture (3).

Ethyl 2,3-Dideoxy-6-O-p-toluenesulfonyl-α-D-erythro-hex-2-enopyranoside, ***12***

The diol **11** (5.00 g, 28.8 mmol) was dissolved in a mixture of pyridine (120 ml) and methylene chloride (120 ml) and cooled in a dry ice–isopropanol bath to −75 °C. *p*-Toluenesulfonyl chloride (5.48 g, 28.8 mmol) was dissolved in methylene chloride (70 ml) and added dropwise to the cold solution over 1 h with continuous stirring. After an additional hour at −75 °C the mixture was left in the freezer compartment of a refrigerator (−40 °C) for 2 days and finally at ambient temperature for 1 day. The pyridine was removed by evaporation, water was added, and the mixture extracted with diethyl ether. (The water layer yielded 1.3 g of starting material, **11**). The ether layer was washed with saturated sodium bicarbonate solution, then with water, dried (Na_2SO_4), and evaporated to syrup, which showed two products R_f 0.53 and 0.30 (EtOAc – petroleum ether 35–60 °C (1:1)). These were isolated by silica column chromatography using the same solvent system. The slower-running material proved to be **12**, 6.0 g, 64% yield based on unrecovered starting material: nmr ($CDCl_3$) δ 4.90 (1H, br s, J_{12} < 1.5 Hz, H-1), 5.68 (1H, dd, J_{23} = 10 Hz, H-2), 5.92 (1H, d, H-3), 3.2–4.2 (4H, m, OCH_2CH_3, H-4, H-5), 4.3 (2H, m, H-6, H-6′), 3.0 (1H, br s, OH), 2.42 (3H, s, $SO_2C_6H_4CH_3$), 1.17 (3H, t, J = 7 Hz, OCH_2CH_3), centered at 7.57 (4H, AB, $SO_2C_6H_4CH_3$).

The syrupy **12** was characterized as the acetate **18** which was crystallized from ether – petroleum ether; mp 89.5–90.5 °C, $[\alpha]_D^{23}$ +92.5° (*c* 2.51, $CHCl_3$). *Anal.* calcd. for $C_{17}H_{22}O_7S$: C 55.12, H 5.99, S 8.66; found: C 55.17, H 6.05, S 8.89. Nuclear magnetic resonance ($CDCl_3$) δ 4.96 (1H, br s, H-1), 5.85 (2H, br s, H-2, H-3), 5.07 (1H d, J = 10 Hz, H-4), 3.2–4.3 (3H, m, H-5, OCH_2CH_3), centered at 4.2 (2H, m, H-6, H-6′), 1.19 (3H, t, J = 7 Hz, OCH_2CH_3), 2.00 (3H, s, OAc), 2.43 (3H, s, $SO_2C_6H_4CH_3$), 7.62 (4H, AB, $SO_2C_6H_4CH_3$).

2-(D-Glycero-1-hydroxy-2-iodoethyl)furan, ***13***

(*a*) The syrupy tosylate **12** (0.190 g, 0.58 mmol) and sodium iodide (0.161 g, 1.07 mmol) were dissolved in methyl ethyl ketone (9 ml) and the solution refluxed with stirring for 8 h. The precipitated salts were removed by filtration and the filtrate evaporated. The resulting residue was dissolved in ether, washed with water and sodium thiosulfate solution, and then dried (Na_2SO_4). Examination by nmr indicated the ratio of **3** to **13** as 2:3. These were isolated by silica column chromatography: 48 mg **3** and 40 mg of **13**.

For **3**: ν_{max} 875 cm^{-1} (11); λ_{max} 225 nm; $[\alpha]_D^{23}$ + 21.2° (*c* 2.74, $CHCl_3$); R_f 0.60 (EtOAc – petroleum ether (1:1)); M^+ 238 (see Scheme 3); nmr ($CDCl_3$) δ 4.81 (1H, t, $J_{1'2'}$ = 6.0 Hz, H-1′), 3.53 (2H, d, H-2′), 3.25 (1H, br s, exchanges D_2O, OH), 6.40 (2H, d, $J_{(3,4),5}$ = 1.2 Hz, H-3, H-4), 7.43 (1H, t, H-5). Irradiation of H-1′ (4.81) col-

[6]We are indebted to Professor Dr. A. Zamojski (3) for providing us with nmr spectra of compounds in this series.

Can. J. Chem. Downloaded from www.nrcresearchpress.com by 210.87.254.5 on 09/05/12
For personal use only.

lapses H-2′ (3.53) to a singlet and vice versa. Irradiation of H-3,4 (6.40) collapses H-5 (7.43) to a singlet.

For the mass spectrum of **13**; *m/e* 238(M^+), 221 ($C_4H_3O\ C^+HCH_2I$), 171($HOCHCH_2I$), 141(CH_2I), 111 ($C_4H_3O\ CHOHCH_2^+$), 97($C_4H_3O\ C^+HOH$), 67 ($C_4H_3O^+$).

Acetylation of **13** gave **14**. R_f in EtOAc – petroleum ether 35–60 °C (50%) is 0.70; nmr ($CDCl_3$) δ 5.96 (1H, t, $J_{1'2'}$ = 6.0 Hz, H-1′), 3.55 (2H, d, H-2′), 2.08 (3H, s, OAc), 6.40 (2H, m, H-3, H-4), 7.41 (1H, d, H-5).

(*b*) The furan-diol **15** from hydrolysis of **11** in aqueous acetic acid (12) (1.44 g, 11.3 mmol) was dissolved in dry pyridine (25 ml), cooled in ice, and *p*-toluenesulfonyl chloride (2.15 g, 11.3 mmol) added gradually over 1 h. After 1 day at 2 °C, the mixture was processed as described for **12**. The syrupy product **16** weighed 1.76 g (55% yield), and had an R_f of 0.51 in EtOAc – petroleum ether 35–60 °C (50%): nmr ($CDCl_3$) δ 4.92 (1H, dd, $J_{1'2'}$ = 5.2, 6.6 Hz, H-1′), 4.22 (2H, d, H-2′), 3.5 (1H, br s, OH), 6.24 (2H, m, H-3, H-4), 7.3 (1H, m, H-5), centered at 7.67 (4H, AB, $SO_2C_6H_4CH_3$), 2.37 (3H, s, $SO_2C_6H_4CH_3$).

The tosylate **16** (1.28 g, 4.5 mmol) was dissolved in butanone (35 ml) and sodium iodide (1.26 g, 8.4 mmol) added. The solution was refluxed with stirring for 4.5 h and then processed as described in part *a*. The material had R_f and spectral features like those obtained in part (*a*), but it could not be obtained crystalline as it readily decomposed to a greenish-black polymer with evolution of a gas!

*Ethyl 6-Iodo-2,3,6-trideoxy-α-D-erythro-hex-2-enopyranoside, **3**, and its Acetate, **19***

The iodinolysis of tosylate **12** was done as described in part *a* above except that 3 equiv. of pyridine were added to the solution *before* the sodium iodide was introduced. After a reaction time of 11 h, the mixture was processed as described above. Compound **13** was the only product (89% yield), R_f = 0.45 (EtOAc – petroleum ether (1:1)): nmr ($CDCl_3$) δ 5.03 (1H, br s, $J_{12} < 1.5$ Hz, H-1), centered at 5.85 (2H, AB, J_{23} = 10 Hz, H-2, H-3), 3.1–4.3 (6H, m, H-4, H-5, H-6, H-6′, OCH_2CH_3), 2.62 (1H, br s, OH), 1.24 (3H, t, J = 7 Hz, OCH_2CH_3).

For characterization, compound **13** was treated with acetic anhydride and pyridine in the usual way to give the acetate **19** which was crystallized and recrystallized from ether – petroleum ether (35–60 °C): mp 56–56.5 °C; $[\alpha]_D^{23}$ +104.0° (*c* 5.76, $CHCl_3$). *Anal.* calcd. for $C_{10}H_{15}O_4I$: C 36.83, H 4.63, I 38.91; found: C 36.53, H 3.77, I 39.87: nmr ($CDCl_3$) δ 5.11 (1H, s, H-1), 5.85 (2H, s, H-2, H-3), 5.16 (1H, d, J_{45} = 10 Hz, H-4), 3.0–4.2 (5H, m, H-5, H-6, H-6′, OCH_2CH_3), 1.26 (3H, t, J = 7 Hz, OCH_2CH_3), 2.11 (3H, s, OAc).

*Ethyl 2,3,6-Trideoxy-α-D-erythro-hex-2-enopyranoside, **1b***

W-2 Raney nickel (~2 g) was boiled in acetone (15 ml) with stirring for 2 h. Iodide **3** (0.101 g, 0.36 mmol) was then added and reflux continued for 20 h when tlc indicated that the reaction was incomplete. A further amount of deactivated Raney nickel was added and after an additional 4 h, when the hydrogenolysis was seen to be complete, the mixture was filtered through celite and the solvent evaporated to give 0.050 g (90% yield) of **1***b*. R_f = 0.33 (EtOAc – petroleum ether 35–60 °C (1:1)). The nmr spectra of **1***b* and **1***a* (described above) were identical except for the aglycon resonances: nmr ($CDCl_3$) δ 4.97 (1H, d, J_{12} = 2 Hz, H-1), 5.71 (1H, dd, H-2), 5.97 (1H, d, H-2 and H-3 form an AB, H-3), 3.3–4.2 (4H, m, H-4, H-5, OCH_2CH_3), 1.20 (3H, d, J_{56} = 6 Hz, H-6), 2.46 (1H, br s, OH), 1.24 (3H, t, J = 8 Hz, OCH_2CH_3).

*Ethyl 2,3,6-Trideoxy-α-D-glycero-hex-2-enopyranosid-4-ulose, **2b***

(*a*) The alcohol **1***b* (75 mg, 0.47 mmol) was dissolved in chloroform (25 ml) and manganese dioxide (0.65 g) added with stirring. After 20 h another quantity (0.65 g) of manganese dioxide was added. Upon completion of the reaction (~60 h total) as indicated by tlc, the solution was filtered through celite and the solvent evaporated to give 0.063 g (85% yield) of **2***b*. R_f = 0.60 (EtOAc – petroleum ether (1:1)); $[\alpha]_D^{23}$ +24.4° (*c* 3.33, $CHCl_3$).

(*b*) The ketone **20** (16) (0.344 g, 2.0 mmol) was dissolved in dry dimethylformamide (10 ml) and stirred under dry nitrogen in a three necked flask. To this solution was added triphenoxyphosphonium methiodide (1.80 g, 4.0 mmol). After 30 min at room temperature, tlc indicated that all of the starting material had disappeared and a new compound **21**, R_f 0.60 (EtOAc – petroleum ether (1:1)) had been formed. At this time methanol (1 ml) was added and reaction stirred for a further 30 min. The reaction mixture was poured into a separatory funnel and diluted with ether (50 ml). The ether solution was washed with a dilute solution of sodium thiosulfate and water, dried (Na_2SO_4), filtered, and evaporated. The residue obtained was dissolved in reagent acetone (10 ml) and this solution was added to Raney nickel W-2 (2 teaspoons) which had previously been deactivated by refluxing in acetone (30 ml) for 3 h (18).[7]

The reaction mixture was refluxed for 6 h and at this time tlc indicated that no starting material remained and a new compound R_f 0.60 EtOAc – petroleum ether 35–60 °C (1:1) was present along with other uv active material which did not char. The reaction mixture was filtered through Celite and evaporated. The residue obtained was purified by column chromatography and the required product (**2***b*) was obtained (0.131 gm, 42% overall yield).

The nmr spectrum of **2***b* was identical with that of **2***a* (3)[5] except for the aglycon resonances. $[\alpha]_D^{23}$ +24.4° (*c* 3.33, $CHCl_3$): nmr ($CDCl_3$) δ 5.22 (1H, d, J_{12} = 4 Hz, H-1), 6.87 (1H, dd, J_{23} = 10 Hz, H-2), 6.08 (1H, d, H-3), 4.58 (1H, q, J_{56} = 6 Hz, H-5), 1.39 (3H, d, H-6), 3.4–4.1 (2H, m, OCH_2CH_3), 1.27 (3H, t, J = 7 Hz, OCH_2CH_3). Since the enone **2***b* could not be induced to form either a 2,4-dinitrophenylhydrazone or a semicarbazone, it was hydrogenated over paladium on charcoal and the dihydro compound characterized as the semicarbazone after recrystallization from methanol, mp 180.5–181 °C. *Anal.* calcd. for $C_9H_{17}O_3N_3$: C 50.21, H 7.96, N 19.52; found: C 50.21, H 8.09, N 19.44.

Acknowledgements

We want to thank the National Research Council of Canada and Bristol Laboratories (Syracuse) for financial assistance.

[7]If Raney nickel was not deactivated prior to use some hydrogenation of the olefinic double bond was observed.

1. J. S. BRIMACOMBE, L. W. DONER, and A. J. ROLLINS. J. Chem. Soc. C, 2977 (1972).
2. K. BOCK, J. K. CHRISTIANSEN, and C. PEDERSEN. Carbohydr. Res. **20**, 73 (1971).
3. O. ACHMATOWICZ, JR., P. BUKOWSKI, B. SZECHNER, Z. ZWIERZCHOWSKA, and A. ZAMOJSKI. Tetrahedron, **27**, 1973 (1971).
4. S. HANESSIAN. Adv. Carbohydr. Chem. **21**, 143 (1966); S. HANESSIAN and T. H. HASKELL. *In* The carbohydrates. Vol. IIA. *Edited by* W. Pigman and D. Horton. Academic Press, New York and London. 1970.
5. S. Y-K. TAM and B. FRASER-REID. Tetrahedron Lett. 4897 (1974); B. FRASER-REID, S. Y-K. TAM, and B. RADATUS. Can. J. Chem. **53**, 2005 (1975).
6. J. HONEYMAN and J. W. W. MORGAN. J. Chem. Soc. 3660 (1955).
7. S. HANESSIAN and N. R. PLESSAS. J. Org. Chem. **34**, 1035 (1969); **34**, 1045 (1969); S. HANESSIAN. Methods in Carbohydr. Chem. **6**, 183 (1972).
8. R. S. TIPSON and A. COHEN. Carbohydr. Res. **1**, 338 (1965).
9. B. FRASER-REID and B. BOCTOR. Can. J. Chem. **47**, 393 (1969).
10. N. L. HOLDER and B. FRASER-REID. Can. J. Chem. **51**, 3357 (1973).
11. K. NAKANISHI. Infrared absorption spectroscopy. Holden-Day, San Francisco. 1962. p. 213.
12. E. ALBANO, D. HORTON, and T. TSUCHIYA. Carbohydr. Res. **2**, 349 (1966); **3**, 257 (1966).
13. S. HANESSIAN, M. M. PONPIPOM, and P. LAVALEE. Carbohydr. Res. **24**, 45 (1972).
14. A. ZAMOJSKI, M. CHMIELEWSKI, and A. KONOWAL. Tetrahedron, **26**, 183 (1970).
15. G. B. SPERO, A. V. MCINTOSH, and R. H. LEVIN. J. Am. Chem. Soc. **70**, 1907 (1948).
16. B. FRASER-REID, A. MCLEAN, E. W. USHERWOOD, and M. B. YUNKER. Can. J. Chem. **48**, 2877 (1970).
17. S. R. LANDAUER and H. N. RYDON. J. Chem. Soc. 2224 (1953).
18. H. G. KUIVILA and E. J. WALSH. J. Am. Chem. Soc. **88**, 571 (1966).
19. B. FRASER-REID *et al.* Tetrahedron Lett. 297 (1975).

Can. J. Chem. Downloaded from www.nrcresearchpress.com by 210.87.254.5 on 09/05/12
For personal use only.

The mechanism of the reaction of lead tetraacetate – hydrogen fluoride with 1-octene[1]

DENNIS D. TANNER AND PETER VAN BOSTELEN
Department of Chemistry, University of Alberta, Edmonton, Alta., Canada T6G 2G2

Received January 27, 1976

DENNIS D. TANNER and PETER VAN BOSTELEN. Can. J. Chem. **54**, 2417 (1976).

The reaction of 1-octene with the lead tetraacetate – hydrogen fluoride reagent led to products resulting from the Markovnikov addition of lead and its ligand (fluoro or acetoxy) to the olefinic double bond. Displacement of lead from the organometalic intermediate via three separate pathways could be distinguished; displacement concomitant with hydride migration alkyl migration, or direct displacement by an external ligand. The pathways for the formation of the product difluorides, fluoroacetates, and diacetate could be followed by an analysis of the products obtained from carrying out the reaction using 1-octene-*1*-^{13}C as substrate. The major pathways to product formation resulting from either hydride or alkyl migration could be rationalized as proceeding through the intermediacy of a resonance stabilized α-fluorocarbonium ion.

DENNIS D. TANNER et PETER VAN BOSTELEN. Can. J. Chem. **54**, 2417 (1976).

La réaction de l'octène-1 avec le réactif tétraacétate de plomb – fluorure d'hydrogène conduit aux produits résultant de l'addition, suivant Markovnikov, du plomb et de son ligand (fluoro ou acétoxy) sur la double liaison. On peut distinguer trois chemins séparés pour le déplacement du plomb de son intermédiaire organométallique; il s'agit du déplacement accompagné d'une migration d'hydrure, d'une migration d'un groupe alkyle ou du déplacement direct par un ligand externe. On a pu suivre les chemins de formation des produits difluorés, fluoroacétates et diacétates grâce à une analyse des produits obtenus en faisant réagir l'octène-1 ^{13}C-*1* comme substrat. On peut rationaliser les chemins majeurs conduisant à la formation de produits résultant soit d'une migration d'hydrure ou de groupe alkyle comme se produisant par l'intermédiaire d'un ion α-fluorocarbonium stabilisé par résonance.

[Traduit par le journal]

Introduction

The mechanism of the oxidation of bicyclic olefins with the lead tetraacetate – hydrogen fluoride reagent (LTA–HF) has been proposed to proceed via the *cis* molecular addition of lead and its ligand across the carbon–carbon double bond to yield a transient organometalic intermediate. Stereospecific displacement of lead leads to the oxidation products observed (1, 2). Consistent with this proposal, it has recently been reported (3) that the reagent, $PbF_2(OAc)_2$, when allowed to react with pregnenolone yielded a relatively stable organometalic addition product (4), $C_{25}H_{38}F_2O_6Pb$. Concomitant with the displacement of the lead a number of molecular rearrangements have been observed (1, 2, 4–7). In several of these reactions where it was structurally possible to form fluorocarbonium ions ($=\overset{+}{C}-F$) by the rearrangement-displacement of lead the formation of such intermediates seems mechanistically to be a reasonable proposal (1, 4, 6, 7). The stability of the fluorocarbonium ion has been used previously to rationalize the rate of substitution and the *ortho–para* directing influence of a fluorine substituent during electrophilic aromatic substitution. However, other rationales, electrostatic in nature, have been suggested (8). The intermediate fluorocarbonium ion has been generated and its nmr spectra (^1H, ^{19}F, and ^{13}C) have been reported (9, 10). From a comparison of the difference in the ^{13}C nmr chemical shifts of the fluoro, chloro, and bromo carbonium ions with those of model compounds, the authors concluded that back donation of the nonbonded electron pairs on the halogen was more effective with fluorine than with the other halogens (10).

In order to expand the synthetic utility of the reagent and to test the proposal that a fluoro substituent will stabilize a carbonium ion centre the reaction of LTA–HF with 1-octene was investigated. By analogy, a mechanism con-

[1]Taken in part from the Ph.D. dissertation of Peter Van Bostelen, University of Alberta, Edmonton, Alberta, 1972.

Can. J. Chem. Downloaded from www.nrcresearchpress.com by 210.87.254.42 on 09/05/12
For personal use only.

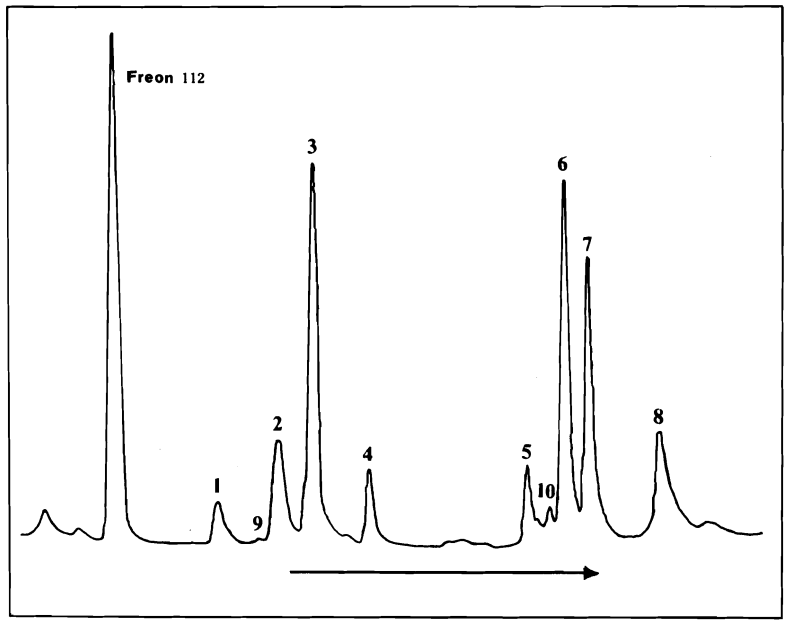

FIG. 1. Gas–liquid partition chromatographic chart of the products obtained from the reaction of LTA–HF with 1-octene.

sistent with that previously proposed for the reaction of 1,1-diphenylethylene (1), norbornene (1), and ethenoanthracene (2), although the stereochemical course of the addition has not been established for nonstrained systems (1, 2), would predict, for the reaction of 1-octene if rearrangement did occur, the intermediary of a primary fluorocarbonium ion. To propose the intermediacy of a terminal cation of this structure implies a large degree of stabilization by the substituent fluorine.

Results

A methylene chloride solution of 1-octene, **1**, and an internal standard, Freon 112, was allowed to react (0 °C) with the preformed LTA–HF reagent. The isolated product mixture was subjected to glpc analysis and seven major products (>2%) and a number of minor products (<2% each) were detected, see Fig. 1.

The major products (**2-8**) and two of the minor products (**9-10**) were isolated by preparative glpc. The structures assigned to the isolated products and their yields as determined by glpc analysis are listed in Table 1.

The structures of compounds **2** and **8** were assigned by a comparison of their ir and nmr spectra and glpc retention times with those of the authentic materials prepared by known methods. Compound **7** was assigned the structure 2-fluoro-1-acetoxyoctane, on the basis of its microanalysis, ir, and nmr (^1H, ^{19}F) spectra and by a comparison of its physical constants with those reported in the literature. The structures of compounds **3** and **4** were assigned on the basis of their microanalysis and nmr (^1H, ^{19}F) spectra.

The geminal fluoroacetates **5** and **6** were both found to decompose during their isolation by preparative glpc, when large amounts of materials were injected on the glpc column. Their decomposition products were collected. The decomposition product formed from **5** was shown to be 2-octanone. Lithium aluminum

TABLE 1. Products from the reaction of 1-octene with LTA–HF

Compound	Yield (%)
2,2-Difluorooctane (**2**)	13
1,1-Difluorooctane (**3**)	34
1,2-Difluorooctane (**4**)	6
2-Fluoro-2-acetoxyoctane (**5**)	3
1-Fluoro-1-acetoxyoctane (**6**)	15
2-Fluoro-1-acetoxyoctane (**7**)	12
1,2-Diacetoxyoctane (**8**)	7
2-Fluoro-1-octene (**9**)	0.5
1-Acetoxy-2,2-difluorooctane (**10**)	0.5

Can. J. Chem. Downloaded from www.nrcresearchpress.com by 210.87.254.42 on 09/05/12
For personal use only.

TABLE 2. Comparison of carbonyl and carbon–oxygen stretching frequencies for some substituted and unsubstituted acetates[a]

Compound	Carbonyl stretch[b] (cm^{-1})	Δ[c]	Carbon–oxygen stretch[b] (cm^{-1})	Δ[c]
1-Acetoxy-1,2-diphenyl ethane[d]	1740	20	1240	29
1-Fluoro-1-acetoxy-1,2-diphenylethane[d]	1760		1211	
2-Acetoxyoctane	1735	35	1243	18
2-Acetoxy-2-fluorooctane (**5**)	1770		1225	
1-Acetoxyoctane	1740	30	1235	17
1-Acetoxy-1-fluorooctane (**6**)	1770		1218	
1-Acetoxy-2-fluorooctane (**7**)	1745		1230	
1-Acetoxy-2,2-difluorooctane (**10**)	1755		1243	
1,2-Diacetoxyoctane (**8**)	1740		1225	
			1240	

[a]Spectra were taken as 1.5% CCl_4 solutions in 0.5 mm NaCl cells on a Perkin-Elmer 337 grating spectrometer.
[b]Frequencies were calibrated against the 1601.4 cm^{-1} peak of polystyrene.
[c]The difference in wave numbers between the geminal substituted and unsubstituted acetates.
[d]Taken from ref. 1.

hydride reduction of 2-octanone yielded 2-octanol, while 1-octanol was obtained from the reduction of the decomposition product of **6**. The ^1H nmr of **5** was consistent with its assigned structure. Its ir spectrum showed a carbonyl absorption frequency at 1770 cm^{-1} and a carbon–oxygen stretching frequency at 1225 cm^{-1}. The shift to a higher wave number for the carbonyl frequency and to a lower wave number for the carbon–oxygen stretching frequency, compared to the frequencies observed for 2-acetoxyoctane, seems to be diagnostic of a geminal acetoxy-fluoroalkane (see Table 2). One fluorine substituent β to an acetoxy group (compound **7**, Table 2) does not appear to greatly affect the acetoxy absorption frequencies, although two β-substituents (compound **10**, Table 2) show a similar effect (although somewhat smaller), as does a geminal fluorine substituent. A similar shift in the acetate absorption frequencies was noted for compound **6**. The structural assignment made for **6** was further confirmed on the basis of its microanalysis and nmr (^1H and ^{19}F) spectra.

The two minor products **9** and **10** were synthesized in the following manner.

$$C_6H_{13}CH{=}CH_2 \xrightarrow{BrF} C_6H_{13}\underset{F}{\underset{|}{C}}H-\underset{Br}{\underset{|}{C}}H_2 \xrightarrow[MeOH]{NaOCH_3} C_6H_{13}\underset{F}{\underset{|}{C}}{=}CH_2$$

9

$$C_6H_{13}\underset{F}{\underset{|}{C}}{=}CH_2 \xrightarrow{LTA\text{–}HF} C_6H_{13}\underset{F}{\underset{|}{\overset{OAc}{\overset{|}{C}}}}-CH_2$$

9 **10**

Their structures were assigned on the basis of their microanalysis and ir and nmr (^1H, ^{19}F) spectra. The glpc retention times of the synthesized materials were identical with those found for **9** and **10** formed in the LTA–HF reaction of 1-octene. A sample of **10** from the LTA–HF reaction with 1-octene could be isolated by preparative glpc under conditions where compounds **5** and **6** had undergone decomposition. Its ir and nmr (^1H, ^{19}F) spectra were identical to those of the synthesized material. Compound **9** could only be obtained by preparative glpc admixed with **2**. The ir and nmr spectra of this mixture, however, contained the same absorption bands found in a synthetic mixture of the two compounds. In the reaction of **9** with LTA–HF no **2** was formed (glpc); however, another compound (~30%), presumably 1,2,2-trifluorooctane, was also found.

In order to establish the mechanistic pathway for the formation of the above products from the reaction of LTA–HF with 1-octene the reaction was carried out with ^{13}C labelled olefin, 1-octene-*1*-^{13}C. The specifically labelled material was synthesized by the method outlined in Scheme 1. The position of the label in the olefin was confirmed by ^{13}C nmr spectroscopy. The ^{13}C labelled olefin was allowed to react with the

Can. J. Chem. Downloaded from www.nrcresearchpress.com by 210.87.254.42 on 09/05/12
For personal use only.

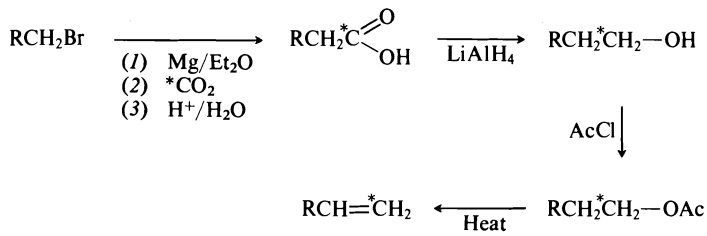

R = *n*-hexyl *indicates the ^{13}C label.

SCHEME 1

TABLE 3. Structures assigned and yields of products from the reaction of 1-octene-*1*-^{13}C with LTA–HF.

Compound[a,b]	Number[b]	Yield (%)
$RCF_2{}^*CH_3$	**2***	13
$R^*CH_2CHF_2$	**3***	34
$RCHF^*CH_2F$	**4***	6
$RCF(OAc)^*CH_3$	**5***	3
$R^*CH_2CHF(OAc)$	**6***	15
$RCHF^*CH_2(OAc)$	**7***	12
$RCH(OAc)CH_2(OAc)$[c]	**8**	7

[a]R = *n*-hexyl.
[b]*indicates ^{13}C enriched atom.
[c]The position of the label in this compound was not determined; however, using mechanistic considerations (see Discussion) the label can be assigned to the C-1 position.

LTA–HF reagent under the same conditions as were used for the unenriched material. The major reaction products, **2**, **3**, **4**, and **7** and the two isomeric alcohols from the reduction of the decomposition products of **5** and **6** were obtained and their ^{13}C spectra were recorded. The position of the enriched atom in six of the seven major products was clearly established from an examination of these spectra (see Table 3).

Discussion

The reaction of 1,1-diphenylethylene has been found to yield initially two compounds 1,1-difluoro-1,2-diphenylethane and a compound (an unstable precursor to desoxybenzoin) tentatively assigned either the structure 1,1-diacetoxy-1,2-diphenylethane or 1-fluoro-1-acetoxy-1,2-diphenylethane (1). The mechanism suggested for the formation of the products formed is given in Scheme 2 (1). Although, 1,1-difluoro-1,2-diphenylethane (Z and Y = F) was stable to the reaction conditions no information was available as to the stability of either of the compounds which were proposed as structures for the desoxybenzoin precursor (Z, Y = OAc or Z = F, Y = OAc). Since, under the reaction conditions 1-acetoxy-1,2-diphenylethylene (nor, presumably, its protonated form **i**) does not lead to the production of desoxybenzoin, the more attractive pathway for the formation of desoxybenzoin is via the intermediacy of a fluorocarbonium ion (**ii**). The intermediate **ii** could be formed conceivably, ultimately from either of the two proposed precursors. The capture of the

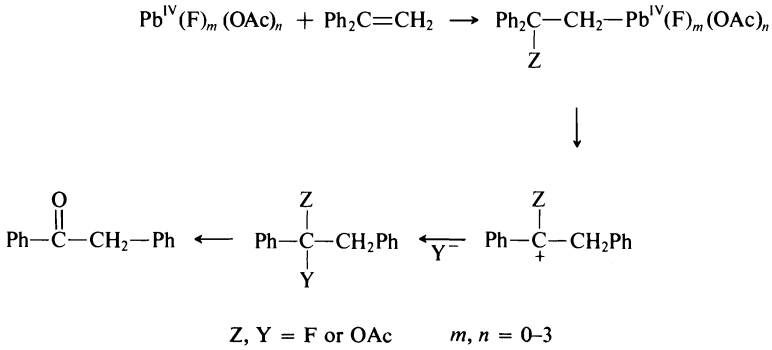

SCHEME 2

Can. J. Chem. Downloaded from www.nrcresearchpress.com by 210.87.254.42 on 09/05/12
For personal use only.

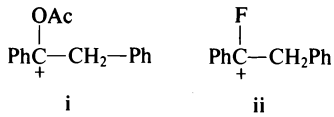

i ii

fluorocarbonium ion **ii** by adventitious water present in the system (1) accommodates the formation of desoxybenzoin.

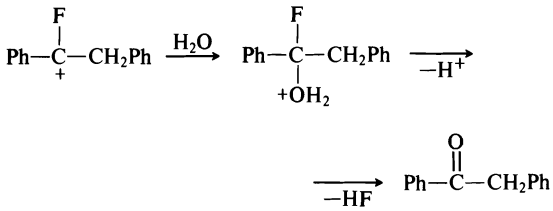

The observation that **5**, produced from the reaction of 1-octene, was unstable and led to the production of 2-octanone gives support to the suggestion that the precursors to the ketonic products in both reactions were geminal fluoroacetates. By analogy the decomposition product from **6** was 1-octanal.

An analogous mechanism to that proposed to explain the reaction of 1,1-diphenylethylene with LTA–HF can be suggested to explain the products formed and the position of the label found in these products for the reaction of 1-octene-*1*-^{13}C with LTA–HF (see Scheme 3).

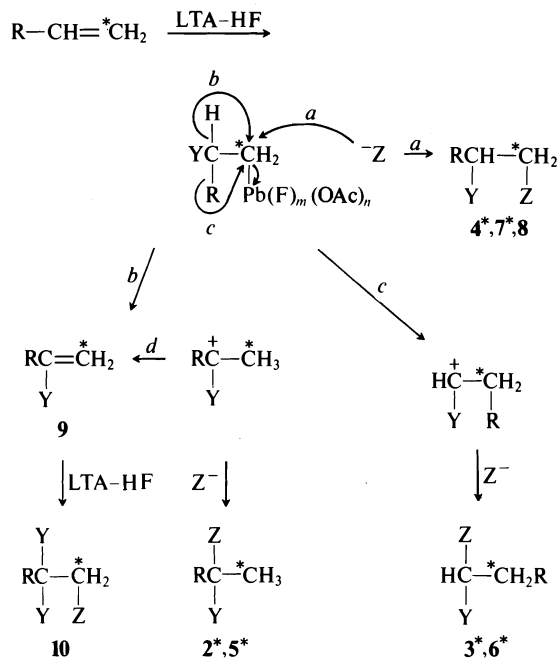

R = *n*-hexyl *indicates ^{13}C enriched atom
Z, Y = F or OAc
m, *n* = 0–3

SCHEME 3

From the products formed and the position of the label in the products three distinct mechanistic pathways for the decomposition of the organometallic addition intermediate can be recognised: path *a* direct substitution, path *b* hydride migration, and path *c* alkyl group migration. These pathways were likewise proposed to explain the stereochemistry of the products observed in the reactions of LTA–HF with norbornene (1). Direct displacement of lead on the primary carbon center led to the formation of three of the major products **4**, **7**, and **8** and was the only reasonable process available to explain the production of *1*-^{13}C labelled products **4***, **7***, and presumably **8**. A competitive 1,2-hydride shift (path *b*) and the migration of the alkyl group (path *c*) are sufficient to rationalize the formation of the remaining major products **2*** and **5*** (path *b*) and **3*** and **6*** (path *c*), and to explain consistently the position of the label in these products (see Scheme 3). The products formed from alkyl migration are favoured over those arising from hydride rearrangement by approximately 3:1. The major portion of both of these processes proceeds via the intermediacy of a fluorocarbonium ion to form **3** (~R) and **2** (~H). The minor portion of each pathway forms **6** (~R) or **5** (~H) via the fluorocarbonium ion or an α-acetoxonium ion, depending upon the sequence of reactions which form these geminal fluoroacetates. Apparently, the driving force for the major portion of the reaction by either rearrangement-displacement pathways, (*b* or *c*), was the formation of a resonance stabilized fluorocarbonium ion.

In the reaction of norbornene with LTA–HF minor amounts of products arising from the loss of a proton from the resonance stabilized 3-fluoronorbornyl cation were observed (1). The production of **9**, similarly, by proton loss from an intermediate cation would not be unexpected (path *d*). Further reaction of **9** with the reagent was shown to yield **10** as its major product.

Experimental

Materials

Lead tetraacetate (Alpha Inorganics, reagent grade)

Can. J. Chem. Downloaded from www.nrcresearchpress.com by 210.87.254.42 on 09/05/12
For personal use only.

Can. J. Chem. Downloaded from www.nrcresearchpress.com by 210.87.254.42 on 09/05/12
For personal use only.

was recrystallized several times from acetic acid containing 4% of acetic anhydride and the white crystals were washed with solvent and air dried.

Anhydrous hydrogen fluoride (Matheson) was distilled and condensed into an open polyethylene flask cooled to −80 °C, and was used without further purification. When used in this manner it could no longer be considered anhydrous.

Methylene chloride was distilled from phosphorous pentoxide prior to use.

Freon 112 (Dupont, research chemicals) was distilled prior to use, bp 90.5 °C/710 torr.

1-Octene (Phillips Petroleum Co., research grade, >99.73 mol% pure) was used without further purification.

^{13}C enriched barium carbonate (61.2 atom% ^{13}C, Bio-Rad Laboratories) was used to prepare the labelled carbon dioxide used in the preparation of 1-octene-*1*-^{13}C.

Gas–Liquid Partition Chromatographic Analysis

Both the analytical results and the preparative collections were carried out on a 10 ft × 0.25 in. glass column packed with 10% SE-30 on Chromosorb WA/W. The column was fitted to a Carlo Erba Fractovap glpc instrument using the terminal conductivity detector and was programmed from 80–275 °C (8 °C per min), see Fig. 1. The molar quantities of products were determined by the use of standard calibration curves constructed using 1,1-difluorooctane and Freon 112 (for the fluorinated materials), and 1-acetoxy-2-fluorooctane and Freon 112 (for the acetate and fluoroacetates).

Reaction of 1-Octene with LTA–HF

A methylene chloride solution (200 ml) of LTA (40 g, 0.09 mol) and hydrogen fluoride (5.4 ml, 0.27 mol) was placed in a polyethylene reaction flask protected from additional moisture by a calcium chloride drying tube. The mixture was stirred (Teflon coated magnetic stirring bar) at 0 °C for 1 h to preform the reagent. To this mixture was added, in one portion, a 50 ml precooled (0 °C) methylene chloride solution of 1-octene (5.01 g, 0.0446 mol) and Freon 112 (3.71 g, 0.0182 mol). The resultant mixture was stirred at 0 °C for 30 min and then quenched by pouring into a cold (0 °C) saturated solution of potassium carbonate. The organic layer was filtered through 'Celite Filter Aid', the aqueous layer was extracted with methylene chloride, the combined organic phases were washed in succession with water, saturated sodium bicarbonate, water, and finally dried over anhydrous sodium sulphate. The reaction mixture was then subjected to glpc analysis. From the ratio of 1-octene to Freon 112 determined before and after the reaction, it was determined that 0.0433 mol (97%) of the olefin had reacted. The yields of the products obtained are listed in Table **1.**

2,2-Difluorooctane ***(2)***

The yield of compound **2** was 0.0057 mol (13.2% based on the consumption of **1**). An authentic sample of compound **2** was prepared by the addition of HF to 1-octyne at −78 °C as described by Grosse and Linn (11). Compound **2** is a colourless liquid: bp 136 °C/700 torr (lit. (12) 136 °C/760 torr); n_D^{20} 1.3776 (lit. (12) n_D^{20} 1.3766); nmr ($CFCl_3$) τ 8.1 (m, 2H), 8.48 (t, J = 18 Hz, 3H), 8.65 (m, 8H), 9.09 (t, J = 5 Hz, 3H); ^{19}F nmr ($CFCl_3$) 126.99 ppm (sextet, J = 18 Hz).

The glpc retention time and the spectral data of synthetic **2** were found to be identical to those of a sample of compound **2** isolated from the reaction of LTA–HF with **1**.

1,1-Difluorooctane ***(3)***

The yield of compound **3** was 0.0148 mol (34.2%). Compound **3** is a colourless liquid: bp 133 °C/690 torr; n_D^{20} 1.3831; nmr (CCl_4) τ 4.29 (t of t, J = 57 Hz, J = 5 Hz, 1H), 8.1 (m, 2H), 8.7 (m, 10H), 9.11 (t, J = 5 Hz, 3H). In a spin decoupling experiment, irradiation of the multiplet at τ 8.1 caused the absorption at τ 4.29 to collapse into a triplet (J = 57 Hz). The ^{19}F nmr (CCl_4) showed only one signal, a doublet of triplets centered at 116.37 ppm (ppm from $CFCl_3$) (J_d = 57 Hz, J_t = 17 Hz); *m/e* 150.1220 (calcd. for $C_8H_{16}F_2$: 150.1220). *Anal.* calcd for $C_8H_{16}F_2$: C 63.92, H 10.73; found: C 63.56; H 10.70.

1,2-Difluorooctane ***(4)***

The yield of compound **4** was 0.0024 mol (5.5%). Compound **4** is a colourless liquid: bp 147 °C/690 torr; n_D^{20} = 1.3929; nmr (CCl_4) τ 5.5 (m), 5.62 (d of d of d, J = 49 Hz, J = 22 Hz, J = 4.5 Hz, the combined signals at τ 5.5 and 5.62 integrated for 3H), 8.35 (m, 2H), 8.62 (m, 8H), 9.08 (t, J = 5 Hz, 3H). The ^{19}F (CCl_4) spectrum of **4** showed two signals, a multiplet centered at 189.5 ppm and a twelve line signal centered at 230.7 ppm (J_t = 49 Hz, J_d = 22 Hz, J_d = 15 Hz). *Anal.* calcd. for $C_8H_{16}F_2$: C 63.92, H 10.73; found: C 64.17, H 10.94.

2-Acetoxy-2-fluorooctane ***(5)***

The yield of compound **5** was 0.0013 mol (3.0%). Compound **5** is a colourless unstable liquid; ir (CCl_4) see Table 2; nmr (CCl_4) τ 8.00 (s, 3H), 8.34 (d, J = 19 Hz, 3H), 8.70 (m, 10H), 9.10 (t, J = 5 Hz, 3H).

When neat **5** was reinjected on the glpc column (180 °C) it completely decomposed to a new compound. The decomposition product was isolated and shown to be 2-octanone by comparison of its ir and nmr spectra with those of an authentic sample.

1-Acetoxy-1-fluorooctane ***(6)***

The yield of compound **6** was 0.0065 mol (15.0%). Compound **6** is a colourless liquid: n_D^{20} 1.4101; ir (CCl_4) see Table 2; nmr (CCl_4) τ 3.77 (d of t, J_d = 56 Hz, J_t = 5 Hz, 1H), 7.96 (s, 3H), 8.30 (m, 2H), 8.70 (m, 10H), 9.12 (t, J = 5 Hz, 3H). The ^{19}F nmr (CCl_4), 128.62 ppm (d of t, J_d = 56 Hz, J_t = 17 Hz). *Anal.* calcd. for $C_{10}H_{19}FO_2$: C 63.13, H 10.07; found: C 62.91, H 9.78.

1-Acetoxy-2-fluorooctane ***(7)***

The yield of compound **7** was 0.0053 mol (12.2%). Compound **7** is a colourless liquid: n_D^{25} 1.4144 (lit. (13) n_D^{25} 1.4134); ir (CCl_4) see Table 2; nmr (CCl_4) τ 5.5 (d of m, J = 50 Hz, 1H), 5.95 (d of d, J = 23 Hz, J = 3 Hz, 2H), 7.97 (s, 3H), 8.30 (m, 2H), 8.7 (m, 8H), 9.11 (t, J = 5 Hz, 3H); ^{19}F nmr (CCl_4) 187.38 ppm ($CFCl_3$) (m). *Anal.* calcd. for $C_{10}H_{19}FO_2$: C 63.13, H 10.07; found: C 63.40, H 10.17.

1,2-Diacetoxyoctane ***(8)***

The yield of **8** from the reaction of LTA–HF with 1-octene was 0.0029 mol (6.7%). Its glpc retention time and ir and nmr spectra were identical to an authentic sample prepared by the acylation of 1,2-octanediol. 1-Octene was oxidized to 1,2-octanediol with hydrogen peroxide according to the method described by Swern *et al.* (14); bp 135–136 °C/9 torr, (lit (14) 135–136 °C/10 torr); n_D^{20} 1.4494; ir (neat) ν 3450, 1075, 1040 cm^{-1}; nmr (CCl_4)

Can. J. Chem. Downloaded from www.nrcresearchpress.com by 210.87.254.42 on 09/05/12
For personal use only.

τ 5.44 (m, 2H), 6.54 (m, 3H), 8.67 (m, 10H), 9.11 (t, J = 5 Hz, 3H).

To 2 g (0.014 mol) of the diol, prepared above, dissolved in 30 ml of benzene, was added 4.8 g (0.056 mol) of freshly fused sodium acetate and 5 ml (0.050 mol) of acetic anhydride. This mixture was heated on a steam bath for 5 h and then heated under reflux for an additional hour. The reaction mixture was cooled and poured into water. Enough sodium carbonate was added to neutralize the mixture. The mixture was transferred into a separatory funnel, the layers were separated, the aqueous layer was extracted with benzene, the combined organic portions were washed with water, and dried over anhydrous sodium sulphate. The benzene was removed by distillation through an 8 in. Vigreaux column to yield 2.7 g (84%) of **8**. Compound **8** was further purified by preparative glpc, n_D^{20} 1.4304; ir (CCl_4) see Table 2; nmr (CCl_4) τ 5.05 (m, 1H), 5.97 (m, 2H), 8.02 (s, 6H), 8.70 (m, 10H), 9.12 (t, J = 5 Hz, 3H). *Anal.* calcd. for $C_{12}H_{22}O_4$: C 62.58, H 9.63; found: C 62.90, H 9.38.

*1-Acetoxy-2,2-difluorooctane (**10**)*

Both compounds **5** and **6** decomposed when the glpc column flooded. When this happened, compound **10** could be isolated (see Fig. 1). Compound **10** is a clear colourless liquid; ir (CCl_4) see Table 2; nmr (CCl_4) τ 5.84 (t, J = 12 Hz, 2H), 7.93 (s, 3H), 8.5 (m, 2H), 8.7 (m, 8H), 9.12 (t, J = 5 Hz, 3H). The ^{19}F nmr (CCl_4) showed a single absorption centered at 105.35 ppm (m.) The glpc retention time and ir and nmr spectra of **10** were identical to those of a sample of **10** prepared by the reaction of **9** with the LTA–HF reagent.

*2-Fluoro-1-octene (**9**)*

Compound **9** could only be isolated admixed with **2**. The ir spectrum of the mixture showed absorption attributed to **9** at ν 1660 cm^{-1} and an nmr spectrum (CCl_4) of the mixture showed besides the absorption of **2** the added absorption of the CH_2 protons of **9** τ 5.48 (d, J = 2 Hz) and τ 6.03 (d of d, J = 34 Hz, J = 2 Hz). The glpc retention time and ir and nmr absorptions observed were identical to those of a synthetic sample of **9**.

*Preparation of 2-Fluoro-1-octene (**9**)*

1-Bromo-2-fluorooctane

The bromofluoride was prepared by the method described by Pattison *et al.* (13), and gave a 53% yield of 1-bromo-2-fluorooctane: bp 89–91 °C/12 torr (lit. (13) 90 °C/16 torr); n_D^{25} 1.4437 (lit. (13) n_D^{25} 1.4423); nmr (CCl_4) τ 5.47 (d of m, J = 48 Hz, 1H), 6.60 (d of d, J = 18 Hz, J = 6 Hz, 2H), 8.1 (m, 2H), 8.65 (m, 8H), 9.08 (t, J = 5 Hz, 3H); ^{19}F nmr (CCl_4) 185.99 ppm ($CFCl_3$) (m).

2-Fluoro-1-octene

To 10 g (0.047 mol) of 1-bromo-2-fluorooctane was added 2.8 g (0.052 mol) of sodium methoxide and 15 ml of methanol. This mixture was heated to reflux with stirring for 8 h. The reaction mixture was cooled, diluted with water, and extracted with ether. The aqueous phase was saturated with sodium chloride and extracted with ether. The combined ether fractions were washed with water and dried over anhydrous sodium sulfate. The glpc analysis revealed that 85% of the 1-bromo-2-fluorooctane had undergone reaction (estimated from peak area measurements) and two products were formed in a 1:1 ratio. The product with the shorter retention time was isolated by preparative glpc and shown to be 2-fluoro-1-octene: bp 132 °C/690 torr; n_D^{25} 1.4011; ir (CCl_4) ν 1660 cm^{-1}; nmr (CCl_4) τ 5.48 (d, J = 2 Hz, 1H), 6.03 (d of d, J = 34 Hz, J = 2 Hz, 1H), 7.86 (d of t, J_d = 16 Hz, J_t = 6 Hz, 2H), 8.65 (m, 8H), 9.08 (t, J = 5 Hz, 3H); ^{19}F nmr (CCl_4) 93.48 ppm ($CFCl_3$) (m). *Anal.* calcd for $C_8H_{15}F$: C 73.79, H 11.61; found: C 73.57, H 11.58.

*Reaction of 2-Fluoro-1-octene (**9**) with LTA–HF*

This reaction was run in an identical manner to that described for the reaction of 1-octene with LTA–HF. By this procedure, a solution of 0.99 g (0.0076 mol) **9** and 0.98 g (0.0048 mol) 'Freon 112' in 10 ml of dry methylene chloride, precooled to 0 °C, was added to a stirred solution of 7 g (0.016 mol) LTA and 1 ml (0.05 mmol) HF in 35 ml of dry methylene chloride at 0 °C. The resultant mixture was stirred at 0 °C for 30 min, then quenched and treated as previously described. The glpc analysis revealed that all of compound **9** had reacted and that two compounds were formed. The larger component (70% by peak area measurement) had an identical glpc retention time and nmr spectrum as the sample of 1-acetoxy-2,2-difluorooctane (**10**) isolated from the reaction of 1-octene with LTA–HF. *Anal.* calcd. for $C_{10}H_{18}F_2O_2$: C 57.67, H 8.71; found: C 58.00, H 9.17. The smaller component (30% by peak area measurement) had an nmr spectrum which is consistent for 1,2,2-trifluorooctane: nmr (CCl_4) τ 5.67 (d of t, J_d = 57 Hz, J_t = 11 Hz, 2H), 8.2 (m, 2H), 8.65 (m, 8H), 9.09 (t, J = 5 Hz, 3H).

Preparation of 1-Octene-1-^{13}C

1-Acetoxyoctane-1-^{13}C

To 0.9 g (0.038 g atom) magnesium turnings was added dropwise, with stirring, a solution of 5.4 g (0.030 mol) 1-bromoheptane in 100 ml of anhydrous ether. The Grignard reagent thus formed was carbonated with the carbon dioxide released from 3 g (0.015 mol) of ^{13}C enriched barium carbonate when it was treated with concentrated sulfuric acid. The procedure used for the carbonation reaction was the same as that reported for the synthesis of acetic acid-*1-^{14}C* (15). Upon completion of the carbonation reaction, the reaction mixture was hydrolysed by the addition of 10 ml of concentrated sulfuric acid. The etherial layer was separated and washed several times with water. The aqueous wash was saturated with sodium chloride and extracted with ether. The combined ether fractions were extracted with saturated sodium bicarbonate solution. The aqueous extract was neutralized with concentrated hydrochloric acid, saturated with sodium chloride, and extracted with ether. The ether solution was dried over anhydrous sodium sulfate.

The above procedure was repeated until a total of 15 g (0.075 mol) of ^{13}C enriched barium carbonate had been converted to octanoic acid-*1-^{13}C*. The octanoic acid was not isolated.

The ethereal solution (300 ml) of octanoic acid, obtained above, was added dropwise, with stirring, to 5.2 g (0.14 mol) of lithium aluminum hydride (LAH) dissolved in 400 ml of anhydrous ether. When addition was completed, the reaction mixture was heated under reflux for 4 h and then allowed to stand overnight. The excess LAH was destroyed by dropwise addition, with stirring, of water saturated ether. The reaction mixture was then treated with 200 ml of 6 *N* hydrochloric acid solution.

Can. J. Chem. Downloaded from www.nrcresearchpress.com by 210.87.254.42 on 09/05/12
For personal use only.

The organic phase was separated and washed in succession with water, saturated sodium bicarbonate solution, water, and finally dried over anhydrous sodium sulfate. The bulk of the ether was removed by distillation through an 8 in. Vigreaux column.

The alcohol formed was not isolated but was treated with 9.7 ml (0.13 mol) of acetyl chloride added in a dropwise manner. When the initial reaction had subsided, enough of an aqueous 20% sodium hydroxide solution was added, in a dropwise fashion, to render the reaction mixture just alkaline to litmus. The layers were separated and the aqueous layer was extracted with ether. The combined ether portions were washed with water and dried over anhydrous sodium sulfate. Removal of the ether by distillation through an 8 in. Vigreaux column resulted in 12 g (92% based on barium carbonate) of 1-acetoxyoctane-*1*-^{13}C; ir (neat) ν 1740, 1235 cm^{-1}.

1-Octene-1-^{13}C

The acetate was subjected to pyrolysis using the procedure reported by Wibaut and Van Pelt (16). By this method, 3.7 g (47%) 1-octene-*1*-^{13}C was isolated. The glpc retention time and the ir spectrum of the enriched olefin were found to be identical to those of an authentic sample of 1-octene.

Compound **1** showed proton decoupled natural abundance ^{13}C resonances at 139.63, 114.65, 34.50, 32.45, 29.61, 29.51, 23.22, and 14.29 ppm. The ^{13}C nmr of 1-octene-*1*-^{13}C showed only one proton decoupled ^{13}C resonance at 114.65 ppm. This signal appeared as a nominal triplet (J = 154 Hz) in the proton coupled ^{13}C nmr spectrum thereby confirming that the ^{13}C enriched carbon was in the C-1 position.

Reaction of 1-Octene-1-^{13}C with LTA–HF

The reaction was run in an identical manner to that described for the unlabelled material. Thus a solution of 3.7 g (0.033 mol) of 1-octene-*1*-^{13}C in 40 ml of dry methylene chloride was added to a cold (0 °C), stirred solution of 30 g (0.066 mol) of LTA and 3.9 ml (0.2 mol) of HF in 150 ml of dry methylene chloride. The reaction was quenched after 30 min reaction time and the products were isolated in the usual manner. The glpc analysis revealed that the product distribution was identical to that obtained from the reaction carried out with unlabelled material. The bulk of the solvent was removed by distillation through an 8 in. Vigreaux column. Upon standing, this solution changed color from pale yellow to dark brown. The glpc analysis of the dark brown solution revealed that the signals corresponding to compounds **5** and **6** had disappeared. A new signal having a retention time of about 1 min longer than that of compound **4** (see Fig. 1) had appeared. The decomposition products were isolated, but not separated, by preparative glpc.

Isolation of 2-Octanol-1-^{13}C and 1-Octanol-2-^{13}C

To 200 mg (5 mmol) of LAH dissolved in 5 ml of anhydrous ether, was added dropwise, with stirring, a solution of 252 mg of the decompcsition products, described above, in 15 ml of anhydrous ether. The reaction mixture was treated in the manner described for the unenriched material. The glpc analysis revealed that two volatile products had been formed. The area ratio of the 2-octanol to the 1-octanol was found to be the same as the area ratio, before decomposition, of compound **5** to compound **6**. The reduction products were isolated by preparative glpc and their nmr spectra were recorded.

The ^{1}H nmr of 2-octanol-*1*-^{13}C showed a doublet of doublets centered at τ 8.83 (J = 125 Hz, J = 6 Hz).

The ^{1}H nmr of 1-octanol-*2*-^{13}C shows a doublet of multiplets centered at τ 8.40 ($2CH_2$, $J_{gem\ ^{13}C-H}$ = 125 Hz).

^{13}C Nuclear Magnetic Resonance Studies

^{13}C nmr spectra were determined using a Bruker Scientific HFX-8 spectrometer operating in conjunction with a Frabri-Tek-1074/PDP-8L fast Fourier transform signal averager. The samples, isolated from glpc, were dissolved in deuteriochloroform, and tetramethylsilane (TMS) was added as an internal reference. Chemical shifts were calculated relative to the internal TMS signal and for purposes of comparison may be converted to the benzene scale (TMS to benzene, 128.54 ppm).

*2,2-Difluorooctane-1-^{13}C (**2***)*

The proton decoupled ^{13}C nmr spectrum showed a triplet centered at 23.25 ppm (J = 28 Hz). The proton coupled ^{13}C nmr spectrum showed a quadruplet of triplets (J_q = 128 Hz, J_t = 28 Hz). The multiplicity and the magnitude (17) of the coupling constants indicate that there are three protons directly attached to the enriched carbon.

*1,1-Difluorooctane-2-^{13}C (**3***)*

The proton-decoupled ^{13}C nmr spectrum of compound **3*** showed resonances at 131.30 (t, J = 237 Hz), 34.41 (t, J = 19 Hz), 32.06 (s), 29.09 (s), 29.07 (t, J = 32 Hz), 22.90 (s), 22.42 (t, J = 5 Hz), and 14.14 (s) ppm. The proton-decoupled spectrum of ^{13}C enriched compound **3*** showed that only the resonance at 34.41 ppm was enhanced.

*1,2-Difluorooctane-1-^{13}C (**4***)*

The proton decoupled nmr spectrum of **4*** showed a doublet of doublets centered at 84.45 ppm (J = 174 Hz, J = 24 Hz). The proton coupled spectrum showed 10 lines in the intensity ratio of 1:1:2:3:1:1:3:2:1:1. The ^{13}C resonance in **4*** was split into a doublet by a geminal fluorine (J = 174 Hz), each branch of which was further split into a triplet by the two geminal protons (J = 150 Hz), each branch of which was still further split into a doublet by the vicinal fluorine atom (J = 24 Hz).

*1-Acetoxy-2-fluorooctane-1-^{13}C (**7***)*

The proton decoupled ^{13}C nmr spectrum of **7*** showed a doublet centered at 65.83 ppm (J = 23 Hz). The proton coupled ^{13}C nmr spectrum showed a triplet of doublets (J_t = 147 Hz, J_d = 23 Hz). The large coupling constant was assigned to the ^{13}C resonance split by the two hydrogens directly attached to the enriched carbon, while the small coupling was assigned to the vicinal ^{13}C fluorine interaction.

Acknowledgements

The authors wish to thank the National Research Council of Canada and the University of Alberta for their generous support of this work. One of the authors (D.D.T.) is also grateful to the administration of the University of St. Andrews and the Faculty of the Department of Chemistry at St. Andrews for their hospitality during the period in which this manuscript was prepared.

1. D. D. TANNER and P. VAN BOSTELEN. J. Am. Chem. Soc. **94**, 3187 (1972).
2. D. D. TANNER, P. VAN BOSTELEN, and M. LAI. Can. J. Chem. **54**, 2004 (1976).
3. J. BORNSTEIN and L. SKARLOS. J. Am. Chem. Soc. **90**, 5044 (1968).
4. M. EPHRITIKHINE and J. LEVISALLES. Chem. Comm. 429 (1974).
5. J. BORNSTEIN and M. R. BORDEN. Chem. Ind. London, 441 (1958).
6. J. LEVISALLES and J. MOLIMARD. Bull. Soc. Chim. Fr. 2037 (1971).
7. P. W. KENT, J. E. G. BARNETT, and K. R. WOOD. Tetrahedron Lett. 1345 (1963).
8. W. A. SHEPPARD and C. M. SHARTS. Organic fluorine chemistry. W. A. BENJAMIN, New York, N.Y. 1969. p. 34.
9. G. A. OLAH and M. B. COMISAROW. J. Am. Chem. Soc. **91**, 2955 (1969).
10. G. A. OLAH, Y. K. MO, and Y. HALPERN. J. Am. Chem. Soc. **94**, 3551 (1972).
11. A. V. GROSSE, and C. B. LINN. J. Am. Chem. Soc. **64**, 2289 (1942).
12. M. W. RENOLL. J. Am. Chem. Soc. **64**, 1115 (1942).
13. F. L. M. PATTISON, D. A. V. PETERS, and F. H. DEAN. Can. J. Chem. **43**, 1693 (1965).
14. D. SWERN, G. N. BILLEN, and J. T. SCANLAN. J. Am. Chem. Soc. **68**, 1505 (1946).
15. M. CALVIN, C. HEIDELBERGER, J. C. REID, B. M. TOLBERT, and P. E. YANKWICH. Isotopic carbon. John Wiley and Sons, Inc., New York, N.Y. 1949. p. 178.
16. J. P. WIBAUT and A. J. VAN PELT, JR. Recl. Trav. Chem. **57**, 1055 (1938).
17. J. W. EMSLEY, J. FEENEY, and L. H. SUTCLIFFE. High resolution nuclear magnetic resonance. Vol. 2. Pergamon Press, Inc., London. 1966. pp. 1011–1028.

Can. J. Chem. Downloaded from www.nrcresearchpress.com by 210.87.254.42 on 09/05/12
For personal use only.

Coordination properties of β-alanine: new complexes with some transition metals cobalt(II), nickel(II), and copper(II)

GIUSEPPE MARCOTRIGIANO

Cattedra di Chimica, Facoltà di Medicina Veterinaria, University of Bari, 70126 Bari, Italy

AND

LEDI MENABUE AND GIAN CARLO PELLACANI

Istituto di Chimica Generale e Inorganica, University of Modena, 41100 Modena, Italy

Received December 16, 1975

GIUSEPPE MARCOTRIGIANO, LEDI MENABUE, and GIAN CARLO PELLACANI. Can. J. Chem. **54**, 2426 (1976).

The neutral six-coordinated tetragonal $Co(\beta\text{-ala})_2 \cdot 2H_2O$ complex (β-ala = $NH_2CH_2CH_2CO\text{-}O^-$) was prepared. In this complex β-alanine acts as an O,N-chelating agent, as in the known $Cu(\beta\text{-ala})_2 \cdot 6H_2O$ and $Ni(\beta\text{-ala})_2 \cdot 3H_2O$ complexes. We also prepared some complexes of a type that is new for β-alanine, with stoichiometries such as $M(\beta\text{-alaH})_2X_2$, $M(\beta\text{-alaH})_4(ClO_4)_2$ (M = Co and Ni), $Cu(\beta\text{-alaH})_3(ClO_4)_2$, and $Cu(\beta\text{-alaH})Cl_2$ (β-alaH = $\overset{+}{N}H_3CH_2CH_2COO^-$), in which the ligand acts as a zwitterion and coordinates toward the carboxy group as a formally neutral ligand. The possibility of formulating the complexes as $H_2[M(\beta\text{-ala})_2X_2]$ is discussed. The electronic spectra and the magnetic moments of the halide complexes are in accord with pseudo-tetrahedral, octahedral, and tetragonal stereochemistry for the cobalt(II), nickel(II), and copper(II) ions, respectively, while those of the perchlorate complexes are in accord with pseudooctahedral stereochemistry. The β-alanine hydrohalide salts and the bis(β-alaninium)-tetrachlorocuprate complex were also prepared and are discussed.

GIUSEPPE MARCOTRIGIANO, LEDI MENABUE et GIAN CARLO PELLACANI. Can. J. Chem. **54**, 2426 (1976).

On a préparé le complexe neutre hexacoordonné tétragonal $Co(\beta\text{-ala})_2 \cdot 2H_2O$ (β-ala = $NH_2CH_2CH_2COO^-$). Dans ce complexe, la β-alanine agit comme un agent chélatant par l'oxygène et l'azote; ce comportement est aussi connu dans les complexes $Cu(\beta\text{-ala})_2 \cdot 6H_2O$ et $Ni(\beta\text{-ala})_2 \cdot 3H_2O$. On a aussi préparé quelques complexes d'un type nouveau pour la β-alanine et possédant des stoechiométries telles que $M(\beta\text{-alaH})_2X_2$, $M(\beta\text{-alaH})_4(ClO_4)_2$ (M = Co et Ni), $Cu(\beta\text{-alaH})_3(ClO_4)_2$ et $Cu(\beta\text{-alaH})Cl_2$ (β-alaH = $\overset{+}{N}H_3CH_2CH_2COO^-$), dans lesquels le ligand, neutre d'une façon formelle et agissant comme un zwitterion, est coordonné par le groupe carboxyle. On discute de la possibilité de représenter les complexes par la formule $H_2[M(\beta\text{-ala})_2X_2]$. Les spectres électroniques et les moments magnétiques des halogénures complexes sont en accord avec des stéréochimies pseudotétraédrique, octaédrique et tétragonale respectivement pour les ions cobalt(II), nickel(II) et cuivre(II); par ailleurs les propriétés des complexes perchlorates correspondent à des stéréochimies pseudooctaédriques. On a aussi préparé et on discute des complexes de sels halohydriques de la β-alanine et du bis(β-alaninium) tétrachlorocuprate.

[Traduit par le journal]

Introduction

Our understanding of the nature of metal-binding sites in proteins owes much to the study of models involving metal complexes with amino acids and small peptides. The coordinating power of amino-acid side chains towards metals, particularly copper(II), has been the object of a great deal of investigation and has been taken into account in many discussions of metal-binding sites in proteins.

Many simple amino-acids have been complexed with a large number of transition metal ions, and a recent review (1) collects the data relating to interactions between transition metal ions and α-amino acids which, formally, act as tridentate ligands.

In this work we study the interactions of the cobalt(II), nickel(II), and copper(II) ions with β-alanine.

The crystal structure (2) and the esr spectra (3–5) of the $Cu(\beta\text{-ala})_2 \cdot 6H_2O$ complex and the electronic and vibrational spectra of the bis-hydrate and anhydrous $Ni(\beta\text{-ala})_2$ complex (6) are known. Also, the rate constants for the formation of Co^{2+}, Ni^{2+} (7), and Cu^{2+} (8) complexes with β-alanine have been measured by

Can. J. Chem. Downloaded from www.nrcresearchpress.com by 210.87.254.105 on 09/05/12
For personal use only.

Can. J. Chem. Downloaded from www.nrcresearchpress.com by 210.87.254.105 on 09/05/12
For personal use only.

temperature-jump and stopped-flow methods.

This study represents an extension of our previous research in which we have investigated the complexes of some transition metal ions with some amino-acids, such as *N*-acetylglycine and *N*-benzoylglycine, and their amine adducts (9).

Experimental

All the reagents were of pure commercial grade.

Preparation of the Complexes

Co(β-ala)$_2$·2H$_2$O was obtained by adding 4×10^{-3} mol of freshly prepared $Co(OH)_2 \cdot nH_2O$ to 10^{-2} mol of β-alanine in 10 ml of H_2O with stirring at 40–50 °C. The unreacted cobalt salt was filtered off and the wine-red solution was cooled at 4–5 °C overnight to yield a pink crystalline compound.

Co(β-alaH)$_4$(ClO$_4$)$_2$ and *Cu(β-alaH)$_3$(ClO$_4$)$_2$*. Solid β-alanine (8×10^{-3} mol) were slowly added with stirring to a 60–70 °C methanolic solution containing 2×10^{-3} mol of $M(ClO_4)_2 \cdot 6H_2O$. The undissolved β-alanine was rapidly filtered off. The lilac cobalt compound was separated by cooling the wine-red solution. The copper(II) compound was separated by concentrating the blue solution, adding diethyl ether until a blue oil was obtained, and cooling the oil at 4–5 °C overnight.

Ni(β-alaH)$_4$(ClO$_4$)$_2$. β-Alanine (1×10^{-2} mol) was suspended in a methanolic solution (15 ml) of $Ni(ClO_4)_2 \cdot 6H_2O$ (2.5 mol) and refluxed for 2 h on a water bath. By concentrating (5 ml) the solution and adding an acetone – diethyl ether (1:1) solution a blue oil separated out. The oil crystallized by cooling in an ice bath overnight. This compound was also recrystallized by dissolving it in methanol and adding acetone as precipitating agent.

M(β-alaH)$_2$X$_2$ (M = Cu, Ni and X = Cl, Br; M = Co and X = Cl, Br, I). The complexes were prepared by refluxing 4×10^{-3} mol of solid β-alanine suspended in a methanolic solution of anhydrous cobalt(II) or nickel(II) halide or in an ethanolic solution of anhydrous copper(II) halide (2×10^{-3} mol in 30 ml) at 70–80 °C until a limpid solution was obtained. Acetone was added until incipient precipitation and then the solution was cooled in an ice bath. The cobalt(II) halide complexes are blue, $Co(\beta\text{-alaH})_2I_2$ is olive-green, and the nickel(II) complexes are green.

Cu(β-alaH)Cl$_2$ was prepared by the reaction of 2×10^{-3} mol of $CuCl_2 \cdot 2H_2O$ in absolute ethanol (20 ml) with 2×10^{-3} mol of β-alanine, as described above.

CuCl$_4$(β-alaH$_2$)$_2$. β-Alanine hydrochloride (2×10^{-3} mol) in 10 ml of absolute ethanol were added with stirring to a 50–60 °C ethanolic solution (15 ml) of $CuCl_2 \cdot 2H_2O$. By cooling the solution at 4–5 °C, a yellow crystalline product was obtained.

The compounds prepared cannot be recrystallized, they are hygroscopic, particularly the cobalt(II) complexes, and decompose in air. They are insoluble in apolar solvents and fairly soluble, with decomposition, in methanol.

Physical Measurements

The electronic spectra of the solid compounds were recorded on a Beckman DK 1A spectrophotometer. The samples were prepared by grinding the complexes using a filter paper as support and a filter paper as reference. Since these compounds are highly hygroscopic the instrument was flushed with dry nitrogen before and during use. The infrared spectra of KBr pellets were recorded with a Perkin-Elmer 521 (4000–250 cm^{-1}) spectrophotometer. The room-temperature magnetic moments were measured by the Gouy method using $Ni(en)_3S_2O_3$ as calibrant and correcting for diamagnetism with the appropriate Pascal constants. The conductivities of the complexes in methanol were measured with a WTW conductivity bridge.

Analyses

Nitrogen, carbon, and hydrogen were analysed by Mr. Giuseppe Pistoni on a Perkin-Elmer 240 elemental analyzer. The halides were analysed by titration with the Volhard method after disgregation of the compound with the alkali metal fusion method (10).

Results and Discussion

The compounds are listed in Table 1. Their preparations and general properties are described in the Experimental section.

We were unable to determine molecular weights, because the compounds were insufficiently soluble or were unstable in suitable solvents (*e.g.* methanol).

The conductivity measurements of some compounds are reported in Table 1. The values obtained are in the range proposed for 2:1 electrolytes (11), but the electronic spectra of the solution (10^{-3} *M*) are indicative of a decomposition of the compounds in solution. In particular very concentrated solutions of the blue cobalt(II) complexes are pink, while 10^{-3} *M* solution of all the compounds are colourless.

In the near-ir region β-alanine shows bands at 4310, 4650, 5130, 5710, and 6070 cm^{-1}, which also appear in all the complexes in virtually the same positions with the same intensities, with the exception of the band at 4650 cm^{-1}, which is shifted to higher energies (4950–4780 cm^{-1}) and is enhanced in intensity only in the $M(\beta\text{-ala})_2 \cdot xH_2O$ ($x = 2$ for M = Co, $x = 3$ for M = Ni, and $x = 6$ for M = Cu) complexes. This band may thus be used to recognize this type of complexes.

The *d–d* bands of the complexes are reported in Table 2. The electronic spectra of the metal halide complexes are typical of octahedral nickel(II) ion, six-coordinate copper(II) ion, and pseudotetrahedral cobalt(II) ion, respectively, and suggest in all these complexes halide co-

TABLE 1. Analytical, magnetic, and conductivity data[a]

Compound	C		H		N		X		μ_{eff} (B.M.)	λ_M 10^{-3} M (MeOH)
	Calcd.	Found	Calcd.	Found	Calcd.	Found	Calcd.	Found		
$Co(\beta\text{-ala})_2\cdot 2H_2O$	26.56	26.48	5.95	6.10	10.33	10.06			5.10	
$Co(\beta\text{-alaH})_2Cl_2$	23.38	24.02	4.58	4.77	9.09	8.88	23.02	22.47	4.93	
$Co(\beta\text{-alaH})_2Br_2$	18.14	18.05	3.56	4.24	7.06	6.33	40.27	39.99	4.75	
$Co(\beta\text{-alaH})_2I_2$	14.79	14.80	2.90	3.63	5.75	5.13			4.61	
$Co(\beta\text{-alaH})_4(ClO_4)_2$	23.45	24.26	4.59	5.13	9.12	8.77	11.55	10.91	4.31	
$Ni(\beta\text{-alaH})_2Cl_2$	23.39	23.88	4.59	5.69	9.10	8.24	23.04	22.69	3.20	123
$Ni(\beta\text{-alaH})_2Br_2$	18.15	17.97	3.56	4.13	7.06	6.61	40.27	40.08	3.26	143
$Ni(\beta\text{-alaH})_4(ClO_4)_2$	23.46	23.58	4.60	4.68	9.13	8.34	11.52	10.93	[b]	138
$Cu(\beta\text{-alaH})_2Cl_2$	23.03	22.90	4.51	4.42	8.96	8.07	22.69	22.22	1.82	111
$Cu(\beta\text{-alaH})Cl_2$	16.11	16.40	3.16	3.38	6.27	6.18	31.73	31.77	1.72	
$Cu(\beta\text{-alaH})_2Br_2$	17.93	17.96	3.51	3.68	6.98	6.57	39.81	39.37	1.99	139
$Cu(\beta\text{-alaH})_3(ClO_4)_2$	20.39	20.11	4.00	4.23	7.93	7.28	13.39	13.01	1.97	183
$CuCl_4(\beta\text{-alaH}_2)_2$	18.77	19.05	3.68	4.29	7.30	7.21	36.98	36.63	1.95	

[a]Abbreviations: β-ala = $NH_2\cdot CH_2CH_2\cdot COO^-$; β-alaH = $NH_3^+\cdot CH_2\cdot CH_2\cdot COO^-$; β-alaH$_2$ = $NH_3^+\cdot CH_2\cdot CH_2\cdot COOH$.
[b]Not measured, for packing difficult, the compound being highly hygroscopic.

TABLE 2. *d–d* transitions (cm^{-1}) of the complexes in the solid state

Compound	Transition (cm^{-1})									
$Co(\beta\text{-ala})_2\cdot 2H_2O$		8 330		10 530sh	20 410sh	21 510				
$Co(\beta\text{-alaH})_2Cl_2$	5 350sh	5 880	6 990	8 620sh	14 710	15 270sh	16 000	17 240sh	20 000sh	
$Co(\beta\text{-alaH})_2Br_2$		5 130	5 790	8 330sh	14 230	14 600sh	15 150	15 750sh	16 750sh	18 870sh
$Co(\beta\text{-alaH})_2I_2$					12 990	14 290sh	15 880sh	19 610	26 320	
$Co(\beta\text{-alaH})_4(ClO_4)_2$		6 800		8 130	18 020	19 230sh				
$Ni(\beta\text{-alaH})_2Cl_2$				8 770	14 700	25 320				
$Ni(\beta\text{-alaH})_2Br_2$				8 550	14 280	25 000				
$Ni(\beta\text{-alaH})_4(ClO_4)_2$				9 710	16 130	26 670				
$Cu(\beta\text{-alaH})_2Cl_2$					13 880					
$Cu(\beta\text{-alaH})_2Br_2$				10 530sh	12 820					
$Cu(\beta\text{-alaH})Cl_2$				10 200sh	12 500					
$Cu(\beta\text{-alaH})_3(ClO_4)_2$				12 500sh	15 630					
$CuCl_4(\beta\text{-alaH}_2)_2$					12 650					

ordination, as the energy order of the *d–d* bands is Cl > Br > I, in accordance with the spectrochemical series. Their magnetic moments agree with the proposed stereochemistries.

The absorption peaks in the nickel-complex spectra (Fig. 1) indicate a fairly symmetrical octahedral field. The low energy band, which represents the average ligand field strength (12), is broad.

In the spectra of the cobalt(II) halide complexes (Fig. 2) the splitting for the $^4T_1(F)$ term suggests a marked effect of a low symmetry component of the crystal field (13).

The electronic spectrum of the nickel(II) perchlorate complexes (Fig. 1) is similar to those of the nickel(II) halide complexes, suggesting an octahedral environment. The energy of the *d–d* bands of the halide complexes which is lower than that of the perchlorate complex depends on the donor strength of the halides.

The electronic spectra of the $Co(\beta\text{-ala})_2\cdot 2H_2O$ and of the $Co(\beta\text{-alaH})_4\cdot(ClO_4)_2$ complexes (Fig. 2) show a weak intensity band split into two components in the near ir region and a more intense multiple band in the 18 000–22 000 cm^{-1} region. The absorption band regions are characteristic of six-coordinate cobalt(II) derivatives, as is confirmed by their magnetic moments, but the splitting of the near-ir band also suggests the existence of distortion from a regular octahedral structure in both the complexes (14).

In the $Co(\beta\text{-ala})_2\cdot 2H_2O$ complex, as in the hydrate nickel and copper β-alaninate complexes, the β-ala ligands have a *trans*, square-

Can. J. Chem. Downloaded from www.nrcresearchpress.com by 210.87.254.105 on 09/05/12
For personal use only.

Can. J. Chem. Downloaded from www.nrcresearchpress.com by 210.87.254.105 on 09/05/12
For personal use only.

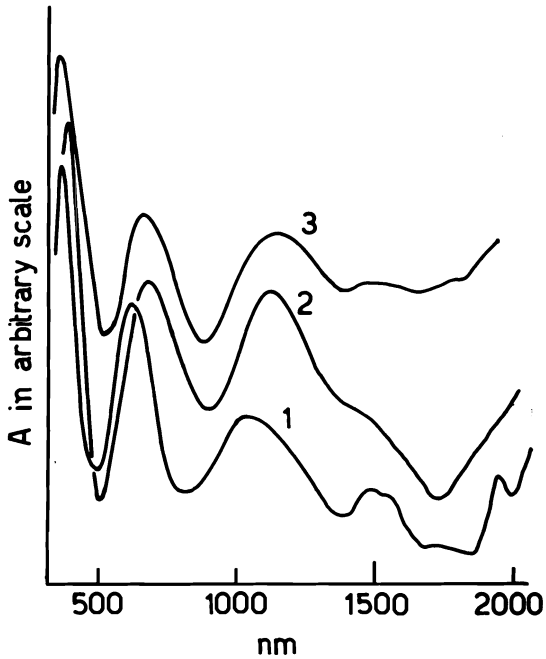

FIG. 1. Examples of electronic spectra of the Ni(β-alaH)$_4$(ClO$_4$)$_2$ (*1*), Ni(β-alaH)$_2$Cl$_2$ (*2*), and Ni(β-alaH)$_2$Br$_2$ (*3*) complexes.

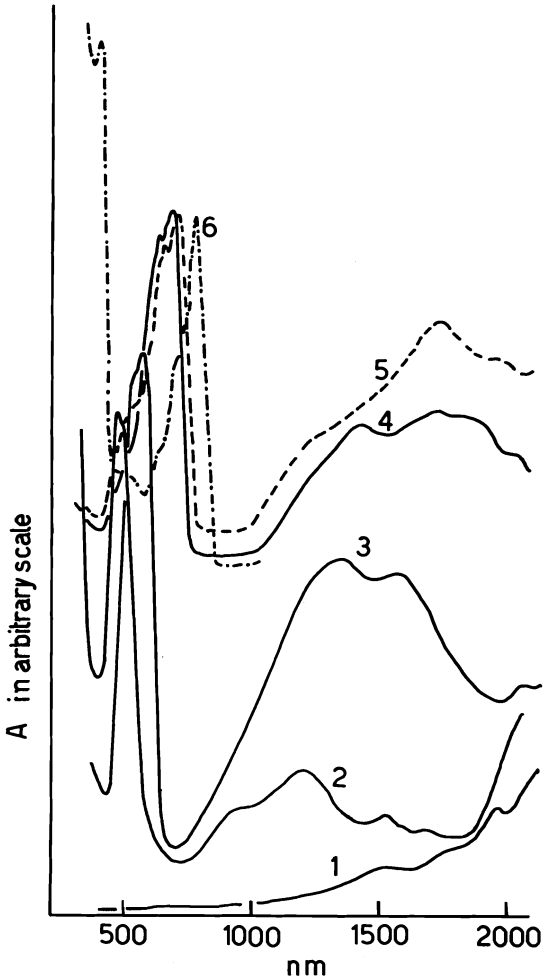

FIG. 2. Examples of electronic spectra of the β-alanine (*1*) and of the Co(β-ala)$_2$.2H$_2$O (*2*), Co(β-alaH)$_4$(ClO$_4$)$_2$ (*3*), Co(β-alaH)$_2$X$_2$ (X = Cl (*4*), Br (*5*) and I (*6*)).

planar arrangement about the metal atom, and the octahedral coordination completed by two water molecules (15).

The assignment of all the bands of the ir spectra of the β-alanine has not been made, but those of NH stretching and antisymmetric and symmetric carboxy stretching frequencies are straightforward. Of primary concern for determining the nature of coordination is the positions of the antisymmetric and symmetric carboxy stretching frequencies and their separations. These are listed in Table 3.

The bands at 1720–1689 and 1236–1190 cm^{-1} and their separation in the β-alanine hydrohalide salts are consistent with those of other amino acids and their hydrohalide salts in which the —COOH group is present (16, 17). The infrared spectra of all the other compounds show a single peak, except the cobalt(II) and copper(II) perchlorate complexes, in the 1610–1545 cm^{-1} region. The absence of absorption at higher wave numbers indicates that no uncomplexed —COOH groups are present (18–20).

In the M(β-ala)$_2\cdot x$H$_2$O (M = Co, Ni, and Cu) complexes of known structure (15), the asymmetric carboxy stretching vibration and the $\Delta\nu$ separation are assumed to typify a monodentate carboxyl group coordination, being also in the range found for other monocoordinated carboxyl group amino acid (6). The energy order of the ν(COO)$_a$ is Ni > Co > Cu.

In the Cu(β-alaH)$_2$X$_2$ complexes, which show $\Delta\nu$ and ν(COO)$_a$ similar to those of the above mentioned complexes, a similar monodentate coordination of the carboxyl group may be proposed.

In the Cu(β-alaH)X$_2$ and M(β-alaH)$_2$X$_2$ (M = Co and Ni) complexes the position of the ν(COO)$_a$, which is in the order Ni > Co > Cu, similar to that found for the M(β-ala)$_2\cdot x$H$_2$O

Can. J. Chem. Downloaded from www.nrcresearchpress.com by 210.87.254.105 on 09/05/12
For personal use only.

TABLE 3. Some ir absorption frequencies (cm^{-1}) of the complexes[a]

Compound	ν(NH)	$\nu(COO)_{as}$	$\nu(COO)_s$	$\Delta\nu$
β-ala	2800–2640vs	1623vs	1386vs	237
β-alaH$_2$·Cl	3170s	1720vs	1190vs	530
β-alaH$_2$·Br	3170s	1700vs	1210vs	490
β-alaH$_2$·I	3140s	1689vs	1236vs	453
$CuCl_4$(β-alaH$_2$)$_2$	3100vsb	1702vs	1230vs	472
Co(β-ala)$_2$·2H$_2$O	3303ms 3250m	1590vs	1402vs	188
Ni(β-ala)$_2$·3H$_2$O[b]	3330–3160	1598	1411	187
Cu(β-ala)$_2$·6H$_2$O	3310s 3170s 3100s	1585vs	1400vs	185
Co(β-alaH)$_2$Cl$_2$	3200sh 3120sb	1560vsb	1420vs	140
Co(β-alaH)$_2$Br$_2$	3200sh 3100sb	1560vsb	1420vs	140
Co(β-alaH)$_2$I	3180sh 3100sb	1550vsb	1420vs	130
Co(β-alaH)$_4$(ClO$_4$)$_2$	3250m 3120m	1612vs 1570vs	1400vs	212(170)
Ni(β-alaH)$_2$Cl$_2$	3200sh 3100sb	1570vsb	1422vs	148
Ni(β-alaH)$_2$Br$_2$	3208sh 3080sb	1570vsb	1420vs	150
Ni(β-alaH)$_4$(ClO$_4$)$_2$	3225m 3140mb	1590vsb	1396vs	194
Cu(β-alaH)Cl$_2$	3190s 3100s	1545vs	1424vs	121
Cu(β-alaH)$_2$Cl$_2$	3235m 3135w	1610vs	1426vs	184
Cu(β-alaH)$_2$Br$_2$	3160sh 3090ms	1610vs	1421vs	189
Cu(β-alaH)$_3$(ClO$_4$)$_2$	3300ms	1600vs 1560vs	1402vs	198(158)

[a]The values reported for the M(β-alaH)$_2$X$_2$ (M = Co and Ni) complexes are the average of a rather broad band probably containing also the δ(NH) vibration. These complexes and the perchlorate ones show a broad band at 3480–3350 which may be due to the absorption of moisture when the KBr pellets of these compounds are prepared.
[b]Reference 6.

complexes, and the $\Delta\nu$ separation are reduced compared with those of the complexes containing a monodentate coordinated carboxyl group. This reduction was also found in the acetate (21) and in the haloacetate (22) complexes of cobalt(II), nickel(II), and copper(II), for which a bidentate coordination of the carboxyl group is proposed.

The ν(NH) bands of these complexes, lower than those of the M(β-ala)$_2$·xH$_2$O complexes which are also coordinated toward the nitrogen atom (15), are in the range of the ν(NH) found in the β-alanine hydrohalide salts and in other hydrochloride salts of amino acids in which the NH_3^+ group is present (16, 17).

All these data indicate that the ligand may be zwitterionic and coordinate as formally neutral ligand, as

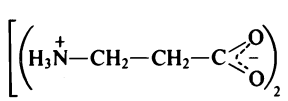

M = Co, Ni, or Cu
X = Cl, Br for Ni and Cu
Cl, Br, I for Co

The presence of the O and X atom in the coordination sphere of the metal ion is justified by the low energy *d–d* bands of these complexes.

An alternative hypothesis is suggested by the fact that in these complexes the presence of uncomplexed —COO^- groups is not precluded, since they absorb in the same region as carboxyl groups which are coordinated (20) and by the fact that the ν(NH) bands are also in the range expected for coordinated NH_2 groups (23). This would permit the formulation of the halide complexes as H$_2$[M(β-ala)$_2$X$_2$], in which the ligand is only coordinated toward the nitrogen atom.

We prefer the first hypothesis which also permits the interpretation of the perchlorate complexes. If the ligand is in the zwitterionic form coordinated toward the oxygen atom, the two ν(COO) bands in the cobalt(II) and copper(II) perchlorate complexes suggest the presence of mono and bidentate carboxyl groups. The ν(NH) bands, higher than those of the halide complexes, may be explained as due to the interaction of the NH_3^+ group with the ClO_4^- anions. In fact the ir bands of the ClO_4^- ions correspond to a slight deformation of this ion from T_d symmetry (24).

The electronic spectrum of the $CuCl_4$(β-alaH$_2$)$_2$ complex, for which no thermochromic behaviour was observed in the 290–370 K temperature range, suggests near square-planar configuration

of the $CuCl_4^{2-}$ anion (25, 26), which indicates the prevailing effect of the crystal field stabilization, since extensive N—H···Cl hydrogen bonding reduces the effective charge on the chlorine atoms (27, 28). The red shift of the ν(NH) band of this complex, as distinct from that of the β-alanine hydrohalide supports this hypothesis. The ir and far-ir spectra of this complex closely resemble those of the β-alanine hydrochloride salt, except for three bands at 270vs, 282sh and 200s, assignable to metal–chlorine vibration in D_{2h} symmetry (28).

Acknowledgement

The authors are grateful to the Istituto di Chimica Generale e Inorganica of the University of Modena which has supplied us the instruments.

1. S. T. Chow and C. A. McAuliffe. Prog. Inorg. Chem. **19**, 51 (1975).
2. K. Tomita. Bull. Chem. Soc. Jpn. **34**, 297 (1961).
3. A. D. Semenov, V. G. Zaletov, and I. M. Semenova. Teor. Exsp. Khim. **5**, 523 (1969).
4. H. Yokoi, M. Otagiri, and T. Isobe. Bull. Chem. Soc. Jpn. **44**, 2395 (1971).
5. H. Yokoi, M. Sai, T. Isobe, and S. Ohsawa. Bull. Chem. Soc. Jpn. **45**, 2189 (1972).
6. C. A. McAuliffe and W. D. Perry. J. Chem. Soc. (A), 634 (1969).
7. R. F. Pasternack, M. Angwin, L. Gipp, and R. Reingold. J. Inorg. Nucl. Chem. **34**, 2329 (1972).
8. W. B. Makinen, A. F. Pearlmutter, and J. E. Stuehr. J. Am. Chem. Soc. **91**, 4083 (1969).
9. G. Marcotrigiano and G. C. Pellacani. Can. J. Chem. **52**, 3607 (1974); Z. Anorg. Allgem. Chem. **413**, 171 (1975); Inorg. Nucl. Chem. Lett. **11**, 643 (1975); Z. Anorg. Allgem. Chem. **415**, 268 (1975).
10. A. Steyermark. Quantitative organic microanalysis. Academic Press, New York, N.Y. 1961. p. 333.
11. W. J. Geary. Coord. Chem. Rev., **7**, 81 (1971).
12. R. S. Drago. Physical methods in inorganic chemistry. Reinhold, New York, N.Y. 1965. Chapt. 6.
13. B. B. Garrett, V. L. Goedken, and J. V. Quagliano. J. Am. Chem. Soc. **92**, 489 (1970).
14. A. B. P. Lever. Inorganic electronic spectroscopy. Elsevier Publ. Co., New York, N.Y. 1968. p. 318.
15. H. C. Freeman. Advan. Protein Chem. **22**, 257 (1967).
16. C. N. R. Rao. Chemical applications of infrared spectra. Academic Press Inc., New York, N.Y. 1963. pp. 246, 255.
17. L. J. Bellamy. The infrared spectra of complex molecules. J. Wiley and Sons, Inc., New York, N.Y. 1959. p. 165.
18. F. D. Dwyer and F. L. Garvan. J. Am. Chem. Soc. **82**, 4823 (1960).
19. J. A. Neal and N. J. Rose. Inorg. Chem. **12**, 1226 (1973).
20. R. E. S. Sievers and J. C. Bailar, Jr. Inorg. Chem. **1**, 174 (1962).
21. N. F. Curtis. J. Chem. Soc. (A), 1579 (1968).
22. A. B. P. Lever and D. Ogden. J. Chem. Soc. (A), 2041 (1967).
23. G. F. Svatos, C. Curran, and J. V. Quagliano. J. Am. Chem. Soc. **77**, 6159 (1955).
24. I. M. Procter, B. J. Hathaway, and P. Nicholls. J. Chem. Soc. (A), 1678 (1968).
25. R. D. Willett. J. Chem. Phys. **44**, 39 (1966).
26. R. D. Willett and O. L. Liles, Jr. Inorg. Chem. **6**, 1666 (1967).
27. G. Felsenfeld. Proc. Roy. Soc. (London) A**236**, 506 (1956).
28. R. D. Willett, J. R. Ferraro, and M. Choca. Inorg. Chem. **13**, 2919 (1974).

Can. J. Chem. Downloaded from www.nrcresearchpress.com by 210.87.254.105 on 09/05/12
For personal use only.

The stereochemistry of 1,3,5-trimethyl-4-piperidone and its 4-phenylalcohol derivatives

P. HANISCH AND ALAN J. JONES[1]

Department of Chemistry, University of Alberta, Edmonton, Alta., Canada T6G 2G2

Received December 23, 1975

P. HANISCH and ALAN J. JONES. Can. J. Chem. **54**, 2432 (1976).

The configurations in solution of the three diastereoisomeric alcohols obtained from the reaction of phenyllithium on 1,3,5-trimethyl-4-phenylpiperidone have been determined unequivocally using ^{13}C and ^{1}H magnetic resonance methods.

P. HANISCH et ALAN J. JONES. Can. J. Chem. **54**, 2432 (1976).

Faisant appel à la résonance magnétique nucléaire du ^{1}H et du ^{13}C, on a déterminé sans équivoque les configurations en solution des trois alcools diastéréoisomères obtenus par réaction du phényllithium sur la triméthyl-1,3,5 phényl-4 pipéridone.

[Traduit par le journal]

The isolation of the three isomeric 1,3,5-trimethyl-4-phenyl-4-piperidinols from a phenyllithium reaction on the corresponding ketone was originally described by Sorokin (1). The structures of the three isomers were assigned as **α**, **β**, and **γ** on the basis of their ease of esterification. No spectroscopic evidence was presented. Sorokin (1) also showed that the propionic ester hydrochlorides of the α- and β-isomers (*cis* Me–Me) were analgesically inactive, while the

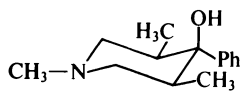

α

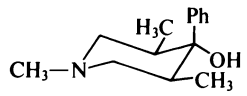

β

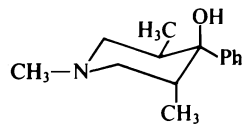

γ

ester hydrochloride of the γ-isomer (*trans* Me–Me) was as potent as promedol (2). It was suggested that the inactivity of the *cis*-isomers may be due to the equatorial methyl groups hindering the formation of a drug–receptor complex. The inverted chair form of the γ-isomer in which the phenyl group is axially oriented occurs only to the extent of 15% (3).

In previous papers we have exhibited the value of nmr studies in assigning stereochemistry in active analgesic compounds (4–7). In particular, we have shown that the preferred conformations of the four diastereoisomers in the analogous 1,2,5-trimethyl (promedol) derivatives (5) had been assigned incorrectly. It, therefore, seemed desirable to repeat Sorokin's synthesis and to determine the configuration of the α-, β-, and γ-1,3,5-isomers unequivocally using nmr methods.

Results

The ^{13}C and ^{1}H nmr data for 1,3,5-trimethyl-4-piperidone **1** and its 4-phenylalcohol α-, β-, and γ-isomers and their hydrochlorides are summarised in Tables 1 and 2, respectively. The conventional labelling system for the piperidine ring is employed. Carbon atoms in substituents are identified by a prime symbol for the number appropriate to the position of substitution on the piperidine ring. Phenyl ring carbon atoms are labelled C-*q*, C-*o*, C-*m*, and C-*p*, corresponding to the quaternary, *ortho*, *meta*, and *para*-carbon sites, respectively.

In the above compounds symmetry is exhibited by the ^{13}C nmr spectra in all but the γ-isomer. In the α- and β-isomers the double intensity of the resonances due to the equivalent carbons

[1]Address correspondence to this author: The National NMR Centre, Australian National University, Canberra, A.C.T., 2600, Australia.

Can. J. Chem. Downloaded from www.nrcresearchpress.com by 210.87.254.6 on 09/05/12
For personal use only.

TABLE 1. ^{13}C chemical shifts[a] of 1,3,5-trimethyl-4-piperidone, the α-, β-, and γ-4-phenyl-4-ol derivatives and their corresponding hydrochlorides

Compound	Carbon position											
	C-2	C-3	C-4	C-5	C-6	C-1′	C-3′	C-5′	C-*q*	C-*o*	C-*m*	C-*p*
1	64.3_5	43.6_9	210.6_6	43.6_9	64.3_5	45.0_4	11.4_3	11.4_3				
1*a*	60.4_2	41.0_5	205.2_1	41.0_5	60.4_2	43.2_6	10.9_5	10.9_5				
1*a**[c]	59.5_1	41.0_5	209.2_1	41.0_5	59.5_1	43.3_3	10.3_2	10.3_2				
	(57.5_2)[b]	(39.2_8)	(93.0_1)	(39.2_8)	(57.5_2)		(9.5_0)	(9.5_0)				
α	58.9_1	40.8_3	75.9_6	40.8_3	58.9_1	46.1_2	12.2_4	12.2_4	145.6_0	128.0_7	126.3_4	125.1_6
α-HCl	55.8_3	38.7_9	74.6_1	38.7_9	55.8_3	43.4_3	11.9_8	11.9_8	142.9_6	128.2_3	126.9_4	124.5_8
β	60.2_6	43.9_7	76.6_6	43.9_7	60.2_6	45.6_9	13.2_7	13.2_7	141.5_6	127.7_4	127.3_1	126.5_0
β-HCl	57.9_4	41.2_1	74.5_0	41.2_1	57.9_4	43.6_4	12.5_2	12.5_2	139.2_4	129.4_2	128.2_3	127.2_6
γ	58.4_8	42.1_9	76.2_8	31.5_0	59.4_5	46.5_6	16.6_2	12.8_4	145.4_9	128.0_2	126.7_7	126.3_4
γ-HCl	56.2_1	41.0_5	74.9_7	30.1_6	56.2_1	44.5_6	15.9_7	12.5_9	143.0_6	128.2_8	126.4_5	127.4_7

[a]Given in ppm downfield from TMS. Solvent $CDCl_3$ except * in which D_2O was employed.
[b]Values in parentheses are approximately 10% the intensity of the parent resonance.
[c]Data converted using $\delta_C^{dioxane} = 66.7_4$ ppm.

C-2,6, C-3,5, and C-3′,5′ enable their distinction compared to the single intensity of the resonances due to C-1′ and C-4. Typical low field shifts for a carbonyl resonance (~200 ppm) distinguish the C-4 carbonyl carbon, while in the phenyl-alcohol isomers the C-4 resonance was identified using the modulated off-resonance method (see for example ref. 8). The off-resonance decoupled spectrum (8) exhibited the characteristic triplet pattern about the lower field methylene resonance and doublet for the methine carbon resonance (40–43 ppm). Quartets about the highest field resonances (10–13 ppm) characterised the C-3′,5′ methyl carbon atoms. The aromatic carbon atom assignments were made on the basis of the lower intensity exhibited by the quaternary and *para*-carbons compared with the *ortho*- and *meta*-carbons. Distinction between the former pair was achieved by off-resonance decoupling. Ambiguities still remain for the assignments of the C-*o* and C-*m* atoms in all cases. However, the lower field resonance was assigned to the *ortho* position comparable to previous assignments in the 4-phenyl-4-piperidinols (5, 6).

For the γ-isomer and its hydrochloride salt the absence of symmetry gave rise to equally intense resonances for all of the ring carbon atoms. Off-resonance and modulated off-resonance techniques enabled distinction of C-4, the quaternary carbon atom, and the methyl, methylene, and methine carbons. Complete assignments were made by consideration of substituent parameters and trends observed upon protonation as described in earlier studies (4–7).

TABLE 2. Proton chemical shifts[a] and coupling constants[b] of the N—Me and C—Me protons in the α-, β-, and γ-free bases and hydrochlorides

	N—Me	C—Me
α	2.3_0	0.5_7(6.0 Hz)
α-HCl	2.8_5(5.0 Hz)	0.6_7(5.5 Hz)
β	2.3_9	0.6_3(6.5 Hz)
β-HCl	3.0_4(4.5 Hz)	0.7_8(6.5 Hz)
γ	2.2_7	0.7_6(6.5 Hz) eq; 0.8_2(7.3 Hz) ax
γ-HCl	2.8_3(5.0 Hz)	0.9_0(4.5 Hz) eq; 1.1_0(8.0 Hz) ax

[a]Given in ppm downfield from TMS. Solvent $CDCl_3$.
[b] $^3J_{HH}$ values given in parentheses.

Discussion

Comparison of the ^{13}C chemical shifts in 1,3,5-trimethyl-4-piperidone and 1,3-dimethyl-4-piperidone (6) enables determination of the substituent effects of the equatorial methyl group (α, +3.1 ppm; β, +8.1 ppm). These values compare favourably with those observed generally in piperidine rings (+3.7 and +7.9 ppm, respectively) (4). The β-effect of the equatorial methyl on the carbonyl resonance induces an attenuated downfield shift (2.9 ppm). This attenuated effect was also noted by Jones and Hassan (4) and attributed to the electronic compensating effect of the carbonyl oxygen atom.

The pmr spectrum of the 1,3,5-trimethyl-4-piperidone hydrochloride salt was determined in both $CDCl_3$ and D_2O. In the former, the *N*-methyl signal appeared as a doublet (J_{HH} = 7 Hz) centered at 2.93 ppm and the ring methyl appeared as a doublet (J_{HH} = 6 Hz) centered at 1.09 ppm. In the latter solvent there was no

Can. J. Chem. Downloaded from www.nrcresearchpress.com by 210.87.254.6 on 09/05/12
For personal use only.

Can. J. Chem. Downloaded from www.nrcresearchpress.com by 210.87.254.6 on 09/05/12
For personal use only.

change in the ring methyl shift but the *N*-methyl signal occurred as a singlet at 3.11 ppm due to deuterium exchange of the N—H proton with the solvent. Other examples of coupling of the *N*-methyl signal in $CDCl_3$ solvent were observed in the pmr spectra of the α-, β-, and γ- hydrochloride derivatives (Table 2). The ^{13}C spectrum of the hydrochloride determined in D_2O gave duplicate resonances for the C-2,6, C-3,5 and C-3′,5′ carbon atoms. The 'new resonances' represent about 10% of the total concentration and are attributed to the 4,4-dideuteroxy compound **1***a* since a concomitant resonance was observed at 93 ppm, typical of a dihydroxy substituted carbon (C-4). Other examples of hydration of the C-4 carbonyl have been reported by Hassan and Casy (9) for the hydrochloride salt of 1,2,5-trimethyl-4-piperidone.

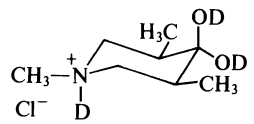

1a

The configuration of the α-isomer is identical to that proposed by Sorokin (1). The single ^{13}C resonance at 12.2_4 ppm characterises the equatorial methyl group (5). The C-*q* aromatic carbon at 145.6 ppm compares favourably with the equivalent carbon in the α-isomer of 1,3-dimethyl-4-phenyl-4-piperidinol (6) (147.5 ppm) if one considers the additional γ-shielding effect of the C-5 methyl group. In the 1,3-dimethyl system the phenyl group is established as having the equatorial orientation (6).

In the β-isomer the C-3,5 and C-3′,5′ carbon positions are deshielded by 3.1 ppm and 1.1 ppm, respectively, compared to the α-isomer. Similar effects (+3.0 and +2.4 ppm) were observed at the analogous C-5 and C-5′ carbon positions in the β-isomer of the 1,2,5-trimethyl-4-phenylpiperidin-4-ol in which the phenyl group is established as axial (5). The configuration of the phenyl group is also defined by the shift of the phenyl C-*q* carbon atom. In the 1,2,5-trimethyl- and 1,2-dimethyl-4-phenylpiperidin-4-ols this carbon is shielded by 2.3 and 3.8 ppm, respectively, compared to the isomer where the phenyl group is equatorial (5, 6). In the 1,3,5-trimethyl β-isomer the effect is similar (−4.0 ppm) and suggests similar conformations in the 1,2- and 1,3,5-systems. The attenuated value in the 1,2,5-isomer may be attributed to a change in the relative orientation of the phenyl ring.

The assignment of the ^{13}C chemical shifts in the γ-isomer was aided by the empirical additivity relationships derived from 1-methyl-4-phenylpiperidin-4-ol and α-1,3-dimethyl-4-phenylpiperidin-4-ol and applied to β-1,3-dimethyl-4-phenylpiperidin-4-ol (*i.e.*, α, +2.4; β_{C-q}, +3.3; β_{C-2}, 7.4 ppm) (6). The calculated shifts agree well for the C-4 and C-6 carbon atoms but deviate by 2.4 ppm at C-5. Evidently the α-substituent effect is compensated for by the possible 1,4-*gauche* interaction between the phenyl-*ortho* and the C-5 carbon positions. The C-1′ carbon resonance was assigned by a proton selective decoupling experiment and the chemical shift (46.56 ppm) is identical to that in the β-1,3-dimethyl system (46.49 ppm) (6). The methyl resonances at 16.6_2 ppm and 12.8_4 ppm are attributed to the axial and equatorial carbons, respectively. The high field methyl resonance compares favourably with that in the α-1,3,5-isomer (12.24 ppm). The low field shift of the axial methyl may be attributed to removal of the hydroxyl group γ-*gauche* effect. This hydroxyl γ-*gauche* effect is characterised between *cis*- and *trans*-2-*tert*-butyl-5-methyl-1,3-dioxane where the identical geometric relationship occurs between the axial C-5′ methyl group which is deshielded by 3 ppm compared to that in the equatorial isomer (10). Recently, Eliel *et al.* (11) have described a hyperconjugative type interaction arising between the free electron pairs centered on the hetero atom with the C_α—C_β bond, which is accompanied by a subsequent alternation of the electron density at the γ-antiperiplanar carbon (*i.e.*, the equatorial methyl group) to explain this effect. The shielding of the equatorial methyl groups in α-1,3-dimethyl- and γ-1,3,5-trimethyl-4-phenylpiperidin-4-ol compared with the axial methyl groups in β-1,3- and γ-1,3,5-trimethyl-4-phenylpiperidin-4-ol is thus accounted for. It also seems probable that the relative shifts of the equatorial and axial methyls in these systems may, at least in part, be due to contributions from the nitrogen lone pair (5, 6).

Comparison of the methyl carbon shifts in 1,3,5-trimethyl-4-phenylpiperidone **1** with those in α- and β-1,3-dimethyl-4-phenylpiperidine-4-ol (6) enables derivation of the *gauche–trans* and *trans–trans* δ-effects. The *gauche–trans* δ-effect is small and deshielding (+0.3 ppm) but in the

Can. J. Chem. Downloaded from www.nrcresearchpress.com by 210.87.254.6 on 09/05/12
For personal use only.

hydrochloride has a shielding value of −1.0 ppm (*cf.* ref. 12). The *trans–trans* δ-effect is small and shielding, −0.5 and −0.1 ppm in the 1,3,5- and α-1,2-systems, respectively.

As expected, protonation of the nitrogen atom results in upfield shifts at all piperidine ring carbons (4). Two features arise from the protonation additivity effects derived by comparing the free base and corresponding hydrochloride salt chemical shifts. (*i*) The equatorial methyl β-deshielding effect is attenuated by 2 ppm at the C-6 carbon in the hydrochlorides relative to the free bases. Presumably the positive charge on the nitrogen restricts the positive character of the adjacent carbon atom. (*ii*) The γ-effect at C-3 is increased by 2 ppm when the methyl groups are *trans* oriented in the free base of the γ-isomer compared to the *cis*-diequatorial methyls of the α-isomer.

The proton chemical shifts for the *N*-methyl and *C*-methyl proton resonances in the α-, β-, and γ-1,3,5-trimethyl free bases and hydrochlorides are given in Table 2. The pmr data for the γ-isomer clearly differentiate the axial and equatorial methyls (assigned on the basis of the observed $^3J_{HH}$ coupling constants compared with that observed in the α- and β-isomers). The hydrochlorides of all three isomers show coupling between the $\overset{+}{N}$—H and *N*-methyl protons of approximately 5 Hz.

Conclusions

The cmr and pmr spectral evidence enables unambiguous assignment of the configurations of the three isomers, α-, β-, and γ-1,3,5-trimethyl-4-phenyl-4-piperidinol. It is highly probable that these configurations also apply to the corresponding ester derivatives as was shown in the case of the 1,2,5-series (5). Thus the analgesic potency of the γ-isomer does not appear to depend on the axial orientation of the 4-phenyl group.

Experimental

1,3,5-Trimethyl-4-phenylpiperidin-4-ol (α-Isomer)

The procedure described by Sorokin (1) was followed and the product isolated as a white solid; mp 130–131 °C (lit (1) mp 131.5–132 °C); ir (Nujol) 3220 cm^{-1} (OH str.); ms parent ion *m/e* 219; hydrochloride mp 221–223 °C (lit. (1) mp 222–222.5 °C).

1,3,5-Trimethyl-4-phenylpiperidin-4-ol (β-Isomer)

The α-isomer was isolated by crystallisation as above and the mother liquors subjected to chromatography on alumina, eluting with chloroform followed by methanol. Residual α-isomer was eluted with chloroform and the β-isomer by methanol. Evaporation of the solvent gave a white solid, mp 117–121 °C, (lit. (1) mp 121–121.5 °C); ir (Nujol) 3300 cm^{-1} (OH str.); ms parent ion *m/e* 219; hydrochloride mp 222–224 °C (lit. (1) mp 223–225.5 °C).

1,3,5-Trimethyl-4-phenylpiperidin-4-ol (γ-Isomer)

The procedure described by Sorokin (1) was followed with the modification that isolation of the title compound was carried out by column chromatography on alumina. Removal of the maximum amount of α-isomer by crystallisation followed by chromatography of the mother liquors eluting with Skelly 'B' – benzene (1:3), 4 × 100 ml; benzene–chloroform (3:1), 4 × 100 ml; (3:1.5), 4 × 100 ml, (1:3), 4 × 100 ml resulted in separation of three bands. The lower band was eluted with chloroform and rechromatographed, yielding a white solid, mp 130–135 °C, (lit. (1) mp 134–135 °C); ir (Nujol) 3300 cm^{-1} (OH str.); ms parent ion *m/e* 219; hydrochloride mp 240–241 °C, (lit. (1) mp 241–242 °C).

^{13}C nmr spectra were determined on a Bruker HFX-90 spectrometer operating at 22.63 MHz. All samples were contained in precision ground 10 mm, o.d. tubes. The spectrometer was used in the cross-coil configuration. On average an 8 μs pulse, corresponding to an approximate tilt angle of 45°, was employed. The delay between pulses was 0.8 s, for an average spectral width of 5000 Hz. Accumulation time averaged 20 min, over 8K data points for concentrations of the order of 0.27 *M*. For off-resonance coupled spectra this time was approximately doubled.

Proton nmr spectra were determined on a Varian HA100 spectrometer.

1. O. I. Sorokin. Izv. Akad. Nauk. SSR. Otd. Khim. Nauk. **3**, 460 (1961).
2. A. F. Casy and K. M. J. McErlane. J. Chem. Soc. Perkin Trans. **1**. 334 (1972).
3. P. Portoghese. J. Pharm. Sci. **55**, 865 (1966).
4. A. J. Jones and M. M. A. Hassan. J. Org. Chem. **37**, 2332 (1972).
5. A. J. Jones, C. P. Beeman, A. F. Casy, and K. M. J. McErlane. Can. J. Chem. **51**, 1790 (1973); Tetrahedron Lett. 1727 (1972).
6. A. J. Jones, A. F. Casy, and K. M. J. McErlane. Can. J. Chem. **51**, 1782 (1973).
7. A. J. Jones, C. P. Beeman, A. F. Casy, M. M. Hassan, and M. U. Hasan. Can. J. Chem. **54**, 126 (1976).
8. A. J. Jones and M. H. Benn. Can. J. Chem. **51**, 486 (1973).
9. M. M. A. Hassan and A. F. Casy. Org. Magn. Reson. **2**, 197 (1970).
10. A. J. Jones, E. L. Eliel, D. M. Grant, M. C. Knoeber, and W. G. Bailey. J. Am. Chem. Soc. **93**, 4772 (1971).
11. E. L. Eliel, W. F. Bailey, L. D. Kopp, R. L. Willer, D. M. Grant, R. Bertrand, K. A. Christensen, D. K. Dalling, M. W. Duch, E. Wenkert, F. M. Schnell, and D. W. Cochran. J. Am. Chem. Soc. **97**, 322 (1975).
12. S. H. Grover, J. P. Guthrie, J. B. Stothers, and C. T. Tan. J. Magn. Reson. **10**, 227 (1973).

Equilibrium protonation of the 1,3,5-trinitrobenzene–phenoxide σ-complex

ERWIN BUNCEL AND WALTER EGGIMANN
Department of Chemistry, Queen's University, Kingston, Ont., Canada K7L 3N6

Received February 19, 1976

ERWIN BUNCEL and WALTER EGGIMANN. Can. J. Chem. **54**, 2436 (1976).

The protonation behavior of the trinitrobenzene–phenoxide σ-complex has been determined in aqueous sulfuric acid, aqueous hydrochloric acid, and ethanolic hydrogen chloride. The conjugate acid of the σ-complex, a nitronic acid, exhibits acidic properties similar to those of picric acid and the cyanocarbon acids. The acidity (pK_a) of the nitronic acid has been evaluated with the aid of various acidity function techniques and using the Bunnett–Olsen method. The nitronic acid is *ca.* 1 p*K* unit stronger than picric acid. However, both the nitronic acid and picric acid are considerably weaker acids in ethanolic than in aqueous media (ΔpK *ca.* 4 units). The results provide a preliminary H_- acidity function scale for aqueous and ethanolic hydrogen chloride.

ERWIN BUNCEL et WALTER EGGIMANN. Can. J. Chem. **54**, 2436 (1976).

On a déterminé le comportement du complexe σ phénolate–trinitrobenzène lors de sa protonation en solution acide sulfurique aqueux, acide chlorhydrique aqueux et chlorure d'hydrogène en solution éthanolique. L'acide conjugué du complexe σ, un acide nitronique, présente des propriétés acides similaires à celles de l'acide picrique et des acides cyanocarbonés. On a déterminé, à l'aide de diverses techniques de fonction d'acidité et utilisant la méthode de Bunnett–Olsen, l'acidité (pK_a) de l'acide nitronique. L'acide nitronique est environ une unité de p*K* plus fort que l'acide picrique. Toutefois les deux acides, nitronique et picrique, sont des acides beaucoup plus faibles en solution éthanolique qu'en solution aqueuse ($\Delta pK \sim 4$ unités). Ces résultats fournissent une échelle préliminaire, de la fonction d'acidité H_- pour le chlorure d'hydrogène en solution aqueuse et éthanolique.

[Traduit par le journal]

Meisenheimer compounds obtained from nucleophilic addition to polynitroarenes have received increasing interest during the last few years (1). Recently (2) we reported on the formation of the 1,3,5-trinitrobenzene–phenoxide σ-complex (**1**) as the major product of the reaction between 1,3,5-trinitrobenzene (TNB) and potassium phenoxide, representing the first case of phenoxide ion acting as an ambident nucleophile in SNAr systems (3). A preliminary examination of the protonation of **1** in acidic methanolic DMSO solutions suggested the existence of the equilibrium given in [1]. The quinoid resonance

[1] 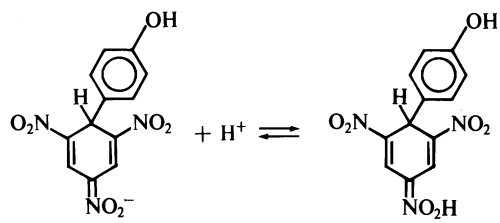

1 **2**

form, which is assumed to be the dominant form of the σ-complex (4), can be regarded as a nitronate anion whose conjugate acid is thought to be the nitronic acid **2**. Nitronic acids are considered to be rather unstable species (5), though some relatively stable compounds of this type have been prepared (6, 7).

It was of interest to investigate the protonation of **1**, since typical Meisenheimer σ-complexes derived from nucleophilic attack on the nitroaromatics by oxygen or nitrogen bases (8, 9) are decomposed by acid. In the present work we have evaluated quantitatively the equilibrium 1 and have compared the results with those obtained in the protonation of picrate ion, [2], and

[2] 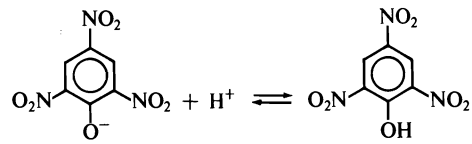

3 **4**

of the cyano-substituted carbanions, [3]. It is

[3] 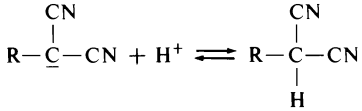

5 **6**

Can. J. Chem. Downloaded from www.nrcresearchpress.com by 210.87.254.105 on 09/05/12
For personal use only.

TABLE 1. Spectral data for TNB–phenoxide/nitronic acid equilibrium (**1** ⇄ **2**) and for picrate ion/picric acid equilibrium (**3** ⇄ **4**)

	1		**2**	
Solvent	λ_{max}	ϵ	λ_{max}	ϵ
H_2O (0.04% EtOH)	470 540–560(sh)	21000		
H_2O/H_2SO_4, H_2O/HCl			366	14400
EtOH	465 545	25000 10400		
EtOH/HCl			368	17600
DMSO	468 570	31600 15400	—[a]	

	3		**4**	
Solvent	λ_{max}	ϵ	λ_{max}	ϵ
H_2O	356	14000		
H_2O/H_2SO_4, H_2O/HCl			338	5400
EtOH/EtO^-	359	16800		
EtOH/HCl			325(sh) 280(sh)	4900 8900

[a]Up to 3.6 *M* H_2SO_4 no protonation occurs, but decomposition of TNB–phenoxide complex sets in.

recalled that the equilibrium 3 has been used to set up an H_- acidity function scale for aqueous perchloric acid and aqueous sulfuric acid (10). To date there are only scant H_- data pertaining to ionization of relatively strong acids, though H_- scales in strongly basic systems pertaining to ionization of weak acids are well established (11). Since, in the present work, aqueous H_2SO_4, aqueous HCl, as well as ethanolic HCl media have been used, the results allow an estimate of an H_- scale for aqueous and ethanolic hydrogen chloride.

Results

The TNB–phenoxide σ-complex **1** has a characteristic spectrum in the visible region, namely an absorption maximum at *ca.* 470 nm with a broad shoulder at *ca.* 550 nm. There is a moderate solvent dependence in these spectral characteristics, as shown in Table 1 for aqueous and ethanolic media.

In media of increasing acid concentration certain spectral changes are observed, namely a gradual decrease in the absorptions at 470 and 550 nm and the growth of a new peak at 356 nm. These spectral changes are indicative of the protonation equilibrium according to [1], in which **1** gives rise to the nitronic acid **2**. Though complete conversion to the nitronic acid can be effected in media of sufficiently high acidity, the species **2** undergoes slow decomposition as evidenced by a gradual decrease in the absorption at 356 nm. Hence, spectra were recorded immediately on preparation of the solutions and the spectral scans were, in general, taken over a limited wavelength interval. Under these conditions a somewhat diffuse isosbestic point was obtained for the interconversion of the two species, as illustrated in Fig. 1 for ethanolic hydrogen chloride solutions.

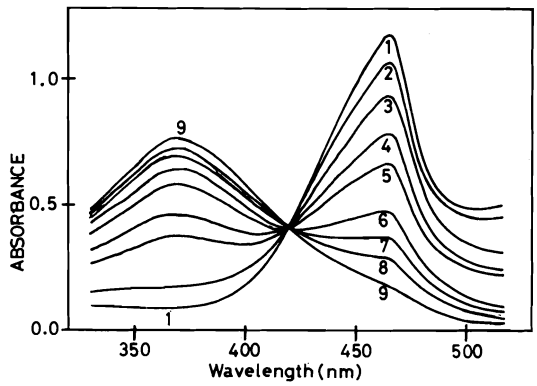

FIG. 1. Spectral curves illustrating the equilibrium protonation of the TNB–phenoxide σ-complex **1** in EtOH–HCl. Curve *1*, [HCl] = 0, curve *2* [HCl] = 1.18×10^{-4} *M*, curve *5* [HCl] = 1.68×10^{-3} *M*, curve *8* [HCl] = 3.36×10^{-2} *M*, curve *9* [HCl] = 0.42 *M*.

The degree of protonation could be calculated

Can. J. Chem. Downloaded from www.nrcresearchpress.com by 210.87.254.105 on 09/05/12
For personal use only.

Can. J. Chem. Downloaded from www.nrcresearchpress.com by 210.87.254.105 on 09/05/12
For personal use only.

from the extinction coefficient values of the anionic (A^-) and protonated (AH) species. The ionization ratio

$$I = [A^-]/[AH] = (\epsilon - \epsilon_{AH})/(\epsilon_{A^-} - \epsilon)$$

was calculated using extinction (or absorbance) data corresponding to the absorption maxima of the anionic and the protonated species. The latter values have a larger associated uncertainty, in part due to the slow decomposition of **2** and in part due to the smaller overall change in absorbance at this wavelength. The complete results (absorbances and ionization ratios for **1** $\rightleftarrows$ **2** in aqueous H_2SO_4, aqueous HCl, and EtOH–HCl) are available.[1]

The acidity constant of the nitronic acid **2** in aqueous H_2SO_4 has been estimated by several methods, as outlined below. (*1*) A plot of the absorbance A at λ_{A^-} and λ_{AH} *vs.* H_- (10) gave sigmoid plots and the H_- values at the inflexion points yielded pK_a values of -1.1 ± 0.1 and -1.2 ± 0.1, respectively. The related Davis–Geissman plot (12), namely $A_{A^-} - A_{AH}$ *vs.* H_-, was likewise sigmoid yielding $pK_a = -1.2 \pm 0.1$. (*2*) The plot of log I *vs.* H_- (10) showed good linearity and the H_- value at log $I = 0$ gave $pK_a = -1.16 \pm 0.02$. The significance of the 'Hammett slope' value of 0.64 ± 0.01 in this plot will be considered in the Discussion. (*3*) The Bunnett–Olsen method (13) has been applied by plotting log I − log C_{H^+} *vs.* H_0 + log C_{H^+} where H_0 is the acidity function for primary anilines and C_{H^+} is the molarity of acid. The intercept of the linear plot yielded $pK_a = -0.91 \pm 0.06$ and the slope gave the parameter $\phi = -0.26 \pm 0.03$.

The data for the protonation of **1** in aqueous hydrochloric acid are not readily interpretable at this stage since Boyd's results for this medium were quite limited (10). However, Phillips (14) has presented an H_- function for aqueous HCl based on the protonation of phosphorus oxyanion bases such as **7**. The plot of log I for [1] *vs.* this H_- function was linear, with an H_- value of 0.22 at log $I = 0$, and a slope of 0.52 ± 002. The value 0.22 is far removed from the .pK_a values estimated using the H_- function of Boyd (-1.16) and by the Bunnett–Olsen method (-0.91). This consideration, as well as the small Hammett slope of 0.52, dictate against the use of Phillips' H_- function to describe the protonation of nitronate ion. The charge localized oxyanion **7** differs greatly from the anions **1**, **3**, and **5**, so that the divergence from Phillips' H_- function is to be expected.

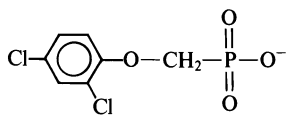

7

Measurements have also been made for the picrate ion – picric acid equilibrium, [2], for purposes of comparison with the 2,4,6-trinitrocyclohexadienate – nitronic acid equilibrium, [1]. The picrate ion – picric acid equilibrium was also included by Boyd in his study of the cyanocarbanion – carbon acid equilibria, [3]. The process in [2] serves to bridge the equilibria represented by [1] and [3]. In fact, our results for equilibrium 2 in aqueous sulfuric acid and in aqueous hydrochloric acid agree closely with Boyd's. Hence these data and their treatment for evaluation of pK_a values will not be presented here in full, though the spectral characteristics for **3** and **4** are included in Table 1. The ionization data for [2] in ethanolic hydrogen chloride solutions have not been recorded previously and these are available.[1]

Discussion

Validity of Methods and pK_a's

Quantitative treatments of acid–base equilibria are often prerequisites for the understanding of acid- or base-catalyzed reactions (15). Acidity functions have been of value to this end (16), but in recent years the limitations of acidity function techniques to describe acid–base equilibria have been pointed out by a number of authors (17–22). Several new approaches have been suggested (18–23). Our results further emphasize both the limitations of the general applicability as well as the usefulness of an acidity function to describe the protonation behaviours of structurally related compounds.

Comparison of the response in protonation towards medium acidity of structurally related

[1]The original absorbance and ionization ratio data for the equilibrium protonation of the TNB–phenoxide σ-complex (**1**) and of picrate ion (**3**) are available, at a nominal charge, from the Depository of Unpublished Data, CISTI, National Research Council of Canada, Ottawa, Canada K1A 0S2.

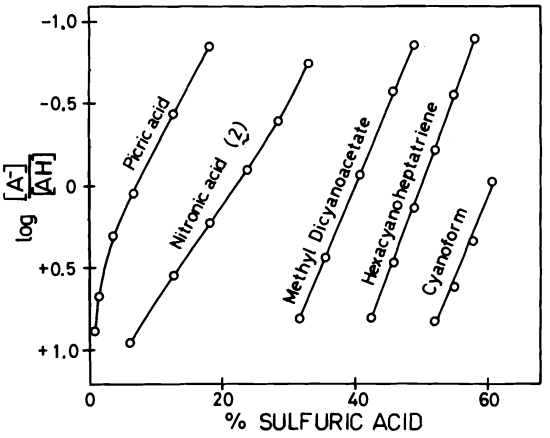

FIG. 2. Plots of log (ionization ratio) *vs.* % H_2SO_4 for picric acid and nitronic acid (this work), contrasting with the behaviour of Boyd's (10) cyanocarbon acid indicators.

compounds can be made by means of plots of the ionization ratio I *vs.* a solvent acidity parameter such as acid concentration. Such a plot is shown in Fig. 2 for the protonation equilibria of [1]–[3] in the sulfuric acid system. A plot of this type is basically the overlapping indicator method, first introduced by Hammett in the 1930's (24). Although in Hammett's original studies, as well as a number of subsequent ones, indicators of a given charge type but of varying functional character were used, it is now realized that the method is strictly applicable only to a given family of indicators, *i.e.* with invariant functionality. Thus the degree of divergence from parallel of the various curves reflects the divergence from a common response to acidity of the indicators, and arises from a differential medium effect on species activity coefficients (*vide infra*).

For a series of well behaved indicators the vertical displacements of the curves in such a figure represent the differences in the pK_a's of the respective indicators. Using an 'anchor' pK_a value of 0.23 for picric acid,[2] one thus obtains for the nitronic acid **2** an average pK_a value of -0.76. This can be compared with the value -1.16 obtained by applying the H_- acidity function technique as outlined in the Results.

The slope of a log I *vs.* H plot gives a measure of whether a given substrate follows a particular H function; for a 'Hammett indicator' the slope should be unity. In Table 2 are given the slopes of the pertinent log I *vs.* H_- (10) plots. The cyanocarbon acid indicators have slope values close to unity, with the exception of hexacyanoheptatriene. Picric acid with a slope of 0.84 deviates somewhat, while the nitronic acid with slope 0.64 deviates appreciably from the H_- acidity function as set up for the cyanocarbon acid equilibrium [3]. These divergences from unit slope reflect the fact that the ratio f_{A^-}/f_{AH} in [4] cannot be assumed to be invariant,

$$[4] \qquad H_- = -\log a_{H^+}(f_{A^-}/f_{AH})$$

at a given solvent composition, for the protonation of anions with even slightly different structures (*cf.* **1**, **3**, **5**). It is not surprising that protonation of a carbanion should be subject to different acidity dependence compared to an oxygen anion. However, it is noteworthy that the oxygen anions **1** and **3** differ appreciably in this regard, even though both represent delocalized aromatic systems with charge distributed largely over nitro groups.

$$[5] \quad \log I - \log C_{H^+} = pK_a + (\phi - 1)(H_0 + \log C_{H^+})$$

The ϕ value in the Bunnett–Olsen equation [5] is also a measure of the response of the ionization ratio to changing acid concentration. Recently, Levi *et al.* (26) have listed ϕ values for the ionization of a number of bases in aqueous sulfuric acid, emphasizing that bases of similar structure generally have similar ϕ values. We have calculated ϕ values for the cyanocarbanion equilibria [3], as well as for the picric acid [2], and nitronic acid equilibria [1], and the results are given in Table 2. It is seen that ϕ generally assumes slightly negative values, except for *p*-(tricyanovinyl)phenyldicyanomethane and cyanoform. Noting that for primary anilines $\phi = 0$ (by definition), the slightly negative ϕ values might be ascribed to the role of hydrogen bonding as a strong form of solvation, as this is also shown on comparison of primary and tertiary aromatic amines where the ϕ values decrease from 0 to -0.3 (27). The fact that the H_- function for ionization of cyanocarbon acids (10) is very similar to H_0 might also be reflected by ϕ values which differ little from zero.

[2]This pK_a value for picric acid is the average of the reported pK_a value 0.25 (10) and the value 0.21 obtained in our work from log I *vs.* H_- plots in the aqueous H_2SO_4 system.

Can. J. Chem. Downloaded from www.nrcresearchpress.com by 210.87.254.105 on 09/05/12
For personal use only.

Can. J. Chem. Downloaded from www.nrcresearchpress.com by 210.87.254.105 on 09/05/12
For personal use only.

TABLE 2. pK_a and slope parameters for equilibria 1–3 in aqueous H_2SO_4 by acidity function and Bunnett–Olsen methods

	Acidity function method		Bunnett–Olsen method	
	pK_a[a]	Slope[a]	pK_a[b]	ϕ[b]
p-(Tricyanovinyl)phenyl-dicyanomethane	0.62	1.02±0.04	0.16	−0.86
Picric acid	0.21	0.84±0.03	−0.10	−0.14
Nitronic acid	−1.16	0.64±0.01	−0.91	−0.26
Methyl dicyanoacetate	−2.92	0.99±0.01	−2.80	−0.20
Hexacyanoheptatriene	−3.89	1.13±0.02	−3.57	−0.08
Cyanoform	−4.98	0.96±0.08	−4.04	0.15
Bis(tricyanovinyl)amine	−5.98	1.00±0.01	−6.15	−0.04

[a]Intercepts (pK_a) and slopes of log I *vs.* H_- (10) plots.
[b]Intercepts (pK_a) and slopes (ϕ-1) in plots (13) of log I − log C_{H^+} *vs.* H_0 + log C_{H^+}.

The H_- Function in Hydrochloric Acid Media

We have used the equilibria of [1] and [2] to generate a preliminary H_- scale in aqueous and in ethanolic hydrogen chloride. In these experiments the known pK_a value of picric acid in the two media is used to obtain pK_a values for the nitronic acid, from which H_- values can then be calculated.

The protonation of the σ-complex **1** and of picrate ion **3** was determined in media of different HCl concentrations. Plots of log I *vs.* [HCl] were constructed and were found to be similar in nature to Fig. 2; the pK_a values of the nitronic acid were obtained from the average vertical displacement of the two curves. One thus obtains for equilibrium 1 in aqueous hydrochloric acid $pK_a = -0.71$, using the reported pK_a value for picric acid of 0.29 (25). In ethanolic hydrogen chloride the pK_a for [1] is 3.01 using a pK_a value for picric acid in ethanol of 3.66 (28). Thus, there is a decrease in the acidity of the nitronic acid, from water to ethanol, of *ca.* 4 pK units, which is also found to be the case for picric acid.

H_- values were obtained from the pK_a and log I values by means of [6], in which n takes the inverse of the slope obtained in the log I *vs.* H_- plots referred to previously (see Table 2). Thus for nitronic acid $n = 1/0.64 = 1.56$ and for

TABLE 3. H_- data for aqueous HCl based on the nitronate – nitronic acid equilibrium [1] and the picrate – picric acid equilibrium [2]

Indicator	pK_a	[HCl] (M)	H_-[c]
Nitronic acid (**2**)	−0.71[a]	0.97	0.507
		1.93	0.148
		2.90	0.648
		3.87	−1.16
		4.84	−1.66
		5.80	−2.30
Picric acid (**4**)	0.29[b]	0.10	1.32
		0.24	0.897
		0.48	0.564
		0.97	0.147
		1.45	−0.162
		1.93	−0.221

[a]Determined by using picric acid as the 'anchor', pK_a = 0.29 (25).
[b]Reference 25.
[c]Calculated using [6], with n = 1.56 for the nitronate – nitronic acid equilibrium [1] and n = 1.19 for the picrate – picric acid equilibrium [2], as determined for the aqueous H_2SO_4 system.

TABLE 4. H_- data for ethanolic HCl based on the nitronate – nitronic acid equilibrium [1] and the picrate – picric acid equilibrium [2]

Indicator	pK_a	[HCl] (M)	H_-[c]
Nitronic acid (**2**)	3.01[a]	1.18×10^{-4}	4.35
		3.36×10^{-4}	3.73
		8.40×10^{-4}	3.26
		1.68×10^{-3}	2.92
		5.04×10^{-3}	2.39
		8.40×10^{-3}	2.20
		1.18×10^{-2}	2.06
		1.68×10^{-2}	1.92
		3.36×10^{-2}	1.67
		5.04×10^{-2}	1.47
Picric acid (**4**)	3.66[b]	0	4.02[d]
		1.18×10^{-4}	3.78
		3.36×10^{-4}	3.62
		8.40×10^{-4}	3.14
		1.68×10^{-3}	2.82
		5.04×10^{-3}	2.31

[a]Determined by using picric acid as the 'anchor', pK_a = 3.66 (28).
[b]Reference 28.
[c]As in Table 3, footnote *c*.
[d]Picric acid was found to be dissociated in ethanol to the extent of 70% for a 10^{-4} M solution (see also ref. 28).

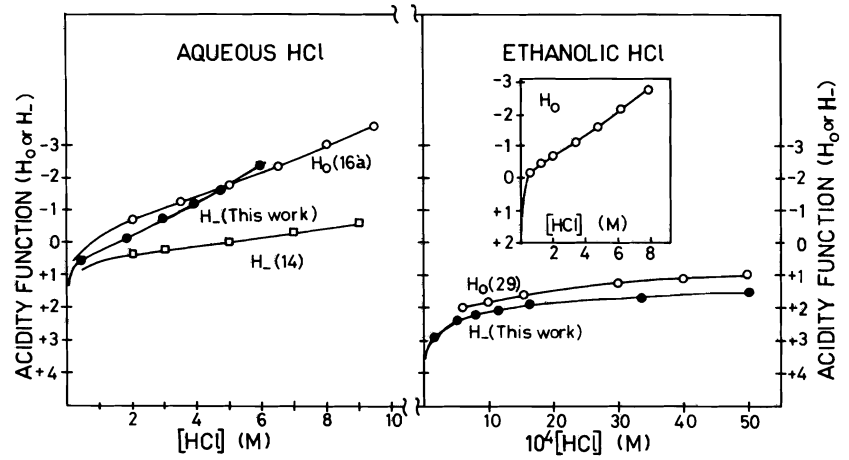

FIG. 3. Comparison of H_- (this work) with the H_- (14) and H_0 (16*a*) acidity functions for aqueous HCl, and with the H_0 function for the ethanolic HCl (29) systems. Note that inset diagram represents H_0 (29) over the whole acid region.

picric acid $n = 1/0.84 = 1.19$. The results are given in Tables 3 and 4. In Fig. 3 a comparison is drawn between H_- and H_0 for aqueous and ethanolic media.

[6] $$H_- = pK_a + n \log I$$

Some exploratory measurements were carried out to determine the effect of water on the equilibrium 1. The results, given in Table 5, show that addition of water up to 0.4 vol% to an acidic ethanolic medium (0.034 *M* HCl) decreases considerably the ionization ratio *I*. A similar effect was observed by Nahlovsky and Chvalovsky (29) in the case of aniline indicators governed by H_0 and signifies an increased medium acidity of the partly aqueous solutions.

Structural Aspects

In [1] the protonation of the σ-complex has been formulated as yielding a nitronic acid, **2**,[3] whereas an alternative structure can also be

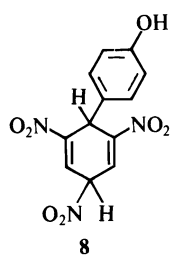

8

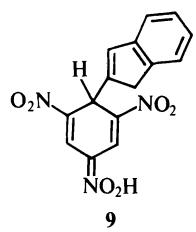

9

[3]In addition, one can formulate a nitronic acid structure in which one of the *ortho* nitro groups becomes protonated, and there will also be a corresponding nitro tautomer.

TABLE 5. Effect of water content on the ionization ratio of the TNB–phenoxide/nitronic acid equilibrium in a 3.36×10^{-2} *M* ethanolic hydrochloric acid solution

Water (% v/v)	A_{465}	I_{465}[a]	log I_{465}
0	0.275	0.163	−0.786
0.1	0.360	0.288	−0.541
0.2	0.430	0.411	−0.386
0.3	0.505	0.573	−0.242
0.4	0.570	0.745	−0.127

[a] $I = [A^-]/[AH] = (A - A_{AH})/(A_{A^-} - A)$ calculated at 465 nm using $A_{AH} = 0.130$ and $A_{A^-} = 1.160$.

formulated, namely **8**.[3] In general, nitro tautomers are thermodynamically more stable than the nitronic acid tautomers (5, 30). However, it can be noted that in the present case there is more extensive conjugation in species **2** than in **8**. Also, our assignment is in agreement with that given by Wennerström for the case of structure **9** (7). The latter was found to be formed on protonation of the σ-complex derived from nucleophilic addition of indenylsilver to TNB (addition of 2,6-dimethylsilver to TNB gave the corresponding σ-complex (6)).

The above structural assignment is supported by nmr and ir evidence. The nmr results, given in Table 6, show that while there is no measurable difference in chemical shift for the H_β signal on protonation, H_α undergoes an upfield shift of 0.38 ppm. There is close agreement between these results and those obtained by Wennerström (7), as seen in Table 6. In addition, if protonation had yielded structure **8**, then the H—C—NO_2

Can. J. Chem. Downloaded from www.nrcresearchpress.com by 210.87.254.105 on 09/05/12
For personal use only.

TABLE 6. Nuclear magnetic resonance parameters for nitronate ions and nitronic acids

Compound		Solvent	H_α	H_β	H_γ	J
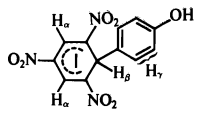	(1)	CH_3OD	8.48	5.60	7.20/7.07/ 6.70/6.55	$J(H_\alpha-H_\beta)$ = 0.3 Hz
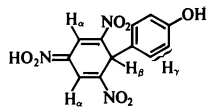	(2)	CH_3OD/D_2SO_4[a]	8.10	5.60	7.13/7.00/ 6.74/6.58	[b]
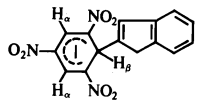	(ref. 7)	Acetone-d_6	8.66	6.08		
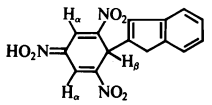	(ref. 7)	Acetone-d_6	8.29	6.11		

[a]See Experimental section for method.
[b]See Discussion for upper limit on $J(H_\alpha-H_\beta)$ value.

proton should have been detectable, but our spectra did not reveal an appropriate peak.[4] Also, the H_α signal for structure **8** would be expected to be significantly affected by spin–spin coupling.[4] However, the experimentally observed signal for H_α was somewhat broadened due to the decomposition process (see Experimental), which precluded the observation of a coupling constant less than *ca.* 0.5 Hz. In the σ-complex **1**, the H_α–H_β coupling constant was found to be 0.3 Hz. The ir spectrum of the protonated material shows broad absorption in the OH region with a peak at *ca.* 2900 cm^{-1}, characteristic of the NO_2H function (5, 6, 34), and a peak at *ca.* 1625 cm^{-1} indicative of C=N. (The unprotonated σ-complex **1** has a corresponding band at 1610–1615 cm^{-1}.)

It is interesting that Strauss (1*a*) has reported several examples of the reaction sequence shown in [7] which gives rise to a nitro compound as the product rather than a nitronic acid tautomer. In these reactions, however, the $C{=}NO_2^-$ function does not form part of a conjugated system, so that protonation now yields the thermodynamically more stable nitro tautomer. Some related observations on nitronates have been made by Baer *et al.* (35).

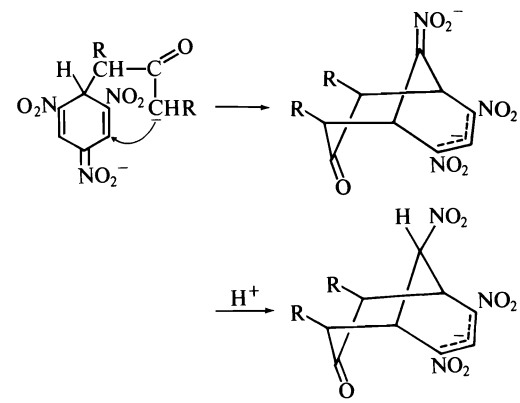

[7]

[4]For 1-nitroindene a H—C—NO_2 proton resonance of 7.6 ppm with a spin–spin coupling constant of 2 Hz has been reported (31). In addition, a long range coupling constant of 7.4–11 Hz has been observed (32) for 1,4-dihydrobenzene derivatives between the 1- and the 4-protons, depending on the stereochemical relationship (boat *vs.* chair, see also ref. 33).

Experimental

Picric acid was crystallized from water. Ethanol was dried by a standard method (36). Sulfuric acid solutions of different concentration were made up by dilution of concentrated sulfuric acid in volumetric flasks. The concentration of the diluted aqueous sulfuric acids was checked by titration with standardized aqueous potassium hydroxide. Hydrochloric acid solutions in water were prepared similarly by diluting concentrated hydrochloric acid and titrating with aqueous potassium hydroxide. Hydrochloric acid solutions in anhydrous ethanol were prepared by dilution of saturated ethanolic HCl. Satu-

Can. J. Chem. Downloaded from www.nrcresearchpress.com by 210.87.254.105 on 09/05/12
For personal use only.

Can. J. Chem. Downloaded from www.nrcresearchpress.com by 210.87.254.105 on 09/05/12
For personal use only.

rated hydrochloric acid in ethanol was prepared by introducing anhydrous hydrogen chloride (Matheson) into ethanol in an absorption trap cooled to 0 °C. The stream of hydrogen chloride was dried with H_2SO_4. In this manner, a saturated solution of hydrogen chloride in ethanol of 11.25 *M* was obtained, from which several stock solutions were prepared by dilution (down to 2×10^{-3} *M*) and standardized.

The TNB–phenoxide complex **1** was prepared as previously (2). For the uv–visible spectral measurements, 5×10^{-3} *M* aqueous and ethanolic solutions were prepared. Due to its limited solubility in water, 1 ml ethanol was first added to the solid complex, and the red solution was diluted with water to 25 ml. Under the conditions that the uv–visible measurements were performed, the volume percent of the organic co-solvent was reduced by a factor 100, to 0.04%.

Ultraviolet–visible measurements were performed on a Unicam SP800B spectrophotometer at room temperature. For measurement of the absorption curves of the complex in different acid solvents, 3.0 ml of the appropriate stock acid solution was transferred in a 1 cm quartz cell, and 30 μl of the 5×10^{-3} stock solution of the σ-complex was added using a micropipet. Initial absorbance readings were taken 30 s after mixing. The error caused by decomposition was checked by recording spectra at a fixed wavelength as a function of time and was found to be negligible under the operating conditions. All spectra were run twice under constant conditions.

For the ir measurements, 20 mg of **1** was dissolved in 50 μl CD_3CN (or CH_3OD), 1 ml of $CDCl_3$ and 1 ml of 40% (v/v) H_2SO_4 were added, and the mixture shaken thoroughly. The yellow chloroform phase was removed, and stored over molecular sieves in dry ice. This extraction procedure yielded a concentration in nitronic acid of *ca.* 2×10^{-2} *M* (from the uv–visible spectrum). Spectra were taken on a Beckmann Acculab 6 and a Perkin Elmer 180 spectrophotometer.

For the nmr measurements, 30 mg of **1** was dissolved in 0.5 ml methanol-*O-d*, 30 μl of concentrated D_2SO_4 was added, and after vigorous shaking the spectrum was taken. Alternatively, the $CDCl_3$-extraction procedure described for the ir measurements was also used. The instrument used was a Bruker 60 MHz HFX-60 model.

The ir and nmr measurements with the nitronic acid were hampered by a relatively facile decomposition process which led to precipitation of a brown solid. The decomposition rate could be slowed down at low temperatures.

Acknowledgment

This research was supported financially by the National Research Council of Canada.

1. (*a*) M. J. Strauss. Acc. Chem. Res. **7**, 181 (1974); (*b*) M. J. Strauss. Chem. Rev. **70**, 667 (1970); (*c*) M. R. Crampton. Adv. Phys. Org. Chem. **7**, 211 (1969); (*d*) E. Buncel, A. R. Norris, and K. E. Russell. Q. Rev. **22**, 123 (1968); (*e*) R. Foster and C. A. Fyfe. Rev. Pure Appl. Chem. **16**, 16 (1966).
2. E. Buncel, A. Jonczyk, and J. G. K. Webb. Can. J. Chem. **53**, 3761 (1975).
3. E. Buncel and J. G. K. Webb. J. Am. Chem. Soc. **95**, 8470 (1973).
4. (*a*) P. Caveng, P. B. Fischer, E. Heilbronner, A. L. Miller, and H. Zollinger. Helv. Chim. Acta, **50**, 848 (1967); (*b*) H. Wennerström and O. Wennerström. Acta Chem. Scand. **26**, 2883 (1972).
5. A. T. Nielsen. *In* The chemistry of the nitro and nitroso groups. Part I, *Edited by* H. Feuer. Interscience, New York. 1969.
6. O. Wennerström. Acta Chem. Scand. **25**, 2341 (1971); **25**, 2355 (1971).
7. C. Moberg and O. Wennerström. Acta Chem. Scand. **25**, 2871 (1971).
8. E. Buncel and J. G. K. Webb. Can. J. Chem. **52**, 630 (1974).
9. E. Buncel, A. R. Norris, K. E. Russell, P. J. Sheridan, and H. Wilson. Can. J. Chem. **53**, 1750 (1974).
10. R. H. Boyd. J. Phys. Chem. **67**, 737 (1963).
11. (*a*) K. Bowden. Chem. Rev. **66**, 119 (1966); (*b*) C. H. Rochester. Acidity functions. Academic Press, London. 1970; (*c*) E. Buncel, E. A. Symons, D. Dolman, and R. Stewart. Can. J. Chem. **48**, 3354 (1970).
12. C. T. Davis and T. A. Geissman. J. Am. Chem. Soc. **76**, 3507 (1954).
13. J. F. Bunnett and F. P. Olsen. Can. J. Chem. **44**, 1899 (1966).
14. J. N. Phillips. Aust. J. Chem. **14**, 183 (1961).
15. R. P. Bell. The proton in chemistry. 2nd. ed. Cornell University Press, Ithaca, New York. 1973.
16. (*a*) M. A. Paul and F. A. Long. Chem. Rev. **57**, 1 (1957); (*b*) F. A. Long and M. A. Paul. Chem. Rev. **57**, 935 (1957).
17. L. P. Hammett. Physical organic chemistry. 2nd ed. McGraw Hill, New York. 1970.
18. J. F. Bunnett and F. P. Olsen. Can. J. Chem. **44**, 1917 (1966).
19. E. M. Arnett and G. Scorrano. Adv. Phys. Org. Chem. In press.
20. R. Cox and R. Stewart. J. Am. Chem. Soc. **98**, 488 (1976).
21. M. M. Kreevoy and E. H. Baughman. J. Am. Chem. Soc. **95**, 8178 (1973).
22. G. Modena and G. Scorrano. *Euchem conference on* Anions and cations in acid media. La Grande Motte, France. May 27 – June 1, 1975.
23. R. F. Cookson. Chem. Rev. **74**, 1 (1974).
24. L. P. Hammett and A. J. Deyrup. J. Am. Chem. Soc. **54**, 2721 (1932).
25. R. G. Bates and G. Schwarzenbach. Experientia, **10**, 482 (1954).
26. A. Levi, G. Modena, and G. Scorrano. J. Am. Chem. Soc. **96**, 6585 (1974).
27. E. M. Arnett and G. W. Mach. J. Am. Chem. Soc. **86**, 2671 (1964).
28. M. Castagnolo, A. de Giglio, A. Dell'Atti, and G. Petrella. Can. J. Chem. **53**, 1651 (1975).
29. B. Nahlovsky and V. Chvalovsky. Collect. Czech. Chem. Commun. **33**, 3122 (1968).

30. E. BUNCEL. Carbanions. Mechanistic and isotopic aspects. Elsevier. Amsterdam. 1975.
31. R. C. KERBER and M. HODOS. J. Org. Chem. **33**, 1169 (1968).
32. L. J. DURHAM, J. STUDEBAKER, and M. J. PERKINS. Chem. Commun. 456 (1965).
33. A. L. BEGBIE, W. R. BOWMAN, M. T. GOLDING, and W. P. WATSON. Chem. Commun. 645 (1974).
34. S. S. NOVIKOV, V. I. SLOVETSKII, A. A. FAINZILBERG, S. A. SHEVELEV, V. A. SHLYAPOCHNIKOV, and V. A. TARTAKOVSKII. Tetrahedron, Suppl. 1, **20**, 119 (1964).
35. H. H. BAER, D. C. SHIELDS, and G. G. DAWSON. Can. J. Chem. **51**, 2843 (1973).
36. A. I. VOGEL. Practical organic chemistry. 3rd ed. Longmans, London. 1964. p. 167.

Can. J. Chem. Downloaded from www.nrcresearchpress.com by 210.87.254.105 on 09/05/12
For personal use only.

The interaction of α-diazoketones with hydroxylic solvents

ROSARIO CATALIOTTI, SALVATORE SORRISO, AND GIULIO PALIANI
Istituto di Chimica Fisica, Università degli Studi, Via Elce di Sotto, 10, 06100 Perugia, Italy
Received January 13, 1976

ROSARIO CATALIOTTI, SALVATORE SORRISO, and GIULIO PALIANI. Can. J. Chem. **54**, 2445 (1976).

The diazo and carbonyl stretching bands of four diazoketones were studied in CCl_4/MeOH mixtures as solvent, where the amount of hydroxylic solvent was linearly varied. The analogous behaviour afforded by the C—O band, either where *cis*/*trans* conformers are present (diazoacetone) or when conformational equilibria are hindered by chemical and/or steric reasons (the other three molecules), clearly indicates that local vibrator–solvent interactions are operative, probably via hydrogen bonding. Some minor effects due to the bulk dielectric constant of the medium were also observed.

ROSARIO CATALIOTTI, SALVATORE SORRISO et GIULIO PALIANI. Can. J. Chem. **54**, 2445 (1976).

On a étudié les bandes de vibration du diazo et du carbonyle de quatre diazocétones dans un mélange de CCl_4/MeOH comme solvant dans lequel les quantités de solvant hydroxylé variaient d'une façon linéaire. Le fait que la bande C—O présente un comportement semblable dans les cas où des conformères *cis* et *trans* sont présents (diazocétone) comme dans les cas où l'équilibre conformationnel est empêché par des raisons chimiques ou stériques (les trois autres molécules), indique clairement que les interactions locales vibrateur/solvant sont en opération probablement par l'intermédiaire de ponts hydrogènes. On a aussi observé quelques effets mineurs dus à la constante diélectrique globale du milieu.

[Traduit par le journal]

Introduction

The behaviour of the uv absorption of α-diazoketones in mixed nonpolar/hydroxylic solvents in which the proportion of hydroxylic component is increased linearly was interpreted by Miller and White (1) as caused by the setting up of keto–enol or diazo–isodiazo tautomeric equilibria, favoured by the protolytic medium. Later, Fahr (2) demonstrated that other mechanisms must be invoked to explain this behaviour. The reason given for this conclusion was that isobestic points in mixed-solvent uv spectra are also given by diazoketones not containing transposable hydrogens. Fahr's explanation of these effects is similar to that previously put forward by us to explain the ir behaviour of the C—O stretching mode of merocyanines in mixed solvents (3). The assumption is made that local vibrator–solvent interactions are operating and these allow an equilibrium to be set up between the 'free' form of solute molecules (presumably that solvated by the nonpolar solvent) and an associated form responsible for the red shift observed in both the uv and ir absorption.

An alternative explanation of the above behaviour has recently been put forward (4, 5) which invokes the presence of conformational equilibria in mixed nonpolar/polar solvent, as shown in [1]:

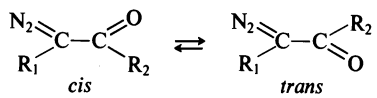

However, although it is true that the solvent may influence the position of a conformational equilibrium via its polarity (6), especially if the two rotamers have very different electric dipole moments, this effect should become evident only via a variation in the relative population of the two isomeric forms with percentage change in polar component in the solvent mixture. In other words, if factors attributable to *cis–trans* equilibrium of α-diazoketones are present in the uv or ir absorption (7, 8) in a nonpolar solvent alone, then an increase in polar solvent in the mixture should lead to an increase in the absorption intensity of only the more polar conformer. In addition, it may be predicted that in those cases where the conformational equilibrium is not established because of steric and/or chemical effects, there should be no spectral variations caused by the solvent when the solvent polarity is varied by gradual addition of bonding solvent. Finally, if the conformational equilibrium in

Can. J. Chem. Downloaded from www.nrcresearchpress.com by 210.87.254.6 on 09/05/12
For personal use only.

TABLE 1. Frequency values of the N—N and C—O stretching vibrations of some α-diazoketones in CCl_4/CH_3OH mixtures

Solvent mixture		Diazoacetone		Diazoacetophenone		Bis-*tert*-butyl diazoacetone		3-Diazocamphor	
		ν_{N-N}	ν_{C-O}	ν_{N-N}	ν_{C-O}	ν_{N-N}	ν_{C-O}	ν_{N-N}	ν_{C-O}
CCl_4	100%	2108 *cis* 2090 *trans*	1660	2106	1632	2059	1635	2072	1695
CCl_4	98%	2108 *cis* 2090 *trans*	1658 1634	—	—	—	—	—	—
CCl_4	95%	2108	1658 1633	2106	1632 1616	2059	1635 1621	2073	1694 1682
CCl_4	90%	2109	1657 1632	2107	1631 1614	2059	1635 1617	2074	1692 1678
CCl_4	80%	2110	1656 1631	2108	1630 1612	2060	1635 1614	2076	1691 1675
CCl_4	60%	2111	1656 1630	2109	1629 1611	2060	1635 1613	2077	1689 1674
CCl_4	40%	2111	1656 1630	2110	1627 1609	2062	1635 1612	2077	1689 1672
CCl_4	20%	2112	1656 1629	2111	1627 1608	2064	1635 1612	2078	1689 1671
CH_3OH	100%	2113	1628	2111	1608	2065	1634.5 1612	2078	1670

α-diazoketones shows itself via the ir absorptions of the N—N and C—O stretching modes, it may be assumed that the above-mentioned medium effects, whenever present, should be apparent on both absorption bands and should always be greater for that absorption which gives a larger splitting of the band components.

To further clarify these effects, we have studied the behaviour in CCl_4/CH_3OH mixtures of the diazo band and the C—O band of diazoacetone, for which the existence of a conformational equilibrium has been established (7–10), and also of diazoacetophenone, $Me_3CCOCCMe_3N_2$, and 3-diazocamphor,[1] for which the equilibrium is hindered for steric and chemical reasons.

Experimental

The compounds were prepared by literature methods (11, 12), except 3-diazocamphor, which was kindly supplied by Dr. Trazza.[2] They were purified by standard methods before carrying out measurements and their purity was checked by glc. Measurements were carried out in the wavenumber range of the N—N (2200–2000 cm^{-1}) and C—O (1750–1600 cm^{-1}) vibrations, on a Perkin-Elmer Model 521 grating spectrometer. Cells with NaCl windows of optical path length 100 μ were utilised. The solvents were Carlo Erba RS grade suitable for spectrophotometry. Attempts to obtain *n*-hexane/methanol mixtures were unsuccessful because of the only slight miscibility of the two components. Because of this a CCl_4/CH_3OH mixture was used, the components being completely miscible in the composition range investigated *i.e.* 2–100% v/v CH_3OH. The solute concentration was in all cases *ca.* 5×10^{-2} *M*.

[1]3-Diazocamphor is a molecule whose structure is

[2]The authors are greatly indebted for this compound to Dr. A. Trazza of the Electrochemistry and Chemical Physics center of CNR, Rome (Italy).

Results

Table 1 reports the frequency values for the N—N and C—O stretching bands of the four compounds studied, in various mixtures having different bonding-solvent content.

Figure 1 shows the situation of the C—O stretching band for all four molecules in pure CCl_4 and pure MeOH and in the CCl_4/MeOH solvent mixtures containing 40% MeOH. The results will be illustrated for each individual case and then discussed together so as to underline analogies in the observed spectroscopic behaviour.

Can. J. Chem. Downloaded from www.nrcresearchpress.com by 210.87.254.6 on 09/05/12
For personal use only.

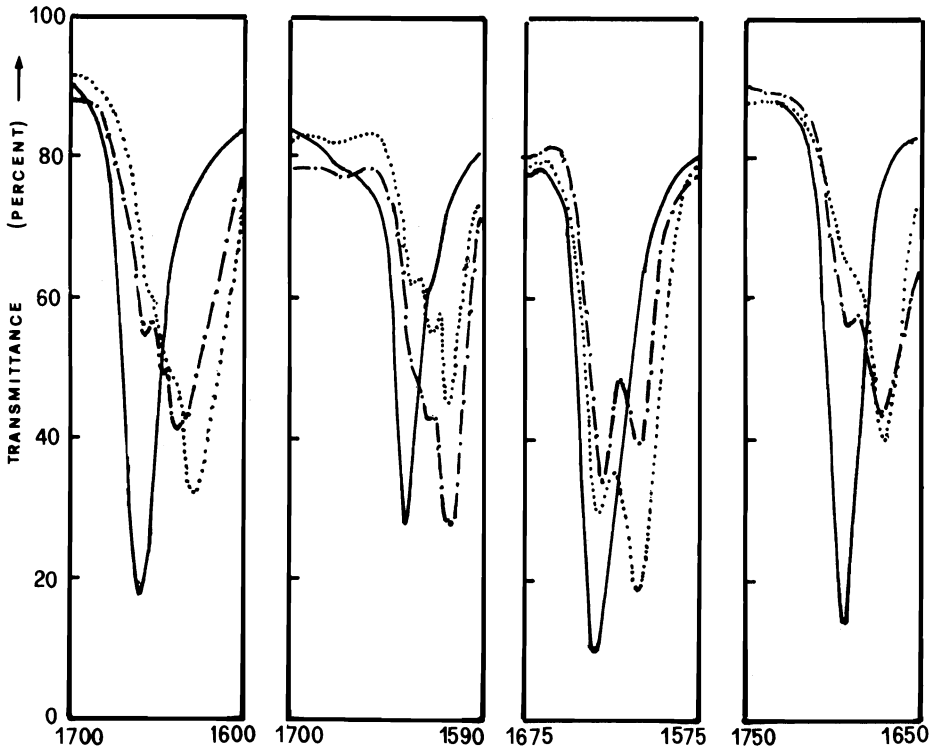

FIG. 1. Carbonyl stretching band of diazoacetone, diazoacetophenone, bis-*tert*-butyl diazoacetone and 3-diazocamphor in pure CCl_4 (solid line), pure methanol (dotted line), and 40% methanol–CCl_4 mixture (dot–dash line).

Diazoacetone

We previously reported (7, 8) that the two absorptions of the N—N vibration at 2108 (vs) and 2090 (w) cm^{-1} in CCl_4 are attributable to the *cis* and *trans* forms, respectively. An increase in temperature shifts the equilibrium in favour of the form less stable at room temperature, *i.e.* the *trans* form. The C—O group gives a single band, at 1660 cm^{-1}, in CCl_4, having only a slight asymmetry on the low-frequency side. It is probable that this shoulder is due to the *trans* form, but the closeness to the main band means that it is not possible to follow its behaviour with change in temperature (8).

The spectrum of the CCl_4/*Me*OH mixture containing 2% MeOH shows a strong diazo band at 2108 cm^{-1} with only a weak shoulder at 2090 cm^{-1}. This shoulder disappears in mixtures having 5% MeOH, and further continuous variation of the proportion of hydroxylic solvent leads to a shift of the main absorption to higher frequency (2113 cm^{-1} in *Me*OH). The behaviour of the carbonyl band in the solvent mixtures is different. There is a change from a single band (at 1660 cm^{-1} in pure CCl_4) to two absorptions (1658 (vs) and 1634 (sh) cm^{-1}) in mixtures containing only 2% v/v *Me*OH. On increasing the proportion of hydroxylic solvent, the absorption at *ca.* 1658 cm^{-1} smoothly decreases in intensity and frequency, while the shoulder at 1634 cm^{-1} develops into a strong band which in pure methanol becomes predominant as an intense peak at 1628 cm^{-1}.

Diazoacetophenone

If this molecule is considered to be planar, then we know that the *cis–trans* interconversion must pass a barrier height of 39.2 $kcal/mol^{-1}$. Consequently there is no conformational equilibrium set up at room temperature, unless rotation of the phenyl group about the Ar—CO bond is admitted, with loss in coplanarity of the phenyl group itself with respect to the diazocarbonyl fragment (10). The reasons why the latter has not been observed experimentally have been discussed by us previously (7). The only con-

Can. J. Chem. Downloaded from www.nrcresearchpress.com by 210.87.254.6 on 09/05/12
For personal use only.

Can. J. Chem. Downloaded from www.nrcresearchpress.com by 210.87.254.6 on 09/05/12
For personal use only.

former existing at room temperature is the *cis* form, as deduced from electric dipole moments (13). This form gives rise to clear absorptions at 2106 (ν_{N-N}) and 1632 (ν_{C-O} cm^{-1}) in pure CCl_4 (the respective values in *n*-hexane are 2105 and 1639 cm^{-1}). Now, while the diazo vibration shifts only slightly to higher frequency with increase in the content of hydroxylic solvent in the mixtures (ν_{N-N} 2111 cm^{-1} in pure MeOH) the carbonyl vibration shifts greatly in position, going to 1608 cm^{-1} in pure MeOH. In addition, the behaviour of both relative intensities and absorption band frequencies of the two absorptions in CCl_4/MeOH is very similar to that described for diazoacetone. This indicates that the solute–solvent interactions must be very similar in both cases, despite the presence of only a single conformer in diazoacetophenone.

Bis-tert-butyl Diazoacetone

For this molecule, spectroscopic and dipole moment evidence (14) suggest the presence of a single conformer having a skew structure, which is understandable given the steric hindrance present. The diazo band again shows gradual shifts to higher frequency on going from CCl_4 (2059 cm^{-1}) to MeOH (2065 cm^{-1}). However, the behaviour of the C—O band is very different from that in the other molecules studied, in terms of the amount of bonding solvent necessary before changeover in the relative intensities of the two components of the carbonyl absorption. Thus, whereas in the other cases 20% MeOH in the mixture already produces spectra showing a clear predominance of the component at lower frequency, in this compound alcohol percentages of 80% are necessary before the low-frequency component becomes more intense. In addition, even 100% MeOH gives a spectrum in which the higher-frequency component is still rather intense. In other words, apart from the normal red shift of the C—O absorption from 1635 to 1612 cm^{-1}, a weak absorption at 1635 cm^{-1} remains, even in pure MeOH; this fact is in some way connected with the considerable steric hindrance produced in the molecule by the two *tert*-butyl groups.

3-Diazocamphor

This compound cannot, of course, give rise to *cis–trans* conformational equilibria (10) for structural reasons. Nevertheless, its behaviour in the solvent mixture is completely analogous to that of the other molecules. The N—N vibration gives rise to a band at 2072 cm^{-1} in CCl_4, which shifts to the blue, going to 2078 cm^{-1}, in MeOH. The carbonyl band, which absorbs at 1695 cm^{-1} in CCl_4, already presents considerable absorption at 1678 cm^{-1} in 10% MeOH, which becomes a single peak at 1670 cm^{-1}, with only a slight asymmetry at high frequency, in pure methanol. Consequently, we are again in the presence of two components in the mixtures, the relative intensities and frequencies of which are a function of the percentage bonding solvent present. The higher-frequency component undergoes shifts of a magnitude similar to those observed in the other molecules, whereas the absorption at low frequency moves further towards the red in this series of molecules.

Discussion

The results described clearly show that the behaviour of the bands attributable to ν_{N-N} and ν_{C-O} vibrations is substantially similar in these solvent mixtures, both when a conformational equilibrium is present and when it is impeded for steric or chemical reasons. We will first discuss the reasons for believing that the participation of solvent-stabilised conformational isomers may be excluded as an interpretation of the uv and ir spectra in solvent mixtures.

(*i*) Whereas the absorptions attributed to the two rotamers lie at very near frequencies in the ir (see ν_{N-N} in diazoacetone), in the uv there are frequency differences of some 50–60 nm. These seem to be too large to be attributable to transitions arising from the same molecular species, even in different conformational situations. This has already been pointed out by Csizmadia *et al.* (10) who calculated the uv transition energies for the two conformers of diazoacetone and diazoacetophenone. This calculation led to the conclusion that each of the bands observed in *n*-heptane arises from the overlap of two very close absorptions due to individual conformers.

That the behaviour in dioxan/water mixtures may be attributed to the presence of *cis* and *trans* conformers, which react differently in the formation of hydrogen bonds, is excluded by the observation of analogous behaviour for molecules in which *trans* conformers are not present, such as 2-diazocyclohexanone, 3-diazonorcamphor, and 3-diazocamphor (see refs. 10 and 13).

Can. J. Chem. Downloaded from www.nrcresearchpress.com by 210.87.254.6 on 09/05/12
For personal use only.

(*ii*) If the hydroxylic solvent acts in some way on the position of the conformational equilibrium, only changes in relative intensity would be expected, the absorption frequencies remaining substantially uninfluenced by the medium. Both the uv data (2, 4, 5) and the present ir results show, instead, that an increase in the percentage of bonding solvent in the mixture causes appreciable red shifts in the band positions.

(*iii*) For diazoacetone, the only molecule among those studied here for which the presence of a *cis–trans* equilibrium has been securely established, it has been found that the *cis* conformer is the more polar (15). Consequently, an increase of polar solvent in the mixture will decrease the intensity of the absorption due to the *trans* form. Since the less intense component of the diazo band doublet has been assigned to the latter form, the disappearance of the absorption at 2090 cm^{-1} in only 5% MeOH indicates that the molecule exists entirely in the *cis* form. Therefore, the second absorption clearly visible on the C—O band in all the CCl_4/MeOH mixtures cannot be attributed to conformational effects, given that, for all practical purposes, a single isomer remains in solution as the absorbing species.

(*iv*) As mentioned above, the behaviour of the N—N and C—O stretching vibrations and of the uv transitions is virtually identical in the mixtures, while the presence of a *cis/trans* equilibrium has been established for only one of the compounds.

The molecules studied here are, on the other hand, systems particularly adapted to taking part in local interactions with hydroxylic solvents. Thus, the diazocarbonyl conjugation may lead to limiting forms having high dipole character, such as **2** which could contribute greatly to the molecular ground state.

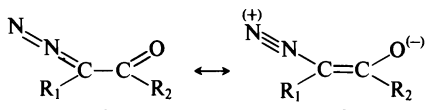

1 **2**

It seems clear that both the N—N and the C—O vibrational frequencies will depend on the relative weight that the charge-separated structure exerts. This will be higher the more this structure is stabilised by a solvent capable of forming hydrogen bonds, such as methanol.

We therefore suggest that there is an equilibrium between noninteracting molecules (those contributing to the ground state with structures not having charge separation and therefore having a higher C—O bond order) and interacting molecules, which presumably occurs via hydrogen bonding. A gradual increase in the amount of methanol in the mixture shifts the equilibrium towards species having charge separation. This increases the intensity of the absorption at lower frequency. Since the decrease in bond order of the C—O vibrator leads to a concomitant increase in the bond order of the diazo group, this would rationalise even the very small increase in N—N frequency.

Fahr's suggestion that to a lower C—O bond order must correspond a larger solvent effect, though consistent with the vibrator–solvent interaction mechanism suggested here, may not always be true. The data for the *tert*-butyl compound clearly indicate that in this molecule the C—O bond order is at least as low as that in diazoacetophenone. However, the two *tert*-butyl groups in the molecule cause such a large steric hindrance that a vibrator, which is inherently strongly polarized, is not allowed to freely interact with the bonding solvent. The fact that the high-frequency component changes little with variation in the bulk dielectric constant of the medium (see below) and the presence of considerable quantities of 'free' molecules in pure methanol may then be attributed to screening of the C—O vibrator by the *tert*-butyl groups, which impedes close approach by the bonding solvent.

While the amount of diazocarbonyl conjugation is probably responsible for the C—O bond orders in diazoacetone, diazoacetophenone, and 3-diazocamphor, in the *tert*-butyl derivative both the relatively low N—N vibrational frequency and the presumably skew configuration (13) indicate that this probably contributes little to the C—O bond order. The low C—O bond order presumably receives contributions from the strong inductive effect of the two *tert*-butyl groups.

Even a small frequency shift in the absorption due to the carbonyl and that due to the 'bonded' carbonyl with increase in methanol content may, at first, seem surprising. Effects due to the change in total dielectric constant of the medium may be responsible for this. Indeed, these shifts are more marked for both components of this

absorption the less shielded is the C—O vibrator (*e.g.* diazocamphor). This indicates that the dielectric constant of the medium acts according to the Onsager cavity model.

As a final point, in all the cases examined, with the exception of the *tert*-butyl derivative, there are weak absorptions at frequencies between those of the C—O vibration and that of the bonded carbonyl-hydrogen. There are not sufficient data to allow definite conclusions to be drawn as to the solute–solvent interactions or solvation complexes responsible for these absorptions. Nevertheless, since they undergo only slight shifts in frequency with little intensity change, in all solvent mixtures, the implication is that the equilibrium between 'free' carbonyl and 'bonded' carbonyl is shifted towards the latter at the expense only of the free species. In pure methanol this gives rise to two types of associated species, of which that interacting via a hydrogen bond predominates.

1. F. A. Miller and W. B. White. J. Am. Chem. Soc. **79**, 5974 (1957).
2. E. Fahr. Chem. Ber. **92**, 398 (1959).
3. R. Cataliotti, A. Poletti, and A. Foffani. Spectrochim. Acta Part A, **25**, 543 (1969).
4. C. Pecile, A. Foffani, and S. Ghersetti. Tetrahedron, **20**, 823 (1964).
5. L. L. Levepson and C. W. Thomas. Tetrahedron, **22**, 209 (1966).
6. G. Paliani, R. Cataliotti, and A. Poletti. J. Chem. Soc. Perkin Trans. II. Submitted for publication.
7. R. Cataliotti, G. Paliani, and S. Sorriso. Spectrosc. Lett. **7**, 449 (1974).
8. G. Paliani, S. Sorriso, and R. Cataliotti. J. Chem. Soc. Perkin Trans II, 707 (1976).
9. F. Kaplan and G. K. Meloy. J. Am. Chem. Soc. **88**, 950 (1966).
10. I. G. Csizmadia, S. A. Houlden, O. Meresz, and P. Yates. Tetrahedron, **25**, 2121 (1969).
11. F. Arndt and J. Amende. Ber. Dtsch. Chem. Ges. **61**, 1122 (1928).
12. M. S. Newmann and A. Arkell. J. Org. Chem. **24**, 385 (1959).
13. S. Sorriso, G. Piazza, and A. Foffani. J. Chem. Soc. B, 805 (1971).
14. S. Sorriso and A. Foffani. J. Chem. Soc. Perkin Trans. II, 2142 (1973).
15. G. Piazza, S. Sorriso, and A. Foffani. Tetrahedron, **24**, 4751 (1968).

Can. J. Chem. Downloaded from www.nrcresearchpress.com by 210.87.254.6 on 09/05/12
For personal use only.

Infrared study of the C—H stretching region of five-membered heterocyclic compounds

ROSARIO CATALIOTTI AND GIULIO PALIANI

Istituto di Chimica Fisica, Università degli Studi, Via Elce di Sotto, 10, 06100 Perugia, Italy

Received December 23, 1975

ROSARIO CATALIOTTI and GIULIO PALIANI. Can. J. Chem. **54**, 2451 (1976).

An infrared analysis of the C—H stretching region of some five-membered heterocyclic molecules (pyrrole, furan, thiophene, selenophene, and tellurophene) has been carried out. Spectra were obtained for gas, liquid, solution (CCl_4), and crystal samples. Polarised infrared radiation was employed for crystalline oriented films. Band profiles in the gas phase and polarisation values for the crystal spectra have been used in order to get new assignments for this spectral region.

ROSARIO CATALIOTTI et GIULIO PALIANI. Can. J. Chem. **54**, 2451 (1976).

On a effectué une analyse infrarouge de la région de vibration C—H de quelques molécules hétérocycliques à cinq membres (pyrrole, furanne, thiophène, sélénophène et tellurophène). On a obtenu les spectres pour des échantillons à l'état gazeux, liquide, en solution (CCl_4) et sous forme cristalline. On a utilisé une radiation infrarouge polarisée pour des films cristallins orientés. On a utilisé des profils de bande en phase gazeuse et des valeurs de polarisation pour les structures cristallines de façon à obtenir de nouvelles attributions pour cette région spectrale.

[Traduit par le journal]

Can. J. Chem. Downloaded from www.nrcresearchpress.com by 210.87.254.6 on 09/05/12
For personal use only.

Introduction

Although the vibrational spectra of pyrrole (1–7), furan (6–11, 24), thiophene (6, 10, 12–18), and selenophene (19–23) have been extensively investigated, considerable discrepancies in the assignment of the 3200–3000 cm^{-1} region exist. This is due to a number of factors: (*i*) four fundamentals (two A_1 and two B_2) must be assigned, but only two sharp peaks are usually observed both in the infrared and in the Raman spectra; (*ii*) the band profiles of the gas spectra are not well defined, especially in the case of pyrrole and furan; (*iii*) the Raman polarisation data are scanty and seem to be reliable only for thiophene (14) and selenophene (21).

We have re-investigated the 3200–3000 cm^{-1} region of these molecules with the intention of arriving at definitive assignments for the C—H motions. The infrared spectra of gas, liquid, solution, and crystal phases have been measured. The crystal infrared spectra have been analysed by means of polarised radiation.

Experimental

Pyrrole, furan, and thiophene were high-purity Fluka products and were used without further purification. Samples of selenophene (99.2% glc) and tellurophene (99.7% glc) were kindly supplied by Prof. F. Fringuelli, Institute of Organic Chemistry of this University. The measurements, in the region 3200–3000 cm^{-1}, were carried out on a Perkin-Elmer Model 521 spectrometer. Spectra of vapour, liquid, solution, and solid (100 K) phases were recorded with standard cells equipped with KBr and NaCl windows. For other experimental details see ref. 25.

The spectra are shown in Figs. 1–3. Frequencies (accurate to ± 0.5 cm^{-1}) and assignments are collected in Table 1.

Discussion

Most previous authors did not attempt to locate the four C—H stretching frequencies exactly, assigning two of them to each of the two observed infrared and Raman bands. Trombetti and Zauli (21), and subsequently Magdesieva (22), proposed an assignment for selenophene which gave the higher frequency mode as ν_{C-H} of both A_1 and B_2 species, while, for the two remaining ν_2 and ν_{13} modes, these authors attributed two different frequencies to the two different vibrations.

We shall review such assignments starting with a discussion of the band profiles in the gas phase. The principal moments of inertia for the molecules are reported in Table 2. The minor axis of inertia always coincides with the C_2 symmetry axis; the intermediate one is perpendicular to the minor axis in the plane of the ring and the major axis is always perpendicular to this plane.

Pyrrole and furan are oblate asymmetric tops,

Can. J. Chem. Downloaded from www.nrcresearchpress.com by 210.87.254.6 on 09/05/12
For personal use only.

TABLE 1. Infrared frequencies of the C—H stretchings of five-membered heterocyclic molecules[a]

Molecules	Gas[b]	Liquid	Solution (CCl_4)	Crystal (100 K)	Assignments
Pyrrole	3145(m)	3130(s)	3130(s)	3128(s)	ν_1 (A_1)
	3127(s)	3112(sh)	3115(sh)	3113(s)	ν_2 (A_1)
	3118(m)	3102(s)	3105(s)	3091(m)	ν_{12} (B_2)
	3088(w)				ν_{13} (B_2)
Furan	3162(m)	3159(s)	3152(s)	3147(s)	ν_1 (A_1)
	3139(s)	3136(sh)	3129(sh)	3125(s)	ν_{12} (B_2)
	3132(m)	3129(s)	3121(s)	3116(m)	ν_2 (A_1)
	3123(w)	(3120)[c]			ν_{13} (B_2)
Thiophene	3126(m)	3116(s)	3112(s)	3115(w)	ν_1 (A_1)
				3100(s)	ν_{12} (B_2)
	3098(s)	3088(sh)	3083(sh)	3079(m)	ν_2 (A_1)
	3086(m)	3080(s)	3075(s)	3072(w)	ν_{13} (B_2)
Selenophene	3120(s)	3101(s)	3108(s)	3099(s)	ν_1 (A_1)
	3083(vs)	3067(sh)	3070(sh)	3067(w)	ν_2 (A_1)
	3062(m)	3058(s)	3060(s)	3053(m)	ν_{13} (B_2)
Tellurophene	3106(s)	3084(vs)	3093(s)	3080(s)	ν_1 (A_1)
				3066(m)	ν_{12} (B_2)
	3064(vs)	3045(s)	3054(s)	3042(s)	ν_2 (A_1)
	3047(m)	3030(s)	3041(m)	3030(m)	ν_{13} (B_2)

[a]Entries are in cm^{-1}.
[b]Gas-frequencies are those of the Q branch for A-type bands and those of the center of band for B-type ones.
[c]Band position inferred from the gas–liquid frequency shift.

TABLE 2. Principal moments of inertia (g $cm^2 \times 10^{-40}$) of the five-membered heterocyclic molecules

Compounds	I_z	I_y	I_x	Ref.
Pyrrole	55.3610	56.1568	111.5335	26
Furan	53.5126	54.6720	108.2304	27
Thiophene	62.8568	93.2944	156.2164	28
Selenophene	66.5327	149.4125	216.0331	22
Tellurophene	71.4123	199.7763	271.1886	25

whereas the other molecules are prolate asymmetric tops.

The experimental band profiles of the infrared rotation–vibration vapour bands, resulting from the C—H stretching motions, are of type A (weak Q branch) for the A_1 modes and of type B (without a Q branch) for the B_2 ones.

The same situation arises for furan and pyrrole even though it is not theoretically foreseeable that in these cases there exists a difference between the contours of the A- and B-type bands (these molecules being nearly oblate symmetric top). The assignments of the A- and B-type bands have, however, been confirmed by measuring the P–R submaxima distances.

Pyrrole

The most recent assignments for pyrrole are those of Scott (7). This author gives values as 3145 and 3129 cm^{-1} for the A_1 and B_2 C—H stretchings.

The infrared spectrum of gaseous pyrrole (Fig. 1) shows that two clear Q branches emerge from the broad general envelope at frequencies of 3145 and 3127 cm^{-1}. Further, there are two weak B-type absorptions centred at 3118 and 3088 cm^{-1}, which we assign to the two expected B_2 motions.

The liquid spectrum of pyrrole shows two strong peaks at 3130 and 3102 cm^{-1} and a shoulder at 3112 cm^{-1}. In CCl_4 solution these absorptions are at 3130, 3105, and 3115 cm^{-1}, respectively. If the 3145 cm^{-1} frequency in the gas phase is associated with the strong band at 3130 cm^{-1} in the liquid, there is a gas–liquid frequency shift of 15 cm^{-1}. The same shift results if the 3127 and the 3118 cm^{-1} bands in the gas phase are associated with the absorptions at 3112 and at 3102 cm^{-1} in the liquid-state spectrum. In the infrared crystal spectrum of pyrrole at 100 K (24) we observe three intense

Can. J. Chem. Downloaded from www.nrcresearchpress.com by 210.87.254.6 on 09/05/12
For personal use only.

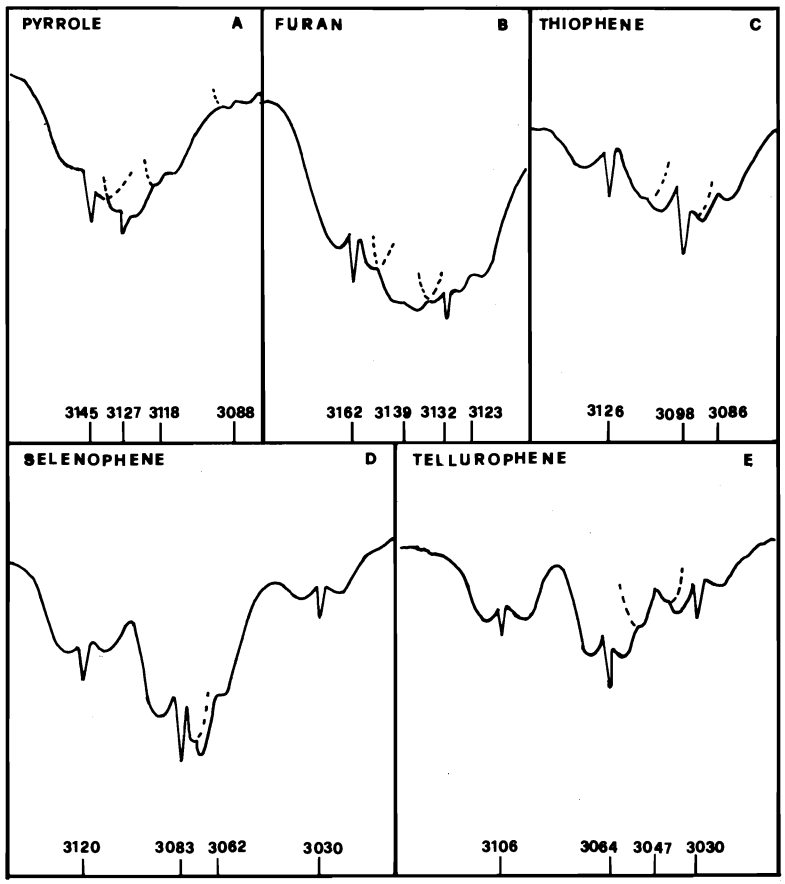

FIG. 1. Gas-phase spectra of the molecules, in the C—H stretching region. The numbers (cm^{-1}) indicate the position of bands discussed in the text.

peaks at 3128, 3113, and 3048 cm^{-1} and a medium-strong peak at 3091 cm^{-1} (see Fig. 3). All the three intense absorptions have low-frequency side peaks at 3122, 3105, and 3042 cm^{-1} respectively, due to factor-group splitting effects (24). Using polarised radiation it is easily seen that the peaks at 3128, 3113, and 3048 cm^{-1} have the same dichroic behaviour, whereas that at 3091 cm^{-1} has opposite dichroic character. Thus, the first three peaks belong to the A_1-type vibrations and that at 3091 cm^{-1} to the B_2 species. Since we must assign only two A_1 fundamentals, we believe that the peak at 3048 cm^{-1} results from the overtone of the 1528 cm^{-1} mode (24). Using these criteria, we propose a modification of the assignments already reported for the C—H stretching mode of pyrrole (1, 2, 6, 7) as follows: $\nu_1(A_1) = 3145\ cm^{-1}$; $\nu_2(A_1) = 3127\ cm^{-1}$; $\nu_{12}(B_2) = 3118\ cm^{-1}$; and $\nu_{13}(B_2) = 3088\ cm^{-1}$ (the frequency values are those for the gas-phase spectrum).

Furan

For the C—H stretching of furan, we start with a discussion of the assignment proposed by Rico *et al.* (8, 9). These authors give values of 3167 (calculated by the complete isotopic rule) and 3140 cm^{-1} for the A_1 C—H motions and values of 3161 and 3129 cm^{-1} for the B_2 ones. These values are all referred to the gas-phase infrared spectrum. The gas spectrum recorded by us shows a clear *R–Q–P* envelope with the *Q* peak centred at 3162 cm^{-1}. We prefer, therefore, to change Rico's assignment and take this band as ν_{C-H} of the A_1 species. In agreement with this assignment, the corresponding strong Raman line at 3154 cm^{-1} is polarised (9).

The second A_1 mode is then assigned at

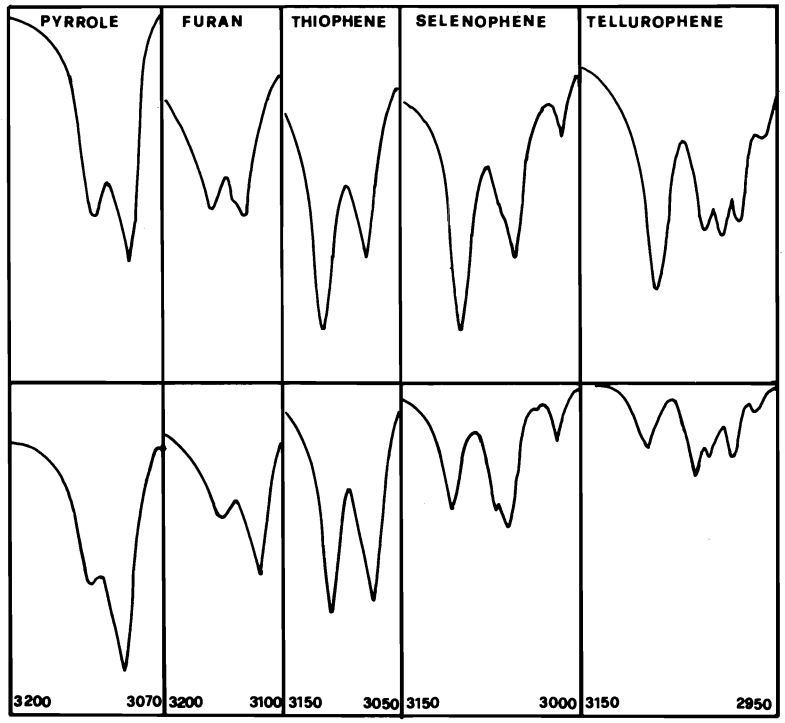

FIG. 2. Liquid-phase (upper) and solution (lower) spectra of the molecules studied, in the C—H stretching region.

3132 cm^{-1}, where the Q branch of another band having R–Q–P structure is found. The two B_2 modes are assigned to the bands at 3139 and 3123 cm^{-1} which lack Q peaks.

In the liquid spectrum we observe two intense bands at 3159 and 3129 cm^{-1} and an evident shoulder at 3136 cm^{-1}. Assuming the liquid–gas modes are assigned to the bands at 3139 and 3129–3132, the three modes will have the same gas–liquid shift of 3 cm^{-1}.

The spectrum in the solid state shows four intense peaks at 3147, 3125, 3116, and 3088 cm^{-1}. Using polarised radiation it is found that the peaks at 3147, 3116, and 3088 cm^{-1} have the same dichroic character and therefore must belong to analogous symmetry species. We attribute the 3147 and 3116 cm^{-1} peaks to the A_1 C—H vibrations, the 3088 cm^{-1} band to the overtone of the 1552 cm^{-1} mode, and the band at 3125 cm^{-1}, having opposite polarisation, to the B_2 mode absorbing at 3136 cm^{-1} in the liquid-state spectrum. Unfortunately, there is no indication of the 4th mode position, from the solid-state spectrum.

Thiophene

The vibrational spectrum of thiophene and of several deuterated derivatives has been extensively investigated by Rico *et al.* (14). Later, Loisel and Lorenzelli (6), Tranchant and Guerin (17), and Paliani *et al.* (18) reported the solid-state infrared spectrum of this molecule, making minor changes in the assignments.

For the C—H vibrations, the frequencies reported by Rico *et al.* for the gas-phase spectrum are 3126 and 3098 cm^{-1} for the ν_1 and ν_2 modes of A_1 species and 3125 (calculated), 3098 cm^{-1} for the ν_{12} and ν_{13} B_2 motions. As in the case of the pyrrole molecule, the same frequency was used twice to assign vibrations belonging to different symmetries.

We agree with the assignment of the A_1 modes since two A-type bands are in our gas spectrum at 3126 and 3098 cm^{-1}. We observe a band, without a Q branch, centred at 3086 cm^{-1}, which is certainly one of the two expected B_2 C—H motions.

The liquid spectrum has two peaks at 3116 (3112 in CCl_4) and at 3080 cm^{-1} (3075 in CCl_4).

Can. J. Chem. Downloaded from www.nrcresearchpress.com by 210.87.254.6 on 09/05/12
For personal use only.

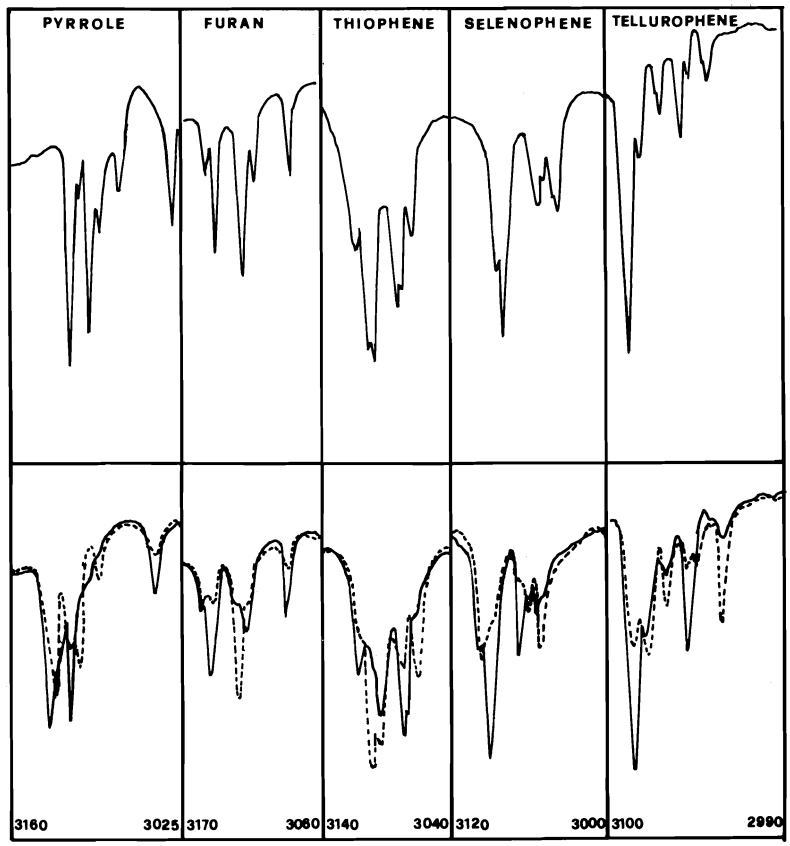

FIG. 3. Crystal ir spectra (upper) and polarised crystal ir spectra (lower) of the heterocyclic molecules, in the C—H stretching region.

In addition, there is an obvious shoulder at 3088 cm^{-1} (3083 in CCl_4). Since the Raman lines at 3107 and 3084 cm^{-1} in the liquid have been shown to be polarised (14), it is clear that they must correspond to the A_1 C—H stretchings and therefore must correlate with the bands having *R–Q–P* structure in the gas. The following correlation of frequencies between gas and liquid spectra supports the proposed assignment: 3126–3116 ($\Delta\nu$ = 10 cm^{-1}; 3098–3088 ($\Delta\nu$ = 10 cm^{-1}); 3086–3080 ($\Delta\nu$ = 6 cm^{-1}). Thus, there is the same shift for motions attributable to the A_1 symmetry species and a smaller shift for the B_2 vibrations.

In our previous paper on the ir spectrum of solid thiophene (18), we were able to discriminate between A_1 and B_2 motions, on the basis of their different dichroic behaviour. We gave frequencies of 3100 and 3072 cm^{-1} for the ν_{12} and ν_{13} B_2 vibrations and the doublet 3079, 3078 cm^{-1} for the ν_2 A_1 mode. The ν_1 vibration was assigned by Tranchant and Guerin (17) at 3112 cm^{-1}, from the spectrum of the 4th solid modification of the molecule. The present crystal study reveals only a small peak perpendicularly polarised at 3115 cm^{-1}. This fact seems quite surprising since the ν_1 mode is the most intense one in the other phases. However, in view of its polarisation, analogous to that of the 3079 cm^{-1} peak, we agree with Tranchant and Guerin that the small absorption at 3115 cm^{-1} might be the ν_1 mode of the 4th phase of solid thiophene.

Selenophene

The assignments of the C—H stretchings of selenophene are well established from previous studies (21, 22). Recently, we reported the ir spectrum and molecular dynamics of selenophene in the solid state (23).

Liquid selenophene has three sharp absorp-

Can. J. Chem. Downloaded from www.nrcresearchpress.com by 210.87.254.6 on 09/05/12
For personal use only.

Can. J. Chem. Downloaded from www.nrcresearchpress.com by 210.87.254.6 on 09/05/12
For personal use only.

tions at 3101, 3067, and 3058 cm^{-1} in the infrared. These correspond to lines in the liquid Raman spectrum lines at 3106, 3071, and 3061 cm^{-1}, respectively. Since the first two lines are polarised whereas the latter is depolarised (21), the assignment is straightforward, considering also that the correspondence with the ir gas spectrum gives two *A*-type bands at 3120 and 3083 cm^{-1}, and a *B*-type band at 3062 cm^{-1}. The absorption at 3030 cm^{-1} (type-*A* contour) is the first overtone of the ν_{14} ring stretching (21–23). In the solid-state ir spectrum there are two doublets at 3099–3103 and at 3067–3064 cm^{-1} with sharp perpendicular polarisation, and a third doublet at 3052, 3054 cm^{-1} with opposite polarisation. Our assignment is therefore the following: the two bands at higher frequencies (3101 and 3067 cm^{-1} in the ir liquid spectrum) are the ν_1 and ν_2 modes of the A_1 species and the remaining one at 3058 cm^{-1} is the ν_{13} motion of the B_2 species (23).

There is no indication, from the spectra in the various phases, of the position of the second B_2 mode, ν_{12}, so that we agree with previous workers that this motion is either accidentally degenerate with one of those described above, or is so weak as to be hidden by another, more intense, band.

Tellurophene

For this molecule we have recently reported an in-depth vibrational study of the normal motions (25). There is thus sufficient experimental data, also for the deuterated species, to allow a reliable assignment of the C—H stretches.

Starting with the gas-phase ir spectrum, we note that in the range 3110–3000 cm^{-1} there are three intense *A*-type bands and a *B*-type one. Since two arise from A_1 and one from B_2 motions, we believe that the band at lower frequency, *i.e.* that at 3030 cm^{-1}, should be a combination arising from the ring mode at 1512 cm^{-1} (25). Thus, peaks at 3106 and 3064 cm^{-1}, with definite *R–Q–P* branches, are the ν_1 and ν_2 motions of the A_1 species, whereas the absorption centred at 3047 cm^{-1}, having no *Q* structure, should be correlated with one of the B_2 vibrations.

The liquid and solution spectra give the same information, because there are secure polarisation data for three Raman lines whose frequencies agree well with the infrared ones. Thus, the lines at 3082 and 3046 cm^{-1} are strongly polarised, whereas that at 3029 cm^{-1} is depolarised. Moreover, in both the infrared and Raman spectrum of solid tellurophene at 100 K, there is a peak at 3066 cm^{-1} which in the ir crystal spectrum has the same polarisation as the other B_2 mode. We therefore assign this peak as ν_{12} and suggest that, as for selenophene, two vibrational energies (*e.g.* ν_1 and ν_{12}) may be close together so that only the narrowing of the bands at liquid nitrogen temperature allows them to be distinguished in frequency.

Concluding Remarks

The present study shows that the liquid state is the least adaptable for spectroscopic investigations on the C—H stretching region for five-membered heterocyclic molecules.

Gas-phase or solid-state ir spectra are much more useful for this kind of study. From these spectra it is possible to arrive at a complete vibrational assignment of the four C—H normal vibrations. However, although the assignments represent an improvement over previous studies, they are still not definitive because some *P–Q–R* contours are difficult to interpret. Unfortunately, in the case of selenophene, only three of these modes produce infrared absorption and Raman scattering in all the physical states, probably because of an accidental degeneracy between two of these vibrational levels.

Acknowledgements

This work was supported in part by the Italian Consiglio Nazionale delle Ricerche, Roma. We sincerely thank Prof. F. Fringuelli, Institute of Organic Chemistry of this University, for the gift of samples of very pure selenophene and tellurophene.

1. R. C. Lord, Jr. and F. A. Miller. J. Chem. Phys. **10**, 328 (1942).
2. P. Mirone. Gazz. Chim. Ital. **86**, 165 (1965).
3. J. Morcillo and J. M. Orza. An. R. Soc. Esp. Fis. Quim. Ser. B, **56**, 231 (1960).
4. J. M. Orza, M. Rico, and M. Barrachina. J. Mol. Spectrosc. **20**, 233 (1966).
5. A. M. Prima. Opt. Spectrosk. Mol. Spectrosc., Suppl. 3, 157 (1967); Opt. Spectrosc. USSR, 79 (1968).
6. J. Loisel and V. Lorenzelli. Spectrochim. Acta Part A, **23**, 2903 (1967).
7. D. W. Scott. J. Mol. Spectrosc. **37**, 77 (1971).
8. M. Rico, M. Barrachina, and J. M. Orza. An. R. Soc. Esp. Fis. Quim. Ser. A, **61**, 141 (1965).
9. M. Rico, M. Barrachina, and J. M. Orza. J. Mol. Spectrosc. **24**, 133 (1967).

10. H. W. THOMPSON and R. B. TEMPLE. Trans. Faraday Soc. **41**, 27 (1945).
11. B. BAK, S. BRODERSEN, and L. HANSEN. Acta Chem. Scand. **9**, 749 (1955).
12. J. LECOMTE. Bull. Soc. Chim. Fr. **13**, 415 (1946).
13. A. HIDALGO. J. Phys. Radium, **16**, 366 (1955).
14. M. RICO, J. M. ORZA, and J. MORCILLO. Spectrochim. Acta, **21**, 689 (1965).
15. K. W. KOHLRAUSCH and H. SCHREINER. Acta Phys. Austriaca, **1**, 373 (1948).
16. G. WADDINGTON, J. C. SMITH, and H. M. HUFFMAN. J. Am. Chem. Soc. **71**, 797 (1949).
17. F. TRANCHANT and R. GUERIN. C. R. Acad. Sci. Ser. B, **274**, 795 (1972).
18. G. PALIANI, A. POLETTI, and R. CATALIOTTI. Chem. Phys. Lett. **18**, 525 (1973).
19. H. GERDING, G. MILAZZO, and H. H. ROSSMARK. Rec. Trav. Chim. **72**, 957 (1953).
20. E. G. TRESHCHOVA, D. EKKHARDT, and Yu. K. YURLEY. Zh. Fiz. Khim. **38**, 159 (1964).
21. A. TROMBETTI and C. ZAULI. J. Chem. Soc. A, 1106 (1967).
22. N. N. MAGDESIEVA. *In* Advances in heterocyclic chemistry. Vol. 12. *Edited by* A. R. Katritzky and A. J. Boulton. Academic Press, N.Y. 1970. p. 1.
23. A. POLETTI, R. CATALIOTTI, and G. Paliani. Chem. Phys. **5**, 291 (1975).
24. R. CATALIOTTI, P. GALLINA, and G. PALIANI. Spectrosc. Lett. **8**, 799 (1975).
25. G. PALIANI, R. CATALIOTTI, A. POLETTI, F. FRINGUELLI, A. TATICCHI, and M. G. GIORGINI. Spectrochim. Acta (1976). In press.
26. B. BAK, D. CHRISTIANSEN, L. HANSEN, and J. RASTRUP-ANDERSEN. J. Chem. Phys. **24**, 720 (1956).
27. B. BAK, D. CHRISTENSEN, W. B. DIXON, L. HANSEN-NYGAARD, J. R. ANDERSEN, and M. SCHOTTLÄNDER. J. Mol. Spectrosc. **9**, 124 (1962).
28. B. BAK, D. CHRISTIANSEN, J. RASTRUP-ANDERSEN, and E. TANNENBAUM. J. Chem. Phys. **25**, 892 (1956).

Can. J. Chem. Downloaded from www.nrcresearchpress.com by 210.87.254.6 on 09/05/12
For personal use only.

Complex hydrogen bonded cations. The imidazole/imidazolium complex cation

D. H. BONSOR, B. BORAH, R. L. DEAN, AND J. L. WOOD[1]

Department of Chemistry, Imperial College of Science and Technology, London, SW7 2AY, England

Received December 17, 1975

D. H. BONSOR, B. BORAH, R. L. DEAN, and J. L. WOOD. Can. J. Chem. **54**, 2458 (1976).

The salts $(ImH^+)X^-$, Im = imidazole, $X^- = PF_6^-$, BF_4^-, or ClO_4^- have been prepared in solution, and the perchlorate salt has been crystallised. The molecularity implied by the formula is confirmed in solution by Job's method, and for the crystals gravimetrically. In MeCN the association constant is $\sim 8\ M^{-1}$. Infrared spectra of solution and crystals are similar, independent of counter ion, and indicate an asymmetric single minimum proton potential. The pronounced doublet in the NH stretching band of the H bridged complex, and replaced by a single band in the D bridged analogue, is not indicative of proton tunnelling. The X-ray structure is compatible with this interpretation of the spectra.

D. H. BONSOR, B. BORAH, R. L. DEAN et J. L. WOOD. Can. J. Chem. **54**, 2458 (1976).

On a préparé, en solution, les sels $(ImH^+)X^-$, Im = imidazole, $X^- = PF_6^-$, BF_4^- ou ClO_4^- et le sel perchlorate a été cristallisé. La molécularité impliquée par la formule est confirmée en solution par la méthode de Job et pour les cristaux d'une façon gravimétrique. Dans le MeCN, la constante d'association est approximativement $\sim 8\ M^{-1}$. Les spectres infrarouges en solution et sous forme de cristaux sont similaires, indépendants de l'anion et indiquent la présence pour le proton d'un potentiel asymétrique comportant un seul minimum. Le doublet très prononcé dans la bande NH d'élongation du complexe ponté avec l'hydrogène qui est remplacé par une bande unique dans l'analogue ponté avec du deutérium, n'indique pas la présence d'un effet de tunnel du proton. La structure déterminée par rayons-X est compatible avec cette interprétation du spectre.

[Traduit par le journal]

Introduction

Many organic bases hydrogen bond with their conjugate cations to give formally symmetric complex cations, of the type $(BH\cdots B)^+$. The infrared spectra show a remarkable doublet in the ν_s (NH stretching) band, when B is a heterocyclic base, which is replaced by a single band in the D bridged analogues (1, 2). Although this behaviour is a notable theoretical consequence of proton tunnelling in a double minimum potential, a number of other features of the spectra suggests that the lower frequency component involves Fermi resonance (1*d*, 2*b*). X-Ray determination of the structure of these complexes should help to resolve this question. Although several complexes have been prepared in the solid state (2*b*, 2*d*, 3), we had not previously been able to obtain crystals suitable for X-ray analysis. Recently Glowiak and coworkers have determined the crystal structures of two related systems containing chains of $NH\cdots N$ bonds in polycations; polytriethylamine diammonium and polypyrazinium salts (4).

Zundel and Muhlinghaus (5) examined the infrared spectra of concentrated (720.8 mg/ml) aqueous solutions of imidazole, partially neutralised with gaseous HCl. A variety of hydrogen bonded species will be present and contribute to the spectra in these solutions. To delimit the species to which the spectra refer, we have used solvents and counterions which are inert in hydrogen bonding, as judged by the absence of spectroscopic effects.

Experimental

Preparations

Three simple imidazole salts, the perchlorate, fluoroborate, and fluorophosphate were prepared, in each case by the addition of an aliquot of aqueous acid at 0 °C to the cooled solution in analar ethanol of the recrystallised base. The hexafluorophosphate precipitates immediately, the other two salts after removal of excess water with the pump. The salts were recrystallised from ethanol. Analyses are mainly within 0.1%, and in no case outside 0.3% of theoretical.

Deuteration of the base, and the perchlorate salt was effected by repeated dissolution in D_2O. The possibility of exchange of hydrogen attached to C was checked by

[1]To whom correspondence should be addressed.

Can. J. Chem. Downloaded from www.nrcresearchpress.com by 210.87.254.5 on 09/05/12
For personal use only.

Can. J. Chem. Downloaded from www.nrcresearchpress.com by 210.87.254.5 on 09/05/12
For personal use only.

nmr in the case of salt. No indication of exchange was found.

Complexes were prepared in solution by dissolving free base in the dry solvent (CH_3CN, CH_2Cl_2, or CH_3NO_2) and adding salt.

The solid complex was obtained by warming equimolar anhydrous base and perchlorate salt[2] in a mortar until fusion occurred (~60 °C), and allowing to cool after thorough stirring. Single crystals for X-ray analysis were obtained by co-dissolving base and perchlorate in dry nitromethane to give a solution 1.5 *M* in both. On slow evaporation of the solvent in a N_2 atmosphere, crystals of base deposit, followed a few days later by crystals of complex. By adding a trace of EtOH larger crystals were obtained. Moisture was excluded at all times by drybox and vacuum handling techniques. The analysis of this sample is C 31.03, H 3.81, N 24.11, Cl 14.62. $Im_2H^+ClO_4^-$ requires C 30.46, H 3.83, N 23.68, Cl 14.98.

Spectroscopy

Infrared spectra above 400 cm^{-1} were recorded with a Grubb-Parsons Spectromaster or Perkin-Elmer 325. For solutions CaF_2, NaCl or AgCl windows were used. Path length = 0.05 mm. Both fused and crystalline solids were examined as Nujol and HCBD mulls, using NaCl or AgCl windows.

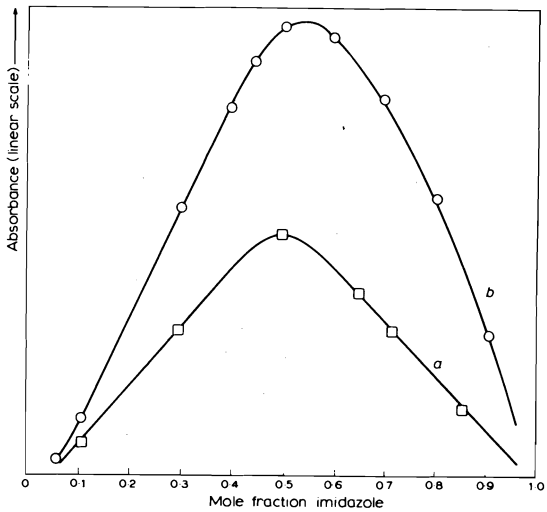

FIG. 1. Job plot for the association of imidazole and imidazolium, using the complex band at ~2 000 cm^{-1}. The BF_4^- salt was examined.

Results

Nature of the Complexes

Imidazole can function as both proton donor and proton acceptor in hydrogen bonding; as a result the crystalline free bases are extensively self-hydrogen bonded (6). The simple cations are bifunctional proton donors. There is thus the opportunity for a cation to complex with more than one base molecule forming a complex cation of general formula $(B_nH)^+$. The possible occurrence of oligomeric cations, which cannot arise in the previously examined monofunctional bases, was therefore investigated. Figure 1 shows Job's method (7) plots for total [Im] + [ImH^+] of 0.75 *M* (*a*) and 1.5 *M* (*b*) using the absorbance of the band at 2000 cm^{-1} (in MeCN solution) as a measure of the amount of complex. Absorption by the individual components is minimal at this frequency. The plot (*a*) is symmetric, with maximum at the equimolar composition, indicating that the $(Im_2H)^+$ complex predominates, with no evidence of polymeric species. The maximum is displaced to ~55 mol% base in plot (*b*), indicating that at higher concentration some polymeric cations, *e.g.*, $(Im_3H)^+$ are present. The close similarity of the spectra of the crystalline and fused solids whose composition is established analytically and from the structure, and those of the equimolar solutions, and the solutions obtained by redissolving the solids indicates that all refer to the species $(Im_2H)^+$.

From the data shown in the lower curve of Fig. 1, the association constant *K* of the complex is obtainable. If *A* is the initial concentration of salt, *B* is the initial concentration of base, *C* is the concentration of complex at equilibrium, then

$$[1] \qquad K = C/(A - C)(B - C)$$

Let *I* be the absorbance of the 2000 cm^{-1} band, and taking $C = \alpha I$

$$[2] \qquad K = \alpha I/(A - \alpha I)(B - \alpha I)$$

or

$$[3] \quad AB/I^2 - \alpha(A + B + K^{-1})/I + \alpha^2 = 0$$

Thus a plot of AB/I^2 against $1/I$ should give a straight line of slope $\alpha(A + B + K^{-1})$ and intercept $-\alpha^2$, so giving *K*. The data of plot (*a*) gives a value of $K = \sim 8\ M^{-1}$. Since K^{-1} is small compared to $A + B$, the method only gives a rough estimate of *K*.

In view of the extensive role in biochemical systems of hydrogen bonding involving imidazole, it is interesting that the occurrence of the present complex, which is at an optimum at a p*H* equal to the p*K* of the base, 6.95 (8), will be near neutrality in aqueous solution.

[2]Note possible explosion hazard.

TABLE 1. Infrared spectra of the imidazole complex cation and the free base and simple cation for comparison (frequencies in cm^{-1})*

Assignment (ImH^+)	$ImH^+ClO_4^-$ solid	$ImH^+ClO_4^-$ ... BF_4^- ... PF_6^- solution	$(Im)_2H^+$ complex Solid	$(Im)_2H^+$ complex Solution	Im Solid	Im Solution	Assignment (Im)
ν_{N-H}	3260s,br	3250s,br	3370s,br	3300s,br	3400sh 2850br	3350s 3000br	$\nu_{N-H(monomer)}$ $\nu_{N-H(associated)}$
ν_{N-H}			2500s,br 1900s,br	2500s,br 1950s,br			ν_{N-H}
R_1	1585s	1586s	1598s,br	1586s	1582w		
R_2	1525m	1534vw					
			1531s	1532m	1543s	1527m	R_1
			1500sh		1498s		
			1480m	1482m	1480s	1480m	R_2
R_3	1448m	1445m	1439m	1450sh,br			
R_4	1420m	1427m	1425m	1430s			
					1448s	1440sh	$R_{3(associated)}$
						1420m	$R_{3(monomer)}$
			1330m	1329s	1329m	1329s	R_4
					1322m	1326sh	
δ_{C-H}	1250m	1250vw	1255m	1257m	1263m	1256s	δ_{C-H}
					1244m	1240sh	$\delta_{N-H(associated)}$
R_5	1193m	1193m					
					1175m		?
δ_{N-H}	Obscured by counterion	1175sh	1210sh	1205w	R_5		
			1161s	1160m	or	1165w	$\delta_{N-H(monomer)}$
		1110sh		1125w	δ_{NH}		
			Obscured		1145s	1140m	R_5
δ_{C-H}		1097s	by	1092s	1099s	1090s	δ_{C-H}
δ_{C-H}		1045s	counterion	1060s	1053s	1060s	δ_{C-H}
		930w	937s	936m,br	935s	933m	R_6
R_6	923w	922w	943sh		921sh	920sh	γ_{NH}
			918m	919s			
		905w		904sh	895s	902w	R_7
R_7	862w		854sh				
					837s	830m	γ_{C-H}
					830m		
γ_{N-H}		815br	843s	846br			
		764s	756sh	760s,br	757s	754s	
γ_{C-H}	748s	748sh	748sh	722,sh,w			γ_{C-H}
						665s	$R_{8(monomer)}$
			650s	658s	658s	661s	$R_{8(associated)}$
			633m	635m			
R_8	615vs	627s					
			609s	613s	618s	621m	$R_{9(associated)}$
						610s	$R_{9(monomer)}$

*Im = imidazole, ImH^+ = imidazolium ion, br = broad, sh = shoulder, s = strong, m = medium, w = weak.

Spectroscopic Observations

It was first confirmed that after allowance for specific bands, the spectra in solution are independent of counterion or the solvent used (MeCN, $MeNO_2$, or CH_2Cl_2).

Throughout the interpretation of the spectra allowance is made for the proportion of free base or salt present, typically about 25% when total base and salt were each 2 *M*. The effect of complexing is most notable in the high frequency range (Fig. 2). In the mid-frequency range, the 665 cm^{-1} band of imidazole, and the 667 cm^{-1} and 942 cm^{-1} bands of d_1-imidazole clearly shift on complexing, as do the 627 and 815 cm^{-1} bands of ImH^+. Many bands in the mixture coincide in frequency with bands of either free base or salt. However, their intensity compared to the residue of base or salt bands which do shift in

Can. J. Chem. Downloaded from www.nrcresearchpress.com by 210.87.254.5 on 09/05/12
For personal use only.

TABLE 2. Infrared spectra of the deuterated imidazole complex cation, and of the deuterated base and simple cation, for comparison (all spectra relate to solution, frequencies in cm^{-1})*

Assignment (d_1-ImD$^+$)	d_1-ImD$^+$$ClO_4^-$ d_1-ImD$^+$$BF_4^-$	(d_1-Im)$_2$D$^+$ complex	d_1-Im	Assignment (d_1-Im)
ν_{N-H}	2430s 2380s,br	2470s,br 1950s,br	2500s,br 2250s,br	$\nu_{N-H(monomer)}$ $\nu_{N-H(associated)}$
R_1	1568m	1567vw		
R_2	1547s	1546s 1540w		
		1512m	1505s	R_1
		1480s	1477s	R_2
R_3	1398m	1398w		
R_4	1367s	1365s		
		1357sh	1355s 1350sh	R_3
		1330w	1334vw	R_4
		1320vw	1320s	
δ_{C-H}	1260w	1260sh		
		1250s	1250s	δ_{C-H}
	1200sh,w			
	Obscured by counterion	Obscured by counterion	1135m	R_5
			1100s	δ_{C-H}
			1062s	δ_{C-H}
			950m,br	$\delta_{N-D(associated)}$
		953s,br	942m	R_6
R_7	932m	932m	930w	R_7
δ_{N-D}	930m,br			
		915vw 900vw	910vw	$\delta_{N-D(monomer)}$
δ_{N-D}	865m	870br		
γ_{C-H}	845m	840s,br	832m	γ_{C-H}
γ_{C-H}	762vs	760s	754s	γ_{C-H}
		662s	667s	R_8
R_8	627vs	627vs		
		620w	621w	$R_{9(associated)}$
			617w	$R_{9(monomer)}$
γ_{N-D}	600m,br			
		540 590 v,br		

*d_1-Im = imidazole-(d_1)-1; d_1-ImD$^+$ = imidazolium-(d_2)-1,3.

the complex often indicates that in the mixture the band cannot arise from the unassociated species. Thus all the bands shown in column 5 of Table 1 are ascribed to the complex, although many coincide with bands shown in columns 3 and 7.

Many coincidences between complex and component bands also occur in the solid state spectra, but the absence of base bands at 895 and 1448 cm^{-1}, and salt bands at 615 and 1585 cm^{-1}, reflects the completeness of complexing shown by the crystal structure.

In the spectrum of the deuterated complex, only examined in solution (Table 2), the majority of the complex bands nearly coincide with either base or salt bands, but may be distinguished by intensity comparison of the effect of altering the salt/base ratio, as before.

Discussion

A most notable observation is the similarity of the spectra of the complex in the solid state and in solution. This is apparent in the ν_s band of the H bridged systems (Fig. 2), particularly as this band is sensitive to the nature of the hydrogen bonding. Another indication of the similarity is that the new bands characteristic of the complex occur at closely similar frequencies in the two phases. Examples are the bands at 635 and 919 cm^{-1}.

Can. J. Chem. Downloaded from www.nrcresearchpress.com by 210.87.254.5 on 09/05/12
For personal use only.

Can. J. Chem. Downloaded from www.nrcresearchpress.com by 210.87.254.5 on 09/05/12
For personal use only.

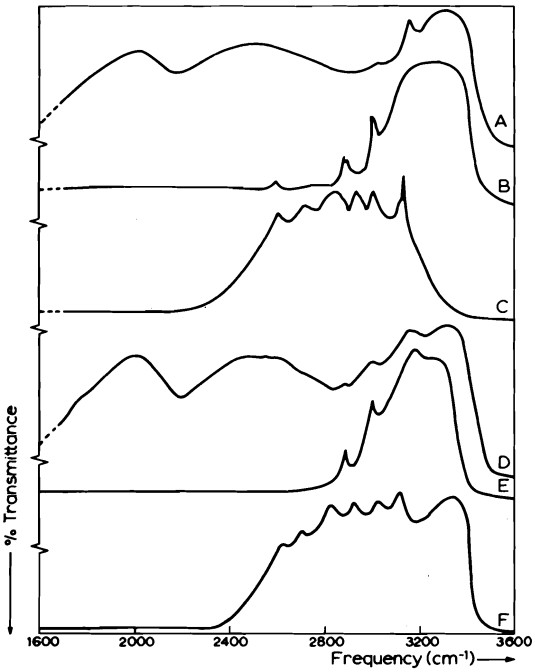

FIG. 2. Infrared spectra in the NH stretching range. (*A*) solid $(Im)_2H^+ClO_4^-$, (*B*) solid $ImH^+ClO_4^-$, (*C*) solid Im, (*D*) $ImH^+ClO_4^-$ + Im in solution each 2 *M*, (*E*) $ImH^+ClO_4^-$ in solution (2 *M*), (*F*) Im in solution (2 *M*). Solvent and counterion bands have been omitted.

The NH and ND Stretching Bands

The very pronounced doublet (Fig. 2) in the ν_s band of the H bridged systems has a very similar appearance in the spectra of other $(B_2H)^+$ complex cations, B being a heterocyclic base (1, 2), particularly the *N*-methylimidazole one (2*a*). The rounded bands at 3300 cm^{-1} (solution), or 3370 cm^{-1} (solid), are close in frequency to similar features in the spectra of the simple salts (9), but as they remain in the presence of excess base, are due to the complex, and arise from stretching of the outer NH groups.

In the deuterated complex, which has only been examined in solution, the stretching of the outer ND groups gives the strong rounded band at 2470 cm^{-1} (Fig. 3), again close to the position in the simple salts (8), while the ν_s band is now represented by only a single broad feature, extending from ~1760 to ~2150 cm^{-1}.

The possibility that proton tunnelling associated with a double minimum potential could give rise to the ν_s band doublet, with the splitting greatly reduced in the D bridged species, has been extensively discussed (10). However, this origin for the appearance of the ν_s band in the spectra of related $(B_2H)^+$ cations was rejected (2*b*), since several other spectroscopic features implied by a double minimum potential were not present. Again in the present system it is unlikely for the ν_s band to be related to proton tunnelling, and Fermi resonance would seem to be the most probable cause of the ν_s doublet, both in the crystal and solution spectra.

The Mid-frequency Range

Two features of the mid-frequency range spectra throw light on the form of the proton potential. The first is the possible duplication of the internal modes of the base, one set corresponding to the proton donor, and the other to the proton acceptor. The vibrational spectra of both imidazole (6), and its salts (9) have been examined in considerable detail by Bellocq and co-workers. Even a cursory examination of the complex bands listed in Tables 1 and 2 shows that the spectrum contains many more bands than either free base or cation alone, and also that many can be related to those of the free cation (proton donor) or base (proton acceptor) *e.g.*, R_1, R_2, R_3, R_4. The spectrum of the deuterated complex displays similar behaviour.

Even though the assignment, shown in the final columns of Tables 1 and 2 and which generally follows the work of Bellocq, is tentative, it can clearly be inferred that the two base molecules in the complex are spectroscopically distinguishable. Although the internal modes could be duplicated in a complex of, *e.g.*, C_{2v}

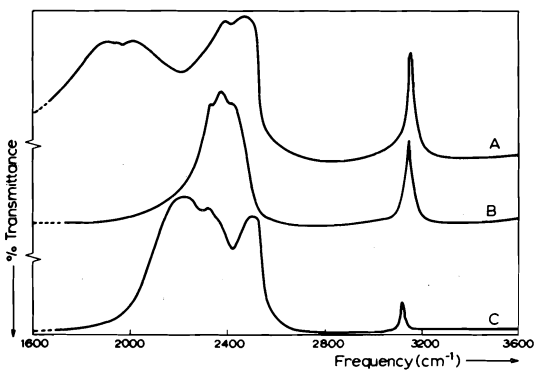

FIG. 3. Infrared spectra in the ND stretching range. (*A*) d_1-$ImD^+ClO_4^-$ + d_1-Im in solution each 2 *M*, (*B*) d_1-$ImD^+ClO_4^-$ in solution (2 *M*), (*C*) d_1-Im in solution (2 *M*). Solvent and counterion bands have been omitted.

Can. J. Chem. Downloaded from www.nrcresearchpress.com by 210.87.254.5 on 09/05/12
For personal use only.

overall symmetry, with identical bases, as a consequence of mechanical interaction, it is unlikely that in both the H and D bridged species the complex modes would relate so well with those of free base or cation.

The second feature of the mid-range spectra indicative of the proton potential is the frequencies of the NH bending modes (1*d*). We can expect the following pattern for the three in-plane modes if the present complexes are asymmetric or have a high barrier, *i.e.*, are effectively cation···base: (*i*) a mode with frequency around the mean of the frequencies of the two modes in the free cation, localised in the outer NH of the cationic moiety, (*ii*) a mode with frequency in the vicinity of that of the free base, localised in the outer NH of the acceptor base, (*iii*) a mode at higher frequency due to the bridging NH group. A guide to the upward shift can be sought in the effect of hydrogen bonding on the NH bending of the base itself.

In contrast, for a complex with a central bridging proton, we are likely to see only a single band developed from the two outer NH groups, and a mode at much higher frequency arising from the central proton.

The situation in the undeuterated systems is complicated by the presence of the ring mode R_5 of both base and salt in the range 1100–1200 cm^{-1} where the NH bending modes are expected. In the deuterated systems the present spectra suggest some revision of the previous assignment of these modes of the base and cation. We take the weak band at 910 cm^{-1} (Fig. 4) to be the bending mode of the free base, and the broader band around 950 cm^{-1}, whose intensity varies with the concentration, to represent the associated base. The previous assignment (6*b*) is of a strong band of the solid (and therefore associated) base at 914 cm^{-1} to this mode. In the free cation a broad rounded band underlies the sharp internal mode band at 932 cm^{-1}, and we take this to be the second ND bending mode, rather than the previously assigned (9) band at 845 cm^{-1} which appears to correspond to the band in the free base at 832 cm^{-1} assigned to a γ CH mode. We concur with the previous assignment of the shoulder at ~865 cm^{-1} to the other ND bend. In the complex, this band remains, as does a weak feature corresponding to that of the free base at 910 cm^{-1}, but a third band cannot be distinguished; it may well underlie the strong band, ascribed to an internal mode, R_6, at 953 cm^{-1}.

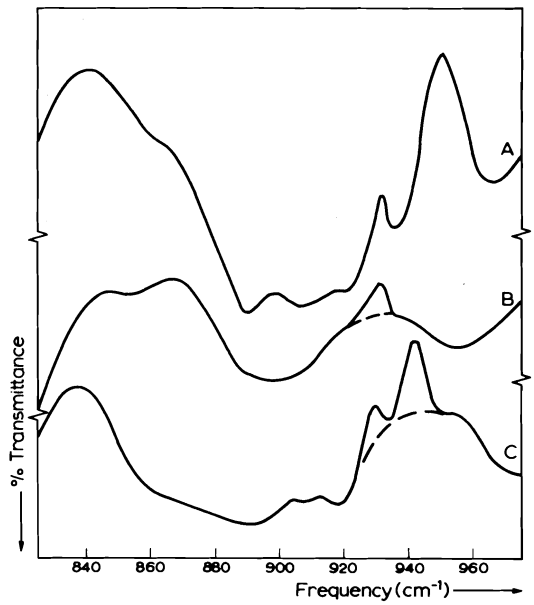

FIG. 4. The infrared spectra in the ND in-plane bending region. (*A*) d_1-ImD$^+$ClO$_4$ + d_1-Im in solution each 2 *M*, (*B*) d_1-ImD$^+$ClO$_4$ in solution (2 *M*), (*C*) d_1-Im in solution (2 *M*). Dotted lines indicate the broad bending mode bands deemed to underlie internal (R) modes in spectra (*B*) and (*C*).

Thus, in general, the in-plane ND bending modes fit an asymmetric position for the bridging proton.

Although in principle the out-of-plane NH (ND) bending modes can be similarly used to assess the bridging proton position, it has not proved feasible to distinguish the modes well enough for this purpose.

Conclusion

The spectra show that the two base molecules in the complex are distinguishable, one having proton acceptor, or free base character, the other cation or proton donor character. This distinction is present both in the crystalline state and in solution. On the vibrational time scale, an asymmetric single minimum potential for the proton is implied. In the solid state this may be the permanent structure, but in solution, over a sufficiently long period of time, the roles of the base molecules must change, corresponding to a high proton barrier. As will be discussed in the following paper, this indicates that the proton

motion, in solution, is coupled with that of the environment.

The data for the present complex also clearly demonstrate that the occurrence of a doublet structure in the ν_s band, converging towards a single maximum in the D bridged analogues, cannot be taken as proof of proton tunnelling through a low barrier (10). Other factors may produce this ν_s band behaviour in systems which are effectively asymmetric. For the same reason, the use of isotopic shifts in the ν_s band as an indicator of the proton potential (10*d*) can also be misleading.

Further discussion of the proton potential in this and closely related systems will be included in the accompanying report on the benzimidazole complex.

1. (*a*) R. CLEMENTS and J. L. WOOD. J. Mol. Struct. **17**, 265 (1973). (*b*) R. CLEMENTS and J. L. WOOD. J. Mol. Struct. **17**, 283 (1973). (*c*) R. CLEMENTS, R. L. DEAN, and J. L. WOOD. J. Mol. Struct. **17**, 291 (1973). (*d*) J. L. WOOD. J. Mol. Struct. **17**, 307 (1973).
2. (*a*) R. L. DEAN and J. L. WOOD. J. Mol. Struct. **26**, 197 (1975). (*b*) R. L. DEAN and J. L. WOOD. J. Mol. Struct. **26**, 215 (1975). (*c*) R. L. DEAN and J. L. WOOD. J. Mol. Struct. **26**, 237 (1975). (*d*) A. QUICK, D. J. WILLIAMS, B. BORAH, and J. L. WOOD. Chem. Commun. 891 (1974).
3. E. GRECH and M. SZAFRAN. Rocz. Chem. Ann. Soc. Chim. Polonorum, **46**, 2365 (1972).
4. T. GLOWIAK, L. SOBCZYK, and E. GRECH. Chem. Phys. Lett. **34**, 292 (1975); **36**, 106 (1975).
5. G. ZUNDEL and J. MUHLINGHAUS. Z. Naturforsch. **26**b, 546 (1971).
6. (*a*) A. M. BELLOCQ, C. PERCHARD, A. NOVAK, and M. L. JOSIEN. J. Chim. Phys. **62**, 1334 (1965). (*b*) C. PERCHARD, A. M. BELLOCQ, and A. NOVAK. J. Chim. Phys. **62**, 1334 (1965). (*c*) C. PERCHARD and A. NOVAK. J. Chim. Phys. **48**, 3079 (1968).
7. P. JOB. Ann. Chim. **9**, 113 (1928).
8. J. L. WOOD. Biochem. J. **143**, 775 (1974).
9. A. M. BELLOCQ and C. GARRIGOU-LAGRANGE. Sp Acta, **27**a 1091 (1971).
10. (*a*) R. L. SOMORJAI and D. F. HORNIG. J. Chem. Phys. **36**, 1980 (1962). (*b*) J. LAANE. Appl. Spectrosc. **24**, 73 (1970). (*c*) J. LAANE. Quart. Rev. Chem. Soc. **25**, 533 (1971). (*d*) J. LAANE. J. Chem. Phys. **55**, 2514 (1971). (*e*) M. D. HARMONY. Chem. Soc. Rev. **1**, 211 (1972).

Can. J. Chem. Downloaded from www.nrcresearchpress.com by 210.87.254.5 on 09/05/12
For personal use only.

The crystal structure of the complex salt imidazole imidazolium perchlorate

ANDREW QUICK AND DAVID J. WILLIAMS[1]

Chemical Crystallography Laboratory, Imperial College, London SW7 2AY, England

Received December 17, 1975

ANDREW QUICK and DAVID J. WILLIAMS. Can. J. Chem. **54**, 2465 (1976).

The crystal structure of imidazole imidazolium perchlorate has been determined at room temperature from three-dimensional diffractometer data, and refined by full-matrix least-squares to a final $R = 0.051$. The planar imidazole rings are linked by a N···N hydrogen bond of length 2.73 Å and rotated with respect to each other about this bond by an angle of 50°. The analysis has failed to give conclusive evidence as to the position of the hydrogen atom between the two imidazoles.

ANDREW QUICK et DAVID J. WILLIAMS. Can. J. Chem. **54**, 2465 (1976).

On a déterminé, à température de la pièce, à partir de données diffractrométriques, la structure cristalline du perchlorate de l'imidazolium de l'imidazole et on l'a affinée par les méthodes des moindres carrés (matrice complète) jusqu'à une valeur finale de $R = 0.051$. Les cycles imidazoles plans sont liés par un lien N···N d'une longueur de 2.73 Å et ils forment l'un par rapport à l'autre autour de ce lien, un angle de 50°. L'analyse n'a pas permis d'obtenir des données concluantes concernant la position de l'atome d'hydrogène entre les deux imidazoles.

[Traduit par le journal]

Can. J. Chem. Downloaded from www.nrcresearchpress.com by 210.87.254.105 on 09/05/12
For personal use only.

Introduction

The successful production of crystals of the $(ImHIm)^+ClO_4^-$ (Im = imidazole) complex suitable for X-ray analysis, offered the opportunity to relate the detailed structure of the ImHIm unit to its infrared spectrum, and to investigate the spectroscopic inference of an asymmetric hydrogen bond between the imidazole molecules. Spectroscopic and preparative aspects of the structure are described in the preceding paper.

Experimental

The complex crystallises as colourless plates which are exceedingly sensitive to moisture. They can, however, be kept for a period of a few days under thoroughly dried liquid paraffin.

Accurate lattice parameters were obtained by least-squares refinement of 24 high-angle reflections measured (at 10 °C) on a diffractometer using Cu-K_α radiation. The crystal data are:

$C_6H_9N_4.ClO_4$ mol. wt. = 236.6

Monoclinic, $a = 5.0994(3)$, $b = 8.7333(5)$, $c = 11.8228(5)$ Å, $\beta = 98.691(5)°$, $U = 520.5$ Å^3, $Z = 2$, $D_c = 1.51$ g cm^{-3}, $F(000) = 244$. Space group $P2_1$. Cu-K_α radiation, $\lambda = 1.5418$ Å, μ(Cu-K_α) = 33.5 cm^{-1}.

A crystal *ca.* $0.6 \times 0.3 \times 0.3$ mm^3 was sealed in a tight fitting Lindemann tube under a minimum quantity of dried liquid paraffin, and mounted along its *a* direction. Data were measured on a Siemens off-line four-circle diffractometer using Ni-filtered Cu-K_α radiation and following procedures described in detail elsewhere (1). A total of 1064 independent reflections were measured (to $\theta = 70°$) and of these, 10 reflections had $I < 2.58\sigma(I)$ and were classed as unobserved (1). The net count of the 054 reflection, measured as a reference every 50 reflections, did not alter significantly during the data collection (*ca.* 2 days) indicating that no deterioration of the crystal had occurred. The data were brought to a uniform arbitrary scale by use of this reflection (1), and Lorentz and polarisation corrections were applied. No absorption corrections were applied.

Solution and Refinement of the Structure

The structure was solved by direct methods by an application of the program MULTAN (2) to 189 reflections with normalised structure factors (E's) ≥ 1.33. An E map, calculated for the phase solution with the highest 'combined figure of merit', gave plausible positions for the atoms of the perchlorate ion and for one of the imidazole rings. The positions of these atoms were refined and a difference electron-density map computed which gave the positions for the atoms of the other ring. The structure was refined anisotropically by full-matrix least-squares to $R = 0.064$, $(R = \sum||F_o| - |F_c||/\sum|F_o|)$ after omission of four reflections which had $|F_o| \ll |F_c|$ and were suspected of being affected by extinction; they are identified in the F list.

A difference map gave plausible positions for all the ring hydrogens, although some of the peaks were rather diffuse. In the region between N(2) and N(3) there were peaks, attributable to hydrogen atoms, ~1 Å distant from both N(2) and N(3) but with peak heights in a ratio of approximately 2:1, the stronger being close to N(2). Isotropic refinement of the hydrogen positions was not wholly successful for, surprisingly, some of the parameters of apparently well resolved atoms failed to converge. The refinement of the larger weight hydrogen attached to N(2) was also not entirely convincing; the convergence

[1]To whom correspondence should be addressed.

Can. J. Chem. Downloaded from www.nrcresearchpress.com by 210.87.254.105 on 09/05/12
For personal use only.

was not decisive and it had a rather large isotropic temperature factor ($B \approx 13$ Å^2). This may possibly reflect a genuine partial occupancy, but in the circumstances refinement with fractional weight atoms was not considered realistic and refinement was terminated at a final $R = 0.051$.[2] A final difference map still showed a small peak (0.13 e/Å^3) near N(3) but also appreciably more residual electron density (up to 0.5 e/Å^3) in the region of the perchlorate ion. This latter suggests that the assumption of a rather large anisotropic thermal motion may not be adequate; some disorder may also occur but cannot be assessed or allowed for. Unit weights were used throughout the refinements. Atomic scattering factors were taken from ref. 3 with the exception of those for hydrogen which were taken from ref. 4.

The computations were carried out on the Imperial College CDC 6400 and the University of London CDC 6600 and 7600 computers, using in the main programs belonging to the X-ray 70 system (5).

Results and Discussion

The final fractional atomic coordinates and thermal parameters for the non-hydrogen atoms together with their estimated standard deviations are listed in Tables 1 and 2. Figure 1 shows a perspective view (ORTEP (6)) of the asymmetric unit of the structure with thermal ellipsoids scaled to enclose 30% probability. The figure also shows the numbering scheme used. Table 3 lists the bond lengths and bond angles and their estimated standard deviations. Table 4 gives selected intergroup contacts ≤ 3.50 Å.

The structure is comprised of endless chains of molecules, loosely hydrogen bonded and running perpendicular to *b*. The two imidazole rings are connected by a hydrogen bond (N(2)$\cdots$N(3) = 2.73(1) A) and these units are in turn linked by weaker hydrogen bonds (3.03 and 2.86 Å) to their counterparts in adjacent cells via the oxygens O(1) and O(3) of the perchlorate. Figure 2 shows the [010] projection of the hydrogen bonding arrangement. Figure 3 shows a stereoscopic view (ORTEP) of the packing of the molecules in the cell. The packing of the screw-related chains of molecules is fairly tight with several contacts between them of less than 3.5 Å (Table 4).

Figure 4 shows a comparison of the bond lengths and angles for the two imidazole rings. Both rings show notable and possibly significant differences in bond lengths: N(1)—C(2) *cf.* N(4)—C(6) and C(1)—N(1) *cf.* C(4)—N(4), each equivalent to $\sim 2.8\sigma$. Larger differences can be seen, however, in the angles *e.g.* 113° at C(4) and 104° at N(3), *cf.* 109° at C(2) and N(1); both differences are $> 3.5\sigma$ and probably statistically significant. Each ring displays a marked and similar asymmetry about the bonds flanking N(2) and N(3), a possible reflection of the nature of the hydrogen bond between them. The two rings are planar, with a maximum displacement from the least-squares plane of 0.015 Å, and are rotated with respect to each other about the N$\cdots$N hydrogen bond by an angle of 50°. Table 5 gives the equations of the ring planes and the displacements of the various atoms from them.

There are notable similarities between the values obtained here and those for the various determinations of the structure of imidazole (7–9), though the symmetry about a plane bisecting the C—C bond is not so pronounced here. This is particularly noticeable if one compares N(3)—C(5) with N(4)—C(6), a difference

TABLE 1. Fractional coordinates ($\times 10^4$) for the non-hydrogen atoms with estimated standard deviations in parentheses

Atom	*x*	*y*	*z*
C(1)	8964(18)	4894(9)	3417(6)
C(2)	10492(21)	2597(10)	3913(8)
C(3)	8316(22)	2449(11)	3155(8)
N(1)	10949(13)	4153(8)	4055(5)
N(2)	7355(10)	3883(7)	2864(4)
C(4)	3756(17)	3841(14)	18(7)
C(5)	1497(17)	5478(13)	772(6)
C(6)	463(17)	5361(14)	−332(6)
N(3)	3613(13)	4455(10)	1005(5)
N(4)	1949(15)	4337(10)	−784(5)
Cl	6651(2)	3563	6563(1)
O(1)	9500(6)	3568(8)	6783(3)
O(2)	5663(12)	2067(7)	6273(7)
O(3)	5740(12)	4567(7)	5624(5)
O(4)	5696(10)	4126(11)	7538(4)

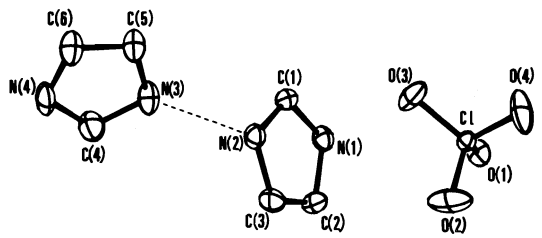

FIG. 1. Perspective view of the imidazole imidazolium complex and the numbering scheme employed.

[2]Tables of observed and calculated structure factors are available at a nominal charge from the Depository of Unpublished Data, CISTI, National Research Council of Canada, Ottawa, Canada K1A 0S2.

Can. J. Chem. Downloaded from www.nrcresearchpress.com by 210.87.254.105 on 09/05/12
For personal use only.

TABLE 2. Final anisotropic thermal parameters* ($\times 10^4$) for the non-hydrogen atoms, with standard deviations in parentheses

Atom	β_{11}	β_{22}	β_{33}	β_{12}	β_{13}	β_{23}
C(1)	503(33)	112(11)	74(6)	−4(16)	15(11)	5(6)
C(2)	713(55)	132(12)	94(7)	89(22)	46(16)	21(8)
C(3)	821(63)	124(12)	99(7)	−71(21)	45(16)	−12(8)
N(1)	387(23)	171(10)	67(4)	8(12)	1(8)	−12(5)
N(2)	435(22)	159(13)	67(4)	−21(12)	−1(7)	−1(5)
C(4)	640(41)	252(23)	97(7)	41(24)	41(13)	−18(10)
C(5)	656(42)	277(18)	69(5)	6(24)	33(12)	0(9)
C(6)	595(41)	312(21)	80(6)	2(25)	5(13)	3(10)
N(3)	580(29)	284(15)	64(4)	−25(19)	−30(9)	−7(7)
N(4)	828(41)	259(14)	55(4)	−158(21)	−10(11)	−17(7)
Cl	319(4)	112(2)	53(1)	15(4)	6(1)	4(1)
O(1)	294(13)	186(7)	87(3)	6(14)	−8(5)	−16(7)
O(2)	575(29)	121(8)	304(12)	−88(13)	−133(15)	−13(9)
O(3)	670(29)	202(11)	116(5)	−79(15)	−97(9)	75(7)
O(4)	633(25)	568(27)	70(3)	171(21)	54(8)	−58(8)

*In the form: $\exp[-(\beta_{11}h^2 + \beta_{22}k^2 + \beta_{33}l^2 + 2\beta_{12}hk + 2\beta_{13}hl + 2\beta_{23}kl)]$.

TABLE 3. Bond lengths and bond angles with standard deviations in parentheses

Bond	Length (Å)	Bonds	Angle (deg)
C(1)—N(1)	1.334(10)	C(1)—N(1)—C(2)	107.9(7)
N(1)—C(2)	1.385(12)	N(1)—C(2)—C(3)	106.6(8)
C(2)—C(3)	1.323(14)	C(2)—C(3)—N(2)	108.2(8)
N(2)—C(3)	1.370(11)	C(3)—N(2)—C(1)	108.5(6)
C(1)—N(2)	1.311(10)	N(2)—C(1)—N(1)	108.6(7)
Cl—O(1)	1.437(3)	O(1)— Cl —O(2)	111.0(4)
Cl—O(3)	1.435(6)	O(1)— Cl —O(4)	108.4(3)
C(4)—N(4)	1.293(11)	O(2)— Cl —O(4)	111.4(5)
N(4)—C(6)	1.335(13)	C(4)—N(4)—C(6)	108.4(7)
C(5)—C(6)	1.335(10)	N(4)—C(6)—C(5)	106.2(8)
N(3)—C(5)	1.396(12)	C(6)—C(5)—N(3)	108.8(8)
C(4)—N(3)	1.296(11)	C(5)—N(3)—C(4)	103.6(6)
Cl—O(2)	1.423(6)	N(3)—C(4)—N(4)	113.0(9)
Cl—O(4)	1.406(6)	O(1)— Cl —O(3)	109.8(3)
		O(2)— Cl —O(3)	108.3(4)
		O(3)— Cl —O(4)	108.0(4)

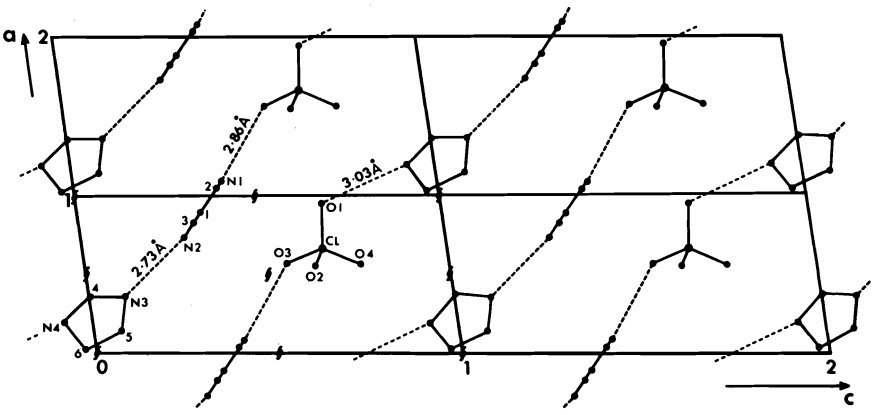

FIG. 2. System of hydrogen bonding in the structure (4 unit cells illustrated), with screw related molecules omitted for clarity.

Can. J. Chem. Downloaded from www.nrcresearchpress.com by 210.87.254.105 on 09/05/12
For personal use only.

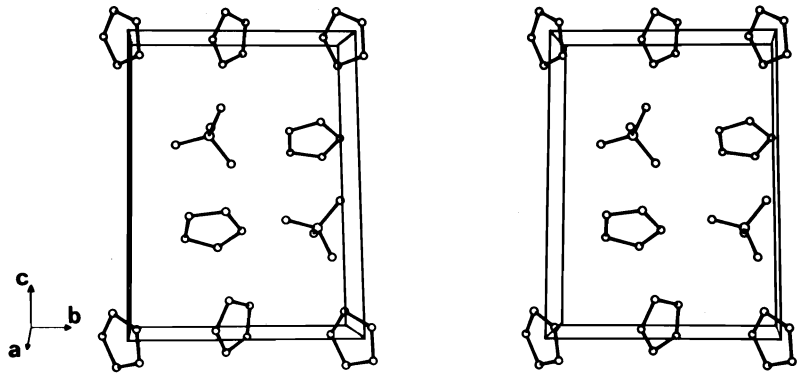

FIG. 3. Stereoscopic view of the packing of the molecules in the unit cell.

TABLE 4. Selected intergroup contacts ≤ 3.5 Å

Contact*	Distance (Å)	Contact*	Distance (Å)
O(3)–C(1)	3.30	O(3)–N(1)	3.48
O(1)–N(1)	3.45	N(3)–N(2)	2.73
O(4)–C(6)^{I}	3.40	O(1)–N(4)^{I}	3.03
O(4)–N(4)^{I}	3.50	N(1)–O(3)^{II}	2.86
O(1)–O(4)^{II}	3.19	O(4)–C(4)^{III}	3.24
O(4)–N(4)^{III}	2.96	O(3)–C(2)^{IV}	3.27
C(1)–O(1)^{IV}	3.32	C(1)–O(2)^{IV}	3.31
N(1)–O(2)^{IV}	3.13	C(1)–O(2)^{V}	3.09
N(2)–O(2)^{V}	3.41	O(3)–O(2)^{V}	3.14

*Symmetry relationships: $^{I}1+x, y, 1+z$; $^{II}1+x, y, z$; $^{III}x, y, 1+z$; $^{IV}2-x, \frac{1}{2}+y, 1-z$; $^{V}1-x, \frac{1}{2}+y, 1-z$; $^{VI}-1+x, y, -1+z$ (see Table 5).

of 0.06 Å, whereas the maximum difference in the imidazole structure is 0.03 Å (in the room temperature determination (8)). The asymmetry about N(2), in ring A, is seen also in the room temperature imidazole structure but not, however, in the low-temperature study (7). The hydrogen bond which links the rings in the complex is distinctly shorter than in the imidazole structure where observed values range from 2.81 Å for room temperature to 2.86 Å for low temperature. The spectra also supported the presence of a stronger hydrogen bond in the complex.

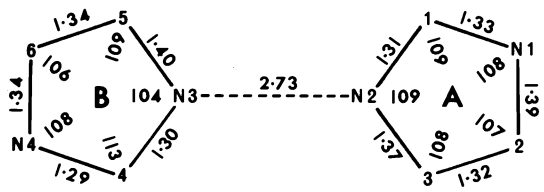

FIG. 4. Comparison of bond lengths and angles for the two imidazole rings.

TABLE 5. Least-squares planes through various sets of atoms

(*a*) Displacements (Å) of atoms from the planes

Ring A		Ring B	
Atom	Displacement	Atom	Displacement
C(1)	0.006	C(4)	0.005
C(2)	0.015	C(6)	−0.010
C(3)	−0.012	C(5)	0.012
N(1)	−0.013	N(4)	0.003
N(2)	0.003	N(3)	−0.010
N(3)*	−0.606	N(2)*	0.209
O(3)^{II}*	−0.048	O(1)^{VI}*	−0.426

*Non-defining atoms.

(*b*) Equations of planes (in terms of fractional coordinates)

Plane	Equation
A	$-3.347x - 0.110y + 9.988z = 0.352$
B	$3.349x + 6.329y - 3.609z = 3.678$

As stated above, it is not possible to be precise about the position of the hydrogen atom between N(2) and N(3). The N—N distance is too long for a symmetric single minimum of potential. There are, however, three other possible configurations, each compatible with the observed N···N bond length: a symmetric double minimum,[3] an asymmetric double minimum, and an asymmetric single minimum potential. The indication from the electron density is that the proton position is asymmetric, but whether there is a double or a single minimum depends on the significance to

[3]In a recent structural example of a proposed symmetric double minimum potential (10), a longer N···N hydrogen bond of length 2.79 Å was found.

be attached to the electron density evidence for a partial atom attached to N(3). If one accepts this evidence the potential distribution has an asymmetric double minimum.

The inability to obtain more precise details of the structure is due, in part, to the difficult experimental conditions, but probably more to the dominance of the diffraction data by the perchlorate group whose atoms are subject either to large thermal vibrations, *e.g.* the large values for β_{33} for O(2) and β_{22} for O(4) (Table 2), or to some degree of disorder which cannot be allowed for satisfactorily.

Acknowledgements

We wish to thank Professor D. Rogers for helpful discussions, the Science Research Council for equipment, and the staffs of the Computer Units of Imperial College and the University of London for their co-operation.

1. F. H. Allen, D. Rogers, and P. G. H. Troughton. Acta Crystallogr. Sect. B, **27**, 1325 (1971).
2. G. Germain. P. Main, and M. M. Woolfson. Acta Crystallogr. Sect. A, **27**, 368 (1971).
3. P. A. Doyle and P. S. Turner. Acta Crystallogr. Sect. A, **24**, 390 (1968).
4. R. F. Stewart, E. R. Davidson, and W. T. Simpson. J. Chem. Phys. **42**, 3175 (1965).
5. J. M. Stewart. F. A. Kundell, and J. C. Baldwin. X-Ray "63" system of crystallographic programs. University of Maryland Technical Report TR646, revised version. 1970.
6. C. K. Johnson. ORTEP Report ORNL-3794, Oak Ridge National Laboratory, Oak Ridge, Tennessee. 1965.
7. S. Martinez-Carrera. Acta Crystallogr. **20**, 783 (1966).
8. G. Will. Z. Kristalloger. **129**, 211 (1969).
9. Yu. A. Omel'chenko and Yu. D. Kondrashev. Kristallographia, **16**, 115 (1971).
10. H. L. Ammon and U. Mueller Westerhoff. Tetrahedron, **30**, 1437 (1974).

Can. J. Chem. Downloaded from www.nrcresearchpress.com by 210.87.254.105 on 09/05/12
For personal use only.

Complex hydrogen bonded cations. The benzimidazole benzimidazolium cation

B. BORAH AND J. L. WOOD[1]

Department of Chemistry, Imperial College of Science and Technology, London, SW7 2AY, England

Received December 17, 1976

B. BORAH and J. L. WOOD. Can. J. Chem. **54**, 2470 (1976).

The complex salts $(Bz_2H)^+Y^-$, Bz = benzimidazole, Y = PF_6^- or BF_4^- have been identified in solution, and the molecularity of the fluoroborate, which has been crystallised, confirmed gravimetrically. Infrared and Raman spectra, together with those of the deuterated systems, indicate a similar structure in solution and the crystal, *viz.*, an asymmetric single minimum bridging proton potential, in conformity with the X-ray structure, proving that the pronounced doublet observed in the ν_s band of the H bridged system is *not* due to proton tunnelling. The origin of the asymmetric structure is discussed.

B. BORAH et J. L. WOOD. Can. J. Chem. **54**, 2470 (1976).

On a identifié en solution les sels complexes $(Bz_2H)^+Y^-$, Bz = benzimidazole, Y = PF_6^- ou BF_4^- et on a confirmé gravimétriquement la molécularité du fluoroborate qui a été cristallisé. Les spectres infrarouges et Raman de ces complexes de même que ceux des systèmes deutérés correspondants indiquent que la structure est similaire en solution et à l'état cristallin à savoir la présence d'un potentiel asymétrique, comportant un pont de proton et un seul minimum; ceci est en accord avec la structure déduite de rayon-X; ces résultats prouvent que le doublet prononcé observé dans la bande ν_s du système hydrogène ponté n'est pas due à un effet tunnel du proton. On discute de l'origine de la structure asymétrique.

[Traduit par le journal]

Introduction

The vibrational spectra of solutions containing both benzimidazole and its cation show many indications of complexing between these species. In particular the ν_s (NH stretching) infrared band has a notable doublet contour, which is replaced by a single band in the D bridged species, a behaviour similar to that in many other $(BHB)^+$ complexes involving heterocyclic bases. However, although this has often been taken as a characteristic consequence of proton tunnelling in a double minimum potential (1), such a cause of the ν_s band doubling in the complexes previously examined was rejected, since several other spectroscopic features do not tally with this model. Instead, an asymmetric single minimum potential for the hydrogen bond (on the vibrational time scale) was proposed (2). Previous attempts to obtain a direct check on this inference by crystallisation of the complexes and consequent structure determination have met the difficulty that solutions containing the complex yielded crystals of either the base or the free salt. However, crystals of the complex benzimidazole salt suitable for X-ray analysis have been obtained. The spectra of the crystalline complex and of the complex in solution are discussed in this report, and the crystal structure reported in the accompanying paper. A preliminary account of the present results has been given (3).

[1]To whom correspondence should be addressed.

Experimental

Preparations

Benzimidazole fluoroborate and fluorophosphate were obtained by adding concentrated aqueous acid to solutions of the free base in methanol, and cooling. Analyses are given in Table 1. Complexing occurs in solution on mixing. On fusing equimolar proportions of the free base, and simple salt at ~120 °C, under N_2, and cooling, the solid complex results. The crystals, however, are not suitable for structure analysis. Although at room temperature the solubility of the base in CH_3CN is only ~0.5 *M*, and the fluoroborate salt ~1.0 *M*, a solution containing 1.5 *M* in both components is formed. On cooling, good crystals of the complex precipitate. The analysis (Table 1) conforms to the formula $Bz_2H^+BF_4^-$. Deuteration of both base and salt was effected by direct exchange with D_2O. The difficulties previously reported (4) were not encountered.

Spectra

Solution spectra were examined in CH_3CN or CD_3CN. Concentrations were usually 1.5 *M* in each component. AgCl and CaF_2 windows were used for solution infrared spectra, path = 0.05 mm while for the solids H.C.B.D. or Nujol mulls employed with NaCl and AgCl windows.

Can. J. Chem. Downloaded from www.nrcresearchpress.com by 210.87.254.6 on 09/05/12
For personal use only.

TABLE 1. Gravimetric analyses of simple and complex benzimidazole salts

Salt	C		H		N		P	
	Found	Required	Found	Required	Found	Required	Found	Required
$BzH^+BF_4^-$	40.74	40.78	3.42	3.39	13.51	13.58		
$BzH^+PF_6^-$	32.01	31.81	2.82	2.65	10.49	10.60	11.53	11.74
$Bz_2H^+BF_4^-$ (fused)	52.39		4.04		18.02			
$Bz_2H^+BF_4^-$ (ppt)	52.03	51.88	4.22	4.01	17.38	17.28		

Infrared spectra were recorded with a Grubb Parsons Spectrometer or a P.E. 325 spectrometer, and Raman spectra obtained with a Cary 81 instrument, using 5682 Å radiation from a Kr ion laser.

Results

It was first observed that the spectra of the benzimidazole systems are independent of counterion, after allowance for specific anion modes. Independence of the solvent was not examined, only CH_3CN or CD_3CN being employed. The presence of a second base site in benzimidazole introduces the possibility of associating several base molecules with a cation to form complexes of formula $(Bz_nH)^+$. However, in solutions containing base:salt in the proportion of 2:1, the only bands in addition to those present in 1:1 mixtures could be accounted for by uncomplexed base. It therefore appears that in solution the1:1 complex predominates.

The ν_s band (NH···N stretching) of the crystalline complex (Fig. 1) displays a very pronounced doublet with maxima at ~2500 and 1900 cm^{-1}. The rounded band at 3300 cm^{-1} can be confidently assigned to the outer NH groups, the frequency indicating that hydrogen bonding to the counterion is weak. In the simple salts this band is at ~3330 cm^{-1}.

In the mid-frequency range, complexing in the solid is manifested by the disappearance of numerous bands in the infrared spectra of the free base (*e.g.* 958, 1135, and 1480 cm^{-1}) and of the simple salt (*e.g.*, 939, 951, 1150, 1229, 1280, 1383 cm^{-1}), and by the appearance of several new bands, *e.g.*, 850, 902, 948, 1258, and 1490 cm^{-1} (Table 2). The Raman spectra (Fig. 2) also display the disappearance of several of the bands of the free base and simple salt in the complex, and the appearance of new bands (Table 3). However, there are many bands of base or salt which are unchanged in the complex, due to insensitive internal modes.

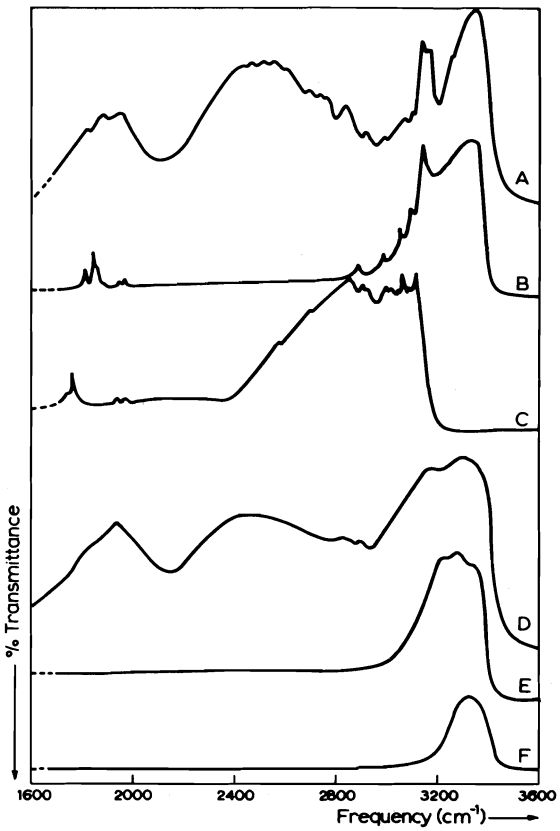

FIG. 1. Infrared spectra in the NH stretching range of (*A*) solid $Bz_2H^+BF_4^-$ (*B*) solid $BzH^+BF_4^-$ (*C*) solid Bz (*D*) $BzH^+BF_4^-$ + Bz (1.5 *M* each) in solution (*E*) $BzH^+BF_4^-$ (1 *M*) in solution (*F*) Bz (0.5 *M*) in solution. Solvent and counterion bands have been omitted.

Extensive complexing is present in solutions containing both base and salt, as witnessed by the ν_s band (Fig. 1) similar to that in the crystalline complex. Numerous new bands appear in the middle range infrared spectrum, *e.g.*, at 626,

Can. J. Chem. Downloaded from www.nrcresearchpress.com by 210.87.254.6 on 09/05/12
For personal use only.

Can. J. Chem. Downloaded from www.nrcresearchpress.com by 210.87.254.6 on 09/05/12
For personal use only.

TABLE 2. Infrared spectra to 500 cm^{-1} of the Bz_2H^+ complex cation, and of Bz and BzH^+ for comparison (counterion bands have been omitted, frequencies in cm^{-1})*

$BzH^+BF_4^-$ or $BzH^+PF_6^-$		$Bz_2H^+BF_4^-$		Bz	
Solid	Solution	Solid	Solution	Solid	Solution
3333s,br	3350	3300s,br	3300s,br		3333w,br
	3275s,br				
	3175	3176s			
		3156s			
3145s		3145s			
				3110s	
3095w					
3060w		3060vw		3060s	
2990w		2995vw	2995w		
2875w					
				2800s,br	
		2500s,br	2500s,br		
		1900m,br	1950s,br		
1622s	1622s	1622s	1622s	1622w	1622w
		1590w	1592w	1590s	1590vw
1536w	1535m	1534w	1535m		
1498s	1502m	1504vw	1500sh		
		1498m	1495s,br	1497w	1496m
		1490s			
				1480s	1485w
		1460sh	1460sh	1459s	1457s
1451vs	1451vs	1456s	1450s		
		1414vs	1410s,br	1409vs	1404s
1400vw	1395sh			1392sh	1395sh
1383s	1383s				
1367sh		1366m	1367vw	1366s	1366w
1353w		1348w	1353w	1350vw	1355w
				1347w	
		1303s	1304s	1302s	1304s
1295s					
1280s		1274sh		1274s	
1270s	1267s	1268m	1267s		1267s
		1258s	1253s		1255s
		1247s		1247vs	
1229s	1232w		1245sh		
		1201w	1200vw	1203s	
1185w	1179w	1181w			
1165w		1165w			
1150w	1145w				
1127s	1111w	1122s		1135s	
		Obscured by BF_4^-	Obscured by BF_4^-		
1007w	1006w	1007w	1005vw	1004s	1005w
988m		986sh			
951m				958m	
		948s	956m		
939s	936w	941sh	936w	933w	936vw
928s		929m			
		902s,br	904vw	897vw	
878vw	882vw	885s	886w,br	888s	880w,br
				882sh	
864vw		866w			
790s,br	805br	850w	850br	847vw	820vw,br
		800vw,br	810w,br		
				778sh	
776w	774sh	773w	774sh	773w	774sh

TABLE 2 (*Concluded*)

$BzH^+BF_4^-$ or $BzH^+PF_6^-$		$Bz_2H^+BF_4^-$		Bz	
Solid	Solution	Solid	Solution	Solid	Solution
766s		768s	768sh	769s	770m
760s	755s	759s			
755sh		749, 745 s,br	752s,br	752s 745s	750s
	660w,br		685s,br		660w,br
		634vw	626w	634m	
623m	621s	625s		626m	
		618s,br		616w	
607s	602m	608s	608s,br		600w,br
		575m	573w	577w	570w
540s	540w	540s	540w	540w	
525s		526s			
		516m			

*BzH^+ = benzimidazolium ion, Bz = benzimidazole, sh = shoulder, br = broad, s = strong, m = medium, w = weak, v = very.

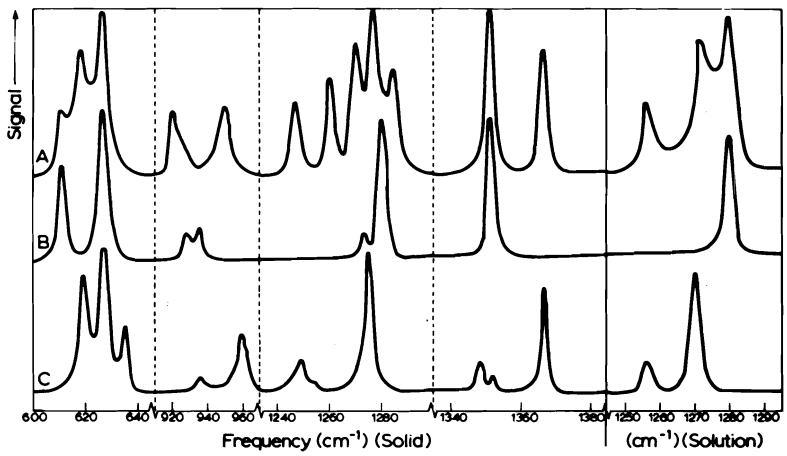

FIG. 2. Selected parts of the Raman spectra of the complex (*A*), the simple salt (*B*) and the free base (*C*) illustrating the presence of new bands, and the disappearance of component bands in the complex, and also the resolution of bands derived from both base and salt, in the complex spectrum.

850, 904, 956, and 1410 cm^{-1} (Table 2) while some bands of the components, *e.g.*, 1404 and 1457 cm^{-1} of the base and 602 and 1383 cm^{-1} of the salt are much weaker, and can be suppressed by addition of excess of the second component. However, numerous bands ascribed to the complex closely coincide with bands of one or other component (Table 2); these have not decreased in intensity on complexing in proportion to free base or salt bands, nor are they suppressed by addition of the second component.

Similar behaviour is shown in the Raman spectra of solutions (Table 3), again some bands clearly shift on complexing, while intensity comparisons and subsidiary experiments show others are retained at effectively the same frequency.

In the deuterated solid complex, the ν_s infrared band no longer has the broad doublet structure, but is represented by a single broad band, with some detailed additional structure. The centre is at $\sim$1950 cm^{-1} in the crystals. In solution, the appearance is similar, the maximum being some 50 cm^{-1} lower in frequency (Fig. 3). The band at 2460 cm^{-1}, present in both solid and solution, represents the stretching of the outer ND groups

Can. J. Chem. Downloaded from www.nrcresearchpress.com by 210.87.254.6 on 09/05/12
For personal use only.

TABLE 3. Raman spectra of benzimidazole (Bz), benzimidazolium ion (BzH^+) and their 1:1 complex as solid and in acetonitrile solution (1700–600) cm^{-1} range (frequencies in cm^{-1})

$BzH^+BF_4^-$		$(Bz)_2H^+BF_4^-$		Bz	
Solid	Solution	Solid	Solution	Solid	Solution
1620s	1624w	1626s	1626w		
		1593s	1596w	1593m	1592m
		1571w			
		1534w			
1505sh		1507w			
1498s	1504s	1500m	1500s	1498w	1498m
		1492w			
				1481w	1486w
1452s	1452s	1456m	1456m		
1440w					
				1422m	
		1418s	1418m,br		
1388vw		1408sh		1412m	1408w
		1368s	1368m	1367s	1366m
1352s	1351s	1352s	1352s		1356m
		1306w	1306w	1304w	1305m
		1286s			
1281s	1280s	1277s	1278s		
1273w		1271s	1271m	1274vs	1270s
		1261m	1257m		1256m
		1248m		1249w	
				1206w	1192w
		1188m			
		1184sh			
1176m	1170w				
1156w		1160w			
1151sh	1146w	1141w	1148w	1138m	
1121vw		1121sh			
		1116w	1118w	1110w	
1010s	1009s	1009s	1009s	1006s	1007s
990w				961w	
		950w	956vw		
936vw	940w			936vw	940w
928vw		920w			
				892vw	
		888vw		884vw	
		868vw			
		856w		850vw	
779vs	776vs	779vs	777vs	779vs	775s
760vw	765w	768sh	768sh		
		747w	752sh	748w	
				636w	
626s	623s	626s	626m	627m	624w
		618s	619sh	619m	
612m		610w			

of the complex cation. The ND stretching mode in the simple salts is at almost the same frequency.

The mid-range spectra of the deuterated systems also display many effects of complexing. Numerous bands of the solid base (*e.g.* 756, 996, 1326, and 1341 cm^{-1}), and of the solid salt (*e.g.* 755, 1271, 1295, 1467 cm^{-1}) are absent in the solid complex, which has new bands at *e.g.* 1227, 1347, and 1379 cm^{-1}. Again the complex also has many bands unchanged in frequency from those of the free base or simple salt.

The mid-range infrared spectra of solutions of the deuterated systems afford similar evidence of complexing (Table 4). New bands are observed at 1227, 1347, 1382, and 1478 cm^{-1} in the mix-

Can. J. Chem. Downloaded from www.nrcresearchpress.com by 210.87.254.6 on 09/05/12
For personal use only.

TABLE 4. Infrared spectra, to 500 cm^{-1}, of the $(d_1\text{-Bz})_2D^+$ complex cation, and of d_1-Bz and d_1-BzD^+ for comparison (counterion bands have been omitted, frequencies in cm^{-1})

d_1-$BzDBF_4^-$ or d_1-$BzD^+PF_6^-$		$(d_1\text{-Bz})_2D^+BF_4^-$		d_1-Bz	
Solid	Solution	Solid	Solution	Solid	Solution
3160sh	3160sh	3160sh			
3145s	3140m	3145s	3140m,br		
3120s					
		3118w		3110w	
3095w		3090w			
3060w		3060w	3060sh	3062vw	
				3054s	
3044m	3040vw	3040w	3040sh	3040w	
3010m	3010vw	3010vw			
2930m	2930vw				
2870w					
2780w	2780vw				
2735w	2735vw				
2660s	2660vw	2660vw			
2500vs,br					2500w,br
2440s,br	2430s,br	2460s,br	2460s,br		
	2350s,br	1950br	1900br	2180s,br	
2360sh					
2340sh					
1969w		Obscured by ν_{N-D}	Obscured by ν_{N-D}		
1930w					
1830m	1830vw				
1810w					
1734w					
Mid-frequency range (1700–500) cm^{-1}					
1630vw	1615sh	1614sh	1615sh		
1610s	1609m	1610m	1607w	1608vw	1610vw
		1590sh	1590w	1590sh	1585vw
1532s	1530m	1531w	1527vw		
				1502m	
1490s	1490s	1490s	1490s		
		1481sh		1484s	
		1479s	1478w	1478m	
1467s	1466s				
		1454s	1458s	1454s	1455m
1440w	1442vw				
		1440s	1443s	1430s	1434s
		1415sh		1411w	
1406vs	1408s	1408s	1406m		
		1379m	1382m		
		1364vw		1366w	
1350m		1350sh,w			
		1347s	1347m		
				1341s	1340sh
1337s	1333s	1333s	1333s		
				1326s	1322s
		1300w	1305w	1303w	
1295m					
	1285w	1285w	1285w	1283s	
				1276sh	1276sh
1271m					
		1264sh	1265w	1264w	1265vw
1259s	1256s	1260s	1255s		
				1253m	

Can. J. Chem. Downloaded from www.nrcresearchpress.com by 210.87.254.6 on 09/05/12
For personal use only.

TABLE 4 (*Concluded*)

d_1-BzDBF$_4^-$ or d_1-BzD$^+$PF$_6^-$		$(d_1\text{-Bz})_2$D$^+$BF$_4^-$		d_1-Bz	
Solid	Solution	Solid	Solution	Solid	Solution
		1242w		1240w	
		1227m	1227m		
		1221sh		1221s	1215m
		1192w		1186w	
1173w		1172sh			
1161w	1143w	1160w		1159w	
1127m		1125m		1112vw	
	1112w				
		Obscured by BF_4^-	Obscured by BF_4^-		
1007w	1006w	1007w	1006w	1004w	1006w
				996s	
989m		989w			
964m		964sh	966vw,br		
960sh		957vw			
951s	950sh,br	951vw	950vw,br		
		944sh		942s,br	
925sh		928w		920vw	
		909			
897vw	898w	898 } w,br			
892vw		887		887w	
865sh	860w,br				
856m		857 } m	856w,br		
843s		845 } m,br			
		839 } sh	832sh		
808vw,br					
767s	762sh	767s	764sh	769m	770m
				764w	
759vs	756vs	759m	754vs,br	756s	754s
755w				750m	
		742vs,br		740s	740s
	680vw,br				
			650vw,br	638vw,br	640w,br
				627w	
		623w			
619w	618s	619sh	618w		
			610m,br	614w	610vw,br
607w	604w	609sh			
				584s	588vw
		582			
571s,vbr	580w,br	} m	586w,br		
		575			
				557w	572vw,br
		549w	542sh		
535w	536m	540w	538w	538w	
524s		523s			

*d_1-Bz = benzimidazole-d_1 (1); d_1-BzD$^+$ = benzimidazolium-d_2 (1, 3).

ture, while again, using intensity comparisons and the effect of excess of either component, bands in the complex which do not shift in frequency are distinguished from free base or salt bands.

Discussion

The gravimetric analysis and the X-ray structural data establish the basic unit of the complex as ($Bz_2H^+X^-$). The great overall similarity of the solid and solution vibrational spectra show that the form of association is similar.

The occurrence of a pronounced doublet in the ν_s band of a formally symmetric H-bridged system, condensing to a single (or much less

Can. J. Chem. Downloaded from www.nrcresearchpress.com by 210.87.254.6 on 09/05/12
For personal use only.

split) band in the D-bridged analogue, has often been taken as the most notable indication of proton tunnelling in a low barrier double minimum potential (1). However, a detailed examination of the spectra of an extensive series of $(BHB)^+$ complex cations indicated that although the ν_s band had a closely similar appearance to that of the present complex, it was not due to proton tunnelling (2). From the mid-frequency and far-infrared spectra of these systems it was inferred that the proton potential was an asymmetric single minimum on the vibrational time scale.

This interpretation is now fully confirmed by the data on the benzimidazole system.

Even without making a detailed assignment of the mid-range spectra of the present complex, it is obvious that many more bands are present in the spectra of the complex than in either that of base or salt alone. Further, numerous complex bands are the counterparts of either base or salt bands. A particularly effective demonstration of this is provided by the Raman spectra; in solution the complex has bands related to both 1270 cm^{-1} of the base and 1280 cm^{-1} of the salt, and in the solid, the complex has bands derived from both 1352 cm^{-1} of the salt and 1367 cm^{-1} of the base (Fig. 3).

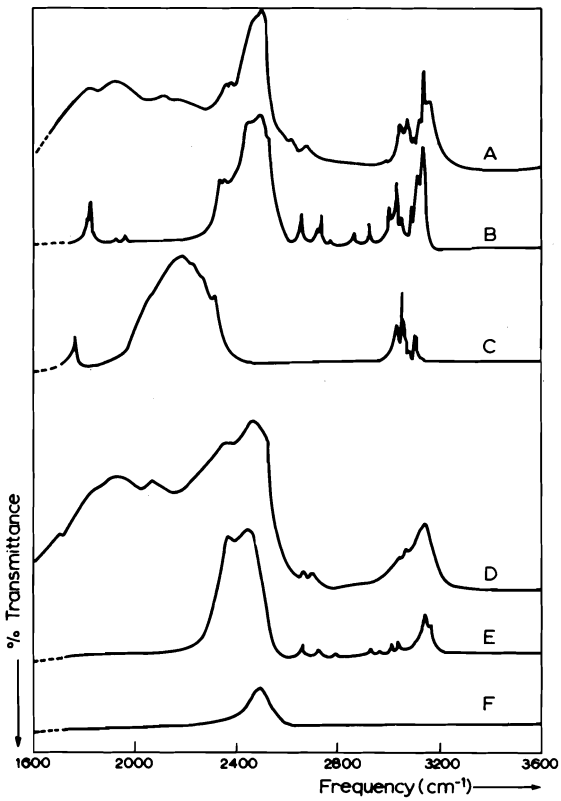

FIG. 3. Infrared spectra in the ND stretching range of the deuterated systems corresponding to those of Fig. 1. Solvent and counterion bands have been omitted.

It is apparent that the complex contains two vibrationally distinct base moieties, one with a cationic or proton donor role, the other with a base-like or proton acceptor role. This distinction in the solid is borne out by the crystal structure determination reported in the accompanying paper. The spectra show that the distinction is retained in solution.

The pattern of the NH bending modes has also been used as an indication of the proton potential in formally symmetric complexes (5). The presence of two basic N atoms in benzimidazole makes the situation somewhat less simple than in previous systems, in which only monofunctional bases were employed. As in the imidazole complex discussed in the accompanying report, for an asymmetric complex $(BzH\cdots Bz)^+$ we expect three NH in-plane bending modes, one around the mean of the frequencies in the free cation, one near the frequency in the free base, and one at higher frequency, comparable to that, for instance, in the base hydrochloride, due to the bridging NH group. A similar pattern is expected for the out-of-plane modes. All would be infrared active. It is difficult to identify the in-plane bending modes in either benzimidazole of its simple salts; probably NH bending is mixed into several modes (4). The bands at 1232 and 1383 cm^{-1} of the simple cation, which appear to shift to 1245 cm^{-1} and 1410 cm^{-1} in the complex, and which are much weaker in the Raman than the infrared spectrum, are possible candidates. The shifts are consistent with an asymmetric model. The situation is rather more promising for the out-of-plane bending modes. A band, at $\sim$660 cm^{-1} weak but broad in the infrared (Fig. 4) spectrum of benzimidazole but not observed in the Raman, and absent in the infrared spectra of d_1-benzimidazole, is a probable choice for this mode. The simple cation should have only one infrared active out-of-plane bending mode, which is very probably represented by the band at $\sim$805 cm^{-1}, absent in the infrared spectrum of the deuterated salt, and in the Raman spectrum. The complex has two, and possibly three, bending mode bands in its infrared spectrum, at $\sim$685, 810, and 850 cm^{-1}

Can. J. Chem. Downloaded from www.nrcresearchpress.com by 210.87.254.6 on 09/05/12
For personal use only.

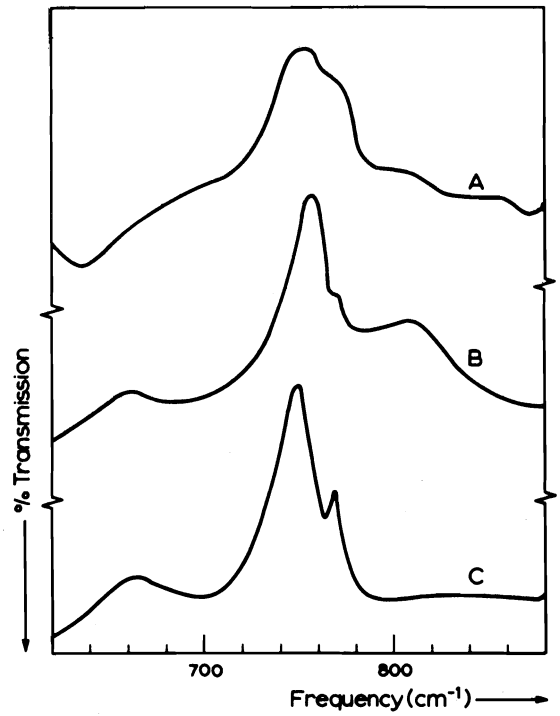

FIG. 4. Infrared spectra in the NH out-of-plane bending range, of (*A*) $BzH^+BF_4^-$ + Bz (1.5 *M* each) (*B*) $BzH^+BF_4^-$ (0.8 *M*) (*C*) Bz (0.6 *M*). All in CH_3CN solution.

(Fig. 4), all absent in the deuterated complex. Though less decisive than one might wish, the pattern of bands in the complex is consistent with the asymmetric structure.

Form and Origin of the Proton Potential

There is a direct connection between the length of the hydrogen bond and the form of the potential. A symmetric single minimum potential is only expected in a short bond, *e.g.* 2.4 Å. A double minimum requires a longer bond, and for the observed length of 2.79 Å, a shallow barrier between the minima could be accommodated. Why does the longer bond occur in the present system? Perhaps we may reframe the question by considering the requisite conditions for the occurrence of a short bond. These are only found linking highly electronegative atoms, as in FHF^- (6) or in OHO^- systems (7). The bond electrons are held in tightly to the electronegative atoms, reducing their repulsion, and so permitting the short hydrogen bond between them (8). In the present systems BH is not a strong acid, and there is less electrostatic advantage in forming the complex than in *e.g.* FHF^-, so the conditions favouring a short bond are lacking. The observed value is typical of NHN bonds (9).

The crystal data indicate an asymmetric potential; any occupation of a second minimum by the proton is below the detectable level. The close similarity of the solid and solution spectra indicate that an asymmetric potential is also present in the latter. There is a distinction, however. In the crystal the asymmetry is permanent, whereas in the solution it is only on the vibrational time scale. On a longer time scale the two bases must be indistinguishable in solution, and this is shown by nmr measurements on similar complex cations.

In a formally symmetric cation, the development, in solution, of asymmetry is at first sight surprising. Zundel has pointed out that a system with a symmetric double minimum potential is highly polarisable (10). This suggests an explanation for the presence of asymmetry in solution. The environment, counterion and solvent, stabilises at any particular instant the proton in one of the minima. If the proton moves to the other, equivalent position in the N···N bond, the environment is not able to rearrange in the time scale of the proton motion, and the vibrational spectra correspond to an effective asymmetric potential, with only one minimum. On the longer time scale of nmr measurements, either as a result of the solvent or counterion rearranging, the two positions become equivalent.

The proton potential can then be taken as a function of two coordinates, θ representing the arrangement of the environment and $x = r_{N_1H} - r_{N_2H}$ the position of the proton between N_1 and N_2. Since the time scale for the change in θ is slow, a Stepanov (11) or Born-Oppenheimer separation of the low frequency motion in θ, and the high frequency motion in the x coordinate is possible. As far as the ν_s band is concerned, the proton can be regarded as moving in a one-dimensional potential at fixed θ, and the presence of the second minimum disregarded. Figure 5 (*a*) to (*c*) show three profiles, at fixed θ, taken through the energy minimum of the corresponding potentials shown in the contour diagrams Fig. 5 (*d*)–(*f*), which also display the symmetry implicit in a longer time scale.

Although a wide range of asymmetric potentials will occur in solution, those shown in

Can. J. Chem. Downloaded from www.nrcresearchpress.com by 210.87.254.6 on 09/05/12
For personal use only.

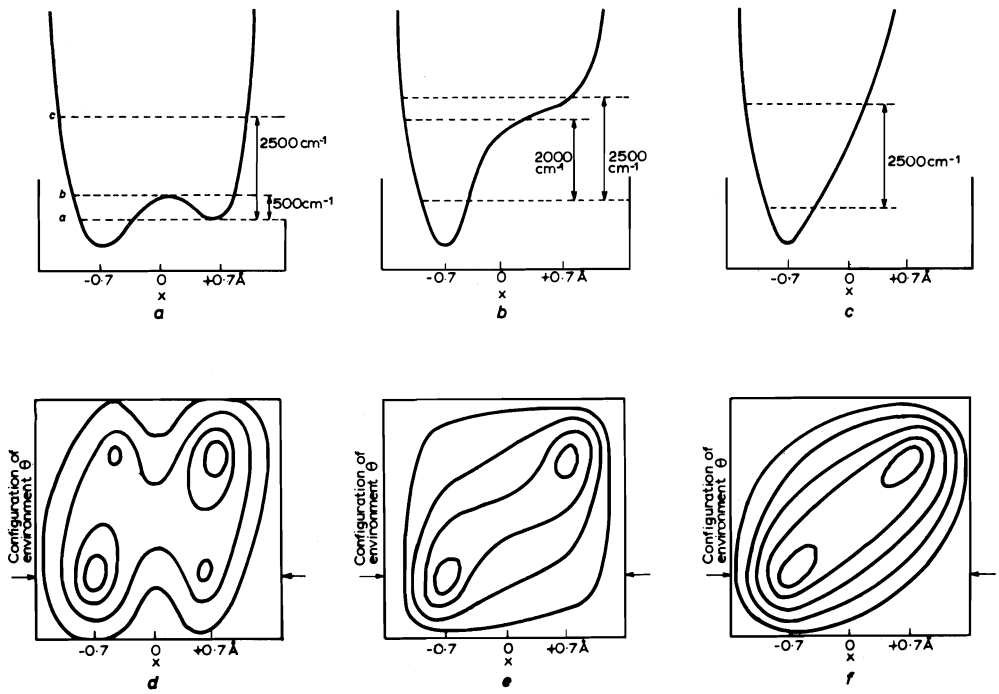

FIG. 5. Some possible asymmetric potentials: (*a*)–(*c*) illustrate increasing asymmetry due to the environment, and represent profiles through the two dimensional energy contours shown in (*d*)–(*f*) respectively, along the line θ = constant, as indicated. Approximate energy levels are shown in (*a*)–(*c*). It should be noted that the splitting of ν_s is *not* considered to arise from the potentials of (*a*) or (*b*), for reasons given in the text.

Fig. 5 (*a*) and (*b*) have been chosen because they illustrate certain special points which will now be discussed.

The approximate positions of the energy levels are indicated in the figures. All transitions will be infrared allowed. The particular points now discussed do not imply the rejection of any potentials in the range, but relate to possible causes of the ν_s band splitting.

Referring to the potential shown in Fig. 5(*a*), the possibility that the lower frequency component arises from the transition $b \rightarrow c$ can be rejected on two grounds. First, low temperature studies on similar complexes[2] show that the two components of ν_s cannot originate from levels which differ in energy by 500 cm^{-1}, and secondly, this origin would imply an increased splitting in the deuterated system.

A further point of interest arises with the potential shown in Fig. 5(*a*). The level *c* (the upper level of the ν_s transition $a \rightarrow c$) is in this case well above the asymmetry introduced by the environment or the internal barrier. The width of the potential well in the *x* coordinate at the height of level *c* will be several tenths of an Å greater than at the corresponding position in FHF^- or OHO^- systems, by virtue of the long N···N bond. In FHF^- or OHO^- systems, ν_s can be as low in frequency as 600–1500 cm^{-1} (6, 7). The reason that the ν_s transition is not still lower in the potential 5*a*, despite the greater breadth, is that different transitions are involved. With potential 5*a*, two lower levels *a* and *b* are present. The presence of the level *b* pushes up the level *c*, and in this case the ν_s band corresponds to the $a \rightarrow c$ transition, in contrast to those cases where a short hydrogen bond is present, when the ν_s transition is between adjacent levels.

If the level *b* is $\sim$500 cm^{-1} above *a*, a value which could reasonably be expected from the effect of the environment, then the transition $a \rightarrow b$ could be responsible for the weak, broad band observed in the infrared spectra of several BHB^+ cations (*e.g.* $PyHPy^+$) in this range. The

[2]R. Clements and J. L. Wood, unpublished observations.

Can. J. Chem. Downloaded from www.nrcresearchpress.com by 210.87.254.6 on 09/05/12
For personal use only.

Can. J. Chem. Downloaded from www.nrcresearchpress.com by 210.87.254.6 on 09/05/12
For personal use only.

unusual rise in the frequency of this band on deuteration would then be explicable (12). With the potential 5*a* the population of level *b* would be too small to show up directly.

The potential example shown in Fig. 5*b* is also *not* deemed to be the origin of the ν_s band splitting. Although this potential would produce a much smaller splitting in the deuterated system, and also the remaining features of the spectra, there are two arguments against this origin for the ν_s band splitting. The first is that on passing to increasingly asymmetric complexes $^1BH^2B^+$, where ^1B and ^2B are differing heterocyclic bases, as the difference in pK increases, the lower frequency member of ν_s falls in intensity, while the upper member evolves to become the regular single ν_s band in highly asymmetric systems (2). With the situation shown in Fig. 5*b*, the lower component would have become dominant, while the upper became the ν_s overtone. A second argument against such an origin for the ν_s band appearance, which also applies to the potential 5*a*, is that it would require a closely similar potential in all the systems BHB^+ whatever the heterocyclic base, counterion (if inert), or solvent. This seems most unlikely.

A potential of the type shown in Fig. 5*c* would also be compatible with the spectra. It does, however, imply a difference in the environmental stabilisation of the proton in the two positions, only some 0.7 Å apart of ~50 kJ/mol, which seems rather large.

To summarise, the splitting of the ν_s band is not considered to be the result of any special form of the potentials illustrated. A wide range of potentials seems likely to occur in solution, since the asymmetry arises from external factors. The arguments given above against a specific origin of the splitting arising from the potentials 5*a*, and 5*b*, do not imply that these potentials do not occur along with others over the range of asymmetry. At present it is not possible to be more exact about the possible range of potentials.

Conclusion

One of the principal results of the present study is in the interpretation of the ν_s band contour in hydrogen bonded systems. Thus the presence of a doublet in this band in formally symmetric systems with a greatly diminished or absent splitting in the deuterated analogues, which has been frequently discussed as the most notable spectroscopic indication of proton tunnelling though a low barrier between equivalent minima, must be reconsidered. The decisive establishment of the asymmetric structure of the crystalline benzimidazole complex shows that this spectroscopic behaviour does not necessarily imply a symmetric double minimum potential. This was also inferred from the spectroscopic examination of several similar complexes (2), *e.g.* of Me imidazole or thiazole, although in these cases no direct confirmation from the X-ray structure was available.

Throughout the series of complexes, the primary cause of the ν_s band doublet is considered to be Fermi resonance involving the δ_{NH} overtone. Consequently great caution should be exercised in attempting to infer the form of the proton potential from the ν_s band contour, or from the shift of the ν_s frequency on deuteration (1*d*).

Referring to Fig. 5, one sees that although the distance over which the proton moves may be quite small, the barrier separating the two proton positions is wide, and involves the movement of a heavier mass. As a result, the effective barrier is much greater than would have been anticipated from the proton displacement alone (13). In some of the systems previously examined, distinctive base and cation bands were only resolved when the parent modes were separated by 20 cm^{-1} or more. This suggests a time scale for the exchange. In the present complex, the solution Raman spectra show resolved pairs of bands, one derived from the cation moiety, and the other from the base moiety, at a smaller separation. If these correspond to the same vibrational mode, it would indicate a slower exchange in the present complex.

Another implication of the proposed model is that, in solution, the barrier, depending as it does on the effect of the surroundings, will vary considerably. Thus the effective barrier determining kinetics of proton transfer will not be a fixed parameter, but will show statistical fluctuation, both in time, and from system to system. The energy levels particularly of the NH stretch will also vary, with consequent band broadening. Numerous other causes for the broadening of the ν_s band have been identified (10, 14, 15) and may also operate in the present case. The environmental effect suggested here

does not seem to have previously been considered. The kinetic consequences of the model discussed here are being examined in further detail.

Another point of interest concerning the hydrogen bonding in the BHB^+ cations is that it is sharply pH dependent (16), having an optimum at the pK_a of the base. This is close to neutrality in both imidazole and benzimidazole; whether this plays a biochemical role remains to be discovered.

1. (*a*) R. L. Somorjai and D. F. Hornig. J. Chem. Phys. **36**, 1980 (1962). (*b*) J. Laane. Appl. Spectrosc. **24**, 73 (1970). (*c*) J. Laane. Quart. Rev. Chem. Soc. **25**, 533 (1971). (*d*) J. Laane. J. Chem. Phys. **55**, 2514 (1971).
2. R. L. Dean and J. L. Wood. J. Mol. Struct. **26**, 215 (1975).
3. A. Quick, D. J. Williams, B. Borah, and J. L. Wood. Chem. Commun. 891 (1974).
4. M. M. Cordes and J. L. Walter. Spectrosc. Acta, **24A**, 1421 (1968).
5. J. L. Wood. J. Mol. Struct. **17**, 307 (1963).
6. B. L. McGraw and J. A. Ibers. J. Chem. Phys. **39**, 2677 (1963).
7. (*a*) D. Hadzi and A. Novak. Spectrosc. Acta, **18**, 1059 (1962). (*b*) D. Hadzi, A. Novak, and J. E. Gordon. J. Phys. Chem. **67**, 1118 (1963).
8. (*a*) L. J. Bellamy and R. J. Pace. Spectrosc. Acta, **25A**, 319 (1969). (*b*) L. J. Bellamy and A. J. Owen. Spectrosc. Acta, **25A**, 329 (1969).
9. S. C. Wallwork. Acta Cryst. **15**, 758 (1962).
10. R. Janoschek, E. G. Weidmann, H. Pfeiffer, and G. Zundell. J. Am. Chem. Soc. **94**, 2387 (1972).
11. (*a*) B. I. Stepanov. Zh. Fiz. Khim. **19**, 507 (1945); (*b*) **20**, 408 (1948).
12. J. L. Wood. J. Mol. Struct. **17**, 307 (1973).
13. J. Brickmann and H. Zimmermann. J. Chem. Phys. **50**, 608 (1969).
14. J. L. Wood. *In* Spectroscopy and structure of molecular complexes. *Edited by* J. Yarwood, Plenum Press. 1972. p. 321.
15. N. Sheppard. *In* Hydrogen bonding. *Edited by* A. Hadzi. Pergamon Press, Oxford. 1959. p. 85.
16. J. L. Wood. Biochem. J. **143**, 775 (1974).

Can. J. Chem. Downloaded from www.nrcresearchpress.com by 210.87.254.6 on 09/05/12
For personal use only.

The crystal structure of the complex salt: benzimidazole benzimidazolium fluoroborate

ANDREW QUICK AND DAVID J. WILLIAMS[1]

Chemical Crystallography Laboratory, Imperial College, London SW7 2AY, England

Received December 17, 1975

ANDREW QUICK and DAVID J. WILLIAMS. Can. J. Chem. **54**, 2482 (1976).

The crystal structure of benzimidazole benzimidazolium fluoroborate has been determined at room temperature from three-dimensional diffractometer data, and refined by block-diagonal least-squares to a final $R = 0.050$. The planar benzimidazole rings are inclined at 7.6° to each other and linked by a hydrogen bond of 2.787(3) Å with the proton in an asymmetric single minimum. The asymmetric siting of the hydrogen atom has produced characterising effects on the bond lengths and angles of the ring to which it is attached.

ANDREW QUICK et DAVID J. WILLIAMS. Can. J. Chem. **54**, 2482 (1976).

On a déterminé, à température de la pièce, à partir des données diffractométriques tridimensionnelles, la structure cristalline du fluoroborate du benzimidazolium de benzimidazole et on a affiné la structure par la méthode des moindres carrés (blocs diagonaux) jusqu'à une valeur finale de $R = 0.050$. Les cycles benzimidazoles planaires sont inclinés de 7.6° les uns par rapport aux autres et sont liés par un pont hydrogène de 2.787(3) Å avec le proton dans un minimum asymétrique simple. L'emplacement asymétrique de l'atome d'hydrogène conduit à des effets qui caractérisent les longueurs de liaison et les angles du cycle auquel il est attaché.

[Traduit par le journal]

Introduction

The infrared spectrum of the complex salt $(ImHIm)^+ClO_4^-$ (Im = imidazole) has been interpreted as indicating the existence of an asymmetric hydrogen bond between the imidazoles (1), but an X-ray structure analysis (2) failed to give conclusive evidence for the nature of the proton potential distribution. Concurrent spectroscopic measurements of the $(BzHBz)^+BF_4^-$ complex (Bz = benzimidazole) were also interpreted as indicating an asymmetric single minimum proton potential. As this complex crystallises to give stable well formed crystals, an X-ray analysis was undertaken to investigate the nature of the hydrogen bond in the system. Details of the preparation and of the spectroscopic analysis are given in the preceding paper. A preliminary account of this investigation has been reported (3).

Experimental

The crystals are long colourless laths. Accurate lattice parameters were obtained by least-squares refinement of 23 high-angle reflections measured (at 10 °C) on a diffractometer using Cu-K_α radiation. The crystal data are:

$C_{14}H_{13}N_4.BF_4$ mol. wt. = 324.1

Monoclinic, $a = 5.797(1)$, $b = 9.231(1)$, $c = 27.480(3)$ Å, $\beta = 90.060(5)°$, $U = 1470.5$ Å^3, $D_m = 1.45(2)$ g cm^{-3} (by flotation), $Z = 4$, $D_c = 1.46$ g cm^{-3}, $F(000) = 664$. Space group $P2_1/n$. Cu-K_α radiation, $\lambda = 1.5418$ Å, μ(Cu-K_α) = 11.1 cm^{-1}.

A crystal *ca.* $0.9 \times 0.2 \times 0.1$ mm^3 was mounted along its *a* direction. Data were measured on a Siemens off-line four-circle diffractometer using Ni-filtered Cu-K_α radiation. A total of 2778 independent reflections were measured (to $\theta = 70°$) using the θ–2θ scan technique with the 'five-value' (4) measuring procedure. Of these, 348 reflections had $I < 2.58\sigma(I)$ and were classed as unobserved (4). The net count of the 0 1 21 reflection, measured as a reference every 50 reflections, did not alter significantly during the data collection (*ca.* 5 days) indicating that no deterioration of the crystal had occurred. The data were brought to a uniform arbitrary scale by use of this reflection (4), and Lorentz and polarisation corrections were applied. No absorption corrections were applied.

Solution and Refinement of the Structure

The structure was solved by direct methods by application of the program MULTAN (5) to 250 reflections with normalised structure factors (E's) ≥ 1.67. An E map, calculated for the phase solution with the highest 'combined figure of merit', gave plausible positions for all the non-hydrogen atoms in the structure.

These atoms were refined anisotropically, by full-matrix least-squares, to give a residual $R = 0.084$ ($R = \sum||F_o| - |F_c||/\sum|F_o|$). A difference map contained sharp peaks corresponding to all the ring hydrogens: also a well defined peak showing the position of the inter-ring hydrogen attached to N(12). The whole structure was refined by block-diagonal least-squares, the hydrogen atoms isotropically, the rest anisotropically. The posi-

[1]To whom correspondence should be addressed.

Can. J. Chem. Downloaded from www.nrcresearchpress.com by 210.87.254.5 on 09/05/12
For personal use only.

Can. J. Chem. Downloaded from www.nrcresearchpress.com by 210.87.254.5 on 09/05/12
For personal use only.

tional and thermal parameters of all the hydrogen atoms converged satisfactorily and R dropped to 0.055. Two reflections which had $|F_o| \ll |F_c|$ were suspected of being affected by extinction and therefore removed: they are identified in the F list. Subsequent refinement reduced R to a final value of 0.050.[2] A final difference map showed no significant peaks, the maximum residual electron density being ~ 0.2 e/Å^3, in the region of the fluoroborate group. Unit weights were used throughout the refinements. Atomic scattering factors were taken from ref. 6 with the exception of those for hydrogen which were taken from ref. 7.

The computations were carried out on the Imperial College CDC 6400 and the University of London CDC 6600 and 7600 computers using, in the main, programs belonging to the X-ray 70 system (8).

Results and Discussion

The final fractional atomic coordinates and anisotropic thermal parameters for the non-hydrogen atoms together with their estimated standard deviations are listed in Tables 1 and 2. Those for the hydrogen atoms with their isotropic temperature factors are given in Table 3. Table 4 lists the bond lengths and bond angles and estimated standard deviations. Table 5 gives selected intergroup contacts ≤ 3.50 Å.

The structure is made up of discrete columns of parallel sheets of molecules inclined at *ca.* 35° to *a* and separated by a unit-cell translation in *a*. Each sheet comprises two BzHBz and two BF_4 units related by a centre of symmetry. Each BzHBz unit contains a N—H···N bridge 2.787(3) Å long, and they are linked via N—H···F bonds (2.866(3) and 2.901(3) Å) to form a closed loop that is nearly planar (see Table 6). Figure 1 shows a perspective view (ORTEP (9)) of this hydrogen bonded ring of molecules and gives, also, the numbering scheme used. The normal separation of the sheets is 3.3 Å with closest atomic intersheet benzimidazole contacts being between C(13) and C(22) (3.38 Å), and between N(12) and N(21) (3.37 Å). Each column is related to its neighbours by the crystallographic n glide and 2_1 screws, there being only van der Waals contacts between them.

Figure 2*a* shows a comparison of the bond lengths and some of the angles for the two benzimidazole groups (excluding hydrogens). Each molecule can be seen to be markedly asymmetric about a line passing through the apical imidazole carbon and bisecting the opposite bond. This is most pronounced in the imidazole ring of molecule B where the difference between the C(27)—N(21) and C(27)—N(22) bonds is 0.058 Å, compared with only 0.013 A for the corresponding bonds in molecule A. This reflects the siting of the intra-benzimidazole proton near molecule A, the resulting double-bond nature of C(27)—N(22), and the large measure of resonance in the imidazole ring of A. There is also an associated difference of 4° in the apical angle of the imidazoles. There is very little asymmetry, however, in the angles, the only significant difference (3°) being in the internal imidazole angles of molecule B at C(21) and C(22). The aromatic ring of molecule A contains a short C—C bond length of 1.345(4) Å.

There have been two consistent determinations of the structure of benzimidazole (10, 11). Figure 2*b* shows, for comparison, the bond lengths obtained for these two determinations. As can be seen they are virtually identical to those we have found for molecule B, and again reflect the absence of a hydrogen atom at N(22). The N···N hydrogen bond in benzimida-

TABLE 1. Fractional coordinates ($\times 10^4$) for the non-hydrogen atoms with estimated standard deviations in parentheses

Atom	x	y	z
C(11)	4941(4)	6251(3)	672(1)
C(12)	3441(4)	6376(3)	1068(1)
C(13)	3720(4)	5581(3)	1483(1)
C(14)	5566(5)	4651(3)	1500(1)
C(15)	7089(5)	4532(3)	1101(1)
C(16)	6815(5)	5311(3)	692(1)
C(17)	2278(5)	7888(3)	495(1)
N(11)	4142(4)	7207(3)	328(1)
N(12)	1816(3)	7413(2)	938(1)
C(21)	−4949(4)	9088(3)	1936(1)
C(22)	−2889(4)	8280(3)	1911(1)
C(23)	−2327(4)	7312(3)	2275(1)
C(24)	−3837(4)	7172(3)	2664(1)
C(25)	−5886(4)	7982(3)	2682(1)
C(26)	−6480(4)	8942(3)	2324(1)
C(27)	−3049(4)	9594(3)	1266(1)
N(21)	−4991(3)	9918(2)	1522(1)
N(22)	−1748(3)	8632(2)	1480(1)
B	−8200(5)	11929(3)	621(1)
F(1)	−9946(3)	11065(2)	441(1)
F(2)	−8337(3)	13277(2)	426(1)
F(3)	−8332(3)	11937(2)	1123(1)
F(4)	−6085(3)	11313(2)	492(1)

[2]Tables of observed and calculated structure factors are available at a nominal charge from the Depository of Unpublished Data, CISTI, National Research Council of Canada, Ottawa, Canada K1A 0S2.

Can. J. Chem. Downloaded from www.nrcresearchpress.com by 210.87.254.5 on 09/05/12
For personal use only.

TABLE 2. Anisotropic thermal parameters* ($\times 10^4$) for the non-hydrogen atoms with standard deviations in parentheses

Atom	β_{11}	β_{22}	β_{33}	β_{12}	β_{13}	β_{23}
C(11)	306(8)	135(4)	13(1)	−28(4)	16(1)	−5(1)
C(12)	242(7)	116(3)	11(1)	−9(4)	7(1)	−2(1)
C(13)	326(9)	141(4)	13(1)	13(5)	9(1)	3(1)
C(14)	411(11)	151(4)	20(1)	31(5)	−5(2)	7(1)
C(15)	329(10)	155(4)	28(1)	54(5)	6(2)	−7(1)
C(16)	333(9)	171(4)	20(1)	0(5)	28(2)	−14(1)
C(17)	393(10)	161(4)	13(1)	−8(5)	−4(1)	6(1)
N(11)	442(9)	191(4)	11(1)	−35(5)	20(1)	2(1)
N(12)	281(6)	137(3)	12(1)	8(4)	5(1)	1(1)
C(21)	250(7)	109(3)	12(1)	2(4)	−4(1)	−1(1)
C(22)	229(7)	117(3)	12(1)	3(4)	1(1)	−1(1)
C(23)	278(8)	132(4)	15(1)	25(4)	−4(1)	2(1)
C(24)	370(9)	138(4)	13(1)	−2(5)	−3(1)	6(1)
C(25)	341(9)	153(4)	13(1)	−9(5)	12(1)	1(1)
C(26)	266(8)	139(4)	15(1)	14(4)	10(1)	−3(1)
C(27)	327(9)	159(4)	12(1)	−8(5)	6(1)	5(1)
N(21)	271(6)	137(3)	14(1)	24(4)	−1(1)	6(1)
N(22)	268(6)	156(3)	14(1)	14(4)	10(1)	4(1)
B	280(9)	148(4)	12(1)	26(5)	9(1)	3(1)
F(1)	529(7)	252(3)	18(1)	−79(4)	−10(1)	3(1)
F(2)	560(7)	174(3)	23(1)	33(4)	18(1)	19(1)
F(3)	417(5)	219(3)	12(1)	68(3)	8(1)	−1(1)
F(4)	439(6)	295(4)	20(1)	139(4)	44(1)	18(1)

*In the form: $\exp[-(\beta_{11}h^2 + \beta_{22}k^2 + \beta_{33}l^2 + 2\beta_{12}hk + 2\beta_{13}hl + 2\beta_{23}kl)]$.

TABLE 3. Fractional coordinates ($\times 10^3$) and isotropic thermal parameters for the hydrogen atoms with estimated standard deviations in parentheses*

Atom	x	y	z	B(Å^2)
H(13)	275(4)	575(3)	178(1)	6.1(7)
H(14)	595(4)	407(3)	180(1)	6.6(7)
H(15)	825(5)	386(3)	114(1)	7.0(7)
H(16)	762(5)	523(3)	40(1)	7.0(7)
H(17)	140(4)	864(3)	28(1)	6.7(7)
H(N11)	449(5)	733(3)	4(1)	7.4(8)
H(N12)	86(5)	779(4)	114(1)	8.8(9)
H(23)	−81(4)	666(3)	226(1)	5.7(6)
H(24)	−348(4)	648(3)	293(1)	4.9(6)
H(25)	−664(4)	785(3)	301(1)	6.3(7)
H(26)	−787(4)	958(3)	232(1)	5.6(6)
H(27)	−281(4)	995(3)	94(1)	4.6(5)
H(N21)	−606(4)	1061(3)	139(1)	6.0(7)

*The numbering of the hydrogen atoms is that of the atoms to which they are bonded.

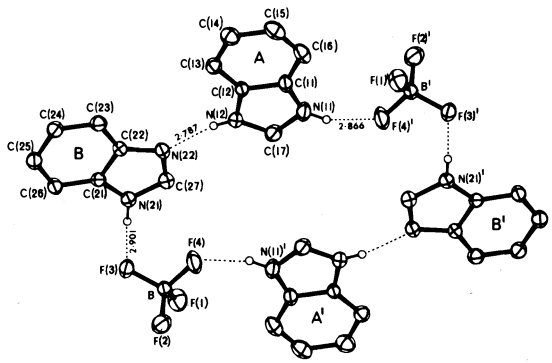

FIG. 1. Perspective view of one of the hydrogen bonded sheets of molecules in the structure, showing also the numbering scheme used. The thermal ellipsoids enclose 30% of the electronic charge.

zole is significantly longer at 2.86 Å, *cf.* 2.787(3) Å for this complex.

Table 6 lists the equations of some selected least-squares planes and the displacements of atoms from them. Both molecules A and B are planar, with standard deviations from planarity of 0.008 and 0.007 Å respectively. The maximum deviants from each plane are C(11) and C(22), each deviating by 0.01 Å. The two benzimidazoles are not coplanar, but are inclined at 7.6° to each other. Despite the small angle between the two molecules, each sheet (Fig. 1), excluding the BF_4's, approximates to a plane passing through a centre of symmetry with a maximum displacement (N(22)) of 0.23 Å, and a standard deviation from planarity of 0.10 Å. Both F(2) and F(3) are within 0.2 Å of this

Can. J. Chem. Downloaded from www.nrcresearchpress.com by 210.87.254.5 on 09/05/12
For personal use only.

TABLE 4
(*a*) Bond lengths (Å) with standard deviations in parentheses

Bond	Length $R = 1$ (Molecule A)	Length $R = 2$ (Molecule B)
C(R1)—C(R2)	1.397(3)	1.409(3)
C(R2)—C(R3)	1.367(3)	1.380(3)
C(R3)—C(R4)	1.372(4)	1.387(3)
C(R4)—C(R5)	1.413(4)	1.405(4)
C(R5)—C(R6)	1.345(4)	1.367(4)
C(R6)—C(R1)	1.391(4)	1.395(3)
C(R1)—N(R1)	1.374(3)	1.372(3)
N(R1)—C(R7)	1.333(4)	1.364(3)
C(R7)—N(R2)	1.320(3)	1.306(3)
N(R2)—C(R2)	1.389(3)	1.395(3)
C(R3)—H(R3)	1.00(3)	1.02(3)
C(R4)—H(R4)	1.00(3)	1.00(2)
C(R5)—H(R5)	0.92(3)	1.01(3)
C(R6)—H(R6)	0.93(3)	1.00(3)
C(R7)—H(R7)	1.04(3)	0.97(2)
N(R1)—H(NR1)	0.82(3)	0.96(3)
N(R2)—H(NR2)	0.87(3)	—
B—F(1)	1.380(3)	
B—F(2)	1.357(4)	
B—F(3)	1.381(3)	
B—F(4)	1.398(3)	

TABLE 4 (*Concluded*)
(*b*) Bond angles (degrees) with standard deviations in parentheses

Bonds	Angle $R = 1$ (Molecule A)	Angle $R = 2$ (Molecule B)
C(R1)—C(R2)—C(R3)	122.2(2)	120.6(2)
C(R2)—C(R3)—C(R4)	117.1(2)	118.0(2)
C(R3)—C(R4)—C(R5)	120.7(3)	120.8(2)
C(R4)—C(R5)—C(R6)	122.3(3)	122.1(2)
C(R5)—C(R6)—C(R1)	117.2(3)	116.9(2)
C(R6)—C(R1)—C(R2)	120.6(2)	121.7(2)
C(R1)—C(R2)—N(R2)	106.2(2)	108.7(2)
C(R3)—C(R2)—N(R2)	131.6(2)	130.8(2)
C(R2)—N(R2)—C(R7)	109.1(2)	105.5(2)
N(R2)—C(R7)—N(R1)	109.0(2)	113.2(2)
C(R7)—N(R1)—C(R1)	109.8(2)	106.9(2)
N(R1)—C(R1)—C(R2)	105.9(2)	105.8(2)
N(R1)—C(R1)—C(R6)	133.6(2)	132.6(2)
C(R2)—C(R3)—H(R3)	122(2)	122(1)
C(R4)—C(R3)—H(R3)	121(2)	120(1)
C(R3)—C(R4)—H(R4)	122(2)	120(1)
C(R5)—C(R4)—H(R4)	117(2)	119(1)
C(R4)—C(R5)—H(R5)	114(2)	110(2)
C(R6)—C(R5)—H(R5)	123(2)	128(2)
C(R5)—C(R6)—H(R6)	128(2)	126(1)
C(R1)—C(R6)—H(R6)	114(2)	117(1)
C(R1)—N(R1)—H(NR1)	132(2)	134(2)
C(R7)—N(R1)—H(NR1)	118(2)	120(2)
C(R2)—N(R2)—H(NR2)	123(2)	
C(R7)—N(R2)—H(NR2)	127(2)	
N(22)—H(N12)—N(12)	167(3)	
N(11)—H(N11)—F(4)′	148(3)	
N(21)—H(N21)—F(3)	177(2)	
F(1)—B—F(2)	110.3(2)	
F(1)—B—F(3)	108.6(2)	
F(1)—B—F(4)	108.5(2)	
F(2)—B—F(3)	112.7(2)	
F(2)—B—F(4)	108.9(2)	
F(3)—B—F(4)	107.7(2)	

plane, but F(4) is displaced by 0.6 Å, producing appreciable bending of the N(11)···F(4)′ hydrogen bond (see Table 4).

Conclusions

The main objective of this analysis, the investigation of the nature of the hydrogen bond in the $(BzHBz)^+$ cation, has, within the limits of accuracy of the analysis, been conclusively achieved. The hydrogen of the N···N hydrogen bond (2.787(3) Å) has been found unambiguously and solely at 0.87(3) Å from its parent nitrogen (*i.e.* it lies in an asymmetric single

TABLE 5. Selected intergroup contacts ≤3.5 Å*

Atom pairs	Distance (Å)	Atom pairs	Distance (Å)
C(27)–F(4)	3.183	N(21)–F(3)	2.901
N(21)–F(4)	3.173	N(12)–N(22)	2.787
C(16)–F(2)^{I}	3.459	C(15)–F(2)^{I}	3.439
C(13)–C(22)^{II}	3.383	C(14)–C(23)^{II}	3.473
N(12)–N(21)^{II}	3.367	C(17)–F(1)^{II}	3.207
C(27)–F(1)^{II}	3.197	C(17)–F(4)^{II}	3.301
C(11)–F(2)^{III}	3.407	N(11)–F(4)^{IV}	2.866
C(16)–F(2)^{IV}	3.451	N(11)–F(2)^{IV}	3.227
C(17)–F(1)^{V}	3.062	F(1)–F(1)^{VI}	3.121
C(25)–F(3)^{VII}	3.455		

*Symmetry relationships: I, $2 + x, -1 + y, z$; II, $1 + x, y, z$; III, $1 + x, -1 + y, z$; IV, $-x, -y, -z$; V, $-1 - x, -y, -z$; VI, $-2 - x, -y, -z$; VII, $-1\frac{1}{2} - x, -\frac{1}{2} + y, \frac{1}{2} - z$.

Can. J. Chem. Downloaded from www.nrcresearchpress.com by 210.87.254.5 on 09/05/12
For personal use only.

TABLE 6. Least-squares planes through various sets of atoms

(*a*) Displacements (Å) of atoms definining the planes

(*i*) Molecules A and B

Molecule A		Molecule B	
Atom	Displacement	Atom	Displacement
C(11)	−0.012	C(21)	0.009
C(12)	−0.008	C(22)	0.010
C(13)	−0.006	C(23)	0.001
C(14)	0.004	C(24)	−0.001
C(15)	0.007	C(25)	−0.007
C(16)	0.003	C(26)	−0.003
C(17)	0.009	C(27)	−0.008
N(11)	−0.004	N(21)	0.004
N(12)	0.007	N(22)	−0.006
N(22)*	0.212	F(3)*	−0.104
F(4)'*	0.484	N(12)*	−0.546
H(N12)*	−0.11	H(N12)*	−0.29
H(N11)*	0.16	H(N21)*	0.00

*Non-defining atoms.

(*ii*) Molecule A + molecule B + molecule A' + molecule B'*

Atom	Displacement	Atom	Displacement
C(11)	−0.05	C(21)	0.01
C(12)	−0.01	C(22)	0.12
C(13)	0.04	C(23)	0.09
C(14)	0.05	C(24)	−0.06
C(15)	0.02	C(25)	−0.18
C(16)	−0.03	C(26)	−0.16
C(17)	−0.06	C(27)	0.18
N(11)	−0.09	N(21)	0.05
N(12)	−0.02	N(22)	0.23

*A' and B' refer to molecules related by the centre of symmetry at (010).

TABLE 6 (*Concluded*)

(*b*) Equations of planes in terms of fractional coordinates

Plane	Equation
A	$3.320x + 6.676(y - 1) + 10.591z = -0.138$
B	$2.807x + 6.728(y - 1) + 13.292z = 0.562$
A + B + A' + B'	$3.294x + 6.543(y - 1) + 11.472z = 0$

minimum in concordance with the spectroscopic conclusions) and has produced characterising effects on the geometry of the benzimidazole molecule to which it is attached. There are two possible ways of detecting and estimating partial occupancy of another site by this hydrogen atom (an asymmetric double minimum for example); either from a change in the C—N bond length in the imidazole ring, or by detection of a partial peak in the difference electron density, a possibility that arose in the determination of the analogous imidazole structure (2). The level in the final $\Delta\rho$ map in the region of the hydrogen bond was of the order of 10% of that observed for the hydrogen atom. Consequently, for significant detection of an alternative site the occupancy would have to be much greater than 10%. Alternatively, taking the dimensions of the free base to represent the unperturbed (0% site occupancy) configuration, and assuming a linear relationship between changes in the differences between equivalent bond lengths in the imidazole and hydrogen site occupancy, we see that a 10% occupancy would produce a change of length only of the order of 1σ (at the currently achieved level of accuracy of bond-length determination) and consequently could not be considered as significant. Thus both considerations indicate that it is unlikely that it would be possible to detect, with statistical significance, a site occupancy of less than ~20%.

Acknowledgements

We wish to thank Professor D. Rogers for

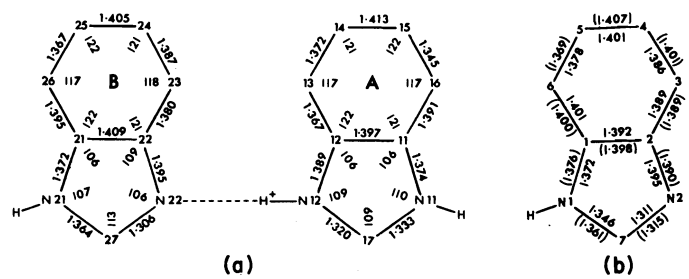

FIG. 2. (*a*) Values of some of the bond lengths and angles for the two benzimidazole molecules in the complex. (*b*) Values of the bond lengths reported for the structure of benzimidazole. Those in parentheses are from ref. 11; the others from ref. 10.

helpful discussions, the Science Research Council for equipment, and the staffs of the Computer Units of Imperial College and the University of London for their co-operation.

1. D. H. BONSOR, B. BORAH, R. L. DEAN, and J. L. WOOD. Can. J. Chem. This issue.
2. A. QUICK and D. J. WILLIAMS. Can. J. Chem. This issue.
3. A. QUICK, D. J. WILLIAMS, B. BORAH, and J. L. WOOD. Chem. Commun. 891 (1974).
4. F. H. ALLEN, D. ROGERS, and P. G. H. TROUGHTON. Acta Crystallogr. **B27**, 1325 (1971).
5. G. GERMAIN, P. MAIN, and M. M. WOLFSON. Acta Crystallogr. **A27**, 368 (1971).
6. P. A. DOYLE and P. S. TURNER. Acta Crystallogr. **A24**, 390 (1968).
7. R. F. STEWART, E. R. DAVIDSON, and W. T. SIMPSON. J. Chem. Phys. **42**, 3175 (1965).
8. J. M. STEWART, F. A. KUNDELL, and J. C. BALDWIN. X-Ray "63" System of Crystallographic Programs, University of Maryland Technical Report TR 646, revised version. 1970.
9. C. K. JOHNSON. ORTEP Report ORNL-3794, Oak Ridge National Laboratory, Oak Ridge, Tennessee. 1965.
10. C. J. DIK-EDIXHOVEN, H. SCHENK, and H. VAN DER MEER. Crystal Struct. Commun. **2**, 23 (1973).
11. A. ESCANDE and J. L. GALIGNÉ. Acta Crystallogr. **B30**, 1647 (1974).

Can. J. Chem. Downloaded from www.nrcresearchpress.com by 210.87.254.5 on 09/05/12
For personal use only.

L'étude de l'adsorption des halogenures d'ammonium quaternaire à l'interface mercure–solution

HUGUES MÉNARD ET FRANK M. KIMMERLE[1]

Département de chimie, Université de Sherbrooke, Sherbrooke (Qué.), Canada J1K 2R1

Reçu le 27 octobre 1975[2]

HUGUES MÉNARD et FRANK M. KIMMERLE. Can. J. Chem. **54**, 2488 (1976).

On a examiné l'adsorption des 16 sels R_4NX (où R = CH_3, C_2H_5, n-C_3H_7 et n-C_4H_9 et où X = F^-, Cl^-, Br^- et I^-) à la surface mercure – électrolyte aqueux. A partir des courbes électrocapillaires on a établit Γ^{Δ}, l'excès de surface structural, qu'on interprète en fonction d'interactions ion–ion et solvant–ion analogues à celles constatées en coeur de solution. Le parallélisme se confirme jusqu'à la valeur de l'énergie d'adsorption si on admet qu'au potentiel de charge E_{pcn} nulle le mercure se comporte comme une surface hydrophobe de rayon infini.

HUGUES MÉNARD and FRANK M. KIMMERLE. Can. J. Chem. **54**, 2488 (1976).

We examined the adsorption of 16 tetraalkylammonium halides, R_4NX, (where R = CH_3, C_2H_5, n-C_3H_7, and n-C_4H_9 and X = F^-, Cl^-, Br^-, I^-), at the mercury – aqueous electrolyte interface. From electrocapillary data we defined Γ^{Δ}, the structural surface excess, which was interpreted in terms of the same ion–ion and ion–solvent interactions proposed for homogeneous solutions. If we treat mercury at the E_{pcn} as a hydrophobic surface having infinite curvature, this parallelism extends even to the numerical calculation of the free energy of adsorption.

Introduction

On trouve dans la littérature, depuis les premiers travaux de Grahame (1), des études plus ou moins systématiques de l'adsorption des sels d'halogénures alcalins à l'interface mercure – solution aqueuse. Ces études, récemment passées en revue par Payne (2), avaient comme but d'élucider des phénomènes de la double couche électrique et se distinguent facilement des études relatives à l'adsorption de molécules organiques. Celles-ci traitent généralement d'une couche interne peuplée par des espèces organiques ayant remplacées des molécules de l'eau adsorbées sur la surface. Celles-là traitent plutôt de solutions de sels simples et de l'adsorption dite "spécifique" de l'anion et l'adsorption dite "électrostatique" du cation.

L'étude de l'adsorption à l'interface mercure–solution d'une série particulière de sels, celle des halogénures d'ammonium quaternaire, peut également fournir des renseignements utiles. Grahame (3) a suggéré que leur comportement pourrait être probablement interprété comme étant dû à l'adsorption "spécifique" du cation volumineux. A la lumière des résultats expérimentaux relatif à la série complète R_4NX (où R = n-butyl, n-propyl, éthyl et méthyl et où X = I^-, Br^-, Cl^- et F^-) nous constatons que cette prédiction s'avère insuffisante à interpréter l'ensemble des comportements.

Devanathan et Fernando (4) furent les premiers à entreprendre une telle étude avec les quatre iodures de tétraalkyl ammonium. Malheureusement même si leurs conclusions globales appuyaient l'argument de Grahame, les calculs incluaient une erreur dans l'interprétation des coefficients d'activité (5). Le traitement des données expérimentales comportait en plus une hypothèse fondamentale qui fut adoptée subséquemment par plusieurs auteurs, à savoir que l'adsorption des cations et anions pouvait être traitée indépendamment et que l'adsorption "spécifique" de I^- en solution de KI était identique à l'adsorption de I^- en solution de R_4NI à concentration et charge équivalentes. L'école de Verdier (6, 7) de la même manière étudia le comportement des bromures de cinq tétraalkyl ammonium, et dans une récente communication (8) adopta une interprétation similaire à celle que nous avions proposée pour les différents halogénures de tétraméthyl ammonium (9).

Plusieurs études traitent du problème de l'adsorption des cations R_4N^+ en solution relativement concentrée d'un électrolyte inerte. Bien que cette approche a des applications immédiates dans l'interprétation de la cinétique des réactions électrochimiques, sa valeur est limitée en ce qui

[1]A qui adresser la correspondance.

[2]Revision reçue le 3 mai 1976.

Can. J. Chem. Downloaded from www.nrcresearchpress.com by 210.87.254.40 on 09/05/12
For personal use only.

Can. J. Chem. Downloaded from www.nrcresearchpress.com by 210.87.254.40 on 09/05/12
For personal use only.

concerne l'élucidation de la structure de la double couche électrique. On peut en conclure que l'adsorption augmente avec la grosseur du cation et que l'anion influence l'adsorption surtout aux charges positives. Comme le montre une récente étude dans 0.1 *M* $HClO_4$ et H_2SO_4 (10), la nature du contre-ion influence l'adsorption du cation. Dans le but d'identifier le rôle de l'anion, il devient nécessaire de faire varier sa concentration indépendamment de celle du cation. Ainsi, il devient nécessaire d'étudier l'adsorption dans les systèmes ternaires.

L'étude de l'adsorption spécifique simultanée des anions et des cations fut entreprise en utilisant des solutions de deux sels ayant un ion commun: soit à un rapport molaire fixe en fonction de la force ionique totale (11), soit à force ionique totale fixe en fonction du rapport molaire (12). Les traitements thermodynamiques supposent que les coefficients d'activité soient connus dans de tels mélanges de sel (par exemple xM $R_4NBr + (y - x)M$ R_4NF, où x et y sont pratiquement limités par la solubilité). Afin de postuler une distribution spatiale (12, 13), il faut admettre qu'au moins un ion, (ici F^-) n'est pas adsorbé spécifiquement et que le rapport de distribution des contre-ions (ici $[Br^-]/[F^-]$) dans la couche diffuse est déterminé par des équations statistiques qui ne tiennent aucun compte de leur nature chimique. Une telle étude indique pour le NH_4Br un comportement qui dépend de la force ionique (14) alors que pour le chlorure de guanidine (15) il est différent de celui normalement observé pour des cations organiques. Avec le traitement de Lakshmanan et Rangarajan (11) appliqué à des solutions de mélange de sels (par exemple xM KBr/xM R_4NBr) il reste à déterminer si le rapport de distribution des contre ions, (ici $[K^+]/[R_4N^+]$), dans la couche diffuse est fonction de la force ionique ou non. Aucune étude expérimentale n'a été entreprise à cette date.

Nous avons récemment démontré que la mesure du temps de formation d'une goutte de mercure, donne des valeurs de tension interfaciale γ tout à fait en accord avec celles de l'électromètre de Lippmann (16) et nous avons décrit le traitement des données recueillies (9). Il n'est donc pas utile de répéter ici les détails de cette méthode, ni d'énumérer les hypothèses du modèle de Gouy–Chapman–Stern (*cf.* Delahay (17) et Mohilner (18)). Notre but se limite essentiellement à la présentation des résultats expérimentaux et la discussion de la signification de deux paramètres thermodynamiques: $\Gamma^+(q_M)$, l'excès de surface ionique; et $(\partial\Gamma^+/\partial q_M)$, le coefficient d'Esin Markov et examiner sa variation en fonction de la charge de l'électrode, q_M. Nous procéderons ensuite à un calcul de $\Delta\bar{G}_{ads}$ à partir de deux isothermes simples. Nous proposerons enfin une interprétation du comportement des sels R_4NX selon un modèle structural en accord avec celui proposé par Desnoyers et Jolicoeur (19) pour des solutions homogènes concentrées, sans toutefois présenter un traitement mathématique quantitatif explicant les contributions anioniques et cationiques.

Partie expérimentale

Les solutions de chlorures, de bromures et d'iodures de tétraalkylammonium sont préparées à partir des sel (Eastman Kodak Co. et J. T. Baker Chemical Co.) recristallisés, selon les méthodes proposées par Conway *et al.* (20), et de l'eau bidistillée sur le permanganate de potassium alcalin. Les solutions concentrées de fluorures sont fabriquées en neutralisant des hydroxydes de tétraalkyl ammonium avec de l'acide fluorhydrique. Les solutions sont désoxygénées en y barbotant de l'azote immédiatement avant l'usage.

Le mercure utilisé nécessite une purification méticuleuse. Environ 500 ml de mercure (Mallenckrodt, tridistillé) sont lavés dans une solution KOH 1 *M* dans un ballon de 1 litre en aspirant de l'air pendant 24 h. Après rincage avec de l'eau bidistillée le traitement est répété plusieurs fois avec une solution HNO_3 1 *M* saturée en $HgNO_3$. Le mercure est séché par passage dans une colonne verticale contenant du CCl_4 et une solution aqueuse HNO_3 1 m*M*. Il est ensuite distillé sous une faible pression obtenue en aspirant de l'oxygène pur à travers un tube capillaire plongeant dans le mercure. Il est finalement soumis à une triple distillation sous vide.

Les valeurs de la tension interfaciale sont calculées à partir du temps de formation d'une goutte de mercure, mesuré tous les 25 mV pour des solutions variant de 10^{-3} à 1 *M*. L'instrumentation nécessaire (16, 21) consiste d'un tensiomètre dynamique, d'un potentiostat et d'un compteur d'intervalle. La cellule de mesure elle-même est fabriquée à partir d'un tube en pyrex de diamètre légèrement supérieur à celui du capillaire polarographique qui y plonge. Ainsi le volume mort constitue moins que 0.5 ml. La solution apportée par une canalisation en Teflon, s'écoule à un débit d'environ 0.5 ml min^{-1} à travers la cellule. Quand la goutte de mercure tombe, elle interrompt un faisceau lumineux émanant d'un faisceau de fibres optiques, ce qui déclenche un signal émis par une photodiode RCA 3062. Le potentiel de la goutte est contrôlé par un potentiostat à trois électrodes, dont une nappe de mercure qui agit comme électrode auxiliaire. Le potentiel de la goutte est mesuré par rapport à une électrode au calomel saturé (E.C.S.) séparée de la solution par un pont agar-agar saturé en KCl.

Can. J. Chem. Downloaded from www.nrcresearchpress.com by 210.87.254.40 on 09/05/12
For personal use only.

Les potentiels de charge nulle par rapport à une électrode E.C.S. ($E_{pcn}^{E.C.S.}$) ou une électrode reversible aux anions (E_{pcn}^{-}) sont mesurés séparément avec l'aide d'une électrode à jet de mercure (9). Ce n'est que lorsque l'écart ($E_{pcn}^{E.C.S.} - E_{pcn}^{-}$) est en accord avec la mesure directe $E_{-}^{E.C.S.}$ et si $E_{pcn}^{E.C.S.}$ est en accord avec le potentiel calculé par différentiation des courbes électrocapillaires qu'on considère que les mesures sont valables. Toutes les mesures au tensiomètre dynamique a l'appareil à jet de mercure sont effectuées à 25.0 ± 0.1 °C.

Les valeurs de la tension interfaciale obtenues sont exploitées selon la méthode présentée précédemment (9), en utilisant les valeurs des coefficients d'activité de Lindenbaum et Boyd (22) et Wen *et al.* (23). Les programmes d'ordinateur déjà décrits (24) sont utilisés dans le traitement des données expérimentales. La reproductibilité est supérieure à $\Delta(q_M) \pm 0.05\ \mu C\ cm^{-2}$ pour la charge d'électrode, $\Delta(F\Gamma_{\pm}) \pm 0.2\ \mu C\ cm^{-2}$ pour l'excès de surface cationique ou anionique et $\Delta(\gamma) \pm 0.3$ dyne cm^{-1} pour la tension interfaciale.

Résultats

Les courbes électrocapillaires ont l'allure prévue et des résultats typiques sont indiqués dans la fig. 1. Il y a coincidence des courbes γ en fonction de E_{-} pour des fluorures de tétraméthyl, tétraéthyl, tétra-*n*-propyl et tétra-*n*-butyl ammonium aux potentiels positifs. La tension interfaciale diminue du côté négatif dans l'ordre $Me_4N^+ < Et_4N^+ < n\text{-}Pr_4N^+ < n\text{-}Bu_4N^+$ et le E_{pcn}^{-} est déplacé vers des potentiels plus positifs à mesure que la dimension du cation augmente.[3] D'autre part, pour un cation donné lorsque la nature de l'anion varie nous retrouvons (fig. 2) un comportement inverse: aux concentrations 0.01 *M* les différents halogénures de tétraéthyl ammonium semblent être adsorbés à peu près de la même façon à des potentiels négatifs par rapport à E_{pcn} mais différemment, selon la nature de l'anion, aux potentiels plus positifs. Le même comportement a déjà été signalé pour les halogénures de tétraméthyl ammonium à 0.1 *M*

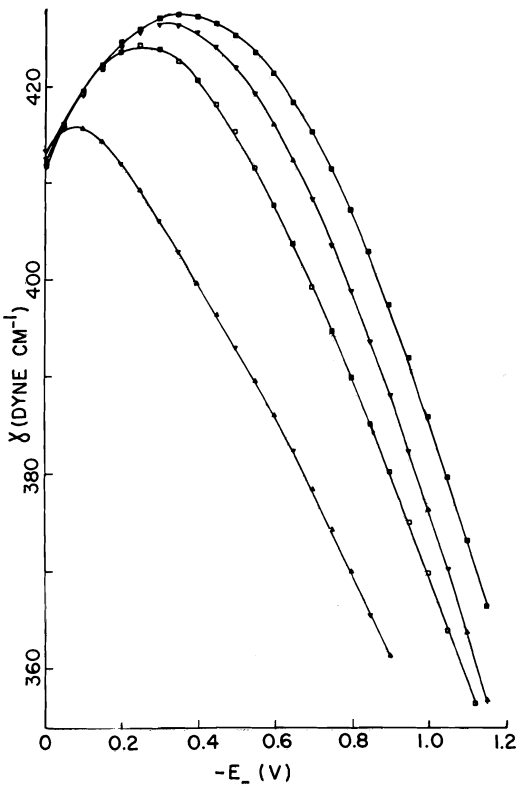

FIG. 1. Tension interfaciale en fonction du potentiel E_{-}; courbe type pour les solutions 0.01 *M*: (■) Me_4NF, (▲) Et_4NF, (□) Pr_4NF, (△) Bu_4NF.

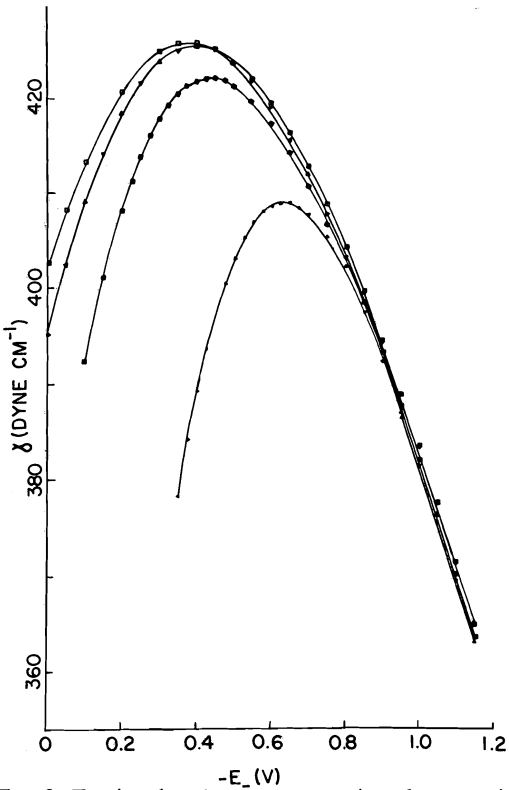

FIG. 2. Tension interfaciale en fonction du potentiel E_{-}; courbe type pour les solutions 0.01 *M*: (□) Et_4NF, (△) Et_4NCl, (■) Et_4NBr, (▲) Et_4NI.

[3]Les données expérimentales $\gamma - E_{E.C.S.}$ peuvent être obtenues à un prix nominal, en s'adressant au Dépôt de données non publiées, ICIST, Conseil national de recherches du Canada, Ottawa, Canada K1A 0S2.

Can. J. Chem. Downloaded from www.nrcresearchpress.com by 210.87.254.40 on 09/05/12
For personal use only.

(9). Aux potentiels plus négatifs que -1.2 V par rapport au $E_{E.C.S.}$ nous avons observé occasionnellement de brusques variations de temps de formation de la goutte de mercure. Quoique nous avons essayé de vérifier les résultats de Hayter et Hunter (25) qui ont identifié de brusques changements de capacité aux alentours de -1.6 V avec un changement d'orientation dans la double couche, notre technique ne le permettait pas. Aux potentiels les plus négatifs le dégagement de bulles d'hydrogène devenait visible et provoquait la chute prématurée de la goutte.

Ces résultats indiquent un comportement similaire des différents sels renfermant le même anion aux charges positives et un comportement similaire des différents sels renfermant le même cation aux charges négatives. On retrouve ce comportement simple pour les sels Me_4NX jusqu'à la concentration 0.1 M, pour les sels n-Pr_4NX jusqu'à 0.001 M et pour les sels n-Bu_4NX seulement aux concentrations plus faible que 0.0001 M où les données expérimentales deviennent trop imprécises pour être fiables. Lorsque les concentrations sont plus élevées que 10^{-1}, 10^{-2}, 10^{-3} et 10^{-4} M respectivement pour des sels Me_4NX, Et_4NX, n-Pr_4NX et n-Bu_4XN, les courbes électrocapillaires sont déplacées verticalement selon la nature de l'anion, même lorsque $q_M \ll 0$. De même, aux concentrations plus élevées que 10^{-1}, 10^{-2}, 10^{-3} et 10^{-4} M, on trouve que les courbes sont déplacées verticalement selon la nature du cation, même lorsque $q_M \gg 0$.

Dans le tableau 1 sont présentées les coordonnées du point de charge nulle (soit E_{pen}^- et γ_{pen}) pour les différents sels étudiés. Le domaine de concentration était dans certains cas limitée par la solubilité et dans d'autres cas par le temps disponible pour atteindre l'équilibre soit 5 s. Ces données permettront au lecteur non seulement le calcul de l'excès de surface, et du déplacement de E_{pen} mais également la comparaison avec les mesures de capacitances dès que celles-ci deviendront disponibles.

Effet Esin Markov

La variation du potentiel E^- en fonction du potentiel chimique nous donne le coefficient de Esin et Markov:[4]

$$\left(\frac{\partial E^-}{\partial \mu}\right)_{T,p,q_M} = -\left(\frac{\partial^2 \gamma}{\partial q_M \partial \mu}\right)_{T,p,E} = -\left(\frac{\partial \Gamma^+}{\partial q_M}\right)_{T,p,\mu}$$

Selon Parsons (26) les pentes des courbes E^- en fonction de μ dépendent peu de la charge q_M si le cation ou l'anion est seul à être adsorbé. E_{pen}^- se déplace vers des potentiels plus négatifs ou positifs quand il s'agit respectivement de l'adsorption spécifique de l'anion ou du cation. Si tous les deux sont fortement adsorbés, le déplacement peut changer de direction à concentration croissante.

Sur les figs 3, 4, 5 et 6 sont données les variations du potentiel de la goutte de mercure (à une charge donnée) par rapport à une électrode réversible aux anions. Nous remarquons que pour le potentiel à charge nulle E_{pen}^- les résultats du tensiomètre s'accordent à ± 3 mV avec les résultats de la méthode de l'électrode à jet de mercure. On notera également que la valeur de $E_{E.C.S.}^- = E_{pen}^- - E_{pen}^{E.C.S.}$ correspond parfaitement aux différences de potentiel mesurées directement entre l'E.C.S. et les électrodes spécifiques.

Les fluorures présentent des variations considérables dans leur comportement. Comme nous l'avons déjà remarqué (9) celui des solutions

TABLEAU 1. Coordonnée du maximum électrocapillaire

Concentration C/mol l^{-1}	Potentiel $-E$/V	Tension interfaciale γ/dyne cm^{-1}
	$(Et)_4NF$	
0.0017	0.388	427.5
0.0033	0.358	427.3
0.0049	0.337	427.1
0.0066	0.328	426.6
0.010	0.321	426.3
0.0166	0.297	425.6
0.033	0.276	424.7
0.049	0.259	424.0
0.100	0.234	422.1
0.271	0.173	414.6
0.543	0.131	410.8
	$(Pr)_4NF$	
0.001	0.355	426.2
0.0016	0.345	425.7
0.0024	0.327	425.4
0.0039	0.299	425.2
0.005	0.287	425.1
0.01	0.253	423.9
0.023	0.196	422.7
0.060	0.144	419.7
0.100	0.116	416.6

[4]Notre symbolisme suit les conventions proposées par Delahay (17) et employées précédemment (9).

Can. J. Chem. Downloaded from www.nrcresearchpress.com by 210.87.254.40 on 09/05/12
For personal use only.

TABLEAU 1 (*Suite*)

Concentration C/mol l^{-1}	Potentiel $-E$/V	Tension interfaciale γ/dyne cm^{-1}
0.157	0.091	414.1
0.236	0.072	412.1
	$(Bu)_4NF$	
0.001	0.238	423.3
0.0015	0.194	421.8
0.0034	0.145	419.4
0.0068	0.102	417.0
0.010	0.077	415.6
0.034	0.016	409.8
0.068	−0.022	406.3
0.10	−0.053	403.4
0.34	−0.084	395.3
	$(Et)_4NCl$	
0.001	0.564	427.5
0.002	0.547	427.2
0.003	0.537	426.9
0.005	0.522	426.4
0.007	0.512	426.2
0.01	0.504	425.7
0.02	0.485	424.7
0.03	0.474	423.7
0.05	0.459	422.6
0.07	0.448	421.5
0.10	0.438	420.4
0.20	0.420	417.4
0.30	0.411	415.4
0.50	0.398	412.9
1.00	0.381	408.5
	$(Pr)_4NCl$	
0.002	0.508	425.0
0.003	0.488	424.5
0.010	0.438	422.1
0.020	0.406	419.8
0.030	0.388	417.7
0.05	0.365	415.6
0.100	0.341	411.6
0.200	0.322	407.4
0.300	0.310	404.9
0.500	0.302	401.4
1.000	0.285	396.8
	$(Bu)_4NCl$	
0.001	0.425	418.2
0.002	0.406	415.5
0.005	0.384	409.3
0.01	0.377	404.3
0.02	0.364	399.4
0.05	0.355	393.6
	Et_4NBr	
0.001	0.446	426.4
0.002	0.426	425.7
0.003	0.418	425.2
0.005	0.408	423.9
0.007	0.400	422.9
0.01	0.390	422.3
0.05	0.386	414.5
0.1	0.384	409.8

TABLEAU 1 (*Suite et fin*)

Concentration C/mol l^{-1}	Potentiel $-E$/V	Tension interfaciale γ/dyne cm^{-1}
0.2	0.377	404.6
0.3	0.372	401.3
0.7	0.373	393.9
	Pr_4NBr	
0.001	0.415	424.6
0.002	0.396	423.5
0.003	0.379	421.8
0.005	0.361	419.9
0.007	0.351	418.3
0.01	0.338	416.7
0.02	0.323	412.1
0.03	0.316	409.3
0.05	0.303	405.1
0.07	0.308	402.4
0.10	0.303	400.6
0.200	0.309	395.3
0.300	0.304	392.2
0.500	0.307	388.4
0.700	0.309	385.5
	Bu_4NBr	
0.001	0.300	416.6
0.002	0.295	411.8
0.003	0.277	408.6
0.005	0.271	405.2
0.007	0.266	403.0
0.01	0.259	400.6
0.02	0.259	394.9
0.03	0.257	391.7
0.07	0.260	385.2
0.10	0.256	382.7
	Et_4NI	
0.003	0.366	417.9
0.005	0.362	413.5
0.008	0.362	411.2
0.01	0.357	409.1
0.014	0.357	406.1
0.087	0.338	390.6
0.145	0.331	386.6
0.290	0.326	379.9
	Pr_4NI	
0.001	0.348	421.4
0.002	0.351	416.5
0.0025	0.349	415.0
0.005	0.346	409.3
0.008	0.340	405.3
0.01	0.334	402.9
0.025	0.315	394.7
0.05	0.301	388.4
0.1	0.292	382.4
	Bu_4NI	
0.001	0.308	399.9
0.002	0.298	393.4
0.0025	0.284	391.8
0.005	0.265	385.9
0.01	0.254	380.1
0.025	0.244	373.4

Can. J. Chem. Downloaded from www.nrcresearchpress.com by 210.87.254.40 on 09/05/12
For personal use only.

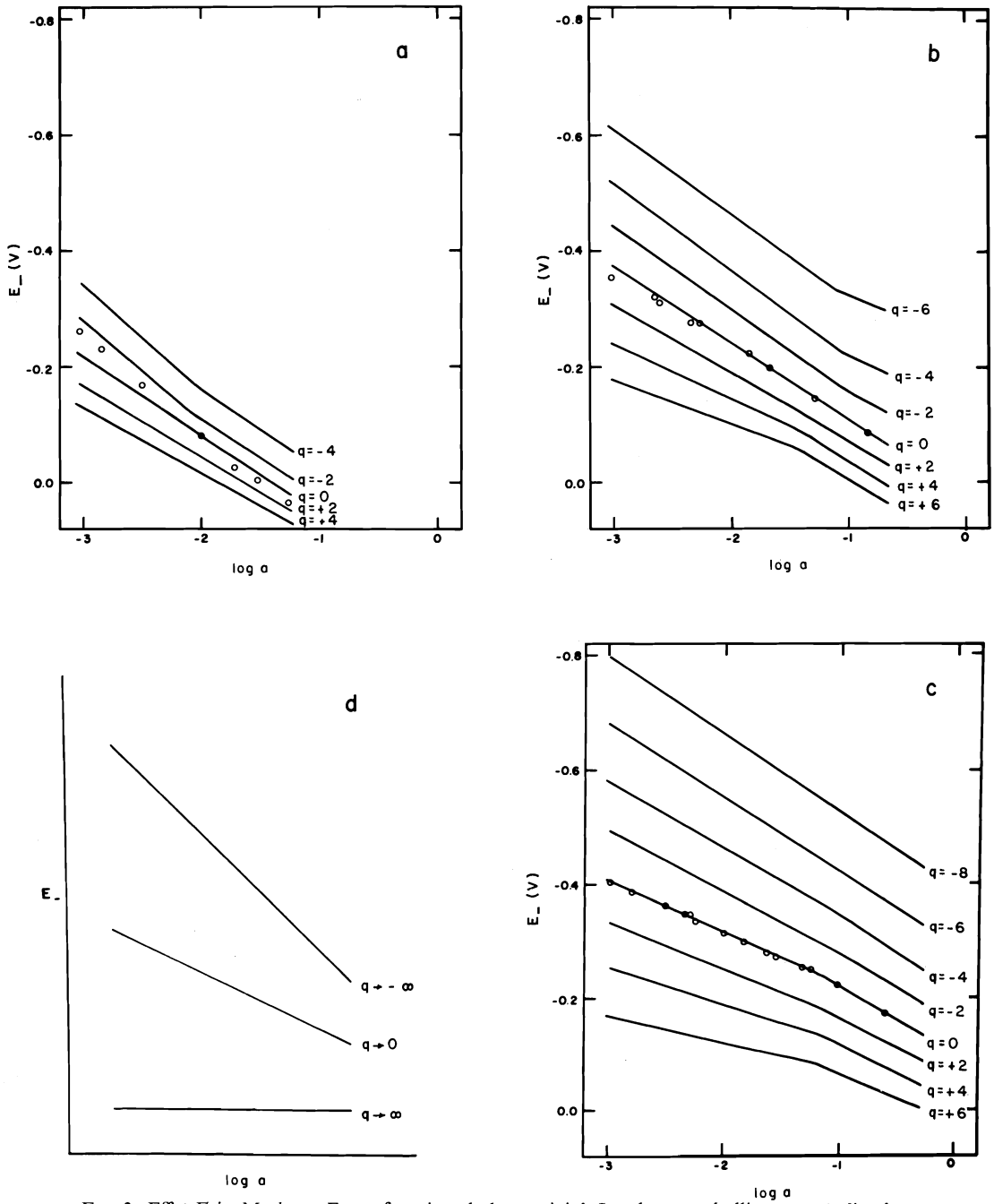

FIG. 3. Effet Esin Markov. E_- en fonction de log activité. La charge métallique est indiquée en $\mu C\ cm^{-2}$. (○) E_{pzc} valeurs obtenues par la méthode d'une électrode de jet de mercure: (*a*) Bu_4NF, (*b*) Pr_4NF, (*c*) Et_4NF, (*d*) courbes théoriques en absence d'adsorption spécifique.

Me_4NF est peu différent des solutions KF, même si une légère pente subsiste à $q_M = +6$ $\mu C\ cm^{-2}$. Les pentes varient dans l'ordre prévu par un modèle électrostatique: $\partial F\Gamma^+/\partial q_M \simeq 0$, -0.5_5 et -1.0 pour $q_M \gg 0$, $q_M = 0$ et $q_M \ll 0$. Par contre, les solutions Bu_4NF présentent des

Can. J. Chem. Downloaded from www.nrcresearchpress.com by 210.87.254.40 on 09/05/12
For personal use only.

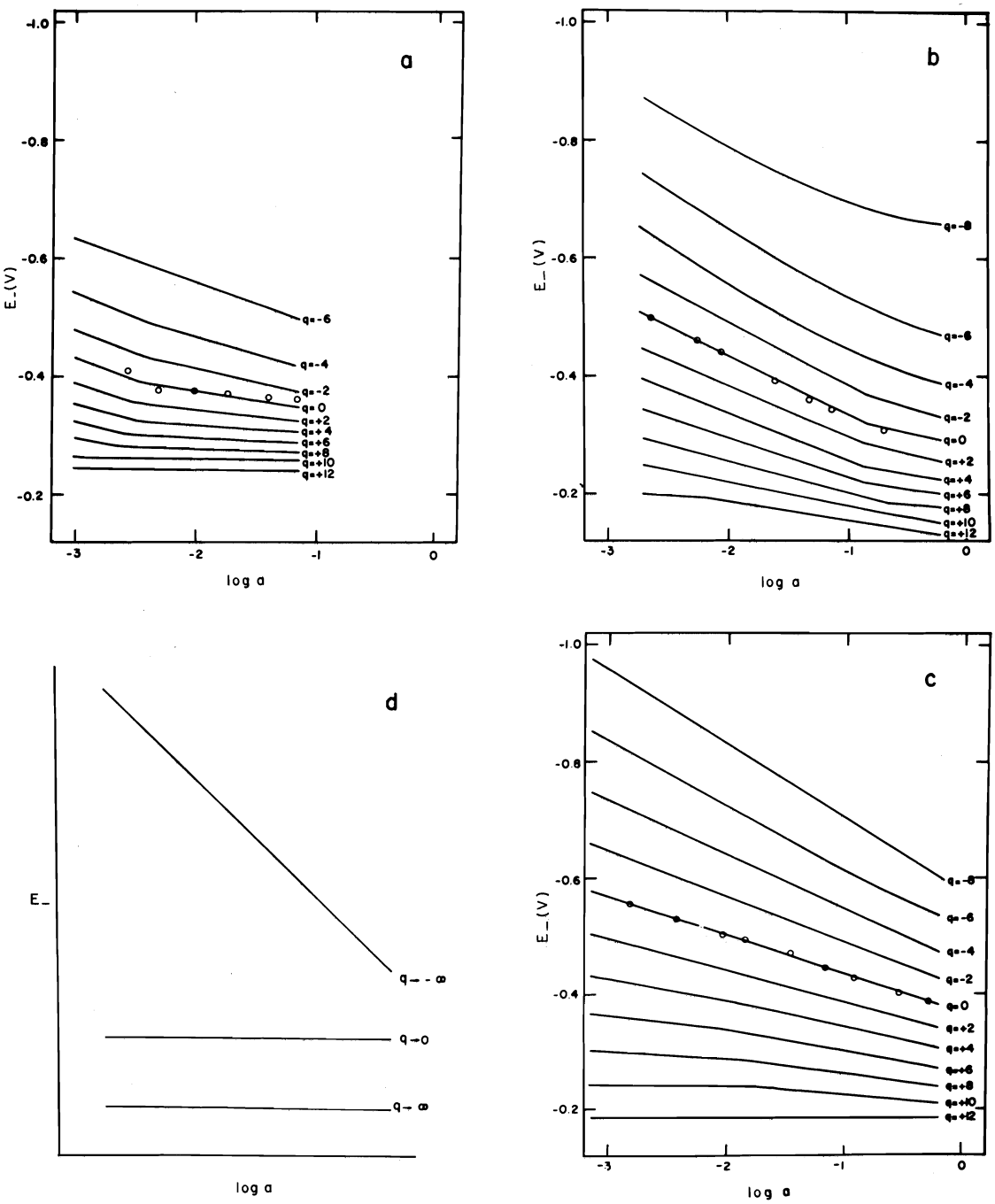

FIG. 4. Effet Esin Markov. Coordonnées identiques à celles de la fig. 3: (*a*) Bu_4NCl, (*b*) Pr_4NCl, (*c*) Et_4NCl, (*d*) courbes théoriques en supposant l'adsorption spécifique de l'anion.

courbes quasi parallèles et très rapprochées. Donc une légère variation du potentiel électrique entraîne une énorme variation de la structure de la double couche, soit analogue à celui déjà constaté pour des solutions de KI (26). Pour des solutions de Et_4NF et Pr_4NF nous trouvons un

Can. J. Chem. Downloaded from www.nrcresearchpress.com by 210.87.254.40 on 09/05/12
For personal use only.

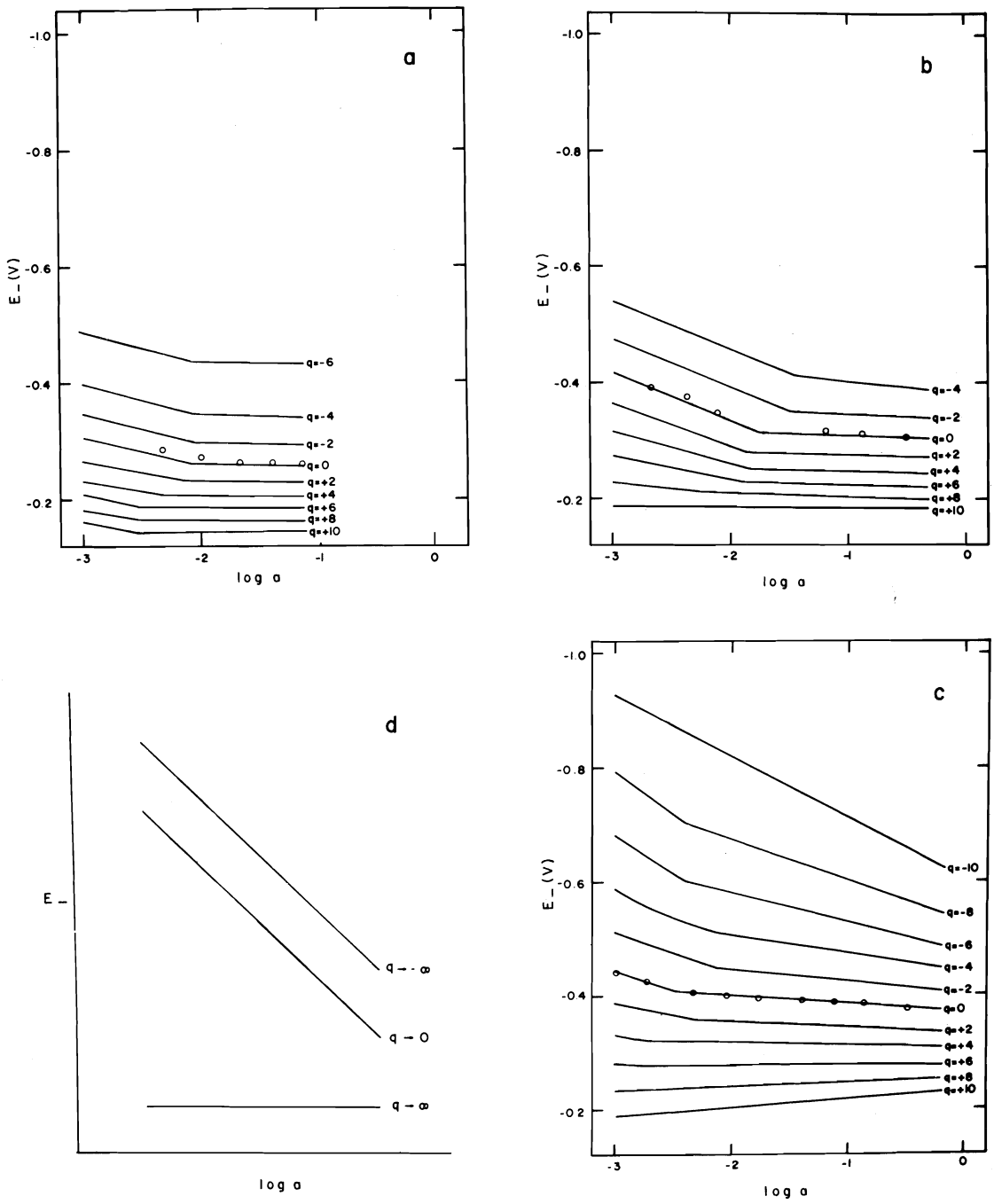

FIG. 5. Effet Esin Markov. Coordonnées identiques à celles de la fig. 3: (*a*) Bu_4NBr, (*b*) Pr_4NBr, (*c*) Et_4NBr, (*d*) courbes théoriques en supposant l'adsorption du cation.

comportement intermédiaire avec de légères variations de la pente en fonction de la concentration. Aux concentrations élevées, les pentes tendent à être égales (ce qui peut être attribué à l'adsorption du cation) tandis qu'aux concentrations faibles, elles varient comme prévu (fig. 3*d*).

Can. J. Chem. Downloaded from www.nrcresearchpress.com by 210.87.254.40 on 09/05/12
For personal use only.

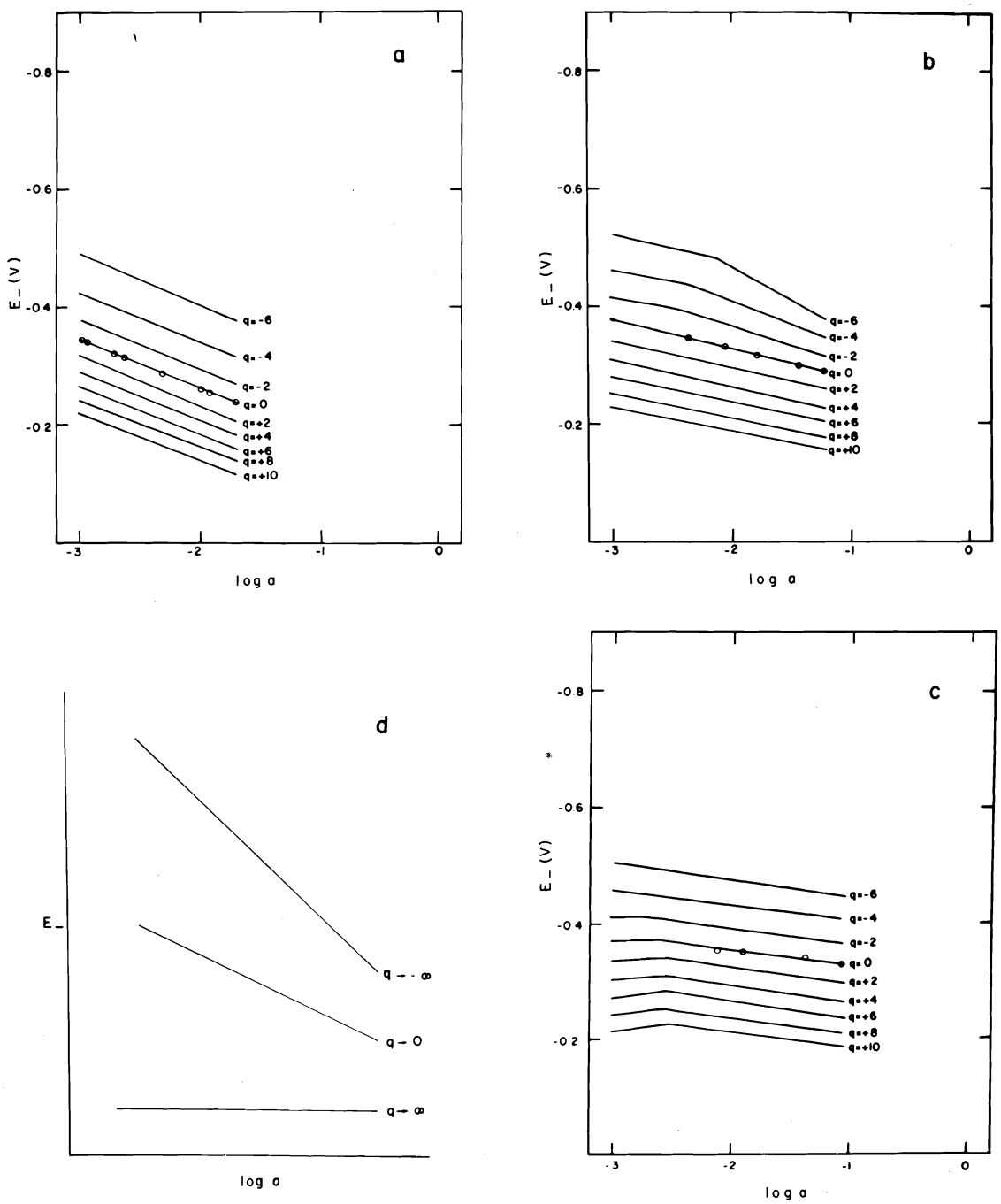

FIG. 6. Effet Esin Markov. Coordonnées identiques à celles de la fig. 3: (*a*) Bu_4NI, (*b*) Pr_4NI, (*c*) Et_4NI, (*d*) courbes théoriques en supposant l'adsorption simultanée de l'anion et du cation.

Pour les fluorures Bu_4NF et Pr_4NF à concentration élevée le comportement se rapproche de celui illustré dans la fig. 5*d* schématisant le cas hypothétique où il y a seulement l'adsorption spécifique du cation.

Les solutions de Me_4NCl (10), et de Et_4NCl,

Can. J. Chem. Downloaded from www.nrcresearchpress.com by 210.87.254.40 on 09/05/12
For personal use only.

(fig. 4*c*) ainsi que celles de Pr_4NBr aux faibles concentrations (fig. 5*b*) se comportent comme prévu par le modèle électrostatique, (fig. 3*d* ou le modèle fig. 6*d*). Aux concentrations plus élevées nous trouvons des courbures plus ou moins prononcées, suivies d'un changement de pente. Dans certains cas le comportement se rapproche de celui illustré en fig. 4*d*. Néanmoins, dans chaque cas, une plus grande étendue de potentiel est nécessaire pour obtenir un Δq_M constant aux fortes concentrations que l'étendue prévue par l'extrapolation des résultats à faible concentration. S'il faut donc augmenter plus que prévu le champs électrostatique, c'est vraisemblablement parce que les forces non-électrostatiques deviennent plus importantes aux fortes concentrations.

Pour les bromures et les iodures Me_4NBr (7, 9), Me_4NI (9), Et_4NBr, (fig. 5*c*) et Et_4NI (fig. 6*c*), le comportement à faible concentration et à $q_M > 0$ ressemble à celui de la fig. 4*d* illustrant le cas hypothétique où il y a seulement l'adsorption spécifique de l'anion. Aux concentrations élevées, l'adsorption pour les bromures, *n*-Pr_4NBr et *n*-Bu_4NBr, semble devenir indépendante du potentiel et donc $(\partial\Gamma^+/\partial q_M) \simeq 0$, tandis que pour les iodures, *n*-Pr_4NI et *n*-Bu_4NI, surtout quand $q_M > 0$, $(\partial\Gamma^+/\partial q_M)$ est constant.

En considérant les 16 sels étudiés nous remarquons donc une transition monotone du comportement quasi-électrostatique de Me_4NF, Et_4NCl et Pr_4NBr (à faible concentration) d'une part vers des sels accusant une forte contribution du cation tels que Bu_4NI, Bu_4NBr, Bu_4NCl, Bu_4NF et Pr_4NF, (à concentration élevée) et d'autre part, vers des sels accusant une forte contribution de l'anion tels que, Et_4NI, Et_4NBr, Me_4NI, Me_4NBr (à faible concentration). Cette tendance est schématisée à la fig. 7.

Excès de surface ionique

L'excès de surface cationique, $F\Gamma^+$, l'axe verticale de la fig. 8 est présenté en trois dimensions afin de bien montrer l'influence des deux paramètres qui l'affectent. Nous avons porté sur l'axe *Y*, le logarithme de la concentration (mol/l), et sur l'axe *X*, la charge sur l'électrode ($\mu C\ cm^{-2}$). Nous avons choisi d'une part la concentration (qui est une valeur expérimentale ne faisant intervenir aucun modèle) plutôt que l'activité et d'autre part la charge plutôt que le potentiel comme paramètre électrique, celle-ci

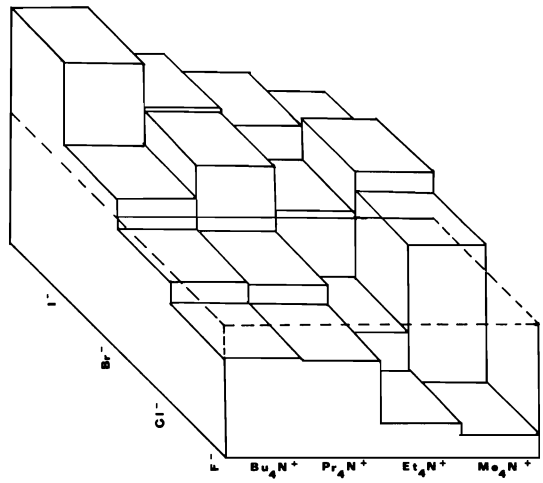

FIG. 7. Schématisation de l'adsorption structurale. La hauteur et la direction des cubes données selon l'expression empirique $(\Gamma^{\Delta}(q_M) - \Gamma^{\Delta}(-q_M))/|q_M|$ pour q_M 0 à $\sim 10\ \mu C\ cm^{-2}$ et $[R_4NX]$ de 10^{-2} à 10^{-1} *M*. Les symboles sont définis dans le texte.

ne dépendant pas de la nature de l'électrode de référence.

Ainsi qu'il a été indiqué précédemment pour Me_4NF, l'excès de surface cationique devient négatif aux charges $q_M > 0$, aux concentrations de 10^{-3} à 1 *M*. Pour les trois autres sels de fluorure, Γ^+, est négatif seulement aux faibles concentrations. Γ^+ continue d'augmenter en fonction de la concentration et en fonction de la charge à l'exception du Bu_4NF où Γ^+ semble plafonner. Nous signalons que les valeurs $\Gamma^+ < 0$ sont (dans certains cas) plus négatives que prévu par la théorie de Gouy–Chapman–Stern. Afin d'expliquer le comportement des cations à $q_M < 0$, il ne suffit pas de supposer qu'ils sont expulsés de la région interfaciale par des forces électrostatiques. Nous avons présenté une explication qualitative pour le cas des solutions de Me_4NF (9); nous développeront des arguments semblables pour les autres quinze sels.

Comme nous l'avons démontré pour le Me_4NF, il est possible, du moins en principe, de calculer q_+^i, la charge due aux ions R_4N^+ adsorbés sur le mercure, si l'on admet que les ions F^- restent hydratés et ne peuvent pas s'approcher de l'électrode pour y être absorbés "spécifiquement". Un tel traitement mathématique suppose d'une façon implicite que l'ion F^- ne subit que des influences analogues aus petits ions alcalins K^+ et Na^+. Cependant, Wen *et al.* (23) ont mis en

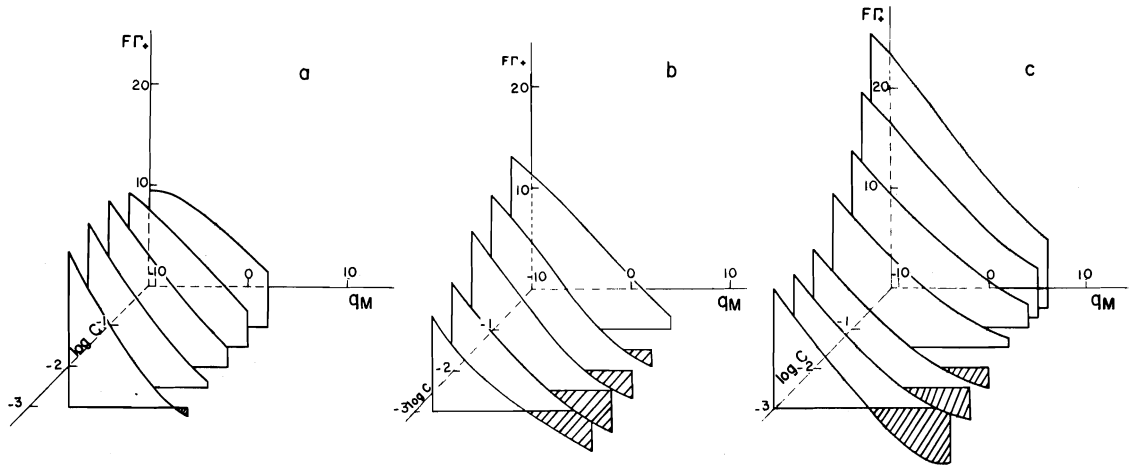

FIG. 8. L'excès ionique de surface $\Gamma^{+}/\mu C\ cm^{-2}$ en fonction de log (concentration/mol l^{-1}) et de la charge métallique $q_M/\mu C\ cm^{-2}$: (*a*) Bu_4NF, (*b*) Pr_4NF, (*c*) Et_4NF. La surface hachurée représente les valeurs négatives de $F\Gamma^{+}$.

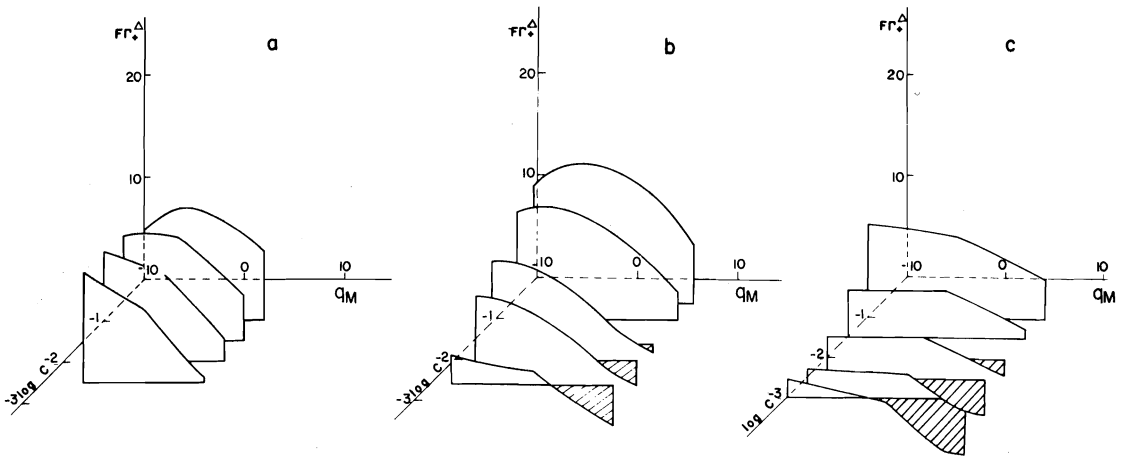

FIG. 9. Excès ionique structural $F\Gamma^{\Delta}/\mu C\ cm^{-2}$ défini selon l'éq. 1 en fonction de log (concentration/mol l^{-1}) et la charge métallique $q_M/\mu C\ cm^{-2}$: (*a*) Bu_4NF, (*b*) Pr_4NF, (*c*) Et_4NF. La surface hachurée représente des valeurs négatives de $F\Gamma^{\Delta}$.

évidence il y a quelques années déjà les propriétés structurantes des fluorures de tétraalkyl ammonium. Il est légitime de supposer que cette influence structurante joue également un rôle dans la double couche électrique. Non seulement peut-elle attirer dans cette région des ions ou molécules ayant des couches de solvatation compatibles ($\Gamma_{\pm} > \Gamma_{\pm}$ électrostatique) mais également repousser de cette région des ions ayant des couches de solvatation non compatibles ($\Gamma_{\pm} < \Gamma_{\pm}$ électrostatique).

Afin de faire ressortir cet argument nous présentons à la fig. 9 l'excès de surface "structural" défini par

$$[1] \qquad F\Gamma^{\Delta} \equiv F\Gamma_{+}{}^{\Delta} \equiv F\Gamma_{-}{}^{\Delta} = F\Gamma_{\pm} - q_{\pm}{}^{d}$$

où $q_{\pm}{}^{d}$ est la composante de charge calculée à partir de la théorie électrostatique (*cf.* éq. 7, réf. 9). La fig. 9 présente alors la différence entre $\Gamma^{+}{}_{sel}$(expérimental) et $\Gamma^{+}{}_{sel}$(théorique) sans toutefois attribuer une distribution spatiale précise à l'excès (au déficit) structural dans la couche électrique.

On observe que Γ^{Δ} augmente avec la dimen-

Can. J. Chem. Downloaded from www.nrcresearchpress.com by 210.87.254.40 on 09/05/12
For personal use only.

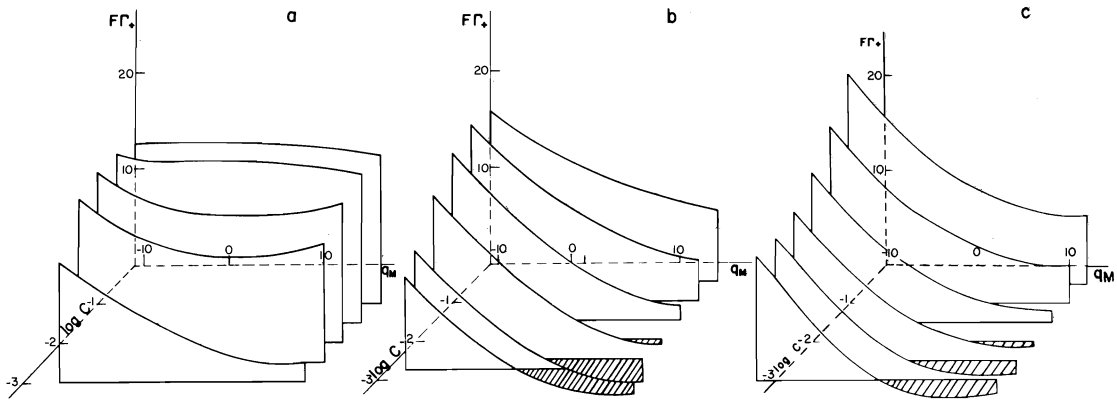

FIG. 10. Excès ionique de surface: coordonnées identiques à celles de la fig. 8: (*a*) Bu_4NCl, (*b*) Pr_4NCl, (*c*) Et_4NCl.

sion et la concentration du cation, quand $q_M > 0$ (pour Et_4NF et Pr_4NF, aux faibles concentrations, $\Gamma^\Delta < 0$) et quand $q_M < 0$ (pour Bu_4NF et Pr_4NF, aux concentrations élevées, Γ^Δ passe par un maximum entre 0.1 et 0.3 *M*). Ces deux dernières observations sont en accord avec un modèle qui suppose des "répulsions" entre la couche d'hydratation hydrophobe de l'ion Bu_4N^+ ou Pr_4N^+ et la couche d'hydratation hydrophile de l'ion F^- en plus de la "répulsion" mutuelle des ions F^-. Par "répulsion" nous entendons, dans l'esprit de Desnoyers et Jolicoeur, l'augmentation au delà des prédictions coulombiennes de l'énergie libre du système quand on approche les ions. Il est évident qu'il y a en solution près des surfaces portant une charge positive, un excès d'ions F^- par rapport aux cations, c'est-à-dire $\Gamma_{F^-}/\Gamma_{R_4N^+} > 1$. Il y a donc un plus grand nombre d'interactions de type $F^- \leftrightarrow F^-$ et $F^- \leftrightarrow R_4N^+$ que d'interactions du type $R_4N^+ \rightarrowtail\!\!\!\!\!\!\leftarrow R_4N^+$. Au stade actuel, en accord avec Friedman et coll. (27) nous ne pouvons attribuer des valeurs absolues à ces interactions, mais il est évident, comme le montre l'étude thermodynamique des solutions homogènes (28) que les deux premières interactions sont fortement répulsive. Il s'ensuit que l'attraction des fluorures dans la double couche due au champ électrostatique du métal chargé est opposée aux forces de répulsion structurale.

De même que la théorie de Gouy–Chapman a dû être modifiée pour tenir compte d'une distance d'approche minimum, il nous semble logique de modifier la théorie de Gouy–Chapman–Stern en admettant l'existence de forces autre qu'électrostatiques entre ions dans la double couche. Un tel traitement ne comporte pas de nouveauté profonde et de nombreux chercheurs en ont examiné l'un ou l'autre de ses aspects. A cet égard, les sels R_4NX constituent une série où ces interactions non-électrostatiques ont des valeurs particulièrement élevées et où des traitements simplifiés s'avèrent inadéquats.

La fig. 10 présente l'excès de surface cationique des sels R_4NCl. Une plus grande étendue de charge peut être atteinte expérimentalement, mais à première vue, il n'existe pas de grandes différences avec le comportement des fluorures (fig. 8). Une comparaison plus attentive indique que l'anion Cl^- augmente d'une façon appréciable l'adsorption, non seulement aux $q_M > 0$ mais aussi aux $q_M < 0$! La fig. 11, qui explicite l'excès structural, Γ^Δ, fait ressortir davantage cette observation.

L'adsorption $\Gamma^\Delta_{Me_4NCl}$ au delà de celle prédite par la théorie G.C.S., est énorme comparée à $\Gamma^\Delta_{Me_4NF}$. Tandis que pour Me_4NF il y a désorption aux $q_M > 0$, ici nous observons que $\Gamma^\Delta_{Me_4NCl}$ ($q_M > 0$) $> \Gamma^\Delta_{Me_4NCl}$ ($q_M < 0$). Pour Et_4NCl à concentration élevée $\Gamma^\Delta_{Et_4NCl}$ est quasi indépendant de la charge tandis que pour Pr_4NCl, comme pour Pr_4NF, l'adsorption est favorisée aux $q_M < 0$. Remarquons qu'il existe peu de différence entre $\Gamma^\Delta_{Bu_4NF}$, $\Gamma^\Delta_{Bu_4NCl}$ et encore moins entre $\Gamma^\Delta_{Pr_4NF}$, $\Gamma^\Delta_{Pr_4NCl}$. Dans ces deux cas, les interactions entre ions semblent quasi indépendantes de la nature de l'anion excepté à $q_M \gg 0$. Ici la valeur de $\Gamma^\Delta_{Pr_4NCl}$ pourrait refléter le fait que les ions chlorures subissent une

Can. J. Chem. Downloaded from www.nrcresearchpress.com by 210.87.254.40 on 09/05/12
For personal use only.

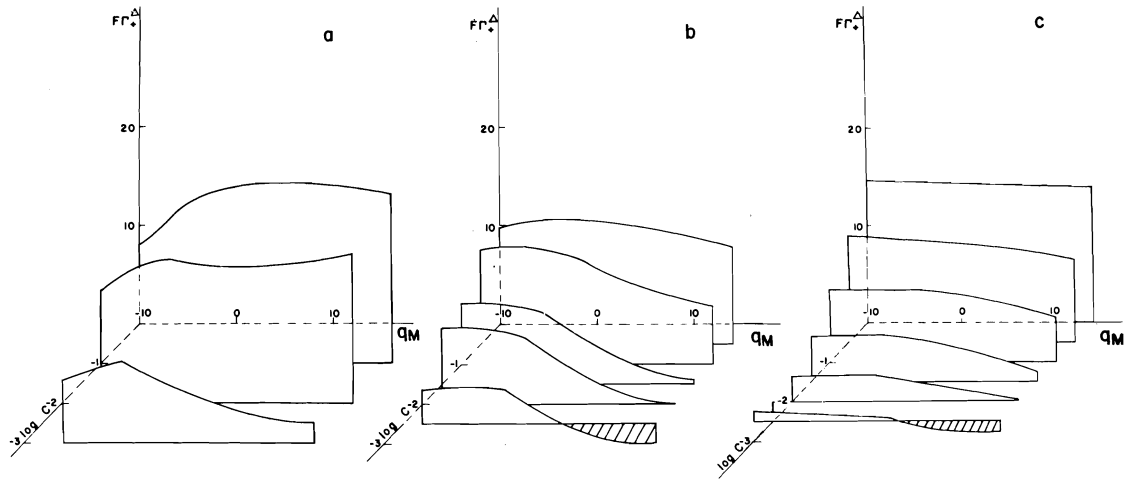

FIG. 11. Excès ionique structural; coordonnées identiques à celles de la fig. 9: (*a*) Bu_4NCl, (*b*) Pr_4NCl, (*c*) Et_4NCl.

FOR ERRATA SEE
V54(20)1976...P3303-re: figure 12.

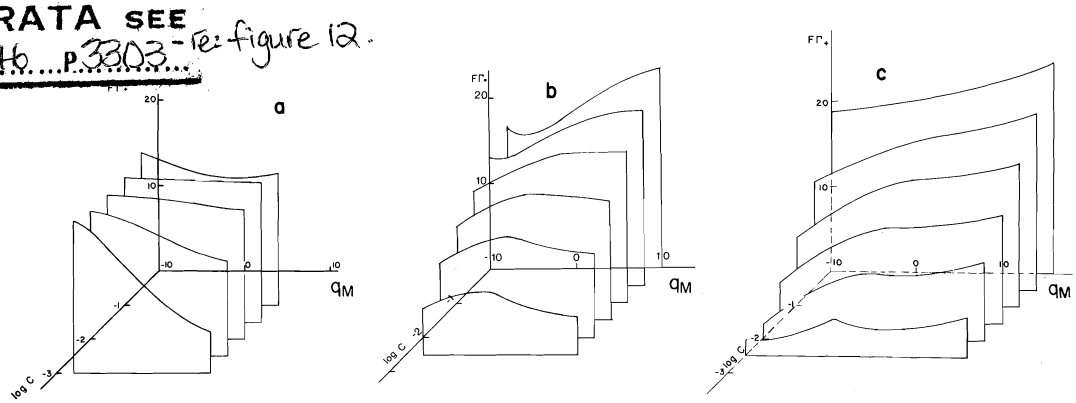

FIG. 12. Excès ionique de surface; coordonnées identiques à celles de la fig. 8: (*a*) Bu_4NBr, (*b*) Pr_4NBr, (*c*) Et_4NBr.

répulsion structurale moins forte que les fluorures.

La fig. 12 indique l'influence prédominante de l'anion bromure sur l'excès de surface. Pour *n*-Pr_4NBr et Et_4NBr $\Gamma^+(q_M > 0) < \Gamma^+(q_M < 0)$ tandis que pour Me_4NBr l'inverse semble se produire aux faibles concentrations. Quoiqu'on ne puisse exclure la possibilité d'erreur expérimentale, ces mêmes tendances ont été observées par Piro *et al.* (8). Selon eux $\Gamma^+(Bu_4NBr)$ croit lorsque $q_M < -10\,\mu C\,cm^{-2}$ et $\Gamma^+(Pr_4NBr)$ plafonne pour $q_M < -10\,\mu C\,cm^{-2}$. Comme nous l'avons démontré (9), par des calculs détaillés, en milieu Me_4NI, Γ^+ ne peut pas être expliqué simplement en termes d'adsorption spécifique simultanée de l'anion et du cation. Un examen qualitatif des graphiques présentés ci-dessus mène à la même conclusion.

Admettons pour le KBr 0.1 *M*, (réf. 17, figs. 4, 5) une valeur de $\Gamma^{\Delta}_{KBr} \simeq 6\,\mu C\,cm^{-2}$ au E_{pcn}, et pour le KCl 0.1 *N* un $\Gamma^{\Delta}_{KCl} \simeq 2\,\mu C\,cm^{-2}$ et supposons un instant avec Verdier (7) que $\Gamma^{\Delta}_{Br^-}$ est dû uniquement aux anions Br^-. La comparaison des figs 8*a*, 10*a* et 12*a* ou 8*b*, 10*b* et 12*b* à $q_M = 0$ indique que l'écart $(\Gamma^+_{R_4NBr} - \Gamma^+_{R_4NF})$ ou l'écart $(\Gamma^+_{R_4NCl} - \Gamma^+_{R_4NF})$ n'égale pas $6\,\mu C\,cm^{-2}$ ou $2\,\mu C\,cm^{-2}$ respectivement. Autrement dit, quand tous les deux ions sont tensioactifs, l'excès de surface n'est pas additif contrairement à ce que laisse supposer le travail de Devanathan et Fernando (4).

L'examen de la fig. 13 conduit à admettre que

Can. J. Chem. Downloaded from www.nrcresearchpress.com by 210.87.254.40 on 09/05/12
For personal use only.

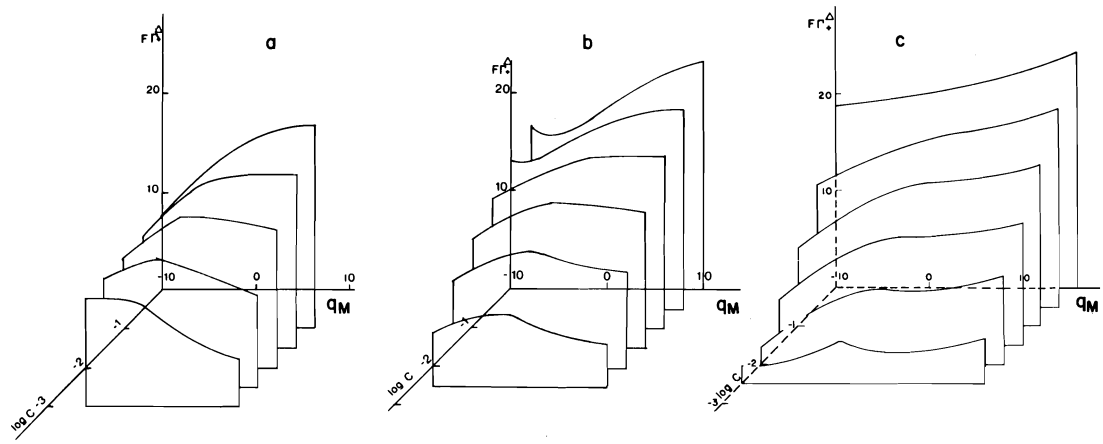

FIG. 13. Excès ionique structural; coordonnées identiques à celles de la fig. 9: (*a*) Bu_4NBr, (*b*) Pr_4NBr, (*c*) Et_4NBr.

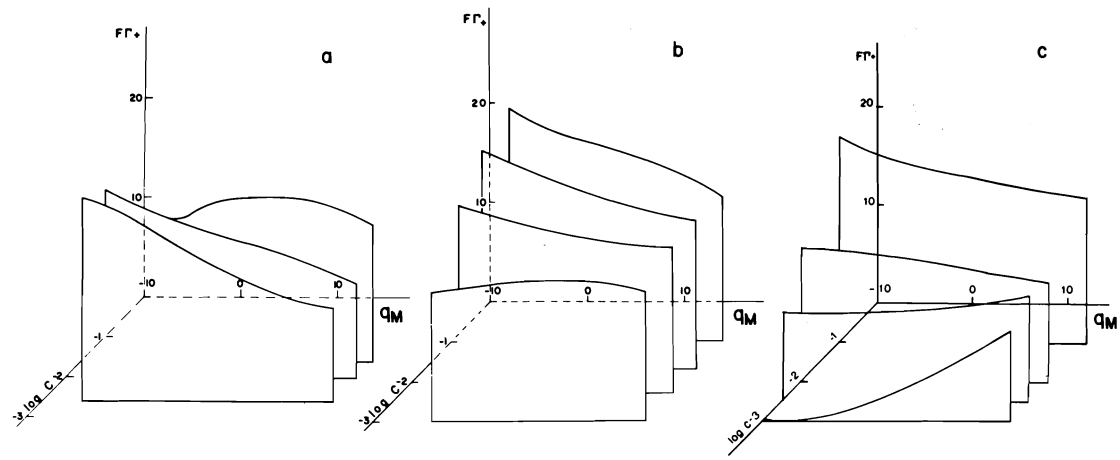

FIG. 14. Excès ionique de surface; coordonnées identiques à celles de la fig. 8: (*a*) Bu_4NI, (*b*) Pr_4NI, (*c*) Et_4NI.

l'adsorption est très élevée aux $q_M > 0$ et apparemment indépendante de la nature du cation. Aux $q_M < 0$, Γ^{Δ} croît avec la dimension du cation mais plus lentement qu'avec R_4NCl ou R_4NF. Une comparaison des figs 9*a*, 11*a* et 13*a*; 9*b*, 11*b* et 13*b*; et 9*c*, 11*c* et 13*c*; à $q_M = 0$ indique que $\Gamma^{\Delta}_{R_4NX} \neq \Gamma^{\Delta}_{R_4NF} + \Gamma^{\Delta}_{KX}$. Des calculs détaillés appuient cette conclusion pour $q_M < 0$, et $q_M > 0$ tandis que pour $q_M \gg 0$ l'approximation $\Gamma^{\Delta}_{R_4NX} \simeq \Gamma^{\Delta}_{KX}$ semble être raisonnable.

Les figs 14 et 15 illustrant $\Gamma^{+}_{R_4NI}$ et $\Gamma^{\Delta}_{R_4NI}$ constituent les cas extrêmes de la série. Pour une solution 10^{-1} *M* on remarque que Γ^{+} croît très peu avec la taille du cation; même à 10^{-2} *M*, si $\Gamma_{Et_4NI} \simeq \Gamma_{Pr_4NI} \simeq \Gamma_{Bu_4NI}$, le déplacement du Γ_{max} vers $q_M < 0$ est évident. $\Gamma^{\Delta}_{Et_4NI}$ semble indiquer un déficit à 10^{-3} *M* pour $q_M \simeq 10\ \mu C\ cm^{-2}$, mais ces régions correspondent aux conditions expérimentales les plus imprécises. Les différences majeures de la fig. 14 se retrouvent surtout aux faibles concentrations où les différences dans l'activité de surface de plusieurs sels peuvent être remarquées. Pratiquement dans tous les cas, Γ^{Δ} passe par un maximum autour de $q_M = 0$. Aux concentrations plus grandes que 10^{-2} *M* on s'approche du recouvrement maximum surtout pour Pr_4NI et Bu_4NI. Ce recouvrement maximum, Γ^{Δ}_{max}, décroît avec la dimension du cation 2.35, 2.20, 2.16, et 1.85 10^{-10} mol cm^{-2}. On doit donc supposer que Γ^{Δ}_{max} est limité non pas par l'adsorbabilité des

Can. J. Chem. Downloaded from www.nrcresearchpress.com by 210.87.254.40 on 09/05/12
For personal use only.

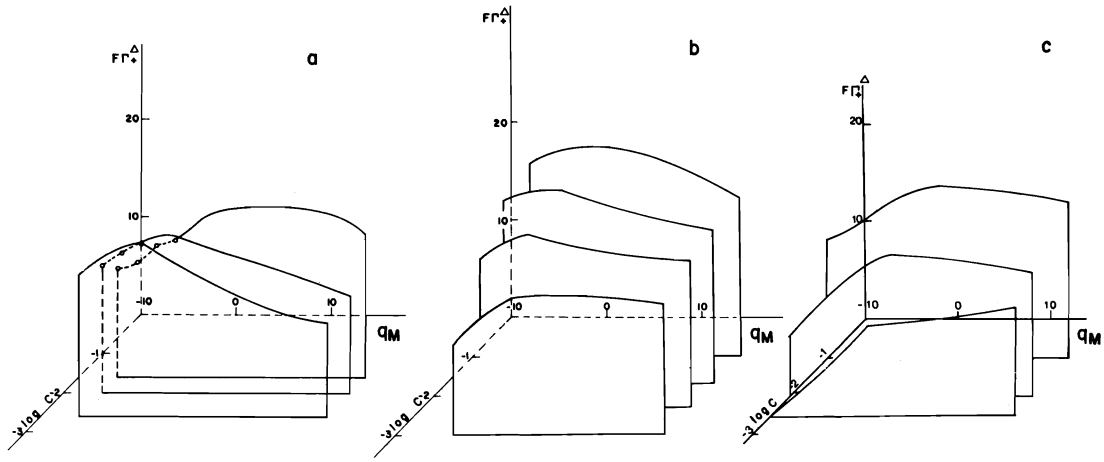

FIG. 15. Excès ionique structural; coordonnées identiques à celles de la fig. 9: (*a*) Bu_4NI, (*b*) Pr_4NI, (*c*) Et_4NI.

différents sels mais par la taille des ions adsorbés en monocouche. (*cf.* tableau 1, réf. 29).

Discussion

Afin d'attribuer des valeurs numériques à l'activité de surface des différents sels, sans toutefois introduire de paramètres arbitraires, il serait utile de pouvoir comparer le comportement dans la double couche avec le comportement en solutions homogènes. Des calculs préliminaires indiquent qu'une telle comparaison s'avère fructueuse. Au point de charge nulle, l'énergie libre d'adsorption peut être attribuée aux interactions soluté–solvant et soluté–soluté (similaires à celles observées en solution concentrée) et aux interactions soluté–électrode (similaires à celles qui régissent pour l'adsorption des espèces neutres). Nous pouvons écrire:

$$\Delta\overline{G}_{ads} = \Delta\overline{G}_{ion-ion} + \Delta\overline{G}_{cation-électrode} + \Delta\overline{G}_{anion-électrode}$$

Nous avons calculé $\Delta G_{ion-ion}$ à partir des données de Wen et de Lindenbaum et de l'expression

$$\overline{G}^{ex} = G^{ex}/m = \nu RT[(1 - \phi) + \ln\gamma]$$

où γ est le coefficient d'activité, ϕ est le coefficient osmotique et ν le nombre d'ions libérés par la dissociation d'un sel de molalité m.

Ces auteurs considèrent que pour des solutions de sels d'ammonium quaternaire $\overline{G}^{ex}$ est essentiellement déterminée par des effets de type Gurney. Gierst *et al.* (30) démontrèrent en 1965 que pour l'adsorption des sels tetraalkyl ammonium les interactions les plus importantes étaient celles entre anions et cations. Il a été également confirmé que la surface de l'électrode à des valeurs de $q_M \simeq -2\ \mu C\ cm^{-2}$ est recouverte par des molécules d'eau orientées d'une façon plus ou moins aléatoire (29). Aux alentours du pcn la surface constitue en quelque sorte un ion hydrophobe ayant un rayon de courbure infiniment grand et une densité de charge infiniment petite.

En conséquence, on pourrait traiter l'interaction non-électrostatique anion-électrode comme étant semblable à l'interaction non coulombienne anion–cation hydrophobe en solution. Cependant ces interactions impliquent, selon des considérations géométriques, environ deux fois le "covolume". L'énergie d'interaction $\Delta\overline{G}_{cation-électrode}$ serait alors donnée par

$$\Delta\overline{G}_{cation-électrode} = \Delta\overline{G}_{ads} - 3\overline{G}^{ex}$$

et devrait varier selon l'aire projeté du cation.

$\Delta\overline{G}_{ads}$ peut être calculé à partir de divers isothermes d'adsorption (31) y compris, au pcn, l'isotherme de Langmuir. A cet effet il est nécessaire de déterminer le taux de recouvrement de la surface, $\theta = \Gamma^{\Delta}/\Gamma^{\Delta}_{max}$ en fonction de la concentration du sel en solution. Γ^{Δ} est obtenu à partir des isothermes d'adsorption (figs. 9, 11, 13 et 15). Γ^{Δ}_{max} dépend de la dimension du cation: nous avons utilisé les valeurs 2.35, 2.20, 2.16 et 1.85 10^{-10} mol cm^{-2} citées ci-dessus. $\overline{G}^{ex}$ peut être calculée en considérant que les co-

Can. J. Chem. Downloaded from www.nrcresearchpress.com by 210.87.254.40 on 09/05/12
For personal use only.

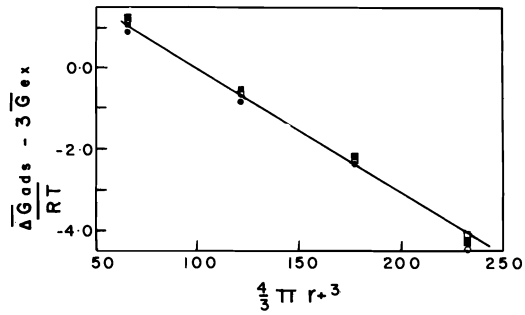

FIG. 16. Energie libre calculée $\Delta\overline{G}_{\text{cation-électrode}}$ en fonction du volume/Å^3 du cation: (○) F^-, (■) Cl^-. (□) Br^-, (●) I^-.

efficients d'activité et les coefficients osmotiques dans la double couche électrique sont les mêmes qu'en solution à concentration équivalente. Il est donc nécessaire de déterminer la concentration locale, Γ^Δ/δ. Pour l'épaisseur effective, δ, nous avons adopté des valeurs $\delta = 2r_+ + \omega$ où "r_+" est le rayon d'après la "Scaled Particle Theory', et "ω" le diamètre d'une molécule de l'eau, c'est-à-dire, 2.76 Å (19, 29). Quoique quelque peu arbitraire, la définition de δ est consistante avec le modèle de Langmuir adopté et l'observation qu'en aucun cas $\Gamma^\Delta{}_{max}$ ne dépasse les valeurs calculées pour le recouvrement de l'électrode par une monocouche de cations. Malheureusement les concentrations locales, même pour $\theta \ll 1$, dépassent souvent les concentrations de solution homogène pour lesquelles des valeurs de $\overline{G}^{ex}$ ont été rapportées. Néanmoins, à $q_M = 0$ pour $\theta = \Gamma/\Gamma_{max} = 0.2$ nous trouvons (fig. 16) une relation linéaire entre $\Delta\overline{G}_{\text{cation-électrode}}$ et le volume du cation. La pente est égale à $1.3kT$ par molécule d'eau déplacée de la surface. Cette valeur numérique est en excellent accord avec $\Delta\overline{G}_{H_2O}$, l'énergie nécessaire pour renverser l'orientation d'une molécule d'eau adsorbée (32). Elle est conforme également à celle calculée à partir des forces imagés, confirmée récemment par Barradas et Sedlak (33).

Bien que nos calculs reflètent plusieurs simplifications concernant la distribution des ions, un nombre suffisant de sels a été examiné afin de pouvoir tirer quelques conclusions générales. Le rapport $\Delta\overline{G}_{\text{cation-électrode}}/\Delta\overline{G}_{H_2O}$ vaut respectivement $5(Bu_4N^+)$, $3(Pr_4N^+)$, $1(Et_4N^+)$ et $-1(Me_4N^+)$. Il est généralement admis que l'ion Bu_4N^+ en solution est entouré d'une couche d'eau plus structurée que l'eau pure, et que la surface de mercure au pcn est recouverte d'une couche de molécules d'eau peu orientées.

Il ne semble pas illogique de supposer que l'adsorption d'un cation volumineux perturbe un certain nombre de molécules d'eau initialement adsorbées à la surface de telle manière qu'elles soient en mesure de solvater à la fois l'ion et l'électrode. Pour les trois premiers cations il y aurait une certaine compatibilité des couches de solvatation, analogue à celle observée en solution entre deux ions hydrophobes. L'adsorption du Me_4N^+ par contre, semble nécessiter une réorientation des molécules d'eau vers l'ion et causer ainsi une perturbation de l'électrode initialement solvatée par sa couche d'hydratation hydrophobe.

Quoique l'analyse de l'isotherme d'adsorption aux différentes charges fasse l'objet d'une communication ultérieure, quelques remarques générales sur la nature des interactions non-électrostatiques dans la région interfaciale nous paraissent utiles en relation avec la fig. 7. Sa présentation, de caractère schématique et empirique, est basée sur les différences $\Gamma^\Delta(q_M) - \Gamma^\Delta(-q_M)$ à diverses charges. La population local des ions dans la région de l'interface accuse un rapport $[R_4N^+]/[X^-] > 1$ pour $q_M < 0$ et $[R_4N^+]/[X^-] < 1$ pour $q_M > 0$. Il est donc évident que dans le premier cas il y a un plus grand nombre d'interactions cation–cation et cation–électrode et que dans le deuxième cas on trouve un plus grand nombre d'interactions de type anion–anion et anion–électrode. Sur le plan qualitatif nous pouvons alors déduire de la coordonnée verticale qu'il y a la prédominance des attractions non-électrostatiques de type $X^- - X^-$ sur celles de type de $R_4N^+ - R_4N^+$ pour les iodures et à un moindre degré pour les bromures. Nous pouvons également conclure que les fluorures accusent une forte répulsion et les chlorures une répulsion beaucoup moins forte.

Il est prématuré de tenter d'interpréter ces tendances par des calculs numériques tant qu'un modèle acceptable de la distribution des ions dans la région interfaciale ne sera pas établi et que des mesures expérimentales des interactions analogues en solution ne deviennent disponibles. Néanmoins le parallélisme est évident et mérite d'être analysé ultérieurement.

Conclusion

L'effet d'Esin Markov, et les valeurs de l'excès

Can. J. Chem. Downloaded from www.nrcresearchpress.com by 210.87.254.40 on 09/05/12
For personal use only.

de surface ionique, de l'énergie d'adsorption et de la pression de surface indiquent que l'activité de surface de seize halogénures de tétraalkyl ammonium, R_4NX, varie dans le sens que présentent les interactions structurales en solution homogène. Nous en concluons que les mêmes forces responsables des variations de l'activité, γ, des sels en solution déterminent la variation de l'excès de surface Γ au E_{pcn}. A priori, il ne semble pas nécessaire de postuler des interactions électrode–soluté particulières ni de limiter les interactions non-électrostatiques à une monocouche recouvrant la surface de l'électrode. Si la couche d'hydratation est compatible avec une hydratation hydrophobe de l'électrode Γ^{Δ} est positif. Si les couches d'hydratation sont non-compatibles et les interactions non coulombiennes entre ions sont non-compatibles Γ^{Δ} est négatif. Si l'une ou l'autre des interactions est répulsive l'effet global dépend de leur importance relative. C'est ainsi qu'on observe sur une surface non-chargée un accroissement monotone de Γ^{Δ} avec la taille de l'anion et avec celle du cation. Les valeurs numériques de Γ^{Δ} s'accordent bien avec des calculs effectués en utilisant l'énergie d'excès trouvé indépendamment en solution homogène à partir des considérations géométriques simples.

Remerciements

Les auteurs sont reconnaissants d'un octroi de recherche du CNRC et d'une bourse d'étude du M.E.Q. qui ont rendu ce travail possible. Nous tenons également à remercier les Drs. Desnoyers et Jolicoeur pour des discussions fructueuses et l'intérêt qu'ils ont porté à ce travail.

1. D. C. Grahame. Chem. Rev. **41**, 441 (1947).
2. R. Payne. J. Electroanal. Chem. **41**, 277 (1973).
3. D. C. Grahame. Z. Electrochem. **59**, 773 (1955).
4. M. A. V. Devanathan et M. S. Fernando. Trans. Faraday Soc. **58**, 368 (1962).
5. H. S. Frank. J. Chem. Phys. **67**, 1554 (1963).
6. G. H. Naficy. Thèse 3e cycle Academie de Montpellier. Montpellier, France. 1972.
7. E. Verdier, G. H. Naficy et P. Vanel. J. Chim. Phys. **1**, 368 (1973).
8. J. Piro, R. Bennes et E. Bou Karam. J. Electroanal. Chem. **57**, 399 (1974).
9. F. M. Kimmerle et H. Ménard. J. Electroanal. Chem. **54**, 101 (1974).
10. J. Kuta et I. Smoler. Coll. Czech. Chem. Commun. **40**, 225 (1975).
11. S. Lakshmanan et S. K. Rangarajan. J. Electroanal. Chem. **27**, 127 (1970).
12. E. Dutkiewicz et R. Parsons. J. Electroanal. Chem. **11**, 100 (1966).
13. H. D. Hurwitz. J. Electroanal. Chem. **10**, 35 (1965).
14. G. J. Hills et R. M. Reeves. J. Electroanal. Chem. **42**, 355 (1973).
15. L. M. Bough et R. Parsons. J. Electroanal. Chem. **58**, 229 (1975).
16. F. M. Kimmerle, H. Ménard, B. E. Conway et H. P. Dhar. Electrochim. Acta, **19**, 883 (1974).
17. P. Delahay. Double layer and electrode kinetics. John Wiley & Sons, Inc. New York 1965.
18. D. M. Mohilner. *Dans* Electroanalytical Chemistry. Vol. I. *Edité par* A. J. Bard. New York. 1966. p. 241.
19. J. E. Desnoyers et C. Jolicoeur. *Dans* Modern aspects of electrochemistry. Vol. 5. *Edité par* J. O'M. Bockris et B. E. Conway. Plenum Press, New York. 1969.
20. B. E. Conway, R. E. Verrall et J. E. Desnoyers. Trans. Faraday Soc. **62**, 2738 (1966).
21. H. Ménard et F. M. Kimmerle. J. Electroanal. Chem. **47**, 375 (1973).
22. S. Lindenbaum et G. G. Boyd. J. Phys. Chem. **68**, 911 (1964).
23. W. Y. Wen, S. Saito et C. M. Lee. J. Phys. Chem. **70**, 1244 (1964).
24. R. G. Barradas, F. M. Kimmerle et E. M. L. Valeriote. J. Pol. Soc. **13**, 30 (1967).
25. J. B. Hayter et R. J. Hunter. J. Electroanal. Chem. **37**, 81 (1972).
26. R. Parsons. *Dans* Modern aspects of electrochemistry. Vol. 1. *Edité par* J. O'M. Bockris. Butterworths, London. 1954. pp. 103–179.
27. I. S. Ramanathan, C. V. Krishnan et H. L. Friedman. J. Solution Chem. **1**, 217 (1972).
28. W. Y. Wen. J. Solution Chem. **2**, 253 (1973).
29. F. M. Kimmerle et H. Ménard. *Dans* Chemistry and physics of aqueous gas solutions. *Edité par* W. A. Adams. The Electrochemical Society, Princeton, New York. 1975. p. 337.
30. L. Gierst, J. Tondeur et E. Nicolas. J. Electroanal. Chem. **10**, 397 (1965).
31. S. Trasatti. J. Electroanal. Chem. **53**, 335 (1974).
32. J. O'M. Bockris, K. Muller, H. Wroblova et Z. Kovac. J. Electroanal. Chim. **10**, 416 (1965).
33. R. G. Barradas et J. M. Sedlak. Electrochimica Acta, **17**, 683 (1972).
34. R. Parsons. Proc. R. Soc. Ser. A, **261**, 79 (1961).

Can. J. Chem. Downloaded from www.nrcresearchpress.com by 210.87.254.40 on 09/05/12
For personal use only.

Metals intercalated in graphite. IV. Intercalation from CCl_4 solution and extraction of intercalated species

JEAN MARC LALANCETTE, LINDA ROY, AND JEANNINE LAFONTAINE

Département de chimie, Université de Sherbrooke, Sherbrooke (Qué.), Canada J1K 2R1

Received March 15, 1976

JEAN MARC LALANCETTE, LINDA ROY, AND JEANNINE LAFONTAINE. Can. J. Chem. **54**, 2505 (1976).

Some chlorides, mainly of transition elements, can be intercalated in graphite from a solution of carbon tetrachloride if their solubility is in the range of 1 to 4 mg/ml in CCl_4, at reflux temperature, in the presence of chlorine.

The rate of extraction of intercalated salts with solvents has been compared to the rate of solution of these salts in the same solvents.

JEAN MARC LALANCETTE, LINDA ROY et JEANNINE LAFONTAINE. Can. J. Chem. **54**, 2505 (1976).

Certains chlorures dérivés principalement des métaux de transition ont pu être insérés dans le graphite, en présence du chlore et à la température de reflux, à partir de leurs solutions dans le tétrachlorure de carbone lorsque leurs solubilités se situaient dans la région 1 à 4 mg/ml de CCl_4.

La vitesse d'extraction des sels insérés par certains solvants a été comparée à la vitesse de dissolution de ces sels dans les mêmes solvants.

A great variety of elements or compounds can be intercalated in graphite (1). These intercalated species can be held by different types of bonding within the lattice of graphite. For example, fluorine, under appropriate experimental conditions, will react with graphitic carbon to give a compound of formula $(C_4F)_x$. In this case, there is a covalent bond formed between graphite and fluorine, the combination is irreversible, and the fluorinated graphite shows no fluorine vapor pressure until the decomposition temperature is reached (2). In other instances, with certain transition metal salts there may be a true coordination bonding between the intercalated salt and the π-electron system of graphite, as shown recently by Volpin (3). In some cases, the bonding between the intercalated species and graphite can be very weak. This situation is well illustrated by the case of bromine intercalates. Bromine can be intercalated in graphite up to a composition of C_8Br. But the larger part of the intercalated bromine can be removed simply by aeration at room temperature (4).

In fact, it can be said that, providing a weak type of bonding between an intercalated salt and graphite and appropriate volatility of the intercalated species exist, there may be an equilibrium between the intercalated state and the vapor state of the intercalated substrate. A similar situation will prevail if the substrate is in solution, as shown by the use of solvent techniques for intercalation (5). This paper, as a part of a study on the chemistry of intercalated metals (6), describes intercalations achieved by means of carbon tetrachloride solutions and indicates interesting aspects of equilibrium between a solvent and an intercalated species.

We have investigated the behavior of several chlorides, known to be intercalated by the standard method of heating a mixture of salt and graphite in an atmosphere of chlorine in order to see if these salts could be intercalated when dissolved in carbon tetrachloride. Results are presented in Table 1. Intercalation can be done with solutions of appropriate salts in CCl_4 if an atmosphere of chlorine is present. Otherwise the intercalation is much slower or absent (7). We interpret this observation as an indication that carbon tetrachloride is not able to promote the opening of the lattice and that the small amount of chlorine present in the refluxing carbon tetrachloride, by itself or combined with the salt, is sufficient to allow the intercalation to proceed.

In this study, we have used a graphite that was 20 mesh or finer. Hooley (5) has shown the

Can. J. Chem. Downloaded from www.nrcresearchpress.com by 210.87.254.42 on 09/05/12
For personal use only.

Can. J. Chem. Downloaded from www.nrcresearchpress.com by 210.87.254.42 on 09/05/12
For personal use only.

TABLE 1. Intercalation of chlorides in graphite from carbon tetrachloride solutions

Starting chloride	Duration of reflux	Solubility[b] (mg/ml) (T °C)	Intercalation (%)	Analysis of intercalates: % by weight of metal[c]	Analysis of intercalates: % by weight of chlorine
$AlCl_3$	3	4.5 (61)	40	8.0	32.0
$AlCl_3$[a]	3	—	<1	—	—
$FeCl_3$	24	5.3 (63)	20	6.8	13.2
$NiCl_2$	72	3.6 (65)	24.5	11.0	13.5
$PtCl_4$	24	1.3 (67)	14	8.1	5.9
$PdCl_2$	48	1.5 (64)	3.7	2.2	1.5
$CuCl_2$	48	2.0 (68)	22	10.5	11.5
$RhCl_3$	70	1.6 (71)	1.2	0.6	0.6
UCl_4	72	1.3 (63)	10	6.2	3.9
$MoCl_5$	48	14.5 (63)	<1	—	—
WCl_6	48	30.4 (—)	<1	—	—
$FeCl_3$ and $AlCl_3$	3	—	9.5 ($AlCl_3$)[d] 11 ($FeCl_3$)	—	—
$FeCl_3$ and $AlCl_3$	24	—	9.4 ($AlCl_3$)[d] 12 ($FeCl_3$)	—	—

[a]Absence of chlorine.
[b]Solubility of the salt at temperature (T) in CCl_4 saturated with Cl_2.
[c]Iron and aluminum have been determined by gravimetry. All the other metals have been determined by atomic absorption, using a Varian instrument, model AA-6.
[d]Determined by the ratio of metals in the intercalate.

relation between the size of particles and intercalation phenomena with graphite. With this size of particles, we have observed intercalation with either standard methods or the solvent method.

We have noted that a very important factor concerning the ability of a carbon tetrachloride solution to promote intercalation is the solubility of the salt in this solvent saturated with chlorine, at reflux temperature. The intercalation will proceed if the salt has a low solubility in the halogenated solvent. With the salts that we have tried, too high a solubility or no solubility led to no intercalation. With the experimental conditions that we have used, intercalation proceeded well with solubilities in the range of 1 to 5 mg/ml. With higher values there was very little intercalation. It is also to be noted that with the mixture $AlCl_3$–$FeCl_3$ dissolved in carbon tetrachloride, both components of the mixture were intercalated simultaneously.

The equilibrium of an intercalated salt which is not very strongly bonded to graphite with a solvent can lead to the complete extraction of the salt from graphite, if the salt is soluble in the solvent and if the solvent is not saturated with the intercalated salt. However, under similar conditions of temperature and concentration, the rate of extraction of an intercalated salt from the lattice of graphite is much slower than the rate of solution of the same salt in a free state, present on the surface of graphite for example. This difference in the rate of extraction *vs.* rate of solution can be used to remove excess nonintercalated salt from a re-

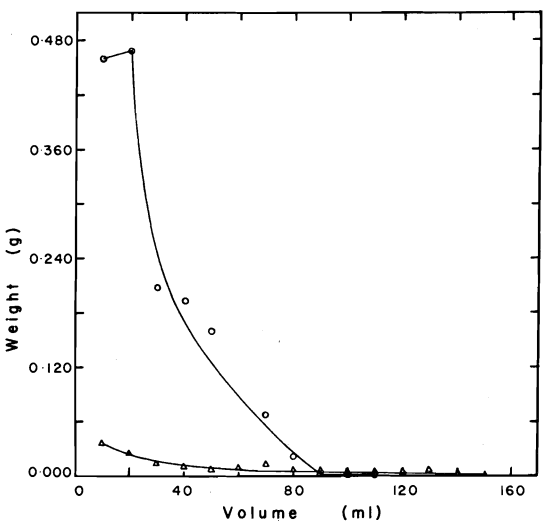

FIG. 1. Weight of $AlCl_3$ eluted by anhydrous tetrahydrofuran from a 10% intercalate of $AlCl_3$ in graphite (△) and from a 10% mixture of $AlCl_3$ with graphite (○).

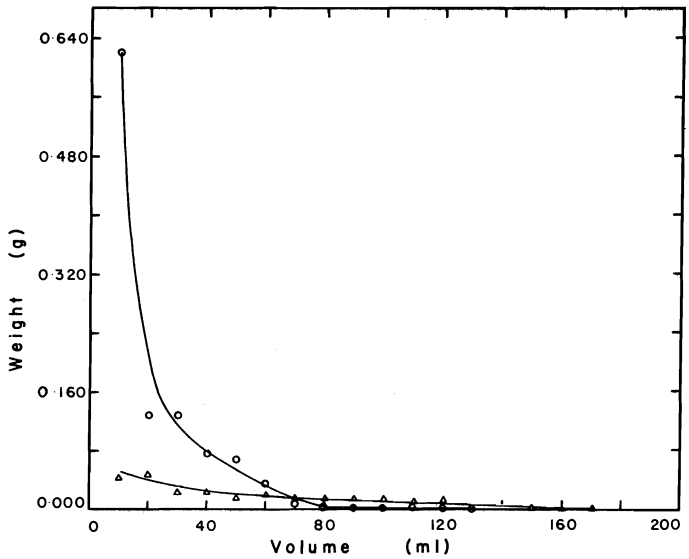

FIG. 2. Weight of $FeCl_3$ eluted by 1% hydrochloric acid from a 15% intercalate of $FeCl_3$ in graphite (△) and from a 15% mixture of $FeCl_3$ with graphite (○).

action mixture if the rate of extraction of a given intercalated salt with a given solvent is known. In fact, by measuring the rate of extraction, it is possible to estimate, in a first approximation, if a salt is intercalated or not. Such a technique is definitely not a substitute to formal X-ray diffraction or DTA analysis, but offers interesting possibilities for a rapid preliminary evaluation of a given intercalate. Typical curves of extractions and solutions are presented in Fig. 1 and Fig. 2 for aluminum chloride and ferric chloride.

Experimental

(1) Intercalation of $AlCl_3$ from a CCl_4 Solution

In a three-necked flask of 500 ml, 20.0 g of well-dried graphite was suspended in 250 ml of CCl_4 dried over alumina (Woehm, grade I). Graphite was of spectroscopic grade and ground to pass through a 20 mesh sieve. Then 8.0 g of anhydrous aluminum chloride (Fisher, Reagent grade) was added and the reaction mixture, under good stirring, was heated to reflux temperature, a slow stream of chlorine being bubbled through the boiling CCl_4 (5 ml/min). Chlorine was Matheson Research grade 99.96% Cl_2 and was used without purification. After a reflux of 3 h, the system was filtered and the residue washed with 500 ml of boiling CCl_4. Any nonintercalated $AlCl_3$ was then removed by heating the intercalate to constant weight under 1.0 torr at 198 °C for 18 h. Under such conditions, any nonintercalated aluminum chloride was eliminated by sublimation. The intercalated aluminum chloride was analyzed as reported before (*6b*), for aluminum and chlorine.

A similar technique was used for other intercalations reported in Table 1. With nonvolatile salts, the amount of salt under experiment was adjusted to remain below the maximum concentration that could be dissolved in the CCl_4 present. The presence of intercalation was verified by differential thermal analysis and comparison of these measurements with a similar analysis on samples prepared by heating the salts and graphite in an atmosphere of chlorine. For the determination of the intercalated metals, the intercalates were digested in concentrated sulfuric acid, followed by treatment of the filtrate by aqua regia and determination of the concentration of metals by atomic absorption. The results of these analyses are presented in Table 1.

(2) Rate of Extraction of Intercalated Salts and Salts Mixed with Graphite

A 10 g sample of a 10% intercalate of aluminum chloride in graphite was placed in a 100 ml burette used as a column. Anhydrous tetrahydrofuran was flowed through the sample at a rate of 30 ml/h. Aliquots were taken at every 10 ml. A plot was made of the weight of $AlCl_3$ extracted against volume of solvent. This gave the curve indicated by the triangles in Fig. 1. A similar experiment was made using a mixture of $AlCl_3$, and graphite instead of intercalate, the concentration of $AlCl_3$ in the mixture being the same as the concentration of $AlCl_3$ in the intercalate. This led to the curve bearing the circular points in Fig. 1. A similar pattern was observed using other concentrations of $AlCl_3$ and $FeCl_3$ intercalates or mixtures, the extraction from the mixture being much more rapid than the extraction from the intercalate. Elutions with ethyl ether, or in the case of $FeCl_3$ with 1% HCl, also gave a similar pattern as shown in Fig. 2. In the case reported in Fig. 1, $AlCl_3$ was recovered as an etherate of aluminum chloride. The amount of aluminum recovered was determined as aluminum

Can. J. Chem. Downloaded from www.nrcresearchpress.com by 210.87.254.42 on 09/05/12
For personal use only.

oxide by hydrolysis and calcination at high temperature. A similar pattern was observed with $FeCl_3$ (Fig. 2), the etherate being hydrolyzed and the amount of metal recovered determined as Fe_2O_3.

Acknowledgment

The authors thank the National Research Council of Canada for financial assistance.

1. W. RUDORFF. Z. Anorg. Chem. **245**, 383 (1941).
2. M. E. VOLPIN, YU. N. NOVIKOV, N. D. LAPKINA, V. I. KASATOCHKIN, YU. T. STRUCHKOV, M. E. KAZAKOV, R. A. STUKAN, V. A. POVITSKIJ, UY. S. DARIMOV, and A. V. ZVARIKINA. J. Am. Chem. Soc. **97**, 3366 (1975).
3. W. RUDORFF and G. RUDORFF. Chem. Ber. **80**, 413 (1947).
4. L. C. F. BLACKMAN, J. F. MATHEWS, and A. R. UBBELOHDE. Proc. Roy. Soc. London, **258**, 339 (1960).
5. J. G. HOOLEY. Carbon, **10**, 155 (1972).
6. (*a*) J. M. LALANCETTE, G. ROLLIN, and J. P. DUMAS. Can. J. Chem. **50**, 3058 (1972); (*b*) J. M. LALANCETTE, M. J. FOURNIER-BREAULT, and R. THIFFAULT. Can. J. Chem. **52**, 589 (1974); (*c*) J. M. LALANCETTE and R. ROUSSEL. Can. J. Chem. **54**, 2110 (1976).
7. M. L. CZURUS and G. R. HENNIG. J. Am. Chem. Soc. **79**, 1051 (1957).

Can. J. Chem. Downloaded from www.nrcresearchpress.com by 210.87.254.42 on 09/05/12
For personal use only.

Phase transformation studies on anthranilic acid by thermal analysis, infrared absorption, and X-ray diffraction methods

KRISHNAN RAJESHWAR AND ETALO A. SECCO[1]

Chemistry Department, St. Francis Xavier University, Antigonish, N.S., Canada B0H 1C0

Received February 27, 1976

KRISHNAN RAJESHWAR and ETALO A. SECCO. Can. J. Chem. **54**, 2509 (1976).

The kinetic, structural, and thermodynamic aspects of the phase transition, orthorhombic I → orthorhombic II, in anthranilic acid (o-$C_6H_4NH_2COOH$) were investigated by thermal analysis, infrared absorption, and X-ray diffraction methods.

KRISHNAN RAJESHWAR et ETALO A. SECCO. Can. J. Chem. **54**, 2509 (1976).

On a étudié, par des méthodes d'analyse thermique, d'absorption infrarouge et de diffraction à rayon-X, les aspects cinétiques, structuraux et thermodynamiques de la transition de phase orthorhombique I → orthorhombique II pour l'acide anthranilique (o-$C_6H_4NH_2COOH$).

[Traduit par le journal]

Can. J. Chem. Downloaded from www.nrcresearchpress.com by 210.87.254.42 on 09/05/12
For personal use only.

Introduction

Anthranilic acid (o-$C_6H_4NH_2COOH$) has been shown to exist in three polymorphic forms (1). Early crystal-growth experiments (2) indicated the crystal form to be highly sensitive to variations in crystallization conditions. The structures of the three polymorphs have been described (1, 3) (two orthorhombic and a third monoclinic) and their infrared spectra have also been reported (4–6).

The stable room-temperature phase, orthorhombic I transforms to an orthorhombic II modification (7) at 100 °C; details on the nature of this transition are not available in the literature. The purpose of this study was, therefore, to examine the kinetic, structural, and thermodynamic aspects of this phase transition using thermal analysis, infrared absorption, and X-ray diffraction methods.

Experimental

The source of anthranilic acid used in this study was Eastman Organic Chemicals, Rochester, N.Y. (recrystallized grade, 99% purity). X-Ray diffraction patterns were obtained on a Norelco diffractometer Model X-86 using CuK_α radiation (8). Infrared spectra were recorded on a Perkin-Elmer Model 180 spectrophotometer using both the mull and KBr disc matrix techniques.

DTA traces were obtained on a duPont 990 Thermal Analyzer in a flowing N_2 (ultrapure) atmosphere using ignited Al_2O_3 as reference material. The precision of a transition temperature measurement was better than ±1 °C. The enthalpy of transformation was evaluated with the DSC accessory to the 990 DTA module using stearic acid fusion as a standard. The anthranilic acid sample, in all cases, was polycrystalline and since particle size affects the transition temperature (9), comparative DTA traces were always recorded on samples of the same particle size. Thermal gradients across the samples were minimized by a small constant mass (~18 mg) and care was taken to ensure a uniform sample distribution.

Pre-compression of the sample was done on a hydraulic pellet press fitted with a calibrated gauge and a stainless steel die. The pelleting procedure and sample preparation after pre-treatment is described elsewhere (10).

Results and Discussion

Crystal Structure Analysis

The X-ray diffraction pattern obtained for the untreated supplier's sample was indexed to an orthorhombic unit cell with dimensions a_0 = 16.05 Å, b_0 = 11.65 Å, and c_0 = 7.20 Å; the observed $\sin^2\theta$ and related parameter values (Table 1) are placed with the Depository of Unpublished Data.[2] The compound fits the orthorhombic modification (3) obtained by evaporation of a saturated alcoholic solution of anthranilic acid at room temperature. The DTA heating trace of this sample exhibits an asymmetric sharp endothermic peak at 99 °C.

The X-ray diffraction pattern at room temperature of the preannealed sample is distinctly different. The pattern was indexed to an orthorhombic unit cell with dimensions a_0 = 12.80 Å, b_0 = 10.78 Å, and c_0 = 9.40 Å; the observed $\sin^2\theta$ and related parameter

[1]To whom correspondence should be addressed.

[2]Complete set of data may be obtained at a nominal charge, upon request, from the Depository of Unpublished Data, CISTI, National Research Council of Canada, Ottawa, Canada K1A 0S2.

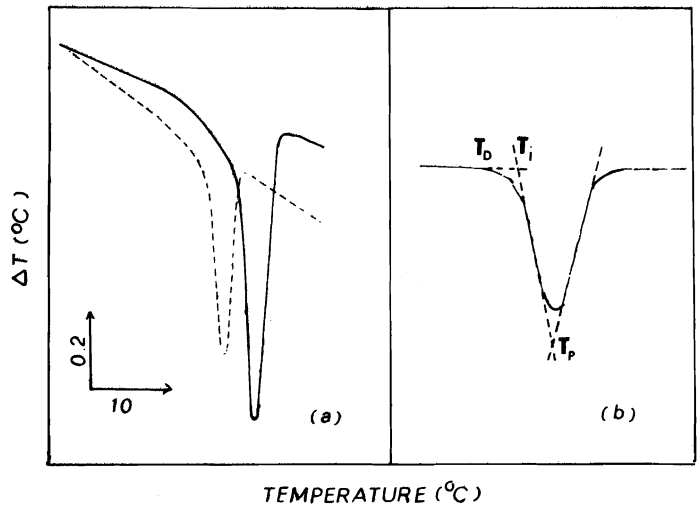

FIG. 1. Typical DTA traces on anthranilic acid; (*a*) —, heating rate 2 °C/min. ---, heating rate 0.5 °C/min. (*b*) Identification of endotherm characteristic temperatures.

values (Table 2) are placed with the Depository of Unpublished Data.[2] The DTA heating trace of the preannealed sample did not reveal the expected endotherm at 99 °C.

The endotherm at 99 °C is interpreted to represent the orthorhombic I → orthorhombic II transformation in anthranilic acid. The orthorhombic II persists as a metastable phase on cooling to room temperature; the metastable phase reverts to the stable room temperature orthorhombic I modification after one month as confirmed by its X-ray diffraction pattern.

The infrared spectra reveal a shift in the $\nu_s(NH_2)$ and $\nu_a(NH_2)$ frequencies from 3230 and 3320 cm^{-1} for phase I to 3360 and 3480 cm^{-1} for phase II respectively. Phase II ν_s and ν_a frequencies are within 10 cm^{-1} of the NH_2 frequencies recorded for p-$C_6H_4NH_2COOH$. The latter exhibits no solid phase transformation and the correlation strongly suggests a rupture of intramolecular hydrogen bonding involving the NH_2 species in the I → II transition.

Thermodynamic Properties

The transformation enthalpy ΔH_t was determined as 1230 ± 60 cal/mol yielding the ΔS_t of 3.35 ± 0.15 cal deg^{-1} mol^{-1}. The molar volume of orthorhombic I is calculated as 101.10 cm^3, with eight molecules per unit cell, and the molar volume of orthorhombic II is 97.83 cm^3; $-\Delta V$ of 3.27 cm^3 mol^{-1} is associated with the I → II transformation. The dT/dP term in the Clausius–Clapeyron equation is negative and a pressure increase would, therefore, shift the I → II transformation to lower temperatures.

TABLE 3. Specific temperatures and activation energies associated with polymorphic transformation

Heating rate (°C/min)	T_d (°C)	T_i (°C)	T_p (°C)	E_a (kcal/mol)
10	82	87.5	99	92
5	82	87.5	98	92
2	83	93	95	83
1	83	91.5	93.5	101
0.5	84	90	91.5	92
				Ave. 92

Phase Transformation Kinetics

Typical DTA heating traces for various heating rates are shown in Fig. 1. The specific T values, the peak temperature T_p, the departure temperature T_d, and the intersection temperature T_i were evaluated as indicated and are presented in Table 3.

The activation energy, E_a, was calculated from the equation (11)

$$\ln \Delta t = C - \frac{E_a}{RT}$$

Can. J. Chem. Downloaded from www.nrcresearchpress.com by 210.87.254.42 on 09/05/12
For personal use only.

Can. J. Chem. Downloaded from www.nrcresearchpress.com by 210.87.254.42 on 09/05/12
For personal use only.

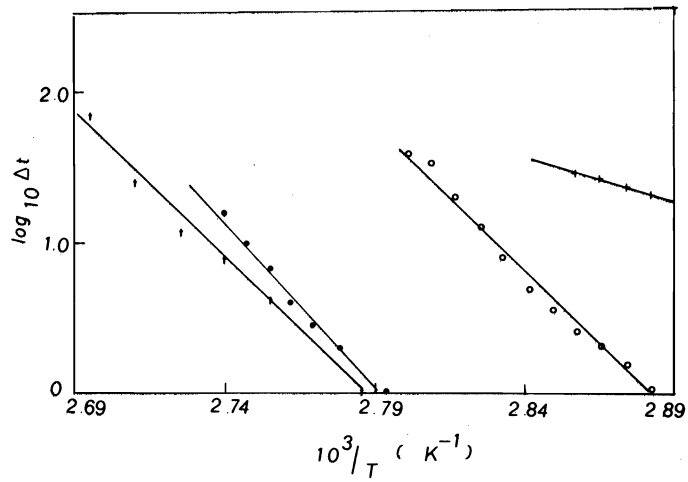

FIG. 2. Representative Arrhenius plots for I → II transformation for heating rates at 10 °C/min (-†-†-†) and 1 °C/min (·····) on uncompressed sample; also on sample pre-compressed at 2500 kg/cm² (-○-○-○) and 25 000 kg/cm² (-+-+-+) with heating rate at 5 °C/min.

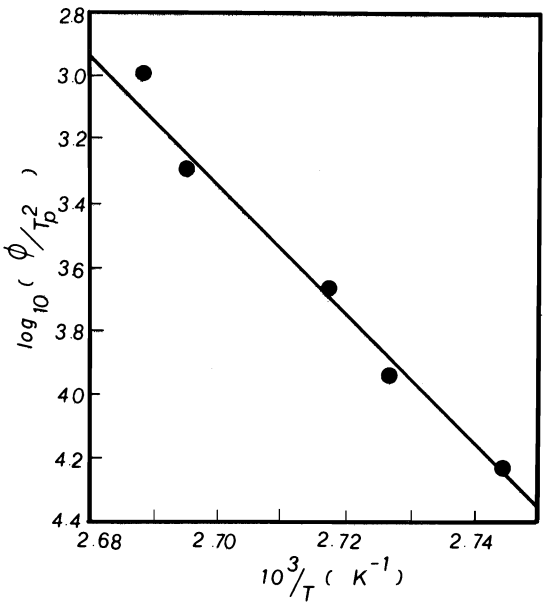

FIG. 3. Plot of log ϕ/T_p^2 *vs.* $1/T$ K.

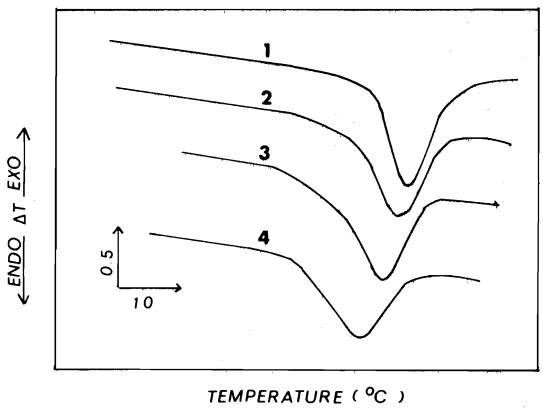

FIG. 4. Effect of sample pre-compression on endotherm profile and characteristic temperatures, curve *1*, 2 500 kg/cm², curve *2*, 5 000 kg/cm², curve *3*, 10 000 kg/cm², curve *4*, 25 000 kg/cm².

where Δt is the peak height at a specific temperature T and C is a constant. Typical linear plots of log Δt *vs.* $1/T$ (K)$^{-1}$ are given in Fig. 2; the slope of the linear plot yields the activation energy E_a whose values are tabulated in Table 3. Caution must be exercised in assessing the values of E_a obtained from dynamic methods of analysis since these values may vary by $\pm 20\%$ with parallel evaluations by isothermal methods. In spite of this discrepancy, it was, nevertheless, worthwhile to make an internal assessment of E_a values in a related series of experiments. The consistent linear Arrhenius plots in Fig. 2 and reproducible E_a values in Table 3 suggest that meaningful E_a values can be extracted from this method of analysis.

The E_a was also evaluated by the method (12) of plotting log ϕ/T_p^2 *vs.* $1/T$(K)$^{-1}$, where T_p is the peak temperature for the specific heating rate ϕ. The plot yields a straight line, Fig. 3, whose slope corresponds to 92 kcal/mol. The reproducible value of 92 kcal/mol obtained by

Can. J. Chem. Downloaded from www.nrcresearchpress.com by 210.87.254.42 on 09/05/12
For personal use only.

TABLE 4. Specific temperatures, activation energies and slope ratios associated with polymorphic transformation*

Pre-compressed pressure (kg/cm²)	T_d (°C)	T_i (°C)	T_p (°C)	E_a (kcal/mol)	Slope ratio
0	82	87.5	98	92	0.62
2 500	74	80	85	92	1.08
5 000	69	76.5	84	54	1.11
10 000	66	73	82	41	1.28
15 000	66	72	81	37	1.26
20 000	66	69	81	41	1.60
25 000	65	67	78.5	32	1.35

*Heating rate 5 °C/min.

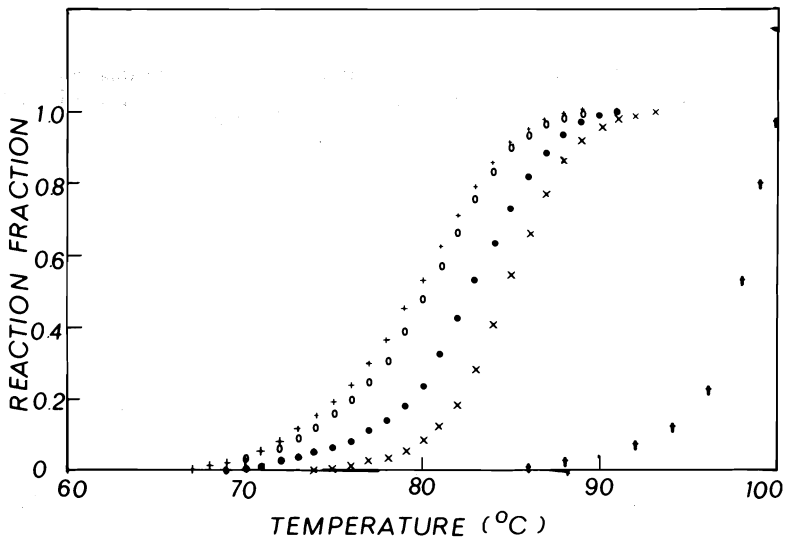

FIG. 5. Effect of sample pre-compression on the transformation rate †, uncompressed; ×, 2 500 kg/cm²; ●, 5 000 kg/cm²; ○ 10 000 kg/cm²; +, 15 000 kg/cm².

two independent analytical methods establishes a high confidence index for E_a.

The effect of pressure pretreatment on transformation was also investigated; the DTA heating curves at various pressures are given in Fig. 4. The shift in peak temperature and variation in peak profile are evident. The effect of pressure on T_p values, E_a values and the symmetries of the DTA peaks as measured by the slope ratios (13) are tabulated in Table 4. The trend in parameter values listed in Table 4 reveals an increase in the slope ratios and a decrease in T_p and E_a with increasing pre-compression pressure values. The reaction fraction *vs.* temperature is plotted in Fig. 5 for various pressure pretreatments of anthranilic acid followed under constant heating rate conditions; the reaction fraction is the ratio of the DTA peak area at a specific temperature to the total peak area. The enhanced reaction rate dependence on pressure is consistent with parallel behavior observed in phase transformation and thermal decomposition rates (14–16).

A simplified model of the I → II orthorhombic phase transformation of anthranilic acid is visualized as a rupture of intramolecular hydrogen bonding, most likely —N—H ··· O=C—. The shift in ν_s and ν_a frequencies to higher values by 160 cm^{-1} and the ΔH_t value of 1.2 kcal are consistent with the model. The enthalpy of transition is assigned to the net contribution of

the intramolecular hydrogen-bond energy and van der Waals energy associated with the transformation.

The direct dependence of the transformation rate on pressure pretreatment is correlated with increased stresses within the solid. Such stresses are expected to enhance the generation of nucleation sites required for the transformation reaction.

Acknowledgments

Grateful acknowledgment is made to the National Research Council of Canada and the University Council for Research for financial support of this research program, and to Dr. M. Natarajan for suggesting the topic for study.

1. W. C. McCrone, J. Whitney, and I. Corvin. Anal. Chem. **21**, 1016 (1949).
2. A. F. Wells. Phil. Mag. (7) **37**, 184 (1946).
3. G. S. R. Krishnamurthi. Indian J. Phys. **31**, 611 (1957).
4. A. A. Ebert, Jr. and H. B. Gottlieb. J. Am. Chem. Soc. **74**, 2806 (1952).
5. A. Theoret. Spectrochim. Acta, **27A**, 11 (1971).
6. D. Hadzi and L. Premru. Bull. Sci. Fac. Chim. Ind. Bologna, **18**, 148 (1960).
7. C. J. Brown. Proc. Roy. Soc. A**302**, 185 (1968).
8. E. A. Secco. Can. J. Chem. **42**, 2143 (1964).
9. M. Natarajan, A. R. Das, and C. N. R. Rao. Trans. Faraday Soc. **65**, 3081 (1969).
10. K. Rajeshwar and V. R. Pai Verneker. J. Solid State Chem. **17**, 27 (1976).
11. G. O. Piloyan, I. D. Ryabchikov, and O. S. Novikova. Nature, **212**, 1229 (1966).
12. W. W. Wendlandt. J. Chem. Educ. **38**, 571 (1961); H. E. Kissinger. Anal. Chem. **29**, 1702 (1957).
13. W. J. Smothers and Yao Chiang. Handbook of differential thermal analysis. Chemical Publishing Co. Inc., New York, 1966. p. 57.
14. A. F. Boyer. Bull. Soc. Fr. Mineral. **77**, 1116 (1954); C. A. **49**:3740; R. J. W. McLaughlin. Am. J. Sci. **252**, 555 (1954).
15. J. H. Burns and M. A. Bredig. J. Chem. Phys. **25**, 1281 (1956); J. Kubo, M. Kato, Y. Mitarai, T. Takahashi, and K. Ohkura. Kogyo-Kagahu Zasshi, **66**, 318 (1963).
16. K. Rajeshwar and V. R. Pai Verneker. J. Phys. Chem. Solids, **37**, 63 (1976).

Can. J. Chem. Downloaded from www.nrcresearchpress.com by 210.87.254.42 on 09/05/12
For personal use only.

Can. J. Chem. Downloaded from www.nrcresearchpress.com by 210.87.254.6 on 09/05/12
For personal use only.

Redox potentials of metal phthalocyanines in non-aqueous media

A. B. P. LEVER AND J. P. WILSHIRE

Department of Chemistry, York University, 4700 Keele Street, Downsview, Ont., Canada M3J 1P3

Received April 21, 1976

A. B. P. LEVER and J. P. WILSHIRE. Can. J. Chem. **54**, 2514 (1976).

A study of the redox potentials of a range of metal phthalocyanines in non-aqueous media compared with analogous data for some porphyrin complexes provides evidence for extensive back donation in metallophthalocyanines. The potentials for some couples are exceedingly sensitive to axial ligation. It is suggested that this sensitivity may be used to 'tune' a redox couple for a specific purpose such as designing a reversible oxygen breathing system.

A. B. P. LEVER et J. P. WILSHIRE. Can. J. Chem. **54**, 2514 (1976).

Une étude des potentiels redox d'une série de métallophtalocyanines en milieu non-aqueux comparée avec des données analogues pour certains complexes de porphyrines amène l'évidence d'une forte rétrodonation dans les métallophtalocyanines. Les potentiels pour certains couples sont excessivement sensibles à la coordination axiale. Il est suggéré que cette sensibilité peut être utilisée pour adapter un couple redox à un but spécifique tel que l'élaboration d'un système réversible de respiration d'oxygène.

[Traduit par le journal]

Redox processes play a critical role in living systems and frequently involve metalloporphyrins (1). Fairly subtle biological events can influence electron transfer chains by modifying the redox couples of their cytochrome components (*e.g.* ref. 2). There is a gross understanding of how variation of solvent (3) (or environment (4)) and of axial ligation (5) can affect redox couples, but many fine details remain to be elucidated. The ability to bind molecular oxygen is also related to the redox couple but in an ill-defined way. The phthalocyanines represent a class of compounds of similar structure (6) to the porphyrins, but whose redox characteristics, as will be demonstrated here, exhibit greater sensitivity towards the factors mentioned above. They may be conveniently used as a probe to gain a more detailed understanding of the electronic processes involved.

The results of this study are surveyed in this communication. Details of the electrode processes, electron transfer rates, etc. will be presented elsewhere (7).

Experimental

Cyclic voltammetric data were obtained with a McKee-Pedersen modular electronic electrochemical system. Solvents and carrier electrolytes were purified by standard techniques to electrochemical purity (1, 8, 9). Mid-point potentials reported in Table 1 are averages obtained over a series of scan rates from 0.005–100 V/s, and over several different runs. The mean deviation from this average is small (less than 5 mV). A three-electrode configuration was employed using platinum wires as working and auxiliary electrodes and an sce as reference. The sce was separated from the solution by a double bridge containing saturated KCl adjacent to the sce, and the solvent and carrier adjacent to the solution.

Results

Representative data presented in Table 1 emphasize iron and manganese because of their intrinsic interest and because they have been comparatively neglected in previous studies (10, 11). Also included, for comparative purposes, are data for some analogous porphyrin complexes. Certain conclusions may be drawn.

(*i*) Chromium(II) phthalocyanine (low spin in pyridine) is exceptionally more stable towards oxidation than a chromium porphyrin analog.

(*ii*) Manganese(II) phthalocyanine (low spin) is significantly more stable towards oxidation to the trivalent state than (high spin) porphyrin analogs. The redox couples of manganese phthalocyanine do not depend greatly upon either solvent or counter ion (carrier).

(*iii*) Low spin iron(II) phthalocyanine, *i.e.* dissolved in DMSO or particularly in pyridine, is much more resistant towards oxidation than is

Can. J. Chem. Downloaded from www.nrcresearchpress.com by 210.87.254.6 on 09/05/12
For personal use only.

TABLE 1. Redox couples for metallophthalocyanines and metalloporphyrins

Complex	Solvent/carrier	M(III)/M(II) (V)	M(II)/M(I)[a] or M(II)/M(II)L^{-}[b] (V)	Ref.
Chromium				
OEP	DMSO/ClO_4^-	−1.14	−1.35[b]	19
Pc	Py/ClO_4	0.52		tw
Manganese				
TPP(Cl)	(hs) Py/ClO_4^-	−0.32		tw
OEP(OH)	(hs) DMSO/ClO_4^-	−0.42	−1.6	19
Pc	(ls) Py/ClO_4^-	0.01	−0.77	tw
	DMSO/ClO_4^-	−0.08		tw
	DMSO/Br^-	−0.09	−0.73	tw
	DMSO/Cl^-	−0.13	−0.86	tw
	DMF/ClO_4^-	−0.14		tw
Iron				
TPP(Cl)	(hs) DMF/ClO_4^-	−0.196	−1.029	20
$(IM)_2$TPP(Cl)	(ls) DMF/ClO_4^-	−0.115	−1.201	20
PIX(Cl)	(hs) DMF/ClO_4^-	−0.307	−1.163	20
$(his)_2$PIX(Cl)	(ls) DMF/ClO_4^-	−0.300	−1.31	20
Pc	(sq) Clnap/ClO_4	0.19	nr	10
	(sq) DMF/ClO_4^-	0.39	−0.56	tw

Complex	Solvent/carrier	M(III)/M(II) or M(II)L^+/M(II)[c] (V)	M(II)/M(I)[a] or M(II)/M(II)L^-[b] (V)	Ref.
Iron	(sq) DMF/Cl	0.01	−0.50	tw
	(ls) Py/ClO_4^-	0.70	−1.12[a]	tw
	(ls) DMSO/ClO_4^-	0.47	−0.77	tw
	(ls) DMSO/Br^-	0.42	−0.70	tw
	(ls) DMSO/Cl^-	0.26	−0.72	tw
Cobalt				
TPP	(ls) DMSO/ClO_4^-	0.06	−0.85[a]	21
	(sq) CH_2Cl_2/ClO_4^-	0.75	nr	21
	(ls) DMSO/Py/ClO_4^-	−0.26	−0.99[a]	21
Pc	(sq) ClNap/ClO_4^-	0.77	nr	10
	(ls) Py/ClO_4^-	0.22	−0.615	tw
Zinc				
TPP	PhCN/ClO_4^-	0.79[c]	nr	10
	DMSO/ClO_4^-	nr	−1.31[b]	22
Pc	Py/ClO_4^-	0.68[c]	−0.89[b]	tw
	Clnap/ClO_4^-	0.68[c]	nr	10

NOTES: The carriers are generally tetraethyl- or tetrabutylammonium salts. The solvents are: Py = pyridine, DMSO = dimethylsulfoxide, DMF = dimethylformamide, Clnap = 1-chloronaphthalene, PhCN = benzonitrile; referring to the divalent species, ls = low spin, hs = high spin, sq = square; for the ligands, TPP = tetraphenylporphyrin, OEP = octaethylporphyrin, Pc = phthalocyanine, PIX = protoporphyrin IX; nr = not recorded, ni = not identified. The identification of the first reduction as reduction of ligand or metal has not always been unequivocally determined. Im = imidazole, his = histidine, tw = this work. Examination of the ferrocinium/ferrocene couple shows that the junction potentials do not vary much among the above solvent/carrier systems.

intermediate spin ($S = 1$) square planar iron(II) phthalocyanine, *i.e.* dissolved in chloronaphthalene. The Fe(III)Pc/Fe(II)Pc couple is influenced both by solvent and counter ion with ease of oxidation increasing with the expected stabilisation of the iron(III) state, in the sequence $Cl^- > Br^- > ClO_4^-$. The Fe(II)Pc/Fe(I)Pc couple is sensitive to solvent, much more so than Mn(II)Pc/Mn(II)Pc$^-$, but insensitive, as would be expected, to counter ion. Porphyrin redox potentials for iron are relatively insensitive to the spin state of the metal except when unusual ligands such as CO (5) are employed.

(*iv*) Square planar cobalt(II) porphyrins are much more resistant to oxidation than low spin octahedral cobalt(II) porphyrins in accord with

Can. J. Chem. Downloaded from www.nrcresearchpress.com by 210.87.254.6 on 09/05/12
For personal use only.

simple cobalt(II) chemistry and conventional ligand field concepts. Cobalt(II) phthalocyanine behaves in a very similar fashion though the low spin octahedral form (in pyridine) is more stable in the divalent state relative to the porphyrins.

(*v*) Oxidation of zinc(II) phthalocyanine involves formation of a phthalocyanine radical cation (12, 13) and the potential is comparable to that for the porphyrin analogs. Reduction to the anion radical, however, is much more facile in the phthalocyanine series.

Porphyrins are known to be strong σ donors. They may be π acceptors or donors depending upon the metal (14) but their overall π capability is minimal. In agreement their ligand field strength is relatively low for a macrocyclic ligand; many of their metal complexes are high spin. Mild bases will deprotonate phthalocyanines (15) but not porphyrins, implying that the former are weaker σ donors than the latter. The redox data presented here provide compelling evidence that phthalocyanines are exceptionally good π acceptors. The considerable stabilisation of low spin iron(II) (t_{2g}^6) and chromium(II) (t_{2g}^4) must be associated with considerable π back donation into the phthalocyanine ring. The ability to oxidise PcFe(II) lies in the sequence DMF > DMSO > pyridine, which is the order of donicity (16) of the axial solvent ligand, enhancing π back donation. Because of the extra stability of the PcFe(II) state with the most strongly donating solvents, the ability to reduce to PcFe(I) will follow the *reverse* sequence of solvents as is evident in Table 1. This results in the spectacular existence range for PcFe(II) in pyridine of 1.82 V, compared with less than a volt for DMF. Square planar Fe(II)Pc, with only two electrons in orbitals of appropriate π symmetry (17), is much less stabilised. Furthermore the comparative ease of reduction to the Pc^- state illustrates the greater acceptor character of the phthalocyanines, as does the fact that they are necessarily high ligand field molecules in that *all* their metal complexes are low spin, where the distinction can be drawn. The stabilisation of cobalt(II) is less dramatic because the electron which is lost is of high energy (σ^*, z^2) and a low spin (t_{2g}^6) configuration is generated. It is clear that variation of solvent and counter ion permits 'tuning' of the Fe(III)Pc/Fe(II)Pc couple over a comparatively wide range (Table 1). The Cr(III)Pc/Cr(II)Pc couple can be similarly tuned (7). Since the ability to bind molecular oxygen depends, at least in part, on the redox potential (18) this procedure permits the design of systems capable of reversibly binding oxygen. Whilst it seems that the redox potentials of iron porphyrins are less sensitive to the environment than those of iron phthalocyanine, dramatic changes can still be observed (23). Thus the 'tuning' mechanism may have a biological role through, for example, protein bound groups moving closer to, and further away from, the metal ion, with conformational change.

Acknowledgments

We are indebted to the National Research Council of Canada (Ottawa) and the Atkinson Foundation for financial support.

1. L. E. Bennett. Prog. Inorg. Chem. **18**, 1 (1973).
2. J. H. Wang and S. Tu. Rec. Adv. Phytochem. **5**, 1 (1972).
3. D. T. Sawyer and J. L. Roberts, Jr. Experimental electrochemistry for chemists. John Wiley, New York. 1974.
4. R. J. Kassner. Proc. Nat. Acad. Sci. **69**, 2263 (1972); J. Am. Chem. Soc. **95**, 2674 (1973).
5. G. M. Brown, F. R. Hopf, T. J. Meyer, and D. G. Whitten. J. Am. Chem. Soc. **97**, 5385 (1975).
6. A. B. P. Lever. Adv. Inorg. Chem. Radiochem. **7**, 27 (1965).
7. A. B. P. Lever and J. P. Wilshire. To be published.
8. C. K. Mann. Electroanal. Chem. **3**, 57 (1969).
9. L. Meites. Polarographic techniques. 2nd ed. Interscience, New York. 1965.
10. A. Wolberg and J. Manassen. J. Am. Chem. Soc. **92**, 2982 (1970).
11. L. D. Rollman and R. T. Iwamoto. J. Am. Chem. Soc. **90**, 1455 (1968).
12. D. Lexa and M. Reix. J. Chim. Phys. **71**, 511 (1974).
13. J. F. Myers, G. W. Rayner-Canham, and A. B. P. Lever. Inorg. Chem. **14**, 461 (1975).
14. G. N. La Mar and F. A. Walker. J. Am. Chem. Soc. **97**, 5103 (1975).
15. D. L. Ledson and M. V. Twigg. Inorg. Chim. Acta, **13**, 43 (1975).
16. V. Gutmann. Coordination chemistry in non-aqueous solutions. Springer-Verlag, New York. 1968.
17. M. J. Stillman and A. J. Thompson. J. Chem. Soc. Faraday Trans. II, **70**, 790 (1974).
18. C. J. Weschler, B. M. Hoffman, and F. Basolo. J. Am. Chem. Soc. **97**, 5278 (1975).
19. J.-H. Fuhrhop, K. M. Kadish, and D. G. Davis. J. Am. Chem. Soc. **95**, 5140 (1973).
20. D. Lexa, M. Momenteau, J. Mispelter, and J. M. Lhoste. Bioelectrochem. Bioenerg. **1**, 108 (1974).
21. L. A. Truxillo and D. G. Davis. Anal. Chem. **47**, 2260 (1975).
22. K. M. Kadish and D. G. Davis. Ann. N.Y. Acad. Sci. **206**, 495 (1973).
23. L. A. Constant and D. G. Davis. Anal. Chem. **47**, 2253 (1975).

Can. J. Chem. Downloaded from www.nrcresearchpress.com by 210.87.254.5 on 09/05/12
For personal use only.

Canadian Journal of Chemistry

Published by
THE NATIONAL RESEARCH COUNCIL OF CANADA

Journal canadien de chimie

Publié par
LE CONSEIL NATIONAL DE RECHERCHES DU CANADA

Volume 54 Number 16 August 15, 1976 Volume 54 numéro 16 15 août 1976

Proton magnetic resonance and Raman spectroscopic studies of methylmercury(II) complexes of inorganic anions

DALLAS L. RABENSTEIN, M. COREEN TOURANGEAU, AND CHRISTOPHER A. EVANS
Department of Chemistry, University of Alberta, Edmonton, Alta., Canada T6G 2G2

Received February 9, 1976

DALLAS L. RABENSTEIN, M. COREEN TOURANGEAU, and CHRISTOPHER A. EVANS. Can. J. Chem. **54**, 2517 (1976).

Complexation of methylmercury(II) by sulfate, selenate, carbonate, sulfite, selenite, thiocyanate, selenocyanate, sulfide, and selenide in aqueous solution has been studied by proton magnetic resonance and Raman spectroscopy. Formation constants were determined for the SO_4^{2-}, SeO_4^{2-}, CO_3^{2-}, SO_3^{2-}, SeO_3^{2-}, SeO_3H^-, SCN^-, and $SeCN^-$ complexes from the p*H* dependence of the chemical shift and the ^{199}Hg–^1H spin–spin coupling constant of the methyl group of $CH_3Hg(II)$ in solutions containing both $CH_3Hg(II)$ and ligand. The chemical shift and the ^{199}Hg–^1H spin–spin coupling constant of the $CH_3Hg(II)$ in each of the complexes were also obtained from the same measurements. Proton magnetic resonance parameters were measured for several complexes with sulfide and selenide. The ligand donor atom in each of the complexes was identified using the formation constants, the ^{199}Hg–^1H spin–spin coupling constant of the complexed methylmercury and the Raman spectral data. It is of particular interest that, in the selenite complex, the methylmercury is bonded to an oxygen atom whereas sulfur is the donor atom in the sulfite complex.

DALLAS L. RABENSTEIN, M. COREEN TOURANGEAU et CHRISTOPHER A. EVANS. Can. J. Chem. **54**, 2517 (1976).

On a étudié, par rmn et par spectroscopie Raman, la complexation du méthylmercure(II) par les ions sulfate, sélénate, carbonate, sulfite, sélénite, thiocyanate, sélénocyanate, sulfure et sélénure en solution aqueuse. On a déterminé les constantes de formation des complexes du SO_4^{2-}, SeO_4^{2-}, CO_3^{2-}, SO_3^{2-}, SeO_3^{2-}, SeO_3H^-, SCN^- et $SeCN^-$ à partir de la dépendance des déplacements chimiques sur le p*H* et des constantes de couplage spin–spin ^{199}Hg–^1H des groupes méthyles du $CH_3Hg(II)$ dans des solutions contenant à la fois du $CH_3Hg(II)$ et du ligand. On a aussi obtenu, à partir des mêmes mesures, les déplacements chimiques et les constantes de couplage spin–spin ^{199}Hg–^1H du $CH_3Hg(II)$ dans chacun des complexes. On a mesuré les paramètres rmp de plusieurs complexes avec le sulfure et le sélénure. On a identifié, dans chaque complexe, l'atome agissant comme ligand donneur en faisant appel aux constantes de formation, aux constantes de couplage spin–spin ^{199}Hg–H^1 du méthylmercure complexé et aux données des spectres Raman. Il est important de noter que dans le complexe sélénite, le méthylmercure est lié à l'atome d'oxygène alors que le soufre est l'atome donneur dans le complexe sulfite.

[Traduit par le journal]

Introduction

The coordination chemistry of the methylmercury(II) cation, CH_3Hg^+, is dominated by its unifunctional nature (1); the tendency to linear two-coordination typical of divalent mercury is greatly accentuated when one ligand is an organic radical. This absence of complications from chelating effects renders this cation an excellent probe. In addition, the solution chemistry of the methylmercury(II) species has

Can. J. Chem. Downloaded from www.nrcresearchpress.com by 210.87.254.5 on 09/05/12
For personal use only.

become a subject of interest (2–7) with the recognition of its importance in environmental pollution by mercury.

As part of a continuing study of the coordination chemistry of methylmercury, we have investigated the methylmercury complexes of several inorganic ligands, including some in which sulfur and selenium are potential coordination sites. These complexes were studied in aqueous solution by proton magnetic resonance and Raman spectroscopy with the objective of characterizing the complexes at the molecular level. In labile systems such as those studied here, the methyl protons of methylmercury give rise to a single averaged resonance pattern whose chemical shift and ^{199}Hg ($I = 1/2$, 16.9% natural abundance) – proton coupling constant are the weighted averages of those of the several species present in the solution. The distribution between the various species is p*H*-dependent and thus formation constants can be obtained from the averaged chemical shift and coupling constant. The value of the coupling constant provides some measure of the nature of the ligating atom (2, 4, 6, 7). The individual species present in solution can be observed directly by Raman spectroscopy, from which structural information can be obtained.

Recently, Ganther and co-workers demonstrated that selenium added as Na_2SeO_3 to the diets of rats decreased methylmercury toxicity in rats and suggested that the decreased toxicity of methylmercury to Japanese quail on diets containing tuna may also result from selenium in the tuna (8). Earlier studies had shown that Na_2SeO_3 decreases the toxicity of $HgCl_2$ injected into rats, possibly by complexation of mercury in the blood (9, 10).

Experimental

Methylmercuric hydroxide[1] (Alpha Inorganics) was purified and a stock solution was prepared as described previously (2). The stock solution was standardized by titration of aliquots with a standard sodium chloride solution in an acidified ethanolic medium; the endpoint was located potentiometrically with a Ag/AgCl indicating electrode (6).

Sodium sulfate (Allied Chemical) and sodium selenate (Alpha Inorganics) were used as the source of the sulfate and selenate ligands, respectively. Sodium sulfate (99%) was used without purification. The sodium selenate was recrystallized from ammoniacal solution to remove traces of acetate which coprecipitated from water. Stock solutions of sodium sulfate and sodium selenate were standardized by a precipitation titration with standard lead nitrate in a faintly acidic 80% acetone medium; dithizone was used to locate the endpoint (11). Sodium selenite (Alpha Inorganics) was purified by recrystallization from water and a stock solution prepared and standardized by p*H* titration with standard HNO_3. Sodium sulfite (Shawnigan Chemicals) or sodium bisulfite (B.D.H.) were used as sources of the sulfite ligand. The solids were analyzed by oxidation with excess iodine solution and back-titration with standard thiosulfate. Stock solutions of potassium thiocyanate (Baker A.R.) were standardized by titration with silver nitrate solution. Potassium selenocyanate and sodium selenide (Alpha Inorganics) were used as received. Sodium sulfide (Fisher) solutions were standardized by titration with standard thiosulfate after oxidation with excess standard iodine.

pH Measurements

All p*H* measurements were made at 25 ± 1 °C with an Orion Model 801 p*H* meter equipped with a standard glass electrode and a fiber-junction, saturated calomel reference electrode. The meter was standardized at 25 °C with Fisher certified standard solutions of p*H* 4.00, 7.00, and 10.00.

p*H* measurements were converted to hydrogen ion concentrations using activity coefficients calculated with the Davies equation (12).

Spectroscopy

Proton magnetic resonance spectra were obtained on a Varian A60-D high resolution spectrometer at a probe temperature of 25 ± 1 °C. Spectra were recorded at sweep rates of 0.1 Hz s^{-1} for the chemical shift measurements and 0.5 Hz s^{-1} for the spin–spin coupling constant measurements. Reported results are the average of three scans. Chemical shifts were measured relative to the *tert*-butyl resonance of internal *tert*-butyl alcohol, as described previously (6), but are reported relative to the methyl resonance of sodium 2,2-dimethyl-2-silapentane-5-sulfonic acid (DSS). Positive shifts correspond to resonances of protons less shielded than the methyl protons of DSS. The *tert*-butyl resonance of *tert*-butyl alcohol is 1.243 ppm downfield from the methyl resonance of DSS. Raman spectra were excited with the 4880 Å line of a Coherent Radiation Model 52 Ar laser, which produced *ca.* 200 mW at the sample. The Raman scattering was dispersed with a Spex 1401 double monochromator and detected with an RCA C31034 photomultiplier tube.

Solution Preparation

Proton Magnetic Resonance Experiments

Solutions used in the pmr measurements were prepared in distilled water from the requisite amounts of methylmercuric hydroxide and ligand stock solutions. The sulfite, selenocyanate, and selenide ligands are sensitive to air and their solutions were prepared in an argon or nitrogen atmosphere using appropriate amounts of crystalline salt, and spectra were obtained immediately after preparation.

For chemical shift or spin–spin coupling constant measurements as a function of p*H*, solutions of methyl-

[1]It is probable that this ill-defined solid is partially-hydrated bis(methylmercuric)oxide.

TABLE 1. Formation constants of methylmercury complexes[a]

Ligand	Donor atom	$[CH_3Hg(II)]_{Total}$	$[Ligand]_{Total}$	pH range	log K_f
SO_4^{2-}	O	0.0532 *M*	0.213 *M*	1.5–5.5	0.94±0.02
SeO_4^{2-}	O	0.0521	0.208	1.5–6	1.12±0.02
CO_3^{2-}	O	0.190	0.380	8–12	6.10±0.10
SO_3^{2-}	S	0.0546, 0.0617	0.546, 0.0617	9.5–12	7.96±0.02
SeO_3^{2-}	O	0.112	0.224	7–11.5	6.46±0.02
SeO_3H^-	O	0.112	0.224	1–6	2.70±0.05
SCN^-	S	0.05	0.13	8.5–10.5	6.05±0.01
$SeCN^-$	Se	0.06	0.015	8.5–9.5	6.79±0.01

[a]Concentration constants at 25 °C. Uncertainties are the standard deviations of from four to ten values.

mercury-to-ligand ratios varying from 1:4 to 4:1 were prepared. The solution was brought initially to pH ≈ 1 and samples withdrawn at approximately 0.4 pH unit intervals as base was added up to approximately pH 12. In this way the solution ionic strength remains almost constant throughout. Concentrated nitric acid or potassium hydroxide were used to change the pH. Typically, 20–30 samples were taken over this pH range.

In mole ratio experiments, the pH was maintained constant by addition of acid or base while a number of samples of varying methylmercury-to-ligand ratio were prepared. In these experiments, the ionic strength varies more between different samples than in the pH studies.

Raman Experiments

Solutions, typically 0.2 *M*, were prepared in distilled water from the requisite amounts of methylmercuric hydroxide stock solution and ligand (usually crystalline). Solutions containing sulfite were prepared from degassed solutions under an argon blanket. The mole ratios and solution pH's chosen were those which, based on calculations using the formation constants derived from the pmr experiments, contained a maximum concentration of the desired methylmercury species. The samples were sealed into glass capillaries (o.d. 1.5 mm).

Results and Discussion

Determination of Formation Constants

The formation constants listed in Table 1 were calculated from the chemical shift and coupling constant of the methyl protons of methylmercury in solutions containing known amounts of methylmercury and the ligand. For example, Fig. 1 shows the chemical shift of the methyl protons of methylmercury as a function of pH in aqueous solution and in aqueous solution containing sodium selenate. Figures 2 and 3 show the chemical shift and coupling constant in solutions containing sodium selenite.

The pH dependence of the chemical shift in aqueous solution is due to the following pH-dependent equilibria:

$$[1]\quad CH_3HgOH_2^+ + OH^- \rightleftarrows CH_3HgOH + H_2O$$

$$K_1 = \frac{[CH_3HgOH]}{[CH_3HgOH_2^+][OH^-]} = 1.97 \times 10^9$$

$$[2]\quad CH_3HgOH_2^+ + CH_3HgOH \rightleftarrows (CH_3Hg)_2OH^+$$

$$K_2 = \frac{[(CH_3Hg)_2OH^+]}{[CH_3HgOH_2^+][CH_3HgOH]} = 2.02 \times 10^2$$

Equations 1 and 2 represent the generally accepted aqueous solution model (1) for methylmercury, although it has been shown that at high methylmercury concentrations the tris(methylmercuric)oxonium cation $[(CH_3Hg)_3O^+]$ is present in detectable amounts around neutral pH (5). At the methylmercury concentrations used in this work, the concentration of $(CH_3Hg)_3O^+$ is negligible.

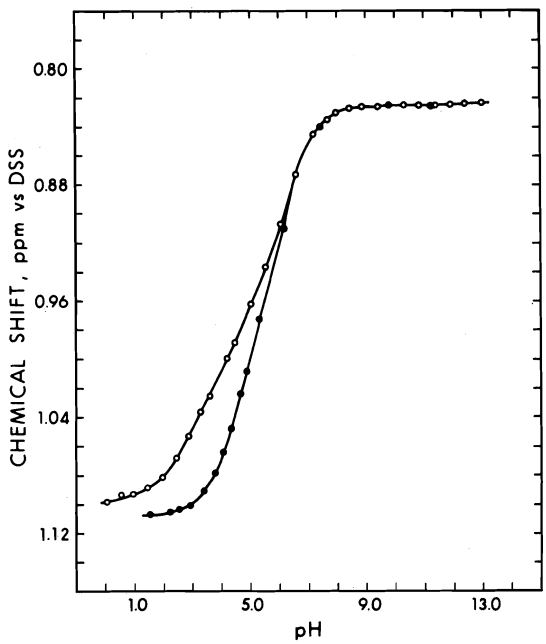

FIG. 1. pH-dependence of the chemical shift of the methyl protons of methylmercury in an aqueous solution containing 0.100 *M* methylmercury (○) and in an aqueous solution containing 0.0521 *M* methylmercury and 0.208 *M* Na_2SeO_4 (●).

Can. J. Chem. Downloaded from www.nrcresearchpress.com by 210.87.254.5 on 09/05/12
For personal use only.

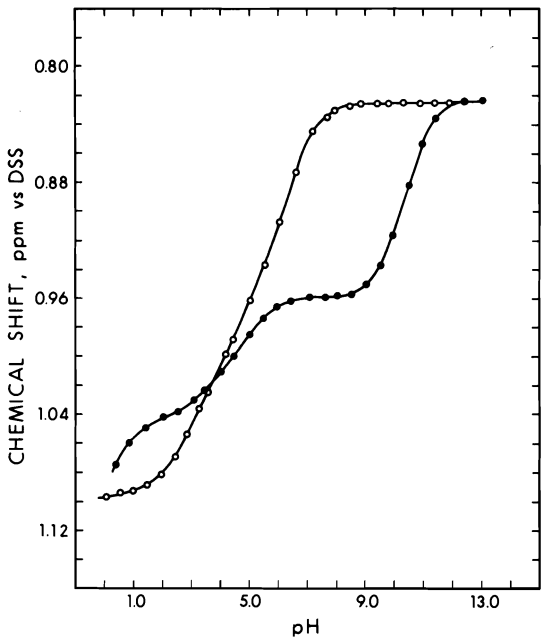

FIG. 2. p*H*-dependence of the chemical shift of the methyl protons of methylmercury in an aqueous solution containing 0.100 *M* methylmercury (○) and in an aqueous solution containing 0.112 *M* methylmercury and 0.224 *M* Na_2SeO_3 (●).

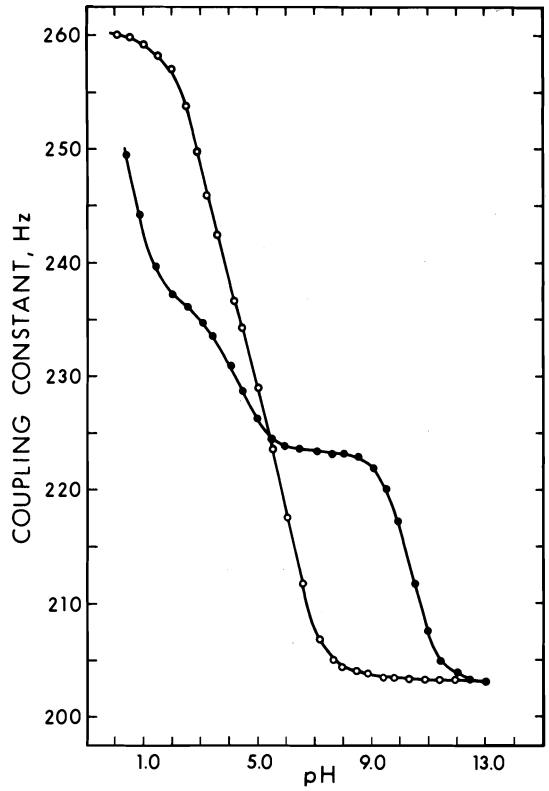

FIG. 3. p*H*-dependence of the mercury-proton spin–spin coupling constant of methylmercury in an aqueous solution containing 0.100 *M* methylmercury (○) and in an aqueous solution containing 0.112 *M* methylmercury and 0.224 *M* Na_2SeO_3 (●).

The different chemical shift curves below p*H* 8 in Fig. 1 indicate some complexation by selenate; above p*H* 8, the methylmercury is completely complexed by hydroxide ion. The coupling constant shows a similar p*H* dependence and yields the same conclusions. The formation constants of the sulfate and selenate complexes, defined by eq. 3, were calculated from chemical shift and coupling constant data,

[3] $$CH_3Hg^+ + SO_4^{2-} \rightleftarrows CH_3HgOSO_3^-$$

$$K_f = \frac{[CH_3HgOSO_3^-]}{[CH_3Hg^+][SO_4^{2-}]}$$

of which that in Fig. 1 is representative. For solutions containing methylmercury and the ligands studied in this work, a single resonance pattern was observed indicating fast exchange of methylmercury on the nmr time scale, although some broadening of the central resonance and the downfield satellite was observed in the selenate (p*H* 4.9) and sulfate (p*H* 3.8–5.8) systems. At each data p*H* where the observed chemical shift indicated complexation, the concentrations of each of the methylmercury-containing species and thus the formation constant were calculated from the observed shift and the observed coupling constant. The method used to obtain the formation constant from the averaged chemical shift will be described; the method used to obtain the formation constant from the averaged coupling constant was identical, and the necessary equations can be obtained from those that follow by replacing δ by J.

The observed chemical shift, δ_{obs}, is the sum of the chemical shifts of the various methylmercury species present, weighted according to the relative concentrations of the various species, as described by eq. 4.

[4] $$\delta_{obs} = P_{CH_3Hg^+}\,\delta_{CH_3Hg^+} + P_{(CH_3Hg)_2OH^+} \times \delta_{(CH_3Hg)_2OH^+} + P_{CH_3HgOH}\,\delta_{CH_3HgOH} + P_{CH_3HgSO_4^-}\,\delta_{CH_3HgSO_4^-}$$

where δ is the chemical shift and P the fraction

Can. J. Chem. Downloaded from www.nrcresearchpress.com by 210.87.254.5 on 09/05/12
For personal use only.

TABLE 2. Proton magnetic resonance parameters of methylmercury complexes

Species	Donor atom	Chemical shift of complex[a] (ppm from DSS)	$^2J(^{199}Hg-^1H)$ of complex[a] (Hz)
$CH_3HgOSO_3^-$	O	1.104	251.4
$CH_3HgOSeO_3^-$	O	1.115	248.5
$CH_3HgOCO_2^-$	O	0.955	221.4
CH_3HgSO_3	S	0.834	172.4
$CH_3HgOSeO_2^-$	O	0.961	223.5
$CH_3HgOSeO_2H$	O	1.036	234.6
CH_3HgSCN	S	1.031	203.0
CH_3HgS^-	S	—	146.2[b]
$(CH_3Hg)_2S$	S	—	156.0[c]
$(CH_3Hg)_3S^+$	S	—	202.0[d]
$CH_3HgSeCN$	Se	1.120	200.4
CH_3HgSe^-	Se	—	143.1[b]

[a]Calculated simultaneously with the formation constants in Table 1 as described in the text unless otherwise indicated.
[b]Measured directly; aqueous solution.
[c]Measured directly; pyridine solution. Reference 13 reports 156.6 Hz under similar conditions. In CS_2 solution $(CH_3Hg)_2Se$ has a coupling constant of 146 Hz (14).
[d]From a mole ratio study at p*H* 1 and $CH_3Hg(II)$/sulfide ratios of 5.0–8.2, assuming that methylmercury is solely in the forms $(CH_3Hg)_3S^+$ or $CH_3HgOH_2^+$ in these conditions. In CD_3CN solution, $(CH_3Hg)_3Se^+$ has a coupling constant of 196 Hz (14).

of methylmercury present as the species indicated. The sum of the fractions is unity. $\delta_{CH_3Hg^+}$, $\delta_{(CH_3Hg)_2OH^+}$, and δ_{CH_3HgOH} have been reported previously (2, 5). Equation 4 can also be written as

$$[5] \qquad \delta_{obs} = P_F\delta_F + P_c\delta_c$$

where P_F, the fraction of methylmercury not associated with SO_4^{2-}, is given by

$$[6] \quad P_F = P_{CH_3Hg^+} + P_{(CH_3Hg)_2OH^+} + P_{CH_3HgOH}$$

and P_c indicates the fraction of complexed methylmercury ($1 = P_F + P_c$). Rearrangement of eq. 5 gives

$$[7] \qquad P_c = \frac{\delta_{obs} - \delta_F}{\delta_c - \delta_F}$$

With eq. 7, P_c and thus the concentrations of free and complexed methylmercury were calculated from δ_{obs}. At the start of a calculation, δ_F is not known; it is dependent on the total concentration of free methylmercury because of the nonsymmetrical nature of the reaction represented by eq. 2. δ_c also is not known since solutions containing the complex also contain free methylmercury. Thus the iterative procedure described previously (2) was used to simultaneously determine K_f and the chemical shifts.

The formation constants of the CH_3Hg^+ complexes of SO_3^{2-}, SeO_3^{2-}, CO_3^{2-}, SCN^-, and $SeCN^-$ were calculated by a modification of the above procedure. These complexes form at higher p*H* values where the free methylmercury is essentially all present as CH_3HgOH, as illustrated in Figs. 2 and 3 for the SeO_3^{2-} complex. Thus $\delta_F = \delta_{CH_3HgOH}$ and the iteration step to find δ_F was not necessary. It was determined from the p*H* dependence of the pmr data for the $CH_3Hg(II)$–selenite system (Figs. 2 and 3) that a CH_3Hg^+ complex with SeO_3H^- forms below p*H* 6. The formation constant of this complex was determined by a procedure similar to that described above for the sulfate complex.

The formation constants and the pmr parameters of the complexes are listed in Tables 1 and 2.

Raman Spectra

The positions and assignments of bands in the Raman spectrum of an aqueous solution of $CH_3HgSO_3^-$ are listed in Table 3. The Raman spectra of the other complexes will be described in the following discussion of the individual complexes.

A considerable amount of information on the vibrational spectra of methylmercury complexes has been published making possible the correlation of the position of certain modes with the nature of the ligating atom. Table 4 lists the positions of the CH_3 symmetric deformation vibration, the mercury–carbon stretching vibration, and the mercury–X stretching vibration for

Can. J. Chem. Downloaded from www.nrcresearchpress.com by 210.87.254.5 on 09/05/12
For personal use only.

Can. J. Chem. Downloaded from www.nrcresearchpress.com by 210.87.254.5 on 09/05/12
For personal use only.

TABLE 3. Raman spectrum of $[CH_3—Hg—SO_3]^-$[a]

Frequency	Description	$[NH_3—Hg—SO_3]$[b]	SO_3^{2-}
2928m[c]	CH_3 stretch (sym.)	(3120)	
1190s,br,pol	CH_3 deformation (sym.)	(1299)	
1100w,br,dp	SO_3 stretch (asym.)	1109	933
997m,pol	SO_3 stretch (sym.)	997	967
785vw,dp	CH_3 rock	(732)	
649w,pol	SO_3 deformation (sym.)	640	620
541vs,pol	Hg—C stretch	(462)	
510w,sh,dp	SO_3 deformation (asym.)	511	469
206vs,pol	Hg—S stretch	[c]	
105s,dp	SO_3 rock	[c]	

[a]Sample prepared under argon from 0.44 *M* CH_3HgOH and an equivalent amount of solid $NaHSO_3$.
[b]Infrared spectrum from ref. 16; values in parentheses are comparable to those in $CH_3HgSO_3^-$ but involve the NH_3 group. The assignment of the bands at 1109 and 997 cm^{-1} has been reversed from that in the original work because the band at 997 cm^{-1} in $CH_3HgSO_3^-$ is polarized.
[c]Not measured.

TABLE 4. Some Raman bands of methylmercuric complexes, CH_3HgX

Complex	Ligating atom	Frequency of vibration: CH_3 deformation (sym.)	Frequency of vibration: Hg—C stretch	Frequency of vibration: Hg—X stretch	Reference
CH_3HgOH	O	1211	577	511	17
$CH_3HgOH_2^+$	O	1207	570	463	18
CH_3HgNO_3	O	1204	566	292	18
$CH_3HgSO_4^-$	O	1207	566	272	19
$(CH_3Hg)_3O^+$	O	1206	563	132[d]	20
CH_3HgSCN	S	1186	540	283	21
$CH_3HgcysH_2^+$	S	1190	544	328	[e]
CH_3HgSCH_3	S	1177	537	329	22
$(CH_3Hg)_3S^+$	S	1176[c]	544	281	20
$CH_3HgS(CH_3)_2^+$	S	1187	546	302	18, 23
$CH_3HgSeCN$[a]	Se	1177, 1164	540, 536	[b]	24
CH_3HgF	F	1209	573	414	25
CH_3HgCl	Cl	1203	556	334	26
CH_3HgBr	Br	1193	546	228	26
CH_3HgI	I	1183	535	181	26

[a]Infrared spectrum of solid $CH_3HgSeCN$.
[b]Spectrum in this region not reported.
[c]Infrared spectrum; maxima of 1185, 1176, 1161 cm^{-1}; ref. 27.
[d]D_{3h} structure, discussion in ref. 20.
[e]D. L. Rabenstein and C. A. Evans, unpublished results. cys = cysteinate.

a number of complexes of methylmercury with various ligating atoms, X. The first two bands are among the most intense features in the Raman spectrum of methylmercuric species, and as examination of Table 4 shows, their positions are a good indication of whether oxygen or sulfur atoms are bound to mercury. Complexes with other first row element ligating atoms appear to exhibit similar frequencies to those for oxygen. The Hg—X stretching frequencies are a less sensitive indication of the nature of the ligating atom, probably because of coupling of this vibration with motion within the ligand itself. Such motion does not markedly affect the frequency of vibration in the CH_3—Hg unit, presumably because of the great mass of the mercury atom. These correlations are used in the identification of the ligating atom in several of the complexes.

Sulfate and Selenate

Clarke and Woodward (19) have studied the stoichiometry and dissociation of the methylmercury–sulfate complex in aqueous solution, by Raman spectroscopy. The complex was shown to be $CH_3HgOSO_3^-$ by comparison with

Can. J. Chem. Downloaded from www.nrcresearchpress.com by 210.87.254.5 on 09/05/12
For personal use only.

the spectra of aqueous sulphuric acid solutions and from intensity measurements of the spectral bands at various mole fractions of methylmercury and sulfate. They concluded from measurements of the free sulfate concentration in solutions containing $CH_3HgOSO_3^-$ that the degree of dissociation of $CH_3HgOSO_3^-$ is 'approximately equal to that of HSO_4^-.' A concentration formation constant of 3 can be estimated from their results, in reasonable agreement with the value of 8.7 determined in this work from pmr data. As in sulfuric acid solutions, where H_2SO_4 molecules are not detectable at concentrations less than 1 *M*, no Raman evidence for the presence of $(CH_3Hg)_2SO_4$ molecules was obtained up to 0.8 *M*.

The basicity of SeO_4^{2-} and $HSeO_4^-$ to protons is similar (15) to that of SO_4^{2-} and HSO_4^-, and by analogy the behavior of selenate towards methylmercury cations is expected to be similar to that of sulfate. The formation constants listed in Table 1 for the sulfate and selenate complexes indicate this to be the case. The selenate complex forms sufficiently weakly, and the selenate moiety is a sufficiently weak Raman scatterer relative to CH_3—Hg—, that the complete Raman spectrum of the complex was not observed. Careful choice of solution conditions, however, enable five shifts attributable to the complex to be observed. Two solutions were prepared, the first at p*H* 3.0 containing 0.8 *M* selenate and 0.2 *M* $CH_3Hg(II)$ and the second 0.5 *M* $CH_3Hg(II)$ and 0.125 *M* selenate at p*H* 2.4. Frequencies for the CH_3—Hg moiety were derived from the spectrum of the first sample, where calculations show that 87% of the $CH_3Hg(II)$ is complexed, and likewise frequencies for the SeO_4 moiety came from the spectrum of the second sample, where 72% of the selenate is complexed. The p*H*'s were chosen in each case to maximize the concentration of the complex.

The symmetric CH_3 deformation at 1203 cm^{-1}, the mercury–carbon stretch at 565 cm^{-1}, and a band of 290 cm^{-1} assigned to mercury–oxygen stretching are all typical of the CH_3—Hg—O grouping and provide additional support for the correlation illustrated in Table 4. Frequencies assigned to SeO_3 stretching, at 856 cm^{-1} in the complex, and SeO_3 deformation, at 503 and 460 cm^{-1} in the complex are close to those for SeO_4^{2-} ion and $HSeO_4^-$ quoted in ref. 15, and confirmed in this work. In particular the SeO_3 stretching frequency observed in this work falls nicely between the ν_1 frequency of SeO_4^{2-} (835 cm^{-1}) and the most intense band in the spectrum of $HSeO_4^-$ (867 cm^{-1}).

Sulfite

The formation constant of the sulfite complex is orders of magnitude larger than those of the sulfate and selenate complexes. For comparison with the results of this work, Schwarzenbach and Schellenberg (1) reported log K_f = 8.11 for the sulfite complex. In addition, the ^{199}Hg–^1H coupling constant of 172 Hz for the complex is much less than those for the oxygen-bound methylmercury in the SO_4^{2-}, SeO_4^{2-}, and CO_3^{2-} complexes and in carboxylate complexes (2), but similar to those found for sulfhydryl-bound methylmercury in sulfur-containing amino acids (6), indicating that the methylmercury is sulfur bound in the sulfite complex. The sulfur-bound structure is supported by the Raman spectrum. The assignments in Table 3 are straightforward and closely follow the known frequencies of the $CH_3Hg(II)$ species in other complexes, the isoelectronic molecule NH_3HgSO_3 (16) and the free and complexed SO_3^{2-} anion (28, 29). The mercury–carbon stretching frequency of 541 cm^{-1} is, as shown in Table 4, typical for complexes with a sulfur atom bound to mercury. The mercury–sulfur stretching frequency is lower than observed for other sulfur ligands but not unreasonably so, and may to some extent correlate with the rather low formation constant.

Selenite

The value of the formation constant of the SeO_3^{2-} complex is much closer to that of the SO_3^{2-} complex than those of the SO_4^{2-} and SeO_4^{2-} complexes, which might be taken to indicate that selenium is the donor atom. However, the mercury–proton coupling constant of the selenite complex (223.5 Hz) is much larger than that observed for sulfur or selenium ligands (typically 140–200 Hz) but comparable to that observed for carboxylic acid complexes (2) and nearly equal to that for the carbonate complex (221.4 Hz) suggesting that an oxygen atom is the ligating atom. Also the formation constant of the selenite complex is similar to that of the carbonate complex. The large value for the formation constant is apparently related to the large pK_A (pK_A = 8.18), in the same manner as

Can. J. Chem. Downloaded from www.nrcresearchpress.com by 210.87.254.5 on 09/05/12
For personal use only.

observed previously for the carboxylic acid complexes (2).

The Raman spectra of 1:1 solutions at various p*H*'s provides confirmation of oxygen bonding in the selenite complex. The symmetric CH_3 deformation (1207 cm^{-1}) and the mercury–carbon stretch (568 cm^{-1}) are typical for oxygen-bonded methylmercury. Other bands in the spectrum are of low intensity relative to these, and the complete spectrum for the complex was not observed. The most intense band from selenium–oxygen stretching in the complex is at 835 cm^{-1}, intermediate in frequency between the strongest bands in SeO_3^{2-}, at 808 cm^{-1}, and $HSeO_3^-$, at 855 cm^{-1}. A medium intensity band at 290 cm^{-1} may be from mercury–oxygen stretching, as its frequency is close to that assigned to similar vibrations in other complexes of oxy-anions, or may be from a deformation mode of complexed selenite. Other bands are at 730 cm^{-1} (Se—O stretch) and 365 cm^{-1} (Se—O deformation). The spectra of aqueous solutions of SeO_3^{2-} and $HSeO_3^-$ (p*H* 5) recorded in the present work are in excellent agreement with those reported by Walrafen (15).

The coupling constant for the SeO_3H^- complex indicates oxygen bonding in this complex also. Its small formation constant relative to that of the SeO_3^{2-} complex correlates with the decreased basicity of SeO_3H^- (2).

The relatively small formation constant of the selenite complex as compared to those of sulfhydryl (31) and nucleoside (32) complexes indicates that the decreased toxicity of methylmercury in diets containing selenite (8) may be by some mechanism other than complexation of the methylmercury by SeO_3^{2-}.

Thiocyanate and Selenocyanate

Formation constants were calculated for CH_3HgSCN and $CH_3HgSeCN$ from chemical shift titration curves using only data at high p*H* where the methylmercury is present as CH_3HgOH or the complex. The results are listed in Table 1. For comparison, Schwarzenbach and Schellenberg (1) reported log $K_f = 6.05$ for CH_3HgSCN while Barbieri and Bjerrum (33) reported log $K_f = 6.11$.

The mercury–proton coupling constants of CH_3HgSCN and $CH_3HgSeCN$ (Table 2) are remarkably similar and larger than usually observed for heavy donor atoms such as Se or S. However, as shown by the Raman spectral data in Table 4 the ligating atoms are indeed sulfur and selenium respectively. The coupling constant of CH_3HgSCN has been previously measured in pyridine (208.0 Hz) (34) and methanol (205.6 Hz) (35) solution.

Sulfide and Selenide

As with oxide, multinuclear methylmercury complexes form readily with sulfide (1), although the complexes are present in slightly different forms in aqueous solution due to the greater acidity of sulfur-bound protons. The sulfide complexes and their formation constants are: CH_3HgS^-, log $K_f = 21.2$; $(CH_3Hg)_2S$, log $K_f = 16.3$; and $(CH_3Hg)_3S^+$, log $K_f \approx 7$ (1). The corresponding oxide complexes are: CH_3HgOH, $(CH_3Hg)_2OH^+$,[2] and $(CH_3Hg)_3O^+$.

The ^{199}Hg–^1H coupling constants of the three sulfide complexes and of CH_3HgSe^- were determined. Precipitation of $(CH_3Hg)_2S$ from aqueous solution limits the region of study to high p*H* with a moderate excess of sulfide over CH_3Hg(II). At p*H* 13.2, both the methyl proton chemical shift and the coupling constant remained invariant in a series of seven solutions having CH_3Hg(II) to sulfide ratios in the range 0.2–0.7. This is taken to indicate that essentially all the methylmercury is bound to sulfide, in the form CH_3HgS^-. The coupling constant, 146.2 Hz, is considerably smaller than observed for substituted sulfides, *e.g.* cysteinate (6), where values around 170 Hz are found, which supports the formulation as CH_3HgS^- rather than CH_3HgSH.

A similar experiment, using sodium selenide at 3- to 5-fold excess over CH_3Hg(II) and at p*H* 13.5 yielded comparable results with the coupling constant being 143.1 Hz. Breitinger and Morell (14) reported coupling constants for $(CH_3Hg)_2Se$ in CS_2 (146 Hz) and $[(CH_3Hg)_3Se]NO_3$ in CD_3CN (196 Hz). The vibrational spectra of $(CH_3Hg)_2Se$ and $[(CH_3Hg)_3Se]NO_3$ were also reported by Breitinger and Morell (14). Our attempts to obtain Raman spectra of CH_3HgSe^- were unsuccessful because of decomposition in the laser beam.

The Raman spectrum of a solution of CH_3HgS^- prepared as described above showed 5 bands, at 2913 ms, 2574 vvw, 1188 ms, 537 vs, and 353

[2] $(CH_3Hg)_2O$ exists in the solid state and in non-aqueous solvents (36).

Can. J. Chem. Downloaded from www.nrcresearchpress.com by 210.87.254.5 on 09/05/12
For personal use only.

cm^{-1}. For a molecule of the C_{3v} point group, 8 frequencies ($4a_1 + 4e$) are expected and presumably the four strong bands are from the a_1 modes. The nonobservance of the e fundamentals in the Raman spectrum is reminiscent of the situation in the isostructural halides (26). The frequencies are assigned as follows: 2913, CH_3 stretch (sym); 1188, CH_3 deformation (sym); 537, Hg—C stretch; and 353, Hg—S stretch. The last three frequencies are in accord with the values in Table 4 for the sulfur-bonded CH_3Hg moiety. The band at 2574 cm^{-1}, in the range for S—H stretching vibrations, was observable only under very high instrument gain and is assigned to a small amount of HS^-. The vibrational spectrum of $(CH_3Hg)_3S^+$ has been reported by Clarke and Woodward (20) and Green (27).

After exposure to the laser beam, or more slowly on standing, the solution of CH_3HgS^- yielded a gas and a black precipitate, presumably mercuric sulfide. The Raman spectrum of the supernatent has a band at 349 cm^{-1} but no bands from methyl groups or mercury–carbon vibrations. These observations are accountable in terms of the equilibrium

$$2CH_3Hg(II) \rightleftarrows Hg(II) + (CH_3)_2Hg$$

being moved to the right by formation of insoluble mercuric sulfide and gaseous dimethylmercury, as discussed by Fagerstrom and Hernelov (37). The formation of HgS_2^{2-} from HgS and excess sulfide is shown by the Raman band at 349 cm^{-1} from the symmetric mercury–sulfur stretching vibration, in agreement with authentic samples and solid cinnabar (38).

Acknowledgements

This research was supported in part by the National Research Council of Canada. We are grateful to Dr. S. Libich for determining the formation constant of the carbonate complex.

1. G. Schwarzenbach and M. Schellenberg. Helv. Chim. Acta, **48**, 28 (1965).
2. S. Libich and D. L. Rabenstein. Anal. Chem. **45**, 118 (1973).
3. S. Mansy, T. E. Wood, J. C. Sprowles, and R. S. Tobias. J. Am. Chem. Soc. **96**, 1762 (1974).
4. D. L. Rabenstein, R. Ozubko, S. Libich, C. A. Evans, M. T. Fairhurst, and C. Suvanprakorn. J. Coord. Chem. **3**, 263 (1974).
5. D. L. Rabenstein, C. A. Evans, M. C. Tourangeau, and M. T. Fairhurst. Anal. Chem. **47**, 338 (1975).
6. D. L. Rabenstein and M. T. Fairhurst. J. Am. Chem. Soc. **97**, 2086 (1975).
7. M. T. Fairhurst and D. L. Rabenstein. Inorg. Chem. **14**, 1413 (1975).
8. H. E. Ganther, C. Goudie, M. L. Sunde, M. J. Kopecky, P. Wagner, S. Oh, and W. G. Hoekstra. Science, **175**, 1122 (1972).
9. J. Parizek and I. Ostadalova. Experientia, **23**, 142 (1967).
10. J. Parizek, I. Ostadalova, J. Kalouskova, A. Babicky, L. Pavlik, and B. Bibr. J. Reprod. Fert. **25**, 157 (1971).
11. W. J. Blaedel and V. W. Meloche. Elementary Quantitative Analysis, 2nd ed. Harper and Row. 1963. p. 290.
12. L. Meites. Handbook of analytical chemistry. McGraw-Hill, New York, N.Y. 1963, pp. 1–8.
13. R. Scheffold. Helv. Chim. Acta, **50**, 1419 (1967).
14. D. Breitinger and W. Morell. Inorg. Nucl. Chem. Lett. **10**, 409 (1974).
15. G. E. Walrafen. J. Chem. Phys. **39**, 1479 (1963).
16. K. Brodersen. Chem. Ber. **57**, 2703 (1957).
17. P. L. Goggin and L. A. Woodward. Trans. Faraday Soc. **56**, 1591 (1960).
18. P. L. Goggin and L. A. Woodward. Trans. Faraday Soc. **58**, 1495 (1962).
19. J. H. R. Clarke and L. A. Woodward. Trans. Faraday Soc. **64**, 1041 (1968).
20. J. H. R. Clarke and L. A. Woodward. Spectrochim. Acta, Part A, **23**, 2077 (1967).
21. R. P. J. Cooney and J. R. Hall. Aust. J. Chem. **22**, 2117 (1969).
22. R. A. Nyquist and J. R. Mann. Spectrochem. Acta, Part A, **28**, 511 (1972).
23. P. L. Goggin, R. J. Goodfellow, S. R. Haddock, and J. G. Eary. J. Chem. Soc. Dalton Trans. 648 (1972).
24. E. E. Aynsley, N. N. Greenwood, and M. J. Sprague. J. Chem. Soc. 2395 (1965).
25. D. Breitinger, A. Zober, and M. Neubauer. J. Organomet. Chem. **30**, C49 (1971).
26. P. L. Goggin and L. A. Woodward. Trans. Faraday Soc. **62**, 1423 (1966).
27. J. H. S. Green. Spectrochim. Acta, Part A, **24**, 863 (1968).
28. G. P. Syrtsova, Y. Y. Kharitonov, and T. S. Bolgar. Russ. J. Inorg. Chem. **17**, 1425 (1972).
29. B. Nyberg and R. Larson. Acta Chem. Scand. **27**, 63 (1973).
30. G. E. Walrafen. J. Chem. Phys. **36**, 90 (1962).
31. R. B. Simpson. J. Am. Chem. Soc. **83**, 4711 (1961).
32. R. B. Simpson. J. Am. Chem. Soc. **86**, 2059 (1964).
33. R. Barbieri and J. Bjerrum. Acta Chem. Scand. **19**, 469 (1965).
34. J. V. Hatton, W. G. Schneider, and W. Siebrand. J. Chem. Phys. **39**, 1330 (1965).
35. J. Relf, R. P. J. Cooney, and H. F. Henneike. J. Organomet. Chem. **39**, 75 (1972).
36. J. Lorbeth and F. Weller. J. Organomet. Chem. **32**, 145 (1971).
37. T. Fagerstrom and A. Hernelov. Water Res. **6**, 1193 (1972).
38. D. M. Adams. Metal–ligand and related vibrations. Edward Arnold, London. 1967. p. 324.

A theoretical study on the stereochemistry and protonation of $^{-}$:CH_2—NO_2

P. G. MEZEY, A. J. KRESGE, AND I. G. CSIZMADIA
Department of Chemistry, University of Toronto, Toronto, Ont., Canada M1C 1A4

Received October 6, 1975[1]

P. G. MEZEY, A. J. KRESGE, and I. G. CSIZMADIA. Can. J. Chem. **54**, 2526 (1976).

The molecular conformation of $^{-}$:CH_2NO_2 is found to be planar with an extremely shallow potential curve to pyramidal inversion. This suggests that suitable substituents could conceivably perturb the system into a pyramidal configuration corresponding to double minimum on the potential surface and that a chiral carbanion might therefore exist. Rotating the NO_2 group out of planarity by 90° raises the barrier to inversion at carbon by an appreciable amount.

A Mulliken population analysis gives a charge distribution in which a substantial portion of the negative charge has shifted from carbon to oxygen; this is consistent with the well-known tendency of nitronate ions to undergo simultaneous competitive protonation on carbon and oxygen.

P. G. MEZEY, A. J. KRESGE et I. G. CSIZMADIA. Can. J. Chem. **54**, 2526 (1976).

On a trouvé que la conformation moléculaire de l'ion $^{-}$:CH_2NO_2 est plane avec une courbe de potentiel extrêmement faible vers l'inversion pyramidale. Ces résultats suggèrent que les substituants appropriés pourraient éventuellement perturber le système et l'amener vers une configuration pyramidale correspondant à un double minimum sur la surface de potentiel impliquant qu'un carbanion chiral pourrait alors exister. En amenant le groupe NO_2 perpendiculaire au plan de la molécule, il y a une augmentation appréciable de la barrière d'inversion au niveau du carbone.

Une analyse de population de Mulliken conduit à une distribution de charge dans laquelle une partie importante de la charge négative s'est déplacée du carbone vers l'oxygène; ceci est en accord avec la tendance bien connue des ions nitronates à subir des protonations compétitives simultanées sur le carbone et l'oxygène.

[Traduit par le journal]

Introduction

An adjacent nitro group exerts a powerful acidifying effect upon carbon-hydrogen bonds. The pK_a of CH_3NO_2, for example, is 10.22 (1), which makes it a stronger acid than the parent hydrocarbon, CH_4, by at least 30 pK units.

This effect is generally ascribed to the ability of NO_2 to stabilize negative charge, and it is of interest, therefore, to inquire into the details of the charge distribution in nitronate ions. This matter is of added current significance inasmuch as the charge distribution in these anions, and departures from it in the proton transfer transition states, has recently been used to rationalize exceptional kinetic behavior in the neutralization of simple nitroalkanes (the 'nitroalkane anomaly') (2).

Of further interest is the conformational structure of nitronate ions, especially whether or not these substances are pyramidal and therefore chiral species. There are reports in the early literature to the effect that optically active 2-nitrobutane and 2-nitrooctane, upon treatment with sodium methoxide followed by bromine, give optically active products (3, 4). It was later demonstrated that impurities in these 2-nitroalkanes could have been responsible for the observed optical activity, but the existence of chiral nitronate anions was not ruled out (5).

These results motivated our present *ab initio* study of the conformational and electronic structure of CH_3NO_2 and its conjugate base :$CH_2NO_2^{-}$. We also investigated the two possible protonation reactions of the anion, *i.e.* C-protonation and O-protonation, and to this end we performed separate calculations on the aci-nitro tautomer of nitromethane, CH_2NO_2H.

Method

Throughout the optimization of the geometries of various species and generation of potential energy surfaces and cross sections an STO-3G basis set, as contracted to an minimal basis (6) was used. In order to obtain more reliable charge distribution and energy differences associated with various protonation reactions, the optimum

[1]Revision received April 14, 1976.

Can. J. Chem. Downloaded from www.nrcresearchpress.com by 210.87.254.42 on 09/05/12
For personal use only.

Can. J. Chem. Downloaded from www.nrcresearchpress.com by 210.87.254.42 on 09/05/12
For personal use only.

structures were recalculated using an extended STO-4-31G basis set (7). The calculations were performed on an IBM 370/165 computer using a version of the Gaussian 70 Program System (7).

Results

Though experimental structural data are available for CH_3NO_2 (8), in order to maintain the comparability of the energy values calculated for the given Gaussian function representation, it seemed essential to carry out full geometry optimization for all molecular systems, $CH_2NO_2^-$, CH_3NO_2 and CH_2NO_2H, at their respective most stable conformation (absolute minimum). In addition, selected points on the topomerization energy surface of $CH_2NO_2^-$ and the maximum along the rotational coordinate for CH_3NO_2, were also optimized.

The structural parameters for the optimum

TABLE 1. Optimum geometries of $^-$:CH_2—NO_2 conformers

Structural parameter[a]	Conformation 1*a*	1*b*	1*c*
CN	1.350	1.457	1.575
NO_1	1.337	1.286	1.282
NO_2	1.337	1.286	1.290
CH	1.071	1.059	1.110
CNO_1	120.35	121.74	119.99
CNO_2	120.35	121.74	121.77
HCN	119.13	116.45	99.81
HCNO	0.00	90.00	H_1CNO=H_2CNO

[a]Symbols AB, ABC and ABCD denote bond length in Å, bond angle in degrees and torsion angle in degrees, respectively.

TABLE 2. Optimum geometries of CH_3NO_2 conformers

Structural parameter[a]	Conformation 2*a*	2*b*
CN	1.529	1.531
NO_1	1.279	1.278
NO_2	1.279	1.279
CH_1	1.091	1.090
CH_2	1.091	1.091
CNO_1	117.58	117.67
CNO_2	117.58	117.50
H_1CN	108.06	107.59
H_2CN	108.06	108.23
H_1CNO_1	90.00	0.00

[a]Symbols AB, ABC and ABCD denote bond length in Å, bond angle in degrees and torsion angle in degrees, respectively.

TABLE 3. Optimum geometry of CH_2NO_2H

Structural parameter[a]	Conformation 3
CN	1.310
NO_1	1.403
NO_2	1.333
O_1H_1	0.998
CH_2	1.083
CH_3	1.079
CNO_1	111.60
CNO_2	116.87
NO_1H_1	99.12
H_2CN	118.39

[a]Symbols AB and ABC denote bond length in Å and bond angle in degrees, respectively.

for a total of six structures including three conformations for $^-CH_2NO_2$ (**1***a*, **1***b*, **1***c*), two conformations for CH_3NO_2 (**2***a*, **2***b*) and one conformation for CH_2NO_2H (**3**) are listed in Tables 1, 2 and 3, respectively. The molecular structures associated with these six geometries are shown in Fig. 1. The total energies are calculated with the minimum basis set, and those of the optimum structures as recalculated with the extended basis are listed in Table 4. In addition, total energies of optimum structures of CH_2-CHO^-, CH_3CHO, CH_2F^-, CH_3F, CH_3^-, and CH_4 as calculated with the extended basis are also included in Table 4 for later comparison of

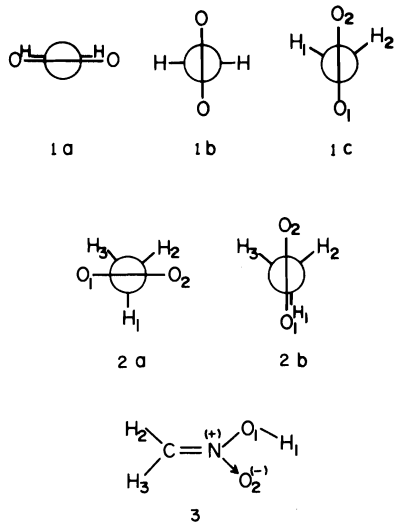

FIG. 1. Schematic representation of the six optimum structures (**1***a*, **1***b*, **1***c*, **2***a*, **2***b*, **3**).

Can. J. Chem. Downloaded from www.nrcresearchpress.com by 210.87.254.42 on 09/05/12
For personal use only.

TABLE 4. Total energies of various species (in hartrees) calculated with minimum and extended basis sets

Minimum basis			Extended basis		
Structure		Total energy (au)	Structure		Total energy (au)
$CH_2NO_2^-$	**1***a*	−239.667260	$CH_2NO_2^-$	**1***a*	−242.687257
	1*b*	−239.596244	CH_3NO_2	**2***b*	−243.263034
	1*c*	−239.641927	CH_2NO_2H	**3**	−243.253247
CH_3NO_2	**2***a*	−240.424609	CH_2CHO^-		−152.060964
	2*b*	−240.424650	CH_3CHO		−152.684601
CH_2NO_2H	**3**	−240.394931	CH_2F^-		−138.154327
			CH_3F		−138.856005
			CH_3^-		−39.400455
			CH_4		−40.139734

TABLE 5. Computed energy values[a] for the rotation–inversion surface: $E = E(\theta,\phi)$ of $^-$:CH_2—NO_2

ϕ Bond angle	γ Inversion angle	Energy, $E = -239.0 - X$, X listed in au			
		$\theta = 0°$	$\theta = 30°$	$\theta = 60°$	$\theta = 90°$
120.0000	90.0000	0.667260*	0.652575	0.618551	0.596243*
119.8562	92.1820	0.667157*	—	—	—
118.6238	96.7860	0.667113*	—	—	—
115.2155	102.8309	0.666901*	0.654848	0.627884	0.611500*
99.8137	117.9516	0.659781*	0.655373	0.646312	0.641927*
90.0000	125.2644	0.641959*	0.587128	0.585605	0.634514*

[a]The points marked with an asterisk were fully optimized with respect to geometry for the given pair of bond angle ϕ and torsional angle θ. For the rest of the points the geometries were obtained by linear interpolation.

protonation energies. The definition of the conformational coordinates for $CH_2NO_2^-$ is given in Fig. 2. For computational reasons the (pyramidal) inversion angle γ as measured from the pyramidal axis was used rather than bond angle ϕ. Where relevant, however, values for ϕ are also presented.

The topomerization surface, corresponding to the simultaneous rotation (θ) – inversion (γ) process:

$$E = E(\gamma,\theta)$$

was generated in three distinct stages. In the *first part* the structures **1***a* and **1***c* were optimized fully. In the *second part* the pyramidal angle γ was systematically varied and at each value of γ the independent geometrical parameters were optimized. The energy values obtained from these two stages are marked by asterisks in Table 5. It should perhaps be pointed out that the cross section corresponding to $\theta = 0°$ was found to have a very shallow potential curve, and several reoptimizations were necessary to obtain the final values reported. Another point of interest is that the minimum at the second cross section investigated ($\theta = 90°$) corresponds to the saddle point of the conformational energy surface, consequently the pyramidal angle of this minimum ($\gamma = 117.85°$ or $\phi = 99.94°$) was also included in the cross section corresponding to $\theta = 0°$. In summary all these optimized points (asterisked values in Table 5) represent

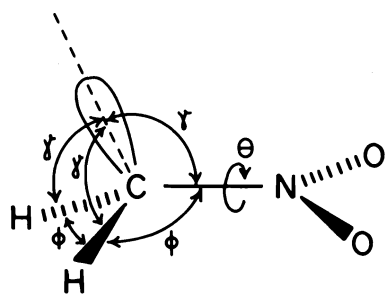

FIG. 2. Definition of topomerization coordinates for $^-$:CH_2—NO_2. Planar structure corresponds to $\gamma = 90°$ ($\phi = 120°$), $\theta = 0°$. $\cos\phi = \frac{1}{2}(3\sin^2(\gamma - 90) - 1)$.

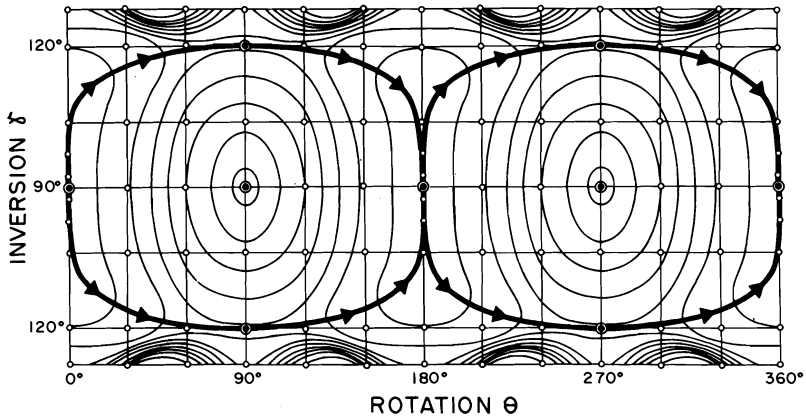

FIG. 3. Topomerization energy surface $E = E(\gamma,\theta)$ associated with the rotation (θ) and inversion (γ) process of $^{-}$:CH_2—NO_2.

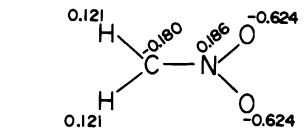

1 a

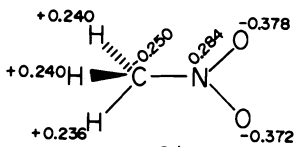

2 b

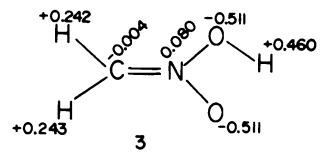

3

FIG. 4. Gross atomic charges of structures **1***a*, **1***b*, **1***c*, **2***a*, **2***b*, and **3**.

the end result of three consecutive sets of full optimization, consequently, the geometries reported are very close to the best geometries that can be obtained within the limitations of the basis set. In the *third part* of the study of the conformational energy surface the intermediate points were computed (values without asterisk in Table 5). For these computations the geometries were obtained from linear interpolations of all geometrical parameters of the starred conformations at a given γ value.

The conformational surface is shown in Fig. 3. The results of Mulliken's population analysis, as calculated with the extended basis, are summarized in Fig. 4.

Discussion

Conformation of $^{-}$:CH_2—NO_2

The most stable conformation of $^{-}$:CH_2—NO_2 is computed to be a fully planar one in accordance with the traditional VB rationalization:

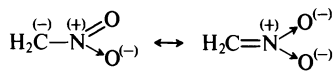

4*a* **4***b*

This conjugative stabilization completely disappears, however, when the —NO_2 moiety is rotated out of the plane. The barrier to rotation occurs at 90° torsional angle (θ = 90°) and the barrier height is found to be 44.6 kcal/mol. As illustrated in Fig. 5 the torsional potential has a two-fold symmetry in contrast to the six-fold symmetry of the torsional potential of CH_3—NO_2 which has a calculated barrier of 0.026 kcal/mol, consistent with the experimentally observed low barrier to rotation (0.006 kcal/mol) (9). This rotational barrier in CH_3—NO_2 corresponds to a typical low value that is characteristic to six-fold barriers. However, the barrier to rotation of the planar $^{-}$:CH_2—NO_2 is much too high for a two-fold barrier. This is because in the **1***a* → **1***b* interconversion **1***a* represents the energy minimum while **1***b* is the energy maximum of the

Can. J. Chem. Downloaded from www.nrcresearchpress.com by 210.87.254.42 on 09/05/12
For personal use only.

Can. J. Chem. Downloaded from www.nrcresearchpress.com by 210.87.254.42 on 09/05/12
For personal use only.

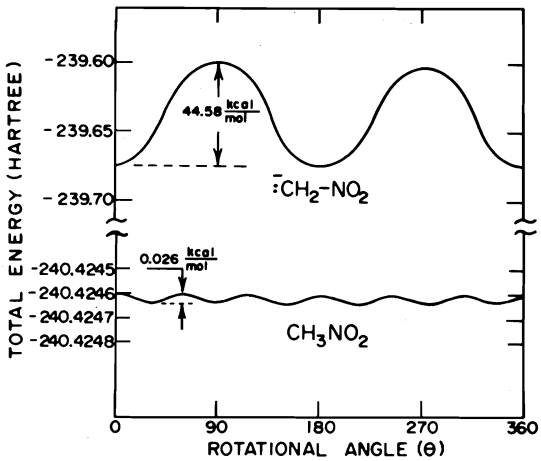

FIG. 5. Rotation potential curve for CH_3—NO_2 and rotation cross section of the topomerization energy surface for $^-$:CH_2—NO_2 at $\phi = 120°$ ($\gamma = 90°$).

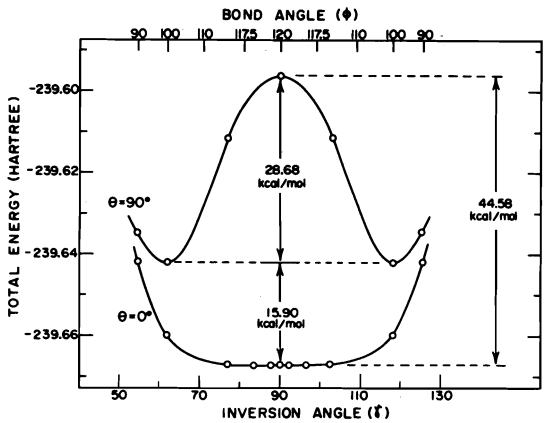

FIG. 6. Inversion cross sections of the topomerization energy surface for $^-$:CH_2—NO_2 at $\theta = 0°$ and $\theta = 90°$.

conformational energy surface (*cf.* Fig. 3). Consequently not all of 44.6 kcal/mol can be attributed to resonance stabilization. This value may only be regarded as the 'upper limit' or the maximum of the conjugative stabilization.

The change in (pyramidal) bond angle about the carbanion centre is also of some importance. By distorting the planar structure of the $^-$:CH_2-moiety in **1***a* a very shallow energy increase is noticed. This is clearly shown in the lower part of Fig. 6. The shallowness of this potential raises the question of substitution at carbon. It is conceivable that with suitably chosen substituents $R_1R_2\ddot{C}^-$—NO_2 may become pyramidal corresponding to a chiral carbanion centre. In contrast to **1***a* the change of the same pyramidal angle in **1***b* leads to a double well potential as shown by the upper potential curve in Fig. 6, implying chirality when the —NO_2 group is rotated by 90°. The minimum point of this curve is that of structure **1***c* (*cf.* Fig. 1) and it is in fact the saddle point of the conformational energy surface (*cf.* Fig. 3). The energy difference between structures **1***a* and **1***c* is 15.9 kcal/mol. This value can be regarded as the 'lower limit' or the minimal value of the conjugative stabilization. Also this value is within the range computed with the basis set used for a typical two-fold rotational potential. For this reason the topomerization of $^-H_2\ddot{C}$—NO_2 occurs *via* a simultaneous rotation inversion as indicated by the heavy line in Fig. 3 and characterized by the following equation

$$\mathbf{1}a \rightleftarrows [\mathbf{1}c]^{\ddagger} \rightleftarrows \mathbf{1}a$$

where $[\mathbf{1}c]^{\ddagger}$ symbolizes the transition state. The topomerization occurs with the omission of structure **1***b* that corresponds to the maximum on the energy surface (*cf.* Fig. 3).

It is of considerable interest to compare the present results with the effect of a carbonyl group on the inversion potential of an adjacent carbanionic center, inasmuch as C=O is also capable of conjugative stabilization. An earlier study has predicted that $^-$:CH_2—CHO is planar in its most stable conformation (10). In order to maintain the comparability of the energetics the calculations on $^-$:CH_2—CHO were repeated using the present basis set. The results are shown in Fig. 7, providing the maximum and minimum values of conjugative stabilization as summarized in Table 6.

In addition to groups that are capable of conjugative stabilization there are groups that exhibit conjugative destabilization. These are groups that have lone electron pairs and the halogen atoms are the simplest of such functional groups. For this reason we included H_3C—F and $H_2\ddot{C}^-$—F in this study for the sake of comparison. The inversion potential of $H_2\ddot{C}F^-$ together with that of $\ddot{C}H_3^-$ are compared to those inversion potentials of $^-H_2\ddot{C}$—NO_2 and $^-H_2\ddot{C}$—CHO where no conjugative stabilization is possible due to the 90° rotation of the —NO_2 and —CHO groups. As may be seen from Fig. 8 there is no increase in barrier height for —NO_2 and —CHO with respect to —H as would have been expected due to the inductive effect of

Can. J. Chem. Downloaded from www.nrcresearchpress.com by 210.87.254.42 on 09/05/12
For personal use only.

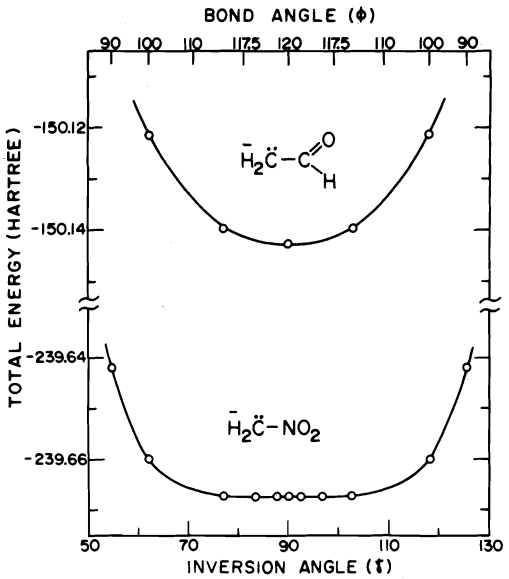

FIG. 7. Comparison of inversion potential curves of $^-$:CH_2—NO_2 ($\theta = 0°$) and $^-$:CH_2—CHO ($\theta = 0°$).

TABLE 6. Conjugative stabilization

	Conjugative stabilization (kcal/mol)	
Group	Maximum	Minimum
—NO_2	44.6	15.9
—CHO	47.5	28.5

TABLE 7. Effects of conjugative stabilization on the bond length[a]

	C—X bond length (Å)		
Group X	H_3C—X	$^-$:CH_2—X	Δr_{C-X}
—NO_2	1.531	1.350	−0.181
—CHO	1.540	1.381	−0.159
—F	1.366	1.440	+0.074

[a]All bond lengths listed were obtained by full geometry optimization.

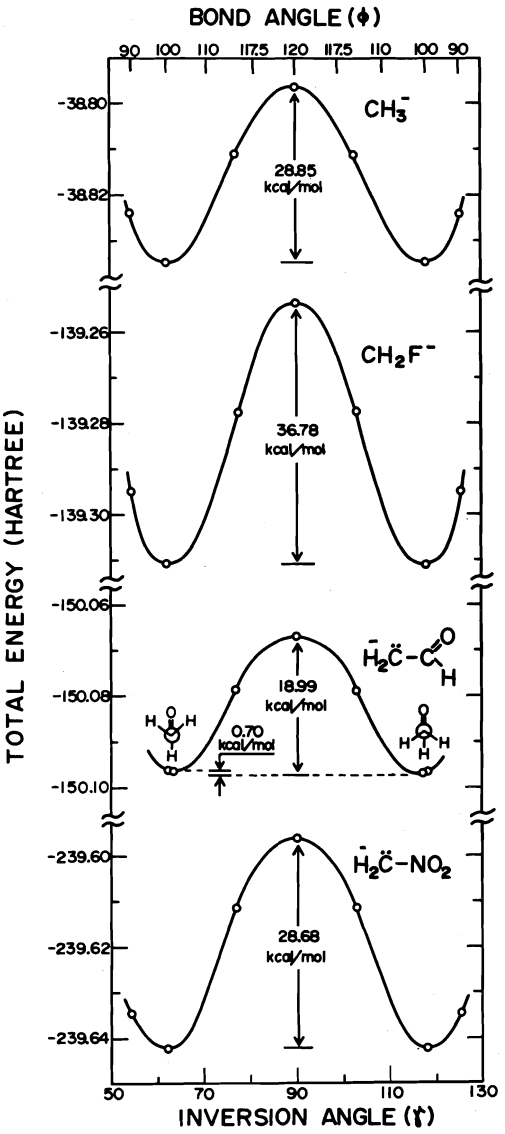

FIG. 8. Comparison of inversion potential curves of $^-$:CH_2F, $^-$:CH_3; $^-$:CH_2—NO_2 ($\theta = 90°$) and $^-$:CH_2—CHO ($\theta = 90°$).

these groups. In fact, there is an actual decrease in barrier height for —CHO. However, the increase of barrier in $H_2\ddot{C}F^-$ with respect to that of $:CH_3^-$ is due to the combined effect of inductive electron withdrawing and resonance releasing (*i.e.* conjugative destabilization). It should be noted that these results are to be interpreted with certain caution as the numerical values obtained with the minimum basis are less reliable. In particular, the calculated barrier for CH_3^- is much too high (11), though it is well known (12) that small basis calculations rarely give inversion barriers less than 10 kcal/mol. Consequently, only the qualitative conclusions based on these data can be accepted.

Another parameter besides energy that may be related to conjugative stabilization and destabilization is the change in bond length,

Can. J. Chem. Downloaded from www.nrcresearchpress.com by 210.87.254.42 on 09/05/12
For personal use only.

Δr_{C-X}, in the protonation–deprotonation process:

$$H_3C{-}X \rightleftarrows H^+ + {}^-H_2C{-}X$$

These results are summarized in Table 7.

Protonation of $^-:CH_2{-}NO_2$

The results of Mulliken's population analysis of the $H_2\ddot{C}^-{-}NO_2$ ion (**1***a*), as calculated with the extended basis and summarized in Fig. 4, shows a marked shift of charge from the less electronegative carbon towards the oxygen atoms. This shift in net negative charge would suggest, in accordance with the **4***a* and **4***b* resonance stabilization, that there are two sites of protonation in $^-:CH_2{-}NO_2$ as indicated below:

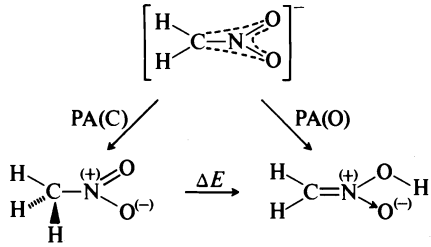

2 **3**

These two processes may be characterized by two proton affinity values: PA(C) and PA(O). The calculations using both the minimal and the extended basis sets indicate that the protonation at carbon (PA(C)) is more exothermic than the protonation at oxygen (PA(O)). In other words $|PA(C)| > |PA(O)|$ as illustrated in Fig. 9. Using the larger basis set the difference in the proton affinities gives the energy separation of the two tautomers to be $\Delta E = PA(O) - PA(C) = 6.1$ kcal/mol. The positive sign indicates that tautomer **2** is more stable than tautomer **3**. In spite of the fact that these calculations are directly comparable with results of gas phase measurements only, the 6.1 kcal/mol stability computed with the extended basis set compares favorably with the thermodynamic stability ($-\Delta G = 9.5$ kcal/mol) observed in solution (1).

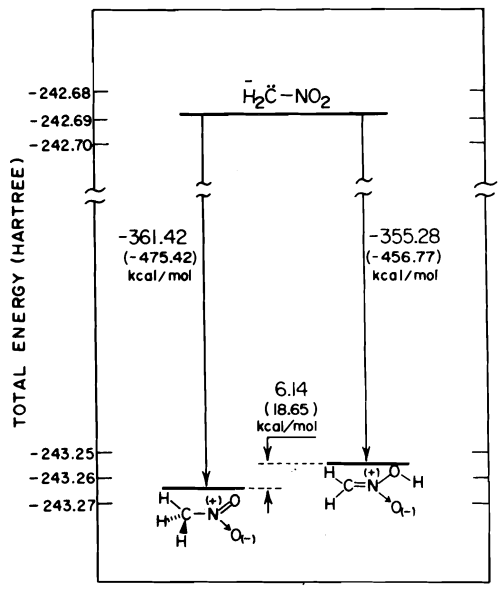

FIG. 9. Proton affinities associated with C— and O— protonation of $^-:CH_2{-}NO_2$, as calculated with extended basis set. Minimum basis set results are in parenthesis.

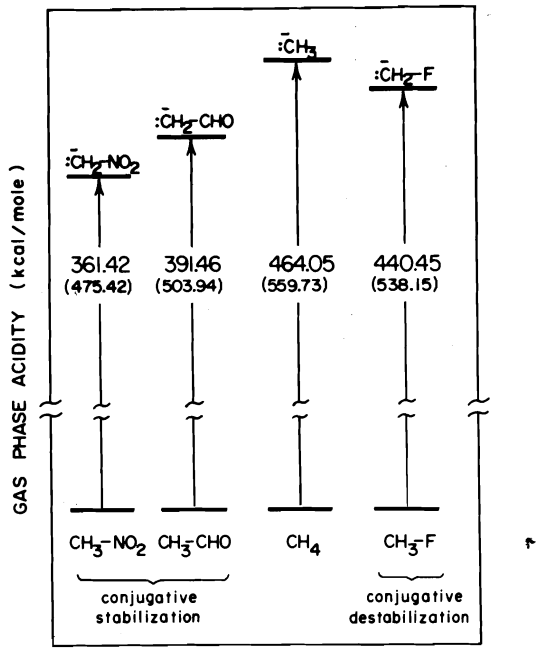

FIG. 10. Gas phase acidities of substituted methanes, as calculated with extended basis set. Minimum basis set results are in parenthesis. The conjugate bases are grouped according to conjugative stabilization and conjugative destabilization.

The calculated proton affinities of the other conjugate bases discussed in this paper are shown in Fig. 10. In both Figs. 9 and 10 the energy differences as calculated with the minimum basis are also indicated in parentheses. Though there are considerable differences between the minimum and extended basis set results, in all cases both support the same qualitative interpretation. It perhaps should be emphasized that not only

$H_2C—NO_2^-$ is capable of protonation at two different sites. In fact, the same can be said for $H_2C—CHO^-$ as well.

$$H_3C—NO_2 \leftarrow H_2C—NO_2^- \rightarrow H_2C=NO_2H$$

$$H_3C—CHO \leftarrow H_2C—CHO^- \rightarrow H_2C=CHOH$$

In agreement with the qualitative prediction of resonance theory the topology of the calculated energy hypersurface clearly implies that the two neutral tautomeric forms of nitromethane (and similarly for acetaldehyde) have only one conjugate base that is common to both.

1. R. G. Pearson and R. L. Dillon. J. Am. Chem. Soc. **75**, 2439 (1953).
2. A. J. Kresge. Can. J. Chem. **52**, 1897 (1973).
3. R. Kuhn and H. Albrecht. Ber. **60**, 1297 (1927).
4. R. L. Shriner and J. H. Young. J. Am. Chem. Soc. **52**, 3332 (1930).
5. N. Kornblum, N. N. Lichtin, J. T. Patton, and D. C. Iffland. J. Am. Chem. Soc. **69**, 307 (1947).
6. R. Ditchfield, W. J. Hehre, and J. A. Pople. J. Chem. Phys. **54**, 724 (1971).
7. W. J. Hehre, W. A. Lathan, R. Ditchfield, M. D. Newton, and J. A. Pople. GAUSSIAN 70, Quantum Chemistry Program Exchange, Indiana University, Bloomington, Indiana.
8. E. Tannenbaum, R. D. Johnson, R. J. Myers, and W. D. Gwinn. J. Chem. Phys. **22**, 949 (1954).
9. E. Tannenbaum, R. J. Myers, and W. D. Gwinn. J. Chem. Phys. **25**, 42 (1956).
10. S. Wolfe, H. B. Schlegel, I. G. Csizmadia, and F. Bernardi. Can. J. Chem. **53**, 3365 (1975).
11. R. E. Kari, and I. G. Csizmadia. J. Chem. Phys. **56**, 4337 (1970).
12. S. Wolfe, L. M. Tel, J. H. Liang, and I. G. Csizmadia. J. Am. Chem. Soc. **94**, 1361 (1972).

Can. J. Chem. Downloaded from www.nrcresearchpress.com by 210.87.254.42 on 09/05/12
For personal use only.

Studies on inorganic ion exchangers. II. Synthesis, ion exchange properties, and applications of ferric arsenate

J. P. RAWAT AND J. P. SINGH
Department of Chemistry, Aligarh Muslim University, Aligarh, U.P., India
Received October 9, 1975

J. P. RAWAT and J. P. SINGH. Can. J. Chem. **54**, 2534 (1976).

A new inorganic ion exchanger, ferric arsenate, has been prepared under varied conditions. The product formed by the homogeneous precipitation method is most stable. Ion exchange selectivity with different metal ions (alkali metal and alkaline earth metal ions) is different and depends upon the hydrated radii of the exchanging cation. A straight line is obtained for the plot of capacity against hydrated radii of the cation in the same group. Some important separations are achieved quantitatively on the columns of ferric arsenate.

J. P. RAWAT et J. P. SINGH. Can. J. Chem. **54**, 2534 (1976).

On a préparé, sous diverses conditions, un nouvel échangeur inorganique d'ions, l'arsénate ferrique. Le produit formé par la méthode de précipitation homogène est très stable. La sélectivité lors de l'échange ionique avec différents ions métalliques (les ions des métaux alcalins et des alcalino-terreux) est différent et dépend du rayon hydraté du cation produisant l'échange. On obtient une ligne droite lorsque l'on dresse un graphique de la capacité d'échange en fonction du rayon hydraté du cation dans un même groupe. On a obtenu quantitativement quelques séparations importantes sur les colonnes d'arsénate ferrique.

[Traduit par le journal]

Introduction

Synthetic inorganic ion exchangers are undergoing rapid development. Walton (1) reviewed the applications of these exchangers in the analytical field. Most of them are prepared by direct precipitation. Most of the studies on inorganic ion exchangers are concerned with zirconium phosphate (2). Arsenates should also follow the same trend as phosphates. Arsenates of zirconium (3), titanium (4), chromium (5), tin (6), thorium (7), and cerium (8) have been synthesized and used for various column and paper chromatographic purposes. Ferric arsenate has not been studied as an ion exchanger so far. Therefore, we decided to synthesize this material under varying conditions of mole ratio, temperature, and p*H* and to study its ion exchange behavior. The product formed by homogeneous precipitation showed the maximum stability. Therefore most of the work is reported on this sample. Some analytically important separations are achieved. Efforts are made to correlate ion exchange capacity with hydrated radii.

Experimental

Reagents

Arsenic acid (B.D.H.) (75% w/v), sodium arsenate dibasic (Riedel), sodium *meta* arsenite, and ferric nitrate (B.D.H.) were used. All other reagents were of Analar grade.

Apparatus

An Elico p*H* meter model L1-10, Bausch and Lomb Spectronic-20, temperature controlled SICO shaker, conductivity bridge Model Phillips PR 9500, and Sargent Oscillometer type (V) were used for p*H* measurements, spectrophotometry, shaking, conductometry, and high frequency titrations respectively.

Synthesis Procedure

Ten samples of ferric arsenate were prepared by mixing 0.1 *M* solutions of sodium arsenate (or arsenic acid) (A) and 0.1 *M* solutions of ferric nitrate (B) in different ratios. The solution of sodium arsenate or arsenic acid was added to the solution of ferric nitrate. (Solution A was added in small increments to solution B in a flask and the reaction mixture was continuously shaken; this process was called 'regular mixing'.) Sample No. 11 was prepared by mixing B with 0.1 *M* sodium arsenite in the ratio 3:4 and p*H* 1 was adjusted by adding HNO_3 and sodium hydroxide solution. No precipitation took place at this stage. Hydrogen peroxide was added in sufficient excess and the reaction mixture was heated for an hour for complete precipitation (here arsenite changes to arsenate by a slow process and arsenate reacts with ferric nitrate to form ferric arsenate). Sample No. 12 was prepared by refluxing the mother liquor of sample No. 2 for 24 h. The precipitates so formed were allowed to settle for 24 h at room temperature and then washed with distilled water several times by decantation until the p*H* of the supernatant liquid was 4–5. This was then filtered and the residue was dried at 40 °C in an incubator. The dried product broke down into small particles when immersed

Can. J. Chem. Downloaded from www.nrcresearchpress.com by 210.87.254.5 on 09/05/12
For personal use only.

TABLE 1. Synthesis and properties of ferric arsenate

Sample No.	Experimental: Molar concentration Ferric	Arsenate	Mixing volume ratio $Fe^{3+}:AsO_4^{3-}$	p*H* of final solution	Method applied	Results: Appearance	Chemical analysis Fe/As	Ion exchange capacity (mequiv./g) for Na^+
1	0.1	0.1 AA*	1:1	1.2	Mixing regular	Gray	1:1.40	0.60
2	0.1	0.1 AA	1:7	1.0	Mixing regular	White	1:1.80	0.60
3	0.1	0.1 AA	1:7	2.0	Mixing regular	White	1:1.72	0.61
4	0.1	0.1 SA	1:1	3.0	Mixing regular	Gray	1:1.0	0.47
5	0.1	0.1 SA	1:2	4.0	Mixing regular	Gray	1:1.30	0.46
6	0.1	0.1 AA	1:7	1.5	Mixing regular	White	1:1.05	0.54
7	0.1	0.1 AA	1:7	2.5	Mixing regular	White	1:1.08	0.30
8	0.1	0.1 AA	1:7	2.0	Mixing regular	White	1:1.59	0.70
9	0.1	0.1 SA	3:8	5.0	Mixing regular	Gray	1:3.46	0.56
10	0.1	0.1 SA	6:8	4.0	Mixing regular	Gray	1:2.19	0.75
11	0.1	0.1 SA^0	6:8	1.0	Homogeneous precipitation	Gray	1:2.56	0.80
12	0.1	0.1 AA*	1:7	1.0	Reflux	White powder	1:1.81	—

*AA, arsenic acid; SA, sodium arsenate; SA^0, sodium arsenite.

in water. It was converted into the hydrogen form by repeated treatment with 1 *M* nitric acid. The excess acid was washed with demineralized water and the granules were dried at 40 °C. The material was now ready for column operation. For distribution studies the sample was sized by sieving to get a product of 100–200 mesh. The conditions of preparation are summarized in Table 1.

Ion Exchange Capacity

The ion exchange capacity was determined by using some mono- and divalent ions. The ion exchange capacity was determined by taking 1 g of the exchanger in the H^+ form (converted according to procedure given in synthesis) in a column, and passing 1 *M* solutions of different mono- and divalent ions over it. The liberated H^+ was titrated with standard sodium hydroxide solution. The effluent collected in each case was 400 ml.

To check whether the exchangers, as synthesized, contained replaceable sodium ions, they were treated in columns with excess 1 *M* nitric acid and washed; the hydrogen ions were then displaced by passing 1 *M* sodium nitrate as before. Again the capacity was found to be 0.79 mequiv./g. The ion exchange capacity of ferric arsenate (sample No. 11) by 1 *M* $NaNO_3$ was determined at room temperature after drying the exchanger at different temperatures in a muffle furnace for 2 h in every case.

*p*H *Titrations*

p*H* titrations of 0.5 g of ferric arsenate sample No. 11 with 0.1 *M* solutions of lithium hydroxide, sodium hydroxide, and potassium hydroxide were performed by the method of Topp and Pepper (9). In titrations with added salts, 0.1 *M* solutions of salts were added to the above-mentioned alkalies. The p*H* of the solution after shaking with the reaction mixture for 4 h was noted.

Chemical Analysis

The exchanger (0.5 g) was dissolved in concentrated HNO_3 and then iron was precipitated as hydroxide (10, p. 532). The arsenic in the filtrate and iron in the precipitate were determined volumetrically with ammonium thiocynate (10, p. 117) and sodium thiosulfate solutions.

Chemical Stability

(*a*) *Equilibrium Studies for Dissolution*

Ferric arsenate (500 mg) in H^+ form (No. 11) was shaken with 50 ml of water in a shaker for different time intervals. The amount of material dissolved in each case was determined by noting the absorbance of the solution after developing the color for the determination of iron. The absorbance was 0.09, 0.14, 0.14, and 0.14 when the shaking time was 1, 2, 3, and 4 h. This shows that equilibrium is reached in 2 h and hence any time more than 2 h will be suitable for the dissolution studies.

(*b*) *Colorimetric Determinations*

The chemical stability of ferric arsenate in H^+ form (No. 11) was studied in water, 0.1 *M* HNO_3, and 0.1 *M* acetic acid by shaking the exchanger (0.5 g) with 50 ml of the solvent concerned in a shaker for 6 h. The undissolved portion of ferric arsenate was filtered off. The ferric and arsenate contents in the filtrate were determined spectrophotometrically by the potassium thiocyanate (12, p. 286) and hydrazine sulfate – ammonium molybdate method (12, p. 524).

Hydrolysis

Hydrolysis of all the samples in H^+ form was studied by using 0.5 g of the exchanger in the hydrolysis apparatus (Visser's method) (14). For this purpose an apparatus was assembled in which the agitated sample was washed continuously with conductivity water (p*H* 6.5–7.0). The flow rate of the effluent was 6–8 drops/min. Effluent 10 ml portions were titrated with 0.01 *M* NaOH until the p*H* approached the value of pure water.

Conductometric and Oscillometric Titrations

To get the optimum combining ratio of ferric and

Can. J. Chem. Downloaded from www.nrcresearchpress.com by 210.87.254.5 on 09/05/12
For personal use only.

TABLE 2. Ion exchange capacities of some mono- and divalent cations on ferric arsenate sample No. 11

Metal ion	Salt solution used	p*H* of solution	Ion exchange capacity (mequiv./g)	Hydrated radii (Å)
Li^+	Lithium nitrate (2 *M*)	5.9	0.63	3.40
Na^+	Sodium nitrate (2 *M*)	6.0	0.80	2.76
K^+	Potassium nitrate (2 *M*)	6.0	0.88	2.32
Mg^{2+}	Magnesium nitrate (1 *M*)	6.6	0.33	7.00
Ca^{2+}	Calcium nitrate (1 *M*)	6.7	0.56	6.30
Sr^{2+}	Strontium nitrate (1 *M*)	6.7	0.60	—
Ba^{2+}	Barium nitrate (1 *M*)	6.7	0.69	5.90

arsenate, high frequency and conductometric titrations of ferric with arsenate were performed. For high frequency titrations 2 ml of the 0.1 *M* solution of sodium arsenate was taken in the cell, diluted to 100 ml, and a 0.1 *M* solution of ferric nitrate was added from the burette. For the conductometric titration 20 ml of 0.1 *M* sodium arsenate solution was taken in the cell, diluted to 50 ml with conductivity water, and titrated with 0.1 *M* ferric nitrate. Both titrations showed breaks at a mole ratio of 3:4. This ratio was taken for the preparation of sample Nos. 10 and 11.

Separations

For separation studies a 30 cm high glass column having a diameter of 0.39 cm was used. Ferric arsenate (2.0 g) was placed in the column with a glass-wool support. The column was washed with demineralized water and the amount of cation added to the column was less than 3% of the experimental ion exchange capacity of the exchanger. The flow rate of the effluent was 8–9 drops/min. All the cations were eluted with 10^{-3} *M* HNO_3; finally barium and aluminum were eluted with 1% NH_4NO_3 and 0.1 *M* phenol. The cations were determined by EDTA titration. In the case of NH_4NO_3 the effluent was evaporated to dryness and then titrated with EDTA. Separations of Ba(II) from Mg(II), Ca(II), Sr(II), Pb(II) and Al(III) from Ga(III) have been achieved.

Results and Discussion

The results of ion exchange capacity studies of various samples of ferric arsenate are presented in Table 1. These results show that the material works as a weak cation exchanger. Ion exchange capacities were measured with different mono- and divalent ions. The results summarized in Table 2 indicate that the ion exchange selectivity of ferric arsenate is different for different cations. The ion exchange capacities are related to the abilities of the different cations to displace hydrogen ions from the exchanger (ferric arsenate). This ability is of course the affinity or the selectivity. The selectivity observed with ferric arsenate is in the same order as given by Hofmeister's lyotropic row (15). Further the ion exchange selectivity depends upon the hydrated radii of these cations and a plot of hydrated radii against ion exchange capacity is a straight line for cations in the same group (Fig. 5). Thus for Li, Na, and K one straight line is obtained; another straight line is obtained for Ba, Sr, Mg, and Ca. These results reveal that the higher the hydrated radii the smaller is the ion exchange capacity. Such a plot is useful because it may be applied for the calculation of hydrated radii.

The ion exchange capacity of the material after drying at different temperatures was 0.8, 0.35, 0.28, 0.20, 0.14, 0.10, 0.05, 0.02, and 0.0 mequiv./g at drying temperatures 25, 100, 150, 200, 300, 400, 500, 600, and 700 °C. These results reveal that by increasing temperature the capacity decreases.

The p*H* titration curves with and without added salts are given in Figs. 1 and 2. These results again confirm that ferric arsenate works as a weak acid.

The results of the chemical analyses presented in Table 1 indicate that the composition of the material depends highly on the conditions of preparation. The mole ratio of Fe:As obtained by chemical analysis does not coincide with the ratio obtained by the conductometric and high frequency titrations. A similar result was observed for stannic molybdate (11). The determination of the chemical stability of ferric arsenate in water, 0.1 *M* HNO_3, and 0.1 *M* CH_3COOH reveals that the dissolution of iron is 3.0, 2.8, 47 mg/l and that of arsenic is 0.2, 0.2, 0.0 mg/l in water, 0.1 *M* CH_3COOH, and 0.1 *M* HNO_3. Hence, selective dissolution of iron during washing of the precipitate may account for a lower Fe:As ratio than 3:4 in the final sample.

According to the composition of 3:4 predicted

Can. J. Chem. Downloaded from www.nrcresearchpress.com by 210.87.254.5 on 09/05/12
For personal use only.

Can. J. Chem. Downloaded from www.nrcresearchpress.com by 210.87.254.5 on 09/05/12
For personal use only.

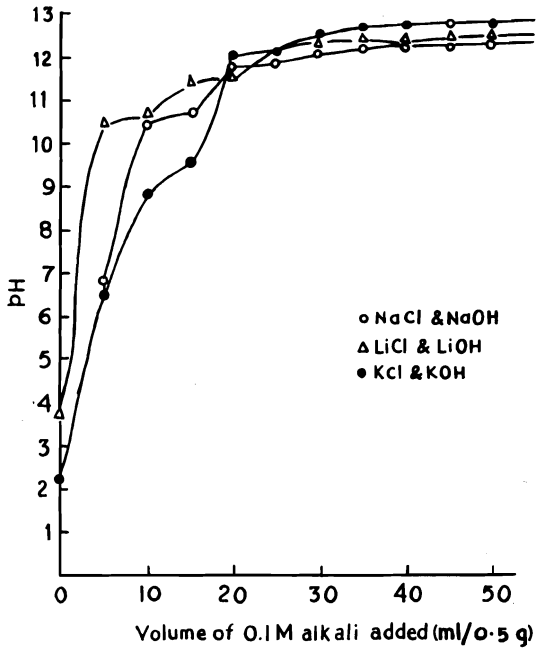

FIG. 1. p*H* titration curves with added salts for ferric arsenate sample No. 11.

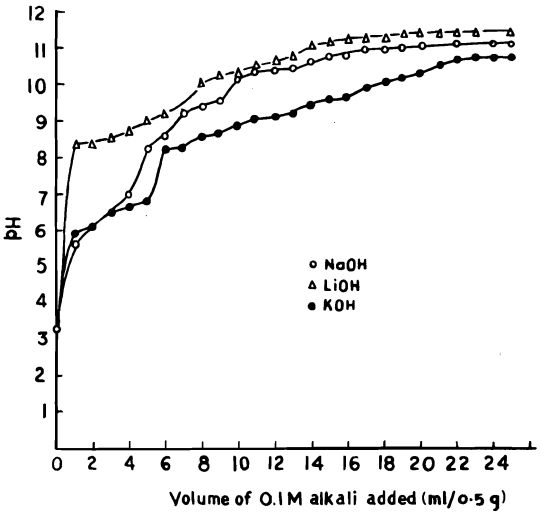

FIG. 2. p*H* titration curves without added salts for ferric arsenate sample No. 11.

from high frequency and conductometric titrations the formula may be given as $Fe_3H_3(AsO_4)_4 .nH_2O$ where $n = 30$, which gives a capacity of about 2.5 mequiv./g if all $3H^+$ were dissociated. However, the experimental value of 0.8 mequiv./g is nearly 1/3 of the theoretical value, probably due to only 1 replaceable hydrogen ion of the 3.

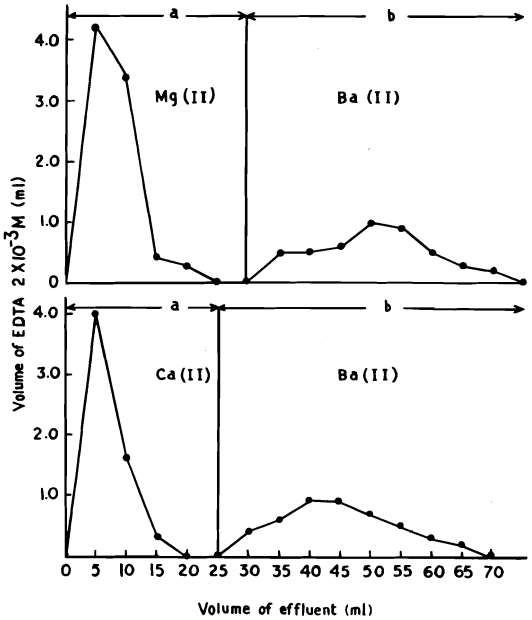

FIG. 3. Separation of Mg(II) from Ba(II) and Ca(II) from Ba(II) on ferric arsenate columns: (*a*) 10^{-3} *M* HNO_3; (*b*) 1% NH_4NO_3.

The hydrolysis results indicated that all the 12 samples undergo hydrolysis. However, samples 6 and 11 show greater resistance to hydrolysis than the others. The ion exchange capacity of sample No. 11 (0.80 mequiv./g) is greater than that of sample No. 6 (0.54 mequiv./g). Sample No. 11 is prepared in the molar ratio as predicted by conductometry and high frequency titrations. Therefore, most of the studies are reported for this sample No. 11.

Sample No. 11 was prepared by homogeneous precipitation. The method is similar to that of Jump and Sherwood (13) who claimed to have prepared zirconium arsenate (crystalline) by homogeneous precipitation following the oxidation of arsenite to arsenate by nitric acid. We have preferred hydrogen peroxide to nitric acid, since excess of hydrogen peroxide does not affect the p*H* of the solution. Thus, either hydrogen peroxide oxidizes arsenite to arsenate slowly on heating and arsenate ion reacts with ferric ion to produce a precipitate of ferric arsenate or it is also possible that arsenite first reduces Fe(III) to Fe(II) and then H_2O_2 reoxidizes Fe(II).

The approximate K_d values for 26 metal ions in nitric acid and phenol are in the following order.

Can. J. Chem. Downloaded from www.nrcresearchpress.com by 210.87.254.5 on 09/05/12
For personal use only.

TABLE 3. Separation of Ba(II) from Mg(II), Ca(II), Sr(II), Pb(II), and Al(III) from Ga(III) on ferric arsenate columns, sample No. 11

Mixture separated	Eluent	Volume of effluent (ml)	Taken (μg)	Found (μg)	% error
Ca^{2+}	10^{-3} *M* HNO_3	20	469	472	0.6
Ba^{2+}	1% NH_4NO_3	70	1236	1236	0.0
Mg^{2+}	10^{-3} *M* HNO_3	25	401	403	0.5
Ba^{2+}	1% NH_4NO_3	80	1236	1220	−1.3
Pb^{2+}	10^{-3} *M* HNO_3	30	2189	2196	0.3
Ba^{2+}	1% NH_4NO_3	80	1236	1236	0.0
Sr^{2+}	10^{-3} *M* HNO_3	35	811	806	−0.6
Ba^{2+}	1% NH_4NO_3	85	1236	1247	0.9
Al^{3+}	0.1 *M* phenol	30	440	441	0.2
Ga^{3+}	10^{-3} *M* HNO_3	70	1264	1268	0.3

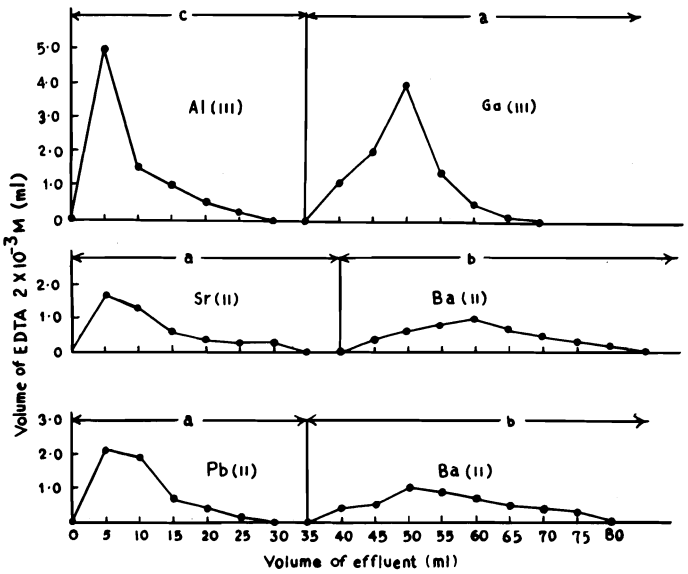

FIG. 4. Separation of Sr(II) from Ba(II), Pb(II) from Ba(II), and Al(III) from Ga(III) on ferric arsenate columns: (*a*) 10^{-3} *M* HNO_3; (*b*) 1% NH_4NO_3; (*c*) 0.1 *M* phenol.

10^{-3} *M* HNO_3

$Ba^{2+} > Mn^{2+} > Sr^{2+} > Ca^{2+} > Hg^{2+} > Ga^{3+} = Nd^{3+} > Ce^{3+} > Cu^{2+} > Lu^{3+} > Ni^{2+} > Mg^{2+} > Hf^{4+} > Cd^{2+} > Pb^{2+} = Dy^{3+} > Eu^{3+} > Er^{3+} > Tb^{3+} > Al^{3+} > Pr^{3+} > Zn^{2+} > Yb^{3+} > Sm^{3+} = Ho^{3+}$

0.1 *M* Phenol

$Ga^{3+} > Nd^{3+} > Pb^{2+} > Ba^{2+} = Ce^{3+} > Lu^{3+} > Zn^{2+} > Hg^{2+} > Cd^{2+} > Cu^{2+} > Ni^{2+} = Ca^{2+} > Al^{3+} > Hf^{4+} > Sr^{2+} = Er^{3+} > Dy^{3+} > Sm^{3+} > Pr^{3+} > Mg^{2+} > Ho^{3+} > Eu^{3+} > Gd^{3+} = Tb^{3+} > Yb^{3+}$

These results indicate the order of selectivity in two solvent systems as a qualitative ranking of affinity towards various metal ions. The separations achieved on the columns of ferric arsenate are presented in Figs. 3 and 4. Ba(II) is completely adsorbed on the exchanger and hence this can be separated from the other 22 metal ions. Ca, Sr, and Ba belong to the same group, therefore, the separations of Mg(II), Ca(II), and Sr(II) from Ba(II) are important. The separations of Ba(II) and Pb(II) and of Al(III) from Ga(III) are also important for various reasons. The quantitative results of separations are given in

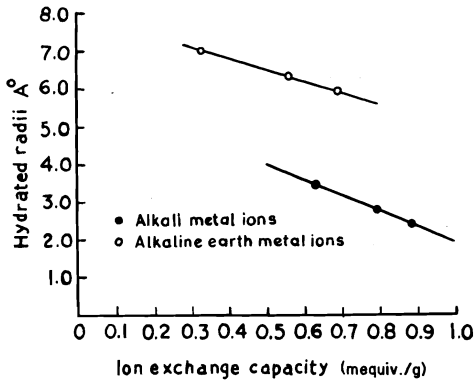

FIG. 5. Ion exchange capacity as a function of hydrated radii.

Table 3. These results reveal that the above-mentioned separations are quantitative within the experimental error range (−1.3 to +0.9%). The separations are sharp, as is clear from Figs. 3 and 4.

Acknowledgments

The authors are grateful to Prof. W. Rahman for providing research facilities. One of us (J. P. Singh) is also thankful to C.S.I.R. (India) for financial assistance.

1. H. F. WALTON. Anal. Chem. **46**, 398R (1974).
2. M. QURESHI, S. Z. QURESHI, J. P. GUPTA, and H. S. RATHORE. Sep. Sci. Rev. **7**(6), 615 (1972).
3. S. BATANERO, P. RODRIQUEZ, P. M. BURRIEL, and F. MART. Inf. Quim. Anal. **26**, 84 (1972); **26**, 262 (1972).
4. M. QURESHI, J. P. RAWAT, and V. SHARMA. Talanta, **20**, 267 (1973).
5. M. QURESHI, R. KUMAR, and H. S. RATHORE. Talanta, **19**, 1377 (1972).
6. M. QURESHI, and S. D. SHARMA. Anal. Chem. **45**, 1283 (1973).
7. G. ALBERTI and M. A. MASSUCCI. J. Inorg. Nucl. Chem. **32**, 1719 (1970).
8. G. ALBERTI, V. COSTANTINO, F. DIGREGONO, and E. TORRACCA. J. Inorg. Nucl. Chem. **31**, 3195 (1969).
9. N. E. TOPP and K. W. PEPPER. J. Chem. Soc. 3299 (1949).
10. N. H. FURMAN. Standard methods of chemical analysis. 6th ed. D. van Nostrand Company, Inc., Princeton, N.J. 1962.
11. M. QURESHI and J. P. RAWAT. J. Inorg. Nucl. Chem. **30**, 305 (1968).
12. E. B. SANDELL. Colorimetric determination of traces of metals. 3rd ed. Mack Printing Co., Easton, Pa. 1959.
13. J. R. JUMP and G. R. SHERWOOD. Analyst, **22**, 496 (1950).
14. E. M. LARSEN and D. R. VISSERS. J. Phys. Chem. **64**, 1732 (1960).
15. J. INCZEDY. Analytical applications of ion exchangers. Pergamon Press, London, Engl. 1966. p. 27.

Can. J. Chem. Downloaded from www.nrcresearchpress.com by 210.87.254.5 on 09/05/12
For personal use only.

Kinetic study of formation of nickel(II)-isoquinoline complex in water and nonaqueous solvents

PRAPHULLA KUMAR CHATTOPADHYAY AND BYRON KRATOCHVIL
Department of Chemistry, University of Alberta, Edmonton, Alta., Canada T6G 2E1

Received February 23, 1976

PRAPHULLA KUMAR CHATTOPADHYAY and BYRON KRATOCHVIL. Can. J. Chem. **54**, 2540 (1976).

Rate constants and activation parameters for the formation of the monocomplex of nickel(II) with isoquinoline in water, methanol, dimethylsulfoxide, and *N*,*N*-dimethylformamide were obtained from measurements by stopped-flow spectrophotometry. The data are compared with previously reported work by other authors for substitution at nickel(II) with related monodentate and multidentate ligands. The results in all solvents except dimethylsulfoxide are consistent with an I_d mechanism. In dimethylsulfoxide substitution at nickel(II) proceeds in a similar way for all monodentate ligands but whether the mechanism is I_d or D cannot be ascertained.

PRAPHULLA KUMAR CHATTOPADHYAY et BYRON KRATOCHVIL. Can. J. Chem. **54**, 2540 (1976).

Faisant appel à la spectrophotométrie par flux stoppé, on a effectué des mesures permettant d'obtenir les constantes de vitesse et les paramètres d'activation pour la formation de monocomplexes du nickel(II) avec l'isoquinoline dans l'eau, le méthanol, le diméthylsulfoxyde et la *N*,*N*-diméthylformamide. On compare ces données avec celles rapportées antérieurement par d'autres auteurs pour la substitution au niveau du nickel(II) par des ligands mono et multidentates. Les résultats dans tous les solvants, excepté le diméthylsulfoxyde, sont en accord avec un mécanisme I_d. Dans le diméthylsulfoxyde, la substitution au niveau du nickel(II) procède par une voie similaire pour tous les ligands monodentates; on ne peut toutefois déterminer si le mécanisme est I_d ou D.

[Traduit par le journal]

Introduction

The volume of data collected on kinetics of ligand substituted reactions in the past 15 years indicates that the gross features of formation of many labile complexes of nickel(II) in water (1), methanol (2), and ethanol (3) are consistent with an I_d mechanism in which the rates of formation of the complexes are controlled by the rates of exchange of solvent molecules between the inner sphere of the nickel ion (NiS_6^{2+}, where S is a solvent molecule) and the bulk solvent. It has been shown (4*a*) that formation of the monocomplexes of nickel(II), cobalt(II), and iron(II) with many monodentate ligands in acetonitrile as solvent can be accommodated within the framework of the I_d mechanism. Apparent 'anomalous' results observed in reactions of nickel(II) with various multidentate ligands (4) could also be rationalized to fit into the structure of the I_d mechanism when effects of different possible types of solute–solvent interactions involving metal ion, ligand and solvent molecules, both in the inner sphere and outer sphere of the metal ion, were considered.

The pathways of the I_d mechanism with nickel(II) and a monodentate ligand L can be represented by

$$[1]\qquad NiS_6 + L \underset{}{\overset{K_{12}}{\rightleftharpoons}} S\text{-}NiS_5,\ L \underset{k_{32}}{\overset{k_{23}}{\rightleftharpoons}} L\text{-}NiS_5,S$$

$$\qquad\qquad\qquad\qquad I \qquad\qquad II$$

in which the rate-determining step for the formation of the inner sphere complex (process II, forward rate constant k_{23}) is preceded by rapid formation of an outer sphere complex (process I, equilibrium formation constant K_{12}). Charges on the metal ion and ligand have been omitted for convenience. For 'normal' types of substitution, when $K_{12}[L] \ll 1$, the second order rate constant k_f for formation of the complex is given by

$$[2]\qquad k_f = K_{12}k_{23}$$

In testing whether substitution is 'normal', the ratio (5) R, given by

$$[3]\qquad R = \frac{4k_{23}}{3k_{ex}} = \frac{4}{3}\frac{k_f}{k_{ex}K_{12}}$$

Can. J. Chem. Downloaded from www.nrcresearchpress.com by 210.87.254.105 on 09/05/12
For personal use only.

Can. J. Chem. Downloaded from www.nrcresearchpress.com by 210.87.254.105 on 09/05/12
For personal use only.

should be close to unity. Here k_{ex} is the first-order rate constant for exchange of solvent molecules between the inner sphere of the metal ion and bulk solvent at the corresponding temperature. Values of k_{ex} and the thermodynamic quantities associated with solvent exchange are generally measured by nmr spectroscopy, and data in several solvents are available (6). The equilibrium constant K_{12} is estimated from the theoretical relationship (7)

$$[4] \qquad K_{12} = \frac{4\pi Na^3}{3 \times 10^3} e^{-U(a)/kT}$$

where

$$[5] \qquad U(a) = \frac{z_1 z_2 e^2}{Da} - \frac{z_1 z_2 e^2 \kappa}{D(1 + \kappa a)}$$

'a' is the closest distance of approach of the center of the ligand to the center of the solvated metal ion.

The kinetic behavior of ligand substitution reactions of nickel(II) in water and, to some extent, in methanol, is insensitive to the nature of the ligand, but in dipolar aprotic solvents like acetonitrile and dimethylsulfoxide, apparently divergent behavior may be observed owing to different types of solute–solvent interactions with a change in the ligand (4*b*), particularly with complex multidentate ligands. As a result it often is difficult to determine the effect of different types of interactions on the overall mechanism of a reaction. The usual method of identifying the mechanism of a reaction is to compare activation parameters of the ligand substitution reaction with those for solvent exchange at the metal ion. Comparison of rates at one temperature from a mechanistic point of view, however, is often speculative and may be misleading. Fine details of the mechanism often may be better understood from consideration of the thermodynamic activation parameters.

Since for a neutral monodentate ligand the change in enthalpy associated with K_{12} (ΔH_{12}) will be close to zero, for a 'normal' substitution the enthalpy of activation for formation ($\Delta H_f^{\ddagger}$) will be close to the corresponding quantity for solvent exchange ($\Delta H_{ex}^{\ddagger}$). Unfortunately the thermodynamic activation parameters reported by various authors for solvent exchange at nickel(II) ion in any given solvent tend to be widely divergent, and it is extremely difficult to select one representative value for comparison. However, systematic measurement of the thermodynamic properties of ligand substitution reactions of metal ions with the same 'simple' monodentate ligand in a series of solvents, including water, can be expected to provide information about the gross features of the mechanism of substitution at the metal ion in those solvents. Except for a study of substitution at nickel(II) by thiocyanate ion (8), systematic investigations of this kind have not yet been reported. On the basis of limited information it has been suggested that substitution reactions by simple monodentate ligands such as pyridine or ammonia proceed normally even in acetonitrile and dimethylsulfoxide according to an I_d mechanism without any specific solute–solvent interactions.

Isoquinoline differs from pyridine structurally by a fused benzene ring. Although the addition of a fused benzene ring to pyridine does not change the pK_a of the pyridine nitrogen, the activation parameters of ligand substitution reactions of nickel(II) with isoquinoline in acetonitrile differ slightly from the expected value, whereas pyridine behaves normally. This apparent slight deviation from normal behavior was explained as being caused by the effect of the benzene ring on the stability of the outer sphere complex of nickel(II) in acetonitrile (4*a*). If this specific interaction is absent in other solvents, isoquinoline could also be expected to behave normally as pyridine does. However, owing to a lack of data on substitution at nickel(II) with isoquinoline in other solvents, it has not been possible to determine conclusively whether this effect of a benzene ring on the stability of the outer sphere complex of nickel(II) is unique in acetonitrile.

In this work we report rate constants and activation parameters for formation of the monocomplex of isoquinoline with nickel(II) in water, methanol, dimethylsulfoxide, and *N*,*N*-dimethylformamide, and compare the results with previous work. There is a particular dearth of information in dimethylformamide, and our present knowledge of possible mechanisms for the formation of labile complexes is this solvent is slight.

Experimental Section

Solvents

Acetonitrile (Aldrich, 99%) was fractionally distilled

Can. J. Chem. Downloaded from www.nrcresearchpress.com by 210.87.254.105 on 09/05/12
For personal use only.

from calcium hydride (Ventron, Lot #J4169A) in an argon atmosphere after pretreatment by the method of O'Donnell, Ayers, and Mann (9), except that the decantation after addition of sulfuric acid was replaced by a fractional distillation at atmospheric pressure. Dimethylsulfoxide (J. T. Baker) was purified according to the previous procedure (*4b*) except that the middle fraction from the first distillation was dried over 3-Å molecular sieves (Linde Division, Union Carbide Corporation) for one day before the final distillation from calcium hydride. Methanol (J. T. Baker, Baker Instra-Analyzed Spectrophotometric Quality) was dried over 3-Å molecular sieves (Linde) for a day, and then distilled fractionally from Mg over N_2. *N,N*-Dimethylformamide (MBW Chemicals, Spectrar Grade), after being dried over 3-Å molecular sieves (Linde) for one day, was decanted onto dry KOH and stirred vigorously for 12 h. It next was decanted onto dry P_2O_5 and stirred for 2 days, fresh P_2O_5 (approximately 15 g/2 l) being added after each day. Finally it was distilled fractionally from dry P_2O_5 under vacuum at 40 °C with an N_2 bleed. The middle fraction was collected and distilled twice more from P_2O_5, the middle fraction being collected each time. Before each distillation the cycle of treatment with KOH and P_2O_5 was repeated. Deionized water was distilled from alkaline $KMnO_4$.

Reagents

Nickel(II) was introduced as the perchlorate salt. For the work in dimethylsulfoxide as solvent, it was the corresponding hexasolvate (10). For acetonitrile hexakis(acetonitrile)nickel(II) perchlorate (11) was used. For dimethylformamide either hexakis(acetonitrile)nickel(II) perchlorate, or nickel(II) perchlorate monohydrate obtained from recrystallized hexahydrate (G. F. Smith) by heating under vacuum at 90 ± 5 °C, was employed. Both samples gave the same results. Nickel(II) perchlorate monohydrate was used for work in methanol and water as solvents. The concentration of the nickel(II) solutions was determined by EDTA titration with murexide indicator after dilution with water and buffering to p*H* 10 with ammonia – ammonium chloride. Isoquinoline (Aldrich, mp 26–28 °C, bp 242 °C) was fractionally distilled from KOH under vacuum at 45 °C.

Instrumentation and Experimental Procedure

All nonaqueous solvents were used within 3 days after purification except dimethylformamide, which was used within 24 h. All nonaqueous solutions were prepared and dispensed in a dry box (Kewaunee Scientific) under dry N_2, using glassware that had been oven dried at 110 °C for several days. All other standard procedures for handling nonaqueous solutions were followed. In all solvents, kinetic experiments for formation rate constants of the complex were carried out at 325 nm.

Kinetic measurements were made with a stopped-flow spectrophotometer (Durrum Instrument Co., Model D-110). A description of the instrument, along with modifications for better temperature control, has been given previously (12). The temperature of the thermostat bath and the cell were controlled to within ±0.03 °C, the temperature being recorded by a calibrated quartz thermometer (Hewlett Packard, Model 2801 A). Changes in transmission with time were recorded either by a combination of a storage oscilloscope (Tektronix, Model R564B) and an oscilloscope Land Camera (Tektronix, Model C-12) or by a waveform recorder (Biomation, Model 805) interfaced to a strip chart recorder (Hewlett Packard, Model 7101 B). In dimethylformamide and water, changes in transmission with time were recorded by both devices, and the two sets of results agreed within ±1% in each solvent.

Kinetic measurements for formation rate constants were made under pseudo-first-order conditions. The concentration of isoquinoline was kept constant at 2×10^{-4} *M* and the concentration of nickel(II) was varied through four to five values, typically from 2.5×10^{-3} to 15.0×10^{-3} *M* in water and methanol, from 2.5×10^{-3} to 10.0×10^{-3} *M* in dimethylsulfoxide, and from 2.5×10^{-3} to 7.5×10^{-3} *M* in dimethylformamide. Other experimental procedures were the same as previously described (5).

Results

Rate constants for formation (k_f) of the mono-complex of isoquinoline with nickel(II) at various temperatures are presented in Table 1. As an additional check on the purity of dimethylformamide, from which traces of dimethylamine are difficult to remove, and on the measurements of k_f and $\Delta H_f^{\ddagger}$ for the reaction of nickel(II) with isoquinoline, we repeated the study by Bennetto and Caldin (*6b*) of bipyridine with nickel(II) in this solvent. Our results for k_f and $\Delta H_f^{\ddagger}$ agreed with his values within ±1%.

TABLE 1. Rate constants for formation of mono-complex of isoquinoline with nickel(II) at various temperatures

Solvent	Rate constant (k_f) × 10^{-3} [a] (l mol^{-1} s^{-1})				
	15 °C	20 °C	25 °C	30 °C	35 °C
Water	1.03	1.61	2.04	3.23	4.26
Methanol	0.0378	0.0620	0.0965	0.154	0.243
Dimethylsulfoxide	[b]	2.67	3.37	4.20	—
N,N-Dimethylformamide	1.03[c]	1.68	2.42	—	4.85

[a]Reproducibility is ±2%; one additional significant figure given.
[b]Additional values: 2.51 at 19 °C and 2.94 at 22 °C.
[c]Additional value: 0.497 at 5 °C.

Can. J. Chem. Downloaded from www.nrcresearchpress.com by 210.87.254.105 on 09/05/12
For personal use only.

TABLE 2. Comparison of rate constants and activation parameters for ligand substitution at nickel(II) with those for solvent exchange[a]

Solvent	Ligand	k_f or k_{ex}	R	$\Delta H_f^{\ddagger}$ or $\Delta H_{ex}^{\ddagger}$	$\Delta S_f^{\ddagger}$ or $\Delta S_{ex}^{\ddagger}$	$k_{23}=k_f/K_{12}$	$\Delta H_{23}^{\ddagger}$	Donor No.	Reference
Water	Water	2.7×10^4	—	11.6	+0.6	—	—	18.0	6*c*
	Pyridine	*ca.* 4×10^3	0.6	*ca.* 11	−5.0	—	—	—	15*b*
	Isoquinoline	2.07×10^3	0.32	11.7±0.7	−4 ±2	6.46×10^3	11.7±0.7	—	This work
	Terpyridine	1.49×10^3	0.22	12.3±0.1	−3.0	—	—	—	5
	Thiocyanate[b]	3.0×10^4	[c]	12.1	+3.1	—	—	—	8
Methanol	Methanol	1.0×10^3	—	15.8	+8.0	—	—	9[d]	6*f*
	Isoquinoline	9.65×10	0.24	15.8±0.1	+3.5±0.3	1.77×10^2	15.8±0.1	—	This work
	Terpyridine	4.6×10	0.12	16.8	+1.0	—	—	—	5
	Thiocyanate	8.6×10^4	[c]	19.5	+31.2	—	—	—	8
Dimethylsulfoxide	Dimethylsulfoxide	5.2×10^3	—	12.1±0.3	−1.5±0.5	—	—	29.6	6*d*
	Pyridine	*ca.* 2×10^3	*ca.* 0.6	*ca.* 4	*ca.* −30	—	—	—	5
	4-Phenylpyridine	1.64×10^3	0.36	9.0±2	−14 ±7	—	—	—	13*b*
	Isoquinoline	3.37×10^3	1.00	7.6±0.2	−16.9±0.7	3.89×10^3	7.6±0.2	—	This work
	Thiocyanate[e]	9.0×10^4	0.85	7.8±0.6	−10 ±2	3.3×10^3	8.4±0.6	—	16
	Bipyridine	6.9×10	0.02	12.6±0.1	−8	—	—	—	5
	Terpyridine	2.5×10	0.007	15.0±0.7	−2	—	—	—	5
N,*N*-Dimethylformamide	*N*,*N*-Dimethylformamide	3.8×10^3	—	15.0	+8	—	—	26.8	6*e*
	Isoquinoline	2.42×10^3	0.98	12.4±0.4	−2 ±1	2.80×10^3	12.4±0.4	—	This work
	Bipyridine	5.4×10^2	0.22	12.7±0.2	−3.3	—	—	—	6*b*
	Thiocyanate[b]	1.3×10^5	[c]	16.5	+21.5	—	—	—	8
Acetonitrile	Acetonitrile	2.7×10^3	—	15.0	+8.5	—	—	14.1	6*g*
	Pyridine	8.3×10^2	0.39	14.7±0.4	+4.0	—	—	—	5
	Isoquinoline	1.24×10^3	0.57	11.9	−5.0	1.16×10^3	11.9	—	4
	Thiocyanate[b]	1.5×10^5	[c]	17	+22	—	—	—	8

[a]All measurements made at 25 °C unless otherwise noted. Units: s^{-1} for k_{ex}, l mol^{-1} s^{-1} for k_f, s^{-1} for k_{23}, kcal mol^{-1} for all $\Delta H^{\ddagger}$ values, cal mol^{-1} deg^{-1} for all $\Delta S^{\ddagger}$ values. Values for donor numbers of solvents taken from ref. 21 except where otherwise noted.
[b]Measurements made at 20 °C.
[c]Ionic strength not reported.
[d]Unpublished results of P. K. Chattopadhyay and B. Kratochvil.
[e]Data corrected to ionic strength = 0.

TABLE 3. Intercepts of pseudo-first-order plots for formation of monocomplex of isoquinoline with nickel(II)

Solvent	Intercept (k_b) [a] (s^{-1})				
	15 °C	20 °C	25 °C	30 °C	35 °C
Water	12.2	21.0	29.6	52.3	78.4
Methanol	0.5_6	1.0_6	1.9_4	3.5_5	6.1
Dimethylsulfoxide	[b]	65	110[c]	190[c]	—
N,*N*-Dimethylformamide	9.6[d]	13.7	19.5	—	46.8

[a]Reproducibility ±5%, error in absolute values ±10% unless otherwise noted.
[b]Additional values: 54 at 19 °C and 87 at 22 °C.
[c]Error limits between 10 and 40%. See text.
[d]Additional value: 2.7 at 5 °C.

In Table 2 rate constants at 25 °C and activation parameters for formation are compared with the corresponding quantities for solvent exchange at nickel(II). The intercepts observed in the pseudo-first-order plots for formation of the complex with isoquinoline are listed in Table 3. Values of the intercept are sometimes used to obtain values of k_b, the rate constant for the reverse reaction (13). But when observed pseudo-first-order rate constants for a reaction fall in the range of 100 to 300 s^{-1}, the experimental conditions are near the limits of the stopped-flow method, and therefore any error in recording of time on the order of a fraction of a millisecond will greatly affect values of K_{obs}. A constant uncertainty in K_{obs} may give an incorrect intercept; this is not uncommon in nonaqueous solvents (6*b*) owing to the presence of traces of impurities. Values of k_f, however, being calculated by least-squares fit from the slope of a line drawn through the experimental points, are not affected by constant error in K_{obs} (4*b*, 6*b*). The uncertainty in k_f is on the order of ±2% for the measurements made in this work. Values for k_b obtained from intercepts of plots of K_{obs} against $[Ni^{2+}]$ for water at 15 °C and dimethylsulfoxide at 30 °C are 12.2 and 190 (Fig. 1 and Table 3). These compare with preliminary values of about 12 and 150 obtained by us through direct measurement on these systems.

The pK_a of isoquinoline in aqueous solution is 5.4 (14). From consideration of the limited experimental information available on the thermodynamic properties of solvents (4, 5, 15) isoquinoline is not expected to be protonated in any of the solvents studied in this work. On the basis of the kinetic data discussed below and also as expected from previous results in acetonitrile (4), it was concluded that only the monocomplex is formed under the experimental conditions employed.

Formation Rate Constant (k_f)

Pseudo-first-order plots in water as solvent are shown in Fig. 1. Second order rate constants for formation (k_f) are calculated from the slopes of the plots. In all solvents studied, as shown for water in Fig. 1, the plots (*a*) are linear with concentration of nickel(II) and (*b*) give an intercept that increases with increasing temperature, in-

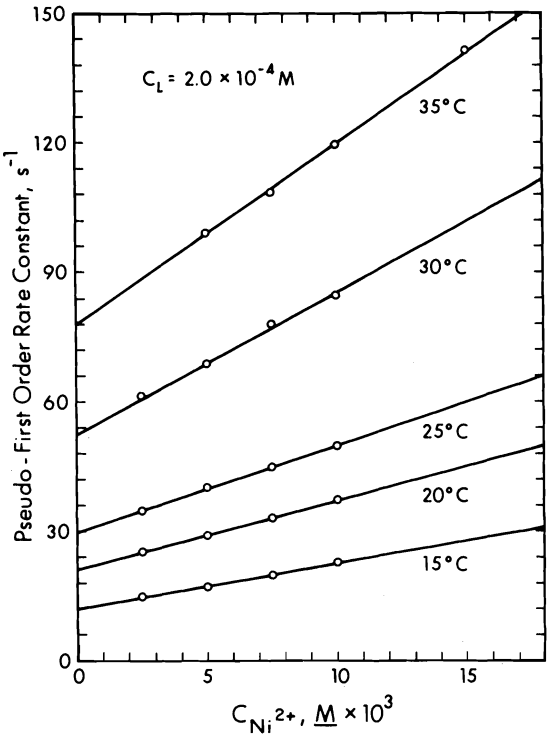

FIG. 1. Pseudo-first-order rate constants for formation of monocomplex of nickel(II) with isoquinoline in water as solvent.

Can. J. Chem. Downloaded from www.nrcresearchpress.com by 210.87.254.105 on 09/05/12
For personal use only.

Can. J. Chem. Downloaded from www.nrcresearchpress.com by 210.87.254.105 on 09/05/12
For personal use only.

dicating that (*a*) only one complex is formed and (*b*) its formation is not complete.

Discussion

From our results in Table 2 for the reaction of nickel(II) with isoquinoline, the following conclusions can be drawn: (*1*) Values of R at 25 °C and activation parameters associated with k_f seem reasonably 'normal' in water, methanol, acetonitrile, and dimethylformamide as solvents. (*2*) In dimethylsulfoxide the activation energy associated with k_f for isoquinoline is similar to the corresponding quantities reported for other monodentate ligands, as summarized in Table 2. Values of R at 25 °C for all monodentate ligands seem reasonably 'normal'.

Considering first the results of formation rate constants and associated activation parameters in dimethylsulfoxide as solvent, we see that any mechanistic discussion of the results in this solvent is complicated by the following conflicting observations:

(1) Values of $\Delta H_{ex}^{\ddagger}$ for solvent exchange at nickel(II) ranging from 6 to 13 kcal have been reported (Table 2); values of k_{ex} at 25 °C vary from 3×10^3 to 14×10^3 s^{-1}. Recently Coetzee and Hsu (16) proposed an I_d mechanism for the substitution reaction at nickel(II) by thiocyanate ion in dimethylsulfoxide as solvent using 8 to 9 kcal as the value of $\Delta H_{ex}^{\ddagger}$ for solvent exchange at nickel(II) in this medium.

(2) For substitution reactions at nickel(II) with many monodentate ligands, values of R seem reasonably 'normal' and $\Delta H_f^{\ddagger}$ values for all the monodentate ligands studied so far (charged or neutral) are in the neighbourhood of 8 to 9 kcal.

(3) With multidentate ligands additional factors such as steric effects influence values of k_f and $\Delta H_f^{\ddagger}$. For substitution reactions at nickel(II) with bipyridine, terpyridine and phenanthroline, $\Delta H_f^{\ddagger}$ values for the formation of monocomplexes could be fitted within the framework of the I_d mechanism by considering 'ring closure', that is, formation of the final bond between ligand and metal ion, to be the rate-limiting step, and substitution with pyridine to be 'normal' (4*b*). Recently a wide range of formation rates and associated activation parameters in reactions of nickel(II) with bidentate substituted pyridine ligands have been observed by Moore and Buck (17).

It is difficult to speculate on and assess correctly the nature, much less the magnitude, of possible solute–solvent interactions involving multidentate ligands, metal ions, and solvent dipoles. Therefore it may be more realistic to discuss gross features of the mechanism that controls substitution reactions in dimethylsulfoxide by considering the activation parameters, not rate constants at one temperature, to yield more useful information concerning reactions with monodentate ligands.

From the above observations it can be concluded that either (*a*) ligand substitution reactions at nickel(II) in dimethylsulfoxide are controlled by an I_d mechanism, and $\Delta H_{ex}^{\ddagger}$ for solvent exchange at nickel(II) in this solvent is 8 to 9 kcal as reported by some authors, or (*b*) a pure I_d mechanism for substitution reactions at nickel(II) is of questionable validity and $\Delta H_{ex}^{\ddagger}$ is about 13 kcal. If an I_d mechanism is operative in this system, the lower values of $\Delta H_f^{\ddagger}$ observed for reactions of nickel(II) with many pyridine-type monodentate ligands can be explained by assuming formation of a stabilized outer-sphere complex in which the ring nitrogen is an electron pair donor toward the sulfur atom of a dimethylsulfoxide molecule coordinated to nickel. A complex of this type has been proposed by Gutmann and Schmid (18). This could explain why pyridine-type monodentate ligands of similar basicity yield similar values of $\Delta H_f^{\ddagger}$ in this solvent.

Of the alternative mechanisms, an associative (A) mechanism seems unlikely because of the absence of evidence for seven-coordinated nickel(II) in dimethylsulfoxide. This may be a result of the bulkiness of six coordinated dimethylsulfoxide molecules about nickel(II); also, as mentioned above, $\Delta H_f^{\ddagger}$ values for substitution reactions with many monodentate pyridine-type ligands in dimethylsulfoxide are similar. An I_a mechanism also seems unlikely in this system for the same reasons.

The possibility of a dissociative (D) type mechanism cannot be ruled out. Evidence for five-coordinated nickel(II) in dimethylsulfoxide has been presented (19). Also, the similarity of the $\Delta H_f^{\ddagger}$ values for several pyridine-type ligands, but differing from $\Delta H_{ex}^{\ddagger}$, supports a D-type mechanism. Further evidence in this direction might be obtained by use of high-pressure techniques to measure $\Delta V^{\ddagger}$ values for this and

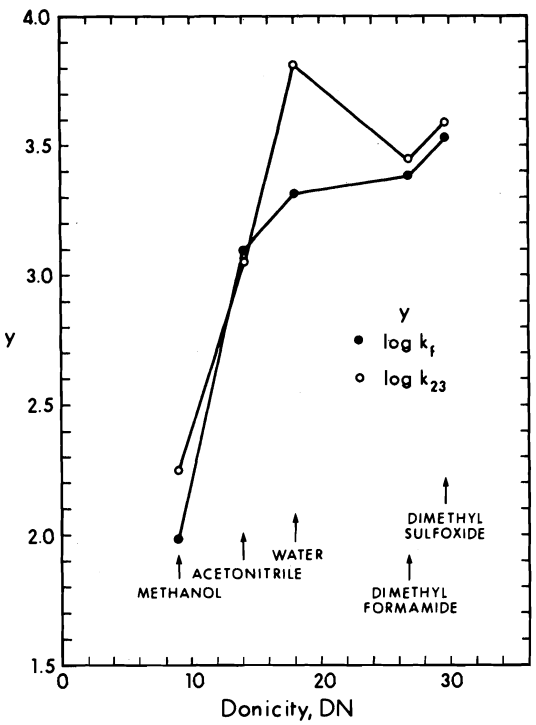

FIG. 2. Enthalpy of activation for formation of monocomplex of nickel(II) with isoquinoline in several donor solvents.

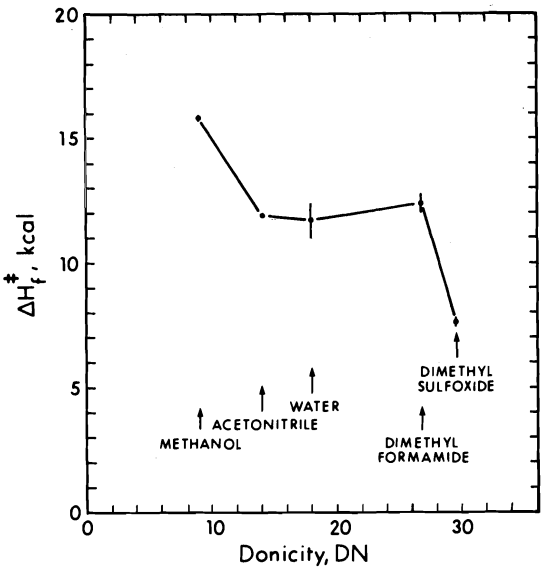

FIG. 3. Rate constants for formation of monocomplex of nickel(II) with isoquinoline in several donor solvents.

similar reactions, as has been done for nickel(II) in water (20). In summary, we conclude from our results that the gross features of the mechanism for substitution at nickel(II) with isoquinoline in dimethylsulfoxide solution are similar to those with other monodentate ligands. A definite conclusion as to whether the mechanism is D or I_d cannot be made, however, at the present time.

Turning to the results in water and methanol, the values of R indicate that substitution is normal in these two solvents, and that $\Delta H_f^{\ddagger}$ is, as expected for an I_d mechanism, close to the values found for solvent exchange. In dimethylformamide only reactions of thiocyanate (8) and bipyridine (6*b*) with nickel(II) have been reported. Values of R indicate that substitution is also normal in this solvent, although the value of $\Delta H_f^{\ddagger}$ is somewhat lower than the corresponding value for solvent exchange. This may be the result of a system similar to that observed in acetonitrile (4) where the value of R for the nickel–isoquinoline system was normal, and the value of $\Delta H_f^{\ddagger}$ was also somewhat lower than that found for solvent exchange.

Recently Dickert, Hoffmann, and Janjic (8) measured rate constants and associated activation parameters for the formation and dissociation of the mono- and bis-complexes of nickel(II) with thiocyanate ion in several solvents. Because isoquinoline is a monodentate ligand like thiocyanate ion, our results in Table 2 for formation of the 1:1 nickel(II)–isoquinoline complex can be compared from a mechanistic point of view with results for the corresponding nickel(II) complex with thiocyanate ion (8). Constants represented by the symbols k_{12} and k_1 in Dickert, Hoffman, and Janjic's results are represented by k_f and k_{23} in this work. They observed a linear relation between solvent donicity and rate constants for formation of the nickel(II)–thiocyanate complex. Donicity is defined as the negative value of the enthalpy of the Lewis acid–base reactions between a dilute solution of antimony(V) chloride and the solvent in dichloromethane (21). A similar relation between rate and equilibrium constants has been observed by Hoffmann for other ligands of -1 charge (22).

From Fig. 2 it is seen that there is no correlation between donicity of the solvent and values of either k_f or k_{23} for the nickel–isoquinoline system in the solvents studied. Similarly, Fig. 3 shows that $\Delta H_f^{\ddagger}$ cannot be related in a systematic way to solvent donicity. Therefore the correlation between donicity and formation rate

Can. J. Chem. Downloaded from www.nrcresearchpress.com by 210.87.254.105 on 09/05/12
For personal use only.

constants observed for the nickel–thiocyanate system cannot be extended to the system studied here. Further study of the kinetic and thermodynamic parameters of uncharged ligands should provide useful information in this area.

In summary, we conclude that the exact nature of the mechanism, whether D or I_d, for formation of the monocomplex of nickel(II) with isoquinoline in dimethylsulfoxide cannot be ascertained at this stage. Results in water, methanol, and dimethylformamide can be accommodated within the framework of an I_d mechanism, but with the caveat that any discussion of details of the mechanism in dimethylformamide must be guarded at this time.

Acknowledgements

Financial support by the National Research Council of Canada and the University of Alberta is gratefully acknowledged.

1. (*a*) M. Eigen and R. G. Wilkins. Adv. Chem. Ser. **49**, 55 (1965); (*b*) R. G. Wilkins. Acc. Chem. Res. **3**, 408 (1970).
2. (*a*) R. G. Pearson and P. Ellegen. Inorg. Chem. **6**, 1379 (1967); (*b*) F. Dickert, H. Hoffmann, and W. Jaenicke. Ber. Bunsenges Phys. Chem. **74**, 500 (1970).
3. M. L. Sanduja and W. M. Smith. Can. J. Chem. **50**, 3861 (1972).
4. (*a*) P. K. Chattopadhyay and J. F. Coetzee. Anal. Chem. **46**, 2014 (1974); (*b*) P. K. Chattopadhyay and J. F. Coetzee. Inorg. Chem. **12**, 113 (1973).
5. J. Neely and R. Connick. J. Am. Chem. Soc. **92**, 3476 (1970).
6. (*a*) C. H. Langford and T. R. Stengle. Ann. Rev. Phys. Chem. **19**, 193 (1968); (*b*) H. P. Bennetto and E. F. Caldin. J. Chem. Soc. (A), 2191 (1971); 2198 (1971); (*c*) T. J. Swift and R. E. Connick. J. Chem. Phys. **37**, 307 (1962); (*d*) N. S. Angermann and R. B. Jordan. Inorg. Chem. **8**, 259 (1969); (*e*) N. A. Matwiyoff. Inorg. Chem. **5**, 788 (1966); (*f*) Z. Luz and S. Meiboom. J. Chem. Phys., **40**, 2686 (1964); (*g*) I.D. Campbell, J. P. Carver, R. A. Dwek, A. J. Nrumelin, and R. E. Richards. Mol. Phys. **20**, 913 (1971).
7. (*a*) M. Eigen. Z. Phys. Chem. (Frankfurt am Main), **1**, 176 (1954); (*b*) R. M. Fuoss. J. Am. Chem. Soc. **80**, 5059 (1958).
8. F. Dickert, H. Hoffmann, and T. Janjic. Ber. Bunsenges Phys. Chem. **78**, 712 (1974).
9. J. F. O'Donnell, J. T. Ayers, and C. K. Mann. Anal. Chem. **37**, 1161 (1965).
10. J. Selbin, W. E. Bull, and L. H. Holmes, Jr. J. Inorg. Nucl. Chem. **16**, 219 (1961).
11. A. E. Wickenden and R. A. Krause. Inorg. Chem. **4**, 404 (1965).
12. P. K. Chattopadhyay and J. F. Coetzee. Anal. Chem. **44**, 2117 (1972).
13. (*a*) C. H. Langford and H. G. Tsiang. Inorg. Chem. **9**, 2346 (1970); (*b*) P. Moore and D. M. W. Buck. J. Chem. Soc. Dalton Trans. 1602 (1973).
14. D. D. Perrin. Dissociation constants of organic bases in aqueous solutions: supplement 1972. Butterworth and Co., London. 1972.
15. (*a*) I. M. Kolthoff. Pure Appl. Chem. **25**, 305 (1971); R. A. Holyer, C. D. Hubbard, S. F. Kettle, and R. G. Wilkins. Inorg. Chem. (*b*) **4**, 929 (1965); (*c*) **5**, 522 (1966).
16. J. F. Coetzee and E. Hsu. J. Solution Chem. **4**, 46 (1975).
17. D. M. W. Buck and P. Moore. J. Chem. Soc. Dalton Trans. 2082 (1974).
18. V. Gutmann and R. Schmid. Coord. Chem. Rev. **12**, 263 (1974).
19. (*a*) C. H. Langford and H. G. Tsiang. Inorg. Chem. **9**, 2346 (1970); (*b*) P. A. Cook, C. E. Cottrell, and R. K. Boyd. Can. J. Chem. **50**, 402 (1972).
20. E. F. Caldin, M. W. Grant, and B. B. Hasinoff. Chem. Commun. 1351 (1971); J. Chem. Soc. Faraday I, 2247 (1972); 1648 (1973).
21. V. Gutmann. Topics Curr. Chem. **27**, 59 (1972).
22. H. Hoffmann. Pure Appl. Chem. **41**, 327 (1975).

Can. J. Chem. Downloaded from www.nrcresearchpress.com by 210.87.254.105 on 09/05/12
For personal use only.

Seven-coordinate metal carbonyl derivatives of *cis*-$(CH_3)_2AsC(CF_3)=C(CF_3)As(CH_3)_2$

WILLIAM R. CULLEN AND LYNN M. MIHICHUK

Chemistry Department, University of British Columbia, Vancouver, B.C., Canada V6T 1W5

Received January 12, 1976

WILLIAM R. CULLEN and LYNN M. MIHICHUK. Can. J. Chem. **54**, 2548 (1976).

The seven-coordinate complexes (L—L)$M(CO)_3X_2$ (M = Mo, W; X = Br, I; (L—L) = *cis*-$(CH_3)_2AsC(CF_3)=C(CF_3)As(CH_3)_2$) were prepared and characterized. ^1H and ^{13}C nmr studies at 25 and −70 °C suggest that the complexes are nonrigid. Similarly ^1H nmr studies indicate the seven-coordinate (L—L)$LMo(CO)_2Br_2$ complexes are also nonrigid. The (L—L)-$L_2Mo(CO)Br_2$ complexes (L is a monodentate phosphite or phosphine) are rigid at 25 °C and nonrigid at higher temperatures. Activation parameters are calculated for the motion of two of the complexes and possible mechanisms are discussed.

WILLIAM R. CULLEN et LYNN M. MIHICHUK. Can. J. Chem. **54**, 2548 (1976).

On a préparé et caractérisé les complexes heptacoordonnés (L—L)$M(CO)_3X_2$ (M = Mo, W; X = Br, I; (L—L) = $(CH_3)_2AsC(CF_3)=C(CF_3)As(CH_3)_2$-*cis*). Des études de rmn du ^1H et du ^{13}C à 25 et à −70 °C suggèrent que les complexes ne sont pas rigides. De la même manière des études rmn du proton indiquent que les complexes heptacoordonnés (L—L)$LMo(CO)Br_2$ ne sont pas rigides. Les complexes (L—L)$L_2Mo(CO)Br_2$ (L est un phosphite ou un phosphine monodentate) sont rigides à 25 °C et non rigides à des températures plus élevées. On a calculé les paramètres d'activation pour les mouvements de deux des complexes et on discute des mécanismes possibles.

[Traduit par le journal]

In the course of studies on seven-coordinate complexes of metal carbonyls (1, 2) we became interested in related tertiary arsine derivatives of molybdenum and tungsten. There are two main methods of preparation of this type of complex as summarized in eqs. 1 and 2. The first method was developed by Nyholm and co-workers (3–6) and the second by Colton and associates (7–14). (M = Mo, W; X = Cl, Br, I; 2L can be a bidentate ligand.)

$$[1] \qquad M(CO)_6 \xrightarrow{2L} L_2M(CO)_4 \xrightarrow{X_2} L_2M(CO)_3X_2$$

$$[2] \qquad M(CO)_6 \xrightarrow{X_2} M(CO)_4X_2 \xrightarrow{2L} L_2M(CO)_3X_2$$

These products are nonelectrolytes and their solid state structures are generally based on a distorted octahedron with a carbonyl group capping one face (15–18) (*e.g.* Fig. 1). An alternative seven-coordinated structure based on a capped trigonal prism is found in related cations (19). Structures which are intermediate between a capped octahedron and a capped trigonal prism are also found (20).

In solution many seven-coordinate complexes are stereochemically non-rigid (21–24) as judged by their nmr spectra, and this paper reports primarily on this aspect of the new complexes prepared from the six-coordinate derivatives (L—L)$M(CO)_4$ (25) where (L—L) is the fluorocarbon-bridged ligand $(CH_3)_2AsC(CF_3)=C(CF_3)$-$As(CH_3)_2$.

Experimental

Air-sensitive starting materials were handled in a nitrogen atmosphere. A standard vacuum system was used for the manipulation of volatile reactants. Infrared spectra were recorded on a Perkin-Elmer 457 spectrophotometer and calibrated using polystyrene and cyclohexane. Nuclear magnetic resonance (nmr) spectra were run on Varian T-60, XL-100, HA-100, and CFT-20 spectrometers with chemical shifts given in ppm downfield from internal TMS for ^1H spectra and upfield from internal $CFCl_3$ for ^{19}F spectra. The HA-100 instrument, equipped with a Varian V-4343 variable temperature unit calibrated against ethylene glycol standard, was used for temperature variation studies.

The synthesis of the ligand *cis*-2,3-bis(dimethylarsino)-1,1,1,4,4,4,-hexafluorobut-2-ene, (L—L), has been previously described (25, 26).

Microanalyses were performed by Peter Borda of this department. Analytical and spectroscopic data for all new compounds are listed in Tables 1 and 2.

Preparation of the (L—L)$M(CO)_3X_2$ Complexes (M = Mo, W; X = Br, I)

These complexes were prepared by the slow addition of the halogen in dichloromethane (25 ml) to a vigorously stirred solution, same solvent, of an equimolar amount of

Can. J. Chem. Downloaded from www.nrcresearchpress.com by 210.87.254.40 on 09/05/12
For personal use only.

TABLE 1. Analytical and preparative data for new complexes[a]

Compound	Colour	Yield % (reaction) time, h)	Analyses Calcd. C	Calcd. H	Calcd. Br	Found C	Found H	Found Br
(L—L)$Mo(CO)_3I_2$	Orange	70	16.38	1.49	31.51(I)	16.20	1.61	31.28(I)
(L—L)$Mo(CO)_3Br_2$	Yellow	73	18.54	1.69	22.47	18.62	1.71	22.35
(L—L)$W(CO)_3I_2$	Orange	72	14.76	1.35	28.41(I)	14.64	1.21	28.25(I)
(L—L)$W(CO)_3Br_2$	Yellow	50	16.50	1.50	20.00	16.54	1.53	20.05
(L—L)^b(L—L)$^m Mo(CO)_2Br_2$[b]	Pale yellow	60	20.46	2.27	15.15	20.50	2.40	14.87
(L—L)$(C_5H_5N)Mo(CO)_2Br_2$[c]	Yellow	60	23.59	2.23		23.52	2.42	
(L—L)$[P(OCH_2CH_3)_3]Mo(CO)_2Br_2$	Yellow	59	22.59	3.18	18.82	22.76	3.40	19.10
(L—L)$[P(C_6H_5)_3]Mo(CO)_2Br_2$	Orange	65	35.52	2.85	16.91	35.35	2.73	16.70
(L—L)$[P(CH_3)(C_6H_5)_2]Mo(CO)_2Br_2$	Yellow	54	31.22	2.83	18.09	31.40	3.06	17.87
(L—L)$[P(CH_3)_2(C_6H_5)]Mo(CO)_2Br_2$	Yellow	58	26.28	2.80	19.46	26.34	2.88	19.14
(L—L)$[P(OCH_3)_3]Mo(CO)_2Br_2$	Yellow	59	19.31	2.60	19.80	19.21	2.70	19.64
(L—L)$[P(OCH_3)_2(C_6H_5)]Mo(CO)_2Br_2$	Yellow	56	25.29	2.69	18.74	25.44	2.70	18.46
(L—L)$_2Mo(CO)Br_2$	Brown	60(0.5)	19.84	2.34	15.56	19.87	2.56	15.28
(L—L)$[P(OCH_2CH_3)_3]_2Mo(CO)Br_2$	Orange	72(14)	25.51	4.25	16.19	25.48	4.10	15.86
(L—L)$[P(OCH_3)_3]_2Mo(CO)Br_2$	Orange	63(1.25)	19.91	3.32	17.55	19.93	3.61	17.70
(L—L)$[P(OCH_3)_2(C_6H_5)]_2Mo(CO)Br_2$	Orange	60(24)	30.12	3.41	16.06	30.23	3.50	15.80
(L—L)$[P(CH_3)_2C_6H_5)]_2Mo(CO)Br_2$	Orange	51(24)	32.19	3.65	17.15	32.47	3.76	17.00

[a]All complexes decomposed without melting above 120 °C.
[b]Superscript b and m indicate that (L—L) is bidentate or monodentate, respectively.
[c]Analysis for N gave 1.82% (calcd. 1.83%).

(L—L)$M(CO)_4$ (25 ml). Temperature control is important. Thus the additions to (L—L)$W(CO)_4$ were performed at 0 °C, after which the solution was stirred for 1 h at 25 °C. Iodination of (L—L)$Mo(CO)_4$ was performed entirely at 0 °C and bromination entirely at −78 °C. In all cases the solution was filtered and most of the solvent removed (5 ml). Addition of degassed hexane (10 ml) and cooling to −20 °C yielded the crystalline (L—L)$M(CO)_3X_2$ complexes.

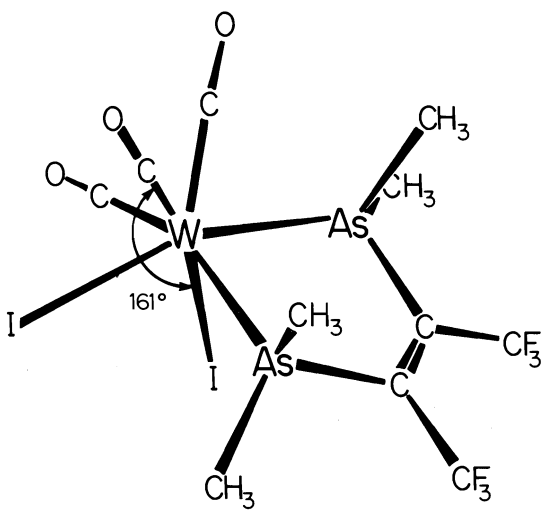

FIG. 1. Crystal structure of (L—L)$W(CO)_3I_2$ (18).

Preparation of the (L—L)$LMo(CO)_2Br_2$ Complexes (L = Monodentate Ligand)

In general the dicarbonyl complexes were prepared by the addition of L to an equimolar amount of (L—L)$Mo(CO)_3Br_2$ in dichloromethane (5 ml) at 25 °C under a nitrogen atmosphere. The orange solution was filtered and concentrated (3 ml) under reduced pressure. Addition of degassed hexane (6 ml) and cooling to −20 °C afforded the crystalline (L—L)$LMo(CO)_2Br_2$ complexes.

Preparation of the (L—L)$L_2Mo(CO)Br_2$ Complexes

All reactions between excess L and (L—L)$Mo(CO)_3Br_2$ were carried out in refluxing benzene (for the time indicated in Table 1) under a nitrogen atmosphere, except for (L—L)$_2Mo(CO)Br_2$ which was synthesized by warming a benzene solution (50 °C) of (L—L)$_2Mo(CO)_2Br_2$ for 30 min. The following experimental details are typical.

(L—L)$Mo(CO)_3Br_2$ (0.30 g, 0.41 mmol) and trimethyl phosphite (0.120 g, 0.96 mmol) in dry degassed benzene (15 ml) were refluxed under nitrogen for 75 min. The ir spectrum of the solution indicated complete reaction of (L—L)$Mo(CO)_3Br_2$. The deep red-orange solution (initially orange) was filtered and the benzene removed under reduced pressure. Recrystallization of the red oil from a degassed dichloromethane–hexane mixture at −20 °C afforded orange plates of (L—L)$[P(OCH_3)_3]_2Mo(CO)Br_2$ (0.24 g, 63%); mp 150 °C (decom).

Results and Discussion

(L—L)$M(CO)_3X_2$ Complexes

Satisfactory preparation of the tricarbonyl complexes requires slow dropwise addition of

Can. J. Chem. Downloaded from www.nrcresearchpress.com by 210.87.254.40 on 09/05/12
For personal use only.

Can. J. Chem. Downloaded from www.nrcresearchpress.com by 210.87.254.40 on 09/05/12
For personal use only.

TABLE 2. Infrared and nuclear magnetic resonance spectroscopic data for new complexes

Compound	^{1}H (ppm)[a]	^{19}F (ppm)[b]	ν(CO) (cm^{-1})[b]
(L—L)Mo(CO)$_3$I$_2$	2.17[c]	51.1	2056(s), 1985(vs), 1927(s)
(L—L)Mo(CO)$_3$Br$_2$	2.05[c]	52.6	2076(s), 1993(vs), 1925(s)
(L—L)W(CO)$_3$I$_2$	2.23[c]	52.4	2052(s), 1971(vs), 1917(s)
(L—L)W(CO)$_3$Br$_2$	2.10[c]	53.2	2068(s), 1977(vs), 1911(s)
(L—L)^b(L—L)^{m}Mo(CO)$_2$Br$_2$	2.47, 2.25	51.2	1981(vs), 1913(s)
(L—L)(C$_5$H$_5$N)Mo(CO)$_2$Br$_2$	2.08, multiplets centred at 7.47, 7.82, and 9.02 (C$_5$H$_5$N)	51.2	1957(vs), 1883(s)
(L—L)[P(OCH$_2$CH$_3$)$_3$]Mo(CO)$_2$Br$_2$	1.98, triplet centred at 1.33 (P—OCH$_2$*CH$_3$*) J(H,H) = 7.0 Hz. Pentet centred at 4.25 (P—*OCH$_2$*CH$_3$), J(H,H) = 7.0 Hz, J(H,P) = 7.0 Hz	51.6	1959(vs), 1879(s)
(L—L)[P(C$_6$H$_5$)$_3$]Mo(CO)$_2$Br$_2$	1.87, multiplets centred at 7.40 and 7.83 (P—C$_6$H$_5$)	51.4	1951(vs), 1869(s)
(L—L)[P(CH$_3$)(C$_6$H$_5$)$_2$]Mo(CO)$_2$Br$_2$	1.70, doublet centred at 2.48 (P—CH$_3$) J(H,P) = 10.0 Hz Multiplets centred at 7.50 and 7.80 (P—C$_6$H$_5$)	51.4	1951(vs), 1869(s)
(L—L)[P(CH$_3$)$_2$(C$_6$H$_5$)]Mo(CO)$_2$Br$_2$	1.83, doublet centred at 2.12 (P—CH$_3$) J(H,P) = 11.0 Hz Multiplets centred at 7.43 and 7.80 (P—C$_6$H$_5$)	51.4	1951(vs), 1867(s)
(L—L)[P(OCH$_3$)$_3$]Mo(CO)$_2$Br$_2$	1.98, doublet centred at 3.88 (P—OCH$_3$) J(H,P) = 11.2 Hz	51.2	1965(vs), 1883(s)
(L—L)[P(OCH$_3$)$_2$(C$_6$H$_5$)]Mo(CO)$_2$Br$_2$	1.85, doublet centred at 3.80 (P—OCH$_3$) J(H,P) = 11.5 Hz Multiplets centred at 7.47 and 7.80 (P—C$_6$H$_5$)	51.6	1957(vs), 1875(s)
(L—L)$_2$Mo(CO)Br$_2$	1.98	50.8	1829
(L—L)[P(OCH$_2$CH$_3$)$_3$]$_2$Mo(CO)Br$_2$[e]	Singlets at 2.07 and 1.50 (As—CH$_3$) Triplet centred at 1.28 (P—OCH$_2$*CH$_3$*) Multiplet centred at 4.25 (P—O*CH$_2$*CH$_3$)	52.4	1841
(L—L)[P(OCH$_3$)$_3$]$_2$Mo(CO)Br$_2$	Singlets at 2.08 and 1.50 (As—CH$_3$) 'Virtual triplet' centred at 3.90 (P—OCH$_3$) $\lvert J$(H,P) + J'(H,P')$\rvert$ = 10.0 Hz	52.2	1843
(L—L)[P(OCH$_3$)$_2$(C$_6$H$_5$)]$_2$Mo(CO)Br$_2$	Singlets at 1.88 and 1.53 (As—CH$_3$) 'Virtual triplet' centred at 3.44 (P—OCH$_3$) $\lvert J$(H,P) + J'(H,P')$\rvert$ = 10.5 Hz and 3.59 (P—OCH$_3$) $\lvert J$(H,P) + J'(H,P')$\rvert$ = 10.0 Hz Multiplets centred at 7.37 and 7.70 (P—C$_6$H$_5$)	52.4	1829
(L—L)[P(CH$_3$)$_2$(C$_6$H$_5$)]$_2$Mo(CO)Br$_2$[d]	Quartets centred at 2.32 (As—CH$_3$) J(H,F) = 2.5 Hz and 0.907 (As—CH$_3$) J(H,F) = 2.0 Hz, singlet at 1.00 (As—CH$_3$) Doublets centred at 2.07 (P—CH$_3$) J(H,P) = 9.75 Hz 1.85 (P—CH$_3$) J(H,P) = 8.25 Hz 1.27 (P—CH$_3$) J(H,P) = 7.75 Hz and 0.912 (P—CH$_3$) J(H,P) = 8.75 Hz Multiplets centred at 7.12 and 7.85 (P—C$_6$H$_5$)	Quartets centred 51.4 and 53.2 (CF$_3$) J(F,F) = 15.0 Hz	1792

[a]CDCl$_3$ solution unless otherwise indicated. Absorptions are singlets unless indicated to the contrary. 'Virtual triplet' refers to a pattern consisting of a broad absorption lying between two peaks of a 1:1 doublet. The doublet separation is given by $\lvert J$(H,P) + J'(H,P')$\rvert$.
[b]CH$_2$Cl$_2$ solution. Absorptions are singlets unless otherwise indicated.
[c]CH$_2$Cl$_2$ solution.
[d]The ^{1}H nmr spectrum of this complex was obtained from C$_6$D$_6$ solution.
[e]See Results and Discussion for coupling constants.

Can. J. Chem. Downloaded from www.nrcresearchpress.com by 210.87.254.40 on 09/05/12
For personal use only.

the halogen to a vigorously stirred solution of the chelate complex. The seven-coordinate complexes are crystalline orange or yellow, nonionic[1] solids considerably more soluble in polar solvents than in nonpolar ones. They appear to decolourize in the solid state after a few months and are quite unstable in oxygenated solvents. The stability of these complexes[2] which is enhanced in nitrogen-saturated solvents decreases in the order tungsten $\gg$ molybdenum, for a given halogen, with the iodides more stable than the bromides. The complexes $M(CO)_3(dmpe)I_2$ also have the stability order W > Mo (24).

The crystal structure of $(L—L)W(CO)_3I_2$, which is very similar to that of $(C_6H_5)_2P(CH_2)_2P(C_6H_5)_2Mo(CO)_3Br_2$, is shown in Fig. 1 (17, 18). The tungsten atom is seven-coordinate with a distorted capped octahedral environment, the capping group being a carbonyl. The capped face consists of the two remaining carbonyl groups and one of the arsenic atoms from the bidentate ligand.

The nmr spectra of the tungsten complex are not in accord with its X-ray crystal structure. The ^1H spectrum at 25 °C and −70 °C exhibits *one* arsenic methyl singlet assignable to the chelating ligand and the ^{19}F spectrum *one* trifluoromethyl singlet. The ^{13}C nmr spectrum at room temperature consists of one singlet for the dimethylarsino groups (^1H decoupled), one quartet for the trifluoromethyl groups ($J(C,F) = 285$ Hz), a broad absorption for the olefinic carbons (due to long range coupling to the fluorine atoms), and *one* singlet for the carbonyl groups.

No static model built from these ligands exists in agreement with these data, which indicates that in solution the whole molecule has a nonrigid structure at 25 °C on an nmr time scale. The ^1H and ^{19}F nmr spectra are consistent with the molecule having this nonrigid structure down to −70 °C. Rapid independent scrambling of the three carbonyl groups could possibly explain the appearance of one absorption in the ^{13}C nmr spectrum (27–31). However, this would not explain the ^1H and ^{19}F spectra since the two arsenic atoms would still be in an asymmetric environment. Thus it seems that the rearrangement process involves rapid scrambling of the carbonyl groups and iodine atoms, and simultaneous migration of the capping group over the faces of the $[As_2C_2I_2]$ octahedron. The sharpness of the spectra at −70 °C indicates that a limiting spectrum corresponding to the solid state structure would be reached only at much lower temperatures. It is possible that this scrambling process is catalyzed by dissociation into ions, since the conductivity of the molecule is not zero although it is in the range of values found for all the nonionic seven-coordinate complexes. A truly ionic complex in this system would have the formula $[(L—L)M(CO)_4X]X$.

The ^1H and ^{19}F nmr spectra of the other halotricarbonyl derivatives are very similar to those of $(L—L)W(CO)_3I_2$ suggesting they also are nonrigid in solution in the manner discussed above. Their ir spectra in the carbonyl region are similar to other characterized seven-coordinate Group VI tricarbonyl derivatives (4, 13, 14).

Henrick and Wild (23) found that the *meso* and racemic isomers of the ligand *o*-phenylene bis(methylphenylarsine) give the seven-coordinate iodo complexes $o\text{-}C_6H_4[As(CH_3)(C_6H_5)]_2Mo(CO)_3I_2.CHCl_3$. These have a crystal structure consisting of a capped trigonal prism with an iodine atom above one of the square faces. Both complexes fail to afford the expected ^1H nmr spectrum at 35 °C; instead only a single line is obtained. Cooling the solution of the *meso* ligand complex results only in line broadening. The spectrum of the other complex eventually (−90 °C) becomes the anticipated doublet (As—CH_3 region) in agreement with the solid state structure. The $\Delta G^{\ddagger}$ for the process is 10.6 kcal mol^{-1} and the authors suggest that the averaging of the arsenic methyl signals is due to motion of the iodine from one square face to another. This process would seem to give an isomer and consequently no coalescence of the nmr absorptions should be expected. A much more drastic motion seems to be required to account for the observed results.

(L—L)LMo(CO)$_2$Br$_2$ Complexes

Facile replacement of a carbonyl group by phosphites and phosphines (L) from (L—L)Mo-

[1]For example, $(L—L)Mo(CO)_3I_2$ has a molar conductivity of 0.9 ohm^{-1} cm^2 in nitrobenzene; 1:1 electrolytes show conductivities of 20–30 ohm^{-1} cm^2 in the same solvent (4).

[2]Refluxing a sample of $(L—L)Mo(CO)_3I_2$ in dichloromethane under a nitrogen atmosphere for 6 h results in complete decomposition. Similar results are obtained after stirring a solution at room temperature for 39 h.

Can. J. Chem. Downloaded from www.nrcresearchpress.com by 210.87.254.40 on 09/05/12
For personal use only.

$(CO)_3Br_2$ yields the crystalline seven-coordinate $(L—L)LMo(CO)_2Br_2$ complexes which are considerably more stable and more soluble than their parent tricarbonyl derivatives.

The nmr spectra of the dicarbonyl complexes indicate a symmetric environment for the ligands and are similar to those of the $(L—L)M(CO)_3X_2$ complexes. Thus, they too are nonrigid in solution, and it seems that all ligands are involved.

Connor *et al.* (24) have recently reported fluxional seven-coordinate molybdenum and tungsten iododicarbonyl cations $[(CH_3)_2PCH_2CH_2P(CH_3)_2]_2M(CO)_2I^+$. They explain the nmr spectra in terms of a migration of the iodine over the faces of a static trigonal prism. However, this could well be a very simplistic explanation, although in this case an ionic pathway seems less likely.

The $(L—L)^b(L—L)^mMo(CO)_2Br_2$ complex provides an interesting example where the nmr data suggest that an additional exchange process is occurring in solution. Even at -80 °C two equal area arsenic methyl resonances are seen. A static structure should give at least two well separated resonances for the monodentate arsenic ligand and one or two for the chelated one. Thus it appears that in addition to a scrambling process involving $(L—L)^m$ and all the other groups, exchange is occurring between the 'free' and coordinated end of $(L—L)^m$.

Exchange between mono- and bidentate ligands has been observed in a similar seven-coordinate complex (32). The suggested mechanism involves the unlikely assumption that the remaining ligands are not involved in any scrambling process.

The ir spectra of all the dicarbonyl complexes in the carbonyl region are very similar and indicate that the carbonyl groups possibly possess a *cis* orientation (24).

$(L—L)L_2Mo(CO)Br_2$ Complexes

The monocarbonyl complexes, which seem to be a new class, are stable in the solid state but unstable in air-saturated solvents (the corresponding $(L—L)LMo(CO)_2Br_2$ complex can be isolated as one of the decomposition products). They show a great tendency to crystallize as dichloromethane adducts, but the solvent of crystallization is readily removed *in vacuo*. The $(L—L)L_2Mo(CO)Br_2$ complexes containing monodentate phosphines or phosphites are carbon monoxide carriers:

$$(L—L)L_2Mo(CO)Br_2 \underset{80\ °C}{\overset{CO}{\rightleftharpoons}} (L—L)LMo(CO)_2Br_2 + L$$

The nmr spectra of the $(L—L)L_2Mo(CO)Br_2$ complexes (L is monodentate) indicate that the species are rigid at room temperature and are nonrigid at higher temperatures. This is in contrast with the tricarbonyl and dicarbonyl derivatives described above.

The $(L—L)[P(OCH_3)_3]_2Mo(CO)Br_2$ and $(L—L)[P(OCH_3)_2(C_6H_5)]_2Mo(CO)Br_2$ complexes are examples of $H_9PP'H_9'$ and $H_6PP'H_6'$ spin systems. The theory of nuclear spin systems of this type, $H_nPP'H_n'$, has been developed by Harris (33, 34) who has shown that the methyl resonance appears as an unresolved, broad resonance lying between a 1:1 doublet of separation $|J(H,P) + J'(H,P')|$ when ^{31}P–^{31}P coupling is intermediate between large and small. The two monocarbonyl complexes exhibit this type of 'triplet' resonance pattern for the methoxy groups.

The ^1H nmr spectrum of the trimethyl phosphite derivative at room temperature can be interpreted in terms of a static seven-coordinate capped octahedral structure **A** ($P = P(OCH_3)_3$) with a carbonyl group in the capping position above the $[P_2Br]$ face. The arsenic methyl groups

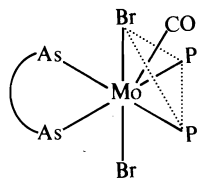

A

on one side of the $[As_2P_2]$ plane experience a different environment from those on the other side and are thus seen as two singlets. **A**, ($P = P(OCH_3)_3$), has a temperature dependent ^1H nmr spectrum shown in Fig. 2. As the temperature is increased the two initially sharp arsenic methyl singlets broaden, collapse, and coalesce into a single line which sharpens as the temperature is further increased. This indicates that at higher temperatures all the arsenic methyl groups are equivalent on an nmr time scale and suggests that the molecule is fluxional in the manner indicated in [3] ($P = P(OCH_3)_3$) where a capping CO group migrates over two octahedral faces via a pentagonal bipyramidal intermediate. It should be pointed out that migration of the capping

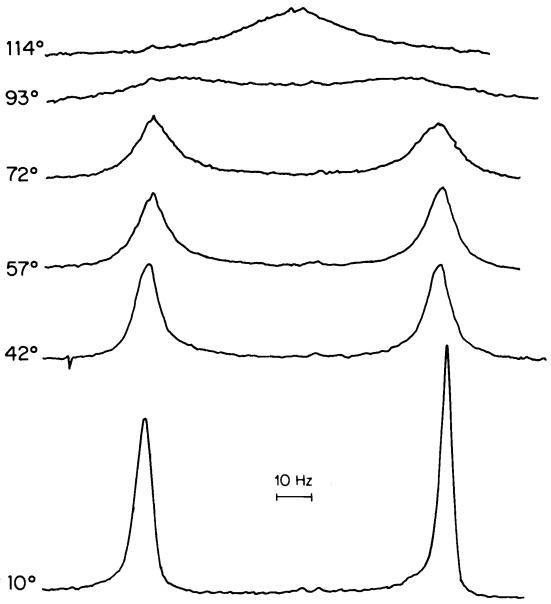

FIG. 2. Variable temperature ^{1}H nmr spectra of (L—L)[P(OCH$_3$)$_3$]$_2$Mo(CO)Br$_2$ in benzene solution. The figure shows the arsenic methyl region.

[3]

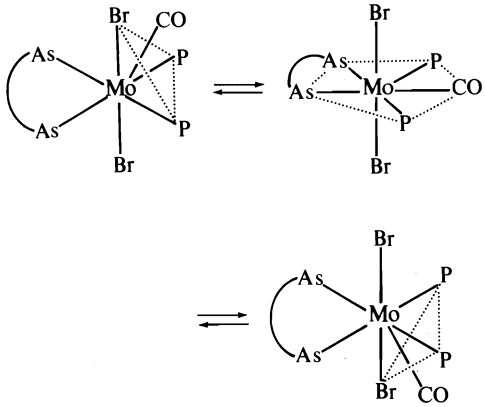

group over all the faces would be indistinguishable.

The ambient temperature nmr spectra of (L—L)[P(OCH$_3$)$_2$C$_6$H$_5$)]$_2$Mo(CO)Br$_2$ indicate the molecule has structure **A** (P = P(OCH$_3$)$_2$(C$_6$H$_5$)). The two downfield 'virtual triplet' patterns are assigned to the diastereotopic (35) methoxy methyl groups on each phosphorus atom (Fig. 3).[3]

The ^{1}H nmr spectrum of **A** (P = P(OCH$_3$)$_2$-(C$_6$H$_5$)) is also temperature dependent. The two arsenic methyl singlets broaden, collapse, and

[3]The ^{31}P nmr spectrum consists of a single multiplet 59.5 ppm upfield from external P$_4$O$_6$.

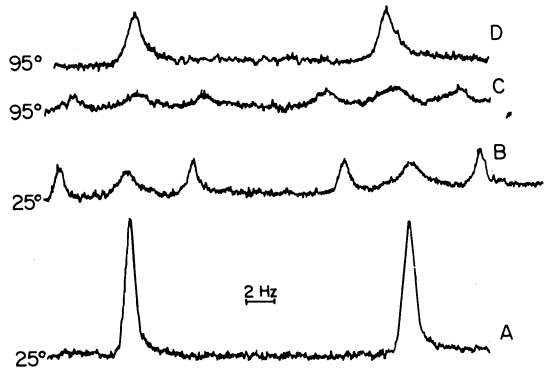

FIG. 3. Variable temperature ^{1}H nmr spectra of (L—L)[P(OCH$_3$)$_2$(C$_6$H$_5$)]$_2$Mo(CO)Br$_2$ in benzene solution. The methoxy methyl region is shown. *A* and *D* are phosphorus decoupled spectra.

coalesce as the temperature is increased. However, there is no equilibration of the two diastereotopic methyl resonances. The high temperature spectra can be accounted for in terms of the same process [3] described above for **A** (P = P(OCH$_3$)$_3$).

Thermodynamic parameters calculated for the motion, using the Gutowsky and Holm procedure (36) are listed in Table 3.

The large negative entropy value indicates a symmetrical transition state as is suggested in [3]. However, the possibility that the capping group migrates over all faces cannot be eliminated without a knowledge of the barriers involved in cap–cap migration above or below the As$_2$P$_2$ plane, and cap–cap migration through the plane. One of these latter paths is that shown in [3].

Dissociative processes such as phosphonite dissociation can be eliminated by the fact that the methoxy methyl groups remain virtually coupled over the entire high temperature range. Dissociation of one end of the chelated ligand would probably require a much higher barrier than observed. For example, Meakin and coworkers (21) report an activation energy of 12.8 kcal mol^{-1} for an exchange process involving dissociation of one end of a ditertiary alkylphosphine ligand in a seven-coordinate tantalum carbonyl complex and suggest that a polytopal rearrangement would possibly have a much lower barrier than observed as is found in our work. Small $\Delta H^{\ddagger}$ and large negative $\Delta S^{\ddagger}$ values (~ -30 eu) have been reported by Jack and Powell (37, 38) for some solvent assisted ex-

Can. J. Chem. Downloaded from www.nrcresearchpress.com by 210.87.254.40 on 09/05/12
For personal use only.

TABLE 3. Thermodynamic parameters for (L—L)L_2Mo(CO)Br_2 complexes

Compound	$\Delta H^{\ddagger}$ (kcal mol^{-1})	$\Delta S^{\ddagger}$ (cal mol^{-1} deg^{-1})	T_c (K)[a]
(L—L)[$P(OCH_3)_2(C_6H_5)]_2$Mo(CO)Br_2	6.7 ± 0.6	-29 ± 2	368 ± 3
(L—L)[$P(OCH_2CH_3)_3]_2$Mo(CO)Br_2	4.9 ± 0.6	-35 ± 2	368 ± 3

[a] T_c is the coalescence temperature of the arsenic methyl resonances.

change process in bridged carboxylate complexes of platinum and palladium. Thus solvent assistance or ionization could be possible in our case. However, the isomerization of the seven-coordinate complexes (h^5-C_5H_5)Mo(CO)$_2$(PR_3)X (X = halogen) appears to be a non-dissociative unimolecular process (39) with $\Delta H^{\ddagger} \approx 23$ kcal mol^{-1} and $\Delta S^{\ddagger}$ small but negative. Again these high $\Delta H^{\ddagger}$ values seem to argue against a dissociative process in our case. Moreover, large negative $\Delta S^{\ddagger}$ values are possible for sterically and electronically restricted transition states (40, 41).

Unfortunately, there is not enough information in the spectra to come to a definite conclusion about the pathway of the process. This is not an unusual situation (31).

The nmr spectra of the triethylphosphite derivative in the (L—L) region is identical with the other two complexes. However, a more detailed examination of the ^{1}H nmr spectrum of the phosphite group shows that with proton decoupling in the CH_3 region, the broad methylene absorption collapses to two doublets with H–P coupling constants of 6.0 and 4.0 Hz. With broad band phosphorus decoupling, the methylene multiplet collapses to two equal area quartets (J(H,H) = 7.0 Hz). In accordance with the two chemically inequivalent sets of methylene protons, the ^{31}P nmr spectrum (two multiplets) indicates the phosphorus atoms are in an asymmetric environment.

These spectra can be interpreted in terms of a seven-coordinate capped octahedral structure **B** (P = $P(OCH_2CH_3)_3$) with the phosphite groups

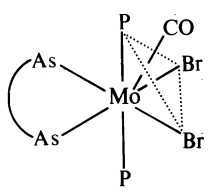

B

in a *trans* position. This complex has a similar temperature dependent ^{1}H nmr spectrum to **A** (P = $P(OCH_3)_3$, $P(OCH_3)_2(C_6H_5)$). At the temperature corresponding to coalescence of the arsenic methyl singlets the two methylene quartets (phosphorus decoupled) collapse into one quartet.

Thermodynamic parameters calculated for the motion (Table 3) are very similar to those of **A** (P = $P(OCH_3)_2(C_6H_5)$) suggesting the two complexes behave in an analogous manner at high temperatures.

The nmr spectra of the (L—L)[$P(CH_3)_2$-$(C_6H_5)]_2$Mo(CO)Br_2 complex differ considerably from the other monocarbonyl complexes as is seen in Fig. 4. The 1:1:2 arsenic methyl ratio is presumably due to an accidental superposition of peaks in benzene since four equal area absorptions appear in deuterochloroform. The ^{19}F and ^{31}P nmr spectra suggest the two trifluoromethyl groups and two phosphorus atoms are in an unsymmetrical environment.

Possible configurations for the complex, consistent with the room temperature nmr spectra are shown in **C** and **D** (P = $P(CH_3)_2(C_6H_5)$). In either configuration the capping carbonyl group is above the [AsPBr] face.

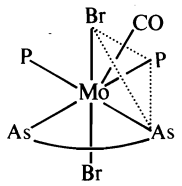

C

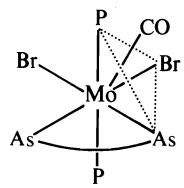

D

The variable temperature ^{1}H nmr spectrum (Fig. 4) is unlike the other complexes in that it was not possible to obtain a limiting high temperature spectrum in benzene solution. The broad high temperature resonance possibly is due to arsenic and phosphine methyl absorptions. Also at high temperatures there is no equilibration of the two phosphorus atoms; however, the two trifluoromethyl quartets broaden, collapse, and coalesce into a single broad peak.

The structure shown in **D** (P = $P(CH_3)_2$-

Can. J. Chem. Downloaded from www.nrcresearchpress.com by 210.87.254.40 on 09/05/12
For personal use only.

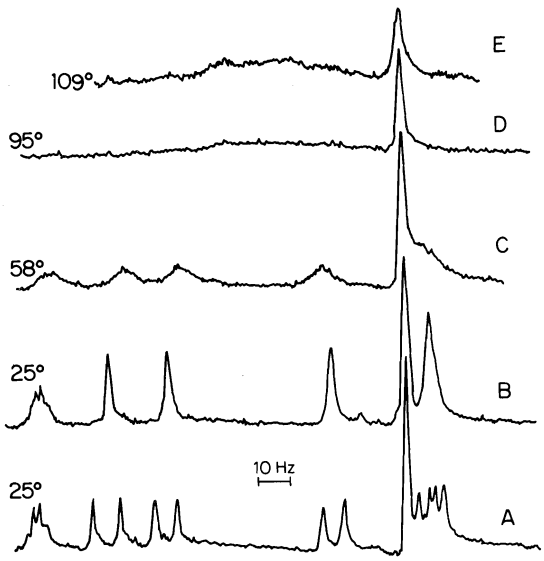

FIG. 4. Variable temperature ^1H nmr spectra of (L—L)[$P(CH_3)_2(C_6H_5)$]$_2$Mo(CO)Br_2 in benzene solution. The methyl region is shown. *A* is the normal spectrum *B*, *C*, *D*, and *E* are phosphorus decoupled.

(C_6H_5)) would allow carbonyl migration over the octahedral faces to equilibrate the trifluoromethyl groups but not the phosphorus atoms.[4] The same motion in a structure like **C** would equilibrate both the trifluoromethyl groups and the phosphorus atoms.

The nmr spectra of (L—L)$_2$Mo(CO)Br_2 cannot be interpreted in terms of a static polyhedron, and a limiting slow exchange spectrum was not reached at −70 °C.

Each of the monocarbonyl complexes shows one carbonyl stretching frequency in its ir spectrum. This is considerably lowered in frequency relative to the dicarbonyl species reflecting the fact that the remaining carbonyl group is sharing a much greater proportion of the available metal *d*-electron density.

Acknowledgments

The authors are grateful to the National Research Council of Canada for financial support of this work in the form of an operating grant (W.R.C.) and scholarships (L.M.M.).

1. W. R. CULLEN, R. K. POMEROY, J. R. SAMS, and T. B. TSIN. J. Chem. Soc. Dalton Trans. 1216 (1975).

[4]Providing the BrBrAsAs plane is not crossed.

2. W. R. CULLEN and R. K. POMEROY. Inorg. Chem. **14**, 939 (1975).
3. C. D. COOK, R. S. NYHOLM, and M. L. TOBE. J. Chem. Soc. 4194 (1965).
4. H. L. NIGAM, R. S. NYHOLM, and M. H. B. STIDDARD. J. Chem. Soc. 1806 (1960).
5. J. LEWIS and R. WHYMAN. J. Chem. Soc. 5486 (1965).
6. J. LEWIS, R. S. NYHOLM, C. S. PANDE, and M. H. B. STIDDARD. J. Chem. Soc. 3600 (1963).
7. R. COLTON and I. B. TOMKINS. Aust. J. Chem. **19**, 1143 (1966).
8. R. COLTON and I. B. TOMKINS. Aust. J. Chem. **19**, 1519 (1966).
9. M. W. ANKER, R. COLTON, and I. B. TOMKINS. Aust. J. Chem. **20**, 9 (1967).
10. J. A. BOWDEN and R. COLTON. Aust. J. Chem. **21**, 2657 (1968).
11. R. COLTON and C. J. RIX. Aust. J. Chem. **22**, 305 (1969).
12. M. W. ANKER, R. COLTON, and I. B. TOMKINS. Aust. J. Chem. **21**, 1159 (1968).
13. M. W. ANKER, R. COLTON, C. J. RIX, and I. B. TOMKINS. Aust. J. Chem. **22**, 1341 (1969).
14. R. COLTON and C. J. RIX. Aust. J. Chem. **23**, 441 (1970).
15. M. G. B. DREW and J. D. WILKINS. J. Chem. Soc. Dalton Trans. 626 (1972).
16. M. G. B. DREW, A. W. JOHANS, A. P. WALTERS, and I. B. TOMKINS. Chem. Commun. 819 (1971).
17. M. G. B. DREW. J. Chem. Soc. Dalton Trans. 1329 (1972).
18. A. MERCER and J. TROTTER. Can. J. Chem. **52**, 3331 (1974).
19. M. G. B. DREW and J. D. WILKINS. J. Chem. Soc. Dalton Trans. 2664 (1973).
20. M. G. B. DREW and J. D. WILKINS. J. Chem. Soc. Dalton Trans. 1654 (1974).
21. P. MEAKIN, L. J. GUGGENBERGER, F. N. TEBBE, and J. P. JESSON. Inorg. Chem. **13**, 1025 (1974).
22. A. P. GINSBERG and M. E. TULLY. J. Am. Chem. Soc. **14**, 4749 (1973).
23. K. HENRICK and S. B. WILD. J. Chem. Soc. Dalton Trans. 2500 (1974).
24. J. A. CONNOR, G. K. MCEWEN, and C. J. RIX. J. Chem. Soc. Dalton Trans. 589 (1974).
25. W. R. CULLEN and L. M. MIHICHUK. Can. J. Chem. **53**, 3401 (1975).
26. J. P. CROW, W. R. CULLEN, F. G. HERRING, J. R. SAMS, and R. L. TAPPING. Inorg. Chem. **10**, 1616 (1971).
27. G. DEGANELLO. J. Organometal. Chem. **59**, 329 (1973).
28. G. RIGATTI, G. BOCCALON, A. CECCON, and G. GIACOMETTI. Chem. Commun. 1165 (1972).
29. F. A. COTTON, L. KRUCZYNSKI, B. L. SHAPIRO, and L. F. JOHNSON. J. Am. Chem. Soc. **94**, 6191 (1972).
30. B. F. G. JOHNSON, J. LEWIS, and T. W. MATHESON. Chem. Commun. 441 (1974).
31. R. D. ADAMS, F. A. COTTON, W. R. CULLEN, D. L. HUNTER, and L. M. MIHICHUK. Inorg. Chem. **14**, 1395 (1975).
32. M. W. ANKER, R. COLTON, and C. J. RIX. Aust. J. Chem. **24**, 1157 (1971).

Can. J. Chem. Downloaded from www.nrcresearchpress.com by 210.87.254.40 on 09/05/12
For personal use only.

33. R. K. HARRIS. Can. J. Chem. **42**, 2275 (1964).
34. R. K. HARRIS. Inorg. Chem. **5**, 701 (1966).
35. K. MISLOW and M. RABIN. Topics in stereochemistry. Vol. 1. *Edited by* N. L. Allinger and E. L. Eliel. Wiley-Interscience, New York, N.Y. 1967. p. 1.
36. H. S. GUTOWSKI and C. H. HOLM. J. Chem. Phys. **25**, 1228 (1956).
37. T. R. JACK and J. POWELL. Can. J. Chem. **53**, 2558 (1975).
38. J. POWELL and T. R. JACK. Inorg. Chem. **11**, 1039 (1972).
39. J. W. FALLER and A. S. ANDERSON. J. Am. Chem. Soc. **92**, 5852 (1970).
40. R. W. MURRAY, P. R. STORY, and M. L. KAPLAN. J. Am. Chem. Soc. **88**, 526 (1966).
41. M. H. AKHTAR, R. S. MCDANIEL, M. FESER, and A. C. OEHLSCHLAGER. Tetrahedron, **24**, 3899 (1968).

Can. J. Chem. Downloaded from www.nrcresearchpress.com by 210.87.254.40 on 09/05/12
For personal use only.

The reactivity of cyclic germoxycarbene complexes of manganese and rhenium towards nucleophiles[1]

M. J. WEBB[2] and W. A. G. GRAHAM
Department of Chemistry, University of Alberta, Edmonton, Alberta T6G 2E1

Received October 2, 1975

M. J. WEBB and W. A. G. GRAHAM. Can. J. Chem. **54**, 2557 (1976).

Several acylate salts and noncyclic carbene complexes of manganese and rhenium, containing organogermanium ligands, have been prepared via the reactions of the cyclic germoxycarbene complexes of empirical formula $Ph_2GeM(CO)_4COMe$ (M = Mn, Re) with the nucleophiles methyllithium or methoxide ion. In each case the observed product could be rationalized in terms of nucleophilic attack at germanium. Treatment of $Ph_2GeRe(CO)_4COMe$ with methyllithium, followed by ethylation with aqueous Et_3OBF_4, afforded *cis*-$Ph_2MeGeRe(CO)_4C(OEt)Me$. The manganese analog of this product could be obtained if excess methyllithium were used in the first step. The use of a deficit of methyllithium, however, followed by ethylation, yielded *cis*-$Ph_2FGeMn(CO)_4C(OEt)Me$. Solution infrared spectra have indicated that lithium methoxide and lithium bromide impurities in the methyllithium are involved in this reaction. The reaction of $Ph_2GeMn(CO)_4COMe$ with sodium methoxide is presumed to involve nucleophilic attack at germanium to give a methoxygermanium species. Subsequent treatment with aqueous tetraethylammonium bromide gave the hydroxygermanium complex, [*cis*-$Ph_2(HO)GeMn(CO)_4C(O)Me$][Et_4N]. Ethylation of the same species with aqueous Et_3OBF_4 afforded *cis*-$Ph_2FGeMn(CO)_4C(OEt)Me$.

M. J. WEBB et W. A. G. GRAHAM. Can. J. Chem. **54**, 2557 (1976).

On a préparé plusieurs sels acylates et plusieurs complexes de carbène non cyclique du manganèse et du rhénium contenant des ligands organogermanium en faisant intervenir les réactions de complexes de germoxycarbène cyclique de structure brute $Ph_2GeM(CO)_4COMe$ (M = Mn, Re) avec les nucléophiles méthyllithium ou ion méthylate. Dans chaque cas, le produit observé peut être rationalisé en terme d'une attaque nucléophile au site du germanium. La réaction du $Ph_2GeRe(CO)_4COMe$ avec le méthyllithium suivi par une réaction d'éthylation avec le Et_3OBF_4 aqueux conduit au $Ph_2MeGeRe(CO)_4C(OEt)Me$ *cis*. On peut aussi obtenir l'analogue avec du manganèse de ce composé si l'on utilise un excès de méthyllithium dans la première étape. L'utilisation d'une quantité déficiente de méthyllithium suivie par une éthylation conduit toutefois au $Ph_2FGeMn(CO)_4C(OEt)Me$ *cis*. Des spectres infrarouges en solution indiquent que des impuretés de méthylate de lithium et de bromure de lithium dans le méthyllithium sont impliqués dans cette réaction. On fait l'hypothèse que la réaction du $Ph_2GeMn(CO)_4COMe$ avec le méthylate de sodium implique une attaque nucléophile au niveau du germanium pour conduire à des espèces méthoxygermanium. Un traitement ultérieur avec du bromure de tétraéthylammonium aqueux conduit au complexe hydroxygermanium [$Ph_2(OH)GeMn(CO)_4C(O)Me$ *cis*][Et_4N]. L'éthylation des mêmes espèces avec du Et_3OBF_4 aqueux conduit au $Ph_2FGeMn(CO)_4C(OEt)Me$ *cis*.

Traduit par le journal]

Introduction

In recent papers we have described the synthesis and characterisation of a number of carbene complexes of manganese and rhenium which also contain organogermanium or organotin ligands. A number of compounds with an unusual cyclic structure of the type **1** have been prepared (1, 2), and in some cases have been shown by nmr spectroscopy to exist as equilibrium mixtures of dimeric and monomeric forms in solution (3, 4). A series of complexes with noncyclic structures of the type **2** has also been

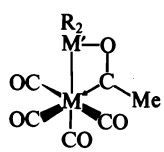

1

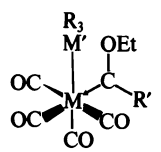

2

[1]Organometallic Compounds Having Metal–Metal Bonds, Part XXX. Part XXIX: ref. 5.

[2]Present address: Department of Chemistry, Memorial University of Newfoundland, St. John's, Newfoundland A1C 5S7.

Can. J. Chem. Downloaded from www.nrcresearchpress.com by 210.87.254.42 on 09/05/12
For personal use only.

Can. J. Chem. Downloaded from www.nrcresearchpress.com by 210.87.254.42 on 09/05/12
For personal use only.

obtained (5). In this paper we present the synthesis of further noncyclic compounds prepared by the reaction of cyclic germoxycarbene complexes with nucleophiles.

Transition metal carbene complexes are known to react with nucleophiles such as phosphines (6–8) and phenyllithium (9), with attack occurring at the carbene carbon atom. Such behaviour might also be expected for the cyclic germoxycarbene complexes of the type **1**. However, the products of reactions with methyllithium or methoxide ion can be rationalized in terms of nucleophilic attack at the germanium atom in the ring.

Experimental

Reactions were carried out under a static nitrogen atmosphere, using solvents previously saturated with nitrogen. Diethyl ether, dichloromethane, and methanol were dried by distillation from calcium hydride, phosphorus pentoxide, and magnesium, respectively.

Solutions of methyllithium in ether and lithium wire (0.01% Na) were obtained from the Ventron Corporation (Alfa Products), Beverly, Mass.; tetraethylammonium bromide and chloride were supplied by Eastman Organic Chemicals, Rochester, N.Y.; sodium methoxide and lithium bromide were obtained from Fischer Scientific Company, Fair Lawn, N.J.; Et_3OBF_4 was purchased from Fluka AG, Switzerland; sodium sulphate (anhydrous) and chromatographic alumina (calcined) were obtained from BDH Chemicals Ltd., Poole, England, and BDH (Canada) Ltd., Toronto, respectively. The compounds $Ph_2GeMn(CO)_4COMe$ and $Ph_2GeRe(CO)_4COMe$ were prepared as described elsewhere (2). Lithium methoxide was prepared by dissolving lithium wire in methanol, followed by removal of excess methanol *in vacuo*.

Microanalyses were performed in the Microanalytical Laboratory of this Department. Melting points, and infrared, mass, and ^1H nmr spectra were recorded as described previously (2).

Where approximate p*H* values are mentioned in the following reactions, they were measured using 'pHydrion' indicator papers, purchased from the Micro Essential Laboratory, Brooklyn, N.Y.

Reaction of $Ph_2GeRe(CO)_4COMe$ with (1) MeLi, (2) Et_3OBF_4

To $Ph_2GeRe(CO)_4COMe$ (0.19 g, 0.33 mmol) in diethyl ether (15 ml) was added from a syringe a solution of 1.5 *M* MeLi in ether (0.23 ml, 0.34 mmol). An immediate colour change from colourless to pale yellow was observed. An infrared spectrum taken after 5 min reaction time indicated complete disappearance of the rhenium starting material and generation of an anion. After removal of the solvent *in vacuo*, the pale yellow, oily residue was extracted with water (10 ml). After filtration, the yellow solution was treated with excess aqueous Et_3OBF_4, which was added dropwise until the p*H* decreased to approximately 2. Addition of the ethylating agent was accompanied by cloudiness in the solution and precipitation of a pale yellow oil. Extraction from the aqueous solution with *n*-pentane (75 ml), removal of the solvent by rotary evaporation, and drying of the product *in vacuo* overnight resulted in the isolation of a yellow oil. Crystallization from *n*-heptane at −78 °C yielded as a white solid *cis*-$Ph_2MeGeRe(CO)_4C(OEt)Me$ (90 mg).

Reaction of $Ph_2GeMn(CO)_4COMe$ with (1) excess MeLi, (2) Et_3OBF_4

The features of this reaction are similar to those above. The complex $Ph_2GeMn(CO)_4COMe$ (0.65 g, 1.49 mmol) in diethyl ether (25 ml) was treated with excess 1.5 *M* MeLi in ether (5.5 ml, 8.25 mmol). The brown, oily residue, after solvent removal, was extracted with water (50 ml) and filtered to give a clear, yellow–orange solution. (Caution: water should be added to the brown oil slowly, since a vigorous reaction occurs with the excess methyllithium.) The dropwise addition of excess aqueous Et_3OBF_4 until a p*H* of about 2 was reached produced a yellow oil, which was extracted with *n*-pentane (150 ml). Removal of the solvent by rotary evaporation and drying *in vacuo* yielded the crude product *cis*-$Ph_2MeGeMn(CO)_4C(OEt)Me$ as a yellow oil (0.20 g). Attempts at crystallization from *n*-pentane and acetone–water yielded only oils. Slow sublimation (55 °C/0.01 mm) on to a water-cooled probe gave a yellow oil, whose infrared spectrum indicated partial decomposition of the *cis*-$Ph_2MeGeMn(CO)_4C(OEt)Me$ product to other carbonyl-containing compounds.

Reaction of $Ph_2GeMn(CO)_4COMe$ with (1) excess MeLi, (2) Et_4NCl

To $Ph_2GeMn(CO)_4COMe$ (1.20 g, 2.74 mmol) in diethyl ether (40 ml) was added 1.5 *M* MeLi (3.7 ml, 5.55 mmol), producing a brown solution. An infrared spectrum, recorded in ether after a few minutes, indicated complete reaction of the manganese starting material and formation primarily of *cis*-$Ph_2MeGeMn(CO)_4C(OLi)Me$, plus small quantities of the other anions mentioned in the discussion. (Larger excesses of MeLi lead to the observation of the only *cis*-$Ph_2MeGeMn(CO)_4C(OLi)Me$, as in the preceding reaction.) Subsequent treatment in water (30 ml) with excess aqueous Et_4NCl (0.66 g, 4.0 mmol) produced a yellow–brown, oily precipitate. An attempt at crystallization from acetone–ether was unsuccessful. Extraction of the oil with ether (300 ml), reduction of the solution volume to 100 ml under reduced pressure, and cooling in the refrigerator yielded pale yellow crystals of [*cis*-$Ph_2MeGeMn(CO)_4C(O)Me$][Et_4N] (35 mg).

Reaction of [cis-$Ph_2MeGeMn(CO)_4C(O)Me$][Et_4N] with Et_3OBF_4

The ether extraction from the crude product in the preceding reaction left a large proportion of the product in the brown, oily residue. This residue was dissolved in dichloromethane (30 ml), and treated with Et_3OBF_4. The progress of the reaction was monitored by infrared spectroscopy as small portions of the ethylating agent were added. Removal of the solvent by rotary evaporation, and extraction of the residue with *n*-pentane, gave a yellow solution. Solvent removal by rotary evaporation yielded an impure yellow oil, whose infrared and mass spectra identified it as *cis*-$Ph_2MeGeMn(CO)_4C(OEt)Me$.

Reaction of $Ph_2GeMn(CO)_4COMe$ with (1) deficit of MeLi, (2) Et_3OBF_4

A solution of two anions (see Discussion) can be gener-

Can. J. Chem. Downloaded from www.nrcresearchpress.com by 210.87.254.42 on 09/05/12
For personal use only.

ated by the reaction of $Ph_2GeMn(CO)_4COMe$ with MeLi in ether in an approximately 2:1 mole ratio. For example, treatment of $Ph_2GeMn(CO)_4COMe$ (0.475 g, 0.95 mmol) with 1.5 *M* MeLi (0.30 ml, 0.45 mmol) gives a pale yellow solution containing two anionic intermediates, neither of which is *cis*-$Ph_2MeGeMn(CO)_4C(OLi)Me$. (This behaviour can be contrasted with a reaction in which MeLi is in excess, *vide supra*.) Removal of solvent and extraction with water leaves a residue of unreacted $Ph_2GeMn(CO)_4COMe$. Treatment of an aqueous solution of the anions with excess aqueous Et_3OBF_4, until the p*H* is approximately 2, yields a yellow oil. Decantation of the aqueous solution, washing with a small amount of water, and drying *in vacuo* yields a yellow oil, whose infrared and mass spectra identify it as impure *cis*-$Ph_2FGeMn(CO)_4C(OEt)Me$.

Reaction of $Ph_2GeMn(CO)_4COMe$ with (1) NaOMe, (2) Et_3OBF_4

To $Ph_2GeMn(CO)_4COMe$ (0.30 g, 0.69 mmol) in methanol (20 ml) was added sodium methoxide (0.038 g, 0.70 mmol). The solution was stirred for 19 h. Removal of the solvent by rotary evaporation yielded a yellow oil, whose infrared spectrum in dichloromethane indicated an anionic material (ν(CO) 2040(m), 1959(s, sh), 1935(vs)) as well as a little residual starting material. Extraction with water (15 ml), and filtration were followed by the dropwise addition of excess aqueous Et_3OBF_4, until the p*H* was approximately 2. A yellow oil was precipitated, and this was extracted with *n*-pentane (2 × 60 ml). The *n*-pentane extract was dried over anhydrous Na_2SO_4 overnight in the refrigerator. Filtration, and removal of the solvent by rotary evaporation, yielded a yellow oil. This was adsorbed on to alumina (*ca.* 2 g), and chromatographed on a column packed with alumina (50 g, 16 cm column height), using *n*-heptane as eluent. A single yellow fraction (*ca.* 50 ml) was collected, the volume reduced (to *ca.* 10 ml), and the solution cooled in the refrigerator. Colourless crystals of *cis*-$Ph_2FGeMn(CO)_4C(OEt)Me$ (45 mg) were obtained.

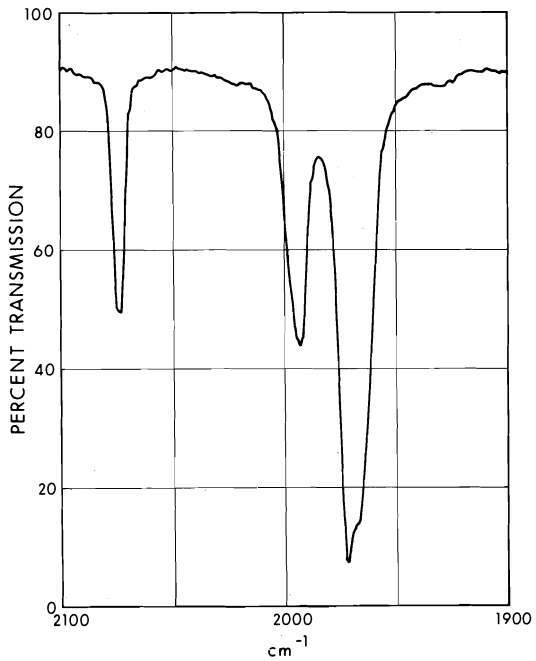

FIG. 1. Infrared spectrum (ν(CO) region) of *cis*-$Ph_2MeGeRe(CO)_4C(OEt)Me$ in cyclohexane.

Reaction of $Ph_2GeMn(CO)_4COMe$ with (1) NaOMe, (2) Et_4NBr

The reaction of $Ph_2GeMn(CO)_4COMe$ with NaOMe in methanol was repeated, using excess NaOMe to avoid residual starting material. $Ph_2GeMn(CO)_4COMe$ (0.30 g, 0.69 mmol) and NaOMe (0.076 g, 1.4 mmol) were stirred in methanol (20 ml) for 24 h. After removal of methanol by rotary evaporation the residue was extracted with water (20 ml) and filtered. Subsequent treatment with excess aqueous Et_4NBr in water precipitated a pale yellow oil. The aqueous solution was decanted and the residue washed with water (20 ml). Drying *in vacuo* overnight, and crystallization from acetone–ether yielded pale yellow crystals of [*cis*-$Ph_2(HO)GeMn(CO)_4C(O)Me$]-[Et_4N] (0.20 g).

Results and Discussion

The Reaction of $Ph_2GeRe(CO)_4COMe$ with MeLi

The cyclic complex of empirical formula $Ph_2GeRe(CO)_4COMe$ reacts[3] rapidly with a slight excess of methyllithium in ether to give a lithium acylate presumed to be *cis*-$Ph_2MeGeRe(CO)_4C(OLi)Me$. Subsequent treatment with Et_3OBF_4 in water yields the novel carbene complex formulated as *cis*-$Ph_2MeGeRe(CO)_4C(OEt)Me$. The suggested formulation of the product

$$Ph_2GeRe(CO)_4COMe + MeLi \xrightarrow{\text{ether}}$$

$$\textit{cis}\text{-}Ph_2MeGeRe(CO)_4C(OLi)Me \xrightarrow[\text{water}]{Et_3OBF_4}$$

$$\textit{cis}\text{-}Ph_2MeGeRe(CO)_4C(OEt)Me$$

is fully consistent with its mass and infrared spectra, and with analytical data (see Tables 1 and 2 and Fig. 1). The attachment of a methyl group to germanium in the final product is further supported by a ^1H nmr spectrum, which reveals a methyl singlet at τ 9.10 (see Table 3). This can be compared with values of τ 8.93 and τ 9.41 respectively for methyl groups bound to germanium in the complexes $Me_2GeRe(CO)_4COMe$ and $Me_3GeRe(CO)_5$ (2). Thus, the reaction product appears to result from methyllithium attack at germanium.

The Reaction of $Ph_2GeMn(CO)_4COMe$ with MeLi

The reaction of $Ph_2GeMn(CO)_4COMe$ with

[3]In reactions of this type it is not known whether the cyclic carbene complexes undergo nucleophilic attack in their monomeric or dimeric forms, or both.

Can. J. Chem. Downloaded from www.nrcresearchpress.com by 210.87.254.42 on 09/05/12
For personal use only.

TABLE 1. Carbonyl stretching frequencies and mass spectral parent ions

Compound	Mass spectral parent ion (m/e)[a]	Carbonyl stretching frequencies (cm^{-1})[e,f]
cis-$Ph_2MeGeRe(CO)_4C(OEt)Me$	612[b]	2074(m), 1994(m), 1971(vs), 1966(s,sh)
cis-$Ph_2MeGeMn(CO)_4C(OEt)Me$	482[c]	2052(m), 1984(m), 1965(vs), 1959(s,sh)
cis-$Ph_2FGeMn(CO)_4C(OEt)Me$	486[d]	2066(m), 1995(m), 1978(vs), 1974(s,sh)
[*cis*-$Ph_2MeGeMn(CO)_4C(O)Me$][Et_4N]	—	2019(m), 1930(vs), 1917(vs), 1897(s)
[*cis*-$Ph_2(HO)GeMn(CO)_4C(O)Me$][Et_4N]	—	2025(m), 1943(s,sh), 1931(vs), 1910(s,sh)

[a]Most abundant peak of isotope combination pattern of parent ion reported. Parent ions show expected isotope combination patterns.
[b]The spectrum, recorded at a source temperature of 45 °C, reveals the presence of an impurity of higher molecular weight; the observed spectrum is, therefore, complex. Intense peaks at m/e 597 due to loss of a methyl group from the parent ion, and at m/e 243 due to Ph_2MeGe^+ are observed.
[c]Shows competing losses of carbonyls and a methyl group from the parent ion. Stepwise loss of four carbonyl groups observed. Very intense peak at m/e 243 due to Ph_2MeGe^+.
[d]Recorded at a source temperature of 85 °C. Spectrum showed competing losses of a fluorine atom and carbonyl groups from the parent ion. Stepwise loss of four carbonyl groups observed. At a source temperature of 60 °C spectrum of volatile impurities observed, with the two peaks of highest mass at m/e 442 and 454. For that at m/e 442, peaks due to loss of one, three, and five carbonyl groups from this parent can be assigned; an intense peak at m/e 247, due to Ph_2FGe^+, further suggests that the peak at m/e 442 might be due to $Ph_2FGeMn(CO)_5$. The ion at m/e 454 corresponds to the mass of $Ph_2(MeO)GeMn(CO)_5$, but this ion shows only the loss of two, three, and four carbonyl groups.
[e]Cyclohexane solvent for neutral complexes, dichloromethane for salts.
[f]Abbreviations: m = medium, s = strong, v = very, sh = shoulder.

TABLE 2. Analytical data, colours, melting points, and yields

Compound	Colour	Melting point (°C)	% yield	Analyses (%) Calculated C	Calculated H	Found[a] C	Found[a] H
cis-$Ph_2MeGeRe(CO)_4C(OEt)Me$	White	54–57	44	41.20	3.46	40.19	3.38
cis-$Ph_2MeGeMn(CO)_4C(OEt)Me$	Yellow	Oil	28	52.45	4.40	50.55	4.23
cis-$Ph_2FGeMn(CO)_4C(OEt)Me$	Colourless	62–64	14	49.54	3.74	49.44	3.95
[*cis*-$Ph_2MeGeMn(CO)_4C(O)Me$][Et_4N][b]	Pale yellow	89–91	2	55.71	6.23	54.36	6.30
[*cis*-$Ph_2(HO)GeMn(CO)_4C(O)Me$][Et_4N][c]	Pale yellow	98–100	50	53.47	5.87	55.08	5.81

[a]C, H, N analyses carried out in duplicate by the Microanalytical Laboratory of this Department (mean value given).
[b]Calculated: N, 2.41; found: N, 2.69.
[c]Calculated: N, 2.40; found: N, 2.64.

TABLE 3. ^1H nmr data

Compound	Chemical shift (τ)[a,b] C—CH_3[c]	Ge—CH_3[c]	O—CH_2—CH_3[d]	O—CH_2—CH_3[e]	Solvent
cis-$Ph_2MeGeRe(CO)_4C(OEt)Me$	7.68	9.10	6.10	8.67	$CDCl_3$
cis-$Ph_2MeGeMn(CO)_4C(OEt)Me$	7.58	9.05	6.18	8.62	$CDCl_3$
cis-$Ph_2FGeMn(CO)_4C(OEt)Me$	7.19	—	5.88	8.62	$CDCl_3$
[*cis*-$Ph_2(HO)GeMn(CO)_4C(O)Me$][Et_4N][f]	7.62	—	—	—	$(CD_3)_2CO$

[a]Relative to internal TMS at 10 τ. Peak integrals consistent with suggested formulations.
[b]Ph resonance complex multiplet at *ca.* 2.5–3.0 τ in all cases.
[c]Singlet.
[d]Quartet.
[e]Triplet.
[f]O—*H* at τ 5.74 (singlet); N—CH_2—CH_3 at τ 6.66 (quartet); N—CH_2—CH_3 at τ 8.72 (triplet of triplets).

methyllithium is rather more complex. The use of a 5.5:1 mole ratio of MeLi to $Ph_2GeMn(CO)_4COMe$ in ether, followed by treatment with Et_3OBF_4 in water, yields exclusively *cis*-$Ph_2MeGeMn(CO)_4C(OEt)Me$ as a yellow oil, in a reaction analogous to the rhenium case described above. Repeated attempts have failed to provide a sample of the highest analytical purity, but infrared and mass spectra, and particularly a ^1H nmr spectrum have allowed an unambiguous structural assignment to be made. The ^1H nmr spectrum reveals a singlet at τ 9.05 due to the

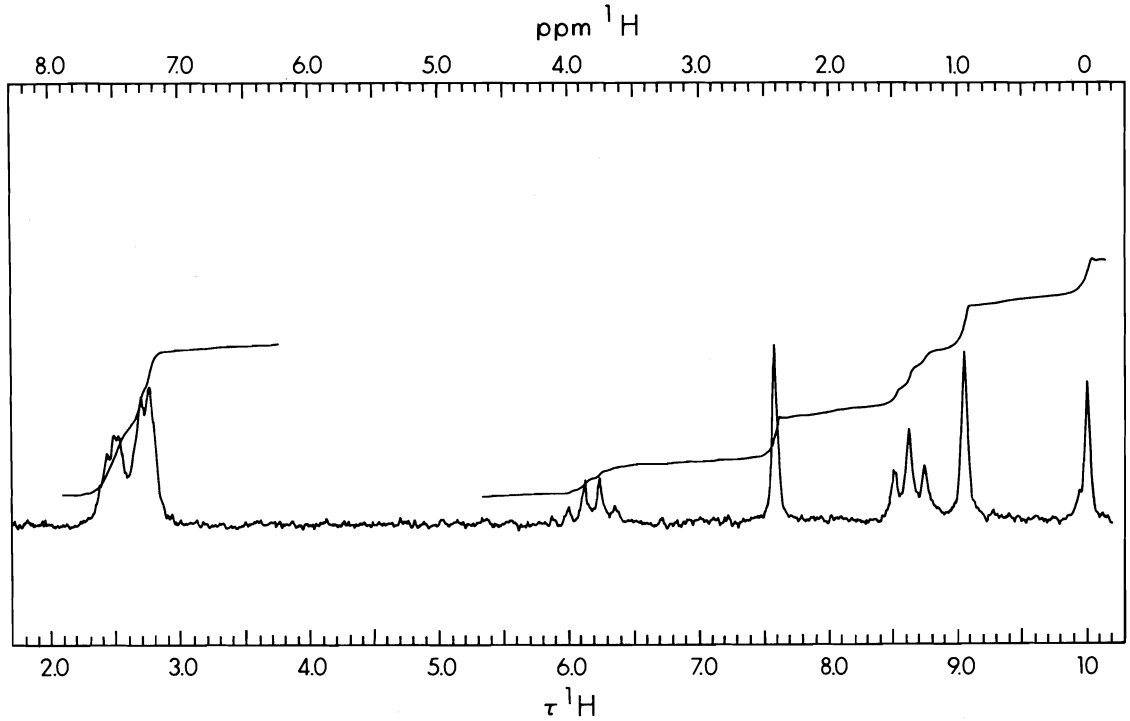

FIG. 2. ^{1}H nmr spectrum of *cis*-$Ph_2MeGeMn(CO)_4C(OEt)Me$ in $CDCl_3$.

methyl group attached to germanium (see Fig. 2). The acylate precursor to the final product has been isolated in low yield as a tetraethylammonium salt, [*cis*-$Ph_2MeGeMn(CO)_4C(O)Me$]-[Et_4N], whose infrared spectrum resembles that of the complex [*cis*-$Ph_3GeMn(CO)_4C(O)Me$]-[Et_4N] described elsewhere (5). Treatment of [*cis*-$Ph_2MeGeMn(CO)_4C(O)Me$][Et_4N] with Et_3OBF_4 in dichloromethane yields *cis*-$Ph_2MeGeMn(CO)_4C(OEt)Me$.

If an equimolar quantity of methyllithium is added to $Ph_2GeMn(CO)_4COMe$ in ether, infrared bands due to three anionic species are observed. Most of the infrared bands overlap, but the highest energy band of each species is clearly visible. These peaks are observed at 2047, 2041, and 2029 cm^{-1} in diethyl ether, and that at 2029 cm^{-1} is known to belong to *cis*-$Ph_2MeGeMn(CO)_4C(OLi)Me$.[4] Addition of a less-than-equimolar quantity of methyllithium to $Ph_2GeMn(CO)_4COMe$ in ether leaves some unreacted starting material and increasingly favours the formation of the anions showing bands at 2047 and 2041 cm^{-1}. The latter peak is always the more intense, with the former appearing as a shoulder. Upon further addition of methyllithium these anions are converted into *cis*-$Ph_2MeGeMn(CO)_4C(OLi)Me$. Treatment of the two anions with aqueous Et_3OBF_4 yields an impure yellow oil, whose infrared and mass spectra closely resemble those of a sample of *cis*-$Ph_2FGeMn(CO)_4C(OEt)Me$, a novel complex whose synthesis by another route is described below.

The Reaction of $Ph_2GeMn(CO)_4COMe$ with NaOMe

The reaction of $Ph_2GeMn(CO)_4COMe$ with

[4]Anionic species with their highest energy infrared bands at 2047 and 2041 cm^{-1} can be generated in diethyl ether by the reactions of $Ph_2GeMn(CO)_4COMe$ with lithium bromide and lithium methoxide, respectively. These anions presumably result from nucleophilic attack at germanium. Thus it seems very likely that lithium bromide and lithium methoxide are present as impurities in the commercial samples of methyllithium used for these reactions. A recent paper has described problems arising in organic syntheses from the presence of lithium bromide in solutions of methyllithium supplied by the Ventron Corporation (10).

Can. J. Chem. Downloaded from www.nrcresearchpress.com by 210.87.254.42 on 09/05/12
For personal use only.

Can. J. Chem. Downloaded from www.nrcresearchpress.com by 210.87.254.42 on 09/05/12
For personal use only.

excess sodium methoxide in methanol proceeds cleanly, and infrared spectra recorded in dichloromethane after removal of the methanol solvent indicate formation of an anion. If an equimolar quantity of sodium methoxide is employed, the same anion is produced and some starting material remains. Treatment of the anion with tetraethylammonium bromide in water *does not* yield [*cis*-$Ph_2(MeO)GeMn(CO)_4C(O)Me][Et_4N]$, but a complex believed to be the first hydroxygermanium – transition metal derivative, [*cis*-$Ph_2(HO)GeMn(CO)_4C(O)Me][Et_4N]$.[5] It seems feasible that the reaction of sodium methoxide with $Ph_2GeMn(CO)_4COMe$ might initially result in a methoxygermyl derivative and that subsequent reaction with water replaces a methoxy group by a hydroxy group.

$$Ph_2GeMn(CO)_4COMe + MeONa \xrightarrow{MeOH}$$
$$[cis\text{-}Ph_2(MeO)GeMn(CO)_4C(ONa)Me] \xrightarrow[water]{Et_4NBr}$$
$$[cis\text{-}Ph_2(HO)GeMn(CO)_4C(O)Me][Et_4N]$$

The presence of an O—H group in the molecule is confirmed by a ^1H nmr spectrum in acetone-d_6 which reveals a signal at τ 5.74, integrating as one proton, which disappears upon treatment with D_2O. An infrared spectrum in Nujol shows bands at 3290 and 1570 cm^{-1} assignable to ν(OH) and ν(C—O^-).

The methoxygermyl intermediate postulated above, upon treatment with Et_3OBF_4 in water, yields the novel carbene complex *cis*-$Ph_2FGeMn(CO)_4C(OEt)Me$. It is of course possible, based on the reaction of this same intermediate with aqueous tetraethylammonium bromide, that the reactive species involved here

$$[cis\text{-}Ph_2(MeO)GeMn(CO)_4C(ONa)Me] \xrightarrow[water]{Et_3OBF_4}$$
$$cis\text{-}Ph_2FGeMn(CO)_4C(OEt)Me$$

could be a hydroxygermyl complex generated by reaction with water prior to addition of the Et_3OBF_4. It has been shown by Marks and Seyam (12, 13) that the BF_4^- ion can act as a fluorine source when $AgBF_4$ is used as a reagent. However, it is also possible that impurities in the Et_3OBF_4, *e.g.*, HF, might be responsible for fluorination of the germanium atom.

It is apparent from the results described above that the reaction products can be rationalized in all cases in terms of nucleophilic attack at germanium. On the basis of these results it is hoped that the reactions of cyclic carbene complexes with other nucleophiles, both anionic and neutral, will yield further interesting products.

[5]The first hydroxysilyl – transition metal complex, $(\eta\text{-}C_5H_5)Fe(CO)_2SiMe_2(OH)$, was recently prepared in this laboratory (11).

Acknowledgements

We thank the National Research Council of Canada for financial support and for a Postgraduate Scholarship to M.J.W., and Professor J. Hooz of this Department for helpful discussions.

1. M. J. Webb, R. P. Stewart, Jr., and W. A. G. Graham. J. Organomet. Chem. **59**, C21 (1973).
2. M. J. Webb and W. A. G. Graham. Can. J. Chem. To be published.
3. M. J. Webb, M. J. Bennett, L. Y. Y. Chan, and W. A. G. Graham. J. Am. Chem. Soc. **96**, 5931 (1974).
4. M. J. Webb and W. A. G. Graham. Can. J. Chem. To be published.
5. M. J. Webb, R. P. Stewart, Jr., and W. A. G. Graham. To be published.
6. F. R. Kreissl and W. Held. J. Organomet. Chem. **86**, C10 (1975).
7. F. R. Kreissl, C. G. Kreiter, and E. O. Fischer Angew. Chem. Int. Ed. Engl. **11**, 643 (1972).
8. F. R. Kreissl, E. O. Fischer, C. G. Kreiter, and H. Fischer. Chem. Ber. **106**, 1262 (1973).
9. C. P. Casey and T. J. Burkhardt. J. Am. Chem. Soc. **95**, 5833 (1973).
10. R. R. Fraser, T. B. Grindley, and S. Passannanti. Can. J. Chem. **53**, 2473 (1975).
11. E. Wood. Ph.D. Thesis, University of Alberta, Edmonton, Alberta. 1974.
12. T. J. Marks and A. M. Seyam. J. Organomet. Chem. **31**, C62 (1971).
13. T. J. Marks and A. M. Seyam. Inorg. Chem. **13**, 1624 (1974).

Studies related to antitumor antibiotics. Part VII. Synthesis of streptonigrin analogues and their single strand scission of DNA

J. WILLIAM LOWN AND SOO-KHOON SIM[1]

Department of Chemistry, University of Alberta, Edmonton, Alta., Canada T6G 2G2

Received March 23, 1976

J. WILLIAM LOWN and SOO-KHOON SIM. Can. J. Chem. **54**, 2563 (1976).

The syntheses of a group of 2-(*o*-nitrophenyl)- and 2-(*o*-aminophenyl)-5,8-quinolinediones which are structurally related to the antitumor antibiotic streptonigrin are described. Ambiguities in the position of required nucleophilic displacements are resolved by independent synthesis. The rates of single strand cleavage of PM2 ccc-DNA (covalently-closed circular-DNA) induced by these compounds are compared, which correlates with antitumor activity. The 2-(*o*-nitrophenyl) derivatives give consistently more rapid DNA cleavage than the 2-(*o*-aminophenyl) compounds. The autoxidations of the dihydroxyquinolines are subject to selective catalysis by Cu^{2+} ion. 2-(*o*-Aminophenyl)-7-amino-6-methoxy-5,6-quinolinedione which has a substitution pattern most closely resembling streptonigrin also closely parallels the rate of scission of DNA of the latter in the presence of NADPH.

J. WILLIAM LOWN et SOO-KHOON SIM. Can. J. Chem. **54**, 2563 (1976).

On décrit la synthèse d'un groupe de (*o*-nitrophényl)-2 et (*o*-aminophényl)-2 quinolinedione-5,8 qui sont reliées d'une façon structurale avec l'antibiotique antitumorale de streptonigrin. On a résolu, par une synthèse indépendante, les ambiguités relatives à la position des déplacements nucléophiles requis. On compare les taux de rupture des hélices simples de l'ADN-ccc PM2 (ADN circulaire fermé d'une façon covalente) qui sont induites par ces composés; ces vitesses sont reliées avec l'activité antitumorale. Les dérivés *o*-nitrophénylés en 2 donnent d'une façon systématique des coupures plus rapides de l'ADN que les composés *o*-aminophénylés en 2. L'autooxydation des dihydroxyquinolines est sujette à une catalyse sélective par l'ion Cu^{2+}. La distribution des substituants dans l'(*o*-aminophényl)-2 amino-7 méthoxy-6 quinolinedione-5,6 est celle qui ressemble le plus à celle de la streptonigrin; cette dione donne un taux de scission de l'ADN qui est très parallèle à celui de ce dernier en présence de NADPH.

[Traduit par le journal]

Streptonigrin (SN) **1** is an antitumor antibiotic produced by *Streptomyces flocculus* (1). It is of interest as a potential chemotherapeutic agent since it exhibits a broad spectrum of inhibition of various tumors *e.g.* carcinoma 755, sarcoma 180, Lewis lung carcinoma, Walker 256 carcinosarcoma, Ridgeway osteogenic sarcoma, and certain types of lymphomas (2–4). The evidence to date indicates streptonigrin has as its principal cell target site the nucleic acids and exerts its antitumor action by extensive degradation of DNA causing disruption of the replicative mechanism of the cell (5). We recently reported that streptonigrin in the presence of NADH induces single strand scission in PM2 ccc-DNA (covalently-closed circular-DNA) by generating superoxide anion and hydrogen peroxide (6). The latter react together to produce hydroxyl radicals which cleave the DNA by a process strongly reminiscent of that induced by ionizing radiation.

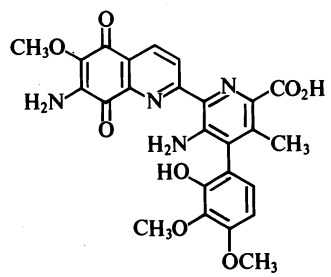

1

The 5,8-quinolinequinone moiety is the principal structural feature required for antineoplastic activity (6). A series of substituted 5,8-quinolinequinones in the presence of NADH cleave PM2 ccc-DNA at different rates and a good correlation is observed between rate of cleavage and percentage tumor weight inhibition of Walker carcinosarcoma 256 induced by these compounds (7). In continuation of our studies in

[1]NRCC Postdoctorate Fellow 1973–1975, National Cancer Institute of Canada Postdoctoral Fellow 1975 to present.

Can. J. Chem. Downloaded from www.nrcresearchpress.com by 210.87.254.42 on 09/05/12
For personal use only.

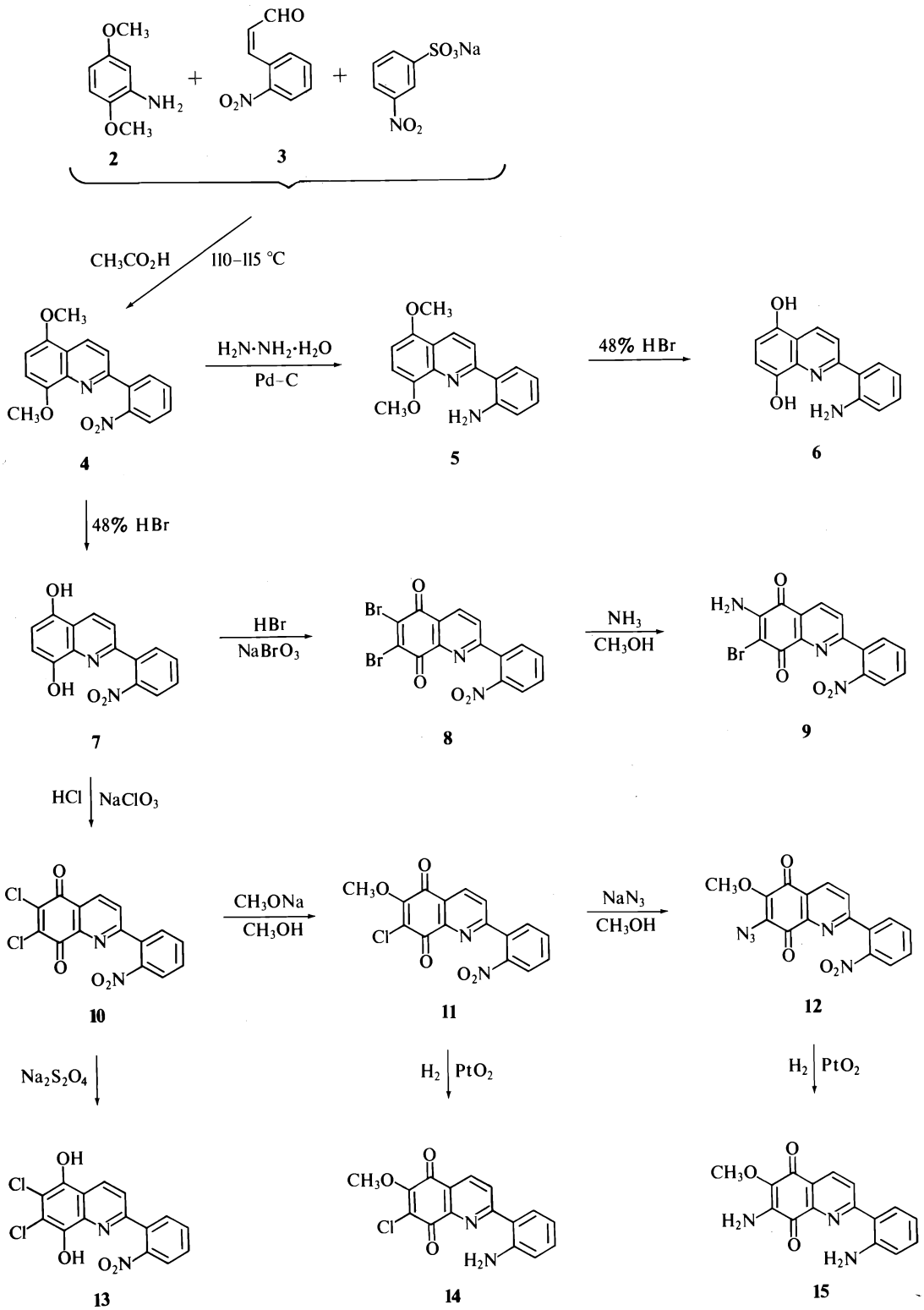

Can. J. Chem. Downloaded from www.nrcresearchpress.com by 210.87.254.42 on 09/05/12
For personal use only.

Can. J. Chem. Downloaded from www.nrcresearchpress.com by 210.87.254.42 on 09/05/12
For personal use only.

this area we report the synthesis of several new analogues of the antibiotics bearing a 2-*o*-substituted aryl moiety on the basic 5,8-quinolinequinone and an examination of the effects of these structural changes on the rate of DNA scission. The syntheses of somewhat different streptonigrin analogs have been reported but no attempt was made to examine their reactions with nucleic acids (8, 9).

2-(*o*-Nitrophenyl)-5,8-dimethoxyquinoline **4** was prepared by a modified Skraup synthesis (10) condensing 2,5-dimethoxyaniline with *o*-nitrocinnamaldehyde in the presence of sodium *m*-nitrobenzenesulfonate. Treatment of **4** with 48% hydrobromic acid afforded 2-(*o*-nitrophenyl)-5,8-dihydroxyquinoline **7** in 40% yield. Reaction of the latter with hydrogen bromide in the presence of sodium bromate (12) effected 6,7-dibromination as well as oxidation to the quinone to afford **8**. This reaction can also be accomplished with bromine in the presence of sodium acetate. Treatment of the latter with ammonia in methanol afforded a single isomer of 2-(*o*-nitrophenyl)-6-amino-7-bromo-5,8-quinolinedione **9**. Independent structure proof for the position of substitution in **9** is provided below.

Reduction of the nitro groups in **4** was effected with hydrazine hydrate in the presence of palladium-on-charcoal to give 2-(*o*-aminophenyl)-5,8-dimethoxyquinoline **5** in 36% yield. Cleavage of the methoxy groups in **5** was effected by treatment with 48% hydrobromic acid giving 2-(*o*-aminophenyl)-5,8-dihydroxyquinoline **6** in 72% yield.

2-(*o*-Nitrophenyl)-6,7-dichloro-5,8-quinolinedione **10** was prepared by reaction of **7** with hydrochloric acid and sodium chlorate (12) in 77% yield. Nucleophilic displacement of the 6-chloro substituent occurred preferentially with sodium methoxide in methanol to give 2-(*o*-nitrophenyl)-7-chloro-6-methoxy-5,8-quinolinedione **11** in 86% yield. As in the case of **9**, independent structure proof for the position of displacement in **11** is discussed below. Reaction of **11** with sodium azide in methanol gives partial displacement of the chloro substituent by azide (13) to afford a mixture of **11** and **12**. This mixture was more conveniently separated at the next reduced stage after hydrogenation over platinum oxide. Chromatographic separation over silica gel gave pure 2-(*o*-aminophenyl)-7-chloro-6-methoxy-5,8-quinolinedione **14** and 2-(*o*-aminophenyl)-7-amino-6-methoxy-5,8-quinolinedione **15**. Although many of the hydroquinone forms were very unstable to air oxidation some proved to be isolable. Thus reduction of the 6,7-dichloro-5,8-quinolinedione **10** with sodium dithionite in aqueous tetrahydrofuran gave 2-(*o*-nitrophenyl)-6,7-dichloro-5,8-dihydroxyquinoline **13** in 90% yield.

In order to prove unambiguously the orientation of the substituents in compounds **9**, **11**, **12**, **14**, and **15**, 2-(*o*-nitrophenyl)-6,8-dimethoxyquinoline **17** was prepared by condensation of 2,4-dimethoxyaniline **16** and *o*-nitrocinnamaldehyde in the presence of sodium *m*-nitrobenzenesulfonate. Oxidation of **17** with nitric acid in acetic acid gave 2-(*o*-nitrophenyl)-6-methoxy-5,8-quinolinedione **18**, in addition to the nitration product 2-(*o*-nitrophenyl)-6,8-dimethoxy-5-nitroquinoline **24**. The hydroquinone **19** corresponding to **18** was prepared by dithionite reduction at room temperature. With the same reagent under refluxing conditions one obtains 2-(*o*-aminophenyl)-6-methoxy-5,8-dihydroxyquinoline **27** which was readily air oxidized to 2-(*o*-aminophenyl)-6-methoxy-5,8-quinolinedione **20**. Treatment of compound **18** with a solution of chlorine in chloroform gave 2-(*o*-nitrophenyl)-6-methoxy-7-chloro-5,8-quinolinedione **11** identical with that produced by nucleophilic substitution of **10**.

The 6-methoxy group in compound **18** could be replaced by an amino group by treatment with ammonia in methanol affording 2-(*o*-nitrophenyl)-6-amino-5,8-quinolinedione **21** in 35% yield. Catalytic reduction of the latter over platinum oxide gave 2-(*o*-aminophenyl)-6-amino-5,8-quinolinedione **23** in 70% yield. Treatment of **18** with bromine in chloroform gave 2-(*o*-nitrophenyl)-6-methoxy-7-bromo-5,8-quinolinedione **22** in 53% yield and reaction of the latter with ammonia in methanol afforded 2-(*o*-nitrophenyl)-6-amino-7-bromo-5,8-quinolinedione **9** in 80% yield identical with that formed by nucleophilic displacement in compound **8**. Catalytic reduction of **9** with palladium-on-charcoal in the presence of hydrazine hydrate afforded 2-(*o*-aminophenyl)-7-bromo-6-amino-5,8-quinolinedione **25**.

Comparison of Efficiency of Single Strand Scission of DNA by Streptonigrin Analogues

Experiments were performed at 37 °C in 0.05

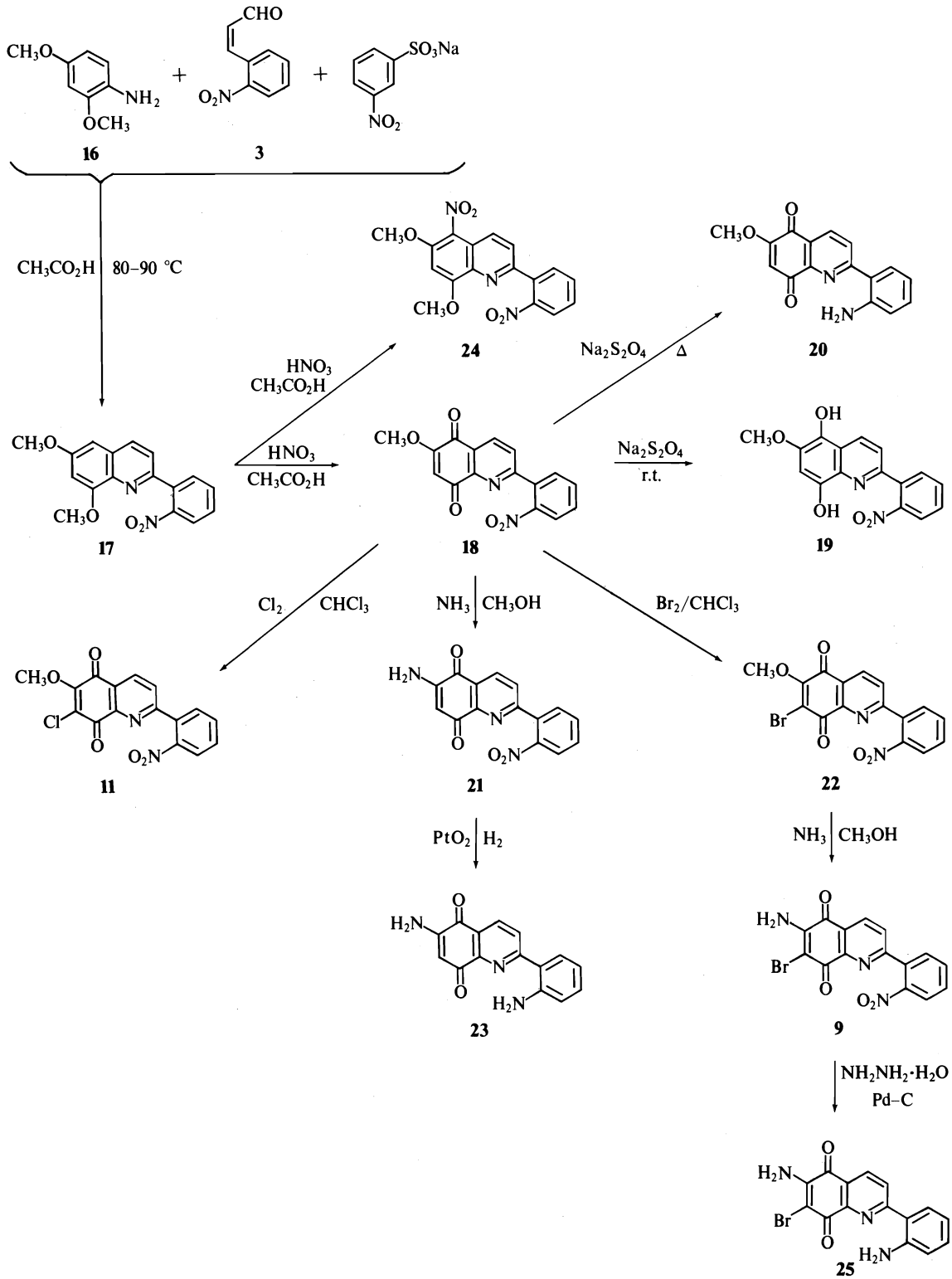

Can. J. Chem. Downloaded from www.nrcresearchpress.com by 210.87.254.42 on 09/05/12
For personal use only.

Can. J. Chem. Downloaded from www.nrcresearchpress.com by 210.87.254.42 on 09/05/12
For personal use only.

M potassium phosphate buffer p*H* 7.0 with $1–4 \times 10^{-4}$ *M* solutions of substrate in the presence of PM2 phage ccc-DNA and a reducing agent. The conversion of ccc-DNA to nicked circular DNA results in a 30% increase in fluorescence intensity of the added intercalative dye ethidium bromide, and 100% loss of fluorescence after a heating and cooling cycle since the strands of the DNA are now separable. The basis and techniques of this assay have been described previously (6, 11).

The reaction pathway leading to DNA strand scission requires initial reduction of the 5,8-quinolinedione (QD) and subsequent reoxidation with the production of superoxide and hydroxyl radicals which then effect strand scission (6, 7).

$$[1] \quad QD + NADH \xrightarrow{H^+} QDH_2 + NAD^+$$

$$[2] \quad QDH_2 + O_2 \rightarrow QDH^{\cdot} + HO_2^{\cdot}$$

$$[3] \quad HO_2^{\cdot} \rightleftarrows O_2^{\cdot-} + H^+$$

$$[4] \quad 2O_2^{\cdot-} + 2H^+ \rightarrow H_2O_2 + O_2$$

$$[5] \quad O_2^{\cdot-} + H_2O_2 \rightarrow HO^{\cdot} + HO^- + O_2$$

In order to examine the effects of substituents in the new streptonigrin analogues on the rate of DNA cleavage, reaction conditions were selected so that (*i*) reduction of QD was rate limiting using NADH or NADPH and (*ii*) reduction of QD was rapid and complete with sodium borohydride so that oxidation of QDH_2 to the semiquinone was rate limiting.

Table 1 compares the rates of DNA cleavage for three analogues using the coenzyme NADH for reduction. The 6,7-dihalo-5,8-quinolinediones which are more readily reduced cleave DNA more efficiently.

TABLE 1. Rate of cleavage of PM2 ccc-DNA by 2-(*o*-nitrophenyl)-6,7-disubstituted-5,8-quinolinediones*

Substrate	[Substrate] (*M*)	[NADH] (*M*)	$t_{1/2}$ (min)†
6,7-Dichloro	1×10^{-4}	2.5×10^{-4}	6.5
6,7-Dibromo	1×10^{-4}	2.5×10^{-4}	8.5
6-Methoxy-7-chloro	1×10^{-4}	2.5×10^{-4}	43.0

*The concentration of PM2 ccc-DNA was 1.0 OD.
†$t_{1/2}$ represents the time required to produce 50% cleavage of PM2 DNA.

Table 2 compares the rate of PM2 DNA cleavage for nine analogues under conditions of very rapid reduction as shown by the instantaneous discharge of the absorption at 340–380 nm characteristic of the 5,8-quinolinedione system. Under these conditions the 2-(*o*-nitrophenyl) derivatives give consistently more rapid DNA cleavage than the 2-(*o*-aminophenyl) compounds.

The 2-(*o*-aminophenyl)-6-methoxy-7-amino-5,8-quinolinedione which approximates most closely to the substituent pattern of the parent antibiotic is close to SN in reactivity. This behaviour was also found in the simpler substituted 5,8-quinolinediones (7). Figure 1 shows that the rate of cleavage of DNA by this substance (I) in the presence of NADPH closely parallels that of the parent antibiotic. The small amount of cleavage induced by NADPH in the control is due to its autoxidation and slow production of hydrogen peroxide followed by a Fenton's reaction of the latter with traces of metal ions (6).

Previous studies with simple 5,8-quinolinediones in the presence of reducing agent and selected metal ions showed a pronounced catalytic effect of Cu^{2+} on the rate of PM2 strand scission and minimal effect due to Co^{2+}. In the present work the isolation of a stable 2-(*o*-

TABLE 2. Rate of cleavage of PM2 ccc-DNA by (2-aryl)-6,7-disubstituted 5,8-quinolinediones with sodium borohydride*

Substrate	[Substrate] (*M*)	[$NaBH_4$] (mg/ml)	$t_{1/2}$ (min)
2(*o*-Nitrophenyl)-6-amino-7-bromo	2×10^{-4}	0.1	$\ll1$
2(*o*-Nitrophenyl)-6-methoxy-7-bromo	2×10^{-4}	0.1	<1
2(*o*-Nitrophenyl)-7-amino	4×10^{-4}	0.1	<1
2(*o*-Nitrophenyl)-7-methoxy	2×10^{-4}	0.1	<1
2(*o*-Aminophenyl)-7-methoxy	2×10^{-4}	0.1	1
2(*o*-Aminophenyl)-6-methoxy-7-amino	2×10^{-4}	0.1	5
2(*o*-Aminophenyl)-6-methoxy-7-chloro	2×10^{-4}	0.1	7

*The concentration of PM2 ccc-DNA was 1.0 OD.

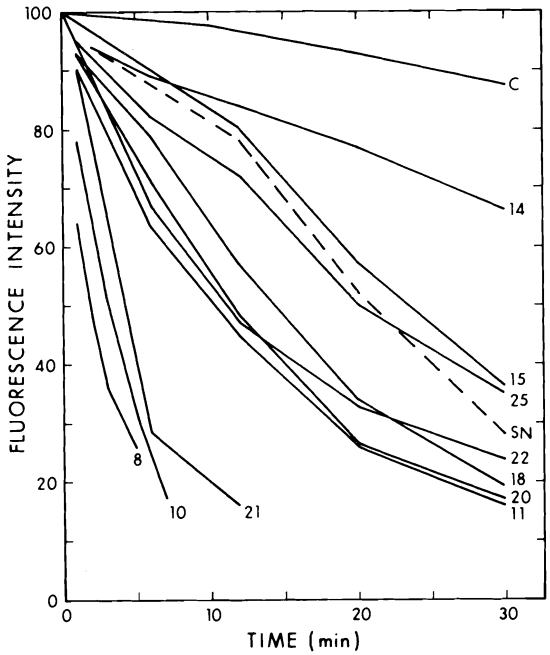

FIG. 1. Comparison of rates of DNA scission by streptonigrin and substituted 5,8-quinolinediones at 37 °C in a total volume of 200 μl buffered with 0.05 *M* potassium phosphate p*H* 7.0. Reaction solutions had a concentration of 1.0 A_{260} of PM2 ccc-DNA, 2 mg/ml of NADPH and 5% acetonitrile, and 1×10^{-4} *M* in the indicated 5,8-quinolinequinones; SN = streptonigrin, C = NADPH control.

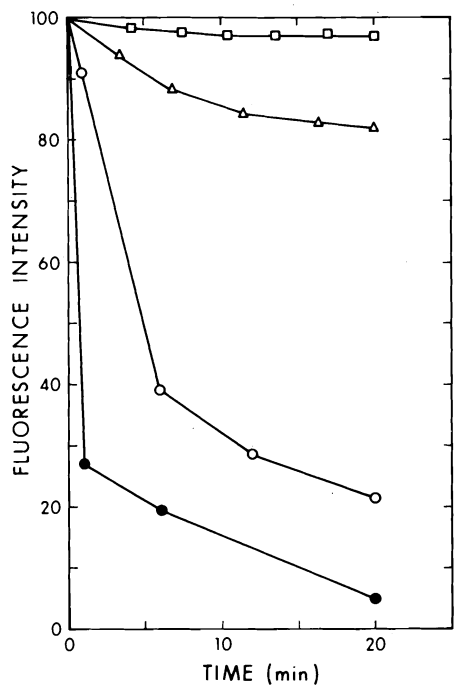

FIG. 2. Single strand scission of PM2 ccc-DNA by 10^{-4} *M* 2-(*o*-aminophenyl)-5,8-dihydroxyquinoline in the presence of metal ions at 37 °C in a total volume of 200 μl buffered with 0.5 *M* potassium phosphate p*H* 7.0 containing 1.0 A_{260} units of PM2 DNA and 5% acetonitrile. Additional components were ○—○ none; ●—● 2×10^{-4} *M* cuprous acetate; △—△ 10^{-4} *M* cobaltous acetate; □—□ 2×10^{-4} *M* cuprous acetate or cobaltous acetate in the absence of **6**.

aminophenyl)-5,8-dihydroxyquinoline allows the examination of the effects of selective bidentate metal chelation on the rate of DNA scission in the absence of a reducing agent. It is seen from Fig. 2 that addition of Cu^{2+} produces a marked acceleration of cleavage whereas Co^{2+} produces no increase in the rate and in fact is somewhat inhibitory. This result is in keeping with the finding that addition of EDTA in the administration of streptonigrin inhibits its antitumor activity (5).

Experimental

Melting points were determined on a Fisher–Johns apparatus and are uncorrected. The ir spectra were recorded on a Perkin-Elmer 421 spectrophotometer and only the principal sharply defined peaks are reported. The nmr spectra were recorded on Varian A-60, and A-100 spectrometers employing 10–15% solutions in $CDCl_3$ with tetramethylsilane as an internal standard. DMSO-d_6 was used for less soluble samples. Line positions are reported in ppm from the reference. Mass spectra were determined on Associated Electrical Industries MS-2 and MS-9 double focussing high resolution mass spectrometers. The ionization energy, in general, was 70 eV. Peak measurements were made by comparison with perfluorotributylamine at a resolving power of 15 000. Microanalyses were carried out by Mrs. D. Mahlow of this department.

Materials

Ethidium bromide and NADH were purchased from Sigma Chemical Co. The NADH was always made up fresh in 50 m*M* phosphate p*H* 7.5. The λ and PM2 DNAs were prepared as before. Streptonigrin was obtained from the U.S. National Cancer Institute, Washington, D.C.

2-(o-Nitrophenyl)-5,8-dimethoxyquinoline (4)

o-Nitrocinnamaldehyde (35.4 g, 0.2 mol) was added over 15 min to a well stirred solution of 30.6 g (0.2 mol) of 2,5-dimethoxyaniline and 67.0 g (0.3 mol) of sodium *m*-nitrobenzenesulfonate in 700 ml of glacial acetic acid at 60–70 °C. The mixture was then heated at 110–115° for 1½ h, then poured over chipped ice. The resulting precipitate was collected, taken up in methylene chloride, and the organic layer washed successively with water and saturated sodium bicarbonate solution and dried ($MgSO_4$). Concentration of the dried solution gave the crude

Can. J. Chem. Downloaded from www.nrcresearchpress.com by 210.87.254.42 on 09/05/12
For personal use only.

Can. J. Chem. Downloaded from www.nrcresearchpress.com by 210.87.254.42 on 09/05/12
For personal use only.

product which was purified by chromatography on 500 g of alumina eluting with 2:1 hexane – methylene chloride affording 2-(*o*-nitrophenyl)-5,8-dimethoxyquinoline **4** as a yellow solid, mp 142–144 °C (10 g, 15% yield) (from methylene chloride – hexane). *Anal.* calcd. for $C_{17}H_{14}N_2O_4$ (mol. wt. 310.0954): C 65.81, H 4.52, N 9.03; found (310.0947, mass spectrum): C 65.80, H 4.58, N 8.79.

The ir spectrum ν_{max} ($CHCl_3$) 1515, 1340 cm^{-1} (NO_2). The nmr spectrum δ_{TMS} ($CDCl_3$) 3.91 (s, 3H, CH_3O), 3.98 (s, 3H, CH_3O), 6.88 (dd, 2H, H6, H7, J = 8 Hz), 7.2–8.1 (m, 5H, aromatic), 8.63 (d, 1H, H4, J_{34} = 8 Hz).

2-(o-Nitrophenyl)-5,8-dihydroxyquinoline (7)

A solution of 500 mg (1.6 mmol) 2-(*o*-nitrophenyl)-5,8-dimethoxyquinoline in 14 ml of 48% hydrobromic acid was heated under reflux for 5 h and then cooled. The black precipitate was removed by filtration and the filtrate neutralized with sodium hydrogen carbonate solution. The yellow precipitate was collected and dried giving 2-(*o*-nitrophenyl)-5,8-dihydroxyquinoline **7** as a yellow solid, (200 mg; 40% yield). The mass spectrum showed a molecular ion peak at 282. Since purification resulted in substantial loss of material, the crude **7** was used immediately to prepare the 6,7-dihalo-5,8-quinolinediones.

2-(o-Nitrophenyl)-6,7-dibromo-5,8-quinolinedione (8)

Method (i)

To a solution of 1.48 g (5 mmol) of 2-(*o*-nitrophenyl)-5,8-dihydroxyquinoline in 20 ml of glacial acetic acid was added 200 mg of sodium acetate followed by 800 mg (5 mmol) of bromine. After stirring at room temperature overnight the mixture was diluted with water and the resulting precipitate collected. The product was purified by chromatography on Florisil eluting with methylene chloride giving 2-(*o*-nitrophenyl)-6,7-dibromo-5,8-quinolinedione **8** as a yellow solid, mp 224–225 °C (1.1 g, 50% yield) (from ethyl acetate). *Anal.* calcd. for $C_{15}H_6N_2O_4Br_2$ (mol. wt. 435.9633): C 41.10, H 1.37, N 6.39, Br 36.53; found (435.9603, mass spectrum): C 41.20, H 1.44, N 6.54, Br 36.73.

The nmr spectrum δ_{TMS} [$(CD_3)_2SO$] 7.86 (m, 3H, aromatic), 8.10 (m, 1H, aromatic), 8.16 (d, 1H, H3, J_{43} = 8 Hz), 8.56 (d, 1H, H4, J_{34} = 8 Hz). The absorption spectrum λ_{max} (CH_3CN, C, 4.6×10^{-5} M) 345 nm (ϵ 2600), 300 nm (ϵ 4400).

Method (ii)

Sodium bromate (200 mg) was added to a solution of 1 g (3.6 mmol) of 2-(*o*-nitrophenyl)-5,8-dihydroxyquinoline **7** in 50 ml of 48% hydrobromic acid. After warming on the steam bath for 5–10 min, the mixture was set aside at room temperature overnight. It was diluted with water, neutralized with sodium hydrogen carbonate, and extracted with ethyl acetate. Concentration of the solution deposited **8** as a yellow solid, mp 224–225 °C (0.68 g, 50% yield).

2-(o-Nitrophenyl)-6,7-dichloro-5,8-quinolinedione (10)

Sodium chlorate (2 g) was added to a suspension of 1.0 g (3.5 mmol) of crude 2-(*o*-nitrophenyl)-5,8-dihydroxyquinoline in 5 ml of concentrated hydrochloric acid at 0–5 °C. After stirring for 24 h at room temperature crude **10** was collected as a yellow solid, 950 mg (77% yield). The analytical sample was obtained by chromatography on silica gel eluting with 1:1 methylene chloride – hexane, mp 231–233 °C. *Anal.* calcd. for $C_{15}H_6N_2O_4Cl_2$: C 51.58, H 1.72, N 8.02, Cl 20.35; found C 51.36, H 2.06, N 7.75, Cl 20.11.

The ir spectrum ν_{max} (Nujol) 1690, 1670 (C=O), 1525, 1370 cm^{-1} (NO_2). The nmr spectrum δ_{TMS} [$(CD_3)_2SO$] 7.86 (m, 3H, aromatic), 8.08 (m, 1H, aromatic), 8.19 (d, 1H, H3, J_{43} = 8 Hz), 8.59 (d, 1H, H4, J_{34} = 8 Hz). The absorption spectrum λ_{max} (CH_3CN, C, 2.8×10^{-5} M), 340 nm (ϵ 3200), 290 nm (ϵ 24 000).

2-(o-Nitrophenyl)-7-chloro-6-methoxy-5,8-quinolinedione (11)

(*a*) Sodium methoxide in methanol (0.6 ml of 1 M) was added to a solution of 210 mg (0.6 mmol) 2-(*o*-nitrophenyl)-6,7-dichloro-5,8-quinolinedione **10** in 40 ml of cold methanol. The solution was stirred at room temperature for 1 h and the solvent was evaporated. The residue was taken up in methylene chloride, washed with water, and the solution concentrated to 20 ml. Upon addition of hexane compound **11** deposited as yellow crystals, mp 180–182 °C (180 mg, 86% yield).

(*b*) Alternatively, to a cold solution of 160 mg (0.5 mmol) 2-(*o*-nitrophenyl)-6-methoxy-5,8-quinolinedione **18** in 30 ml of chloroform was added 46 ml of cold chloroform saturated with chlorine. The solution was kept at 0–5 °C for 2 h. The solvent was removed *in vacuo* and the residue recrystallized from methanol to give **11** as yellow crystals, mp 179–181 °C (144 mg, 84% yield). Mixture melting point with the product prepared from 2-(*o*-nitrophenyl)-6,7-dichloro-5,8-quinolinedione showed no depression. *Anal.* calcd. for $C_{16}H_9N_2O_5Cl$ (mol. wt. 344.0197): C 55.73, H 2.61, N 8.13, Cl 10.31; found (344.0194, mass spectrum): C 55.50, H 2.56, N 7.88, Cl 10.99.

The nmr spectrum δ_{TMS} [$(CD_3)_2SO$] 4.75 (s, 3H, CH_3O), 7.84 (m, 3H, aromatic), 8.10 (m, 1H, aromatic), 8.13 (d, 1H, H3, J_{43} = 8 Hz), 8.50 (d, 1H, H4, J_{34} = 8 Hz). The ir spectrum ν_{max} (Nujol): 1665 (C=O), 1525 cm^{-1} (NO_2). The absorption spectrum λ_{max} (CH_3CN, C, 5.6×10^{-5}), 340 nm (ϵ 2000), 290 nm (ϵ 18 000).

2-(o-Aminophenyl)-7-amino-6-methoxy-5,8-quinolinedione (15) and 2-(o-Aminophenyl)-7-chloro-6-methoxy-5,8-quinolinedione (14)

Sodium azide (200 mg, 3 mmol) was added to a solution of 200 mg (0.58 mmol) of 2-(*o*-nitrophenyl)-7-chloro-6-methoxy-5,8-quinolinedione **11** in 10 ml of methanol and the mixture stirred at room temperature for 12 h. The solvent was evaporated and the residue recrystallized twice from methylene chloride – hexane to give 26 mg of 2-(*o*-nitrophenyl)-7-azido-6-methoxy-5,8-quinolinedione **12** as red crystals, mp 133–135 °C.

The ir spectrum ν_{max} (Nujol) 1640, 1665 (CO), 1520 (NO_2), and 2010 cm^{-1} (N_3). The nmr spectrum δ_{TMS} [$(CD_3)_2SO$] 4.08 (s, 3H, CH_3O), 7.84 (m, 3H, aromatic), 8.10 (m, 1H, aromatic), 8.12 (d, 1H, H3, J_{43} = 8 Hz), 8.46 (d, 1H, H4, J_{34} = 8 Hz).

The mother liquor from the above recrystallization was evaporated to dryness. The residue was taken up in methanol and hydrogenated over 30 mg of platinum oxide at room temperature and 1 atm pressure for 2 h. The catalyst was removed by filtration, the solvent evaporated, and the residue purified by chromatography on silica gel, eluting with chloroform to give two products.

Can. J. Chem. Downloaded from www.nrcresearchpress.com by 210.87.254.42 on 09/05/12
For personal use only.

The first product eluted was recrystallized from methylene chloride – hexane giving 2-(*o*-aminophenyl)-7-chloro-6-methoxy-5,8-quinolinedione, **14** mp 162–165 °C (30 mg, 17% yield). *Mol. Wt.* calcd. for $C_{16}H_{11}N_2O_3Cl$: 314.0458; found (mass spectrum): 314.0451.

The ir spectrum ν_{max} (Nujol), 1665 (C=O), 3430 cm^{-1} (NH_2). The absorption spectrum λ_{max} (CH_3CN, *C*, 1×10^{-4} *M*) 490 nm (ϵ 900), 380 nm (ϵ 3700), 310 nm (ϵ 6200), 290 nm (ϵ 9000).

The second compound eluted was the 2-(*o*-aminophenyl)-7-amino-6-methoxy-5,8-quinolinedione **15**. Recrystallization from methylene chloride – hexane yielded 50 mg (28% yield) of **15** as a purple solid mp 213–215 °C. *Anal.* calcd. for $C_{16}H_{13}N_3O_3$ (mol. wt. 295.0957): C 65.08, H 4.41, N 14.24; found (295.0952, mass spectrum): C 64.89, H 4.42, N 14.32.

The ir spectrum λ_{max} (Nujol) 1670 (C=O), 3240, 3320, 3420 cm^{-1} (NH_2). The nmr spectrum δ_{TMS} (pyridine-d_5) 4.02 (s, 3H, CH_3O), 6.72–7.90 (m, 4H, aromatic), 8.08 (d, 1H, H3, J_{43} = 8 Hz), 8.42 (d, 1H, H4, J_{34} = 8 Hz). The absorption spectrum λ_{max} (CH_3CN, *C*, 10^{-5} *M*), 500 nm (ϵ 3000), 380 nm (ϵ14 000), 320 nm (ϵ 21 000).

*2-(o-Nitrophenyl)-6,8-dimethoxyquinoline (**17**)*

A modified Skraup synthesis similar to that described for **4** was carried out with 16 g (0.1 mol) of 2,4-dimethoxyaniline, 25 g (0.11 mol) of sodium *m*-nitrobenzenesulfonate, and 17.7 g (0.1 mol) of *o*-nitrocinnamaldehyde in 250 ml of glacial acetic acid at 80–90 °C and gave 7.2 g (23% yield) of 2-(*o*-nitrophenyl)-6,8-dimethoxyquinoline **17** as a yellow solid mp 204–206 °C (methanol). *Anal.* calcd, for $C_{17}H_{14}N_2O_4$ (mol. wt. 310.0954): C 65.81, H 4.52, N 9.02; found (310.0945, mass spectrum): C 65.52, H 4.57, N 8.98.

The ir spectrum ν_{max} (Nujol) 1340, 1515 (NO_2) cm^{-1}. The nmr spectrum δ_{TMS} ($CDCl_3$) 3.90(s, 3H, CH_3O), 4.00 (s. 3H, CH_3O), 6.70 (AB quartet, 2H, H5, H7, $J_{5,7}$ = 3 Hz), 7.46 (d, 1H, H3, J_{43} = 8 Hz), 7.50–8.00 (m, 4H, aromatic), 8.06 (d, 1H, H4, J_{34} = 8 Hz).

*2-(o-Nitrophenyl)-6-methoxy-5,8-quinolinedione **18** and 2-(o-Nitrophenyl)-6,8-dimethoxy-5-nitroquinoline (**24**)*

A solution of 1.6 g (5 mmol) of 2-(*o*-nitrophenyl)-6,8-dimethoxyquinoline **17** in 20 ml of 5:1 acetic acid – fuming nitric acid was heated at 40–50 °C for 1 h. The solution was poured into chipped ice, neutralized with saturated sodium hydrogen carbonate, and then extracted with chloroform. The chloroform solution after drying and concentration gave 1.4 g of a mixture. Recrystallization from methylene chloride gave 300 mg **24**. The residue was chromatographed on silica gel, eluting with methylene chloride. The first compound eluted was 2-(*o*-nitrophenyl)-6,8-dimethoxy-5-nitroquinoline **24**, 853 mg, mp 208–210 °C. *Anal.* calcd. for $C_{17}H_{13}N_3O_6$ (mol. wt. 355.0791): C 57.46, H 3.66, N 11.83; found (355.0792, mass spectrum): C 57.65, H 3.71, N 12.01.

The ir spectrum ν_{max} (Nujol) 1350, 1520 cm^{-1} (NO_2). The nmr spectrum δ_{TMS} [$(CD_3)_2SO$] 4.12 (s, 3H, CH_3O), 4.14 (s, 3H, CH_3O), 7.24 (s, 1H, H7), 7.84 (m, 3H, aromatic), 7.94 (d, 1H, H3, J_{34} = 8 Hz), 8.08 (m, 1H, aromatic), 8.26 (d, 1H, H4, J_{43} = 8 Hz).

Further elution with methylene chloride gave 200 mg (13% yield) of 2-(*o*-nitrophenyl)-6-methoxy-5,8-quinolinedione **18** mp 235–237 °C. *Anal.* calcd. for $C_{16}H_{10}N_2O_5$ (mol. wt. 310.0591): C 61.94, H 3.23, N 9.03; found (310.0591, mass spectrum): C 61.81, H 3.28, N 9.17.

The ir spectrum ν_{max} (Nujol) 1680, 1660 (C=O), 1520 cm^{-1} (NO_2). The nmr spectrum δ_{TMS} [$(CD_3)_2SO$] 3.90 (s, 3H, CH_3O), 6.48 (s, 1H, H7), 7.84 (m, 3H, aromatic), 8.10 (m, 1H, aromatic), 8.10 (d, 1H, H3, J_{43} = 8 Hz), 8.32 (d, 1H, H4, J_{34} = 8 Hz). The absorption spectrum λ_{max} (CH_3CN, *C*, 2×10^{-5} *M*) 340 nm (ϵ 2100), 290 nm (ϵ 54 000).

*2-(o-Nitrophenyl)-7-bromo-6-methoxy-5,8-quinolinedione (**22**)*

A solution of 53 mg (0.17 mmol) 2-(*o*-nitrophenyl)-6-methoxy-5,8-quinolinedione **18** in chloroform was treated with excess of bromine. After stirring at room temperature for 1 h, the solution was washed with saturated sodium hydrogen carbonate solution. The organic layer was removed and again treated with a few drops of bromine. The bromination and neutralization procedure was repeated four times after which tlc showed very little starting material was left. The solvent was evaporated and the residue recrystallized from methanol giving 35 mg (53% yield) of **22** as yellow crystals, mp 195–197 °C. *Anal.* calcd. for $C_{16}H_9N_2O_5Br$ (mol. wt. 387.9695): C 49.36, H 2.32, Found: (387.9694, mass spectrum): C 49.34, H 2.12.

The ir spectrum ν_{max} (Nujol) 1520 (NO_2), 1675, 1660 (C=O) cm^{-1}. The nmr spectrum δ_{TMS} [$(CD_3)_2CO$] 4.52 (s, 3H, CH_3O), 7.82 (m, 3H, aromatic), 8.02 (m, 1H, aromatic), 8.06 (d, 1H, H3, J_{43} = 8 Hz), 8.54 (d, 1H, H4, J_{34} = 8 Hz). The absorption spectrum λ_{max} (CH_3CN, *C*, 2.7×10^{-5} *M*), 390 nm (ϵ 1800), 294 nm (ϵ 13 000).

*2-(o-Nitrophenyl)-6-amino-7-bromo-5,8-quinolinedione (**9**)*

A solution of 50 mg (0.13 mmol) of 2-(*o*-nitrophenyl)-7-bromo-6-methoxy-5,8-quinolinedione **22** in methanol was saturated with ammonia and kept at room temperature for 5 h. The resulting precipitate was collected to give 40 mg (80% yield) of **9**, mp 265–268 °C. *Anal.* calcd. for $C_{15}H_8N_3O_4Br$ (mol. wt. 372.9698): C 48.13, H 2.14, N 11.23; found (372.9696, mass spectrum): C 47.84, H 2.19, N 11.13.

The ir spectrum ν_{max} (Nujol) 1520 (NO_2), 1676 (C=O), 3340, 3460 cm^{-1} (NH_2). The nmr spectrum δ_{TMS} [$(CD_3)_2SO$] 7.60 (br s, 2H, NH_2), 7.82 (m, 3H, aromatic), 8.02 (d, 1H, H3, J_{43} = 8 Hz), 8.08 (m, 1H, aromatic), 8.46 (d, 1H, H4, J_{34} = 8 Hz). The absorption spectrum λ_{max} (CH_3CN, *C*, 10^{-5} *M*) 450 nm (ϵ 20 000), 300 nm (ϵ 170 000).

A similar reaction between 2-(*o*-nitrophenyl)-6,7-dibromo-5,8-quinolinedione **8** with ammonia in methanol gave 2-(*o*-nitrophenyl)-6-amino-7-bromo-5,8-quinolinedione **9** as the major product in 80% yield. Recrystallization from methanol yielded a reddish solid mp 264–266 °C. Mixed melting point with the compound prepared from 2-(*o*-nitrophenyl)-7-bromo-6-methoxy-5,8-quinolinedione showed no depression.

*2-(o-Nitrophenyl)-6-amino-5,8-quinolinedione (**21**)*

A solution of 62 mg (0.2 mmol) 2-(*o*-nitrophenyl)-6-methoxy-5,8-quinolinedione **18** in methanol was saturated with ammonia and kept at room temperature for 12 h. The solvent was evaporated and the residue dissolved in methylene chloride. Addition of ether deposited 20 mg (35%) of **21** as a reddish solid mp 149–152 °C. *Mol. Wt.*

Can. J. Chem. Downloaded from www.nrcresearchpress.com by 210.87.254.42 on 09/05/12
For personal use only.

calcd. for $C_{15}H_9N_3O_4$: 295.0593; found (mass spectrum): 295.0597. The absorption spectrum λ_{max} (CH_3CN, *C*, 2×10^{-5} *M*), 420 nm (ϵ 2200), 280 nm (ϵ 45 000).

2-(o-Aminophenyl)-6-amino-5,8-quinolinedione (23)

A solution of 40 mg (0.14 mmol) of 2-(*o*-nitrophenyl)-6-amino-5,8-quinoline **21** in methanol was hydrogenated over 10 mg of platinum oxide at room temperature and at atmospheric pressure for 1 h. The catalyst was removed by filtration and the filtrate upon concentration deposited 26 mg (70% yield) of **23** as a reddish solid, mp 220 °C (dec.). *Mol. Wt.* calcd. for $C_{15}H_{11}N_3O_2$: 265.0851; found: 265.0848. The ir spectrum ν_{max} ($CHCl_3$) 1670 (C=O). 3400, 3500 cm^{-1} (NH_2).

2-(o-Aminophenyl)-7-bromo-6-amino-5,8-quinolinedione (25)

To a solution of 50 mg (0.13 mmol) of 2-(*o*-nitrophenyl)-7-bromo-6-amino-5,8-quinolinedione **9** in 20 ml of methanol at 60 °C was added 20 mg of palladium-on-carbon catalyst, followed by 0.1 ml of hydrazine hydrate. After refluxing for ½ h the catalyst was collected and the solvent evaporated. The residue was chromatographed on Florisil eluting with 1% methanol in methylene chloride giving 10 mg (23% yield) of **25** as a purple solid, mp 243–245 °C. *Mol. Wt.* calcd. for $C_{15}H_{10}N_3O_2Br$: 342.9802; found: 342.9803.

2-(o-Aminophenyl)-5,8-dimethoxyquinoline (5)

In a similar manner to that described for **25**, a solution of 1.55 g (5 mmol) of 2-(*o*-nitrophenyl)-5,8-dimethoxyquinoline **4** in 100 ml of ethanol was treated with 20 mg of palladium-on-charcoal and 1 ml of hydrazine hydrate and heated under reflux for ½ h. The catalyst was removed by filtration and the solvent evaporated. The residue was chromatographed through alumina eluting with 2:1 hexane – methylene chloride to give 510 mg (36% yield) of **5** as a pale yellow solid, mp 130–131 °C (from methylene chloride – hexane). *Anal.* calcd. for $C_{17}H_{16}N_2O_2$ (mol. wt. 280.1212): C 72.86, H 5.72, N 10.00; found (280.1206, mass spectrum): C 72.59, H 5.70, N 9.92.

The ir spectrum ν_{max} ($CHCl_3$) 3240, 3470 cm^{-1} (NH_2). The nmr spectrum δ_{TMS} ($CDCl_3$) 3.87 (s, 3H, CH_3O), 3.95 (s, 3H, CH_3O), 6.38 (br s, 2H, NH_2), 6.53–7.85 (m, 6H, aromatic), 7.86 (d, 1H, H3, J_{43} = 8 Hz), 8.50 (d, 1H, H4, J_{34} = 8 Hz).

2-(o-Aminophenyl)-5,8-dihydroxyquinoline (6)

A solution of 400 mg (1.43 mmol) of 2-(*o*-aminophenyl)-5,8-dimethoxyquinoline **5** in 12 ml of 48% hydrobromic acid was refluxed for 5 h under N_2. The solution was diluted with water and neutralized with sodium bicarbonate solution. The resulting precipitate was collected and recrystallized from ethanol giving the hydrobromide salt of **6** as a yellow solid, (350 mg, 72% yield) mp 240 °C (dec.). *Anal.* calcd. for $C_{15}H_{13}N_2O_2Br$: C 54.05, H 3.90, N 8.41, Br 24.03; found: C 53.94, H 4.08, N 8.15, Br 24.31.

The free amine was obtained by dissolving the hydrobromic acid salt in methanol and treating with an equimolar quantity of sodium acetate in methanol. Addition of water precipitated the free amine as a brown solid mp 190 °C (dec.). *Mol. Wt.* calcd. for $C_{15}H_{12}N_2O_2$: 252.1108; found (mass spectrum): 252.1108.

The nmr spectrum δ_{TMS} (CD_3OD) 7.00 (AB quartet, 2H, H6, H7, J_{67} = 8 Hz), 7.48 (m, 3H, aromatic), 7.92 (m, 1H, aromatic), 8.04 (d, 1H, H3, J_{34} = 8 Hz), 8.84 (d, 1H, H4, J_{34} = 8 Hz).

Preparation of Hydroquinones from Quinones

A solution of the 5,8-quinolinediones in tetrahydrofuran was treated with an aqueous solution of sodium dithionite and stirred at room temperature for 1 h. The tetrahydrofuran was removed *in vacuo* and the residue extracted with methylene chloride. The 5,8-dihydroxyquinoline was then precipitated by addition of hexane.

New compounds prepared by this procedure:

(*i*) 2-(*o*-Nitrophenyl)-7-chloro-6-methoxy-5,8-dihydroxyquinoline **26** in 80% yield, mp 192–195 °C. *Mol. Wt.* calcd. for $C_{16}H_{11}N_2O_5Cl$: 346.0351; found (mass spectrum): 346.0351.

(*ii*) 2-(*o*-Nitrophenyl)-6-methoxy-5,8-dihydroxyquinoline **19** in 75% yield, mp 205–208 °C. *Anal.* calcd. for $C_{16}H_{12}N_2O_5$ (mol. wt. 312.0745 : C 61.54, H 3.85, N 8.98; found (312.0746, mass spectrum): C 61.58, H 4.14, N 8.82.

(*iii*) 2-(*o*-Nitrophenyl)-6,7-dichloro-5,8-dihydroxyquinoline **13** in 90% yield mp 190–192 °C. *Mol. Wt.* calcd. for $C_{15}H_8N_2O_4Cl_2$: 349.9861; found: (mass spectrum): 349.9819.

(*iv*) 2-(*o*-Aminophenyl)-6-methoxy-5,8-dihydroxyquinoline **27**. This compound was prepared by refluxing a solution of 2-(*o*-nitrophenyl)-6-methoxy-5,8-quinolinedione **18** with sodium dithionite in tetrahydrofuran for 3 h. The crude product was recrystallized from methanol giving 60% yield of a purple solid mp 225–227 °C. *Mol. Wt.* calcd. for $C_{16}H_{14}N_2O_3$: 282.1004; found (mass spectrum): 282.1002. The absorption spectrum λ_{max} (CH_3CN, *C*, 2.5×10^{-5} *M*) 470 nm (ϵ 10 000), 360 nm (ϵ 3100), 290 nm (ϵ 20 000).

General Procedure for the Determination of Cleavage of PM2 ccc-DNA with 5,8-quinolinequinones

The 5,8-quinolinequinones were added as a 2 m*M* solution in acetonitrile and PM2 DNA as an aqueous solution. Reaction mixtures were buffered with 1 *M* potassium phosphate buffer at p*H* 7.0. The quinolinequinones were reduced in the reaction solutions by an aqueous solution (2 mg/ml) of NADH or sodium borohydride (10 mg/ml).

Experiments were performed at 37 °C in a total volume of 200 μl buffered with 0.05 *M* potassium phosphate, p*H* 7.0. Reaction solutions had concentrations of 1.0 OD_{260} units of PM2 DNA, 2×10^{-4} *M* of quinolinequinone, and 0.4 mg/ml of NADH. Aliquots (20 μl) were removed at timed intervals and analyzed by the fluorescence assay described previously (6, 11). The conversion of PM2 ccc-DNA to nicked circular DNA results in a 30% increase in fluorescence intensity in the alkaline ethidium assay solution, and 100% loss of fluorescence after a heating and cooling cycle since the strands of DNA are now separable.

A control reaction mixture prepared as above but containing no quinolinequinone was run with each experiment. Analysis of the control reaction showed constant fluorescence and approximately 90% return of fluorescence after heating in each case. These results were identical to those obtained by analyzing a pure aqueous solution of PM2 DNA by the same fluorescence assay.

Acknowledgements

This research was supported by grants to J.W.L. from the National Cancer Institute of Canada, the National Research Council of Canada, and by the Department of Chemistry, University of Alberta. We thank Dr. A. Hogg and Mr. R. Swindelhurst for the mass and nmr spectra.

1. K. V. RAO, K. BIEMANN, and R. B. WOODWARD. J. Am. Chem. Soc. **85** 2532 (1963).
2. K. V. RAO. Cancer Chemother. Rep. **4**, 11 (1974).
3. J. J. OLESON, L. A. CALDERELLA, A. R. REITH, R. S. THIE, and I. TOPLIN. Antibiot. Chemother. **11**, 158 (1961).
4. H. C. REILLY and K. SUGIURA. Antibiot. Chemother. **11**, 174 (1961).
5. B. K. BHUYAN. *In* Antibiotics 1: mechanism of action. *Edited by* D. Gottlieb and P. D. Shaw. Springer-Verlag, New York. 1967. p. 175.
6. R. CONE, S. K. HASAN, J. W. LOWN, and A. R. MORGAN. Can. J. Biochem. **54**, 219 (1976).
7. J. W. LOWN and S. K. SIM. Can. J. Biochem. **54**, 446 (1976).
8. (*a*) K. V. RAO, J. Heterocycl. Chem. **12**, 725 (1975); (*b*) K. V. RAO and P. VENKATESWARLU. J. Heterocycl. Chem. **12**, 731 (1975).
9. T. KAMETANI and K. OGASAWARA. Yakugaku Zasshi, **85**, 985 (1965); **86**, 55 (1966); **86**, 815 (1966); **87**, 260 (1967); **87**, 1189 (1967); **87**, 1195 (1967); **91**, 1068 (1971); **93**, 406 (1973).
10. R. H. F. MANSKE and M. KULKA. Org. React. **7**, 59 (1953).
11. A. R. MORGAN and D. E. PULLEYBLANK. Biochem. Biophys. Res. Commun. **61**, 346 (1974).
12. C. W. SCHELL-HAMMER and S. PETERSON. Ann. **624**, 108 (1959).
13. T. K. LIAO and C. C. CHANG. Angew. Chem. Int. Ed. Engl. **6**, 82 (1967).

Can. J. Chem. Downloaded from www.nrcresearchpress.com by 210.87.254.42 on 09/05/12
For personal use only.

Carbon kinetic isotope effects in the oxidation of oxalate by permanganate in aqueous solutions of sulfuric acid

ROBERT H. BETTS AND WAYNE D. BUCHANNON
Department of Chemistry, University of Manitoba, Winnipeg, Man., Canada R3T 2N2

Received January 19, 1976

ROBERT H. BETTS and WAYNE D. BUCHANNON. Can. J. Chem. **54**, 2573 (1976).

Fractionation of the carbon isotopes occurs during the oxidation of oxalate by permanganate in aqueous sulfuric acid. The isotope effect, expressed as k_{12}/k_{13}, rises from near unity in the very early stages of the reaction, to reach a value of 1.037 ± 0.001 after completion of the induction period. Addition of fluoride prolongs the induction period, and reduces the isotope effect to values near 1.000. These observations are consistent with there being two essentially independent paths for formation of carbon dioxide. The first, operative in the early stages, involves rate-controlling electron transfers from Mn(VI) or Mn(IV) to the oxalate ion, while the second involves oxidative decomposition of an oxalate complex of Mn(III), for which the rate-controlling step is C—C bond rupture.

ROBERT H. BETTS et WAYNE D. BUCHANNON. Can. J. Chem. **54**, 2573 (1976).

Il se produit une fractionnement des isotopes de carbone durant l'oxydation de l'oxalate par le permanganate en solution aqueuse d'acide sulfurique. L'effet isotopique, exprimé sous forme de k_{12}/k_{13}, augmente d'une valeur pratiquement égale à l'unité au tout début de la réaction jusqu'à une valeur de 1.037 ± 0.001 une fois que la période d'induction est complétée. L'addition d'ions fluorures prolonge la période d'induction et réduit l'effet isotopique à des valeurs près de 1.000. Ces observations sont en accord avec l'existence de deux chemins essentiellement indépendants pour la formation du dioxyde de carbone. Le premier qui agit au début de la réaction implique un transfert d'électron du Mn(VI) ou Mn(IV) vers l'ion oxalate dans l'étape déterminante de la réaction alors que le deuxième chemin implique la décomposition oxydante du complexe oxalate de Mn(III) pour lequel l'étape déterminante est la rupture du lien C—C.
[Traduit par le journal]

Can. J. Chem. Downloaded from www.nrcresearchpress.com by 210.87.254.40 on 09/05/12
For personal use only.

Introduction

The oxidation of oxalate to CO_2 by permanganate has been the subject of many studies, well summarized by Noyes (1) and by Adler and Noyes (2). While there have been several more recent publications confirming or elaborating points of the mechanism (3, 4), the definitive study appears to be that of Adler and Noyes, published 20 years ago. As is well known, the reaction has the overall stoichiometry:

$$5C_2O_4^{2-} + 2MnO_4^- + 16H^+ \rightarrow 10CO_2 + 2Mn^{2+} + 8H_2O$$

The reaction is characterized by an induction period, the extent of which is rather variable, followed by a much faster process. There is general agreement that the rate-controlling step in the latter stage involves the oxidative decomposition of 1:1, 1:2, or 1:3 Mn(III) oxalate chelates (here illustrated for the 1:1 complex [1]).

[1] 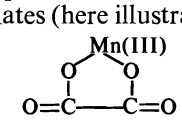 $\rightarrow$ Mn(II) + CO_2 + CO_2^-

Noyes (2) adduces evidence to support the proposal that in the initial stage, quite different (and slower) processes are involved in the formation of CO_2. These require a two-electron transfer to MnO_4^{2-} (Mn(VI)) from oxalate, and also a similar process involving Mn(IV):

[2] $$Mn(VI) + C_2O_4^{2-} \rightarrow Mn(IV) + 2CO_2$$

and

[3] $$Mn(IV) + C_2O_4^{2-} \rightarrow Mn(II) + 2CO_2$$

In this paper, we report measurements of $^{12}C/^{13}C$ isotope effects which support the mechanism outlined by Adler and Noyes (2). A much earlier study (5) of this aspect showed that $^{12}CO_2$ is formed in preference to $^{13}CO_2$ (k_{12}/k_{13} = 1.017–1.030) but the effect was somewhat irreproducible. The addition of Mn(II) to the reaction mixture, which minimizes the induction period, gave values of k_{12}/k_{13} in the range 1.032–1.036 (5).

Can. J. Chem. Downloaded from www.nrcresearchpress.com by 210.87.254.40 on 09/05/12
For personal use only.

TABLE 1. Isotope effects for oxidation of 0.05 *M* oxalate with 0.02 *M* $KMnO_4$*

Fraction of oxalate reacted†	k_{12}/k_{13}‡			
	Run 1	Run 2	Run 3	Run 4
0–0.0016	—	—	—	1.0290
0.0016–0.0032	—	—	—	1.0318
0–0.0032	1.0306	1.0305	1.0303	—
0.0032–0.0048	—	—	—	1.0336
0.0032–0.0064	1.0345	1.0338	1.0330	—
0.0048–0.0064	—	—	—	1.0357
0.0064–0.0096	1.0363	1.0363	1.0357	1.0351
0.0096–0.0128	1.0389	1.0372	1.0367	1.0358
0.0128–0.0160	1.0382	—	1.0370	—
0.0160–0.0192	—	—	1.0370	—
0.0192–0.0224	—	—	1.0374	—
0.0224–0.0256	—	—	1.0373	—
0.0256–0.0288	—	—	1.0376	—
0.0288–0.0320	—	—	1.0375	—

*The data in the table may be converted to percentage isotope effect by the expression: % isotope effect = $(k_{12}/k_{13} - 1)$ 100, *e.g.*, the first entry would be 2.9%, and similarly for the other entries.

†All solutions were initially 0.05 *M* $Na_2C_2O_4$, 0.9 *M* H_2SO_4, at 2 °C, and maintained air free at all times.

‡Average of last 16 entries = 1.0369 ± 0.0010 (s.d.).

Experimental

Analytical reagents were used without further purification. The water used was doubly distilled. The same source of reagents ($Na_2C_2O_4$, H_2SO_4, $KMnO_4$) was used in all experiments. In addition, to minimize the effect of variable amounts of Mn(II), a fresh batch of aqueous permanganate was prepared for each experiment.

Sufficient $Na_2C_2O_4$ was added to 0.9 *M* H_2SO_4 to give 0.05 *M* $Na_2C_2O_4$. This solution was thoroughly out-gassed under vacuum, and maintained thereafter at 2 °C. Successive known volumes of 0.02 *M* aqueous $KMnO_4$ (previously standardized with $Na_2C_2O_4$) were added to the oxalate – sulfuric acid solution. All the carbon dioxide evolved for each addition of $KMnO_4$ was collected separately by vacuum transfer before the next batch of $KMnO_4$ was added. In each case, the collected CO_2 was purified for mass analysis by suitable vacuum transfers.

The reference CO_2 for mass analysis was prepared by complete conversion of a sample of the same batch of $Na_2C_2O_4$ to CO_2 by reaction with excess $KMnO_4$. The $^{13}C/^{12}C$ ratio was obtained from measurement of the abundance of mass 45 ($^{13}C^{16}O^{16}O$) relative to the sum of the abundances of masses 44 + 46 + 47 + 48. A Varian Mat GD-150 isotope ratio mass spectrometer was used. Correction for the contribution of ^{17}O (as $^{12}C^{16}O^{17}O$) to the mass 45 abundance was made assuming a random distribution of oxygen isotopes amongst the species concerned.

Results

The results are summarized in Table 1. The kinetic isotope effect is expressed as the ratio: k_{12}/k_{13} for the processes[1]

$$^{12}C^{12}CO_4^{2-} \xrightarrow{k_{12}} 2\,^{12}CO_2$$

$$^{12}C^{13}CO_4^{2-} \xrightarrow{k_{13}} {}^{12}CO_2 + {}^{13}CO_2$$

We have neglected the species $^{13}C_2O_4^{2-}$. Runs 1 to 3 in Table 1 were made to determine the degree of reproducibility of the measurements, with the addition that in run 3, measurements were made on samples taken to a greater extent of reaction. Run 4 is essentially a repetition of the earlier runs, except that the first samples were taken nearer the start of the reaction.

The reproducibility of the data is very satisfactory. For example, as shown in the footnote to Table 1, the average of the last 16 entries (all for conversions >0.5%) gives $k_{12}/k_{13} = 1.0369$, with a standard deviation of ±0.0010. The reproducibility of the values of k_{12}/k_{13} determined within a run is considerably better than this, *e.g.*, for run 3, the average of the last seven values (covering the range of oxidation from 1.0% to 3.0%) is 1.0370 ± 0.0001 (s.d.).

Table 1 shows that for each run, the value of k_{12}/k_{13} rises appreciably as the reaction proceeds, and then levels off after ~0.5% of the oxalate is

[1]As a very satisfactory approximation, $k_{12}/k_{13} = R_x/R_s$, where R_x = ratio $^{12}C^{16}O_2/^{13}C^{16}O_2$ in the sample, and R_s = corresponding ratio for reference sample. The *R* values were obtained from the measured ratio: mass 45/(mass (44 + 46 + 47 + 48)), assuming random distribution of the oxygen isotopes. Allowance was made, where required, for the relative depletion of ^{12}C in the remaining oxalate as the reaction proceeded.

Can. J. Chem. Downloaded from www.nrcresearchpress.com by 210.87.254.40 on 09/05/12
For personal use only.

consumed. This conclusion is strengthened by a comparison of the data for one run with those for other runs, *e.g.*, the average of the first two results for run 4 is in quantitative agreement with the first result in each of the other three experiments. Similarly, the third entry for run 4 falls satisfactorily between the first and second entries for the other runs.

Discussion

As pointed out above, this reaction is characterized by an induction period, which for the conditions used here, extends to ~0.5% conversion of oxalate. The evidence previously cited establishes very clearly that the rate-controlling step after the completion of the induction period is the decomposition of a Mn(III)–oxalate complex (eq. 1 above), this process being followed by a rapid reaction of the CO_2^- thus formed with Mn(III). The trivalent Mn(III) complexes involved are relatively stable, and can be observed directly by conventional spectrophotometry, the equilibrium constant for formation of $Mn(C_2O_4)_3^{3-}$ from $Mn(C_2O_4)_2^- + C_2O_4^{2-}$ having been determined in this way (2, 6).

We feel it reasonable to ascribe the value of $k_{12}/k_{13} = 1.0370$ to the process shown in [1] above, which involves C—C bond rupture, accompanied by intramolecular electron transfer.

On the other hand, the rate-controlling steps for formation of CO_2 in the induction period appear to be quite different. The initiating step is:

[4] $Mn(II) + MnO_4^- \rightarrow Mn(III) + MnO_4^{2-}(Mn(VI))$

The rate constant for reaction 4 is quite favourable (3), but the intrinsic rate of this step is limited initially by the very low concentration of Mn(II). Moreover, this reaction does not itself involve oxidation of oxalate to CO_2. According to Noyes (2) reactions 2 and 3 are responsible for CO_2 production at this stage. As the overall reaction proceeds through the induction period, the concentration of Mn(II) increases, via the concurrent processes:

$$Mn(VI) + Mn(II) \rightarrow 2Mn(IV)$$

and

$$Mn(IV) + Mn(II) \rightarrow 2Mn(III)$$

followed by reaction 1. As these conditions develop, the process responsible for CO_2 formation will become, predominantly, that shown in [1].

We have then, according to this analysis, two kinds of processes, with markedly different rate-controlling steps, for the production of CO_2. The first, in the earlier stages, involves two-electron transfers from oxalate to Mn(VI) or Mn(IV), while the second involves C—C bond rupture with concomitant single electron transfer within the Mn(III)–oxalate complex. Of course, one would not expect an abrupt transition from one mechanism to the other, or indeed, even in the induction period, the presence of only one of these processes.[2]

Our data support these general conclusions. We would expect the electron transfer processes (eqs. 2 and 3) to show very little or even zero difference in the rate constants for reaction of the isotopic species $^{12}C_2O_4^{2-}$ and $^{12}C^{13}CO_4^{2-}$. On the other hand, the process indicated by [1] allows the full development of isotopic discrimination. Certainly the value of $k_{12}/k_{13} = 1.037$ is typical of carbon isotope effects for processes in which C—C bond rupture is rate-controlling (8).

We conclude therefore that formation of CO_2 during the induction period proceeds, at least in part, by processes 2 and 3, with increasing contribution from process 1 as the reaction proceeds. These conclusions have led us to examine $^{12}C/^{13}C$ fractionation for other processes, involving decomposition of oxalate to CO_2, for which one may reasonably expect C—C bond rupture not to be rate-determining. In a subsequent publication, we describe such a process, involving photolysis of the Fe(III)–oxalate complex in aqueous solution (9).

Acknowledgment

Financial support by the National Research Council of Canada is gratefully acknowledged.

[2]It is known (7) that addition of fluoride (as NaF) prolongs the induction period indefinitely, presumably by fluoride competing successfully with oxalate for Mn(III), and thereby inhibiting or stopping reaction 1. However it is not obvious that fluoride should inhibit reaction 2, as it involves MnO_4^{2-} reacting with $C_2O_4^{2-}$. We have accordingly done one further experiment, not shown in Table 1, in which a large excess of NaF was added initially. We found that the induction period was indeed prolonged indefinitely. More importantly, the CO_2 which continues to be formed slowly had initially an isotopic composition corresponding to $k_{12}/k_{13} = 0.997$ to 1.008. This result provides a striking confirmation of the hypotheses outlined in the body of this paper.

1. R. M. NOYES. Trans. N. Y. Acad. Sci. **13**, 314 (1951).
2. S. J. ADLER and R. M. NOYES. J. Am. Chem. Soc. **77**, 2036 (1955).
3. J. I. MORROW and S. PERLMAN. Inorg. Chem. **12**, 2453 (1973).
4. M. WRONSKA and T. ERNST. Z. Phys. Chem. Leipzig, **244**, 144 (1970).
5. C. A. BUNTON and D. R. LLEWELLYN. Research, **5**, 443 (1952).
6. G. H. CARTLEDGE and W. P. ERICKS. J. Am. Chem. Soc. **58**, 2065 (1936).
7. H. F. LAUNER and D. M. YOST. J. Am. Chem. Soc. **56**, 2571 (1934).
8. J. G. LINDSAY, D. E. MCELCHERAN, and H. G. THODE. J. Chem. Phys. **17**, 589 (1949).
9. R. H. BETTS and W. D. BUCHANNON. Can. J. Chem. This issue.

Can. J. Chem. Downloaded from www.nrcresearchpress.com by 210.87.254.40 on 09/05/12
For personal use only.

The dependence on wavelength of ^{13}C isotope effects in photolysis of aqueous solutions of ferric oxalate

ROBERT H. BETTS AND WAYNE D. BUCHANNON
Department of Chemistry, University of Manitoba, Winnipeg, Man., Canada R3T 2N2

Received February 13, 1976

ROBERT H. BETTS and WAYNE D. BUCHANNON. Can. J. Chem. **54**, 2577 (1976).

The formation of carbon dioxide by photolysis of aqueous solutions of ferric oxalate is accompanied by carbon isotopic fractionation. ^{12}C appears preferentially in the evolved CO_2, but the isotope effect depends markedly on the wavelength of the light used. Fractionation is essentially zero ($k_{12}/k_{13} = 1.001$) at 366 nm, and increases with wavelength, reaching 1.050 at 520 nm. It is proposed that this variation of isotopic discrimination arises from the differing properties of the excited levels formed by photochemical activation.

ROBERT H. BETTS et WAYNE D. BUCHANNON. Can. J. Chem. **54**, 2577 (1976).

La formation du dioxyde de carbone par photolyse de solutions aqueuses d'oxalate ferrique est accompagnée par une fractionnement isotopique du carbone. Il semble que le $^{12}CO_2$ apparait d'une façon préférentielle; toutefois l'effet isotopique dépend d'une façon marquée sur la longueur d'onde de la lumière utilisée. A 366 nm, la fractionnement est pratiquement zéro ($k_{12}/k_{13} = 1.001$); toutefois il augmente avec la longueur d'onde et atteint 1.050 à 520 nm. On propose que la variation dans la discrimination isotopique provient de propriétés différentes au niveau excité formé par une activation photochimique.

[Traduit par le journal]

Introduction

Aqueous solutions of ferric oxalate are widely used for chemical actinometry (1, 2). The usually accepted description of the photochemical process is:

[1] $[Fe(III)(C_2O_4)_3]^{3-} + h\nu \rightarrow [Fe(II)(C_2O_4^{\cdot-})(C_2O_4)_2]^{3-} \rightarrow Fe(II) + C_2O_4^{\cdot-} + 2C_2O_4^{2-}$

followed by:

[2] $C_2O_4^{\cdot-} + Fe(III) \rightarrow Fe(II) + 2CO_2$

The overall reaction is thus:

[3] $2[Fe(III)(C_2O_4)_3]^{3-} + h\nu \rightarrow 2Fe(II) + 2CO_2 + 5C_2O_4^{2-}$

The quantum yield for decomposition of the oxalate ion varies gradually with wavelength, from 0.64 at 250 nm to 0.46 at 470 nm, and then drops rapidly to 0.03 at 545 nm, and is essentially zero at wavelengths beyond 580 nm (2).[1] As is implied by [3], the quantum yield for formation of Fe(II) is exactly twice as large as that for decomposition of the oxalate ion.

Porter *et al.* (3) have discussed the nature of the photoabsorption and the events which follow. They suggest that the intense ultraviolet absorption band, which extends with diminishing intensity into the visible, represents an electron transfer event associated with the first step in [1] above. The subsequent fate of the species $[Fe(II)(C_2O_4^{\cdot-})(C_2O_4)_2]^{3-}$ includes primary dissociation:

[4] $[Fe(II)(C_2O_4^{\cdot-})(C_2O_4)_2]^{3-} \rightarrow Fe(II) + C_2O_4^{\cdot-} + 2C_2O_4^{2-}$

followed by reaction 2 of the radical ion $C_2O_4^{\cdot-}$. There is also the possibility that $C_2O_4^{\cdot-}$ might dissociate within the primary cage to CO_2 and $CO_2^{\cdot-}$, *i.e.*, prior to the diffusion separation process implied by [4]. This would be followed by electron transfer from the species $CO_2^{\cdot-}$ to a second Fe(III) complex (4).

In addition to these pathways, there must be other very fast internal conversion processes to allow the primary photoexcited species to return to the ground state without chemical decomposition. Presumably these involve some form of vibrational relaxation since fluorescence activity, if present at all, is very weak (3).

Porter (3) is of the opinion that the much less intense absorption band at longer wavelengths involves ligand field excitation, in contrast to electron transfer at short wave lengths. Absorption in this band involves promotion of an

[1]Other data are given in column 4 of Table 1, and these are from ref. 2.

Can. J. Chem. Downloaded from www.nrcresearchpress.com by 210.87.254.6 on 09/05/12
For personal use only.

Can. J. Chem. Downloaded from www.nrcresearchpress.com by 210.87.254.6 on 09/05/12
For personal use only.

electron from a nonbonding to an anti-bonding orbital. Because this process also leads to photodecomposition (albeit with much lower quantum efficiency), Porter suggests that there may be radiationless transitions from the ligand field states to charge transfer states, followed by chemical decomposition.

Our interest in these processes arises from a recent study of ^{13}C isotope effects in the chemical oxidation of oxalate to CO_2 by aqueous $KMnO_4$ (5). It occurred to us, as a result of speculations about the mechanism described in (5), that a rate-controlling step which led ultimately to decomposition of oxalate, but which did *not* involve C—C bond breakage, might well be expected to show a small or even zero ^{13}C isotope effect. For example, if every photoexcited oxalate ion decomposed to CO_2, then one would expect ^{13}C isotope effects to be zero, apart from differences in the optical spectrum of the isotopic species. In general, such differences undoubtedly exist, but must be extremely small, especially for species dissolved in a condensed phase, and exposed to light which, as in the present work, is not markedly monochromatic. It was also thought of interest, in view of Porter's description (3) of the light absorption processes, to determine whether or not ^{13}C isotope effects vary with the wavelength of the exciting radiation.

Experimental

$K_3Fe(C_2O_4)_3 \cdot 3H_2O$ was prepared by the method of Hatchard and Parker (2). Sufficient of this compound was dissolved in 0.25 *M* H_2SO_4 to give a solution 0.012 *M* Fe(III). Air-free solutions were exposed to light of the desired wavelength, and the CO_2 produced was collected by vacuum transfer, dried, purified, and its isotopic composition determined as described previously (5). In each case less than 1% decomposition of the oxalate occurred, so that no correction was made for possible changes in the isotopic composition of the remaining material. A sample of the original $K_3Fe(C_2O_4)_3 \cdot 3H_2O$ was converted quantitatively to CO_2 with excess $KMnO_4$, and the recovered CO_2 used as a reference standard for isotopic comparison.

Two light sources were used. For all wavelengths except 366 nm, the source was a 500 W CZX DAB lamp with three focussing lenses, and with a 2.5 cm water filter between the last two lenses. The output from this assembly was intercepted by a Jena interference wedge mounted 1 cm from the last lens, with the vessel containing the oxalate solution 5 cm from the wedge. The wedge setting was changed as required to produce the desired wavelength. The spectral distribution for each setting of the wedge was determined using a Zeiss PMQ II spectrophotometer. The band width (*i.e.*, the full width at half maximum intensity) was 24 nm for all wavelengths shown in Table 1 (except for the 366 nm source). There was negligible output of wavelengths extending more than ±20 nm on each side of the peak.

The light source for the irradiations at 366 nm was a 200 W 901B Hanovia Hg–Xe lamp with suitable power supply and filters. An analysis with the Zeiss spectrophotometer of the radiation used from this source showed it to be 366.5 nm, with a band width of 1.6 nm.

TABLE 1. ^{13}C isotope effects in photolysis of ferric oxalate solutions

λ (nm)	$^{13}C/^{12}C$*	k_{12}/k_{13}†	Quantum yield‡
—	0.011205	(Reference CO_2)	—
		$T = 19 \pm 1$ °C	
366	0.011193	1.001_0	0.60
366	0.011193	1.001_0	0.60
403	0.011038	1.015_1	0.55
403	0.011035	1.015_4	0.55
403	0.011039	1.015_0	0.55
403	0.011011	1.017_6	0.55
403	0.011000	1.018_6	0.55
410	0.011028	1.016_0	0.54
441	0.010915	1.026_6	0.51
481	0.010782	1.039_2	0.42
507	0.010682	1.048_9	0.23
520	0.010673	1.049_8	0.07
		$T = 2 \pm 1$ °C	
403	0.011028	1.016_0	0.50
441	0.010882	1.029_7	0.50
481	0.010778	1.039_6	0.40
520	0.010623	1.054_8	0.05

*$^{13}C/^{12}C$ is ratio of isotope abundance in CO_2 produced.
†$k_{12}/k_{13} = (^{12}C/^{13}C)_{sample}/(^{12}C/^{13}C)_{ref}$.
‡Quantum yields by interpolation of the data in ref. 2. These values uncertain by ~ ±0.02. Average of five entries for 403 nm for $k_{12}/k_{13} = 1.0163 \pm 0.0014$.

Results

Table 1 summarizes the results of this investigation. The reproducibility of the data may be judged from the fact that the five measurements shown for 403 nm represent quite separate determinations, done on different days, and which were interspersed with measurements at other wavelengths. The average value of $^{13}C/^{12}C$ for these five measurements is 0.01102_5 with an average deviation of $\pm 0.00001_5$.

Table 1 shows that the ^{13}C isotope effect varies in a striking manner with the wavelength of the light used to effect the decomposition, and indeed varies approximately inversely with the quantum yield. Thus, when the quantum yield approaches its maximum, the ^{13}C isotope effect is essentially zero ($k_{12}/k_{13} = 1.001$), while at the longest

wavelength examined, where the quantum yield is 0.07 (2), the isotope effect is 1.050. Results for wavelengths between these extremes show a similar correlation. Similar effects are apparent for the less extensive results at 2 °C, shown in the lower part of Table 1.

Discussion

We are able to account for the results in Table 1 by proposing two quite different kinds of intermediate levels for photodecomposition. The first kind, A_1, which dominates at short wavelengths, decays without isotopic fractionation to two lower levels A_2 and A_3. One of these latter in turn provides a route for return to the original ground state without chemical change, while the second leads *only* to chemical decomposition of the oxalate:

[5] $[Fe(III)(C_2O_4)_3]^{3-} + h\nu \rightarrow$

$$\text{---}A_1 \begin{cases} \xrightarrow{k_1} A_2 \rightarrow [Fe(III)(C_2O_4)_3]^{3-} \\ \xrightarrow{k_2} A_3 \rightarrow Fe(II) + 2CO_2 \end{cases}$$

We propose that all processes leading to A_2 and A_3 do so without isotopic discrimination, which seems not unreasonable, since no C—C bonds are broken. The consequence of this would be that the CO_2 formed must necessarily have the same isotopic composition as the original oxalate. This scheme provides for a quantum yield which cannot be greater than $k_2/(k_1 + k_2)$, *i.e.*, less than unity. Such a mechanism also provides a rationale for the results of Yankwich and Buddemeier (6) on uranyl oxalate photodecomposition. Their results imply no ^{13}C intermolecular isotope effect for decomposition of uranyl oxalate (the end products in this system are CO and CO_2, rather than $2CO_2$). However, decomposition of an intermediate like A_3, while allowing no intermolecular discrimination, would permit intramolecular fractionation of carbon isotopes between CO and CO_2, as observed by these authors (6).

The second kind of excited level proposed may be described as follows:

[6] $[Fe(III)(C_2O_4)_3]^{3-} + h\nu \rightarrow$

$$\text{---}B \begin{cases} \xrightarrow{k_3} [Fe(III)(C_2O_4)_3]^{3-} \\ \xrightarrow{k_4} Fe(II) + 2CO_2 \end{cases}$$

This kind of level must have a reasonably long lifetime (*i.e.*, at least in the microsecond range) and offer alternate and competing modes of reaction; one mode leads to the original ground state, and the other leads to formation of CO_2. With these properties, the rate constant k_4 in [6] would be expected to display an isotope effect of the usual kind, *i.e.*, $C^{12}C^{12}O_4^{2-}$ reacting with higher probability than $C^{12}C^{13}O_4^{2-}$, because the rate-controlling step involves C—C bond rupture. The excess of ^{13}C which would accumulate in level B would find its way back to the ground state via the k_3 route shown in [6]. Also, in conformity with experiment, the quantum yield for this process could not be greater than $k_4/(k_3 + k_4)$, and may well be less, if alternate pathways exist for loss of photoexcitation by radiationless transitions, and not involving levels of type B.

We also propose that the two processes indicated by [5] and [6] contribute in varying proportions to the observed yield of CO_2 as the wavelength of the exciting radiation is changed. At short wavelengths, A-type intermediates dominate, and at long wavelengths, B-type levels are dominant.

While it is tempting to ascribe the B-type levels as arising from ligand field excitation, and the A-type to electron transfer processes, such an assumption is not warranted. Indeed the relatively low extinction coefficients for the ligand field band, especially on its short wavelength side (7), would appear insufficient to account for the change in ^{13}C isotope effects with wavelength. For this reason, levels of type B may well be populated by absorption in the longer wavelength tail of the electron transfer band, as implied by Porter (3).

It may be thought that these proposals are unnecessarily complex, and that [6] is sufficient to account for the present results, by allowing the ratio k_3/k_4 to vary with wavelength. Such a description does indeed predict an isotope effect which varies with wavelength as observed, but is quantitatively untenable, because it would require the quantum efficiency to be 1.00 when the isotope effect was zero. Such a quantum yield is contrary to the results of the very careful work of Hatchard and Parker (2), and we have therefore rejected this simpler scheme.

A referee has very kindly suggested that we might with profit discuss our results in terms of the mechanisms proposed by Endicott and his

Can. J. Chem. Downloaded from www.nrcresearchpress.com by 210.87.254.6 on 09/05/12
For personal use only.

collaborators, which have been developed to describe the analogous photo-redox behaviour of Co(III) complexes (see *e.g.*, refs 8 and 9).

Endicott's description (8) of the photo-activation steps, while more detailed and precise, is not essentially different to that described by Porter (3). To account for the variation of quantum efficiency with wavelength, a number of energy-dependent transition probabilities are postulated, and a similar kind of explanation undoubtedly applies to the ferric oxalate system. In ref. 8, Endicott postulates only one exit channel leading to chemical decomposition, *i.e.*, a smooth relaxation along a single photoreaction coordinate. This is satisfactory when only one reaction product, or reaction mode, is experimentally observable. In the paper cited (8) this is the appearance of Co(II) as a photoreaction product. In a subsequent paper (9) where more than one reaction product is observed, Endicott postulates a reaction path for each product. Our description of the variation of the ^{13}C isotope effect with wavelength is therefore formally consistent with that of Endicott's for multi-path processes.

Acknowledgments

Financial support by the National Research Council of Canada is gratefully acknowledged. We are also indebted to our colleagues Dr. J. L. Charlton and Dr. A. Queen for the loan of the light sources used in this work.

1. C. A. PARKER. Proc. R. Soc. Ser. A, **220**, 104 (1953).
2. C. G. HATCHARD and C. A. PARKER. Proc. R. Soc. Ser. A, **235**, 518 (1956).
3. G. B. PORTER, J. G. W. DOERING, and S. KARANKA. J. Am. Chem. Soc. **84**, 4027 (1962).
4. S. J. ADLER and R. M. NOYES. J. Am. Chem. Soc. **77**, 2036 (1955).
5. R. H. BETTS and W. D. BUCHANNON. Can. J. Chem. This issue.
6. P. E. YANKWICH and R. W. BUDDEMEIER. J. Chem. Phys. **30**, 861 (1959).
7. C. A. PARKER. Trans. Faraday Soc. **50**, 1213 (1954).
8. J. F. ENDICOTT, G. J. FERRAUDI, and J. R. BARBER. J. Phys. Chem. **79**, 630 (1975).
9. G. J. FERRAUDI, J. F. ENDICOTT, and J. R. BARBER. J. Am. Chem. Soc. **97**, 6406 (1975).

Can. J. Chem. Downloaded from www.nrcresearchpress.com by 210.87.254.6 on 09/05/12
For personal use only.

Study on the preparation of 3α-hydroxy-5α-cholestan-6-one and -7-one by stereoselective catalytic hydrogenation

MASAYOSHI ISHIGE, MICHIO SHIOTA, AND FUMIYO SUZUKI
Chemical Laboratory, Ochanomizu University, Otsuka, Bunkyo-ku, Tokyo, Japan

Received March 15, 1976

MASAYOSHI ISHIGE, MICHIO SHIOTA, and FUMIYO SUZUKI. Can. J. Chem. **54**, 2581 (1976).

The title compounds are conveniently obtained from the corresponding diones by the stereoselective hydrogenation with Urushibara nickel A catalyst in cyclohexane.

MASAYOSHI ISHIGE, MICHIO SHIOTA et FUMIYO SUZUKI. Can. J. Chem. **54**, 2581 (1976).

On peut obtenir facilement les composés mentionnés dans le titre en partant des diones correspondantes et en les soumettant à une hydrogénation stéréosélective en présence d'un catalyseur de nickel A d'Urushibara dans le cyclohexane.

[Traduit par le journal]

Can. J. Chem. Downloaded from www.nrcresearchpress.com by 210.87.254.105 on 09/05/12
For personal use only.

Introduction

3α-Hydroxy-5α-cholestan-6-one (**3**) may be prepared by various routes (1–6) but the yields are always quite low even if the experiments are done carefully. There is little information about 3α-hydroxy-5α-cholestan-7-one (**5**) in the literature (7, 8) and a convenient preparation is not available.

We have reported earlier (9) that epicholestanol (5α-cholestan-3α-ol) and epicholesterol (5-cholesten-3α-ol) are readily prepared from the corresponding steroidal ketones in good yields by the nickel catalyzed hydrogenation in hydrocarbon solvents at low temperature under high pressure. It is of interest that the more stable equatorial 3β-ol is not the predominant product. We attempted to apply this reduction method for the preparation of the title compounds.

Results

The hydrogenation of 4-cholestene-3,6-dione (**1**), which is easily prepared from cholesterol by oxidation, was effected by maintaining a mixture of the substrate and Urushibara nickel A (abbreviation U-Ni-A) in cyclohexane at 35 °C under high hydrogen pressure. The product was chromatographed on silica gel and recrystallized from ethanol to give **3** in a 70% yield; mp 163–164 °C.

In *tert*-butyl alcohol solvent, the yield of the desired material **3** was decreased not only because of the low stereoselectivity for the 3α-hydroxy ketone but also because of an increased yield of by-products.

On the other hand, under ambient temperature

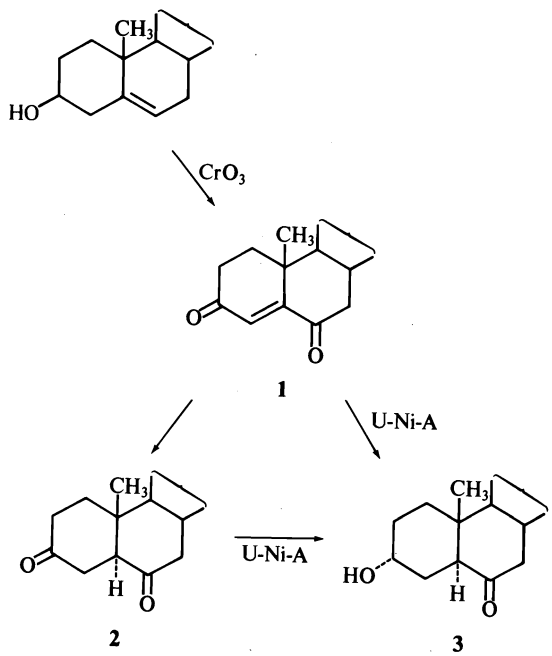

and pressure, the diketone **1** underwent the hydrogenation to **3** in a good yield in *tert*-butyl alcohol. However, the reduction under such conditions was very sensitive to the activity of the catalyst; if the catalytic activity was slightly lowered, 5α-cholestane-3,6-dione (**2**) was a major product. A similar trend to yield the dione **2** was also observed in cyclohexane medium under atmospheric pressure.[1] Therefore, the

[1]Moffatt reported that the palladium catalyzed hydrogenation of 4-cholestene-3,6-dione in ethanol forms mainly 5α-cholestane-3,6-dione and its 5β-isomer in the ratio of 2:1 (10).

Can. J. Chem. Downloaded from www.nrcresearchpress.com by 210.87.254.105 on 09/05/12
For personal use only.

preparation should be carried out under high pressure.

When PtO_2 and Raney Ni catalysts were used, the product mixture was complex, containing the diols and some other materials.

The fact that 5β-cholestan-3α-ol is obtained from 4-cholesten-3-one with U-Ni-A in cyclohexane, suggests that the catalyst attacks predominantly the 4,5-double bond from the β-face of the conjugated ketone. In the present reduction, it is, therefore, inferred that 3α-hydroxy-5α-cholestan-6-one may be derived by the rapid isomerization of the corresponding 5β-isomer, which is formed as an intermediate from the β-side attack of the catalyst on the C=C and C=O bonds of the starting ketone. Moreover, this consideration explains the highly stereoselective formation of the axial 3α-hydroxyl group of this 5α-steroid.

The reduction of 5α-cholestane-3,6-dione (**2**) was also found to lead to the 3α-hydroxy ketone **3**. However, preliminary experiments demonstrated that the 3,6-dione **2** was hydrogenated only very slowly. Consequently it was necessary to allow the reaction to proceed for a long time and to use a larger quantity of the catalyst under slightly more drastic conditions. Gas chromatographic analysis showed that the product thus obtained consisted of 3α-hydroxy-5α-cholestan-6-one (82%) and its 3β-isomer (18%). Compound **3** was isolated in a 77% yield when the product was chromatographed on silica gel.

It is evident that, in the reactions with U-Ni-A, the 3-oxo group is smoothly reduced while the 6-oxo group remains almost intact. In this connection, we have observed that 5α-cholestan-6-one and 3β-hydroxy-5α-cholestan-6-one cannot be hydrogenated in cyclohexane with U-Ni-A, though the latter ketone is known to be easily converted into the 3β,6β-diol in ethanol with U-Ni-B, which is prepared by base treatment (11). Therefore, it is supposed that U-Ni-A is not sufficiently active to reduce the 6-oxo group at the more hindered position.

Similarly, 3α-hydroxy-5α-cholestan-7-one (**5**) was easily obtained from 5α-cholestane-3,7-dione (**4**). The reduction product was chromatographed on silica gel and recrystallized from methanol to give 77% of **5**; mp 197–198 °C.

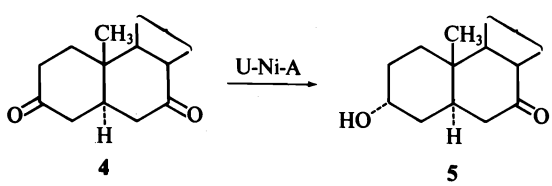

4 **5**

As in the case of **1**, a high hydrogen pressure was desirable not only for favorable formation of the 3α-hydroxyl group but for reproducibility of the result.

In *tert*-butyl alcohol medium, the 3,7-dione gave considerable amounts of the 3,7-diols, and the amount of the 3α-hydroxy compound decreased.

The present hydrogenations of the diketones are uniquely attained in a hydrocarbon medium in the presence of U-Ni-A. These reactions are characterized by the exclusive reduction of the 3-oxo group as well as the highly stereoselective formation of the 3α-hydroxyl group.

Experimental

4-Cholestene-3,6-dione (1)

The compound **1** was prepared according to the procedure described in the literature (12) with some modifications. To an ice cooled solution of cholesterol (1 g) in acetone (150 ml), previously cooled Kiliani reagent (6 ml) was added in small portions with stirring. The temperature was not allowed to rise above 15 °C during the addition. The solution was stirred for 2 h at about 10 °C. After the oxidation was complete, excess oxidizing reagent was decomposed by adding 100 ml of 5% $NaHSO_3$. The mixture was poured into 1.5 l of water and the precipitate was filtered, washed free from acid, and recrystallized from methanol. Yield 750 mg (73%); mp 121–123 °C (lit. (12) mp 122–124 °C).

5α-Cholestane-3,6-dione (2)

Freshly prepared U-Ni-A (from 1 g of precipitated nickel) was prereduced in cyclohexane (20 ml) for about 1 h. 4-Cholestene-3,6-dione (100 mg) was added and the hydrogenation was carried out for 4 h at ambient temperature and pressure. After the removal of the catalyst by filtration, the solution was worked-up as usual and the product was purified by recrystallization from ethanol. Yield 79 mg (80%); mp 171–172 °C (lit. (13) mp 172 °C).

5α-Cholestane-3,7-dione (4)

The compound **4** was prepared by a literature procedure (13). The crude 3,7-dione was purified by recrystallization from ethanol and then twice from acetone; mp 189–190 °C (lit. (13) mp 190 °C).

U-Ni-A Catalyst

U-Ni-A was prepared according to the procedure described previously (9).

Hydrogenation of 4-Cholestene-3,6-dione

According to the method described in the earlier paper (9), the ketone (70 mg) was hydrogenated in cyclohexane (3 ml) with U-Ni-A (freshly prepared from 1 g of precipitated nickel) at 35 °C for 3 h under a hydrogen

pressure of 100 kg/cm². The resulting mixture was worked-up as usual. The product was chromatographed on silica gel (10 g) with hexane–ether (8:2) and then recrystallized from ethanol to give pure 3α-hydroxy-5α-cholestan-6-one (**3**) (49 mg, 70%); mp 163–164 °C (lit. (1) mp 159–160.5 °C); ir (KBr) 3300, 1708, 1032, and 1000 (sharp, strong) cm^{-1}; nmr ($CDCl_3$, TMS) δ 4.15 (3β-H, $W_{1/2}$ *ca.* 8 Hz); cd $[\theta]_{313}$ -2.40×10^3, $[\theta]_{303}$ -3.76×10^3, $[\theta]_{294}$ -3.52×10^3, $[\theta]_{287}$ -2.68×10^3 (*c* 0.0857, cyclohexane, 26 °C). The acetate of **3**; mp 106–107 °C (lit. (1) mp 107–108 °C); ir (KBr), 1735, 1708, 1260, 1238, and 1018 cm^{-1}; nmr ($CDCl_3$, TMS) δ 5.10 (3β-H, $W_{1/2}$ *ca.* 8 Hz) and 2.00 ($OCOCH_3$).

Hydrogenation of 5α-Cholestane-3,6-dione

The hydrogenation of **2** (70 mg) was carried out in cyclohexane (3 ml) with U-Ni-A (from 3 g of precipitated nickel) at 45 °C for 12 h at 120 kg/cm² pressure. The yield of **3** isolated was 54 mg (77%).

Hydrogenation of 5α-Cholestane-3,7-dione

5α-Cholestane-3,7-dione (70 mg) was reduced by the same procedure as in the case of the compound **1**. 3α-Hydroxy-5α-cholestan-7-one was isolated by column chromatography on silica gel (10 g) with hexane–ether (8:2) and then by recrystallization from methanol. The yield was 54 mg (77%); mp 197–198 °C; ir (KBr) 3300, 1708, 1020, and 1003 (sharp, strong) cm^{-1}; nmr ($CDCl_3$, TMS) δ 4.10 (3β-H, $W_{1/2}$ *ca.* 8 Hz); cd $[\theta]_{312}$ -7.45×10^2, $[\theta]_{302}$ -1.18×10^3, $[\theta]_{295}$ -1.26×10^3 (*c* 0.0422, cyclohexane, 26 °C) (lit. (8) λ_{max} 291 nm in ethanol, $\Delta\epsilon$ −0.72); *m/e*, 402 (M^+). The acetate of **5**; mp 93–94 °C (lit. (14) mp 95–96 °C); ir (KBr) 1732, 1708, 1244, 1233, and 1021 cm^{-1}; nmr ($CDCl_3$, TMS) δ 5.00 (3β-H, $W_{1/2}$ *ca.* 8 Hz) and 1.97 ($OCOCH_3$); *m/e*, 444 (M^+).

1. R. M. Dodson and B. Riegel. J. Org. Chem. **13**, 424 (1948).
2. M. Shiota and K. Mori. Nippon Kagaku Zasshi, **76**, 1192 (1955).
3. H. B. Henbest and T. I. Wrigley. J. Chem. Soc. 4765 (1957).
4. J. M. Coxon, M. P. Hartshorn, C. N. Muir, and K. E. Richards. Tetrahedron Lett. 3725 (1967).
5. J. M. Coxon, M. P. Hartshorn, and C. N. Muir. Tetrahedron, **25**, 3925 (1969).
6. D. N. Jones, R. Grayshan, A. Hinchcliffe, and D. E. Kime. J. Chem. Soc. C, 1208 (1969).
7. R. Breslow, S. Baldwin, T. Flechtner, P. Kalicky, S. Liu, and W. Washburn. J. Am. Chem. Soc. **95**, 3251 (1973).
8. J. Hudec and G. P. Powell. Chem. Commun. 806 (1971).
9. M. Ishige and M. Shiota. Can. J. Chem. **53**, 1700 (1975).
10. J. S. Moffatt. J. Chem. Soc. 812 (1947).
11. S. Nishimura. Nippon Kagaku Zasshi, **77**, 340 (1956).
12. T. Nishina and M. Kimura. Yakugaku Zasshi, **84**, 390 (1964).
13. D. H. R. Barton and J. D. Cox. J. Chem. Soc. 783 (1948).
14. A. R. Davies and G. H. R. Summers. J. Chem. Soc. C, 1227 (1967).

Can. J. Chem. Downloaded from www.nrcresearchpress.com by 210.87.254.105 on 09/05/12
For personal use only.

Les systèmes eau/ester. I. Etude calorimétrique des systèmes eau/acétate d'alcoyle

DOMINIQUE RICHON ET ANDRÉ VIALLARD

Laboratoire de Thermodynamique et Cinétique Chimique, Groupe de Chimie Physique, U.E.R. des Sciences Exactes et Naturelles, B.P. 45, 63170 Aubière, France et Ecole Nationale Supérieure de Chimie, Boulevard Côte-Blatin 63000, Clermont-Ferrand, France

Reçu le 29 juillet 1975[1]

DOMINIQUE RICHON et ANDRÉ VIALLARD. Can. J. Chem. **54**, 2584 (1976).

Une étude calorimétrique des systèmes binaires eau/acétate d'alcoyle a été réalisée dans tout le domaine de composition des mélanges en milieu homogène et hétérogène. Signe, intensité et évolution dans la série homologue des enthalpies d'excès et des valeurs des solubilités sont discutées.

Les valeurs des enthalpies molaires d'excès pour les mélanges eau/ester sont utilisées à la détermination des enthalpies molaires partielles d'excès et des enthalpies de "solvatation" à dilution infinie.

De l'évolution des valeurs de ces grandeurs thermodynamiques dans une série homologue, les auteurs déduisent des conclusions quant aux interactions eau/acétate d'alcoyle.

DOMINIQUE RICHON and ANDRÉ VIALLARD. Can. J. Chem. **54**, 2584 (1976).

A calorimetric study of alkyl acetate/water systems has been carried out in the complete homogeneous and heterogeneous domain of mole fractions. The sign, intensity, and trends of excess enthalpies and mutual solubilities are discussed.

Values of the excess enthalpies for ester/water homogeneous mixtures are used for the determination of partial molar excess enthalpies and enthalpies of "solvation" at infinite dilution.

The trends of the thermodynamic quantities in this homologous series are discussed in terms of ester/water interactions.

Dans un précédent travail (1), nous avons proposé d'utiliser les courbes d'enthalpie molaire d'excès des systèmes binaires hétérogènes à des fins analytiques. Ici, nous interpréterons en termes d'interactions moléculaires, les formes de ces courbes dans le cas des systèmes "eau/acétate".

Partie expérimentale

Le calorimètre

Le calorimètre utilisé est un calorimètre Setaram, type C.R.M.T. L'expérience nous a montré que ce type de calorimètre est parfaitement adapté à l'étude calorimétrique des systèmes hétérogènes liquide/liquide. Il possède en effet un mécanisme permettant le retournement de la cellule, donc l'agitation du milieu, avec une fréquence choisie à l'avance. Même pour des mélanges conduisant à de faibles effets thermiques, la correction d'agitation alors relativement très importante, est toujours très facilement déterminée, à condition de maintenir cette agitation durant toute la durée de l'expérience. Cette remarque est de la plus haute importance. Il semble en effet que les difficultés rencontrées par certains auteurs, lors de mesures en milieu liquide/liquide, soient dues à un mauvais contrôle de l'effet thermique d'agitation. Un calorimètre à flux thermique, capable d'intégrer tous les effets thermiques produits dans la cellule calorimétrique est naturellement indispensable.

L'effet thermique à déterminer est obtenu alors à partir de la différence des aires des surfaces limitées par les courbes enregistrées, premièrement au cours de l'opération de mélange, deuxièmement au cours d'une opération d'agitation du mélange, réalisée après le mélange. Les produits: (*i*) l'eau est distillée; (*ii*) les esters sont des produits du commerce purifiés par chromatographie en phase vapeur. La colonne utilisée est une colonne Carbowax 30% sur Chromosorb 45/60 mesh.

La précision, estimée sur les valeurs expérimentales des enthalpies molaires d'excès, dépend de l'effet thermique observé. Pour un effet thermique d'environ 400 J mol^{-1}, elle est meilleure que 1%.

Résultats

Les valeurs des enthalpies molaires d'excès h^E des mélanges (eau/acétate) apparaissent dans les tableaux 1 à 4. Les concentrations sont exprimées en fraction molaire de l'ester, X_B.

Les acétates étudiés sont les acétates de méthyle, éthyle, butyle et amyle.

Sur toutes les figures: X_B représente la fraction molaire de l'ester dans le mélange, la phase α représente la phase aqueuse et la phase β la phase organique.

[1]Revision reçue le 3 mai 1976.

Can. J. Chem. Downloaded from www.nrcresearchpress.com by 210.87.254.105 on 09/05/12
For personal use only.

Can. J. Chem. Downloaded from www.nrcresearchpress.com by 210.87.254.105 on 09/05/12
For personal use only.

TABLEAU 1. Enthalpie molaire d'excès: mélange eau/acétate de méthyle à 25 °C

X_{ester}	h^E_{exp} / J mol^{-1}	$\frac{X(1-X)}{h^E_{exp}}$ / J^{-1} mol $\times 10^{-6}$	h^E_{calc} / J mol^{-1} Milieu homogène	h^E_{calc} / J mol^{-1} Milieu hétérogène
0.00038	−2.51	−150.0	−3.29	
0.00414	−33.6	−122.6	−32.5	
0.00666	−48.6	−136.0	−49.0	
0.01104	−74.2	−147.1	−73.1	
0.01427	−85.9	−163.7	−87.9	
0.01570	−91.1	−169.7	−93.8	
0.02862	−136.5	−203.6	−134.3	
0.04051	−158.2	−245.7	−158.1	
0.04938	−170.7	−274.9	−170.8	
0.09428	−121.9			−121.7
0.14574	−48.0			−48.6
0.17964	−1.2			−0.38
0.19689	24.9			24.1
0.36729	265.2			266.4
0.60643	609.2			606.4
0.67650	704.0			706.0
0.73746	778.4	248.7		
0.76558	775.6	231.4	779.5	
0.79774	758.5	212.7	750.3	
0.81940	578.2	167.4	566.8	
0.94482	360.1	144.7	358.2	
0.96808	225.2	137.2	229.6	
0.94444	44.4	124.6	45.3	

La fig. 1 montre la forme des courbes d'enthalpie molaire d'excès pour ces différents systèmes.

Expression analytique des courbes $h^E(X)$

En milieu hétérogène

Nous avons établi précédemment (1, 2) que l'enthalpie molaire d'excès h^E varie linéairement avec la fraction molaire X de l'un des constituants. Nous pouvons donc écrire:

[1] $$h^E(X) = aX + b$$

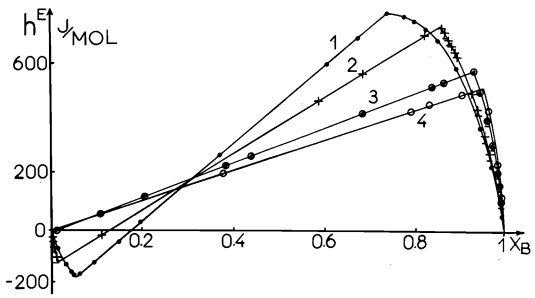

FIG. 1. Courbes d'enthalpie molaire d'excès pour les mélanges (eau/ester) à 25 °C (*1*) acétate de méthyle, (*2*) acétate d'éthyle, (*3*) acétate de butyle, (*4*) acétate d'amyle.

Une méthode de moindres carrés permet de calculer les coefficients a et b à partir des résultats expérimentaux. Les valeurs ainsi obtenues sont reportées dans le tableau 5, ainsi que l'écart quadratique moyen, σ, entre valeurs expérimentales de h^E (voir tableaux 1 à 4) et valeurs calculées à partir des coefficients a et b obtenus par "moindres carrés".

En milieu homogène

L'habitude veut que les courbes $h^E(X)$ soient représentées par une expression purement analytique, par exemple du type:

$$h^E(X) = X(1 - X)(A + BX + CX^2 + \ldots)$$

On notera que les différentes théories des solutions conduisent elles à des expressions qui leur sont propres. C'est ainsi, par exemple, que celles se situant dans le domaine dit de "l'approximation zéro" (3, 4, 5) conduisent à une expression de l'enthalpie d'excès pouvant se mettre sous la forme:

[2] $$h^E = \frac{X(1 - X)}{a'X + b'}$$

Can. J. Chem. Downloaded from www.nrcresearchpress.com by 210.87.254.105 on 09/05/12
For personal use only.

TABLEAU 2. Enthalpie molaire d'excès: mélange eau/acétate d'éthyle à 25 °C

X_{ester}	h^E_{exp} / J mol^{-1}	$\frac{X(1-X)}{h^E_{exp}}$ / J^{-1} mol $\times 10^{-6}$	h^E_{calc} / J mol^{-1}	
			Milieu homogène	Milieu hétérogène
0.00219	−20.4	−106.8	−20.6	
0.00602	−53.2	−112.6	−52.6	
0.01360	−104.0	−129.1	−104.3	
0.03394	−38.3			−38.2
0.3203	195.9			194.2
0.5920	470.0			472.5
0.6934	578.1			576.3
0.8281	714.1			714.3
0.8585	713.2	163.4	755.5	
0.8711	719.8	155.9	716.8	
0.8767	696.0	155.3	698.5	
0.8818	670.3	155.5	680.9	
0.8938	643.0	147.6	636.6	
0.8970	688.1	147.1	624.1	
0.9238	510.4	137.9	505.9	
0.9244	507.3	137.7	502.9	
0.9402	433.4	129.7	420.4	
0.9552	333.3	128.4	332.5	
0.9645	272.8	125.5	272.5	
0.9863	110.7	121.6	113.7	
0.9987	61.7	117.4	62.3	

TABLEAU 3. Enthalpie molaire d'excès: mélange eau/acétate de butyle à 25 °C

X_{ester}	h^E_{exp} / J mol^{-1}	$\frac{X(1-X)}{h^E_{exp}}$ / J^{-1} mol $\times 10^{-6}$	h^E_{calc} / J mol^{-1}	
			Milieu homogène	Milieu hétérogène
0.000195	−1.8	−109.6	−1.796	
0.000386	−3.5	−109.7	−3.49	
0.000654	−5.8	−112.3	−5.76	
0.000955	−8.1	−117.5	−8.18	
0.0099	−2.8			−2.9
0.1089	−57.8			58.5
0.2055	119.1			118.4
0.3860	229.9			230.3
0.4417	264.1			264.9
0.6865	419.8			416.7
0.8381	511.5			510.7
0.8630	523.4			526.1
0.9281	567.7	117.7	567.2	
0.9395	493.3	115.2	498.5	
0.9556	394.3	107.6	389.6	
0.9654	315.0	106.2	316.0	
0.9796	201.3	99.4	197.6	
0.9895	103.8	99.8	105.6	

Can. J. Chem. Downloaded from www.nrcresearchpress.com by 210.87.254.105 on 09/05/12
For personal use only.

TABLEAU 4. Enthalpie molaire d'excès: mélange eau/acétate d'amyle à 25 °C

X_{ester}	h^E_{exp} / J mol^{-1}	$\frac{X(1-X)}{h^E_{exp}}$ / J^{-1} mol × 10^{-6}	h^E_{calc} / J mol^{-1} Milieu homogène	h^E_{calc} / J mol^{-1} Milieu hétérogène
0.000167	−1.15			
0.3782	207.1			207.0
0.7854	431.9			432.1
0.8300	456.2			456.8
0.8983	495.3			494.6
0.9544	424.0	102.6	424.5	
0.9782	221.6	96.4	220.8	
0.9826	179.2	95.4	179.0	
0.9898	107.1	93.9	107.7	

Ballet (6) a montré qu'une représentation intéressante des enthalpies d'excès pour ces solutions consistait à tracer les courbes:

$$\frac{X(1-X)}{h^E} = f(X)$$

car alors $f(X)$ est une fonction linéaire. Tout écart à la linéarité peut alors être interprété comme un écart à l'approximation zéro.

Nous avons utilisé une telle représentation et constaté que, dans les domaines homogènes considérés, une loi linéaire est parfaitement représentative des variations de l'enthalpie d'excès (voir figs 2 et 3).

Pour l'instant, à défaut d'une investigation plus poussée, la relation:

$$[3] \qquad \frac{X(1-X)}{h^E} = a'X + b'$$

sera pour nous une simple façon commode de représenter les résultats expérimentaux. Elle s'est d'ailleurs avérée la plus satisfaisante de toutes celles essayées. Nous n'en tirerons donc ici aucune conclusion quant à sa signification, car la linéarité observée l'est dans un domaine relativement restreint de concentrations, et de ce fait est peut-être purement fortuite.

Les coefficients a' et b' ont été eux aussi calculés par une méthode de "moindres carrés" (voir tableau 6). L'écart quadratique moyen σ a été calculé comme précédemment.

TABLEAU 5. Coefficients de l'équation des droites $h^E(X)$ en milieu hétérogène (éq. 1)

Mélange	a / J mol^{-1}	b / J mol^{-1}	σ / J mol^{-1}
Eau/AcMe	1422	−256	1.5
Eau/AcEt	1025	−134	1.6
Eau/AcBu	620.1	−9.01	1.6
Eau/AcAm	553.0	−2.17	0.51

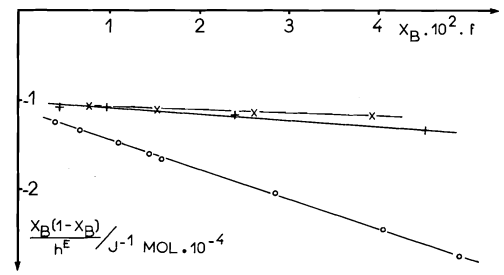

FIG. 2. Représentation des courbes enthalpiques en milieu homogène, phase α: ○ eau/acétate de méthyle $f = 1$, + eau/acétate d'éthyle $f = 25$, × eau/acétate de butyle $f = 250$.

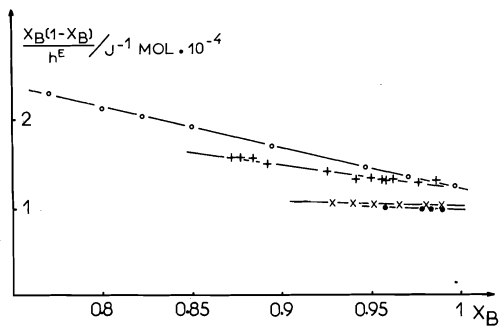

FIG. 3. Représentation des courbes enthalpiques en milieu homogène, phase β: ○ eau/acétate de méthyle, + eau/acétate d'éthyle, × eau/acétate de butyle, ● eau/acétate d'amyle.

TABLEAU 6. Coefficients de l'équation des courbes $h^E(X)$ en milieu homogène (éq. 3)

Mélange	Milieu riche en eau			Milieu riche en ester		
	$a' \times 10^4$ / J^{-1} mol	$b' \times 10^4$ / J^{-1} mol	σ / J mol^{-1}	$a' \times 10^4$ / J^{-1} mol	$b' \times 10^4$ / J^{-1} mol	σ / J mol^{-1}
Eau/AcMe	−32.74	−1.13	1.4	−4.72	5.92	8.3
Eau/AcEt	−19.80	−1.02	0.34	−3.32	4.45	6.3
Eau/AcBu	−106.9	−1.06	0.058	−3.18	4.12	3.1
Eau/AcAm				−2.49	3.40	0.57

Discussion

(a) Interprétation des formes des courbes d'enthalpie molaire d'excès

Ces courbes possèdent trois régions distinctes: une partie centrale rectiligne séparant deux parties courbes.

Nous constatons que la phase riche en eau donne, pour toute la série des esters étudiée, des enthalpies molaires d'excès négatives, tandis que la phase riche en ester donne des enthalpies molaires d'excès positives.

Les enthalpies molaires d'excès observées résultent de deux effets: (*1*) démolition des structures de chaque constituant du mélange. Ce processus met en jeu, d'une part les liaisons hydrogène de l'eau, d'autre part les forces dipôle–dipôle et de dispersion de l'ester. (*2*) restructuration du milieu avec mise en place de nouvelles liaisons: liaisons hydrogène (eau/ester et eau/eau) dipôle–dipôle, dipôle–dipôle induit et liaisons par forces de dispersion.

Analysons ce qui se passe dans les domaines des phases homogènes.

Côté riche en eau

L'introduction de molécules d'ester, à l'intérieur du réseau très ordonné de l'eau, va conduire à la rupture de nombreuses liaisons ester/ester relativement peu énergétiques et de quelques liaisons eau/eau. Puis, de nouvelles liaisons hydrogène relativement fortes, eau/ester, eau/eau vont s'établir, les premières sur le carbonyle de l'ester ou l'oxygène éther-oxyde, les secondes entre molécules d'eau, spontanément ou par liaison hydrophobe (7) à cause de la partie hydrocarbonée de la molécule d'ester. Ces interactions sont fortes et exothermiques, ces derniers effets compenseraient donc largement les précédents, d'où un bilan enthalpique global négatif et d'autant plus intense, pour une composition donnée, que s'allongerait la chaîne hydrocarbonée de l'ester (voir fig. 1).

A X_B donnée, un allongement de la chaîne se traduit par une diminution de l'enthalpie molaire d'excès de l'ester, la différence $h_B{}^E = h_B - h_B{}^+$ où h_B et $h_B{}^+$ sont respectivement les enthalpies molaires partielles de l'ester dans la solution et dans le corps pur.

C'est dire que h_B croît moins vite que $h_B{}^+$ avec le nombre n' d'atomes de carbone de la chaîne alcoyle. Cet "effet de chaîne" pourrait être dû en partie à la contribution exothermique des interactions hydrophobes, d'autant plus importantes que s'allonge la chaîne alcoyle.

A dilution infinie: l'enthalpie molaire partielle d'excès ($h_B{}^\infty - h_B{}^+$) est expérimentalement sensiblement indépendante de la longueur de chaîne, c'est dire que $h_B{}^\infty$ et $h_B{}^+$ varient sensiblement de la même façon. Mais la précision expérimentale dans ce domaine ne permet pas de l'affirmer, les quantités d'ester utilisées sont en effet très faibles, les esters sont très volatils.

Côté riche en ester

L'introduction de molécules d'eau entre les molécules d'ester (milieu peu organisé) nécessite la rupture des liaisons hydrogène de l'eau et de quelques liaisons ester/ester, d'où une consommation importante d'énergie. Ensuite, des liaisons hydrogène plus faibles et moins nombreuses que celles rompues se créent entre les molécules d'eau et d'ester.

Le résultat global de ce réarrangement se traduit par une valeur positive de l'enthalpie molaire d'excès d'autant plus grande que s'allonge la chaîne alcoyle de l'ester (voir fig. 1) pour une composition donnée.

A dilution infinie, même "effet de chaîne": une diminution de l'importance des interactions eau/ester par liaisons hydrogène quand s'allonge la chaîne hydrocarbonée pourrait ici contribuer à cet effet de chaîne.

Can. J. Chem. Downloaded from www.nrcresearchpress.com by 210.87.254.105 on 09/05/12
For personal use only.

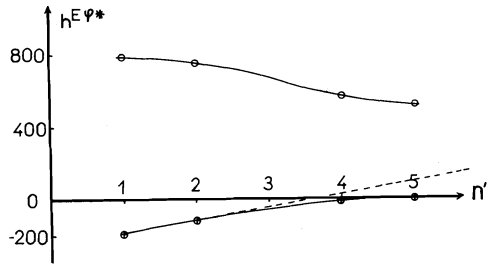

FIG. 4. Enthalpies molaires d'excès à saturation $h^{E\phi*}$ pour les phases: $\phi = \alpha$(phase aqueuse), $\phi = \beta$(phase ester): ○ $h^{E\beta*}$, ⊕ $h^{E\alpha*}$.

(b) Propriétés des phases à saturation

(1) Enthalpies molaires d'excès

En phase aqueuse saturée—Si l'on désigne par n' le nombre d'atomes de carbone de la partie R′ de l'ester RCOOR′, on constate (fig. 4) qu'en valeur absolue ces enthalpies diminuent quand n' croît. Le cas de l'acétate d'amyle est particulièrement intéressant, car, bien que très faible, l'enthalpie molaire d'excès est elle aussi négative, en dépit d'une loi d'évolution initiale (n' faible) qui aurait pu laisser supposer qu'elle fût positive pour $n' = 5$.

Ce résultat montre clairement que les molécules d'ester peuvent être assimilées (pour un nombre donné d'atomes de carbone appartenant à des chaînes hydrocarbonées) à des molécules d'hydrocarbures "solubilisées" par le groupement fonctionnel $-C\lesssim^{O}_{O}$ dont l'importance relative diminue très rapidement lorsque s'allonge la chaîne. On voit en effet que le comportement de ces molécules d'ester tend vers un comportement d'hydrocarbure lorsque s'allonge la chaîne R′ de l'alcool puisque, à saturation, l'enthalpie d'excès tend pour n' croissant vers des valeurs qui restent négatives.

En phase ester saturée—Nous constatons une diminution de la valeur de l'enthalpie d'excès à saturation (voir fig. 4). Il semble que l'on tende, ici encore, pour n' suffisamment grand, vers une loi limite qui pourrait être celle des hydrocarbures. Malheureusement, la pauvreté de la littérature dans ce domaine n'autorise pas actuellement une tentative de vérification de cette hypothèse.

(2) Compositions

En phase aqueuse—Il apparaît, à la lumière de nos résultats, que la solubilité des acétates peut être représentée convenablement par une loi du type

$$\log s = An' + B \quad \left.\begin{array}{r}\text{où } A = -1.36\\ B = \ \ 0.28\end{array}\right\} \text{à } 25\ ^\circ\text{C}$$

lorsque la solubilité s de l'ester est exprimée en mol/100 g d'eau et où n' est le nombre d'atomes de carbone de la chaîne alcoyle de l'ester.

La possibilité d'insérer les molécules d'ester dans le réseau très ordonné des molécules de l'eau liquide diminue donc rapidement avec la taille de la molécule.

En phase ester—La diminution de solubilité de l'eau observée lorsque s'allonge la chaîne pourrait résulter d'une plus grande tendance de l'eau à se structurer au sein de l'ester par liaison hydrophobe (7) conduisant ainsi plus vite, lorsque la teneur en eau croît, à l'apparition d'une structure de phase aqueuse.

Remarque—Un fait intéressant est à noter: la solubilité de l'eau dans les esters est beaucoup plus grande que celle des esters dans l'eau. Cette différence de solubilité augmente très rapidement avec l'allongement de la chaîne de l'ester.

Nous avons comparé (2) ce comportement à celui des systèmes (eau/hydrocarbure) et là encore, comme avec les enthalpies d'excès à saturation, apparaît une similitude de comportement frappante entre hydrocarbures et esters de masse moléculaire suffisamment élevée.

On trouvera, fig. 5, les courbes représentatives de l'évolution de la quantité $\log_{10}(X_{eau}{}^{i*}/X_i^{eau*})$ en fonction du nombre N d'atomes de carbone dans la molécule où $X_{eau}{}^{i*}$ est la fraction molaire de l'eau dans le solvant i à saturation (*) et X_i^{eau*} celle du soluté i dans l'eau à saturation.

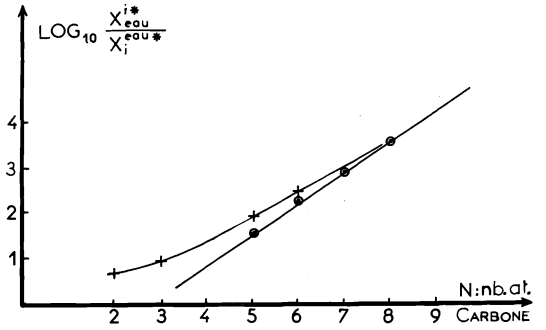

FIG. 5. Solubilités relatives des systèmes eau/acétate et eau/hydrocarbure à 25 °C: + esters, ⊙ hydrocarbures.

Can. J. Chem. Downloaded from www.nrcresearchpress.com by 210.87.254.105 on 09/05/12
For personal use only.

Can. J. Chem. Downloaded from www.nrcresearchpress.com by 210.87.254.105 on 09/05/12
For personal use only.

TABLEAU 7. Enthalpies molaires partielles d'excès estimées à dilution infinie à 25 °C et sous 1 atm

Ester (acétates de)	$h_A^{E\infty}$/kJ mol^{-1}	$h_B^{E\infty}$/kJ mol^{-1}
Méthyle	8.37	−8.83
Ethyle	8.78	−9.82
Butyle	10.5	−9.39
Amyle	11.0	

Seuls les atomes de carbone appartenant à des chaînes hydrocarbonées sont comptabilisés. Les esters considérés sont les acétates.

Les valeurs de solubilité corrélées sont celles obtenues par Polak et Lu (8), pour les systèmes eau/hydrocarbure.

(c) Grandeurs thermodynamiques à dilution infinie

Nous avons vu à la partie *a* combien l'interprétation des courbes $h^E(X)$, trop globales, est difficile car, comme nous l'avons souligné, elles dépendent de trop de facteurs.

Une première étape dans l'interprétation passe donc nécessairement par une réduction du nombre des paramètres. Une bonne simplification consiste à s'intéresser aux solutions infiniment diluées. Nous nous sommes donc attachés, dans ce qui suit, à une étude de quelques grandeurs thermodynamiques à dilution infinie dans la série homologue des acétates.

(1) Enthalpies d'excès à dilution infinie

Nous avons calculé précédemment les valeurs des coefficients a' et b' de l'équation 3.

Par dérivation de $h^E(X)$ et passage aux limites: $X \rightarrow 0$ et $X \rightarrow 1$, nous obtenons les enthalpies molaires partielles d'excès à dilution infinie des constituants

$$[4a] \qquad h_B^{E\infty} = \frac{1}{b'}$$

$$[4b] \qquad h_A^{E\infty} = \frac{1}{a' + b'}$$

où les indices A et B sont affectés respectivement à l'eau et à l'ester.

Des valeurs de a' et b' précédemment déterminées et des relations [4*a*] et [4*b*], on déduit les valeurs des enthalpies molaires partielles d'excès à dilution infinie des constituants i: $h_i^{E\infty}$.

On voit ainsi, tableau 7, que: (*i*) $h_A^{E\infty}$ est positive et croît avec l'allongement de la chaîne alcoyle; (*ii*) $h_B^{E\infty}$ est négative et peut être considérée comme pratiquement constante, à la précision expérimentale près et en tout cas voisine de -9.3 ± 0.4 kJ mol^{-1}.

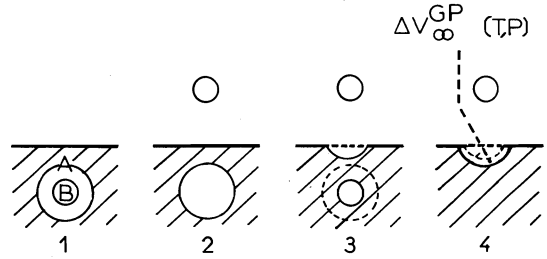

FIG. 6. Composantes de l'enthalpie de transfert à dilution infinie: Δh_∞^{GP}.

(2) Enthalpie de "solvatation" à dilution infinie

Considérons une solution infiniment diluée à la température T et sous la pression P.

L'enthalpie molaire de transfert $\Delta h_\infty^{GP}(T, P)$ du soluté depuis la solution infiniment diluée jusqu'à l'état de gaz parfait (à T et P) peut être décomposée en trois parties (voir schéma de la fig. 6). C'est au signe près ce que certains auteurs appellent l'enthalpie molaire de "solvatation" à dilution infinie. Nous lui préférons le terme plus thermodynamique, donc plus clair, d'enthalpie de transfert.

On aura alors:

$$[5] \qquad \Delta h_\infty^{GP} = \Delta h_1^2 + \Delta h_2^3 + \Delta h_3^4$$

où Δh_1^2 traduit l'enthalpie d'interaction soluté–solvant. Δh_2^3 est associée à la restructuration du solvant qui entourait les molécules de soluté. C'est par exemple le terme associé aux liaisons "hydrophobes" que certains auteurs (7) ont cherché à évaluer dans les systèmes eau/hydrocarbure. Δh_3^4 provient de l'effondrement de la cavité laissée dans l'état 3 après restructuration du solvant.

On notera au passage que la représentation du volume molaire de transfert $\Delta v_\infty^{GP}(T, P)$ utilisée fig. 6 est ici purement symbolique.

On peut simplifier l'expression de Δh_∞^{GP} en utilisant un terme unique, plus global, associé à la création de cavité, soit alors:

$$\Delta h_\infty^{GP} = \Delta h_1^2 + \Delta h_2^4$$

Pour rappeler la signification de ces deux termes, nous écrirons:

$$[6] \qquad \Delta h_\infty^{GP} = \Delta h^i + \Delta h^c$$

Cette enthalpie de transfert est reliée très simplement à l'enthalpie de transfert pour le

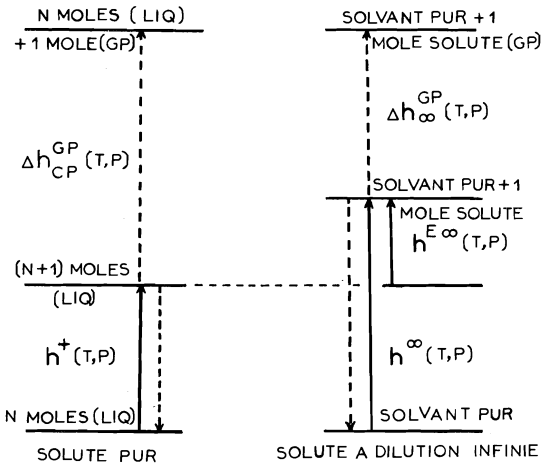

FIG. 7. Relations entre grandeurs thermodynamiques du corps pur et du soluté à dilution infinie: enthalpie molaire de transfert à dilution infinie Δh_{∞}^{GP}, enthalpie molaire de transfert du corps pur: Δh_{CP}^{GP}, enthalpie molaire du corps pur: h^{+}, enthalpie molaire partielle du soluté à dilution infinie: h^{∞}, enthalpie molaire partielle d'excès du soluté à dilution infinie: $h^{E\infty}$.

soluté à l'état de corps pur Δh_{CP}^{GP} et à l'enthalpie molaire d'excès du soluté à dilution infinie $h^{E\infty}$ par la relation:

$$[7] \qquad \Delta h_{\infty}^{GP} = \Delta h_{CP}^{GP} - h^{E\infty}$$

Le schéma de la fig. 7 apporte une justification de cette relation.

Remarques: (*i*) Cette grandeur traduit l'énergie nécessaire pour extraire une mole de soluté d'une quantité infinie de solvant et la faire passer à l'état de gaz parfait. Ici, seules interviennent donc les interactions soluté–solvant à dilution infinie et les interactions solvant–solvant mises en jeu lors de sa restructuration. (*ii*) On voit que, si l'on a toutes les données nécessaires au calcul de Δh_{CP}^{GP}, la détermination calorimétrique de $h^{E\infty}$ permet alors d'accéder à l'enthalpie de transfert. L'évolution de cette grandeur dans une série homologue est susceptible, comme nous le verrons, d'apporter des informations intéressantes concernant les interactions soluté–solvant.

(d) Enthalpie de transfert de l'eau à dilution infinie dans les acétates d'alcoyle

Des calculs faisant appel aux données de la littérature (9, 10) relatives aux différentes grandeurs thermodynamiques nécessaires pour obtenir la variation d'enthalpie accompagnant le passage de l'eau liquide à 25 °C sous une atmosphère à l'eau vapeur à 100 °C, sous une atmosphère, et à l'expression du second coefficient du viriel donnée par Keyes (4) nous ont conduit à la valeur suivante de l'enthalpie molaire de transfert de l'eau de l'état de corps pur à celui de gaz parfait à 25 °C et sous une atmosphère

$$\Delta h_{CP}^{GP}(H_2O) = 44.0 \text{ kJ/mol}$$

A partir des valeurs expérimentales de $h^{E\infty} = h_A^{E\infty}$ (ici) contenues dans le tableau 7 et en utilisant la relation [7], on déduit les enthalpies molaires de transfert de l'eau à dilution infinie dans différents esters (voir tableau 8).

TABLEAU 8. Enthalpie molaire de transfert de l'eau à dilution infinie dans différents esters. Solvant RCOOR′

	R′			
	CH_3	C_2H_5	C_4H_9	C_5H_{11}
$\Delta h_{\infty}^{GP}(H_2O)$ (kJ mol^{-1})	35.6	35.2	33.5	33.0

De l'examen des valeurs de ces enthalpies, nous déduisons qu'il est d'autant plus facile d'extraire une molécule d'eau à dilution infinie dans l'ester que la chaîne alcoyle de l'ester est plus longue. De plus, cette enthalpie de transfert est inférieure à celle nécessaire à l'extraction d'une molécule d'eau de l'eau pure. Comment interpréter ce résultat?

Discussion

Nous avons vu précédemment que

$$\Delta h_{\infty}^{GP} = \Delta h^{c} + \Delta h^{i}$$

Des deux termes de droite, le premier (création de cavité) est nécessairement négatif, le second est positif, c'est donc lui qui impose son signe. C'est dire que l'énergie mise en jeu par les interactions est supérieure à celle nécessaire à la création des cavités.

Si donc l'on admet que l'enthalpie de création de cavité pour loger une molécule d'eau est sensiblement la même dans les différents esters, ce qui paraît raisonnable, puisqu'il s'agit dans tous les cas de loger une même molécule dans des solvants chimiquement identiques, c'est donc que l'enthalpie d'interaction décroît avec la longueur de la chaîne.

Ceci peut être interprété en supposant que les sites "actifs" de la molécule d'ester avec lesquels ont lieu les interactions eau/ester (probablement, pour l'essentiel, les atomes d'oxygène des groupe-

Can. J. Chem. Downloaded from www.nrcresearchpress.com by 210.87.254.105 on 09/05/12
For personal use only.

Can. J. Chem. Downloaded from www.nrcresearchpress.com by 210.87.254.105 on 09/05/12
For personal use only.

TABLEAU 9. Enthalpies molaires de vaporisation de quelques esters dans l'eau à 25 °C. Solvant RCOOR'

	R'		
	CH_3	C_2H_5	C_4H_9
Δh^{+vap}(ester)/kJ mol^{-1}	33.2	36.3	39.6
Δh_∞^{GP}(ester)/kJ mol^{-1} (approchée)	42.5	45.6	49.0

ments carbonyle liés par liaison hydrogène) sont d'autant moins accessibles aux molécules d'eau que la molécule d'ester est de plus grandes dimensions ou que l'intensité des liaisons mises en jeu diminue.

L'enthalpie molaire d'interaction diminuerait donc, soit par diminution de l'énergie de liaison, soit par diminution du nombre de liaisons échangées, soit par variation des deux à la fois.

(e) Enthalpies molaires de transfert des acétates d'alcoyle à dilution infinie dans l'eau

Dans ce cas, nous ne disposons pas de toutes les données nécessaires au calcul de Δh_∞^{GP}. Aussi, par nécessité, nous avons dû assimiler les vapeurs d'esters à des gaz parfaits.

Les enthalpies de vaporisation des esters purs à 25 °C ont été calculées à partir des courbes de pression de vapeur (9), les valeurs sont rassemblées dans le tableau 9, ainsi que les valeurs approchées des enthalpies de transfert des esters à dilution infinie dans l'eau calculées par le procédé indiqué précédemment.

Remarque: La valeur négative de l'enthalpie molaire partielle d'excès à dilution infinie fait que, pour l'ensemble des esters, l'enthalpie de transfert à dilution infinie dans l'eau est supérieure à celle des corps purs. C'est dire que la molécule d'ester est plus liée dans l'eau qu'au sein du liquide ester pur.

Nous avons toujours:

$$\Delta h^{GP} = \Delta h^c + \Delta h^i$$

mais, ici, l'enthalpie de création de cavité va dépendre du nombre d'atomes de carbone de l'ester. On a:

$$\Delta h^c = \Delta h_2^3 + \Delta h_3^4$$

Δh_3^4 est <0 et décroît avec la taille de la molécule d'ester qu'il faut insérer dans le réseau de l'eau. Δh_2^3 est >0 (destructuration de l'eau) et croît avec la taille de la molécule. Δh^i est >0 et décroît sans doute légèrement lorsque croît la taille de la molécule comme semblent l'indiquer les résultats obtenus ci-dessus pour l'enthalpie de transfert à dilution infinie de l'eau dans l'ester.

Nous sommes donc, ici, dans une situation plus complexe que précédemment lorsque l'eau était soluté, car nous ne sommes pas encore en mesure d'expliciter correctement les trois termes enthalpiques en présence, ni même d'apprécier les ordres de grandeur de certains d'entre eux, Δh_1^2 par exemple. Aussi, il semble difficile de juger à priori de leur importance respective.

L'enthalpie de transfert des acétates à dilution infinie dans l'eau apparaît donc, globalement, comme une fonction monotone du nombre d'atomes de carbone traduisant la longueur de la chaîne alcoyle, c'est tout ce que l'on peut dire.

Les travaux les plus récents, tels que ceux de Hermann (11) donnent une idée des difficultés rencontrées dans l'estimation quantitative des interactions hydrophobes, même lorsque, comme le fait cet auteur, on se limite à l'étude de solutés aussi simples que les hydrocarbures.

Conclusion

Il ressort de cette étude, tout d'abord, que les systèmes hétérogènes liquide/liquide peuvent être étudiés par calorimétrie tout aussi bien que les systèmes homogènes, moyennant le respect de certaines conditions expérimentales. Ces courbes enthalpiques complètes ont pu être établies pour des systèmes eau/ester, particulièrement eau/ester de la série homologue des acétates.

L'étude calorimétrique réalisée ici montre que les molécules d'esters étudiées doivent être considérées comme des molécules d'hydrocarbures plus ou moins solubilisées par le groupement fonctionnel ester. Le comportement enthalpique de ces systèmes, variable avec la longueur de la chaîne provenant de l'alcool, résulte de la compétition des différents types d'interaction.

L'évolution de la solubilité réciproque observée, avec l'allongement de la chaîne alcoyle dans les systèmes eau/ester étudiés est à rapprocher de celle des systèmes eau/hydrocarbure à la même température, la solubilité de l'eau dans ces solvants étant supérieure à celle de ces "solvants" dans l'eau, ceci à 25 °C.

On a vu également, en considérant l'évolution de l'enthalpie de "solvatation" à dilution infinie de l'eau dans l'ester, pour la série des acétates

d'alcoyle, que cette évolution peut être interprétée comme une conséquence d'une diminution de l'importance des interactions par liaison hydrogène entre molécules d'eau et molécules d'ester lorsque s'allonge la chaîne hydrocarbonée en provenance de l'alcool.

1. M. WOYCICKA, D. RICHON et A. VIALLARD. C.R. Acad. Sci. Ser. C, **276**, 983 (1973).
2. D. RICHON. Thèse de Spécialité (Chimie Physique), Université de Clermont-Ferrand. 1974.
3. E. A. GUGGENHEIM. Mixtures. Clarendon Press, Oxford. 1952.
4. J. H. HILDEBRAND. Regular and related solutions. Van Nostrand, Reinhold Co. (1970).
5. H. KEHIAIAN, K. SOSNKAWSKA-KEHIAIAN et R, HRYNIEWICZ. J. Chim. Phys. Physicochim. Biol. **68**. 922 (1971).
6. D. BALLET. Thèse de Spécialité (Chimie Physique), Université de Clermont-Ferrand. 1972.
7. (*a*) G. NÉMETHY et H. A. SCHERAGA. J. Chem. Phys. **36**, 3382 (1962); (*b*) G. NÉMETHY et H. A. SCHERAGA. J. Chem. Phys. **36**, 3401 (1962).
8. J. POLAK et B. C-Y. LU. Can. J. Chem. **51**, 4018 (1973).
9. R. C. WEAST (*Editor*). Handbook of Chemistry and Physics. 47° ed. The Chemical Rubber Co., Cleveland, Ohio. 1966.
10. D. EISENBERG et W. KAUZMANN. The structure and properties of water. Clarendon Press, Oxford. 1959.
11. R. B. HERMANN. J. Phys. Chem. **79**, 163 (1975).

Can. J. Chem. Downloaded from www.nrcresearchpress.com by 210.87.254.105 on 09/05/12
For personal use only.

Binding energies and stabilities of potassium ion complexes with ethylene diamine and dimethoxyethane (glyme) from measurements of the complexing equilibria in the gas phase[1]

W. R. DAVIDSON AND P. KEBARLE
Chemistry Department, University of Alberta, Edmonton, Alta., Canada T6G 2E1

Received March 23, 1976

W. R. DAVIDSON and P. KEBARLE. Can. J. Chem. **54**, 2594 (1976).

The temperature dependence of the gas phase equilibria $K^+(en)_{n-1} + en \rightleftharpoons K^+(en)_n$ where en = ethylene diamine were measured for $n = 1$ to $n = 3$. The equilibrium K^+ + dimethoxyethane $\rightleftharpoons$ K^+(dimethoxyethane) was also determined. The measurements were made with a high ion source pressure mass spectrometer equipped with a thermionic potassium ion emitter. The resulting $\Delta H°$, $\Delta G°$, and $\Delta S°$ values are compared with the corresponding values for monodentate ligands like H_2O, NH_3, CH_3OCH_3 etc. determined in earlier work. As expected, the bidentate ligands lead to considerably stronger (0,1) interactions. Dimethoxyethane leads to a stronger complex than ethylene diamine. The third molecule of ethylene diamine leads to much weaker binding than is observed for the first two molecules. Explanation of the observed effects is given on basis of electrostatic and steric arguments.

W. R. DAVIDSON et P. KEBARLE. Can. J. Chem. **54**, 2594 (1976).

On a mesuré la dépendance sur la température de l'équilibre en phase gazeuse $K^+(en)_{n-1}$ + en $\rightleftharpoons$ $K^+(en)_n$ (où en = l'éthylènediamine) pour $n = 1$ jusqu'à $n = 3$. On a aussi déterminé l'équilibre K^+ + diméthoxyéthane $\rightleftharpoons$ K^+(diméthoxyéthane). On a fait les mesures avec un spectrometre de masse muni d'une source d'ions à haute pression et d'un émitteur thermoionique d'ions potassium. On a comparé les valeurs de $\Delta H°$, de $\Delta G°$ et de $\Delta S°$ qui en résultent avec les valeurs correspondantes déterminées antérieurement pour H_2O, NH_3, CH_3OCH_3 etc. Comme on pouvait s'y attendre, les ligands bidentates conduisent à des interactions (0,1) beaucoup plus fortes. Le diméthoxyéthane conduit à un complexe plus fort que celui de l'éthylènediamine. La troisième molécule d'éthylènediamine conduit à une fixation beaucoup plus faible que celle observée avec les deux premières molécules. On donne une explication des effets observés en se basant sur les arguments électrostatiques et stériques.

[Traduit par le journal]

Introduction

A program of studies based on ion–molecule equilibria determinations in the gas phase was initiated in the present laboratory several years ago (1–3). An important part of this research was studies of alkali ion–solvent molecule equilibria. Results for the alkali ions and water molecules (4) and acetonitrile (5) have been published. Recently also a survey was made of the binding energies and stabilities of complexes containing the potassium ion and one basic molecule M (= ammonia, amines, aniline, pyridine, ethers) (6).

The present work, in which the equilibria $(n - 1,n)$ of the potassium ion with ethylene diamine (en) and dimethoxyethane were determined is a continuation of these studies.

$$K^+(en)_{n-1} + en \rightleftharpoons K^+(en)_n \qquad (n - 1,n)$$

In solution, complexes of the transition metal ions with multidentate ligands like ethylene diamine and polyethers represent an important branch of chemistry. Complexes involving chelating agents and the alkali ions have received less attention. Some of the reasons for this must be the weaker binding involved and the lack of spectroscopic transitions (colour) and paramagnetic properties. However, more recently considerable interest in the coordination chemistry of alkali ions and particularly Na^+ and K^+ has originated with the synthesis of cyclic polyethers which by complexing can be agents in cation selective transport through biological membranes (7–9). Other research groups have also become interested (10) in alkali ion coordination because of its importance to the metabolism of plants.

The present work which provides the first binding energies and stabilities of bidendate complexes in the absence of solvent should be

[1]Based on the Ph.D. Thesis of W.R.D.

Can. J. Chem. Downloaded from www.nrcresearchpress.com by 210.87.254.6 on 09/05/12
For personal use only.

Can. J. Chem. Downloaded from www.nrcresearchpress.com by 210.87.254.6 on 09/05/12
For personal use only.

useful in clarifying the intrinsic forces involved. Of course, gas phase thermodynamic data by themselves are of limited use. Fortunately, theoretical methods and particularly *ab initio* molecular orbital calculations can provide binding energies for ion–molecule complexes which are in good agreement with the results from gas phase thermodynamics.

The theoretical calculations however also predict the stabilities of the various possible structures. The theoretical treatments can also be extended to evaluation of free energy and entropy changes by means of the Monte Carlo method (11). For example, the experimental (1–4) gas phase thermodynamic determinations for the $M^+(OH_2)_n$, $X^-(H_2O)_n$, and $H^+(H_2O)_n$ species were followed by many theoretical calculations (11–15) which provided detailed structural predictions of great interest. It can be hoped that a somewhat similar development will also occur in the area of polydentate ligands.

Experimental

The measurements were done with an alkali ion source capable of operating at neutral gas pressures up to 4 torr. The ion source used is similar to that described earlier (16) but incorporated a few modifications (5, 17), made to increase the leaktightness of the source and the temperature homogeneity of the gas in the equilibration chamber.

The principle of the experimental method is as follows. Potassium ions are produced by thermionic emission from a heated platinum filament coated with potassium alumosilicate melt. Weak electric fields drift the ions through the gas into a thermostated equilibration chamber which is free of electrical fields. The ion–molecule reactions reach equilibrium in this chamber. A probe of the gas plus ions bleeds continuously through a small slit out of the chamber into an evacuated space where the gas is pumped out and the ions accelerated, magnetically mass analyzed, and detected. The relative intensities of the detected ions K^+ and K^+M_n are taken to be equal to the relative equilibrium concentrations $[K^+]$ and $[K^+M_n]$ in the equilibrium chamber, where M stands for ethylene diamine and dimethoxyethane.

Some specific problems were encountered in the present study. The (0,1) equilibria with ethylene diamine and dimethoxyethane could be studied with pure ethylene diamine, dimethoxyethane respectively. However, the (1,2) and (2,3) equilibria did not give equilibrium quotients which remained constant with pressure, when the pure compound was used. The equilibrium quotients were observed to fall off above about 0.3 torr. It appeared that this fall-off at high pressure was caused by collisional dissociation of $K^+(M_n)$ to $K^+(M_l)$, where $l < n$ outside the ion source. The occurrence of this effect has been described and analyzed in earlier work (ref. 1, and see section Effect of collisional dissociation of clusters outside ion source, of ref, 18). It appears that the effect is more serious when large, high molecular weight molecules M are used. Equilibrium quotients which were independent of the pressure of M could be obtained if gas mixtures were used where M = (ethylene diamine) was the minor gas (10–150 mtorr) and N_2 or some other inert gas was the major gas at pressures in the torr range. Total pressures in the torr range are required to provide efficient thermal activation and deactivation of the reaction and to slow down diffusion of the ions to the wall.

Results and Discussion

The equilibrium constants were determined at a given constant temperature and several different pressures of M. An example of the pressure range covered at the different temperatures is shown in Fig. 1 which gives the equilibrium constants for the (1,2) reaction with ethylene diamine. The van't Hoff plots for the potassium – ethylene diamine (0,1), (1,2), and (2,3) equilibria are given in Fig. 2. Equilibria with higher n were not determined. The van't Hoff plot for the (0,1) potassium–dimethoxyethane equilibrium is shown in Fig. 3. The van't Hoff plots of several (0,1) equilibria involving K^+ and other

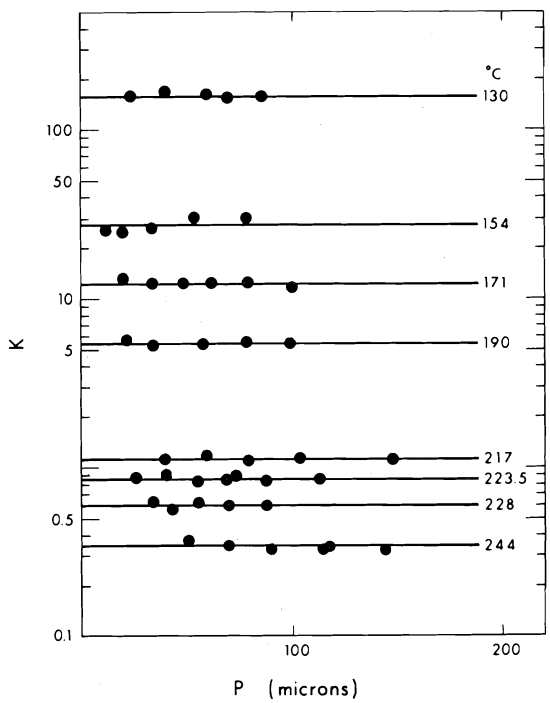

FIG. 1. Equilibrium constant K for reaction: $K^+(en) + en \rightleftarrows K^+(en)_2$ where en = ethylene diamine. Pressure shown corresponds to partial pressure of en. N_2 gas at ~1 torr used as third body.

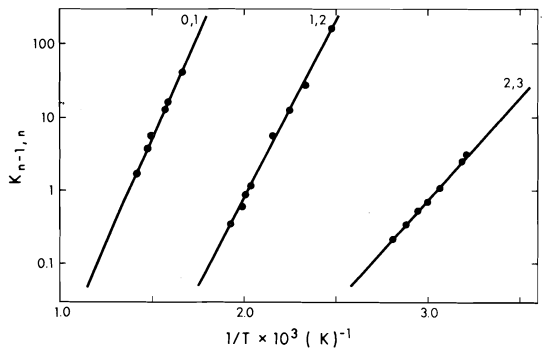

FIG. 2. Van't Hoff plots of reactions $(n-1,n)$: $K^+(en)_{n-1} + en \rightleftharpoons K^+(en)_n$ where en = ethylene diamine. Results show that third molecule of en is accommodated quite poorly.

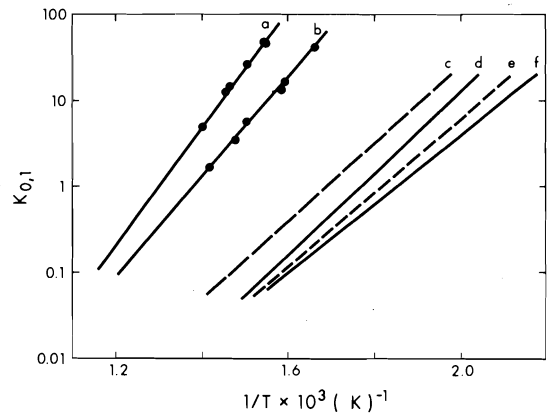

FIG. 3. Van't Hoff plots of reactions (0,1): $K^+ + M \rightleftharpoons K^+M$; (*a*) dimethoxyethane, (*b*) ethylene diamine, (*c*) diethyl ether, (*d*) propylamine, (*e*) dimethyl ether, (*f*) ammonia. Results show that bidendate ligands lead to much stronger interactions; (*a*), (*b*), present work, (*c*), (*e*), Y. Lau and P. Kebarle, unpublished work, (*d*), (*e*), see ref. 6.

molecules are included in Fig. 3 for comparison purposes. The $\Delta H°$, $\Delta G°$, and $\Delta S°$ data resulting from the van't Hoff plots are given in Table 1. This table also includes results for the monodentate ligands OH_2, NH_3, CH_3NH_2, and CH_3OCH_3. These results which were obtained earlier (6, 16) are given for comparison.

The most direct information on changes of stability with number of ligand molecules is obtained from examination of the van't Hoff plots. Recalling that the higher the position of a van't Hoff line the higher the stability of the given cluster we notice in Fig. 2 that an appreciable drop between the lines (0,1) and (1,2) is followed by a much larger drop between (1,2) and (2,3). This shows that the addition of the third ethylene diamine molecule is very much less favorable than the addition of the first and the second molecule. The results for the $\Delta H^0_{n-1,n}$ and $\Delta G^0_{n-1,n}$ changes in Table 1 reproduce this trend in greater detail. Thus one sees that while $-\Delta H_{0,1}$ and $-\Delta H_{1,2}$ do not change much, *i.e.* from 26 to 22 kcal/mol, $-\Delta H_{2,3} = 13$ kcal/mol is very much lower. When three dimensional

TABLE 1. Thermodynamic data for reactions $(n-1,n)$: $K^+M_n + M = K^+M_n$ from gas phase

M	Reaction	Equilibria measurements $-\Delta H^{0a}$ (kcal/mol)	$-\Delta G^{0a}$ (kcal/mol)	$-\Delta S^0$ (eu)
$(CH_2NH_2)_2$[b]	0,1	25.7±0.5	19.0±0.5	22.3±0.8
	1,2	22.2±0.5	12.7±0.6	32.0±1.1
	2,3	12.9±0.3	5.1±0.4	26.3±0.9
$(CH_3OCH_2)_2$[b]	0,1	30.8±1.1	22.8±1.2	26.8±1.6
NH_3[c]	0,1	17.9	11.8	20.0
CH_3NH_2[c]	0,1	19.1	12.7	21.8
CH_3OCH_3[d]	0,1	22.2	14.2	26.8
OH_2[e]	0,1	16.9[c], 17.9[e]	11.0[c], 11.4[e]	19.9[c], 21.6[e]
	1,2	16.1	8.9	24.2
	2,3	13.2	6.3	23.0
	3,4	11.8	4.4	29.7

[a]Standard state 1 atm, ΔG^0 at 298 K, errors given represent standard deviation from least-squares treatment of van't Hoff plots. Actual error believed to be larger. Estimated at ±1 kcal/mol for ΔH and ΔG and ±2 or 3 eu for ΔS.
[b]Present work.
[c]Reference 6.
[d]Unpublished results by Y. Lau and P. Kebarle.
[e]Reference 16.

Can. J. Chem. Downloaded from www.nrcresearchpress.com by 210.87.254.6 on 09/05/12
For personal use only.

Can. J. Chem. Downloaded from www.nrcresearchpress.com by 210.87.254.6 on 09/05/12
For personal use only.

models (Leybold atom models) of ethylene diamine molecules are placed around a sphere scaled to the size of the potassium ion (radius 1.3–1.5 Å) one finds that two molecules can be fitted easily but that an arrangement of three molecules all with two point attachment to K^+, while just possible, is very crowded. The very low $-\Delta H_{2,3}$ is thus in line with the scale model.

The *ab initio* MO calculations of alkali ion water complexes (12, 15) have shown that the bonding is almost purely electrostatic since there is essentially no net transfer of electrons from the water molecule to the alkali ion. For this reason the results from the earlier study (6) of K^+M complexes were interpreted in simple electrostatic terms. The situation with the bidentate ligands of the present work should be similar. Therefore in the further discussion mostly simple qualitative electrostatic arguments are used.

It is interesting to compare the $-\Delta H_{0,1}$ of the bidentate ethylene diamine with the enthalpy changes for the monodentate NH_3 and CH_3NH_2 which were published earlier (6). These $-\Delta H_{0,1}$ are 17.9 and 19.1 kcal/mol which is smaller than the value for the bidentate ethylene diamine $-\Delta H_{0,1}$ of 25.7 kcal/mol. Using the $\Delta H_{n-1,n}$ values for H_2O as a guide (see Table 1) one can estimate that $-\Delta H_{1,2}$ for CH_3NH_2 should be somewhere around 16.5 kcal/mol which means that the addition of two CH_3NH_2 molecules $(-\Delta H_{0,1} + -\Delta H_{1,2})$ would release some 35 to 36 kcal/mol. This is much more than the $-\Delta H_{0,1} = 25.7$ kcal/mol for the bidentate ethylene amine. However this difference is not surprising if one considers that the two isolated CH_3NH_2 molecules can go to opposite ends of the potassium ion to minimize dipole–dipole repulsions. This is not possible in the diamine where the CH_2NH_2 groups are tied closely together. In addition to the large permanent dipole repulsion there will be a field effect which is best visualized if one divides the attachment of the ethylene diamine molecule into two steps. The attachment of the first NH_2 group to K^+ is accompanied with considerable internal polarization of the total molecule by which electronic charge is shifted to the nitrogen atom involved. This leaves the second nitrogen relatively electron deficient. The resulting second interaction of this atom with K^+ is thus much weaker.

The stability of the dimethoxyethane K^+ complex is seen to be considerably larger than that of the ethylene diamine. Both the $-\Delta G_{0,1}$ and the $-\Delta H_{0,1}$ values are larger for the oxygen compound. Some of this difference can be explained by the presence of the methyl groups in the oxygen compound. As discussed in the earlier work (6), which dealt with monodentate complexes K^+M, methyl substitution decreases the permanent dipole moment and the net electronic charge on the hetero atom (N or O). However, the increased polarizability of the CH_3 relative to H is a bigger effect which overrides the lower dipole and leads to somewhat stronger interactions with the methyl substituted compound (see NH_3 and CH_3NH_2 in Table 1). The monodentate ligands serve also as a guide of the relative role of the nitrogen and oxygen atoms. As pointed out in the earlier work (6) the oxygen compounds have the higher permanent dipoles but the lower polarizability. For small ions up to and including K^+ the nitrogen analogue gives the stronger interaction (see H_2O, NH_3 in Table 1). For larger ions the oxygen compound with its higher permanent dipole leads to the stronger bond. The situation with the bidentate ligands should be similar but the oxygen compounds should become the stronger ligands already for ions of radius smaller than that of K^+. This follows from the following considerations. When monodentate ligands are put on the ion, one by one, the average ion–ligand distance increases because of repulsive interactions between the ligands. Considering further that a vicinal bidentate ligand gives weaker binding than two separate monodentate ligands, we conclude that the ion – bidentate ligand distance will be significantly larger than the ion – single monodentate ligand distance. At larger distances the permanent dipole becomes more important, *i.e.* oxygen is favored over nitrogen. There might be also an additional reason that favors oxygen in bidentate ligand bonding. The higher polarizability of nitrogen may be not as effective in a bidentate ligand (like ethylene diamine) because of the close proximity of the two nitrogen groups and the efficient transfer of the field through the N—C—C—N bonds.

The entropy changes $-\Delta S_{0,1}$ of 22.3 and 26.8 eu for the reaction of ethylene diamine and dimethoxyethane with K^+ are larger than the entropy changes of the reactions of NH_3 and OH_2 with K^+, the latter being $\sim$20 eu (see

Can. J. Chem. Downloaded from www.nrcresearchpress.com by 210.87.254.6 on 09/05/12
For personal use only.

Table 1). If we separate the bidentate attachment into two stages: single point attachment followed by double point attachment then it would be reasonable to assume that ΔS_s for the single point attachment (second group assumed not to interact with the ion) should be similar to $\Delta S_{0,1}$ for monodentate ligands of similar strength and that the ΔS_c for single to double point attachment should be negative and not negligible since in the quasi-cyclization that occurs at least two internal degrees of rotational freedom (around C—C bond and around C—N bond) are lost. Measurements (19) of the entropy of cyclization of protonated ethylene diamine gave a value of $-\Delta S_{cycl} = 12.7$ eu. Of course the loss of freedom on cyclization of protonated ethylene diamine should be much larger than the expected entropy loss, ΔS_c, in the potassium – ethylene diamine complex. However, a choice of $\Delta S_c = -5$ to -8 eu would appear reasonable, yet the experimental results indicate a change of only -2 to -4 eu. The possibility of experimental error cannot be excluded particularly when considering that the temperature interval in the van't Hoff plots is somewhat narrow. We cannot resolve this difficulty at the present time but conclude that if the experimental entropies are right then the entropy loss with bidentate ligands turns out to be surprisingly close to that for (similar) monodentate ligands.

The $-\Delta S^0_{1,2} = 32.0$ eu for ethylene diamine is considerably larger than $-\Delta S^0_{0,1} = 22.3$ eu. This should be due to the more restricted geometry of the K^+ $(en)_2$ complex. It is interesting to note that $-\Delta S^0_{2,3} = 26.3$ eu is smaller than $-\Delta S^0_{1,2}$. It was mentioned earlier that scale models show that the $K^+(en)_3$ complex is very crowded if two point contact for all three ligands is to be achieved. The smaller $-\Delta S^0_{2,3}$ taken at face value could mean that one of the ethylene diamine molecules makes only single point contact.

In solution it is generally observed that the stability constant $K_{0,1}$ for complexing with a single bidentate ligand is larger than the stability constant $K_{0,2} = K_{0,1}K_{1,2}$ for complexing with two monodentate ligands which have functional groups which are of the same kind as the groups of the bidentate ligand. For example in the complexing of nickel(II) by ammonia and ethylene diamine one finds (20) that $K_1 = 10^5$ while $K_2 = 10^{7.5}$.

[1] $$Ni^{2+}_{(aq)} + 2NH_{2\,(aq)} \rightleftharpoons Ni^{2+}(NH_3)_{2\,(aq)}$$

[2] $$Ni^{2+}_{(aq)} + en_{(aq)} \rightleftharpoons Ni^{2+}(en)_{(aq)}$$

This greater stability of the complex containing the chelate over the complex with the two monodentate ligands is called the 'chelate effect'. A qualitative explanation of the chelate effect is given (20) on the basis of entropy changes. When two monodentate ligands react as in [1] two molecules are immobilized, on the other hand the reaction of the bidentate ligand [2] leads to immobilization of only one molecule. Therefore the entropy change of the two monodentate reaction 1 should be more unfavorable than that for type [2].

The situation regarding entropy changes in the gas phase is quite similar and in fact simpler and more tractable since entropy changes due to the solvent need not be considered. The entropy change in the gas phase is dominated by the translational entropies of the reactants and the translational entropy loss for [3] and [4] should be roughly twice as large as that for [5]. On these

[3] $$K^+ + 2NH_3 \rightleftharpoons K^+(NH_3)_2$$

[4] $$K^+ + 2CH_3NH_2 \rightleftharpoons K^+(CH_3NH_2)_2$$

[5] $$K^+ + en \rightleftharpoons K^+(en)$$

grounds one might have expected that a 'chelate effect' should be observed also in the gas phase. However, the data in Table 1 show that this is not the case. A comparison of the equilibrium constants involved in [3]–[5] is more conveniently done with the related ΔG^0_{298} values. The $\Delta G^0_3 = \Delta G^0_{0,2}(NH_3) = \Delta G^0_{0,1}(NH_3) + \Delta G^0_{1,2}(NH_3)$ while $\Delta G^0_4 = \Delta G^0_{0,1}(CH_3NH_2) + \Delta G^0_{1,2}(CH_3NH_2)$. Unfortunately values for $\Delta G^0_{1,2}$ of these compounds have not been determined. However an inspection of Table 1 and some general considerations indicate that $\Delta G^0_{1,2}(NH_3) \approx \Delta G^0_{1,2}(CH_3NH_2) \approx \Delta G^0_{1,2}(H_2O) = -9$ kcal/mol. This assumption leads to $-G^0_3 \approx 20.8$ kcal/mol and $-\Delta G^0_4 \approx 21.7$ kcal/mol. Both of these are larger than $-\Delta G^0_5 = \Delta G^0_{0,1}(en) = 19$ kcal/mol (see Table 1). Thus the 'chelate effect' does not operate in the gas phase. It was pointed out earlier in the discussion that $-\Delta H_{0,2}$ for the monodentate ligands CH_3NH_2 is probably much larger than $-\Delta H_{0,1}(en)$. Thus the chelate effect in the gas phase does not operate since the enthalpy change with the two monodentate ligands is so much larger that it overcomes the unfavorable entropy change. The reasons why

two monodentate ligands should give a larger enthalpy lowering were already considered. These were lower permanent dipole repulsions and the absence of an internal field effect. The occurrence of a chelate effect in solution and its absence in the gas phase should be due to the different importance of the field effect in the two media. In a continuum model approximation the field effect will be inversely proportional to the dielectric constant of the medium. Thus in solution an appreciable reduction of the field effect will occur even though dielectric saturation near the ion will effectively reduce the dielectric constant. In the gas phase experiments such a reduction of the field will not be experienced and the bonding of the bidentate ligand will be poorer.

1. A. M. HOGG and P. KEBARLE. J. Chem. Phys. **43**, 449 (1965).
2. P. KEBARLE. Ions and ion solvent molecule interactions in the gas phase. *In* Ions and ion pairs in organic reactions, Vol. 1. *Edited by* M. Szwarc, Wiley, New York. 1972.
3. P. KEBARLE. Gas phase ion equilibria and ion solvation. *In* Modern aspects of electrochemistry. Vol. 9. *Edited by* B. E. Conway and J. O'M. Bockris. Plenum Press. 1974.
4. I. DZIDIC and P. KEBARLE. J. Phys. Chem. **74**, 1975 (1970).
5. W. R. DAVIDSON and P. KEBARLE. J. Am. Chem. Soc. In press.
6. W. R. DAVIDSON and P. KEBARLE. J. Am. Chem. Soc. In press.
7. C. J. PEDERSEN. J. Am. Chem. Soc. **89**, 7017 (1967); **92**, 386 (1970).
8. R. M. IZATT, D. P. NELSON, J. H. RYTTING, B. L. HAYMORE, and J. J. CHRISTENSEN. J. Am. Chem. Soc. **93**, 1619 (1971).
9. H. K. FRENSDORFF. J. Am. Chem. Soc. **93**, 4684 (1971).
10. A. K. BANERJEE, A. J. LAYTON, R. S. NYHOLM, and M. R. TRUTER. J. Chem. Soc. A, 2536 (1969).
11. M. R. MRUZIK, F. F. ABRAHAM, D. E. SCHREIBER, and G. M. POUND. A Monte-Carlo study of ion water clusters. I.B.M. report 965-03. 1975.
12. G. H. DIERCKSEN and W. P. KRAEMER. Theoret. Chem. Acta, Berlin, **23**, 387 (1972); **23**, 393 (1972); **27**, 265 (1972).
13. W. P. KRAEMER and G. H. F. DIERCKSEN. Chem. Phys. Lett. **5**, 463 (1970); **5**, 570 (1970).
14. M. D. NEWTON and S. EHRENSON. J. Am. Chem. Soc. **93**, 4971 (1971).
15. E. CLEMENTI and H. POPKIE. J. Chem. Phys. **57**, 1077 (1972); H. KISTENMACHER, H. POPKIE, and E. Clementi. J. Chem. Phys. **58**, 1689 (1973); **59**, 5892 (1973).
16. S. K. SEARLES and P. KEBARLE. Can. J. Chem. **47**, 2620 (1961).
17. W. R. DAVIDSON. Ph.D. Thesis, Department of Chemistry, University of Alberta, Edmonton, Alberta. 1975.
18. K. HIRAOKA and P. KEBARLE. J. Am. Chem. Soc. **97**, 4179 (1975).
19. R. YAMDAGNI and P. KEBARLE. J. Am. Chem. Soc. **95**, 3504 (1973).
20. F. A. COTTON and G. WILKINSON. Advanced inorganic chemistry. 2nd ed. Interscience Publishers, New York. 1966. p. 156.

Can. J. Chem. Downloaded from www.nrcresearchpress.com by 210.87.254.6 on 09/05/12
For personal use only.

Studies of metal–organic interactions in model systems pertaining to natural waters

ROBERT D. GUY AND C. L. CHAKRABARTI[1]

Department of Chemistry, Carleton University, Ottawa, Ont., Canada K1S 5B6

Received February 26, 1976

ROBERT D. GUY and C. L. CHAKRABARTI. Can. J. Chem. **54**, 2600 (1976).

The interactions of Cu(II), Pb(II), Cd(II), and Zn(II) with humic and tannic acids were studied to evaluate the possibility of metal speciation using a combination of dialysis/atomic absorption spectroscopy, and the p*H* characteristics of the metal–organic species. The stability constants of metal–organic complexes were found to decrease in the order Pb(II) > Cu(II) > Cd(II) > Zn(II) and EDTA > humic acid > tannic acid. Scatchard plots for the metal – humic acid systems indicated two types of binding sites with a difference in stability constants of about 10. Ultrafiltration of metal – humic acid solutions indicated that the metal ions were concentrated in the large molecular size fractions (> 3.1 nm). Separation by dialysis was used to investigate the release of metal from model sediment components by the organic acids (the metal–organic complexes were non-dialyzable). For release of copper from bentonite, it was found that the amount of copper released depended on both the concentration of ligand and the stability constant of metal complex, with the ratio of metal release to complexing sites decreasing in the order EDTA > humic acid > tannic acid. Release of metal from the solids decreased in the order: bentonite > MnO_2 > humic acid. Release of metal from the hydrous oxides via a redox decomposition of the oxide by natural organics was investigated using pyrogallol, gallic, and tannic acids. At natural water p*H* levels (6–8), 20 μg/ml solutions of the organic acids released 20 μmol manganese per 100 ml solutions whereas at p*H* 2, 60 μmol manganese were released. The p*H* behaviour of the organic acids has been explained in terms of formation of oxalic acid at p*H* < 5, which then reduces the hydrous oxide.

ROBERT D. GUY et C. L. CHAKRABARTI. Can. J. Chem. **54**, 2600 (1976).

Faisant appel à une combinaison de spectroscopie atomique, de dialyse ainsi qu'aux caractéristiques de p*H* des espèces organométalliques, on a étudié les interactions de Cu(II), de Pb(II), de Cd(II) et de Zn(II) avec les acides humique et tannique dans le but d'évaluer la possibilité de spéciation des métaux. On a trouvé que les constantes de stabilité des complexes organométalliques décroissent dans l'ordre Pb(II) > Cu(II) > Cd(II) > Zn(II) et EDTA > acide humique > acide tannique. Les courbes de Scatchard pour les systèmes acide humique/métal indiquent qu'il y a deux types de sites de couplage et que la différence entre leurs constantes de stabilité est d'environ 10. L'ultrafiltration de solutions de métal/acide humique indique que les ions métalliques sont concentrés dans les fractions de grands poids moléculaires (> 3.1 nm). On a utilisé la séparation par dialyse pour examiner la libération, par les acides organiques (les complexes organométalliques ne sont pas dialysables), des métaux attachés à des composants modèles de sédiments. Pour la libération du cuivre de la bentonite, on a trouvé que la quantité de cuivre libéré dépend à la fois de la concentration des ligands et de la constante de stabilité du complexe métallique avec un rapport de libération du métal par rapport aux sites complexants qui diminue dans l'ordre EDTA > acide humique > acide tannique. La libération des métaux à partir des solides décroît dans l'ordre bentonite > MnO_2 > acide humique. On a étudié la libération des métaux à partir des oxydes hydratés par l'intermédiaire d'une décomposition rédox de l'oxyde par les composés organiques naturels en utilisant le pyrogallol et les acides gallique et tannique. Au p*H* naturel de l'eau (6–8), les solutions à 20 μg/ml d'acides organiques libèrent environ 20 μmol de manganèse par 100 ml de solution alors qu'à p*H* 2, il y a une libération de 60 μmol de manganèse. Le comportement en fonction du p*H* des acides organiques est expliqué en termes de formation d'acide oxalique à p*H* < 5 qui réduit alors l'oxyde hydraté.

[Traduit par le journal]

Introduction

Metal ions in natural waters may be found in different physicochemical forms, for example, as simple aquated ions, metal–inorganic anion complexes, metal–organic complexes, and metal ions sorbed onto organic and inorganic colloids. Several authors (1–3) have reviewed the distribution of metal ions between sediment and

[1]To whom correspondence should be addressed.

Can. J. Chem. Downloaded from www.nrcresearchpress.com by 210.87.254.40 on 09/05/12
For personal use only.

Can. J. Chem. Downloaded from www.nrcresearchpress.com by 210.87.254.40 on 09/05/12
For personal use only.

solution; Leland *et al.* (1) concluded that organic matter and hydrous oxides control metal concentrations in sediment; Jenne (2) concluded that the hydrous oxides of manganese and iron were the principal sediment components to sorb ions, whereas Sanchez and Lee (3) found that in calcareous sediments copper was bound in the sediment by replacement of Ca^{2+} and Mg^{2+} in the sedimentary carbonates. These conclusions are based on investigations of real sediments in which all possible components are present, and since natural sediments are difficult to characterize, all possible variables that may determine the metal distribution cannot be controlled in studies in which natural sediments are employed. A more definitive approach is to employ model systems to investigate the metal distribution between solution and solid phases. Several studies have been made on the components individually, for example, MnO_2 (4–6), iron oxides (7, 8), clays (9), and humic substances (10). More comprehensive studies (11–13) have been done comparing the different solids under controlled experimental conditions. For example, McClaren and Crawford (11) found that for copper the adsorption capacity decreased in the order: MnO_2 > humic material > iron oxide > clay minerals; Kharkar *et al.* (12) found for selenium the adsorption decreased in the order: $Fe(OH)_3$ > MnO_2 > clay > peat; Gardiner (13) reported that the order of adsorption for cadmium was humic acid > silica > kaolin. The discrepancies in the relative adsorption capacities stem largely from the different modes of preparation of the hydrous oxide, and the type of organic material employed; however, a relative order of hydrous oxide > humic substances > clay is indicated.

The studies reported to date serve to emphasize that metal ions are concentrated in the sedimentary material but ignore the effects of complexing agents in the solution phase. Guy *et al.* (14) have described a model system composed of bentonite, solid and soluble humic acid, MnO_2, tannic acid, and $NaHCO_3$ that may be employed to investigate metal ion distributions between solution (with and without complexing agents) and sediment. This paper describes the application of the above model to investigate: (*1*) the competition between Cu^{2+}, Pb^{2+}, Cd^{2+}, and Zn^{2+} for the complexing sites of humic acid in solution; (*2*) the relationship between the concentration of complexing agent in solution and the amount of metal ion released from the sediment.

There are several techniques for investigating the metal ion distribution in solution: anodic stripping voltammetry (ASV) (15–17), ion selective electrodes (18, 19), and dialysis or ultrafiltration (20, 21). Guy and Chakrabarti (22) have compared ASV and size separation procedures and concluded that, since the adsorption of organic substances onto the hanging mercury drop electrode makes the interpretation of stripping voltammograms difficult, the size separation procedures were more convenient. Dialysis separations are unable to differentiate between small species; for example, between $CuCO_3^0$ and aquated copper ions; therefore, an additional technique specific to free copper (aquated copper ions) must be employed. It was decided, therefore, to use a combination of ion selective electrodes (to determine aquated copper ions), and dialysis/atomic absorption spectroscopy (to differentiate simple hydroxy and carbonate complexes from large organic complexes) in the present study of the metal distribution in solution.

Experimental

Apparatus

Potentiometric measurements were made with an Orion Digital Voltmeter, Model 801A, equipped with copper and lead ion selective electrodes, models 94-29A and 94-82A, respectively. The reference electrodes were a single junction electrode model 90-01 for the copper electrode, and a double junction electrode model 90-02-00 was used in conjunction with the lead electrode. An Orion platinum electrode, model 96-78, was used for E_h measurements.

Size separations were made using Amicon ultrafilters (filters UM2, PM10, PM30, XM50, and XM100) and an Amicon ultrafiltration assembly, model 201. Dialysis tubings were Spectrapor membranes, No. 1, 2 and 3. The tubing was treated with a 0.1% (w/v) Na_2S solution at 60 °C, rinsed with distilled water, and acidified with 1% H_2SO_4 (v/v) before use to remove sulphur impurities.

A Varian, model AA-5, atomic absorption spectrophotometer equipped with an air–acetylene premix burner, Techtron Model AB51, was used for all flame atomic absorption determinations. A Perkin-Elmer, model 503, atomic absorption spectrometer equipped with a Heated Graphite Atomizer, model 2000, was used for all nonflame atomic absorption determinations.

Reagents

Stock solutions (1000 μg/ml) of metals were prepared by dissolving the appropriate quantity of copper metal (99.9% pure), $Pb(NO_3)_2$ (99.9% pure), zinc metal (99.9% pure), and $CdCO_3$ (99.9% pure) in nitric acid and diluting

Can. J. Chem. Downloaded from www.nrcresearchpress.com by 210.87.254.40 on 09/05/12
For personal use only.

to appropriate volume with ultrapure water (Millipore Corporation). KNO_3 and $NaHCO_3$ solutions were prepared from reagent grade chemicals.

The humic acid (Aldrich) was leached with dilute nitric acid to remove metal impurities. The elemental composition of the treated humic acid was C 46.92%, H 5.76%, N 0.93%, and the ir spectrum agreed with the published spectra for soil humic acid. The clay bentonite (Fisher Chemical Co.) was converted to the potassium form using the method prescribed by van Olphen (23); its cation exchange capacity (measured at p*H* 5.2 using ammonium acetate) was 0.59 mequiv./g. Hydrous manganese dioxide was prepared using the reaction:

$$3Mn^{2+} + 2MnO_4^- + 2H_2O \rightarrow 5MnO_2 + 4H^+$$

under basic conditions. The collected precipitate was washed with 0.1 *M* KNO_3, and then with distilled water, and then air-dried. The solid had a surface area of 147 m^2/g, as determined by BET adsorption of N_2.

Procedure

The chelating capacity of the solutions was determined by a procedure reported by Ramamoorthy and Kushner (24) using the copper ion selective electrode. A calibration curve was prepared by adding aliquots of 1000 μg/ml copper to 100 ml of 0.010 *M* KNO_3 (at p*H* 3.5). The chelating capacity of a solution was then determined by titrating it with the standard copper solution and determining the concentration of free copper. A plot of $(C_A - C_M)/C_A$ *vs.* C_A (C_A is the added metal concentration and C_M is the measured copper concentration) shows a definite break at the endpoint. The chelating capacity of EDTA, tannic acid, humic acid, and natural water samples was thus determined.

The distribution of metal in solution was studied using separation by dialysis and flame atomic absorption spectroscopy. The following two types of experiments were performed.

(1) The competition between complexing agents for metal ions was studied as follows. A dialysis bag (molecular weight cutoff ~14 000) was used to separate the metal species associated with humic and tannic acids from the simple carbonate and EDTA complexes. The dialysis bag containing 20 ml of ultrapure water was equilibrated with 200 ml of solution containing 0.01 *M* KNO_3, 5 μg/ml metal ion, 20 μg/ml humic acid (or tannic acid), 1.0×10^{-4} *M* EDTA, and 1.0×10^{-3} *M* $NaHCO_3$. The systems were equilibrated for 24 h. The metal concentration inside the dialysis bag was taken as the concentration of metal–EDTA complex.

(2) The competition for complexing sites between the heavy metal ions, Cu^{2+}, Pb^{2+}, Cd^{2+}, and Zn^{2+} was studied as follows. Solutions containing 20 μg/ml humic or tannic acid and 1.57×10^{-5} *M* each of the metal ions were dialyzed for 24 h. The concentration of metal ion inside the dialysis bag was taken as the concentration of free metal ions.

Solutions of 20 μg/ml humic and tannic acid were titrated with standard solutions of metal ions and dialyzed for 24 h. The concentration of metal ion inside the dialysis bag is that of the uncomplexed metal ion (M_F), and the difference between the concentration of uncomplexed and added metal (M_A) is the concentration of bound metal (M_B). A plot of M_F *vs.* M_A was used to determine the chelating capacity of the solutions based on size separation.

Ultrafiltration separations were used to determine the size distribution of Cu^{2+}, Fe^{3+}, Pb^{2+}, and Mn^{2+} in humic and tannic acid solutions as well as several samples of natural waters. The solutions consisted of 20 μg/ml of complexing agent and 50 ng/ml each of Cu^{2+}, Pb^{2+}, and Fe^{3+}, and 25 ng/ml of Mn^{2+}. The metal concentrations in the filtrate were determined using graphite-furnace atomic absorption spectroscopy. To prevent cross contamination between filters, a fresh 100 ml of solution was used for each filtration.

The release of copper ions from clay, humic acid, and hydrous manganese dioxide was investigated by equilibrating solutions of complexing agents with solid components spiked with copper ions. The concentration of total metal released and the concentration of dialyzable (through the 3000 MW membrane) metal were determined to determine free and complexed forms of the metal. An additional study to determine the feasibility of reduction of MnO_2 by organics was undertaken by adding 20 μg/ml solutions of gallic acid, tannic acid, and pyrogallol to solid MnO_2 and the redox potential measured using the Pt/Ag–AgCl electrode.

Results and Discussion

The distribution of a metal ion between different soluble species is governed by a number of equilibria

$$[1] \qquad M^{n+} + R^{m-} \overset{K}{\rightleftharpoons} MR^{(m-n)-}$$

where M^{n+} is the free metal ion and R^{m-} may be carbonate, sulfide, hydroxide, chloride, humic acids, etc. The determination of a solution's chelating capacity by titration with heavy metal ions will depend both on the magnitude of *K* and the sensitivity of detection technique for the free metal ion. The ion selective electrode is responsive only to the free metal ion, and therefore a theoretical titration curve may be obtained by calculating the free metal concentration for different *K* and concentrations of M^{n+} and R^{m-}. Figure 1 shows the titration curve calculated for a species MR with a stability constant of 10^7 and a concentration of R^{2-} of 1.0×10^{-6} *M*. The titration error for $K = 10^7$ is 32%, for $K = 10^8$ is 10%, $K = 10^9$ is 2%, and $K = 10^{10}$ is 0%. In natural waters, metal species have stability constants of the order of 10^8; therefore, considerable errors can occur in the determination of the ligand concentration. Table 1 presents the measured chelating capacities for several model ligands and natural waters. For weak metal–organic complexes in natural waters, the complexing or binding capacity as determined by

Can. J. Chem. Downloaded from www.nrcresearchpress.com by 210.87.254.40 on 09/05/12
For personal use only.

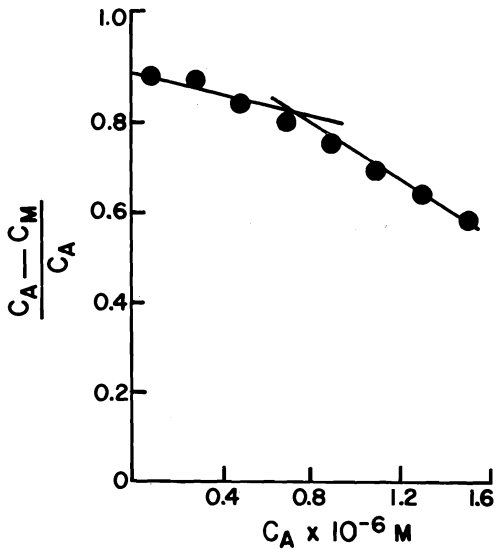

FIG. 1. Theoretical titration curve for a ligand concentration of 1.0×10^{-6} M and a stability constant, $K = 1.0 \times 10^{7}$.

titration will be low, and perhaps a better characterization of the water sample would be the plot of free metal concentration *vs.* total metal concentration plots. There are two reasons for the suggested characterization scheme: first, the toxic metal species in natural waters is generally regarded to be the free metal ion (19), and secondly, such a plot would be useful in evaluating the effect of sudden additions of metal ions to the watercourse from a foreign source.

The determination of the metal species in natural waters is a difficult problem that requires some definition before meaningful results are possible. The problem of analysis of metal ions in natural waters can be attacked from two points of view: the ideal case where the concentration of every species is determined (including identification of that species), or the practical case where the total concentration is determined by atomic absorption spectroscopy or neutron activation analysis. The ideal speciation scheme is not available; the total metal concentrations do not provide the biologically significant fractions of the metal species for the purpose of evaluating the toxicity of natural waters to living beings (for example, the work of Hutchinson and Stokes (25) indicates no relationship between total copper concentration and toxicity to algae).

TABLE 1. Binding capacity of model solutions

Solution	Binding capacity (μM)
20 μg/ml humic acid	50.4±0.5
3.0×10^{-5} M EDTA	30.0±0.1
10 μg/ml tannic acid	22.0±0.5
Rideau River water	49 ±2
Meach Lake water	29 ±1
Pinks Lake water	23 ±1

If one considers, however, that the metal species are distributed along a size continuum, then a differentiation by size, for example 'small' (free ions and inorganic complexes), 'medium' (organic complexes), and 'large' (colloids), in conjunction with the chemical behaviour of the size groups (such as distribution changes due to variation in the pH and metal concentration) may serve as a definitive speciation scheme. To test this hypothesis, the chemical characteristics of humic and tannic complexes of metal ions were evaluated with respect to pH, metal concentration, and competition with synthetic ligands (EDTA).

The requirements for a good size separation by dialysis are that the membrane be impermeable to metal–organic species, permeable to free copper ion, $CuCO_3$, and simple inorganic complexes (*e.g.*, $CuEDTA^{2-}$), and the time necessary to reach equilibrium should be a minimum. Figure 2 shows dialysis curves for the model species for the two dialysis membranes. It is evident that a combination of Spectrapor 2 and 3 will serve to differentiate between the different species where Spectrapor 2 is permeable to the metal–EDTA complexes but not the humic

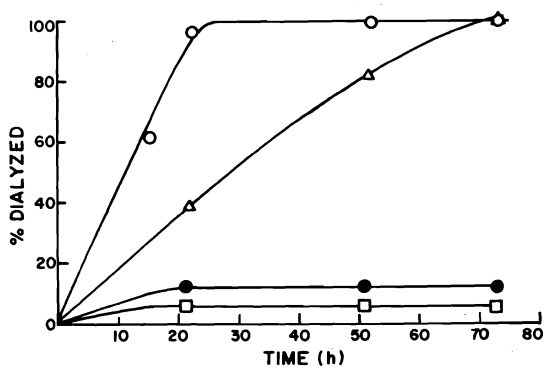

FIG. 2. Dialysis as a function of time: ○ $CuEDTA^{-2}$, Spectrapore 2, △ $CuEDTA^{-2}$, Spectrapore 3, ● copper/humic acid, Spectrapore 3, □ copper/tannic acid, Spectrapore 3.

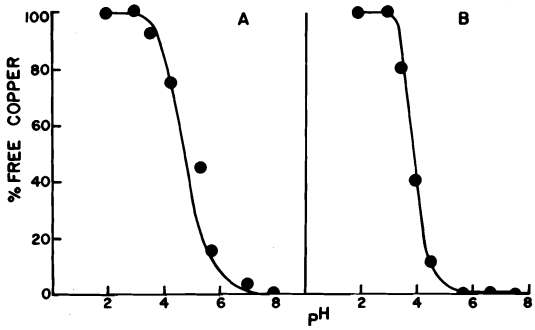

FIG. 3. Concentration of free copper ion as a function of p*H*. (*A*) Copper – humic acid. (*B*) Copper – Rideau River water.

TABLE 2. p*H* characteristics of metal–organic species

Metal ion	Organic*	100% dialysis (p*H*)	50% dialysis (p*H*)
Copper	TA	5.0	6.0
Copper	HA	3.1	4.6
Lead	TA	5.0	6.0
Lead	HA	2.9	4.4
Cadmium	TA	4.9	6.2
Cadmium	HA	3.4	4.8
Zinc	TA	5.4	5.6
Zinc	HA	4.0	5.5
Manganese	TA	5.4	6.0
Manganese	HA	3.5	6.0

*HA = humic acid, TA = tannic acid.

and tannic complexes, and the Spectrapor 3 membrane is permeable to the free metal ion and the metal carbonate complex. In Fig. 2, the time required to reach equilibrium was 24 h.

The Spectrapor 3 membrane is permeable only to the smaller metal species, and since the metal organic reaction in reaction 1 is p*H* dependent, a plot of dialysis *vs.* p*H* would be a valid characterization of the metal species. Figure 3 shows the copper distribution as a function of p*H* for solutions of humic acid and Rideau River water. Table 2 is a summary of the results of dialysis studies for the different metal ions investigated. In Table 2, from a comparison of the humic and tannic acids it is evident that the humic acid can bind the metal ions at lower p*H* than the tannic acid. The principal reason for this difference is the different pK_a values for the two acids (humic acid has a $pK_a \approx 4$ whereas tannic acid has a $pK_a \approx 6$) if the stability constants of the two complexes are similar then the differences in pK_a would result in a shift in the metal distribution curves.

In natural waters, two forms of competition are of interest: the competition for complexation sites between metal ions, and the competition between different ligands for the same metal ion. Figure 4 presents a plot of free metal ion *vs.* p*H* for equal concentrations of copper, lead, cadmium, and zinc in a humic acid solution. In the p*H* range 6–7, copper and lead are fully complexed (within the experimental error), and the order of stability is: $Pb^{2+} \sim Cu^{2+} > Cd^{2+} \sim Zn^{2+}$; at p*H* 5 the concentration of free metal ions increases in the order: $Pb^{2+} < Cu^{2+} < Cd^{2+} < Zn^{2+}$. In Fig. 4, pronounced minima in the concentration of free metal ions occur at p*H* 6–7, whereas in Fig. 3, for copper – humic acid, no minimum is observed. The concentrations of bound metals, 45.1 and 31.0 μM, at p*H* 6.9 and 7.6, respectively, indicate that the competition for binding sites is not responsible for the minima. The reason for the difference between Figs. 3 and 4 is that in Fig. 4, $NaHCO_3$ is also present, and hence, three competing equilibria are present:

$$[2] \qquad Cu^{2+} + H_2Org \overset{K_1}{\rightleftharpoons} CuOrg + 2H^+$$

$$[3] \qquad Cu^{2+} + H_2O \overset{K_2}{\rightleftharpoons} CuOH^+ + H^+$$

$$[4] \qquad Cu^{2+} + HCO_3^- \overset{K_3}{\rightleftharpoons} CuCO_3 + H^+$$

Comparison of reactions 3 and 4 indicates that Cu^{2+} and $CuCO_3$ predominate at $pH < 6$ and $6 < pH < 9.3$, respectively; therefore, only the competition between reactions 2 and 4 need be

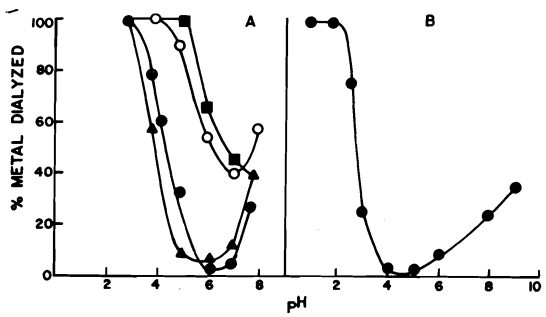

FIG. 4. Dialysis of metal as a function of p*H* in a humic acid solution. (*A*) Competition between metal ions for complexation sites: ● copper, ▲ lead, ○ cadmium, ■ zinc. (*B*) Theoretical curve for copper in humic acid – $NaHCO_3$ solution.

Can. J. Chem. Downloaded from www.nrcresearchpress.com by 210.87.254.40 on 09/05/12
For personal use only.

TABLE 3. Stability constants for the theoretical curve (Fig. 4*B*)

1.	$Cu^{2+} + Org^{2-} \rightleftharpoons CuOrg$	$\log K = 7.0$
2.	$Cu^{2+} + CO_3^{2-} \rightleftharpoons CuCO_3$	$\log K' = 6.77$
3.	$H_2Org \rightleftharpoons HOrg^- + H^+$	$\log K_1 = -3.30$
4.	$HOrg^- \rightleftharpoons Org^{2-} + H^+$	$\log K_2 = -9.0$
5	$H_2CO_3 \rightleftharpoons HCO_3^- + H^+$	$\log K_1' = -6.35$
6.	$HCO_3^- \rightleftharpoons H^+ + CO_3^{2-}$	$\log K_2' = -10.33$
7.	$C_T = [H_2Org] + [HOrg^-] + [Org^{2-}] = 5 \times 10^{-5}\ M$	
8.	$C_T' = [H_2CO_3] + [HCO_3^-] + [CO_3^{2-}] = 5 \times 10^{-4}\ M$	
9.	$[Org^{2-}] = C_T\alpha_2;\ [CO_3^{2-}] = C_T'\alpha_2'$	
10.	$\alpha_2 = \left(\frac{[H^+]^2}{K_1K_2} + \frac{[H^+]}{K_2} + 1\right)^{-1}$	
11.	$\alpha_2' = \left(\frac{[H^+]^2}{K_1'K_2'} + \frac{[H^+]}{K_2'} + 1\right)^{-1}$	
12.	$\log \frac{[CuOrg]}{[CuCO_3]} = \log K_4 - \log C_T' + \log C_T - \log \alpha_2' + \log \alpha_2$	
13.	$CuCO_3 + Org^{2-} \rightleftharpoons CuOrg + CO_3^{2-}$	$\log K_4 = 0.23$

considered. In the pH range 6–9, the equilibrium is represented by:

$$[5] \qquad CuCO_3 + Org^{2-} \overset{K_4}{\rightleftharpoons} CuOrg + CO_3^{2-}$$

from which eq. 6 may be derived as follows.

$$[6] \quad \log \frac{[CuOrg]}{[CuCO_3]} = \log K_4 - \log [CO_3^{2-}] + \log [Org^{2-}]$$

Equation 6 was evaluated using the constants given in Table 3, and the theoretical dialysis – pH curve is shown in Fig. 4*B*. The theoretical curve in Fig. 4*B* indicates that the competition between carbonate and humic acid will indeed cause the concentration of dialyzable metal to increase at p$H > 6.5$.

Humic acid can complex metal ions using salicylic type groups:

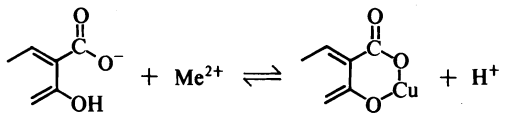

Also, tannic acid has similar functional groups. The competition between EDTA, tannic acid, and humic acid for copper ions indicated that the metal–organic complexes were much weaker than the respective metal–EDTA complex; for example, 5 μg/ml Cu^{2+} ion in 20 μg/ml humic acid was nondialyzable, whereas after the addition of EDTA all the copper was found to be dialyzable. To calculate the stability constant of a metal complex, the equilibrium concentrations of the free metal ion, complexed ion, and free ligand are required. Figure 5 presents a plot of the concentration of dialyzable copper against the total copper concentration for a 20 μg/ml humic acid solution at pH 6.8 (adjusted with KOH). If one assumes that the only species that is dialyzable is uncomplexed copper (both Cu^{2+} and $CuOH^+$), then a titration provides the concentration of

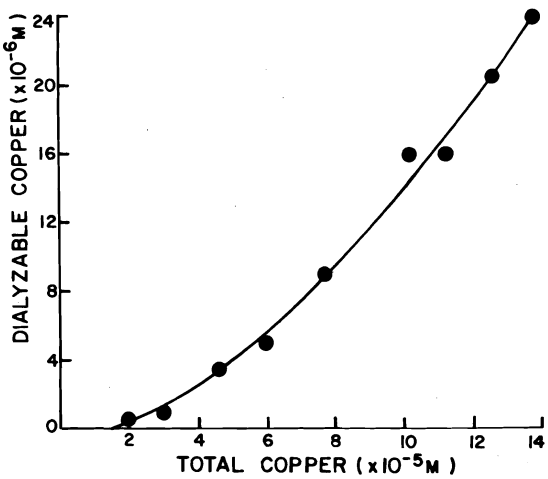

FIG. 5. Dialyzable copper as a function of total metal concentration in 20 μg/ml humic acid at pH 6.8.

Can. J. Chem. Downloaded from www.nrcresearchpress.com by 210.87.254.40 on 09/05/12
For personal use only.

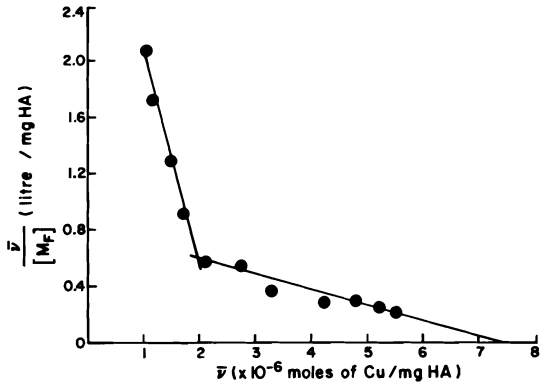

FIG. 6. Scatchard plot for binding of Cu(II) by humic acid at p*H* 6.8.

both bound and unbound copper; the stability constant can be readily evaluated. Mantoura and Riley (26) have used a gel filtration procedure to determine the stability constants of natural organics – metal ion complexes. They employed the equation:

$$[7] \qquad \frac{\bar{\nu}}{M_F} = K_i(n_i - \bar{\nu})$$

where $\bar{\nu}$ = bound metal/humic acid, K_i is the stability constant of the complex i, and n_i is the number of binding sites per molecule of the acid with stability constant K_i. Figure 6 presents a plot of $\bar{\nu}/M_F$ *vs.* $\bar{\nu}$ for a 20 μg/ml humic acid solution at p*H* 6.8 (derived from Fig. 5). Figure 6 shows that two types of binding sites are present. Table 4 presents the values of K_i and n_i for the four metals and two ligands studied. The stability constants obtained were evaluated for the concentration of humic acid in units of weight per unit volume because a molecular weight of humic substances is not available because of its uncertain composition (an estimate of the molecular weight from dialysis membrane cutoffs or ultrafiltration separations would not be valid because the separations are based on size and charge characteristics and not molecular weight). The stability constant obtained is a conditional constant for the p*H* and ionic strength conditions employed. Inspection of the values in Table 4 does indicate that the order of stability is: $Pb^{2+} > Cu^{2+} > Cd^{2+} > Zn^{2+}$, in agreement with the results of the competition method.

Dialysis separates the metal species into 'small' and 'large' size, whereas ultrafiltration permits

TABLE 4. Stability constants for metal–organic complexes

Metal ion	Ligand	K_i	n_i (mmol/g)
Copper	HA	1.6×10^6	2
		1.2×10^5	5.5
Cadmium	HA	1.1×10^5	3.0
Zinc	HA	1.0×10^5	4
Lead	HA	3.4×10^6	2
		2.0×10^5	6
Copper	TA	2.2×10^5	11
Lead	TA	2.4×10^5	11
Zinc	TA	1.8×10^4	11
Cadmium	TA	1.8×10^4	11

TABLE 5. Distribution of metal in humic acid

Size (nm)	Metal in the fraction (%)							
	p*H* 2				p*H* 6			
	Pb	Cu	Fe	Mn	Pb	Cu	Fe	Mn
>5.1	—	—	—	—	64	32	43	24
>3.2	—	—	—	—	36	67	45	30
>2.4	—	—	—	—	—	—	—	16
>1.9	—	—	—	—	—	—	—	14
<1.9	100	100	100	100	—	—	11	16

the fractionation of metal species into several different size groupings. Table 5 presents the results of ultrafiltration for 50 ng/ml Cu^{2+}, Fe^{3+}, Pb^{2+}, and 25 ng/ml Mn^{2+} in humic acid solution at two p*H* values. The results show two important points: at p*H* 2, all the metal is present as small species (in agreement with the results of p*H*/dialysis studies), and at natural water p*H* (p*H* > 6), the metal ions are bound in the species with sizes greater than 5.0 nm.

The solid–solution interface of the particulate can be considered as an impermeable membrane, that is, if a clay, humic acid, or hydrous oxide particulate with adsorbed metal ions was added to distilled water, the adsorbed metal ions would remain on the particulate because the 'fixed' negative surfaces cannot pass across the interface to maintain electroneutrality in solution (this is an example of Donnan Membrane equilibrium). Metal ions can be released from the particulate by one of three mechanisms: (*1*) ion exchange where a cation from the solution passes across the interface releasing an adsorbed cation into the solution; (*2*) solubilization of the matrix, for example, a humic acid particulate may redissolve; or, (*3*) the organic acids decompose the particulate matrix. Table 6 presents results for

Can. J. Chem. Downloaded from www.nrcresearchpress.com by 210.87.254.40 on 09/05/12
For personal use only.

Can. J. Chem. Downloaded from www.nrcresearchpress.com by 210.87.254.40 on 09/05/12
For personal use only.

TABLE 6. Release of copper from spiked particulates

Solution	Copper released (μmol)	
	Clay	Humic acid
Distilled water	0	0
1.0×10^{-3} *M* $NaHCO_3$	0.78	0.89
20 μg/ml Ca^{2+}	0.02	0.09
40 μg/ml Ca^{2+}	0.04	0.23
60 μg/ml Ca^{2+}	0.06	0.44

mechanisms *1* and *2* for clay and humic acid. The copper released by 1.0×10^{-3} *M* $NaHCO_3$ was not dialyzable, and therefore, was released as the humic acid complex whereas, in the presence of calcium ion, all copper released was by ion exchange. A comparison of the amount of metal ion released with the amount of calcium sorbed indicated that for both clay and humic acid, the ratio was not 1:1. The reason for this is that both particulates were not saturated with copper ion. The number of binding sites on the particulates is constant (0.45 mmol/g for humic acid and 0.29 mmol/g for the clay). A comparison of the amount of calcium adsorbed, copper released, and number of binding sites possible indicated that most of the calcium exchanged with the sites not occupied by Cu^{2+} but with K^+. For example, the humic acid system has 2.30×10^{-5} binding sites of which 6.8×10^{-6} sites were initially occupied by Cu^{2+}; after equilibration, 1.66×10^{-5} sites were occupied by Ca^{2+}; therefore, 0.4×10^{-6} mol of copper must be released, which is in good agreement with the value reported in Table 6.

The results presented in Table 6 show that metal ions can be released from particulates via ion exchange. Several authors (27, 28) have proposed that the metal transport mechanism involves mainly fulvic and humic acids. This indicates that two equilibria are operative:

$$[8] \qquad \text{Cu-clay} + 2K^+ \overset{K_1}{\rightleftharpoons} K_2\text{clay} + Cu^{2+}$$

$$[9] \qquad Cu^{2+} + Org^{2-} \overset{K_2}{\rightleftharpoons} CuOrg$$

where the presence of the organic acid will shift the ion exchange equilibrium to the right, thus increasing the concentration of soluble metal. Equilibria 8 and 9 are the same as those considered in the determination of stability constant of the complex, using the ion exchange method

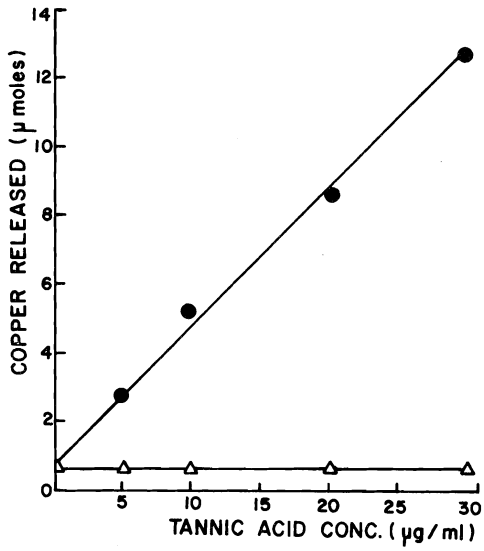

FIG. 7. Copper release from bentonite as a function of tannic acid concentration: ● total copper released, △ dialyzable copper.

(29), where the increase in the concentration of soluble metal depends on K_2 and the concentration of organic ligand. Figure 7 shows the amount of copper released from bentonite as a function of the concentration of tannic acid. Two points are worth noting: (*1*) with no tannic acid present some copper is released by ion exchange and this copper is dialyzable; and (*2*) as the concentration of tannic acid is increased more copper is released but the concentration of dialyzable copper remains constant. This is direct evidence for the coupling of equilibria 8 and 9. Table 7 presents the relationship between the copper released, the ligand concentration, and the stability constant of the copper complex. The copper–EDTA complex has a stability

TABLE 7. Release of metal from copper bentonite

Solution	Complexing sites (μ*M*)	Metal released (μ*M*)	Dialysis (%)
2.5×10^{-5} *M* EDTA	25	25.8	100
20 μg/ml TA	220*	62.5	6
20 μg/ml HA	150*	17.6	0
Rideau River water	—	22.0	48
Lac Phillippe water	—	39.2	43
Pinks Lake water	—	22.7	76
Meach Lake water	—	29.6	62

*Calculated using n_i values from Table 6.

TABLE 8. Fractionation of metal released from bentonite

Size (A)	Copper in the fraction (%)				
	HA*	HA	Rideau River 1†	Rideau River 2†	Meach Lake
>51	32	79	29	11	80
>31	67	11	—	—	—
>24	—	—	10	—	—
>19	—	10	—	—	—
<19	—	—	65	89	20
Total concentration (μM)	79	7.66	13.5	11.8	17.3

*50 ppb Cu^{2+} in 50 μg/ml humic acid solution at pH 6.
†The two Rideau River sites are 25 miles apart. All experiments performed in triplicate; experimental error in all cases was less than ± 10%.

constant of $\sim 10^{18}$, and therefore, all the complexing sites are occupied, whereas the copper–humic or tannic acid complexes have much smaller stability constants and the ratio of the copper released to the number of complexing sites is not 1:1.

Table 7 also presents the copper released from bentonite by several natural waters. In the case of the natural waters, appreciable concentrations of copper are present in small species. To investigate this effect, three more water samples were equilibrated with bentonite–copper, and then fractionated by ultrafiltration. Table 8 presents the results of ultrafiltration for a humic acid sample as well as for these three samples of natural waters. It is evident that in the humic acid solutions, the metal is released to the large size fraction (in agreement with the results of the earlier distribution for Cu^{2+} + humic acid) but an increase in the fraction >5.1 nm is noted. This increase can arise from two sources: in the fractionation of Cu^{2+} + humic acid, the concentration of Cu^{2+} was only 7.86×10^{-7} M whereas in the fractionation of the Cu/clay/humic acid solution the concentration was 7.66×10^{-6} M, and therefore, more of the sites on the large molecules are occupied. The second explanation is that there could be peptization of the clay particles by humic acid; however, fractionation of humic acid and copper at higher concentrations showed the same distribution as shown for humic acid equilibrated with clay. The equilibration of natural waters with copper sorbed onto bentonite indicated that the metal is present in two fractions, one >5.1 nm and the other <1.9 nm, indicating release by ion exchange with some complexation by large species.

A comparison of the release of copper from MnO_2, humic acid, and clay is presented in Table 9. The results in Table 9 show that when the solubilization of manganese is accounted for, the order of release is: clay > MnO_2 > humic acid, which is the same as observed by McClaren and Crawford (30) for isotope exchangeable copper. This order of metal release reflects the effect of K_1 in equilibria 8 and 9, that is, the amount of metal solubilized depends on the relative magnitudes of K_1 and K_2. Table 9 contains one other interesting piece of information, for the release of copper from humic acid, the ratio of copper released to EDTA present is less than 1, contrary to what would be expected from a comparison of the stability constants of metal–organic complexes. This can be explained in terms of the sorption of the EDTA onto the humic acid:

[10] $$Cu\text{–}HA + EDTA \rightleftharpoons HA\text{–}Cu\text{–}EDTA$$

by formation of a complex with copper bound to the humic acid (*i.e.*, ligand exchange where EDTA replaces water molecules bound to the Cu – humic acid complex).

Release of metal from the sediments via decomposition of the components may be an important mechanism for the hydrous oxides of manganese and iron. The chemical decomposition can occur via two mechanisms: (*1*) the formation of iron or manganese complexes with

TABLE 9. Release of copper from particulates

Ligand	Copper released (μmol)		
	MnO_2*	Humic acid	Clay
1.8 μmol EDTA	0.51 (0.78)	0.51	1.80
7.5 μmol HA	0.32 (2.08)	0.35	0.88
16.0 μmol TA	0.19 (1.70)	0.04	1.95

*The value in parentheses is the amount of manganese released (in μmol).

Can. J. Chem. Downloaded from www.nrcresearchpress.com by 210.87.254.40 on 09/05/12
For personal use only.

TABLE 10. Release of manganese from MnO_2

Ligand*	pH	Mn^{2+} concentration ($\times 10^{-5}$ M)	pε	
			Calculated	Measured
Pyrogallol	8	1.78	6.78	6.9±0.1
Pyrogallol	2.1	63.7	17.8	11.4±0.1
Tannic acid	8	3.25	6.66	6.8±0.1
Tannic acid	2.1	50.0	17.9	11.4±0.1
Gallic acid	8	5.71	6.54	6.6±0.1
Gallic acid	2.1	64.2	17.8	11.5±0.1
HCO_3^-	8	0.89	6.94	8.4±0.2
HNO_3	2.1	2.80	18.5	11.3±0.1
40 ppm Mn^{2+}	2.1	72.8	17.8	11.7±0.1
Quinone/hydroquinone	8	54.5	—	—

*The organic acids were present at 20 μg/ml; the quinone/hydroquinone system contained 0.02 M each.

organic acids (for example Baker (27) found that 100 ml of 0.1% (w/v) humic acid solubilizes 340 μg of iron and 2100 μg of manganese from haematite and pyrolusite, respectively), and consequently, releasing sorbed ions; or (2) reduction of the hydrous oxides to soluble species (for example, Hem (31) and Theis and Singer (32) have noted that tannic substances can reduce Fe(III) to Fe(II)). The question that arises is: which mechanism is operative in metal release from sediments?

Consider, for example, the equilibrium between MnO_2 and Mn^{2+}:

[11] $$MnO_2 + 4H^+ + 2e^- \rightleftharpoons Mn^{2+} + 2H_2O$$

where the relation between pε and Mn^{2+} concentration is (33):

[12] $$p\epsilon = 20.42 + \tfrac{1}{2}\log\frac{[H^+]^4}{[Mn^{2+}]}$$

where pε is the negative logarithm of the activity of electron (similar to pH for acid–base reactions.) Inspection of [12] indicates that the $[Mn^{2+}]$ increases if the pH or pε decrease. If some species that can lower the pε is present in natural waters, then the hydrous MnO_2 will be decomposed; it is well known that polyhydric phenols such as pyrogallol 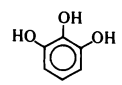 , gallic acid 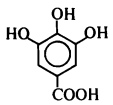 and tannic acid may reduce compounds via formation of quinones:

[13] 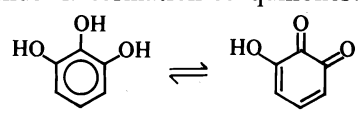

Consider, for example, the quinone/hydroquinone reaction:

[14] $$C_6H_4O_2 + 2H^+ + 2e^- \rightleftharpoons C_6H_4(OH)_2$$

with a standard potential of 0.6992 V. The expression for pε is:

[15] $$p\epsilon = 11.85 + \tfrac{1}{2}\log\frac{[C_6H_4O_2][H^+]^2}{[C_6H_4(OH)_2]}$$

The MnO_2/Mn^{2+} reaction at a concentration of 3.25×10^{-5} M Mn^{2+} at pH 8 gives a pε of 6.66 corresponding to $[C_6H_4O_2]/[C_6H_4(OH)_2] = 4.57 \times 10^5$, that is, all the hydroquinone will be oxidized (and Mn^{2+} released from the hydrous oxide). Table 10 presents results for the solubilization of MnO_2 by pyrogallol, gallic, and tannic acids, and includes the measured and calculated pε values (calculated by using [12]). Table 10 indicates that the organic reducing agents release manganese into solution. The pε values measured at pH 8 agree well with the calculated values; however, the values at pH 2 do not. For the platinum electrode to measure the correct pε value of the solution, it must respond to the half-reaction given in eq. 11. The platinum electrode, however, is not a good indicator electrode; for example, the pε of aerated water measured by the platinum electrode does not agree with calculated value of ~13; the measured pε is considerably smaller. The reason for this is that the following reaction controls the potential (34)

[16] $$Pt{-}O + 2H^+ + 2e \rightleftharpoons Pt + H_2O$$

[17] $$p\epsilon = 14.9 - 1.01\,pH$$

and if the pH values of the organic solutions are substituted into eq. 17, then at pH 2.1, pε = 12.8,

Can. J. Chem. Downloaded from www.nrcresearchpress.com by 210.87.254.40 on 09/05/12
For personal use only.

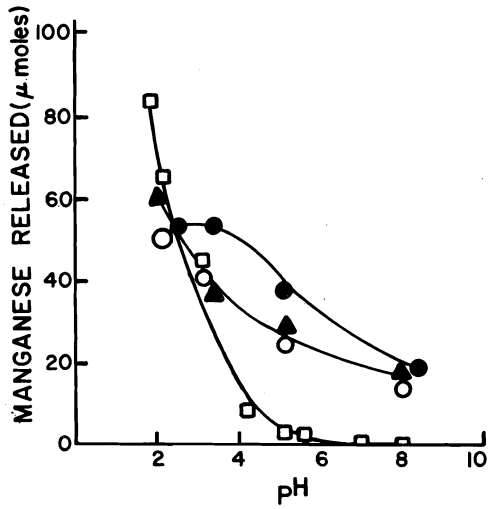

FIG. 8. Release of manganese by organic acids: ● 20 g/ml gallic acid, ▲ 20 g/ml pyrogallol, ○ 20 g/ml tannic acid, □ 1.0×10^{-3} *M* oxalic acid.

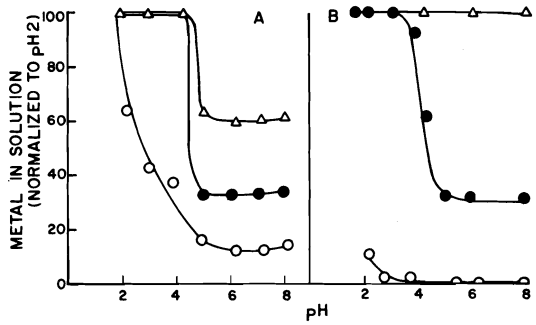

FIG. 9. Distribution of metal in MnO_2 Cu(II) systems as a function of p*H*. (*A*) MnO_2 – Cu(II) – tannic acid system: ● dialyzable Cu(II), △ total soluble Cu(II), ○ manganese in solution. (*B*) MnO_2–Cu(II)–$NaHCO_3$ system: △ dialyzable Cu(II), expressed as % of soluble Cu(II), ● total Cu(II), ○ manganese in solution.

and at p*H* 8.0, $p\epsilon = 6.82$, which are in reasonable agreement with the experimental values. It is evident that the $p\epsilon$ values measured by the Pt-electrode are of no value for monitoring the $MnO_2 - Mn^{2+}$ – organic acid system. The mechanism of the release of manganese from MnO_2 must be deduced from considerations other than $p\epsilon$ measurements. A comparison of the manganese released by 0.01 *M* quinone/0.01 *M* quinhydrone at p*H* 8.0 with the different acids is also presented in Table 10. It is evident that the polyhydric phenols can release similar amounts of manganese as the quinhydrone/quinone reaction. The effect of p*H* on the release of manganese from MnO_2 in the presence of organics is shown in Fig. 8. Figure 8 indicates that at lower p*H* values, the amount of manganese released by gallic acid, pyrogallol, and tannic acid increases and the behaviour is similar to that of oxalic acid. The shape of the curve can be explained as follows: at p*H* values greater than 6, polyhydric phenol is oxidized to quinone, and it has been reported (35) that peroxide oxidizes gallic acid to oxalic acid. As the p*H* is lowered below 5, the phenols may be oxidized to oxalic acid by HNO_3 (36), and the oxalic acid reduces the MnO_2 to Mn(II) releasing more manganese.

Figure 9 presents a study of the $Cu^{2+} - MnO_2$ – tannic acid system as a function of p*H*. Two conclusions can be drawn from this figure: (*1*) copper is maintained at a higher concentration in solution by a copper – tannic acid complex; (*2*) a comparison of Fig. 9 *A* and 9 *B* shows that the concentration of free copper ion is the same in both cases, that is, the increase in the concentration of soluble copper results from the complexation of copper and not from the reduction of MnO_2 by tannic acid. In this case, copper ion is not released from the particulate via reduction of MnO_2 because of the presence of a large amount of MnO_2.

Conclusions

These studies indicate that metal species in solution can be characterized by a combination of dialysis (to separate the species into different size groupings) and determination of the chemical properties of the metal species. Humic acids in solution and natural complexing agents in river waters can maintain metal ions in a bound form at a p*H* as low as 3, and in the case of humic acid, the metal ions are concentrated in species larger than 3.1 nm. The release of metal ions from sediments is by a combination of ion exchange and complex formation where the stability constant of the metal–organic complex determines the amount of metal solubilized. The hydrous oxides of manganese can be solubilized via reduction to Mn^{2+} with organic acids, especially, the polyhydric phenols.

Acknowledgement

The authors are grateful to the National Research Council of Canada for financial support of this research.

Can. J. Chem. Downloaded from www.nrcresearchpress.com by 210.87.254.40 on 09/05/12
For personal use only.

1. H. V. LELAND, S. S. SHUKLA, and N. F. SHIMP. *In* Trace metals and metal–organic interactions in natural waters. *Edited by* P. C. Singer. Ann Arbor Science, Ann Arbor, Michigan. 1973. p. 89.
2. E. A. JENNE. *In* Trace inorganics in water. *Edited by* Robert F. Gould. Adv. Chem. Ser. No. 73, Washington, D.C. 1968. p. 389.
3. ISAAC SANCHEZ and G. F. LEE. Water Res. **7**, 587 (1973).
4. H. S. POSSELT, F. J. ANDERSON, and W. J. WEBER. Environ. Sci. Technol. **2**, 1087 (1968).
5. J. B. GABANO, P. ETIENNE, and J. F. LAURENT. Electrochim. Acta, **10**, 947 (1965).
6. J. W. MURRAY. Geochim. Cosmochim. Acta, **39**, 505 (1975).
7. R. RAO GADDE and H. A. LAITINEN. Anal. Chem. **46**, 2022 (1974).
8. R. RAO GADDE and H. A. LAITINEN. Environ. Lett. **5**, 223 (1973).
9. J. E. BITTELL and R. J. MILLER. J. Environ. Qual. **3**, 250 (1974).
10. M. A. RASHID. Soil Sci. **111**, 298 (1971).
11. R. G. MCCLAREN and D. V. CRAWFORD. J. Soil Sci. **24**, 443 (1973).
12. D. P. KHARKAR, K. K. TUREKIAN, and K. K. BERTINE. Geochim. Cosmochim. Acta, **32**, 285 (1968).
13. J. GARDINER. Water Res. **8**, 157 (1974).
14. R. D. GUY, C. L. CHAKRABARTI, and L. L. SCHRAMM. Can. J. Chem. **53**, 661 (1975).
15. W. R. MATSON. Ph.D. Thesis, Massachusetts Institute of Technology, Boston, Massachusetts. 1968.
16. Y. K. CHAU, and K. LUM-SHUE-CHAN. Water Res. **8**, 383 (1974).
17. R. ERNST, H. E. ALLEN, and K. H. MANCY. Water Res. **9**, 969 (1975).
18. J. GARDINER. Water Res. **8**, 23 (1974).
19. M. J. STIFF. Water Res. **5**, 171 (1971).
20. P. BENEŠ and E. STEINNES. Water Res. **8**, 947 (1974).
21. J. E. SCHINDLER, J. J. ALBERTS, and K. R. HONICK. Limnol. Oceanogr. **17**, 952 (1972).
22. R. D. GUY and C. L. CHAKRABARTI. Proceedings of International Conference on Heavy Metals in the Environment, Toronto, Canada. 1975. In press.
23. H. VAN OLPHEN. An introduction to clay colloid chemistry. Interscience, New York. 1963.
24. S. RAMAMOORTHY and D. J. KUSHNER. Nature, **256**, 399 (1975).
25. T. C. HUTCHINSON and P. M. STOKES. *In* Water quality parameters. *Edited by* S. Barabas. ASTM Special Technical Publication 573. Philadelphia, Pa. 1975.
26. R. F. C. MANTOURA and J. P. RILEY. Anal. Chim. Acta, **78**, 195 (1975).
27. W. E. BAKER. Geochim. Cosmochim. Acta, **37**, 269 (1973).
28. NG SIEW KEE and C. BLOOMFIELD. Geochim. Cosmochim. Acta, **24**, 206 (1961).
29. M. SCHNITZER and S. U. KHAN. Humic substances in the environment. Marcel Dekker, New York. 1972.
30. R. G. MCCLAREN and D. V. CRAWFORD. Soil Science, **25**, 111 (1974).
31. J. D. HEM. Complexes of ferrous iron with tannic acid. Geological Survey Water-Supply Paper 1459-D, U.S. Government Printing Office, Washington. 1960.
32. T. L. THEIS and P. C. SINGER. Environ. Sci. Technol. **8**, 569 (1974).
33. W. STUMM and J. J. MORGAN. Aquatic chemistry. Interscience, New York. 1970. p. 306.
34. W. G. BRECK. J. Mar. Res. **30**, 121 (1972).
35. D. SLAWINSKA and J. SLAWINSKI. Anal. Chem. **47**, 2101 (1975).
36. W. A. DAVIS and S. S. SADTLER. Allen's commercial organic analysis. Vol. 5. P. Blakiston's Son & Co., Philadelphia, Pa. 1910. p. 20.

Can. J. Chem. Downloaded from www.nrcresearchpress.com by 210.87.254.40 on 09/05/12
For personal use only.

On the constitutions of silver iodine dibenzoates (Simonini complexes)

NIGEL J. BUNCE AND MARY HADLEY

Guelph–Waterloo Centre for Graduate Work in Chemistry, University of Guelph, Guelph, Ont., Canada N1G 2W1

Received April 6, 1976

NIGEL J. BUNCE and MARY HADLEY. Can. J. Chem. **54**, 2612 (1976).

Infrared and conductance measurements on three Simonini complexes (silver iodine dibenzoates) indicate a symmetrical structure. $Ag^+ (ArCO_2)_2I^-$ is considered a limiting constitution, but the substance is an extremely weak electrolyte. The constitution is discussed in terms of the observed chemistry and the stabilizing role of the silver cation.

NIGEL J. BUNCE et MARY HADLEY. Can. J. Chem. **54**, 2612 (1976).

Des mesures infrarouges et de conductivité sur trois complexes Simonini (dibenzoate d'iodure d'argent) suggèrent qu'ils existent sous forme de structure symétrique. On considère que le $Ag^+ (ArCO_2)_2I^-$ est une constitution limitante mais la substance est un électrolyte extrêmement faible. On discute de la constitution en terme de la chimie observée et du rôle stabilisant du cation argent.

[Traduit par le journal]

Interaction of a silver carboxylate with a half molar quantity of iodine at room temperature leads to the Simonini complex [1].

[1] $$2RCO_2Ag + I_2 \rightarrow (RCO_2)_2AgI + AgI$$

In many cases, especially when R is an aryl group, these complexes are isolable and their gross constitutions have been confirmed by elemental analysis. However, their structures have been debated since their first isolation (1), most recently by Beattie and Bryce-Smith (2), whose proposed formulation is shown as **1**.

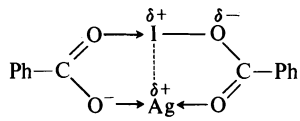

1

A reason for the interest in the structures of these compounds is their varied chemistry (3), with which any proposed formulation must be consistent. Beattie and Bryce-Smith (2) noted that silver iodine dibenzoate is soluble in *N,N*-dimethylformamide, DMF, from which it may be recovered unchanged. Such solutions precipitate AgI when treated with I^-, but not with Ag^+, implying that Ag^+ (but not I^-) may be made readily available, in accord with their proposed structure. These observations led us to consider the completely ionic formulation Ag^+ [PhC(=O)—O—I—O—C(=O)Ph]$^-$, **2**, for silver iodine dibenzoate; such a structure would be the analogue of the trihalide anions such as ICl_2^- whose chemistry is well known (4). The observations reported here are an attempt to evaluate this proposal.

Infrared Studies

Structure **1** for the Simonini complex tends to emphasize the molecular association between the silver carboxylate and the acyl hypoiodite. Structures of this sort would be expected to exhibit two carbonyl stretching sequences, the carboxylate anion near 1600 cm^{-1} (5) and the acyl hypohalite at high frequency.[1] In fact (see Table 1) both silver iodine dibenzoate and two nitro analogues show only one carbonyl absorption, consistent with a symmetrical structure such as **2**.

By contrast, addition of a half molar quantity of iodine to nitrobenzene solutions of silver acetate or trifluoroacetate (9) gives solutions with several absorptions in the carbonyl region. Despite the problems of using nitrobenzene as solvent, no absorption near 1700 cm^{-1} is observed, and these solutions thus appear to be mixtures of silver salt and acyl hypoiodite. No Simonini complex could be isolated from these solutions under our conditions, so that the stability of any such complex must be limited at

[1]Attachment of an electronegative atom or group to a carboxyl moiety generally leads to a high frequency carbonyl absorption, *cf.* diacyl peroxides and carboxylic peresters (10).

Can. J. Chem. Downloaded from www.nrcresearchpress.com by 210.87.254.5 on 09/05/12
For personal use only.

Can. J. Chem. Downloaded from www.nrcresearchpress.com by 210.87.254.5 on 09/05/12
For personal use only.

TABLE 1. Carbonyl ir absorptions of Simonini complexes and related compounds

Compound	Phase	ν_{max}(cm^{-1})
$(C_6H_5CO_2)_2AgI$	Nujol mull	1705
$(m\text{-}NO_2C_6H_4CO_2)_2AgI$	Nujol mull	1695
$(p\text{-}NO_2C_6H_4CO_2)_2AgI$	Nujol mull	1700
$ArCO_2^-$	Ref. 5	1610–1550
CH_3CO_2Br	CCl_4, Ref. 6	1790
CH_3CO_2I	CCl_4	1750
CH_3CO_2Cl	Ref. 7	1798
FCO_2F	Ref. 8	1930
$CF_3CO_2Ag + \frac{1}{2}I_2$	Nitrobenzene	1950, 1840*
$CH_3CO_2Ag + \frac{1}{2}I_2$	Nitrobenzene	1750, 1790*

*Nitrobenzene bands obscure the region below ~1720 cm^{-1}.

best. Whatever the constitution of the Simonini complex, it appears that equilibria corresponding to [2] are involved, and that the equilibrium constant differs according to the identity of the group R (and possibly the solvent).

[2] $$(RCO_2)_2AgI \rightleftharpoons RCO_2Ag + RCO_2I$$

The chemistry of the Simonini complexes is readily explained by this proposal. Dissociation into silver salt and acyl hypoiodite, followed by radical chain decomposition of the latter, adequately explains the formation of alkyl iodides and Simonini esters in aliphatic systems, as well as the production of iodides, esters, and biaryls in the aromatic series (11). Dissociation, followed by addition to an alkene and the subsequent reactions of such adducts, accounts for the Prévost group of products (3), while substitution of terminal alkynes probably follows the reaction sequence [3]–[4].

[3] $$RCO_2Ag + R'C{\equiv}CH \rightarrow RCO_2H + R'C{\equiv}CAg$$

[4] $$R'C{\equiv}CAg + RCO_2I \rightarrow R'C{\equiv}CI + RCO_2Ag$$

Conductance Studies

For reasons of solubility, DMF was the solvent employed. The method of purification was that of Brummer (12), which gave solvent with specific conductance in the range $1\text{–}3 \times 10^{-7}$ ohm^{-1} cm^{-1}; this was better than we could achieve by other methods (13). Freshly distilled solvent was always used, as its conductance was found to increase after 1–2 days' storage. Reliable results could not be obtained from single point determinations or by using a technique of successive dilutions, presumably because of the difficulty of protecting the solutions from the moist air of the laboratory. Measurements were therefore taken by adding aliquots of stock solutions of complex from a volumetric burette into the conductance cell, which already contained pure solvent.

At relatively high concentrations of the complex in DMF ($> 10^{-2}$ *M*) reprecipitation (2) gave back unchanged material. At lower concentrations, reprecipitation failed to occur, and removal of the solvent under reduced pressure was so slow that decomposition always resulted. Measurements were taken within 30 min or so of preparing the stock solution, since the solutions decomposed on standing, first to precipitate silver benzoate, while after several hours, the solution became yellow. Silver benzoate solutions in DMF themselves become yellow, slowly at room temperature, but rapidly at 100 °C when a silver mirror is deposited within 10 min.

The conductance results indicate the presence of a weak electrolyte in solution. At 10^{-3} *M*, the equivalent conductance is consistently below 10 ohm^{-1} cm^2 mol^{-1}, compared with the limiting conductances of the order of 85–90 ohm^{-1} cm^2 mol^{-1} obtained by Prue and Sherrington (14) and the range of 65–90 ohm^{-1} cm^2 mol^{-1} suggested by Geary (15) as being typical of 1:1 electrolytes in DMF at such concentrations.

Plots of Λ *vs.* $C^{1/2}$ were curved, and did not permit extrapolation to infinite dilution. Likewise, the $C\Lambda$ *vs.* Λ^{-1} plots of Kraus (16) had intercepts too close to zero to be useful, and the Λ^{-1} *vs.* $C^{1/2}$ plot due to Shedlovsky (17) also required too long an extrapolation. Consequently, no good value of Λ_0 could be obtained, neither could a test be made of whether the species present obeyed the Onsager relationship as a 1:1 electrolyte. Failure to obtain Λ_0 is unfortunate in that whereas most 1:1 electrolytes have limiting conductance of the order of 85–90 ohm^{-1} cm^2 mol^{-1} (14), potassium triiodide has been reported as 57 ohm^{-1} cm^2 mol^{-1} (18). It would be of interest to study other large anions such as the one postulated here, since this result implies a limiting ionic conductance as low as 26 ohm^{-1} cm^2 mol^{-1} for the triiodide ion (based on $\lambda = 30.8$ ohm^{-1} cm^2 mol^{-1} for K^+ (14)), only half the value observed for other anions.

Despite the various techniques recently devised to permit better extrapolation, we consider the quality of our data insufficient to warrant their use. Among the experimental problems to be considered are: (*i*) The Simonini complex is

Can. J. Chem. Downloaded from www.nrcresearchpress.com by 210.87.254.5 on 09/05/12
For personal use only.

TABLE 2. Average equivalent conductance *vs.* concentration for Simonini complexes

Benzoate, runs 1–3		Benzoate, runs 4–6		*m*-Nitrobenzoate	
c*	Λ†	c	Λ	c	Λ
2.5	15.5±5.0	2.5	26 ±10	2.5	41 ±17
5.0	10.7±2.5	5.0	16.5± 4.2	5.0	27 ±10
7.5	8.3±1.7	7.5	13.5± 2.3	7.5	20 ± 6
10.0	7.5±1.3	10.0	12.0± 1.7	10.0	17.0± 4.7
12.5	6.7±0.5	12.5	11.2± 1.0	12.5	14.5± 3.0
15.0	6.6±0.4	15.0	10.8± 0.7	15.0	13.7± 3.0
20	6.4±0.5	20	10.4± 0.5	20	12.4± 2.6
50	5.9±0.4	30	10.0± 0.4	30	10.2± 1.4
100	5.8±0.4	50	9.3± 0.3	40	9.4± 1.3
200	5.8±0.3	70	8.5± 0.3	60	8.6± 1.0

*Concentrations are 10^5 *M*.
†Equivalent conductance values are the average values of three runs, interpolated from graphs of c *vs.* Λ.

susceptible to hydrolysis (19) so that even traces of water will seriously affect the conductance data. Although Prue and Sherrington (14) concluded that minor amounts of water probably do not cause large deviations in conductance in DMF, their studies involved substrates not liable to hydrolysis. For this reason, we regard 10^{-4} *M* as a lower reliable limit for concentration and, at that concentration, the equivalent conductance is far from limiting. (*ii*) Ionic impurities could be present in the Simonini complex preparations. We used a new preparation for each run. Nevertheless, we note a consistent difference in values between runs 1–3 and 4–6 on the benzoate derivative (Table 2). These employed different preparations of silver benzoate. (*iii*) It is not clear what dissociation is occurring at the lower concentrations. Clearly, the substance is a weak electrolyte, and it is possible that equilibrium 5 is involved. However, it is also conceivable that equilibrium 2, for which as noted above there is chemical evidence, is responsible for the conductance which, in that case, would be due to silver benzoate.

[5] $(PhCO_2)_2AgI \rightleftharpoons Ag^+ + (PhCO_2)_2I^-$

Contributing to the lack of dissociation of the complex may be the presence of the silver ion. Although Ag^+ in $AgClO_4$ exhibits normal behaviour in DMF, silver nitrate behaves as a relatively weak electrolyte (14). Another approach to the problem of the limiting equivalent conductance would be to prepare another salt of $(ArCO_2)_2I^-$, taking advantage of the Kohlrausch law of independent ionic migration, which is known to hold in DMF (14). The tetraethylammonium salt was chosen, and reaction 6 attempted, but without success at separating a stable material.

[6] $(PhCO_2)_2AgI + Et_4NCl \rightarrow AgCl + Et_4N^+(PhCO_2)_2I^-$

Conclusions

The conductance measurements demonstrate that the two Simonini complexes studied are at best very weak electrolytes ($K_{diss} < 10^{-4}$ M). This observation, coupled with the failure of the synthesis represented by [6], demonstrates the importance of the silver ion in stabilizing the complex. Our results thus confirm this aspect of the Beattie and Bryce-Smith structure **1**, although on the basis of the infrared results, we suggest a more symmetrical version of it, such as **3**. We would expect the eight membered ring to be symmetrical and essentially planar as it is, for example, in the dimers of salts of carboxylic acids (20). Unfortunately, like Beattie and Bryce-Smith (2), we have been entirely unsuccessful in preparing crystalline material for an X-ray crystallographic study.

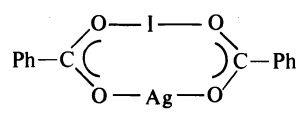

3

Quite possibly, silver(I) is an ideal cation to stabilize this structure, with its two coordinate linear geometry complementing that of the linear, two coordinate iodine(I). Only relatively polarizable ligands normally seem to be capable

Can. J. Chem. Downloaded from www.nrcresearchpress.com by 210.87.254.5 on 09/05/12
For personal use only.

of stabilizing iodine(I): thus, the stability of trihalide ions increases from ICl_2^- through I_3^- (21); other examples of related species are the recently observed $I(SCN)_2^-$ (22) and the iodine(I) dipyridine cation (23). Among oxygen donor atoms, very few complexes of iodine(I) have been reported. Tertiary amine complexes of acyl hypoiodites are known (24, 25), but not all oxygen donors can stabilize the central iodine atom; $I(NO_3)_2^-$ compounds are very unstable (26), while an attempt (27) to prepare $I(ClO_4)_2^-$ was unsuccessful. Thus the role of the silver ion in the Simonini complex may well be to prevent the dissociation, and hence decomposition, of the $I(ArCO_2)_2^-$ ion, and it is for this reason that the substances studied are such weak electrolytes.

Experimental

Preparation of Silver Salts

Equimolar quantities of the benzoic acid and silver nitrate were dissolved in aqueous ethanol. A solution containing 95% of the theoretical amount of sodium hydroxide in water was added with vigorous stirring. The silver salt was filtered with suction, washed repeatedly with water then acetone, and dried at 60 °C for several days.

Silver Iodine Dibenzoate

Typically, to a well stirred mixture of silver benzoate (1.00 g) and dry benzene (75 ml) was added a solution of iodine (0.554 g) in dry benzene (50 ml). The flask was stoppered to exclude moisture and the mixture stirred until the colour of iodine was discharged (about 1 h). Suction filtration through a glass sinter of porosity E to remove silver iodide, and evaporation *in vacuo* of the solvent from the filtrate left the complex as a cream coloured powder. *Mol. Wt.* calcd. for $C_{14}H_{10}IO_4Ag$ (iodometric): 477; found: 474 ± 4 (three determinations). A new preparation was made for each experiment.

Infrared Studies

A Beckman model IR 12 was used throughout. The Simonini complex was run as a mull in the range 200–4000 cm^{-1} using NaCl or polyethylene plates as appropriate. For solution work, NaCl solutions cells could not be used due to attack by the substrates, and 1 mm polyethylene cells, constructed in our laboratory, were used instead. Carbonyl stretching frequencies of the compounds studied are given in Table 1. Acetyl hypoiodite was made by treatment of a cooled slurry of silver acetate and iodine with excess I_2 (*cf.* ref. 28).

Conductance Studies

The conductivity bridge was a Beckman model RC16-B2 A.C. The cell was a Beckman fill type with platinized electrodes, having a cell constant of 0.217 cm^{-1} determined using standard KCl solutions from the data of Jones and Bradshaw (29). Into the central ground glass opening of the cell fitted a 10 ml volumetric burette, equipped in our laboratories with a matching ground glass taper and pressure equalizing device, so that the solutions were not exposed to the air of the laboratory during a run. At the beginning of a run, the cell was charged with 10.00 ml of DMF, freshly distilled under reduced pressure following several treatments with activated molecular sieves (12). This volume covered the electrodes. A stock solution of the complex in DMF was added in small portions from the burette, and the conductance read each time after the contents had been mixed by manual shaking. No temperature control was maintained; the solutions were equilibrated to the temperature of the laboratory, which was consistently 21–23 °C. At the end of each run, the cell was thoroughly rinsed with purified DMF and stored full of DMF. Other apparatus was washed conventionally, and finally rinsed with distilled water then with water redistilled from alkaline permanganate, and dried at 110 °C. Results of the conductance experiments are given in Table 2.

The results in Table 2 are interpolated values that are the average in each case of three separate runs. Each run used a new preparation of the Simonini complex, whose purity was checked by iodometric titration. Only samples having molecular weight (average of three titrations) within 1% of the nominal value were used. For the benzoate derivative, two different silver benzoate samples were employed. These gave different results, reported in Table 2 as the average of runs 1–3 and of runs 4–6.

Not reported in Table 2 are some preliminary experiments with silver iodine di-*p*-nitrobenzoate, R = *p*-$NO_2C_6H_4$. This compound was less soluble than the *m*-nitro analogue and was not studied in detail. Equivalent conductances were 3.4, 5.2, and 6.5 $ohm^{-1}\,cm^2\,mol^{-1}$ at 3.2×10^{-3}, 1.9×10^{-3}, and 1.8×10^{-3} *M*, all based on single data points.

Aged solutions of the complex in DMF became yellow and deposited a solid. The solid was shown to be silver benzoate (insoluble in DMF, soluble in NH_4OH, with KI a precipitate which redissolved in excess of the reagent; ir spectrum; the same as authentic material). Discolouration of the solutions was probably due to oxidation of the solvent by Ag(I); treatment of DMF with silver benzoate at 100 °C produced rapid discolouration, and after 10 min a silver mirror was deposited.

Acknowledgments

We thank the National Research Council of Canada for financial support, Dr. R. G. Goel for use of the conductivity bridge, and Mr. J. C. Curry for help with some of the preparations.

1. A. Simonini. Monatsch. **13**, 320 (1892); **14**, 81 (1893).
2. I. R. Beattie and D. Bryce-Smith. Nature, **179**, 577 (1957).
3. D. D. Tanner and N. J. Bunce. *In* The chemistry of acyl halides. *Edited by* S. Patai, Wiley-Interscience. 1972. p. 455.
4. A. I. Popov. *In* Halogen chemistry. Vol. I. *Edited by* V. Gutmann. Academic Press, London. 1967. p. 225.
5. D. H. Williams and I. Fleming. Spectroscopic methods in organic chemistry. McGraw-Hill, London. 1966.

6. J. J. REILLY, D. J. DUNCAN, T. P. WUNZ, and R. A. PATSIGA. J. Org. Chem. **39**, 3291 (1974).
7. J. C. EVANS, G. Y-S. LO, and Y-L. CHANG. Spectrochim. Acta, **21**, 973 (1965).
8. R. L. CAUBLE and G. H. CADY. J. Am. Chem. Soc. **89**, 5161 (1967).
9. R. N. HASZELDINE and A. G. SHARPE. J. Chem. Soc. 993 (1952).
10. K. NAKANISHI. Infrared absorption spectroscopy. Holden-Day, San Francisco. 1962; P. D. BARTLETT and R. R. HIATT. J. Am. Chem. Soc. **80**, 1398 (1958).
11. N. J. BUNCE and N. G. MURRAY. Tetrahedron, **27**, 5323 (1971).
12. S. B. BRUMMER. J. Chem. Phys. **42**, 1636 (1965).
13. D. P. AMES and P. G. SEARS. J. Phys. Chem. **59**, 16 (1955); C. M. FRENCH and K. H. GLOVER. Trans. Faraday Soc. **51**, 1418 (1955).
14. J. E. PRUE and P. J. SHERRINGTON. Trans. Faraday Soc. **57**, 1795 (1961).
15. W. G. GEARY. Coord. Chem. Rev. **7**, 81 (1971).
16. J. ROBBINS. Ions in solution. Clarendon Press, Oxford. 1972. p. 22.
17. T. SHEDLOVSKY. J. Franklin Inst. **225**, 739 (1938).
18. E. Y. GORENBEIN and A. E. GORENBEIN. Electrokhim. Acta, **5**, 119 (1969).
19. D. BRYCE-SMITH and P. CLARKE. J. Chem. Soc. 2264 (1956).
20. A. E. BLAKESLEE and J. L. HOARD. J. Am. Chem. Soc. **78**, 3029 (1956).
21. F. EPHRAIM. Ber. **50**, 1069 (1917); *cf.* H. W. CREMER and D. R. DUNCAN. J. Chem. Soc. 2243 (1931).
22. C. LONG and D. A. SKOOG. Inorg. Chem. **5**, 206 (1966).
23. S. G. W. GINN and J. L. WOOD. Trans. Faraday Soc. **62**, 777 (1966).
24. A. J. DOWNS and C. J. ADAMS. Comprehensive inorganic chemistry. Vol. 2. *Edited by* A. F. Trotman-Dickenson. Pergamon, Oxford. 1973, p. 475; F A. COTTON and G. WILKINSON. Advanced inorganic chemistry. 2nd Ed. Wiley–Interscience, New York. p. 580.
25. H. CARLSOHN. Ber. **68**, 2209 (1935); **68**, 2212 (1935).
26. M. LUSTIG and J. K. RUFF. Inorg. Chem. **5**, 2124 (1966).
27. K. O. CHRISTE and C. J. SCHACK. Inorg. Chem. **11**, 1682 (1972).
28. T. R. BEEBE, B. A. BARNES, K. A. BENDER, A. P. HALBERT, R. D. MILLER, M. L. RAMSAY, and M. W. RIDENOUS. J. Org. Chem. **40**, 1992 (1975).
29. G. JONES and B. C. BRADSHAW. J. Am. Chem. Soc. **55**, 1780 (1933).

Can. J. Chem. Downloaded from www.nrcresearchpress.com by 210.87.254.5 on 09/05/12
For personal use only.

Predictions of adiabatic Joule–Thomson coefficients based on modern potentials for noble gases

VIJAY P. S. NAIN AND RONALD A. AZIZ[1]

Department of Physics, University of Waterloo, Waterloo, Ont., Canada N2L 3G1

Received January 5, 1976

VIJAY P. S. NAIN and RONALD A. AZIZ. Can. J. Chem. **54**, 2617 (1976).

The predictions of the Joule–Thomson coefficient for the inert gases on the basis of numerous intermolecular potentials are calculated and compared with directly measured experimental data and derived values from p–V–T measurements. For all systems, the agreement is good except for TFD potentials derived by Gustafsson for He and Ne. We have also shown that the kinetic energy corrections in the low pressure region are not as high as those suggested by Gustafsson. Inversion temperatures are also calculated and recommended values are presented. Also presented are empirical relations which give as a function of temperature, second virial coefficients including the first two quantum corrections for many of the realistic potentials.

VIJAY P. S. NAIN et RONALD A. AZIZ. Can. J. Chem., **54**, 2617 (1976).

On a calculé les prédictions des coefficients de Joule–Thomson pour des gaz inertes en se basant sur de nombreux potentiels intermoléculaires et on les a comparés avec les données expérimentales mesurées directement et dérivées de valeurs provenant de mesures p–V–T. Dans tous les systèmes, il y a une bonne concordance excepté pour les potentiels TFD dérivés par Gustafsson pour He et Ne. On a aussi trouvé que les corrections, pour l'énergie cinétique dans la région de basse pression, ne sont pas aussi hautes que celles suggérées par Gustafsson. On a aussi calculé des températures d'inversion et on présente des valeurs recommandées. On présente aussi des relations empiriques qui donnent, en fonction de la température, les coefficients viriels seconds y compris les deux premières corrections quantiques de plusieurs potentiels réalistes.

[Traduit par le journal]

Can. J. Chem. Downloaded from www.nrcresearchpress.com by 210.87.254.5 on 09/05/12
For personal use only.

The Joule–Thomson coefficients in the zero pressure limit can be used as measures of the deviations from ideality arising from interactions involving pairs of molecules. These first order deviations are able to yield useful information on the nature of the intermolecular forces if reliable data on Joule–Thomson coefficients (J–T coefficients) can be obtained experimentally or derived through thermodynamically consistent relations.

The J–T coefficients have proved widely useful in such areas as: the computation of the thermostatic tables (*e.g.* steam), calculation of the imperfect gas correction in gas thermometry, the Linde process for liquefaction of gases, etc. Thus, the Joule–Thomson effect is not only of interest to the chemists as a probe of the potential function but also to the engineer for its applied aspects.

The objective of this work is to generate data for the second virial coefficients and hence Joule–Thomson coefficients which are more difficult to measure, on the basis of a number of intermolecular potentials recently proposed for the inert gas atoms. Invariably in the derivation or testing of these potentials, J–T coefficients were not used. While the J–T coefficient is more sensitive than the second virial coefficient as a probe of the potential function, the former, when derived from p–V–T data, has an inherent error. Moreover, directly measured values of the J–T coefficient are rare and an error of 1% was found (1) to be the limiting error required to mask the sensitivity of the property to the potential. In the present work we examine the various potentials as to their ability to predict the J–T coefficient and arrive at some interesting conclusions as described in the next section.

[1]To whom correspondence should be addressed.

The Joule–Thomson Coefficient

The zero-pressure Joule–Thomson coefficient μ_0 can be defined most simply as the numerical value of the gradient of an isenthalpic T–p curve in the limit of zero pressure. That is,

$$[1]\quad \mu_0 = \left[\frac{\partial T}{\partial p}\right]_H = \frac{1}{c_{p\to 0}}\left[T\left[\frac{\partial V}{\partial T}\right]_{p\to 0} - V\right]$$

Can. J. Chem. Downloaded from www.nrcresearchpress.com by 210.87.254.5 on 09/05/12
For personal use only.

Here, T, p, V, and H are the temperature, pressure, molar volume, and enthalpy of the gas system, respectively and $c_{p\to 0} = c_p^0$ is the molar heat capacity in the zero density limit of the gas. This definition in conjunction with the virial equation of state can be written in the following form

$$[2] \qquad \mu_0 = \frac{1}{c_p^0}\left[T\frac{dB(T)}{dT} - B(T)\right]$$

where $B(T)$ is the second virial coefficient. The higher virial coefficients are neglected for the obvious reason that, under these conditions, only the binary interactions play a dominant role.

The Data

Data may be determined directly as measured in a porous plug experiment or may be derived from p–V–T data.

(i) Directly Measured Data

Roebuck (2) observed that experimental data must be corrected for kinetic energy effects. Gustafsson (3), in a statistical analysis of the porous plug experiment, concluded that, due to these effects, true μ_0 values are lower than those actually measured. Grindley (4) observed, however, that the correct trend of μ *vs.* p is maintained down to $\frac{1}{2}$ atm. In extrapolating to the zero pressure limit, we have used the tangent to the μ–p curve drawn from the lowest experimentally measured point. The experimental data used in our comparison are listed in Table 1 with the appropriate references.[2]

(ii) Derived Data

A number of p–V–T determinations have been analysed to provide derived μ_0 values. These data are listed in Table 2.[2]

More recently, Kestin *et al.* (5) and Kestin and Mason (ref. 6, p. 137) have presented an extended law of corresponding states. The law of corresponding states is based on the assumption that the potential function for gases, whose molecular pairs interact through centrally-symmetric forces, has the same reduced form:

$$[3] \qquad \phi^* = \frac{\phi}{\varepsilon} = f(r/r_m, \alpha_i)$$

[2]Tables 1 and 2 are available, at a nominal charge, from the Depository of Unpublished Data, CISTI, National Research Council of Canada, Ottawa, Canada K1A 0S2.

The shape parameters α_i are the same for all gases in a group which obey the law of corresponding states. Any two gases in the group differ only by the value of a length parameter r_m and an energy parameter ε. By an analysis involving graphical and numerical procedures of a carefully selected set of data on the second virial and transport coefficients, they were able to determine universal functionals of these properties which are unique functions of reduced temperature $T^*(=T/(\varepsilon/k))$. Values of scaling parameters are presented in Table 3*a*. The universal functional for the second virial coefficient has the form

$$[4] \qquad B^*(T^*) = \frac{\exp(1/T^*)}{\sqrt{T^*}} \sum_{i=0}^{4} A_i(\ln T^*)^i$$

where $0.5 < T^* < 100$. From this functional and the appropriate scaling parameters, the values of the second virial coefficient and its derivative with respect to temperature could be determined and, hence μ_0 could be derived from eq. 2. These derived data are presented in Figs. 1, 3, 4, 5, and 6.

Theoretical Calculations

The classical second virial coefficient and its first two quantum corrections are computed from the equations (6.5-3 to 6.5-6) as given by Hirschfelder, Curtiss, and Bird (7*a*). The correction term for non-classical statistics, $B^0(T)$ $(= \mp(h^2/m)^{3/2}]B_0(T))$, in eq. 6.5-3 is not necessary in semi-classical approximations to the second virial coefficient for realistic intermolecular potentials and is thus omitted in the present calculations (7*b*). Using eq. 6.5-3 of ref. 7*a* we calculate $B^*(T^*)$ for He, Ne, Ar, Kr, and Xe on the basis of a number of modern pair potential energy functions at approximately 90 different values of T^* ranging from 0.2 to 100. The resulting values of $B^*(T^*)$ are fitted by multi-parametric numerical least square analysis to a relationship of the form of eq. 4. The resulting expression for a particular energy function together with the appropriate energy and length parameters are used to determine $B(T)$ and $dB(T)/dT$ and, hence μ_0 from eq. 2. (c_p^0 is equal to the ideal gas value of $\frac{5}{2}R$ where R is the gas constant.)

For many years, the Lennard-Jones 12-6 potential has been extensively used as a pair

TABLE 3
(*a*) Scaling parameters for Kestin–Mason correlation

Gas	ε/K (K)	σ (Å)
He	11.29	2.556
Ne	45.58	2.707
Ar	153.61	3.291
Kr	211.33	3.518
Xe	285.27	3.848

(*b*) Potential parameters

System	Potential	Potential parameters ε/k (K)	Potential parameters r_m (Å)	Reference
He–He	Beck	10.369	2.969	9
	ESMSV	11.0	2.963	10
Ne–Ne	11-6-8	45.83	3.0018[a]	12
	ESMSV I	42.73	3.11	13
	ESMSV III	42.01	3.102	14
Ar–Ar	11-6-8	152.8	3.67438	12
	MSV III	140.734	3.760	15
	BFW	142.095	3.7612	16
	ESBFW	142.095	3.7612	17
Kr–Kr	11-6-8	215.8	3.91511	12
	Buck *et al.*	200.0	4.03	18[b]
	M.S.	199.2	4.02	19[b]
	Barker *et al.*	201.9	4.0067	20[b]
Xe–Xe	11-6-8	294.6	4.28288	12
	Barker *et al.*	281.0	4.3623	20
	BP	280.53	4.4002	22

[a]See ref. 22.
[b]In a recent study, Aziz and Kocay (21) have shown that these potentials for Kr, as well as predicting microscopic properties, describe dilute bulk gas properties very well.

potential model for the inert gas atoms in the dilute gas phase. It has been known for some time that this potential is inadequate in its ability to predict dilute gas properties over a wide range of temperature. Much progress has been made, however, over the past three or four years in determining realistic potentials which are now considered to be accurate to within 1–2% of the real ones. These potentials have been largely derived empirically and in a number of ways. In most, the long range attraction has been constrained to be consistent with the semi-empirical calculations of the dispersive energy. In some, the short range interaction has been chosen to be in general agreement with *ab initio* calculations of the exchange energy. At intermediate ranges, an assumed potential form was fit to one or more experimental properties: molecular beam data, transport data, spectroscopic data (of dimers), and solid state data. In some cases, semi inversion techniques were applied with success to viscosity and virial data.

The specific potentials (9–22) used in these studies, details of which may be found in the Appendix,[3] are referred to in Table 3*b*. The calculated values of μ_0 based on Gustafsson's TFD potential (11) as reported in this work for the noble gases are taken from his tabulations of this physical quantity. Other TFD potentials are not considered (*e.g.* ref. 26) because they are very difficult to fit to an analytical form required

[3]Appendix is available, at a nominal charge, from the Depository of Unpublished Data, CISTI, National Research Council of Canada, Ottawa, Canada K1A 0S2.

Can. J. Chem. Downloaded from www.nrcresearchpress.com by 210.87.254.5 on 09/05/12
For personal use only.

TABLE 4. Parameters for eq. 4 for various potentials

Gas system	Potential	A_0	A_1	A_2	A_3	A_4	T^*
He	Beck	−0.37105	0.34565	0.16463	−0.02730	0.00157	≥6.0
	ESMSV	−0.71168	0.55983	0.08628	−0.00654	−0.00067	≥8.0
Ne	11-6-8	−0.40960	0.18876	0.28189	−0.05277	0.00386	
	ESMSV I	−0.47553	0.18966	0.30949	−0.05840	0.00387	
	ESMSV III	−0.480742	0.18574	0.31044	−0.05847	0.00386	
Ar	11-6-8	−0.48292	0.23078	0.30747	−0.05842	0.00436	
	MSV III	−0.52570	0.20199	0.30915	−0.06027	0.00352	
	BFW	−0.53082	0.20863	0.31456	−0.06024	0.00309	
	ESBFW	−0.53067	0.21017	0.31572	−0.06104	0.00413	
Kr	(11-6-8)	−0.48526	0.23287	0.30638	−0.05811	0.00433	
	Buck *et al.*	−0.51245	0.21206	0.30514	−0.06054	0.00370	
	M.S.	−0.53770	0.20657	0.31314	−0.06157	0.00370	
	Barker *et al.*	−0.50456	0.21747	0.30553	−0.06101	0.00462	
Xe	(11-6-8)	−0.48586	0.23343	0.30608	−0.05802	0.00432	
	Barker *et al.*	−0.50844	0.22082	0.30667	−0.06049	0.00459	
	Barker–Pompe	−0.49171	0.21616	0.29549	−0.05831	0.00320	
Kestin–Mason universal functional		−0.7035	0.3217	0.4828	−0.1016	0.0069	

for the calculations of the equilibrium properties and these potentials have ε/k and r_m values which seem too unrealistic compared to those derived from the spectroscopic and molecular beam scattering experiments.

Results and Discussion

Second virial coefficients including the first two quantum corrections may be calculated using an expression of the form of eq. 4 for all the potentials studied in this paper. The required fitting parameters A_i resulting from our analysis are listed for each potential in Table 4. The ε/k and r_m parameters for the various potentials given by the original authors and used in the present analysis are recorded in Table 3*b*.

The Joule–Thomson coefficients calculated on the basis of the various potentials are displayed for each system in Figs. 1–6 along with the experimental and derived data. Average absolute percentage deviations (AAPD) between calculated and experimental data are presented in Table 5. We will now discuss the results for each system in detail.

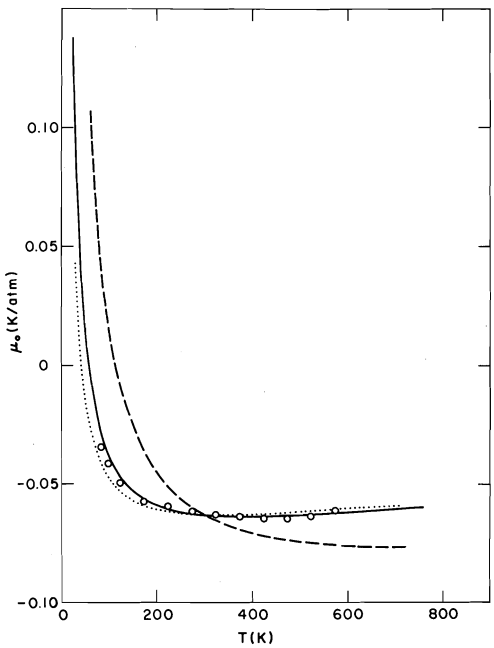

FIG. 1. Comparison of experiment and theoretical predictions of μ_0: --- Gustafsson, --- Beck, — (Kestin–Mason) experimental data; ○ (Roebuck *et al.* (Mage)).

Helium

μ_0 values for helium were measured by Roebuck and Osterberg (23). Their experimental data, as corrected and reanalysed by Mage (24) and Roebuck (25) are considered here. In addition we present derived data based on the correlation of Kestin and Mason (ref. 6, p. 145).

Can. J. Chem. Downloaded from www.nrcresearchpress.com by 210.87.254.5 on 09/05/12
For personal use only.

Can. J. Chem. Downloaded from www.nrcresearchpress.com by 210.87.254.5 on 09/05/12
For personal use only.

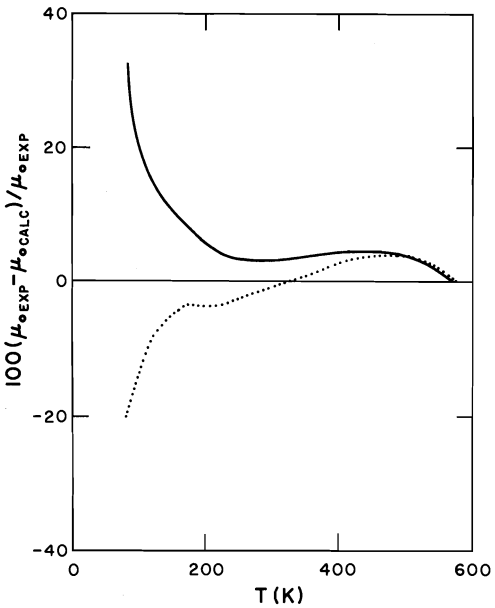

FIG. 2. Deviation curves between experimental and calculated μ_0 for He: --- Beck, — ESMSV.

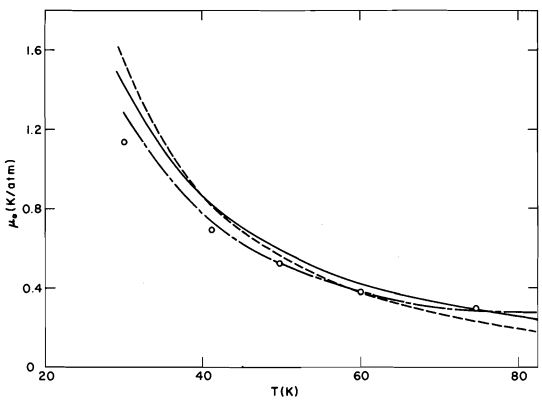

FIG. 3. Comparison of experiment and theoretical predictions of μ_0 for Ne: ----- ESMSV I, --- Gustafsson, — (Kestin–Mason) experimental data; ○ (Gladun).

Calculated values of μ_0 based on various potentials are also plotted in Fig. 1. The experimental data of Roebuck and the derived data are in close agreement for most of the temperature range displaying the mutual consistency of the two methods of obtaining μ_0 data. The μ_0 values derived on the basis of Gustafsson's TFD potential deviate substantially from the experimental data. Typically they differ by more than 200% at 83 K, 125% at 98 K, and 80% at 123 K. Gustafsson has suggested that, had quantum

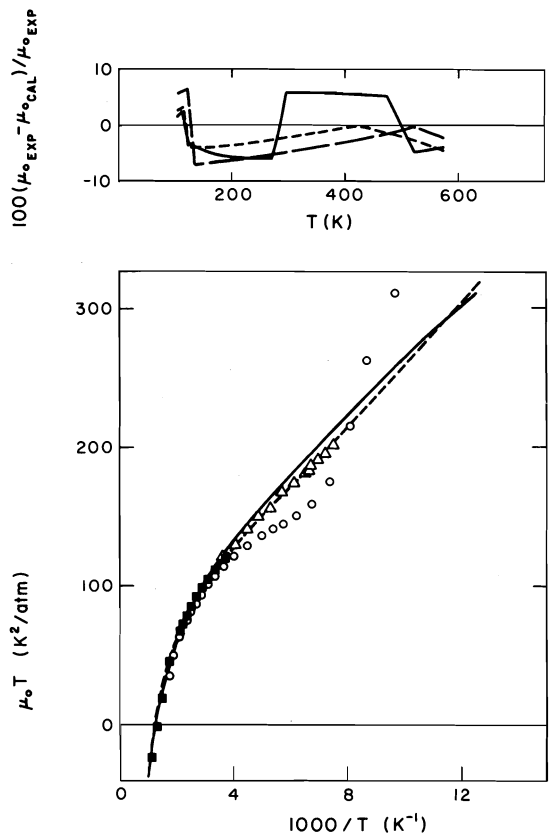

Fig 4. Comparison of experiment and theoretical predictions of μ_0 for Ar. Upper part: --- BFW, — (11-6-8), --- MSV III, experimental data: (Kestin–Mason). Lower part: --- BFW, experimental data: ○ (Roebuck and Osterberg), ■ (Whalley), △ (Michels *et al.*), — (Kestin–Mason).

corrections been taken into account, there would have been better agreement. In support of his argument, he indicated that the quantum contribution to μ_0 values on the basis of the Lennard-Jones 12-6 potential are 86, 28, and 6% at 80.9, 116.8, and 297.5 K respectively. Even if one makes the crude approximation that Gustafsson's potential resembles the Lennard-Jones 12-6 potential, we still cannot account for the observed discrepancy between experimental and calculated values. This falls in line with the conclusion of Gordon and Kim (27) and Toennies (28) that the TFD derived potentials are not valid in the intermediate region where the potential has its minimum. To examine this point further, we fitted classical $B(T)$ values on the basis of Beck's

Can. J. Chem. Downloaded from www.nrcresearchpress.com by 210.87.254.5 on 09/05/12
For personal use only.

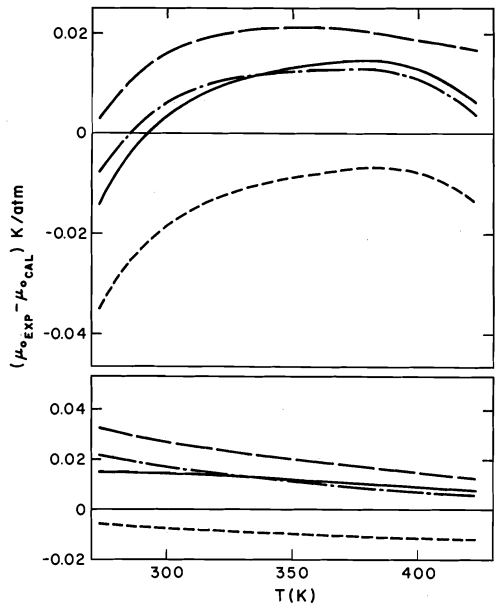

FIG. 5. Comparison of experiment and theoretical predictions of μ_0 for Kr. Upper part: — (11-6-8), -·-·- Buck *et al.*, --- M.S., – – – Barker *et al.*, experimental data: (Trappeniers *et al.*). Lower part: — (11-6-8), -·-·- Buck *et al.*, --- M.S., – – – Barker *et al.*, experimental data (Kestin–Mason).

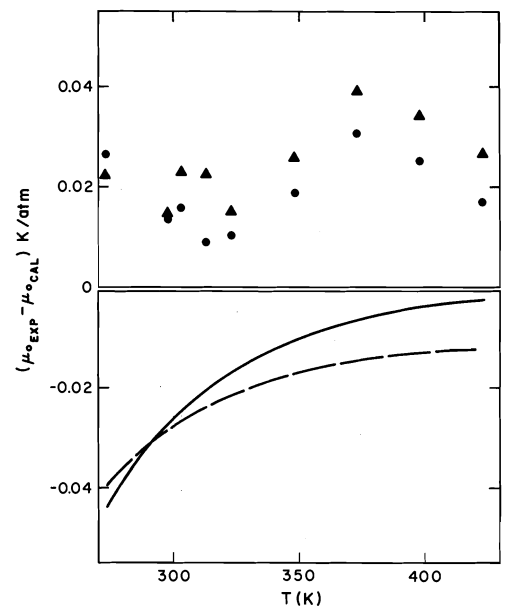

FIG. 6. Comparison of experiment and theoretical predictions of μ_0 for Xe: ▲ (11-6-8), ● Barker *et al.*, — (11-6-8), --- Barker *et al.*, experimental data: (Kestin–Mason).

potential (9) to eq. 4 and calculated μ_0. In case of this potential, the average absolute percentage deviation (AAPD) is found to be 25.4% over the temperature range 83 to 573 K for which direct experimental data on μ_0 are available. When quantum corrections are introduced, the agreement between experimental and predicted values is better (AAPD = 5.6%). We have compared the prediction of the ESMSV potential (10) with experiment and found that the deviation (AAPD) is three times larger than it is in the case of the Beck potential. The chief deviation, as one might expect, is in the low temperature range. We have avoided plotting all of the results in Fig. 1 to maintain clarity. Instead we present a deviation plot in Fig. 2 for the Beck and ESMSV potentials and tabulate the deviation in Table 5. Thus, the Beck potential best describes the Joule–Thomson coefficient. This is in agreement with the conclusions of Taylor and Keller (29, 30). Moreover, from the indicated agreement between theory and experiment, we can conclude that the kinetic energy contribution to μ_0 at low pressures suggested by Gustafsson is not large.

Neon

The only experimental data on neon are the direct measurements of Gladun (31) in the temperature range from 30 to 75 K. These are presented in Fig. 3. The correlation of Kestin and Mason (6) is based on $B(T)$ data at temperatures above 75 K and 'extrapolated' values of μ_0 derived from this condition may be in doubt. We nevertheless plot these derived values for the sake of completeness in the figure. Calculated values of μ_0 on the basis of the ESMSV I and Gustafsson's potentials are also shown. Calculated values on the basis of Hanley and Klein's 11-6-8 potential (12) using the parameters of Neufeld and Aziz (22) almost coincide with the derived values from Kestin and Mason's correlation. The discrepancy between these calculated values and those of Gladun suggests that the choice of the value of $\gamma = 3$ which gives rise to the exponent '11' in the 11-6-8 potential is incorrect for neon. The predictions of the ESMSV I and III potentials, on the other hand, lie in close agreement with Gladun's values above 40 K but are higher below this temperature.

The values of μ_0 calculated on the basis of

Can. J. Chem. Downloaded from www.nrcresearchpress.com by 210.87.254.5 on 09/05/12
For personal use only.

TABLE 5. Average absolute percentage deviations between experimental direct/derived data and the calculated μ_0 values

Gas	Number of experimental/ derived points	Temperature range (K)	Reference experimental/ derived data	Gustafsson's TFD potentials	Average absolute percentage deviations (AAPD)			
						Beck	ESMSV	
He	12	83–573	24	48.48		5.63	14.13	
	12	83–573	6, p. 137	51.32		8.60	6.48	
					(11-6-8)	ESMSV I	ESMSV III	
Ne	5	30–75	31	12.56	10.60	4.81	5.57	
	5	30–75	6, p. 137	8.99	19.62	9.80	12.48	
					(11-6-8)	MSV III	BFW	ESBFW
Ar	47	100–873	23, 32, 33	175.74	11.02	14.12	13.95	14.20
	21	100–573	23	26.49	7.19	7.86	10.03	9.50
	26	133–873	32, 33	103.99	13.92	19.06	17.35	17.56
	23	133–573	32, 33	18.51	2.88	2.08	0.86	0.89
	47	133–873	6, p. 137	80.12	6.49	10.08	7.53	7.63
	44	133–573	6, p. 137	17.76	5.08	4.95	2.70	2.68
					(11-6-8)	Buck *et al.*	M.S.	Barker *et al.*
Kr	7	273–423	35	4.64	1.88	1.65	1.98	2.91
	7	273–423	6, p. 137	4.78	1.83	1.79	1.60	3.28
					(11-6-8)	Barker *et al.*		Barker–Pompe
Xe	9	273–423	36	0.38	1.71	1.35		2.30
	9	273–423	6, p. 137	2.73	1.01	1.39		4.19

Can. J. Chem. Downloaded from www.nrcresearchpress.com by 210.87.254.5 on 09/05/12
For personal use only.

Gustafsson's potential are lower above 60 K and higher below this temperature. This departure at low temperatures cannot be accounted for by the omission of quantum corrections as suggested by Gustafsson for the following reason. The quantum contribution to μ_0 at 30 K as calculated by Gladun (31) is about 8%. At this temperature, the deviation between Gustafsson's TFD results and the experimental data is about four and one-half times this amount. At 74 K, the deviation is about 23%. Once again, a TFD derived potential fails to adequately describe the μ_0 data for neon. Perhaps, as Gustafsson suggests, TFD derived potentials are not applicable to low atomic number systems so far as equilibrium properties, *viz.* $B(T)$ and μ_0 are concerned.

Argon

The experimental data for argon are by far the most extensive. Firstly there are the porous plug experimental data of Roebuck and Osterberg (23) and Mage (24) which cover the range from 103.15 to 573.15 K. Secondly there are the p–V–T derived data of μ_0 due to Whalley (32) (133–273 K) and Michels *et al.* (33) (273–873 K). Finally, we have μ_0 values derived from Kestin and Mason's correlations. The derived data from all these three sources are consistent. The directly measured data are consistent with the derived data above 275 K. Below this temperature the direct data values are lower than the derived ones down to 125 K. We will examine the direct and derived data separately and compositely.

The Ar–Ar interaction is the most extensively studied one in the literature. Very refined and flexible potential functions are available due to Barker and co-workers. The Barker–Fisher–Watts (BFW) (16) and MSV III potential of Lee and co-workers (15), though derived differently, possess almost identical shapes. The BFW potential was fine tuned by Aziz (17). He developed a new potential (ESBFW) with a repulsive wall steeper than that for the BFW potential. This change is needed to characterize high temperature isotopic thermal diffusion and thermal conductivity (34).

The other potentials investigated are Hanley and Klein's 11-6-8 and Gustafsson's TFD potentials. The former potential, while not too realistic, is an excellent correlating potential. Only the predictions of BFW potential are shown in Fig. 4 (lower part) along with the experimental data (23, 24) and the p–V–T derived data (32, 33) in the form of $\mu_0 T$ *vs.* T. The deviation plots for the BFW, MSV III, and (11-6-8) potentials from the derived data of the Kestin–Mason correlation (ref. 6, p. 145) are also displayed in the upper part of Fig. 4. The predictions of the ESBFW potential are not displayed because they are essentially equivalent with those of the BFW potential. Table 5 lists the deviations for the Ar–Ar system in detail. The deviations between predictions and derived data seem to be unduly high for all potentials when the whole temperature range is considered. Omission of just three data points between 673 and 873 K lessen the AAPD markedly. In this temperature region which contains the inversion temperature, the values of μ_0 are very small and the percentage deviations are very large. As a consequence we will only consider values up to a temperature of 573 K. In case of the directly determined data of Roebuck and Osterberg (23) the best predictions are given by the 11-6-8 potential. In case of the derived data of Kestin and Mason (ref. 6, p. 145), Whalley (32), and Michels *et al.* (33), the BFW and ESBFW are definitely superior to the 11-6-8 and MSV III potentials. Below 275 K where the derived data values are higher than the directly measured ones, the predictions of all potentials are more consistent with the derived values. Furthermore, the predictions of all potentials are more consistent with the data of Michels *et al.* than with those of Whalley. The predictions on the basis of Gustafsson's TFD potential seem to be somewhat too low above 250 K and too high below that temperature.

Krypton

There are no directly determined values of μ_0 for this system. Trappeniers *et al.* (35) have derived μ_0 values for krypton from their p–V–T measurements. As is clear from Fig. 5 and Table 5 all the potentials, namely the Hanley–Klein 11-6-8 (12), Buck *et al.* (18), Gough *et al.* M.S. (19), Barker *et al.* (20), and TFD of Gustafsson, predict values within the experimental uncertainty. Because all but the last mentioned potential have used $B(T)$ measurements in their determination, this result is not altogether surprising.

Can. J. Chem. Downloaded from www.nrcresearchpress.com by 210.87.254.5 on 09/05/12
For personal use only.

Xenon

As in the case of krypton, there are no direct measurements for xenon. Michels *et al.* (36) have derived μ_0 values from their p–V–T data. As seen from Fig. 6 and Table 5, predictions on the basis of the 11-6-8, Barker *et al.*, and Gustafsson TFD potentials, are all within experimental error.

Inversion Temperatures

The maximum inversion temperature T_i^{max} is the temperature below which cooling will take place as a result of Joule–Thomson expansion in the zero-pressure limit.

We have calculated this temperature for each gas on the basis of all potentials considered in this study. We have also derived values of T_i^{max} from Kestin and Mason's correlations (KM). These values are presented in Table 6 along with experimental and derived values appearing in the literature. We further tabulate the inversion temperature presented by Levelt Sengers *et al.* (37) (LKG). They critically analysed existing $B(T)$ data, fitted a correlating 18-6 potential to the data and evaluated inversion temperatures.

For helium Gustafsson's value is unduly high. For all of the other gases, his predicted values of the inversion temperature are low especially for neon but seem to approach the experimental values (KM and LKG) as the molecular weight of the system increases. For neon the predictions of the 11-6-8 and ESMSV I and III potential are practically identical with the derived values (KM and LKG). For argon and krypton, all potentials except Gustafsson's compare favorably with the derived values. For xenon, Gustafsson's value follows the usual trend of predicting a low value for the T_i^{max} but is closer to the derived values than either of the predictions of the 11-6-8 and Barker *et al.* potentials.

Our recommendations, as listed in Table 6, for the inversion temperature values of Ar, Kr, and Xe are heavily weighted towards the predictions of the realistic intermolecular potential functions (17, 20) rather than those derived from the fitting of the experimental data on $B(T)$ by Kestin and Mason (ref. 6, p. 137) and Levelt Sengers *et al.* (37). The above choice is supported by the evidence of the real discrepancies (20, 38) between the experimental and the predicted values by the realistic potential functions for the second virial coefficients of Ar and Kr at low temperatures. This has been experimentally verified subsequently in case of Ar (39) and also the new low temperature $B(T)$ data for Xe (40) are in excellent agreement with the predictions of the improved Barker type potential (41) for this system.

Conclusions

Inversion temperatures as predicted by various realistic potentials are in reasonable agreement with one another and probably are better estimates than those available in the literature. The empirical relations defined by eq. 4 almost exactly reproduce the second virial coefficients including the first two quantum corrections for all the modern intermolecular pair potential energy functions considered in the present study. This greatly reduces the computing time and effort required in obtaining the derived data on the second virial and J–T coefficients without loss of accuracy even outside the temperature range over which the experimental data for both these physical quantities are available.

Directly measured experimental data on μ_0 are consistent with derived values from p–V–T measurements. This indicates that the derived data have not suffered from loss of accuracy to the extent of not being useful as a probe of the potential. For He, Ne, and Ar where direct data exist, the potentials can be put to a stringent test. The Beck potential for He, the ESMSV I and III potentials for Ne, and the BFW and ESBFW potentials for Ar describe the μ_0 data fairly well. It should be pointed out that the ESMSV I and III potentials for Ne predict μ_0 values which agree with direct data in the temperature range 30–60 K, even though this is outside the range of the virial data used in the determination of the potentials. This confirms the findings of Aziz (14) who established that the latter potential is the most realistic potential yet devised for neon. The Barker *et al.* (20) potentials for Kr and Xe describe the derived data very well. However, more accurate experimental data over an extensive temperature range are needed.

The TFD potentials derived by Gustafsson do not adequately describe direct μ_0 data on He and Ne. Other potentials described above are

Can. J. Chem. Downloaded from www.nrcresearchpress.com by 210.87.254.5 on 09/05/12
For personal use only.

TABLE 6. Inversion temperatures (K)

Gas	Inversion temperature (K)									
	Gustafsson					(Kestin–Mason)	NBS (Levelt Sengers *et al.*)	Other sources	Reference	Present recommendations
He	113	ESMSV 61	Beck 48			57	—	51	42, 43	55 ± 5
Ne	133	ESMSV I 233	ESMSV III 223		11-6-8 234	232	231	270	44	230 ± 4
Ar	606	MSV III 806	BFW 803	ESBFW 804	11-6-8 790	783	780	723	23	800 ± 5
Kr	841	Buck *et al.* 1154	M.S. 1196	Barker *et al.* 1144	11-6-8 1162	1077	1070	1050	44	1152 ± 10
Xe	1418	Barker *et al.* 1546	Barker–Pompe 1519	L-J(12-6) 1430	11-6-8 1535	1453	1456	1290	44	1540 ± 10

definite improvements over Gustafsson's. The mutual consistency in the values of the inversion temperature based on different potentials except those of Gustafsson further supports our conclusion.

The kinetic energy corrections in the zero pressure limit for μ_0 do not seem to be as high as those suggested by Gustafsson.

Acknowledgments

This work was carried out with the assistance of a grant in aid of research from the National Research Council of Canada. We would like to thank Mr. H. H. Chen for some assistance in the computations.

1. H. J. M. Hanely. U.S. National Bureau of Standards Technical Note 360 (1967).
2. J. R. Roebuck. Proc. Am. Acad. Arts Sci. **60**, 537 (1925).
3. O. Gustafsson. Ark. Fys. **40**, 481 (1970).
4. J. H. Grindley. Philos. Trans. R. Soc. London Ser. A, **194**, 1 (1900).
5. J. Kestin, S. T. Ro, and W. Wakeham. Physica, **58** 165 (1972).
6. J. Kestin and E. A. Mason. A.I.P. Conference Proceedings No. 11, *Edited by* J. Kestin. American Institute of Physics, New York, 1973.
7. (*a*) J. O. Hirschfelder, C. F. Curtiss, and R. B. Bird. Molecular theory of gases and liquids. Wiley and Sons, New York. 1964. (*b*) P. R. Certain, and L. W. Bruch. Intermolecular forces. MTP International Review of Science, Physical Chemistry Series 1, Vol. 1. MTP Co., Butterworth & Co. Publishers Ltd., London, England. 1972.
8. J. deBoer and A. Michels. Physica, **5**, 945 (1938).
9. D. E. Beck. Mol. Phys. **14**, 311 (1968); **15**, 332 (1968).
10. J. M. Farrar, T. P. Schafer, and Y. T. Lee. A.I.P. Conference Proceedings No. 11, *Edited by* J. Kestin. American Institute of Physics, New York. 1973. p. 279.
11. O. Gustafsson. Ark. Fys. **40**, 465 (1970).
12. H. J. M. Hanley and M. Klein. J. Phys. Chem. **76**, 1743 (1972).
13. J. M. Farrar, Y. T. Lee, V. V. Goldman, and M. L. Klein. Chem. Phys. Lett. **19**, 359 (1973).
14. R. A. Aziz. Mol. Phys. **30**, 1409 (1975).
15. J. M. Parson, P. E. Siska, and Y. T. Lee. J. Chem. Phys. **56**, 1511 (1972).
16. J. A. Barker, R. A. Fisher, and R. O. Watts. Mol. Phys. **21**, 657 (1971).
17. R. A. Aziz. Chem. Phys. Lett. **28**, 47 (1974).
18. U. Buck, M. J. Dondi, U. Valabusa, M. L. Klein, and G. Scoles. Phys. Rev. **8**, 2409 (1973).
19. D. W. Gough, E. B. Smith, and G. C. Maitland. Mol. Phys. **27**, 867 (1974).
20. J. A. Barker, R. O. Watts, J. K. Lee, T. P. Schafer, and Y. T. Lee. J. Chem. Phys. **61**, 3081 (1974).
21. R. A. Aziz and W. L. Kocay. Mol. Phys. **30**, 857 (1975).
22. P. D. Neufeld and R. A. Aziz. J. Chem. Phys. **59**, 2234 (1973).
23. J. R. Roebuck and H. Osterberg. Phys. Rev. **43**, 60 (1933); **46**, 785 (1934); Smithsonian Physical Tables Publication 4169. Smithsonian Institute, Washington, D.C. 1954.
24. D. T. Mage. J. Chem. Phys. **42**, 2977 (1965).
25. J. R. Roebuck. Collection of experimental records. The University of Michigan Library. Ann Arbor, Michigan.
26. J. S. Cohen and R. T. Pack. J. Chem. Phys. **61**, 2372 (1974).
27. R. G. Gordon and Y. S. Kim. J. Chem. Phys. **56**, 3122 (1972).
28. J. P. Toennies. Chem. Phys. Lett. **20**, 238 (1973).
29. W. L. Taylor and J. M. Keller. J. Chem. Phys. **54**, 647 (1971).
30. J. M. Keller and W. L. Taylor. J. Chem. Phys. **51**, 4829 (1969).
31. A. Gladun. Thesis, Technical University of Dresden, Dresden, East Germany. 1966; A. Gladun. Cryogenics, **6**, 31 (1966).
32. E. Whalley. Can. J. Technol. **33**, 111 (1955).
33. A. Michels, J. M. Levelt, and G. J. Wolkers. Physica, **24**, 769 (1958).
34. V. P. S. Nain, R. A. Aziz, P. C. Jain, and S. C. Saxena. J. Chem. Phys. In press.
35. N. J. Trappeniers, T. Wassenaar, and G. J. Wolkers. Physica, **32**, 1503 (1966).
36. A. Michels, T. Wassenaar, G. J. Wolkers, and J. Dawson. Physica, **22**, 17 (1956).
37. J. M. H. Levelt Sengers, M. Klein, and J. S. Gallagher. NBS Report No. AEDC-TR-71-39, March 1971.
38. H. J. M. Hanley, J. A. Barker, J. M. Parson, Y. T. Lee, and M. Klein. Mol. Phys. **24**, 11 (1972).
39. B. Schramm and U. Hebgen. Chem. Phys. Lett. **29**, 137 (1974).
40. R. Hahn, K. Schafer, and B. Schramm. Ber. Bunsenges. Phys. Chem. **78**, 287 (1974).
41. J. A. Barker. J. Chem. Phys. **63**, 2767 (1975).
42. F. G. Keyes. Temperature. Reinhold, New York. 1941. p. 45.
43. W. H. Keesom. Helium. Elsevier, Amsterdam. 1942.
44. H. H. Hollis and G. A. Cook. Argon, helium, and the rare gases. Vol. II. *Edited by* G. A. Cook. Interscience Publishers, New York. 1961. Chapt. XIV. p. 546.

Can. J. Chem. Downloaded from www.nrcresearchpress.com by 210.87.254.5 on 09/05/12
For personal use only.

Réaction oscillante de Belousov. 1. Cinétique de la réaction bromate–céreux

CLAUDE HERBO, GUY SCHMITZ ET MARTINE VAN GLABBEKE

Faculté des Sciences Appliquées, Université Libre de Bruxelles, 1050 Bruxelles, Belgique

Reçu le 10 juin 1975[1]

CLAUDE HERBO, GUY SCHMITZ et MARTINE VAN GLABBEKE. Can. J. Chem. **54**, 2628 (1976).

Au cours de l'oxydation de l'acide malonique par le bromate de potassium catalysée par le couple céreux-cérique en solution sulfurique, on observe des oscillations des concentrations en ions cériques et bromures. Cette réaction, découverte par Belousov peut être décomposée en deux réactions partielles: la réduction du bromate par les ions céreux et l'oxydation de l'acide malonique par les ions cériques. La première présente des caractéristiques cinétiques très particulières et son mécanisme est à la base de l'explication des oscillations. Elle est autocatalytique mais inhibée par les ions bromures. Nous avons donc repris son étude en faisant varier non seulement les concentrations initiales en bromate et en cerium mais également en bromure. Le mécanisme que nous proposons comporte, outre les pas classiques de la réaction bromate–bromure, l'oxydation des ions céreux par le radical $BrO_2^{\cdot}$ formé suivant

$$HBrO_2 + Br_2O_2 = 2BrO_2^{\cdot} + Br^- + H^+$$

CLAUDE HERBO, GUY SCHMITZ, and MARTINE VAN GLABBEKE. Can. J. Chem. **54**, 2628 (1976).

During the oxidation of malonic acid by potassium bromate catalyzed by the Ce(III)–Ce(IV) couple in a sulfuric acid solution, concentration oscillations of ceric and bromide ions are observed. This reaction, discovered by Belousov, can be resolved into two parts: reduction of bromate by cerous ions and oxidation of malonic acid by ceric ions. The former shows very unusual kinetic features and its mechanism is the basis of the explanation of the oscillations. It is autocatalytic but inhibited by bromide ions. We have thus reinvestigated this reaction varying not only the initial concentrations of bromate and of cerium but also that of bromide. The mechanism suggested involves, besides the classic steps of the bromate–bromide reaction, the oxidation of cerous ions by $BrO_2^{\cdot}$ radicals produced by the step

$$HBrO_2 + Br_2O_2 = 2BrO_2^{\cdot} + Br^- + H^+$$

Introduction

L'oxydation de l'acide malonique par le bromate de potassium en solution sulfurique ne se produit avec une vitesse mesurable que si elle est catalysée par un couple redox tel que le couple Ce(III)–Ce(IV). Alors qu'en général dans un tel système chimique, le rapport entre les formes oxydées et réduites du catalyseur tend vers une valeur quasi-stationnaire, ici au contraire il existe un domaine de concentration des réactifs dans lequel ce rapport varie de façon périodique au cours du temps. Ce type de système oscillant a été découvert en 1958 par Belousov (1). Depuis lors de nombreux travaux y ont été consacrés; citons principalement ceux de Zhabotinskii et coll. (2–4), de Degn (5), de Kasperek et Bruice (6) et de Noyes et coll. (7–9).

Les deux phases de la réaction oscillante correspondent à deux groupes de réactions partielles: l'oxydation du Ce(III) par le bromate et la réduction du Ce(IV) par l'acide malonique ou bromomalonique.

Kasperek et Bruice (6) ont étudié ces réactions séparement et ont obtenu la loi cinétique de la réduction du Ce(IV). Par contre l'étude de la réaction bromate–céreux s'est révelée beaucoup plus difficile et ne leur a pas permis d'en déduire le mécanisme.

Noyes, Field et Thompson (10) ont proposé le mécanisme suivant:

$$[1'] \quad BrO_3^- + HBrO_2 + H^+ \rightleftharpoons 2BrO_2^{\cdot} + H_2O$$

$$[2'] \quad BrO_2^{\cdot} + Ce^{3+} + H^+ \rightleftharpoons HBrO_2 + Ce^{4+}$$

$$[3'] \quad BrO_2^{\cdot} + Ce^{4+} + H_2O \rightarrow BrO_3^- + Ce^{3+} + 2H^+$$

$$[4'] \quad 2HBrO_2 \rightarrow BrO_3^- + HOBr + H^+$$

Basé sur les résultats obtenus par Thompson (11) travaillant avec un excès de Ce(III) par rapport au bromate, ce mécanisme n'est pas en accord avec l'ensemble des résultats obtenus si l'on utilise un excès de bromate comme dans le

[1]Revision reçue le 13 janvier 1976.

Can. J. Chem. Downloaded from www.nrcresearchpress.com by 210.87.254.6 on 09/05/12
For personal use only.

Can. J. Chem. Downloaded from www.nrcresearchpress.com by 210.87.254.6 on 09/05/12
For personal use only.

cas de la réaction oscillante. La première partie de nos travaux concernant la réaction de Belousov a donc été consacrée à une nouvelle étude cinétique de la réaction bromate–céreux.

Stoechiométrie de la réaction bromate–céreux

A partir des potentiels d'oxydo–réduction donnés par Latimer (12)

$$BrO_3^- + 6H^+ + 5e = \tfrac{1}{2}Br_2(aq.) + 3H_2O \quad 1.51\ V$$

$$BrO_3^- + 5H^+ + 4e = HOBr + 2H_2O \quad 1.49\ V$$

$$Ce^{4+} + e = Ce^{3+}\ (H_2SO_4, 1\ M) \quad 1.44\ V$$

$$Br_2 + 2e = 2Br^- \quad 1.087\ V$$

on voit que le Ce(III) en milieu sulfurique peut réduire le bromate à l'état de brome ou d'acide hypobromeux mais pas de bromure.

Utilisant les constantes cinétiques de Eigen et Kustin (13) on vérifie que dans nos conditions expérimentales, l'équilibre [I] n'est quasi pas perturbé.

$$[I] \qquad Br_2 + H_2O = HOBr + Br^- + H^+$$

On en déduit que la réaction de réduction du bromate produira soit du brome soit de l'acide hypobromeux suivant la concentration du bromure dans le système. Lors de la plupart de nos expériences nous introduisons initialement de petites quantités de bromure mais même sans addition intentionnelle il est présent en traces comme impureté du bromate (*cf.* partie expérimentale). Le système général est donc tri-stoechiométrique: outre l'équilibre [I] on peut écrire les réactions de réduction du bromate sous la forme correspondant aux milieux pauvres en bromure:

$$[II] \qquad BrO_3^- + 2Br^- + 3H^+ = 3HOBr$$

$$[III] \quad BrO_3^- + 4Ce^{3+} + 5H^+ = HOBr + 4Ce^{4+} + 2H_2O$$

La constante d'équilibre [I] est bien connue (14):

$$K[I] = \frac{[HOBr][Br^-][H^+]}{[Br_2]} = 5.8 \times 10^{-9} \text{ à } 25\ ^\circ C$$

A partir des potentiels d'oxydo–réduction on calcule les deux autres constantes d'équilibre:

$$K[II] = 2 \times 10^{10} \quad K[III] = 2.5 \times 10^3$$

Ces valeurs ne sont cependant qu'approximatives, non seulement par la nature de ce type de calcul, mais aussi par l'utilisation de potentiels standards pour les dérivés du brome et d'un potentiel en milieu sulfurique molaire pour le cérium.

Dans les milieux riches en bromure les réactions [II] et [III] sont remplacées par:

$$[II'] \qquad BrO_3^- + 5Br^- + 6H^+ = 3Br_2 + 3H_2O$$

$$[III'] \quad BrO_3^- + 5Ce^{3+} + 6H^+ = \tfrac{1}{2}Br_2 + 5Ce^{4+} + 3H_2O$$

Considerons un exemple type de conditions initiales réalisées lors de nos expériences:

$$[H^+] = 1; \quad [BrO_3^-] = 0.1;$$

$$[Ce^{3+}] = 2 \times 10^{-4}; \quad [Br^-] = 10^{-5}$$

A l'équilibre on calcule les valeurs suivantes:

$$[BrO_3^-] = 0.1; \quad [HOBr] = 6.4 \times 10^{-5};$$

$$[Br_2] = 1.2 \times 10^{-7}; \quad [Br^-] = 10^{-11};$$

$$[Ce^{4+}] = 2 \times 10^{-4}; \quad [Ce^{3+}] = 4 \times 10^{-6}$$

Au début de la réaction on forme du brome suivant [II'] et [III'] mais il se dismute ensuite et à l'équilibre on a formé quasi uniquement de l'acide hypobromeux suivant les stoechiométries [II] et [III]. Remarquons également que l'oxydation des ions céreux est quasi totale.

Technique expérimentale

Le réacteur, contenant environ 100 ml de solution, est thermostatisé et pourvu d'une agitation magnétique. Une pompe péristaltique dérive une faible fraction de son volume vers la cuvette d'un spectrophotomètre également thermostatisée. On mesure ainsi en continu l'absorbance de la solution à 320 nm, maximum du spectre des ions cériques en milieu sulfurique. Dans la zone de concentrations utilisée on n'observe qu'une très faible influence de l'acide sulfurique sur la courbe d'étalonnage. Cette courbe doit être déterminée point par point car la loi de Beer–Lambert n'est pas vérifiée pour des concentrations en ions cériques supérieures à 2×10^{-4} ion g/l. Pour quelques expériences faites avec une concentration initiale en bromure élevée, le calcul de la concentration en ions cériques tient compte d'une petite correction sur l'absorption à 320 nm due à la formation transitoire de brome. On peut alors déterminer les concentrations en cérique et en brome au cours d'une même expérience en mesurant l'absorbance de la solution à 320 et 395 nm.

La concentration en ions bromures est mesurée par une électrode spécifique Orion. L'électrode de référence au calomel est reliée à la solution par un pont au sulfate de potassium, les ions chlorures pouvant influencer la vitesse de la réaction. On a vérifié que dans nos conditions expérimentales cette électrode est très sélective et a un temps de réponse suffisamment court (quelques secondes).

Les courbes d'étalonnages sont semblables à celles obtenues par Koros et Burger (15). La limite de sensibilité

Can. J. Chem. Downloaded from www.nrcresearchpress.com by 210.87.254.6 on 09/05/12
For personal use only.

de l'électrode est de 10^{-6} ion g/l. Nous pensons cependant que, dans nos milieux réactionnels, son potentiel reste au moins qualitativement relié à la concentration en ions bromures au delà de cette limite. Nous nous sommes assurés que la présence de l'électrode n'a aucune influence sur la vitesse de formation des ions cériques.

Les réactifs utilisés sont des produits commerciaux 'pour analyse'. La seule impureté pouvant avoir une influence sur la vitesse de la réaction est le bromure présent en traces dans le bromate de potassium. Il est possible qu'il soit à l'origine de l'irréproductibilité de la période d'induction observée par Kasperek et Bruice (6). Lors de nos expériences nous avons toujours ajusté la concentration initiale en ions bromures. La composition de la solution stock de bromate est connue par simple pesée. La solution de sulfate céreux est standardisée par une méthode en retour à l'aide d'EDTA.

Toutes les expériences ont été faites en solution normale en acide sulfurique et à 22 °C. On a fait varier systématiquement les concentrations initiales en ions bromures (de 10^{-6} à 10^{-3} ion g/l) et céreux (de 10^{-4} à 2×10^{-3} ion g/l) en présence d'un excès de bromate de potassium (de 10^{-2} à 10^{-1} ion g/l).

Au cours d'une expérience les concentrations macroscopiques qui ne sont pas mesurées directement peuvent être calculées. $[Ce^{3+}]$ est donné par une équation de bilan: $[Ce^{3+}] = [Ce^{3+}]_0 - [Ce^{4+}]$ l'indice '$_0$' indiquant la valeur initiale. Le bromate étant en large excès par rapport aux autres réactifs on admet

$$[BrO_3^-] = [BrO_3^-]_0$$

[HOBr] et $[Br_2]$ sont calculés en admettant que l'équilibre [I] n'est pas perturbé et en utilisant l'équation de bilan:

$$2[HOBr] + 5[Br_2] = 3[[Br^-]_0 - [Br^-]] + \tfrac{1}{2}[Ce^{4+}]$$

On obtient

$$[HOBr] = \frac{3[[Br^-]_0 - [Br^-]] + \frac{1}{2}[Ce^{4+}]}{2 + 5[Br^-][H^+]/K[I]}$$

Nous avons vu que pour des expériences faites avec une concentration initiale en bromure élevée on peut également suivre $[Br_2]$ par spectrophotométrie.

Des tests préliminaires ont montré que les résultats sont indépendants de la vitesse d'agitation dans le réacteur et du débit dérivé vers le spectrophotomètre à condition que ces paramètres soient suffisamment grands. Nous avons vérifié également que dans nos conditions il n'y a pas d'effet photochimique ni d'influence de l'oxygène dissous.

Résultats expérimentaux

La fig. 1 reproduit un exemple caractéristique d'évolution des concentrations en fonction du temps. On y distingue trois périodes de la réaction.

1. Période d'induction

On produit très peu ou pas du tout d'ions cériques. La vitesse de disparition du bromure est quasi identique à celle que l'on obtient avec

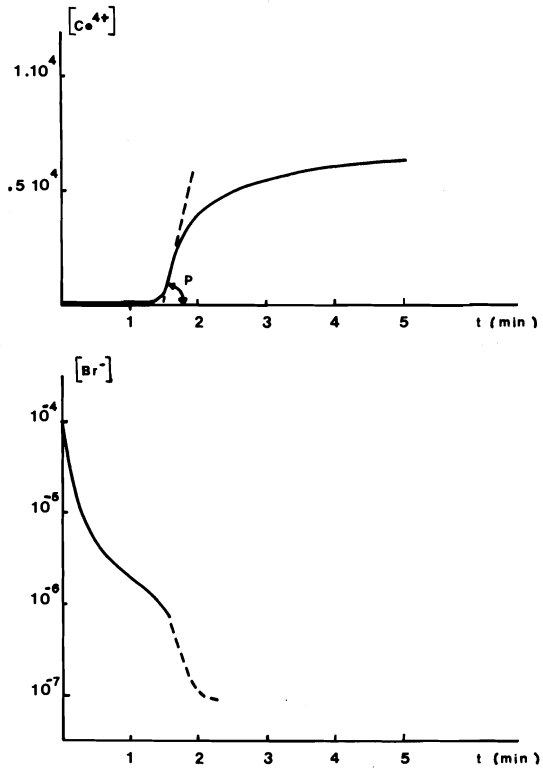

FIG. 1. Exemple d'évolution des concentrations en fonction du temps. $[BrO_3^-]_0 = 5 \times 10^{-2}$; $[Br^-]_0 = 10^{-4}$; $[Ce^{3+}]_0 = 1.68 \times 10^{-4}$.

les mêmes concentrations en bromate et bromure mais en l'absence d'ions céreux.

La durée de cette période augmente légèrement avec la concentration initiale en bromure (fig. 2*a*), varie très rapidement avec la concentration en bromate (fig. 2*b*) mais ne dépend quasi pas de la concentration en ions céreux. Pour confirmer ce dernier point nous avons fait les expériences suivantes.

On ajoute d'abord le bromure au bromate, ce qui marque le temps zéro, et ensuite le sulfate céreux après un temps variable. Si ce temps est inférieur à la période d'induction obtenue par addition du sulfate céreux au temps zéro, cette période ne change pas, si par contre on a dépassé cette période le démarrage de la réaction est immédiat.

La concentration en ions bromures atteinte à la fin de la période d'induction est de l'ordre de 10^{-6} ion g/l. Elle augmente avec la concentration initiale en bromate et en bromure mais ne semble pas dépendre de la concentration en

Can. J. Chem. Downloaded from www.nrcresearchpress.com by 210.87.254.6 on 09/05/12
For personal use only.

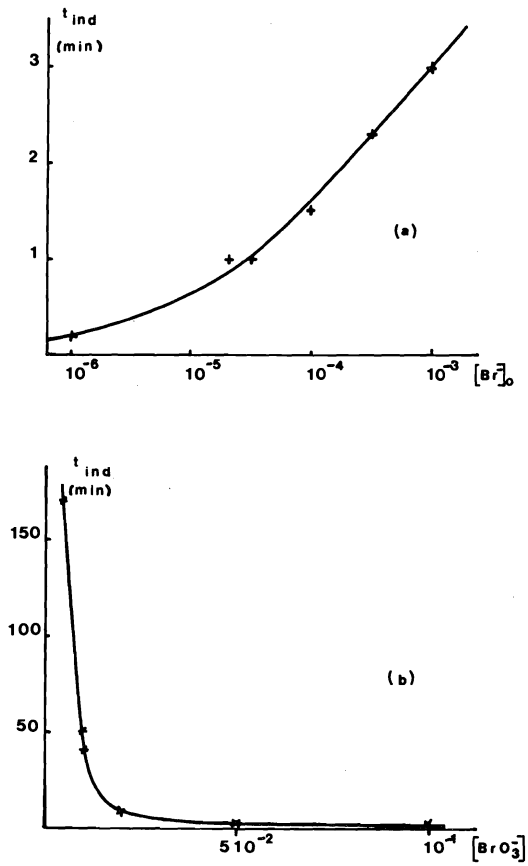

FIG. 2. Effet des concentrations initiales sur la durée de la période d'induction. (*a*) $[BrO_3^-]_0 = 5 \times 10^{-2}$; $[Ce^{3+}]_0 = 1.68 \times 10^{-4}$. (*b*) $[Br^-]_0 = 10^{-4}$; $[Ce^{3+}]_0 = 1.68 \times 10^{-4}$.

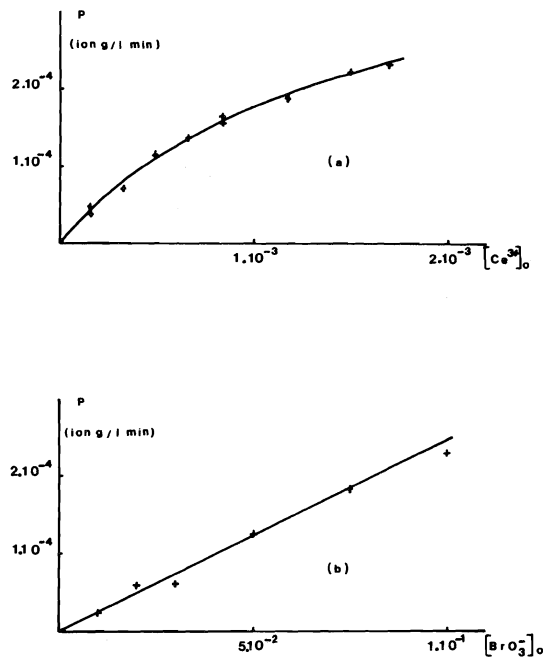

FIG. 3. Effet des concentrations initiales sur la vitesse maximum (*p*) de production des ions cériques. (*a*) $[BrO_3^-]_0 = 10^{-2}$; $[Br^-]_0 = 10^{-5}$. (*b*) $[Br^-]_0 = 10^{-4}$; $[Ce^{3+}]_0 = 1.68 \times 10^{-4}$.

sulfate céreux. Ces conclusions ne sont que qualitatives car on est à la limite de sensibilité de l'électrode indicatrice.

2. Période de réaction 'rapide'

Après la période d'induction la concentration en ions bromures diminue rapidement et cesse d'être mesurable. Simultanément on a une production rapide d'ions cériques. La pente *p* de la courbe de production en son point d'inflexion (fig. 1) dépend de façon complexe des différentes concentrations et il n'a pas été possible d'exprimer cette dépendance sous forme d'une loi empirique.

L'ordre par rapport à la concentration en ions céreux est en général compris entre 0 et 1. Il tend vers zéro lorsque la concentration en ions céreux augmente (fig. 3*a*) et est d'autant plus grand que la concentration initiale en bromure est grande.

L'ordre par rapport à la concentration en bromate est voisin de 1 (fig. 3*b*).

Le bromure ayant été quasi totalement oxydé au cours de la période d'induction l'influence de sa concentration initiale sur la vitesse de production des ions cériques traduit celle des concentrations en brome et en acide hypobromeux au moment de la réaction. Lorsque l'on augmente la concentration initiale en bromure, on augmente sa concentration pendant la période de réaction rapide, on allonge cette période et on diminue légèrement la pente *p*. La frontière avec la période suivante devient de moins en moins marquée et correspond à une concentration en ions cériques de plus en plus grande.

3. Période de réaction 'lente'

Après la période de réaction rapide et alors que l'on est encore loin de l'équilibre on observe un très net ralentissement de la production d'ions cériques qui ne peut être expliqué par la diminution de la concentration des ions

Can. J. Chem. Downloaded from www.nrcresearchpress.com by 210.87.254.6 on 09/05/12
For personal use only.

céreux. Alors qu'au début de la période de réaction rapide l'allure de la réaction était autocatalytique, elle est maintenant auto-inhibée. Par exemple dans les conditions de la fig. 1, 25% des ions céreux sont oxydés après 2 min mais il faut plusieurs heures pour approcher de l'équilibre thermodynamique. Il n'existe pas de frontière bien définie entre les périodes de réaction rapide et de réaction lente. La distinction que nous introduisons ici se justifie par une modification évidente des caractéristiques cinétiques du système avec le passage progressif de l'une à l'autre.

Le pourcentage d'ions céreux oxydés au moment du ralentissement augmente si l'on diminue la concentration initiale en sulfate céreux ou si l'on augmente les concentrations initiales en bromate et en bromure. Les résultats quantitatifs se rapportant à cette période de la réaction seront donnés lors de l'étude du modèle cinétique.

Pour terminer soulignons une observation qualitative remarquable: si au cours de la période de réaction lente on rajoute du bromure à la solution on observe, après une période d'induction, une nouvelle accélération temporaire de la production d'ions cériques.

Modèle cinétique

Le modèle proposé par Noyes et coll. (10) permet de rendre compte de certains faits expérimentaux mais ne peut cependant être adopté pour les raisons suivantes.

L'ordre 2 par rapport au bromate a été observé par Thompson en présence d'un excès d'ions céreux. En présence d'un excès de bromate, ce qui est le cas pour la réaction oscillante, nous avons trouvé un ordre 1.

Le modèle peut expliquer l'action inhibitrice des ions bromures pendant la période d'induction, ceux-ci empêchant l'acide bromeux de s'accumuler dans le système à cause de la réaction $HBrO_2 + Br^- + H^+ \rightarrow 2HOBr$. Cependant il ne rend pas compte des effets observés de la concentration initiale en bromure sur le déroulement ultérieur de la réaction. En particulier il n'explique pas que l'addition de bromure pendant la période de réaction lente provoque une nouvelle accélération de la réaction.

Le pas [3′] de leur modèle étant identique à la somme des pas [−1′] et [−2′] on a: $k_1'k_2'k_3' = k_{-1}'k_{-2}'k_{-3}'$. A partir de cette égalité on montre que le modèle ne permet pas de justifier l'effet inhibiteur des ions cériques.

En conséquence nous avons recherché un nouveau modèle cinétique.

Pendant la période d'induction le bromate oxyde le bromure en brome et en acide hypobromeux. D'autre part on sait que les réactions halogénates–halogénures font intervenir des complexes du type X_2O_2 de structure non précisée et probablement hydratés (16, 17). Nous écrivons donc le mécanisme de la réaction bromate–bromure sous la forme

[1] $$BrO_3^- + Br^- + 2H^+ \rightleftharpoons Br_2O_2 + H_2O$$

[2] $$Br_2O_2 + H_2O \rightleftharpoons HBrO_2 + HOBr$$

[3] $$HBrO_2 + Br^- + H^+ \rightarrow 2HOBr$$

[4] $$HOBr + Br^- + H^+ \rightleftharpoons Br_2 + H_2O$$

Pour condenser nous ne faisons pas apparaître explicitement les équilibres acide–base mais les incluons dans l'écriture des étapes élémentaires. Même en tenant compte de cette restriction le pas [3] n'est pas une étape élémentaire. Cela n'a cependant aucune incidence sur la suite du raisonnement car nous admettons que, dans nos conditions, ce pas est irréversible. Cette hypothèse est justifiée par la très petite valeur de la vitesse de retour calculée en utilisant la constante cinétique $k_{-3} = 0.42$ l/mol h déterminée par Betts et MacKenzie (18).

A ce schéma nous ajoutons l'oxydation des ions céreux par le radical $BrO_2^{\cdot}$

[5] $$HBrO_2 + Br_2O_2 \rightleftharpoons 2BrO_2^{\cdot} + Br^- + H^+$$

[6] $$BrO_2^{\cdot} + Ce^{3+} + H^+ \rightleftharpoons HBrO_2 + Ce^{4+}$$

Le pas [5] est analogue à celui qui a été admis dans le mécanisme de formation du bioxyde de chlore (19). Le pas [6] se retrouve dans le modèle de Noyes et coll. Dans le milieu considéré le cérium est complexé par les ions sulfates. Cela n'influence cependant pas la forme des équations cinétiques, d'ou la simplification d'écriture adoptée. L'oxydation du bromure par le Ce(IV) formé ne doit pas être considérée, sa vitesse étant, dans nos conditions expérimentales tout à fait négligeable (20).

1. Equations générales

En exprimant que $HBrO_2$, Br_2O_2, et $BrO_2^{\cdot}$ sont des labiles on obtient les trois stoechiométries considérées précédemment, la stoechio-

métrie [I] s'identifiant au pas [4]. Désignons par r_i la vitesse globale vers la droite du pas d'indice i, par a la vitesse de consommation du bromate suivant la stoechiométrie [II] et par b cette vitesse suivant [III]. La quasi-stationnarité des labiles donne

$$r_1 = a + b$$

$$r_2 = a - b$$
$$r_3 = a + b$$
$$r_5 = 2b$$
$$r_6 = 4b$$

Il vient, en incluant la concentration en H^+ dans les constantes cinétiques et en posant $X = b/(a + b)$

$$k_2[Br^-]\frac{k_1[BrO_3^-] - k_3[HBrO_2]}{k_{-1}} - k_{-2}[HBrO_2][HOBr] = (1 - 2X)k_3[Br^-][HBrO_2]$$

$$k_5[HBrO_2]\frac{k_1[BrO_3^-] - k_3[HBrO_2]}{k_{-1}} - k_{-5}[BrO_2^\cdot]^2 = 2Xk_3[HBrO_2]$$

$$k_6[BrO_2^\cdot][Ce^{3+}] - k_{-6}[HBrO_2][Ce^{4+}] = 4Xk_3[Br^-][HBrO_2]$$

d'ou l'on déduit

$$[HBrO_2] = \frac{k_1k_2}{k_{-1}}\frac{[BrO_3^-][Br^-]}{k_3\left(1 - 2X + \frac{k_2}{k_{-1}}\right)[Br^-] + k_{-2}[HOBr]} = \frac{\frac{k_1k_5}{k_{-1}k_3}[BrO_3^-] - 2X}{\frac{k_{-5}}{k_3}\left[\frac{k_{-6}[Ce^{4+}] + 4Xk_3[Br^-]}{k_6[Ce^{3+}]}\right]^2 + \frac{k_5}{k_{-1}}}$$

On obtient ainsi une équation reliant X aux concentrations des constituants non labiles du système. Cette équation est trop lourde pour qu'il soit utile de l'expliciter par rapport à X et nous n'envisagerons que ses dégénérescences. Elle permet cependant de voir dans le cas général que *X est une fonction décroissante de $[Br^-]$*. Si $[Br^-]$ est très grand $X \ll 1$, c'est à dire $b \ll a$, et l'on a quasi uniquement la réaction bromate–bromure. C'est la période d'induction. Ensuite $[Br^-]$ diminuant X augmente et la vitesse d'oxydation du Ce[III] ne deviendra mesurable que lorsque la concentration en bromure sera devenue suffisamment petite.

2. Période d'induction

Le résultat obtenu ci-dessus à partir des équations générales peut être exprimé de façon plus intuitive: on a quasi uniquement la réaction bromate–bromure aussi longtemps que la concentration en bromure est suffisamment grande pour que le pas [3] maintienne $[HBrO_2]$ et $[BrO_2^\cdot]$ petits. L'étape [2] est alors déterminante tandis que l'étape [1] est pratiquement à l'équilibre (16). En introduisant dans les équations générales

$$b \ll a; \quad k_2 \ll k_{-1}; \quad k_{-2}[HOBr] \ll k_3[Br^-]$$

on obtient l'équation cinétique classique de cette réaction la concentration $[H^+]$ étant inclue dans les constantes cinétiques.

$$a = \frac{k_1k_2}{k_{-1}}[BrO_3^-][Br^-]$$

Conformément aux résultats expérimentaux la concentration initiale en sulfate céreux n'a pas d'influence sur la cinétique pendant cette période.

Tant que la réaction produit quasi uniquement du brome on a

$$d[Br^-]/dt = -5a$$

et le bromate étant quasi constant, car en large excès, on doit obtenir une droite en portant log $[Br^-]$ en fonction du temps. On constate que l'on s'écarte rapidement de cette droite alors que l'on est encore très loin de l'équilibre du système bromate–bromure–brome. Cet écart est du à l'hydrolyse du brome. Si l'on produit de l'acide hypobromeux la relation ci-dessus devient

$$\frac{d[Br^-]}{dt} = -5a + \frac{d[HOBr]}{dt}$$

La loi linéaire cesse d'être suivie dès que $[HOBr]$ cesse d'être négligeable devant $[Br^-]$ et l'écart peut être très important alors même que l'on a $[Br_2] \gg [HOBr]$. En effet on a égale-

Can. J. Chem. Downloaded from www.nrcresearchpress.com by 210.87.254.6 on 09/05/12
For personal use only.

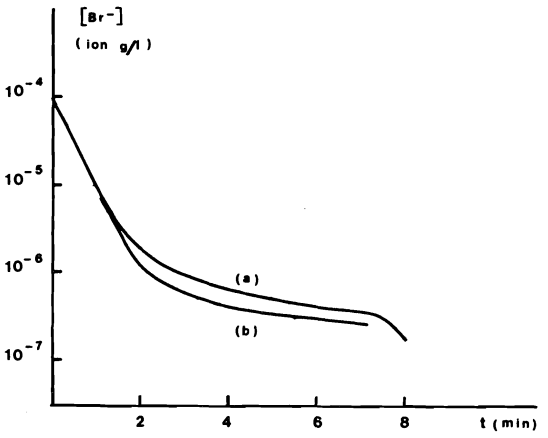

FIG. 4. Evolution de la concentration en ions bromures au cours de la période d'induction: $[BrO_3^-]_0 = 2 \times 10^{-2}$; $[Br^-]_0 = 10^{-4}$; $[Ce^{3+}]_0 = 1.68 \times 10^{-4}$; (*a*) courbe expérimentale; (*b*) courbe calculée.

ment $[Br_2] \gg [Br^-]$ et un petit déplacement de l'équilibre d'hydrolyse du brome correspond à une variation relativement importante de la concentration du bromure. Pendant cette période la relation de bilan donnant [HOBr] se réduit à

$$[HOBr] = \frac{3K[I]}{5[H^+]}\left[\frac{[Br^-]_0}{[Br^-]} - 1\right]$$

et l'on peut intégrer la loi cinétique qui devient

$$\ln \frac{[Br^-]_0}{[Br^-]} + \frac{3K[I][Br^-]_0}{10[H^+]}\left[\frac{1}{[Br^-]^2} - \frac{1}{[Br^-]_0^2}\right] = 5\frac{k_1k_2}{k_{-1}}[BrO_3^-]_0 t$$

La fig. 4 donne un exemple de comparaison de nos résultats avec cette loi. La deuxième ionisation de l'acide sulfurique pouvant être négligée on a $[H^+] = 0.5$ mol/l. La partie linéaire de la courbe expérimentale permet de calculer le coefficient de t

$$\frac{k_1k_2}{k_{-1}}[BrO_3^-]_0 = 0.5$$

Pour la loi cinétique sous la forme classique

$$a = k[BrO_3^-][Br^-][H^+]^2$$

Cette valeur donne $k = 100$ en parfait accord avec les résultats de Bray et Liebhafsky (21) pour une force ionique de 0.5.

Comme nous mesurons des concentrations, pour calculer le premier membre de loi intégrée il faut tenir compte des coefficients d'activité. Ceux-ci sont malheureusement mal connus dans notre milieu fortement acide et nous avons adopté l'estimation de Noyes (8): 0.7 pour des ions monovalents. En prenant pour $K[I]$ la valeur donné par Liebhafsky (14) on obtient l'équation de la courbe calculée de la fig. 4:

$$-\ln 10^4[Br^-] + 7.1 \times 10^{-13}[[Br^-]^{-2} - 10^8] = 2.5t$$

La concordance avec la courbe expérimentale est tout à fait satisfaisante, l'écart observé résultant probablement de la non linéarité de la réponse de l'électrode indicatrice pour des concentrations en bromure de l'ordre de 10^{-6} ion g/l. Remarquons également que cet écart serait réduit si l'on adoptait une valeur plus faible pour les coefficients d'activité.

3. Transition

La diminution de la concentration $[Br^-]$ entraine l'augmentation de X. Lorsque l'on cesse d'avoir $X \ll 1$, $[HBrO_2]$ augmente de façon autocatalytique du fait des pas [5] et [6]. La vitesse d'oxydation des ions céreux est rapidement croissante. Comme simultanément $[Br_2O_2]$ diminue et [HOBr] augmente, le rapport

$$k_{-2}[HBrO_2][HOBr]/k_2[Br_2O_2]$$

devient de plus en plus grand et l'étape [2] cesse d'être quasi irréversible. La vitesse globale r_2 diminue, passe par zéro pour $X = 0.5$ ($a = b$) puis devient négative. *C'est cette inversion du sens de l'étape [2] qui est la clef du changement de stoechiométrie du système.*

Il est possible qu'à ce moment la vitesse de variation de $[HBrO_2]$ soit telle que l'on ne puisse plus utiliser l'approximation de la stationnarité. Cette remarque ne nuit cependant pas à la généralité du raisonnement car $[HBrO_2]$ atteint très rapidement la valeur quasi-stationnaire correspondant à la période suivante de la réaction. Les équations générales établies ci-dessus redeviennent alors valables.

On constate que pour obtenir $X = 0.5$ il faut non seulement que $[Br^-]$ soit petit mais également que [HOBr] soit suffisamment grand. Ceci explique l'existence d'une période d'induction quelle que soit la concentration initiale en bromure.

Can. J. Chem. Downloaded from www.nrcresearchpress.com by 210.87.254.6 on 09/05/12
For personal use only.

Can. J. Chem. Downloaded from www.nrcresearchpress.com by 210.87.254.6 on 09/05/12
For personal use only.

4. Période de réaction rapide

Suite à l'inversion du pas [2] on a $0.5 < X \leqslant 1$. La diminution de $[Br^-]$ continue provisoirement à entrainer l'augmentation de $[HBrO_2]$ et donc de la vitesse d'oxydation des ions céreux. Au moment ou cette vitesse est maximale (pente p sur la fig. 1) nous admettons que les conditions suivantes sont satisfaites.

L'inversion du pas [2] est totale:

$$k_{-2}[HBrO_2][HOBr] \gg k_2[Br_2O_2]$$

Les équations générales permettent alors de calculer X

$$X = \tfrac{1}{2} + \frac{k_{-2}[HOBr]}{2k_3[Br^-]}$$

La concentration en bromate est telle que

$$\frac{k_1k_5}{k_{-1}k_3}[BrO_3^-] \gg 2X$$

On peut voir que cette condition implique que le déroulement de la réaction ne perturbe pas l'équilibre de l'étape [5].

La quantité de Ce(IV) produite est suffisamment faible pour que l'on puisse négliger la réversibilité de l'étape [6]. Dans ces conditions on obtient

$$\frac{d[Ce^{4+}]}{dt} = \frac{2k_1k_5k_6^2[BrO_3^-][k_3[Br^-] + k_{-2}[HOBr]][Ce^{3+}]^2}{4k_{-1}k_{-5}[k_3[Br^-] + k_{-2}[HOBr]]^2 + k_3k_5k_6^2[Ce^{3+}]^2}$$

Cette vitesse dépend non seulement de concentrations mesurables ou calculables mais également de la concentration du bromure qui devient inférieure à la limite de sensibilité de l'électrode indicatrice. En outre, malgré les hypothèses simplificatrices adoptées, l'expression obtenue est trop complexe pour qu'une comparaison quantitative avec nos mesures soit possible. Montrons néanmoins qu'il y a un accord qualitatif parfait entre le modèle et l'expérience.

On obtient l'ordre 1 pour le bromate. L'ordre par rapport à $[Ce^{3+}]$ est compris entre 0 et 2 suivant l'importance relative des deux termes du dénominateur. Pour un taux de conversion donné, il diminue si l'on augmente la concentration initiale du sulfate céreux ou si l'on diminue celle du bromure et par conséquent la somme $k_3[Br^-] + k_{-2}[HOBr]$.

L'ordre zéro correspond à l'étape [1] déterminante, l'ordre deux à cette étape à l'équilibre. Lorsque les deux termes du dénominateur sont d'importance comparable on obtient un ordre voisin de 1 pour $[Ce^{3+}]$ et un effet très faible de la concentration initiale en bromure sur la vitesse de réaction.

Au cours de cette période $[Br^-]$ diminue et [HOBr] augmente. La somme $k_3[Br^-]$ et et $k_{-2}[HOBr]$ qui diminuait pour X voisin de 0.5 finit donc toujours par augmenter (X voisin de 1). Dans nos conditions expérimentales ce n'est cependant pas cette augmentation qui provoque la diminution de la vitesse de réaction (effet inhibiteur de HOBr) mais bien la réversibilité de l'étape [6] (effet inhibiteur de Ce^{4+}). Cet effet apparait lorsque l'on cesse d'avoir $k_{-6}[Ce^{4+}] \ll 4k_3[Br^-]$ et l'on comprend ainsi que le ralentissement de la réaction se produise pour une concentration en ions cériques d'autant plus grande que la concentration initiale en bromure était grande.

5. Période de réaction lente

La diminution très nette de la vitesse de réaction est due à l'apparition de la réversibilité de l'étape [6]. Après une période intermédiaire où les équations cinétiques sont trop complexes pour être confrontées avec l'expérience, $[Br^-]$ devient suffisamment petit et $[Ce^{4+}]$ suffisamment grand pour que l'on ait

$$k_{-6}[Ce^{4+}] \gg 4k_3X[Br^-]$$

A ce moment le pas [6] est pratiquement à l'équilibre. De plus $[Br^-]$ étant microscopique la stoechiométrie [II] est négligeable:

$$a \ll b \text{ ou } X = 1$$

On admet, comme précédemment, que le pas [5] est à l'équilibre

$$\frac{k_1k_5}{k_{-1}k_3}[BrO_3^-] \gg 2$$

Ayant $k_{-1} \gg k_2$ il peut exister, et nous allons voir qu'il existe effectivement, une période où

$$\frac{k_{-1}}{k_3}\frac{k_{-5}k_{-6}^2[Ce^{4+}]^2}{k_5k_6^2[Ce^{3+}]^2} \gg 1 \gg \frac{k_2}{k_3}\frac{k_{-5}k_{-6}^2[Ce^{4+}]^2}{k_5k_6^2[Ce^{3+}]^2}$$

On constate que ces hypothèses reviennent à admettre que lorsque la vitesse de réaction

Can. J. Chem. Downloaded from www.nrcresearchpress.com by 210.87.254.6 on 09/05/12
For personal use only.

TABLEAU 1. Invariance de k_v au cours de la période de réaction lente

t	$[Ce^{4+}]$ ($\times 10^4$)	$\frac{[Ce^{4+}]}{[Ce^{3+}]}$	$\frac{d[Ce^{4+}]}{dt}$ ($\times 10^4$)	k_v
A. $[BrO_3^-]_0 = 10^{-2}$; $[Br^-]_0 = 10^{-6}$; $[Ce^{3+}]_0 = 16.8 \times 10^{-4}$				
1.66	1.1	0.070	0.39	(17.7)
2.0	1.2	0.077	0.26	13.7
2.33	1.3	0.084	0.23	13.9
2.66	1.38	0.089	0.20	13.3
3.0	1.45	0.094	0.18	13.1
4.5	1.68	0.111	0.14	13.1
				k_v moyen 13.4
B. $[BrO_3^-]_0 = 10^{-2}$; $[Br^-]_0 = 10^{-6}$; $[Ce^{3+}]_0 = 1.7 \times 10^{-4}$				
2.0	0.20	0.133	0.085	(29.6)
3.0	0.21	0.141	0.034	12.9
4.0	0.23	0.156	0.034	15.4
8.0	0.28	0.197	0.024	15.9
15.0	0.35	0.259	0.015	15.8
				k_v moyen 15.0
C. $[BrO_3^-]_0 = 10^{-1}$; $[Br^-]_0 = 10^{-4}$; $[Ce^{3+}]_0 = 1.7 \times 10^{-4}$				
2.0	0.59	0.531	0.159	(17.5)
2.33	0.61	0.560	0.099	12.1
2.5	0.64	0.604	0.093	13.2
3.0	0.67	0.650	0.077	12.6
4.0	0.75	0.789	0.061	14.6
4.5	0.78	0.848	0.047	13.0
				k_v moyen 13.1

NOTE: Unités: mol/l et min.

diminue l'équilibre du pas [1], qui avait été perturbé pendant la période de réaction rapide, se rétablit tandis que le pas [−2] reste irréversible.

Sous ces conditions les équations générales deviennent[2]

$$\frac{d[Ce^{4+}]}{dt} = 4k_3\frac{k_1k_5k_6^2[Ce^{3+}]^2}{k_{-1}k_{-5}k_{-6}^2[Ce^{4+}]^2}[BrO_3^-][Br^-]$$

[2]On peut être surpris par les équations obtenues qui impliquent que l'étape [3] soit devenue déterminante. Cela se comprend plus intuitivement si l'on remarque que pendant cette période les hypothèses faites permettent d'écrire le mécanisme conduisant à la stoechiométrie [III] sous la forme:

$$[1]\quad BrO_3^- + Br^- + 2H^+ \overset{\text{(équilibre)}}{\rightleftharpoons} Br_2O_2 + H_2O$$

$$[5] + 2[6]\quad Br_2O_2 + 2Ce^{3+} + H^+ \overset{\text{(équilibre)}}{\rightleftharpoons} HBrO_2 + Br^- + 2Ce^{4+}$$

$$[3]\quad HBrO_2 + Br^- + H^+ \rightarrow 2HOBr$$

$$[-2]\quad HBrO_2 + HOBr \rightarrow Br_2O_2 + H_2O$$

et

$$k_{-2}[HOBr] = k_3[Br^-]$$

La relation de bilan donnant [HOBr] devient, en négligeant le premier terme du dénominateur,

$$[HOBr] = K[I]\frac{6[Br^-]_0 + [Ce^{4+}]}{10[H^+][Br^-]}$$

et l'on obtient finalement

$$\frac{d[Ce^{4+}]}{dt} = \frac{k_1k_5k_6^2}{k_{-1}k_{-5}k_{-6}^2}(1.6k_{-2}k_3K[I]/[H^+])^{1/2} \times [BrO_3^-]\frac{[Ce^{3+}]^2}{[Ce^{4+}]^2}(6[Br]_0 + [Ce^{4+}])^{1/2}$$

Cette équation est vérifiée par nos résultats expérimentaux, compte tenu d'une certaine imprécision sur les mesures de vitesses, celles-ci étant obtenues en traçant les tangentes aux courbes $[Ce^{4+}]$ en fonction du temps. Dans les

TABLEAU 2. Invariance de k_v pour différentes concentrations initiales

$[BrO_3^-]_0$	$[Br^-]_0$	$[Ce^{3+}]_0$ ($\times 10^4$)	$[Ce^{4+}]$ ($\times 10^4$)	$\frac{d[Ce^{4+}]}{dt}$ ($\times 10^4$)	k_v
10^{-2}	10^{-6}	0.84	0.084	0.037	12.0
10^{-2}	10^{-6}	1.7	Voir tableau 1		15.0
10^{-2}	10^{-6}	5.0	0.50	0.086	14.2
10^{-2}	10^{-6}	8.4	0.84	0.087	11.3
10^{-2}	10^{-6}	13.4	1.34	0.147	15.3
10^{-2}	10^{-6}	16.8	Voir tableau 1		13.4
10^{-1}	5×10^{-5}	1.7	0.65	0.75	15.0
10^{-1}	10^{-4}	1.7	Voir tableau 1		13.1
10^{-1}	3×10^{-4}	1.7	0.65	1.70	15.1
10^{-1}	5×10^{-4}	1.7	0.65	1.66	11.5
10^{-1}	10^{-3}	1.7	0.65	2.55	12.5

NOTE: Unités: mol/l et min.

tableaux 1 et 2 nous donnons quelques valeurs de

$$k_v = \frac{10^4}{[BrO_3^-]_0(6[Br^-]_0 + [Ce^{4+}])^{1/2}} \frac{[Ce^{4+}]^2}{[Ce^{3+}]^2} \frac{d[Ce^{4+}]}{dt}$$

pour des conditions initiales variables. Dans le tableau 1 on voit qu'après la période de réaction rapide k_v devient constant au cours du temps. Pour des temps supérieurs à ceux indiqués la variation relative de $[Ce^{4+}]$ devient trop faible et la vitesse de réaction n'est plus mesurable. Les valeurs du tableau 2 montrent que conformément au modèle k_v ne dépend pas des concentrations initiales même pour une variation de la concentration initiale en bromure d'un facteur 1000!

La vitesse augmentant avec $[Br^-]_0$ on interprète aisément la nouvelle accélération de la production d'ions cériques provoquée par une addition de bromure au cours de cette période.

6. *Comparaison avec les résultats d'autres auteurs*

Thompson (11) a étudié la réaction en présence d'un excès de Ce(III) par rapport au bromate et avec des concentrations initiales en Ce(III) beaucoup plus grandes que les nôtres. Dans ces conditions on peut admettre qu'après la période d'induction on a toujours

$$\frac{k_5}{k_{-1}} \gg \frac{k_{-5}}{k_3}\left[\frac{k_{-6}[Ce^{4+}] + 4Xk_3[Br^-]}{k_6[Ce^{3+}]}\right]^2$$

On constate que les concentrations $[Ce^{3+}]$ et $[Ce^{4+}]$ ainsi que les constantes cinétiques k_6 et k_{-6} disparaissent des équations générales. Ceci explique que Thompson ait obtenu des vitesses indépendantes de la concentration et de la nature de l'agent réducteur.

Les résultats présentés par Kasperek et Bruice (6) sont parfaitement en accord avec ce travail. Ils ont notamment observé l'effet inhibiteur d'une addition de Ce(IV). Ayant constaté qu'un barbotage d'oxygène, d'azote ou de dioxyde de carbone diminue la vitesse pendant la période de réaction lente, ils ont attribué un caractère hétérogène à cette réaction. Nous proposons plutôt l'explication suivante: $K[I]$ étant très petit la concentration en brome du système n'est pas négligeable. Le barbotage entrainant le brome déplace son équilibre d'hydrolyse et la relation de bilan utilisée au paragraphe 5 n'est plus valable. La concentration en bromure devient beaucoup plus petite ce qui explique la diminution de la vitesse de réaction.

Conclusion

Le mécanisme proposé permet de rendre compte de l'ensemble des faits expérimentaux relatifs à la réaction bromate–céreux. En présence d'un excès de bromate l'évolution du système réactionnel peut être décomposée en trois phases.

Can. J. Chem. Downloaded from www.nrcresearchpress.com by 210.87.254.6 on 09/05/12
For personal use only.

1. Lorsque la concentration en bromure est grande la réaction bromate–céreux est inhibée. La réaction principale est

$$BrO_3^- + 5Br^- + 6H^+ \rightarrow 3Br_2 + 3H_2O$$

couplée avec l'équilibre d'hydrolyse du brome. L'étape 2 du schéma est déterminante.

2. La concentration en bromure diminuant, BrO_2H augmente, le sens du pas [2] s'inverse et la réaction bromate–céreux prend une allure autocatalytique. La concentration en bromure devient microscopique et la réaction principale est alors

$$BrO_3^- + 5Ce^{3+} + 6H^+ \rightarrow \tfrac{1}{2}Br_2 + 5Ce^{4+} + 3H_2O$$

(toujours couplée avec l'équilibre d'hydrolyse). Les étapes [−2] et [6] sont irréversibles. L'équilibre de l'étape [1] est perturbé ou non suivant la concentration en Ce(III).

3. Lorsque le rapport entre les concentrations en ions cériques et bromures devient suffisamment grand, la réversibilité du pas [6] apparait et la réaction devient auto-inhibée.

En complétant ce mécanisme avec les réactions des acides maloniques et bromaloniques il est possible d'expliquer les oscillations de la réaction de Belousov. Les travaux à ce sujet feront l'objet d'une publication ultérieure.

1. B. P. Belousov. Sborn Referat Radiats Meditsin zo 1958, Medzig, Moscow. 1959.
2. A. M. Zhabotinskii. Dokl. Akad. Nauk SSSR, **157**, 392 (1964).
3. A. M. Zhabotinskii. Biofizika, **9**, 306 (1964).
4. V. A. Vavilin et A. M. Zhabotinskii. Kinet. Katal. **10**, 83 (1969); **10**, 657 (1969).
5. H. Degn. Nature (London), **213**, 589 (1967).
6. G. J. Kasperek et T. C. Bruice. Inorg. Chem. **10**, 382 (1971).
7. R. M. Noyes, R. J. Field et E. Koros. J. Am. Chem. Soc. **94**, 1394 (1972).
8. R. J. Field, E. Koros et R. M. Noyes. J. Am. Chem. Soc. **94**, 8649 (1972).
9. R. J. Field et R. M. Noyes. J. Chem. Phys. **60**, 1877 (1974).
10. R. M. Noyes, R. J. Field et R. C. Thompson. J. Am. Chem. Soc. **93**, 7315 (1971).
11. R. C. Thompson. J. Am. Chem. Soc. **93**, 7315 (1971).
12. W. M. Latimer. Oxidation potentials. 2nd ed. Prentice Hall, New York. 1952.
13. H. Eigen et K. Kustin. J. Am. Chem. Soc. **84**, 1355 (1962).
14. H. A. Liebhafsky. J. Am. Chem. Soc. **56**, 1500 (1934).
15. E. Koros et M. Burger. Ion-selective electrodes. Symposium de Matrofûred, 1972. *Edité par* E. Pungor. Akademian Kiado, Budapest. 1973.
16. J. Sigalla. J. Chim. Phys. **55**, 758 (1958).
17. A. F. M. Barton et G. A. Wright. J. Chem. Soc. A, **4**, 1747 (1968).
18. R. H. Betts et A. N. MacKenzie. Can. J. Chem. **29**, 666 (1951).
19. H. Rooze. Thèse. Vrije Universiteit, Brussel. 1972.
20. E. L. King et M. L. Pandow. J. Am. Chem. Soc. **75**, 3063 (1953).
21. W. C. Bray et H. A. Liebhafsky. J. Am. Chem. Soc. **57**, 51 (1935).

Can. J. Chem. Downloaded from www.nrcresearchpress.com by 210.87.254.6 on 09/05/12
For personal use only.

Evidence for one-bond cleavage in the thermolysis of (−)-(*S*)-1-diphenylmethyl-2-(2-butyl)diazene and of 1-diphenylmethyl-2-phenyldiazene[1]

KARL R. KOPECKY, PETER M. POPE,[2] AND JUAN A. LOPEZ SASTRE

Department of Chemistry, University of Alberta, Edmonton, Alta., Canada T6G 2E1

Received February 5, 1976

KARL R. KOPECKY, PETER M. POPE, and JUAN A. LOPEZ SASTRE. Can. J. Chem. **54**, 2639 (1976).

Thermolysis of (−)-(*S*)-1-diphenylmethyl-2-(2-butyl)diazene (−)-(*S*)-**1** at 100 °C in benzene and in benzene containing 1 *M* butanethiol produces (−)-(*R*)-1,1-diphenyl-2-methylbutane (−)-(*R*)-**6** with 2 and 6% net inversion of configuration, respectively. These results indicate that the rate determining step is a one-bond cleavage to give diphenylmethyl and 2-butyldiazenyl radicals because a two-bond cleavage process cannot produce a coupling product with net inversion of configuration. The cage effect is at least 13% on thermolysis of (±)-**1** at 100 °C in benzene containing 1 *M* butanethiol. (−)-(*R*)-**6** is not thought to be formed by a displacement reaction of the diphenylmethyl radical on the (*S*)-2-butyldiazenyl radical. An estimate for the lifetime of the latter radical is $\sim 10^{-10}$ s or less. There is a small viscosity effect on the rate of thermolysis, *k*, of (±)-**1**. At 77.6 °C in cumene, octane, and hexadecane k = 4.48, 4.28, and 3.95 × 10^{-5} s^{-1}, respectively. At 77.6 °C in cumene $\Delta H^{\ddagger}$ = 30.5 ± 1.3 kcal/mol and $\Delta S^{\ddagger}$ = 8.1 ± 4.0 eu for thermolysis of (±)-**1**.

No emission or enhanced absorption due to the methine proton of the diphenylmethyl group of (±)-**1** was detected in the nmr spectrum of the thermolysis at 120 °C in hexadecane.

Enhanced absorption of the corresponding proton was observed in the nmr spectrum of thermolysis in hexadecane of 1-diphenylmethyl-2-phenyldiazene **7** at 180 °C which indicates one-bond cleavage occurs in this system. No evidence for the formation of crossed azo products was obtained when concentrated solutions of **7** and its tri-*p-tert*-butyl derivative were thermolized for one half-life (25 s) at 190 °C. This indicates that the phenyldiazenyl radical does not survive long enough to encounter a diphenylmethyl radical produced from another molecule of azo compound.

KARL R. KOPECKY, PETER M. POPE et JUAN A. LOPEZ SASTRE. Can. J. Chem. **54**, 2639 (1976).

La thermolyse du (−)-(*S*)-diphénylméthyl-1 (butyl-2)-2 diazène, le (−)-(*S*)-**1**, à 100 °C dans le benzène et dans une solution molaire de butanethiol dans le benzène donne le (−)-(*R*)-diphényl-1,1 méthyl-2 butane, le (−)-(*R*)-**6**, avec inversion de configuration nette de 2 et 6% respectivement. Ces résultats démontrent que l'étape limitante est une rupture d'une seule liaison donnant les radicaux diphénylméthyl et butyl-2 diazényle, parce qu'une rupture simultanée de deux liaisons ne peut donner de produit de couplage avec une inversion nette de configuration.

L'effet de cage est au moins 13% dans la thermolyse de (±)-**1** à 100 °C dans une solution molaire de butanethiol dans la benzène. On ne pense pas que le (−)-(*R*)-**6** est formé par une réaction de déplacement du radical diphénylméthyle sur le radical (*S*)-butyl-2 diazényle. Nous estimons que ce dernier a une durée de vie d'environ 10^{-10} s, ou moins. Il y a un léger effet de viscosité sur la vitesse de la thermolyse, *k*, du (±)-**1**. A 77.6 °C dans le cumène, l'octane et l'hexadécane k = 4.48, 4.28 et 3.95 × 10^{-5} s^{-1}, respectivement. A 77.6 °C dans le cumène $\Delta H^{\ddagger}$ = 30.5 ± 1.3 kcal mol^{-1} et $\Delta S^{\ddagger}$ = 8.1 ± 4 cal deg^{-1} mol^{-1} pour la thermolyse du (±)-**1**.

Aucune émission ni d'absorption renforcée due au proton méthinique du groupe diphénylméthyle du (±)-**1** n'est détectée dans le spectre rmn de la thermolyse à 120 °C dans le hexadécane.

L'absorption renforcée du proton correspondant est observée dans le spectre rmn de la thermolyse dans l'hexadécane du diphénylméthyl-1 phényl-2 diazène, **7**, à 180 °C ce qui indique qu'il y a rupture d'une seule liaison pour ce système. Aucune évidence de formation de produits azo croisés n'est obtenue lors de la thermolyse à 190 °C de solutions concentrées de **7** et de son dérivé tri-*p-tert*-butylé pour une periode égale à la durée de demi-vie (25 s). Ceci indique que le radical phényldiazényle ne survit pas assez longtemps pour rencontrer un radical diphénylméthyle résultant d'une autre molécule de composé azo.

---

[1]Presented in part at the 56th Canadian Chemical Conference of the Chemical Institute of Canada, Montreal, P.Q. June 1973. Abstract 209.

[2]Holder of a National Research Council of Canada Studentship, 1969–1971.

Can. J. Chem. Downloaded from www.nrcresearchpress.com by 210.87.254.6 on 09/05/12
For personal use only.

Can. J. Chem. Downloaded from www.nrcresearchpress.com by 210.87.254.6 on 09/05/12
For personal use only.

Introduction

The results of the earlier studies of the thermolysis of the optically active azoalkanes (−)-(*S*)-1-(1-phenylethyl)-2-benzyldiazene[3] (2) and (−)-(*R*)-1-(2-phenyl-2-butyl)-2-benzyldiazene (3) as well as of (−)-(*S*,*S*)-1,2-bis(1-phenylethyl)diazene (4) are consistent with the assumption that in these compounds both C—N bonds are breaking simultaneously in the rate determining steps, [1]. There has already been other evidence which is still accumulating, that

[1] $$R{-}N{=}N{-}R' \rightarrow R\cdot\ N_2\ R'\cdot$$

such a concerted cleavage occurs on thermolysis of a number of acyclic (5) and cyclic (refs. 6*a*–*d*; however, for a different interpretation of some of these reactions see refs. 6*e*–*g*) azoalkanes. In most of these systems R· and R′· are radicals of similar stability.

At the time we initiated studies in this area we began also to examine azoalkanes that might provide stereochemical evidence for one-bond cleavage (7) as indicated by racemization of optically active starting material, [2], in which R· is a much more stable radical than is R′·. However, the first two compounds investigated,

[2] $$(+)\text{-}R{-}N{=}N{-}R' \rightleftarrows R\cdot\ \cdot N{=}N{-}R' \rightleftarrows (-)\text{-}R{-}N{=}N{-}R'$$

(+)-(*S*)-1-(2-phenyl-2-butyl)-2-(2-propyl)diazene (8) and (−)-(*R*)-1-(2-phenyl-2-butyl)-2-(4-nitrophenyl)diazene,[4] were both recovered without loss of optical activity after having been heated for one half-life of decomposition.

In the meantime, stereochemical evidence for one-bond cleavage during thermolysis of optically active azo compounds has been obtained with several compounds (9). Other evidence for one-bond cleavage has been obtained from kinetic (10), pressure (11), and nmr (12) studies of, and the observation of isomerization (13) in, the thermolysis of azo compounds.

The present paper reports the results of a somewhat different stereochemical approach for the detection of one-bond cleavage: a study of the thermolysis of (−)-(*S*)-1-diphenylmethyl-2-(2-butyl)diazene (−)-(*S*)-**1**. One-bond cleavage of this compound would give a diphenylmethyl radical and the (*S*)-(2-butyl)diazenyl radical. If the latter radical had a significant lifetime it would undergo numerous rotations or perhaps even diffuse away to some extent from the initial solvent cage before losing nitrogen. This could result in a smaller amount of net retention in the cage coupling product than had been observed before (1–3) and in a smaller cage effect.

The observations made in this study prompted some experiments with 1-diphenylmethyl-2-phenyldiazene and its tri-*tert*-butyl derivative which are also reported here.

Results

Absolute Configurations of Starting Material and Product

Two routes were used to prepare (±)-**1** in quantity. Diphenylmethylhydrazine, readily prepared in 80% yield by treatment of diphenylmethyl chloride with excess hydrazine in dimethyl sulfoxide, was converted to the hydrazone with butanone. This was hydrogenated, using Adam's catalyst, to the hydrazine which was in turn oxidized by air to (±)-**1**. Alternatively, the disubstituted hydrazine could be prepared from the isomeric hydrazone (which was made by the treatment of diphenyldiazomethane with 2-butylmagnesium chloride) by reduction with sodium amalgam at 120 °C in ethylene glycol.

The preparations of (−)-(*S*)-**1** and the coupling product expected from its decomposition, both of known absolute configuration, are shown in Scheme 1. The rotations given are for optically pure materials. A convenient preparation of the azo compound with known absolute configuration was the conversion (14) of (+)-(*S*)-2-butylamine (+)-(*S*)-**2** (15) to (+)-(*S*)-*N*-2-butylsydnone (+)-(*S*)-**3** followed by hydrolysis (16) of the sydnone to (−)-(*S*)-2-butylhydrazine (−)-(*S*)-**4** and conversion of this hydrazine to (−)-(*S*)-**1** by successive treatment with benzophenone, sodium amalgam in hot ethylene glycol, and air. A sample of (+)-(*R*)-**1**, 91% optically pure, prepared by a completely independent route had $[\alpha]_D^{21}$ 2.1° (*c* 5.0) (see Experimental). Thus, no racemization occurred during the synthesis of (−)-(*S*)-**1**.

The absolute configuration of the product of coupling of the diphenylmethyl and 2-butyl radicals, 1,1-diphenyl-2-methylbutane **6**, was

[3]The nomenclature used in this paper is based on the proposals of Huang and Kosower (1).

[4]Unpublished studies by Dr. J. A. Barry.

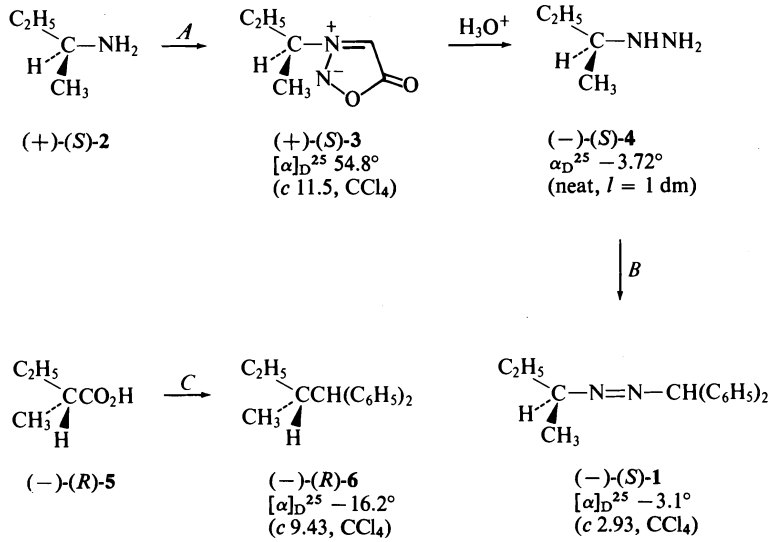

SCHEME 1. *Reagents*: *A*. (*i*) $ClCH_2CO_2C_2H_5$, (*ii*) HO^-, (*iii*) HNO_2, (*iv*) $(CH_3CO)_2O$. *B*. (*i*) $(C_6H_5)_2CO$, (*ii*) Na(Hg), $(HOCH_2)_2$, 120 °C, (*iii*) O_2. *C*. (*i*) $SOCl_2$, (*ii*) C_6H_5MgBr, (*iii*) NH_4^+, (*iv*) $Na/NH_3/C_2H_5OH$. Rotations given are for optically pure materials. Actually, (+)-(*S*)-**2** of 89% optical purity and (−)-(*R*)-**5** of 85% optical purity were used.

determined by the conversion (17) of (−)-(*R*)-2-methylbutanoic acid (−)-(*R*)-**5** (18) to (−)-(*R*)-1,1-diphenyl-2-methyl-1-butanol followed by reduction of the latter compound to (−)-(*R*)-**6** with sodium and alcohol in ammonia (19). The recent direct conversion of (+)-(*S*)-**5** to (+)-(*S*)-**2** (20) puts the relative configurations of (−)-(*R*)-**6** and (−)-(*S*)-**1** on a very firm footing.

Rate and Products of Thermolysis of 1

The rates of thermolysis, determined by monitoring the evaluation of gas, of (±)-**1** in several solvents are shown in Table 1. Less gas than expected was produced. Since some butenes and butane should have been formed (no search was made for these products) in thermolyses carried out in cumene, more than 1 mol of gas per mole of (±)-**1** should have been evolved. The reason for this discrepancy was not pursued. A 10-fold change in the initial concentration of (±)-**1** had no effect on the rate of thermolysis. Thus, little, if any, induced decomposition can be occurring.

There appears to be some effect of viscosity on the rate of thermolysis of (±)-**1** as the rate in hexadecane is ~8% smaller than that in octane. This is a smaller difference than that, 15%, observed for thermolysis of 1-(4-nitrophenyl)-2-triphenylmethyldiazene in the two solvents (10*a*).

The energy of activation for the thermolysis of (±)-**1**, 31.2 kcal/mol, is somewhat lower

TABLE 1. Rates[a] of thermolysis of (±)-**1**

Temperature (°C)	Solvent	Concentration (*M*)	$k_d \times 10^5$ (s^{-1})	Moles of gas[b]
97.3	Cumene	0.5	48.1 ±0.6[c]	0.92
97.3	Cumene	0.06	48.9 ±0.1[c]	0.97
77.6	Cumene	0.5	4.48±0.06[c]	0.92
77.6	Octane	0.5	4.28	
77.6	Hexadecane	0.5	3.95±0.05[c]	

[a]At 77.6 °C in cumene $\Delta H^{\ddagger}$ = 30.5 ± 1.3 kcal/mol, $\Delta S^{\ddagger}$ = 8.1 ± 4.0 eu. The uncertainties were calculated by assuming a 5% error in the rate constants.
[b]Moles of gas per mole of (±)-**1**.
[c]Average of two runs with average error.

Can. J. Chem. Downloaded from www.nrcresearchpress.com by 210.87.254.6 on 09/05/12
For personal use only.

TABLE 2. Thermolysis of 0.1 *M* (−)-(*S*)-**1**[a] in benzene at 100 °C

(−)-(*S*)-**1** (mg)	[C_4H_9SH] (*M*)	(−)-(*R*)-**6** (mg)	$[\alpha]_D^{25}$ (deg)	Net inversion (%)
700	—	92	−0.32	2
500	1	34	−0.90	6

[a]The (−)-(*S*)-**1** used was 89% optically pure.

than that, 34.9 kcal/mol, of 1-diphenylmethyl-2-phenyldiazene **7** (*5b*). The difference is in the direction expected if conjugation of the phenyl group with the azo linkage results in a stronger diphenylmethyl–N bond in **7** (*5b*, 21).

A detailed study of the products of thermolysis of (±)-**1** was not made. Attention was focused on the compounds containing the diphenylmethyl group, diphenylmethane, (±)-**6**, and tetraphenylethane. At 100 °C in benzene these were formed in a 15:56:29 molar ratio in 60% total yield together with a ~10% yield of several other products which were assumed to contain the diphenylmethyl fragment on the basis of their gc retention times. Only traces of the product of coupling of two 2-butyl radicals, 3,4-dimethylhexane, were detected. When 1 *M* butanethiol was present the known materials were formed in a 62.5:27.5:10 molar ratio in 46% total yield. About 0.25 mol of dibutyldisulfide per mole of (±)-**1** was formed as well as a ~20% yield of two products which were eluted from the gc column nearly together and had retention times slightly longer than that of (±)-**6**. Presumably both contain the diphenylmethyl group. Neither was characterized but one may be diphenylmethyl 1-butyl sulfide and the other may be the mixed azine of benzophenone and butanone. It has been noted in previous studies (1, 3, 22) that the thermolysis of diazenes in the presence of thiols produces appreciable amounts of azines.

The relative amount of diphenylmethane formed was greatly increased when butanethiol was present but a small amount, 5%, of tetraphenylethane was also still produced. This shows that the diphenylmethyl radicals which escape from the primary cage are not completely scavenged by 1 *M* butanethiol. This observation is consistent with the report that thiophenol catalyzes the hydrogen exchange of diphenylmethyl radicals with diphenylmethane (23). Since butanethiol scavenges completely free 1-phenylethyl (2) and 2-phenyl-2-butyl (3) radicals it must scavenge all the 2-butyl radicals which escape from the cage in the present system. Thus, the 13% of coupling product (±)-**6** which was formed in the presence of butanethiol must all have been formed in the primary solvent cage.

The yield of (±)-**6** is reduced by over 50% in the presence of butanethiol. This indicates that considerable coupling between diphenylmethyl and 2-butyl radicals occurs outside the primary solvent cage in the absence of butanethiol. However, little coupling between two 2-butyl radicals occurs as only traces of 3,4-dimethylhexane are formed. Thus, the steady state concentration of the diphenylmethyl radical must be considerably higher than that of the 2-butyl radical.

The observation of a significant cage effect makes it worthwhile to attempt to study the stereochemistry of the coupling reaction. The thermolysis of (−)-(*S*)-**1** at 100 °C in benzene and in benzene containing 1 *M* butanethiol produces (−)-(*R*)-**6** with 2 and 6% net inversion of configuration, respectively, Table 2.

CIDNP Studies

It will be shown below that the formation of (−)-(*R*)-**6** from (−)-(*S*)-**1** with net inversion of configuration is good evidence that (−)-(*S*)-**1** thermolizes by a one-bond cleavage process. In an unsuccessful attempt to obtain more evidence for one-bond cleavage the thermolysis of (+)-**1** was monitored by nmr spectroscopy at 120 °C in hexadecane solvent. Emission and enhanced absorption signals were seen in various regions of the spectrum, but the signal due to the methine proton of the diphenylmethyl group of (±)-**1** decreased monotonously in intensity during the decomposition.

The failure to observe the appropriate spin polarization effect may be due to the extremely short lifetime of the 2-butyldiazenyl radical (see

Can. J. Chem. Downloaded from www.nrcresearchpress.com by 210.87.254.6 on 09/05/12
For personal use only.

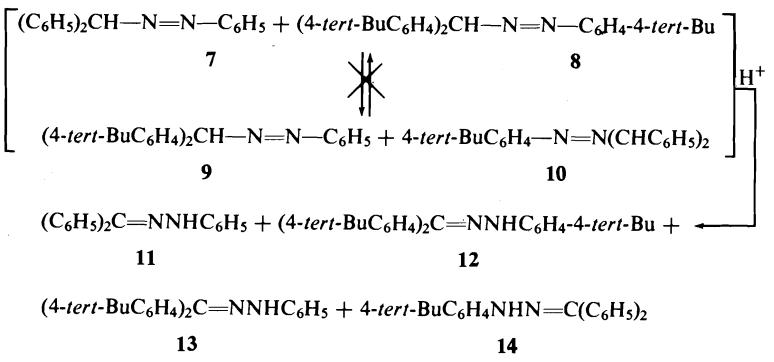

SCHEME 2

below). A diphenylmethyl azo compound which would decompose to give a more stable substituted diazenyl radical was then examined. Nuclear magnetic resonance spectroscopic evidence was obtained for one-bond cleavage in the thermolysis of **7** at 180 °C in hexadecane solvent. The signal due to the methine proton of **7** first increased somewhat and then decreased in intensity as the thermolysis of **7** progressed. In a typical run the relative areas of the signal were 1:2.5:1.3 in the first three sweeps taken at ~30 s intervals through this region of the spectrum shortly after the sample had been inserted into the probe.

Attempted Radical Exchange Reactions

The detection of the appropriate spin polarization during thermolysis of **7** is good evidence that the phenyldiazenyl radical lives long enough at this temperature to escape from the solvent cage. Unsuccessful attempts were made to obtain chemical evidence for one-bond cleavage in this molecule. These attempts involved heating mixtures of **7** and the corresponding tri-*tert*-butyl derivative 1-(4,4′-di-*tert*-butyldiphenylmethyl)-2-(4-*tert*-butylphenyl)diazene **8** to partial decomposition to try to produce some of the mixed azo compounds, 1-(4,4′-di-*tert*-butyldiphenylmethyl)-2-phenyldiazene **9** and 1-diphenylmethyl-2-(4-*tert*-butylphenyl)diazene **10**, Scheme 2. Thus, hexadecane solutions containing about 50% by volume of an equimolar mixture of **7** and **8**, preheated to 90 °C, were placed in a bath at 190 °C for 25 s and then quickly cooled. About 50% decomposition of the two azo compounds had occurred. The reaction mixture was then treated with *p*-toluenesulfonic acid to isomerize the azo compounds to the corresponding hydrazones which were then separated by column chromatography. The only hydrazones isolated were benzophenone phenylhydrazone **11**, 44%, and 4,4′-di-*tert*-butylbenzophenone 4-*tert*-butylphenylhydrazone **12**, 56%. Neither of the mixed hydrazones, 4,4′-di-*tert*-butylbenzophenone phenylhydrazone **13** or benzophenone 4-*tert*-butylphenylhydrazone **14**, was detected. Control experiments showed that the hydrazones could be separated by the methods used and that 1% of either of the mixed hydrazones **13** or **14** could have been detected in the reaction mixtures.

Discussion

Stereochemical Evidence for One-bond Cleavage

The formation of coupling product with net inversion of configuration in the thermolysis of (−)-(*S*)-**1** cannot be the result only of a process in which simultaneous cleavage of both C—N bonds to produce directly diphenylmethyl and 2-butyl radicals is followed by coupling of these radicals. Such a process must lead either to product with net retention of configuration or, in the limit where the effective rate of rotation of the 2-butyl radical with respect to the diphenylmethyl radical is very much greater than the rate of combination, to racemic product if any coupling takes place within the initial solvent cage. This is evident from [3] (2),

$$[3] \qquad \left(\frac{\text{retention}}{\text{inversion}}\right)_{\text{cage}} = 1 + k_t/k_r$$

where k_t represents the sum of the rate constants for combination, disproportionation, and diffusion of the two radicals and k_r is the rate

Can. J. Chem. Downloaded from www.nrcresearchpress.com by 210.87.254.6 on 09/05/12
For personal use only.

Can. J. Chem. Downloaded from www.nrcresearchpress.com by 210.87.254.6 on 09/05/12
For personal use only.

constant for rotation of the 2-butyl radical about an axis perpendicular to the line joining the radical centers of the caged pair.

The formation of coupling product with net inversion of configuration could be reconciled with a concerted two-bond cleavage process if some of the product were formed by a backside displacement of a diphenylmethyldiazenyl radical from (−)-(*S*)-**1** by a diphenylmethyl radical. However, it is unlikely that such an induced decomposition is taking place: there appears to be no precedent for it in alkyldiazene chemistry; a 10-fold change in concentration has no effect on the rate of thermolysis of (±)-**1** and relatively more inverted product is formed in the presence of butanethiol. While butanethiol does not scavenge all the diphenylmethyl radicals which escape from the initial solvent cage their steady state concentration must be decreased from what it is in the absence of butanethiol. This is indicated by the much smaller relative amount of tetraphenylethane formed when butanethiol is present. If a coupling product with inverted configuration were formed by induced decomposition of (−)-(*S*)-**1** relatively less, not more, of it should have been formed in the presence of butanethiol. Thus, (−)-(*R*)-**6** is formed in the initial solvent cage by a process which begins with one-bond cleavage of (−)-(*S*)-**1**.

Coupling product formed outside the initial solvent cage must be racemic, so that a greater proportion of product with inverted configuration should be produced in the presence of butanethiol than in benzene alone. This is observed and the stereochemical results indicate that about twice as much coupling product is formed outside the solvent cage as is formed in it, in reasonable agreement with the results of the product studies.

Cage Effect

On the other hand there is an appreciable cage effect in the thermolysis of **1**. In benzene at 100 °C it is at least 13% (the absolute yield of (±)-**6** formed in the presence of 1 *M* butanethiol) and could be as large as 24–28%. The latter values are obtained by noting that ~35–45% of the diphenylmethyl fragments are unaccounted for (this amount of (±)-**1** may be consumed in side reactions that do not give diphenylmethyl radicals) and by assuming that the same ratio of diphenylmethane/(±)-**6** is formed in the solvent cage as is formed in the unscavenged decomposition of (±)-**1**, namely, 0.27. Even the minimum value of 13% for the cage effect does not differ in any remarkable way from the values of the cage effect found in benzene with other azo compounds which are believed to decompose by a concerted cleavage of both C—N bonds: 22% (extrapolated to 100 °C from data obtained at lower temperatures) for 1,2-bis(2-phenyl-2-propyl)diazene (24), 28% (105 °C) for 1,2-bis(1-phenylethyl)diazene (4, 25), and 25–30% (110 °C) for 1-(1-phenylethyl)-2-benzyldiazene (2). The magnitude of the cage effect in the thermolysis of (±)-**1** suggests that either the diphenylmethyl–2-butyl radical pair is formed from the initial diphenylmethyl–2-butyldiazenyl radical pair with a rate that competes well with the rate of diffusion from the cage or that the coupling product is formed as readily from the initial radical pair by displacement of nitrogen as are caged products from azo compounds that cleave by a concerted two-bond mechanism. However, the displacement mechanism cannot contribute significantly to cage product formation because the displacement would presumably occur with inversion, and from thermolysis of (−)-(*S*)-**1** the cage product is formed with only a small amount of net inversion. Thus, the lifetime of the 2-butyldiazenyl radical must be equal to or less than the time of diffusion of the radical pair, about 10^{-10} s or less (26). This estimate of the lifetime of the 2-butyldiazenyl radical is consistent with the knowledge that decomposition of this radical must be very exothermic (6*g*) and with the estimate that the lifetime of the methyldiazenyl radical is $\sim 2 \times 10^{-10}$ s at 161 °C (7).

Mechanism of Formation of Cage Coupling Product

A likely mechanism for the formation of the cage coupling product is shown in Scheme 3. Diffusion and disproportionation processes are not indicated. *A* and *B* represent the initial arrangement and its rotational complement of the diphenylmethyl–2-butyldiazenyl radical pair. *C*, *D*, *E*, and *F*, which can interconvert most simply as indicated, represent extreme rotational arrangements of the diphenylmethyl–2-butyl radical pair. The nitrogen molecule is

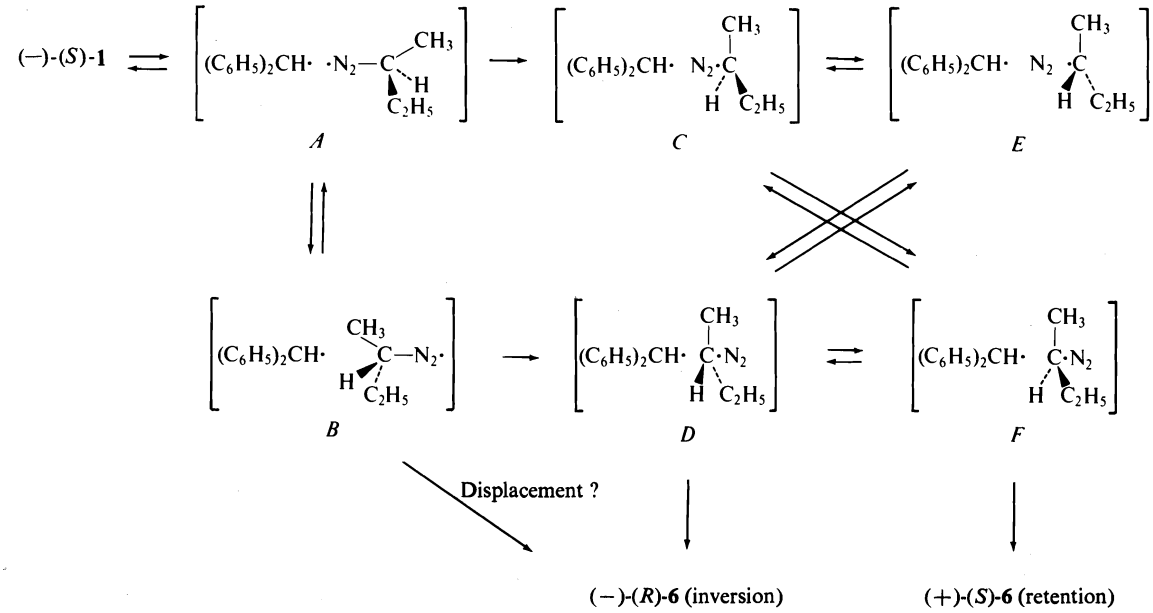

SCHEME 3. The 2-butyl radicals are assumed to be either planar as indicated or pyramidal and inverting rapidly.

effectively between the two radicals or not. Coupling product arising from the diphenylmethyl–2-butyl radical pairs which are formed initially with arrangement *C* (the arrangement that would have been formed had (−)-(*S*)-**1** undergone a concerted two-bond cleavage) would probably be formed with ~10–15% net retention of configuration by analogy with the previously studied systems (2–4). Coupling product arising from the radical pairs formed initially with arrangement *D* is likely to be formed with a larger amount of net inversion (with respect to (−)-(*S*)-**1**) than this, because *D*, in contrast to *C*, has no intervening nitrogen molecule. In *C*, this must move away before coupling can occur. Even if a considerably smaller number of the radical pairs were born initially in the effective arrangement *D* than in the effective arrangement *C* the overall result could still be the formation of coupling product with inversion of configuration. The rate of rotation of the 2-butyldiazenyl radical could thus be somewhat slower than the rate of its decomposition. In this way the formation of coupling product with some net inversion of configuration can be accounted for without requiring that inverted product be formed by a backside displacement of the nitrogen molecule in the radical pair *B*, although it is possible that some (−)-(*R*)-**6** may be formed in this way.

CIDNP Studies

Although stereochemical evidence for one-bond cleavage of (−)-(*S*)-**1** was obtained, attempts to obtain confirmatory evidence for this mode of decomposition by searching for the appropriate emission or enhanced absorption signals in the nmr spectra of hot solutions of (±)-**1** were unsuccessful. Perhaps the rapid decomposition of the 2-butyldiazenyl radical prevents any significant amount of spin polarization from occurring and also allows only a small fraction of the initial radicals to recombine. This would allow only a small effect of viscosity on the rate of decomposition of (±)-**1** as is observed.

The enhanced absorption of the methine proton of **7** observed in the nmr spectrum in hexadecane at 180 °C is good evidence that thermolysis of **7** occurs by way of one-bond cleavage. Equation 4 predicts that enhanced absorption

$$[4] \qquad \Gamma_{ne} = \underset{-+}{\mu\varepsilon}\Delta g \underset{+-}{a} = +$$

of the methine proton of **7** should be observed if cage recombination is occurring (27). The

Can. J. Chem. Downloaded from www.nrcresearchpress.com by 210.87.254.6 on 09/05/12
For personal use only.

Can. J. Chem. Downloaded from www.nrcresearchpress.com by 210.87.254.6 on 09/05/12
For personal use only.

relevant signs are placed below each symbol. Those for μ and ε are given (27), that for a is known (28), and that for Δg is assigned from the fact that the g value, <2.001, for the phenyldiazenyl radical (29) is much less than that for a carbon centered radical (12).

Thus, the phenyldiazenyl radical survives long enough to escape from the initial solvent cage at 180 °C as well as at ~40 °C (12). An attempt to determine whether it can survive long enough at 190 °C to combine with a radical from another molecule of azo compound did not yield positive results. No evidence for the formation of any **9** was detected on thermolysis for one half-life of a concentrated mixture of **7** and **8** at this temperature. The lack of success is not due to the more rapid decomposition of one of these azo compounds because the rate constants for thermolysis of 1,2-bis(2-phenyl-2-propyl)diazene and that of its 4,4′-di-*tert*-butyl derivative are indistinguishable (30). The free phenyldiazenyl radical either loses nitrogen or undergoes abstraction and addition reactions before it encounters a substituted diphenylmethyl radical from **8**. At 190 °C the latter reactions must be very rapid in the solution used.

Experimental

Melting points and boiling points are uncorrected. The former were taken on a Reichert Austria melting point apparatus. Infrared spectra were recorded on a Perkin Elmer 421 grating spectrophotometer. Nuclear magnetic resonance spectra were recorded on Varian analytical spectrometers, models A-60 and A-56/60, using tetramethylsilane as internal standard with ~10% solutions of substrate. No peak assignments are given as these are evident from either the positions, relative intensities, or multiplicities. Solution optical rotations were measured on a Perkin-Elmer 141 polarimeter and neat optical rotations were taken on a Rudolf polarimeter, model 80. Refractive indices were taken on a Bausch and Lomb Abbe-3L refractometer. Gas chromatography was carried out with an Aerograph 202 fractometer using a 6 ft × $\frac{1}{4}$ in. stainless steel column packed with 20% SF-96 on 60/80 Chromosorb P for preparative work and a 10 ft × $\frac{1}{4}$ in. stainless steel column packed with 4% SF-96 on 60/80 Chromosorb P for analytical work. Solvents were dried with magnesium sulfate except as indicated. Elemental analyses were carried out by Mrs. Darlene Mahlow and Mrs. Andrea Dunn.

Benzene, cumene, octane, and hexadecane were purified by shaking repeatedly with sulfuric acid, three times with saturated sodium bicarbonate, and three times with water. After drying, the solvents were distilled and the middle third was collected for use. Commercial 1-butanethiol was distilled through a 10 cm Vigreux column and the middle fraction was collected and stored in the dark.

Glassware with which azo compounds came into contact was cleaned with chromic acid, rinsed with distilled water, then immersed in concentrated ammonia for several hours and finally baked at 130 °C for 10 h.

Diphenylmethylhydrazine

A solution of 70 g (0.35 mol) freshly distilled diphenylmethyl chloride in 50 ml dimethyl sulfoxide was added dropwise over a 20 min period to a stirred mixture of 50 g (1.56 mol) anhydrous hydrazine and 30 g (0.4 mol) sodium bicarbonate in 150 ml dimethyl sulfoxide under a nitrogen atmosphere. The resulting mixture was heated to 50 °C for 2 h and then poured into 200 ml of ice water. This mixture was shaken with three 100 ml portions of methylene chloride. The combined extracts were washed with water, dried, and concentrated. The residual oil was distilled to give 55 g (80%) of an oil, bp 122–124 °C/0.2 torr, which crystallized to a white solid upon standing, mp 50–53 °C (lit. (31) mp 55–60 °C).

Butanone Diphenylmethylhydrazone

A mixture of 23 g (0.12 mol) of diphenylmethylhydrazine, 50 g (0.7 mol) of butanone, and 20 g of anhydrous magnesium sulfate was stirred under a nitrogen atmosphere at 50 °C for 2 h and then at 22 °C overnight. The resulting mixture was filtered and concentrated and the residue distilled to give 16.8 g (60%) of an oil, bp 133–134 °C/0.15 torr, which formed a white solid on standing; mp 33–35 °C; ir (CCl_4) 1610 cm^{-1}; nmr (CCl_4) τ 2.78 (m, 9.9H), 4.56 (s, 1.0H), 5.31 (br, 1.0H, N—H), 7.95 (q, J = 7 Hz, 1.9H), 8.47 (s, 3.0H), 9.06 (t, J = 7 Hz, 2.9H). *Anal.* calcd. for $C_{17}H_{20}N_2$: C 80.91, H 7.99, N 11.10; found: C 80.72, H 80.02, N 11.38.

(±)-Benzophenone 2-Butylhydrazone

Method A

A solution of crude diphenyldiazomethane (prepared from 39.7 g (0.2 mol) of benzophenone hydrazone and 44 g yellow mercuric oxide (32)) in 75 ml ether was added over a 30 min period to a Grignard reagent made from 30 g (0.33 mol) of 2-chlorobutane and 12 g (0.5 mol) of magnesium in 250 ml ether. The resulting red mixture was allowed to stand overnight after which the solution was colorless over a yellow precipitate. This mixture was hydrolyzed with ice and saturated ammonium chloride. The resulting ether layer was separated and the aqueous layer was extracted with ether. The combined ether fractions were dried over calcium chloride, concentrated, and the residual oil was distilled to give 36.4 g (72%) of a viscous yellow oil which darkened rapidly upon exposure to air; bp 86–89 °C/0.05 torr; n_D^{30} 1.5987; ir (neat) 1670 cm^{-1}; nmr (CCl_4) τ 2.75 (m, 10.5H), 5.05 (br, 1.0H, NH), 6.75 (m, 1.0H), 8.50 (m, 2.1H), 8.87 (d, J = 6.5Hz, 3.2H), 9.15 (t, J = 6.5 Hz, 3.0H). *Anal.* calcd. for $C_{17}H_{20}N_2$: C 80.91, H 7.99, N 11.10; found: C 80.94, H 8.12, N 10.46.

Method B

A solution of 6.0 g (0.033 mol) of benzophenone and 8.0 g (0.09 mol) of 2-butylhydrazine in 15 ml 1-butanol was heated under reflux for 24 h under nitrogen. The solution was then concentrated and the residue distilled to give 2.5 g (30%) of the hydrazone with an nmr spectrum identical to that of the product produced in method *A*.

Can. J. Chem. Downloaded from www.nrcresearchpress.com by 210.87.254.6 on 09/05/12
For personal use only.

(+)-(S)-2-Butylamine (+)-(S)-2

Resolution of 2-butylamine was achieved by modification of a reported procedure (33). A solution of 40% aqueous *d*-tartaric acid was stirred into a cooled solution of 48 g (±)-**2** in 25 ml water until the latter solution was neutral to litmus. Then an equal volume of additional *d*-tartaric acid solution was added. The resulting solution was concentrated to 265 g and then allowed to stand overnight at 10 °C. The crystals which formed were filtered, dried, and taken up in 1.2 g water per g of salt. This material was allowed to stand at ~23 °C for a day and at 10 °C for 3 days. The crystals which formed were recrystallized in the same way from 1 g water per g of salt to give 30 g of crystals.

A total of 1200 g salt from 40 batches was dissolved in a minimum amount of water. Excess sodium hydroxide was added to the resulting solution. A mixture of amine and water was distilled from the basified solution. Sodium hydroxide pellets were added to the distillate until no more water was extracted into the lower phase. The organic layer was heated under reflux over sodium hydroxide pellets for 1 h and then distilled. This operation was repeated on the distillate to give 220 g of product; n_D^{25} 1.3925; $[\alpha]_D^{25}$ + 7.21° (*l* 1 dm, neat) (lit. (34) n_D^{25} 1.3930, $[\alpha]_D^{25}$ + 8.1 (neat) for (+)-(*S*)-**2** with the highest reported rotation). Thus, our preparation of (+)-(*S*)-**2** is 89% optically pure.

(±)-2-Butylhydrazine (±)-4

Method A

A procedure (16) for hydrolysis of sydnones was adapted for the hydrolysis of *N*-(2-butyl)sydnone (±)-**3**. A mixture of 150 ml (1.8 mol) concentrated hydrochloric acid and 50 g (0.35 mol) (±)-**3** (14) was heated under reflux for 2.5 h at which time the evolution of gas, initially rapid, had ceased. The reaction mixture was cooled in an ice bath while 320 g of 25% aqueous sodium hydroxide (2.0 mol) were added. The resulting mixture was distilled until 150 ml distillate had been collected. Potassium hydroxide pellets were added to the distillate until the organic phase no longer decreased in volume. The organic phase was distilled to give 20.2 g (65%) of colorless oil; bp 102–105 °C/700 torr; n_D^{25} 1.4024; ir (neat) 3350 cm^{-1} (br); nmr (CCl_4) τ 6.47 (br, 3.1H), 7.46 (m, 0.95H), 8.30–9.30 (m, 8.0H). This material has been prepared previously and was characterized as the hydrochloride salt (35).

Method B

The procedure was adapted from the general method (36) for obtaining alkyl hydrazines. A mixture of 28 g (0.11 mol) of benzophenone 2-butylhydrazone, prepared according to method *A*, 60 ml absolute ethanol, and 40 ml (0.48 mol) of concentrated hydrochloric acid was allowed to stand at ~23 °C under nitrogen overnight. The resulting mixture was concentrated to remove ethanol and the residue was shaken with 2 × 50 ml ether. The aqueous layer was treated in an ice bath with 90 g (0.48 mol) of 25% aqueous sodium hydroxide. Further work-up as described in method *A* produced 6.4 g of (±)-**4** whose nmr spectrum was identical to that of (±)-**4** made by method *A*.

(−)-(S)-2-Butylhydrazine (−)-(S)-4

This material was prepared by hydrolysis as described above for (±)-**3** of (+)-(*S*)-*N*-(2-butyl)sydnone (+)-(*S*)-**3**, $[\alpha]_D^{25}$ 48.8° (*c* 11.5, CCl_4) which had been prepared (16) from (+)-(*S*)-**2** of $[\alpha]_D^{25}$ 7.21 (*l* 1 dm, neat). This sample of (−)-(*S*)-**4** had α_D^{25} −3.35° (*l* 1 dm, neat) and an nmr spectrum identical to that of (±)-**4**.

(±)-1-Diphenylmethyl-2-(2-butyl)diazene (±)-1

Method A

A mixture of 1.5 g butanone diphenylmethylhydrazone and 200 mg of platinum oxide in 20 ml methanol was stirred under 1 atm of hydrogen. After 1 h 1 equiv. of hydrogen had been taken up and the catalyst and solvent were removed. The residue was taken up in 100 ml ether and the resulting solution was stirred in an unstoppered flask for 6 h. The solution was dried over sodium sulfate, concentrated, and the residual oil was adsorbed on a 1.5 cm diameter column of 5 g Florisil, 100–200 mesh. The azo compound was eluted with 50 ml pentane. Removal of the pentane left 0.38 g (25%) of a pale yellow oil; n_D^{25} 1.5454; ir (neat) 1603 cm^{-1}, nmr (CCl_4) τ 2.77 (m, 10.0H), 4.48 (s, 10H), 6.54 (m, 0.95H), 8.35 (m, 2.0H), 8.84 (d, J = 6.5 Hz, 3.1H), 9.26 (t, J = 7 Hz, 3.1H).

Method B

A solution of 2.5 g (0.01 mol) of benzophenone 2-butylhydrazone in 20 ml ether was added over a 1 h period to a slurry of 0.51 g lithium aluminum hydride in 100 ml ether. The resulting mixture was stirred and heated under reflux for 2 days and then hydrolyzed by adding successively 1 ml water, 6 ml 10% potassium hydroxide solution, and 1 ml water. The mixture was filtered and the filtrate stirred in air and worked up as described under method *A* to give 0.5 g (20%) of a pale yellow oil whose nmr spectrum was identical to that of (±)-**1** formed by method *A*.

Method C

A solution of 2.0 g (0.01 mol) of benzophenone 2-butylhydrazone in 150 ml ethylene glycol was stirred vigorously at 110 °C under nitrogen while 46 g (0.023 mol) of 4% sodium amalgam (37) was added portionwise over a 15 min period. After 30 min a second 46 g batch of amalgam was added in the same way. After another 30 min stirring the mixture was cooled and extracted with 3 × 100 ml ether. The combined ether extracts were dried and then stirred under air and worked up as described under method *A* to give 0.3 g (15%) of a pale yellow oil whose nmr spectrum was identical to that of (±)-**1** formed by method *A*.

(−)-(S)-1-Diphenylmethyl-2-(2-butyl)diazene (−)-(S)-1

(−)-(*S*)-**4**, α_D^{25} −3.35° (*l* 1 dm, neat), was converted to the benzophenone hydrazone which was in turn converted without isolation to the azo compound using the procedure of method *C* for the preparation of (±)-**1**. The product had $[\alpha]_D^{25}$ −2.8° (*c* 2.93, CCl_4) and an nmr spectrum identical to that of (±)-**1**.

(±)-1,1-Diphenyl-2-methyl-1-butanol

This material was prepared in 60% yield by the described procedure (17); bp 113–114 °C/0.3 torr (lit. (17) bp 126 °C/1.0 torr); n_D^{25} 1.5630; ir (neat) 3580 cm^{-1} (sharp); nmr (CCl_4) τ 2.72 (m, 9.8H), 7.60 (m, 1.0H) 8.07 (s, 1.05H), 8.4–9.3 (m, 7.8H).

(−)-(*R*)-*1,1-Diphenyl-2-methyl-1-butanol*

This material was prepared using the procedure (17)

Can. J. Chem. Downloaded from www.nrcresearchpress.com by 210.87.254.6 on 09/05/12
For personal use only.

for the preparation of the racemic compound from (−)-(*R*)-2-methylbutanoic acid (38) of $[\alpha]_D^{24}$ −16.4° (*l* 1 dm, neat), 85% optically pure (38). The product had mp 33–38 °C, $[\alpha]_D^{25}$ −20.2° (*c* 9.3, CCl_4) and an nmr spectrum identical (except for the position of the OH peak) to that of the racemic material.

*(±)-1,1-Diphenyl-2-methylbutane (±)-***6**

A stirred solution of 7.0 g (0.03 mol) of (±)-1,1-diphenyl-2-methyl-1-butanol and 3.0 g (0.05 mol) of ethanol in 150 ml liquid ammonia was treated with 1.5 g (0.07 mol) of small pieces of sodium. The ammonia was allowed to evaporate and water was added to the solid residue. The resulting mixture was shaken with 2 × 50 ml of ether. The combined ether extracts were shaken with 3 × 50 ml water, dried, and concentrated. The residue was distilled to give 5.8 g (88%) of colorless oil, bp 86–87 °C/0.15 torr; n_D^{25} 1.5501; nmr (CCl_4) τ 2.82 (m, 10.0H), 6.50 (d, J = 10.5 Hz, 1.0H), 7.80 (m, 1.0H), 8.5–9.3 (m, 8.0H). *Anal.* calcd. for $C_{17}H_{20}$: C 91.01, H 8.99; found: C 91.29, H 8.99.

*(−)-(R)-1,1-Diphenyl-2-methylbutane (−)-(R)-***6**

Reduction of (−)-(*R*)-1,1-diphenyl-2-methyl-1-butanol, $[\alpha]_D^{25}$ −20.2° (*c* 9.3, CCl_4), in the manner described for the preparation of (±)-**6** produced (−)-(*R*)-**6**, α_D^{25} −12.8° (neat, *l* = 1 dm), $[\alpha]_D^{25}$ −13.8° (*c* 9.43, carbon tetrachloride), whose nmr spectrum was identical to that of (±)-**6**.

1-Diphenylmethyl-2-phenyldiazene

A 20 g quantity of benzophenone phenylhydrazone was reduced as described (5*b*). All operations involving the hydrazine were carried out under nitrogen. The hydrazine was isolated from the hydrolyzed ether extract of the reaction mixture as the hydrochloride, mp 182–185 °C (lit. (5*b*) mp 178–180 °C), from which the hydrazine was recovered by treatment with 20% sodium hydroxide. The hydrazine was crystallized from ethanol to give 6.6 g (33%) of light yellow crystals; mp 84–85 °C (lit. (5*b*) mp 115 °C); nmr (CCl_4) τ 6.8 (br, 1.7H), 5.05 (s, 0.9H), and 3.67 (m, 15H). The melting point did not change on repeated recrystallization. The previous workers (5*b*) appear to have isolated a mixture of hydrazine and hydrazone.

A solution of the hydrazine in ether was stirred under oxygen overnight (39). A 60% yield of **7** was isolated; mp 74–75 °C (lit. (5*b*) mp 73–75 °C); nmr (CCl_4) τ 2.68 (m, 15H) and 4.12 (s, 1H).

4-tert-Butylaniline

A mixture of 90 g (0.46 mol) 4-*tert*-butylbenzoyl chloride (40) and 35.5 g (0.55 mol) sodium azide in 1 litre benzene was stirred under reflux for 96 h and then cooled. The mixture was filtered and 300 ml concentrated hydrochloric acid was added to the filtrate. The resulting mixture was heated under reflux for 3 h, cooled, and filtered. The precipitate was washed with dilute hydrochloric acid and with water and dried to give 76 g of the hydrogen chloride salt, mp 272–275 °C (lit. (41) mp 270–274 °C). Concentration of the aqueous layer of the filtrate yielded 4 g of product (total yield 95%). Treatment of the salt with 20% sodium hydroxide solution yielded the free amine; bp 114–115 °C/10 torr (lit. (40) bp 248–250 °C); nmr (CCl_4) τ 2.92 (m, 2H), 3.60 (m, 2H), 6.72 (s, 2.1H), and 8.77 (s, 8.5H). *Anal.* calcd. for $C_{10}H_{15}N$: C 80.46, H 9.38, N 10.16; found: C 80.32, H 9.56, N 9.86.

4-tert-Butylphenylhydrazine

A 45.5 g (0.3 mol) quantity of 4-*tert*-butylaniline was diazotized (42) and the resulting cold solution was poured slowly into a stirred solution of 24 g sodium carbonate, 100 g (0.79 mol) sodium sulfite, and 152 ml water which was kept at 0 °C. A red oil appeared which solidified to a yellow orange precipitate when half the diazotized solution had been added. After the addition was complete a solution of 20 g (0.19 mol) sodium bisulfite in 50 ml water was added to the well stirred suspension. The resulting mixture was heated with stirring on the steam bath. All the material had gone into solution at 70 °C. The solution was heated to 80 °C, 500 ml concentrated hydrochloric acid was added slowly, and stirring was continued for another hour. The mixture, containing a yellow-brown precipitate, was cooled slowly to 0 °C and filtered. The precipitate was washed with 5% hydrochloric acid, dried under vacuum, washed with ether, and dried again to 32 g of white crystals, mp 164–165 °C after recrystallization from methanol (lit. (42) mp 221–222 °C).

The precipitate was shaken with 150 ml 20% sodium hydroxide and the mixture was extracted with ether. The ether layer was washed with water, dried, and concentrated. The residual solid was recrystallized from petroleum ether to give 13 g (26%) of a white solid; mp 72–74 °C; nmr (CCl_4) τ 2.91 (m, 2H), 3.47 (m, 2H), 6.09 (s, 3.1H), and 8.74 (s, 9H). *Anal.* calcd. for $C_{10}H_{16}N_2$: C 73.13, H 9.87, N 17.05; found: C 73.21, H 9.77, N 16.87.

4,4′-Di-tert-butylbenzophenone 4-tert-Butylphenylhydrazone **12**

A mixture of 14.1 g (0.047 mol) of 4,4′-di-*tert*-butylbenzophenone (43), 7.7 g (0.047 mol) of 4-*tert*-butylphenylhydrazine, and 4 ml acetic acid in 40 ml ethanol were heated on the steam bath for 45 min. The solution was cooled and the product filtered off and recrystallized from ethanol–benzene to give 15 g (72%) of the hydrazone, mp 180–181 °C; nmr (CCl_4) τ 2.4–3.3 (m, 13H) 8.62 (s, 9H), 8.72 (s, 9H) and 8.74 (s, 9H). *Anal.* calcd. for $C_{31}H_{40}N_2$: C 84.49, H 9.15, N 6.36; found: C 84.37, H 9.21, N 6.39.

1-(4,4′-Di-tert-butyldiphenylmethyl)-2-(4-tert-butylphenyl)hydrazine Dihydrochloride

A solution of 15 g (0.034 mol) of the hydrazone in 325 ml benzene was added over a 2 h period to a mixture of 3.5 g (0.09 mol) of lithium aluminum hydride in 325 ml ether which had been stirred under reflux for 4 h. Ether was evaporated until the internal temperature of the mixture reached 50 °C. The mixture was stirred at 50 °C for 8 h, cooled, and then hydrolyzed by slow addition of 28 g sodium potassium tartrate in 100 ml water. The hydrazine was taken up in ether and then was precipitated as the dihydrochloride by passing hydrogen chloride through the dried ether solution. Evaporation of the ether left a solid which was washed several times with ether and dried to give 14.8 g (84%) of white crystals, mp 220–225 °C after recrystallization from benzene–petroleum ether.

Can. J. Chem. Downloaded from www.nrcresearchpress.com by 210.87.254.6 on 09/05/12
For personal use only.

Anal. calcd. for $C_{31}H_{44}Cl_2N_2$: C 71.79, H 9.14, Cl 13.67, N 5.40; found: C 71.95, H 9.02, Cl 13.42, N 5.65.

Several attempts were made to prepare the free hydrazine but these all resulted in the formation of sticky yellowish solids.

1-(4,4'-Di-tert-butyldiphenylmethyl)-2-(4-tert-butylphenyl)diazene **8**

A mixture of 8 g of the above dihydrochloride, 100 ml 20% sodium hydroxide, and 100 ml ether was shaken under nitrogen until the solid had all dissolved. The ether layer was washed with water twice and then added to 100 ml benzene. The resulting solution was stirred under air for 24 h. The solvent was then removed under reduced pressure and the residue was crystallized from methanol–benzene to give 5.2 g (76%) of crystals mp 152–154 °C (dec.); nmr (CCl_4) τ 2.3–2.9 (m, 12H), 5.75 (s, 1H), and 9.30 (s, 27H). *Anal.* calcd. for $C_{31}H_{40}N_2$: C 84.49, H 9.15, N 6.36; found: C 84.22, H 9.19, N 6.09.

4,4'-Di-tert-butylbenzophenone Phenylhydrazone **13**

This material was prepared from 4,4'-di-*tert*-butylbenzophenone and phenylhydrazine following the procedure for the formation of **12**. Recrystallization from ethanol–benzene gave either needles, mp 144.5–145.5 °C, or plates, mp 95–100 °C which resolidified at 120 °C and remelted at 144.5–145.5 °C; nmr (CCl_4) τ 2.4–3.4 (m, 13H), 8.61 (s, 9H), and 8.72 (s, 9H). *Anal.* calcd. for $C_{27}H_{32}N_2$: C 84.32, H 8.28, N 7.40; found: C 83.92, H 8.37, N 7.36.

Attempted Preparation of Benzophenone 4-tert-Butylphenylhydrazone **14**

Benzophenone and 4-*tert*-butylphenylhydrazine were allowed to react in the manner described for the preparation of **12**. All of the numerous attempts resulted in the formation of viscous oils which could not be induced to crystallize and could not be purified by column chromatography although the other three hydrazones **11**, **12** and **13** survived chromatography without decomposition. Nuclear magnetic resonance (CCl_4) τ 2.3–3.2 (m, 15H) and 8.73 (s, 9H).

Kinetic Studies

The rates of evolution of gas from solutions of (±)-**1** were measured using an apparatus and a procedure similar to that described (44). The solutions were flushed with purified nitrogen for 10 min before being placed in the heating bath. Final volume readings were taken after 10 half-lives of decomposition. Unimolecular rate constants were calculated from the slopes of plots of log (V_∞-V_t) *vs.* time and are summarized in Table 1.

Product Analyses from Thermolysis of (±)-1

About 0.5 ml of 0.2 *M* solutions of (±)-**1** in benzene or in 1 *M* butanethiol in benzene were placed in test tubes made from 9 mm glass tubing and degassed with three freeze–thaw cycles under 0.02 torr pressure. The tubes were sealed and placed in a preheated oven maintained at 100 ± 1 °C or 80 ± 1 °C for 10 half-lives of decomposition. The tubes were then cooled to −70 °C, opened, and the contents analyzed by gc. Samples were injected at a column temperature of 80 °C which was then increased to 220 °C over 15 min. Gas flow was 60 ml/min helium at 80 °C. Duplicate analyses were made for each sample. Calibrations were made using solutions containing known amounts of diphenylmethane, (±)-**6**, and the tetraphenylethane. Unidentified compounds assumed to contain a diphenylmethyl fragment were arbitrarily assigned a response factor equal to that of (±)-**6**.

Thermolysis of (−)-(S)-1

About 0.7 g of (−)-(*S*)-**1** in 20 ml solvent was placed in a stainless steel pressure bomb which had been treated as had the glassware used to handle the azo compounds. The solution was flushed with purified nitrogen for 10 min. The bomb was closed and placed in a preheated oven at 100 ± 1 °C overnight, about 15 half-lives of decomposition. The bomb was then cooled, opened, and the contents concentrated to a small volume. The residue was injected in 10 μl portions into the gc and (−)-(*R*)-**6** was collected from the effluent stream. The results are given in Table 2.

Thermolysis of (±)-1 in the Nuclear Magnetic Resonance Probe

About 0.1 g of (±)-**1** was added to an nmr sample tube, followed by 0.5 ml hexadecane which had been preheated to 120 °C. The tube was plugged with cotton, shaken, and placed in an nmr probe which was heated at 120 °C. The spectrum was scanned repeatedly from τ 2 to 6 for as long as emission and enhanced absorption effects in various regions of the spectrum could be observed, about 6 min. The magnitude of the signal due to the methine proton decreased monotonously during this time while other emission and enhanced absorption signals first increased and then decreased in intensity.

Thermolysis of Mixtures of 1-Diphenylmethyl-2-phenyldiazene **7** *and 1-(4,4'-Di-tert-butyldiphenylmethyl)-2-(4-tert-butylphenyl)diazene* **8**

An intimate mixture of 1.0 g (0.0040 mol) of **7** and 1.53 g (0.0035 mol) of **8** was divided equally among 15 very thin walled test tubes. To each was added 15 drops of hexadecane and the mixture was heated at 90 °C until solution had taken place. The tubes were then placed in a bath at 190 °C for 25 s and then quickly cooled. The contents of each tube were dissolved in ether and 0.030 g of *p*-toluenesulfonic acid was added to the combined solutions which had a volume of ~90 ml. After 1 h the ether was removed, and the residue dissolved in warm hexane and chromatographed on 300 g activated alumina in a 25 mm column using 10% ether in hexane as eluent. A total of 0.444 g of pure **11** and 0.853 g of pure **12** was recovered together with a mixture of hydrocarbons. No evidence for the presence of the mixed hydrazones **13** and **14** was detected. The hydrazone **12** was eluted more rapidly.

Control experiments showed that the hydrazones **13** and **14** eluted together in fractions separated from those containing **11** and **12**, and that had 1% of **13** or **14** been formed they would have been detected.

Thermolyses carried out in this way for 20 s and 30 s and subsequent work-up resulted in the recovery of somewhat greater and smaller quantities, respectively, of the two hydrazones **11** and **12**. When the thermolysis was carried out for 70 s no hydrazone could be recovered.

Can. J. Chem. Downloaded from www.nrcresearchpress.com by 210.87.254.6 on 09/05/12
For personal use only.

Thermolysis of **7** *in the Nuclear Magnetic Resonance Probe*

An nmr sample tube containing 0.1 g **7** in 0.5 ml hexadecane was heated to 80 °C and then placed in the probe of an nmr spectrometer at 180 °C. The region between τ 3 and 5 was scanned repeatedly for as long as emission and enhanced absorption effects could be detected, about 3 min. The signal due to the methine proton of **7** was observed to increase and then decrease in intensity during this time before disappearing entirely. In a typical run the relative areas of the signal on the first three scans (~30 s intervals) were 1:2.5:1.3.

Methyl 2-Diphenylmethylhydrazinecarboxylate

A solution of 6.35 g (0.067 mol) methyl chloroformate in 100 ml ether was added slowly to a stirred solution of 15 g (0.075 mol) diphenylmethylhydrazine and 21 g (0.2 mol) triethylamine in 700 ml ether at 0 °C under nitrogen. The resulting mixture was allowed to stand at 20 °C overnight and then filtered. The oil remaining on removal of the ether was crystallized from benzene–hexane to give 12 g (70%) product, mp 80–92 °C. Two crystallizations afforded the analytical sample mp 101–102.5 °C; ir (CCl_4) 3458, 3320, 1730 cm^{-1}; nmr (CCl_4) τ 2.77 (s, 10H), 3.52 (d, J = 5.5 Hz, 1H, NH), 4.78 (s, 1H, CH), 5.66 (d, J = 5.5 Hz, 1H, NH), 6.48 (s, 3H). *Anal.* calcd. for $C_{15}H_{16}N_2O_2$: C 70.31, H 6.29, N 10.92; found: C 70.57, H 6.33, N 10.98.

(±)-Methyl 1-(2-Butyl)-2-diphenylmethylhydrazinecarboxylate

A solution of 5.0 g (0.023 mol) 2-butyl *p*-toluenesulfonate (45) in a little ether was added quickly to a stirred solution of 50 ml of anhydrous dimethyl sulfoxide at 20 °C which contained 6 g (0.023 mol) methyl 2-diphenylmethylhydrazinecarboxylate and 1.5 g (0.026 mol) dry sodium ethoxide. The resulting solution warmed slightly and was allowed to stand under nitrogen for 2 h. The reaction mixture was then poured into ice water and the product extracted with ether. The ether was dried and concentrated to an oil which was chromatographed on silica gel using benzene–hexane as eluent to give 3.2 g (44%) of a viscous oil that was oxidized slowly in air; ir (CCl_4) 3290, 1696 cm^{-1}; nmr (CCl_4) τ 2.71 (s, 10H), 4.78 (d, J = 2 Hz, 1H), 5.50 (d, J = 2 Hz, 1H, NH), 6.30 (s, 3H), 6.4 (m, 1H), 8.7 (m, 2H), 9.29 (d, J = 7 Hz, 3H), 9.38 (t, J = 6 Hz, 3H). *Anal.* calcd. for $C_{19}H_{24}N_2O_2$: C 73.05, H 7.74, N 8.97; found: C 72.98, H 7.71, N 8.73.

(+)-Methyl (R)-1-(2-Butyl)-2-diphenylmethylhydrazinecarboxylate

This material was prepared as described for the racemic compound except that the alkylating agent used was (+)-(*S*)-2-butyl-4-bromobenzenesulfonate (45) $[\alpha]_D^{21}$ 9.3° (*c* 13.2, $CHCl_3$) which had been prepared from (+)-(*S*)-2-butanol (Norse) $[\alpha]_D^{21}$ 12.6° (neat, l = 1 dm) (lit. (46) $[\alpha]_D^{21}$ 13.83° (neat, l = 1 dm). The starting alcohol was thus 91% optically pure. The product had $[\alpha]_D^{21}$ 12.3°, $[\alpha]_{578}^{21}$ 13.3°, $[\alpha]_{546}^{21}$ 15.6°, $[\alpha]_{436}^{21}$ 29.2° (*c* 1.53, CCl_4).

Conversion of (+)-Methyl (R)-1-(2-Butyl)-2-diphenylmethylhydrazinecarboxylate to the Diazene (+)-(R)-1

A solution of 1.0 g of the title ester and 1.0 g potassium hydroxide in 10 ml methanol was heated under nitrogen at 125 °C for 4 h in a stainless steel bomb. After cooling, the reaction mixture was acidified with hydrochloric acid. The resulting mixture was diluted with 20 ml water and extracted with ether. The aqueous layer was made basic and extracted with ether. The ether layer was shaken vigorously with 5% aqueous sodium hypochlorite, dried, and concentrated under vacuum to give 0.3 g of an oil whose nmr spectrum was identical with that of (±)-**1** prepared by method *A*; $[\alpha]_D^{21}$ +2.1°, $[\alpha]_{546}^{21}$ +4.2°, $[\alpha]_{436}^{21}$ +41° (*c* 5.0, CCl_4).

Acknowledgments

We thank the National Research Council of Canada for financial support and Dr. D. D. Tanner for helpful discussions.

1. P. C. Huang and E. S. Kosower. J. Am. Chem. Soc. **90**, 2362 (1968).
2. K. R. Kopecky and T. Gillan. Can. J. Chem. **47**, 2371 (1969).
3. T. Gillan. Ph.D. Thesis. University of Alberta. 1969.
4. F. D. Greene, M. A. Berwick, and J. C. Stowell. J. Am. Chem. Soc. **92**, 867 (1970).
5. (*a*) H. C. Ramsperger. J. Am. Chem. Soc. **51**, 2134 (1929); (*b*) S. G. Cohen and C. H. Wang. J. Am. Chem. Soc. **77**, 3628 (1955); (*c*) C. G. Overberger and A. V. DiGuilio. J. Am. Chem. Soc. **81**, 2154 (1959); (*d*) S. Seltzer. J. Am. Chem. Soc. **83**, 2625 (1961); (*e*) S. Seltzer. J. Am. Chem. Soc. **85**, 15 (1963); (*f*) S. Seltzer and S. G. Mylonakis. J. Am. Chem. Soc. **89**, 6584 (1967); (*g*) J. Hinz, A. Oberlinner, and C. Rüchardt. Tetrahedron Lett. 1975 (1973); (*h*) T. R. Lynch, F. N. MacLachlan, and J. L. Suschitzky. Can. J. Chem. **51**, 1378 (1973).
6. (*a*) R. J. Crawford and A. Mishra. J. Am. Chem. Soc. **87**, 3768 (1965); (*b*) R. J. Crawford and D. M. Cameron. Can. J. Chem. **45**, 691 (1967); (*c*) B. H. Al-Sader and R. J. Crawford. Can. J. Chem. **46**, 3301 (1968); (*d*) K. R. Kopecky and J. Soler. Can. J. Chem. **52**, 2111 (1974); (*e*) W. R. Roth and M. Martin. Ann. **702**, 1 (1967); (*f*) P. B. Condit and R. G. Bergman. Chem. Commun. 4 (1971); (*g*) S. W. Benson and H. E. O'Neal. Natl. Stand. Data Ref. Ser. Natl. Bur. Stand. **21**, 31 (1970).
7. S. Seltzer and F. T. Dunne. J. Am. Chem. Soc. **87**, 2628 (1965).
8. T. Mojelski. M.Sc. Thesis. University of Alberta. 1968.
9. (*a*) A. Tsolis, S. Mylonakis, M. Nieh, and S. Seltzer. J. Am. Chem. Soc. **94**, 829 (1972); (*b*) R. A. Johnson and S. Seltzer. J. Am. Chem. Soc. **95**, 938 (1973); (*c*) N. Porter and L. J. Marnett. J. Am. Chem. Soc. **95**, 4361 (1973).
10. (*a*) W. A. Pryor and K. Smith. J. Am. Chem. Soc. **92**, 5403 (1970); (*b*) K. Takagi and R. J. Crawford. J. Am. Chem. Soc. **94**, 7406 (1972); (*c*) A. W. Garner, J. W. Timberlake, P. S. Engel, and R. A. Melaugh. J. Am. Chem. Soc. **97**, 7377 (1975).
11. R. C. Neuman, Jr., G. D. Lockyer, Jr., and M. J. Amrich. Tetrahedron Lett. 1221 (1972).

12. (*a*) N. A. PORTER, L. J. MARNETT, C. H. LOCKMÜLLER, G. L. CLOSS, and M. SHOBATAKI. J. Am. Chem. Soc. **94**, 3664 (1972); (*b*) N. A. PORTER, J. G. GREEN, and G. R. DUBAY. Tetrahedron Lett. 3363 (1975).
13. N. A. PORTER and M. O. FUNK. Chem. Commun. 263 (1973).
14. C. V. GRECO, W. H. NYBERG, and C. C. CHENG. J. Med. Pharm. Chem. **5**, 861 (1962).
15. P. BREWSTER, F. HIRON, E. D. HUGHES, C. K. INGOLD, and P. A. D. S. RAO. Nature, **166**, 179 (1950).
16. J. FUGGER, J. M. TIEN, and I. M. HUNSBERGER. J. Am. Chem. Soc. **77**, 1843 (1955).
17. R. C. HUSTON and R. I. JACKSON. J. Am. Chem. Soc. **63**, 541 (1941).
18. K. FREUDENBERG and W. LWOWSKI. Ann. **594**, 76 (1955).
19. A. J. BIRCH. J. Chem. Soc. 809 (1945).
20. A. KJER and S. E. HANSEN. Acta Chem. Scand. **11**, 898 (1957).
21. S. G. COHEN, F. COHEN, and C. H. WANG. J. Org. Chem. **28**, 1479 (1963).
22. A. F. BICKEL and E. C. KOOYMAN. Nature, **170**, 211 (1952).
23. S. G. COHEN and C. H. WANG. J. Am. Chem. Soc. **77**, 4435 (1955).
24. S. F. NELSON and P. D. BARTLETT. J. Am. Chem. Soc. **88**, 143 (1966).
25. S. SELTZER and E. J. HAMILTON, JR. J. Am. Chem. Soc. **88**, 3775 (1966).
26. F. W. LAMPE and R. M. NOYES. J. Am. Chem. Soc. **76**, 2140 (1954).
27. R. KAPTEIN. Chem. Comm. 732 (1971).
28. D. R. DALTON and S. A. LIEBMAN. J. Am. Chem. Soc. **91**, 1194 (1969).
29. J. J. WINDLE, A. K. WIERSEMA, and A. L. TAPPEL. J. Chem. Phys. **41**, 1996 (1964).
30. J. R. SHALTON, C. K. LIANG, and P. KOVACIC. J. Am. Chem. Soc. **90**, 354 (1968).
31. S. G. COHEN and S. G. WANG. J. Am. Chem. Soc. **77**, 2457 (1955).
32. L. I. SMITH and K. L. HOWARD. *In* Organic synthesis. Coll. Vol. 3. Wiley, New York. 1955. p. 351.
33. A. FLEURY-LARSONNEAU. Bull. Soc. Chim. Fr. **6**, 1576 (1939).
34. H. E. SMITH, S. L. COOK, and M. E. WARREN. J. Org. Chem. **29**, 2265 (1964).
35. K. A. TAIPALE and P. V. USACHEV. J. Russ. Phys. Chem. Soc. **62**, 1241 (1930); Chem. Abstr. **25**, 2415 (1931).
36. P. A. S. SMITH, J. M. CLEGG, and J. LAKRITZ. J. Org. Chem. **23**, 1595 (1958).
37. L. F. FIESER and M. FIESER. Reagents for organic synthesis. Wiley. New York. 1967. p. 1030.
38. G. ODHAM. Ark. Kemi, **20**, 507 (1963).
39. K. R. KOPECKY and S. EVANI. Can. J. Chem. **47**, 4041 (1969).
40. R. C. FUSON and R. TULL. J. Am. Chem. Soc. **71**, 2543 (1949).
41. B. W. LARNER and A. T. PETERS. J. Chem. Soc. 680 (1952).
42. I. M. HUNSBERGER, E. R. SHAW, J. FUGGER, R. KETCHAM, and D. LEDNICER. J. Org. Chem. **21**, 394 (1956).
43. N. P. BUU-HOI, R. ROYER, N. D. XUONG, and K. V. THANG. Bull. Soc. Chim. Fr. 1204 (1955).
44. R. C. PETERSEN, J. H. MARKGRAF, and S. D. ROSS. J. Am. Chem. Soc. **83**, 3819 (1961).
45. L. F. FIESER and M. FIESER. Reagents for organic synthesis. Vol. 1. Wiley. New York. 1967. p. 1180.
46. J. KENYON, H. PHILLIPS, and V. P. PITTMAN. J. Chem. Soc. 1072 (1935).

Can. J. Chem. Downloaded from www.nrcresearchpress.com by 210.87.254.6 on 09/05/12
For personal use only.

Organic sulfur mechanisms. 19. Sulfene – tertiary amine zwitterions and base size effects in sulfene condensations[1]

JAMES FREDERICK KING AND DAVID ROGER KAY HARDING

Department of Chemistry, University of Western Ontario, London, Ont., Canada N6A 5B7

Received January 29, 1976

JAMES FREDERICK KING and DAVID ROGER KAY HARDING. Can. J. Chem. **54**, 2652 (1976).

The effect of changing the size of the tertiary alkylamine has been investigated in two systems: (*a*) the reaction of phenylmethanesulfonyl chloride with a tertiary amine, and (*b*) the formation of the β-sultone from the reaction of chloral, ethanesulfonyl chloride, and a tertiary amine. In the first reaction the yield of stilbene (**3**) or stilbene episulfone (**4**) increases and that of the thiobenzoyl chloride *S*-oxides (**5**) decreases as the size of the base decreases, as expected for a mechanism involving a tertiary amine – sulfene zwitterion in the formation of the stilbene products. In the second reaction the yield of the β-sultone is much enhanced by the use of a small amine; the latter observation precludes a simple sulfene–chloral cycloaddition mechanism and points to a zwitterionic intermediate derived from the amine and either the sulfene or chloral.

JAMES FREDERICK KING et DAVID ROGER KAY HARDING. Can. J. Chem. **54**, 2652 (1976).

On a étudié l'effet, sur deux types de réactions, d'un changement de grosseur d'alkylamine tertiaire: (*a*) la réaction du chlorure de phénylméthanesulfonyle avec une amine tertiaire et (*b*) la formation d'une β-sultone à partir du chloral, du chlorure d'éthanesulfonyle et d'une amine tertiaire. Dans la première réaction, le rendement en stilbène (**3**) ou en épisulfone de stilbène (**4**) augmente alors que celui des *S* oxydes du chlorure de thiobenzoyle (**5**) diminue à mesure que la grosseur de la base diminue; ces résultats correspondent à ceux attendus sur la base d'un mécanisme impliquant un zwitterion amine tertiaire/sulfène lors de la formation des produits de type stilbène. Dans la deuxième réaction, le rendement de la β-sultone augmente beaucoup par l'utilisation d'une amine qui est petite; cette dernière observation élimine un mécanisme de cycloaddition simple sulfène–chloral et indique que la réaction se produit par un intermédiaire de nature zwittérionique dérivé de l'amine et soit du sulfène ou du chloral.

[Traduit par le journal]

Introduction

In earlier papers (1, 2) we have presented evidence for the reversible formation of a zwitterionic species such as **1**, by reaction of a sulfene with a tertiary amine, *e.g.*:

$$CH_2{=}SO_2 + NMe_3 \rightleftharpoons \bar{C}H_2SO_2\overset{+}{N}Me_3$$

1

Presumably such zwitterions are involved also in the formation of the coupled zwitterions (3–5) first reported by Opitz *et al.* (3) and which evidently lead to the further products described by Grossert (6, 7). We report herein our efforts to see if such species are intermediates in other reactions as well.

In our multiexchange experiments (1) a key feature was the effect of changing the steric requirements of the amine. Extensive multiexchange was found with those tertiary amines such as trimethylamine, quinuclidine, and 1,4-diazabicyclo[2.2.2]octane (DABCO), in which the vicinity of the nitrogen is uncluttered. As ethyl groups replaced the methyls in trimethylamine, the extent of multiexchange progressively dropped until essentially no multiexchanged product was found with triethylamine. It seemed, therefore, that the intermediacy of sulfene – tertiary amine zwitterions might be betrayed by variations in product composition with change in 'size' of the base.[2] The effect of base size on two different sulfene processes has been investigated, and is reported here.

Results and Discussion

Stilbene Formation from Phenylmethanesulfonyl Chloride

The first of these two processes is the formation of stilbene and other products by the action

[1]For part 18; see ref. 23.

[2]In this paper, we refer to the relative inaccessibility of the free electron pairs of the amine (as deduced from multiexchange experiments) as the 'size' of the amine. Those which behave like trimethylamine are termed 'small', and those like triethylamine are called 'large'.

Can. J. Chem. Downloaded from www.nrcresearchpress.com by 210.87.254.5 on 09/05/12
For personal use only.

Can. J. Chem. Downloaded from www.nrcresearchpress.com by 210.87.254.5 on 09/05/12
For personal use only.

of tertiary amines on phenylmethanesulfonyl chloride (**2**). This reaction has historical interest because it was in the discussion of this reaction that Wedekind and Schenk in 1911 (8) made the first proposal of sulfene formation that has withstood subsequent investigation. It has become evident, however, that the original Wedekind and Schenk mechanism for the further transformation of phenylsulfene via phenylcarbene to stilbene is incorrect (9, 10), and although other suggestions have been made in reviews (9, 11), there has not been sufficient information to warrant further discussion.

Work in this laboratory some years ago (12) showed that the stoichiometry and products of the reaction of **2** and triethylamine may be summarized by [1] and [2]:

[1] $2PhCH_2SO_2Cl + 2Et_3N \longrightarrow 2Et_3\overset{+}{N}H\overset{-}{Cl} +$

2

$(1-x)$ 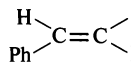 $+ x$ 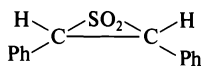

trans-**3** *cis*-**4**

[2] $2PhCH_2SO_2Cl + 2Et_3N \longrightarrow Et_3\overset{+}{N}H\overset{-}{Cl} +$

2

$(1-y)$ 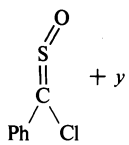 $+ y$ 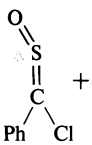 $+ Et_3\overset{+}{N}H\ \overset{-}{O}_3SCH_2Ph$

cis-**5** *trans*-**5**

Reaction [1] was found to be the principal process in the more polar solvents used (methylene chloride and ether), whereas [2] was the chief route in cyclohexane. Substantial amounts of the products of both pathways were obtained when the reaction was run in benzene, and this solvent was therefore chosen for our study of the effect of base size on product ratios.[3]

Phenylmethanesulfonyl chloride (**2**) was treated in benzene solution with each of the tertiary amines in Table 1. The work-up converted *cis*-**4** to *cis*-stilbene (*cis*-**3**) and the isomeric stilbenes were separated chromatographically from the chlorosulfines (**5**); the two columns labelled 'stilbenes' and 'sulfines' thus indicate the relative amounts of products formed via reactions [1] and [2], respectively. These data clearly show an increase in the proportion of the products from reaction [1] as

TABLE 1. Effect of base size on the reaction of phenylmethanesulfonyl chloride (**2**) with tertiary alkylamines*

Amine	Yield (%) Stilbenes (**3**)	Sulfines (**5**)
Trimethylamine	70	21
Triethylamine	21	63
Tributylamine	2	81
N-Ethyl-*N*,*N*-diisopropylamine	~0	< 50

*In dry benzene at room temperature, initial concentrations: **2**, 0.6 *M*; amine 0.9 *M*.

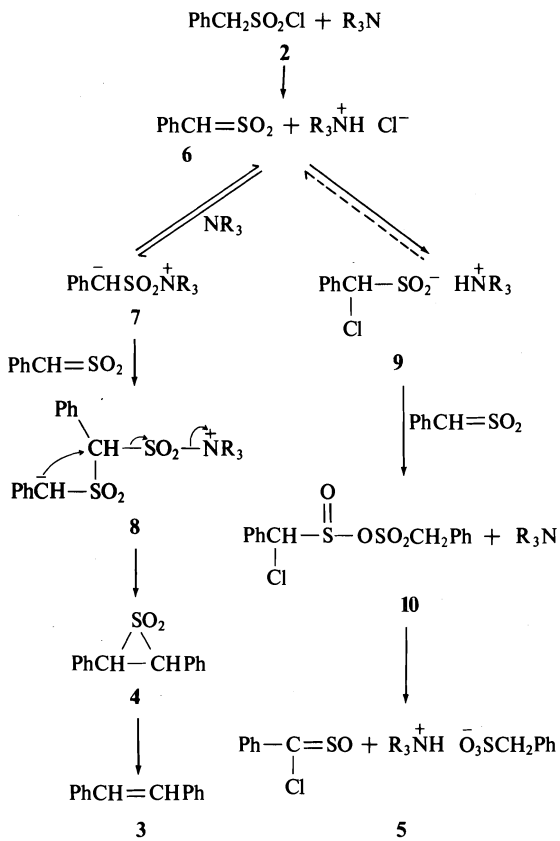

SCHEME 1

[3]It should perhaps be explicitly noted that because sulfenes are formed in the rate determining step and react in a subsequent fast step (in all examples studied to date), simple rate studies give no information about the mechanisms by which sulfenes react; to obtain this one must study competition experiments in a kinetically controlled system.

Can. J. Chem. Downloaded from www.nrcresearchpress.com by 210.87.254.5 on 09/05/12
For personal use only.

the base size decreases, a result which is nicely consistent with the mechanisms suggested in Scheme 1. The primary effect of smaller size of the tertiary amine is, by this mechanism, to increase the equilibrium amount[4] of the zwitterion (**7**) and hence the rate of formation of **3** relative to that of **5**. This, of course, would hold only if the rate of the process **6** → **5** is much less dependent on base size than **6** ⇌ **7** → **3**, a condition which may be seen to be entirely reasonable from the following argument. Though **6** → **5** is irreversible under these conditions, it is not known which reaction in Scheme 1 is rate determining. If it is formation of **9** from **6**, then since this step does not involve the base, obviously **6** → **5** would be unaffected by base size. If, however, either the formation or consumption of **10** is rate determining, the base is presumably involved but only to transfer a proton, a process which is normally found to be much less sensitive to base size effects than nucleophilic attack on a sulfene.[5]

The mechanisms in Scheme 1 are also consistent with the increase in yield of **3** and **4** with greater solvent polarity, since the equilibrium amount of the zwitterion (**7**) should be increased by increasing the polarity of the medium. Formation of **9**, on the other hand, involves conversion of a neutral species (**6**) plus an ion pair into another ion pair in which the negative charge is shared primarily between two atoms rather than one, and hence is not facilitated at all by increasing solvent polarity. Also, reaction of **9** with **6** to form **10** converts an ion pair plus a neutral molecule into neutral species and should accelerate as solvent polarity is lowered. The final step (**10** → **5**), however, leads to ionic products, suggesting that the observed solvent effect is more easily accounted for if an earlier step in the sequence is rate determining.

The other steps in the conversion **2** → **3** merit brief comment. The formation of the sulfene (**6**) in similar circumstances has been adequately proved (see ref. 10 for a review) and need not be discussed further. The step **7** → **8** is well-precedented in the formation of the Opitz zwitterion ($CH_3SO_2\bar{C}HSO_2\overset{+}{N}Me_3$) (3, 4), of the oligomers of sulfene described by Grossert and Bharadwaj (7), and of mesylmesylate esters ($CH_3SO_2CH_2SO_2OR$) on reaction of 'easy mesyl' ($CH_3SO_2\overset{+}{N}MeEt_2\ FSO_3^-$) with hindered alcohols (2). The cyclization **8** → **4** is very similar to the key step proposed by Bordwell and Cooper (14) for the Ramberg–Bäcklund rearrangement. Whether the $-SO_2\overset{+}{N}R_3$ group is displaced directly or not cannot be specified at present. Such a process is not unreasonable in the light of the existence of S_N2 displacements of benzylic $-SO_2Cl$ and $-SO_2Br$ groups (15), but it is also possible that the $-SO_2\overset{+}{N}R_3$ is modified before the cyclization to **4**.[6] That *trans*-stilbene arises from *trans*-**4** follows from the work of Bordwell *et al.* (16). The sequence **6** → **7** → **8** → **4** cannot be regarded as proved, but rather as a reasonable suggestion which satisfactorily accounts for (*a*) the formation of the observed products by invoking only processes with satisfactory precedents, (*b*) the effect of solvent change, and (*c*) the effect of change in base size described in this work.

[4]We have noted (1) that **2** with DABCO in *tert*-butyl alcohol leads to partial exchange of the second hydrogen of the methylene group; it is therefore highly likely that formation of **7** from **6** is reversible under the conditions that lead to **3** or **5**.

[5]In contrast to the base size effect found with formation of **1** from sulfene, it has been found (13) that formation of sulfene from methanesulfonyl chloride shows an excellent correlation with base strength with these amines, *i.e.* there are no base size effects in the proton removal step that do not equally affect the (equilibrium) base strength in that medium.

[6]A referee has asked why **8** does not give the diphenyl analogue of the Opitz zwitterion, *i.e.* $PhCH_2SO_2\text{-}\bar{C}PhSO_2\overset{+}{N}R_3$, which as far as we know has never been observed. In reply to this interesting query we conjecture that the following factors may contribute. (*a*) The favored conformation for the Ramberg–Bäcklund-type reaction of **8** is obtained either directly or very easily on combination of **6** and **7**. (*b*) Conversion of **8** to $PhCH_2SO_2\bar{C}PhSO_2\overset{+}{N}R_3$, on the other hand, may be comparatively difficult for conformational reasons. Formation of the zwitterion by intramolecular proton transfer could be difficult because any arrangement of **8** which places the proton close enough to the carbanion either has some very strong steric repulsions or does not allow the proton to be in what is believed to be the preferred arrangement for proton transfer, viz. with the proton simultaneously synclinal to at least one set of sulfonyl oxygens (see, for example, ref. 24 (especially pp. 105ff)). Another imaginable route to the 'diphenyl Opitz zwitterion' would be via protonation of **8** followed by deprotonation. To facilitate the latter step the proton can be placed synclinal to all four sulfonyl oxygens, but this leads to severe nonbonding repulsions involving the phenyl group; such interactions are lacking in the formation of the Opitz zwitterion itself.

Can. J. Chem. Downloaded from www.nrcresearchpress.com by 210.87.254.5 on 09/05/12
For personal use only.

β-Sultone Formation from Chloral and Related Compounds

The second reaction in which we have looked at the effect of base size is the formation of β-sultones by the reaction of sulfonyl halides with trialkylamines and perhalogenated ketones or aldehydes (17–20):

$$CH_3SO_2Cl + Cl_3CCHO \xrightarrow{Et_3N} Cl_3C-CH(CH_2-SO_2)-O$$

11

Although this reaction is formally a cycloaddition, comparison with other reactions of sulfenes reveals an anomaly in that all other reactions of simple sulfenes show the sulfene to be acting as an electrophilic reagent. This is evident not only in reactions with amines and alcohols and the like, but also in cycloadditions with substituted olefins; enamines, ketene acetals and aminals react readily, vinyl ethers less readily, and simple alkenes not at all. With formation of β-sultones, however, the reaction takes place only with highly electrophilic carbonyl compounds such as chloral and various perhaloacetones; by contrast acetone and *p*-nitroacetophenone do not give β-sultones under these conditions (19).

It appeared to us that this difference could be accounted for simply by postulating the intermediacy of zwitterions as, for example, in Scheme 2, and we therefore looked at the effect of changing the base size on this reaction. Control experiments showed that the methylated sulfone **14***b* was much more stable to standing in the presence of a tertiary amine than **14***a*, and so the base size effect was tested on the reaction with ethanesulfonyl chloride and chloral. The results (Table 2) indicate a strong correlation between the yield of **14***b* and the 'smallness' of the base, in excellent accord with the mechanism shown in Scheme 2. On this basis, as the base size is decreased the steady state concentration of the sulfene (**12**) is lowered (and that of the zwitterion (**13**) raised), the net result being to favour formation of **14** relative to reaction of **13** with **12** to form oligomers; the latter reaction is believed to be the normal way in which sulfenes are consumed in the absence of competing sulfene trapping reactions (*cf.* ref. 7). It should be noted that, in accord with this picture, the reaction of trimethylamine in the presence of added triethylamine gives a good yield of **14***b*; this shows that the poor yield obtained with triethylamine does not derive from any destructive effect of triethylamine in the formation of **14***b*.

TABLE 2. Base size effects in the reaction of ethanesulfonyl chloride, chloral, and tertiary alkylamines*

Base	Yield of **14***b* (%)
Tributylamine	0
Triethylamine	10
DABCO	50
Trimethylamine	54
Trimethylamine (0.25 mol)	67
Trimethylamine plus triethylamine (0.07 mol)	69

*Except as otherwise indicated, using 0.1 mol each of chloral, ethanesulfonyl chloride, and amine in ether at 0 °C.

It must be pointed out that these data, though in agreement with the sulfene–amine zwitterion mechanism, can also be explained by assuming the intermediacy of a *chloral*–amine zwitterion, $\bar{O}-CH(CCl_3)-\overset{+}{N}R_3$; such a species is presumably an intermediate in the tertiary amine catalyzed polymerization of chloral (21, 22). We have no evidence to distinguish between

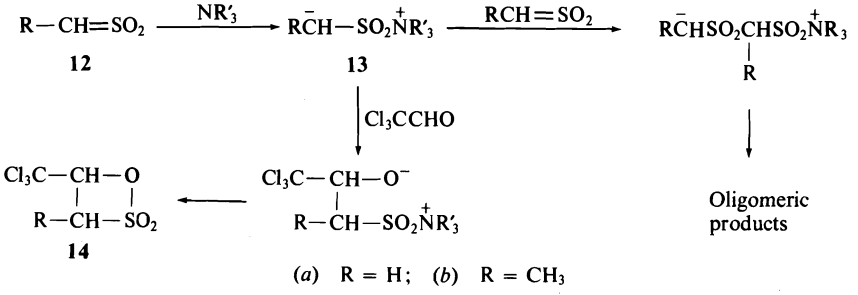

(*a*) R = H; (*b*) R = CH_3

SCHEME 2

TABLE 3. Nuclear magnetic resonance spectra* of 3-substituted 4-trichloromethyl-1,2-oxathietane 2,2-dioxides (**14**)

R	δ (ppm) C-3H	C-4H	Others	Coupling constants (Hz)
H(**14***a*)	4.76, 4.82	5.07		J_{gem} = 13.6 $J_{3,4}$ = 6 and 7 (respectively)
CH_3 (**14***b*)	5.24	5.08	CH_3 1.88	$J_{3,4}$ = 8.4 $J_{3,Me}$ = 7.2
CH_3CH_2	5.00	5.08	CH_3 1.19 CH_2: H_A 2.21 H_B 2.68	$J_{3,4}$ = 8.8 $J_{3,A}$ = 3.7, $J_{3,B}$ = 8.8 J_{AB} = 15 $J_{Me,A(B)}$ = 7.2
Ph	5.96	5.12	Ph 7.3–7.7	$J_{3,4}$ = 6.5

*Of $CDCl_3$ solutions determined with a Varian HA-100 spectrometer. Values were assigned by first-order analysis (aided by proton decoupling experiments as required).

these possibilities. What the present results do show, however, is that the formation of β-sultones in this reaction is not a simple [2 + 2] cycloaddition, thereby removing an apparent mechanistic anomaly.

These experiments also provide a serviceable practical improvement in the formation of β-sultones from sulfenes. The yield of **14***b* has been increased from a previously reported 5% (16) to 65–70%. In extension of this we tried the previously unreported reactions of chloral with 1-propanesulfonyl and phenylmethanesulfonyl chlorides using DABCO as the base, and in single experiments obtained the 3-ethyl and 3-phenyl derivatives of **11** in 46% and 13% yields respectively.

Table 3 gives nmr data for the four β-sultones encountered in this work; the agreement between the nmr spectra and the assigned structures is good. With either crude or recrystallized samples of the three 3-substituted materials no sign was seen of any more than one of the two possible diastereomers. Though the nmr data do not, in our view, allow an unambiguous assignment of the configurations of these sultones, a *trans* orientation of the substituents is suggested by both a simple conformational picture of β-sultone formation following Scheme 2 and the observation of the greater stability of **14***b* over **14***a* on standing with triethylamine. Among the more likely routes for the decomposition of **14***a* under those conditions is ring opening via *anti* elimination of the C-3 hydrogen and the sulfonate function. This would be particularly inhibited by a *trans* orientation of the methyl and trichloromethyl groups, since this makes the C-3 hydrogen quasi-axial and hence clinal to the heterocyclic oxygen. This assignment of stereochemistry is, of course, highly tentative.

Experimental

Infrared spectra were obtained with Beckman IR-10 and IR-20A spectrometers using 0.1 mm NaCl cells. Nuclear magnetic resonance spectra were obtained with Varian T-60 and HA-100 instruments using tetramethylsilane as internal standard. Melting points were determined on a Kofler hot stage and are uncorrected. Benzene, triethylamine, tributylamine, and diisopropylethylamine were dried by refluxing over calcium hydride and distilling, and stored under nitrogen. Anhydrous trimethylamine was Eastman White Label grade, 1,4-diaza[2.2.2]bicyclooctane (DABCO) that supplied by the Aldrich Chemical Company, and dry ether Mallinckrodt anhydrous reagent.

*Reaction of Phenylmethanesulfonyl Chloride (**2**) with Tertiary Amines in Benzene*

Phenylmethanesulfonyl chloride (Eastman, recrystallized from CCl_4, 604 mg, 3.2 mmol) was dissolved in dry benzene (45 ml) under nitrogen. The tertiary amine (4.7–4.9 mmol) in dry benzene (5 ml) was added from a syringe with stirring as fast as possible through a serum cap and the resulting mixture stirred for 1 h. The solvent was then removed under reduced pressure and the residue worked-up by ether extraction, washing with 3 *M* HCl, drying over $MgSO_4$, and removing the solvent under reduced pressure. The residue was chromatographed on silica gel (BDH 60–120 mesh, 10 g), eluting the stilbenes (**3**) with petroleum ether (bp 30–60 °C) and the chlorosulfines (**5**) with methylene chloride. The composition of the products was checked by ir and nmr. The weights (mg) of the amine, stilbene fractions, and sulfine fraction are, respectively: trimethylamine, 290, 199, 58; triethylamine, 475, 60, 173; tributylamine, 880, 7, 222; diisopropylethylamine, 615, 0, 126.

Can. J. Chem. Downloaded from www.nrcresearchpress.com by 210.87.254.5 on 09/05/12
For personal use only.

Can. J. Chem. Downloaded from www.nrcresearchpress.com by 210.87.254.5 on 09/05/12
For personal use only.

Reaction of Ethanesulfonyl Chloride, Chloral, and Tertiary Amines

Chloral (10 ml, 0.1 mol) and the tertiary amine were dissolved in dry ether (100 ml) under dry nitrogen and the mixture cooled to about −15 °C in a dry ice – acetone bath. Ethanesulfonyl chloride (Eastman, 9.5 ml, 0.1 mol) in dry ether (50 ml) was added dropwise with stirring over 30 min, and the mixture stirred at <0 °C for 1 h. The solid obtained after removal of the solvent under reduced pressure was dissolved in CH_2Cl_2, and this solution washed with water, 3 *M* HCl, saturated $NaHCO_3$, and brine, and dried over $MgSO_4$. Removal of the solvent gave a sticky solid mass which was slurried with pentane (100 ml) and the white crystalline 3-methyl-4-trichloromethyl-1,2-oxathietane 2,2-dioxide (**14***b*) collected by vacuum filtration. These materials were identical in nmr spectrum to the product obtained in 4% yield (3% yield after recrystallization from ether, mp 118–120 °C) by following the procedure of Truce and Liu (19); ir (CH_2Cl_2) ν_{max} 1370, 1208 cm^{-1}. The quantities of the amine and product in each of these experiments were as follows: trimethylamine (9.5 ml) gave 12.9 g (54%), 25 ml gave 15.9 g (67%); trimethylamine (9.5 ml) and triethylamine (10 ml) gave 16.5 g (69%); DABCO (12 g) gave 11.8 g (50%) in one experiment and 11.4 g (48%) in another run carried out at room temperature; triethylamine (10.5 g) gave an oily crude product (5.6 g) estimated by nmr to be a mixture of the sultone (**14***b*) and ethanesulfonyl chloride in a molar ratio of 2:1; tributylamine, also gave an oily crude product the nmr of which showed no sign of any **14***b*.

*Stability of the Sultones **14a** and **14b** to Triethylamine*

A sample of each sultone (1 g) in dry ether (10 ml) was treated with stirring with triethylamine (0.5 g, 5 mmol) and the mixture stirred at room temperature for 2 h. The sultone was recovered (by taking up in ether–CH_2Cl_2, washing with 3 *M* HCl, saturated $NaHCO_3$ and brine, drying over $MgSO_4$, and evaporation of the solvent) to the extent of 0.9 g (90%) with **14***b* and 0.62 g (62%) with **14***a*.

3-Ethyl-4-trichloromethyl-1,2-oxathietane 2,2-Dioxide

Propanesulfonyl chloride (Eastman, 14.3 g, 0.1 mol) in ether (40 ml) was added dropwise with stirring over about 30 min to a solution at 0 °C under N_2 of chloral (10 ml, 0.1 mol) and DABCO (20 g, 0.18 mol) in ether (100 ml). After stirring for 1 h the mixture was worked-up as above to give a brownish solid (14.7 g) which, after extraction with pentane, left tan colored crystals (11.6 g, 46%) melting at 78–80 °C. The analytical specimen was obtained by recrystallization from ether–pentane, mp 80–82 °C; ir (CH_2Cl_2) ν_{max} 1368, 1188 cm^{-1}. *Anal.* calcd. for $C_5H_7Cl_3O_3S$: C 23.68, H 2.78, Cl 41.95, S 12.65; found: C 23.73, H 2.86, Cl 41.68, S 12.70.

3-Phenyl-4-trichloromethyl-1,2-oxathietane 2,2-Dioxide

Phenylmethanesulfonyl chloride (9.5 g, 50 mmol) in ether (25 ml) and tetrahydrofuran (15 ml) was added over 30 min to a mixture of chloral (5 ml, 50 mmol) and DABCO (10 g, 85 mmol) in ether (50 ml) at about −15 °C under N_2 with stirring. The mixture was stirred a further 1 h at 0 °C and worked-up as above. The solid obtained (7 g) was extracted with ether. The ether-soluble solid was extracted with pentane to give *trans*-stilbene (1.3 g, 29%). The ether-insoluble white solid, mp 132–134 °C (1.9 g, 13%), appeared to be mostly the sultone. Two recrystallizations from CCl_4 gave the analytical sample; ir (CH_2Cl_2) ν_{max} 1365, 1185 cm^{-1}. *Anal.* calcd. for $C_9H_7Cl_3O_3S$: C 35.85, H 2.34, Cl 35.27, S 10.63; found: C 36.12, H 2.06, Cl 35.19, S 10.55.

Acknowledgment

We thank the National Research Council of Canada for financial support.

1. J. F. King, E. A. Luinstra, and D. R. K. Harding. J. Chem. Soc. Chem. Commun. 1313 (1972).
2. J. F. King and J. R. du Manoir. J. Am. Chem. Soc. **97**, 2566 (1975).
3. G. Opitz, M. Kleeman, D. Bücher, G. Walz, and K. Rieth. Angew. Chem. Int. Ed. Engl. **5**, 594 (1966).
4. G. Opitz and D. Bücher. Tetrahedron Lett. 5263 (1966).
5. L. I. Ragulin, P. P. Ropalo, G. A. Sokol'skii, and I. L. Knunyants. Izv. Akad. Nauk SSR Ser. Khim. 1045 (1971).
6. J. S. Grossert. Chem. Commun. 305 (1970).
7. J. S. Grossert and M. M. Bharadwaj. J. Chem. Soc. Chem. Commun. 144 (1974).
8. E. Wedekind and D. Schenk. Ber. **44**, 198 (1911).
9. G. Opitz. Angew. Chem. Int. Ed. Engl. **6**, 107 (1967).
10. J. F. King. Acc. Chem. Res. **8**, 10 (1975).
11. T. J. Wallace. Q. Rev. **20**, 67 (1966).
12. J. F. King and T. Durst. Can. J. Chem. **44**, 819 (1966).
13. E. A. Luinstra. Ph.D. Thesis, University of Western Ontario, London, Ontario. 1971.
14. F. G. Bordwell and G. D. Cooper. J. Am. Chem. Soc. **73**, 5187 (1951).
15. J. F. King and D. J. H. Smith. J. Am. Chem. Soc. **89**, 4803 (1967).
16. F. G. Bordwell, J. M. Williams, jr., E. B. Hoyt, jr., and B. B. Jarvis. J. Am. Chem. Soc. **90**, 429 (1968).
17. D. Borrmann and R. Wegler. Chem. Ber. **99**, 1245 (1966).
18. F. I. Luknitskii and B. A. Vovsi. Dokl. Akad. Nauk SSR, **172**, 1327 (1967).
19. W. E. Truce and L. K. Liu. Chem. Ind. London, 457 (1969).
20. J. R. Norell. Chem. Commun. 1291 (1969).
21. O. Bayer. *In* Methoden der organischen Chemie (Houben-Weyl). Vol. 7. Part 1. 4th ed. Georg Thieme Verlag, Stuttgart. 1954. p. 430.
22. O. F. Vogl. U. S. Patent 3 454 527 (July, 1969); Chem. Abstr. **71**, P82057b (1969).
23. J. F. King and D. R. K. Harding. J. Am. Chem. Soc. **98**, 3312 (1976).
24. D. J. Cram. Fundamentals of carbanion chemistry. Academic Press, New York. 1965.

Conformational changes accompanying electronic excitation of trifluoronitrosomethane

R. D. GORDON, S. C. DASS, J. R. ROBINS, H. F. SHURVELL, AND R. F. WHITLOCK

Department of Chemistry, Queen's University, Kingston, Ont., Canada K7L 3N6

Received March 31, 1976

R. D. GORDON, S. C. DASS, J. R. ROBINS, H. F. SHURVELL, and R. F. WHITLOCK. Can. J. Chem. **54**, 2658 (1976).

The 690 nm absorption spectrum of CF_3NO has been studied in the gas phase at various temperatures and in the condensed phase at 77 K, and assigned to an ($n\pi^*$) transition. Analysis of the vibrational structure shows that, while only the eclipsed conformer is stable in the ground state, there are two stable isomers of comparable energy in the excited electronic state. One has an eclipsed conformation, but with the CF_3 group tilted away from the oxygen atom. The other has a staggered conformation. In both of the excited state isomers the barrier to internal rotation is higher than in the ground state.

R. D. GORDON, S. C. DASS, J. R. ROBINS, H. F. SHURVELL et R. F. WHITLOCK. Can. J. Chem. **54**, 2658 (1976).

Le spectre d'absorption à 690 nm de CF_3NO a été étudié en phase gazeuse à différentes températures et en phase condensée à 77 K et il fut assigné à une transition ($n\pi^*$). L'analyse de la structure vibrationnelle montre, qu'alors qu'il n'y a que le conformère éclipsé de stable à l'état fondamental, il y a deux isomères stables d'énergie comparable dans l'état électronique excité. L'un possède une conformation éclipsée mais avec le groupe CF_3 incliné dans la direction opposée de l'atome d'oxygène. L'autre possède une conformation décalée. Pour les deux isomères à l'état excité la barrière de rotation interne est plus élevée qu'à l'état fondamental.

[Traduit par le journal]

Introduction

CF_3NO, a blue gas, owes its colour to a weak ($f = 2.4 \times 10^{-4}$), structured absorption near 690 nm, shown in Fig. 1. Further weak absorption occurs at 270 nm and strong absorption begins near 240 nm. Mason (1) assigned the 690 nm system to an ($n\pi^*$) transition on the basis of its energy, intensity, and behaviour in different solvents. She was unable, however, to identify an electronic origin or to carry out a satisfactory vibrational analysis. CF_3NO belongs to group C_s and ($n\pi^*$) transitions are allowed with symmetry $A'' \leftarrow A'$. Similar $\tilde{A}^1A''$ ($n\pi^*$) $\leftarrow \tilde{X}^1A'$ transitions have been observed in other nitroso compounds such as HNO (2) and CH_3NO (3), and have been predicted theoretically (4, 5).

We have re-examined the 690 nm absorption spectrum of CF_3NO, in the gas phase at various temperatures and in the condensed phase at 77 K, and found that many of the vibrational bands record transitions involving the torsional mode, ν_{12}. Analysis shows that electronic excitation is accompanied by striking conformational changes, including a change in the phase of the barrier to internal rotation.

The ground state structure of CF_3NO has been determined by electron diffraction (6). The NO group is eclipsed by one of the CF bonds. Eleven of the twelve ground state fundamentals were assigned in a recent study of the infrared and Raman spectra (7), and combination and hot bands were used to estimate a frequency of about 50 cm^{-1} for ν_{12}'', the torsional mode. Attempts to observe the microwave spectrum of CF_3NO have failed (8).

Experimental Methods

CF_3NO was obtained from Penninsular Chemresearch Inc. Previous studies (7) showed that further purification was unnecessary.

Low resolution gas phase spectra (Fig. 1) were obtained on a Cary 14 spectrometer using a jacketed 10 cm cell maintained at five different temperatures in the range 205 to 358 K.

Medium resolution spectra (Fig. 2) were photographed on Kodak High Speed Infrared film, using a Bausch and Lomb 1.5 m grating spectrograph with resolution better than 0.5 cm^{-1}, and a 50 cm cell cooled by a Dry Ice/acetone bath. The vacuum wavenumbers listed in Table 1 were measured from these spectra which were calibrated by the emission from an iron/neon hollow cathode lamp (9).

A viscous liquid film (7) was produced when the gas was sprayed onto a CsI window cooled by liquid nitrogen

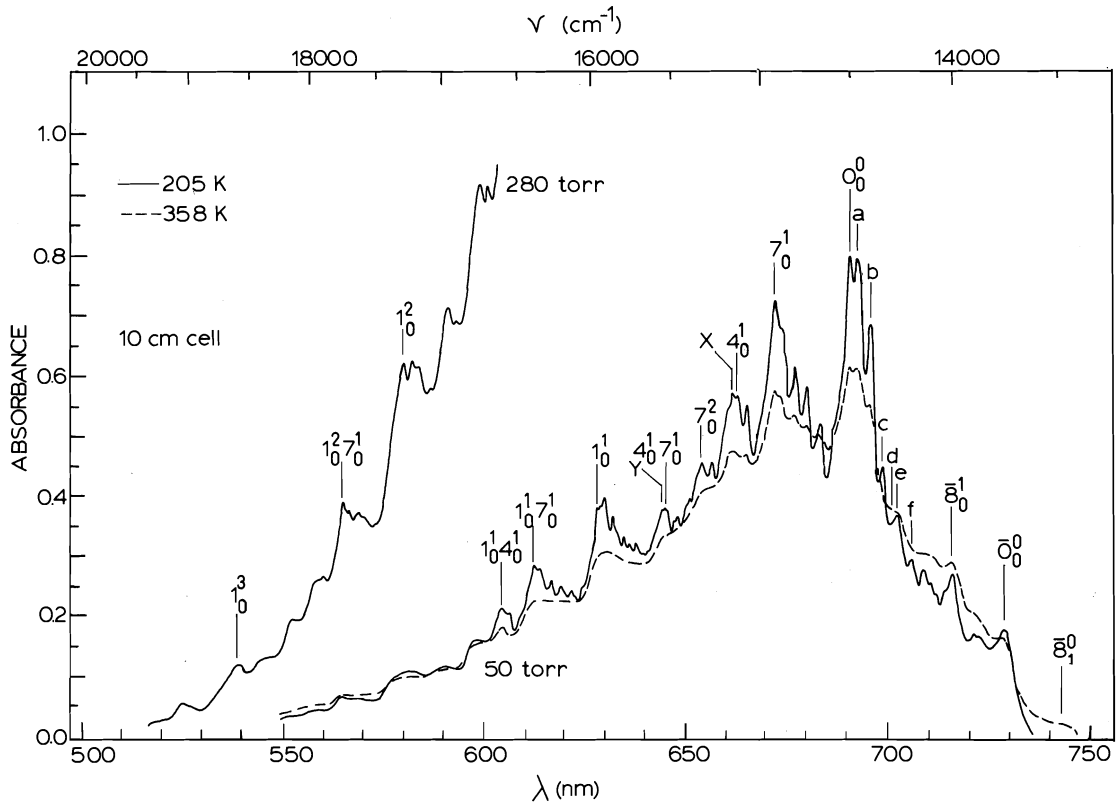

FIG. 1. Low resolution absorption spectrum of CF_3NO gas at 205 and 358 K.

in an Air Products and Chemicals Inc. Cryotip refrigerator. The spectrum of this film (Fig. 3) was recorded on a (single-beam) Perkin-Elmer E14 spectrometer. For comparison, a gas phase spectrum and a blank run were recorded at room temperature with the same cell, window, and spectrometer.

Upon prolonged exposure to fluorescent lights, or irradiation for several hours with a 150 W Xe lamp, CF_3NO gas changes irreversibly from blue, to green, and finally to yellow. The 690 nm system disappears and is replaced by new absorption (λ_{max} = 380 nm) between 540 and 340 nm. The continuous part of the new spectrum has been attributed (10) to the dimer $(CF_3)_2NONO$; superimposed on it are discrete bands attributable (11) to NO_2. The CF_3NO was shielded from room light, and protected by 0Y10 or Corning 2408 filters during absorption experiments. Under these conditions photodecomposition was slow, and in any case would not produce spurious absorption in the 550 to 750 nm region being studied.

Description of the Spectrum and Vibrational Analysis

The 690 nm absorption of CF_3NO gas, recorded under low resolution at 205 and 358 K, is shown in Fig. 1. Absorption maxima and their assignments are listed in Table 1 where the notation used is defined. A number of parent bands, labelled $N^{v'}_{v''}$, are each accompanied by a group of satellite bands. The parent bands are assigned to two systems, I and II, and those belonging to System I are distinguished by super bars. Vibrational frequencies in the ground and excited electronic states are collected in Table 2.

Portions of the medium resolution spectrum are shown in Fig. 2 where the low resolution maxima are seen to consist of groups of sharp features. This fine structure is irregular and differs from band to band. For example, the maximum 0^0_0 at 14 494 cm^{-1} is resolved into an unsymmetrical doublet with components at 14 492 and 14 496 cm^{-1}, while the maximum 7^1_0 consists of a triplet with components at 14 895, 14 899, and 14 905 cm^{-1}. The 'absorption maxima' listed in Table 1 are the estimated centers of these differently structured multiplets and uncertainties in defining their centers may contribute errors of several cm^{-1} to the listed

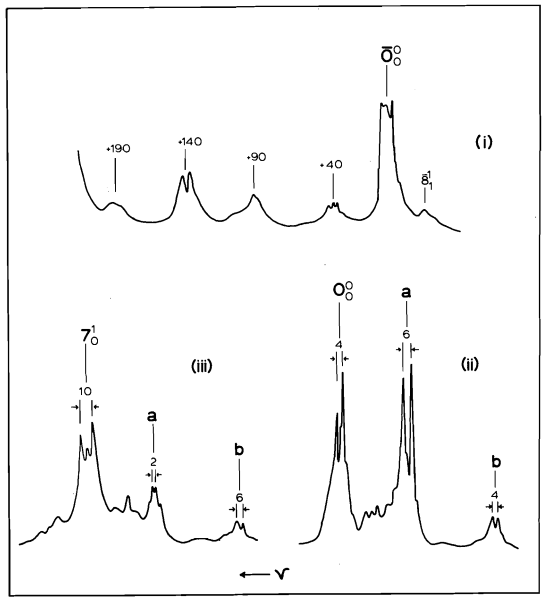

FIG. 2. Densitometer traces of parts of the medium resolution spectrum of CF_3NO gas. (*i*) System I origin and satellite bands. (*ii*) System II origin and (*iii*) 7_0^1 band and some of their satellites. Separations of multiplet components are given in cm^{-1}.

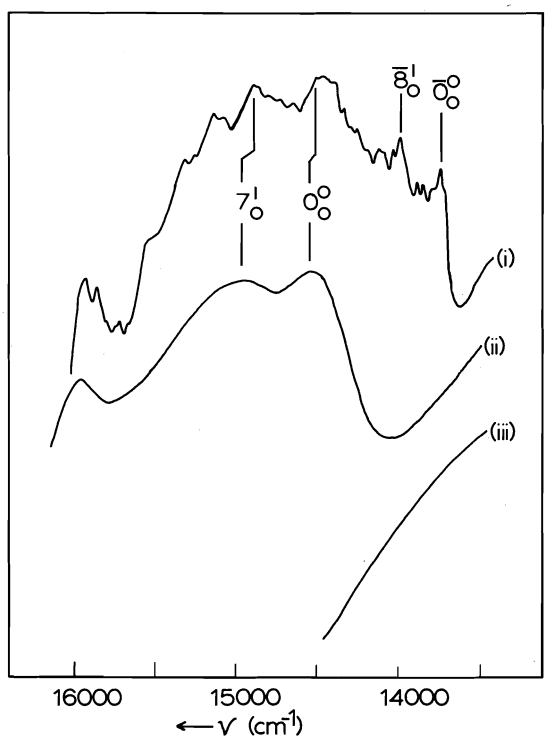

FIG. 3. Absorption of CF_3NO. (*i*) Gas phase, room temperature. (*ii*) Condensed (glassy liquid) phase, 77 K. (*iii*) Blank run with empty cell. Note that the photomultiplier response falls off sharply towards lower energies.

values. The observed features broaden at higher energies and above 15 200 cm^{-1} the multiplet structure is no longer resolved. There is every indication that additional fine structure could be observed under higher resolution conditions, but the present paper will deal only with the absorption maxima listed in Table 1.

The parent bands above 14 494 cm^{-1} (System II) are each accompanied by a group of satellite bands degraded towards *lower* energies and labelled *a–f*, corresponding to separations of approximately −50, −115, −180, −235, −255, and −320 cm^{-1}, respectively, from their parents. A weak feature 30 cm^{-1} to higher energies is assigned as satellite *g*. These satellites become more intense, relative to their parents, as the temperature is increased. However, this temperature dependence is small and precludes their assignment to sequences involving ground

TABLE 1. Absorption maxima in the 690 nm spectrum of CF_3NO (cm^{-1})

	*ν**	Assignment†		*ν**	Assignment†
w	13425	$\bar{8}_2^1$?		15520	Y ($\bar{1}_0^1\,\bar{7}_0^1$?)
	13455	$\bar{8}_1^0$ ($\bar{0}_0^0$ − 277)		15540	Y + 20
	13490	$\bar{8}_1^0$ + 40	w	15590	Y + 70
	13545	$\bar{8}_1^0$ + 90		15625	$1_0^1 f$
	13590	$\bar{8}_1^0$ + 140		15685	$1_0^1 e$
w	13706	$\bar{8}_1^1$?		15720	$1_0^1 d$; $7_0^2\,4_0^1 c$
	13732	$\bar{0}_0^0$ (System I Origin)		15755	$1_0^1 c$
	13769	$\bar{0}_0^0$ + 40	w	15795	$7_0^2\,4_0^1 b$
	13823	$\bar{0}_0^0$ + 90		15825	$1_0^1 b$
	13869	$\bar{0}_0^0$ + 140	w	15875	$7_0^2\,4_0^1 a$
	13920	$\bar{0}_0^0$ + 190		15885	$1_0^1 a$

TABLE 1. (*Concluded*)

	ν^*	Assignment†		ν^*	Assignment†
w	13953	$\bar{8}_1^2$?	w	15920	$7_0^2 4_0^1$
	13979	$\bar{8}_0^1 (\bar{0}_0^0 + 247)$		15940	$1_0^1 (0_0^0 + 1446)$
	14017	$\bar{8}_0^1 + 40$	w	16040	$1_0^1 7_0^1 f$
	14070	$\bar{8}_0^1 + 90$		16085	$1_0^1 7_0^1 e$
	14103	$\bar{7}_0^1$? $(\bar{0}_0^0 + 371)$		16165	$1_0^1 7_0^1 c$
	14122	$\bar{8}_0^1 + 140$		16225	$1_0^1 7_0^1 b$
	14170	$0_0^0 f$; $\bar{8}_0^1 + 190$		16300	$1_0^1 7_0^1 a$
	14238	$0_0^0 e$	w	16320	$7_0^3 4_0^1$
	14265	$0_0^0 d$		16350	$1_0^1 7_0^1$
	14317	$0_0^0 c$		16500	$1_0^1 4_0^1 a$
	14378	$0_0^0 b$		16550	$1_0^1 4_0^1$
w	14415	$8_1^1 a$?		16675	$1_0^1 7_0^2 a$
	14442	$0_0^0 a$		16730	$1_0^1 7_0^2$
w	14470	8_1^1 ?		16885	$1_0^1 4_0^1 7_0^1 a$
	14494	0_0^0 (System II Origin)		16940	$1_0^1 4_0^1 7_0^1$
w	14530	$0_0^0 g$	w	17070	$1_0^2 e$
	14579	$7_0^1 f$		17150	$1_0^2 c$
	14645	$7_0^1 e$		17210	$1_0^2 b$
	14665	$7_0^1 d$		17275	$1_0^2 a$
	14717	$7_0^1 c$		17330	$1_0^2 (1_0^1 + 1390)$
	14778	$7_0^1 b$	w	17470	$1_0^2 7_0^1 e$
w	14810	$7_0^1 8_1^1 a$?		17560	$1_0^2 7_0^1 c$
	14845	$7_0^1 a$		17610	$1_0^2 7_0^1 b$
	14870	$7_0^1 8_1^1$?		17675	$1_0^2 7_0^1 a$
	14900	$7_0^1 (0_0^0 + 406)$		17730	$1_0^2 7_0^1$
w	14925	$7_0^1 g$; $4_0^1 c$		17880	$1_0^2 4_0^1 a$
	14980	$4_0^1 b$		17930	$1_0^2 4_0^1$
	15045	$4_0^1 a$		18120	$1_0^2 7_0^2$
	15100	$4_0^1 (0_0^0 + 606)$		18540	$1_0^3 b$
	15135	X $(\bar{1}_0^1$?; $\bar{0}_0^0 + 1403)$		18600	$1_0^3 a$
w	15160	X + 25		18660	$1_0^3 (1_0^2 + 1330)$
	15245	$7_0^2 a$		19010	$1_0^3 7_0^1 a$
	15305	7_0^2		19060	$1_0^3 7_0^1$
	15325	$4_0^1 7_0^1 c$		19260	$1_0^3 4_0^1$
	15370	$4_0^1 7_0^1 b$		19450	$1_0^3 7_0^2$
	15445	$4_0^1 7_0^1 a$		19930	$1_0^4 (1_0^3 + 1270)$
	15500	$4_0^1 7_0^1$		20350	$1_0^4 7_0^1$

*The absorption maxima appear as single peaks or shoulders under low resolution (Fig. 1), but between 13 700 and 15 200 cm^{-1} most of them can be resolved into multiplets under medium resolution (Fig. 2), and the frequencies listed correspond to the centers of these multiplets. An uncertainty of 1–3 cm^{-1} is probably involved in estimating the centers of the multiplets. At higher and lower energies multiplet structure is no longer resolved and the frequencies listed are accurate only to ± 5–10 cm^{-1}. Bands marked w are weak relative to their immediate neighbours.

†$N_{v''}^{v'}$ denotes a ($v' \leftarrow v''$) transition in mode N, using the numbering of ref. 7. Fundamental frequencies are listed in Table 2. A super bar distinguishes bands of System I. Assignments marked ? are tentative. Letters a–g denote satellites in System II, separated from their parents by approximately -50, -115, -180, -235 (shoulder), -255, -320, and $+30$ (weak) cm^{-1}, respectively.

state levels higher than 125 cm^{-1}. Since the lowest ground state fundamental, other than the torsional mode, is 296 cm^{-1} (7), we associate these satellites with the torsional mode and discuss them in the following section.

A different pattern of satellite bands, degraded towards *higher* energies, accompanies the parent bands below 14 000 cm^{-1} (System I), and this is one of the reasons for assigning them to a separate system. These satellites, best

TABLE 2. Totally-symmetric fundamentals active in the 690 nm spectrum of CF_3NO (cm^{-1})

Description	Ground state*	Excited state†	
		System I	System II
ν_1 NO stretch	1594	1403?	1446‡
ν_4 (CN stretch)	810	—	606
ν_7 (skeletal bend)	427	371?	406
ν_8 CF_3 rock	296, 277†§	247	—

*Infrared and Raman, from ref. 7. Since there is extensive mixing of symmetry coordinates in ν_4 and ν_7, the descriptions in parentheses are only approximate.
†This work. Tentative assignments are marked ?.
‡Successive intervals are 1446, 1390, 1330, and 1270 cm^{-1}.
§Hot band in electronic spectrum.

seen in Fig. 2*i*, are separated from their parents by approximately 40, 90, 140, and 190 cm^{-1}. Their temperature dependence seems to be greater than that of their counterparts in System II, but this effect is probably due to underlying hot bands of the stronger System II.

Temperature dependence studies of the parent bands show that only the weak band at 13 455 cm^{-1} can be assigned to a hot transition, and that it involves a ground state level excited by 280 ± 50 cm^{-1}. Since its separation from the lowest-energy cold band at 13 732 cm^{-1} is close to ν_8'', it is assigned as $\bar{8}_1^0$. The 13 732 cm^{-1} band is taken as the origin ($\bar{0}_0^0$) of System I, and a band 247 cm^{-1} to higher energies is assigned $\bar{8}_0^1$.

A quite different vibrational pattern begins with the strong band at 14 494 cm^{-1} which is taken as the origin (0_0^0) of System II. Progressions in 1446 (ν_1'), 606 (ν_4'), and 406 cm^{-1} (ν_7') are observed, but the 247 cm^{-1} interval $\bar{\nu}_8'$ is not found.

Two distinct absorption systems have been assigned in this region on the basis of differing vibrational structures and satellite band patterns. Further evidence is shown in Fig. 3 which compares the spectrum of the gas at 295 K to that of the glassy liquid at 77 K. In the condensed phase the bands assigned to System II broaden and are blue-shifted by 50 to 100 cm^{-1}, but System I disappears completely. Extrapolation to 77 K of the gas-phase temperature dependence studies shows that this is not merely a temperature effect; bands $\bar{0}_0^0$ and $\bar{8}_0^1$ are not hot. Rather, we believe that a medium-dependent (gas-glassy liquid) shift occurs, and that it is much larger (>600 cm^{-1}) for System I than for System II.

Walsh's rules (ref. 12 and following articles), *ab initio* calculations (4), and the observed spectra of HNO (2) and CH_3NO (3) all suggest that ($n\pi^*$) excitation of CF_3NO should lead to a lengthening of the NO bond, an opening of the C—N—O angle, and perhaps a small shortening of the CN bond, and that the corresponding vibrations should be active in the spectrum. These expectations are borne out in System II. The main progression, successive members of which are separated by 1446, 1390, 1330, and 1270 cm^{-1}, must record the excited state NO stretching mode, ν_1'. A reduction in frequency from the ground state value of 1594 cm^{-1} is consistent with bond lengthening, and a simple one-dimensional Franck–Condon analysis (13), ignoring anharmonicity, suggests a change of 0.03 to 0.04 Å in r_{NO}. (Compare 0.03 Å in HNO (2).)

Shorter progressions in 606 and 406 cm^{-1} are assigned to ν_4' and ν_7', respectively. A normal coordinate analysis of the ground state (7) indicates that these modes involve substantial C—N—O angle bending and C—N bond stretching as well as motions within the CF_3 group. Since extensive mixing of these coordinates is likely also in the excited state, no Franck–Condon analysis was attempted.

An unexpected observation in System I is the activity of ν_8, the a' CF_3 rocking mode, which suggests that the angle θ (Fig. 6) between the CN bond and the symmetry axis of the CF_3 group changes upon excitation. A Franck–Condon calculation (13), assuming the ground

state normal coordinates (7), suggests that the change may be as large as 5 to 8 deg.

Higher-frequency modes of System I can be assigned only tentatively because of the onset of stronger absorption due to System II. Bands at 14 103, 15 135 (labelled X), and 15 520 cm^{-1} (labelled Y) could be assigned as $\overline{7}_0^1$, $\overline{1}_0^1$, and $\overline{1}_0^1\overline{7}_0^1$ respectively, yielding values of 371 cm^{-1} for $\bar{\nu}_7'$ and 1403 cm^{-1} for $\bar{\nu}_1'$. Bands X and Y occur within the System II absorption region, but lack the satellites characteristic of System II parent bands. Rather, each is accompanied by diffuse features at higher energies. If these assignments are correct, excitation in System I must be accompanied by geometrical changes similar to those described above for System II.

Satellite Band Structure and the Barriers to Internal Rotation in the Ground and Excited Electronic States

Computational Methods

The temperature dependence of the satellite bands indicates that they record transitions involving torsional levels. In order to explore this hypothesis, the expected energies and intensities of such transitions were calculated.

If interaction with other types of motion is neglected, internal rotation in CF_3NO is governed by the Schrödinger equation (14)

$$[1] \qquad \left[-F\frac{d^2}{d\phi^2} + U - E_{v\sigma}\right]\psi_{v\sigma} = 0$$

where $U = \frac{1}{2}V_3(1 - \cos 3\phi) + \frac{1}{2}V_6(1 - \cos 6\phi) + \cdots$, ϕ is the torsional angle, F is the reduced rotational constant for internal rotation (14), and V_3 is the height of the barrier to internal rotation. The second and higher terms in the potential U are usually small and have been neglected here. The allowed torsional states are labelled[1] by their vibrational quantum numbers $v = 0, 1, \ldots$, and symmetry species $\sigma = a$ or e.

[1]If internal rotation is considered to be a 'feasible' operation, the non-rigid (15) molecule CF_3NO can be assigned to a group isomorphous with C_{3v}, and its torsional levels assigned to species $\sigma = a_1$, a_2, or e. For even values of v, $\sigma = a_1$ or e; for odd v, $\sigma = a_2$ or e. Since only a_1–a_1, a_2–a_2, and e–e transitions are allowed in the electronic spectrum, the simplified notation $(v'\ v'')_\sigma$ is used to label transitions. Note that for even values of Δv both a (*i.e.* a_1–a_1 or a_2–a_2) and e transitions are allowed, but for odd Δv only e transitions are permitted.

Following the method of Lewis *et al.* (16), the Hamiltonian matrix corresponding to eq. [1] was set up in terms of sine and cosine basis functions and diagonalized to yield energies $E_{v\sigma}$ and wave functions $\psi_{v\sigma}$ for assumed values of the parameters F and V_3. Transition energies $(E' - E'')$ and relative intensities $[|\langle\psi'|\psi''\rangle|^2 \exp(-E''/kT)]$ were then calculated for various transitions $(v'\ v'')_\sigma$. Although the e levels are doubly degenerate, consideration of nuclear spin statistics for the CF_3 group shows that a and e levels should be assigned equal weights.

An internal rotation constant $F'' = 2.44\ cm^{-1}$ can be calculated from the known ground state structure (6). ($r_{CF} = 1.321$, $r_{CN} = 1.555$, $r_{NO} = 1.171$ Å; F—C—F = 111.9°, C—N—O = 121.0°; the symmetry axis of the CF_3 group makes a small angle $\theta = +1.3$ deg with the CN bond (Fig. 6); F is independent of the torsional angle ϕ.) Various F' values, ranging from 2.0 to 3.1 cm^{-1} and all corresponding to plausible excited state structures, were used in trial calculations. A likely excited state structure ($r_{NO} = 1.20$ Å, $r_{CF} = 1.324$ Å, C—N—O = 129°, $\theta = 0°$, other parameters as in the ground state) yields $F' = 2.80\ cm^{-1}$.

Trial calculations revealed the satellite band patterns to be expected. Typical energy levels and transitions are illustrated in Figs. 4, 5, and 6.

If the barriers V_3' and V_3'', in the excited and ground electronic states respectively, are in phase (eclipsed conformation in both states), the most important transitions form a $\Delta v = 0$ sequence as would be expected from simple Franck–Condon considerations. The spacings between successive satellite bands are differences between excited and ground state intervals. If $V_3' > V_3''$, the satellites degrade towards *higher* energies. If $V_3' < V_3''$, they degrade to *lower* energies and, since V_3'' must then be fairly large, the intensities of successive bands decrease rapidly because of their low Boltzmann factors (Fig. 4*i*).

If, on the other hand, the barriers are out of phase (staggered conformation in the excited state), progressions rather than sequences are expected as illustrated in Fig. 4*ii*. The strongest transition in absorption is from $v'' = 0$ to a level just above the summit of the excited state barrier. Satellite bands run to *lower* energies, each recording transitions with a given value of Δv, and their separations correspond to vibra-

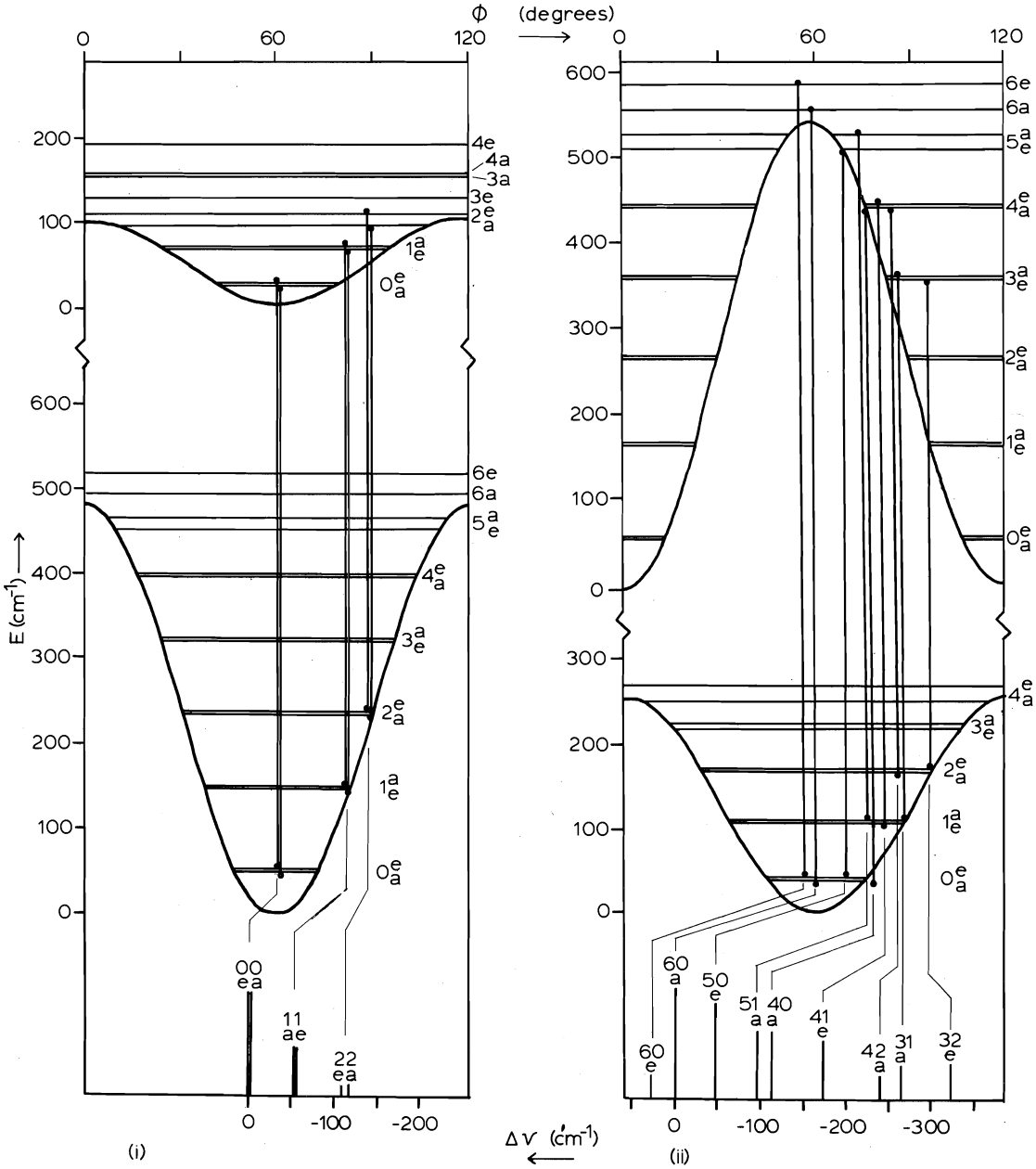

FIG. 4. Potential curves, energy levels, principal transitions, and calculated satellite band structure for electronic transitions involving the torsional mode in CF_3NO. Torsional angles ϕ of 0, 120, 240 deg correspond to a staggered conformation; 60, 180, 300 deg correspond to an eclipsed conformation. (*i*) Barriers in phase. $V_3' = 100$, $F' = 2.80$, $V_3'' = 480$, $F'' = 2.44$ cm^{-1}. (*ii*) Barriers out of phase. $V_3' = 550$, $F' = 2.80$, $V_3'' = 250$, $F'' = 2.44$ cm^{-1}.

tional intervals rather than the differences between vibrational intervals. Since V_3'' need not be large, the intensities of successive bands need not decrease too rapidly.

System II

An extensive pattern of satellites, degraded towards *lower* energies with an average separation of 60 cm^{-1}, is attached to each of the

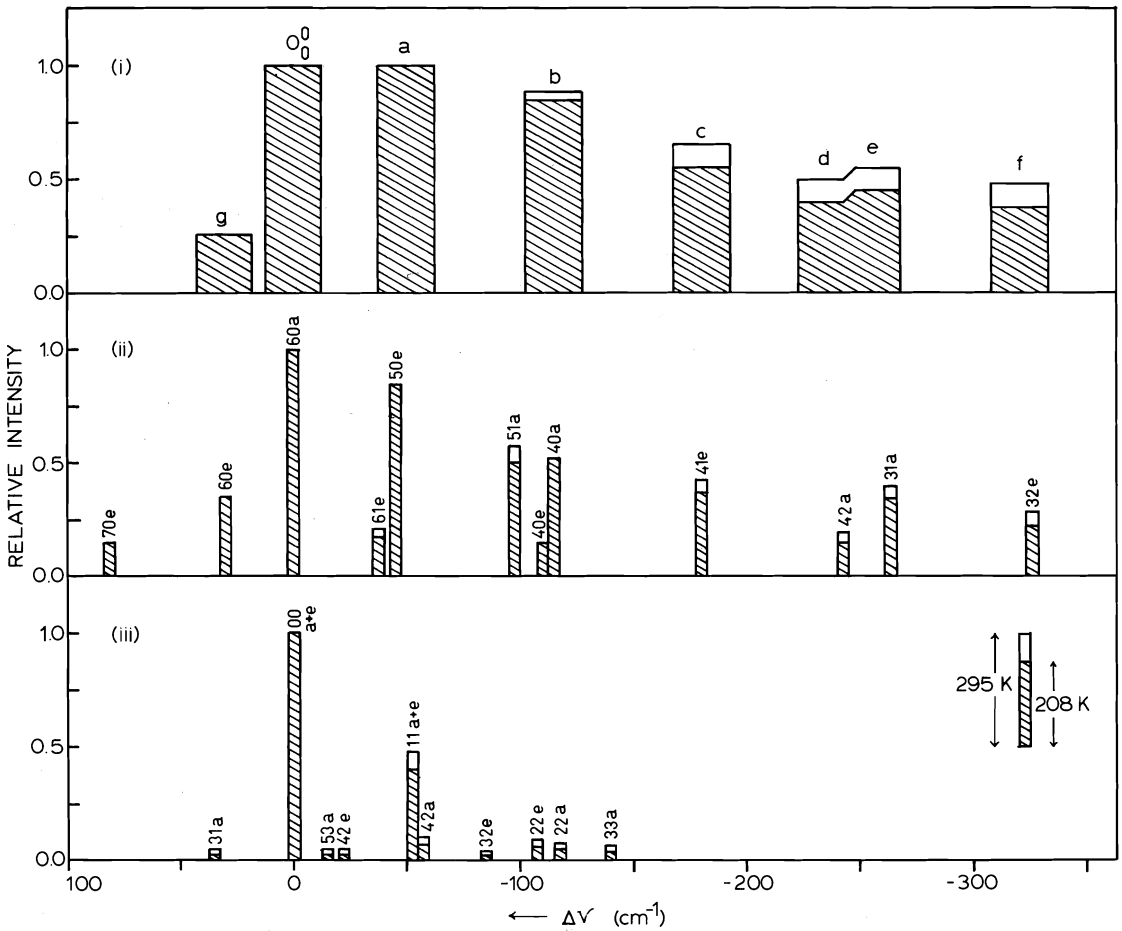

FIG. 5. Observed and calculated satellite band structure in system II of CF_3NO at 208 and 295 K. Intensities are relative to those of the parent band. (*i*) Observed satellites attached to 0_0^0. (*ii*) Calculated spectrum barriers, out of phase. $V_3' = 550$, $F' = 2.80$, $V_3'' = 250$, $F'' = 2.44$ cm^{-1}. A few weak transitions are predicted at energies lower than those plotted, but these, as well as the weak $7O_e$ transition at $+81$ cm^{-1}, would be hidden under stronger features belonging to other parent bands. (*iii*) Calculated spectrum, barriers in phase. $V_3' = 100$, $F' = 2.80$, $V_3'' = 480$, $F'' = 2.44$ cm^{-1}.

parent bands of System II. The pattern observed at 208 and at 295 K is depicted in Fig. 5*i*.

If the ground and excited state barriers are in phase, V_3'' must be considerably larger than V_3' to account for the degradation to lower energies and the fairly wide band spacings. The energy levels and spectrum calculated for $V_3' = 100$, $F' = 2.80$, $V_3'' = 480$, and $F'' = 2.44$ cm^{-1} are shown in Figs. 4*i* and 5*iii* where it can be seen that the calculated intensities decrease much more rapidly than is observed. A less rapid decline might be expected for lower values of both barriers, but as V_3' approaches zero, many weak, irregularly spaced, $\Delta v \neq 0$ transitions are predicted to accompany the strong $(0\ 0)_{a+e}$ band, again contrary to observation. Using a wide range of parameters, we were unable to calculate a satellite spectrum having the observed spacings, yet with significant intensity in more than two of its members; hence we reject the assumption of in-phase barriers.

Better agreement can be obtained if the barriers are assumed to be out of phase. Trial calculations showed that the strongest transition must be $(v'_{max},0)_a^e$ (upper and lower symmetry species for odd or even values of v'_{max}, respectively) where level $v'_{max_a}{}^e$ lies just above the sum-

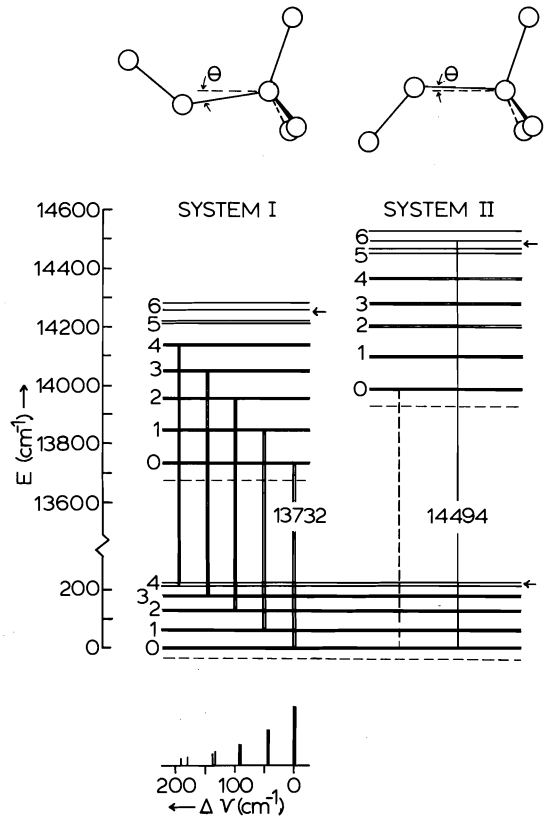

FIG. 6. Top left: CF_3NO in the eclipsed conformation with large θ. Top right: staggered conformation with small θ. Angle θ is considered positive if the CF_3 symmetry axis intersects the NO bond. Bottom left: calculated energy levels and satellite spectrum for System I. $V_3' = 575$, $F' = 2.80$, $V_3'' = 250$, $F'' = 2.44$ cm^{-1}, barriers in phase, temperature = 208 K. Horizontal broken lines mark the minima of the potential curves and arrows the tops of the barriers. The 13 732 cm^{-1} transition is $\bar{0}_0^0$. Bottom right: calculated energy levels for System II plotted on the same scale, using the parameters of Fig. 4*ii*. The 14 494 cm^{-1} transition has been referred to as 0_0^0, but is really 12_{0a}^{6a}. The true origin, which was not observed, is shown by the broken line transition.

mit of the excited state barrier. Furthermore, satellite *a*, 50 cm^{-1} lower in energy, must include transition $(v'_{max} - 1,0)_e^a$. These constraints served to fix $v'_{max} = 6$, and limit V_3' to the range 500 to 600 cm^{-1} depending on the value chosen for F'. Finally, transitions $(5\ 1)_a$ and $(4\ 1)_e$ are expected to make important contributions to satellites *b* and *c* respectively, thus fixing $V_3'' \approx 250$ cm^{-1} for $F'' = 2.44$ cm^{-1}.

The calculated energy levels and spectrum for $V_3' = 550$, $F' = 2.80$, $V_3'' = 250$, and $F'' = 2.44$ cm^{-1} are shown in Figs. 4*ii* and 5*ii* where it can be seen that agreement with experiment is much better. Satisfactory fits could, in fact, be obtained for a rather wide range of parameters: V_3' 525 to 625 cm^{-1} for F' between 3.0 and 2.5 cm^{-1}, and V_3'' 225 to 275 cm^{-1} for $F'' = 2.44$ cm^{-1}. Thus we conclude that the equilibrium conformation of CF_3NO changes from eclipsed in the ground state to staggered in the excited state of System II. The barrier to internal rotation increases from about 250 to about 550 cm^{-1} upon excitation, but these values may be in error as much as 20%.

The value $V_3'' \approx 250$ cm^{-1} corresponds to a separation of 68 cm^{-1} between the $v = 1$ and $v = 0$ torsional levels of the ground state, chosen to match the observed spectrum. A value of 50 cm^{-1} was estimated for the same interval from combination and hot bands in the infrared and Raman spectra (7), corresponding to a barrier height $V_3'' \approx 150$ cm^{-1}. In view of the uncertainties in both these observed quantities, the two estimates for V_3'' are not irreconcilable.

It should be noted that, according to the interpretation above, band 0_0^0 is not the true origin of System II, but rather is transition 12_{0a}^{6a}. The true origin, which is Franck–Condon forbidden and was not observed, would lie near 14 000 cm^{-1} as shown by the broken line transition in Fig. 6.

The spectrum calculated above accounts for the gross structure of the satellite bands in System II, but not for the finer details shown in Fig. 2*ii* and *iii*. A more detailed interpretation would have to consider not only torsion/internal rotation but also end-over-end rotation and the interaction between these motions. These interactions would be particularly strong and complicated for levels close to the top of the torsional barrier and their treatment is beyond the scope of this paper. The observed difference in fine structure between a satellite attached to 0_0^0 and its counterpart attached to 7_0^1 suggests that interactions with other vibrational modes are also important.

System I

The parent bands of System I are accompanied by satellites running to higher energies and separated by 40 to 50 cm^{-1} intervals as shown in Fig. 2*i*. Positive-running satellites are

expected only if the ground and excited state barriers are in phase and $V_3' > V_3''$. The observed spacings can be reproduced on this assumption as shown on the left of Fig. 6, calculated for $V_3' = 575\ cm^{-1}$, $F' = 2.80\ cm^{-1}$, and the previously determined ground state parameters. However, the observed intensities do not fall off smoothly towards higher energies as predicted; in particular, the $+140\ cm^{-1}$ satellite, assigned to the $(3\ 3)_{a+e}$ transition, is unexpectedly strong. It is too close to its parent to record a new fundamental, especially since the lowest frequency a' mode, ν_8', has already been assigned. And although hot bands of System II must contribute to the background absorption in this region, no strong hot band is expected to coincide with one of the $+140\ cm^{-1}$ satellites.

A more plausible explanation for the anomalous intensity of this satellite is perturbation by low-lying torsional levels of System II. As shown in Fig. 6, the $v' = 3$ torsional level of System I should lie just above the lowest level of System II, their exact relative positions depending on the parameters chosen. If this explanation is correct, the low-lying levels of System II should also be perturbed, but this could not be checked since transitions to the $v' = 0$, and 1 levels of System II were not observed.

Thus we conclude that the excited state of System I has an eclipsed conformation and a barrier V_3' of approximately $575\ cm^{-1}$. The eclipsed conformation is at first surprising since the staggered conformation of System II suggests that ($n\pi^*$) excitation favours an increase in the shorter O...F distance. However, this distance can also be increased by tilting the CF_3 group away from the oxygen atom, as shown on the top left of Fig. 6, and a substantial change in the angle θ has already been inferred from the activity of ν_8.

The Nature of the Two Band Systems

Ab initio calculations for the related molecules HNO (4) and CH_3NO (5) predict only one excited electronic state ($^1A''$, $n\pi^*$) in the 14 000 cm^{-1} region, and for each molecule only one electronic transition has been observed (2, 3). Furthermore, the calculations predict unusually large gaps between this state, the next higher excited state, and the very low-lying ($^3A''$, $n\pi^*$) state. Thus it would be surprising if two excited electronic states, separated by only about $250\ cm^{-1}$, were to occur near $14\ 000\ cm^{-1}$ in CF_3NO.

We suggest instead that Systems I and II record transitions to *two different conformational isomers* of a single excited electronic state, as shown at the top of Fig. 6. The potential surface in this state would have two inequivalent sets of minima, differing in energy by approximately $250\ cm^{-1}$, and corresponding, respectively, to an eclipsed conformation with a moderately large angle θ, and to a staggered conformation with θ close to its ground state value of 1.3°.

Two isomers of comparable energy can reasonably be expected in the excited state since there are two ways in which relatively long O...F distances can be achieved. In the ground state, however, where a shorter O...F distance is favoured, only one conformation (eclipsed, small θ) is suitable, and only one isomer has been observed (6). The spectrum of the glassy liquid (Fig. 3) suggests that the eclipsed excited state isomer is destabilized in the condensed phase.

Conclusions

The 690 nm absorption of CF_3NO leads to an ($n\pi^*$) excited state with two stable isomers. The lower energy isomer has an eclipsed conformation, as in the ground state, but the CF_3 group is tilted away from the oxygen atom by an angle θ which may be as large as 5–8 deg. The second isomer, approximately $250\ cm^{-1}$ (0.7 kcal/mol) higher in energy, has a staggered conformation and a small or zero tilt angle θ. Excitation is also accompanied by a lengthening of r_{NO}, and probably also by changes in r_{CN} and angle C—N—O, as would be expected.

The observed spectra can be reproduced by assuming barrier heights V_3 of $250\ cm^{-1}$ (0.7 kcal/mol) in the ground state, and 575 and $550\ cm^{-1}$ ($\sim$1.6 kcal/mol), respectively, in the lower and higher energy isomers of the excited state; these values, however, may be in error by 20% or more.

To our knowledge, a change in the phase of the barrier to internal rotation upon electronic excitation has not previously been observed experimentally. Dixon and Kroto (3) mentioned such a possibility in their study of the 670 nm spectrum of CH_3NO but rejected it as unlikely.

However, a subsequent microwave determination (17) of the ground state barrier conflicts with their interpretation, and a re-examination of the CH_3NO spectrum is in progress in this laboratory. Theoretical calculations, however, indicate that conformational changes can be expected to accompany electronic excitation. A study of FCH_2OH (18) predicts both a change in phase of the barrier to internal rotation and an increase in the number of minima in the potential surface.

NOTE ADDED IN PROOF: After this work had been submitted for publication, the microwave spectrum of CF_3NO was reported (19). The ground state barrier V_3'' was determined to be 770 ± 50 cal mol^{-1} (269 ± 17 cm^{-1}), in excellent agreement with the value (250 cm^{-1}) reported here.

Acknowledgments

The authors are grateful to the National Research Council of Canada and to Queen's University for financial support.

1. J. MASON. J. Chem. Soc. 3904 (1957).
2. F. W. DALBY. Can. J. Phys. **36**, 1336 (1958). M. J. Y. CLEMENT and D. A. RAMSAY. Can. J. Phys. **39**, 205 (1961). J. L. BANCROFT, J. M. HOLLAS, and D. A. RAMSAY. Can. J. Phys. **40**, 322 (1962).
3. R. N. DIXON and H. W. KROTO. Proc. Roy. Soc. Ser. A, **283**, 423 (1964).
4. A. A. WU, S. D. PEYERIMHOFF, and R. J. BUENKER. Chem. Phys. Lett. **35**, 316 (1975).
5. T.-K. HA and U. P. WILD. Chem. Phys. **4**, 300 (1974).
6. M. I. DAVIS, J. E. BOGGS, D. COFFEY, JR., and H. P. HANSON. J. Phys. Chem. **69**, 3727 (1965).
7. H. F. SHURVELL, S. C. DASS, and R. D. GORDON. Can. J. Chem. **52**, 3149 (1974).
8. J. E. BOGGS, D. COFFEY, JR., and J. C. DAVIS, JR. J. Phys. Chem. **68**, 2383 (1964).
9. H. M. CROSSWHITE. J. Res. Nat. Bur. Stand. **79A**, 17 (1975).
10. R. N. HAZELDINE and J. H. MATTISON. J. Chem. Soc. 1741 (1957). J. MASON. J. Chem. Soc. 4351 (1963); 4537 (1963).
11. T. C. HALL and F. E. BLACET. J. Chem. Phys. **20**, 1745 (1952).
12. A. D. WALSH. J. Chem. Soc. 2260 (1953).
13. J. B. COON, R. E. DEWAMES, and C. M. LOYD. J. Mol. Spectrosc. **8**, 285 (1962).
14. D. R. HERSCHBACH. J. Chem. Phys. **31**, 91 (1959). K. D. MÖLLER and W. G. ROTHSCHILD. Far-infrared spectroscopy. Wiley-Interscience, New York. 1971.
15. H. C. LONGUET-HIGGINS. Mol. Phys. **6**, 445 (1963).
16. J. D. LEWIS, T. B. MALLOY, JR., T. H. CHAO, and J. LAANE. J. Mol. Struct. **12**, 427 (1972).
17. D. COFFEY, JR., C. O. BRITT, and J. E. BOGGS. J. Chem. Phys. **49**, 591 (1968).
18. S. WOLFE, L. M. TEL, W. J. HAINES, M. A. ROBB, and I. G. CSIZMADIA. J. Am. Chem. Soc. **95**, 4863 (1973).
19. P. H. TURNER and A. P. COX. Chem. Phys. Lett. **39**, 585 (1976).

Organometallic peroxy radicals. Part II. A kinetic electron spin resonance study of some organogermylperoxy radicals[1,2]

JAMES ANTHONY HOWARD AND JOHN CHARLES TAIT[3]

Division of Chemistry, National Research Council of Canada, Ottawa, Canada K1A 0R9

Received March 4, 1976

JAMES ANTHONY HOWARD and JOHN CHARLES TAIT. Can. J. Chem. **54**, 2669 (1976).

Trimethylgermylperoxy and triphenylgermylperoxy have been prepared and their kinetic behaviour investigated by electron spin resonance techniques. At low temperatures (< -50 °C) these radicals exist in equilibrium with the tetroxide. The thermodynamic parameters for this equilibrium ($-\Delta H^0 \approx 11.5$ kcal mol^{-1} and $-\Delta S^0 \approx 26.5$ cal deg^{-1} mol^{-1}) are the same, within experimental error, for both radicals. Above -50 °C $(CH_3)_3GeO_2$ and $(C_6H_5)_3GeO_2$ decay irreversibly by a unimolecular process. $(C_6H_5)_3GeO_2$ is slightly less stable than $(CH_3)_3GeO_2$ although both radicals appear to fit an Arrhenius equation of the approximate form log $(k_{epr}{}^1/s^{-1}) \approx 5 - 6/\theta$ where $\theta = 2.303RT$ kcal mol^{-1}.

JAMES ANTHONY HOWARD et JOHN CHARLES TAIT. Can. J. Chem. **54**, 2669 (1976).

On a préparé les radicaux triméthylgermylperoxy et triphénylgermylperoxy et on a étudié leur comportement cinétique par les techniques de résonance paramagnétique électronique. A basse température (< -50 °C) ces radicaux existent en équilibre avec le tétraoxyde. Dans les limites des erreurs expérimentales, les paramètres thermodynamiques pour cet équilibre ($-\Delta H^0 \approx 11.5$ kcal mol^{-1} et $-\Delta S^0 \approx 26.5$ cal deg^{-1} mol^{-1}) sont les mêmes pour les deux radicaux. Au dessus de -50 °C les radicaux $(CH_3)_3GeO_2$ et $(C_6H_5)_3GeO_2$ se décomposent d'une façon irréversible par un processus unimoléculaire. Le $(C_6H_5)_3GeO_2$ est un peu moins stable que le radical $(CH_3)_3GeO_2$; il semble toutefois que la décomposition des deux radicaux suit une équation d'Arrhénius de la forme approximative log $(k_{epr}{}^1/s^{-1}) \approx 5 - 6/\theta$ où $\theta = 2.303RT$ kcal mol^{-1}.

[Traduit par le journal]

Introduction

Hydrocarbon peroxy radicals have been thoroughly studied by kinetic electron spin resonance spectroscopy (KESR) and the kinetics and mechanisms for their self-reaction are now reasonably well understood (1–6). There has, however, been only one preliminary report of the related Group IVb organometallic peroxy radicals and that was concerned primarily with their preparation and esr spectra (7). We now report the results of a detailed KESR study of the decay of two typical organogermylperoxy radicals, $(CH_3)_3GeO_2$ and $(C_6H_5)_3GeO_2$. This study has revealed some intriguing differences in the kinetic behavior of hydrocarbon peroxy and organogermylperoxy radicals.

Experimental

Materials

Trimethylgermane was prepared by reduction of trimethylgermyl bromide (Pierce Chem. Co.) with tri-*n*-butyltin hydride (Ventron, Alfa Products). Triphenylgermane was prepared from the bromide (Alfa Inorganics Inc.) by reduction with lithium aluminum hydride. The crude product was recrystallized from *n*-pentane; mp 47 °C, lit. (8) mp 42.5–45 °C. Tetramethylgermane was obtained from Ventron, Alfa Products. Triphenylgermyl hydroperoxide was prepared from triphenylgermyl bromide by the method of Dannley and Farrant (9).

Radical Production

Trimethylgermylperoxy and triphenylgermylperoxy radicals were produced in a silica tube (Suprasil, 4 mm o.d.) directly in the cavity of a Varian E-4 ESR spectrometer by photolyzing di-*t*-butyl peroxide (5%) in oxygen saturated toluene, cyclopropane, or cyclopentane containing the organogermyl hydride.

$$t\text{-BuOOBu-}t \xrightarrow{h\nu} t\text{-BuO}^\cdot$$

$$t\text{-BuO}^\cdot + R_3GeH \rightarrow t\text{-BuOH} + R_3Ge^\cdot$$

$$R_3Ge^\cdot + O_2 \rightarrow R_3GeO_2$$

where R is CH_3 or C_6H_5.

Trimethylgermylperoxyl was also prepared from trimethylgermyl bromide and sodium atoms in a matrix of cyclopentane in a rotating cryostat (10).

Kinetic Procedure

Kinetic and thermodynamic parameters for irreversible and reversible radical decays were determined by kinetic electron spin resonance techniques (2–6).

[1]For Part I see ref. 7.

[2]NRCC No. 15330.

[3]NRCC Research Associate 1975–1976.

Can. J. Chem. Downloaded from www.nrcresearchpress.com by 210.87.254.105 on 09/05/12
For personal use only.

Can. J. Chem. Downloaded from www.nrcresearchpress.com by 210.87.254.105 on 09/05/12
For personal use only.

Results

Trimethylgermylperoxyl

A broad singlet esr spectrum centered at $g = 2.0245$ was obtained when a mixture of trimethylgermane and di-*t*-butyl peroxide (DTBP) was photolyzed in an oxygenated solvent at −90 °C, which was attributed to $(CH_3)_3GeO_2$ (7). At this temperature the radical did not decay irreversibly when the light was shuttered. As the temperature was raised gradually the radical concentration increased and did not decay until about −55 °C. In the temperature range −55 to −120 °C the radical concentration could be increased by raising the temperature and decreased by lowering the temperature with no irreversible radical decay. Typical radical concentrations obtained in this temperature range are presented in Table 1. Trimethylgermylperoxyl is, therefore, analogous to *t*-butylperoxyl in its behavior at low temperatures and must exist in equilibrium with bis-trimethylgermyl tetroxide.

[1] $$2(CH_3)_3GeO_2 \rightleftharpoons (CH_3)_3GeO_4Ge(CH_3)_3$$

The equilibrium constant K_1 for this process is given by

[2] $$K_1 = \frac{[(CH_3)_3GeO_4Ge(CH_3)_3]}{[(CH_3)_3GeO_2]^2}$$

and the variation of K_1 with temperature by an integrated form of the van't Hoff relation,

[3] $$\ln K_1 = \frac{\Delta S^0}{R} - \frac{\Delta H^0}{RT}$$

where ΔS^0 and ΔH^0 are the changes in the standard entropy and enthalpy.

Values of K_1 can only be calculated if the radical concentration at complete dissociation, $[(CH_3)_3GeO_2]_{max}$, can be measured since

[4] $$[(CH_3)_3GeO_4Ge(CH_3)_3] = \tfrac{1}{2}\{[(CH_3)_3GeO_2]_{max} - [(CH_3)_3GeO_2]\}$$

Unfortunately, $[(CH_3)_3GeO_2]_{max}$ could not be estimated because the radical began to decay irreversibly before the tetroxide was completely dissociated.

There are two methods of estimating ΔS^0 and ΔH^0 in this situation. First, values of $[(CH_3)_3GeO_2]_{max}$, ΔH^0, and ΔS^0 which give the best fit between experimental and predicted curves for the variation of $[(CH_3)_3GeO_2]$ with temperature can be computed (3).

A plot of the experimental and calculated data is presented in Fig. 1 with the solid line representing the calculated curve for $\Delta H^0 = -11.4$ kcal mol^{-1} and $\Delta S^0 = -31.1$ cal deg^{-1} mol^{-1}. Thermodynamic parameters estimated by this procedure are, however, subject to

TABLE 1. The concentration of $(CH_3)_3GeO_2$ in the dark as a function of temperature[a]

Temperature (°C)	$10^6[(CH_3)_3GeO_2]$ (M)
−87	2.26
−99	0.9
−119	0.16
−103	0.52
−109	0.25
−78	4.2
−82	3.3
−69	8.0
−74	5.5
−62	12.4
−58	13.8
−98	0.81
−114	0.11

[a]In cyclopropane. The radical was generated by photolysis at −87 °C, the light was then switched off and the temperature changed randomly.

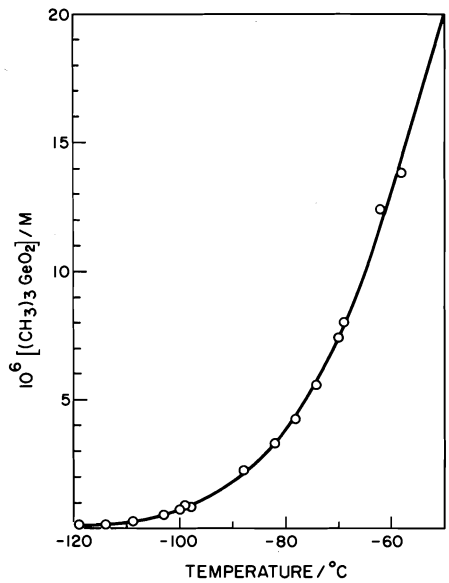

FIG. 1. Variation of the concentration of $(CH_3)_3GeO_2$ with temperature in the range where irreversible radical decay does not occur.

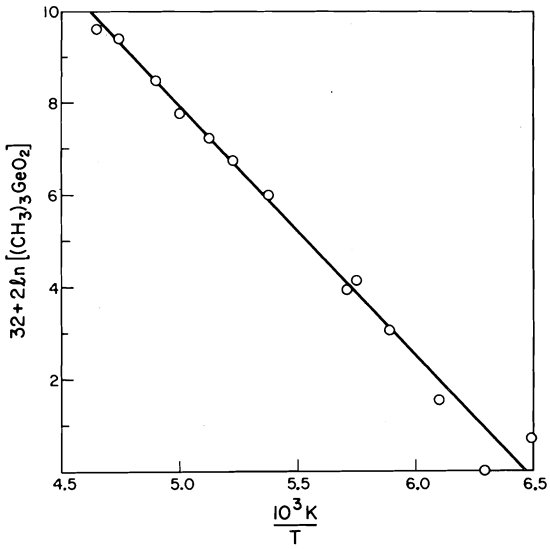

FIG. 2. A plot of 2 ln $[(CH_3)_3GeO_2]$ as a function of the reciprocal of the absolute temperature in the range where irreversible radical decay does not occur.

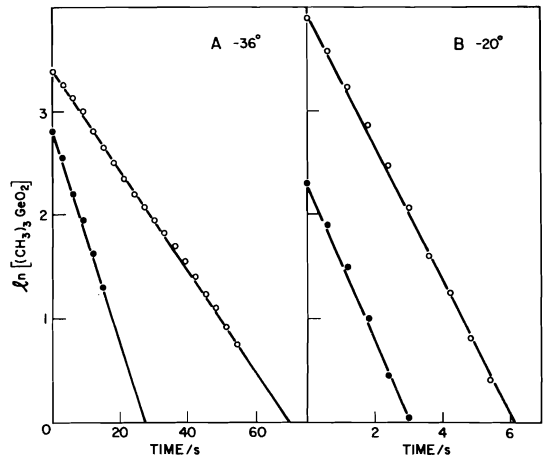

FIG. 3. Plots of ln $[(CH_3)_3GeO_2]$ against time at -36 and -20 °C. The open and filled circles represent decays of radicals that were generated with 100% and 3% light intensity, respectively.

fairly substantial errors because the shape of the plot of $[(CH_3)_3GeO_2]$ *vs.* temperature in the region $T < -80$ °C is rather insensitive to small changes in ΔH^0 and $[(CH_3)_3GeO_2]_{max}$. We do, however, believe that ΔH^0 is accurate to ± 0.5 kcal mol^{-1} and ΔS^0 to ± 4 cal deg^{-1} mol^{-1}.

The alternative approach is to assume that at the lowest temperature most of the radicals exist as tetroxide. The slope of a plot of 2 ln $[(CH_3)_3GeO_2]$ against $1/T$ then gives ΔH^0. Such a plot for $(CH_3)_3GeO_2$ is shown in Fig. 2 and the slope of this plot yields an enthalpy change of -10.5 kcal mol^{-1}, in good agreement with the value obtained by the first procedure. Since $[(CH_3)_3GeO_2]_{max}$ must be greater than the highest concentration of radicals that could be regenerated (1.5×10^{-5} *M*) ΔS^0 must be < -32 cal deg^{-1} mol^{-1}.

We have previously reported (7) that trimethylgermylperoxy radicals prepared in a rotating cryostat in cyclopropane disappeared immediately the solvent melted and did not reappear upon warming the sample to -40 °C. We have carefully repeated this experiment using cyclopentane as solvent. We now find that $(CH_3)_3GeO_2$ can be detected when the solvent melts and is indefinitely persistent up to -50 °C. Below -50 °C temperature jump experiments confirmed that this radical exists in equilibrium with a diamagnetic dimer. Our previous failure to observe the equilibrium in cyclopropane may be due to the difficulties associated with using this solvent as a matrix for rotating cryostat studies.

Above -50 °C photochemically generated trimethylgermylperoxyls decayed irreversibly when the light was shuttered. Plots of the reciprocal of the radical concentration against time exhibited pronounced curvature while plots of the logarithm of the concentration against time were linear.

These results imply that radical decays were *first-order* rather than second-order. The slopes of the first-order plots at the lower temperatures were, however, dependent on the initial radical concentration, increasing slightly when the initial radical concentration was decreased by a factor of *ca.* 30 (see Fig. 3*A*). This difference in slopes was less marked at the higher temperatures (Fig. 3*B*) and decays were truly first-order over the entire concentration range. Typical 'apparent' first-order rate constants (k_{epr}^1) are presented in Table 2.

In the first-order decay region plots of the logarithm of the steady-state radical concentration against the logarithm of the intensity of the initiating light gave an intensity exponent of 1.0, the value expected for truly first order decay (Fig. 4).

Interestingly trimethylgermylperoxyl was the only radical that could be detected during photolysis of DTBP and tetramethylgermane in

Can. J. Chem. Downloaded from www.nrcresearchpress.com by 210.87.254.105 on 09/05/12
For personal use only.

Can. J. Chem. Downloaded from www.nrcresearchpress.com by 210.87.254.105 on 09/05/12
For personal use only.

TABLE 2. Rate constants (k_{epr}^{1}) for irreversible first-order decay of $(CH_3)_3GeO_2$ at different temperatures[a]

Temperature (°C)	k_{epr}^{1} (s)
−50	0.10
−40	0.19
−30	0.31
−20	0.47
−10	0.83
0	1.22

[a]The initial radical concentration was about 10^{-6} M in toluene.

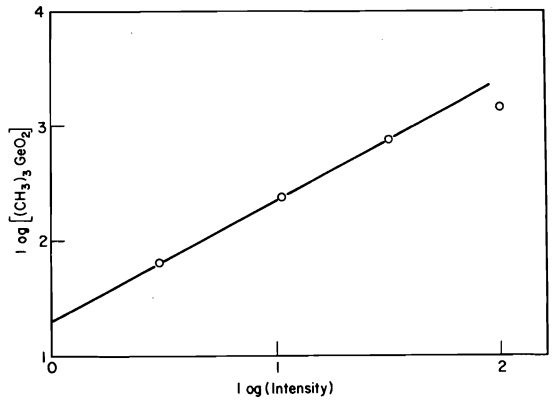

FIG. 4. A plot of the logarithm of the steady-state concentration of $(CH_3)_3GeO_2$ against the logarithm of the light intensity.

oxygen-saturated cyclopropane. This radical was identified by its g-factor (2.024), its first-order irreversible decay parameters (*e.g.* $k_{epr}^{1}(-40\ °C) \approx 0.2\ s^{-1}$) and the thermodynamic parameters for reversible dimerization ($\Delta H^0 \approx -10$ kcal mol^{-1}; $\Delta S^0 < -30$ cal deg^{-1} mol^{-1}).

In the absence of oxygen trimethylgermylmethyl, $(CH_3)_3GeCH_2^{\cdot}$ is the only radical that can be detected (11). The peroxy radical derived from this radical would have a g-factor similar to the characteristic value for alkylperoxy radicals, *i.e.* ≈2.015 (12). Furthermore, it should behave kinetically like other primary alkylperoxy radicals and be relatively short-lived (1). The detection of an organogermylperoxy radical in the presence of oxygen implies that organogermyl radicals are formed although, because of the long lifetime of $(CH_3)_3GeO_2$, they may be a very small fraction of the total radical concentration.

There are two possible mechanisms for the production of a germyl radical in this system

(*i*) Non-terminating interactions of $(CH_3)_3GeCH_2O_2$ would give trimethylgermylmethoxy radicals which could undergo β-scission to give $(CH_3)_3Ge^{\cdot}$ and formaldehyde:

[5] $2(CH_3)_3GeCH_2O_2 \rightarrow 2(CH_3)_3GeCH_2O^{\cdot} + O_2$

$(CH_3)_3GeCH_2O^{\cdot} \rightarrow (CH_3)_3Ge^{\cdot} + CH_2O$

This mechanism is not unreasonable when one considers that Ingold (13) has found rate constants of about 10^4 M^{-1} s^{-1} for the peroxy radicals produced by photolysis of *t*-butylacetyl peroxide in an oxygen-saturated solvent. By analogy with other primary alkylperoxy radicals $(CH_3)_3CCH_2O_2$ should have a termination rate constant $\sim 10^8$ M^{-1} s^{-1} (1). A rate constant four orders of magnitude below the expected value could be indicative of interference from $(CH_3)_3CO_2$.

(*ii*) Self-destruction of $(CH_3)_3GeCH_2O_2$ by the Russell mechanism (14) would lead to the formation of trimethylgermylcarbinol and trimethylgermylcarboxaldehyde

$2(CH_3)_3GeCH_2O_2 \longrightarrow$

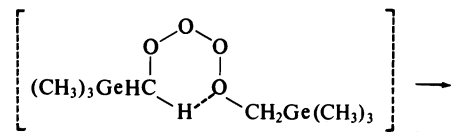

$\longrightarrow (CH_3)_3GeCHO + O_2 + (CH_3)_3GeCH_2OH$

Reaction of *t*-butoxy radicals with $(CH_3)_3GeCHO$ would give $(CH_3)_3GeC(O)$ which could either decarbonylate or add oxygen:

[6] $(CH_3)_3CO^{\cdot} + (CH_3)_3GeCHO \rightarrow (CH_3)_3COH$

$$+ (CH_3)_3GeC(O)^{\cdot} \begin{cases} \xrightarrow{O_2} (CH_3)_3GeC(O)O_2 \\ \longrightarrow (CH_3)_3Ge^{\cdot} + CO \end{cases}$$

$(CH_3)_3GeC(O)O_2$ could also give $(CH_3)_3Ge^{\cdot}$ by the following series of reactions:

[7] $2(CH_3)_3GeC(O)O_2 \rightarrow 2(CH_3)_3GeC(O)O^{\cdot}$

$\rightarrow 2(CH_3)_3Ge^{\cdot} + CO_2$

At the present time we are inclined to favor the first mechanism because tetraethylgermane and tetra-*n*-butylgermane both give germylperoxy radicals[4] when photolyzed in the presence

[4]The yield of germylperoxy radicals in these systems was, however, quite low relative to the yield of alkylperoxy radicals.

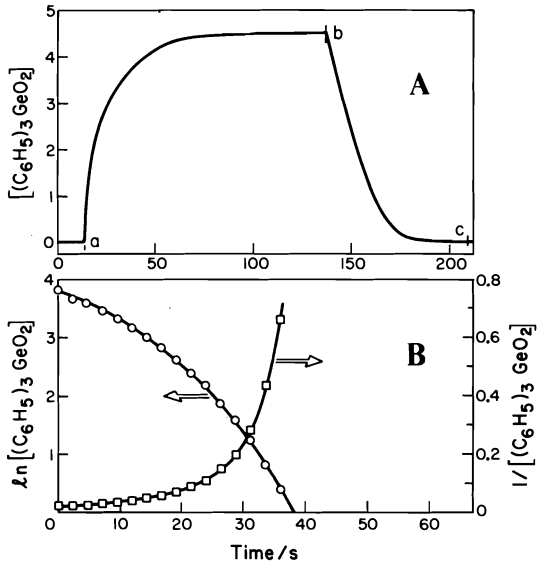

FIG. 5. (*A*) The variation of the concentration of triphenylgermylperoxy radicals with time during continuous photolysis, *a* to *b*; and after the light was shuttered, *b* to *c*. (*B*) First- and second-order plots for the decay of $(C_6H_5)_3GeO_2$.

of DTBP and O_2. The alkylperoxy radicals from these substrates give ketones by Russell termination, compounds that would not be expected to yield trialkylgermyl radicals.

$$[8]\quad 2R_3GeCHO_2 \rightarrow R_3GeC(R')=O + R_3GeCH(R')OH + O_2$$

where R = C_2H_5 or n-C_4H_9 and R′ = CH_3 or n-C_3H_7.

Triphenylgermylperoxy

Photolysis of DTBP and triphenylgermane in oxygen saturated cyclopropane and toluene at −96 °C gave $(C_6H_5)_3GeO_2$ (broad singlet, g = 2.0245). At this temperature this radical decayed rapidly when photolysis was interrupted and plots of the reciprocal radical concentration against time were linear. The intensity exponent for the steady state radical concentration was 0.5. Triphenylgermylperoxyl must, therefore, decay at −96 °C by a second-order process. The bimolecular rate constant (k_{epr}^2) was determined at two initial radical concentrations (1.6×10^{-7} and 4.8×10^{-7} M) and the average value of k_{epr}^2 was 5.35×10^7 M^{-1} s^{-1}.

Triphenylgermylperoxy radicals were regenerated when the temperature was increased from −96 °C and temperature jump experiments indicated that this radical exists in equilibrium with bistriphenylgermyl tetroxide.

$$[9]\quad 2(C_6H_5)_3GeO_2 \underset{k_{-5}}{\overset{k_5}{\rightleftharpoons}} (C_6H_5)_3GeO_4Ge(C_6H_5)_3$$

The bimolecular rate constant measured at −96 °C must, therefore, be the rate constant for combination of $(C_6H_5)_3GeO_2$ to give $(C_6H_5)_3GeO_4Ge(C_6H_5)_3$, *i.e.*, $k_{epr}^2 \equiv k_9$. The only other rate constant that has been reported for dimerization of peroxyl radicals is the value of 6×10^6 M^{-1} s^{-1} obtained by Simic and Hayon for the peroxy radical derived from dihydrothymine (15).

As with $(CH_3)_3GeO_2$ equilibrium constants for reaction 9 could not be calculated because $(C_6H_5)_3GeO_2$ decayed irreversibly before complete dissociation of the tetroxide. A plot of 2 ln $[(C_6H_5)_3GeO_2]$ *vs.* $1/T$, however, yielded $\Delta H^0 = -11$ kcal mol^{-1} and $\Delta S^0 < -30$ cal deg^{-1} mol^{-1}; parameters almost identical with those for $(CH_3)_3GeO_2$.

Above −60 °C triphenylgermylperoxyls decayed irreversibly (see *e.g.*, Fig. 5 *A*). Plots of ln $[(C_6H_5)_3GeO_2]$ and $1/[(C_6H_5)_3GeO_2]$ against time were not linear (Fig. 5*B*) indicating that rates of radical decay were neither first- nor second-order. In fact the overall reaction appeared to have a radical concentration exponent of 0.5. If, however, very low initial radical concentrations were generated, radical decays followed first-order kinetics. At higher temperatures radical decays were first-order over the entire concentration range and the intensity exponent was exactly 1.0. First-order rate constants (k_{epr}^1) were independent of the concentration of hydride and oxygen and were identical in toluene and *t*-butylbenzene. The values of k_{epr}^1 did, however, depend on the concentration of DTBP, decreasing by almost a factor of two when the concentration of DTBP was increased from 0.5 to 10 *M*. A decrease in k_{epr}^1 of this magnitude going from 10% DTBP to nearly 100% DTBP can probably be attributed to a solvent effect. Typical values of k_{epr}^1 for $(C_6H_5)_3GeO_2$ are presented in Table 3.

$(C_6H_5)_3GeO_2$ was also generated by photolysis of deoxygenated toluene containing triphenylgermyl hydroperoxide. The kinetic behavior of $(C_6H_5)_3GeO_2$ produced in this way was identical

Can. J. Chem. Downloaded from www.nrcresearchpress.com by 210.87.254.105 on 09/05/12
For personal use only.

Can. J. Chem. Downloaded from www.nrcresearchpress.com by 210.87.254.105 on 09/05/12
For personal use only.

TABLE 3. Values of the first-order rate constant k_{epr}^{1} for $(C_6H_5)_3GeO_2$[a] as a function of temperature

Temperature (°C)	k_{epr}^{1} (s)
−30	1.8
−20	2.7
−10	4.2

[a]Produced by photolyses of DTBP (0.5 *M*) in oxygenated toluene containing triphenylgermyl hydride (0.01 *M*).

with that described above for the radical formed from $(C_6H_5)_3GeH$, DTBP and O_2.

Discussion

Radical–Dimer Equilibrium

$(CH_3)_3GeO_2$ and $(C_6H_5)_3GeO_2$ at low temperatures exist in equilibrium with the appropriate tetroxide. In this respect they are analogous to tertiary alkylperoxy radicals such as $(CH_3)_3CO_2$ which exists in equilibrium with di-*t*-butyl tetroxide.

Enthalpy changes for dimerization of $(CH_3)_3GeO_2$ and $(C_6H_5)_3GeO_2$ are about 11 kcal mol^{-1} and are at least 3 kcal mol^{-1} larger than values of ΔH^0 for alkylperoxyls (1). If the activation energy for dimerization of peroxyls is small (*vide infra*) this enthalpy difference suggests that the central O–O bond in organogermyl tetroxides is at least 3 kcal mol^{-1} stronger than the corresponding bond in alkyl tetroxides.

Entropy changes for dimerization of $(CH_3)_3GeO_2$ and $(C_6H_5)_3GeO_2$ are about 30 cal deg^{-1} mol^{-1} and are similar to the value of ΔS^0 for *t*-butylperoxyl. Entropy changes of this magnitude are consistent with a radical–radical dimerization process.

The rate constant for dimerization of $(C_6H_5)_3GeO_2$ of $\sim 5 \times 10^7$ M^{-1} s^{-1} is about two orders of magnitude below the diffusion controlled limit. A rate constant of this magnitude suggests an activation energy for dimerization of about 1.5 kcal mol^{-1}.

Irreversible Decays

Above −50 °C organogermylperoxyls decay irreversibly with rates that are not a simple function of the radical concentration. At low initial radical concentrations and higher temperatures decays are, however, first-order.

Most free-radicals (R·), including alkylperoxyls, undergo self-reaction by a second-order process (16), *i.e.*, $-d[R\cdot]/dt \propto [R\cdot]^2$. There are, however, a number of persistent radicals which decay by first-order kinetics, *i.e.* $-d[R\cdot]/dt \propto [R\cdot]$(17–20). These unusual kinetics have been attributed to the occurrence of a rapid but reversible, dimerization of the radicals, *i.e.* $R\cdot + R\cdot \rightleftharpoons R_2$, where R_2 is the dimer (17, 18). If the equilibrium lies to the right and the radical concentration is high, $-d[R\cdot]/dt$ can be proportional to $[R\cdot]$. Irreversible decays of organogermylperoxyls are unique compared with other radical decays because the concentration exponent is < 1.0 at high radical concentrations becoming first-order at low radical concentrations. These observations would fit the third situation envisaged by Brokenshire, Roberts, and Ingold (18) to account for first-order decay kinetics. Thus if the radicals are in equilibrium with a dimer and decay irreversibly by a true unimolecular reaction, *i.e.*,

$$2R \underset{k_{-10}}{\overset{k_{10}}{\rightleftharpoons}} R_2 \qquad [10]$$

$$R\cdot \xrightarrow{k_{11}} \text{Stable molecular products} \qquad [11]$$

the rate of radical decay is given by

$$\frac{-d[R\cdot]}{dt} = \frac{k_{11}[R\cdot]}{1 + 4K_{10}[R\cdot]} \qquad [12]$$

Clearly if $4K_{10}[R\cdot] \gg 1$, $-d[R\cdot]/dt$ is independent of $[R\cdot]$ whereas if $4K_{10}[R\cdot] \ll 1$, $-d[R\cdot]/dt \propto [R\cdot]$.

Decays of organogermylperoxyls are certainly consistent with eq. 12 and the non-integral decay curves exhibited by $(CH_3)_3GeO_2$ and $(C_6H_5)_3GeO_2$ can be constructed from the integrated form of eq.12 with measured values of k_{epr}^{1} and values of $-\Delta H^0$ of 11–12 kcal mol^{-1} and $-\Delta S^0$ of 23–30 cal deg^{-1} mol^{-1}. Furthermore steady-state radical concentrations were directly proportional to the light intensity, good evidence for a true unimolecular radical decay (18).

There would, therefore, appear to be compelling kinetic evidence that $(CH_3)_3GeO_2$ and $(C_6H_5)_3GeO_2$ decay unimolecularly. The most obvious unimolecular reaction is decomposition to give a germyl radical and oxygen.

$$R_3GeO_2 \rightarrow R_3Ge\cdot + O_2 \qquad [13]$$

Organogermylperoxy radicals are, however,

unlikely to undergo this reaction at subambient temperatures because of the strength of the Ge—O bond. Furthermore, the organogermyl radical formed in reaction 13 would disappear by scavenging R_3GeO_2.

[14] $R_3GeO_2 + R_3Ge^{\cdot} \rightarrow R_3GeO_2GeR_3$

Reactions 13 and 14, even if [13] is reversible and the peroxy radicals are in reversible equilibrium with tetroxide, do not give a rate expression that can be zero-order in R_3GeO_2.

There are several alternative modes of unimolecular decomposition of hydrocarbon peroxy radicals (12). These reactions are, however, only important at elevated temperatures. At the present time we are actively engaged in an investigation of the products of decomposition of organogermylperoxy radicals in the hope that they will help to explain their unusual kinetic behavior.

Acknowledgment

We thank Professor A. G. Davies and Dr. K. U. Ingold for their simultaneous suggestions that $(CH_3)_3GeO_2$ may be formed from $(CH_3)_3GeCH_2O^{\cdot}$.

1. J. A. HOWARD. Adv. Free Radical Chem. **4**, 49 (1972).
2. J. E. BENNETT, D. M. BROWN, and B. MILE. Trans. Faraday Soc. **66**, 386 (1970).
3. J. E. BENNETT, D. M. BROWN, and B. MILE. Trans. Faraday Soc. **66**, 397 (1970).
4. K. ADAMIC, J. A. HOWARD, and K. U. INGOLD. Can. J. Chem. **47**, 3803 (1969).
5. J. A. HOWARD, K. ADAMIC, and K. U. INGOLD. Can. J. Chem. **47**, 3793 (1969).
6. J. A. HOWARD and J. E. BENNETT. Can. J. Chem. **50**, 2374 (1972).
7. J. E. BENNETT AND J. A. HOWARD. J. Am. Chem. Soc. **94**, 8244 (1972).
8. M. DUB (*Editor*). Organometallic compounds. Vol. II. Springer-Verlag, N.Y. 1967.
9. R. L. DANNLEY and G. C. FARRANT. J. Org. Chem. **34**, 2428 (1969).
10. J. E. BENNETT, B. MILE, A. THOMAS, and B. WARD. Adv. Phys. Org. Chem. **8**, 1 (1970).
11. P. J. KRUSIC and J. K. KOCHI. J. Am. Chem. Soc. **91**, 6161 (1969).
12. K. U. INGOLD. Acc. Chem. Res. **2**, 1 (1969).
13. K. U. INGOLD. Private communication.
14. G. A. RUSSELL. J. Am. Chem. Soc. **79**, 3871 (1957).
15. M. SIMIC and E. HAYON. FEBS Lett. **44**, 334 (1974).
16. K. U. INGOLD. Free radicals, **I**, 37 (1973).
17. S. A. WEINER and L. R. MAHONEY. J. Am. Chem. Soc. **94**, 5039 (1972).
18. J. L. BROKENSHIRE, J. R. ROBERTS, and K. U. INGOLD. J. Am. Chem. Soc. **94**, 7040 (1972).
19. J. R. ROBERTS and K. U. INGOLD. J. Am. Chem. Soc. **95**, 3228 (1973).
20. V. MALATESTA and K. U. INGOLD. J. Am. Chem. Soc. **96**, 3949 (1974).

Can. J. Chem. Downloaded from www.nrcresearchpress.com by 210.87.254.105 on 09/05/12
For personal use only.

Excess volumes of binary mixtures of an alcohol + diethylketone

KALLURU S. REDDY, MURARI VENKATA P. RAO, AND PULIGUNDLA R. NAIDU
Sri Venkateswara University Chemical Laboratory, Tirupati 517502, India

Received February 23, 1976

KALLURU S. REDDY, MURARI VENKATA P. RAO, and PULIGUNDLA R. NAIDU. Can. J. Chem. **54**, 2676 (1976).

Excess volumes of mixtures of 1-propanol+, 1-butanol+, 1-pentanol+, and 1-hexanol + diethylketone have been measured at 303.15 and 313.15 K. Of the four mixtures included here 1-propanol + diethylketone shows an inversion in sign in V^E at 313.15 K. V^E becomes more positive with increase in temperature.

KALLURU S. REDDY, MURARI VENKATA P. RAO et PULIGUNDLA R. NAIDU. Can. J. Chem. **54**, 2676 (1976).

On a mesuré, à 303.15 et à 313.15 K, les volumes d'excès de mélange de propanol-1 +, de butanol-1 +, de pentanol-1 + et d'hexanol-1 + pentanone-3. Parmi les quatre mélanges examinés dans cette étude, il existe une inversion dans le signe de V^E à 313.15 K pour le mélange propanol-1 + pentanone-3. Dans ce cas V^E devient plus positif lorsqu'on augmente la température.

[Traduit par le journal]

Can. J. Chem. Downloaded from www.nrcresearchpress.com by 210.87.254.105 on 09/05/12
For personal use only.

Introduction

In continuation of earlier work on excess volumes of binary mixtures of alcohols in a common solvent (1), V^E values for mixtures of 1-propanol+, 1-butanol+, 1-pentanol+, and 1-hexanol + diethylketone at 303.15 and 313.15 K are reported here. A literature survey showed that no one has reported V^E data for the mixtures of the four alcohols with the ketone.

Experimental

Excess volumes of the four binary mixtures were measured using the dilatometer described by Rao and Naidu (1). The values are accurate to ± 0.003 cm^3 mol^{-1}. The alcohols were purified by the methods described by Rao and Naidu (1). Diethylketone was dried over potassium carbonate for 3 days then boiled for 2 h and distilled (2). The purity of diethylketone was checked by comparing the values of density ρ and boiling temperature T_b with those reported in the literature: ρ(303.15 K) = 0.80455 g cm^{-3} (lit. 0.80461 g cm^{-3} (3)); T_b = 375.05 K (lit. 375.15 K (3)).

Results

Excess volumes at 303.15 and 313.15 K of the four binary mixtures are given in Figs. 1 to 4.[1] These results may be represented by an empirical equation of the form

$$[1]\quad V^E/x_A x_B \text{ cm}^3 \text{ mol}^{-1} = a_0 + a_1(x_A - x_B) + a_2(x_A - x_B)^2$$

the values of a_0, a_1, and a_2 obtained by the method of least-squares are given in Table 1 along with the standard deviation $\sigma(V^E)$. This fit was not attempted in the case of 1-butanol+, 1-pentanol + diethylketone at 303.15 K as their V^E values were very small.

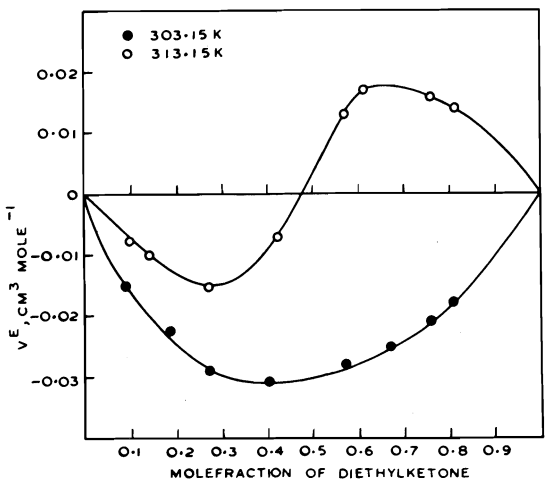

FIG. 1. Plot of V^E as a function of composition for diethylketone and 1-propanol system.

[1]Photocopies of the data are available, upon request, at a nominal charge from the Depository of Unpublished Data, CISTI, National Research Council of Canada, Ottawa, Canada K1A 0S2.

TABLE 1. Standard deviation $\sigma(V^E)$ and values of the constants in eq. 1

System	Temperature (K)	a_0	a_1	a_2	$\sigma(V^E)$ (cm^3 mol^{-1})
Diethylketone + 1-propanol	303.15	−0.1315	0.0511	0.0488	0.004
Diethylketone + 1-hexanol	303.15	0.0529	−0.0069	0.0281	0.001
Diethylketone + 1-propanol	313.15	0.0130	0.1448	0.0079	0.005
Diethylketone + 1-butanol	313.15	0.0614	0.0323	0.0165	0.001
Diethylketone + 1-pentanol	313.15	0.0608	0.0033	−0.0159	0.001
Diethylketone + 1-hexanol	313.15	0.1287	0.1035	0.0215	0.002

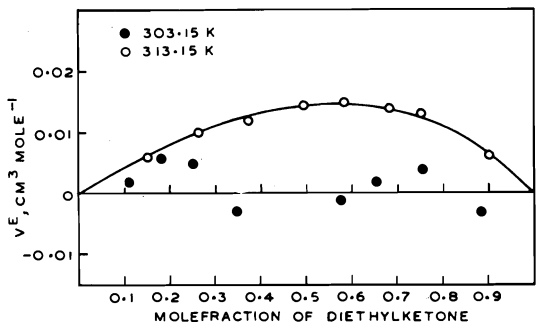

FIG. 2. Plot of V^E as a function of composition for diethylketone and 1-butanol system.

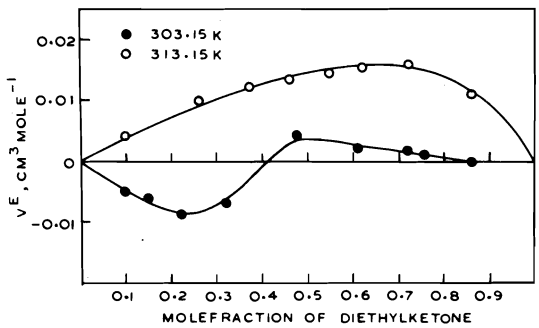

FIG. 3. Plot of V^E as a function of composition for diethylketone and 1-pentanol system.

Discussion

The values of V^E at 303.15 K are negative over the entire range of composition for 1-propanol + diethylketone. The values of V^E of 1-butanol+, 1-pentanol + diethylketone are within the experimental error. The values of V^E of 1-hexanol + diethylketone are positive over the entire range of composition. The function V^E at 313.15 K shows an inversion in sign at about 0.45 mole fraction of ketone in the case of 1-propanol + diethylketone. The V^E values of the other three mixtures are positive over the entire range of composition. A comparison between the V^E values at 303.15 and 313.15 K shows that V^E becomes more positive with increase in temperature in the four mixtures. The results of the four systems fall in the order:

1-propanol < 1-butanol ≈ 1-pentanol < 1-hexanol.

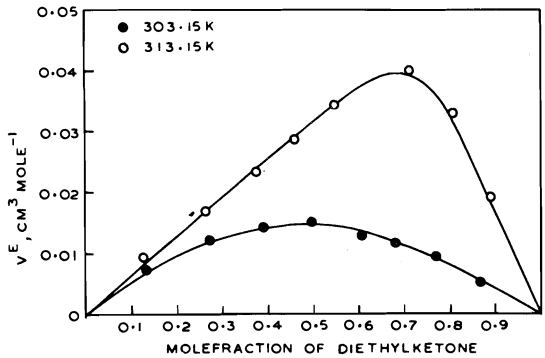

FIG. 4. Plot of V^E as a function of composition for diethylketone and 1-hexanol system.

Acknowledgment

One of the authors (M.V.P.R.) is thankful to Council of Scientific and Industrial Research, New Delhi, for the award of a post-doctoral fellowship.

1. M. V. P. RAO and P. R. NAIDU. Can. J. Chem. **52**, 788 (1974).
2. P. R. NAIDU. Aust. J. Chem. **23**, 967 (1970).
3. J. TIMMERMANS. Physico-chemical constants of pure organic compounds. Elsevier Publishing Co., Amsterdam. 1950.

Can. J. Chem. Downloaded from www.nrcresearchpress.com by 210.87.254.105 on 09/05/12
For personal use only.

Erratum: Thermodynamics of ester and orthoester formation from trifluoroacetic acid

J. PETER GUTHRIE
Department of Chemistry, University of Western Ontario, London, Ont., Canada N6A 5B7

Received June 4, 1976

(Ref.: Can. J. Chem. **54**, 202 (1976))

On page 208, the first sentence in the left-hand column should read ". . . but a negligible effect upon hydration of carboxyl compounds is quite mysterious".

Can. J. Chem. Downloaded from www.nrcresearchpress.com by 210.87.254.105 on 09/05/12
For personal use only.

Can. J. Chem. Downloaded from www.nrcresearchpress.com by 210.87.254.105 on 09/05/12
For personal use only.

[4]Annulene. Comments on its infrared spectrum[1]

SATORU MASAMUNE, YOSHIKAZU SUGIHARA, KAZUHIKO MORIO, AND JOHN E. BERTIE
Department of Chemistry, University of Alberta, Edmonton, Alta., Canada T6G 2G2

Received May 17, 1976

SATORU MASAMUNE, YOSHIKAZU SUGIHARA, KAZUHIKO MORIO, and JOHN E. BERTIE. Can. J. Chem. **54**, 2679 (1976).

A photo-precursor (**4**) of [4]annulene (**1**) has been irradiated at 4–10 K in argon. The infrared spectrum of the photolysate shows two strong bands at 1240 cm^{-1} and 570 but, in contradiction to an earlier claim, one at 650 cm^{-1} is missing. The discrepancy between this and the earlier observation is explained, and comments on the infrared spectrum of **1** are made.

SATORU MASAMUNE, YOSHIKAZU SUGIHARA, KAZUHIKO MORIO et JOHN E. BERTIE. Can. J. Chem. **54**, 2679 (1976).

On a irradié, à 4–10 K dans l'argon, un photoprécurseur (**4**) du [4]annulène (**1**). Le spectre infrarouge du photolysat présente deux bandes intenses à 1240 et 570 cm^{-1}; toutefois par opposition avec une prétention antérieure, la bande à 650 cm^{-1} est absente. La différence entre cette observation et celle rapportée antérieurement est expliquée et on fait des commentaires sur le spectre infrarouge de **1**.

[Traduit par le journal]

Recent intense studies on [4]annulene (cyclobutadiene) (**1**) and its derivatives have substantially enriched the knowledge of this intriguing system (for recent reviews see ref. 1). The full characterization of an appropriately[2] substituted crystalline derivative (**2**) has led to the unambiguous demonstrations, (*i*) that the ground state of **2** is singlet (2*a*, 2*b*) and (*ii*) that

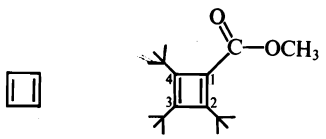

1 **2**

the geometry of **2** is definitely not square, but a slightly distorted rectangle (2*c*). The successful isolation of the parent species (**1**) in an argon matrix has allowed an infrared spectrum of **1** to be obtained (3), and trapping of **1** in an organic matrix has made possible the recording of its ultraviolet spectrum (4).

The conclusion that **1** possesses square geometry (D_{4h}) (*cf.* that of **2**), drawn from the analysis of the infrared spectrum of **1** generated from α-photopyrone (**3**), is almost entirely based on the observation of four bands at 3040 cm^{-1},

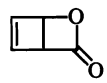

3

1240 (or 1236), 650 (or 653), and 570 (or 573). Group theory predicts four infrared-active fundamentals for D_{4h} symmetry and more than four for less symmetrical [4]annulenes. While we could reproduce the results published by two other groups (3), we wished to confirm that our [4]annulene precursor (**4**) utilized for the ultraviolet spectral measurement (*vide supra*) (4) yields the same infrared spectrum of **1** as that reported, if photolyzed at 4–10 K in argon. It was found that the photo-induced cleavage of **4** proceeded more efficiently by far than that of other

4 **5**

known precursers such as **3**, **5** (5), **6**, and **7** (6), as expected from the structure of **4**. Photolysis

[1]Supported by a National Research Council of Canada grant.

[2]The substitution pattern in **2** is such that C(1)—C(2) and C(1)—C(4) can attain equivalence if the π-electrons are fully delocalized. The first crystalline derivative was elegantly synthesized by Kimling and Krebs (2*d*).

Can. J. Chem. Downloaded from www.nrcresearchpress.com by 210.87.254.105 on 09/05/12
For personal use only.

(2537 Å) of **4** was indeed essentially complete in 1 h without side reactions such as the formation of acetylene (3*b*), as evidenced by the chemical analysis of the products. The infrared spectrum clearly showed the two strong bands at 1240 cm^{-1} and 570,[3] but, in contradiction to the earlier observation, the one at 650 cm^{-1} was missing. In the region between 690 cm^{-1} (where a weak band due to a vibration of phthalan appears) and 570 cm^{-1}, there was absolutely no absorption. Professor Maier recently informed us that in attempts to generate **1** from pyridine

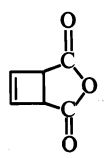

6

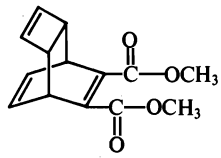

7

(via **5** (3*b*)) in his laboratory, only the two bands at 1240 cm^{-1} and 570 were observable, but none at the 650 cm^{-1}, and that **6** exhibited after irradiation the four bands previously reported (*vide supra*) with a small splitting (4 cm^{-1}) of the band at 1240 cm^{-1} (1*b*).[4] Therefore, it is reasonable to conclude that the band at 650 cm^{-1} is NOT attributable to a vibration of **1** but appears only when CO_2 is a formal by-product of the photolysis.

Maier has accumulated convincing evidence that **1** has the strong propensity to form a charge-transfer complex whenever a species possessing acceptor properties exists in the neighborhood of **1** (1*b*). Therefore, it is probable that CO_2 generated from **3** and **6** upon photolysis interacts weakly with **1**, thus causing a weak splitting (650 cm^{-1} and 660) of the band associated with the degenerate bending vibration of CO_2. Phthalan does not act as an acceptor. Thus the earlier assignments and discussions of the band near 660 cm^{-1} (3*b*, 3*d*) are now redundant, and the only bands attributable to [4]annulene are at 1240 cm^{-1} and 570, as well as the weak band (3*b*) at 3040 cm^{-1}. The conclusion (3) that [4]annulene has D_{4h} symmetry, in contrast to the rectangular ring of **2** (2*c*), rests mainly on the appearance of just one apparent C—C stretching vibration at 1240 cm^{-1}. Additional experimental evidence to ensure that the assignments of the infrared bands of **1** are correct is highly desirable. A suggestion has already been made to this end (1*a*) and experiments are in progress.[5,6]

[3]The C—H stretching band of **1** at 3040 cm^{-1} (3) is masked by a band of phthalan which formed concomitantly with **1**.

[4]Private communication from Professor G. Maier.

1. (*a*) S. Masamune. Pure Appl. Chem. **44**, 861 (1975); (*b*) G. Maier. Angew. Chem. Int. Ed. Engl. **13**, 425 (1974).
2. (*a*) S. Masamune, N. Nakamura, M. Suda, and H. Ona. J. Am. Chem. Soc. **95**, 8481 (1973); (*b*) R. S. Brown and S. Masamune. Can. J. Chem. **53**, 972 (1975); (*c*) L. T. J. Delbaere, M. N. G. James, N. Nakamura, and S. Masamune. J. Am. Chem. Soc. **97**, 1973 (1975); (*d*) H. Kimling and A. Krebs. Angew. Chem. Int. Ed. Engl. **11**, 932 (1972).
3. (*a*) C. Y. Lin and A. Krantz. J. Chem. Soc. Chem. Commun. 1111 (1972); (*b*) O. L. Chapman, C. L. McIntosh, and J. Pacansky. J. Am. Chem. Soc. **95**, 614 (1973); (*c*) O. L. Chapman, D. De La Cruz, R. Roth, and J. Pacansky. J. Am. Chem. Soc. **95**, 1337 (1973); (*d*) A. Krantz, C. Y. Lin, and M. D. Newton. J. Am. Chem. Soc. **95**, 2744 (1973).
4. (*a*) S. Masamune, M. Suda, H. Ona, and L. M. Leichter. J. Chem. Soc. Chem. Commun. 1268 (1972); (*b*) G. Maier and B. Hoppe. Tetrahedron Lett. 861 (1973).
5. K. E. Wilzbach and D. J. Rausch. J. Am. Chem. Soc. **92**, 2178 (1970).
6. E. Hedaya, R. D. Miller, D. W. McNeil, P. E. D'Angelo, and P. Schissel. J. Am. Chem. Soc. **91**, 1875 (1969).

[5]It may be noted that the available data permit two interpretations of D_{4h} symmetry for [4]annulene. First, the potential energy surface may have its minimum at this geometry, so that the ring is square. Second, the potential surface of the singlet state may have two minima, which correspond to the two rectangular (D_{2h}) conformers, and the barrier at the square geometry between these two conformers may be lower than the zero-point energy of the B_{1g} normal vibration (under D_{4h}) which causes this change in geometry. The frequency of the B_{1g} vibration is probably close to that of the infrared-active E_u mode, 1240 cm^{-1}. If this is so, the maximum height of the above barrier must be about 2 kcal/mol. In this case the molecular symmetry can be termed 'quasi-D_{4h}', and the ring 'quasi-square'.

[6]We thank Professor G. Maier for sending us, prior to publication, a preprint of his manuscript that has prompted us to disclose our findings as a preliminary, interim report of the project. We are also grateful to Professor G. Closs for his valuable suggestions.

Can. J. Chem. Downloaded from www.nrcresearchpress.com by 210.87.254.40 on 09/05/12
For personal use only.

Canadian Journal of Chemistry

Published by
THE NATIONAL RESEARCH COUNCIL OF CANADA

Journal canadien de chimie

Publié par
LE CONSEIL NATIONAL DE RECHERCHES DU CANADA

Volume 54 Number 17 September 1, 1976 Volume 54 numéro 17 1 septembre 1976

The pseudobase behaviour of 1,3-disubstituted-1,2-dihydro-2-oxopyrimidinium cations

OSWALD S. TEE AND MASAKI ENDO

Department of Chemistry, Sir George Williams Campus, Concordia University, Montreal, P.Q., Canada H3G 1M8

Received August 5, 1975[1]

OSWALD S. TEE and MASAKI ENDO. Can. J. Chem. **54**, 2681 (1976).

The title cations form pseudobases in aqueous solution as shown by their uv and pmr spectra. Of the two potential pseudobases possible when the substitution is unsymmetrical, the preferred one is that having the hydroxyl group adjacent to the less bulky substituent. Aside from this steric influence, the pK_{ROH} values for the pseudobases are determined by simple electronic effects since they give reasonable correlations with Taft's σ^* values.

OSWALD S. TEE et MASAKI ENDO. Can. J. Chem. **54**, 2681 (1976).

Les cations ci-haut mentionnés forment des pseudobases en solution aqueuse tel que démontré par leurs spectres uv et rmp. Lorsque la substitution est nonsymétrique, deux pseudobases potentielles sont possibles et celle qui est préférée est celle qui possède le groupement hydroxyle adjacent au substituant le moins volumineux. A part cette influence stérique, les valeurs de pK_{ROH} pour les pseudobases sont déterminées par les effets électroniques simples vu qu'ils donnent des corrélations raisonnables avec les valeurs σ^* de Taft.

[Traduit par le journal]

Introduction

The concept of pseudobase formation by quaternary heterocyclic cations was first put forward at the turn of the century by Hantzsch (1). Since that time it has entered the folklore of heterocyclic chemistry, and yet it is only recently that quantitative studies have been made. More particularly, it is only within the last decade that the effects of substituents upon equilibrium pseudobase formation have been considered to any great extent.

Cooksey and Johnson (2) have measured equilibrium constants (K_{ROH}) for pseudobase formation by *N*-cyanoquinolinium cations bearing substituents mainly in the benzenoid ring. For the equilibrium [1] between the quaternary heterocyclic cation (Q^+) and its pseudobase (QOH) the equilibrium constant $K_{ROH} = [QOH][H^+]/[Q^+]$. Usually this is used in its logarithmic form pK_{ROH} $(= -\log_{10} K_{ROH})$ which is on the same scale as the pK_a values of Brønsted acids. For equilibria of the type **1** ⇄ **2**, Cooksey and Johnson (2) found a good correlation between pK_{ROH} and the constant σ_p (3) for the substituent Y, with a ρ value of -6.16. For substituents at other positions in the benzenoid ring of **1** (Y = H) they obtained correlations using a combination of substituent constants, and ρ values also around -6.

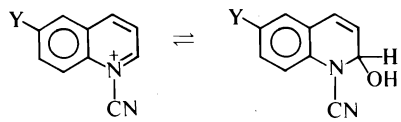

1 **2**

More recently, Bunting and Meathrel (4) have

[1] $Q^+ + H_2O \rightleftarrows QOH + H^+$

[1]Revision received May 3, 1976.

studied various quinolinium, isoquinolinium, and 1,8-naphthyridinium cations bearing different substituents on the quaternary nitrogen. Their data give reasonable correlations with Taft's σ^* substituent constant (5). For equilibria of the type **3** $\rightleftarrows$ **4** they found that for various

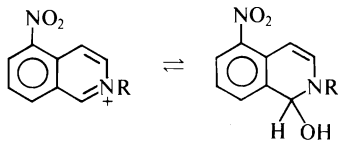

3 **4**

substituents R, $pK_{ROH} = -3.7\sigma^* + 11.6$, and for equilibria **5** $\rightleftarrows$ **6** they found that $pK_{ROH} = -4.9\sigma^* + 12.5$. In addition, they point out that

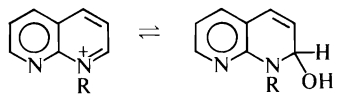

5 **6**

Lindquist and Cordes (6) obtained a value of $\rho^* = -3.7$ for the formation of 1,4-dihydro adducts between cyanide ion and *N*-substituted 3-carbamoyl pyridinium cations.

We have studied the formation of pseudobases from 1,2-dihydro-2-oxopyrimidinium cations **7** and find that their pK_{ROH} values also correlate reasonably well with σ^* and give ρ^* values around -4.

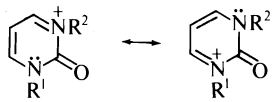

7*a* **7***b*

Results and Discussion

We chose to study cations of the structure **7** for three reasons. Firstly, the dimethyl cation **7** ($R^1 = R^2 = Me$) has a value of pK_{ROH} about 7 (7), and so wide variations in the substituents R^1 and R^2 might still result in pK_{ROH} values accessible in the normal p*H* range. Secondly, such cations are readily synthesized by condensation of an appropriate 1,3-disubstituted urea with malondialdehyde (8). Thirdly, for cations **7** where the substituents R^1 and R^2 are different, there is the possibility of the formation of two distinct pseudobases **8***a* and **8***b*, and the proportions of these might give some insight into the importance of steric factors in pseudobase formation.

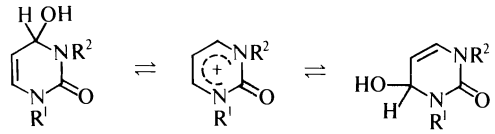

8*a* **7** **8***b*

We have synthesized 21 salts containing 13 different cations **7** by a method previously reported by us (8). Two distinct series of **7** were made: one in which $R^1 = R^2$; one in which $R^2 = Me$, R^1 = various. For both series we were able to observe pseudobase formation in all cases by uv and pmr spectroscopies. In most cases we were also able to measure pK_{ROH} values for the formation of pseudobases **8***a* and/or **8***b*.

Ultraviolet Spectral Studies

The uv spectral data obtained for salts of the cations **7** in an acid medium (1 *N* H_2SO_4, p*H* = 0.29) and in a basic medium (borate buffer, p*H* = 9.18) are presented in Table 1.

In the acidic medium the cations **7** exist as such and their absorption spectra show two distinct bands (9): an intense band below 210 nm due to a $\pi \rightarrow \pi^*$ transition, and a less intense band about 320 nm due to the $n \rightarrow \pi^*$ transition. Where the salt contains iodide ion as the counterion there is an additional band about 225 nm, which is also present in spectra taken in the basic medium. The $n \rightarrow \pi^*$ band ($\sim$320 nm) shows little variation in intensity over the range of substituents covered.

In the basic medium the cations **7** are present as pseudobases **8***a* and/or **8***b* which give rise to two entirely different bands at about 238 and 300 nm. In some cases the former band is obscured by the more intense 225 nm band due to iodide ion. The band around 238 nm is consistent with the proposed pseudobase structures **8** in that the similar structures **9** and **10** have similar uv absorptions of similar intensity. In methanol **9** shows $\lambda_{max} = 236$ nm, log ϵ =

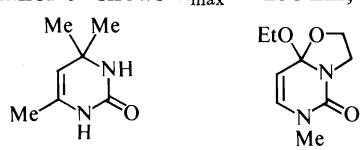

9 **10**

Can. J. Chem. Downloaded from www.nrcresearchpress.com by 210.87.254.40 on 09/05/12
For personal use only.

TABLE 1. Ultraviolet spectral data of cation **7** salts and pseudobases **8**

			Cation (p*H* 0.29)[a]				Pseudobase (p*H* 9.18)[b]			
R^1	R^2	Anion	λ	log ε	λ	log ε	λ	log ε	λ	log ε
Me	Me	HSO_4			316	3.93	239	3.93	296	2.70
Me	Et	I	225	4.16	316	3.93	228	4.23	296	3.27
Me	*i*-Pr	HSO_4			317	3.92	238	3.76	298	3.02
Me	*t*-Bu	HSO_4			316	3.92	236	3.61	308	3.22
Me	c-Hex	I	223	>4.00	319	3.96	227	4.16	300	3.21
Me	Ph	Cl			326	3.91	235	3.85	335	1.66
Me	Ph	I	225	4.15	325	3.95	227	4.33	338	2.00
Me	$PhCH_2$	HSO_4			318	3.95	239	3.69	299	2.51
Et	Et	Cl			317	3.91	238	3.71	300	2.84
Et	Et	HSO_4			317	3.92	238	3.69	300	2.83
Et	Et	I	223	>4.00	317	3.90	225	>4.00	299	3.12
Pr	Pr	I	223	4.09	320	3.89	227	>4.00	303	3.50
i-Pr	*i*-Pr	$EtSO_4$			319	3.95	237	3.62	305	3.31
n-Bu	*n*-Bu	HSO_4			319	3.95	240	3.61	301	2.88
$PhCH_2$	$PhCH_2$	HSO_4			321	3.99[c]	241	—[c]		
c-Hex	c-Hex	$EtSO_4$			322	4.02[c]	239	3.73[c]		

[a]1.00 *N* sulfuric acid.
[b]Sodium borate buffer.
[c]In 95% ethanol.

3.51 (10), whereas in an aqueous medium of p*H* 5 it shows λ_{max} = 246 nm, log ε = 3.28 (11). The structure **10**, which resembles our pseudobases **8** even more closely, shows λ_{max} = 235 nm, log ε = 3.81 (12) (*cf.* Table 1).

The band at ~300 nm which is shown by the pseudobases is probably due to an $n \rightarrow \pi^*$ transition. In keeping with this, its intensity is markedly diminished by an *N*-phenyl group which can involve the nitrogen lone pair in conjugation.

The pseudobases **8** ($R^1 = R^2$ = c-Hex or $PhCH_2$) precipitate from aqueous solution, and so their uv spectra were taken in 95% ethanol. Isolation of these pseudobases enabled us to obtain mass spectral evidence for their structure.

Mass Spectral Studies[2]

To a concentrated aqueous solution of the pyrimidinium salt **7** ($R^1 = R^2 = PhCH_2$) bisulphate 1 *N* sodium hydroxide solution was added dropwise until precipitation was complete. The pale sticky yellow precipitate was collected and dried in air to give a glassy solid which we were unable to recrystallize. Mass spectra[2] of this material, the pseudobase **8** ($R^1 = R^2 = PhCH_2$), showed a small peak due to the parent molecular ion at *m/e* 294, a sizeable peak at *m/e* 292 (*M* − 2), and a large peak at *m/e* 277 (*M* − 17) corresponding to loss of OH and the formation of the cation **7** ($R^1 = R^2 = PhCH_2$). The largest peak in the spectra was always at *m/e* 91 and is almost certainly due to the benzyl/tropylium ion manifold.

The pseudobase **8** ($R^1 = R^2$ = c-Hex) was isolated in an analogous manner from the salt **7** ($R^1 = R^2$ = c-Hex) ethyl sulphate (8). Its mass spectra[2] also showed a relatively small parent molecular ion peak at *m/e* 278, and a large peak at *m/e* 261 corresponding to loss of hydroxyl and the formation of the cation **7** ($R^1 = R^2$ = c-Hex).

Proton Magnetic Resonance Spectral Studies

Pseudobase formation by all of the cations we have made (8) is readily observed by pmr (see Tables 2–5). The ring protons of the 2-oxopyrimidinium cations give characteristically simple spectra. When $R^1 = R^2$ the cation **7** is symmetrical about the C_2–C_5 axis, so that the 4 and 6-protons are magnetically equivalent, and thus a simple first-order spectrum is observed in which the 4,6-protons appear as a doublet $\delta \sim 9$, and the 5-proton as a triplet $\delta \sim 7$ (Table 2). When $R^1 \neq R^2$ the cation **7** is no longer symmetrical and more complex spectra would be anticipated (Table 3). However, in the cations **7** (R^1 = Me, R^2 = Et or $PhCH_2$) the effect of

[2]We thank Dr. R. T. B. Rye for kindly running mass spectra.

Can. J. Chem. Downloaded from www.nrcresearchpress.com by 210.87.254.40 on 09/05/12
For personal use only.

TABLE 2. Proton magnetic resonance spectral data of cation **11** salts in D_2O/DSS

R	Anion	Shifts[a] (δ) 4,6-H	5-H	Other
Me	Cl	8.90	7.00	3.82(NMe)
Me	HSO_4	8.95	7.12	3.85(NMe)
Et	Cl	8.97	7.08	1.45(CH_3), 4.28(CH_2)
Et	HSO_4	8.95	7.07	1.47(CH_3), 4.27(CH_2)
Et	I	9.00	7.10	1.48(CH_3), 4.28(CH_2)
Pr	Cl	8.97	7.20	0.98(CH_3), 1.80(CH_2), 4.17(NCH_2)
Pr	I	8.94	7.00	0.97(CH_3), 1.80(CH_2), 4.15(NCH_2)
i-Pr	$EtSO_4$	8.99	7.18	1.30($CH_3CH_2SO_4$), 1.55(CH_3), 4.10($CH_3CH_2SO_4$), 5.06(CH)
n-Bu	HSO_4	8.95	7.08	0.95(CH_3), 4.23(NCH_2)
$PhCH_2$	HSO_4	9.24	7.15	5.34(NCH_2), 7.42(Ph)
c-Hex	$EtSO_4$	8.88	7.09	1.30(CH_3), 4.08(CH_2)

[a]Coupling constant $J_{5,6} = J_{4,5} = 6.5$ Hz.

TABLE 3. Proton magnetic resonance spectral data of cation **18** salts in D_2O/DSS

R	Anion	Shifts[a] (δ) 4-H	6-H	5-H	NMe	Other
Me	Cl	8.90	8.90	7.00	3.82	
Me	HSO_4	8.95	8.95	7.05	3.85	
Et	Cl	9.02	9.02	7.12	3.88	1.49(CH_3), 4.31(CH_2)
Et	HSO_4	9.02	9.02	7.10	3.86	1.47(CH_3), 4.29(CH_2)
Et	I	9.02	9.02	7.10	3.87	1.47(CH_3), 4.30(CH_2)
i-Pr	HSO_4	9.02m[c]		7.15	3.88	1.56(CH_3), 5.08(CH)
t-Bu	HSO_4	9.00m[c]		7.03	3.82	1.75(CH_3)
c-Hex	I	8.95m[c]		7.06	3.82	
Ph	Cl[b]	9.23	9.62	7.21	3.80	7.62(Ph)
Ph	I[b]	9.18	9.37	7.23	3.78	7.65(Ph)
$PhCH_2$	HSO_4	9.03	9.03	7.10	3.84	5.42(CH_2), 7.53(Ph)

[a]Coupling constants $J_{4,5} = J_{5,6} = 6.5$ Hz; $J_{4,6} = 2$ Hz where observable.
[b]In DMSO-d_6 (reference TMS).
[c]m, multiplet.

the alkyl groups is so similar that their spectra closely resemble those of symmetrical cations. Presumably in these cases the contributions by the canonical structures *7a* and *7b* are very nearly equal. In the remaining cases the 4 and 6-protons are no longer equivalent and appear as a multiplet at $\delta \sim 9$. For the cation **7** (R^1 = Me, R^2 = Ph) the signals of the 4 and 6-protons are well separated, each appearing as a doublet of doublets due to $J_{4,5} = J_{5,6} = 6.5$ Hz and $J_{4,6} = 2$ Hz. In all cases the coupling constants $J_{4,5}$ and $J_{5,6}$ are essentially equal and so the 5-proton always appears as a triplet, though sometimes slightly broadened.

When 1 or 2 drops of 40% NaOD–D_2O are added to D_2O solutions of the cations **7** their characteristic spectra are removed and replaced by peaks at higher field attributable to pseudobases **8** (Tables 4, 5). For the symmetrical cations **11** only one pseudobase **12** is possible and so simple spectra are obtained (Table 4). For each pseudobase **12** the 4-proton appears as a doublet at $\delta \sim 5.3$ split by the 5-H ($J_{4,5} = 4.5$ Hz), the

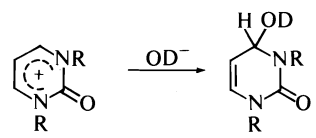

11 **12**

6-proton as a doublet at $\delta \sim 6.4$ split by the 5-H ($J_{5,6} = 8$ Hz) also, and the 5-H as a doublet of doublets at $\delta \sim 5.0$ ($J_{4,5} = 4.5$ Hz, $J_{5,6} = 8$ Hz). Appropriate signals are seen for the groups R in **12**.

The spectra of the pseudobases **12** (R = *i*-Pr

Can. J. Chem. Downloaded from www.nrcresearchpress.com by 210.87.254.40 on 09/05/12
For personal use only.

TABLE 4. Proton magnetic resonance spectral data of the pseudobases **12** in NaOD/D_2O/DSS

R	Shifts[a] (δ) 6-H	4-H	5-H	Other
Me	6.25	5.39	5.07	3.04(N_1-Me), 2.97(N_3-Me)
Et	6.39	5.48	5.11	3.49, 3.45(CH_2), 1.17, 1.13(CH_3)
Pr	6.44	5.47	5.17	0.98, 0.86(CH_3)
i-Pr	6.50	5.48	5.23	1.36, 1.30(N_3-CH_3), 1.17, 1.13(N_1-CH_3)
n-Bu[b]	6.34	5.34	4.93	
$PhCH_2$[b]	6.42	5.21	4.93	7.28, 7.25(Ph), 4.67(N_1-CH_2), 5.22, 4.97, 4.45, 4.20(N_3-CH_2)[c]
c-Hex[b]	6.41	5.33	4.99	

[a]Coupling constant $J_{4,5}$ = 4.5 Hz; $J_{5,6}$ = 8 Hz.
[b]These pseudobases precipitate from aqueous solution. For R = $PhCH_2$, spectrum was run in DMSO-d_6. For R = *n*-Bu, c-Hex, spectra run in acetone-d_6 (TMS).
[c]AB quartet, $\Delta\delta_{AB}$ = 0.72 ppm, J_{AB} = 15 Hz.

TABLE 5. Proton magnetic resonance spectral data of the pseudobases **19***a* and **19***b* in NaOD/D_2O/DSS

R	**19***a* or **19***b*	Shifts[a] (δ) 6-H	4-H	5-H	N-Me	Other	Ratio[b] **19***a*:**19***b*
Me	**19***a* = **19***b*	6.25	5.39	5.07	2.97	3.04(CH_3)	50:50
Et	**19***a*	6.30	5.38	5.10	2.97	1.11(CH_3)	68:32
	19*b*	6.27	5.38	5.08	3.03	1.14(CH_3)	
i-Pr	**19***a*	6.55	5.41	5.18	3.02	1.20, 1.17(CH_3)	93:7
	19*b*	6.53	?	?	3.08		
t-Bu	**19***a*	6.58	5.27	5.04	2.94	1.43(CH_3)	>99:1
c-Hex	**19***a*	6.59	5.43	5.17	3.03		94:6
	19*b*	?	?	?	3.10		
Ph	**19***a*	6.30	Complex		3.04	7.42(Ph)	60:40
	19*b*	6.33			3.11	7.38(Ph)	
$PhCH_2$[d]	**19***a*	6.41	5.22	4.88	2.90	7.26(Ph), 4.63(CH_2)	67:33
	19*b*	6.37	5.13	4.86	3.03	7.26(Ph), 5.17, 4.92, 4.38, 4.12(CH_2)[c]	

[a]Coupling constant $J_{4,5}$ = 4.5 Hz; $J_{5,6}$ = 8 Hz where observable.
[b]Ratio determined from peak heights of N-Me signals in **19***a* and **19***b*.
[c]AB quartet, $\Delta\delta_{AB}$ = 0.74 ppm, J_{AB} = 15 Hz.
[d]In DMSO-d_6.

or $PhCH_2$) are interesting in that they show diastereotopic nuclei (13). In the case of **12** (R = $PhCH_2$) the methylene protons of one benzyl group appear as a slightly broadened singlet (area 2) at δ 4.67, whereas those of the other give rise to four peaks[3] at δ 4.20, 4.45, 4.97, and 5.22 corresponding to an AB quartet (14) centered at δ 4.71 with a chemical shift difference of 0.72 ppm and a geminal coupling constant J_{AB} = 15 Hz. We suggest that the AB quartet results from diastereotopic methylene protons in the benzyl group closest to the asymmetric centre in the pseudobase **13**. Clearly from structure **14** the environment of the two benzylic protons is quite different. Moreover, the shift

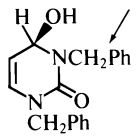

13

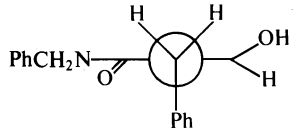

14

difference and coupling constant are very close to those found by other workers (15, 16)[4] for structurally related systems. Molecules of type **15** (X ≠ H) show diastereotopic benzylic pro-

[3]The peaks at δ 4.97 and δ 5.22 overlap with those of the 4-H and 5-H, but from the shape of the manifold in this region, and its integrated area it is clear that these peaks are truly there.

[4]L. D. Colebrook and F. H. Hund, unpublished results.

Can. J. Chem. Downloaded from www.nrcresearchpress.com by 210.87.254.40 on 09/05/12
For personal use only.

Can. J. Chem. Downloaded from www.nrcresearchpress.com by 210.87.254.40 on 09/05/12
For personal use only.

tons due to restricted rotation about the aryl-N bond. For **15** (X = Me) there is an AB quartet centred at δ 4.73, with a shift difference of 0.83 ppm and geminal coupling constant of 14 Hz (15). Colebrook and Hund (16)[4] studied

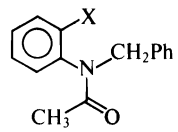

15

several molecules **15** (X = Me, Cl, Br, Ph) and found shift differences of 0.79–1.82 ppm and J_{AB} = 13.9–15.7 Hz.

The pseudobase **12** (R = *i*-Pr) shows diastereotopism in *both* isopropyl groups. Each isopropyl methyl doublet shows further splitting, one by ~3 Hz (0.05 ppm), the other by ~1.5 Hz. Presumably the larger of these splittings is associated with the isopropyl adjacent to the hydroxyl group, while the smaller is that of the more distant isopropyl group. The latter group, though farther removed from the asymmetric centre, should have diastereotopic methyls (see **16** and **17**).

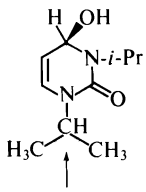

16

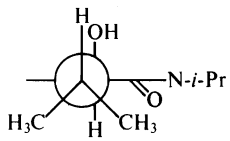

17

From the unsymmetrical cations **18** two pseudobases **19***a* and **19***b* may possibly be formed, and from the pmr spectra (Table 5) it is evident that in most instances both are formed, though in unequal amounts. The problem is to decide which set of signals belongs to which pseudobase. However, if we assume that *N*-methyl protons

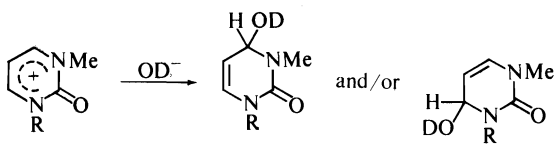

18 **19***a* **19***b*

adjacent to the hydroxyl group normally occur to higher field of those distant from it (see **20**), then a consistent pattern of behaviour emerges.

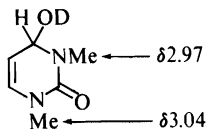

20

Given this assumption it appears that the predominant pseudobase is **19***a* formed by preferential hydroxide attack adjacent to the less bulky methyl group of **18** (see Table 5).

For example, from the cation **18** (R = Et) the major pseudobase **19***a* (R = Et) has the N-Me signal at δ 2.97, whereas the minor pseudobase **19***b* (R = Et) has it at δ 3.03. From the cation **18** (R = *i*-Pr) one pseudobase greatly exceeds the other, with the major one (93%) having N-Me at δ 3.02, and the minor one (7%) having N-Me at δ 3.08. Added confirmation of the structure of the major pseudobase as **19***a* (R = *i*-Pr) is afforded by the splitting of the isopropyl methyl signals due to diastereotopism (*vide supra*). The magnitude of this splitting (~1.5 Hz) is consistent with the isopropyl group being distant from the hydroxyl group as in **19***a* (R = *i*-Pr).

A similar situation arises for the pseudobases derived from the methyl benzyl cation **18** (R = CH_2Ph). The major component **19***a* (R = CH_2Ph) (67%) shows *N*-methyl at δ 2.90 and a singlet at δ 4.63 for the benzylic methylene. The minor component **19***b* (R = CH_2Ph) shows *N*-methyl at δ 3.03, and its benzylic protons appear as an AB quartet (δ 4.13, 4.38, 4.92, 5.17) centred at δ 4.65, with a shift difference of 0.74 ppm and J_{AB} = 15 Hz due to the diastereotopism induced by the adjacent asymmetric centre (*vide supra*). The proportions of these two pseudobases (**19***a*:**19***b* = 2:1) may be determined by kinetic rather than thermodynamic factors since they precipitated from aqueous solution as a mixture of oils whose pmr spectra were taken in DMSO-d_6 where equilibration between them may be much slower.

Both pseudobases derived from the cation **18** (R = Ph) are observable, and again the major one **19***a* (R = Ph) is that bearing the OH next to *N*-methyl. For the remaining cations **18** (R = *tert*-Bu, c-Hex) only one pseudobase is clearly observable which is assumed to be **19***a* (R = *tert*-Bu, c-Hex). However, a small signal at δ 3.10 may be due to a small amount (6%) of the

TABLE 6. pK_{ROH} values of cation **7** salts in aqueous solution at 24 °C

R^1	R^2	Anion	pK_{ROH}	σ^* for R^2
Me	Ph	Cl	4.87±0.02(8)[a]	0.6[b]
Me	Ph	I	4.86±0.03(11)	0.6
Me	$PhCH_2$	HSO_4	6.49±0.02(6)	0.215
Me	Me	Cl	7.03±0.05(6)[c]	0.0
Me	Me	HSO_4	7.11±0.03(8)	0.0
Me	Et	I	7.21±0.03(11)	−0.1
Me	*i*-Pr	HSO_4	7.49±0.05(12)	−0.19
Me	c-Hex	I	7.62±0.04(13)	−0.15
Me	*t*-Bu	HSO_4	8.41±0.02(18)	−0.3
Et	Et	HSO_4	7.49±0.03(12)	−0.1
Et	Et	I	7.52±0.04(12)	−0.1
n-Pr	*n*-Pr	I	7.42±0.03(12)	−0.115
n-Bu	*n*-Bu	HSO_4	7.58±0.02(9)	−0.13
i-Pr	*i*-Pr	$EtSO_4$	7.94±0.02(7)	−0.19

[a]Quoted errors are the greatest deviation from the average. Number in parentheses is the number of values from which average was calculated.
[b]σ^* values from Taft (5).
[c]From ref. 7, at 20 °C.

pseudobase **19***b* (R = c-Hex) derived from the methyl cyclohexyl cation **18** (R = c-Hex).

In summary, it appears that where two conceivable pseudobases may arise from **18**, the preferred one derives from hydroxide attack adjacent to the less bulky substituent. Moreover, there is a reasonable correlation between the proportion of the preferred pseudobase **19***a* and the bulkiness of the substituent R.

Equilibrium Constants and Substituent Effects

In aqueous solution the cations **7** behave as weak acids due to the equilibria with their pseudobases **8** [1], and so values of K_{ROH} and pK_{ROH} may be determined by conventional techniques (17). In Table 6 are shown pK_{ROH} values for all of the cations **7** except for $R^1 = R^2$ = c-Hex and $R^1 = R^2 = PhCH_2$. These could not be determined properly since the corresponding pseudobases precipitate from solution during titration.

The trends evident in the data in Table 6 are easily rationalized in terms of the electronic and steric effects of the substituents. Progressively larger alkyl groups increase the value of pK_{ROH} for two reasons. Firstly, the increasing electron-releasing ability of the substituent serves to stabilize the cation **7**. Secondly, the increasing steric size of the substituent serves to destabilize the pseudobase **8** when the substituent is adjacent to the hydroxyl group.

Reasonable correlations exist between the data and Taft's substituent constant σ^* which is a measure of the ability of the substituents to release (or withdraw) electron density inductively (5). For the series of cations **18** (R = Ph, $PhCH_2$, Me, Et, c-Hex, *i*-Pr, *tert*-Bu) least-squares fitting of the data gives

$$[2] \qquad pK_{ROH} = -3.6\sigma^* + 7.1$$

with a correlation coefficient of 0.985 for seven values. The value of $\rho^* = -3.6$ is very close to those found by Bunting and Meathrel (4), and by Lindquist and Cordes (6). Both our value and those of Bunting and Meathrel must involve a steric component. However, in our case, since the cation **18** has the choice to form a pseudobase **19***a* with OH away from the bulky group R, the most that a pK_{ROH} value might be elevated by, due to a steric effect, is the statistical factor log 2 = 0.3. In view of the uncertainties in the pK_{ROH} values and, more particularly, in the proportions of **19***a* and **19***b* derived from pmr peak heights (Table 5), we have not attempted to dissect out separate pK_{ROH} values for the formation of **19***a* and **19***b*.

The data for the symmetrical cations **11** is more limited than intended. We were unable to prepare **11** (R = Ph or *tert*-Bu) (8), and as mentioned earlier, we could not determine pK_{ROH} for **11** (R = c-Hex or $PhCH_2$) due to precipitation of the pseudobases. The remaining five symmetrical cations **11** (R = Me, Et, *n*-Pr, *n*-Bu, *i*-Pr) have pK_{ROH} values which approxi-

Can. J. Chem. Downloaded from www.nrcresearchpress.com by 210.87.254.40 on 09/05/12
For personal use only.

mately fit [3] with a correlation coefficient of 0.964.

$$[3] \qquad pK_{ROH} = -4.2\sigma^* + 7.1$$

The more negative $\rho^* = -4.2$ is due to steric effects since the OH group of the pseudobase **12** is necessarily next to the substituent R. Again, however, the value is close to those found by other workers (4, 6).

We have also measured pK_{ROH} for the 5-bromo cation **21** (X = Br) (18) and find it to be 3.08, *i.e.* 4.04 units lower than that of the parent

		X = H	X = Br
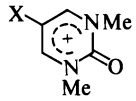 **21**	pK_{ROH}	7.12	3.08
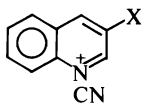 **22**	pK_{ROH}	−1.05	−5.19

21 (R = H). This difference is very close to the value of 4.14 found for the cations **22** (R = H and Br) by Cooksey and Johnson (2). If the pK_{ROH} values for such cations as **21** and **22** correlate with σ_m^+ (3), the values given above correspond to a ρ value of −10. This large ρ may also contain a substantial steric component.

Experimental

The preparations of the compounds used in this work have been described elsewhere (8, 18). Ultraviolet spectra were taken on a Cary 14 instrument. Proton magnetic resonance spectra were obtained at 60 MHz on a Varian A-60 spectrometer. Mass spectra were run on a Perkin-Elmer–Hitachi RMU-6E mass spectrometer.

The pK_{ROH} values were determined using the potentiometric method (17). A 25 ml portion of 0.01 *M* solution of the cation salt was titrated against standard (0.05 *N* or 0.01 *N*) KOH solution using a Metrohm Herisau Potentiograph E436 previously calibrated using standard buffer solutions. Lack of hysterisis, reproducibility, and reversibility were checked by back titration against standard 0.01 *N* hydrochloric acid solution. From the titration data values of pK_{ROH} were calculated (17) using a BASIC computer program written by Dr. S. Banerjee.

Acknowledgements

The work was supported by a grant from the National Research Council of Canada. We thank Professor J. W. Bunting for informing us of the progress of his work, and Prof. L. D. Colebrook for discussions about diastereotopism. We are also grateful to Prof. J. G. Dick for the use of the Metrohm Potentiograph.

1. A. Hantzsch. Chem. Ber. **32**, 575 (1899); A. Hantzsch and M. Kalb. Chem. Ber. **32**, 3109 (1899).
2. C. J. Cooksey and M. D. Johnson. J. Chem. Soc. B, 1191 (1968).
3. J. E. Leffler and E. Grunwald. Rates and equilibria of organic reactions. Wiley, New York. 1963.
4. J. W. Bunting and W. G. Meathrel. Can. J. Chem. **52**, 962 (1974).
5. R. W. Taft. Steric effects in organic reactions. *Edited by* M. S. Newman. Wiley, New York. 1956. Chapt. 13.
6. R. N. Lindquist and E. H. Cordes. J. Am. Chem. Soc. **90**, 1269 (1968).
7. A. R. Katritzky, M. Kingsland, and O. S. Tee. Chem. Commun. 289 (1968); J. Chem. Soc. B, 1484 (1968).
8. O. S. Tee and M. Endo. J. Heterocycl. Chem. **11**, 441 (1974).
9. D. J. Brown. The pyrimidines. *In* The chemistry of heterocyclic compounds. Vol. 16. *Edited by* A. Weissberger. Interscience, New York. 1962. Chapt. 13.
10. H. Hatt and C. K. Triffett. Chem. Commun. 439 (1965).
11. T. Inoi, T. Okamoto, and Y. Koizumi. J. Org. Chem. **31**, 2700 (1966).
12. D. Lipkin and E. G. Lovett. J. Org. Chem. **40**, 1713 (1975).
13. K. Mislow and M. Raban. *In* Topics in stereochemistry. Vol. 1. *Edited by* N. L. Allinger and E. L. Eliel. Interscience, New York. 1967. p. 1.
14. J. D. Roberts. An introduction to the analysis of spin–spin splitting in nuclear magnetic resonance. Benjamin, New York. 1962. pp. 49–60.
15. Y. Shvo, E. C. Taylor, K. Mislow, and M. Raban. J. Am. Chem. Soc. **89**, 4910 (1967); T. H. Siddall and C. A. Prohaska. J. Am. Chem. Soc. **88**, 1172 (1966).
16. F. H. Hund. Ph.D. Thesis, University of Rochester, Rochester, N.Y. 1971.
17. A. Albert and E. P. Serjeant. Ionization constants of acids and bases. Methuen, London. 1962.
18. O. S. Tee and S. Banerjee. Chem. Commun. 1032 (1972); Can. J. Chem. **52**, 451 (1974).

Can. J. Chem. Downloaded from www.nrcresearchpress.com by 210.87.254.40 on 09/05/12
For personal use only.

Oligoribonucleotide synthesis. X.[1,2] An improved synthesis of the anticodon loop region of methionine transfer ribonucleic acid from *E. coli*

E. S. WERSTIUK AND THOMAS NEILSON
Department of Biochemistry, McMaster University, Hamilton, Ont., Canada L8S 4J9

Received April 12, 1976

E. S. WERSTIUK and THOMAS NEILSON. Can. J. Chem. **54**, 2689 (1976).

Nonaribonucleotide, GpCmpUpCpApUpApApC, was synthesized using a block phosphotriester method. Its sequence corresponds to that of the anticodon loop of transfer RNA_f^{Met} (*E. coli*). Protected tetramer, GCmUC and pentamer nucleotides, AUAAC, assembled stepwise from nucleoside derivatives, were joined together to give protected nonamer which on deblocking, gave the free nonaribonucleotide in milligram amounts. The superior internucleotide coupling efficiency of mesitylenesulfonyl triazolide (MST) over triisopropylbenzenesulfonyl chloride (TPS) is demonstrated.

E. S. WERSTIUK et THOMAS NEILSON. Can. J. Chem. **54**, 2689 (1976).

Le nonaribonucléotide GpCmpUpCpApUpApApC, a été synthétisé en utilisant une méthode séquencée au phosphotriester. Sa séquence correspond à celle de la boucle de l'anticodon du ARN_f^{Met} de transfert (*E. coli*). Le tétramère GCmUC et les nucléotides pentamères, AUAAC protégés, assemblés un à un à partir de dérivés nucléosides, ont été reliés ensemble pour donner le nonamère bloqué, lequel, après déblocage, a conduit au nonaribonucléotide libre à l'échelle du milligramme. L'efficacité supérieure du couplage internucléotide du triazole mésitylènesulfonyle (MST) sur le chlorure de triisopropylbenzènesulfonyle (TPS) est démontrée.

[Traduit par le journal]

Continuous conformational change in transfer RNA is believed responsible for the various enzymic interactions which occur during protein biosynthesis. Identification and characterization of each of these sites have proven difficult on a complete native molecule (3). Specific interactions may be determined, however, using oligoribonucleotide 'fragments' corresponding to part of the primary sequence. Several partial RNAse T_1 digestions (4) provided fragments which have been studied for recognition by codons or the aminoacyl-tRNA synthetases.

Since fragments from enzymic digests are controlled by specific cleavage points in a polynucleotide chain, only a limited number of oligonucleotides of known length and sequence are currently available. Chemical synthesis on the other hand is theoretically capable of providing all possible oligoribonucleotides. Should a particular sequence within a transfer RNA molecule be considered a possible functional site, a 'tailor-made' oligoribonucleotide could be prepared and tested for recognition. Subsequent substitution of bases may determine the exact points of interactions. Two such syntheses, the duplex stem region of yeast $tRNA^{Ala}$ (5) and the duplex dihydrouridine loop neck region of several tRNAs (1) have been carried out.

In this communication we report an improved synthesis (2) of the nonaribonucleotide, GpCmpUpCpApUpApApC, which corresponds to the anticodon loop of $tRNA_f^{Met}$ from *E. coli* (6) using a phosphotriester fragment coupling procedure (7). Oligoribonucleotide synthesis using intermediates containing phosphotriester internucleotide linkage has recently been reviewed (8) and is now recognized as offering many advantages, especially scale.

In our preliminary studies (2) this nonaribonucleotide was assembled from three protected dinucleotides and one trinucleotide using three fragment coupling steps. Since yields of both 5′-selective deblockings and fragment couplings were low, a reduction in the number of those steps was desirable. Scheme 1 shows an outline of the synthesis of GpCmpUpCpApUpApApC which consists of stepwise assembly of protected tetranucleotide (**8**) and protected pentanucleotide (**15**) and their subsequent coupling. Internucleotide coupling reactions using triisopropylbenzenesulfonyl chloride (TPS) are frequently

[1]For part IX, see ref. 1.
[2]For a preliminary account of this synthesis, see ref. 2.

Can. J. Chem. Downloaded from www.nrcresearchpress.com by 210.87.254.6 on 09/05/12
For personal use only.

sluggish and highly coloured, probably the result of pyridine hydrochloride generation. In an effort to overcome these practical difficulties, the coupling agent, mesitylenesulfonyl 1,2,4-triazolide (MST) (9) was used in all later phosphorylation and coupling reactions.

Suitably protected nucleosides, **1** (10), **4** (11) **6**, **11** (12), and **9** (13), had been prepared previously. Each heterocyclic base (except uracil) carried a benzamido grouping and each ribofuranoside 2′-hydroxyl was protected by a tetrahydropyranyl group. 5′-Trityloxyacetates

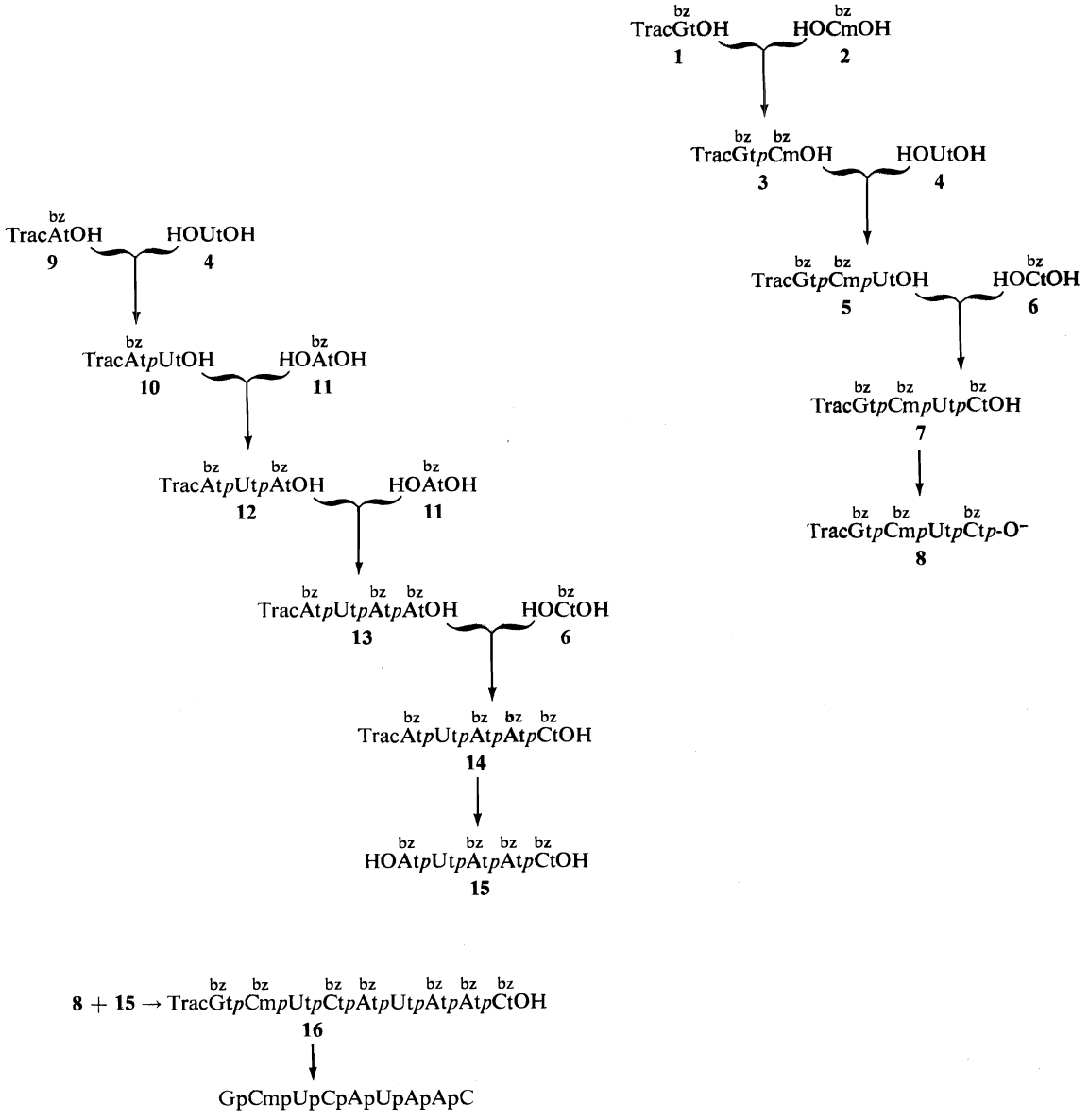

SCHEME 1. Abbreviations are as suggested by the IUPAC–IUB commission. Trac is 5′-*O*-triphenylmethoxyacetyl, t is 2′-*O*-tetrahydropyranyl, m is 2′-*O*-methyl, bz represents a benzoyl modification of the base amino function, *p* between characters *e.g.* At*p*Ut, indicates a 3′–5′ (2,2,2-trichloroethyl)phosphotriester internucleotide linkage and *p*-O is 3′-*O*-(2,2,2-trichloroethyl) phosphate.

Can. J. Chem. Downloaded from www.nrcresearchpress.com by 210.87.254.6 on 09/05/12
For personal use only.

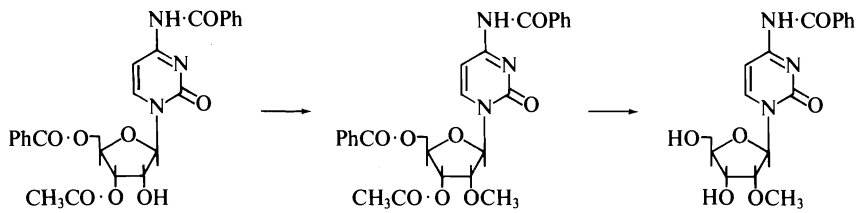

17 18 2

1 and **9** were the starting points for stepwise synthesis of protected tetranucleotide derivative **8** and protected pentanucleotide derivative **15**. Protected oligomer, AUA (**12**) has been described earlier (13).

The 5′-trityloxyacetyl group was employed for three reasons (7). It could be selectively removed using very mild basic conditions. Any compound containing the trityl group could be conveniently detected on thin layer chromatography using an acid spray. The lipophilic nature of this group allowed organic phase extraction of any compound containing this group from aqueous solution *even* if that compound contained one negative charge.

N^4-Benzoyl-2′-*O*-methylcytidine (**2**) was prepared from 3′-*O*-acetyl-N^4-5′-*O*-dibenzoylcytidine (**17**) (12). Diazomethane treatment of **17** gave the corresponding 2′-*O*-methyl ether (**18**) in 87% yield. Carefully controlled de-*O*-acylation of **18** gave **2** in 85% yield.

Coupling between protected nucleosides was a two-step procedure. Phosphorylation of the 3′-hydroxyl of 5′-*O*-trityloxyacetylnucleoside derivative with pyridinium mono-2,2,2-trichloroethylphosphate in the presence of activating agents, TPS or MST, gave the corresponding nucleotide derivative. Condensation of this nucleotide, activated by a fresh portion of appropriate coupling agent, with the 5′-hydroxyl of the next nucleoside in the sequence, completed the internucleotide linkage. Isolation and purification was accomplished after each two-step process using silica gel chromatography with methanol – methylene chloride mixtures. Sequences up to tetranucleotide derivative **7** and pentanucleotide **14** were assembled stepwise starting from their 5′-terminus by adding each protected nucleoside derivative one at a time. Yields for the two-step coupling using TPS (Table 1) were in the 50–70% range with one exception (GCmU + C). Corresponding yields using MST were on the average 10% higher and the products were less coloured.

Before block coupling between **7** and **14** could be effected, the 5′-trityloxyacetyl group of **14** was selectively removed to give protected pentanucleotide derivative **15**, and **7** was phosphorylated to give protected 3′-phosphate derivative **8**. **8** was then activated with a fresh portion of TPS or MST and coupled to the 5′-terminus of **15** to give protected nonaribonucleotide **16** in 40% and 48% yield respectively, over two steps. No evidence for undesirable 3′–3′ linkages was detected in any of the coupling reactions. Bulky 2′-*O*-tetrahydropyranyl groups appear to shield their neighbouring 3′-hydroxyls from any nucleotide phosphorylation.

Table 2 summarizes the efficiencies of coupling agents, TPS and MST. Some earlier data (synthesis of protected AUA) (13) has been included. Coupling with MST is, on the average, 10% more efficient than with TPS in the present series of reactions. In an earlier communication (1) we reported that MST-activated couplings were 50–100% better than the corresponding TPS reactions, however, it should be emphasized that most of these internucleotide couplings involved the purine base, guanine. In addition to the increase in yield, reaction times are shortened (*ca.* 50%) and the products were free from colouration, after routine column chromatography of the reaction mixture.

Complete deblocking of all protected oligomers was carried out after the addition of each new nucleoside derivative and after the fragment coupling. To eliminate the possibility that residual copper and zinc ions may be associated with free oligomers further purification steps were introduced (1) into the normal three-step deblocking procedure (14). After the first two steps, deprotection with Cu/Zn couple and 7 *M* methanolic ammonia, treatment with Chelex 100 (NH_4^+ form) rather than Dowex 50W-X8

Can. J. Chem. Downloaded from www.nrcresearchpress.com by 210.87.254.6 on 09/05/12
For personal use only.

Can. J. Chem. Downloaded from www.nrcresearchpress.com by 210.87.254.6 on 09/05/12
For personal use only.

TABLE 1. Summary of preparation of protected oligoribonucleotides

(a) TPS as condensing agent

Reactants						Product		
	Quantity			Quantity			Quantity	
No.	mg	mmol	No.	mg	mmol	No.	mg	%
1	400	0.54	**2**	288	0.80	**3**	450	62
3	544	0.33	**4**	164	0.50	**5**	320	52
5	300	0.16	**6**	108	0.24	**7**	125	31
12	505	0.26	**11**	180	0.39	**13**	437	65
13	400	0.15	**6**	98	0.23	**14**	265	56
14	190	0.06				**15**	140	82
7	100	0.04	**15**	140	0.05	**16**	95	40

(b) MST as condensing agent

Reactants						Product		
	Quantity			Quantity			Quantity	
No.	mg	mmol	No.	mg	mmol	No.	mg	%
1	640	0.82	**2**	430	1.2	**3**	715	71
3	675	0.51	**4**	255	0.77	**5**	500	55
5	300	0.162	**6**	108	0.24	**7**	150	38
12	1000	0.54	**11**	370	0.80	**13**	1120	82
13	900	0.35	**6**	225	0.52	**14**	705	70
14	500	0.156				**15**	330	84
7	123	0.05	**15**	220	0.075	**16**	140	48

TABLE 2. Comparison of TPS and MST as condensing agents in oligoribonucleotide synthesis

Reactants	Yield (%) TPS†	MST‡
1+ **2** (G+Cm)*	62	71
3+ **4** (GCm+U)	52	55
5+ **6** (GCmU+C)	31	38
9+ **4** (A+U)	66	78
10+**11** (AU+A)	58	60
12+**11** (AUA+A)	65	82
13+ **6** (AUAA+C)	56	70
7+**15** (GCmUC+AUAAC)	40	48

*G + Cm represents the following reactions:

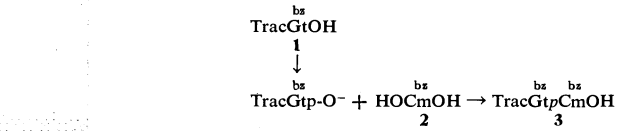

†Phosphorylation with cyclohexylammonium salt of mono-2,2,2-trichloroethyl phosphate.

‡Phosphorylation with free acid of mono-2,2,2-trichloroethyl phosphate.

(NH_4^+) was carried out. After removal of the resin, the filtrate was evaporated *in vacuo* and the residue subjected to preparative Whatman 40 paper chromatography in system *A*. Since the oligomers still were protected by 2′-*O*-tetrahydropyranyl groups, their mobility was quite high. The bands were cut out, desalted in absolute ethanol for 1 h, dried in ether, and eluted with distilled water. Eluates were then adjusted to p*H* 2 with 2 *N* hydrochloric acid solution to give free oligomers which were isolated using a similar preparative paper chromatographic procedure. Characterization by enzymic analysis is shown in Table 3. This modified procedure gave very pure, biological active (to be published elsewhere) material, especially for longer sequences. Unfortunately the yields are not as high as reported in our earlier communication, apparently the Chelex treatment and the additional paper chromatography contribute to loss.

Thus the present synthesis of nonaribonucleotide, GpCmpUpCpApUpApApC, has suggested three improvements which will have major consequence in future oligoribonucleotide synthesis using phosphotriester intermediates.

(*i*) Stepwise assembly is convenient for oli-

TABLE 3. Characterization of free oligoribonucleotides

Compound	Yield (%) for complete deprotection*	R_{Gp} pc$_A$	tlc$_A$	pc$_B$	pe	Enzymic analysis from SVD and spleen digestions
GCm	39	5.10	6.20	1.54	0.29	G:Cm (0.95:1.0)
GCmU	30	2.45	2.68		0.60	G:Cm:U (1.0:1.0:1.0)
GCmUC	35	0.82	0.84	0.61	0.82	G:Cm:C:U (1.0:1.1:1.1:1.0)
AUA	40	0.85	0.95	0.88	0.55	A:U (2.1:1.0)
AUAA	37	0.40	0.35		0.63	A:U (3.1:1.0)
AUAAC	37	0.27	0.20	0.70	0.88	A:C:U (3.1:0.9:1.0)
GCmUCAUAAC	25	0.21	0.05	0.18	0.89	G:Cm:A:C:U (1.0:1.1:2.9:2.1:2.0)
Gp		1.00	1.00	1.00	1.00	
U					0.00	

*Calculated from ultraviolet spectrophotometric data assuming a hypochromicity factor of 90%.

gomers up to five residues and subsequent fragment coupling leads to oligomers of longer sequences.

(*ii*) Mesitylenesulfonyl 1,2,4-triazolide is now the established coupling agent.

(*iii*) An improvement deblocking procedure suitable for longer sequences has been developed.

Experimental

Proton magnetic resonance spectra were recorded on a Varian T60 or Varian HA-100 spectrometer in 10–15% (w/v) DMSO-d_6–D_2O solutions and line positions are reported in ppm from the reference (TMS).

Silica gel (Baker Analyzed Reagent) was used for column chromatography; Analtech prescored silica gel plates were employed for tlc. The plates were usually developed in 5 or 10% methanol in methylene chloride mixtures. The tlc detection was carried out using a ceric sulfate spray (1 g $H_4Ce(SO_4)_4$ in 10% aqueous sulfuric acid solution) and followed by heating the plates at 300–400 °F. Compounds containing a trityl group develop as yellow spots, while others appear as brown coloration.

Paper chromatography was performed using the descending technique on Whatman No. 1 or 40 paper. Analtech precoated cellulose plates (Avicel F) were used for tlc of deblocked nucleotides. The solvent systems employed for pc on Whatman No. 1 and tlc on cellulose were (*A*) ethanol – 1 *M* ammonium acetate, p*H* 7.5 (7:3, v/v) and (*B*) 1-PrOH – concentrated NH_4OH – H_2O (55:10:35, v/v) respectively. Paper electrophoresis was performed at 1400 V/66 cm using Whatman 3 MM paper and (*C*) 0.05 *M* triethylammonium bicarbonate, p*H* 8.0. A short uv lamp was used for detection.

It was essential that moisture be excluded from all coupling reactions. After evaporation *in vacuo* of the pyridine solution, normal pressure was restored with dry nitrogen and not atmospheric air. All such evaporations were carried out in the temperature range of 30–40 °C. Emulsions, frequently obtained during methylene chloride extractions of aqueous pyridine solutions, were broken by the addition of a few millilitres of saturated sodium chloride solution.

*3′-O-Acetyl-N⁴-5′-O-dibenzoyl-2′-O-methylcytidine (**18**)*

Diazomethane (prepared from *N*-methyl-*N*′-nitro-*N* nitrosoguanidine, 2.0 g) in dry ether (15 ml) was added at 0 °C to a stirred suspension of 3′-*O*-acetyl-*N*⁴-5′-*O*-dibenzoylcytidine (**17**) (12) (1.96 g, 4 mmol, R_F 0.63 in 10% CH_3OH–CH_2Cl_2) in dry tetrahydrofuran (40 ml). The reaction mixture was stirred at 0 °C for 2 days, then a second portion of ethereal diazomethane solution (from 2.0 g of *N*-methyl-*N*′-nitro-*N*-nitrosoguanidine) (15 ml) was added. Stirring was continued for further 2 days at 0 °C. Thin layer chromatography of the resulting solution indicated *ca.* 90% conversion into a major product of R_F 0.73 in 10% CH_3OH–CH_2Cl_2. Excess diazomethane was removed by bubbling air through the yellow solution, and the colourless solution so obtained was evaporated to dryness *in vacuo*. Crude reaction mixture was purified by chromatography on silica gel (30 g) in methylene chloride. Pure 3′-*O*-acetyl-*N*⁴-5′-*O*-dibenzoyl-2′-*O*-methylcytidine (1.75 g, 87%, R_F 0.73 in 10% CH_3OH–CH_2Cl_2) was obtained by elution with 1.0–1.5% methanol–methylene chloride mixtures. Crystallization from methylene chloride – petroleum ether (40–60 °C) provided an analytical sample of mp 53–55 °C.

The pmr spectrum showed signals (δ TMS) at 8.28–7.27 (12H, m, two C_6H_5CO—, and 6, 5-cytidine protons), 6.20 (1H, d, $J \sim 4$ Hz, 1′-anomeric proton), 3.35 (3H, s, —OCH_3 protons), and 2.05 ppm (3H, sharp s, —$COCH_3$ protons). *Anal.* calcd. for $C_{26}H_{25}N_3O_8$ (mol. wt. 507. 48): C 61.53, H 4.97, N 8.28; found: C 62.17, H 5.53, N 7.71.

*N⁴-Benzoyl-2′-O-methylcytidine (**2**)*

A solution of 3′-*O*-acetyl-*N*⁴-5′-*O*-dibenzoyl-2′-*O*-methylcytidine (**18**) (1.8 g, 3.6 mmol, R_F 0.73 in 10% CH_3OH–CH_2Cl_2) in methanolic ammonia (100 ml, 0.75 *N*, prepared by twenty-fold dilution of concentrated ammonia with methanol) was stirred at room temperature. Progress of reaction was followed by tlc which after 4 h indicated *ca.* 90% conversion into a major product of R_F 0.34 in 10% CH_3OH–CH_2Cl_2. The solution was then evaporated to dryness *in vacuo*, and the colourless glass obtained was purified by chromatography on silica gel (30 g) in methylene chloride. Elution with 1.5% methanol – methylene chloride mixtures yielded some unreacted starting material (0.35 g, R_F 0.73 in 10% CH_3OH–CH_2Cl_2). Pure *N*⁴-benzoyl-2′-*O*-methylcytidine (0.85 g,

Can. J. Chem. Downloaded from www.nrcresearchpress.com by 210.87.254.6 on 09/05/12
For personal use only.

Can. J. Chem. Downloaded from www.nrcresearchpress.com by 210.87.254.6 on 09/05/12
For personal use only.

85%, R_F 0.34 in 10% CH_3OH–CH_2Cl_2) was obtained on further elution with 3.0–3.5% methanol – methylene chloride mixtures (500 ml + 500 ml). Crystallization from ethyl acetate provided an analytical sample of mp 82–84 °C (sublimed) (0.65 g, 65%). The pmr spectrum showed signals (δ TMS) at 8.20–7.35 (12H, m, two C_6H_5CO—, and 6, 5-cytidine protons), 6.45 (1H, d, $J \sim 4$ Hz, 1′-anomeric proton), and 3.45 ppm (3H, s, —OCH_3 protons). *Anal.* calcd. for $C_{17}H_{19}O_6N_3$ (mol. wt. 361.352): C 56.50, H 5.30, N 11.63; found: C 56.16, H 5.27, N 11.75.

N^2-Benzoyl-2′-O-tetrahydropyranyl-5′-O-triphenylmethoxyacetylguanylyl[3′-(2,2,2-trichloroethyl)-5′]N^4-benzoyl-2′-O-methylcytidine (3)

(*a*) *TPS-Coupling*

Biscyclohexylammonium mono-2,2,2-trichloroethyl phosphate (15) (480 mg, 1.08 mmol) was dissolved in anhydrous pyridine (25 ml) with warming and converted into its pyridinium salt by repeated evaporation *in vacuo*, and solution in pyridine (5 × 30 ml). TPS (655 mg, 2.16 mmol) was then added to the solution of pyridinium salt in pyridine (15 ml), and the reaction mixture sealed under dry nitrogen. After 1 h a pyridine solution (15 ml) of N^2-benzoyl-2′-O-tetrahydropyranyl-5′-O-triphenylmethoxyacetylguanosine (**1**) (10) (400 mg, 0.54 mmol, R_F 0.66 in 10% CH_3OH–CH_2Cl_2) was added to the activated pyridinium salt, and the reaction mixture sealed under dry nitrogen and set aside at room temperature in the dark. After 3 days tlc indicated complete conversion into a product of R_F 0.0–0.20 in 10% CH_3OH–CH_2Cl_2. Ice (5 g) was then added, the quenched reaction left for 30 min, then poured into ice water (40 ml) and repeatedly extracted with methylene chloride (5 × 25 ml). The combined organic extracts were washed with water (3 × 20 ml), and evaporated *in vacuo*. The residue was dissolved in anhydrous pyridine, (25 ml) and evaporated from pyridine (3 × 25 ml). TPS (182 mg, 0.60 mmol) was added to the pyridine solution containing the blocked guanylate derivative, and activation was allowed to proceed for 1 h at room temperature. A pyridine solution (15 ml) containing N^4-benzoyl-2′-O-methylcytidine (**2**) (288 mg, 0.80 mmol, 1.5 equiv., R_F 0.37 in 10% CH_3OH–CH_2Cl_2) was added to the activated guanylate derivative and the reaction mixture sealed under nitrogen and stored at room temperature for 6 days in the dark. Further portions of TPS (3 × 50 mg) were added till all the blocked guanylate derivative had reacted. After 6 days tlc indicated *ca.* 80% conversion into a product of R_F 0.70 in 10% CH_3OH–CH_2Cl_2. Ice (5 g) was then added, and after 30 min the reaction mixture was poured into ice water (30 ml) and repeatedly extracted with methylene chloride (4 × 25 ml). Combined organic extracts were washed with water (2 × 25 ml), and evaporated *in vacuo*. The last traces of pyridine were removed by co-distillation with toluene (3 × 15 ml), and the product isolated by column chromatography on silica gel (30 g) in methylene chloride. Elution with 1–1.5% methanol – methylene chloride mixtures removed some fast moving impurities. On further elution with 2.0–2.5% methanol – methylene chloride mixtures **3** was obtained as a mixture of diastereoisomers (450 mg, 62%).

(*b*) *MST-Coupling*

The free acid of mono-2,2,2-trichloroethyl dihydrogen phosphate (1) (360 mg, 1.64 mmol) was converted to its pyridinium salt by solution in anhydrous pyridine and repeated evaporation *in vacuo* (3 × 25 ml). MST (9) (800 mg, 3.20 mmol) was added to the pyridine solution (*ca.* 10 ml), and the reaction mixture sealed under dry nitrogen. Gentle heating (40 °C) was required to redissolve the pyridinium trichloroethyl phosphate, and complete the activation. After 1 h pyridine solution (5 ml) containing N^2-benzoyl-2′-O-tetrahydropyranyl-5′-O-triphenylmethoxyacetylguanosine (**1**) (10) (640 mg, 0.82 mmol) was added to the clear solution of the activated phosphate, and the reaction mixture sealed under dry nitrogen, and set aside at room temperature in the dark. After 3 days tlc indicated that the phosphorylation was complete (R_F 0.66 → 0.0 – 0.20 in 10% CH_3OH–CH_2Cl_2). The reaction was quenched with ice (2 g), poured into ice water (40 ml) and repeatedly extracted with methylene chloride. Combined organic extracts were washed with water (3 × 20 ml), and evaporated *in vacuo* to a light yellow foam. This residue containing the blocked guanylate derivative was repeatedly evaporated *in vacuo* from anhydrous pyridine (4 × 25 ml, final volume *ca.* 5 ml) and MST (225 mg, 0.90 mmol) was added. After 1 h a pyridine solution of N^4-benzoyl-2′-O-methylcytidine (**2**) (430 mg, 1.20 mmol, 1.5 equiv.) was added, and the reaction mixture set aside at room temperature under nitrogen. Thin layer chromatography indicated that the reaction was complete after 4 days (R_F 0.0 – 0.20 → 0.70 in 10% CH_3OH–CH_2Cl_2). The reaction was quenched, and worked-up in the usual manner, and the light yellow foam obtained was purified by silica gel chromatography (30 g) in methylene chloride. Elution with 2.0–2.5% methanol – methylene chloride mixtures gave **3** as a mixture of diastereoisomers (615 mg, 61%). Further elution with 3.0% methanol – methylene chloride mixtures yielded a mixture of **3** and **2** (210 mg). 'Back tritylation' of this mixture with *p*-methoxytrityl chloride (100 mg, 3.33 mmol), and subsequent silica gel chromatography yielded further 100 mg of **3**, (total yield 715 mg, 71%).

Guanylyl(3′–5′)2′-O-methylcytidine (GpCm)

A solution of N^2-benzoyl-2′-O-tetrahydropyranyl-5′-O-triphenylmethoxyacetylguanylyl[3′-(2,2,2-trichloroethyl)-5′]-N^4-benzoyl-2′-O-methylcytidine (**3**) (20 mg, R_F 0.70 in 10% CH_3OH–CH_2Cl_2) in *N*,*N*-dimethylformamide (1.0 ml) was stirred at 50 °C with Cu–Zn couple (*ca.* 30 mg). After 2 h tlc indicated complete conversion of starting material into a product of R_F 0 (origin) in 10% CH_3OH–CH_2Cl_2. Methanol (2 ml) and concentrated ammonia (2 ml) were added, and the reaction mixture stirred at room temperature for 72 h. Ammonia solution (1 ml, 1 *N*) was added, and the Cu–Zn couple filtered off, and washed well with *N* ammonia. Combined filtrate and washings were carefully concentrated *in vacuo* and the p*H* of the solution adjusted to *ca.* 9.0. Chelex 100 (*ca.* 1 g, 100–200 mesh, NH_4^+ form) was added and the mixture stirred at room temperature for 30 min. The resin was filtered off, and washed well with water. Combined filtrate and washings were concentrated *in vacuo* to a

Can. J. Chem. Downloaded from www.nrcresearchpress.com by 210.87.254.6 on 09/05/12
For personal use only.

small volume (<1 ml), and applied to Whatman 40 paper. Descending paper chromatography in solvent *A*, yielded a uv absorbing band which was cut out and the band desalted with absolute ethanol for 1 h, dried with diethyl ether for 15 min, and eluted with distilled water overnight (R_F 0.80, *ca.* 150 A_{260}). The p*H* of the eluate was adjusted to 2.0 with 2 *N* hydrochloric acid and stored at room temperature. Hydrolysis of the tetrahydropyranyl ethers was followed by tlc on Avicel F plates, in solvent *A*, R_F 0.80 → 0.52. After 48 h the solution was neutralized with concentrated ammonium hydroxide, evaporated *in vacuo* to a small volume (<1 ml), and applied to Whatman 40 paper. Descending paper chromatography in solvent *A* gave a uv absorbing band of R_F 0.60. This band was desalted, dried, and eluted with distilled water as described above.

Removal of blocking groups yielded GCm (100 A_{260}, 39%, R_{Gp} 5.10 in solvent *A*) which was characterized by enzymic analysis. Snake venom phosphodiesterase in NaOAc–$Mg(OAc)_2$ (0.1 *M*, p*H* 8.80) showed complete digestion, and gave the desired products G + pCm. Spleen phosphodiesterase in sodium succinate (0.1 *M*, p*H* 6.5) gave the expected products Gp + Cm. Products of enzymatic digestion were identified by paper chromatographic and tlc analysis in system *A*.

Similar procedures for the removal of protecting groups were used for all protected oligoribonucleotides. Enzymic analysis of longer sequences required the use of a second system, *B*. The results are summarized in Table 3.

N^2-Benzoyl-2′-O-tetrahydropyranyl-5′-O-triphenylmethoxyacetylguanylyl[3′-(2,2,2-trichloroethyl)-5′]N^4-benzoyl-2′-O-methylcytidylyl[3′-(2,2,2-trichloroethyl)-5′]2′-O-tetrahydropyranyluridine ***(5)***

Similar phosphorylation (as described above for **3**, MST-coupling) of blocked GpCm (675 mg, 0.51 mmol, R_F 0.70 in 10% CH_3OH–CH_2Cl_2) and subsequent coupling with the low R_F diastereoisomer of 2′-*O*-tetrahydropyranyluridine (**4**) (11) (255 mg, 0.77 mmol, R_F 0.45 in 10% CH_3OH–CH_2Cl_2) gave the desired product **5** as a solid foam (500 mg, R_F 0.67 in 10% CH_3OH–CH_2Cl_2) in 55% yield. Complete deblocking of **5** as described above gave GpCmpU in 30% yield; R_{Gp} 2.45 in solvent *A*. GpCmpU was completely digested by snake venom diesterase to give G, pCm, and pU in the ratio of 1:1:1.

N^2-Benzoyl-2′-O-tetrahydropyranyl-5′-O-triphenylmethoxyacetylguanylyl[3′-(2,2,2-trichloroethyl)-5′]N^4-benzoyl-2′-O-methylcytidylyl[3′-(2,2,2-trichloroethyl-5′]2′-O-tetrahydropyranyluridylyl[3′-(2,2,2-trichloroethyl)-5′]N^4-benzoyl-2′-O-tetrahydropyranylcytidine ***(7)***

Similar phosphorylation (as described for **3**, MST-coupling) of blocked GpCmpU (**5**, 300 mg, 0.162 mmol, R_F 0.67 in 10% CH_3OH–CH_2Cl_2) and subsequent coupling with the high R_F diastereoisomer of N^4-benzoyl-2′-*O*-tetrahydropyranylcytidine (**6**) (12) (108 mg, 0.24 mmol, R_F 0.48 in 10% CH_3OH–CH_2Cl_2) gave tetramer **7** as a mixture of diastereoisomers (150 mg, R_F 0.48 in CH_3OH–CH_2Cl_2) in 38% yield. Complete deblocking of **7** as described above gave GpCmpUpC in 35% yield; R_{Gp} 0.82 in solvent *A*. GpCmpUpC was completely digested by snake venom diesterase to give G, pCm, pU, and pC in the expected ratio.

N^6-Benzoyl-2′-O-tetrahydropyranyl-5′-O-triphenylmethoxyacetyladenylyl[3′-(2,2,2-trichloroethyl)-5′]2′-O-tetrahydropyranyluridylyl[3′-(2,2,2-trichloroethyl)-5′]N^6-benzoyl-2′-O-tetrahydropyranyladenylyl-[3′-(2,2,2-trichloroethyl)-5′]N^6-benzoyl-2′-O-tetrahydropyranyladenosine ***(13)***

Phosphorylation of blocked ApUpA (**12**) (13) (as described for **3**, MST-coupling) (1.0 g, 0.54 mmol, R_F 0.66 in 10% CH_3OH–CH_2Cl_2) and subsequent coupling with N^6-benzoyl-2′-*O*-tetrahydropyranyladenosine (**11**) (12) (370 mg, 0.80 mmol, R_F 0.48 in 10% CH_3OH–CH_2Cl_2) gave the desired product as a mixture of diastereoisomers (1.12 g, R_F 0.60–0.65 in 10% CH_3OH–CH_2Cl_2) in 82% yield. Complete deblocking gave ApUpApA in 37% yield; R_{Gp} 0.40 in solvent *A*. ApUpApA was completely digested by snake venom diesterase to give A, pU, and pA in the ratio of 1:1:2.

N^6-Benzoyl-2′-O-tetrahydropyranyl-5′-O-triphenylmethoxyacetyladenylyl[3′-(2,2,2-trichloroethyl)-5′]2′-O-tetrahydropyranyluridylyl[3′-(2,2,2-trichloroethyl)-5′]N^6-benzoyl-2′-O-tetrahydropyranyladenylyl-[3′(2,2,2-trichloroethyl)-5′]N^6-benzoyl-2′-O-tetrahydropyranyladenylyl[3′(2,2,2-trichloroethyl)-5′]N^4-benzoyl-2′-O-tetrahydropyranylcytidine ***(14)***

Phosphorylation of blocked ApUpApA (**13**) (as described for **3**, MST-coupling) (900 mg, 0.35 mmol, R_F 0.65 in 10% CH_3OH–CH_2Cl_2) and subsequent coupling with the high R_F diastereoisomer of N^4-benzoyl-2′-*O*-tetrahydropyranylcytidine (**6**) (12) (225 mg, 0.52 mmol, R_F 0.48 in 10% CH_3OH–CH_2Cl_2) gave the protected pentanucleotide as a mixture of diastereoisomers (705 mg, R_F 0.60–0.68 in 10% CH_3OH–CH_2Cl_2) in 70% yield. Complete deblocking gave ApUpApApC in 37% yield; R_{Gp} 0.27 in solvent *A*. ApUpApApC was completely digested by snake venom diesterase to give A + pU + pA + pC in 1:1:2:1 ratio.

N^6-Benzoyl-2′-O-tetrahydropyranyladenylyl[3′-(2,2,2-trichloroethyl)-5′]2′-O-tetrahydropyranyluridylyl-[3′-(2,2,2-trichloroethyl)-5′]N^6-benzoyl-2′-O-tetrahydropyranyladenylyl[3′-(2,2,2-trichloroethyl)-5′]N^6-benzoyl-2′-O-tetrahydropyranyladenylyl[3′-(2,2,2-trichloroethyl)-5′]N^4-benzoyl-2′-O-tetrahydropyranylcytidine ***(15)***

A solution of ApUpApApC (**14**) (500 mg, 0.156 mmol, R_F 0.60–0.68 in 10% CH_3OH–CH_2Cl_2) in methanolic ammonia (0.15 *N*, 50 ml) was stirred at room temperature, and the progress of reaction followed by tlc. After 2 h, tlc indicated *ca.* 90% hydrolysis of the Trac group of the starting material (**14**), R_F 0.62–0.68 (yellow) → 0.48–0.54 (black). The reaction was quenched by evaporation *in vacuo*, and the resulting foam was purified by column chromatography on silica gel (25 g) in methylene chloride. Elution with 3% methanol – methylene chloride mixtures gave some unreacted **14** (70 mg). Continued elution with 4.0% methanol – methylene chloride mixtures yielded the desired pentanucleotide derivative **15** (330 mg, R_F 0.54 in 10% CH_3OH–CH_2Cl_2) in 84% yield.

*N^2-Benzoyl-2'-O-tetrahydropyranyl-5'-O-triphenylmethoxyacetylguanylyl[3'-(2,2,2-trichloroethyl)-5']N^4-benzoyl-2'-O-methylcytidylyl[3'-(2,2,2-trichloroethyl)-5']2'-O-tetrahydropyranyluridylyl[3'-(2,2,2-trichloroethyl)-5']N^4-benzoyl-2'-O-tetrahydropyranylcytidylyl[3'-(2,2,2-trichloroethyl)-5']N^6-benzoyl-2'-O-tetrahydropyranyladenylyl[3'-(2,2,2-trichloroethyl)-5']2'-O-tetrahydropyranyluridylyl[3'-(2,2,2-trichloroethyl)-5']N^6-benzoyl-2'-O-tetrahydropyranyladenylyl-[3'-(2,2,2-trichloroethyl)-5']N^6-benzoyl-2'-O-tetrahydropyranyladenylyl[3'-(2,2,2-trichloroethyl)-5']N^4-benzoyl-2'-O-tetrahydropyranylcytidine (**16**)*

Blocked GpCmpUpC (**7**) (123 mg, 0.05 mmol, R_F 0.48 in 10% CH_3OH–CH_2Cl_2) was phosphorylated, using the free acid of mono-2,2,2-trichloroethyl phosphate (70 mg, 0.30 mmol) preactivated with MST (150 mg, 0.60 mmol). Progress of the reaction was followed by tlc. Further portions of MST were added (3 × 40 mg) until reaction was complete. (R_F 0.48 → 0.0 – 0.45 in 10% CH_3OH–CH_2Cl_2). After 8 days blocked GpCmpUpCp (**10**) was isolated by extraction with methylene chloride (as described for **3** MST-coupling), converted into its pyridinium salt by repeated evaporations from pyridine (3 × 10 ml), activated with MST (25 mg, 0.10 mmol), sealed under dry nitrogen, and set aside at room temperature in the dark. After 2 h the blocked pentanucleotide derivative **15** (220 mg, 0.75 mmol, R_F 0.54 in 10% CH_3OH–CH_2Cl_2) in pyridine (5 ml) was added, the reaction mixture sealed under dry nitrogen, and allowed to proceed in the dark. Further portions of MST (4 × 40 mg) were added to ensure completion of reaction. After *ca.* 8–10 days tlc indicated *ca.* 75% conversion into a new product of R_F 0.66–0.76 in 10% CH_3OH–CH_2Cl_2. Ice (2 g) was then added and 30 min later the reaction mixture was poured into ice water (10 ml), and repeatedly extracted with methylene chloride (5 × 15 ml). The combined organic extracts were washed with water (3 × 10 ml), and evaporated to dryness *in vacuo*. The last traces of pyridine were removed by co-distillation with toluene, and the residual yellow foam was purified by column chromatography on silica gel (20 g) in methylene chloride. Elution with 2.0–2.5% methanol – methylene chloride mixtures removed some impurities (R_F 0.85 black). Pure protected nonanucleotide **16** was isolated by elution with 3.0–4.0% methanol – methylene chloride mixtures, as a diastereoisomeric mixture (140 mg, R_F 0.68–0.74 in 10% CH_3OH–CH_2Cl_2) in 48% yield. Complete deblocking gave GpCmpUpCpApUpApApC in 25% yield; R_{Gp} 0.21 in solvent *A*.

Acknowledgment

Financial assistance from the Medical Research Council of Canada is acknowledged.

1. T. E. England and Thomas Neilson. Can. J. Chem. **54**, 1714 (1976).
2. T. Neilson and E. S. Werstiuk. J. Am. Chem. Soc. **96**, 2295 (1974).
3. H. G. Zachau. Frontiers of biology. Vol. 27. The mechanisms of protein synthesis and its regulation. American Elsevier Publishing Co., New York. 1972. Chapt. 7, p. 173.
4. (*a*) B. F. C. Clark, S. K. Dube, and K. A. Marcker. Nature, **219**, 484 (1968); (*b*) R. W. Chambers. Prog. Nucleic Acid Res. Mol. Biol. **11**, 489 (1971).
5. E. Ohtusuka, M. Ubasawa, S. Marioka, and M. Ikehara. J. Am. Chem. Soc. **95**, 4725 (1973).
6. S. K. Dube, K. A. Marcker, B. F. C. Clark, and S. Corey. Nature, **218**, 232 (1968).
7. E. S. Werstiuk and T. Neilson. Can. J. Chem. **50**, 1283 (1972).
8. H. Kössel and H. Seliger. Recent advances in polynucleotide synthesis. *In* Progress in the chemistry of organic natural products. **32**, 297 (1975).
9. N. Katagiri, K. Itakua, and S. A. Narang. J. Chem. Soc. Chem. Commun. 325 (1974).
10. T. Neilson, E. V. Wastrodowski, and E. S. Werstiuk. Can. J. Chem. **51**, 1068 (1973).
11. B. E. Griffin, M. Jarman, and C. B. Reese. Tetrahedron, **24**, 639 (1968).
12. T. Neilson and E. S. Werstiuk. Can. J. Chem. **49**, 493 (1971).
13. T. Neilson, K. V. Deugau, T. E. England, and E. S. Werstiuk. Can. J. Chem. **53**, 1093 (1975).
14. T. Neilson and E. S. Werstiuk. Can. J. Chem. **49**, 3004 (1971).
15. F. Eckstein. Chem. Ber. **100**, 2228 (1967).

Can. J. Chem. Downloaded from www.nrcresearchpress.com by 210.87.254.6 on 09/05/12
For personal use only.

[LM(CO)$_{3,4}$X] complexes of manganese(I) and rhenium(I) with phosphino- and thiophosphinatopyrazole ligands

JAMES HOYANO AND LOUIS K. PETERSON

Department of Chemistry, Simon Fraser University, Burnaby, B.C., Canada V5A 1S6

Received October 16, 1975[1]

JAMES HOYANO and LOUIS K. PETERSON. Can. J. Chem. **54**, 2697 (1976).

A series of complexes [LM(CO)$_3$X] (L = ϕ_xP(R$_2$pz)$_{3-x}$, R$_2$pz = pyrazolyl, or 3,5-dimethylpyrazolyl, x = 0–2; M = Mn, X = Cl; M = Re, X = Br) and [(ϕ_2P(S)(R$_2$pz))Re(CO)$_3$Br] were prepared by the reaction of the appropriate ligand with [M(CO)$_5$X] or [M(CO)$_4$X]$_2$, and were characterized by elemental analysis, solution molecular weight, and infrared, mass, and nmr spectroscopic data. The products are formed via tetracarbonyl intermediates, of which the phosphorus bonded derivative [(ϕ_2P(pz))Re(CO)$_4$Br] was isolated and characterized. The tricarbonyl complexes [LM(CO)$_3$X] and [(ϕ_2P(S)(R$_2$pz))Re(CO)$_3$Br] adopt a *cis*-octahedral configuration, in which the ligands form four-, five-, or six-membered chelate structures, via (*i*) the P atom and the 2-N site of the pyrazolyl moiety, with ϕ_2P(R$_2$pz), (*ii*) the sulphur and 2-N atoms, with ϕ_2P(S)(R$_2$pz), (*iii*) the 2-N atoms of two pyrazolyl rings, with ϕP(R$_2$pz)$_2$, and (*iv*) the 2-N atoms of three pyrazolyl rings, resulting in a bicyclic system, with P(R$_2$pz)$_3$.

The reactions of [CH$_3$Re(CO)$_5$] with ϕ_xP(R$_2$pz)$_{3-x}$ require forcing conditions, resulting in the simultaneous elimination of carbon monoxide and methane, and yielding a variety of products, including tetracarbonyl, tricarbonyl, and ring-metalated species.

JAMES HOYANO et LOUIS K. PETERSON. Can. J. Chem. **54**, 2697 (1976).

Une série de complexes [LM(CO)$_3$X] (L = ϕ_xP(R$_2$pz)$_{3-x}$, R$_2$pz = pyrazolyle, ou diméthyl-3,5 pyrazolyle, x = 0–2; M = Mn, X = Cl; M = Re, X = Br) et [(ϕ_2P(S)(R$_2$pz))Re(CO)$_3$Br] ont été préparés par la réaction du ligand approprié avec [M(CO)$_5$X] ou [M(CO)$_4$X]$_2$ et ont été caractérisés par analyse des éléments, détermination du poids moléculaire en solution, infrarouge, spectrométrie de masse et rmn. Les produits sont formés par voie d'intermédiaires tétracarbonylés, parmi lesquels le dérivé lié au phosphore [(ϕ_2P(pz))Re(CO)$_4$Br] a été isolé et caractérisé. Les complexes tricarbonylés [LM(CO)$_3$X] et [(ϕ_2P(S)(R$_2$pz))Re(CO)$_3$Br] adoptent une configuration octaédrique *cis*, dans laquelle les ligands forment des structures chélatées tétragonales, pentagonales ou hexagonales en passant par (*i*) l'atome de phosphore et le site azoté 2-N de la partie pyrazolyle, avec ϕ_2P(R$_2$pz), (*ii*) les atomes de soufre et d'azote 2-N, avec ϕ_2P(S)(R$_2$pz), (*iii*) les deux atomes d'azote 2-N des deux noyaux pyrazolyles avec ϕP(R$_2$pz)$_2$, et (*iv*) les trois atomes d'azote 2-N des trois noyaux pyrazolyles, conduisant à un système bicyclique, avec P(R$_2$pz)$_3$.

Les réactions de [CH$_3$Re(CO)$_5$] avec ϕ_xP(R$_2$pz)$_{3-x}$ demandent des conditions forcées, aboutissant à l'élimination simultanée de monoxyde de carbone et de méthane et conduisant à une variété de produits, comprenant les espèces tétracarbonylées et tricarbonylées ainsi que l'espèce cyclique comprenant le métal.

[Traduit par le journal]

Introduction

The chemistry of transition metal complexes containing phosphine ligands has been extensively documented (1). We have synthesized a series of azolylphosphines, where an aromatic, heterocyclic moiety other than phenyl is bonded to the phosphorus centre via nitrogen (2, 3), and have studied the coordinating properties of these ligand systems toward Cr(III), Mo(0), Mn(I), Re(I), Pd(II), Cu(I), and Hg(II). We report here our investigations of complexes of manganese and rhenium. Coordination chemistry with other metals will be reported elsewhere.[2]

Discussion

A number of complexes [LM(CO)$_3$X] (L = ϕ_xP(R$_2$pz)$_{3-x}$, x = 0–2, R$_2$pz = pyrazolyl or 3,5-dimethylpyrazolyl) of manganese(I) and rhenium(I) were prepared by the reaction of the pentacarbonyl halide [M(CO)$_5$X] or the tetracarbonyl halide dimer [M(CO)$_4$X]$_2$ (M = Mn, X = Cl; M = Re, X = Br) with the appropriate

[1]Revision received April 20, 1976.

[2]S. Fischer and L. K. Peterson, unpublished results.

Can. J. Chem. Downloaded from www.nrcresearchpress.com by 210.87.254.6 on 09/05/12
For personal use only.

Can. J. Chem. Downloaded from www.nrcresearchpress.com by 210.87.254.6 on 09/05/12
For personal use only.

TABLE 1. Infrared ν(CO) stretching frequencies of pyrazolylphosphine complexes of Mn(I) and Re(I)[a,b]

Complex	Frequency (cm^{-1})	Complex	Frequency (cm^{-1})
$[(\phi_2Ppz)Re(CO)_3Br]$[c]	2043s, 1958s, 1913s[f]		
$[(\phi_2P(Me_2pz))Re(CO)_3Br]$[c]	2040s, 1952s, 1910s	$[(\phi_2P(Me_2pz))Mn(CO)_3Cl]$	2038s, 1967s, 1915
$[(\phi P(pz)_2)Re(CO)_3Br]$[d,e]	2033s, 1935s, 1903s		
$[(\phi P(Me_2pz)_2)Re(CO)_3Br]$[d,e]	2030s, 1922s, 1902(s)	$[(\phi P(Me_2pz)_2)Mn(CO)_3Cl]$	2040s, 1970s, 1930s
$[(P(pz)_3)Re(CO)_3Br]$[d,e]	2038s, 1927s,br		
$[(P(Me_2pz)_3)Re(CO)_3Br]$[d,e]	2033s, 1925s,br	$[(P(Me_2pz)_3)Mn(CO)_3Cl]$	2040s, 1948s,br
$[(\phi_2P(S)pz)Re(CO)_3Br]$[c,d]	2032s, 1940s, 1905s		
$[(\phi_2P(S)(Me_2pz))Re(CO)_3Br]$[c,d]	2030s, 1932s, 1900s		
$[(\phi_2Ppz)Re(CO)_4Br]$[d,g]	2115m, 2034s, 2015s, 1963ms	$[(\phi_2Ppz)Mn(CO)_4Cl]$[h]	2100m, 2030s, 2020s, 1970ms
$[(\phi_2P(Me_2pz))Re(CO)_4Br]$[d,g,h]	2110m, 2030s, 2005s, 1960m		
$[(\phi_3PRe(CO)_4Br]$[d,g]	2110m, 2030s, 2005s, 1953ms		

[a] pz = pyrazolyl, $C_3H_3N_2$; Me_2pz = 3,4-dimethylpyrazolyl, $C_5H_7N_2$.
[b] The given data is for spectra recorded using chloroform solutions in cells of 0.1 mm path length and fitted with sodium chloride windows.
[c] As in footnote *b*, but with hexane as solvent.
[d] As in footnote *b*, but with toluene as solvent.
[e] As in footnote *b*, but with ether as solvent.
[f] s = strong, ms = medium strong, m = medium, br = broad; bands positions are accurate to ± 3 cm^{-1}.
[g] Data for *cis* isomers of the tetracarbonyls.
[h] Observed in solution; too unstable to be isolated.

Can. J. Chem. Downloaded from www.nrcresearchpress.com by 210.87.254.6 on 09/05/12
For personal use only.

ligand, in benzene solution, at temperatures varying from 50–100 °C (eqs. 1 and 2). Rhenium(I) complexes containing the pentavalent phosphorus derivatives $\phi_2P(S)(R_2pz)$ were also obtained, again by the direct reaction of the ligand with $[Re(CO)_4Br]_2$ in solution [3]. The evolved carbon monoxide was monitored and pure products were obtained in high yield, according to the given stoichiometries (eqs. 1–3).

$$[1]\quad [M(CO)_5X] + \phi_xP(R_2pz)_{3-x} \xrightarrow[50\text{–}100\ ^\circ C]{C_6H_6} [(\phi_xP(R_2pz)_{3-x})M(CO)_3X] + 2CO$$

$$[2]\quad [M(CO)_4X]_2 + 2\phi_xP(R_2pz)_{3-x} \xrightarrow[50\text{–}100\ ^\circ C]{C_6H_6} 2[(\phi_xP(R_2pz)_{3-x})M(CO)_3X] + 2CO$$

$$[3]\quad [Re(CO)_4Br]_2 + 2\phi_2P(S)(R_2pz) \xrightarrow[80\ ^\circ C]{C_6H_6} 2[(\phi_xP(S)(R_2pz))Re(CO)_3Br] + 2CO$$

The dimers $[M(CO)_4X]_2$ react more easily than the mononuclear pentacarbonyls $[M(CO)_5X]$, the manganese derivatives being considerably more reactive than corresponding rhenium ones.

The formulations of products as $[LM(CO)_3X]$ are based upon reaction stoichiometry, elemental analysis, solution molecular weight, and infrared, mass, and nmr spectroscopic data. The complexes, once obtained pure, are moderately air stable crystalline solids, contrasting with the oxidative and hydrolytic instability of the free ligands (2, 3*a*). The dimethylpyrazolyl derivatives $[(\phi_xP(Me_2pz)_{3-x})M(CO)_3X]$ are more soluble than their unsubstituted pyrazolyl analogs $[\phi_xP(pz)_{3-x})M(CO)_3X]$, and solubility decreases with an increasing number of azole groups on phosphorus.

The products $[LM(CO)_3X]$ are formed via a tetracarbonyl intermediate $[LM(CO)_4X]$. Unstable $[(\phi_2P(pz))Re(CO)_4Br]$ was isolated from the mild reaction of $\phi_2P(pz)$ with $[Re(CO)_4Br]_2$, but was readily converted by gentle warming, to $[(\phi_2P(pz))Re(CO)_3Br]$, via further loss of CO. Infrared evidence (Table 1) showed the presence of analogous tetracarbonyl intermediates in the reactions of $\phi_2P(Me_2pz)$ with rhenium(I) carbonyls, and of ϕ_2Ppz with manganese(I) carbonyls, but such compounds were too unstable to be isolated. The proximity of a second donor site to the metal centre in $[LM(CO)_4X]$ leads to facile displacement of CO, concomitant with the formation of the tricarbonyl compounds $[LM(CO)_3X]$. This clear indication of chelation by the ligands was confirmed by spectroscopic studies. By comparison, the complex *cis*-$[(\phi_3P)Re(CO)_4Br]$, containing monodentate triphenylphosphine, is thermally stable, but suffers displacement of a second CO molecule on further treatment with ϕ_3P, to yield $[(\phi_3P)_2Re(CO)_3Br]$ (4). Attempts to prepare the corresponding bis(pyrazolylphosphine) complex $[(\phi_2P(pz))_2Re(CO)_3Br]$ were unsuccessful, the preferred product being $[(\phi_2P(pz))Re(CO)_3Br]$. Furthermore, the strongly coordinating ligand ϕ_3P, and CO, are displaced from $[(\phi_3P)Re(CO)_4Br]$ by reaction with $P(Me_2pz)_3$, the product being $[(P(Me_2pz)_3)Re(CO)_3Br]$. Indeed, the chelate structures of $[LM(CO)_3X]$ appear to be stable against ring opening or further substitution reactions with other ligands; $[(\phi_2P(Me_2pz))Re(CO)_3Br]$, for example, failed to react with ϕ_3P in refluxing benzene, or with carbon monoxide, over a period of several days.

Complexes of Diphenylphosphinopyrazoles $\phi_2P(R_2pz)$

The application of group theoretical principles to the elucidation of the structures of six-coordinate octahedral carbonyl complexes is well established (5, 6). Thus, the four ir bands observed in the ν(CO) region for the tetracarbonyl complexes $[(\phi_2P(R_2pz))Re(CO)_4Br]$ (see Table 1), and the similarity of the band patterns to that of *cis*-$[(\phi_3P)Re(CO)_4Br]$, indicate coordination via phosphorus rather than the 2-N site of the pyrazolyl ring, as in the *cis*-octahedral structure **1**. The phosphorus atom of $\phi_2P(R_2pz)$

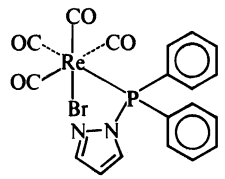

1

is also the preferential site for coordination of alkyl CH_3 and BF_3 species (3*a*). The highest frequency, lowest intensity band (2115–2100 cm^{-1}) of the tetracarbonyl system can be assigned to the symmetric stretching vibration of the two mutually *trans* carbonyl groups; this band is absent in the tricarbonyl derivatives $[(\phi_2P(R_2pz))M(CO)_3X]$.

On the basis of their coordinatively saturated

Can. J. Chem. Downloaded from www.nrcresearchpress.com by 210.87.254.6 on 09/05/12
For personal use only.

character, their solubility in benzene, toluene, and chloroform, the absence of polynuclear species in their mass spectra, and their monomeric molecular weights in solution, the tricarbonyl derivatives $[(\phi_2P(R_2pz))M(CO)_3X]$ (M = Mn, X = Cl; M = Re, X = Br) are mononuclear and six-coordinate, while ir data (ν(CO) region) are readily interpreted on the basis of an octahedral configuration. The three observed ν(CO) bands are symmetrical and of equal intensity, indicating the *cis*-octahedral pseudo C_{3v} structure **2***a* and/or its stereoisomer **2***b*, rather than the pseudo C_{2v} structure **3***a* and/or **3***b*. The latter would be expected to give rise to one low intensity high energy band, and two equal intensity bands of lower energy. Attempts to detect the presence of isomers of any kind by ir studies, using various solvents, were unsuccessful. Complexes analogous to our $[LM(CO)_3X]$ systems have been reported, with comparable ν(CO) spectra, and with *cis*-octahedral configurations (7).

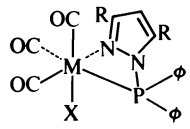

2*a*

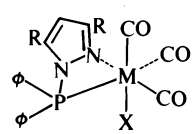

2*b*

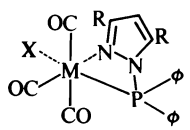

3*a*

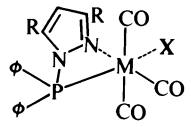

3*b*

The ^{31}P proton decoupled FT nmr spectra of the complexes $[(\phi_2P(R_2pz))M(CO)_3X]$ consist of single resonances with appreciable negative coordination chemical shifts (*i.e.* the ^{31}P resonance moves to lower field on coordination), as has been observed in many monodentate and polydentate organophosphine complexes (8, 9), thus corroborating phosphorus-to-metal bonding.

The ^1H nmr spectrum of $[(\phi_2P(Me_2pz))Re(CO)_3Br]$ showed singlet resonances for the 3-CH_3, 5-CH_3 and 4-H protons; thus the isomeric forms **2***a* and **2***b*, if present in solution, were not distinguishable by the spectroscopic methods employed. The preliminary results of a single-crystal X-ray structure determination of $[(\phi_2P(Me_2pz))Mn(CO)_3Cl]$, however, indicate an equal distribution of the chelated *cis*-octahedral enantiomorphic stereoisomers **2***a* and **2***b*.[3]

Complexes of Diphenylthiophosphinatopyrazoles $\phi_2P(S)(R_2pz)$

The mass spectrum of $[(\phi_2P(S)(Me_2pz))Re(CO)_3Br]$ exhibits the mononuclear parent ion, and its room temperature ^1H nmr spectrum indicates one kind of environment for the pyrazolyl ring. The ^{31}P nmr spectra of both analogues $[(\phi_2P(S)(R_2pz))Re(CO)_3Br]$ consist of single resonances with significant negative coordination shifts (Table 2). The ν(CO) ir spectra of both complexes, in various solvents, consist of three intense, symmetric bands, similar to the ν(CO) region of $[(\phi_2P(R_2pz))M(CO)_3X]$ (Table 1). The enantiomorphic five-membered chelate ring structures **4***a* and **4***b*, with essentially identical ir and nmr characteristics, are consistent with the above observations.

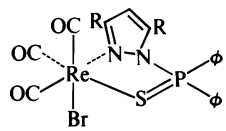

4*a*

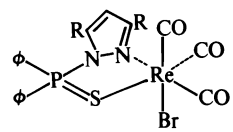

4*b*

Complexes of Bis(pyrazolyl)phenylphosphines $\phi P(R_2pz)_2$

The complexes $[(\phi P(R_2pz)_2)M(CO)_3X]$ all show three strong, symmetric ir bands in the ν(CO) region, without evidence of splittings that the presence of isomers might be expected to cause. The ^{31}P nmr resonances are broad singlets; the coordination shifts are sensitive to substituents on the pyrazole rings and to the nature of the central metal of the complex, being slightly negative for $[(\phi P(Me_2pz)_2)Mn(CO)_3Cl]$ and $[(\phi P(pz)_2)Re(CO)_3Br]$ and slightly positive for $[(\phi P(Me_2pz)_2)Re(CO)_3Br]$ (Table 2). The ^1H nmr spectrum (Table 3) of $[(\phi P(Me_2pz)_2)Re(CO)_3Br]$ consisted of an equal intensity doublet for the 4-H protons, a methyl singlet, and an equal intensity methyl doublet; the ^{31}P decoupled ^1H spectrum consisted of singlets, in a 1:3:3 intensity ratio, indicating equivalent pyrazole rings. Thus a structure such as **5**, where one

[3]R. Cobbledick and F. W. B. Einstein, personal communication.

TABLE 2. ^{31}P nmr data for pyrazolylphosphine complexes of Mn(I) and Re(I)

Complex	Chemical shifts[a]		
	Ligand	Complex	Coordination[b]
$[(\phi_2P(pz))Re(CO)_3Br]$	59.63	75.30	−15.67
$[(\phi P(pz)_2)Re(CO)_3Br]$	77.04	97.65	−20.61
$[(P(pz)_3)Re(CO)_3Br]$[c]	65.19	—	—
$[(\phi_2P(Me_2pz))Re(CO)_3Br]$	44.69	55.55	−10.86
$[(\phi P(Me_2pz)_2)Re(CO)_3Br]$	66.67	64.69	+1.98
$[(P(Me_2pz)_3)Re(CO)_3Br]$	77.53	25.43	+52.10
$[(\phi_2P(Me_2pz))Mn(CO)_3Cl]$	44.69	99.26	−54.57
$[(\phi P(Me_2pz)_2)Mn(CO)_3Cl]$	66.67	109.38	−42.71
$[(P(Me_2pz)_3)Mn(CO)_3Cl]$	77.53	24.69	+52.84
$[(\phi_2P(S)(pz))Re(CO)_3Br]$	68.64	79.25	−10.61
$[(\phi_2P(S)(Me_2pz))Re(CO)_3Br]$	67.41	76.67	−9.26
$[(\phi_2P(pz))Re(CO)_4Br]$	59.63	66.30	−6.67
$[(\phi_2P(Me_2pz))Re(CO)_4Br]$	44.69	62.72	−18.03
$[(\phi_3PRe(CO)_4Br]$	0.00	4.94	−4.94

[a]In ppm; data for the free ligand and the complex are downfield from external ϕ_3P, in toluene solution. To convert to values relative to H_3PO_4, subtract 5.90 ppm.
[b]The coordination chemical shift is (δ(free ligand) − δ(complex)).
[c]Very low solubility.

TABLE 3. ^1H nmr data for 3,5-dimethylpyrazolylphosphines and their complexes with rhenium (I) carbonyl compounds[a]

Compound	Chemical shifts (τ)[b]	
	3-Me and 5-Me	4-H
$\phi_2P(Me_2pz)$	7.57(s), 7.78(s)	4.10(s,br)
$[(\phi_2P(Me_2pz))Re(CO)_3Br]$	7.70(s), 7.97(s)	4.02(s,br)
$\phi P(Me_2pz)_2$	7.65(s), 7.72(s)	4.08(s)
$[(\phi P(Me_2pz)_2)Re(CO)_3Br]$	7.22(s), 7.42(d)[c]	3.76(d)[d]
$P(Me\ pz)_3$	7.82(s), 7.85(s)	4.05(s)
$[(P(Me_2pz)_3)Re(CO)_3Br]$	7.12(q),[e] 7.37(s)	3.61(d)[f]
$\phi_2P(S)(Me_2pz)$	7.63(s), 7.85(s)	4.03(m,br)
$[(\phi_2P(S)(Me_2pz))Re(CO)_3Br]$	7.32(s), 8.35(s)	3.77(s)

[a]Spectra were measured in $CDCl_3$, using TMS as internal standard.
[b]s = singlet, d = doublet, q = quartet, m = multiplet, br = broad.
[c]J_{P-H} = 2 Hz.
[d]J_{P-H} = 5.0 Hz.
[e]1:1:1:1 quartet, (doublet of doublets, peak separation = 1 Hz; J_{P-H} = 2.0, J_{H-H} = 1.0 Hz).
[f]J_{P-H} = 4.2 Hz.

pyrazolyl ring is coordinated while the second ring is free, is excluded. An alternative structure **6** would probably show a significant negative ^{31}P coordination shift, and is further eliminated on the grounds that the mass spectrum of $[(\phi P(Me_2pz)_2)Re(CO)_3Br]$ does show the molecular ion, together with ions corresponding to the stepwise loss of the three carbonyl groups from the parent, without loss of Br. The combined spectral information suggests structure **7**, in which preferential coordination occurs through the 2-N sites of the two pyrazolyl rings; the reduced basicity of phosphorus may be attributed to the electron-withdrawing effect of the two azole rings (3*a*). The large ring structure **7**[4] is common among complexes of pyrazolylborate ligand systems (10).

Complexes of Tris(pyrazolyl)phosphines $P(R_2pz)_3$

The infrared spectra of the $[(P(R_2pz)_3)M(CO)_3X]$ complexes all show only two strong ir bands in the ν(CO) region, a sharp high-fre-

[4]We thank a referee for pointing out the possibility of geometrical and conformational isomerism in structure 7.

Can. J. Chem. Downloaded from www.nrcresearchpress.com by 210.87.254.6 on 09/05/12
For personal use only.

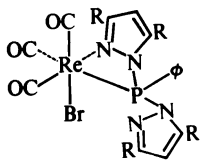

5

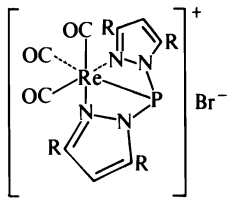

6

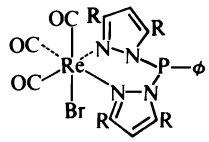

7

quency band and a slightly broadened but symmetrical lower frequency band. No evidence for splitting or broadening of either band was observed in various solvents. The occurrence of only two ν(CO) bands may mean that the compounds have only two infrared active vibrational modes, or that the lower frequency band is composed of two accidentally degenerate vibrational modes.

The ^{31}P nmr resonances for both complexes [$(P(Me_2pz)_3)M(CO)_3X$] (M = Mn, Re; X = Cl, Br) are very broad on account of the quadrupolar relaxation of three N nuclei attached to phosphorus, and show large positive coordination shifts. This is in marked contrast to the tricarbonyl complexes of $\phi_2P(R_2pz)$, suggesting that the phosphorus centre, as in [$(\phi P(R_2pz)_2)M(CO)_3X$] is not coordinated to the metal, consistent with the decreasing basicity of P with increasing pyrazolyl substitution (*3a*). Increased pyrrolyl substitution in a series of phenyl(pyrrolyl)phosphines causes a similar decrease in the coordination properties of the phosphorus centre (*3b*).[5]

The ^{1}H nmr spectrum of [$(P(Me_2pz)_3)Re(CO)_3Br$] exhibits an equal intensity doublet for the 4-H protons, a methyl singlet, and an equal intensity methyl quartet. On decoupling from phosphorus, the 4-H resonance collapsed to a singlet, and the methyl multiplet to a single broad band; further decoupling from 4-H sharpened the latter band (an unresolved doublet) into a narrow singlet. These observations establish that the pyrazolyl rings are equivalent. ^{1}H nmr spectra for [$(P(Me_2pz)_3)Re(CO)_3Br$] were recorded at temperatures down to −60 °C ($CDCl_3$ solution) and −90 °C (acetone-d_6 solution); the absence of spectral changes at the lowest temperature suggests the absence of exchange between coordinated and uncoordinated pyrazolyl rings. The combined ir and nmr data are consistent with the ion pair formulation in structure **8**, where the cationic species has essentially C_{3v} symmetry, and in which all three pyrazolyl rings are coordinated to the metal. Only two ir active bands are expected for such a structure. The mass spectrum of [$(P(Me_2pz)_3)Re(CO)_3Br$] provides further evidence for this formulation; the largest observed ion is the cation [$(P(Me_2pz)_3)Re(CO)_3]^+$, and Br is not present in any of the smaller fragments. The conductivity of [$(P(Me_2pz)_3)Re(CO)_3Br$] in nitrobenzene is low, and solubility (soluble in chloroform, slightly soluble in benzene and toluene, insoluble in hexane) and solution molecular weight data are consistent for an intimate ion-pair combination. Structures analogous to

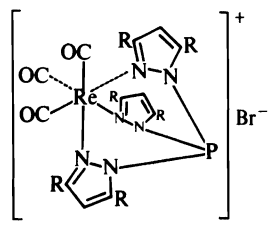

8

the cation of **8** have been postulated for the neutral pyrazolylborate complexes [$RB(R_2pz)_3Mn(CO)_3$] and [$B(R_2pz)_4Mn(CO)_3$]; only two strong ν(CO) bands were observed, corresponding closely with the bands for [$P(R_2pz)_3Mn(CO)_3Cl$], and temperature independence of the ^{1}H nmr spectra indicated spectroscopic identity for the three coordinated pyrazolyl groups (11).

Reactions of Pentacarbonylmethylrhenium with Pyrazolylphosphine Ligands

To elucidate further the structural implications described above, syntheses of methyl analogs [$LM(CO)_{3,4}(CH_3)$] were attempted. The first method, involving direct reaction between [$CH_3Re(CO)_5$] and $\phi_xP(R_2pz)_{3-x}$ in solution in xylene,

[5] J. Hoyano, unpublished observations.

Can. J. Chem. Downloaded from www.nrcresearchpress.com by 210.87.254.6 on 09/05/12
For personal use only.

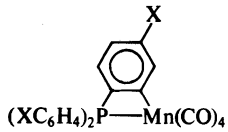

X = H, CH_3, F

11

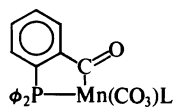

L = CO, ϕ_3P

12

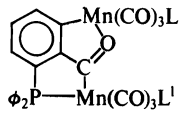

L,L¹ = CO or ϕ_3P

13

required forcing conditions (120–140 °C) and gave a complex mixture of products as a result of elimination of CO and CH_4. The tetracarbonyl [$LRe(CO)_4(CH_3)$] was observed spectroscopically, together with other carbonyl species, in the reaction mixtures. The loss of CH_4 along with the carbon monoxide was due to an intramolecular metalation process, at least in the case of the reaction of $\phi_2P(Me_2pz)$ with [$CH_3Re(CO)_5$] [8] where the products **9** and **10** were painstakingly separated and characterized by infrared, mass spectral, and nmr spectral studies; metalation of the phenyl, rather than of the pyrazolyl ring in product **10** was clearly indicated. Methane evolution was also observed, however, in reactions involving $P(Me_2pz)_3$ and [$CH_3Re(CO)_5$],

[8] $[CH_3Re(CO)_5] + \phi_2P(Me_2pz) \xrightarrow[120\text{–}140\ °C]{\text{Xylene}}$

cis-[$(\phi_2P(Me_2pz))Re(CO)_4(CH_3)$]

9

+ [$(\phi(Me_2pz)(C_6H_4)P)Re(CO)_4$]

10

+ Other products

the 5-methyl substituent being the most likely site for the metalation reactions. Methane formation as a result of thermal decomposition of [$CH_3Re(CO)_5$] was shown to be insignificant, in a separate study, where the complex was heated in xylene at a temperature of 150 °C for 24–48 h.

A recent study, by Kaesz and co-workers (12), has shown that various metalation products arise from the reaction of alkyl- and arylphosphines and phosphites with [$CH_3M(CO)_5$] (M = Mn, Re); for example, products **11**, **12**, and **13** were isolated following the thermolysis of [((*p*-$XC_6H_4)_3P)Mn(CO)_4(CH_3)$].

The second approach to the methyl analogs, involving the reaction of [$(\phi_2P(Me_2pz))Re(CO)_3Br$] with methyllithium in ether, did not yield meaningful products, apparently due to a cleavage of the ligand. Likewise, attempted reductions of the bromo derivative with sodium borohydride, resulted in some destruction of the ligand.[6]

Experimental

Experimental operations were performed under anhydrous conditions, using high vacuum or dry, inert atmosphere systems. Solvents were dried by standard methods, distilled, and deaerated prior to use. The pyrazolylphosphine ligands $\phi_xP(R_2pz)_{3-x}$ (x = 0–2, R_2pz = pyrazolyl or 3,5-dimethylpyrazolyl) and $\phi_2P(S)(R_2pz)$ (2, 3), and the following transition metal complexes were prepared according to published methods: [$Re(CO)_5Br$] (13), [$Mn(CO)_5Cl$] (14), [$Re(CO)_4Br]_2$ (15), [$CH_3Re(CO)_5$] (16). The preparations *a*–*k* described below were performed in heavy walled glass tubes (~50 ml capacity) equipped with vacuum tight teflon valves and standard ground glass joints. Except in cases where reactions were carried out under nitrogen, the solutions were degassed in a series of three freeze–pump–thaw cycles; following the completion of reaction, the vessel was cooled to −196 °C and noncondensible products (carbon monoxide, methane) were collected and measured by means of a Sprengel pump.

Elemental analyses were performed by the university analyst, Simon Fraser University. ^1H and ^{31}P nuclear magnetic resonance spectra were obtained using Varian A56/60 and XL100 instruments, the latter having Fourier transform and proton decoupling facilities. Infrared spectra were recorded with a Perkin-Elmer 457 spectrophotometer and were calibrated against standard polystyrene film. Mass spectra were determined with the double focussing Hitachi–Perkin-Elmer RMU-6E instrument (Table 4). Molecular weights in solution were measured using the Hitachi–Perkin-Elmer model 115 molecular weight osmometer.

(a) Preparation of [($\phi_2P(pz)$)Re(CO_4)Br]

A mixture of $[Re(CO)_4Br]_2$ (0.60 mmol), ϕ_2Ppz (1.21 mmol), and benzene (10 ml) was stirred at room temperature for 8 days. The clear solution was evaporated to

[6]NOTE ADDED IN PROOF—A single crystal diffraction study of [$(\phi P(Me_2pz)_2)Re(CO)_3Br$] has substantiated the main features of the suggested structure **7**. The rhenium atom is octahedrally coordinated, with the three CO groups arranged *facially*, and the atoms of the six-membered ring (see **7**) define a boat configuration (L. R. J. Dowdell and F. W. B. Einstein, personal communication).

Can. J. Chem. Downloaded from www.nrcresearchpress.com by 210.87.254.6 on 09/05/12
For personal use only.

TABLE 4. Mass spectral fragmentation data for pyrazolylphosphine complexes of rhenium

Compound	Probe temperature (°C)	Positive fragment ions[a]
$[(P(pz)_3)Re(CO)_3Br]$	140	$M - CO - pz$ (8.0), $M - 2CO - pz$ (10.0), $M - 3CO - pz$ (3.1)
$[(P(Me_2pz)_3)Re(CO)_3Br]$	300	$M - Br$ (10.0), $M - Br - 3CO$ (7.0)
$[(\phi P(Me_2pz)_2)Re(CO)_3Br]$	200	M (1.4), $M - CO$ (1.7), $M - 2CO$ (0.2), $M - 3CO$ (10.0)
$[(\phi_2P(Me_2pz))Re(CO)_3Br]$	160	M (2.6), $M - CO$ (6.2), $M - 2CO$ (0.7), $M - 3CO$ (10.0)
$[(\phi_2P(S)(Me_2pz))Re(CO)_3Br]$	250	M (2.0), $M - CO$ (5.0), $M - 2CO$ (3.0), $M - 3CO$ (10.0)

[a]Fragment ions containing Re, with an identifiable isotope pattern, are given; relative intensities on an arbitrary scale (0–10.0) are given in parentheses. Fragments due to the ligands are not included.

dryness under vacuum, giving a residue which was crystallized from chloroform–hexane and identified as $[(\phi_2P(pz))Re(CO)_4Br]$; white crystals, yield 79%. *Anal.* calcd. for $C_{19}H_{13}BrN_2O_4PRe$: C 36.20, H 2.08, N 4.44; found: C 36.0, H 2.11, N 4.22. The infrared spectrum (ν(CO) region) confirmed the tetracarbonyl formulation (see Table 1).

(b) Preparation of $[(\phi_2P(pz))Re(CO)_3Br]$

The tetracarbonyl $[(\phi_2P(pz))Re(CO)_4Br]$ (0.23 mmol) and benzene (10 ml) were heated at 80–90 °C for 50 h. The evolved carbon monoxide (0.19 mmol) was collected, the solution was evaporated to dryness under vacuum, and the residue was crystallized from chloroform–hexane, to yield white crystals identified as $[(\phi_2P(pz))Re(CO)_3Br]$ (yield, 73%). *Anal.* calcd. for $C_{18}H_{13}BrN_2O_3PRe$: C 35.89, H 2.18, N 4.65; found: C 35.8, H 2.16, N 4.33. *Mol. Wt.* calcd. 602.4; found: ($CHCl_3$): 660, 680.

(c) Preparation of $[(P(pz)_3)Re(CO)_3Br]$

A solution of $[Re(CO)_5Br]$ (0.85 mmol) and $P(pz)_3$ (0.85 mmol) in benzene (20 ml) was heated under reflux for 5 h; a white precipitate formed on cooling to room temperature. The solid was filtered off, dried under vacuum (100 °C/10^{-3} torr), and identified as $[(P(pz)_3)Re(CO)_3Br]$; yield 61%; mp 175–178 °C. *Anal.* calcd. for $C_{12}H_9BrN_6O_3PRe$: C 24.7, H 1.79, N 14.4; found: C 24.8, H 1.64, N 13.1. *Mol. Wt.* calcd. 582.4; found (in $CHCl_3$): 650, 700.

(d) Preparation of $[(\phi_2P(Me_2pz))Re(CO)_3Br]$

In a preliminary experiment, an equimolar mixture of $[Re(CO)_4Br]_2$ and $\phi_2P(Me_2pz)$ (1 mmolar scale) in benzene was stirred for 8 days; the solvent was removed, and the residue was crystallized from chloroform–hexane and identified by infrared spectral analysis as a mixture of $[(\phi_2P(Me_2pz))Re(CO)_4Br]$ (~60%) and $[(\phi_2P(Me_2pz))Re(CO)_3Br]$ (~40%).

A mixture of $[Re(CO)_4Br]_2$ (0.31 mmol) and $\phi_2P(Me_2pz)$ (0.63 mmol) in benzene (10 ml) was heated at 75 °C for 16 h. The evolved carbon monoxide (0.61 mmol) was determined, and the solution was evaporated to dryness under vacuum, giving a residue which was crystallized from chloroform–hexane and identified as $[(\phi_2P(Me_2pz))Re(CO)_3Br]$; white crystals, yield 76%; mp 90–92 °C. *Anal.* calcd. for $C_{20}H_{17}BrN_2O_3PRe$: C 38.11, H 2.72, N 4.44; found: C 38.1, H 2.70, N 4.35. Mass spectrum M calcd. (m/e): 630.1; found: 630; species corresponding to the successive loss of three CO groups were observed.

(e) Preparation of $[(\phi P(Me_2pz)_2)Re(CO)_3Br]$

A mixture of $[Re(CO)_4Br]_2$ (0.19 mmol) and $\phi P(Me_2pz)_2$ (0.38 mmol) in benzene (10 ml) was heated at 95–100 °C for 8 h. The evolved carbon monoxide (0.36 mmol) was determined and the solution was evaporated to dryness under vacuum to give a residue which was recrystallized twice from chloroform–hexane and identified as $[(\phi P(Me_2pz)_2)Re(CO)_3Br]$; yield 62%; mp 146–150 °C. *Anal.* calcd. for $C_{19}H_{19}BrN_4O_3PRe$: C 35.19, H 2.95, N 8.64; found: C 35.3, H 2.90, N 8.42. Mass spectrum, M calcd.: 648.1; found: 648; species corresponding to the stepwise loss of three CO groups were observed.

(f) Preparation of $[(P(Me_2pz)_3)Re(CO)_3Br]$

A mixture of $[Re(CO)_4Br]_2$ (0.19 mmol) and $P(Me_2pz)_3$ (0.39 mmol) in benzene (10 ml) was heated at 95–100 °C for 16 h. The evolved carbon monoxide was determined (0.38 mmol) and the solution was evaporated to dryness under vacuum yielding a white solid which was crystallized from chloroform–hexane and identified as $[(P(Me_2pz)_3)Re(CO)_3Br]$; yield 79%. *Anal.* calcd. for $C_{15}H_{21}BrN_6O_3PRe$: C 32.43, H 3.15, N 12.61; found: C 32.0, H 2.79, N 12.0.

(g) Preparation of $[(\phi_2P(Me_2pz))Mn(CO)_3Cl]$

A mixture of $[Mn(CO)_5Cl]$ (0.386 mmol) and $\phi_2P(Me_2pz)$ (0.39 mmol) in benzene (6 ml) was heated at 80 °C for 1 h, giving an orange solution. The evolved carbon monoxide (0.64 mmol) was collected (some loss of CO at room temperature was observed during the degassing stage); the solution was evaporated to dryness, the residue was crystallized from chloroform–hexane, and was identified as $[(\phi_2P(Me_2pz))Mn(CO)_3Cl]$; orange needles; yield 74%; mp 98–100 °C. *Anal.* calcd. for $C_{20}H_{17}ClMnN_2O_3P$: C 52.83, H 3.77, N 6.16; found: C 52.6, H 3.73, N 6.11. The complex decomposed into free ligand and other species in the mass spectrometer at the temperature (160 °C) required to cause volatilization.

(h) Preparation of $[(\phi P(Me_2pz)_2)Mn(CO)_3Cl]$

A stirred mixture of $[Mn(CO)_5Cl]$ (0.37 mmol) and

Can. J. Chem. Downloaded from www.nrcresearchpress.com by 210.87.254.6 on 09/05/12
For personal use only.

$\phi P(Me_2pz)_2$ (0.37 mmol) in benzene (8 ml) was heated at 50 °C for 2 h. The solvent was removed under vacuum and the residue was crystallized from chloroform–hexane and identified as $[(\phi P(Me_2pz)_2)Mn(CO)_3Cl]$; orange crystals; yield 69%; mp 72–74 °C. *Anal.* calcd. for $C_{19}H_{19}ClMnN_4O_3P$: C 48.27, H 4.05, N 11.9; found: C 48.2, H 4.40, N 10.8.

(i) Preparation of $[(\phi_2P(S)pz)Re(CO)_3Br]$

A solution of $[Re(CO)_5Br]$ (0.59 mmol) and $\phi_2P(S)pz$ (0.59 mmol) in benzene (25 ml) was heated under reflux, under nitrogen, for 2 h. Infrared spectral measurements (ν(CO) region) showed that reaction was complete. The solvent was removed under vacuum, giving a residue which was crystallized twice from chloroform–hexane, pumped dry under high vacuum, and identified as $[(\phi_2P(S)pz)Re(CO)_3Br]$; white crystals, 74% yield; mp 205 °C. *Anal.* calcd. for $C_{18}H_{13}BrN_2O_3PReS$: C 34.07, H 2.07, N 4.42; found: C 34.8, H 2.08, N 4.25. *Mol. Wt.* calcd.: 634.5; found ($CHCl_3$): 660, 690.

(j) Preparation of $[(\phi_2P(S)(Me_2pz))Re(CO)_3Br]$

A mixture of $[Re(CO)_4Br]_2$ (0.11 mmol) and $\phi_2P(S)(Me_2pz)$ (0.21 mmol) in benzene (5 ml) was heated at 80–90 °C for 3 h. The evolved carbon monoxide (0.19 mmol) was collected, the solvent was removed under vacuum, and the product was crystallized from chloroform–hexane and identified as $[(\phi_2P(S)(Me_2pz))Re(CO)_3Br]$; white crystals, 72% yield; mp 197–200 °C. *Anal.* calcd. for $C_{20}H_{17}BrN_2O_3PReS$: C 36.26, H 2.59, N 4.23; found: C 35.9, H 2.66, N 4.35. Mass spectrum: M calcd.: 662; found: 662 (weak); species due to stepwise loss of three CO groups, and to free ligand, were observed.

(k) Reaction of $[(\phi_3P)Re(CO)_4Br]$ *with* $P(Me_2pz)_3$

A mixture of $[(\phi_3P)Re(CO)_4Br]$ (0.20 mmol) and $P(Me_2pz)_3$ (0.20 mmol) in benzene was heated at 80–90 °C for 48 h. The evolved carbon monoxide (0.19 mmol) was collected, and the solvent was removed under vacuum. The ir spectrum (ν(CO) region, 2035(s), 1925 (br s) cm^{-1} in solution in $CHCl_3$) and the ^{31}P spectrum (two singlet resonances at 25.18 and 0.00 ppm relative to external ϕ_3P, in toluene) of the solid residue were measured, and indicated the formation of $[(P(Me_2pz)_3)Re(CO)_3Br]$ and free ϕ_3P. The product was recrystallized and analyzed, confirming $[(P(Me_2pz)_3)Re(CO)_3Br]$.

Acknowledgment

The authors acknowledge the financial support of the National Research Council of Canada.

1. C. A. McAuliffe. Transition metal complexes of phosphorus, arsenic, and antimony ligands. Wiley. 1973, and cited references.
2. S. Fischer, L. K. Peterson, and J. F. Nixon. Can. J. Chem. **52**, 3981 (1974).
3. (*a*) S. Fischer, J. Hoyano, and L. K. Peterson. Can. J. Chem. This issue; (*b*) S. Fischer, J. Hoyano, I. Johnson, and L. K. Peterson. Can. J. Chem. This issue.
4. E. W. Abel and G. Wilkinson. J. Chem. Soc. 1501 (1959).
5. L. E. Orgel. Inorg. Chem. **1**, 25 (1962).
6. M. A. El-Sayed and H. D. Kaesz. J. Mol. Spectrosc. **9**, 310 (1962); Inorg. Chem. **2**, 158 (1963).
7. N. Flitcroft, J. M. Leach, and F. J. Hopton. J. Inorg. Nucl. Chem. **32**, 137 (1970).
8. S. O. Grim, R. L. Keiter, and W. McFarlane. Inorg. Chem. **6**, 1133 (1967).
9. R. B. King and J. C. Cloyd. Inorg. Chem. **14**, 1550 (1975).
10. S. Trofimenko. Chem. Rev. **72**, 497 (1972), and references cited therein.
11. S. Trofimenko. J. Am. Chem. Soc. **91**, 588 (1969).
12. R. J. McKinney, R. Hoxmeier, and H. D. Kaesz. J. Am. Chem. Soc. **97**, 3059 (1975); R. J. McKinney and H. D. Kaesz. J. Am. Chem. Soc. **97**, 3066 (1975), and references therein.
13. E. W. Abel and G. Wilkinson. J. Chem. Soc. 1501 (1959).
14. E. O. Brimm, M. A. Lynch, Jr., and W. J. Sesny. J. Am. Chem. Soc. **76**, 3831 (1954).
15. E. W. Abel, G. B. Hargreaves, and G. Wilkinson. J. Chem. Soc. 3149 (1958).
16. W. Hieber and G. Braun. Z. Naturforsch. Teil **B**, **14**, 132 (1959); Inorg. Chem. **4**, 389 (1965).

Can. J. Chem. Downloaded from www.nrcresearchpress.com by 210.87.254.6 on 09/05/12
For personal use only.

Syntheses and properties of phosphino- and phosphinatopyrroles

SVEN FISCHER, JAMES HOYANO, IAN JOHNSON, AND LOUIS K. PETERSON
Department of Chemistry, Simon Fraser University, Burnaby, B.C., Canada V5A 1S6

Received December 22, 1975

Can. J. Chem. Downloaded from www.nrcresearchpress.com by 210.87.254.105 on 09/05/12
For personal use only.

SVEN FISCHER, JAMES HOYANO, IAN JOHNSON, and LOUIS K. PETERSON. Can. J. Chem. **54**, 2706 (1976).

The syntheses of P—N bonded pyrrolyl- and 2,5-dimethylpyrrolylphosphines $\phi_x P(py)_{3-x}$ and $\phi_x P(Me_2py)_{3-x}$ ($x = 0$–2) and the oxy derivatives py_3PO and $(Me_2py)_2P(O)Cl$ by the reaction of potassium pyrrolide or 2,5-dimethylpyrrolide with an appropriate chlorophosphine or with $POCl_3$ are described. Molecular structures were inferred from spectroscopic data. The P—N bonded phosphines are stable to solvolytic attack by water or alcohols and do not undergo insertion reactions with CS_2, but they are oxidised by oxygen and suffer nucleophilic displacement of the azole moiety by strong base. The Lewis acid BCl_3 cleaves the P—N bond and CH_3I reacts with only one member, $\phi_2P(py)$, to form a phosphonium salt. Hindered rotation about the P—N bond was detected in the (2,5-dimethylpyrrolyl)phosphine series, but not among the corresponding oxy derivatives. The nature of the P—N bond and trends in the basicity of the phosphorus atom are discussed.

SVEN FISCHER, JAMES HOYANO, IAN JOHNSON et LOUIS K. PETERSON. Can. J. Chem. **54**, 2706 (1976).

On décrit les synthèses de pyrrolyl et de diméthyl-2,5 pyrrolyl phosphines $\phi_x P(py)_{3-x}$ et $\phi_x P(Me_2py)_{3-x}$ ($x = 0$–2) contenant des liens P—N et des dérivés oxy py_3PO et $(Me_2py)_2P(O)Cl$ par la réaction du pyrrolure de potassium ou du diméthyl-2,5 pyrrolure de potassium avec une chlorophosphine appropriée ou avec $POCl_3$. On a proposé les structures moléculaires à partir des données spectroscopiques. Les phosphines contenant un lien P—N sont stables aux attaques solvolytiques de l'eau ou des alcools et ne subissent pas de réactions d'insertion avec le CS_2; ils sont toutefois oxydées par l'oxygène et subissent des déplacements nucléophiles de la portion azole sous l'influence de bases fortes. L'acide de Lewis BCl_3 coupe le lien P—N et le CH_3I réagit uniquement avec le $\phi_2P(py)$ conduisent à un sel de phosphonium. On a détecté un empêchement à la rotation autours du lien P—N dans la série diméthyl-2,5 pyrrolyl phosphine; ce n'est toutefois pas le cas dans les dérivés oxy correspondants. On discute de la nature du lien P—N et des tendances dans la basicité de l'atome de phosphore.

[Traduit par le journal]

Introduction

The *N*-pyrrolylphosphines and phosphine oxides are members of the azole phosphine class of compounds, where a heteroaromatic system is bonded via nitrogen to phosphorus (1). Modifications of the chemistry of the P—N bond and of the coordination properties of the phosphorus centre, as compared to dialkylaminophosphine and tris(aryl)phosphine systems, may be expected. In this paper the syntheses and reactions of pyrrolylphosphines are described. A study of metal coordination complexes will be reported later.

Discussion

The P—N bonded pyrrolylphosphines (**1**–**6**) listed in Table 1 were prepared by the reaction of potassium pyrrolide (K^+py^-) or 2,5-dimethylpyrrolide ($K^+Me_2py^-$) with an appropriate chlorophosphine in ether.

$$(3 - x)K^+py^- + \phi_x PCl_{3-x} \rightarrow \phi_x P(py)_{3-x} + (3 - x)KCl \qquad x = 0\text{–}2$$

The analogous reaction of potassium pyrrolide with phosphorus oxychloride yields tris(pyrrolyl)-phosphine oxide **7**, whereas potassium 2,5-dimethylpyrrolide gives the partially substituted bis(2,5-dimethylpyrrolyl)chlorophosphine oxide **8**.

The *N*-pyrrolylphosphines are low melting solids or colorless, viscous liquids, which have been characterised by analysis and mass, ir, and nmr spectral measurements. In all cases the pyrrolylphosphines prepared via the potassium salt have structures based upon the P—N bonded formulations **I** and **II**, as evidenced by the absence of N—H bonds in the infrared spectrum, and by ^1H nmr spectra (see Table 2). The ^{13}C FT nmr spectrum of **3** corroborates this structural assignment, indicating that the alternative P—C_α structure postulated by Issleib and Brack (2) for

TABLE 1. Pyrrolyl- and 2,5-dimethylpyrrolylphosphines and oxyphosphines

Compound		Method of purification	mp (°C)	Analytical data: Observed C	H	N	Calculated C	H	N	Parent ion *m/e*
ϕ_2Ppy	1	Vacuum distillation ~100 °C/1 torr	Colorless oil	76.6	5.98	5.85	76.5	5.62	5.57	251
ϕP(py)$_2$	2	Vacuum distillation ~180 °C/0.001 torr	Colorless oil	70.1	5.55	11.5	70.0	5.40	11.7	240
P(py)$_3$	3	Crystallization from methanol	43–44[a]	—	—	—	—	—	—	—
ϕ_2P(Me$_2$py)	4	Vacuum distillation ~140 °C/0.001 torr	47–50[b]	77.6	6.61	5.67	77.4	6.55	5.02	279
ϕP(Me$_2$py)$_2$	5	Vacuum distillation ~140 °C/0.001 torr	60–65[b]	73.2	7.20	9.33	73.0	7.09	9.46	296
P(Me$_2$py)$_3$	6	Sublimation ~100 °C/0.001 torr	60–65[b]	68.9	7.81	13.1	69.0	7.67	13.4	313
(py)$_3$PO	7	Crystallization from ethanol	80	58.7	5.14	16.4	58.8	4.93	17.1	245
(Me$_2$py)$_2$P(O)Cl[c]	8	—	Oil	—	—	—	—	—	—	270[d] 272

[a]Literature value, 45 °C (2).
[b]Strong tendency to form a glass on cooling.
[c]Attempts to prepare (Me$_2$py)$_3$PO by refluxing **8** with K$^+$(Me$_2$py)$^-$ in toluene were unsuccessful.
[d]The intensity ratio, 3:1, was characteristic of a monochloride.

tris(pyrrolyl)phosphine, also prepared via the potassium salt, is incorrect. Using decoupled

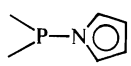

I

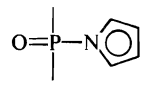

II

spectra, a partial analysis of couplings was possible (see Table 2). Our ^{1}H-assignments are consistent with those proposed for pyrrole itself (3, 4).

The reaction of pyrrolyl–Grignard compounds with chlorophosphines leads mainly to P—C$_\alpha$ structures, pyrrolylmagnesium bromide and POCl$_3$ giving tris(α-pyrrolyl)phosphine oxide (5) which is distinguishable on spectroscopic evidence from tris-(*N*-pyrrolyl)phosphine oxide **7**.

The ^{1}H-nmr spectra (Table 2) for the ϕ_xP(Me$_2$py)$_{3-x}$ series indicate restricted rotation about the P—N bond, resulting in separate resonances for the 2-methyl and 5-methyl protons. In the case of ϕ_2P(Me$_2$py) the two signals are only observed at low temperatures and coalesce on warming to −50 °C, whereas for ϕP(Me$_2$py)$_2$ and P(Me$_2$py)$_3$ the restriction to rotation attributable to the methyl substituents was observed at temperatures up to +130 °C. Steric hindrance to rotation is not observed in the unsubstituted pyrrolyl series ϕ_xP(py)$_{3-x}$ at room temperature. In the oxyphosphine series ϕ_xP(O)(Me$_2$py)$_{3-x}$ and in (Me$_2$py)$_2$P(O)Cl, however, all the methyl resonances are singlets, implying equivalent 2- and 5-methyl substituents. Apparently, the widening of the bond angle about phosphorus upon conversion of phosphine to phosphine oxide eliminates the steric barrier to rotation.

In contrast to the facile solvolysis of the P—N bond of most alkylaminophosphines (6) by protic reagents, the pyrrolylphosphines are stable to water and alcohols. Also the typical insertion of CS$_2$ into the P—N bond of alkylaminophosphines (6) is not observed with pyrrolylphosphines. Because of involvement of the lone pair in the π-electron sextet of the heterocyclic ring (7) the nitrogen is not available for electrophilic attack. This chemical anomaly misled the earlier workers in their assignment of the structure of tris(pyrrolyl)phosphine **3** (2). Phenylphosphinoamines of the type ϕP(NR$_2$)$_2$ are immiscible with water and show no obvious

Can. J. Chem. Downloaded from www.nrcresearchpress.com by 210.87.254.105 on 09/05/12
For personal use only.

TABLE 2. ^{1}H nmr data for pyrrolyl- and 2,5-dimethylpyrrolylphosphines and oxyphosphines[a]

Compound		2-R, 5-R R = H or CH_3	3-H, 4-H	$-C_6H_5$	J (Hz)
ϕ_2Ppy	**1**	3.30 d of t's	3.83 d of t's	2.79–2.90	$^3J_{H_2H_3} = {}^4J_{H_2H_4} = 2$ $^3J_{PH} = {}^4J_{PH} = 0.4$
ϕP(py)$_2$	**2**	3.28 q	3.65 q	2.6 –2.8	$^3J_{H_2H_3} = {}^4J_{H_2H_4} = 22$
P(py)$_3$[b]	**3**	3.23 q	3.68 t		$^3J_{PH} = 4.5$ $^4J_{PH} = 0.3$
ϕ_2P(Me$_2$py)[c]	**4**	8.02 s	4.13 br	2.6 –2.8	
ϕP(Mepy)$_2$	**5**	8.02 s 8.00 s	4.7 br	2.5 –2.6	
P(Me$_2$py)$_3$[d]	**6**	8.02 s 8.04 s	4.1 br		
OP(py)$_3$	**7**	3.20 sextet	3.55 septet		$^3J_{H_2H_3} = 2.9$ $^4J_{H_2H_4} = 1.9$ $^3J_{PH} = 2.9$ $^4J_{PH} = 5.0$
Cl(O)P(Me$_2$py)$_2$	**8**	7.77 s	4.06 d		$^4J_{PH_{3,4}} = 5.5$

[a] τ-values, in $CDCl_3$ with TMS as internal standard.
[b] ^{13}C-spectrum: α-C, δ 122.6 ppm downfield from TMS, $^2J_{PC} = 14$ Hz; β-C, δ 112.8 ppm, $^3J_{PC} = 4.5$ Hz.
[c] Low temperature studies, in $(CD_3)_2CO$, showed that the methyl resonance is a doublet at -78 °C, which coalesces to a singlet by -48 °C.
[d] Variable temperature studies, in bromobenzene, indicated two distinct methyl resonances at temperatures up to +130 °C.

TABLE 3. ^{31}P chemical shifts of azolylphosphines[a]

az[b]	Pyrrolyl	2,5-Dimethylpyrrolyl	Pyrazolyl[c]	3,5-Dimethylpyrazolyl[c]
ϕ_2P(az)	52.59	39.57	59.63	44.69
ϕP(az)$_2$	63.46	73.58	77.04	66.67
P(az)$_3$	83.95	90.72	65.69[d]	77.53

[a] Proton-decoupled spectra, in toluene solution, in ppm downfield from external ϕ_3P dissolved in toluene; to relate to external H_3PO_4, subtract 5.9 ppm from the given values.
[b] az = azolyl = pyrrolyl, 2,5-dimethylpyrrolyl, pyrazolyl, or 3,5-dimethylpyrazolyl.
[c] Reference 10.
[d] This apparently anomalous value may be attributed to exchange effects (1).

tendency for hydrolysis or alcoholysis (8). The absence of typical P—N bond reactions among (trifluoromethyl)phosphinoamines is also attributed to the reduced basicity of the N-atom due, in this case, to N → P π-bonding effects (9).

BX_3 electrophiles readily cleave the P—N bond in pyrrolylphosphines, BCl_3 and ϕ_2Ppy yielding ϕ_2PCl and unstable pyrrolylchloroboranes. Reaction with methyl iodide is limited to ϕ_2Ppy which forms a phosphonium salt according to ^{1}H nmr evidence (CH_3-resonance, doublet, $J_{PCH_3} = 13$ Hz). The failure of other members of the series to react with CH_3I reflects the decreasing basicity of the phosphorus centre with an increasing number of pyrrolyl substituents, in parallel with the trends in ^{31}P chemical shifts for the series ϕ_xP(py)$_{3-x}$ and ϕ_xP(Me$_2$py)$_{3-x}$. Phenyl(pyrazolyl)phosphines behave in a similar fashion (see Table 3),[1] whereas the bis- and tris-(dialkylamino)phosphines, as well as the monoamino derivatives give phosphonium salts with methyl iodide (6*a*, 8).

Strong nucleophiles readily displace the pyrrolyl moiety, for example ϕ_2Ppy being converted to ϕ_3P by reaction with phenyllithium. The pyrrolylphosphines are oxidised by oxygen to phosphine oxides, contrasting with the stability of phenylphosphinoamines in air (8). *N*-Alkylpyrroles isomerize on heating to α-substituted derivatives, but tris(pyrrolyl)phosphine **3** and tris(pyrrolyl)phosphine oxide **7** are thermally stable, being recovered unchanged after 2 h at 180 °C.

Experimental

Experimental operations were performed under anhydrous conditions, using dry inert atmosphere systems. Solvents were dried by standard methods and distilled prior to use. Elemental analyses were performed by the university analyst, Simon Fraser University. ^{1}H and ^{31}P

[1] I. Johnson and L. K. Peterson, unpublished results.

Can. J. Chem. Downloaded from www.nrcresearchpress.com by 210.87.254.105 on 09/05/12
For personal use only.

Can. J. Chem. Downloaded from www.nrcresearchpress.com by 210.87.254.105 on 09/05/12
For personal use only.

nuclear magnetic resonance spectra were obtained using Varian A56/60 and XL100 instruments, the latter having Fourier transform and proton decoupling facilities. Infrared spectra were recorded with a Perkin Elmer 457 spectrophotometer and were calibrated against standard polystyrene film. Mass spectra were determined with a double focussing Hitachi–Perkin-Elmer RMU-6E instrument.

Preparation of Pyrrolylphosphines

The pyrrolyl- and 2,5-dimethylpyrrolylphosphines (compounds **1–6**) and oxyphosphines (**7**, **8**) listed in Table 1 were prepared on a 5–10 mmolar scale, by adding an ethereal solution of the appropriate chlorophosphine (ϕ_2PCl, ϕPCl_2, or PCl_3) or phosphorus oxychloride to an ethereal suspension of 20% excess potassium pyrrolide. Reaction times varied from 12–24 h. The precipitate of KCl and excess potassium pyrrolide was filtered off and the solvent was removed under vacuum, leaving pyrrolyl phosphorus derivatives which were purified by crystallization, sublimation, or fractional distillation under vacuum and characterized on the basis of analytical, melting point, and mass, infrared, and nmr spectral data (see Tables 1 and 2). The yields are between 70 and 95%.

Reactions of the Pyrrolylphosphines

(a) With Water

The pyrrolylphosphine (ϕ_2Ppy, **1**; $P(py)_3$, **3**; $\phi_2P(Me_2py)$, **4**; $\phi P(Me_2py)$, **5**; $P(Me_2py)_3$, **6**;) (~0.5 mmol scale) was dissolved in ether and treated with a twofold excess of water. After 1 h, the solvent was removed under vacuum, leaving unchanged starting material, as evidenced by nmr and mass spectral examination.

(b) With Oxygen

The pyrrolylphosphine ($\phi_2P(Me_2py)$, **4**; $\phi P(Me_2py)_2$, **5**; $P(Me_2py)_3$, **6**;) (~0.5 mmol) was dissolved in ether, (~5 ml), through which a slow stream of dry oxygen was passed for 3–4 h. The solvent was removed under vacuum, leaving a residue consisting mostly of starting material, as evidenced by nmr and mass spectral examinations, together with new species corresponding to the oxides $\phi_xP(O)(Me_2py)_{3-x}$. The new, distinct resonances (at τ 8.2) attributable to the methyl protons of $(Me_2py)_3PO$, $\phi_2P(O)(Me_2py)$, and $\phi P(O)(Me_2py)_2$ were singlets in all cases.

(c) With Alcohol (Methanol or Ethanol)

The pyrrolylphosphine (~0.5 mmol) was dissolved in an excess of the alcohol. $P(py)_3$ **3**, and $OP(py)_3$ **5**, in EtOH; $\phi_2P(Me_2py)$ **4**, $P(Me_2py)_3$ **6**, and $\phi P(Me_2py)_2$ **5** in CH_3OH and allowed to stand for several hours. The solvent was removed, leaving a residue giving a ^1H nmr spectrum corresponding to unchanged starting material.

(d) With CS_2

The pyrrolylphosphine (~0.5 mmol) ($\phi_2P(py)$, **1**; $P(py)_3$, **3**; $\phi_2P(Me_2py)$, **4**) was dissolved in benzene (~5 ml), and treated with tenfold excess of carbon disulphide and heated under reflux for several hours. The CS_2 and solvent were removed under vacuum, leaving a residue giving the same mass spectrum as the starting material.

(e) With Phenyllithium

Solutions of ϕ_2Ppy, **1**, (0.59 mmol) in ether and phenyllithium (0.98 mmol) in benzene–ether (70:30) were mixed and allowed to stand for two days. Colorless crystals of Li-pyrrolide, mp 197 °C were precipitated and filtered off. The nmr spectrum in CD_3OD–D_2O demonstrated the presence of the pyrrolyl moiety. The filtrate was washed with water until neutral, dried over sodium sulphate, and cooled to 0 °C to yield ϕ_3P (70%) identified by mass spectra and mixture melting point measurements.

(f) With Methyl Iodide

ϕ_2Ppy, **1**, (~0.5 mmol) in ether was treated with a 25-fold excess of methyl iodide. After 3 days, the white precipitate (46% yield) was filtered off and identified as $[\phi_2P(py)CH_3^+]I^-$, mp 150 °C (dec.). *Anal.* calcd. for $C_{17}H_{17}NPI$: C 51.9, H 4.32, N 3.56; found: C 51.6, H 4.21, N 3.46. ^1H nmr ($CDCl_3$) τ 2.18–2.32 (phenyl) 2.95 (m, 2-H and 5-H of pyrrole ring) 3.35 (m, 3-H and 4-H of pyrrole ring) 6.42 (d, methyl, J_{PCH_3} = 13 Hz). Compound $P(py)_3$, **3**, failed to react with methyl iodide under the conditions described above.

(g) With BCl_3

ϕ_2Ppy, **1** (0.20 mmol) in $CDCl_3$ was treated with an equivalent amount of BCl_3 and after several hours a brown oil separated out. The solvent was removed and a mass spectral analysis of the residue showed the presence of ϕ_2Ppy and ϕ_2PCl. The molecular ions for $pyBCl_2$, py_2BCl, or py_3B were not observed.

Acknowledgement

The financial support of the National Research Council of Canada is gratefully acknowledged.

1. S. Fischer, L. K. Peterson, and J. F. Nixon. Can. J. Chem. **52**, 3981 (1974).
2. K. Issleib and A. Brack. Z. Anorg. Allgem. Chem. **292**, 245 (1957).
3. G. F. Katekar and A. G. Moritz. Aust. J. Chem. **22**, 1199 (1969).
4. J. F. Page, J. D. Alger, and D. U. Grant. J. Am. Chem. Soc. **87**, 5333 (1965).
5. (*a*) C. E. Griffin, R. P. Peller, K. R. Martin, and J. A. Peters. J. Org. Chem. **30**, 97 (1965); (*b*) R. H. Kemp, W. A. Thomas, M. Gordon, and C. E. Griffin. J. Chem. Soc. B, 527 (1969).
6. (*a*) E. Fluck. *In* Topics in phosphorus chemistry. Vol. 4. *Edited by* M. Grayson and E. J. Griffith. Interscience, New York. 1966; (*b*) L. A. Hamilton and P. S. Landis. *In* Organic phosphorus compounds. Vol. 4. *Edited by* G. M. Kosolapoff and L. Maier. Wiley–Interscience. 1972. p. 504.
7. (*a*) A. R. Katritzky and J. M. Lagowski. *In* The principles of heterocyclic chemistry. Methuen and Co., London. 1967; (*b*) R. Fessenden and D. F. Crowe. J. Org. Chem. **25**, 598 (1960).
8. G. Ewart, D. S. Payne, A. L. Porte, and A. P. Lane. J. Chem. Soc. 3984 (1962).
9. A. B. Burg and J. Heners. J. Am. Chem. Soc. **87**, 3092 (1965).
10. S. Fischer, L. K. Peterson, and J. Hoyano. Can. J. Chem. This issue.

Syntheses and properties of phosphino- and phosphinatopyrazoles

SVEN FISCHER, JAMES HOYANO, AND LOUIS K. PETERSON
Department of Chemistry, Simon Fraser University, Burnaby, B.C., Canada V5A 1S6

Received December 22, 1976

SVEN FISCHER, JAMES HOYANO, and LOUIS K. PETERSON. Can. J. Chem. **54**, 2710 (1976).

The new P—N bonded phosphino- and phosphinatopyrazoles $\phi P(Me_2pz)_2$, $(pz)_3PO$, $(Me_2pz)_3PO$, $\phi_2P(S)(Me_2pz)$, $(pz)_3PS$, and $(C_2H_5)_2P(pz)$ and the arsenic derivative $(pz)_3As$ have been prepared and characterized (pz = pyrazolyl, Me_2pz = 3,5-dimethylpyrazolyl).

The reactivity of the P—N bond in phosphinopyrazoles towards electrophiles and nucleophiles is discussed. HCl, H_2O, CH_3OH, and BCl_3 cleave the P—N bond, presumably via attack at the 2-N site. BF_3 forms 1:1 adducts bonded to phosphorus which are reasonably stable in the solid state. CH_3I forms a phosphonium salt with diphenyl(pyrazolyl)phosphine while other members of the series do not react. All members are inert toward CS_2. Nucleophiles like sodium methoxide or phenyllithium displace the pyrazolyl moiety by attack at the phosphorus. Comparisons are made with the P—N bond in dialkylaminophosphines.

SVEN FISCHER, JAMES HOYANO et LOUIS K. PETERSON. Can. J. Chem. **54**, 2710 (1976).

On a préparé et caractérisé les nouveaux phosphino et phosphinatopyrazoles $\phi P(Me_2pz)_2$, $(pz)_3PO$, $(Me_2pz)_3PO$, $\phi_2P(S)(Me_2pz)$, $(pz)_3PS$ et $(C_2H_5)_2P(pz)$ contenant des liens P—N et le dérivé $(pz)_3As$ de l'arsenic (pz = pyrazolyle, Me_2pz = diméthyl-3,5 pyrazolyle).

On discute de la réactivité du lien P—N des phosphinopyrazoles vis-à-vis des électrophiles et des nucléophiles. HCl, H_2O, CH_3OH et BCl_3 coupent le lien P—N probablement par une attaque au niveau du 2-N. BF_3 conduit à des adduits 1:1 liés par le phosphore qui sont assez stables à l'état solide. CH_3I forme un sel de phosphonium avec la diphényle(pyrazolyle)phosphine alors que les autres termes de la série ne réagissent pas. Tous les termes sont inertes vis-à-vis le CS_2. Des nucléophiles comme méthylate de sodium et le phénylithium déplacent la partie pyrazolyle par une attaque au niveau du phosphore. On fait des comparaisons avec le lien P—N des dialkylaminophosphines.

[Traduit par le journal]

Introduction

A number of synthetic routes to phosphino- and phosphinatopyrazoles have been described (1). In this paper we report the preparation of further new members and studies of the chemical behaviour of this class of compound. The coordination properties of pyrazolylphosphines in carbonyl complexes of manganese and rhenium have been reported (2), and the synthesis of complexes of Mo(0), W(0), Co(0), Pd(II), Cu(I), and Hg(II) will be described later.[1]

Discussion

P—N bonded pyrazolylphosphines can be prepared by the reaction of a chlorophosphine with: (*i*) pyrazole in ether in the presence of triethylamine, (*ii*) potassium pyrazolide suspended in ether or benzene, (*iii*) trimethylsilylpyrazole in the absence of solvent. Phosphinato derivatives are conveniently prepared: (*iv*) by the reaction of $POCl_3$ or $PSCl_3$ with potassium pyrazolide in ether or benzene, (*v*) by sulphur oxidation of a pyrazolylphosphine in refluxing toluene.

Using these methods the following compounds were prepared in good yield and characterized on the basis of melting point, elemental analysis, mass, ir, and nmr spectral data: $P(pz)_3$ and $P(Me_2pz)_3$ by methods (*ii*) and (*iii*) (1), $\phi P(Me_2pz)_2$ (*i*), $(pz)_3PO$ and $(Me_2pz)_3PO$ (*iv*), $\phi_2P(S)(Me_2pz)$ (*v*), $(pz)_3PS$ (*iv*) and $(C_2H_5)_2P(pz)$ (*i*) (pz = pyrazolyl, Me_2pz = 3,5-dimethylpyrazolyl).

Whereas PCl_3 and K^+pz^- give $P(pz)_3$ at room temperature, $AsCl_3$ has to be refluxed in benzene with K^+pz^- to obtain $As(pz)_3$. $AsCl_3$ does not react with pyrazole in the presence of triethylamine. The main product of the reaction of $AsCl_3$ with K^+pz^- in ether or with Me_3Sipz at 60 °C is the partially substituted $(pz)_2AsCl$. Similarly, the derivative $(Et_2N)_2AsCl$ does not react further with $Me_3Si(NEt_2)$ (3). The reaction of Me_3Sipz with $P(S)Cl_3$ stops at $(pz)_2P(S)Cl$, a useful intermediate in further syntheses.

Potassium 3,5-dimethylpyrazolide and $POCl_3$ give $(Me_2pz)_3PO$, whereas the analogous reaction of potassium 2,5-dimethylpyrrolide stops at

[1]S. Fischer and L. K. Peterson, unpublished results.

Can. J. Chem. Downloaded from www.nrcresearchpress.com by 210.87.254.105 on 09/05/12
For personal use only.

Can. J. Chem. Downloaded from www.nrcresearchpress.com by 210.87.254.105 on 09/05/12
For personal use only.

the partially substituted $(Me_2py)_2P(O)Cl$, presumably on account of steric hindrance (4).

The reactivity of the P—N bond in *N*-phosphinopyrazoles was investigated by reactions with various electrophiles and nucleophiles. The planarity of the heteroaromatic ring has been confirmed by X-ray structural studies for $P(pz)_3$,[2] implying sp^2 hybridization for the phosphorus bonded nitrogen atom. The P—N bond is cleaved readily by HCl, H_2O, CH_3OH, or BCl_3 and slowly by BF_3. In contrast pyrrolylphosphines (4) and pyrrolyl silanes (5) are stable towards H_2O and CH_3OH because of involvement of the nitrogen lone pair in the π-electron sextet of the ring (6). Apparently in *N*-phosphinopyrazoles the P—N bond cleavage by protic species and by BX_3 Lewis acids follows a mechanistic route involving electrophilic attack at the lone pair of the 2-N site [1]. A similar route should apply for the cleavage of *N*-phosphinoimidazoles by water, where the 3-N site is the obvious center for electrophilic attack.

[1] 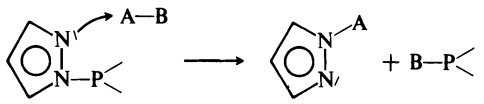

A—B = H—OH, H—OCH_3, H—Cl, BCl_2—Cl, BF_2—F

Nucleophilic attack at the phosphorus center by water or methanol seems unlikely in view of the observed stability of *N*-pyrrolylphosphines towards these agents (4).

CS_2 does not insert into the P—N bond of pyrrolyl- and pyrazolylphosphines, contrasting with the behaviour of the more strongly basic dialkylaminophosphines (7, 8) [2]. In dialkylaminophosphines the nitrogen is sufficiently basic to allow electrophilic attack by species (AB) such as H_2O, ROH, HX, BCl_3, and BF_3, resulting in P—N cleavage [3] (7).

[2] 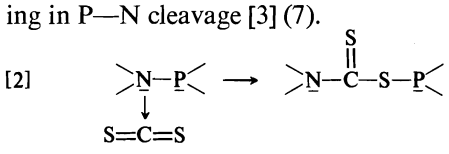

[3] 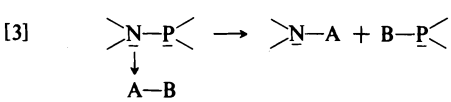

A—B = H—OH, H—OR, H—X, BCl_2—Cl, BF_2—F

Mavel and co-workers (9) observed stepwise alcoholysis of $(Me_2N)_3P$, using nmr methods. Bis(diethylamino)phenylphosphine, however, does not react with alcohols or water, due, it is suggested, to N → P π-bonding effects and the reduced basicity of the nitrogen atoms (10). For similar reasons perfluoroalkylaminophosphines resist P—N bond cleavage in the gas phase with HCl, BCl_3, BF_3, and NH_3 (11). The phosphorus atom in pyrazolylphosphines is less basic than in triphenylphosphine. The basicity decreases with an increasing number of azole groups, as suggested by the trends in ^{31}P chemical shifts and by the inability of members beyond $\phi_2P(pz)$ to react with methyl iodide. Similar ^{31}P chemical shift trends were observed in the pyrrolylphosphine series where reaction with methyl iodide is likewise restricted to the monopyrrolyl derivatives (4). Thus the methyl iodide studies indicate phosphonium, rather than ammonium salt formation, and bonding of CH_3 to phosphorus is further confirmed by ^1H and ^{31}P nmr data for $[\phi_2P^+(CH_3)(pz)]I^-$, $[\phi_2P^+(CH_3)(py)]I^-$ (4) and $[\phi P^+(CH_3)(NEt_2)_2]I^-$ (10); in each case, the $^1H(PCH_3)$ resonance is a doublet with chemical shift (τ 6.4–7.8) and $^2J_{PH}$ values (11.5–14.0 Hz) characteristic for the $(CH_3)P^+$ group (9*b*).

The pyrazolylphosphines $\phi_xP(pz)_{3-x}$ form, 1:1 adducts with BF_3 that are reasonably stable when isolated in the solid state, but decompose in solution into products indicative of P—N bond cleavage. From nmr evidence the phosphorus atom is the site for attachment of BF_3, resulting in ^{31}P coupled doublets in the ^{19}F spectra and ^{19}F coupled 1:2:2:1 quartets in the ^{31}P spectra. The $^2J_{P-F}$ coupling constants in the series $\phi_xP(pz)_{3-x}BF_3$ increase with increasing azolyl-substitution ($^2J_{PF}$ = 45, 53, and 60 Hz for x = 2, 1, 0) in line with the expected increase in the *s*-character of the P—B bond (12, 13). P—B and B—F couplings were not detected. These observations contrast with the relatively large $^2J_{PF}$ (229 Hz), $^1J_{PB}$ (174 Hz), and $^1J_{BF}$ (51 Hz) couplings observed for the adduct $(CH_3)_3PBF_3$ (14). The origin of such decouplings is a matter of some controversy, and may be due to exchange effects (15, 16), to autoionization (14), or to specific quadrupolar relaxation effects at the boron nucleus.[3] Reaction via BF_3 attack at the 2-N site would provide a route for the observed

[2]F. W. B. Einstein and R. Cobbledick, personal communication.

[3]E. J. Wells, private communication.

Can. J. Chem. Downloaded from www.nrcresearchpress.com by 210.87.254.105 on 09/05/12
For personal use only.

P—N bond cleavage (see eq. 1 and earlier discussion).

In dialkylaminophosphines the preferential coordination of BH_3 to phosphorus, rather than to nitrogen, is attributed to an enhanced basicity of the former centre by $N \rightarrow P$ π-bonding (7, 17, 18). Alkyl halides (7, 10, 19), trialkylboranes (20, 21) and metal complexes (22, 23) also coordinate preferentially at phosphorus.

From ^1H nmr and mass spectroscopic evidence, the P—N bond in pyrazolylphosphines is rapidly cleaved by BCl_3, giving products consistent with [4] and [5]: similar (pyrazolyl)chloroborane derivatives were observed in the mass spectra of the products obtained by treating BCl_3 with K^+pz^-.

[4] $$\phi_2P(pz) + BCl_3 \rightarrow \phi_2PCl + [(pz)BCl_2]_2$$

[5] $$P(pz)_3 + BCl_3 \rightarrow (pz)_2PCl + (pz)PCl_2 + [(pz)BCl_2]_2 + [(pz)_3B]_2$$

The azolide moiety in pyrazolyl- and pyrrolylphosphines (4) is readily displaced by sodium methoxide and phenyllithium in a nucleophilic substitution at phosphorus. The electron-withdrawing influence of the attached azole and the absence of N—P π-bonding effects in azolylphosphines would facilitate such nucleophilic attack. Similar arguments apply for the conversion of diphenyl(pyrazolyl)phosphine oxide into triphenylphosphine oxide by phenyllithium.

The compound $Et_2P(pz)$ was prepared for examination of possible fluxional behaviour (24, 25). The 3- and the 5-H resonances of the pyrazole ring were not sufficiently separated to permit a ^1H variable temperature study.

Experimental

For general procedures see previous publication (4).

Preparations

(a) $P(pz)_3$ and $P(Me_2pz)_3$

A solution of PCl_3 (15 mmol) in ether was slowly added to a stirred suspension of K^+pz^- (62 mmol) (26) in ether. The mixture was stirred for 12 h, the precipitate filtered off and washed with ether, and the solvent evaporated from the filtrate. The residue was purified by sublimation; yield 85%. This is an alternative to the earlier reported method using PCl_3 and trimethylsilylpyrazole (1).

The analogous reaction of PCl_3 with potassium 3,5-dimethylpyrazolide in ether gave a mixture of partially substituted products; several treatments of this mixture with $Me_3Si(Me_2pz)$ (24, 27), with intermittent removal of Me_3SiCl, were necessary in order to effect complete replacement of halogen. The products $P(pz)_3$ and $P(Me_2pz)_3$ were purified by sublimation (1).

(b) $\phi P(Me_2pz)_2$

An ethereal solution of ϕPCl_2 (0.5 mmol) was added slowly to a stirred solution of 3,5-dimethylpyrazole (1 mmol) and triethylamine (1.05 mmol) in ether; a white precipitate formed immediately. After several hours the precipitate was filtered off and washed with ether. The solvent was removed under vacuum and the residue was purified by distillation at 140 °C/10^{-3} torr; mp 60–62 °C; yield 90%. *Anal.* calcd. for $C_{16}H_{19}N_4P$: C 64.4, H 6.42, N 18.7; found: C 64.5, H 6.52, N 18.5. Mass spectrum: M calcd. (*m/e*): 298; found: 298; nmr spectrum ($CDCl_3$) τ 2.55–2.73 (phenyl), 4.09 (s, 4-H), 7.64 (br s, 5-CH_3), 7.72, (br s, 3-CH_3); intensity ratio 5:2:6:6.

(c) $(pz)_3As$

A benzene solution of arsenic trichloride (1.96 mmol) was added dropwise to a stirred suspension of potassium pyrazolide (12 mmol) in benzene and the mixture was heated under reflux for 15 h. The precipitate was filtered and the solvent distilled off, leaving a white solid which was sublimed at 90 °C/10^{-3} torr; mp 144–146 °C. *Anal.* calcd. for $C_9H_9N_6As$: C 39.1, H 3.26, N 30.4; found: C 40.2, H 3.49, N 30.8. Mass spectrum: the parent ion M (calcd) (*m/e*) (276) appeared very weakly; major fragments were $(pz)_2As$ (208), pzAs (142); nmr ($CDCl_3$) τ 2.19, (br, not resolved, 3-H), 2.47 (br, not resolved, 5-H), 3.54 (t, 4H, $^3J_{H_3H_4} = {}^3J_{H_4H_5} = 2$ Hz).

The treatment of an ethereal solution of pyrazole and $(C_2H_5)_3N$ with $AsCl_3$ gave the adduct $(C_2H_5)_3NAsCl_3$ without promoting halogen substitution, and the room temperature reaction of an excess of K^+pz^- with $AsCl_3$ in ether gave partially substituted products, with no evidence for $(pz)_3As$.

Arsenic trichloride (3.7 mmol) and trimethylsilylpyrazole (~16 mmol) were heated in a sealed ampoule at 60 °C for 12 h. The products were separated by fractional distillation on a vacuum line. A mass spectral analysis of the appropriate fraction indicated the formation of $(pz)_2AsCl$ (*m/e* 244) and $(pz)AsCl_2$ (*m/e* 212).

(d) $(pz)_3PO$ and $(Me_2pz)_3PO$

A benzene solution of $POCl_3$ (4.7 mmol) was added dropwise to a stirred suspension of potassium pyrazolide (18.6 mmol) in benzene; the mixture was heated under reflux for 24 h, cooled, and filtered. The solvent was removed from the filtrate, yielding a white residue which was sublimed at 160 °C/10^{-3} torr; yield 91%; mp 76–78 °C. *Anal.* calcd. for $C_9H_9N_6OP$: C 43.5, H 3.60, N 33.8; found: C 43.5, H 3.64, N 34.2. Mass spectrum, M calcd.: (*m/e*) 248; found: 248; nmr ($CDCl_3$) τ 2.05 (m, 3H and 5H) 3.50 (m, 4H).

$(Me_2pz)_3PO$ was prepared in the same way. For purification it was sublimed at 160–165 °C/10^{-3} torr; yield 65%; mp 115–118 °C. *Anal.* calcd. for $C_{15}H_{21}N_6OP$: C 54.2, H 6.37, N 25.2; found: C 54.6, H 6.68, N 24.9. Mass spectrum (*m/e*), M calcd.: 332; found: 332; nmr spectrum ($CDCl_3$) τ 4.00 (d, 4-H, $^4J_{PH} = 4.0$ Hz), 7.73 (d, 5-Me, $^3J_{PH} = 0.5$ Hz), 7.82 (s, 3-Me).

(e) $(pz)_3PS$

An ethereal solution of thiophosphoryl chloride (8.35 mmol) was added to an ethereal suspension of a twofold excess of potassium pyrazolide, and the mixture stirred

Can. J. Chem. Downloaded from www.nrcresearchpress.com by 210.87.254.105 on 09/05/12
For personal use only.

for 1 day. The precipitate was filtered off and the solvent removed from the filtrate, leaving a white residue which was sublimed at 130 °C/10^{-3} torr; yield 75%; mp 149–151 °C. *Anal.* calcd. for $C_9H_9N_6PS$: C 40.9, H 3.43, N 31.8; found: C 40.0, H 3.33, N 31.5. Mass spectrum, M calcd. (*m/e*): 264; found: 264; nmr ($CDCl_3$) τ 1.98 (m, 3H and 5H), 3.49 (m, 4H).

Attempts to prepare $SP(pz)_3$ by the reaction of thiophosphorylchloride with trimethylsilylpyrazole gave an oil consisting mainly of bis(pyrazolyl)thiophosphoryl chloride, according to mass spectral analysis; further treatments of this product with $Me_3Si(pz)$ in sealed tubes at 100 °C failed to effect substitution of the halogen moiety.

(f) $\phi_2P(S)(Me_2pz)$

A toluene solution of $\phi_2P(Me_2pz)$ (0.5 mmol) was heated for several hours under reflux with an equivalent amount of sulphur, until conversion to $\phi_2P(S)(Me_2pz)$ was complete, as monitored by ^1H nmr spectroscopy. The solvent was removed and the product, $\phi_2P(S)(Me_2pz)$ was sublimed at 80 °C/10^{-3} torr; yield 95%. *Anal.* calcd. for $C_{17}H_{17}N_2PS$: C 65.3, H 5.49, N 8.97; found: C 65.9, H 5.20, N 8.74 Mass spectrum, calcd (*m/e*): 312; found: 312; nmr ($CDCl_3$) τ 2.0–2.7 (complex m's, phenyl), 4.02 (m, 4-H), 7.63 (br s, 5-CH_3), 7.85 (s, 3-CH_3).

(g) Et_2Ppz

An ethereal solution of Et_2PCl (8.67 mmol) was added dropwise to a stirred solution of pyrazole (8.67 mmol) and triethylamine (~9 mmol) in ether, giving an immediate white precipitate After 6 h, the mixture was filtered and the solvent was removed under vacuum from the filtrate, leaving an oil which was distilled at 35 °C/10^{-3} torr; yield 99%. *Anal.* calcd. for $C_7H_{13}N_2P$: C 53.8, H 8.38, N 18.6; found: C 53.8, H 8.39, N 17.9. Mass spectrum, M calcd. (*m/e*): 156; found: 156; nmr ($CDCl_3$) τ 2.37 (m, 3H and 5H), 3.80 (m, 4H), 7.6–8.7 (m, methylene), 8.8–9.4 (m, methyl).

Reactions of Pyrazolylphosphines

(a) With Water

Distilled water (1.20 mmol) was added to an ethereal solution of ϕ_2Ppz, $\phi_2P(Me_2pz)$, and $\phi_2P(imid)$ (1) (0.60 mmol); after three days, the volatile products were removed under vacuum, leaving a residue giving the nmr and mass spectral characteristics of the azole and of diphenylphosphinous acid, $\phi_2P(O)H$ (28) (imid = imidazolyl).

(b) With Methanol

A mixture of ϕ_2Ppz and methanol in a 1:2 molar ratio in ether underwent only partial hydrolysis over a period of 3 days. A mixture of ϕ_2Ppz (3.6 mmol) and excess methanol (~80 mmol) gave, after 3 days, a mixture of pyrazole and ϕ_2POCH_3. M calcd.: 216; found: 216; nmr τ 2.65–2.85 (phenyl), 6.45 (d, CH_3O, $^3J_{PH}$ = 14 Hz).

(c) With Anhydrous HCl

$\phi_2P(pz)$ (1.40 mmol) in benzene-d_6 was allowed to react with an equivalent amount of anhydrous HCl, giving a white precipitate which was identified by nmr (in D_2O) as pyrazole hydrochloride. The nmr spectrum of the benzene-d_6 solution showed resonances due to phenyl and pyrazolyl moieties; the solvent was removed, leaving a residue consisting of ϕ_2PCl and unreacted $\phi_2P(pz)$, according to mass spectral measurements.

(d) With $Na^+OCH_3^-$

$\phi_2P(pz)$ (3.52 mmol) in ether was stirred with sodium methoxide (3.80 mmol) over a period of 3 days. The precipitate was filtered off, dried, and dissolved in D_2O; the ^1H nmr spectrum indicated the pyrazolyl moiety. The ethereal filtrate was evaporated leaving an oil which was distilled *in vacuo* and characterized as ϕ_2POCH_3 by ir. mass, and nmr spectroscopy; there was no evidence of unreacted $\phi_2P(pz)$.

(e) With Phenyllithium

An ethereal solution of $\phi_2P(pz)$ (1.32 mmol) was treated with a benzene–ether solution of phenyllithium (1.70 mmol). After 2 days, the mixture was hydrolyzed and the ethereal phase isolated, dried over sodium sulphate, and evaporated *in vacuo*. The residue was recrystallized from ethanol and characterized as ϕ_3P (yield 72%) by mixed melting point and ir spectral measurements.

The reaction of $\phi_2P(O)(pz)$ with phenyllithium was studied in the manner described above, resulting in the formation of ϕ_3PO, as evidenced by mixed melting point, ir, and nmr measurements.

(f) With Methyl Iodide

An ethereal solution of $\phi_2P(pz)$ (1.53 mmol) was treated with a 25-fold excess of CH_3I, yielding a yellow precipitate over a period of 5 days. The precipitate was filtered off, washed with ether, and characterized as the adduct $\phi_2P^+(pz)CH_3I^-$; yield 28%; mp 140–155 °C (dec.). *Anal.* calcd. for $C_{16}H_{16}N_2PI$: C 48.8, H 4.09, N 7.10; found: C 48.6, H 4.06, N 7.57. The nmr spectrum consisted of a multiplet (τ 1.72–2.50, 3H, 5H, phenyl envelope), a second multiplet (τ 3.24, 4H) and a doublet (τ 6.39, $^2J_{PH}$ = 13.5 Hz, CH_3 group), with relative intensities consistent for a 1:1 adduct.

Various attempts, including sealed tube reactions at 80 °C failed to induce adduct formation between $\phi P(pz)_2$ or $P(pz)_3$ and methyl iodide.

(g) With CS_2

Samples (~0.5 mmol) of $\phi_2P(pz)$ and $P(pz)_3$ in benzene solution were heated under reflux for several hours with an excess of carbon disulphide. After removing the volatile components the starting materials were recovered unchanged, as evidenced by mass and nmr spectral analysis.

(h) With BCl_3

Solutions of $\phi_2P(pz)$ (~0.5 mmol) and an equivalent amount of BCl_3 in $CDCl_3$ were mixed in an nmr tube and the reaction was followed spectroscopically. Within 1 h new resonances attributable to new pyrazolyl products were observed, at lower fields than the resonances due to the 3-H, 4-H and 5-H protons of $\phi_2P(pz)$ itself. A mass spectrometric analysis was performed. Species assigned as $(pzBCl_2)_2$ (294) and ϕ_2PCl (220) were observed. There was no evidence for unreacted $\phi_2P(pz)$.

The reaction of $P(pz)_3$ with BCl_3 was studied in the manner described above. New nmr multiplets in the region for the 4-H proton were observed. The mass spectrum showed species assigned as $[(pz)_3B]_2$ (422), $(pzBCl_2)_2$ (294), $(pz)_2PCl$ (200), and $pzPCl_2$ (168). There was no evidence for unreacted $P(pz)_3$.

(i) With BF_3

A solution of ϕ_2Ppz (1.44 mmol) in hexane–ether (2:1)

Can. J. Chem. Downloaded from www.nrcresearchpress.com by 210.87.254.105 on 09/05/12
For personal use only.

was treated with BF_3 (1.44 mmol) and allowed to stand at room temperature. The volatile components were removed under vacuum, leaving a white precipitate identified as $\phi_2P(pz)\cdot BF_3$; yield quantitative; mp 88–90 °C. *Anal.* calcd. for $C_{15}N_{13}N_2BF_3$: C 62.3, H 4.53, N 9.69; found: C 62.2, H 4.66, N 8.20. The ^{19}F spectrum, in $CDCl_3$, consisted of a doublet ($^2J_{PF}$ = 44 Hz). The ^{31}P spectrum, in $CDCl_3$, was a 1:2:2:1 quartet ($^2J_{PF}$ = 45 Hz), which collapsed to a broad singlet upon irradiating at the ^{19}F frequency. The product described above was also obtained from preparations using 2 mol of BF_3 per mole of ϕ_2Ppz.

The compound $\phi P(pz)_2\cdot BF_3$ (mp 94–96 °C) was prepared in the manner described above, using 1 mol of BF_3 per mol of $\phi P(pz)_2$. The ^{19}F spectrum consists of a doublet ($J \sim 53$ Hz). Upon standing in solution resonances due to new fluorine containing products appeared.

The reaction of $P(pz)_3$ with BF_3 was studied in the way described above; $P(pz)_3\cdot BF_3$ in $CDCl_3$ gave a ^{19}F spectrum consisting of a doublet ($J \sim 60$ Hz).

The ^{19}F chemical shifts, downfield from $CFCl_3$ were: ϕ_2PpzBF_3 (272.6), $\phi P(pz)_2BF_3$ (273.4), $P(pz)_3BF_3$ (152.0).

Acknowledgement

The financial support of this research work by the National Research Council of Canada is gratefully acknowledged.

1. S. Fischer, L. K. Peterson, and J. F. Nixon. Can. J. Chem. **52**, 3981 (1974).
2. J. Hoyano and L. K. Peterson. Can. J. Chem. This issue.
3. E. W. Abel and D. A. Armitage. J. Organomet. Chem. **5**, 326 (1966).
4. S. Fischer, J. Hoyano, I. Johnson, and L. K. Peterson. Can. J. Chem. This issue.
5. R. Fessenden and D. F. Crowe. J. Org. Chem. **25**, 598 (1960).
6. (*a*) K. Schofield. *In* Hetero-aromatic nitrogen compounds. Plenum Press, New York. 1967; (*b*) T. L. Jacobs. Pyrazoles and related compounds. *In* Heterocyclic compounds. Vol. 5. *Edited by* R. C. Elderfield. J. Wiley and Sons, New York. 1957; (*c*) R. Fusco. Pyrazoles, pyrazolines, pyrazolidines, indazoles and condensed rings. *In* The chemistry of heterocyclic compounds. *Edited by* A. Weissberger. Interscience, New York. 1967; (*d*) A. R. Katritzky and J. M. Lagowski. The principles of heterocyclic chemistry. Methuen and Co., London. 1967.
7. (*a*) E. Fluck. *In* Topics in phosphorus chemistry. Vol. 4. *Edited by* M. Grayson and E. J. Griffith. Interscience Publishers, New York. 1966; (*b*) G. M. Kosolapoff and L. Maier. *In* Organic phosphorus compounds. Vol. 4. *Edited by* G. M. Kosolapoff and L. Maier. Interscience Publishers. 1972.
8. H.-J. Vetter and H. Noth. Chem. Ber. **96**, 1308 (1963).
9. (*a*) R. Burgada, G. Martin, and G. Mavel. Bull. Soc. Chim. Fr. 2154 (1963); (*b*) G. Mavel. *In* Progress in NMR spectroscopy. Vol 1. *Edited by* J. W. Emsley, J. Feeney, and L. H. Sutcliffe. Pergamon, Oxford. 1966.
10. G. Ewart, D. S. Payne, A. L. Porte, and A. P. Lane. J. Chem. Soc. 3984 (1962).
11. A. B. Burg and J. Heners. J. Am. Chem. Soc. **87**, 3092 (1965).
12. H. A. Bent. J. Inorg. Nucl. Chem. **19**, 43 (1961).
13. H. A. Bent. Can. J. Chem. **38**, 1235 (1960).
14. C. W. Heitsch. Inorg. Chem. **4**, 1019 (1965).
15. J. G. Verkade, R. W. King, and C. W. Heitsch. Inorg. Chem. **3**, 884 (1964).
16. T. D. Coyle and F. G. A. Stone. J. Am. Chem. Soc. **83**, 4138 (1961).
17. T. Reetz and B. Katlafsky. J. Am. Chem. Soc. **82**, 5036 (1960).
18. H. Noth and H.-J. Vetter. Chem. Ber. **96**, 1298 (1963).
19. A. B. Burg and P. J. Slota. J. Am. Chem. Soc. **80**, 1107 (1958).
20. R. R. Holmes and R. P. Carter. Inorg. Chem. **2**, 1146 (1963).
21. R. R. Holmes and R. P. Wagner. J. Am. Chem. Soc. **84**, 357 (1962).
22. J. G. Verkade and K. J. Coskran. *In* Organic phosphorus compounds. Vol. 2. *Edited by* G. M. Kosolapoff and L. Maier. Interscience Publishers, New York. 1972.
23. R. B. King. Inorg. Chem. **2**, 936 (1963).
24. V. N. Torochesnikov, N. M. Sergeyev, N. A. Viktorov, G. S. Goldin, V. G. Poddubny, and A. N. Kultsova. J. Organomet. Chem. **70**, 347 (1974).
25. F. A. Cotton and D. J. Ciappenelli. Synth. Inorg. Metal-Org. Chem. **2**, 197 (1972).
26. G. R. Clemo and G. R. Ramage. J. Chem. Soc. 49 (1931).
27. D. H. O'Brien and C.-P. Hrung. J. Organomet. Chem. **27**, 185 (1971).
28. K. Moedritzer, L. Maier, and L. C. D. Groenweghe. J. Chem. Eng. Data, **7**, 307 (1962).

Crystallographic studies on neuroleptics of the benzocycloheptapyridoisoquinoline series. The crystal structure of butaclamol hydrobromide and the absolute configuration and crystal structure of dexclamol hydrobromide

P. H. BIRD

Chemistry Department, Sir George Williams Campus, Concordia University, Montreal, Que., Canada H3G 1M8

AND

F. T. BRUDERLEIN AND L. G. HUMBER

Chemistry Department, Ayerst Research Laboratories, Montreal, Que., Canada H4R 1J6

Received December 15, 1975

P. H. BIRD, F. T. BRUDERLEIN, and L. G. HUMBER. Can. J. Chem. **54**, 2715 (1976).

The compound butaclamol hydrobromide crystallizes in space group $P2_1/c$ with cell dimensions; a = 14.38(3), b = 13.31(3), c = 12.07(3) Å, β = 101.64(8)°. The structure was solved by Patterson methods and non-hydrogen atoms have been refined isotropically using a full-matrix least-squares to an R value of 0.17 for 779 observed reflections.

The compound dexclamol hydrobromide crystallizes in space group $P2_12_12_1$ with a = 8.412(2), b = 24.392(7), c = 10.465(2) Å. Refinement of non-hydrogen atoms using isotropic thermal parameters and rigid aromatic rings converted at R = 0.090 using 1249 observed reflections, for the preferred enantiomorph, and R = 0.099 for the other enantiomorph.

Both compounds have their hydroxy groups in the axial position, and both adopt conformations of the seven membered ring such that the C13*b* hydrogen atom experiences a flagpole-bowsprit interaction with a hydrogen atom of C9.

P. H. BIRD, F. T. BRUDERLEIN et L. G. HUMBER. Can. J. Chem. **54**, 2715 (1976).

Le bromhydrate de butaclamol cristallise dans le groupe d'espace $P2_1/c$ avec des dimensions de maille a = 14.38(3), b = 13.31(3), c = 12.07(3) Å, β = 101.64(8)°. On a résolu la structure par les méthodes de Patterson et on a affiné les atomes autres que les atomes d'hydrogène d'une façon isotrope utilisant la méthode des moindres carrés (matrice complète) jusqu'à une valeur de R de 0.17 pour 779 réflexions qui avaient été observées.

Le bromhydrate de dexclamol cristallise dans le groupe d'espace $P2_12_12_1$ avec a = 8.412(2), b = 24.392(7), c = 10.465(2) Å. L'affinement des atomes autres qu'hydrogène utilisant des paramètres thermiques isotropes et des cycles aromatiques rigides convergent à une valeur de R = 0.090 utilisant 1249 réflexions observées pour l'énantiomorphe préféré et une valeur de R = 0.099 pour l'autre énantiomorphe.

Dans chacun des composés, les groupes hydroxyles sont en position axiale et dans chaque cas ils adoptent une conformation du cycle à sept membres telle que l'atome d'hydrogène en C13*b* et l'atome d'hydrogène en position C9, subissent des interactions mât-beaupré.

[Traduit par le journal]

Introduction

Recent studies have demonstrated that various compounds containing the novel benzo[6,7]cyclohepta[1,2,3-*de*]pyrido[2,1-*a*]-isoquinoline system possess useful psychopharmacological properties (1–4). In particular, the *tert*-butyl carbinol (±)-**1**.HCl, butaclamol hydrochloride, [1,2] is an antipsychotic agent whose efficacy in man has been demonstrated (5). The relative configurations at positions 3,4*a* and 13*b* have been assigned

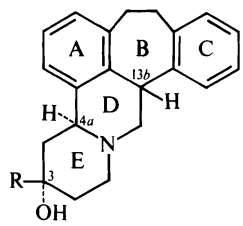

(±)-**1**, R = *tert*-butyl (butaclamol)
(+)-**2**, R = 2-propyl (dexclamol)

[1]Nonproprietary name selected by the U.S. Adopted Names Council.

[2]This compound is also known by the Ayerst code number AY-23,028.

Can. J. Chem. Downloaded from www.nrcresearchpress.com by 210.87.254.105 on 09/05/12
For personal use only.

Can. J. Chem. Downloaded from www.nrcresearchpress.com by 210.87.254.105 on 09/05/12
For personal use only.

on the basis of nmr spectroscopy and by mechanistic considerations (2, 3). The first aim of the present investigation was to verify these previous stereochemical assignments and to determine the conformations of rings B and E. We thus describe the crystal structure of (±)-**1**.HBr (mp 307–309 °C).

After the crystal structure of (±)-**1**.HBr had been completed, the resolution of butaclamol was achieved (6), and it was found that the pharmacological activity of the racemate was due solely to the *dextro*-enantiomer (6–9). Resolution of the related 2-propyl carbinol, (±)-**2**, also revealed that neuroleptic activity resided only in the *dextro*-enantiomer, (+)-**2**, dexclamol,[1,3] a drug with potential utility as a neuroleptanalgesic agent (10). The second aim of this investigation was to determine the absolute configurations at the chiral centers of (+)-**2**, and to redetermine the conformations of rings B and E. Thus, the crystal structure of (+)-**2**.HBr (mp 265–267 °C) has been determined.

Neuroleptic agents such as dexclamol, (+)-**2**, exert their effects through a series of events initiated by a blockage of the biological receptor in the brain with which the neurotransmitter dopamine (3,4-dihydroxyphenethylamine) interacts (11). The capacity of (+)-**1** and (+)-**2** to block the central dopamine receptor has been demonstrated by *in vivo* and/or *in vitro* studies (6–9) while the corresponding *laevo*-enantiomers are entirely devoid of such properties. (+)-**1** and (+)-**2** are thus the first dopamine receptor antagonist which display absolute optical specificity with respect to the dopamine receptor. 6*aR*(−)-Apomorphine, in contrast, is a potent dopamine receptor agonist (11) whose absolute configuration (12) and molecular geometry (13) are known and which similarly displays absolute optical specificity towards the dopamine receptor, since its *dextro*-enantiomer is completely devoid of such actions (14).

(+)-**2** and (−)-apomorphine thus constitute a unique pair of dopamine receptor ligands in that they exhibit opposite biological activities, and are semi-rigid, chiral molecules of known absolute configuration and molecular geometry. (−)-Apomorphine's dopaminergic activity has been conclusively demonstrated to be due to the presence of its 3,4-dihydroxyphenethylamine moiety (11), while the antidopaminergic activity of (+)-**2** has been ascribed to the presence of an extended phenethylamine moiety in this molecule (6) (see Fig. 3). These dopamine receptor ligands, by virtue of their possession of this common structural feature, can serve as independent probes of the topography of the dopamine receptor. A third aim of the present study is to identify and define relevant parameters of the molecular structures of (+)-**2** and of (−)-apomorphine which will permit a quantitative comparison of the topographies of the extended phenethylamine moieties of these ligands.

Experimental

*Crystallographic Study of Butaclamol Hydrobromide, (±)-**1**.HBr;(±)-(4a,13b-trans)-(3-hydroxy-13b(H)-trans)-3-tert-butyl-2,3,4,4a,8,9,13b,14-octahydro-1H-benzo[6,7]cyclohepta[1,2,3-de]pyrido[2,1-a]isoquinolin-3-ol Hydrobromide*

The crystal data are as follows:

$C_{25}H_{31}NO.HBr$ fw = 442.4

Monoclinic, a = 14.38(3), b = 13.31(3), c = 12.07(2) Å, β = 101.64(8)°, V = 2262.7 Å^3, Z = 4, ρ_c = 1.299, ρ_o = 1.30(2) g cm^{-3}, $F(000)$ = 928 (20 °C, MoKα, λ = 0.71069 Å, μ = 19.4 cm^{-1}). Absent reflections: $0k0$, $k \neq 2n$ and $h0l$, $l \neq 2n$ uniquely define $P2_1/c$ (C_{2h}^5, No. 14).

Crystal dimensions: (100) to ($\bar{1}$00) 0.002 mm, (010) to (0$\bar{1}$0) 0.05 mm, and (001) to (00$\bar{1}$) 0.20 mm; diffractometer ϕ axis parallel to c^*; estimated transmission factors 0.90 to 0.99. No absorption correction was applied.

The structure was solved by conventional Patterson and Fourier methods using diffractometer data. The structure was refined isotropically using 779 'observed' reflections to R = 0.17 and R_w = 0.13. No further attempt was made to improve the model, the objective of the study having been realized. A final difference synthesis showed no significant residual electron density.

The final atomic parameters are given in Table 1. Measured and calculated structure factors have been placed in the Depository of Unpublished Data.[4]

*Crystallographic Study of Dexclamol Hydrobromide, (+)-**2**.HBr;(+)-(4a,13b-trans)-(3-hydroxy-13b(H)-trans-3-(2-propyl)-2,3,4,4a,8,9,13b,14-octahydro-1H-benzo[6,7]cyclohepta[1,2,3-de]isoquinoline-3-ol Hydrobromide*

The crystal data are as follows:

$C_{24}H_{29}NO.HBr$ fw = 428.4

Orthorhombic, a = 8.412(2), b = 24.392(7), c = 10.462(2) Å, V = 2147.3 Å^3, Z = 4, ρ_c = 1.323, ρ_o = 1.34(2) g cm^{-3}, $F(000)$ = 896 (20 °C, MoKα, λ = 0.71069 A, μ = 20.4 cm^{-1}). Absent reflections: $h00$, $h \neq 2n$, 0k0,

[3]This compound is also known by the Ayerst code number AY-24,169.

[4]The structure factor table is available at a nominal charge, from the Depository of Unpublished Data, CISTI, National Research Council of Canada, Ottawa, Canada K1A 0S2.

Can. J. Chem. Downloaded from www.nrcresearchpress.com by 210.87.254.105 on 09/05/12
For personal use only.

TABLE 1. Final atomic coordinates and isotropic thermal parameters for (±)-**1**.HBr (with estimated standard deviations in parentheses)*

Atom	*x/a*	*y/b*	*z/c*	*B*
Br	111.0(5)	107.4(5)	−223.3(5)	3.1(2)
O	−143(3)	414(3)	−125(3)	3.7(9)
N	073(3)	306(3)	−083(3)	1.8(9)
C1	000(4)	288(4)	−010(4)	1.6(9)
C2	−087(4)	255(4)	−078(4)	2.3(9)
C3	−130(4)	317(4)	−181(4)	1.5(9)
C4	−051(4)	341(4)	−251(4)	1.1(9)
C4*a*	032(4)	382(5)	−176(4)	2.5(10)
C4*b*	123(5)	395(5)	−240(5)	2.4(9)
C5	090(5)	449(5)	−348(5)	2.2(9)
C6	165(5)	456(5)	−410(5)	2.2(9)
C7	249(5)	421(5)	−380(5)	2.9(9)
C7*a*	287(5)	370(5)	−272(5)	3.5(9)
C8	396(7)	330(5)	−249(6)	5.6(12)
C9	405(4)	252(5)	−148(4)	4.2(10)
C9*a*	417(5)	325(5)	−036(5)	4.1(9)
C10	512(5)	348(5)	−018(5)	4.1(10)
C11	518(4)	412(5)	−122(4)	4.2(14)
C12	437(5)	447(5)	144(5)	5.1(14)
C13	337(5)	424(5)	087(5)	5.1(13)
C13*a*	341(5)	353(5)	−014(5)	5.1(14)
C13*b*	234(4)	321(4)	−083(3)	1.3(9)
C13*c*	206(5)	360(4)	−205(4)	3.7(10)
C14	163(4)	336(4)	−013(3)	1.3(9)
C1′	−226(4)	278(4)	−259(4)	1.8(11)
C2′	−205(5)	177(5)	−311(4)	3.9(13)
C3′	−271(4)	358(4)	−352(4)	4.3(13)
C4′	−301(5)	267(5)	−181(5)	5.0(15)

*Fractional coordinates have been multiplied by 10^3.

$k \neq 2n$; $00l$, $l \neq 2n$ uniquely define $P2_12_12_1$ (D_2^4, No. 19).

The sample crystal, mounted with a^* parallel to the rotation axis had dimensions: (100) to ($\bar{1}00$), 0.25; (010) to ($0\bar{1}0$), 0.12; and (001) to ($00\bar{1}$), 0.12 mm. Preliminary photographs were used to establish the space group and approximate unit cell data. The diffraction spots showed minimal mosaic spread and unexpectedly low intensities.

The crystal was transferred to a Picker Nuclear FACS-1 diffractometer equipped with a molybdenum target tube, graphite monochromator, scintillation counter, and a pulse height analyzer adjusted to accept 100% of the MoK_α peak. The Picker Disc Operating System was used to control alignment and data collection operations. Twelve reflections, widely separated in reciprocal space, were automatically centered at both positive and negative 2θ values. Their setting angles were used to obtain the cell parameters and the orientation matrix by least-squares refinement. The θ-2θ scan technique was employed for data collection with a 1 deg min^{-1} scan speed, a base scan width of 2° in 2θ, and 20 s background measurements at the initial and final scan positions. A check reflection, remeasured every 30 cycles, varied randomly in intensity over about 5%. Intensity data were collected in two octants; limited to positive or zero h, k, and l, and $4° < 2\theta < 45°$, and the other limited to negative h, k, and l with $4° < 2\theta < 30°$. Net intensities were computed as: $I = S - B(t_S/t_B)$, where S is the scan count accumulated in time t_S, and B is the total background count measured over a time t_B: $\sigma(I) = [S + B(t_S/t_B)^2 + (0.02S)^2]^{1/2}$. Of a total of 2146 reflections collected, 1249 with $I > 3\sigma(I)$ were retained after data processing: the two octants were, of course, not merged. The data were corrected for absorption:[5] transmission factors ranged between 0.74 and 0.87.

The positions of the bromide ion were determined from a three-dimensional Patterson synthesis, and the remaining non-hydrogen atoms were located from the subsequent structure factor calculation and Fourier synthesis.[6] The positional and isotropic parameters were refined using a full-matrix least-squares with the following constraints: no hydrogen atoms were included in the model; non-hydrogen atoms were refined with individual isotropic thermal parameters; and the two aromatic rings were refined as rigid groups, with a C—C bond length of 1.39 Å. The anomalous dispersion correction for bromine (ref. 16, p. 216) was applied to the scattering factors during refinement. At convergence after 5 cycles, the residuals for the first enantiomorph (chosen arbitrarily at

[5]Using a modified version of GNABS, a general absorption correction program by Burnam (15).

[6]Fourier and Patterson calculations were performed using FORDAP by Zalkin. Structure factor calculations and least-squares refinements were obtained using NUCLS in its rigid body version of Ibers. Scattering factors were taken from the compilation of Ibers (ref. 16, p. 202).

Can. J. Chem. Downloaded from www.nrcresearchpress.com by 210.87.254.105 on 09/05/12
For personal use only.

TABLE 2. Final atomic positions and isotropic thermal parameters for (+)-**2**.HBr (with estimated standard deviations in parentheses)*

Atom	*x/c*	*y/b*	*z/c*	*B*
Br	−0032(5)*	−0045(1)	0821(3)	4.84(8)
O	−1963(21)	−4271(7)	0003(20)	3.7(5)
N	1407(19)	−5141(7)	0193(16)	1.9(4)
C1	1049(26)	−4596(9)	0988(24)	2.8(6)
C2	0865(27)	−4093(10)	0088(25)	2.4(6)
C3	−0602(26)	−4212(9)	−0781(26)	2.7(6)
C4	−0391(25)	−4737(8)	−1586(19)	1.4(6)
C4*a*	0023(36)	−5281(6)	−0657(20)	1.9(5)
C4*b*	0381(20)	−5783(5)	−1427(15)	2.7(6)†
C5	−0364(17)	−5851(6)	−2602(17)	3.3(6)†
C6	0078(21)	−6282(7)	−3396(11)	2.8(5)†
C7	1265(22)	−6643(6)	−3016(16)	3.7(7)†
C7*a*	2010(15)	−6574(6)	−1841(18)	3.1(6)†
C8	3368(34)	−7005(11)	−1616(28)	4.9(8)
C9	4452(28)	−6960(9)	−0417(23)	4.4(8)
C9*a*	3345(18)	−7028(9)	0808(13)	3.9(6)†
C10	3377(18)	−7504(7)	1539(20)	4.2(7)†
C11	2431(23)	−7546(6)	2623(18)	5.4(7)†
C12	1453(19)	−7113(9)	2978(13)	3.8(7)†
C13	1421(18)	−6637(6)	2248(19)	3.1(7)†
C13*a*	2367(22)	−6595(6)	1163(16)	2.8(7)†
C13*b*	2383(34)	−6055(12)	0337(27)	2.8(8)
C13*c*	1568(18)	−6143(7)	−1047(12)	2.0(5)†
C14	1664(28)	−5602(10)	1110(25)	1.6(6)
C1′	−0747(29)	−3704(10)	−1801(25)	4.0(7)
C2′	−2134(35)	−3860(12)	−2738(27)	4.6(8)
C3′	−1138(32)	−3189(11)	−1038(28)	5.4(8)

*Fractional coordinates have been multiplied by 10^4.
†These atoms are part of aromatic rings refined as rigid planar regular hexagonal groups with C—C = 1.39 Å.

the Patterson solution stage) were $R = 0.090$ and $R_w = 0.111$ ($R = \sum(||F_o| - |F_c||)/\sum|F_o|$; $R_w = [\sum w(|F_o| - |F_c|)^2/\sum w|F_o|^2]^{1/2}$, where $w = [\sigma(F_o)])^{-2}$ and $\sigma(F_o) = \sigma(I)/2Lp|F_o|$). The signs of all coordinates were reversed to generate the other enantiomorph, and the refinement was repeated (2 cycles), yielding $R = 0.099$ and $R_w = 0.116$. A final difference Fourier showed no significant residual electron density.

The final atomic parameters for the first enantiomorph are given in Table 2. Measured and calculated structure factors have been placed in the Depository of Unpublished Data.[4]

Results and Discussion

The crystal packing of butaclamol hydrobromide is shown in Fig. 1, intermolecular contacts were found to be normal within the (rather large) estimated standard deviations.

The molecular structure of butaclamol hydrobromide (±)-**1**.HBr (Fig. 2) confirms the previously assigned relative configurations at position 3, 4*a*, and 13*b* (2, 3), and reveals that in the solid state that (*a*) ring E (Fig. 3) assumes a

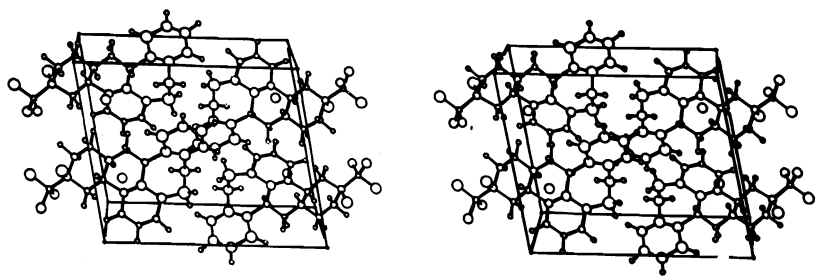

FIG. 1. Molecular packing of butaclamol hydrobromide, (±)-**1**.HBr (hydrogen atoms are shown in calculated positions).

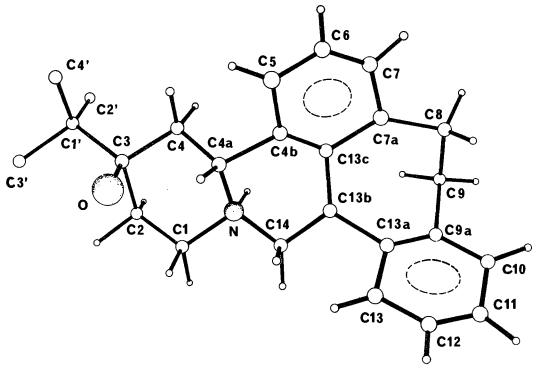

FIG. 2. The cation of butaclamol hydrobromide, (±)-**1**.HBr.

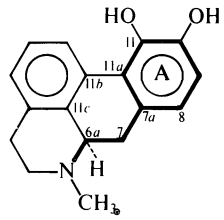

(−)-Apomorphine

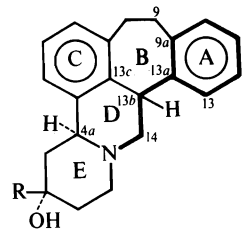

(+)-**1**, R = *tert*-butyl
(+)-**2**, R = 2-propyl

FIG. 3. Extended phenethylamine groupings in (−)-apomorphine, (+)-**1** and (+)-**2**.

conformation in which the *tert*-butyl group is attached equatorially, and (*b*) ring B adopts a conformation in which one of the C9-hydrogens experiences a flagpole-bowsprit type interaction with the lone hydrogen at C13*b*.

The crystal packing of dexclamol hydrobromide is shown in Fig. 4 while bond distances and angles are collected in Table 3. Again, no abnormal intermolecular contacts were observed. The difference in *R* factors obtained after refinement of the enantiomers is significant by

TABLE 3. Distances and angles with estimated standard deviations for (+)-**2**.HBr

Bond*	Length (Å)	Bonds	Angles (deg)
C1—C2	1.58(3)	N—C1—C2	110(2)
C2—C3	1.54(3)	C1—C2—C3	106(2)
C3—O	1.44(3)	C2—C3—C4	113(2)
C3—C1′	1.63(3)	C2—C3—O	107(2)
C3—C4	1.53(3)	C2—C3—C1′	105(2)
C4—C4*a*	1.68(3)	C4—C3—O	111(2)
C4*a*—C4*b*	1.49(3)	C4—C3—C1′	107(2)
C4*a*—N	1.51(3)	O—C3—C1′	111(2)
C7—C8	1.57(3)	C3—C4—C4*a*	111(2)
C8—C9	1.59(3)	C4—C4*a*—N	108(2)
C9—C9*a*	1.59(3)	C4—C4*a*—C4*b*	112(2)
C13*a*—C13*b*	1.57(3)	C4*b*—C4*a*—N	109(2)
C13*b*—C13c	1.63(4)	C4*a*—C4*b*—C13*c*	121(2)
C13*b*—C14	1.50(4)	C13*c*—C7*a*—C8	129(2)
C14—N	1.51(3)	C3—C1′—C2′	107(2)
N—C1	1.60(3)	C3—C1′—C3′	106(2)
C1′—C2′	1.51(4)	C13*c*—C7*a*—C7	111(2)
C1′—C3′	1.58(4)	C7*a*—C8—C9	118(2)
		C8—C9—C9*a*	107(2)
		C9—C9*a*—C10	120(2)
		C9—C9*a*—C13*a*	120(2)
		C13—C13*a*—C13*b*	122(2)
		C9*a*—C13*a*—C13*b*	118(2)
		C13*a*—C13*b*—C13*c*	112(2)
		C13*a*—C13*b*—C14	108(2)
		C13*c*—C13*b*—C14	114(2)
		C13*b*—C14—N	105(2)
		C14—N—C1	108(2)
		C14—N—C4*a*	109(2)
		C1—N—C4*a*	110(2)
		C2′—C1′—C3′	111(2)

*All C—C distances in benzene rings are 1.39 Å.

Can. J. Chem. Downloaded from www.nrcresearchpress.com by 210.87.254.105 on 09/05/12
For personal use only.

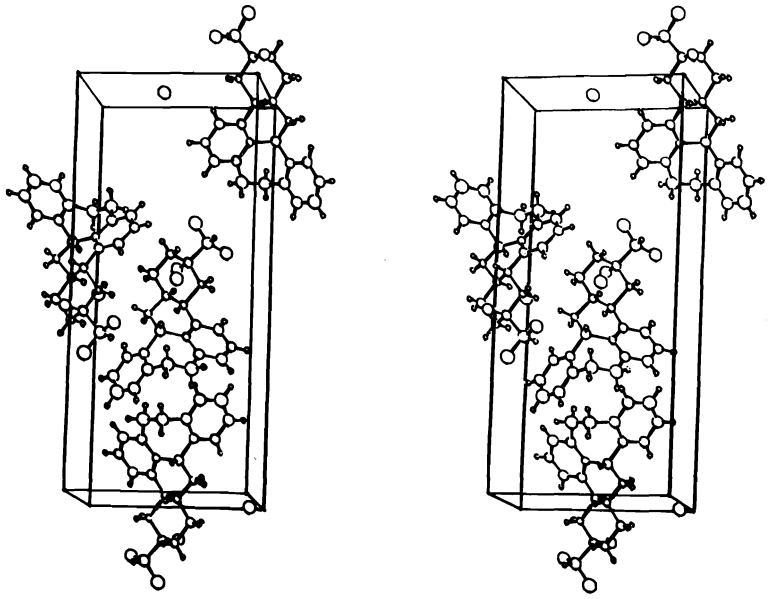

FIG. 4. Molecular packing of dexclamol hydrobromide, (+)-**2**.HBr (hydrogen atoms are shown in calculated positions).

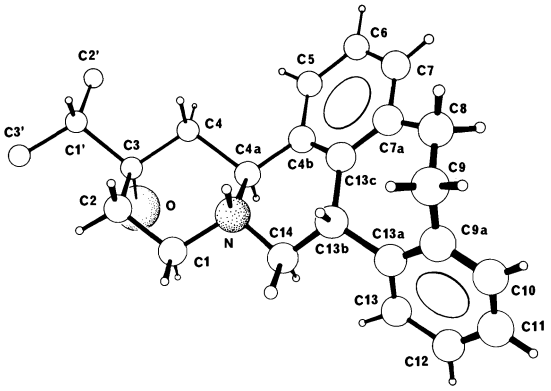

FIG. 5. The cation of dexclamol hydrobromide, (+)-**2**.HBr (hydrogen atoms are shown in calculated positions).

Hamilton's test (17) at better than the 0.005 level, thus the absolute configuration of dexclamol, (+)-**2**, is virtually certainly that pictured in Fig. 5, that is 3*S*, 4*aS*, 13*bS*.

The biologically active enantiomer of butaclamol, (+)-**1**, is also assigned 3*S*, 4*aS*, and 13*bS* absolute configurations on the basis of a comparison of molecular rotations of (+)-**1** and (+)-**2** (see Table 4).

The crystal structure of dexclamol hydrobromide, (+)-**2**.HBr, Fig. 5, reveals that the ring E and ring B conformations are the same as those observed with butaclamol hydrobromide, (+)-**1**.HBr.

TABLE 4. Molecular rotations, [M], of (+)-**1** and (+)-**2**

Wavelength (nm)	[M]		$[\alpha]_D^{25}$	
	(+)-**1**	(+)-**2**	(+)-**1**	(+)-**2**
365	3146	3190	790.4	831.5
435	1859	1847	467.2	481.2
547	1030	1022	258.9	266.3
580	897	892	225.3	232.3
590	856	850	215.1	221.3

For purposes of comparing the topographies of the extended phenethylamine moieties of dexclamol and apomorphine, the four parameters described below are considered to be of relevance. The position of the nitrogen atom with respect to the phenyl ring A as defined by the two angles X_1 and X_2 is shown in Fig. 6. These angles as well as the conventional torsion angles, are, collected in Table 5. The out-of-plane displacements of the nitrogen atom are also collected in Table 5: a positive displacement implies that the nitrogen atom is above the plane of phenyl ring A, with the molecules oriented as in Fig. 3. The distance of the nitrogen atom from the center of ring A has been calculated and these values are collected in Table 5.

Can. J. Chem. Downloaded from www.nrcresearchpress.com by 210.87.254.105 on 09/05/12
For personal use only.

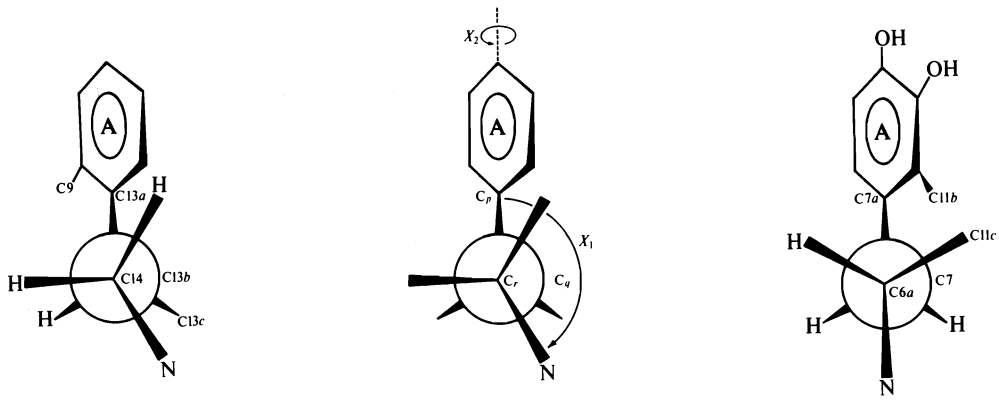

Dexclamol, (+)-2 (−)-Apomorphine

FIG. 6. Definition of the angles used to describe the phenethylamine moiety in dexclamol and (−)-apomorphine.

TABLE 5. Parameters associated with the conformation of the phenethylamine moiety in (+)-dexclamol [(+)-**2**], and (−)-apomorphine

Parameter	(+)-**2**, Conformer A C9–H, C13–H eclipsed	(+)-**2**, Conformer B C8–H, C13–H eclipsed*
X_1‡	169°	155°
Torsion angle C13*a*—C13*b*—C14—N	−169°	−155°
X_2‡	73°	85°
Torsion angle C13—C13*a*—C13*b*—C14	17°	5°
Distance of N from the plane of ring A	0.19 Å	−0.9 Å
Distance of N from the centre ring A	5.10 Å	5.1 Å

Parameter	Value for (−)-apomorphine†	
X_1	−178,	−178°
Torsion angle C7*a*—C7—C6*a*—N	178,	178°
X_2	56,	45°
Torsion angle C8—C7*a*—C7—C6*a*	−146,	−135°
Distance of the N from the plane of ring A	−0.90,	−1.23 Å
Distance of the N from the centre of ring A	5.12,	5.09 Å

*Values estimated from Dreiding models.
†Values calculated for the two crystallographically independent molecules in the unit cell.
‡See Fig. 6 for definition of these parameters.

The conformation of ring B in (+)-**1** (and in (±)-**2**) is one in which there is a C9–H, C13*b*–H interaction, and this rotamer is designated 'conformer A'. The alternative rotamer, with a C8–H, C13*b*–H interaction, designated 'conformer B' is not observed in the solid state, but this conformation may be assumed on the interaction of (+)-**2** with a biological receptor.[7]

[7]The probability that ring E of (+)-**2** may undergo a conformational change is considered unlikely since, in the resulting conformer, ring E would be a boat with an axial 2-propyl group.

The values for the parameters collected in Table 5 are derived from the crystal structure data for (+)-**2**, conformer A, from Dreiding models for (+)-**2**, conformer B, and from the recently published crystal structure data for apomorphine (13).

The data in Table 5 permit a comparison of the topographies of the extended phenethylamine moieties of 6*aR*(−)-apomorphine with those of conformers A and B of dexclamol, (+)-**2**. In essence, it is apparent from a consideration of Fig. 3 and the data in Table 5 that it is possible to

Can. J. Chem. Downloaded from www.nrcresearchpress.com by 210.87.254.105 on 09/05/12
For personal use only.

align the phenethylamine groups of (−)-apomorphine and of dexclamol, conformer B, with their phenyl rings coplanar and concentric, and with their nitrogen atoms essentially coincident. It is also seen from the data that both conformers A and B of dexclamol, as well as apomorphine, have virtually identical distances between their nitrogen atoms and the center of ring A, and that therefore this parameter alone is not of relevance for identifying topographical similarities between these ligands.

The finding that there are major areas of topographical similarity between dexclamol, conformer B, and (−)-apomorphine has provided a basis for a proposed mode of interaction between these ligands and the central dopamine receptor (6). In addition, it has permitted the assignment of a biological significance to the unique chirality of dexclamol, in terms of the topography of the macromolecule of which the dopamine receptor is a part (6).

1. K. VOITH and F. HERR. Abstracts of Papers, 5th Int. Congress of Pharmacology, San Francisco, 1972, Abstract No. 1457, p. 243.
2. F. BRUDERLEIN, L. HUMBER, and K. PELZ. Can. J. Chem. **52**, 2119 (1974).
3. F. BRUDERLEIN, L. HUMBER, and K. VOITH. J. Med. Chem. **18**, 185 (1975).
4. K.VOITH and F. HERR. Psychopharmacologia, **42**, 11 (1975).
5. D. H. MIELKE, D. M. GALLANT, T. OELSNER, C. M. KESSLER, W. K. TOMLINSON, and G. H. COHEN. Discuss. Nervous System, **36**, 7 (1975).
6. L. HUMBER, F. BRUDERLEIN, and K. VOITH. Mol. Pharmacol. **11**, 833 (1975).
7. K. VOITH and J. CUMMINGS. Abstracts of Papers, 6th Int. Congress of Pharmacology, July 1975, Helsinki, Finland.
8. W. LIPPMANN, T. PUGSLEY, and J. MERKER. Life Sci. **16**, 213 (1975).
9. R. J. MILLER, A. S. HORN, and L. L. IVERSEN. J. Pharm. Pharmacol. **27**, 212 (1975).
10. J. JARAMILLO. Can. J. Physiol. Pharmacol. In press.
11. L. IVERSEN. Science, **188**, 1084 (1975).
12. H. CORRODI and E. HARDEGGER. Helv. Chim. Acta, **38**, 2038 (1955).
13. J. GIESECKE. Acta Crystallogr. B**29**, 1785 (1973).
14. W. S. SAARI, S. W. KING, and V. LOTTI. J. Med. Chem. **16**, 171 (1973).
15. C. W. BURNAM. Am. Mineral, **51**, 159 (1966).
16. International Tables for X-Ray Crystallography. Vol. III. Kynoch Press, Birmingham, England. 1962.
17. W. C. HAMILTON. Acta Crystallogr. **5**, 60 (1952).

Can. J. Chem. Downloaded from www.nrcresearchpress.com by 210.87.254.105 on 09/05/12
For personal use only.

Crystal structures of phenacylkojate (2-(hydroxymethyl)-5-phenacyloxy-4*H*-pyran-4-one) and its complex with sodium chloride: bis(phenacylkojate)sodium chloride

SIMON E. V. PHILLIPS AND JAMES TROTTER

Department of Chemistry, University of British Columbia, Vancouver, B.C., Canada V6T 1W5

Received April 2, 1976

SIMON E. V. PHILLIPS and JAMES TROTTER. Can. J. Chem. **54**, 2723 (1976).

The structures of the title compounds have been determined by three dimensional X-ray crystal structure analysis.

Crystals of anhydrous phenacylkojate are monoclinic, space group $P2_1/c$, with unit cell dimensions $a = 9.087(4)$, $b = 11.764(3)$, $c = 12.714(4)$ Å, $\beta = 116.57(2)°$, $Z = 4$. The structure was solved by direct methods and refined by full-matrix least-squares to $R = 0.044$ for 1225 independent diffractometer observations. The crystal structure is held together by hydrogen bonding between carbonyl and hydroxyl groups and C—H···O interactions.

Crystals of the sodium chloride complex are monoclinic, space group $C2/c$, with unit cell dimensions $a = 11.3714(6)$, $b = 15.796(1)$, $c = 14.487(1)$ Å, $\beta = 97.241(5)°$, $Z = 4$. The structure was solved by heavy atom and Fourier methods and comparison with the previously determined structure of the potassium iodide complex. It was refined to $R = 0.040$ for 1670 independent diffractometer observations. The structure closely resembles that of the potassium iodide complex ($P2_1/n$), but in $C2/c$, the alkali metal ion being eight co-ordinate in each. Na^+—O distances are in the range 2.558–2.674 Å and the $Cl^-\cdots O$ hydrogen bonded distance is 3.266 Å.

SIMON E. V. PHILLIPS et JAMES TROTTER. Can. J. Chem. **54**, 2723 (1976).

Les structures des composés ci-haut mentionnés ont été déterminées par analyse tridimensionnelle de la structure cristalline en rayon-X.

Les cristaux du kojate de phénacyle anhydre sont monocliniques, groupe d'espace $P2_1/c$, avec des dimensions de la maille de $a = 9.087(4)$, $b = 11.764(3)$, $c = 12.714(4)$ Å, $\beta = 116.57(2)°$, $Z = 4$. La structure a été résolue par méthode directe et affinée par moindres carrés (matrice complète) jusqu'à $R = 0.044$ pour 1225 réflexions indépendantes. Les molécules sont maintenues entre elles dans le cristal par des liens hydrogènes entre les groupements carbonyles et hydroxyles et les interactions C—H···O. Les cristaux du complexe de chlorure de sodium sont monocliniques, groupe d'espace $C2/c$, avec des dimensions de la maille de $a = 11.3714(6)$, $b = 15.796(1)$, $c = 14.487(1)$ Å, $\beta = 97.241(5)°$, $Z = 4$. La structure a été résolue par les méthodes d'atome lourd et de Fourier et en comparaison avec la structure précédemment déterminée du complexe d'iodure de potassium. Le facteur d'accord final est $R = 0.040$ pour 1670 réflexions indépendantes. La structure ressemble étroitement à celle du complexe d'iodure de potassium ($P2_1/n$), mais dans $C2/c$; l'ion alcalin du métal a huit liaisons de coordination dans chacun d'eux. Les distances Na^+—O s'étendent dans l'écart de 2.558–2.674 Å et la distance du lien hydrogène $Cl^-\cdots O$ est de 3.266 Å.

[Traduit par le journal]

Introduction

Alkali metal halides form complexes with phenacylkojate (1), (pak), in one of two stoichiometries, $MX(pak)_2$ or MX(pak), depending on the radius sum $r_{M^+} + r_{X^-}$ (2). Crystal structures have been determined for examples of both cases (3, 4) and for the hydrated form of the free ligand (5).

The structure of $NaCl(pak)_2$ was investigated because its unit cell dimensions ($C2/c$) and crystal morphology resembled those of the $KI(pak)_2$ complex ($P2_1/n$). This observation suggested that the structure might contain eight-co-ordinate sodium rather than the more usual sixfold co-ordination found in $NaI(pak)_2.2H_2O$ (6). If the structure of $NaCl(pak)_2$ is similar to that of $KI(pak)_2$, this would show that the $MX(pak)_2$ complexes, that occur in both $P2_1/c$ and $C2/c$ (7), all have the same structure. The structure of pak itself was elucidated to confirm that the conformation of the molecule is planar even when the two carbonyl oxygen atoms are not interacting with a metal cation or water molecule.

Can. J. Chem. Downloaded from www.nrcresearchpress.com by 210.87.254.42 on 09/05/12
For personal use only.

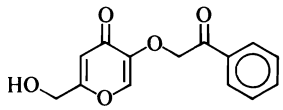

pak

Experimental

Pak

Slow cooling and evaporation of a solution of pak in warm methanol gave a mixture of colourless needles, (pak).H_2O, and plates (pak). A well-formed plate with dimensions *ca.* 0.003 × 0.020 × 0.048 cm was chosen for data collection and mounted on a Datex-automated G.E. XRD-6 three circle diffractometer with the ϕ axis through $\bar{1}02$. Accurate cell dimensions were obtained by least-squares refinement from 2θ settings of 20 manually centred reflections. Crystal data are:

$C_{14}H_{12}O_5$ f.w. = 260.2

Monoclinic, a = 9.087(4), b = 11.764(3), c = 12.714(4) Å, β = 116.57(2)°, V = 1215.4(7) Å^3, ρ_m = 1.42 (flotation), Z = 4, ρ_c = 1.42 g ml^{-1}, $F(000)$ = 544. Space group $P2_1/c$ (20 °C; Cu-K$_\alpha$, λ = 1.5418 Å, μ = 9.3 cm^{-1}).

Intensities were collected in shells of reciprocal space for all independent reflections with $2\theta < 120°$. Scanning was carried out at 2° min^{-1} and backgrounds counted for 10 s at the ends of each scan. Reflection 122 was measured at intervals of 50 reflections and its intensity fluctuated randomly between limits of ±4% throughout the data collection. The variations were used to scale the observed intensities. The total number of unique reflections collected was 1805. Lorentz and polarization factors (LP) were applied and standard deviations ($\sigma(I)$) calculated from $\sigma^2(I) = S + B + (0.05S)^2$, where S = scan and B = background count. A total of 1225 reflections was considered observed with intensity $(I) > 3\sigma(I)$ above background.

Structure Determination

The 221 reflections having $E > 1.5$ were used in the structure solution. Sign determination was carried out with a computer program (8) using a multisolution approach and applying $\sum_2$ relationships in an iterative procedure. The starting set consisted of seven reflections, three defining the origin, and the others having various

TABLE 1
(I) Final positional parameters for pak (fractional × 10^4, H × 10^3) with estimated standard deviations in parentheses

Atom	x	y	z
C(1)	5487(4)	1661(3)	−58(3)
C(2)	6383(4)	1506(3)	−687(3)
C(3)	7805(4)	881(3)	−208(3)
C(4)	8357(5)	404(3)	890(3)
C(5)	7453(4)	538(3)	1511(3)
C(6)	6007(4)	1167(3)	1045(2)
C(7)	5073(4)	1295(3)	1750(3)
C(8)	3597(4)	2067(3)	1277(3)
O(9)	2884(2)	2025(2)	2069(2)
C(10)	1474(4)	2638(3)	1761(2)
C(11)	735(4)	3257(3)	788(3)
O(12)	−694(3)	3853(2)	531(2)
C(13)	−1382(4)	3773(3)	1271(3)
C(14)	−700(4)	3169(3)	2258(3)
C(15)	808(4)	2563(3)	2606(3)
C(16)	−2952(5)	4442(4)	826(4)
O(17)	−3714(4)	4273(3)	1563(3)
O(18)	1511(3)	2032(2)	3541(2)
O(19)	5487(3)	794(2)	2673(2)
H(1)	453(4)	209(3)	−37(3)
H(2)	600(4)	182(3)	−150(3)
H(3)	846(5)	76(3)	−64(3)
H(4)	947(4)	−4(3)	128(3)
H(5)	787(4)	26(3)	230(3)
H(8*a*)	281(3)	183(2)	51(3)
H(8*b*)	395(4)	288(3)	123(3)
H(11)	103(4)	336(3)	15(3)
H(14)	−120(3)	312(2)	273(2)
H(16*a*)	−273(4)	520(3)	75(3)
H(16*b*)	−372(5)	420(3)	−2(4)
H(17)	−399(6)	491(4)	171(4)

Can. J. Chem. Downloaded from www.nrcresearchpress.com by 210.87.254.42 on 09/05/12
For personal use only.

TABLE 1 (*Concluded*)

(*II*) Final thermal parameters and their estimated standard deviations*
(*a*) Anisotropic thermal parameters ($U_{ij} \times 10^3$ Å^2)

Atom	U_{11}	U_{22}	U_{33}	U_{12}	U_{13}	U_{23}
C(1)	41(2)	45(2)	42(2)	2(2)	24(2)	2(2)
C(2)	58(2)	57(2)	44(2)	5(2)	35(2)	7(2)
C(3)	56(2)	54(2)	59(2)	8(2)	43(2)	3(2)
C(4)	53(2)	53(2)	60(2)	16(2)	38(2)	9(2)
C(5)	48(2)	43(2)	44(2)	6(2)	26(2)	7(2)
C(6)	37(2)	33(2)	36(2)	−4(1)	22(1)	−4(1)
C(7)	41(2)	42(2)	35(2)	−5(2)	21(1)	−3(1)
C(8)	39(2)	56(2)	34(2)	1(2)	27(2)	1(2)
O(9)	42(1)	68(2)	39(1)	8(1)	29(1)	5(1)
C(10)	35(2)	46(2)	36(2)	−4(2)	21(1)	−3(1)
C(11)	46(2)	58(2)	40(2)	4(2)	32(2)	5(2)
O(12)	50(1)	59(2)	47(1)	7(1)	33(1)	12(1)
C(13)	46(2)	40(2)	43(2)	−4(2)	30(2)	−8(2)
C(14)	44(2)	48(2)	38(2)	−6(2)	30(2)	−8(2)
C(15)	36(2)	49(2)	32(2)	−7(2)	21(1)	−5(1)
C(16)	54(2)	46(2)	71(3)	6(2)	38(2)	4(2)
O(17)	80(2)	82(2)	92(2)	25(2)	66(2)	6(2)
O(18)	53(2)	83(2)	33(1)	8(1)	26(1)	9(1)
O(19)	62(2)	77(2)	44(1)	14(1)	35(1)	17(1)

(*b*) Isotropic thermal parameters ($U \times 10^3$)

Atom	U (Å^2)	Atom	U (Å^2)	Atom	U (Å^2)
H(1)	57(10)	H(5)	71(11)	H(14)	39(8)
H(2)	78(12)	H(8*a*)	39(8)	H(16*a*)	60(11)
H(3)	77(12)	H(8*b*)	57(10)	H(16*b*)	82(13)
H(4)	63(10)	H(11)	49(9)	H(17)	112(19)

*Anisotropic thermal parameters in the expression: $f = f^0 \exp\,[-2\pi^2(U_{11}h^2a^{*2} + U_{22}k^2b^{*2} + U_{33}l^2c^{*2} + 2U_{12}hka^*b^* + 2U_{13}hla^*c^* + 2U_{23}klb^*c^*)]$.

sign combinations. The most probable set of signs with a consistency (8) of 87% was used to calculate an *E*-map, but the molecule could not be located. The next set with consistency 85% gave an *E*-map clearly showing all the non-hydrogen atoms. One cycle of full-matrix least-squares isotropic refinement using program BUCILS for all non-hydrogen atoms with unit weights and observed data gave $R = 0.25$.[1] Two further cycles with anisotropic temperature factors and weights $w = 1/\sigma^2(F)$, where $\sigma(F)$ values were derived from the previously calculated $\sigma(I)$ values, gave $R = 0.081$ and a difference Fourier map clearly showed all the hydrogen atoms. Two further cycles with the hydrogen atoms refined isotropically gave $R = 0.048$. At this point extinction effects became apparent in the data and a correction parameter $\boldsymbol{E}$ was introduced and refined. F_c was replaced in the calculations by F_{corr}, where $F_{corr} = F_c/(1 - \boldsymbol{E}I_o)$ (10), I_o being the uncorrected intensity. The weighting statistics from the $\sigma^2(F)$ values gave constant values of $\langle w\Delta^2 \rangle$ (weight $\times$ $(|F_o| - |F_c|)^2$), and two final cycles of refinement were carried out including the anomalous scattering contributions for C, O. The final R, R' were 0.044, 0.056 for observed data only, and 0.066, 0.056 for all data. The extinction parameter $\boldsymbol{E}$ refined to $5.8(7) \times 10^{-7}$ and the highest peak on the difference map was 0.27 e Å^{-3}. Bond lengths and angles with errors were calculated, by the program ORFFE,[2] with use of the variance–covariance matrix of the final cycle of refinement. Scattering factor curves were taken from ref. 12 for H atoms and ref. 13 for C and O atoms. $\Delta f'$ and $\Delta f''$ for O and C atoms were taken from ref. 14. Final positional and thermal parameters are given in Table 1. Measured and calculated structure factors have been placed in the Depository of Unpublished Data.[3]

NaCl(pak)$_2$

Crystals of NaCl(pak)$_2$ were obtained by dissolving

[1]BUCILS is a local version of the full-matrix least-squares program NUCILS by R. J. Doedens and J. A. Ibers.

[2]Interatomic distances and errors program ORFFE by W. R. Busing and H. A. Levy.

[3]The structure factor table is available, at a nominal charge, from the Depository of Unpublished Data, CISTI, National Research Council of Canada, Ottawa, Canada K1A 0S2.

Can. J. Chem. Downloaded from www.nrcresearchpress.com by 210.87.254.42 on 09/05/12
For personal use only.

Can. J. Chem. Downloaded from www.nrcresearchpress.com by 210.87.254.42 on 09/05/12
For personal use only.

NaCl and pak in 1:2 molar ratio in warm methanol and allowing the solution to cool and evaporate slowly. An irregular crystal fragment, with approximate dimensions $0.05 \times 0.03 \times 0.01$ cm was mounted with the goniometer ϕ axis through 101. The 2θ values of the CuK_{α_1} and K_{α_2} peaks of thirteen reflections were used to refine the cell parameters. Crystal data are:

$(C_{14}H_{12}O_5)_2NaCl$ f.w. = 578.8

Monoclinic, $a = 11.3714(6)$, $b = 15.796(1)$, $c = 14.487(1)$ Å, $\beta = 97.241(5)°$, $V = 2581.4(3)$ Å^3, $\rho_m = 1.46$(flotation), $Z = 4$, $\rho_c = 1.49$ g ml^{-1}, $F(000) = 1200$. Space group $C2/c$ (from absences and structure refinement) (20 °C; Cu-K_α, $\lambda = 1.5418$ Å, $\mu = 20.1$ cm^{-1}).

Data collection proceeded as for pak. The standard reflection, 424, varied ±3% and the total number of reflections was 1910, of which 1670 were considered observed at the 3σ level.

Structure Determination

The symmetry of the space group requires the Cl^- and Na^+ ions to be lying on special positions. With the assumption that the complex is isostructural with $KI(pak)_2$, the ions were placed at the positions observed for K^+ and I^- in $P2_1/n$. Na^+ lies on a two-fold axis at $1/2,y,1/4$ and Cl^- on a centre of symmetry at $1/4,1/4,1/2$. Refinement of the isotropic temperature factors and the y co-ordinate of Na^+ gave $R = 0.61$, and the Fourier electron density map showed most of the non-hydrogen atoms in the pak molecule in positions close to those found in $KI(pak)_2$. Anisotropic refinement of Cl^- and Na^+ ($U_{12} = U_{23} = 0$ for Na^+ due to symmetry (15)) and isotropic refinement of C and O atoms with unit weights led to $R = 0.12$. With all atoms anisotropic and weights based on $\sigma^2(F)$, R dropped to 0.071 and a difference map clearly showed all the hydrogen atoms. Isotropic refinement of the hydrogen atoms led to $R = 0.042$, but examination of the weighting statistics showed extinction effects and the need for an improved weighting scheme to produce constant values of $\langle w\Delta^2 \rangle$. An extinction correction was introduced as for pak and the weighting scheme used was: $\sqrt{w} = |F_o|/15.0$ where $|F_o| \leq 15.0$ and $\sqrt{w} = 15.0/|F_o|$ where $|F_o| > 15.0$. The refinement converged to $R = 0.040$, $R' = 0.050$ for observed data and 0.046, 0.052 respectively for all data. The extinction

TABLE 2

(*I*) Final positional parameters for $NaCl(pak)_2$ (fractional $\times 10^4$, Cl and Na $\times 10^5$, H $\times 10^3$) with estimated standard deviations in parentheses

Atom	*x*	*y*	*z*
Cl	25000	25000	50000
Na	50000	42047(7)	25000
C(1)	1619(2)	5260(2)	−520(2)
C(2)	542(2)	5184(2)	−1079(2)
C(3)	63(3)	4406(3)	−1269(2)
C(4)	633(3)	3691(3)	−903(2)
C(5)	1712(2)	3755(2)	−315(2)
C(6)	2206(2)	4550(1)	−130(1)
C(7)	3355(2)	4619(1)	475(1)
C(8)	3933(2)	5484(1)	573(1)
O(9)	5014(1)	5385(1)	1178(1)
C(10)	5599(2)	6107(1)	1484(1)
C(11)	5293(2)	6891(1)	1218(1)
O(12)	5900(1)	7585(1)	1589(1)
C(13)	6855(2)	7464(1)	2231(1)
C(14)	7227(2)	6697(1)	2520(1)
C(15)	6608(2)	5941(1)	2192(1)
C(16)	7360(2)	8302(1)	2571(2)
O(17)	8471(2)	8220(1)	3122(1)
O(18)	6848(1)	5223(1)	2487(1)
O(19)	3833(1)	4014(1)	885(1)
H(1)	191(3)	582(2)	−44(2)
H(2)	12(3)	571(2)	−135(3)
H(3)	−66(3)	437(2)	−169(2)
H(4)	40(3)	317(3)	−96(2)
H(5)	213(2)	330(2)	−4(2)
H(8*a*)	410(2)	567(1)	−3(2)
H(8*b*)	341(2)	587(1)	83(1)
H(11)	463(2)	705(2)	80(2)
H(14)	785(2)	666(1)	294(2)
H(16*a*)	676(2)	857(2)	292(2)
H(16*b*)	746(2)	863(2)	203(2)
H(17)	835(3)	802(2)	359(2)

TABLE 2 (*Concluded*)

(*II*) Final thermal parameters and their estimated standard deviations
(*a*) Anisotropic thermal parameters ($U_{ij} \times 10^3$, Na and Cl $\times 10^4$ Å^2)

Atom	U_{11}	U_{22}	U_{33}	U_{12}	U_{13}	U_{23}
Cl	573(5)	467(5)	515(5)	−90(4)	−190(4)	8(3)
Na	510(7)	411(7)	543(7)	0	−119(5)	0
C(1)	42(1)	66(2)	43(1)	−11(1)	−4(1)	7(1)
C(2)	46(1)	95(2)	54(2)	−18(1)	−8(1)	13(1)
C(3)	55(2)	110(3)	55(2)	−29(2)	−7(1)	−2(2)
C(4)	68(2)	87(2)	78(2)	−46(2)	13(2)	−32(2)
C(5)	59(2)	58(2)	57(2)	−20(1)	11(1)	−14(1)
C(6)	41(1)	52(1)	33(1)	−14(1)	4(1)	−9(1)
C(7)	42(1)	40(1)	32(1)	−2(1)	4(1)	−7(1)
C(8)	35(1)	39(1)	34(1)	−2(1)	−6(1)	−2(1)
O(9)	37(1)	35(1)	46(1)	−2(1)	−13(1)	−5(1)
C(10)	30(1)	36(1)	30(1)	−2(1)	0(1)	−4(1)
C(11)	33(1)	38(1)	37(1)	−1(1)	−8(1)	2(1)
O(12)	41(1)	32(1)	45(1)	−3(1)	−12(1)	4(1)
C(13)	30(1)	42(1)	31(1)	−2(1)	0(1)	1(1)
C(14)	28(1)	40(1)	36(1)	0(1)	−6(1)	−2(1)
C(15)	32(1)	36(1)	32(1)	4(1)	0(1)	−1(1)
C(16)	46(1)	39(1)	54(1)	−10(1)	−10(1)	0(1)
O(17)	52(1)	53(1)	62(1)	−15(1)	−17(1)	1(1)
O(18)	51(1)	34(1)	49(1)	6(1)	−10(1)	2(1)
O(19)	55(1)	37(1)	55(1)	0(1)	−5(1)	−1(1)

(*b*) Isotropic thermal parameters ($U \times 10^3$)

Atom	U (Å^2)	Atom	U (Å^2)	Atom	U (Å^2)
H(1)	78(9)	H(5)	54(7)	H(14)	42(6)
H(2)	103(11)	H(8*a*)	37(5)	H(16*a*)	64(8)
H(3)	81(9)	H(8*b*)	34(5)	H(16*b*)	59(7)
H(4)	95(11)	H(11)	54(7)	H(17)	62(10)

parameter E refined to $3.6(9) \times 10^{-8}$, and the highest peak on the final difference map was 0.30 e Å^{-3}. Bond length calculations and scattering factor curves were as for pak, $\Delta f'$ and $\Delta f''$ for Na^+ and Cl^- being taken from ref. 14. Final positional and thermal parameters are given in Table 2. Measured and calculated structure factors have been placed in the Depository of Unpublished Data.[3]

Thermal Motion Analysis

The mean C—C distances in the phenyl rings for pak and NaCl(pak)$_2$ are 1.382(3) and 1.385(6) Å respectively, rather shorter than the expected value of about 1.394 Å (16), indicating the possibility of apparent bond shortening due to thermal motion.

The thermal motion has been analysed in terms of the rigid body modes of translation, libration, and screw motion (17) using the computer program MGTLS. The individual rings and immediate substituents behave as rigid bodies, but the chains joining the two rings do not. Bond lengths within the rigid bodies have been corrected for libration (18, 19) with shape parameter 0.08 for all atoms. The C(16)—O(17) bond was further corrected for independent motion based on the ΔU_{ij} values (20, 21). Bond lengths, corrected lengths, and angles are given in Table 3. The corrected mean C—C bond lengths in the phenyl rings are 1.388(4) and 1.390(6) Å, still a little short, but not significantly different from the typical value.

Computing

All calculations were carried out using the IBM 370/168 at this university. Thermal ellipsoid plots were made using the program ORTEP.[4]

Results and Discussion

The Structure of pak

The arrangement of the pak molecules (see Fig. 1 for formula and crystallographic numbering scheme) in the structure is dependent on O—H···O hydrogen bonding, C—H···O interactions and van der Waals contacts between stacked phenyl and pyranone rings. The latter interactions, which occur with interplanar spacings of about 3.5 Å as found for (pak).H_2O (5), link parallel molecules. There are two different

[4]Thermal ellipsoid program ORTEP by C. K. Johnson.

Can. J. Chem. Downloaded from www.nrcresearchpress.com by 210.87.254.42 on 09/05/12
For personal use only.

Can. J. Chem. Downloaded from www.nrcresearchpress.com by 210.87.254.42 on 09/05/12
For personal use only.

TABLE 3

(*I*) Bond lengths (Å) in the pak molecules before and after thermal motion corrections with standard deviations in parentheses

Bond	pak		$NaCl(pak)_2$	
	Uncorr.	Corr.	Uncorr.	Corr.
C(1) —C(2)	1.385(4)	1.389	1.385(3)	1.389
C(1) —C(6)	1.391(4)	1.400	1.389(3)	1.397
C(2) —C(3)	1.370(5)	1.375	1.359(5)	1.365
C(3) —C(4)	1.374(5)	1.384	1.374(5)	1.383
C(4) —C(5)	1.379(5)	1.383	1.406(4)	1.410
C(5) —C(6)	1.389(4)	1.396	1.388(3)	1.395
C(6) —C(7)	1.493(4)	1.497	1.483(3)	1.488
C(7) —C(8)	1.505(5)	1.512	1.514(3)	1.522
C(7) —O(19)	1.213(3)	1.219	1.216(3)	1.222
C(8) —O(9)	1.421(3)	—	1.426(2)	—
O(9) —C(10)	1.366(4)	1.369	1.365(2)	1.368
C(10)—C(11)	1.330(4)	1.336	1.330(3)	1.335
C(10)—C(15)	1.453(4)	1.461	1.463(3)	1.471
C(11)—O(12)	1.380(4)	1.383	1.368(2)	1.372
O(12)—C(13)	1.346(3)	1.353	1.352(2)	1.358
C(13)—C(14)	1.330(4)	1.337	1.333(3)	1.340
C(13)—C(16)	1.501(5)	1.504	1.500(3)	1.503
C(14)—C(15)	1.429(4)	1.433	1.437(3)	1.441
C(15)—O(18)	1.237(3)	1.242	1.231(3)	1.235
C(16)—O(17)	1.406(4)	1.412	1.413(3)	1.416

(*II*) Bond angles (deg) in the pak molecules with standard deviations in parentheses. Values corrected for thermal motion are not significantly different and are not shown

Bonds	Angle	
	pak	$NaCl(pak)_2$
C(2) —C(1) —C(6)	120.3(3)	120.8(3)
C(1) —C(2) —C(3)	119.7(3)	120.0(3)
C(2) —C(3) —C(4)	120.9(3)	120.5(3)
C(3) —C(4) —C(5)	119.6(3)	120.5(3)
C(4) —C(5) —C(6)	120.6(3)	118.9(3)
C(1) —C(6) —C(5)	118.9(3)	119.4(2)
C(1) —C(6) —C(7)	122.3(3)	121.6(2)
C(5) —C(6) —C(7)	118.8(3)	119.0(2)
C(6) —C(7) —C(8)	117.7(3)	117.5(2)
C(6) —C(7) —O(19)	121.1(3)	122.5(2)
C(8) —C(7) —O(19)	121.0(3)	120.1(2)
C(7) —C(8) —O(9)	107.6(3)	106.8(2)
C(8) —O(9) —C(10)	116.4(2)	117.1(1)
O(9) —C(10)—C(11)	125.1(3)	125.8(2)
O(9) —C(10)—C(15)	113.8(3)	112.6(2)
C(11)—C(10)—C(15)	121.2(3)	121.5(2)
C(10)—C(11)—O(12)	121.9(3)	122.1(2)
C(11)—O(12)—C(13)	118.8(3)	118.6(2)
O(12)—C(13)—C(14)	122.1(3)	122.7(2)
O(12)—C(13)—C(16)	111.1(3)	110.1(2)
C(14)—C(13)—C(16)	126.8(3)	127.2(2)
C(13)—C(14)—C(15)	122.5(3)	121.9(2)
C(10)—C(15)—C(14)	113.6(3)	113.1(2)
C(10)—C(15)—O(18)	122.3(3)	121.9(2)
C(14)—C(15)—O(18)	124.1(3)	125.0(2)
C(13)—C(16)—O(17)	110.1(3)	112.5(2)

TABLE 3 (*Concluded*)

(*III*) Bond angles (deg) involving hydrogen atoms differing by more than 3σ from normal values

Bond	Angle	
	pak	$NaCl(pak)_2$
H(4) —C(4) —C(3)	—	129(2)
H(4) —C(4) —C(5)	—	111(2)
H(11)—C(11)—C(10)	129(2)	127(2)
H(11)—C(11)—O(12)	109(2)	111(2)

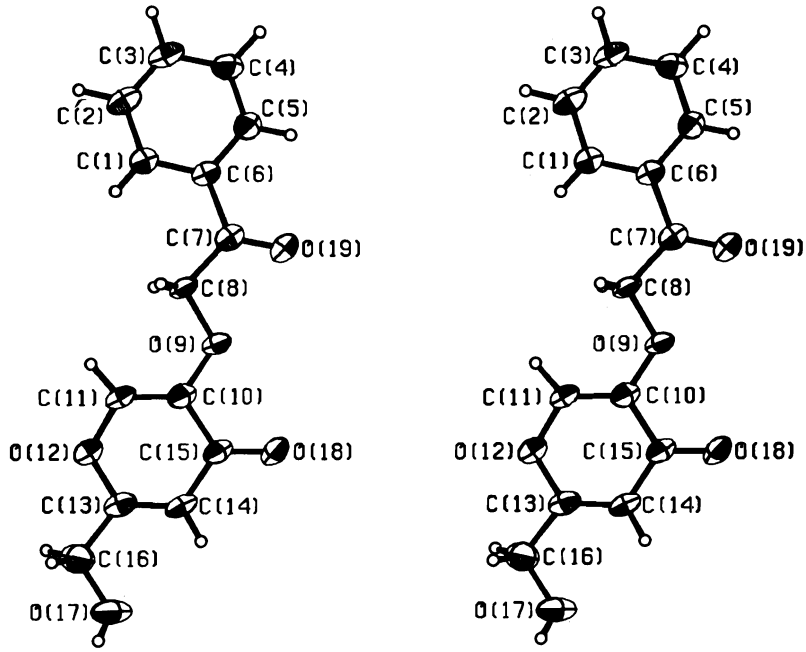

FIG 1. Stereo view of the pak molecule with 50% probability vibration ellipsoids for non-hydrogen atoms.

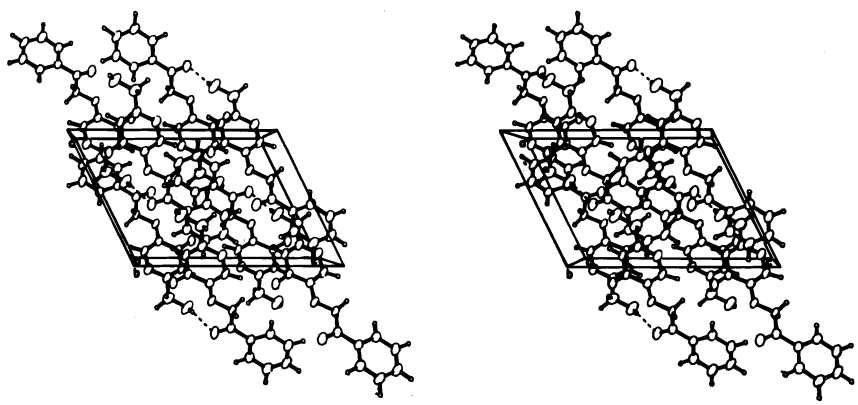

FIG. 2. *y*-projection of pak structure. Broken lines indicate hydrogen bonds.

Can. J. Chem. Downloaded from www.nrcresearchpress.com by 210.87.254.42 on 09/05/12
For personal use only.

Can. J. Chem. Downloaded from www.nrcresearchpress.com by 210.87.254.42 on 09/05/12
For personal use only.

TABLE 4. Geometry of the hydrogen bond and C—H···O interactions in pak

(*I*) Bond distances

Bond	Distance (Å)
O(17)—H(17)	0.84(5)
O(17)···O(19^{I})	2.854(4)
H(17)···O(19^{I})	2.17(5)
C(16)—H(16*a*)	0.93(4)
C(16)····O(18^{I})	3.272(4)
H(16*a*)···O(18^{I})	2.40(4)
C11—H(11)	0.97(3)
C(11)···O(18^{II})	3.252(4)
H(11)···O(18^{II})	2.32(3)

(*II*) Bond angles at hydrogen atoms*

Bonds	Angle (deg)
O(17)—H(17)···O(19^{I})	146(4)
C(11)—H(11)···O(18^{II})	160(2)
C(16)—H(16*a*)···O(18^{I})	155(2)

(*III*) Interatomic distances in $NaCl(pak)_2$

(*a*) Na^+—O co-ordination distances

Bond	Distance (Å)
Na—O(9)	2.674(2)
Na—O(17^{III})	2.579(2)
Na—O(18)	2.649(2)
Na—O(19)	2.558(2)

(*b*) Hydrogen bond geometry

Bond	Distance (Å)
Cl···O(17^{III})	3.266(2)
Cl···H(17^{III})	2.51(3)
O(17)—H(17)	0.77(3)

Bonds	Angle (deg)
Cl···H(17^{III})—O(17^{III})	168(3)°

*Roman numeral superscripts refer to other asymmetric units as follows: I, $-x$, $1/2 + y$, $1/2 - z$; II, x, $1/2 - y$, $-1/2 + z$; III, $-1/2 + x$, $-1/2 + y$, z.

orientations of the molecular planes, which alternate along the *c* axis and are related by the *c* glide plane (see Fig. 2 for packing diagram). Interactions between non-parallel molecules are due to hydrogen bonding. There is a hydrogen bond between the hydroxyl group and the O(19) carbonyl oxygen of a neighbouring molecule with an O···H separation of 2.17(5) Å and favourable geometry (see Table 4). This distance is greater than the corresponding one in $(pak).H_2O$ (5) of 1.98(3) Å, involving the water molecule, and this is reflected in the ν(OH) frequencies in the infrared spectra, which are observed at 3490 and 3470 cm^{-1} for pak and $(pak).H_2O$ respectively. Other interactions are of the C—H···O type and whether these can be classified as true hydrogen bonds has been discussed elsewhere (23). The geometry of the two most significant of these interactions is given in Table 4 and both qualify as hydrogen bonds according to the conditions given in ref. 23. Several others occur with borderline geometry, for instance H(1)···O(18^{II}) at 2.67 Å, but these are not given in Table 4. The interaction of the carbonyl groups with C—H groups replaces the O···M^+ and O···HOH interactions found in other pak structures.

The Structure of NaCl (pak)$_2$

The crystal structure of $NaCl(pak)_2$ is directly analogous to that of $KI(pak)_2$ (3), except that the approximate two-fold symmetry of the latter is exact for the sodium complex. The packing of the two structures in the unit cell is almost identical, as long as $KI(pak)_2$ is considered in the non-standard space group $P2_1/n$.

The co-ordination shell of the sodium (see Fig. 3) contains eight oxygen atoms, a higher co-ordination number than is usual for this ion, with Na^+—O distances in the range 2.558–2.674 Å and a weighted mean value of 2.62(3) Å (see Table 4). These distances are in agreement with those found for other complexes containing eight-co-ordinate sodium. Some other examples are $NaBr(dibenzo\text{-}18\text{-}crown\text{-}6).2H_2O$ (9) with Na^+—O in the range 2.27–2.89 Å and mean 2.65 Å, and $NaBr(dicyclohexyl\text{-}18\text{-}crown\text{-}6).2H_2O$ (11) with Na^+—O in the range 2.349–2.975 and mean 2.69 Å. An eight-co-ordinate sodium cryptate has also been reported (22) with Na^+—O 2.582, 2.566 Å and Na^+—N 2.782, 2.722 Å, the mean of the Na^+—O and Na^+—N distances being 2.66 Å. In all these cases, however, the co-ordination number is determined by at least six of the co-ordinating atoms belonging to the same ligand and each complex contains definite long and short co-ordination distances. $NaCl(pak)_2$ is different in that the conformation of the ligand does not impose particular co-ordination geometries on the sodium. This is supported by the

Can. J. Chem. Downloaded from www.nrcresearchpress.com by 210.87.254.42 on 09/05/12
For personal use only.

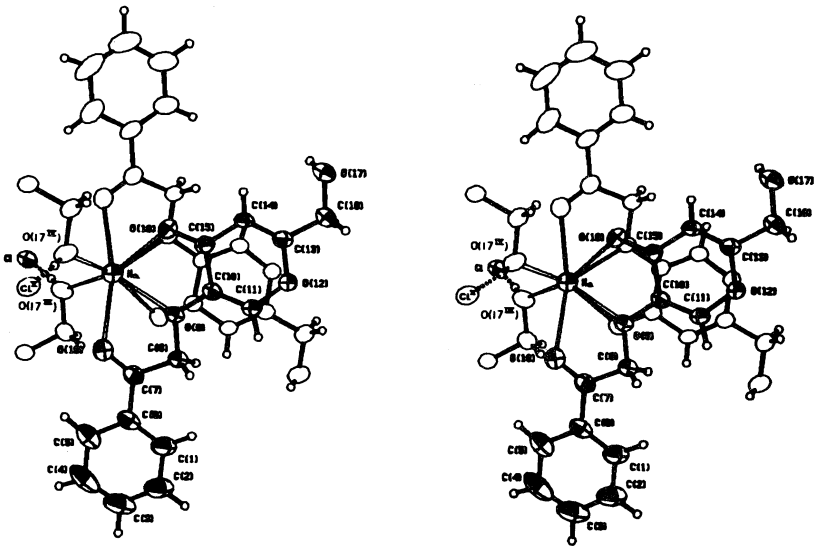

FIG. 3. The environment of the sodium ion in $NaCl(pak)_2$ showing the co-ordinated pak molecules and neighbouring chloride ions. Hollow bonds show Na^+—O contacts and broken lines indicate the O—H···Cl^- hydrogen bonds. Shaded ellipsoids show atoms in the asymmetric unit and plain ones symmetry related atoms. Roman numeral superscripts refer to other asymmetric units as follows: III, $-1/2 + x$, $-1/2 + y$, z; IV, $1 - x$, $1 - y$, $1 - z$; V, $1/2 + x$, $1/2 - y$, $-1/2 + z$.

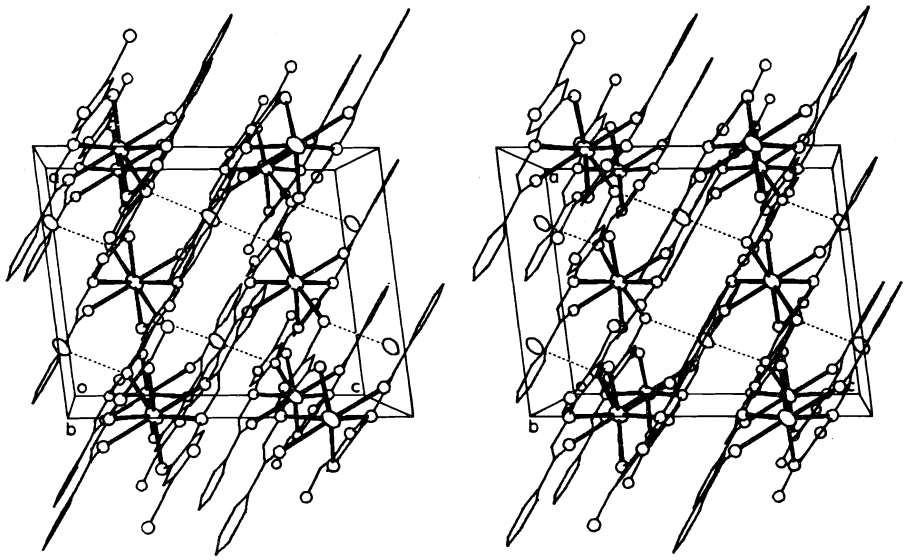

FIG. 4. y-projection of $NaCl(pak)_2$ structure. Na^+ and Cl^- ions are shown as ellipsoids and O atoms as circles. Heavy bonds show Na^+—O co-ordination and broken lines O—H···Cl^- hydrogen bonds.

distorted octahedral configuration found in $NaI(pak)_2.2H_2O$. Also the range of Na^+—O distances is much smaller than in the other complexes. The deviation of the sodium ion from the plane defined by O(9), O(18), and O(19) is 0.999 Å. The co-ordination geometry has already been described for $KI(pak)_2$ (3).

The crystal packing (see Fig. 4) is the same as

Can. J. Chem. Downloaded from www.nrcresearchpress.com by 210.87.254.42 on 09/05/12
For personal use only.

for $KI(pak)_2$ but location and refinement of hydrogen atoms has confirmed the existence of the $Cl^- \cdots O(17)$ hydrogen bond (see Table 4 for geometry) and thus the proposed $I^- \cdots O(17)$ hydrogen bond in $KI(pak)_2$. The parallel stacking of phenyl rings across centres of symmetry occurs as before with an interplanar separation of 3.42 Å.

It is possible that the stability of the three-dimensional crystal lattice stabilizes the eight-fold co-ordination of the sodium ion. The similarity of the 1:2 complexes, all occurring in space groups $P2_1/c$ or $C2/c$, suggests that this structure is common to them all.

Pak Molecules

The bonds and angles in pak are normal and follow trends found in other pak structures (5). Bond lengths in $NaCl(pak)_2$ follow the mean values given in ref. 5 more closely than those of pak itself. This suggests that the geometry found in the pak structure is closer to that of the free molecule than that of $(pak).H_2O$. The only bond length that differs by more than 3σ between the two molecules in Table 3 is C(4)—C(5) and the difference is maintained after correction for thermal motion. Variations in bond length around the phenyl ring are probably a real effect dependent on the adjacent carbonyl group. Bond angles are much the same as before with the angle at O(9) again being closer to trigonal rather than tetrahedral. Mean C—H bond distances for pak and $NaCl(pak)_2$ are 0.98(2), 0.97(1) Å respectively for H—C(sp^3) and 0.97(2), 0.93(2) Å for H—C(sp^2). Most bond angles involving hydrogen are as expected, except for those at C(11) (see Table 3) where the deviations correspond to those found in the other pak structures. The anomalous C—C—H angles at C(4) in $NaCl(pak)_2$ are probably the result of poor refinement of the position of H(4).

A mean plane calculation for the free pak molecule shows it to be slightly, but significantly, non-planar. The complexed molecule, however, shows the slight arching observed in the other complexes. In both cases the hydroxyl oxygen atom, O(17), is close to the plane. The position of O(17) found in all the pak structures studied, except $(pak).H_2O$, may be the result of a weak interaction with H(14), the distance $O(17) \cdots H(14)$ being 2.49 and 2.57 Å respectively for pak and $NaCl(pak)_2$.

Acknowledgments

We thank Dr. M. R. Truter for originally suggesting the problem and supplying the sample of phenacylkojate, the National Research Council of Canada for financial support, and the University of British Columbia Computing Centre for assistance.

1. C. D. Hurd and R. J. Sims. J. Am. Chem. Soc. **71**, 2240 (1949).
2. D. E. Fenton. J. Chem. Soc. Dalton, 1380 (1973).
3. D. L. Hughes, S. E. V. Phillips, and M. R. Truter. J. Chem. Soc. Dalton, 907 (1974).
4. S. E. V. Phillips and M. R. Truter. J. Chem. Soc. Dalton, 2517 (1974).
5. S. E. V. Phillips and M. R. Truter. J. Chem. Soc. Dalton, 1071 (1975).
6. S. E. V. Phillips and M. R. Truter. J. Chem. Soc Dalton, 1066 (1975).
7. S. E. V. Phillips. Ph.D. Thesis. University of London, London, England. 1974.
8. R. E. Long. Ph.D. Thesis. University of California at Los Angeles, Los Angeles, California. 1965.
9. M. A. Bush and M. R. Truter. J. Chem. Soc. (B), 1440 (1971).
10. G. H. Stout and L. H. Jensen. X-Ray structure determination. Macmillan, New York. 1968. pp. 409–412.
11. M. Mercer and M. R. Truter. J. Chem. Soc. Dalton, 2215 (1973).
12. R. F. Stewart, E. R. Davidson, and W. T. Simpson. J. Chem. Phys. **42**, 3175 (1965).
13. D. T. Cromer and J. B. Mann. Acta Crystallogr. A**24**, 321 (1968).
14. D. T. Cromer and D. Liberman. J. Chem. Phys. **53**, 1891 (1970).
15. W. J. A. M. Peterse and J. H. Palm. Acta Crystallogr. **20**, 147 (1966).
16. Chem. Soc. Special Publ. No. 18, 1965.
17. V. Schomaker and K. N. Trueblood. Acta Crystallogr. B**24**, 63 (1968).
18. D. W. J. Cruickshank. Acta Crystallogr. **9**, 747 (1956); **9**, 754 (1956).
19. D. W. J. Cruickshank. Acta Crystallogr. **14**, 896 (1961).
20. W. R. Busing and H. A. Levy. Acta Crystallogr. **17**, 142 (1964).
21. C. K. Johnson. *In* Crystallographic computing. Munksgaard, Copenhagen. 1970. pp. 207–226.
22. D. Moras and R. Weiss. Acta Crystallogr. B**29**, 396 (1973).
23. D. J. Sutor. J. Chem. Soc. (B), 1105 (1963).

Solvent, concentration, and temperature dependence of the platinum–phosphorus nuclear magnetic resonance coupling constants in *cis*- and *trans*-$[PtCl_2(PBu_3^n)_2]$

KEITH R. DIXON,[1] MARTIN FAKLEY, AND ALAN PIDCOCK
School of Molecular Sciences, University of Sussex, Brighton, England BN1 9QJ

Received April 12, 1976

KEITH R. DIXON, MARTIN FAKLEY, and ALAN PIDCOCK. Can. J. Chem. **54**, 2733 (1976).

Studies of the effects of solvent, concentration and temperature on the ^{31}P nmr parameters of *cis*- and *trans*-$[PtCl_2(PBu^n_3)_2]$ are reported. The coupling constants, $^1J_{Pt-P}$, are markedly dependent upon all three variables but, in contrast to previous studies on non-coordination compounds, very little corresponding variation in chemical shifts is found. Results are discussed in terms of a solvent cavity model using reaction field, Stark and Macrae effects but it is concluded that a more specific model involving competitive solvation at platinum gives a better interpretation of the data.

KEITH R. DIXON, MARTIN FAKLEY et ALAN PIDCOCK. Can. J. Chem. **54**, 2733 (1976).

Une étude sur les effets du solvant, de la concentration et de la température sur les paramètres du rmn ^{31}P du $[PtCl_2(PBu^n_3)_2]$ *cis* et *trans* est rapportée. Les constantes de couplage $^1J_{Pt-P}$ dépendent d'une façon marquée des trois variables mais contrairement à des études précédentes sur des composés de non-coordination, on ne trouve qu'une très petite correspondance dans la variation des déplacements chimiques. Les résultats sont discutés en terme d'un modèle de cage de solvant utilisant les effets de champs de réaction et les effets de Stark et Macrae toutefois, on en conclue qu'un modèle plus spécifique impliquant une solvatation compétitive du platine donne une meilleure interprétation des résultats.

[Traduit par le journal]

Introduction

The marked solvent dependence of many nuclear magnetic resonance chemical shifts has been known for a long time. Only more recently has the solvent dependence of coupling constants been recognized and investigated. Several review articles have been published (1–3), the most extensive compilation being that by Smith (4). However, there seem to be no studies on co-ordination complexes with the exception of a small amount of data (published subsequent to the completion of our studies) on $^1J_{Pt-P}$ in *cis*-$[PtCl_2(PBu^n_3)_2]$ and *trans*-$[PtI_2(PBu^n_3)_2]$ (5). Indeed the only extensive data on metal containing complexes of any type relates to $^2J_{MH}$ couplings in tin, lead, mercury, and thallium alkyls (6–9). The introduction of fast Fourier transform techniques has made ^{31}P nmr spectroscopy a tool of increasing importance for the characterisation of co-ordination complexes containing tertiary phosphine ligands and it has also found extensive application in the study of *trans* influence phenomena (10, 11). Very few examples of solvent dependent couplings involving ^{31}P have been studied; the only examples being $^1J_{PH}$ in PH_3, $PH(OCH_3)_2$, and $PH(CF_3)_2$, $^2J_{PF}$ in the last compound (12–14), and the limited $^1J_{Pt-P}$ data mentioned above (5). We therefore considered it of interest to examine the effect of the usual laboratory variables in the nmr experiment (*i.e.* solvent, temperature, and concentration) on the spectrum of a typical tertiary phosphine complex. The objectives of the study were to determine the likely effect of these variables on the validity of characterisation of complexes by ^{31}P nmr, on *trans* influence series compiled by nmr and on any related type of project. We also wished to compare the results with previous studies on simpler (non-co-ordination) compounds. The complex *trans*-$[PtCl_2(PBu^n_3)_2]$ was chosen for the study because of its high solubility in a wide range of solvents and because square planar platinum complexes are commonly used in *trans*-influence studies. For comparison purposes, some experiments were also carried out with *cis*-$[PtCl_2(PBu^n_3)_2]$.

[1]Author to whom correspondence should be addressed. Permanent address: Department of Chemistry, University of Victoria, Victoria, British Columbia, Canada V8W 2Y2.

Can. J. Chem. Downloaded from www.nrcresearchpress.com by 210.87.254.105 on 09/05/12
For personal use only.

TABLE 1. Solvent dependence of $^1J_{Pt-P}$ in *cis*- and *trans*-$[PtCl_2(PBu^n_3)_2]$

Solvent	Dielectric constant[a]	Refractive index[a]	Nmr parameters: *trans* $^1J_{Pt-P}$[b] (Hz)	*trans* δ[c] (ppm)	*cis* $^1J_{Pt-P}$[b] (Hz)	*cis* δ[c] (ppm)
1 *n*-Hexane	1.88	1.372	2459.7	135.95		
2 Cyclohexane	2.01	1.427	2457.9	135.80		
3 Cyclohexene	2.22[d]	1.447	2445.1	135.92		
4 Diethyl ether	4.18	1.352	2440.8	136.10		
5 Carbon tetrachloride	2.22	1.459	2424.9	135.39		
6 Butyric acid	2.99	1.396	2412.1	136.02		
7 Benzene	2.27	1.498	2412.1	136.01	3479.6	139.81
8 Acetone	20.4	1.357	2399.3	136.10	3491.8	139.69
9 Pyridine	12.2	1.507	2387.1	135.69	3491.2	139.33
10 Dichloromethane	8.79	1.424	2384.6	135.74	3510.1	139.49
11 Methanol	32.0	1.326	2383.4	136.22	3523.6	139.09
12 Dimethylformamide	36.7[d]	1.431	2382.8	135.47	3491.8	139.06
13 Chloroform	4.67	1.444	2379.8	135.71	3519.9	139.16
14 Acetonitrile	38.8[d]	1.342	2375.5	135.89	3502.8	139.28

[a]Values from ref. 17. Dielectric constants corrected to nmr probe ambient temperature (28 °C) wherever possible.
[b]Values for *trans*- and *cis*-$[PtCl_2(PBu^n_3)_2]$ at 50 mg ml^{-1} concentration in the indicated solvents at 28 °C. For comments on likely accuracy, see Experimental section.
[c]In ppm upfield from $P(OMe)_3$ external reference.
[d]Value at 25 °C.

Results

Coupling Constants

Results for the variation of $^1J_{Pt-P}$ in *trans*-$[PtCl_2(PBu^n_3)_2]$ with change of solvent and concentration are presented in Table 1 and Fig. 1. The total spread (~3.5%) of solvent induced changes is roughly comparable with the previously reported range (4) of 1–5% for one-bond coupling constants but is unusually large for a non-polar solute. If we assume that values obtained in solvents such as *n*-hexane are close to the unperturbed ('gas phase') coupling constants, then it is clear that two groups of solvents cause a substantial lowering of the coupling constant: (*a*) Solvents (*e.g.* CH_2Cl_2 and $CHCl_3$) in which the solubility of this type of complex is known to be especially high. *trans*-$[PtCl_2(PBu^n_3)_2]$ is, in fact, almost completely miscible with these solvents. (*b*) Solvents (*e.g.* CH_3CN, $HCON(CH_3)_2$ and CH_3OH) of high dielectric constant or good donor properties.[2] In general the solubility of *trans*-$[PtCl_2(PBu^n_3)_2]$ in these solvents is rather low (*ca.* 50 mg/ml).

With the single exception of butyric acid (see Discussion), the positions of the other solvents in the series are consistent with a combination of these two effects. The overall series shows some similarities to previous series obtained for non-co-ordination compounds but there are important differences. Firstly, in the literature series (4) the chlorinated solvents generally occupy a position which is consistent with their comparatively low dielectric constants whereas in our series they cause a lowering of coupling constant comparable with that produced by the high dielectric solvents. Secondly, the effects in our series are the inverse of those normally observed. Smith (4) has pointed out that one-bond coupling constants generally increase in the absolute sense in solvents of greater polarity or higher refractive index. $^1J_{Pt-P}$ is known to be positive (15) and hence decreases in these solvents. Thirdly, the coupling constant changes are not accompanied by corresponding variations in chemical shift (see Discussion).

In order to assess the importance of the moisture content of our solvents we deliberately added water to some of the solutions. The results are easily rationalized in terms of an increase in the dielectric/donor properties of the medium. For example, use of diethyl ether saturated with water gives $^1J_{Pt-P}$ = 2437.1 Hz (δ = 136.09 ppm), 3.7 Hz lower than the value in thoroughly dried ether. Similarly, acetone containing ~10%

[2]It is not possible to make a clear distinction between dielectric and donor properties for the present group of solvents.

Can. J. Chem. Downloaded from www.nrcresearchpress.com by 210.87.254.105 on 09/05/12
For personal use only.

Can. J. Chem. Downloaded from www.nrcresearchpress.com by 210.87.254.105 on 09/05/12
For personal use only.

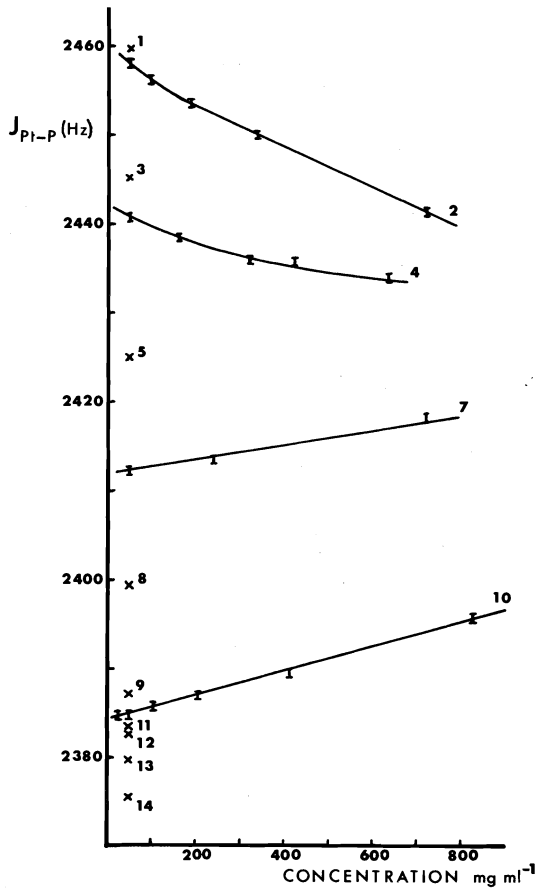

FIG. 1. Solvent and concentration dependence of $^1J_{Pt-P}$ in *trans*-$[PtCl_2(PBu^n_3)_2]$. Solvents are identified by numbers corresponding to those used in Table 1.

water gives $^1J_{Pt-P}$ = 2391.4 Hz (δ = 136.04), 7.9 Hz lower than the value in dry acetone. These results also demonstrated that variations due to traces of water in these solvents are not significant within our experimental errors ($\pm$0.6 Hz) and in consequence rigorous drying of the other solvents was unnecessary. The single exception to this statement was methanol. The solubility of *trans*-$[PtCl_2(PBu^n_3)_2]$ in methanol decreases sharply if traces of water are present and thorough drying was essential to obtain a 50 mg ml^{-1} solution.

The variation of $^1J_{Pt-P}$ with concentration may also be interpreted in terms of the solvation/dielectric ideas presented above. Thus, in cyclohexane and diethyl ether, which may be regarded as having poorer solvating/dielectric properties than *trans*-$[PtCl_2(PBu^n_3)_2]$ itself, $^1J_{Pt-P}$ falls as the concentration of *trans*-$[PtCl_2(PBu^n_3)_2]$ increases. The reverse occurs in benzene and dichloromethane, solvents presumably having better solvating/dielectric properties than the solute, and the plots should therefore converge on the value $^1J_{Pt-P}$ for pure liquid *trans*-$[PtCl_2(PBu^n_3)_2]$ (mp 65 °C). Extrapolation of Fig. 2*c* to 28 °C, the probe temperature for the concentration dependence studies, gives 2433 Hz, in reasonable agreement with the approximate convergence point (2425–2430 Hz) of the concentration plots. The effect is similar to that observed previously for $^1J^{13}_{C-H}$ in solutions of haloethylenes in cyclohexane or dimethylformamide (16).

The range of solvents for which $^1J_{Pt-P}$ in *cis*-$[PtCl_2(PBu^n_3)_2]$ can be studied is more restricted owing to the limited solubility of the complex. The results (Table 1) suggest a tendency for the order of solvent effects to be in opposite directions for the *cis* and *trans* isomers but the correlation coefficient is only 0.68. It is probable that this partial reversal of solvent order is due to opposition of reaction field and specific solvation effects in the *cis* isomer (see Discussion). The comparatively low solubility of *cis*-$[PtCl_2(PBu^n_3)_2]$ also prevented us from measuring concentration dependence in a range of solvents but in CH_2Cl_2 the variation was the inverse of that observed for the *trans* isomer, being approximately linear from 3510.1 Hz at 50 mg ml^{-1} to 3501.0 Hz at 825 mg ml^{-1}. The recent report (5) of solvent dependence of $^1J_{Pt-P}$ in *cis*-$[PtCl_2(PBu^n_3)_2]$ does not specify the concentrations used. The data include only three solvents (CH_2Cl_2, $CHCl_3$, and $(CH_3)_2CO$, $^1J_{Pt-P}$ = 3505, 3508, and 3487 respectively) in common with our study and in each case the coupling constants are slightly lower than those given in Table 1. This probably means that the solutions used were more concentrated than the 50 mg ml^{-1} employed in the present work.

Results for the temperature variation of $^1J_{Pt-P}$ are shown in Fig. 2 for both *cis*- and *trans*-$[PtCl_2(PBu^n_3)_2]$. As is the case with the solvent effects, the temperature variations are in the reverse direction to those observed previously for $^1J_{P-H}$ in phosphine (12). It is possible that variation of dielectric constant is a factor in these temperature effects since the change in $^1J_{Pt-P}$ for *trans*-$[PtCl_2(PBu^n_3)_2]$ is largest in CH_2Cl_2, which also has a large temperature

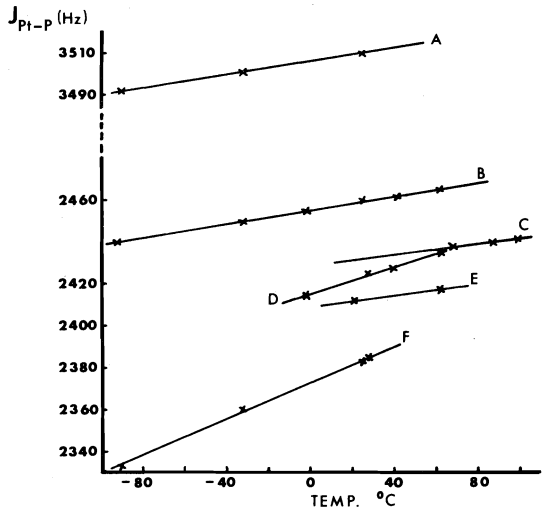

FIG. 2. Temperature dependence of $^1J_{Pt-P}$. (*A*) *cis*-$[PtCl_2(PBu^n_3)_2]$, 50 mg ml^{-1} in CH_2Cl_2; (*B*) *trans*-$[PtCl_2(PBu^n_3)_2]$, 50 mg ml^{-1} in *n*-hexane; (*C*) *trans*-$[PtCl_2(PBu^n_3)_2]$, neat liquid; (*D*) *trans*-$[PtCl_2(PBu^n_3)_2]$, 50 mg ml^{-1} in CCl_4; (*E*) *trans*-$[PtCl_2(PBu^n_3)_2]$, 50 mg ml^{-1} in butyric acid; (*F*) *trans*-$[PtCl_2(PBu^n_3)_2]$, 50 mg ml^{-1} in CH_2Cl_2.

dependence of its dielectric constant (*ca.* -0.06 deg^{-1}), and smallest in butyric acid, chosen because its dielectric constant increases with temperature (*ca.* $+0.002$ deg^{-1}) (17). However, there are clearly other factors involved (see Discussion) since the temperature dependence of $^1J_{Pt-P}$ is not reversed in butyric acid and there is also marked temperature dependence of $^1J_{Pt-P}$ in hexane and CCl_4 which have very small (*ca.* -0.002 deg^{-1}) temperature variation of dielectric.

Chemical Shifts

Solvent induced changes in coupling constants are normally parallelled by changes in chemical shifts as is expected if the changes are due to reaction field or solvent Stark effects. Inspection of Table 1 shows that this is not the case for the present results. The total variation of chemical shift induced by solvent changes is only $\sim 0.6\%$ and there is no correlation with $^1J_{Pt-P}$.

During the concentration variation studies, small, regular changes of chemical shift were noted. Thus the coupling constant variations illustrated in Fig. 1, plots 2, 4, 7, and 10, were accompanied by changes of chemical shift from 135.88 to 135.54 (plot 2, cyclohexane), from 136.09 to 135.70 (plot 4, diethyl ether), from 136.03 to 135.67 (plot 7, benzene) and from 135.74 to 135.56 (plot 10, dichloromethane). In each case the first chemical shift quoted corresponds to the lowest concentration point plotted in Fig. 1 and the second shift to the highest concentration point. A similar variation was observed for *cis*-$[PtCl_2(PBu^n_3)_2]$ in dichloromethane from 139.46 (50 mg ml^{-1}) to 139.12 (825 mg ml^{-1}). The changes in chemical shift are approximately linear[3] with coupling constant but whereas the direction of the latter change varies, the shifts are always in a downfield direction with increasing concentration.

Similar small variations of chemical shift (0.1–0.3 ppm) occurred during temperature dependence and mixed solvent studies, but in these cases no particular trends or correlations emerged. In general, although the chemical shifts were determined to an instrumental accuracy of ± 0.61 Hz ($\equiv 0.015$ ppm), the necessity of using $P(OMe)_3$ in an external reference capillary probably means that the real errors are considerably greater. It would therefore be unwise to attach much significance to the small variations of chemical shift reported in the above paragraphs.

Discussion

The results discussed above enable us to arrive at some conclusions on the likely significance of solvent, concentration, and temperature variations in the routine use of ^{31}P nmr in coordination chemistry. It is clear that within the usual range of ambient probe temperatures, temperature dependence is unlikely to be an important factor. The variation of ~ 0.5 Hz deg^{-1} found for *trans*-$[PtCl_2(PBu^n_3)_2]$ in methylene chloride is, however, large enough that it might find application as a temperature calibration standard for variable temperature ^{31}P studies. Concentration effects will be more serious but with the usual routine range of instrument conditions (*e.g.* 8192 data points ($\equiv$ 4096 real time points) in a 10 kHz sweep giving resolution of 2.44 Hz) they will lie within experimental error for concentrations < 100 mg/ml, *i.e.* ~ 0.15 *M*. For most spectra this concentration would give adequate signal/noise after a few hundred pulses. The most serious variations are those due to changes of solvent and these indicate a need for caution in the use of

[3]There is evidence of curvature in some cases but it is small compared with experimental error.

Can. J. Chem. Downloaded from www.nrcresearchpress.com by 210.87.254.105 on 09/05/12
For personal use only.

Can. J. Chem. Downloaded from www.nrcresearchpress.com by 210.87.254.105 on 09/05/12
For personal use only.

^{31}P for complex characterization. Inspection of Table 1 shows that the variation of chemical shift is much smaller than the variation of coupling constant and the former parameter may actually be more reliable in some cases. In applications such as *trans*-influence studies where the range of coupling constant variation may be very large (11), solvent effects would be unlikely to affect the gross features of a series but could change detailed interpretation.

It is of interest to examine the causes of the observed coupling constant variations in more detail. Previous authors have generally used a model featuring a solute molecule in a cavity in a continuous solvent medium and have interpreted their results in terms of a solvent reaction field, solvent Stark effects, and the Macrae term (4). Although our results show no overall correlations with any of these parameters, their application to the problem may be discussed using Fig. 3, which shows a plot of $^1J_{Pt-P}$ for *trans*-$[PtCl_2(PBu^n{}_3)_2]$ against the square root of solvent dielectric constant. It is clear that high solvent dielectric constant is one factor which can cause a substantial lowering of $^1J_{Pt-P}$ and for the group of solvents; *n*-hexane, cyclohexane, cyclohexene, diethyl ether, acetone, methanol, dimethylformamide, and acetonitrile, a roughly linear correlation with $\sqrt{\epsilon}$ is apparent. Although a reaction field effect is not expected for a nonpolar solute, solvent Stark effects remain a possible explanation of this correlation. The remaining solvents, which all lower $^1J_{Pt-P}$ to a much greater extent than is expected from their dielectric constants, are either chlorinated or aromatic species.[4] An important factor here may be dispersion forces since the order of decreasing $^1J_{Pt-P}$ in *n*-hexane, cyclohexane, cyclohexene, carbon tetrachloride, and benzene is the same as the order of increasing refractive index (17). Moreover, chloroform, dichloromethane and pyridine are also solvents of relatively high refractive index. We note however, that cyclohexane and dimethylformamide have refractive indices similar to chloroform and yet lie on the dielectric plot (Fig. 3). Moreover, as with the dielectric effects, the order of these refractive index effects is the reverse of that observed for

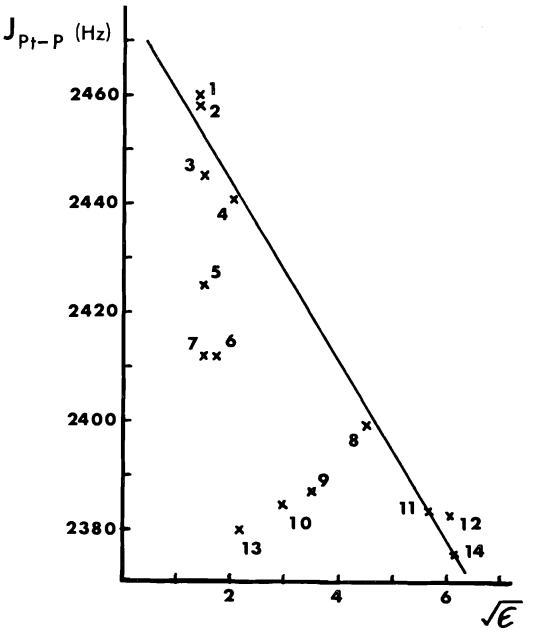

FIG. 3. Dependence of $^1J_{Pt-P}$ in *trans*-$[PtCl_2(PBu^n{}_3)_2]$ on solvent dielectric constant. Solvents are identified by numbers corresponding to those used in Table 1. The significance of the solid line is discussed in the text. It is not intended to imply an overall correlation!

organic solutes and their magnitude is unusually large. In view of these difficulties, we consider that a more intimate model of the interactions may provide a better interpretation than the solvent cavity approach used in deriving reaction field, Stark and Macrae terms. For the square planar *trans*-$[PtCl_2(PBu^n{}_3)_2]$, occupation of axial positions by solvent molecules is an obvious possibility. Results for solvent mixtures (see Fig. 4) show that specific formation of six co-ordinate species {*e.g.* $[PtCl_2(Py)_2(PBu^n{}_3)_2]$} does not occur[5] but the curvature of the plots does suggest a more specific interaction than simple averaging of electric field effects. Thus a competitive solvation, occurring primarily in the plane perpendicular to P—Pt—P and including Cl—Pt—Cl, is a possible explanation. This would cause partial rehybridisation at Pt with a subsequent loss of *s* character in the Pt—P bonds leading to a fall in $^1J_{Pt-P}$. The effect would be greatest for good donor solvents (generally those with high dielectric constant) and the effects of chlorinated and aromatic solvents can be under-

[4]With the exception of butyric acid. A possible explanation of this anomaly is disruption by the solute of the solvent hydrogen bonded dimers, thus causing the solvent to have greater effective dielectric/donor properties than the dielectric constant would suggest.

[5]Specific six co-ordination would lead to a very rapid change in $^1J_{Pt-P}$ on the addition of 2 molar equivalents of polar solvent (*ca.* 0.02 vol.%).

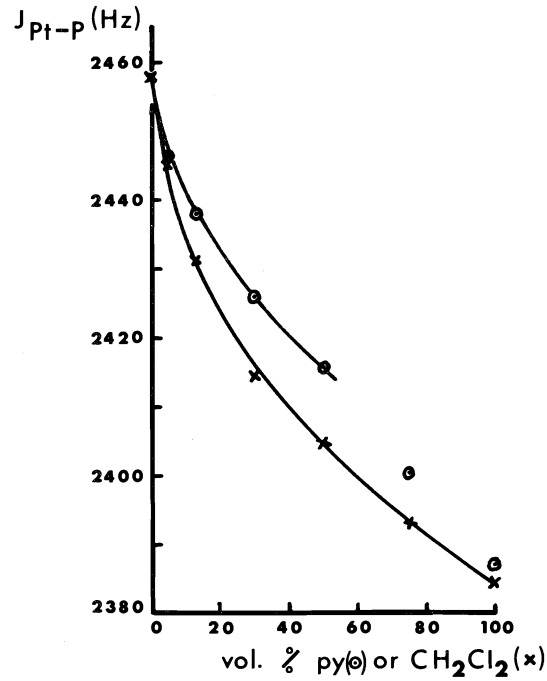

FIG. 4. Variation of $^1J_{Pt-P}$ for 50 mg ml^{-1} of *trans*-$[PtCl_2(PBu^n_3)_2]$ in solvent mixtures; cyclohexane plus CH_2Cl_2 or pyridine. (In the pyridine case two phases were present for mixtures >60% pyridine.)

stood in terms of their polarizability and their known ability to be highly effective at solvating this type of complex. The effect would decrease with temperature as thermal agitation removes molecules from the solvation sphere, thus explaining the unusual (relative to previous studies) increase of $^1J_{Pt-P}$ with increasing temperature. Other important evidence for this model is the lack of solvent effect on the phosphorus chemical shift. Smith has noted (4) that in virtually every instance solvent induced changes in coupling constants parallel changes in chemical shifts. Consequently, the lack of variation in the present instance is strong evidence against generalized field effects and in favour of a more specific interaction at platinum, changing $^1J_{Pt-P}$ via the 6*s* orbital, and having relatively little effect on the overall electron density at phosphorus. Finally, for *cis*-$[PtCl_2(PBu^n_3)_2]$, the possibility of reaction field effects for the polar solute may be responsible for the partial reversal of the order of solvent effects.

Experimental

cis- and *trans*-$[PtCl_2(PBu^n_3)_2]$ were prepared and purified as previously described (18). Solvents were of spectroscopic grade and were normally used as received. Methanol was dried over magnesium methoxide and diethyl ether over sodium but special drying procedures were not employed for the other solvents after experiments indicated that traces of water did not cause serious errors (see Discussion).

Nuclear magnetic resonance spectra were recorded in 8 mm tubes using a JEOL PFT 100 Fourier transform spectrometer operating at 40.482 MHz. External deuterium lock and phosphorus reference signals were provided by a capilliary insert containing C_6D_6 and trimethylphosphite, and all chemical shifts are quoted as ppm upfield from this reference. Protons were decoupled by broad band (2.5 kHz) 'noise' irradiation and 16 384 data points were used in a sweep width of 5000 Hz, giving resolution of 0.6 Hz. The reported coupling constants and chemical shifts are therefore subject to errors of this magnitude. All results are reported for a probe temperature of 28 °C unless otherwise noted. Concentrations are given in mg per ml *of solution*.

Acknowledgements

We thank the University of Victoria for the granting of study leave to K.R.D. and the University of Sussex for the provision of research facilities during this leave.

1. M. BARFIELD and M. D. JOHNSTON, JR. Chem. Rev. **73**, 53 (1973).
2. P. LASZLO. *In* Progress in nmr spectroscopy. Vol. 3. *Edited by* J. W. Emsley, J. Feeney, and L. H. Sutcliffe. Pergamon Press, New York. 1967. Chapt. 6
3. J. RONAYNE and D. H. WILLIAMS. Ann. Rev. N.M.R. Spectrosc. **2**, 83 (1969).
4. S. L. SMITH. Top. Current Chem. **27**, 119 (1972).
5. P. H. KREUTZER, K. T. SCHORPP, and W. BECK. Z. Naturforsch. **30**b, 544 (1975).
6. P. LASZLO and A. SPEERT. J. Mag. Res. **1**, 291 (1969).
7. J. V. HATTON, W. G. SCHNEIDER, and W. SIEBRAND. J. Chem. Phys. **39**, 1330 (1963).
8. G. D. SHIER and R. S. DRAGO. J. Organomet. Chem. **5**, 330 (1966).
9. G. D. SHIER and R. S. DRAGO. J. Organomet. Chem. **6**, 359 (1966).
10. J. F. NIXON and A. PIDCOCK. Ann. Rev. N.M.R. Spectrosc. **2**, 345 (1969).
11. T. G. APPLETON, H. C. CLARK, and L. E. MANZER. Co-ord. Chem. Rev. **10**, 335 (1973).
12. E. A. V. EBSWORTH and G. M. SHELDRICK. Trans. Faraday Soc. **63**, 1071 (1967).
13. R. FIELDS, M. GREEN, and A. JONES. J. Chem. Soc. (A), 2740 (1969).
14. Y. L. KLAIMAN, N. V. MORKOVIN, and B. I. IONIN. J. General Chem. (USSR), **37**, 2661 (1967).
15. W. MCFARLANE. J. Chem. Soc. (A), 1922 (1967).
16. V. S. WATTS, J. LOEMBER, and J. H. GOLDSTEIN. J. Mol. Spectrosc. **17**, 348 (1965).
17. R. C. Weast (*Editor*). Handbook of chemistry and physics. Chemical Rubber Co., Cleveland, Ohio. 1970.
18. G. B. KAUFFMAN and L. A. TURNER. Inorg. Synth. **7**, 245 (1963).

Can. J. Chem. Downloaded from www.nrcresearchpress.com by 210.87.254.105 on 09/05/12
For personal use only.

The effect of monolayers on the rate of evaporation of H_2O and solution of O_2 in H_2O

R. N. O'Brien and A. I. Feher
Department of Chemistry, University of Victoria, P.O. Box 1700, Victoria, B.C., Canada V8W 2Y2
AND
K. L. Li and W. C. Tan
Lester B. Pearson College of the Pacific, Pedder Bay, B.C., Canada

Received December 29, 1975

R. N. O'Brien, A. I. Feher, K. L. Li, and W. C. Tan. Can. J. Chem. **54**, 2739 (1976).

The well-known effect of the retardation of evaporation by monolayers of surfactants has been investigated by laser interferometry and the appropriate conventional apparatus. The temperature drop caused by evaporation has been calibrated for several surfactants in general use for conserving reservoir waters and for lecithins considered to be part of living membranes. Rate of ingress of oxygen has been treated in the same way. The best performance was about 60% retardation of evaporation for the molecules that pack well. The behaviour for O_2 ingress retardation was very similar. The lecithins were suitably permeable to be able to act as a bilamellar layer cell membrane.

R. N. O'Brien, A. I. Feher, K. L. Li et W. C. Tan. Can. J. Chem. **54**, 2739 (1976).

L'effet bien connu du ralentissement de l'évaporation par des monocouches de surfactants a été étudié par interférométrie de laser et par un appareillage conventionnel approprié. La baisse de température causée par l'évaporation a été calibrée pour plusieurs surfactants utilisés couramment pour la conservation des eaux en réservoir et pour les lécithines qui sont considérées comme faisant partie des membranes vivantes. Le taux d'imprégnation de l'oxygène a été traité de la même façon. Le meilleur rendement observé fut un retardement de l'évaporation de 60% pour les molécules qui se tassent bien entre elles. Un comportement similaire a été observé pour le retardement de l'imprégnation d'O_2. Les lécithines se sont avérées suffisamment perméables pour pouvoir agir comme une paroi cellulaire à couche bilamellaire.

[Traduit par le journal]

Introduction

Since the pioneering work of Langmuir and Langmuir (1) and Rideal (2) it has been accepted that the resistance to evaporation of water afforded by a monolayer was simply the added resistance to a diffusive evaporation process. Many others have contributed both theory and results to these studies (3). Recently Wu (4) has suggested that the smoothing of surface ripples by a monolayer results in a decrease of wind shear over large water surfaces and that this is the controlling factor in evaporation retardation. His suggestion has been disputed by both Mansfield and Mysels (5) but Wu has rebutted (5). In this publication we wish to add some helpful data in this area. Our data were collected by a new technique for measuring evaporation retardation by monitoring the surface cooling in water with an interferometer.

To the best of our knowledge only two studies have been carried out on the effect of monolayers on gas dissolution into water (6, 7). In this study we have also applied interferometric techniques to the measurement of oxygen diffusion into water in the presence of a monolayer. In the present era of environmental concern it is clearly important to investigate the effects of monolayers (or oil spills) on the rate of oxygen absorption into the underlying waters. If oxygen dissolution were hindered in natural bodies of water the oxygen-dependent organisms would become depleted.

Experimental

Five different monolayer forming substances were used: stearyl alcohol (ultra high purity, Hormel, University of Minnesota), stearic acid (ultra high purity, Hormel), oleic acid (99.9%, K & K), dipalmitoyl phosphotidyl choline (saturated synthetic lecithin, K & K), and soybean lecithin (unsaturated natural lecithin, Hormel).

The molecular areas of these surfacants (Table 1) were determined at their equilibrium spreading pressures in a standard calibrated Langmuir–Wilhelmy trough. All necessary precautions were taken with regard to cleanliness of apparatus, chemicals, spreading solvent (hexane) and water (8).

Can. J. Chem. Downloaded from www.nrcresearchpress.com by 210.87.254.40 on 09/05/12
For personal use only.

Can. J. Chem. Downloaded from www.nrcresearchpress.com by 210.87.254.40 on 09/05/12
For personal use only.

The water evaporation and oxygen dissolution measurements were carried out in a Fabry–Perot interferometer specially designed for high pressure gas dissolution work. The details of its design have been previously published (9). Briefly, this interferometer was made of stainless steel, was thermostatically jacketed, and was capable of withstanding 10 atm of pressure without distortion. The interference fringes produced by the two 90% reflecting windows (of flatness $\lambda/20$ and set 5 cm apart) had a coefficient of finesse (10) of approximately 7. This was sufficient to allow the fringe centres to be located with a reproducibility of between 1/20 and 1/50 of the fringe spacing (10).

Figure 1 is a schematic diagram of the interferometer as used for measuring the rate of evaporation of water. Figure 1*a* gives the general construction details of the cell showing the direction of propagation of the laser light (Spectra Physics 132; 632.8 nm), the level of the water, and the gas flow arrangements. Figure 1*b* is an end-on representation of the appearance of the fringes in the air and water separated by the meniscus. Figure 1*c* shows the simple arrangement used to determine the gas flow rate through the interferometer.

In the experiments on water evaporation this interferometer was used as a thermometer to measure the temperature profile of the surface water layers. The gas flow over the water was selected to be 10 cc s^{-1} at 1 atm and, from the cell geometry, this corresponded to a gas stream flowing at 10 cm s^{-1} over the water. The gas used was either high purity compressed air or nitrogen and both gave the same cooling at the surface.

The water evaporating into the gas stream lowered the surface temperature which in turn raised the density and refractive index of the surface layers. Natural convection began as the cooler water began to sink and the warmer began to rise. Within about 60 s a dynamic equilibrium was established such that a 2 mm layer of water had a steady temperature gradient in it. The refractive index profile in this 2 mm water layer was manifested by the smoothly curved set of interference fringes shown in Fig. 2*a*. There appears to be a fringe shift of about 0.92 fringes (*i.e.* the top of the fringe system is displaced 0.92 times the original spacing in the bulk). Using previously published calibrations (9–12) this fringe shift is known to be equivalent to a temperature drop of 0.38 °C below that of the bulk.

At the same gas flow rate as above a monolayer was spread and after 60 s another interferogram was recorded. Figure 2*b* shows the effect of stearyl alcohol on the surface temperature of water. The fringe shift is now 0.38 and the surface temperature drop is only 0.16 °C below that of the bulk.

The oxygen ingress experiments (using high purity compressed oxygen) were started without a monolayer. About 4 atm of oxygen were rapidly applied to the water previously equilibrated with 1 atm of oxygen. After 60 s an interferogram was recorded. In the next experiment a monolayer was spread and when the new steady state diffusion under the same O_2 pressure was established (60 s) another interferogram was recorded. A specially designed gas diffuser at the inlet stage was used to prevent gross distortions of the water surface as the pressure was rapidly increased (9, 12). The compression of the gas above the water and the accompanying condensation of water vapour contributed to an initial temperature rise in the water surface; this relaxed in about 1 s (9, 12).

The refractive index of water solutions of oxygen has a negative slope of -2.69×10^{-3} (refractive index per molarity). Oxygen solutions in water have a lower density and refractive index than pure water. Previous calibrations have shown (9, 12) that a pressure of 4 atm of oxygen over water gives a fringe shift of 2.2 in the opposite direction to the previous water evaporation and hence cooling experiments. (For a comprehensive explanation of interferometric calculations the reader is referred to O'Brien (10).)

All the interferograms were recorded on video tape by a Sony AV-3650 recorder using a Sony AVC-3210 video camera. Fields (or 'frames') were selected from the video tape and displayed on a television monitor and photographed with a 35 mm camera. The developed 35 mm negatives were then projected onto a 'light table' and the fringe spacings and shifts were measured. The image magnification so obtained was in general not less than 53×.

Results and Discussion

The analysis of the interferograms obtained in the water evaporation experiments are summarized in Table 1. In that table the term 26% retardation by both lecithins, for example, means that the fringe shift was only about 3/4 that for a monolayer free surface under the same conditions of gas flow over the surface. A number of assumptions are involved in equating these observations to a 26% evaporation retardation.

The first is that the temperature dependence of the refractive index of water is linear over the temperature interval involved 20.0–20.5 °C. This is a valid assumption (11). It is further assumed that the heat necessary for the evaporation of the top layers is supplied by the bulk water through convection and conduction, and that the elapsed time of the experiment is not sufficient to appreciably reduce the bulk water temperature. This is also a reasonable assumption, for if the bulk temperature had changed then the fringe spacing would also have changed noticeably. Furthermore, if the bulk water temperature had changed then heat would have been supplied by the surroundings, most likely the bottom of the cell. It has been our experience that when this occurs erratic convective flows arise which distort the fringe pattern in characteristic (spectacular) ways. Absence of these convective flows results in smoothly bent fringes (Fig. 2) produced by the integrating effect of the fringes on the refractive index over all the very small Liesegang (Bénard) convective cells in the water.

Can. J. Chem. Downloaded from www.nrcresearchpress.com by 210.87.254.40 on 09/05/12
For personal use only.

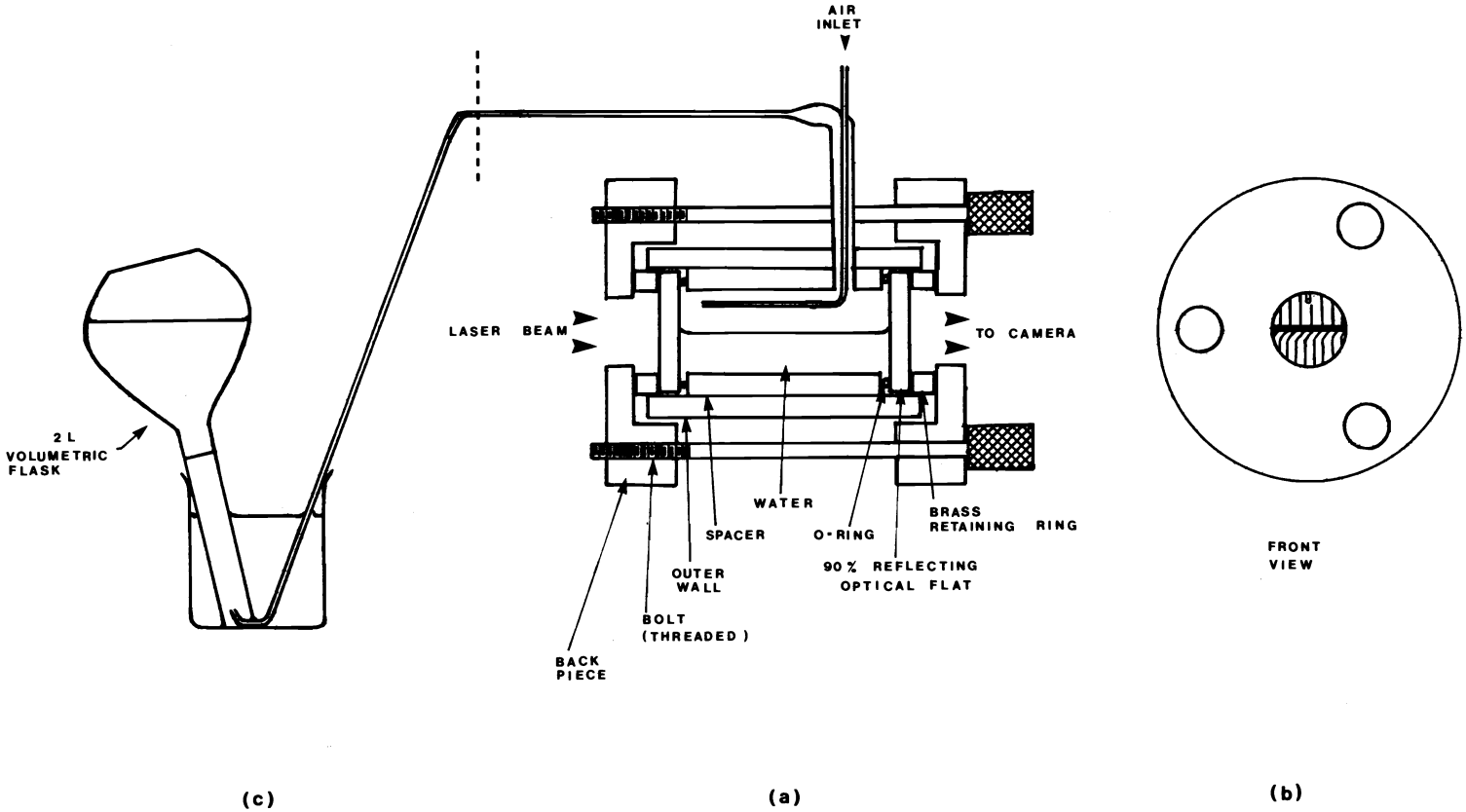

FIG. 1. Diagram of the interferometer cell, the flow measuring apparatus, and a schematic view of a typical front view fringe pattern.

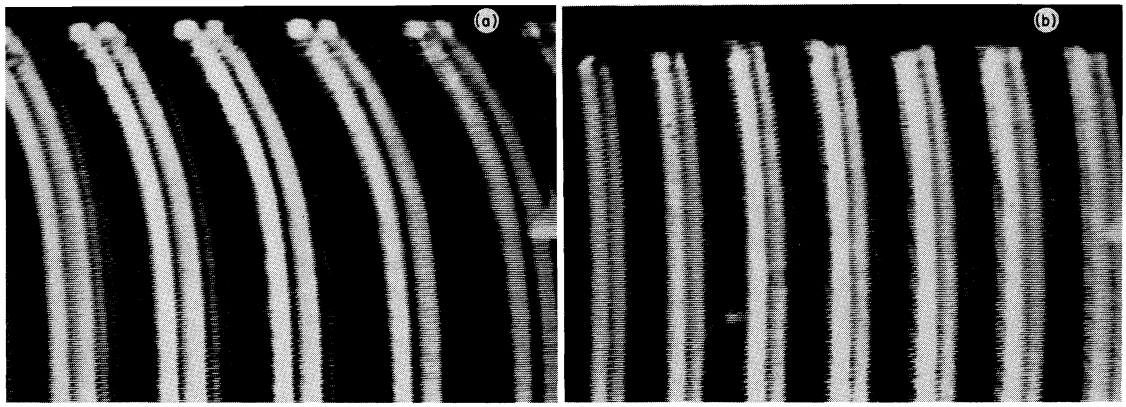

FIG. 2. Two interferograms: (*a*) air flow over a bare water surface; (*b*) over a monolayer covered surface.

TABLE 1. Retardation of evaporation by monolayers on water

Compound	% retardation	Area (Å² molecule)
Lecithins (both)	20	40–45
Oleic acid (*cis*-9-octadecanoic)	5	28
Stearic acid (octadecanoic)	28	24
Stearic alcohol (octadecanol)	59	22

The difference in surface temperature at constant gas flow (or wind speed) over the surface both with (Fig. 2*b*) and without (Fig. 2*a*) a monolayer of stearic alcohol is striking. The wind does not produce as much cooling in, or evaporation from, the surface in the presence of the monolayer. In both cases thermal diffusion alone cannot account for the heat transfer necessary for the evaporation. If diffusion alone were operative then the temperature profiles (fringe profiles) would fit the error function solution of Fick's second law. Analysis of similar temperature reductions that accompany the leading edge of a spreading monolayer (13) has shown that the thermal changes are too rapid for diffusion alone, so some convection must also be present.

The third and most important assumption is that the temperature changes in the water surface are taken to be directly proportional to the changes in the evaporation rate of water. This must be true for very thin films of water that are thermally isolated. It should also be true for volumes of water which are very large in relation to the volume of water evaporated per unit time, or to the rate at which heat must be supplied. This case corresponds to one of the boundary conditions for the solution of the differential equation for diffusion: that the cell be semi-infinite, or that the diffusion gradient reach zero inside the bulk of the water. Since the fringe bends occurred to a depth of only 3 mm and the total depth of water was 20 mm the above condition is met. It is therefore reasonable to expect a linear relationship between the surface temperature change and the change in evaporation rate.

The experiments on the rate of dissolution of oxygen through a monolayer depend on prior knowledge of the refractive index of oxygen solutions. The previously published values of O'Brien and Hyslop (9) were used in this study. Analyses of the interferograms in terms of oxygen concentrations in water with the different monolayers are shown in Fig. 3.

The monolayer free surface reached about 6×10^{-3} *M* in O_2 in 60 s, the oleic acid covered surface was 5×10^{-3} *M* in O_2, the stearic acid about 4.5×10^{-3} *M* in O_2, and the stearyl alcohol about 3×10^{-3} *M* in O_2. In terms of retardation of oxygen ingress this is 16% for oleic acid, 25% for stearic acid, and 50% for stearyl alcohol. The lecithins tended to dissolve (without a spreading solvent) when the oxygen pressure was applied which resulted in poor optical resolution of the fringes. It is estimated that their resistance to oxygen ingress was about the same as for stearic acid. After a few seconds, visible particles attached to gas bubbles appeared.

The plot of oxygen dissolving in clean water has been found to fit the error function depend-

Can. J. Chem. Downloaded from www.nrcresearchpress.com by 210.87.254.40 on 09/05/12
For personal use only.

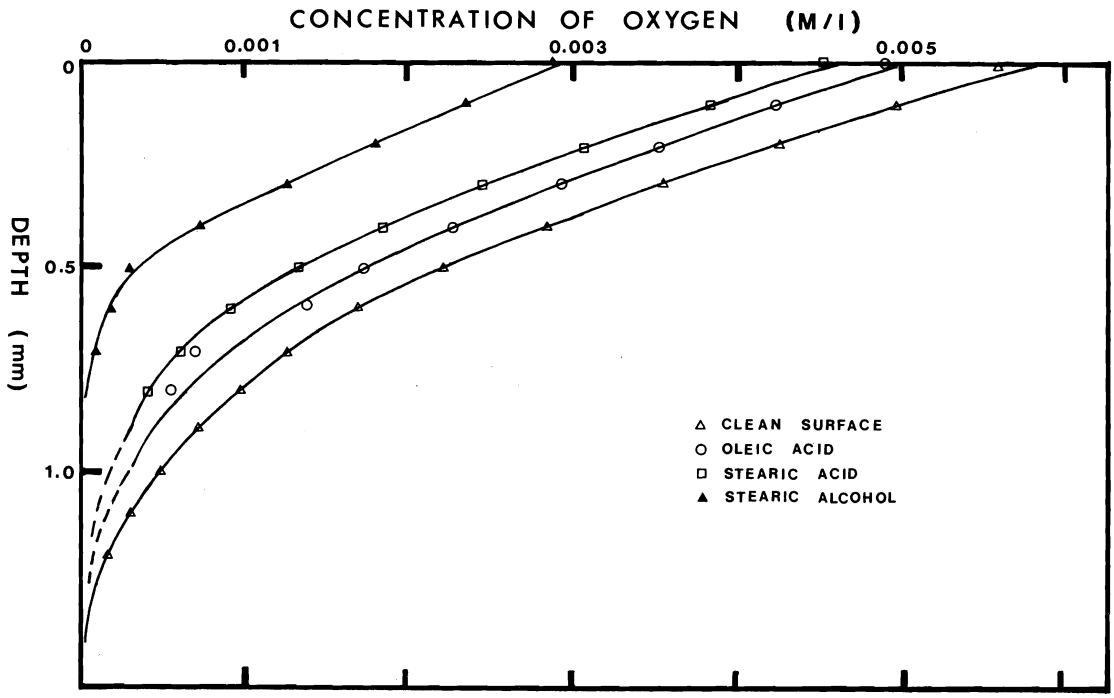

FIG. 3. Retardation of O_2 dissolving in water by a monolayer.

ence expected (9, 12) because in this case the gas solution has a lower density than pure water (no convection). Within 60 s a detectable diffusion gradient existed down to about 1.5 mm. All the plots should give zero concentration at the same depth; however, concentrations below 2×10^{-4} M O_2 are difficult to measure accurately since this represented a fringe shift at the limits of detection.

Conclusions

In general it appears that the area covered by a molecule in a compact monolayer is a good indication of the degree to which it retards evaporation of water. This is in agreement with previous findings (14).

Retardation of oxygen penetration into water by the monolayers showed the same general trend as for evaporation retardation. The acids and the lecithins which do not form highly compact monolayers give the least resistance to both oxygen and water. These surfactants also have a relatively large hydrophilic group which may also contribute to their low resistances. On the other hand the stearyl alcohol forms a compact monolayer and has a small hydrophilic group which would interact very favourably with the surface water layers and perhaps form a denser array at the interface compared with the free water surface.

Both lecithins were found to be highly permeable to oxygen and water despite the fact that the synthetic sample had saturated hydrocarbon chains, suggesting that it is the large hydrophilic group which has the greater effect on permeability. The lecithins in the monolayer state are considered to form 1/2 of the widely accepted bilamellar layer model of a cell membrane and it appears that they are sufficiently permeable to give the rapid transport of oxygen and water that is known to occur in living cells such as erythrocytes.

Acknowledgements

Our thanks are due to R. J. Raine for assistance with the experimental work and to J. Leja for helpful discussions.

This work was supported by the National Research Council of Canada and Environment Canada under contract No. OST4-0186 to whom our thanks are due.

1. I. LANGMUIR and D. B. LANGMUIR. J. Phys. Chem. **31**, 1719 (1927).

Can. J. Chem. Downloaded from www.nrcresearchpress.com by 210.87.254.40 on 09/05/12
For personal use only.

2. E. K. RIDEAL. J. Phys. Chem. **29**, 1585 (1925).
3. V. K. LAMER (*Editor*). Retardation of evaporation by monolayers. Academic Press, N.Y. 1962.
4. J. WU. Science, **174**, 283 (1971).
5. W. W. MANSFIELD. Science, **176**, 944 (1972). K. J. MYSELS. Science, **176**, 944 (1972). J. WU. Science. **176**, 945 (1972).
6. J. G. HAWKE and A. E. ALEXANDER. *In* Retardation of evaporation by monolayers. *Edited by* V. K. LaMer. Academic Press, N.Y. 1962. p. 67.
7. M. BLANK. *In* Retardation of evaporation by monolayers. *Edited by* V. K. LaMer. Academic Press, N.Y. 1962. p. 75.
8. G. L. GAINES, JR. Insoluble monolayers at gas/liquid interfaces. Interscience, N.Y. 1965. pp. 30–75.
9. R. N. O'BRIEN and W. F. HYSLOP. Symposium on physics and chemistry of gas solutions. *Edited by* W. A. Adams. The Electrochemical Society, Princeton, N.J. 1975.
10. R. N. O'BRIEN. Rev. Sci. Instrum. **35**, 803 (1964). R. N. O'BRIEN. *In* Techniques in chemistry, physical methods. Part IIIA. *Edited by* A. Weissberger and B. W. Rossiter. Wiley, N.Y. 1974. Chapt. I.
11. R. N. O'BRIEN. Chem. Eng. Data, **13**, 2 (1968). R. N. O'BRIEN. Chem. Eng. Data, **18**, 144 (1973).
12. W. F. HYSLOP. Ph.D. Dissertation, Department of Chemistry, University of Victoria, Victoria, B.C. 1975.
13. R. N. O'BRIEN, A. I. FEHER, and J. LEJA. J. Colloid Interface Sci. **51**, 366 (1975).
14. G. T. BARNES, T. I. QUICKENDEN, and J. E. SAYLOR. J. Colloid Interface Sci. **33**, 236 (1970).

Can. J. Chem. Downloaded from www.nrcresearchpress.com by 210.87.254.40 on 09/05/12
For personal use only.

A catalyst for ester hydrolysis showing electrostatic and hydrophobic binding properties

J. Peter Guthrie[1] and Yasutsugu Ueda

Department of Chemistry, University of Western Ontario, London, Ont., Canada N6A 5B7

Received October 1, 1975[2]

J. Peter Guthrie and Yasutsugu Ueda. Can. J. Chem. **54**, 2745 (1976).

The steroid 17β-(4-imidazolyl)-5α-androstane-3β,11β-diamine, **1***a*, R = H, acts as a catalyst for the hydrolysis of aryl esters. For a series of aryl acetates, **2***a–h*, at 1 *M* ionic strength, log k_2 for **1***a* catalyzed hydrolysis is linearly related to log k_2 for imidazole catalyzed hydrolysis, with only **2***d*, 4-acetoxy-3-nitrobenzoate, deviating: at zero ionic strength, all anionic substrates show positive deviations, and a cationic substrate shows a negative deviation. This is interpreted in terms of a stringent geometrical requirement for strong electrostatic catalysis. With favorable geometry, a 1:1 electrostatic attraction can lead to a 15 fold rate enhancement (μ = 0). For a series of arylpropionate esters **3***a–c*, rate constants for **1***a* catalyzed hydrolysis show a small but progressive increase with increasing size of the aryl group: after correcting for substrate reactivity and electrostatic interactions, this hydrophobic effect is independent of the leaving group. **1***b* (R = isopropyl) was prepared to determine the rate of reaction at N-3 of the steroidal imidazole ring: this is the more hindered nitrogen but also the more suitable for hydrophobic binding. **1***b* was markedly less reactive than **1***a*, but showed larger hydrophobic effects. Detailed analysis suggests that the potential hydrophobic rate enhancement for the interaction of a phenanthryl group with the lower surface of a steroid is about 160-fold. This study provides guidelines for the design of enzyme models of greater catalytic efficiency.

J. Peter Guthrie et Yasutsugu Ueda. Can. J. Chem. **54**, 2745 (1976).

Le stéroïde (imidazolyl-4)-17β androstane-5α diamine-3β,11β, **1***a*, R = H, agit comme catalyseur pour l'hydrolyse d'esters d'aryle. Pour une série d'acétates d'aryle, **2***a–h*, à force ionique de 1 *M*, le log k_2 pour l'hydrolyse catalysée par **1***a* est linéairement relié au log k_2 pour l'hydrolyse catalysée par l'imidazole, avec seulement l'acétoxy-4 nitro-3 benzoate **2***d* qui dévie: à force ionique 0, tous les substrats anioniques montrent des déviations positives et un substrat cationique montre une déviation négative. Ceci est interprété en terme d'une exigence géométrique rigoureuse pour une catalyse électrostatique forte. Avec une géométrie favorable, une attraction électrostatique 1:1 peut conduire à une augmentation de vitesse par un facteur de 15 (μ = 0). Pour une série d'esters propionate d'aryle **3***a–c*, les constantes de vitesse pour l'hydrolyse catalysée par **1***a* montrent une augmentation petite mais progressive avec l'augmentation de la taille du groupement aryle: après correction pour la réactivité du substrat et les interactions électrostatiques, cet effet hydrophobe est indépendant du groupe partant. Le composé **1***b* (R = isopropyle) a été préparé pour déterminer la vitesse de réaction à l'azote N-3 du cycle imidazole du stéroïde: celui-ci est l'azote le plus encombré mais aussi le plus approprié pour une liaison hydrophobe. Ce composé **1***b* s'est avéré passablement moins réactif que **1***a* mais a montré des effets hydrophobes plus grand. Une analyse détaillée suggère que l'augmentation potentielle de la vitesse due aux effets hydrophobes est environ de 160 fois pour l'interaction d'un groupe phénanthryle avec la surface inférieure d'un stéroïde. Cette étude fournit un guide pour l'élaboration de modèles d'enzymes ayant une plus grande efficacité catalytique.

[Traduit par le journal]

Introduction

As an approach to the problem of a rationally designed artificial enzyme, it seemed obligatory to devise catalysts which were rigid, monomeric, well-defined species interacting with simple, proven stoichiometry with their substrates in aqueous solution, so that observed rate enhancements could be attributed to particular, defined interactions. In this way one could obtain reliable information concerning the requirements for binding and catalysis and so lay a foundation for the design of systems showing large catalytic effects. The free energy of binding of substrates to enzymes is believed to arise in large measure from hydrophobic and sometimes electrostatic interactions (1). Both of these interactions are very weak when calculated per pair

[1]Alfred P. Sloan Fellow, 1975–1977.

[2]Revision received May 3, 1976.

Can. J. Chem. Downloaded from www.nrcresearchpress.com by 210.87.254.42 on 09/05/12
For personal use only.

Can. J. Chem. Downloaded from www.nrcresearchpress.com by 210.87.254.42 on 09/05/12
For personal use only.

of interacting atoms, so that they are difficult to evaluate in small molecule systems.

Numerous studies (2–7) have been reported in which rate enhancements of ester reactions result from hydrophobic interactions of catalyst and substrate. However, these have almost all been of systems where it is impossible to specify in any detail the conformation of the transition state, so that it has not been possible to interpret the rate enhancements observed in terms of geometrical requirements (2–5). Furthermore, most of these studies used linear alkyl chains as binding groups (2–6): it has recently been shown that compounds with long alkyl chains are aggregated at much lower concentrations than had been believed (8, 9), so that there is some doubt about the interpretation of the large rate enhancements reported for these compounds (10). Enzyme models based upon cyclodextrins circumvent some of these difficulties, in that both binding constants and rate constants for reaction within the complex are measureable (11–18). Unfortunately, only limited variation of either the binding group of the substrate or of the cyclodextrin is possible, and it is difficult to generalize from the behavior of these systems because of the rather heterogeneous chemical nature of the inner surface of the cyclodextrin binding cavity.

The present paper describes experiments with an enzyme model, **1***a* (19–22), based upon a steroid ring system, which has provided unambiguous evidence concerning the magnitude of hydrophobic and electrostatic interactions with rather well specified geometry.

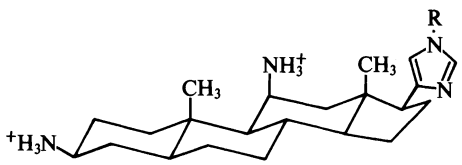

1*a* R = H
1*b* R = $CH(CH_3)_2$

Results

Titration

Potentiometric titration of the steroid, **1***a*, Fig. 1, revealed a well-defined inflection point corresponding to a pK_a of 7.18 attributed to the imidazole. The pK_a's of the two amino groups are less well-defined, but values of 9.69 and10.68 are consistent with the curve. The imidazole pK_a is almost unperturbed by the rest of the steroid: titration of imidazole itself under the same conditions gave a pK_a of 7.14. Of the two amino group pK_a's, that of 9.69 is attributed to the 11-amino group by analogy with the work of Bird and Cookson (23) who showed that hindered steroidal amines were less basic than unhindered amines. There will be an additional base weakening effect due to electrostatic interaction with the 3-ammonium group.

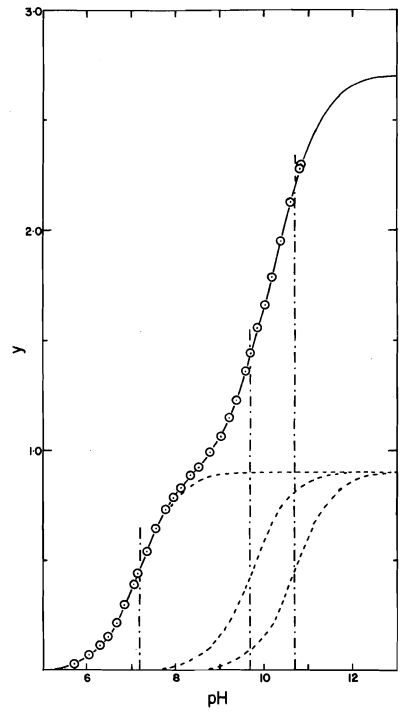

FIG. 1. Potentiometric titration of **1***a*; *y* is the difference in the volume of base required to produce a given p*H* in the presence and absence of sample. The points are experimental, the solid line is calculated using parameters evaluated by least squares and the dashed lines are calculated for the individual pK_a's: pK_1 = 7.18, pK_2 = 9.69, and pK_3 = 10.68.

pH Rate Profile

The steroid **1***a* shows p*H* rate profiles indicative of a kinetically significant pK_a of *ca.* 7.2, but other features complicate the interpretation of the profile, see Table 1 and Fig. 2. For the substrate *p*-nitrophenyl acetate, **2***a*, there is superimposed upon the simple titration curve for the imidazole what is apparently a hydroxide catalyzed process. For the substrate, **2***d*, there is a fall off in rate above p*H* 8.5 which presumably reflects deprotonation of the 11-am-

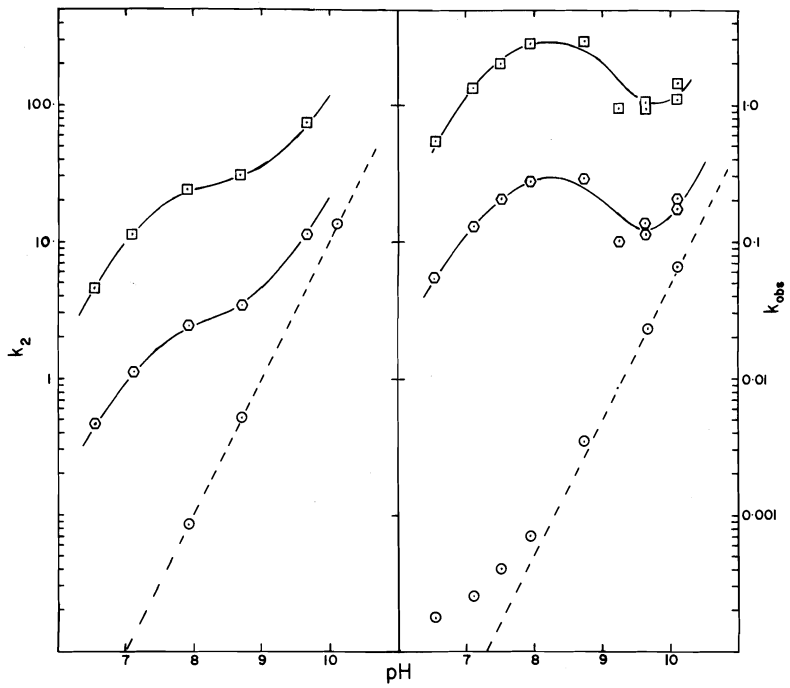

FIG. 2. p*H* rate profiles for **1***a* catalyzed hydrolysis of **2***a* and **2***d*. Left hand ordinate: k_{obs}, the pseudo first-order rate constant for phenoxide release. Right hand ordinate, k_2, the apparent second-order rate constant for **1***a* catalysis. (○) Buffer alone: lines are of unit slope. (⬡) k_{obs} with 0.00097 *M* **1***a*; lines are the sum of the catalyzed and uncatalyzed reactions. (□) k_2 for **1***a*; lines are calculated using parameters evaluated by least squares.

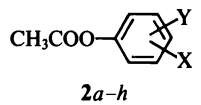

2*a–h*

a	X = H, Y = 4-NO_2
b	X = H, Y = 3-NO_2
c	X = 2-NO_2, Y = 4-NO_2
d	X = 3-CO_2^-, Y = 6-NO_2
e	X = 4-CO_2^-, Y = 6-NO_2
f	X = 4-SO_3^-, Y = 6-NO_2
g	X = 4-NMe_3^+, Y = 6-NO_2
h	X = 3-CO_2Me, Y = 6-NO_2

monium group and loss of electrostatic binding of the substrate (*vide infra*); the apparent kinetic pK_a is *ca.* 9.5 which is consistent with this interpretation. There is a suggestion of a hydroxide catalyzed reaction at high p*H*. To extend the p*H* rate profiles into more alkaline solutions would have required much higher steroid concentrations to overcome the rapidly increasing uncatalyzed hydrolysis rate, and this seemed sure to lead to problems of micellization of the catalyst (which indeed may be occurring at p*H* 10). In any event p*H* 8 appears to be optimal for a study of the substrate specificity of **1***a*.

Micellization

The steroid **1***a* was designed to be monomeric at p*H* 8 where it is dicationic. To test whether this is the case, the effect of varying steroid concentration upon the rate constant for steroid catalyzed hydrolysis was tested, using *p*-nitrophenyl hexanoate as substrate. Menger and McCreery have shown (24) that bile salt micelles bind *p*-nitrophenyl hexanoate, and so protect it from hydroxide catalyzed hydrolysis. It seemed to us that the hexanoate is the optimum ester for this purpose, since it is hydrophobic enough to bind strongly to micelles, yet (as previous work in this laboratory had shown), the hexanoate ester itself was not aggregated until much higher concentrations than were used in the present experiments. It was conceivable that micellization of the steroid would lead to either enhanced or reduced reactivity toward the ester, but seemed improbable that it would have no effect. In fact from 10^{-4} to 10^{-2} *M* steroid the second-order rate constant is concentration independent within experimental error.[3] We conclude that at

[3]The apparent second-order rate constants (M^{-1} min^{-1}) were (**1***a*) k_2: 0.968 × 10^{-2} *M*, 18.3; 0.968 × 10^{-3} *M*, 18.2; 0.968 × 10^{-4} *M*, 19.7.

Can. J. Chem. Downloaded from www.nrcresearchpress.com by 210.87.254.42 on 09/05/12
For personal use only.

concentrations of steroid **1***a* less than or equal to 10^{-2} *M* micelle formation does not occur. For bile salts, cmc values range from 10^{-3} to 10^{-2} *M*.[4]

Electrostatic Catalysis (22b)

Rate constants for imidazole and **1***a* catalyzed hydrolysis of a series of aryl acetates were measured in buffers of varying ionic strength; these values are found in Table 2. A plot of log k_2 for **1***a* catalyzed hydrolysis *vs.* log k_2 for imidazole catalyzed hydrolysis of these esters using data at $\mu = 1.0$ *M* for the ionic esters and any ionic strength for the neutral esters gives a good straight line of slope 0.80 with only the point for **2***d* deviating; see Fig. 3. Extrapolation to $\mu = 0$ was possible by plotting log k_2 *vs.* log $\gamma_\pm$ calculated from the Davies equation (25). Figure 4 shows typical plots of this type. The points for zero ionic strength shown on Fig. 3 (for the neutral esters rate constants were independent of ionic strength) reveal that all of the ionic substrates deviate in the predicted manner, but that the magnitude of the deviations for **2***d* is greater than for any others. Thus, the electrostatic interaction of **2***d* with **1***a* in the transition state for **1***a* catalyzed hydrolysis of **2***d* must be particularly favorable. Examination of space filling molecular models shows that for the transition state involving **2***d*, and only for this substrate, it is possible for the transition state to adopt a conformation in which there is contact between the carboxylate of the substrate and the 11-ammonium of the catalyst and simultaneously hydrogen bonding between these groups (22*b*).

[4]For ionic strength *ca.* 0.2, typical values are (24): bile salt, cmc (*M*); cholic acid, 0.012; deoxycholic acid, 0.006; chenodeoxycholic acid, 0.006; taurocholic acid, 0.009; glycocholic acid, 0.007; taurodeoxycholic acid, 0.008; glycodeoxycholic acid, 0.0012.

TABLE 1. p*H* rate profile data[a]

(*a*) Substrate **2***d* (0.975×10^{-4} *M*)

p*H*	Buffer	$10^2 \times$[Buffer] (*M*)	Catalyst	$10^3 \times$[Catalyst] (*M*)	$10^2 \times k_{obs}$ (min^{-1})	k_2^{app} (M^{-1} min^{-1})[b]
The following data fit the equation $k_{obs} = 1.7 \times 10^{-4} + 4.7 \times 10^2[OH^-]$[c]						
6.51	Phosphate	5.75			0.0176	
7.09	Phosphate	4.02			0.0256	
7.92	Tris	0.968			0.0716	
8.64	Tris	0.968			0.348	
9.74	Carbonate	5.53			2.64	
10.15	Carbonate	4.75			6.60	
10.18	Carbonate	4.82			6.79	
The following data fit the equation $k_2^{app} = (59.1 \pm 1.0)/(1 + [H^+]/10^{-7.14\pm0.02})$[d]						
6.70	Phosphate	5.74	Imidazole	9.68	15.4	15.9
7.23	Phosphate	4.02		9.68	31.8	32.8
7.62	Phosphate	3.41		9.68	41.6	43.0
7.94	Tris	0.968		9.68	50.9	52.5
8.85	Tris	0.968		0.968	5.94	55.8
10.12	Carbonate	4.32		9.68	63.1	58.4
10.14	Carbonate	4.75		0.968	12.8	60.0
The following data fit the equation $k_2^{app} = \dfrac{(3.87 \pm 0.52) \times 10^2}{\dfrac{[H^+]}{10^{-7.38\pm0.11}} + 1 + \dfrac{10^{-9.1\pm0.12}}{[H^+]}} + \dfrac{(7.18 \pm 1.14) \times 10^{-9}}{[H^+]}$[d]						
6.55	Phosphate	5.74	**1***a*	0.915	5.32	58.0
7.12	Phosphate	4.02	**1***a*	0.915	12.9	133
7.51	Phosphate	3.41	**1***a*	0.915	19.2	210
7.96	Tris	0.968	**1***a*	0.915	27.2	296
8.73	Tris	0.968	**1***a*	0.915	29.0	313
9.24	Carbonate	6.82	**1***a*	0.915	13.0[e]	132[e]
9.69	Carbonate	5.52	**1***a*	0.915	11.5	100
9.69	Carbonate	5.52	**1***a*	0.915	12.5[e]	112[e]
10.10	Carbonate	4.32	**1***a*	0.915	20.4	150
10.10	Carbonate	4.32	**1***a*	0.915	17.1	114

Can. J. Chem. Downloaded from www.nrcresearchpress.com by 210.87.254.42 on 09/05/12
For personal use only.

TABLE 1 (*Concluded*)
(*b*) Substrate **2***a* (0.96×10^{-4} *M*)

p*H*	Buffer	$10^2 \times$[Buffer] (*M*)	Catalyst	$10^3 \times$[Catalyst] (*M*)	$10^2 \times k_{obs}$ (min^{-1})	k_2^{app} (M^{-1} min^{-1})[b]
The following data fit the equation $k_{obs} = 956 \times [OH^-]$[c]						
7.95	Tris	0.968			0.0854	
8.74	Tris	0.968			0.508	
9.71	Carbonate	5.51			5.45	
10.18	Carbonate	4.75			13.3	
The following data fit the equation $k_2^{app} = (29.9 \pm 1.4)/(1 + [H^+]/10^{-7.12\pm0.05})$[d]						
6.72	Phosphate	5.74	Imidazole	9.68	7.96	8.20
7.25	Phosphate	4.02	Imidazole	9.68	17.0	17.6
7.9	Tris	0.968	Imidazole	9.68	26.5 ± 0.8[f]	27.3 ± 0.9[f]
8.92	Tris	0.968	Imidazole	9.68	3.57	28.0
10.14	Carbonate	4.75	Imidazole	9.68	16.6	34
The following data fit the equation $k_2^{app} = (28.8 \pm 1.1)/(1 + [H^+]/10^{-7.25\pm0.03}) + (9.90 \pm 0.67) \times 10^{-9}/[H^+]$[d]						
6.55	Phosphate	5.74	**1***a*	0.915	0.467	4.86
7.12	Phosphate	4.02	**1***a*	0.915	1.13	12.1
7.9	Tris	0.968	**1***a*	0.915	2.57 ± 0.02[g]	25.6 ± 0.2[g]
8.72	Tris	0.968	**1***a*	0.915	3.45	32.2
9.68	Carbonate	5.52	**1***a*	0.915	11.5	76.5

[a] In aqueous solution, 25.0 ± 0.1 °C, with 0.64 *M* acetonitrile, ionic strength adjusted with KCl to 0.097 *M*.
[b] Apparent second-order rate constants calculated from the observed pseudo first-order rate constants (corrected for uncatalyzed hydrolysis) by dividing by the total catalyst concentration.
[c] Calculated ignoring the contributions of buffer catalysis terms, since these are always small relative to the contributions of the imidazole containing catalysts. The apparent rate constant for hydroxide ion is made spuriously large by this procedure.
[d] Calculated by least squares.
[e] The pseudo first-order plot was slightly curved.
[f] Average of eight runs (Table 3).
[g] Average of three runs (Table 3).

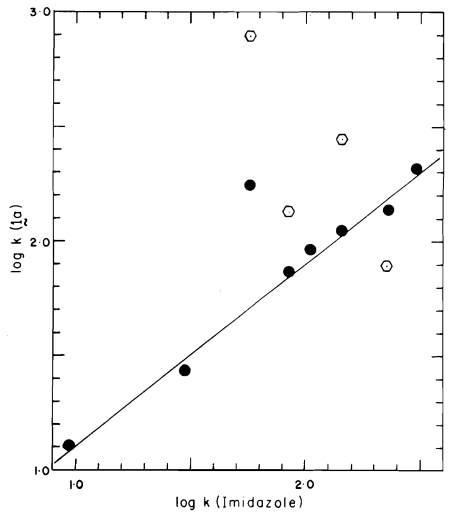

FIG. 3. Electrostatic effects upon rate constants for **1***a* catalyzed hydrolysis of aryl acetates. Log k_2 for **1***a* catalyzed reaction of **2***a–g* is plotted *vs.* log k_2 for imidazole catalyzed reaction of these esters. (●) Reaction at $\mu = 0.88$ *M* (KCl); (○) (hypothetical) reaction at $\mu = 0$; rate constants calculated by extrapolation of log k_2 *vs.* log $\gamma_\pm$. The line is calculated using parameters evaluated by least squares using data for $\mu = 0.88$ *M* for all esters but **2***d* (slope = 0.80).

For the other anionic substrates, close electrostatic contact requires desolvation of one of the ammonium hydrogens *without* any compensating hydrogen bond formation (22*b*). This is doubtless sufficient to render such close contact prohibitive. If the charged groups remain farther apart, the electrostatic interaction is smaller, and can be wiped out by high ionic strength, as was observed.

Arylpropionates (22a)

3-Arylpropionic acids were expected to be good substrates for the steroid on the basis of examination of space filling models which showed that two methylenes provided sufficient flexibility (22*a*) for the aromatic rings to make contact with the steroid while the imidazole was bonded to the ester carbonyl. The results (Tables 3 and 4) show that indeed there is a marked catalysis of the hydrolysis of **3***a–c*: toward **3***c*, **1***a* is nearly twice as effective a nucleophile as hydroxide ion, and twenty times as effective as imidazole.

Clearly a significant part of the observed rate enhancement will result from electrostatic catalysis; this must be taken into account in order to assess the rate enhancement attributable to

Can. J. Chem. Downloaded from www.nrcresearchpress.com by 210.87.254.42 on 09/05/12
For personal use only.

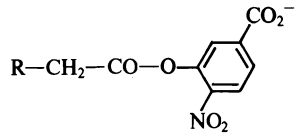

2d R = H
3a R = CH_2–(benzyl)
3b R = CH_2–(naphthyl)
3c R = CH_2–(phenanthryl)

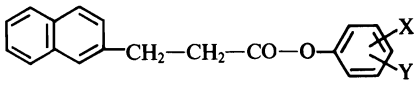

3b X = 3-CO_2^-, Y = 6-NO_2
4a X = H, Y = 4-NO_2
4b X = 4-NMe_3^+, Y = 6-NO_2

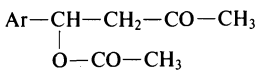

7a Ar = (phenyl)
7b Ar = (naphthyl)
7c Ar = (phenanthryl)

hydrophobic binding of the aromatic ring system to the steroid. The procedure which we employ is to calculate the ratio, R_1, of the rate constant for steroid catalyzed hydrolysis of a substrate to the rate constant for the analogous imidazole catalyzed reaction. This procedure cancels any difference in inherent reactivity of the substrate. Then we calculate the ratio, R_2, of this ratio for a substrate to the ratio for the corresponding acetate. This cancels any difference in inherent reactivity between the steroidal imidazole and imidazole itself, and also any interactions between steroid and leaving group. The only structural feature which remains as a variable is the arylmethyl substituent; the effect of this variable is revealed by the magnitude of the ratio. The logarithms of these ratios are plotted as a function of π (26, 27) in Fig. 5. Two features are clear: first, the hydrophobic rate enhancements are small; second, the arylpropionate esters are *less* reactive than might be anticipated if the hydrophobic effect were simply additive, since the line fitting the points for phenyl, naphthyl, and phenanthryl propionates extrapolates to a value well below that observed for acetate. Since the three aryl groups produce rate enhancements linear in π, it seems clear that they interact with the steroid in a way which *stabilizes* the transition

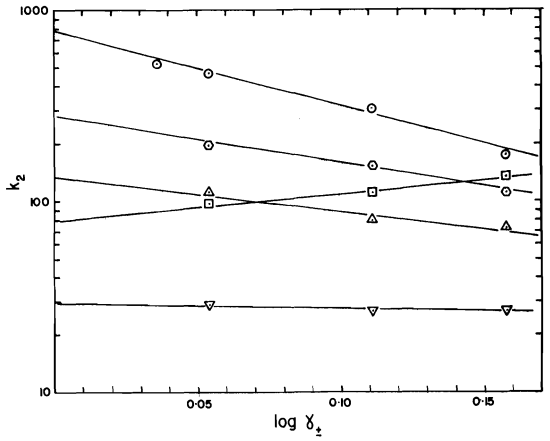

FIG. 4. Ionic strength dependence of rate constants for **1***a* catalyzed hydrolysis. Log k_2 *vs.* log $\gamma_\pm$ calculated using the Davies equation, as described in the text. (○), **2***d*; (△), **2***e*; (⬡), **2***f*; (□), **2***g*; (▽), **2***a*.

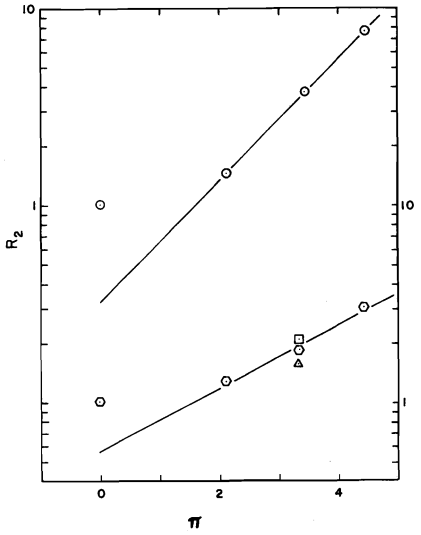

FIG. 5. Log R_2, the ratio of the relative rate constants (**1***a* or **1***b* *vs.* imidazole as standard) for an aryl propionate ester to the relative rate constants for the corresponding acetates as a function of π, the Hansch hydrophobicity parameter of the aryl group. (⬡) negative substrates, (□) positive substrates, (△) neutral substrates, **1***a* as catalyst, right hand ordinate; (○) negative substrates, **1***b* as catalyst, left hand ordinate.

Can. J. Chem. Downloaded from www.nrcresearchpress.com by 210.87.254.42 on 09/05/12
For personal use only.

TABLE 2. Electrostatic effects in the hydrolysis of aryl esters.[a] Rate constants[b] (M^{-1} min^{-1}) as a function of ionic strength

Substrate	Catalyst	Ionic strength 0.88 *M*	0.097 *M*	0.015 *M*	0.0062 *M*
2*a*	Imidazole[c]	29.8	28.2	28.6	
	1*a*[d]	27.0	26.6	28.2	
2*b*	Imidazole[c]		9.44		
	1*a*[d]		12.7		
2*c*	Imidazole[c]		306		
	1*a*[d]		209		
2*d*	Imidazole[c]	57.5	54.6	55.5	56.9
	1*a*[d]	174	305	463	525
2*e*	Imidazole[c]	85.4	69.6	75.6	
	1*a*[d]	72.5	79.8	111	
2*f*	Imidazole[c]	145	135	133	
	1*a*[d]	111	152	196	
2*g*	Imidazole[c]	234	232	252	
	1*a*[d]	137	111	97	
2*h*	Imidazole[c]		105		
	1*a*[d]		92		

[a]In aqueous solution, p*H* 7.9, 25.0 ± 0.1 °C, with 0.64 *M* acetonitrile, 0.0097 *M* Tris buffer, ionic strength adjusted with KCl.
[b]Apparent second-order rate constants calculated from the observed pseudo first-order rate constants (corrected for uncatalyzed hydrolysis) by dividing by the total catalyst concentration.
[c]0.0097 *M*.
[d]0.00097 *M*.

state. Since the line extrapolates to a point lower that that observed for the acetate ester, it seems probable that there is a significant *destabilization* to be overcome if the aryl group is to be positioned so that it can interact with the steroid.

In order to assess the magnitude of the hydrophobic effect, we extrapolate a plot of log R_2 *vs.* π for the *aryl* group to $\pi = 0$, and take the value of R_2 so obtained as representing that for the unsubstituted propionate ester reacting by a transition state with the conformation suitable for hydrophobic binding of the aryl group. In this way, are calculated rate factors of: phenyl, 2.34; naphthyl, 3.31; phenanthryl, 5.55. These ratios are distinctly smaller than was originally anticipated and led to a reexamination of the question of which nitrogen of the imidazole ring is reacting with the substrate; *vide infra*. These ratios are apparently independent of the leaving group (as they must be if the analysis is valid); using naphthyl propionate esters of *p*-nitrophenol **4***a*, $R_2 = 2.01 \pm 0.43$; and of 2-nitro-4-trimethylammoniophenol **4***b*, $R_2 = 1.78 \pm 0.49$; these are within experimental error of the value for **3***b*, $R_2 = 1.90 \pm 0.10$.

N-Isopropyl-1

In the original idea upon which this work was based, it was anticipated that the hydrophobic rate enhancements would be larger than were actually found. This anticipation was based upon the large rate effects reported for other systems (5, 6). Thus there was a hope that the benefits of hydrophobic binding, which models suggested very strongly would be better for reaction at N-3 (the more hindered imidazole nitrogen) than at N-1 (the unhindered), would overcome whatever steric hindrance was present. The rather modest rate enhancements observed cast doubt upon this hope. Accordingly we prepared a derivative of the steroid alkylated at N-1, to force reaction with the substrates to occur at N-3. The route employed is that shown in Scheme 1; although the transformations are prosaic, the resistance of **6** to alkaline hydrolysis was quite astonishing: although trifluoroacetamides are normally hydrolyzed under very mild conditions, typically methanolic sodium carbonate at room temperature (28) (which indeed unblocked the 3-amine), the 11β-amide was unaffected by methanolic NaOH at 105 °C for 4 days! Although alkaline

Can. J. Chem. Downloaded from www.nrcresearchpress.com by 210.87.254.42 on 09/05/12
For personal use only.

Can. J. Chem. Downloaded from www.nrcresearchpress.com by 210.87.254.42 on 09/05/12
For personal use only.

TABLE 3. Rate data for hydrophobic substrates[a]

Substrate	$10^4 \times$ [Substrate] (M)	Catalyst	$10^3 \times$ [Catalyst] (M)	$10^2 \times k_{obs}$ (min^{-1})	k_2^{app} (M^{-1} min^{-1})[b]
2*d*	0.193	Imidazole	0.968	5.36	54.6
	0.193	Imidazole	4.83	25.9	53.4
	0.195	Imidazole	9.68	55.2	56.9
	0.957	Imidazole	9.68	50.9	52.5
	0.968	Imidazole	9.68	50.5	52.0
	0.975	Imidazole	9.68	52.5	54.2
					Av. 53.9 ± 1.3
	0.193	**1***a*	0.0968	2.94	296
	0.193	**1***a*	0.0968	3.13	316
	0.201	**1***a*	0.202	6.23	305
	0.957	**1***a*	0.915	27.2	296
					Av. 304 ± 7
	0.193	**1***b*	0.903	0.990	10.1
	0.193	**1***b*	0.830	0.960	10.7
					Av. 10.4 ± 0.3
3*a*	0.0200	—		0.058	
	0.0200	Imidazole	4.83	28.6	59.0
	0.0200	**1***a*	0.0333	1.56	450
	0.0200	**1***b*	0.0286	0.104	16
3*b*	0.50	—		0.0666	
	0.0200	Imidazole	5.00	27.8	55.7
	0.0500	Imidazole	5.00	29.4	58.6
	0.100	Imidazole	5.00	28.5	56.8
	0.193	Imidazole	4.83	27.4	56.5
	0.200	Imidazole	5.00	27.9	55.6
	0.500	Imidazole	5.00	30.4	60.6
					Av. 57.3 ± 1.5
	0.0500	**1***a*	0.0333	2.16	633
	0.100	**1***a*	0.0333	2.01	589
	0.200	**1***a*	0.0333	2.12	620
					Av. 614 ± 17
	0.0200	**1***b*	0.0286	0.179	39.2
3*c*	0.0200	—		0.0646	
	0.0100	Imidazole	5.00	31.3	62.4
	0.0200	Imidazole	4.83	29.6	61.0
	0.0200	Imidazole	1.00	5.78	57.2
					Av. 60.2 ± 3.0
	0.0100	**1***a*	0.0333	3.17	934
	0.0100	**1***a*	0.0333	4.07	1200
	0.0200	**1***a*	0.0200	2.26	1100
	0.0200	**1***a*	0.0333	3.86	1140
	0.0200	**1***a*	0.0333	3.52	1040
					Av. 1080 ± 101
	0.0100	**1***b*	0.0286	3.15	87.5 ± 17.7
4*a*	0.0200	—		0.124	
	0.00667	Imidazole	9.68	23.5	24.2
	0.0200	Imidazole	9.68	23.5	24.2
					Av. 24.2
	0.0200	**1***a*	0.0602	0.400	45.8

[a]In aqueous solution, pH 7.9, 25.0 ± 1 °C, with 0.64 M acetonitrile, 0.0097 M Tris buffer, ionic strength adjusted with KCl to 0.097 M.

[b]Apparent second-order rate constants calculated from the observed pseudo first-order rate constants (corrected for uncatalyzed hydrolysis) by dividing by the total catalyst concentration.

TABLE 4. Hydrolysis of aryl esters: hydrophobic effects[a]

Substrate	Catalyst and rate constant: None $10^4 \times k_0$[b]	Imidazole k_2[c]	**1***a* k_2[c]	**1***b* k_2[c]
2*d*	7.16	53.9 ± 1.3	304 ± 7	10 ± 2
3*a*	5.8	59 ± 6	450 ± 43	16 ± 3
3*b*	6.66	57.3 ± 1.5	614 ± 17	39 ± 8
3*c*	6.46	60.2 ± 3.0	1080 ± 80	87 ± 18
2*a*	8.54	27.2 ± 0.7	25.5 ± 0.1	0.94 ± 0.09
4*a*	12.4	24.2 ± 2	45.8 ± 9	
2*g*	46.9	242 ± 6	101 ± 10	
4*b*	42.8[d]	316 ± 60[d]	234 ± 40[d]	

[a]In aqueous solution, p*H* 7.9, 25.0 ± 0.1 °C, with 0.64 *M* acetonitrile, 0.01 *M* Tris buffer, μ = 0.1 *M* (KCl).
[b]Observed pseudo first-order rate constants (min^{-1}).
[c]Apparent second-order rate constant; $k_2 = (k_{obs} - k_0)/[catalyst]_{total}$ (M^{-1} min^{-1}).
[d]Reference 20.

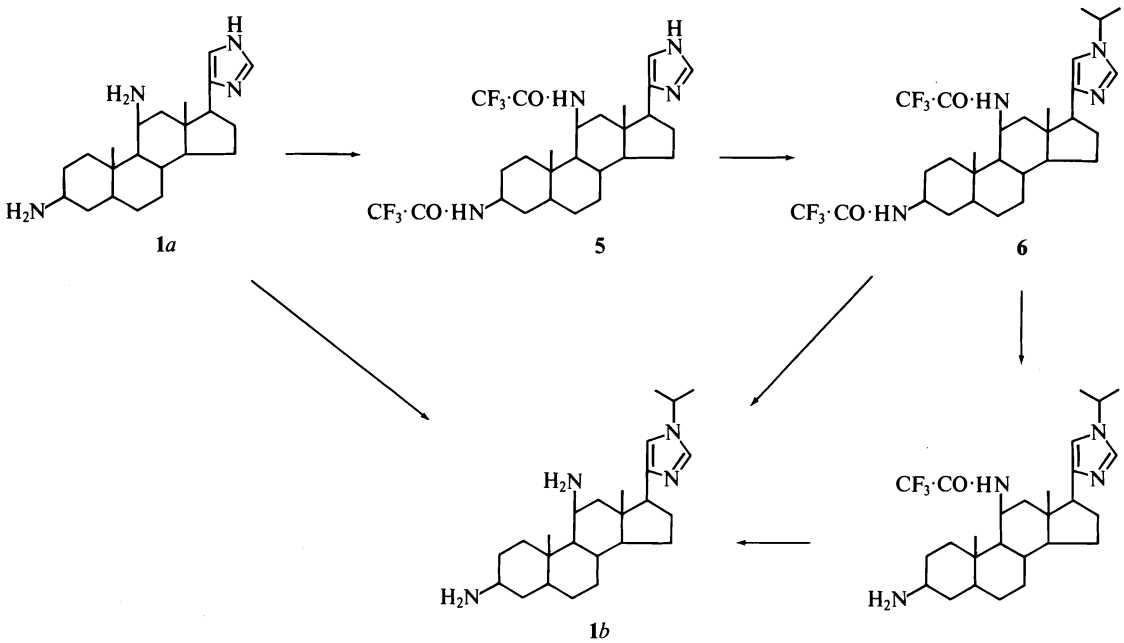

SCHEME 1

conditions were ineffective, acid hydrolysis was relatively facile. The imidazole ring is expected to react with a bulky alkylating agent preferentially at the less hindered nitrogen (29); in fact, only one product was obtained. The structure was confirmed by examination of the nmr spectrum: the cross ring coupling constant for the imidazole CH protons was of the magnitude expected for the isomer alkylated in N-1 (30).

By analogy with numerous experiments using *N*-methyl imidazole and imidazole as nucleophilic catalysts for ester hydrolysis (ref. 1, p. 68), we anticipate that the rate constants observed for **1***b* will be very similar to those for reaction of **1***a* at N-3. The experimental values are recorded in Table 4. Clearly N-3 is *much* less reactive than N-1; judging from the reaction of **2***a*, the steric hindrance results in a rate retardation of 30-fold. R_2 values, calculated as for **1***a* are shown in Fig. 5*b*. Once again log R_2 is a

Can. J. Chem. Downloaded from www.nrcresearchpress.com by 210.87.254.42 on 09/05/12
For personal use only.

Can. J. Chem. Downloaded from www.nrcresearchpress.com by 210.87.254.42 on 09/05/12
For personal use only.

linear function of π for the phenyl, naphthyl, and phenanthryl propionate esters. The extrapolated value for $\pi = 0$ is only 0.32 times the value observed for the acetate ester. Thus, in addition to the simple steric effect of crowding at N-3, there is an additional price to be paid if the productive binding conformation of the substrate is formed. The slope of the log R_2 *vs.* π plot for **1***b* is markedly steeper than that observed for **1***a*, being 0.25. This implies that once the disadvantages of reaction at N-3 have been overcome, the anticipated superior hydrophobic interaction is observed. Values of the rate enhancement may be calculated for **1***a* as: phenyl, 4.5; naphthyl, 11.8; phenanthryl, 24.0.

Discussion

Electrostatic Interactions

Electrostatic effects on reaction rates are normally rather small unless one or both of the reactants are polyelectrolytes (1). The effect observed for the reaction of **1***a* or **1***b* with **2***d* is then of particular interest because it is so large at low ionic strength. The contrast between the behaviour of **2***d* and **2***e* requires that there be a marked geometrical requirement for strong electrostatic binding, and this may explain why so few examples have been found to date. There is a strong implication that electrostatic binding can be very useful in enzyme model systems if the geometrical requirements can be met.

It is curious that the electrostatic effects are not reciprocal, in that the non-optimal anionic substrates **2***e* and **2***f* are accelerated by a smaller factor than **2***g* is retarded by, yet the interacting charges will be no farther apart, and indeed should be closer for the anionic substrates. A possible rationalization is that the cationic substrate, **2***g*, has an $-N(CH_3)_3^+$ group which is inefficiently solvated, so that little charge dispersal occurs, whereas the anionic substituents, $-COO^-$ or $-SO_3^-$, in **2***e* or **2***f* should be efficiently solvated by water, with attendent dispersal of charge onto solvent molecules. This charge dispersal would lessen the effective charge interacting with the $-NH_3^+$ group of the steroid. One would expect the transition state for the reaction of **1***a* with **2***g* to have a conformation with the cationic substituents as far apart as possible. The transition states for the reactions of **2***e* or **2***f* with **1***a* would be expected to have the oppositely charged substituents closer to each other than this maximum separation, but still, as was argued above, to have them separated by at least one layer of water molecules. Since this close contact requires loss of rotational freedom, this would be the predominant conformation only if there were a strong compensating electrostatic interaction. Direct interaction of the ionic substituents along the shortest line joining them will be the overwhelming contribution to the electrostatic potential energy when the groups are in contact, but will decline rapidly in importance as the thickness of the intervening layer of water increases. (It has been suggested that electrostatic interactions through the solvent can be neglected once there is more than one intervening layer of water molecules (32)). Interaction of the ionic groups through the rest of the reacting molecules, which constitutes a low dielectric constant path between the charges, will be rather insensitive to relative orientation; this would be expected to be the dominant contribution to the electrostatic interaction except when the charges are very close in space, and the magnitude of this contribution would depend principally upon the effective charges. The analysis just presented suggests that: for the transition states for **1** catalyzed reaction of **2***e* or **2***f*, there is very little tendency for the interacting charges to be particularly close; for the transition state for the reaction of **2***d*, the preferred conformation has the $-COO^-$ and $-NH_3^+$ groups in hydrogen bonded contact; the magnitude of the rate enhancement observed for **2***d* represents a lower limit to the potential electrostatic interaction free energy because of the loss in rotational freedom consequent upon taking up this one conformation.

Hydrophobic Interactions

The pattern exhibited by the rate constants for the reactions of **1***a* and **1***b* with **3***a–c* clearly requires that the transition states be stabilized by hydrophobic interactions. The net effect is small even for **1***b*, where the simple analysis given above leads to a factor of 25 fold for phenanthrene as binding group. It is disturbing that this is quite different from the factor (110-fold) deduced by an analogous argument based on rates of **1***a* catalyzed elimination from substrates **7***a–c* (33). We will now show that these two sets of results actually lead to an internally consistent

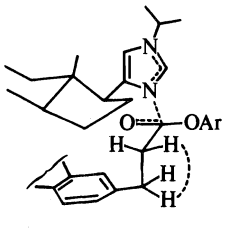

8

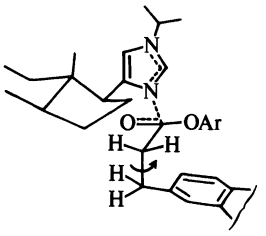

9

interpretation when they are examined in more detail.

Although **1***b* is constrained to react at only one of the imidazole nitrogens, there are two modes of reaction possible. These are indicated in structures **8** and **9**. It was observed that a plot of log k_2^{app} *vs.* π for the reaction of **1***b* with **3***a–c* led to an extrapolated rate for the hypothetical substrate, with no benzene ring but the same transition state geometry, considerably slower than the experimental value for the acetate ester. Thus transition state **8** which permits hydrophobic interactions between steroid and aromatic ring systems, has some destabilizing interactions over and above those present in the transition state for reaction with the acetate. These may, at least in part, be recognized as a partially eclipsing interaction of the methylene hydrogens indicated by the dotted line in **8**. The alternative transition state **9**, which differs from **8** by rotation about a C—C bond (indicated by an arrow in **9**) can have a completely staggered conformation about the bond joining the methylenes. This transition state should be virtually identical in free energy, relative to starting materials, to that for the reaction with the acetate. Although **8** and **9** differ only by rotation about a single bond, they are separated by a free energy barrier which includes, besides the intrinsic rotational barrier, the barrier to deplacing solvent molecules as the bulky side chain is swung through *ca.* 180°, and the barrier imposed by the solvent reorientation as hydrophobic contact is made.

We will assume that the rate of reactions proceeding by way of transition state **9** is equal to the rate of the acetate reaction. The observed second-order rate constant will be the sum of two rate constants $k^{H\phi}$ for reaction by transition state **8**, and $k^{non\ H\phi}$ for reaction by transition state **9**.

$$k_2^{app} = k^{H\phi} + k^{non\ H\phi}$$

In addition to the hydrophobic interactions between **1***b* and **3***a–c*, there is an electrostatic stabilization. That this would be of the same magnitude for **1***a* and **1***b* was anticipated from examination of space filling models, since for both steroids, conformations of the transition state exist with contact (and hydrogen bonding) of carboxylate and ammonium. This expectation was confirmed by the ratio of rate constants for **2***a* and **2***d* with the two steroids. For **1***a*, $k_{2d}/k_{2a} = 11.9$; for **1***b*, $k_{2d}/k_{2a} = 11.1$. These values are, within experimental error, the same: it should be noted that this ratio reflects both the electrostatic stabilization of the transition states for the **2***d* reactions, and the inherently greater reactivity of **2***d*. Since **1***a* and **1***b* show the same electrostatic stabilization in their reactions with **2***d*, the magnitude of this effect for **1***b* may be taken from Fig. 3 which is based on experiments with **1***a*. The value so obtained is a factor of 6.0 ± 1.3 in rate. Division of $k^{H\phi}$ by this factor gives a rate constant which we will call $k^{H\phi}_{corr}$ which is now corrected for this constant electrostatic contribution. This rate constant $k^{H\phi}_{corr}$ refers to the hypothetical reaction proceeding by transition state **8** of neutral analogs of **3***a–c*. In the case of **3***c* a neutral analog would be extremely insoluble, so that experimental measurement of such a process is probably impossible. Values of $k^{H\phi}_{corr}$ for the reaction of **1***b* with **3***a–c* are: **3***a*, 1.1 ± 0.4; **3***b*, 4.8 ± 1.1; **3***c* 12.9 ± 4.0; (all in M^{-1} min^{-1}). A plot of log $k^{H\phi}_{corr}$ *vs.* π is satisfactorily linear, with a slope of 0.47 ± 0.15. Taking the intercept at $\pi = 0$ (*i.e.*, no aromatic ring system) as the reference point, the rate enhancement attributable to hydrophobic interactions of the phenanthrene ring of **3***c* with **1***b* may be calculated as $10^{2.0\pm0.5}$.

A similar analysis should of course be applied to the data reported for the enolization reaction (33), although the effects will be much smaller in this case, since the steric demands of transition states for general base catalyzed reactions are expected to be much less than for nucleophilic catalysis (34), and the relative rate constants for steroid *vs.* imidazole as catalyst are larger. The enolization substrates were neutral, so that there is no complication from electrostatic interactions. The size of the aryl group does affect the rates of reaction of the elimination substrates, and therefore relative rate constants must be used.

We make the assumption used before (33) that the inherent reactivity of **1***a* is the same as that of imidazole, and an assumption analogous to that

Can. J. Chem. Downloaded from www.nrcresearchpress.com by 210.87.254.42 on 09/05/12
For personal use only.

Can. J. Chem. Downloaded from www.nrcresearchpress.com by 210.87.254.42 on 09/05/12
For personal use only.

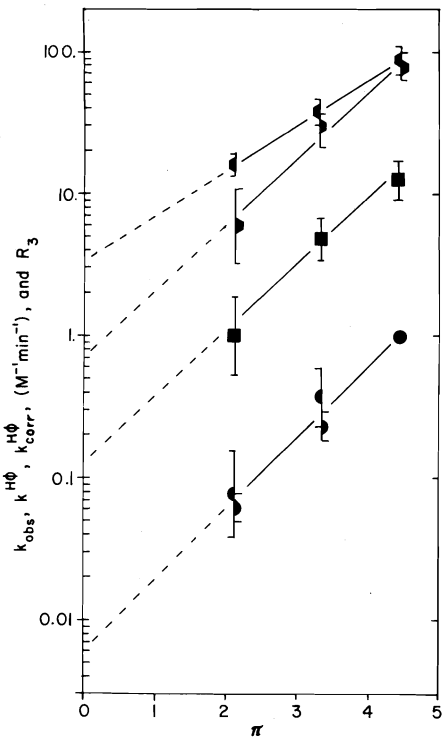

FIG. 6. Hydrophobic effect for reaction at nitrogen-3 of a steroidal imidazole. Reaction of **1***b* with **3***a–c*: (◖) k_{obs}; (◗) $k^{H\phi}$; (■) $k^{H\phi}_{corr}$; (◖) R_3. (◗) R_3 for the enolization of **7***a–c* catalyzed by **1***a*. (For definitions, see the text). The abscissa is the Hansch π value for the aryl group in the substrate.

made above for the reaction of **1***b* with **3***a–c*, that there are two transition states possible, one with hydrophobic contact, and one with no hydrophobic contact (for which the rate will be identical to that for imidazole).

We can then write for the directly calculated relative rate constants, k^{app}_{rel},

$$k^{app}_{rel} = k^{H\phi}_{rel} + 1$$

From a plot of log $k^{H\phi}_{rel}$ *vs.* π we obtain a rate enhancement of $10^{2.38\pm0.26}$ for a phenanthrene group.

In order to plot the results from the two reactions on a single graph, we calculate ratios, with the phenanthryl derivative as standard. These ratios, R_3, permit comparison of both reactions on the same scale. Figure 6 shows a plot of log R_3 *vs.* π, and confirms that both sets of data define a single line within the experimental uncertainty. This line has a slope of 0.49 and leads to a potential hydrophobic rate enhancement of 156 for phenanthrene bound to a steroid. This value is obtained from an extrapolation, on a logarithmic plot, of a line based on points derived from extended calculations, so that propagation of errors leads to considerable uncertainty. The hydrophobic rate enhancement should be reliable within a factor of two.

The analysis presented above is rather lengthy, but it gains support from the close agreement found for initially discordant appearing results. Although **1***b* is not a good 'artificial enzyme' study of this compound has made clear (*a*) that there are potentially important hydrophobic rate enhancements for hydrocarbon contacts of the sort studied here, but (*b*) that much of this potential can be masked if the transition state imposes steric requirements which work against hydrophobic contact.

Experimental

Materials

Glass distilled water was used for preparing solutions. Acetonitrile for stock solutions of substrates was Eastman spectrograde, freed of nucleophilic impurities by passage through a column of Woelm neutral alumina (grade I). *p*-Nitrophenyl acetate and hexanoate were commercial materials, used without further purification. Imidazole was recrystallized prior to use. Inorganic salts were reagent grade used without further purification. The steroid **1***a* was prepared and purified as previously described (19). Some samples of **1***a*, though homogeneous to tlc and nmr were less active catalysts for the hydrolysis of *p*-nitrophenyl acetate than the original analytical sample. Potentiometric titration of the trihydrochloride salt with NaOH, and kinetic assay using the *p*-nitrophenyl acetate reaction gave results which were in satisfactory agreement. We attribute the discrepancy to inorganic salts which coprecipitated with **1***a*. Stock solutions of **1***a* were assayed using the *p*-nitrophenyl acetate reaction, and a value for the second-order rate constant of 28.1 M^{-1} min^{-1}.

17-β-(1-Isopropyl-4-imidazolyl-)-5α-androstane-3β,11β-diamine, **1***b*

To a stirred, ice cold solution of **1***a*, as the trihydrochloride, (140 mg, 0.3 mmol) in dry pyridine (5.2 ml) was added trifluoroacetic anhydride (1.5 ml) drop wise. After 1 h at room temperature the reaction mixture was poured into ice water and extracted with ethyl acetate (3 × 20 ml). The combined extracts were washed with saturated aqueous sodium chloride, dried (Na_2SO_4) and evaporated. Crystallization from ethyl acetate gave 139 mg of the bistrifluoroacetamide, **5**.

A suspension of **5** (55 mg, 0.1 mmol) and isopropyl iodide (32 mg) in acetonitrile (1.7 ml) was refluxed for 3 days, treated with an additional 30 mg of isopropyl iodide, and refluxed 3 more days. The reaction mixture was

Can. J. Chem. Downloaded from www.nrcresearchpress.com by 210.87.254.42 on 09/05/12
For personal use only.

evaporated to dryness, basified with methanolic ammonia, and evaporated to dryness. Preparative layer chromatography (plc) (silica gel, $CHCl_3$–CH_3OH, 4:1 as eluant) gave 40 mg crude **6** (68%) as the fastest band. This on crystallization from acetonitrile gave 31 mg **6**, mp 298–301 °C; nmr ($CDCl_3$, 100 MHz), 0.66 (3H, s, 18-CH_3), 0.88 (3H, s, 19-CH_3), 1.47 (6H, d, J = 6.5 Hz, $(CH_3)_2CH$), 3.7 (1H, br s, 3-CH(α)), 4.36 (1H, septet, J = 6.5 Hz, $(CH_3)_2CH$—), 4.5 (1H, br s, 11-C*H*(α)), 6.4 (2H, d of d, amide NH), 6.66 (1H, br s, $\Delta\nu_{1/2}$ = 2.7 Hz, 5′C*H*), 7.58 (1H, d, J = 1.2 Hz, 2′C*H*). Unreacted **5** (16 mg, 29%) was recovered as the second band on plc.

A suspension of **6** (50 mg, 0.085 mmol) in 6 *N* aqueous HCl (20 ml) was refluxed for 2 days, cooled, basified with 2 *N* KOH (70 ml), brought to saturation with NaCl, and extracted with ethyl acetate containing 10% methanol (4 × 30 ml). The aqueous layer was maintained at p*H* 10–12 during this extraction by the addition of KOH as needed. The combined organic layers were washed with saturated aqueous sodium chloride, dried (Na_2SO_4), and evaporated to give **1***b*. Crude **1***b* was purified by plc (silica gel, 3 *M* ammonia in methanol as eluant), dissolved in 1:1 methanol–isopropanol, treated with a slight excess of aqueous 1 *N* HCl and evaporated to dryness to give the trihydrochloride of **1***b* as a white powder. Treatment with active charcoal and filtration of concentrated aqueous and methanolic solutions to remove traces of insoluble material gave analytically pure powder; nmr (D_2O, DSS as reference, 100 MHz) δ 0.70 (3H, s, C*H*$_3$-18), 0.98 (3H, s, C*H*$_3$-19) 1.15 (3H, d, J = 6 Hz, $\frac{1}{2}$(CH_3)$_2$CHOH), 1.52 (6H, d, J = 7 Hz, (CH_3)$_2$C*H*—N), 2.82 (1H, br t, J = 8.5 Hz, C*H*-17β), 3.21 (1H, br t, $\Delta\nu_{1/2}$ = 20 Hz, C*H*-3α), 4.00 (1H, br, $\Delta\nu_{1/2}$ = 10 Hz, C11α-H), 7.46 (1H, br s, $\Delta\nu_{1/2}$ = 2.7 Hz, C*H*-5 imidazole) 8.65 (1H, s, C*H*-2 of imidazole). *Anal.* calcd. for $C_{25}H_{45}N_4Cl_3 \cdot \frac{1}{2}(C_3H_8O) \cdot 3H_2O$: C 53.75, H 9.36; found: C 53.36, H 9.27.

Substrates

Compounds **2***b–g* were prepared by published procedures and had mp in satisfactory agreement with the literature values (35–38). **2***h* was prepared by reaction of **2***d* with CH_2N_2 in diethyl ether, and recrystallized from petroleum ether: mp 72–73.5 °C. *Anal.* calcd. for $C_{10}H_9NO_6$: C 50.22, H 3.80; found: C 50.58, H 3.91. **3***a–c* were prepared from the corresponding aryl propionic acids by the procedure employed for **3***b* (20). **4***b* was prepared as described previously (20). **4***a* was prepared from 3-(2-naphthyl)propionic acid by the ethyl chloroformate procedure and crystallized from 95% ethanol; mp 126–128 °C. *Anal.* calcd. for $C_{19}H_{15}NO_4$: C 71.02, H 4.71; found: C 70.74, H 4.97. 3-(3-Phenanthryl)propionic acid was prepared starting from 3-acetyl phenanthrene, mp 68–72 °C (lit. (39) mp 72 °C) which was oxidized (ClO^-) to phenanthrene-3-carboxylic acid (39), which in turn was reduced ($LiAlH_4$, tetrahydrofuran, 3 h reflux) to 3-phenanthrylcarbinol. This was oxidized (CrO_3–pyridine in CH_2Cl_2 solution (40)) to phenanthrene-3-carboxaldehyde, which after passage through a short column of silicic acid (eluting with benzene) and crystallization from benzene–hexane had mp 77–79 °C (lit. (41) mp 79.5–80 °C). Knoevenagel condensation with malonic acid followed by reduction using sodium amalgam gave 3-(3-phenanthryl)-propionic acid, mp 158–160 °C, (lit. (42) mp 158.5–159.5 °C).

Kinetics

Solutions were brought to the desired calculated ionic strength with KCl. The p*H* was determined at the end of each run. Reactions were initiated by injecting suitable volumes of substrate solutions in acetonitrile (using a microliter syringe) to buffer solutions containing imidazole or steroid in quartz cuvettes, equilibrated in the thermostatted cell compartment of a Gilford model 240 spectrophotometer, and mixed by inversion. Reactions were followed at suitable wavelengths near 400 nm. Infinity points were taken after ten half-lives; pseudo first-order rate constants were calculated from first-order plots which were normally linear for at least three half-lives.

Potentiometric Titration

Amine hydrochloride (0.02 mmol) and potassium chloride (2 mmol) were dissolved in carbonate-free glass-distilled water (20 ml) in a three necked flask with magnetic stirrer, nitrogen inlet, buret and combination electrode. While the solution was stirred under nitrogen at 25 ± 1 °C, 0.02 *N* sodium hydroxide solution was added dropwise, from a burette which could be read to 0.005 ml. Readings of volume and p*H* (using a Radiometer p*H* meter 25 SE with a GK2301C combination electrode) were taken after each addition. A similar titration was carried out on a sample of 0.1 *M* potassium chloride (20 ml).

The titration data were analyzed by calculating the difference in the amount of base required to reach a given p*H* in the presence and absence of amine hydrochloride (43). This quantity, y, was then fitted to the theoretical expression

$$y = a(\sum_i 1/(1 + 10^{-pH}/K_i))$$

where a is the volume of base corresponding to one equivalent of amine and the sum is over all titratable groups. A non-linear weighted least-squares procedure (44) was used to fit the data to the appropriate expression using a computer program. For imidazole the pK_a so obtained was 7.14 ± 0.06 (lit. (31) 7.10 at μ = 0.12); for cyclohexylamine, the pK_a was 10.76 ± 0.11 (lit. (31) 10.66 at μ = 0.01). For **1***a*, the pK_a's were 7.18 ± 0.04, 9.69 ± 0.09, and 10.68 ± 0.24. The error limits are those calculated by the computer program, and reflect the degree of scatter of experimental points about the calculated line.

Acknowledgment

We thank the National Research Council of Canada for financial support of this work.

1. W. P. Jencks. Catalysis in chemistry and enzymology. McGraw-Hill, New York. 1969. p. 393.
2. T. Maugh II and T. C. Bruice. J. Am. Chem. Soc. **93**, 6584 (1971).
3. C. A. Blyth and J. R. Knowles. J. Am. Chem. Soc. **93**, 3017 (1971); **93**, 3021 (1971).
4. R. G. Shorenstein, C. S. Pratt, C. J. Hsu, and T. E. Wagner. J. Am. Chem. Soc. **90**, 6199 (1968).
5. D. Oakenfull. J. Chem. Soc. Perkin Trans. II, 1006 (1973).

6. R. HERSHFIELD and M. L. BENDER. J. Am. Chem. Soc. **94**, 1376 (1972).
7. C. ASO, T. KUNITAKE, and S. SHINKAI. Chem. Commun. 1983 (1968); Bull. Chem. Soc. Jpn. **43**, 1109 (1970); **43** 2581 (1970).
8. J. P. GUTHRIE. Chem. Commun. 897 (1972); Can. J. Chem. **51**, 3494 (1973).
9. R. SMITH and C. TANFORD. Proc. Natl. Acad. Sci. U.S. **70**, 289 (1973).
10. J. P. GUTHRIE and Y. UEDA. J. Chem. Soc. Chem. Commun. 991 (1974).
11. F. CRAMER and W. KAMPE. J. Am. Chem. Soc. **87**, 1115 (1965).
12. N. HENNRICH and F. CRAMER. J. Am. Chem. Soc. **87**, 1121 (1965).
13. F. CRAMER, W. SAENGER, and H. CH. SPATZ. J. Am. Chem. Soc. **89**, 14 (1967).
14. H. R. L. VAN ETTEN, J. F. SEBASTION, G. A. CLOWES, and M. L. BENDER. J. Am. Chem. Soc. **89**, 3242 (1967); **89**, 2253 (1967).
15. R. BRESLOW and P. CAMPBELL. J. Am. Chem. Soc. **91**, 3085 (1969).
16. D. E. TUTT and M. A. SCHWARTZ. J. Am. Chem. Soc. **93**, 767 (1971).
17. R. BRESLOW and L. E. OVERMAN. J. Am. Chem. Soc. **92**, 1075 (1970).
18. T. S. STRAUB and M. L. BENDER. J. Am. Chem. Soc. **94**, 8875 (1972); **94**, 8881 (1972).
19. J. P. GUTHRIE. Can. J. Chem. **50**, 3993 (1972).
20. J. P. GUTHRIE and Y. UEDA. Can. J. Chem. **51**, 3936 (1973).
21. J. P. GUTHRIE and Y. UEDA. Fed. Proc. Fed. Am. Soc. Exp. Biol. **32**, 628 (1973).
22. J. P. GUTHRIE and Y. UEDA. Chem. Commun. (*a*) 898 (1973); (*b*) 111 (1974).
23. C. W. BIRD and R. C. COOKSON. J. Chem. Soc. 2343 (1960).
24. F. M. MENGER and M. J. MCCREERY. J. Am. Chem. Soc. **96**, 121 (1974).
25. R. A. ROBINSON and R. H. STOKES. Electrolyte solutions. Academic Press, New York. 1955. p. 231.
26. T. FUJITA, J. IWASA, and C. HANSCH. J. Am. Chem. Soc. **86**, 5175 (1964).
27. M. S. TUTE. Adv. Drug. Res. **6**, 1 (1971).
28. H. NEWMAN. J. Org. Chem. **30**, 1287 (1965).
29. J. B. JONES and D. W. HYSERT. Can. J. Chem. **49**, 3012 (1971).
30. H. R. MATTHEWS and H. RAPOPORT. J. Am. Chem. Soc. **95**, 2297 (1973).
31. D. D. PERRIN. Dissociation constants of organic bases in aqueous solution. Butterworths, London. 1965.
32. H. A. SCHERAGA. Adv. Phys. Org. Chem. **6**, 130 (1968).
33. J. P. GUTHRIE and S. O'LEARY. Can. J. Chem. **53**, 2150 (1975).
34. F. COVITZ and F. H. WESTHEIMER. J. Am. Chem. Soc. **85**, 1773 (1963).
35. F. D. CHATTAWAY. J. Chem. Soc. 2495 (1931).
36. J. R. A. POLLOCK and R. STEVENS (*Editors*). Dictionary of organic chemistry. Eyre and Spottiswoode, London. 1965.
37. C. G. OVERGERGER, T. ST. PIERRE, N. VORCHEIMER, J. LEE, and S. YAROSLAVSKY. J. Am. Chem. Soc. **87**, 296 (1965).
38. T. C. BRUICE, J. KATZHENDLER, and L. R. FEDOR. J. Am. Chem. Soc. **90**, 1333 (1968).
39. E. MOSETTIG and J. VAN DE KAMP. J. Am. Chem. Soc. **52**, 3704 (1930).
40. R. RATCLIFFE and R. RODEHORST. J. Org. Chem. **35**, 4000 (1970).
41. E. MOSETTIG and J. VAN DE KAMP. J. Am. Chem. Soc. **55**, 2996 (1933).
42. W. E. BACKMAN and M. C. KLOETZEL. J. Am. Chem. Soc. **59**, 2207 (1937).
43. T. V. PARKE and W. W. DAVIS. Anal. Chem. **26**, 642 (1954).
44. W. E. WENTWORTH, J. Chem. Educ. **42**, 96 (1965); **42**, 162 (1965); W. E. DEMING. Statistical adjustment of data. Dover, New York, N.Y. 1964.

Can. J. Chem. Downloaded from www.nrcresearchpress.com by 210.87.254.42 on 09/05/12
For personal use only.

Alcoxy-2, aryloxy-2, acyloxy-2 cyclohexanones. Synthèse et étude de leur équilibre conformationnel

D. CANTACUZENE ET M. TORDEUX

C.N.R.S.-C.E.R.C.O.A., 2 rue Henri Dunant, Thiais 94320 France

Reçu le 16 février 1976

D. CANTACUZENE et M. TORDEUX. Can. J. Chem. **54**, 2759 (1976).

On montre qu'il existe une corrélation de Hammett dans l'équilibre conformationnel des aryloxy-2 cyclohexanones quand le substituant X situé en *para* sur le noyau benzénique est attracteur. Ceci permet de prévoir la position équatoriale du substituant dans les acyloxy-2 cyclohexanones. L'équilibre conformationnel des alcoxy-2 cyclohexanones (R = CH_3 à $C(CH_3)_3$) est également étudié.

D. CANTACUZENE and M. TORDEUX. Can. J. Chem. **54**, 2759 (1976).

We show a linear Hammett correlation in the conformational equilibrium of 2-aryloxycyclohexanones when the X substituent located *para* on the phenyl ring is electron withdrawing. This leads to the prediction of the equatorial position of the substituent in the 2-acyloxycyclohexanones. The conformational equilibria of 2-alcoxycyclohexanones (R = CH_3 to $C(CH_3)_3$) also are examined.

Can. J. Chem. Downloaded from www.nrcresearchpress.com by 210.87.254.6 on 09/05/12
For personal use only.

L'équilibre conformationnel des halogéno-2 cyclohexanones est désormais bien connu. Il a été suggéré que la stabilisation de la forme axiale était dûe à l'intervention d'une forme mésomère de type V provenant d'une interaction entre la liaison σ C—X avec l'orbitale antiliante π^* du carbonyle (1, 2). Néanmoins des calculs effectués sur la fluoro-2 cyclohexanone (où la liaison C—F est peu polarisable) montrent que dans ce cas il est préférable de considérer le recouvrement d'un doublet libre du fluor avec l'orbitale antiliante du carbonyle (3) pour expliquer l'équilibre observé. Cette hypothèse avait déjà été envisagée dans le cas des aryl-2 cyclohexanones (4, 5).

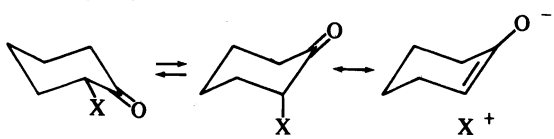

I II V

Cependant, dans cette série il est difficile de séparer l'influence, sur l'équilibre **I** $\rightleftarrows$ **II**, des effets stériques de celle des effets électroniques. Par contre dans les cyclohexanones présentant en position 2 une fonction aryloxy (OR = OC_6H_4X: X variant de NEt_2 à NO_2) le facteur stérique doit être considéré comme constant, ce qui permet d'accéder directement à l'étude des effets électroniques influençant la position de l'équilibre **III** $\rightleftarrows$ **IV**.

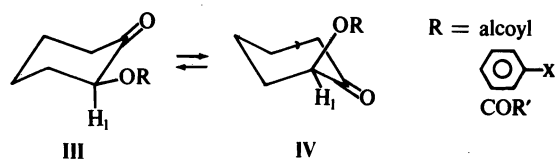

III IV

Nous montrerons, d'autre part, la variation de l'équilibre conformationnel des alcoxy-2 cyclohexanones en fonction du degré de substitution du groupement R (R variant de CH_3 à $C(CH_3)_3$). Les acyloxy-2 cyclohexanones seront également examinées.

La méthode de dosage choisie pour ces systèmes à échange conformationnel rapide est la mesure par rmn, de la largeur du signal du proton H_l situé au pied du groupement OR.[1] Nous avons utilisé les *tert*-butyl-4 cyclohexanones comme modèles figés de référence: ceci nous permet d'atteindre les valeurs extrêmes de la largeur du signal (somme des constantes de couplage) pour un proton H_l axial et pour un proton H_l équatorial (6, 7). Dans le cas des alcoxy-2 cyclohexanones, le signal dû au proton H_l est masqué par les signaux des groupements alcoxy (OCH_3, OC_2H_5, $OCH(CH_3)_2$). Nous avons donc été amenés à synthétiser les perdeutério alcoxy-2 cyclohexanones (OR = OCD_3, OC_2D_5, $OCD(CD_3)_2$).

[1]Voir la partie expérimentale pour la discussion sur le choix de la largeur du signal.

Can. J. Chem. Downloaded from www.nrcresearchpress.com by 210.87.254.6 on 09/05/12
For personal use only.

Synthèses

tert-Butyl-4 alcoxy-2 et phénoxy-2 cyclohexanones

Les *tert*-butyl-4 méthoxy-2 et *tert*-butoxy-2 cyclohexanones ont été synthétisées à partir des sels d'immonium α bromés (schéma 1).

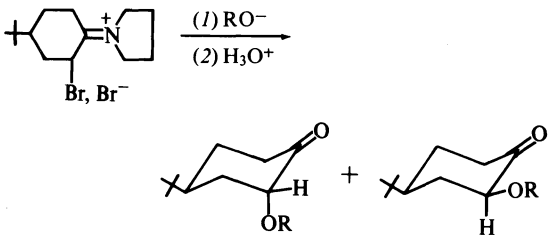

R = CH_3 **1***a* **1***e*
R = *t*-butyl **2***a* **2***e*

SCHÉMA 1

Les *tert*-butyl-4 phénoxy-2 cyclohexanones *cis* et *trans* (**3***e* et **3***a*) s'obtiennent par action du phénate sur la chloro-2 *tert*-butyl-4 cyclohexanone.

Alcoxy-2 cyclohexanones

Elles ont été synthétisées à partir d'énamines à halogène allylique suivant une méthode mise au point au laboratoire (8) (schéma 2).

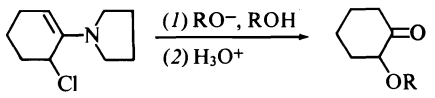

R = CD_3 **4**
R = C_2D_5 **5**
R = $CD(CD_3)_2$ **6**
R = $C(CH_3)_3$ **7**

SCHÉMA 2

Les rendements sont bons (cétones **4**–**6**: rdt 65%) ou acceptables (cétone **7**: rdt 35%).

Aryloxy-2 cyclohexanones

Elles ont été synthétisées par action des phénates *p*-XC_6H_4ONa sur la chloro-2 cyclohexanone selon une méthode décrite (9). Une difficulté s'est présentée lors de la synthèse du *p-NN*-diéthylaminophénol puisque toutes les synthèses décrites (10) ont échoué. Nous avons finalement utilisé une méthode de réduction de l'acétate du *p-NN*-diacétylaminophénol par l'hydrure de lithium et d'aluminium (schéma 3).

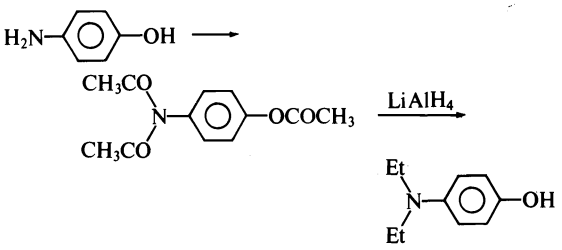

SCHÉMA 3

Acyloxy-2 cyclohexanones

Elles ont été préparées par action des sels d'argent $R(COO)_2Ag$ sur le chloro-6 pyrrolidino-1 cyclohexène (schéma 4).

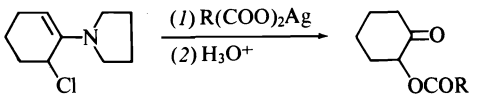

R = CH_3 **19**
R = C_6H_5 **20**
R = $C_6H_4OCH_3$ **21**

SCHÉMA 4

Résultats

Aryloxy-2 cyclohexanones

Les aryloxy-2 cyclohexanones, en solution dans un solvant polaire se trouvent toutes dans un même équilibre, très fortement déplacé vers la forme **III** équatoriale (85%) (tableau 1). Dans un solvant non polaire, l'équilibre conformationnel dépend de la nature du substituant X situé en *para* sur le noyau benzénique. En effet dans le cas de groupements attracteurs nous voyons apparaître une variation très nette de l'équilibre conformationnel en fonction du substituant X: dans tous les cas la forme équatoriale est favorisée. Par exemple pour X = NO_2, il y a 80% de forme équatoriale dans CCl_4. On notera que l'on observe une bonne corrélation entre les énergies conformationnelles ΔG dans CCl_4 et les σ de Hammett (figs. 1 et 3). Dans cette série (X attracteur), on remarque par ailleurs une dépendance de la valeur $\Delta G_{CH_3CN} - \Delta G_{CCl_4}$ avec le groupement X. Par contre si X est donneur (X = H, CH_3, OCH_3, OC_6H_5, NEt_2) l'équilibre est le même quelque soit X (55% de forme axiale **IV**). D'autre part, la différence $\Delta G_{CH_3CN} - \Delta G_{CCl_4}$ est sensiblement la même pour les différents substituants donneurs, soit 1.15 ± 0.14 kcal/mol.

TABLEAU 1. Energie conformationnelle des aryloxy-2 cyclohexanones

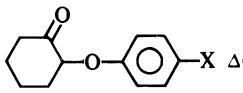

$$\Delta G = -RT \log \frac{ax}{eq} \text{ (kcal/mol)}$$

Cétone	X	σ^a	CCl_4 Axial (%)	CCl_4 ΔG	CH_3CN Axial (%)	CH_3CN ΔG	$\Delta G_{CH_3CN} - \Delta G_{CCl_4}$
8	NO_2	0.778	17±2	0.93±0.09	15	1.04±0.11	0.1 ±0.2[b]
9	$COCH_3$	0.502	31±2	0.48±0.05	15	1.04±0.11	0.56±0.15
10	CHO	0.45	28±2	0.56±0.06	15	1.04±0.11	0.48±0.15
11	Br	0.23	41±2	0.22±0.02	15	1.04±0.11	0.82±0.12
12	Cl	0.227	41±2	0.22±0.02	15	1.04±0.11	0.82±0.12
13	F	0.062	47±2	0.08±0.01	15	1.04±0.11	0.96±0.12
14	H	0	51±2	−0.02±0.01	15	1.04±0.11	1.06±0.12
15	CH_3	−0.170	54±2	−0.10±0.01	15	1.04±0.11	1.14±0.12
16	OCH_3	−0.268	54±2	−0.10±0.01	15	1.04±0.11	1.14±0.12
17	OC_6H_5	−0.32	52±2	−0.05±0.01	15	1.04±0.11	1.09±0.12
18	NEt_2	−0.8	54±2	−0.10±0.01	15	1.04±0.11	1.14±0.12

[a]Références 11 et 12.
[b]On voit nettement par rmn que la proportion de forme axiale dans CCl_4 est légèrement plus importante que dans CH_3CN; le calcul d'erreur n'a ici aucune signification.

TABLEAU 2. Energie conformationnelle ΔG des alcoxy-2 cyclohexanones

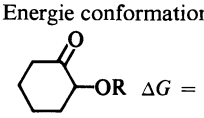

$$\Delta G = -RT \log \frac{ax}{eq} \text{ (kcal/mol)}$$

Cétone	R[a]	CCl_4 Axial (%)	CCl_4 ΔG	CH_3CN Axial (%)	CH_3CN ΔG	$\Delta G_{CH_3CN} - \Delta G_{CCl_4}$
4	CD_3	63.5±2	−0.33±0.03	20±2	0.82±0.08	1.15±0.11
5	C_2D_5	67.5±2	−0.44±0.04	24±2	0.68±0.07	1.12±0.11
6	$CD(CD_3)_2$	74 ±2	−0.63±0.06	30±2	0.50±0.05	1.13±0.11
7	$C(CH_3)_3$	80.5±2	−0.82±0.08	37±2	0.30±0.03	1.12±0.11

[a]R = H: la molécule est bloquée en position équatoriale du fait de la présence d'une liaison hydrogène entre le carbonyle et l'hydroxyle.

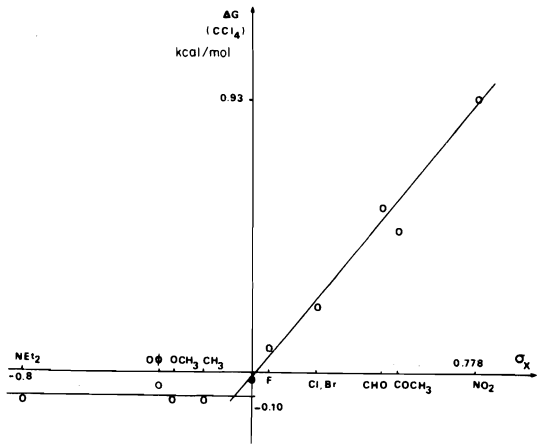

FIG. 1. Energie conformationnelle des p_X-phénoxy-2 cyclohexanones en fonction du σ_X de Hammett.

Alcoxy-2 cyclohexanones

Dans un solvant polaire (CH_3CN) les alcoxy-2 cyclohexanones prennent la conformation la plus polaire c'est-à-dire celle où le substituant est équatorial. On notera cependant que plus le groupement R est substitué plus la forme axiale est favorisée (tableau 2). Par exemple, la *tert*-butoxy-2 cyclohexanone **7** se trouve à 37% en position axiale alors que la méthoxy-2 cyclohexanone **4** se trouve seulement à 20% en axial. Cette même tendance vers une plus grande proportion de forme axiale si le substituant est encombré se retrouve si l'on examine l'equilibre conformationnel dans un solvant non polaire (CCl_4).

D'autre part, l'examen de la variation de l'équilibre conformationnel en fonction de la

Can. J. Chem. Downloaded from www.nrcresearchpress.com by 210.87.254.6 on 09/05/12
For personal use only.

Can. J. Chem. Downloaded from www.nrcresearchpress.com by 210.87.254.6 on 09/05/12
For personal use only.

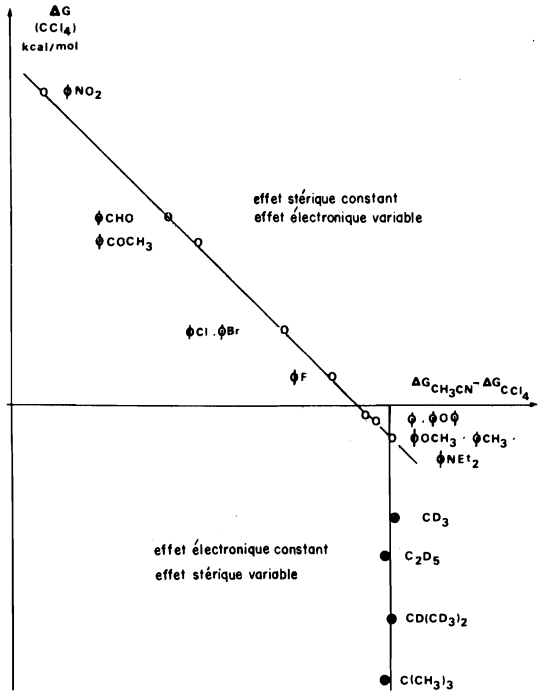

FIG. 2. Energie conformationnelle des alcoxy-2 et des aryloxy-2 cyclohexanones en fonction de $\Delta G_{CH_3CN} - \Delta G_{CCl_4}$.

polarité du solvant montre que, quelque soit le substituant R, la différence entre l'énergie conformationnelle dans CH_3CN et celle dans CCl_4 est pratiquement constante ($\Delta G_{CH_3CN} - \Delta G_{CCl_4} = 1.13 \pm 0.13$ kcal/mol) (fig. 2).

Acyloxy-2 cyclohexanones

Les trois acyloxy-2 cyclohexanones étudiées se trouvent toutes déjà en position équatoriale dans le tétrachlorure de carbone. Il n'est donc pas possible dans ce cas d'étudier l'influence du groupement R sur l'équilibre conformationnel.

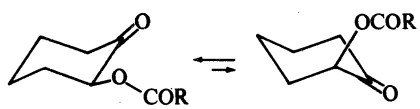

R = CH_3
C_6H_5
$C_6H_4OCH_3$

Discussion

Le cas des aryloxy-2 cyclohexanones est particulièrement intéressant. Le facteur stérique pouvant être considéré comme constant dans toute cette série, nous avons mis en évidence une dépendance directe de l'équilibre conformationnel en fonction de facteurs purement électroniques, ce qui à notre connaissance n'avait jamais été signalé.

La corrélation linéaire observée, quand X est attracteur, entre l'énergie conformationnelle ΔG dans CCl_4 et les σ de Hammet pouvait nous laisser prévoir les résultats obtenus avec les acyloxy-2 cyclohexanones (OCOR: 100% en équatorial) puisque dans ce cas le groupement attracteur est directement attaché à l'oxygène et les effets électroniques sont donc renforcés.

Les groupements donneurs conduisent toujours au même équilibre (tableau 1). Il apparaît ici un nivellement analogue à celui observé quand on mesure l'acidité des phénols (11). On remarque, d'autre part que ce phénomène met en défaut l'hypothèse selon laquelle la forme limite de stabilisation pour la forme axiale serait de type énolique (V) (schéma 5).

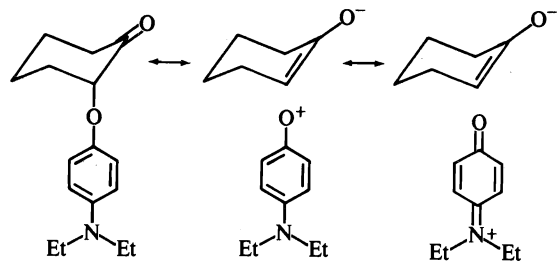

SCHÉMA 5

En effet, dans cette hypothèse le substituant le plus donneur (NEt_2) stabiliserait au maximum la forme axiale, ce qui est contraire à ce que l'on observe.

Dans le cas des alcoxy-2 cyclohexanones, il n'est pas raisonnable de tenter une corrélation entre l'énergie conformationnelle et les σ^* de Taft puisque pour les groupes alcoyles ces valeurs ont été très controversées (13).

Cependant le fait que la différence entre l'énergie conformationnelle dans CH_3CN et celle dans CCl_4 soit constante laisse supposer que la contribution électronique des groupements R, dans la variation de l'équilibre des alcoxy-2 cyclohexanones, est faible. En effet, en admettant que la contribution stérique (interactions de type van der Waals) est sensiblement la même quel que soit le solvant, on peut écrire que l'énergie électronique E de chacune des deux formes dépend du solvant selon (14, 15):

$$E_{\text{solvant}} = E^{e}_{\text{vide}}/D + E^{i}_{\text{vide}}/D = E_{\text{vide}}/D$$

où E^e = énergie électrostatique : interaction dipole–dipole, E^i = énergie d'interaction dipole–dipole induit et D = constante diélectrique du solvant. Soit:

$$E^{eq}_{CH_3CN} = \frac{E^{eq}_v}{D_1} \qquad D_1 = D_{CH_3CN}$$

$$E^{eq}_{CCl_4} = \frac{E^{eq}_v}{D_2} \qquad D_2 = D_{CCl_4}$$

$$E^{eq}_{CH_3CN} - E^{eq}_{CCl_4} = E^{eq}_v \left(\frac{I}{D_1} - \frac{I}{D_2}\right)$$

$$E^{ax}_{CH_3CN} - E^{ax}_{CCl_4} = E^{ax}_v \left(\frac{I}{D_1} - \frac{I}{D_2}\right)$$

ou encore:

$$\Delta E^{eq-ax}_{CH_3CN} - \Delta E^{eq-ax}_{CCl_4} = \Delta E^{eq-ax}_v \left(\frac{I}{D_1} - \frac{I}{D_2}\right)$$

Le terme $\Delta E^{eq-ax}_{CH_3CN} - \Delta E^{eq-ax}_{CCl_4}$ étant constant quelque soit R cela signifie que ΔE^{eq-ax}_v est indépendant de R, c'est-à-dire que la contribution électronique est la même quel que soit R. Par conséquent, c'est le facteur stérique qui détermine la différence dans la position de l'équilibre conformationnel des alcoxy-2 cyclohexanones.

Par ailleurs, pour les aryloxy-2 cyclohexanones comportant un groupement X donneur, on peut raisonnablement supposer que la contribution électronique du groupement R = XC_6H_4 est négligeable puisque l'on retrouve également la valeur 1.14 kcal/mol pour la différence $\Delta G_{CH_3CN} - \Delta G_{CCl_4}$. Ceci est bien en accord avec le fait que l'on n'observe aucune variation dans la position de l'équilibre conformationnel quand on passe de X = CH_3 à X = NEt_2.

Conclusion

En minimisant l'influence du facteur stérique dans la série des aryloxy-2 cyclohexanones nous avons pu mettre directement en évidence l'influence de facteurs électroniques sur l'équilibre conformationnel des cyclohexanones. Les résultats sont très nets: plus le groupement X est attracteur plus la forme équatoriale est favorisée et à la limite, le groupe acyloxy est uniquement équatorial.

Partie expérimentale

Les spectres de rmn ont été enregistrés à 60 MHz sur un appareil JEOL C60 HL avec le TMS comme référence interne et à 250 MHz sur un appareil CAMECA; les spectres ir ont été pris dans CCl_4 sur un spectrophotomètre Perkin-Elmer 457. Les différentes manipulations et distillations ont été faites sous atmosphère d'azote. Les analyses élémentaires des composés obtenus sont en accord avec les formules proposées (la marge d'erreur acceptée est de 0.2% pour C, H, O, N et de 0.4% pour les halogènes).

Choix de la largeur du signal en résonance magnétique nucléaire

Le problème de la mesure de la largeur du signal du proton situé au pied du groupement Y dans un système cyclohexanique en équilibre rapide a déjà été discuté (6, 7).

Nous sommes en présence d'un système ABX: la partie X est représentée par un triplet quand H est équatorial (**1***a* et **2***a*) et par un doublet dédoublé quand H est axial (**1***e* ou **2***e*): dans le cas de **3***a* et **3***e* les signaux sont mal résolus et nous avons pris les largeurs à mi-hauteur comme mesure de la somme des constantes de couplage. Par la suite nous avons également pris les largeurs à mi-hauteur pour comparer les différents systèmes en équilibre, les valeurs indiquées proviennent d'une moyenne entre sept mesures. Même si elles ne sont pas rigoureusement exactes, la variation dans une même série (celle des aryloxy-2 cyclohexanones par exemple) est très significative et reproductible. Pratiquement on prend comme référence la cétone **8** (X = NO_2) ou **16** (X = OCH_3) et on mesure la variation de la largeur à mi-hauteur des signaux des cétones **9** à **18** à partir de la référence choisie (**8** ou **16**) (les aires des signaux doivent être sensiblement les mêmes pour que l'on puisse superposer les spectres) (fig. 3). Pour les cétones **15**, **16** et **18** (aryloxy-2 cyclohexanones avec X donneur) on constate une excellente superposition des spectres et donc aucune variation de l'équilibre conformationnel avec X.

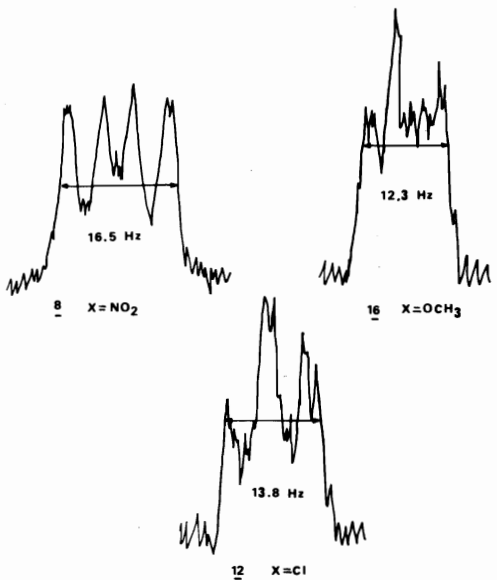

FIG. 3. Spectres rmn du proton H_1, à 250 MHz, obtenus pour les aryloxy-2 cyclohexanones (dans CCl_4).

Can. J. Chem. Downloaded from www.nrcresearchpress.com by 210.87.254.6 on 09/05/12
For personal use only.

TABLEAU 3. Caractéristiques physicochimiques des aryloxy-2 cyclohexanones

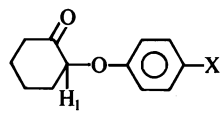

			rmn[a]						
			CCl_4[b,c]			CH_3CN			ir(CCl_4, cm^{-1})
Cétone	X	pf (°C)	δH_1	WH_1	δX	δH_1	WH_1	δX	ν(CO)[d]
8	NO_2	106	4.72	16.5		5.0	17		1730–1737[ep]
9	$COCH_3$	105	4.54	15	2.42	4.90	17	2.48	1727–1738[ep]
10	CHO	73	4.65	15.3	10.6	4.92	17	9.70	1728–1738[ep]
11	Br	87	4.56	13.8		4.80	17		1730–1738[ep]
12	Cl	87	4.56	13.8		4.75	17		1728–1738[ep]
13	F	82	4.44	13.1		4.80	17		1728–1738[ep]
14	H	59	4.50	12.6		4.80	17		1728–1737[ep]
15	CH_3	80	4.54	12.3	2.33	4.80	17	2.50	1730–1737[ep]
16	OCH_3	77	4.34	12.3	3.71	4.75	17	3.75	1730–1738[ep]
17	OC_6H_5	117	4.41	12.5		4.75	17		1729–1738[ep]
18	NEt_2	63	4.30	12.3	1.1	4.60	17	1.0	1728–1736[ep]
					3.23			3.25	

[a]Les spectres rmn ont été enregistrés à la concentration de 8.9×10^{-3} mol/l, à 250 MHz.
[b]Les déplacements chimiques sont exprimés en ppm (réf. TMS).
[c]La largeur W du massif dû au proton H_1 est exprimée en Hz.
[d]ep = épaulement.

tert-Butyl-4 méthoxy-2 cyclohexanone ***1***

On verse goutte à goutte 12 g (0.066 mol) de brome dans 17.8 g (0.066 mol) de *tert*-butyl-4 pyrrolidino-1 cyclohexène dilué dans 100 ml de pentane; on chasse le pentane sous vide puis on ajoute 100 ml d'une solution de méthylate de sodium (6 g, 0.01 mol) dans le monoglyme. On porte à reflux pendant 4 h. On chasse le monoglyme puis on hydrolyse par H_2SO_4 à 20%. On extrait à l'éther, on effectue un lavage basique et on sèche la solution éthérée sur sulfate de magnésium. Les deux isomères *cis* et *trans* sont obtenus purs après passage sur colonne de silice (éluant benzène): après éliminations des fractions de tête contenant en particulier la bromo cyclohexanone n'ayant pas réagi, l'isomère *trans* **1***a* passe en premier (ir ν(CO) 1723 cm^{-1}); puis vient l'isomère *cis* **1***e* (ir ν(CO) 1733 cm^{-1}; rdt global 30%; *cis*/*trans* = 2:1). Les caractéristiques rmn sont rassemblées dans le tableau 4.

tert-Butyl-4 t-butyoxy-2 cyclohexanone ***2***

On opère de la même manière que précédemment. L'immonium bromé (0.066 mol) est mis à refluer dans une solution de *tert*-butylate de potassium (0.09 mol) dans 100 ml de monoglyme. Après les traitements habituels, on sépare les deux isomères *trans* **2***a* (ir ν(CO) 1723 cm^{-1}) et *cis* **2***e* (ir ν(CO) 1733 cm^{-1}) par chromatographie sur colonne de silice (éluant benzène; rdt global 20%; *cis*/*trans* = 2:1). Les caractéristiques rmn sont rassemblées dans le tableau 4.

tert-Butyl-4 phénoxy-2 cyclohexanone ***3***

La *tert*-butyl-4 bromo-2 cyclohexanone (12 g) est mis à reflux pendant 4 h dans 50 ml de benzène contenant 5.8 g de phénate de sodium. On traite le mélange par de la soude diluée. On obtient après extraction à l'éther et traitement habituel un mélange de *tert*-butyl-4 phénoxy-2 cyclohexanones *cis* et *trans* (rdt 70%).

L'isomère axial (*trans*) **3***a* est séparé par chromatographie sur colonne de silice (éluant benzène; ir ν(CO) 1728 cm^{-1}). Il est liquide et se transforme rapidement en isomère *cis*; l'isomère équatorial **3***e* (*cis*) cristallise dans un mélange benzène–éther (pf = 75 °C, ir ν(CO) 1738 cm^{-1}); les caractéristiques rmn sont rassemblées dans le tableau 4).

Alcoxy-2 cyclohexanones

Le principe de la méthode a été décrit précédemment (8). Nous avons utilisé l'énamine dérivant de la chloro-2 cyclohexanone comme produit de départ (16). Pour R = $CH(CH_3)_2$ et R = *tert*-butyl nous n'avons pas trouvé d'autres méthodes décrites dans la littérature.

Perdeutériométhoxy-2, éthoxy-2 cyclohexanones ***4*** *et* ***5***

Le chloro-6 pyrrolidino-1 cyclohexène (5 g, 0.027 mol) (15) est mis à reflux pendant 2 h dans 10 ml de perdeutériométhanol dans lequel on a fait préalablement réagir 0.65 g (0.028 at/g) de sodium et le mélange est ensuite hydrolysé par de l'acide sulfurique normal. On extrait à l'éther la phase aqueuse acide, on rince la solution éthérée par une solution de soude et sèche sur sulfate de magnésium. On obtient ainsi 2.1 g (0.017 mol) de perdeutériométhoxy-2 cyclohexanone **4** après distillation (rdt 60%); le même mode opératoire permet d'obtenir la perdeutérioéthoxy-2 cyclohexanone **5** avec un rendement de 65%.

Perdeutérioisopropanoxy-2 cyclohexanone ***6***

Le chloro-6 pyrrolidino-1 cyclohexène (5 g 0.027 mol) est mis à reflux pendant 2 h dans 10 ml de perdeutérioisopropanol contenant 0.06 g (0.0027 at/g) de sodium. Après les traitements habituels, on extrait la perdeutérioisopropanoxy-2 cyclohexanone **6** de la phase aqueuse acide (0.017 mol; 2.6 g; rdt 65%; p $éb_{15}$ = 85 °C; ir

Can. J. Chem. Downloaded from www.nrcresearchpress.com by 210.87.254.6 on 09/05/12
For personal use only.

TABLEAU 4. Caractéristiques rmn des *tert*-butyl-4 aryloxy et alcoxy-2 cyclohexanones[a]

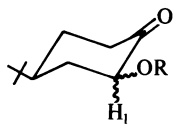

Cétone	R		CCl_4		CH_3CN	
			δH_1	WH_1	δH_1	WH_1
1*e*	CH_3	eq	3.70	18.0	3.83	18.4
1*a*		ax	3.74	7.0	3.43	7.2
2*e*	*t*-Butyl	eq	3.84	18.2	4.10	18.6
2*a*		ax	3.70	7.0	3.82	7.2
3*e*	C_6H_5	eq	4.63	18.5	4.91	18.7
3*a*		ax	4.34	7.0	4.58	7.2

[a]Mêmes remarques que dans le tableau 3.

TABLEAU 5. Caractéristiques rmn des alcoxy-2 et acyloxy-2 cyclohexanones[a]

Cétone	R	CCl_4		CH_3CN	
		δH_1	WH_1	δH_1	WH_1
4	CD_3	3.42	11.0		16.25
5	C_2D_5	3.58	10.5		15.75
6	$CD(CD_3)_2$	3.65	9.8		15.1
7	$C(CH_3)_3$	3.75	9		14.25
19	$COCH_3$	5.05	18.0	5.1	18.5
20	COC_6H_5	5.0	19.0	5.4	19.0
21	$COC_6H_4OCH_3$	5.18	19.0	5.34	19.0

[a]Concentration: 2×10^{-2} mol/l.

ν(CO) 1722–1732 (ep) cm^{-1}). Les caractéristiques rmn sont données dans le tableau 5.

tert-Butoxy-2 cyclohexanone **7**

Le chloro-6 pyrrolidino-1 cyclohexene (5 g, 0.027 mol) est mis à reflux pendant 4 h dans 10 ml de *tert*-butanol contenant 0.06 g de sodium. Après traitement habituel on obtient la *tert*-butoxy-2 cyclohexanone **7** (1.4 g; rdt 30%; p $éb_{0.15}$ = 48 °C; ir ν(CO) 1723–1733 (ep) cm^{-1}).

*Aryloxy-2 cyclohexanones (**8** à **18**)*

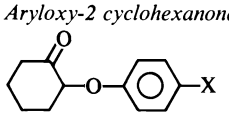

X = H,F,Cl,Br,CHO,$COCH_3$, NO_2,CH_3,OCH_3,OC_6H_5

Les aryloxy-2 cyclohexanones ont été préparées selon la méthode de Mousseron *et al.* (9). On ajoute 0.1 mol de phénol substitué en *para* à une solution de 2.3 g de sodium dans 100 ml de méthanol anhydre. On porte le mélange à ébullition puis on chasse le méthanol sous vide. Le phénate broyé est mis en suspension dans 50 ml de benzène et on ajoute alors 0.1 mol (13.2 g) de chloro-2 cyclohexanone. On chauffe au reflux du benzène pendant 4 h; après refroidissement, on ajoute de la soude diluée et on extrait à l'éther. On rince la phase éthérée à la soude diluée puis à l'eau et on sèche sur sulfate de magnésium. On chasse les solvants sous vide: il reste un produit noirâtre que l'on reprend par 50 ml d'éther. On récupère la partie soluble dans l'éther à laquelle on ajoute 50 ml de pentane et on obtient ainsi l'aryloxy-2 cyclohexanone qui précipite. Elle est recristallisée dans un mélange 50:50 benzène–éther de pétrole. Les rendements sont de l'ordre de 65%. Les caractéristiques des aryloxy-2 cyclohexanone sont rassemblées dans le tableau 3.

Les phénols X—ϕ—OH sont commerciaux sauf celui où X = NEt_2, X = H, NO_2, CH_3 (Aldrich); X = F, Cl, Br, CHO, $COCH_3$ (Fluka); X = OCH_3 (Schuchardt); X = OC_6H_5 (Kodak).

para-Diéthylaminophénoxy-2 cyclohexanone **18**

(a) para-N,N-Diéthylaminophénol—Le *p*-aminophénol (20 g) est mis à reflux dans 120 ml d'anhydride acétique pendant 4 h. On distille ensuite l'anhydride et l'acide acétique formés et on obtient alors un mélange d'acétate de *p-N*-acétylaminophénol *A* et d'acétate de p-*N*,*N*-diacétylaminophénol *B*. On ajoute 500 ml d'éther que l'on porte à reflux. Après refroidissement, l'acétate *A* cristallise, on le filtre; l'acétate de *N*,*N*-diméthylaminophénol *B* est obtenu en chassant l'éther du filtrat (rdt 65%, pf = 74 °C, ir ν(CO) 1710–1760 cm^{-1}; rmn ($CDCl_3$) 2.26 ppm (9H), 7.15 ppm (4H)).

A 9 g d'hydrure de lithium et d'aluminium dans 100 ml d'éther au reflux on ajoute 20 g de l'acétate *B* dissous dans

Can. J. Chem. Downloaded from www.nrcresearchpress.com by 210.87.254.6 on 09/05/12
For personal use only.

500 ml d'éther. L'addition terminée, on ajoute goutte à goutte 50 ml d'eau puis 100 ml d'acide sulfurique à 20%. On sépare la couche supérieure; la couche inférieure est neutralisée par le bicarbonate de sodium puis extraite à l'éther. On chasse l'éther jusqu'à ce qu'il en reste 50 ml. Placé au congélateur, le *N*-éthylaminophénol, produit secondaire précipite; on le filtre et on utilise le *para-N,N*-diéthylaminophénol restant sans autre purification, le composé s'oxydant très rapidement (4.7 g; rdt 65%; rmn ($CDCl_3$) 1 (6H), 3.2 (4H), 6.2 ppm (4H).

(b) para-Diéthylaminophénoxy-2 cyclohexanone ***18***—A 4.7 g de *p*-diéthylaminophénol dans 20 ml de monoglyme, on ajoute 0.6 g de sodium; on attend 4 h. On décante sous azote la solution de phénate et on fait réagir 6 g de chloro-2 cyclohexanone à reflux du monoglyme pendant 2 h; le solvant est chassé sous vide, le résidu est traité par 1 *N* H_2SO_4 et lavé à l'éther pour éliminer la chloro-2 cyclohexanone n'ayant pas réagi. La solution est ensuite alcalinisée, extraite à l'éther et séchée sur $MgSO_4$. La *p-N,N*-diéthylaminophénoxy-2 cyclohexanone est recristallisée dans un mélange éther–pentane (2.1 g; rdt = 18%) (tableau 3).

*Acyloxy-2 cyclohexanones (**19**, **20**, **21**)*

Les sels d'argent des acides acétique, benzoïque, *p*-méthoxybenzoïque sont obtenus par action du nitrate d'argent sur l'acide, dans l'eau. Le sel d'argent précipite, est recristallisé dans l'eau et séché sous vide.

Le chloro-6 pyrrolidino-1 cyclohexène (5 g, 0.027 mol), en solution dans 50 ml de benzène est mis à réagir avec le sel d'argent en quantité stoechiométrique au reflux pendant 4 h. Le mélange réactionnel est hydrolysé par de l'acide sulfurique normal, extrait à l'éther et séché sur sulfate de magnésium.

L'acétoxy-2 cyclohexanone **19** est distillée (p $éb_{0.35}$ = 55 °C; rdt 70%; ir ν(CO) 1734–1755 cm^{-1}.

Les benzoxy-2 cyclohexanone **20** et *p*-méthoxybenzoxy-2 cyclohexanone **21** sont recristallisées dans un mélange benzène–éther (rdt 75%). R = $OCOC_6H_5$ **20**: pf = 89 °C; ir ν(CO) 1727–1737 (ep) cm^{-1}; $OCOC_6H_4OCH_3$ **21**: pf = 75 °C; ir ν(CO) 1723–1737 (ep) cm^{-1}. Les caractéristiques rmn sont rassemblées dans le tableau 5.

Remerciements

Nous remercions très vivement M. Welwart pour de fructueuses discussions.

1. E. J. Corey et H. J. Burke. J. Am. Chem. Soc. **77**, 5418 (1955); N. L. Allinger, J. Chow Tai et M. A. Miller, J. Am. Chem. Soc. **88**, 4495 (1966); C. Y. Chen et R. J. Lefevre. J. Chem. Soc. 3700 (1965).
2. J. Cantacuzene, R. Jantzen et D. Ricard. Tetrahedron, **26**, 717 (1972).
3. O. Eisenstein, N. Trong Anh, Y. Jean, A. Devaquet, J. Cantacuzene et L. Salem. Tetrahedron, **30**, 1717 (1974).
4. R. C. Cookson et N. S. Wariayar. J. Chem. Soc. 2302 (1956).
5. H. Labhart et C. Wagniere. Helv. Chim. Acta, **42**, 2219 (1959).
6. Y. H. Pan et J. B. Stothers. Can. J. Chem. **45**, 2943 (1967); J. Cantacuzene et R. Jantzen. Tetrahedron, **26**, 2429 (1970).
7. H. Booth. Tetrahedron, **20**, 2211 (1964).
8. D. Cantacuzene et M. Tordeux. Tetrahedron Lett. 4807 (1971).
9. M. Mousseron, R. Jacquier et A. Fontaine. Bull. Soc. Chim. Fr. 767 (1952).
10. G. Chuchani et A. Frohlich. J. Chem. Soc. B, 1417 (1971); F. Minisci, R. Galli et M. Perchinunno. Org. Prep. Proced. **1**, 87 (1969); M. Sekiya, M. Tomie et N. J. Leonard. J. Org. Chem. **33**, 318 (1968).
11. L. P. Hammett. Physical Organic Chemistry, 2ème éd. McGraw-Hill, New York. 1970. p. 347.
12. A. A. Humffray, J. J. Ryan, J. P. Warren et Y. H. Yung. Chem. Commun. **23**, 610 (1965).
13. J. Shorter. Q. Rev. Chem Soc. **24**, 433 (1970).
14. E. L. Eliel, N. L. Allinger, J. J. Angyal et G. A. Morrison (*Editors*). Conformational analysis. Interscience. 1965. p. 159.
15. N. L. Allinger, J. Allinger, L. A. Freiberg, R. Czaja et N. A. Lebel. J. Am. Chem. Soc. **82**, 5876 (1960).
16. J. C. Blazejewski, D. Cantacuzene et C. Wakselman. Tetrahedron, **29**, 4233 (1973).

Can. J. Chem. Downloaded from www.nrcresearchpress.com by 210.87.254.6 on 09/05/12
For personal use only.

Isotope effects in the gas phase radiolysis of H_2S and D_2S[1]

ROBERT D. MCALPINE, O. A. MILLER, AND A. W. BOYD

Physical Chemistry Branch, Chalk River Nuclear Laboratories, Atomic Energy of Canada Limited, Chalk River, Ont., Canada K0J 1J0

Received March 17, 1976

ROBERT D. MCALPINE, O. A. MILLER, and A. W. BOYD. Can. J. Chem. **54**, 2767 (1976).

Gas phase radiolysis studies have been carried out on mixtures of H_2S and D_2S using as irradiation sources, either a Gammacell or a Febetron 705 pulsed electron accelerator. Separation factors ($\alpha = (H/D)_{prod} \div (H/D)_{react}$) were obtained for various values of x_D (the mole fraction of D_2S), dose rate and temperature, as well as with the addition of SF_6. All of the observed α values, for $0.2 \leq x_D \leq 0.8$, fall on the following empirical straight line.

[1] $$\alpha(x_D) = (1.18 \pm 0.04) + (1.07 \pm 0.09)x_D$$

The addition of neon to a D_2S/H_2S mixture gives a value of α which decreases as the partial pressure of neon increases. For a 70% D_2S/30% H_2S mixture, $\alpha = 1.9 \pm 0.1$ for the pure mixture and 1.28 ± 0.08 when 90 kPa of neon has been added to 10 kPa of the mixture. The α values described by eq. 1 are interpreted as arising from kinetic isotope effects in the reactions of (translationally) hot H or D atoms with H_2S, HDS, or D_2S to form H_2, HD or D_2.

Hydrogen yields from the gas phase radiolysis of pure H_2S and pure D_2S have been determined for dose rates from 4×10^{16} to 2×10^{28} eV g^{-1} s^{-1}. Using dose rates of up to 2×10^{27} eV g^{-1} s^{-1}, $\Delta G = G(H_2) - G(D_2) = 0.5$. For the highest dose rate used (2×10^{28} eV g^{-1} s^{-1}), $\Delta G = 1.5$. The larger value of ΔG at very high dose rates is thought to arise from the dissociative neutralization processes. A possible mechanism is discussed.

ROBERT D. MCALPINE, O. A. MILLER et A. W. BOYD. Can. J. Chem. **54**, 2767 (1976).

Des études de radiolyse en phase gazeuse ont été faites sur des mélanges de H_2S et D_2S en utilisant comme source d'irradiation, soit un Gammacell soit un accélérateur d'électrons à impulsion Febetron 705. Les facteurs de séparation [$\alpha = (H/D)_{prod.} \div (H/D)_{react.}$] ont été obtenus pour différentes valeurs de x_D (la fraction molaire de D_2S), de taux d'irradiation et de températures, aussi bien qu'avec l'addition de SF_6. Toutes les valeurs α observées, pour $0.2 \leq x_D \leq 0.8$, se situent sur la droite empirique suivante:

[1] $$\alpha(x_D) = (1.18 \pm 0.04) + (1.07 \pm 0.09)x_D$$

L'addition de néon à un mélange de D_2S/H_2S donne une valeur α qui diminue comme la pression partielle du néon augmente. Pour un mélange D_2S/H_2S, 70:30, $\alpha = 1.9 \pm 0.1$ pour le mélange pur et 1.28 ± 0.08 quand 90 kPa de néon a été ajouté à 10 kPa du mélange. Les valeurs α décrites par l'éq. 1 sont interprétées comme venant des effets cinétiques dans les réactions d'atomes H ou D, riches en énergie de translation, avec H_2S, HDS ou D_2S pour former H_2, HD ou D_2. Les rendements en hydrogène de la radiolyse en phase gazeuse de H_2S pur et D_2S pur ont été déterminés pour des taux d'irradiation de 4×10^{16} eV g^{-1} s^{-1} à 2×10^{28} eV g^{-1} s^{-1}. Utilisant des taux d'irradiation jusqu'à 2×10^{27} eV g^{-1} s^{-1}, $\Delta G = G(H_2) - G(D_2) = 0.5$. Pour le plus grand taux d'irradiation utilisé (2×10^{28} eV g^{-1} s^{-1}), $\Delta G = 1.5$. On croit que la plus grande valeur de ΔG à des taux d'irradiation très élevés est attribuable aux processus dissociatifs de neutralisation. Un mécanisme possible est discuté.

[Traduit par le journal]

Introduction

The radiation chemistry of H_2S has been studied using γ, α and pulsed electron sources and a general understanding of many of the processes which lead to the production of hydrogen has evolved. The hydrogen yield, $G(H_2)$, has been observed to vary according to the rate at which the dose is absorbed. At the low dose rates which are typical of Gammacells ($10^{14} - 10^{18}$ eV g^{-1} s^{-1}), $G(H_2) = 7.0 - 7.9$ (1–4). Electron scavengers such as SF_6 or N_2O are found to have no effect on this yield. With pulsed electron sources, the hydrogen yield is found to vary from $G(H_2) = 11.1$ for a dose rate of 10^{26} eV g^{-1} s^{-1} to $G(H_2) = 13.0$ for a dose rate of 2×10^{28} eV g^{-1} s^{-1} (5, 6). Electron scavengers reduce these yields to values comparable with those obtained using low dose rates.

[1]AECL No. 5487.

Can. J. Chem. Downloaded from www.nrcresearchpress.com by 210.87.254.5 on 09/05/12
For personal use only.

Can. J. Chem. Downloaded from www.nrcresearchpress.com by 210.87.254.5 on 09/05/12
For personal use only.

The major difference in yields between low and high dose rate experiments is thought to arise from the quenching of dissociative neutralization processes at low dose rates (6). For $10^{14} - 10^{18}$ eV g^{-1} s^{-1}, products that act as electron scavengers (probably the polysulphanes H_2S_n, $n > 2$) are able to compete with dissociative neutralization processes. However, with short high intensity electron pulses these products do not reach sufficient concentration during the pulse to compete effectively with dissociative neutralization. Using these pulses, in excess of 30% of the hydrogen produced results from dissociative neutralization (5, 6). It has been suggested (5) that the variation of $G(H_2)$ at high dose rates may be explained in terms of competition between the dissociative neutralizations of various clustered ions such as $H_3S^+(H_2S)$ and $H_3S^+(H_2S)_n$ where $n > 1$. Boyd, Willis, and Miller (5) suggest that $H_3S^+(H_2S)$ may give two H atoms per neutralization, while the more highly clustered ions ($n > 1$) give less than two. Dissociative neutralization and clustering are parallel reactions with the rate constants for dissociative neutralization being $\sim 10^3$ times those for clustering (5). Increasing the dose rate (and hence the concentration of the electrons) will favour dissociative neutralization over clustering. Consequently, using high dose rates, dissociative neutralization will occur for smaller clusters and as a result the overall hydrogen yield will correspondingly increase. As the zero point energy of clustered ions such as $D_3S^+(D_2S)_n$ is somewhat lower than the corresponding protio species, $H_3S^+(H_2S)_n$, one might expect the more highly clustered species to be more numerous in D_2S than in H_2S. At a given dose rate, this effect could result in a lower value of $G(D_2)$ than of $G(H_2)$. The effect of deuteration on the hydrogen yield could provide further insight into the role that dissociative neutralization and clustering plays in the radiolysis of H_2S.

In addition to dissociative neutralization processes, other primary and secondary processes can give rise to isotope effects. These effects are difficult to determine *a priori*; however they can provide detailed information about various important processes which is difficult to obtain in other ways. In this paper, we present the results of a study of isotope effects on the radiolysis of gas phase mixtures of H_2S and D_2S.

Experimental

The H_2S used for most of these experiments was Matheson CP grade. In addition MG-4 grade high purity H_2S obtained from M.G. Scientific was used for a few experiments. Comparable results were obtained using both samples of H_2S. Mixtures of H_2S and D_2S (Merck, Sharpe and Dohme) were sealed in quartz cells and were subjected to a number of freeze–thaw cycles in an effort to assure that the samples had reached exchange equilibrium. Samples were then irradiated using either a Febetron 705 or a Febetron 706 at sample temperatures of 195 or 300 K. For experimental details, see refs. 5 and 6. The hydrogen produced was stripped off and was analysed on a CEC Model 21-610 mass spectrometer to obtain separation factors ($\alpha = (H/D)_{prod} \div (H/D)_{react}$). Mixtures containing less than 20% or more than 80% D_2S were not studied since they produced H_2, HD, and D_2 mixtures which are difficult to analyse accurately because of memory effects in the mass spectrometer (7). The G values from Febetron irradiations were obtained relative to N_2O dosimetry with $G(N_2) = 12.4$ (8).

A number of experiments were performed in which a mixture of 70% D_2S, 30% H_2S was added to various partial pressures of neon (Matheson research grade) to give a total pressure (mixture plus neon) $\approx$ 100 kPa ($\sim$1 atm). The samples were then pulsed up to ten times using a Febetron 705 until H_2, HD, D_2 mixtures sufficiently large for analysis were obtained. The repetitive pulses were necessary since neon has a lower stopping power for electrons than H_2S.

Results and Discussion

G Values

The isotope effect on the G values for the production of hydrogen from pure H_2S or D_2S is shown in Table 1. At Gammacell dose rates, $G(H_2)$ is 7% higher than $G(D_2)$. This difference could arise from an isotope effect for the primary formation of H or D (or H_2 or D_2), or it could arise in one or more of the complex secondary processes. Studies at Gammacell dose rates using H atom scavengers have shown that no more than 7% of the hydrogen produced at these dose rates is due to a primary unimolecular yield of hydrogen molecules (3). Once the H atoms are formed, they virtually all react with H_2S to give H_2, since abstraction is much faster than other possible H atom reactions in the system. Thus abstraction by H or D cannot lead to an isotope effect in the total G values, *i.e.*, $(G(H_2) + G(HD) + G(D_2))$. Since dissociative neutralization processes are not important for Gammacell dose rates, we can also rule these out as a source of the observed isotope effect in the yields.

TABLE 1. Dose rate dependence of the G values for H_2 and D_2 from Febetron and Gammacell irradiations of pure H_2S and pure D_2S

Line	Parameter	Value at dose rate in eV g^{-1} s^{-1}			
		4×10^{16}	10^{26}	2×10^{27}	2×10^{28}
1	Pure H_2S $G(H_2)$	7.3[a] ±0.3	11.1 ±0.4	11.8 ±0.4	13.0 ±0.4
2	Pure D_2S $G(D_2)$	6.8[b] ±0.3	10.8 ±0.4	10.9 ±0.4	11.5 ±0.4
3	$G(D_2) + 0.5$[c]	7.3 ±0.3	11.3 ±0.4	11.4 ±0.4	12.0 ±0.4
4	ΔG = Line 1 − Line 2	+0.5	+0.3	+0.9	+1.5
5	$(\Delta G)_{corr}$ = Line 1 − Line 3	0	−0.2	+0.4	+1.0

[a]Assumed from Febetron yields for H_2S + S (see ref. 5).
[b]Measured in a Gammacell compared to $G(H_2) = 7.3$.
[c]$G(H_2) - G(D_2)$ at Gammacell dose rates.

For dose rates 10^{26} and 2×10^{27} eV g^{-1} s^{-1} we observe $\Delta G = G(H_2) - G(D_2) = 0.3$ and 0.9 respectively (line 4, Table 1). In addition to the mechanisms which lead to isotope effects in the low dose rate experiments, new mechanisms may give rise to isotope effects when higher dose rates are employed. In order to determine whether new mechanisms are operating, we subtract the observed Gammacell isotope effects from the higher dose rate results (line 5, Table 1). For dose rates 10^{26} and 2×10^{27} eV g^{-1} s^{-1}, this gives $(\Delta G)_{corr} = \Delta G - 0.5 = -0.2$ and 0.4 respectively. Within experimental error, there is no evidence of new isotope effects for the G values (other than those observed for Gammacell dose rates) for dose rates up to 2×10^{27} eV g^{-1} s^{-1}.

For the highest dose rate used, 2×10^{28} eV g^{-1} s^{-1}, $\Delta G = 1.5$ and $(\Delta G)_{corr} = 1.0$. The observed change here in $(\Delta G)_{corr}$ compared to lower dose rate experiments is larger than experimental error, and a new source of isotope effects on the yield is evident. These results are consistent with the suggestion of Boyd, Willis, and Miller (5), that competition between clustered ions of various sizes in the dissociative neutralization processes is responsible for the observed variation of $G(H_2)$ at very high dose rates.

Separation Factors

As shown in Fig. 1 and Table 2, the separation factors, α, were obtained for various values of x_D (the mole fraction of D_2S before exchange equilibration), dose rate and temperature, as well as with the addition of SF_6. All of the observed α values appear to fall on the same empirical straight line for $0.2 \leq x_D \leq 0.8$.

$$[1] \quad \alpha(x_D) = (1.18 \pm 0.04) + (1.07 \pm 0.09)x_D$$

Since both the addition of SF_6 and the use of low dose rates result in a quenching of the dissociative neutralization processes, we conclude that the α values measured cannot be characteristic of these processes alone. As discussed, the Gammacell yields have shown a 7% isotope effect for pure H_2S compared to pure D_2S. This would lead to $\alpha = 1.07$ only. This isotope effect could be associated with the primary formation of H or D (or H_2 or D_2). Except for values $x_D \approx 0$, we conclude that the observed α values described by eq. 1 are not due to any selectivity in the primary yields of H or D (or H_2 or D_2); but rather, are due to isotope effects in the secondary reactions of H and D.

A normal kinetic isotope effect, in a zeroth

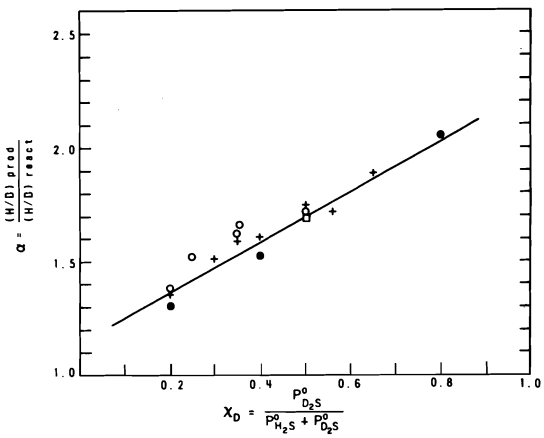

FIG. 1. Separation factors for the gas phase radiolysis of H_2S/D_2S mixtures. Experiments were carried out under the following conditions: +, 300 K, dose rate 2×10^{27} eV g^{-1} s^{-1} (runs 1–6); □ 300 K, dose rate 2×10^{27} with 1% SF_6 added (run 7); ●, 300 K dose rate 4×10^{15} (runs 9–11); ○, 195 K, dose rate 2×10^{27} eV g^{-1} s^{-1} (runs 12–16).

Can. J. Chem. Downloaded from www.nrcresearchpress.com by 210.87.254.5 on 09/05/12
For personal use only.

Can. J. Chem. Downloaded from www.nrcresearchpress.com by 210.87.254.5 on 09/05/12
For personal use only.

TABLE 2. Isotopic separation factors for various H_2S/D_2S mixtures

Run No.	x_D[a]	T (K)	Dose rate (eV g^{-1} s^{-1})	Other details	α[b]
1	0.20	300	2×10^{27}	Pure mixture	1.36
2	0.30	300	2×10^{27}	Pure mixture	1.51
3	0.35	300	2×10^{27}	Pure mixture	1.59
4	0.40	300	2×10^{27}	Pure mixture	1.61
5	0.50	300	2×10^{27}	Pure mixture	1.75
6	0.57	300	2×10^{27}	Pure mixture	1.72
7	0.65	300	2×10^{27}	Pure mixture	1.88
8	0.50	300	2×10^{27}	~1% SF_6 added	1.65
9	0.20	300	4×10^{15}	Pure mixture	1.30
10	0.40	300	4×10^{15}	Pure mixture	1.52
11	0.80	300	4×10^{15}	Pure mixture	2.05
12	0.20	195	2×10^{27}	Pure mixture	1.38
13	0.25	195	2×10^{27}	Pure mixture	1.52
14	0.35	195	2×10^{27}	Pure mixture	1.62
15	0.36	195	2×10^{27}	Pure mixture	1.66
16	0.50	195	2×10^{27}	Pure mixture	1.72

[a] $x_D = P_{D_2S}^0/(P_{H_2S}^0 + P_{D_2S}^0)$; $P_{D_2S}^0$ and $P_{H_2S}^0$ are the initial partial pressures of D_2S and H_2S respectively before exchange equilibration.
[b] $\alpha = (H/D)_{prod}/(H/D)_{react}$.

order approximation involving the breaking of an S—H bond ($\bar{\nu} \approx 2000\ cm^{-1}$), would be expected to show α values which are at least 20% larger at 195 than at 300 K. The lack of such a temperature effect in our results might be expected if the H atoms are formed translationally hot (symbolized H*) and they react with H_2S before having an opportunity to be moderated. In order to test this hypothesis we have performed a series of experiments which are summarized in Fig. 2. The separation factor, α, was observed as a function of the partial pressure of an added gas

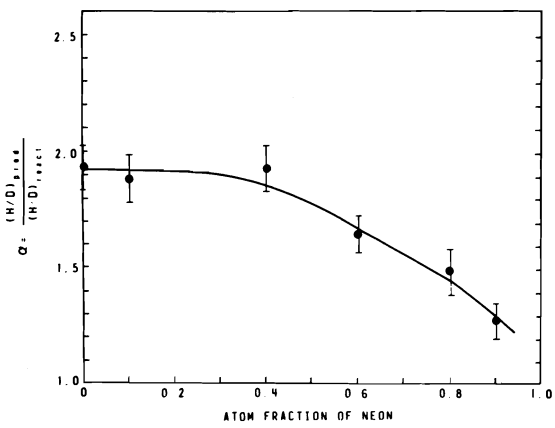

FIG. 2. Separation factors for a 70% D_2S/30% H_2S mixture as a function of the atom fraction of added neon at 300 K and for a dose rate of 2×10^{27} eV g^{-1} s^{-1}.

(neon) which could act as a moderator for H* and D*. Since both the ionization potential (21.4 eV) and the lowest excited state (16.7 eV) of neon are well above the ionization potential of H_2S, the irradiation energy absorbed initially by the neon will be transferred to the H_2S/D_2S mixture where it will cause processes similar to those occurring in the direct irradiation of the H_2S/D_2S mixture (9). In the case of the most neon-rich sample, the H* or D* atoms will now collide with ~9 neon atoms for every H_2S (or HDS or D_2S) encountered. Thus the H* or D* atoms will be somewhat moderated before they have an opportunity to react. Figure 2 clearly shows that α decreases as the degree of moderation is increased, indicating that the enrichment of hydrogen over deuterium for the pure H_2S–D_2S mixture is due to isotope effects in the reaction of H* and D*.

It has long been recognized from photolysis experiments (10–23) that, when energy is introduced into levels of H_2S lying above the bond dissociation energy (~4 eV (18)), the excess energy goes into kinetic energy of the H atoms. In addition there is evidence that hot hydrogen atoms are important in radiolysis experiments (4). The hot hydrogen atoms can react while still hot

$$H^* + H_2S \rightarrow H_2 + SH \qquad [2a]$$

or they can be moderated to thermal energies

Can. J. Chem. Downloaded from www.nrcresearchpress.com by 210.87.254.5 on 09/05/12
For personal use only.

through non-reactive collisions with H_2S or some other added gas.

[3] $$H^* + M \rightarrow H + M$$

The thermalized H atoms can then react with H_2S

[2*b*] $$H + H_2S \rightarrow H_2 + SH$$

The reaction rate of [2*b*] has been measured by esr and flash photolysis techniques (19–23). In these studies the reaction was found to proceed too quickly to be measured unless moderators were added. These results indicate that H_2S reacts with H* more quickly than it moderates H* and further that reaction 2*a* is faster than reaction 2*b*. This is consistent with the results obtained in the present experiments. The α values measured in pure H_2S/D_2S mixtures are characteristic of reactions of H* and D*. When a moderator is added and reaction 3 is allowed to compete with [2*a*], we find that different α values, which are presumably more characteristic of [2*b*], are obtained.

Rate constants have not been measured for reaction 2*a* and all of the various isotopic permutations of this reaction. The isotope separation factors depend in a complex way on the competition between these various reactions and it is not possible to relate them in a simple way to a single branching ratio. The evidence in this present work indicates that the isotope effect does not arise in the initial distribution of H* and D*, but rather from whether H* reacts to form HD or H_2 and whether D* reacts to form HD or D_2. Previous studies (18) have indicated that the initial kinetic energy distribution for H* and D* should be very similar. However, the D* atoms are travelling with velocities 40% less than those of H*. This means that D* undergoes less collisions in a given time than H*. In addition D* will probably lose slightly more energy per non-reactive collision than will H*. The result of this will be that the kinetic energy distribution of H* and D* will no longer be the same after they have had an opportunity to either react or undergo several non-reactive collisions. This means that the isotopic separation factors measured will not only derive from a complex array of different isotopic reactions, but also possibly from the relative effects of kinetic energy on the cross sections of these reactions.

An isotope effect has been reported for the displacement (exchange) reaction of a translationally hot tritium atom replacing either H or D in CX_3H and CX_3D respectively. The lighter H atom is more easily displaced than D leading to $k_H/k_D = 1.25$ (24). If displacement reactions are occurring in the H_2S system, these could also contribute to α. It is interesting to note that α decreases when a moderator is added (Fig. 2). This could be interpreted as a larger kinetic isotope effect for reactions of the type [2*a*] than for [2*b*]. Alternatively, this could be explained in terms of displacement reactions competing favourably with abstraction for atoms with high kinetic energy. If the kinetic energy threshold for displacement reactions is higher than for abstraction, this competition would favour abstraction for low kinetic energies and any isotope effect introduced by displacement reactions would tend to disappear when moderators are added. However there appears to be no independent evidence to indicate that displacement reactions are important in this system.

Conclusions

The separation factor for the hydrogen produced in pulsed electron or Gammacell irradiation of mixtures of H_2S and D_2S is empirically found to increase linearly with x_D, at least over the range $0.2 \leq x_D \leq 0.8$. Variation in temperature and dose rate or the addition of SF_6 is found to have no effect on these separation factors. The addition of a moderator to the reaction mixture sharply reduces the α values indicating that the α values in pure H_2S/D_2S mixtures arise from the reactions of hot hydrogen or deuterium atoms with H_2S, D_2S, or HDS.

The hydrogen yields of pure H_2S compared to pure D_2S show an isotope effect of $\Delta G = 0.5$ for dose rates up to 2×10^{27} eV g^{-1} s^{-1}. Using higher dose rates, an additional isotope effect is observed (to give $\Delta G = 1.5$ for a dose rate of 2×10^{28} eV g^{-1} s^{-1}) which appears to arise from the dissociative neutralization processes. This result is consistent with the suggestion that, for a given dose rate, the D_3S^+ ions are more highly clustered in D_2S than are the H_3S^+ ions in H_2S, leading to the formation of less D atoms per dissociative neutralization in D_2S than H atoms per dissociative neutralization in H_2S.

Acknowledgement

The authors would like to thank Mr. F. K. McClusky for technical help with some of the experimental work.

1. D. W. HUYTON and T. W. WOODWARD. Trans. Faraday Soc. **66**, 1648 (1970).
2. M. FORYS and K. WOJCIECHOWSKI. Radiochem. Radioanal. Lett. **10**, 277 (1972).
3. D. W. HUYTON and T. W. WOODWARD. J. Chem. Soc. Faraday Trans. I, **69**, 257 (1973).
4. D. W. HUYTON and T. W. WOODWARD. J. Chem. Soc. Faraday Trans I, **69**, 1049 (1973).
5. A. W. BOYD, C. WILLIS, and O. A. MILLER. Can. J. Chem. **51**, 1228 (1973) and references therein.
6. C. WILLIS, A. W. BOYD, and O. A. MILLER. Can. J. Chem. **49**, 1677 (1971).
7. A. W. BOYD, C. WILLIS, and C. G. LALOR. Can. J. Chem. **50**, 83 (1972).
8. C. WILLIS, A. W. BOYD, and P. E. BINDNER. Can. J. Chem. **50**, 1557 (1972).
9. C. J. WOOD and R. A. MASCALL. J. Chem. Soc. Faraday Trans. I, **71**, 1678 (1975).
10. B. DE B. DARWENT and R. ROBERTS. Discuss. Faraday Soc. **14**, 55 (1953).
11. R. G. GANN and J. DUBRIN. J. Chem. Phys. **47**, 1867 (1967).
12. B. DE B. DARWENT, R. L. WADLINGER, and M. J. ALLARD. J. Phys. Chem. **71**, 2346 (1967).
13. B. G. OZANTIEV and A. V. SHISHKOV. Khim. Vys. Energ. **1**, 192 (1967).
14. R. L. WADLINGER and B. DE B. DARWENT. J. Phys. Chem. **71**, 2057 (1967).
15. L. E. COMPTON, J. L. GOLE, and R. M. MARTIN. J. Phys. Chem. **73**, 1158 (1969).
16. G. R. WOOLLAY and R. J. CVETANOVIĆ. J. Chem. Phys. **50**, 4697 (1969).
17. G. P. STURM and J. M. WHITE. J. Chem. Phys. **50**, 5035 (1969).
18. L. E. COMPTON and R. M. MARTIN. J. Chem. Phys. **52**, 1613 (1970).
19. D. PERNER and TH. FRANKEN. Ber. Bunsenges. Phys. Chem. **73**, 897 (1969).
20. D. MIHELCIC and R. N. SCHINDLER. Ber. Bunsenges. Phys. Chem. **74**, 1280 (1970).
21. M. J. KURYLO, N. C. PATERSON, and W. BRAUN. J. Chem. Phys. **54**, 943 (1971).
22. J. N. BRADLEY, S. P. TRUEMAN, D. A. WHYTOCK, and T. A. ZALESKI. J. Chem. Soc. Faraday Trans. I, **69**, 416 (1973).
23. R. D. PENZHORN, E. LISSI, I. RIVAS, and H. IOTO. Z. Phys. Chem. **83**, 200 (1973).
24. T. SMAIL and F. S. ROWLAND. J. Phys. Chem. **72**, 1845 (1968).

Can. J. Chem. Downloaded from www.nrcresearchpress.com by 210.87.254.5 on 09/05/12
For personal use only.

Molecular reorientation in crystalline thiophene and furan[1]

W. E. SANFORD AND R. K. BOYD

Guelph-Waterloo Centre for Graduate Work in Chemistry, Guelph Campus, Ont., Canada N1G 2W1

Received December 22, 1975

W. E. SANFORD and R. K. BOYD. Can. J. Chem. **54**, 2773 (1976).

Molecular reorientation processes in crystalline thiophene and furan have been studied using pulse nmr techniques, over a range of temperature. The results obtained have been evaluated in the context of literature data on the heat capacities and crystal structures of these systems; this evaluation has been facilitated by the use of potential energy calculations for a molecule in the crystal lattice, based upon the empirical atom–atom approximation for the intermolecular interactions. In the case of furan, all available data can be reconciled in a self-consistent picture of the dynamic structure of the crystal. In the case of thiophene, however, various inconsistencies suggest that the published crystal structure determination should be repeated, and that further work on the pulse nmr at lower temperatures is necessary.

W. E. SANFORD et R. K. BOYD. Can. J. Chem. **54**, 2773 (1976).

On a étudié, à l'aide des techniques de rmn pulsé, à plusieurs températures, les processus de réorientation moléculaire dans du thiophène et du furanne cristallins. On a évalué les résultats obtenus à la lumière des données existant dans la littérature pour les capacités calorifiques et les structures cristallines de ces systèmes; cette évaluation a été facilitée par l'utilisation de calcul d'énergie potentielle pour une molécule dans le réseau cristallin qui était basé sur des approximations empiriques atome-atome pour des interactions intermoléculaires. Dans le cas du furanne, toutes les données disponibles peuvent être conciliées avec une image autocohérente de la structure dynamique du cristal. Toutefois dans le cas du thiophène, diverses inconsistences suggèrent que les déterminations de structures cristallines qui ont été publiées devraient être répétées; de plus d'autres travaux de rmn pulsé à des températures plus basses sont nécessaires.
[Traduit par le journal]

Introduction

The occurrence of rapid molecular reorientation in organic crystals has been well established (1, 2); in the case of non-symmetrical molecules, such reorientations introduce disorder into the crystal, which will show up in measurements of heat capacities (order–disorder transitions) and in studies of the crystal structure via diffraction of X-rays or of neutrons. In many cases, the time-scale for these reorientations is such that the rates may be studied by a variety of magnetic resonance methods, and in suitable cases by dielectric measurements.

The aim of the present work was to examine all available data on some simple molecular crystals, in which molecular reorientation was thought to occur, in an attempt to obtain a more complete understanding of the dynamic structures of these crystals. To this end, a pulse nmr spectrometer has been built, suitable for measurements of spin–lattice relaxation times (T_1) of solids, and also for measurements of characteristic times for relaxation of dipolar order (T_{1D}); the latter technique is well suited (3) to the detection of relatively slow motional processes, to which the more conventional T_1 methods are essentially insensitive. In addition, empirical calculations of potential energy profiles for reorientation of a molecule in the crystal lattice have been performed. These are based upon the atom–atom approximation first introduced by Kitaigorodskii (4), and subsequently adapted (5) to the present purpose for the case of aromatic hydrocarbons.

Experimental

(i) Nuclear Magnetic Resonance Pulse Spectrometer

A block diagram of the pulse spectrometer is shown in Fig. 1. The pulse programmer was assembled from modular units (Farnell Instruments Ltd., Wetherby, Yorkshire, U.K.); pulse widths, pulse delays, and pulse sequence repeat times are all continuously adjustable over several decades. A 'Racal' Universal Counter (Type 835) was used to accurately time the pulse delays within a given sequence, and also to check the pulse sequence repeat times. The rf oscillator used an 18.5 MHz quartz

[1]Taken from the M.Sc. thesis of W.E.S., 1975. Presented in part at the 57th Annual Conference, Chemical Institute of Canada, Regina, Sask., 1974.

Can. J. Chem. Downloaded from www.nrcresearchpress.com by 210.87.254.42 on 09/05/12
For personal use only.

Can. J. Chem. Downloaded from www.nrcresearchpress.com by 210.87.254.42 on 09/05/12
For personal use only.

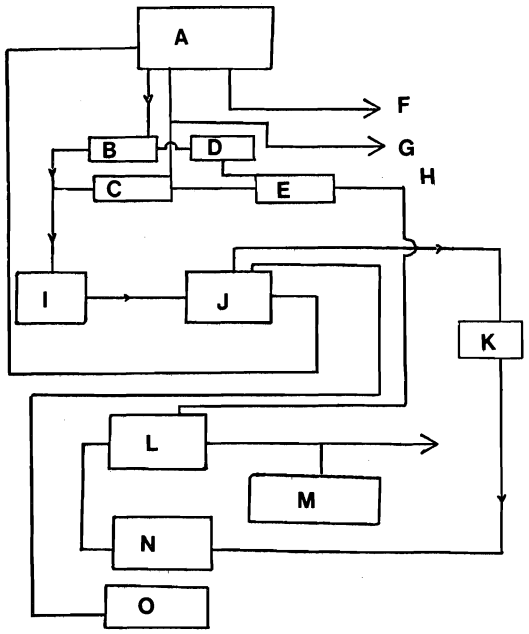

FIG. 1. Block diagram of spectrometer: A, Farnell pulse generator; B, switch No. 1; C, switch No. 2; D, phase shifter; E, 18.5 MHz oscillator; F, scope external trigger; G, counter; H, reference; I, rf power amplifier; J, rf transmitter; K, probe; L, phase sensitive detector; M, box car integrator; N, receiver 18.5 MHz; Q, regulated dc power supply.

crystal; the rf signal from this oscillator was fed to the rf gates, to the phase shifter, and to the phase-sensitive detector, via cathode followers. The rf gates used were Type S-11 wideband rf switches (F & H Instruments. Gaithersburg, Md), with rise and fall times of 100 ns. The phase shifter (Type P-12) and phase-sensitive detector (Type P-10) were also supplied by F & H Instruments. The broad-band rf power amplifier was a model 310L amplifier from Electronic Navigation Industries, Rochester, N.Y.

The power transmitter was based upon the design of Lowe and Tarr (6), with rise and fall times both less than 0.1 μs. The rf probe was a single-coil design, again based upon a design by Lowe and Tarr (7); the magnet used was that of a Brüker esr spectrometer, Model B-ER414. The receiver was a two stage tunable wide-band amplifier, with 75 ohm input and 50 ohm output impedances, and an overall gain of approximately 6. The boxcar integrator is a modified version of a design due to Samuelson and Ailion (8). The linearity of the digitiser/averager section of this device was checked, and found to be excellent over the entire range used in the present work. The transmitter, probe, receiver, and boxcar integrator were all constructed at the University of Guelph. This equipment is capable of measuring T_1 using any of the 180°–t–90°, 90°–t–90°, or 90° saturation pulse sequences; also, the 'spin-locking' sequence for $T_{1\rho}$ measurements and the pulse sequence for T_{1D} first suggested by Jeener and Broekhart (9) can be generated. Relaxation times can be evaluated either from the boxcar integrator, or directly from oscilloscope photographs; the latter technique was used periodically throughout this work as a check on the boxcar integrator.

Temperature control of the sample within the probe was achieved by the usual gas-flow type of equipment, in which the signal from a thermocouple junction immersed in the flowing nitrogen, close to the sample, was compared against a standard voltage. The null detector was a 'Fluke' Model 845 AR High Impedance Voltmeter/Null Detector; the actual temperature of the sample was measured using a Systron-Donner Model 7004 Digital Multimeter.

(ii) Materials

The thiophene was reagent grade, purchased from British Drug Houses Ltd.; it was purified by drying followed by fractional freezing (15 cycles). The furan was practical grade purchased from Eastman Chemicals, and was purified in a similar fashion.

(iii) Computations

The basic method of computation of the potential energy profiles has been described previously (5). Additional features introduced in the present work are best described for each appropriate case.

Results

(i) Benzene

It was decided to check the present experimental equipment and technique by making measurements of T_1 and of T_{1D} for benzene at 18.5 MHz; the former data were obtained using the 90°–t–90° pulse sequence, and the latter using the technique proposed previously (9). The results are shown in Fig. 2; the curve drawn through the T_1 data represents a least-squares computer fit of the data to the equation:

$$[1] \quad T_1^{-1} = C\left[\frac{\tau_c}{1+\omega_0^2\tau_c^2} + \frac{4\tau_c}{1+4\omega_0^2\tau_c^2}\right]$$

where the temperature dependence of the motional correlation time τ_c was assumed to have an Arrhenius form:

$$[2] \quad \tau_c = \tau_0 \exp(E_a/RT)$$

The best values of the parameters for benzene were found to be:

$$\tau_0 = 1.675 \times 10^{-14}\ \text{s}$$

$$C = 3.159 \times 10^{9}\ \text{s}^{-2}$$

$$E_a = 4.16 \pm 0.01\ \text{kcal mol}^{-1}$$

The T_{1D} data for benzene have a temperature dependence very similar to that found previously by Van Steenwinkel (10); above 230 K, the

Can. J. Chem. Downloaded from www.nrcresearchpress.com by 210.87.254.42 on 09/05/12
For personal use only.

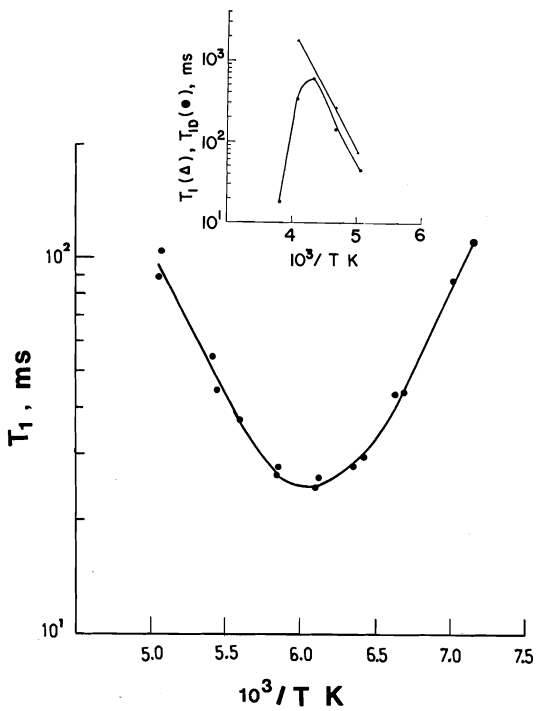

FIG. 2. The variation of T_1 in ms *vs.* the reciprocal of absolute temperature for crystalline benzene. The points represent the experimental data and the continuous curve represents the 'theoretical fit' obtained from a least squares fit of the experimental T_1 data. The insert represents the variation of $T_{1\rho}$ in ms *vs.* the reciprocal of absolute temperature for crystalline benzene.

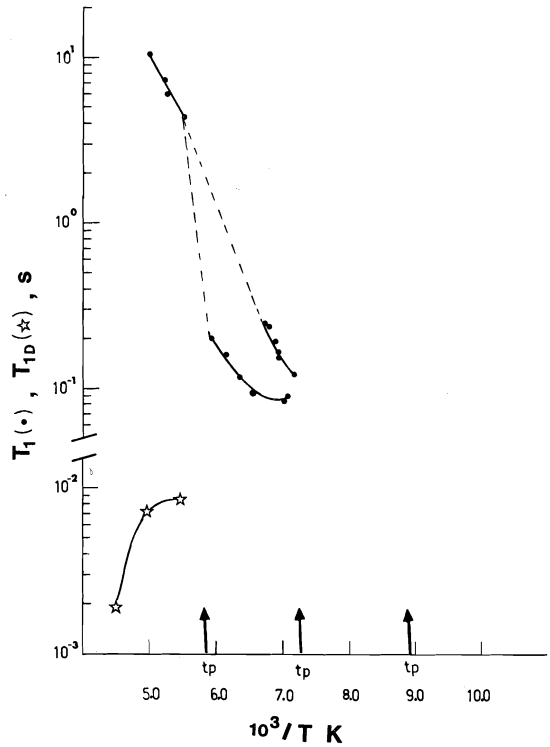

FIG. 3. The variation of T_1 (●) and T_{1D} (★) *vs.* the reciprocal of absolute temperature for crystalline thiophene. The arrows indicate the three solid–solid phase transitions of crystalline thiophene (11).

slope of the curve is consistent with an activation energy of about 21 kcal mol^{-1}.

The computation of a potential energy profile for the in-plane rotation of a benzene molecule in its crystal lattice gave results identical to those reported previously (5). In addition, an attempt was made in the present work to discover a motional process which might correspond to the higher activation energy process detected by the T_{1D} measurements (Fig. 2). Various out-of-plane motions were considered, with cooperative motions of surrounding molecules to alleviate the short contacts. However, no such cooperative motion, involving the centre-of-mass of each molecule fixed at its lattice site, was discovered with an activation energy less than about 300 kcal mol^{-1}. While the present computer search was not exhaustive, it is felt that a different type of motional process must be invoked to account for the observed effect (Fig. 2); this point is discussed further below.

(ii) Thiophene

The present result, obtained at 18.5 MHz, for T_1 and T_{1D} for thiophene, are shown in Fig. 3. Considerable difficulty was experienced in obtaining reproducible data in this case, and the problem was associated with the thermal history of the sample. Measurements of the heat capacity of crystalline thiophene (11) down to 11.7 K indicate three thermal anomalies with maxima at 112, 138, and 171.6 K; these transition temperatures are indicated by the arrows in Fig. 3. Between 171.6 K and the melting point (11) of 234.95 K (Phase I), the T_1 data were reproducible and in essential agreement with earlier results obtained by Anderson (12); the data in this region yield an activation energy of 3.7 kcal mol^{-1}. However, in Phase II between 138 and 171.6 K, the T_1 results obtained in the present work split into two categories (Fig. 3). The higher set of data are believed to correspond to a phase resulting from supercooling of Phase I, or some other metastable phase; evidence for this con-

Can. J. Chem. Downloaded from www.nrcresearchpress.com by 210.87.254.42 on 09/05/12
For personal use only.

clusion arises from the general observation that slow, careful cooling through the transition at 171.6 K almost always yielded a phase with T_1 values on the lower curve in Fig. 3. In particular, in one experiment the thiophene sample in the nmr tube was maintained at 143 K in a *n*-pentane slush bath for 7 h, then transferred quickly to the nmr probe which had been pre-cooled to 160 K; after stabilising in the probe for a further hour, T_1 was measured at 152 K, yielding a value of 102 ms, very close to the lower curve in Fig. 3.

In Phases III and IV (between 112 and 138 K, and below 112 K, respectively), the data were even more irreproducible, and are not reported here. Presumably the lower temperatures involved slowed down the equilibration processes sufficiently that the times required were too long to be readily obtainable in the present controlled gas flow equipment. However, a series of experiments using unpurified thiophene yielded a T_1 curve which was very similar to, though not exactly identical with, that obtained previously by Anderson (12).

The T_{1D} data for thiophene (Fig. 3) were fairly difficult to obtain, due to a combination of fairly low signal level and rather long T_1 values; the latter determine the pulse sequence repeat times, since about $5 \times T_1$ was allowed between sequences to ensure complete magnetic recovery before repeating the measurement. This made severe demands on the long-term drift stability of the present electronic equipment. However, as shown in Fig. 3, there is a clear indication of an additional motional process in Phase I, similar to that observed for benzene (Fig. 2); the activation energy for this additional process is estimated at >6 kcal mol^{-1}, although this is based upon only two measured points.

The computations of potential energy profiles for in-plane rotation of a thiophene molecule in its crystal lattice involved three additional features not necessary in the earlier work (5) for aromatic hydrocarbons. First, the presence of a hetero-atom (sulphur) in the molecule necessitated the inclusion of three new sets of potential parameter; the potential functions chosen for the sulphur–sulphur, sulphur–carbon, and sulphur–hydrogen interactions were Lennard-Jones 6-12 functions, as parametrised by Nyburg (13). The other necessary parameters used were those (14) determined previously (5) to give the best account of the sublimation energies and reorientation barriers observed for aromatic hydrocarbons.

The second complication in these computations arises from the fact that the crystal structure of thiophene in Phase I, as determined by Abrahams and Lipscomb (15) using X-ray diffraction, indicates a high degree of orientation disorder of the thiophene molecule at its lattice site. The model finally chosen by these authors (15) involves a four-fold disorder; however, a model involving two-fold disorder was equally consistent with the data (15), each model giving an *R*-factor of about 26%. The atomic coordinates from this X-ray work are correspondingly uncertain, but fortunately there are good microwave data available (16) for gaseous thiophene; the bond lengths and angles from this latter work (16) differ but slightly from those found in the X-ray paper, and it was fairly easy to devise an 'idealised' crystal structure using molecular dimensions from the microwave work (16), plus crystal packing from the X-ray results (15). The orientations (one particular choice out of four (15) possibilities) for each of the molecules surrounding that molecule whose in-plane rotation was considered, was chosen by a suitably normalised random number generator. Each computation of a potential energy profile was repeated at least once, using a different set of such randomly chosen orientations, to ensure that the qualitative features of a given profile were not an artifact of the particular set of orientations.

The third additional complication in these computations arose from the permanent electrical polarisation of the thiophene molecule, due to the high electronegativity of the sulphur atom. The electrostatic contribution to the total energy was estimated by converting the electron densities calculated by a molecular orbital method (17) to (assumed) point charges on each atom. A simple Coulomb potential function, using a dielectric constant of unity, then permitted estimation of the electrostatic energy; it would certainly be wrong to use the bulk dielectric constant of solid thiophene for these calculations, as only a small number of molecules is involved. In any event, the electrostatic contributions were invariably very small ($\leq 2\%$ of total energy), and were not an important factor

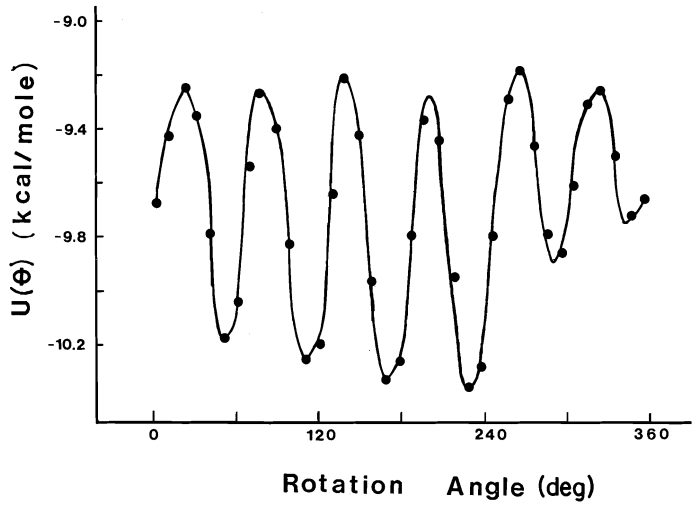

FIG. 4. The variation of intermolecular potential U (kcal/mol), with rotation angle for in-plane motion of thiophene based on X-ray structure at 218 K (15).

in determining the general shape of the potential profile. Thus, uncertainties in this respect are not important.

The first such profile computed assumed a four-fold random disorder of the molecules, as suggested by the X-ray data (15). However, this model invariably produced a potential profile for the central molecule with *six* potential minima. Accordingly, to make the computation self-consistent at least, the computer generated a model lattice with six-fold random disorder. A typical profile computed using this model is shown in Fig. 4; the qualitative shape of the profile is dominated by those interactions involving the peripheral hydrogen atoms, as was found previously (5).

(iii) Furan

The present results for T_1 and T_{1D} for furan, obtained at 18.5 MHz, are shown in Fig. 5. Below 150 K, the T_1 values are large, and vary but slightly with temperature; this behaviour is consistent with a lattice in which the furan molecules are essentially rigid, with no dipolar relaxation due to molecular motion. At 150 K there is a gross discontinuity in the T_1 curve; this temperature corresponds to that of an almost isothermal (first-order), or possibly very narrow lambda (higher-order) thermal transition, observed (18) in the heat capacity data for solid furan. Above the phase transition the T_1 values are much shorter, and vary with temperature in a fashion consistent with a molecular motion with an activation energy of 2.7 kcal mol^{-1}.

The general behaviour of the T_{1D} results for furan near the melting point (Fig. 5) is very similar to that observed for benzene (Fig. 2) and for thiophene (Fig. 3). The high-temperature limiting slope of the T_{1D} curve is consistent with an activation energy of about 14 kcal mol^{-1}.

The crystal structures of furan, both above and below the thermal transition at 150 K, have been well characterised through the work of Fourme (19), and this facilitated the potential energy calculations. Below the transition the structure is completely ordered (19), and this is consistent with the behaviour of the T_1 data in this region. Above the transition, the molecular packing is different, and there is a four-fold orientational disorder observed (19) for each molecule at its lattice site. Thus, the potential profile calculations for in-plane rotation are similar to those described previously (5) for the low-temperature phase, and to those described above for thiophene, for the high-temperature phase. The charge densities on the atoms in furan were taken from the literature (20). The potential functions involving oxygen atoms were Lennard-Jones 6-12 functions; two sets of parameters were tried, those proposed by Giglio (21) and those by Scheraga (22), the latter proving to be more satisfactory in general.

Can. J. Chem. Downloaded from www.nrcresearchpress.com by 210.87.254.42 on 09/05/12
For personal use only.

Can. J. Chem. Downloaded from www.nrcresearchpress.com by 210.87.254.42 on 09/05/12
For personal use only.

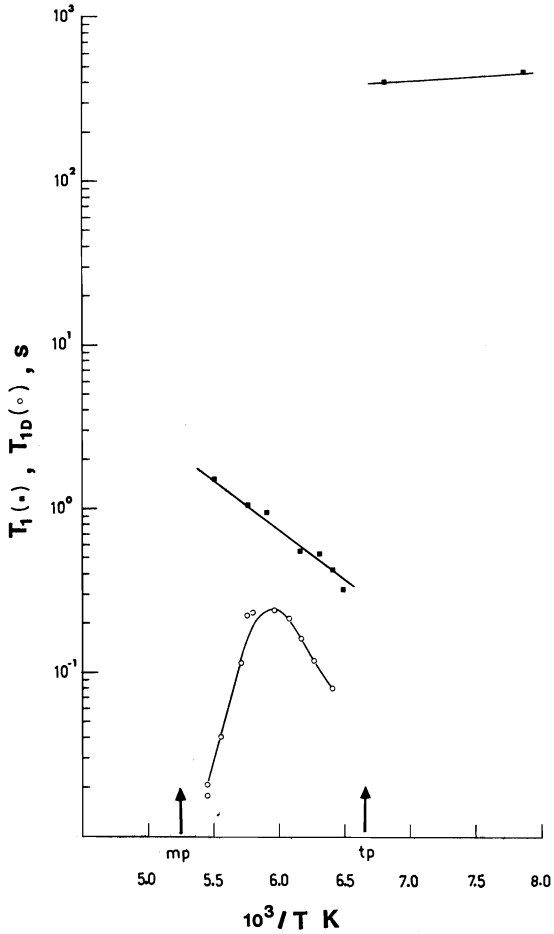

FIG. 5. The variation of T_1 (■) and T_{1D} (○) *vs.* the reciprocal of absolute temperature for crystalline furan. The arrows indicate the melting point (mp) and the solid–solid phase transition (tp) of crystalline furan (18).

Typical results of these computations are shown in Fig. 6 for the low-temperature phase, and in Fig. 7 for the high-temperature phase. Again, the electrostatic contributions are small, and the general shape of the profiles is dominated by the interactions of the peripheral hydrogen atoms. In the case of the disordered phases of both furan and thiophene, the centres of rotation are defined by the crystallographic space-group requirements; for the ordered, low-temperature phase of furan, however, the centre of rotation is open to choice, though the molecular symmetry clearly requires that it lie on the C_2 symmetry axis. A calculation of the interaction energy for the approach of a hydrogen atom along this axis, from each direction, gave a 'centre of repulsion' almost identical (within 0.02 Å) with the crystallographic centre defined by the disordered-phase space-group. This was true for both thiophene and furan, and this result gave further confidence in the present approach to computing these potential energy profiles.

Discussion

(i) Benzene

The present T_1 data for benzene yield an activation energy of 4.2 kcal mol^{-1} in good agreement with recent determinations of this parameter of 4.4 (10), 4.2 (23) and 3.95 (24), all in kcal mol^{-1}. The T_{1D} data are consistent with an activation energy of 21 kcal mol^{-1}, though there is considerable uncertainty in this value due to the lack of data points (Fig. 2); the disagreement with the value of 16 kcal mol^{-1} found previously (10) is probably only marginally significant. Attempts to characterise this slower motion in crystalline benzene, using the present, potential energy computations, were unsuccessful (see Results section). However, it is interesting to note that a study of self-diffusion in benzene (25), using the isotopic tracer technique, yielded an activation energy of 23.1 kcal mol^{-1} for this process. Further work along these lines seems necessary.

(ii) Thiophene

In Phase I, above 171.6 K, the present T_1 results for thiophene are in fair agreement with those of Anderson (12), when the difference in rf frequencies is taken into account. However, at temperatures below the transition at 171.6 K, the results obtained in the two investigations are qualitatively different. In the present work, results generally similar to the earlier data (12) were obtained using unpurified thiophene, with little attention paid to thermal equilibration. For this reason, it is presently felt that the low-temperature results of Anderson (12) probably refer to a metastable phase of crystalline thiophene. Similar problems were encountered in the heat capacity measurements (11), and there seems little doubt that it is fairly simple to supercool Phase I below 171.6 K.

This conclusion is fairly important, since it is known (11) that the third-law entropy for thiophene vapor, obtained from the calorimetric data (11), is in excellent agreement with the absolute entropy calculated from spectroscopic

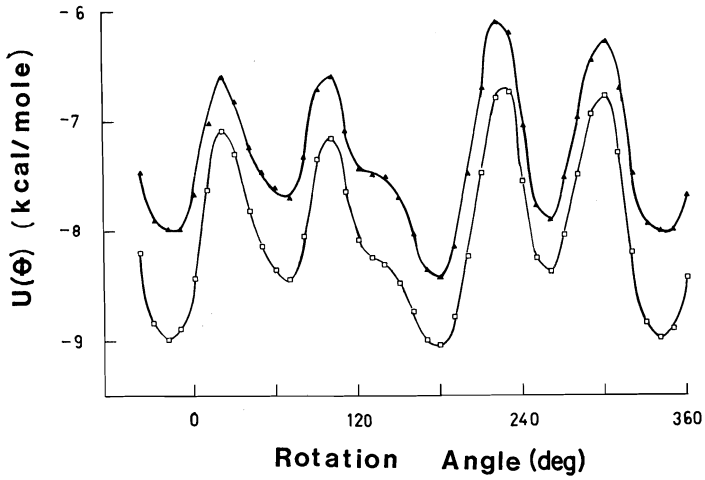

FIG. 6. The variation of intermolecular potential U (kcal/mol), with rotation angle for in-plane motion of furan based on X-ray structure at 123 K (19). Upper curve, oxygen parameters from Giglio (21), lower curve from Scheraga (22).

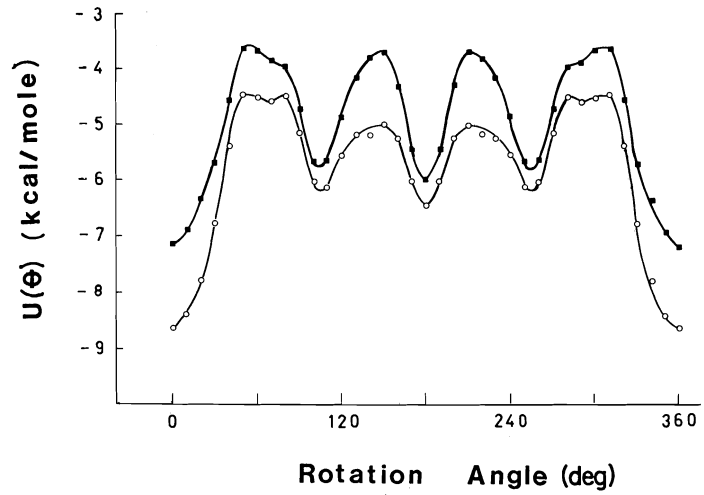

FIG. 7. The variation of intermolecular potential U (kcal/mol), with rotation angle for in-plane motion of furan based on X-ray structure at 152 K (19). Upper curve, oxygen parameters from Giglio (21), lower curve from Scheraga (22).

data. This implies that the thiophene sample used in the calorimetry experiments (11) formed a completely ordered lattice at the lowest temperatures used, 11.7 K. Between this temperature and 112 K, there is no evidence (11) of an order–disorder transition. Nonetheless, the T_1 results of Anderson (12) indicate a fairly rapid molecular motion in crystalline thiophene as low as 85 K; in view of the limited degree of symmetry in the thiophene molecule, it is difficult to conceive of a molecular motion which would be possible at such low temperatures, and which would *not* introduce orientational disorder into the crystal. The only conceivable motion not subject to such an objection would be motion about the molecular C_2 axis. No crystal structure is available for the low-temperature phases of thiophene, but in the typical 'herring-bone' crystal structure found (15) for Phase I, such a motion would involve an impossibly high activation energy. In addition, a measurement (12) of the second moment of the cw signal for thiophene at the lowest temperatures suggests that the motion is, in fact, an in-plane motion. It seems much more

Can. J. Chem. Downloaded from www.nrcresearchpress.com by 210.87.254.42 on 09/05/12
For personal use only.

Can. J. Chem. Downloaded from www.nrcresearchpress.com by 210.87.254.42 on 09/05/12
For personal use only.

likely that the present conclusion is correct, *i.e.* the low-temperature T_1 data of Anderson (12) refer to a different (metastable) phase from that obtained in the calorimetric experiments (11). Such a conclusion is easy to understand, in view of our own difficulties in equilibrating the thiophene sample in the spectrometer probe.

The present potential energy computations (Fig. 4) refer only to Phase I. The calculated lattice energy is in good agreement with the experimental (11) enthalpy of sublimation of 10.1 kcal mol^{-1}, measured at the melting point. The computed barriers to molecular rotation are about 1.2 kcal mol^{-1}, appreciably lower than the experimental activation energy of 3.7 kcal mol^{-1}. This disagreement is almost certainly a reflection of uncertainties in the crystal structures, as well as of the approximations inherent in the present computational model.

More important, however, is the qualitative feature of the computed potential profile (Fig. 4) of *six* potential wells. These are not, of course, all of the same depth, and those depicted in Fig. 4 merely reflect one typical set of orientations of the molecules surrounding that central molecule whose reorientation is under consideration. A properly ensemble-averaged version of Fig. 4 would presumably indicate six equivalent potential wells; however, such a calculation was far beyond our computational resources. Nonetheless, the present suggestion of a six-fold disorder for thiophene in Phase I must be critically examined in view of the experimentally determined crystal structure (15).

Abrahams and Lipscomb (15) finally settled on a model involving four-fold disorder (space group *Bmab*); however, the non-centrosymmetric space group *B2ab* involving a two-fold disorder, gave a slightly better *R*-factor, (27% as opposed to 28%). Accordingly, the observed (15) structure factors were presently fitted to our six-fold disorder model, and also, as a check, on the straightforward four-fold disorder model (15).[2] The two models yielded identical *R*-factors. Thus, the available X-ray data are unable to distinguish between two-fold, four-fold, or six-fold disorder for thiophene at its lattice site, in Phase I. It should be stressed that this X-ray investigation (15) was an early attempt at a difficult problem of a type rarely undertaken, and that elucidation of the general features of the crystal structure represents a considerable achievement. A repetition of this work (15) using more modern techniques should yield a more definitive answer, although such cases as thiophene will probably always present problems. Thus, as emphasized by Welberry (26) in a recent study of the disordered phase of acenaphthalene, the concept of a space-group becomes somewhat tenuous in such cases; the systematic absences of reflections used, in practice, to determine the space-group, are defined by the translational elements of the space-group (27), and the degree of molecular disorder at a fixed lattice site has little effect, as is well exemplified by the findings (15) for thiophene. While the present work was in course of preparation for publication there appeared a paper by Gavezzotti and Simonetta (32) on the computation of potential barriers for molecular reorientation in several crystals, including thiophene and furan. These workers (32) also concluded that a six-fold disorder model is perfectly consistent with the available X-ray data (15).

Two further comments on this proposed six-fold disorder seem appropriate. First, the angles between the vectors joining the centre of rotation of the thiophene molecule to each of the hydrogen atoms, are all very nearly 60°. Thus, since the overall shape of the profile is dominated by the interactions of these peripheral hydrogen atoms, it is qualitatively clear why there is a potential well every 60° or so in Fig. 4. The second comment concerns the possible interpretation (28) of the excess entropy of the thermal transitions in terms of N_1 and N_2 the numbers of distinguishable orientations above and below the transitions, respectively, via:

$$[3] \qquad \Delta S_{\text{excess}} = R \ln (N_1/N_2)$$

The pitfalls in the uncritical use of this relationship are well documented (28). By drawing the most obvious baseline through the heat capacity data (11), an estimate of ΔS_{excess} was obtained which corresponds to $(N_1/N_2) = 1.7$. With $N_2 = 1$ (perfectly-ordered low temperature phase), this estimate of N_1 is clearly too low to account for any of the models proposed for the crystal structure, although it must be noted that any given molecule is not presently predicted to have

[2]We are greatly indebted to Dr. W. C. Marsh and Professor G. Ferguson, of this university, for this computation.

Can. J. Chem. Downloaded from www.nrcresearchpress.com by 210.87.254.42 on 09/05/12
For personal use only.

six *equivalent* wells, so that the effective value predicted for N_1 is considerably less than 6. Further experimental work, particularly X-ray crystal analysis, seems necessary to resolve this problem. An attempt was made to establish a baseline using heat capacity data for tetrahydrothiophene, but this was much too ambiguous, particularly for the transition at 177.6 K with its very small $\Delta S \approx 0.9$ eu.

The T_{1D} data for Phase I of thiophene (Fig. 3) are unfortunately sparse, but indicate the onset of an additional, slower motion near the melting point, similar to that observed for benzene. By analogy with the suggestion made in the latter case, this new motional process could be diffusion, but at present this suggestion is purely speculative.

A referee has drawn our attention to the work of Jaffrain (33), who reports evidence of five distinct dielectric relaxation processes in solid thiophene between 50 and 150 K, with activation energies 1.9, 2.6, 3.2, 3.9 and 24 kcal mol^{-1}. It is possible that the four lowest activation energies correspond to barriers to in-plane rotation, of the type dominating the T_1 relaxation measurements, while the high barrier of 24 kcal mol^{-1} corresponds to a motional process related to that giving rise to the T_{1D} relaxation. However, in view of the rather low temperature range employed in the dielectric work (33), the exact relationship of these results to the present nmr data for Phase I remains unclear. It is possible that a systematic investigation of the linewidths and second moments, of both purified and unpurified samples, could help to elucidate the behaviour of solid thiophene as the temperature is lowered below 177.6 K.

(iii) Furan

The present T_1 data for furan (Fig. 5) are in excellent overall agreement with those obtained previously by Ripmeester and Dunell (29), who used the adiabatic rapid passage technique at a rf frequency of 8 MHz. Both T_1 and broadline nmr (30) measurements indicate that the furan lattice is rigid below the thermal transition (18) at 150 K; above the transition, the present data suggest an activation energy of 2.7 kcal mol^{-1}, in reasonable agreement with the value obtained previously (29) of 2.35 kcal mol^{-1}, and with a value of 2 kcal mol^{-1} obtained (31) from dielectric studies. All of these findings are entirely consistent with the X-ray studies (19).

The potential energy computations for the high-temperature phase of furan (Fig. 7) indicate four potential wells, again not all equivalent, the differences being a few tenths of a kilocalorie; however, an ensemble average corresponding to the observed crystal would presumably reproduce the observed (19) four-fold disorder. By extrapolating the enthalpy of vaporisation data well out of the experimental (18) temperature range, it is possible to estimate the enthalpy of sublimation near the melting point as 8.7 kcal mol^{-1}. The parametrisation of the oxygen atom potential functions due to Scheraga (22) appears to give the better account of this quantity; the same is true of the potential barriers, which are predicted to be about 1.9 kcal mol^{-1} by Scheraga's potentials.

The positions of the potential minima in Fig. 7 are not identical with the crystallographically determined orientations. It was thought that this might be due to directional effects associated with the lone pair of electrons on the oxygen atom, assuming one lone pair to be delocalised into the ring. A calculation along these lines produced no qualitative changes in the profiles (Fig. 7).

The low-temperature potential profile (Fig. 6) is qualitatively similar, but now the crystallographically observed orientation (0° rotation) lies about 3 kcal mol^{-1} deeper than the other three orientations, using the Scheraga potentials (22); below 150 K, the equilibrium populations of these metastable minima are negligible, in agreement with the observed crystal structure (19). Also, the energy barriers are increased to about 4.5 kcal mol^{-1}, which is *not* an impossibly high activation barrier for such motions at these temperatures (*cf.* benzene). Thus the observed rigidity of the low-temperature phase of furan must be due to the factor τ_0 in eq. 2 being very small. In turn, this can probably be ascribed to the necessity for a 360° jump in furan, to reach the next stable potential well, as opposed to only 60° for benzene; however, our model is incapable at present of accounting quantitatively for this effect.

Thus the dynamic structures of crystalline furan are reasonably well understood, relative to the situation for thiophene, for example. It is possible to give a reasonable partial interpretation of the phase transition consistent with these

potential energy calculations and experimental results. Thus, a completely ordered low temperature phase ($N_2 = 1$) and a high temperature phase in which there is *four*-fold disorder of each molecule $N_1 = 4$ (see above) would predict:

$$\Delta S_{\text{excess}} = R \ln \left(\frac{N_1}{N_2}\right) = R \ln \left(\frac{4}{1}\right) = 2.75 \text{ cal deg}^{-1} \text{ mol}^{-1}$$

which is significantly less than the experimental value, 3.26 eu. However the transition is not a simple order–disorder phenomenon dominated by purely configurational changes, but also involves a change in molecular packing so that the purely configurational entropy change should be a lower limit. What is still unclear is the nature of the driving force behind this phase transition which involves a qualitative change in crystal packing.

Acknowledgements

The active assistance and cooperation of Dr. C. A. Fyfe, in all aspects of the present work, are gratefully acknowledged. Dr. K. R. Jeffrey provided a great deal of advice and practical assistance in the design and construction of the pulse spectrometer, large portions of which were made by Mr. D. Sproat. Financial support of this research by the National Research Council of Canada is gratefully acknowledged, as is an NRCC Scholarship awarded to W.E.S.

1. D. Fox, M. M. Labes, and A. Weissberger (*Editors*). Physics and chemistry of the organic solid state. Vol. 1. Interscience, New York, N.Y., 1963.
2. C. A. Fyfe. *In* Molecular complexes. *Edited by* R. Foster. Logos Press, London. 1973.
3. D. C. Ailion. Adv. Magn. Reson. **5**, 177 (1971).
4. A. I. Kitaigorodskii. (*a*) Tetrahedron, **14**, 230 (1961); (*b*) Acta Cryst. **18**, 585 (1965); (*c*) J. Chim. Phys. **63**, 6 (1966); (*d*) Molecular crystals and molecules, Academic Press, New York, N.Y. 1973.
5. R. K. Boyd, C. A. Fyfe, and D. A. Wright. J. Phys. Chem. Solids, **35**, 1355 (1974).
6. I. J. Lowe and C. E. Tarr. J. Phys. E. **1**, 604 (1968).
7. I. J. Lowe and C. E. Tarr. J. Phys. E. **1**, 320 (1968).
8. G. L. Samuelson and D. C. Ailion. Rev. Sci. Instr. **40**, 676 (1969).
9. J. Jeener and P. Broekhart. Phys. Rev. **157**, 232 (1967).
10. R. Van Steenwinkel. Naturforsch, **24***a*, 1526 (1969).
11. G. Waddington, J. W. Knowlton, D. W. Scott, G. D. Oliver, S. S. Todd, W. N. Hubbard, J. C. Smith, and H. M. Huffman. J. Am. Chem. Soc. **71**, 797 (1949).
12. J. E. Anderson. Mol. Cryst. Liq. Cryst. **11**, 343 (1970).
13. S. C. Nyburg. Trans. Am. Crystallogr. Soc. **6**, 95 (1970).
14. D. E. Williams. J. Chem. Phys. **45**, 3770 (1966).
15. S. C. Abrahams and W. N. Lipscomb. Acta Crystallogr. **5**, 93 (1952).
16. B. Bak, D. Christensen, L. Hansen-Nygaard, and J. Rastrup-Andersen. J. Mol. Spectrosc. **7**, 58 (1961).
17. M. J. S. Dewar and N. Trinajstic. J. Am. Chem. Soc. **92**, 1453 (1970).
18. G. B. Guthrie, D. W. Scott, W. N. Hubbard, C. Katz, J. P. McCullough, M. E. Gross, K. D. Williamson, and G. Waddington. J. Am. Chem. Soc. **74**, 4662 (1952).
19. R. Fourme. Acta Crystallogr. B**28**, 2984 (1972).
20. M. J. S. Dewar, A. J. Harget, N. Trinajstic, and S. D. Worley. Tetrahedron, **26**, 4505 (1970).
21. E. Giglio. Nature, **222**, 339 (1963).
22. H. A. Scheraga. Adv. Phys. Org. Chem. **6**, 103 (1969).
23. J. A. Ripmeester. Ph.D. Thesis. University of British Columbia, Vancouver, B.C. 1970.
24. Y. I. Rosenberg and N. E. Ainbinder. Sov. Phys. Solid State, **12**, 641 (1970).
25. R. Fox and J. N. Sherwood. Trans Faraday. Soc. **67**, 3364 (1971).
26. T. R. Welberry. Proc. Roy. Soc. A**334**, 19 (1973).
27. G. H. Stout and L. H. Jensen. X-Ray structure determination, a practical guide. MacMillan. 1968.
28. J. A. Ripmeester and B. A. Dunell. Can. J. Chem. **52**, 191 (1972).
29. F. Fried. C. R. Acad. Sci. Paris, **262**, 1497 (1966).
30. F. Fried and B. Lassier. J. Chim. Phys. **63**, 75 (1966).
31. A. Gavezzotti and M. Simonetta. Acta Cryst. A**31**, 645 (1975).
32. M. Jaffrain. J. Chim. Phys. **63**, 77 (1966).

Can. J. Chem. Downloaded from www.nrcresearchpress.com by 210.87.254.42 on 09/05/12
For personal use only.

Nematic phase nuclear magnetic resonance studies of the structure and orientation of 1,5- and 2,6-naphthyridines

Y. P. Lee and D. F. R. Gilson

Department of Chemistry, McGill University, P.O. Box 6070, Station A, Montreal, Que., Canada H3C 3G1

Received February 23, 1976

Y. P. Lee and D. F. R. Gilson. Can. J. Chem. **54**, 2783 (1976).

The proton magnetic resonance spectra of 1,5- and 2,6-naphthyridine dissolved in the nematic liquid crystal MBBA have been analysed. The proton geometries do not give good fits to the ring skeleton structure but it appears that the carbon–hydrogen bond lengths are not all of equal length and the bond angles indicate some bending of the C—H bonds toward the adjacent nitrogen atom. The probability functions for orientation of diazanaphthalenes in nematic solvents show that nitrogen atoms in the ring framework affect the direction of principal orientation, which does not follow either the maximum molecular dimension or the inertial axis.

Y. P. Lee et D. F. R. Gilson. Can. J. Chem. **54**, 2783 (1976).

Les spectres de résonance magnétique du proton des naphtyridine-1,5 et -2,6 en solution dans le cristal liquide nématique MBBA ont été analysés. La géométrie des protons n'est pas en bon accord avec la structure du squelette cyclique mais il semble que les longueurs des liens carbone–hydrogène ne soient pas toutes égales et que les angles de valence indiquent une certaine inclinaison des liens C—H vers l'atome d'azote adjacent. Les fonctions de probabilité pour l'orientation des diazanaphtalènes dans des solvants nématiques montrent que les atomes d'azote dans le squelette cyclique affectent le sens de l'orientation principale qui ne suit ni la dimension moléculaire maximum ni l'axe d'inertie.

[Traduit par le journal]

Introduction

Nuclear magnetic resonance spectroscopy of solute molecules partially oriented in a liquid crystal solvent has been applied to the determination of the relative proton structures of a wide variety of molecules (1). Although numerous benzene derivatives have been studied there are only few reported cases of condensed aromatics and only naphthalene (2), 1-chloronaphthalene (3), 1,4-naphthoquinone (4), coumarine (5), and the nitrogen heterocyclic derivatives, phthalazine (6), quinoxaline (7), and 2,7-naphthyridine (8) have been investigated. The diazanaphthalenes are an interesting series since ten possible isomers exist and a study of these compounds should provide information regarding the structural and orientational consequences of replacing C—H groups by nitrogen atoms. Phthalazine and quinoxaline have both nitrogen atoms in the same ring. In the present study, we report on the nematic phase nmr studies of 1,5- and 2,6-naphthyridines in which the nitrogen atoms are in different rings.

Experimental

1,5- and 2,6-naphthyridines were obtained as gifts from Professor A. Taurins. Proton spectra were obtained for 8 mol% and 7 mol% solutions respectively in MBBA (*p*-methoxybenzylidene *p*-*n*-butylaniline) at the Canadian 220 MHz NMR Centre, Sheridan Park, Ontario. Probe temperature was 18 °C. The spectra were analysed with the computer program SPECFIT (9) and the geometry which provided the best fit to the experimental direct dipole coupling obtained using the program GEOFIT (9)

Results

The spectrum of the 2,6-isomer spanned over 7 kHz but the spectrum of 1,5-naphthyridine was less than half this width, reflecting in part the difference in the degree of orientation in the nematic solvent. The experimental direct dipole coupling constants are given in Table 1. Iteration upon the indirect dipole coupling constants, J_{ij}, gave values which agreed, within experimental error, with literature values obtained from isotropic spectra (10–13). For 1,5-naphthyridine the rms deviation between calculated and experimental line positions was 1.1 Hz for 90 lines and for 2,6-naphthyridine the rms deviation was 2.4 Hz for 119 lines. The numbering system and axis system are shown in Fig. 1.

Discussion

Nine direct dipole coupling constants are

Can. J. Chem. Downloaded from www.nrcresearchpress.com by 210.87.254.40 on 09/05/12
For personal use only.

Can. J. Chem. Downloaded from www.nrcresearchpress.com by 210.87.254.40 on 09/05/12
For personal use only.

TABLE 1. Spectral parameters for 1,5- and 2,6-naphthyridines

Parameter	1,5-Naphthyridine	2,6-Naphthyridine
ν_1 (Hz, TMS)	—	1779.75±0.68
ν_2	1856.17±0.25	—
ν_3	1519.17±1.05	1712.87±0.58
ν_4	1714.60±1.09	1470.28±0.34
D_{13} (Hz)	—	+63.88±0.51
D_{14}	—	+119.40±1.42
D_{15}	—	−37.52±1.33
D_{17}	—	−455.94±0.72
D_{18}	—	−3029.21±2.85
D_{23}	−569.23±2.81	—
D_{24}	−243.27±2.44	—
D_{26}	−74.80±0.30	—
D_{27}	−74.02±0.57	—
D_{28}	−158.87±0.79	—
D_{34}	−1583.90±1.15	−2531.83±3.44
D_{37}	−38.34±0.69	−112.68±1.28
D_{38}	−38.12±0.25	−97.00±1.44
D_{48}	−30.71±0.76	+39.27±0.67
J_{13}	—	+0.02±0.54
J_{14}	—	+0.63±0.81
J_{15}	—	+1.34±1.11
J_{17}	—	−0.38±1.26
J_{18}	—	+1.36±0.48
J_{23}	+3.94±1.56	—
J_{24}	−1.24±1.73	—
J_{26}	−0.18±0.30	—
J_{27}	+1.56±0.61	—
J_{28}	+1.06±0.61	—
J_{34}	+8.45±0.46	+6.0
J_{37}	+0.55±0.65	+1.63±1.01
J_{38}	−0.59±0.25	+0.93±0.86
J_{48}	+0.70±0.64	−0.17±0.74

obtained for each isomer. The proton geometry can be described by six independent parameters, see Fig. 1, but since only ratios of distances are involved at least one of these distances must be assumed. These naphthyridine isomers have limited symmetry and three independent motional constants or orientation parameters (1) are required to relate the degree of orientation of the molecule-fixed axis system to the nematic liquid crystal axis. Thus a total of eight parameters are to be determined from the nine direct dipole coupling constants. The previous studies on naphthalene and its derivatives (2, 6, 7) have compared the ratios of interproton distances relative to the distance between the protons in the β-positions in the unsubstituted ring but the substitution pattern in the naphthyridine compounds does not provide a suitable common distance for a similar comparison. The ring atom coordinates for both naphthyridines have been determined by Brufani and co-workers (14–16) by X-ray methods and the proton positions were fitted to these structures with the assumption of the coordinates of H_3 in 1,5-naphthyridine and H_4 in 2,6-naphthyridine. These protons are not adjacent to the nitrogen atom and are presumed to undergo least perturbation. Adopting the coordinates in this way is equivalent to assuming two of the distance parameters. The C—H bond length was assumed to be 1.085 Å and lying along the bisector of the ring angle, and the resulting distance parameters (see caption to Fig. 1) are given in Table 2. Fitting the proton positions to the rest of the carbon atom positions gave unacceptable C—H bond lengths for both compounds; in 1,5-naphthyridine C_2—H_2 = 1.033 Å and is displaced 2.3° toward the nitrogen atom away from the ring angle bisector, C_4—H_4 = 1.101 Å and is displaced 1.9° in the opposite sense (*i.e.* clockwise in Fig. 1); in 2,6-naphthyridine C_1—H_1 = 1.053 Å, angular displacement 0.1° away from the nitrogen atom, C_3—H_3 = 1.038 Å displaced 2.1° towards nitrogen. This structure is obviously unacceptable

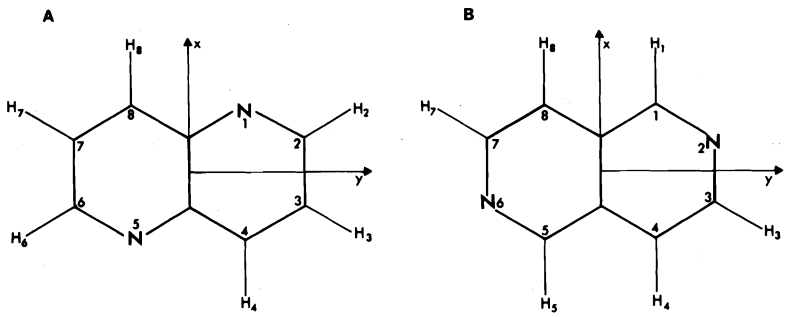

FIG. 1. (*A*) 1,5-Naphthyridine: distance parameters referred to in the text are: $d_1 = y_2$, $d_2 = x_2$, $d_3 = y_3$, $d_4 = x_3$, $d_5 = y_4$, $d_6 = x_4$. (*B*) 2,6-Naphthyridine: distance parameters $d_1 = y_1$, $d_2 = x_1$, $d_3 = y_3$, $d_4 = x_3$, $d_5 = y_4$, $d_6 = x_4$.

TABLE 2. Distance parameters (Å) for 1,5- and 2,6-naphthyridines*

Parameter	1,5-Naphthyridine I	1,5-Naphthyridine II	2,6-Naphthyridine I	2,6-Naphthyridine II
d_1 (Å)	3.1295	3.0929	1.2509	1.2557
d_2	1.4073	1.5140	2.4192	2.4454
d_3	(3.3792)	(3.4243)	3.3184	3.3526
d_4	(1.0665)	(0.9592)	1.0820	1.0286
d_5	1.2960	1.3799	(1.2887)	(1.3078)
d_6	2.4435	2.4084	(2.4551)	(2.4744)
ΔD_{ij}(rms,Hz)	0.51	0.51	1.10	1.10
S_{zz}	−0.1237	−0.1250	−0.1503	−0.1545
$(S_{yy} - S_{xx})$	0.0370	0.0325	0.2650	0.2720
S_{xy}	−0.0365	−0.0380	−0.0337	−0.0348

*Assumed distances in parentheses.

TABLE 3. C—H bond lengths and C—C—H bond angle deviations

	1,5-Naphthyridine Bond length (Å)	1,5-Naphthyridine Angle*		2,6-Naphthyridine Bond length (Å)	2,6-Naphthyridine Angle*
C_2—H_2	1.071	−8.1	C_1—H_1	1.080	+0.1
C_3—H_3	1.085	−6.2	C_3—H_3	1.070	−2.9
C_4—H_4	1.071	−2.5	C_4—H_4	1.105	−1.0

*Positive angle indicates clockwise rotation in Fig. 1.

and therefore the restriction that H_3 and H_4 should lie along the ring bisector was removed and the bond lengths of all carbon–proton bonds allowed to vary within reasonable limits. The distance parameters obtained from this treatment, but still based on the positions of H_3 and H_4 in 1,5- and 2,6-naphthyridine respectively, are given in columns II of Table 2. Smaller variations in bond length in 1,5-naphthyridine were obtained at the expense of larger angular deviations, Table 3. The direction of these angular displacements is, however, consistent in each molecule in being towards the adjacent nitrogen atom. It also appears that the C—H bonds at different ring positions may not be of the same length. The effects of vibrational averaging upon the geometry have been ignored but a more extensive analysis of the results is scarcely warranted in view of the difficulty of fitting the proton structure to the ring skeleton. For this reason, an analysis of probable errors has also been omitted.

In their study of 2,7-naphthyridine, Danieli *et al.* (8) compared the ratios of the interproton distances with the corresponding ratios for two pyridine rings fused together at the appropriate C—C bond. They concluded that no appreciable distortions of the pyridine rings resulted from such fusion. Similar comparisons for 1,5- and 2,6-naphthyridines lead to the same result. However, we do not believe that this necessity indicates a negligible modification of the pyridine ring structure since the X-ray investigations of the naphthyridines (14–17) showed bond lengths which differ significantly from the fused ring model. A degree of 'bond fixation' occurs in fused ring compounds and is well illustrated by a comparison of naphthalene *vs.* two fused benzene rings.

The orientation of a solute molecule in a liquid crystal solvent can be described by the probability function $P(\theta, \phi)$ [1].

$$[1]\quad P(\theta,\phi) = (4\pi)^{-1}\{1 + (\tfrac{5}{2})[S_{zz}(3\cos^2\theta - 1) + (S_{xx} - S_{yy})\sin^2\theta\cos 2\phi + 4S_{xz}\sin\theta\cos\theta\cos\phi + 4S_{yz}\sin\theta\cos\theta\sin\phi + 2S_{xy}\sin^2\theta\sin 2\phi]\}$$

where θ and ϕ relate the liquid crystal axis to the molecule-fixed Cartesian coordinates. These functions are plotted in Fig. 2 for 1,5- and 2,6-naphthyridine. The rotations of the principal

Can. J. Chem. Downloaded from www.nrcresearchpress.com by 210.87.254.40 on 09/05/12
For personal use only.

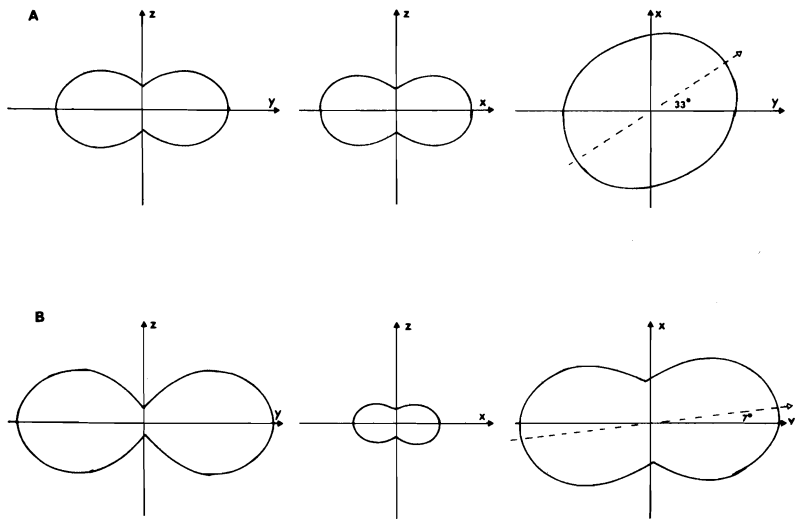

FIG. 2. Orientation probability functions $P(\theta,\phi)$ for (*A*) 1,5-naphthyridine, (*B*) 2,6-naphthyridine.

axes of orientation from the molecule fixed axes are 33° and 7° respectively, indicating the influence of nitrogen substitution upon the orientation. The usual orientation of a solute molecule is with the longest molecular dimension parallel to the liquid crystal axis but pyridine, for example, aligns with the C_2 axis parallel to the solvent axis whereas benzene has no preferred orientation in the *xy* plane. Various parameters have been suggested as suitable descriptions of the anisotropy of orientation (18–20). Anderson has used the parameter $(S_{yy} - S_{xx})/S_{zz}$ and correlated this function with the anisotropy of the principal moments of inertia (19). The naphthyridines, however, do not correlate their principal orientation axes with their inertial axes since the latter are rotated by only small amounts from the molecule fixed axes; 1,5-naphthyridine 2.5°; 2,6-naphthyridine 1.4°. Orrell and Sik (20) have used a similar parameter, $(S_{yy} - S_{xx})/3S_{zz}$, to compare the orientations of substituted pyridines and to derive a substituent additive model for pyridines *vs.* their benzene analogues. This parameter has limiting values of ± 1 but the sign depends only on the choice of *x* and *y* axes. In the present work, we have used the ratio of the probability functions from [1] for the maximum and minimum values in the *xy* plane. The choice of axes also affects this function and we adopt the convention $S_{yy} > S_{xx}$, *i.e.* the principal orientation axis lies along, or closer to, the molecule fixed *y* axis, and the limiting values are from 1 to 8. Table 4 gives the probability function ratios for various naphthalene-related derivatives. Substitution in the α-positions of naphthalene, *i.e.* an '*x*-axis substituent', reduces the anisotropy of orientation in 1,5-naphthyridine, quinoxaline, 1,4-naphthoquinone, and 1-chloronaphthalene, whereas β-substitution, closer to the direction of the largest molecular dimension, maintains, and in 2,6-naphthyridine increases, the orientational anisotropy relative to naphthalene. Saupe has shown that localized bond contributions to the free energy of orientation can account quantitatively for the orientation of solute molecules in nematic solvents (21, 22). On this basis, the contributions from a nitrogen atom and two carbon–nitrogen bonds exceed those of a C—H bond and two carbon–carbon bonds.

TABLE 4. Orientation probability ratios in naphthalene derivatives

	P_{max}/P_{min}
Naphthalene	2.434
1,5-Naphthyridine	1.254
2,6-Naphthyridine	3.052
2,7-Naphthyridine	2.116
Phthalazine	2.101
Quinoxaline	1.301
1-Chloronaphthalene	1.137
1,4-Naphthoquinone	1.329
Coumarine	2.115

Can. J. Chem. Downloaded from www.nrcresearchpress.com by 210.87.254.40 on 09/05/12
For personal use only.

Acknowledgements

The authors thank Professor A. Taurins for the naphthyridine compounds. This work was supported by grants from the National Research Council of Canada.

1. P. DIEHL and C. L. KHETRAPAL. *In* NMR basic principles and progress. Vol. 1. *Edited by* P. Diehl, E. Fluck, and R. Kosfeld. Springer Verlag. 1969.
2. J. M. DEREPPE, J. DEGELAEN, and M. VAN MEERSCHE. J. Mol. Struct. **17**, 225 (1973).
3. P. DIEHL and J. VOGT. Org. Magn. Reson. **6**, 33 (1974).
4. J. M. DEREPPE, J. DEGELAEN, and M. VAN MEERSCHE. Org. Magn. Reson. **4**, 551 (1972).
5. E. CAPELLI, A. DINOLA, and A. L. SEGRE. Mol. Phys. **27**, 1385 (1974).
6. C. L. KHETRAPAL, A. SAUPE, and A. C. KUNWAR. Mol. Cryst. Liq. Cryst. **17**, 121 (1972).
7. C. L. KHETRAPAL and A. C. KUNWAR. Mol. Cryst. Liq. Cryst. **15**, 363 (1972).
8. R. DANIELI, L. LUNAZZI, and C. A. VERACINI. J. Chem. Soc. Perkin Trans. II, 19 (1976).
9. K. C. COLE. Ph.D. Thesis, McGill University, Montreal. 1974.
10. G. GIACOMELLO, F. GUATTIORI, F. M. RICCIORI, and M. L. STEIN. Tetrahedron Lett. 1117 (1965).
11. R. TAN and A. TAURINS. Tetrahedron Lett. 2737 (1965).
12. A. H. GAMER and B. P. DAILEY. J. Chem. Phys. **43**, 2658 (1965).
13. W. W. PAUDLER and T. J. KRESS. J. Org. Chem. **33**, 1384 (1968).
14. M. BRUFANI, D. DURANTI, and G. GIACOMELLO. Gazz. Chim. Ital. **89**, 2328 (1959).
15. M. BRUFANI, D. DURANTI, G. GIACOMELLO, and L. ZAMBONELLI. Gazz. Chim. Ital. **91**, 287 (1961).
16. M. BRUFANI, W. FEDELI, G. GIACOMELLO, F. M. RICCIERI, and A. VIACIAGO. Atti. Accad. Naz. Lincei, Cl. Sci. Fis., Mat. Nat. Rend. **40**, 187 (1966). *Reported in* Physical methods in heterocyclic chemistry. Vol. 5. *Edited by* A. R. Katritzky. Academic Press. 1972.
17. A. CLEARFIELD, M. J. SIMS, and P. SINGH. Acta Cryst. Sect. B, **28**, 350 (1972).
18. J. C. ROBERTSON, C. T. YIM, and D. F. R. GILSON. Can. J. Chem. **49**, 2345 (1971).
19. J. M. ANDERSON. J. Magn. Reson. **4**, 231 (1971).
20. K. G. ORRELL and V. SIK. J. Chem. Soc. Faraday Trans. II, **71**, 1360 (1975).
21. A. SAUPE. Mol. Cryst. **1**, 527 (1966).
22. J. NEHRING and A. SAUPE. Mol. Cryst. Liq. Cryst. **8**, 403 (1969).

Can. J. Chem. Downloaded from www.nrcresearchpress.com by 210.87.254.40 on 09/05/12
For personal use only.

Nematic phase nuclear magnetic resonance spectra and vibrationally averaged structures of cyclopropyl chloride, bromide, and cyanide

K. C. COLE[1] AND D. F. R. GILSON[2]

Department of Chemistry, McGill University, P.O. Box 6070, Station A, Montreal, Que., Canada H3C 3G1

Received April 8, 1976

K. C. COLE and D. F. R. GILSON. Can. J. Chem. **54**, 2788 (1976).

The nmr spectra of partially oriented cyclopropyl chloride, bromide, and cyanide have been analysed and the relative proton structure corrected for vibrational effects. The proton structures provide indirect evidence in support of Hoffmann's theory of substituent effects in cyclopropane rings. The distance between protons on the same side of the ring as the substituent is less than the corresponding distance on the other side. The direction of the principal orientation axis in two nematic solvents EBBA and MBBA is the same but the anisotropy of alignment is less in MBBA.

K. C. COLE et D. F. R. GILSON. Can. J. Chem. **54**, 2788 (1976).

Les spectres de rmn du chlorure, du bromure et du cyanure de cyclopropyle partiellement orientés ont été analysés et la structure relative aux protons a été corrigée pour les effets vibrationnels. Les structures dues aux protons fournissent une évidence indirecte appuyant la théorie d'Hoffmann sur les effets de substituants dans les noyaux cyclopropaniques. La distance entre les protons du même côté du cycle que le substituant est moindre que la distance correspondante de l'autre côté du cycle. La direction de l'axe d'orientation principal dans deux solvants nématiques, le EBBA et le MBBA, est la même mais l'anisotropie de l'alignement est moindre dans le MBBA.

[Traduit par le journal]

Introduction

The Walsh model (1) of bonding in the cyclopropane molecule has been extended by Hoffmann to include substituent-induced effects (2). The antisymmetric occupied ring orbital is bonding for the carbon–carbon bonds adjacent to the substituent but antibonding for the bond opposite. Thus a suitably oriented acceptor orbital on the substituent group can withdraw electron density from the ring orbital leading to a lengthening of the adjacent bonds and a shortening of the opposite bond. A π electron donor substituent should cause a weakening of all ring bonds, relative to cyclopropane, since the appropriate Walsh orbital is totally antibonding. Unfortunately only a few accurate structure determinations of cyclopropyl derivatives have been reported. Penn and Boggs (3) have analysed the available microwave data and concluded that a consistent shortening, by an average of about 0.015 Å, occurs for the bond opposite an unsaturated substituent. An r_s determination[3] of the ring bond lengths in cyclopropyl cyanide (4) gave values of 1.528 ± 0.005 Å and 1.500 ± 0.002 Å for the adjacent and opposite bonds respectively. (The bond length in cyclopropane is 1.510 Å (5).) Thus in the case of acceptor orbitals the theory has some experimental support. The situation is less clear for the saturated or donor substituents. From Penn and Boggs' analysis (3) there is little change in ring bond lengths relative to cyclopropane and an r_s determination of the structure of cyclopropyl chloride (6) indicated ring bond lengths to be unchanged from cyclopropane within experimental error. In cyclopropylamine (7) the adjacent bonds are longer, 1.535 ± 0.006 Å but the opposite bond length, 1.513 ± 0.003 Å is essentially the same as cyclopropane. For 1,1-difluorocyclopropane (8) the adjacent bonds were found to be significantly shorter at 1.464 ± 0.002 Å but the opposite bond longer at 1.553 ± 0.001 Å. A similar result was obtained for 1,1-dichlorocyclopropane (9). An X-ray crystal structure study of 1,1-dichloro-2,2-diphenylcyclopropane and the dibromo analogue also gave bond lengths in conflict with the predictions of the theory (10).

The analysis of nuclear magnetic resonance

[1]1967 Science Scholarship 1969–1973.

[2]Author to whom correspondence should be addressed.

[3]For definitions and discussion of the various distance parameters see ref. 29.

Can. J. Chem. Downloaded from www.nrcresearchpress.com by 210.87.254.40 on 09/05/12
For personal use only.

Can. J. Chem. Downloaded from www.nrcresearchpress.com by 210.87.254.40 on 09/05/12
For personal use only.

spectra of molecules partially oriented in nematic liquid crystal solvents can provide additional structural information, particularly with regard to the relative proton positions in a molecule (11). However, proper comparisons between structural data derived by different experimental methods should take into account the manner in which the interatomic distances are affected by the averaging over vibrational motions. Lucas (12, 13) has shown how vibrationally averaged r_z structures can be derived from nematic phase nmr results and notably how the allowance for vibrational effects improves the agreement between the electron diffraction and nematic phase nmr structures of cyclopropane (14). The method involves an expansion of the expression for the direct dipole coupling constant, D_{ij}, as a Taylor series involving the mean square amplitudes of the harmonic vibrational motion. These amplitudes can be obtained from a normal coordinate analysis of the vibrational spectrum.

In this paper the results of an analysis of the nematic phase nmr spectra of cyclopropyl chloride, bromide, and cyanide are reported together with vibrationally averaged structural parameters for the proton positions.

Experimental

Spectra were recorded at 220 MHz at the Canadian 220 MHz NMR Centre, Sheridan Park, Ontario, and analysed using the program SPECFIT, a modified version of LAOCN3. Sample concentrations, etc., are given in Table 1. The geometry which provided the best fit to the experimental direct dipole coupling constants were computed with the program GEOFIT. Calculations of the mean square amplitudes of vibration were based upon the W-matrix transformation method of Schachtschneider and Snyder (15).

Results

The spectra of the cyclopropyl derivatives were similar to each other; a central part due to the proton on the same carbon atom as the substituent, and two widely separated regions due to the remaining four protons. The large separation is due to the large geminal dipolar coupling constant. The spectrum of cyclopropyl bromide in MBBA is illustrated in Fig. 1 and spectral parameters for all compounds are listed in Table 1. The numbering system corresponds to that shown in Fig. 2. For cyclopropyl chloride and bromide the spectra were analysed with the indirect coupling constants, J_{ij}, fixed for one spectrum at the literature values for isotropic spectra (16) and for other spectra allowed to vary in the analysis. The change in substituent group from halide to cyanide altered the average orientation in the nematic solvent to the extent that D_{13} and D_{14} are small. The indirect coupling constants are not well defined in the analysis and therefore were fixed at the isotropic values. The actual assignment of the coupling constants is not unique since the same spectra are obtained if ν_1 and ν_2, J_{15} and J_{25}, and D_{15} and D_{25} are interchanged. However, the present assignment is the one for which the D_{ij} values are consistent with the geometry. Thus J_{15} is greater than J_{25}, which confirms the assumption made in the analysis of the isotropic spectra (16).

The vibrational spectra of cyclopropyl chloride, bromide, and cyanide have been reported (17–20). Approximate force fields were derived for these compounds using the procedure of Cyvin and co-workers (21, 22) whereby an initial force field is based upon known force constants transferred from closely related compounds and used to calculate a set of frequencies. A comparison between these frequencies and the experimental values then permits adjustments to the force field such that an exact fit to the experimental frequencies can be obtained. A quadratic force field for cyclopropane itself has been derived by Duncan and Burns (23) and was transformed from their set of symmetrized internal coordinates to the coordinates used for the nematic phase nmr results.

For cyclopropyl chloride and bromide the present assignments are in agreement with those of Aleksanyan *et al.* (19) rather than those reported earlier (17, 18). In cyclopropyl cyanide the bands at 1044 and 1124 cm^{-1} were attributed to the C—CN stretch and the A′ ring deformation modes respectively (20). In the present analysis the 739 cm^{-1} band is assigned to the C—CN stretch (which occurs at 738 cm^{-1} in 2-propyl cyanide (24)) and thus some reassignment of frequencies was necessary.

Discussion

The cyclopropyl compounds studied in the present work possess a single plane of symmetry and therefore three motional constants are required to describe the average orientation (25). By choosing the axis system shown in Fig. 2, where H_1, H_2, H_3, and H_4 all lie in the *yz* plane

Can. J. Chem. Downloaded from www.nrcresearchpress.com by 210.87.254.40 on 09/05/12
For personal use only.

TABLE 1. Spectral parameters for cyclopropyl derivatives

Parameter	Cyclopropyl chloride		Cyclopropyl bromide			Cyclopropyl cyanide
	Spectrum I	Spectrum II	Spectrum I	Spectrum II	Spectrum III	
Solvent	EBBA	EBBA	EBBA	EBBA	MBBA	EBBA
Concentration (mol%)	19.3	15.9	20.6	19.2	10.6	20.5
Temperature (°C)	18	18	18	18	18	18
ν_1* (Hz)	169.46 ± 0.48	177.11 ± 0.19	183.87 ± 0.47	194.16 ± 0.52	—	143.21 ± 0.18
ν_2	239.41 ± 0.41	254.78 ± 0.17	238.43 ± 0.44	251.53 ± 0.43	ν_1 + 40.92 ± 0.35	279.42 ± 0.17
ν_3	778.93 ± 0.42	799.75 ± 0.17	750.90 ± 0.44	765.97 ± 0.48	ν_1 + 526.76 ± 0.39	416.30 ± 0.17
J_{12}†	(−6.01)	−6.10 ± 0.24	(−6.12)	−6.47 ± 0.77	−5.92 ± 0.53	(−4.72)
J_{13}	(+10.26)	+9.90 ± 0.41	(+10.16)	+11.11 ± 1.06	+10.32 ± 0.89	(+9.18)
J_{14}	(+7.14)	+7.15 ± 0.18	(+7.01)	+7.43 ± 0.52	+7.79 ± 0.38	(+7.08)
J_{15}	(+7.01)	+6.85 ± 0.28	(+7.13)	+6.64 ± 0.88	+6.33 ± 0.74	(+8.43)
J_{24}	(+10.72)	+10.31 ± 0.46	(+10.45)	+11.49 ± 1.28	+9.65 ± 0.90	(+9.65)
J_{26}	(+3.58)	+4.00 ± 0.43	(+3.80)	+1.29 ± 1.38	+3.50 ± 1.18	(+5.12)
D_{12}	+2252.16 ± 0.38	+2504.99 ± 0.23	+2208.43 ± 0.40	+2383.22 ± 0.69	+1655.02 ± 0.65	+1677.71 ± 0.20
D_{13}	−110.41 ± 1.08	−121.92 ± 0.46	−100.31 ± 1.15	−107.09 ± 1.25	−89.63 ± 0.95	−2.17 ± 0.41
D_{14}	+124.18 ± 0.46	+138.95 ± 0.18	+122.52 ± 0.44	+134.04 ± 0.52	+88.33 ± 0.42	+122.18 ± 0.25
D_{15}	−619.29 ± 0.53	−690.78 ± 0.52	−603.17 ± 0.58	−652.46 ± 1.67	−450.58 ± 1.54	+493.58 ± 0.26
D_{24}	−123.67 ± 0.89	−135.15 ± 0.38	−112.52 ± 0.95	−119.15 ± 1.03	−98.50 ± 0.78	−9.89 ± 0.42
D_{25}	+338.97 ± 0.68	+375.82 ± 0.52	+320.80 ± 0.73	+348.01 ± 1.65	+237.02 ± 1.49	+425.92 ± 0.39
No. of lines used	60	49	53	52	64	49
rms deviation (Hz)	1.79	0.51	1.75	1.54	1.41	0.73

*Chemical shifts in Hz from TMS (except cyclopropyl bromide spectrum III).
†Assumed parameters in parentheses.

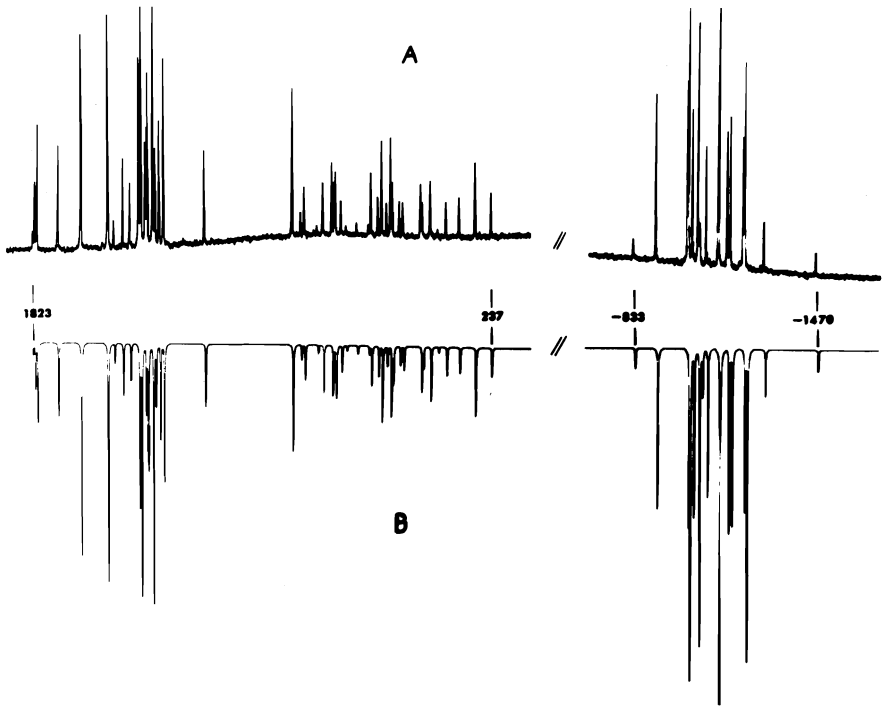

FIG. 1. Nuclear magnetic resonance spectrum of partially oriented cyclopropyl bromide (10.6 mol% in MBBA; temperature 18 °C): (*A*) experimental, (*B*) computed spectrum.

with H_1 and H_3 on the y axis, the three motional constants are $C_{3z^2-r^2}$, $C_{x^2-y^2}$, and C_{xz}, and the proton geometry can be specified by five distances; y_3 $(= -y_1)$, y_4 $(= -y_2)$, z_4 $(= z_2)$, x_5, and z_5. Thus with one parameter assumed in order to scale the relative geometry, there are seven parameters to be determined from only six

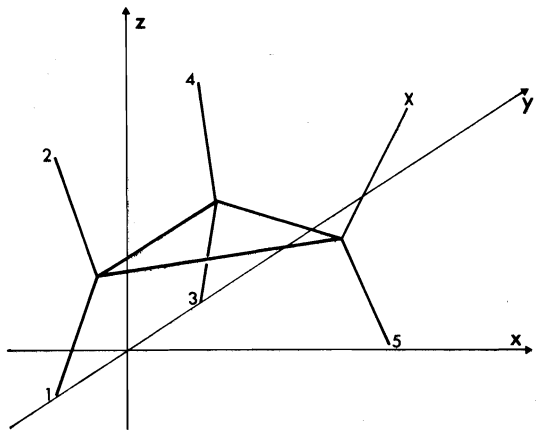

FIG. 2. Molecule fixed axis system for cyclopropyl derivatives.

experimental direct dipole coupling constants and one additional assumption is necessary. If vibrational effects are neglected initially then the four coupling constants D_{12}, D_{13}, D_{14}, and D_{24} are independent of the motional constant C_{xz} in the chosen coordinate system. If, for example, z_4 is fixed for scaling purposes, then y_3, y_4, $C_{3z^2-r^2}$ and $C_{x^2-y^2}$ can be determined without further assumptions. In order to determine the coordinates of H_5 and the value of C_{xz} either x_5 or z_5 must be assumed. The structural calculations were performed with z_4 fixed at 1.8400 Å and with different values of z_5, in Tables 2–4. For cyclopropyl chloride and bromide, where two and three spectra respectively were analysed, small differences in structures and motional constants were obtained but the differences were within experimental error. The values given in the final column of Tables 2 and 3 are averages weighted inversely according to the squares of the probable errors. In cyclopropyl cyanide where the average orientation was such that D_{13} and D_{14} had small values these coupling constants cannot be used to derive accurate structural information and the distance param-

Can. J. Chem. Downloaded from www.nrcresearchpress.com by 210.87.254.40 on 09/05/12
For personal use only.

TABLE 2. Structural results for cyclopropyl chloride*†

Parameter	No vibrational correction (weighted average)	Vibrational correction		
		Spectrum I	Spectrum II	Weighted average
y_3 (Å)	1.2740	1.2840 ± 0.0031	1.2810 ± 0.0012	1.2814 ± 0.0011
y_4 (Å)	1.2305	1.2529 ± 0.0027	1.2547 ± 0.0010	1.2545 ± 0.0010
z_4 (Å)	(1.8400)	(1.8400)	(1.8400)	(1.8400)
$C_{3z^2-r^2}$	—	−0.1369 ± 0.0001	−0.1522 ± 0.0001	—
$C_{x^2-y^2}$	—	+0.0592 ± 0.0001	+0.0662 ± 0.0001	—
x_5 (Å)	2.1297	2.1948 ± 0.0033	2.1959 ± 0.0015	2.1957 ± 0.0014
z_5 (Å)	(0.0000)	(0.0000)	(0.0000)	(0.0000)
C_{xz}	—	+0.1550 ± 0.0008	0.1724 ± 0.0004	—
x_5 (Å)	—	2.1341	2.1353	2.1351
z_5 (Å)	—	(−0.0500)	(−0.0500)	(−0.0500)
C_{xz}	—	+0.1442	+0.1604	—
x_5 (Å)	—	2.2545	2.2555	2.2553
z_5 (Å)	—	(+0.0500)	(+0.0500)	(+0.0500)
C_{xz}	—	+0.1662	+0.1849	—

*Assumed parameters in parentheses.
†See Fig. 2 for proton numbering.

TABLE 3. Structural results for cyclopropyl bromide*†

Parameter	No vibrational correction (weighted average)	Vibrational correction			
		Spectrum I	Spectrum II	Spectrum III	Weighted average
y_3 (Å)	1.2769	1.2841 ± 0.0037	1.2887 ± 0.0036	1.2816 ± 0.0034	1.2847 ± 0.0021
y_4 (Å)	1.2330	1.2558 ± 0.0032	1.2563 ± 0.0031	1.2551 ± 0.0030	1.2557 ± 0.0018
z_4 (Å)	(1.8400)	(1.8400)	(1.8400)	(1.8400)	(1.8400)
$C_{3z^2-r^2}$	—	−0.1450 ± 0.0001	−0.1344 ± 0.0001	−0.1007 ± 0.0001	—
$C_{x^2-y^2}$	—	+0.0646 ± 0.0001	+0.0595 ± 0.0001	+0.0422 ± 0.0001	—
x_5 (Å)	2.1391	2.2125 ± 0.0037	2.2083 ± 0.0038	2.2012 ± 0.0055	2.2087 ± 0.0024
z_5 (Å)	(0.0000)	(0.0000)	(0.0000)	(0.0000)	(0.0000)
C_{xz}	—	+0.1640 ± 0.0012	+0.1505 ± 0.0008	+0.1096 ± 0.0009	—
x_5 (Å)		2.1523	2.1483	2.1430	2.1489
z_5 (Å)		(−0.0500)	(−0.0500)	(−0.0550)	(−0.0500)
C_{xz}		+0.1526	+0.1400	+0.1020	—
x_5 (Å)		2.2718	2.2673	2.2587	2.2675
z_5 (Å)		(+0.0500)	(+0.0500)	(+0.0500)	(+0.0500)
C_{xz}		+0.1760	+0.1615	+0.1175	—

*Assumed parameters in parentheses.
†See Fig. 2 for proton numbering.

eters in Table 4, while giving adequate fits to the D_{ij} values, are unacceptable. It was necessary therefore to assume an additional distance parameter and the coordinate y_3 was set at 1.2830 Å, the average of the cyclopropyl chloride and bromide values.

The application of Lucas' method (12–14) to derive the vibrationally averaged r_z distances requires the inclusion of the motional constant C_{xz} in the expansions of D_{12}, D_{13}, D_{14}, and D_{24}. The same coordinate system was used and the same distance parameters assumed. The results are given in Tables 2, 3, and 4 with the values obtained from the analysis of each spectrum as well as the weighted average. Small differences in structure and motional constants are evident but these are within experimental error. The error limits quoted in these tables are derived from the experimental errors in the D_{ij} values (26).

There are obvious differences between the uncorrected distances, r_d, derived directly from the direct dipole coupling constants and the

Can. J. Chem. Downloaded from www.nrcresearchpress.com by 210.87.254.40 on 09/05/12
For personal use only.

TABLE 4. Structural results for cyclopropylcyanide*†

Parameter	No vibrational correction	Vibrational correction	
y_3 (Å)	1.7112	2.8558	(1.2830)
y_4 (Å)	1.0324	1.1260	1.2354±0.0016
z_4 (Å)	(1.8400)	(1.8400)	(1.8400)
$C_{3z^2-r^2}$	−0.1340	−0.6011	−0.1020±0.0001
$C_{x^2-y^2}$	+0.0764	+0.3506	+0.0588±0.0001
x_5 (Å)	1.7975	3.1733	2.2247±0.0008
z_5 (Å)	(0.0000)	(0.0000)	(0.0000)
C_{xz}	+0.1093	+0.7325	+0.1946±0.0003
x_5 (Å)			2.1264
z_5 (Å)			(−0.0500)
C_{xz}			+0.1785
x_5 (Å)			2.3199
z_5 (Å)			(+0.0500)
C_{xz}			+0.2117

*Assumed parameters in parentheses.
†See Fig. 2 for proton numbering.

TABLE 5. Proton distance ratios in cyclopropyl derivatives

		r_{13}/r_{34}	r_{24}/r_{34}	r_{13}/r_{24}	Reference
Cyclopropane	r_z	1.378	1.378	1.000	14
	r_d	1.359	1.359	1.000	14
Cyclopropyl chloride	r_z	1.393	1.366	1.021	This work
	r_d	1.385	1.338	1.035	This work
	r_s	1.388	1.358	1.022	6
Cyclopropyl bromide	r_z	1.396	1.365	1.024	This work
	r_d	1.388	1.340	1.036	This work
	r_s	1.404	1.396	1.033	27
Cyclopropyl cyanide	r_z	1.395	1.343	1.039	This work
1,1-Dichlorocyclopropane	r_z	1.399	1.399	1.000	9
	r_d	1.385	1.385	1.000	9
1,1-Difluorocyclopropane	r_s	1.376	1.376	1.000	8

corrected distances, r_z, obtained by the Lucas method. For cyclopropyl chloride the r_z distances show generally better agreement with the microwave r_s structure (6) than do the r_d values. The structures of the chloride and bromide derivatives are quite similar and the present results favour structure I of the two alternatives given by Lam and Dailey (27) for cyclopropyl bromide. The position of H_5 in each compound is subject to some uncertainty and it is not possible to draw firm conclusions regarding the coordinates of this atom. It is, however, apparent that coordinate x_5 in each case is greater than the corresponding value for cyclopropane (2.178 Å) and is largest for cyclopropyl cyanide. This is consistent with a lengthening of the ring bonds adjacent to the substituent and thus provides some indirect evidence in support of the Hoffmann theory.

Proton distance ratios are compared in Table 5 where results for other cyclopropyl compounds are also included. An interesting feature for the monosubstituted derivatives is the larger value of r_{13} relative to r_{24}. This may be due to a longer C—H bond but the microwave structure of cyclopropyl chloride showed little difference in C—H bond lengths and it is more probable that the C_1–C_2–H_1 and C_1–C_2–H_2 bond angles differ such that the protons *cis* to the substituent are displaced towards the substituent (or, conversely, the *trans* protons displaced in the opposite direction).

The probability that the applied field direction (or the nematic liquid crystal axis if these are

Can. J. Chem. Downloaded from www.nrcresearchpress.com by 210.87.254.40 on 09/05/12
For personal use only.

Can. J. Chem. Downloaded from www.nrcresearchpress.com by 210.87.254.40 on 09/05/12
For personal use only.

TABLE 6. Angle of principal orientation and orientation anisotropy

	θ_{max}	$\frac{P(\theta,\phi)_{max}}{P(\theta,\phi)_{min}}$
Cyclopropane*	90	1.22
Cyclopropyl chloride I	66.9	2.47
II	66.9	2.79
Cyclopropyl bromide I	67.0	2.63
II	67.1	2.41
III	67.3	1.94
Cyclopropyl cyanide	60.6	2.58

*From data in ref. 14.

assumed to be parallel) makes spherical polar angles θ and ϕ to the molecule-fixed axis system is given (25) by [1]

$$[1]\quad P(\theta,\phi)=(4\pi)^{-1}\Big[1+C_{3z^2-r^2}\frac{\sqrt{5}}{2}(3\cos^2\theta-1)+C_{x^2-y^2}\frac{\sqrt{15}}{2}\sin^2\theta\cos 2\phi+C_{xz}\sqrt{15}\sin\theta\cos\theta\cos\phi+C_{xy}\frac{\sqrt{15}}{2}\sin^2\theta\sin 2\phi+C_{yz}\sqrt{15}\sin\theta\cos\theta\sin\phi\Big]$$

The monosubstituted cyclopropanes orient preferentially with their symmetry planes parallel to the liquid crystal axis and rotated about the molecule-fixed y axis by angles given by [2]

$$[2]\qquad \tan 2\theta=\frac{2C_{xz}}{\sqrt{3}C_{3z^2-r^2}-C_{x^2-y^2}}$$

These angles are given in Table 6 and show that cyclopropyl chloride and bromide have about the same orientation but cyclopropyl cyanide is rotated slightly more. For cyclopropyl bromide the principal orientation direction is essentially unchanged in the two solvents EBBA and MBBA. The anisotropy of alignment in the xz plane can be expressed as the ratio between the maximum and minimum values of $P(\theta, \phi)$. The ratios are also given in Table 6, and are very similar for all solutions in EBBA, including cyclopropyl cyanide, but it is significantly lower for cyclopropyl bromide in MBBA. The order parameter of the nematic solvent, for the pure material and for solutions, can be expressed as a universal function of reduced temperature (28) and the lower degree of solute orientation and low anisotropy for the cyclopropyl bromide/MBBA system reflects the higher reduced temperature and lower solvent order.

Acknowledgments

This work was supported by grants from the National Research Council of Canada. The authors thank Professor V. W. Laurie for details of the structure of cyclopropyl cyanide.

1. A. D. WALSH. Trans. Faraday Soc. **45**, 179 (1949).
2. R. HOFFMANN. Tetrahedron Lett. **33**, 2907 (1970).
3. R. E. PENN and J. E. BOGGS. J. Chem. Soc. Chem. Commun. **11**, 666 (1972).
4. R. PEARSON, A. CHOPLIN, and V. W. LAURIE. J. Chem. Phys. **62**, 4859 (1975).
5. O. BASTIANSEN, F. N. FRITSCH, and K. HEDBERG. Acta Crystallogr. **17**, 538 (1964).
6. R. H. SCHWENDEMAN, G. D. JACOBS, and T. M. KRIGAS. J. Chem. Phys. **40**, 1022 (1964).
7. M. D. HARMONY, R. E. BOSTROM, and D. K. HENDRICKSEN. J. Chem. Phys. **62**, 1599 (1975).
8. A. T. PERRETTA and V. W. LAURIE. J. Chem. Phys. **62**, 2469 (1975).
9. K. C. COLE and D. F. R. GILSON. J. Mol. Struct. **28**, 385 (1975).
10. J. W. LAUHER and J. A. IBERS. J. Am. Chem. Soc. **97**, 561 (1975).
11. P. DIEHL and C. L. KHETRAPAL. *In* NMR basic principles and progress. Vol. 1. *Edited by* P. Diehl, E. Fluck, and R. Kosfeld. Springer Verlag. 1969.
12. N. J. D. LUCAS. Mol. Phys. **22**, 147 (1971).
13. N. J. D. LUCAS. Mol. Phys. **23**, 825 (1972).
14. N. J. D. LUCAS. Mol. Phys. **22**, 233 (1971).
15. J. H. SCHACHTSCHNEIDER and R. G. SNYDER. Spectrochim. Acta, **19**, 117 (1963).
16. K. M. CRECELY, V. S. WATTS, and J. H. GOLDSTEIN. J. Mol. Spectrosc. **30**, 184 (1969).
17. M. I. KAY. Ph.D. Thesis, Rensselaer Polytechnic Institute, Troy, N.Y. 1962.
18. W. G. ROTHSCHILD. J. Chem. Phys. **44**, 3875 (1966).
19. V. T. ALEKSANYAN, V. M. SHOSTAKOVSKII, S. M. SHOSTAKOVSKII, and O. M. NEFEDOV. Izv. Akad. Nauk SSSR, Ser. Khim. 772 (1973).
20. L. H. DALY and S. E. WIBERLEY. J. Mol. Spectrosc. **2**, 177 (1958).
21. I. L. ANDRESEN, S. J. CYVIN, B. LARSEN, and O. TORSET. Acta Chem. Scand. **25**, 473 (1971).
22. B. N. CYVIN and S. J. CYVIN. Acta Chem. Scand. **26**, 3943 (1972).
23. J. L. DUNCAN and G. R. BURNS. J. Mol. Spectrosc. **30**, 253 (1969).
24. P. KLABOE. Spectrochim. Acta, Ser. A, **26**, 87 (1970).
25. L. C. SNYDER. J. Chem. Phys. **43**, 4041 (1965).
26. K. C. COLE and D. F. R. GILSON. Can. J. Chem. **52**, 281 (1974).
27. F. M. K. LAM and B. P. DAILEY. J. Chem. Phys. **49** 1588 (1968).
28. B. KRONBERG, D. F. R. GILSON, and D. PATTERSON. J. Chem. Soc. Faraday Trans. In press.
29. G. A. SIM and L. E. SUTTON (*Editors*) Molecular structure by diffraction methods, Specialist Periodical Reports, The Chemical Society, London. Vol. 1. 1973.

Studies in the usnic acid series. I. The condensation of (+)-usnic acid with aliphatic and aromatic amines

JAMES P. KUTNEY AND IGNACIO H. SANCHEZ

Department of Chemistry, The University of British Columbia, 2075 Wesbrook Place, Vancouver, B.C., Canada V6T 1W5

Received April 22, 1976

JAMES P. KUTNEY and IGNACIO H. SANCHEZ. Can. J. Chem. **54**, 2795 (1976).

Detailed investigations concerned with the reaction of usnic acid (**1**) and dihydrousnic acid (**14**) with a variety of aliphatic and aromatic amines are described. Extensive analyses of the characteristic spectroscopic data allow structural assignments for all the isolated products. The correctness of these assignments is established by an X-ray analysis of one of the products resulting from the reaction of usnic acid with ammonia.

JAMES P. KUTNEY et IGNACIO H. SANCHEZ. Can. J. Chem. **54**, 2795 (1976).

Des études détaillées concernant la réaction de l'acide usnique (**1**) et de l'acide dihydrousnique (**14**) avec divers amines aliphatiques et aromatiques sont décrites. L'analyse approfondie des données spectroscopiques caractéristiques permet l'assignation de la structure à chacun des produits isolés. L'exactitude de ces assignations a été établie par l'analyse aux rayons-X de l'un des produits résultant de la réaction de l'acide usnique avec l'ammoniaque.

[Traduit par le journal]

Can. J. Chem. Downloaded from www.nrcresearchpress.com by 210.87.254.42 on 09/05/12
For personal use only.

During the synthetic investigations that were required for our studies on the biodegradation of the lichen antibiotic (+)-usnic acid (**1**) (1–4), it became essential to prepare usnic acid derivatives in which the highly reactive β-triketone system, characteristic of this series of compounds, was fully protected.

Of the several possibilities available for the protection of β-di- and β-triketones, (5) the one arising from the formation of stable heterocyclic systems, generated in the reaction of these ketones with amine reagents, seemed appropriate for our purpose and was therefore considered. However, since only brief reports have appeared (6–11) on the condensation of **1** with aliphatic or aromatic amines and in view of the obvious complications implied, we felt that a thorough study of such condensations was required. This article presents our results in this area.

When (+)-usnic acid (**1**) was reacted with a series of aliphatic and aromatic amines, various condensation products could be isolated and characterized (Fig. 1). Some of these (**2**, **3**, **5** and **12**) represent preferential attack of the amine function at the chelated acetyl side chain of the β-triketone system to provide novel β,β′-diketo enamine structures which are different from the structures proposed by earlier workers (8–11). Condensation of the amine with the aromatic methyl ketone, as shown in **4** and **6**, occurs as a secondary reaction and furnishes the expected imine derivative. The latter reaction can be suppressed by regulating the amount of amine added. Although the formation of vinylogous amides has been demonstrated during amination studies in the alicyclic β-triketone series (12, 13), such condensation products had not been recognized in the usnic acid series.

The general procedure employed in our study is essentially that of Schopf and co-workers (10, 11) consisting of treating a suspension of (+)-usnic acid (**1**) in absolute ethyl alcohol with an appropriate amine followed by heating to reflux under a nitrogen atmosphere for several hours. It is appropriate to mention here that the well known thermal racemization of usnic acid derivatives (14–16) is not observed under these conditions.

The structural assignments of these various products were based on extensive analyses of the spectroscopic data obtained. The correctness of these assignments was subsequently established when an X-ray analysis (see later) of one of the products (**2**) was completed. This substance was of pivotal importance in this and related studies and consequently was selected for the X-ray determination. It is appropriate to discuss below the most salient features of the spectroscopic characteristics exhibited by the various compounds.

Can. J. Chem. Downloaded from www.nrcresearchpress.com by 210.87.254.42 on 09/05/12
For personal use only.

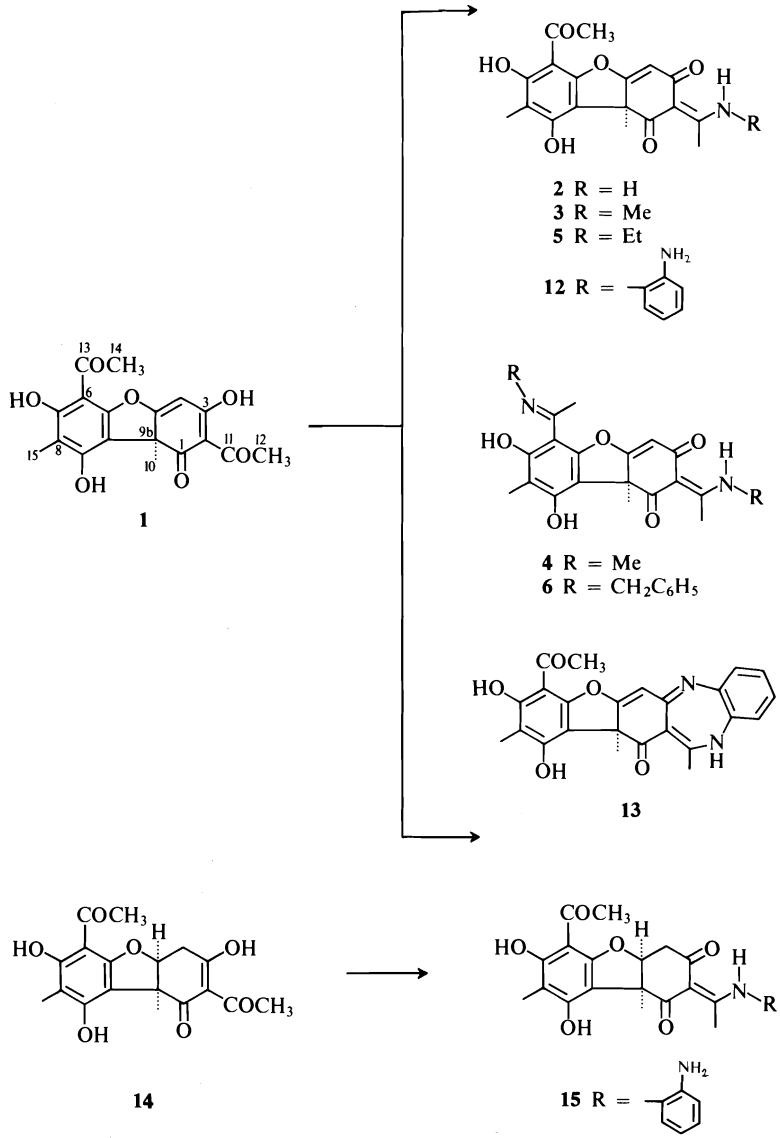

FIG. 1. The condensation of (+)-usnic acid (**1**) and (−)-dihydrousnic acid (**14**) with aliphatic and aromatic amines.

An analysis of the ultraviolet absorption spectra (Table 1) revealed that these data could be employed to distinguish between the series of products resulting from the condensation of 1 mol of amine with the aliphatic acetyl side chain in ring C of usnic acid (for example, **2**, **3**, **5** and **12**) and the series in which condensation at both the aliphatic side chain and the aromatic carbonyl has occurred (for example, **4** and **6**). The former series exhibited absorption maxima at 345, 293, and 223 nm, while the latter revealed maxima at 300, 250, and 234 nm.

The infrared spectra, typical of the series, provide valuable information regarding the type of substitution present in ring C. While the C-1 carbonyl absorption appears consistently at 1695–1700 cm^{-1} for both series, thereby indicating little or no conjugation with the adjacent β-ketoenamino system, the absorption of the unsaturated vinylogous amide (1560–1570 cm^{-1})

TABLE 1. Some physical data on the condensation products of (+)-usnic acid (**1**) and (−)-dihydrousnic acid (**14**) with aliphatic and aromatic amines

Compound	mp (°C)	$[\alpha]_D^{27}$* (deg)	Ultraviolet data: λ_{max} (nm) and log ϵ (in parentheses)	Solvent*
1	202–204	+493 (*A*)	328(3.61), 285(4.08), 231(4.12)	(*A*)
14	150–151	−83 (*B*)	337(3.44), 283(4.38), 227(4.19)	(*A*)
2	252–254	−230 (*A*)	333(3.38), 291(4.18)	(*B*)
3	209–211	−344 (*A*)	345(3.39), 293(4.19), 223(4.07)	(*A*)
5	133–134	+365 (*A*)	348(3.56), 294(4.38)	(*B*)
12	185–186	+266 (*B*)	349(3.76), 293(4.20), 228(4.24)	(*B*)
15	179–181	−279 (*B*)	342(3.76), 293(4.21), 230(4.15)	(*B*)
13	180 (dec)	+920 (*B*)	370(3.09), 305(4.13), 288(4.13), 226(4.10)	(*B*)
4	198–200	+94 (*A*)	300(4.13), 250(3.96), 234(4.05)	(*B*)
6	197–198	+262 (*A*)	301(4.23)	(*B*)

*The solvent used is indicated in parentheses: *A*, CH_3OH; *B*, CH_3CN.

TABLE 2. Infrared absorption frequencies of (+)-usnic acid – amine condensation products (cm^{-1})

Compound	Functionality/frequency: C=O (C-1)	C=O (C-3)	C=X (C-13)
1	1680	—	1625 (X = O)
2	1697	1570	1630 (X = O)
3	1700	1560	1630 (X = O)
4	1700	1560	1630 (X = NCH_3)
5	1705	1570	1630 (X = O)
6	1695	1560	1620 (X = NCH_2Ph)
12	1695	1540	1625 (X = O)

reflects the effect of both unsaturation and strong intramolecular hydrogen bonding when compared with the normal absorption range of vinylogous amides (1615–1642 cm^{-1}) (17, 18). Similarly the chelated aromatic methyl ketone shows a strong absorption band at 1630 cm^{-1}, a position comparable to that found in the spectrum of (+)-usnic acid itself (19, 20) (Table 2).

Our previous detailed study of the mass spectrometric fragmentations in the usnic acid series (21) proved invaluable in applying this technique as a structural aid in these investigations. The characteristic fragmentation pattern is exemplified for (−)-$\Delta^{2,11}$-enaminousnic acid (**2**) (Fig. 2). Thus, the base peak arises from the *retro* Diels–Alder cleavage of ring C to produce the benzofuranylketene intermediate ***a*** which, in turn, fragments further by loss of carbon monoxide and of methyl radical to provide significant fragments at *m/e* 232 and 217. These data clearly reveal the reaction of ammonia with usnic acid in ring C rather than at the aromatic methyl ketone. Also of importance is the low relative abundance of fragments arising from the alternate β-imino ketoenolic tautomer which is believed to produce ions ***b*** and ***c***. The loss of methyl radical (ion ***d***) is usually observed from the molecular ion. The postulated fragmentation pathways shown in Fig. 2 are applicable to all the compounds isolated from the various reactions. Thus, in the products **4** and **6**, where condensation of the amine has occurred at the aromatic carbonyl, one observes ions corresponding to those indicated but with the appropriate increase in mass units due to the nitrogenous portion.

Table 3 provides a summary of selected pmr data obtained with the aliphatic amine – usnic acid condensation products. These data reveal that throughout the series the signal for the C-11 methyl group appears consistently at higher field than that for the methyl group at the 13-position. The products involving condensation with 2 mol of amines (**4** and **6**) show, in addition, a noticeably low-field signal for the enamino proton (δ 16.92 and 16.85) as compared to this signal in

Can. J. Chem. Downloaded from www.nrcresearchpress.com by 210.87.254.42 on 09/05/12
For personal use only.

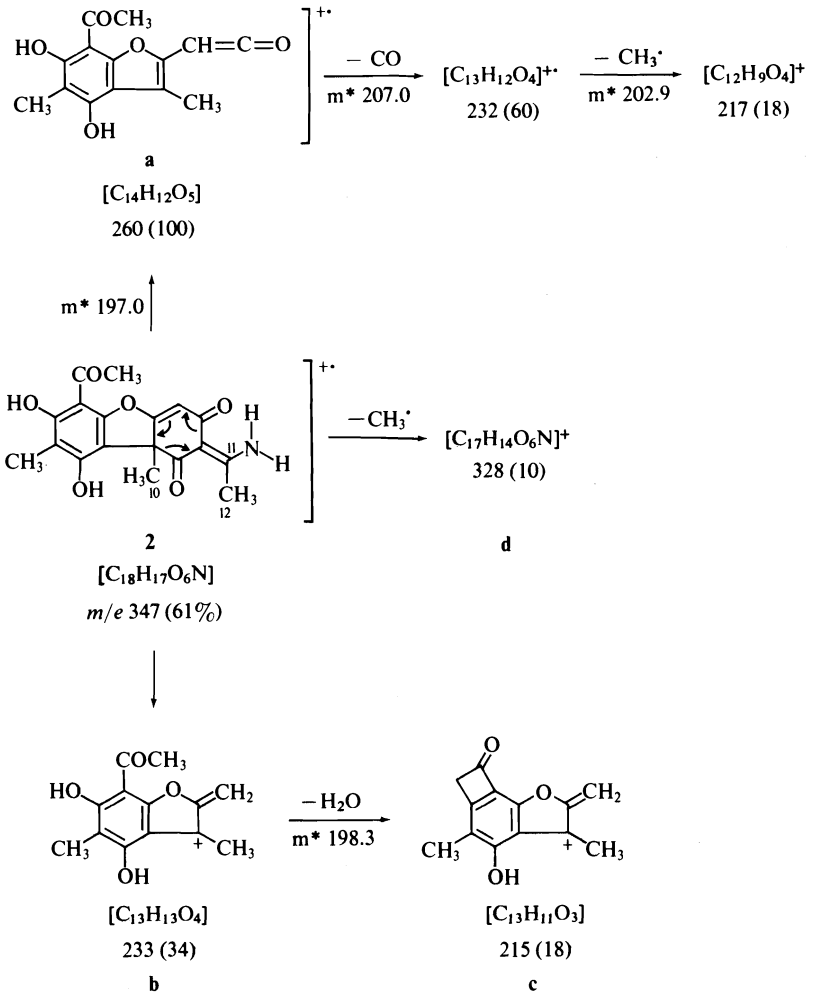

FIG. 2. The postulated fragmentation pattern of (−)-$\Delta^{2,11}$-enaminousnic acid (**2**) in the mass spectrometer.

the spectra of the series exemplified by **2**, **3** and **5**.

Clearly the structural assignments, as summarized in Fig. 1, relied heavily on spectroscopic analyses. It appeared desirable to establish conclusively, by means of X-ray analysis, the structure of one of the products which was of central importance in this and related studies. The crystalline product obtained from the condensation of ammonia at the aliphatic acetyl side chain in ring C of usnic acid was selected for this purpose. The X-ray determination was performed by Professor Jon C. Clardy at Iowa State University and the details of this study will be published elsewhere. It is sufficient to indicate here the computer generated structure for this compound as shown in **2***a* (Fig. 3), and therefore this substance could be given the name, $\Delta^{2,11}$-enaminousnic acid (**2**, Fig. 1). The absolute configuration shown is an assumed one. The bond distances obtained in the X-ray study suggest that the best single representation is that shown by **2** with important contributions from **7**.

The X-ray result established the novel en-

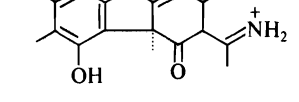

7

Can. J. Chem. Downloaded from www.nrcresearchpress.com by 210.87.254.42 on 09/05/12
For personal use only.

TABLE 3. Summary of selected proton magnetic resonance data for the aliphatic amine – usnic acid series (ppm, δ scale)

Amine	Compound	C_{9b}-CH_3	C_{11}-CH_3	C_{13}-CH_3	N-CH_2-R	N′-CH-R	N-H	C_9-OH	C_7-OH	C_4-H
Ammonia	**2**	1.66	2.59	2.65	—	—	9.56	11.72	13.35	5.75
Methylamine	**3**	1.70	2.64	2.66	3.16 (R = H)	—	13.20	11.90	13.30	5.77
Ethylamine	**5**	1.65	2.59	2.61	3.52 ($R = CH_3$)	—	13.26	11.91	13.30	5.72
Methylamine	**4**	1.70	2.56	2.66	3.18 (R = H)	3.30 (R = H)	16.92	11.40	13.32	5.80
Benzylamine	**6**	1.68	2.55	2.65	4.65 ($R = C_6H_5$)	4.76 ($R = C_6H_5$)	16.85	11.35	11.95	5.72

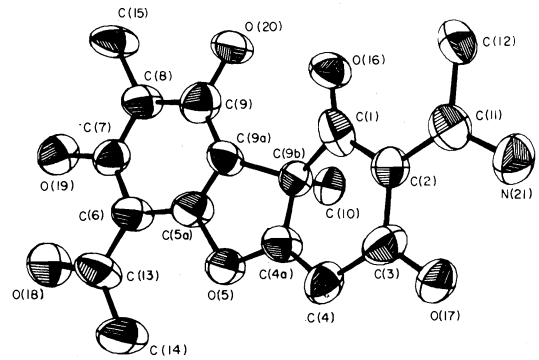

2a

FIG. 3. The computer generated structure for compound **2**.

aminodiketo system in ring C of the usnic acid – amine adducts, a structural feature already suggested from the spectral data discussed earlier. The close similarities in the spectroscopic features of the various products when compared to those exhibited by **2** left no doubt about the correctness of the structural assignments as presented in Fig. 1.

We then decided to evaluate the behavior of (+)-usnic acid (**1**) when treated with aromatic amines. Although the work performed in this area has been somewhat more extensive (6–8), earlier work was directed exclusively towards the analysis of the antimicrobial and antimycotic properties of the crude materials (6, 7), thus furnishing no conclusive structural evidence or spectroscopic characteristics. Although Seshadri and co-workers (8) were able to postulate ring C as the active condensation site, they failed to recognize both the β,β'-diketoenamine system characteristic of the series and the role of the chelated aromatic methyl ketone in its reaction with the amine. They postulated that condensation of the second mole of amine took place at the C-3 carbonyl group in ring C. A close scrutiny of the reported pmr data (8) (Table 4) for the aromatic amine – usnic acid adducts allowed us to deduce the correct structures **8–11**.

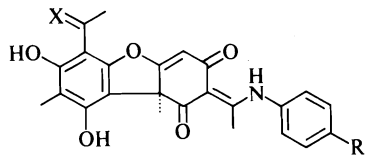

8 R = $COCH_3$; X = O
9 R = COOH; X = O
10 R = $COOCH_2CH_3$; X = O
11 R = $COCH_3$; X = *p*-N—C_6H_4—$COCH_3$

As a means of preparing protected β-diketone systems (23) we studied, as well, the condensation of **1** with *o*-phenylenediamine, a system previously considered by Seshadri and co-workers (8) and indeed we obtained the expected monocondensation product **12**, mp 185–186 °C (lit. (8) mp 185–186 °C), $[\alpha]_D^{27}$ (CH_3CN) +266°, showing infrared absorption characteristics (1695, 1625, 1540 cm^{-1}) comparable to those recorded in Table 2 for the aliphatic series. Although compound **12** would not be cyclized under the described conditions (8), this novel 1,5-benzodiazepine derivative **13** can be obtained in 82% yield by treating **12** with concentrated hydrochloric acid in absolute ethyl alcohol at room temperature. The importance of such a system for our purposes was enhanced by the known stability of 1,5-benzodiazepines towards a variety

Can. J. Chem. Downloaded from www.nrcresearchpress.com by 210.87.254.42 on 09/05/12
For personal use only.

TABLE 4. Selected proton magnetic resonance data for the aromatic amine – usnic acid adducts (8) (values are quoted in the δ scale)

Compound	C_{9b}-CH_3	C_{11}-CH_3	C_{13}-CH_3	N-H	C_9-OH	C_7-OH	C_4-H
8	1.75	2.62	2.62	15.40	11.63	13.38	5.92
9	1.74	2.55	2.58	—	11.78	13.38	5.96
10	1.78	2.60	2.65	15.20	11.76	13.40	5.70
11	1.75	2.42	2.66	—	10.83	13.23	5.83

of experimental conditions and by the possibility of regenerating or further transferring the 1,3-dicarbonyl systems (22–28) at appropriate stages in our synthetic work.

Finally studies with dihydrousnic acid (10, 11, 29) (**14**) were performed to determine whether removal of the double bond in ring C had any effect on the reaction with amines. Thus **14** was treated with *o*-phenylenediamine in alcoholic solution and the isolated crystalline product (95% yield) was determined, by its characteristic spectral data, to be **15** thereby revealing a similar reaction course to that in the normal usnic acid series.

In conclusion these studies have provided a clarification of the results obtained with the reactive and highly functionalized usnic acid molecule and various amines. These results have proved invaluable for studies related to the biodegradation of usnic acid to be published in subsequent publications.

Experimental

Melting points were determined on a Kofler block and are uncorrected.

Ultraviolet (uv) spectra were recorded on a Cary 15 spectrophotometer in methanol solution (unless otherwise noted) and the absorption maxima are reported in nm.

Infrared (ir) spectra were measured in chloroform solution on Perkin-Elmer model 710 or 457 spectrophotometers and the absorption maxima are quoted in wave numbers (cm^{-1}).

Proton magnetic resonance (pmr) spectra were measured in deuterochloroform ($CDCl_3$) solution (unless otherwise indicated) at room temperature. Routine spectra were recorded at 60 MHz on a Varian T-60 spectrometer, and analytical or comparison spectra at 100 MHz on either a Varian HA-100 or a Varian XL-100 spectrometer. All pmr spectra obtained via the Fourier Transform (FT) technique are so noted and were recorded on a Varian XL-100 spectrometer. Line positions are given in the δ (ppm) scale using tetramethylsilane (TMS) as internal standard. The integrated peak areas, multiplicity, and proton assignments are indicated in parentheses.

Low resolution mass (ms) spectra were determined at 70 eV on either an AEI-902 or an Atlas CH-4B mass spectrometer, while high resolution mass spectra were recorded exclusively on an AEI-MS-902 mass spectrometer.

Circular dichroism (cd) spectra were obtained on a Jasco model J-20 spectropolarimeter in methanol solution (unless otherwise indicated). The wavelength of the absorption maxima is reported in nm. The differential molar extinction coefficient ($\Delta\epsilon$) and the sign of the observed Cotton effect are indicated in parentheses.

Optical rotations ($[\alpha]_D$) were measured on a Perkin-Elmer model 141 polarimeter at the sodium D line in chloroform solution (unless otherwise noted) using cells with a 0.1 dm path.

Microanalyses were performed by Mr. P. Borda of the Microanalytical Laboratory, University of British Columbia.

Merck silica gel G (acc. to Stahl) impregnated with oxalic acid (2%) and with 2% fluorescent indicator added, was used as adsorbent for thin layer chromatography (tlc), unless otherwise noted. The tlc plates were activated in an oven at 90 °C for 4 h before use. For qualitative chromatography, layers of 0.3 mm thickness were used and the spots were visualized by viewing under ultraviolet (uv) light or spraying with a 1% ethanolic ferric chloride solution. For preparative (plc) chromatography large (20 × 20 and 20 × 60 cm) plates with a thicker layer (0.7 mm) were used. The developing systems were *A*, petroleum ether (30–60 °C) – acetone (4:1), and *B*, chloroform – ethyl acetate (3:2), unless otherwise indicated.

Column chromatography was performed on either Mackerey–Nagel (0.2–0.5 mm grain size) or Merck 60 (0.063–0.2 mm grain size) silica gel.

The usnic acid utilized throughout the course of this study was obtained from Koch-Light Laboratories, England, as the optically active dextrorotatory isomer, (+)-usnic acid, isolated from lichen sources (*Usnea barbata*).

In order to present in a coherent manner the characteristic spectroscopic data for those compounds that are formally derived from usnic acid and retain its basic skeletal features, we have decided to maintain through the course of this work the numbering system recommended for the parent molecule (*i.e.* the approved dibenzofuran numbering (30)) instead of using those arising from the corresponding systematic names. In all other instances the latter numbering systems will be used.

*Condensation of (+)-Usnic Acid (**1**) with Amines*

*I. Aqueous Ammonia. Preparation of (−)-$\Delta^{2,11}$-Enaminousnic Acid (**2**) (Usnic Acid Amide (9)) (6-Acetyl-7,9-dihydroxy-8,9bα-dimethyl-2-ethylid-2,11-ene-11-amino-1,9b,2,3-tetrahydro-1,3-dioxodibenzofuran)*

A suspension of (+)-usnic acid (**1**) (600 mg, 1.744

Can. J. Chem. Downloaded from www.nrcresearchpress.com by 210.87.254.42 on 09/05/12
For personal use only.

Can. J. Chem. Downloaded from www.nrcresearchpress.com by 210.87.254.42 on 09/05/12
For personal use only.

mmol) in a mixture of dry benzene (2 ml) and absolute ethyl alcohol (4 ml) was treated with concentrated ammonium hydroxide (0.8 ml) and refluxed under nitrogen atmosphere for 2 h. After cooling in an ice bath the yellow solution was concentrated to approximately one third the original volume, acidified with 1 *N* hydrochloric acid, and extracted with ethyl acetate (2 × 20 ml). The combined extracts were thoroughly washed with water and brine solution, dried over anhydrous sodium sulfate, and evaporated under reduced pressure. The residue (525 mg) was crystallized from chloroform to produce pale yellow plates of (−)-$\Delta^{2,11}$-enaminousnic acid (**2**) (495 mg, 1.443 mmol, 82%), mp 252–254 °C (lit. (9) mp 248 °C); $[\alpha]_D^{26}$ −230° (*c* 0.099); uv (CH_3CN) λ_{max} (log ϵ) 333 (3.38), 291 (4.18); ir ν_{max} 3475 (N—H), 3400–2500 (OH, NH, chelated), 1697 (C=O, ketoenamine system), 1630 (C=O, chelated acetyl grouping; C=C, enol ether, aromatic ring), 1570 (C=O, chelated ketoenamine system); pmr ($CDCl_3$–DMSO-d_6) δ 1.66 (3H, s, C_{9b}-CH_3), 2.00 (3H, s, C_8-CH_3), 2.59 (3H, s, C_{11}-CH_3), 2.65 (3H, s, C_6-$COCH_3$), 5.75 (1H, s, C_4-H), 9.56 (1H, br, N-H), 11.72 (1H, br, C_9-OH), 12.05 (1H, s, N-H), 13.35 ppm (1H, s, C_7-OH); ms *m/e* 343 (M^+), 328 (*M* − 15) 260 (base peak), 232, 217, 215. *Anal.* calcd. for $C_{18}H_{17}O_6N$: C 62.97, H 4.95, N 4.08; found: C 62.90, H 5.10, N 4.09. High resolution molecular weight determination: calcd.: 343.106; found: 343.108.

*II. Methylamine. Formation of (−)-N-Methyl-$\Delta^{2,11}$-enaminousnic Acid (**3**) (6-Acetyl-7,9-dihydroxy-8,9bα-dimethyl-2-ethylid-2,11-ene-1,9b,2,3-tetrahydro-11-N-methylamino-1,3-dioxodibenzofuran) and (+)-N′-Methylimino-N-methyl-$\Delta^{2,11}$-enaminousnic Acid (**4**) (7,9-Dihydroxy-8,9bα-dimethyl-6-ethyl-2-ethylid-2,11-ene-1,9b,2,3-tetrahydro-13-N-methylimino-11-N-methylamino-1,3-dioxodibenzofuran)*

A suspension of (+)-usnic acid (**1**) (500 mg, 1.453 mmol) in absolute ethyl alcohol (10 ml) was treated with 40% aqueous methylamine solution (0.5 ml) and heated to reflux under nitrogen atmosphere for 1.5 h. The reaction mixture was acidified with glacial acetic acid (3 ml), concentrated under reduced pressure, and diluted with cold distilled water (10 ml). The precipitate was filtered, air dried, and recrystallized from ethyl alcohol to produce pale yellow prisms of (−)-*N*-methyl-$\Delta^{2,11}$-enaminousnic acid (**3**) (380 mg, 1.064 mmol; 73%), mp 209–211 °C; $[\alpha]_D^{26}$ −344° (*c* 0.0545); uv λ_{max} (log ϵ) 345 (3.39), 293 (4.19), 223 (4.07); ir ν_{max} 3200–2500 (OH, NH, chelated), 1700 (C=O, ketoenamine system), 1630 (C=O, chelated acetyl grouping; C=C, enol ether, aromatic ring), 1560 (C=O, chelated ketoenamine system); pmr δ 1.70 (3H, s, C_{9b}-CH_3), 2.10 (3H, s, C_8-CH_3), 2.64 (3H, s, C_{11}-CH_3), 2.66 (3H, s, C_6-$COCH_3$), 3.16 (3H, d, J = 5 Hz, N-CH_3), 5.77 (1H, s, C_4-H), 11.90 (1H, s, C_9-OH), 13.20 (1H, br, N-H), 13.30 ppm (1H, s, C_7-OH); ms *m/e* 357 (M^+, base peak), 342 (*M* − 15), 260, 233, 232, 217, 215. *Anal.* calcd. for $C_{19}H_{19}O_6N$: C 63.87, H 5.32, N 3.92; found: C 63.91, H 5.49, N 3.62. High resolution molecular weight determination: calcd.: 357.121; found: 357.121.

Preparative layer chromatography (silica gel, ethyl acetate) purification of the mother liquors yielded a second compound, (+)-*N*′-methylimino-*N*-methyl-$\Delta^{2,11}$-enaminousnic acid (**4**) (12 mg, 0.032 mmol; 2%), bright yellow prisms from ethyl alcohol, mp 198–200 °C; $[\alpha]_D^{26}$ +94° (*c* 0.04215); uv (CH_3CN) λ_{max} (log ϵ) 300 (4.13), 250 (3.96), 234 (4.05); ir ν_{max} 3600–3100 (OH, NH, chelated), 1700 (C=O, ketoenamine system), 1630 (C=N, chelated; C=C, enol ether, aromatic ring), 1560 (C=O, chelated ketoenamine system); pmr δ 1.70 (3H, s, C_{9b}-CH_3), 2.14 (3H, s, C_8-CH_3), 2.56 (3H, s, C_{11}-CH_3), 2.66 (3H, s, C_{13}-CH_3), 3.18 (3H, d, J = 5 Hz, N-CH_3), 3.30 (3H, s, N′-CH_3), 5.80 (1H, s, C_4-H), 11.90 (1H, s, C_9-OH), 13.20 (1H, br, N-H), 13.30 ppm (1H, s, C_7-OH); ms *m/e* 370 (M^+), 355 (*M* − 15), 273 (base peak), 245, 230, 228. *Anal.* calcd. for $C_{20}H_{22}O_5N_2$: C 64.84, H 5.98, N 7.56; found: C 64.59, H 5.91, N 7.49. High resolution molecular weight determination: calcd.: 370.153; found: 370.153.

*III. Ethylamine. Formation of (+)-N-Ethyl-$\Delta^{2,11}$-enaminousnic Acid (**5**) (6-Acetyl-7,9-dihydroxy-8,9bα-dimethyl-2-ethylid-2,11-ene-1,9b,2,3-tetrahydro-11-N-ethylamino-1,3-dioxodibenzofuran)*

A suspension of (+)-usnic acid (**1**) (500 mg, 1.453 mmol) in absolute ethyl alcohol (10 ml) was treated with 70% aqueous ethylamine (0.3 ml), and heated to reflux under nitrogen atmosphere for 1.5 h. The reaction mixture was concentrated under reduced pressure, acidified with 1 *N* hydrochloric acid, and extracted with ethyl acetate (3 × 15 ml). The combined extracts were washed with water (2 × 20 ml), dried over anhydrous sodium sulfate, and evaporated to produce a yellow glassy material (527 mg) which showed several spots on tlc. Purification of this material by preparative layer chromatography on silica gel – oxalic acid (solvent system *B*) afforded (+)-*N*-ethyl-$\Delta^{2,11}$-enaminousnic acid (**5**) (380 mg, 1.024 mmol; 70.5%), pale yellow plates from chloroform–methanol, mp 133–134 °C; $[\alpha]_D^{26}$ +365° (*c* 0.14825); uv (CH_3CN) λ_{max} (log ϵ) 348 (3.56), 294 (4.38); ir ν_{max} 3700–2500 (OH, NH, chelated), 1705 (C=O, ketoenamine system), 1630 (C=O, chelated aromatic acetyl), 1600 (C=C), 1570 (C=O, chelated ketoenamine system); pmr δ 1.38 (3H, t, J_{AM} = 7.5 Hz, J_{AX} = 0 Hz, —CH_2—CH_3), 1.65 (3H, s, C_{9b}-CH_3), 2.03 (3H, s, C_8-CH_3), 2.59 (3H, s, C_{11}-CH_3), 2.61 (3H, s, C_6-$COCH_3$), 3.52 (2H, octet, J_{AM} = 7.5 Hz, J_{MX} = 5 Hz, —CH_2—CH_3), 5.72 (1H, s, C_4-H), 11.91 (1H, s, C_9-OH), 13.26 (1H, br, N-H), 13.30 ppm (1H, s, C_7-OH); ms *m/e* 371 (M^+), 356 (*M* − 15), 260 (base peak), 232, 217, 113. *Anal.* calcd. for $C_{20}H_{21}O_6N$: C 64.69, H 5.70, N 3.77; found: C 64.51, H 5.64, N 3.79. High resolution molecular weight determination: calcd.: 371.137; found: 371.134.

*IV. Benzylamine. Formation of (+)-N′-Benzylimino-N-benzyl-$\Delta^{2,11}$-enaminousnic Acid (**6**) (7,9-Dihydroxy-8,9bα-dimethyl-6-ethyl-2-ethylid-2,11-ene-1,9b,2,3-tetrahydro-13-N-benzylimino-11-N-benzylamino-1,3-dioxodibenzofuran)*

A suspension of (+)-usnic acid (**1**) (1.0 g, 2.906 mmol) in absolute ethyl alcohol (20 ml) was treated with 98% benzylamine (1.2 ml, 8.684 mmol) and refluxed under nitrogen for 3 h. The reaction mixture was then diluted with distilled water (5 ml) and the precipitate filtered. Recrystallization from chloroform – ethyl alcohol produced (+)-*N*′-benzylimino-*N*-benzyl-$\Delta^{2,11}$-enaminousnic acid (**6**) (1.25 g, 2.394 mmol; 82%); bright yellow needles, mp 197–198 °C; $[\alpha]_D^{26}$ +262° (*c* 0.058); uv (CH_3CN) λ_{max} (log ϵ) 301 (4.23); ir ν_{max} 3600–2500 (OH, NH, chelated), 1695 (C=O, ketoenamine system), 1620 (C=N, chelated), 1590 (C=C, aromatic rings), 1560 (C=O, chelated ketoenamine system); pmr δ 1.68 (3H, s, C_{9b}-CH_3), 2.08 (3H, s, C_8-CH_3), 2.55 (3H, s, C_{11}-CH_3),

Can. J. Chem. Downloaded from www.nrcresearchpress.com by 210.87.254.42 on 09/05/12
For personal use only.

2.65 (3H, s, C_{13}-CH_3), 4.65 (2H, d, J = 6 Hz, N—CH_2—C_6H_5), 4.76 (2H, s, N′—CH_2—C_6H_5), 5.72 (1H, s, C_4-H), 7.37 (10H, s, N,N′—CH_2—C_6H_5), 11.35 (1H, s, C_9-OH), 11.95 (1H, br, C_7-OH), 16.85 ppm (1H, br, N-H); ms *m/e* 522 (M^+), 349 (base peak), 216, 202, 188, 187, 174, 134, 106, 91. *Anal.* calcd. for $C_{32}H_{30}O_5N_2$: C 73.54, H 5.85, N 5.36; found: C 73.06, H 5.79, N 5.39. High resolution molecular weight determination: calcd.: 522.309; found: 522.311.

V. o-Phenylenediamine. Preparation of (+)-N-1′-(2′-Aminophenyl)-$\Delta^{2,11}$-enaminousnic Acid ***(12)*** *(6-Acetyl-7,9-dihydroxy-8,9bα-dimethyl-2-ethylid-2,11-ene-1,9b,2,3-tetrahydro-11-N-1′-(2′-aminophenyl)-1,3-dioxodibenzofuran)*

A suspension of (+)-usnic acid (**1**) (1.0 g, 2.906 mmol) in absolute ethyl alcohol (40 ml) was treated with *o*-phenylenediamine (0.320 g, 2.962 mmol) and heated to reflux under nitrogen atmosphere for 4 h. The reaction mixture was concentrated under reduced pressure and the precipitate filtered. Recrystallization from chloroform – ethyl alcohol and purification of the resulting mother liquors by preparative chromatography (silica gel – oxalic acid plates, ethyl acetate) produced (+)-*N*-1′-(2′-aminophenyl)-$\Delta^{2,11}$-enaminousnic acid (**12**) (1.191 g, 2.744 mmol; 94%), pale yellow crystals, mp 185–186 °C; $[\alpha]_D^{27}$ (CH_3CN) +266° (*c* 0.030); uv (CH_3CN) λ_{max} 349 (3.76), 293 (4.20), 228 (4.24); ir ν_{max} 3500, 3415 (Ar-NH_2), 3300–2400 (OH, NH, chelated), 1695 (C=O, ketoenamine system), 1625 (C=O), chelated aromatic acetyl; C=C of enol ether, aromatic ring), 1540 (C=O, chelated ketoenamine system); pmr δ 1.70 (3H, s, C_{9b}-CH_3), 2.07 (3H, s, C_8-CH_3), 2.56 (3H, s, C_{11}-CH_3), 2.65 (3H, s, C_6-$COCH_3$), 4.09, (2H, br, N—C_6H_4—NH_2), 5.79 (1H, s, C_4-H), 6.90 (4H, m, N—C_6H_4—NH_2), 11.62 (1H, s, C_9-OH), 13.30 (1H, s, C_7-OH), 14.39 ppm (1H, br, N-H); ms *m/e* 434 (M^+), 419 (M − 15), 302, 260, 232, 217, 214, 201, 175, 133 (base peak), 92, 77, 65. *Anal.* calcd. for $C_{24}H_{22}O_6N_2$: C 66.34, H 5.10, N 6.64; found: C 66.19, H 5.25, N 6.41. High resolution molecular weight determination: calcd.: 434.148; found: 434.145.

VI. o-Phenylenediamine. Preparation of (+)-1H-[Benzodiazepino[3,4-b]usnic Acid ***(13)*** *(14-Acetyl-11,13-dihydroxy-2a,9a,10,10a-tetrahydro-9,10aα,12-trimethyl-10-oxo-1H-[1,5]benzodiazepino[3,4-b]-dibenzofuran*

A suspension of (+)-*N*-2′-(1′-aminophenyl)-$\Delta^{2,11}$-enaminousnic acid (**12**) (100 mg, 0.230 mmol) in absolute ethyl alcohol (9 ml) was treated with concentrated hydrochloric acid (1 ml) and allowed to stand at room temperature with occasional shaking for 4 h. The resulting deep red reaction mixture was poured into cold saturated sodium bicarbonate solution (20 ml) and the product isolated by extraction with ethyl acetate (3 × 15 ml). The combined extracts were washed with water, dried over anhydrous sodium sulfate, and evaporated under reduced pressure. The red residue (87 mg) was recrystallized twice from ethyl acetate – ethyl alcohol to produce bright red needles of (+)-1*H*-[1,5]benzodiazepino[3,4-*b*]usnic acid (**13**) (78.5 mg, 0.188 mmol; 82%), which decompose without melting at 180 °C; $[\alpha]_D$ (CH_3CN) +920° (*c* 0.025); uv (CH_3CN) λ_{max} (log ϵ) 370 (3.09), 305 (4.13), 288 (4.13), 226 (4.10); ir ν_{max} 3340 (N-H), 3050–2800 (OH, chelated), 1700 (C=O), 1630 (C=O, chelated aromatic acetyl; C=C, enol ether, aromatic ring), 1580 (C=C, aromatic ring); pmr ($CDCl_3$–DMSO-d_6) δ 1.65 (3H, s, C_{9b}-CH_3), 2.03 (3H, s, C_{11}-CH_3), 2.66 (3H, s, C_6-$COCH_3$), 6.16 (1H, s, C_4-H), 7.00 (4H, m, C_6H_4), 9.72 (1H, br, N-H), 12.25 (1H, s, C_9-OH), 13.35 ppm (1H, s, C_7-OH); ms *m/e* 416 (M^+, base peak), 401 (M − 15), 387, 373, 284, 241, 133, 83, 77, 67. *Anal.* calcd. for $C_{24}H_{20}O_5N_2$: C 69.21, H 4.84, N 6.72; found: C 69.71, H 4.80, N 6.59. High resolution molecular weight determination: calcd.: 416.137; found: 416.135.

Condensation of (−)-Dihydrousnic Acid ***(14)*** *with o-Phenylenediamine. Formation of (−)-N-1′-(2′-Aminophenyl)-$\Delta^{2,11}$-enaminodihydrousnic Acid* ***(15)*** *(6-Acetyl-7,9-dihydroxy-8,9bα-dimethyl-2-ethylid-2,11-ene-1,9b,2,3,4,4a-hexahydro-11-N-1′-(2′-aminophenyl)-1,3-dioxodibenzofuran)*

A suspension of (−)-dihydrousnic acid (**14**) (250 mg, 0.722 mmol) in absolute ethyl alcohol (20 ml) was treated with *o*-phenylenediamine (80 mg, 0.740 mmol), and heated to reflux under nitrogen atmosphere for 2.75 h. Upon concentration of the reaction mixture precipitation was observed. The solid material was then removed by filtration and purified by repeated crystallizations from chloroform – ethyl ether to yield pure (−)-*N*-1′-(2′-aminophenyl)-$\Delta^{2,11}$-enaminodihydrousnic acid (**15**) (300 mg, 0.688 mmol; 95%), rectangular pale yellow prisms, mp 179–181 °C; $[\alpha]_D^{27}$ (CH_3CN) −279° (*c* 0.0715); uv (CH_3CN) λ_{max} 342 (3.76), 293 (4.21), 230 (4.15); ir ν_{max} 3500, 3400 (Ar-NH_2), 3000–2890 (OH, NH, chelated), 1660 (C=O, ketoenamine system), 1620 (C=O, chelated aromatic acetyl; C=C, aromatic ring), 1545 (C=O, chelated ketoenamine system); pmr δ 1.70 (3H, s, C_{9b}-CH_3), 2.05 (3H, s, C_8-CH_3), 2.48 (3H, s, C_{11}-CH_3), 2.60 (3H, s, C_6-CH_3), 3.01 (2H, d, J = 5 Hz, C_4-H_2), 3.80 (2H, br, N—C_6H_4—NH_2), 4.86 (1H, t, J = 5 Hz, $C_{4a\alpha}$-H), 6.92 (4H, m, C_6H_4), 10.30 (1H, s, C_9-OH), 13.40 (1H, s, C_7-OH), 14.20 ppm (1H, br, N-H); ms *m/e* 436 (M^+), 421 (M − 15), 276, 233, 203, 133 (base peak), 131, 92. *Anal.* calcd. for $C_{24}H_{24}O_6N_2$: C 66.04, H 5.54, N 6.41; found: C 65.95, H 5.62, N 6.34. High resolution molecular weight determination: calcd.: 436.163; found: 436.161.

Preparation of (−)-Dihydrousnic Acid ***(14)*** *(2,6-Diacetyl-8,9bα-dimethyl-1,9b,4,4a-tetrahydro-3,7,9-trihydroxy-1-oxodibenzofuran)*

(+)-Usnic acid (**1**) (2.0 g, 5.813 mmol) was dissolved in dry tetrahydrofuran (80 ml) and hydrogenated over Palladium-black catalyst (400 mg) at atmospheric pressure. After the uptake of 1 equiv. hydrogen, the reaction mixture was filtered through Celite, the solvent evaporated under reduced pressure, and the residue crystallized from ethyl alcohol to produce pure (−)-dihydrousnic acid (**14**) 2.01 g, 5.809 mmol; 99%), mp 150–151 °C (lit. (31) mp 149 °C); $[\alpha]_D^{27}$ (CH_3CN) −83° (*c* 0.30) (lit. (31) $[\alpha]_D^{24}$ −85°); uv λ_{max} (log ϵ) 337 (3.44), 283 (4.38), 227 (4.19); ir ν_{max} 3600–2900 (OH, chelated), 1680, 1635 (C=O, enone system), chelated aromatic acetyl; C=C, aromatic ring); pmr (60 MHz) δ 1.70 (3H, s, C_{9b}-CH_3), 2.06 (3H, s, C_8-CH_3), 2.60 (3H, s, C_2-$COCH_3$), 2.64 (3H, s, C_6-$COCH_3$), 3.10 (2H, d, J = 5 Hz, C_4-H_2), 4.86 (1H, t, J = 5 Hz, $C_{4a\alpha}$-H), 9.50 (1H, s, C_9-OH), 13.45 (1H, s, C_7-OH), 18.25 ppm (1H, br, C_3-OH); ms *m/e* 346 (M^+,

base peak), 318, 233, 220, 215, 205, 177. *Anal.* calcd. for $C_{18}H_{18}O_7$: C 62.42, H 5.23; found: C 62.49, H 5.30. High resolution molecular weight determination: calcd.: 346.105; found: 346.105.

Acknowledgement

Financial aid from the National Research Council of Canada is gratefully acknowledged. One of us (I.H.S.) wishes to thank the NRCC for a scholarship during the period of this study.

1. Y. ASAHINA and S. SHIBATA. Chemistry of lichen substances. Japan society for the promotion of science. Tokyo, Japan. 1954. p. 171.
2. F. M. DEAN. Naturally occurring oxygen ring compounds. Butterworths, London. 1963. p. 148.
3. C. F. CULBERSON. Chemical and botanical guide to lichen products. The University of North Carolina Press, Chapel Hill, North Carolina. 1969. p. 171.
4. C. F. CULBERSON. Bryologist, **73**, 201 (1970).
5. J. F. W. MCOMIE. Advances in organic chemistry: methods and results. Vol. 3. Interscience Publishers, New York, N.Y. 1963. p. 191.
6. O. E. VIRTANEN, H. VIITANEN, and A. E. KORTEKANGAS. Suom. Kemistil. B, **27**, 18 (1954).
7. O. E. VIRTANEN and M. VAHATAB. Suom. Kemistil. B, **29**, 30 (1956).
8. S. K. MANAKTALA, S. NEELAKANTAN, and T. R. SESHADRI. Ind. J. Chem. **5**, 29 (1967).
9. O. WIDMAN. Ann. **324**, 139 (1902).
10. C. SCHOPF and K. HEUCK. Ann. **459**, 233 (1927).
11. C. SCHOPF and F. ROSS. Ann. **546**, 1 (1941).
12. A. A. AKHREM, A. M. MOISEENKOV, F. A. LACHWICZ, M. B. ANDABURSKA, A. V. MCHITARYAN, T. N. SEDLETSKAYA, and V. A. PETUCHOV. Izv. Akad. Nauk. SSSR, Ser. Khim. 594 (1971).
13. A. A. AKHREM, A. M. MOISEENKOV, A. I. POSELIONOV, V. A. PETOCHOV, and V. S. BOGDANOV. Izv. Akad. Nauk. SSSR, Ser. Khim. 1746 (1971).
14. S. MACKENZIE. J. Am. Chem. Soc. **77**, 2214 (1955).
15. G. STORK. Chem. Ind. (London), 915 (1955).
16. L. BERTILSSON and C. A. WACHTMEISTER. Acta Chem. Scand. **22**, 1791 (1968).
17. S. GHOSAL, R. K. CHAUDHURI, M. P. TIWARI, A. K. SINGH, and F. W. WEHRLI. Tetrahedron Lett. 403 (1974).
18. G. BUCHI and J. VEDERAS. J. Am. Chem. Soc. **94**, 9128 (1972).
19. S. FORSEN, M. NILSSON, and C. A. WACHTMEISTER. Acta Chem. Scand. **16**, 583 (1962).
20. R. K. SHARMA. Diss. Abstr. **24**, 4417 (1964).
21. J. P. KUTNEY, I. H. SANCHEZ, and T. YEE. Org. Mass Spectrom. **8**, 129 (1974).
22. F. D. POTT and A. C. NOBLE. Adv. Heterocycl. Chem. **8**, 21 (1967).
23. S. GARATTIRI, E. MUSSINI, and L. O. RANDALL. The benzodiazepines. Raven Press, New York, N.Y. 1973.
24. J. THIELE and G. STEIMMIG. Chem. Ber. **40**, 935 (1907).
25. W. RIED and W. HOHNE. Chem. Ber. **87**, 1801 (1954).
26. I. L. FINAR. J. Chem. Soc. 4094 (1958).
27. J. A. BARLTROP, C. G. RICHARDS, D. M. RUSSELL, and G. RYBACK. J. Chem. Soc. 1132 (1959).
28. T. KAMETANI, M. IHARA, and K. TAKAHASHI. Chem. Pharm. Bull. Jpn. **20**, 1588 (1972).
29. Y. ASAHINA, M. YANAGITA, and S. MAYEDA. Chem. Ber. **70**, 1500 (1937); **70**, 2462 (1937).
30. A. M. PATTERSON, L. T. CAPELL, and D. F. WALKER. The ring index. 2nd ed. American Chemical Society, Washington, D.C. 1960. p. 388.
31. S. SHIBATA, K. TAKAHASHI, and Y. TANAKA. Chem. Pharm. Bull. Jpn. **4**, 65 (1956).

Can. J. Chem. Downloaded from www.nrcresearchpress.com by 210.87.254.42 on 09/05/12
For personal use only.

8-Oxo-8*H*-1,2,4,-oxadiazolo[2,3-*i*]purines

JOHN P. DEVLIN
Pharma Research Canada Ltd., Pointe Claire, Que., Canada H9R 1G8

Received May 20, 1975[1]

JOHN P. DEVLIN. Can. J. Chem. **54**, 2804 (1976).

The preparation of 8-oxo-8*H*-1,2,4-oxadiazolo[2,3-*i*]purines (**1**) and their mass spectral fragmentation patterns are described. Novel imidazol-5-yl-4*H*-1,2,4-oxadiazol-5-ones (**5**) are formed upon acid hydrolysis of **1**.

JOHN P. DEVLIN. Can. J. Chem. **54**, 2804 (1976).

On décrit la synthèse des oxo-8 8*H*-oxadiazolo-1,2,4 [2,3-*i*]purines (**1**) ainsi que leurs patrons de fragmentation en spectrométrie de masse. Par hydrolyse en milieu acide de **1** on obtient de nouvelles imidazole-5-yl 4*H*-oxadiazole-1,2,4 ones-5 (**5**).

[Traduit par le journal]

Studies directed at the development of potential immunosuppressive agents have led us to investigate novel modifications of the purine base, adenine. To this end we have prepared 8-oxo-8*H*-1,2,4-oxadiazolo[2,3-*i*]purine (**1***a*) by the condensation of adenine-1-*N*-oxide (1) with ethyl chloroformate in pyridine. The chemistry and spectral properties of this compound and the 3-benzyl analogue (**1***b*) is herein presented.

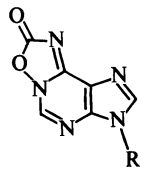

1*a* R = H
1*b* R = $C_6H_5CH_2$

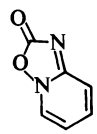

2

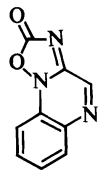

3

6-Oxo-1,2,4-oxadiazolo[2,3-*a*]pyridine (**2**) has been prepared (2) by thermolysis of 2-(ethoxycarbamoyl)pyridine-1-oxide at 150 °C; 2-oxo-1,2,4-oxadiazolo[2,3-*a*]quinoxaline (**3**) was similarly obtained (3). The oxadiazolo-purines (**1**) were formed directly from the appropriate adenine-1-*N*-oxide in high yield by reaction with ethyl chloroformate in pyridine.

4-Aminoimidazole-5-carboxamidoxime (**4**) is rapidly and quantitatively formed (4) by heating adenine-1-*N*-oxide in hydrochloric acid under reflux. With this behaviour in mind we were encouraged to investigate the acid stability of the oxadiazolo-purines (**1**). At room temperature in dilute aqueous acid **1***a* yielded 3-(4-formamidoimidazol-5-yl)-4*H*-1,2,4-oxadiazol-5-one (**5***a*) which subsequently provided **5***b* when heated under reflux in methanolic hydrogen chloride. Compound **1***b* was unaffected by dilute aqueous acid; however, in methanolic hydrogen chloride the oxadiazole **5***c* was formed in low yield. The identities of these degradation products were established by spectral and analytical data as well as by the positive (imidazoyl derivatives) Pauly tests (5) which were observed.

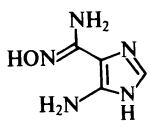

4

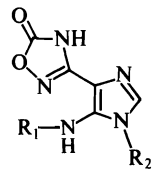

5*a* R_1 = CHO R_2 = H
5*b* R_1 = H R_2 = H
5*c* R_1 = H R_2 = $C_6H_5CH_2$

The relative intensities of the higher mass ions in the mass spectra of compounds **1***a* and **1***b* are presented in Table 1. The fragmentation pattern outlined in Scheme 1 is suggested. The formation of the $M - 16$ fragment is of interest in that both the intermediary ions **6** and **7** may be considered.

Experimental

Melting points were determined on a Reichert Kofler Micro Heating Stage and are uncorrected. Ultraviolet

[1]Revision received May 21, 1976.

Can. J. Chem. Downloaded from www.nrcresearchpress.com by 210.87.254.5 on 09/05/12
For personal use only.

Can. J. Chem. Downloaded from www.nrcresearchpress.com by 210.87.254.5 on 09/05/12
For personal use only.

spectra were recorded in ethanol solution on a Bausch and Lomb Spectronic 505 and ir spectra (KBr pellet) on a Perkin-Elmer 237B spectrophotometer. Nuclear magnetic resonance spectra were taken on a Varian T-60 spectrometer. Tetramethylsilane was used as an internal standard. Mass spectra were recorded by Morgan Schaeffer Corporation, Montreal, Quebec, with a Hitachi–Perkin-Elmer RMU-6D spectrometer at an ionization potential of 70 eV using the direct probe technique. Elemental analyses were determined by Microanalyses Laboratories Ltd., Toronto.

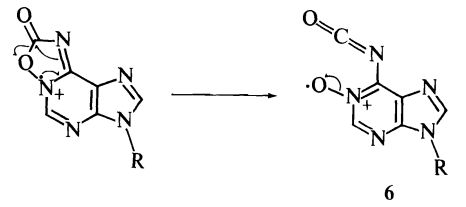

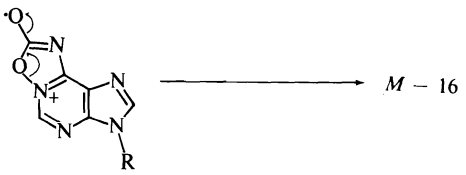

TABLE 1. Higher mass ions in the mass spectra of compounds **1***a* and **1***b*

Compound **1***a*		Compound **1***b*		
m/e	%*	*m/e*	%*	Assignment†
177	15	267	100	M^+
161	3	251	3	*a*
		250	2	*a* − H
135	100	225	37	*b*
		224	38	*b* − H
119	4	209	2	*c*
108	35	198	1	*b* − CN
92	3	182	8	*c* − CN

*Relative abundance.
†See Scheme 1.

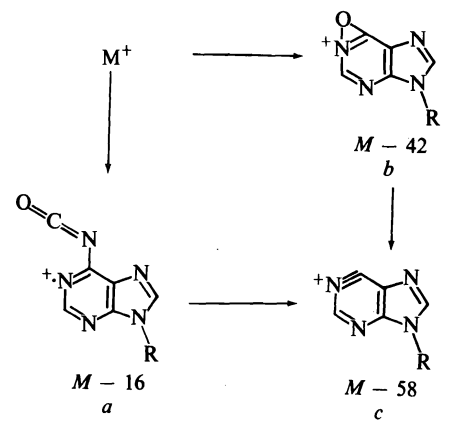

SCHEME 1

*8-Oxo-8H-1,2,4-oxadiazolo[2,3-i]purine (**1a**)*

Ethyl chloroformate (40 g, 0.46 mol) was added dropwise to a vigorously stirred suspension of adenine-1-*N*-oxide (30 g, 0.32 mol) in pyridine (750 ml) while the temperature was kept below 20 °C with external cooling. When the addition was complete (15 min), the reaction mixture was stirred at room temperature for 24 h, after which the gelatinous mass was heated to 95 °C and maintained at this temperature for 2 h. The resulting red solution was concentrated to 200 ml and cooled. The insoluble material was collected and washed with cold pyridine (20 ml) and ether (2 × 50 ml). The crude product was shaken with water (150 ml) and the insoluble solid was collected and air dried to provide the title compound (52 g, 92%). Recrystallization from dimethylformamide–ethanol afforded colorless prisms, mp 248–249 °C, λ_{max} 260 (log ϵ 4.03), 277 nm (log ϵ 4.05); ν_{max} 1802, 1775, 1640 cm^{-1}; nmr (CD_3SOCD_3) δ 8.59 (s, 1H), 9.42 (s, 1H). *Anal.* calcd. for $C_6H_3O_2N_5$: C 40.69, H 1.71, N 39.54; found: C 41.13, H 1.78, N 39.40.

*3-Benzyl-8-oxo-8H-1,2,4-oxadiazolo[2,3,-i]purine (**1b**)*

The title compound (9.0 g, 90%), mp 195–198 °C (from acetone), was obtained when 9-benzyladenine-1-*N*-oxide (6) (9.0 g, 0.038 mol) in pyridine was treated with ethyl chloroformate (4.85 g, 0.045 mol) in the manner described for the synthesis of compound **1***a*. λ_{max} 260 (log ϵ 4.00), 270 (log ϵ 4.20), 277 nm (log ϵ 4.18); ν_{max} 1815, 1655, 1545, 1512, 1499 cm^{-1}; nmr (CD_3SOCD_3) δ 5.57 (s, 2H), 7.38 (s, 5H), 8.73 (s, 1H), 9.48 (s, 1H). *Anal.* calcd. for $C_{13}H_9O_2N_5$: C 58.42, H 3.39, N 26.21; found: C 58.59, H 3.45, N 26.60.

*3-(4-Formamidoimidazol-5-yl)-4H-1,2,4-oxadiazol-5-one (**5a**)*

A suspension of compound **1***a* (13.0 g, 0.0735 mol) in 0.1 *N* hydrochloric acid (1000 ml) was stirred at room temperature for 24 h. The insoluble solid was collected and washed with water (50 ml) and acetone (50 ml). Recrystallization from dimethylformamide provided the title compound as colorless needles (9.1 g, 64%), mp > 350 °C; ν_{max} 1775, 1760, 1675, 1630 cm^{-1}; nmr (CD_3SOCD_3) δ 7.68 (s, 1H, C2-H), 8.33 (s, 1H, CHO). *Anal.* calcd. for $C_6H_5N_5O_3$: C 36.93, H 2.58, N 35.89; found: C 37.06, H 2.43, N 35.61.

*3-(4-Aminoimidazol-5-yl)-4H-1,2,4-oxadiazol-5-one (**5b**)*

A suspension of compound **5***a* (7.0 g, 0.036 mol) in methanol (250 ml) containing hydrogen chloride (1.5 g, 0.041 mol) was heated under reflux for 1 h. The reaction mixture was cooled and the insoluble solid (5.8 g) was collected and recrystallized from methanol–ether to provide the title compound, as the hydrochloride (4.0 g, 55%), mp 200 °C (chars); λ_{max} 276 nm (log ϵ 3.99); ν_{max} 1775, 1730, 1650, 1635 cm^{-1}; nmr (CD_3SOCD_3) δ 8.75

(s, 1H, C2-H). *Anal.* calcd. for $C_5H_5N_5O_2 \cdot HCl$: C 29.49, H 2.97, N 34.40, Cl 17.42; found: C 29.64, H 3.11, N 34.20, Cl 16.80.

*3-(3-Benzyl-4-aminoimidazol-5-yl)-4H-1,2,4-oxadiazol-5-one (**5c**)*

A suspension of compound **1***b* (2.8 g, 0.0105 mol) in methanol (100 ml) containing hydrogen chloride (0.44 g, 0.012 mol) was heated under reflux for 1 h. The resulting solution was cooled, filtered, and evaporated to dryness. The residue was recrystallized from acetone to provide the title compound, mp 211–214 °C (0.6 g, 22%); λ_{max} 276 nm (log ϵ 4.24); ν_{max} 1745, 1630, 1596 cm^{-1}; nmr (CD_3SOCD_3) δ 4.83 (br s, 2H, $—NH_2$), 5.17 (s, 2H, $—CH_2—$), 5.73 (br s, 1H, —CONH—), 7.31 (s, 5H, $C_6H_5—$), 7.38 (s, 1H, C2-H). *Anal.* calcd. for $C_{12}H_{11}O_2N_5$: C 56.02, H 4.31, N 27.23; found: C 56.01, H 4.42, N 27.39.

Acknowledgment

The author gratefully acknowledges the technical assistance of Mrs. I. Guse.

1. M. A. Stevens, D. I. Magrath, H. W. Smith, and G. B. Brown. J. Am. Chem. Soc. **80**, 2755 (1958).
2. A. R. Katritzky. J. Chem. Soc. 2063 (1956); 4385 (1957).
3. R. A. Burrell, J. M. Cox, and E. G. Savins. J. Chem. Soc. 2707 (1973).
4. M. A. Stevens and G. B. Brown. J. Am. Chem. Soc. **80**, 2759 (1958).
5. H. Pauly. Z. Physiol. Chem. **42**, 508 (1904).
6. T. Fujii, C. C. Wu, T. Itaya, and S. Yamada. Chem. Ind. 1598 (1966).

Can. J. Chem. Downloaded from www.nrcresearchpress.com by 210.87.254.5 on 09/05/12
For personal use only.

Pulse radiolytic formation of solvated electrons in hydrazine[1]

WILLIAM ARTHUR SEDDON, JOHN WALLACE FLETCHER, AND FRED CHARLES SOPCHYSHYN

Physical Chemistry Branch, Atomic Energy of Canada Limited, Chalk River Nuclear Laboratories, Chalk River, Ont., Canada K0J 1J0

Received April 20, 1976

WILLIAM ARTHUR SEDDON, JOHN WALLACE FLETCHER, and FRED CHARLES SOPCHYSHYN. Can. J. Chem. **54**, 2807 (1976).

The spectrum and yield of solvated electrons in anhydrous hydrazine have been investigated by pulse radiolysis. At room temperature the optical absorption band has a maximum at 1.22 eV (1015 nm) with a molar extinction coefficient of $2.2 \pm 0.1 \times 10^4 M^{-1}$ cm^{-1} and a temperature coefficient of 1.5×10^{-3} eV deg^{-1} from 7–45 °C. The oscillator strength is estimated to be 0.6. The optical transition energy is in reasonable agreement with an empirical correlation of solvent properties proposed by Freeman provided that only the polarisability of the nitrogen lone-pair electrons contribute to E_{max}. Comparisons are made with liquid amides which also have lone-pair polarisable groups and with water and liquid ammonia which have physiçal properties very similar to hydrazine. Electron yields increase from $G_{e_s^-} = 2.35 \pm 0.15$ in pure hydrazine to 2.65 ± 0.15 in basic solutions containing $\geqslant 0.1$ *M* sodium hydrazide.

WILLIAM ARTHUR SEDDON, JOHN WALLACE FLETCHER et FRED CHARLES SOPCHYSHYN. Can. J. Chem. **54**, 2807 (1976).

Le spectre et le rendement des électrons solvatés dans l'hydrazine anhydre ont été étudiés par radiolyse à impulsion. A température de la pièce la bande d'absorption optique présente un maximum à 1.22 eV (1015 nm) avec un coefficient d'extinction molaire de $2.2 \pm 0.1 \times 10^4 M^{-1}$ cm^{-1} et un coefficient de température de 1.5×10^{-3} eV deg^{-1} entre 7 et 45 °C. La force d'oscillateur est évaluée à 0.6. L'énergie de la transition optique donne un accord raisonnable avec une corrélation empirique des propriétés du solvant proposée par Freeman, pourvu que seulement la polarisabilité de la paire d'électrons libres de l'azote contribue au E_{max}. Des comparaisons sont faites avec des amides liquides qui ont aussi des groupements polarisables à doublets libres et avec l'eau et l'ammoniac liquide qui ont des propriétés physiques très similaires à l'hydrazine. Les rendements des électrons augmentent de $G_{e_s} = 2.35 \pm 0.15$ dans l'hydrazine pure à 2.65 ± 0.15 en solution basique contenant des quantités $\geqslant 0.1$ *M* d'hydrazide de sodium.

[Traduit par le journal]

Introduction

Optical properties of solvated electrons are now well established in a wide range of solvents of differing molecular structure and dielectric properties (1–4). Hydrazine is an interesting solvent in that its physical properties resemble both water and liquid ammonia. It is a highly polar solvent with a dielectric constant of 51.7 and a dipole moment of 1.85 D (6.17×10^{-24} C m) at 25 °C (5, 6). Alkali metals are readily soluble in hydrazine but unlike liquid ammonia (3, 4, 7, 8) do not produce stable blue solutions. However, on dissolution an intense blue color is observed at the surface of an alkali metal indicating the transient formation of solvated electrons. Surprisingly, little information exists on the optical properties of e_s^- in hydrazine although an absorption band with no clearly defined maximum below 1100 nm has been reported (9). This paper discusses our observations on the spectrum and properties of e_s^- in hydrazine and compares the data with an empirical correlation proposed by Freeman (10).

Experimental

Details of the pulse radiolysis facilities and solution handling techniques have been described elsewhere (11–13). Hydrazine (>95%, Eastman Kodak Co.) was dried over BaO, redistilled under vacuum, and followed by further reaction with sodium until an intense blue color persisted at the metal surface. After a further distillation the hydrazine was assumed to be anhydrous.

Results and Discussion

Spectrum

Figure 1 shows the transient optical spectrum observed at 20 °C immediately after a 0.3 μs pulse in pure hydrazine and in solutions containing 0.1 *M* sodium hydrazide. Within experi-

[1]AECL No. 5489.

Can. J. Chem. Downloaded from www.nrcresearchpress.com by 210.87.254.5 on 09/05/12
For personal use only.

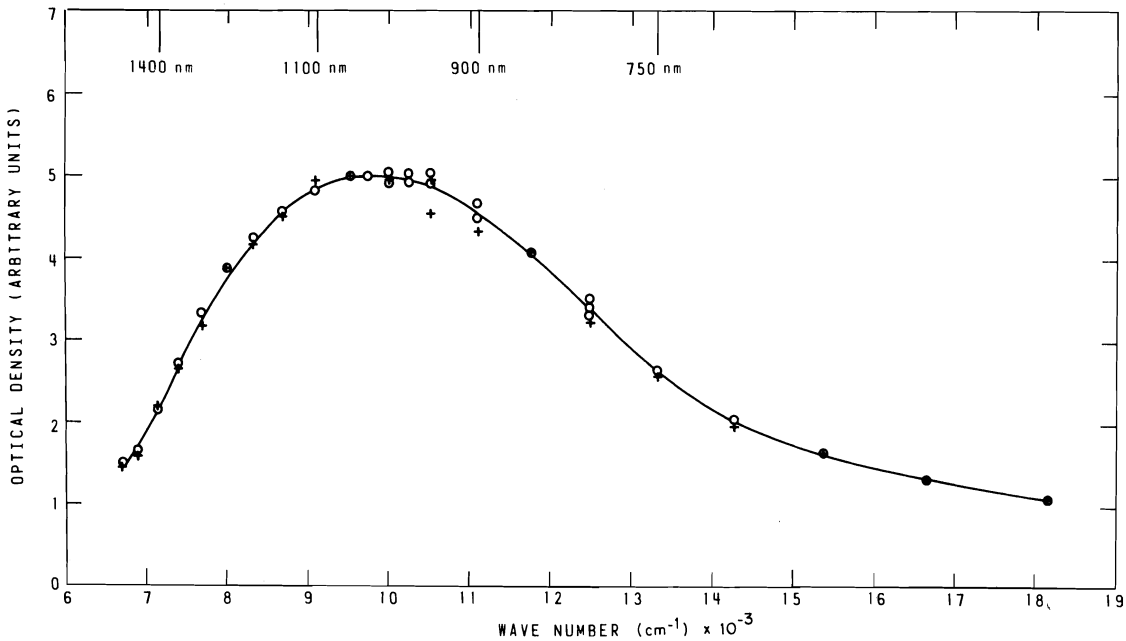

FIG. 1. Optical absorption spectrum observed immediately after the pulse in hydrazine: ○, pure hydrazine; + solutions containing 0.1 *M* sodium hydrazide.

mental error, identical spectra were obtained at intermediate concentrations of the solvent base or in solutions saturated with NaOH. The band maxima occurs at 9850 cm^{-1} (1015 nm) with a width at half height, $\Delta\nu_{1/2}$, of 6100 $\pm$ 100 cm^{-1}. Increasing the temperature shifts the maximum towards lower energies with a temperature coefficient of $-1.5 \pm 0.2 \times 10^{-3}$ eV deg^{-1} (-12 ± 2 cm^{-1} deg^{-1}) over the range 7–45 °C. In the presence of biphenyl as an electron scavenger the absorption band is eliminated completely with the concomitant formation of the biphenyl radical anion.

The above behaviour is characteristic of e_s^- in a variety of polar solvents (14–21) and taken in conjunction with the earlier report (9) leaves little doubt that the spectrum in Fig. 1 arises from e_s^- in hydrazine.

Freeman (10) has correlated the optical absorption maximum, E_{max} (eV), for e_s^- in a number of amines, ethers, alcohols, ammonia, and water with the expression $D_s d g_k^3 \alpha_p$ where D_s is the static dielectric constant of the liquid, d is the density, g_k is the Kirkwood correlation parameter (22, 23), and α_p is the polarisability of the polar group in the molecule. The factor g_k indicates the extent to which molecules align themselves with respect to their neighbours. A value greater than 1 indicates a greater local polarity in the microscopic regions of the liquid than would be expected simply from the dipole moment. Values of g_k are calculated from [1] (10).

$$[1] \quad [(D_s - 1)(2D_s + 1)/9D_s](M/d) = 4\pi N/3[\alpha + (g_k\mu^2/3kT)]$$

where M is the molecular weight, N is Avogadro's number, α is the molecular polarisability, μ is the molecular dipole moment in the liquid phase, k is Boltzmann's constant, and T is the absolute temperature. Liquid-phase values of μ are estimated via [2].

$$[2] \quad \mu = \frac{(2D_s + 1)(n^2 + 2)}{3(2D_s + n^2)}\mu_g$$

where μ_g is the vapor phase dipole moment and n the refractive index of the liquid (24, 25). Bond refraction data (26–28) were used to calculate α for hydrazine.

Figure 2 shows a plot of E_{max} *vs.* $D_s d g_k^3 \alpha_p$ for hydrazine and the various liquids considered by Freeman. If, in the case of hydrazine, α_p is taken to be equivalent to α then the correlation

Can. J. Chem. Downloaded from www.nrcresearchpress.com by 210.87.254.5 on 09/05/12
For personal use only.

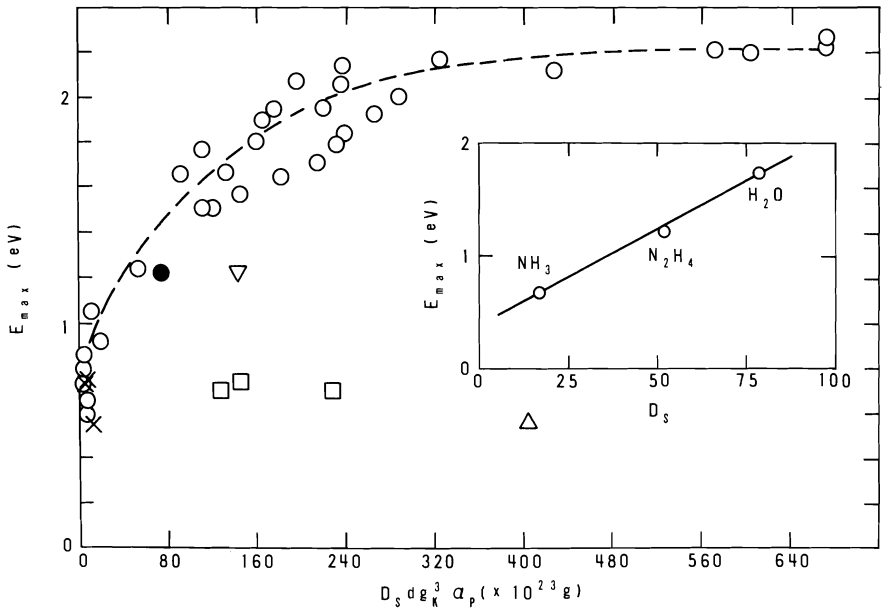

FIG. 2. Freeman correlation of optical absorption maxima with solvent properties: ○, water, alcohols, ethers, ammonia, and amines (10); ●, hydrazine using α_p for N—H bond; ▽, hydrazine using α_p for —NH_2 bonds; □, amides (29); △, HMPA (30); ×, revised values for amides and HMPA using μ (D) and α_p (see Table 1 and text). Inset shows the correlation of optical absorption maxima with D_s for NH_3, N_2H_4, and H_2O.

fails. However, if α_p is governed only by the polarisability of the N—H bond (which incorporates the polarisability of the nitrogen lone-pair electrons (26)) then reasonable agreement with Freeman's data is achieved. Alternatively, since g_k only emphasizes the importance of solvent structure and local ordering in determining E_{max}, it may be that the exponent for hydrazine is <3. The inset also shows a simple correlation between E_{max} and D_s for NH_3, N_2H_4, and H_2O at room temperature.

It is worth noting here that the results obtained by Dorfman and co-workers for the liquid amides (29) and hexamethylphosphoramide (HMPA) (30) were also considered anomalous (see Fig. 2). Again, in these cases α_p was taken as equivalent to α, an assumption which seems inconsistent with the premise that the significant e_s^-–solvent interactions responsible for E_{max} are short range and associated with the polar groups of the molecule (10). Furthermore, the dipole moments which significantly affect g_k were apparently not corrected to the liquid values. By analogy with hydrazine it would therefore seem more reasonable to utilize the N—C bond polarisabilities to estimate α_p for the amides and HMPA. Data revised in this manner are in accord with Freeman's correlation and are presented in Fig. 2 and Table 1 along with the comparative values for hydrazine, NH_3, and H_2O.

Although this approach is purely empirical the use of bond polarisabilities is entirely consistent with the mounting evidence that short-range interactions are largely responsible for the binding and transition energies of e_s^- (31–34). The revised correlation with respect to the amides suggests as in HMPA (20, 33, 34) that the electron is situated in the alkane-like environment of the positive ends of the molecular dipoles with, as in the branched alkyl alcohols (34), the optimum configuration of e_s^- being sensitive to steric hindrance.

Yield, Extinction Coefficient, and Oscillator Strength

In common with our other studies (14) both the yield and extinction coefficient were determined by comparison with $G\varepsilon$ (anion) in the presence of biphenyl (B) as an electron scavenger. Because of limited solubility biphenyl concentrations were $\leqslant 10^{-3}$ M. For each con-

Can. J. Chem. Downloaded from www.nrcresearchpress.com by 210.87.254.5 on 09/05/12
For personal use only.

TABLE 1. Solvated electron transition energies and solvent properties at ~25 °C[a]

Parameter	Value						
	N_2H_4	NH_3	H_2O	DMF	DMA	DEF	HMPA
E_{max} (eV)	1.22	0.67	1.73	0.74	0.69	0.70	0.56
D_s	51.7	16.9	78.5	36.7	40.2	29.6	30
d (g/cm^3)	1.004	0.603	0.997	0.945	0.937	0.903	1.024
n	1.47	1.33	1.33	1.428	1.437	1.434	1.457
μ_g (D)	1.85	1.46	1.85	4.13	4.60	4.30	5.30
μ (D)	2.54	1.70	2.31	5.45	6.15	5.72	7.15
α ($\times 10^{24}$ cm^3)	3.50	2.16	1.46	7.84	9.69	11.54	18
α_p ($\times 10^{24}$ cm^3)	0.70	2.16	1.46	1.77	1.77	1.77	3.54
g_k	2.74	1.64	2.70	1.03	1.05	1.08	1.05
$D_s d g_k^3 \alpha_p$ ($\times 10^{23}$ g)	74.7	9.7	225	6.7	7.7	6.0	12.6[b]

[a]See refs. 10, 29, 30, 45 and text for further details.
[b]Including N—P bonds this value increases to 17.8.

centration yields were calculated from linear plots of optical density against the energy absorbed per pulse for doses $\leqslant 1 \times 10^{20}$ eV l^{-1} assuming the extinction coefficients $\varepsilon_{B^-} = 4 \times 10^4$ and 1.25×10^4 M^{-1} at 410 and 640 nm, respectively (35). On this basis we find that $G_{e_s^-} = 2.35 \pm 0.15$ and by comparison with $G\varepsilon$ at 1015 nm in the absence of B, then $\varepsilon_{1015nm} = 2.2 \pm 0.1 \times 10^4$ M^{-1} cm^{-1}. The addition of base, either as 0.1 M sodium hydrazide or in solutions saturated with sodium hydroxide, enhances the yield to $G_{e_s^-} = 2.65 \pm 0.15$. This value is identical to that observed in aqueous solutions (15) but less than $G_{e_{am}^-} = 3.2$ obtained in liquid ammonia (14, 19, 36, 37).

It has been indicated recently that the maximum extinction coefficient for B^- is solvent dependent (38). Absolute values of 1.9 and 3.1×10^4 M^{-1} cm^{-1} have been reported for the 400 nm band in water (39) and NH_3 (38), respectively. These differ considerably from that assumed in this and previous work (14) on the basis of conventional spectrophotometric techniques (35). We have re-examined the B^- spectrum in both pure and basic solutions of ND_3, methylamine, ethylamine (40), and hydrazine and normalized such spectra relative to those reported in NH_3 (38) and tetrahydrofuran (THF) (35). Apart from slight (±2–3 nm) shifts in band maxima excellent overlap was obtained for NH_3, ND_3, and THF solutions. For ethylamine, methylamine, and hydrazine solutions the shoulder at ~375 nm was not clearly resolved but otherwise the B^- spectra are, within experimental error, also superimposable on the ammonia and THF spectra. Furthermore the relative extinction coefficient for the 400 to 630 nm bands corresponds to 3.2 ± 0.1 in excellent agreement with the ratio reported in THF (35) and isopropanol (41). Consequently we find no evidence for a significant difference in the extinction coefficients of B^- with a change in solvent. Since independent measurements of $G_{e_{am}^-}$ in liquid ammonia, in the presence or absence of B, are all self-consistent (14, 19, 36, 37, 42), this supports the assumption that ε_{B^-} (400 nm band) is 4×10^4 M^{-1} cm^{-1}.

The oscillator strength, f, of the e_s^- absorption band in hydrazine can be estimated from the approximation (43).

$$f \sim 4.32 \times 10^{-9}\, \varepsilon_{max} \Delta\nu_{1/2}$$

Substituting the values for ε_{max} and $\Delta\nu_{1/2}$ deduced above gives $f = 0.58$. Assuming the spectrum is described by a Gaussian-Lorenztian shape function (44) and then correcting for the internal field of the solvent (16) gives a comparable value $f = 0.61$. This oscillator strength is in accord with the values of 0.65, 0.62, 0.68, and 0.54 ± 0.15 for e_s^- in water and ND_3 (16), ethers (44), and HMPA (45), respectively, all corrected for the influence of the internal field.

Decay of e_s^- and Reaction with Biphenyl

The half-life of e_s^- in hydrazine decreases with increasing dose per pulse and increases in basic solutions. At doses ranging from ~3–25×10^{19} eV l^{-1} initial half-lives decrease from ~7 to 3 μs in pure hydrazine and in 0.3 M sodium hydrazide solutions from ~20 to 12 μs. The overall decay kinetics are complex

Can. J. Chem. Downloaded from www.nrcresearchpress.com by 210.87.254.5 on 09/05/12
For personal use only.

Can. J. Chem. Downloaded from www.nrcresearchpress.com by 210.87.254.5 on 09/05/12
For personal use only.

and have not been investigated in any detail. However, it is clear that mixed first and second order processes are involved with the latter becoming more dominant in basic solutions at the higher doses. This behaviour is typical of other systems involving reactions of e_s^- with impurities, radiolytically produced radicals, and positive ions (45).

Since in basic solutions initial half-lives are dose dependent and exceed 50 μs at doses $< 1 \times 10^{19}$ eV l^{-1} it is evident that the reaction of e_s^- with hydrazine itself is extremely slow. Since a blue color is observed on dissolution of an alkali metal we estimate, using the mathematical model described previously (46), that $k(e_s^- + N_2H_4) \leqslant 3 \times 10^{-2}$ and $k(e_s^- + e_s^-) \leqslant 3 \times 10^3$ M^{-1} s^{-1}, respectively. Such rate constants are orders of magnitude less than the corresponding values of 16 and 6×10^9 M^{-1} s^{-1} observed in water (15), but apparently greater than in liquid ammonia where blue solutions due to the presence of e_s^- are extremely stable (3, 4, 7, 8). The very slow rate of reaction of e_s^- with hydrazine is also in accord with previous observations in liquid ammonia (47).

The reaction of e_s^- with biphenyl was monitored by observing the decay of e_s^- at 1015 nm and the corresponding growth of B^- at 410 nm. Excellent agreement between both sets of data gave $k(e_s^- + B) = 2.2 \pm 0.2 \times 10^{10}$ M^{-1} s^{-1} which can be compared with values of 8×10^{10} and 1.2×10^{10} M^{-1} s^{-1} determined with NH_3 (38) and water (39) respectively.

1. R. F. Gould (*Editor*). Solvated electron. *In* Advances in chemistry series. Vol. 50. 1965.
2. A. K. Pikaev. The solvated electron in radiation chemistry. Eng. Transl. 1971. Available U.S. Dept. of Commerce. Tech. Info. Service.
3. J. Jortner and N. R. Kestner (*Editors*). Electrons in fluids. Springer-Verlag, Berlin. 1973.
4. B. Crawford, Jr. (*Editor*). Electrons in fluids – the nature of metal – ammonia solutions. Colloque Weyl IV. J. Phys. Chem. **79**, 2789 (1975).
5. L. F. Audrieth and B. A. Ogg. The chemistry of hydrazine. J. Wiley and Sons Inc., New York. 1951.
6. A. F. Trotman-Dickenson (*Executive Editor*). Comprehensive inorganic chemistry. Vol. 2. Pergamon Press, N.Y. 1973. p. 250.
7. G. Lepoutre and M. J. Sienko (*Editors*). Metal–ammonia solutions. Colloque Weyl I. W. A. Benjamin Inc., New York. 1964.
8. J. J. Lagowski and M. J. Sienko (*Editors*). Metal–ammonia solutions. Colloque Weyl II, Int. Union Pure Appl. Chem. Butterworths, London. 1970.
9. N. A. Slavinskaya, B. M. Kozlov, N. V. Petrukhin, S. A. Kamenetskaya, and S. Ya. Pshezhetskii. High Energy Chem. **8**, 57 (1974).
10. G. R. Freeman. J. Phys. Chem. **77**, 7 (1973).
11. W. A. Seddon, C. Willis, M. Young, and E. B. Selkirk. Atomic Energy of Canada Ltd. Report AECL-3853.
12. J. W. Fletcher, W. A. Seddon, and F. C. Sopchyshyn. Can. J. Chem. **51**, 2975 (1973).
13. W. A. Seddon, E. B. Selkirk, and J. W. Fletcher. Int. J. Radiat. Phys. Chem. **5**, 323 (1973).
14. W. A. Seddon, J. W. Fletcher, F. C. Sopchyshyn, and J. Jevcak. Can. J. Chem. **52**, 3269 (1974).
15. E. J. Hart and M. Anbar. The hydrated electron. Wiley-Interscience, N.Y. 1970.
16. K. N. Jha, G. L. Bolton, and G. R. Freeman. J. Phys. Chem. **76**, 3876 (1972).
17. D. F. Burow and J. J. Lagowski. Adv. Chem. Ser. **50**, 125 (1965)
18. I. Hurley, T. R. Tuttle, Jr., and S. Golden. Metal–ammonia solutions. Colloque Weyl II, Int. Union Pure Appl. Chem. *Edited by* J. J. Lagowski and M. J. Sienko. Butterworths, London. 1970. p. 503.
19. W. A. Seddon, J. W. Fletcher, J. Jevcak, and F. C. Sopchyshyn. Can. J. Chem. **51**, 3653 (1973).
20. H. Nauta and C. Van Huis. J. Chem. Soc. Faraday Trans. I, 647 (1972).
21. S. Arai and L. M. Dorfman. J. Chem. Phys. **41**, 2190 (1964).
22. G. Oster and J. G. Kirkwood. J. Chem. Phys. **11**, 175 (1943).
23. N. E. Hill, W. E. Vaughan, A. H. Price, and M. Davies. *In* Dielectric properties and molecular behavior. *Edited by* T. M. Sugden. Van Nostrand Reinhold Co., London. 1969. p. 24.
24. L. Onsager. J. Am. Chem. Soc. **58**, 1486 (1936).
25. N. E. Hill. *In* Dielectric properties and molecular behavior. *Edited by* T. M. Sugden. Van Nostrand Reinhold Co., London. 1969. p. 30.
26. R. J. W. LeFèvre. Adv. Phys. Org. Chem. **3**, 1 (1965).
27. R. J. W. LeFèvre. Rev. Pure Appl. Chem. **20**, 67 (1970).
28. A. H. Price. *In* Dielectric properties and molecular behavior. *Edited by* T. M. Sugden. Van Nostrand Reinhold Co., London. 1969. p. 232.
29. J. F. Gavlas, F. Y. Jou, and L. M. Dorfman. J. Phys. Chem. **78**, 2631 (1974).
30. L. M. Dorfman and J. F. Gavlas. *In* Radiation research. Proc. Fifth Int. Congr. Radiat. Res. *Edited by* O. F. Nygaard, H. I. Adler, and W. K. Sinclair. Academic Press Inc., New York. 1975. p. 326.
31. I. A. Taub and K. Eiben. J. Chem. Phys. **49**, 2499 (1968).
32. A. Gaathon, G. Czapski, and J. Jortner. J. Chem. Phys. **58**, 2648 (1973).
33. R. R. Hentz and G. A. Kenney-Wallace. J. Phys. Chem. **76**, 2931 (1972).
34. R. R. Hentz and G. A. Kenney-Wallace. J. Phys. Chem. **78**, 514 (1974).
35. J. Jagur-Grodzinski, M. Feld, S. L. Yang, and M. Szwarc. J. Phys. Chem. **69**, 628 (1965).
36. Farhataziz and L. M. Perkey. J. Phys. Chem. **79**, 1651 (1975).

37. FARHATAZIZ, L. M. PERKEY, and R. R. HENTZ. J. Chem. Phys. **60**, 4383 (1974).
38. FARHATAZIZ and L. M. PERKEY. J. Phys. Chem. **80**, 122 (1976).
39. K. SEHESTED and E. J. HART. J. Phys. Chem. **79**, 1639 (1975).
40. W. A. SEDDON and J. W. FLETCHER. Unpublished results.
41. S. ARAI, H. UEDA, R. F. FIRESTONE, and L. M. DORFMAN. J. Chem. Phys. **50**, 1072 (1969).
42. J. BELLONI, P. CORDIER, and J. DELAIRE. Chem. Phys. Lett. **27**, 241 (1974).
43. J. G. CALVERT and J. N. PITTS, JR. Photochemistry. John Wiley and Sons, Inc., New York. 1966. p. 172.
44. F. Y. JOU and L. M. DORFMAN. J. Chem. Phys. **58**, 4715 (1973).
45. E. A. SHAEDE, L. M. DORFMAN, G. J. FLYNN, and D. C. WALKER. Can. J. Chem. **51**, 3905 (1973).
46. J. W. FLETCHER and P. J. RICHARDS. Can. J. Chem. **49**, 2275 (1971).
47. J. BELLONI. Int. J. Radiat. Phys. Chem. **1**, 441 (1969).

Can. J. Chem. Downloaded from www.nrcresearchpress.com by 210.87.254.5 on 09/05/12
For personal use only.

Thermal pressure and energy–volume coefficients for the acetonitrile + water system

DAVID F. GRANT-TAYLOR[1] AND DIGBY D. MACDONALD[2]

Department of Chemistry, Victoria University of Wellington, Wellington, New Zealand

Received March 10, 1976

DAVID F. GRANT-TAYLOR and DIGBY D. MACDONALD. Can. J. Chem. **54**, 2813 (1976).

Densities and thermal pressure coefficients for the acetonitrile + water system at temperatures from 298.15 to 328.15 K are reported. These data are used to derive expansivities, energy–volume coefficients, cohesive energy densities, isothermal compressibilities, and derivatives of entropy with respect to pressure. The variation of these parameters with composition and temperature is described.

DAVID F. GRANT-TAYLOR et DIGBY D. MACDONALD. Can. J. Chem. **54**, 2813 (1976).

On rapporte les densités et les coefficients de pression thermique du système acétonitrile + eau à des températures allant de 298.15 à 328.15 K. On utilise ces données pour dériver les expansivitées, les coefficients énergie–volume, les densités d'énergie cohésive, les compressibilités isothermes et les dérivés de l'entropie par rapport à la pression. On décrit la variation de ces paramètres avec la composition et avec la température.

[Traduit par le journal]

Can. J. Chem. Downloaded from www.nrcresearchpress.com by 210.87.254.6 on 09/05/12
For personal use only.

Introduction

The acetonitrile + water system has been frequently used as a medium for the study of both kinetic and equilibrium phenomena. Recent investigations (1–3, 22) have shown that this system exhibits a number of unusual features in the variation of the excess functions of mixing with composition. Thus, at 298.15 K the excess Gibbs energy and enthalpy of mixing are both positive, whereas the excess volume of mixing is negative, over the entire range of composition. Furthermore, the excess entropy of mixing at constant pressure is negative at acetonitrile mole fractions less than 0.65, but is positive for higher organic compositions. In contrast, the acetone + chloroform system (4), which exhibits strong intercomponent hydrogen bonding, is characterized by negative values for all four excess functions over the entire range of composition. The *tert*-butanol + water system (5), on the other hand, exhibits positive and negative values for G^E and (TS_P^E, V^E), respectively, at all compositions, but H^E changes from negative to positive as the mole fraction of *tert*-butanol is increased through 0.45. The excess function of mixing behavior suggests, therefore, that the acetonitrile + water system occupies a position intermediatory between the strong intercomponent interaction case of the acetone + chloroform system and the entropy dominated hydrophobic *tert*-butanol + water system.

As part of our continuing study of the PVT properties of binary systems, we report in this paper thermal pressure coefficients ($\beta = (\partial p/\partial T)_V$) and densities for the acetonitrile + water system. Previous work in this series (6–9) has demonstrated that β, and the derived energy–volume coefficient are sensitive to

$$[1] \qquad (\partial U/\partial V)_T = T\beta - p$$

changes in the 'structure' of a binary system as the composition is changed. Accordingly, these parameters, together with the temperature derivative of β, are well suited as probes for the study of binary liquid mixtures.

Experimental

Materials

A.R. acetonitrile was distilled from a mixture containing $KMnO_4$ and Na_2CO_3, as described by O'Donnell *et al.* (10), with the fore and aft 10% cuts being discarded. The distillate was then fractionally distilled through a 30 cm Vigreux column with the cut boiling at (354.9 ± 0.1) K being retained and stored under nitrogen in amber bottles for later use. The purified acetonitrile was degassed immediately before use and exhibited the following properties: Boiling temperature: (354.9 ± 0.1) K at 0.1 MPa; this compares with literature values of 353.3 K (11) and 355.2 K (10) at 0.1004 MPa. Refractive index:

[1]Present address: Chemistry Division, Department of Scientific and Industrial Research, Petone, New Zealand.

[2]Present address: Department of Chemistry, University of Calgary, Calgary, Alberta, Canada. To whom correspondence should be addressed.

TABLE 1. Isobaric coefficients of thermal expansion (α) for the acetonitrile + water system

	$\alpha/10^{-4}$ K^{-1}			
X_{CH_3CN}	298.15 K	308.15 K	318.15 K	328.15 K
0.0000	2.60 (2.57)[a]	3.43 (3.46)[a]	4.19 (4.23)[a]	4.90 (4.91)[a]
0.0401	2.61	3.75	5.19	6.49
0.1942	8.21	8.09	8.82	9.75
0.2840	9.15	9.61	10.11	10.74
0.3736	9.91	10.75	11.27	11.24
0.4431	11.07	11.39	11.66	12.34
0.5438	11.88	12.34	12.48	13.00
0.6750	11.48	11.80	11.86	12.60
0.7809	13.53	13.84	13.89	14.13
0.8832	13.92	14.12	14.31	14.68
1.0000	13.71	14.31	14.78	14.85

[a]Values in parentheses taken from ref. 15.

n(293.15 K) = 1.3442; literature values range from 1.34338 (12) to 1.3444 (2). Density, ρ = 777.8 kg m^{-3} at 298.15 K; literature values range from 776.7 (13) to 785.6 (11) kg m^{-3} at 293.15 K. The latter value is equivalent to 781.3 kg m^{-3} at 298.15 K. Analysis by glc showed less than 0.1% by weight impurity, calculated as water.

Double distilled water was degassed by the freeze–pump–thaw method immediately before use. All acetonitrile + water mixtures were prepared by weight.

Apparatus and Method

The constant volume cell and associated apparatus for the measurement of the thermal–pressure coefficients of liquid systems has been described (7, 9). Pressure/temperature isochores were measured over the 0.1 to 40 MPa pressure range with data being collected in both the ascending and descending directions. The temperature of the pressure vessel contents, including the constant volume cell, was measured with a calibrated platinum resistance thermometer encapsulated in a high temperature epoxy resin. The previously described (7, 9) procedures were adopted to ensure thermal equilibration of the cell contents with the pressurising and thermostat fluids.

Volumes of the liquid mixtures were measured over the 298.15 to 328.15 K temperature range using a mercury displacement dilatometer similar in design to that described by Gibson and Loeffler (14). The dilatometer was thermostatted in a water bath to better than ±0.005 K at 298.15 K and ±0.01 K at 323.15 K. All weighings of the dilatometer and contents, and the displaced mercury, were corrected to masses. The dilatometer was calibrated using degassed double distilled water and triple distilled mercury. The precision of the calibrated volume was ±0.002% as determined by multiple measurement.

Results

Coefficients of Thermal Expansion

The dilatometric technique employed in this work yielded volume/temperature data directly. These data were then used to calculate mean expansivities over the temperature interval T_1 to T_2 ($T_2 - T_1$ = 10 K) according to eq. 2.

$$[2] \qquad \langle\alpha\rangle = (V_2 - V_1)/\langle V\rangle(T_2 - T_1)$$

where $\langle V\rangle = (V_1 + V_2)/2$. This procedure is numerically equivalent to that described by Gibson and Loeffler (14), although it is without the refinement of separating out the second order V/T coefficient. The V *vs.* T curves for fixed compositions were sufficiently monotonic that the difference between $\langle\alpha\rangle$, as calculated using eq. 2, and the true expansivity $\alpha = (\partial V/\partial T)/V$ is small, and well within experimental error. Numerical values for $\langle\alpha\rangle$ are listed in Table 1 for four temperatures over the range 298.15 to 328.15 K. The precision of the values is estimated to be better than ±2%. Liquid densities were calculated from the volume/mass data and are given in Table 2. The values have an estimated precision of ±0.01%.

Thermal Pressure Coefficients

Plots of applied pressure *vs.* temperature for apparent constant volume of the system were found to be linear and reproducible with respect to ascending and descending pressure/temperature changes. Therefore, the $(p,T)_V$ data were fitted with the equation

$$[3] \qquad p = \beta_{app}T + C$$

where β_{app} is the observed thermal pressure coefficient. The β_{app} values were then corrected for the finite expansion and compression of glass in the usual manner (7, 8, 16).

Corrected thermal–pressure coefficients for the acetonitrile + water system are listed in Table 3 as a function of temperature and composition. In view of the probable errors in temperature (±0.01 K) and in pressure

Can. J. Chem. Downloaded from www.nrcresearchpress.com by 210.87.254.6 on 09/05/12
For personal use only.

Can. J. Chem. Downloaded from www.nrcresearchpress.com by 210.87.254.6 on 09/05/12
For personal use only.

TABLE 2. Densities (ρ) for various acetonitrile + water mixtures as a function of temperature

	$\rho/10^3$ kg m^{-3}			
X_{CH_3CN}	298.15 K	308.15 K	318.15 K	328.15 K
0.0000	0.99708	0.99406	0.99025	0.98573
0.0408	0.9753	0.9721	0.9679	0.9621
0.0852	0.9538	0.9489	0.9439	0.9378
0.1942	0.9212	0.9138	0.9072	0.8996
0.2840	0.8964	0.8889	0.8800	0.8711
0.3736	0.8733	0.8642	0.8548	0.8452
0.4431	0.8583	0.8488	0.8392	0.8291
0.5438	0.8372	0.8274	0.8172	0.8067
0.6750	0.8146	0.8053	0.7958	0.7862
0.7809	0.7998	0.7893	0.7782	0.7673
0.8832	0.7889	0.7779	0.7669	0.7558
1.0000	0.7778	0.7669	0.7557	0.7447

TABLE 3. Thermal–pressure coefficients (β) for the acetonitrile + water system

T/K	$\beta/10^5$ Pa K^{-1}	T/K	$\beta/10^5$ Pa K^{-1}	T/K	$\beta/10^5$ Pa K^{-1}
	0.000[a]		0.044		0.109
305.05	7.10 (7.13)[b]	300.65	11.69	301.55	14.67
308.15	7.78 (7.75)[b]	317.45	13.60	315.95	15.10
325.65	10.92 (10.70)[b]	322.65	14.70	323.95	15.38
342.25	13.20 (13.40)[b]				
	0.180		0.315		0.408
300.65	15.75	297.55	16.95	300.15	15.06
320.65	16.45	318.15	16.60	306.95	14.66
328.15	15.61	330.45	16.36	322.45	13.72
338.15	16.57				
	0.484		0.502		0.694
298.45	14.75	297.15	15.30	299.65	13.79
317.45	13.80	313.65	14.62	309.75	13.69
327.95	13.63	328.35	13.75	327.35	12.74
	0.785		1.000		
301.25	13.20	298.15	12.07		
318.15	12.78	308.15	11.88		
325.15	11.97	326.35	10.92		

[a]Mole fraction acetonitrile.
[b]Values in parentheses taken from ref. 4.

(± 0.02 MPa) the precision of the thermal–pressure coefficients is better than $\pm 2\%$. Good agreement is found with data taken from the literature.

Plots of β against T for various compositions of the binary system were found to be linear. Values for $(\partial\beta/\partial T)_p$ were calculated directly from the plots and are listed in Table 4.

Energy–Volume Coefficients and Cohesive Energy Densities

The energy–volume coefficient of the system can be related to the cohesive energy density, $\Delta U_V/V$, by

$$[4] \qquad (\partial U/\partial V)_T = n(\Delta U_V/V)$$

where ΔU_V is the energy of vaporization of the mixture to the perfect gas state, and n is an empirical parameter which is equal to one for a van der Waals fluid (17). The energy of vaporization of a real liquid mixture to the perfect gas state may be calculated using the following expression (7)

$$[5] \quad \Delta U_V \simeq x_1\Delta H_{V,1} + x_2\Delta H_{V,2} - H^E - RT$$

Can. J. Chem. Downloaded from www.nrcresearchpress.com by 210.87.254.6 on 09/05/12
For personal use only.

TABLE 4. Thermal–pressure coefficients (β), energy–volume coefficients ($(\partial U/\partial V)_T$), cohesive energy densities ($\Delta U_v/V$), parameter n, and values for $(\partial\beta/\partial T)_p$ for the acetonitrile + water system at 298.15 K

Mole fraction acetonitrile	β[a] 10^5 Pa K^{-1}	$(\partial U/\partial V)_T$ 10^8 Pa	$(\Delta U_V/V)$ 10^9 Pa	n	$(\partial\beta/\partial T)$[b] 10^5 Pa K^{-2}
0.000	5.76	1.71	2.242	0.077	0.22_6
0.044	11.40	3.40	2.074	0.160	0.11_5
0.109	14.61	4.35	1.838	0.237	0.03_0
0.180	15.90	4.74	1.530	0.310	0.02_0
0.315	16.93	5.05	1.232	0.410	-0.00_2
0.408	15.28	4.55	0.990	0.460	-0.04_4
0.502	15.32	4.57	0.899	0.508	-0.05_0
0.694	13.97	4.16	0.708	0.588	-0.04_2
0.785	13.46	4.01	0.658	0.610	-0.04_5
1.000	12.05	3.59	0.595	0.603	-0.03_3

[a]Estimated precision ±2%.
[b]Estimated uncertainty = $\pm 0.015 \times 10^5$ Pa K^{-2}.

TABLE 5. Coefficients of isothermal compressibility (κ) for the acetonitrile + water system

X_{CH_3CN}	$\kappa/10^{-9}$ Pa^{-1} 298.15 K	318.15 K
0	0.45_1 (0.4524)[a]	0.44_1 (0.4415)[a]
0.10	0.38_2	0.45_0
0.20	0.48_8	0.54_9
0.30	0.55_6	0.62_8
0.40	0.65_6	0.76_0
0.50	0.75_7	0.87_5
0.60	0.84_8	0.96_3
0.70	0.93_5	1.03_9
0.80	1.01_5	1.12_0
0.90	1.08_7	1.20_0
1.00	1.15_4	1.30_0

[a]Values given in ref. 15.

where $\Delta H_{V,1}$ and $\Delta H_{V,2}$ are the enthalpies of vaporization of components 1 and 2, respectively, to the perfect gas state, and H^E is the excess enthalpy per mole of mixture. Enthalpy of vaporization (18) and mixing (19) data were combined with molar volumes calculated from the densities given in Table 2 to yield the values for $(\Delta U_V/V)$ listed in Table 4. These data were then combined with the energy–volume coefficients (Table 4) to yield values for the parameter n (Table 4) using eq. 4.

Isothermal Compressibility

Coefficients of isothermal compressibility, $\kappa = -(\partial \ln V/\partial p)_T$, were calculated using eq. 6 from interpolated values for β and α at temperatures of 298.15 and 318.15 K

$$\kappa = \alpha/\beta \qquad [6]$$

and are given in Table 5. The values are considered accurate to ±3%. The compressibilities obtained in this work for water ($0.45_1 \times 10^{-9}$ and $0.44_1 \times 10^{-9}$ Pa^{-1} at 298.15 and 318.15 K, respectively) are in excellent agreement with the values of 0.4524×10^{-9} and 0.4415×10^{-9} Pa^{-1} quoted in the literature (15) for the same temperatures.

Discussion

Energy–Volume Coefficients and Cohesive Energy Densities

The energy–volume coefficients, cohesive energy densities, and values for n, for the acetonitrile + water system at 298.15 K are plotted as a function of composition in Fig. 1.

Both β (Table 4) and the energy–volume coefficient (Fig. 1) are found to pass through a maximum at $x \approx 0.3$, *i.e.* at this composition the internal energy and entropy of the system are most susceptible to isothermal increase in volume. Other aqueous-organic mixtures, including methanol + water (8), dimethyl sulfoxide + water (7), and *tert*-butanol + water (8) exhibit similar maxima in the highly aqueous region of composition. On the other hand, dimethyl sulfoxide + methanol system (9) exhibits a maximum in $(\partial U/\partial V)_T$ at x(DMSO) = 0.5, as well as a temperature dependent minimum at a slightly higher DMSO mole fraction.

Both the cohesive energy density, $(\Delta U_V/V)_T$

Can. J. Chem. Downloaded from www.nrcresearchpress.com by 210.87.254.6 on 09/05/12
For personal use only.

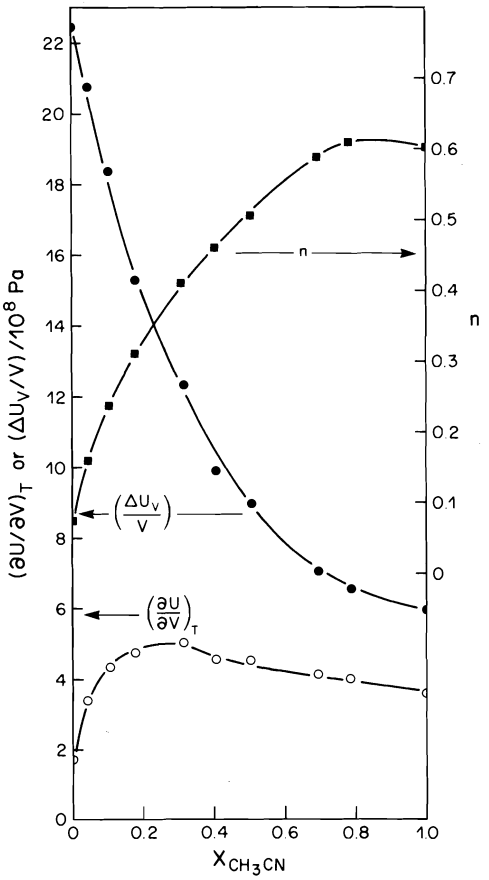

FIG. 1. Energy–volume coefficients, $(\partial U/\partial V)_T$, cohesive densities, $(\Delta U_v/V)$, and values for the parameter n, eq. 4, plotted as a function of composition at 298.15 K.

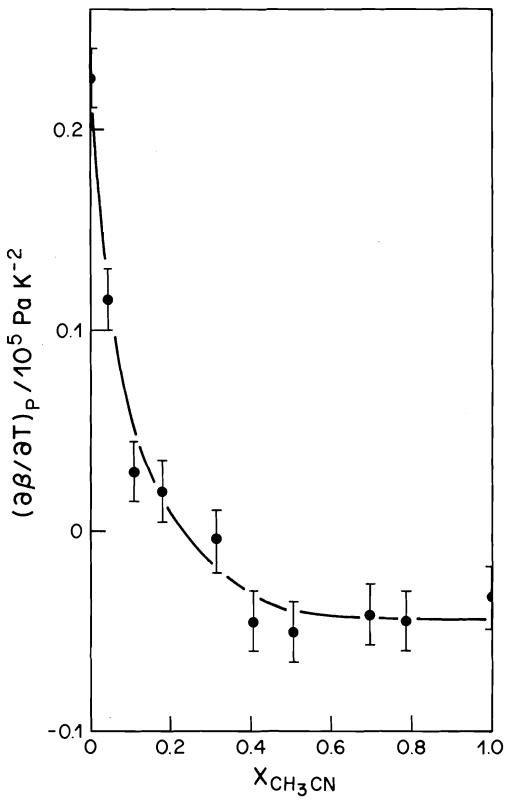

FIG. 2. Plot of $(\partial\beta/\partial T)_p$ *vs.* composition for the acetonitrile + water system at 298.15 K.

and n show monotonic variations with composition, with the possibility of a small maximum in the latter quantity at high acetonitrile mole fractions. It is evident from the data plotted in Fig. 1 that the maximum in $(\partial U/\partial V)_T$ arises from the non-compensatory behavior of the cohesive energy density and n. Thus, on the water-rich side of the maximum, the dominant term on the right hand side of eq. 4 is n, whereas at higher mole fractions the energy–volume coefficient behavior of the system is determined principally by the cohesive energy density.

Previous work by a number of investigators (20, 21) has shown that $n \simeq 1$ for those liquids which are generally regarded as weakly interacting and approximate to the van der Waals model. On the other hand, strongly interacting systems are characterised by small values for n, particularly those liquids which are extensively hydrogen bonded (*i.e.* the alcohols and water). Thus, the data plotted in Fig. 1 suggest that in the higher aqueous region of composition (*i.e.* on the aqueous side of the maximum) the behavior of $(\partial U/\partial V)_T$ reflects principally changes in the extent of hydrogen bonding in the system. At higher mole fractions, the effect of the addition of the acetonitrile cosolvent upon the cohesive energy density of the system (which reflects contributions to the energy of the system from all types of interactions) is more than sufficient to dominate cosolvent induced changes in the state of hydrogen bonding.

The temperature dependence of $\beta\{(\partial\beta/\partial T)_p = [\partial(\partial S/\partial V)_T/\partial T]_p\}$ at 298.15 K is plotted as a function of composition in Fig. 2. This parameter is seen to decrease rapidly upon the addition of acetonitrile from an initial value of 0.226×10^5 Pa K^{-2} for pure water and changes sign at approximately 30 mol% acetonitrile. Further addition of cosolvent has little effect upon $(\partial\beta/\partial T)_p$, and in this respect the acetonitrile +

Can. J. Chem. Downloaded from www.nrcresearchpress.com by 210.87.254.6 on 09/05/12
For personal use only.

TABLE 6. Numerical values for $(\partial S/\partial p)_T$ for acetonitrile + water mixtures at various temperatures

	$-(\partial S/\partial p)_T 10^{-9}$ J mol^{-1} K^{-1} Pa^{-1}[a]			
X_{CH_3CN}	298.15 K	308.15 K	318.15 K	328.15 K
0.000	4.70	6.23	7.62	8.96
0.0408	5.07	7.31	10.2	12.8
0.1942	20.0	19.9	21.9	24.4
0.2840	25.1	26.5	28.2	30.3
0.3736	30.2	33.1	35.1	35.4
0.4431	36.4	37.9	39.2	42.0
0.5438	43.3	45.6	46.6	49.2
0.6750	47.3	49.2	50.0	53.8
0.7809	60.9	63.1	64.3	66.3
0.8832	67.7	69.6	71.6	74.5
1.000	72.4	76.6	80.3	81.9

[a]Estimated precision ±2%.

water system is similar to the other organic cosolvent + water systems which have been studied (6–9).

There is no need to stress here the abnormal behavior of liquid water, as this topic has been treated in detail elsewhere (23). A number of modern theories (23) propose that liquid water consists of a dynamic equilibrium involving open 'flickering cluster' configurations of hydrogen bonded water molecules. Because of the tetrahedral hydrogen bonding capabilities of individual water molecules, the open 'flickering clusters' are not favored at small volumes, and for these configurations $(\partial S/\partial V)_T$ is negative. With increasing temperature, however, the clusters tend to break down, and their contribution to the total $(\partial S/\partial V)_T$ of the liquid is less negative, *i.e.* the clusters contribute a positive component to the overall $(\partial\beta/\partial T)$ term for the system.[3] With the addition of 'structure breaking' acetonitrile, the cluster contribution is reduced since the clusters are broken down (24), either by direct intermolecular interaction with the cosolvent or by the bulk dilution effect which will tend to shift the cluster-size distribution towards smaller configurations. Thus, the added cosolvent will decrease the cluster contribution, such that at 30 mol% acetonitrile this positive contribution is balanced by the negative one which arises from 'normal' intermolecular interaction (7, 8). It is apparent, therefore, that the cluster contribution dominates in determining the sign of $(\partial\beta/\partial T)$ for water and for acetonitrile + water mixtures with less than approximately 30 mol% acetonitrile. In this respect, these systems may be described as 'essentially aqueous' in nature, whereas mixtures containing greater amounts of acetonitrile exhibit the same type of behavior as the 'normal' non-aqueous systems mentioned above.

The effect of pressure on the structure of a liquid may be examined using the derivative $(\partial S/\partial p)_T = -\alpha V$, where α is the isobaric coefficient of thermal expansion. Numerical values for $(\partial S/\partial p)_T$ for various mixtures of acetonitrile and water at four temperatures in the range 298.15 to 328.15 K are given in Table 6. The values at all temperatures are negative, *i.e.* the entropy of the system decreases with increasing pressure, and increase monotonically with composition. Furthermore, the derivative $[\partial(\partial S/\partial p)/\partial T]_p$ is also negative for all mixtures studied and, again, tends to increase with x. Similar trends were found for the methanol + DMSO (9), although in this case it appears that $[\partial(\partial S/\partial p)/\partial T]_p$ is positive for low DMSO mole fractions.

Compressibility

The coefficients of isothermal compressibility listed in Table 5 for $T = 298.15$ K exhibit an initial decrease upon the addition of acetonitrile to water. At mole fractions of cosolvent greater than 0.1, however, κ increases monotonically with composition. The initial decrease in κ upon the addition of organic cosolvent to water is generally observed for other aqueous-organic solvent systems (25). At 318.15 K, κ increases monotonically with cosolvent mole fraction over the entire range of composition.

The isothermal compressibility of a thermodynamically ideal mixture is given as (9)

$$[7]\quad \kappa^{id} = x_1(\kappa_1{}^0 V_1{}^0/V_m{}^{id}) + x_2(\kappa_2{}^0 V_2{}^0/V_m{}^{id})$$

where $V_1{}^0$ and $V_2{}^0$ are the molar volumes of components 1 and 2, respectively, and $V_m{}^{id}$ is the volume of the ideal mixture at mole fraction composition x_1, $x_2 = 1 - x_1$. Therefore, the excess isothermal compressibility is defined as

[3]It is important to note that the cluster contribution is not dominant in determining the sign of β at 298.15 K, since the observed thermal pressure coefficient is positive. However, for water in the temperature range 273.15 to 277.13 K, β is negative. In this case, few of the 'flickering cluster' configurations have been disrupted by thermal agitation, and the sign of $(\partial S/\partial V)_T$ for the system is determined by the influence of volume change on the stability (and hence the entropy) of the water clusters.

Can. J. Chem. Downloaded from www.nrcresearchpress.com by 210.87.254.6 on 09/05/12
For personal use only.

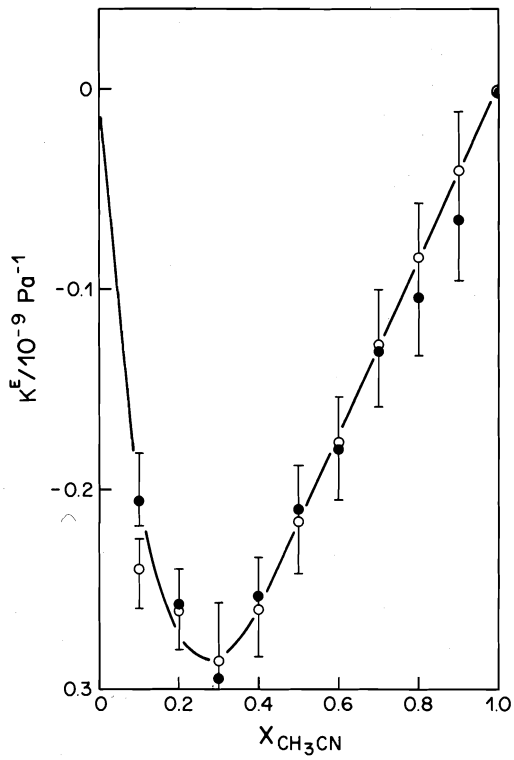

FIG. 3. Plot of the excess isothermal compressibility (κ^E) as a function of composition for the acetonitrile + water system at 298.15 and 318.15 K.

$$[8] \qquad \kappa^E = \kappa - \kappa^{id}$$

and is plotted as a function of composition in Fig. 3 for temperatures of 298.15 and 318.15 K. At both temperatures κ^E is negative, and passes through an extremum at $x \simeq 0.3$, in contrast to the composition of ≤ 10 mol% acetonitrile at which κ was observed to pass through a minimum at 298.15 K. The negative maximum in κ^E occurs at the same composition as the extrema in $(\partial U/\partial V)_T$, $S_P{}^E$ (negative maxima) (1), and the excess volume of mixing (1, 22).

Finally, temperature is found to have remarkably little effect upon the excess compressibility of the acetonitrile + water system (Fig. 3), even though the compressibility itself is clearly temperature dependent over the entire range of composition (Table 5).

1. D. GRANT-TAYLOR. M. Sc. Thesis, Victoria University of Wellington, Wellington, New Zealand. 1974.
2. A. L. VIERK. Z. Anorg. Chem. **261**, 283 (1950).
3. K. W. MORCOM and R. W. SMITH. J. Chem. Thermodyn. **1**, 503 (1969).
4. J. S. ROWLINSON. Liquids and liquid mixtures, 2nd ed. Butterworths, London. 1969. p. 166.
5. J. KENTTAMAA, E. TOMMILA, and M. MARTTI. Ann. Acad. Sci. Fenn. Ser. A, **93**, 1 (1959).
6. D. D. MACDONALD, J. B. HYNE, and F. L. SWINTON. J. Am. Chem. Soc. **92**, 6355 (1970).
7. D. D. MACDONALD and J. B. HYNE. Can. J. Chem. **49**, 611 (1971).
8. D. D. MACDONALD and J. B. HYNE. Can. J. Chem. **49**, 2636 (1971).
9. K. M. CHAPMAN and D. D. MACDONALD. J. Chem. Thermodyn. In press.
10. J. F. O'DONNELL, J. T. AYRES, and G. K. MANN. Anal. Chem. **37**, 1161 (1965).
11. A. J. PARKER. Chem. Rev. **69**, 1 (1969).
12. G. J. JANZ and S. S. DANYLUCK. J. Am. Chem. Soc. **81**, 3846 (1959).
13. D. F. EVANS, C. ZAWOYSKI, and R. L. KAY. J. Phys. Chem. **69**, 3878 (1965).
14. R. E. GIBSON and O. H. LOEFFLER. J. Am. Chem. Soc. **61**, 2515 (1939).
15. Handbook of Chemistry and Physics, 51st ed. Chemical Rubber Company, Cleveland, Ohio. 1971.
16. C. F. LAU, G. N. MALCOLM, and D. V. FENBY. Aust. J. Chem. **22**, 855 (1969).
17. H. S. FRANK. J. Chem. Phys. **13**, 493 (1945).
18. D. R. STULL, E. F. WESTRUM, and G. E. SINKE. The chemical thermodynamics of organic compounds. Wiley, New York. 1969.
19. I. M. KOLTHOFF and J. F. COETZEE. J. Am. Chem. Soc. **79**, 870 (1957).
20. J. H. HILDEBRAND. Phys. Rev. **34**, 984 (1929).
21. G. ALLEN, G. GEE, and G. J. WILSON. Polymer, **1**, 456 (1960).
22. D. A. ARMITAGE, M. J. BLANDAMER, M. J. FOSTER, N. J. HIDDEN, K. W. MORCOM, M. C. R. SYMONS, and M. J. WOOTTEN. Trans. Faraday Soc. **64**, 1193 (1968).
23. F. FRANKS (*Editor*). Water, a comprehensive treatise. Vols. 1 to 4. Plenum Press, New York. 1973.
24. G. WADA and S. UMEDA. Bull. Chem. Soc. Jpn. **35**, 1797 (1962).
25. K. H. JUNG and J. B. HYNE. Can. J. Chem. **48**, 2423 (1970).

^{13}C T_1 nuclear magnetic resonance study of molecular motion: rotational barriers in hindered methyl groups

DAVID E. AXELSON AND CLIVE E. HOLLOWAY

Department of Chemistry, York University, Downsview, Ont., Canada M3J 1P3

Received March 23, 1976

DAVID E. AXELSON and CLIVE E. HOLLOWAY. Can. J. Chem. **54**, 2820 (1976).

Analysis of spin–lattice relaxation (T_1) data can give information on restricted rotation which is otherwise inaccessible. This study investigates the influence of substituents on the rotation of a neighbouring methyl group in a series of related polycyclic compounds.

DAVID E. AXELSON et CLIVE E. HOLLOWAY. Can. J. Chem. **54**, 2820 (1976).

Une analyse des données de relaxation spin–réseau (T_1) peut fournir de l'information, qui serait par ailleurs inacessible, sur des rotations empêchées. Le présent travail étudie l'influence des substituants sur la rotation d'un groupe méthyle voisin dans une série de composés polycycliques analogues.

[Traduit par le journal]

Can. J. Chem. Downloaded from www.nrcresearchpress.com by 210.87.254.6 on 09/05/12
For personal use only.

Introduction

The *tert*-butyl moiety has been studied numerous times by proton nmr to obtain activation energies for rotation about the sp^3 bond (1–5). More recently, interest has centered on the dynamic behaviour of the individual methyl groups in hindered environments (6–13). Proton nmr is complicated in these instances by the tightly coupled A_2B or ABC spin system characteristic of a methyl group in such a situation. Also, in many cases, the activation energy involved is too low to permit freezing out of the rotation at temperatures within the range of many instruments. A study by Nakanishi *et al.* (3) investigated the restricted rotation of methyl groups within a rigidly held *tert*-butyl group and found that temperatures as low as −133 °C were necessary to observe line broadening. Another study by Anderson and Rawson (10) indicated a barrier to rotation of 7.2 kcal mol^{-1} from the complete nmr line shape analysis of a sterically hindered $-CD_2H$ group.

Spin–lattice T_1 relaxation studies (7, 8, 14) offer a simplifying alternative to the line shape studies, particularly where rotational barriers are too low to be conveniently obtained from line shape analysis. Provided that certain approximations can be made, useful information on rates of rotation can be extracted from such studies. In systems where the rotating moiety is attached to a molecule of a reasonable size, three simplifying steps in the interpretation of ^{13}C T_1 data can be made. First, the relaxation time behaviour of the molecule as a whole will probably be dominated by the dipole–dipole interaction (14). This is important because the relevant calculations are related to the dipolar relaxation rate alone, and the identification and factoring out of secondary mechanisms can be difficult. Second, the motion of the entire molecule tends to become essentially isotropic which results in a further reduction in the complexity of the calculations. Finally, the determination of the isotropic diffusion constant D for the molecule is obtainable from the T_1 values of the peripheral rigid backbone carbons. By contrast, in small molecules with few distinctly different carbon atoms it may be necessary to estimate D from temperature dependent density and viscosity data, or from dielectric relaxation times (7).

A freely rotating methyl group attached to an isotropically reorienting rigid molecule can have a spin rotation (SR) contribution to T_1. Examples of this effect can be found in the study by Lyerla and Grant (*7a*) of methyl rotational barriers in small molecules. Measurement of this contribution to T_1 can be used to estimate energy barriers, as shown by the work of Zens and Ellis (18). In the present cases the SR contribution was not important because of the large molecular size, longer correlation times, and hence faster relaxation rates. Thus, measured T_1 values can be used without correction in the calculation of energy barriers for either

Can. J. Chem. Downloaded from www.nrcresearchpress.com by 210.87.254.6 on 09/05/12
For personal use only.

the random jump or stochastic diffusion models (15). The former involves a methyl group jumping randomly between its three minimum energy positions, while the latter assumes a Gaussian probability distribution for the orientation of the group.

For a system behaving isotropically, the relaxation rate $(T_1\mathrm{dd})^{-1}$ from the random jump model is related to the internal methyl jumping rate K by eq. 1:

$$[1]\quad (T_1\mathrm{dd})^{-1} = \frac{3\gamma_H^2\gamma_c^2\hbar^2}{2r^6}D^{-1} \times \left[\frac{A_1 + B_1 + C_1}{6} + \frac{A_2 + A_3 + B_2 + B_3 + C_2 + C_3}{6 + KD^{-1}}\right]$$

where the isotropic diffusion constant is given by 2:

$$[2]\qquad D = \tfrac{1}{6}[\gamma_H^2\gamma_c^2\hbar^2 T_1^* r^{-6}]$$

The backbone methine carbons have an average relaxation time of T_1^*, and the geometric factors A_i, B_i, and C_i are discussed elsewhere (15).

The resultant value of K can be related to the internal rotation barrier (V_r) by:

$$[3]\qquad K = K_0 \exp(-V_r/RT)$$

where K_0 = three-halves times the rate of reorientation of a methyl moiety in the gas phase, $1.3 \times 10^{13}\ \mathrm{s}^{-1}$.

In the stochastic diffusion model K_0 is just two-thirds times this value and the relaxation rate is related to the methyl diffusion rate (K') by the equation.

$$[4]\qquad T_1^{-1} = \frac{3\gamma_H^2\gamma_c^2\hbar^2}{2r^6}D^{-1}\left[\frac{A_1 + B_1 + C_1}{6} + \frac{A_2 + B_2 + C_2}{6 + K'/D} + \frac{A_3 + B_3 + C_3}{6 + 4K'/D}\right]$$

Theory predicts (15, 16) that a freely rotating sp^3 methyl carbon attached to an isotropically reorienting rigid molecule, satisfying the extreme narrowing condition and having only one degree of internal freedom, will have a T_1 three times that of a methine carbon located on the backbone. Conversely, an immobile methyl under such conditions may have a T_1 of one-third of that of the backbone methine carbon. Relaxation rates between these extremes will be observed for intermediate rates of rotation (16), and under these conditions energy barriers may be obtained.

Experimental

The compounds studied were prepared and purified by methods published elsewhere (17). Solutions for nmr were prepared in $CDCl_3$ and not degassed unless otherwise noted. All spectra were obtained on a Varian CFT-20 FT nmr spectrometer at 20 MHz with an 8K 620L-100 computer. Sealed sample tubes (8 mm o.d.) were used at ambient temperatures (*ca.* 36 °C). Complete, noise modulated, proton decoupling was employed. Chemical shifts were internally referenced to the $CDCl_3$ lock, corrected, and reported relative to TMS. For each T_1 some 10 to 18 spectra were used and each run repeated at least three times. Very short T_1 values were measured by the inversion–recovery technique (19) with a $(180°-\tau-90°-\mathrm{delay})_n$ pulse sequence. Longer T_1 values were more conveniently obtained from the progressive saturation technique (20), $(90°-\tau)_n$. For very long T_1 values, particularly quaternary carbons, the intensity-ratio modification (21) of the progressive saturation method was employed. The advantages of and errors in such measurements have been discussed by Levy and Peat (22). The estimated errors in this work range from ±15% in dilute solutions to ±5% in the most concentrated.

Values of T_1 were determined from a linear least-squares fit of intensity data to eq. 5:

$$[5]\qquad \ln(M_0 - M_\tau) = -\tau/T_1$$

M_0 being the equilibrium intensity $(\tau \geqslant 5T_1)$ of a given resonance and M_τ is the intensity at a pulse delay time of τ. In the calculation, allowance was made for the fact that for τ values much longer than $2T_1$ the M_τ values used should be given less importance than those of shorter τ values (22). Calculations were performed on a Hewlett-Packard 2100-A minicomputer or an IBM 370/158 with programs written in Fortran IV.

Nuclear Overhauser enhancements (nOe) were measured using the gated decoupling technique (23) from integrated intensities.

Peak assignments were made using observed shifts, proton coupling patterns, and T_1 values. Methylene (sp^3) carbons were readily located in the region 64–72 ppm by off-resonance decoupling. Methine carbons were usually found in the region of 39–56 ppm with T_1 values similar to those of the aromatic carbons and twice as long as those of the methylene carbons. The protonated carbons of the tosylate groups were identifiable from their relaxation times. The increased internal motion of this unit, relative to the rigid backbone structure, results in significantly longer T_1 values. Comparison with *p*-toluene sulphonyl chloride also assisted in the assignment.

The *tert*-butyl methyl and quaternary carbons have similar shifts in these compounds, but are readily differentiated by off resonance decoupling. Other methyl substituents were invariably found in the region 14–16 ppm and confirmed by their very short T_1 values and proton coupling patterns.

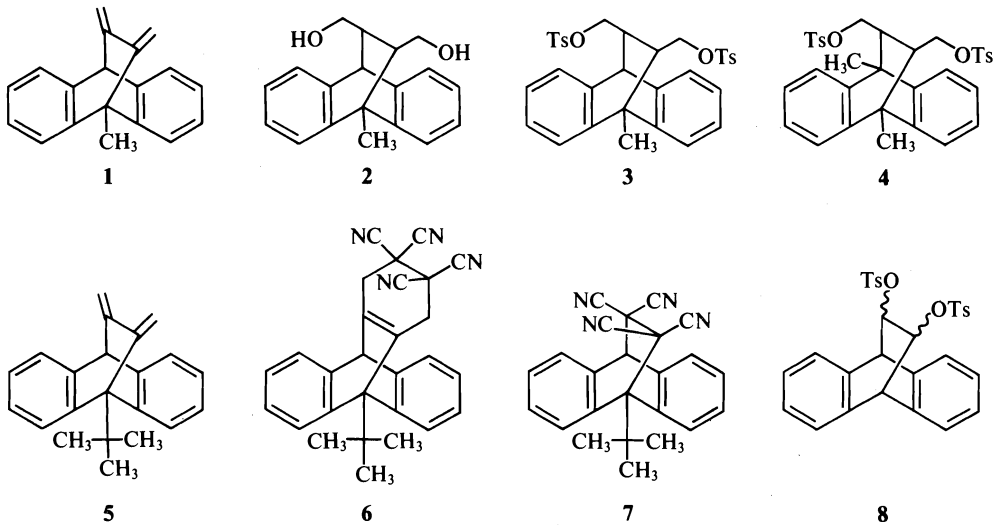

FIG. 1. Structures of compounds discussed.

Results and Discussion

The measured relaxation rate in any experiment will be a sum of the relaxation rates due to the various possible mechanisms for the ^{13}C nucleus (24):

$$[6] \quad T_1^{-1}(\text{obs}) = T_1^{-1}(\text{dd-inter}) + T_1^{-1}(\text{dd-intra}) + T_1^{-1}(\text{SR}) + T_1^{-1}(\text{CSA}) + T_1^{-1}(\text{SC}) + T_1^{-1}(\text{e})$$

where the terms correspond respectively to dipole–dipole inter- and intramolecular, spin rotation, chemical shift anisotropy, scalar coupling, and electron–nuclear dipolar interactions. In the present study the predominant mechanism is the intramolecular dipolar one (14, 25), since for each protonated carbon a maximum nOe (26) was observed within experimental error. Thus the eq. 1–4 introduced above can be used directly with the observed T_1 values.

The compounds are shown and numbered in Fig. 1. The relevant chemical shift and relaxation data are given in Table 1 together with calculated isotropic diffusion constants. These constants were obtained from the average T_1 of the protonated sp^2 carbons of the backbone and eq. 2 with appropriate values for the constants, assuming all sp^2 carbon–hydrogen bond lengths to be identical. In fact, in these systems, inclusion of all protonated backbone carbons makes only minor changes in the end results, even without correction for variations in C—H bond length. For backbone carbons of identical bond length the T_1 values should reflect only the number of bonded hydrogens, to a good degree of approximation. Variations greater than experimental error, such as seen in compound **1** for example, can probably be ascribed to anisotropy of motion. A more detailed description of the motions of this and similar molecules are the subject of a separate study, but for this work the averaged T_1 value was used as if the molecule were reorienting isotropically.

Intramolecular dipole–dipole relaxation involving hydrogens not bonded directly to the carbon under study should also be considered here. The r^{-6} dependence of this relaxation mechanism suggest that such contributions will be comparatively small even in these fairly congested molecules. Although such contributions have been therefore ignored in these systems, there are some small differences in T_1 values which need further comment. The olefinic methylene carbons of compounds **1** and **5** can be separately identified because of a small long-range coupling on one of them to the neighboring bridgehead proton. In both compounds there are small differences in the two methylene T_1 carbons, 1.44 *vs.* 1.21 seconds for compound **1** and 1.13 *vs.* 0.91 seconds for compound **5**. The longer T_1 is associated with the methylene carbon showing the long-range proton coupling. Deviation from isotropic motion will permit the

Can. J. Chem. Downloaded from www.nrcresearchpress.com by 210.87.254.6 on 09/05/12
For personal use only.

Can. J. Chem. Downloaded from www.nrcresearchpress.com by 210.87.254.6 on 09/05/12
For personal use only.

TABLE 1. Chemical shift (δ, ppm) and relaxation data (T_1,s)

	1		2		3		4		5		6		7		8 *trans*		8 *cis*	
Assignment	δ	T_1	δ	T_1	δ	T_1	δ	T_1	δ	T_1	δ	T_1	δ	T_1	δ	T_1	δ	T_1
Aromatic and	146.7	—	145.8	—	144.9	—	145.4	7.60	148.6	—	145.9	—	136.9		145.0	—	145.0	—
olefinic	144.8	—	143.9	—	144.7	—	144.9	7.28	147.1	—	144.2	—	136.5		142.1	—	142.2	—
quaternary	143.5	—	142.9	—	142.5	—	142.3	5.68	144.8	—	142.2	—		—	139.2	—	139.5	—
and tosylate	142.5	—	141.2	—	141.6	—			142.8	—	138.2	—		—	132.7	—	132.7	—
quaternary					139.5	—			141.2	—	110.4							
					132.7	—	132.7	6.81	136.1	—	110.3	—						
					132.5	—												
Tosylate					129.8	0.33	129.9	1.00							129.6	0.94	130.0	0.95
aromatic CH					127.7	0.34	127.9	0.98							127.9	0.79	127.8	1.18
					127.5	0.35												
Aromatic	125.7	2.88	125.8	1.06	126.1	0.10	126.1	0.36	126.8	2.20	126.2	0.91	129.2	1.27	126.6	0.35	126.3	0.47
backbone —CH	122.7	3.37	125.7	0.99	126.0	0.10			125.9	2.07	124.8	0.82	128.9	1.22	126.2	0.39	125.4	0.52
	120.4	4.08	124.6	1.20	125.2	0.11			125.0	2.06	124.4	0.89	128.4	1.22	125.6	0.41		
			123.2	0.98	123.4	0.16	122.5	0.44	123.6	1.89	123.3	0.93	127.3	1.32	123.6	0.32	123.6	0.49
			122.3	1.05	122.4	0.11												
			120.6	1.05	120.6	0.14	120.8	0.46										
Tosylate (*para* CH_3)					21.4	1.02	21.7	3.05							21.7	—	21.6	1.87
Bridge subst.	103.8	1.44	66.6	0.56	71.4	0.07	71.4	0.28	109.4	1.13	35.4	0.57			71.4	0.21	69.1	0.23
CH_2,	102.2	1.21	64.2	0.53					102.9	0.91	35.2	0.55						
Bridge and	55.1	3.96	47.4	0.93	45.8	0.13	48.3	0.37	56.5	2.76	55.6	0.99	52.6	1.36	44.8	0.39	45.6	0.53
bridgehead CH			46.5	0.92	44.3	0.11									42.1	0.42	39.8	0.53
					44.1	0.11												
Bridgehead	48.1	—	44.0	—	43.7	—	43.4	5.17	64.1	—	68.4	—						
quaternary																		
tert-Butyl																		
quaternary									33.9	—	33.2	—	37.2	—				
Parameter																		
NT_1(Av)	3.18		1.02		0.12		0.42		2.05		0.97		1.29		0.39		0.51	
τ_c(s)	1.5×10^{-11}		4.6×10^{-11}		4.0×10^{-10}		1.1×10^{-10}		2.2×10^{-11}		5.2×10^{-11}		3.7×10^{-11}		1.2×10^{-10}		9.2×10^{-11}	
$D(s^{-1})$	1.1×10^{10}		3.7×10^{9}		4.0×10^{8}		1.52×10^{9}		7.6×10^{9}		3.2×10^{9}		4.5×10^{9}		1.4×19^{9}		1.8×10^{9}	

TABLE 2. Methyl rotational barriers

Compound	T_1^{calc} (s) Locked	T_1^{calc} (s) Free	T_1^{obs}	Chemical shift	V_r (kcal mol^{-1}) Random jump	V_r (kcal mol^{-1}) Stochastic diffusion
1	1.06	9.54	1.15	14.2	4.5[c]	—
2	0.34	3.06	0.38	15.7	5.5[c]	—
3	0.04	0.36	0.06	15.3	7.5[c]	—
4	0.14	1.26	0.14	15.9	6.5[c]	—
5	0.68	6.15	4.55 6.02	33.2[a] 33.0[b]	1.7 Free	1.8 Free
6	0.32	2.91	3.16 3.33	34.2[a] 33.6[b]	Free Free	Free Free
7	0.43	3.87	2.12 3.34	33.4[a] 33.0[b]	2.5 Free	2.7 Free

[a]See Fig. 2*a*.
[b]See Fig. 2*b*.
[c]Lower limit estimate.

C—H vector of the respective methylene groups to have different cosines with respect to the principal axes of diffusion, and would thus cause differences in relaxation rate (27). Examination of the aromatic methine carbon relaxation times suggests that anisotropy of motion is more severe in compound **1** than **5**, but without a detailed analysis the actual effect on the methylene protons cannot be predicted. Looking for similar effects in the bridge substituents of the other molecules is hampered by the lack of chemical shift differences in all but compound **2**. However, in this system it is clear that the differences in T_1 for the bridge CH (0.93 and 0.92 s) and the substituent —CH_2OH (0.56 and 0.53 s) are negligible. By contrast, the *tert*-butyl analogue of compound **2**, which is not reported here in detail, does show a 20% difference in T_1 for the —CH_2OH groups and is thus comparable with compound **5**.

It is interesting to note that the CH_2O groups attached to the bridge of these compounds do not appear to exhibit significant internal rotation as far as any effect on their T_1 values is concerned. Thus the carbon atom of this group is relaxing essentially twice as fast as the average relaxation rate of the corresponding backbone carbons, which is consistent with the presence of two C—H bonds *vs.* one. By contrast, the influence of additional motion on the T_1 values of the tosylate aromatic ring and methyl group is quite marked. The ring of the tosylate group is clearly in a position to move fairly unrestrictedly, and this is of course a considerable aid in the identification of its resonances. The apparent lack of significant extra motion of the CH_2O moiety also appears in the system which does not contain a substituent in the bridgehead position, compound **8**. Both the *cis*- and *trans*-isomers of this derivative have been examined and reveal no significant differences in the T_1 parameters, although there are differences in chemical shifts.

Barriers to Rotation

The observed T_1 values for the bridgehead methyl groups of compounds **1** to **4** indicate correlation times essentially determined by the tumbling of the overall system. This implies that the methyl groups are not freely rotating. Molecular models (Dreiding) indicate that in the staggered conformation the hydrogens of the methyl group are approximately 2.4 Å from the *peri*-hydrogens of the aromatic ring. Rotation about the C—C bond would bring two methyl protons to within the estimated van der Waal's radii of these *peri*-hydrogens, while the bridge part of the molecule provides a further nonbonding interaction with the third proton. Thus resistance to free rotation is not unexpected. The symmetry of the 'locked' environment in these cases should provide an A_2B proton nmr spectrum, however at temperatures accessible in this study (to −70 °C) only

Can. J. Chem. Downloaded from www.nrcresearchpress.com by 210.87.254.6 on 09/05/12
For personal use only.

Can. J. Chem. Downloaded from www.nrcresearchpress.com by 210.87.254.6 on 09/05/12
For personal use only.

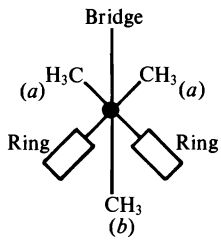

FIG. 2. Newman projection of *tert*-butyl group about the C_9—C_{t-Bu} bond.

a single line averaged spectrum was obtained. From the observed T_1 values it is possible to compute a minimum energy barrier preventing free rotation and these are given in Table 2. The values obtained are similar in magnitude to the 7.2 kcal mol^{-1} obtained by Anderson and Rawson (10) in a related system. The difference in values between compounds **3** and **4**, which should be effectively identical, reflect differences in concentration (**3** was more concentrated) and error limits. Errors are discussed further below.

Compounds **5**, **6**, and **7** all contain a *tert*-butyl group at the bridgehead position, and in each case the group is effectively locked in a staggered configuration relative to the rest of the molecule (Fig. 2). Symmetry requires two of the methyl groups to be identical (Fig. 2*b*), and both the ^1H and ^{13}C nmr spectra show two methyl group resonances in the ratio of 2:1. The weaker line in the ^{13}C spectrum is to high field and can be assigned to the methyl bisecting the angle described by the aromatic rings. In each case this carbon atom has a relaxation rate typical of a free rotor. The remaining identical carbons show varying rates of rotation depending on the substituents at the bridge position. Calculation of these barriers, using eqs. 1–4 are given in Table 2. Using the random jump model, the highest barrier of 2.5 kcal mol^{-1} is observed for **7** which represents the most sterically crowded system of this series. The lowest barrier is found in **6** which corresponds to effectively free rotation. Nakanishi *et al.* (3) have observed differential proton resonance broadening for the three methyl groups of a locked *tert*-butyl moiety, and assumed this to infer different rates of rotation within each methyl. The present results confirm that this does indeed occur and furthermore is much easier to observe using T_1 measurements.

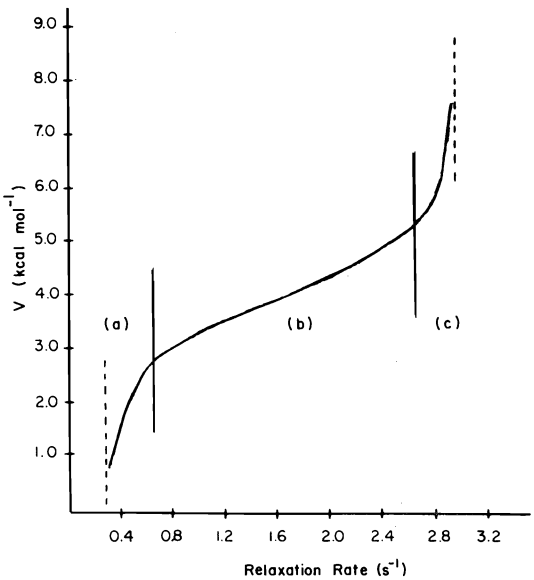

FIG. 3. Plot of the barrier to methyl rotation *vs.* relaxation rate for the random jump model.

The *tert*-butyl analogs of compounds **1** to **4** have three different methyl sites, and initial studies indicate, as expected, three different energy barriers to methyl rotation.

The difference in energy barriers calculated from the random jump and stochastic diffusion models is a systematic one, the latter being consistently higher.

Comments on Errors

For a given situation, a diffusion constant D and correlation time τ_c is obtained from the rigid isotropically reorienting backbone of the molecule. Using eq. 1 a plot of energy barrier *vs.* relaxation rate can then be obtained and a typical result is shown in Fig. 3. The curve has three regions. In (*a*) and (*c*) the calculated barriers asymptotically approach zero and infinity respectively, and in these regions very accurate relaxation data is necessary to obtain any meaningful information. In region (*b*) the restrictions are much less severe. The precision of the relaxation data alone is not sufficient to estimate errors since changes in geometry also affect the calculation. The results of possible errors in diffusion constant D, relaxation rate T_1^{-1}, and the C—H bond angle α on the calculated energy barrier V_r are shown in Table 3. In the region

TABLE 3. Error analysis: effect of changes in relaxation rate, isotropic diffusion constant, and geometry on calculated random jump barriers V_r

	$R + \Delta R^a$		$D + \Delta D^b$		α^c	
V_r	−10%	+15%	−10%	+15%	107.8	113.0
0.72	[d]	1.48	[d]	1.40	[d]	1.83
1.09	[d]	1.64	[d]	1.55	[d]	1.91
1.65	1.35	1.94	1.08	1.99	1.29	2.05
2.64	2.45	2.86	2.51	2.77	2.47	2.89
3.11	2.98	3.28	3.00	3.20	3.04	3.23
5.29	4.80	[d]	4.86	[d]	5.28	5.32

[a]Relaxation rate.
[b]Isotropic diffusion constant.
[c]See text for definition of this angle.
[d]Outside theoretical limits.

where the curve approaches a limit asymptotically the errors are severely magnified as expected. In general, for barriers much below 2 kcal mol^{-1} or above 6 kcal mol^{-1} relatively large errors can be anticipated using the T_1 method. Between these extremes errors of ± 10 to 15% are probable, depending on the reliability of the T_1 data and the available geometric parameters. The error factors have been calculated here only for the random jump model since they are essentially identical in both models.

Acknowledgments

We wish to thank Dr. D. N. Butler and Dr. R. A. Snow for providing the compounds used in this study. One of us (D.E.A.) thanks the National Research Council of Canada for a postgraduate scholarship, and financial support from the NRCC in support of this study is also gratefully acknowledged.

1. (*a*) F. A. L. ANET, M. ST. JACQUES, and G. N. CHMURNY. J. Am. Chem. Soc. **90**, 5243 (1968); (*b*) A. RICKER and H. KERSLER. Tetrahedron Lett. 1227 (1969); (*c*) J. E. ANDERSON and H. PEARSON. J. Chem. Soc. B, 1209 (1971); (*d*) C. H. BUSHWELLER, G. U. RAO, W. G. ANDERSON, and P. E. STEVENSON. J. Am. Chem. Soc. **94**, 4744 (1972).
2. M. OKI and M. SUDA. Bull. Chem. Soc. Jpn. **44**, 1876 (1971).
3. H. NAKANISHI, D. YAMAMOTO, M. NAKAMURA, and M. OKI. Tetrahedron Lett. 727 (1973).
4. F. SUZUKI, M. OKI, and H. NAKANISHI. Bull. Chem. Soc. Jpn. **46**, 2858 (1973).
5. M. NAKAMURA, M. OKI, and H. NAKANISHI. Tetrahedron, **30**, 543 (1974).
6. I. MORISHIMA and T. IIZUKA. J. Am. Chem. Soc. **96**, 7365 (1974).
7. (*a*) J. R. LYERLA and D. M. GRANT. J. Phys. Chem. **76**, 3213 (1972); (*b*) K. F. KUHLMANN and D. M. GRANT. J. Chem. Phys. **55**, 2998 (1971).
8. T. D. ALGER, D. M. GRANT, and R. K. HARRIS. J. Phys. Chem. **76**, 281 (1972).
9. M. NAKAMURA, M. OKI, H. NAKANISHI, and O. YAMAMOTO. Bull. Chem. Soc. Jpn. **47**, 2415 (1974).
10. J. E. ANDERSON and D. I. RAWSON. Chem. Commun. 830 (1973).
11. G. C. LEVY and G. L. NELSON. J. Am. Chem. Soc. **94**, 4897 (1972).
12. K. D. BARTLE, P. M. G. BAVIN, D. W. JONES, and R. L'AIME. Tetrahedron, **26**, 911 (1967).
13. J. P. N. BREWER, H. HEANEY, and B. A. MARPLES. Chem. Commun. 27 (1967).
14. (*a*) A. ALLERHAND, D. DODDRELL, and R. KOMOROSKI. J. Chem. Phys. **55**, 189 (1971); (*b*) K. F. KUHLMANN, D. M. GRANT, and R. K. HARRIS. J. Chem. Phys. **52**, 3439 (1970).
15. D. E. WOESSNER, B. S. SNOWDEN, JR., and G. H. MEYER. J. Chem. Phys. **50**, 719 (1969).
16. D. DODDRELL, V. GLUSHKO, and A. ALLERHAND. J. Chem. Phys. **56**, 3683 (1972).
17. R. A. SNOW. Ph.D. Thesis, York University, Toronto, Ontario. 1976.
18. A. P. ZENS and P. D. ELLIS. J. Am. Chem. Soc. **97**, 5685 (1975).
19. R. L. VOLD, J. S. WAUGH, M. P. KLEIN, and D. E. PHELPS. J. Chem. Phys. **48**, 3831 (1968).
20. R. FREEMAN and H. D. W. HILL. J. Chem. Phys. **54**, 3367 (1971).
21. R. FREEMAN, H. D. W. HILL, and R. KAPTEIN. J. Magn. Reson. **6**, 84 (1972).
22. G. C. LEVY and I. R. PEAT. J. Magn. Reson. **18**, 500 (1975).
23. O. A. GANSOW and W. SCHITTENHELM. J. Am. Chem. Soc. **93**, 4294 (1971).
24. G. C. LEVY and G. L. NELSON. Carbon-13 nuclear magnetic resonance for organic chemists. Wiley, New York. 1972.
25. K. F. KUHLMANN and D. M. GRANT. J. Am. Chem. Soc. **90**, 7355 (1968).
26. E. BREITMAIER, K. H. SPOHN, and S. BERGER. Angew. Chem. Int. Ed. Engl. **14**, 144 (1975).
27. D. E. WOESSNER. J. Chem. Phys. **37**, 647 (1962).

Can. J. Chem. Downloaded from www.nrcresearchpress.com by 210.87.254.6 on 09/05/12
For personal use only.

Metal complexes of sulfur-nitrogen chelating agents. V. 2-*N*-Ethylaminocyclopentene-1-dithiocarboxylic acid complexes of Ni(II), Pd(II), Pt(II), Co(II), Co(III), and Cu(I)

K. NAG AND D. S. JOARDAR

Department of Inorganic Chemistry, Indian Association for the Cultivation of Science, Calcutta 700032, India

Received February 5, 1976

K. NAG and D. S. JOARDAR. Can. J. Chem. **54**, 2827 (1976).

2-*N*-Ethylaminocyclopentene-1-dithiocarboxylic acid (EACDA) acts as an ambidentate ligand toward several metal ions. Bis-chelates have been obtained with Ni(II), Pd(II), Pt(II), and Co(II), and tris-chelate with Co(III). Cu(I) forms a 1:1 complex. The bonding sites involved in the metal chelates and their stereochemistry have been ascertained from electronic, infrared and nmr spectra, magnetic moment, and thermal analysis. In the Co(II) and Co(III) chelates bonding takes place from (S,S^-) donor sites, whereas in the Ni(II), Pd(II), and Pt(II) chelates (N,S^-) type bonding occurs. The Cu(I) complex appears to be polymeric in nature.

K. NAG et D. S. JOARDAR. Can. J. Chem. **54**, 2827 (1976).

L'acide *N*-éthylamino-2 cyclopentènedithiocarboxylique-1 (EACDA) agit comme un ligand ambidentate vis-à-vis plusieurs ions métalliques. On a obtenu des bis-chélates avec le Ni(II), le Pd(II), le Pt(II) et Co(II) et des tris-chélates avec le Co(III). Le Cu(I) forme un complexe 1:1. On a déterminé les sites de complexations impliqués dans les chélates métalliques et leur stéréochimie à partir des spectres électroniques, ir et rmn, des moments magnétiques et de l'analyse thermique. Dans les chélates du Co(II) et du Co(III), la liaison se fait par les sites donneurs (S,S^-) alors que dans les chélates Ni(II) et Pd(II) et Pt(II), il se produit une liaison du type (N,S^-). Il semble que le complexe Cu(I) soit de nature polymérique.

[Traduit par le journal]

Introduction

In contrast to aminocarboxylic acid complexes of various metal ions, complexes of aminodithiocarboxylic acids are strikingly lacking. In view of the interesting role played by aminocarboxylic acid complexes in body systems and also because of the current interest in metal–sulfur compounds in biological molecules delineation of the nature of metal ion binding and stereochemistry in aminodithiocarboxylic acid complexes seems desirable. To serve this purpose we used (1–3) 2-aminocyclopentene-1-dithiocarboxylic acid (ACDA) as the chelating agent. This ligand contains the back bone $NH_2-C=C-\overset{\overset{S}{\|}}{C}-S^-$ which has some similarity with derivatives of dithiocarbazic acid $-\overset{|}{N}-\overset{|}{N}-\overset{\overset{S}{\|}}{C}-S^-$. Metal dithiocarbazates have been adequately investigated in recent years (4–7). These types of ligands are ambidentate in nature. With ACDA for a large number of metal ions (N,S^-) bonding sites are involved in bond formation (1, 2), whereas with Co(II), Co(III), and Cr(III) disulfur chelation takes place (3). The phenomenon of geometrical isomerism is also observed in Ni(II), Pd(II), and Pt(II) complexes. In dithiocarbazic acid derivatives it has been observed (4, 5) that while with the parent acid itself and some of its N(2) substituted derivatives (N,S^-) type chelation takes place, on the other hand N(3) substituted products prevent *N*-coordination regardless of the electron-releasing or electron-withdrawing ability of the substituents, thus indicating a strong steric effect for the substituents. This prompted us to investigate the coordination behavior of 2-*N*-ethylaminocyclopentene-1-dithiocarboxylic acid (EACDA) with some metal ions.

Experimental

Chemicals

Chemicals and solvents used were the same as described earlier (1–3).

EACDA

The ligand was prepared by the amine exchange reaction between 2-aminocyclopentene-1-dithiocarboxylic acid and ethylamine adopting the procedure of Bordas *et al.* (8) with slight modification. When the neutralization is accomplished with 2 *N* HCl under ice cooled condition instead of acetic acid a better yield is obtained (90%). The compound was recrystallized from air-free acetone at room temperature. The ligand was converted to its ammonium salt in a similar way described previously (1).

Can. J. Chem. Downloaded from www.nrcresearchpress.com by 210.87.254.42 on 09/05/12
For personal use only.

TABLE 1. Analytical and magnetic data

Compound	Color	M Calcd.	M Found	N Calcd.	N Found	S Calcd.	S Found	μ_{eff} (B.M.)
NiL_2	Dark red	13.6	13.7	6.5	6.6	29.7	29.5	Diamagnetic
PdL_2	Yellow	22.2	22.1	5.8	5.9	26.7	26.8	Diamagnetic
CuL	Chocolate	25.5	25.3	5.6	5.6	25.6	25.5	Diamagnetic
CoL_2	Snuff	13.7	13.6	6.5	6.5	29.7	29.5	2.66
CoL_3	Deep Brown	9.5	9.5	6.8	6.9	31.1	31.2	Diamagnetic
PtL_2*	Vermilion	—	—	4.9	5.0	—	—	Diamagnetic

*Calcd.: C, 33.9; H, 4.2. Found: C, 33.8; H, 4.2.

$Ni(EACDA)_2$

An aqueous solution of the ammonium salt of the ligand (4 mmol) was added dropwise with stirring to an aqueous solution of hydrated nickel chloride (2.1 mmol). After stirring the mixture for *ca.* 1 h, the precipitated compound was filtered, washed thoroughly with water and finally with acetone. The compound was substantially pure and could not be recrystallized due to the lack of proper solvent; yield 90%.

$Pd(EACDA)_2$

This compound was prepared in a similar way from sodium tetrachloropalladate (II); yield 85%.

$Pt(EACDA)_2$

The reaction between potassium tetrachloroplatinite(II) and the ammonium salt of the ligand being somewhat slow, the stirring of the mixture in this case was continued for 4 h. The compound separated was filtered and washed first with water, then with warm water till the filtrate was free from chloride, and finally with acetone; yield 80%.

$Co^{II}(EACDA)_2$

An aqueous solution of the ligand (4 mmol) was allowed to drip slowly into a stirred aqueous solution containing hydrated cobalt nitrate (2.1 mmol) and ammonium nitrate (2 g) in a current of nitrogen. After stirring the mixture for 30 min, the slurry was filtered through a fine porosity glass frit and washed successively with water and acetone–water mixture (1:1). The compound was recrystallized from chloroform (under nitrogen atmosphere), dried and stored *in vacuo*; yield 80%.

$Co^{III}(EACDA)_3$

To an aqueous solution of the ligand (6.4 mmol) an aqueous solution of hexaminocobaltic nitrate (2 mmol) was added with stirring. The mixture, after stirring for 30 min, was filtered and washed liberally with water and finally with acetone. The compound was recrystallized from chloroform; yield 80%.

$Cu^{I}(EACDA)_2$

By treating the ammonium salt of EACDA in equimolar proportion with cuprous iodide (dissolved in excess of potassium iodide solution) this compound was obtained in 80% yield.

Physical Measurements

Ultraviolet and visible spectra were recorded in Hilger UV-spek or Spectro MOM 201 spectrophotometer. For Co(II) and Co(III) complexes chloroform solutions (10^{-5}–10^{-3} *M*) were used and for Ni(II) and Cu(I) complexes saturated solutions in chloroform were used. The mull spectra of Ni(II), Pd(II), and Pt(II) complexes were also recorded. Infrared spectra (in Nujol mull) were recorded in the range 4000–200 cm^{-1} in a Perkin-Elmer Model 621 spectrophotometer. Nuclear magnetic resonance spectra of EACDA and $Co(EACDA)_3$ were recorded on a Varian 60 MHz spectrometer, at room temperature, in CCl_4 and $CDCl_3$ solutions respectively using TMS as the internal reference. Magnetic measurements were performed on a Guoy balance and thermal analysis was carried out with a MOM Derivatograph.

Results and Discussion

Table 1 shows color, composition, and magnetic moment of the compounds. All but the Co(II) and the Co(III) compounds are practically insoluble in common organic solvents. Ni(II) and Cu(I) complexes are slightly soluble in chloroform. Co(II) and Co(III) complexes are fairly soluble in acetone, chloroform, and benzene. Except for the Co(II) complex, which shows a room temperature magnetic moment of 2.66 B.M., the compounds are diamagnetic. In low-spin octahedral complexes of Co(II), the magnetic moments are close in the range 1.8–2.0 B.M. (9), whereas for Co(II) complexes

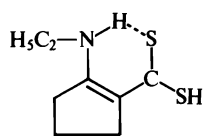

1

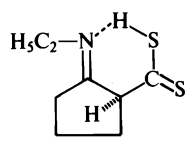

2

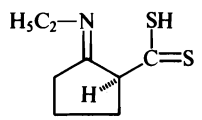

3

Can. J. Chem. Downloaded from www.nrcresearchpress.com by 210.87.254.42 on 09/05/12
For personal use only.

TABLE 2. Nuclear magnetic resonance data

Compound	Solvent	Chemical shift*					
		N-Ethyl					
		CH_3	CH_2	$CH_{2(4)}$	$CH_{2(3,5)}$	SH	NH
EACDA	CCl_4	1.33(6 cps)	3.40(6 cps)	1.86(7 cps)	2.66	4.60	12.1
$Co(EACDA)_3$	$CDCl_3$	1.24(6 cps)	3.30(6 cps)	1.84(6 cps)	2.68	—	8.66

*Chemical shift values refer to δ scale (ppm).

having definite square planar configuration the values fall in the range 2.1–2.8 B.M. (9, 10).

The ligand in principle may exist in several tautomeric forms. Among these, the zwitterionic form may be excluded since a sharp medium intensity band due to sulfhydryl is observed at 2440 cm^{-1} and no band due to ν(N—H) could be observed. The tautomeric forms **2** and **3** also appear unlikely on the basis of nmr spectrum of EACDA, whose chemical shifts (Table 2) are consistent with the structure **1**.

The nmr spectrum of $Co(EACDA)_3$ in $CDCl_3$ shows a triplet due to —CH_3 and a quintet due to —CH_2— group in the *N*-ethyl substituent at δ 1.24 ppm and δ 3.30 ppm, respectively. It may be seen that the chemical shifts due to these groups remain practically unchanged in the complex with respect to the ligand (Table 2). This means that the ligand is not bound with Co(III) through the nitrogen atom. Had this been the case, there would have been large shift particularly of the CH_2 protons in the down field. In fact CH_3 and CH_2 protons have suffered a slight up field shift by *ca.* 0.10 ppm. The signal due to the NH proton appears at δ 8.66 ppm and is slowly exchanged with D_2O. The large chemical shift of the NH proton (by *ca.* 3.44 ppm) in the up field region may be regarded as a positive evidence for (S,S^-) type bonding in the complex. Table 2 shows that the other resonances in the complex remain unaffected.

Table 3 summarizes the bands observed in the electronic spectra of the ligand and its chelates. In the ligand three bands are observed in the range 25–40 kK, their high intensities indicate π–π^* type transitions. In the Co(II) complex altogether four bands are observed, among these the bands at 25.1 and 32.8 kK appear almost at the same energies as observed in the ligand. The highest energy band in the complex at 37 kK suffers considerable red shift with respect to the ligand band (at 39.2 kK). To our knowledge there is little information available in the literature on the electronic spectra of (N,S^-) type or (S,S^-) type low-spin square planar complexes of Co(II). Everett and Holm (11) reported a narrow band at 8.5 kK and a strong band at 20 kK in the low-spin complexes with the $[CoO_2N_2]$ chromophore. Few other square planar complexes of Co(II) are also reported (12, 13) to exhibit a band around 23–20 kK due to $^1A_{1g} \rightarrow {}^1T_{1g}$ transition. In $Co(EACDA)_2$ no band could be detected in the lower energy range. The band at 21.5 kK is of very high intensity, consequent to this we assume it to be due to both charge-transfer (CT) and d–d transition. In the Co(III) complex apart from the three bands due to internal ligand transitions, two other bands appear at 15.6 and 21.4 kK. The latter one may be regarded as due to $^1A_{1g} \rightarrow {}^1T_{2g}$ transition coupled with CT, and the former one as due to $^1A_{1g} \rightarrow {}^1T_{1g}$ transition. Although the 10 *Dq* value in this complex could not be evaluated, however, the energy of the first spin-allowed transition suggests it to be a disulfur chelated species. It has been indicated (3, 14, 15) that for a large number of Co(III) complexes having $[CoS_6]$ chromophore the first spin-allowed transition occurs in the range 15–16 kK, whereas in compounds having $[CoN_3S_3]$ chromophore the corresponding band energy is 17.5–18.5 kK. In the Ni(II) complex three bands are observed in chloroform solution and two bands in the mull spectrum. The band at 18.2 kK may be regarded as arising due to $^1A_{1g} \rightarrow {}^1A_{2g}$ transition. It is likely that the $^1A_{1g} \rightarrow {}^1B_{1g}$ transition is swamped by the ligand band at 26.3 kK. Since in complexes having $[NiS_4]$ chromophore $^1A_{1g} \rightarrow {}^1A_{2g}$ transition appears in the range 15–17 kK, and with $[NiN_2S_2]$ chromophore this band energy is ~18 kK (4), so in $Ni(EACDA)_2$ bonding seems

Can. J. Chem. Downloaded from www.nrcresearchpress.com by 210.87.254.42 on 09/05/12
For personal use only.

Can. J. Chem. Downloaded from www.nrcresearchpress.com by 210.87.254.42 on 09/05/12
For personal use only.

TABLE 3. Electronic absorption spectra

Compound	Medium	λ_{max} (cm^{-1})	log ε	Assignment
EACDA	Chloroform	25 000	4.39	
		32 260	4.10	
		32 890	4.11	
		39 220	3.82	
$Co(EACDA)_2$	Chloroform	21 510	4.36	CT + $^1A_{1g} \rightarrow {}^1T_{1g}$
		25 130	4.42	$L \rightarrow L^*$
		32 790	4.01	$L \rightarrow L^*$
		37 040	3.91	$L \rightarrow L^*$
$Co(EACDA)_3$	Chloroform	15 630	2.72	$^1A_{1g} \rightarrow {}^1T_{1g}$
		21 370	4.71	CT + $^1A_{1g} \rightarrow {}^1T_{2g}$
		25 190	4.79	$L \rightarrow L^*$
		32 570	4.40	$L \rightarrow L^*$
		36 630	4.19	$L \rightarrow L^*$
$Ni(EACDA)_2$	Chloroform*	(18 350)	—	CT + ($^1A_{1g} \rightarrow {}^1A_{2g}$)
		26 320	—	$L \rightarrow L^*$ + ($^1A_{1g} \rightarrow {}^1B_{1g}$)
		35 340	—	$L \rightarrow L^*$
$Ni(EACDA)_2$	Nujol	18 180	—	CT + ($^1A_{1g} \rightarrow {}^1A_{2g}$)
		25 970	—	$L \rightarrow L^*$ + ($^1A_{1g} \rightarrow {}^1B_{1g}$)
$Pd(EACDA)_2$	Nujol	21 740	—	CT + $L \rightarrow L^*$
		27 780	—	CT
$Pt(EACDA)_2$	Nujol	19 610	—	CT + $L \rightarrow L^*$
		28 570	—	CT
Cu(EACDA)	Chloroform*	26 530	—	$L \rightarrow L^*$
		37 740	—	$L \rightarrow L^*$

*Saturated solutions of these complexes were used.

TABLE 4. Infrared data

Ligand	Infrared frequency (cm^{-1})					Assignment
	NiL_2	PdL_2	PtL_2	CoL_2	CoL_3	
—	3270(w)	3265(w)	3280(w)	3300(w,b)	3260(w)	ν(N—H)
—	3160(vw)	3150(w)	—	—	—	—
2440(m)	—	—	—	—	—	ν(S—H)
1600(vs)	1580(vs)	1590(vs)	1590(vs)	1565(s)	1570(vs)	δ(N—H) + ν(C=C)
1500(s)	1490(s)	1500(vs)	1500(vs)	—	—	ν(C=C)
1325(s)	1338(s)	1350(vs)	1350(s)	1325(s)	1338(m)	ν(C—N) + ν(C=S)
1280(s)	1280(s)	1280(s)	1278(s)	1275(m)	1268(m)	ν(C=S) + ν(C—N)
870(s)	900(s)	896(s)	892(m)	—	—	ν(Assym. CSS)
—	880(w)	878(w)	878(vw)	—	—	—
—	855(s)	850(m)	850(m)	850(w)	852(m)	—
630(w,b)	655(s)	650(vs)	640(s)	640(b)	640(m)	ν(Sym. CSS)
—	485(m)	485(m)	481(m)	—	—	ν(M—N)
—	388(vs)	338(vs)	342(s)	355(m)	357(m)	ν(M—S)
—	—	—	—	328(w)	328(w)	—

to take place from (N,S^-) donor sites of the ligand.

In Table 4 some of the important infrared bands of the ligand and the metal chelates have been listed. It has already been pointed out that no band due to ν(N—H) could be located in the ligand but the frequency due to ν(S—H) appears at 2440 cm^{-1}. In the complexes ν(N—H) is

present but ν(S—H) is absent. Ni(II), Pd(II), and Pt(II) complexes show two bands at 3270 and 3160 cm^{-1}. If bonding takes place from the dithiocarboxylate moiety only the secondary amino group then remains free and consequently ν(N—H) should appear at higher energy. In fact Co(II) and Co(III) complexes display a broad band in the range 3480–3260 cm^{-1} which supports the inference drawn already from nmr and electronic spectra. The basis for assignment of the other bands summarized in Table 4 has already been discussed (1, 3). In the case of dithiocarbamates (16, 17) and dithiocarbazates (4, 6) it is observed that when disulfur chelation takes place the band due to assymetric CSS^- stretching (at 1000 cm^{-1}) remains unsplit, whereas unidentate sulfur bonding causes this band to split. EACDA does not show any band around 1000 cm^{-1} but the strong band at 870 cm^{-1} appears to be due to CSS^- assymetric vibration. Ni(II), Pd(II), and Pt(II) chelates display three band heads at 900, 880, and 850 cm^{-1}; however, in the case of Co(II) and Co(III) chelates only a single band is observed at 850 cm^{-1}. This leads us to infer that in the former metal chelates (N,S^-) type bonding is operative, whereas in the latter type dithiocarboxylate ion binds the metal ions. The frequency due to symmetric CSS^- stretching or C—S stretching is observed in the range 655–640 cm^{-1} in the metal chelates. By screening the frequencies appearing in the lower energy range due to the ligand, a band around 485 cm^{-1} in the d^8 metal chelates has been assigned due to M—N stretching. Another band due to M—S stretching appears at 388 cm^{-1} in the Ni(II) chelate and at ~340 cm^{-1} in the Pd(II) and Pt(II) chelates. In the Co(II) and Co(III) chelates ν(M—S) appears as a doublet at 357 and 328 cm^{-1}. The two types of complexes may be represented by the structures **4** and **5**.

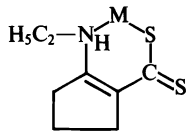

4

M = Ni(II), Pd(II), Pt(II)

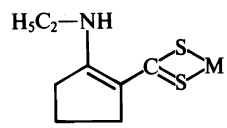

5

M = Co(II), Co(III)

So far we have not commented over the Cu(I) complex. While the electronic spectrum and the magnetic datum are not useful criteria to ascertain the nature of metal–ligand binding, the infrared spectra of the Cu(I) complex is highly unresolved which probably suggests it to be a polymeric species.

Thermal analysis of $Ni(EACDA)_2$ and $Co(EACDA)_2$ shows that the former decomposes above 210 °C and the latter is stable up to 125 °C. This difference in thermal stability is in keeping with the donor sites involved in these metal chelates, since a four-membered disulfur chelated species should be less stable than a six-membered ring involving sulfur and nitrogen.

Acknowledgment

The courtesy extended by Professor S. E. Livingstone, University of New South Wales in obtaining the ir spectra is gratefully acknowledged.

1. K. Nag and D. S. Joardar. Inorg. Chim. Acta, **14**, 133 (1975).
2. K. Nag and D. S. Joardar. Z. Naturforch., **30***b*, 107 (1975).
3. K. Nag and D. S. Joardar. Inorg. Chim. Acta, **17**, 111 (1976).
4. C. Battistoni, G. Mattogno, A. Monaci, and F. Tarli. J. Inorg. Nucl. Chem. **33**, 3915 (1971).
5. C. Battistoni, G. Mattogno, A. Monaci, and F. Tarli. Inorg. Nucl. Chem. Lett. **7**, 1081 (1971).
6. M. Akbar Ali, S. E. Livingstone, and D. J. Phillips. Inorg. Chim. Acta, **5**, 119 (1971).
7. M. F. Iskander and L. El-Sayed. J. Inorg. Nucl. Chem., **33**, 4253 (1971).
8. B. Bordas, P. Sohar, G. Matolcsy, and P. Berencsi. J. Org. Chem. **37**, 1727 (1972).
9. R. L. Carlin. Transition Met. Chem. **1**, 28 (1965).
10. B. N. Figgis and J. Lewis. Prog. Inorg. Chem., **6**, 192 (1964).
11. G. W. Everett, Jr. and R. H. Holm. J. Am. Chem. Soc. **87**, 5266 (1965).
12. M. Nicolini, C. Pecile, and A. Turco. Coord. Chem. Rev. **1**, 133 (1966).
13. A. B. P. Lever, J. Lewis, and R. S. Nyholm. J. Chem. Soc. 2552 (1963).
14. C. K. Jorgensen. Inorg. Chim. Acta Rev. **2**, 65 (1968).
15. K. K. W. Sun and R. A. Haines. Can. J. Chem. **48**, 2327 (1970).
16. M. L. Shankarnaryana and C. C. Patel. Spectrochim. Acta, **21**, 95 (1965).
17. F. Bonati and R. Ugo. J. Organomet. Chem. **10**, 257 (1967).

Can. J. Chem. Downloaded from www.nrcresearchpress.com by 210.87.254.42 on 09/05/12
For personal use only.

Can. J. Chem. Downloaded from www.nrcresearchpress.com by 210.87.254.6 on 09/05/12
For personal use only.

Canadian Journal of Chemistry

Published by
THE NATIONAL RESEARCH COUNCIL OF CANADA

Journal canadien de chimie

Publié par
LE CONSEIL NATIONAL DE RECHERCHES DU CANADA

Volume 54 Number 18 September 15, 1976 Volume 54 numéro 18 15 septembre 1976

Reactions of metal carbonyl complexes. VIII.[1] Kinetics and mechanisms of the substitution reactions of *cis*-$Mn(CO)_4LBr$ (L = PPh_3, $AsPh_3$, $SbPh_3$) with group VA bidentate ligands[2]

I. S. BUTLER AND H. K. SPENDJIAN

Department of Chemistry, McGill University, P.O. Box 6070, Station A, Montreal, P.Q., Canada H3C 3G1

Received April 21, 1976

I. S. BUTLER and H. K. SPENDJIAN. Can. J. Chem. **54**, 2833 (1976).

The substitution reactions of *cis*-$Mn(CO)_4LBr$ (L = PPh_3, $AsPh_3$, $SbPh_3$) with diphos, diarsine, and dipy (A—A) take place with the loss of one CO group and L to form *fac*-$Mn(CO)_3$(A—A)Br. The observed reaction rates in $CHCl_3$ solution are first order in substrate but depend on the nature of L and A—A, and in some cases the concentration of A—A as well. When L = PPh_3 and A—A = diphos, and when L = $AsPh_3$ and A—A = diphos, diarsine, or dipy, the rates are independent of [A—A]. For these reactions, an S_N1 dissociative mechanism involving the rupture of one of the Mn—CO bonds as the rate-determining step is proposed. The observed positive entropies of activation (~10 e.u.) for these reactions are supportive of the proposed mechanism. The reactions of *cis*-$Mn(CO)_4(SbPh_3)Br$ with A—A are essentially independent of both the nature and the concentration of A—A. However, for these reactions, an S_N1 dissociative mechanism involving the rupture of the Mn—$SbPh_3$ bond as the rate-determining step is proposed; the observed positive $\Delta S^{\neq}$ values (~12 e.u.) are in accord with such a mechanism. The rates when L = PPh_3 and A—A = diarsine or dipy are dependent on both the nature and the concentration of A—A. A mechanism involving rapid pre-equilibrium steps between the parent molecule and the intermediates, $Mn(CO)_3(PPh_3)Br$ and $Mn(CO)_4Br$, is proposed to account for the complex kinetic behaviour found for these reactions. These results are particularly noteworthy because octahedral first-row transition metal complexes generally undergo substitution reactions which are independent of the concentrations of the entering nucleophiles.

I. S. BUTLER et H. K. SPENDJIAN. Can. J. Chem. **54**, 2833 (1976).

Les réactions de substitution des $Mn(CO)_4LBr$ *cis* (L = PPh_3, $AsPh_3$, $SbPh_3$) avec le diphos, la diarsine et le dipy (A—A) se produisent avec la perte d'un groupe CO et de L pour former $Mn(CO)_3$(A—A)Br *fac*. Les vitesses de réaction observées en solution dans le $CHCl_3$ sont de premier ordre en substrat mais dépendent de la nature de L et de A—A et dans certains cas de la concentration de (A—A) aussi. Quand L = PPh_3 et A—A = diphos et lorsque L = $AsPh_3$ et A—A = diphos, diarsine ou dipy, les vitesses sont indépendantes de [A—A]. Pour ces réactions, un mécanisme de dissociation S_N1 impliquant la rupture de l'un des liens Mn—CO comme étape déterminante de la vitesse est proposé. Les entropies positives d'activation observées (~10 u.e.) pour ces réactions appuient le mécanisme proposé. Les réactions des $Mn(CO)_4(SbPh_3)Br$ *cis* avec A—A sont essentiellement indépendantes et de la nature et de la concentration de A—A. Toutefois, pour ces réactions, un mécanisme de dissociation S_N1 comprenant la rupture du lien Mn—$SbPh_3$ comme étape déterminante de la vitesse est proposé; les valeurs positives observées de $\Delta S^{\neq}$ (~12 u.e.) sont en accord avec un tel mécanisme. Lorsque L = PPh_3 et A—A = diarsine ou dipy les vitesses dépendent et de la nature et de la concentration de A—A. Un

[1]Part VII. See ref. 10.

[2]Taken in part from the Ph.D. thesis of H. K. Spendjian, McGill University, 1970.

mécanisme, comprenant des étapes de pré-équilibre rapides entre la molécule initiale et les intermédiaires, $Mn(CO)_3(PPh_3)Br$ et $Mn(CO)_4Br$, est proposé pour expliquer le comportement cinétique complexe trouvé pour ces réactions. Ces résultats sont particulièrement intéressants à cause des complexes octaédriques des métaux de transition de la première série qui subissent généralement des réactions de substitution qui sont indépendantes des concentrations des nucléophiles.

[Traduit par le journal]

Can. J. Chem. Downloaded from www.nrcresearchpress.com by 210.87.254.6 on 09/05/12
For personal use only.

Introduction

Several years ago, while attempting to synthesize octahedral manganese(I) dicarbonyl complexes by reacting *cis*-$Mn(CO)_4LBr$ (L = PPh_3, $AsPh_3$, $SbPh_3$) with group VA bidentate ligands (A—A) such as 1,2-bis(diphenylphosphino)-ethane ($Ph_2PCH_2CH_2PPh_2$, diphos), we noticed that instead of displacing two CO groups, the bidentate ligands invariably eliminated one CO group and L to give *fac*-$Mn(CO)_3(A—A)Br$ (eq. 1).

[1] *cis*-$Mn(CO)_4LBr + A—A \rightarrow$

fac-$Mn(CO)_3(A—A)Br + CO + L$

These reactions differ from those of the related *mer*-$[P(OPh)_3]_2Mn(CO)_3X$ (X = Cl, Br) derivatives with A—A which yield two products, *viz.* *cis*-$(CO)_2Mn[P(OPh)_3](A—A)X$ and *fac*-$Mn(CO)_3(A—A)X$ (1). Angelici and Basolo (2) have studied the kinetics of the reactions of several *cis*-$Mn(CO)_4LX$ complexes with monodentate ligands (L′) to give *fac*-$Mn(CO)_3LL'X$, and have proposed an S_N1 dissociative mechanism involving the loss of one CO group as the rate-determining step. Our preliminary kinetic investigations of reaction 1, however, showed that in certain cases the rates were dependent on both the nature and the concentration of the entering A—A ligand, suggestive of an S_N2 displacement mechanism. Second-order kinetics are extremely rare for first-row octahedral transition metal carbonyl complexes and the only known examples for manganese(I) are the reactions of $Ph_3EMn(CO)_5$ (E = Ge, Sn) with monodentate ligands (L′) to give *cis*-$Mn(CO)_4(EPh_3)L'$ (3). In addition, there have been remarkably few kinetic studies of metal carbonyl substitution reactions involving bidentate ligands. Of interest in the present context are the reactions of $Re(CO)_5X$ with A—A (4, 5).

In view of the above observations, we decided to carry out a detailed kinetic study of reaction 1 and report here the results of this investigation.

Experimental

The *cis*-$Mn(CO)_4LBr$ (L = PPh_3, $AsPh_3$, $SbPh_3$) complexes were prepared and purified according to the literature method (2). As a check on the purity of the complexes, the PPh_3 derivative was analyzed (Schwarzkopf Microanalytical Laboratory). *Anal.* calcd. for $C_{22}H_{15}O_4PMnBr$: C 51.9, H 2.97, Br 15.7; found: C 52.1, H 3.09, Br 15.6. Spectrograde $CHCl_3$ was dried over $CaCl_2$ and distilled under nitrogen before use. Diphos, 1,2-bis(diphenylarsino)ethane ($Ph_2AsCH_2CH_2AsPh_2$, diarsine), and 2,2′-dipyridyl [$(C_5H_4N)_2$, dipy] were used as purchased from Strem Chemicals Inc.

Kinetic Studies

(*a*) *Product Identification*

A mixture of *cis*-$Mn(CO)_4(PPh_3)Br$ (0.081 g, 0.16 mmol) and diphos (0.068 g, 0.17 mmol) in $CHCl_3$ (10 ml) was allowed to stand at room temperature for 5 h. The volume of the solution was then reduced to ~2 ml in a stream of air. Addition of *n*-hexane (40 ml) to the concentrated solution caused precipitation of *fac*-$Mn(CO)_3$-(diphos)Br as a yellow solid which was then washed with *n*-hexane and dried *in vacuo* (yield 0.069 g, 70%). *Anal.* calcd. for $C_{29}H_{24}O_3P_2MnBr$: C 56.4, H 3.92, Br 12.9; found: C 56.7, H 4.09, Br 12.7. The ir spectrum of the complex in $CHCl_3$ solution in the ν(CO) region exhibited three strong bands at 2025, 1959, and 1919 cm^{-1}, at identical positions with the bands of the product obtained from the direct reaction of $Mn(CO)_5Br$ with diphos. The authenticity of the other two products was established by the similarity of their ir spectra in $CHCl_3$ solution in the ν(CO) region to that of the diphos product, *viz.* *fac*-$Mn(CO)_3$(diarsine)Br (2026s, 1957s, and 1919s cm^{-1}) and *fac*-$Mn(CO)_3$(dipy)Br (2033s, 1945s, and 1924s cm^{-1}).

(*b*) *Determination of Rates*

Kinetic data were obtained by monitoring the rate of disappearence of the highest energy ν(CO) band of each substrate in $CHCl_3$ solution at ~2100 cm^{-1} in a manner similar to that described earlier for the C_8H_{14} substitution reactions of $(\eta^5\text{-}C_5H_5)Mn(CO)(CS)(C_8H_{14})$ (6). All the kinetic runs were carried out under pseudo-first-order conditions and the resulting plots of ln $(A - A_\infty)$ *vs.* t were linear to at least 75% completion, except for the reactions of *cis*-$Mn(CO)_4(AsPh_3)Br$ with diarsine which showed significant deviations after about 50% completion. The rate constants were reproducible to within ±10%; the activation parameters were calculated using a standard least-squares program on an IBM 360/75 IBM computer.

Results and Discussion

The observed pseudo-first-order rate constants (k_{obsd}) for the three substrates are given in

TABLE 1. Rates of reaction of *cis*-$Mn(CO)_4LBr$ with various bidentate ligands (A—A) in $CHCl_3$ solution*

A—A	T (°C)	[A—A] (M)	$k_{obsd} \times 10^5$ (s^{-1})	A—A	T (°C)	[A—A] (M)	$k_{obsd} \times 10^5$ (s^{-1})
Rates for *cis*-$Mn(CO)_4(PPh_3)Br$				Rates for *cis*-$Mn(CO)_4(AsPh_3)Br$			
Diphos[d]	25.0	0.039	19	Diphos[e]	30.0	0.024	9.2[b]
		0.051	18		35.0	0.028	19
	30.0	0.022	40[b]			0.037	20
	35.0	0.055	80		40.0	0.029	42[b]
		0.063	82[c]				
		0.079	81	Diarsine[f]	30.0	0.038	8.8[b]
		0.104	81		35.0	0.025	17[b]
		0.124	83			0.057	19
					40.0	0.035	36
Diarsine	30.4	0.039	5.5			0.055	36
		0.066	7.8				
		0.078	8.5	Dipy[g]	30.0	0.074	11
	35.0	0.039	13			0.136	11
		0.042	11[c]		35.0	0.044	21[b]
		0.057	19		40.0	0.051	43[b]
		0.077	23		46.0	0.105	46[b]
		0.096	25				
		0.116	30	Rates for *cis*-$Mn(CO)_4(SbPh_3)Br$			
	40.0	0.038	18	Diphos[h]	30.0	0.032	3.2[b]
		0.058	25		35.0	0.013	6.9
		0.074	27			0.047	6.9
						0.074	7.0
Dipy	30.4	0.045	0.66		40.0	0.075	14[b]
		0.074	0.74				
		0.107	0.88	Diarsine[i]	30.0	0.038	2.1[b]
		0.163	1.2		35.0	0.038	4.7[b]
		0.219	1.2		40.0	0.040	10
	35.0	0.055	1.5			0.052	10
		0.114	2.1			0.060	10
		0.160	2.5				
		0.216	2.6	Dipy[j]	30.0	0.065	3.2
	40.0	0.049	2.5			0.136	3.3
		0.091	3.0		35.0	0.085	7.1[b]
		0.134	3.9		40.0	0.076	15
		0.178	4.4			0.21	15
		0.232	5.1				

*[a]The concentrations of the substrates in all cases was ≤ 0.004 M. [b]Average value of at least two duplicate runs. [c]In the presence of ~ 0.035 M PPh_3. [d]$\Delta H^{\ddagger} = 27 \pm 1$ (1 standard deviation) kcal mol^{-1}; $\Delta S^{\ddagger} = 11$ e.u. [e]$\Delta H^{\ddagger} = 29 \pm 1$ kcal mol^{-1}; $\Delta S^{\ddagger} = 13$ e.u. [f]$\Delta H^{\ddagger} = 27 \pm 1$ kcal mol^{-1}; $\Delta S^{\ddagger} = 7$ e.u. [g]$\Delta H^{\ddagger} = 26 \pm 1$ kcal mol^{-1}; $\Delta S^{\ddagger} = 6$ e.u. [h]$\Delta H^{\ddagger} = 28 \pm 1$ kcal mol^{-1}; $\Delta S^{\ddagger} = 9$ e.u. [i]$\Delta H^{\ddagger} = 29 \pm 1$ kcal mol^{-1}; $\Delta S^{\ddagger} = 13$ e.u. [j]$\Delta H^{\ddagger} = 29 \pm 1$ kcal mol^{-1}; $\Delta S^{\ddagger} = 13$ e.u.

Table 1. For *cis*-$Mn(CO)_4(PPh_3)Br$, the rates at comparable temperatures decrease with changes in A—A in the order diphos > diarsine > dipy. However, when A—A = diphos, the rates are independent of [diphos], but for the other two bidentate ligands the rates are dependent on [A—A]. For *cis*-$Mn(CO)_4(AsPh_3)Br$, the rates are independent of both the nature and the concentration of A—A. Finally, for *cis*-$Mn(CO)_4(SbPh_3)Br$, the rates are independent of [A—A], but when A—A = diarsine they are significantly slower than those with the other two bidentate ligands. These results may be explained by the mechanistic steps shown in Fig. 1.

Applying the steady-state approximation to the concentrations of the intermediates (**2**) and (**4**) yields the following rate law for the disappearance of *cis*-$Mn(CO)_4LBr$ (**1**).

$$[2] - \frac{d[1]}{dt} = \left\{\frac{k_1k_3[A—A]}{k_2[CO] + k_3[A—A]} + \frac{k_4k_6[A—A]}{k_5[L] + k_6[A—A]}\right\}[1]$$

or

Can. J. Chem. Downloaded from www.nrcresearchpress.com by 210.87.254.6 on 09/05/12
For personal use only.

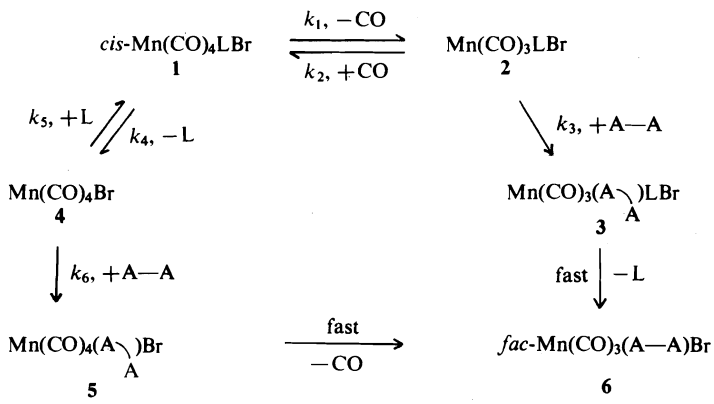

FIG. 1. Proposed steps in the mechanism of the reactions of *cis*-$Mn(CO)_4LBr$ with bidentate ligands (A—A). Note that (A⌒A) means that only one of the two coordinating atoms in the bidentate ligands is attached to the manganese.

$$[3]\quad k_{obsd} = \frac{k_1k_3[A—A]}{k_2[CO] + k_3[A—A]} + \frac{k_4k_6[A—A]}{k_5[L] + k_6[A—A]}$$

The k_{obsd} values for the reactions of *cis*-$Mn(CO)_4LBr$ (L = PPh_3, $AsPh_3$) with diphos are of the same order of magnitude as those reported by Angelici and Basolo (2) for the analogous reactions with $P(OBu^n)_3$. However, since the literature results are for C_2Cl_4 solution, we re-examined the same two reactions in $CHCl_3$ solution. The observed rate constants[3] proved to be the same, within experimental error, as those reported here for the diphos reactions. Thus, it seems reasonable to conclude that the same S_N1 dissociative mechanism is operative in both cases, *viz.* the loss of one CO group in the rate-determining step to give a five-coordinate intermediate $Mn(CO)_3LBr$ which then reacts rapidly with the incoming ligand. Referring to Fig. 1, these conditions would obtain when there is no step **1** → **4** and so $k_4 = k_5 = k_6 = 0$, and when $k_3[A—A] \gg k_2[CO]$, *i.e.* eq. 3 reduces to $k_{obsd} = k_1$. The other [A—A] independent reactions mentioned above, except those of *cis*-$Mn(CO)_4(SbPh_3)Br$ (*vide infra*), presumably follow the same S_N1 dissociative mechanism. Further support for the proposed mechanism comes from the close similarity of the activation parameters for the reactions of the $AsPh_3$ derivative with diphos and $P(OBu^n)_3$: diphos ($\Delta H^{\ddagger} = 29 \pm 1$ kcal mol^{-1}, $\Delta S^{\ddagger} = 13$ e.u.), $P(OBu^n)_3$ ($\Delta H^{\ddagger} = 30 \pm 1$ kcal mol^{-1}, $\Delta S^{\ddagger} = 18$ e.u. (2)). The slight difference in $\Delta S^{\ddagger}$ presumably arises because of the different solvents used. Furthermore, addition of excess PPh_3 in the reaction of *cis*-$Mn(CO)_4(PPh_3)Br$ with diphos does not retard the observed reaction rate. It should also be mentioned that CO exchange of the PPh_3 derivative with $C^{18}O$ apparently occurs by the preferential loss of one of the two *trans* CO groups (7), and the same may be true for all the related reactions discussed here.

From our earlier ir study of the reaction of *cis*-$Mn(CO)_4(SbPh_3)Br$ with $C^{18}O$ (7), it is apparent that both $SbPh_3$ and CO are replaced by $C^{18}O$ to give initially $Mn(CO)_4(C^{18}O)Br$ and *cis*-$Mn(CO)_3(C^{18}O)(SbPh_3)Br$. Moreover, the loss of $SbPh_3$ is appreciably faster than the loss of CO. Consequently, for the reactions of *cis*-$Mn(CO)_4(SbPh_3)Br$ with A—A, we favour an S_N1 dissociative path involving the loss of $SbPh_3$ as the major rate-determining step to give $Mn(CO)_4Br$ which then reacts rapidly with A—A to afford *fac*-$Mn(CO)_3(A—A)Br$. Under these conditions, $k_{obsd} = k_4$; however, if the CO dissociative path does contribute to the disappearence of *cis*-$Mn(CO)_4(SbPh_3)Br$, $k_{obsd} = k_1 + k_4$. The observed positive entropies of activation (~12 e.u.) are supportive of a dissociative mechanism. Perhaps when A—A = diarsine, step **1** → **2** (k_1) does not play an important role and this is the reason why the

[3]The k_{obsd} values for these reactions in $CHCl_3$ solution are approximately twice those reported for C_2Cl_4 solution. The reaction of *cis*-$Mn(CO)_4(SbPh_3)Br$ with $P(OBu^n)_3$ was also studied but, contrary to the literature (2), the ir spectra of the reaction mixtures in the ν(CO) region indicated the formation of *both* *fac*-$Mn(CO)_3LL'Br$ and *cis*-$Mn(CO)_4L'Br$.

Can. J. Chem. Downloaded from www.nrcresearchpress.com by 210.87.254.6 on 09/05/12
For personal use only.

Can. J. Chem. Downloaded from www.nrcresearchpress.com by 210.87.254.6 on 09/05/12
For personal use only.

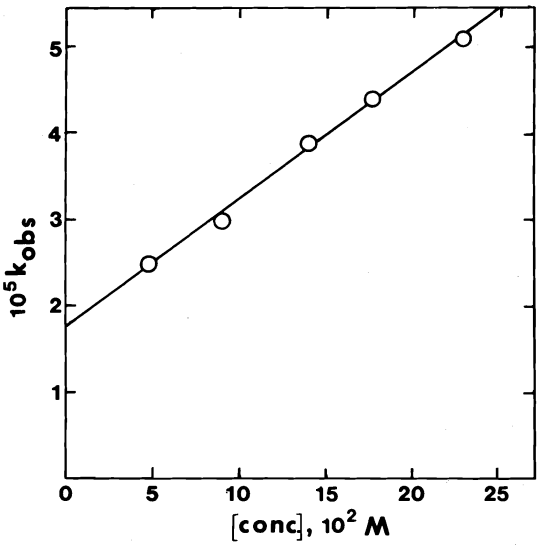

FIG. 2. Plot of the observed rate constants *vs.* the concentration of dipy for the reaction of *cis*-$Mn(CO)_4(PPh_3)Br$ with dipy in $CHCl_3$ solution at 40 °C.

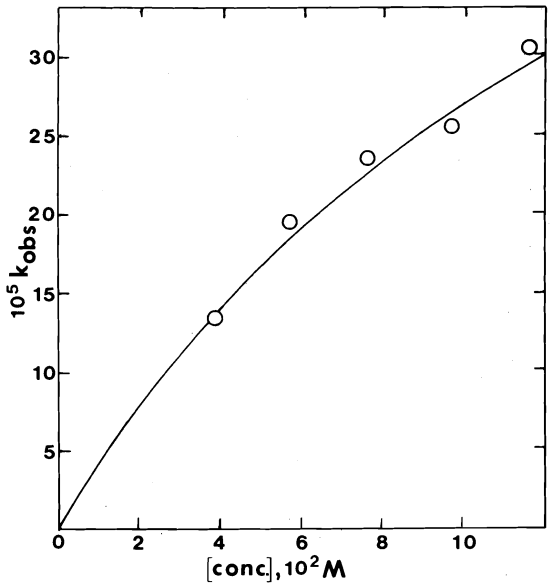

FIG. 3. Plot of the observed rate constants *vs.* the concentration of diarsine for the reaction of *cis*-$Mn(CO)_4(PPh_3)Br$ with diarsine in $CHCl_3$ solution at 35 °C.

rates with this ligand are significantly slower than with diphos and dipy.

When k_{obsd} for the reactions of *cis*-$Mn(CO)_4(PPh_3)Br$ with dipy and diarsine are plotted against [A—A], almost linear plots are obtained for dipy, while those for diarsine tend towards limiting rates at high [A—A] (Figs. 2, 3). There are definitely non-zero intercepts for the dipy reactions; however, for the diarsine reactions the curves apparently pass through the origin.

Two different mechanisms may be responsible for the [A—A] dependence. The first is an S_N2 displacement mechanism (eq. 4),

$$[4]\quad cis\text{-}Mn(CO)_4(PPh_3)Br \xrightarrow[\text{slow}]{+A-A} Mn(CO)_4(A\underset{A}{\diagdown})(PPh_3)Br \xrightarrow{\text{fast}} fac\text{-}Mn(CO)_3(A-A)Br \quad (-CO,\ -PPh_3)$$

while the second involves the rapid pre-equilibrium steps **1** → **2** and **1** → **4** shown in Fig. 1. The linear dependence on [dipy] for the dipy reactions, together with the non-zero values for the intercepts, suggest a mixed S_N1 and S_N2 mechanism such as that found for $M(CO)_6$ (M = Cr, Mo, W) (8). However, if this is true, then the intercepts should correspond to the k_1 values for the [A—A] independent reactions of the same substrate with diphos. Since this is not the case, we feel that we can rule out the mixed-order mechanism.

If there is competition for the intermediates **2** and **4** such that either $k_2[CO] \simeq k_3[A—A]$ and $k_6[A—A] \gg k_5[L]$ or $k_2[CO] \ll k_3[A—A]$ and $k_5[L] \simeq k_6[A—A]$, then [3] will reduce to equations of the approximate form $k_{obsd} = k' + k''[A—A]$, *viz.*

$$[5]\quad k_{obsd} = k_4 + \frac{k_1 k_3[A—A]}{2k_2[CO]}$$

(for the former case)

and

$$[6]\quad k_{obsd} = k_1 + \frac{k_4 k_6[A—A]}{2k_5[L]}$$

(for the latter case)

Both [5] and [6] describe the behaviour observed for the reactions of *cis*-$Mn(CO)_4(PPh_3)Br$ with dipy. However, since the intercepts do not correspond at all with the k_1 values found for the [A—A] independent reactions with diphos, we favour the mechanism indicated by [5]. Further support for this proposal comes from the fact that when the reaction of *cis*-$Mn(CO)_4(PPh_3)Br$ with dipy is carried out under an atmosphere of CO, the reaction rate is unchanged, while in the

Can. J. Chem. Downloaded from www.nrcresearchpress.com by 210.87.254.6 on 09/05/12
For personal use only.

presence of only excess PPh_3, the rate is appreciably slower.

The presence of excess PPh_3 in the reaction of the PPh_3 derivative with diarsine decreases the observed rate slightly, as does the presence of CO. This suggests that both loss of PPh_3 and CO contribute to the observed rates of disappearence of the substrate. Equation 3 predicts a dependence of k_{obsd} on [A—A] and furthermore, at very high [A—A], k_{obsd} should reach a limiting value of $k_1 + k_4$, while when [A—A] = 0, k_{obsd} should be equal to zero. These predictions seem to be borne out by the data for the diarsine reactions.

From the above discussion, all the varied kinetic behaviour of the *cis*-$Mn(CO)_4LBr$ complexes upon reaction with bidentate ligands A—A can be accounted for in terms of the interplay of the steps given in Fig. 1. In general, these reactions follow the same S_N1 dissociative mechanism proposed earlier (2) for the reactions of these substrates with monodentate ligands. However, for *cis*-$Mn(CO)_4(SbPh_3)Br$, the reactions proceed via S_N1 $SbPh_3$ dissociation rather than CO dissociation, although it is possible that both paths contribute to the observed rates. In the case of the PPh_3 derivative, the mechanism followed depends markedly upon the nature of the entering bidentate ligand. Since phosphines are usually considered to be better nucleophiles than arsines and pyridines (9), it is probable that diphos is much more effective in capturing the intermediate $Mn(CO)_3(PPh_3)Br$ species than are the other two bidentate ligands. The net result is that with diphos, the normal S_N1 dissociative behaviour is observed, while in the reactions with diarsine and dipy, the reverse steps $\mathbf{2} \rightarrow \mathbf{1}$ and $\mathbf{4} \rightarrow \mathbf{1}$ (Fig. 1) play a more important role in determining the mechanistic path followed. In any event, [A—A] dependence for the reactions of *cis*-$Mn(CO)_4(PPh_3)Br$ with diarsine and dipy is unexpected and suggests that it might be worthwhile investigating the kinetics of the substitution reactions of other octahedral first-row transition metal carbonyl complexes with polydentate ligands to ascertain whether or not this is a fairly general phenomenon. It would be particularly interesting to study the reactions of *cis*-$Re(CO)_4LX$ with A—A, since direct S_N2 behaviour might also occur for these systems.

Acknowledgments

This research was supported by grants from the National Research Council of Canada and the Quebec Department of Education. One of us (H.K.S.) thanks the National Research Council of Canada for the award of a graduate fellowship. We thank Dr. K. R. Plowman for drawing the figures.

1. I. S. Butler, N. J. Coville, and H. K. Spendjian. J. Organometal. Chem. **43**, 185 (1972).
2. R. J. Angelici and F. Basolo. Inorg. Chem. **2**, 728 (1963).
3. G. R. Dobson and E. P. Ross. Inorg. Chim. Acta, **5**, 199 (1971).
4. F. Zingales, M. Graziani, F. Faraone, and U. Belluco. Inorg. Chim. Acta, **1**, 172 (1967).
5. D. A. Brown and R. T. Sane. J. Chem. Soc. A, 2088 (1971).
6. I. S. Butler and A. E. Fenster. Inorg. Chim. Acta, **7**, 79 (1973).
7. I. S. Butler and H. K. Spendjian. J. Organometal. Chem. **101**, 97 (1975).
8. J. R. Graham and R. J. Angelici. J. Am. Chem. Soc. **88**, 3658 (1966); Inorg. Chem. **6**, 2082 (1967).
9. F. Basolo and R. G. Pearson. Mechanisms of inorganic reactions. A study of metal complexes in solution. 2nd ed. Wiley and Sons, Inc., New York. 1967. Chapt. 7.
10. I. S. Butler and T. Sawai. Inorg. Chem. **14**, 2703 (1975).

Charge distributions and chemical effects. XII. A unifying concept

SÁNDOR FLISZÁR

Department of Chemistry, University of Montreal, Montreal, P.Q., Canada H3C 3V1

Received January 14, 1976

SÁNDOR FLISZÁR. Can. J. Chem. **54**, 2839 (1976).

Major inconsistencies which are currently acknowledged in discussions involving atomic charges, inductive effects, ^{13}C nmr shifts, and stability of carbonium ions are removed (*i*) by the use of an appropriate definition of charges and (*ii*) by the recognition that in alkanes and alkyl carbonium ions any decrease in positive charge at carbon atoms results in a downfield ^{13}C shift. Methyl appears to be less electron withdrawing than hydrogen, and stability of carbonium ions is associated with dispersion of positive charge at the carbonium center, in line with the more traditional views which are repeatedly challenged in recent literature.

SÁNDOR FLISZÁR. Can. J. Chem. **54**, 2839 (1976).

Les contradictions majeures qui sont couramment mentionnées dans les discussions concernant les charges atomiques, les effets inductifs, les déplacements en rmn ^{13}C et la stabilité des ions carbonium, sont éliminés (*i*) en utilisant une définition appropriée des charges et (*ii*) en reconaissant que dans les alcanes et dans les ions alkyles carbonium n'importe quelle diminution de charge positive sur les atomes de carbone résulte à un déplacement en ^{13}C vers les champs faibles. Le méthyle apparait être moins attracteur d'électrons que l'hydrogène, et la stabilité des ions carbonium est associée à la dispersion de la charge positive au centre de l'ion carbonium, conformément avec les vues les plus traditionnelles qui sont fréquemment remises en question dans la littérature récente.

[Traduit par le journal]

Major inconsistencies are currently acknowledged in discussions involving charge distributions, inductive effects, stability of carbonium ions, and ^{13}C nmr shifts. Confusion is at its best when these four topics are elements of a same study.

Theoretical calculations have contributed a great deal to this state of affairs by providing different and often conflicting information, depending upon the choice of the method for calculating charges. For example, the spectrum of results obtained for the carbon net atomic charge of methane ranges from $+0.60$ to -1.07 electron; just the sort of results likely to undermine one of the most popular concepts in chemistry, that of charge distributions in molecules.

The interpretation of inductive effects has also suffered from the blank acceptance of theoretical charges. For example, Hoffmann (1) noted that his results are at odds with the widely held assumption that a methyl group is a better electron donor than hydrogen. Incidentally, most of the results (both, semi-empirical and *ab initio*) presented earlier (2) would suggest the same conclusion.[1]

In turn, extended Hückel (1) and *ab initio* calculations (3) predict the correct order of carbonium ion stability, even though a methyl group would appear to be electron withdrawing with respect to hydrogen. Now, molecular energies and atomic charges are distinct matters of calculations as, for the latter, simple changes in the type of population analysis shuffle considerably the results for charges (4, 5)[2] leaving, of course, the energy results unaltered. One aspect in the cited (1, 3) carbonium ion calculations is that increasing methyl substitution at the C^+ center increases its positive charge. This, of course, is at variance with common views which would, on the contrary, associate increasing stability (*e.g.*, tertiary *vs.* secondary carbonium ion) with dispersion of the positive charge on the carbonium center by electron release from the methyl groups.

Finally, current interpretations of ^{13}C nmr shifts also suggest that the cationic center of the isopropyl ion has a lower net positive charge than that of the tertiary carbon in the *tert*-butyl ion (6), again in contradiction with the fact that tertiary alkyl ions are more stable than secondary ions and with the usual view that methyl groups are better electron donors than hydrogen.

[1]Indeed, most results indicate a C^-H^+ polarity. Therefore, writing methane as CH_3—H, positive hydrogen atoms indicate that methyl withdraws electronic charge from H.

[2]A number of attempts for defining appropriate criteria guiding population analyses are listed in ref. 5.

Can. J. Chem. Downloaded from www.nrcresearchpress.com by 210.87.254.5 on 09/05/12
For personal use only.

TABLE 1. Inductive and optimized STO-3G net charges in alkanes

Molecule	Atom	Inductive charges: $f(n)$, rel. un.	Inductive charges: $n=1.3325$ $Q=-20.96$ me	Optimized STO-3G (me)
Methane	C	$4(n+1)/3n$	−48.92	−48.92
Ethane	C	1.000	−20.96	−20.96
Propane	C_{prim}	$(3n+0.55)/3n$	−23.84	−23.81
	C_{sec}	$(2n-3.8)/3n$	5.95	5.94
	H_{prim}*	$(0.15-n)/3n$	6.20	6.23
	H_{sec}	$(0.9-n)/3n$	2.27	2.20
Isobutane	C_{prim}	$(3n+1.03)/3n$	−26.36	−26.39
	C_{tert}	$(n-7.7)/3n$	33.39	33.36
	H_{prim}*	$(0.29-n)/3n$	5.47	5.50
	H_{tert}	$(2-n)/3n$	−3.50	−3.53
Neopentane	C_{prim}	$(n+0.49)/n$	−28.67	−28.66
	C_{quat}	$-4/n$	62.92	62.92
	H	$(0.51-n)/3n$	4.31	4.31

*Weighted average of nonequivalent H atoms.

Further accumulation of disturbing inconsistencies in the area to which the above observations refer is of little use. We wish now to proceed with an analysis which, hopefully, will contribute to clarify this subject.

Charge Analyses in Alkanes

The trends in atomic populations obtained from a variety of theoretical methods have been examined (2) in terms of the usual order of electron releasing ability

$$tert\text{-}C_4H_9 > iso\text{-}C_3H_7 > C_2H_5 > CH_3$$

of the alkyl groups. This type of analysis can be justified by considering that propane can be viewed as an ethyl group attached to a methyl group. Therefore, provided that the above inductive order is reflected in the electron populations of ground state molecules, it should be expected that each methyl group in propane carries a net negative charge. Direct experimental evidence (7) has indicated that the propane methyl groups carry, indeed, the negative ends and, hence, that ethyl is a better electron donor than methyl. This is typically a situation which, in principle, should be reflected by quantum theory, if any meaning at all is to be given to theoretical charges.

Assuming now that Taft's polar σ^* constants (8) of alkyl groups represent an adequate scaling for their electron releasing abilities, net atomic charges in a number of alkanes can be expressed in terms of one single parameter, n,[3] in a scale of relative units defined by setting the carbon net charge in ethane equal 1 arbitrary unit (2). Multiplication of these relative charges by the scale factor, Q = carbon net charge in ethane, yields the corresponding results in charge units. A comparison (Table 1) of these inductive charges with their *ab initio* (optimized STO-3G) counterparts (9) reveals a near perfect agreement with $n = 1.3325$ and $Q = -20.96$ millielectron (me).

Good agreement between inductive and quantum mechanical charges (both, *ab initio* and semi-empirical) is quite general (2): the inductive equations represent a summary of theoretical results, where each method simply corresponds to definite n and Q values. This means that *inductive effects are correctly reproduced by theoretical charges as far as alkyl groups are concerned.* However, though important, this type of coherence between theoretical charges and inductive effects is not sufficient, as for now the position of H in the scale of electron releasing

[3]These charges are derived from the inductive Taft-like equations $q_H = a\sigma^* + b$ (for H net charges in R—H compounds) and $q(CH_3) = a\sigma^*$ (for methyl net charges in R—CH_3 alkanes), where $a = -10/3n$ measures, in a way, the sensitivity of partial charge transfers to substituent effects. If inductive effects were nonexistent, the charges would be those corresponding to $n = \infty$, *i.e.*, $a = 0$.

Can. J. Chem. Downloaded from www.nrcresearchpress.com by 210.87.254.5 on 09/05/12
For personal use only.

Can. J. Chem. Downloaded from www.nrcresearchpress.com by 210.87.254.5 on 09/05/12
For personal use only.

abilities still remains to be defined. This question is linked to the definition of the 'true' n value. The general concepts underlying this analysis can be summarized as follows.

In current practice,[4] atomic charges (such as those presented in Table 1) are calculated following Mulliken's population analysis method (11) which implies the half-and-half partitioning of all overlap population terms among the centers k, l, . . . involved, *i.e.*, in standard notation,

$$[1] \quad N(k) = 2\sum_{i}\sum_{r} (c_{ir_k}^2 + \sum_{l \neq k} c_{ir_k} c_{is_l} S_{r_k s_l})$$

where $N(k)$ = population of center k. Then, on occasion, these charges are used in studies of property–charge relationships without questioning the implications contained in this particular type of population analysis. This is looking for trouble, although the definition expressed by eq. 1 can be regarded as approximately valid. Indeed, while the usual half-and-half assignment is easy to defend in situations involving partners of equal nature, this may be a less good approximation in cases involving dissimilar atoms. Assuming now a more sophisticated mode of distributing overlap population (12, 13) one obtains

$$[2] \quad N(k) = 2\sum_{i}\sum_{r} (c_{ir_k}^2 + \sum_{l \neq k} c_{ir_k} c_{is_l} S_{r_k s_l} \lambda_{r_k s_l})$$

where the weighting factor $\lambda_{r_k s_l}$, whose value remains to be defined, causes the departure from the usual halving of the overlap terms.

Under these circumstances, it appears most convenient (*i*) to use Mulliken's scheme for calculating charge distributions, thus providing sets of results in a well-defined standard of reference; then (*ii*) to evaluate modifications in terms of departures from this standard of reference. In the modified population analysis (4) which does not allocate half of the C—H overlap to each carbon and hydrogen, the hydrogen and carbon net charges are

$$[3] \quad q_H = q_H^0 - p$$

$$[4] \quad q_c = q_c^0 + Np$$

where q_H^0 and q_c^0 are Mulliken's charges, N the number of H atoms bonded to C, and p the departure from the usual halving of the C—H overlap population, for one C—H bond. Equations 3 and 4 are simplified and convenient forms derived from eq. 2, whereby

$$2\sum_{i}\sum_{r}\sum_{l=k} c_{ir_k} c_{is_l} S_{r_k s_l} (1 - \lambda)_{r_k s_l} = Np$$

(sum over H atoms bonded to C). The advantage resulting from our approximation, eq. 4, proceeds from its link to the inductive formulas. Indeed, if n^0 and Q^0 are the parameters corresponding to a Mulliken set of charges, $\{q^0\}$, and n, Q the parameters for the modified set, $\{q\}$, it is (4)

$$[5] \quad Q/n = Q^0/n^0$$

$$[6] \quad p = (Q - Q^0)/3$$

Equations 3–6 enable the calculation[5] of modified charges, $\{q\}$, for any n value of our choice from an original set of Mulliken charges, $\{q^0\}$. Conversely, *adoption of charge definitions following eq. 2, rather than eq. 1, simply corresponds to an appropriate change in the value of n.* This raises the question about the 'true' value of n, an indirect but convenient way of assessing the appropriate value of p.

Here we take advantage of the fact that carbon net charges calculated for different n values are not linearly related one to another. Consequently, *if a property is expected to correlate with C net charges, it is imperative that the latter correspond to the 'proper' n value: the use of any theoretical set of charges corresponding to an n value other than the 'proper' one is bound to fail in showing the expected correlation.* This is to say that properties, P, should be compared either with inductive charges, $\{f(n)\}$, treating n as an unknown or, else, with C charges, eq. 4, leaving now p to be determined by experiment. In case of a linear P–q_c relationship, for example, the 'proper' p value can be deduced from the equation

$$[7] \quad P = a(q_c^0 + Np) + b$$

which uses as sole inputs the set of P values and the set of C net charges resulting from a Mulliken

[4]A critical discussion of point charge analyses is presented in ref. 10.

[5]In this example we calculate the C charge of cyclohexane for $n = -4.4122$ from that corresponding to $n = 1.3325$, which is $q_c = 2.76$ me (14). First, $Q(n = -4.4122)$ is calculated by means of [5]: $Q = -4.4122(-20.96/1.3325) = 69.40$ me. Then (eq. 6), it is found that $p = 30.12$ me and (eq. 4) $q_c = 2.76 + 2p = 63.00$ me. In the scale of relative units, this charge is $q_c(\text{rel}) = 63.00/Q = 0.9078$.

Can. J. Chem. Downloaded from www.nrcresearchpress.com by 210.87.254.5 on 09/05/12
For personal use only.

TABLE 2. Charge distributions in alkanes, corrected for $n = -4.4122$, from the optimized STO-3G basis

Molecule	Atom	Net charge (me)
Methane	C	71.56
Ethane	C	69.40
Propane	C_{prim}	66.55
	C_{sec}	66.18
	H_{prim}*	−23.89
	H_{sec}	−27.92
Isobutane	C_{prim}	63.97
	C_{tert}	63.48
	H_{prim}*	−24.62
	H_{tert}	−33.65
Neopentane	C_{prim}	61.70
	C_{quat}	62.92
	H	−25.81

*Weighted average of nonequivalent H atoms.

population analysis. This truly amounts to an experimental calibration of the appropriate mode of partitioning C—H overlap populations.

While, in principle, the 'true' n value should be determined from an examination of property–charge relationships involving experimental results, there is a particular value for n which merits attention, *i.e.*, that which corresponds to a condition of 'most even electron distribution' (4). For the set of alkane molecules, a possible formulation can be derived from the condition that the various C atoms of the set be as similar as possible, which is met by $n \approx -4.4$. This n value now appears to correspond to real physical situations, albeit its generality is presently difficult to assess; indeed, comparisons of experimental results with carbon net charges indicate $n = -4.4122$ (from ^{13}C nmr shifts (4)), $n = -4.4083$ (from ionization potentials (15)), and $n \approx -4.41$ (from enthalpies of formation (16)). Consequently, *it can be assumed with a reasonable degree of confidence that* $n \approx -4.4$ *best describes the atomic populations in saturated hydrocarbons*. The charges for $n = -4.4122$, derived from the optimized STO-3G (Mulliken) results of Table 1, are indicated in Table 2. These results are deduced from eqs. 3 and 4, with $p = 30.12$ me.[5]

Contrasting with the Mulliken set of charges (Table 1) which predicts a C^-—H^+ polarity in terms of atomic populations, the final results (Table 2) indicate a C^+—H^- polarity in alkane molecules, a result which is in line with the view that hydrogen is certainly more electronegative than carbon, as Mulliken and Roothaan have pointed out (17). Since then, the C^+—H^- polarity has been advocated in various occasions, *e.g.*, by Julg (18), Bader and Preston (19), and Jug and co-workers (5, 20), but has also been overshadowed by numerous theoretical calculations, in fact by all those for which $n > 0$ (2).

We can now focus attention on the interpretation of inductive effects of alkyl groups in terms of population analyses.

Inductive Effects

The set of charges derived in the spirit of eq. 2 (Table 2) reflects the inductive charges, $\{f(n)\}$, and, hence, the usual inductive effects of alkyl groups (one relative to another) just as well as their original counterparts, $\{q^0\}$. In addition they also account for the proper partitioning of C—H overlap terms. The change in trends resulting from our definition of charges can be grasped from an examination of methane, written as CH_3—H. Electron deficient H atoms indicate that CH_3 is electron withdrawing with respect to H. It follows, therefore, that increasing methyl substitution at a carbon center renders this carbon more positive (Table 1). This type of behavior is typical for any set of alkane charges showing a C^-—H^+ polarity (2). In the modified set of charges, of course, the C^+—H^- polarity is coherent with the usual concept that methyl is a better electron donor than H, in agreement with a vast body of chemical evidence.

Although it can now be concluded that the well known disturbing contradictions between theoretical atomic charges and the customary inductive effects have vanished with the use of appropriate definitions of charges, the following descriptive interpretation may help in clarifying several aspects relating inductive effects to the C^+—H^- polarity.

This polarity suggests, in a way, that hydrogen atoms 'retain' electrons in CH_N groups. This retention within the group decreases as the number of H atoms in the group decreases, *i.e.*, partial charge transfers occur in the direction of the hydrogen richer CH_N groups (*e.g.*, $CH_2 \rightarrow CH_3$ as in propane).

Isobutane is chosen as an example for examining the effect of α-methyl substitution on a

'central' C atom (C_{tert} in this case) and on a 'central' CH_N group (*i.e.* C—H_{tert}). This molecule may be described as in **1**, using the results of Table 2 or, alternatively, as in **2**; a representation which is somewhat misleading.

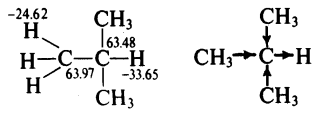

1 **2**

In **2** the arrow C→H suggests correctly that the tertiary H atom gains electronic charge. The arrows $CH_3 \rightarrow C_{tert}$ suggest that the central C gains electrons as the number of CH_3 groups replacing H is increased. This is in line with common views and is, indeed, reflected by the population analyses of Table 2. Nevertheless, the arrow $CH_3 \rightarrow C$ is misleading in another respect, in that it may suggest that the methyl group loses charge to the remainder of the molecule, whereas all calculations indicate the reverse, *i.e.*, a net negative charge for each methyl group when attached to a better electron donor (i-C_3H_7, in this example). Reversal of the arrow ($CH_3 \leftarrow$ C), intending to account for $q(CH_3)$ negative, is no better because then it would seem that the central atom becomes increasingly positive as the number of methyl substituents is increased, which is false. The apparent conflict between the facts (*i*) that the central C atom gains electrons with increasing number of methyl substituents and (*ii*) that the methyl groups themselves withdraw electronic charge is easily resolved by observing that although each methyl group pulls electrons from the i-C_3H_7 group ($q(CH_3) = -9.89$ me), it attracts less electrons than the H atom which has been replaced by it (q_H(sec) in propane $= -27.92$ me). This, of course, means that H is a better attractor than CH_3, which is reflected in methane, $(CH_3)^+$—H^-, *i.e.*, by the C^+—H^- polarity. Similar arguments also apply to other molecules. In short, *the central C atom and the central CH_N group become increasingly negative (i.e., less positive) as the number of α-methyl substituents is increased not because methyl itself pushes electrons toward the central C atom (or CH_N group) but because it withdraws less electrons than the H atom for which it has been substituted.*

As a whole, we recognize here many of the familiar pictures and aspects of the customary interpretation of the inductive effects of alkyl groups and their coherence with atomic charges derived from our analysis.

^{13}C Nuclear Magnetic Resonance Shifts

It is usually understood that one of the major factors governing the shielding of a specific nucleus is its local electron density. On these premises, considerable and often frustrating efforts have been devoted to attempts to correlate chemical shifts with charges (21). The most accurate relationship between ^{13}C nmr shifts, δ_c, and carbon net charges is that found for alkanes (4), *i.e.*,

$$[8] \qquad \delta_c = -237.1 q_c + 242.64 \text{ ppm}$$

from TMS, where the C net charges are expressed in the scale of relative units defined by setting q_c(ethane) = 1. Choosing now ethane as reference compound for defining chemical shifts, eq. 8 takes the form

$$[9] \qquad \delta_c = -237.1(q_c - 1) \text{ ppm from ethane}$$

which has the merit of expressing clearly that the *only* empirical parameter arising from the correlation between chemical shifts and carbon net charges is the slope, −237.1 ppm/relative charge unit. These equations are obtained from the comparison of ^{13}C shifts with inductive charges, $\{f(n)\}$, thus determining $n = -4.4122$ or, else, from eq. 7 using the *ab initio* results of Table 1, whereby $p = 30.12$ me. In a range of ~40 ppm, the standard deviation (0.3 ppm) is small in comparison with the error (~2.4 ppm) in δ_c which would result from a 1% error in the estimate of q_c. As a consequence of this agreement, eq. 8 can be used to calculate accurately C net charges in saturated hydrocarbons (Table 3).

Equations like [8] and [9] involving carbon charges expressed in charge units (*i.e.*, q_c(rel)·Q) would be impractical because the corresponding slope, $-237.1/Q$, would then depend upon the scale factor, Q, whose 'true' value is not known, hence, upon the basis used for calculating charges (4). One major advantage of eqs. 8 and 9 is precisely that they require only the knowledge of the proper relative scaling of carbon charges, which, of course, is independent of Q. Moreover, *eqs. 8 and 9 represent the only possible monotonic dependence of the δ_c's on carbon charges since the use of any set of C charges corresponding to an n*

Can. J. Chem. Downloaded from www.nrcresearchpress.com by 210.87.254.5 on 09/05/12
For personal use only.

TABLE 3. Carbon net charges, in the relative scale defined by q_c(ethane) = 1, for $n = -4.4122$, *viz.* $p = 30.12$ me

Molecule	Atom	q_c from Ind. Th.	STO-3G*	^{13}C shift	δ_c
Methane	C	1.031	1.031	1.032	−2.1
Ethane	C	1.000	1.000	0.999	5.8
Propane	C_{prim}	0.958	0.959	0.958	15.6
	C_{sec}	0.954	0.954	0.955	16.1
Butane	C_{prim}	0.968		0.968	13.2
	C_{sec}	0.920		0.918	25.0
Pentane	C_{centr}	0.878		0.878	34.5
Isobutane	C_{prim}	0.922	0.922	0.921	24.3
	C_{tert}	0.915	0.915	0.917	25.2
Neopentane	C_{prim}	0.889	0.889	0.891	31.5
	C_{quat}	0.907	0.907	0.906	27.9
Cyclohexane	C		0.908	0.907	27.7
Adamantane	C_{sec}		0.862	0.862	38.24
	C_{tert}		0.896	0.902	28.75

*The optimized STO-3G results are extracted from refs. 14 (cyclohexane), 22 (adamantane), and 9 (other compounds).

value other than ~ −4.4 would destroy the monotonicity (linear or otherwise).

These δ_c–q_c relationships further indicate that *δ_c increases (downfield shift) as q_c decreases, i.e., with decreasing positive character of the carbon atom*, which is at variance with common views. There appears to be no means of reconciling the latter with present results because Q is necessarily positive (meaning that the sign of C net charges in units of charge is that of the relative charges, *i.e.*, positive),[6] unless reversing the argument that ethyl is a better electron donor than methyl. Reversal of this argument would, however, be at odds with experimental evidence (7) indicating that the methyl ends in propane carry net negative charges. In conclusion, noting that all alkane C atoms are positive, eqs. 8 and 9 indicate that *their ^{13}C shifts are farther downfield as the C atoms are closer to electroneutrality.*

This behavior is possibly related to Grant's analysis (23) of the local paramagnetic screening constant (σ_p) for orbitals centered entirely on carbon, and its dependence on charge. This treatment predicts, in line with common views, that *addition* of electronic charge to a neutral carbon atom results in an upfield shift because the contribution of σ_p to the overall screening constant becomes less deshielding. Upon *removal* of electronic charge from a neutral C atom, however, this contribution of σ_p is more deshielding only up to a certain point, after which any further increase of net positive charge at the C atom in question results in a decrease of the σ_p contribution and, hence, in an increase in shielding. This latter trend is observed with alkanes, whose carbon atoms are, indeed electron deficient. In spite of this encouragement, it would be premature at this stage to assess the merits of a tentative interpretation in terms of Grant's analysis because (*i*) of the approximations involved in it, (*ii*) the uncertainty about the point at which inversion of trends would occur, which is linked to the definition of the 'effective nuclear charge parameter', and (*iii*) because we ignore the absolute values of carbon charges (*i.e.*, Q).[7]

Now these reservations should not obscure the fact that carbon charges which are derived from

[6]The demonstration that n and Q are necessarily opposite in sign is given in ref. 2. This point can also be inferred from relative charges calculated from the inductive formulas of Table 1, for $n = -4.4122$. If Q were negative, then the methyl groups in propane would carry net positive charges, at variance with experiment (7).

[7]Moreover, the significance or generality of correlations like eq. 8 is not known, and ^{13}C shifts should not be indiscriminantly interpreted as being strictly linearly related to electron density in *all* systems.

Can. J. Chem. Downloaded from www.nrcresearchpress.com by 210.87.254.5 on 09/05/12
For personal use only.

Can. J. Chem. Downloaded from www.nrcresearchpress.com by 210.87.254.5 on 09/05/12
For personal use only.

chemical shifts are virtually in perfect agreement with their theoretical counterparts which, moreover, reflect in detail inductive effects in their current acceptation, *i.e.*, . . . $C_2H_5 > CH_3 > H$. In saturated hydrocarbons and in comparable situations any downfield shift occurring upon substitution of H by CH_3 is, therefore, interpreted as an electron withdrawal from the carbon of interest, which is less pronounced with the methyl substituent than with hydrogen.

Stability of Carbonium Ions

Chemical shift is a property of the interaction of charge density with an external magnetic field. Consequently, it depends not only on the value of the integrated charge density (or 'charge') in the neighborhood of a nucleus but also on the magnetic susceptibility of that charge. It must be understood, therefore, that any δ_c–q_c correlation, such as eq. 8, is only applicable within series of closely related compounds. Carbonium ions are, hence, compared only among themselves.

The trends can reasonably be expected to be similar to those described for alkanes, *i.e.*, the inductive order of electron releasing ability, . . . $C_2H_5 > CH_3 > H$, and a downfield trend in chemical shifts for positive carbon atoms gaining some electronic charge, thus tending in part towards electroneutrality. The latter trend, involving only the inductive effect of ethyl *vs.* that of methyl, is illustrated by the comparison of ions **3** and **4**

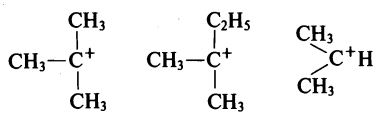

3 **4** **5**

where the positive charge on the C^+ center is expected to be lesser in **4** than in **3**. Indeed, the shift for the carbonium center in **4** (333.8 ppm) is downfield with respect to that in **3** (330.0 ppm) (24). Moreover, turning now to the inductive effect of methyl *vs.* that of hydrogen, the nmr shift of the carbonium center in the trimethylcarbonium ion is 10.4 ppm farther downfield than that of the dimethylcarbonium ion (319.6 ppm) (24). Hence, it follows from the trend noticed above for ethyl *vs.* methyl that the carbonium center in **3** is less positive than that of **5**. This, of course, agrees with the previous results for alkanes indicating that methyl is a better electron donor than H (or less electron withdrawing than H) and, consequently, with traditional concepts which associate stability of carbonium ions with inductive dispersion of positive charge at the carbonium center.

These three carbonium ions are at the center of the interpretative difficulties which were hitherto encountered in attempts to reconcile theoretical charges with usual inductive effects and stability of carbonium ions (25). The present analysis indicates that the most traditional views of organic chemists turn out to be the correct ones. It is unfortunate that extended Hückel (1) and *ab initio* (3) calculations indicating that the positive charge at a C^+ center increases with the number of methyl substituents were widely used in discussions of carbonium ion chemistry without proper consideration of the implications contained in the Mulliken population analysis adopted in these calculations. Appropriate '*p* corrections' (eq. 4) cannot be disregarded in the evaluation of meaningful orders for atomic charges, or, more generally, an appropriate definition of charges in terms of eq. 2.

There is a more general aspect relating stability with dispersion of positive charge on carbon atoms and higher (downfield) δ_c values. Enthalpies of formation, ΔH_f^0, of acyclic alkanes are correlated to ^{13}C shifts, δ^{eth} (relative to ethane), by the equation (16)

$$[10]\quad \Delta H_f^0 = \Delta H_f^0(C_2H_6) + \nu(N-2) + \lambda\sum(N_{cc}+1)\delta^{eth}$$

where N now represents the number of C atoms, N_{cc} = the number of C—C bonds formed by the C atom to which δ^{eth} refers, and ν, λ are parameters determined from comparisons with experimental ΔH_f^0 values. This equation covers compounds ranging from methane (−17.89 kcal/mol) to nonanes (∼−60 kcal/mol) with a mean deviation of 0.27 kcal/mol. The point is that λ is negative (−0.04657 kcal/mol). This, of course, means that *thermodynamic stability is increased as the δ^{eth} values become larger*. While this is particularly evident in comparisons of isomers, the above rule is quite general. Indeed, it has been applied on an empirical basis by Perlin and Koch (26) in a study of ^{13}C and proton chemical shifts of cyclohexanes in relation to interaction energy. Now it makes sense that any increase in stability parallels situations whereby

C atoms come closer to their electroneutrality, as electron removal from neutral C atoms certainly costs work. These alkane results are, thus, coherent with those presented above for carbonium ions, *i.e.*, larger δ_c values indicate loss of positive charge and increase in stability.

This study never intended to be exhaustive in any of the topics considered. Its primary goal was to pin-point the sources of disturbing conceptual difficulties. Their removal hopefully discloses easier paths for future research, within a frame of beneficial coherence.

Acknowledgement

Generous support received from the National Research Council of Canada is gratefully acknowledged.

1. R. HOFFMANN. J. Chem. Phys. **39**, 1397 (1963).
2. S. FLISZÁR, G. KEAN, and R. MACAULAY. J. Am. Chem. Soc. **96**, 4353 (1974).
3. L. RADOM, J. A. POPLE, and P. VON RAGUÉ-SCHLEYER. J. Am. Chem. Soc. **94**, 5935 (1972).
4. S. FLISZÁR, A. GOURSOT, and H. DUGAS. J. Am. Chem. Soc. **96**, 4358 (1974).
5. P. O. LÖWDIN. J. Chem. Phys. **21**, 374 (1975); D. PETERS. J. Chem. Soc., London, 2015 (1963); P. ROS and G. C. A. SCHUIT. Theor. Chem. Acta, **4**, 1 (1966); M. POLLAK and R. REIN. J. Chem. Phys. **47**, 2045 (1967); E. R. DAVIDSON. J. Chem. Phys. **46**, 3320 (1967); C. A. COULSON and G. DOGGETT, Int. J. Quant. Chem. **2**, 825 (1968); E. W. STOUT and P. POLITZER. Theor. Chim. Acta, **12**, 379 (1968); G. DOGGETT. J. Chem. Soc. A, 229 (1969); P. POLITZER and R. R. HARRIS. J. Am. Chem. Soc. **92**, 6451 (1970); K. JUG. Theor. Chim. Acta, **31**, 63 (1973).
6. G. A. OLAH, A. M. WHITE, J. R. DEMEMBER, A. COMMEYRAS, and C. Y. LUI. J. Am. Chem. Soc. **92**, 4627 (1970).
7. V. W. LAURIE and J. S. MUENTER. J. Am. Chem. Soc. **88**, 2883 (1966).
8. R. W. TAFT. *In* Steric effects in organic chemistry. *Edited by* M. S. Newman. Wiley, New York, N.Y., 1956; R. W. TAFT. J. Am. Chem. Soc. **75**, 4231 (1953).
9. G. KEAN and S. FLISZÁR. Can. J. Chem. **52**, 2772 (1974).
10. A. JULG. Topics in Current Chem. **58**, 1 (1975).
11. R. S. MULLIKEN. J. Chem. Phys. **23**, 1833 (1955); **23**, 1841 (1955); **23**, 2338 (1955); **23**, 2343 (1955).
12. P. O. LÖWDIN. J. Chem. Phys. **18**, 365 (1950).
13. R. DAUDEL and A. LAFORGUE. Compt. Rend. **233**, 623 (1951).
14. R. ROBERGE and S. FLISZÁR. Can. J. Chem. **53**, 2400 (1975).
15. H. HENRY and S. FLISZÁR. Can. J. Chem. **52**, 3799 (1974).
16. H. HENRY, A. JULG, and S. FLISZÁR. Can. J. Chem. **54**, 2085 (1976).
17. R. S. MULLIKEN and C. C. J. ROOTHAAN. Chem. Rev. **41**, 219 (1947).
18. A. JULG. J. Chim. Phys. 548 (1956).
19. R. F. W. BADER and H. J. T. PRESTON. Theor. Chim. Acta, **17**, 384 (1970).
20. K. JUG, G. KEAN, and S. FLISZÁR. Unpublished results.
21. D. G. FARNUM. *In* Advances in physical organic chemistry. Vol. 11. Academic Press, New York, N.Y. 1975. p. 123.
22. G. KEAN, D. GRAVEL, and S. FLISZÁR. J. Am. Chem. Soc. In press.
23. R. J. PUGMIRE and D. M. GRANT. J. Am. Chem. Soc. **90**, 697 (1968).
24. G. A. OLAH and A. M. WHITE. J. Am. Chem. Soc. **91**, 5801 (1969).
25. G. M. KRAMER. *In* Advances in physical organic chemistry. Vol. 11. Academic Press, New York, N.Y. 1975. p. 177.
26. A. S. PERLIN and H. J. KOCH. Can. J. Chem. **48**, 2639 (1970).

Can. J. Chem. Downloaded from www.nrcresearchpress.com by 210.87.254.5 on 09/05/12
For personal use only.

Stereochemical properties of 1,3-bissulfonium salts and 1,3-bissulfonium ylides

SAUL WOLFE, PETER CHAMBERLAIN, AND TIMOTHY F. GARRARD
Department of Chemistry, Queen's University, Kingston, Ont., Canada K7L 3N6

Received August 19, 1975[1]

SAUL WOLFE, PETER CHAMBERLAIN, and TIMOTHY F. GARRARD. Can. J. Chem. **54**, 2847 (1976).

Ten acyclic and two cyclic 1,3-bissulfonium bistetrafluoroborates have been synthesized by appropriate modification of the literature procedures for the preparation of such compounds. The acyclic salts are deprotonated readily by one molar-equivalent of potassium hydroxide to give 1,3-bissulfonium ylides. However, under the same conditions, the cyclic salts decompose. Hydrogen exchange experiments reveal that the C2 hydrogens of the cyclic salts are significantly less acidic than the C2 hydrogens of the acyclic salts. The relative acidities of the C2 hydrogens of the cyclic salts depend upon the medium and upon the configuration and conformation of the molecule, and preliminary attempts have been made to associate the kinetic and thermodynamic acidities of these hydrogens with their specific stereochemical environments.

Deprotonation of a 1,3-bissulfonium salt is accompanied by a decrease of at least 5 kcal/mol in the barrier to pyramidal inversion at sulfur. However, attempts to establish the static and dynamic behaviour at the carbanionic centre were not successful.

SAUL WOLFE, PETER CHAMBERLAIN et TIMOTHY F. GARRARD. Can. J. Chem. **54**, 2847 (1976).

Dix dérivés bistétrafluoroborate de bissulfonium-1,3 acycliques et deux cycliques ont été synthétisés par des modifications appropriées des procédés décrits dans la littérature pour la préparation de tels composés. Les sels acycliques sont déprotonés facilement par un équivalent molaire d'hydroxyde de potassium pour donner des ylures de bissulfonium-1,3. Cependant, sous les mêmes conditions, les sels cycliques se décomposent. Des expériences d'échange d'hydrogène révèlent que les hydrogènes en C2 des sels cycliques sont passablement moins acide que les hydrogènes en C2 des sels acycliques. Les acidités relatives des hydrogènes en C2 des sels cycliques dépendent du milieu et de la configuration et de la conformation de la molécule. Des essais préliminaires ont été faits pour associer les acidités cinétiques et thermodynamiques de ces hydrogènes avec leurs environnements stéréochimiques spécifiques.

La déprotonation d'un sel de bissulfonium-1,3 est accompagnée d'un abaissement d'au moins 5 kcal/mol dans la barrière d'inversion pyramidale à l'atome de soufre. Cependant, les essais pour établir le comportement statique et dynamique au site carbanionique n'ont pas eu de succès.

[Traduit par le journal]

Introduction

The use of sulfonium ylides in synthesis has developed rapidly in recent years (1). Their possible intervention in certain highly stereospecific biosynthetic processes has also been discussed (2), and there is evidence that, even under non-enzymatic conditions, these compounds can serve as vehicles for the introduction of chirality at carbon (3).

A full understanding of such results requires a knowledge of the static and dynamic stereochemical properties of sulfonium ylides. The following problems can be recognized. (*i*) What is the nature of the bond between sulfur and carbon? (*ii*) What is the geometry at sulfur? (*iii*) What is the geometry at carbon? (*iv*) What is the dihedral angle about the carbon–sulfur bond? (*v*) What is the barrier to rotation about the carbon–sulfur bond? (*vi*) What is the barrier to pyramidal inversion at carbon, and how is the barrier to inversion of a 'simple' carbanion affected by the attachment of a sulfonium substituent? (*vii*) What is the barrier to pyramidal inversion at sulfur, and how is the barrier to inversion of a 'simple' sulfonium cation affected by the attachment of a carbanionic substituent?

In the present work, an attempt is made to answer some of these questions in terms of a heuristic analysis of the stereochemical capabilities of sulfonium ylides. The most evident structural feature of such compounds is the presence of two directly bonded tricoordinate atoms, each of which carries an unshared electron pair. In the present analysis, the assumption is

[1]Revision received April 6, 1976.

Can. J. Chem. Downloaded from www.nrcresearchpress.com by 210.87.254.40 on 09/05/12
For personal use only.

Can. J. Chem. Downloaded from www.nrcresearchpress.com by 210.87.254.40 on 09/05/12
For personal use only.

made that these electron pairs are localized on sulfur and carbon, as indicated in structure **1**.

The stereochemical requirements of adjacent electron pairs affect both the static and the dynamic properties of systems which contain this structural unit (4). The effect upon static properties takes the form of a '*gauche* effect' (5), *i.e.*, a tendency of the system to exist preferentially in that conformation that has the maximum number of *gauche* interactions between the adjacent electron pairs. The effect upon dynamic properties is manifested most demonstrably upon barriers to pyramidal inversion (6) when the nuclei bearing the electron pairs are tricoordinate. In the absence of electronegativity effects, the attachment of $R_1R_2\ddot{M}$— to —$\ddot{Q}R_3R_4$ leads to an increase in the barriers to inversion at M and Q, as compared to those observed in R_1R_2MH and HQR_3R_4 (7). Electronegativity effects may either complement or oppose electron pair – electron pair effects according to whether there is electron release to or electron withdrawal from the pyramidal centres in question (8). Electron-withdrawing substituents increase the barrier, and electron-releasing substituents decrease the barrier.

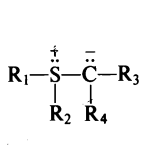

1

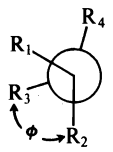

2

Extension of such observations to the case of the ylide **1**, leads to the following predictions:[2] (*i*) both sulfur and carbon should have pyramidal configurations; (*ii*) the stable conformation should have a dihedral angle ϕ in the range 80–120° (see **2**); (*iii*) the electron-withdrawing sulfonium substituent should cause the barrier to inversion at the adjacent carbanionic centre to be greater than that in a simple carbanion (2–6 kcal/mol (9)); the electron-releasing carbanionic substituent should cause the barrier to inversion at the adjacent sulfonium centre to be lower than that in a sulfonium salt (*ca.* 30 kcal/mol (10)).

These predictions are susceptible to experimental test. Proof of pyramidal sulfur in sulfonium ylides was first obtained by nmr (11) and, subsequently, by the resolution of the ylide **3** (12). Proof of pyramidal carbon in sulfonium ylides was obtained by Fava and Eliel and their co-workers (13), who observed the stereoselective transformation **4** → **5**.[3] Darwish and Tomilson demonstrated (12) that the barrier to inversion at sulfur in the ylide **3** is at least 6 kcal/mol lower than in the parent sulfonium salt. Whether the torsional behaviour about the C—S bond of a sulfonium ylide is in harmony with the postulate of the *gauche* effect is not yet settled, because the intermediate in transformations such as **4** → **5** cannot be observed directly, and conclusions derived from kinetic observations of hydrogen isotope exchange do not necessarily apply to thermodynamic stabilities (13, 17).

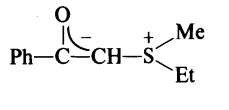

3

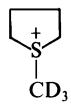

4

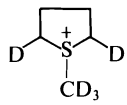

5

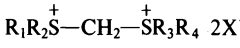

10

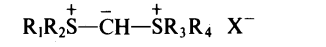

11

Lillya (18) and Gosselck (19) and their co-workers have described the synthesis of 1,3-bissulfonium salts (10) and their derived ylides (11). These compounds appeared to be particularly suitable for a study of the static and dynamic properties of sulfur ylides because both **10** and **11** are relatively stable at room temperature, a range of structural types is readily synthesized by appropriate modification of Lillya and Miller's procedures, and extension of the predictions made above from a system contain-

[2]These predictions first appeared in ref 5.

[3]It could be argued that the difference in the kinetic acidities of the prochiral α-methylene protons of **4** is a consequence of steric approach control in the quenching of a planar carbanion. However, steric approach control is not apparent in the related transformations **6** → **7** (14) and **8** → **9** (15), although the nature of the intermediate in these latter reactions is not yet clear (16).

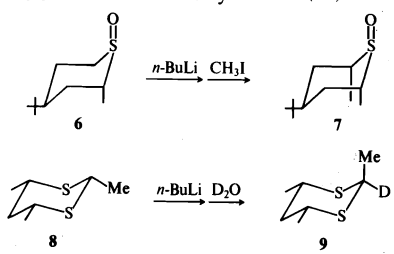

6 **7** **8** **9**

Can. J. Chem. Downloaded from www.nrcresearchpress.com by 210.87.254.40 on 09/05/12
For personal use only.

ing two adjacent electron pairs to one containing three adjacent electron pairs is straightforward. In addition, it was hoped that the presence of two electron-withdrawing sulfonium substituents on the ylide carbon atom would stabilize the pyramidal configuration at this centre, and allow measurement of the barrier to pyramidal inversion of a 'positively charged carbanion'.

Experimental

Synthesis of 1,3-Bissulfonium Tetrafluoroborates

The 1,3-bissulfonium salts were prepared by one of three routes, exemplified below as Method *A*, Method *B*, and Method *C*. In all cases, the salts were crystalline, and showed no peaks in their nmr spectra inconsistent with the assigned structures. The nmr spectra at 60 MHz were obtained on a Varian A60 spectrometer, with TMS or DSS as internal standards, according to the solvent employed. Spectra at 100 MHz were obtained on a Varian HA100 spectrometer at the University of Toronto through the generous cooperation of Professor W. F. Reynolds. Data in the exerimental section are recorded in τ values.

Method A

Triethyloxonium fluoroborate was prepared from freshly distilled epichlorohydrin and boron trifluoride etherate, and converted to trimethyloxonium fluoroborate by the usual procedures (20). To silver fluoroborate (1.27 g, 6.5 mmol) was added a solution of ethyl bromomethylsulfide (1.14 g, 6.5 mmol) in tetrahydrothiophene (7 ml). A white solid formed immediately and much heat was generated. The solid slowly dissolved, and the solution was stirred overnight at room temperature. The next day, methylene chloride (25 ml) was added, whereupon a yellow precipitate of silver bromide separated. This was removed, and the filtrate was evaporated to dryness. The residue was triturated twice with petroleum ether (30–60 °C), and then three times with ether until the product crystallized. The yield of **12** was 1.5 g: nmr (D_2O) 5.55 (2H, s), 6.4 (4H, m), 7.1 (2H, q), 7.6 (4H, m), 8.6 (3H, t).

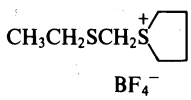

BF_4^-

12

This salt (1.5 g) and triethyloxonium fluoroborate (2.2 g) were mixed in methylene chloride (10 ml), and the mixture was stirred at room temperature overnight. The solvent was then decanted and the residue washed with petroleum ether (30–60 °C), methylene chloride, and ethanol, and then recrystallized by slow addition of ethanol to an aqueous solution. The yield of **13***a* was 620 mg, mp 134–136 °C.

For the preparation of the 1,1-dimethyl-3,3-diethylbissulfonium salt **15***a*, silver fluoroborate (1.27 g, 6.5 mmol) was added to a solution of ethyl bromomethylsulfide (1.14 g, 6.5 mmol) in dimethylsulfide (10 ml). The reaction, which was very exothermic in its early stages, was allowed to proceed for 2 h. Then methylene chloride was added, the mixture was filtered, and the filtrate was evaporated to dryness to give the salt **14** (1.8 g) as a light brown viscous oil. nmr (CH_2Cl_2) 5.2 (2H, s), 4.75 (6H, s), 4.86 (2H, q), 8.34 (3H, t).

$$CH_3CH_2SCH_2\overset{+}{S}(CH_3)_2\ BF_4^-$$

14

This oil (1.8 g) and triethyloxonium fluoroborate (6 g) were mixed in methylene chloride (10 ml), and the mixture was stirred overnight at room temperature. It was then treated with 5 ml of methanol, stirred for 0.5 h, and evaporated to dryness. The oily solid residue was washed with ether, dissolved in water, and absolute ethanol was added to the cloud point. Crystallization was allowed to proceed at 10 °C to give 1.05 g (50% in the two steps) of the bissulfonium salt **15***a*, mp 107–109 °C.

Method B

Formaldehyde dimethylthioacetal, bp 149–151 °C, and formaldehyde diethylthioacetal, bp 75–78 °C, were prepared in 35% and 73% yields, respectively (21). Reaction of the dimethylthioacetal with trimethyloxonium fluoroborate, and of the diethylthioacetal with triethyloxonium fluoroborate, according to Miller (22), afforded **17***a* and **16***a*, the 1,1,3,3-tetramethyl (yield 68%, mp 171–172 °C) and 1,1,3,3-tetraethyl (yield 54%, mp 151–152 °C) bissulfonium tetrafluoroborate salts, respectively. Reaction of the dimethylthioacetal with triethyloxonium fluoroborate (22), or the diethylthioacetal with trimethyloxonium fluoroborate produced, in 63% and 75% yields, respectively, the same substance, **18***a*, methylenebis-(methylethylsulfonium)fluoroborate, mp 125–126 °C; mixture melting point 125–126 °C. The spectroscopic properties and the melting point of the material were unchanged following recrystallization from acetone, acetone–ether, ethyl acetate, or dimethyl sulfoxide – ethanol.

Method C

Hydrogen chloride gas was passed, during 3 h at −10 °C, into a stirred mixture of thiophenol (27.5 g, 0.25 mol) and paraformaldehyde (7.5 g, 0.23 mol). At the end of this time, the paraformaldehyde had dissolved and water was present in the reaction mixture. Calcium chloride was added and, after 20 h at 0 °C, the mixture was filtered, and the filtrate distilled. Phenyl chloromethylsulfide (13.6 g, 34%) was collected at 108–110 °C: nmr ($CDCl_3$) 2.7 (m, 5H), 5.15 (s, 2H).

Sodium hydroxide (2 g, 50 mmol) was added to absolute ethanol (30 ml), the mixture was cooled to 0 °C, and methanethiol was introduced until the sodium hydroxide had dissolved. Then phenyl chloromethylsulfide (7.9 g, 50 mmol) was added dropwise during 5 min. A heavy white precipitate formed. The mixture was warmed to 40 °C to distil out excess methanethiol, and it was left overnight. The solvent was then removed under reduced pressure, and the residue was shaken with water and ether. The ether phase was dried over anhydrous magnesium sulfate and evaporated to give 8.1 g (95%) of phenylmethyldithiomethane: nmr ($CDCl_3$) 2.8 (m, 5H), 6.08 (s, 2H), 7.85 (s, 3H).

Reaction of phenyl chloromethylsulfide with ethanethiol, in the manner just described, gave phenylethyl-

TABLE 1. Melting points of the 1,3-bissulfonium salts $[R_1R_2\overset{+}{S}CH_2\overset{+}{S}R_3R_4]^{2+}\ 2BF_4^-$ synthesized in this work

Compound	R_1	R_2	R_3	R_4	Method	Melting Point (°C) This work	Literature
13*a*	Et	Et	$(CH_2)_4$		*A*	134 –136	
15*a*	Me	Me	Et	Et	*A*	107 –109	
16*a*	Et	Et	Et	Et	*B*	151 –152	152–158 (22)
17*a*	Me	Me	Me	Me	*B*	171 –172	187–194 (22)
18*a*	Me	Et	Me	Et	*B*	125 –126	131–133 (22)
19*a*	Ph	Me	Me	Me	*C*	128.5–129.5	
20*a*	Ph	Et	Et	Me	*C*	109 –111	
21*a*	Ph	Me	Et	Me	*C*	112 –113	
22*a*	Me	Me	$(CH_2)_4$		*A*	151 –152	
23*a*	Et	Me	Me	Me	*A*	56 – 57	
24*a*					*B*	208 –211	186 (23)
25*a*					*B*	108 –110	114 (23)

dithiomethane: nmr ($CDCl_3$) 2.8 (m, 5H), 6.00 (2H, s), 7.30 (2H, q), 8.75 (3H, t).

Phenylmethyldithiomethane (1.1 g, 6.5 mmol) and trimethyloxonium fluoroborate (2.9 g, 19.6 mmol) were mixed in a dry box under nitrogen, and the mixture was shaken at room temperature. When a semi-solid paste had formed, methylene chloride (3 ml) was added, the flask was sealed, and stirring was continued for 24 h. The light brown solid mass was collected by filtration, triturated with anhydrous ether followed by methylene chloride, and then dissolved in the minimum amount of water. Ethanol was added to the cloud point, and crystallization was allowed to proceed at 10 °C. The crystals were collected, washed with absolute ethanol, and dried *in vacuo* at 25 °C. The yield of the 1,3,3-trimethyl-1-phenylbissulfonium fluoroborate, **19***a*, mp 128.5–129.5 °C, was 1.6 g (66%).

In a different preparation, phenylmethyldithiomethane (1.1 g, 7.2 mmol) and triethyloxonium fluoroborate (6.0 g, 31 mmol) were mixed in a dry box under nitrogen. The reaction flask was then sealed and shaken at room temperature for 44 h. The resulting dark brown oil was triturated with three 10 ml portions of anhydrous ether and then dissolved in methylene chloride and precipitated with ether. This procedure was repeated once and the black oil was then dissolved in absolute methanol and reprecipitated with ether. Repetition of this latter procedure caused crystallization of the compound. Three triturations with 10 ml portions of methanol afforded an off-white solid. This was dissolved in water (3 ml), ethanol (50 ml) was added to the cloud point, and crystallization was allowed to proceed at 10 °C. The compound was collected, washed with ethanol, and dried *in vacuo* at 25 °C. The yield of white crystalline 1-phenyl-1-ethyl-3-methyl-3-ethylbissulfonium salt, **20***a*, was 0.4 g (18%), mp 109–111 °C.

The reaction of phenylethyldithiomethane with trimethyloxonium fluoroborate in the same manner as described in the above two paragraphs afforded a semi-solid mass. This was triturated with a large excess of absolute ethanol to give an off-white solid whose nmr spectrum (see Discussion) indicated the presence of predominantly one diastereoisomer. Recrystallization in the usual manner from aqueous ethanol yielded the 1-methyl-1-phenyl-3-methyl-3-ethylbissulfonium salt, **21***a*, mp 112–113 °C. *Anal.* calcd. for $C_{11}H_{18}S_2 \cdot 2BF_4$: C 34.05, H 4.67; found: C 34.25, H 4.40.

Preparation of the 1,3-Diethylbissulfonium Salt of 1,3-Dithiane

1,3-Dithiane (0.87 g, 7.53 mmol) and triethyloxonium fluoroborate (5.01 g, 26.4 mmol) were dissolved in methylene chloride, and the flask was sealed in a dry box and allowed to stand overnight at room temperature. The solvent was then decanted from the heavy oil which had precipitated, and the oil was triturated a number of times with dry ether and then evacuated overnight at 0.01 torr. At this point, the compound crystallized upon the addition of absolute methanol to give 1.22 g (66.5%) of the salt **25***a*. Recrystallization from aqueous ethanol gave material melting at 108–110 °C (lit. (23) mp 114 °C). *Anal.* calcd. for $C_8H_{18}S_2 \cdot 2BF_4$: C 27.35, H 5.15; found: C 27.52, H 4.99. The nmr (TFA-*d*) 4.70 (d, 12 Hz), 4.72 (s), 5.05 (d, 12 Hz, $\overset{+}{S}$-CH_2-$\overset{+}{S}$, see text), 6.10 (8H, q, $\overset{+}{S}$-CH_2), 6.97 (2H, m, CH_2-CH_2-CH_2), 8.26 (6H, t, CH_3).

The 1,3-dimethylbissulfonium salt **24***a*, mp 208–211 °C (lit. (23) mp 186 °C), prepared analogously from 1,3-dithiane, had the following nmr spectrum in TFA: 4.79 (2H, s, $\overset{+}{S}$-CH_2-$\overset{+}{S}$), 6.12 (4H, m, $\overset{+}{S}$-CH_2), 6.69 (6H, s, CH_3), 7.08 (2H, m, CH_2—CH_2—CH_2). In D_2O, two peaks were observed in the methyl region: 4.82 (2H, s, exchanges), 6.20 (4H, m), 6.68 (2.4H, s), 6.72 (3.6H, s), 7.13 (2H, m).

Table 1 lists the various salts synthesized by appropriate choice of methods *A–C*, and the melting points of these salts. Table 2 contains proton chemical shift data for these compounds.

Can. J. Chem. Downloaded from www.nrcresearchpress.com by 210.87.254.40 on 09/05/12
For personal use only.

Can. J. Chem. Downloaded from www.nrcresearchpress.com by 210.87.254.40 on 09/05/12
For personal use only.

TABLE 2. Proton chemical shifts[a] of dithiomethanes $R_1SCH^B{}_2SR_2$, 1,3-bissulfonium salts $R_1R_2\overset{+}{S}CH^B{}_2\overset{+}{S}R_3R_4$[b], and 1,3-bissulfonium ylides $R_1R_2\overset{+}{S}\overset{-}{C}H^B\overset{+}{S}R_3R_4$[b]

Compound	Substituent				Proton observed	Salt		Ylide		Dithiomethane ($CDCl_3$)
	R_1	R_2	R_3	R_4		TFA	D_2O	D_2O	CH_2Cl_2	
15*a,b*	$CH^A{}_3$	$CH^A{}_3$	$CH_3CH^{A'}{}_2$	$CH_3CH^{A'}{}_2$	A	[c]	196	168	168	
					A′		222	176.4, 185.6[d]	170.4, 179.6[d]	
					B		[e]	[e]	138	
16*a,b*	$CH_3CH^A{}_2$	$CH_3CH^A{}_2$	$CH_3CH^A{}_2$	$CH_3CH^A{}_2$	A	205	229	180.6, 183.4[d]	178.6, 181.4[d]	
					B	285	[e]	[e]	128	
17*a,b*	$CH^A{}_3$	$CH^A{}_3$	$CH^A{}_3$	$CH^A{}_3$	A	[c]	194	166	167	
					B		[e]	[e]	154	
18*a,b*	$CH^A{}_3$	$CH_3CH^{A'}{}_2$	$CH^A{}_3$	$CH_3CH^{A'}{}_2$	A	174[f]	194	179	162	
					A′	206	225	195[d,g]	179[d,g]	
					B	288	[e]	[e]	137	
19*a,b*	Ph	$CH^A{}_3$	$CH^{A'}{}_3$	$CH^{A''}{}_3$	A	192	215	[c]	185	
					A′	161	179		170	
					A″	169	184		173	
					B	300	[e]		130	
20*a,b*	Ph	$CH_3CH^A{}_2$	$CH_3CH^{A'}{}_2$	$CH^{A''}{}_3$	A	222.5				
					A′	190				
					A″	169, 156.5		168, 164		
					B	300				
21*a,b*	Ph	$CH^A{}_3$	$CH_3CH^{A'}{}_2$	$CH^{A''}{}_3$	A	215[h]	220	[c]	182	
					A′	205	212		175[d,g]	
					A″	179	187		170, 168[i]	
					B	332	[e]		148	

Can. J. Chem. Downloaded from www.nrcresearchpress.com by 210.87.254.40 on 09/05/12
For personal use only.

TABLE 2 (*Concluded*)

Compound	Substituent				Proton observed	Salt		Ylide		Dithiomethane ($CDCl_3$)
	R_1	R_2	R_3	R_4		TFA	D_2O	D_2O	CH_2Cl_2	
22*a,b*	$CH^A{}_3$	$CH^A{}_3$	$—CH^{A'}{}_2(CH_2)_2CH^{A'}{}_2—$		A	181			173	
					A′	220			218	
					B	285				
23*a,b*	$CH_3CH^A{}_2$	$CH^{A'}{}_3$	$CH^{A''}{}_3$	$CH^{A''}{}_3$	A	210	225	175[d,g]	175[d,g]	
					A′	179	194	158	161	
					A″	182	197	162	165	
					B	296	[e]	[e]	144	
13*a,b*	$CH_3CH^A{}_2$	$CH_3CH^A{}_2$	$—CH^{A'}{}_2(CH_2)_2CH^{A'}{}_2—$		A	216			180	
					A′	228			212	
					B	291				
39*a*	$CH^A{}_3$	$CH^A{}_3$			A					127
					B					216
39*b*	Ph	$CH^A{}_3$			A					129
					B					235
39*c*	$CH_3CH^A{}_2$	$CH_3CH^A{}_2$			A					160
					B					221

[a]Spectra were obtained as 10% solutions at 30 °C on a Varian A60 spectrometer, and were temperature independent except where mentioned in the text. All chemical shifts are reported in Hz downfield from internal TMS or DSS, as appropriate.
[b]The anion is tetrafluoroborate.
[c]The compound is insoluble in this solvent.
[d]An ABX_3 spectrum was observed.
[e]These protons undergo rapid hydrogen–deuterium exchange.
[f]The same substance, mp 125–126 °C, is obtained by methylation of diethyldithioacetal or ethylation of dimethyldithioacetal.
[g]The ABX_3 spectrum was not analyzed; the chemical shift quoted is for the centre of the absorption.
[h]These data are for the single diastereomer (see text).
[i]These are the A″ shifts of the two diastereomers; the CH_3 protons of the ethyl group appear as two triplets centred at 69 and 79 Hz.

Can. J. Chem. Downloaded from www.nrcresearchpress.com by 210.87.254.40 on 09/05/12
For personal use only.

Deprotonation of Acyclic 1,3-Bissulfonium Salts

The ylides **13***b*, **15***b*–**23***b* were generated from the salts **13***a*, **15***a*–**23***a* in greater than 90% yield by treatment with 1 mol equiv. of methanolic potassium hydroxide, followed by evaporation of the solvent, trituration of the residue with methylene chloride, and reevaporation. The tetramethylbissulfonium ylide **17***b* was a white crystalline compound, mp 103.5–104.5 °C (lit. (22) mp 104 °C). All others were pale yellow oils.

Recrystallization of **17***b* from a mixture of methanol – methylene chloride – ether gave large prisms which, unfortunately, proved to be unsuitable for crystallographic work.[4] It had been hoped that such a study would provide direct evidence concerning the geometry of the ylide carbon in the solid state. Although this was not successful, it is important to note that the crystal structure of dehydromethionine (**i**), which is isoelectronic to a sulfonium ylide, has been found to have pyramidal geometry at nitrogen (24).

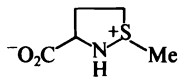

i

Results and Discussion

Preparation of 1,3-Bissulfonium Salts

Ten acyclic 1,3-bissulfonium salts (**13***a*, **15***a*–**23***a*; see Table 1) were prepared by appropriate reaction sequences, termed Method *A* [1], Method *B* [2], and Method *C* [3]. These afforded an array

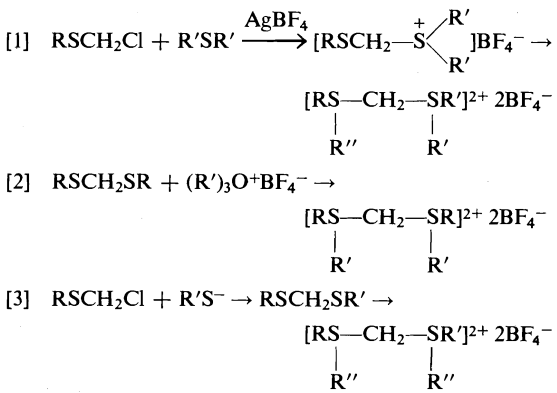

of symmetrically and unsymmetrically substituted 1,3-bissulfonium salts bearing phenyl, methyl, ethyl, and tetrahydrothiophenyl substituents. Attempts to prepare compounds having one or two *S*-benzyl groups, 1,3-diphenyl substitution, or a substituted central methylene group were unsuccessful.

The two cyclic 1,3-bissulfonium salts **24***a* and **25***a* were prepared by alkylation of 1,3-dithiane (23). In each case the salt was obtained as a mixture of geometrical isomers; **24***a* was a 60:40 mixture of isomers, based upon integration of the *S*-methyl signals. In CF_3COOH (TFA-*h*), the spectrum of the 1,3-diethylbissulfonium salt **25***a* was more informative, and it allowed a determination of the proportions of the *cis* and *trans* isomers (*cis*:*trans* = 62:38). The C2 methylene protons of the *cis* isomer **26** appeared as a quartet (τ_e = 4.70; τ_a = 5.05; J_{ea} = 12 Hz), and those of the *trans* isomer **27** as a singlet (τ 4.72). Since **26** is conformationally constrained (anancomeric) (25), H_{2e} and H_{2a} are anisochronous, but rapid ring inversion of **27** averages the signals of these protons. It should be noted that **26** exemplifies the class of *meso* compounds $X_+CH_2X_-$, and **27** exemplifies a *dl* isomer of the type $X_+CH_2X_+$ (and $X_-CH_2X_-$), in which X_+ and X_- are enantiomeric chiral ligands. The methylene protons in $X_+CH_2X_-$ are diastereotopic, and those in $X_+CH_2X_+$ (and $X_-CH_2X_-$) are homotopic. This fact has been employed to assign structures to the *meso* and *dl* isomers of 2,4-dithiapentane 2,4-dioxide (26).

The assignment of the H_{2e} and H_{2a} chemical shifts of **26** was based initially upon the observation of broadening of the low field half of the quartet ($W_{1/2}$ = 9 Hz *vs.* $W_{1/2}$ = 3 Hz for the upfield half of the quartet), and was confirmed by double irradiation experiments in the region of the C4 and C6 protons at τ 6.10. The broadening of H_{2e} is the result of a W effect (27) with the equatorial ring protons at C4 and C6.

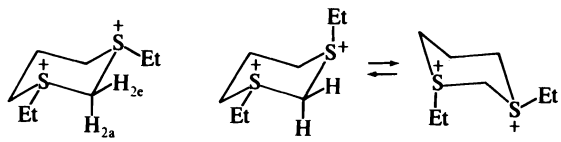

26 **27**

Deprotonation of 1,3-Bissulfonium Salts

Each of the acyclic salts was converted without difficulty to the 1,3-bissulfonium ylide upon treatment with 1 mol equiv. of methanolic potassium hydroxide. However, this procedure led to decomposition in the case of the cyclic salts **24***a* and **25***a*.

Hydrogen–deuterium exchange studies helped to clarify this behaviour. Following the preparation of 10% solutions in D_2O, all of the acyclic salts and ylides underwent extremely rapid exchange (<0.5 min) of the C2 proton(s). On

[4] G. I. Birnbaum, personal communication.

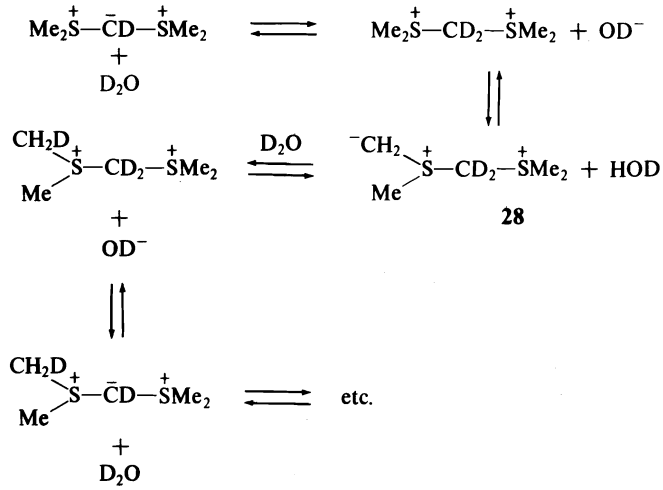

SCHEME 1

further standing in D_2O, the methyl protons of the ylide **17***b* also exchanged within 20 min at 30 °C, but those of the salt **17***a* did not. In H_2O, back-exchange of perdeuterio **17***b* occurred, with regeneration of the starting material.

The simplest explanation for the exchange of the methyl protons of **17***b* under these conditions is shown in Scheme 1. This assumes the existence of a tautomer **28**, which may be present to a small extent in aqueous solution.[5] Since **17***a* has a pK_a of 9.0 (18), the assumption that hydrogen–deuterium exchange proceeds solely via sulfonium ylide intermediates allows the calculation that the rates of exchange of the methyl protons of 0.1 *M* solutions of **17***a* and **17***b* should differ by a factor of 10^4.

The methyl protons of the ylide **17***b* also exchanged completely in CD_3OD solvent (75 min for a 0.1 *M* solution at 30 °C). Isolation of the perdeuterio compound and dissolution in CH_3OH led to recovery of **17***b*. Repetition of this experiment with the phenyltrimethylbissulfonium ylide **19***b* revealed that the methyl group at 215 Hz exchanged more rapidly than the two methyl groups at 179 and 184 Hz (see Table 2). This permitted the synthesis of the selectively deuterated compounds **29** and **30**, by appropriate sequences of exchange. As expected for a process involving the formation of an intermediate carbanion, the methylene protons of the *S*-ethyl groups of **15***b* and **18***b* did not exchange in D_2O or CD_3OD in the time required to achieve complete exchange of the methyl groups.

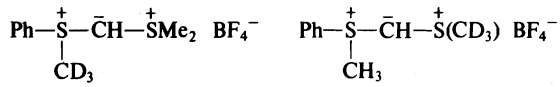

29 **30**

A methylene chloride solution of **29** showed no scrambling of deuterium during 17.5 h at room temperature. Similarly a 1:1 mixture of **19***b* and perdeuterio **17***b* in methylene chloride showed no evidence of scrambling during 5 days. These results demonstrate that tautomeric equilibria involving intra- and intermolecular carbon–hydrogen transfer reactions are unimportant in these acyclic ylides.

The kinetic acidities of the C2 protons of the cyclic 1,3-bissulfonium salts were found to be substantially less than those of the corresponding protons of the acyclic salts. For example, at 30 °C the exchange of the C2 protons of **24***a* (10% in D_2O) required 20 min for completion. Addition of 0.1 mol equiv. of NaOD to such a solution led to rapid exchange of the methyl protons (10 min). It seems likely that this reduced kinetic acidity of the cyclic salts permits base-promoted hydrolysis to become a competitive process which leads to decomposition (Scheme 2).

[5]One cannot *a priori* rule out the existence of a 'diylide', *i.e.*,

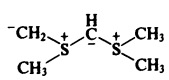

Can. J. Chem. Downloaded from www.nrcresearchpress.com by 210.87.254.40 on 09/05/12
For personal use only.

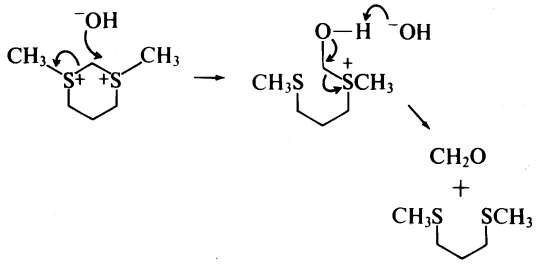

SCHEME 2

Under controlled conditions, in which decomposition was largely avoided, the two isomers of **24***a* displayed different reactivities towards base. In a typical experiment, six 0.25 *M* H_2O solutions of **24***a* were prepared and equilibrated at 30 °C. To these solutions were added 2.5, 5.0, 7.5, 10.0, 12.5, and 15.0 μl (0.1–0.6 mol equiv.) of 10 *N* NaOH. In each case, the chemical shifts of the *S*-methyl groups (199 and 197 Hz for the minor and major isomers of the salt, respectively) were recorded before the addition of the base, immediately after the addition of the base, and again after the addition of sufficient TFA to regenerate the salt. Some decomposition was evident following reprotonation of the solution containing 0.6 mol equiv. of base, but the other mixtures were stable under these conditions. As the amount of added base was increased progressively, the chemical shift of the methyl groups of the major isomer remained constant, but that of the minor isomer shifted upfield by 2.0, 6.5, 11.5, 14.5, and 16.5 Hz for 0.1–0.5 mol equiv. of base, respectively. The ratio of the major and minor isomers remained the same, in the presence of the base and after the reprotonation. As will be seen in the next section, these upfield shifts are consistent with the preferential formation of a bissulfonium ylide of the minor isomer. If the stereochemical course of methylation and ethylation of 1,3-dithiane is the same, then the minor isomer of **24***a* is the *trans* compound **31**.[6] In this compound, one of the C2 protons is anticoplanar to one 'lone pair' and *gauche* to the other; the other C2 proton is *gauche* to both 'lone pairs'. In the *cis* isomer **32**, one of the C2 protons is anticoplanar to both 'lone pairs' and the other is *gauche* to both 'lone pairs'.

These various observations show that the

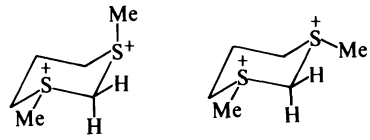

31 **32**

thermodynamic acidities of protons flanked by two sulfonium substituents, like the kinetic acidities of protons adjacent to one sulfonium substituent (13), are subject to very subtle conformational effects. If it is now assumed that, in acyclic 1,3-bissulfonium salts, staggered conformations are more stable than eclipsed conformations, **33** appears to be the only fully staggered conformation which cannot be attained by the cyclic salts. In this conformation, each of the C2 protons is *gauche* to one 'lone pair' and anticoplanar to the other. We therefore suggest tentatively that, in water solvent, the relationship between conformation and acidity is **33** > **31** > **32**.

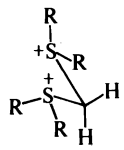

33

However, it is known (17) that the kinetic acidities of protons adjacent to sulfur are subject to both conformational and medium effects. Experiments with the 1,3-diethyl compound **25***a* demonstrated this point in the present system. In rigorously purified TFA-*d* (29), **25***a* was stable for at least 2 days at 30 °C, and there was no exchange of any of the protons. Addition of the base D_2O to this solution led to exchange of the C2 protons but not of the other methylene protons, and the compound remained stable. Careful adjustment of the proportions of TFA-*d* and D_2O allowed the exchange of the C2 protons to be followed by nmr as a function of time.

Initial, qualitative, observations in various TFA-*d* – D_2O mixtures indicated that the C2 quartet of the *cis* isomer **26** disappeared more rapidly than the C2 singlet of the *trans* isomer **27**. Therefore, in this solvent system, the relative kinetic acidities of the geometrical isomers are the reverse of the thermodynamic acidities observed in D_2O alone. More significantly, the

[6]Attempts to confirm this structural assignment by cmr have not been successful (28).

Can. J. Chem. Downloaded from www.nrcresearchpress.com by 210.87.254.40 on 09/05/12
For personal use only.

Can. J. Chem. Downloaded from www.nrcresearchpress.com by 210.87.254.40 on 09/05/12
For personal use only.

exchange of the diastereotopic C2 protons of **26** was stereoselective. As the quartet disappeared, a peak at τ 5.04, corresponding to **34**, grew in intensity and then slowly disappeared. The diastereomer **35** could not be observed at any time under a variety of conditions (5% of this compound would have been detected).

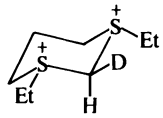

34

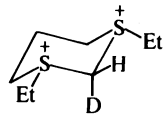

35

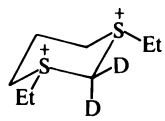

36

In an attempt to obtain more quantitative data, a 0.41 *M* solution of the 1,3-diethyl-1,3-dithianylbissulfonium salts (0.16 *M* in the *trans* isomer **27**), in TFA-*d* – D_2O (73:27) (D_2O:**25***a* = 64), was allowed to undergo exchange for 15 min at 30 °C until the quartet of **26** had disappeared but not the singlet of **34**. The singlet of **27** was then integrated as a function of time using the 8-proton CH_2 multiplet and the 6-proton triplet of the methyl groups as internal standards. After 20, 30, 40, 50, and 60 min, the singlet of **27** corresponded to 0.61, 0.55, 0.48, 0.43, and 0.38 hydrogen. These data correspond closely to pseudo first-order kinetic behaviour, with a rate constant under these conditions of 0.12 min^{-1}.[7]

In a second experiment, a 0.29 *M* solution of the 1,3-diethyl-1,3-dithianylbissulfonium salts was allowed to exchange in TFA-*d* – D_2O (89:11) (D_2O:**25***a* = 16), and the integrals of the singlet of **34** at 5.04 and the upfield half of the quartet of **26** were recorded as a function of time. These integrals were then normalized to initial values of zero protons and two protons for **34** and **26**, using the six-proton triplet of the methyl groups as an internal standard, and assuming that the proportions of **26** and **27** remain the same during the course of the exchange of the C2 protons (see below).

When the exchange of diastereotopic protons H_A and H_B is performed under pseudo first-order conditions, and the observed process is $H_AH_B \rightarrow D_AH_B \rightarrow D_AD_B$, a plot of $\ln [H_AH_B]$ *vs.* time gives $(k_A + k_B)$. In the latter stages of the reaction, when H_AH_B has disappeared, a plot of $\ln [D_AH_B]$ *vs.* time gives k_B (neglecting the secondary isotope effect), so that both k_A and k_B can be estimated. For the experiment just described, the data gave $k_A = k_B = 0.04$ min^{-1}, *i.e.*, H_{2e} and H_{2a} of **26** have almost the same kinetic acidity.

This is an important result. If H_{2e} and H_{2a} have the same kinetic acidity, the stereoselective formation of **34** as an intermediate requires the conclusion that H_{2e} exchanges with net *retention* of configuration, and H_{2a} exchanges with net *inversion* of configuration. Although stereoselective exchange of diastereotopic methylene protons is a well established phenomenon (see, *e.g.*, ref. 13), all previous work on sulfur-containing systems has found this stereoselectivity to originate in a difference in the kinetic acidities of prochiral protons adjacent to sulfur. When these kinetic acidities differ significantly, there is no doubt (13*a*, 17) that the fast exchange must occur with retention of configuration. Inversion of configuration in the slow exchange can be anticipated (13*a*, 17), when the transition states for proton abstraction are higher than the activation energy associated with the interconversion of diastereomeric carbanions (**37** ⇄ **38** in the present case). There has been no previous determination of the stereochemical course of exchange at both sites, to assess the relative contributions to the overall process of these kinetic and thermodynamic effects. However, if it is accepted that protonation of the carbanion is the microscopic reverse of its formation by proton abstraction, it can be seen, upon reflection, that *no combination of kinetic and thermodynamic effects can lead to equal kinetic acidities and different stereochemical results at the two sites*. If we are invoking microscopic reversibility, the above statement must also include the circumstance that the carbanion is planar and is subject to 'steric approach control' (or 'stereoelectronic approach control') in the reprotonation step (see *e.g.*, ref. 30).

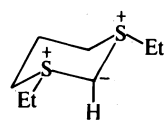

37

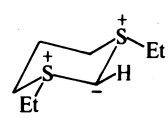

38

It is therefore necessary to suggest that the observed pseudo first-order rate constant for the abstraction of H_{2e} of **26** is lower than the true rate constant. This could be the result of a

[7]Extrapolation to zero time leads to a calculated initial integral for the C2 singlet of 0.80. This corresponds to a 60:40 mixture of **26** and **27**, and agrees with the initial ratio of **26** and **27** obtained by integration of the quartet and singlet.

Can. J. Chem. Downloaded from www.nrcresearchpress.com by 210.87.254.40 on 09/05/12
For personal use only.

significant contribution to the exchange process of 'internal return' (31), with this being more pronounced for H_{2e} than H_{2a}. Because of its high acidity, trifluoroacetic acid can hardly be regarded as a typical medium for the formation of a carbanion. Yet there is no doubt that hydrogen exchange of **26** takes place in the TFA–D_2O mixture. It is noteworthy that despite its acidity, TFA is a solvent of low polarity. Its dielectric constant (8.4–8.5 at 20 °C (32)) is less than that of methylene chloride, a solvent in which isoracemization (33) can be observed (34). On the other hand, Fraser and his co-workers (personal communication) have found that internal return is barely perceptible in the exchange of benzyl methyl sulfoxide in NaOD–D_2O. A decision on whether a TFA-D_2O medium containing 11% of D_2O can sustain internal return in the exchange of a 1,3-bissulfonium salt will have to await additional, more detailed, experimental studies.

The treatment of the data just discussed depends upon the assumption that interconversion of **26** and **27** is not important under the conditions of the exchange of the C2 protons. A mechanism for such interconversion is pyramidal inversion at sulfur in the various ylides, which are present in a low equilibrium concentration (for an account of a similar situation, see footnote 18 of ref. 13*b*). That this process is not rapid in the present case was already evident from the aqueous deprotonation–reprotonation experiments described above, in which the *cis*:*trans* ratio of **24***a* remained the same, and from the observation recorded in footnote 7. However, a change in the *cis*:*trans* ratio of **25***a*, from 62:38 to 50:50 could be observed in aqueous TFA after extended periods (10–20 h).[8]

Proton Chemical Shifts of Acyclic 1,3-Bissulfonium Salts and Ylides

Table 2 displays the chemical shifts of various protons in the acyclic 1,3-bissulfonium bistetrafluoroborates and their derived ylides. The chemical shifts of three dithiomethanes are included in this table for comparison.

Neglecting for the present the various examples of anisochronous methyl and/or methylene protons which are found in this table (see next section for a discussion of this phenomenon), it is seen that the conversion of a dithioacetal **39** into a 1,3-bissulfonium salt is accompanied by a downfield shift of the A protons, by 65–69 Hz. The B protons are shifted downfield by 64–72 Hz. A downfield shift is expected in both cases, because the transformation **39** → **40** converts a neutral molecule into a dication. Similarly, the conversion of the neutral molecule **39** into the *mono*-cation **41** leads to downfield shifts of the A protons (19–22 Hz and 35–39 Hz for R = H and CH_3, respectively). But the B protons are shifted *upfield* by 67–93 Hz. Thus, deprotonation of a 1,3-bissulfonium salt causes an upfield shift of the A protons of 30–40 Hz; and for the B protons the upfield shift is 131–165 Hz. These chemical shifts seem quite compatible with the charge localized structure shown in **41** and elsewhere in this paper.[9,10]

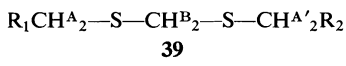

39

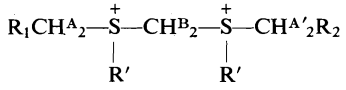

40

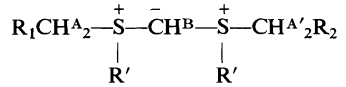

41

Dynamic Behaviour of 1,3-Bissulfonium Salts and Ylides

The isolation of the cyclic salts **24***a* and **25***a* as distinguishable (by nmr) mixtures of diastereomers demonstrates that 1,3-bissulfonium salts, like simpler monosulfonium salts (11, 12), have a pyramidal configuration at sulfur and a relatively high barrier to pyramidal inversion at this

[8]The possibility that, in some solvents, the *cis* isomer, with one axial substituent, has equal or slightly greater thermodynamic stability than the *trans* isomer, will be the subject of a separate communication (*cf.* refs. 28 and 35).

[9]Whether the chemical shifts are also compatible with a charge-delocalized representation **42** is not clear. In the case of phosphonium salts and ylides, the use of chemical shift data to distinguish between ylide and ylene representations has led to considerable controversy (36).

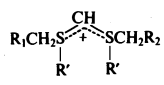

42

[10]Attempts to record cmr spectra and ^{13}C–H coupling constants of the C2 protons of the salts and ylides were not successful. We thank Professors J. B. Stothers and A. S. Perlin for their cooperation.

Can. J. Chem. Downloaded from www.nrcresearchpress.com by 210.87.254.40 on 09/05/12
For personal use only.

centre. In agreement with this result, the salts **20***a* and **21***a*, which have two chiral sulfur atoms, were each found to be approximately 1:1 mixtures of isomers.

One of the isomers of **21***a* could be obtained in pure form by fractional crystallization. After standing at −10 °C for 75 h, an aqueous solution of this compound showed the presence of *ca.* 12% of the second isomer. Since the 1:1 mixture of isomers showed no change in composition during this interval, it seems reasonable to assume that the proportion of the diastereomers at equilibrium is 1:1. If it is also assumed that the isomerization proceeds by pyramidal inversion at sulfur, an approximate rate constant k_1 (see Scheme 3) of 4.7×10^{-7} s^{-1} can be calculated for this process, corresponding to a free energy of activation at −10 °C of 25 kcal/mol. This is a minimum value because, as will be seen, $k_2 > k_1$ so that, depending on the relative values of k_a, k_{-a}, and k_2, some or all of the observed interconversion could have occurred via pyramidal inversion at sulfur in the ylide. It should be noted that, since **21***a* has two chiral centres, and inversion at either centre will cause interconversion of the diastereomers, 25 kcal/mol is a minimum value for the lower barrier at sulfur. However, it is known (10, 12) that barriers to inversion of monosulfonium salts are relatively insensitive to the nature of the substituents.

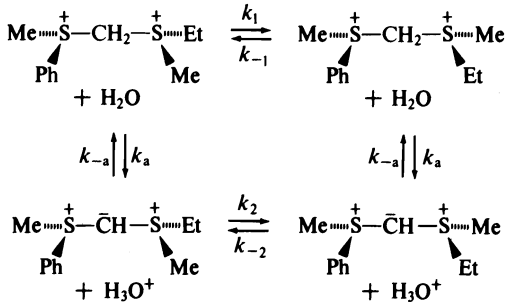

SCHEME 3

The phenyltrimethylbissulfonium salt **19***a* shows three methyl singlets. In principle, this observation might be interpreted in terms of planar configurations at S_1 and S_2 and restricted rotation about the C—S_1 and C—S_2 bonds; or pyramidal configurations at sulfur and diastereotopic A′ and A″ protons. We prefer the second explanation for three reasons: (*i*) the evidence for pyramidal sulfur atoms in these compounds, already discussed; (*ii*) the achiral salts **15***a*–**17***a* show isochronous methyl and/or ethyl groups; (*iii*) the nmr spectrum of **19***a* showed no change in the temperature range 30–80 °C.[11] Any dynamic process which might cause coalescence of the A′ and A″ peaks must therefore have a barrier $\Delta G^{\ddagger} > 25$ kcal/mol (37). It seems very unlikely that C—S bond rotation could have such a high barrier, although a pronounced preference for a particular conformation (*e.g.* **33**) could vitiate this latter argument.

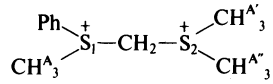

19*a*

The phenyltrimethylbissulfonium ylide **19***b* also shows three methyl singlets. In this case, reversible changes in the nmr spectrum were observed in DMSO-d_6 in the range 40–85 °C, with a coalescence of the A′ and A″ signals occurring at 80 °C. The assumption that this coalescence is the result of a dynamic process permits the calculation (37) of a free energy of activation for this process of 19.8 kcal/mol at 80 °C.

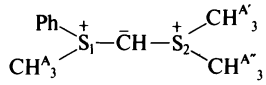

19*b*

At least six explanations can be offered for these results, *viz.* (*i*) there is restricted rotation about the C—S_1 and C—S_2 bonds, as in **42**; (*ii*) the A′ and A″ protons are diastereotopic with respect to an asymmetric centre at S_1; (*iii*) the A′ and A″ protons are diastereotopic with respect to an asymmetric centre at C2; (*iv*) asymmetry exists on the nmr time scale at both sulfur and carbon, with accidental coincidence of the A′ and A″ protons of the two diastereomers; (*v*) preferential formation of only one of the two possible diastereomers; (*vi*) loss of asymmetry at one chiral centre by a mechanism not involving pyramidal inversion.

The first explanation seems unlikely, because of the observation of equivalent methyl and/or ethyl groups in the ylides **16***b*–**18***b*. The fourth explanation is ruled out by the observation that

[11]In DMSO-d_6; above 80 °C, the compound decomposed rapidly.

Can. J. Chem. Downloaded from www.nrcresearchpress.com by 210.87.254.40 on 09/05/12
For personal use only.

the chemical shift difference between the A′ and A″ protons of **19***b* decreases slightly, but the relative intensities of the two peaks (1:1) remain the same as the temperature is lowered from +40 to −45 °C. Had this explanation been viable, the relative amounts (and thus the relative intensities of the A′ and A″ absorptions) of the two diastereomers should have been temperature dependent. To provide a mechanism for interconversion of diastereomers, these low temperature studies were performed in methylene chloride saturated with water. This medium would be expected to facilitate interconversion by a protonation–deprotonation sequence since Caserio and her co-workers (38) have observed that an intermolecular exchange reaction between an ylide and trace amounts of water affects the appearance and position of the methine signal (see also ref. 39).

The fifth explanation might be valid if **43** (*cf.* **33** and **37**) were the preferred conformation of the ylide. However, this argument is speculative at the present time.

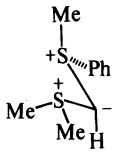

43

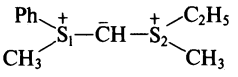

44

Using the single diastereomer of **21***a* it was possible to differentiate between explanations (*ii*) and (*iii*). Deprotonation of this salt afforded an ylide **44** whose nmr spectrum indicated that it was a mixture of at least two compounds. Reprotonation of **44** regenerated *both diastereomers* of **21***a*. Therefore, the mixture of ylides could not have been epimeric at carbon since, in this event, the single diastereomer would have been regenerated. Consequently, **44** must have a barrier to inversion at *sulfur* which, at 30 °C, is high on the nmr time scale, allowing more than one compound to be observed, but low on the isolation time scale. The (first-order) rate constant associated with stereomutation at sulfur in **44** was found, by reprotonation at various times, to be 1.1×10^{-3} s^{-1} at 2.4 °C, corresponding to a free energy of activation at this temperature of 19.7 kcal/mol. In DMSO-d_6 the nmr spectrum of **44** underwent reversible temperature dependent changes, and coalescence of the S_2—CH_3 signals [12] was observed at 66 °C, corresponding to a free energy of activation at this temperature of 19.3 kcal/mol.

The close agreement between the chemical and dnmr measurements on **19***b* and **44** suggest that all three activation energies are associated with the same dynamic process, *viz.*, pyramidal inversion at sulfur. Therefore, the deprotonation of a 1,3-bissulfonium salt is accompanied by a decrease of at least 5 kcal/mol in the barrier to inversion at sulfur.

Finally, although the salts **13***a*, **15***a*, **16***a*, **18***a*, and **23***a* showed no detectable non-equivalence of the methylene protons of the ethyl groups (at 60 or 100 MHz), each of the derived ylides had ABX_3 patterns for these ethyl groups. Analysis of these patterns gave $\Delta\nu = 2.8$ Hz for the tetraethyl ylide **16***b*, and 9.2 Hz[13] for the 1,1-dimethyl-3,3-diethyl ylide **15***b*.

Summary and Conclusion

The static, dynamic, and chemical properties of 1,3-bissulfonium ylides are consistent with a charge-localized structure in which both sulfur atoms and the ylide carbon have pyramidal configurations. The kinetic and thermodynamic acidities of the C2 protons of 1,3-bissulfonium salts are not the same, and these acidities depend upon both the orientation of the C—H bond(s) with respect to the substituents on the sulfur atoms and on the nature of the solvent. Further, more detailed, kinetic studies will be necessary to delineate the stabilities associated with a system containing three adjacent lone pairs.

Deprotonation of a 1,3-bissulfonium salt causes a decrease of at least 5 kcal/mol in the barrier to pyramidal inversion at sulfur, as expected from the generation in this reaction of an electron-releasing carbanionic centre. However, no quantitative data have been obtained concerning the geometry at the ylide carbon, although it is possible that more detailed kinetic studies of hydrogen exchange in the cyclic salt **26** might provide such data. Except for the ylide **17***b*, which was crystalline, all of the ylides were found to be hygroscopic and it was not

[12]Various other peaks in the spectrum also displayed coalescence behaviour. The changes associated with the S_2—CH_3 signals of the two diastereomers were followed most conveniently.

[13]These $\Delta\nu$ values refer to 60 MHz. The value for **16***b* is based on analysis of the 100 MHz spectrum.

Can. J. Chem. Downloaded from www.nrcresearchpress.com by 210.87.254.40 on 09/05/12
For personal use only.

possible to be certain that all of the water had been removed prior to the various measurements reported herein. In the presence of trace amounts of water, a reaction

$$[R_2S{-}CH{-}SR_2]^+ + H_2O \rightleftarrows [R_2S{-}CH_2{-}SR_2]^{2+} + OH^-$$

would cause effective loss of any asymmetry that may have been present at the ylide carbon (38).[14] This corresponds to the sixth explanation proposed to explain the nmr spectrum of **19***b*, and it cannot be excluded.

In view of this uncertainty concerning the configurational stability at carbon of the 1,3-bissulfonium ylides, attempts were made to observe the formation of diastereomeric compounds following the exchange of the tetrafluoroborate anion of **15***a* by a chiral anion (40). Exchange by chiral carboxylic acids was not successful. Sulfonic acid salts could be prepared, but the nmr spectrum of the salt of **15***b* with *d*-camphorsulfonate was too complicated to analyze. Attempts to prepare the chiral sulfonic acid **45** have so far been unsuccessful, but these experiments are continuing.

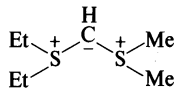

15*b*

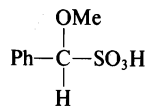

45

Acknowledgment

We thank the National Research Council of Canada for financial support of this work.

1. B. M. Trost and L. S. Melvin, Jr. Sulfur ylides. Emerging synthetic intermediates. Academic Press, New York. 1975.
2. (*a*) J. W. Cornforth, R. H. Cornforth, C. Donninger, and G. Popjak. Proc. R. Soc. B, **163**, 492 (1966); (*b*) B. M. Trost, P. Conway, and J. Stanton. Chem. Commun. 1639 (1971).
3. (*a*) B. M. Trost and W. D. Biddlecom. J. Org. Chem. **38**, 3438 (1973); (*b*) B. M. Trost and R. F. Hammen. J. Am. Chem. Soc. **95**, 962 (1973).
4. S. Wolfe, A. Rauk, L. M. Tel, and I. G. Csizmadia. J. Chem. Soc. B, 136 (1971).
5. S. Wolfe. Acc. Chem. Res. **5**, 102 (1972).
6. (*a*) J. M. Lehn. Top. Curr. Chem. **15**, 311 (1970); (*b*) A. Rauk, L. C. Allen, and K. Mislow. Angew. Chem. Int. Ed. Engl. **9**, 400 (1970); (*c*) J. B. Lambert. Top. Stereochem. **6**, 19 (1971).
7. (*a*) J. E. Anderson, D. L. Griffith, and J. D. Roberts. J. Am. Chem. Soc. **91**, 6371 (1969); (*b*) M. J. S. Dewar and B. Jennings. J. Am. Chem. Soc. **91**, 3655 (1969); (*c*) H. Kessler and D. Leibfritz. Tetrahedron Lett. 4297 (1970).
8. (*a*) K. Mislow. Trans. N.Y. Acad. Sci. Ser. 11, **35**, 227 (1973); (*b*) I. G. Csizmadia, A. H. Cowley, M. W. Taylor, and S. Wolfe. J. Chem. Soc. Chem. Commun. 432 (1974).
9. R. E. Kari and I. G. Csizmadia. J. Chem. Phys. **46**, 4585 (1967).
10. D. Darwish. Mech. React. Sulfur Compd. **3**, 33 (1968).
11. (*a*) K. W. Ratts. Tetrahedron Lett. 4707 (1966); (*b*) A. F. Cook and J. G. Moffatt. J. Am. Chem. Soc. **90**, 740 (1968).
12. D. Darwish and R. L. Tomilson. J. Am. Chem. Soc. **90**, 5938 (1968).
13. (*a*) G. Barbarella, A. Garbesi, A. Boicelli, and A. Fava. J. Am. Chem. Soc. **95**, 8051 (1973); (*b*) O. Hofer and E. L. Eliel. J. Am. Chem. Soc. **95**, 8045 (1973).
14. S. Bory, R. Lett, B. Moreau, and A. Marquet. Tetrahedron Lett. 4921 (1972).
15. A. A. Hartmann and E. L. Eliel. J. Am. Chem. Soc. **93**, 2572 (1971); E. L. Eliel, A. A. Hartmann, and A. G. Abatjoglou. J. Am. Chem. Soc. **96**, 1807 (1974).
16. R. Lett and A. Marquet. Tetrahedron Lett. 1579 (1975).
17. R. R. Fraser, F. J. Schuber, and Y. Y. Wigfield. J. Am. Chem. Soc. **94**, 8795 (1972).
18. C. P. Lillya and P. Miller. J. Am. Chem. Soc. **88**, 1559 (1966); **88**, 1560 (1966).
19. I. Stahl, M. Hetschko, and J. Gosselck. Tetrahedron Lett. 4077 (1971); I. Stahl and J. Gosselck. Tetrahedron Lett. 989 (1972); I. Stahl and J. Gosselck. Tetrahedron **29**, 2323 (1973).
20. Organic syntheses. Coll. Vol. V. 1080 (1973); 1096 (1973).
21. H. Böhme and R. Marx. Chem. Ber. **74**, 1667 (1941).
22. P. Miller. Ph.D. Thesis. University of Massachusetts, Amherst, Mass. 1968.
23. H. Böhme and W. Krack. Ann. Chem. **758**, 143 (1972).
24. R. S. Glass and J. R. Duchek. J. Am. Chem. Soc. **98**, 965 (1976).
25. M. Anteunis, D. Tavernier, and F. Borremans. Bull. Soc. Chim. Belg. **75**, 396 (1966).
26. R. Louw and H. Nieuwenhuyse. Chem. Comm. 1561 (1968).
27. L. M. Jackman and S. Sternhell. Applications of nuclear magnetic resonance in organic chemistry. Second Ed. Pergamon Press. 1969. p. 334.
28. E. L. Eliel, R. L. Willer, A. T. McPhail, and K. D. Onan. J. Am. Chem. Soc. **96**, 3021 (1974).
29. H. C. Brown and W. R. Wirkkala. J. Am. Chem. Soc. **88**, 1447 (1966).
30. S. Wolfe, H. B. Schlegel, I. G. Csizmadia, and F. Bernardi. Can. J. Chem. **53**, 3365 (1975).
31. A. Streitwieser, Jr., P. H. Owens, G. Sonnichsen, W. K. Smith, G. R. Ziegler, H. M. Niemeyer, and T. L. Kruger. J. Am. Chem. Soc. **95**, 4254 (1973).

[14]Attempts to deprotonate 1,3-bissulfonium salts under aprotic conditions (NaH, LiH or *n*-butyllithium in DMSO) led to decomposition.

32. W. DANNHAUSER and R. H. COLE, JR. J. Am. Chem. Soc. **74**, 6105 (1952); F. E. HARRIS and C. T. O'KONSKI. J. Am. Chem. Soc. **76**, 4317 (1954).
33. D. J. CRAM. Fundamentals of carbanion chemistry. Academic Press, New York. 1965. pp. 98–103.
34. S. WOLFE, W. S. LEE, and R. MISRA. J. Chem. Soc. D, 833 (1970).
35. (*a*) R. J. ABRAHAM, H. D. BANKS, E. L. ELIEL, O. HOFER, and M. KALOUSTIAN. J. Am. Chem. Soc. **94**, 1913 (1972); (*b*) E. L. ELIEL and S. A. EVANS, JR. J. Am. Chem. Soc. **94**, 8587 (1972).
36. H. SCHMIDBAUR and W. TRONICH. Chem. Ber. **101**, 595 (1968); **101**, 3556 (1968).
37. G. BINSCH. Top. Stereochem. **3**, 97 (1968).
38. S. H. SMALLCOMBE, R. J. HOLLAND, R. H. FISH, and M. C. CASERIO. Tetrahedron Lett. 5987 (1968).
39. H. SCHMIDBAUR and W. TRONICH. Chem. Ber. **101**, 604 (1968).
40. M. RABAN and K. MISLOW. Top. Stereochem. **2**, 199 (1967).

Can. J. Chem. Downloaded from www.nrcresearchpress.com by 210.87.254.40 on 09/05/12
For personal use only.

Synthesis of pencolide and corroboration of its revised stereochemistry

GEORGE M. STRUNZ AND WU-YUN REN

Maritimes Forest Research Centre, Canadian Forestry Service, P.O. Box 4000, Fredericton, N.B. Canada E3B 5G4

Received May 1, 1975 [1]

GEORGE M. STRUNZ and WU-YUN REN. Can. J. Chem. **54**, 2862 (1976).

A synthesis of the fungal metabolite pencolide from citraconic anhydride and threonine is described. Evidence is presented which corroborates the *Z* configuration recently assigned to the metabolite.

GEORGE M. STRUNZ et WU-YUN REN. Can. J. Chem. **54**, 2862 (1976).

On décrit la synthèse du métabolite pencolide à partir de l'anhydride citraconique et de thréonine. On présente des évidences qui confirment la configuration *Z* récemment attribuée au métabolite.

Isolation of the metabolite pencolide, **1**, from cultures of *Penicillium multicolor* Grigorieva-Manilova and Poradielova (N.R.R.L. 4036) was reported by Birkinshaw *et al.* in 1963 (1). The *E* configuration was subsequently assigned to the double bond on the basis of pmr arguments (2), however Olsen and collaborators have revised the geometry to *Z* in a recent publication (3). It was suggested (1) that the biosynthetic precursors of pencolide might be citraconic acid and threonine or a related amino acid.

We describe herein a facile synthesis of the metabolite, based on this biosynthetic concept, as well as additional evidence which corroborates the revised geometry (**2**, R = OH) of pencolide (3).

The synthesis was effected by heating citraconic anhydride with L-threonine (or racemic *allo*-threonine) at 150 °C without a solvent. Chromatography of the product furnished, in yields greater than 40%, a crystalline compound identified as pencolide on the basis of its physical and chemical characteristics.[2]

Reexamination of the reaction of the metabolite with diazomethane, first described in the original study (1), has provided independent support for the amended (*Z*) stereochemistry. Treatment of pencolide with this reagent "until effervescence ceased" was reported to result in "addition of diazomethane, presumably to a double bond, in addition to methylation" (esterification) (1). On repeating the reaction it was found that the simple methyl ester **2** (R = OMe) or the pyrazoline ester **3** (*cf.* ref. 4) could be obtained by using the appropriate amounts of diazomethane (excess reagent resulted in further attack at the Δ^2 double bond.

While the spectra of **2** (R = OMe) were unremarkable, a recrystallized, analytically pure sample of pyrazoline **3**, $C_{11}H_{13}N_3O_4$ (apparently homogeneous on tlc) showed broadening and duplication of signals in the 220 MHz pmr spectrum; based on the methyl ester signals, the presence of two isomers in the approximate ratio 14:10 was indicated. That the doubling of signals

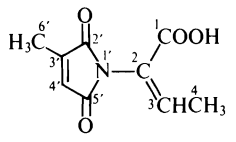

1

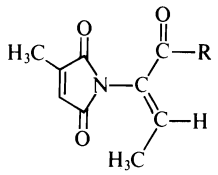

2

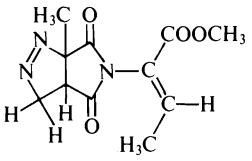

3

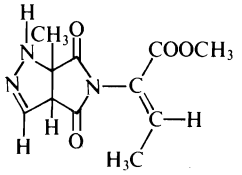

4

was not due to loss of stereochemical integrity of the Δ^2 double bond, but rather to conformational effects, became clear from variable temperature studies. Thus, when the spectrum was run at −50 °C, peaks were dramatically sharpened and complete first-order analysis of the two interlacing spectra (ratio now *ca.* 18:10) became possible (5). Furthermore, the spectrum of the isomerized pyrazoline **4** (*vide infra*) at ambient

[1]Revision received May 10, 1976.

[2]Direct comparison of synthetic material with an authentic sample of pencolide kindly provided by Professor Sir Derek Barton confirmed their identity.

Can. J. Chem. Downloaded from www.nrcresearchpress.com by 210.87.254.42 on 09/05/12
For personal use only.

Can. J. Chem. Downloaded from www.nrcresearchpress.com by 210.87.254.42 on 09/05/12
For personal use only.

temperature similarly displays duplication of signals associated with conformational isomerism, and these signals coalesced in a spectrum recorded at 50 °C.

In the low temperature spectrum of **3**, the signals corresponding to the C-4 methyl and the methyl ester hydrogens of the preferred conformer occur respectively at δ 1.59 and 3.80 ppm, while for the minor conformer, these are observed at δ 1.82 and 3.70 ppm. Significantly, the chemical shifts of the C-3 olefinic hydrogen do not differ appreciably in the major and minor conformers (overlapping quartets at δ 7.32 and 7.37 ppm respectively).

Inspection of space-filling (Courtauld's) models of pencolide derivatives indicates considerable non-bonded interaction between double bond substituents and the imide oxygen atoms on rotation about the N-1′, C-2 bond, *i.e.* a substantial energy barrier can be predicted for interconversion of the rotamers. Somewhat similar phenomena are well documented for *N′,N′*-diacyl-*N*-amino imides (6). This suggests that the duplication of signals in the spectrum of **3** is a manifestation of such restricted rotation, and it is apparent that the 0.23 ppm separating the signals for the C-4 hydrogens in the two conformers results from shielding of this methyl group, in the preferred conformation, by the pyrazoline system. A chemical shift difference of 0.10 ppm for the methyl ester signals of the major and minor rotamers, with the *latter* appearing upfield, is in consonance with this interpretation. Accordingly, the relative constancy of the C-3 olefinic proton quartet demonstrates that the latter hydrogen is outside the shielding influence of the pyrazoline, and the *Z*-configuration, **2** (R = OH) is indicated for pencolide, in agreement with Olsen's assignment (3).

On heating **3** in chloroform solution under reflux, it underwent gradual rearrangement to **4** (the reaction appeared to be accelerated by the presence of traces of acid). In the 220 MHz pmr spectrum of **4**, restricted rotation was again manifested as doubling of some signals (ratio *ca.* 19:10). The duplicate signals (specifically those due to the methyl ester and the C-4 methyl protons) coalesced above ambient temperature as previously noted. Although the long-range shielding effect associated with the pyrazoline system of **4** is smaller in the region of interest than that of **3**, the C-4 methyl doublet for the major rotamer still appears slightly upfield from that of the minor conformer. The chemical shift of the C-3 olefinic proton (coincident quartets for the two conformers) is again essentially unaffected by the pyrazoline ring, behavior consistent with the assigned *Z*-stereochemistry.

Experimental

Melting points were determined on a hot-stage apparatus and are uncorrected. Infrared spectra were recorded on a Beckmann IR-10 spectrophotometer. Ultraviolet spectra were obtained using a Perkin-Elmer 402 spectrophotometer. Nuclear magnetic resonance spectra at 60 MHz were recorded for solutions in deuteriochloroform with a Varian T-60 instrument employing tetramethylsilane as internal standard; the 220 MHz nmr spectra were measured on a Varian HR-220 instrument at the Canadian 220 MHz NMR Center, Ontario Research Foundation. Mass spectra were obtained with an Hitachi–Perkin-Elmer RMU-6D mass spectrometer. Microanalyses were performed by Spang Microanalytical Laboratory, Ann Arbor, Michigan.

Synthesis of Pencolide

A mixture of L-threonine (300 mg, 2.52 mmol) and citraconic anhydride (0.35 ml, 436 mg, 3.89 mmol) was heated with stirring at 150 °C for 3 h. Preparative layer chromatography of the resulting brown oil on silica gel plates (benzene–acetone, 4:1) afforded crude pencolide, which crystallized from ether–*n*-hexane to give 208 mg colorless crystals (42% based on L-threonine), mp 133–138 °C; ir (KBr) *inter alia*, 2600–2200, 1780(w), 1715, 1690, 1650, 1405, 1380, 1330, and 1300 cm^{-1}; ir ($CHCl_3$) 3600–2200, 1780(w), 1720, and 1660 cm^{-1}; uv λ_{max} (H_2O) 215 nm (ϵ19 200); pmr ($CDCl_3$, 60 MHz) δ 1.83 (3H, d, $J \sim 7$ Hz), 2.16 (3H, d, $J \sim 2$ Hz), 6.52 (1H, q, $J \sim 2$ Hz), 7.48 (1H, q, $J \sim 7$ Hz), 11.37 (1H, br s); mass spectrum, *inter alia*, *m/e* 195 (M^+), 177 (base peak) $(M - H_2O)^+$. *Anal.* calcd. for $C_9H_9NO_4$: C 55.38, H 4.65, N 7.18; found: C 55.46, H 4.71, N 7.26.

In the same manner *allo*-threonine (racemic) (280 mg, 2.35 mmol) and citraconic anhydride (0.3 ml, 374 mg, 3.34 mmol) gave 190 mg (41%) of crystalline pencolide indistinguishable from the above material.

Direct comparison of synthetic material with an authentic sample of natural pencolide confirmed their identity (see footnote 2).

Reaction of Pencolide with Diazomethane (cf. ref. 1).

Treatment of a suspension of pencolide in ether with an ethereal diazomethane solution of known concentration gave either the simple methyl ester **2** (R = OMe) or the pyrazoline ester **3** depending on the molar ratios employed. The ester **2** (R = OMe) (which was also prepared by treatment of the acid chloride with methanol) was obtained as a colourless oil from chromatography of the crude product on preparative layer plates of silica gel; ir ($CHCl_3$) 1780(w), 1720, and 1665 cm^{-1}; nmr ($CDCl_3$, 60 MHz) δ 1.79 (3H, d, $J \sim 7$ Hz), 2.16 (3H, d, $J \sim 2$ Hz), 3.79 (3H, s), 6.52 (1H, q, $J \sim 2$ Hz), 7.34 (1H, q, $J \sim 7$ Hz); mass spectrum, *inter alia*, *m/e* 209 (M^+), 177 $(M - CH_4O)^+$, 96 (base peak) $(C_5H_4O_2)^+$, and 68

$(C_4H_4O)^+$. *Mol Wt.* calcd. for $C_{10}H_{11}NO_4$:209.0688; found (M^+): 209.0688.

In the cycloaddition reaction, the pyrazoline ester **3** could be obtained without chromatography in 42% yield by crystallization of the crude product from ether–*n*-hexane: colorless crystals, mp 117–120 °C, ir (KBr) *inter alia*, 1795(w), 1735(sh), 1725, and 1665 cm^{-1}; uv λ_{max}(EtOH) <210 nm; nmr ($CDCl_3$, 220 MHz) δ 1.57 (0.60 methyl, d, $J \sim 7$ Hz), 1.78 and 1.80 [1.42 methyl, d (at δ 1.79) $J \sim 7$ Hz, superimposed on singlet(s)], 2.99–3.12 (1H, m), 3.69 (0.42 methyl, s), 3.79 (0.58 methyl, s), 4.84–5.21 (2H, 8 peak m), 7.22–7.36 (1H, 5 peak m); pmr ($CDCl_3$, 220 MHz, −50 °C) (peaks sharpened and resolved: overlapping spectra corresponding to two rotamers, ratio *ca.* 18:10); *major rotamer*: δ 1.59 (d, $J \sim 7$ Hz, C-4 methyl), 1.81? (s, angular methyl), 3.19 (dd, $J \sim 9.5$ and 2.5 Hz, X part of AMX), 3.80 (s, ester methyl), 4.95 (dd, $J \sim 19$ and 9.5 Hz, M part of AMX), 5.24 (dd, $J \sim 19$ and 2.5 Hz, A part of AMX), 7.32 (q, $J \sim 7$ Hz, C-3 hydrogen); *minor rotamer*: δ 1.82 (d, $J \sim 7$ Hz, C-4 methyl), 1.84? (s, angular methyl), 3.10 (dd, $J \sim 9.5$ and 3.5 Hz, X part of AMX), 3.70 (s, ester methyl), 5.04 (dd, $J \sim 19$ and 9.5 Hz, M part of AMX), 5.21 (dd, $J \sim 19$ and 3.5 Hz, A part of AMX), 7.37 (q, $J \sim 7$ Hz, C-3 hydrogen); mass spectrum, *inter alia*, *m/e* 251 (M^+), 223 probably $(M - N_2)^+$, 191 (base peak) $(M - N_2 - CH_4O)^+$. *Anal.* calcd. (sample mp 110–113 °C) for $C_{11}H_{13}N_3O_4$: C 52.58, H 5.22, N 16.73; found: C 52.66, H 5.27, N 16.71.

Pyrazoline **4**

A solution of pyrazoline **3** (42 mg, 0.167 mmol) in chloroform (10 ml) containing *p*-toluenesulfonic acid (0.5 mg) was heated under reflux for 12 h. The resulting solution was washed with brine, dried over magnesium sulfate, and evaporated to dryness, furnishing **4** as a colorless oil in quantitative yield: ir ($CHCl_3$) 3380, 1795(w), 1730 and 1665 cm^{-1}; uv λ_{max}(EtOH) <210 nm; nmr ($CDCl_3$, 220 MHz) δ 1.68 and 1.72 (1.65 methyl, s at δ 1.68, superimposed on doublet (δ 1.70), $J \sim 7$ Hz), 1.77 (0.35 methyl, d, $J \sim 7$ Hz), 3.74 (0.35 methyl, s), 3.79 (0.65 methyl, s), 4.04 (1H, br s with shoulder at δ 4.02), 6.30 and 6.40 (together 1H, br singlets, exchangeable with D_2O), 6.79 (1H, d, $J \sim 2$ Hz), 7.32 (1H, q, $J \sim 7$ Hz); in a spectrum run at 50 °C, the duplicate signals corresponding to the C-4 methyl group and the methyl ester protons coalesced to a doublet ($J \sim 7$ Hz) and a singlet respectively; mass spectrum, *inter alia*, *m/e* 251 (base peak) (M^+), 223 (*ca.* 6%) probably $(M - N_2)^+$, 191 $(M - N_2 - CH_4O)^+$. *Mol. Wt.* calcd. for $C_{11}H_{13}N_3O_4$: 251; found: *m/e* 251.

Acknowledgments

We thank Ms. M. Austria, University of New Brunswick for the mass spectra, and Dr. A. Grey, Canadian 220 MHz NMR Centre for his helpful co-operation in the variable temperature nmr studies. The interest of Mr. D. Greatbanks, I.C.I. Pharmaceuticals Division, Alderley Park, Cheshire, in various aspects of this problem is gratefully acknowledged.

1. J. H. Birkinshaw, M. G. Kalyanpur, and C. E. Stickings. Biochem. J. **86**, 237 (1963).
2. A. G. Brown and T. C. Smale. Chem. Commun. 1489 (1969).
3. A. Srinivasan, K. D. Richards, and R. K. Olsen. Tetrahedron Lett. 891 (1976).
4. W. I. Awad, S. M. Abdel, R. Omran, and M. Sobhy. J. Org. Chem. **26**, 4126 (1961).
5. L. M. Jackman and S. Sternhell. Applications of nuclear magnetic resonance spectroscopy in organic chemistry. Pergamon Press, Oxford. 1969.
6. B. H. Korsch and N. V. Riggs. Tetrahedron Lett, 5897 (1966); S. M. Verma and C. K. Rao. Tetrahedron, **28**, 5029 (1972); S. M. Verma, K. O. P. Sinha, and C. K. Rao. Can. J. Chem. **52**, 2399 (1974).

Can. J. Chem. Downloaded from www.nrcresearchpress.com by 210.87.254.42 on 09/05/12
For personal use only.

Polybrominated derivatives of 5α-androstane and 5α-estrane 3-ketones: cyclopropanol formation

J. F. TEMPLETON AND C. W. WIE
Faculty of Pharmacy, University of Manitoba, Winnipeg, Man., Canada R3T 2N2
AND
F. E. HRUSKA
Department of Chemistry, University of Manitoba, Winnipeg, Man., Canada R3T 2N2

Received March 11, 1976

J. F. TEMPLETON, C. W. WIE, and F. E. HRUSKA. Can. J. Chem. **54**, 2865 (1976).

Bromohydrin acetates from sodium borohydride reduction of di- and tribrominated 17β-hydroxy-5α-androstan-3-one and 17β-hydroxy-5α-estran-3-one have been prepared and their structures determined by spectroscopic methods. Some 220 MHz proton magnetic resonance data are reported for structure determination. The formation of cyclosteroid derivatives by 1,3-elimination of bromine with zinc–copper couple is discussed.

J. F. TEMPLETON, C. W. WIE et F. E. HRUSKA. Can. J. Chem. **54**, 2865 (1976).

Des acétates de bromohydrines ont été préparés à partir de la réduction par le borohydrure de sodium de produits di- et tribromés de l'hydroxy-17β androstane-5α one-3 et de l'hydroxy-17β estrane-5α one-3 et leurs structures ont été déterminées par des méthodes spectroscopiques. Quelques données de résonance magnétique du proton à 220 MHz sont rapportées pour la détermination des structures. La formation de dérivés cyclostéroïdes par élimination-1,3 de brome à l'aide du couple zinc–cuivre est discutée.

Traduit par le journal]

Can. J. Chem. Downloaded from www.nrcresearchpress.com by 210.87.254.40 on 09/05/12
For personal use only.

Introduction

In the course of preparing the secondary 2β,4β-cyclosteroid 3-alcohols in the 5α-androstane and 5α-estrane series by the 1,3-elimination method previously reported (1), we investigated the bromohydrin products from the reduction of the di- and tribrominated 3-ketones. The bromination of 3-oxo-5α-steroids has been extensively studied (2, 3*a*), mainly to establish the stereochemistry of the products as determined in the reaction by kinetic or thermodynamic control. The bromohydrin derivatives of the polybrominated ketones have not been so thoroughly investigated. In this paper, the bromohydrin derivatives prepared from di- and tribrominated 17β-hydroxy-5α-androstan-3-one and 17β-hydroxy-5α-estran-3-one are reported and their structure determined by proton magnetic resonance spectroscopy. Cyclopropanol formation is also discussed.

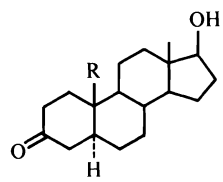

1*a*, R = CH_3
b, R = H

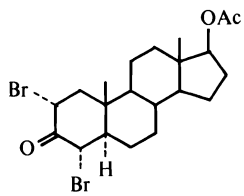

2

Results and Discussion

Dibromination of 17β-hydroxy-5α-androstan-3-one (**1***a*) with bromine in acetic acid yielded 2α,4α-dibromo-17β-acetoxy-5α-androstan-3-one (**2**) (4). Sodium borohydride reduction of **2** in ethanol proceeded rapidly to give a mixture of the epimeric 2α,4α-dibromo-5α-androstane-3α,-17β- and 3β,17β-diol 17-acetates at room temperature (1). Rapid reduction is consistent with conclusions reached concerning the sodium borohydride reduction of 2α-bromo-5α-cholestan-3-one in that interactions between the dipoles of the ketone and the bromine destabilize the bromo ketone (5). The mixture of dibromo alcohols obtained from the reduction was acetylated to give the more stable dibromo acetates (**3***a* and **4**) which were chromatographically separated. The isomeric dibromo acetates were obtained in an approximate ratio of 8:2 (3α:3β), showing that sodium borohydride reduction of the dibromo ketone **2** led predominately to the axial alcohol.

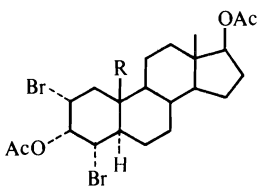

3*a*, R = CH_3
b, R = H

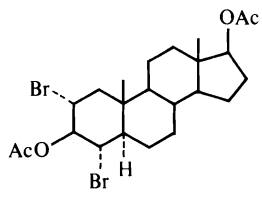

4

The stereochemistry of metal hydride reduction of the 3-oxosteroids has generally (6) led to results in agreement with the original observation of Barton (7) that reduction of sterically hindered ketones yields an increased proportion of the axial over the equatorial alcohol. The usual epimeric ratio (a:e) (1:9) of the unsubstituted A-ring 3-oxosteroids (6) on monobromination at C-2 is altered to 4:6 (8). The a:e ratio obtained on reduction of the α,α'-dibromo-3-oxosteroid (**2**) (8:2) (estimated from yields on chromatographic separation) while reversing the epimeric ratio of the major product, is consistent with the excepted result of an increased steric effect. A similar ratio has been obtained on reduction of 2α-bromo-19β,28-epoxy-24-nor-18α-oleanan-3-one (9) which is an α-bromo-α'-methyl 3-ketone. The factors affecting the stereochemistry of metal hydride reduction of ketones has been the subject of considerable interest (10). The high yields of the equatorial dibromo acetates (**3***a* and **4**) show that the bromine atoms are in a *cis*-1,3-relationship. Since the conformation of the A-ring of 2α,4α-dibromo-17β-acetoxy-5α-androstan-3-one (**1***a*) has not been determined, it is not meaningful to rationalize the stereochemical result of the reduction (3*b*, 6).

The structures of **3***a* and **4** were determined by their pmr spectra, which showed a triplet at 5.70 ($J_{2\beta,3\beta} = J_{3\beta,4\beta} = 2.5$ Hz) and 5.27 ($J_{2\beta,3\alpha} = J_{3\alpha,4\beta} = 10.0$ Hz) for the C-3 equatorial and the C-3 axial protons, respectively. The multiplet centered at 4.33 ($J_{1\alpha,2\beta} = 13.0$; $J_{1\beta,2\beta} = 4.5$; $J_{2\beta,3\beta} = 2.5$ Hz) is assigned to the C-2 axial proton of **3***a* and the quartet at 4.16 ($J_{4\beta,5\alpha} = 11.0$; $J_{3\beta,4\beta} = 2.5$ Hz) to the C-4 axial proton. Similarly, the multiplet centered at 4.28 ($J_{1\alpha,2\beta} = 13.0$; $J_{2\beta,3\alpha} = 10.0$; $J_{1\beta,2\beta} = 4.4$ Hz) is assigned to the C-2 axial proton of **4** and the quartet at 3.92 ($J_{4\beta,5\alpha} = 11.7$; $J_{3\alpha,4\beta} = 10.0$ Hz) to the C-4 axial proton of **4**.

Tribromination of 17β-hydroxy-5α-androstan-3-one (**1***a*) yielded a mixture of bromo ketones which, without further purification, was reduced with sodium borohydride. Acetylation of the bromo alcohols followed by chromatography gave a tribromo acetate which showed a doublet at 5.39 δ ($J_{3\alpha,4\beta} = 10.0$ Hz) assigned to the C-3 axial proton and a quartet at 4.14 δ ($J_{4\beta,5\alpha} = 12.0$; $J_{3\alpha,4\beta} = 10.0$ Hz) assigned to the C-4 axial proton; no proton signal of the 2β-H type was observed. The presence of two doublets centered at 3.15 δ ($J_{gem} = 15.0$ Hz) and 2.60 δ ($J_{gem} = 15.0$ Hz) corresponding to the C-1 equatorial and C-1 axial protons, respectively, further supported the formation of 2,2,4α-tribromo-5α-androstane-3β,17β-diol diacetate (**5***a*). A substantial amount of the 2α,4α-dibromo-5α-androstane-3α,17β-diol diacetate (**3***a*) and an unsaturated tribromo acetate (**6**) was also obtained (11). The pmr spectrum of **6** showed a doublet at 5.87 δ ($J_{2\beta,3\alpha} = 9.0$ Hz) due to the C-3 axial proton; an octet similar in pattern to the 2β-H of 2α,4α-dibromo-5α-androstane-3β,17β-diol diacetate at 4.37 δ ($J_{1\alpha,2\beta} = 13.8$; $J_{2\beta,3\alpha} = 9.0$; $J_{1\beta,2\beta} = 3.5$ Hz) is assigned to the C-2 axial proton. A quartet at 5.59 δ ($J = 4.4$ and 2.1 Hz) is assigned to the 6α-proton. The configuration of the bromine atom at C-6 was further confirmed by comparison of the estimated (12, 13) chemical shifts of the 19-methyl protons in 6α-bromo (1.23 δ) and 6β-bromo (1.47 δ) derivatives with the experimental value 1.52 δ. The results establish the structure of 2α,4,6β-tribromo-androst-4-ene-3β,17β-diol diacetate (**6**).

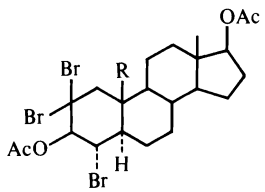

5*a*, R = CH_3
b, R = H

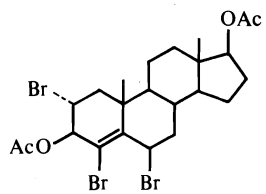

6

The formation of the above dibromo, tribromo and unsaturated tribromo derivatives may be rationalized as follows. Treatment of **1***a* with 3 equiv. of bromine gives a mixture of the 2α,4α-dibromo ketone (**2**) and the 2,2,4α-tribromo ketone similar to that obtained from the tribromination of 16β-hydroxy-3-oxo-5α-pregnane-20-carboxylic acid lactone (11). The unstable

Can. J. Chem. Downloaded from www.nrcresearchpress.com by 210.87.254.40 on 09/05/12
For personal use only.

Can. J. Chem. Downloaded from www.nrcresearchpress.com by 210.87.254.40 on 09/05/12
For personal use only.

tribromo ketone may eliminate hydrogen bromide to give the 2,2-dibromo-4-en-3-one, which, by further addition of bromine across the C-4 double bond, may give rise to a tetrabromo ketone similar to the 2,2,4ξ,5ξ-tetrabromo-5α-cholestan-3-one isolated from dibromination of either 2,2-dibromo- or 2α,4α-dibromo-5α-cholestan-3-one (14). Elimination of hydrogen bromide from the tetrabromo ketone can lead to the 2,2,4-tribromo-17β-acetoxyandrost-4-en-3-one from which the C-2 axial bromine atom can rearrange to the allylic C-6 position. Rearrangement of C-2 axial bromine atom to the allylic C-6 position has been shown to occur (15).

In the 19-nor-3-oxo-5α-steroids, the stereochemical outcome of the bromination is complicated by the removal of the 19-methyl group which leads to partial formation of the 3-enol (16). Dibromination of 17β-hydroxy-5α-estran-3-one (**1***b*) led to a mixture of dibromo ketones (**7***a*) which was reduced with sodium boro-

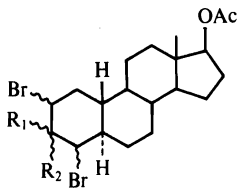

7*a*, R_1R_2 = O
b, R_1 = H; R_2 = OH

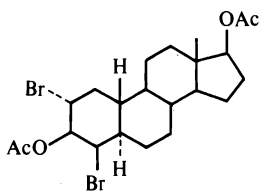

8

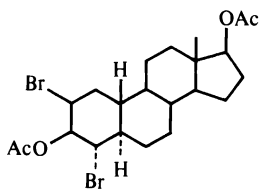

9

hydride and followed by acetylation. The resulting dibromo acetates on chromatography gave a mixture which was recrystallized from ether to afford two compounds. The pmr spectrum of compound **3***b* showed a triplet at 5.71 δ ($J_{2\beta,3\beta}$ = $J_{3\beta,4\beta}$ = 2.5 Hz) due to the C-3 equatorial proton, an octet at 4.10 δ ($J_{1\alpha,2\beta}$ = 12.5; $J_{1\beta,2\beta}$ = 4.5; $J_{2\beta,3\beta}$ = 2.5 Hz) due to the C-2 axial proton, and a quartet at 3.87 δ ($J_{4\beta,5\alpha}$ = 11.5; $J_{3\beta,4\beta}$ = 2.5 Hz) due to the C-4 axial proton. These proton signals were similar in pattern to those of **3***a* and were consistent with the structure of 2α,4α-dibromo-5α-estrane-3α,17β-diol diacetate (**3***b*). Compound **8** showed a quartet centered at 4.78 δ ($J_{2\beta,3\alpha}$ = 10.8; $J_{3\alpha,4\alpha}$ = 3.3 Hz) for the C-3 axial proton and another quartet at 4.47 δ ($J_{3\alpha,4\alpha}$ = 3.5; $J_{4\alpha,5\alpha}$ = 1.9 Hz) for the C-4 equatorial proton. The octet centered at 4.39 δ ($J_{1\alpha,2\alpha}$ = 11.6; $J_{2\beta,3\alpha}$ = 10.4; $J_{1\beta,2\beta}$ = 5.0 Hz) which partly overlaps with the 4α-proton signal was consistent with the expected C-2 axial proton in 2α,4β-dibromo-5α-estrane-3β,17β-diol diacetate (**8**).

Further chromatography gave 2β,4α-dibromo-5α-estrane-3β,17β-diol diacetate (**9**) which was identified by the following evidence. A quartet at 4.81 δ ($J_{3\alpha,4\beta}$ = 10.0; $J_{2\alpha,3\alpha}$ = 3.8 Hz) is similar to the 3α-proton in **8** and was therefore assigned to the C-3 axial proton; an unresolved multiplet at 4.66 δ which overlaps with the lower field signal of the 17α-proton triplet is assigned to the C-2 proton. The band width of the C-2 proton precludes any axial–axial coupling interaction and since the C-3 proton is axially orientated, the C-2 proton must be equatorial (17). A triplet at 4.09 δ ($J_{3\alpha,4\beta}$ = $J_{4\beta,5\alpha}$ = 10.5 Hz) corresponds to the C-4 axial proton.

Tribromination of 17β-hydroxy-5α-estran-3-one (**1***b*) followed by reduction with sodium borohydride and acetylation of the tribromo alcohol formed gave on chromatography over neutral alumina a tribromo acetate. No other bromo acetates were detected in the mother liquor by pmr determination. The tribromo acetate showed a doublet at 5.30 δ ($J_{3\alpha,4\beta}$ = 10.0 Hz) assigned to the C-3 axial proton and a triplet at 3.91 δ ($J_{3\alpha,4\beta}$ = $J_{4\beta,5\alpha}$ = 10.5 Hz) assigned to the C-4 axial proton, in the pmr spectrum. These results are consistent with the formation of 2,2,4α-tribromo-5α-estrane-3β,17β-diol diacetate (**5***b*) by comparison with the pmr spectrum of **5***a*.

The numbers of bromine atoms present in the bromo acetates were further confirmed by elemental analysis and mass spectrometric analysis. The isomeric 2α,4α-dibromo acetates (**3***a* and **4**) showed a weak molecular ion signal at *m/e* 472, 474, 476; signals at 393, 395, and 333; 335 corresponded to the elimination of acetic acid and bromine consecutively from the molecular ion. The dibromo acetates of the 5α-estrane series (**3***b*, **8** and **9**) contained no molecular ion. Elimination of acetic acid from the molecular

Can. J. Chem. Downloaded from www.nrcresearchpress.com by 210.87.254.40 on 09/05/12
For personal use only.

ion was the primary fragmentation process. The mass spectrum of the 2,2,4α-tribromo-5α-androstane-3β,17β-diol diacetate (**5***a*) and 2,2,4α-tribromo-5α-estrane-3β,17β-diol diacetate (**5***b*) showed no molecular ion; the ion of highest mass arose from elimination of acetic acid from the molecular ion. The elimination of bromine from the molecular ion was also a primary process in this molecule. The molecular ion of the unsaturated tribromo acetate (**6**) was not observed in its mass spectrum and elimination of bromine became the sole primary fragmentation process. This is consistent with the presence of an allylic bromine atom in the molecule.

Treatment of a mixture of the 2ξ,4ξ-dibromo-5α-estrane-3ξ,17β-diol 17-acetate (**7***b*) with zinc–copper couple gave three main products by tlc. Extraction of the crude reaction product with petroleum ether, which was successful with the androstane derivatives (1), failed to separate these substances. The total crude mixture was converted to the more stable acetate derivatives for chromatographic separation.

The major and least polar fraction (by tlc) was a mixture of 17β-acetoxy-5α-estr-2- and 3-ene (**10**) as shown by ir, pmr, and mass spectrum analysis. One of the more polar fractions, after recrystallization from methanol, afforded

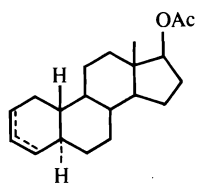

10

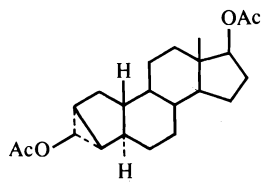

11

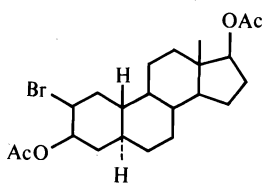

12

a compound in very low yield identified as 2β,4β-cyclo-5α-estrane-3β,17β-diol diacetate (**11**) which showed cyclopropyl C—H stretching at 3040 cm^{-1} in the ir spectrum. No olefinic proton signal was observed in the pmr spectrum, however, the presence of an unresolved triplet at 3.61 δ (J_{trans} = 1 Hz) was consistent with the 3α-proton (18). The remaining fraction, upon crystallization from ethanol, gave 2β-bromo-5α-estrane-3β,17β-diol diacetate (**12**). The assignment of this structure is consistent with the presence of a broad multiplet at 4.64 δ for the axial proton at C-3 (17) and an unresolved multiplet at 4.52 δ for the equatorial proton at C-2 similar to that in **9**. Mass spectrum and elemental analysis showed that **12** was a monobrominated derivative. The corresponding 3α-cyclopropanol derivative was not obtained from the reaction. The proportion of cyclopropane to olefin formed by 1,3- as opposed to 1,2-elimination in the debromination step is dependent upon the stereochemical relationship between the bromine and the hydroxyl substituents as shown previously in the 5α-androstane series (1). The three 2,4-dibromo acetates of the 5α-estrane series have an axial–equatorial relationship between a bromine atom and the C-3 oxygen function. This would be expected to increase the ease of 1,2-elimination and thereby olefin formation. In the 5α-androstane series the analogous 2- or 4-axial bromine is destabilized by the 1,3-diaxial interaction with the C-19 methyl group and only the equatorial bromine derivatives are isolated.

Experimental

General experimental details and apparatus are reported in ref. 19. Unless otherwise stated, ir spectra are recorded in carbon tetrachloride (Perkin-Elmer model 267), pmr spectra in deuterochloroform, and specific rotations in chloroform (23 °C). Neutral alumina is prepared by the ethyl acetate treatment of Fieser and Fieser (20). All pmr spectra were recorded at 220 MHz by the Canadian 220 MHz NMR Centre, Ontario Research Foundation, Sheridan Park, Ontario. Elemental analyses were performed by Mr. George Crouch, Microanalytical Laboratory, School of Pharmacy, University of London, England. The acetylation procedure is given in ref. 1.

*2α,4α-Dibromo-5α-androstane-3α,17β- and -3β,17β-diol Diacetates (**3***a* and **4**)*

To 2α,4α-dibromo-17β-acetoxy-5α-androstan-3-one (**2**) (2 g) in ethanol (100 ml) was added a solution of sodium borohydride (130 mg) in ethanol (10 ml). The mixture was stirred at room temperature for 5 min during which time dissolution occurred. The reaction was poured into excess cold dilute sulfuric acid followed by dichloromethane extraction. The crude dibromo alcohols were acetylated and the crude product chromatographed on neutral alumina. Elution with 15–25% benzene – petro-

Can. J. Chem. Downloaded from www.nrcresearchpress.com by 210.87.254.40 on 09/05/12
For personal use only.

leum ether gave 2α,4α-dibromo-5α-androstane-3α,17β-diol 17-acetate (**3***a*), (1.7 g), mp 228–229 °C; pmr δ 5.70 (1, t, J = 2.5 Hz, 3β-proton), 4.58 (1, t, J = 8.0 Hz, 17α-proton), 4.33 (1, o, J = 13.0, 4.5, and 2.5 Hz, 2β-proton), 4.16 (1, q, J = 11.0 and 2.5 Hz, 4β-proton), 2.18 (3, s) and 2.02 (3, s, 3- and 17-acetoxy methyl), 0.90 (3, s, 19-methyl), 0.76 (3, s, 18-methyl) ppm.

Elution with benzene gave 2α,4α-dibromo-5α-androstane-3β,17β-diol diacetate (**4**) (517 mg), mp 217–218 °C; pmr δ 5.27 (1, t, J = 10.0 Hz, 3α-proton), 4.60 (1, t, J = 8.0 Hz, 17α-proton), 4.28 (1, o, J = 13.0, 10.0 and 4.4 Hz, 2β-proton), 3.92 (1, q, J = 11.7 and 10.0 Hz, 4β-proton), 2.42 (1, q, J = 13.0 and 5.0 Hz, 1β-proton), 2.12 (3, s) and 2.01 (3, s, 3- and 17-acetoxy methyl), 0.88 (3, s, 19-methyl), 0.76 (3, s, 18-methyl) ppm.

*Tribromination of 17β-Hydroxy-5α-androstan-3-one (**1a**)*

17β-Hydroxy-5α-androstan-3-one (**1***a*) (1.0 g) in glacial acetic acid (100 ml) was treated overnight with phenyltrimethylammonium perbromide (4.27 g) (4). The crude product (2 g) was reduced with sodium borohydride (130 mg) in ethanol (80 ml) by the procedure described above. The crude product was acetylated with acetic anhydride (10 ml) in dry pyridine (20 ml). The diacetates (2 g) were adsorbed from 5% benzene – petroleum ether onto neutral alumina. The fractions from 5% benzene – petroleum ether (650 mg) were recrystallized from acetone to give 2,2,4α-tribromo-5α-androstane-3β,17β-diol diacetate (**5***a*), mp 256–260 °C; $[\alpha]_D$ −15°; ir ν_{max} 1761, 1736 (ester C=O), 1238, 1211 (ester C—O) cm^{-1}; pmr δ 5.39 (1, d, J = 10.0 Hz, 3α-proton), 4.59 (1, t, J = 8.0 Hz, 17α-proton), 4.14 (1, q, J = 12.0 and 10.0 Hz, 4β-proton), 3.15 (1, d, J = 15.0 Hz, 1β-proton), 2.60 (1, d, J = 15.0 Hz, 1α-proton), 2.26 (3, s) and 2.05 (3, s, 3- and 17-acetoxy methyl), 1.20 (3, s, 19-methyl), 0.80 (3, s, 18-methyl) ppm; ms *m/e* 550, 552, 554, 556 (M^+ – HOAc). *Anal.* calcd. for $C_{23}H_{33}O_4Br_3$: C 45.04, H 5.42; found: C 45.20, H 5.44.

Elution with 5–10% benzene – petroleum ether gave crystalline material (543 mg) which was recrystallized from ether to give 2α,4α-dibromo-5α-androstane-3α,17β-diol diacetate (**3***a*), mp 227–228 °C.

Elution with 25–50% benzene – petroleum ether gave a fraction (337 mg) which was recrystallized from acetone to afford the 2α,4,6β-tribromo-androst-4-ene-3β,17β-diol diacetate (**6**) (128 mg), mp 202–203 °C; $[\alpha]_D$ −250°; ir ν_{max} 1754, 1736 (ester C=O), 1235, 1211 (ester C—O) cm^{-1}; pmr δ 5.87 (1, d, J = 9.0 Hz, 3α-proton), 5.59 (1, q, J = 4.4 and 2.1 Hz, 6α-proton), 4.61 (1, t, J = 8.3 Hz, 17α-proton), 4.37 (1, o, J = 13.8, 9.0 and 3.5 Hz, 2β-proton), 2.38 (1, q, J = 13.0 and 4.0 Hz, 1β-proton), 2.19 (3, s) and 2.05 (3, s, 3- and 17-acetoxy methyl), 1.52 (3, s, 19-methyl), 0.88 (3, s, 18-methyl) ppm; ms *m/e* 529, 531, 533 (M^+ – Br). *Anal.* calcd. for $C_{23}H_{31}O_4Br_3$: C 45.19, H 5.11, Br 39.22; found: C 45.37, H 5.11, Br. 39.21.

*Dibromination of 17β-Hydroxy-5α-estran-3-one (**1b**)*

To a solution of 17β-hydroxy-5α-estran-3-one (**1***b*) (3.7 g) in glacial acetic acid (370 ml) was added solid phenyltrimethylammonium perbromide (11.1 g). The solution was allowed to stir at room temperature overnight and poured into ice water (4 l). The precipitate was collected and dissolved in ether. The ether solution was washed with saturated sodium bicarbonate solution and water and dried. Evaporation of the ether under reduced pressure afforded an epimeric mixture of 2ξ,4ξ-dibromo-17β-acetoxy-5α-estran-3-one (**7***a*) (6.4 g), pmr δ 4.64 (1, t, 17α-proton), 4.50–4.30 (2, m, 2ξ- and 4ξ-proton), 2.30 (3, s, 17-acetoxy methyl), 0.83 (3, s, 18-methyl) ppm. To 2ξ,4ξ-dibromo-17β-acetoxy-5α-estran-3-one (**7***a*) (6.3 g) in ethanol (100 ml) was added a solution of sodium borohydride (507 mg) in ethanol (10 ml) and the product isolated as described above for **2**.

2ξ,4ξ-Dibromo-5α-estrane-3ξ,17β-diol Diacetates

A portion (1.3 g) of the epimeric mixture from the reduction of **1***b* was acetylated. The acetylated product was adsorbed from petroleum ether onto neutral alumina. Fractions from 10% benzene–petroleum ether (237 mg) were recrystallized from ether to give 2α,4α-dibromo-5α-estrane-3α,17β-diol diacetate (**3***b*) (40 mg), mp 270–273 °C (dec.); $[\alpha]_D$ −13°; ir ν_{max} 1759, 1732 (ester C=O), 1235, 1215 (ester C—O) cm^{-1}; pmr δ 5.68 (1, t, J = 2.5 Hz, 3β-proton), 4.59 (1, t, J = 8.0 Hz, 17α-proton), 4.09 (1, o, J = 12.5, 4.5, and 2.5 Hz, 2β-proton), 3.85 (1, q, J = 11.5 and 2.5 Hz, 4β-proton), 2.20 (3, s) and 2.03 (3, s, 3- and 17-acetoxy methyl), 0.79 (3, s, 18-methyl) ppm; ms *m/e* 458, 460, 462 (M^+ – HOAc). *Anal.* calcd. for $C_{22}H_{32}O_4Br_2$: C 50.78, H 6.20, Br 30.72; found: C 50.64, H 6.20, Br 31.16.

Further recrystallization of the mother liquor from ether gave 2α,4β-dibromo-5α-estrane-3β,17β-diol diacetate (**8**) (41 mg), mp 179–180 °C; $[\alpha]_D$ −29°; ir ν_{max} 1735 (ester C=O), 1224 (ester C—O) cm^{-1}; pmr δ 4.78 (1, q, J = 10.8 and 3.3 Hz, 3α-proton), 4.60 (1, t, J = 8.0 Hz, 17α-proton), 4.47 (1, q, J = 3.5 and 1.9 Hz, 4α-proton), 4.39 (1, o, J = 11.6, 10.4, and 5.0 Hz, 2β-proton), 2.62 (1, q, J = 10.0 and 5.0 Hz, 1β-proton), 2.16 (3, s) and 2.04 (3, s, 3- and 17-acetoxy methyl), 0.80 (3, s, 18-methyl) ppm; ms *m/e* 458, 460, 462 (M^+ – HOAc). *Anal.* calcd. for $C_{22}H_{32}O_4Br_2$: C 50.78, H 6.20, Br 30.72; found: C 51.00, H 6.41, Br 30.42.

Elution with 50% benzene – petroleum ether (376 mg) on recrystallization from ether afforded 2β,4α-dibromo-5α-estrane-3β,17β-diol diacetate (**9**) (94 mg), mp 214–215 °C; $[\alpha]_D$ +39°; ir ν_{max} 1736 (ester C=O), 1224 (ester C—O) cm^{-1}; pmr δ 4.81 (1, q, J = 10.0 and 3.8 Hz, 3α-proton), 4.66 (1, unresolved m, $W_{1/2} \sim 10$ Hz, 2α-proton), 4.61 (1, t, J = 8.5 Hz, 17α-proton), 4.09 (1, t, J = 10.5 Hz, 4β-proton), 2.45–2.30 (2, m, 1α- and 1β-proton), 2.16 (3, s) and 2.05 (3, s, 3- and 17-acetoxy methyl), 0.81 (3, s, 18-methyl) ppm; ms *m/e* 458, 460, 462 (M^+ – HOAc). *Anal.* calcd. for $C_{22}H_{32}O_4Br_2$: C 50.78, H 6.20, Br 30.72; found: C 50.77, H 6.24, Br 30.82.

*Tribromination of 17β-Hydroxy-5α-estran-3-one (**1b**)*

17β-Hydroxy-5α-estran-3-one (**1***b*) (1.1 g) in glacial acetic acid (110 ml) was treated with phenyltrimethylammonium perbromide (4.95 g) by the method described above. The crude product was reduced with sodium borohydride (150 mg) in ethanol (80 ml) as above, acetylated, and chromatographed on neutral alumina. Elution with 10–25% benzene – petroleum ether gave a fraction (1.28 g) which on recrystallization from acetone yielded 2,2,4α-tribromo-5α-estrane-3β,17β-diol diacetate (**5***b*) (650 mg), mp 247–249 °C (dec.); $[\alpha]_D$ +61°; ir ν_{max} 1764, 1736

(ester C=O), 1230, 1209 (ester C—O) cm^{-1}; pmr δ 5.30 (1, d, J = 10.0 Hz, 3α-proton), 4.61 (1, t, J = 8.5 Hz, 17α-proton), 3.91 (1, t, J = 10.5 Hz, 4β-proton), 3.04 (1, q, J = 14.8 and 2.5 Hz, 1β-proton), 2.24 (3, s) and 2.05 (3, s, 3- and 17-acetoxy methyl), 0.81 (3, s, 18-methyl) ppm; ms m/e 536, 538, 540, 542 (M^+ − HOAc). *Anal.* calcd. for $C_{22}H_{31}O_4Br_3$: C 44.09, H 5.22, Br 40.01; found: C 44.09, H 5.34, Br 39.78.

Debromination of Crude 2ξ,4ξ-Dibromo-5α-estrane-3ξ,17β-diol 17-Acetate (7b) with Zinc–Copper Couple

The mixture of dibromo alcohols (**7b**) (3.4 g) obtained from reduction of the dibromination product of 17β-hydroxy-5α-estran-3-one (**1b**) was stirred in ethanol (100 ml) with zinc–copper couple (23 g) for 15 min at room temperature (1). The reaction was filtered and the filtrate poured into excess cold aqueous sodium bicarbonate and ether extracted. Recrystallization of this product gave no pure compounds. The crude product was acetylated and chromatographed over neutral alumina. Elution with petroleum ether gave material (800 mg) which was not further purified and consisted of a mixture of 17β-acetoxy-5α-estr-2- and 3-ene (**10**); ir ν_{max} 3021 (vinylic C—H), 1733 (ester C=O), 1238 (ester C—O) cm^{-1}; pmr δ (CCl_4) 5.67–5.24 (2, m, olefinic proton), 4.62 (1, t, J = 8.0 Hz, 17α-proton), 1.98 (3, s, 17-acetoxy methyl), 0.80 (3, s, 18-methyl) ppm; ms m/e 302 (M^+).

Elution with 5% benzene – petroleum ether gave a fraction (300 mg) which was recrystallized from methanol to afford 2β,4β-cyclo-5α-estrane-3β,17β-diol diacetate (**11**) (55 mg), mp 117–118 °C; $[\alpha]_D$ +16°; ir ν_{max} 3040 (cyclopropyl C—H), 1739 (ester C=O), 1227 (ester C—O) cm^{-1}; pmr δ 4.58 (1, t, J = 8.5 Hz, 17α-proton), 3.61 (1, poorly resolved t, $J_{trans} \sim 1$ Hz, 3α-proton), 2.02 (3, s) and 1.98 (3, s, 3- and 17-acetoxy methyl), 0.77 (3, s, 18-methyl) ppm; ms m/e 318 ($M^+ - CH_2CO$), 300 (M^+ − HOAc). *Anal.* calcd. for $C_{22}H_{32}O_4$: C 73.30, H 8.95; found: C 73.39, H 9.07.

The later fractions (662 mg) eluted from the column gave on recrystallization from ethanol 2β-bromo-5α-estrane-3β,17β-diol diacetate (**12**) (203 mg), mp 129–130 °C; $[\alpha]_D$ −1°; ir ν_{max} 1733 (ester C=O), 1235 (ester C—O) cm^{-1}; pmr δ 4.64 (1, br m, 3α-proton), 4.59 (1, t, J = 8.0 Hz, 17α-proton), 4.52 (1, unresolved m, $W_{1/2}$ = 6 Hz, 2α-proton), 2.09 (3, s) and 2.03 (3, s, 3- and 17-acetoxy methyl), 0.80 (3, s, 18-methyl) ppm; ms m/e 380, 382 (M^+ − HOAc), 320, 322 (M^+ − 2HOAc), 301 [M^+ − (Br + HOAc)]. *Anal.* calcd. for $C_{22}H_{33}O_4Br$: C 59.86, H 7.54, Br 18.11; found: C 60.19, H 7.57, Br 18.40.

Acknowledgments

Financial assistance from the Research Board, University of Manitoba and the Medical Research Council of Canada is gratefully acknowledged.

1. J. F. Templeton and C. W. Wie. Can. J. Chem. **53**, 1693 (1975).
2. C. C. Beard. *In* Organic reactions in steroid chemistry. Vol. 1. *Edited by* J. Fried and J. A. Edwards. Van Nostrand Reinhold Company, New York. 1972. p. 267.
3. D. N. Kirk and M. P. Hartshorn. Steroid reaction mechanisms. Elsevier Publishing Company, New York. 1968 (*a*) p. 163; (*b*) p. 135.
4. J. B. Jones and S. Ship. Biochim. Biophys. Acta, **258**, 800 (1972).
5. J. L. Mateos. J. Org. Chem. **24**, 2034 (1959).
6. D. M. S. Wheeler and M. M. Wheeler. *In* Organic reactions in steroid chemistry. Vol. 1. *Edited by* J. Fried and J. A. Edwards. Van Nostrand Reinhold Company, New York. 1972. Chapt. 2.
7. D. H. R. Barton. J. Chem. Soc. 1027 (1953).
8. L. F. Fieser and W. Y. Huang. J. Am. Chem. Soc. **75**, 4837 (1953).
9. J. Klinot, M. Horejsi, M. Budesinsky, and A. Vystrcil. Coll. Czech. Chem. Commun. **40**, 3712 (1975).
10. D. N. Kirk. *In* Terpenoids and steroids. Vol. 5. The Chemical Society, London, England. 1975. p. 246.
11. S. Kaufmann. J. Org. Chem. **26**, 5197 (1961).
12. N. S. Bhacca and D. H. Williams. Applications of NMR spectroscopy in organic chemistry. Illustration from the steroid field. Holden-Day, Inc., San Francisco. 1964. p. 51.
13. D. B. Cowell, A. K. Davis, D. W. Mathieson, and P. D. Nicklin. J. Chem. Soc. Perkin Trans. I, 1505 (1974).
14. C. W. Shoppee, R. E. Lack, and J. Scott. J. Chem. Soc. 2233 (1962).
15. A. Butenandt and G. Schramm. Chem. Ber. **69**, 2289 (1936).
16. B. Berkoz, E. P. Chanez, and C. Djerassi. J. Chem. Soc. 1323 (1962).
17. A. Hassner and C. Heathcock. J. Org. Chem. **29**, 1350 (1964).
18. U. Schöllkopf and H. Kuppers. Tetrahedron Lett. 105 (1963).
19. J. F. Templeton and C. W. Wie. Can. J. Chem. **49**, 3636 (1971).
20. L. F. Fieser and M. Fieser. Reagents for organic synthesis. Vol. 1. John Wiley and Sons, Inc., New York. 1967. p. 19.

Can. J. Chem. Downloaded from www.nrcresearchpress.com by 210.87.254.40 on 09/05/12
For personal use only.

Ditertiary(phosphines and arsines) with perfluoro-(bi-1-cycloalken-1-yl) bridging groups. Preparation and properties including a solid state structure of a tetracarbonylmolybdenum derivative

WILLIAM R. CULLEN AND ANTHONY W. WU
Chemistry Department, University of British Columbia, Vancouver, B.C., Canada V6S 1W5
AND
ALAN R. DAVIS, FREDERICK W. B. EINSTEIN, AND JOHN D. HAZLETT
Chemistry Department, Simon Fraser University, Burnaby, B.C., Canada V5A 1S6

Received April 29, 1976

WILLIAM R. CULLEN, ANTHONY W. WU, ALAN R. DAVIS, FREDERICK W. B. EINSTEIN, and JOHN D. HAZLETT. Can. J. Chem. **54**, 2871 (1976).

The bi-1-cycloalken-1-yl compounds $ClC{=}C(CF_2)_n\ C{=}CCl(CF_2)_n$ react with arsines and phosphines R_2EH to yield $R_2EC{=}C(CF_2)_n\ C{=}CCl(CF_2)_n$ $n = 2$, $R_2E = (CH_3)_2As$, **1**; $n = 2$, $R_2E = (C_6H_5)_2P$, **2**; $n = 3$, $R_2E = (CH_3)_2As$, **3**; and $(C_6H_5)_2PC{=}C(CF_2)_3\ C{=}CCl(CF_2)_3$. Methyl diphenylphosphite affords $(C_6H_5)_2P(O)C{=}C(CF_2)_3\ C{=}CCl(CF_2)_3$. The ditertiary phosphine **2** is photochromic in the solid state. It reacts with $M(CO)_6$ (M = Cr, Mo, W) to give $(L{-}L)M(CO)_4$. Similar compounds are obtained from the ditertiary arsines **1** and **3**. The solid state structure of the $Mo(CO)_4$ derivative of **3** has been determined from three-dimensional single crystal data. The compound crystallizes in the orthorhombic space group *Pbcn* with a = 16.26(1) Å, b = 11.55(1) Å, c = 13.34(1)Å, and there are four molecules in the unit cell. The coordinates of the heavy atoms were determined by vector space methods. All other atomic parameters were obtained by full matrix least-squares refinement to a final R factor of 10.1% for 715 reflections. The ligand is chelated to the molybdenum atom and the resulting seven-membered ring is considerably puckered. The As—Mo—As angle is 89.6(0.2)°.

WILLIAM R. CULLEN, ANTHONY W. WU, ALAN R. DAVIS, FREDERICK W. B. EINSTEIN et JOHN D. HAZLETT. Can. J. Chem. **54**, 2871 (1976).

Les composés bicycloalcène-1 yl-1 $ClC{=}C(CF_2)_n\ C{=}CCl(CF_2)_n$ réagissent avec les arsines et les phosphines R_2EH pour donner $R_2EC{=}C(CF_2)_n\ C{=}CCl(CF_2)_n$ $n = 2$, $R_2E = (CH_3)_2As$, **1**; $n = 2$, $R_2E = (C_6H_5)_2P$, **2**; $n = 3$, $R_2E = (CH_3)_2As$, **3**; et $(C_6H_5)_2PC{=}C(CF_2)_3\ C{=}CCl(CF_2)_3$. Le diphénylphosphite de méthyle conduit à $(C_6H_5)_2P(O)C{=}C(CF_2)_3\ C{=}CCl(CF_2)_3$. La phosphine ditertiaire **2** est photochromique en phase solide. Elle réagit avec $M(CO)_6$ (M = Cr, Mo, W) pour donner $(L{-}L)M(CO)_4$. Des produits semblables sont obtenus à partir des arsines ditertiaires **1** et **3**. La structure cristalline du dérivé $Mo(CO)_4$ de **3** a été déterminée à l'aide des données tri-dimensionnelles d'un cristal unique. Le composé cristallise dans le groupe d'espace orthorhombique *Pbcn* avec a = 16.26(1) Å, b = 11.55(1) Å, c = 13.34(1) Å, et il y a quatre molécules dans la maille élémentaire. Les coordonnées des atomes lourds ont été déterminées par des méthodes de vecteurs d'espace. Tous les autres paramètres atomiques ont été obtenus par la méthode des moindres carrés (matrice complète) pour être affiné à un facteur d'accord final R de 10.1% pour 715 réflexions. Le ligand est chélaté à l'atome de molybdène et le cycle à sept chaînons résultant est considérablement plissé. L'angle As—Mo—As est de 89.6(0.2)°.

[Traduit par le journal]

The reactions of phosphines and arsines with 1,2-dihaloperfluorocycloalkenes afford a number of interesting ditertiary(phosphines and arsines), eq. 1:

$$\text{[1]}\quad XC{=}CX + 2HER_2 \rightarrow R_2EC{=}CER_2 + 2HX$$

(HER_2 = $HAs(CH_3)_2$ or $HP(C_6H_5)_2$; n = 2, 4, 6; X = F (usually), Cl (1–3). The products of

Can. J. Chem. Downloaded from www.nrcresearchpress.com by 210.87.254.6 on 09/05/12
For personal use only.

[1] such as $(CH_3)_2AsC{=}CAs(CH_3)_2CF_2CF_2$, $f_4$fars, have been investigated with regard to their ability to form complexes with transition metal derivatives, particularly with metal carbonyls (1). Thus derivatives such as $f_4farsMn_2(CO)_8$, $f_4farsFe_3(CO)_{10}$, $f_4farsCo_2(CO)_6$ have been isolated and characterized.

The recent synthesis of fluorobialicyclic compounds (4), eq. 2, provided a suitable starting

[2] $$ClC{=}Cl + 2Cu + IC{=}CCl \rightarrow ClC{=}C{-}C{=}CCl + 2CuI$$

material for the preparation of ditertiary(phosphines and arsines) with bialicyclic, 'butadiene', bridging groups.

In this paper we report on the success of this endeavour and also on some of the metal carbonyl complexes obtained from these new ligands. Impetus was given to this work by the discovery that a complex with this type of bridging group can be isolated when $f_4farsCo_2(CO)_6$ is warmed in solution (5, 6).

Experimental

A standard vacuum system was used for the manipulation of volatile reactants. All reactions were carried out either in sealed evacuated Carius tubes or conventional reaction flasks. Infrared spectra were recorded on a Perkin-Elmer 457 spectrophotometer and calibrated using polystyrene. Nuclear magnetic resonance spectra were run on a Varian T-60 spectrometer. Chemical shifts are given in ppm downfield from internal TMS for ^1H and upfield from internal $CFCl_3$ for ^{19}F spectra. Melting points were determined using a Gallenkamp melting point apparatus and are uncorrected. Microanalyses were performed by Mr. P. Borda, Chemistry Department, University of British Columbia, and data for all new compounds are listed in Table 1.

The hexacarbonyls, $M(CO)_6$ (M = Cr, Mo, W), were obtained commercially and used without further purification. Benzene was distilled over $LiAlH_4$ prior to use. 2,2′-Dichlorooctafluoro-(bi-1-cyclobuten-1-yl) was prepared as indicated in [2] (4) as was the dodecafluoro(bi-1-cyclopenten-1-yl) analogue.

Preparation of 2,2′-Bis(dimethylarsino)octafluoro-(bi-1-cyclobuten-1-yl)

Dimethylarsine (0.42 g, 4 mmol) and 2,2′-dichlorooctafluoro-(bi-1-cyclobuten-1-yl) (0.64 g, 2 mmol) in dry benzene (5 ml) were sealed in a Carius tube. The tube was shaken for 1 day at 25 °C, opened, and the solvent was removed at reduced pressure. The resulting yellow oil was dissolved in a small amount of dichloromethane and chromatographed on Florisil. Elution with dichloromethane afforded a light yellow band of the desired compound. The product was recrystallized from hexane to yield 0.60 g (65%) of needle-like crystalline product.

Preparation of 2,2′-Bis(diphenylphosphino)octafluoro-(bi-1-cyclobuten-1-yl)

In a 100 ml three-necked round bottom flask fitted with N_2 inlet, stirrer, and pressure-equalized dropping funnel was placed 2,2′-dichlorooctafluoro-(bi-1-cyclobuten-1-yl) (0.64 g, 2 mmol) in 25 ml of anhydrous diethyl ether. Diphenylphosphine (0.75 g, 4 mmol) in 25 ml of diethyl ether was added dropwise at room temperature over a period of 60 min. After the addition was completed, the resulting green solution was left at room temperature for 24 h before the solvent was removed at reduced pressure. The solid residue was dissolved in a small volume of dichloromethane and chromatographed on Florisil. The desired product, 2,2′-bis(diphenylphosphino)octafluoro-(bi-1-cyclobuten-1-yl), was eluted as a bright yellow band with dichloromethane. After removal of solvent, bright yellow crystals were obtained which were purified by recrystallization from hexane to give 1.1 g (86%) of the product.

Preparation of 2,2′-Bis(dimethylarsino)dodecafluoro-(bi-1-cyclopenten-1-yl)

Dimethylarsine (0.42 g, 4 mmol) and 2,2′-dichlorododecafluoro-(bi-1-cyclopenten-1-yl) (0.84 g, 2 mmol) in dry benzene (5 ml) were sealed in a Carius tube. After heating for 2 days at 60 °C the tube was opened and the solvent was removed at reduced pressure. The remaining residue was dissolved in dichloromethane and chromatographed on Florisil. Elution with dichloromethane afforded a light yellow band of the desired product. After removal of solvent, a yellow oil was obtained. The oil solidified upon addition of petroleum ether. Recrystallization from hexane yielded 0.62 g of 2,2′-bis(diphenylarsino)dodecafluoro-(bi-1-cyclopenten-1-yl) (56%).

Preparation of 2-Chloro-2′-diphenylphosphinododecafluoro-(bi-1-cyclopenten-1-yl)

Diphenylphosphine (0.75 g, 4 mmol) and 2,2′-dichlorododecafluoro-(bi-1-cyclopenten-1-yl) (0.84 g, 2 mmol) were heated at 60 °C in a sealed Carius tube for 2 days. At the end of the reaction period, the tube was opened and a gummy dark red reaction product was extracted with CH_2Cl_2. The red solution was concentrated at reduced pressure and chromatographed on Florisil. Removal of solvent gave 0.36 g (32%) of white 2-chloro-2′-diphenylphosphinododecafluoro-(bi-1-cyclopenten-1-yl).

Preparation of 2,2′-Bis(diphenylphosphinyl)octafluoro-(bi-1-cyclobuten-1-yl)

In a 50 ml round bottom flask fitted with stirrer and condenser was placed 2,2′-bis(diphenylphosphino)octafluoro-(bi-1-cyclobuten-1-yl) (0.62 g, 1 mmol) and 10 ml 30% H_2O_2 in 25 ml of acetone. The solution was refluxed for 5 h and then poured into cold water. Ferrous sulfate was added to destroy the excess peroxide and the mixture was extracted three times with ether. The combined extracts were dried over $MgSO_4$. The solvent was removed at reduced pressure to give a white solid (0.26 g, 41%) which was identified as 2,2′-bis(diphenylphosphinyl)octafluoro-(bi-1-cyclobuten-1-yl), mp 178 °C. The ir spectrum shows a P=O stretching absorption at 1230

Can. J. Chem. Downloaded from www.nrcresearchpress.com by 210.87.254.6 on 09/05/12
For personal use only.

TABLE 1. Analytical data for new compounds

	Compound*	Color	Melting point (°C)	Analyses (%) C Calcd.	C Found	H Calcd.	H Found
1	$(CH_3)_2AsC{=}CCF_2CF_2C{=}CAs(CH_3)_2CF_2CF_2$	White	63	31.4	31.2	2.62	2.85
2	$(C_6H_5)_2PC{=}CCF_2CF_2C{=}CP(C_6H_5)_2CF_2CF_2$	Yellow†	126	62.1	62.3	3.23	3.37
3	$(CH_3)_2AsC{=}C(CF_2)_3C{=}CAs(CH_3)_2(CF_2)_3$	White	25	30.1	30.0	2.15	2.10
4	$(C_6H_5)_2PC{=}C(CF_2)_3C{=}CCl(CF_2)_3$	White	150	46.5	46.3	1.76	1.80
5	$(C_6H_5)_2P(O)C{=}C(CF_2)_3C{=}CCl(CF_2)_3$	White	145	45.2	45.0	1.72	1.80
6	$bif_8farsCr(CO)_4$	Dark red	110–112	30.9	30.9	1.93	1.97
7	$bif_8farsMo(CO)_4$	Orange red	98–99	28.8	28.7	1.80	1.84
8	$bif_8farsW(CO)_4$	Red	100–102	25.2	25.6	1.60	1.62
9	$bif_8fosCr(CO)_4$	Dark purple	204–206	55.2	55.7	2.56	2.70
10	$bif_8fosMo(CO)_4$	Dark purple	201	52.3	52.2	2.42	2.48
11	$bif_8fosW(CO)_4$	Dark purple	203–205	47.3	47.0	2.19	2.21
12	$bif_{12}farsCr(CO)_4$	Red	98	29.9	30.0	1.66	1.66
13	$bif_{12}farsMo(CO)_4$	Orange red	145	28.2	28.4	1.57	1.58
14	$bif_{12}farsW(CO)_4$	Orange red	158	25.3	25.3	1.41	1.37

*Abbreviations used are as follows: bif_8fars = **1**, bif_8fos = **2**, $bif_{12}fars$ = **3**.
†The compound is photochromic and yellow is the 'dark' color.

cm^{-1} and ν(C=C) at 1600(w) cm^{-1}. The mass spectrum shows a molecular ion at m/e = 650.

Preparation of 2-Chloro-2'-diphenylphosphinyldodecafluoro-(bi-1-cyclopenten-1-yl)

In a 50 ml three-necked round bottom flask fitted with condenser, dropping funnel, and stirrer was placed 2,2'-dichlorododecafluoro-(bi-1-cyclopenten-1-yl) (0.84 g, 2 mmol) in 20 ml of dry tetrahydrofuran. Methoxydiphenylphosphine (0.44 g, 2 mmol) in 10 ml tetrahydrofuran was added dropwise. After the addition, the solution was refluxed for 3 h. The solvent was then removed at reduced pressure to give a white residue. Recrystallization from hexane–dichloromethane gave a white crystalline product (0.3 g, 50%) identified as 2-chloro-2'-diphenylphosphinyldodecafluoro-(bi-1-cyclopenten-1-yl). The ir spectrum shows a P=O stretching absorption at 1215 cm^{-1}. The mass spectrum shows a molecular ion at m/e = 584.

Preparation of Group VI Metal Carbonyl Complexes

A general method of preparation of the new complexes is outlined below. Conditions used for a specific complex are shown in Table 3.

A benzene solution (5–10 ml) containing a 1:1 mole ratio of ligand to hexacarbonyl was heated at 150 °C in an evaculated Carius tube for 24 h. At the end of the reaction period, the tube was opened and the colored products were immediately chromatographed on a Florisil column using dichloromethane as eluting solvent. The solvent was then removed at reduced pressure, and the crude mixture was sublimed under vacuum to remove the unreacted hexacarbonyl. The residue was recrystallized from hexane to give the brightly colored crystalline complexes.

TABLE 2. Spectroscopic data for new phosphines and arsines

Compound	ν(C=C) (cm^{-1}) (CH_2Cl_2)	^1H*	^{19}F†
1	1605w	1.38	107.2 110.0
2	1605w	7.28(m)	107.2 109.6
3	1580w	1.40	109.2 116.8 134.0
4	1590w	7.32(m)	106.8 109.6
	1600w		111.2 115.2
	1680m		130.0 131.8
5	1590m 1600m 1670w	7.68(m), 7.72(m)	

*All resonances are singlets in $CDCl_3$ solution unless indicated as a multiplet (m).
†All resonances are multiplets and are of equal area for a particular compound.

Can. J. Chem. Downloaded from www.nrcresearchpress.com by 210.87.254.6 on 09/05/12
For personal use only.

TABLE 3. Preparative and spectroscopic data for new complexes

Reactants	Conditions T (°C)	Time (h)	Product	Yield (%)	^{1}H*†	$_{19}$F*‡	ν(CO)(cm^{-1})(cyclohexane)
1+Cr(CO)$_6$	150	5	**6**	85	1.83	109.2 112.8	2020m 1942s 1925s 1918s
1+Mo(CO)$_6$	150	8	**7**	81	1.84	109.3 113.5	2030m 1948s 1932s 1922s
1+W(CO)$_6$	150	12	**8**	75	1.84	109.2 112.8	2020m 1940s 1926s 1918s
2+Cr(CO)$_6$	100	12	**9**	75	7.42m	107.6 111.4	2015s 1945w 1926m 1920s
2+Mo(CO)$_6$	120	18	**10**	80	7.46m	107.4 111.2	2023m 1953m 1933m 1927s
2+W(CO)$_6$	150	24	**11**	70	7.45m	107.6 111.4	2020m 1948m 1928s 1920s
3+Cr(CO)$_6$	150	12	**12**	69	1.68 1.75	12 peaks between 101.6–139.2	2020m 1941s 1937s 1927s
3+Mo(CO)$_6$	150	18	**13**	73	1.70 1.78 (triplet)	12 peaks between 101.6–139.2	2020m 1950s 1935s 1927s
3+W(CO)$_6$	150	24	**14**	71	1.76 1.85 (triplet)	12 peaks between 101.6–139.2	2020m 1942s 1929s 1918s

*Spectra run in $CDCl_2$ except **7** and **10** for which the solvent was CD_3COCD_3.
†All peaks are singlets unless otherwise indicated.
‡All peaks, multiplets unless otherwise indicated and multiplets are equal area for a given complex.

TABLE 4. Principal bond lengths and angles in (dif$_{12}$fars)Mo(CO)$_4$. Least-squares estimated errors are given in parentheses

Bond	Lengths (Å)	Bonds	Angles (deg)
Mo—C6	2.12(4)	AsMoAs′	89.6(0.2)
Mo—C7	1.90(4)	C7MoC7′	84(2)
Mo—As	2.585(5)	AsMoC6	89(1)
As—C8	1.92(4)	C7MoC6	90(2)
As—C9	2.03(4)	MoAsC1	113.3(0.8)
As—C1	1.98(3)	MoAsC8	117(1)
C1—C2	1.51(5)	MoAsC9	121(1)
C1—C5	1.34(4)	C8AsC9	100(2)
C2—C3	1.52(5)	AsC1C5	126(2)
C3—C4	1.53(5)	C1C5C5′	127(2)
C4—C5	1.47(5)	C1C2C3	106(3)
C5—C5′	1.42(6)	C2C3C4	101(3)
C2—F21	1.32(4)	C3C4C5	109(3)
C2—F22	1.39(4)	C4C5C1	108(3)
C3—F31	1.31(4)	F21C2F22	105(3)
C3—F32	1.36(4)	F31C3F32	109(3)
C4—F41	1.37(4)	F41C4F42	101(3)
C4—F42	1.38(4)		

Structural Analysis of (dif$_{12}$fars)Mo(CO)$_4$

The crystal data are summarized below:

$C_{18}H_{12}O_4F_{12}As_2Mo$ fw = 765.87

Orthorhombic, a = 16.26(1) Å, b = 11.55(1) Å, c = 13.34(1) A, V = 2505 A^3, ρ_m = 2.04 g/ml (by flotation), Z = 4, d_x = 2.03 g/ml; space group *Pbcn*; Mo Kα radiation (λ = 0.70926 Å), μ(Mo Kα) = 35.9 cm^{-1}, T = 22 °C.

The complex is obtained as red oblong crystals elongated along the c axis. The intensities of 1171 independent reflections were measured in two shells ($0° < 2\theta < 20°$ and $20° < 2\theta < 50°$) using a Picker FACS-1 computer-controlled diffractometer; 715 of these reflections were classed as observed ($>2.3\sigma$). No absorption corrections were applied. The coordinates of the heavy atoms were determined by vector space methods. All other atomic parameters were obtained from several series of full matrix, least-squares refinement and subsequent Fourier and difference maps. The final R factor was 10.1% (only Mo and As atoms were permitted anisotropic thermal motion parameters).

Crystallographic computer programs used in this determination have been cited elsewhere (7).

Final atomic parameters and thermal parameters are listed in Table 4. Principal bond lengths and angles are given in Table 5. Standard deviations in both tables are in parentheses as units in the least significant figure.

Table 6, a listing of structure factor amplitudes, has been deposited with the Depository of Unpublished Data.[1]

[1]Table 6 is available, at a nominal charge, from the Depository of Unpublished Data, CISTI, National Research Council of Canada, Ottawa, Canada K1A 0S2.

Can. J. Chem. Downloaded from www.nrcresearchpress.com by 210.87.254.6 on 09/05/12
For personal use only.

Can. J. Chem. Downloaded from www.nrcresearchpress.com by 210.87.254.6 on 09/05/12
For personal use only.

TABLE 5. Fractional atomic coordinates and thermal motion parameters

a Fractional atomic coordinates ($\times 10^4$ for Mo and As; $\times 10^3$ for all other atoms) in crystalline $dif_{12}farsMo(CO)_4$. Least-squares estimated errors are given in parentheses

Atom type	*x*	*y*	*z*
Mo	0	217(4)	2500
As	926(2)	1805(3)	1736(3)
F21	207(1)	260(2)	367(2)
F22	237(1)	393(2)	260(2)
F31	126(2)	405(2)	474(2)
F32	207(1)	531(2)	403(2)
F41	94(2)	591(2)	281(2)
F42	16(1)	537(2)	401(2)
O6	113(2)	16(2)	447(2)
O7	104(2)	−179(2)	153(2)
C1	100(2)	321(3)	257(2)
C2	174(2)	349(4)	320(3)
C3	151(2)	452(3)	386(3)
C4	73(2)	494(4)	334(3)
C5	40(2)	400(2)	271(2)
C6	76(2)	20(4)	379(3)
C7	65(2)	−100(4)	197(3)
C8	206(2)	143(2)	151(3)
C9	64(2)	261(4)	43(3)
H81	243	203	172
H82	214	130	80
H83	219	73	188
H91	109	315	35
H92	12	300	48
H93	63	206	12

b Thermal motion parameters ($\times 10^3$ Å^2) in crystalline $dif_{12}farsMo(CO)_4$

Atom type	U_{11}	U_{22}	U_{33}	U_{12}	U_{23}	U_{13}
Anisotropic atoms (expressed in the form $\exp[-2\pi^2(ha^{*2}\,U_{11} \cdots + 2hka^*b^*U_{12} + \cdots)]$)						
Mo	34(3)	42(3)	17(2)	0	−3(2)	0
As	39(2)	42(2)	15(2)	6(2)	4(2)	1(2)

Atom type	*U*	Atom type	*U*	Atom type	*U*
Isotropic atoms					
F21	70(7)	C1	25(8)	H81	47
F22	72(7)	C2	55(11)	H82	47
F31	75(8)	C3	44(11)	H83	47
F32	64(7)	C4	51(11)	H91	57
F41	74(7)	C5	15(7)	H92	57
F42	50(6)	C6	50(11)	H93	57
O6	79(9)	C7	60(13)		
O7	86(10)	C8	49(12)		
		C9	59(12)		

Results and Discussion

The vinylic halogens of dihaloperfluorocycloalkenes are easily displaced by —OR, —SR, and ER_2 groups as illustrated in [1] (1). It is expected that the corresponding reactions of 2,2′-dihaloperfluoro-(bi-1-cycloalken-1-yl) would be equally facile. Wu (8) has studied their reactions with nucleophiles such as amines and alkoxides and finds this to be the case. The present work extends these investigations to the reactions of phosphines, arsines, and phosphites.

We find that both dimethylarsine and diphenylphosphine react easily with the bicyclobuten-1-yl derivative at 25 °C, eq. 3, $n = 2$. Only

$$[3]\quad ClC{=}C{-}\overset{(CF_2)_n}{\overset{\frown}{C}}{=}\overset{(CF_2)_n}{\overset{\frown}{C}}{-}C{=}CCl + HER_2 \rightarrow R_2EC{=}C{-}\overset{(CF_2)_n}{\overset{\frown}{C}}{=}\overset{(CF_2)_n}{\overset{\frown}{C}}{-}C{=}CER_2 + 2HCl$$

the disubstituted derivatives are obtained even if the mole ratio of, say, phosphine to fluorocarbon is 1:1. We have reason to believe that monosubstituted products may be isolated if the reactions are carried out at lower temperatures.

In the case of the dichloro(bicyclopenten-1-yl) derivatives the ditertiary arsine is produced at 60 °C (reaction is very slow at 25 °C), eq. 3, $n = 3$, but reaction with diphenylphosphine at the same temperature or even at 150 °C affords only the monosubstituted derivative. Maximum yields are obtained at 60 °C.

When $n = 3$, eq. 3, there is no reaction with either dimethylarsine or diphenylphosphine even under forcing conditions.

The mechanism of these substitution reactions is not known although likely candidates appear to involve addition–elimination sequences or carbanion intermediates. The reactivity pattern follows the same sequence found for cycloalkenyl compounds, eq. 1, namely $n = 2 > n = 3 > n = 4$ (1, 3). This primary effect is consistent with the ring strain arguments used by Stockel and co-workers (9, 10). However, a major difference seems to be in the result that only the monosubstituted product is obtained from diphenylphosphine and the bicyclopenten-1-yl derivative, whereas dimethylarsine gives the ditertiary arsine, eq. 3, $n = 3$. In the corresponding alkene series, reaction with diphenylphosphine more readily affords disubstitution. For example, eq. 1, when $n = 2$ and X = F, *only*

Can. J. Chem. Downloaded from www.nrcresearchpress.com by 210.87.254.6 on 09/05/12
For personal use only.

disubstitution has ever been obtained with diphenylphosphine (1, 11) (the product is known as $f_4$fos) yet dimethylarsine gives monosubstitution at 25 °C and disubstitution at 150 °C (2, 11).

Frank (12–14) found that phosphites react with fluorocyclopentenes to give cyclopentenyl-

$$[4]\quad (C_6H_5)_2P(OC_2H_5) + ClC(CF_2)_3C=CCl \rightarrow (C_6H_5)_2P(O)C(CF_2)_3C=C(O)P(C_6H_5)_2 + 2C_2H_5Cl$$

$$[5]\quad (C_6H_5)_2P(OCH_3) + ClC(CF_2)_3C(CF_2)_3C=CCl \rightarrow (C_6H_5)_2P(O)C(CF_2)_3C(CF_2)_3C=CCl + CH_3Cl$$

phosphonates, for example, eq. 4. Monosubstitution is also achievable. The bicyclopenten-1-yl compound reacts in the same way, eq. 5. This reaction has not yet been studied extensively so it is not known if disubstitution will occur. The anticipated product of such a reaction involving the dihalo-(bicyclobuten-1-yl) derivative can be obtained by oxidation of 2,2′-bis(diphenylphosphino)octafluoro-(bicyclobuten-1-yl) with 30% hydrogen peroxide.

The analytical and spectroscopic data for the new fluorocarbon derivatives of phosphorus and arsenic are in accord with their formulation, and the mass spectra all show the expected molecular ion. The solid state structure of **2** has been determined (14). The molecule has the *cisoid* arrangement of double bonds with the rings twisted approximately 35° away from planarity.

One of the remarkable features of this ditertiary phosphine is its photochromism. Very large crystals of the yellow form (~5 mm^3) can be easily obtained in the dark. When these are exposed to sunlight they turn bright orange-red. The process is reversible, but at a slower rate, on removing the light source provided the exposure has not been too great. The color change is confined to the solid and red crystals give yellow solutions which are light stable. At the moment we have no explanation for the phenomenon. The bis(phosphine oxide) is colorless which suggests that the phosphorus lone pairs are involved. It is not even clear why the compound should be colored at all. These aspects are currently under investigation.

The new ligands **1**, **2**, and **3** all react with Group VI metal hexacarbonyls with displacement of two carbonyl groups and the formation of the highly colored, crystalline, chelate complex. The derivatives have the usual four bands in the carbonyl stretching region of the infrared spectrum and the frequencies are similar to those obtained for similar complexes of $f_4$fos and related ligands (15). The mass spectra show parent ions followed by loss of four carbonyl groups. The colors of the complexes of **2** are unusual.

The chelate complexes contain a seven-membered ring as in **A** and Fig. 1. This has been

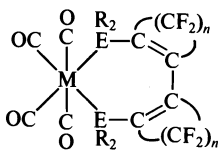

A

established for the molybdenum derivatives of both ditertiary arsines (16) one of which is described in detail below. The seven-membered ring is puckered in the solid state in both cases and the arsenic methyl groups are not equivalent. The nmr spectra of the derivatives of **1** show only one resonance in the As—CH_3 region indicating that the ring is fluxional in the nmr time scale. This is also found for complexes containing certain five- and six-membered chelate rings (17–19). Similar remarks may be made about the ^{19}F nmr spectra of these complexes and the derivative of **2**.

The nmr spectra of the complexes containing **3** are more complicated. The singlet/triplet pattern in the As—CH_3 region indicates two different environments for As—CH_3 groups possibly involving some stereospecific methyl–fluorine coupling as is found in some ditertiary arsine derivatives of chromium carbonyl containing a five-membered chelate ring (19). The complexity of the ^{19}F nmr spectra of these derivatives of **3** also points to some rigidity of the puckered ring in solution. However, at lower temperatures the singlet and triplet collapse together resulting in one adsorption at −80 °C.

The solid state structure of bif$_{12}$farsMo(CO)$_4$ is illustrated in Fig. 1. Structural parameters are listed in Tables 4 and 5.

Coordination about the central metal is very nearly octahedral, with the molecule having a

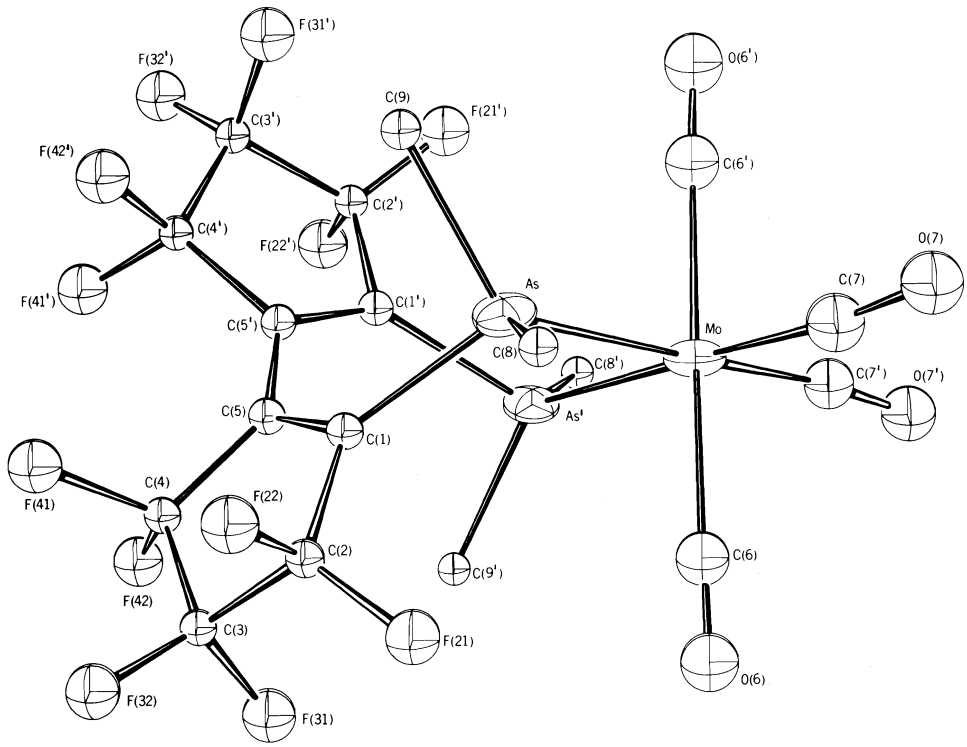

FIG. 1. Perspective view of $(bif_{12}fars)Mo(CO)_4$, indicating thermal motion ellipsoids (50%). Hydrogen atoms have been omitted for clarity.

crystallographic twofold axis of symmetry. The symmetry axis relates two pairs of carbonyl groups, and the two halves of the chelating ligand. Considerable puckering of the seven-membered ring formed by chelation is evident. This puckering can be described in terms of the dihedral angles formed between planes defined by the following trios of atoms: As′,Mo,As and Mo,As,C1(147(1)°); Mo,As,C1 and As,C1,C5-(72(3)°); As,C1,C5 and C1,C5,C5′(1(5)°).

The two different environments for the As—CH_3 groups as observed in the nmr spectrum are seen clearly in the solid state. Non-bonded methyl carbon to fluorine contacts are much shorter for C8 (C8···F21 = 3.19(5) Å, and C8···F22 = 3.26(5) Å), and are likely to remain short in solution, than for C9 (C9···F31′ = 3.75(5) Å, and C9···F21′ = 4.55(5) Å).

The As—Mo—As bond angle is not unusual (89.6°).

Acknowledgments

We wish to thank the National Research Council of Canada for financial support of this work.

1. W. R. CULLEN. Adv. Inorg. Chem. Radiochem. **15**, 332 (1972).
2. L. S. CHIA and W. R. CULLEN. Can. J. Chem. **50**, 1421 (1972).
3. W. R. CULLEN, P. S. DHALIWAL, and G. E. STYAN. J. Organometal. Chem. **6**, 364 (1966).
4. R. L. SOULEN, S. K. CHOI, and J. D. PARK. J. Fluorine Chem. **3**, 141 (1973/74).
5. F. W. B. EINSTEIN and R. D. G. JONES. J. Chem. Soc. Dalton Trans. 2568 (1972).
6. W. R. CULLEN and A. J. T. JULL. Can. J. Chem. **51**, 1521 (1973).
7. F. W. B. EINSTEIN and R. D. G. JONES. Inorg. Chem. **11**, 395 (1972).
8. A. W. WU, Ph.D. Thesis, University of Colorado, Boulder, Colorado. 1973.
9. R. F. STOCKEL, F. MEGSON, and M. R. BEACHEM. J. Org. Chem. **33**, 4395 (1968).
10. N. S. ZEFINOV and V. I. SOKOLOV. Russ. Chem. Rev. **36**, 90 (1967).
11. W. R. CULLEN, D. S. DAWSON, and P. S. DHALIWAL. Can. J. Chem. **45**, 683 (1967).
12. A. W. FRANK. J. Org. Chem. **31**, 1917 (1966).
13. A. W. FRANK. J. Org. Chem. **31**, 1521 (1966).

Can. J. Chem. Downloaded from www.nrcresearchpress.com by 210.87.254.6 on 09/05/12
For personal use only.

14. A. W. FRANK. J. Org. Chem. **31**, 1920 (1966).
15. S. RETTIG and J. TROTTER. Unpublished results.
16. A. R. DAVIS, F. W. B. EINSTEIN and J. D. HAZLETT. Acta Crystallogr. To be published.
17. W. R. CULLEN, D. F. DONG, and J. A. J. THOMPSON. Can. J. Chem. **47**, 4671 (1969).
18. W. R. CULLEN, L. D. HALL, J. T. PRICE, and G. SPENDJIAN. J. Am. Chem. Soc. **96**, 410 (1974).
19. W. R. CULLEN, L. D. HALL, and J. E. H. WARD. J. Am. Chem. Soc. **96**, 3422 (1974).
20. W. R. CULLEN, L. D. HALL, and J. E. H. WARD. J. Am. Chem. Soc. **94**, 5702 (1972).

Can. J. Chem. Downloaded from www.nrcresearchpress.com by 210.87.254.6 on 09/05/12
For personal use only.

Deuterium isotope effects on the ionization of the lower carboxylic acids in water and deuterium oxide

JAN BRON
University of Natal, Department of Chemistry, Durban, South Africa

Received February 9, 1976

JAN BRON. Can. J. Chem. **54**, 2879 (1976).

To facilitate the interpretation of isotope effects on the ionization of weak acids in water and deuterium oxide, a comparison of these quantities with that for a standard acid is proposed. Therefore, a quantity K_r has been defined by the equation $K_r = (K_H/K_D)/(K_H'/K_D')$. The equilibrium constants K_H and K_D refer to the ionization constants in water and deuterium oxide respectively. The equilibrium constant K_X'(X = H, D) refers to the acid used as a reference. An equation is derived from which it may be concluded, that for a series of acids closely similar in geometry and force field around the acidic group, a value of K_r close to unity should be obtained. To test this prediction the values of K_H/K_D for a series of *n*-alkanoic acids (N = 3–6) are compared experimentally with the value of K_H/K_D of acetic acid (25 °C). An emf method has been used in these measurements (quinhydrone electrode). In agreement with the theory a value for K_r close to unity has been observed.

JAN BRON. Can. J. Chem. **54**, 2879 (1976).

Pour faciliter l'interprétation des effets isotopiques sur l'ionisation des acides faibles dans l'eau et dans l'oxyde de deutérium, une comparaison de ces données avec celle d'un acide standard est proposée. Par conséquent, un terme K_r a été défini par l'équation $K_r = (K_H/K_D)/(K_H'/K_D')$. Les constantes d'équilibre K_H et K_D se réfèrent respectivement aux constantes d'ionisation dans l'eau et dans l'oxyde de deutérium. La constante d'équilibre K_X'(X = H, D) se réfère à l'acide utilisé comme référence. Une équation est dérivée et à partir de celle-ci on peut conclure que pour une série d'acides de géométrie et de champs de force très similaires dans le voisinage du groupement acide, une valeur de K_r près de l'unité devrait être obtenue. Pour vérifier cette prédiction, les valeurs de K_H/K_D pour une série d'acides *n*-alcanoiques (N = 3–6) sont comparées expérimentalement avec la valeur de K_H/K_D de l'acide acétique (25 °C). On a utilisé une méthode de fem dans ces mesures (électrode à la quinhydrone). En accord avec la théorie, une valeur de K_r près de l'unité a été observée.

[Traduit par le journal]

Introduction

It has been stated that the deuterium isotope effect on the ionization of weak acids in water and deuterium oxide is not clearly understood (1). The main problems are the lack of an adequate knowledge of all solvated species involved and the structures of water and deuterium oxide. This paper is an attempt to clarify some points on the subject by theoretical considerations and an experimental study.

The ionization of a weak acid XA (X = H, D) in X_2O can be represented by the equilibria

[1] $HA(H_2O) + H_2O(liq) \rightleftharpoons A^-(H_2O) + H_3O^+(H_2O)\ (K_H)$

$DA(D_2O) + D_2O(liq) \rightleftharpoons A^-(D_2O) + D_3O^+(D_2O)\ (K_D)$

All species are solvated by the solvent indicated in parentheses. In terms of partition functions the ratio K_H/K_D, or the isotope effect, may be written as (2)

$$[2] \qquad \frac{K_H}{K_D} = \frac{q(DA)}{q(HA)} \cdot \frac{q(H_3O^+)}{q(D_3O^+)} \cdot \frac{q(D_2O)}{q(H_2O)}$$

In [2] q is the molecular canonical partition function of the solvated species indicated in parentheses. It has been assumed that the partition function of A^- in H_2O and D_2O are the same. Also, implicit in [2] is the assumption that the molecules in the condensed phase can be represented by a system of non-interacting particles or the ideal gas phase. It is not surprising that some theoretical studies based on [2] are not always considered satisfactory (1). However, these two assumptions mentioned above may sound more reasonable if they are rephrased into the single statement: that the contributions of forces that cause the differences between species in the gas phase and condensed phase tend to cancel in ratios like [2] for molecules only differ-

Can. J. Chem. Downloaded from www.nrcresearchpress.com by 210.87.254.6 on 09/05/12
For personal use only.

Can. J. Chem. Downloaded from www.nrcresearchpress.com by 210.87.254.6 on 09/05/12
For personal use only.

ing in isotopic substitution. The difficulty still remains as to how to represent the X_2O and X_3O^+ molecules and several attempts have been made to evaluate K_H/K_D for a number of acids (3–5) with varying degrees of success.

The computational and conceptual problems in the evaluation of the isotope effect, K_H/K_D, for weak acids, can be eliminated by comparing the values of K_H/K_D for certain acids at a particular temperature with the value of K_H/K_D of a standard acid at the same temperature. The advantage of this is that all K_H/K_D values for the various acids have the ratio R

$$[3] \qquad R = \frac{q(H_3O^+)}{q(D_3O^+)} \cdot \frac{q(D_2O)}{q(H_2O)}$$

in common. Arithmetically this means to define a ratio K_r such that

$$[4] \qquad K_r = \frac{K_H}{K_D}\left(\frac{K_H'}{K_D'}\right)^{-1} = \frac{q(DB)}{q(HB)} \cdot \frac{q(HA)}{q(DA)}$$

The quantity $q(HA)/q(DA)$ refers to the standard acid, say acetic acid, and may be estimated (6) by using the observed gas phase frequencies of vibration.

The constant K_r can be written, in terms of the harmonic approximation (7), as

$$[5] \qquad K_r = \prod_{i=1}^{3N-6} \frac{[u_i^{-1} \sinh(\tfrac{1}{2}u_i)]_{HB}}{[u_i^{-1} \sinh(\tfrac{1}{2}u_i)]_{DB}} \times \prod_{j=1}^{18} \frac{[u_j^{-1} \sinh(\tfrac{1}{2}u_j)]_{AcOD}}{[u_j^{-1} \sinh(\tfrac{1}{2}u_j)]_{AcOH}}$$

in which u_i has the usual meaning of $hc\omega_i/kT$. It may be noted that K_r is expressed by using acetic acid as the reference acid. The quantity K_r cannot be evaluated for most acids, since for only a few the vibrational frequencies are known. For the formic–acetic acid pair the experimental value for K_r can be deduced (8) and the vibrational frequencies are known (9, 10). For this acid pair the experimental value for K_r at 20 °C is 0.87 and the theoretical value, computed by means of [5], is 0.83 at the same temperature. In this case the agreement between theory and experiment is encouraging.

If the vibrational frequencies of the acids HB and DB are not known, [5] has a more limited value. Equation 5 can be used, however, to predict or explain trends in K_r for a series of structurally similar acids. In fact, the high temperature forms of [5] are particularly suitable (11). For high temperatures or small values of u_i and u_j, [5] can be expanded (12). The result is

$$[6] \qquad K_r \simeq 1 + \frac{1}{24}\left[\sum_i (u_{iH}^2 - u_{iD}^2)_{BX} - \sum_j (u_{jH}^2 - u_{jD}^2)_{AcOX}\right]$$

Only the first two terms in the expansion have been retained. Equation 6 can also be written in terms of Wilson's **F**, **G** matrix elements (12–14).

$$[7] \qquad K_r \simeq 1 + \kappa T^{-2}\left[\sum_i \sum_j F_{ij}(G_{ij}^{(H)} - G_{ij}^{(D)})_{BX} - \sum_k \sum_l F_{kl}(G_{kl}^{(H)} - G_{kl}^{(D)})_{AcOX}\right]$$

The constant κ is equal to $(h/2\pi k)^2(24)^{-1}$. It is interesting to note that the classical limit ($T \to \infty$) of K_r is unity. Therefore, the second (temperature dependent) terms in the expansions 6 and 7 are called first quantum corrections (15).

Equation 7 has a restricted quantitative value, especially in the lower temperature region. For qualitative purposes [7] is more useful (14). Equation 7 has the advantage that trends in K_r can be discussed in such basic quantities as force constants (F_{ij}) and **G** matrix elements.

It can be seen immediately from the form of [7] that only those **G** matrix elements in the species BX (and AcOX) are affected and contribute to K_r, if, as a necessary condition, *both* the corresponding internal coordinates contain the centre of isotopic substitution in their definitions (13, 14). Hence, considering that the definitions of the usual internal coordinates never exceed four atoms, this suggests that in model calculations of isotope effects, the molecule can be abbreviated, or paraphased, only that part of the molecule in the immediate neighbourhood of the centre of isotopic substitution determines the value of K_r or an isotope effect in general. An obvious conclusion is that acids with similar geometry and force constants as the reference acid should give values of K_r close to unity, if [7] is of any qualitative value. The fact that a molecule can be abbreviated in model calculations of isotope effects has been concluded by Wolfsberg and Stern (12) in their calculations of *kinetic* isotope effects in nucleophilic substitution reactions. Their calculations were based on transition state or pseudo equilibrium theory and equations of type [5].

Can. J. Chem. Downloaded from www.nrcresearchpress.com by 210.87.254.6 on 09/05/12
For personal use only.

It may then be anticipated that straight chain carboxylic acids, with reference to acetic acid, should give K_r values close to unity. It was decided to test this expectation experimentally and use the carboxylic acids as a test of the qualitative value of [7].

Experimental

The isotope effect K_r can be written as

$$[8] \qquad K_r = \frac{K_H(HB)}{K_H(AcOH)} \cdot \frac{K_D(AcOD)}{K_D(DB)}$$

The ratios of the equilibrium constants, $K_H(HB)/K_H(AcOH)$ and $K_D(AcOD)/K_D(DB)$, can be measured by using the method of Everett *et al.* (ELP). These workers measured (16) the emf of a symmetrical cell, containing buffers of organic acids, by means of the hydrogen electrode. If the acids are half neutralised, the emf of the cell is then, at 25 °C

$$[9] \qquad E\,(\text{mV}) = 59.16 \log \left[\frac{K_X(AcOX)}{K_X(XB)}\right]$$

Rather than using the X_2 electrode it was decided to use the quinhydrone (Q,QX_2) electrode and the cell used to measure the equilibrium constant ratios can be represented by

$$[10] \quad \text{Pt} \;\Big|\; \begin{matrix} 0.025\ M\ \text{AcOX} \\ 0.025\ M\ \text{AcONa} \\ 0.0045\ M\ \text{Q,QX}_2 \\ 0.15\ M\ \text{KCl} \\ \text{X}_2\text{O} \end{matrix} \;\Big\|\; \begin{matrix} 0.025\ M\ \text{XB} \\ 0.025\ M\ \text{NaB} \\ 0.0045\ M\ \text{Q,QX}_2 \\ 0.15\ M\ \text{KCl} \\ \text{X}_2\text{O} \end{matrix} \;\Big|\; \text{Pt}$$

The reasons for using the quinhydrone electrode were convenience and the elimination of the need for (expensive) D_2. A detailed discussion of the quinhydrone electrode has been given by Ives and Janz (17).

The glass emf cell recommended by ELP was found inconvenient to use. Hence another and also *symmetrical* cell of an H shape was designed. Electrical contact between the two legs of the cell was secured by a sintered glass disk of very fine porosity. The disk should be of very fine porosity, otherwise mixing of the different solutions in the legs takes place. At the bottom of the two legs sintered glass disks of medium porosity were fused and through these disks slow streams of purified nitrogen (strongly alkaline pyrogallol) were introduced into the solutions to remove dissolved oxygen and to stir the solutions. The electrodes were two 1 cm^2 platinum disks with long platinum stems with the ends fused in glass. The cell was emerged in a thermostat bath at 25.00 ± 0.05 °C.

The electrodes were cleaned with warm (60–70 °C) chromic acid and thoroughly rinsed before use. The electrodes were not dried before use, but, after shaking off the water, were inserted immediately into the solutions. The cell was tested with the acetic acid – benzoic acid buffer pair and the emf was as expected. Also the zero of the cell was tested by using the same solutions in both legs. The result was 0 ± 10 μV. The emf was measured with a Keithley digital multimeter (Model 171).

The chemicals were obtained from various commercial sources. The quinhydrone was recrystallized from ethanol before use (17). The purities of the straight chain carboxylic acids (acetic to *n*-hexanoic acid), as found by acid–base titration, were, after distillation, 99.7% or better. The deuterium oxide had a purity of 99.8%. The potassium chloride was dried before use.

To minimise any impurity effects, stock solutions of quinhydrone and KCl in X_2O were prepared and added to a volume of half neutralised acids. The concentrations of the stock solutions were such as to obtain the concentrations as shown in [10] to within 1% after mixing. Readings of the emf were taken after one hour of equilibration. It has been implied in [9] and [10] that the acids are exactly half neutralised. Half neutralization was accomplished by the addition of a carbonate free solution of NaOX to known quantities of the acids. Since the standard volumetric techniques used always involve errors, six of these half neutralised solutions were prepared to generate the 2 × 6 determinations as listed in Table 1. Repeated measurements of the emf of the *same* pair of solutions gave results differing by not more than 0.1 mV.

The results of the measurements are given in Table 1. The isotope effect, K_r, can be deduced from [9] and the following definition

$$[11] \quad \Delta E\,(\text{mV}) = E_H - E_D = -59.16 \log K_r$$

The errors in ΔE and K_r have been computed by means of the formula (18)

$$[12] \qquad \delta Y = \left[\sum_i \left(\frac{\partial Y}{\partial x_i}\right)^2 (\delta x_i)^2\right]^{1/2}$$

The quantity δY is the most probable error in Y and δx_i is the error in x_i. No attempt has been made to measure K_r at various ionic strengths (to obtain K_r at zero ionic strength), since it has been found by ELP that the dependence of the emf on the ionic strength, in measurements of this type, is negligible.

Results and Discussion

The results in Table 1 show that the isotope effects (K_r) are indeed small for all acids as predicted by [7]. The constant K_r increases from 0.995 for propionic acid to 1.020 for *n*-pentanoic acid. The values of K_r for *n*-hexanoic acid are essentially the same, so K_r seems to reach its maximum value at *n*-pentanoic acid. However, it should be pointed out that the differences in the values of K_r for the various acids are statistically not very significant.

Formic acid, with K_r equal to 0.87 and only one carbon atom, is too different to be defined as 'structurally similar' to its higher homologs. From the above discussion of [7] and the experimental results it seems to follow, that as a

TABLE 1. Some properties of cell at 25 °C

Parameter	Value			
	C_3H[a]	C_4H	C_5H	C_6H
Electromotive force of cell in H_2O				
Experiment 1	7.68	4.45	5.25	6.39
2	7.40	—	4.70	6.49
3	7.30	4.38	5.05	6.66
4	7.12	4.63	4.88	6.78
5	7.28	4.28	5.13	7.02
6	7.29	4.31	4.92	6.68
Average[b]	7.35±0.19	4.41±0.14	4.99±0.20	6.67±0.22
Literature[c]	7.12	3.68	5.15	5.98
Electromotive force of cell in D_2O				
Experiment 1	6.73	4.32	5.55	7.05
2	7.46	4.54	5.70	7.22
3	7.40	4.06	5.11	6.98
4	7.18	4.31	5.65	7.37
5	7.34	4.83	5.38	7.14
6	7.19	4.49	5.64	6.99
Average	7.22±0.26	4.43±0.26	5.51±0.22	7.13±0.15
ΔE	0.13±0.32	−0.02±0.30	−0.52±0.30	−0.46±0.27
K_r	0.995±0.012	1.001±0.012	1.020±0.012	1.018±0.011

[a]The symbol C_nH stands for the *n*-alkanoic acid containing *n* carbon atoms.
[b]Arithmetic mean and standard deviation, the electromotive force is expressed in mV.
[c]Computed from Table 2 in ref. 16, where no error limits have been given.

good approximation, the C—COOX grouping is the important part of the *n*-alkanoic acids. This implies that, in fact, the acids do not need to be straight chain alkanoic acids, but may have side chains. In order to test this, the value of K_r for trimethyl acetic acid was also determined at 25 °C. The result for K_r for trimethyl acetic acid was 0.974 ± 0.017 at 25 °C.

By comparing the value of K_r for trimethyl acetic acid with the one for formic acid it can be seen that the isotope effect is still small. Hence, it seems that chain branching does not make K_r considerably different from unity. At this point it is reasonable to ask: do all carboxylic acids, when compared to acetic acid, have K_r close to unity? To take benzoic acid as an example, it is found that, by using literature data (19, 20), the K_r value for this acid is 0.86 at 25 °C. Therefore, the answer to the above question is negative, even though benzoic acid has the C—COOX unit in common with the *n*-alkanoic acids. The term 'structurally similar', which refers mainly to force constants, seems to be the key to small K_r values when an acid is compared to a standard acid. The approach used in this paper can also be applied to explain isotope effects on the dissociation constants for weak *bases* in H_2O and D_2O.

Acknowledgement

The author would like to thank Miss V. Peters for technical assistance.

1. R. P. BELL. The proton in chemistry. Chapman and Hall, London. 1973.
2. T. L. HILL. An introduction to statistical thermodynamics. Addison-Wesley Publishing Company, Reading (U.S.A.). 1962.
3. C. A. BUNTON and V. J. SHINER. J. Am. Chem. Soc. **83**, 42 (1961); **83**, 3207 (1961); **83**, 3214 (1961).
4. C. G. SWAIN and R. F. W. BADER. Tetrahedron, **10**, 182 (1960); **10**, 200 (1960).
5. R. A. MORE O'FERRALL, G. W. KOEPPL, and A. J. KRESGE. J. Am. Chem. Soc. **93**, 1 (1971).
6. J. BRON. Can. J. Chem. **52**, 3078 (1974).
7. I. BRON, CHEN FEE CHANG, and M. WOLFSBERG. Z. Naturforsch. **28a**, 129 (1973).
8. G. SCHWARZENBACH, A. EPPRECHT, and H. ERLENMEYER. Helv. Chim. Acta, **19**, 1292 (1936).
9. S. J. CYVIN, I. ALFHEIM, and G. HAGEN. Acta Chem. Scand. **24**, 3038 (1970).

Can. J. Chem. Downloaded from www.nrcresearchpress.com by 210.87.254.6 on 09/05/12
For personal use only.

10. I. ALFHEIM and S. J. CYVIN. Acta Chem. Scand. **24**, 3043 (1970); **24**, 3049 (1970).
11. J. BIGELEISEN and M. WOLFSBERG. Adv. Chem. Phys. **1**, 15 (1958).
12. M. WOLFSBERG and M. STERN. Pure Appl. Chem. **8**, 225 (1964).
13. E. B. WILSON, J. C. DECIUS, and P. C. CROSS. Molecular vibrations. McGraw-Hill Book Company, Toronto. 1955.
14. J. BRON. Can. J. Chem. **54**, 160 (1976).
15. H. S. JOHNSTON. Gas phase reaction rate theory. The Ronald Press Company, New York. 1966.
16. D. H. EVERETT, D. A. LANDSMAN, and B. R. W. PINSENT. Proc. Roy. Soc. **215A**, 403 (1952).
17. D. J. G. IVES and G. J. JANZ. Reference electrodes. Academic Press, New York. 1961.
18. H. W. SALZBERG, J. I. MORROW, S. R. COHEN, and M. E. GREEN. Physical chemistry: a modern laboratory course. Academic Press, New York. 1969.
19. B. M. LOWE and D. G. SMITH. J. Chem. Soc. Faraday I, **71**, 389 (1975).
20. R. GARY, R. G. BATES, and R. A. ROBINSON. J. Phys. Chem. **69**, 2750 (1965).

Can. J. Chem. Downloaded from www.nrcresearchpress.com by 210.87.254.6 on 09/05/12
For personal use only.

Spectroscopic studies in olefins. VI. The valence angle dependence of interproton nuclear magnetic resonance coupling constants

FRANS H. A. RUMMENS AND LEE KASLANDER
Department of Chemistry, University of Regina, Regina, Sask., Canada S4S 0A2

Received March 3, 1976

FRANS H. A. RUMMENS and LEE KASLANDER. Can. J. Chem. **54**, 2884 (1976).

INDO–MO calculations have been performed for all the proton–proton coupling constants in ethylene, propylene, and *cis*- and *trans*-2-butene, both at their equilibrium geometry and at geometries deviating from equilibrium, thus resulting in $dJ/d\phi$ parameters for all coupling constants as a function of all valence angles ϕ. It is shown that such valence angle effects can be appreciable, particularly for two- and three-bond couplings. The valence angle effects are demonstrated to be independent and additive. The calculated data, in combination with the exact geometrical data and experimental values for the coupling constants allow the separation of (inductive) substitution and rehybridization effects. It is also shown that for three-bond couplings the effects of *in*-path C—C—H bond angle changes are minor in comparison to the *exo*-path C=C—C valence angle effects. The new data provide a consistently good model to explain certain empirical trends in two- and three-bond coupling constants as a function of the size of the substituents, assuming a simple steric hindrance induced rehybridization mechanism. On the other hand it is also found that such a mechanism cannot account for similar trends in the H—C=C—CH_3 allylic and the CH_3—C=C—CH_3 homoallylic coupling constants.

FRANS H. A. RUMMENS et LEE KASLANDER. Can. J. Chem. **54**, 2884 (1976).

On a effectué des calculs INDO-MO pour toutes les constantes de couplage proton–proton de l'éthylène, du propylène et des butène-2 *cis* et *trans* dans leur géométrie d'équilibre et à des géométries qui dévient de l'équilibre; ceci nous a permis d'évaluer les paramètres $dJ/d\phi$ pour toutes les constantes de couplage en fonction de tous les angles de valence ϕ. On a montré que de tels effets d'angles de valence peuvent être importants principalement pour les couplages à travers deux et trois liaisons. On a démontré que les effets d'angles de valence sont indépendants et additifs. Les valeurs calculées, de concert avec des données de géométrie exacte et des valeurs expérimentales pour les constantes de couplage, permettent de séparer les effets de substitution (inductif) et de réhybridation. On a aussi montré que, pour les couplages à travers trois liaisons, les effets de changement d'angles de liaison C—C—H "*endo*-trajet" sont peu importants par rapport aux effets d'angles de valence C=C—C "*exo*-trajet". Des nouvelles données permettent d'établir un bon modèle qui peut expliquer d'une façon consistante certaines tendances empiriques dans les constantes de couplage à travers deux et trois liaisons en fonction de la grosseur des substituants invoquant un mécanisme de réhybridation induit par un empêchement stérique simple. Par ailleurs on a aussi trouvé qu'un tel mécanisme ne peut expliquer les tendances similaires dans les constantes de couplage allylique H—C=C—CH_3 et homoallylique CH_3—C=C—CH_3.

[Traduit par le journal]

Introduction

It is well known that proton–proton coupling constants depend strongly on the number and the nature of the intervening atoms, the hybridization state of the latter, the conformation of the bonds forming the H···H coupling path, and the nature of the substituents, their electronegativity in particular. Beyond these gross effects there are others, which, although they appear to be more subtle, may nevertheless account for substantial changes in the various coupling constants. Karplus (1), for example, calculated the effect of changes $\Delta\theta$ and $\Delta\theta'$ of the H—C= angles for the *cis*-coupling ^3J_c in H—C_{sp2}—C_{sp2}—H as well as the similar effects on $^3J_{s-cis}$ and $^3J_{s-trans}$ in H—C_{sp3}—C_{sp3}—H systems. Ranft (2) has carried out similar calculations on the valence angle effects of ^3J_v of H—C_{sp2}—C_{sp3}—H fragments. Based on the above mentioned calculations, Rummens and de Haan (3) showed how steric hindrance, especially between *cis* alkyl groups in olefins, via rehybridization of the sp^2 carbon atoms and the associated valence angle changes, could qualitatively account for observed trends in ^3J_c, ^3J_t, ^3J_v, $^4J_{ca}$, and $^4J_{ta}$ (subscripts referring, respectively to *cis*-, *trans*-, *vicinal*-, *cisoid allylic*-, and *transoid allylic*-couplings). The extension to four-

Can. J. Chem. Downloaded from www.nrcresearchpress.com by 210.87.254.40 on 09/05/12
For personal use only.

Can. J. Chem. Downloaded from www.nrcresearchpress.com by 210.87.254.40 on 09/05/12
For personal use only.

bond coupling constants was made without the benefit of any calculations, however. A similar extrapolation, this time for $^5J_{cha}$ and $^5J_{tha}$ (subscripts referring to *cisoid homoallylic*- and *transoid homoallylic*-couplings respectively), was used by Rummens and Kaslander (4) in their study of the *cis*- and *trans*-2-butenes. Further discussion by Rummens (5) regarding steric interaction and rehybridization appeared to confirm the general validity of the concept.

Cooper and Manatt (6) have since applied much the same steric hindrance *cum* geometrical distortions to coupling constants (mainly ^3J_c) in aromatics, benzocycloalkenes and cycloalkenes. They discussed in particular the effects of steric crowding on C=C and C—H bond lengths, the C=C—H bond angle, and out-of-plane bendings. The bond length effects on ^3J_c may be very considerable if molecules with different C=C bond order are compared, but they found that the sterically induced bond length changes have almost no effect on ^3J_c. Out-of-plane bending was found to have a possible effect on ^3J_c of about 0.03 Hz per degree, so that this effect can only be substantial if there is a very severe twisting of the molecule. This type of distortion should lead to a decrease in ^3J_c, but Cooper and Manatt found that in heavily crowded condensed aromatics the ^3J_c of twisted H—C=C—H fragments was substantially *larger* than those of equivalent but planar fragments. These authors also found that the C=C—H bond angle effect can be substantial, and they ascribed, for example, the differences in ^3J_c of cyclohexene and cyclopentene entirely to the C=C—H angle changes, leading to an estimate of $d^3J_c/d\phi$ of between 0.4 and 0.8 Hz per degree. It should be noted however, that these authors did not consider the effect of C—C=C bond angle changes.

Angular distortions in substituted butadienes have been discussed by Albriktsen *et al.* (7) and by Bacon and Maciel (8), confirming the view that the observed variations in coupling constants could well be due to rehybridization and its subsequent changes in valence angles.

The geminal coupling ^2J_g has been shown by Karplus and Grant (9), Gutowsky *et al.* (10), and Banwell and Sheppard (11) to be approximately linearly dependent on changes in H—C—H bond angle, but since ^2J_g also relates linearly to the electronegativity of the substituents, it is not clear whether there is indeed a separable bond angle effect.

The present study was prompted by a number of considerations. Firstly, it was realized that the steric rehybridization model was only qualitative and that it was therefore necessary to perform some quantitative calculations on molecules for which both the geometry and the coupling constants were very accurately known. Secondly, it was realized that in virtually all the discussions on bond angle dependence of coupling constants it has been taken for granted that the bond angle changes of interest are those that are entirely in the coupling path, ignoring the possibility that bonds which have only one atom in common with the coupling path may have an important effect on the couplings. Lastly, the extrapolations of the steric hindrance *cum* rehybridization model to allylic (3, 4) and homoallylic (4) coupling constants were made without the benefit of any calculations to provide a rationale for the validity of such an extension. This has become even more urgent since recent theoretical and experimental work of Barfield and co-workers (12–14) on four- and five-bond couplings now provide a much better understanding of the mechanisms of these couplings.

It was therefore decided to calculate all coupling constants of ethylene, propylene, and *cis*- and *trans*-2-butene as a function of all valence angles, the angle between C_{sp2}—C_{sp3} bond and the rotational axis of the CH_3 groups as well as of (in one case) the twist angle between the two sp^2 planes of the carbon atoms constituting the C=C bond.

INDO–MO Calculations

Coupling constants were calculated by the finite perturbation method in the INDO approximation (15). Geometries used to calculate atomic coordinates were taken from gas phase electron diffraction results for ethylene (16) and *trans*-2-butene (17) and from microwave spectroscopy results for propylene (18) and *cis*-2-butene (19). Bond angle definition and equilibrium values of the bond angles are given in Table 1.

Initial calculations were carried out for each molecule using the equilibrium geometry. Then for each structure the calculations were repeated while varying one angle over $\pm 2°$ from the equilibrium value, by increments of 1°, while all other angles were held at their equilibrium value.

TABLE 1. Angle parameters in substituted ethylenes

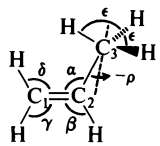

	α	β	γ	δ	ε	ρ*	Reference
Ethylene	121.7	121.7	121.7	121.7	—	—	16
Propylene	124.3	119.0	121.5	120.5	107.7	0.0	18
cis-2-Butene	126.7	117.3	117.3	126.7	109.5	−0.9(?)	19
trans-2-Butene	123.8	121.5	121.5	123.8	110.0	0.6	17

*ρ is taken to be negative in the configuration shown.

The procedure was then repeated while varying one other angle, until all angular variations were considered one at a time. In a few cases two angles were varied simultaneously; the results obtained were so closely equal to the added results of the calculations on single bond angle changes that it was generally concluded that the effect of bond angle changes on coupling constants is strictly additive in the sense that cross terms are negligible and contribute no more than 1×10^{-3} Hz over the range studied. In those molecules having equivalent angles (*e.g.* α and δ for *cis*-2-butene) all such equivalent angles were varied equally and simultaneously. For propylene and the two butenes only the preferred methyl conformation (*i.e.* with one C—H bond of the methyl group eclipsing the C=C bond (17–19)) was used in the calculations. For *cis*-2-butene a series of calculations of coupling constants was carried out for geometries in which the C=C bond was twisted. A twist angle of up to 20° led to no significant change in the calculated coupling constants. Therefore, variance of the C=C twist angle was not pursued any further.

Convergence criteria used in the calculations were those described by Wasylishen and Schaefer (20). According to these authors these criteria lead to a computation error in individual coupling constants no greater than 1×10^{-5} Hz where convergence is obtained. For all but one perturbation, convergence was obtained in fewer than seventy SCF iteration cycles. In the one exception no complete convergence was obtained after 100 iterations; however, near the 100th iteration all coupling constants were changing by less than 1×10^{-3} Hz per iteration.

Whereas for ethylene it is sufficient to put a perturbation on only one atom in order to obtain all coupling constants, for the other three molecules at least three independent calculations with the peturbations on different atoms were required. As a result many coupling constants were obtained more than once from these independent calculations. It was found that such degenerate results differed by as much as 1×10^{-3} Hz. This variation therefore seems to be a more realistic computational error limit. For the above two reasons the results from the one calculation where the convergence was not complete are nevertheless considered acceptable and these were indeed included. For the vicinal and allylic couplings only the average couplings $\langle J \rangle = (J_{\phi=0} + 2J_{\phi=120})/3$ are reported; the reported data for homoallylic couplings refer to the similar average over the six individual couplings.

All calculations were carried out on an IBM 360/50 computer.

Results and Discussion

The coupling constants of ethylene, *cis*- and *trans*-2-butene, and propylene as calculated at their equilibrium bond distances and bond angles are given in Table 2, together with the experimental values of these coupling constants. Most calculated coupling constants are reasonably close to the experimental ones, except perhaps for the calculated ^3J_t couplings which are about twice too large. Although the agreement of calculated *vs.* experimental is not perfect it still seems a reasonable assumption that calculated dependencies of J on valence angles should yield at least a semi-quantitive estimate of the magnitude of these effects.

Table 3 summarizes the results obtained. They

Can. J. Chem. Downloaded from www.nrcresearchpress.com by 210.87.254.40 on 09/05/12
For personal use only.

TABLE 2. Calculated and experimental proton–proton coupling constants in Hz

Molecule		^2J_g	^3J_c*	^3J_t*	^3J_v*	$^4J_{ca}$	$^4J_{ta}$	$^5J_{cha}$	$^5J_{tha}$
Ethylene	Exptl. (21)	2.5	11.6	19.1					
	Calcd.†	2.51	10.33	27.77					
Propylene	Exptl. (22)	2.08	10.02	16.81	6.40	−1.75	−1.33		
	Calcd.†	4.39	10.77	29.10	9.00	−2.23	−1.52		
cis-2-Butene	Exptl. (4)		10.80		6.76		−1.85	1.20	
	Calcd.†		14.45		9.52		−2.04	2.52	
trans-2-Butene	Exptl. (4)			14.99	6.44	−1.72			1.59
	Calcd.†			29.17	8.74	−2.30			2.44

*Signs assumed positive.
†All calculations refer to the exact equilibrium geometries.

TABLE 3. Calculated angular dependencies in Hz per degree of the proton–proton coupling constants

Coupling constant	Molecule	$dJ/d\alpha$	$dJ/d\beta$	$dJ/d\gamma$	$dJ/d\delta$	$dJ/d\epsilon$	$dJ/d\rho$
^2J_g	Ethylene			−0.690 ($\alpha+\beta+\gamma+\delta$)		—	—
	Propylene	−0.099	−0.049	−0.237	−0.250	+0.015	+0.008
^3J_c	Ethylene			+0.381 ($\alpha+\beta+\gamma+\delta$)		—	—
	Propylene	+0.288	−0.056	+0.075	+0.241	−0.002 (3ϵ)	−0.032
	cis-2-Butene	+0.613 ($\alpha+\delta$)	−0.129 ($\beta+\gamma$)			−0.004 ($3\epsilon+3\epsilon'$)	−0.024 ($\rho+\rho'$)
^3J_t	Ethylene			+0.634 ($\alpha+\beta+\gamma+\delta$)			
	Propylene	+0.392	+0.037	+0.308	−0.013	+0.002 (3ϵ)	−0.043
	trans-2-Butene	+0.828 ($\alpha+\gamma$)	+0.093 ($\beta+\delta$)			+0.005 ($3\epsilon+3\epsilon'$)	−0.081 ($\rho+\rho'$)
^3J_v	Propylene	+0.139	−0.000	+0.010	−0.002	−0.095 (3ϵ)	+0.022
	cis-2-Butene	+0.143 ($\alpha+\delta$)	+0.009 ($\beta+\gamma$)			−0.084 ($3\epsilon+3\epsilon'$)	+0.025 ($\rho+\rho'$)
	trans-2-Butene	+0.143 ($\alpha+\gamma$)	−0.000 ($\beta+\delta$)			−0.077 ($3\epsilon+3\epsilon'$)	+0.027 ($\rho+\rho'$)
$^4J_{ca}$	Propylene	+0.002	−0.005	−0.004	+0.004	+0.022 (3ϵ)	−0.002
	trans-2-Butene	−0.005 ($\alpha+\gamma$)	−0.006 ($\beta+\gamma$)			+0.017 ($3\epsilon+3\epsilon'$)	−0.008 ($\rho+\rho'$)
$^4J_{ta}$	Propylene	−0.063	−0.006	+0.007	+0.004	+0.001 (3ϵ)	−0.001
	cis-2-Butene	−0.036 ($\gamma+\delta$)	−0.007 ($\beta+\gamma$)			−0.006 ($3\epsilon+3\epsilon'$)	−0.003 ($\rho+\rho'$)
$^5J_{cha}$	*cis*-2-Butene	+0.017 ($\alpha+\delta$)	−0.000 ($\beta+\gamma$)			−0.049 ($3\epsilon+3\epsilon'$)	+0.002 ($\rho+\rho'$)
$^5J_{tha}$	*trans*-2-Butene	−0.002 ($\alpha+\gamma$)	−0.000 ($\beta+\delta$)			−0.046 ($3\epsilon+3\epsilon'$)	+0.002 ($\rho+\rho'$)

are essentially best least-squares slopes over five points, assuming a linear relation between J and valence angle. The slight curvature which was apparent in some J *vs.* angle plots were therefore mostly ignored (*vide infra*). The simultaneous change of equivalent bond angles is indicated in parentheses such as $(\alpha + \gamma)$ to indicate that in *trans*-2-butene both the H—C= angles were

Can. J. Chem. Downloaded from www.nrcresearchpress.com by 210.87.254.40 on 09/05/12
For personal use only.

TABLE 4. Group contributions to $dJ/d\phi$ in Hz/deg. for the angles $\phi = \alpha, \beta, \gamma, \delta, \epsilon$, and ρ

	α(H)	β(H)	γ(H)*	δ(H)	α(C)	γ(C)	δ(C)	3ϵ(H) (α)†	3ϵ(H) (γ, δ)	ρ (α)	ρ (γ, δ)
^2J_g	−0.085	−0.085	−0.244	−0.244	−0.099	—	—	+0.015	—	+0.008	—
^3J_c	+0.227	−0.066	−0.066	+0.227	+0.282	—	+0.282	−0.002	−0.002	−0.019	+0.019
^3J_t	+0.275	+0.032	+0.275	+0.032	+0.418	+0.418	—	+0.002	+0.002	−0.041	−0.041
$^3J_g(\alpha)$†	—	+0.000	+0.009	−0.002	+0.139	+0.004	+0.004	−0.095	+0.015	+0.022	+0.004
$^4J_{ca}$	—	−0.007	−0.004	+0.003	+0.002	−0.007	—	+0.022	−0.005	−0.002	−0.006
$^4J_{ta}$	—	−0.005	+0.004	+0.004	−0.063	—	+0.028	+0.001	−0.008	−0.001	−0.002
$^5J_{cha}$	—	0.000	0.000	—	+0.008	—	+0.008	−0.024	−0.024	+0.001	+0.001
$^5J_{tha}$	—	0.000	—	0.000	−0.001	−0.001	—	−0.023	−0.023	+0.001	+0.001

*γ(H) is the symbol for $dJ/d\gamma$ if there is an H atom on the γ position.
†The first CH_3 substituent is placed at the α-position.

changed in the same calculation. The effect on the coupling constant in question may or may not be twice the effect of a single angle change, however.

General Observations

(*i*) It appears that bond angle effects may be of substantial magnitude with some as large as 0.8 Hz/deg. Since even rather minor substituent changes may result in bond angle changes of several degrees (compare the geometries of *cis*- and *trans*-2-butene), coupling constant effects of several Hz in three-bond H···H couplings seem indicated. In relative terms, coupling constant changes of up to 5% per degree of (some) bond angle change are found.

(*ii*) Angle dependencies of J coupling can approximately be considered as an additive property of group contributions, the latter almost independent of substitutions. The most direct example of this is the fact that in propylene $d^2J/d\delta$ is virtually the same as $d^2J/d\gamma$. Also in *trans*-2-butene $d^3J_t/d\alpha = 0.828$ or 0.414 per changing angle, since this is calculated for the two angles α and $\gamma = \alpha$ changing simultaneously. This value of 0.414 is very close to the value of 0.392 for $d^3J_t/d\alpha$ in propylene. Similarly, $d^3J_t/d\beta$ in *trans*-2-butene per angle is +0.046, close to the +0.037 for $d^3J_t/d\beta$ in propylene. In *cis*-2-butene half of $d^3J_c/d\alpha$ is equal to 0.306 as compared to $d^3J_c/d\alpha = 0.288$ in propylene; also $\frac{1}{2}d^3J_c/d\beta = -0.064$ in *cis*-2-butene *vs.* $d^3J_c/d\beta = -0.056$ in propylene.

The additivity aspect of these group contributions could be tested as follows: the $d^2J/d\alpha$ in ethylene consists of two equal contributions due to the angular changes in γ and δ, for which one can take twice the average of $d^2J/d\gamma$ and $d^2J/d\delta$ in propylene, and two equal contributions from the angles α and β for which one can take twice the $d^2J/d\beta$ of propylene. Adding these terms together one finds +0.586, *vs.* +0.690 from the direct calculation on ethylene. Also the $d^3J_t/d\alpha$ in ethylene can be thought of as consisting of two equal contributions from α and γ, and using twice $d^3J_t/d\gamma$ of propylene. Adding the appropriate terms from propylene one finds 0.590 *vs.* $d^3J_t/d\alpha = 0.634$ from direct calculations on ethylene.

(*iii*) This additivity is useful in estimating certain contributions that could not be calculated directly. For example, in *cis*-2-butene the angles α and δ are equivalent in terms of molecular symmetry resulting in $d^4J_{ta}/d(\alpha + \delta) = -0.036$. But this is now the sum of two *un*equal contributions because α and δ are nonequivalent with respect to the four-bond *transoid* coupling. Since $d^4J_{ta}/d\alpha = -0.063$ for propylene, one can assume that this would also be the correct value of $d^4J_{ta}/d\alpha$ in *cis*-2-butene-2, resulting in $d^4J_{ta}/d\delta = +0.027$. Since some of the $dJ/d\phi$ data are not constants but slightly ϕ dependent, the above comparison of different geometries may not be entirely valid. However, by using angle dependent $dJ/d\phi$ data and inserting the equilibrium ϕ value of the molecule in question, it was established that the above noted additivity was even improved. In Table 4 the group contributions obtained for normalized angles C=C—H equal 120° and angles C=C—C equal to 125° are given. Where more than one relation was available, least-squares 'best' values are reported.

(*iv*) A rather unexpected phenomenon is revealed by Table 4. It appears quite generally that *in*-path valence angle changes are substantially

Can. J. Chem. Downloaded from www.nrcresearchpress.com by 210.87.254.40 on 09/05/12
For personal use only.

Can. J. Chem. Downloaded from www.nrcresearchpress.com by 210.87.254.40 on 09/05/12
For personal use only.

less important than those which have only one leg in the coupling path (*exo*-path). For example the *in*-path contributions of angles β and γ in ^3J_c is -0.066 Hz/deg *i.e.* only one third of the effects of changes in the angles α and δ. The effect is even more pronounced for ^3J_t. Also for the ^3J_v it can be seen that $dJ/d\alpha$ is fairly large, whereas changes in the C_{sp3}—C_{sp2}—H angle have a zero effect on ^3J_v if α is kept constant. Similar results also pertain to $^4J_{ca}$, but apparently not to $^4J_{ta}$ where the *in*-path $dJ/d\alpha$ is the largest effect.

The Effect of Substitution

Substitution, even that by CH_3 or other alkyl groups, can change the value of the coupling constants quite considerably (see Table 2). While a large part of these changes may be due to inductive (electronegativity) effects, basically controlled by electron densities on the carbon atoms of the coupling pathway, our above quoted results do indicate that a substantial part of these changes can be due to hybridizational changes which accompany the substitution but which in themselves produce no electron density changes on the rehybridizing carbon atoms. Thus these two effects should be separable.

If one takes, for example, ethylene and substitutes one H atom by CH_3 to form propylene, quite substantial valence angle changes occur; $\Delta\alpha = +2.6°$, $\Delta\beta = -2.7°$, $\Delta\gamma = -0.2°$, and $\Delta\delta = -1.2°$. If one now calculates the change ^3J_c due to these valence angle changes using the data from Table 4 and adds these together, one finds ^3J_c(hybridization) $= +0.65$ Hz. Since the experimental change is -1.58 Hz it is concluded that the inductive term $^3J_c(\chi_C) = -2.23$ Hz where χ_C is the electronegativity of carbon relative to H. Calculations for propylene show that only the electron density at C_2 is substantially different from that of ethylene, whereas on C_1 there is only a minor change; the substitution effect appears therefore to be primarily limited to the carbon atom at which the substitution takes place. This conclusion allows one to check the above calculated $\Delta^3J_c(\chi_C)$ effect by comparing ethylene and *cis*-2-butene. The calculated Δ^3J_c(rehyb.) is found to be $+3.63$ Hz which, combined with the experimental change of -0.8 Hz, leads to $\Delta^3J_c(\chi_C) = -2.21$ Hz per CH_3 group. This agrees well with the earlier mentioned -2.23 Hz. Similarly $\Delta^3J_t(\chi_C)$ values of -3.17 Hz (comparing ethylene to propylene) and -2.91 Hz (comparing ethylene to *trans*-2-butene) were obtained. The comparison Δ^2J_g of ethylene to propylene gave a calculated Δ^2J_g(rehyb.) $= +0.223$ Hz *vs.* an experimental difference of -0.42 Hz which would result in $\Delta^2J_g(\chi_C) = -0.64$ Hz.

It can therefore be stated that studies on electronegativity effects on coupling constants are incomplete and to a considerable extent (about 30% in the above quoted cases) in error unless the effect of bond angle changes are taken into account.

Similar CH_3 substitution effect calculations on $^4J_{ca}$ using propylene and *trans*-2-butene and taking into account changes in α, β, γ, δ, ϵ, and ρ produced a calculated Δ^4J_{ca}(rehyb.) $= +0.02$ Hz basically because the ϵ-effect off-sets the effects of changes of the β and γ angles. Since the experimental difference is $+0.03$ Hz, it appears that the electronegativity effect on $^4J_{ca}$ is virtually nil. In spite of the fact that the electronegativity effect of a C_1 substituent is apparently somewhat smaller and of opposite sign for $^4J_{ca}$ than for $^4J_{ta}$ (14), it is felt that the CH_3 electronegativity effect on $^4J_{ta}$ can also be assumed to be negligible. The calculated rehybridization effect in going from propylene to *cis*-2-butene can be estimated to be maximally -0.02 Hz (by assuming that $\rho = +4°$ rather than $\rho = -0.9°$ as indicated by Kondo *et al.* (19)). The smallness of Δ^4J_{ta}(rehyb.) is due to the almost quantitative off-set of the $\Delta\alpha$ and $\Delta\gamma$ effects. The sum of rehybridization and electronegativity effect should therefore be approximately zero. Since the experimental difference is -0.52 Hz it seems indicated that an extra mechanism contributing to this $^4J_{ta}$ coupling is involved.

The Geminal Coupling ^2J_g

The only systematic study available is that by Bothner-By and co-workers (22, 23) on monoalkylated ethylenes. For $H_2C{=}CHR$, all coupling constants remain virtually unchanged for R = CH_3, C_2H_5, *n*-C_4H_9, and *i*-C_3H_7, including the ^2J_g which was found to be 2.0 ± 0.2 Hz (the actual variations probably being due to error in the spectral analysis). However, for R = CH_2(*tert*-Bu) and R = CH(*tert*-Bu)$_2$ the ^2J_g found were 2.37 and 2.65 Hz respectively. It can also be shown that all data of Bothner-By *et al.* are quantitatively consistent with the view

Can. J. Chem. Downloaded from www.nrcresearchpress.com by 210.87.254.40 on 09/05/12
For personal use only.

that in the latter two compounds the only populated conformer(s) has (have) the C_3 proton(s) *anti* to the olefinic hydrogen at C_2. In these conformations the *tert*-butyl groups will have a strong steric effect on the C_2 hydrogen; rehybridization to alleviate this strain will reduce the angle β (and perhaps also α) which, according to Table 4 will result in an *increase* in ^2J_g, as is indeed observed.

The Olefinic Couplings ^3J_c and ^3J_t

In the same series of compounds as discussed above, ^3J_c and ^3J_t are virtually constant at 10.2 ± 0.2 and 17.1 ± 0.1 Hz but they appear to be somewhat smaller for R = CH(*tert*-Bu)$_2$ with values of 9.97 and 17.01 Hz. (22, 23) This can be explained perhaps by the fact that $d^3J_c/d\alpha$ and $d^3J_t/d\alpha$ are now *positive* and fairly large, so that any small decrease in α and the resulting decrease in ^3J_c and ^3J_t is likely going to outweigh the steric effects on the β angle. It was also observed (3) that in going from monoalkylated to 1,2-dialkylated ethylenes ^3J_c increases while ^3J_t decreases. This can now be rationalized as follows: comparing the geometries of propylene and *cis*-2-butene and using the data of Table 4 one calculates Δ^3J_c(rehyb.) = +3.02 Hz which combined with the earlier established value of $\Delta^3J_c(\chi_C) = -2.22$ Hz results in a prediction that ^3J_c in *cis*-2-butene should be 0.80 Hz larger than in propylene which is in exact agreement with the experimental difference. Similarly, the geometry changes in going from propylene to *trans*-2-butene and the data of Table 4 give Δ^3J_t(rehyb.) = +0.91 Hz, which combined with the previously obtained average result of $\Delta^3J_t(\chi_C) = -3.04$ Hz would predict that ^3J_t in *trans*-2-butene is 2.13 Hz *lower* than in propylene in good agreement with the experimental difference of −1.82 Hz.

Rummens and de Haan (3) explained these effects by assuming that the increase in angles α and δ in the *cis*-dialkylated ethylenes would, by reflex-rehybridization, decrease the angles β and γ, and that this decrease would be responsible for the increase of ^3J_c. It is now clear that their model gave the correct trends but for the wrong reason; the *exo*-path contributions of changes in α and δ, while working in the same direction as those of the reflex changes in β and γ, are quantitatively much more important. It has also been observed (5) that ^3J_t is constant at 15.1 ± 0.1 Hz for all those *trans*-dialkylated ethylenes that have at least one proton on C_3 and C_4, but that $^3J_t = 15.6 \pm 0.1$ if one of the alkyl groups is *tert*-butyl and $^3J_t = 16.1$ Hz for di-*tert*-butyl ethylene. It is surmized that this is due to a change in electronegativity effect, $\Delta^3J_t(\chi_C)$ being −3.04 Hz for substituents like methyl, ethyl, and isopropyl, but rather equal to −2.54 Hz if the alkyl substituent is *tert*-butyl. This hypothesis seems reasonable because (*i*) all data refer to aprotic, nonpolar solvents thus ruling out differences in solvation, (*ii*) the effect is strictly additive, which rules out a hyperconjugative mechanism, (*iii*) since the steric hindrance between a *tert*-butyl methyl and the C_1 proton must be considerably less than the *cisoid* interaction in *cis*-2-butene, even in the most unfavorable conformation where only one methyl group would eclipse the C=C bond, a steric rehybridization explanation is very unlikely, and (*iv*) the cyclotron resonance results on the gas phase reaction $Cl^- + RBr \rightarrow Br^- + RCl$ show that the reaction rate constant for R = *tert*-Bu is an order of magnitude less than for R = methyl, ethyl, and isopropyl,[1] thus indicating that the quarternary carbon atom in *tert*-butyl has a reduced electron-donating effect as compared to carbons with one or more hydrogens directly attached to them. If the above hypothesis is correct then also $\Delta^3J_c(\chi_C)$ will be smaller, in the same ratio, for *tert*-butyl substituents, leading to $\Delta^3J_c(\chi_{tert\text{-butyl}}) = -1.84$ Hz or a change of +0.38 Hz. However, ^3J_c in *cis*-dialkylated ethylenes is 12.0 Hz and 14.2 Hz if one or both alkyl groups respectively are *tert*-butyl (22), increases therefore above those of *cis*-2-butene of +1.2 Hz and +3.4 Hz respectively. It appears therefore that in these compounds there is a further rehybridization leading to larger angles α and δ and thereby to corresponding increases of ^3J_c. From Table 4 it can be seen that extra increases of $\Delta\alpha = \Delta\delta = +5°$ combined with $\Delta\beta = \Delta\gamma = -3°$ would be sufficient to cause such extra increases in ^3J_c, which appears reasonable.

It is also clear that earlier results on ^3J_c in cycloalkenes and benzocycloalkenes (6) need now to be reinterpreted in terms of changes in C=C—C angles, rather than in C=C—H angles.

[1]M. A. Heney and R. T. McIver. Unpublished results quoted in ref. 24.

Can. J. Chem. Downloaded from www.nrcresearchpress.com by 210.87.254.40 on 09/05/12
For personal use only.

The Vicinal Coupling ^3J_v

A complication arises here, as well as with the allylic and homoallylic couplings to be discussed, in as much as rehybridization at the sp^3 carbons can have an appreciable effect (see Table 4). However, it can be shown in a manner quite parallel to that used for sp^2 rehybridization (25), that for an sp^3 carbon there are two possible fundamental modes of distortion which can proceed, in the first order approximation, without energy loss. One of these is mostly appropriate to CH_2 fragments and consists of pinching one angle (say H—C—H) while simultaneously increasing the opposing (C—C—C) angle or reverse. The second is an umbrella-type of distortion increasing (or decreasing) all three angles C—C—H simultaneously. This is the geometry change assumed in our calculations on methyl groups, and which is also assumed to be operative when steric effects might induce a rehybridization. As a corollary it is assumed that any asymmetrical steric hindrance does not alter the basic C_{3v} symmetry of the methyl group, but rather, apart from changing all angles ϵ to the same extent, causes a bond bending as indicated by the angle ρ.

It has been observed (3–5) that ^3J_v for =CH—CH_3 fragments in *cis*-ethylenes is always somewhat larger than in the corresponding *trans*-isomers. Since in this case this cannot be due to a change in rotamer population, it has been proposed (3) that this is due to the reflex decrease in angles β and γ, which in turn are caused by the sterically induced increases in α and δ. As can be seen from Table 4, however, the effects $d^3J_v/d\beta$ and $d^3J_v/d\gamma$ are negligible. *Cisoid* steric interaction can be assumed to increase α, decrease ϵ and possibly increase the angle ρ; all these three effects act to increase ^3J_v. The total calculated increase in ^3J_v in going from *trans*- to *cis*-2-butene, using the known geometries and the data of Table 4 is +0.47 Hz, which is in reasonable agreement with the experimental differences of +0.36 Hz for the 2-butenes and also for the *cis*- and *trans*-crotonic acids (3). With bulkier *cisoid* counter groups such as *tert*-butyl or phenyl larger effects can be expected as has indeed been found (3).

The Allylic Couplings $^4J_{ca}$ *and* $^4J_{ta}$

Only averaged allylic couplings of the type H—C=C—CH_3 will be discussed here. In examples with a hydrogen *cis* to the CH_3 group, it has always been found that $^4J_{ta}$ is less negative than $^4J_{ca}$. For example, in propylene $^4J_{ta}$ = −1.33 Hz (calculated by INDO–FPT (12) as −1.20 Hz) and $^4J_{ca}$ = −1.75 (calculated by INDO–FPT (12) as −2.05 Hz). However, in dialkyl-substituted ethylenes the reverse is observed (3–5). It must be noted that now $^4J_{ta}$ and $^4J_{ca}$ are found in two different molecules (the *cis*- and *trans*-isomer respectively) but as discussed above, geometry differences between *cis*- and *trans*-2-butene cannot have any substantial effect. Nevertheless the effect is very clear: with R denoting the substituent in H—CR=CH—CH_3 one has: $^4J_{ta}$ = −1.85, $^4J_{ca}$ = −1.72 Hz for R = CH_3 (4), $^4J_{ta}$ = −1.85, $^4J_{ca}$ = −1.30 Hz for R = *i*-C_3H_7,[2] $^4J_{ta}$ = −1.85, $^4J_{ca}$ = −1.06 Hz for R = *i*-C_4H_9,[2] $^4J_{ta}$ = −1.82, $^4J_{ca}$ = −1.66 Hz for R = *tert*-C_4H_9 (3) and $^4J_{ta}$ = −1.81, $^4J_{ca}$ = −1.51 Hz for R = C_6H_5 (3). The constancy of $^4J_{ta}$ in this series should be noted, which is the more remarkable since with R = *tert*-C_4H_9 and R = C_6H_5 the *cisoid* steric interaction must be distinctly larger as is duly reflected in ^3J_c and ^3J_v. The explanation is likely to be found in the fact that the α(C) and δ(C) effects are of opposite sign (see Table 4). Calculations on the 2-butenes so far have not reproduced the reversal in magnitude. INDO–FPT calculations by Barfield *et al.* (14) at standard valence angles gave $^4J_{ta}$ = −1.31, $^4J_{ca}$ = −1.71 Hz; these calculations repeated while using the exact molecular geometries gave $^4J_{ta}$ = −1.50, $^4J_{ca}$ = −1.71 Hz (14); our own INDO calculations (see Table 2) gave $^4J_{ta}$ = −2.04, $^4J_{ca}$ = −2.30 Hz. Whereas it appears that part of the problem is in the calculations, particularly for $^4J_{ta}$, no explanation at all seems to be available for the large spread in experimental data for $^4J_{ca}$ as quoted above. Particularly for R = CH_3, *i*-C_3H_7, and *i*-C_4H_9 the geometries of these *trans*-configurational molecules must be very similar. Furthermore Table 4 shows that all valence-angle dependencies for $^4J_{ca}$ are almost negligibly small. It is clear, however, that the earlier view that the difference in $^4J_{ta}$ and $^4J_{ca}$ in *cis–trans* pairs is related to the steric cisoid strain (3, 4) must be abandoned, although no satisfactory alternative model can be offered.

[2]J. W. de Haan, private communication.

The Homoallylic Couplings $^5J_{cha}$ and $^5J_{tha}$

In restricting the discussion to the fully averaged couplings of $CH_3—C{=}C—CH_3$ systems, only *cis*- and *trans*-2-butene are of relevance. Recent INDO–SCF–MO calculations of Barfield and Sternhell (13) resulted in $^5J_{cha} = +1.30$ and $^5J_{tha} = +1.60$ Hz. These calculations were done, assuming standard trigonal and tetrahedral angles, however. Table 4 shows that only the ϵ effect and (for $^5J_{cha}$) possibly the effect of α(C) and δ(C) are potentially of any magnitude (13). Using Table 4, Barfield and Sternhell's calculated data can be modified to take into account the correct geometries. This results in $^5J_{cha} = +1.41$ and $^5J_{tha} = +1.62$ Hz, which values are still in good agreement with the experimental results. From the smallness of the above corrections in spite of the sizable angle changes ($\Delta\alpha = \Delta\delta = +6.7°$), it can be concluded that sterically induced hybridization changes are of no significant effect on $CH_3—C{=}C—CH_3$ homoallylic coupling constants.

Acknowledgements

We are indebted to Drs. J. B. Rowbotham, R. E. Wasylishen, and T. Schaefer of the University of Manitoba who supplied us with an IBM listing of CNINDO (20) which included the finite perturbation subroutine INDO. The financial support of the National Research Council of Canada and of the University of Regina is also gratefully acknowledged.

1. M. KARPLUS. J. Am. Chem. Soc. **85**, 2870 (1963).
2. J. RANFT. Ann. Phys. **8**, 322 (1961); **9**, 124 (1962); Proc. Xth Colloq. Ampère, Leipzig. 1961. p. 224.
3. F. H. A. RUMMENS and J. W. DE HAAN. Org. Magn. Reson. **2**, 351 (1970).
4. F. H. A. RUMMENS and L. KASLANDER. Can. J. Spectrosc. **17**, 99 (1972).
5. F. H. A. RUMMENS. J. Magn. Reson. **6**, 550 (1972).
6. M. A. COOPER and S. L. MANATT. J. Am. Chem. Soc. **91**, 6325 (1969); Org. Magn. Reson. **2**, 511 (1970); J. Am. Chem. Soc. **92**, 1605 (1970); **92**, 4646 (1970).
7. P. ALBRIKTSEN, A. V. CUNLIFFE, and R. K. HARRIS. J. Magn. Reson. **2**, 150 (1970).
8. M. BACON and G. E. MACIEL. Mol. Phys. **21**, 257 (1971).
9. M. KARPLUS and D. M. GRANT. Proc. Natl. Acad. Sci. (U.S.A.), **45**, 1269 (1959).
10. H. S. GUTOWSKY, M. KARPLUS, and D. M. GRANT. J. Chem. Phys. **31**, 1278 (1959).
11. C. N. BANWELL and N. SHEPPARD. Mol. Phys. **3**, 351 (1960); Discuss. Faraday Soc. **34**, 115 (1962).
12. M. BARFIELD, A. M. DEAN, C. J. FALLICK, R. J. SPEAR, S. STERNHELL, and P. W. WESTERMAN. J. Am. Chem. Soc. **97**, 1482 (1975).
13. M. BARFIELD, and S. STERNHELL. J. Am. Chem. Soc. **94**, 1905 (1972).
14. M. BARFIELD, R. J. SPEAR, and S. STERNHELL. Chem. Rev. In press.
15. J. A. POPLE and D. L. BEVERIDGE. Approximate molecular orbital theory. McGraw-Hill, Toronto. 1970.
16. K. KUCHITSU. J. Chem. Phys. **44**, 906 (1966).
17. A. ALMENNINGEN, I. M. ANFINSEN, and A. HAALAND. Acta Chem. Scand. **24**, 43 (1970).
18. D. R. LIDE and D. CHRISTENSEN. J. Chem. Phys. **35**, 1374 (1961).
19. S. KONDO, Y. SAKURAI, E. HIROTA, and Y. MORINO. J. Mol. Spectrosc. **34**, 231 (1970).
20. R. WASYLISHEN and T. SCHAEFER. Can. J. Chem. **50**, 1852 (1972).
21. R. M. LYNDEN-BELL and N. SHEPPARD. Proc. R. Soc. London, Ser. A, **269**, 385 (1962).
22. A. A. BOTHNER-BY and C. NAAR-COLLIN. J. Am. Chem. Soc. **83**, 231 (1961).
23. A. A. BOTHNER-BY, C. NAAR-COLLIN, and H. GUENTHER. J. Am. Chem. Soc. **84**, 2748 (1962).
24. J. D. BALDESCHWIELER and S. S. WOODGATE. Acc. Chem. Res. **4**, 114 (1971).
25. F. H. A. RUMMENS. Recl. Trav. Chim. Pays Bas, **84**, 5 (1965).

Can. J. Chem. Downloaded from www.nrcresearchpress.com by 210.87.254.40 on 09/05/12
For personal use only.

The alkaloids of *L. magellanicum* and the structure of magellanine

MARIANO CASTILLO, LUIS A. LOYOLA,[1] AND GLAUCO MORALES [1]
Facultad de Ciencias, Departamento de Quimica, Universidad de Chile, Santiago, Chile
AND
ISHWAR SINGH,[2] CRISPIN CALVO, HERBERT L. HOLLAND, AND DAVID B. MACLEAN
Department of Chemistry, McMaster University, Hamilton, Ont., Canada L8S 4M1

Received March 5, 1976

MARIANO CASTILLO, LUIS A. LOYOLA, GLAUCO MORALES, ISHWAR SINGH, CRISPIN CALVO, HERBERT L. HOLLAND, and DAVID B. MACLEAN. Can. J. Chem. **54**, 2893 (1976).

Examination of the alkaloids of *Lycopodium magellanicum* (Palisot de Beauvois) has revealed the presence of five alkaloids of established structure and a previously unreported alkaloid, magellanine ($C_{17}H_{25}NO_2$). The ring system of magellanine, deduced from an examination of its spectroscopic properties, is identical with that of paniculatine. The structure of magellanine has been confirmed, and its relative stereochemistry established, in an X-ray crystallographic study.

MARIANO CASTILLO, LUIS A. LOYOLA, GLAUCO MORALES, ISHWAR SINGH, CRISPIN CALVO, HERBERT L. HOLLAND et DAVID B. MACLEAN. Can. J. Chem. **54**, 2893 (1976).

L'examen des alcaloides du *Lycopodium magellanicum* (Palisot de Beauvois) a montré la présence de cinq alcaloïdes de structure connue et d'un autre alcaloïde encore non rapporté, la magellanine ($C_{17}H_{25}NO_2$). Le système cyclique de la magellanine, déduit à partir de l'examen des propriétés spectroscopiques, est identique à celui de la paniculatine. La structure de la magellanine a été confirmée, et sa stéréochimie relative établie par une étude cristallographique aux rayons-X.

[Traduit par le journal]

Can. J. Chem. Downloaded from www.nrcresearchpress.com by 210.87.254.6 on 09/05/12
For personal use only.

Examination of the alkaloids of *L. magellanicum* collected in the spring revealed the presence of three alkaloids of established structure, lycopodine, fawcettiine, and deacetylfawcettiine, and a new alkaloid that we have named magellanine (for recent reviews, see refs. 1–3). Examination of the same species collected in early summer yielded lycopodine, α-obscurine, clavolonine, and deacetylfawcettiine; no fawcettiine was found and magellanine was present only in traces. Here we describe the extraction and isolation procedures and discuss the structure and properties of magellanine.

The molecular formula of magellanine, ($C_{17}H_{25}NO_2$), was established through combustion analysis of the free base and its methobromide and through high resolution mass spectrometry on the free base.

The infrared spectrum of magellanine had ν_{max} (KBr) 3330, 3150–2400, and 1650 cm^{-1} while its ultraviolet spectrum showed λ_{max} (EtOH) 237 nm, (log ϵ 3.8). These data are compatible with the presence of an α,β-unsaturated ketone and a hydroxy group. It is now apparent that magellanine is tetracyclic. The ^1H nmr spectrum of magellanine (220 MHz) is shown in Fig. 1. A singlet of area 3 at 2.23 δ is assigned to an *N*-methyl group and a singlet of area 3 at 1.94 δ attributed to a vinylic methyl group. The signal of area 1 at 5.88 δ ($W_{1/2}$ = 6 Hz), has been assigned to a vinylic hydrogen. An apparent triplet of area 1 at 4.21 δ has been assigned to a hydrogen geminal to OH in a secondary hydroxy group. Decoupling experiments have established the presence of the part structure >CH—C(CH_3)=CH—CO— in magellanine. Irradiation at 1.94 δ (*C*-methyl) caused the signal at 5.88 δ to sharpen to a cleanly resolved doublet, J = 2 Hz. Conversely, irradiation at 5.88 δ caused sharpening of the *C*-methyl signal and a line shape change at 2.6 δ which was attributed to the removal of long-range coupling to an allylic hydrogen. In confirmation, it was found that irradiation at 2.6 δ caused sharpening of the signal of the vinylic hydrogen ($W_{1/2}$ = 3.8 Hz on irradiation).

The apparent triplet of 4.21 δ was found to be coupled to hydrogens resonating at 2.6 δ and at 1.66 δ. Irradiation at 2.6 δ caused the signal at

[1]On leave of absence from Departamento de Quimica, Universidad de Chile, Sede Antofagasta.

[2]Present address: Department of Chemistry, Mohawk College, Hamilton, Ontario.

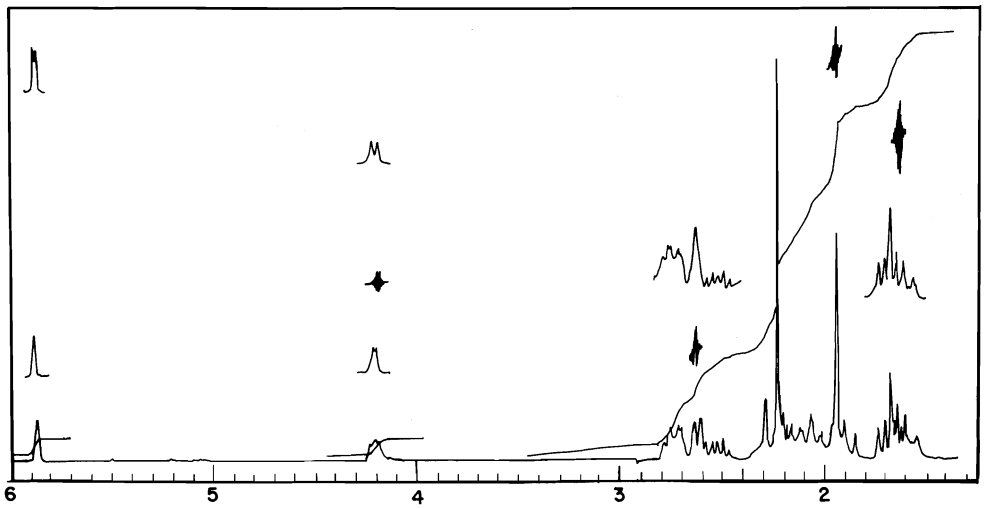

FIG. 1. The 220 MHz proton magnetic resonance spectrum of magellanine.

4.21 δ to collapse to a doublet, $J = 4$ Hz, while irradiation at 1.66 δ also gave a doublet, $J = 6$ Hz. Since it is now known (see below) that the CHOH group is flanked on one side by a methine and on the other by methylene, one of the three hydrogens must be so disposed that it does not couple with the hydrogen resonating at 4.21 δ.

The mass spectrum of magellanine has many ions in common with that of paniculatine (**1**), (4, 5). The mass spectral data (discussed below) along with the other spectroscopic data already discussed, suggest that magellanine has structure **2**, a structure confirmed by the X-ray study (*vide infra*). The numbering system of magellanine is analogous to that of lycopodine.

In the mass spectrum of magellanine the nitrogen-containing ions at *m/e* 57, 58, 70, 71, 96, 97, 110, and 111 are identical in composition with those of paniculatine. Their derivation from magellanine may be considered to proceed through the same bond cleavages that were postulated to lead to the corresponding ions in the spectrum of paniculatine as shown in Scheme 1 (*cf.* Scheme 1 of ref. 5).

The ions shown in Scheme 2 are considered to arise through a cleavage adjacent to the carbonyl group followed by C7–C8 or C8–C15 cleavage. Similar ions are formed from paniculatine (*cf.* Scheme 2 of ref. 5). Surprisingly the most intense C_{13} ion in the spectrum of magellanine is at *m/e* 204 rather than at *m/e* 206 as expected in analogy with paniculatine. The C_{12} ion at *m/e* 192, however, arises in the same way as the *m/e* 190 ion of paniculatine.

It is evident that the ring system found in paniculatine and in magellanine has a distinctive fragmentation pattern and may be differentiated

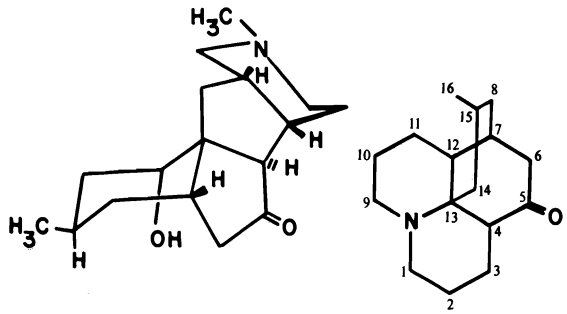

1

Lycopodine

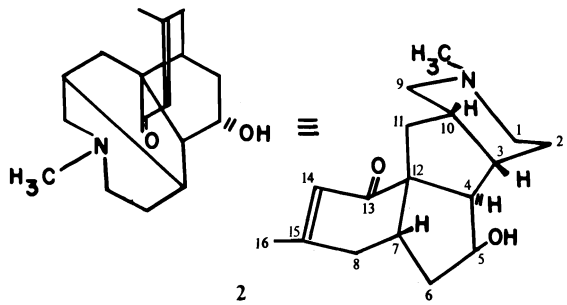

2

Magellanine and paniculatine are given the same conformation in these formulas. However magellanine methobromide and paniculatine hydrobromide in the solid state differ in conformation at the juncture of rings A and B. The absolute configuration of the alkaloids is not known and is not implied in these formulas.

Can. J. Chem. Downloaded from www.nrcresearchpress.com by 210.87.254.6 on 09/05/12
For personal use only.

by mass spectrometry from other ring systems found in the *Lycopodium* family.

Since supplies of both paniculatine and magellanine were minuscule it was not possible to correlate the two by chemical methods. We therefore undertook an X-ray examination of magellanine methobromide, which confirmed our deductions based on the spectroscopic

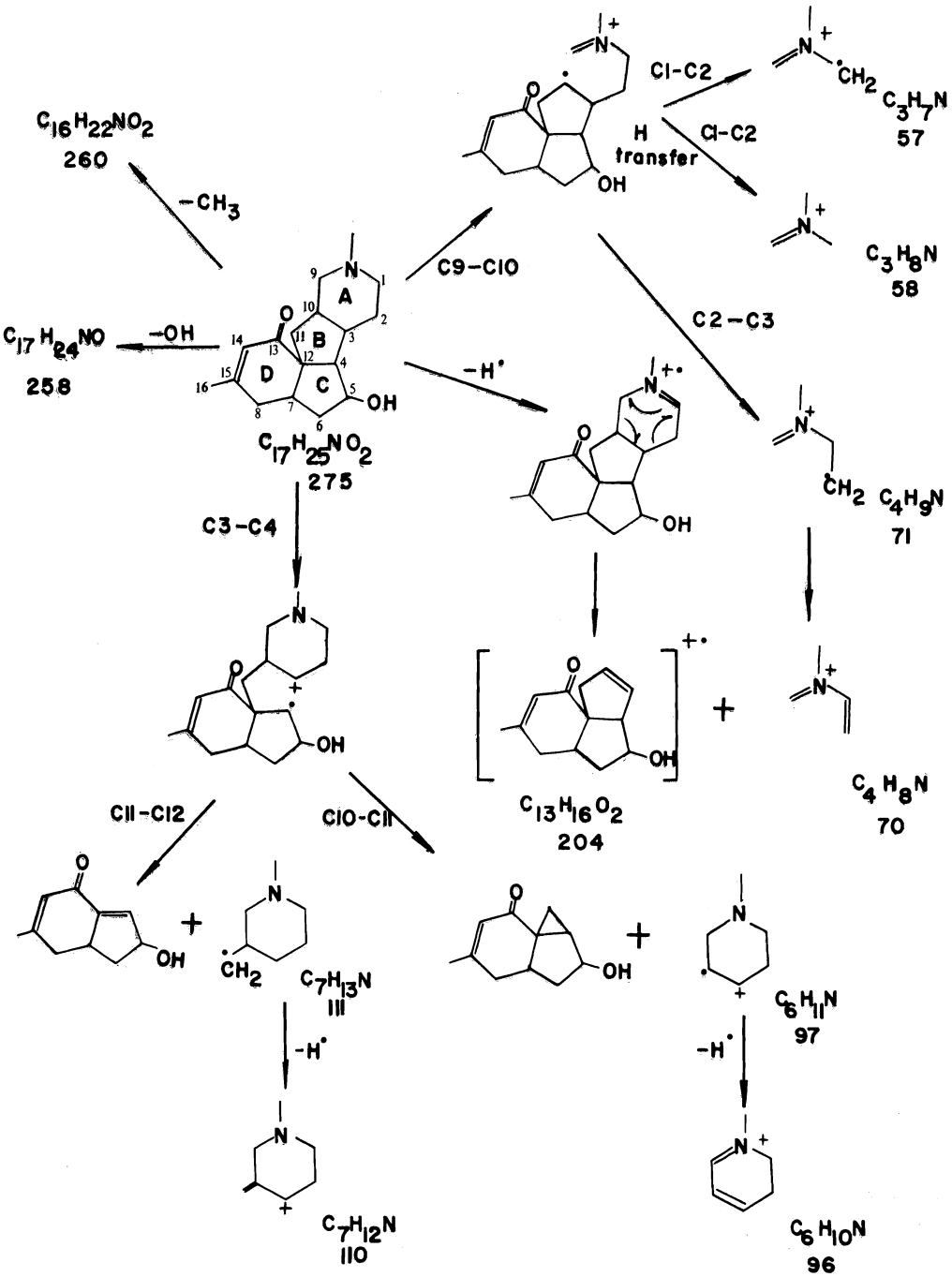

SCHEME 1. The fragmentation of magellanine upon electron impact. Nitrogen-containing ions of low *m/e*.

Can. J. Chem. Downloaded from www.nrcresearchpress.com by 210.87.254.6 on 09/05/12
For personal use only.

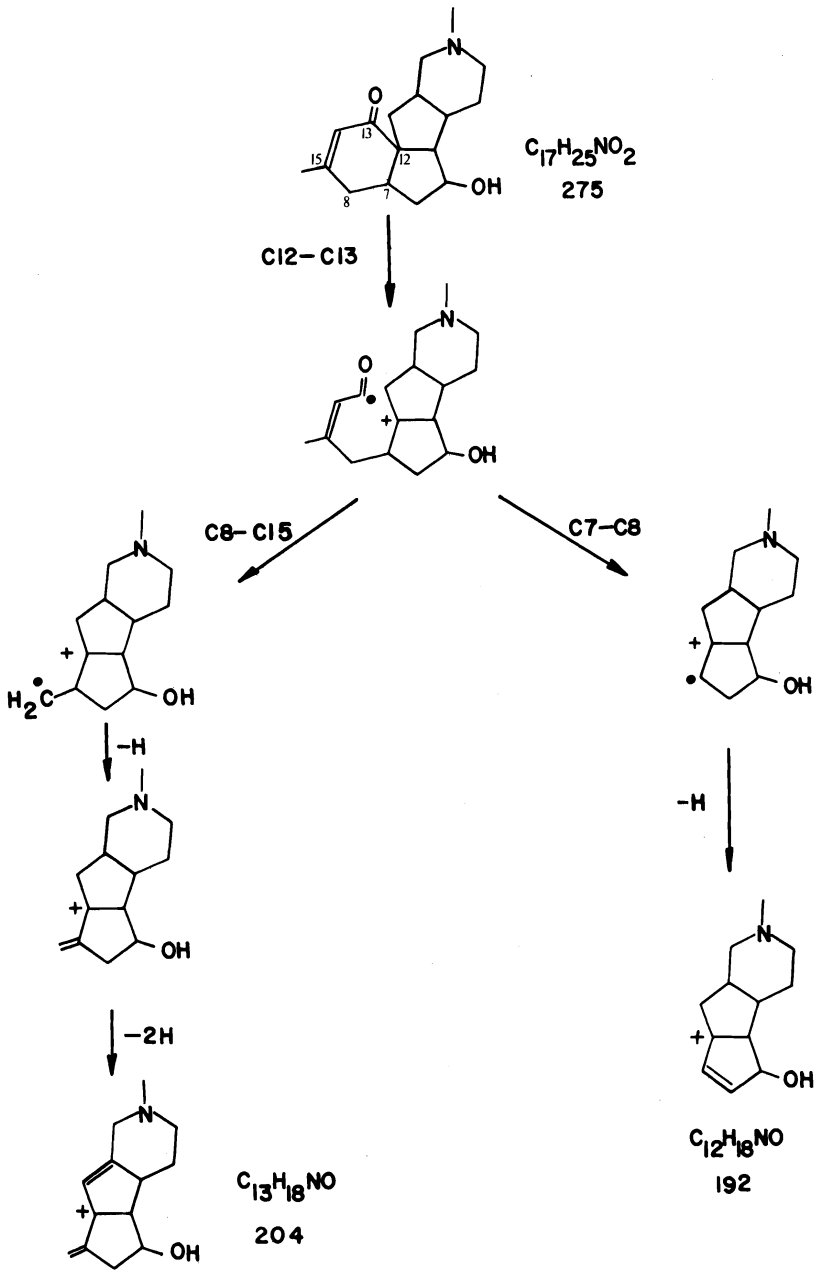

SCHEME 2. The fragmentation of magellanine upon electron impact. Nitrogen-containing ions of high *m/e*.

studies, and defined the relative stereochemistry of magellanine.

The atomic parameters derived from the X-ray study are shown in Table 1 and the bond angles and bond distances in Table 2. C12, the only carbon atom bonded to four other carbons, showed the lowest thermal parameter. Bond lengths lay within one to two standard deviations of their respective standard values. A view of the molecule is seen in Fig. 2. The skeleton of the

Can. J. Chem. Downloaded from www.nrcresearchpress.com by 210.87.254.6 on 09/05/12
For personal use only.

Can. J. Chem. Downloaded from www.nrcresearchpress.com by 210.87.254.6 on 09/05/12
For personal use only.

TABLE 1. Atomic parameters of magellanine methobromide

Atom	x	y	z	U^* (Å)^2
$\bar{Br}$	0.0513(3)	0.2500	1.3071(3)	†
C1	0.534(3)	0.1676(8)	0.843(3)	4.1(5)
C2	0.570(3)	0.0958(7)	0.858(2)	3.1(4)
C3	0.702(3)	0.0778(8)	1.100(3)	2.7(4)
C4	0.712(3)	0.0066(8)	1.120(2)	2.8(4)
C5	0.928(3)	−0.0224(8)	1.303(3)	5.0(5)
C6	0.854(3)	−0.0759(8)	1.399(2)	3.6(4)
C7	0.655(3)	−0.0467(7)	1.430(2)	3.0(4)
C8	0.530(3)	−0.0910(8)	1.504(3)	4.2(5)
C9	0.508(3)	0.1682(7)	1.210(3)	3.4(4)
C10	0.589(2)	0.0983(7)	1.248(2)	2.6(4)
C11	0.409(3)	0.0473(7)	1.219(2)	3.5(5)
C12	0.529(2)	−0.0124(7)	1.204(2)	1.8(4)
C13	0.369(3)	−0.0542(8)	1.040(3)	3.5(5)
C14	0.298(3)	−0.1141(8)	1.100(3)	3.0(4)
C15	0.369(3)	−0.1315(8)	1.311(3)	3.7(5)
C16	0.297(3)	−0.1900(9)	1.375(3)	4.9(6)
C17	0.386(2)	0.2548(13)	0.962(2)	4.7(4)
C18	0.157(3)	0.1614(8)	0.845(2)	3.6(5)
N	0.388(2)	0.1875(6)	0.962(2)	3.6(4)
O1	1.034(2)	0.0263(5)	1.466(2)	4.6(4)
O2	0.285(2)	−0.0399(7)	0.842(2)	6.0(4)

*U and U_{ij} have been multiplied by 100. The anisotropic thermal factor is: exp $-2\pi^2$ ($U_{11}h^2b_1^2$ + --- + $2U_{12}hkb_1b_2$ + ---) where b_i are reciprocal vectors.

†Anisotropic thermal components for bromide ion are:

U_{11}	U_{22}	U_{33}	U_{12}	U_{13}	U_{23}
4.0(1)	5.3(1)	4.2(1)	0.5(2)	1.5(1)	0.2(2)

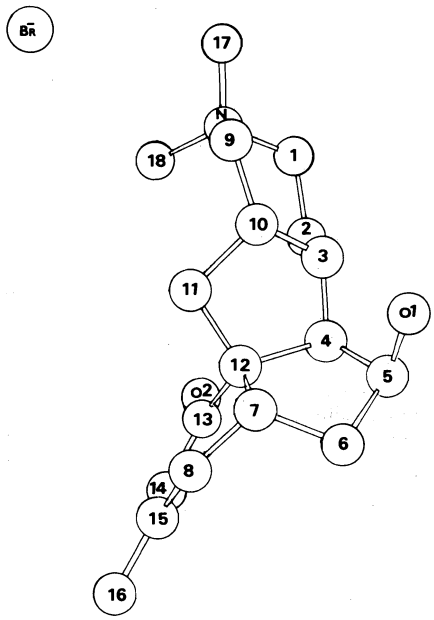

FIG. 2. The structure of magellanine methobromide.

TABLE 2. Bond distances and angles in magellanine methobromide

Bond	Bond lengths (Å)	Bonds	Angle (deg)
C1—C2	1.56(2)	N—C1—C2	111(2)
C1—N	1.56(3)		
C2—C3	1.53(2)	C1—C2—C3	109(1)
C3—C4	1.54(2)	C2—C3—C4	109(1)
C3—C10	1.55(3)	C2—C3—C10	112(1)
		C4—C3—C10	104(2)
C4—C5	1.59(2)	C3—C4—C5	117(1)
C4—C12	1.60(3)	C3—C4—C12	106(1)
		C5—C4—C12	103(1)
C5—O1	1.46(2)	C4—C5—O1	107(1)
C5—C6	1.50(3)	C4—C5—C6	105(2)
		C6—C5—O1	112(2)
C6—C7	1.57(3)	C5—C6—C7	102(1)
C7—C8	1.49(3)	C6—C7—C8	115(1)
C7—C12	1.57(2)	C6—C7—C12	102(1)
		C8—C7—C12	118(1)
C8—C15	1.56(2)	C7—C8—C15	112(2)
C9—C10	1.58(2)	N—C9—C10	114(1)
C9—N	1.56(2)		
C10—C11	1.59(2)	C9—C10—C11	116(1)
		C9—C10—C3	114(1)
		C11—C10—C3	106(1)
C11—C12	1.55(2)	C10—C11—C12	101(1)
C12—C13	1.47(2)	C4—C12—C11	108(1)
		C4—C12—C7	106(1)
		C7—C12—C11	114(1)
		C7—C12—C13	111(1)
C13—C14	1.49(3)	C12—C13—O2	120(2)
C13—O2	1.24(2)	C14—C13—O2	117(1)
		C12—C13—C14	123(1)
C14—C15	1.34(2)	C13—C14—C15	120(1)
C15—C16	1.48(3)	C14—C15—C16	122(1)
		C14—C15—C8	122(2)
		C8—C15—C16	117(1)
N—C17	1.45(3)	C9—N—C17	105(1)
N—C18	1.52(2)	C9—N—C18	114(1)
		C1—N—C9	108(1)
		C17—N—C18	111(1)
		C1—N—C17	106(1)
		C1—N—C18	111(1)

molecule is made of two fused five-membered rings each of which in turn is fused to a six-membered ring. The six-membered ring containing quaternary nitrogen has a conformation close to the chair form of piperidine (6) with C17 and C18 bonded equatorially and axially to the nitrogen, respectively. This is evidenced by the fact that C17 is 0.48 Å and C18 1.75 Å away from the plane defined by N, C1, C2, C3, C9, and C10. C4 is equatorial at C3 and C11 is axial at C10. The least-squares plane defined by C3, C4, C10, C11, C12 makes an acute angle of 56° with the six-membered ring plane, and the

Can. J. Chem. Downloaded from www.nrcresearchpress.com by 210.87.254.6 on 09/05/12
For personal use only.

fusion of the 5–6 system at C3 and C10 is *cis*. This last five-membered ring is puckered and has a conformation close to the half-chair conformation of the cyclopentane molecule. The second five-membered ring defined by C4, C5, C6, C7, and C12 has a similar conformation (see Fig. 3 and Table 3).[3] The acute angle between the two fused five-membered rings is 55° and the fusion at C4 and C12 is *cis*, as seen by the out-of-plane distances of 1.02 and 0.90 Å for C3 and C11, respectively. O1 is 1.67 Å away from this plane and is on the same side as C3 and C11 but opposite to C8, C13, and O2. The fusion between the five and six-membered rings at C7 and C12 is also *cis*. The conformation of the six-membered ring defined by C7, C8, C12, C13, C14, and C15 can be best described as an envelope with C7 0.40 Å out of the plane defined by O2, C13, C14, C15, and C16. The plane defined by C7, C8, and C12 makes an angle of 146° with this last plane. This conformation is similar to the conformation reported in the structure of dimedone (7).

There is evidence that the molecules of magellanine methobromide are hydrogen bonded to each other in the solid state. The interatomic distance between the hydroxy oxygen, O1, of the asymmetric unit and the carbonyl oxygen, O2, of the molecule generated by the symmetry operation $x + 1$, y, $z + 1$ is 2.76 Å and the angles C5—O1---O2, and C13—O2---O1 are 103° and 158°, respectively. The $\overset{+}{N}$---$\overset{-}{Br}$ distance is 4.08 Å and other distances involving bromide ion are, 3.83, 3.84, and 3.93 Å, respectively, for C9---$\overset{-}{Br}$, C17---$\overset{-}{Br}$, and C18---$\overset{-}{Br}$.

Experimental

Apparatus, Methods, and Materials

The apparatus and methods used were identical with those described previously (5).

The plant material was collected near Osorno, Chile, in the spring of 1973. It was identified by G. Looser as *Lycopodium magellanicum* (Palisot de Beauvois) Swartz. A voucher specimen is on file in the Herbarium of the Faculty of Sciences, University of Chile, Santiago.

The X-ray data were collected on a crystal 0.02 × 0.02 × 0.03 cm mounted along the *b* axis. Preliminary photographs showed monoclinic symmetry. The cell parameters were obtained by least-squares fitting to eight 2θ values measured on a P1 Syntex automatic diffractometer.

$C_{18}H_{28}\overset{+}{N}O_2\overset{-}{Br}$ fw = 370

$a = 6.748(2)$, $b = 21.532(8)$, $c = 6.657(2)$ Å, $\beta = 114.8(2)°$, $Z = 2$, $d_{calcd} = 1.40$ g cm^{-3}, $\lambda(MoK_\alpha) = 0.71069$ Å, $\mu = 25.73$ cm^{-1}.

Systematic absences, observed only for $0k0$ indicated that the space group $P2_1$ was the only possibility consistent with the optical activity of the molecule. A total of 1636 unique reflections lying in the range $0 < 2\theta \leq 50°$ were measured on the Syntex diffractometer using graphite monochromatized MoK_α radiation. Reflections were scanned in the θ–2θ mode at a rate between 8 and 24° per min depending on the peak intensity. Backgrounds were recorded on either side of the peak and used to determine the integrated intensity together with an estimated standard deviation based upon counting statistics. Those reflections whose intensity was less than 3σ, 421 in number, were regarded as unobserved. The data were corrected for Lorentz and polarization effects but not absorption. The XRAY-71 package of programs for X-ray crystallography published by the University of Maryland as adopted for use with the CDC 6400 by H. D. Grundy of this institution was used for all computations.

A three-dimensional Patterson function showed clear $\overset{-}{Br}$–$\overset{-}{Br}$ vectors in the section $P(u, \frac{1}{2}, w)$, confirming the space group as $P2_1$. Structure factors calculated with $\overset{-}{Br}$ ion alone gave $R = 34.2\%$. Fourier and difference maps calculated with bromide phases showed the usual centrosymmetric ambiguity. However, atomic co-ordinates for four bonded atoms were recognized and these positions were further used for locating other atoms of the molecule by the successive use of full matrix least-squares refinement, Fourier, and difference Fourier methods. These initial positions were refined with their individual isotropic temperature factors and a scale-factor. This yielded a minimum R of 0.13. The atomic scattering curves for the bromide ions, C and O atoms were obtained from the International Tables for X-ray Crystallography (8). Further refinements were carried out, using the anisotropic temperature factor for bromide ions and the isotropic temperature factors for the other atoms. Weights were given by $\omega = [2.10 - 0.03F_o]^{-1/2}$. These weights were chosen so that $\omega|F_o - F_c|^2$ would be locally independent of F_o, the observed structure factor. The unobserved reflections were weighted as were the observed and also included in the refinement. The final refinement resulted in a minimum R of 0.103 and $R\omega = (\sum\omega|F_o - F_c|^2/\sum\omega|F_o|^2)^{1/2}$ equal to 0.093. The average shift/error in the final cycle of refinement was 0.31 with a maximum of 2.1. A final difference Fourier map showed no missing structural features although peaks of 0.25 of a carbon atom were noted. The final atomic parameters are listed in Table 1 and the observed and calculated structure factors are in Table 4.[3] A list of bond lengths and angles with standard deviations calculated from the standard errors derived from the least-squares matrix is given in Table 2.

Extraction and Isolation of the Alkaloids

Dried plant material (*L. magellanicum*, 11 kg), collected in spring, was ground and extracted in the manner described for *L. paniculatum* (5). The crude alkaloid

[3]Figure 3 and Table 3 (least-squares planes and out-of-plane distances) and Table 4 (observed and calculated structure factors) are available, at a nominal charge, from the Depository of Unpublished Data, CISTI, National Research Council of Canada, Ottawa, Canada K1A 0S2.

fraction (26 g) was dissolved in chloroform and extracted several times with a phosphate–citrate buffer of p*H* 7. Evaporation of the chloroform gave the 'weak bases' (5.5 g). The p*H* of the aqueous phase was then raised to p*H* 11 by addition of aqueous sodium hydroxide solution. A second extraction with chloroform gave the 'strong bases' (17.5 g).

The strong bases were adsorbed on a column of basic alumina (600 g, activity I) and eluted in seven fractions; eluant and amount are given for each as follows: (*1*) ether, 0.7 g; (*2*) ether, 0.9 g; (*3*) ether–chloroform (1:1), 4.36 g; (*4*) chloroform, 1.68 g; (*5*) chloroform–methanol (99:1), 2.70 g; (*6*) chloroform–methanol (99:1), 0.60 g; (*7*) chloroform–methanol (98:2), 4.5 g.

Fraction *1* contained lycopodine (500 mg), identical in tlc behaviour, mp, and spectral properties with an authentic specimen.

Fraction *2* comprised several components (tlc analysis) but a separation was not achieved.

Fraction *3* was adsorbed on a column of basic alumina (200 g, Activity III) and eluted first with chloroform and then with chloroform–methanol. The chloroform eluate on evaporation and crystallization from acetone afforded fawcettiine (550 mg), mp 170–171 °C, identical with an authentic specimen. The chloroform–methanol eluate yielded magellanine (160 mg) which, after crystallization from ethyl acetate, melted at 165–166 °C. Spectral data: ir ν_{max} (KBr) 3300, 3150–2400, 1650 cm^{-1}; uv λ_{max} 237 nm (log ϵ 3.8); pmr included signals at δ 1.94 (3H, s, C-CH_3), 2.23 (3H, s, N-CH_3), 4.21 (t, J = 3.7 Hz, C*H*OH), 5.88 (br s, $W_{1/2}$ = 5 Hz, olefinic CH); ms (*m/e*, %) 275(100), 260(25), 258(21), 204(4), 202(3), 192(6), 111(6), 110(16), 97(3), 96(15), 71(12), 70(20), 58(11), 57(8). *Anal.* calcd. for $C_{17}H_{25}NO_2$: C 74.14, H 9.15, N 5.09; found: C 74.24, H 8.99, N 5.01.

Magellanine methobromide was obtained by addition of cold methyl bromide (2 ml) to a solution of magellanine (26 mg) in acetone. Repeated crystallization from ethanol–ether yielded colorless crystals melting at 274 °C. *Anal.* calcd. for $C_{18}H_{28}NO_2Br$: C 58.38, H 7.62, N 3.78, Br 21.58; found: C 58.61, H 7.48, N 3.76, Br 21.88.

Fractions *4* and *5* yielded further amounts of fawcettiine (400 mg) along with other uncharacterized bases.

Fraction *6* contained fawcettiine, magellanine, and at least two other unidentified components.

Fraction *7* contained mainly deacetylfawcettiine (4 g) which was identified by comparison of its melting point and infrared spectrum with those of an authentic sample.

The 'weak bases' were shown by tlc to contain several components among which was lycopodine, but have not been carefully examined.

Acknowledgments

Part of this work was made possible through grants 147 and 1524 from the Oficina Técnica de Desarrollo Cientifico y Creación Artística, Universidad de Chile. The work at McMaster was supported through grants from the National Research Council of Canada.

1. D. B. MacLean. *In* The alkaloids. Vol. 10. *Edited by* R. H. F. Manske. Academic Press, New York. 1967. p. 305.
2. D. B. MacLean. *In* The alkaloids. Vol. 14. *Edited by* R. H. F. Manske. Academic Press, New York. 1973. p. 347.
3. W. A. Ayer. *In* Alkaloids. *Edited by* K. Wiesner. MTP International Review of Science, Organic Chemistry, Series 1, Vol. 9. Butterworths, London. 1973. p. 1.
4. M. Castillo, G. Morales, L. A. Loyola, I. Singh, C. Calvo, H. L. Holland, and D. B. MacLean. Can. J. Chem. **53**, 2513 (1975).
5. M. Castillo, G. Morales, L. A. Loyola, I. Singh, C. Calvo, H. L. Holland, and D. B. MacLean. Can. J. Chem. This issue.
6. C. Rerat. Acta Crystallogr. **13**, 72 (1960).
7. I. Singh and C. Calvo. Can. J. Chem. **53**, 1046 (1975).
8. International Tables for X-ray Crystallography. Vol. III. Kynoch Press, Birmingham, England. 1962.

Can. J. Chem. Downloaded from www.nrcresearchpress.com by 210.87.254.6 on 09/05/12
For personal use only.

The alkaloids of *L. paniculatum* and the structure of paniculatine

MARIANO CASTILLO, GLAUCO MORALES,[1] AND LUIS A. LOYOLA[1]
Facultad de Ciencias, Departamento de Quimica, Universidad de Chile, Santiago, Chile

AND

ISHWAR SINGH,[2] CRISPIN CALVO, HERBERT L. HOLLAND, AND DAVID B. MACLEAN
Department of Chemistry, McMaster University, Hamilton, Ont., Canada L8S 4M1

Received March 5, 1976

MARIANO CASTILLO, GLAUCO MORALES, LUIS A. LOYOLA, ISHWAR SINGH, CRISPIN CALVO, HERBERT L. HOLLAND, and DAVID B. MACLEAN. Can. J. Chem. **54**, 2900 (1976).

Seven alkaloids have been isolated from *Lycopodium paniculatum* Desvaux. Three of these, lycopodine, dihydrolycopodine, and acetyldihydrolycopodine are alkaloids of established structure. Of the four new alkaloids the structure of one, paniculatine, has been clarified. Its structure, elucidated through an X-ray crystallographic study of its hydrobromide, is different from other alkaloids of the *Lycopodium* family. The spectral properties of paniculatine are interpreted in the light of its structure.

MARIANO CASTILLO, GLAUCO MORALES, LUIS A. LOYOLA, ISHWAR SINGH, CRISPIN CALVO, HERBERT L. HOLLAND et DAVID B. MACLEAN. Can. J. Chem. **54**, 2900 (1976).

Sept alcaloïdes ont été isolés du *Lycopodium paniculatum* Desvaux. Trois d'entre eux, la lycopodine, la dihydrolycopodine et l'acétyldihydrolycopodine sont des alcaloïdes de structure connue. Parmi les quatre nouveaux alcaloïdes, la structure de l'un d'entre eux, la paniculatine, a été clarifiée. Sa structure, élucidée à l'aide d'une étude cristallographique aux rayons-X du bromhydrate s'est avérée différente de celles des autres alcaloïdes de la famille du *Lycopodium*. Les propriétés spectrales de la paniculatine sont interprétées à la lumière de sa structure.
[Traduit par le journal]

Examination of *L. paniculatum* has led to the isolation and characterization of seven alkaloids. Included among these are three alkaloids of established structure, lycopodine, dihydrolycopodine, and acetyldihydrolycopodine (1, 2) and four new alkaloids designated P2, P4, P5, and paniculatine. The structure of the latter was recently communicated (3). In this paper we present the isolation procedure and the physical and spectral data obtained for P2, P4, and P5, and provide a fuller discussion of our work leading to the assignment of structure **1** to paniculatine.

The alkaloids were extracted by conventional procedures and separated into ether-soluble and chloroform-soluble fractions. Each of these was subjected to counter-current distribution and the resulting fractions chromatographed on alumina. The crystalline alkaloids isolated from each fraction represented a relatively small proportion of the total. Examination of the amorphous fractions is still in progress and it is anticipated that other alkaloids will be found in these.

The molecular formula of paniculatine, $C_{17}H_{27}NO_2$, was established by high resolution mass spectrometry and by combustion analysis. Its infrared spectrum in $CHCl_3$ showed absorption at 3620, 3600–3000, 1720, and 1040 cm^{-1} indicative of the presence of hydroxy and carbonyl functions, the absorption of the latter suggesting the presence of a cyclopentanone unit. From these observations it is apparent that paniculatine is tetracyclic.

The ^1H nuclear magnetic resonance spectrum of paniculatine, shown in Fig. 1, was obtained at 220 MHz. A sharp singlet at 2.18 δ corresponding in area to three hydrogens indicated the presence of an *N*-methyl group while a doublet of equivalent area of 0.90 δ (J = 6.5 Hz) showed that a CH—CH_3 group was present. The complex multiplet corresponding to one hydrogen at 3.78 δ ($W_{1/2}$ = 8 Hz) was assigned to a hydrogen geminal to a hydroxy group. The multiplicity of this signal suggested that it was coupled to at least two other hydrogens. Through double irradiation experiments the presence of the part structure, —$CH(CH_3)CH_2CH(OH)$— was in-

[1]On leave of absence from Departamento de Quimica, Universidad de Chile, Sede Antofagasta.

[2]Present address: Department of Chemistry, Mohawk College, Hamilton, Ontario.

Can. J. Chem. Downloaded from www.nrcresearchpress.com by 210.87.254.5 on 09/05/12
For personal use only.

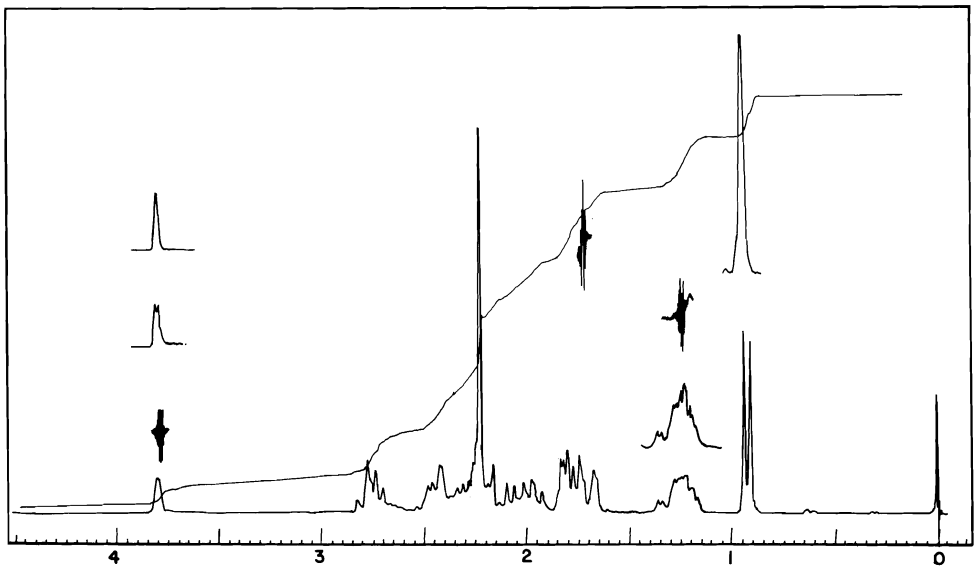

FIG. 1. The 220 MHz pmr spectrum of paniculatine.

ferred. Irradiations centred either at 1.70 δ or at 1.22 δ caused the signal of the hydrogen geminal to the hydroxy group to sharpen to $W_{1/2} = 5$ Hz indicating that this hydrogen was adjacent to a methylene group whose hydrogens were non-equivalent. Irradiation at 1.70 δ also caused the *C*-methyl signal at 0.90 δ to collapse to a singlet implying that the methine hydrogen geminal to the *C*-methyl also resonates at or near 1.70 δ. The double irradiation experiments are also subject to other interpretations, and it was not until the X-ray examination was completed that these experiments were unambiguously interpreted.

Both the broad-band and off-resonance ^{13}C nmr spectra of paniculatine were recorded. Although there were a number of overlapping signals, the spectra clearly indicated the presence in paniculatine of carbonyl, C—CH_3, N—CH_3, and CHOH groups. It also indicated that the N—CH_3 was flanked by methylene groups.

An interpretation of the spectrum was not feasible until the structure was established. Now, however, the assignments shown in Fig. 2 may be tentatively advanced. 1,3,4-Trimethylpiperidine serves as a convenient model of ring A, 2,2,3,5-tetramethylcyclohexanol for ring D, and 2-methylcyclopentanone for the carbonyl of ring C (ref. 4, p. 290).

The calculated chemical shifts of the carbon atoms of the model compounds are also shown in Fig. 2. The spectrum of 2,2,3,5-tetramethylcyclohexanol was calculated as follows. 1,1-Dimethylcyclohexane was taken as the reference

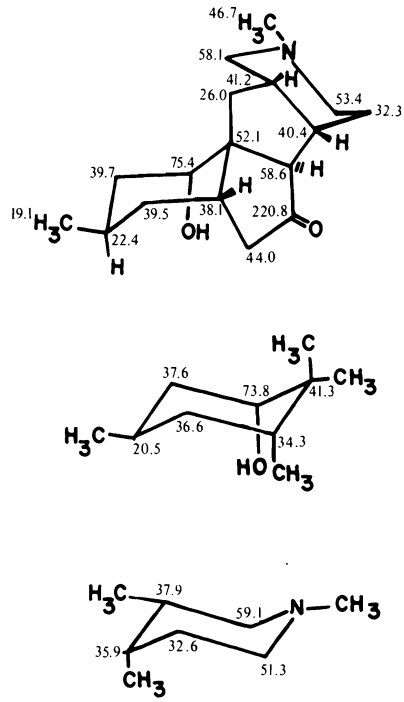

FIG. 2. Assignment of the ^{13}C signals in the spectrum of paniculatine.

Can. J. Chem. Downloaded from www.nrcresearchpress.com by 210.87.254.5 on 09/05/12
For personal use only.

compound. The shifts resulting from placing an axial methyl at C2, an equatorial methyl at C4, and an axial hydroxyl at C6 were then calculated. The substitutant parameters for axial and equatorial methyl were those reported by Stothers (ref. 4, p. 65) and those for an axial hydroxy

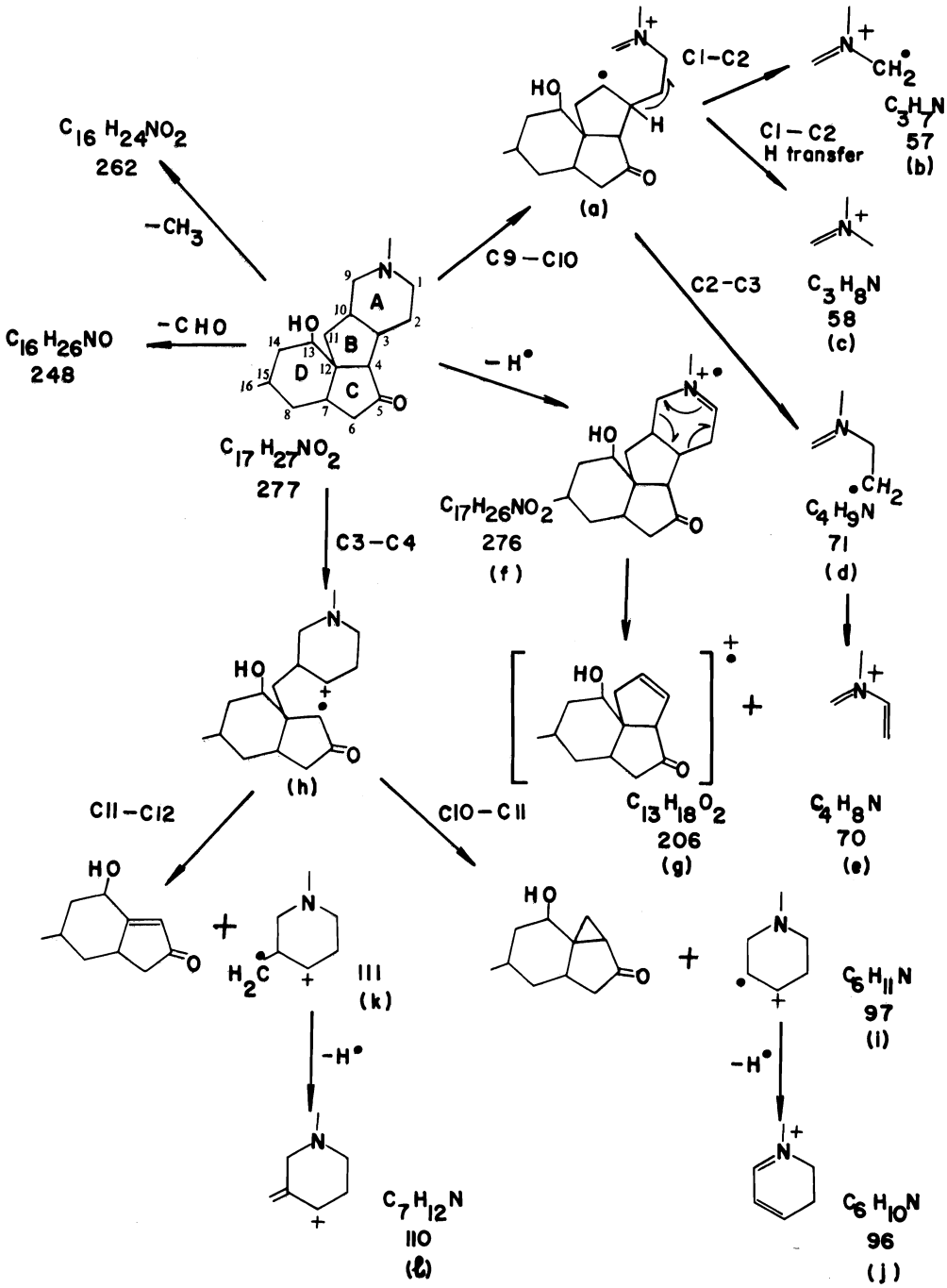

SCHEME 1. The fragmentation of paniculatine upon electron impact. Nitrogen-containing ions of low *m/e*.

Can. J. Chem. Downloaded from www.nrcresearchpress.com by 210.87.254.5 on 09/05/12
For personal use only.

Can. J. Chem. Downloaded from www.nrcresearchpress.com by 210.87.254.5 on 09/05/12
For personal use only.

group were based on the chemical shift differences between *cis*-4-*tert*-butylcyclohexanol (ref. 4, p. 163) and *tert*-butylcyclohexane (ref. 4, p. 67).

The spectrum of 1,3,4-trimethylpiperidine was calculated from the reported spectrum of piperidine. The same shift parameters for the methyl groups were used as before. The calculations were made for an axial methyl at position 4 and equatorial methyls at 1 and 3.

The calculated chemical shifts of the carbons in the model compounds are of the same order as those of the corresponding carbons of paniculatine, except at the bridging carbons. Thus they lend credence to the assignments made for paniculatine.

The methylene of ring C may be differentiated from that of ring B because of its proximity to the carbonyl group. The assignments of the methine carbons, C3, C4, C7, and C10 and the quaternary carbon at C12, are not secure and the methylenes, C8 and C14, cannot be differentiated.

The mass spectrum of paniculatine is characterized by a series of nitrogen-containing ions of low mass. Such ions are found in piperidine derivatives (5) and in alkaloids containing a single saturated nitrogen-containing ring (6). The spectrum is sufficiently different from other alkaloids of this family (1, 2) that it suggested that the structure of paniculatine was different from any of the *Lycopodium* alkaloids of established structure. With the structure now known the mass spectrum may be interpreted as shown in Schemes 1 and 2.[3]

The loss of methyl and of carbon monoxide plus hydrogen from the molecular ion are predictable and require no further comment. A major fragmentation pathway may be considered to begin by cleavage of the C9–C10 bond producing ion **a**. Subsequent cleavage of the C1–C2 bond can lead directly to **b** (*m/e* 57) or with accompanying hydrogen transfer to **c** (*m/e* 58), while cleavage of the C2–C3 bond will provide **d** (*m/e* 71) which may undergo loss of hydrogen yielding **e**. Ion **f**, derived from the molecular ion by loss of hydrogen, may undergo a retro Diels–Alder fragmentation providing another route to **e** or, if charge is retained on the nitrogen free fragment, yielding the ion **g** of *m/e* 206. The latter is also derivable from **a** by C2–C3 cleavage when the charge remains with the nitrogen-free fragment.

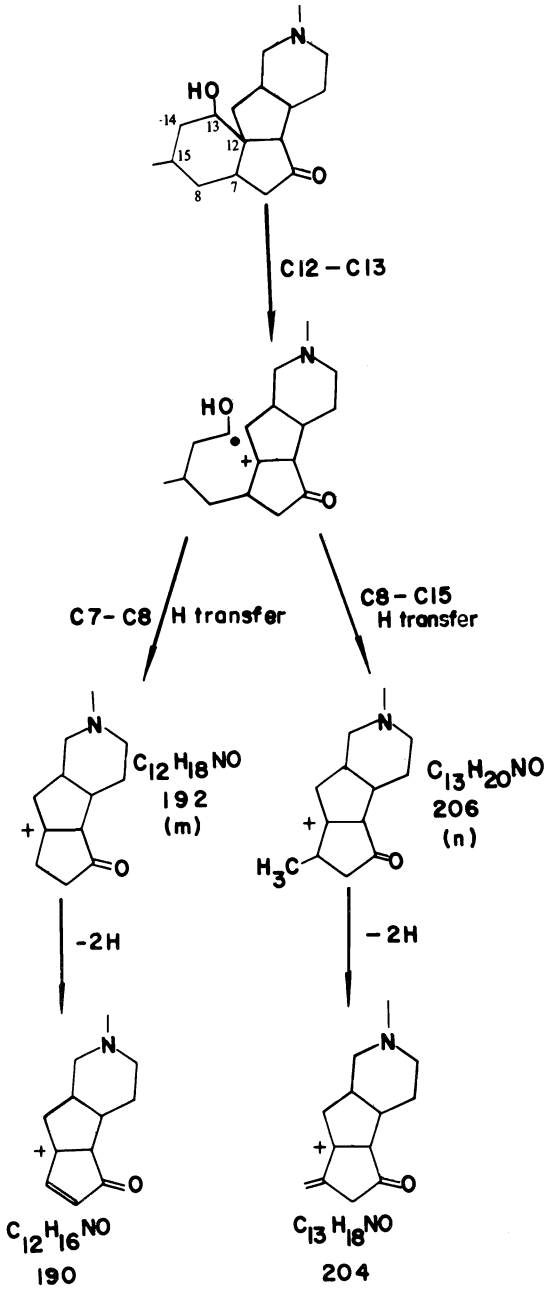

SCHEME 2. The fragmentation of paniculatine upon electron impact. Nitrogen-containing ions of high *m/e*.

Other nitrogen-containing ions may be derived in a series of steps initiated by C3–C4 bond cleavage yielding the ion formulated as **h**. By

[3]The composition of all ions was established by high resolution mass spectrometry. The calculated masses agreed with those observed within 0.005 amu.

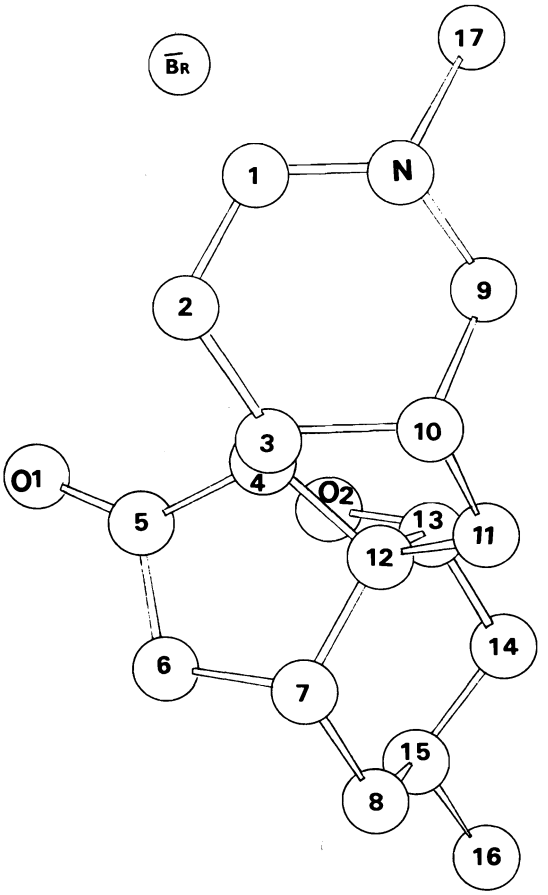

FIG. 3. The structure of paniculatine hydrobromide.

TABLE 1. Atomic parameters of paniculatine hydrobromide*

Atom	x	y	z	U^* (Å)^2
Br	−0.0174(2)	0.7500	0.7264(3)	†
C1	−0.011(2)	0.277(4)	0.884(2)	3.4(7)
C2	0.118(2)	0.338(4)	0.949(2)	4.5(6)
C3	0.246(2)	0.282(3)	0.869(2)	2.9(5)
C4	0.244(2)	0.081(3)	0.874(2)	2.8(5)
C5	0.333(2)	0.023(4)	0.997(2)	3.8(6)
C6	0.461(2)	0.005(3)	0.971(2)	2.5(5)
C7	0.451(2)	0.098(4)	0.836(2)	3.9(6)
C8	0.547(2)	0.030(4)	0.760(2)	4.8(7)
C9	0.046(2)	0.254(6)	0.669(2)	3.6(5)
C10	0.177(2)	0.320(4)	0.726(2)	4.2(6)
C11	0.268(2)	0.210(4)	0.666(2)	4.8(7)
C12	0.318(2)	0.061(4)	0.762(2)	3.6(6)
C13	0.292(2)	−0.121(3)	0.696(2)	3.6(6)
C14	0.390(2)	−0.176(4)	0.620(2)	4.7(7)
C15	0.522(2)	−0.169(4)	0.714(2)	4.6(7)
C16	0.614(3)	−0.216(7)	0.628(3)	8.2(11)
C17	−0.170(2)	0.283(4)	0.681(2)	3.6(6)
N	−0.043(2)	0.334(3)	0.743(2)	4.4(5)
O1	0.305(2)	−0.014(3)	1.096(2)	5.9(5)
O2	0.292(1)	−0.256(4)	0.797(2)	5.2(4)

*U and U_{ij} have been multiplied by 100. The anisotropic thermal factor is: $\exp -2\pi^2 (U_{11}h^2b_1^2 + \text{---} + 2U_{12}hkb_1b_2 + \text{---})$ where b_i are reciprocal vectors.

†Anisotropic thermal components for bromide ion are:

U_{11}	U_{22}	U_{33}	U_{12}	U_{13}	U_{23}
4.3(1)	4.0(1)	8.4(2)	0.4(2)	2.1(1)	0.1(2)

breaking the C10–C11 bond of **h** ion **i** is formed, which may then lose hydrogen yielding **j**. In a further fragmentation, cleavage at C11–C12 will lead to **k** and it in turn to ***l*** through loss of hydrogen.

The nitrogen-containing ion **m** at *m/e* 192 may form from the molecular ion by fission of the C12–C13 bond followed by C7–C8 fission, with the latter accompanied by hydrogen transfer, as shown in Scheme 2. Similarly the ion **n** at *m/e* 206, may be derived by C12–C13 cleavage followed by C8–C15 cleavage and accompanied by H transfer. Both **m** and **n** lose two hydrogens yielding the ions at *m/e* 190 and 204, respectively.

The skeleton of paniculatine as derived from the structure of paniculatine hydrobromide consists of a six-membered ring with a protonated tertiary nitrogen in the ring, fused to a five-membered ring which in turn is fused to another five-membered ring containing a carbonyl (O1). The latter ring is in turn fused to a six-membered ring which bears methyl and hydroxy (O2) substituents as shown in Fig. 3. The atomic parameters of paniculatine hydrobromide derived from the X-ray data are listed in Table 1 and the bond lengths and bond angles in Table 2. The hydroxy oxygen and methyl are *trans* to each other with the hydroxy group at C13 in the axial and the methyl at C15 in the equatorial position. The six-membered ring containing the hydroxy group is not a perfect chair as seen by the out-of-plane deviations for atoms C7, C8, C12, C13, C14, and C15 which also are used to define the plane (Table 3, Fig. 4).[4] The five-membered ring containing carbonyl is fused to the six-membered ring in a *cis* fashion with C6 in the axial and C4 in the equatorial position, as evidenced by the fact that C6 is 1.56 Å and C4 is 0.71 Å away from

[4]Table 3 and Fig. 4 (least-squares and out-of-plane distances) and Table 4 (observed and calculated structure factors of paniculatine hydrobromide) are available, at a nominal charge, from the Depository of Unpublished Data, CISTI, National Research Council of Canada, Ottawa, Canada, K1A 0S2.

Can. J. Chem. Downloaded from www.nrcresearchpress.com by 210.87.254.5 on 09/05/12
For personal use only.

Can. J. Chem. Downloaded from www.nrcresearchpress.com by 210.87.254.5 on 09/05/12
For personal use only.

TABLE 2. Bond distances and angles in paniculatine hydrobromide

Bond	Bond length (Å)	Bonds	Angle (deg)
C1—N	1.52(3)	N—C1—C2	111(2)
C1—C2	1.52(3)	C1—C2—C3	112(2)
C2—C3	1.56(3)	C2—C3—C4	114(2)
C3—C4	1.55(3)	C2—C3—C10	114(2)
C3—C10	1.51(3)	C4—C3—C10	104(2)
C4—C5	1.52(3)	C3—C4—C5	114(2)
C4—C12	1.59(3)	C3—C4—C12	102(2)
C5—O1	1.19(3)	C4—C5—C6	111(2)
C5—C6	1.52(3)	C4—C5—O1	124(2)
C6—C7	1.56(3)	O1—C5—C6	125(2)
C7—C8	1.55(4)	C5—C6—C7	103(2)
C7—C12	1.55(3)	C6—C7—C8	113(2)
C8—C15	1.58(4)	C6—C7—C12	105(2)
C9—N	1.51(4)	C8—C7—C12	112(2)
C9—C10	1.54(3)	C7—C8—C15	112(2)
C10—C11	1.55(4)	N—C9—C10	110(2)
C11—C12	1.53(4)	C3—C10—C9	111(2)
C12—C13	1.53(4)	C3—C10—C11	104(2)
C13—O2	1.45(4)	C9—C10—C11	109(2)
C13—C14	1.56(4)	C10—C11—C12	108(2)
C14—C15	1.59(3)	C4—C12—C7	102(2)
C15—C16	1.56(5)	C4—C12—C11	104(2)
N—C17	1.49(3)	C4—C12—C13	109(2)
		C7—C12—C13	117(2)
		C12—C13—C14	112(2)
		C12—C13—O2	110(2)
		C14—C13—O2	107(2)
		C13—C14—C15	108(2)
		C14—C15—C8	107(2)
		C14—C15—C16	105(2)
		C8—C15—C16	107(3)
		C1—N—C17	111(2)
		C1—N—C9	110(2)
		C17—N—C9	110(2)

the plane defined by C7, C13, and C15 and also C6 is 1.84 Å and C4 is 0.84 Å away from the plane defined by C8, C12, and C14. Similarly C11 is axial at C12 with respect to the six-membered ring and equatorial at C10. C4 lies underneath C3 and is axial to it. Thus the two five-membered rings are *cis* to each other and the five-membered ring defined by C3, C4, C10, C11, and C12 is *cis* to the six-membered ring containing nitrogen. The five-membered ring defined by C3, C4, C10, C11, and C12 is puckered and is close to the half-chair form of cyclopentane as shown by the out-of-plane deviations given in Fig. 4.[4] The second five-membered ring defined by C4, C5, C6, C7, and C12 is also puckered and the conformation is that of a half-chair as seen by comparing with the half-chair conformation of cyclopentane (7) in Fig. 4. The acute angle between the two five-membered rings is 53°. The equations for various planes and other out of plane deviations supporting the stereochemistry described are given in Table 3.[4]

The protonated tertiary amino nitrogen is hydrogen bonded to a bromide ion with $\overset{+}{N}\text{---}\overset{-}{Br}$ equal to 3.15 Å. Each bromide ion also interacts with one hydroxy group 3.4 Å away (3). The angle, $O2\text{---}\overset{-}{Br}\text{---}\overset{+}{N}$ is 94°, the angle, C13—$O2\text{---}\overset{-}{Br}$, is 89° and angles C1—$\overset{+}{N}\text{---}\overset{-}{Br}$, C9—$\overset{+}{N}\text{---}\overset{-}{Br}$, and C17—$\overset{+}{N}\text{---}\overset{-}{Br}$ are about 108°.

The quantities of P2, P4, and P5 obtained were insufficient to permit a complete structural elucidation. However, the mass spectra of all compounds have $M - 57$ as their most intense peak suggesting that they are related in structure to lycopodine (8). In that case the bridge in all three compounds does not carry a substituent. From the nmr data and the mass spectral data it may be deduced that P2 has one acetoxy and one hydroxy group, that P4 has two hydroxy groups, and that P5 may have a double bond and a hydroxy group. When more material becomes available we plan to carry out further structural investigations on the three compounds, all of which appear to be new alkaloids.

Paniculatine represents a new structural type among the *Lycopodium* alkaloids. Its formal relationship to lycopodine **2** is implicit in the numbering system shown in the formulas for the two alkaloids. Paniculatine is, however, more closely related to fawcettimine **3**, shown here in its open-chain rather than carbinolamine form. It is, in fact, easy to envisage the formation of paniculatine from a fawcettimine derivative such as **4**. The biosynthesis of paniculatine has not been studied but it is likely that it is derived by a modification of the pathway already suggested for lycopodine (9).

Experimental

Apparatus, Methods, and Materials

The infrared spectra were determined on a Perkin-Elmer 700 or Beckmann IR 5 spectrophotometer. The pmr spectra were run at 100 MHz on a Varian HA 100 instrument or at 220 MHz on a Varian HR-220 instrument.[5] The ^{13}C magnetic resonance spectra were determined in chloroform solution on a Brucker WH 90 instrument at 22.62 MHz. Chemical shifts are reported in ppm (δ) from TMS, the symbols s (singlet), d (doublet),

[5]The 220 MHz spectra were recorded at the Canadian 220 MHz NMR Centre, Sheridan Park, Ontario.

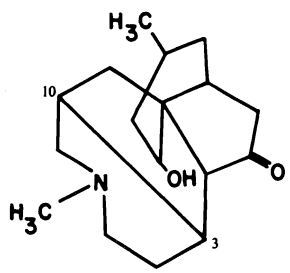

1

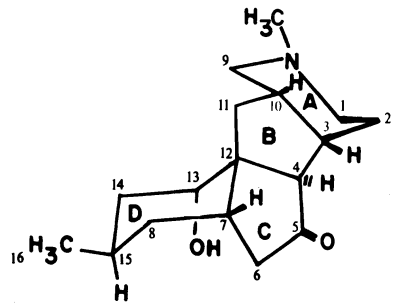

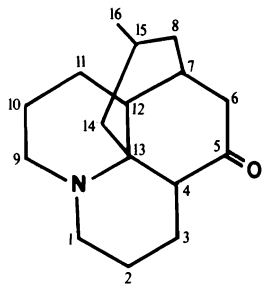

2

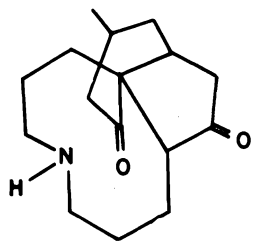

3

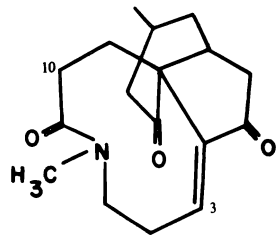

4

t (triplet), and m (multiplet) being used to denote the multiplicity of the signals. Mass spectra were obtained with a CEC 21-110 B mass spectrometer at an ionizing voltage of 80 eV and at a source temperature of 150–200 °C. High resolution mass measurements were performed by the method already described (10).

Melting points are uncorrected. Thin layer chromatography was carried out on alumina GF_{254} plates which were dried for 1 h at 110 °C and developed with Dragendorff's reagent or with iodine vapor. The solvent systems used were chloroform or chloroform–methanol, 95:5.

The microanalyses were performed by Gygli Microanalytical Laboratory, Toronto, Ontario.

The plant material was collected near Osorno, Chile in October 1973 and identified as *L. paniculatum* Desvaux by G. Looser of the Academia Chilena de Ciencias Naturales. A voucher specimen is on file in the Herbarium of the Faculty of Sciences at Santiago.

In the X-ray experiments a crystal of paniculatine hydrobromide with dimensions $0.02 \times 0.02 \times 0.04$ cm and a Syntex $P\bar{1}$ automatic diffractometer with graphite monochromatized MoK_α ($\lambda = 0.71069$ Å) radiation were used throughout the investigation. Unit cell parameters were determined by least squares methods from 11 values of 2θ. The crystal data are as follows:

$C_{17}H_{27}NO_2 \cdot HBr$ fw = 358

$a = 11.27(2)$, $b = 7.520(8)$, $c = 10.58(2)$ Å, $\beta = 102.2(2)°$, $V = 876.52$ Å^3 at 23 °C, $Z = 2$, $d_{calcd} = 1.36$ g/cm^3, $\mu = 26.30$ cm^{-1}, monoclinic space group $P2_1$ (C_2^2) determined from systematic absences and optical activity of the alkaloid.

A total of 1310 unique reflections lying in the range $0 < 2\theta \leq 45°$ were measured. Reflections were scanned in the θ–2θ mode at a rate between 8° and 24° per min depending on the peak intensity. Background was recorded on either side of the peak and used to determine the integrated intensity together with an estimated standard deviation based upon counting statistics. Those reflections whose intensity was less than 3σ, 347 in number, were regarded as unobserved. The data were corrected for Lorentz and polarization effects but not absorption. The XRAY-71 package of programs for X-ray crystallography, published by the University of Maryland and adopted for use with the CDC 6400 by H. D. Grundy of this Institution, were used for all computations.

The $\bar{Br}$–$\bar{Br}$ vector was located in the Harker sections at $2x$, $\frac{1}{2}$, $2z$ in the Patterson map. The phases based upon the bromide ion position were used for finding the other atoms by the successive use of full matrix least-squares, Fourier, and difference Fourier methods. In the beginning all the other atoms were considered as carbon atoms. The peak heights in the Fourier and difference map and the temperature factors of the atoms helped to distinguish between C, N, and O atoms. These atomic positions were refined with their individual isotropic temperature factors and a scale factor. This yielded a minimum R of 0.12. The atomic scattering curves for bromide ion, C and O atoms were obtained from the International Tables for X-ray Crystallography (11). Further refinements with unit weights were carried out using the anisotropic temperature factor for bromide ion and isotropic temperature factors for the other atoms.[6] The thermal parameter for

[6]During refinement the y coordinate of the bromide ion was fixed at 0.25.

Can. J. Chem. Downloaded from www.nrcresearchpress.com by 210.87.254.5 on 09/05/12
For personal use only.

Can. J. Chem. Downloaded from www.nrcresearchpress.com by 210.87.254.5 on 09/05/12
For personal use only.

C16 was significantly larger than that of the remaining atoms. All the bond lengths and angles lay within 1–2 standard deviations of their expected values. The final R value was 0.085 for observed reflections only, and 0.112 when the unobserved reflections were included. The average shift/error in the final refinement cycle was 0.092 with a maximum of 0.42. A final difference synthesis showed no missing structural features although peaks of 0.25 of a carbon atom were noted.

The final atomic parameters are given in Table 1, and observed and calculated structure factors are compared in Table 4.[4] Table 2 contains a list of the pertinent bond lengths and angles with standard deviations calculated from the standard errors derived from the least-squares matrix.

Extraction and Isolation of the Alkaloids

The dried plant material (*L. paniculatum*, 28 kg) was ground and extracted with ethanol for 72 h in a large Soxhlet apparatus. The extract was concentrated under reduced pressure and the residue digested with aqueous hydrochloric acid (5%) and filtered. The insoluble residue was digested again with an additional portion of aqueous hydrochloric acid (10%) and again filtered. The combined acidic extract was washed with ether (5 × 500 ml) and the washings discarded. The aqueous solution was basified with 10% sodium hydroxide to pH 11, and then extracted with chloroform until the extracts gave a negative test with Dragendorff's reagent. Removal of the chloroform under reduced pressure gave the crude alkaloids (202 g).

The crude alkaloids (202 g) were treated with hydrochloric acid (2 l, 10%). The mixture was filtered from suspended solid and the latter washed with an additional 2 l of 10% hydrochloric acid (residual solid, 31 g). The filtrate was brought to pH 10 by addition of sodium hydroxide solution and the mixture extracted first with ether (the ether-soluble fraction) and then with chloroform (the chloroform-soluble fraction) until the extracts gave a negative test with Dragendorff's reagent.

Examination of the Ether-soluble Fraction

The ether extract was dried and evaporated yielding a residue (92 g) which was dissolved in acetone and placed in a refrigerator for several days. A white solid (6.2 g) separated which was identified as dihydrolycopodine by comparison with authentic samples as both the free base and the hydrochloride.

The mother liquor was evaporated to dryness and dissolved in chloroform. A distribution was then carried out in 13 separatory funnels between the chloroform solution and McIlvane's buffer (the moving phase) of pH 7. The distributed material was then divided into four fractions on the basis of thin layer chromatographic behaviour. Fraction A (69.0 g) was comprised of acetyldihydrolycopodine (25 g), lycopodine (10 g), a number of unidentified bases, and 20 g of neutral material. Fraction B (4.7 g) was adsorbed on a column of basic alumina (210 g, activity II). The fraction (3.0 g) eluted with chloroform–methanol (95:5) showed two components on tlc and glc. The sample was dissolved in ethanol and made just acidic with hydrobromic acid and evaporated to dryness. The residue was dissolved in an ethanol–ether mixture and set aside to crystallize. There separated 600 mg of colorless crystals melting at 247–249 °C. The base derived from the hydrobromide was allowed to crystallize from acetone and melted at 65–66 °C. This fraction, now referred to as P2, has the following spectral properties: ir ν_{max} (KBr) 3500–3100, 2930–2840, 1740, 1240 cm^{-1}; pmr included signals at δ 0.94 (3H, d, J = 6 Hz, CH—CH_3), 2.04 (3H, s, $COCH_3$), 5.11 (t, J = 6 and 6 Hz, CHOAc); ms (m/e (%), composition) 307(25) $C_{18}H_{29}NO_3$, 264(6) $C_{15}H_{22}NO_3$, 250(100) $C_{14}H_{20}NO_3$, 208(10) $C_{12}H_{18}NO_2$, 206(8) $C_{12}H_{16}NO_2$, 190(22) $C_{12}H_{16}NO$, 172(11) $C_{12}H_{14}N$. Hydrobromide, ir ν_{max} (KBr) 3250, 2950, 2700–2500, 1739, 1240 cm^{-1}.

The basic fraction liberated from the mother liquors after the separation of P2 hydrobromide was adsorbed on a column of basic alumina (30 g, activity II–III) and the column eluted with ether. The fraction so obtained was evaporated to dryness and the residue sublimed and crystallized from acetone. The colorless crystals (20 mg) melted at 175–185 °C (dec.). This compound designated P5, has the following peaks in its mass spectrum: ms (m/e (%), composition) 247(20) $C_{16}H_{25}NO$, 204(8) $C_{13}H_{18}NO$, 190(100) $C_{12}H_{16}NO$, 172(63) $C_{12}H_{14}N$; pmr included signals at δ 0.90 (3H, d, J = 7 Hz, CHCH_3), 5.4 (1H, m, $W_{1/2}$ = 9 Hz, olefinic H); ir ν_{max} (KBr) 3250–3190, 2950–2850, 1070 cm^{-1}.

Fraction C (6.2 g) was adsorbed on a column of basic alumina (300 g, activity II). The fraction, eluted with chloroform–methanol (99:1), yielded paniculatine (0.8 g), mp 181 °C (acetone). Spectral data: ir ν_{max} ($CHCl_3$) 3620, 3600–3000, 1720, 1250–1200, 1040 cm^{-1}; pmr included signals at δ 0.90 (3H, d, J = 6.5 Hz, CHCH_3), 2.18 (3H, s, NCH_3), 3.78 (1H, broad s, $W_{1/2}$ = 8 Hz, CHOH); ms (m/e, %) 277(18), 276(22), 262(10), 248(5), 206(5), 204(29), 192(17), 190(3), 180(5), 111(4), 110(11), 97(3), 96(21), 71(25), 70(27), 58(100), 57(30). *Anal.* calcd. for $C_{17}H_{27}NO_2$: C 73.61, H 9.81, N 5.05; found: C 73.64, H 9.70, N 5.04.

Paniculatine hydrobromide was prepared from the base and hydrobromic acid in the usual manner. The colorless solid so obtained was recrystallized from ethanol–ether and melted at 310 °C. It had the following properties: ir ν_{max} (KBr) 3370, 2800–2400, 1725, 1200, 1040 cm^{-1}. *Anal.* calcd. for $C_{17}H_{28}NO_2Br$: C 56.98, H 7.88, N 3.91, Br 22.30; found: C 56.75, H 7.78, N 3.86, Br 22.11.

Fraction D was subjected to a 58 tube counter current distribution between chloroform and Borax–HCl (the moving phase), pH 8.8, yielding the following fractions: tubes 1–6 (2.2 g), a non-resolvable mixture, tubes 7–36 (9.9 g), dihydrolycopodine, and tubes 37–56 (1.8 g), P4 (600 mg from acetone), *vide infra*.

Examination of the Chloroform-soluble Fraction

The chloroform solution was evaporated yielding a residue of 30 g which was partitioned in eight funnels between chloroform (stationary phase) and McIlvane's buffer (pH 7). The distributed material was divided as a result of tlc examination into three fractions, E, F, and G, containing 11.0, 1.8, and 11.6 g, respectively. Fraction G was adsorbed on a column of basic alumina (300 g, activity II). Elution of the column with ether gave a fraction of 30 mg which melted at 217 °C after crystallization from acetone. This substance, hereinafter referred to as P4, has the following properties: ir ν_{max} (Nujol) 3500,

3200, 2950–2850 cm^{-1}; pmr included signals at δ 0.85 (3H, d, J = 6 Hz, $CHCH_3$), 3.86 (1H, d, J = 6 Hz, $CHOH$); ms (m/e (%), composition 265(16) $C_{16}H_{27}NO_2$, 222(4) $C_{13}H_{20}NO_2$, 208(100) $C_{12}H_{18}NO_2$, 190(7) $C_{12}H_{16}NO$, 162(2) $C_{11}H_{16}N$ and $C_{10}H_{12}NO$.

The other portion of fraction *G* has not yet yielded any characterizable compounds. Fractions *E* and *F* have not yet been examined.

Acknowledgments

Part of this work was made possible through grants 147 and 1524 from the Oficina Técnica de Desarrollo Cientifico y Creación Artística, Universidad de Chile. The work at McMaster was supported through grants from the National Research Council of Canada.

1. D. B. MacLean. *In* The alkaloids. Vol. 10. *Edited by* R. H. F. Manske. Academic Press, New York. 1967. p. 305.
2. D. B. MacLean. *In* The alkaloids. Vol. 14. *Edited by* R. H. F. Manske. 1973. p. 347.
3. M. Castillo, G. Morales, L. A. Loyola, I. Singh, C. Calvo, H. L. Holland, and D. B. MacLean. Can. J. Chem. **53**, 2513 (1975).
4. J. B. Stothers. Carbon-13 NMR spectroscopy. Academic Press, New York. 1972.
5. H. Budzikiewicz, C. Djerassi, and D. H. Williams. Mass spectrometry of organic compounds. Holden-Day, Inc., San Francisco. 1967. pp. 313–315.
6. H. J. Veith, M. Hesse, and H. Schmid. Helv. Chim. Acta, **53**, 1355 (1970).
7. E. L. Eliel. Stereochemistry of carbon compounds. McGraw Hill, New York. 1962. p. 250.
8. D. B. MacLean. Can. J. Chem. **41**, 2654 (1963).
9. W. D. Marshall, T. T. Nguyen, D. B. MacLean, and I. D. Spenser. Can. J. Chem. **53**, 41 (1975).
10. C. K. Yu and D. B. MacLean. Can. J. Chem. **49**, 3025 (1971).
11. International Tables of X-ray Crystallography. Vol. III. Kynoch Press, Birmingham, England. 1962.

Can. J. Chem. Downloaded from www.nrcresearchpress.com by 210.87.254.5 on 09/05/12
For personal use only.

The synthesis and spectroscopic characterization of Indulin 6B tetrasulfonate

W. E. SOLODAR AND A. R. MONAHAN
Xerox Webster Research Center, Webster, N.Y., U.S.A. 14580

Received December 11, 1975

W. E. SOLODAR and A. R. MONAHAN. Can. J. Chem. **54**, 2909 (1976).

An unambiguous synthetic route to pure forms of Indulin 6B base and Indulin 6B tetrasulfonate is described. The visible electronic spectrum of each compound was examined in solution and the solid state. The longest wavelength electronic transition observed for both compounds is a $\pi - \pi^*$ state possessing a considerable amount of intramolecular charge transfer character. Indulin 6B tetrasulfonate was found to self-associate in water with a dimerization constant of $(1.84 \pm 0.22) \times 10^2\ M^{-1}$. The nature of the intermolecular interactions between Indulin dye molecules in solution and the solid state is discussed.

W. E. SOLODAR et A. R. MONAHAN. Can. J. Chem. **54**, 2909 (1976).

Une voie de synthèse non ambigue des formes pures de la base Induline 6B et du tétrasulfonate d'Induline 6B est décrite. Le spectre électronique visible de chacun de ces composés a été examiné en solution et en phase solide. La transition électronique de plus grande longueurs d'onde observée pour ces deux composés est un état $\pi - \pi^*$ possédant une proportion considérable d'un caractère de transfert de charge intramoléculaire. Le tétrasulfonate d'Induline 6B s'associe avec lui-même dans l'eau avec une constante de dimérisation de $(1.84 \pm 0.22) \times 10^2\ M^{-1}$. La nature des interactions intramoléculaires entre les molécules de colorant Induline en solution et en phase solide est discutée.

[Traduit par le journal]

Introduction

The indulin dye of commerce is solubilized by sulfonation of a mixture of insoluble indulin colorants. This mixture, or 'indulin melt', is obtained by the fusion of aniline hydrochloride with sodium nitrite (1); the aminoazobenzene thus produced reacting with more aniline hydrochloride to form Indulin 3B, Indulin 6B, and numerous by-products (2, 3).

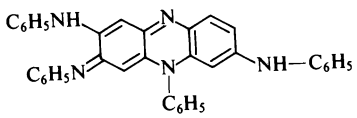

Indulin 3B

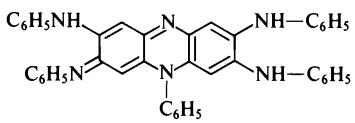

Indulin 6B

Indulin 6B, the principal component of the mixture, has been prepared from Indulin 3B (4) and from 2-amino-3,7,8-trianilino-5-phenylphenazine (5). The sulfonated product has never been purified and characterized. The objectives of the work were to synthesize Indulin 6B base in pure form by an unambiguous route, to convert the base to a single sulfonated product, and to identify and spectroscopically characterize that product. Our synthetic route is indicated in Scheme 1.

This scheme is an adaptation of Kehrmann's (4, 5) general method, with the following modifications. *Step 1*: 4,5-dianilino-1,2-benzoquinone was prepared by the procedure given in ref. 8. *Step 2*: 5-chloro-2-aminodiphenylamine hydrochloride was prepared by catalytic hydrogenation of 5-chloro-2-nitrodiphenylamine. This was reportedly done by Kottenhahn and co-workers (6) though no data on the reaction was reported. *Step 4*: represents a combination of two of Kehrmann's steps, making it possible to go directly from the chloro indulin (**3**) to Indulin 6B without isolating the intermediate Indulin 3B (Scheme 2).

Additionally, in step *6*, a method was developed for the controlled sulfonation of Indulin 6B, and for the isolation and purification of the product.

Can. J. Chem. Downloaded from www.nrcresearchpress.com by 210.87.254.6 on 09/05/12
For personal use only.

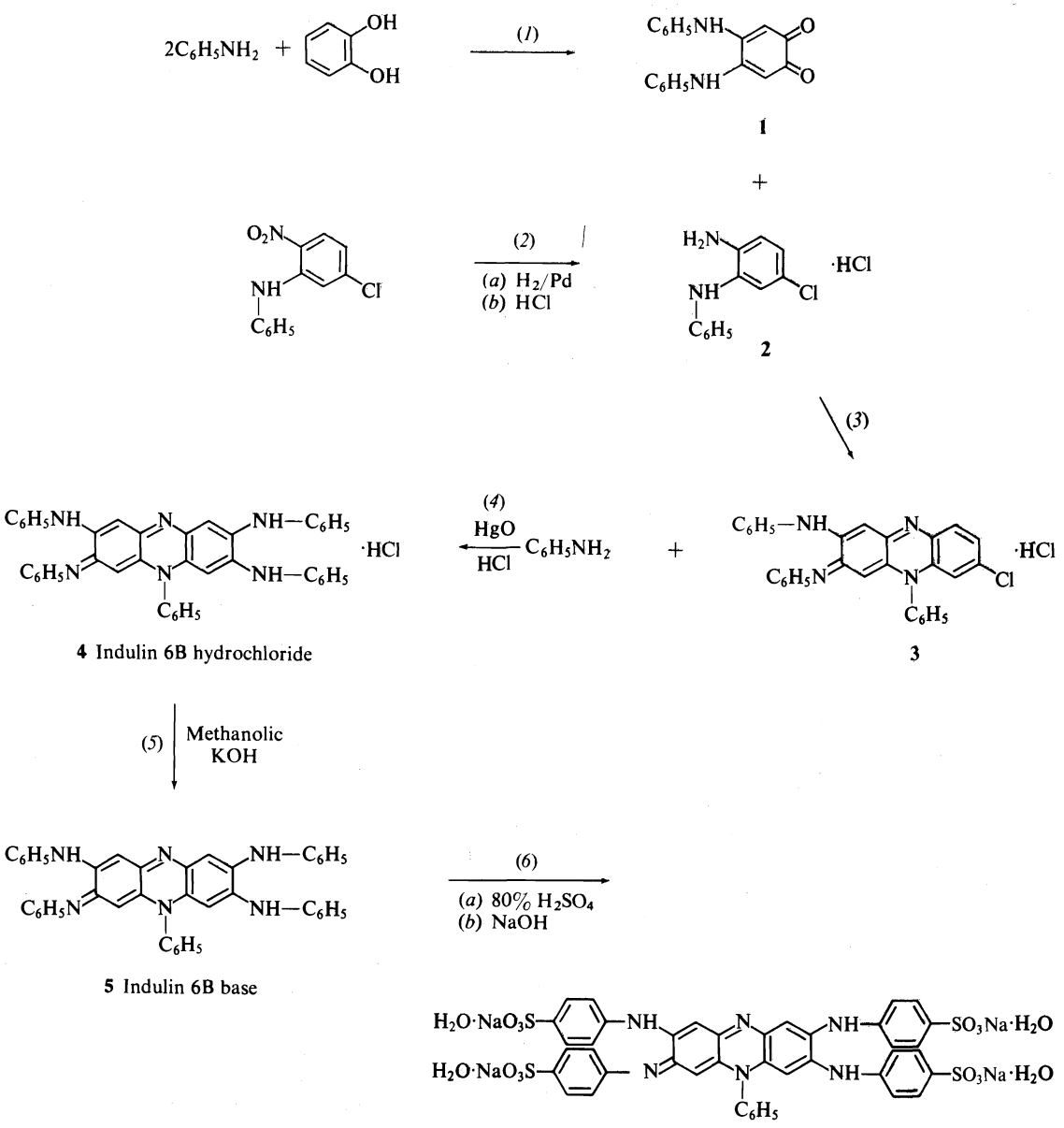

SCHEME 1

Experimental and Results

Synthesis

4,5-Dianilino-1,2-benzoquinone (7) (1)

To a solution of 33 g (0.3 mol) of catechol and 55.8 g (0.6 mol) of aniline in 1350 ml of ethanol in a 4-l beaker was slowly added (30 min) with stirring, a solution of 60 g (0.3 mol) of $NaIO_3$ in 1350 ml of water. The mixture turned reddish and turbid. It was stirred at room temperature for 5.5 h after all the $NaIO_3$ had been added. The reddish-brown precipitate that separated was filtered off, washed with 1 litre warm water, then with 250 ml of methanol. The solid was further purified by transferring it to a beaker and slurrying with 1 litre of methanol for 30 min, after which it was filtered and air dried. Yield of maroon solid, mp 183–185 °C, was 62.1 g (71.5%).

Can. J. Chem. Downloaded from www.nrcresearchpress.com by 210.87.254.6 on 09/05/12
For personal use only.

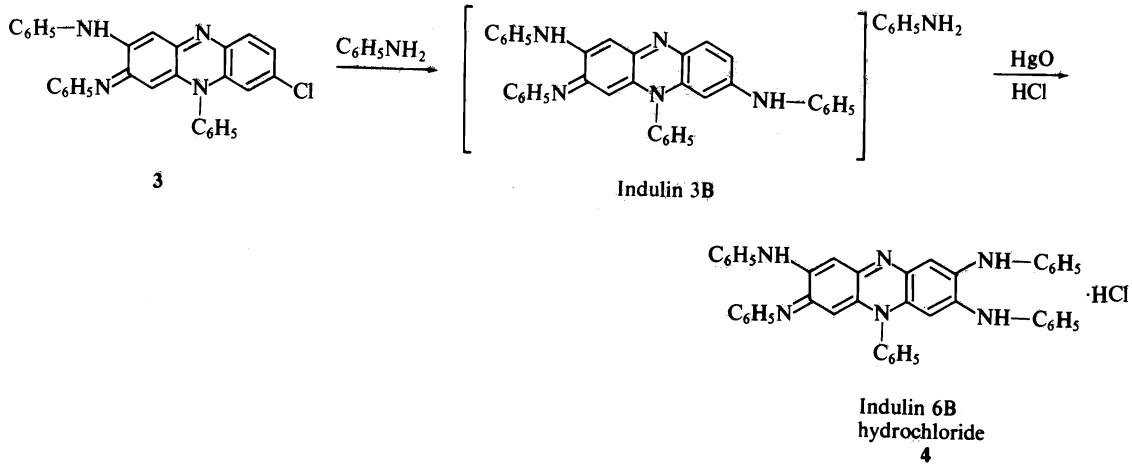

SCHEME 2

5-Chloro-2-aminodiphenylamine Hydrochloride (6, 7) (2)

A suspension of 9.92 g of 5-chloro-2-nitrodiphenylamine (Aldrich Chem., 15 322-2) in 200 ml of acetic acid was hydrogenated over 1.0 g of 5% $Pd/BaSO_4$ catalyst in a Parr shaker overnight under 50 psi hydrogen. Uptake of hydrogen was 11.5 psi, which is 100% of theory. Six millilitres of concentrated HCl was added immediately upon opening the system. The catalyst was filtered off and the acetic acid evaporated *in vacuo*. The residue was triturated with dilute HCl to yield a salmon-colored precipitate that was filtered and desiccated under vacuum over KOH. Yield of pink solid was 8.95 g (88%).

2-Chloro-6,7-dianilino-9-phenylphenazine Hydrochloride (8) (3)

In a 1 litre flask, a mixture of 22.3 g (0.0875 mol) of 5-chloro-2-aminodiphenylamine hydrochloride, 25.4 g (0.0875 mol) of 4,5-dianilino-1,2-benzoquinone, and 500 ml of ethanol was deaerated with nitrogen and then carefully heated to reflux with mechanical stirring. There was an initial exotherm at reflux which was controlled by moderate external cooling as needed. Color of the mixture changed from deep amber to blood red. After several hours of refluxing there was some precipitation. The mixture was refluxed for a total of 6 h, then allowed to cool overnight. The precipitated product was filtered off, washed with ethanol, and air dried. Yield of crude product, lustrous green crystals melting at 270–274 °C (dec.), was 35.3 g (79.5%). The product was further purified by digesting it in 500 ml of boiling ethanol. After cooling the mixture, filtering, and drying the product, 33.8 g (76% yield) of lustrous green crystals, melting at 276–279 °C (dec.), was recovered.

2,3,6,7-Tetraanilino-9-phenylphenazine Hydrochloride Indulin 6B Hydrochloride (4) (4)—A mixture of 5.1 g (0.01 mol) of **3**, 50 ml of aniline and 10 g of aniline hydrochloride was stirred and refluxed for 15 min. The color of the solution changed from magenta to deep blue. The mixture was cooled slightly below the reflux temperature and 2.17 g (0.01 mol) of yellow mercuric oxide was introduced to the mixture. The mixture was refluxed for 6 h, then allowed to cool overnight. The solidified mass was rewarmed and decanted from metallic mercury; the flask was rinsed with ethanol several times and added to the reaction product. The above mixture was diluted to 150 ml with ethanol, then filtered through a medium porosity filter to recover 4.47 g of bronze crystals (63.2% yield). A sample, purified by treatment with boiling ethanol, decomposed above 300 °C and gave the following analysis. *Anal.* calcd. for $C_{42}H_{33}N_6Cl$: C 76.75, H 5.06, N 12.79, Cl 5.39; found: C 77.17, H 5.09, N 12.53, Cl 5.20.

Indulin 6B Base (5)—To a suspension of 8 g of Indulin 6B hydrochloride in 450 ml of methanol was added a solution of 2 g of KOH in 20 ml of methanol. The mixture was stirred and refluxed for 4.5 h, then concentrated under vacuum to *ca.* 100 ml and diluted with water. The base was filtered off and desiccated in vacuum over P_2O_5 to give 6.4 g of black solid, mp 294–300 °C. A sample purified by treatment with boiling xylene, melted at 300–304 °C (Kehrmann reported 286–288 °C) and gave the following analysis. *Anal.* calcd. for $C_{42}H_{32}N_6$: C 81.26, H 5.20, N 13.54; found: C 81.16, H 5.30; N 13.60.

Indulin 6B Sodium Tetrasulfonate (6)—To a mixture of 15 ml of concentrated H_2SO_4 and 5 ml of water at 100 °C was gradually added, with stirring, 4 g of Indulin 6B base. The addition took 30 min. The temperature was raised to 120 °C and the mixture stirred at that temperature for an additional 6 h. After cooling, it was poured onto ice in an evaporating dish. The quench was adjusted to p*H* 8 by the careful addition of *ca.* 25 ml of 50% NaOH solution.

Water was evaporated from the neutralized quench by heating on a steam bath in a well-ventilated hood for 5 to 6 h.[1] The residue was dried in a vacuum desiccator over P_2O_5 overnight. The dried residue was extracted in a Soxhlet apparatus with 400 ml of methanol for 24 h. The methanol extract was evaporated to dryness *in vacuo* to give 7.1 g of dark purple solid.

Elemental analysis indicated the presence of sodium sulfate and sodium hydroxide in this material. It was

[1]It was not feasible to evaporate the water under vacuum because of excessive frothing.

Can. J. Chem. Downloaded from www.nrcresearchpress.com by 210.87.254.6 on 09/05/12
For personal use only.

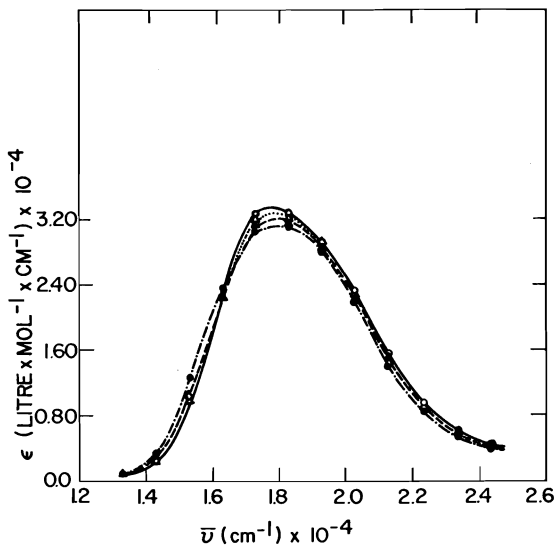

FIG. 1. Series of absorption spectra of Indulin 6B sulfonate in water, showing isosbestic point at 16 300 cm^{-1} (674 nm): —○— $C_T = 5.15 \times 10^{-6}$ M; ··· △ ··· $C_T = 2.06 \times 10^{-5}$ M; ---▲--- $C_T = 1.03 \times 10^{-4}$ M; ···●··· $C_T = 1.03 \times 10^{-3}$ M.

purified by dissolving 4 g in 40 ml of warm water and precipitating the product with 120 ml of ethanol. *Anal.* calcd. for $C_{42}H_{36}N_6S_4O_{16}Na_4$: C 45.82, H 3.30, N 7.63, S 11.65, Na 8.35; found: C 45.67, H 2.95, N 7.24, S 11.28, Na 8.11.[2]

Spectroscopic Measurements

Solution spectra of the Indulin base were determined using solutions of *ca.* 1×10^{-5} M in methanol and cyclohexane (Burdick and Jackson). The visible absorption spectrum of the indulin base exhibits an intense ($\epsilon_{max} = 6.0 \times 10^4$ l mol^{-1} cm^{-1}) transition at 500 nm in cyclohexane. In a polar solvent such as methanol, the transition undergoes a pronounced shift to 605 nm.

This type of transition involving a large bathochromic polar solvent shift and a relatively large molar extinction coefficient has been described as a charge transfer (CT) singlet state. The CT state has both practical (primarily photochemical) and theoretical importance and details of the state have been outlined in other papers (9). In the indulin molecule, excited state charge transfer occurs from the secondary or tertiary amino group to the imino moiety. The solvent effect on the position of the absorption spectrum originates in the differential interaction of solvent molecules on the ground and excited states of the dye molecule. In polar solvents there exists a greater stabilization of the excited state than the ground state, causing a shift to longer wavelengths.

The tetrasulfonate dye which is insoluble in non-polar solvents was investigated spectroscopically in water (pH = 7.5) in the 10^{-6} M to 10^{-3} M concentration range. The water was obtained from a Millipore Super-Q system (18 megohms resistivity). Spectra were measured on a Cary Model 14R automatic spectrophotometer using 0.1-, 1-, 5-, and 10-cm matched quartz cells.

The concentration dependence of the absorption spectra of Indulin 6B tetrasulfonate is shown in Fig. 1. At the most dilute concentration of 5.15×10^{-6} M, the band peak occurs at 17 700 cm^{-1} (565 nm). Successively higher concentrations result in a slight blue shift of this peak with a measurable decrease in the apparent extinction coefficient. Spectral blue shifts are commonly observed for planar dye molecules upon increasing concentration in aqueous solutions (10). An isosbestic point occurs at 16 300 cm^{-1} (674 nm) for the series of absorption spectra in Fig. 1.

Discussion

From the concentration dependent spectra, the calculation of the pure monomer spectrum, pure dimer spectrum, and equilibrium constant was accomplished using a computer procedure which was previously reported (11). In the analysis it was assumed that the monomer concentration C_m and dimer concentration C_d follow the law of mass action

$$[1] \qquad K_{eq} = C_d/C_m^2$$

where K_{eq} is the association (equilibrium) constant for dimer formation. If the total dye concentration (CT) is small so that no higher aggregates are formed, then

$$[2] \qquad C_d = (C_T - C_m)/2$$

Assuming that [1] and [2] are valid, a best-fit monomer spectrum and dimer spectrum can be calculated for a given K_{eq}. By varying K_{eq} systematically, the best-fit ϵ_m, ϵ_d, and K_{eq} are established where ϵ_m and ϵ_d are the molar extinction coefficients of monomer and dimer, respectively. The best-fit ϵ_m and ϵ_d are then used to calculate K_{eq} at each concentration and limits of error on K_{eq} are determined. The result of this calculation with the fitting of the concentrations C_m and C_d to [1] is shown in Fig. 2. The solid line is drawn with a theoretical slope of 2.00, in fulfillment of the demands of [2]. The best-fit monomer and dimer spectra are shown in Fig. 3. The splitting of the dimer band can be explained by the theory of exciton interaction between monomer chromophores in the indulin dimer (10–12). A schematic drawing of the parallel plane dimer and the energy levels of the monomer and dimer are shown in Fig. 4. Both parallel and non-parallel orientations of the transition dipoles can lead to quantum mechanical resonance splitting. The schematic parallel

[2]Galbraith Laboratories, Inc.

Can. J. Chem. Downloaded from www.nrcresearchpress.com by 210.87.254.6 on 09/05/12
For personal use only.

Can. J. Chem. Downloaded from www.nrcresearchpress.com by 210.87.254.6 on 09/05/12
For personal use only.

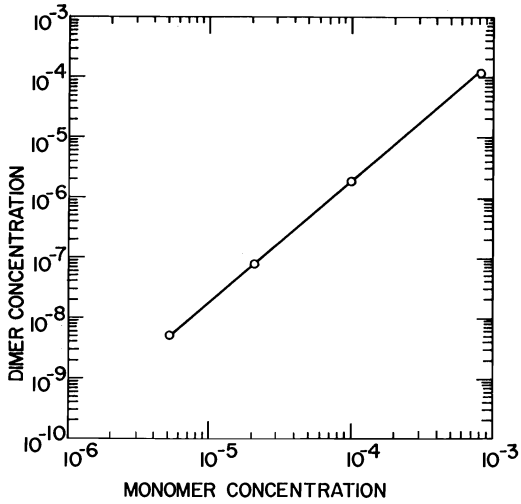

FIG. 2. Plot of monomer concentration *vs.* dimer concentration. Solid line is drawn with a theoretical slope of 2.00, in fulfillment of the demands of [2]. $K_{eq} = (1.84 \pm 0.22) \times 10^2$ l mol^{-1}.

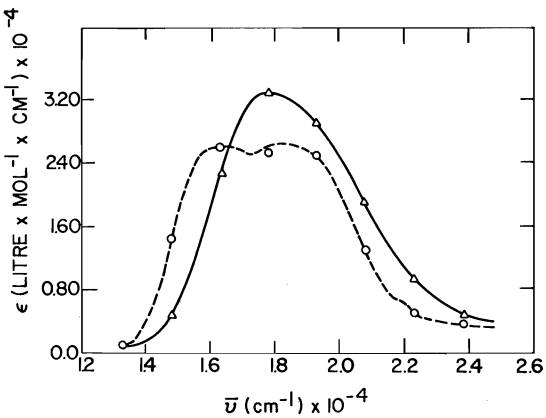

FIG. 3. The best-fit monomer and dimer spectra based on equation [1]: ---○--- ϵ_{dimer}; —△— $\epsilon_{monomer}$.

plane dimer configuration, shown in Fig. 4, was chosen as a plausible structure for the indulin dimer because the dye has an extended planar character and the simple model does yield allowable transitions to both *J*- (16 500 cm^{-1} lower energy transition) and *H*-bands (18 300 cm^{-1} higher energy transition) for $\alpha \neq 0$. The shift in midpoint between the monomer band and high energy and low energy dimer bands is attributable to London dispersion force interactions and to a lesser degree by the overlap of the electron wave function between the two indulin molecules in the dimer. The absorption spectra of solution

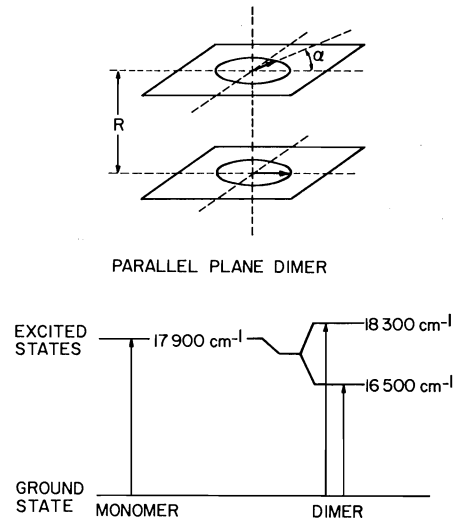

FIG. 4. Schematic drawing of the parallel plane dimer and the energy levels of the monomer and dimer.

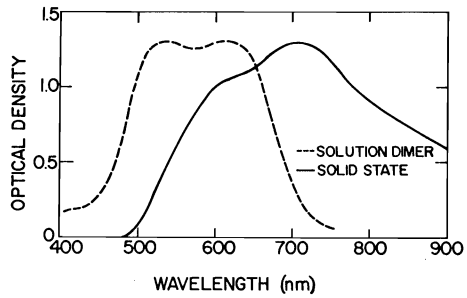

FIG. 5. Absorption spectra of solution dimer and crystalline dye compound: --- solution dimer; — solid state.

dimer and crystalline dye are shown for comparison in Fig. 5. The molecular exciton models can also be used to qualitatively understand differences between dimer spectra and exciton bands in larger molecular aggregates, *i.e.* trimers, tetramers, etc. In a manner similar to the dimer model, exciton theory predicts that a parallel stacking of N transition dipoles or H aggregate can lead to either hypsochromically (*H*-band) or bathochromically shifted (*I*-band) for strictly parallel dipoles ($\angle = 0°$). If the N coupled dye molecules are tilted from their perpendicular position with respect to each other in a structure such that the angle separating the molecules is less than 90°, electronic transitions red shifted (bathochromic) from the monomer or dimer (*J*-aggregate) are predicted by the theory (12).

Therefore the *J*-aggregate state of indulin could be responsible for the electron absorption spectrum in the crystalline state. The exact orientation of the molecules with respect to each other and number of molecules in the aggregate must await a detailed crystal structure of the Indulin tetrasulfonate molecule.

1. DALE and CARO. Brit. Patent No. 3307 (December, (1863).
2. O. FISCHER and E. HEPP. Ber. **20**, 2479 (1887).
3. O. FISCHER and E. HEPP. Z. Farben Text. Chem. **1**, 457 (1902); Chem. Zentr. II, 902 (1902).
4. F. KEHRMANN and W. KLOPFENSTEIN. Ber. **56**, 2396 (1923).
5. F. KEHRMANN and L. STANOYEVITCH. Helv. Chim. Acta, **8**, 663 (1925).
6. A. KOTTENHAHN *et al.* J. Org. Chem. **28**, 3118 (1963).
7. V. BARRY *et al.* U.S. Patent No. 2 948 726 (August, 1960).
8. Brit. Patent No. 824 468 (December, 1959).
9. M. B. LEDGER and P. SUPPAN. Spectrochim. Acta, Ser. A, **23**, 641 (1967).
10. M. KASHA, H. R. RAWLS, and M. A. EL-BAYOUMI. Pure Appl. Chem. **11**, 371 (1965).
11. A. R. MONAHAN and D. F. BLOSSEY. J. Phys. Chem. **74**, 4014 (1970).
12. E. G. MCRAE and M. KASHA. *In* Physical processes in radiation biology. *Edited by* L. Augenstein, B. Rosenberg, and R. Mason. Academic Press, New York. 1964. pp. 21–44.

Can. J. Chem. Downloaded from www.nrcresearchpress.com by 210.87.254.6 on 09/05/12
For personal use only.

^{13}C nuclear magnetic resonance spectra of alkyl indoles including derivatives of hexahydroechinulin

ROBERT R. FRASER AND SALVATORE PASSANNANTI[1]
Department of Chemistry, University of Ottawa, Ottawa, Ont., Canada KIN 6N5
AND
FRANCO PIOZZI
Instituto di Chimica Organica, Universita Di Palermo, Palermo, Italy

Received April 26, 1976

ROBERT R. FRASER, SALVATORE PASSANNANTI, and FRANCO PIOZZI. Can. J. Chem. **54**, 2915 (1976).

Revised structures for 4-bromohexahydroechinulin and 6-nitrohexahydroechinulin have been established using ^{13}C nmr spectroscopy. For this purpose the substituent parameter for the nitro group at a site flanked by two methyl groups has been measured. Inconsistencies in previous data on alkyl indoles in comparison with hexahydroechinulin suggested a reassignment of the C_4 and C_6 signals in 5-methylindole, which we have proven by single frequency spin-decoupling experiments. The original data on methyl indoles has been retabulated to include the above reassignments and others recently reported by Gribble *et al.* A more consistent and reliable set of methyl substituent parameters is thereby obtained.

ROBERT R. FRASER, SALVATORE PASSANNANTI et FRANCO PIOZZI. Can. J. Chem. **54**, 2915 (1976).

Les structures revisées de la bromo-4 hexahydroéchinuline et de la nitro-6 hexahydroéchinuline ont été établies en utilisant la spectroscopie rmn ^{13}C. A cet effet, le paramètre du substituant pour le groupe nitro sur un site bordé de deux groupes méthyles a été mesuré. Des inconsistances dans les données précédentes sur les alkylindoles en comparaison avec l'hexahydroéchinuline ont suggéré une réattribution des signaux des carbones C_4 et C_6 dans le méthyl-5 indole, ce que nous avons démontré par des expériences de découplage de spin à fréquence unique. Les données originales sur les méthylindoles ont été remises en tableau pour inclure les réattributions ci-mentionnées et d'autres valeurs récemment rapportées par Gribble *et al.* On obtient ainsi une série de paramètres plus consistants et plus fiables du substituant méthyle.

[Traduit par le journal]

The extensive studies of Quilico and his coworkers on echinulin, **1**, and its hexahydro derivative, **2**, clearly established their structures by chemical means (1). Prior to this, tentative structures had been proposed for bromohexahydroechinulin, **3**, (2) and nitrohexahydroechinulin, **4**, (3) which were subsequently invalidated by the final result for hexahydroechinulin. In this paper we wish to describe the elucidation of the structure of **3** and **4** by the use of ^{13}C nmr. Since the point to be ascertained was the position of the substituent in the indole nucleus, it was necessary also to study a number of alkylated indoles and to reexamine previous signal assignments in monoalkyl indoles.

A previous study using ^{13}C nmr in this area has been made on echinulin and two other metabolites from the same mould, (4). The metabolites had structures distinctly different from echinulin in that the indole ring lacked substituents at position 5. The complete assignment for all carbon signals was not possible, the major focal point of their study being the assignments for carbons located in the substituent at C_3 of the indole ring.

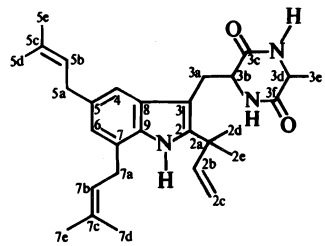

1

The ^{13}C spectra of hexahydroechinulin and its bromo and nitro derivatives each contain 29

[1]Canada Council post-doctoral fellow, 1974–1975.

Can. J. Chem. Downloaded from www.nrcresearchpress.com by 210.87.254.42 on 09/05/12
For personal use only.

TABLE 1. ^{13}C shieldings of indole and some methyl derivatives*

Substituent	C_2	C_3	C_4	C_5	C_6	C_7
H	125.2	102.6	121.3	120.3	122.3	111.8
2-Methyl	[135.7]	100.4	(120.0)	(119.9)	121.1	110.9
3-Methyl	122.7	[111.4]	(119.4)	(119.6)	122.3	111.7
4-Methyl	124.2	101.1	[130.2]	120.1	122.2	109.3
5-Methyl	125.0	102.1	120.8	[128.8]	123.7	111.3
6-Methyl	124.3	102.3	(120.7)	(121.9)	[131.5]	111.6
7-Methyl	124.8	103.0	(118.9)	(120.3)	122.7	[120.9]
1,2-Dimethyl	[138.1]	100.0	(120.0)	(119.6)	120.7	109.2
2,3-Dimethyl	[131.4]	[106.8]	118.4	119.3	121.1	110.7
2,7-Dimethyl	[135.1]	101.0	117.7	119.8	121.7	[119.9]
2,3,7-Trimethyl	[131.2]	[106.3]	118.1	[127.8]	122.5	110.2
2,5,7-Trimethyl	—	100.5	117.1	[128.9]	123.2	[118.9]

*δC, ppm from TMS. All shift data, except for the 2,5,7-trimethyl derivative (0.4 *M* in $CDCl_3$) is that originally reported (5) and converted using δC (CS_2) 192.8. Square brackets indicate substituted carbons. Shifts given in parentheses indicate possible assignment reversal.

signals, not all of which can be unambiguously assigned without the use of exceedingly complex techniques. Those line positions, listed in the Experimental, which can be assigned by using substituent parameters and data from appropriate models, or by analogy with those made for echinulin (4) are so indicated. Of particular interest to us is the problem of assignment of the carbons of the indole nucleus. The twofold greater intensities of the two strongest signals in the indole region of the spectrum of **1** clearly establish these signals as belonging to carbons deriving nOe enhancement from an attached proton, *i.e.* C_4 and C_6. Although the observed signals appeared at 114.6 and 122.4, the shifts predicted from the substituent parameters derived from a study of indole and its monomethyl derivatives (5) were essentially equal for C_4 (120.1) and C_6 (120.3). A second indication that the earlier indole data contained erroneous assignments was a similar deviation in the shifts in 2,5,7-trimethylindole which we have measured as a useful model for hexahydroechinulin. The shifts for C_6 in this compound as given in Table 1 could not be rationalized on the basis of Roberts' data. We therefore reexamined the spectrum of 5-methylindole with a view to checking the assignments for C_4 and C_6 in this compound. Single frequency off-resonance spin-decoupling experiments showed clearly that the resonance at 120.8 is due to the carbon atom whose attached proton appears at lowest field (δ 7.3) in the proton spectrum. Since this proton is readily assigned to position 4 on the basis of its being the only singlet (broadened by long-range splittings), the original assignments to C_4 and C_6 must be reversed. In addition, the recent studies of Gribble *et al.* (6) have revealed another error in the assignments of alkyl indoles.

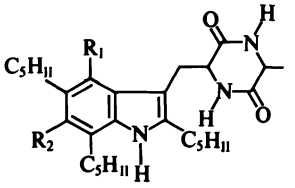

2 $R_1 = R_2 = H$
3 $R_1 = Br, R_2 = H$
4 $R_1 = H, R_2 = NO_2$

They proved that the shifts for C_5 and C_6 are the reverse of those originally given for indole and for 2,3-dialkylindole. The same was proposed to be the case (but not rigorously proven) for all the other indoles in the original study. These two errors have resulted in subsequent erroneous assignments in the work of Roberts' group on Rauwolfia alkaloids (7) and of Wenkert's group (see ref. 8, which contains assignments to the indole ring of seven alkaloids which require C_5 and C_6 to be reversed) on a variety of indole alkaloids. While it is beyond the scope of this paper to reexamine the assignments for all the methylated indoles it would seem worthwhile to clarify the existing indole data in the light of the findings of Gribble and that reported herein.

Revised Shieldings for Indole and its Methyl Derivatives

The shieldings for carbons 4, 5, and 6 in indole, 5-methylindole, and 2,3-dimethylindole are now reassigned the values in Table 1. By assuming that C_5 also appears at higher field

Can. J. Chem. Downloaded from www.nrcresearchpress.com by 210.87.254.42 on 09/05/12
For personal use only.

TABLE 2. Methyl substituent effects in the indole ring system*

	C_2	C_3	C_4	C_5	C_6	C_7
2-Methyl	[10.5]	−2.2	−1.3	−0.4	−1.2	−0.9
3-Methyl	−2.5	[8.8]	−1.9	−0.7	0.0	−0.1
4-Methyl	−1.0	−1.5	[8.9]	−0.2	−0.1	−2.5
5-Methyl	−0.2	−0.5	−0.5	[8.5]	1.4	−0.5
6-Methyl	−0.9	−0.3	(−0.6)	(1.6)	[9.2]	−0.2
7-Methyl	−0.4	0.4	(−2.4)	(0.0)	0.4	[9.1]

*In ppm from indole. Square brackets indicate substituted carbons. Shifts in parentheses are tentative.

than C_6 in all the other methylated indoles the remaining shieldings in Table 1 can be assigned. There are four pairs of assignments remaining in doubt which are so indicated in this table.[2] The set of methyl substituent parameters derived from these new shielding assignments are given in Table 2.[3] It is noteworthy that they now show a narrower range of both α and β effects. Use of these effects now gives good agreement, <0.6 ppm, between the predicted and observed shieldings of 2,3,5- and 2,5,7-trimethylindole. Only C_2 and C_3 of the former deviate by larger amounts, not surprisingly, since they are close to the site of *ortho* disubstitution where additivity effects are known to fail. Furthermore it is interesting to note the reciprocal character of these substituent effects, *i.e.* the effect of introducing a methyl group at position 5 on the shielding of C_4 is similar to that of position 4 on C_5. The revised shielding for the di- and trimethylindoles are also given in Table 1. From this data it is now clear that the signals at 114.6 and 122.4 in hexahydroechinulin belong to the carbons C_4 and C_6 of the indole nucleus, respectively.

Positions of Br and NO_2 Substituents in Hexahydroechinulin

The pioneering work of Lauterbur established the fact that substituent effects on aryl carbon shieldings are additive except in certain *ortho* di- or trisubstituted benzene derivatives. For example, a comparison of the shift at C_3 in 2,6-dimethyliodobenzene (10) with the shift at C_4 of *meta*-xylene shows that the iodo substituent causes a downfield shift of 2.6 ppm, an effect identical (within the precision of that time) to that at the *meta* carbon of iodobenzene *vs.* benzene, 2.9 ppm (10). However, the effect of a nitro group on the *meta* shielding was not the same in benzene *vs.* nitrobenzene as in *meta*-xylene *vs.* 2,6-dimethylnitrobenzene since steric inhibition of resonance is present in the latter case (10, 11). A comparison of these shieldings (C_3 in 2,6-dimethylnitrobenzene is 129.9 (11) *vs.* C_4 in *meta*-xylene at 126.4 (12)) indicates a 3.5 ppm deshielding effect upon introduction of the nitro group. Since this figure involves data obtained by two different investigators using two different solvents and two different references, we have redetermined this effect by measuring the same shifts for 0.5 *M* solutions of *m*-xylene and 2,6-dimethylnitrobenzene in $CDCl_3$ using TMS as internal reference. The effect of a nitro group on the *meta* shielding using our data (see Experimental) is +2.8 ppm in quite good agreement with the +3.5 ppm figure estimated above. The effect of introducing a bromine substituent on a *meta* carbon shift of benzene was found by Spiesecke and Schneider to be +2.2 ppm (13). In view of Lauterbur's demonstration that the iodo substituent parameter is the same in the case of 2,6-dimethyliodobenzene as in iodobenzene, we feel justified in assuming the effects will be the same in bromobenzene as in 2,6-dimethylbromobenzene since both systems lack the complicating influence of steric inhibition of resonance.

Having selected *meta* shielding parameters of 2.2 and 2.8 for the bromo and nitro substituents respectively it remains to determine the position of these substituents in bromohexahydroechinulin and nitrohexahydroechinulin. In Table 3 are given the chemical shifts of the remaining strong

[2]The new shieldings for C-4 *vs.* C-6 of indole in Table 1 are assumed to be in the order established for 5-methylindole although they were not completely proven by Levy and co-workers. The alternative assignment leads to a quite inconsistent set of substituent parameters. For example, if C_6 were at 121.3 the effects of methyl substitution at C_3, C_4, or C_7 would all be positive (deshielding) while for methyl substitution at every other site of the benzene ring they are negative.

[3]It is noteworthy that the original contents of these two tables appear in Stothers' book on ^{13}C nmr (9) along with comments on the limits of their accuracy.

Can. J. Chem. Downloaded from www.nrcresearchpress.com by 210.87.254.42 on 09/05/12
For personal use only.

Can. J. Chem. Downloaded from www.nrcresearchpress.com by 210.87.254.42 on 09/05/12
For personal use only.

TABLE 3. Carbon shieldings in the indole ring of some hexahydroechinulins*

Compound	Observed shifts C_4	Observed shifts C_6	Predicted shifts C_4	Predicted shifts C_6
Hexahydroechinulin	114.6	122.4		
Bromohexahydroechinulin		124.0	116.8	124.6
Nitrohexahydroechinulin	116.6		117.4	125.2

*Shifts in ppm from TMS.

peak in the indole portion of the ^{13}C spectrum of each derivative (the peak which is assigned to the carbon bearing a proton and hence benefitting from intensity enhancement by a combination of Overhauser and relaxation effects). In addition the shifts predicted from the observed shieldings of C_4 and C_6 in hexahydroechinulin and the above shielding parameters are presented for comparison.

For each derivative there is agreement to better than 1 ppm as opposed to 7 ppm for the alternative assignment of substituent position which clearly establishes the compounds to be 4-bromohexahydroechinulin and 6-nitrohexahydroechinulin.

Experimental

Compounds

Hexahydroechinulin and its bromo and nitro derivatives have been prepared as described previously (2, 3). A sample of 2,5,7-trimethylindole was obtained as a gift from Dr. O. E. Edwards of the National Research Council of Canada. 5-Methylindole was purchased from Sigma Chemical laboratories.

Nuclear Magnetic Resonance Spectra

The ^{13}C spectra were run on a Varian CFT-20 nmr spectrometer. All chemical shifts in this study were obtained from measurements of 0.25 *M* solutions in $CDCl_3$ relative to internal tetramethylsilane as standard. It is noteworthy that a comparison of the shifts for 5-methylindole obtained from 0.2 and 2.0 *M* solutions showed differences of up to 0.7 ppm with the shifts moving to higher field on dilution. The data quoted in Table 1 for 2,5,7-trimethylindole is thus not strictly comparable with data for other indoles as the spectrum was measured using a 0.4 *M* solution while the remaining data comes from 5 *M* solutions in dioxane (5).

The signals observed for **2**, **3**, and **4** are given with their relative intensities in brackets and the assignments which can be made with reasonable certainty follow using the numbering on formula **1**.

Hexahydroechinulin, **2**—9.4 (32) 2c; 19.9 (38) 3e; 22.6 (100) 5, 7 d, e; 28.0 (65); 28.3 (60); 28.7 (32); 30.1 (36) 3a; 34.1 (34); 36.4 (43); 36.9 (26); 38.9 (33); 41.9 (36); 50.8 (48) 3d; 54.8 (36) 3b; 104.3 (21) 3; 114.7 (38) 4; 122.4 (38) 6; 124.7 (16) 7; 128.9 (15) 5; 131.8 (8) 8; 135.1 (14) 2; 142.6 (14) 9; 168.1 and 169.0 (20) and (28) 3c and 3f.

4-Bromohexahydroechinulin, **3**—9.4 (24) 2c; 19.2 (20) 3e; 22.7 (100) 5, 7, d, e; 28.1 (69); 28.3 (68); 28.7 (26); 34.5 (24); 36.4 (30); 37.3 (17); 38.8 (19); 40.4 (29); 50.8 (26) 3d; 55.1 (14) 3b; 105.8 (8) 3; 112.0 (6) 4; 124.0 (33) 6; 124.2 (13) 7; 133.2 (5) 5; 134.8 (7) 8; 143.4 (6) 2; 143.9 (9) 9; 168.3 and 169.1 (8) and (8) 3c and 3f.

6-Nitrohexahydroechinulin, **4**—9.3 (32) 2c; 20.1 (34) 3e; 22.4 (93) 5, 7 d, e; 25.3 (30); 28.1 (100); 30.0 (76) 3a; 36.3 (36); 37.2 (25); 38.9 (31); 40.8 (33); 50.9 (43) 3d; 55.2 (34) 3b; 105.1 (17) 3; 116.6 (36) 4; 117.7 (12) 5; 126.8 (14) 2 or 7; 129.9 (9) 7 or 2; 130.8 (11) 8; 146.2 (13) 9; 146.7 (5) 6; 168.0 and 168.3 (22) and (19) 3c and 3f.

Acknowledgments

We wish to thank Dr. I. C. P. Smith and Mr. Leo Taylor of N.R.C.C. (Ottawa) who performed the single frequency off-resonance spin-decoupling experiments, as well as running the majority of the regular spectra. We also thank Dr. O. E. Edwards for the sample of 2,5,7-trimethylindole. The financial assistance of the National Research Council of Canada is gratefully acknowledged.

1. G. GASNATI, R. CAVALLERI, F. PIOZZI, and A. QUILICO. Gazz. Chim. Ital. **92**, 105 (1962).
2. A. QUILICO, F. PIOZZI, and M. DUBINI. Gazz. Chim. Ital. **88**, 1308 (1958).
3. A. QUILICO, F. PIOZZI, and C. CARDANI. Gazz. Chim. Ital. **88**, 125 (1958).
4. R. CARDILLO, C. FUGANTI, G. GATTI, D. GHIRINGHELLI, and P. GRASSELLI. Tetrahedron Lett. 3163 (1974).
5. R. G. PARKER and J. D. ROBERTS. J. Org. Chem. **33**, 996 (1970).
6. G. W. GRIBBLE, R. B. NELSON, J. L. JOHNSON, and G. C. LEVY. J. Org. Chem. **40**, 3720 (1975).
7. R. H. LEVIN, J.-Y. LALLEMAND, and J. D. ROBERTS. J. Org. Chem. **38**, 1983 (1973).
8. E. WENKERT, J. S. BINDRA, C.-J. CHANG, D. W. COCHRAN, and F. M. SCHELL. Acc. Chem. Res. **7**, 46 (1974).
9. J. B. STOTHERS. Carbon-13 NMR spectroscopy. Academic Press, New York. 1972. p. 266.
10. P. C. LAUTERBUR. J. Chem. Phys. **38**, 1406 (1963); **38**, 1415 (1963).
11. P. C. LAUTERBUR. J. Chem. Phys. **38**, 1432 (1963).
12. W. R. WOOLFENDEN and D. M. GRANT. J. Am. Chem. Soc. **88**, 1496 (1966).
13. H. SPIESECKE and W. G. SCHNEIDER. J. Chem. Phys. **35**, 731 (1961).

Ion formation in hydrocarbon flames[1]

ARTHUR T. BLADES

Chemistry Division, Physical Sciences Branch, Alberta Research Council, 11315-87th Avenue, Edmonton, Alta., Canada T6G 2C2

Received October 6, 1975[2]

ARTHUR T. BLADES. Can. J. Chem. **54**, 2919 (1976).

While it is generally accepted that ions arise in hydrocarbon flames by the CH—O mechanism, the only indication that this is the sole mechanism is the equal per carbon response of most hydrocarbons in the flame ionization detector. This response feature can equally be attributed to other flame processes and does not apply to C_2H_2 in any case. Comparison of rates of ion formation with CH and As emission intensities indicates that C_2H_2 and CH_4 give abnormal rates of ion formation which can be explained on the basis of one or more additional mechanisms of ion formation.

ARTHUR T. BLADES. Can. J. Chem. **54**, 2919 (1976).

Alors qu'il est généralement accepté que des ions soient formés par un mécanisme CH—O dans une flamme d'hydrocarbure, la seule indication qui dise que ce soit l'unique mécanisme est la réponse égale par carbone de la plupart des hydrocarbures dans le détecteur à ionisation de flamme. La caractéristique de cette réponse peut être attribuée également à d'autres processus de la flamme et ne s'applique pas à C_2H_2 en aucun cas. La comparaison des vitesses de formation des ions avec les intensités d'émission de CH et de As montrent que C_2H_2 et CH_4 donnent des vitesses anormales de formation des ions qui peuvent être expliquées en se basant sur un ou plusieurs mécanismes additionnels de formation des ions.

[Traduit par le journal]

Introduction

The evidence for the chemi-ionization reaction in hydrocarbon flames

[1] $$CH + O \rightarrow CHO^+ + e$$

is now so overwhelming that little serious consideration is given to alternate mechanisms (1–4). A significant feature of this evidence is that it has been obtained from diverse physical systems, including low and high pressure flames, premixed and diffusion flames, atomic flames, and shock tube oxidations, and from measurements of reactant and product concentrations and rates of ion formation, yet no single piece of evidence is, in itself, conclusive. When equivocal evidence is marshalled in favour of a particular mechanism, there is the implicit assumption that only one mechanism exists. Whether this is valid for chemi-ionization in hydrocarbon flames bears re-examination.

Major support for the contention that only one mechanism is operative arises from the observation that the relative sensitivities of hydrocarbons in the flame ionization detector are proportional to their carbon number (5). A major deviant from this generalization is C_2H_2, which has a sensitivity 30% higher than other hydrocarbons and this might imply a second chemi-ionization reaction specific to C_2H_2 (6). A similar 'equal per carbon response' feature has been observed (7) for paraffins in a low pressure flame and, therein, C_2H_2 gives three times as many ions as C_2H_6, indicating that in some flames additional mechanisms of ion formation may be of considerable importance. It might be argued that since an additional mechanism of ion formation need only be considered seriously for C_2H_2, it is not of concern for hydrocarbon flames in general; this is probably true, but most of the evidence for reaction 1 has been obtained from studies of C_2H_2 oxidation. Thus while separate pieces of evidence may be explicable on the basis of this mechanism, they cannot be legitimately considered as cumulative evidence in its favour.

The response characteristics of the flame ionization detector are, in any case, open to alternate or more general explanations. The linear response of the detector over at least 4 decades of hydrocarbon concentration (5) implies that the parent hydrocarbon and its fragments

[1]Contribution No. 782 from Alberta Research Council, Edmonton, Alberta.

[2]Revision received May 27, 1976.

Can. J. Chem. Downloaded from www.nrcresearchpress.com by 210.87.254.40 on 09/05/12
For personal use only.

Can. J. Chem. Downloaded from www.nrcresearchpress.com by 210.87.254.40 on 09/05/12
For personal use only.

undergo first order reactions (in hydrocarbon species) exclusively. The equal per carbon response, on the other hand, may imply that the parent hydrocarbon is totally converted to a single carbon species prior to its oxidation, independent of its original structures (7). This species may be CH and it may subsequently initiate a single chemi-ionization reaction.

The equal per carbon response has been found to apply to the flame ionization detector only when it is operated in its standard mode (8), and the response pattern has been judged to arise from the character of the basic flame rather than from the hydrocarbon itself. It was therefore postulated that in this flame, hydrocarbons in general are totally degraded by H-atom reactions prior to oxidation and that the most reasonable single carbon product of this reaction is CH_3. Subsequent reactions of CH_3 may then produce ions by one, or several, mechanisms independent of the original hydrocarbon structures.

If the equal per carbon response feature fails for a particular hydrocarbon, as is indicated for C_2H_2 (5), the implication would be that it is not totally degraded to CH_3 prior to oxidation. The 'high' level of ion formation from C_2H_2 might have arisen from an alternate mechanism of conversion of C_2H_2 to CH, such as postulated in the oxidation studies of Williamson and Bayes (9). To explore this possibility, Klemm and Blades (6) examined two other consequences of hydrocarbon oxidation in a H_2-in-O_2 diffusion flame which are first order in CH_4 and other hydrocarbon concentrations, and which may depend on the CH concentration, namely CH emission and the hydrocarbon-stimulated emission of As atoms (10, 11). Both these additional parameters indicated low responses for C_2H_2 compared to CH_4, C_2H_6, and C_2H_4, and Klemm and Blades (6) postulated that the excess ion formation from C_2H_2 arises from

$$[2] \qquad C_2H + O_2^* \rightarrow CO + CHO^+ + e$$

Peeters *et al.* (12) have made rate of ion formation and CH emission measurements on a H_2–O_2 premixed flame containing traces of several hydrocarbons and also observe a first order component of CH emission for several hydrocarbons, including CH_4. Excitation of CH is primarily attributed to

$$[3] \qquad CH + H + OH \rightarrow CH^* + H_2O$$

They observe excess CH emission over ion formation for C_2H_2 and C_4H_{10} which they attribute to

$$[4] \qquad C_2 + OH \rightarrow CH^* + CO$$

and/or

$$[5] \qquad C_2H + O \rightarrow CH^* + CO$$

the C_2 and/or C_2H being postulated to arise by processes first order in the parent hydrocarbon. The system does not give good first order dependence, however, nor is the 'equal per carbon response' feature particularly obvious for any class of compounds. The study does indicate the possibility of further discrepancies between ion formation and other indicators of CH concentration and a more extensive study of hydrocarbon oxidations in the H_2-in-O_2 diffusion flame has been undertaken.

Experimental

Measurements of rates of ion formation and emission intensity were carried out simultaneously on a basic H_2-in-O_2 diffusion flame on a modified flame photometry burner (9). About 1 l/min of H_2 entered through an axial jet (0.75 mm) and about 4 l/min of O_2 through an annulus and, with traces of hydrocarbon in the H_2, a stable luminous reaction zone about 4 mm high was formed. With the burner polarized at -150 V, ions were collected on a helix above the luminous zone while emission intensities were observed on an EMI 6255S photomultiplier attached to a Zeiss M 4 Q III spectrometer using photon counting circuitry.

The effect of hydrocarbon concentration on the rates of ion formation or emission intensities was determined by injecting known volumes to the hydrogen stream prior to a 1 l mixing chamber. For comparison of the various hydrocarbons, measurements were carried out with carbon concentrations equivalent to 300 ppm CH_4 in H_2, integrated responses being used to avoid diffusional differences. The deuterated compounds were purified by gas chromatography using an H_2 carrier and were monitored by a katharometer before admission to the mixing chamber. When arsenic was to be added to the flame, a few cc/min of a 1% mixture of AsH_3 in H_2 was added continuously to the H_2 stream. This increased the background emission in the neighborhood of CH (431.5 nm) emission and made it impossible to measure both emissions on the same flame.

Results

The linear dependence of the rate of ion formation and of CH (431.5 nm) emission has previously been established for CH_4, C_2H_6, C_2H_4, and C_2H_2, and data for C_2H_4, C_3H_6, iso-C_4H_{10}, and neo-C_5H_{12} are presented in Figs. 1 and 2.

Can. J. Chem. Downloaded from www.nrcresearchpress.com by 210.87.254.40 on 09/05/12
For personal use only.

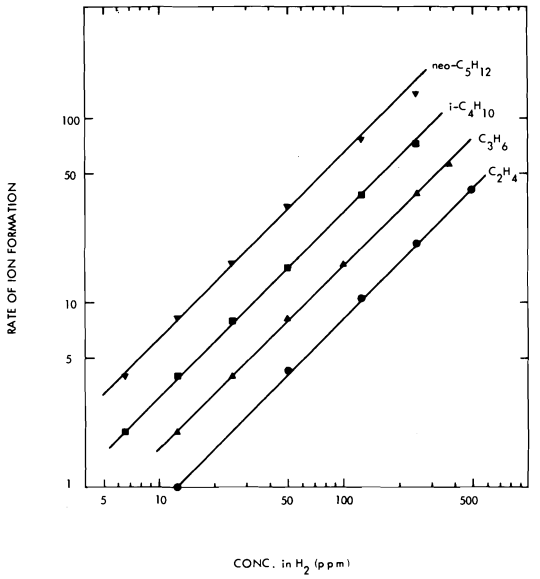

FIG. 1. Rates of ion formation *vs.* concentration (ppm) for various hydrocarbons.

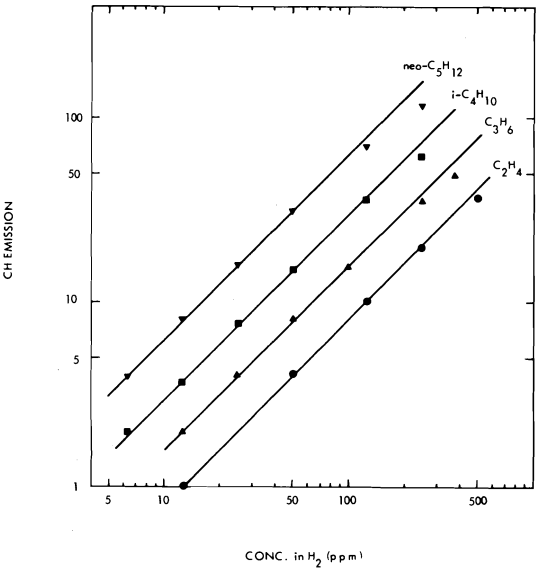

FIG. 2. CH emission (431.5 nm) intensity *vs.* concentration (ppm) for various hydrocarbons.

This linearity appears to be general in the concentration range studied. Data from a comparison of the relative rates of ion formation and CH emission from a variety of hydrocarbons are presented in Table 1 as relative rates on a per carbon basis. Similar data for a comparison of

TABLE 1. Relative rates of ion formation and of CH* emission (431.5 nm) on a per carbon atom basis

Compound	Relative rates of: Ion formation	Relative rates of: CH* emission	Ratio ions:CH*
CH_4	1.02	0.82	1.24
C_2H_6	0.98	0.99	0.99
C_3H_8	0.98	0.99	0.99
n-C_4H_{10}	1.01	1.04	0.97
i-C_4H_{10}	1.00	0.98	1.02
neo-C_5H_{12}	1.04	1.04	1.00
C_2H_4	1.00	0.90	1.11
C_3H_6	0.98	0.96	1.02
1-C_4H_8	1.01	1.00	1.01
cis-C_4H_8	0.98	0.98	1.00
i-C_4H_8	1.01	0.98	1.03
C_2H_2	1.37	0.79	1.73

TABLE 2. Relative rates of ion formation and of As* emission (228.8 nm) on a per carbon atom basis

Compound	Relative rates of: Ion formation	Relative rates of: As* emission	Ratio ions:As*
CH_4	1.07	0.89	1.20
C_2H_6	0.97	0.95	1.02
C_3H_8	0.97	0.96	1.01
n-C_4H_{10}	1.03	1.04	0.99
i-C_4H_{10}	1.03	1.03	1.00
neo-C_5H_{12}	1.04	1.06	0.98
C_2H_4	1.02	0.92	1.11
C_3H_6	0.99	0.99	1.00
1-C_4H_8	1.03	1.04	0.99
cis-C_4H_8	0.98	1.01	0.97
i-C_4H_8	1.01	1.03	0.98
C_2H_2	1.30	0.69	1.88

rates of ion formation and of arsenic emission at 228.8 nm are presented in Table 2. These data have been arbitrarily normalized around the average relative rate of ion formation and the relative CH emission intensity of those compounds for which the ratio was constant within $\pm 3\%$. This meant the exclusion of CH_4, C_2H_4, and C_2H_2 in each case. In Table 3, data for the relative rates of ion formation and CH emission for CH_4, CD_4, C_2D_6, C_2H_2, and C_2D_2 are compared with the rates for C_2H_6. Since CD rather than CH emission at a different wavelength and sensitivity might be expected on the addition of perdeutero compounds to a H_2 flame, it would be desirable to know the relative proportions of

Can. J. Chem. Downloaded from www.nrcresearchpress.com by 210.87.254.40 on 09/05/12
For personal use only.

TABLE 3. Rates of ion formation and of CH* emission (431.5 nm) on a per carbon basis relative to C_2H_6

Compounds	Relative rates of: Ion formation	Relative rates of: CH* emission	Ratio ions:CH*
C_2H_6	1.00	1.00	1.00
C_2D_6	1.14	1.17	0.97
CH_4	1.08	0.85	1.27
CD_4	1.47	0.82	1.79
C_2H_2	1.43	0.79	1.81
C_2D_2	1.47	0.83	1.77

CH and CD emission. It was shown however that, when CH_4 was added to a D_2-in-O_2 flame, only CD emission occurred at CH_4 concentrations in the first order regime. It was therefore assumed that only CH emission arises from deutero compounds in a H_2 flame, although this is much more difficult to establish experimentally.

Discussion

The flame system used in these studies is fundamentally identical to the analytical flame ionization detector (5), *i.e.* the basic flame is a H_2-in-O_2 diffusion flame, and the hydrocarbon being oxidized is introduced into the H_2. The observation of rates of ion formation linear in hydrocarbon concentrations at least up to 500 ppm of C_2H_4, or its equivalent (Fig. 1), was, therefore, not unexpected. Likewise, the fairly constant relative rates of ion formation of various hydrocarbons on a per carbon basis (Table 1) indicate a further similarity of these two systems. In addition, as indicated by Fig. 2, Tables 1 and 2, and previous publications (6, 10), both CH and As emissions are first order in hydrocarbon concentration and exhibit similar equal, per carbon atom intensities for a variety of hydrocarbons. Thus, while the chemical reactions exciting these two emissions are not well established, both would have prompted the proposition of total decomposition of the parent hydrocarbon to a single carbon species as was initially derived from the flame ionization pattern.

As previously found in the more limited studies (6), the equal per carbon response feature is not completely uniform; this is particularly obvious from the ratios of ion formation to CH emission, Table 1, and to As emission, Table 2. The higher precision and the larger number of systems examined now reveals apparent anomalies in the behaviour of CH_4, C_2H_4, and C_2H_2, the ion to emission ratios being apparently high in each case. In order to discuss these anomalies, the reaction pattern dominated by H-atoms (8) has been adopted despite the lack of 'proof' of the total conversion of the additive hydrocarbons to a single carbon fragment (CH_3) because it is the only known mechanism which describes the general response pattern. The behaviour of C_2H_2, C_2H_4, and CH_4 are discussed separately on this basis.

A. C_2H_2

As previously suspected from more limited data (6), C_2H_2 gives a higher rate of ion formation and a lower CH and As emission than the majority of hydrocarbons. It might be argued that the 'low' CH intensity for C_2H_2 is the norm and that the other multi-carbon hydrocarbons give some CH emission via reactions of C_2 or C_2H which arise by processes first order in the parent hydrocarbon and that they, rather than C_2H_2, are abnormal. It is difficult to imagine a class of reactions which would convert hydrocarbons in general to C_2 or C_2H without C_2H_2 being an intermediate, yet doing so equally, on a per carbon basis, for such odd and even carbon atom compounds as C_2H_6 and C_3H_8. Concurrently, it would have to be argued that the 'high' level of ion formation for C_2H_2 is normal and that the majority of other hydrocarbons give equivalent, but low, rates of ion formation. The simultaneous operation of these coincidences seems unlikely.

Alternately, the C_2H_2 anomaly might arise as a result of the complex nature of the flame. If ions arise only by the CH—O reaction, then their formation occurs in that region of the flame where the CH and O concentration profiles overlap. Likewise, on the assumption that CH emission is proportional to the CH ground state concentration, as would apply for thermal excitation of CH or in reaction III, CH emission intensity would depend on the interaction of the CH concentration profile with that of other profiles which are effective in its excitation. Now, if for C_2H_2 the CH profile is shifted to give greater overlap with the O-atom profile and less appropriately for CH excitation, then the 'high' rate of ion formation and the low CH emission would result. The validity of this rationalization

Can. J. Chem. Downloaded from www.nrcresearchpress.com by 210.87.254.40 on 09/05/12
For personal use only.

of the C_2H_2 data can only be tested by a further monitor on the CH concentration. Metal atom chemi-emission in hydrocarbon flames is believed to involve CH (10, 11), and may arise in a variation of the overall process,

[6] $$CH + O + M \rightarrow CHO + M^*$$

The data in Table 2 on As atom emission show the same general features of equal per carbon response as ion formation and CH emission. Most notable, however, is the low value of As emission for C_2H_2 and consequently the fairly good correspondence between As emission, Table 2, and CH emission, Table 1. This is taken to imply that CH and As emission are better monitors of CH concentration than is ion formation and, if the assumptions are correct, that all ions from C_2H_2 do not arise by the CH—O mechanism.

While these observations suggest that other mechanisms for ion formation may be operative for C_2H_2, they in no way indicate why C_2H_2 should be unique or how ions might be formed. It is known that C_2H_2 catalyzes the recombination of H-atoms (13) and it is therefore not unreasonable to expect a portion of the C_2H_2 to avoid H-addition and subsequent C—C bond cleavage as has been assumed to occur with hydrocarbons in general. If this C_2H_2 enters the oxidative zone, it may give rise to ions by reactions of either C_1 or C_2 species arising there. Previously it was suggested that ions might arise by reaction 2 (6). This process is in accord with the mass spectrometric evidence (14) and, if O_2^* is $A^3\Sigma^+_u$, is quite exothermic. In addition, the reaction is analogous to the reaction for ion formation from cyano-compounds in flames (7, 15, 16).

[7] $$CN + O_2^* \rightarrow CO + NO^+ + e$$

On the other hand, C_2H_2 is known to react with O-atoms to give CH_2 (17) and, if O_2^* is a reasonable reactant, a further ion-forming reaction is also possible:

[8] $$CH_2 + O_2^* \rightarrow CHO^+ + OH^-$$

This reaction also suits the mass spectrometric evidence (14) and is exothermic. The ion, OH^-, is commonly observed in hydrocarbon flames (1) but it is generally thought to arise by electron attachment.

There are, therefore, two possible mechanisms of ion formation which might explain excess ion formation over CH emission from C_2H_2, and both depend on the failure of H-atoms to cleave the C≡C bond. If reaction 2 is the origin of this ionization, excess CH emission might also have been expected by reaction 5. The marginally greater CH emission (Table 1) over As emission (Table 2) cannot be attributed to this source with any confidence, and this might be taken as evidence against reaction 2 as the source of ions. This is particularly pertinent in view of the observation of excess CH emission from C_2H_2 by Peeters *et al.* (12). It is important to recognize, however, that, even at their lowest concentration, about 15% of the CH emission in the flame arose from processes judged to be second order in hydrocarbon concentration. Under these circumstances, very little confidence should be attached to the relative values of the coefficients of the first order part of their CH emission. In addition, reaction 5 is a possible, but unproven, source of CH*.

It is interesting to note in Table 3 that there is no significant isotope effect in ion formation or CH emission with C_2H_2. This is consistent with the expectation that H-atom exchange would occur during the catalytic function of C_2H_2 in H-atom recombination.

B. C_2H_4

The data in Tables 1 and 2 indicate a substantial anomaly in the CH and As emission for C_2H_4, both being about 10% lower than the ion formation. In its reactions with H-atoms, C_2H_4 gives about 90% addition and 10% abstraction (18); the C_2H_5 from the former would be predicted to further react with H-atoms to give CH_3, as with hydrocarbons in general, while the C_2H_3 from abstraction would convert to C_2H_2 and thereafter exhibit C_2H_2 type behaviour, *i.e.* high ion to emission ratios, as are observed. Thus, C_2H_4 behaves predictably on the basis of the H-atom fragmentation scheme and the known response of C_2H_2.

C. CH_4

The deviation of CH_4 from the norm established for the majority of hydrocarbons is difficult to accept, particularly since the total conversion of hydrocarbons to CH_3 is the assumed origin of the 'equal-per-carbon' sensitivity feature of the flame (8). In addition, the rate of ion formation is only slightly high. Never-

Can. J. Chem. Downloaded from www.nrcresearchpress.com by 210.87.254.40 on 09/05/12
For personal use only.

theless, CH and As emission are both 'low' and it may be postulated that the relative per carbon CH emission (Table 1) of 0.82 has its origin in the incomplete conversion of CH_4 to CH_3. The rate of abstraction by H-atoms is five times greater for C_2H_6 than for CH_4 (18) and, if CH_4 were 82% converted to CH_3, C_2H_6 would be virtually completely converted to C_2H_5 and, presumably, to CH_3.

This hypothesis was tested by an examination of the hydrogen isotope effects. If CH_4 is incompletely converted to CH_3 by H-atom abstraction, the attack on CD_4 should be substantially less, and the methane anomaly amplified, subject to subsequent isotope effects along the path to ion formation and CH emission. The importance of these latter effects was explored by a comparison of C_2H_6 and C_2D_6; as shown in Table 3, there is about a 15% reverse isotope effect in both ion formation and CH emission. The expected response from CD_4 would therefore be enhanced ion formation as a result of the reduced conversion to CD_3, as judged from the CH_4 ion formation, and a further enhancement from the reverse isotope effect from that portion of the CD_4 converted to CD_3. The CH emission, on the other hand, would be reduced by virtue of the lesser conversion to CD_3, but enhanced by the reverse isotope effect from that converted to CD_3. These predictions are confirmed by the data in Table 3; ion formation from CD_4 is substantially enhanced over CH_4 while CH emission is virtually the same. This evidence supports the proposition that CH_4 is incompletely converted to CH_3 in the pre-oxidative zone. As with C_2H_2, the excess of ion formation over CH emission for CH_4 may reasonably be proposed to arise in ion-forming reactions of CH_4 in the oxidative zone. Equally, it may be attributed to the CH—O reaction, but the As emission data in Table 2 do not support this explanation. It might be attributed to the CH_2—O_2* reaction, 8, and this would require that CH_2 be formed directly from CH_4, without the intermediacy of CH_3 or the subsequent formation of CH. This is an unconventional mechanism for the oxidation of CH_4 (19) but it appears necessary to explain the anomalies observed in ion formation and CH emission from CH_4 in this flame system.

In conclusion, the equal-per-carbon response feature of the flame ionization detector for hydrocarbons is consistent with one or more chemi-ionization reactions and deviations from this pattern are most reasonably explained by additional chemi-ionization processes.

Acknowledgements

The author acknowledges useful discussions with E. M. Bulewicz, P. J. Padley, T. M. Sugden, H. W. Habgood, and D. J. Currie.

1. W. J. Miller. XIV Symposium (Internat.) on Combustion. Combustion Institute. 1973. p. 397.
2. (*a*) A. Fintijn. Progress in reaction kinetics. Vol. 6. *Edited by* K. R. Jennings and R. B. Cundall. Pergamon Press, 1971. p. 75, (*b*) A. Fintijn. Pure Appl. Chem. **39**, 287 (1974).
3. H. F. Calcote and W. J. Miller. Chemical reactions under plasma conditions. Vol. 2. *Edited by* M. Venugopalan. Interscience Publishers. 1971. p. 327.
4. W. J. Miller. Oxidation Combust. Rev. **3**, 97 (1968).
5. J. C. Sternberg, W. S. Gallaway, and D. T. L. Jones. Gas chromatography. *Edited by* N. Brenner, J. E. Callen, and M. D. Weiss. Academic Press, New York. 1962. p. 231.
6. R. F. Klemm and A. T. Blades. Nature, **212**, 920 (1966).
7. E. M. Bulewicz and P. J. Padley. IXth Symposium (Internat.) on Combustion. Academic Press, New York. 1963. pp. 638 and 647.
8. A. T. Blades. J. Chromatog. Sci. **11**, 251 (1973).
9. D. G. Williamson and K. D. Bayes. J. Phys. Chem. **73**, 1232 (1969).
10. A. T. Blades. Can. J. Chem. **49**, 2476 (1971).
11. D. Gutman and S. Matsuda. Can. J. Chem. **49**, 3904 (1971).
12. J. Peeters, J. F. Lambert, P. Hertoghe, and A. Van Tiggelen. XIIIth Symposium (Internat.) on Combustion. Combustion Institute. 1971. p. 321.
13. J. V. Michael and H. Niki. J. Chem. Phys. **46**, 4969 (1967).
14. J. A. Green and T. M. Sugden. IXth Symposium (Internat.) on Combustion. Academic Press, New York. 1963. p. 607.
15. A. T. Blades. J. Chromatog. Sci. **10**, 693 (1972).
16. A. Van Tiggelen, J. Peeters, and C. Vinckier. XIII Symposium (Internat.) on Combustion. Combustion Institute. 1971. p. 311.
17. C. P. Fenimore and G. W. Jones. J. Chem. Phys. **39**, 1514 (1963).
18. K. Schofield. Planet. Space Sci. **15**, 643 (1967).
19. C. P. Fenimore. Chemistry in premixed flames. The Macmillan Co., New York. 1964.

C-Nucleosides and related compounds. VIII. Synthesis of 5-(4′β-hydroxymethyl-2′β,3′α-dihydroxycyclopent-1′β-yl)-6-azauracil

G. JUST[1] AND R. OUELLET[2]

Department of Chemistry, McGill University, Montreal, P.Q., Canada H3C 3G1

Received November 26, 1975

G. JUST and R. OUELLET. Can. J. Chem. **54**, 2925 (1976).

Starting from the Diels–Alder reaction of *trans*-β-bromoacrylic acid with cyclopentadiene, a synthesis of the substituted bicycloheptene **8** is described. The stereochemistry of the substituents is clearly defined. Oxidative cleavage of the double bond in the compound **8***c* afforded an acid keto ester **10** that was treated with thiosemicarbazide. Treatment of the resulting thiosemicarbazone **11** with sodium methoxide gave a 3-thioxo-1,2,4-triazine-5-one compound that was converted into the title compound.

G. JUST et R. OUELLET. Can. J. Chem. **54**, 2925 (1976).

A partir de l'adduit d'acide *trans*-β-bromoacrylique avec le cyclopentadiène, une synthèse du bicycloheptène substitué **8** est décrite. La stéréochimie des substituants est nettement définie. Une coupure oxydative de la double liaison du composé **8***c* a donné un acide céto ester **10** qui a reagi avec la thiosemicarbazide. La thiosemicarbazone **11** obtenue a été traitée avec le methylate de sodium pour donner une triazine-1,2,4 one-5 thioxo-3 qui a été transformée en la triazine désirée.

Can. J. Chem. Downloaded from www.nrcresearchpress.com by 210.87.254.5 on 09/05/12
For personal use only.

The *C*-nucleosides form a class of compounds that are characterized by a carbon–carbon bond between the β-D-ribofuranosyl residue and the heterocyclic aglycone. These are pseudouridine, the constant component of tRNA, and the antibiotics oxazinomycin (or minimycin), formycin, laurusin (or formycin B), oxoformycin B, showdomycin, and pyrazomycin (or pyrazofurin) (1). In order to gain more information on the mode of action of these *C*-nucleosides, many related compounds have been synthesized and their properties studied (for a review see ref. 2).

Interest in the series of *C*-nucleosidic analogues has centered around the preparation of compounds having a ribosyl or an arabinosyl sugar residue linked by a carbon–carbon bond to various heterocyclic rings. Many carbocyclic analogues were also prepared, but none had the 2′,3′-hydroxyl groups *trans* to each other. Our interest in arabino-like carbocyclic analogues of *C*-nucleosides was stimulated by the discovery of aristeromycin (3), a carbocyclic nucleoside, and by the findings that the synthetic arabinofuranosyl analogues of cytosine (4) and adenine (5) exhibited biological activity. It has been reported that 6-azauracil **1***a* inhibited the growth of a number of microorganisms in mice (6). Šorm *et al.* (7) observed the anticancerous action

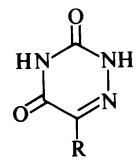

1

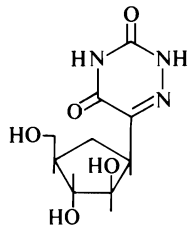

2

a R = H
b R = CH_3
c R = cyclopropyl

of 6-azauracil. The 5-methyl homologue **1***b* of 6-azauracil (6-azathymine) also inhibited the growth of various species of bacteria (8). Many other analogues of 6-azauracil have been published and tested. Recently, a synthesis of 5-cyclopropyl-6-azauracil **1***c* has been described (9).

We now wish to report on the synthesis of a new uracil analogue **2**. The first step consisted of the addition reaction between propiolic acid and hydrobromic acid, giving a mixture of the known geometrical isomers, *cis*- and *trans*-β-bromoacrylic acids (10). Both isomers acted as dienophiles in a Diels–Alder reaction with cyclopentadiene (11).

The bromo acid **3***a* was treated with acid in methanol to give the ester **3***b* that was purified by distillation and fully identified by its spectra and analysis. Epoxidation with *m*-chloroper-

[1]Author to whom inquiries should be addressed.
[2]Holder of an NRCC Scholarship, 1971–1975.

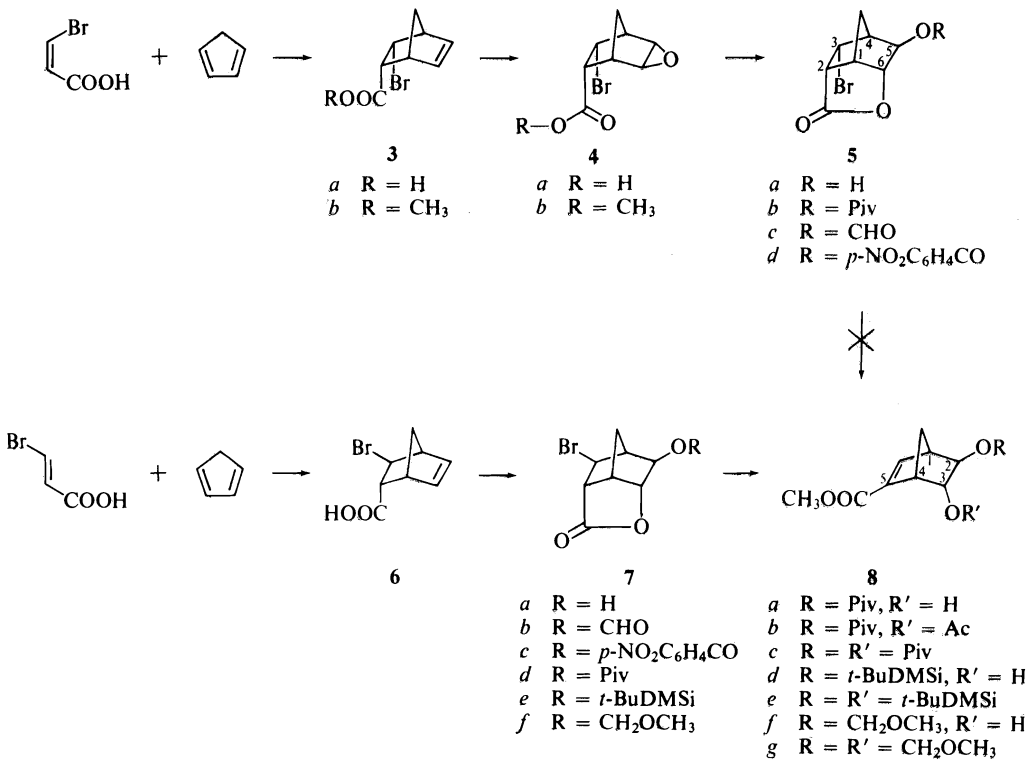

SCHEME 1

benzoic acid afforded the epoxide **4***b*, the *exo* position of which was identified by ir spectroscopy. In similar bicyclic systems, the sharp peak at 850 cm^{-1} has been identified as an *exo* epoxide (12). The compound **4***b* was treated with formic acid to give the hydroxy lactone **5***a* that was pivaloylated to the pivalate **5***b*. The latter compound was also obtained by another route. The adduct **3***a* was treated with hydrogen peroxide in formic acid to give the hydroxy lactone **5***a* and its formate **5***c* (13). The hydroxy lactone **5***a* was formed by a mechanism involving the isomerization of the unstable epoxido intermediate **4***a*. Such intramolecular openings of a three-membered ring by an acid group have received great attention in synthetic chemistry (14). Here, the conformation of the groups (*endo* acid and *exo* epoxide) favoured the internal rearrangement. The alcohol **5***a* was well characterized as its crystalline pivalate **5***b* and *p*-nitrobenzoate **5***d*. The pmr spectra of γ-lactones in similar bicyclo[2.2.1] systems had been of special interest because they exhibited characteristic geminal, vicinal, and long-range coupling constants, as revealed by spin–spin decoupling (15).

The *trans* relationship between the masked hydroxyl functions at C-5 and C-6 in the structure **5***b* is now clearly established from the above reactions. Attempts to open the lactone **5***b* with sodium methoxide and eliminate hydrobromic acid during the same reaction to circumvent relactonization were unsuccessful. On the other hand, when the bromine atom at C-3 was in the *exo* position, the reaction occurred readily. Thus, treatment of the adduct **6** with hydrogen peroxide in formic acid led to the hydroxy lactone **7***a* and its formate **7***b*. Hydrolysis of the formate by a base increased the yield of the hydroxy lactone. On pivaloylation, the alcohol **7***a* afforded the crystalline compound **7***d*. Treatment of this lactone with sodium methoxide resulted in the opening of the lactone function, followed by elimination of hydrobromic acid that neutralized the reagent (1 equiv.) as the reaction proceeded, giving sodium bromide and olefin **8***a*. This product displayed absorptions at 3480 (hydroxyl), 1730 and 1720 (ester carbonyls), and 1610 cm^{-1} (olefin), but no absorption around

Can. J. Chem. Downloaded from www.nrcresearchpress.com by 210.87.254.5 on 09/05/12
For personal use only.

Can. J. Chem. Downloaded from www.nrcresearchpress.com by 210.87.254.5 on 09/05/12
For personal use only.

1790 cm^{-1} (γ-lactone). Its pmr spectrum displayed a one-proton doublet (J = 4 Hz) at δ 7.08 assigned to the H-6 proton, a singlet at δ 3.78 (methyl ester), and an exchangeable proton at δ 3.06 (hydroxyl). The mass spectrum indicated the complete removal of the bromine atom.

Acetylation afforded the oily acetate **8***b* that also displayed the one-proton doublet (J = 4 Hz) at δ 7.07 for the H-6 proton. Treatment of the compound **8***a* with pivaloyl chloride in pyridine produced in high yield the crystalline dipivalate **8***c*.

Similar bicyclic systems having base-stable hydroxyl protecting groups were also prepared. These protecting groups were *tert*-butyl dimethylsilyl and methoxy methyl ethers. Reaction of the alcohol **7***a* with *tert*-butyl dimethylsilyl chloride (16) and imidazole in DMF led to the silyl derivative **7***e* in almost quantitative yield. This derivative was completely identified by its pmr spectrum that was quite similar to the spectra of many other γ-lactones in the bicyclo[2.2.1] series. The lactone **7***e* was then converted into the olefin alcohol **8***d* by a process involving

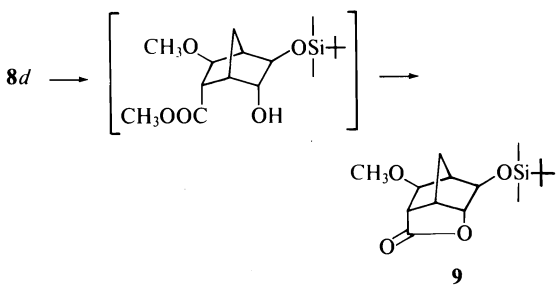

9

firstly the attack of sodium methoxide on the lactone and secondly the elimination of hydrobromic acid to give the product and sodium bromide. Also obtained was a side-product to which the structure **9** was assigned. It arose from the addition of methanol (or sodium methoxide, since a greater excess of it increased the amount of **9**) on the olefin **8***d*, with subsequent relactonization. A closely related reaction is the addition of methanol, catalyzed by base, on 2-carbomethoxynorbornadiene (17). The alcohol **8***d* was then protected by another *tert*-butyl dimethylsilyl group to afford the bicyclo[2.2.1] heptene **8***e*.

Similarly, the alcohol **7***a* was protected as a methoxy methyl ether, using dimethoxymethane and phosphorus pentoxide (18). This method provided the product **7***f* in a quantitative yield. An advantage of the methoxy methyl ether over other protecting groups (*e.g.*, the tetrahydropyranyl group) is the easy identification of the product by pmr spectroscopy. Besides, the reagent is readily available and the reaction is fast (1–2 h). Treatment of the lactone **7***f* with sodium methoxide (1 equiv.) resulted in the opening of the lactone group and the elimination of hydrobromic acid to give the desired compound **8***f*, the alcoholic function of which was protected as another methoxy methyl ether to give the compound **8***g*.

The dipivalate intermediate **8***c* was chosen to prepare the triazine **2**. Oxidative cleavage of this olefin **8***c* afforded the acid keto ester **10***a*. In its ir spectrum, it displayed a broad absorption band between 2500 and 3240 cm^{-1} (acid) and a broad peak at 1750 cm^{-1} (carbonyls). Reaction of the keto ester **10***a* with 2,4-dinitrophenylhydrazine in DMF (19) gave the derivative **10***b*. The derivatives **10***c* and **10***d* were also prepared. Treatment of α-keto ester **10***a* with thiosemicarbazide gave the derivative **11***a* in excellent yield, which was fully characterized as its methyl ester **11***b*. This compound was also obtained on treatment of the dimethoxy ester **10***c* with thiosemicarbazide, confirming that the stereochemistry of the four cyclopentyl substituents was preserved.

The cyclization of thiosemicarbazones **11***a* and **11***b* afforded the 1,2,4-triazines **12***a* and **12***b*, respectively. In the case of compound **11***a*, the reaction with sodium methoxide (2 equiv.) occurred readily at ambient temperature. The resulting cyclized product was transformed into its methyl ester **12***b* which proved to be identical with the product obtained on the treatment of the thiosemicarbazone **11***b* with sodium methoxide (1 equiv.). The latter result indicated that the cyclization of the thiosemicarbazone was a much faster reaction than the isomerization of the carbomethoxyl group at C-4′.

The uv spectra of these 1,2,4-triazines showed maxima around 272 nm in methanol (log ϵ 4.2 $\pm$ 0.1) and their mass spectra exhibited an abundant molecular ion peak (M^+). The acid **12***a* was treated with diborane in a tetrahydrofuran solution to afford the corresponding alcohol from which the acetate **13***a* was prepared. The hydroxyl-protecting groups were removed by

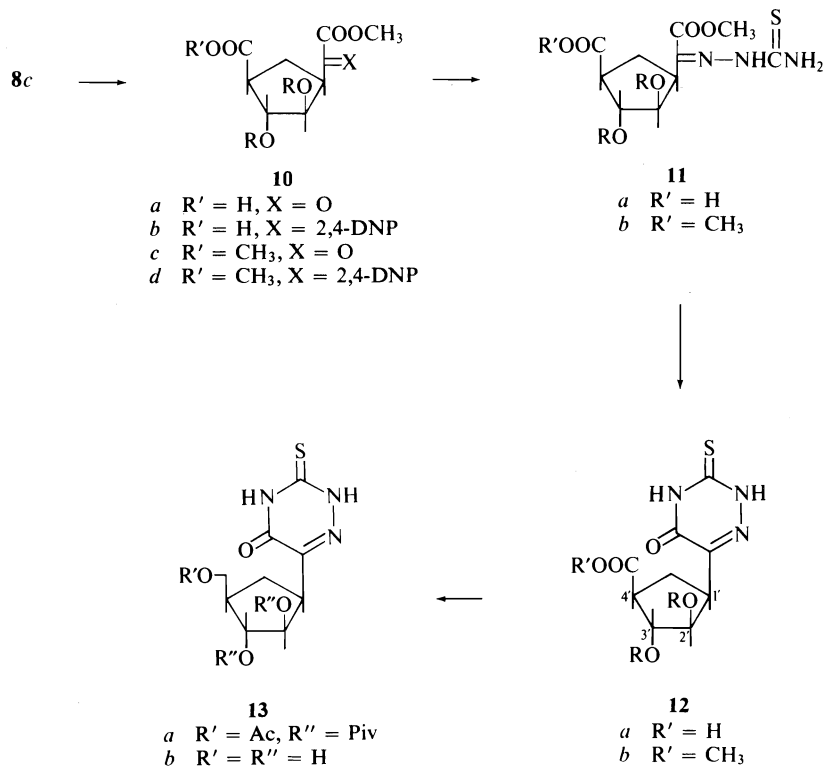

SCHEME 2

sodium hydroxide, leaving the triol **13***b*. In the uv region, this compound absorbed at 272 nm (log ϵ 4.23) like the other 5-oxo-3-thioxo-1,2,4-triazine rings in this series. The replacement of the sulfur atom by an oxygen atom was accomplished by the method of Bobek *et al.* (20). Thus the thioxo compound **13***b* was treated with methyl iodide giving a methyl thiol intermediate that was hydrolyzed by acid to the end product **2**. The uv spectrum of this compound showed an absorption at 265 nm.

An overall view of this synthesis indicated that it was quite simple and straightforward. Starting from the dipivalate **8***c*, the acid keto ester **10***a* was obtained. Without purification, it was converted into its thiosemicarbazone **11***a* and the latter was cyclized to a 1,2,4-triazine ring **12***a*. Reduction of the carboxylic acid function, followed by acetylation, led to **13***a* which was sequentially treated with methyl iodide and acid to give 6-azapseudouridine (21).

Experimental

Solvents were reagent grade. Pyridine and dimethylformamide were dried over Linde 3A molecular sieves. All evaporations were done under reduced pressure (water aspirator) with a bath temperature of 45 °C unless otherwise noted. Melting points were determined on a Gallenkamp block in open capillary tubes and were uncorrected. The following spectrometers were used: ir, Unicam SP1000 and Perkin-Elmer 257; uv, Pye Unicam SP-800; pmr, Varian T-60. Chemical shifts are given in the δ scale (ppm) using the tetramethylsilane signal as internal standard and the solvent was deuteriochloroform unless otherwise mentioned. In the descriptions of the pmr spectra, 's' means singlet; 'd' doublet; 't', triplet; 'q' quartet; 'm', complex multiplet whose center is given; 'b', broad.

Mass spectra were taken on an AEI-MS-902 mass spectrometer using the direct sample inlet system with a 70 eV ionization energy, at the indicated temperatures.

Thin layer chromatography was run on Eastman Chromagram sheets 6060 silica gel plates with fluorescent indicator. Woelm alumina and silica gel were used for column chromatography. Brinkmann silica gel $HF_{254,366}$ was used for thick layer chromatography (1 mm) on glass plates.

Can. J. Chem. Downloaded from www.nrcresearchpress.com by 210.87.254.5 on 09/05/12
For personal use only.

Can. J. Chem. Downloaded from www.nrcresearchpress.com by 210.87.254.5 on 09/05/12
For personal use only.

Elemental analyses for all new crystalline compounds were performed by C. Daessle, Montreal, Heterocyclic Chemical Corporation, Missouri, or Chemalytics Inc, Arizona.

β-Bromoacrylic Acids

(*a*) A solution of 25 g of 98% propiolic acid in 100 ml of 48% aqueous hydrobromic acid was stirred for 2 h at 80 °C (preheated bath) and then allowed to cool overnight. Crystals were filtered and washed with cold water to afford 20.1 g of *trans*-β-bromoacrylic acid with mp 116–117 °C (lit. (11) 121 °C). The filtrate was saturated with sodium chloride and the other isomer was extracted with chloroform (4 times). The extracts were dried over sodium sulfate and the solvent was evaporated to leave 28.9 g of *cis*-β-bromoacrylic acid, with mp 54–55 °C (lit. (11) 55 °C). The total yield of the addition products was 92.5%.

(*b*) A solution of propiolic acid (100 g) in 48% aqueous hydrobromic acid (400 ml) was stirred for 2 h at 100 °C (preheated bath) and the reaction mixture processed as above. At this temperature, 153.3 g (71%) of *trans*-β-bromoacrylic acid were obtained and the amount of the *cis*-isomer was therefore considerably reduced. If the temperature was increased far above 100 °C, the reaction mixture darkened rapidly due to extensive decomposition of propiolic acid.

endo-2-Bromobicyclo[2.2.1]hept-5-ene-endo-3-carboxylic Acid **3***a*

To a solution of 20 g of *cis*-β-bromoacrylic acid in benzene (80 ml) was added freshly distilled cyclopentadiene (30 ml), and the resulting solution was refluxed for 1 h. An additional 10-ml portion of cyclopentadiene was added and the mixture was refluxed for 0.5 h. The solvent was evaporated. The residue formed a precipitate on addition of petroleum ether. The precipitate was filtered and washed with petroleum ether to give 14.8 g (52%) of adduct **3***a* with mp 174–175 °C from chloroform–hexanes (lit. (11) 179 °C); ir ν_{max} (Nujol) 1710 (carbonyl), 2500–3200 cm^{-1} (hydroxyl); pmr δ 1.52 (q, 2H, J = 9 Hz, CH_2), 3.20 (m, 3H), 4.60 (dd, 1H, J = 4 Hz, J = 9 Hz, CHBr), 6.15 (m, 1H), 6.46 (m, 1H), 10.2 (bs, 1H, OH).

exo-2-Bromobicyclo[2.2.1]hept-5-ene-endo-3-carboxylic Acid **6**

To a solution of 15 g of *trans*-β-bromoacrylic acid in benzene (80 ml) was added freshly distilled cyclopentadiene (30 ml) and the resulting solution was refluxed for 1 h. Then an extra 10-ml portion of cyclopentadiene was added, followed by 0.5 h reflux. Solvent and excess cyclopentadiene were evaporated *in vacuo*. Added petroleum ether (bp 37–51 °C) was coevaporated with the residual reagent. This procedure was repeated three times. The precipitate was filtered, washed with petroleum ether, and vacuum-dried to give 16.1 g (75%) of adduct **6**, with mp 133–134 °C from methylene chloride – petroleum ether (lit. (11) 134 °C); ir ν_{max} ($CHCl_3$) 3520, 2500–3200 (hydroxyl), 1725 cm^{-1} (carbonyl); pmr δ 1.98 (q, 2H, J = 10 Hz, CH_2), 3.40 (m, 3H), 4.14 (m, 1H, CHBr), 6.36 (bs, 2H, HC=CH), 10.8 (bs, 1H, OH).

endo-3-Bromo-endo-2-carbomethoxybicyclo[2.2.1]hept-5-ene **3***b*

A mixture of 10 g (46 mmol) of acid **3***a* in methanol (100 ml) and concentrated sulfuric acid (4 ml) was refluxed for 4 h. The residue from solvent removal was partitioned between chloroform and 5% aqueous sodium bicarbonate. The extracts were dried over sodium sulfate and the solvent was evaporated to leave a liquid. Distillation (bp 73–76 °C/0.1 torr) afforded the analytically pure product (8.9 g, 84%) that solidified on cooling, mp 29–30 °C; ir ν_{max} (neat) 1748 cm^{-1} (carbonyl); pmr δ 1.53 (q, 2H, J = 9 Hz, CH_2), 3.24 (m, 3H), 3.74 (s, 3H, methyl ester), 4.66 (dd, 1H, J = 4 Hz, J = 9 Hz, CHBr), 6.16 (m, 1H), 6.60 (m, 1H); ms (40 °C) *m/e* 230, 232 (M^+, ^{79}Br, ^{81}Br), 199 ($M^+ - OCH_3$), 171 ($M^+ - COOCH_3$), 165, 151 ($M^+ - Br$). *Anal.* calcd. for $C_9H_{11}BrO_2$: C 46.75, H 4.76, Br 34.63; found C 46.50, H 4.79, Br 34.22.

endo-3-Bromo-endo-2-carbomethoxy-exo-5,6-epoxidobicyclo[2.2.1]heptane **4***b*

To a solution of the olefin **3***b* (8 g, 34.6 mmol) in chloroform (30 ml) was added by portions a solution of 85% *m*-chloroperbenzoic acid (7.77 g, 38.8 mmol) in chloroform (100 ml) and the mixture was stirred for 3 h at 35 °C. Excess reagent was decomposed by addition of a saturated sodium bisulfite solution. The organic phase was washed with 10% aqueous sodium bicarbonate (3 times) and water, and dried over sodium sulfate. Solvent removal left 8.2 g (96%) of an oil that solidified on cooling (mp 77–78 °C); ir ν_{max} (KBr) 1745 (carbonyl) and 850 cm^{-1} (*exo* epoxide); pmr δ 1.18 (q, 2H, $J_{7a,7b}$ = 11 Hz, CH_2), 2.90 (m, 2H), 3.27 (dd, 1H, $J_{3exo,4}$ = 4 Hz, $J_{2exo,3exo}$ = 10 Hz, CHBr), 3.54 (d, 1H, J = 4 Hz), 3.75 (s, 3H, methyl ester), 4.03 (d, 1H, J = 4 Hz), 4.56 (dd, 1H, $J_{1,2exo}$ = 4 Hz, $J_{2exo,3exo}$ = 10 Hz, CHC=O); ms (70 °C) *m/e* 246, 248 (M^+, ^{79}Br, ^{81}Br), 215 ($M^+ - OCH_3$), 167 ($M^+ - Br$), 139 ($M^+ - Br - CO$). An analytical sample was recrystallized from petroleum ether. *Anal.* calcd. for $C_9H_{11}BrO_3$: C 43.77, H 4.99, Br 32.35; found: C 43.58, H 4.64, Br 32.62.

endo-3-Bromo-exo-5-formoxy-endo-6-hydroxybicyclo-[2.2.1]heptane-endo-2-carboxylic Acid γ-Lactone **5***c*

A mixture of 1 g (4.6 mmol) of bromoacid **3***a* in 98% formic acid (20 ml) and 30% hydrogen peroxide (6 ml) was stirred for 1 h at 50 °C. Evaporation of the solvent left an oil that was applied on silica gel plates and eluted with chloroform giving two major bands. The less polar compound was identified as the formate **5***c* by ir and pmr spectra. It was a syrup (0.25 g); ir ν_{max} (Nujol) 1800 (lactone carbonyl), 1730 cm^{-1} (formate carbonyl); pmr δ 1.73–2.33 (m, 2H, CH_2), 2.74–3.14 (m, 2H), 3.33 (m, 1H), 4.26–4.76 (m, 2H), 5.27 (d, 1H, J = 2 Hz), 8.10 (s, 1H, CHO).

The more polar compound was the free alcohol **5***a*; ir ν_{max} 3440 (hydroxyl), 1795 cm^{-1} (lactone carbonyl). It was characterized as its *p*-nitrobenzoate **5***d* (*vide infra*).

endo-3-Bromo-endo-6-hydroxy-exo-5-pivaloyloxybicyclo-[2.2.1]heptane-endo-2-carboxylic Acid γ-Lactone **5***b*

(*a*) A mixture of 1 g (4.6 mmol) of bromo acid **3***a* in 98% formic acid (20 ml) and 30% hydrogen peroxide (6 ml) was stirred for 1 h at 50 °C. Solvent removal left an oil (tlc, chloroform, two spots under iodine). A mixture of this oil in anhydrous pyridine (10 ml) and pivaloyl chloride (4 ml) was stirred overnight at room temperature. Water (10 ml) and concentrated sulfuric acid (0.5 ml) were added at 0 °C. The product was extracted with

Can. J. Chem. Downloaded from www.nrcresearchpress.com by 210.87.254.5 on 09/05/12
For personal use only.

chloroform. The extracts were washed with 5% sulfuric acid and 10% sodium hydroxide, and dried over sodium sulfate. Solvent removal afforded 0.4 g of compound **5***b*, with mp 138–139 °C from methylene chloride – hexanes; ir ν_{max} (Nujol) 1800 (lactone carbonyl), 1735 cm^{-1} (ester carbonyl); pmr δ 1.22 (s, 9H, *tert*-butyl), 1.87 (m, 1H), 1.97 (m, 1H), 2.77 (d, 1H, J = 4 Hz, H-4), 2.88 (dd, 1H, J = 5 Hz, J = 10 Hz, CHCO), 3.30 (m, 1H, H-1), 4.40 (dd, 1H, J = 4 Hz, J = 10 Hz, CHBr), 4.60 (d, 1H, J = 5 Hz), 5.14 (d, 1H, J = 2 Hz); ms (100 °C) *m/e* 316, 318 (M^+, ^{79}Br, ^{81}Br), 237 ($M^+ - Br$), 209 ($M^+ - Br - CO$), 184.3 (M*, 237 → 209), 153, 85, 57. *Anal.* calcd. for $C_{13}H_{17}BrO_4$: C 49.21, H 5.36; found: C 49.31, H 5.09.

(*b*) *Preparation of* **5***b from* **4***b*

A solution of 1 g (4 mmol) of ester **4***b* in 98% formic acid (5 ml) was stirred for 1 h at 50 °C (preheated bath). Formic acid was evaporated completely. A mixture of the residual oil in pyridine (10 ml) and pivaloyl chloride (2 ml) was stirred overnight at ambient temperature. Solvent was evaporated *in vacuo* and the residue was partitioned between chloroform and 10% hydrochloric acid. The chloroform extracts were washed with 10% aqueous sodium hydroxide and water, and dried over sodium sulfate. Solvent removal left a crude product that was purified on dry column silica gel (2.5 g) using benzene as eluent (20 ml). Evaporation of benzene afforded 0.5 g (39%) of the pivalate **5***b* (mp 137–138 °C, undepressed on the admixture with the sample prepared above); ir and pmr spectra were also superimposable with the spectra obtained in part *a*.

Attempted Opening of Lactone **5***b*

A mixture of 0.19 g of lactone **5***b* in methanol (6 ml) and 0.4 *M* methanolic sodium methoxide (1.6 ml) was refluxed for 1 h. The reagent was decomposed with Rexyn 102(H). After filtration of the resin, the reaction mixture was concentrated and chloroform was added. No sodium bromide precipitated. The solvent was evaporated completely. The pmr spectrum of the residue did not show the olefinic proton and the ir spectrum showed a lactone peak. It was mainly the starting material. The pivalate group was slightly attacked by the base.

endo-3-Bromo-endo-6-hydroxy-exo-5-p-nitrobenzoyloxybicyclo[2.2.1]heptane-endo-2-carboxylic Acid γ-Lactone **5***d*

(*a*) A solution of 0.18 g (0.83 mmol) of bromo acid **3***a* in 98% formic acid (5 ml) and 30% hydrogen peroxide (2 ml) was stirred for 1 h at 45–50 °C. Solvent removal left a colourless oil. A solution of this oil and *p*-nitrobenzoyl chloride (0.17 g) in anhydrous pyridine (2 ml) was stirred overnight at room temperature. Water (10 ml) and concentrated sulfuric acid (0.5 ml) were added. The precipitate was filtered, washed with a 5% aqueous sodium hydroxide solution, and partitioned between water and chloroform. The extracts were dried over sodium sulfate and the solvent was evaporated to give 0.17 g of crude product **5***d* that was purified on silica gel plates, eluting twice with chloroform to give a product with mp 229–230 °C; ir ν_{max} (Nujol) 1795 (lactone carbonyl), 1735 cm^{-1} (benzoate carbonyl); ms (195 °C) *m/e* 381, 383 (M^+, ^{79}Br, ^{81}Br), 302 ($M^+ - Br$), 233, 231, 150. *Anal.* calcd. for $C_{15}H_{12}BrNO_6$: C 47.12, H 3.14, Br 20.94, N 3.67; found: C 47.41, H 3.15, Br 21.16, N 3.60.

(*b*) The compound **5***a*, isolated from plates (see above), was mixed with *p*-nitrobenzoyl chloride (1.1 equiv.) in pyridine (3 ml) and the mixture was stirred overnight at room temperature. Solvent was evaporated and the product was recrystallized from methanol–water leaving 0.24 g of a white solid, with mp and mmp 229–230 °C. The ir spectrum was also superimposable with the compound obtained in part *a*.

exo-3-Bromo-exo-5,endo-6-dihydroxybicyclo[2.2.1]heptane-endo-2-carboxylic Acid γ-Lactone **7***a and its Formate* **7***b*

To a mixture of 20 g (92 mmol) of adduct **6** in 98% formic acid (150 ml) at 45–50 °C (preheated bath) was added over 2 h, 80 ml of 30% hydrogen peroxide (exothermic reaction). The adduct gradually dissolved on addition of hydrogen peroxide. The reaction temperature should be rigorously controlled. After the addition, the resulting solution was stirred for an additional 2 h at 45–50 °C. The solvent was evaporated completely. The product was crystallized from chloroform–hexanes giving 12.5 g (62%) of **7***a*. An analytical sample was recrystallized from chloroform–hexane, giving a compound with mp 121–122 °C. Evaporation of the first filtrate left an oil that contained the formate **7***b*. A solution of this oil in methanol (15 ml) and water (2.5 ml) was stirred 15 min at room temperature. Filtration afforded 2.8 g of **7***b* with mp 86–87 °C; data for alcohol **7***a*: ir ν_{max} (Nujol) 3420 (hydroxyl) and 1770 cm^{-1} (carbonyl); pmr δ 2.24 (s, 2H, CH_2), 2.57 (s, 1H, OH), 2.70 (bs, 1H), 2.97 (m, 1H, CHCOO), 3.20 (m, 1H), 3.72 (s, 1H, C*H*OH), 4.00 (s, 1H, CHBr), 4.42 (d, 1H, J = 5 Hz, CHOC=O); ms (120 °C) *m/e* 232, 234 (M^+, ^{79}Br, ^{81}Br), 153 ($M^+ - Br$), 125 ($M^+ - Br - CO$), 102.1 (M*, 153 → 125). *Anal.* calcd. for $C_8H_9BrO_3$: C 41.23, H 3.89, Br 34.29; found: C 41.36, H 3.90, Br 34.25.

Data for formate **7***b*: ir ν_{max} (Nujol) 1730 (formate carbonyl) and 1795 cm^{-1} (lactone carbonyl); pmr δ 2.26 (m, 2H, CH_2), 2.90–3.07 (m, 2H), 3.34 (m, 1H), 4.16 (s, 1H, CHBr), 4.56–4.71 (m, 2H), 8.05 (s, 1H, CHO); ms (95 °C) *m/e* 260, 262 (M^+, ^{79}Br, ^{81}Br), 231 ($M^+ - CHO$), 180 ($M^+ - HBr$), 152 ($M^+ - HBr - CO$), 128.3 (M*, 180 → 152). *Anal.* calcd. for $C_9H_9BrO_4$: C 41.38, H 3.45, Br 30.65; found: C 41.54, H 3.44, Br 30.69.

p-Nitrobenzoate **7***c*

A solution of 0.35 g (1.5 mmol) of alcohol **7***a* and *p*-nitrobenzoyl chloride (0.37 g, 2 mmol) in pyridine (2 ml) was stirred overnight at ambient temperature, followed by the addition of water (5 ml) containing 0.1 ml of concentrated sulfuric acid. The precipitate was filtered and washed with 5% sodium bicarbonate and water. The product was purified on silica gel plates, eluting with chloroform and giving a solid (80%) with mp 205–206 °C; ir ν_{max} (Nujol) 1795 (lactone carbonyl), 1730 (ester carbonyl), 1610 (C=C), 1530 cm^{-1} (nitro); ms (160 °C) *m/e* 381, 383 (M^+, ^{79}Br, ^{81}Br), 351 ($M^+ - NO$), 302 ($M^+ - Br$), 231 ($M^+ - p\text{-}NO_2C_6H_4CO$), 150 ($p\text{-}NO_2C_6H_4CO^+$). *Anal.* calcd. for $C_{15}H_{12}BrNO_6$: C 47.15, H 3.17, Br 20.92, N 3.67; found: C 46.84, H 3.25, Br 21.12. N 3.76.

exo-3-Bromo-endo-6-hydroxy-exo-5-pivaloyloxybicyclo-[2.2.1]heptane-endo-2-carboxylic Acid γ-Lactone **7***d*

To a solution of 10 g (43 mmol) of alcohol **7***a* in pyridine (20 ml) was added pivaloyl chloride (10 ml), and

Can. J. Chem. Downloaded from www.nrcresearchpress.com by 210.87.254.5 on 09/05/12
For personal use only.

the resulting solution was stirred overnight at ambient temperature. A precipitate (py·HCl) appeared during the reaction. Pyridine and excess pivaloyl chloride were evaporated. The residue was partitioned between chloroform and 10% hydrochloric acid. The organic phase was washed twice with 10% hydrochloric acid and once with water, and dried over sodium sulfate. Solvent removal left a solid residue that was chromatographed through 5 g of silica gel, grade I, eluting with benzene, to give 12.65 g (93%) of product **7***d*, with mp 114–115 °C; ir ν_{max} (Nujol) 1790 (lactone carbonyl) and 1740 cm^{-1} (pivalate carbonyl); pmr δ 1.18 (s, 9H, *tert*-butyl), 2.15 (q, 2H, J = 12 Hz, CH_2), 2.77 (bs, 1H), 3.00 (bs, 1H, CHC=O), 3.24 (m, 1H), 4.08 (bs, 1H, CHBr), 4.50 (m, 2H, two CH—O); ms (120 °C) *m/e* 316, 318 (M^+, ^{79}Br, ^{81}Br), 237 (M^+ − Br), 236 (M^+ − HBr), 209 (M^+ − Br − CO), 208 (M^+ − HBr − CO), 184.3 (M^*, 236 → 208), 153, 85, 57. *Anal.* calcd. for $C_{13}H_{17}BrO_4$: C 49.25, H 5.41, Br 25.21; found: C 49.35, H 5.36, Br 25.28.

5-Carbomethoxy-endo-3-hydroxy-exo-2-pivaloyloxybicyclo[2.2.1]hept-5-ene **8***a*

To a solution of 1 g (3.16 mmol) of lactone **7***d* in dry methanol (20 ml) was added 0.4 *M* methanolic sodium methoxide (8.4 ml, 3.36 mmol) and the mixture was stirred for 1 h at 25 °C. The excess of reagent was decomposed by Rexyn 102(H) previously washed with methanol. The resin was filtered and methanol was evaporated. Chloroform was added to the residue and the precipitate was filtered off (NaBr, 0.27 g, 83%). Solvent was evaporated leaving an oily product (0.85 g) that was purified through dry column silica gel (2 g) eluting with chloroform (30 ml) to give 0.70 g (82.5%) of syrup **8***a*; ir ν_{max} (neat) 3480 (hydroxyl), 1730, 1720 (carbonyls), 1610 cm^{-1} (olefin); pmr δ 1.23 (s, 9H, *tert*-butyl), 1.83 (bs, 2H. CH_2), 3.00 (m, 1H), 3.06 (s, 1H), 3.30 (m, 1H, H-4), 3.78 (s, 3H, methyl ester), 4.15 (m, 2H), 7.08 (d, 1H, $J_{1,6}$ = 4 Hz, C=CH); ms (150 °C) *m/e* 268 (M^+), 237 (M^+ − OCH_3), 236, 209 (M^+ − $COOCH_3$), 183 (M^+ − $(CH_3)_3$-CCO), 125, 85 ($(CH_3)_3CCO^+$), 57, ($(CH_3)_3C^+$).

endo-3-Acetoxy-5-carbomethoxy-exo-2-pivaloyloxybicyclo-[2.2.1]hept-5-ene **8***b*

A mixture of 0.85 g (3.17 mmol) of alcohol **8***a* in pyridine (4 ml) and acetic anhydride (3 ml) was stirred overnight at 25 °C. The excess of anhydride was hydrolyzed by slowly adding 10% hydrochloric acid to the chilled solution. The product was extracted with chloroform and the extracts washed with 10% hydrochloric acid and dried over sodium sulfate. Solvent removal left a yellow oil that was filtered through dry column alumina (4 g) eluting with benzene to give 0.98 g (100%) of syrup **8***b*; ir ν_{max} (neat) 1730 cm^{-1} (carbonyls); pmr δ 1.25 (s, 9H, *tert*-butyl), 1.90 (m, 2H, CH_2), 1.97 (s, 3H, CH_3CO), 3.00 (m, 1H), 3.47 (m, 1H), 3.75 (s, 3H, methyl ester), 4.54 (s, 1H), 5.10 (d, 1H, J = 4 Hz), 7.07 (d, 1H, $J_{1,6}$ = 4 Hz, C=CH); ms (140 °C) *m/e* 310 (M^+), 268, 226, 194, 125, 85, 57.

5-Carbomethoxy-exo-2,endo-3-dipivaloyloxybicyclo-[2.2.1]hept-5-ene **8***c*

A mixture of 0.87 g (3.24 mmol) of alcohol **8***a* in dry pyridine (8 ml) and pivaloyl chloride (1.5 ml) was stirred overnight at 25 °C during which time a white precipitate was formed (py·HCl). Solvent was evaporated *in vacuo*. Toluene was used as a chaser. The residue was partitioned between chloroform and 10% hydrochloric acid. The chloroform extracts were dried over sodium sulfate. Evaporation gave a residue which was filtered through dry column silica gel (1 g) washing with benzene (20 ml). Evaporation of benzene left 1.02 g (90%) of a syrup that solidified on standing, mp 69–70 °C. An analytical sample was sublimed at 48 °C/0.05 torr; ir ν_{max} (neat) 1735 (carbonyls) and 1610 cm^{-1} (C=C); pmr δ 1.12 and 1.23 (s, 9H each, *tert*-butyls), 1.90 (m, 2H, CH_2), 2.98 (m, 1H), 3.44 (m, 1H), 3.74 (s, 3H, methyl ester), 4.44 (s, 1H), 5.10 (d, 1H, J = 4 Hz), 7.10 (d, 1H, $J_{1,6}$ = 4 Hz); ms (120 °C): *m/e* 352 (M^+) 321 (M^+ − OCH_3), 268, 236, 152, 125, 85, 57. *Anal.* calcd. for $C_{19}H_{28}O_6$: C 64.75, H 8.01; found: C 64.64, H 8.03.

exo-3-Bromo-endo-6-hydroxy-exo-5-tert-butyl Dimethylsiloxybicyclo[2.2.1]heptane-endo-2-carboxylic Acid γ-Lactone **7***e*

A mixture of 5 g (21.5 mmol) of alcohol **7***a*, *tert*-butyl dimethylsilyl chloride (5 g) and imidazole (3.5 g, 52 mmol) in dry dimethylformamide (20 ml) was stirred for 1 day at 40 °C. The solvent and excess silane were evaporated. The residue was dissolved in chloroform, washed with water (5 times), and dried over sodium sulfate. Solvent removal left a white oil (7.11 g, 95%) that solidified on standing. An analytical sample was passed through dry column silica gel, eluting with benzene to give a product with mp 67–68 °C; ir ν_{max} (neat) 1800 cm^{-1} (lactone carbonyl); pmr δ 0.10 (s, 6H, $Si(CH_3)_2$, 0.90 (s, 9H, $SiC(CH_3)_3$), 2.20 (bs, 2H, CH_2), 2.58 (m, 1H), 2.94 (s, 1H), 3.12 (m, 1H, C-1 H), 3.58 (s, 1H), 4.00 (s, 1H, CHBr), 4.32 (m, 1H, CHOCO); ms (170 °C) *m/e* 346, 348 (M^+, ^{79}Br, ^{81}Br), 333, 331, 291, 289, (M^+ − *tert*-butyl), 181, 151, 115. *Anal.* calcd. for $C_{14}H_{23}BrO_3Si$: C 48.42, H 6.63, Br 23.05; found: C 48.51, H 6.82, Br 23.01.

5-Carbomethoxy-endo-3-hydroxy-exo-2-tert-butyl Dimethylsiloxybicyclo[2.2.1]hept-5-ene **8***d*

A mixture of 1 g (3 mmol) of lactone **7***e* in dry methanol (20 ml) and 7.8 ml of a 0.4 *M* methanolic sodium methoxide solution was stirred for 1 h at room temperature. Excess reagent was decomposed with Rexyn 102(H). The resin was filtered out and methanol was evaporated completely. To the residue was added chloroform and sodium bromide (0.24 g, 78%) was filtered out. Solvent removal gave an oil that was purified through a silica gel dry column (22) (30 cm length × 3 cm flat diameter), eluting with methylene chloride till 60 ml of eluate were collected. The eluate was kept for the identification of the byproduct (see below). The product **8***d* (0.54 g, 60%), detected on the nylon column by a 254 nm light, was extracted with chloroform. It solidified on scratching, mp 74–75 °C; ir ν_{max} (neat) 3540 (hydroxyl), 1720 (ester carbonyl), 1616 cm^{-1} (C=C); pmr δ 0.10 (s, 6H, dimethylsilyl), 0.92 (s, 9H, *tert*-butyl), 1.85 (d, 1H, J = 2 Hz), 1.98 (m, 2H, CH_2), 2.77 (m, 1H), 3.17 (m, 1H), 3.47 (m, 1H, CHOSi), 3.75 (s, 3H, methyl ester), 4.12 (m, 1H), 7.04 (d, 1H, J = 3 Hz, C=CH); ms (60 °C) *m/e* 298 (M^+), 201, 194, 165, 85. *Anal.* calcd. for $C_{15}H_{26}O_4Si$: C 60.40, H 8.72; found: C 60.22, H 8.55.

The eluate was freed from solvent and the oily residue, **9**, analyzed by ir and pmr spectra; ir ν_{max} (neat), no hydroxyl peak, no olefinic peak, 1800 cm^{-1} (lactone carbonyl); pmr δ 3.32 (s, 3H, $COCH_3$).

Can. J. Chem. Downloaded from www.nrcresearchpress.com by 210.87.254.5 on 09/05/12
For personal use only.

5-Carbomethoxy-exo-2,endo-3-di-tert-butyl Dimethylsiloxybicyclo[2.2.1]hept-5-ene **8e**

A mixture of 0.2 g (0.66 mmol) of alcohol **8d**, imidazole (0.13 g, 1.9 mmol), and *tert*-butyl dimethylsilyl chloride (0.13 g, 0.9 mmol) in dry dimethylformamide (6 ml) was stirred for 1 day at 40 °C. Solvent was evaporated *in vacuo* and the residue dissolved in chloroform, washed with water (3 times), and dried over sodium sulfate. Solvent removal left an oil that solidified on scratching. It was purified through 1.7 g of silica gel (activity III), eluting with benzene (10 ml) to give 0.24 g (87%) of product **8e**, with mp 50–51 °C. It was stored at −10 °C; ir ν_{max} (Nujol) 1730 (ester carbonyl) and 1615 cm^{-1} (C=C); pmr δ 0.08 (s, 12H, two dimethylsilyl's), 0.85 and 0.92 (s, 9H each, *tert*-butyl's), 1.92 (m, 2H, CH_2), 2.72 (m, 1H), 3.10 (m, 1H), 3.47 (m, 1H), 3.74 (s, 3H, methyl ester), 4.12 (d, 1H, J = 4 Hz), 7.07 (d, 1H, J = 3 Hz, C=CH); ms (130 °C) m/e 412 (M^+), 397, 381, 355 (M^+ − *tert*-butyl), 288, 231, 115. *Anal.* calcd. for $C_{21}H_{40}O_4Si_2$: C 61.17, H 9.71; found: C 61.08, H 10.01.

exo-3-Bromo-exo-5,endo-6-dihydroxy-5-O-methoxymethylbicyclo[2.2.1]heptane-endo-2-carboxylic Acid γ-Lactone **7f**

To a solution of 1 g of alcohol **7a** in chloroform (dried over phosphorus pentoxide) were added methylal (1 ml) and phosphorus pentoxide (2–3 g), and the mixture was shaken for 1.5 h at room temperature. The solution was poured into an ice-cooled sodium carbonate solution and the residue in the flask was washed with 5% sodium carbonate solution. The chloroform extracts were dried over sodium sulfate and freed from solvent, leaving 1.18 g (99%) of a syrup; pmr δ 2.10 (bs, 2H, C—CH_2—C), 2.70–2.87 (m, 2H), 3.10 (d, 1H, J = 4 Hz), 3.27 (s, 3H, OCH_3), 3.46 (s, 1H), 3.97 (s, 1H), 4.36 (d, 1H, J = 4 Hz), 4.54 (s, 2H, OCH_2O).

5-Carbomethoxy-exo-2,endo-3-dihydroxy-2-O-methoxymethylbicyclo[2.2.1]hept-5-ene **8f**

A mixture of 1.18 g (4.3 mmol) of lactone **7f** in methanol and 5.5 ml of a 0.8 *M* sodium methoxide solution was stirred for 1 h at room temperature and worked-up as usual. The product was purified on silica gel plates eluting with chloroform – ethyl acetate (9:1). It was isolated in 70% yield; ir ν_{max} (neat) 3450 (hydroxyl), 1720 (carbonyl), and 1608 cm^{-1} (C=C); pmr δ 1.20 (d, 1H, J = 3 Hz), 1.83 (m, 2H, C−CH_2−C), 2.86–3.14 (m, 3H), 3.30 (s, 3H, OCH_3), 3.64 (s, 3H, $COOCH_3$), 4.10 (d, 1H, J = 4 Hz), 4.59 (s, 2H, OCH_2O), 6.86 (d, 1H, J = 4 Hz, C=CH).

5-Carbomethoxy-exo-2,endo-3-dihydroxy-2,3-O-methoxymethylbicyclo[2.2.1]hept-5-ene **8g**

The alcohol **8f** was treated with methylal and phosphorus pentoxide in dry chloroform, as described above, and gave the product **8g** in a quantitative yield; ir ν_{max} (neat) 1730 (carbonyl) and 1612 cm^{-1} (C=C); pmr δ 1.28 (m, 1H), 1.83 (bs, 2H, C—CH_2—C), 2.92 (m, 1H), 3.30 and 3.32 (s, 3H each, OCH_3), 3.44 (bs, 1H), 3.64 (s, 3H, methyl ester), 4.10 (d, 1H, J = 3 Hz), 4.54 (q, 2H, J = 6 Hz, *endo* OCH_2O), 4.61 (s, 2H, *exo* OCH_2O), 6.85 (d, 1H, J = 4 Hz, C=CH).

Methyl 2-(4β-Carboxy-2β,3α-dipivaloyloxycyclopent-1β-yl)glyoxylate **10a**

A mixture of sodium periodate (4 g) and potassium permanganate (0.1 g) in water (50 ml) and 1 g (3 mmol) of olefin **8c** in acetone (20 ml) was stirred for 3 h at ambient temperature. The mixture was filtered through celite and the residue on celite washed with chloroform. The filtrate was extracted with chloroform (3 times). The extracts were washed with brine, dried over sodium sulfate, and freed of solvent. The product **10a**, obtained as an oil, crystallized slowly from methylene chloride–hexanes. Recrystallization was best carried out with seeding to give 0.5 g (45%) of a product with mp 90–91 °C; ir ν_{max} (Nujol) 2500–3240 (acid) and 1750 cm^{-1} (carbonyls); pmr δ 1.08 and 1.23 (s, 9H each, *tert*-butyls), 2.00–3.00 (m, 4H), 3.87 (s, 3H methyl ester), 5.46 (m, 2H), 10.06 (bs, 1H, COOH); ms (200 °C) m/e 341 (M^+ − $COOCH_3$), 313 (M^+ − $COOCH_3$ − CO), 287.3 (M*, 341 → 313), 299, 298, 257, 239, 214, 211, 196, 193, 85, 57. *Anal.* calcd. for $C_{19}H_{28}O_9$: C 56.99, H 7.07; found: C 57.08, H 7.00.

Preparation of 2,4-Dinitrophenylhydrazone **10b**

A mixture of 0.4 g (1 mmol) of acid keto ester **10a** in dimethylformamide (4 ml), 2,4-dinitrophenylhydrazine (0.2 g, 1 equiv.), and concentrated hydrochloric acid (0.2 ml) was shaken some minutes and left 2 h at room temperature. The precipitate was filtered, washed with 10% hydrochloric acid, water, and ethanol–water (1:5), and dried under vacuum to give 0.60 g of the product **10b** that was recrystallized from chloroform–hexanes (mp 235–236 °C); uv λ_{max} (EtOH) 362 nm (log ϵ 4.41); ir ν_{max} (KBr) 3200–2500 (acid), 1750, 1730, 1715 (carbonyls), 1624 (C=C), 1585 (C=N), 1510 cm^{-1} (nitro); pmr (DMSO-d_6) δ 1.02 and 1.25 (s, 9H each, *tert*-butyls), 3.93 (s, 3H, $COOCH_3$); ms (290 °C) m/e 580 (M^+), 478, 376, 183, 85, 57. *Anal.* calcd. for $C_{25}H_{32}N_4O_{12}$: C 51.72, H 5.52, N 9.66; found: C 51.81, H 5.74, N 9.86.

Methyl 2-(4β-Carbomethoxy-2β,3α-dipivaloyloxycyclopent-1β-yl)glyoxylate 2,4-Dinitrophenylhydrazone **10d** *from* **10b**

A mixture of the acid **10b** in ether was treated with a solution of diazomethane in ether for 1 h at 0 °C. The solvent was evaporated, leaving the product (100%) that was recrystallized from methanol, mp 194–195 °C; uv λ_{max} (EtOH) 360 nm (log ϵ 4.18); ir ν_{max} (KBr) 3220, 3120 (NH), 1750, 1730 (carbonyls), 1625 (C=C, C=N), 1510–1530 cm^{-1} (nitro); pmr δ 1.03 and 1.27 (s, 9H each, *tert*-butyls), 2.00–3.06 (m, 4H), 3.80 (s, 3H, $COOCH_3$). 4.00 (s, 3H, $COOCH_3$), 5.43 (m, 2H), 8.25 (s, 1H), 8.40 (m, 1H), 9.20 (m, 2H); ms (195 °C) m/e 594 (M^+), 564 (M^+ − NO), 492, 407, 390, 373, 358, 345, 331, 131, 57. *Anal.* calcd. for $C_{26}H_{34}N_4O_{12}$: C 52.52, H 5.76, N 9.42; found: C 52.73, H 5.98, N 9.70.

Methyl 2-(4β-Carboxy-2β,3α-dipivaloyloxycyclopent-1β-yl)glyoxylate Thiosemicarbazone **11a**

(*a*) A mixture of 0.45 g (1.1 mmol) of keto ester **10a**, thiosemicarbazide (0.2 g), and concentrated hydrochloric acid (0.2 ml) in methanol (10 ml) was stirred for 2 h at room temperature during which time thiosemicarbazide gradually dissolved and the product precipitated. It was filtered and washed with water and methanol to afford 0.5 g (94%) of the thiosemicarbazone **11a**. An analytical sample (mp 243–244 °C) was recrystallized from methanol; uv λ_{max} (THF) 326 nm (log ϵ 4.10); ir ν_{max} (Nujol) 3400 (hydroxyl), 1750 (ester

Can. J. Chem. Downloaded from www.nrcresearchpress.com by 210.87.254.5 on 09/05/12
For personal use only.

carbonyls), 1718 (acid carbonyl), 1620 cm^{-1} (C=N); ms (250 °C) *m/e* 473 (M^+), 458, 414 (M^+ − CSNH), 401, 362.4 (M*, 473 → 414), 330, 310, 300, 198, 85, 57. *Anal.* calcd. for $C_{20}H_{31}N_3O_8S$: C 50.73, H 6.60, N 8.88, S 6.77; found: C 50.81, H 6.48, N 8.87, S 6.85.

(*b*) The same product was also prepared from olefin **8***c*. To a solution of sodium periodate (4 g) and powdered potassium permanganate (0.1 g) in water (50 ml) was added 1 g (3 mmol) of olefin **8***c* in acetone (20 ml), and the mixture was stirred for 3 h at room temperature. It was filtered through celite and the residue on celite was washed with chloroform. The product in the filtrate was extracted with chloroform (3 times). The extracts were washed with brine and dried over sodium sulfate. Solvent removal left an oil that was dissolved in methanol (15 ml), and thiosemicarbazide (0.28 g) and concentrated hydrochloric acid (0.2 ml) were added to the solution. The mixture was vigorously stirred for 2 h at room temperature. The precipitate was filtered, to give 0.5 g of white solid **11***a*. The filtrate was concentrated to half its volume and water (2 ml) was added. After standing 3 h, the precipitate was filtered and washed with methanol to give an additional 0.18 g of product identical in all respects to the product prepared in part *a* (total yield 0.68 g, 50% from olefin **8***c*).

Methyl 2-(4β-Carbomethoxy-2β,3α-dipivaloyloxycyclopent-1β-yl)glyoxylate Thiosemicarbazone ***11b***

(*a*) A mixture of 0.68 g (1.4 mmol) of acid **11***a* in methanol (50 ml) and 0.1 ml of concentrated sulfuric acid was refluxed for 2.5 h (or longer if dissolution was incomplete). The mixture was cooled, concentrated to half its volume, and the precipitate was filtered, to give 0.36 g of product. The filtrate was freed of solvent, the residue was partitioned between chloroform and 10% sodium bicarbonate, and it was worked-up as usual, giving a product (0.14 g) that was recrystallized from benzene–hexanes (total yield, 0.5 g, 72%, mp 194–195 °C); uv λ_{max} (THF) 328 nm (log ε 4.09); ir ν_{max} (Nujol) 3300, 3200 (NH), 1750 (carbonyls), 1610 cm^{-1} (C=N); pmr δ 1.07 and 1.20 (s, 9H each, *tert*-butyls), 2.54 (m, 4H), 3.68 and 3.84 (s, 3H each, $COOCH_3$), 5.37 (m, 2H), 6.74 (m, 2H), 7.84 (m, 1H); ms (200 °C) *m/e* 487 (M*), 428 (M^+ − CSNH), 376.1 (M*, 487 → 428), 344, 326, 242, 160, 85, 57. *Anal.* calcd. for $C_{21}H_{33}N_3O_8S$: C 51.74, H 6.82, N 8.62, S 6.57; found: C 51.78, H 6.94, N 8.66, S 6.55.

(*b*) *Preparation of* ***11b*** *from* ***10c***

A mixture of 0.1 g (0.24 mmol) of ketone **10***c* in methanol (2 ml) and thiosemicarbazide (0.03 g) in water (2 ml) was stirred at room temperature and processed as usual, to give a product that was identical (ir, pmr, and mmp) to the compound prepared in part *a*.

6-(4′β-Carboxy-2′β,3′α-dipivaloyloxycyclopent-1′β-yl)-3-thioxo-2,3,4,5-tetrahydro-1,2,4-triazine-5-one ***12a***

To a suspension of 2.41 g (5.1 mmol) of thiosemicarbazone **11***a* in dry methanol (25 ml) was added 16 ml (12.8 mmol) of a 0.8 *M* methanolic sodium methoxide solution and the mixture was stirred for 1 h at room temperature (yellow solution). It was then acidified with 1 *N* aqueous hydrochloric acid (14 ml), stirred for 10 min and the precipitate was filtered, giving 1.77 g (79%) of product **12***a* that melted above 250 °C (with decomposition). The filtrate was freed from methanol. The residue was partitioned between ethyl acetate and water, and the organic phase was washed twice with water and dried over sodium sulfate. The residue from solvent removal was recrystallized from methanol–water to give an additional portion (0.2 g) of **12***a*; uv λ_{max} (MeOH) 272 nm (log ε 4.19); ir ν_{max} (Nujol) 3200–2500 (acid), 1750 (ester carbonyl), 1710 (acid carbonyl), 1630 cm^{-1} (C=N); ms (210 °C) *m/e* 441 (M^+), 339, 254, 190.3 (M*, 339 → 254), 85, 57.

6-(4′β-Carbomethoxy-2′β,3′α-dipivaloyloxycyclopent-1′β-yl)-3-thioxo-2,3,4,5-tetrahydro-1,2,4-triazine-5-one

(*a*) *Preparation of* ***12b*** *from* ***11b***

A mixture of 0.5 g (1 mmol) of thiosemicarbazone **11***b* in methanol (20 ml) and 0.8 *M* methanolic sodium methoxide solution (1.3 ml) was stirred for 20 min at 40 °C. The mixture was neutralized with Dowex 50W-X8(H), the resin filtered out, and the solvent was evaporated giving 0.4 g (86%) of product **12***b* with mp 195–196 °C from benzene–hexanes; uv λ_{max} (MeOH) 269 nm (log ε 4.33); ir ν_{max} (Nujol) 3230 (NH), 1740 (ester carbonyl), 1620 cm^{-1} (C=N); pmr (acetone-d_6) δ 1.07 and 1.20 (s, 9H each, *tert*-butyls), 2.20–3.14 (m, 4H), 3.64 (s, 3H, methyl ester), 5.27 (m, 2H); ms (220 °C) *m/e* 455 (M^+), 424, 353, 268, 203.5 (M*, 353 → 268), 85, 57.

(*b*) *Preparation of* ***12b*** *from* ***12a***

A mixture of 0.1 g (0.21 mmol) of acid **12***a* in methanol and concentrated hydrochloric acid (0.05 ml) was stirred for 3 h at room temperature. The solvent was evaporated and the residue partitioned between chloroform and water. The product was extracted with chloroform and the extracts dried over sodium sulfate. Solvent removal left a solid (0.08 g) with mp 193–195 °C from benzene–hexanes; uv λ_{max} (MeOH) 269 nm (log ε 4.32). A mixture mp with the product prepared in part *a* showed no depression.

6-(4′β-Acetoxymethyl-2′β,3′α-dipivaloyloxycyclopent-1′β-yl)-3-thioxo-2,3,4,5-tetrahydro-1,2,4-triazine-5-one ***13a***

A mixture of 1.53 g (3.5 mmol) of acid **12***a* in dry tetrahydrofuran (20 ml) and 5 ml of a 1 *M* diborane solution in tetrahydrofuran was stirred for 1 h at 0 °C. Water was added to decompose excess reagent and the solvent was evaporated. Boric acid was removed as methyl borate by several evaporations with methanol. To the residue were added acetic anhydride (2 ml) and pyridine (4 ml), and the mixture was stirred overnight at room temperature. Solvent and reagent were evaporated, and chloroform was added. The solution was washed three times with 5% hydrochloric acid and water, and the solution was dried over sodium sulfate. Solvent removal left the crude product that was applied on seven silica gel plates and eluted with chloroform – ethyl acetate (8:2). The product, at r_f 0.5, was extracted with ethyl acetate to give 0.67 g (41%) of a white solid with mp 190–192 °C from chloroform–hexanes; uv λ_{max} (MeOH) 272 nm (log ε 4.30); ir ν_{max} (Nujol) 3240 (NH) and 1710–1750 cm^{-1} (ester carbonyls); pmr δ 1.13 and 1.25 (s, 9H each, *tert*-butyls), 2.20 (s, 3H, CH_3CO), 2.24–3.00 (m, 4H), 4.20 (d, 2H, J = 6 Hz, CCH_2O), 5.04 (m, 1H), 5.26 (m, 1H), 10.8–12.0 (m, 2H); ms (240 °C) *m/e* 469 (M^+), 368, 282,

85, 57. *Anal.* calcd. for $C_{21}H_{31}N_3O_7S$: C 53.72, H 6.66, N 8.95, S 6.82; found: C 53.58, H 6.65, N 9.09, S 6.81.

6-(4′β-Hydroxymethyl-2′β,3′α-dihydroxycyclopent-1′β-yl)-3-thioxo-2,3,4,5-tetrahydro-1,2,4-triazine-5-one ***13b***

A mixture of 0.63 g (1.34 mmol) of **13***a* in methanol (6 ml) and 8 ml of a 1 *N* aqueous sodium hydroxide solution was stirred overnight at ambient temperature. The solution was neutralized with Dowex 50W-X8(H). The resin was filtered and solvents were evaporated. The product was recrystallized from ethanol–chloroform, leaving 0.28 g (81%) of white solid **13***b* with mp 204–205 °C (tlc AcOEt–MeOH(1:1), r_f 0.5); λ_{max} (MeOH) 272 nm (log ϵ 4.23); ir ν_{max} (Nujol) 3100–3400 (OH and NH), 1715 cm^{-1} (carbonyl); ms (200 °C) *m/e* 259 (M^+), 241, 212, 156. *Anal.* calcd. for $C_9H_{13}N_3O_4S$: C 41.70, H 5.06, N 16.21, S 12.34; found: C 41.71, H 4.96, N 16.41, S 12.18.

5-(4′β-Hydroxymethyl-2′β,3′α-dihydroxycyclopent-1′β-yl)-6-azauracil ***2***

A mixture of 0.15 g (0.58 mmol) of thioxo compound **13***b* in water (20 ml) was heated, under a reflux condenser, with methyl iodide (0.3 ml) for 6 h in an oil bath maintained at 55 °C, according to the method of Bobek *et al.* (20). Excess methyl iodide was allowed to evaporate under normal pressure at 55 °C by removing the condenser. The solution was neutralized with Dowex 1-X8(OH). The resin was filtered. The uv spectrum ($\lambda_{max} \sim 240$ nm) indicated that the methyl thiol intermediate was present and no starting material remained. The solution was then heated at 100 °C for 1 h with Dowex 50W-X8(H). Water was evaporated completely. The product **2** was recrystallized from ethanol–chloroform (50 mg, mp 208–210 °C); uv λ_{max} (H_2O) 265 nm (log ϵ 3.75).

The same product was obtained on treatment of thioxo compound **13***b* with chloroacetic acid (4 h reflux in water), as described with model compounds (23).

Acknowledgment

The authors wish to thank the National Research Council of Canada for financial assistance.

1. K. Gerzon, D. C. DeLong, and J. C. Cline. Pure Appl. Chem. **28**, 489 (1971).
2. R. Ouellet. Ph.D. Thesis, McGill University, Montreal, P.Q. 1975. pp. 1–20.
3. T. Kishi, M. Muroi, T. Kusaka. M. Nishikawa, K. Kamiya, and K. Mizuno. Chem. Commun. 852 (1967).
4. S. S. Cohen. *In* Progress in nucleic acid research and molecular biology. Academic Press, New York. 1966. pp. 1–88.
5. A. P. Kimball, B. Bowman, P. S. Bush, J. Herriot, and G. A. LePage. Cancer Res. **26**, 1337 (1966).
6. F. Šorm and J. Škoda. Collect. Czech. Chem. Commun. **21**, 487 (1956); R. Schindler and A. D. Welch. Science, **125**, 548 (1957); R. E. Handschumacher. Biochim. Biophys. Acta, **23**, 428 (1957).
7. F. Šorm, A. Jakubovič, and L. Šlechta. Experientia, **12**, 271 (1956).
8. W. H. Prusoff, W. L. Holmes, and A. D. Welch. Cancer Res. **14**, 570 (1954).
9. I. Bašnák and J. Farkaš. Collect. Czech. Chem. Commun. **40**, 1038 (1975).
10. J. Niwa and H. Kasiwagi. Bull. Chem. Soc. Jpn. **36**, 1414 (1963); W. R. Vaughan, R. L. Craven, R. Q. Little, Jr., and A. C. Shoenthaler. J. Am. Chem. Soc. **77**, 1596 (1955).
11. K. Alder, F. Brochhagen, C. Kaiser, and W. Roth. Ann. **593**, 1 (1955); E. E. van Tamelen and M. Shamma. J. Am. Chem. Soc. **76**, 2315 (1954); H. Brouwer and J. B. Stothers. Can. J. Chem. **49**, 2152 (1971).
12. H. Kwart and H. G. Vosburgh. J. Am. Chem. Soc. **76**, 5400 (1954); H. B. Henbest and B. Nicholls. J. Chem. Soc. C, 221 (1959); J. A. Berson and S Suzuki. J. Am. Chem. Soc. **80**, 4341 (1958).
13. A. Roebuck and H. Adkins. Org. Syntheses. Coll. Vol. **3**, 217 (1955).
14. R. M. Moriarty, H. G. Walsh, and H. Gopal. Tetrahedron Lett. 4363 (1966); R. M. Moriarty and H. Gopal. Tetrahedron Lett. 347 (1972); J. B. Hendrickson. J. Am. Chem. Soc. **84**, 653 (1962).
15. R. M. Moriarty, H. Gopal, H. G. Walsh, K. C. Ramey, and D. C. Lini. Tetrahedron Lett. 4555 (1966); K. C. Ramey, D. C. Lini, R. M. Moriarty, H. Gopal, and H. G. Welsh. J. Am. Chem. Soc. **89**, 2401 (1967).
16. E. J. Corey and A. Venkateswarlu. J. Am. Chem. Soc. **94**, 6190 (1972).
17. S. W. Baldwin and J. C. Tomesch. J. Org. Chem. **39**, 2382 (1974).
18. K. Fuji, S. Nakano, and E. Fujita. Synthesis, 276 (1975).
19. J. Parrick and J. W. Rasburn. Can. J. Chem. **43**, 3453 (1965).
20. M. Bobek, J. Farkaš, and F. Šorm. Collect. Czech. Chem. Commun. **32**, 3572 (1967).
21. M. Bobek, J. Farkaš and F. Šorm. Tetrahedron Lett. 1543 (1968).
22. B. Loev and K. M. Snader. Chem. Ind. London, 15 (1965); H. Brockmann and H. Schodder. Ber. B, **74**, 73 (1941).
23. J. Gut. Collect. Czech. Chem. Commun. **23**, 1588 (1958).

Can. J. Chem. Downloaded from www.nrcresearchpress.com by 210.87.254.5 on 09/05/12
For personal use only.

C-Nucleosides and related compounds. XI. The synthesis of the 2-deoxy carbocyclic analogue of D,L-pyrazofurin A

GEORGE JUST AND SUNGGAK KIM[1]

Department of Chemistry, McGill University, Montreal, P.Q., Canada H3C 3G1

Received March 22, 1976

GEORGE JUST and SUNGGAK KIM. Can. J. Chem. **54**, 2935 (1976).

The title compound has been synthesized in an eleven-step sequence, starting from the known Diels–Alder adduct **7**.

GEORGE JUST et SUNGGAK KIM. Can. J. Chem. **54**, 2935 (1976).

Le composé du titre a été synthétisé en une séquence de onze étapes en commençant par le produit **7** connu de la réaction Diels–Alder.

Can. J. Chem. Downloaded from www.nrcresearchpress.com by 210.87.254.5 on 09/05/12
For personal use only.

Pyrazofuran A (pyrazomycin) **16** is a *C*-nucleoside bearing a pyrazol ring which possesses marked antiviral activity (1). As part of a program to synthesize pyrazofurin (pyrazomycin) analogues, we recently reported the synthesis of the carbocyclic analogue of pyrazofurin A (2).

We now wish to describe the synthesis of its 2-deoxy analogue **15**, based on a similar reaction scheme in which an olefin ester of type **4** is the key intermediate.

The known Diels–Alder adduct (3) between cyclopentadiene and (*E*)-β-bromoacrylic acid was esterified to give ester **1** (4). Hydroboration of ester **1**, followed by oxidation with alkaline hydrogen peroxide, gave two compounds in a ratio of 57:43. The major compound **2** had the expected composition and formed a crystalline *p*-nitrobenzoate **2***a*. Elimination of hydrogen bromide by reaction with DBU gave the olefin **6**. The position of the hydroxy group in **2** was proven by lactonizing its mesylate **2***b*, with formic acid to produce the lactone **5**.

The spectral data for the minor compound **3** indicated that it did not contain a hydroxy group and had lost bromine.

Since hydroboration of olefin **1** most likely led to two isomeric boranes, it is probable that the borane in which the boron atom is attached to the 5-position (see **1**) gave tricyclic **3** by intramolecular displacement of bromide (5).

Since the desired olefin **4** could not be obtained by this procedure, the Diels–Alder reaction was repeated using (*Z*)-β-bromoacrylic acid and cyclopentadiene. It was thought that displacement of the bromine by borane attached to C-5 could not take place readily with expected *endo*

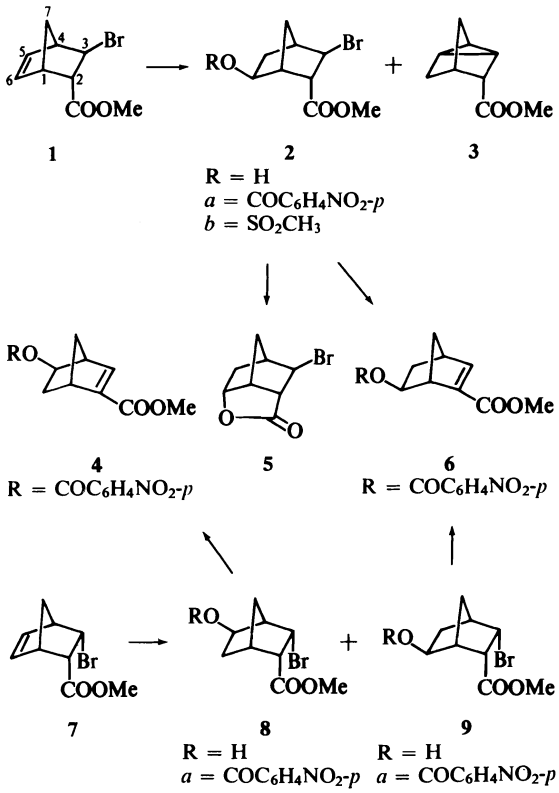

bromo derivative **7**. Olefin **7** was hydroborated and the product oxidized with alkaline hydrogen peroxide. The resulting alcohols (60:40 by nmr) could not be separated by either distillation or chromatography. Fractional crystallization of the *p*-nitrobenzoates of the alcohol mixture gave **8***a* and **9***a* in 45% and 25% yield respectively. Elimination of hydrogen bromide by DBU from the minor isomer **9***a* gave **6**, which was identical with **6** obtained from **2***a*. The analogous elimina-

[1]Holder of a McConnell Fellowship, 1974–1976.

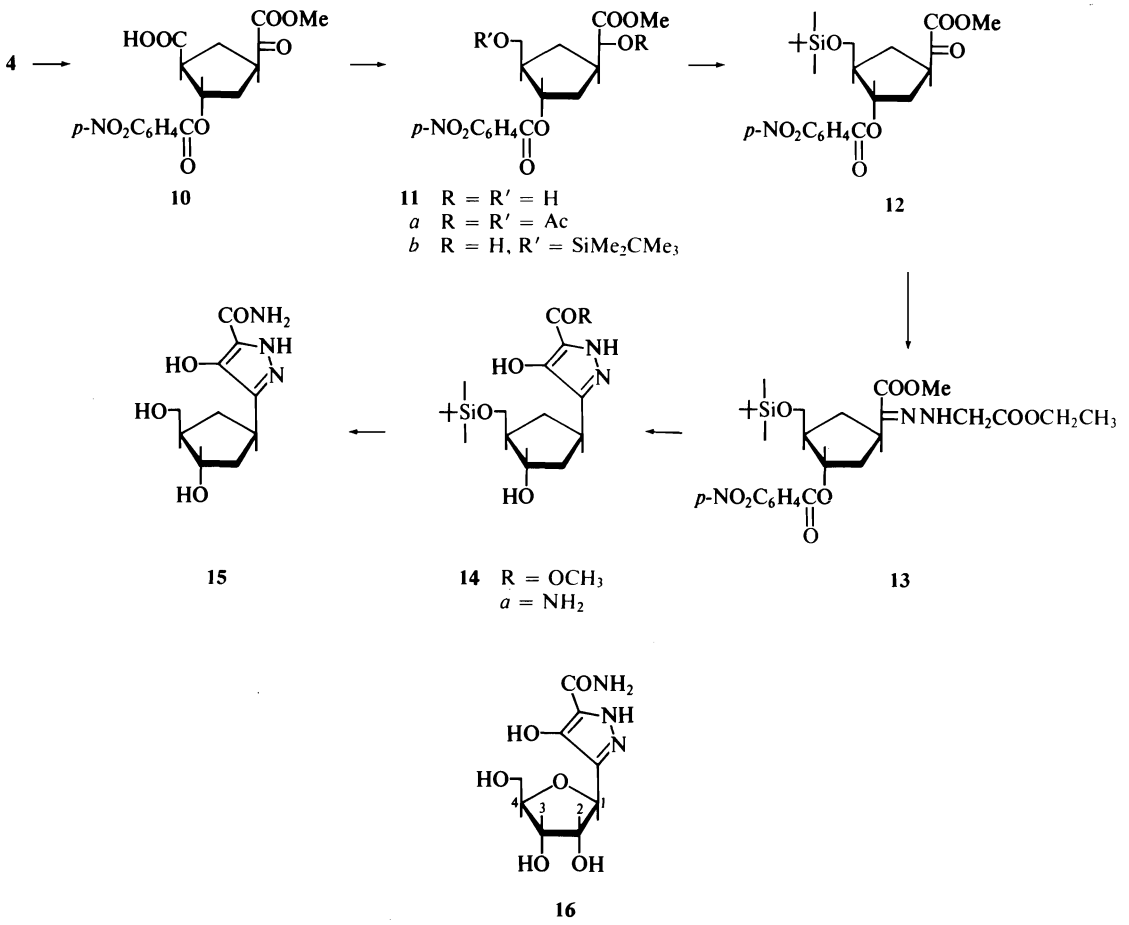

tion reaction was carried out on the major compound **8***a* and gave the desired bicyclic olefin **4** in an overall yield of 30%, based on (*Z*)-β-bromoacrylic acid.

Permanganate – sodium periodate oxidation (6) of the olefin **4** gave the keto acid **10**. Selective reduction of the keto acid with diborane could not be achieved. Instead the diol **11** was obtained and characterized as its diacetate **11***a*. Selective silylation of **11** with *tert*-butyldimethylchlorosilane and imidazole (7) gave **11***b* in 83% yield after purification by tlc. Oxidation with ruthenium dioxide – sodium periodate (8) gave the keto ester **12** in essentially quantitative yield. The keto ester was unstable to silica gel and could not be purified. It was transformed to the hydrazone **13** by means of ethyl hydrazinoacetate in aqueous methanol. Cyclization, using sodium methoxide in methanol, gave **14** in 20% yield. Treatment of **14** with methanolic ammonia at room temperature for a week afforded the amide **14***a* in 80% yield after chromatographic purification. Treatment of **14***b* with 50% aqueous trifluoroacetic acid at room temperature for 30 min gave the desired 2-deoxy derivative **15** in 60% yield.

Experimental

Melting points were determined on a Gallenkamp block and are uncorrected. Mass spectra were obtained on an AE1-MS-902 mass spectrometer at 70 eV using a direct-insertion probe. Nuclear magnetic resonance spectra were recorded on a Varian Associates T-60 spectrometer. Infrared spectra were obtained on a Unicam SP1000 and a Perkin-Elmer 257 ir spectrophotometer. Ultraviolet spectra were determined with a Unicam SP-800 spectrophotometer. Microanalyses were carried out by Dr. C. Daessle, Montreal and Heterocyclic Chemical Corp., Harrisonville, MO U.S.A.

*exo-3-Bromo-endo-2-carbomethoxy-exo-6-hydroxybicyclo[2.2.1]heptane (**2**) and endo-3-Carbomethoxytricyclo[2.2.1.0]heptane (**3**)*

To **1** (9.80 g) in tetrahydrofuran (20 ml) was added 1.0

Can. J. Chem. Downloaded from www.nrcresearchpress.com by 210.87.254.5 on 09/05/12
For personal use only.

Can. J. Chem. Downloaded from www.nrcresearchpress.com by 210.87.254.5 on 09/05/12
For personal use only.

M diborane (1 mol/l, 16 ml) in tetrahydrofuran in an ice bath and the reaction mixture was stirred for 1 h. The excess diborane was destroyed by adding a few drops of water. The trialkylborane was oxidized by the addition to the stirred reaction mixture of 3 *N* sodium hydroxide (15 ml), followed by the dropwise addition of 30% hydrogen peroxide (15 ml) in an ice bath. The reaction mixture was stirred for an additional 30 min, saturated with sodium chloride, and then the tetrahydrofuran layer formed was separated and washed with saturated sodium chloride solution. Distillation gave 4.80 g of **2** (bp 126 ~ 130 °C/0.7 torr) and 2.21 g of **3** (bp 49 ~ 52 °C/0.7 torr). Major product (**2**): nmr ($CDCl_3$) δ 4.20 (m, 1H), 3.73 (s, 3H, COOMe), 3.70 (b, 1H), 3.20 (m, 1H), 2.57 (m, 2H), 2.40 (bs, 1H, OH), 1.20–2.00 (m, 4H); ir (film) 3200, 3600, 1740 cm^{-1}; ms *m/e* 250, 248 (M^+, ^{81}Br, ^{79}Br), 169 ($M^+ - Br$). Minor product (**3**): nmr ($CDCl_3$) δ 3.63 (s, 3H, COOMe), 2.40 (bs, 1H), 2.03 (b, 1H), 1.60 ~ 1.00 (m, 7H); ir (film) 1740, 1440 cm^{-1}; ms (70 eV) *m/e* 152 (M^+), 121 ($M^+ - OMe$), 120 ($M^+ - CH_3OH$), 93 ($M^+ -$ COOMe).

exo-3-Bromo-endo-2-carbomethoxy-exo-6-p-nitrobenzoylbicyclo[2.2.1]heptane

Compound **2** (500 mg), *p*-nitrobenzoyl chloride (380 mg), and pyridine (210 mg) were dissolved in methylene chloride (20 ml). After stirring at room temperature overnight, the solution was washed three times with water and once with saturated salt solution. The methylene chloride layer was dried over sodium sulfate and evaporated to give a crystalline compound. The compound obtained was recrystallized from carbon tetrachloride – petroleum ether to give **2***a* (560 mg) in 70% yield, mp 141 ~ 143 °C; nmr ($CDCl_3$) δ 8.23 (s, 4H), 4.82 (m, 1H), 4.30 (m, 1H), 3.83 (s, 3H, COOMe), 3.33 (m, 1H), 2.80 (m, 2H), 2.25 ~ 1.40 (m, 4H); ir (KBr) 1740, 1620, 1555 cm^{-1}; ms (70 eV) *m/e* 399, 397 (M^+, ^{81}Br, ^{79}Br), 367, 365 ($M^+ - CH_3OH$), 318 ($M^+ - Br$), 249, 247 ($M^+ - p\text{-}NO_2C_6H_4CO$).

exo-2-Bromo-endo-2-carbomethoxy-exo-6-mesylbicyclo-[2.2.1]heptane

To a cooled solution of **2***b* (788 mg) and triethylamine (358 mg) in methylene chloride (15 ml) in a dry ice bath was added dropwise mesyl chloride (400 mg) in methylene chloride (10 ml). The reaction mixture was stirred for an additional hour and was then poured into water. The methylene chloride layer was washed twice with water, dried over sodium sulfate, and evaporated to give an oily compound (870 mg) in 85% yield; nmr ($CDCl_3$) δ 4.35 (m, 1H), 4.10 (m, 1H), 3.70 (s, 3H), 3.27 (m, 1H), 3.00 (s, 3H), 2.30 ~ 2.87 (b, 2H), 1.13 ~ 2.20 (m, 4H); ir (film) 1745, 1460, 1390 cm^{-1}; ms (70 eV) *m/e* 297, 295 ($M^+ - OCH_3$, ^{81}Br, ^{79}Br), 247 ($M^+ - Br$), 215 ($M^+ - CH_3OH - Br$).

exo-3-Bromo-endo-6-hydroxybicyclo[2.2.1]heptane-endo-2-carboxylic Acid γ-Lactone

Compound **2***b* (320 mg) was dissolved in formic acid (10 ml). The solution was heated at 60–65 °C for 2 h, evaporated under reduced pressure to remove most of formic acid, and ethyl acetate was then added to the residue. The solution was washed once with 0.5 *M* sodium bicarbonate solution and washed once with saturated salt solution. The ethyl acetate layer was dried over sodium sulfate and then evaporated to give an oily compound. Purification of crude product on silica gel plates using chloroform as an eluant gave **5** (188 mg) in 80% yield; nmr ($CDCl_3$) δ 4.80 (m, 1H), 4.17 (bs, 1H), 3.20 (m, 1H), 2.97 (m, 1H), 2.67 (b, 1H), 2.40 ~ 1.20 (m, 4H); ir ($CHCl_3$) 1790, 1370 cm^{-1}; ms (70 eV) *m/e* 218, 216 (M^+, ^{81}Br, ^{79}Br), 137 ($M^+ - Br$), 107 ($M^+ - Br - CO$). *Anal.* calcd. for $C_8H_9O_2Br$: C 44.24, H 4.15, Br 36.82; found: C 44.48, H 4.32, Br 37.07.

2-Carbomethoxy-exo-6-p-nitrobenzoylbicyclo[2.2.1]-hept-2-ene

Compound **2***a* (320 mg) was dissolved in anhydrous ethyl ether (20 ml) and 1,5-diazabicyclo[5.4.0.]undec-5-ene (DBU) (180 mg) in anhydrous ethyl ether (10 ml) was added dropwise with cooling in an ice bath and with vigorous stirring of the ether solution. After all the DBU was added, the solution was stirred for an additional 30 min and the white precipitate was filtered off and washed several times with ether. The ether solutions were combined and washed three times with 0.5 *M* hydrochloric acid and once with saturated salt solution. Drying over sodium sulfate and evaporation gave a pale yellow oil (230 mg) in 90% yield which crystallized on standing; mp 62–63 °C; nmr ($CDCl_3$) δ 8.23 (s, 4H), 7.20 (d, J = 2 Hz, 1H), 5.03 (m, 1H), 3.80 (s, 3H, COOMe), 3.50 (bs, 1H), 3.13 (bs, 1H), 2.25 ~ 1.40 (m, 4H); ir ($CHCl_3$)1730. 1620, 1540 cm^{-1}; ms (70 eV) *m/e* 317 (M^+), 285 ($M^+ -$ MeOH), 167 ($M^+ - p\text{-}NO_2C_6H_4CO$).

endo-3-Bromo-endo-2-carbomethoxy-exo-5-hydroxybicyclo[2.2.1]heptane ***(8)*** *and endo-3-Bromo-endo-2-carbomethoxy-exo-6-hydroxybicyclo[2.2.1]heptane* ***(9)***

To **7** (10.60 g) in tetrahydrofuran (20 ml) was added diborane (1 mol/l, 18 ml) in tetrahydrofuran in an ice bath and the reaction mixture was stirred for 1 h. Excess diborane was destroyed by adding a few drops of water. The trialkylborane was oxidized by the addition to the stirred reaction mixture of 3 *N* solution of sodium hydroxide (15 ml), followed by the dropwise addition of 30% hydrogen peroxide (15 ml) in an ice bath. The reaction mixture was stirred for an additional 30 min and then saturated with sodium chloride. The tetrahydrofuran layer formed was separated and washed with saturated sodium chloride solution. Distillation at 124–126 °C/0.5 torr gave 9.70 g (85%) of **8** and **9**; nmr ($CDCl_3$) δ 5.00 ~ 4.23 (m, 2H), 3.80 (s, 3H, COOMe), 3.60 ~ 2.50 (m, 5H), 1.20 ~ 2.30 (m, 3H); ir (film) 3200 ~ 3600, 1740, 1450 cm^{-1}; ms (70 eV) *m/e* 250, 248 (M^+, ^{81}Br, ^{79}Br), 219, 217 ($M^+ - OMe$), 169 ($M^+ - Br$), 137 ($M^+ - Br - CH_3OH$).

endo-3-Bromo-endo-2-carbomethoxy-exo-5-p-nitrobenzoylbicyclo[2.2.1]heptane ***(8a)*** *and endo-3-Bromo-endo-2-carbomethoxy-exo-6-p-nitrobenzoylbicyclo[2.2.1]-heptane* ***(9a)***

The mixture of **8** and **9** (910 mg) and *p*-nitrobenzoyl chloride (680 mg) were dissolved in pyridine (2 ml) and methylene chloride (10 ml). After stirring at room temperature overnight, the solution was evaporated under reduced pressure to remove most of the pyridine. Chloroform (20 ml) was added to the residue and the solution was washed with water and once with saturated sodium chloride solution. The chloroform layer was then dried over sodium sulfate and evaporated to give two crystalline compounds. Major product **8***a* was recrystallized from carbon tetrachloride – petroleum ether (7:3) to give 650

Can. J. Chem. Downloaded from www.nrcresearchpress.com by 210.87.254.5 on 09/05/12
For personal use only.

mg (45%); mp 151 ~ 153 °C; nmr ($CDCl_3$) δ 8.33 (s, 4H), 5.67 (bd, J = 5 Hz, 1H), 4.67 (d of d, J = 12 and 4 Hz, 1H), 3.77 (s, 3H, COOMe), 3.40 ~ 2.50 (m, 4H), 2.20 ~ 1.20 (m, 3H); ir (KBr) 1740, 1730, 1610, 1540 cm^{-1}; ms (70 eV) m/e 399, 397 (M^+, ^{81}Br, ^{79}Br), 367, 365 ($M^+ - CH_3OH$), 318 ($M^+ - Br$), 286 ($M^+ - Br - CH_3OH$), 249, 247 ($M^+ - p$-$NO_2C_6H_4CO$). *Anal.* calcd. for $C_{16}H_{16}O_6NBr$: C 48.24, H 4.05, N 3.52; found: C 48.47, H 4.20, N 3.56. Minor product **9***a* was recrystallized from chloroform – petroleum ether (1:1) to give 360 mg (25%); mp 101 ~ 103 °C; nmr ($CDCl_3$) δ 8.33 (s, 4H), 6.27 (bd, J = 5 Hz, 1H), 4.70 (d of d, J = 12 and 4 Hz, 1H), 3.77 (s, 3H, COOMe), 3.40 (d of d, J = 12 and 4 Hz, 1H), 2.80 (m, 2H), 2.33 ~ 1.40 (m, 4H); ir (KBr) 1740, 1730, 1610, 1540 cm^{-1}; ms (70 eV) m/e 399, 397 (M^+, ^{81}Br, ^{79}Br), 367, 365 ($M^+ - CH_3OH$), 318 ($M^+ - Br$), 286 ($M^+ - Br - CH_3OH$), 249, 247 ($M^+ - p$-$NO_2C_6H_4CO$).

2-Carbomethoxy-exo-5-p-nitrobenzoylbicyclo[2.2.1]-hept-2-ene

To **8***a* (310 mg) in methylene chloride (20 ml) was added DBU (200 mg) and the reaction mixture was refluxed for 2 h. The reaction mixture was washed three times with 0.5 *M* hydrochloric acid and once with saturated salt solution. Drying over sodium sulfate and evaporation gave a crystalline compound (220 mg) in 90% yield; mp 118–119 °C; nmr ($CDCl_3$) δ 8.25 (s, 4H), 7.00 (d, J = 2 Hz, 1H), 3.12 (m, 1H), 3.80 (s, 3H, COOMe), 3.33 (b, 2H), 2.20 ~ 1.60 (b, 4H); ir (KBr) 1740, 1610, 1540 cm^{-1}; ms (70 eV) m/e 317 (M^+), 285 ($M^+ - CH_3OH$); *Anal.* calcd. for $C_{16}H_{15}O_6N$: C 60.56, H 4.77, N 4.41; found: C 60.51, H 5.04, N 4.51.

2-Carbomethoxy-exo-6-p-nitrobenzoylbicyclo[2.2.1]-hept-2-ene

Compound **9***a* (250 mg) was treated as above with DBU to give **6** (170 mg) in 85% yield. The mp and spectral data (nmr, ir, and ms) were identical with **6** which was prepared from **2***a*.

Methyl-2-(4β-carboxy-3α-p-nitrobenzoylcyclopent-1β-yl)-glyoxylate

A mixture of sodium periodate (1.80 g) and potassium permanganate (100 mg) in p*H* 7 phosphate buffer (15 ml) and **4** (600 mg) in acetone (20 ml) was stirred at room temperature for 4 h. The reaction mixture was filtered through Celite and the residue on Celite washed with acetone. The filtrate was extracted with chloroform. The chloroform layer was washed with water and saturated salt solution, dried over sodium sulfate, and then evaporated under reduced pressure to give **10** (620 mg) in 90% yield; nmr δ 10.76 (bs, 1H, COOH), 8.20 (s, 4H), 5.60 (m, 1H), 3.90 (s, 3H, COOMe), 3.20 (m, 1H), 3.00 ~ 2.00 (m, 5H); ir ($CHCl_3$) 3500 ~ 3100, 1750, 1630, 1550 cm^{-1}; ms (70 eV) m/e 320 ($M^+ - COOH$), 306 ($M^+ - COOMe$), 215 ($M^+ - p$-$NO_2C_6H_4CO$).

Methyl-2-(3α-p-nitrobenzoyl-4β-hydroxymethylcyclopent-1β-yl)glycolate

To a cooled solution of **10** (250 mg) in tetrahydrofuran (5 ml) in an ice bath was added 1.0 *M* diborane (1.00 ml) in tetrahydrofuran. The reaction mixture was stirred in an ice bath for 1 h. Water was added and solvents were evaporated. Boric acid was removed by several coevaporations with methanol under reduced pressure. Purification on silica gel plates using chloroform – ethyl acetate (1:1) as an eluant gave **11** (192 mg) in 79% yield: nmr ($CDCl_3$) δ 8.27 (s, 4H), 5.33 (b, 1H), 4.23 (d, 1H, J = 4 Hz), 3.83 (s, 3H), 3.70 (d, 2H, J = 5 Hz), 3.33 (bs, 2H, OH), 2.80 ~ 1.20 (m, 6H); ir ($CHCl_3$) 3650 ~ 3200, 1740, 1620, 1550 cm^{-1}; ms (70 eV) m/e 353 (M^+), 294 ($M^+ - COOMe$), 276 ($M^+ - COOMe - H_2O$), 203 ($M^+ - p$-$NO_2C_6H_4CO$). *Anal.* calcd. for $C_{16}H_{19}O_8N$: C 54.39, H 5.42, N 3.96; found: C 54.09, H 5.58, N 3.84.

*Preparation of Diacetate **11***a* *from **11***

Compound **11** (85 mg) was dissolved in pyridine (1 ml) and acetic anhydride (5 drops). The solution was stirred at room temperature overnight and evaporated under reduced pressure. Purification on a silica gel plate using chloroform – ethyl acetate (1:1) as an eluant gave **11***a* (98 mg) in 93% yield; nmr ($CDCl_3$) 8.27 (s, 4H), 5.33 (m, 1H), 5.00 (d, 1H, J = 4 Hz), 4.23 (d, 2H, J = 5 Hz), 3.80 (s, 3H, COOMe), 2.20 (s, 3H), 2.07 (s, 3H), 3.00 ~ 1.20 (m, 6H); ir ($CHCl_3$) 1750, 1740, 1620, 1550 cm^{-1}; ms (70 eV) m/e 406 ($M^+ - OCH_3$), 394 ($M^+ - CH_3CO$), 378 ($M^+ - COOMe$).

Methyl-2-(3α-p-nitrobenzoyl-4β-tert-butyldimethyl-siloxymethylcyclopent-1β-yl)glycolate

Compound **11** (320 mg), *tert*-butyldimethylchlorosilane (150 mg), and imidazole (155 mg) were dissolved in dimethylformamide (5 ml). After stirring at room temperature for 24 h, the solution was evaporated under reduced pressure to remove most of the dimethylformamide. Chloroform (30 ml) was added to the residue and the solution was washed three times with water. The chloroform layer was dried over sodium sulfate, evaporated to dryness, and following purification on silica gel plates using chloroform – ethyl acetate (2:1) gave **11***b* (350 mg) in 83% yield; nmr ($CDCl_3$) δ 8.23 (s, 4H), 5.30 (m, 1H), 4.13 (m, 1H), 3.77 (s, 3H, COOMe), 3.66 (d, 2H, J = 4 Hz), 3.13 (b, 1H, OH), 2.60 ~ 1.30 (m, 6H), 0.85 (s, 9H), 0.05 (s, 6H); ir ($CHCl_3$) 3650 ~ 3100, 1740, 1620, 1540 cm^{-1}; ms (70 eV) m/e 467 (M^+), 408 ($M^+ - COOMe$). *Anal.* calcd. for $C_{22}H_{33}O_3NSi$: C 56.52, H 7.12, N 3.00; found: C 56.53, H 7.34, N 3.04.

Methyl-2-(3α-p-nitrobenzoyl-4β-tert-butyldimethyl-silyloxymethylcyclopent-1β-yl)glyoxylate

Sodium metaperiodate (280 mg) and a catalytic amount of ruthenium dioxide (10 mg) were dissolved in water (20 ml). The p*H* of the mixture was controlled between 6 and 7 by the addition of a small amount of sodium bicarbonate. The solution of **11***b* (280 mg) in carbon tetrachloride (30 ml) was added to the mixture, with vigorous stirring, at room temperature. The end of the reaction, after about 4 h, was indicated by a change in color from black to yellow. The carbon tetrachloride layer was separated, washed with water, ruthenium tetroxide was destroyed by the addition of a few drops of isopropyl alcohol, and the mixture was filtered. The carbon tetrachloride layer was dried over sodium sulfate and evaporated under reduced pressure to give **12** (260 mg) in 93% yield: nmr ($CDCl_3$) δ 8.23 (s, 4H), 5.30 (m, 1H), 3.87 (s, 3H, COOMe), 3.70 (b, 2H), 2.77 ~ 1.40 (m, 6H), 0.93 (s, 9H), 0.05 (s, 6H); ir ($CHCl_3$) 1740, 1620, 1550 cm^{-1}; ms (70 eV) m/e 465 (M^+), 408 ($M^+ - C(CH_3)_3$), 406 ($M^+ - COOMe$), 300 ($M^+ - CH_3 - p$-$NO_2C_6H_4CO$).

Can. J. Chem. Downloaded from www.nrcresearchpress.com by 210.87.254.5 on 09/05/12
For personal use only.

*Preparation of Hydrazone **13** from **12***

Compound **12** (140 mg), ethyl hydrazinoacetate hydrochloride (54 mg), and sodium acetate (30 mg) were dissolved in aqueous methanol (10 ml). The reaction mixture was stirred at room temperature overnight, evaporated under reduced pressure to remove methanol, and then extracted twice with methylene chloride. The methylene chloride layer was washed with water, dried over sodium sulfate, and evaporated to dryness. Purification on a silica gel plate using chloroform – ethyl acetate (3:1) as an eluant gave **13** (150 mg) in 88% yield; nmr ($CDCl_3$) δ 10.17 (t, NH, J = 4 Hz), 8.20 (s, 4H), 6.43 (t, NH, J = 4 Hz), 5.33 (m, 1H), 4.53 ~ 3.97 (m, 4H), 3.77 (s, 3H, COOMe), 3.70 (b, 2H), 2.66 ~ 1.50 (m, 6H), 1.27 (t, 3H, J = 7 Hz), 0.90 (s, 9H), 0.05 (s, 6H); ir ($CHCl_3$) 3250 ~ 3650, 1740, 1730, 1620, 1550 cm^{-1}; uv λ_{max} (EtOH) 266 nm (log ϵ 3.93), 292 nm (log ϵ 3.74); ms (70 eV) *m/e* 565 (M^+), 506 (M^+ – COOMe). *Anal.* calcd. for $C_{26}H_{39}O_9N_3Si$: C 55.21, H 6.95, N 7.43; found: C 55.40, H 6.98, N 7.20.

3(5)-(3α-Hydroxy-4β-tert-butyldimethylsiloxymethylcyclopent-1β-yl)-5(3)-carbomethoxy-4-hydroxypyrazole

To the solution of **13** (570 mg) in methanol (10 ml) was added 0.62 *M* sodium methoxide (3.5 ml). The reaction mixture was refluxed for 2 h, evaporated under reduced pressure, acidified with hydrochloric acid after water was added to the residue, and then extracted with ethyl acetate. The organic layer was dried over sodium sulfate and evaporated to dryness. Separation on silica gel plates using ethyl ether as an eluant gave **14** (75 mg) in 20% yield; nmr ($CDCl_3$) δ 6.60 (b, 2H), 4.33 (m, 1H), 3.93 (s, 3H, COOMe), 3.90 ~ 3.37 (m, 3H), 2.50 ~ 1.50 (m, 5H), 0.93 (s, 9H), 0.07 (s, 6H); ir ($CHCl_3$) 3460, 1720, 1690, 1590 cm^{-1}; uv λ_{max} (0.1 *N* HCl) 228 nm (log ϵ 3.28) and 275 nm (log ϵ 3.66); λ_{max} (0.1 *N* NaOH) 238 nm (log ϵ 3.87) and 320 nm (log ϵ 3.91); ms (70 eV) *m/e* 370 (M^+), 355 ($M^+ - CH_3$), 339 ($M^+ - OCH_3$), 313 ($M^+ - C(CH_3)_3$), 281 ($M^+ - C_4H_9 - CH_3OH$).

3(5)-(3α-Hydroxy-4β-tert-butyldimethylsiloxymethylcyclopent-1β-yl)-5(3)-carboxamide-4-hydroxypyrazole

Compound **14** (150 mg) was added to methanol (10 ml) saturated with ammonia. The solution was allowed to stand at room temperature for a week. Evaporation and purification on a silica gel plate using ethyl acetate as an eluant gave **14***a* (115 mg) in 80% yield: ir ($CHCl_3$) 3580, 3440, 1690, 1630, 1600 cm^{-1}; ms (70 eV) *m/e* 355 (M^+), 288 ($M^+ - C(CH_3)_3$), 281 ($M^+ - C(CH_3)_3 - NH_3$); uv λ_{max} (0.1 *N* HCl) 220 nm (log ϵ 3.77) and 268 nm (log ϵ 3.57); λ_{max} (0.1 *N* NaOH) 235 nm (log ϵ 3.69) and 315 nm (log ϵ 3.78). *Anal.* calcd. for $C_{16}H_{29}N_3O_4Si$: C 54.08, H 8.17, N 11.83; found: C 54.19, H 8.24, N 11.60.

3(5)-(3α-Hydroxy-4β-hydroxymethylcyclopent-1β-yl)-5(3)-carboxamide-4-hydroxypyrazole

To the solution of **14***a* (140 mg) in methanol (2 ml) was added 50% aqueous trifluoroacetic acid (2 ml). The solution was stirred at room temperature for 30 min and then evaporated under reduced pressure. The crude product was crystallized from methanol – ethyl ether to give **15** (58 mg) in 60% yield; mp 138 ~ 141 °C; ir (KBr) 3100 ~ 3600, 1690, 1640 cm^{-1}; ms (70 eV) *m/e* 241 (M^+), 224 ($M^+ - NH_3$), 223 ($M^+ - H_2O$), 206 ($M^+ - H_2O - NH_3$); uv λ_{max} (0.1 *N* HCl) 220 nm (log ϵ 3.76) and 268 nm (log ϵ 3.64); λ_{max} (0.1 *N* NaOH) 235 nm (log ϵ 3.77) and 314 nm (log ϵ 3.90).

Acknowledgments

We wish to thank the National Research Council of Canada and Eli Lilly and Company for financial support.

1. R. J. SUHADOLNIK. Nucleosides antibiotics. Wiley–Interscience, New York. 1970. p. 390, and references therein.
2. G. JUST and S. G. KIM. Tetrahedron Lett. 1063 (1976).
3. K. ALDER, R. HARTMANN, and W. ROTH. Ann. Chem. **613**, 6 (1958).
4. G. JUST and G. READER. Tetrahedron Lett. 1521 (1973).
5. H. C. BROWN and K. J. MURRAY. J. Am. Chem. Soc. **81**, 4108 (1959).
6. R. U. REMIEUX and E. VON RUDLOFF. Can. J. Chem. **23**, 1701 (1955).
7. E. J. COREY and A. VENKATESWARLU. J. Am. Chem. Soc. **94**, 6190 (1972).
8. V. M. PARIKH and J. K. N. JONES. Can. J. Chem. **43**, 3452 (1965).

Syntheses of *C*-nucleosides. IX. Reactions of D,L-3,4-di-*O*-isopropylidene-2,5-anhydroallose with Wittig reagents. Syntheses of bis-homo anhydro-*C*-nucleosides.

GEORGE JUST, MOHABIR RAMJEESINGH, AND TENG JIAM LIAK
Department of Chemistry, McGill University, Montreal, P.Q., Canada H3C 3G1

Received March 15, 1976

GEORGE JUST, MOHABIR RAMJEESINGH, and TENG JIAM LIAK. Can. J. Chem. **54**, 2940 (1976).

The nmr spectra of the two anomers of 1-*O*-acetyl-3,4-di-*O*-isopropylidene-2,5-anhydro-D,L-allose (**2***a*, **2***b*) are discussed. The reactions of D,L-3,4-di-*O*-isopropylidene-2,5-anhydroallose (**1**) with carbethoxymethylenetriphenylphosphorane, bromocarbethoxymethylenetriphenylphosphorane and ethyl triphenylphosphoranylidene pyruvate to give respectively the olefin derivatives **7**, **9**, and **10** and an internal Michael addition product **11** are described. From **11**, two bis-homo anhydro-*C*-nucleosides having 6-azauracil (**15**) and 4-hydroxy-5-carboxamidopyrazole (**19**) bases were synthesized.

GEORGE JUST, MOHABIR RAMJEESINGH, et TENG JIAM LIAK. Can. J. Chem. **54**, 2940 (1976).

Les spectres rmn des deux anomères du *O*-acétyl-1 di-*O*-isopropylidène-3,4 anhydro-2,5 D,L-allose (**2***a*, **2***b*) sont rapportés et discutés. On décrit aussi les réactions du di-*O*-isopropylidène-3,4 anhydro-2,5 D,L-allose avec le carbéthoxyméthylène triphénylphosphoranne, le bromocarbéthoxyméthylène triphénylphosphoranne et le triphénylphosphorannylidène pyruvate d'éthyle donnant respectivement les dérivés oléfiniques **7**, **9**, **10** et le produit de condensation interne de Michael **11**. A partir du composé **11**, on a synthétisé deux bis-homo anhydro-*C*-nucléosides ayant les bases aza-6 uracile **15** et hydroxy-4 carboxamidopyrazole-5 **19**.

In previous papers (1, 2), we reported a synthesis of D,L-3,4-di-*O*-isopropylidene-2,5-anhydroallose (**1**) and its use for *C*-nucleoside syntheses. In this paper we wish to present a study of the reactions of D,L-3,4-di-*O*-isopropylidene-2,5-anhydroallose with Wittig reagents and the syntheses of two bis-homo anhydro-*C*-nucleosides.

In our synthesis of D,L-3,4-di-*O*-isopropylidene-2,5-anhydroallose, both the α and β anomers were obtained in approximately equal amounts. This conclusion was based on their nmr spectral data in which the anomeric protons of both anomers have different chemical shifts. They appeared at 5.08 and 5.21 ppm and their approximate intensity was half a proton each.

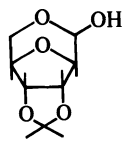

1

It was possible to separate the α and β forms of the acetate derivative (**2***a*, **2***b*) by thin layer chromatography eluting with ether–hexane (1:2). The two anomers with $R_f = 0.45$, mp 64.5–65.6 °C, and $R_f = 0.4$, mp 140.5–141.5 °C, had virtually identical infrared and mass spectra but different nmr spectra. Structural assignment of the two anomers were based on their nmr data. Generally for sugars, an equatorial anomeric proton produces a signal at lower field by approximately 25 Hz than an axial proton (3). On this basis, the anomer ($R_f = 0.45$) with the

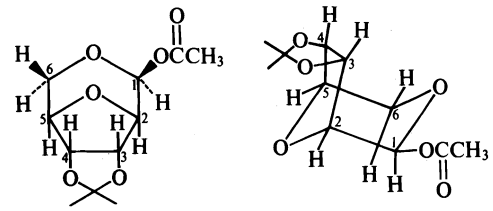

2*a*

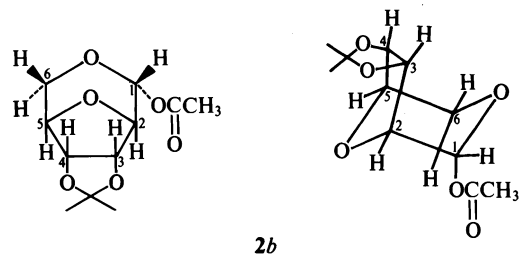

2*b*

Can. J. Chem. Downloaded from www.nrcresearchpress.com by 210.87.254.6 on 09/05/12
For personal use only.

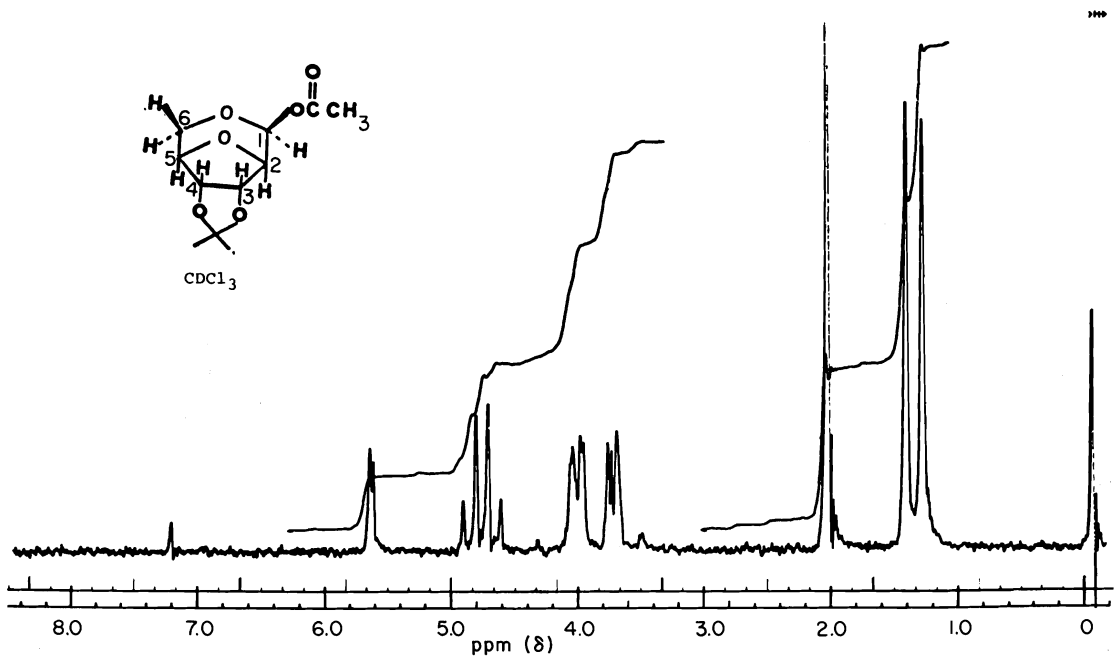

FIG. 1. Nuclear magnetic resonance spectrum of the β anomer **2***a*.

proton on C-1 6 Hz higher than the other (in deuteropyridine) was assigned the β configuration (**2***a*). The other isomer (R_f = 0.40, Fig. 2) was therefore the α anomer (**2***b*).

A major difference between the two spectra were the signals for the protons at C-3 and C-4. In the α anomer (Fig. 2) they appeared as a singlet at 4.80 ppm whereas for the β anomer, (Fig. 1) they gave an AB pattern (J = 6 Hz). In addition both protons on C-6 in the **2***a* and **2***b* were found to have distinctly different chemical shifts, a feature which is much more pronounced in **2***b* (Fig. 2). This is easily explainable since the axial substituent in **2***b* was in close proximity to the axial proton on C-6 thus causing the latter to be in a different chemical environment than its equatorial counterpart. Hence, one of them appeared as part of an AB system at 3.50 ppm and the other as the other part of the AB system at 4.13 ppm (J_{AB} = 11 Hz). The latter was also coupled to the proton on C-5 with J = 2 Hz. Using the Karplus curve (4) which predicts a small coupling constant for the equatorial proton having a dihedral angle of about 30° with C-5 H, the signal at 4.13 was assigned to this equatorial proton. The axial proton which had a dihedral angle of about 90° with C-5 H was assigned to the signal at 3.50 ppm.

For the β anomer **2***a* (Fig. 1), on the other hand, the substituent was now equatorial and was pointing away from the two protons on C-6. Hence these two protons on C-6 did not show the same large difference in chemical shift, appearing as an AB system at 3.74 (H_a) and 3.95 ppm (H_e).

The reaction of the 2,5-anhydroallose **1** with 2 equiv. each of triphenylphosphine, carbon tetrabromide, and zinc dust (5) at 23 °C in dry methylene chloride did not give the dibromoolefin **3**. Starting material was quantitatively recovered. Another variation of this reaction

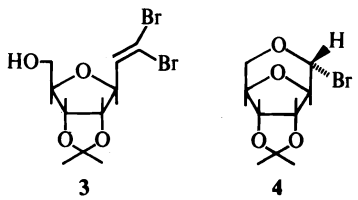

3 **4**

(5), namely reaction of **1** with 4 equiv. of triphenylphosphine and 2 equiv. of carbon tetrabromide, was equally unsuccessful. Instead the crystalline 1-bromocompound **4** mp 144–145 °C, was isolated in 75% yield. Only one stereoisomer

Can. J. Chem. Downloaded from www.nrcresearchpress.com by 210.87.254.6 on 09/05/12
For personal use only.

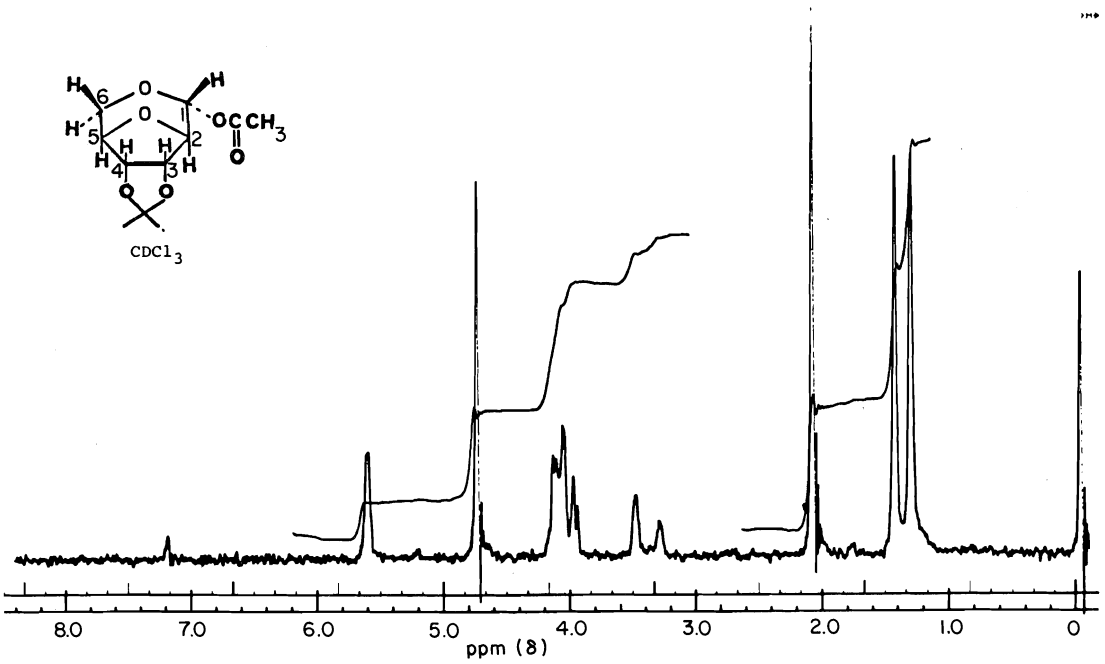

FIG. 2. Nuclear magnetic resonance spectrum of the α anomer **2***b*.

was obtained and its nmr spectrum was very similar to that of (**2***b*). Protons on C-3 and C-4 appeared as a singlet at 4.75 ppm. Protons on C-6 had very different chemical shifts and were geminally coupled. They appeared at 3.50 ppm and 4.18 ppm with a coupling constant of 13 Hz. As in the case of **2***b* these nmr data were characteristic of an axial substituent at the C-1 position. The formation of only one isomer was not surprising since it is well known that for 1,4-dioxane systems, halogen atoms were found to prefer the axial orientation because of the anomeric effect (for a review on the anomeric effect in 1,4-dioxane systems, see ref. 6) (7). This stereochemistry was favoured by several kcal/mol[2].

The formation of **4** was most probably due to the bromination of anhydroallose **1** by triphenylphosphine dibromide **5**. It is known that the latter is produced as a side product in this method of generating the ylide **6** (8).

$$2Ph_3P + CBr_4 \rightarrow \underset{\mathbf{6}}{Ph_3PCBr_2} + \underset{\mathbf{5}}{Ph_3PBr_2}$$

It is also known that triphenylphosphine dibromide generally brominates alcohols and phenols to the aryl and alkyl halides (9).

The reaction of the 2,5-anhydroallose **1** with carbethoxymethylenetriphenylphosphorane in DMF for 6 h at 90 °C gave exclusively the oily *trans* olefin **7** in up to 75% yield. These conditions were similar to those employed in the condensation of galactose (10) with the ylide. The *trans* isomer was expected in this case since on steric grounds, the *threo* struction of the intermediate betaine was probably more stable than the *erythro* structure which leads to the *cis* olefin (11). The unsaturated ester **7** showed

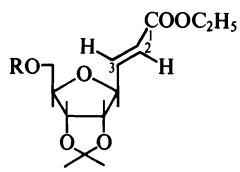

7 R = H
a R = Ac
b R = $(CH_3)_3CSi(CH_3)_2$

vinyl protons absorption as an AB system at 5.73 and 6.70 ppm (J = 14 Hz), characteristic of a *trans* olefin (4).

A crystalline side product, mp 123–124 °C, was also isolated in less than 8% yield from this reaction. Its nmr spectrum showed the presence

Can. J. Chem. Downloaded from www.nrcresearchpress.com by 210.87.254.6 on 09/05/12
For personal use only.

Can. J. Chem. Downloaded from www.nrcresearchpress.com by 210.87.254.6 on 09/05/12
For personal use only.

of any ethyl group and the absence of olefinic protons. The infrared spectrum showed a carbonyl absorption at 1740 cm^{-1} and the mass spectrum gave a molecular ion peak at 272 showing it to be an isomer of **7**. This side product was assigned structure **8** and was most likely formed from **7** by an internal Michael type addition. The yield of **8** was found to increase with higher temperature and longer reaction time.

Both stereoisomers[1] of **8** were obtained. One isomer was more soluble in hexane than the other. Using this fractional solubilization technique, fairly pure samples of both isomers (**8***a*

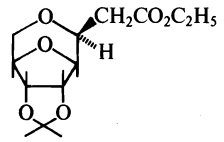

8*a*

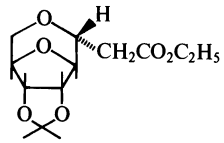

8*b*

and **8***b*) could be obtained. Their nmr showed the same characteristic differences as in the case for **2***a* and **2***b*. For the α isomer **8***b* which was analogous to **2***b*, the two protons on C-6 had different chemical shifts, appearing as an AB system at 3.40 ppm and at 4.0 ppm with a coupling constant (J_{AB}) of 11 Hz. The β isomer **8***a* had nearly the same chemical shift for the two C-6 protons which appeared as a complex signal at 3.65 ppm. Moreover, it was found that for the β isomer,[1] protons (C-2′) of the side chain appeared as a doublet at higher field, 2.42 ppm (J = 6 Hz), whereas, for the α isomer[1] they appeared as doublet of doublets at lower field (2.82 ppm, J = 8 Hz, J = 3 Hz).

Acetylation of **7** gave a monoacetate **7***a* which again was not crystalline. Silylation of **7** with *tert*-butyldimethylsilyl chloride in dimethylformamide (12) gave the oily monosilyl derivative **7***b*. Both of these compounds were important intermediates in our synthesis of *C*-nucleosides (13).

In the large scale preparation of **7***a*, it was found expedient to acetylate directly the crude product obtained from the Wittig reaction after evaporation of dimethylformamide. Work-up followed by filtration through a silica gel column (activity 3) eluting with ether–hexane (1:1) effectively separated the product **7***a* (R_f = 0.8) from triphenylphosphine oxide, and gave an 80% overall yield of **7***a*, based on 2,5-anhydroallose (**1**).

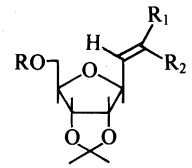

9*a* R = H, R_1 = Br, R_2 = CO_2Et
b R = H, R_1 = CO_2Et, R_2 = Br
c R = Ac

Reaction of bromocarbethoxymethylenetriphenylphosphorane (14) with the 2,5-anhydroallose **1** in DMF at 95 °C gave the oily olefin **9**, in less than 20% yield. Both possible isomers in which the proton on C-3 and the bromine substituent were both *cis* **9***a* and *trans* **9***b* were obtained. Since the *cis* deshielding parameter of bromine is roughly 0.5 ppm smaller than that of the carbethoxy group (15), one would expect the C-3 proton of **9** to be at markedly higher field. Hence the doublet of the C-3 proton at 6.64 ppm (J = 7 Hz) was assigned to the *cis* isomer **9***a* and that at 7.25 ppm (J = 5 Hz) was assigned to the *trans* isomer **9***b*. The ratio of *cis* to *trans* isomers was variable with a predominance of the *trans* isomer. This mixture was further characterized as the acetate derivative **9***c*.

The reaction of the 2,5-anhydroallose **1** with ethyl triphenylphosphoranylidene pyruvate (16) at 90 °C for 2 days did not give the α,β-unsaturated keto ester **10**. Instead an oil (**11**) which

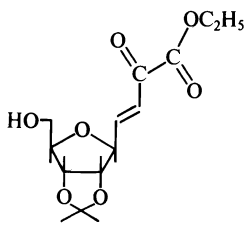

10

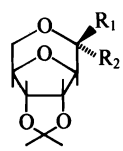

11*a* R_1 = H, R_2 = CH_2COCO_2Et
b R_1 = CH_2COCO_2Et, R_2 = H

turned out to be the internal Michael addition (17) product of **10** was obtained. Milder reaction conditions did not give any product.

Both stereoisomers[1] **11***a* and **11***b* were ob-

[1]By analogy with **2***a* and **2***b*, the stereochemistry of the substituent at the C-1 position of this and other similar bicyclic compounds will be denoted by the letters α or β. When the substituent is axial or equatorial with respect to the 1,4-dioxane ring, the compound will be referred to as the α isomer or the β isomer respectively.

Can. J. Chem. Downloaded from www.nrcresearchpress.com by 210.87.254.6 on 09/05/12
For personal use only.

tained as a mixture. The nmr spectrum of the mixture was similar to that of **8** except for the chemical shifts of the methylene protons of the side chain. For the β isomer[1] (**11***b*) the methylene protons appeared as a multiplet at 3.0 ppm and for the α isomer[1] as a multiplet at 3.50 ppm, thus following the same pattern as in **8** in which the methylene protons of the α isomer (**11***a*) were more downfield than those of the β isomer[1].

Acetylation of the isomeric mixture **11***a* and **11***b* with acetic anhydride in pyridine gave on work-up the vinyl acetate derivative **12** as a

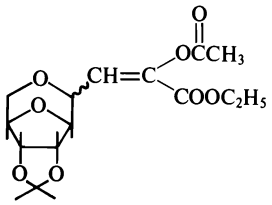

12

mixture of isomers. The olefinic proton appeared as a doublet at 6.30 ppm (J = 7 Hz). The infrared spectrum showed strong bands at 1780 cm^{-1} (enol acetate) and 1740 cm^{-1} (ester) and a medium intensity band at 1680 cm^{-1} (C=C). Its mass spectrum showed a molecular ion peak at 342. The structure was confirmed by microanalysis.

The reaction of the isomeric mixture **11***a* and **11***b* with semicarbazide hydrochloride gave the semicarbazones **13***a* and **13***b*. One isomer, mp

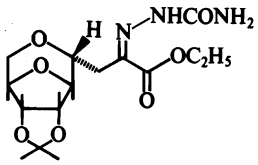

13*a*

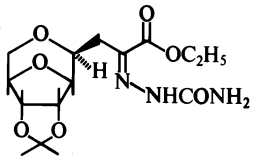

13*b*

218–220 °C, crystallized out from the reaction mixture. The other isomer obtained by extraction of the mother liquor was crystallized from ether – petroleum ether as a white powder, mp 82–84 °C. The nmr spectra of both isomers[1] showed the same characteristic differences as was discussed for **8***a* and **8***b*. The one isomer, mp 218–220 °C, had a chemical shift of 2.68 ppm for the methylene protons on C-3′, and showed an AB quartet for the protons on C-3 and C-4 of the bicyclic ring. It was assigned structure **13***a*. The other isomer had a chemical shift of 2.90 ppm for its methylene protons of C-3′ and showed a singlet at 4.48 ppm for the protons on C-3 and C-4 of the bicyclic ring. This isomer was assigned structure **13***b*. The mass spectra of both isomers were identical.

Cyclization of **13***a* with methanolic sodium hydroxide gave the 6-azauracil derivative **14***a* (18), mp 170 °C. It had a uv absorption characteristic for azauridine at 253 nm (ϵ 6900) in ethanol (18). Its mass spectrum showed a molecular ion peak at 311.

Cleavage of the acetonide with 50% aqueous trifluoroacetic acid gave the crystalline bishomo anhydro-*C*-nucleoside **15***a*.

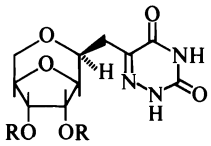

14*a* R,R = $C(CH_3)_2$
15*a* R,R = H

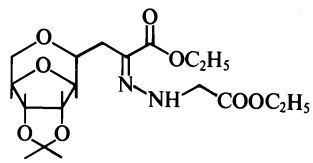

16

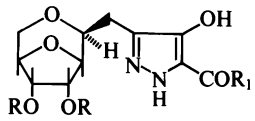

17*a* R,R = $C(CH_3)_2$, R_1 = OCH_3
18*a* R,R = $C(CH_3)_2$, R_1 = NH_2
19*a* R,R = H, R_1 = NH_2

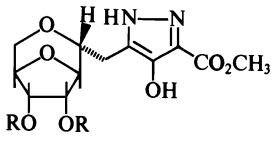

17*b*

Condensation of the isomeric mixture **11***a* and **11***b* with ethyl hydrazinoacetate hydrochloride gave the corresponding isomeric oily hydrazone **16**. Cyclization of **16** with sodium methoxide gave the 4-hydroxy pyrazole derivative as a mixture of isomers **17***a* and **17***b* (19), which was obtained as a powder after purifica-

Can. J. Chem. Downloaded from www.nrcresearchpress.com by 210.87.254.6 on 09/05/12
For personal use only.

tion by tlc using ethyl acetate – methanol, (10:1) giving the isomeric mixture (**17***a* and **17***b*) (R_f = 0.7) as a white powder. A portion of this product was soluble in chloroform and from its nmr turned out to be the β isomer[1] **17***a* mp 82–84 °C. The chloroform insoluble fraction crystallized from methanol–chloroform, mp 173–175 °C. Based on its nmr data, it was assigned structure **17***b*. Both compounds displayed characteristic uv absorptions of a 4-hydroxy-5-carbomethoxypyrazole derivative (19) at 238 nm (ε 6300), 328 nm (ε 8100) in 0.1 *N* NaOH and at 228 nm (ε 6900), 273 nm (ε 5000) in 0.1 *N* HCl.

The β isomer **17***a* was converted to the carboxamide derivative **18***a* which, upon cleavage of the isopropylidene protecting group with 80% aqueous trifluoroacetic acid, yielded the bis-homo anhydro-*C*-nucleoside **19***a*.

Experimental

For general procedures, see preceding paper (13).

1-O-Acetyl-2,5-anhydro-3,4-O-isopropylidene-D,L-allose (2a and 2b)

Anhydroallose (**1**) (202 mg, 1 mmol) was acetylated overnight with 4 ml of acetic anhydride and 5 ml of pyridine. Work-up gave a quantitative yield of the crystalline mixture of **2***a* and **2***b*. Separation on silica gel plates, 20 × 20 cm × 1 mm eluting with ether–hexane (1:2) gave two bands, R_f = 0.45 and R_f = 0.40. Extraction of the bands gave 105 mg of **2***a* (β anomer) mp 64.5–65.5 °C, and 115 mg of **2***b* (α anomer) mp 140–141 °C; ir ($CHCl_3$), 1750 (OAc), 1385 cm^{-1} (acetonide); nmr (**2***a*) ($CDCl_3$), δ 1.38 (s, 3H), 1.51 (s, 3H), 2.14 (s, 3H), 3.74 (d, J_{AB} = 12 Hz, 1H), 3.94 (d of d, J_{AB} = 12 Hz, J = 2 Hz, 1H), 4.05 (d, J = 2 Hz, 1H), 4.15 (s, 1H), 4.85 (AB quartet, J_{AB} = 6 Hz, 2H), 5.73 (d, J = 2 Hz, 1H); nmr (**2***b*) ($CDCl_3$), δ 1.38 (s, 3H), 1.51 (s, 3H), 2.14 (s, 3H), 3.50 (d, J = 12 Hz, 1H), 4.17 (bs, 1H), 4.20 (s, 1H), 4.86 (s, 2H), 5.73 (d, J = 2 Hz, 1H); ms 229 ($M^+ - CH_3$). *Anal.* calcd. for $C_{11}H_{16}O_4$: C 54.09, H 6.60; found: C 54.03, H 6.59.

1-Deoxy-1α-bromo-D,L-2,5-anhydro-3,4-O-isopropylidene-allose 4

Carbon tetrabromide (0.665 g, 2 mmol) and triphenylphosphine (1.08 g, 4 mmol) were dissolved in 15 ml of dry methylene chloride. Anhydroallose (**1**) (202 mg, 1 mmol) in 10 ml of methylene chloride was added slowly to this solution. The reaction mixture was stirred at 0 °C for ½ h. Evaporation of solvent and passage through a silica gel column (activity 3) eluting with ether–hexane (1:1) gave 310 mg of **4**, mp 144–145 °C, yield 84%; ir (Nujol) 1390 cm^{-1} (acetonide); nmr ($CDCl_3$) δ 1.32 (s, 3H), 1.50 (s, 3H), 3.55 (d, J = 12 Hz, 1H), 4.18 (d, J = 12 Hz, 1H), 4.25 (2H), 4.80 (s, 2H), 6.15 (s, 1H); ms 256 (M^+, ^{81}Br), 254 (M^+, ^{79}Br), 185 (M^+ – Br). *Anal.* calcd. for $C_9H_{13}O_4Br$: C 40.7, H 4.9, Br 30.20; found: C 40.6, H 4.9, Br 30.15.

Ethyl trans-3-(5β-Hydroxymethyl-3α,4α-dihydroxy-di-O-isopropylidenefuran-1β-yl)acrylate (7)

Carbethoxymethylenetriphenylphosphorane (600 mg, 1.725 mmol) was added to the anhydroallose **1** (300 mg, 1.48 mmol) in 15 ml of dimethylformamide. The solution was heated at 95 °C for 6 h, cooled, and stripped of solvent by evaporation under high vacuum. The residue was triturated with ether and the white crystalline material that precipitated was filtered off. The filtrate was evaporated to dryness and chromatographed on 20 × 20 cm silica gel plates. Elution with methylene chloride – ether (2:3) gave 250 mg of colorless oily product, yield 66%; ir (film) 3500 (OH), 1730 (ester), 1670 (C=C), 1380 cm^{-1} (*gem*-dimethyl); nmr ($CDCl_3$) δ 1.20 (t, 3H, J = 7 Hz), 1.30 (s, 3H), 1.52 (s, 3H), 2.02 (s, O–H), 3.5 to 4.52 (m's, 8H), 5.73 (d, 1H, J = 14 Hz), 6.70 (dd, 1H, J = 14 Hz, J = 4 Hz); ms (70 eV) *m/e* 272 (M^+), 257 ($M^+ - CH_3$), 227 ($M^+ - CH_3 - CH_2O$), 214 ($M^+ - CH_3 - CH_3COO$), 167, 129, 85. *Anal.* calcd. for $C_{13}H_{20}O_6$: C 57.35, H 7.35; found: C 56.61, H 7.66.

Ethyl trans-3-(5β-tert-Butyldimethylsilyl-O-methyl-3α,4α-dihydroxy-di-O-isopropylidenefuran-1β-yl)acrylate (7b)

The acrylic ester **7** (230 mg, 0.85 mmol) was silylated using *tert*-butyldimethylsilyl chloride (300 mg, 2.3 equiv.) and imidazole (290 mg, 5 equiv.) in 15 ml of dimethylformamide at 40 °C for 14 h. Evaporation of solvent and separation on a silica gel column eluting with ether–hexane (1:1) gave 290 mg of colourless oil, yield 90%; ir ($CHCl_3$) 1735 (ester), 1680 (C=C), 1385 cm^{-1} (acetonide); nmr ($CDCl_3$) δ 0.12 (s, 6H), 0.92 (s, 9H), 1.28 (t, 3H), 1.36 (s, 3H), 1.55 (s, 3H), 3.73 (d, J = 4 Hz, 2H), 4.60 (q, 2H), 4.8–5.2 (4H), 6.08 (dd, J = 16 Hz, J = 5 Hz); ms 386 (M^+), 371 ($M^+ - CH_3$), 329 ($M^+ - C(CH_3)_3$), 271 (M^+ – *tert*-butyl-Si$(CH_3)_2$), 241, 184. *Anal.* calcd. for $C_{19}H_{34}O_6Si$: C 59.02, H 8.75; found: C 58.96, H 8.75.

D,L-1-Deoxy-1α,β-carbethoxymethylene-2,5-anhydro-3,4-O-isopropylideneallose (8a, 8b)

Anhydroallose (**1**) (202 mg, 1 mmol) was heated at 110 °C with carbethoxymethylenetriphenylphosphorane (400 mg, 1.14 mmol) in 12 ml of dimethylformamide for 48 h. Evaporation of solvent, and passage of the crude through a silica gel column (activity 3) eluting with ether–hexane (1:1) gave 245 mg of crystalline material, yield 90%. Addition of 10 ml of hexane to the product, and filtration gave 85 mg of the β isomer, mp 128 °C. Evaporation of the filtrate, addition of a small volume of hexane to the residue, followed by filtration and evaporation of the filtrate gave 64 mg of the fairly pure α isomer, mp 85–86.5 °C; ir (Nujol) 1740 (ester), 1385 cm^{-1} (acetonide); nmr (β isomer) (pyridine-d_5) δ 1.05 (t, 3H), 1.32 (s, 3H), 1.53 (s, 3H), 2.42 (d, J = 7 Hz, 2H), 3.60 (m, 2H), 4.02 (q, 2H), 4.05–4.40 (3H), 4.65 (s, 2H); nmr (α isomer) (pyridine-d_5) δ 1.05 (t, 3H), 1.32 (s, 3H), 1.53 (s, 3H), 2.82 (m, 2H), 3.40 (d, J_{AB} = 13 Hz, 1H), 3.98 (d of d, J_{AB} = 13 Hz, J = 2 Hz, 1H), 4.15 (q, 2H), 4.18–4.40 (3H), 4.14 (s, 2H); ms 257 ($M^+ - CH_3$), 227 (M^+ – OEt), 185 ($M^+ - CH_2CO_2Et$). *Anal.* calcd. for $C_{13}H_{20}O_6$: C 57.34, H 7.40; found: C 57.31. H 7.30.

Ethyl trans-3-(5β-Acetoxymethyl-3α.4α-dihydroxy-di-O-isopropylidenefuran-1β-yl)acrylate (7a)

Crude or pure ester **7** (200 mg) was acetylated using

Can. J. Chem. Downloaded from www.nrcresearchpress.com by 210.87.254.6 on 09/05/12
For personal use only.

5 ml of acetic anhydride in 6 ml of pyridine stirring for 6 h at room temperature. The mixture was then evaporated to dryness under high vacuum. The oily product was purified on a silica gel column (activity 3), eluting with ether–hexane (1:1). When intermediate **7** was not isolated, the overall yield based on **1** is 80%; ir (film) 1745 (acetate), 1725 (ethyl ester), 1660 (C=C), 1380 cm^{-1} (acetonide); nmr ($CDCl_3$) δ 1.24 (t, 3H, J = 7 Hz), 1.33 (s, 3H), 2.10 (s, 3H), 4.0–4.52 (m's, 8H), 6.18 (d, 1H, J = 16 Hz), 6.95 (dd, 1H, J = 16 Hz, J = 5 Hz); ms (70 eV) *m/e* 314 (M^+), 299 ($M^+ - CH_3$), 256 (299 − CH_3CO), 211, 196, 86.

*Ethyl 2-Bromo-3-(2,3-di-O-isopropylidene-5-O-acetyl-1β-ribofuranosyl)acrylate (**9c**)*

Carbethoxybromomethylenetriphenylphosphorane (450 mg, 1.28 mmol) was added to a solution of the anhydroallose (**1**) (202 mg, 1 mmol) in 15 ml dimethylformamide. The solution was heated at 95 °C for 24 h, cooled, and evaporated to dryness under high vacuum. Toluene and absolute ethanol were used as chaser. The residue was directly acetylated using 5 ml of pyridine and 3 ml of acetic anhydride with stirring for 8 h. Evaporation of excess pyridine and acetic anhydride yielded a brown oily residue. This was chromatographed on a silica gel column (activity 3). Elution with ethyl ether – hexane (1:1) gave 75 mg of the isomeric mixture of product, an oil, yield 19%; ir (film) 1745 (acetate), 1710 (ethyl ester), 1640 and 1680 (C=C), 1380 cm^{-1} (acetonide); nmr ($CDCl_3$) δ 1.32 (s, 3H), 1.4 (t, 3H, J = 7 Hz), 1.55 (s, 3H), 2.1 (s, 3H), 4.0–4.6 (7H), 4.8 (d of d, J = 7 Hz. J = 3 Hz, 0.6H), 5.10 (d of d, J = 7 Hz, J = 3Hz, 0.4H), 6.64 (d, J = 7 Hz, 0.6H), 6.73 (d, J = 7 Hz, 0.4H); ms 394 (M^+, ^{81}Br), 392 (M^+, ^{79}Br), 379 (394 − CH_3), 397 (392 − CH_3), 318, 316, 276, 274, 229. *Anal.* calcd. for $C_{15}H_{21}O_7Br$: C 47.33, H 5.61, Br 14.77; found: C 47.32, H 5.48, Br 14.70.

*1-Deoxy-1α,β-ethoxalylmethylene-2,5-anhydro-3,4-O-isopropylidene-D,L-allose (**11**)*

Ethyl triphenylphosphoranylidene pyruvate (515 mg, 1.35 mmol) was added to anhydroallose (**1**) (202 mg, 1 mmol) in 15 ml of dimethylformamide. The solution was heated at 95 °C for 26 h, cooled, and stripped of solvent by evaporation under high vacuum. Separation of the crude product on a silica gel column eluting with ether–hexane (1:1) gave 195 mg of **11** as an oil, yield 65%; ir 1745 (strong, ketoester), 1395 cm^{-1} (acetonide); nmr ($CDCl_3$) δ 1.35 (t, 3H), 1.38 (s, 3H), 1.51 (s, 3H), 3.0 (m, CH_2 of β), 3.45 (m, CH_2 of α), 3.8 (m, 2H), 4.0–4.6 (5H), 4.02 (s, 2H of α), 4.05 (2H of β). *Anal.* calcd. for $C_{15}H_{20}O_7$: C 55.99, H 6.71; found: C 55.89, H 6.67.

*1-Deoxy-1α,β-ethoxalylmethylene-2,5-anhydro-3,4-O-isopropylidene-D,L-allose Semicarbazone (**13a**, **13b**)*

The keto ester **11** (350 mg, 1.1 mmol) in 5 ml of ethanol was added to semicarbazide hydrochloride (114 mg, 1.5 mmol) and sodium acetate (130 mg, 1.55 mmol) dissolved in 4 ml of water. The resulting solution was heated on a hot plate to boiling and was then allowed to cool slowly. The crystals obtained (β isomer) (**12a**) (165 mg), mp 218–220 °C, were filtered off and to the resulting filtrate an additional 10 ml of water was added and then extracted with 3 × 10 ml of chloroform. Drying of the organic layer with sodium sulfate and evaporation gave 196 mg of a white powder (α isomer, **12b**) mp 82–84 °C; total yield 86%; ir (KBr disc) 3500, 3385 (NH_2), 1720 (keto ester), 1700 (amide), 1590 (C=N), 1390 cm^{-1} (acetonide); nmr (β isomer) (DMSO-d_6) δ 1.21 (t, 3H), 1 32 (s, 3H), 1.37 (s, 3H), 2.68 (m, 2H), 3.32 (m, 2H), 3.54 (m, 1H), 4.0 (m, 2H), 4.16 (q, 2H), 4.7 (d, J_{AB} = 6 Hz, 1H), 5.0 (d, J_{AB} = 6 Hz, 1H), 6.45 (NH_2), 10.1 (NH); nmr (α isomer) ($CDCl_3$) δ 1.24 (t, 3H), 1.31 (s, 3H), 1.41 (s, 3H), 2.90 (m, 2H), 3.6–4.2 (7H), 4.84 (s, 2H), 6.45 (NH_2), 10.5 (NH); ms 357 (M^+), 342 ($M^+ - CH_3$), 298 ($M^+ - NH_2CONH$), 284 ($M^+ - NH_2CONHN$), 210, 173. *Anal.* calcd. for $C_{15}H_{23}O_7N_3$: C 50.41, H 6.49, N 11.76; found: (β isomer): C 50.60, H 6.58, N 11.77; found (α isomer): C 50.62, H 6.53, N 11.72.

*1-Acetoxy-1-carbethoxy-2-(1-deoxy-2,5-anhydro-3,4-di-O-isopropylidene-D,L-allose-1α,β-yl)ethene (**12**)*

The cyclic keto ester **11** (200 mg) was acetylated with acetic anhydride (2 ml), pyridine (3 ml), and triethylamine (1 ml) overnight. Work-up in the usual way gave a quantitative yield of the crystalline enol–acetate as a mixture of isomers, mp 90.5–92 °C; ir (KBr disc) 1780 (enol–acetate), 1740 (ester), 1680 (C=C), 1385 cm^{-1} (acetonide); nmr ($CDCl_3$) δ 1.28 (t, 3H), 1.31 (s, 3H), 1.53 (s, 3H), 2.25 (s, 3H), 3.65 (m, 2H), 4.10 (bs, 2H), 4.13 (q, 2H), 4.45 (dd, J = 7 Hz, J = 2 Hz, 1H), 4.74 (s, 2H), 6.31 (d, J = 7 Hz, 1H); ms 342 (M^+), 327 ($M^+ - CH_3$). *Anal.* calcd. for $C_{16}H_{22}O_8$: C 56.13, H 6.48; found: C 55.86, H 6.59.

*1-Deoxy-1β-(6-azauracylyl-5-methylene)-2,5-anhydro-3,4-O-isopropylidene-D,L-allose (**14a**)*

The semicarbazone **12a** (175 mg, 0.5 mmol) was stirred at room temperature with 6 equiv. of aqueous sodium hydroxide for 4 h. Neutralization to p*H* 4 followed by rapid extraction with ethyl acetate (3 × 15 ml) gave, after drying, a white powder. Recrystallization from hot ethanol gave 90 mg of pure (**14a**), mp 173–174 °C; yield 60%; ir (KBr disc) 3500–3300 (multiple bands, NH), 1710 (strong, cyclic amide), 1600 (C=N), 1390 cm^{-1} (acetonide); nmr (DMSO-d_6) δ 1.32 (s, 3H), 1.40 (s, 3H), 2.68 (m, 2H), 3.50 (m, 2H), 3.92 (m, 3H), 4.7 (d, J = 6 Hz, 1H), 5.0 (d, J = 6 Hz, 1H), 6.8–7.0 (b, 2H); uv λ_{max} (EtOH) 253 (ϵ 6900); ms 311 (M^+), 296 ($M^+ - CH_3$) 270, 210, 113 (B + 1). *Anal.* calcd. for $C_{13}H_{17}O_6N_3$: C 50.16, H 5.50, N 20.64; found: C 49.98, H 5.53, N 20.61.

*1-Deoxy-1β-(6-azauracylyl-5-methylene)-2,5-anhydro-D,L-allose (**15a**)*

The azauracil derivative **14a** (150 mg) was dissolved in 50% aqueous trifluoroacetic acid and stirred at room temperature for 30 min. Evaporation of the solvent gave a yellow powder. After washing several times with small amounts of methanol, a white powder (**15a**) was obtained, mp 198 °C; ir (KBr disc), 3500–3300 (multiple bands, NH), 1710 (strong, cyclic amide), 1600 (C=N); uv λ_{max}(EtOH) 253 (ϵ 6900). *Anal.* calcd. for $C_{10}H_{13}O_6N_3$: C 44.28. H 4.79, N 15.49; found: C 44.32, H 4.76, N 15.72.

*1-Deoxy-1α,β-(5(3)-carbomethoxy-4-hydroxypyrazolyl-3(5)-methylene)-2,5-anhydro-3,4-O-isopropylidene-D,L-allose (**17a**, **17b**)*

The keto ester **11** (300 mg, 1 mmol) and ethyl hydrazinoacetate hydrochloride (175 mg, 1.15 mmol) was dissolved

Can. J. Chem. Downloaded from www.nrcresearchpress.com by 210.87.254.6 on 09/05/12
For personal use only.

in methanol–water (8:2) and sodium acetate (100 mg, 1.25 mmol) was added. The reaction mixture was stirred overnight. An equal volume of water was then added and the aqueous solution was extracted with chloroform (3 × 15 ml). Drying of the organic extract over sodium sulfate, and evaporation gave a quantitative yield of crude **16**. This crude product was refluxed for 3 h with 4 equiv. of sodium methoxide in methanol. After evaporation of methanol, water was added and the solution carefully neutralized with dilute hydrochloric acid to p*H* 5. Extraction with 4 × 20 ml of ethyl acetate and drying over sodium sulfate gave, after evaporation of solvent, a yellow powder. Purification on silica gel plates (20 × 20 cm × 1 mm) eluting with ethyl acetate – methanol (10:1) gave a broad band, R_f = 0.5–0.7. Extraction with methanol gave a white powder, as a mixture of isomers (175 mg), yield 53%.

The mixture was shaken with 10 ml of chloroform and then filtered. The undissolved powder (α isomer, **17***b*) (60 mg) was recrystallized from methanol–chloroform, mp 173–175 °C. The chloroform filtrate was evaporated to give 115 mg of fairly pure β isomer (**17***a*); mp 82–84 °C; ir (**17***a*) ($CHCl_3$) 3500, 3400 (NH), 1720 (ester), 1610 (C=N), 1400 cm^{-1} (acetonide); ir (**17***b*) (KBr disc) 3450, 3320 (NH), 1720 (ester), 1600 (C=N), 1390 cm^{-1} (acetonide); nmr (**17***a*) (pyridine-d_5) δ 1.31 (s, 3H), 1.53 (s, 3H), 3.10 (d, J = 6 Hz, 2H), 3.65 (m, 2H), 3.80 (s, 3H), 4.45–4.05 (m, 3H), 4.81 (d, J = 6 Hz, 1H), 5.18 (d, J = 6 Hz), 8.9 (1H, exchangeable), 8.5–8 (b, exchangeable); nmr (**17***b*) (pyridine-d_5) δ 1.31 (s, 3H), 1.53 (s, 3H), 3.6 (m, 2H), 3.7 (m, 2H), 3.90 (s, 3H), 4.6–4.25 (3H), 5.06 (s, 2H), 6.7 (b, 2H exchangeable); uv λ_{max} (EtOH) 228 (ϵ 6900), 273 (ϵ 5000), 238 (ϵ 6300), 328 (ϵ 8100); ms (**17***a*), 340 (M^+), 325 ($M^+ - CH_3$), 293 (325 − CH_3OH), 229, 185 ($M^+ - CH_2B$) where B is pyrazole base. The mass spectrum of **17***b* is identical to that of **17***a*. *Anal.* calcd. for $C_{15}H_{20}O_7N_2$: C 52.93, H 5.92, N 8.23; found (**17***a*) C 52.70, H 5.85, N 8.42.

*1-Deoxy-1β-(5(3)-carboxamido-4-hydroxypyrazolyl-3(5)-methylene)-2,5-anhydro-3,4-O-isopropylidene-D,L-allose (**18***a*)*

The β isomer **17***a* (200 mg) was dissolved in methanol and saturated at 0 °C with ammonia. The solution was allowed to stand at room temperature for seven days. Evaporation of the solvent gave a yellow powder. Purification on silica gel plates (20 × 20 cm × 1 mm) eluting with ethyl acetate – methanol (10:1) gave a band with R_f = 0.58. Extraction with methanol gave a white powder (145 mg) mp 178–180 °C; yield 76%; nmr (pyridine-d_5) δ 1.31 (s, 3H), 1.53 (s, 3H), 3.10 (d, J = 6 Hz, 2H), 3.65 (m, 2H), 4.45–4.05 (m, 3H), 4.81 (d, J = 6 Hz, 1H), 6.92–5.82 (b, 3H), 8.6 ~ 8.2 (b, 1H); ir ($CHCl_3$) 3450 (NH), 1690 (amide I band, C=O), 1630 (amide II band, NH), 1600 (C=N), 1400 (acetonide); uv λ_{max} (EtOH) 228 (ϵ 6700), 268 (ϵ 4700), 238 (ϵ 4700), 238 (ϵ 5200), 315 (ϵ 7900); ms 325 (M^+), 310 ($M^+ - 15$), 185 ($M^+ - CH_2B$), 140 (CH_2B).

*1-Deoxy-1β-(5(3)-carboxamido-4-hydroxypyrazolyl-3(5)-methylene)-2,5-anhydro-D,L-allose (**19***a*)*

The protected amide **18***a* (150 mg) was stirred in 4 ml 80% trifluoroacetic acid at room temperature for 20 min. Evaporation to dryness and recrystallization from ethanol–chloroform gave a white powder (107 mg), mp 188–190 °C; yield 81%; ir (KBr disc) 3450 ~ 3200 (OH), 1680 (amide I, C=O), 1675 (amide II, NH); uv λ_{max} (EtOH) 227 (ϵ 6700), 269 (ϵ 4700), 236 (ϵ 5000), 318 (ϵ 7700).

Acknowledgment

We wish to thank the National Research Council of Canada and Eli Lilly and Company for financial support.

1. G. Just and A. Martel. Tetrahedron Lett. 1517 (1973).
2. G. Just, A. Martel, K. Grozinger, and M. Ramjeesingh. Can. J. Chem. **53**, 131 (1975).
3. E. L. Eliel, N. L. Allinger, S. J. Angyal, and G. A. Morrison. Conformational analysis. Wiley Interscience, New York. 1967. p. 398, and references therein.
4. E. D. Becker. High resolution NMR. Academic Press Inc., New York. 1969.
5. E. J. Corey and P. L. Tuchs. Tetrahedron Lett. 3769 (1972).
6. E. L. Eliel and N. L. Allinger (*Editors*). Topics in stereochemistry. Vol. 4. Wiley Interscience, New York. 1969. p. 73.
7. C. B. Anderson and D. T. Stepp. J. Org. Chem. **32**, 607 (1967).
8. F. Ramirez, N. Desai, and N. Mckelvie. J. Am. Chem. Soc. **84**, 1745 (1962).
9. L. F. Fieser and M. Fieser. Reagents for organic syntheses. Wiley Inc., New York. 1967. p. 1247.
10. N. K. Kochetkov and B. A. Dmitriev. Tetrahedron, **21**, 803 (1965).
11. L. D. Bergelson, L. I. Barsukov, and M. M. Shemyakin. Tetrahedron, **23**, 2709 (1967).
12. E. J. Corey and A. Venkateswarlu. J. Am. Chem. Soc. **94**, 6190 (1972).
13. G. Just and M. Ramjeesingh. Tetrahedron Lett. 997 (1975).
14. D. B. Denney and S. T. Ross. J. Org. Chem. **27**, 998 (1962).
15. S. N. Tobey. J. Org. Chem. **34**, 1281 (1969).
16. Y. A. Thdanov and L. A. Uzlova. J. Gen. Chem. USSR, **36**, 1225 (1966).
17. S. Danishefsky, G. Koppel, and R. Levine. Tetrahedron Lett. 2257 (1968).
18. M. Bobek, J. Farkas, and F. Sorm. Tetrahedron Lett. 1543 (1968).
19. J. Farkas and T. Flegelova. Tetrahedron Lett. 1591 (1971).

Complexes of niobium(III) with bidentate ligands

A. D. ALLEN[1] AND S. NAITO[2]

Department of Chemistry, University of Toronto, Toronto, Ont., Canada M5S 1A1

Received April 20,1976

A. D. ALLEN and S. NAITO. Can. J. Chem. **54**, 2948 (1976).

A novel method is reported for the convenient preparation of new niobium(III) chloro complexes containing the ligands SMe_2, $CH_3C(CH_2AsMe_2)_3$, *o*-$C_6H_4(AsMe_2)_2$, and $((C_6H_5)_2P—CH_2—)_2$. Details of the preparation and characterization of the compounds are given. In each case the compounds are diamagnetic, and a dimeric metal–metal bonded structure is proposed.

A. D. ALLEN et S. NAITO. Can. J. Chem. **54**, 2948 (1976).

Une nouvelle méthode est rapportée pour la préparation de nouveaux complexes de chloro niobium(III) contenant les ligands SMe_2, $CH_3C(CH_2AsMe_2)_3$, *o*-$C_6H_4(AsMe_2)_2$ et $((C_6H_5)_2P—CH_2—)_2$. La préparation et la caractérisation de ces composés sont décrites en détail. Dans chacun des cas les composés sont diamagnétiques et une structure de dimère impliquant un lien métal–métal est proposée.

[Traduit par le journal]

Introduction

Although a small number of monomeric cyclopentadiene complexes of niobium(III) have been reported, *e.g.* $(\pi C_5H_5)_2Nb$ H.L., where L = CO, PR_3, C_2H_4 (1) and RC≡CR′ (2), the only simple complexes of niobium(III) halides are $Nb_2X_6(SC_4H_8)_3$ (X = Cl, Br, I), $[Nb_2Cl_8(SC_4H_8)]^{2-}$, and $[Nb_2Cl_9]^{3-}$ (3). The absence of reports of other adducts of niobium(III) halides is at least partly due to experimental difficulties, the anhydrous trihalides being difficult to prepare and too inert for use as starting materials (3).

We have discovered a convenient synthetic route to niobium(III) halo complexes which uses the readily available niobium pentachloride as a starting material. Treatment of this with the borane – dimethyl sulphide complex and a stoichiometric amount of sodium/potassium alloy in toluene at room temperature gives directly in good (30%) yield the product $Nb_2Cl_6(SMe_2)_3$, which can readily be converted into complexes of the form $Nb_2Cl_6(L—L)_2$, where L—L is a chelating diphosphine or diarsine.

Experimental

General

Since many of the reagents and products are sensitive to oxygen and water, all reactions were done using a vacuum line under rigorously purified nitrogen or argon. Solvents were purified and dried by conventional means. They were freshly distilled under nitrogen and degassed by freezing and melting under vacuum and nitrogen. Solid reagents were dried and degassed *in situ* by warming under high vacuum.

Materials

Niobium pentachloride was prepared by direct chlorination of the metal powder (4). To minimize contamination with oxytrichloride the chlorine was first condensed at −80 °C under nitrogen and then allowed to warm slowly in a stream of nitrogen. The bright yellow crystalline product was kept in a sealed flask under nitrogen. Portions were transferred to the reaction vessel under nitrogen using a glove bag.

Ligands

1,1,1-Tris(dimethylarsinomethyl)ethane, (triars) (5), *o*-phenylene bis(dimethylarsine), (diars) (5), and 1,2-bis(diphenylphosphine)ethane, (diphos) (6), were prepared as previously reported.

The borane–dimethylsulphide complex ($BH_3 \cdot SMe_2$) was purchased from the Aldrich Chemical Co. Inc., and was used as supplied. It was kept at 0 °C and the volume of liquid removed (by syringe) for each experiment was replaced by dry nitrogen.

Complexes

$Nb_2Cl_6(SMe_2)_3$

Niobium pentachloride, 7.2 g (26.6 mmol), was added to 200 ml toluene. A dark reddish-brown solution was formed and some solid remained undissolved. Borane–dimethylsulphide, 5.1 ml (53.2 mmol), was added by syringe. Within a few minutes the excess solid dissolved and the solution changed to an orange colour. The orange solution was added to freshly prepared Na/K alloy (26.6 mmol of each metal) and the mixture was stirred at room temperature. During the next 3–5 h the colour of the solution changed from orange to yellow-brown to red and finally to a deep purple. Stirring was continued for about 12 h after the purple colour developed. The mixture was filtered through a Schlenk tube. The dark solid residue was removed and carefully destroyed with alcohol under

[1]To whom correspondence should be addressed.

[2]On leave from The University of Tokyo, Tokyo, Japan.

Can. J. Chem. Downloaded from www.nrcresearchpress.com by 210.87.254.5 on 09/05/12
For personal use only.

TABLE 1. Analyses

Compound	Calculated (%)				Found (%)			
	Nb	Cl	C	H	Nb	Cl	C	H
$Nb_2Cl_6(Me_2S)_2.0.1C_6H_5CH_3$[a]	31.3	35.8	13.5	3.2	31.8	35.2	13.1	3.0
$Nb_2Cl_6(triars)_2.0.7C_6H_5CH_3$	15.1	17.3	26.3	4.8	15.9	17.0	26.4	5.4
$Nb_2Cl_6(diars)_2.0.1C_6H_5CH_3$	19.0	21.7	25.0	3.3	18.1	21.8	24.5	3.2
$Nb_2Cl_6(diphos)_20.7C_6H_5CH_3$	14.8	16.9	54.3	4.3	15.7	16.5	54.1	4.3

[a]Toluene contents calculated from nmr spectrum of sample analysed.

TABLE 2. Proton magnetic resonance spectra[a]

Compound	δ (ppm) and ratio in parentheses
Me_2S	2.12
$Nb_2Cl_6(SMe_2)_3$	2.63 (2) (S—CH_3 terminal); 3.34 (1) (S—CH_3 bridging)
$CH_3C(CH_2As(CH_3)_2)_3$	0.95 (6) (As—CH_3); 1.75 (2) (C—CH_2—As); 1.10 (1) (C—CH_3)
$Nb_2Cl_6(triars)_2$	1.25 (6) (As—CH_3 co-ord.); 1.80 (2) (C—CH_2—As co-ord.); 1.08 (1.5) (C—CH_3)
	0.97 (3) (As—CH_3 free); 1.58 (1) (C—CH_2—As free)
$C_6H_4(AsMe_2)_2$	1.27 (3) (As—CH_3); 7.37 (1) (C_6H_4)
$Nb_2Cl_6(diars)_2$	1.60 (3) (As—CH_3); 7.57 (1) (C_6H_4)

[a]In $CDCl_3$ solution.

TABLE 3. Infrared spectra[a]

Compound	Infrared frequency
$Nb_2Cl_6(SMe_2)_3$	1424(vs), 1328(m), 1310(m), 1030(s, doublet) 980 (s, doublet), 685(m), 355(sh), 345(vs) 322(s), 318(s), 285(w), 238(m).
$Nb_2Cl_6(diars)_2$	1418(m), 1265(w), 1250(m), 1111(m), 1041(w), 909(s) 877(s), 752(s), 613(m), 595(m), 442(m) 355(s), 308(s), 285(s), 244(w).
$Nb_2Cl_6(triars)_2$	1492(w), 1420(m), 1380(w), 1264(m), 1250(m), 905(s) 881(vs), 606(m), 580(m), 489(m), 330(vs), 285(s), 238(m).
$Nb_2Cl_6(diphos)_2$	1590(w), 1574(w), 1485(m), 1435(s), 1193(w), 1080(w), 1070(w), 1030(m), 1000(w), 862(m), 840(w), 741(vs), 730(s), 695(vs), 518(s), 488(m), 474(m) 345(sh), 332(vs), 286(m), 245(w).

[a]In Nujol mulls.

nitrogen in a fume hood. The purple filtrate was evaporated by pumping until a precipitate began to form. Pentane (or petroleum ether) was added to give a purple solid which was separated by filtration. After recrystallization from toluene/pentane the purple product, 2.2 g (28.5%), was dried under vacuum and kept under nitrogen.

$Nb_2Cl_6(triars)_2$

$Nb_2Cl_6(SMe_2)_3$, 1.5 g (2.6 mmol), was dissolved in 200 ml toluene. triars, 2.5 g (6.5 mmol), was added by syringe and the solution was stirred at room temperature for about 10 h, during which time the colour changed from purple to deep-red. After filtration the filtrate was evaporated until a precipitate formed. Addition of pentane, filtration and recrystallization from toluene/pentane gave the red product, 2.6 g (86%).

$Nb_2Cl_6(diars)_2$

$Nb_2Cl_6(SMe_2)_3$, 1.8 g (3.1 mmol), was dissolved in 200 ml toluene. diars, 2.0 g (7.0 mmol), was added and the solution was stirred at room temperature for about 10 h. The colour changed to reddish-purple and a precipitate slowly formed. Addition of pentane gave a red-purple solid product, which was insufficiently soluble in toluene to permit recrystallization. After washing with toluene and pentane and pumping the product, 2.4 g (82%) was obtained.

$Nb_2Cl_6(diphos)_2$

$Nb_2Cl_6(SMe_2)_3$, 1.5 g (2.5 mmol), was dissolved in 150 ml toluene. To this was added a solution of diphos, 3.0 g (7.5 mmol) in 50 ml toluene, and the mixture was stirred at room temperature for about 10 h. A purple precipitate slowly formed, which was too insoluble in toluene to permit recrystallization. After washing with toluene and pentane and pumping, the product, 2.7 g (92%) was obtained.

Analyses and Spectra

Results are given in Tables 1 to 3.

Can. J. Chem. Downloaded from www.nrcresearchpress.com by 210.87.254.5 on 09/05/12
For personal use only.

Can. J. Chem. Downloaded from www.nrcresearchpress.com by 210.87.254.5 on 09/05/12
For personal use only.

C, H, and Cl analyses were done by A.B. Gygli, Toronto. Niobium was determined as Nb_2O_5. Treatment of the complexes with aqueous ammonia under nitrogen gave a dark grey solution and suspension which turned white when air was bubbled through. The surprising stability of the grey colour indicates a significant stability of an oxidation state of less than five for niobium in aqueous ammonia. Any free ligand was removed from the Nb_2O_5 precipitate by washing with benzene, and any remaining phosphorus or arsenic oxides were removed by washing the precipitate with water between ignitions to constant weight. In the case of $Nb_2Cl_6(SMe_2)_3$ it was possible to determine the oxidation state (3.0 ± 0.1) by oxidation with ferric ion (3). For the other complexes oxidation of the ligand interfered with the result. Infrared spectra were done on a Perkin Elmer 337 and 180 spectrometer and nmr spectra on a Varian T-60 spectrometer. Magnetic susceptibilities were measured on a Gouy balance: all the compounds were diamagnetic.

The molecular weight of the triars complex in benzene solution was determined by osmometry. Found M = 1160; calculated for $Nb_2Cl_6(triars)_2$, 1167.

Results and Discussion

Synthetic Procedures

It was almost a year before our attempts to prepare complexes of niobium in low oxidation states starting from niobium pentachloride were successful. We modelled our attempts on the successful reductions of molybdenum (7) and tungsten (8) but were unable to obtain significant yields of products until we changed from oxygen donor solvents (ether, THF) to toluene. With niobium pentachloride and a great variety of heterogeneous reducing agents in toluene black-brown niobium-containing solids were formed, with the occasional development of a pale purple coloration. In our search for a strong reducing agent soluble in toluene we tried several boron hydrides and aluminium alkyls, and finally the borane – dimethyl sulphide complex, which has the advantage of being solvent free. An immediate reaction occurs between this reagent and niobium pentachloride, producing a colour change from red to orange and solubilizing all the niobium pentachloride in the toluene. No further reaction seems to occur and addition of excess strong reducing agent (Na/K alloy) eventually produced a dark brown solid which could not be characterized. There was, however, clear evidence of an intermediate stage in this reaction which gave a deep purple solution. To stop the reaction at the purple stage we used various amounts of alloy corresponding to up to 5 equivalents of reductant and found that 2 equivalents of alloy produced, in 3–4 h, an intense purple solution that then was stable overnight. From this solution the dimethyl sulphide complex could be isolated in about 30% yield. When we used dimethyl sulphide alone instead of the borane complex a slight purple colour developed over 2–3 days, indicating that the reaction does occur to a very small extent in the absence of borane, but that the presence of the borane is essential to the preparation of the solid product in good yield. It seems likely that a niobium pentachloride – borane dimethyl sulphide adduct is formed almost immediately and that this species is more readily reduced than a niobium pentachloridedimethyl sulphide adduct.

When the complex $Nb_2Cl_6(SMe_2)_3$ is reacted with various ligands in toluene it is possible to obtain intermediate products of variable composition that contain both dimethyl sulphide and the new ligand. It seems that the terminal dimethyl sulphides are replaced quite rapidly but that the bridging dimethylsulphide is more inert to substitution. This observation is consistent with the preparation of $[Nb_2Cl_8(SC_4H_8)]^{2-}$, which presumably contains one bridging tetrahydrothiophene (3).

When the purple-red compounds $Nb_2Cl_6(L—L)_2$ are exposed to air they slowly lose their colour. In a few hours they all become white solids. Similarly when air is bubbled through their solutions in toluene the colour slowly changes, usually going through a pink stage, until finally a white precipitate and colourless solution are formed.

Structure

The formulation of these complexes as dimeric species is based primarily on their diamagnetism and on the molecular weight of the triars complex. Far infrared spectra in the νNb—Cl region are consistent with this. The only monomeric niobium(III) species so far reported are those containing cyclopentadiene ligands. These are also diamagnetic, but this is not unexpected on the basis of the orbitals available (9). We assume that an octahedral monomer of niobium(III) would have to be paramagnetic, with the two *d*-electrons unpaired, but that a dimeric structure with a strong metal–metal interaction could account for the diamagnetism. There is, of

course, ample evidence for metal–metal bonds in niobium chemistry (10).

The proposed structure for $Nb_2Cl_6(SMe_2)_3$ is

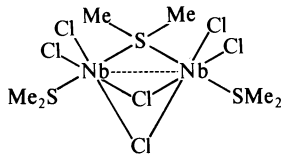

which corresponds to a confacial fusion of two octahedra. The presence of two different kinds of dimethyl sulphide ligand is shown by two S—CH_3 resonances at δ 2.63 and δ 3.34 in the ratio 2:1. The former resonance is assigned to the two terminal dimethyl sulphide ligands, which must be magnetically equivalent. There is no evidence supporting their indicated location *trans* to the bridging dimethylsulphide, except by analogy with the tetrahydrothiophene complex, which is reported to have this structure (3). Also consistent with that report we assign ir bands at 355(sh), 345(vs), and 332(s) cm^{-1} to νNb—Cl, at 318(s) and 285(w) to terminal νNb—S, and at 232(m) to bridging Nb—S—Nb.

For the complexes $Nb_2Cl_6(L—L)_2$ we propose the structure

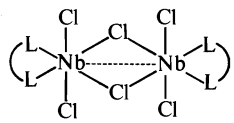

based on two octahedra fused along one edge. The clearest evidence in support of this structure is the nmr spectrum of the diars complex. All 24 As—CH_3 protons are identical, with δ 1.60. The only other structure that could produce this equivalence would be if each diars formed an additional bridge across the two niobiums. This seems most unlikely as the preferred arrangement. A metal–metal bond formed through an octahedral edge is also found, for example, in the diamagnetic niobium tetrachloride, where niobium atoms are in octahedral holes but are clearly linked together in pairs (10).

An additional structural feature of interest is found in the triars complex. For this the nmr spectrum shows clearly that only two of the three arsenic atoms of each ligand are coordinated, the third being in a 'dangling' situation. In the partial structure

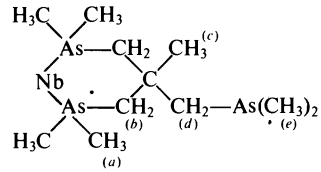

the δ values and ratios for the protons indicated are (*a*) 1.25 (12), (*b*) 1.80 (4), (*c*) 1.08 (3), (*d*) 1.58 (2), and (*e*) 0.97 (6). The coordinated As—CH_3 protons are shifted to lower field by about 0.3 ppm, but the dangling As—CH_3 protons are almost unchanged from those in the free ligand. As with the diars complex the 24 coordinated As—CH_3 protons are equivalent, supporting the symmetrical structure proposed. Nyholm *et al.* (11) observed similar bidentate behaviour for triars in $W(CO)_4$(triars), and $Re(CO_3Cl$(triars), and report similar nmr spectra. The fact that the third arsenic remains uncoordinated indicates that niobium(III) is unwilling to expand its coordination number to greater than six, and also that the chloride bridges (plus the metal–metal interaction) are strong enough to resist cleavage by a strong ligand favorably located. Our search for a monomeric niobium(III) complex must clearly be directed towards use of heavier halogens (to increase the metal–metal distance in the dimer) and even more strongly π accepting ligands L. This search is in progress, but preliminary results indicate that the analogous bromo complexes are also dimeric and diamagnetic.

Because of its low solubility in toluene and its decomposition in chloroform it has not been possible to obtain a good nmr spectrum of the diphos complex. However, from the similarity of its far ir spectrum we believe that this has the same structure as the arsine complexes.

Acknowledgements

The authors are grateful to the Atkinson Charitable Foundation and the National Research Council of Canada for grants in support of this research.

1. F. N. Tebbe and G. W. Parshall. J. Am. Chem. Soc. **93**, 3793 (1971).
2. Jay A. Labinger and Jeffrey Schwartz. J. Am. Chem. Soc. **97**, 1596 (1975).
3. E. T. Maas, Jr. and R. E. McCarley. Inorg. Chem. **12**, 1096 (1973).

Can. J. Chem. Downloaded from www.nrcresearchpress.com by 210.87.254.5 on 09/05/12
For personal use only.

4. K. M. ALEXANDER and F. FAIRBROTHER. J. Chem. Soc. S223 (1949).
5. R. D. FELTHAM, A. KASENALLY, and R. S. NYHOLM. J. Organomet. Chem. **7**, 285 (1967).
6. J. CHATT and F. A. HART. J. Chem. Soc. 1378 (1960).
7. J. CHATT and A. G. WEDD. J. Organomet. Chem. **27**, C15 (1971).
8. B. BELL, J. CHATT, and G. J. LEIGH. J. Chem. Soc. Dalton, 2492 (1972).
9. L. J. GUGGENBERGER, P. MEAKIN, and F. N. TEBBE. J. Am. Chem. Soc. **96**, 5420 (1974).
10. D. L. KEPPERT. The early transition metals. Academic Press, London, 1972. p. 24.
11. R. S. NYHOLM, M. R. SNOW, and M.H. B. STIDDARD. J. Chem. Soc. 6564 (1965).

Can. J. Chem. Downloaded from www.nrcresearchpress.com by 210.87.254.5 on 09/05/12
For personal use only.

Solvation effects on the conductivity of concentrated electrolyte solutions

DOUGLAS E. GOLDSACK, RAYMOND FRANCHETTO, AND ARLENE (ANTTILA) FRANCHETTO

Department of Chemistry, Laurentian University, Sudbury, Ont., Canada P3E 2C6

Received November 10, 1975

DOUGLAS E. GOLDSACK, RAYMOND FRANCHETTO, and ARLENE (ANTTILA) FRANCHETTO. Can. J. Chem. **54**, 2953 (1976).

The Falkenhagen–Leist–Kelbg equation for the conductivity of electrolyte solutions has been extended to include the effect of solvation on the concentration of the salt. Two equations have been derived, both of which have only two freely adjustable parameters at any temperature: Λ_0 the molar conductance of the salt at infinite dilution and H_0, a solvation number parameter for the salt. In one of these equations H_0 is assumed to be independent of concentration. In the other, H_0 is assumed to be dependent on concentration and an explicit concentration dependent formula is derived for H_0. Conductance data for the alkali halide salts in the 0.5 to 10 *m* concentration range and 0 to 60 °C temperature range were found to be adequately reproduced by both these equations, but with the variable hydration parameter equation yielding better fits to the data. The H_0 parameters from the fixed hydration parameter equation are found to be similar to those obtained from the analysis of activity coefficient and other data whereas the variable hydration parameter equation yields H_0 parameters which are much larger.

DOUGLAS E. GOLDSACK, RAYMOND FRANCHETTO et ARLENE (ANTTILA) FRANCHETTO. Can. J. Chem. **54**, 2953 (1976).

On a étendu l'équation de Falkenhagen–Leist–Kelbg s'appliquant à la conductivité des solutions d'électrolyte de façon à inclure l'effet de solvatation sur la concentration du sel. On a dérivé deux équations et chacune ne possède que deux paramètres entièrement ajustables à toutes les températures; Λ_0 la conductivité molaire du sel à dilution infinie et H_0 un paramètre pour le nombre de solvatation du sel. Dans une de ces équations, on fait l'hypothèse que H_0 est indépendant de la concentration. Dans l'autre, on fait l'hypothèse que H_0 dépend de la concentration et on dérive pour H_0 une formule contenant une dépendance explicite sur la concentration. Les données de conductivité pour des sels d'halogénures alcalins à des concentrations de 0.5 à 10 *m* et à des températures de 0 à 60 °C peuvent être reproduites adéquatement par chacune de ces équations; toutefois l'équation incluant des paramètres variables pour l'hydratation fournit une meilleure corrélation avec les données. On a trouvé que les paramètres H_0 pour l'équation avec des paramètres fixes pour l'hydratation sont semblables à ceux obtenus à partir d'une analyse des coefficients d'activité et d'autres données alors que les équations avec les paramètres variables pour l'hydratation conduisent à des paramètres H_0 qui sont beaucoup plus grands.

[Traduit par le journal]

Introduction

It has been shown that one of the fundamental limitations on the efficiency of an electrochemical device is the conductance of the electrolyte solution of the device (1). But, despite intensive work in both the theoretical and experimental areas over several decades (2–6), there still does not exist a satisfactory equation which explains the concentration dependence of the conductivity of simple electrolytes in the high concentration (1–10 *M*) range. Yet it is precisely this range of concentration that is used in practical electrochemical devices.

The theoretical treatment of most conductance data of concentrated solutions has been approached by extending existing electrostatic hydrodynamic theories (2), or in the case of extremely high concentrations by use of a theory based on the available free volume of the solvent in the solution (7–9). All such theories involve the use of two or more freely adjustable parameters for fitting the conductance data.

In the case of the free volume theory as applied by Angell and co-workers (7–9), a three parameter equation is used to describe the temperature or concentration dependence of the conductivity or viscosity of an electrolyte solution. These parameters are not related to intrinsic properties of the electrolyte itself, but to the configurational entropy content of the solvent in the solution and a glass transition temperature for the solution.

Can. J. Chem. Downloaded from www.nrcresearchpress.com by 210.87.254.6 on 09/05/12
For personal use only.

Can. J. Chem. Downloaded from www.nrcresearchpress.com by 210.87.254.6 on 09/05/12
For personal use only.

On the other hand, the parameters of the electrostatic hydrodynamic theories for conductivity are directly related to such properties of the electrolyte as the ion pair formation constant, K, the Debye–Hückel distance of closest approach between two ions, a_0, and the molar conductance of the salt at infinite dilution, Λ_0 (10).

Although it is well known that the fundamental limitations on the electrostatic hydrodynamic conductance equations realistically limit their applications to less than 0.01 M, some success has been attained in applying these equations to the reproduction of data in the high concentration region. It would therefore seem reasonable to pursue this admittedly semi-empirical path to gain further insight into the gross features of the electrolyte solution which are controlling the conductivity of simple electrolytes at high concentrations.

One of the more successful electrostatic hydrodynamic equations for use in interpreting the conductivity of concentrated electrolyte solutions was derived by Falkenhagen, Leist, and Kelbg (11). It can be written in the following form to express the molar conductance Λ_c of a 1:1 electrolyte as a function of concentration:

$$\Lambda_c = \left(\Lambda_0 - \frac{B_2 I^{1/2}}{1 + B_3 a_0 I^{1/2}}\right)\left(1 - \frac{B_1 I^{1/2} F}{1 + B_3 a_0 I^{1/2}}\right) \quad [1]$$

$$F = \frac{e^{0.2929 B_3 a_0 I^{1/2}} - 1}{0.2929 B_3 a_0 I^{1/2}}$$

where $B_1 = 8.2 \times 10^5 (\varepsilon T)^{-3/2}$, $B_2 = 82.5 \times \eta^{-1} (\varepsilon T)^{-1/2}$, $B_3 = 50.29 (\varepsilon T)^{-1/2}$, I is the molar ionic strength of the salt, Λ_0 is the molar conductance of the salt at infinite dilution, ε is the dielectric constant of the solvent, η is the viscosity of the solvent, and T the absolute temperature. The values of B_1, B_2, and B_3 have been tabulated for water from 0 to 100 °C (2).

This equation has two adjustable parameters, a_0, the Debye–Hückel distance, and Λ_0. By choosing suitable values of a_0 and Λ_0, it has been found possible to reproduce the conductivity of some salts up to several molar concentrations. Wishaw and Stokes (12), noting that some salts failed to follow this equation at extremely high concentrations, introduced a relative viscosity correction factor into the equation. For 1:1 electrolytes, where the ionic strength equals the molarity, the equation becomes:

$$\Lambda_c = \frac{\eta_0}{\eta}\left(\Lambda_0 - \frac{B_2 C^{1/2}}{1 + B_3 a_0 C^{1/2}}\right) \times \left(1 - \frac{B_1 C^{1/2} F}{1 + B_3 a_0 C^{1/2}}\right) \quad [2]$$

where C is the molarity of the salt.

Although this equation has had remarkable success in its application to the conductivity of concentrated electrolyte solutions, the introduction of the relative viscosity factor does not give a molecular explanation for its success.

It has been shown by Stokes and Robinson and others (13–17) that the concept of solvation could be usefully appended to the classical Debye–Hückel expression for activity coefficients of electrolytes to reproduce the concentration dependence of activity coefficients at high concentration (1–10 M) in terms of two adjustable parameters; a_0, the Debye–Hückel distance of closest approach of ions to each other and H_0, a solvation number of the salt.

This approach certainly oversimplifies the explanation for the deviations from the Debye–Hückel limiting behaviour for electrolytes at high concentrations. For instance, it ignores the changing dielectric constant of the medium at high concentrations and the possibility of ion pair formation. However the final equations satisfactorily reproduce the data in the high concentration region and do give some added insight into the properties of concentrated electrolyte solutions through the solvation concept.

Because of this, it would seem reasonable to attempt a similar approach to account for the conductance of concentrated electrolyte solutions. The Falkenhagen–Leist–Kelbg equation has been chosen as the starting point for this analysis because of its already noted successes. By introducing the solvation effect on the concentration of the electrolyte, an attempt will be made to eliminate the arbitrary, though useful, application of the relative viscosity factor in the Stokes–Wishaw equation.

Experimental

To provide comparative data at high concentrations and several temperatures, the conductances of solutions

Can. J. Chem. Downloaded from www.nrcresearchpress.com by 210.87.254.6 on 09/05/12
For personal use only.

of LiCl, RbCl, CsCl, NH_4Cl, NaBr, KBr, NH_4Br, and KI were determined at concentrations ranging from 0.5 to 10 *m* and at temperatures from 0 to 60 °C. Data for other salts and temperatures were also culled from the literature.

All salts (Fisher certified) were used as such after drying in a vacuum oven. The solutions were prepared by weight with deionized distilled water from concentrations ranging from 0.5 *m* to approximately saturation for each salt. Solution resistances were determined with a Beckman micro-dip cell ($K = 100$, Model No. BM 0872) with platinized black electrodes and a manually balanced conductivity bridge consisting of a standard Wheatstone bridge with an oscilloscope detector. Results were reproducible to 0.1 ohms. The cell constants were found to be independent of frequency at frequencies less than 1000 Hz. The cell constants at each temperature were determined using the HCl data of Owen and Sweeton (18) and cross checked with KCl standard solutions at 25 °C (3). Temperature control was maintained to better than ±0.02 °C. An IBM 360 computer was used for analysis of the data. A computer program was written to systematically vary the appropriate parameters of the different equations tested as indicated in the discussion. The criterion used to determine the best fit for the observed data to a theoretical curve was that the sum of the absolute deviations of observed from calculated values of the conductance be minimized.

Theory

Although eqs. 1 and 2 for the molar conductance of an electrolyte have two adjustable parameters, Λ_0 and a_0, it will be assumed that the tabulated values of the molar ionic conductances of each ion as given in standard references (2, 3) can be accepted as values that are known to within a few percent error or less. Hence it was assumed that the Λ_0 values for any salt considered in this paper at temperatures from 0 to 60 °C can be obtained from such tabulations and by graphical interpolation. With this assumption in mind, best fit tests of eqs. 1 and 2 for NaCl and LiCl at 25 °C with variable a_0 values were carried out and the results are given graphically in Fig. 1. It can be seen that the Stokes–Wishaw equation adequately represents the data for both salts with a_0 values of 5.67 Å for LiCl and 7.75 Å for NaCl. Without the viscosity correction, Fig. 1 clearly illustrates that the Falkenhagen–Leist–Kelbg equation will not reproduce the molar conductance data even over a wide range of a_0 values at the high concentration limit for LiCl and NaCl. This fact has been noted before for other salts as well. It is noted however that in the case of NaCl a very large value of $a_0 = 7.75$ Å was necessary in order to obtain a satisfactory fit to the data with eq. 2.

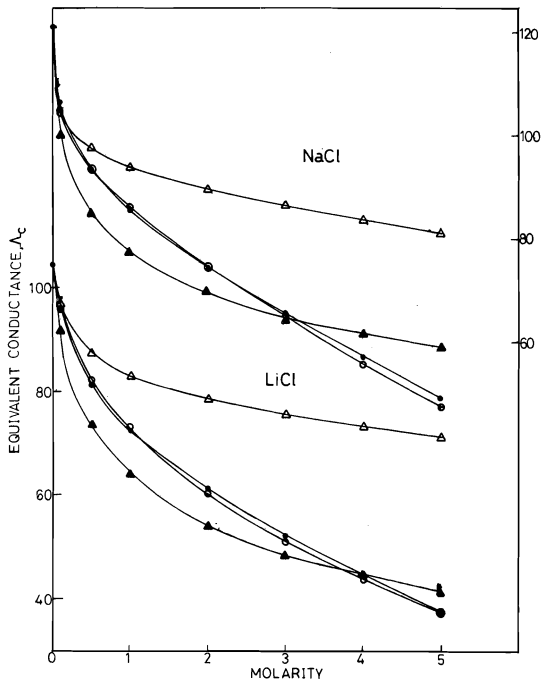

FIG. 1. Test of Falkenhagen–Leist–Kelbg and Stokes–Wishaw equations for NaCl and LiCl at 25 °C with values of a_0 used for the fits to the data.

It is significant that NaCl solutions at high concentrations are much more viscous than KCl or NH_4Cl solutions. This factor may be the cause of the necessity for such a high a_0 value in this case. Furthermore, it has already been ascertained that for some electrolytes which are not as heavily solvated as LiCl and NaCl as judged by activity coefficient data, (*e.g.* KCl and NH_4Cl), the viscosity correction was only necessary at extremely high concentrations of the salt in order to obtain a satisfactory fit to the data with eq. 2 (2). It seems reasonable therefore to assume that there is some correlation between solvation effects and viscosity since the calculated conductances of highly solvated salts such as LiCl and NaCl, which are quite viscous at high concentrations, show very large deviations from the observed conductance values at high concentration without the viscosity correction being included as shown in Fig. 1. These facts led to the following attempt to account for solvation effects on the conductivity of concentrated electrolyte solutions.

If the ionic strength is introduced using the

Can. J. Chem. Downloaded from www.nrcresearchpress.com by 210.87.254.6 on 09/05/12
For personal use only.

molality scale instead of the molarity scale, eq. 1 can be utilized to introduce the ideas of Stokes and Robinson (13). A salt on dissolution becomes solvated to some extent. Hence the molality of the solvated salt will be higher than the molality of the salt taking all the solvent, both bound and free, into account. Designating the apparent molality of the solvated salt as m_s, eq. 1 for 1:1 electrolyte can be re-written as:

$$[3]\quad \Lambda_m = \left(\Lambda_0 - \frac{B_2 m_s^{1/2}}{1 + B_3 a_0 m_s^{1/2}}\right) \times \left(1 - \frac{B_1 m_s^{1/2} F}{1 + B_3 a_0 m_s^{1/2}}\right)$$

$$F = \frac{e^{0.2929\, B_3 a_0 m_s^{1/2}} - 1}{0.2929 B_3 a_0 m_s^{1/2}}$$

Since this equation is a function of molality, the Λ_m values computed are compared with observed molal conductances (*i.e.* the specific conductance of the solution divided by the molality).

By conservation of mass on the solvent, the apparent molality m_s can be related to the total molality m of the salt by:

$$[4]\quad m_s = \frac{55.51m}{55.51 - H_0 m}$$

where m is the total molality of the salt (moles of salt per kg of water), 55.51 is the moles of water per kg of water, and H_0 is the total solvation number parameter of the salt, which is assumed to be a constant and independent of concentration. Equation 4 can be re-written as:

$$[5]\quad m_s = \frac{m}{1 - 0.018 H_0 m}$$

and introduced into eq. 3 to yield:

$$[6]\quad \Lambda_m = \left(\Lambda_0 - \frac{B_2 m^{1/2}}{(1 - 0.018 H_0 m)^{1/2} + B_3 a_0 m^{1/2}}\right)\left(1 - \frac{B_1 m^{1/2} F'}{(1 - 0.018 H_0 m)^{1/2} + B_3 a_0 m^{1/2}}\right)$$

$$F' = \frac{(e^{0.2929 B_3 a_0 m^{1/2}/1 - 0.018 H_0 m^{1/2}} - 1)(1 - 0.018 H_0 m)^{1/2}}{0.2929 B_3 a_0 m^{1/2}}$$

Note that at low concentrations eq. 6 reduces to eq. 1. Equation 6 has two adjustable parameters, the Debye–Hückel distance parameter a_0 and the solvation parameter H_0, if we assume that the Λ_0 values are known. In order to have an equation of comparable usefulness as eq. 2, which has only one adjustable parameter, a_0, it would be necessary to eliminate one of the two independent parameters in eq. 6.

One way of doing this is to introduce the idea of the solvation (19, 20) cospheres associated with each ion to obtain a relation between the Debye–Hückel distance parameter, a_0, and the solvation number parameter, H_0. This distance, a_0, supposedly represents the distance of closest approach of the solvated cation and anion to each other in solution. If it is assumed that a sphere of radius a_0 Å would encompass the total volume of both the anion and cation cospheres together and if the water molecule is assumed spherical with a radius of 1.38 Å (20), then for a cation crystal radius, $R1$, and anion crystal radius, $R2$, and a total number of solvent water molecules, H_0, associated with the total cosphere, the following relationship is obtained:

$$[7]\quad \frac{4}{3}\pi a_0^3 = \frac{4}{3}\pi(R1)^3 + \frac{4}{3}\pi(R2)^3 + \frac{4}{3}\pi(1.38)^3 H_0$$

$$[8]\quad a_0 = ((R1)^3 + (R2)^3 + 2.63 H_0)^{1/3}$$

Equation 8 when combined with eq. 6 yields a one parameter equation in terms of H_0 alone provided the Λ_0 values are assumed known. We will refer to this combination of equations as the fixed solvation parameter equation since it is assumed in eq. 4 that the solvation parameter, H_0, is independent of concentration.

There are, however, two possible problems associated with eqs. 6 and 8. In calculating the parameter, a_0, it has been assumed that the ordinary crystal radii can be used and that the volume of all the water molecules is compressed into a compact sphere along with the cation and anion volumes. This assumes there is no dead-space about a solvated ion between the solvent molecules. Conway *et al.* (21) have in fact shown that a dead space correction to the

TABLE 1. Variation of solvation number parameter, S, with concentration at 25 °C (from ref. 21)

Molality	S_{obs}	S_{calcd}	Molality	S_{obs}	S_{calcd}	Molality	S_{obs}	S_{calcd}
LiCl, $S_0 = 5.5$			NaCl, $S_0 = 6.4$			KCl, $S_0 = 6.7$		
0.10	5.3	5.50	0.10	6.5	6.62	0.17	6.2	6.28
1.02	4.9	5.00	1.02	5.7	5.97	1.03	5.7	5.72
2.09	4.5	4.56	2.09	4.7	5.35	4.57	4.0	4.19
5.56	3.3	3.54	5.75	3.9	3.96			
RbCl, $S_0 = 5.3$			NaBr, $S_0 = 6.2$			NaI, $S_0 = 5.6$		
0.10	5.0	5.25	0.10	6.1	6.13	0.1	5.5	5.54
0.93	4.9	4.87	1.14	5.7	5.50	1.04	4.6	5.07
1.80	4.9	4.52	2.12	5.1	5.01	2.31	4.4	4.54
3.99	4.0	3.84	6.00	3.7	3.71	5.84	3.2	3.52

radius of an ion is an important factor in accounting for the partial molal volumes of ions in solution. They have derived a semi-empirical relation between the effective volume, v_A, of an ion in solution and its crystal radius, r, in Å. The relation is

$$v_A = 2.51r^3 + 3.15r^2 \text{ ml/mol}$$
$$= 4.18r^3 + 5.25r^2 \text{ Å}^3\text{/molecule}$$

Hence the effective radius of the spherical ion including dead space is r_A in Å and is given by

[9] $$r_A = (r^3 + 1.25r^2)^{1/3}$$

If we include the dead space correction, then the equation for the Debye–Hückel distance parameter, a_0, in terms of the solvation parameter, H_0, and the known crystal radii (25) becomes

[10] $$a_0 = ((R1)^3 + (R2)^3 + 1.25((R1)^2 + (R2)^2) + 2.63H_0)^{1/3}$$

The other problem is associated with the form of eq. 6. It is noted that the factor $(1 - 0.018H_0m)^{1/2}$ in eq. 6 may become imaginary when the term $0.018H_0m$ is greater than unity. This limits the application of eq. 6 to salts and molalities where the condition ($H_0m > 55.51$) holds. This restriction seems like an artificial condition and it is. It derives from the assumption that the solvation parameter H_0 is considered to be independent of concentration. In fact, Bockris and Saluja (22) as well as others (23) have shown that the 'solvation number' of a salt decreases with increasing concentration at high concentrations. This is exactly what would be expected to happen at higher molalities where less solvent molecules per mole of salt are available for distribution to the increasing number of ions in solution. Typical data representing this trend are given in Table 3.

To account for this concentration dependence of the solvation number parameter, a simple relationship can be derived as follows. Assume that the ratio of the solvation number parameter, S, to the moles of free solvent available to a salt is a constant. Designating the solvation number parameter at infinite dilution as S_0 and that at any other molality as S, then

[11] $$\frac{S}{55.51 - Sm} = \frac{S_0}{55.51}$$

since there are 55.51 moles of free water available to the salt at infinite dilution and there are $(55.51 - Sm)$ moles of water available to the salt at molality m. This equation can be rearranged to yield an equation for the concentration dependence of the solvation number parameter as:

[12] $$S = \frac{S_0}{1 + 0.018S_0m}$$

Equation 12 can be checked with the ultrasonic data of Bockris and Saluja (22). As shown in Table 1, with the appropriate S_0 value for each salt, eq. 12 reproduces the concentration dependence of the solvation number parameters quite well.

It might be noted at this point that the solvation number parameters, S_0, as determined from the Bockris and Saluja data probably represents the total primary hydration layer of the salt ions. Solvation number parameters obtained from the analysis of transport phe-

Can. J. Chem. Downloaded from www.nrcresearchpress.com by 210.87.254.6 on 09/05/12
For personal use only.

nomena with an emphasis on high concentration data may reflect both primary and secondary solvation layers and may thus be larger (23).

Assuming that the same analysis applies to the solvation parameter, H_0, as well, then we can introduce eq. 12 into eq. 5 to yield a new equation for the apparent molality of the solvated salt as:

$$[13] \qquad m_s = m(1 + 0.018H_0m)$$

It is seen that this relationship eliminates the artificial restriction observed in using eq. 6. Introduction of eq. 13 into eq. 3 gives for the molal conductance of a 1:1 electrolyte:

$$[14] \quad \Lambda_m = \left(\Lambda_0 - \frac{B_2m^{1/2}(1 + 0.018H_0m)^{1/2}}{1 + B_3a_0m^{1/2}(1 + 0.018H_0m)^{1/2}}\right)\left(1 - \frac{B_1F''m^{1/2}(1 + 0.018H_0m)^{1/2}}{1 + B_3a_0m^{1/2}(1 + 0.018H_0m)^{1/2}}\right)$$

$$F'' = \frac{e^{0.2929B_3a_0m^{1/2}(1+0.018H_0m)^{1/2}} - 1}{0.2929B_3a_0m^{1/2}(1 + 0.018H_0m)^{1/2}}$$

Since H_0 is now assumed to vary with concentration according to eq. 12, this also means that the Debye–Hückel distance parameter will vary with concentration, being large at low concentrations, reflecting a large solvation shell about each ion, and becoming smaller at higher concentrations as the solvation shells become smaller. The new equation for a_0 thus becomes:

$$[15] \qquad a_0 = \left((R1)^3 + (R2)^3 + 1.25((R1)^2 + (R2)^2) + \frac{2.63H_0}{1 + 0.018H_0m}\right)^{1/3}$$

We will refer to the combination of eqs. 14 and 15 as the variable solvation parameter equation.

Both the fixed and variable one parameter solvation equations were tested to determine if they could first of all adequately represent the conductance data of simple electrolytes in the high concentration range over a wide temperature range, and secondly to determine if they could account for the relative viscosity correction factor of the Stokes–Wishaw equation.

Results

Table 2 presents the results of an analysis of the conductance data obtained from the literature for the salts LiCl (24), NaCl (24), KCl (24), and NH_4Cl (12) using density and viscosity data from the International Critical Tables. Λ_1 and Λ_2 represent molar conductances calculated using eqs. 1 and 2 respectively and the a_0 values indicated in the table. Λ_3 and Λ_4 represent molar conductances calculated using the fixed hydration parameter equation (eqs. 6 and 10 combined) and the variable hydration parameter equation (eqs. 14 and 15 combined) respectively. Considering the fact that these data were obtained from several sources (viscosity, density, and conductivity), it can be seen that the fixed and variable hydration parameter equations do adequately represent these data, though not as well as the Stokes–Wishaw equation. In the case of the more solvated salts LiCl and NaCl it would seem that the variable hydration parameter equation reproduces the data better than the fixed hydration parameter equation whereas in the case of the less solvated salts KCl and NH_4Cl, there is no major difference between the two equations.

Since the fixed and variable hydration parameter equations are just the Falkenhagen–Leist–Kelbg equation with a change in concentration variable introduced through the solvation concept, then it seems reasonable to attempt a direct comparison between these equations and the Stokes–Wishaw equation, which multiplies the Falkenhagen–Leist–Kelbg equation by a concentration-dependent viscosity ratio. The calculations shown in Table 2 seem to indicate that the hydration parameter equations can account for the viscosity ratio correction factor as used by Stokes and Wishaw.

To corroborate this observation, the results of an extensive study carried out over a wide temperature range and including more salts are given in Table 3 and Figs. 2 through 6. Table 3 gives the observed molal conductances for the salts obtained for this study (LiCl, RbCl, CsCl, NH_4Cl, NaBr, KBr, NH_4Br, KI) at the temperatures indicated. The data for other salts

Can. J. Chem. Downloaded from www.nrcresearchpress.com by 210.87.254.6 on 09/05/12
For personal use only.

Can. J. Chem. Downloaded from www.nrcresearchpress.com by 210.87.254.6 on 09/05/12
For personal use only.

TABLE 2. Comparison of four conductivity equations at 25 °C

	LiCl					NaCl				
Molarity	Λ_c Obs	Λ_1 $a_0 = 5.67$	Λ_2 $a_0 = 5.67$	Λ_3 $H_0 = 4.8$	Λ_4 $H_0 = 27.8$	Λ_c Obs	Λ_1 $a_0 = 7.75$	Λ_2 $a_0 = 7.75$	Λ_3 $H_0 = 7.8$	Λ_4 $H_0 = 26.9$
0.50	81.86	88.36	82.66	80.68	83.91	93.62	98.09	93.78	87.65	89.80
1.00	73.00	83.94	73.51	72.71	75.53	85.76	94.38	86.27	79.72	81.27
2.00	61.74	79.24	60.86	65.22	65.77	74.71	90.02	74.71	71.88	71.44
3.00	52.51	76.19	51.51	60.26	58.11	65.67	86.81	64.73	65.72	63.65
4.00	44.53	73.76	44.09	56.14	51.26	57.23	83.97	55.65	58.80	56.75
5.00	37.65	71.66	37.81	51.92	44.54	49.46	81.29	47.65	45.07	49.74
6.00	31.70	69.73	32.36	46.91	37.54	—	—	—	—	—

	KCl					NH_4Cl				
Molarity	Λ_c Obs	Λ_1 $a_0 = 4.75$	Λ_2 $a_0 = 4.75$	Λ_3 $H_0 = 4.8$	Λ_4 $H_0 = 8.2$	Λ_c Obs	Λ_1 $a_0 = 4.33$	Λ_2 $a_0 = 4.33$	Λ_3 $H_0 = 4.2$	Λ_4 $H_0 = 8.0$
0.50	117.27	117.51	117.86	111.10	111.92	116.80	116.39	117.09	112.87	113.82
1.00	111.87	111.58	112.15	105.20	106.00	111.30	110.18	111.18	105.99	106.92
2.00	105.23	105.28	105.07	97.94	98.25	105.10	103.61	103.82	99.58	99.96
3.00	99.46	101.26	99.17	93.43	93.29	100.20	99.49	100.19	96.36	96.08
4.00	93.46	98.14	93.47	89.17	89.07	95.10	96.34	96.14	93.29	92.65
5.00	—	—	—	—	—	89.40	93.70	92.13	89.28	89.33

Can. J. Chem. Downloaded from www.nrcresearchpress.com by 210.87.254.6 on 09/05/12
For personal use only.

TABLE 3. Experimental and calculated molal conductances
(*a*) At 23, 30, 40, 50, 60 °C

	23 °C		30 °C		40 °C		50 °C		60 °C	
Molality	Obs	Calcd	Obs	Calcd	Obs	Calcd	Obs	Calcd	Obs	Calcd
					NH_4Cl					
1.00	102.3	102.5	122.4	113.5	141.9	134.6	160.8	156.5	179.3	177.4
2.00	91.55	92.48	106.5	102.7	125.2	121.0	140.6	140.1	159.6	158.2
3.00	83.40	85.38	97.37	95.42	111.3	111.5	124.5	128.5	139.0	144.6
4.00	80.28	79.46	93.15	89.62	106.9	103.7	119.2	118.9	135.9	133.3
5.00	74.00	74.16	86.70	84.61	99.02	96.86	109.1	110.3	123.0	123.4
6.00	69.45	69.19	81.25	80.07	91.62	90.07	101.7	102.2	113.3	113.9
7.00	64.37	64.39	74.55	75.82	84.41	84.44	92.96	94.47	102.8	104.8
8.00	—	—	—	—	77.75	78.51	86.91	86.80	95.89	95.89
9.00	—	—	—	—	—	—	79.72	79.08	88.58	86.89
					LiCl					
1.00	72.88	73.36	82.51	82.30	100.8	97.94	112.8	114.9	125.5	131.3
2.00	58.75	62.70	68.55	70.20	82.50	83.37	94.30	97.58	106.7	111.2
3.00	48.40	54.63	56.73	61.14	68.00	72.53	77.83	84.74	90.73	96.33
4.00	42.10	47.68	49.30	53.42	58.98	63.32	67.48	73.86	76.78	83.75
5.00	35.60	41.27	41.26	46.38	49.40	54.96	56.86	63.99	65.64	72.37
6.00	30.83	35.07	36.00	39.66	42.83	47.02	49.15	54.64	56.02	61.60
7.00	26.16	28.88	30.66	33.02	36.39	39.21	42.00	45.46	47.87	51.05
8.00	22.53	22.52	26.29	26.29	31.31	31.32	36.18	36.20	40.48	40.44
9.00	19.22	15.84	22.44	19.31	26.83	23.18	30.92	26.67	34.74	29.53
					RbCl					
1.00	108.3	105.7	124.5	117.7	145.9	138.1	166.2	160.6	189.7	180.7
2.00	99.35	95.52	113.7	106.4	132.0	124.0	149.9	142.7	166.8	160.7
3.00	91.13	88.26	104.4	98.54	119.9	113.8	132.3	130.3	148.7	146.2
4.00	84.88	82.20	96.60	92.12	110.7	105.4	122.4	119.8	136.3	133.9
5.00	78.26	76.75	88.94	86.45	101.4	97.80	111.8	110.2	123.7	122.9
6.00	71.65	71.63	81.25	81.21	92.73	90.67	101.8	101.2	111.4	112.3
7.00	65.10	66.67	73.07	76.22	83.73	83.77	91.16	92.32	100.1	102.0
8.00	—	—	—	—	76.58	76.92	83.44	83.44	91.78	91.66
					CsCl					
1.00	105.6	106.3	124.3	118.3	145.5	139.3	163.1	160.1	180.6	181.0
2.00	95.95	95.51	110.4	106.3	126.6	124.7	141.2	142.5	157.4	160.6
3.00	85.47	87.39	97.70	97.52	112.7	113.9	126.0	129.5	139.6	145.4
4.00	78.15	80.34	88.88	90.04	102.2	104.6	113.1	118.3	125.7	132.4
5.00	72.12	73.75	81.38	83.18	92.28	95.98	102.1	108.1	113.3	120.4
6.00	66.32	67.32	75.82	76.59	86.12	87.64	94.77	97.94	103.9	108.7
7.00	60.36	60.82	69.97	70.06	78.76	79.28	86.71	87.88	95.16	96.93
8.00	54.03	54.11	62.76	63.43	70.60	70.71	77.58	77.55	84.91	84.87
9.00	49.19	47.05	57.13	56.57	64.09	61.74	—	—	76.66	72.22

Can. J. Chem. Downloaded from www.nrcresearchpress.com by 210.87.254.6 on 09/05/12
For personal use only.

TABLE 3 (*Concluded*)
(*b*) At 0, 25, 35, 45, 55 °C

	0 °C		25 °C		35 °C		45 °C		55 °C	
Molality	Obs	Calcd	Obs	Calcd	Obs	Calcd	Obs	Calcd	Obs	Calcd
					NaBr					
0.50	30.78	52.19	94.02	94.68	114.2	114.0	133.7	134.2	154.2	155.1
1.00	46.84	47.62	86.33	86.09	103.8	103.5	120.0	121.6	140.7	140.4
2.00	41.15	41.37	74.02	74.73	89.17	89.67	102.0	105.1	117.7	121.3
3.00	36.24	36.47	64.64	66.07	77.35	79.24	89.31	92.68	102.5	106.9
4.00	31.61	32.07	58.86	58.52	68.24	70.19	77.99	81.90	90.06	94.54
5.00	27.10	27.82	49.44	51.44	59.05	61.76	68.09	71.87	78.66	83.11
6.00	23.57	23.51	43.13	44.48	52.00	53.51	59.69	62.08	69.15	72.02
7.00	20.49	18.99	37.40	37.39	45.21	45.16	52.23	52.18	60.86	60.87
8.00	—	—	32.41	29.97	39.53	36.48	45.65	41.89	53.14	49.36
					KBr					
0.50	67.37	63.91	117.0	113.3	139.9	135.6	159.3	159.5	184.2	182.9
1.00	65.83	59.46	109.6	104.8	129.9	125.1	148.0	146.8	166.9	167.9
2.00	61.81	54.21	101.1	95.05	118.3	112.9	134.4	131.1	151.5	149.2
3.00	58.21	50.56	92.23	88.51	108.7	104.6	121.7	119.8	137.2	135.5
4.00	55.89	47.57	85.72	83.29	99.96	97.76	110.2	110.2	124.2	123.9
5.00	—	—	78.79	78.78	91.80	91.78	100.7	101.5	112.9	113.3
					NH_4Br					
0.50	68.38	62.90	118.4	113.7	140.9	136.6	160.4	160.5	186.3	184.0
1.00	66.45	58.48	110.1	105.2	131.8	126.2	148.6	147.9	173.0	169.1
2.00	62.98	53.62	101.5	95.51	119.2	113.9	134.5	132.3	152.9	150.9
3.00	59.76	50.48	94.75	88.93	110.0	105.2	121.4	120.9	140.2	137.7
4.00	56.62	48.07	87.75	83.62	99.75	98.04	109.8	111.3	128.3	126.6
5.00	53.36	46.03	81.50	78.99	93.68	91.68	101.4	102.6	116.7	116.5
6.00	50.41	44.22	74.86	74.76	85.77	85.73	94.23	94.24	106.1	106.8
7.00	—	—	68.94	70.75	78.76	80.01	86.24	86.00	97.37	97.32
					KI					
0.50	68.52	63.23	117.8	113.5	140.7	135.3	159.0	157.7		
1.00	66.17	58.89	110.6	105.1	130.6	125.1	147.6	145.4		
1.50	64.83	55.98	105.4	99.53	124.3	118.2	139.6	137.2		
2.00	63.49	53.67	101.2	95.09	119.1	112.8	132.8	130.7		
2.50	62.29	51.71	97.40	91.32	113.7	108.1	126.9	125.1		
3.00	61.15	49.96	93.82	87.96	109.4	104.0	121.3	120.2		

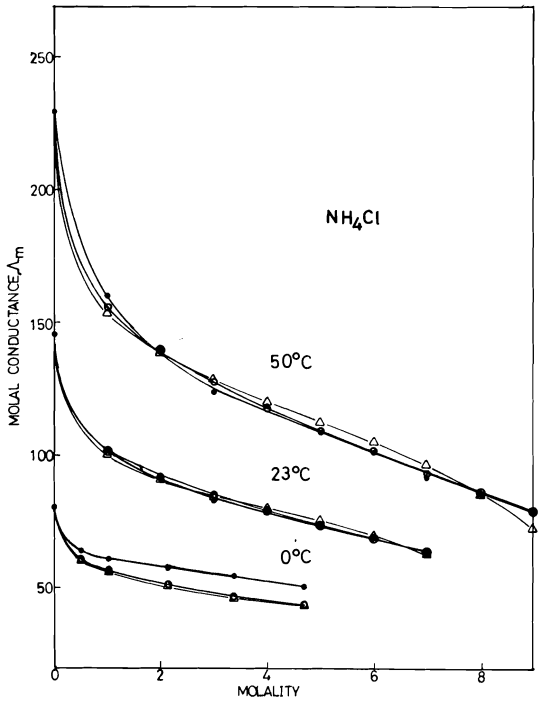

FIG. 2. Molal conductance data for NH_4Cl at three temperatures; ● observed Λ_m values; △ calculated Λ_m values with constant H_0 parameter given in Table 4; ○ calculated Λ_m values with variable H_0 parameter given in Table 4.

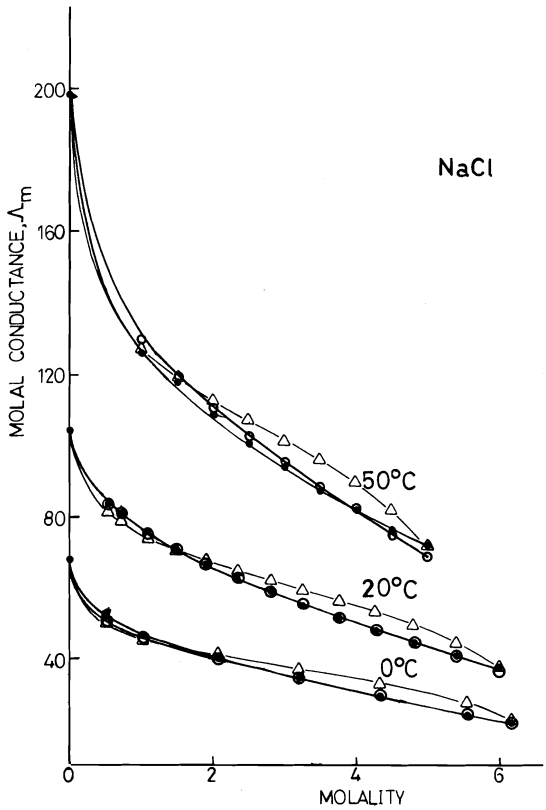

FIG. 3. Molal conductance data for NaCl at three temperatures. Symbols as in Fig. 2.

(NaCl (27), KCl (27), LiBr (28), LiI (28)) and other temperatures (29–31) were obtained from the literature. Table 3 also gives molal conductances calculated with the variable hydration parameter equation and the H_0 values for these salts given in Table 4. Table 3 and Figs. 2 through 6 indicate clearly that both equations adequately represent the conductance data for a large number of salts and temperatures from 0 to 60 °C. Systematic deviations do occur at the low concentration end for most of the salts for both equations.

Although both equations fit the chloride data equally well, Figs. 4 through 6 show that the variable hydration parameter equation reproduces the data better than the fixed hydration parameter equation.

Discussion

Table 4 is a compilation of the hydration parameters, H_0, obtained from the analyses of the conductance data as a function of temperature for both the fixed and variable hydration parameter equations.

Several points should be made before any discussion of the data of Table 4 is undertaken. In extrapolating the usefulness of these extended Falkenhagen–Leist–Kelbg equations into the 1 to 10 *m* regions, many factors have been neglected to keep the analysis as simple as possible. First of all, no ion pair formation has been assumed to occur in these salt solutions at all temperatures. Secondly, the values of B_1, B_2, and B_3 in all these equations are functions of the dielectric constant and viscosity of the solvent. It has been definitively shown (32) that when salts are dissolved in water, the dielectric constant of the medium decreases in a roughly linear manner with the concentration of the salt and this decrease is salt dependent. The viscosity of an electrolyte solution certainly changes substantially as the concentration increases in the 1 to 10 *m* region. It can be argued then that perhaps the bulk dielectric and viscosity values

Can. J. Chem. Downloaded from www.nrcresearchpress.com by 210.87.254.6 on 09/05/12
For personal use only.

Can. J. Chem. Downloaded from www.nrcresearchpress.com by 210.87.254.6 on 09/05/12
For personal use only.

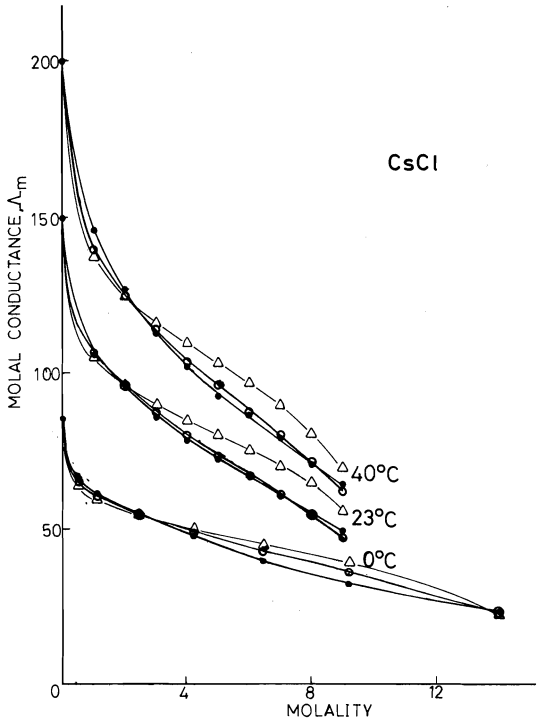

FIG. 4. Molal conductance data for CsCl at three temperatures. Symbols as in Fig. 2.

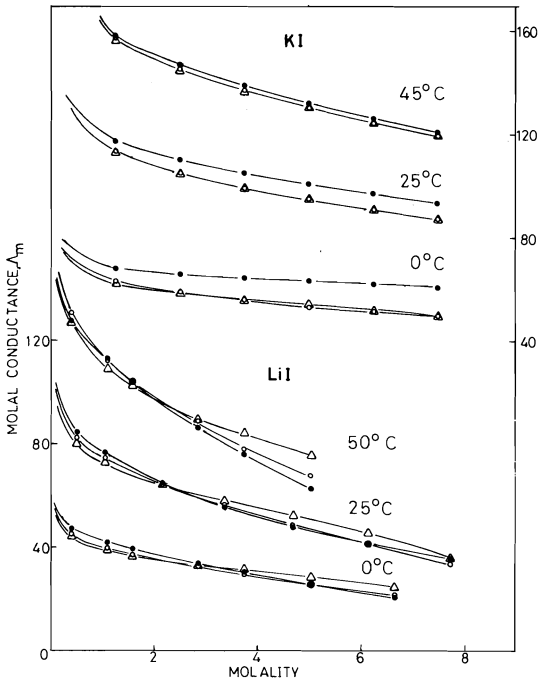

FIG. 6. Molal conductance data for LiI and KI at three temperatures. Symbols as in Fig. 2.

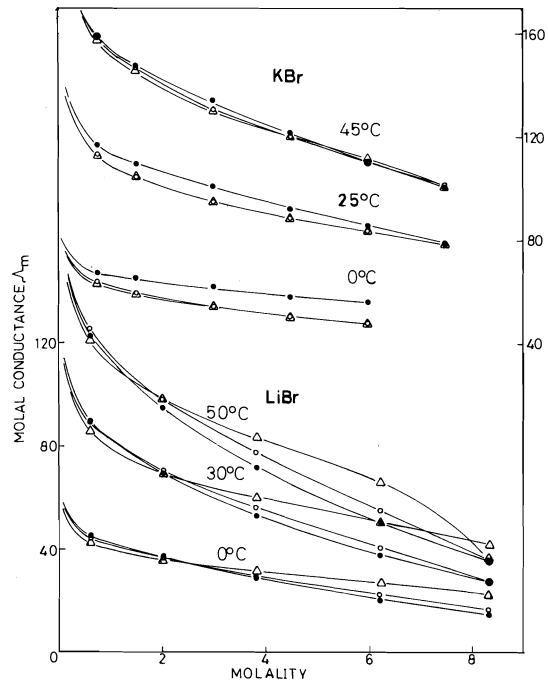

FIG. 5. Molal conductance data for LiBr and KBr at three temperatures. Symbols as in Fig. 2.

should be introduced into the values of B_1, B_2, and B_3.

Each of these factors could indeed be taken into account if it were felt justified. However to do so would involve the introduction of more parameters into the equation. For ion pair formation, an ion pair equilibrium constant K would need to be added to the adjustable parameter set. To account for bulk dielectric changes, a dielectric decrement parameter, δ, could be introduced. And finally the bulk viscosity instead of the solvent viscosity could be used in the value of B_2 and a Stokes–Wishaw-like equation would result.

Finally the above mentioned criticisms all pale beside the criticism that the theoretical basis of the Falkenhagen–Leist–Kelbg equation just does not extend into these higher concentration regions. Hence in essence the fixed and variable hydration parameter equations should be treated primarily as semi-empirical equations which when applied to conductance data yield a solvation parameter which may or may not be related to an actual solvation number of the salt in solution.

Can. J. Chem. Downloaded from www.nrcresearchpress.com by 210.87.254.6 on 09/05/12
For personal use only.

TABLE 4. Fixed and variable H_0 values at several temperatures

(*a*) Chloride

	H_0											
T °C	LiCl		NaCl		KCl		NH_4Cl		RbCl		CsCl	
0	4.9	33.8	7.3	38.2	7.1	13.2	4.1	7.2	—	—	2.8	9.2
20	5.0	35.8	7.3	37.2	—	—	4.8	11.6*	5.0	11.7*	4.2	18.6*
25	4.6	33.9*	7.8	26.9	5.5	9.1	4.2	8.0	7.2	13.2	—	—
30	4.6	31.2	8.5	35.2	5.7	10.6	3.9	6.5	4.8	9.0	4.2	15.3
35	—	—	8.6	39.0	6.6	14.2	—	—	—	—	—	—
40	4.5	29.8	8.5	38.8	6.9	15.1	4.2	9.8	4.5	12.3	4.2	16.8
45	—	—	8.5	38.6	7.3	18.0	—	—	—	—	—	—
50	4.5	29.0	8.4	39.3	7.8	20.4	4.3	11.5	4.7	14.4	4.2	17.7
55	—	—	8.4	39.2	8.5	22.0	—	—	—	—	—	—
60	4.5	28.3	—	—	—	—	4.3	11.7	4.7	14.6	4.1	17.9

(*b*) Bromides and iodides

	H_0											
T °C	LiBr		NaBr		KBr		NH_4Br		LiI		KI	
0	4.0	24.5	6.5	38.4	5.0	11.7	2.2	3.3	4.8	22.9	6.7	10.6
20	3.9	27.9†	—	—	—	—	—	—	4.8	26.8	—	—
25	—	—	5.6	30.6	4.1	10.5	4.2	7.1	5.2	21.2	7.0	11.2
30	3.9	26.9	—	—	—	—	—	—	4.8	24.9	—	—
35	—	—	5.5	38.9	4.8	8.4	4.7	10.2	—	—	7.0	11.6
40	—	—	—	—	5.5	10.4	—	—	—	—	6.1	13.5
45	—	—	5.5	28.4	6.5	14.6	5.2	14.7	—	—	7.1	11.8
50	5.3	27.0	—	—	6.2	13.3	—	—	4.8	23.3	6.7	17.5
55	—	—	5.5	26.5	6.7	16.1	5.1	14.3	—	—	—	—

*T = 23 °C.
†T = 15 °C.

Can. J. Chem. Downloaded from www.nrcresearchpress.com by 210.87.254.6 on 09/05/12
For personal use only.

Taking into consideration the above mentioned criticisms, we can consider the values of the H_0 parameters in Table 4. Several observations can be made. First, the fixed hydration parameter data for the salts are roughly in agreement with hydration parameters obtained by other methods (22, 23) with the same trends being observed. For instance at 25 °C, the LiCl through CsCl variation shows a maximum value with NaCl (7.8) and decreasing values with increasing cation radius. Anion effects are also observed, with the H_0 parameters of the bromides less than that of the chlorides. However, the iodide values are larger than the corresponding bromides and the H_0 values are not additive. Between 25 and 60 °C, only the fixed H_0 parameters for KCl and KBr are strongly temperature dependent, increasing by 50% in that temperature interval.

The variable H_0 parameters are rather high for parameters indicating solvation numbers (23). Although the same rough trends in H_0 values are observed, with lithium and sodium salts having much larger H_0 parameters than potassium or ammonium salts, it is found that the H_0 parameters for CsCl are larger than those for KCl at room temperature, becoming smaller than those for KCl above 50 °C. The temperature dependence of KCl and KBr is again observed, but the variable H_0 parameters of NH_4Cl and NH_4Br also increase with temperature. If the variable H_0 parameters have any meaning, then they may be related to the secondary hydration number of the salt, rather than the primary hydration number. Total hydration numbers of 28 for NaCl, 26 for NaBr, 34 for KCl, and 22 for KBr have been obtained from an analysis of the refractive index of concentrated solutions of these electrolytes (2, p. 121). Such numbers are not too unreasonable when it is realized that within a radius of 4.5 Å around a central water molecule in liquid water, there are 4 nearest neighbour water molecules, 11 second neighbours, and 22 third neighbours (26). Hence the seemingly large hydration parameters of the lithium and sodium salts may only reflect the ability of these small ions to affect the secondary and tertiary layer of water about them as they move in the presence of an electric field. It must also be noted that these variable H_0 parameters represent infinite dilution parameters. At 1 *m* concentration, the values of these parameters are about two-thirds of their infinite dilution value and at 5 *m* about one quarter. At these concentrations the values of the variable H_0 parameter approach those of the fixed H_0 parameters.

In conclusion, it would seem that to a first approximation gross solvation effects on the conductance of simple electrolytes can help to explain the effect of viscosity on the conductance at high concentrations. But, the hydration parameters obtained from the analysis of these data in this manner must be treated with caution. A better understanding of the conductance of simple electrolytes at high concentrations requires first a fundamental formulation of the concentration dependence of other variables of electrolyte solutions, particularly the bulk dielectric constant and viscosity. Otherwise, only the semi-empirical path to the solution of the conductance problem can be followed in the concentrated electrolyte solution region.

Acknowledgments

We thank the National Research Council of Canada for financial support and for a postgraduate scholarship to R.F. We also thank IBM of Canada for financial support of the computer work involved in this paper.

1. C. A. ANGELL. J. Electrochem. Soc. 114 (1967); 1033 (1967).
2. R. A. ROBINSON and R. H. STOKES. Electrolyte solutions. Academic Press, New York. 1959.
3. H. S. HARNED and B. B. OWEN. The physical chemistry of electrolyte solutions. 3rd ed. Reinhold Publishing Corp., New York. 1958.
4. A. N. CAMPBELL and E. M. KARTZMARK. Can. J. Chem. **33**, 887 (1955).
5. A. N. CAMPBELL and R. J. FRIESDEN. Can. J. Chem. **37**, 1288 (1959).
6. A. N. CAMPBELL and L. ROSS. Can. J. Chem. **34**, 566 (1956).
7. C. A. ANGELL. J. Phys. Chem. **70**, 3988 (1966).
8. C. A. ANGELL and R. D. BRESSEL. J. Phys. Chem. **76**, 3244 (1972).
9. A. J. EASTEAL and C. A. ANGELL. J. Phys. Chem. **74**, 3987 (1970).
10. RAYMOND M. FUOSS. J. Phys. Chem. **79**, 525 (1975).
11. H. FALKENHAGEN, M. LEIST, and G. KELBG. Ann. Phys. Lpz. **6**, 51 (1952).
12. B. F. WISHAW and R. H. STOKES. J. Am. Chem. Soc. **76**, 2065 (1954).
13. R. H. STOKES and R. A. ROBINSON. J. Am. Chem. Soc. **70**, 1870 (1948).
14. D. G. MILLER. J. Phys. Chem. **60**, 1296 (1956).
15. E. GLUEKAUF. Trans. Faraday Soc. **51**, 1235 (1955).

16. R. H. STOKES and R. A. ROBINSON. Trans. Faraday Soc. **53**, 301 (1975).
17. R. H. STOKES and R. A. ROBINSON. J. Solution Chem. **2**, 173 (1973).
18. B. B. OWEN and F. H. SWEETON. J. Am. Chem. Soc. **63**, 2811 (1941).
19. R. W. GURNEY. Ionic processes in solution. Dover Publications, New York. 1953.
20. B. E. CONWAY. Physical chemistry. An advanced treatise. Vol. 1XA. Academic Press, New York. 1970. Chapt. 1.
21. B. E. CONWAY, R. E. VERRALL, and J. E. DESNOYERS. Z. Phys. Chem. **230**, 157 (1965).
22. J. O'M. BOCKRIS and P. P. S. SALUJA. J. Phys. Chem. **76**, 2146 (1972).
23. E. S. AMIS and J. F. HINTON. Solvent effects on chemical phenomena. Vol. 1. Academic Press, New York. 1973.
24. M. POSTLER. Coll. Czech. Chem. Comm. **35**, 535 (1975).
25. L. PAULING. The nature of the chemical bond. Cornell U.P. 1960.
26. D. EISENBERG and W. KAUZMANN. The structure and properties of water. Oxford Clarendon Press, London. 1969. p. 168.
27. C. V. SURYANARAYANA and V. K. VENKATESAN. Acta Chim. Hung. **17**, 327 (1958).
28. N. M. BARON and M. U. SCHERBA. Zh. Prik. Khim. **44**, 2118 (1971).
29. International critical tables. Vols. 3 and 5, McGraw-Hill, New York. 1933.
30. J. F. CHAMBERS. J. Phys. Chem. **62**, 1136 (1958).
31. J. F. CHAMBERS, J. M. STOKES, and R. H. STOKES. J. Phys. Chem. **60**, 985 (1956).
32. J. B. HASTED. Aqueous dielectrics, Chapman and Hall, London. 1973.

Can. J. Chem. Downloaded from www.nrcresearchpress.com by 210.87.254.6 on 09/05/12
For personal use only.

Erratum: Tautomeric equilibrium study of thiazolidine-2-thione. Transition metal complexes of the deprotonated ligand

CARLO PRETI AND GIUSEPPE TOSI
Istituto di Chimica Generale ed Inorganica, University of Modena, 41100 Modena, Italy

Received May 21, 1976
(Ref.: Can. J. Chem. **54**, 1558 (1976))

The structures shown on p. 1558 were incorrectly drawn; the correct structures appear below.

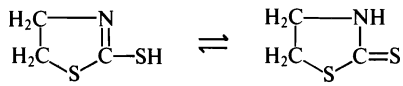

Thiol form ⇌ Thione form

Can. J. Chem. Downloaded from www.nrcresearchpress.com by 210.87.254.5 on 09/05/12
For personal use only.

Can. J. Chem. Downloaded from www.nrcresearchpress.com by 210.87.254.5 on 09/05/12
For personal use only.

Canadian Journal of Chemistry

Published by
THE NATIONAL RESEARCH COUNCIL OF CANADA

Journal canadien de chimie

Publié par
LE CONSEIL NATIONAL DE RECHERCHES DU CANADA

Volume 54 Number 19 October 1, 1976 Volume 54 numéro 19 1 octobre 1976

Nicotinamide coenzyme regeneration. Flavin mononucleotide (riboflavin phosphate) as an efficient, economical, and enzyme-compatible recycling agent[1]

J. BRYAN JONES AND KEITH E. TAYLOR
Department of Chemistry, University of Toronto, Toronto, Ont., Canada M5S 1A1

Received February 18, 1976

J. BRYAN JONES and KEITH E. TAYLOR. Can. J. Chem. **54**, 2969 (1976).

The high cost of nicotinamide coenzymes currently acts as a deterrent to the widespread adoption of alcohol dehydrogenases as chiral catalysts for effecting stereospecific and selective CH(OH) $\rightleftarrows$ C=O oxidoreductions on a preparative scale. Attempts to overcome this problem generally involve using catalytic amounts of coenzyme together with an auxiliary system capable of continuously regenerating its active form *in situ*. Flavin mononucleotide has been found to be an effective, convenient, and inexpensive reagent for *in situ* recycling of NAD^+. Using horse liver alcohol dehydrogenase-catalyzed oxidation of cyclohexanol as a representative process, up to 50-fold NAD^+-regeneration levels have been achieved. This method is the most satisfactory and practical oxidative-mode recycling procedure yet developed for routine laboratory applications.

J. BRYAN JONES et KEITH E. TAYLOR. Can. J. Chem. **54**, 2969 (1976).

Le coût très élevé des coenzymes de la nicotinamide agit actuellement de façon à empêcher une utilisation très grande des déshydrogénases de l'alcool comme catalyseurs chiraux pour effectuer des réactions d'oxydoréductions stéréospécifiques et sélectives du type CH(OH) $\rightleftarrows$ C=O sur une base préparative. Des essais pour surmonter ce problème impliquent généralement l'utilisation de quantités catalytiques de coenzymes avec un système auxiliaire capable de se régénérer continuellement *in situ* sous sa forme active. On a trouvé que la mononucléotide de flavine est un réactif efficace, peu dispendieux et utile pour la régénération *in situ* du NAD^+. Utilisant la réaction d'oxydation du cyclohexanol, catalysée par la déshydrogénase d'alcool du foie de cheval, on a pu atteindre des niveaux de régénération du NAD^+ allant jusqu'à 50 fois. Pour des applications de routine dans le laboratoire, cette méthode est la plus satisfaisante et la plus pratique pour recycler dans le mode oxydant.

[Traduit par le journal]

The asymmetric synthesis potential of alcohol dehydrogenases, which catalyze oxidoreduction reactions of the type represented in [1] with considerable stereospecificity and selectivity, is very great and many such reactions of organic chemical interest have now been documented (2).

The high costs[2] of the nicotinamide coenzymes

[1] $$CH(OH) + NAD(P)^+ \underset{}{\overset{K \sim 10^{-10}\ M}{\rightleftharpoons}} C{=}O + NAD(P)H + H^+$$

required dictate that, in order to permit such

[1]Abstracted from the Ph.D. thesis of K.E.T., University of Toronto, 1973. A preliminary account of some of these data has been published (1).

[2]1976 prices (in dollars) per mole:[3] NAD^+, >2000; NADH, >17 000; $NADP^+$, >60 000; NADPH, >200 000.

TABLE 1. Survey of the NAD^+-regenerating efficiency of FMN, riboflavin, and DCIP in the HLADH-catalyzed oxidation of cyclohexanol*

Recycling agent	$[NAD^+]$ (mM)	Cyclohexanone (% yield)†	$NADH \rightarrow NAD^+$ recycles‡
FMN	0.1	40	23.0
	0.25	63	14.2
	0.5	78	8.4
	0.9	90	5.0
	0.1§	60	35.0
Riboflavin	0.25‖	37	7.9
	1.0‖	60	2.6
DCIP	0.25	37	7.9
	1.0	62	2.7
	1.0§	45	1.7
	1.0¶	70	3.2

*Reactions were carried out for 24 h at 20 °C using stirred solutions of aqueous 0.05 M Tris–HCl buffer pH 9.0, 6.0 mM in cyclohexanol, 12 mM in recycling agent and 4×10^{-7} M in HLADH.
†By glc analysis.
‡The first 'cycle' of coenzyme has not been included since the NAD^+ added initially functions directly in the oxidation.
§30 mM in recycling agent.
‖[Riboflavin] < 2 mM.
¶[DCIP] 6 mM.

enzyme-catalyzed oxidoreductions to be practical, it is necessary to use catalytic quantities only of the desired coenzyme in conjunction with an auxiliary system capable of continuously regenerating it in its active form. Many methods of achieving this end have been investigated (2) but none has yet proven wholly satisfactory. With the equilibrium of [1] being heavily in favour of carbonyl reduction, the coenzyme recycling problem is particularly acute for NAD^+ [3] and $NADP^+$ regeneration in oxidative-mode reactions. In this paper we report on *in situ* chemical regeneration of NAD^+ via FMN[3]-mediated oxidation of NADH as an effective, economical, and convenient means of achieving oxidized nicotinamide coenzyme recycling during alcohol dehydrogenase-catalyzed oxidations of alcohols in laboratory-scale reactions.

Selection of FMN and riboflavin for this purpose was influenced by the fact that FMN is often the natural H-acceptor for many *in vivo* enzyme-catalyzed oxidations of NADH and by the numerous reports detailing nonenzymic H-transfer between dihydropyridines and flavin derivatives (3–7). Furthermore, it was felt that the magnitude of the redox potential difference between FMN or riboflavin and NAD^+ (100 mV(8)) would facilitate the desired H-transfer reaction (7, 9–11). This latter consideration, together with the data on H-transfer between various quinones, dyes, and similar compounds (3–7, 12), prompted a concurrent evaluation of DCIP; the DCIP–NAD^+ system has the largest redox potential difference (532 mV (8)) of the H-transfer redox couples (2–6, 8–10) of potential recycling value.

Results

The practicability of applying FMN, riboflavin, or DCIP to maintain continuous *in situ* $NADH \rightarrow NAD^+$ conversion was evaluated using horse liver alcohol dehydrogenase (HLADH) as the enzyme and cyclohexanol as a typical substrate. The results obtained are summarized in Table 1. In view of the clear superiority of FMN-mediated regeneration, its recycling performance was assessed in more detail. The effects of some variations in reaction conditions on the yield of cyclohexanone and the FMN recycling efficiency are recorded in Table 2. Altering the HLADH concentration within the range $1–4 \times 10^{-7}$ M was without effect on the FMN-recycling efficiency under the Table 1 conditions. The pH dependence of FMN re-

[3]Abbreviations used: NAD^+/H and $NAD(P)^+$/H; oxidized and reduced forms respectively of nicotinamide adenine dinucleotide and its phosphate; FMN, flavin mononucleotide (riboflavin phosphate); DCIP, 2,6-dichlorophenolindophenol; HLADH, horse liver alcohol dehydrogenase.

Can. J. Chem. Downloaded from www.nrcresearchpress.com by 210.87.254.5 on 09/05/12
For personal use only.

TABLE 2. Influence of reaction time and [NAD+] on FMN-recycling efficiency and yield of ketone*

Reaction period (h)	[NAD+] (m*M*)	Cyclohexanone (% yield†)	NADH → NAD+ recycles
1	0.1	5	2.4
2	0.1	17	10.5
3	0.1	21	13.2
6	0.1	30	19.3
9	0.1	40	26.0
22	0.1	61	40.2
70	0.1	75	49.6
1	1.0	32	1.2
2	1.0	50	2.4
3	1.0	59	3.0
6	1.0	73	3.9
9	1.0	82	4.5
22	1.0	94	5.4

*All reactions were carried out at 20 °C in aqueous 0.1 *M* Tris–HCl buffer solution of p*H* 9.0, 6.75 m*M* in cyclohexanol, 13 m*M* in FMN, and 5.4×10^{-7} *M* in HLADH.
†By glc analysis.

cycling was also investigated. As Fig. 1 shows, the overall reaction showed a clear p*H* optimum of 9.

Discussion

The choice of HLADH as the enzyme was a natural one since it is currently the alcohol dehydrogenase of most general asymmetric synthetic utility to organic chemists (2). The substrate used, cyclohexanol, is structurally simple but its HLADH-catalyzed oxidation behaviour is representative of those of many other alcohols of greater complexity and interest (2). The coenzyme-recycling surveys summarized by Table 1 were carried out on reaction mixtures containing up to 1 g of cyclohexanol in order to ensure that truly preparative-scale behaviour was being reflected by the data obtained. The assays were performed at p*H* 9; the use of basic reaction solutions is common for alcohol dehydrogenase-catalyzed oxidations since this helps to ameliorate the unfavourable equilibrium of [1]. Control experiments were carried out to ensure that none of the recycling agents oxidized cyclohexanol in the absence of enzyme or coenzyme and that up to 6 m*M* concentrations of cyclohexanone did not inhibit the reaction.

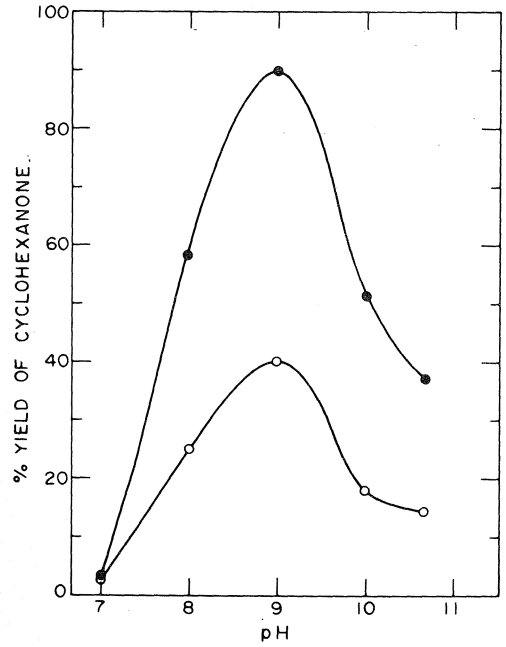

FIG. 1. p*H* dependence of the yield of cyclohexanone from HLADH-catalyzed oxidation of cyclohexanol with FMN regeneration of NAD+ under the Table 1 reaction conditions. ○ [NAD+] 0.1 m*M*, ● [NAD+] 1.0 m*M*.

The limited success observed with DCIP was disappointing, particularly in view of its successful application for a similar purpose in analytical systems (13). Its mediocre performance as a recycling agent under preparative-scale conditions appears to be due to its inhibitory effect on the enzyme; the yield of cyclohexanone and the recycling efficiency both decrease as the DCIP concentration is raised from 6 to 30 m*M*. In contrast, there was no noticeable inhibition of the enzyme by FMN. The poor performance of riboflavin is at least partly due to its very low solubility in the aqueous assay solution. For all

Can. J. Chem. Downloaded from www.nrcresearchpress.com by 210.87.254.5 on 09/05/12
For personal use only.

Can. J. Chem. Downloaded from www.nrcresearchpress.com by 210.87.254.5 on 09/05/12
For personal use only.

the recycling agents of Table 1, the highest levels of NADH → NAD^+ regeneration are achieved at the lowest coenzyme concentrations. This is a common observation with recycling systems (11, 14, 15).

FMN is clearly a very effective NAD^+-recycling agent with good yields of the cyclohexanone product accompanied by high levels of NAD^+ turnover being achieved routinely under the Table 1 conditions. Evaluation of its performance as function of time (Table 2) showed that substantial levels of the ketone product were produced within 3 h at moderate NAD^+ concentrations. While cyclohexanol oxidation was slower at low NAD^+ levels, the yields of cyclohexanone again became very respectable as the reaction period was increased. The p*H* profile for the overall process (Fig. 1) parallels those of HLADH-catalyzed oxidations of alcohols (2) and that of the influence of p*H* on the rates of reduction of riboflavin by dihydropyridines (16).

The data of Table 2, and the observation that reducing the enzyme concentration by up to a factor of 4 does not affect the Table 1 results, indicate that enzyme instability is not a major problem for extended reactions involving FMN recycling. This contrasts the situation encountered with other chemical recycling agents (2, 11, 14). The dependence of the yields of cyclohexanone and the recycling efficiencies (Tables 1 and 2) on factors such as NAD^+ and FMN concentration, and the fact that limited variations in HLADH concentration are without effect, point to H-transfer from NADH to FMN as being partly or wholly rate limiting under many of the conditions applied.

In addition to making the use of nicotinamide coenzymes more economical, oxidative recycling possesses the advantage that it assists in displacing the unfavourable equilibrium of the enzyme-catalyzed oxidations in the desired direction. For example, taking the equilibrium constant of [1] as $\sim 4 \times 10^{-10}$ *M* for HLADH-mediated cyclohexanol oxidation (2), the maximum yields of cyclohexanone attainable under Table 1 conditions *in the absence of recycling agents* are calculated to be 10% for solutions 1.0 m*M* in NAD^+ and merely 41% if the extremely high NAD^+ concentration of 7.2 m*M* was used. This contrasts the 75% yield obtained with only 0.1 m*M* NAD^+ using FMN recycling (Table 2). Another benefit of being able to operate at low NAD^+ concentrations in p*H* 9 reaction solutions is that the rate of elimination of the active coenzyme via pseudobase formation (11, 17) is reduced.

With its up to 50-fold NADH → NAD^+ regeneration capability FMN is already superior to any previous chemical oxidative-mode recycling system (2, 11) and still greater recycling efficiency can be anticipated using higher FMN concentrations and under optimized conditions.[4] Furthermore, FMN has several practical advantages over other oxidative recycling systems (2, 11). It can be used in high concentrations owing to its excellent solubility characteristics; it is very soluble in the aqueous reaction media but is insoluble in the organic solvents used to work up enzymic reactions of this type (2). Also, the reduced FMN produced oxidizes very rapidly in air so that the FMN concentration remains effectively constant under the conditions used. No deleterious effects from the hydrogen peroxide byproduct of the oxidation step have yet been observed.

FMN regeneration of NAD^+ is now in routine use in our laboratory. Examples of its application for this purpose during alcohol dehydrogenase-catalyzed oxidations of alcohol substrates of general organic chemical interest will be reported shortly.

The results of kinetic studies on the FMN–NADH and related reactions are reported in the following paper (18).

Experimental

HLADH (E.C. 1.1.1.1, mol. wt. 84 000, 3 × crystallized) was purchased from Worthington and NAD^+, DCIP, riboflavin, and FMN (commercial grade) from Sigma. Gas–liquid chromatographic analyses were performed using a 2% QF-1 on a Chromosorb G column.

General Recycling Procedure

The recycling studies were carried out in 0.05 or 0.1 *M* Tris–HCl solutions p*H* 9.0 (10–150 ml) containing fixed concentrations of cyclohexanol (6.0 or 6.75 m*M*), NAD^+ (0.1–1.0 m*M*), FMN or DCIP (6–30 m*M*), or riboflavin (2 m*M*), and HLADH ($1–4 \times 10^{-7}$ *M*). The p*H* dependence studies were performed using 0.05 *M* Tris–HCl (p*H* 7–9) and 0.05 *M* carbonate–bicarbonate (p*H* 10–11) buffers. For the routine assays, stock solutions of cyclohexanol (20 m*M*) and NAD^+ (30 m*M*) in p*H* 9 buffer

[4]For the Table 1 and 2 experiments where the oxidation is virtually quantitative (*i.e.* >90%), the low recycling factors recorded obviously do not represent the maximum levels of coenzyme regeneration achievable under the conditions applied.

were used. The corresponding stock solution of HLADH (10^{-5} *M*) was made up in p*H* 7 Tris–HCl buffer; this solution retained >90% of its activity during storage for 1 month at 4 °C. FMN, riboflavin, and DCIP were added in solid form to the reaction mixture. The reactants were combined in stoppered 10–200 ml, pear-shaped flasks in the desired concentrations and the mixtures stirred slowly (avoiding foaming or cavitation) at 20 °C in the dark with a magnetic stirrer. The analytical-scale oxidations were monitored by extracting 3 ml aliquots with chloroform (3 × 3 ml) and analyzing the dried (Na_2SO_4) and concentrated (to 0.3 ml) chloroform extract by glc. This procedure permitted >60% of the cyclohexanol/cyclohexanone to be recovered.

The preparative-scale viability of the FMN process was verified under the best Table 1 and Table 2 conditions using solutions containing up to 1 g of cyclohexanol. When glc analysis indicated total conversion of cyclohexanol (24–72 h) the reaction mixtures were continuously extracted with chloroform and the chloroform solutions dried (Na_2SO_4), evaporated, and distilled to give >60% yields of pure cyclohexanone.

Acknowledgments

This work was supported by a grant from the National Research Council of Canada. The award (to K.E.T.) of an NRCC Scholarship (1969–1973) is gratefully acknowledged.

1. J. B. Jones and K. E. Taylor. Chem. Commun. 205 (1973).
2. J. B. Jones and J. F. Beck. Applications of biochemical systems in organic chemistry. (Techniques of chemistry. Vol. 10.) Part I. *Edited by* J. B. Jones, D. Perlman, and C. J. Sih. 1976. Chapt. 4.
3. H. Sund. Biological oxidations. *Edited by* T. P. Singer. Wiley–Interscience, New York, N.Y. 1968. pp. 603–639.
4. T. C. Bruice and S. J. Benkovic. Bioorganic mechanisms, Vol. 2. W. A. Benjamin, New York, N.Y. 1966 pp. 301–349; M. Brustlein and T. C. Bruice. J. Am. Chem. Soc. **94**, 6548 (1972), and references therein.
5. K. A. Schellenberg. The pyridine nucleotide-dependent dehydrogenases. *Edited by* H. Sund. Springer-Verlag, Berlin. 1970. pp. 15–26.
6. S. Shinkai. Kagaku (Kyoto), **29**, 12 (1974).
7. G. Blankenhorn. Eur. J. Biochem. **50**, 351 (1975); Biochemistry, **14**, 3172 (1975), and references therein.
8. H. A. Sober (*Editor*). Handbook of Biochemistry. Chemical Rubber Co., Cleveland, Ohio. 1968 pp. J31–J32.
9. K. Wallenfels and M. Gellrich. Justus Liebig's Ann. Chem. **621**, 149 (1959).
10. A. R. Battersby, J. Staunton, and M. R. Wiltshire. J. Chem. Soc. Perkin Trans. I, 1156 (1975).
11. K. E. Taylor and J. B. Jones. J. Am. Chem. Soc. **98**. In press (Sept. 1976).
12. J. Hajdu and D. S. Sigman. J. Am. Chem. Soc. **97**, 3524 (1975), and references therein.
13. S. Pinder, J. B. Clark, and A. L. Greenbaum. *In* Methods in enzymology, Vol. 18B. *Edited by* D. B. McCormick and L. D. Wright. Academic Press, New York, N.Y. 1971. pp. 20–45.
14. J. B. Jones, D. W. Sneddon, W. Higgins, and A. J. Lewis. Chem. Commun. 856 (1972).
15. J. R. Wyckes, P. Dunnill, and M. D. Lilly. Biochim. Biophys. Acta, **286**, 260 (1972).
16. C. H. Seulter and D. E. Metzler. Biochim. Biophys. Acta, **44**, 23 (1960).
17. U. Eisner and J. Kuthan. Chem. Rev. **72**, 1 (1972).
18. J. B. Jones and K. E. Taylor. Can. J. Chem. This issue.

Can. J. Chem. Downloaded from www.nrcresearchpress.com by 210.87.254.5 on 09/05/12
For personal use only.

Nicotinamide coenzyme regeneration. The rates of some 1,4-dihydropyridine, pyridinium salt, and flavin mononucleotide hydrogen-transfer reactions[1]

J. Bryan Jones and Keith E. Taylor

Department of Chemistry, University of Toronto, Toronto, Ont., Canada M5S 1A1

Received April 15, 1976

J. Bryan Jones and Keith E. Taylor. Can. J. Chem. **54**, 2974 (1976).

The rates of H-transfer between various 1,4-dihydropyridines and pyridinium salts (including NADH and NAD^+), and from 1,4-dihydropyridines to FMN, have been measured. The reactions are found to be sufficiently slow for H-transfer to be rate-determining to a significant extent when such systems are applied for nicotinamide coenzyme recycling purposes. The rates of H-transfer parallel the magnitudes of the donor–acceptor redox potential differences ($\Delta E_0'$); $\Delta E_0'$ values may therefore be used as qualitative guides in formulating and selecting redox couples of NAD/H recycling value. On the basis of deuterium isotope effects, it is concluded that formation of a complex prior to H-transfer is not rate determining for 1,4-dihydropyridine–NAD^+ reactions. This behavior is in contrast to that of other model alcohol dehydrogenase systems.

J. Bryan Jones et Keith E. Taylor. Can. J. Chem. **54**, 2974 (1976).

On a mesuré les vitesses de transferts d'hydrogène entre diverses dihydro-1,4 pyridines et de sels de pyridinium (incluant NADH et NAD^+) et entre des dihydro-1,4 pyridines et le FMN. On a trouvé que les réactions sont suffisamment lentes pour que le transfert d'hydrogène soit l'étape déterminante pour une partie importante de la réaction quand de tels systèmes sont appliqués pour des besoins de recycler le coenzyme de la nicotinamide. Les vitesses de transferts d'hydrogène sont parallèles aux grandeurs des différences de potentiel redox donneur–accepteur ($\Delta E_0'$); les valeurs de $\Delta E_0'$ peuvent donc être utilisées comme des guides qualitatifs pour formuler et choisir des couples de redox qui sont efficaces pour le recyclage du NAD /H. Sur la base des effets isotopiques du deutérium, on peut conclure que la formation d'un complexe antérieur au transfert d'hydrogène n'est pas l'étape déterminante pour les réactions dihydro-1,4 pyridine – NAD^+. Ce comportement est en opposition avec celui d'autres systèmes modèles d'alcool déhydrogénase.

[Traduit par le journal]

Oxidoreductions involving hydrogen transfer between nicotinamide coenzymes, dihydropyridines and pyridinium salts, and flavins and related compounds have received considerable attention in recent years (1–11). Our interest in such reactions derives from their potential for nicotinamide coenzyme regeneration during preparative-scale applications of alcohol dehydrogenases in asymmetric synthesis (12); the types of redox systems which have been surveyed in this coenzyme recycling context are depicted in [1] and [2].[2] Successful oxidative-mode recycling of NAD^+ was achieved using pyridinium salts **1** of lower redox potential than NAD^+ to displace the equilibrium of [1] to the right.

[1] 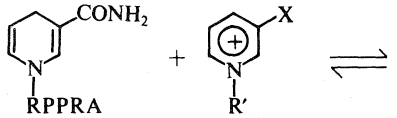

NADH **1***a–g*

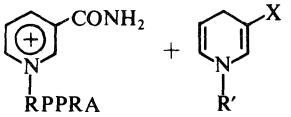

NAD^+ **2***a–g*

a, R′ = $CH_2C_6H_5$, X = $CONH_2$
b, R′ = n-C_3H_7, X = $CONH_2$
c, R′ = α- or β-TAG, X = $CONH_2$
d, R′ = β-TAG, X = $COCH_3$
e, R′ = DCB, X = NO_2
f, R′ = PNB, X = NO_2
g, R′ = $CH_2COC_6H_5$, X = NO_2

[1]Abstracted from the Ph.D. thesis of K.E.T., University of Toronto, 1973.

[2]Abbreviations used: NAD^+/NADH, oxidized and reduced forms respectively of nicotinamide adenine dinucleotide; FMN/FMN·H, oxidized and reduced forms respectively of flavin mononucleotide (riboflavin phosphate); RPPRA (in NAD/H), ribose-phosphate-phosphate-ribose-adenine; RP (in FMN), ribose-phosphate; TAG, α- or β-2,3,4,6-tetraacetyl-D-glucosyl; DCB, 2,6-dichlorobenzyl; PNB, p-nitrobenzyl; HLADH, horse liver alcohol dehydrogenase.

Can. J. Chem. Downloaded from www.nrcresearchpress.com by 210.87.254.5 on 09/05/12
For personal use only.

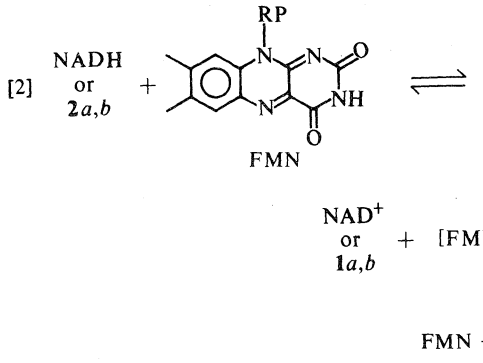

[2]

Conversely, reductive-mode recycling of NADH was effected by driving the equilibrium of [1] in the opposite direction with dihydropyridines **2** of greater redox potential than NADH (12*a*). The selection of FMN, the most successful chemical NAD^+-recycling agent developed so far as described in the preceding paper (12*b*), was guided by similar considerations with displacement of the eq. 2 reactions in the desired direction being greatly assisted by rapid aerial oxidation of the FMNH produced.

For the above systems, it appeared that (*a*) the magnitude of the redox potential difference between an H-acceptor or donor and NAD^+/H could be used as a guide to its effectiveness as a recycling agent and that (*b*) the H-transfer step in these regeneration processes was rate-limiting to some degree (12). The rate studies reported in this paper confirm these conclusions. The data obtained also bear on non-enzymic model alcohol dehydrogenase studies.

Results

For all the reactions studied, the rates of H-transfer were measured under pseudo first-order conditions with the H-acceptor present in excess. Since it is well documented that 1,4-dihydropyridine – pyridinium salt and dihydropyridine–flavin reactions are first-order with respect to each redox component (2, 4, 6, 8, 10, 13–17) the calculation of the corresponding second-order rate constants presented no problem. The kinetics were followed by monitoring the rate of change of absorption at or near the λ_{max} of each dihydropyridine in the range 340–450 nm. In each case, care was taken to ensure that Beer's law was obeyed at the recording wavelength. The results obtained for the rates of H-transfer between various 1,4-dihydropyridine–pyridinium systems in water at neutral p*H* are recorded in Table 1 together with the estimated redox potential differences for each couple. In general, it is seen that the rates of H-transfer increase progressively as the $\Delta E_0'$ values become larger.

TABLE 1. Rate constants for dihydropyridine–pyridinium H-transfer reactions[a]

Donor	Acceptor	k (M^{-1} s^{-1})	$\Delta E_0'$ (mV)[b]
2*a*	NAD^+	$2.15 \pm 0.04 \times 10^{-2}$ [c]	46
2*b*	NAD^+	$5.6 \pm 0.3 \times 10^{-2}$	72
2*b*	**1***c*-α	0.34 ± 0.01	(~90)
NADH	**1***d*	1.49 ± 0.09	93
2*b*	**1***c*-β	1.05 ± 0.02	120
NADH	**1***e*	2.18 ± 0.11[d]	(>120)
NADH	**1***f*	2.60 ± 0.25[d]	(>120)
NADH	**1***g*	2.81 ± 0.21[d,e]	—[f]
2*b*	**1***e*	8.9 ± 0.2[d,e]	(>190)
2*b*	**1***f*	11.7 ± 0.2[d,e]	(>190)
2*b*	**1***g*	16.0 ± 1.1[d,e]	—[f]

[a]Rates were measured at 25 °C in aqueous solutions of p*H* 7 under pseudo first-order conditions using an excess of the acceptor by monitoring changes in dihydropyridine absorption at or near the λ_{max} (360–400 nm range) in each case. The constants recorded are from reactions run for at least 2–3 half lives and repeated 4–6 times; correlation coefficients were > 0.99.

[b]$\Delta E_0'$ is the calculated (or estimated if in parentheses) redox potential difference between the acceptor and the donor at 20 °C (12*a*).

[c]In 0.05 *M* Tris–HCl buffer p*H* 7 containing 1.6% EtOH. Rate constant (corrected for hydration of **2***a*) calculated using the method of Guggenheim (18).

[d]Monitored at 448 nm.

[e]p*H* 6.2.

[f]Not available (12*a*).

That the reactions of Table 1 proceeded as indicated by [1] was verified by uv spectroscopic analysis of the products, and by the formation of coenzymically-active NADH from the reactions utilizing NAD^+ as acceptor (12*a*). It was recognized that the results obtained might be affected by the facility with which 1,4-dihydropyridines undergo hydration (19). Accordingly, the susceptibility to hydration of the dihydropyridines involved was checked under the assay conditions. At p*H* 7, the rates of hydration were significant only for the *N*-benzyl compound **2***a* (k_{hydr} 4.3 and 18.8×10^{-6} s^{-1} in water and 0.05 *M* Tris–HCl respectively) and the *N*-propyl derivative **2***b* (k_{hydr} 17.7×10^{-6} s^{-1} in 0.05 *M* Tris–HCl). The data reported for H-transfers involving these two compounds have been corrected for this side reaction whenever necessary.

The data for dihydropyridine–FMN reactions were obtained in a similar manner except that, owing to the phosphate group of FMN, it was necessary to use 0.05 *M* Tris–HCl buffer solutions in order to enable p*H* 7 to be maintained during the assay period. These results are summarized in Table 2. Again the values of the

Can. J. Chem. Downloaded from www.nrcresearchpress.com by 210.87.254.5 on 09/05/12
For personal use only.

TABLE 2. Rate constants for some dihydropyridine–FMN H-transfer reactions[a]

Donor	Acceptor	k (M^{-1} s^{-1})	$\Delta E_0'$ (mV)[b]
NADH	FMN	0.27 ± 0.02[c] (0.16)[d]	100
2*a*	FMN	20.6 ± 0.7[e]	146
2*b*	FMN	94.9 ± 1.4 (117)[f]	172

[a]The reactions were performed at 25 °C in 0.05 *M* Tris–HCl buffer p*H* 7 as outlined for Table 1. Correlation coefficients were >0.995 for each assay.
[b]$\Delta E_0'$ is the calculated redox potential difference between FMN and the donor at 20 °C (12*b*).
[c]p*H* 6.7.
[d]From ref. 16 at p*H* 6.8, 27 °C.
[e]1.6% EtOH.
[f]From ref. 2*a*, at p*H* 6.7.

second-order rate constants reflect the magnitudes of the respective $\Delta E_0'$ values. H-transfers between dihydropyridines and flavins have been intensively studied (2, 6, 8, 10, 15–19) and the spectral characteristics of the Table 2 reactions were in accord with the process depicted in [2]. Furthermore, it had been established previously that coenzymically-active NAD^+ was produced in the NADH–FMN reaction (12*a*).

Most practical applications of alcohol dehydrogenases involving coenzyme recycling are performed within the p*H* range 7–9. The p*H* dependence of H-transfer reactions of the eq. 1 and 2 types was therefore examined using NADH–**1***d* and NADH–FMN as representative redox couples. The data (Table 3) for both systems show a small decrease in the rates of H-transfer as the p*H* is raised.

Deuterium isotope effects for eq. 1 type H-transfers to NAD^+ were evaluated using the 4,4-dideuterated-1,4-dihydropyridines **2***a*-$[^2H]_2$ and **2***b*-$[^2H]_2$ as representative donors. The results are given in Table 4. The rate constants for deuterium transfer were obtained from the limiting slope of the first-order plots (2*a*) in order to preclude contributions of residual protium transfer to the overall rate. In practice, data from the 25–70% extent of reaction range was used for **2***a*-$[^2H]_2$ (1.92$[^2H]_2$/molecule at C-4) and from the 65–80% range for **2***b*-$[^2H]_2$ (1.65$[^2H]_2$/molecule at C-4). The $k_{[^2H]_2}$ value for the **2***b*-$[^2H]_2$–NAD^+ reaction is an upper limit since a very minor proportion of protium transfer was still evident after 65% reaction.

Discussion

All the pyridinium salts **1** and 1,4-dihydropyridines **2** used were prepared as described previously (12*a*). For the Table 1 reactions, the spectral data required to verify that the products were as expected from an eq. 1 reaction were available for all systems except for those involving the 3-nitro derivatives **1***e–g*. These latter, very electrophilic, compounds were too susceptible to pseudobase formation to permit their evaluation as recycling agents at p*H* 9 (12*a*). Nevertheless, they proved sufficiently stable at p*H* < 6.5 for their performance as H-acceptors to be measured. The 1,4-dihydropyridine products, **2***e*–g, of their reactions with NADH and with **2***b* were isolated in 15–40% yields. The

TABLE 3. Effects of p*H* on H-transfer from NADH[a]

		k (M^{-1} s^{-1})		
Donor	Acceptor	p*H* 7	p*H* 8	p*H* 9
NADH	**1***d*	1.26 ± 0.05	0.71 ± 0.1	0.26 ± 0.02
NADH	FMN	0.27 ± 0.02	0.20 ± 0.01	0.13 ± 0.01

[a]Studies carried out at 25 °C in 0.05 *M* Tris–HCl buffers as described for Table 1.

TABLE 4. Deuterium isotope effects in H-transfers from **2***a* and **2***b* to NAD^+[a]

Donor	Acceptor	$k_{[^2H]_2}$ (M^{-1} s^{-1})	k_H[b]/$k_{[^2H]_2}$
2*a*-$[^2H]_2$	NAD^+	$4.47 \pm 0.24 \times 10^{-3}$[c]	4.8 ± 0.4
2*b*-$[^2H]_2$	NAD^+	$0.13 \pm 0.05 \times 10^{-3}$[d]	4.3 ± 0.4

[a]The kinetics were measured at 25 °C in 0.05 *M* Tris–HCl buffer according to the Table 1 procedure. The data are corrected for hydration of **2***a*,*b*-$[^2H]_2$.
[b]From Tables 1 and 2.
[c]1.6% ethanol.
[d]Calculated by the method of Guggenheim (18) and corrected for the rate of hydration.

Can. J. Chem. Downloaded from www.nrcresearchpress.com by 210.87.254.5 on 09/05/12
For personal use only.

Can. J. Chem. Downloaded from www.nrcresearchpress.com by 210.87.254.5 on 09/05/12
For personal use only.

structure assignments of **2***e*–g were supported by their ir absorptions at ~1678 and ~1608 cm^{-1} (20), their uv maxima of ~430 and ~450 nm in methanol and water respectively,[3] and by the narrow doublets (J = 1.5 Hz) at δ ~ 7.9–8.0 ppm in their nmr spectra (attributed to the unusually strongly deshielded C-2 proton split only by long-range coupling). These data exclude 1,2- but not 1,6-dihydro arrangements. However, in view of the overwhelming evidence for exclusive C-4 H-transfer in such reactions (4, 12*a*, 13, 14), 1,6-dihydro structures cannot be considered serious possibilities.

The susceptibility of each of the 1,4-dihydropyridines of Table 1 towards hydration was evaluated but such side reactions were negligibly slow for all reactants except for **2***a* and **2***b*. The rate constant recorded for **2***a* is of the magnitude expected (2*b*) and the 5-fold difference between the specific rates of hydration of **2***b* in buffer and in water is in accord with the known effect of general acids on this process (2*b*, 22).

Analysis of H-transfer reactions involving FMN was more straightforward. Such reactions have been conclusively shown to be as indicated in [2] and the behavior and spectral characteristics of the Table 2 reactions and products were as expected from the close literature analogies (2, 6, 8, 10, 15–19). Under the aerobic conditions of the assays, the reduced flavin product, FMNH, underwent rapid oxidation (2*a*) and the FMN concentration of the Table 2 reactions thus remained truly constant.

The small, but finite, effects of pH on H-transfer (Table 3) are attributed to the pK_a differences of the various phosphate groups of the reagents (23). The rates of redox reactions of this type are not universally sensitive to pH changes (2*a*).

From Tables 1 and 2 it is seen that the rates of H-transfer parallel the magnitudes of the acceptor–donor redox potential difference.[4] Although this dependence is a qualitative one, it would be unrealistic to expect a more quantitative correlation at this time since some of the $\Delta E_0'$ values are estimates only. Furthermore, structural factors undoubtedly play an important role in some of the Table 2 and 3 reactions. The effects of changes in $\Delta E_0'$ on the specific rates are more dramatic when FMN (Table 2), and not a pyridinium salt (Table 1), is the acceptor. It is recognized that $\Delta E_0'$ differences, being thermodynamic free energy parameters, need not necessarily be reflected in the H-transfer rates. Nevertheless, provided that they are used judiciously within the same reaction series, the current and literature (10*c*, 24, 25) data strongly support their use as guides in formulating redox couples likely to have H-transfer rates high enough to permit efficient NAD/H-regeneration during alcohol dehydrogenase catalyzed oxidoreductions (12*a*).

While the deuterium isotope effect studies of Table 4 were carried out in connection with the preparation of 1-deuterioalcohols via the recycling procedure, the results are relevant to the continuing debate on the mechanisms of dihydropyridine–acceptor H-transfer reactions (1–11). These reactions have been considered to involve formation of an intermediate, possibly charge-transfer, complex as shown in [3] (6, 7) with k_1 usually rate determining. Both $k/k_{[^2H]_2}$ values

$$[3]\quad \text{Donor-H} + \text{Acceptor} \underset{k_{-1}}{\overset{k_1}{\rightleftharpoons}} [\text{Donor-H:Acceptor}] \xrightarrow{k_2} \text{Donor} + \text{Acceptor-H}$$

of Table 4 are very similar but are quite different from those for the reactions of the same donors with, for example, trifluoroacetophenone (1.47 for **2***a*, 1.16 for **2***b* (6)) and *N*-methylacridinium ion (1.46 for **2***b* (7*b*)) and to the 1.75 value observed for the NADH–acetylpyridine–NAD^+ couple (13*b*). On the other hand, the Table 4 isotope effects are of the same order of magnitude as the partition ratios for deuterium transfer from several 1,4-dihydropyridines to various non-flavinoid acceptors (1, 6, 7*b*, 11). These results are in accord either with k_2 (of eq. 3) having become rate determining for the Table 4 reactions (6) or with a mechanism involving direct H-transfer. We attribute this change in the normal rate determining step to the unique structure of the NAD^+ acceptor, which, since it is organized into its own intramolecular complex in solution (26, 27), will either be less inclined to form, or need not form at all, a charge-transfer

[3]These λ_{max} values are at longer wavelengths than for most 1,4-dihydropyridines owing to the presence of the 3-nitro substituent (21).

[4]The limited comparisons which are possible with literature data on other dihydropyridine–pyridinium (13, 14*a*) and –flavin (2*a*) systems are also consistent with this trend.

Can. J. Chem. Downloaded from www.nrcresearchpress.com by 210.87.254.5 on 09/05/12
For personal use only.

complex of the eq. 3 type prior to undergoing reduction. The absence of any significant effect of the *N*-substituents of **2***a*,*b* on the magnitude of $k/k_{[^2H]_2}$ during NAD^+ reduction is consistent with a hydride transfer mechanism (11, 28, 29).

As indicated initially, a major aim of the current study was to ascertain to what extent the H-transfer steps of the reactions of [1] and [2] are rate determining when such systems are used to effect nicotinamide coenzyme recycling on a practical scale. From the rate data of Tables 1 and 2 it is concluded that the H-transfer rate is a major, but not necessarily dominant, factor. The relative rates of reduction of NAD^+ by **2***a*, **2***a*-$[^2H]_2$, and **2***b*, of **1***c*-α and -β by **2***b*, and of **1***d* by NADH are in accord with the relative recycling capabilities of these dihydropyridine and pyridinium compounds (12*a*). Furthermore, for the first 3–4 hours of preparative-scale HLADH-catalyzed oxidation of cyclohexanol (12*b*), the NAD^+-regeneration efficiency of FMN is as calculated for a rate-limiting NADH–FMN reaction. The instability of the enzyme becomes an increasingly important factor as reaction times are extended and, except in the case of the deuterated dihydropyridine reagents, the rates of H-transfer for [1] and [2] systems cease to be preparatively significant when applied to HLADH-catalyzed oxidoreductions taking longer than 24 h.

Experimental

All compounds and materials were obtained as described previously (12).

General Kinetic Procedure

All kinetic studies were carried out under pseudo first-order conditions with the H-donor as the limiting reactant. Reactions were monitored using a Cary 16 instrument equipped with a Varian G2500 chart recorder and a thermostatted cell compartment maintained at 25.0 °C. H-acceptor stock solutions were made up in water or in Tris–HCl buffer of the desired p*H*. Unbuffered aqueous solutions were generally adjusted to p*H* 7.0 before being made up to volume. With the exception of *N*-benzyl-1,4-dihydronicotinamide (**2***a*), which was dissolved in ethanol, H-donor stock solutions were made up in a similar manner but without p*H* adjustment. Most runs were carried out in 1.0 cm pathlength quartz cells using 3.0 ml of acceptor stock solution and 25–200 μl of donor solution. The reference cell was filled with acceptor solution of the same concentration as the final sample cell solution. The sample cell was stoppered immediately after addition of the H-donor, inverted several times to ensure mixing, and then placed in the cell compartment. By this method reliable readings could be obtained within 20 s of initiation of the reaction. In some cases 0.2 or 10.0 cm pathlength cells were used. Assays performed in 10 cm pathlength cells were similarly formulated in the cell with 9.0 ml of H-acceptor stock solution. When 0.2 cm pathlength cells were used, solutions were first mixed in a 10 ml stoppered flask and then an aliquot (*ca.* 0.6 ml) was quickly transferred to the cell. The data obtained after several half-lives were treated by standard first-order regression analysis and the second-order rate constants obtained by dividing each pseudo first-order rate constant by the H-donor concentration. Each run was performed at least in triplicate.

Rates of H-Transfer to Pyridinium Salts

Solutions of the following concentrations were used for all assays except those involving nitropyridinium acceptors. Donors: NADH, $0.4–4.1 \times 10^{-4}$ *M*; **2***a*, $1.6–6.0 \times 10^{-4}$ *M*; **2***b*, $4.0–8.0 \times 10^{-4}$ *M*. Acceptors: NAD^+, $11–26 \times 10^{-3}$ *M*; **1***c*-α and -β, 7.0×10^{-3} *M*; **1***d*, $3.2–7.0 \times 10^{-3}$ *M*. For **1***e*–*f* reactions, the concentrations were: NADH $0.4–2.1 \times 10^{-4}$ *M* and **1***e*–*f*, $0.9–2.4 \times 10^{-3}$ *M*; **2***a*, $3.6–6.2 \times 10^{-6}$ *M* and **1***e*–*f*, $1.5–3.7 \times 10^{-4}$ *M*. Ten centimetre pathlength cells were used for **2***a* – **1***e*–*g* assays; otherwise 1 cm cells were employed throughout. For reactions involving **2***b* as H-donor and NAD^+ and **1***a*–*d* as acceptors, the change in absorption of the H-donor was monitored at 400 nm in order to avoid complications from overlapping absorption of the reduced acceptor product. Although this wavelength was not the absorption maximum, it was established that Beer's law was obeyed in each case. With **1***d* as acceptor, the species monitored was the reduced acceptor and thus infinity readings were necessary. With **2***a* as H-donor the 400 nm absorptions were due to several chromophores and again infinity readings were required. The **2***a*–NAD^+ reaction was assayed at 360 nm. Reactions involving **2***a* were slow and the data analyzed by the method of Guggenheim (18) after determining that the H-transfers were indeed pseudo first-order for three or more half-lives. Where necessary, the observed pseudo first-order rate constant was corrected for the rates of hydration of **2***a* and **2***b*. These were determined by the general kinetic procedure by measuring the rate of disappearance of absorption at 360 nm. A concurrent increase in absorption at the 293 nm λ_{max} of the products was also observed. H-transfers to **1***e*–*g* were followed at 448 nm. (Similar results were obtained by monitoring the absorption changes at 340 nm.) Further details of the assay procedure and of the conditions used for each system are given in Table 1. The effects of p*H* on the NADH–**1***d* reaction (Table 3) were studied in 0.05 *M* Tris–HCl buffers of p*H* 7.0–9.0.

The kinetics of deuterium transfer from **2***a*,*b*-$[^2H]_2$ to NAD^+ were determined in an analogous manner except that the rate constants were calculated from the limiting slope of the first-order plots (**2***a*). Corrections were again made for hydration of **2***a*,*b*-$[^2H]_2$. The results are summarized in Table 4.

The structures of the products of the Table 1 reaction were verified by comparison of their spectra with those of authentic samples of **1***a*–*f* and **2***a*–*d* (12*a*). Also, when NAD^+ was the acceptor, NADH formation was confirmed by the >80% yield of cyclohexanol obtained when a large-scale kinetic run was added to a p*H* 7 solution of cyclohexanone containing HLADH. The

samples of **2***e–f* required to characterize the nitropyridinium salt reduction reactions were prepared as described below.[5]

*N-(2,6-Dichlorobenzyl)-3-nitro-1,4-dihydropyridine (**2***e*)

A solution of *N*-(2,6-dichlorobenzyl)-3-nitropyridinium bromide (**1***e*, 179 mg, 0.49 mmol) and *N*-propyl-1,4-dihydronicotinamide (**2***b*, 83 mg, 0.50 mmol) in p*H* 7.0 buffer (75 ml) was stirred under N_2 for 1 h at 20 °C. The chloroform extract (4 × 75 ml) was slurried with silica gel (7 g), evaporated to dryness, and the silica mixture was dry-packed onto a short dry silica gel column (10 g). Elution with diethyl ether (200 ml) and evaporation yielded a brown solid (73 mg) which was further purified by preparative tlc on 0.5 mm thick silica gel G developed with benzene. The resulting material (40 mg, 29%) was recrystallized from methanol–water (2:1) to give **2***e* as brown needles, mp 185–188 °C; ir ($CHCl_3$) ν_{max} 1680, 1602, 1570, and 1293 cm^{-1}; uv (H_2O containing 1.6% MeOH) λ_{max} 453 nm; (MeOH) 430 nm; (cyclohexane containing 1.6% MeOH) 412 nm; nmr ($C[^2H]Cl_3$) δ 3.47 (m, 2H), 4.82 (s, 2H), 5.20 (m, 2H), 5.97 (d of d, J = 2, 8 Hz, 1H), 7.44 (s plus weaker signals, 4H), 8.00 (d, J = 1.5 Hz, 1H) ppm; mass spectrum m/e 284 ($M^+ - 1$).

*N-(p-Nitrobenzyl)-3-nitro-1,4-dihydropyridine (**2***f*)

N-(*p*-Nitrobenzyl)-3-nitropyridinium bromide (**1***f*; 179 mg, 0.52 mmol) and *N*-propyl-1,4-dihydronicotinamide (**2***b*; 86 mg, 0.52 mmol) were reacted and worked-up as above. The sample of **2***f* (20 mg, 15%) obtained had mp 147–149 °C; ir ($CHCl_3$) ν_{max} 1678, 1608, 1514, 1350, 1311, and 1291 cm^{-1}; uv (H_2O containing 1.6% MeOH) λ_{max} 453 nm; (MeOH) 431 nm; nmr ($C[^2H]Cl_3$) δ 3.50 (m, 2H), 4.60 (s, 2H), 5.25 (m, 1H), 5.80 (d, J = 7.5 Hz, 1H), 7.47 (d, J = 8.5 Hz, 2H), 7.89 (d, J = 1.5 Hz, 1H), 8.30 (d, J = 8.5 Hz, 2H) ppm; mass spectrum m/e 261 (M^+).

*N-Benzoylmethyl-3-nitro-1,4-dihydropyridine (**2***g*)

Treatment of *N*-benzoylmethyl-3-nitropyridinium bromide (**1***g*; 175 mg, 0.54 mmol) and *N*-propyl-1,4-dihydronicotinamide (**2***b*; 91 mg, 0.54 mmol) as above gave **2***g* as an unstable gum (20 mg, 15%); ir ($CHCl_3$) ν_{max} 1700, 1675, 1608, 1350, 1315, and 1290 cm^{-1}; uv (H_2O containing 1.6% MeOH) λ_{max} 448 nm; (MeOH) 431 nm; nmr ($C[^2H]Cl_3$) 3.53 (m, 2H), 4.78 (s, 2H), 5.25 (m, 1H), 5.75 (d, J = 8.0 Hz, 1H), 7.4–8.1 (several signals, large integral) ppm.

Rates of H-Transfer to FMN

The rates of H-transfer to FMN were determined using assay solutions of the following concentrations: donors: NADH, 2.0–4.0 × 10^{-4} M; **2***a*, 2.9–6.0 × 10^{-4} M; **2***b*, 0.4–0.9 × 10^{-4} M; FMN (acceptor) 22–37 × 10^{-4} M (with NADH), 0.3–2.5 × 10^{-4} M (with **2***a* and **2***b*). The NADH, **2***a* and **2***b* reactions were monitored at 340, 355, and 360 nm respectively. All reactions exhibited pseudo first-order kinetics for two or more half-lives of reaction. The results are presented in Table 2. The p*H* dependence of the NADH–FMN H-transfer was studied using 0.05 M Tris–HCl buffers of p*H* 7.0–9.0.

[5]Each of **2***e–f* was too unstable to permit elemental analyses to be obtained. Alternative attempts to prepare **2***e–f* by sodium dithionite reduction of **1***e–f* were unsuccessful.

Acknowledgments

We thank the National Research Council of Canada for financial support of this work and for the award (to K.E.T.) of an NRCC Scholarship for the period 1969–1973.

1. (*a*) D. Mauzerall and F. H. Westheimer. J. Am. Chem. Soc. **77**, 2261 (1955); (*b*) R. H. Abeles, R. F. Hutton, and F. H. Westheimer. J. Am. Chem. Soc. **79**, 712 (1957).
2. (*a*) C. H. Seulter and D. E. Metzler. Biochim. Biophys. Acta, **44**, 23 (1960); (*b*) C. C. Johnson, J. L. Gardner, C. H. Seulter, and D. E. Metzler, Biochemistry, **2**, 689 (1963).
3. D. C. Dittmer and R. A. Fouty. J. Am. Chem. Soc. **86**, 91 (1964).
4. J. Ludoweig and A. Levy. Biochemistry, **3**, 373 (1964).
5. K. A. Schellenberg, G. W. McLean, H. C. Lipton, and P. S. Lietman. J. Am. Chem. Soc. **89**, 1948 (1967).
6. J. J. Steffens and D. M. Chipman. J. Am. Chem. Soc. **93**, 6694 (1971).
7. (*a*) D. J. Creighton and D. S. Sigman. J. Am. Chem. Soc. **93**, 6314 (1971); (*b*) D. J. Creighton, J. Hajdu, G. Mooser, and D. S. Sigman. J. Am. Chem. Soc. **95**, 6855 (1973); (*c*) J. Hajdu and D. S. Sigman. J. Am. Chem. Soc. **97**, 3524 (1975).
8. (*a*) T. C. Bruice, L. Main, S. Smith, and P. Y. Bruice. J. Am. Chem. Soc. **93**, 7327 (1971); (*b*) M. Brustlein and T. C. Bruice. J. Am. Chem. Soc. **94**, 6548 (1972); (*c*) S. Shinkai and T. C. Bruice. J. Am. Chem. Soc. **94**, 8258 (1972); Biochemistry, **12**, 1756 (1973).
9. A. Ohno and N. Kito. Chem. Lett. 369 (1972).
10. (*a*) D. J. T. Porter, G. Blankenhorn, and L. L. Ingraham. Biochem. Biophys. Res. Commun. **52**, 447 (1973); (*b*) G. Blankenhorn. Eur. J. Biochem. **50**, 351 (1975); (*c*) G. Blankenhorn. Biochemistry, **14**, 3172 (1975).
11. L. C. Kurz and C. Frieden. J. Am. Chem. Soc. **97**, 677 (1975).
12. (*a*) K. E. Taylor and J. B. Jones. J. Am. Chem. Soc. **98**. In press, Sept. 1976, and references therein; (*b*) J. B. Jones and K. E. Taylor. Can. J. Chem. This issue.
13. (*a*) M. J. Spiegel, G. R. Drysdale. J. Biol. Chem. **235**, 2498 (1960); (*b*) G. R. Drysdale, M. J. Spiegel, and P. Strittmatter. J. Biol. Chem. **236**, 2323 (1961).
14. (*a*) G. Cilento. Arch. Biochem. Biophys. **88**, 352 (1960); (*b*) G. Cilento and S. Schreier. Arch. Biochem. Biophys. **107**, 102 (1964).
15. T. P. Singer and E. B. Kearney. J. Biol. Chem. **183**, 409 (1950).
16. G. K. Radda and M. Calvin. Biochemistry, **3**, 384 (1964).
17. J. L. Fox and G. Tollin. Biochemistry, **5**, 3865 (1966); **5**, 3873 (1966).
18. E. A. Guggenheim. Philos. Mag. **2**, 538 (1926); *cf.* W. P. Jencks. Catalysis in chemistry and enzymology. McGraw-Hill. New York, N.Y. 1969. p. 562.

Downloaded from www.nrcresearchpress.com by 210.87.254.5 on 09/05/12
For personal use only.

19. N. J. OPPENHEIMER and N. O. KAPLAN. Biochemistry, **13**, 4675 (1974), and references therein.
20. A. LOMBARDO and D. C. DITTMER. Bioorg. Chem. **1**, 400 (1971).
21. T. SEVERIN, H. LERCHE, and D. BÄTZ. Chem. Ber. **102**, 2163 (1969).
22. (*a*) A. G. ANDERSON and G. BERKELHAMER. J. Am. Chem. Soc. **80**, 992 (1958); (*b*) K. S. CHOI and S. G. A. ALIVISATOS. Biochemistry, **7**, 190 (1968); (*c*) C. S. J. KIM and S. CHAYKIN. Biochemistry, **7**, 2339 (1968).
23. W. P. JENCKS. Handbook of Biochemistry. *Edited by* H. A. Sober. Chemical Rubber Co., Cleveland, Ohio. 1968.
24. K. WALLENFELS and M. GELLRICH. Justus Liebig's Ann. Chem. **621**, 149 (1959).
25. A. R. BATTERSBY, J. STAUNTON, and H. R. WILTSHIRE. J. Chem. Soc. Perkin Trans. I, 1156 (1975).
26. D. VOET. J. Am. Chem. Soc. **95**, 3763 (1973).
27. L. J. ARNOLD, JR. and N. O. KAPLAN. J. Biol. Chem. **249**, 652 (1974).
28. C. G. SWAIN, R. A. WILES, and R. F. W. BADER. J. Am. Chem. Soc. **83**, 1945 (1961); C. G. SWAIN, R. F. W. BADER, R. M. ESTEVE, JR., and R. N. GRIFFIN. J. Am. Chem. Soc. **83**, 1951 (1961).
29. J. P. KLINMAN. J. Biol. Chem. **247**, 7977 (1972).

Can. J. Chem. Downloaded from www.nrcresearchpress.com by 210.87.254.5 on 09/05/12
For personal use only.

Pyrolysis of iodobenzene by the toluene carrier technique and determination of $D[C_6H_5-I]$

R. JOHN KOMINAR AND MICHAEL J. KRECH
Chemistry Department, Wilfrid Laurier University, Waterloo, Ont., Canada N2L 3C5

AND

STANLEY JAMES W. PRICE
Chemistry Department, University of Windsor, Windsor, Ont., Canada N9B 3P4

Received April 13, 1976

R. JOHN KOMINAR, MICHAEL J. KRECH, and STANLEY JAMES W. PRICE. Can. J. Chem. **54**, 2981 (1976).

The pyrolysis of C_6H_5I has been studied by the toluene carrier technique over the temperature range 861–955 K using contact times of 0.54–3.28 s and total pressures of 2.5–4.13 kPa. Percent decomposition based on analysis for residual C_6H_5I ranged from 5.6–93.3%. Only trace quantities of I_2 were observed and when HI was trapped out the only other gaseous products were small quantities of hydrogen and methane in about a 2:1 ratio. Within the limits of the experimental method the decomposition was found to be homogeneous and first order.

[1] $$C_6H_5I \rightarrow C_6H_5 + I$$

The Arrhenius equation obtained for reaction 1 is

$$\log k_1\,(s^{-1}) = (15.0 \pm 0.28) - \frac{269\,600 \pm 4\,800}{19.15\,T}$$

Making an approximate correction of the activation energy to 298 K then gives

$$D[C_6H_5—I] = 266.3 \pm 4.8\ \text{kJ mol}^{-1}$$

R. JOHN KOMINAR, MICHAEL J. KRECH et STANLEY JAMES W. PRICE. Can. J. Chem. **54**, 2981 (1976).

La pyrolyse de C_6H_5I a été étudiée à l'aide de la technique du toluène comme gaz porteur sur un écart de température de 861 à 955 K utilisant des temps de contact de 0.54 à 3.28 s et des pressions totales de 2.5 à 4.13 kPa. Le pourcentage de décomposition basé sur l'analyse du C_6H_6I résiduel s'échelonnait de 5.6 à 93.3%. Des quantités de I_2 à l'état de trace seulement furent observées et quand HI fut éliminé par piégeage les seuls autres produits gazeux observés n'étaient que des petites quantités d'hydrogène et de méthane dans un rapport d'environ 2:1. En considérant les limites de la méthode expérimentale, la décomposition fut trouvée homogène et de premier ordre.

[1] $$C_6H_5I \rightarrow C_6H_6 + I$$

L'équation d'Arrhénius obtenue pour la réaction 1 est:

$$\log k_1\,(s^{-1}) = (15.0 \pm 0.28) - \frac{269\,600 \pm 4\,800}{19.15\,T}$$

En faisant une correction approximative de l'énergie d'activation à 298 K on obtient

$$D[C_6H_5—I] = 266.3 \pm 4.8\ \text{kJ mol}^{-1}$$

[Traduit par le journal]

Introduction

A recent paper by two of the present authors on the pyrolysis of C_6F_5I by the toluene carrier technique (1) gave $D[C_6F_5—I] = 277$ kJ mol^{-1}. Previously Szwarc (2) had reported a value of $D[C_6H_5—I]$ of the order of 239 kJ mol^{-1}, indicating that $D[C_6F_5—I]$ was significantly larger than $D[C_6H_5—I]$. However, from a study of the reaction

$$I + C_6H_5I \rightleftharpoons C_6H_5 + I_2$$

Rodgers *et al.* (3) obtained $D[C_6H_5—I] = 272$ kJ mol^{-1}. This result leads to $\Delta H_{f298}^0(C_6H_5, g) = 328.4$ kJ mol^{-1}, a value close to the recently recommended value of 325.1 kJ mol^{-1} (4). The present study was undertaken in an attempt to resolve the discrepancy between the earlier toluene carrier study and the more recent equilibrium work.

Can. J. Chem. Downloaded from www.nrcresearchpress.com by 210.87.254.6 on 09/05/12
For personal use only.

TABLE 1. Selected experimental results for the toluene carrier flow system pyrolysis of iodobenzene

T^* (K)	P (kPa)	t_c (s)	Decomposition (%)	Benzene (mol × 10^4)	Toluene / C_6H_5I molar ratio	k_1 (s^{-1})
954	3.53	1.39	88.4	6.67 (92%)†	153	1.57
953	3.51	1.52	88.3	5.76 (83%)	122	1.41
939p	3.96	1.37	69.1	4.01 (77%)	71	0.858
936p	3.85	1.34	67.7	4.51 (79%)	69	0.844
935	3.95	2.23	81.2	5.86 (92%)	97	0.751
906	3.95	2.33	45.3	—	118	0.260
899	3.95	2.29	39.1	2.23 (77%)	136	0.217
897p	3.91	1.55	27.7	2.07 (79%)	59	0.209
883	3.93	2.66	23.2	1.32 (87%)	104	0.100
873p	3.77	1.49	11.1	0.50 (73%)	50	0.079
866	3.75	2.68	13.5	0.74 (84%)	102	0.059

*p denotes runs in packed reaction vessel, surface-to-volume ratio 17 times that in the unpacked vessel.
†Percent of C_2H_5 released that is found as C_6H_6.

Experimental

Materials

(a) Iodobenzene

The iodobenzene used was obtained from Eastman Kodak, Eastman Organic #152. Analysis by gas chromatography (6 ft Apiezon L on 80–100 mesh chromosorb W, N_2 carrier, 30 cc/min, isothermal for 4 min at 100 °C and temperature programmed from 100–200 °C at 32°/min showed only traces of minor impurities estimated at a maximum of 0.01% of the sample.

(b) Benzene

Analar grade benzene from British Drug House was similarly tested by gas chromatography and the minor impurities were estimated at a maximum of 0.01% of the sample.

(c) Toluene

Toluene from sulfonic acid (Eastman Organic X325) was prepared for use by refluxing over sodium under vacuum and then degassing by bulb-to-bulb distillation.

Apparatus and Procedures

The basic toluene carrier system has been previously described (5). The system was modified to the extent that the quantity of C_6H_5I required for a run was injected via a gas-tight syringe through a silicone rubber septum. It was then subjected to controlled evaporation into the toluene carrier stream. Care was taken to be sure that all parts of the system where C_6H_5I was handled were mercury-free. Pressures were taken by a differential manometer after the C_6H_5I had been removed from the system while only toluene was flowing. The reaction vessel was treated with hot fuming nitric acid before use. Residual acid was baked out under vacuum after the vessel was installed in the system.

Toluene, unreacted C_6H_5I and condensable (at −80 °C) products were collected, sealed in airtight amber-colored sample bottles with Teflon lined tops and analyzed for C_6H_5I and C_6H_6 by gas chromatography (conditions as described under Materials (*a*)).

Results and Discussion

Selected experimental results are given in Table 1 and the Arrhenius plot for the decomposition of C_6H_5I is shown in Fig. 1. The results may be discussed in terms of the following mechanism

[1] $$C_6H_5I \rightarrow C_6H_5 + I$$

[2] $$I + C_6H_5CH_3 \rightarrow C_6H_5CH_2 + HI$$

[3] $$C_6H_5 + C_6H_5CH_3 \rightarrow C_6H_6 + C_6H_5CH_2$$

[4] $$2\,C_6H_5CH_2 \rightarrow \text{dibenzyl}$$

[5] $$2\,C_6H_5 \rightarrow \text{diphenyl}$$

[6] $$C_6H_5 + C_6H_5CH_2 \rightarrow \text{diphenyl methane}$$

Only traces of I_2 were detected. These presumably were formed by reaction 7

[7] $$2I + M \rightarrow I_2 + M$$

in the exit tube of the flow reactor. Since the gas collecting system was not mercury-free no attempt was made to quantitatively determine HI. Large quantities were formed and the characteristic yellow solid Hg_2I_2 was observed when the liquid nitrogen trap was removed and the HI was brought to room temperature in the presence of mercury.

The only other gaseous products observed were hydrogen and methane which were found in about a 2:1 ratio (hydrogen 68 ± 2%, methane 32 ± 2%). The quantities found ranged from about 1×10^{-5} to 1×10^{-4} mol with consistently higher yields for a fixed set of experi-

Can. J. Chem. Downloaded from www.nrcresearchpress.com by 210.87.254.6 on 09/05/12
For personal use only.

Can. J. Chem. Downloaded from www.nrcresearchpress.com by 210.87.254.6 on 09/05/12
For personal use only.

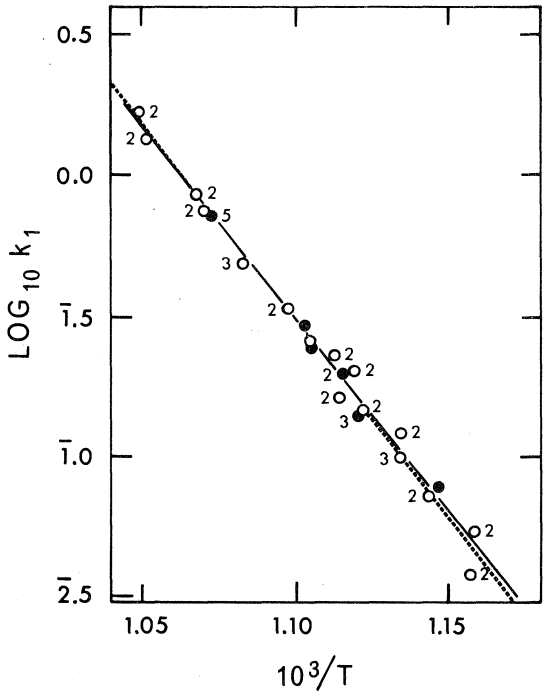

FIG. 1. Arrhenius plot for the decomposition of iodobenzene. Open circles, ○, represent unpacked vessel runs. Full circles, ●, represent packed vessel runs. Numbers beside points indicate the number of experiments averaged to obtain plotted point. Dashed line is the visual line of best fit (see text).

TABLE 2. Tests of the effect of C_6H_5I concentration on k_1

T (K)	Iodobenzene concentration (mol cm^{-3} × 10^9)	k_1 (s^{-1})
899	18.3	0.213
	3.9	0.217
	3.5	0.231
	2.0	0.232
893	19.1	0.149
	7.6	0.142
	7.4	0.150
	7.2	0.144
	6.8	0.179
	3.3	0.162

mental conditions when the packed vessel was used. This is consistent with the slight, predominantly heterogeneous, pyrolysis of toluene expected (6).

The quantitative yield of $H_2 + CH_4$ was, however, up to several times that expected in a conditioned vessel. Runs with toluene alone confirmed the literature data so that it must be inferred that either C_6H_5I or products of its pyrolysis caused a temporary modification of the surface that enhanced the toluene decomposition.

It is also possible that the reaction sequence

[8] $$2HI + M \rightarrow H_2I + I + M$$

[9] $$H_2I + M \rightarrow H_2 + I + M$$

plays a minor role. But formation of any significant quantities of H_2 by reaction 9 would seem to be ruled out by the fact that the observed H_2/CH_4 ratio is nearly identical to that observed in the pyrolysis of toluene (6).

The benzene yields in Table 1 are total amounts but the percentage figures in parentheses are based on the benzene yield from reaction 3, which based on the reaction sequence

[10] $$H + C_6H_5CH_3 \rightarrow C_6H_6 + CH_3$$

[11] $$CH_3 + C_6H_5CH_3 \rightarrow CH_4 + C_6H_5CH_2$$

is presumed to be equal to the total moles benzene minus moles CH_4. In general this correction is somewhat less than 10%. As shown by the percentage figures in parentheses in Table 1 reaction 3 is therefore the major process by which C_6H_5 is removed. Approximately 80% of the remaining C_6H_5 is removed by reaction 5, the residual being found as diphenyl methane.

Reactions 12 and 13

[12] $$H + C_6H_5I \rightarrow HI + C_6H_5$$

[13] $$CH_3 + C_6H_5I \rightarrow CH_3I + C_6H_5$$

which would affect the calculated values of k_1 have been ruled out on two counts. First, values of k_1 are invariant as the toluene/C_6H_5I ratio is changed over a wide range. Secondly, no CH_3I was observed. These reactions, however, might be significant at toluene/C_6H_5I ratios below those used in the present work.

Values of k_1 have been calculated from the usual first-order expression using percent decomposition based on the moles C_6H_5I used and the amount recovered. As shown in Table 2 values of k_1 determined in this way show no significant variation when the C_6H_5I concentration is varied over a range of up to a factor of nine.

Least-squares analysis of the data in Fig. 1 gives

$$\log k_1\,(s^{-1}) = (14.43 \pm 0.28) - \frac{260\,200 \pm 4\,800}{19.15\,T}$$

However, as observed previously in the case of C_6F_5I (1), the least-squares line may not be the best representation of the data. A visual line of best fit (the dashed line in Fig. 1) gives an activation energy of 269.6 kJ mol^{-1} and an A factor of $10^{15.0}$. The fact that this A factor leads to $A_{-1} = 10^{9.7}\ M^{-1}\ s^{-1}$, as opposed to $A_{-1} = 10^{9.1}\ M^{-1}\ s^{-1}$ when the unweighted least-mean-squares treatment is used, seems to suggest that the 'line of best fit' result is to be preferred. On this basis

$$\log k_1\,(s^{-1}) = (15.0 \pm 0.28) - \frac{269\,600 \pm 4\,800}{19.15\,T}$$

Approximate correction of the activation energy to 298 K then gives $D[C_6H_5—I] = 266.3 \pm 4.8$ kJ mol^{-1}. This is considerably higher than the previous toluene carrier result (2) and is in very good agreement with the value of 272 kJ mol^{-1} obtained from the work of Rodgers *et al.*

It would still appear that $D[C_6F_5—I]$ is somewhat larger than $D[C_6H_5—I]$ although the difference is much less than in the case of other C_6F_5X and C_6H_5X compounds (7).

Acknowledgements

This work has been supported in part by the National Research Council of Canada. Two of the authors (R.J.K. and M.J.K.) are also indebted to Wilfrid Laurier University for summer research support. The authors wish to thank Mr. C. Langford for his assistance in computer processing of the experimental data.

1. M. J. Krech, S. J. W. Price, and W. F. Yared. Int. J. Chem. Kinet. **6**, 257 (1974).
2. M. Szwarc. Chem. Rev. **47**, 75 (1950).
3. A. S. Rodgers, D. M. Golden, and S. W. Benson. J. Am. Chem. Soc. **89**, 4578 (1967).
4. G. A. Chamberlain and E. Whittle. Trans. Faraday Soc. **67**, 2077 (1971).
5. M. Krech and S. J. W. Price. Can. J. Chem. **41**, 224 (1963).
6. S. J. W. Price. Can. J. Chem. **40**, 1310 (1962).
7. S. J. W. Price and H. J. Sapiano. Can. J. Chem. **52**, 4109 (1974).

Can. J. Chem. Downloaded from www.nrcresearchpress.com by 210.87.254.6 on 09/05/12
For personal use only.

A reinterpretation of beta, gamma, and delta substituent effects on ^{13}C chemical shifts

HELMUT BEIERBECK AND JOHN K. SAUNDERS
Département de chimie, Université de Sherbrooke, Sherbrooke, P.Q., Canada J1K 2R1

Received January 26, 1976

HELMUT BEIERBECK and JOHN K. SAUNDERS. Can. J. Chem. **54**, 2985 (1976).

It is shown that β-, γ-, and δ-substituent effects on ^{13}C chemical shifts may be better understood by assuming that the upfield shifts caused by *gauche* γ-substituents are not due to nonbonded interactions introduced with the γ-group, but that they are due to the removal of the hydrogen on the β-substituent.

HELMUT BEIERBECK et JOHN K. SAUNDERS. Can. J. Chem. **54**, 2985 (1976).

Il est montré que les effets de substituants β, γ et δ sur les déplacements chimiques du ^{13}C seraient mieux compris en supposant que les déplacements vers les champs forts, causés par des substituants γ *gauches*, ne sont pas dus à des interactions entre atomes non-liées introduites avec le groupement en γ mais sont dus à l'enlèvement de l'hydrogène sur le substituant en β.

[Traduit par le journal]

The upfield shift associated with the introduction of a *gauche* γ-substituent is one of the most useful diagnostic effects in ^{13}C nmr spectroscopy. This upfield shift has been attributed to nonbonded interactions between the hydrogens on the carbon in question and on the γ-substituent (1, 2). However, this interpretation is not very satisfactory, since upfield shifts are also observed if the γ-group does not bear any hydrogen. For example, chlorine shields a *gauche* γ-carbon to the same extent as a methyl group (3).

We were led to a reexamination of *gauche* γ-substituent effects by a report (4) that *syn*-axial δ-substituents cause downfield shifts. If it is accepted that nonbonded hydrogen–hydrogen interactions are the cause of the shielding effect of the γ-group, the observed δ-substituent effect must be considered a δ − γ shift, since a γ-interaction has been displaced by the δ-group (5, 6). The δ-substituent effect itself would then become an upfield shift. Like the δ-shift, the γ-substituent effect is formally the result of two steps, namely removal of a hydrogen from the β-carbon and addition of the γ-group, and the possibility must be considered that both steps contribute to the γ-shift. In order to estimate the contribution of β-hydrogen elimination to the *gauche* γ-effect one must know the role of that hydrogen in the β-substituent effect. It has been shown (6, 7) that the prediction of β-substituent shifts may be based on additivity parameters associated with *gauche* interactions of the β-group X with hydrogen, HX, and carbon, CX (or the more general parameters $2 \times HX \times \cos\phi$ and $2 \times CX \times \cos\phi$, if the dihedral angle ϕ differs from 60°). Consider the stepwise introduction of a β-methyl group, X = C, and a *gauche* γ-methyl group in scheme A → B → C. The second *gauche* interaction is not specified, since only the result of the HC *gauche* interaction between the H-°C hydrogen and the H_β hydrogen of the β-methyl group is pertinent to the argument that follows. Order-of-magnitude values of 5 ppm are given for the β-shift A → B and the *gauche* γ-shift B → C, since only general trends are to be analyzed. The actual numerical values were 4.73 and −4.50 ppm, respectively (7). The chemical shift changes that occur in steps A → B → C may be interpreted in at least two different ways.

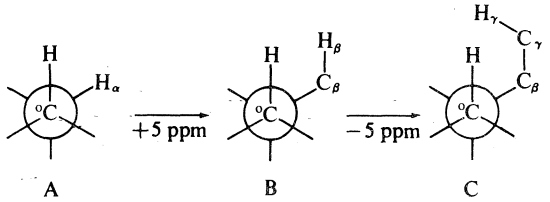

Possibility 1: The introduction of a β-carbon has a deshielding effect regardless of the nature of the attached γ-group, *i.e.* both step A → B and step A → C introduce a 5 ppm downfield shift. In addition the presence of a nonbonded γ-interaction in configuration C causes a −5 ppm upfield shift. According to this interpretation the chemical shift difference B → C is entirely due

Can. J. Chem. Downloaded from www.nrcresearchpress.com by 210.87.254.42 on 09/05/12
For personal use only.

TABLE 1. ^{13}C chemical shifts in ketoandrostanes[a,b]

Item	Ketone	C No.	δ(C=O)	δ(CH)	Sub.	Pred.	B-type	Double bond	Type	Configuration
				Substituent effect at the γ-position						
1	**11**	19	11.9	12.4	−0.5	0	0	0	P	
2	**2**	19	12.4	12.4	0.0	0	0	0	P	
3	**4**	19	13.8	12.4	1.4	0	0	0	P	
4	**6**	19	13.0	12.3	0.7	0	0	0	P	
5	**11**	18	18.1	17.7	0.4	0	0	0	P	
6	**15**	18	18.3	17.7	0.6	0	0	0	P	
7	**16**	18	18.1	17.7	0.4	0	0	0	P	
				Substituent effect at the β-position						
8	**1**	9	49.8	55.1	−5.3	−5	−5	0	T	*syn*
9	**4**	6	20.5	29.1	−8.6	−10	−10	0	S	*syn*
10	**6**	4	26.1	34.5	−8.4	−10	−10	0	S	*syn*
11	**7**	14	50.5	54.8	−4.3	−5	−5	0	T	*syn*
12	**11**	10	35.8	36.4	−0.6	0	0	0	Q	*syn*
13	**12**	17	31.9	40.6	−8.7	−10	−10	0	S	*syn*
14	**15**	8	32.5	36.0	−3.5	−5	−5	0	T	*syn*
15	**17**	12	31.7	39.0	−7.4	−10	−10	0	S	*syn*
16	**1**	19	12.3	12.4	−0.1	0	−5	5	P	*anti*
17	**12**	18	17.7	17.7	0.0	0	−5	5	P	*anti*
18	**17**	18	13.8	17.7	3.9	0	−5	5	P	*anti*
19	**1**	3	28.1	26.8	1.3	0	−5	5	S	*anti*
20	**1**	5	47.2	47.2	0.0	0	−5	5	T	*anti*
21	**2**	4	29.1	29.1	0.0	0	−5	5	S	*anti*
22	**2**	10	40.5	36.4	4.1	5	0	5	Q	*anti*
23	**3**	1	38.7	38.8	−0.1	0	−5	5	S	*anti*
24	**3**	5	46.9	47.2	−0.3	0	−5	5	T	*anti*
25	**4**	2	22.7	22.2	0.5	0	−5	5	S	*anti*
26	**4**	10	42.7	36.4	6.3	5	0	5	Q	*anti*
27	**6**	8	37.9	35.7	2.2	0	−5	5	T	*anti*
28	**6**	10	40.9	36.4	4.5	5	0	5	Q	*anti*
29	**7**	5	47.2	47.2	0.0	0	−5	5	T	*anti*
30	**7**	9	56.6	54.8	1.8	0	−5	5	T	*anti*
31	**11**	8	37.3	35.7	1.8	0	−5	5	T	*anti*
32	**11**	13	44.8	40.9	3.9	5	0	5	Q	*anti*
33	**12**	9	56.4	54.8	1.6	0	−5	5	T	*anti*
34	**12**	14	54.6	54.8	−0.2	0	−5	5	T	*anti*
35	**15**	13	39.2	40.9	−1.7	5	0	5	Q	*anti*
36	**15**	17	35.2	40.6	−5.4	0	−5	5	S	*anti*
37	**16**	13	39.2	40.9	−1.7	5	0	5	Q	*anti*
38	**16**	14	51.9	54.8	−2.9	0	−5	5	T	*anti*
39	**17**	14	51.6	54.8	−3.2	0	−5	5	T	*anti*
40	**17**	15	21.8	25.6	−3.8	0	−5	5	S	*anti*

[a]The 6-ketone is 6-ketocholestanyl acetate. The chemical shifts for 3, 4, 15, 16, and 17-ketoandrostane were taken from ref. 15; the remaining data are unpublished results from this laboratory.

[b]Column headings: δ(C=O), chemical shifts in the ketones. δ(CH), chemical shifts in the corresponding hydrocarbons. These are the A- and B-ring resonances in 17 β-hydroxyandrostane and the C- and D-ring resonances of 3 β-hydroxyandrostane (15). The cholesteryl acetate resonances of ref. 16, as quoted in ref. 1, were used in the case of the 6-ketone. Sub., Substituent effect of the carbonyl group. Pred., The predicted substituent shift is the sum of contributions from the elimination of 1,3-diaxial hydrogen interactions and double bond shielding effects. B-type, the shielding effect due to the elimination of B-type interactions. Double bond, the double bond substituent effect. Type, P = primary, S = secondary, T = tertiary, Q = quaternary.

to the presence of the $H–H_\gamma$ interaction in C, and the removal of the β-hydrogen in B is of no consequence. There is no overall change in chemical shift in step A → C, because upfield and downfield shifts cancel each other.

Possibility 2: The introduction of a β-carbon gives rise to a 5 ppm downfield shift only if it introduces a 1,3-diaxial hydrogen interaction, *i.e.* only in step A → B, but not in step A → C. According to this interpretation the chemical shift difference B → C is entirely due to the removal of the β-hydrogen in B, and the presence of the nonbonded γ-interaction in C is of no consequence. There is no change in chemical

Can. J. Chem. Downloaded from www.nrcresearchpress.com by 210.87.254.42 on 09/05/12
For personal use only.

TABLE 2. ^{13}C chemical shifts in some steroidal olefins[a,b,c]

Item	Olefin	Hydrocarbon	C No.	δ(C=C)	δ(CH)	Sub.	Pred.	B-type	Double bond	Type	Configuration
				Substituent effect of γ,δ double bonds							
41	**11**	**14**	18	10.5	11.3	−0.8	0	0	0	P	
42	**8**	**12**	18	12.1	12.3	−0.2	0	0	0	P	
				Substituent effect of β,γ double bonds							
43	**8**	**7**	10	37.5	37.0	0.5	0	0	0	Q	*syn*
44	**9**	**7**	10	35.5	37.0	−1.5	0	0	0	Q	*syn*
45	**11**	**14**	13	41.3	43.2	−1.9	0	0	0	Q	*syn*
46	**7**	**12**	8	32.5	36.0	−3.5	−5	−5	0	T	*syn*
47	**7**	**12**	9	50.7	54.9	−4.2	−5	−5	0	T	*syn*
48	**8**	**7**	15	23.3	24.9	−1.6	−5	−5	0	S	*syn*
49	**9**	**7**	1	34.3	37.6	−3.3	−5	−5	0	S	*syn*
50	**10**	**13**	1	35.0	38.7	−3.7	−5	−5	0	S	*syn*
51	**11**	**14**	1	33.8	36.1	−2.3	−5	−5	0	S	*syn*
52	**11**	**14**	14	47.6	51.1	−3.5	−5	−5	0	T	*syn*
53	**7**	**12**	19	19.6	12.3	7.3	5	0	5	P	*anti*
54	**10**	**13**	19	17.3	11.5	5.8	5	0	5	P	*anti*
55	**11**	**14**	19	26.1	17.3	8.8	5	0	5	P	*anti*
56	**8**	**12**	19	16.3	12.3	4.0	5	0	5	P	*anti*
57	**9**	**12**	19	18.9	12.3	6.6	5	0	5	P	*anti*
58	**8**	**7**	13	43.3	42.8	0.5	5	0	5	Q	*anti*
59	**7**	**12**	1	37.6	37.2	0.4	0	−5	5	S	*anti*
60	**7**	**12**	3	74.0	73.5	0.5	0	−5	5	T	*anti*
61	**8**	**7**	11	21.4	21.6	−0.2	0	−5	5	S	*anti*
62	**10**	**13**	7	31.2	32.2	−1.0	0	−5	5	S	*anti*
63	**10**	**13**	9	54.4	54.2	0.2	0	−5	5	T	*anti*
64	**11**	**14**	7	31.7	32.2	−0.5	0	−5	5	S	*anti*

[a]The chemical shifts for substrates **7**, **8**, **9**, **10**, **12**, and **14** were taken from ref. 16, as quoted in ref. 1. The resonance values for **11** are unpublished data from this laboratory, and those for substrate **13** were taken from ref. 15.

[b]Column headings: see Table 1.

[c]Structures:

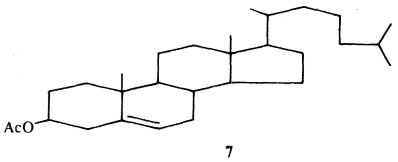

7

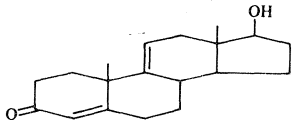

11

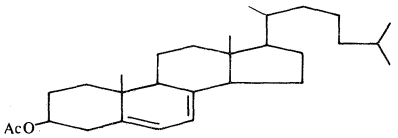

8

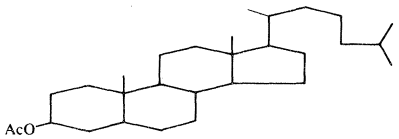

12

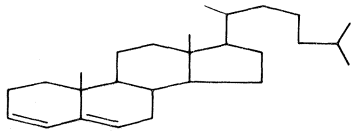

9

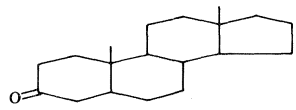

13

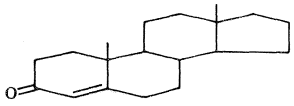

10

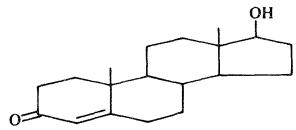

14

Can. J. Chem. Downloaded from www.nrcresearchpress.com by 210.87.254.42 on 09/05/12
For personal use only.

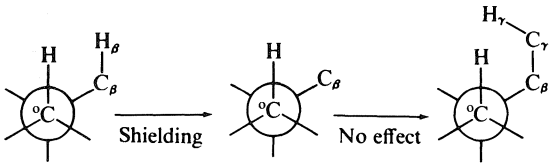

shift in step A → C, since the introduction of the β- and γ-carbons causes neither upfield nor downfield shifts. In this interpretation the hypothesis of steric shielding in configuration C is unnecessary.

In order to decide whether the removal of the β-hydrogen or the addition of the γ-carbon (or γ-heteroatom) are responsible for the γ-shift, or whether both steps contribute, we have studied situations in which a β-hydrogen is eliminated from configuration B, or a γ-hydrogen from configuration C, without replacement by another substituent. The results of these studies led us to conclude that it is indeed hydrogen elimination from B, rather than hydrogen–hydrogen interaction in C, which is responsible for the upfield shift in step B → C. In other words, it appears that the hydrogen on the β-substituent determines the magnitude of the β-substituent shift, and that the often involved steric γ-shift does not exist.

Results

This conclusion is supported by several observations.

(*i*) Elimination of γ-*gauche* hydrogens by C=C or C=O double bond formation does not alter the chemical shifts at the γ-position, whereas the substituent effect of C=C and C=O double bonds at the β-position depends on the number of eliminated 1,3-diaxial hydrogen interactions.

(*ii*) The number of hydrogens on a heteroatom has little influence on its *gauche* γ-substituent effect, but the shielding effect of β-heterosubstituents shows a dependence on inductive σ^* constants if the varying number of H—X bonds is taken into consideration.

(*iii*) Bond rotation to eliminate the 1,3-diaxial hydrogen alignment in configuration B has the same effect as removal of the β-hydrogen from B.

In addition to the shift increments associated with the introduction or elimination of the hydrogen–hydrogen interaction in configuration B, double bond shielding effects and polar shift contributions by heterosubstituents have to be taken into consideration. Again, only the order of magnitude of these parameters is given, since only general shielding trends are to be rationalized. There are not always enough experimental data available to derive reliable average values, and the role of conformational effects is difficult to assess. For instance, substituent effects in the steroidal D-ring do not always correspond to those in the rest of the molecule.

Elimination of the Gauche γ-Hydrogen by Double Bond Formation

The effect of γ-hydrogen elimination in configuration C is illustrated by the methyl group resonances in steroidal ketones and olefins. The γ-hydrogen may be removed either by β,γ or by γ,δ double bond formation. Items 1–7 in Table 1

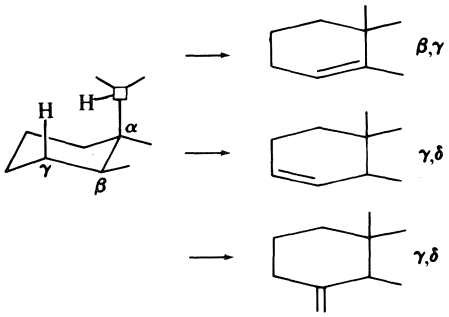

and items 41, 42 in Table 2 show that removal of the *gauche* γ-hydrogen by γ,δ double bond formation has no significant influence on the methyl carbon resonances. The olefinic β,γ double bond, on the other hand, causes a downfield shift of the order of 5 ppm (items 53–57, Table 2). It will be shown in the next section that this displacement is associated with the introduction of the double bond, and not with the removal of the γ-hydrogen.

Elimination of the 1,3-Diaxial β-Hydrogen by Double Bond Formation

The effect of β-hydrogen elimination in configuration B is illustrated by ring carbon resonances in steroidal ketones and olefins. Whereas the double bond substituent effect at the γ-position was insignificant, its effect at the β-position can no longer be neglected. The β-carbon may be *syn* or *anti* with respect to the double bond. In endocyclic olefins the two *anti* positions are not strictly equivalent, but the substituent effects show the same trends at both *anti* positions.

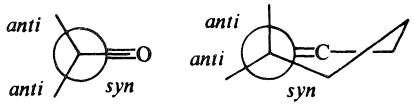

Can. J. Chem. Downloaded from www.nrcresearchpress.com by 210.87.254.42 on 09/05/12
For personal use only.

The double bond substituent shift is directly observed at quaternary carbons, since in these cases β-hydrogen elimination does not remove 1,3-diaxial hydrogen interactions. Items 8, 9, and 12 in Table 1 illustrate the result of introducing a *syn* β,γ carbonyl group. There is essentially no *syn* carbonyl shift. The upfield shifts of −5.3 and −8.6 ppm reflect the removal of one and two 1,3-diaxial hydrogen interactions, respectively.

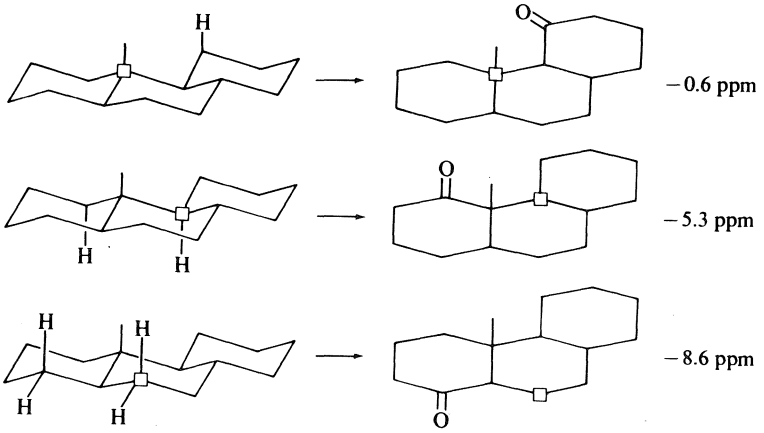

Items 25 and 26 illustrate the *anti* β,γ carbonyl shift of 5 ppm, and the cancelling effect of elimination of a 1,3-diaxial hydrogen interaction.

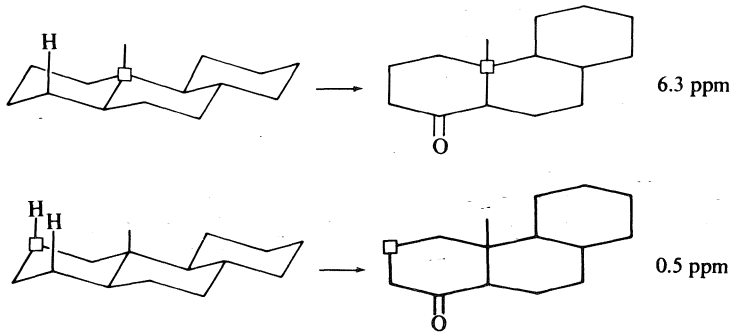

The β-carbon resonances in the olefin series do not follow this scheme quite as well, presumably because of conformational effects associated with the formation of the endocyclic double bond. Item 43 indicates that there is essentially no *syn* β,γ olefin shift, which agrees with the *syn* β,γ carbonyl substituent effect. Item 46 illustrates the superimposed effect of β-hydrogen elimination.

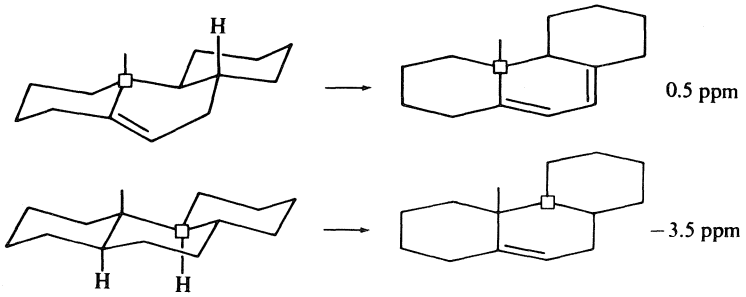

By analogy to the *anti* β,γ carbonyl shift an *anti* olefin shift of 5 ppm might be expected. The only available example of a quaternary *anti* β-carbon, item 58, does not show the expected 5 ppm down-

Can. J. Chem. Downloaded from www.nrcresearchpress.com by 210.87.254.42 on 09/05/12
For personal use only.

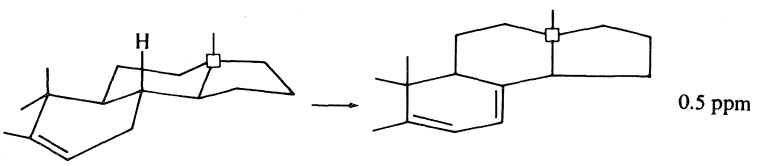

field shift. However, there is indirect evidence that quaternary *anti* carbons are deshielded relative to quaternary *syn* carbons. Consider the three isomeric pimaradienes **1–3** (8). The step from the

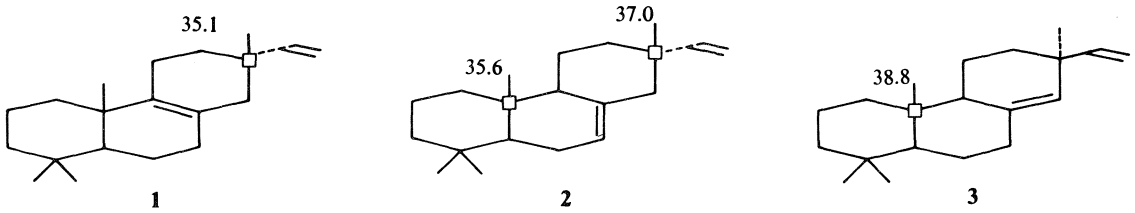

$\Delta^{8,9}$ to the Δ^{7} olefin constitutes a *syn* → *anti* change for C(13), and results in a 1.9 ppm downfield shift. The Δ^{7} and $\Delta^{8,14}$ olefins give a *syn* → *anti* displacement of 3.2 ppm for C(10).

Primary, secondary, and tertiary *anti* β-carbons show substituent effects which are consistent with a 5 ppm double bond shift. For example, item 61 illustrates the result of a 5 ppm olefin

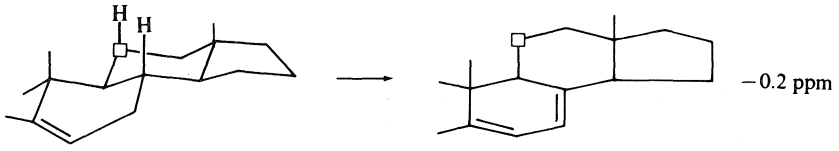

shift and a −5 ppm upfield shift caused by β-hydrogen elimination. A more convincing demonstration of the 5 ppm *anti* olefin shift is provided by steroidal methyl groups. In this case no 1,3-diaxial hydrogen interaction is eliminated and the double bond effect is directly observed.

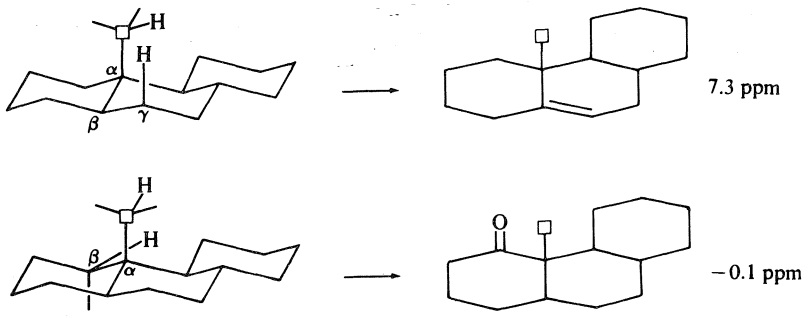

Item 53 may serve as example. This example also illustrates the different effects of *anti* β,γ C=C and C=O groups on angular methyl carbons. The endocyclic C=C bond replaces a C—C bond and only eliminates a γ-hydrogen. The carbonyl group, on the other hand, replaces a C—H bond and therefore eliminates one 1,3-diaxial interaction. Thus, formation of the Δ^{5} double bond (item 53) only shows the double bond shift, whereas formation of the β-ketone (item 16) causes cancelling shift increments due to introduction of the C=O bond and removal of the β-hydrogen.

Variation of the Number of γ-Hydrogens on Gauche γ-Heterosubstituents

An extension of these ideas to heterosubstituents is complicated by the presence of additional shielding contributions due to the polar nature of the C—X bonds and by the uncertainty regarding the orientation of the H—X bonds. Nevertheless, it is quite clear from the *gauche*

Can. J. Chem. Downloaded from www.nrcresearchpress.com by 210.87.254.42 on 09/05/12
For personal use only.

Can. J. Chem. Downloaded from www.nrcresearchpress.com by 210.87.254.42 on 09/05/12
For personal use only.

γ-shifts in 2-substituted adamantanes (9) that there is no relation between the *gauche* γ-shift and the number of γ-hydrogens.

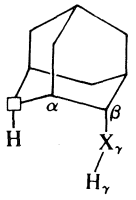

X	δ(X)
F	−6.29
Cl	−6.90
Br	−6.28
I	−4.83
NH_2	−7.03
OH	−6.73
CH_3	−6.48
CN	−4.56
CO_2H	−4.24

Variation of the Number of β-Hydrogens on β-Heterosubstituents

The β-heterosubstituent effects are seen from a new and interesting perspective if the contributions of the β-hydrogens are taken into consideration. It has been shown (10) that antiperiplanar γ-substituent shifts in 1-adamantyl derivatives correlate approximately with inductive σ^* constants, whereas the β-substituent shifts are rather insensitive to the nature of the β-substituent. This is illustrated in Figs. 1 and 2 for the substituents CH_3, NH_2, OH, Cl, and Br. A correlation between β-substituent shifts and the inductive σ^* constants emerges, however, as soon as the varying number of 1,3-diaxial hydrogen interactions is taken into account. Consider the simplifying assumption that every B-type hydrogen–hydrogen interaction makes the same deshielding contribution, whether the γ-hydrogen is on a carbon, nitrogen, or oxygen atom. With the substituents NH_2 and OH this alignment is $\frac{2}{3}$ and $\frac{1}{3}$ as probable as with the CH_3 group. The contributions of hydrogen interactions to the

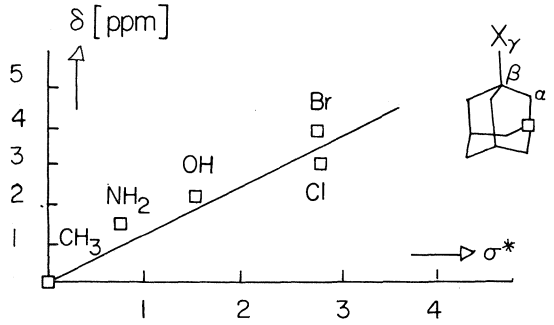

FIG. 1. Chemical shifts of *anti* γ-carbons in a series of 1-adamantyl derivatives, plotted against inductive σ^* constants. Chemical shifts and σ^* constants were taken from ref. 10.

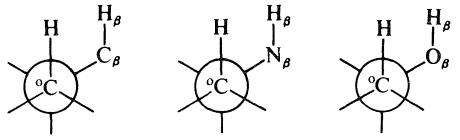

β-shifts of NH_2 and OH groups may therefore be taken to be equal to $\frac{2}{3}$ and $\frac{1}{3}$ of the observed β-methyl substituent shift. The remaining portion of the observed β-effect is then taken to be the polar shielding contribution. The observed substituent effect of the halogens is attributed entirely to the polarity of the C—X bond, since they do not bear any hydrogens. If the β-substituent shifts are plotted after correction for contributions from 1,3-diaxial hydrogen interactions, an approximate σ^* dependence emerges (Fig. 2). While these considerations are not meant as derivations of the polar shift contributions, they offer a simple explanation for the apparent lack of relations between bond polarity and observed β-substituent effects.

Elimination of 1,3-Diaxial Hydrogen Interactions by Bond Rotation

The role of the β-hydrogen may also be tested by bond rotation and elimination of the hydrogen alignment in B, rather than by elimination of the β-hydrogen itself. Molecular deformation would be expected to decrease the efficiency of this deshielding mechanism and result in upfield shifts. For instance, any deviation from the cyclohexane chain form, such as ring flattening, as the result of replacing a methylene group by a heteroatom would cause rotation about the

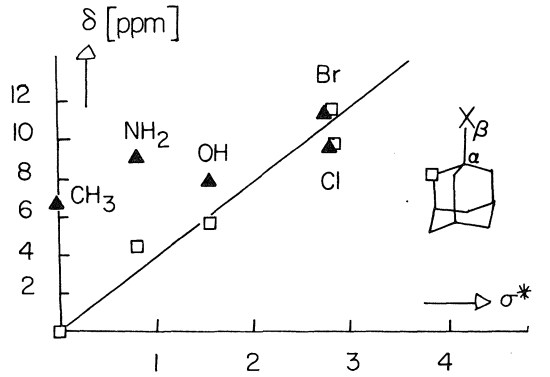

FIG. 2. Chemical shifts of the β-carbons in a series of 1-adamantyl derivatives, plotted against inductive σ^* constants. ▲: observed β-shifts, □: β-shifts corrected for contributions by 1,3-diaxial hydrogen–hydrogen interactions. Chemical shifts and values for the σ^* constants were taken from ref. 10.

carbon–carbon bond adjacent to the heteroatom, and render these hydrogen–hydrogen interactions less effective. This hypothesis provides a

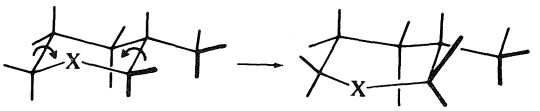

simple explanation for the rather large upfield shifts observed for antiperiplanar γ-carbons in some heterocyclic systems, compared to their cyclohexane analogues (11, 12). Consider, for instance, the three 1,3-dioxane derivatives **4**–**6**.

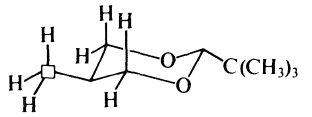

4

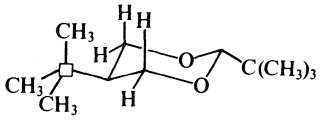

5

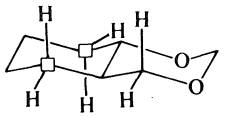

6

The methyl protons in **4** are involved in four B-type interactions which would account for a total downfield shift of *ca.* 20 ppm in the chair form. Rotation about bonds C(4)—C(5) and C(6)—C(5) affects all four B-interactions and readily explains the observed methylcyclohexane–methyldioxane shift difference of −10.9 ppm. The antiperiplanar carbon in derivative **5**, on the other hand, is quaternary and no significant conformational effect on its resonance is expected, since no B-type interactions are present. The two hydrogens on C(5) of *trans*-decalin and its oxygenated derivative **6** are involved in two B-interactions with the hydrogens of C(4). The corresponding deshielding increment of *ca.* 10 ppm may again be partially or completely eliminated by conformational changes in the oxygenated ring. C(8), on the other hand, does not have B-type interactions with the oxygenated ring and its resonance would therefore be expected to be relatively insensitive to conformational effects. It should also be mentioned here that smaller upfield shifts, of the order of −2 ppm, caused by antiperiplanar heteroatoms are quite common. We shall return to this point in the Discussion section.

The effect of bond rotation and partial elimination of shift contributions from B-type interactions may also be observed in hydrocarbons. For example, the resonance of C(8) in steroids was predicted (7) to be 41.6 ppm, but found at 35.7 ppm. The simplest explanation for this discrepancy is the presence of the 5-membered D-ring, and particularly the lack of alignment of the C(8)—H(8) and C(15)—H(15β) bonds, which renders this interaction ineffective and eliminates a 5 ppm deshielding increment.

Discussion

To summarize, the hypothesis that the *gauche* γ-substituent shift is the result of removal of the β-hydrogen, rather than the introduction of steric interactions with the γ-group, is supported by these observations.

(*i*) A γ-group does not have to carry hydrogens in order to cause the usual upfield *gauche* γ-substituent shift, *e.g.* chlorine causes the same displacement as a methyl group.

(*ii*) The elimination of the hydrogen on the β-group, on the other hand, has a pronounced effect on the β-substituent shift. In addition, it is only after consideration of the varying number of hydrogens on a β-group, that a correlation between β-substituent shifts and bond polarity emerges.

(*iii*) Finally, the importance of the hydrogens on the β-substituent is demonstrated by the observation that elimination of the 1,3-diaxial hydrogen alignment by bond rotation has the same effect as hydrogen elimination.

It must be emphasized that only empirical correlations between structural features and carbon resonances are attempted here, and that no interpretation of underlying shielding mechanisms can be given at this time. However, these empirical correlations have some interesting implications for proton nmr spectroscopy and conformational analysis.

According to the present interpretation of β-carbon substituent effects the two 1,3-diaxial hydrogen interactions contribute *ca.* 2 × 5 ppm to the carbon resonance in cyclohexane. If 1,3-diaxial hydrogen interactions shift carbon resonances downfield, it is reasonable to assume that

Can. J. Chem. Downloaded from www.nrcresearchpress.com by 210.87.254.42 on 09/05/12
For personal use only.

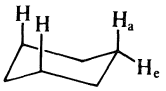

they shift the hydrogen resonances upfield. The axial hydrogens in cyclohexane are engaged in two such interactions, whereas the equatorial hydrogen has none. It is therefore quite likely that the 1,3-diaxial hydrogen alignment contributes to the H_a–H_e shift difference. Thus, the new interpretation of β-substituent shifts in ^{13}C nmr spectroscopy offers at least a partial explanation for the experimental analogies between carbon and hydrogen resonances (17).

A recent reinterpretation of the factors governing equatorial–axial equilibria in cyclohexane derivatives (13) provides an interesting comparison with our view on *gauche* γ-substituent effects. It was suggested that the equatorial cyclohexane derivative predominates, because the ring hydrogen prefers the axial position, and not because the substituent prefers the equatorial orientation (13). It is the equatorial position which is more crowded, and the axial substituent is in the less hindered position. If steric interactions with the axial γ-substituent are not particularly severe, the presence or absence of hydrogens on the *gauche* γ-substituent is not expected to influence carbon resonances significantly. It will be shown at the end of this section that antiperiplanar γ-shifts support the view that equatorial substituents are subject to more severe interactions.

The reinterpretation of the γ-substituent effect leads to the following β-, γ-, and δ-parameters.

β-Parameters—The parameters describing the β-substituent shifts in structures with dihedral angles of 60° are denoted by HX and CX (6, 7). The more general parameters $2 \times HX \times \cos\phi$ and $2 \times CX \times \cos\phi$ are approximately valid for any dihedral angle ϕ (6). It is principally the definition of the HX parameter which changes. Consider first the β-carbon substituent effect, X = C. The parameter HC now specifically denotes a shift increment associated with a β-carbon introducing a 1,3-diaxial hydrogen–hydrogen interaction, whereas before it indicated the displacement caused by any β-carbon, regardless of the nature of the groups attached to it. The exocyclic CC parameter is presumably a shift increment caused by conformational effects related to the presence of exocyclic carbon–carbon interactions. The interpretation of the β-heterosubstituent parameters HX and CX is complicated by the presence of polar shielding effects and the uncertainty regarding the orientation of the H—X bonds. If the polar shift contribution is not considered explicitly, it must be contained in HX and CX. In this case an HX parameter is required even if the β-heteroatom does not introduce 1,3-diaxial hydrogen interactions. There are then two different sets of HX/CX parameters required, depending on whether or not a given heteroatom has an H—X bond in configuration B. For example, a description of the β-nitrogen shift in piperidines and quinolizidines would be expected to give two different sets of HN/CN parameters. Even in the absence of B-type interactions it might be difficult to define the nature of polar shift contributions and to identify additional factors like shift increments associated with carbon–heteroatom *gauche* interactions. Consider, for instance, the possibility that the β-shift consists of a combination of an angle-independent term β, such as an inductive effect, and an angle-dependent term like an electric field effect. The constant β is readily incorporated into the angular terms, and the β-shift would appear to be described adequately by the angular terms alone. For example, the expression

$$\beta(X) = 2 \times HX \times \cos\phi_1 + 2 \times CX \times \cos\phi_2$$

is nearly equivalent to

$$\beta'(X) = (2 \times HX - \beta) \times \cos\phi_1 + (2 \times CX - \beta) \times \cos\phi_2 + \beta$$

since the sum $(\phi_1 + \phi_2)$ is always close to 120° and the sum $(\cos\phi_1 + \cos\phi_2)$ does not vary greatly with ϕ_1 and ϕ_2. Even if it should prove impossible to sort out the various β-shift contributions this would not affect the validity of the empirical parameters for predictive purposes.

γ-Parameters—The principal effect of introducing a *gauche* γ-substituent is the elimination of an HX interaction. However, the observed γ-shift is somewhat larger than the replaced HX increment and a *gauche* γ(X) parameter may still be required. For example, the *gauche* γ-hydroxyl shift, about −6.5 ppm, is nearly 2 ppm larger than the HC parameter (6). The new *gauche* γ-parameters now signify differences between the observed γ-shifts and the removed HX β-shift increments.

Can. J. Chem. Downloaded from www.nrcresearchpress.com by 210.87.254.42 on 09/05/12
For personal use only.

Can. J. Chem. Downloaded from www.nrcresearchpress.com by 210.87.254.42 on 09/05/12
For personal use only.

As mentioned in the Results section, *anti* γ-heterosubstituents generally also cause upfield shifts, of the order of -2 ppm. This was recently demonstrated with a large number of examples and it was noted that the only exceptions to that rule appear to be the downfield shifts observed for bridgehead substituents (12). However, the fact that upfield *anti* γ-shifts are observed far more often than downfield shifts is highly misleading. All examples of antiperiplanar shielding in ref. 12 occurred in structural units characterized by an equatorial substituent on a six-membered ring. One is therefore essentially comparing only two structural features giving rise to shift increments of opposite sign, namely equatorial substituents on six-membered rings causing upfield shifts and bridgehead substituents leading to downfield shifts. These two

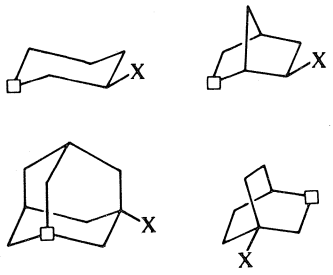

cases must be given equal weight, regardless of the number of ways in which the structural arrangements may be generated. The important difference between the two cases is the possibility of conformational distortions in equatorially substituted rings which is not possible with bridgehead substituents, for reasons of symmetry. In the first case one would therefore expect a combination of conformational and substituent effects, whereas in the second case the *anti* γ-substituent shift itself should be observed. This is borne out firstly by the approximate σ^* dependence of the *anti* γ-shifts in 1-adamantyl derivatives, shown in Fig. 1 (10). Secondly, antiperiplanar γ-shifts involving axial substituents also show downfield shifts. For instance, the methyl carbon in 9-methyldecalin is deshielded by the 1α-hydroxyl group (4), and C(19) in cortisol is deshielded by 9α-halogens (14). This is in agreement with the suggestion (13) that an equatorial substituent is more crowded than an axial group. The observation (12) that γ-halogens do not cause noticeable

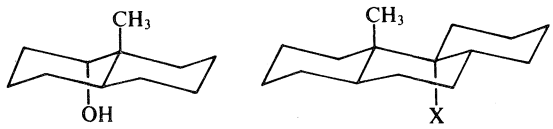

0.4 ppm

X = F 0.8 ppm
Cl 2.1 ppm
Br 2.4 ppm

displacements in situations where oxygen or nitrogen give rise to upfield shifts of the order of -2 ppm also finds a simple explanation. The resonances of the antiperiplanar carbons in 1-adamantyl chloride or bromide occur about 2 ppm to lower field than in the corresponding hydroxyl derivative, in accordance with a σ^* dependence (Fig. 2). If halogens cause conformational changes similar to the hydroxyl group, they would be expected to shift the *anti* γ-carbon resonances 2 ppm to lower field than antiperiplanar oxygen.

While it is clear that there is an antiperiplanar γ-heterosubstituent shift, the choice of an *anti* γ-parameter is difficult, since shielding increments would be required for most predictive purposes, whereas only deshielding increments seem to have a physical basis.

δ-Parameters—Introduction of a *syn*-axial δ-substituent shifts the carbon resonance to lower field. Based on the hypothesis of nonbonded *gauche* γ-interactions this observed displacement had to be considered a δ(X)–γ(C) shift, and δ(X) itself a shielding parameter (5, 6). If it is assumed, on the other hand, that the *gauche* γ-shift has nothing to do with nonbonded interactions involving hydrogens on the γ-substituent, the observed *syn*-axial δ-shift itself is the δ(X) parameter, *i.e.* δ(X) is now deshielding. Whereas previously the γ-shift was larger than the δ-effect, the more severe δ-interaction now seems to be the only steric interaction that needs to be considered. It appears therefore at the moment that steric interactions are deshielding, rather than shielding as was believed previously.

1. J. B. STOTHERS. Carbon-13 NMR spectroscopy. Academic Press, New York. 1972.
2. D. M. GRANT and B. V. CHENEY. J. Am. Chem. Soc. **89**, 5315 (1967).
3. O. A. SUBBOTIN and N. M. SERGEYEV. J. Am. Chem. Soc. **97**, 1080 (1975).
4. S. H. GROVER and J. B. STOTHERS. Can. J. Chem. **52**, 870 (1974).
5. J. G. BATCHELOR. J. Magn. Reson. **18**, 212 (1975).

6. H. BEIERBECK and J. K. SAUNDERS. Can. J. Chem. **54**, 632 (1976).
7. H. BEIERBECK and J. K. SAUNDERS. Can. J. Chem. **53**, 1307 (1975).
8. E. WENKERT and B. L. BUCKWALTER. J. Am. Chem. Soc. **94**, 4367 (1972).
9. G. E. MACIEL, H. C. DORN, R. L. GREENE, W. A. KLESCHICK, M. R. PETERSON, JR., and G. H. WAHL, JR. Org. Magn. Reson. **6**, 178 (1974).
10. T. PEHK, E. LIPPMAA, V. V. SEVOSTJANOVA, M. M. KRAYUSHKIN, and A. I. TARASOVA. Org. Magn. Reson. **3**, 783 (1971).
11. A. J. JONES, E. L. ELIEL, D. M. GRANT, M. C. KNOEBER, and W. F. BAILEY. J. Am. Chem. Soc. **93**, 4772 (1971).
12. E. L. ELIEL, W. F. BAILEY, L. D. KOPP, R. L. WILLER, D. M. GRANT, R. BERTRAND, K. A. CHRISTENSEN, D. K. DALLING, M. W. DUCH, E. WENKERT, F. M. SCHELL, and D. W. COCHRAN. J. Am. Chem. Soc. **97**, 322 (1975).
13. D. H. WERTZ and N. L. ALLINGER. Tetrahedron, **30**, 1579 (1974).
14. D. D. GIANNINI, P. A. KOLLMAN, N. S. BHACCA, and M. E. WOLFF. J. Am. Chem. Soc. **96**, 5462 (1974).
15. J. W. APSIMON, H. BEIERBECK, and J. K. SAUNDERS. Can. J. Chem. **51**, 3874 (1973).
16. H. J. REICH, M. JAUTELAT, M. T. MESSE, F. J. WEIGERT, and J. D. ROBERTS. J. Am. Chem. Soc. **91**, 7445 (1969).
17. E. L. ELIEL, V. S. RAO, F. W. VIERHAPPER, and G. ZUNIGA JUARISTI. Tetrahedron Lett. 4339 (1975).

Can. J. Chem. Downloaded from www.nrcresearchpress.com by 210.87.254.42 on 09/05/12
For personal use only.

Etude des phénomènes de redistribution des groupements monofonctionnels -R, -F, -Cl, -Br, -I, -SCN sur des atomes de bore tricoordonnés

JEAN-PIERRE COSTES, GERARD CROS ET JEAN-PIERRE LAURENT
Laboratoire de Chimie de Coordination du CNRS, B.P. 4142-31030 Toulouse Cedex, France

Reçu le 4 mars 1976

JEAN-PIERRE COSTES, GERARD CROS et JEAN-PIERRE LAURENT. Can. J. Chem. **54**, 2996 (1976).

L'étude par résonance magnétique nucléaire (^{11}B et ^{1}H) des réactions de redistribution entre trihalogénures de bore BX_3 (X = I, Br, Cl, F) et trialkylbore BR_3 (R = C_3H_7, C_4H_9) a permis de montrer qu'à l'équilibre les espèces mixtes sont diversement favorisées. L'influence du caractère acide de Lewis des trihalogénures et des effets stériques sont discutées.

JEAN-PIERRE COSTES, GERARD CROS, and JEAN-PIERRE LAURENT. Can. J. Chem. **54**, 2996 (1976).

A study by ^{11}B and ^{1}H nmr of the scrambling reactions between the boron trihalides BX_3 (X = I, Br, Cl, F) and the trialkylborane BR_3 (R = C_3H_7, C_4H_9) shows that the mixed species, on equilibrium are non uniformly favoured. The effects of Lewis acidity and steric hindrance are discussed.

Dans le domaine de la chimie du bore que nous nous proposons d'aborder, celui des redistributions dans les systèmes BR_3/BX_3, les données expérimentales disponibles (1, 2) présentent un caractère essentiellement qualitatif traduisant les possibilités d'obtention des espèces mixtes $BR_{3-i}X_i$(i = 1 ou 2) à partir des espèces symétriques. Elles ont néanmoins l'avantage de mettre en relief les différences d'aspect revétu par ces réactions suivant la nature de l'halogène (-X) ou même du reste alkylé (-R) et suivant les conditions de leur mise en oeuvre.

Au cours de ce travail nous nous proposons de donner une description quantitative des processus de redistribution dans les systèmes BR_3/BX_3 (R désignant un reste alkylé tel que C_3H_7,[1] C_4H_9[1] et X un halogène ou un pseudohalogène F, Cl, Br, I, SCN).

Cette étude prolonge directement celles que nous avons réalisées des systèmes $B(NMe_2)_3$/-$B(OMe)_3$ (3), $B(NMe_2)_3/B(SMe)_3$ (4), BPr_3/B_2O_3 (5) et BPr_3/BY_3 avec Y = NMe_2, SMe, OMe (6) et destinées à préciser la nature des facteurs intervenant dans ces processus.

Partie expérimentale

Les trihalogénures (BF_3, BCl_3 et BBr_3) ont été purifiés soit par condensation, soit par distillation. Les préparations de BI_3 (7) et de $BuBF_2$ (8) ont été décrites par ailleurs. Les trialkylbore ont été obtenus à l'aide du processus de Johnson *et al.* (9) légèrement modifié (5). Le trinéopentylbore a été préparé et isolé suivant la méthode décrite par McCusker et coll. (10). L'action du thiocyanate d'argent rigoureusement anhydre sur le tribromure de bore au sein du chlorure de méthylène a permis d'obtenir le triisothiocyanate de bore avec un rendement voisin de 80%.

La réalisation des mélanges destinés aux mesures a été effectuée par pesée directe des constituants introduits successivement dans les tubes de rmn en atmosphère d'argon. Les tubes scellés ont été maintenus à une température de 120 °C pendant une semaine, des expériences préliminaires ont en effet montré qu'à cette température l'état d'équilibre est atteint en 4 jours.

L'étude repose essentiellement sur la considération des spectres de résonance des noyaux ^{11}B car l'utilisation des spectres de résonance ^{1}H se heurte en effet à plusieurs difficultés: complexité des spectres de résonance protonique des restes alkylés lourds, grande volatilité de certains composés fluorés et phénomènes d'échange rapide en présence de radicaux méthylés.

Suivant la procédure déjà décrite (3, 6) la composition initiale d'un mélange est représentée par le paramètre $R = [X]/[B]_{total}$, [X] désignant la concentration en groupement halogéné (F, Cl, Br, I ou SCN) et $[B]_{total}$ la concentration totale en bore. Les concentrations (C_r) des différentes espèces $BR_{3-i}X_i$ présentes à l'équilibre sont obtenues par intégration des pics de résonance (^{11}B) correspondants. Elles permettent de calculer les constantes $(K_i)_R$ (i = 1 ou 2) caractérisant les équilibres:

$$2BR_{3-i}X_i \rightleftarrows BR_{3-i+1}X_{i-1} + BR_{3-i-1}X_{i+1}$$

puis les deux constantes $(K_{i_1})_R = 1/(K_1^2K_2)$ et $(K_{1_2})_R = 1/(K_1K_2^2)$ qui se rapportent aux équilibres:

$$iBR_3 + (3 - i)BX_3 \rightleftarrows 3BR_iX_{3-i}$$

Il est possible, ainsi, d'atteindre la variation d'enthalpie libre caractérisant la formation des espèces mixtes:

$$(\Delta G_i)_R = -\frac{RT}{n}\log (K_{i_i})_R$$

[1]Remplacés par Pr et Bu dans le texte.

TABLEAU 1. Caractéristiques rmn (^{11}B, ^{19}F) des composés R_nBX_{3-n}

R	X		BX_3	RBX_2	R_2BX	R_3B
Pr	Cl	$\delta^{11}B$(ppm)*	46.5	62.3	77.2	87.5
Pr	Br		39.4	62.5	78.8	87.5
Pr	I		−7.1	50.5	79.1	87.5
Pr	SCN		4.0	39.5	64.0	87.5
Bu	F	$\delta^{11}B$(ppm)*	11.6	28.2	59.0	87.0
		$\delta^{19}F$(ppm)†	—	3.3	46.0	—
		J_{B-F}(Hz)	—	80	116	—

*$\delta^{11}B$ = 0 ppm pour Et_2OBF_3 (étalon externe).
†$\delta^{19}F$ = 0 ppm pour CF_3COOH (étalon externe).

Suivant l'usage (11), nous comparerons les résultats caractérisant les systèmes réels à ceux d'un système idéal dans lequel les redistributions de substituants monofonctionnels (−R et −X) sur des centres trifonctionnels (−B<) s'effectuent au hasard et pour lequel:

$$(K_1)_S = (K_2)_S = 0.33$$

$$(K_{t_1})_S = (K_{t_2})_S = 27$$

On admet généralement (12) que les variations d'entropie sont identiques dans le système réel et dans le système statistique, ce qui conduit à la relation:

$$(\Delta H_t)_R = -\frac{RT}{n}\log\frac{(K_t)_R}{(K_t)_S}$$

Comme pour le modèle statistique ΔH égale zéro, ces variations d'enthalpies sont une manière de chiffrer l'écart à la non additivité des énergies de liaison ainsi que l'importance des modifications de structure électronique subies par ces mêmes liaisons au cours du processus d'échange.

Les systèmes pour lesquels les espèces mixtes sont favorisées présentent les paramètres caractéristiques suivants:

$$\Delta H > 0 \quad K_t < 0.33 \quad K_t > 27$$

Les spectres de résonance ont été obtenus à l'aide d'un spectrographe Perkin-Elmer R-10 opérant à 19.25 MHz. Les déplacements chimiques exprimés en ppm sont repérés par rapport à un étalon externe de $Et_2O\cdot BF_3$. La détermination de l'aire des pics de résonance a été effectuée à l'aide d'un analyseur de courbes Dupont de Nemours.

La plupart des espèces BR_tX_{3-t} se caractérisent en résonance de ^{11}B par un pic unique. Seuls les composés BRF_2 et BR_2F présentent des spectres plus complexes par suite de l'intervention du couplage B–F. Les valeurs des déplacements $\delta^{11}B$ relatifs aux différents composés $BR_{3-t}X_t$ sont rassemblées dans le tableau 1. On doit noter ici la très faible différence de déplacement existant, d'une façon générale, entre les composés BR_2X et BR_3 se traduisant par un certain recouvrement des pics de résonance qui, dans le cas du système BPr_3/BI_3, ne nous a pas permis de distinguer l'espèce Pr_2BI de l'espèce Pr_3B.

Résultats

Système BPr_3/BBr_3 (tableau 2A)

La faible valeur de K_2 implique que l'espèce dihalogénée est nettement favorisée par rapport au modèle statistique, l'espèce monohalogénée l'étant un peu moins. Quoiqu'il en soit on doit souligner les possibilités offertes par les réactions de redistribution au point de vue synthèse: en négligeant les facteurs cinétiques, les réactions de redistribution permettent d'obtenir les composés $BPrBr_2$ et BPr_2Br avec des rendements voisins de 85%.

Système BPr_3/BI_3 (tableau 2B)

Il apparaît que la concentration (C_r) du terme diodé BRI_2 est nettement plus importante que celle (C_s) qui résulterait d'une redistribution au hasard ce qui conduit à une constante $K_2 = (6.1 \pm 1.0) \times 10^{-3}$. Comme nous l'avons déjà noté, il est plus délicat d'évaluer les concentrations de l'espèce monoiodée par suite du recouvrement de son signal avec celui de l'espèce trialkylée (BPr_3). L'examen du spectre (fig. 1*A*) d'un mélange de composition initiale $R = [I]/[B]_{total} \simeq 1$ montre que l'espèce monosubstituée ($\delta^{11}B \simeq 75$ ppm) est prédominante comme l'est l'espèce disubstituée dans un mélange $R \simeq 2$ (fig. 1*B*); dans ces conditions nous pensons pouvoir attribuer à la constante K_1 une valeur très voisine de celle de K_2 c'est-à-dire de l'ordre de 10^{-3}.

Système BPr_3/BCl_3 (tableau 2C)

Contrairement à ce qui a été observé pour les deux systèmes précédents, les espèces mixtes se caractérisent par des constantes K_i nettement différentes. L'espèce monochlorée présente donc une plus grande stabilité que l'espèce dichlorée ce qui confirme les observations faites en cours de préparation de ces composés (13).

Système BBu_3/BF_3 (tableau 2D)

Compte tenu de la grande volatilité des espèces BF_3 (péb = −100 °C) et $BPrF_2$ (péb =

TABLEAU 2. Composition des mélanges BR_3/BX_3 chauffés à 120 °C

(*A*) BPr_3/BBr_3*

R	BPr_3 (%)	Pr_2BBr (%)	$PrBBr_2$ (%)	BBr_3 (%)
0.70	29.7	68.7	1.6	—
0.72	29.1	68.9	2.0	—
0.87	16.3	79.9	3.8	—
1.02	8.0	81.8	10.2	—
1.30	—	60.0	40.0	—
1.85	—	9.1	87.1	3.8
2.01	—	4.0	87.8	8.2
2.30	—	—	63.0	27.0
2.60	—	—	40.0	60.0

*$K_1 = (1.1 \pm 0.1) \times 10^{-2}$; $K_2 = (4.4 \pm 0.2) \times 10^{-3}$. Système BMe_3/BBr_3 $K_1 = (1.2 \pm 0.8) \times 10^{-2}$ (analysé en rmn ^1H).

(*B*) BPr_3/BI_3*

R	BPr_3 (%)	Pr_2BI (%)	$PrBI_2$ (%)	BI_3 (%)
1.40	—	54.0	46.0	—
1.75	—	21.5	77.0	1.5
1.85	—	15.5	82.0	2.5
1.93	—	10.5	84.5	5.0
2.16	—	—	77.5	22.5
2.30	—	—	64.0	36.0

*($K_1 \simeq 10^{-3}$) (valeur estimée); $K_2 = (6.0 \pm 1.0) \times 10^{-3}$.

(*C*) BPr_3/BCl_3*

R	BPr_3 (%)	Pr_2BCl (%)	$PrBCl_2$ (%)	BCl_3 (%)
0.85	20.0	78.0	2.0	—
0.92	9.5	89.5	1.0	—
1.04	1.0	90.5	8.5	—
1.31	—	58.0	38.5	3.5
1.40	—	52.5	47.5	—
1.83	—	18.0	71.0	11.0
2.12	—	12.5	62.5	25.0
2.42	—	11.5	45.0	43.5

*$K_1 = (3 \pm 2) \times 10^{-3}$; $K_2 = (1.3 \pm 0.7) \times 10^{-1}$.

(*D*) $BBu_3/BuBF_2$*

R	BBu_3 (%)	Bu_2BF (%)	$BuBF_2$ (%)
0.86	33.2	48.1	18.7
1.15	16.4	50.6	33.0
1.20	16.0	48.2	35.8
1.22	14.8	47.9	37.3
1.50	—	36.3	63.7
1.80	—	24.2	75.8
1.92	—	9.5	90.5

*$K_1 = (2.5 \pm 0.5) \times 10^{-1}$; ($K_2 = 10^{-3}$) (valeur estimée).

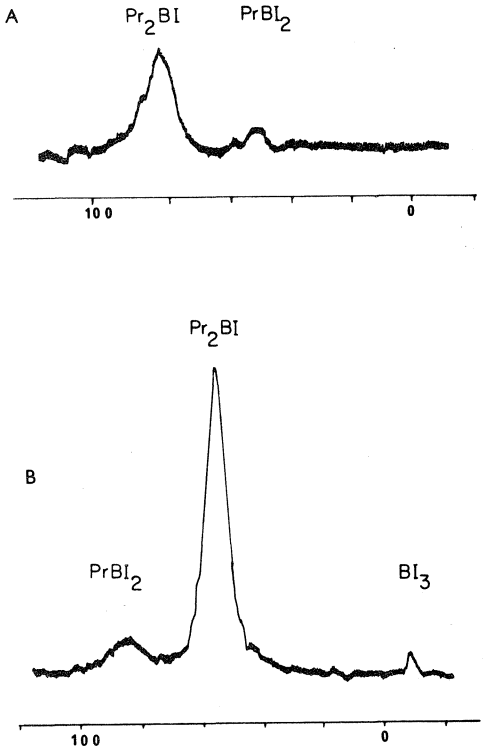

FIG. 1. Système BPr_3/BI_3: rmn ^{11}B (*A*) $R = 1.15$ à l'équilibre à 120 °C; (*B*) $R = 1.83$ à l'équilibre à 120 °C.

10 °C) nous avons été amenés à utiliser des composés présentant des restes alkylés relativement lourds (R = Bu) et à borner notre étude au domaine $R = [F]/[B]_{total}$ compris entre 0 et 2. En fait nous avons envisagé le système $BBu_3/BBuF_2$.

La caractéristique la plus importante de ce système réside dans la forte valeur de la constante K_1, beaucoup plus importante que celles qui ont été obtenues pour les autres systèmes BR_3/BX_3. Ainsi pour le mélange $R = [F]/[B]_{total} = 1.15$: l'espèce monofluorée BBu_2F n'entre que pour 50% dans la composition du mélange à l'équilibre alors que, dans les mêmes conditions, les concentrations des espèces BR_2Cl, BR_2Br ou BR_2I atteignent 80 à 90%.

En examinant la composition à l'équilibre d'un mélange $R = 1.92$, on constate que la concentration en $BBuF_2$ est de dix fois supérieure à celle de BBu_2F; on se trouve donc dans une situation extrêmement voisine de celles observées dans les systèmes BPr_3/BBr_3 et BPr_3/BI_3 pour $R \simeq 2$ et qui accordaient à K_2 une valeur de l'ordre de 5×10^{-3}. Cette valeur que nous

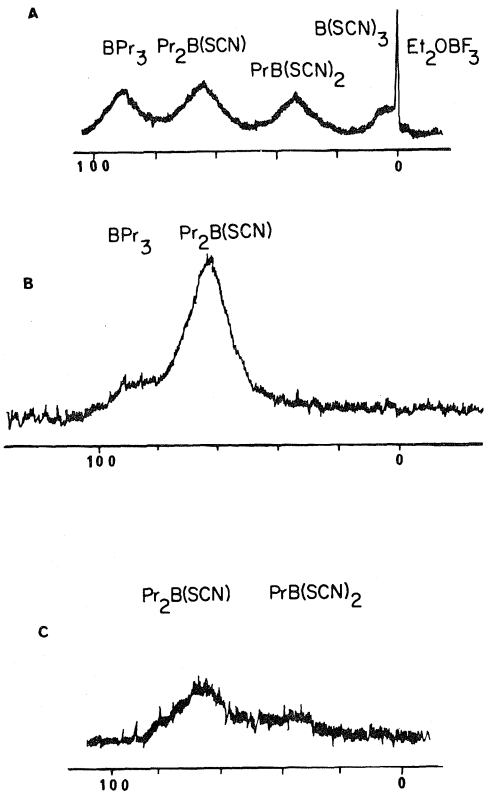

FIG. 2. Système $BPr_3/B(SCN)_3$: rmn ^{11}B (*A*) $R = 1.15$ 2 semaines à 55 °C; (*B*) $R = 1.19$ à l'équilibre à 70 °C; (*C*) $R = 1.65$ à l'équilibre à 70 °C.

retiendrons à titre indicatif accorde à l'espèce $BBuF_2$ une stabilité conforme aux observations de McCusker (14).

Système $BPr_3/B(SCN)_3$

Le spectre d'un mélange défini par $R = [SCN]/[B]_{total} = 1.15$ chauffé 15 jours à 50 °C comporte quatre pics (fig. 2*A*). Les pics extrêmes correspondent aux composés symétriques tandis que les pics intermédiaires peuvent être attribués aux espéces mixtes $BPr(SCN)_2$ et $BPr_2(SCN)$. Il ne nous a pas été possible néanmoins de réaliser une étude complète car les mélanges caractérisés par des compositions R supérieures à 1.75 se polymérisent rapidement à 120 °C. Nous devons nous borner à une description plus qualitative du comportement de ce système.

Pour un mélange $R = 1.19$ l'état d'équilibre atteint après un chauffage à 70 °C pendant 3 semaines se traduit par un spectre comportant deux pics centrés à 64.5 et 86 ppm et correspondant aux composés $BPr_2(SCN)$ (90%) et BPr_3 (10%) (fig. 2*B*). Pour un mélange défini par $R = 1.65$ (fig. 2*C*), le spectre ne comporte que deux pics attribuables aux composés $BPr(SCN)_2$ (70%) et $BPr_2(SCN)$ (30%). Ces deux observations sont en faveur d'un rapprochement entre les systèmes $BPr_3/B(SCN)_3$ et BPr_3/BI_3: dans les deux cas, les espèces mixtes sont très favorisées par rapport à la distribution statistique.

Examen des résultats

Une première constatation importante a trait au comportement du système B(néopentyl)$_3$/-BCl_3 mettant en jeu un radical ramifié et qui, chauffé plusieurs semaines à 120 °C, n'est le siège d'aucune redistribution. Ceci est en accord avec les observations déjà formulées (10) et peut certainement être mis sur le compte d'effets d'ordre stérique.

Dans les autres systèmes, dont les valeurs des paramètres caractéristiques sont rassemblés dans le tableau 3, il y a redistribution et, d'une façon générale, les espèces mixtes sont favorisées par rapport au modèle de redistribution au hasard.

En d'autres termes on peut dire que les stabilités des espèces BR_2X et BRX_2 sont supérieures aux valeurs déduites de l'addition des énergies des liaisons B—C et B—X dans les composés symétriques. Cette non additivité a déjà été observée par voie thermochimique dans les séries $B(OEt)_iCl_{3-i}$ et $B(NMe_2)_iCl_{3-i}$ où les composés mixtes se trouvent également favorisés (15). Pour ce qui nous concerne, l'étude des

TABLEAU 3. BR_3/B trihalogenures*

X	R	K_{t_1}	K_{t_2}	ΔH_1 (kcal)	ΔH_2 (kcal)	ΔG_1 (kcal)	ΔG_2 (kcal)
Cl	Pr	$(8.5\pm6.0)\times10^5$	$(2\pm1)\times10^4$	−2.7	−1.7	−3.6	−2.6
Br	Pr	$(1.9\pm0.4)\times10^6$	$(5\pm1)\times10^6$	−2.9	−3.2	−3.8	−5
I	Pr	(1.7×10^8)	(2.8×10^7)	(∼−4)	(∼−3.5)	(∼−4)	(∼−3.5)
F	Bu	(1.6×10^4)	(4.0×10^6)	(∼−1.5)	(∼−3)	(∼−2.4)	(∼−3.9)

*Les valeurs entre crochets sont des valeurs estimées.

systèmes $B(NMe_2)_3/B(OMe)_3$ et $B(NMe_2)_3/B(SMe)_3$ a conduit à mettre en évidence, au contraire un comportement presque statistique soit:

$$-0.5 \lesssim \Delta H_f \lesssim +0.5 \text{ kcal}$$

Ces résultats permettent de penser dès maintenant que ces réactions sont sous la dépendance de plusieurs facteurs. Le premier d'entre eux est d'ordre stérique et le second résiderait dans le caractère acide (au sens de Lewis) des composés intervenant. A ce point de vue il faut noter que les enthalpies caractérisant les réactions de formation des espèces mixtes à partir des espèces symétriques sont, pour les systèmes BR_3/BX_3 (X = I, Br, Cl, F, SCN) de l'ordre de 3 à 4 kcal c'est-à-dire nettement plus fortes que celles obtenues pour les systèmes $B(NMe_2)_3/B(OMe)_3$ et $B(NMe_2)_3/B(SMe)_3$ ($\simeq$0.5 kcal) dans lesquels interviennent des composés dont le caractère accepteur est très inférieur à celui des trihalogènes. L'influence de l'acidité effective de l'atome de bore dans les édifices BR_3 et BX_3 est très cohérente avec l'hypothèse (16) suivant laquelle les redistributions se feraient à partir d'un intermédiaire ponté.

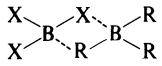

1. P. A. McCusker et J. H. Bright. J. Inorg. Nucl. Chem. **28**, 2261 (1966).
2. V. W. Buls, O. L. Davis et R. I. Thomas. J. Am. Chem. Soc. **74**, 337 (1957).
3. J. P. Laurent, G. Cros, G. Copin et J. Praud. J. Chim. Phys. **4**, 695 (1972).
4. J. P. Costes, G. Cros et J. P. Laurent. C.R. Ser. C, **280**, 665 (1975).
5. G. Cros, J. P. Costes et J. P. Laurent. Org. Magn. Reson. **7**, 78 (1975).
6. J. P. Costes, G. Cros et J. P. Laurent. A paraître.
7. H. Mongeot. Thèse d'Ingénieur Docteur, Lyon, France. 1966.
8. J. P. Tuchagues et J. P. Laurent. Bull. Soc. Chim. Fr. **11**, 4160 (1967).
9. J. R. Johnson, H. R. Snyder et M. G. Van Campen. J. Am. Chem. Soc. **60**, 115 (1938).
10. F. M. Rossi, P. A. McCusker et G. F. Hennion. J. Org. Chem. **32**, 1233 (1967).
11. G. Calingaert et M. A. Beatty. J. Am. Chem. Soc. **61**, 2748 (1939); J. R. Van Wazer. Am. Sci. **50**, 450 (1962).
12. J. R. Van Wazer et K. Moedritzer. J. Inorg. Nucl. Chem. **26**, 737 (1964); J. C. Lockhart. Chem. Rev. **65**, 131 (1965).
13. P. A. McCusker, G. F. Hennion et F. C. Ashby. J. Am. Chem. Soc. **79**, 5192 (1957).
14. P. A. McCusker et L. J. Glunz. J. Am. Chem. Soc. **77**, 4253 (1955).
15. H. A. Skinner et N. B. Smith. J. Chem. Soc. 3930 (1954); H. A. Skinner et N. B. Smith. J. Chem. Soc. 2324 (1954).
16. J. C. Lockhart. Redistribution reactions. Academic Press, New York. 1970.

The crystal and molecular structure of thiamine iodide hydroiodide

WILLIAM EDWARD LEE[1] AND MARY FRANCES RICHARDSON[2]
Department of Chemistry, Brock University, St. Catharines, Ont., Canada L2S 3A1

Received March 31, 1976

WILLIAM EDWARD LEE and MARY FRANCES RICHARDSON. Can. J. Chem. **54**, 3001 (1976).

The X-ray crystal structure of thiamine iodide hydroiodide, $C_{12}H_{18}N_4OSI_2$, has been determined. The unit cell parameters are: $a = 13.835(7)$, $b = 7.442(4)$, $c = 20.243(9)$ Å, $\beta = 120.52(7)°$, monoclinic space group $P2_1/c$, $Z = 4$. A total of 1445 reflections having $F^2 > 2\sigma(F^2)$, $2\theta < 40°$ were collected on a Picker 4-circle diffractometer with MoKα radiation by the 2θ scan technique. The structure was solved by the heavy-atom method. The iodide and sulphur atoms were refined anisotropically; only positional parameters were refined for the hydrogen atoms. Successive full-matrix least-squares refinements yielded an unweighted *R*-factor of 0.054. The pyrimidine ring is protonated on the ring nitrogen opposite the amino group. The relative disposition of the pyrimidine and thiazolium rings is similar to that observed in most other thiamine structures. The β-hydroxyethyl side chain of the thiazolium ring is folded in such a way that there is a short S . . . O contact, 2.97 Å in length. The iodide ions are involved in a number of weak hydrogen bonds.

WILLIAM EDWARD LEE et MARY FRANCES RICHARDSON. Can. J. Chem. **54**, 3001 (1976).

La structure cristalline de l'iodhydrate de l'iodure de thiamine, $C_{12}H_{18}N_4OSI_2$ a été déterminée par rayon-X. Les paramètres de la maille élémentaire sont: $a = 13.835(7)$, $b = 7.442(4)$, $c = 20.243(9)$ Å, $\beta = 120.52(7)°$, groupe d'espace monoclinique $P2_1/c$, $Z = 4$. Un total de 1445 réflexions ayant $F^2 > 2\sigma(F^2)$, $2\theta < 40°$ ont été recueillies sur un diffractomètre Picker à 4 cercles en utilisant MoKα comme source de radiation d'après une technique de balayage de 2θ. La structure a été résolue par la méthode de l'atome lourd. Les atomes de soufre et d'iodure ont été affinés anisotropiquement; seuls les paramètres de position ont été affinés pour les atomes d'hydrogène. Des affinements successifs par la méthode des moindres carrés (matrice complète) ont donné un facteur d'accord non pondéré de 0.054. Le noyau pyrimidine est protoné sur le noyau azoté à l'opposé du groupement amino. La disposition relative des noyaux pyrimidine et thiazolium est semblable à celle observée dans la plupart des structures des thiamines. La chaîne latérale β-hydroxyéthyle du noyau thiazolium est repliée de telle façon qu'il y a un contact S . . . O court, de 2.97 Å de longueur. Les ions iodures sont impliqués dans un certain nombre de liens hydrogènes faibles.

[Traduit par le journal]

Introduction

Thiamine as its pyrophosphate ester, is a coenzyme in a number of decarboxylating enzyme systems which include the α-keto acid decarboxylases and the transketolases. Studies on the enzyme pyruvate decarboxylase have led to a proposed mechanism for the decarboxylation of pyruvic acid to acetaldehyde via a 2-(1-carboxy-1-hydroxyethyl)thiamine pyrophosphate intermediate (1, 2). In order to have a clear stereochemical picture of the enzyme–coenzyme-substrate complex, it is necessary to have well-founded concepts about the conformation of the thiamine molecule itself.

Theoretical calculations on the conformation of thiamine around the central methylene carbon (3) have shown that there is a wide range of conformations available to an isolated thiamine molecule. However, the coenzyme operates in conjunction with a large globular protein in an aqueous medium, and so is hardly an isolated molecule. Enzyme–coenzyme and substrate–coenzyme interactions as well as solvent effects will change the conformational energies, stabilizing some and destabilizing other conformations, with a net result of decreasing the range of conformations likely to be observed.

Thiamine hydrochloride was the first thiamine compound whose X-ray crystal structure was solved (4). In the ensuing years, the number of reported structures of thiamine compounds has risen, but only two different conformations have been observed for these compounds (5–13). In this paper we are reporting the molecular and

[1]Present address: Department of Chemistry, University of Guelph, Guelph, Ontario.

[2]To whom correspondence should be addressed.

Can. J. Chem. Downloaded from www.nrcresearchpress.com by 210.87.254.40 on 09/05/12
For personal use only.

Can. J. Chem. Downloaded from www.nrcresearchpress.com by 210.87.254.40 on 09/05/12
For personal use only.

TABLE 1

(*a*) Positional and thermal parameters of non-hydrogen atoms and their estimated standard deviations in parentheses

Atom	$10^4 x$	$10^4 y$	$10^4 z$	B (Å^2)
I(1)	3929.0(7)	8710(1)	1159.0(5)	[a]
I(2)	790.1(8)	6512(1)	2040.7(5)	[a]
O	−3668(8)	6195(12)	1918(5)	3.6(2)
C(1)	−4081(13)	4474(21)	1862(9)	4.1(3)
C(2)	−4435(11)	3584(18)	1065(8)	3.1(3)
C(3)	−3424(10)	3335(16)	974(7)	2.7(3)
C(4)	−2926(9)	1834(16)	938(7)	2.4(2)
C(5)	−3296(13)	−60(20)	925(10)	3.7(3)
C(6)	−1724(10)	3901(15)	909(7)	2.8(2)
S	−2663(3)	5206(5)	976(2)	[a]
N(1)	−1977(8)	2165(13)	892(5)	2.3(2)
C(7)	−1240(10)	694(17)	874(8)	2.4(2)
C(8)	−164(10)	1395(16)	959(7)	2.7(3)
C(9)	−95(9)	2152(16)	326(7)	2.2(2)
N(2)	−966(9)	2246(14)	−379(6)	3.0(2)
N(3)	892(8)	2810(14)	439(6)	3.0(2)
C(10)	1780(10)	2708(17)	1126(7)	3.2(3)
C(11)	2827(15)	3531(22)	1258(11)	3.9(4)
N(4)	1769(9)	1904(14)	1726(6)	2.9(2)
C(12)	771(10)	1306(15)	1631(7)	2.5(2)

(*b*) Anisotropic thermal parameters[b]

Atom	$10^5 \beta_{11}$	$10^5 \beta_{22}$	$10^5 \beta_{33}$	$10^5 \beta_{12}$	$10^5 \beta_{13}$	$10^5 \beta_{23}$
I(1)	578(9)	1986(25)	265(4)	46(9)	201(5)	53(7)
I(2)	927(10)	1405(23)	203(4)	−199(10)	259(5)	−37(6)
S	765(31)	1043(73)	463(18)	−1(36)	442(20)	−39(27)

[a]Atom refined anisotropically.
[b]The expression for the anisotropic temperature factor is $T_i = \exp(-\beta_{11}h^2 - \beta_{22}k^2 - \beta_{33}l^2 - \beta_{12}hk - \beta_{13}hl - \beta_{23}kl)$.

crystal structure of thiamine hydroiodide. The structure determination was undertaken to help cast additional light on the conformation of thiamine.

Experimental

Crystals of thiamine hydroiodide were prepared by mixing aqueous solutions of thiamine hydrochloride and sodium iodide (1:2 mole ratio) and allowing the solution to evaporate. A single plate-like crystal (1.0 × 0.5 × 0.2 mm) was mounted on a glass fibre with epoxy cement and aligned about the b^* axis on a Picker 4-circle diffractometer. The long dimension of the crystal was approximately parallel to the ϕ axis of the diffractometer. Zirconium-filtered MoKα radiation at a take-off angle of 1.5° was used to measure the 2θ values of the axial and $h0l$ reflections. When the α_1–α_2 doublet was not resolved, the interplanar spacing was calculated from the average MoKα wavelength (λ = 0.7107 Å); when the doublet was resolved, only the α_1 component was used in the determination. The angle β^* was determined from the location of the a* and c^* axes ($\beta^* = \phi_{h00} - \phi_{00l}$) and also from the interplanar spacings of the $h0l$ reflections. The crystal data are:

$C_{12}H_{18}I_2N_4OS$ f.w. = 520.2

Monoclinic, a = 13.835(7), b = 7.442(4), c = 20.243(9) A, β = 120.52(7)°, V = 1795.5 Å^3, Z = 4, ρ_c = 2.02, ρ_{obs} = 1.96 g cm^{-3}, $F(000)$ = 992. MoKα, λ = 0.7107 Å, μ = 37.2 cm^{-1}. Space group $P2_1/c$.

The procedures used for the data collection and reduction to structure factors have been previously described (14). A total of 1865 reflections in the independent quadrant ($2\theta < 40°$) were measured. Of these, 1445 had $F_o^2 > 2\sigma(F_o^2)$ and were classified as observed. The crystal quality did not deteriorate noticeably throughout the course of the data collection and there was no significant decrease in the intensity of the standard reflection, which was measured every 2 h. No corrections were made for either absorption or extinction.

Scattering factors for neutral I, S, O, N, C, and H atoms as well as the real and imaginary parts of the anomalous scattering of iodine were taken from the International Tables for X-Ray Crystallography (15). Major computer programs employed included Zalkin's FORDAP, Busing and Levy's ORFLS, and Busing,

TABLE 2. Positional parameters of hydrogen atoms and estimated standard deviations in parentheses

Atom	$10^2 x$	$10^2 y$	$10^3 z$
H(0)	−43(1)	74(2)	190(9)
H(1C1)	−48(1)	44(2)	187(10)
H(2C1)	−36(1)	33(2)	220(11)
H(1C2)	−48(1)	26(2)	99(8)
H(2C2)	−51(1)	46(2)	63(9)
H(1C5)	−24(1)	−11(2)	154(10)
H(2C5)	−35(1)	−7(2)	42(10)
H(3C5)	−39(1)	−11(2)	101(9)
H(C6)	−9(1)	46(2)	119(8)
H(1C7)	−18(1)	−2(2)	40(9)
H(2C7)	−10(1)	0(2)	136(9)
H(1N2)	−17(1)	18(2)	−42(9)
H(2N2)	−9(1)	24(2)	−88(9)
H(1C11)	28(1)	36(2)	65(11)
H(2C11)	33(1)	37(2)	168(11)
H(3C11)	32(1)	26(2)	127(11)
H(N4)	25(1)	18(2)	233(9)
H(C12)	9(1)	11(2)	222(8)

Martin, and Levy's ORFFE. The computations were performed on a Burroughs 5500 computer. During the least-squares refinements the function minimized was $\sum w\Delta^2$, where the weighting factor $w = 1/\sigma^2(F)$ and $\Delta = ||F_o| - |F_c||$. Unweighted and weighted residuals R_1 and R_2, respectively were calculated at the end of each refinement, where

$$R_1 = \sum\Delta/\sum|F_o|$$
$$R_2 = \sum w\Delta^2/\sum wF_o^2$$

The iodine positions were determined from the three-dimensional Patterson map. A difference Fourier synthesis yielded the positions of all of the atoms heavier than hydrogen. Thermal parameters were converted from isotropic to anisotropic for iodine and sulphur, and anomalous scattering factors were introduced for iodine. Two successive cycles of least-squares refinement of the positional and thermal parameters and the scale factor converged to a value of 0.068 for R_1 and 0.087 for R_2.

By a weighting analysis it was observed that a number of strong reflections with low sin θ/λ values were somewhat overweighted. For (2,0,−6), (3,0,−2), (302), and (310), the weighting scheme was changed so that

$$\sigma(F) = (1/|F_o - F_c|) \cdot \text{scale factor}$$

The weights of these reflections were changed because they were probably affected by extinction. As no corrections were made for extinction, the accuracy of these measurements is diminished so less weight was given to them.

Another difference map yielded the positions of 14 of the 18 hydrogen atoms. The atoms which were not located at this point were H(1C1), H(2C2), H(2N2), and H(3C11). The positions of these hydrogen atoms were calculated by assuming d(C—H) = d(N—H) = 1 Å and the appropriate angles for tetrahedral carbon and trigonal nitrogen. The isotropic thermal parameter for each hydrogen atom was fixed at 1 Å² greater than the thermal parameter of the atom to which it was bonded. The hydrogen positions were included but not refined in the next least squares cycle. The R factors resulting from this refinement were $R_1 = 0.055$ and $R_2 = 0.069$.

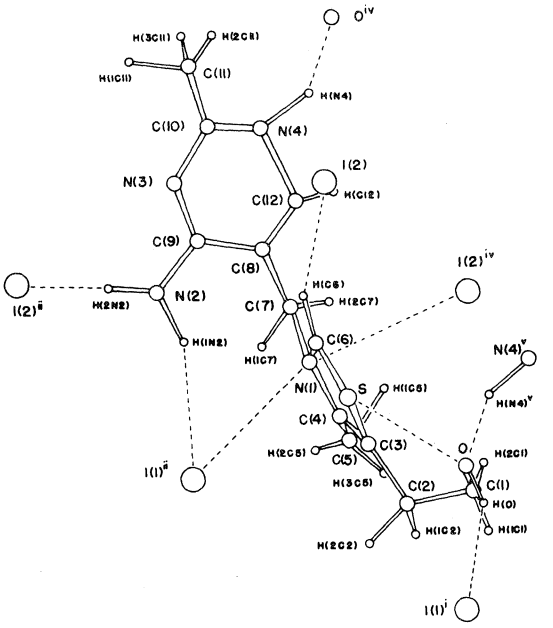

FIG. 1. Projection of thiamine hydroiodide along (010). Symmetry superscripts are as follows: no superscript (x, y, z); i ($x-1$, y, z); ii ($-x$, $1-y$, $-z$); iii (x, $y-1$, z); iv ($-x$, $-\frac{1}{2}+y$, $\frac{1}{2}-z$); v ($-x$, $\frac{1}{2}+y$, $\frac{1}{2}-z$); vi (x, $\frac{1}{2}-y$, $\frac{1}{2}+z$).

In the last cycle the scale factor, positional parameters for all 38 atoms (including hydrogen atoms), anisotropic thermal parameters for iodine and sulphur, and isotropic thermal parameters for the other 17 atoms heavier than hydrogen were refined: a total of 150 parameters. The R factors were $R_1 = 0.054$ and $R_2 = 0.066$. The average (parameter shift)/(e.s.d.) on this cycle was equal to 0.6. The standard error on an observation of unit weight was 1.98. A final difference Fourier synthesis was computed. The highest peak positions, corresponding to ripples around the iodine atoms, were approximately 1 e/Å³. There were no holes in the vicinity of the hydrogen atoms whose positions were calculated. At this point the refinement was considered complete.

The final coordinates and thermal parameters are given in Tables 1 and 2. Table 3 contains the observed and calculated structure factors.[3]

Results and Discussion

Thiamine hydroiodide, THI, is composed of a

[3]The structure factor table is available, at a nominal charge, from the Depository of Unpublished Data, CISTI, National Research Council of Canada, Ottawa, Canada K1A 0S2.

Can. J. Chem. Downloaded from www.nrcresearchpress.com by 210.87.254.40 on 09/05/12
For personal use only.

Can. J. Chem. Downloaded from www.nrcresearchpress.com by 210.87.254.40 on 09/05/12
For personal use only.

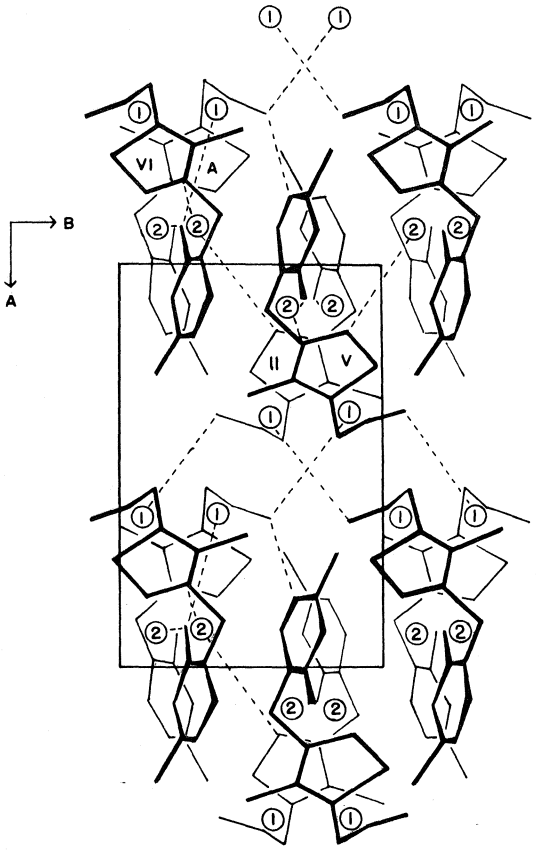

FIG. 2. Molecular packing of thiamine hydroiodide; the projection is along (001). Molecule A is the starting molecule at (x, y, z); other symmetry designations are as listed in the caption for Fig. 1. The numbered circles represent I(1) and I(2). Intermolecular hydrogen bonding is shown by the dashed lines.

divalent thiaminium cation and two monovalent iodide anions (Figs. 1 and 2). One positive charge is associated with the aromatic thiazolium ring, the other results from the protonation of N(4) in the pyrimidine ring. Protonation of N(4) has been observed in all other thiamine structures in which hydrogen atom positions have been determined (4–11). The bond distances and angles of THI are given in Tables 4 and 5, and in Table 6 are presented the equations of the least-squares planes of the thiazolium and pyrimidinium rings. The molecular structure of thiamine hydroiodide closely resembles those of thiamine hydrochloride (4) and hydrobromide (13). The increased size of the anions in THI has only a minor effect on the general molecular conformation, although

TABLE 4. Bond lengths (Å) and estimated standard deviations

Bond	Distance	Bond	Distance
O—C(1)	1.38(2)	O—H(0)	1.2(2)
C(1)—C(2)	1.57(2)	C(1)—H(1C1)	1.0(2)
C(2)—C(3)	1.51(2)	C(1)—H(2C1)	1.1(2)
C(3)—C(4)	1.33(2)	C(2)—H(1C2)	0.8(2)
C(3)—S	1.74(1)	C(2)—H(2C2)	1.2(1)
C(4)—C(5)	1.49(2)	C(5)—H(1C5)	1.5(1)
C(4)—N(1)	1.38(2)	C(5)—H(2C5)	1.0(2)
C(6)—S	1.68(1)	C(5)—H(3C5)	1.2(2)
C(6)—N(1)	1.33(1)	C(6)—H(C6)	1.2(1)
N(1)—C(7)	1.51(2)	C(7)—H(1C7)	1.0(1)
C(7)—C(8)	1.50(2)	C(7)—H(2C7)	1.0(2)
C(8)—C(9)	1.45(2)	N(2)—H(1N2)	1.0(2)
C(8)—C(12)	1.32(1)	N(2)—H(2N2)	1.1(2)
C(9)—N(2)	1.32(1)	C(11)—H(1C11)	1.2(2)
C(9)—N(3)	1.36(2)	C(11)—H(2C11)	0.8(2)
N(3)—C(10)	1.31(1)	C(11)—H(3C11)	0.9(2)
C(10)—C(11)	1.48(3)	N(4)—H(N4)	1.1(1)
C(10)—N(4)	1.36(2)	C(12)—H(C12)	1.1(2)
N(4)—C(12)	1.37(2)		

the overall crystal structure is quite different from the other hydrohalides (4, 13).

The conformation at the methylene carbon is best described in terms of torsion angles ϕ_T, C(8)—C(7)—N(1)—C(6), and ϕ_P, N(1)—C(7),-C(8)—C(9) (11). The thiamine cation in the present structure has $\phi_T = -5.9°$ and $\phi_P = 81.0°$. This conformation is the one most often found in other thiamine structures (4–9, 13), there being only two examples (10, 11) of a conformation with $\phi_T \simeq 105°$, $\phi_P \simeq 140°$.

There are a number of hydrogen bonds in the structure (Fig. 1 and Table 7). The hydrogen bonds involving iodide ions as acceptors are weak, with the H . . . I distances being $\simeq$0.5 Å shorter than the sum of the van der Waals radii for H and I (3.2 Å (16)). This shortening is consistent with the criterion of Hamilton and Ibers for hydrogen bonding (17), namely that the H . . . X distance be at least 0.2 Å shorter than the van der Waals distance.

The positive charge in the thiazolium ring is divided between the nitrogen and sulphur atoms (3, 9). These atoms make several dipolar contacts. The S . . . O distance of 2.97 Å is 0.35 Å shorter than the van der Waals distance, whereas the N(1) . . . I(1)^{ii} and N(1) . . . I(2)^{iv} contacts are slightly longer than the van der Waals distance. The $N^+ \ldots I^-$ contacts in the thiazolium ring are suggestive of charge-transfer interactions. They are significant because such

Can. J. Chem. Downloaded from www.nrcresearchpress.com by 210.87.254.40 on 09/05/12
For personal use only.

TABLE 5. Bond angles and estimated standard deviations

Bonds	Angle	Bonds	Angle
O—C(1)—C(2)	112.0(15)	N(1)—C(7)—C(8)	112.8(10)
C(1)—C(2)—C(3)	110.4(11)	C(7)—C(8)—C(9)	122.7(9)
C(2)—C(3)—C(4)	130.1(13)	C(7)—C(8)—C(12)	119.8(14)
C(2)—C(3)—S	119.8(9)	C(8)—C(9)—N(2)	123.0(12)
C(3)—C(4)—C(5)	127.5(15)	C(8)—C(9)—N(3)	120.3(9)
C(3)—C(4)—N(1)	112.9(12)	C(9)—N(3)—C(10)	118.7(13)
C(5)—C(4)—N(1)	119.6(13)	N(3)—C(10)—C(11)	118.6(15)
S—C(3)—C(4)	109.9(10)	N(3)—C(10)—N(4)	122.9(13)
S—C(6)—N(1)	111.0(11)	C(11)—C(10)—N(4)	118.5(11)
C(3)—S—C(6)	91.7(7)	C(10)—N(4)—C(12)	119.0(9)
C(4)—N(1)—C(6)	114.6(11)	C(8)—C(12)—N(4)	121.3(14)
C(4)—N(1)—C(7)	123.2(10)	N(2)—C(9)—N(3)	116.8(13)
C(6)—N(1)—C(7)	122.1(12)	C(9)—C(8)—C(12)	117.5(13)
H(0)—O—C(1)	111(8)	H(1C7)—C(7)—N(1)	95(10)
H(1C1)—C(1)—O	116(9)	H(1C7)—C(7)—C(8)	119(12)
H(1C1)—C(1)—C(2)	101(9)	H(1C7)—C(7)—H(2C7)	122(12)
H(1C1)—C(1)—H(2C1)	101(16)	H(2C7)—C(7)—N(1)	105(10)
H(2C1)—C(1)—O	127(9)	H(2C7)—C(7)—C(8)	102(9)
H(2C1)—C(1)—C(2)	95(11)	H(1N2)—N(2)—C(9)	113(9)
H(1C2)—C(2)—C(1)	114(13)	H(1N2)—N(2)—H(2N2)	119(11)
H(1C2)—C(2)—C(3)	110(13)	H(2N2)—N(2)—C(9)	126(8)
H(1C2)—C(2)—H(2C2)	105(11)	H(1C11)—C(11)—C(10)	109(8)
H(2C2)—C(2)—C(1)	103(8)	H(1C11)—C(11)—H(2C11)	137(21)
H(2C2)—C(2)—C(3)	114(10)	H(1C11)—C(11)—H(3C11)	77(8)
H(1C5)—C(5)—C(4)	111(7)	H(2C11)—C(11)—C(10)	114(19)
H(1C5)—C(5)—H(3C5)	86(10)	H(2C11)—C(11)—H(3C11)	91(19)
H(1C5)—C(5)—H(2C5)	107(11)	H(3C11)—C(11)—C(10)	103(14)
H(2C5)—C(5)—C(4)	110(11)	H(N4)—N(4)—C(10)	124(10)
H(3C5)—C(5)—C(4)	146(9)	H(N4)—N(4)—C(12)	117(11)
H(2C5)—C(5)—H(3C5)	93(14)	H(C12)—C(12)—N(4)	107(7)
H(C6)—C(6)—S	112(8)	H(C12)—C(12)—C(8)	130(7)
H(C6)—C(6)—N(1)	128(7)		

TABLE 6. Deviations from least squares planes[a]

Atoms used in calculating plane	Deviation (Å)	Atoms not used in calculating plane	Deviation (Å)
Pyrimidine ring: $0.3719X - 0.8972Y - 0.2383Z = -1.766$			
C(8)	0.01	C(7)	0.03
C(9)	−0.02	N(2)	−0.07
N(3)	0.00	H(1N2)	−0.06
C(10)	0.02	H(2N2)	−0.36
N(4)	−0.03	C(11)	0.14
C(12)	0.01		
Thiazolium ring: $-0.0558X + 0.0352Y - 0.9978Z = -1.297$			
C(3)	−0.01	C(2)	0.06
C(4)	0.01	C(5)	0.01
C(6)	−0.01	C(7)	0.06
S	0.01	O	1.49
N(1)	−0.01		

[a]The equations of these unweighted least squares planes have the form $aX + bY + cZ = d$, where X, Y, and Z are the orthogonal coordinates (in Å) of the atoms in a system where the x, y, and z axes are parallel to the a^*, b, and c axes of the unit cell, respectively.

contacts, which are not frequently observed in thiamine structures, have been suggested as a model for thiamine interactions with the apoenzyme in biological systems (18, 19).

The overall molecular packing is shown in Fig. 2. Pairs of glide-related thiamine cations (*e.g.*, molecules A and VI) are separated in the *a*-direction by I(1) anions. The distance between a pair of glide-related molecules is on the order of 10 Å in the *c*-direction, leaving room to sandwich in the I(2) anions. Glide-related molecules are linked in infinite chains in the *c*-direction by a system of I(1) . . . N(2) . . . I(2) . . . N(2) . . . I(1) . . . hydrogen bonds. Hydrogen bonds involving the OH . . . I(1) . . . NH_2 grouping provide a series of linkages in the (001) plane. The packing in the hydroiodide has been compared to that in the hydrochloride and hydrobromide in a recent paper (13).

The most significant conclusion to be drawn from this structure is that no gross molecular

TABLE 7
(*a*) Hydrogen bonding distances and angles[a]

a	*b*	*c*	∠abc (deg)	d_{b-c}, (Å)	d_{a-c}, (Å)
O—H(0)	. . .	I(1)^{i}	145(11)	2.3(2)	3.42(2)
N(2)—H(1N2)	. . .	I(1)^{ii}	153(12)	2.7(2)	3.64(1)
N(2)—H(2N2)	. . .	I(2)^{ii}	170(11)	2.6(2)	3.62(2)
C(6)—H(C6)	. . .	I(2)	162(13)	2.5(1)	3.61(2)
N(4)—H(N4)	. . .	O^{iv}	163(14)	1.6(1)	2.72(2)

(*b*) Selected other short contacts[a]

Atoms	Distance (Å)
S . . . O	2.97(1)
N(1) . . . I(1)^{ii}	3.66(1)
N(1) . . . I(2)^{iv}	3.67(1)

[a]See Fig. 1 for key to symmetry superscripts.

change accompanies the substitution of iodine for chlorine atoms in the lattice even though the molecular packing, and thus the crystal structure, changes. From this and other works (4–9) it may be inferred that the conformation observed is particularly stable as it persists over a wide range of accompanying anions and salts.

Acknowledgement

We thank the National Research Council of Canada for financial support of this research.

1. R. BRESLOW. J. Am. Chem. Soc. **80**, 3719 (1958).
2. J. CROSBY, R. STONE, and G. LIENHARD. J. Am. Chem. Soc. **92**, 2871 (1970).
3. F. JORDAN. J. Am. Chem. Soc. **96**, 3623 (1974).
4. J. KRAUT and H. J. REED. Acta Crystallogr. **15**, 747 (1962).
5. J. PLETCHER, M. SAX, S. SENGUPTA, J. CHU, and C. S. YOO. Acta Crystallogr. B**28**, 2928 (1972).
6. M. R. CAIRA, G. V. FAZAKERLEY, P. W. LINDER, and L. R. NASSIMBENI. Acta Crystallogr. B**30**, 1660 (1974).
7. D. A. CLEMENTE, G. BANDOLI, G. BENETOLLA, and A. MARZOTTO. J. Crystallogr. Mol. Struct. **4**, 1 (1974).
8. I. L. KARLE and K. BRITTS. Acta Crystallogr. **20**, 118 (1966).
9. J. PLETCHER and M. SAX. J. Am. Chem. Soc. **94**, 3998 (1972).
10. M. F. RICHARDSON, K. FRANKLIN, and D. M. THOMPSON. J. Am. Chem. Soc. **97**, 3204 (1975).
11. M. SAX, P. PULSINELLI, and J. PLETCHER. J. Am. Chem. Soc. **96**, 155 (1974).
12. C. H. CARLISLE and D. S. COOK. Acta Crystallogr. B**25**, 1359 (1969).
13. D. M. THOMPSON and M. F. RICHARDSON. Acta Crystallogr. In press.
14. M. F. RICHARDSON. Can. J. Chem. **52**, 3716 (1974).
15. International tables for X-ray crystallography. Vols. III and IV. Kynoch Press, Birmingham. 1968, 1975.
16. A. BONDI. J. Phys. Chem. **68**, 441 (1964).
17. W. C. HAMILTON and J. A. IBERS. Hydrogen bonding in solids. W. A. Benjamin, Inc. New York, New York. 1968. pp. 12–18.
18. J. E. BIAGLOW, J. J. MIEGAL, J. SUCHY, and H. Z. SABLE. J. Biol. Chem. **244**, 4054 (1969).
19. C. P. HEINRICH, D. SCHMIDT, and K. NOACK. Eur. J. Biochem. **41**, 555 (1974).

Can. J. Chem. Downloaded from www.nrcresearchpress.com by 210.87.254.40 on 09/05/12
For personal use only.

^{13}C and $^{33,34}S$ isotope effects on the vapour pressure of liquid carbon disulfide

ROBERT H. BETTS AND WAYNE D. BUCHANNON
Department of Chemistry, University of Manitoba, Winnipeg, Man., Canada R3T 2N2

Received April 12, 1976

ROBERT H. BETTS and WAYNE D. BUCHANNON. Can. J. Chem. **54**, 3007 (1976).

Precision isotope ratio mass spectrometry has been used to determine the relative vapour pressures of the four principal isotopic species of liquid carbon disulfide. Relative to the principal species $^{12}C^{32}S^{32}S = 1.000000$, the vapour pressures of the other species are: $^{12}C^{32}S^{34}S = 0.99985_5$, and $^{13}C^{32}S^{32}S = 1.00162$. A value of 0.99992_7 for $^{12}C^{32}S^{33}S$ is deduced by application of the rule of the geometric mean. The results are invariant with temperature between -20 and $+56$ °C. Qualitatively similar effects have been reported earlier for ^{13}C and ^{18}O substitution in $^{12}C^{16}O_2$, a chemical analogue of CS_2.

ROBERT H. BETTS et WAYNE D. BUCHANNON. Can. J. Chem. **54**, 3007 (1976).

La spectrométrie de masse à rapports isotopiques précis a été utilisée pour déterminer les pressions de vapeur relatives des quatre principales espèces isotopiques du disulfure de carbone liquide. En relation avec l'espèce principale $^{12}C^{32}S^{32}S = 1.000000$, les pressions de vapeur des autres espèces sont: $^{12}C^{32}S^{34}S = 0.99985_5$, et $^{13}C^{32}S^{32}S = 1.00162$. Une valeur de 0.99992_7 pour le $^{12}C^{32}S^{33}S$ est déduite en appliquant la règle de la moyenne géométrique. Les résultats sont constants dans l'écart de température allant de -20 à $+56$ °C. Des effets qualitativement similaires ont été rapportés précédemment pour des substitutions ^{13}C et ^{18}O dans le $^{12}C^{16}O_2$, un analogue chimique de CS_2.

[Traduit par le journal]

Introduction

For a long time it was believed that substitution of a heavier isotope for a lighter isotope in pure polyatomic molecular liquids invariably decreased the vapour pressure of the liquid. This relation between the vapour pressure and molecular weight is usually described as a normal vapour pressure isotope effect (1). While many molecular systems do indeed display normal vapour pressure isotope effects (H_2O and D_2O provide perhaps the best known example), other systems are known which show an inverse isotope effect, *i.e.*, the heavier species has the higher vapour pressure. For example, it is well established that the vapour pressure of $^{13}CH_3OH$ is greater than that of $^{12}CH_3OH$ (2). For some systems, both kinds of effects have been observed for a given element, with the isotope effect changing sign when the temperature is changed. The deutero-methanes are an example of this class (3). Perhaps even more unexpectedly, systems are also known for which an inverse isotope effect is produced by substitution in one part of a polyatomic molecule, and a normal isotope effect by substitution in another part of the same molecule (2, 4, 5).

Carbon dioxide is the best studied example of a molecule which shows both normal and inverse isotope effects, depending on whether O or C is involved. Grootes *et al.* (4) used precision mass spectrometry to measure isotopic fractionation between liquid and gaseous phases of naturally occurring CO_2. For all temperatures examined (220 to 303 K), $^{12}C^{16}O^{18}O$ is less volatile than $^{12}C^{16}O^{16}O$ (a normal isotope effect) while $^{13}C^{16}O^{16}O$ is more volatile than $^{12}C^{16}O^{16}O$ (an inverse isotope effect). Both isotope effects approach zero as the CO_2 critical temperature of 304 K is approached.

More recently, Bilkadi *et al.* (5) used direct manometric comparisons of the vapour pressures of essentially isotopically pure samples of $^{12}C^{16}O_2$, $^{13}C^{16}O_2$, and $^{12}C^{18}O_2$. Their data are mainly for the solid–vapour equilibrium, but extend approximately 0.3 K past the triple point into the liquid–vapour region. For all temperatures, the vapour pressures are in the order: $P_{^{13}C^{16}O_2} > P_{^{12}C^{16}O_2} > P_{^{12}C^{18}O_2}$. In addition, these authors show that their results at the highest temperature examined (217 K) are in good agreement with the measurements of Grootes *et al.*, which were obtained by a very different method

Can. J. Chem. Downloaded from www.nrcresearchpress.com by 210.87.254.5 on 09/05/12
For personal use only.

Can. J. Chem. Downloaded from www.nrcresearchpress.com by 210.87.254.5 on 09/05/12
For personal use only.

with CO_2 of natural isotopic abundance. The authors of ref. 4 and also particularly those of ref. 5 presented an extensive theoretical interpretation of these effects. Broadly speaking, the inverse ^{13}C isotope effect is related to a mass-dependent shift in the internal vibrations in such a way that the intermolecular forces, relative to $^{12}C^{16}O_2$, are somewhat reduced. Hindered translation is the most important aspect of the normal ^{18}O isotope effect in the liquid, and hindered rotation accounts for most of the oxygen isotope effect in the solid–vapour equilibrium.

Carbon disulfide is the sulfur analogue of CO_2. Like CO_2, it is a linear molecule, and has a variety of isotopically distinguishable species. We therefore thought it of interest to determine whether or not the vapour pressure isotope effects found for CO_2 are also exhibited by CS_2. To our knowledge, there are only three very brief references (6–8 and ref. 246 of ref. 1) in the literature on the effect of isotopic substitution on the vapour pressure of CS_2. Reference 6 simply reports that, at some unspecified temperature, $^{13}CS_2$ is more volatile than $^{12}CS_2$. Reference 7 is a summary paper without any experimental detail whatsoever, which reports (as a numerical entry in Table 2, p. 70 of ref. 7) that the vapour pressure of $^{13}CS_2$ is 0.1% higher than that of $^{12}CS_2$, presumably at the normal boiling point, but this is not stated. The original for ref. 8 is unfortunately not available to us, and we have had to rely on ref. 1 as a secondary reference in this case. According to Jancso and Van Hook (ref. 1, p. 706) the work in ref. 8 simply confirms the data already cited from ref. 7.

For natural abundances of the isotopes of C and S (9), the species $^{12}C^{32}S^{32}S$ (mass 76) comprises 89.26% and $^{12}C^{32}S^{34}S$ (mass 78) contributes 7.94%.[1] The two species of mass 77, $^{13}C^{32}S^{32}S$ (41.2% of mass 77) and $^{12}C^{32}S^{33}S$ (58.8% of mass 77) together make up 2.43% of all the isotopic varieties of CS_2. The much rarer species of masses 79 to 82, involving ^{12}C or ^{13}C with ^{33}S, ^{34}S, and ^{36}S, make up the remaining 0.37%.

[1]Mass 78 is actually 99.83% $^{12}C^{32}S^{34}S$, and 0.17% $^{13}C^{32}S^{33}S$ and $^{12}C^{33}S^{33}S$. We have neglected these rare species in our work. In this and the other calculations above of the natural abundances of the isotopic species, we have used the relative abundances of the C and S isotopes given in ref. 9.

In the present work, we have used isotope ratio mass spectrometry to measure the equilibrium distribution of the principal isotopic species between liquid and vapour. Such measurements give, either directly[2] or indirectly, the relative vapour pressures of the pure species $^{12}C^{32}S^{34}S$ (species 1), $^{12}C^{32}S^{32}S$ (species 2), $^{13}C^{32}S^{32}S$ (species 3), and $^{12}C^{32}S^{33}S$ (species 4). As is shown later, the behaviour of species 4 is inferred from those of species 1 and 2 by interpolation.

Experimental

Fisher certified spectranalyzed grade CS_2 was further purified by distillation under vacuum from mercury to remove traces of other sulfides and mercaptans. Thereafter, it was kept in the vacuum system in the absence of light. A sample of approximately 100 ml of the purified liquid was placed in a round-bottomed flask which was attached to a vacuum rack, and the liquid allowed to boil slowly under a suitable pressure of purified argon. Variation of the equilibration temperature (from −20.4 to +56 °C) was achieved by variation of the pressure of argon, with auxiliary external cooling provided as required. The vapour phase was condensed in a side arm arranged in such a way that further fractionation of the liquid in this portion of the system could not occur. The condensed vapour phase, comprising about 3% of the total sample, was returned continuously to the interior of the liquid phase through a small return line. This line was equipped with stop-cocks which allowed a portion of the condensed vapour phase to be removed for mass analysis, without disturbing the remainder of the system. Finally, to insure that a single stage equilibrium had been reached, the liquid phase in the completely closed system was allowed to boil for several hours, with continuous recirculation of the condensed vapour phase before a sample was withdrawn for mass analysis.

A portion of the starting purified liquid was converted completely to vapour to provide a sample for isotopic assay of the liquid phase (invariant for all temperatures). This sample was thus a reference isotopic standard, against which each sample of the vapour phase was

[2]Making the basic assumption that Raoult's Law applies to mixtures of isotopic species, it is easy to show that if P^0_1 and P^0_2 are the vapour pressures of isotopically pure liquids 1 and 2, then:

$$P^0_1/P^0_2 = \left(\frac{^{12}C^{32}S^{34}S}{^{12}C^{32}S^{32}S}\right)_v \Big/ \left(\frac{^{12}C^{32}S^{34}S}{^{12}C^{32}S^{32}S}\right)_1$$

and similarly for the other species. The quantities in parentheses represent the equilibrium ratios of the abundances of the indicated species in the vapour and liquid phases of a system containing both species. Our mass spectrometer measures not mass 78/mass 76, or mass 77/mass 76, but mass 78/masses (76 + 77 + 79 + 80) and mass 77/masses (76 + 78 + 79 + 80), respectively. These latter ratios may be used without significant loss of precision for the desired ratios.

Can. J. Chem. Downloaded from www.nrcresearchpress.com by 210.87.254.5 on 09/05/12
For personal use only.

compared. The procedure was to compare, in succession, the composition of the reference sample with that of each sample of the vapour. Such comparisons were usually made twice for each sample. At some temperatures, several independent samples of the vapour phase were removed for mass analysis.

A Varian-Mat GD-150 isotope ratio mass spectrometer was used for isotopic assay. This spectrometer has a dual gas phase inlet system which permits rapid and alternate intercomparisons between sample and reference standard. In addition, the spectrometer has facilities for precise matching of the inlet pressures of the samples being compared. This adjustment was particularly necessary in this work because of the very small variations in the isotopic composition observed.

Two mass ratios were measured for each sample and reference. The first was mass 78/masses (76 + 77 + 79 + 80). This ratio, referred to as R_{78} in Table 1, is a good measure of the abundance of $^{12}C^{32}S^{34}S$ relative to the other species (mainly $^{12}C^{32}S^{32}S$). The second mass ratio was mass 77/masses (76 + 78 + 79 + 80), referred to as R_{77} below. The GD-150 mass spectrometer does not distinguish between $^{13}C^{32}S^{32}S$ and $^{12}C^{32}S^{33}S$, which together make up mass 77. To determine their relative contributions to the mass 77 abundance, we proceeded as follows:

Let 1 = $^{12}C^{32}S^{34}S$
2 = $^{12}C^{32}S^{32}S$
3 = $^{13}C^{32}S^{32}S$
4 = $^{12}C^{32}S^{33}S$

together with the definitions:

[1] $P^0_3/P^0_2 = R_{3,2}$

[2] $P^0_4/P^0_2 = R_{4,2}$

[3] $P^0_1/P^0_2 = R_{1,2} = (R_{78})_v/(R_{78})_l$

$R_{1,2}$ is given directly from the measured quantities $(R_{78})_v$ and $(R_{78})_l$. $R_{3,2}$ and $R_{4,2}$ cannot be directly measured, but may be deduced from $R_{1,2}$ and R_{77} values by application of the rule of the geometric mean.[3] This rule, which has both experimental and theoretical support, predicts *e.g.*, that:

[4] $P^0_{H_2{}^{17}O} = \sqrt{P^0_{H_2{}^{16}O} \times P^0_{H_2{}^{18}O}}$

and

[5] $P^0_{HDO} = \sqrt{P^0_{H_2O} \times P^0_{D_2O}}$

[3]At first sight we appear to be begging the question by using this rule. We emphasize that we use it only to estimate the effect of $-^{33}S$ additions, as between $-^{32}S$ or $-^{34}S$ addition to the group common to all three species, namely $^{12}C^{32}S-$. This is a logical extension of the rule. It would not, for example, be valid to calculate P^0 for $^{13}C^{32}S^{32}S$ from a knowledge of P^0 values for $^{12}C^{32}S^{32}S$ and $^{12}C^{32}S^{34}S$. In any case a *linear* interpolation gives the same result for $P^0{}_{^{12}C^{32}S^{33}S}$ as does the rule of the geometric mean. We therefore feel confident that our treatment of this point is valid.

TABLE 1. Relative isotopic abundances for masses 76, 77, and 78 in CS_2 vapours in equilibrium with liquid CS_2

T(°C)	R_{77}*	R_{78}*
—	0.0221670 (liquid)	0.075877 (liquid)
−20.4	0.0221841	0.075843
−20.4	0.0221840	0.075891
−20.4	0.0221840	0.075860
−20.4	0.0221800	—
−20.4	0.0221790	—
−14.8	0.0221820	0.075870
−14.8	0.0221819	0.075866
−14.8	0.0221810	0.075862
−14.8	0.0221812	0.075863
18.5	0.0221760	0.075877
18.5	0.0221820	0.075867
56.0	0.0221821	0.075865
56.0	0.0221842	0.075866
56.0	0.0221801	0.075862
56.0	0.0221771	0.075867
56.0	0.0221750	0.075862
56.0	0.0221800	0.075868
	Av. 0.0221808	0.075866
	±0.0000022(a.d.)	±0.000006(a.d.)

*$R_{77} = \frac{\text{Mass 77}}{\text{Masses (76 + 78 + 79 + 80)}}$

$R_{78} = \frac{\text{Mass 78}}{\text{Masses (76 + 77 + 79 + 80)}}$

The most precise data (10, 11) for the systems in [4] and [5] show some slight departure from the rule of the geometric mean. However these deviations are not large, and we feel the rule to be sufficiently precise for our purpose, which is to calculate the value of $R_{4,2}$ from that for $R_{1,2}$. Thus:

[6] $P^0_4 = \sqrt{P^0_1 P^0_2}$

Substitute for P^0_1 in [6] from [3]:

[7] $P^0_4 = P^0_2\sqrt{R_{1,2}}$

Comparison of [7] and [2] leads to the result that:

[8] $R_{4,2} = \sqrt{R_{1,2}}$

This result, together with the measured value of R_{77}, gives $R_{3,2}$ from equation [9]:

[9] $(R_{77})_v/(R_{77})_l = 0.412\ R_{3,2} + 0.588\sqrt{R_{1,2}}$

The factors 0.412 and 0.588 in [9] are the fractional contributions of $^{13}C^{32}S^{32}S$ and $^{12}C^{32}S^{33}S$ to mass 77 for CS_2 composed of naturally occurring isotopic abundances of C and S. The value of $R_{3,2}$ calculated from this equation will depend on the values of these factors, but fortunately this dependence is very slight. Variations of as much as ±2.5% in the factor 0.412 (and corresponding changes in the factor 0.588) altered the value of $R_{3,2}$ = 1.00162 shown in Table 2 by only ±0.00004. A variation of ±2.5% is judged, somewhat arbitrarily, as more than sufficient to allow for the possibility that the CS_2 used

TABLE 2. Relative vapour pressure of some isotopic carbon disulfides*

Species	Relative vapour pressure
$^{12}C^{32}S^{32}S$	1.000000 (Reference)
$^{12}C^{32}S^{33}S$	$0.99992_7 \pm 0.000013$†
$^{12}C^{32}S^{34}S$	$0.99985_5 \pm 0.000026$
$^{13}C^{32}S^{32}S$	1.00162 ± 0.00005‡

*Results are temperature-independent from −20 to 56 °C.
†By interpolation. See text and footnote 3.
‡See text for discussion of the sources of uncertainty for this value.

had C and S isotope abundances which differed from the accepted values (9).

Results

The results are summarized in Tables 1 and 2. Table 1 gives the values of R_{77} and R_{78} for each vapour phase, relative to a fixed value of each ratio for the liquid phase, over a temperature range from −20.4 to 56 °C. Table 2 gives the relative vapour pressures of the principal species of CS_2 derived from the data given in Table 1.

The consistency of the data in Table 1 can be assessed in the following ways. For example, the mean of the six entries for R_{78} at 56 °C is 0.075865, with an average deviation of ± 0.000002 (*i.e.*, ± 2 parts in 75 000). The standard deviation of the mean for these entries is ± 0.000001.

The group of seven values of R_{78} for −14.8 to −20.4 °C, similarly analyzed, gives a mean value of 0.075865 ± 0.000009 (a.d.), and a standard deviation of the mean of ± 0.000005. This constant value of R_{78} for the two sets of temperature extrema leads us to conclude that R_{78} is independent of temperature within the precision of our measurements. We have therefore taken the average of all 15 entries to give $R_{78} = 0.075866 \pm 0.000006$ (a.d.), with a standard deviation of the mean of ± 0.000002. Comparison of this result for the vapour phase with that for the liquid phase (0.075877) shows that:

$$P^0_{^{12}C^{32}S^{34}S} = (0.99985_5 \pm 0.000026)\, P^0_{^{12}C^{32}S^{32}S}$$

This number (0.999855) differs from 1.000000 by 6× the experimental uncertainty. From [8] one calculates:

$$P^0_{^{12}C^{32}S^{33}S} = \sqrt{0.999855}\, P^0_{^{12}C^{32}S^{32}S} = (0.99992_7)\, P^0_{^{12}C^{32}S^{32}S}$$

i.e., this value is calculated by interpolation, using the rule of the geometric mean, as already discussed. These results are recorded in Table 2.

Turning to the data for R_{77} in Table 1, an analysis similar to that described for R_{78} shows that these data also are independent of temperature within the experimental uncertainty. The average value of all 17 entries for R_{77} is 0.0221808 $\pm$ 0.0000022 (a.d.), with a standard deviation of the mean = ± 0.0000006. This mean value, together with R_{77} for the liquid phase (0.0221670) and $\sqrt{R_{1,2}} = 0.99992_7$, leads via [9] to:

$$R_{3,2} = 1.00161_9 \pm 0.000007.$$

To the mass spectrometric error of ± 0.000007 for $R_{3,2}$ must be added a further uncertainty, already pointed out, ascribable to a possible difference in the abundances of ^{13}C and ^{33}S in our sample of CS_2 from the accepted values (9). A generous estimate, involving the factors 0.412 ± 0.020 and 0.588 ± 0.020, leads to a further uncertainty of ± 0.00004 in the value of $R_{3,2}$. These two kinds of errors are combined and shown as ± 0.00005 in Table 2. Thus $P^0_{^{13}C^{32}S^{32}S} = (1.00162)\, P^0_{^{12}C^{32}S^{32}S}$ (Table 2).

Discussion

The data summarized in Table 2 show clearly that $^{13}C^{32}S_2$ is more volatile than $^{12}C^{32}S_2$, whilst substitution of ^{33}S or ^{34}S in $^{12}C^{32}S_2$ reduces the vapour pressure. These results are therefore in qualitative agreement with the effects of ^{13}C or ^{18}O substitution in $^{12}C^{16}O_2$. Moreover the two sets of results are not markedly dissimilar numerically. Thus, depending on the temperature (4):

$$P^0_{^{13}C^{16}O_2} = (1.00014 - 1.00057)\, P^0_{^{12}C^{16}O_2}$$

and

$$P^0_{^{12}C^{16}O^{18}O} = (0.99897 - 0.99994)\, P^0_{^{12}C^{16}O_2}$$

We must however admit to some surprise at the absence of observable temperature effects for CS_2. This liquid has a critical temperature of 279 °C, as compared with 31 °C for liquid CO_2, and the conditions for our measurements are therefore much further from the critical temperature of CS_2 than are those of Grootes *et al.* (4) for CO_2. Certainly vapour pressure isotope effects must disappear, by definition, at the critical temperature. The results for CO_2 suggest that one might reasonably expect the isotope

Can. J. Chem. Downloaded from www.nrcresearchpress.com by 210.87.254.5 on 09/05/12
For personal use only.

effects to increase as the difference in the density of the two phases increases (and as the vapour approaches ideality). On the other hand, the theory (4, 5) does predict two temperature-dependent terms with opposite signs, such that normal and inverse vapour pressure isotope effects can be expected over a sufficiently wide range of temperature. It is conceivable that for the temperature interval examined here, these two effects are in approximate balance, with a fortuitous cancellation of a temperature-dependent behaviour within the limits of the accuracy of our measurements. Examination of this system over a wider temperature range might help to resolve this question.

Finally, we note that the ^{13}C effect in CS_2 is significantly greater than it is for CO_2 (1.0016 *vs.* 1.0004). A referee has suggested that this result may be rationalized in the following way. As pointed out in the Introduction, a normal isotope effect is related to translation, while an inverse isotope effect is associated with internal modes. For CO_2, the translational normal effect is much larger than for CS_2. Thus if the internal effects are similar for the two molecules, the *net* separation factor will be a larger inverse isotope effect for ^{13}C in CS_2 than in CO_2, as observed.

Acknowledgment

The financial support of the National Research Council of Canada is gratefully acknowledged.

1. G. Jansco and W. A. Van Hook. Chem. Rev. **74**, 689 (1974).
2. P. Baertschi, W. Kuhn, and H. Kuhn. Nature, **171**, 1018 (1953).
3. G. T. Armstrong, F. G. Brickwedde, and R. B. Scott. J. Res. Natl. Bur. Stand. **55**, 39 (1955).
4. P. M. Grootes, W. G. Mook, and J. C. Vogel. Z. Physik. **221**, 257 (1969).
5. Z. Bilkadi, M. W. Lee, and J. Bigeleisen. J. Chem. Phys. **62**, 2087 (1975).
6. Ya. D. Zel'venskii, V. E. Sokolov, and V. A. Shalygin. Nauchn. Dokl. Vyssh. Shk. Khim. Khim. Tekhnol. **1**, 388 (1958).
7. J. Kistamaker, J. Bigeleisen, and A. O. C. Nier *Editors*. International Symposium on Isotope Separation. Amsterdam. April 23–27, 1957. North Holland Publishing Co., Amsterdam. 1958.
8. E. Krell and W. Nattermüller. Abh. Dtsch. Akad. Wiss. Berlin Kl. Chem. Geol. Biol. 131 (1965).
9. C. M. Lederer, J. M. Hollander, and I. Perlman. Table of isotopes. 6th ed. John Wiley and Sons, Inc., New York. 1967.
10. S. Szapiro and F. Steckel. Trans. Faraday Soc. **63**, 883 (1967).
11. W. A. Van Hook. J. Phys. Chem. **76**, 3040 (1972).

Can. J. Chem. Downloaded from www.nrcresearchpress.com by 210.87.254.5 on 09/05/12
For personal use only.

Synthesis of sultines via *tert*-butyl hydroxyalkyl sulfoxides

NARENDRA K. SHARMA,[1] FRANÇOIS DE REINACH-HIRTZBACH, AND TONY DURST
Department of Chemistry, University of Ottawa, Ottawa, Ont., Canada K1N 6N5

Received April 6, 1976

NARENDRA K. SHARMA, FRANÇOIS DE REINACH-HIRTZBACH, and TONY DURST. Can. J. Chem. **54**, 3012 (1976).

A general route leading to 5- to 8-membered cyclic sulfinate esters (sultines) is described. The method is based on the reaction of *tert*-butyl hydroxyalkyl sulfoxides with SO_2Cl_2 in an inert solvent.

NARENDRA K. SHARMA, FRANÇOIS DE REINACH-HIRTZBACH et TONY DURST. Can. J. Chem. **54**, 3012 (1976).

Une voie générale d'accès aux ester-sulfinates cycliques (sultines) ayant de 5 à 8 chaînons est décrite. La méthode est basée sur la réaction des *tert*-butylhydroxyalkylsulfoxydes avec le SO_2Cl_2 dans un solvant inerte.

[Traduit par le journal]

Can. J. Chem. Downloaded from www.nrcresearchpress.com by 210.87.254.40 on 09/05/12
For personal use only.

Introduction

Several years ago, as part of our studies on the α-halogenation of sulfoxides, we observed that sulfoxides of the type **1**, upon reaction with SO_2Cl_2 or *N*-chlorosuccinimide (NCS) furnished cyclic sulfinate esters (sultines) in good to excellent yield (1) (Eq. 1). At the time this observation was made, only a very limited number of sultines had been prepared, utilizing routes exemplified by [2]–[6].

Since these methods (eqs. 2–6) do not lend themselves very readily to the preparation of sultines having different ring size and substitution patterns, we decided to investigate the sulfoxide cleavage route [1] in some detail. We have used this new synthesis to prepare a number of specifically substituted 5- to 8-membered ring sultines utilizing simple, readily available starting materials. The availability of a variety of sultines has allowed us to study in some detail the chemical and physical properties of these compounds. The results of the synthetic endeavours are presented in this paper. Some chemical reactions and a description of the conformational properties of the δ-sultines will be described in subsequent publications. Attempts to prepare 4-membered ring sultines via [1] have resulted in the discovery of a sulfur analogue of the Wittig olefin synthesis (6). One example of a stable, crystalline β-sultine (3,3-dimethyl-4,4-diphenyl-1,2-oxathietane-2-oxide) has been obtained (7).

[1] $t\text{-BuS(O)CH}_2(\text{CH}_2)_n\text{CH}_2\text{OH}$ (**1**) $\xrightarrow[CH_2Cl_2]{SO_2Cl_2}$ (ref. 1)

[2] 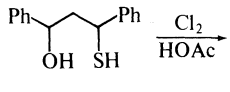 (ref. 2*a*)

[3] 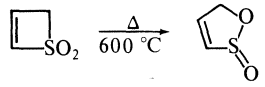 (ref. 3)

[4] 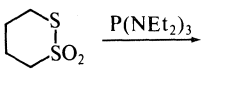 (ref. 4)

[5] 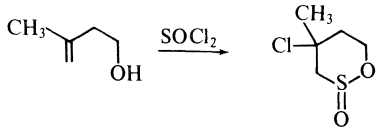 (ref. 5)

[6] 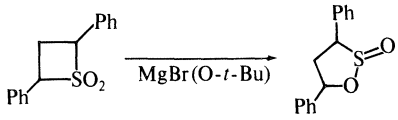 (ref. 2*a*)

Discussion and Results

(*a*) *Synthesis of the Parent 5- to 8-Membered Ring Sultines*

The precursor *tert*-butyl ω-hydroxyalkyl sulfoxides **1–4** required for the synthesis of the unsubstituted sultines **5–8** were readily available from the reaction of potassium *tert*-butylthiolate with the appropriate halohydrins, fol-

[1]Most of the work described herein is taken from the Ph.D. Thesis of N. K. Sharma, University of Ottawa, 1975.

Can. J. Chem. Downloaded from www.nrcresearchpress.com by 210.87.254.40 on 09/05/12
For personal use only.

lowed by oxidation with *tert*-butyl hypochlorite (8) (see eq. 7). Reaction of **1**–**4** with SO_2Cl_2 in methylene chloride for 30 min at room temperature led to the sultines **5**–**8** in isolated yields of 83, 75, 58, and 45% respectively. The above yields decreased as expected in going to the 7- and 8-membered ring systems, but are quite acceptable considering the accessibility of the starting sulfoxides.

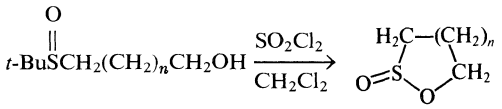

1, $n = 1$ **5**, $n = 1$
2, $n = 2$ **6**, $n = 2$
3, $n = 3$ **7**, $n = 3$
4, $n = 4$ **8**, $n = 4$

The sultines **5**–**8** each showed a strong S=O stretching frequency in the infrared at 1100–1120 cm^{-1}. There appears to be no consistent increase in the S=O frequency in going from the δ to the γ sultines similar to that observed in the corresponding lactones and lactams. The nmr spectra of **5** and **6** were in agreement with those reported earlier by Harpp and Gleason (4, 9) while those of **7** and **8** each showed the expected three areas of absorption: 3.8–4.2 (2H, α to oxygen), 2.6–2.8 (2H, α to sulfur), and 1.2–2.2 (6H and 8H, for **7** and **8** respectively) for the remaining methylene groups. Each of the sultines gave the expected molecular ion in its mass spectrum and was oxidized to the corresponding sultone. The route represented by [1] is thus also of value as a synthesis of sultones, in particular, the 7- and 8-membered species which are very difficult to prepare by the standard routes (10).

(*b*) *Preparation of Substituted Sultines*

The successful synthesis of the parent 5- to 8-membered ring sultines discussed above reduced the problem of the preparation of specifically substituted sultines to that of preparing the appropriately substituted *tert*-butyl hydroxyalkyl sulfoxides. These compounds were obtained from a variety of simple reaction sequences. The most commonly used routes are shown in [7]–[11].

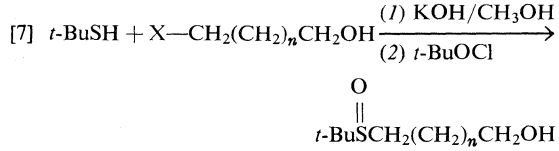

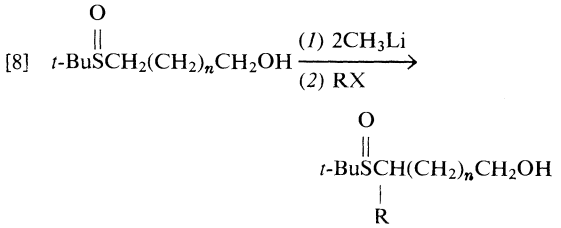

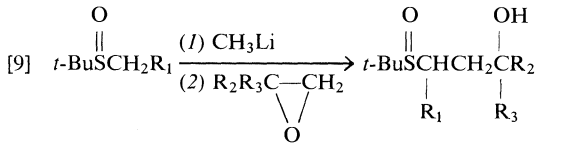

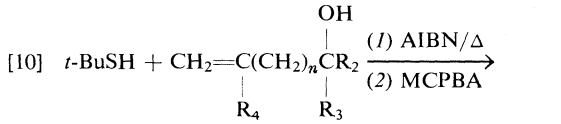

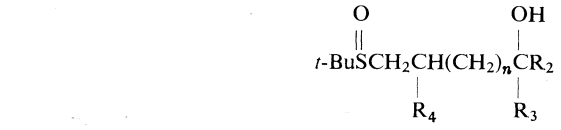

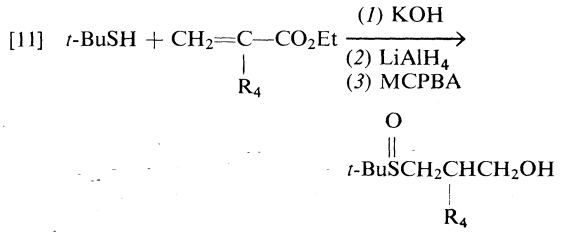

To illustrate the versatility of the sultine synthesis we have, using the cyclization depicted in [1] together with one of the steps [7]–[11], synthesized some 20–25 different sultines. Included are the parent 5- to 8-membered compounds mentioned above, the three possible monomethylated γ sultines, two phenyl substituted γ sultines, four monomethylated δ sultines, several benz-fused sultines, and a number of other disubstituted sultines required for a study of the photochemical, thermal, and conformational behaviour of these compounds. The method of preparation and yields of the precursor hydroxysulfoxides, together with the structure and yields of the sultines produced, are shown in Table 1. Complete nmr data and the position of the S=O frequency in the infrared spectra of the various sultines are given in the Experimental section.

Although only two examples of [8] were car-

Can. J. Chem. Downloaded from www.nrcresearchpress.com by 210.87.254.40 on 09/05/12
For personal use only.

TABLE 1. Preparation of sultines

Entry	Starting materials	Formation of hydroxy sulfoxide intermediate: Method (eq. no.)	Formation of hydroxy sulfoxide intermediate: Yield	Formation of product: Sultine	Formation of product: Yield
1	*t*-BuSH, $Cl(CH_2)_3OH$	7	68	**5**	83
2	*t*-BuSH, $Cl(CH_2)_4OH$	7	53	**6**	75
3	*t*-BuSH, $Cl(CH_2)_5OH$	7	61	**7**	58
4	*t*-BuSH, $Cl(CH_2)_6OH$	7	56	**8**	45
5	*t*-BuS$(CH_2)_3OH$, CH_3I	8	82		72
6*a*	*t*-BuSH, $CH_2{=}C(CH_3)CH_2OH$	10	65		80
6*b*	*t*-BuSH, $CH_2{=}C(CH_3)CO_2Et$	11	63		
7	*t*-BuS$(O)CH_3$, $CH_2{-}CHCH_3$ (O)	9	88	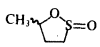	80
8	*t*-BuSH, $PhCH{=}CHCO_2CH_3$	11	25		0
9	*t*-BuSH, $CH_2{=}C(Ph)CH_2OH$	10	51		81
10	*t*-BuS$(O)CH_3$, $CH_2{-}CHPh$ (O)	9	85	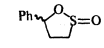	96
11	*t*-BuS$(O)CH_2CH_3$, $CH_2{-}CHCH_3$ (O)	9	90	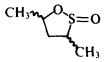	90
12	*t*-BuS$(O)CH_2CH_3$, $CH_2{-}CHPh$ (O)	9	88	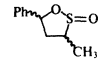	96
13	*t*-BuS$(O)CH_3$,	9	60	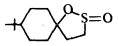	88
14	*t*-BuS$(CH_3)_4OH$, CH_3I	8	80	**21**	78
15	*t*-BuSH, $CH_2{=}C(CH_3)CH_2CH_2OH$	10	68	**20**	80
16	*t*-BuSH, $Cl(CH_2)_3COCH_3$, CH_3I	7	20	**19**	65
17	*t*-BuSH, $Cl(CH_2)_3CCH_3$, $NaBH_4$	7	34	**18***a*	85
18	*t*-BuSH, $CH_2{=}CHCH_2CHPh$ (OH)	10	67	**18***b*	72
19	*t*-BuSH, $CH_2{=}CHCH_2C(CH_3)_2$ (OH)	10	56	**22**	70
20	*t*-BuSH, $CH_2{=}CHCH_2CPh$ (CH_3) (OH)	10	50	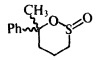	90
21	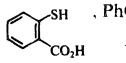 , $PhCHCH_3$ (Br)	7	66	**23**	60
22	*t*-BuSH, 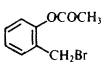	7	74	**25**	See text
23	*t*-BuS$(O)CH_2Li$, 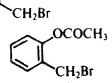		70	**29**	95

Can. J. Chem. Downloaded from www.nrcresearchpress.com by 210.87.254.40 on 09/05/12
For personal use only.

ried out, this route should prove quite useful for the preparation of sultines bearing a variety of alkyl substituents α to sulfur, since α-sulfinyl carbanions can generally be alkylated in good to excellent yield with both primary and secondary alkyl bromides (*1b*). In the dianion **9**, no *O*-alkylation was observed, despite the fact that methyl iodide was used in excess.

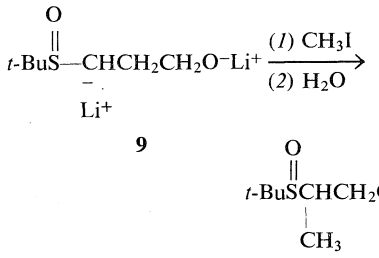

The reaction of α-lithio sulfoxides with epoxides (eq. 9) is an excellent route to γ-hydroxy sulfoxides (entries 7 and 10–13 in Table 1). With the unsymmetrical epoxides employed, complete regiospecificity, resulting from attack of the anion at the least hindered position of the epoxide, was observed.

Many of the prerequisite hydroxy sulfoxides were prepared by free radical addition of *tert*-BuSH to allylic and homoallylic alcohols, followed by oxidation (eq. 10, entries 6*a*, 9, 15, 18–20 in Table 1). The addition to the double bond occurs with high regioselectivity in the expected *anti*-Markownikov sense. Allylic alcohols and homoallylic alcohols thus served as starting materials for γ- and δ-sultines, respectively. Michael addition of *tert*-BuSH to α–β unsaturated esters or ketones, followed by lithium aluminum hydride reduction and *meta*-chloroperbenzoic acid oxidation (eq. 11) was also utilized as a route to the required hydroxy sulfoxides.

The method is not readily applicable to synthesis of sultines bearing either a phenyl group or two alkyl groups α to sulfur. Thus, the attempted synthesis of 3-phenyl-1,2-oxathiolane-2-oxide, **10**, by reaction of either **11***a* or **11***b* with SO_2Cl_2 or NCS was not successful, the only identified reaction product being 1,3-dichloro-1-phenylpropane. Either cleavage of the initial chlorooxosulfonium ion or the cyclic alkoxyoxosulfonium ion (see discussion of the mechanism below) occurred mainly in the undesired direction,[2] or sultines such as **10** are not stable under reaction conditions. In connection with the latter point, we have observed that sultines react very rapidly with excess SO_2Cl_2 to give cleavage products according to [12].[3] A similar cleavage of **10** would lead to **13** which would be expected to decompose to the dichloride **12** (11).

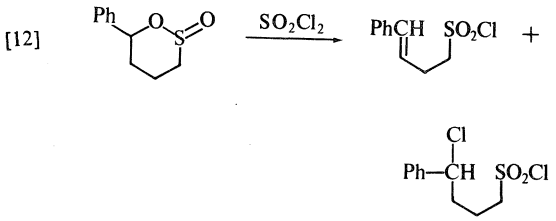

All of the substituted 5-membered ring sultines reported herein were obtained as diastereomeric mixtures after column chromatography or distillation, as judged by the multiplicity of various signals in the nmr spectra. For example, the nmr of 5-methyl-1,2-oxathiolane-2-oxide showed two methyl signals at δ 1.39 and 1.59 (J = 6.0 Hz) and two multiplets from 4.4–4.8 and 4.9–5.3 due to the C-5 hydrogen in addition to very complex absorption from δ 1.0 to 3.4.

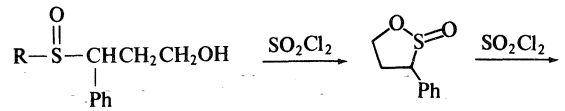

11*a* R = *t*-Bu
11*b* R = $CH_3O—C_6H_4CH_2$

10

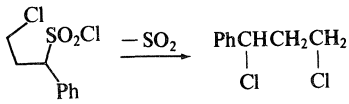

13 **12**

In the case of the 4-phenyl-1,2-oxathiolane-2-oxide, the two diastereomers were readily separated by silica gel chromatography. The tentative structure assignments, **14** and **15** for the faster and slower moving materials obtained in 30 and 51% yields respectively, are based mainly on their ^{13}C and proton nmr spectra. These assignments are supported by the chromatographic behaviour of the two isomers. A number of

[2]The direction of C—S bond cleavage is governed by the relative stability of the two possible carbocations.

[3]F. de Reinach-Hirtzbach, unpublished observations.

Can. J. Chem. Downloaded from www.nrcresearchpress.com by 210.87.254.40 on 09/05/12
For personal use only.

authors have shown that for a pair of isomeric sulfoxides the isomer having its S=O group sterically less accessible for association is eluted more rapidly (12). In the *trans* isomer **14**, the S=O bond is pseudoaxial when the phenyl group is pseudoequatorial and thus sterically less accessible than in the *cis* isomer **15** where both groups may take up the pseudoequatorial positions.

The proton spectrum of the less polar isomer showed multiplets from 2.9–3.2 (2H), 3.4–4.1 (2H), and 4.6–5.0 (1H) while absorption for the more polar one was observed from 3.1–3.5 (2H), 4.1–4.5 (2H), and 5.0–5.2 (1H). The S=O bond is known to deshield *syn*-3-hydrogens in both cyclic sulfoxides (13) and sultines (9). In agreement with this, the benzylic hydrogen when *cis* to S=O, *i.e.*, structure **14**, is shifted downfield by about 0.6 ppm relative to that in **15** which is *trans* to the S=O group.

In the ^{13}C spectra, the absorptions for the ring carbons 3, 4, and 5 occurred at 45.0, 67.4, and 78.9 ppm respectively, for the less polar isomer, and at 42.0, 64.8, and 80.4 ppm for the more polar one. The isomeric 4-phenyl-1,3-dioxathiolane-2-oxides **16** and **17** can be considered as reasonable model compounds for **14** and **15** respectively. The changes in the ^{13}C resonances at C_4 (80.9 ppm) and C_5 (73.5 ppm) in going from the *trans* sulfite **16**, to the *cis* isomer **17** (C_4 at 85.6, C_5 at 71.4 ppm)[4] are qualitatively similar to the differences at C_4 and C_5 in *trans*-**14** (78.9 and 67.4 ppm) *vs.* *cis*-**15** (80.4 and 64.8 ppm). When the sultines were stored at room temperature for several weeks it was observed that **14** was partly converted into **15** and an unknown product, whereas **15** remained unchanged.

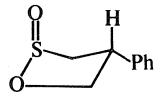

14

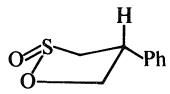

15

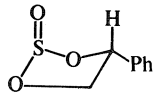

16

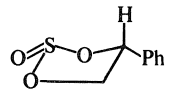

17

In contrast, all monosubstituted δ-sultines were obtained in high diastereomeric purity. Based on the proton and ^{13}C nmr spectra, structures **18–21** were assigned to these compounds.[5]

For example, the proton nmr spectrum of 6-methyl-1,2-oxathiane-2-oxide (**18***a*), showed the methyl group as a doublet at δ 1.08, and multiplets from 1.1–3.0 (3H), 3.3–3.8 (3H), and 4.0–4.6 (1H). These absorptions are as expected for the isomer shown. The 6-axial hydrogen at 4.0–4.6 is strongly deshielded by the *syn*-axial S=O group and is in the same area as the 6-axial hydrogen of the parent δ-sultine (9). A similar deshielding of the 4-axial hydrogen moves it into the 3.3–3.8 region, also occupied by the two protons α to sulfur. The assignment of the S=O bond as axial in the isomers **19–21** and **18***b* was also based on the observation of the strong deshielding on the 4- and 6-axial hydrogens. The C-5 methyl group in **19** was assigned the equatorial position based on a comparison of the methyl ^{13}C resonance, δ 21.8, with those of the equatorial methyl groups of **18***a* and **20**, δ 21.5 and 21.9, respectively.

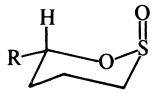

18*a* R = CH_3
18*b* R = Ph

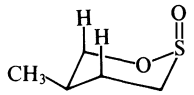

19

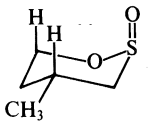

20

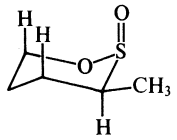

21

The high diastereomer selectivity may be due to both a significant preference for the formation of one of the diastereomers and a possible isomerization of the products under the reaction or isolation conditions. In the mechanism of the formation of 6-membered ring sultines (see part *c*), we suggest the intermediacy of a cyclic alkoxyoxosulfonium salt. Such a salt in the case of these sultines would be expected to show a significant preference for the structure **i** shown below in which both the *tert*-butyl and R group occupy equatorial positions. Cleavage of the *tert*-butyl–sulfur bond in **i** leads to the major observed sultines. Since the stereochemistry at sulfur is readily epimerizable at the intermediate

[4]G. R. Buchanan, private communication.

[5]A more detailed analysis of the conformational behaviour of these compounds will be presented separately.

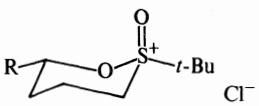

i

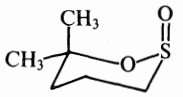

22

chlorooxosulfonium ion stage (14), the intermediate **i** can be formed from either of the two possible diastereomeric *tert*-butyl hydroxyalkyl sulfoxides which were used as starting materials in these reactions.

The nmr spectrum of crude product obtained in the synthesis of **18***a* suggested the possible presence of a second isomer in up to about 15% yield. However, on attempted purification, either via silica gel chromatography or distillation, only the isomer shown was obtained. As shown above, the nmr data for **18**–**21** indicate a very strong preference for the S=O group to adopt the axial conformation. The axial S=O preference is sufficiently strong that **22**, despite the *syn*-1,3-methyl – S=O interaction, exists almost exclusively in the chair conformation, having the S=O bond axial[5]. Isomerization, possibly acid catalyzed, of the various isomers may be sufficiently facile so that our isolation procedures produced only the most stable one. Both sulfites (15) and sulfoxides (16) have been shown to undergo acid-catalyzed epimerization.

A number of benz-fused sultines were also prepared utilizing the sulfoxide cleavage route. 3*H*-2,1-Benzoxathiole-1-oxide (**23**) (17) was obtained in 60% yield, together with α-phenethyl chloride (60%) upon treatment of **24** with SO_2Cl_2. The hydroxy sulfoxide **24** had been prepared from *o*-mercaptobenzoic acid in 70% overall yield via alkylation with α-phenethyl bromide, followed by $LiAlH_4$ reaction and MCPBA oxidation.

The synthesis of the isomeric 3*H*-1,2-benzoxathiole-2-oxide **25** was initially attempted via SO_2Cl_2 or NCS cleavage of the *tert*-butyl sulfoxide **26**, prepared from α-bromo-*o*-cresyl acetate by reaction with *tert*-butyl thiol, followed by oxidation. NCS or SO_2Cl_2 induced C—S bond cleavage in **26** occurred, not altogether unexpectedly, at the benzylic rather than the *tert*-butyl carbon–sulfur bond to furnish an unstable substance, tentatively identified as the open chain ester **27**. It was therefore decided to replace the *tert*-butyl group in **26** by the *p*-methoxybenzyl group with the hope that this might lead to cleavage in the desired direction. Reaction of the phenolic sulfoxide **28** synthesized in the same manner as **26**, gave a crude product whose nmr spectrum was interpreted in terms of an equimolar mixture of the sultine **26**, (δ 4.16 (d, J = 16 Hz), 4.56 (d, J = 16 Hz, 1H), and 7.4 (m, 4H)) and *p*-methoxybenzyl chloride. Unfortunately, despite considerable efforts involving column chromatography or distillation, the isolation of pure **25** was not successful. Chromatography of the crude reaction product on silica gel gave a number of fractions which contained peaks not found in the crude reaction mixture, thus indicating decomposition of the original products. The only pure substance which was isolated from the column was *p*-methoxy benzyl alcohol, presumably formed upon hydrolysis of the chloride.

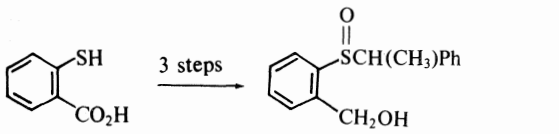

24

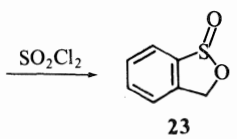

23

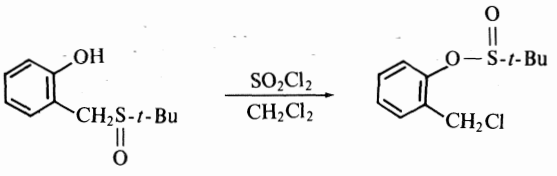

26 27

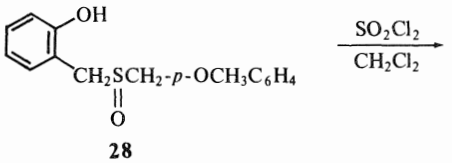

28

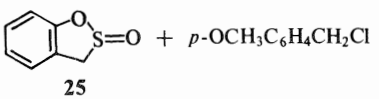

25

The instability of **25** compared to **23** is not surprising. Sultines generally undergo ring opening in the presence of nucleophiles by attack at sulfur followed by cleavage of the S—O bond. In **25**, such a cleavage results in the formation of a phenolic anion compared to an alkoxide anion

Can. J. Chem. Downloaded from www.nrcresearchpress.com by 210.87.254.40 on 09/05/12
For personal use only.

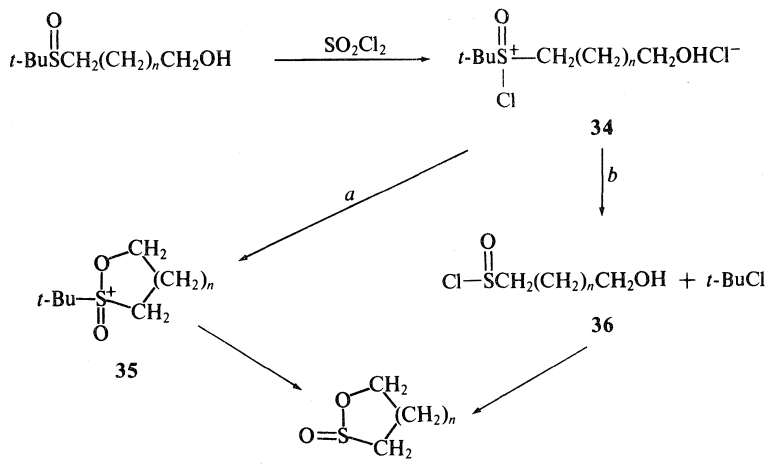

Mechanisms of sultine formation.

in **23**. Givens and Hamilton have reported (*2b*) and we have confirmed the instability of δ-sultine **29**, the homologue of **25**.

Two of the three possible δ benz-fused sultines **29** and **30** were prepared by the present method. Sultine **29**, previously prepared by controlled chlorination of β-(*o*-hydroxyphenyl)ethyl mercaptan in acetic acid, was obtained in greater than 95% crude yield by reaction of the sulfoxide **31** with SO_2Cl_2. The preparation of the sultine **30** via **32** and its extrusion of SO_2 to give *o*-quinodimethane have previously been reported (14).

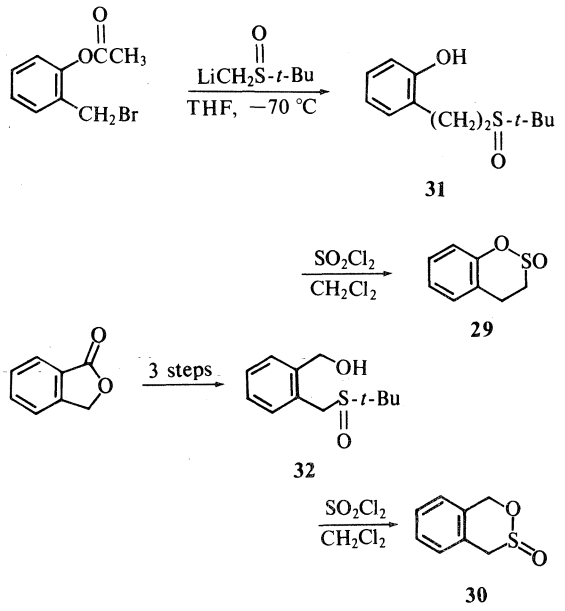

(*c*) *Mechanism of Sultine Formation*

Two possible mechanisms can be suggested for the sultine formation. Both involve initial formation of a chlorooxosulfonium ion, species which have been invoked as intermediates in the chlorination of sulfoxides (see, for example, ref. 18). In mechanism *a*, the chlorooxosulfonium ion **34** is converted to a cyclic alkoxyoxosulfonium ion **35**, via displacement of chloride ion from sulfur by the remote hydroxyl group (17). Subsequent cleavage of the *tert*-butyl carbon–sulfur bond yields the sultine. In mechanism *b*, sulfur–carbon bond cleavage occurs at the chlorooxosulfonium ion stage to yield the hydroxysulfinyl chloride **36** which undergoes subsequent intramolecular esterification to the sultine.

Cyclic alkoxyoxosulfonium ions have been shown to be intermediates in the chlorination of the hydroxyalkyl phenyl sulfoxides **37***a–c*, a reaction which resulted in the formation of the chloroalkyl phenyl sulfones **38** (19). In contrast, the sulfoxides **37***d–e*, on chlorination, yield α-chloro sulfoxides **39** thus showing that the formation of cyclic alkoxyoxosulfonium ions is extremely facile only when 4- to 6-membered rings are produced. It is therefore suggested that the formation of γ- and δ-sultines most probably occurs via mechanism *a* and that of the larger-ring sultines, via *b*.

Experimental

All proton nmr spectra were recorded on either Varian T-60 or HA-100 spectrometers using $CDCl_3$ – 1% TMS as solvent. ^{13}C spectra were obtained at 25.2 MHz, under conditions of complete proton noise decoupling, using a

Can. J. Chem. Downloaded from www.nrcresearchpress.com by 210.87.254.40 on 09/05/12
For personal use only.

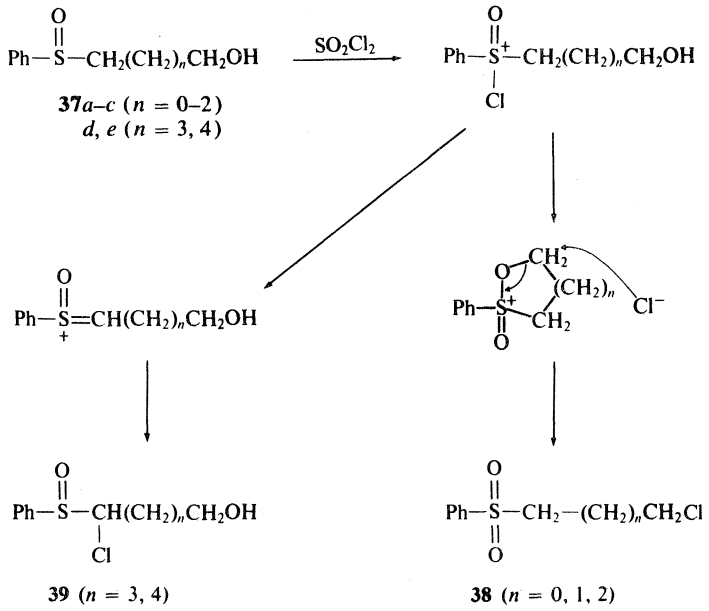

Varian XL-100 spectrometer operating in the Fourier transform mode. Carbon and proton shifts are reported in ppm downfield from TMS.

Usual work-up of reactions refers to partitioning of the reaction solvent between water and CH_2Cl_2, drying of the organic layer with anhydrous magnesium sulfate, and evaporating the solvent using a rotary evaporator.

Preparation of tert-Butyl Hydroxyalkyl Sulfides

Most of the compounds were prepared either by nucleophilic displacement of a halohydrin by potassium *tert*-butylthiolate in methanol (method *A*), or by free-radical addition of *tert*-butyl mercaptan to the appropriate unsaturated alcohol (method *B*). These general procedures are outlined below and the results are presented in Table 2. The sulfides required for the synthesis of the sultines found in entries 6, 8, 16, 17, 21, and 22 were prepared by different routes. Their synthesis is described below. The structures of the sulfides were readily apparent from their nmr spectra and method of synthesis. No elemental analyses were carried out on these materials.

Method A. To a solution of the appropriate thiol in methanol containing 20% excess KOH was added dropwise the appropriate amount of alkyl halide. The reaction mixture was stirred overnight and the precipitate formed was filtered. The filtrate was diluted with an equal volume of H_2O and extracted several times with CH_2Cl_2. The combined organic extract was washed twice with 10% KOH solution, dried, and evaporated. The crude sulfides were generally purified by distillation under reduced pressure.

Method B. Equimolar mixtures of *tert*-butyl mercaptan and alkene were heated with an oil bath at about 70–80 °C in the presence of a small amount of bis(azobutyronitrile) (AIBN) for up to 8 h, or until the nmr spectrum of the reaction mixture indicated the disappearance of the alkene. The desired sulfide was purified by distillation under reduced pressure.

2-Methyl-3-tert-butylthiopropan-1-ol (Entry 6, Table 2)

Methyl methacrylate (10.0 g, 0.1 mol) was added to a solution prepared by the addition of 9.0 g (0.1 mol) of *tert*-BuSH and 6.0 g of KOH to 25 ml of methanol. The reaction was stirred overnight and worked-up in the usual manner to yield 2.2 g of methyl 2-methyl-3-*tert*-butylthiopropanoate and 14.4 g of 2-methyl-3-*tert*-butylthiopropanoic acid. The acid and ester were combined and reduced to 2-methyl-3-*tert*-butylthiopropan-1-ol with lithium aluminum hydride in ether. The overall yield was 68%.

3-Phenyl-3-tert-butylthiopropan-1-ol (Entry 8, Table 2)

Methyl cinnamate (14.8 g, 0.09 mol) was added to a solution of 9.0 g (0.1 mol) of *tert*-butyl thiol and 6 g of KOH in 25 ml of methanol. The reaction mixture was stirred overnight, stripped of methanol, diluted with H_2O, and extracted with CH_2Cl_2. The crude product (12.0 g) obtained after evaporating the organic extracts was immediately reduced with $LiAlH_4$ in ether to afford 10.4 g (68% overall) of 3-phenyl-3-*tert*-butylthiopropan-1-ol.

5-tert-Butylthiopentan-2-ol (Entry 17, Table 2)

5-Chloro-2-pentanone (6.0 g, 0.05 mol) was added to a methanolic KOH solution containing 4.5 g of *tert*-butylthiol (0.05 mol). The reaction mixture was stirred overnight, diluted with water, and then extracted with CH_2Cl_2. The product, bp 110 °C/4 torr, obtained in 45% yield, was reduced with sodium borohydride in methanol. The yield of 5-*tert*-butylthiopent-2-ol was 95%.

2-Methyl-4-tert-butylthiobutan-1-ol (Entry 16, Table 2)

To a solution of 0.04 mol of lithium diisopropylamide in 40 ml of dry THF at −20 °C was added 3.52 g (0.02 mol) of 4-*tert*-butylthiobutanoic acid which had been obtained in 40% yield by reaction of *tert*-BuS^-K^+ with methyl 4-chlorobutanoate. The reaction mixture was stirred for 5 min and then treated with 3 g of methyl iodide. After a further 30 min of reaction the usual work-up gave 3.45 g (90%) of crude 2-methyl-4-*tert*-butanoic

Can. J. Chem. Downloaded from www.nrcresearchpress.com by 210.87.254.40 on 09/05/12
For personal use only.

Can. J. Chem. Downloaded from www.nrcresearchpress.com by 210.87.254.40 on 09/05/12
For personal use only.

TABLE 2. Preparation and nmr spectra of *tert*-butyl sulfides[a]

Entry	Sulfide	Method of preparation	Yield (%)	Boiling point (°C/torr)	nmr data
1	*t*-BuS(CH$_2$)$_3$OH	*A*[b]	90	53–55/0.5	1.33(s, 9H), 1.87(m, 2H), 2.70(t, J = 6 Hz, 2H), 3.8(t, J = 6 Hz, 2H), 1.93(1H, OH)
2	*t*-BuS(CH$_2$)$_4$OH	*A*	70	70/0.1	1.26(s, 9H), 1.3–2.0(m, 4H), 2.0–2.6(m, 2H), 3.2–3.7(m, 3H)
3	*t*-BuS(CH$_2$)$_5$OH	*A*	85	68–70/0.05	1.33(s, 9H), 1.5–2.0(m, 7H), 2.3–2.6(m, 2H), 3.5–3.7(m, 2H)
4	*t*-BuS(CH$_2$)$_6$OH	*A*	80	74–76/0.05	1.33(s, 9H), 1.5–2.0(m, 9H), 2.4–2.7(m, 2H), 3.5–3.7(m, 2H)
6	*t*-BuSCH$_2$CHCH$_2$OH | CH$_3$	*B*[c]*C*[d]	68		0.98(d, J = 7 Hz, 3H), 1.3(s, 9H), 1.5–2.3(m, 2H), 2.3–2.8(m, 2H), 3.5(d, J = 6 Hz, 2H)
8	*t*-BuSCH(CH$_2$)$_2$OH | Ph	*C*	50		1.2(s, 9H), 1.7–2.35(m, 2H), 2.5(1H, OH), 3.3–4.5(m, 3H), 7.0–7.3(m, 5H)
9	*t*-BuSCH$_2$CHCH$_2$OH | Ph	*B*	82	124/5	1.23(s, 9H), 2.13(1H), 2.9(3H), 3.9(2H), 7.2(5H)
15	*t*-BuSCH$_2$CH(CH$_2$)$_2$OH | CH$_3$	*B*	85	95–98/0.4	1.0(d, J = 6 Hz, 3H), 1.3(s, 9H), 1.35–2.2(m, 3H), 2.2–2.7(m, 2H), 2.8(1H, OH), 3.56(t, J = 6 Hz, 2H)
16	*t*-BuS(CH$_2$)$_2$CHCH$_2$OH | CH$_3$	*C*	31		0.95(d, J = 6 Hz, 3H), 1.33(s, 9H), 1.5–2.1(m, 4H), 2.76(t, J = 7 Hz, 2H), 3.5(d, J = 5 Hz, 2H)
17	*t*-BuS(CH$_2$)$_3$CHOH | CH$_3$	*C*	43		1.21(d, J = 6 Hz, 3H), 1.3(s, 9H), 1.4–2.2(m, 5H), 2.3–2.7(m, 2H), 3.6–3.8(m, 1H)
18	*t*-BuS(CH$_2$)$_3$CHPh | OH	*B*	95	60–62/0.1	1.25(s, 9H), 1.5–2.2(m, 4H), 2.3–2.6(m, 3H), 4.5–4.6(m, 1H), 7.3(s, 5H)
19	*t*-BuS(CH$_2$)$_3$C(CH$_3$)$_2$ | OH	*B*	80	88–90/2	1.13(s, 6H), 1.3(s, 9H), 1.4–1.7(m, 5H), 1.9–2.4(m, 2H)
20	*t*-BuS(CH$_2$)$_3$C(CH$_3$)Ph | OH	*B*	83	120–125/0.15	1.25(s, 9H), 1.53(s, 3H), 1.6–2.3(m, 5H), 2.4–2.7(m, 2H), 7.2–7.5(m, 5H)
21	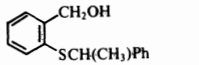	*A*[d]	78		1.6(d, 3H), 2.9(1H, OH), 4.25(q, 1H), 4.9(s, 2H), 7.0–7.4(m, 9H)
22	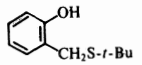	*A*	92		1.33(s, 9H), 3.76(s, 2H), 5.5(1H, OH), 6.5–7.3(m, 4H)

[a]The numbered entries in each table correspond to each other. [b]*tert*-BuS$^-$ + halohydrin. [c]AIBN-catalyzed addition of *tert*-BuSH to unsaturated alcohol. [d]See Experimental section.

Can. J. Chem. Downloaded from www.nrcresearchpress.com by 210.87.254.40 on 09/05/12
For personal use only.

acid which was reduced without further purification with $LiAlH_4$ in ether. The yield of purified 2-methyl-4-*tert*-butylthiobutan-1-ol was 2.8 g (85%).

o-Hydroxymethylphenyl α-Methylbenzylsulfide (Entry 21, Table 2)

o-Mercaptobenzoic acid was alkylated in 85% yield with α-phenethyl bromide and the resultant crude acid was reduced with $LiAlH_4$. The sulfide alcohol was obtained in 92% yield.

tert-Butyl o-Hydroxyphenyl Sulfide (Entry 22, Table 2)

α-Bromo-*o*-cresyl acetate (6.9 g, 0.03 mol) was added to a solution containing 2.7 g of *tert*-butylmercaptan (0.03 mol) and 1.7 g of KOH in 25 ml of CH_3OH. After a 30 min reaction time at room temperature, an additional 1.7 g of KOH were added, and stirring was continued for a further 30 min. The reaction mixture was acidified and extracted to furnish 5.4 g of the desired phenolic sulfide.

Oxidations of the Hydroxysulfoxides

General Procedures

These oxidations were carried out following the literature procedures. Method *A*: *tert*-butyl hypochlorite in CH_3OH at −70 °C (8). Method *B*: *meta*-chloroperbenzoic acid (8). As a variation of method *B*, we have found it advantageous to use ethyl acetate rather than CH_2Cl_2 as solvent. Its use permits relatively large scale oxidation reactions to be run under homogeneous conditions at temperatures of about −30 to −40 °C, conditions which result in very little overoxidation to hydroxy sulfones. The results together with the nmr spectral data of the hydroxy sulfoxides are given in Table 3. The preparation of hydroxy sulfoxides by routes other than by oxidation is described below. Elemental analyses were obtained only on the hydroxy sulfoxides which were crystalline substances and occasionally on the related hydroxy sulfones. The structures of all these compounds were readily identified on the basis of their nmr data and method of synthesis.

Preparation of γ-Hydroxy Sulfoxides via the Reaction of α-Lithio tert-Butyl Sulfoxides and Epoxides (Method C, Table 3)

The nmr spectra of the sulfoxides are described in Table 2.

(*a*) 4-*tert*-Butylsulfinylbutan-2-ol. The α-lithio derivative of *tert*-butyl methyl sulfoxide (30 mmol), prepared by reacting 3.6 g of *tert*-butyl methyl sulfoxide dissolved in 30 ml of dry tetrahydrofuran (THF) at 0 °C with 18.4 ml (33 mmol) of methyllithium for 5 min, was allowed to react with 1.8 g (31 mmol) of propylene oxide for 3 h at 0 °C. The usual work-up gave 4.7 g (88%) of the desired product.

(*b*) 3-*tert*-Butylsulfinyl-1-phenyl-1-propanol. This compound was prepared in 85% yield starting from 3.6 g (30 mmol) of *tert*-butyl methyl sulfoxide and 3.6 g (30 mmol) of styrene oxide as described above. See Table 3.

(*c*) 3-*tert*-Butylsulfinyl-1-phenyl-1-butanol. This compound was prepared as above from *tert*-butyl ethyl sulfoxide (4.0 g) and styrene oxide (3.6 g) in 88% yield. The crude product was recrystallized from ether–pentane to give a colorless crystalline solid, mp 67–69 °C. *Anal.* calcd. for $C_{14}H_{22}O_2S$: C 65.87, H 8.62; found: C 65.66, H 8.49.

(*d*) 4-*tert*-Butylsulfinylpentan-2-ol. Reaction of *tert*-butyl ethyl sulfoxide with 1.1 equiv. of methyllithium followed by 1 equiv. of propylene oxide gave after purification a 90% yield of the title compound as a viscous oil.

(*e*) 1-(β-*tert*-Butylsulfinyl)ethyl-4-*tert*-butylcyclohexanol. To a solution of 0.015 mol of α-lithiomethyl-*tert*-butyl sulfoxide in 25 ml of dry THF at 30 °C was added 2.4 g (0.015 mol) of the epoxide obtained from 4-*tert*-butylcyclohexane and dimethylsulfonium methylide in DMSO (20). The yield of hydroxy sulfoxide, mp 140 °C (dec.) was 60%.

Preparation of 3-tert-Butylsulfinyl-3-methyl-1-propanol

Methyllithium (33 mol) was added via syringe into a solution of 3-*tert*-butylsulfinyl-1-propanol (2.4 g 15 mmol) dissolved in 25 ml of dry THF at 0 °C. The reaction mixture was stirred for 5 min and 2.5 g of methyl iodide were added. The usual work-up, after 1 h of additional reaction time, gave 2.13 g (82%) of the desired hydroxy sulfoxide. After purification by column chromatography, the product showed infrared bands at 3330 (OH) and 1000 (S=O) cm^{-1}. See Table 3 for nmr data.

Preparation of 4-tert-Butylsulfinyl-4-methyl-1-butanol

A solution of 10 mmol of the dilithio salt of 4-*tert*-butylsulfinyl-1-butanol prepared as above was reacted for 1 h with 1.56 g (11 mmol) of methyl iodide. The usual work-up gave 1.5 g (80%) of the title hydroxy sulfoxide as a viscous oil after column chromatography.

Cyclization of Hydroxy Sulfoxides to Sultines

General Procedure

To a solution of hydroxy sulfoxide in CH_2Cl_2 at room temperature, 0 °C, or at −78 °C was added 1.1 equiv. of SO_2Cl_2 (generally neat). The reaction progress was followed by thin layer chromatography. After the disappearance of starting material, the volatile material was removed on the rotary evaporator. The crude product was generally purified by column chromatography, followed by distillation or recrystallization. Because of the instability of some of the sultines, analytical data were not obtained. The structures were assigned on the basis of their mode of preparation, spectroscopic properties, and by oxidation to the corresponding sultones. Infrared, nmr, and analytical data for the sultines is given below. The number in the section below corresponds to that of Table 1.

Spectroscopic Properties of the Sultines

(*1*) 1,2-Oxathiolan-2-oxide (**5**): ir 1110 cm^{-1}; nmr 1.7–3.2 (m, 4H), 4.0–4.7 (m, 2H); ms *Mol. Wt.* calcd: 106; found: 106. Oxidation with *meta*-chloroperbenzoic acid gave 94% of 1,3-propane sultone.

(*2*) 1,2-Oxathiane-2-oxide (**6**): bp 59–60 °C/0.5 torr; ir 1120 cm^{-1}; nmr 1.5–2.2 (m, 3H), 2.2–3.0 (m, 3H), 3.6–3.8 (m, 1H), 4.3–4.7 (m, 1H); ms *Mol. Wt.* calcd: 120.0247; found: 120.0245. Oxidation gave 1,4-butane sultone in 90% yield.

(*3*) 1,2-Oxathiepane-2-oxide (**7**): ir 1110 cm^{-1}; nmr 1.2–2.2 (m, 6H), 2.6–2.8 (m, 2H), 3.8–4.2 (m, 2H); ms *Mol. Wt.* calcd: 134; found: 134. *Anal.* calcd. for $C_5H_{10}O_2S$: C 44.75, H 7.51, S 23.89; found: C 44.84, H 7.41, S 23.04. Oxidation afforded 1,2-oxathiepane-2,2-dioxide (ir 1138, 1150, and 895 cm^{-1}) in 90% yield.

(*4*) 1,2-Oxathiocane-2-oxide (**8**): ir 1110 cm^{-1}; nmr 1.2–2.2 (m, 8H), 2.5–3.0 (m, 2H), 3.8–4.2 (m, 2H); ms 148. *Anal.* calcd. for $C_6H_{12}O_2S$: C 48.64, H 8.16, S 21.60; found: C 48.21, H 8.04, S 22.12.

Can. J. Chem. Downloaded from www.nrcresearchpress.com by 210.87.254.40 on 09/05/12
For personal use only.

TABLE 3. *tert*-Butyl hydroxyalkyl sulfoxides[a]

Entry	Sulfoxide	Method of oxidation	Yield (%)	nmr data
1	*t*-BuS(O)$(CH_2)_3OH$	*A*[b]	75	1.30(s, 9H), 1.8–2.4(m, 2H), 2.5–2.9(m, 2H), 3.75(t, J = 6 Hz, 2H), 3.75(1H, OH)
2	*t*-BuS(O)$(CH_2)_4OH$	*A*	75	1.33(s, 9H), 1.6–2.3(m, 4H), 2.3–2.8(m, 2H), 3.3–4.0(m, 3H)
3	*t*-BuS(O)$(CH_2)_5OH$	*A*	72	1.30(s, 9H), 1.4–2.0(m, 7H), 2.3–2.6(m, 2H), 3.5–3.7(m, 2H)
4	*t*-BuS(O)$(CH_2)_6OH$	*A*	70	1.32(s, 9H), 1.4–2.0(m, 9H), 2.3–2.7(m, 2H), 3.5–3.7(m, 2H)
5	*t*-BuS(O)$CH(CH_2)_2OH$, CH_3	—[e]	82	1.3(s, 9H), 1.30, 1.34(2 d's, 3H), 1.6–2.3(m, 2H), 2.7–3.4(m, 1H), 3.4–4.0(m, 3H)
6	*t*-BuS(O)$CH_2CH(CH_3)CH_2OH$	*A*	70	1.0–1.35(m, 12H), 1.9–3.0(m, 3H), 3.1–3.9(m, 2H), 4.5(1H, OH)
7	*t*-BuS(O)$(CH_2)_2CHCH_3$, OH	*C*[d]	88	1.3–1.4(m, 12H), 1.6–2.9(m, 4H), 3.4(1H, OH), 3.7–4.3(m, 1H)
8	*t*-BuS(O)$CH(CH_2)_2OH$[f], Ph	*B*[c]	50	1.03(s, 9H), 1.9–2.6(m, 3H), 3.3–4.2(m, 3H), 7.2–7.5(m, 5H)
9	*t*-BuS(O)$CH_2CH(Ph)CH_2OH$[g]	*B*	62	Less polar isomer: 1.27(s, 9H), 2.7–3.2(m, 3H), 3.4–3.6(m, 1H), 4.03(d, J = 6 Hz, 2H), 7.33(5H). More polar isomer: 1.26(s, 9H), 2.6–3.1(m, 3H), 3.3–4.0(m, 3H), 7.39(5H),
10	*t*-BuS(O)$(CH_2)_2CHPh$, OH	*C*	85	1.25(s, 9H), 2.0–2.7(m, 4H), 4.3–5.0(m, 2H), 7.0–7.4(m, 5H)
11	*t*-BuS(O)$CH(CH_3)CH_2CHCH_3$, OH	*C*	90	1.0–1.4(m, 15H), 1.5–2.4(m, 3H), 2.9–3.4(m, 1H), 3.2–4.1(m, 1H)
12	*t*-BuS(O)$CH(CH_3)CH_2CHPh$, OH	*C*	88	1.23(s, 9H), 1.3(d, J = 6 Hz, 3H), 1.6–3.3(m, 3H), 3.8(1H, OH), 4.9–5.0(m, 1H), 7.1–7.4(m, 5H)
13	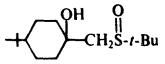	*C*	60	0.9(s, 9H), 1.28(s, 9H), 1.0–2.9(m, 13H), 3.1(1H, OH)

Can. J. Chem. Downloaded from www.nrcresearchpress.com by 210.87.254.40 on 09/05/12
For personal use only.

TABLE 3 (*Concluded*)

Entry	Sulfoxide	Method of oxidation	Yield (%)	nmr data
14	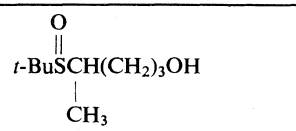	—[e]	80	1.1–1.3(12H), 1.3–2.0(m, 4H), 2.2–2.9(m, 1H), 3.4–3.6(m, 2H), 4.0(1H, OH)
15	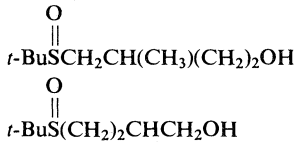	*A*	70	1.0–1.35(d + s, 12H), 1.9–3.0(m, 5H), 3.1–3.9(m, 2H), 4.5(1H, OH)
16	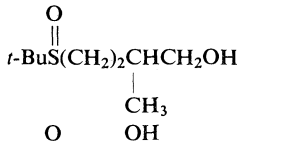	*B*	60	0.94 and 0.95(2d, J = 6 Hz, 3H), 1.25(s, 9H), 1.6–1.9(m, 3H), 1.9–2.4(m, 3H), 3.2(d, J = 5 Hz, 2H)
17	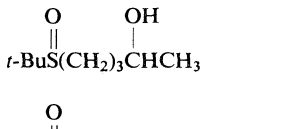	*B*	80	1.2 and 1.26(2d, J = 6 Hz, 3H), 1.25(s, 9H), 1.4-2.2(m, 4H), 2.3–2.9(m, 2H), 3.2–4.0(m, 2H)
18	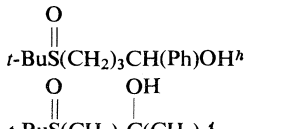	*B*	70	1.20(s, 9H), 1.6–2.0(m, 4H), 2.1–2.7(m, 3H), 4.5–4.7(m, 1H), 7.15(s, 5H)
19	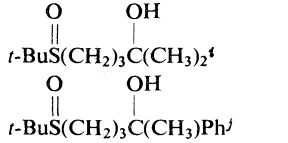	*B*	70	1.14(s, 6H), 1.18(s, 9H), 1.4–2.2(m, 4H), 2.3–2.6(m, 2H), 3.76(1H, OH)
20	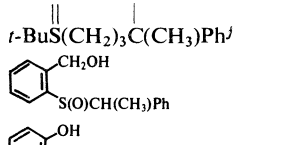	*B*	60	1.13(s, 9H), 1.53(s, 3H), 1.6–2.1(m, 2H), 2.2–2.7(m, 2H), 3.3(1H, OH), 7.1–7.5(m, 5H)
21		*B*	85	1.55(d, J = 7.0 Hz, 3H), 3.5(1H, OH), 3.9–4.7(m, 3H), 6.9–7.5(m, 9H)
22*a*	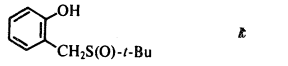 [k]	*B*	80	1.4(s, 9H), 3.86(d, J = 12 Hz, 1H), 4.46(d, J = 12 Hz, 1H), 6.7–7.4(m, 5H, includes OH)
22*b*	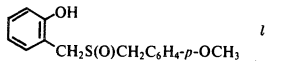 [l]	*B*	60	3.8(s, 3H), 3.6–4.2(m, 4H), 6.7–7.5(m, 9H)
23	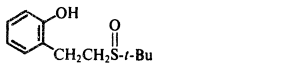	—[e]	70	1.25(s, 9H), 1.6–2.2(m, 4H), 6.9–7.3(m, 5H)

[a] The numbered entries in each table correspond to each other.
[b] Using *tert*-butyl hypochlorite.
[c] Using *meta*-chloroperbenzoic acid.
[d] *tert*-BuS(O)CH_2Li and epoxides.
[e] See Experimental section.
[f] mp 94–96 °C. *Anal.* found: C 64.95, H 8.42, S 13.65.
[g] Less polar isomer: mp 95–96 °C. *Anal.* found: C 64.55, H 8.23. More polar isomer (major product): mp 125–126 °C. *Anal.* found: C 64.17, H 8.35.
[h] mp 56–59 °C. The corresponding sulfone had mp 94–95 °C. *Anal.* found: C 62.63, H 8.46.
[i] mp 47–49 °C. For the sulfone: mp 66–67 °C. *Anal.* found: C 54.38, H 10.37.
[j] mp 80–81 °C. *Anal.* found: C 66.73, H 8.59, S 11.82; mp of the sulfone, 104–105 °C.
[k] mp 154–156 °C. *Anal.* found: C 62.14, H 7.62, S 15.84.
[l] mp 105–107 °C. *Anal.* found: C 65.36, H 5.74, S 11.82.

Can. J. Chem. Downloaded from www.nrcresearchpress.com by 210.87.254.40 on 09/05/12
For personal use only.

(*5*) 3-Methyl-1,2-oxathiolan-2-oxide: ir 1100 cm^{-1}; nmr 1.22 and 1.38 (both d, J = 7 Hz, 3H), 1.75–3.5 (m, 3H), 4.2–4.9 (m, 2H); ms 120. *Anal.* calcd. for $C_4H_8O_2S$: C 39.98, H 6.71; found: C 39.67, H 6.37. Oxidation gave the corresponding dioxide (sultone) in 80% yield (ir 1325, 1130, and 880 cm^{-1}).

(*6*) 4-Methyl-1,2-oxathiolan-2-oxide: ir 1110 cm^{-1}; nmr 1.07 and 1.18 (both d, J = 7 Hz, 3H), 2.2–4.9 (m, 5H). ms 120. *Anal.* calcd. for $C_4H_8O_2S$: C 39.98, H 6.71; found: C 39.76, H 6.75. The corresponding sultone (ir 1340, 1160, and 950 cm^{-1}) was formed in 89% yield.

(*7*) 5-Methyl-1,2-oxathiolan-2-oxide: ir 1120 cm^{-1}; nmr 1.39 and 1.59 (both d, J = 6 Hz, 3H), 2.2–3.4 (m, 3H), 4.7–5.2 (m, 1H); ms 120. *Anal.* calcd. for $C_4H_8O_2S$: C 39.98, H 6.71; found: C 40.00, H 6.47. Peracid oxidation gave 5-methyl-1,2-oxathiolane-2,2-dioxide in 80% yield (ir 1350 and 1160 cm^{-1}).

(*8*) Attempted preparation of 3-phenyl-1,2-oxathiolane-2-oxide (**10**). The reaction of the hydroxy sulfoxides **11***a* or **11***b* with SO_2Cl_2 under the usual conditions gave mixtures of products from which the only isolated material was 1-phenyl-1,3-dichloropropane.

(*9*) 4-Phenyl-1,2-oxathiolan-2-oxide. Less polar isomer (**14**): ir 1100, 1135 cm^{-1}; nmr see text. *Anal.* calcd. for $C_9H_{12}O_2S$: C 59.31, H 5.53, S 17.59; found: C 59.52, H 5.55, S 17.07. More polar isomer (**15**): mp 63–63.5 °C; ir 1110 and 1130 cm^{-1}; nmr see text. *Anal.* found: C 59.27, H 5.63, S 17.71.

The separation of the two isomers was successful using a silica gel column and eluting with a 7:2:1 mixture of hexane, ethyl acetate, and methylene chloride. From 3.2 g of precursor hydroxy sulfoxide was obtained 0.75 g of the less and 1.2 g of the more polar isomer. The ratios depended somewhat on the method, since the less polar isomer isomerized slowly to the more polar one. Overall yield, 81%.

(*10*) 5-Phenyl-1,2-oxathiolan-2-oxide: ir 1110 cm^{-1}; nmr 2.5–3.5 (m, 4H), 5.45–6.0 (m, 1H), 7.2–7.5 (m, 5H); ms 182.

(*11*) 3,5-Dimethyl-1,2-oxathiolane-2-oxide: ir 1105 cm^{-1}; nmr 1.1–1.6 (4 d's, 6H), 1.7–2.7 (m, 2H), 2.8–3.5 (m, 1H); ms 134.

(*12*) 3-Methyl-5-phenyl-1,2-oxathiolan-2-oxide: ir 1105 cm^{-1}; nmr 1.25–1.31 (2 d's, 3H), 2.0–3.0 (m, 2H), 3.3–3.6 (m, 1H), 5.4–6.1 (m, 1H), 7.1–7.4 (m, 5H); ms 196. *Anal.* calcd. for $C_{10}H_{12}O_2S$: C 61.79, H 6.16, S 16.03; found: C 61.95, H 6.44, S 15.41.

(*13*) 7-*tert*-Butyl-1,2-oxathiospiro[4,5]nonane-2-oxide: mp 114–116 °C; ir 1110 cm^{-1}; nmr 0.86 (s, 9H), 1.3–2.5 (m, 11H), 2.95–3.15 (m, 2H); ms 230. *Anal.* calcd. for $C_{12}H_{22}O_2S$: C 62.58, H 9.63, S 11.40; found: C 62.46, H 9.54, S 11.82.

(*14*) 3-Methyl-1,2-oxathiane-2-oxide (**21**): ir 1120 cm^{-1}; nmr 1.08 (d, J = 6 Hz, 3H), 1.1–3.0 (s, 5H), 3.3–3.8 (m, 1H) and 4.0–4.6 (m, 1H); ms 134. *Anal.* calcd. for $C_5H_{10}O_2S$: C 44.75, H 7.51; found: C 44.63, H 7.62.

(*15*) 4-Methyl-1,2-oxathiane-2-oxide (**20**): ir 1120 cm^{-1}; nmr 1.0 (d, J = 6 Hz, 3H), 1.2–1.9 (m, 2H), 2.3–2.8 (m, 3H), 3.75–4.0 (m, 1H), 4.4–4.7 (m, 1H); ms 134.039. *Anal.* calcd. for $C_5H_{10}O_2S$: C 44.75, H 7.51; found, C 44.89, H 7.72.

(*16*) 5-Methyl-1,2-oxathiane-2-oxide (**19**): ir 1105 cm^{-1}; nmr 0.87 (d, J = 6 Hz, 3H), 1.3–3.0 (m, 5H), 3.6–3.8 (m, 1H), 4.0–4.5 (m, 1H); ms 134.040. *Anal.* calcd. for $C_5H_{10}O_2S$: C 44.75, H 7.51; found: C 44.64, H 7.42.

(*17*) 6-Methyl-1,2-oxathiane-2-oxide (**18***a*): ir 1110 cm^{-1}; nmr 1.22 (d, J = 6 Hz, 3H), 1.45–2.0 (m, 3H), 2.3–2.8 (m, 3H), 4.5–4.9 (m, 1H); ms 134.040.

(*18*) 6-Phenyl-1,2-oxathiane-2-oxide (**18***b*): ir 1125 cm^{-1}; nmr 1.2–2.2 (m, 3H), 2.5–2.9 (m, 3H), 5.37 (d of d, J = 9 and 6 Hz, 1H), 7.3 (m, 5H); ms 196.056. *Anal.* calcd. for $C_{10}H_{12}O_2S$: C 61.19, H 6.16; found: C 61.07, H 6.26.

(*19*) 6,6-Dimethyl-1,2-oxathiane-2-oxide (**22**): ir 1135 cm^{-1}; nmr 1.25 (s, 3H), 1.57 (s, 3H), 1.6–1.9 (m, 3H), 2.35–2.75 (m, 3H); ms 148.056. *Anal.* calcd. for $C_6H_{12}O_2S$: C 48.64, H 8.16; found: C 48.14, H 8.31.

(*20*) 6-Methyl-6-phenyl-1,2-oxathiane-2-oxide. Mixture of two isomers. *Anal.* calcd. for $C_{11}H_{14}O_2S$: C 68.82, H 6.71; found: C 62.96, H 6.87. More polar isomer: nmr 1.58 (s, 3H), 1.7–3.2 (m, 6H), and 7.1–7.5 (m, 5H). Less polar isomer: nmr 1.90 (s, 3H), 2 multiplets centred at about 2.25 and 2.75 δ each 3H, 7.2 (s, 5H).

(*21*) 3*H*-2,1-Benzoxathiole-1-oxide (**23**): mp 39–40 °C (lit. mp (17) 39–40 °C); ir 1120 cm^{-1}; nmr 5.42 (d, J = 13.5 Hz, 1H), 5.78 (d, J = 13.5 Hz, 1H), 7.2 (m, 4H).

(*22*) Attempted synthesis of 3*H*-1,2-benzoxathiole-2-oxide (**25**): see text for a discussion of this reaction.

(*23*) 3,4-Dihydro-1,2-benzoxathiin-2-oxide (**29**): this sultine was prepared in 95% crude yield (nmr 2.3–3.5 (m, 4H), 6.8–7.4 (m, 4H)) and oxidized immediately to the corresponding dioxide, (75% yield), mp 108–110 °C, (lit. (2*b*) mp 108–109 °C).

1. (*a*) N. K. Sharma, F. Jung, and T. Durst. Tetrahedron Lett. 2863 (1973); (*b*) F. Jung and T. Durst. Chem. Commun. 4 (1973).
2. (*a*) R. M. Dodson, P. D. Hammen, and R. H. Davis. J. Org. Chem. **36**, 2693 (1973); (*b*) E. N. Givens and L. A. Hamilton. J. Org. Chem. **32**, 2857 (1967).
3. (*a*) D. C. Dittmer, R. S. Henion, and N. Takashina. J. Org. Chem. **34**, 1310 (1969); (*b*) J. F. King, P. de Mayo, C. L. McIntosh, K. Piers, and D. J. H. Smith. Can. J. Chem. **48**, 3704 (1970), and references therein; (*c*) C. R. Hall and D. J. H. Smith. Tetrahedron Lett. 3633 (1974).
4. D. N. Harpp and J. G. Gleason. Tetrahedron Lett. 1447 (1969).
5. (*a*) K. S. Dhami. Chem. Ind. (London), 1004 (1968); (*b*) Indian J. Chem. **12**, 278 (1974); (*c*) K. Henrick and B. L. Johnson. Aust. J. Chem. **25**, 2263 (1972).
6. F. Jung, N. K. Sharma, and T. Durst. J. Am. Chem. Soc. **95**, 3420 (1973).
7. T. Durst and B. Gimbarzevsky. J. Chem. Soc. Chem. Commun. 724 (1975).
8. C. R. Johnson and D. McCants, Jr. J. Am. Chem. Soc. **87**, 1109 (1965).
9. D. N. Harpp and J. G. Gleason. J. Org. Chem. **36**, 1314 (1971).
10. T. Durst and K. C. Tin. Can. J. Chem. **48**, 845 (1970).
11. (*a*) J. L. Kice. *In* The chemistry of organic sulfur compounds. *Edited by* N. Kharasch and C. Y. Meyers. Pergamon Press, Oxford. 1966. Chapt. 5; (*b*) M. S. Kharasch, E. N. May, and F. R. Mayo. J. Org. Chem. **3**, 189 (1940).

12. W. O. SIEGL and C. R. JOHNSON. J. Org. Chem. **35**, 3657 (1970).
13. (*a*) K. W. BUCK, A. B. FOSTER, W. D. PARDOE, M. H. QADIR, and J. M. WEBER. J. Chem. Soc. Chem. Commun. 357 (1966); (*b*) E. JOHNSON and S. HOHNQUIST. Ark. Kemi, **29**, 301 (1968); (*c*) I. SATATY. Org. Magn. Reson. **6**, 8 (1974).
14. F. JUNG, M. MOLIN, R. VAN DEN ELZEN, and T. DURST. J. Am. Chem. Soc. **96**, 935 (1974).
15. L. CAZAUX, G. CHASSAING, and P. MARONI. Tetrahedron Lett. 2517 (1975).
16. K. MISLOW, T. SIMMONS, J. T. MELILLO, and A. L. TERNAY, JR. J. Am. Chem. Soc. **86**, 1452 (1964).
17. J. F. KING, B. L. HUSTON, H. HAWSON, J. KOMERY, D. M. DEAKEN, and R. D. K. HARDING. Can. J. Chem. **49**, 936 (1971).
18. (*a*) S. BORY, R. LETT, B. MOREAU, and A. MARQUET. C.R. Acad. Sci. Ser. C. **276**, 1323 (1973); (*b*) P. CALZAVARA, M. CINQUINI, S. COLONNA, R. FORNASIER, and F. MONTANARI. J. Am. Chem. Soc. **95**, 7431 (1973); (*c*) J. KLEIN and H. STOLLAR. J. Am. Chem. Soc. **95**, 7473 (1973); (*d*) S. IRIUCHIJIMA, M. ISHIBASHI, and G. TSUCHIHASHI. Bull. Chem. Soc. Jpn. **46**, 921 (1973).
19. (*a*) T. DURST, K. C. TIN, and M. J. V. MARCIL. Can. J. Chem. **51**, 1704 (1973); (*b*) F. JUNG and T. DURST. J. Chem. Soc. Chem. Commun. 4, (1973).
20. E. J. COREY and M. CHAYKOVSKY. J. Am. Chem. Soc. **87**, 1345 (1965).

Can. J. Chem. Downloaded from www.nrcresearchpress.com by 210.87.254.40 on 09/05/12
For personal use only.

On the photoelectron and ultraviolet spectra of molecules containing a divalent sulfur atom and a carbonyl group separated by a methylene group

P. R. OLIVATO, H. VIERTLER, AND B. WLADISLAW
Instituto de Quimica, Universidade de São Paulo, São Paulo, Brasil

AND

K. C. COLE AND C. SANDORFY
Département de Chimie, Université de Montréal, Montréal, Qué., Canada H3C 1V1

Received May 10, 1976

P. R. OLIVATO, H. VIERTLER, B. WLADISLAW, K. C. COLE and C. SANDORFY. Can. J. Chem. **54**, 3026 (1976).

Photoelectron spectra show that in $CH_3SCH_2COCH_3$ the sulfur and carbonyl lone pair orbitals ($\bar{S}$,$\bar{O}$) are both stabilized with respect to the compounds containing S or CO only. This is in keeping with the observed values of the basicity constants. The ultraviolet absorption spectra contain the expected $\pi^* \leftarrow \bar{O}$ and $\sigma^* \leftarrow \bar{S}$ bands and give evidence for a significant amount of mixing between the excited orbitals.

P. R. OLIVATO, H. VIERTLER, B. WLADISLAW, K. C. COLE et C. SANDORFY. Can. J. Chem. **54**, 3026 (1976).

Nous avons mis en évidence par la mesure de spectres photoélectroniques que dans la molécule $CH_3SCH_2COCH_3$ les orbitales des doublets libres du soufre et du carbonyle sont toutes deux stabilisées par rapport à leur valeur dans les molécules respectives qui ne contiennent que S ou CO. Cela est en accord avec les valeurs observées des constantes de basicité. Les fréquences des bandes $\pi^* \leftarrow \bar{O}$ et $\sigma^* \leftarrow \bar{S}$ dans le spectre d'absorption ultraviolet indiquent qu'il se produit un mélange appréciable entre les orbitales excitées.

Introduction

The work reported in this paper is an attempt to obtain additional information on the extent to which a divalent sulfur atom and a carbonyl group separated by a $-CH_2-$group interact in the molecular ground state and in the lowest singlet excited states. Previously this problem has been examined by ultraviolet, infrared and nmr spectroscopic measurements (1–6). We now present the He(I) photoelectron spectra of the following molecules:

$CH_3SCH_2CH_2CH_3$ (**1**), $CH_3COCH_2CH_2CH_3$ (**2**), $CH_3SCH_2COCH_3$ (**3**), $CH_3OCH_2COCH_3$ (**4**), $CH_3CH_2CH_2COOCH_3$ (**5**), $CH_3OCH_2COOCH_3$ (**6**), and $CH_3SCH_2COOCH_3$ (**7**).

They will be interpreted together with some of the related ultraviolet spectra.

Experimental

The photoelectron spectra were measured on a Perkin-Elmer PS-16 instrument with a He(I) source. All ionization potentials cited in the paper are vertical values. The ultraviolet absorption spectra were measured in *n*-hexane and 50% (v/v) ethanol–water solutions on a Cary-14 spectrometer and on a Beckman DK-2A spectrometer.

Reagents

Commercial 2-pentanone (BDH) was purified as described elsewhere (7). Methyl *n*-propyl sulfide (8), 4-thiapentan-2-one (9), 4-oxapentan-2-one (10), methyl butanoate (11), methyl 3-oxabutanoate (12), and methyl 3-thiabutanoate (13) were prepared by literature procedures. All compounds were analyzed by glc to assess their purity.

Results and Discussion

The Photoelectron Spectra

The photoelectron (PE) spectrum of 4-thiapentan-2-one (**3**) is given in Fig. 1. Its ionization potential (IP) is 8.84 eV (71 300 cm^{-1}) while the second photoelectron band is at 9.90 eV (79 800 cm^{-1}). Table 1 compares these values to those for the related thioether (**1**) and ketone (**2**) as well as to methyl *n*-propylether and 4-oxapentan-2-one (**4**).

Before drawing conclusions from these data we have to emphasize the dangers of basing arguments on small differences in IP's. First, any such argument uses the orbital concept and supposes the validity of Koopmans' theorem which does not take adequate account of energy changes due to electronic rearrangement upon

Can. J. Chem. Downloaded from www.nrcresearchpress.com by 210.87.254.105 on 09/05/12
For personal use only.

Can. J. Chem. Downloaded from www.nrcresearchpress.com by 210.87.254.105 on 09/05/12
For personal use only.

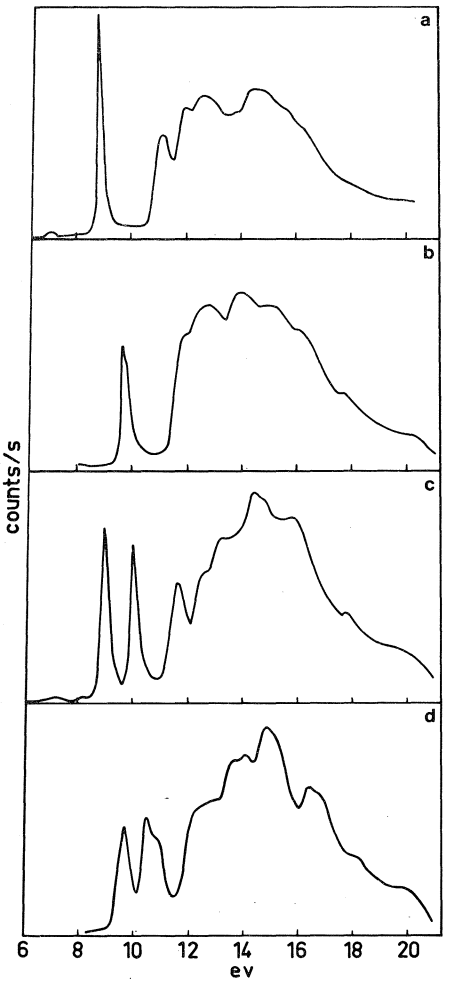

FIG. 1. The He(I) – photoelectron spectra of CH_3SCH_2-CH_2CH_3 (*a*), $CH_3COCH_2CH_2CH_3$ (*b*), $CH_3SCH_2COCH_3$ (*c*), and $CH_3OCH_2COCH_3$ (*d*). Counts s^{-1} against electron volts.

TABLE 1. Lowest photoelectron bands in eV

Compound	Band (eV)	
$CH_3SCH_2CH_2CH_3$	8.49	
$CH_3CH_2CH_2COCH_3$	9.45	
$CH_3SCH_2COCH_3$	8.84	9.90
$CH_3OCH_2CH_2CH_3$	9.74	(estimated)
$CH_3CH_2CH_2COCH_3$	9.45	
$CH_3OCH_2COCH_3$	9.62	10.44
$CH_3CH_2CH_2COOCH_3$	10.29	
$CH_3SCH_2COOCH_3$	8.81	10.54
$CH_3OCH_2COOCH_3$	9.94	~10.9 sh 11.23

ionization. Second, IP's belonging to lone pairs of electrons (and these are most important for the present problem) can be rather sensitive to their environment in the molecule. The data collected in Table 2, taken from the literature, illustrate this point. Therefore it is essential to compare closely related compounds only as we have done in Table 1.

There is no doubt that the first photoelectron band in all these compounds relates to ionization from the sulfur or oxygen lone pair. It is usually more than 1 eV lower for $\bar{S}$ than for $\bar{O}$ (14–20). For the first IP of methyl *n*-propyl sulfide (**1**) we obtained 8.49 eV (68 450 cm^{-1}). This is nearly equal to the arithmetic mean of the IP's of dimethyl sulfide and di-*n*-propyl sulfide, 8.67 and 8.34 eV respectively.

Since no sample of methyl *n*-propyl ether was available to us we estimated its IP from the known values for dimethyl ether, 10.04 eV (21), and diethyl ether, 9.63 eV (22) according to a procedure described by Cocksey, Eland, and Danby (23) who take account of the inductive effect of alkyl groups by comparing the IP's in series of alcohols, ethers, aldehydes, ketones, iodides and several other types of compounds. We obtained 9.74 eV (78 550 cm^{-1}). The IP for 4-thiapentan-2-one (**3**), the molecule of central interest to us, is 8.84 eV (71 300 cm^{-1}) which is higher than that of the sulfide (8.49 eV). The second photoelectron band of (**3**) (9.90 eV or 79 800 cm^{-1}) can only relate to ionization from the carbonyl oxygen lone pair orbital (*cf.* 24–28) which in the ketone (**2**) is related to the IP at 9.45 eV.

We believe that this is a significant result: the presence of both a sulfur and a carbonyl–oxygen lone pair in **3** leads to the stabilization of both with respect to the compounds containing S or CO only.

The interaction between two lone pair orbitals can be discussed in terms of through-space and through-bond contributions as proposed by Hoffmann (29, 30). Most of our present knowledge relates, however, to two identical lone pairs. The problem we have to face for —S—CH_2—CO— is rather more complicated. No definite conclusions can be reached without a refined quantum-mechanical calculation and this is yet to be carried out. A similar observation is made for methyl 3-thiabutanoate (**7**). Both $\bar{S}$ and $\bar{O}$ orbitals shift to higher energies; $\bar{S}$ from

TABLE 2. Vertical ionization potentials in eV

Sulfide	IP	Ref.	Ether	IP	Ref.	Ketone	IP	Ref.
Me_2S	8.67	19	Me_2O	10.04	21	MeCOMe	9.71	24
Et_2S	8.44	19	Et_2O	9.63	22	EtCOMe	9.52	24
$(n\text{Pr})_2S$	8.34	19				*i*BuCOMe	9.42	24
$(i\text{Pr})_2S$	8.26	19				*i*PrCOMe	9.36	24
$(n\text{Bu})_2S$	8.22	19				*i*BuCOMe	9.21	24
$(i\text{Bu})_2S$	8.13	19						
$(t\text{Bu})_2S$	8.07	19						
Tetrahydrothiophene	8.40	19	Tetrahydrofuran	9.73	22	Cyclopentanone	9.25	34
Tetrahydrothiapyran	8.39	36	Tetrahydropyran	9.46	36	Cyclohexanone	9.14	35

8.49 to 8.81 and $\bar{O}$ from 10.29 to 10.54 eV (Fig. 2).

The onset of ionization of the bonding orbitals is at about 10.8–11.2 eV in all these PE spectra. We refrain from dealing with these bands in detail since we have no theoretical basis for assigning them. The IP corresponding to the other (non-carbonyl) ester oxygen is also at these higher energies (25).

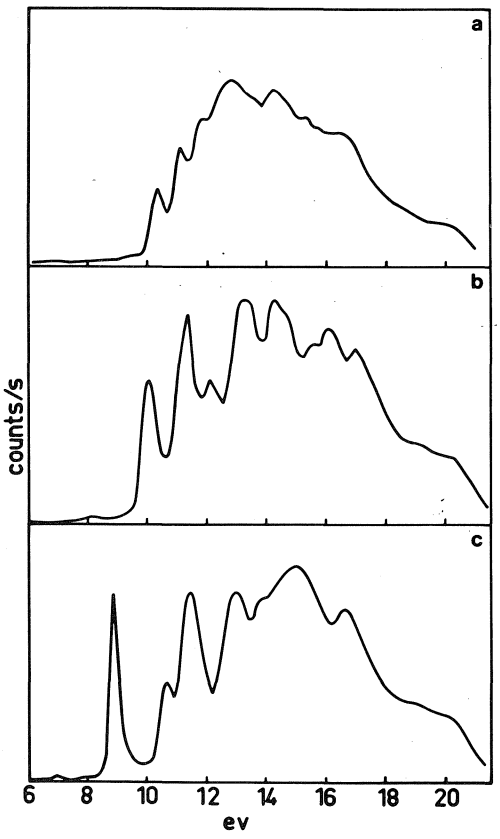

FIG. 2. The He(I) – photoelectron spectra of CH_3CH_2-CH_2COOCH_3 (*a*), $CH_3OCH_2COOCH_3$ (*b*), and CH_3-SCH_2COOCH_3 (*c*). Counts s^{-1} against electron volts.

In the compounds where —O— replaces —S— (Table 1) the carbonyl oxygen lone pair seems to be connected with the first and the ether oxygen lone pair with the second band in the PE spectrum. From available data on ketones and ethers we can deduce that the first IP's for the ethers are always somewhat higher than for carbonyls. The same applies for diethers *vs.* diketones (15, 26). Then we see that the carbonyl $\bar{O}$ is stabilized slightly while the ether $\bar{O}$ is stabilized quite appreciably by the interaction. In methyl 3-oxabutanoate (**6**) at first sight at least both IP's are stabilized: instead of 9.74 we find 9.94 and instead of 10.29 we find a composite band with a shoulder at 10.9 and a peak at 11.23 eV. A switchover of the levels is not entirely ruled out, however, and we will refrain from pushing the argument further. Theoretical work is clearly needed.

The large decrease in basicity constants, observed for the cyclic and open-chain 3-thiaketones (3, 6), is thus parallelled by the trend in the IP's. The slight stabilization of the carbonyl oxygen lone pair in the oxa-ketone is also in agreement with the K_{as} data in the cyclic series (6), which showed that the replacement of the β-methylene in cyclopentanone by oxygen affects only slightly the basicity, much less than replacement by sulfur. This point will be discussed in a later publication.

The Ultraviolet Absorption Spectrum of $CH_3SCH_2COCH_3$

As is well known, aliphatic ketones have only one (singlet–singlet) band at wavelengths longer than 200 nm, the $\pi^* \leftarrow$ n band. In 2-pentanone (**2**) its maximum is at 282 nm (35 500 cm^{-1}) in *n*-hexane and at 273 nm (36 600 cm^{-1}) in 50%

Can. J. Chem. Downloaded from www.nrcresearchpress.com by 210.87.254.105 on 09/05/12
For personal use only.

Can. J. Chem. Downloaded from www.nrcresearchpress.com by 210.87.254.105 on 09/05/12
For personal use only.

(v/v) ethanol–water. As expected 4-oxapentan-2-one (**4**) does not differ significantly from this pattern: the band has its maximum at practically the same wavelength (285 nm in *n*-hexane and 273 nm in 50% (v/v) ethanol–water). A second band appears at 204 nm (49 000 cm^{-1}) in *n*-hexane and 207 nm (48 300 cm^{-1}) in 50% (v/v) ethanol–water.

The spectra of saturated thioethers present some problems (31–39) but recently a satisfactory degree of understanding has been achieved. The pertaining argument has been thoroughly discussed by Robin (40). All the known bands of sulfides are due to transitions from the sulfur lone pair orbital. In H_2S this is $2b_1$, antisymmetrical with respect to reflection in the molecular plane. From there transitions are possible to two empty valence-shell orbitals ($6a_1$ and $3b_2$) which are antibonding combinations of the S—H orbitals (σ^*). However, the 4*s* Rydberg band falls into the same part of the spectrum. The 4*p* band comes in at higher frequencies. The result is that the lowest frequency region of the absorption spectrum receives contributions from the $4s \leftarrow 2b_1$, $6a_1\sigma^* \leftarrow 2b_1$, and $3b_2\sigma^* \leftarrow 2b_1$ transitions. The situation is similar in thioethers, like CH_3SCH_3, or other methyl alkyl sulfides.

The $4s \leftarrow \bar{S}$ band is near 220–230 nm (44 000 – 46 000 cm^{-1}) and it is overlapped by (probably) two bands due to valence-shell transitions. These bands are weak with ϵ values in the hundreds.

The $4p \leftarrow \bar{S}$ manifold (usually two bands) is located between 200 and 190 nm (49 000 – 52 000 cm^{-1}).

The spectrum of 4-thiapentan-2-one (**3**) contains both the carbonyl $\pi^* \leftarrow$ n band and the thioether bands but they are significantly shifted from their 'original' location (Fig. 3). In *n*-hexane solution the band of lowest wavenumber has its maximum at 302 nm (33 100 cm^{-1}; ϵ = 218 l mol^{-1} cm^{-1}) followed by a somewhat more intense band at 241 nm (41 500 cm^{-1}; ϵ = 375) and a strong band at 218 nm (45 900 cm^{-1}). In 50% (v/v) ethanol–water solution the first band shifts to 295 nm (33 900 cm^{-1}); ϵ = 288) and the second one to 243 nm (41 150 cm^{-1}; ϵ = 328).

The relative intensities and wavenumbers of the bands as well as the solvent shifts are in agreement with the assignment of the first band of the carbonyl $\pi^* \leftarrow$ n transition and the second band to transitions from the sulfur lone pair. Indeed, no ketones have bands near 240 nm (43 300 cm^{-1}). The Rydberg (4*s*) band is unlikely to be identifiable since in condensed phases Rydberg bands usually undergo extensive broadening and 'disappear' in the background (41). The gas phase spectra have not been measured yet.

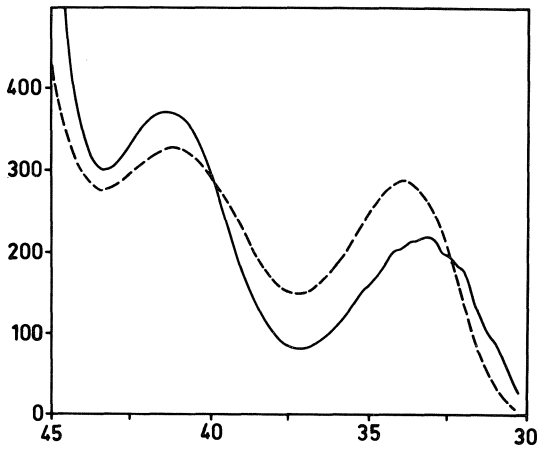

FIG. 3. The ultraviolet absorption spectrum of $CH_3SCH_2COCH_3$. Molar extinction coefficients against wavenumbers in cm^{-1}: —, in *n*-hexane, --- in 50% ethanol–water solution.

Thus we assign the band at 302 nm to the carbonyl $\pi^* \leftarrow$ n band and the band at 240 nm to the valence-shell transitions from the sulfur lone pair orbital. If so the only new fact is the quite sizable bathochromic shifts which both bands underwent. This is made more significant by the fact that as shown by the ionization potentials the orbitals with which these transitions originate were actually stabilized for both. This indicates a high degree of mutual influence between the original π^* and σ^* orbitals, certainly an important fact for the interpretation of these spectra.

These assignments put the carbonyl $\pi^* \leftarrow$ n transition to lower energies than the sulfur $\sigma^* \leftarrow$ n (and 4*s*) bands while the *n* IP's are in the opposite order. It might seem to be possible that the bands have switched places, with the 302 nm band the $\sigma^* \leftarrow \bar{S}$ band and the 240 nm band the carbonyl $\pi^* \leftarrow$ n band. This is rendered very unlikely in view of the observed spectra. A $\sigma^* \leftarrow \bar{S}$ band at 302 nm would be very low and a $\pi^* \leftarrow \bar{O}$ band at 240 nm would be very high indeed. We have little information

Can. J. Chem. Downloaded from www.nrcresearchpress.com by 210.87.254.105 on 09/05/12
For personal use only.

on the relative positions and mixing between the excited orbitals and this interpretation is not entirely ruled out. Only one thing is certain: the band at 302 nm cannot be the $4s \leftarrow \bar{S}$ Rydberg band. It would have a term value of about 37 000 cm^{-1} which is much too high (40). There is no such criterion relating to σ^* and although it is in near-coincidence with $4s$ in all the thioether spectra known to us, it is not *a priori* impossible that they separate from each other in the presence of a β carbonyl. On the other hand it is known that electronic rearrangement is an important factor in carbonyl $\pi^* \leftarrow$ n transitions in placing the band at relatively low energies (42, 43). It probably would be hard for σ^* to come in below π^* and to raise it.

Acknowledgments

This collaboration originated when C.S. visited B.W.'s Laboratory during his sojourn in Brazil in the framework of the Brazil–Canada scientific exchange agreement. We are grateful to the National Research Council of Canada and to the Conselho Nacional de Pesquisas de Brasil for having made this possible. We acknowledge financial help from le Ministère de l'Education du Québec, from the "Fundaçao de Amparo à Pesquisa do Estado de São Paulo" and K.C.C. is indebted for a National Research Council of Canada postdoctorate fellowship.

1. B. Wladislaw, H. Viertler, and E. B. Demant. J. Chem. Soc. (B), 565 (1971).
2. B. Wladislaw, A. Giora, and H. Viertler. Anais Acad. Brasil. Cienc. **43**, 381 (1971).
3. B. Wladislaw, R. Rittner, and H. Viertler. J. Chem. Soc. (B), 1859 (1971).
4. B. Wladislaw, H. Viertler, F. A. C. Andrade, and E. B. Demant. Internat. J. Sulfur Chem. A**2**, 161 (1972).
5. B. Wladislaw, P. R. Olivato, and R. Rittner. Rev. Lat. Am. **5**, 206 (1974).
6. B. T. Buzzi, P. R. Olivato, R. Rittner, C. Trufen, H. Viertler, and B. Wladislaw. J. Chem. Soc. Perkin II, 1294 (1975).
7. D. D. Perrin, W. L. F. Armarego, and D. R. Perrin. Purification of laboratory chemicals. Pergamon Press, Oxford. 1966.
8. D. T. McAllan, T. V. Cullum, R. A. Dean, and F. A. Fidler. J. Am. Chem. Soc. **73**, 3627 (1951).
9. C. K. Bradsher, F. C. Brown, and R. J. Grantham. J. Am. Chem. Soc. **76**, 114 (1954).
10. W. Reppe *et al.* Ann. **596**, 38 (1955).
11. A. I. Vogel. J. Chem. Soc. 624 (1948).
12. R. P. Mariella and E. P. Belcher. J. Am. Chem. Soc. **74**, 4049 (1952).
13. J. M. Carpenter and G. Shaw. J. Chem. Soc. (C), 2016 (1970).
14. K. Watanabe, T. Nakayama, and J. Mottl. J. Quant. Spectrosc. Radiat. Transfer, **2**, 369 (1962).
15. D. A. Sweigart and D. W. Turner. J. Am. Chem. Soc. **94**, 5599 (1972).
16. D. C. Frost, F. G. Herring, A. Katrib, C. A. McDowell, and R. A. N. McLean. J. Phys. Chem. **76**, 1030 (1972).
17. A. D. Bain, J. C. Bünzli, D. C. Frost, and L. Weiler. J. Am. Chem. Soc. **95**, 291 (1973).
18. H. Bock and G. Wagner. Angew. Chem. (Int. Ed.) **11**, 150 (1972).
19. G. Wagner and H. Bock. Chem. Ber. **107**, 68 (1974).
20. A. Schweig and W. Thiel. Mol. Phys. **27**, 265 (1974).
21. S. Cradock and R. A. Whiteford. J. Chem. Soc. Faraday II, 281 (1972).
22. W. C. Tam and C. E. Brion. J. Electron Spectrosc. **3**, 263 (1974).
23. B. J. Cocksey, J. H. D. Eland, and C. J. Danby. J. Chem. Soc. (B), 790 (1971).
24. W. C. Tam, D. Yee, and C. E. Brion. J. Electron Spectrosc. **4**, 77 (1974).
25. D. A. Sweigart and D. W. Turner. J. Am. Chem. Soc. **94**, 5592 (1972).
26. K. N. Houk, L. P. Davis, G. R. Newkome, R. E. Duke, and R. V. Nauman. J. Am. Chem. Soc. **95**, 8364 (1973).
27. W. Schäfer, A. Schweig, G. Maier, and T. Sayrac. J. Am. Chem. Soc. **96**, 279 (1974).
28. J. C. Bünzli, D. C. Frost, and L. Weiler. J. Am. Chem. Soc. **96**, 1952 (1974).
29. R. Hoffmann. Acc. Chem. Res. **4**, 1 (1971).
30. R. Hoffmann, A. Imamura, and W. J. Hehre. J. Am. Chem. Soc. **90**, 1499 (1968).
31. A. A. Planckaert, J. Doucet, and C. Sandorfy. J. Chem. Phys. **60**, 4846 (1974).
32. S. D. Thompson, D. G. Carroll, F. Watson, M. O'Donnell, and S. P. McGlynn. J. Chem. Phys. **45**, 1367 (1976).
33. E. A. Fehnel and M. Carmack. J. Am. Chem. Soc. **71**, 84 (1949); **71**, 2889 (1949).
34. H. P. Koch. J. Chem. Soc. 387 (1949).
35. H. H. Szmant and J. J. McIntosh. J. Am. Chem. Soc. **73**, 4356 (1951).
36. L. B. Clark and W. T. Simpson. J. Chem. Phys. **43**, 3666 (1965).
37. J. Barrett and M. J. Hitch. Spectrochim. Acta, A**24**, 265 (1968).
38. D. R. Williams and L. T. Kontnik. J. Chem. Soc. B, 312 (1971).
39. H. H. Jaffe and M. Orchin. Theory and applications of ultraviolet spectroscopy. Wiley, New York. 1962. p. 474.
40. M. B. Robin. Higher excited states of polyatomic molecules. Vol. I. Academic Press. 1974–1975. pp. 276–296.
41. M. B. Robin and N. A. Kuebler. J. Mol. Spectrosc. **33**, 247 (1970).
42. T. P. Debies and J. W. Rabalais. J. Electron Spectrosc. **1**, 355 (1972/73).
43. J. N. Murrell and R. J. Suffolk. J. Electron Spectrosc. **1**, 471 (1972/73).

The trifluoroacetic acid solvent system. Part V. Cryoscopic measurements

MICHAEL G. HARRISS AND JOHN B. MILNE
Department of Chemistry, University of Ottawa, Ottawa, Canada K1N 6N5

Received January 5, 1976

MICHAEL G. HARRISS and JOHN B. MILNE. Can. J. Chem. **54**, 3031 (1976).

Measurement of freezing point depressions for the non-electrolytes, CCl_4. CH_3SO_2F, and $(CF_3CO)_2O$ permit calculation of the cryoscopic constant for trifluoroacetic acid, HOTFA. Water is shown to give freezing point depressions lower than those for non-electrolytes and this is attributed to association. Freezing point depressions for NaOTFA, KOTFA, and CsOTFA have been measured and accounted for in terms of ion-pair dissociation constants previously determined from electrical conductivity measurements. The results cast doubt on the existence of triple ions in this solvent.

MICHAEL G. HARRISS et JOHN B. MILNE. Can. J. Chem. **54**, 3031 (1976).

La mesure de la dépression du point de congélation pour les non-électrolytes CCl_4, CH_3SO_2F et $(CF_3CO)_2O$ permet de calculer la constante cryoscopique pour l'acide trifluoroacétique, HOTFA. Il est montré que l'eau donne des dépressions du point de congélation plus basses que celles pour les non-électrolytes et ceci est attribué à des phénomènes d'association. Les dépressions du point de congélation pour NaOTFA, KOTFA et CsOTFA ont été mesurées et interprétées en termes de constantes de dissociation des paires d'ions préalablement déterminées par des mesures de conductivité électrique. Ces résultats mettent en doute l'existence des ions triples dans ce solvant.

[Traduit par le journal]

Introduction

The investigation of simple ionic equilibria in trifluoroacetic acid (HOTFA) necessitates the study of low solute concentrations ($\sim 10^{-3}$ mol l^{-1}) (1) as a result of the low dielectric constant of this solvent (8.4) (2). Electrical conductivity studies have shown that ionophores are present as ion-pairs with small concentrations of free ions and ion-triples at concentrations normally studied in the laboratory ($\sim 10^{-1}$ *M*) (1, 3). These findings have been discussed in a recent review concerning this solvent (4). No cryoscopic study of this solvent has been made although the freezing point diagram of HOTFA–H_2O mixtures has been determined (5) and the cryoscopic constant for eutectic HOTFA (10.6 mol% H_2O) has recently been reported (6). It was felt to be of interest to apply the cryoscopic technique to the further study of the nature of ionophores in HOTFA to test the findings of electrical conductivity work (1, 3) especially with regard to the existence of ion-triples and to give a basis for molecular weight determinations in this solvent.

Experimental

Materials

Trifluoroacetic acid (Matheson, Coleman and Bell) was purified by distillation and trifluoroacetic acid anhydride and the sodium, potassium, and cesium trifluoroacetates were prepared as described earlier (1). Spectral grade carbon tetrachloride (Baker) and methanesulfonylfluoride (Eastman) were used without further purification.

Procedure

The apparatus used for the measurement of the freezing points has been described earlier (7). Temperatures were measured with a mercury-in-glass thermometer (Thermoschneider, Wertheim, Germany) which was calibrated by the National Research Council of Canada. The scale was divided into 0.01 °C intervals and, using a magnifier, could be read by interpolation to an accuracy of 0.001 °C.

To carry out an experiment, the apparatus was first assembled without the thermometer or air jacket and flamed out in a stream of dry nitrogen. When the glassware was cool, the thermometer was replaced and solvent was introduced from a weight burette (~70 g HOTFA). A continuous small positive pressure of dry nitrogen was maintained in the cryoscope during the course of the experiment. The freezing point was taken as follows. The liquid was cooled almost to its freezing point by immersing the cryoscope directly in an ice/salt slush bath. The bath was then removed, the air jacket was fitted and surrounded by a second ice/salt bath at a temperature such that the temperature of the HOTFA solution fell at a rate of 0.1–0.2 °C per min. The solvent or solution was supercooled about 1 °C, this temperature was recorded, then a small piece of platinum foil cooled in liquid nitrogen was introduced into the liquid. Crystallization occurred immediately and the latent heat evolved caused the temperature to rise rapidly to a virtually constant

Can. J. Chem. Downloaded from www.nrcresearchpress.com by 210.87.254.105 on 09/05/12
For personal use only.

freezing point. For the freezing points of the solutions, a correction was applied to the solute concentration to allow for the solvent frozen out as a result of the supercooling. The following formula was used

$$m_s = \frac{m^*}{[1 - C_p\Delta T/L]}$$

where m^* is the molality of the original solution, m_s is the molality of the solution in equilibrium with solid solvent, C_p is the specific heat of liquid HOTFA (0.464 cal g^{-1} $°C^{-1}$ (8)), L is the latent heat of fusion of HOTFA (21.14 cal g^{-1}) as calculated from the cryoscopic constant and ΔT is the difference between the temperature at which the solution was seeded and the observed freezing point. The corrections involved were normally of the order of 2%.

Samples to be studied were added as concentrated solutions in HOTFA and allowance for the added solvent was made in the calculation of concentration. All solutions were made up by weight.

Results and Discussion

The freezing point depression, θ, is related to the solute molality, m_s, by an expression similar to that used by Gillespie and Oubridge (9) for sulfuric acid solutions

$$[1]\quad \frac{\theta}{m_s} = \phi\nu\lambda\left\{1 - \left[\frac{1}{T_0} - \frac{\bar{J}}{2\bar{L}_0}\right]\theta\right\}\left\{1 + \frac{(s-\nu)m_s}{m_A}\right\}$$

where ϕ is the osmotic coefficient, ν is the number of moles of ions and molecules formed by one mole of solute, λ is the cryoscopic constant, T_0 is the freezing point of the pure solvent, $\bar{J}$ is the difference between the heat capacities of the solid and liquid solvent, $\bar{L}_0$ is the latent heat of fusion of the pure solvent, s is the solvation number of the solute and m_A is the molality of the pure solvent. The factor $(1/T_0 - \bar{J}/(2\bar{L}_0))\theta$ cannot be evaluated for HOTFA, since the heat capacity of solid HOTFA has not been measured, but it is probably negligible, at least in the concentration range studied in this work. For acetic acid, which is known to have similar structures to those of HOTFA in the solid and liquid phases (4), this factor amounts to 0.0002θ. Thus expression [1] was reduced to:

$$[2]\quad \frac{\theta}{m_s} = \phi'\nu\lambda$$

where

$$[3]\quad \phi' = \phi\left[1 + \frac{(s-\nu)m_s}{m_A}\right]$$

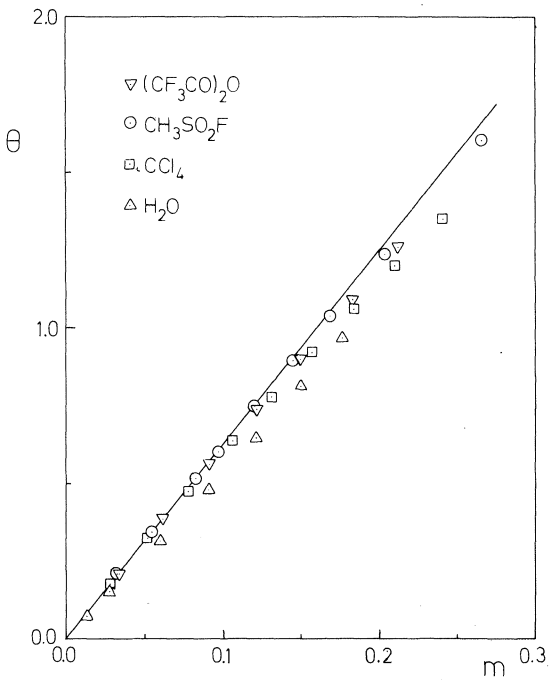

FIG. 1. Freezing point depressions for non-electrolytes in HOTFA. The solid line represents the ideal slope for $\nu = 1$.

Non-electrolytes: The Freezing Point and Cryoscopic Constant of HOTFA

The highest freezing point observed for HOTFA in this work was −15.216 °C and this was taken as the freezing point of the pure acid. The cryoscopic constant was determined from the freezing point data for non-electrolytes given in Table 1 and plotted in Fig. 1. Methanesulfonylfluoride is a non-electrolyte in fluorosulfuric acid (10) and is not expected to behave as an electrolyte in the more weakly acidic HOTFA. Trifluoroacetic acid anhydride is a non-electrolyte in HOTFA (1) and it is unlikely that CCl_4 undergoes any reactions in this solvent. Water is a very weak electrolyte in HOTFA (1). All of the non-electrolytes show negative deviations from ideality with increasing concentration and the cryoscopic constant was evaluated from the limiting maximum slope at low solute molalities where ϕ' approaches unity. Up to a concentration of 0.06 mol kg^{-1} all of the non-electrolytes have points on a straight line which gives a value for λ of 6.25 °C mol^{-1} kg.

Using this value and assuming $\nu = 1$, ϕ' values have been calculated from the freezing point

Can. J. Chem. Downloaded from www.nrcresearchpress.com by 210.87.254.105 on 09/05/12
For personal use only.

TABLE 1. Freezing point depressions (θ) and osmotic coefficients (ϕ') for non-electrolytes

Compound	10^2m (mol kg^{-1})	θ (°C)	ϕ' Obsd	ϕ' Calcd
$(CF_3CO)_2O$	3.34	0.210	1.006	0.996
(fp of pure solvent −15.221 °C)	6.19	0.384	0.993	0.993
	9.19	0.560	0.975	0.990
	12.17	0.737	0.969	0.986
	14.97	0.902	0.964	0.983
	18.28	1.093	0.957	0.979
	21.22	1.260	0.950	0.976
CH_3SO_2F	3.25	0.209	1.029	0.996
(fp of pure solvent −15.261 °C)	5.44	0.343	1.009	0.994
	8.25	0.516	1.001	0.991
	9.70	0.602	0.993	0.989
	12.02	0.749	0.997	0.986
	14.52	0.898	0.990	0.983
	16.85	1.039	0.987	0.981
	20.37	1.237	0.972	0.977
	26.55	1.603	0.966	0.970
CCl_4	2.79	0.178	1.021	0.997
(fp of pure solvent −15.216 °C)	5.23	0.324	0.991	0.994
	7.79	0.472	0.969	0.991
	10.64	0.638	0.959	0.988
	13.11	0.777	0.948	0.985
	15.69	0.922	0.940	0.982
	18.38	1.060	0.923	0.979
	21.00	1.200	0.914	0.976
	24.12	1.348	0.894	0.972
H_2O	1.29	0.072	0.893	—
(fp of pure solvent −15.221 °C)	2.78	0.152	0.874	—
	5.98	0.313	0.837	—
	9.10	0.479	0.842	—
	12.17	0.647	0.851	—
	15.03	0.812	0.864	—
	17.61	0.968	0.880	—

depressions for $(CF_3CO)_2O$, CH_3SO_2F, and CCl_4 and these are listed in Table 1. Theoretical ϕ' values have been calculated from equation [3] assuming $\phi = 1$ and $s = 0$ and these are listed for comparison in Table 1. The assumption that these solutes are unsolvated is consistent with their inert character and the solvent's tendency to form dimers (4) and its weak solvating power (1). The observed ϕ' values are lower than the calculated values and thus the actual osmotic coefficients themselves, ϕ, are less than unity. This may be a result of a positive heat of mixing of solute and solvent (12, p. 243).

The initial slope of the water curve lies below that expected for a non-electrolyte but as the concentration is increased, the slope becomes greater. Water apparently behaves in HOTFA as it does in HF where there is some dimer and perhaps higher oligomer formation (11).

Ionophoric Solutes

The freezing point depressions (θ) for NaOTFA, KOTFA, and CsOTFA are given in Table 2 and plotted in Fig. 2. At low concentrations (<0.03 mol kg^{-1}) the θ values fall on the same straight line with a slope near that expected for a solute with $\nu = 1$. At higher concentrations the curves deviate from each other with the freezing point depressions following the order NaOTFA > KOTFA > CsOTFA.

Deviations from the ideal slope for $\nu = 1$ will be due to both ionic dissociation ($\nu \neq 1$) and changes in ϕ'. The products, $\nu\phi'$, have been calculated from the freezing point depressions

Can. J. Chem. Downloaded from www.nrcresearchpress.com by 210.87.254.105 on 09/05/12
For personal use only.

ERRATA - in equation 6, W_S is the molecular weight of the solute.

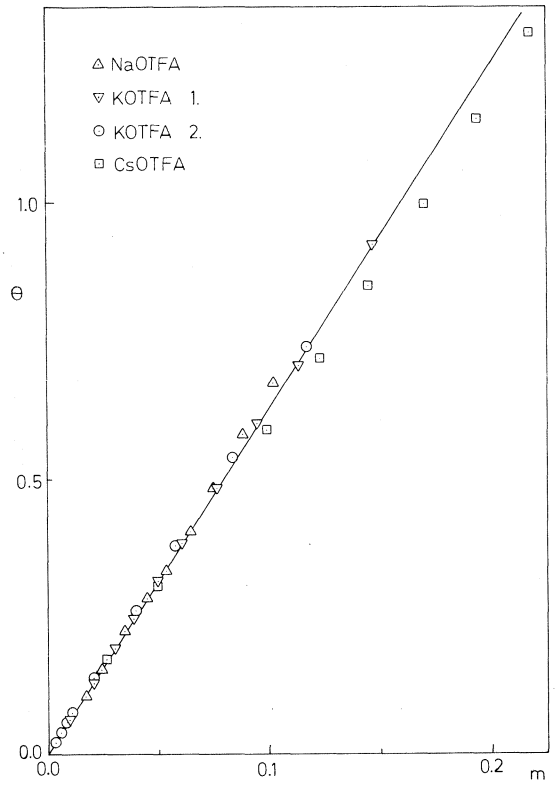

FIG. 2. Freezing point depressions for ionophores in HOTFA. The solid line represents the ideal slope for $\nu = 1$.

and these are listed in Table 5. Assuming that solvation effects may be ignored to a first approximation, $\nu\phi$ values for the case of simple ion-pair dissociation and for the case of ion-pair dissociation and triple ion formation, may be calculated for comparison. In these calculations conversions between molar and molal concentrations were made using the density of pure solvent at -15.216 °C, 1.5732 g ml^{-1} (4). The method of calculation was as follows.

For the case of simple ion-pair dissociation, ν may be calculated from the expression

$$[4] \qquad \nu = \frac{[MX] + 2[M^+]}{c_{MX}}$$

The concentrations $[M^+]$ and $[MX]$ may be calculated by trial and iterative methods from:

$$[5] \qquad K_d = \frac{a_{M^+}{}^2}{[MX]} = \frac{y_\pm{}^2[M^+]^2}{[MX]}$$

$$[6] \qquad y_\pm = \frac{10^{-A\sqrt{I}/(1+Ba_0\sqrt{I})}}{1 + \dfrac{0.001 c_{MX}\nu(W_A - W_s)}{d}}$$

where K_d is the ion-pair dissociation constant; a_{M^+}, the ionic activity; $y_\pm$, the molar activity coefficient; A and B, constants (12); a_0, the distance of closest approach of the cation and anion (1); I, the ionic strength ($= [M^+]$); d, the solvent density; W_A, the molecular weight of the solvent; and W_s, the molecular weight of the solvent.

For the case of ion-pairs, single ions, and triple ions, the number of particles may be calculated from the expression:

$$[7] \qquad \nu = \frac{[MX] + 2[M^+] + 2[M_2X^+]}{c_{MX}}$$

where the assumption has been made that $[M^+] = [X^-]$ and $[M_2X^+] = [MX_2^-]$ (3). All terms in the numerator may be evaluated by trial and iterative methods from the expressions [5] and [6] ($I = [M^+] + [M_2X^+]$) above and

$$[8] \qquad K_d/k_d{}^2 = \frac{a^2{}_{M_2X^+}}{[MX]^3} = \frac{y_\pm{}^2[M_2X^+]^2}{[MX]^3}$$

and

$$[9] \qquad c_{MX} = [MX] + [M^+] + 3[M_2X^+]$$

The calculation of ion concentrations and ν for the both cases proceeds as follows. A value of [MX] is chosen, the corresponding activities calculated from expression [5] and, where triple ions are involved, [8]. An initial corresponding trial $y_\pm$ value is chosen and constant $y_\pm$ and ionic strength arrived at by iteration of [6]. Ion molarities may now be calculated and the trial value of [MX] checked by the mass balance expression. The process is repeated until the proper value of [MX] and the corresponding ion molarities are found.

The ion-pair and triple ion dissociation constants and a_0 values have been measured at 25 °C by electrical conductivity methods (1, 3). The values of the dissociation constants at the freezing point of HOTFA were determined using a scaling factor from the theoretical Fuoss expressions for K_d and k_d (13). The value of the dielectric constant (9.72) was arrived at by a short extrapolation of Harris and O'Konski values quoted in ref. 4. The adjustment was small

Can. J. Chem. Downloaded from www.nrcresearchpress.com by 210.87.254.105 on 09/05/12
For personal use only.

TABLE 2. Freezing point depressions (θ) for ionophores

Compound	10^2m (mol kg^{-1})	θ (°C)
NaOTFA	1.68	0.105
(fp of pure solvent −15.239 °C)	2.42	0.152
	3.44	0.223
	4.45	0.277
	5.35	0.333
	6.42	0.403
	7.50	0.481
	8.83	0.580
	10.18	0.672
KOTFA No. 1	0.97	0.062
(fp of pure solvent −15.250 °C)	2.04	0.129
	2.99	0.192
	3.88	0.246
	4.95	0.315
	6.05	0.383
	7.65	0.483
	9.45	0.599
	11.32	0.703
	14.65	0.923
KOTFA No. 2	0.29	0.020
(fp of pure solvent −15.243 °C)	0.57	0.039
	0.84	0.059
	1.07	0.075
	2.07	0.139
	3.93	0.261
	5.74	0.379
	8.34	0.538
	11.66	0.739
CsOTFA	2.62	0.171
(fp of pure solvent −15.234 °C)	4.92	0.305
	9.91	0.587
	12.30	0.717
	14.47	0.849
	16.96	0.996
	19.32	1.150
	21.70	1.306

due to the compensating effect of temperature and dielectric constant changes. Thus, the factor for converting the equilibrium constant at 25 °C to that at −15.216 °C was 0.9984. The extended Debye–Hückel expression at −15.216 °C is

$$[10] \qquad y_{\pm} = \frac{10^{-14.534\sqrt{I}/(1 + 1.0044a_0\sqrt{I})}}{1 + \dfrac{0.001c_{MX}\nu(114 - W_s)}{1.5732}}$$

The constants, K_d, k_d, and a_0 used for the trifluoroacetates studied are given in Table 4. Calculated ion molarities and ν values for the case of ion-pairs only are given in Table 3.

Osmotic coefficients for the free ions in solution may be calculated from the expression (12, p. 235):

$$[11] \qquad \phi_i = 1 - \frac{e^2|z_1z_2|}{6\epsilon kT}\kappa\sigma(\kappa a_0)$$

where the function σ has the form

$$[12] \qquad \sigma(x) = \frac{3}{x^3}\left[(1 + x) - 2\ln(1 + x) - \frac{1}{1 + x}\right]$$

For HOTFA at the freezing point [11] takes the form

$$\phi_i = 1 - 11.154\sqrt{I}\sigma(1.0044a_0\sqrt{I})$$

Assuming the osmotic coefficient for the ion-pair to be unity, the product of the overall osmotic coefficient, ϕ, and ν is given by:

$$\nu\phi = \frac{[m_{MX} + \phi_i\sum m_i]}{m_s}$$

where m_{MX} is the molal concentration of the ion-pair, MX, $\sum m_i$ is the total free ion concentration and m_s is the stoichiometric molal concentration of the solute. The ionic osmotic coefficients, ϕ_i, for the case of single ions and ion-pairs are given in Table 3. The theoretical $\nu\phi$ products for the both cases and the measured values of $\nu\phi'$ are given in Table 5. Comparison of experimental and theoretical values shows that the results are best interpreted by simple ion-pair dissociation and are not compatible with the presence of triple ions. For the purpose of this comparison, $\phi' \approx \phi$.

Electrical conductivity measurements at 25 °C (3) show a minimum in the equivalent conductivity, Λ, *vs.* concentration plots and this has been interpreted as evidence for the existence of triple ions in HOTFA (3). It is unlikely that the slightly larger dielectric constant at −15.216 °C (9.72) as compared to that at 25 °C (8.40) could account for such a great change in behaviour and the existence of significant amounts of triple ions in HOTFA at 25 °C is therefore doubtful. The minimum in the Λ *vs.* c_{MX} plots for solvents of moderately low dielectric constant has been accounted for by Davies in an alternative way (14), whereby the fall-off in the ionic activity coefficient with increasing solute concentration is sufficiently great to cause an actual increase in the degree of dissociation and, if this effect is large enough, a consequent increase in the

Can. J. Chem. Downloaded from www.nrcresearchpress.com by 210.87.254.105 on 09/05/12
For personal use only.

TABLE 3. Calculated ν values, ion osmotic coefficients, ϕ_i, and degrees of dissociation, α, for the case of ion-pairs and single ions

Compound	m (mol kg^{-1})	c_{MX}[a] (mol l^{-1})	[MX] (mol l^{-1})	[M$^+$] (mol l^{-1})	$y_\pm$	ν	ϕ_i	α
NaOTFA	0.0125	0.01967	0.01954	0.00013	0.694	1.007	0.881	0.0066
	0.0250	0.03933	0.03913	0.00020	0.639	1.005	0.855	0.0051
	0.0500	0.07866	0.07836	0.00030	0.583	1.004	0.826	0.0038
	0.1000	0.15732	0.15683	0.00049	0.508	1.003	0.783	0.0031
KOTFA	0.0125	0.01967	0.01930	0.00037	0.554	1.019	0.811	0.0188
	0.0250	0.03933	0.03872	0.00061	0.477	1.016	0.766	0.0155
	0.0500	0.07866	0.07760	0.00106	0.389	1.013	0.707	0.0135
	0.1000	0.15732	0.15532	0.00200	0.291	1.013	0.625	0.0127
	0.1500	0.23598	0.23284	0.00314	0.227	1.013	0.560	0.0133
CsOTFA	0.0125	0.01967	0.01856	0.00111	0.389	1.056	0.710	0.0564
	0.0250	0.03933	0.03733	0.00200	0.300	1.051	0.640	0.0509
	0.0500	0.07866	0.07426	0.00440	0.196	1.056	0.535	0.0559
	0.1000	0.15732	0.14532	0.01200	0.101	1.076	0.400	0.0763
	0.1500	0.23598	0.21098	0.02500	0.059	1.106	0.319	0.1059
	0.2000	0.31464	0.27204	0.04260	0.039	1.135	0.279	0.1354

[a]Calculated using the density of pure HOTFA at −15.216 °C, 1.5732 g/ml.

TABLE 4. Ion-pair and triple ion dissociation constants at −15.216 °C

Compound	$10^6 K_d$ (mol l^{-1})[a]	k_d (mol l^{-1})[a]	a_0 (Å)
NaOTFA	0.397	0.06	4.04
KOTFA	2.19	0.033	4.63
CsOTFA	10.1	0.017	5.35

[a]Calculated from values at 25 °C (1, 3).

equivalent conductivity. Earlier attempts to reproduce the minimum in Λ using the measured ion-pair dissociation constants and the extended Debye–Hückel expression for $f_\pm$ were unsuccessful (3) but small changes in $f_\pm$ could produce a minimum in the concentration range studied. The present calculations, which are for a concentration range much higher than that at which the conductivity minimum occurs, do indicate a

TABLE 5. Measured and calculated $\nu\phi$ products for the case of ion-pairs and single ions and the case including triple ions

Compound	m (mol kg^{-1})	$\nu\phi$ Ion-pairs and single ions	$\nu\phi$ Ion-pairs, simple and triple ions	Measured $\nu\phi'$[a]
NaOTFA	0.0125	1.004	1.003	0.998
	0.0250	1.003	0.998	0.992
	0.0500	1.003	0.991	1.002
	0.1000	1.002	0.949	1.059
KOTFA	0.0125	1.012	0.993	1.024
	0.0250	1.008	0.961	1.030
	0.0500	1.006	0.831	1.030
	0.1000	1.003	0.544	1.013
	0.1500	1.002	0.406	1.007
CsOTFA	0.0125	1.024	0.854	1.050
	0.0250	1.014	0.745	1.037
	0.0500	1.004	0.544	0.989
	0.1000	0.985	0.396	0.949
	0.1500	0.962	0.341	0.939
	0.2000	0.940	0.319	0.956

[a]Interpolated.

Can. J. Chem. Downloaded from www.nrcresearchpress.com by 210.87.254.105 on 09/05/12
For personal use only.

minimum in the degree of dissociation, α, as shown in Table 3. The use of a more precise expression than [10] for the activity coefficient may reproduce the experimental electrical conductivities in the region of the observed minimum.

Extension of the calculation of osmotic coefficients to allow for solvation and the exact expression of the solvent mole fraction (eq. 3), are not warranted in view of the scatter in experimental points and in the absence of density data.

Acknowledgements

The authors thank the National Research Council of Canada for financial support and M.G.H. thanks the Council for the award of a bursary.

1. M. G. HARRISS and J. B. MILNE. Can. J. Chem. **49**, 1888 (1971).
2. F. E. HARRIS and C. T. O'KONSKI. J. Am. Chem. Soc. **76**, 4317 (1954).
3. M. G. HARRISS and J. B. MILNE. Can. J. Chem. **50**, 3789 (1972).
4. J. B. MILNE. *In* The chemistry of non-aqueous solvents. Vol. V. *Edited by* J. J. Lagowski. Academic Press, New York. 1976.
5. H. H. CADY and G. H. CADY. J. Am. Chem. Soc. **76**, 915 (1954).
6. M. ARDON and G. YAHAV. Inorg. Chem. **15**, 12 (1976).
7. R. J. GILLESPIE, E. D. HUGHES, and C. K. INGOLD. J. Chem. Soc. 2473 (1950).
8. T. SANO, N. TATSUMATO, Y. MENDE, and T. YASUNAGA. Bull. Chem. Soc. Jpn. **45**, 2673 (1972).
9. R. J. GILLESPIE and J. V. OUBRIDGE. J. Chem. Soc. 81 (1956).
10. R. J. GILLESPIE, J. B. MILNE, and R. C. THOMPSON. Inorg. Chem. **5**, 469 (1966).
11. H. H. HYMAN and J. J. KATZ. *In* Non-aqueous solvent systems. *Edited by* T. C. Waddington. Academic Press, New York. 1965.
12. R. A. ROBINSON and R. H. STOKES. Electrolyte Solutions. Butterworths, London. 1961.
13. R. M. FUOSS and F. ACCASCINA. Electrolyte conductance. Interscience, New York. 1959.
14. C. W. DAVIES. Ion association. Butterworths, London. 1962. p. 105.

Can. J. Chem. Downloaded from www.nrcresearchpress.com by 210.87.254.105 on 09/05/12
For personal use only.

The acid cleavage of triphenylvinylmercuric salts

CHOI CHUCK LEE AND PETER J. SMITH

Department of Chemistry and Chemical Engineering, University of Saskatchewan, Saskatoon, Sask., Canada S7N 0W0

Received December 8, 1975[1]

CHOI CHUCK LEE and PETER J. SMITH. Can. J. Chem. **54**, 3038 (1976).

An attempted solvolytic demercuration of triphenylvinylmercuric acetate or bromide (**1**-HgOAc or **1**-HgBr) in HOAc in the presence of $HClO_4$ failed to give the triphenylvinyl cation, but instead gave a high yield of triphenylethylene (**2**). Kinetic studies showed that the formation of **2** from the reaction of **1**-HgOAc with $HClO_4$ in CH_3OH was first order with respect to the substrate and second order with respect to $HClO_4$. Mechanistic implications of these findings are discussed.

CHOI CHUCK LEE et PETER J. SMITH. Can. J. Chem. **54**, 3038 (1976).

Lors d'essais de démercuration solvolytique de l'acétate ou du bromure du triphénylvinylmercure (**1**-HgOAc ou **1**-HgBr) dans AcOH en présence de $HClO_4$, il n'y a pas eu de formation du cation triphénylvinyle mais plutôt un bon rendement en triphényléthylène (**2**). Des études cinétiques ont montré que la formation de **2** par réaction de **1**-HgOAc avec $HClO_4$ dans CH_3OH est du premier ordre par rapport au substrat et du deuxième ordre par rapport à $HClO_4$. On discute des implications mécanistiques de ces résultats.

[Traduit par le journal]

In a study on the acetolysis, formolysis, and trifluoroacetolysis of triphenylvinyl-2-^{14}C triflate (1), it was found that the extent of isotopic scrambling resulting from the degenerate 1,2-phenyl shift was not affected by the presence of the conjugate base of the solvent. This observation suggested that the degenerate rearrangement occurred in the ion-pair stage, since the presence of the conjugate base of the solvent would be expected to suppress the extent of scrambling if the 1,2-phenyl shift were to take place in the free, classical triphenylvinyl cation. It is, therefore, of interest to generate a 'free' triphenylvinyl cation and to ascertain if 1,2-phenyl shifts would take place in such a species. In the solvolytic demercuration of alkylmercuric perchlorates, generally carried out by treating the alkylmercuric acetate in an appropriate solvent in the presence of $HClO_4$, free carbocations are believed to be generated since the loss of Hg^0 from RHg^+ gives no counterion for ion-pair formation (2). In an attempt to generate the triphenylvinyl cation, the possibility of solvolyzing triphenylvinylmercuric acetate (**1**-HgOAc) was studied.

1-HgOAc was prepared from triphenylvinyl bromide (**1**-Br) (1) by the method of Ouellette (3) which involved the reaction of the Grignard reagent from **1**-Br with $HgBr_2$ to give **1**-HgBr, followed by treatment with AgOAc to give **1**-HgOAc. Reaction of **1**-HgOAc in HOAc in the presence of $HClO_4$ gave, instead of the expected **1**-OAc, a high yield of triphenylethylene (**2**). A similar reaction with **1**-HgBr also gave **2**. These observations suggested the occurrence of an electrophilic substitution (4, 5) instead of the formation of a carbocation.

In an attempt to clarify further the electrophilic substitution process, kinetic measurements were carried out in CH_3OH, using a procedure similar to the study of Kreevoy (6) on the acid cleavage of CH_3HgI. Reaction of **1**-HgOAc with $HClO_4$ in CH_3OH also gave **2** as product. A typical set of data on the dependence of the observed pseudo first-order rate constant, k_{ob}, at 61.6 °C, on the $HClO_4$ concentration is given in Table 1. Unlike the results from the study with CH_3HgI (6), division of k_{cb} by $[HClO_4]$ does not give a reasonably constant k_2, expected for a direct S_E2 substitution. However, division of k_{ob} by $[HClO_4]^2$ does give an essentially constant value (Table 1), indicating that k_{ob} varies with the square of the $HClO_4$ concentration.

If the kinetic order with respect to $[HClO_4]$ were x

$$k_{ob}[\textbf{1}\text{-HgOAc}] = k[HClO_4]^x[\textbf{1}\text{-HgOAc}]$$

[1]Revision received June 18, 1976.

Can. J. Chem. Downloaded from www.nrcresearchpress.com by 210.87.254.105 on 09/05/12
For personal use only.

TABLE 1. Dependence of the pseudo first-order rate constant, k_{ob}, on $[HClO_4]$ in the reaction of **1**-HgOAc with $HClO_4$ in CH_3OH at 61.6 °C

Initial [**1**-HgOAc] × 10^4 (mol/l)	$[HClO_4]$ (mol/l)	$k_{ob} \times 10^6$ (s^{-1})	$10^6 k_{ob}/[HClO_4]^2$
6.17	0.96	1.88 ± 0.06	2.0
5.41	1.20	2.45 ± 0.06	1.7
3.40	1.44	3.28 ± 0.08	1.6
3.48	1.92	5.77 ± 0.12	1.6
3.28	2.40	9.53 ± 0.17	1.7
3.45	2.88	13.9 ± 0.2	1.7

Hence

$$k_{ob} = k[HClO_4]^x$$
$$\log k_{ob} = \log k + x \log [HClO_4]$$

Using the data in Table 1, a plot of log k_{ob} *vs.* log $[HClO_4]$ gave a straight line with a slope, generated by the computer, of 2.00 ± 0.05. Similar kinetic experiments at 70 °C over a slightly smaller range of $HClO_4$ concentrations also gave a slope of about 2. These results thus indicate that the rate of formation of **2** in the reaction studied is first order in [**1**-HgOAc] and second order in $[HClO_4]$.

Kreevoy and Kretchmer (7) have also studied the reaction of vinylmercuric iodide with $HClO_4$ or H_2SO_4. It was concluded that the rate-determining step in the cleavage of this substrate to ethylene and HgI^+ was the transfer of a proton from a hydronium ion to carbon. The rate was first order in substrate and roughly proportional to acid concentration up to about 4 *M* $HClO_4$ or H_2SO_4. It was also suggested that the HgI^+, formed in the primary reaction, equilibrated rapidly with more substrate to give HgI_2 and $C_2H_3Hg^+$, which in turn decomposed to acetaldehyde and elemental Hg. The present results from **1**-HgOAc, however, differ from those observed for vinylmercuric iodide in that the rate is not simply proportional to the acid concentration, but rather, it is proportional to $[HClO_4]^2$. Moreover, no substitution product analogous to acetaldehyde was observed.

It is of interest to consider the possible significance of the observed second-order dependence of the rate of cleavage of **1**-HgOAc to **2** on the $HClO_4$ concentration. It is possible that $HClO_4$ solutions in CH_3OH in the 1–3 *M* range may be very non-ideal and deviations of the activity coefficients from unity would render any observed kinetic dependence on $HClO_4$ concentration unreliable as a criterion of reaction mechanism.[2] In that event, no mechanistic conclusions can be made from the present results except for a restatement of the fact that **1**-HgOAc is cleaved by $HClO_4$ to give **2** and that the rate of this reaction increases rapidly with increasing acid concentration.

It may be pointed out once more that in the study with methylmercuric iodide (6) or with vinylmercuric iodide (7), the rate was found to be roughly proportional to $HClO_4$ concentrations of up to about 4 *M*, and this first-order dependence of the rate on acid concentration was taken as an indication that the rate-determining step was a proton transfer to carbon. Since such first-order dependence of the rate on $HClO_4$ concentrations of up to about 4 *M* has been utilized as a criterion on the nature of the rate-determining step, some mechanistic significance for the presently observed second-order dependence on $HClO_4$ concentrations of up to about 3 *M* appears to be justified. If this is the case, the following is one possible mechanism which would fit the observed result of $d[\mathbf{2}]/dt = k[H^+]^2[\mathbf{1}\text{-HgX}]$.

$$(Ph)_2C{=}C(Ph)HgX \underset{}{\overset{H^+}{\rightleftharpoons}} (Ph)_2\overset{+}{C}{-}CH(Ph)HgX$$
1-HgX **3**

$$\xrightarrow[S_E2,\ -HgX^+]{H^+,\ slow} (Ph)_2\overset{+}{C}{-}CH_2Ph \xrightarrow[fast]{-H^+} (Ph)_2C{=}CHPh$$
2

It has been shown that direct S_N2 substitution on vinylic substrates is energetically unfavorable (8) and such a reaction has so far not been observed (9, 10). Possibly, in the present reaction with **1**-HgOAc or **1**-HgBr, a direct S_E2 substitu-

[2]This argument was suggested by a referee.

Can. J. Chem. Downloaded from www.nrcresearchpress.com by 210.87.254.105 on 09/05/12
For personal use only.

tion also could not occur. Instead, a prior protonation would give rise to a relatively stable diphenyl substituted tertiary cation (**3**) which would allow an S_E2 reaction to proceed on saturated carbon (4, 5). Rapid deprotonation following the S_E2 reaction would give the final stable product, **2**. Such a mechanism could also account for the fact that no substitution product derived from the triphenylvinyl cation was observed. Apparently, a facile protonation of **1**-HgX to **3** provided a preferred alternative route to the formation of the triphenylvinyl cation via demercuration.

Experimental

*Triphenylvinylmercuric Bromide (**1**-HgBr)*

The Grignard reagent, prepared from 14.75 g (44 mmol) of triphenylvinyl bromide (1) and 1.12 g (46 mmol) of Mg in 500 ml of anhydrous ether, was quickly poured into an ice-cooled suspension of 15.85 g (44 mmol) of $HgBr_2$ in 15 ml of anhydrous ether. The mixture was stirred under N_2 at ice-bath temperature for 2 h and then stirred at room temperature for an additional 3 h. Water (150 ml) and HOAc (50 ml) were added, the ether layer separated, and the aqueous layer was repeatedly extracted with ether. The combined extract was washed with saturated $NaHCO_3$ solution and finally with water. After drying over $MgSO_4$, concentration of the ethereal solution gave 17.5 g (77%) of product which was recrystallized from ether, mp 165–166 °C, nmr (CCl_4) δ 7.05 (m, 10H), 7.35 (s, 5H). *Anal.* calcd. for $C_{20}H_{15}HgBr$: C 44.47, H 2.85; found: C 44.65, H 2.93.

*Triphenylvinylmercuric Acetate (**1**-HgOAc)*

In a 200 ml round bottom flask, which was painted black, were placed 3.00 g (5.5 mmol) of **1**-HgBr, 0.93 g (5.5 mmol) of AgOAc, and 100 ml of CH_3OH. The flask was stoppered and the suspension was stirred magnetically at room temperature for 24 h. The precipitated AgBr was removed by filtration and washed with CH_3OH. The combined filtrate and washing was concentrated at 45 °C under reduced pressure to about 30 ml, and upon cooling gave 2.65 g (92%) of product which was recrystallized from CH_3OH, mp 156–158 °C, nmr ($CDCl_3$) δ 1.95 (s, 3H), 7.15 (m, 10H), 7.45 (s, 5H). *Anal.* calcd. for $C_{22}H_{18}O_2Hg$: C 51.31, H 3.52; found: C 51.25, H 3.59.

*Acid Cleavage of **1**-HgOAc or **1**-HgBr*

When **1**-HgOAc or **1**-HgBr was treated with $HClO_4$ in HOAc or CH_3OH at reflux temperature for about 20 h, high yields of triphenylethylene were obtained. A typical reaction is as follows.

A solution of 200 mg (0.39 mmol) of **1**-HgOAc in 25 ml of a 1:20 mixture of 70% $HClO_4$:HOAc was heated under reflux overnight and then it was poured into 50 ml of saturated $NaHCO_3$ solution. After extraction with ether (3 × 50 ml), the aqueous layer gave a positive test for Hg^{2+} ion. The combined ether extract was washed with $NaHCO_3$ solution and with H_2O and then dried over $MgSO_4$. Removal of the ether gave 90 mg (91%) of product which, after recrystallization from hexane, was identical with a commercially obtained authentic sample of triphenylethylene, mp 67–68 °C, nmr (CCl_4) δ 7.06 (s, 1H), 7.25 (s, 5H), 7.40 (m, 10H).

Kinetic Studies

In CH_3OH, **1**-HgOAc showed λ_{max} at 235 nm (ϵ 21 600) while **2** showed absorptions at 297 nm (ϵ 21 800) and at 228 nm (ϵ 17 900). The kinetic measurements were made at the λ_{max} of **2** (297 nm). Initially, cold $HClO_4$ was pipetted into a solution of **1**-HgOAc in CH_3OH which was also cooled in an ice bath. The solution was made up to the appropriate volume with cold CH_3OH before being placed in an oil bath at 61.6 °C. At different time intervals, aliquots were withdrawn for uv measurement after appropriate dilution. The pseudo first-order rate constant, k_{ob}, was obtained from the slope of $\log (A_\infty - A_t)$ *vs.* t, using a computer programmed for such determinations.

Acknowledgments

The financial support given by the National Research Council of Canada and the technical assistance of Lorraine Noble are gratefully acknowledged.

1. C. C. Lee, A. J. Cessna, B. A. Davis, and M. Oka. Can. J. Chem. **52**, 2679 (1974).
2. F. R. Jensen, R. J. Ouellette, G. Knutson, D. A. Babbe, and R. Hartgerink. Trans. N.Y. Acad. Sci. **30**, 761 (1968).
3. R. J. Ouellette. Ph.D. Thesis. University of California, Berkeley, California. 1962.
4. G. Köbrich. Angew. Chem. Int. Ed. Engl. **1**, 382 (1962).
5. O. A. Reutov. Russ. Chem. Rev. **36**, 163 (1967).
6. M. M. Kreevoy. J. Am. Chem. Soc. **79**, 5927 (1957).
7. M. M. Kreevoy and R. A. Kretchmer. J. Am. Chem. Soc. **86**, 2435 (1964).
8. D. R. Kelsey and R. G. Bergman. J. Am. Chem. Soc. **93**, 1953 (1971).
9. P. J. Stang. Prog. Phys. Org. Chem. **10**, 205 (1973).
10. L. R. Subramanian and M. Hanack. J. Chem. Educ. **52**, 80 (1975).

Can. J. Chem. Downloaded from www.nrcresearchpress.com by 210.87.254.105 on 09/05/12
For personal use only.

Rearrangement studies with ^{14}C. XLI. Degenerate rearrangements in vinyl cations from triphenylvinyl-2-^{14}C-phenyltriazene and from trianisylvinyl-2-^{14}C-phenyltriazene

CHOI CHUCK LEE AND ERIC C. F. KO

Department of Chemistry and Chemical Engineering, University of Saskatchewan, Saskatoon, Sask., Canada S7N 0W0

Received June 25, 1976

CHOI CHUCK LEE and ERIC C. F. KO. Can. J. Chem. **54**, 3041 (1976).

The triphenylvinyl cation generated from reactions of triphenylvinyl-2-^{14}C-phenyltriazene (**1**) with a number of acids gave no isotopic scrambling from degenerate 1,2-phenyl shifts. The trianisylvinyl cation generated from reaction of trianisylvinyl-2-^{14}C-phenyltriazene (**2**) with HOAc showed about 38% scrambling of the label from C-2 to C-1, attributable to degenerate 1,2-anisyl shifts. When **2** was treated with HOAc containing 1.7 equiv. of NaOAc, the extent of scrambling was decreased to about 17%. Mechanistic implications of these results are discussed.

CHOI CHUCK LEE et ERIC C. F. KO. Can. J. Chem. **54**, 3041 (1976).

Le cation triphénylvinyle produit à partir des réactions du triphénylvinyl-2-^{14}C phényltriazène (**1**) avec un certain nombre d'acides ne conduit à aucune distribution isotopique provenant de déplacements dégénérés 1,2 des groupes phényles. Le cation trianisylvinyle produit par la réaction du trianisylvinyl-2-^{14}C phényltriazène (**2**) avec AcOH conduit à 38% de distribution des isotopes à partir de la position 2 vers la position 1; ce résultat est attribuable à des déplacements dégénérés 1,2 du groupe anisyle. Le traitement de **2** par AcOH contenant 1.7 équiv. de AcONa fournit un produit dans lequel la répartition des isotopes a été diminuée jusqu'à environ 17%. On discute des implications mécanistiques de ces résultats.

[Traduit par le journal]

Can. J. Chem. Downloaded from www.nrcresearchpress.com by 210.87.254.42 on 09/05/12
For personal use only.

Jones and Miller (1) have reported the generation of vinyl cations from reactions of acids with vinyltriazenes. 1,2-Aryl shifts across the double bond were observed, for example, in the rearrangement of the 1-phenyl-2,2-di-*p*-tolylvinyl cation to the 2-phenyl-1,2-di-*p*-tolylvinyl cation (1). Degenerate 1,2-aryl shifts in triarylvinyl cationic systems labeled with ^{14}C or ^{13}C have been investigated in this laboratory (2–5). It is generally agreed that α-anisyl substituted vinyl systems would give rise to open, classical vinyl cations, and degenerate 1,2-anisyl shifts took place in the classical trianisylvinyl cation (4–8). However, ion-pairs might be involved in the degenerate 1,2-phenyl shifts observed in solvolyses of triphenylvinyl-2-^{14}C triflate (2). Since vinyl cations generated from vinyltriazenes arose via vinyldiazonium ions (1) which could not give rise to any counter ion for ion-pair formation, a study on the possibility of degenerate 1,2-phenyl shifts in the triphenylvinyl cation from triphenylvinyl-2-^{14}C-phenyltriazene (**1**) should provide further information on whether ion-pairs are the intermediates involved in such a 1,2-shift. As a comparison, the extent of degenerate 1,2-anisyl shifts in the trianisylvinyl cation from trianisylvinyl-2-^{14}C-phenyltriazene (**2**) was also investigated.

Triphenylvinyl-2-^{14}C bromide (2) and trianisylvinyl-2-^{14}C bromide (4) were converted to the corresponding Grignard reagents and treated with phenyl azide to give triazenes **1** and **2** (1). Reaction of **1** with HOAc, with or without the presence of NaOAc, CF_3COOH, or 90% acetone – 10% H_2O containing 0.1% $HClO_4$ gave the expected products, triphenylvinyl acetate, triphenylvinyl trifluoroacetate, or phenyl diphenylmethyl ketone, respectively. Conversion of these products to 1,2,2-triphenylethanol followed by oxidation to benzophenone as described previously (2) showed no scrambling of the isotopic label from C-2 to C-1 in any of these reactions, the data being summarized in Table 1. On the other hand, reaction of **2** with HOAc gave trianisylvinyl acetate which upon degradation via 1,2,2-trianisylethanol to dianisyl ketone showed about 38% scrambling of the ^{14}C-label from C-2 to C-1. When the same reaction of **2** with HOAc was carried out in the presence of 1.7 equiv. of NaOAc, the extent of scrambling

TABLE 1. Data from reactions of acids with triphenylvinyl-2-^{14}C-phenyltriazene (**1**) and with trianisylvinyl-2-^{14}C-phenyltriazene (**2**)

Triazene	Acid	Specific activity[a] (dpm/mmol) $Ar_2CHCH(Ar)OH$[b] Run 1	$Ar_2CHCH(Ar)OH$[b] Run 2	$ArCOAr$[b,c] Run 1	$ArCOAr$[b,c] Run 2	^{14}C scrambling from C-2 to C-1 (%) Run 1	Run 2
1	HOAc	6 140 000	2 690 000	6 170 000	2 700 000	0	0
1	HOAc 1.7 equiv. NaOAc	1 440 000	2 210 000	1 450 000	2 200 000	0	0
1	CF_3COOH	1 730 000	1 490 000	1 720 000	1 500 000	0	0
1	90% acetone–10% H_2O–0.1% $HClO_4$	1 430 000		1 420 000		0	
2	HOAc	613 000	477 000	381 000	294 000	37.8	38.4
2	HOAc 1.7 equiv. NaOAc	970 000	925 000	805 000	771 000	17.0	16.6

[a]Measured by a liquid scintillation counter.
[b]From **1**, Ar = Ph; from **2**, Ar = An.
[c]Assayed as the oxime.

in the product was decreased to about 17%. These data are also summarized in Table 1.

The decrease in the extent of scrambling, brought about by the presence of NaOAc in the reaction of **2** with HOAc, is in agreement with expectation, the more nucleophilic OAc^- being able to compete better than HOAc with the 1,2-aryl shift in the classical trianisylvinyl cation.

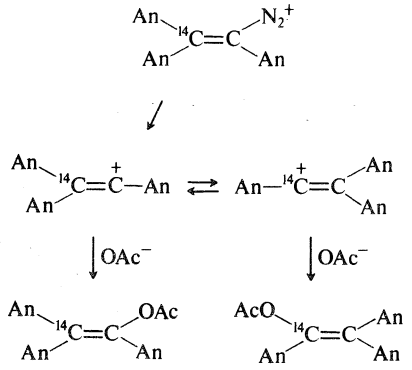

A similar suppression by added OAc^- of rearrangements in vinyl cations from triazenes was observed by Jones and Miller (1).

The lack of 1,2-phenyl shift in the triphenylvinyl cation generated from **1** under a variety of conditions (Table 1) is of interest and is worthy of some discussion. In the solvolyses of triphenylvinyl-2-^{14}C triflate (2), the presence of the conjugate base of the solvent did not affect the extent of isotopic scrambling, suggesting that the observed degenerate 1,2-phenyl shifts occurred via ion-pairs rather than free, classical ions. This conclusion appears to have been confirmed by the present results which show no 1,2-phenyl shift in the free, classical triphenylvinyl cation.

The absence of 1,2-phenyl shifts in the reactions of **1** with various acids, in contrast to the 38% scrambling observed in the reaction of **2** with HOAc, could simply be attributed to a difference in the migratory aptitudes of the phenyl and the anisyl groups. Indeed, from solvolytic studies with *cis*- and *trans*-1,2-diphenyl-2-anisylvinyl bromides (9), it was deduced that the ratios of anisyl to phenyl rearrangements were of the order of 76–120. Although comparisons of 1,2-aryl shifts in the triphenylvinyl and trianisylvinyl systems are not straightforward since the migrating group, migration origin, and migration terminus in the two systems are different, it may still be of interest to compare the scrambling data from the reactions of triphenylvinyl-2-^{13}C bromide (**3**) and trianisylvinyl-2-^{13}C bromide (**4**) with HOAc–AgOAc and the results from **1** and **2** in the present work. The reaction of **4** with HOAc–AgOAc gave 20% scrambling of the label from C-2 to C-1 due to 1,2-anisyl shifts (4), while in the reaction of **2** with HOAc, the scrambling was increased to 38% (Table 1). In contrast, the reaction of **3** with HOAc–AgOAc gave about 7% scrambling (3), but in the reaction of **1** with HOAc, instead of an increase to more than 7% scrambling, no 1,2-phenyl shift was observed. It appears, therefore, that a simple parallel behaviour attributable to migratory aptitudes does not hold in the reactions of **1** and

Can. J. Chem. Downloaded from www.nrcresearchpress.com by 210.87.254.42 on 09/05/12
For personal use only.

Can. J. Chem. Downloaded from www.nrcresearchpress.com by 210.87.254.42 on 09/05/12
For personal use only.

2 with HOAc and in the reactions of **3** and **4** with HOAc–AgOAc. Again, the possibility of 1,2-phenyl shifts occurring only in the ion-pair from **3** and not in the free ion from **1** may account for the observed different behaviours.

It has been pointed out in a recent review (10) that vinyl cations are not basically different from normal trisubstituted carbocations. Since nitrous acid deaminations also give rise to carbocations via diazonium ions, consideration of known data from deaminations in comparison with the present results may be worthwhile. In saturated carbocationic systems from deaminations, the An/Ph migratory ratios have been found to be quite low (about 1.2–2.0) (11–13). Furthermore, Bonner and Putkey (14) have actually observed a lower extent of 1,2-anisyl shift (17%) in the deamination of 1,2,2-trianisylethylamine-*1*-^{14}C than the previously observed 1,2-phenyl shift (26–28%) in the deamination of 1,2,2-triphenylethylamine-*1*-^{14}C. A diminished positive character due to the delocalization of the positive charge at the migration terminus has been suggested as playing an important role in accounting for this reversal in migratory aptitudes (14, 15). If the reactions of **1** and **2** with acids were to behave in similar ways as the deamination reactions of saturated systems, one would expect that the extent of 1,2-phenyl shift in reactions of **1** should be less than the 1,2-anisyl shift in reactions of **2** by a factor of no more than about two. Obviously this was not the case since no 1,2-phenyl shift was observed. The present results may be explained by assuming that in the relatively stable trianisylvinyl cation, the lifetime of the ion is relatively long, and since the anisyl group has a high migratory aptitude, degenerate 1,2-anisyl shifts can occur before the ion is trapped by solvent to give product. With the less stable triphenylvinyl cation, its lifetime is shorter and the migratory aptitude of the phenyl group is lower. Both of these factors would contribute, resulting in the failure of the degenerate 1,2-phenyl shift to compete with product formation.[1]

[1]If the same arguments regarding the stability of trianisyl and triphenyl substituted ions were applied to analogous saturated systems, the deamination of 1,2,2-trianisylethylamine should give more rearrangement than the deamination of 1,2,2-triphenylethylamine, but this was not the case (14, 15). The present results thus indicate that there are interesting differences between the vinylic and saturated analogs.

When the triphenylvinyl substrate can give rise to an ion-pair, the ion-pair may have a longer lifetime, thus allowing some 1,2-phenyl shifts to occur. There is also the possibility of phenyl participation to give the phenyl-bridged cation in the ion-pair formation. Since phenyl-bridging does take place in the 1,2-dimethyl-2-phenylvinyl system (16, 17) while there is no phenyl participation in the 1,2-dianisyl-2-phenylvinyl system (5), it is attractive to consider the possibility of a gradation of mechanisms, with triphenylvinyl systems that can give ion-pairs falling into the borderline region between full phenyl participation and no phenyl participation. Such a possibility, however, remains to be confirmed or rejected by further experimentation.

Experimental

*Triphenylvinyl-2-^{14}C-phenyltriazene (**1**) and Trianisylvinyl-2-^{14}C-phenyltriazene (**2**)*

Triphenylvinyl-*2*-^{14}C bromide (2) or trianisylvinyl-*2*-^{14}C bromide (4) was converted to the corresponding Grignard reagent. The initiation of this reaction was quite slow and prolonged refluxing (1–4 days) in tetrahydrofuran under nitrogen was required to effect the conversion. The Grignard solution was cooled in an ice bath and an equivalent of freshly prepared phenyl azide (18) was added. The reaction mixture was stirred for 1 h, treated with a solution of 10% NH_4OH – 10% NH_4Cl, and then extracted with ether. The extract was washed with H_2O and dried over $MgSO_4$. Removal of the ether under reduced pressure gave a bright yellow oil which was purified by passage through an alumina column, using 90% petroleum ether – 10% ether as eluant. Unreacted phenyl azide and a by-product, triphenylethylene or trianisylethylene, were the first components to be eluted. The desired product, **1** or **2**, was collected last and after recrystallization from hexane, the yields of **1** and **2** were about 50 and 35%, respectively. Compound **1** melted with decomposition at 113–115 °C. *Anal.* calcd. for $C_{26}H_{21}N_3$: C 83.20, H 5.60, N 11.20; found: C 83.12, H 5.26, N 11.04. Compound **2** melted with decomposition at 121–122 °C. *Anal.* calcd. for $C_{29}H_{27}O_3N_3$: C 74.82, H 5.85, N 9.03; found: C 74.57, H 5.88, N 8.71.

*Reactions of **1** or **2** with Acids*

The reactions carried out were between **1** and HOAc, HOAc containing 1.7 equiv. of NaOAc, CF_3COOH, or 0.1% $HClO_4$ in 90% acetone – 10% H_2O, and between **2** and HOAc or HOAc containing 1.7 equiv. of NaOAc. In general, the reactions were effected at room temperature for a period of 10 min. A typical run is described below.

A solution of 200 mg (0.43 mmol) of **2** and 60 mg (0.73 mmol) of NaOAc in 3.0 ml of glacial acetic acid was shaken at room temperature for 10 min. Evolution of N_2 took place as soon as the triazene came into contact with the acid and the gas evolution apparently ceased within about 1 min. Most of the solvent was removed at

room temperature under reduced pressure. The residual oil was dissolved in 30 ml of ether and the solution was washed successively with saturated $NaHCO_3$ solution and with H_2O. After drying over $MgSO_4$, the ether solution containing the acetate product was treated twice successively with $LiAlH_4$ to give 1,2,2-trianisylethanol (4) which was isolated with the aid of added inactive carrier. In preliminary trials with non-labeled materials, the yield of the acetate product was about 85%.

Conversions of various triarylvinyl products to 1,2,2-triarylethanols, followed by oxidative degradation to diaryl ketones, were carried out according to previously described procedures (2).

Acknowledgement

The financial support given by the National Research Council of Canada is gratefully acknowledged.

1. W. M. Jones and F. W. Miller. J. Am. Chem. Soc. **89**, 1960 (1967).
2. C. C. Lee, A. J. Cessna, B. A. Davis, and M. Oka. Can. J. Chem. **52**, 2679 (1974).
3. F. H. A. Rummens, R. D. Green, A. J. Cessna, M. Oka, and C. C. Lee. Can. J. Chem. **53**, 314 (1975).
4. M. Oka and C. C. Lee. Can. J. Chem. **53**, 320 (1975).
5. C. C. Lee and M. Oka. Can. J. Chem. **54**, 604 (1976).
6. Z. Rappoport and A. Gal. J. Am. Chem. Soc. **91**, 5246 (1969).
7. Z. Rappoport and Y. Houminer. J. Chem. Soc. Perkin Trans. II. 1506 (1973).
8. Y. Houminer, E. Noy, and Z. Rappoport. J. Am. Chem. Soc. **98** (1976). In press.
9. Z. Rappoport, E. Noy, and Y. Houminer. J. Am. Chem. Soc. **98**, 2238 (1976).
10. L. R. Subramanian and M. Hanack. J. Chem. Educ. **52**, 80 (1975).
11. L. S. Ciereszko and J. G. Burr. J. Am. Chem. Soc. **74**, 5431 (1952).
12. J. D. Roberts and C. M. Regan. J. Am. Chem. Soc. **75**, 2069 (1953).
13. D. Y. Curtin and M. C. Crew. J. Am. Chem. Soc. **76**, 3719 (1954).
14. W. A. Bonner and T. A. Putkey. J. Org. Chem. **27**, 2348 (1962).
15. M. J. McCall, J. M. Townsend, and W. A. Bonner. J. Am. Chem. Soc. **97**, 2743 (1975).
16. P. J. Stang and T. E. Dueber. J. Am. Chem. Soc. **95**, 2683 (1973).
17. P. J. Stang and T. E. Dueber. J. Am. Chem. Soc. **95**, 2686 (1973).
18. R. O. Lindsay and C. F. H. Allen. Organic syntheses. Coll. Vol. III. John Wiley and Sons, New York. 1955. p. 710.

Can. J. Chem. Downloaded from www.nrcresearchpress.com by 210.87.254.42 on 09/05/12
For personal use only.

The addition of 4-chlorobenzenesulfenyl chloride to phenyl-substituted acetylenes: the structures of the intermediate thiirenium ion[1]

GEORGE H. SCHMID, AGNIESZKA MODRO, DENNIS G. GARRATT, AND KEITH YATES
Department of Chemistry, University of Toronto, Toronto, Ont., Canada M5S 1A1

Received March 17, 1976

GEORGE H. SCHMID, AGNIESZKA MODRO, DENNIS G. GARRATT, and KEITH YATES. Can. J. Chem. **54**, 3045 (1976).

A comparison is made of the effect on the rates and product compositions of substituting a phenyl ring for a hydrogen on ethylene and acetylene and their derivatives. Such a comparison leads to the conclusion that the structure of the intermediate phenyl thiirenium ion, formed by the addition of an arenesulfenyl chloride to phenylacetylenes, is one in which charge is delocalized into the phenyl ring.

GEORGE H. SCHMID, AGNIESZKA MODRO, DENNIS G. GARRATT et KEITH YATES. Can. J. Chem. **54**, 3045 (1976).

On a comparé l'effet, sur les vitesses et la composition des produits, de la substitution par un noyau phényle d'un hydrogène de l'éthylène, de l'acétylène et leurs dérivés. Une telle comparaison nous amène à la conclusion que la structure de l'intermédiaire, l'ion phénylthiirènium formé par l'addition d'un chlorure d'arènesulfényle au phénylacétylène, est celle dans laquelle la charge est délocalisée vers le noyau phényle.

[Traduit par le journal]

The mechanism of the addition of arenesulfenyl chlorides to phenyl substituted acetylenes has been the subject of considerable interest (2–4). On the basis of second-order kinetics and the formation of products by *anti* stereospecific but nonregiospecific addition, a mechanism involving a thiirenium ion (**1**) was proposed for this reaction (2).

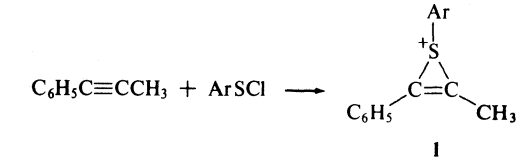

1

Rate determining step

Product determining step

There are two possible structures for the intermediate (**1**). Either the remaining double bond is conjugated with the phenyl ring as in **2** or the thiirenium ion is stabilized by conjugation with

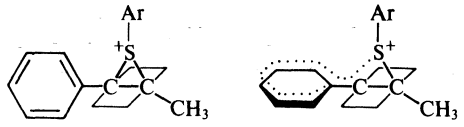

2 **3**

the phenyl ring as in **3**. On the basis of a low ρ value for the effect of substituents in the phenyl ring of the acetylene, it has been concluded that the structure of the intermediate is best represented by **2** (4). We would like to present kinetic and product data which provides additional information on whether the rate determining transition state more clearly resembles structures **2** or **3**.

Results

The rates of addition of 4-chlorobenzenesulfenyl chloride to acetylene (**4**) and four phenyl substituted derivatives were measured by following the disappearance of the 4-chlorobenzenesulfenyl chloride absorption at 392.5 nm in 1,1,2,2-tetrachloroethane at 25 °C. The stopped

[1]Reactions of sulfenyl chlorides and their derivatives. XVI. For part XV see ref. 1.

Can. J. Chem. Downloaded from www.nrcresearchpress.com by 210.87.254.5 on 09/05/12
For personal use only.

Can. J. Chem. Downloaded from www.nrcresearchpress.com by 210.87.254.5 on 09/05/12
For personal use only.

$R^1C{\equiv}CR^2$

	R^1	R^2
4	H	H
5	C_6H_5	H
6	C_6H_5	CH_3
7	C_6H_5	C_2H_5
8	C_6H_5	C_6H_5

flow technique, using a Durrum–Gibson spectrophotometer, was used for all compounds except acetylene whose reaction was monitored by conventional techniques using a Cary 16 spectrophotometer. The addition was found to follow normal second-order kinetics, first-order in both alkyne and sulfenyl halide to 80% completion of the reaction. The second-order specific rate constants are given in Table 1.

The *anti* stereospecific but nonregiospecific addition of arenesulfenyl chlorides to phenyl acetylenes has been convincingly demonstrated several times (2–4). On the basis of the known stereochemistry of the adducts, it is possible to verify several relationships between chemical shift positions and alkene configuration (5–7). The ^{13}C and proton magnetic resonance data are given in Tables 2 and 3 respectively for all four adducts of alkynes **5**, **6** and **7**. The *Z*-isomers were obtained by irradiating the products of addition.

From the data in Table 2, it is clear that the ^{13}C chemical shifts of carbons, attached to a carbon–carbon double bond appear at higher field for the *Z*- than for the *E*-isomer. Furthermore the ^{13}C chemical shift for an olefinic carbon is at lower field when bonded to chlorine than to sulfur.

The following relationships between adduct configuration and proton chemical shift are found in Table 3. The chemical shifts of protons vicinal to chlorine are observed at lower field relative to those vicinal to the arylthio group. Also the chemical shifts of γ-protons in the *Z*-isomers are observed at higher field relative to those in the *E*-isomer.

The kinetically controlled product composition, given in Table 4, could be determined from nonoverlapping peaks in the proton spectrum of the reaction mixture.

TABLE 1. The bimolecular rate constants for the addition of 4-chlorobenzenesulfenyl chloride to alkynes in 1,1,2,2-tetrachloroethane at 25 °C

Alkyne	k_2 (M^{-1} s^{-1})	k_{rel}
HC≡CH	$(2.31 \pm 0.01) \times 10^{-3}$	1.0
$C_6H_5C{\equiv}CH$	0.262 ± 0.001	113
$C_6H_5C{\equiv}CCH_3$	9.11 ± 0.03	3.94×10^3
$C_6H_5C{\equiv}CC_2H_5$	17.8 ± 0.1	7.71×10^3
$C_6H_5C{\equiv}CC_6H_5$	0.268 ± 0.002	116

Discussion

A comparison of the value of ρ for the addition of arenesulfenyl chlorides to 1-phenylpropene ($\rho = -2.68$) (8) and 1-phenylpropyne ($\rho = -1.3$) (4) has been used as the basis for establishing the structure of the thiirenium ion intermediate. Such a comparison implies that $|\rho|$ is a quantitative measure of bridging in the rate determining transition state for electrophilic addition reactions. The available evidence for additions to alkenes and alkynes does not support this view. The values of ρ for hydration

TABLE 2. The observed ^{13}C magnetic resonance parameters for the adducts of 4-chlorobenzenesulfenyl chloride to phenyl substituted alkynes

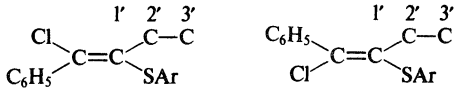

E *Z*

Compound		C_1	$C_{1'}$	$C_{2'}$	$C_{3'}$
$C_6H_5C(Cl){=}C(SAr)CH_3$	*E*	145.62	121.43	19.78	
	Z	—	—	17.78	
$C_6H_5C(SAr){=}C(Cl)CH_3$	*E*	142.62	131.39	22.04	
	Z	143.66	132.45	19.77	
$C_6H_5C(Cl){=}C(SAr)C_2H_5$	*E*	147.56	122.08	29.68	13.07
	Z	—	—	26.38	13.22
$C_6H_5C(SAr){=}C(Cl)C_2H_5$	*E*	140.26	134.09	31.03	12.87
	Z	—	—	28.76	12.39

TABLE 3. The observed proton magnetic resonance for the adducts of 4-chlorobenzenesulfenyl chloride to phenyl substituted alkynes

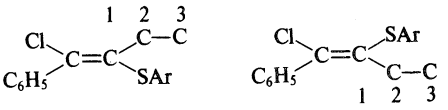

E *Z*

Compound		H_1	H_2	H_3
$C_6H_5C(Cl)=CHSAr$	*E*	6.67s	—	—
	Z		—	—
$C_6H_5C(SAr)=CHCl$	*E*	6.91s	—	—
	Z		—	—
$C_6H_5C(Cl)=C(SAr)CH_3$	*E*		2.12s	—
	Z		1.94s	—
$C_6H_5C(SAr)=C(Cl)CH_3$	*E*		2.51s	—
	Z		2.41s	—
$C_6H_5C(Cl)=C(SAr)C_2H_5$	*E*		2.40q	1.08t
	Z		2.27q	1.12t
$C_6H_5C(SAr)=C(Cl)C_2H_5$	*E*		2.98q	1.11t
	Z		2.67q	1.14t

TABLE 4. Kinetically controlled products of addition of 4-chlorobenzenesulfenyl chloride to unsymmetrical phenylacetylenes

	Percent composition	
R	C_6H_5, Cl, SC_6H_4Cl, R	C_6H_5, ClC_6H_4S, Cl, R
H	100	0
CH_3	61	33
C_2H_5	51	49

bromination, chlorination, and addition of arenesulfenyl chlorides to styrene and phenyl acetylene derivatives decrease in the order $|\rho_{H^+}| \gtrsim |\rho_{Br_2}| > |\rho_{Cl_2}| > |\rho_{ArSCl}|$. On the basis of product studies, salt effects, and amounts of solvent incorporated products, it has been concluded that the importance of bridging in the rate determining transition state decreases in the order $ArSCl \gg Br_2 > Cl_2 > H^+$. Clearly for these four electrophiles, the magnitude of ρ is not simply related to either the extent of bridging or the extent of charge on the carbons in the rate determining transition state.

More meaningful results can be obtained by comparing the effect on the rates and product compositions of substituting a phenyl group for a hydrogen on ethylene and acetylene and their derivatives. These data are given in Table 5. Substituting a phenyl ring for a hydrogen on acetylene results in a rate increase of 113 while a similar substitution on ethylene has little effect. This result indicates that for ethylene the stabilization by the phenyl ring in the transition state is exactly balanced by its ground state stabilization (Fig. 1). For the acetylene, the phenyl ring must stabilize the transition state more than the ground state. This stabilization of the transition state could be due to (*i*) a structure similar to **3** in which the charge is delocalized into the phenyl ring or (*ii*) a structure similar to **2** in which the phenyl is conjugated with the remaining double bond. In the latter case the phenyl ring would be expected to exert an inductive effect upon the rate of addition. Consequently the rates should correlate with the sum of Taft inductive substituent constants ($\sum\sigma^*$). No such correlation exists. This is in contrast to the addition to simple alkyl substituted acetylenes where a good correlation between rate and $\sum\sigma^*$ was found (9).

Furthermore, the phenyl ring is conjugated with one of the double bonds of the acetylene in the ground state. If the rate determining transi-

TABLE 5. Comparison of the second-order rate constants and product composition for the addition of 4-chlorobenzene sulfenyl chloride to alkenes and alkynes in 1,1,2,2-tetrachloroethane at 25 °C

		$R_1CH=CHR_2$				$R_1C\equiv CR_2$			
R_1	R_2	k_2 (M^{-1} s^{-1})	k_{rel}	M (%)	aM (%)	k_2 (M^{-1} s^{-1})	k_{rel}	*E*-M (%)	*E*-aM (%)
H	H	65.1	1.0	—	—	2.31 ±0.02	1.0	—	—
C_6H_5	H	62.0±0.2	0.95	100	0	0.262±0.001	113	100	0
C_6H_5	CH_3	118.3±0.07[a]	1.81	100	0	9.11±0.03	3.94×10^3	61	39
C_6H_5	C_2H_5			—	—	17.8 ±0.1	7.71×10^3	51	49
C_6H_5	C_6H_5	8.5[a]	0.12	—	—	0.268±0.002	116	—	—

[a] *trans*-Isomer.

Can. J. Chem. Downloaded from www.nrcresearchpress.com by 210.87.254.5 on 09/05/12
For personal use only.

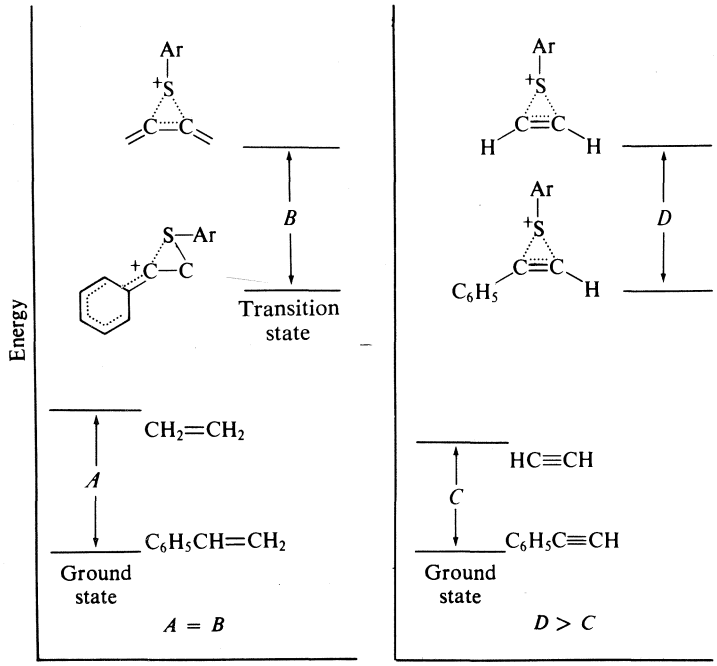

FIG. 1. Effect of phenyl ring on ground and transition states of the addition of 4-chlorobenzenesulfenyl chloride to ethylene and acetylene.

tion state resembles structure **2** there might well be a balancing of the stabilization of the ground and transition states as occurs in the case of styrene. Thus structure **3**, in which the charge is delocalized into the phenyl ring, seems more compatible with the data.

In support of this view, the rate data of Okuyama *et al.* (4) on the addition of 2,4-dinitrobenzenesulfenyl chloride to phenyl substituted 1-phenylpropynes correlates better with σ^+ than σ. Thus, the following correlation is obtained

$$\log k/k_0 = -1.35\sigma^+ - 1.29 \qquad r = 0.989$$

Correlations with σ^+ are usually obtained in systems in which conjugation between the substituents and the reaction center is important.

The regiochemistry of the products provides further evidence for structure **3**. The products of kinetic control of the addition of 4-chlorobenzenesulfenyl chloride to six terminal alkynes are the *E-anti*-Markownikoff and *E*-Markownikoff adducts. For all alkyl substituents the *E-anti*-Markownikoff adduct is the major product (>75% yield). This product regiochemistry

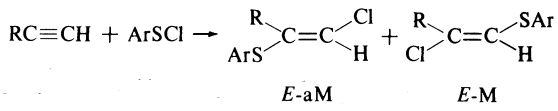

is in accord with a bridged thiirenium-like product determining transition state in which the carbon of the substituent, the thiirenium ring and the attacking chloride ion all lie in one plane. As a result the major effect of the substituent is steric in nature (9).

The steric effect of the phenyl group is different in structures **2** and **3**. In structure **2** the phenyl ring is in the same plane as the thiirenium ring and should sterically hinder any attack at the α-carbon as illustrated in Fig. 2. Thus, attack at the β-carbon would be favored to form products with *E-anti*-Markownikoff orientation. However, only *E*-Markownikoff products are formed by addition to phenylacetylene. This result can be explained only if the effect of the phenyl ring in the product determining step is polar (electron delocalization) rather than steric. This is consistent with **3** rather than **2** as the structure of the intermediate.

The *anti* stereospecific and regiospecific addi-

Can. J. Chem. Downloaded from www.nrcresearchpress.com by 210.87.254.5 on 09/05/12
For personal use only.

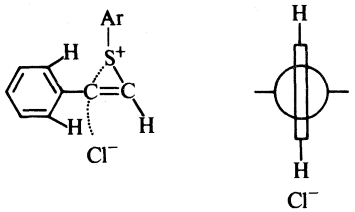

Side view End view

FIG. 2

tion to phenylacetylene suggests that both the intermediate and the product determining transition state have unsymmetrical structures. As the acetylenic hydrogen of phenylacetylene is substituted by methyl and ethyl groups, the addition becomes progressively less regiospecific. This suggests that the structure of the intermediate becomes more symmetrical with the result that both steric and polar effects are important in the product determining transition state.

The effect of solvent upon product regiochemistry is very similar for additions of arenesulfenyl chloride to both phenyl substituted acetylenes and ethylenes. As the acidity of the solvent increases the percent of Markownikoff adduct also increases (10, 11). The similarity in response to such solvent change strongly suggests that the product determining transition states are similar for both reactions. Electron delocalization into the phenyl ring is well established for the addition to styrene derivatives, suggesting that **3** is the structure of the intermediate for the addition to acetylenes.

Finally, replacing the acetylenic hydrogen of phenylacetylene and the β-hydrogen of styrene by a phenyl ring has a similar effect on the relative rates. In the case of tolan, the rate is almost identical to that of phenylacetylene while for *trans*-stilbene the rate is slightly less than that for styrene. Thus, in both systems the introduction of a second phenyl group has little effect on the rate of addition.

The data presented here point clearly to structure **3** as the structure of the thiirenium ion intermediate formed by the addition of 4-chlorobenzenesulfenyl chloride to phenyl substituted acetylenes.

Experimental

The alkynes were obtained commercially and their purity was verified by glc and nmr.

4-Chlorobenzenesulfenyl chloride was prepared as previously described (12).

1,1,2,2-Tetrachloroethane was purified as previously described (12).

Kinetics and product compositions were determined as previously described (12).

Acknowledgements

Continued financial support from the National Research Council of Canada is gratefully acknowledged. A University of Toronto Special Open Fellowship (1973–1974), and an NRCC Postgraduate Scholarship (1974–1976) to DGG are also very much appreciated.

1. G. H. SCHMID, A. MODRO, and K. YATES. J. Org. Chem. In press.
2. G. H. SCHMID and M. HEINOLA. J. Am. Chem. Soc. **90**, 3466 (1968).
3. G. MODENA and G. SCORRANO. Int. J. Sulfur Chem. **3**, 115 (1968).
4. T. OKUYAMA, K. IZAWA, and T. FUENO. J. Org. Chem. **39**, 351 (1974).
5. G. H. SCHMID and D. G. GARRATT. Can. J. Chem. **51**, 2463 (1973).
6. J. R. CAVANAUGH and B. P. DAILEY. J. Chem. Phys. **34**, 1093 (1961).
7. B. P. DAILEY and J. N. SCHOOLERY. J. Am. Chem. Soc. **77**, 3977 (1955).
8. K. IZAWA. Ph.D. Thesis, Osaka University, Japan. 1973.
9. G. H. SCHMID, A. MODRO, F. LENZ, D. G. GARRATT, and K. YATES. J. Org. Chem. **41**, 2331 (1976).
10. G. H. SCHMID and V. M. CSIZMADIA. Can. J. Chem. **50**, 2432 (1972).
11. V. CALO, G. MODENA, and G. SCORRANO. J. Chem. Soc. *C*, 1339 (1968).
12. G. H. SCHMID, V. M. CSIZMADIA, V. J. NOWLAN, and D. G. GARRATT. Can. J. Chem. **50**, 2457 (1972).

Can. J. Chem. Downloaded from www.nrcresearchpress.com by 210.87.254.5 on 09/05/12
For personal use only.

Reactions of *tert*-$C_4H_9^+$, *tert*-$C_5H_{11}^+$, and CH_3-cy-$C_5H_9^+$ ions with pentenes

GUY J. COLLIN

Département des sciences pures, Université du Québec à Chicoutimi, Chicoutimi (Qué.), Canada G7H 2B1

Received April 13, 1976

GUY J. COLLIN. Can. J. Chem. **54**, 3050 (1976).

Total reaction rate constants for the disappearance of *tert*-$C_4H_9^+$ ions with five C_5H_{10} unsaturated hydrocarbons were determined by comparing the rate of formation of isobutane in the radiolysis of neopentane in the presence of various additives. These rate constants are of the order of 5 to 13.5 $\times$ 10^{-10} cm^3 molecule^{-1} s^{-1} depending upon the olefin under investigation. The hydride transfer reaction from 3-methyl-1-butene and *trans*-2-pentene toward the *tert*-$C_4H_9^+$ ion was also observed, as was the proton transfer reaction from the *tert*-$C_4H_9^+$ ion toward 2-methyl-2-butene and 2-methyl-1-butene. In the latter two cases, a significant isomerization of methylbutene is noticed: an isomerization mechanism based upon the reactions of *tert*-$C_5H_{11}^+$ ions is tentatively suggested. Finally, the transfer reaction of an hydrogen molecule between the CH_3-cy-$C_5H_9^+$ ion and the methylbutenes is observed during the radiolysis of methylcyclopentane.

GUY J. COLLIN. Can. J. Chem. **54**, 3050 (1976).

Les constantes de vitesse de réaction des ions *tert*-$C_4H_9^+$ avec cinq isomères insaturés en C_5H_{10} ont été déterminés en comparant les vitesses de formation de l'isobutane dans la radiolyse du néopentane en présence de différents additifs. Ces vitesses sont de l'ordre de 5 à 13.5 $\times$ 10^{-10} cm^3 molecule^{-1} s^{-1} dépendant de l'oléfine ajoutée. Le transfert d'un ion hydrure du méthyl-3 butène-1 et du *trans*-pentène-2 vers l'ion *tert*-$C_4H_9^+$ est observée, de même que le transfert d'un proton de l'ion *tert*-$C_4H_9^+$, vers les méthyl-2 butène-2 et méthyl-2 butène-1. Dans ces deux derniers cas, on observe une isomérisation importante de l'oléfine. On propose un mécanisme en chaîne intégrant l'ion *tert*-$C_5H_{11}^+$ pour rendre compte des observations. Enfin, on propose le transfert d'une molécule d'hydrogène de l'ion CH_3-cy-$C_5H_9^+$ vers les méthylbutènes pour rendre compte de la formation de l'isopentane lors de la radiolyse du méthylcyclopentane.

Introduction

In the study of the photoionization of 3-methyl-1-butene (3M1B) at 10.03 eV (123.6 nm) we pointed out that the parent ion is responsible for the formation of 2-methyl-2-butene (2M2B) and 2-methyl-1-butene (2M1B) (1). This isomerization was also observed in the photoionization of 2M1B and again was explained in terms of ionic reactions (2). In order to obtain data on the ionic mechanism(s) probably involved in that isomerization, we have undertaken a research programme on ion–molecule reactions in various similar systems. This paper covers the study of radiolysis of gaseous neopentane in the presence of C_5H_{10} unsaturated hydrocarbons. This system is a good source of *tert*-$C_4H_9^+$ ions, and because these ions do not react with neopentane we have compared their fate in the presence of various additives. Finally, we have tried to obtain information about the methylbutene isomerization. In particular, we wanted to know if the *tert*-$C_5H_{11}^+$ ions may initiate the observed isomerization. Some photoionization (11.6–11.8 eV, 104.6–106.8 nm) experiments were also performed in order to support certain results.

Experimental

All the hydrocarbons employed were American Petroleum Institute chemicals and were used without further purification (99.9% minimum purity) following vacuum degassing (10^{-6} torr). Oxygen and ammonia (99.99%, Matheson of Canada) were used as received. Samples were prepared in a Pyrex vacuum line (mercury free) equipped with Teflon stopcocks and Wallace and Tiernan metallic membrane manometers. The Pyrex cell volume was 300 $\pm$ 30 cm^3. Oxygen was added to each sample in order to prevent the formation of products by radical mechanisms. γ-Ray irradiations were carried out in an Atomic Energy of Canada Ltd. 220 Gammacell type source. Irradiation times were 400 min and the dose rate chemically measured in gaseous neopentane was 1.6 $\times$ 10^{17} eV mol^{-1} s^{-1} (3). Some irradiations were made in the photoionization region using an argon resonance lamp (11.6–11.8 eV) described in the literature (4) of intensity 1.5 $\times$ 10^{13} photons/s. Analyses were carried out by gas chromatography with a squalane column using a dual flame ionization detector.

Results

The results are recorded in the tables and figures. Radiolytic yields are given as M/N(X) values where M is the number of X molecules formed in comparison with the number of ions N released in the direct radiolysis of neopentane.

Can. J. Chem. Downloaded from www.nrcresearchpress.com by 210.87.254.40 on 09/05/12
For personal use only.

Can. J. Chem. Downloaded from www.nrcresearchpress.com by 210.87.254.40 on 09/05/12
For personal use only.

The M/N values are multiplied by 4.37 (5) in order to obtain the usual G values. Dosimetry was carried out by comparing the yields of the products formed in the irradiation of gaseous neopentane with those found by Lias and Ausloos (3): $M/N(C_2H_4) = 0.07$ and $M/N(C_3H_6) = 0.11$ in the neo-$C_5H_{12} - O_2$ mixtures. In a few cases (see text), some yield values were estimated without carrying out accurate dosimetry. Oxygen at levels of 5 to 10% was added to all samples to act as a free radical scavenger.

Some irradiations were done using an argon resonance lamp 11.6–11.8 eV. Actinometry was carried out in two different ways and both methods provided identical results. In the presence of 5% methylcyclopentane (MCP), it was assumed that all the ions formed in the photoionization of neopentane lead to the formation of isobutane (6–8) (see below). The quantum yield of these ions is known: $\Phi(\text{ion})_{11.6-11.8\text{ eV}} = 0.42$ (2). Such values were verified by comparing the amounts of the products obtained with those formed in the photoionization of 2M1B–O_2 (1.0:0.1 torr) (2).

The following observations should be noted. (*1*) The iso-C_4H_{10} yield was constant ($M/N = 0.040 \pm 0.005$) in the radiolysis of neo-C_5H_{12}–3M1B–O_2 mixture (100:5:5) when the pressure of neopentane ranged between 10 and 300 torr. (*2*) The addition of ammonia (5 torr) to the neo-C_5H_{12}–2M1B–O_2 mixture (40:2:4 torr) increased the radiolytic yield in isobutene from 0.37 to 0.67 and lowered the yield of 2M2B from 1.6 to 0.04. (*3*) The isobutene yield in the photoionization of the neo-C_5H_{12}–MCP–O_2 mixture (100:5:5) increased along with the total pressure: $\Phi(\text{iso-}C_4H_8) = 0.33$ at 5 torr and 0.38 at 40 torr.

Discussion

(A) Radiolysis of Neopentane–Methylcyclopentane–Oxygen Mixtures

The radiolysis of gaseous neopentane in the presence of oxygen (2–4%) is well known (3). *tert*-$C_4H_9^+$ ions are formed with a yield of $M/N(\textit{tert}\text{-}C_4H_9^+) = 0.66$ (7) at a pressure of 40 torr. This value is confirmed by the irradiation of neopentane in the presence of methylcyclopentane where a value of $M/N(\text{iso-}C_4H_{10}) = 0.68_5$ (Table 1) was obtained:

[1] $\textit{tert}\text{-}C_4H_9^+ + CH_3\text{-cy-}C_5H_9 \rightarrow \text{iso-}C_4H_{10} + C_6H_{11}^+$

It is not necessary to take into account the formation of isobutane from iso-$C_4H_8^+$ ions for which the yield is negligible: $M/N(\text{iso-}C_4H_8^+) = 0.025$ (7, 8).

[2] $\text{iso-}C_4H_8^+ + CH_3\text{-cy-}C_5H_9 \rightarrow \text{iso-}C_4H_{10} + C_6H_{10}^+$

Because *tert*-$C_4H_9^+$ ions do not react, or react only very slowly, with neopentane (6, 7), the neopentane system is ideal for investigating the chemistry of these ions.

TABLE 1. Radiolysis of neopentane–additive–oxygen mixtures (40.0:X:2.0 torr)

Additive (X)	$M/N(\text{iso-}C_4H_{10})$	$M/N(\text{iso-}C_4H_8)$
—	0.00_4	0.20
2M2B (2.0)	0.00_7	0.56_5
2M1B (1.0)	0.00_1	0.37
3M1B (2.0)	0.04_2	0.20
n-1-C_5H_{10} (2.0)	0.00	0.20
trans-2-C_5H_{10} (2.0)	0.08	0.20
CH_3-cy-C_5H_9 (5.0)	0.68_5	0.20

(B) Hydride Transfer Reactions of tert-$C_4H_9^+$ Ions with C_5H_{10} Compounds

The reaction first observed when C_5H_{10} olefins are added to neopentane is the hydride transfer reaction between the additive and the *tert*-$C_4H_9^+$ ion, as noticed for saturated hydrocarbons (7). The results presented in Table 1 show the occurrence of such a reaction for *trans*-2-pentene and 3M1B (see also Fig. 1). From the increments in the isobutane yields it is deduced that 12% of the reactive collisions, $R(H^-)$, in the first case,

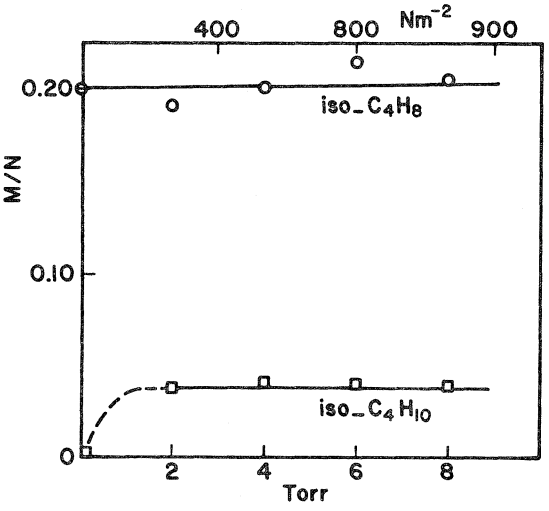

FIG. 1. Effect of the pressure of 3M1B in the radiolysis of neo-C_5H_{12}–oxygen mixtures (40.0:2.0 torr).

Can. J. Chem. Downloaded from www.nrcresearchpress.com by 210.87.254.40 on 09/05/12
For personal use only.

and 6% in the second one, generate isobutane:

$$R(H^-) = \frac{G(\text{iso-}C_4H_{10})}{G(\textit{tert}\text{-}C_4H_9^+)} = \frac{G(\text{iso-}C_4H_{10})}{0.66}$$

[3] $\textit{tert}\text{-}C_4H_9^+ + \textit{trans}\text{-}2\text{-}C_5H_{10} \rightarrow \text{iso-}C_4H_{10} + C_5H_9^+$

[4] $\textit{tert}\text{-}C_4H_9^+ + 3M1B \rightarrow \text{iso-}C_4H_{10} + C_5H_9^+$

where $G(\text{iso-}C_4H_{10})$ is the isobutane yield measured in the presence of olefin. These two reactions are exothermic ($\Delta H = -10$ kcal mol^{-1}) although the enthalpy of formation of some of the ionic species does not seem to be known with great accuracy (10). Moreover, it is likely that the ions formed are stabilized by resonance.

(C) Proton Transfer Reactions of tert-$C_4H_9^+$ Ions with C_5H_{10} Compounds

The second reaction observed is the proton transfer reaction between the *tert*-$C_4H_9^+$ ion and the unsaturated additive. Such a reaction is only observed for 2M1B and 2M2B through the variation of the isobutene yields (Figs. 2 and 3 respectively).

[5] $\textit{tert}\text{-}C_4H_9^+ + 2M1B \rightarrow \text{iso-}C_4H_8 + \textit{tert}\text{-}C_5H_{11}^+$ $\Delta H = -3.3$ kcal mol^{-1}

[6] $\textit{tert}\text{-}C_4H_9^+ + 2M2B \rightarrow \text{iso-}C_4H_8 + \textit{tert}\text{-}C_5H_{11}^+$ $\Delta H = -1.3$ kcal mol^{-1}

The importance, $R(H^+)$, of the proton transfer reaction can be calculated from the increments in isobutene yields (Table 2):

$$R(H^+) = \frac{G(\text{iso-}C_4H_8) - G^0(\text{iso-}C_4H_8)}{G^0(\textit{tert}\text{-}C_4H_9^+)}$$

where G^0 and G are the yields of products measured in the neopentane–oxygen and neopentane–alkene–oxygen mixtures respectively. $R(H^+)$ values are 0.40 for 2M2B and about 0.25 for 2M1B. In the other cases, the ion resulting from the proton transfer reaction would have a secondary structure. Therefore, the corresponding reactions are probably endothermic and are not observed.

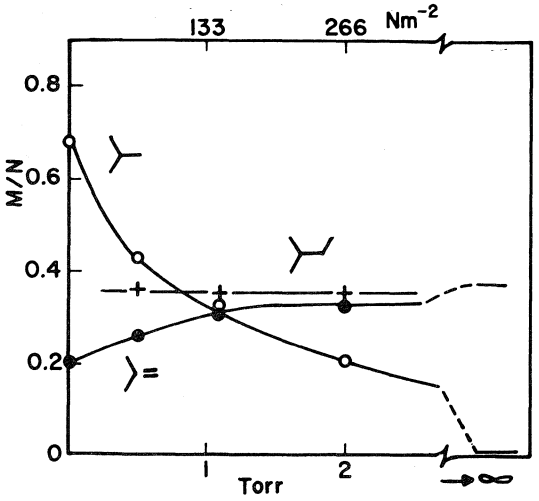

FIG. 2. Effect of the pressure of 2M1B in the radiolysis of neo-C_5H_{12}–CH_3-cy-C_5H_9–O_2 mixtures (40.0:10.0:4.0 torr). Values indicated as $\rightarrow \infty$ were obtained in the radiolysis of neo-C_5H_{12}–2M1B–O_2 mixtures (40.0:1.0:4.0 torr).

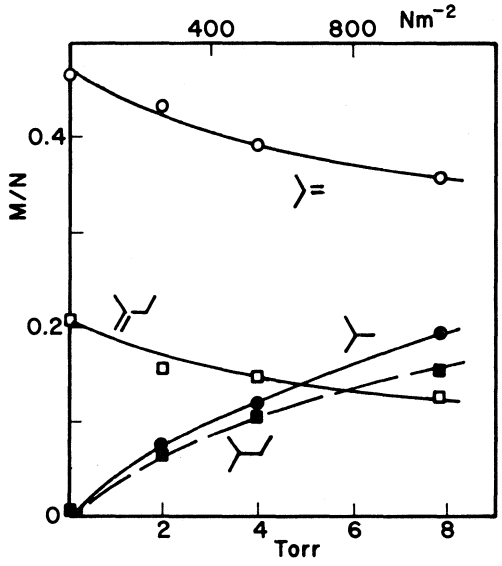

FIG. 3. Effect of the pressure of methylcyclopentane in the radiolysis of neo-C_5H_{12}–2M2B–O_2 mixtures (40.0: 2.0:2.0 torr).

TABLE 2. Total reaction rate constants between the *tert*-butyl ion and hydrocarbons

Hydrocarbon	k (cm^3 molecule^{-1} s^{-1} × 10^{10}) Present work[a]	Literature value (ref.)
Neopentane	—	0.00 (11)
Methylcyclopentane	—	0.74 (11)
2M2B	6.5±0.6	—
2M1B	8.4±0.9	—
3M1B	3.3±0.3	—
n-1-Pentene	4.9±0.5	7 (12)
trans-2-Pentene	5.0±0.7	—

[a]Values are derived from at least five experiments.

Can. J. Chem. Downloaded from www.nrcresearchpress.com by 210.87.254.40 on 09/05/12
For personal use only.

(D) Reaction Rate Constants

In order to determine the total rate constant for the reaction between the *tert*-$C_4H_9^+$ ion and each of the additives, the variation of the formation of isobutane (process 1) was measured in the presence of additive and of various amounts of methylcyclopentane (see Figs. 2 and 3):

$$\frac{k_7}{k_1} = \frac{G^0(\text{iso-}C_4H_{10}) - G(\text{iso-}C_4H_{10})}{G(\text{iso-}C_4H_{10})} \times \frac{[CH_3\text{-cy-}C_5H_9]}{[C_5H_{10}]}$$

where G^0 and G values are measured in the absence or in the presence of the olefin in the neopentane–methylcyclopentane–oxygen mixtures. The rate constant of process 1 was estimated by Ausloos and his collaborators: $k_1 = 0.74 \times 10^{-10}$ cm^3 molecule^{-1} s^{-1} (7, 11). We obviously had to take into account the formation of isobutane through processes 3 and 4. Results are recorded in Table 2. These coefficients represent the total rate constants, and they therefore include hydride and proton transfer, as well as probable addition reactions.

[7] *tert*-$C_4H_9^+ + C_5H_{10} \rightarrow$ Products

The rate constants so determined correspond adequately with those determined for other olefins by Ausloos and his collaborators (7). The total rate constant obtained for *n*-1-pentene is in good agreement with that obtained by Munson in spite of the considerable differences between the techniques used (9, 12).

(E) Reactions of tert-$C_5H_{11}^+$ Ions

The formation of the *tert*-$C_5H_{11}^+$ ion through the proton transfer reaction between *tert*-$C_4H_9^+$ ion and 2M1B or 2M2B has already been mentioned above (processes 3 and 4). In these two cases, the formation in large amounts of a C_5H_{10} isomer is also noted (Figs. 4 and 5). Tentatively, it is interesting to link such a formation to the presence of *tert*-$C_5H_{11}^+$ ions.

[8] *tert*-$C_5H_{11}^+ + 2M1B \underset{k_{-8}}{\overset{k_8}{\rightleftarrows}} 2M2B + tert\text{-}C_5H_{11}^+$

$\Delta H = -1.49$ kcal mol^{-1}

[9] *tert*-$C_5H_{11}^+ + C_5H_{10} \rightarrow$ Product different from C_5H_{10}

At room temperature, the equilibrium constant calculated from thermochemical data for processes -8 and 8 is such that $k_8/k_{-8} \simeq 8$. The formation of 2M2B is then clearly favoured. In the 2M1B system, (Figs. 4 and 5), the k_8/k_9 ratio can then be determined by considering processes 5, 7, 8, and 9 only.[1]

$$k_8/k_9 = k_7/k_5 \times \frac{M/N(2M2B)}{M/N(tert\text{-}C_4H_9^+)} = 7.5 \pm 0.5$$

In the 2M2B system (Fig. 3), the k_{-8}/k_9 ratio is such that

$$k_{-8}/k_9 = k_7/k_6 \times \frac{M/N(2M1B)}{M/N(tert\text{-}C_4H_9^+)} = 1.1 \pm 0.2$$

In both cases, the M/N(2M2B) and the M/N(2M1B) values were corrected for the direct formation of these compounds through the absorption of energy by C_5H_{10} additives (see Table 3 and Fig. 4). This correction is less than

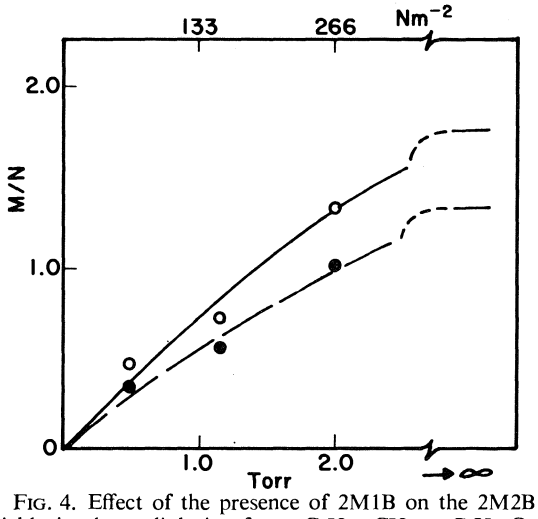

FIG. 4. Effect of the presence of 2M1B on the 2M2B yields in the radiolysis of neo-C_5H_{12}–CH_3-cy-C_5H_9–O_2 mixtures (40:10:4 torr). Values indicated as $\rightarrow \infty$ were obtained in the radiolysis of neo-C_5H_{12}–2M1B–O_2 mixtures (40:1:4 torr); ○ measured values; ● previous values less product formed through the direct irradiations of 2M1B determined in separate experiments.

[1]Assuming $x = k_8/(k_8 + k_9)$, the 2M2B yield formed in the first step, $M/N(2M1B)_1$, is equal to the yield of *tert*-$C_5H_{11}^+$ times x. The *tert*-$C_5H_{11}^+$ ions formed in process 8 lead again to the formation of 2M2B and in the second step the $M/N(2M2B)_2$ is equal to $M/N(tert\text{-}C_5H_{11}^+)x^2$. Then the total 2M2B yield is:

$$M/N(2M2B) = M/N(tert\text{-}C_5H_{11}^+) \times (x + x^2 + x^3 + x^4 + \ldots x^n)$$

and

$$\frac{M/N(2M2B)}{M/N(tert\text{-}C_5H_{11}^+)} = \frac{1}{1-x} - 1 = \frac{k_8}{k_9}$$

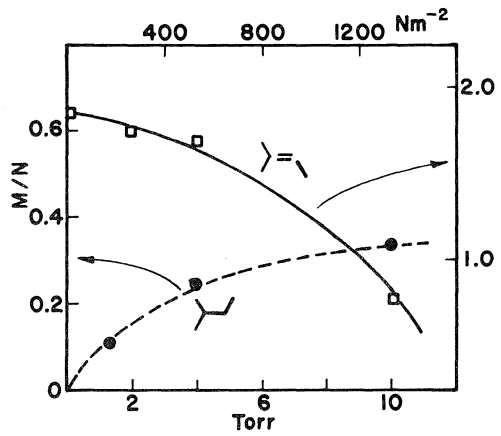

FIG. 5. Effect of the pressure of methylcyclopentane in the radiolysis of neo-C_5H_{12}–2M1B–O_2 mixtures (40.0: 1.0:4.0 torr).

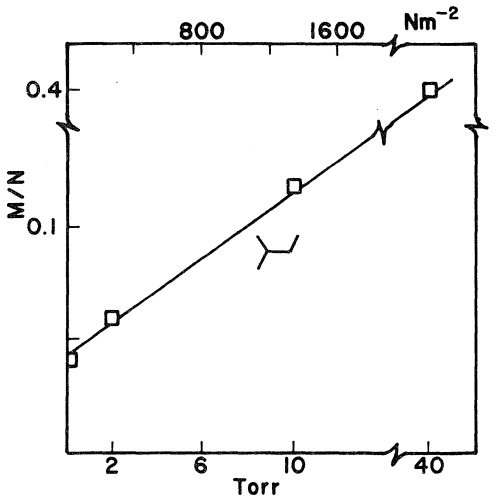

FIG. 6. Effect of the pressure of methylcyclopentane in the radiolysis of neo-C_5H_{12}–3M1B–O_2 mixtures (40.0: 2.0:2.0 torr).

TABLE 3. Gaseous radiolysis of 2-methyl-1-butene in the presence of additives

Mixtures (torr)	M/N values[a]			
	C_3H_6	iso-C_4H_8	iso-C_5H_{12}	2M2B
2M1B–O_2 (1.1:2.0)	1.1	1.6	0.85	9.3
MCP[b]–2M1B–O_2 (10:0.5:1.2)	4.0 (0.2)[c]	1.5	8.0 (0.4)[c]	6.3 (0.3)[c]

[a]Calculated relatively to energy absorbed by 2M1B.
[b]Methylcyclopentane.
[c]Relative to energy absorbed by MCP.

10%. Assuming that k_9 values are the same in both systems, we then obtain $k_8/k_{-8} = 7$. The agreement with the thermodynamic value is satisfactory, although it might be accidental. In systems containing methylcyclopentane, the hydride transfer reaction might be anticipated. However, the k_8/k_9 and k_{-8}/k_9 ratios do not show significant variations between experiments performed in the absence or in the presence of methylcyclopentane. Therefore, k_{10} must be less than $k_8 + k_9$ or $k_{-8} + k_9$ as noted for the corresponding reactions with *tert*-$C_4H_9^+$ (13).

[10] *tert*-$C_5H_{11}^+ + CH_3$-cy-$C_5H_9 \rightarrow$ iso-$C_5H_{12} + C_6H_{11}^+$

(F) Other Reactions

When irradiations are made in the presence of methylcyclopentane, a significant increase of the isopentane yield is noted. The formation of isopentane can be related to a hydrogen molecule or an H_2^- ion transfer reaction.

[11] $3M1B + CH_3$-cy-$C_5H_9^+ \rightarrow$ iso-$C_5H_{12} + C_6H_{10}^+$

[12] $3M1B^+ + CH_3$-cy-$C_5H_9 \rightarrow$ iso-$C_5H_{12} + C_6H_{10}^+$

These reactions were observed with butenes and methylcyclopentane (11). The importance of such reactions will not be discussed here. Nevertheless, the isopentane yield increase, together with the development of methylcyclopentane partial pressure, in the system containing 3M1B can easily be explained on the basis of process 11 (Fig. 6). Without carrying out accurate dosimetry, one can estimate a yield of M/N(process 11) $\simeq 0.35$ with respect to the energy absorbed by methylcyclopentane. For 2M1B, the interpretation is much more difficult (Figs. 2 and 5). However, and again in the absence of accurate dosimetry (Table 4), the M/N(process 11) value can be estimated to 0.35. For 2M2B, (Fig. 3), a similar value is found.

(G) Photoionization at 11.6–11.8 eV

The interpretation given so far takes into account only the *tert*-$C_4H_9^+$ ions formed in the direct radiolysis of neopentane; account is also taken of the reaction of the iso-$C_4H_8^+$ ions. However, other ions are formed in the radiolysis of neopentane (3): $C_2H_3^+$, $C_2H_5^+$, $C_3H_5^+$, and $C_3H_7^+$. These ions react with neopentane by a hydride transfer reaction; a few react at an

Can. J. Chem. Downloaded from www.nrcresearchpress.com by 210.87.254.40 on 09/05/12
For personal use only.

TABLE 4. Photolysis at 11.6–11.8 eV of neo-C_5H_{12}–O_2 (10.0:0.8 torr) in the presence of various additives

Additives (torr)	Quantum yields				
	iso-C_4H_8	iso-C_4H_{10}	iso-C_5H_{12}	2M1B	2M2B
MCP (0.5)[a]	0.36_4	0.42	0.00	0.00	0.00
3M1B (0.6)	0.36	0.02	0.01	0.01	0.01
3M1B (0.5)–MCP (0.5)	0.36	0.08_4	0.02	0.01	0.10
2M1B (0.5)	0.51	0.01	0.03	—	0.93
2M2B (0.45)–He (70)	0.55	0.00	0.00	1.87	—

[a]Methylcyclopentane; Φ(ethylene) = 0.042; Φ(propene) = 0.075.

appreciable rate (11). On the other hand, the yield of these ions is low (3). In order to eliminate completely the possibility that such ions interfere with the mechanism previously suggested, some photoionization (11.6–11.8 eV) experiments of several neopentane–methylbutene mixtures were performed. Only *tert*-$C_4H_9^+$ (89%) and iso-$C_4H_8^+$ (11%) ions are formed (6). Results are recorded in Table 4. Again, no proton transfer reaction is noted for 3M1B. However, if such a transfer reaction takes place for 2M1B, it seems more important (≃35%) than that observed in radiolytic experiments. It is possible that a pressure effect is responsible for the difference. It must also be noted that the energy dispersion is not homogeneous contrary to what is taking place in radiolysis. The neutralization reaction of *tert*-$C_4H_9^+$ ions can then interfere with the suggested mechanism.

The rate constants determined here for the reaction of *tert*-$C_4H_9^+$ ion with the unsaturated additives agree well with those determined in other radiolysis studies. However, the calculation is much less accurate, as the participation of process 2 in the formation of isobutane would have to be known exactly. Finally, the isomerization of 2M1B or 2M2B is again observed.

Acknowledgment

We are indebted to the Chemistry Department of Laval University for the availability of the Cobalt-60 source (Professor J. A. Herman).

1. G. J. COLLIN and C. BERTRAND. J. Photochem. **3**, 123 (1974).
2. H. GAGNON, G. J. COLLIN, and C. BERTRAND. J. Phys. Chem. **78**, 98 (1974).
3. S. G. LIAS and P. AUSLOOS. J. Chem. Phys. **43**, 2748 (1965).
4. R. GORDON, JR., R. E. REBBERT, and P. AUSLOOS. Natl. Bur. Stand. Tech. Note, 496 (1969).
5. T. A. STONEHAM, D. R. ETHRIDGE, and G. G. MEISELS. J. Chem. Phys. **54**, 4054 (1971).
6. L. W. SIECK, S. K. SEARLES, and P. AUSLOOS. J. Res. Natl. Bur. Stand. Sect. A, **75**, 147 (1971).
7. P. AUSLOOS and S. G. LIAS. J. Am. Chem. Soc. **92**, 5037 (1970).
8. J. HERMAN, K. HERMAN, and P. AUSLOOS. J. Chem. Phys. **52**, 28 (1970).
9. C. E. KLOTS. J. Chem. Phys. **56**, 124 (1972).
10. J. L. FRANKLIN, J. G. DILLARD, H. M. ROSENSTOCK, J. T. HERRON, K. DRAXL, and F. H. FIELD. Natl. Stand. Ref. Data Ser. Natl. Bur. Stand. 26 (1969); J. J. SOLOMON and F. H. FIELD. J. Am. Chem. Soc. **95**, 4483 (1973).
11. S. G. LIAS and P. AUSLOOS. *In* Ion–molecule reactions and their role in radiation chemistry. American Chemical Society. 1975. Chapt. 6.
12. M. S. B. MUNSON. J. Am. Chem. Soc. **90**, 83 (1968).
13. G. J. COLLIN. Can. J. Chem. **52**, 2341 (1974).

Can. J. Chem. Downloaded from www.nrcresearchpress.com by 210.87.254.40 on 09/05/12
For personal use only.

Reactions of organolithium compounds with sulfonate esters. A novel sulfone synthesis

W. H. BAARSCHERS

Department of Chemistry, Lakehead University, Thunder Bay, Ont., Canada P7B 5E1

Received March 31, 1976

W. H. BAARSCHERS. Can. J. Chem. **54**, 3056 (1976)

The reaction of a variety of organolithium compounds with sulfonate esters leads to nucleophilic substitution on sulfur, resulting in the formation of sulfones in moderate to high yields. Several new sulfones were prepared by this method.

W. H. BAARSCHERS. Can. J. Chem. **54**, 3056 (1976).

La réaction d'une série de composés organolithiens avec des esters sulfoniques conduit à une substitution nucléophile sur l'atome de soufre pour donner les sulfones correspondantes avec des rendements qui varient de moyens à élevés. Plusieurs nouvelles sulfones furent préparées par cette méthode.

[Traduit par le journal]

Can. J. Chem. Downloaded from www.nrcresearchpress.com by 210.87.254.105 on 09/05/12
For personal use only.

The occasion to treat cyclohexyl methanol tosylate with one molar equivalent of 3-thienyllithium arose during another project in progress in this laboratory. The objective was to effect a displacement of the tosylate with the 3-thienyl moiety, analogous to the reactions reported by Sommer and Korte (1). However, the product of the reaction was 3-thienyl *p*-tolyl sulfone isolated in 55% yield. Similarly a 50% yield of 3-thienyl phenyl sulfone was obtained from cyclohexyl methanol benzene sulfonate.

Although nucleophilic substitution on tetracoordinated sulfur is not all that common (2), the formation of sulfones by such a mechanism is not unknown. However, yields obtained in such reactions are usually (3) from 10–20%, and are thus of little preparative significance. A high yield by direct substitution would be a useful supplement to several existing methods of sulfone formation, and avoids, for example, the strongly acidic conditions of aromatic sulfonylation as well as the oxidative conditions used for the conversion of sulfides and sulfoxides into sulfones.[1] It was therefore decided to investigate further the synthetic utility of this reaction.

It was soon realised that the phenoxy group is a better leaving group, since it excludes such side reactions as β-elimination. Thus, when treatment of phenyl tosylate with *n*-butyllithium, phenyllithium, and 3-thienyllithium respectively gave near quantitative yields of the corresponding *p*-tolyl sulfones a wider selection of phenyl arylsulfonates was used for further study.

At first sight it may seem that such a study could be extended to include the reaction of mesylate esters with organolithium compounds. It was found that cyclohexyl methanol mesylate, on treatment with 3-thienyllithium, led to a quantitative recovery of starting material. It is probable that in this reaction one of the acidic methyl protons is abstracted, resulting in proton exchange after aqueous work-up. Since similar observations have been reported in the literature (4) this reaction was not further investigated.

The reactions are carried out by addition of the appropriate sulfonate to the freshly prepared organolithium compound in an inert atmosphere. Reaction times are generally short (up to 30 min), and products are isolated by benzene extraction after quenching with water. The results, as summarised in Table 1, indicate that a wide variety of sulfones, particularly diaryl sulfones, may be prepared according to the general equation 1.

[1] $ArSO_2OPh + Ar'Li \text{ (or } RLi) \rightarrow ArSO_2Ar' \text{ (or } ArSO_2R) + PhOLi$

A possible rationalization of the reactions of cyclohexyl methanol sulfonates (experiments 1, 2, and 3, Table 1) could be based on the stereochemistry and preferred conformations of these esters. Thus, in a structure like **1**, β-elimination involving the axial hydrogen would be unfavourable, while attack on carbon may be subject to some steric hindrance. Such a rationaliza-

[1]For other methods of sulfone preparation see ref. 17.

TABLE 1. Sulfone syntheses

Experiment no.	Sulfonate ester	Li compound	Sulfone	Yield (%)	mp (°C)
1	*p*-Tolyl.SO_2.O.CH_2.C_6H_{11}	3-Thienyl	*p*-Tolyl.SO_2.3-thienyl[a]	55[b]	136–138
2	*p*-Tolyl.SO_2.O.CH_2.C_6H_{11}	Phenyl	*p*-Tolyl.SO_2.phenyl	38[b]	119–122[e]
3	*p*-Ph.SO_2.O.CH_2.C_6H_{11}	3-Thienyl	Phenyl.SO_2.3-thienyl[a]	50[b]	117–118
4	*p*-Tolyl.SO_2.O.*n*-Bu	*n*-Butyl	*p*-Tolyl.SO_2.*n*-butyl	36[c]	—
5	*p*-Tolyl.SO_2.O.*n*-Bu	Phenyl	*p*-Tolyl.SO_2.phenyl	53[b]	119–122[e]
6	Ph.SO_2.O.Ph	Phenyl	Phenyl.SO_2.phenyl	97[d]	121–123[e]
7	Ph.SO_2.O.Ph	3-Thienyl	Phenyl.SO_2.3-thienyl	85[d]	117–118
8	Ph.SO_2.O.Ph	2-Thienyl	Phenyl.SO_2.2-thienyl	88[b,d]	121.3[f]
9	Ph.SO_2.O.Ph	2-Naphthyl	Phenyl.SO_2.2-naphthyl	46[b]	119–121[g]
10	Ph.SO_2.O.Ph	*p*-OCH_3Ph	Phenyl.SO_2.C_6H_4.*p*-OCH_3[a]	98[d]	85–87
11	Ph.SO_2.O.Ph	α-Picolyl	Phenyl.SO_2.α-picolyl	78[b]	110–111[h]
12	Ph.SO_2.O.Ph	*p*-$(CH_3)_2$NPh	Phenyl.SO_2.C_6H_4.*p*-$N(CH_3)_2$[a]	70[b]	172–174
13	*p*-Tolyl.SO_2.O.Ph	*n*-Butyl	*p*-Tolyl.SO_2.*n*-butyl	85[c]	—
14	*p*-Tolyl.SO_2.O.Ph	Phenyl	*p*-Tolyl.SO_2.phenyl	98[d]	119–122
15	*p*-Tolyl.SO_2.O.Ph	3-Thienyl	*p*-Tolyl.SO_2.3-thienyl	96[d]	136–138
16	*p*-Tolyl.SO_2.O.Ph	α-Picolyl	*p*-Tolyl.SO_2.α-picolyl[a]	67[b]	154–155
17	*p*-Tolyl.SO_2.O.Ph	Allyl	*p*-Tolyl.SO_2.allyl	67[c]	52–53[e]
18	2-Naphthyl.SO_2.O.Ph	*n*-Butyl	2-Naphthyl.SO_2.*n*-butyl	60[c]	—
19	2-Naphthyl.SO_2.O.Ph	Phenyl	2-Naphthyl.SO_2.phenyl	40[b]	119–121
20	2-Naphthyl.SO_2.O.Ph	3-Thienyl	2-Naphthyl.SO_2.3-thienyl[a]	76[b]	123–124
21	*p*-OCH_3.Ph.SO_2.O.Ph	Phenyl	Phenyl.SO_2.C_6H_4.*p*-OCH_3	73[b]	85–87

[a]These compounds have not before been reported in the literature.
[b]Isolated by preparative tlc.
[c]Determination of yield and purification by glc.
[d]Isolated by direct crystallization of crude product.
[e]Identical with an authentic specimen.
[f]Literature mp 123 °C, ref. 14.
[g]Literature mp 115–116 °C, ref. 15.
[h]Literature mp 112 °C, ref. 16.

tion becomes less attractive when one considers the observation that the conformationally more mobile *n*-butyltosylate, which is expected to be more susceptible to β-elimination, also gives an appreciable yield (53%) of phenyl *p*-tolyl sulfone (exp. 5).

But indeed, when these factors are excluded by the use of the phenoxy anion as the leaving group, a substantial increase in yield is obtained (exps. 7, 14, and 15). In fact, all phenyl sulfonates used in this study gave sulfones in yields of 60% and higher, with the exception of 2-naphthyl phenyl sulfone. That the reported low yield of 2-naphthyllithium from 2-bromonaphthalene (5) cannot be the only reason for the low yield in this case (46%, exp. 9) follows from the fact that an interchange of the Ar and Ar′ groups (eq. 1) gives an even lower yield (40%, exp. 19). Presumably the bulky 2-naphthyl group offers a degree of steric hindrance, which can be overcome only by the use of a stronger nucleophile such as 3-thienyllithium (exp. 20). Then again, in the absence of such steric effects, such charge delocalised lithium compounds as allyllithium and α-picolyllithium also give good yields of the corresponding sulfones (exps. 11, 16, and 17).

In some cases published methods for the preparation of the organolithium compounds could be improved. A striking example is the formation of 2-thienyllithium. A halogen metal exchange with 2-bromothiophene was found to be substantially superior, at least in small scale experiments, to a recently reported direct metalation of thiophene (6).

An interesting deviation from the general reaction was observed in the reactions of 3-pyridyllithium with several sulfonate esters. The products, in their infrared spectra, did have the characteristic (7) sulfone bands, but ms and analyses indicated the presence of an 'extra' pyridine ring. The consistent appearance of signals at *m/e* 203 ($C_{10}H_7N_2OS^+$) and at *m/e* 155 ($C_{10}H_7N_2^+$) in the mass spectra of these compounds suggests the presence of a bipyridyl moiety. It is suggested that when the sulfones **2** are initially formed, the introduction of the electron-withdrawing sulfone group into the already electron poor pyridine ring sufficiently

Can. J. Chem. Downloaded from www.nrcresearchpress.com by 210.87.254.105 on 09/05/12
For personal use only.

activates this ring towards further nucleophilic attack by an excess of 3-pyridyllithium. Such a sequence of events, depicted in [2], would explain the formation of the sulfones **3**, in which R is H, Me, and OMe respectively, and which were isolated in 15–30% yields.

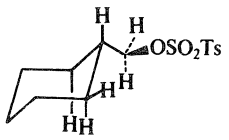

1

[2] 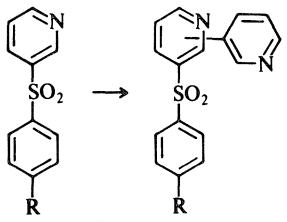

2 **3**

Since mass spectra, in addition to infrared and analyses, were used to characterize the present sulfones, the anomalous mass spectra of the α-picolyl sulfones (exps. 11 and 16, Table 1) must be mentioned. Normally (8) diaryl sulfones give rise to well defined molecular ions, and under electron impact rearrange to sulfinate esters, which fragment further as in [3].

The highest observable peaks in the spectra of the α-picolyl compounds were found at $M^+ - 64$, resulting from the expulsion of SO_2. At the same time fragmentation according to [3] was virtually non-existent. Such an expulsion of SO_2 is not unexpected in view of similar observations reported (9) for some 2-pyridyl ketones. However, the spectra of the α-picolyl sulfones are anomalous because of the complete absence of the molecular ion. A further mass spectrometric study of representative picolyl and pyridyl sulfones is presently in progress.

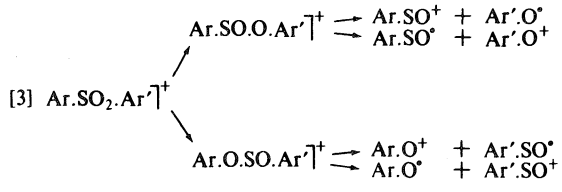

[3]

Experimental

Thin layer chromatograms on silica gel G were developed with benzene or benzene–acetone mixtures. Gas chromatographic separations were carried out with a 2 m × 6 mm glass column, packed with 10% SE 30 on Gaschrom Q, at 235 °C, with N_2 as a carrier gas.

Sulfonate esters were prepared according to Tipson (10). All sulfonate esters and sulfones were characterized by correct analyses (within 0.3% of calculated values),[2] appropriate infrared absorption (7), and mass spectra (for details see ref. 8*b*). In some cases comparison with authentic specimens was made.

Lithium compounds were, in most cases, generated by halogen metal exchange (11), using *n*-butyllithium in hexane (1.5–2.0 *M*, Alfa Products). Allyllithium was obtained by cleavage of allyl phenyl ether (12) and α-picolyllithium resulted from metalation of α-picoline (13). Observations concerning 2-thienyllithium and *p*-anisoyllithium are recorded below.

General Procedure

After the desired lithium compound was prepared (3–5 mmol) in ether (5–10 ml), an ether (10–15 ml) solution of the sulfonate ester (2–3 mmol) was added by syringe, and the mixture stirred for periods up to ½ h or until the mixture had reached room temperature in those cases where the lithium compound was generated at low temperatures (*e.g.* 3-thienyllithium). The reaction mixture was then poured into water and extracted with benzene. The solid sulfones were recrystallised, either directly or after preparative tlc; liquid sulfones were purified by preparative gas chromatography.

2-Thienyl p-Tolyl Sulfone (Experiment 8)

(*i*) To a solution of 2-thienyllithium (4.2 mmol) in tetrahydrofuran (0.29 ml) and benzene (0.7 ml) prepared according to Screttas *et al.* (6) was added phenyl tosylate (580 mg, 2.34 mmol) and the mixture was treated as above. The yield of 2-thienyl sulfone, after preparative tlc was 90.2 mg (16%).

(*ii*) To 2-bromothiophene (0.5 ml, 5.15 mmol) in ether (5 ml) was added *n*-butyllithium (4.8 mmol) at −25 °C. After the mixture reached room temperature (0.5 h) phenyl tosylate (571 mg, 2.3 mmol) in ether (15 ml) was added, and the mixture stirred another 0.3 h. The crude product (655 mg) was recrystallised from benzene to give 399 mg of 2-thienyl *p*-tolyl sulfone. A further 80 mg was obtained by preparative tlc of the mother liquors (total yield, calculated on phenyl tosylate, 87.6%).

Phenyl p-Methoxyphenyl Sulfone (Experiment 10)

(*i*) When phenyl benzene sulfonate (280 mg, 1.25 mmol) was added to an ether solution of *p*-anisoyllithium (3 mmol, from *p*-bromoanisole (561 mg) and *n*-butyllithium (3.2 mmol)) the crude product (419 mg), after preparative tlc, yielded crystalline material (256 mg) containing 8.75% bromine. The formation of bromine containing compounds, arising from hydrogen lithium exchange

[2]Most analyses were performed in this laboratory, using a Perkin-Elmer Model 240 Elemental Analyser. For some of the analyses the author is indebted to Mr. P. Borda, Microanalytical Laboratory, University of British Columbia. Tabulated analytical data are available, at a nominal charge, from the Depository of Unpublished Data, CISTI, National Research Council of Canada, Ottawa, Canada K1A 0S2.

Can. J. Chem. Downloaded from www.nrcresearchpress.com by 210.87.254.105 on 09/05/12
For personal use only.

(ref. 11, p. 349), could be avoided by the following procedure.

(*ii*) To *p*-bromoanisole (187 mg, 1 mmol) in dry pentane (5 ml) was added *n*-butyllithium (1 mmol). After 15 min the pentane was blown off with a stream of dry nitrogen, and ether (5 ml) was added to the dry, yellow *p*-anisoyllithium. Completing the reaction in the normal way with phenyl benzene sulfonate (230 mg, 0.98 mmol) in ether (15 ml) led to the formation of phenyl *p*-methoxyphenyl sulfone in 98% yield.

Reactions with 3-Pyridyllithium

3-Pyridyllithium was generated in quantitative yield (by reaction with benzophenone) from 3-bromopyridine and *n*-butyllithium in ether at −50 °C. To solutions containing approximately 3 mmol of pyridyllithium were added 1–2 mmol of phenyl benzene sulfonate, phenyl tosylate, and phenyl *p*-methoxybenzene sulfonate respectively. The crude reaction products were subjected to preparative tlc and gave 15–30% yields of the corresponding aryl bipyridyl sulfones **3** which had characteristic infrared absorptions (7) at 1120–1160 cm^{-1}, and at 1325 cm^{-1}, and typical mass spectral peaks at *m/e* 203 (—$OSC_5H_3N.C_5H_4N^+$) and at *m/e* 155 (—$C_5H_3NC_5H_4N^+$). The three compounds were further characterized as follows: (*i*) phenyl bipyridyl sulfone (**3**, R = H), mp 204–207 °C, M^+ 296; (*ii*) *p*-tolyl bipyridyl sulfone (**3**, R = CH_3), mp 201–203 °C, M^+ 310; (*iii*) *p*-methoxyphenyl bipyridyl sulfone (**3**, R = OCH_3), mp 173–174 °C, M^+ 326; and analysis results within 0.3% of the values calculated for $C_{16}H_{12}N_2O_2S$, $C_{17}H_{14}N_2O_2S$, and $C_{17}H_{14}N_2O_3S$ respectively.

Acknowledgments

The author thanks the Senate Research Committee of Lakehead University for generous financial support, and Dr. J. P. Kutney, University of British Columbia, Vancouver, B.C. for his hospitality during a sabbatical leave, which enabled the author to complete part of the experimental work. Technical assistance from Mr. T. L. Loh with some preliminary experiments is also acknowledged.

1. L. H. Sommer and W. D. Korte. J. Org. Chem. **35**, 22 (1970).
2. E. Cuiffarin and F. Fava. Prog. Phys. Org. Chem. **6**, 81 (1968).
3. (*a*) M. A. Sabol and K. K. Andersen. J. Am. Chem. Soc. **91**, 3603 (1969); (*b*) A. I. Meyers, A. Nabeya, H. Adickes, and I. Politzer. J. Am. Chem. Soc. **91**, 763 (1969).
4. E. J. Corey and T. Durst. J. Am. Chem. Soc. **88**, 5656 (1966).
5. H. Gilman and F. W. Moore. J. Am. Chem. Soc. **62**, 1843 (1940).
6. C. G. Screttas, J. F. Estham, and C. W. Kamienski. Chimia, **24**, 109 (1970).
7. K. Nakanishi. Infrared absorption spectroscopy. Holden-Day, San Francisco. 1962. p. 54.
8. (*a*) S. Meyerson, H. Drews, and E. K. Fields. Anal. Chem. **36**, 1294 (1964); (*b*) W. H. Baarschers and B. W. Krupay. Can. J. Chem. **51**, 156 (1973).
9. (*a*) E. V. Brown and M. B. Shambhu. Org. Mass. Spectrom. **6**, 479 (1972); (*b*) K. B. Tomer and C. Djerassi. J. Org. Chem. **38**, 4151 (1973).
10. R. S. Tipson. J. Org. Chem. **9**, 235 (1944).
11. R. G. Jones and H. Gilman. Org. React. **6**, 339 (1951).
12. J. J. Eisch and A. M. Jacobs. J. Org. Chem. **28**, 2145 (1963).
13. O. F. Beumel, W. Novis Smith, and B. Rybalka. Synthesis, 43 (1974).
14. M. Burton and W. A. Davey. J. Chem. Soc. 525 (1948).
15. A. Michael and A. Adair. Ber. **10**, 585 (1877).
16. S. Golding, A. R. Katritzky, and H. Z. Kucharska. J. Chem. Soc. 3090 (1965).
17. G. C. Barrett. Organic compounds of sulphur, selenium and tellurium. Chem. Soc. Spec. Period. Rept. Vol. 3. 1975. p. 52.

Can. J. Chem. Downloaded from www.nrcresearchpress.com by 210.87.254.105 on 09/05/12
For personal use only.

Etude des mobilités ioniques dans les mélanges eau–hexaméthylphosphotriamide. I. Cas du HMPT pur à 25 °C

JEAN-CLAUDE BOLLINGER ET THÉOPHILE YVERNAULT

Laboratoire de Chimie Générale et Analytique, U.E.R. Sciences Limoges, 123 Rue Albert Thomas, 87100 Limoges

ET

JEAN-YVES GAL[1] ET FRANÇOISE PERSIN

Laboratoire de Chimie Analytique, Université des Sciences et Techniques du Languedoc, Place E. Bataillon, 34060 Montpellier Cedex

Reçu le 14 mai 1976

JEAN-CLAUDE BOLLINGER, THÉOPHILE YVERNAULT, JEAN-YVES GAL et FRANÇOISE PERSIN. Can. J. Chem. **54**, 3060 (1976).

Nous avons effectué des mesures de mobilités ioniques dans l'hexaméthylphosphotriamide (HMPT) et dans les mélanges eau–HMPT, dans le but d'aborder le problème de la solvatation des ions. Compte tenu du nombre de publications relatives aux études conductométriques effectuées dans le HMPT pur, nous avons pensé qu'il pouvait être intéressant d'en proposer une analyse bibliographique. Dans le présent mémoire, nous présentons l'ensemble de nos résultats dans le HMPT pur, dans le cadre de cette analyse.

JEAN-CLAUDE BOLLINGER, THÉOPHILE YVERNAULT, JEAN-YVES GAL, and FRANÇOISE PERSIN. Can. J. Chem. **54**, 3060 (1976).

Ionic mobilities have been measured in hexamethylphosphotriamide (HMPT) and in water–HMPT mixtures in order to investigate the solvation of ions. In view of the large number of studies of conductivities in pure HMPT, we felt it would be interesting to give a general analysis of these data. Our results in pure HMPT will be presented in the course of this analysis.

Depuis quelques années (1–41), nos laboratoires se sont préoccupés des phénomènes de solvatation des ions dans l'hexaméthylphosphotriamide (HMPT). Une revue de méthodes utilisées pour étudier la solvatation des ions a été faite par Hinton et Amis (2). Nous nous sommes ici plus particulièrement intéressés à la détermination de la solvatation d'ions monovalents, par mesures conductométriques. La méthode consiste à déterminer les conductivités équivalentes limites Λ_0 d'une série d'électrolytes monovalents puis d'atteindre les valeurs λ_0 des conductivités ioniques équivalentes des différents cations et anions considérés. L'application de la loi de Stokes permet alors de déterminer le rayon des ions solvatés et d'envisager de calculer le nombre de molécules solvatantes dans le cas des solvants purs.

La détermination expérimentale des conductivités équivalentes limites ne présente pas de difficultés particulières dans les solvants autres que l'eau si l'on dispose d'un solvant et de sels suffisamment purifiés et d'un matériel fonctionnant correctement dans les milieux fortement résistants. Dans le HMPT pur, nous verrons que cet ensemble de conditions ne semble avoir été obtenu que par Prue et coll. (3).

La détermination des conductivités ioniques équivalentes λ_0 peut être effectuée soit uniquement à partir de données expérimentales, soit le plus souvent à l'aide d'hypothèses. Dans la plupart des cas, les auteurs font alors l'hypothèse de l'égalité des conductivités ioniques équivalentes de l'anion et du cation pour un sel composé de deux ions volumineux:

$$\lambda_0^{A^-} = \lambda_0^{B^+} = \tfrac{1}{2}\Lambda_0^{AB}$$

Fowler et Kraus (4) utilisent le triphényl borofluorure et le triphényl borohydroxyde de tétrabutyl ammonium, Fuoss et Hirsch (5) le tétraphenylborate de tétrabutylammonium, Coplan et Fuoss (6) le tétraphénylborate de triamylbutylammonium dans de nombreux solvants, Coetzee et Cunningham (7) le tétraamylborate de tétraamylammonium, Hansen et Yeager (8)

[1]A qui toute correspondance peut être adressée.

Can. J. Chem. Downloaded from www.nrcresearchpress.com by 210.87.254.40 on 09/05/12
For personal use only.

Can. J. Chem. Downloaded from www.nrcresearchpress.com by 210.87.254.40 on 09/05/12
For personal use only.

cette hypothèse dans le carbonate de propylène, Zipp (9) l'hypothèse de Coplan et Fuoss dans le sulfolane et le méthyl-3 sulfolane, Dubois et coll. celle de Fuoss et Hirsch dans le DMSO (10). Une autre hypothèse consiste à admettre comme Gutmann et coll. (11) que le produit de Walden de l'ion tétrabutylammonium est constant lorsque l'on passe d'un solvant à un autre.

La détermination expérimentale des λ_0 repose sur la mesure du nombre de transport d'un ion judicieusement choisi, les conductivités ioniques équivalentes se déduisant facilement.

La méthode de la frontière mobile a été employée par Spiro et coll. dans le formamide (12) et l'éthylène glycol (13), par Prue dans l'eau et le diméthylformamide (14, 15). La méthode de Hittorf fut appliquée dans le formamide (16–18, 20), le *N*-méthylacétamide (18, 19), le sulfolane (22), le DMSO (23, 24), le diméthylformamide (25–27) et le diméthylacétamide (28). Enfin, Mukherjee *et al.* (29) et Hoare et Wiese (30) ont utilisé des piles de concentration dans le carbonate de propylène.

L'application directe de la loi de Stokes donne un rayon de l'ion solvaté erroné

$$[1] \qquad r_s = \frac{0.82|Z|}{\lambda_0 \eta_0}$$

Ce rayon est un rayon dynamique, il fait intervenir la viscosité du solvant pur et il est toujours inférieur au rayon cristallin r_c. Il faut alors faire une correction qui repose sur l'hypothèse que les ions tétraalkylammonium ne sont pas solvatés (31). Selon les cas, (9, 12, 15, 21, 32, 33) on porte r_c/r_s en fonction de r_s (31) ou r_c en fonction de r_s (42) pour les cations ammonium quaternaires; on choisit la grandeur donnant la meilleure droite. On déduit le rayon solvaté corrigé r_{scor} des autres ions: il correspond au point d'abscisse r_s sur la courbe $r_c/r_s = f(r_s)$ ou sur la courbe $r_c = f(r_s)$.

Le volume de solvatation est alors donné par laformule $V_s = \frac{4}{3}\Pi (r_{scor}^3 - r_c^3)$. Dans le cas d'un solvant pur il suffit de diviser par le volume molaire du solvant pour obtenir le nombre de moles de solvatation.

La valeur d'un tel résultat, compte tenu du mode d'obtention peut être discutée, une étude de ce genre permet néanmoins de comparer de façon simple le pouvoir solvatant de divers solvants.

Détermination des conductivités équivalentes limites dans le HMPT pur à 25 °C

Il semble que Prue (3) soit le seul à indiquer des mesures extrapolées à fréquence infinie.[2]

L'ensemble des résultats obtenus est regroupé dans le tableau 1. Della Monica et coll. (34, 35), Dubois et coll. (10), Fujinaga *et al.* (36), Gutmann et coll. (11), Muller et Siegfried (37) et nous mêmes avons calculé les conductivités équivalentes limites en utilisant l'équation de Fuoss–Onsager. Prue (3) a utilisé l'équation de Fuoss–Hsia et Paul *et al.* (38) l'équation de Fuoss–Onsager–Skinner.

Dans le tableau 2 figurent les constantes caractéristiques du solvant intervenant dans les différents modes de traitement des résultats expérimentaux.

En ce qui nous concerne, nous indiquons principalement les résultats de Moliton-Bouchetout (1) que nous avons vérifiés et rectifiés par des mesures complémentaires.

Si l'on considère l'équation de Fuoss–Onsager (1, 21)

$$[2] \quad \Lambda = \Lambda_0 - SC^{1/2} + EC \log C + J(a)C + J_{3/2}(a)C^{3/2}$$

avec $S = \alpha\Lambda_0 + \beta$ et $E = E_1\Lambda_0 - E_2$ on peut négliger le terme en $C^{3/2}$.

Selon les valeurs de ϵ, η, ρ, nous avons deux groupes de valeurs pour les termes constants (tableau 3). Quoique différentes ces valeurs ne conduisent pas à plus de divergence lorsque l'on traite les résultats expérimentaux d'une même série de mesures que lorsque l'on compare les résultats de plusieurs séries de mesures pour un même sel en utilisant toujours le même ensemble de valeurs. C'est pour cette raison que nous avons regroupé dans une seule colonne du tableau 1 l'ensemble de nos déterminations.

La lecture de ce tableau 1 montre clairement que l'ensemble des travaux publiés n'est pas rigoureusement cohérent si l'on compare ligne par ligne.

Pour un même auteur, on remarque des écarts importants si l'on compare par exemple les sels de deux cations. Ce sont les travaux de Prue qui présentent la plus grande homogénéité bien que

[2]Selon une récente publication (62) les premiers travaux de Dubois (10) avaient eux aussi été extrapolés à fréquence infinie.

TABLEAU 1. Conductivité équivalente limite à 25 °C dans le HMPT en Ω^{-1} cm^2 mol^{-1}

	Della Monica (34, 35)	Dubois (10)	Fujinaga (36)	Gutmann (11)	Prue (3)	Paul (35)	Siegfried (37)	Nous-mêmes*
$LiClO_4$	—		20.7_0		21.243	19.66		20.9_6
$NaClO_4$	21.1_4	21.40	21.3_0		21.456	21.32		21.3_0
$KClO_4$	21.3_5	21.52	21.5_5		21.669	21.60		21.3_0
$RbClO_4$			21.5_5		21.900	22.00		
$CsClO_4$			21.8_8		22.138	28.55		
$AgClO_4$						21.18		
NH_4ClO_4					21.448	21.57		
$MeNH_3ClO_4$						23.39		
Me_3NHClO_4						25.94		
Me_4NClO_4			23.3_7			28.26		
Et_4NClO_4		24.94	24.7_8			24.84		25.1_3
n-Pr_4NClO_4			22.3_1					22.5_2
n-Bu_4NClO_4		21.58	21.3_6	19.3		21.40		21.7_2
Hex_4NClO_4			19.9_7					
$Ca(ClO_4)_2$			24.0_6					
$Sr(ClO_4)_2$			24.1_3					
$Ba(ClO_4)_2$			23.9_2					
$LiNO_3$	24.9_5				25.334			24.9_2
$NaNO_3$	24.0_6				25.470			
KNO_3	24.3_3				25.560			25.8_0
$RbNO_3$	24.4_2							
$AgNO_3$					25.575			25.4_0
NH_4NO_3					25.419			25.9_0
LiI					22.359			
NaI					22.590			22.1_8
KI					22.724			
NH_4I					22.530			22.5_7
Et_4NI					26.249			
n-Pr_4NI	23.5_5							
n-Bu_4NI	22.7_6							
n-Am_4NI	22.3_0							
LiBr				21.2	24.172		24.66	
NaBr	23.8_8				24.389			
KBr					24.615			
NH_4Br					24.342		23.61	23.9_5
n-Pr_4NBr	25.1_0							
n-Bu_4NBr	24.3_9			21.8			24.67	24.3_0
n-Am_4NBr	23.8_8							
LiCl				25.3	25.039	25.90	25.10	25.2_7
NH_4Cl					25.147		23.98	
n-Bu_4NCl				25.5			25.10	
n-Am_4NCl	24.7_1							
NaSCN	25.9_9							
KSCN	26.1_7					25.40		
ϕ_4BNa		11.97						12.4_3
$Bu_4NB\phi_4$		12.25						
Bu_4NBBu_4								12.3_0

*Les copies de ces données seront disponibles, à un prix nominal, en s'adressant au Dépôt des données non publiés, ICIST, Conseil national de recherches du Canada, Ottawa, Canada K1A 0S2.

les écarts $K^+ - Na^+$ passant de 0.09 à 0.226Ω^{-1} cm^2 mol^{-1} par exemple, font penser que les deuxième et troisième décimales sont un peu optimistes. Cependant, il semble bien que cet ensemble de travaux dans l'hexaméthylphosphotriamide pur soit la référence la plus sérieuse.

Remarque—Aux faibles concentrations, la plupart des électrolytes étudiés sont totalement dissociés. Seuls KNO_3, $AgNO_3$, KBr, NH_4Br et Bu_4NBr seraient partiellement associés et NH_4Cl

Can. J. Chem. Downloaded from www.nrcresearchpress.com by 210.87.254.40 on 09/05/12
For personal use only.

Can. J. Chem. Downloaded from www.nrcresearchpress.com by 210.87.254.40 on 09/05/12
For personal use only.

TABLEAU 2. Valeurs de la constante diélectrique, de la viscosité, de la masse volumique, retenues pour les calculs

	Della Monica (34, 35)	Dubois (10)	Fujinaga (36)	Gutmann (11)	Prue (3)	Paul (35)	Siegfried (37)	Nous-mêmes	
								A (1)	*B*
ϵ	29.64 (39)	29.64 (39)	29.64 (39)	29.64 (39)	29.60	29.64 (39)	—	28.32(1)	29.20 (40)
η (cP)	3.34	—	3.23	3.31	3.25	3.11	—	3.22 (1)	3.35 (41)
ρ (g ml^{-1})	1.019 (39)	1.019 (39)	—	—	1.020	1.019 (39)	—	1.019 (39)	1.019_9 (41)

Can. J. Chem. Downloaded from www.nrcresearchpress.com by 210.87.254.40 on 09/05/12
For personal use only.

TABLEAU 3. Valeurs de nos coefficients dans le HMPT

	A (1)	*B**
α	1.057	1.010
β	26.992	26.390
E_1	11.248	11.266
E_2	42.06	39.29

*Valeurs déduites de la colonne *B* du tableau 2.

partiellement dissocié. Dans le tableau 1, nous n'avons pas fait figurer les constantes d'association K_A car les valeurs trouvées diffèrent fortement selon le traitement mathématique utilisé.

Détermination des conductivités ioniques équivalentes limites dans le HMPT pur à 25 °C

Pour déduire les conductivités ioniques équivalentes Dubois et coll. (10) ont utilisé l'hypothèse de Fuoss et Hirsch ils trouvent:

$$\lambda_0{}^{\phi_4B^-} = \lambda_0{}^{NBu_4^+} = 6.1\ \Omega^{-1}\ cm^2\ mol^{-1}$$

Fujinaga (36) et Della Monica (34, 35) ont utilisé cette valeur pour déduire de leurs propres mesures, les valeurs des conductivités ioniques équivalentes qu'ils proposent.

En ce qui nous concerne, nous avons étudié différentes méthodes de mesures des nombres de transport que nous discuterons en interprétant les résultats dans le HMPT pur. Nous avons cependant retenu l'hypothèse (41)

$$\lambda_0{}^{BBu_4^-} = \lambda_0{}^{NBu_4^+} = 6.15\ \Omega^{-1}\ cm^2\ mol^{-1}$$

Cette hypothèse est cohérente avec celle de Dubois et coll. (10).

Gutmann (11) a appliqué au HMPT, au carbonate de propylène et au DMSO l'hypothèse que le produit de Walden de NBu_4^+ était constant, utilisant les valeurs de Mukherjee (29) dans le carbonate de propylène et celles déduites par Arrington et Griswold (57) de l'hypothèse de Fuoss et Hirsch dans le DMSO.

C'est par des mesures de nombre de transport en électrolysant LiCl selon la méthode de Hittorf que Paul (38) a atteint une valeur de $\lambda_0{}^{Li^+}$ qui s'écarte des autres résultats proposés, contrairement aux déterminations de $\lambda_0{}^{K^+}$ par l'électrolyse de KSCN et de $\lambda_0{}^{Ag^+}$ par celle de $AgClO_4$.

Prue (3) a utilisé la méthode de la frontière mobile pour déterminer le nombre de transport de Na^+ dans $NaNO_3$. Il trouve $T^{Na^+} = 0.169$; 0.165 pour $C = 0.0376$; 0.0195 mol l^{-1}. Quel que soit le traitement utilisé pour extrapoler ces valeurs à dilution infinie nous ne retrouvons pas la valeur donnée $\lambda_0{}^{Na^+} = 5.5$, cette valeur semblant tout à fait possible par ailleurs.

TABLEAU 4. Conductivités ioniques équivalentes limites à 25 °C dans le HMPT en Ω^{-1} cm^2 eq^{-1}†

	Della Monica (34, 35) *A*	Dubois (10) *A*	Fujinaga (16) *A*	Gutmann (11) *A*	Prue (3) *B*	Paul (38) *B*	Nous-mêmes *A*
Li^+	6.8		5.2_0	6.8–6.4	5.3	3.63	5.3_9
Na^+	5.9*	5.9	5.8_0		5.5	5.29	5.7_4
K^+	6.1	6.1	6.0_5		5.6	5.57	5.7_3
Rb^+	6.3		6.0_5		5.9	5.97	
Cs^+			6.3_8		6.1	6.52	
Ag^+					5.6	5.15	5.3_0
NH_4^+					5.4	5.54	5.8_0
Me_4N^+			7.8_7			12.23	7.8_0
Et_4N^+	9.4	9.4	9.2_8		9.1	8.81	9.5_6
n-Pr_4N^+	7.1		6.8_1				6.9_5
n-Bu_4N^+	6.4	6.1	5.8_6	7		5.51	6.1_5
n-Am_4N^+	5.9						
ClO_4^-	15.2	15.5	15.5*	12.3	16	16.03	15.5_7
NO_3^-	18.1				20.0		20.1_0
I^-	16.4				17.1		16.7_7
Br^-	18.0			14.8	18.9		18.1_5
Cl^-	18.8			18.5	19.7	22.35	19.8_8
SCN^-	20.1			17.5		19.78	
ϕ_4B^-		6.1					6.7_0
Bu_4B^-							6.1_5

*Empruntés à Dubois.
†*A* Nécessite une hypothèse; *B* Valeurs déduites de mesures de nombre de transport.

Can. J. Chem. Downloaded from www.nrcresearchpress.com by 210.87.254.40 on 09/05/12
For personal use only.

Le tableau 4 regroupe l'ensemble des conductivités ioniques équivalentes limites. Il est bien évident que chaque auteur a dû faire un choix pour écarter les sels conduisant à des résultats trop divergents. Néanmoins, l'ensemble est relativement cohérent et nous permet de penser que, bien que peu sophistiqué, notre appareillage conduit à des résultats dont on peut tenir compte.

Interprétation des résultats

Il est très remarquable de constater pour les valeurs de conductivités ioniques limites équivalentes du tableau 4, que les résultats issus d'une hypothèse sont finalement très peu différents de ceux issus des mesures comme l'avait déjà constaté Della Monica pour le DMSO (23).

Une série d'expériences au laboratoire est en bon accord avec cette observation.

(*a*) En testant une adaptation de la méthode de mesure des nombres de transport de Baca et Hill (49), certains d'entre nous (48) ont été amenés à exposer des résultats parfaitement reproductibles qui faisaient apparaître des mobilités cationiques supérieures à ce qu'on obtenait à l'aide d'une hypothèse. Ces valeurs conduisaient à calculer des nombres de solvatation des anions élevés et non conformes à ce que l'on pouvait envisager. Nous pensons pouvoir interpréter cette série d'expériences. On déterminait le déplacement de la frontière mobile formée entre une solution de LiCl dans le HMPT et une solution de $HgCl_2$ générée par le passage du courant à travers une anode de mercure. En fait, il eut fallu tenir compte de la formation du complexe $HgCl_3^-$ qui avait déjà été mise en évidence par tracé de courbes intensité potentiel (50), et qui a été vérifiée depuis par différentes méthodes électrochimiques (travaux non publiés). Il faut corriger les résultats obtenus, car en première approximation, $\frac{2}{3}$ seulement des cations Li^+ migrent vers la cathode.

Dans ces conditions, on trouve $T_\infty^{Li^+} = 0.247$. On peut comparer cette valeur expérimentale aux différentes valeurs de $T_\infty^{Li^+}$ que l'on déduit du tableau 4. Selon: Della Monica $T_\infty^{Li^+} = 0.266$; Prue $T_\infty^{Li^+} = 0.212$; Nous-mêmes $T_\infty^{Li^+} = 0.213$.

Sans être totalement satisfaisante, cette valeur rectifiée est tout de même plus proche de l'ensemble des résultats que celle trouvée par Paul (38) ($T_\infty^{Li^+} = 0.1385$). Elle permet de considérer que la méthode de Baca et Hill peut fournir des renseignements utiles à condition d'identifier au préalable la réaction électrochimique à l'anode. De plus, il apparaît à la lumière des expériences ultérieures que le chlorure de lithium était mal choisi compte tenu de la difficulté qui existe déjà pour obtenir des valeurs précises et reproductibles de Λ_0^{LiCl} (*cf.* tableau 1).

(*b*) Il nous a semblé intéressant aussi de confronter les valeurs des conductivités ioniques équivalentes limites que nous avons trouvées et les études polarographiques effectuées sur les sels de métaux alcalins. La réduction polarographique des cations alcalins n'est pas contrôlée par la diffusion lorsqu'on opère en présence de perchlorate de tétraalkylammonium (51–53). Par contre, en milieu $LiClO_4$ 0.1 *M* (50) les vagues de réduction des ions Na^+ et K^+ sont des vagues de diffusion de hauteur égale, ce qui est clairement en accord avec la quasi égalité trouvée pour $\lambda_0^{Na^+}$ et $\lambda_0^{K^+}$.

L'application de l'équation d'Ilkovic au courant moyen du palier de diffusion de réduction des ions Na^+ nous permet de calculer le coefficient de diffusion des ions Na^+ en milieu $LiClO_4$ 0.1 *M*.

$$D^{1/2} = \frac{\bar{i}_d}{n607\, m^{2/3}\, t^{1/6}\, C}$$

avec $n = 1$. De D, on déduit:

$$\lambda = \frac{ZF^2}{RT} D \quad (55)$$

avec $Z = 1$.

Pour une solution Na^+ 10^{-2} *M* en utilisant un capillaire de constantes $t^{1/6} = 1.134$ et $m^{2/3} = 1.605$ (travaux non publies), $\bar{i}_d$ est égal à 13.8 μA. On peut calculer $\lambda^{Na^+} = 5.84\ \Omega^{-1}\ cm^2\ mol^{-1}$ en milieu $LiClO_4$ 0.1 *M*. Soit par cette méthode, $\lambda^{Na^+} = \lambda^{K^+} = 5.84\ \Omega^{-1}\ cm^2\ mol^{-1}$. Ce résultat est voisin des valeurs trouvées à dilution infinie, cependant l'ensemble de nos travaux dans le HMPT pur ne nous permet pas d'envisager pouvoir étendre cette étude à de nombreux cations.

(*c*) On peut aussi atteindre d'une façon approchée la mobilité des ions Na^+ en effectuant leur réduction polarographique en l'absence d'électrolyte indifférent.

Dans ce cas, on peut écrire (56):

$$i_t = i_m + i_d$$

Can. J. Chem. Downloaded from www.nrcresearchpress.com by 210.87.254.40 on 09/05/12
For personal use only.

TABLEAU 5. Volume de solvatation et nombre de solvatation h dans le HMPT à 25 °C

	r_c (Å) (42)	r_s (Å)	r_s(corrigé)	$V_{solvatation}$ (Å^3)	h
Li^+	0.60	4.54	5.30	622.7	2.14
Na^+	0.95	4.26	5.10	552.1	1.89
K^+	1.33	4.27	5.11	549.1	1.88
Ag^+	1.26	4.62	5.35	633.0	2.17
NH_4^+	1.48	4.22	5.10	542.1	1.86
Me_4N^+	3.47 (31)	3.14	3.47	0	0
Et_4N^+	4.00 (31)	2.56	4.00	0	0
n-Pr_4N^+	4.52 (31)	3.52	4.52	0	0
n-Bu_4N^+	4.94 (31)	3.98	4.92	0	0
ClO_4^-	2.40 (31)	1.57	3.27	88.6	0.30
NO_3^-	1.88	1.22	3.05	94.0	0.32
I^-	2.16	1.46	3.20	95.0	0.33
Br^-	1.95	1.35	3.12	96.2	0.33
Cl^-	1.81	1.22	3.05	94.0	0.32

avec: i_t courant total; i_m courant de migration; i_d courant de diffusion.

Si on opère à une concentration 0.1 M en Na^+, l'extrapolation de la droite d'étalonnage établie en milieu $LiClO_4$ 0.1 M permet de prévoir un courant de diffusion $i_d = 138\ \mu A$. Comme on mesure un courant total de 190 μA, il vient T^{Na^+} dans $NaClO_4$ 0.1 $M = 190 - 138/190$, soit $T^{Na^+} = 0.273$.

Ce résultat est peu différent de ce que l'on peut calculer à partir des valeurs du tableau 4: à savoir: Della Monica 0.280; Fujinaga 0.272; Prue 0.256; Paul 0.248; nous-mêmes 0.269.

Nombres de solvatation

Nous avons calculé les volumes et les nombres de solvatation des différents ions étudiés (Tableau 5) et nous les comparons dans le tableau 6 aux résultats que l'on peut tirer ou déduire de la bibliographie. Il apparaît que selon les résultats obtenus par la méthode de travail de Robinson et Stokes (31), le HMPT solvate très peu les anions et que en raison de l'encombrement stérique de sa molécule, le nombre de solvatation des cations reste peu important. Ce résultat ne laisse en rien préjuger de la qualité des liaisons ions–solvant que l'on pourrait mieux étudier par une étude de coefficients de transfert. Effectivement, nous n'avons pu trouver une corrélation simple entre les valeurs du tableau 6 et les valeurs de Parker (58, 59) des coefficients de transfert des ions de l'eau à différents solvants.

Il convient d'ajouter que la méthode de Robinson et Stokes nécessite la connaissance des rayons cristallins des cations ammonium quaternaires avec une bonne précision. Selon Desnoyers (63, 65) nous aurions choisi des valeurs trop grandes (31), il faudrait d'attendre à trouver des volumes de solvatation des ions plus faibles que ce que nous avons trouvé. Effectivement le nombre de solvatation de Li^+ (2, 14) peut apparaître comme étant trop grand si l'on considère les travaux de Nakamura (64) sur les complexes Li^+–HMPT dans l'acétonitrile puisque cet auteur a pu mettre en évidence seulement Li^+, HMPT et Li^+, 2HMPT.

Il convient aussi d'ajouter qu'à l'échelle atomique l'environnement d'un ion dans son solvant est régi par des lois d'encombrement comme dans un cristal. Il est donc peu probable que la formule donnant directement h en divisant le volume de solvatation par le volume molaire du solvant soit rigoureuse (65).

Dans un prochain mémoire, nous présenterons les résultats de nos mesures de mobilités ioniques dans les mélanges eau–HMPT et les conclusions que l'on peut déduire de l'ensemble de notre travail en matière de solvatation.

Partie expérimentale

Tous les sels utilisés, de pureté analytique (Prolabo, Carlo Erba, K et K, G. F. Smith, Alfa, Merck) ont été déshydraté par chauffage sous vide à 70 °C; le HMPT est purifié selon la technique déjà décrite (53–60).

Les solutions sont conservées sous argon U à l'abri de la lumière à basse température (60). Selon leur solubilité les sels ont été utilisés en solutions titrées 5×10^{-2} M ou 10^{-1} M, par addition à l'aide d'une microburette de ces solutions mères à un volume de 15 ml de solvant pur initialement placé dans le vase de mesure. Ainsi les

Can. J. Chem. Downloaded from www.nrcresearchpress.com by 210.87.254.40 on 09/05/12
For personal use only.

TABLEAU 6. Nombre de solvatation *h* dans différents solvants

	HMPT			ϕNO_2*	DMSO*	DMF*	DMAC*	$HCONH_2$	CH_3CN*	Sulfolane	CH_3OH*	NMAC	ODPN	H_2O
	Nous	(36)	(38)	(44)	(23)	(15)	(45)	(12)	(46)	(32)	(47)	(19)	(43)	(31)
Li^+	2.14	1.9	3.43		4.74	4.28	4.13†	5.4	3.37	1.4	6.75	5.1	4.84	7.47
Na^+	1.89	1.5	1.75	1.53	3.03	2.84	2.61*	4	3.50	2.0	5.45	3.5	1.76	4.70
K^+	1.88	1.5	1.59	1.25	2.66	2.60	2.67*	2.5	3.07	1.5	4.32	3.3		2.46
Ag^+	2.17		1.83		2.19	1.93	2.34†		2.12		4.65		1.71	2.32
NH_4^+	1.86		1.56	1.15		1.54	1.42†	2.06*		0.9	3.74	2.7		3.67
ClO_4^-	0.30		0.27	0.82	0.65	0.69	0.98* 0.79†	1.43*	1.76	0.27*	2.67		0.84	6.55
NO_3^-	0.32			0.72	0.56	0.65	0.88*	1.52*	1.70		1.02	1.5	0.98	5.50
I^-	0.33			0.79	0.63	0.63	1.04* 0.92†	1.44*	1.69	0.13*	3.01	1.5	0.97	1.10
Br^-	0.33			0.77	0.74	0.71	0.97* 0.94†	1.48*	1.88	0.31*	3.77	1.7	1.17	1.31
Cl^-	0.32		0.27	0.74	0.98	0.68	0.89†	1.59*	2.25	0.45*	4.08	2.1	1.42	1.73

*Calculés selon la méthode de Robinson et Stokes à partir de valeurs de λ_0 indiquées dans les références.
†Calculés par Paul (28).

concentrations étudiées sont comprises entre 2×10^{-4} et 10^{-2} *M*.

Nous avons utilisé un conductomètre Tacussel type CD 7, équipé d'électrodes type GM/02/55 en platine platiné, à la fréquence de 1000 Hz; un courant d'argon U déshydraté permet de dégazer la solution contenue dans le vase thermostaté à 25 ± 0.05 °C.

Les électrodes sont étalonnées par une solution de KCl 10^{-2} *M* en prenant les valeurs de conductivité obtenues par Jones et Bradshaw (61). Les constantes de cellule étaient de l'ordre de 0.6 à 1.1 cm^{-1}.

Remarque

De récentes travaux (54)[3] indiquent une réelle toxicité cancérigène du HMPT au niveau des voies respiratoires du rat. En tout état de cause en raison des mesures de protection que l'on doit prendre pour éviter la peroxydation et l'hydratation du solvant il semble peu probable que les chercheurs soient eux mêmes en danger. Cependant on peut conseiller de toujours distiller le HMPT avec un piège efficace.

1. C. Moliton-Bouchetout. Thèse 3ième cycle, Limoges. 1972.
2. J. F. Hinton et E. S. Amis. Chem. Rev. **71**, 627 (1971).
3. E. M. Hanna, A. D. Pethybridge, J. E. Prue et D. J. Spiers. J. Solution Chem. **3**, 8 (1974).
4. D. L. Fowler et C. A. Kraus. J. Am. Chem. Soc. **62**, 2237 (1940).
5. R. M. Fuoss et E. Hirsch. J. Am. Chem. Soc. **82**, 1013 (1960).
6. M. A. Coplan et R. M. Fuoss. J. Phys. Chem. **68**, 1177 (1964).
7. J. F. Coetzee et G. P. Cunningham. J. Am. Chem. Soc. **87**, 2529 (1965).
8. M. L. Hansen et H. L. Yeager. J. Phys. Chem. **77**, 3089 (1973).
9. A. P. Zipp. J. Phys. Chem. **77**, 718 (1973).
10. C. Atlani, J. C. Justice, M. Quintin et J. E. Dubois. J. Chim. Phys. **66**, 180 (1969).
11. U. Mayer, V. Gutmann et A. Lodzinska. Monatsh. Chem. **104**, 1045 (1973).
12. J. M. Notley et M. Spiro. J. Phys. Chem. **70**, 1502 (1966).
13. M. Carmo Santos et M. Spiro. J. Phys. Chem. **76**, 712 (1972).
14. A. D. Covington et J. E. Prue. J. Chem. Soc. 1567 (1957).
15. J. E. Prue et P. J. Sherrington. Trans. Faraday Soc. **57**, 1795 (1961).
16. L. R. Dawson et C. Berger. J. Am. Chem. Soc. **79**, 4269 (1957).
17. R. Gopal et O. N. Bhatnagar. J. Phys. Chem. **68**, 3892 (1964).
18. G. P. Johari et P. H. Tewari. J. Phys. Chem. **70**, 197 (1966).
19. R. Gopal et O. N. Bhatnagar. J. Phys. Chem. **69**, 2382 (1965).
20. R. C. Paul, J. P. Singla, D. S. Gill et S. P. Narula. Indian J. Chem. **9**, 981 (1971).

[3]M. Baizer, communication personnelle.

21. R. M. Fuoss et F. Accascina. Electrolytic conductance. Interscience, New York. 1959. pp. 191–205, 207–247.
22. M. Della Monica, U. Lamanna et L. Senatore. J. Phys. Chem. **72**, 2124 (1968).
23. M. Della Monica, D. Masciopinto et G. Tessari. Trans. Faraday Soc. **66**, 2872 (1970).
24. R. Gopal et J. S. Jha. J. Phys. Chem. **78**, 2405 (1974).
25. R. C. Paul, J. P. Singla et S. P. Narula. J. Phys. Chem. **73**, 741 (1969).
26. R. C. Paul, J. L. Singla et S. P. Narula. Indian J. Chem. **8**, 63 (1970).
27. R. C. Paul, J. P. Singla, D. S. Gill et S. P. Narula. J. Inorg. Nucl. Chem. **33**, 2953 (1971).
28. R. C. Paul, J. S. Banait et S. P. Narula. Aust. J. Chem. **28**, 321 (1975).
29. J. L. Mukherjee, D. P. Boden et R. Lindauer. J. Phys. Chem. **74**, 1942 (1970).
30. J. P. Hoare et C. R. Wiese. J. Electrochem. Soc. **121**, 83 (1974).
31. R. A. Robinson et R. H. Stokes. Electrolyte solutions. Butterworths, London. 1959. pp. 124–126.
32. M. Della Monica et U. Lamanna. J. Phys. Chem. **72**, 4329 (1968).
33. M. Della Monica et L. Senatore. J. Phys. Chem. **74**, 205 (1970).
34. P. Bruno, M. Della Monica et E. Righetti. J. Phys. Chem. **77**, 1258 (1973).
35. P. Bruno et M. Della Monica. Gazz. Chim. Ital. **104**, 757 (1974).
36. T. Fujinaga, K. Izutsu et S. Sakura. Nippon Kagaku Kaishi, 191 (1973).
37. P. Muller et B. Siegfried. Helv. Chim. Acta, **55**, 2965 (1972).
38. R. C. Paul, J. Banait et S. P. Narula. Z. Phys. Chem. (Frankfurt am Main) **94**, 199 (1976).
39. J. E. Dubois et H. Viellard. J. Chim. Phys. **62**, 699 (1965).
40. J. Jose, R. Philippe et P. Clechet. Can. J. Chem. Eng. **53**, 88 (1975).
41. F. Persin. Thèse 3ième cycle, Montpellier. 1975.
42. E. R. Nightingale, Jr. J. Phys. Chem. **63**, 1381 (1959).
43. M. Persin. Thèse 3ième cycle, Montpellier. 1974.
44. E. G. Taylor et C. A. Kraus. J. Am. Chem. Soc. **69**, 1731 (1947).
45. G. R. Lester, T. A. Gover et P. G. Sears. J. Phys. Chem. **60**, 1076 (1956).
46. A. C. Harkness et H. M. Daggett. Can. J. Chem. **43**, 1215 (1965).
47. E. C. Evers et A. G. Knox. J. Am. Chem. Soc. **73**, 1739 (1951).
48. J. Y. Gal, C. Moliton-Bouchetout et T. Yvernault. C.R. Acad. Sci. Ser. C, **275**, 253 (1972).
49. G. Baca et R. D. Hill. J. Chem. Educ. **47**, 235 (1970).
50. J. Y. Gal. Thèse d'Etat, Limoges. 1972.
51. K. Isutsu, S. Sakura et T. Fujinaga. Bull. Chem. Soc. Jpn. **45**, 445 (1972).
52. K. Isutsu, S. Sakura et T. Fujinaga. Bull. Chem. Soc. Jpn. **46**, 493 (1973).
53. J. Y. Gal et T. Yvernault. Bull. Soc. Chim. Fr. 2770 (1971).

Can. J. Chem. Downloaded from www.nrcresearchpress.com by 210.87.254.40 on 09/05/12
For personal use only.

54. Chem. Anal. Eng. News, September 29, 1975. p. 17.
55. W. NERNST. Z. Phys. Chem. **2**, 613 (1888).
56. G. CHARLOT, J. BADOZ-LAMBLING et B. TREMILLON. Les réactions électrochimiques. Masson. 1959.
57. D. E. ARRINGTON et E. GRISWOLD. J. Phys. Chem. **74**, 123 (1970).
58. A. J. PARKER. Chem. Rev. **69**, 1 (1969).
59. R. ALEXANDER, A. J. PARKER, J. H. SHARP et W. E. WAGHORNE. J. Am. Chem. Soc. **94**, 1148 (1972).
60. J. Y. GAL et T. YVERNAULT. Bull. Soc. Chim. Fr. 839 (1972).
61. G. JONES et B. C. BRADSHAW. J. Am. Chem. Soc. **55**, 1780 (1933).
62. C. ATLANI et J. C. JUSTICE. J. Solution Chem. **4**, 955 (1975).
63. J. E. DESNOYERS et N. DESROSIERS. Can. J. Chem. A paraître.
64. T. NAKAMURA. Bull. Soc. Chim. Jpn. **48**, 1451 (1975).
65. B. E. CONWAY, R. E. VERRAL et J. E. DESNOYERS. Trans. Faraday Soc. **62**, 2738 (1966).

Downloaded from www.nrcresearchpress.com by 210.87.254.40 on 09/05/12
For personal use only.

Molecular weight of lecithin micelles in toluene by osmometry and Brillouin spectroscopy

ROBERT J. BRAEDLEY, DOUGLAS H. GRANT, VINCENT C. REINSBOROUGH, AND PETER A. ROSS
Department of Chemistry, Mount Allison University, Sackville, N.B., Canada E0A 3C0

Received May 3, 1976

ROBERT J. BRAEDLEY, DOUGLAS H. GRANT, VINCENT C. REINSBOROUGH, and PETER A. ROSS. Can. J. Chem. **54**, 3070 (1976).

Number average molecular weights for lecithin micelles in toluene were determined by osmometry at 25 and 40 °C to be 54 000 and 41 900 respectively. The weight average molecular weights were found to be 78 000 and 68 000 for the same two temperatures by Brillouin spectroscopy. This new technique shows promise in determining micelle size.

ROBERT J. BRAEDLEY, DOUGLAS H. GRANT, VINCENT C. REINSBOROUGH et PETER A. ROSS. Can. J. Chem. **54**, 3070 (1976).

On a déterminé, par osmométrie, à 25 et 40 °C, que les masse moléculaire moyenne en nombre des micelles de lécithine dans le toluène sont respectivement de 54 000 et de 41 900. Par spectroscopie Brillouin, on a trouvé que les masse moléculaire moyenne en poids sont de 78 000 et de 68 000 pour les deux mêmes températures. Cette nouvelle technique montre de grandes possibilités pour déterminer les grandeurs des micelles.

[Traduit par le journal]

Can. J. Chem. Downloaded from www.nrcresearchpress.com by 210.87.254.105 on 09/05/12
For personal use only.

Introduction

Lecithin in non-polar solvents forms reverse micelles which apparently can act as catalytically-active micro-centers for biologically important reactions (1). Of obvious significance is the micellar size and this study reports on the molecular weights of lecithin micelles in toluene as determined by osmometry and Brillouin spectroscopy.

While molecular weight determination by osmometry is well established, Brillouin light scattering by contrast has not previously been applied to micellar systems. Miller and co-workers (2, 3) however have developed equations whereby Brillouin spectra can be made to yield molecular weights of polymers and of large complex species in solution in good agreement with conventional techniques. The intensity ratio J of the Rayleigh peak to the two Brillouin peaks is measured and the difference from the intensity ratio of the pure solvent J_0 is related to the concentration C by the linear equation:

$$\frac{BKC}{J - J_0} = \frac{1}{M_2} + 2A_2C$$

where B is a parameter that can be calculated or determined empirically with a solute of known molecular weight, M_2 is the molecular weight of the solute aggregate, A_2 is the second virial coefficient (higher order virial coefficients are neglected) and

$$K = \frac{C_p\left(\frac{\partial n}{\partial C}\right)^2}{RT^2\left(\frac{\partial n}{\partial T}\right)^2}$$

(n is the refractive index). Since these solutions are dilute, C_p and $(\partial n/\partial T)$ are approximated by using the pure solvent values.

This is the relationship that holds in dilute solution in a relaxing solvent. For a normal or 'nonrelaxing' solvent, the value of B is J_0 (2).

Experimental

(a) Osmotic Pressures

Osmotic pressures were measured using a Hewlett–Packard/Mechrolab 501 osmometer fitted with a H-P type 0-8 cellulose membrane. Membrane conditioning was conventional; from water through propanol to toluene in 25% steps, allowing 24 h in each bath. Stock solutions of lecithin (Schwarz–Mann) in toluene (Fisher Certified) were prepared on a w/v basis. Dilutions were prepared by removing known volumes of solution with subsequent refilling with solvent. Measurements of π, as cm of solvent, were made at both 25 and 40 °C. π/C against C plots were analysed by a linear least-squares fit.

(b) Brillouin Spectroscopy

The Brillouin spectrometer has been previously described (4). The lecithin solutions were repeatedly filtered by positive pressure through 0.25 μ asbestos

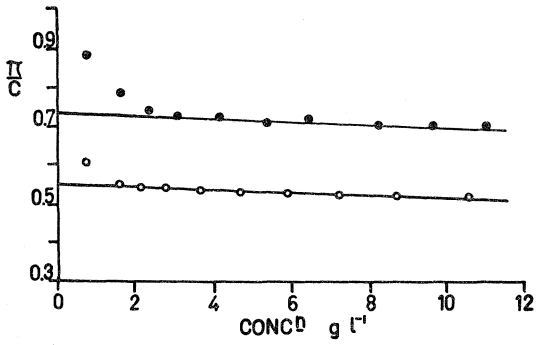

FIG. 1. Osmotic pressures of lecithin in toluene solutions at 25 °C (open circles) and at 40 °C (closed circles).

filters in a dust-free atmosphere since dust can give rise to exaggerated Rayleigh peaks. Aliquots of each solution were evaporated to dryness to obtain the original lecithin concentrations. Scattering measurements were done at 25 and 40 °C with a scattering angle of 90° which spaced all peaks equally apart with no overlap. The 'true' baseline of each peak was determined as proposed by Miller and Lee (5) and then the peaks for five interferometric orders were carefully cut out and weighed. Measurements of $(\partial n/\partial C)$ were obtained with a Hilger interferometer at room temperature and these data were presumed valid at 40 °C.

Results

(a) Osmotic Pressure

Figure 1 shows plots of π/C against C for lecithin in toluene at 25 and 40 °C. Both have distinct upward curvatures at concentrations below 2–3 g l^{-1}, resembling the results reported by Elworthy (6) for lecithin in benzene. Only data for concentrations above 3 g l^{-1}, *i.e.* well into the micelle region, were included in the least-squares analysis, which gave the equations for the lines as:

$$\pi/C = 0.534 - 3.3 \times 10^{-3}\, C \text{ at } 25\,^{\circ}\text{C}$$

and

$$\pi/C = 0.736 - 3.7 \times 10^{-3}\, C \text{ at } 40\,^{\circ}\text{C}$$

These lead to number average molecular weights (M_n) of 54 000 and 41 900 g mol^{-1} and second virial coefficients (A_2) of -1.1×10^{-4} and -1.2×10^{-4} ml mol g^{-2} at 25 and 40 °C, respectively.

These molecular weight values are strikingly similar to the values of 57 000 and 43 000 g mol^{-1} found by Elworthy (6) in benzene. Small, even negative, second virial coefficients are consistent with the idea that micellar structures only form when interaction between solvent and solute is rather 'poor'.

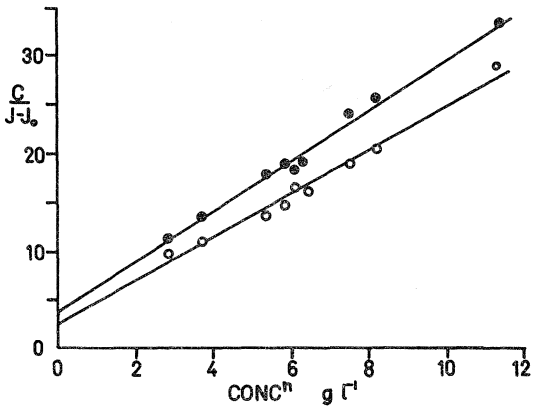

FIG. 2. Concentration dependence of $C/(J - J_0)$ from Brillouin light scattering measurements with lecithin dissolved in toluene at 25 °C (open circles) and at 40 °C (closed circles).

(b) Brillouin Spectroscopy

Figure 2 shows the plot of $C/(J - J_0)$ against C for the Brillouin spectra for lecithin dissolved in toluene at 25 and 40 °C in the 3–12 g l^{-1} concentration range. The osmotic pressure measurements showed this range to be well above the critical micelle concentration (c.m.c.).

The best straight lines by computer fitting were

$$\frac{C}{J - J_0} = 2.50 + 2.43C \quad (25\,^{\circ}\text{C})$$

$$\frac{C}{J - J_0} = 3.09 + 2.68C \quad (40\,^{\circ}\text{C})$$

with C in g l^{-1}. The weight average molecular weights (M_w) calculated from the intercept ($1/BKM_w$) were 78 000 and 68 000. The values of K (0.0142 at 25 and 0.0133 at 40 °C) were obtained from the following pure solvent parameters:

$$C_p = 0.368 \text{ cal ml}^{-1} \text{ deg}^{-1} \text{ (7)}$$

$$B = 0.360 \text{ (2)}$$

and

$$\partial n/\partial T = -5.51 \times 10^{-4} \text{ (2)}$$

The quantity $\partial n/\partial C$ obtained with the Hilger interferometer was 0.0461 ml g^{-1}. The calculated A_2 values were 6.2×10^{-3} and 6.4×10^{-3} ml mol g^{-2} at 25 and 40 °C respectively. The value of J_0 for pure toluene of 0.45 agreed well with literature values of 0.43 (8) and 0.42 (5). The error in $J - J_0$ largely determines the error in M_w and this is approximately 5–10%.

Can. J. Chem. Downloaded from www.nrcresearchpress.com by 210.87.254.105 on 09/05/12
For personal use only.

Ordinarily in light scattering studies in micellar systems, C is replaced by $(C - \text{c.m.c.})$ on both axes (9). The osmotic pressure measurements indicate that the c.m.c. is less than $1\ g\ l^{-1}$ (Elworthy found it to be $0.7\ g\ l^{-1}$ at 40 °C with lecithin dissolved in benzene (6)) so that neglecting this refinement in this system is within experimental error.

Discussion

Since there is no reason to suppose that micelle molecular weights are mono-disperse, the agreement between the molecular weight values obtained by the two methods must be regarded as highly satisfactory. In poly-disperse systems, weight averages will be greater than number averages.

This poly-dispersity will also give rise to different second virial coefficients (A_2) as determined by each method (10). The discrepancy found in the present work between the slightly negative A_2 in osmotic pressure measurements (-1×10^{-4} ml mol g^{-2}) and the large positive value (6×10^{-3} ml mol g^{-2}) in the Brillouin scattering is greater than is found normally for the same solvent. In defense of each, the osmotic pressure A_2 for the only other comparable study in a micellar system was also small and negative (6) while the Brillouin scattering A_2 compares favourably in magnitude with conventional light scattering A_2 values in micellar systems (9). A preliminary Brillouin scattering study in this laboratory in the lecithin–benzene system at 40 °C gave similarly large values for A_2 while yielding a reasonable M_w (50 000) in comparison with Elworthy's M_n value (43 000) (6). The wide difference in A_2 values does not appear to affect adversely the determination of reasonable molecular weights. Osmotic pressure has not been commonly employed to determine micellar weights and an extensive study by this method in several micellar systems in different solvents may provide an explanation.

In comparison with conventional light scattering, Brillouin scattering thus appears an interesting alternative in the determination of micellar size. The chief advantage Brillouin offers over conventional light scattering is that the Rayleigh ratio or turbidity, often difficult to measure because of the difference in magnitude of the intensities being compared, is replaced by the ratio of the relative intensities of the Brillouin and Rayleigh peaks which are of the same order of magnitude. Otherwise, the two methods require the same type of ancillary data.

Acknowledgements

We wish to thank Dr. John Valleau of the University of Toronto for the use of the Brillouin spectrometer. Funds were provided by the National Research Council of Canada.

1. E. J. Fendler, S. A. Chang, J. H. Fendler, R. T. Medary, O. A. El Seoud and V. A. Woods. *In* Reaction kinetics in micelles. *Edited by* E. Cordes. Plenum Press, New York. 1973. p. 127.
2. G. A. Miller, F. I. San Filippo, and D. K. Carpenter. Macromolecules, **3**, 125 (1970).
3. F. I. San Filippo, G. A. Miller, and J. A. Bertrand. Inorg. Chem. **11**, 1433 (1972).
4. V. C. Reinsborough and J. P. Valleau. Can. J. Chem. **50**, 2704 (1972).
5. G. A. Miller and C. S. Lee. J. Phys. Chem. **72**, 4644 (1968).
6. P. H. Elworthy. J. Chem. Soc. 813 (1959).
7. E. B. Freyer, J. C. Hubbard, and D. H. Andrews. J. Am. Chem. Soc. **51**, 759 (1929).
8. H. Z. Cummins and R. W. Gammon. J. Chem. Phys. **44**, 2785 (1966).
9. P. Debye. J. Phys. Chem. **53**, 1 (1949).
10. K. A. Stacey. *In* Light-scattering in physical chemistry. Butterworth, London. 1956. p. 120.

Can. J. Chem. Downloaded from www.nrcresearchpress.com by 210.87.254.105 on 09/05/12
For personal use only.

The interrelationship between partial molal expansibility and the solute induced shift in the temperature of maximum density of water

DIGBY D. MACDONALD AND JAMES B. HYNE
Department of Chemistry, University of Calgary, Clagary, Alta., Canada T2N 1N4

Received April 1, 1976

DIGBY D. MACDONALD and JAMES B. HYNE. Can. J. Chem. **54**, 3073 (1976).

The effect of solutes on the temperature of maximum density (TMD) of water is analysed with emphasis upon the applicability of thermodynamic dissection of the observed change in the TMD ($\Delta\theta_{obs}$) into ideal ($\Delta\theta_{id}$) and structural ($\Delta\theta_{st}$) components. The use of TMD as a probe for examining the effect of dissolved solutes on the structural properties of water is critically compared with methods based upon apparent and partial molal expansibilities.

DIGBY D. MACDONALD et JAMES B. HYNE. Can. J. Chem. **54**, 3073 (1976).

On analyse l'effet des solutés sur la température de densité maximum (TDM) de l'eau en essayant de mettre en évidence la possibilité d'appliquer la division thermodynamique du changement observé dans TDM, ($\Delta\theta_{obs}$), en composants idéaux ($\Delta\theta_{id}$) et structuraux ($\Delta\theta_{st}$). On compare d'une façon critique l'utilisation du TDM comme moyen d'examiner l'effet de solutés dissous sur les propriétés structurales de l'eau avec les méthodes basées sur les expansibilités molales apparentes et partielles.

[Traduit par le journal]

Can. J. Chem. Downloaded from www.nrcresearchpress.com by 210.87.254.42 on 09/05/12
For personal use only.

Introduction

The shift in the temperature of maximum density (TMD) of water that occurs on dissolution of a solute is now recognized as a useful tool for the investigation of solute induced changes in the structure of liquid water (1–13). However, a number of recent papers (6, 10–12) suggest that some confusion exists as to the appropriate interpretation of the data. In particular, a few authors (6, 11, 12) have used the overall experimentally observed shift in the TMD ($\Delta\theta_{obs}$), or parameters derived therefrom (*e.g.* partial molal expansibility), as a measure of change in the structure of water caused by solid solutes. We attempt to show in this paper that care must be exercised in the use and interpretation of these parameters in order to avoid erroneous conclusions as to the effect of solutes on the structure of liquid water.

Thermodynamic and Structural Considerations

Wada and Umeda (3, 4) and later Franks and Watson (5) demonstrated that the observed shift in the TMD of water on dissolution of a solute can be dissected into an ideal contribution, $\Delta\theta_{id}$, and a 'structural' contribution, $\Delta\theta_{st}$, according to eq. 1

$$[1]\quad \Delta\theta_{obs} = \underbrace{-\left[\frac{\chi}{1-\chi}\,\frac{(\partial V_2^0/\partial T)}{2\alpha_1 V_1^*}\right]}_{(\Delta\theta_{id})} \underbrace{-\left[\frac{(\partial \Delta V^M/\partial T)}{2\alpha_1 V_1^*\,(1-\chi)}\right]}_{(\Delta\theta_{st})}$$

where V_2^0 is the molar volume of the solute, V_1^* is the molar volume of water at 3.98 °C, ΔV^M is the excess volume of mixing at solute mole fraction χ, and α_1 is a constant which defines the parabolic variation of the molar volume of water with temperature in the neighbourhood of the TMD. For an ideal mixture ΔV^M is zero at all temperatures, and the observed shift in the TMD is equal to the ideal component, $\Delta\theta_{id}$.

It is convenient to interpret the effect of solutes on the TMD in terms of a model for liquid water which recognizes transient regions of bonded bulkiness and unbonded denseness. The dynamic equilibrium between these states is referred to as the 'structural equilibrium' in the system. Maximum density occurs when the opposing effects of temperature upon the structural equilibrium and upon the volume of the components themselves are balanced. Ideal mixing of a solute with the solvent demands that the molar volume of water in the mixture is the same

Can. J. Chem. Downloaded from www.nrcresearchpress.com by 210.87.254.42 on 09/05/12
For personal use only.

as that in the pure liquid, *i.e.* $\Delta\theta_{id}$ *does not* contain a contribution from a solute induced shift in the structural equilibrium. On the other hand, the non-ideal contribution $\Delta\theta_{st}$, arises principally from solute induced shifts in this equilibrium. Thus, if the solute shifts the equilibrium in the direction of less dense water clusters (positive $\Delta\theta_{st}$) the solute is said to have a 'structure making' effect. Solutes which shift the equilibrium in the reverse direction (negative $\Delta\theta_{st}$) are commonly referred to as 'structure breakers'. Note that we have not specified the exact mechanism by which a solute may induce a shift in the structural equilibrium. However, the analysis presented above does demonstrate that any classification of solutes into structure makers or breakers based upon TMD data can only be made using the non-ideal contribution, $\Delta\theta_{st}$, and not upon the basis of the total observed shifts in the TMD, $\Delta\theta_{obs}$.

Partial Molal Expansibilities

A number of workers (12, 14) have suggested that other volume/temperature relationships may be used as reliable probes for determining the effect of dissolved solutes on the structure of liquid water. We now critically examine this premise in the light of the preceding discussion.

The volume of a solution at temperature T is given as

$$[2] \qquad V = \chi\phi + (1-\chi)V_1^0 = (1-\chi)V_1^0 + \chi V_2^0 + \Delta V^M$$

where χ is the mole fraction of the solute, ϕ is the apparent molal volume of the dissolved species, and ΔV^M is the previously defined excess volume of mixing at composition χ. Differentiation with respect to temperature at fixed composition, and rearrangement, results in an expression for the temperature dependence of the excess volume of mixing, *viz.*

$$[3] \qquad \left(\frac{\partial \Delta V^M}{\partial T}\right)_\chi = \chi\left[\left(\frac{\partial\phi}{\partial T}\right)_\chi - \left(\frac{\partial V_2^0}{\partial T}\right)\right]$$

Substitution of the above relationship into eq. 1 yields

$$[4] \qquad \left(\frac{\partial\phi}{\partial T}\right)_\chi = -2(1-\chi)\alpha_1 V_1^* \left(\frac{\Delta\theta_{obs}}{\chi}\right)_\chi$$

At infinite dilution $(1-\chi)\rightarrow 1$ and $\partial\phi/\partial T \rightarrow \partial\bar{V}_2^0/\partial T$, where $\bar{V}_2^0$ is the partial molal volume of the solute at the temperature of interest. Thus

$$[5] \qquad \left(\frac{\partial\bar{V}_2^0}{\partial T}\right) = -2\alpha_1 V_1^* \left(\frac{\Delta\theta_{obs}}{\chi}\right)_{\chi\rightarrow 0}$$

which in the case of water as solvent yields

$$[6] \qquad \left(\frac{\partial\bar{V}_2^0}{\partial T}\right) = -2.81\times 10^{-4}\left(\frac{\Delta\theta_{obs}}{\chi}\right)_{\chi\rightarrow 0} \text{ ml mol}^{-1}\ K^{-1}$$

The derivation given above is essentially that presented recently by Kuppers (12) and earlier by Lilley and Murphy (11), Neal and Goring (14), and Sakurai *et al.* (7). Kuppers (12) goes on to define the partial molal expansibility of the solute in water as

$$[7] \qquad \bar{\alpha} = \frac{1}{\bar{V}_2^0}\left(\frac{\partial\bar{V}_2^0}{\partial T}\right) = \frac{-2.81\times 10^{-4}}{\bar{V}_2^0}\left(\frac{\Delta\theta_{obs}}{\chi}\right)_{\chi\rightarrow 0}$$

and suggests that this quantity may be useful for investigating the structure of aqueous solutions.

Neal and Goring (14) found that for dilute solutions of hydrophobic solutes, such as 1-butanol, neopentanol, and cyclohexanol, $\phi < V_2^0$, $(\partial\phi/\partial T) < (\partial V_2^0/\partial T)$ and $(\partial^2\phi/\partial T^2) > 0$. On the other hand, typically hydrophilic solutes, such as formamide, exhibit $(\partial\phi/\partial T) > (\partial V_2^0/\partial T)$ and negative values for the second differential $(\partial^2\phi/\partial T^2)$, even though ϕ is still generally less than V_2^0. The above relationships led Neal and Goring to conclude that the quantity $(\partial\phi/\partial T)$ can be used to ascertain the effect of dissolved solutes on the structure of liquid water. Furthermore, they state that "However, the TMD changes sharply with concentration and $\partial\phi/\partial T$ is a more direct measure of the effect of the solute on the structure of water". The fact that $(\partial\phi/\partial T)$ and $(\Delta\theta_{obs}/\chi)$ are linearly related (eq. 4), and since $\Delta\theta_{obs}$ is not simply a measure of structural influence, but includes an ideal term, places the second conclusion of Neal and Goring in some doubt. Therefore, it is concluded that $(\partial\phi/\partial T)$ is no more reliable as an index of solute structure making/breaking ability than is $\Delta\theta_{obs}$.

An illustration of the pitfalls accompanying the use of $\Delta\theta_{obs}$ (and hence $(\partial\phi/\partial T)$) as a structural parameter is afforded by data plotted in

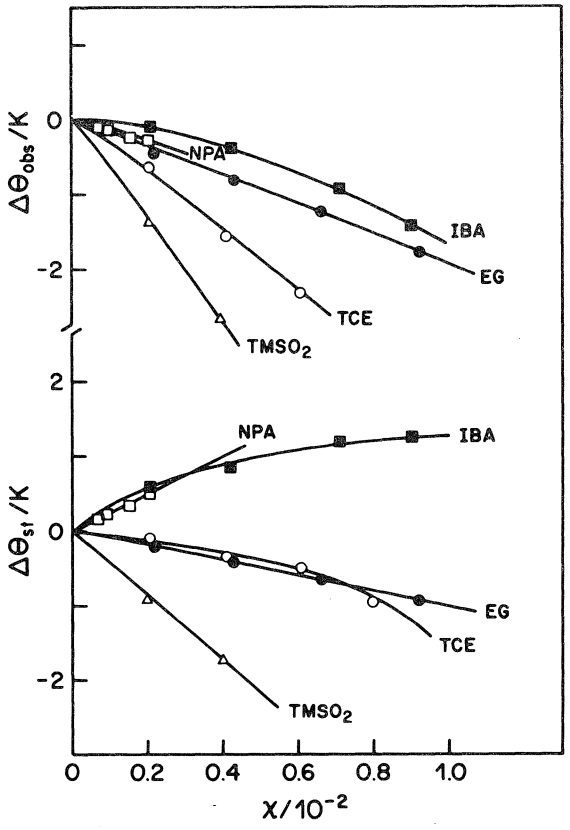

FIG. 1. Plot of the observed shift in the TMD, $\Delta\theta_{obs}$, and the structural contribution, $\Delta\theta_{id}$, against solute mole fraction, χ, for isobutanol (IBA) (13), neopentanol (NPA) (13), ethylene glycol (EG) (13), tetramethylene sulphone ($TMSO_2$) (1), and 2,2,2-trichloroethanol (TCE) (13).

Fig. 1. Thus, for a number of solutes, such as isobutanol (IBA) and neopentanol (NAP), $\Delta\theta_{obs}$ is negative even though the structural contribution, $\Delta\theta_{st}$, is positive, and these solutes are almost certainly structure makers. Structure breaking solutes (*i.e.* negative $\Delta\theta_{st}$), such as ethylene glycol (EG), tetramethylene sulphone ($TMSO_2$), and 2,2,2-trichloroethanol (TCE) also exhibit negative values for $\Delta\theta_{obs}$ and, therefore, positive values for $(\partial\phi/\partial T)$. Consequently, no unambiguous classification of solutes as water structure makers or breakers can be performed on the basis of $(\partial\phi/\partial T)$ data alone. Furthermore, the observation that for hydrophobic solutes $(\partial\phi/\partial T) < (\partial V_2^0/\partial T)$ is equivalent to stating that $\Delta\theta_{st}$ is positive (eqs. 1 and 3); that is the evaluation of the above inequality requires exactly the same experimental information as is required for the dissection of $\Delta\theta_{obs}$ into $\Delta\theta_{id}$ and $\Delta\theta_{st}$, *viz.* the determination of $(\partial V_2^0/\partial T)$. Thus, no conceptual or practical advantages exist in using $(\partial\phi/\partial T)$ instead of TMD data for determining the effect of solutes on the structure of liquid water.

In a recent paper, Kuppers (12) rightly points out that the measurement of $\Delta\theta_{obs}$ provides with relative ease and precision the partial molal expansibility of a solute at infinite dilution at 3.98 °C (eq. 7). He further claims that such data obviate the difficulty of deriving $\Delta\theta_{st}$ data, and hence $(\partial\Delta V^M/\partial T)$, for solutes which are not liquids at temperatures in the region of the TMD. Since the partial molal volumes for organic solutes in water are generally positive, irrespective of whether the solute is a structure maker or breaker, the same argument against the use of $(\partial\phi/\partial T)$ data also apply to the application of partial molal expansibility data in determining the effect of solutes on the structure of liquid water. This then weakens Kuppers' claim for the utility of $\bar{\alpha}$ data.

Finally, it is worthwhile commenting generally upon the relative merits of various parameters which have been used to determine the nature of water in the immediate vicinity of a dissolved solute. A number of parameters, including viscosity, partial molal heat capacity, relaxation time (nmr and dielectric), to name a few, utilize the concept of 'structural temperature' which was first introduced by Bernal and Fowler (15). Unfortunately, as pointed out by Ben-Naim (16), different experimental techniques yield different structural temperatures for the same system. Part of the problem arises from our inability to estimate the contribution to the structural temperature due to ideal mixing. Furthermore, few, if any of these techniques utilize a property (such as TMD) which is unique to liquid water and, consequently, there is no reason to believe that the probes employed do, in fact, respond only to structural changes in the aqueous system. These criticisms do not apply to the use of $\Delta\theta_{st}$, although the first does to the use of $\Delta\theta_{obs}$. Therefore, it seems reasonable to conclude that the extracted $\Delta\theta_{st}$ parameter is probably one of the more useful probes for determining the influence

Can. J. Chem. Downloaded from www.nrcresearchpress.com by 210.87.254.42 on 09/05/12
For personal use only.

of a dissolved solute on the unique three dimensional structure of liquid water.

Acknowledgement

Financial assistance for this work from the National Research Council of Canada is gratefully acknowledged.

1. D. D. MACDONALD, M. D. SMITH, and J. B. HYNE. Can. J. Chem. **49**, 2817 (1971).
2. D. D. MACDONALD, M. E. ESTEP, M. D. SMITH, and J. B. HYNE. J. Soln. Chem. **3**, 713 (1974).
3. G. WADA and S. UMEDA. Bull. Chem. Soc. Jpn. **35**, 646 (1962).
4. G. WADA and S. UMEDA. Bull. Chem. Soc. Jpn. **35**, 1797 (1962).
5. F. FRANKS and B. WATSON. Trans. Faraday Soc. **63**, 329 (1967).
6. A. J. DARNELL and J. GREYSON. J. Phys. Chem. **72**, 3021 (1968).
7. M. SAKURAI, T. KOMATSU, and T. KAKAGAWA. Bull. Chem. Soc. Jpn. **45**, 1038 (1972).
8. M. C. DEPRETZ. Ann. Chim. Phys. **70**, 49 (1830).
9. M. C. DEPRETZ. Ann. Chim. Phys. **73**, 296 (1840).
10. G. WADA and M. MIURA. Bull. Chem. Soc. Jpn. **42**, 2498 (1969).
11. T. H. LILLEY and S. MURPHY. J. Chem. Thermodyn. **5**, 467 (1973).
12. J. R. KUPPERS. J. Phys. Chem. **78**, 1041 (1974).
13. D. D. MACDONALD, B. DOLAN, and J. B. HYNE. J. Soln. Chem. In press.
14. J. L. NEAL and D. A. I. GORING. J. Phys. Chem. **74**, 658 (1970).
15. J. D. BERNAL and R. H. FOWLER. J. Phys. Chem. **1**, 515 (1933).
16. A. BEN-NAIM. *In* Chemistry and physics of aqueous gas solution. *Edited by* W. A. Adams *et al.* The Electrochemical Society, New Jersey. 1975.

Can. J. Chem. Downloaded from www.nrcresearchpress.com by 210.87.254.42 on 09/05/12
For personal use only.

Crystal structure and vibrational spectra of methyl *N,N*-diethyldithiocarbamato mercury(II)

CHUNG CHIEH AND LAURA P. C. LEUNG

Guelph-Waterloo Centre for Graduate Work in Chemistry, Department of Chemistry, University of Waterloo, Waterloo, Ont., Canada N2L 3G1

Received April 21, 1976

CHUNG CHIEH and LAURA P. C. LEUNG. Can. J. Chem. **54**, 3077 (1976).

Reactions of tetraethylthioperoxydicarbonic diamide with methylchloromercury(II) gave two kinds of products of formula CH_3—Hg[$S_2CN(C_2H_5)_2$] and Hg[$S_2CN(C_2H_5)_2$]$_2$. The latter exists in two crystal forms as reported by Iwasaki who obtained these compounds by other reactions. The former compound is a colorless monoclinic crystal with a = 7.155, b = 7.757, c = 18.248 Å, and β = 96.1°.

In methyl *N,N*-diethyldithiocarbamato mercury(II), the mercury is two-coordinated with CH_3—Hg and Hg—S bond distances of 2.04(3) and 2.418(7) Å respectively in a linear fashion. The angle C—Hg—S is 171.2°. The molecule is planar with both CH_3— of the ethyl groups bending toward one side of the plane. Two molecules around the centre of symmetry are loosely

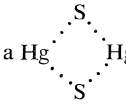

bridged by two sulfur atoms forming a Hg Hg group and the bridging Hg...S distances are 2.964 (intramolecular) and 3.147 Å (intermolecular). There are two bands between 970 and 1000 cm^{-1} due to C=S and these bands become broad upon coordination. The ν_{Hg-CH_3} band is at 522 (ir) and 528 (Raman) cm^{-1}.

CHUNG CHIEH et LAURA P. C. LEUNG. Can. J. Chem. **54**, 3077 (1976).

Les réactions de la diamide tétraéthylthiopéroxydicarbonique avec le chlorure de méthylmercure(II) ont donné deux types de produits de formule CH_3—Hg[$S_2CN(C_2H_5)_2$] et Hg[$S_2CN(C_2H_5)_2$]$_2$. Ce dernier existe sous deux formes cristallines tel que rapporté par Iwasaki qui a obtenu ces composés par d'autres réactions. Le premier composé se présente sous forme de cristaux monocliniques incolores avec a = 7.155, b = 7.757, c = 18.248 Å et β = 96.1°.

Dans le *N,N*-diéthyldithiocarbomato méthylmercure(II), le mercure est deux fois coordonné avec des longueurs de liens CH_3—Hg et Hg—S de 2.04(3) et 2.418(7) Å respectivement, le tout disposé de façon linéaire. L'angle C—Hg—S est de 171.2°. La molécule est planaire avec les deux CH_3— des groupes éthyle déformés vers un côté du plan. Deux molécules autour du centre de symétrie sont pontées faiblement par deux atomes de soufre formant un groupement

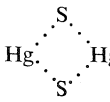

Hg et les distances du pont Hg...S sont 2.964 (intramoléculaire) et 3.147 Å (intermoléculaire). Il apparaît deux bandes entre 900 et 1000 cm^{-1} qui sont dues au C=S; ces bandes deviennent plus larges s'il y a coordination. La bande ν_{Hg-CH_3} est à 522 (ir) et 528 (Raman) cm^{-1}.

[Traduit par le journal]

Introduction

Sulfur plays an important role in biochemistry (1). Interest in the interaction of mercurials with sulfur-containing ligands is high because of the topical problems of mercury poisoning (2). Many sulfur-containing functional groups in the biological system are of the —SS— and —SH type; therefore it is interesting to study the reaction of heavy metals, such as mercurous and mercuric ions, with these groups.

The reaction of methyl mercury chloride with tetraethylthioperoxydicarbonic diamide, which is

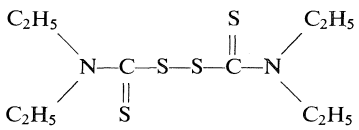

Can. J. Chem. Downloaded from www.nrcresearchpress.com by 210.87.254.5 on 09/05/12
For personal use only.

TABLE 1. Atomic coordinates (fractional $\times 10^4 \pm (x, y, z; x, \frac{1}{2} - y, \frac{1}{2} + z)$) and thermal parameters of the form $\exp\{-2\pi^2(a^{*2}h^2U_{11} + \ldots + 2a^*b^*hkU_{12} + \ldots)\} \times 10^{-3}$ for all atoms but $\times 10^{-4}$ for Hg

Atom	x	y	z	U_{11}	U_{22}	U_{33}	U_{12}	U_{13}	U_{23}
Hg	−2461(2)	−0319(2)	0563(1)	501(6)	494(6)	495(6)	−047(5)	−042(4)	−002(4)
S(1)	1584(10)	0041(7)	1087(4)	51(3)	25(2)	61(4)	06(2)	−05(3)	−00(3)
S(2)	−1508(9)	2647(9)	0772(4)	47(3)	43(3)	63(4)	04(3)	−15(3)	−08(3)
N	1940(27)	3474(25)	1317(10)	44(8)	33(8)	33(8)	−03(8)	04(8)	−08(8)
C(1)	0899(35)	2172(32)	1081(13)	51(9)	42(9)	36(9)	22(8)	07(8)	09(8)
C(2)	4006(37)	3152(47)	1553(20)	32(8)	78(9)	88(9)	−03(9)	−06(9)	10(9)
C(3)	4402(52)	3026(69)	2420(22)	62(8)	141(9)	79(9)	−02(9)	−25(9)	12(9)
C(4)	1275(42)	5275(34)	1334(17)	64(9)	33(8)	69(9)	−22(8)	11(9)	23(9)
C(5)	0371(55)	5728(50)	2044(19)	89(9)	77(8)	56(9)	09(9)	10(9)	−09(9)
C(6)	−3561(60)	2745(36)	0496(9)	168(9)	49(9)	01(7)	−12(8)	−22(8)	01(8)

better known as tetraethylthiuram disulfide (TETD), in basic solution of chloroform and ethanol produced two compounds of formula $Hg[S_2CN(C_2H_5)_2]_2$ and $CH_3Hg[S_2CN(C_2H_5)_2]$. The former exists in two crystal forms (3).

Crystal structure analyses by X-ray diffraction methods revealed the structure of methyl *N*,*N*-diethyldithiocarbamato mercury(II).

The reactions of methyl mercuric chloride, phenyl mercuric chloride, and mercuric halides with TETD produced a variety of crystals depending on the reaction conditions. This is the first report of our effort to understand these reactions.

Experimental

Equal molar amounts of TETD and methyl mercuric chloride dissolved in chloroform and ethanol respectively were mixed at room temperature. No immediate change was observable and the reaction mixture was left in a cold room (0 °C) partly covered. After 2 weeks, two kinds of crystals appeared in the same beaker and they were subjected to X-ray diffraction studies. The brown crystals proved to be the α-form of bis(*N*,*N*-diethyldithiocarbamato)mercury(II) from cell constants and other physical properties. The colorless crystals are monoclinic, with the following crystal data:

$C_6H_{13}HgNS_2$ fw = 363.8

Monoclinic, $a = 7.155(5)$, $b = 7.757(4)$, $c = 18.248(17)$ Å, $\beta = 96.1(1)°$, $V = 1007.1$ Å^3, $D_m = 2.39$, $Z = 4$, $D_x = 2.399$, mp = 141 °C, $\mu_{MoK\alpha} = 158.3$ cm^{-1}. Space group $P2_1/c$.

Systematic absences $h0l$, when l is odd, $0k0$ when k is odd.

The cell constants were estimated from film data and refined by a least-squares method based on the 2θ values of 27 reflections measured on a G.E. diffractometer. Intensities of 2926 reflections with $2\theta \leq 60°$ were measured using the stationary-crystal stationary-counter method which was chosen because the crystal decom poses in the X-ray beam. The counting time was 30 s for each reflection. The crystal used for intensity measurement was mounted with a^* along the goniostat. The dimensions of the crystal used are $0.15 \times 0.06 \times 0.06$ mm along the a, b, and c directions. The average background curve measured as a function of 2θ in several orientations was used. Four strong standard reflections were measured repeatedly between every 100 reflections and their intensity dropped to 80% of their initial values at the end of data collection. The standard reflections were also used to scale the reflections, measured immediately after, to a uniform level. Reflections with $2\theta \leq 40°$ (1145) were measured first and the intensity of standard reflections dropped only slightly (4%). Those data with $I >$ background by $2\sigma_I$ were considered observed and these 1854 reflections were used in the refinement. Lorentz and polarization corrections were made in the usual way to derive the structure amplitude.

The structure was solved using the heavy atom method and refined by full-matrix least-squares. The function minimized was $\sum w(|F_o| - |F_c|)^2$ where $w = (40 + |F_o| + 0.001|F_o|^2)^{-1}$ and the scattering factors used were taken from the International Tables for X-ray Crystallography (4). During the course of refinement, several options had been tried. If the reflections with $2\theta > 40°$ (MoKα) were discarded, an R factor of 0.07 was obtained, but the standard deviations for atomic parameters were considerably higher. Including all data in order to get good resolution, a difference Fourier was calculated. The likely positions for hydrogen atoms had positive electron densities; however, the peaks were not as high as the ripples for the mercury atoms. An effort was made to locate all hydrogen atoms, but not all hydrogen atoms gave reasonable bond distances and angles. Inclusion of hydrogen atoms did not affect the R factor significantly. Because of the high degree of uncertainty, it was decided not to report their coordinates. With the weighting scheme mentioned earlier, the variation of $\sum w\Delta F^2$ *vs.* ranges of F_o was very small. In the final refinement, the average shifts were less than 0.1σ for all parameters. The final R factor is 0.10.[1] The atomic coordinates and temperature factors are shown in Table 1.

Raman and Infrared Spectra

Polycrystalline solid state Raman spectra were excited

[1]Complete set of tables of structure factors is available, at a nominal charge, from the Depository of Unpublished Data, CISTI, National Research Council of Canada, Ottawa, Canada K1A 0S2.

Can. J. Chem. Downloaded from www.nrcresearchpress.com by 210.87.254.5 on 09/05/12
For personal use only.

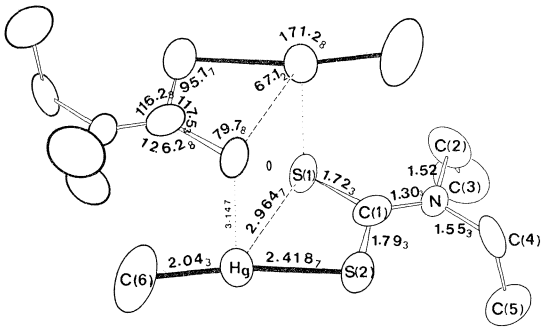

FIG. 1. ORTEP plot of the molecule and the formation of the dimeric grouping of methyl *N*,*N*-diethyldithiocarbamato mercury(II).

with the 514.5 nm line of a Spectra Physics 165 Ar ion laser operating at approximately 350 mW light power and recorded using a Jarrell-Ash Model 400 Raman spectrophotometer. The ir spectra were recorded on a Perkin-Elmer 457 using KBr pellets.

Description of the Structure

The crystal consists of single molecules. The obvious intermolecular contact is the additional S...Hg bridging for two molecules which relate to each other by a centre of symmetry. The molecule and the dimeric grouping is shown in Fig. 1, which includes atomic numbering and bond distances and angles. Dimeric groups can be considered as packing units. The packing diagram, looking along the *b* direction, is given in Fig. 2. The molecules pack as layers in the *ac* plane. The next layer of molecules is directly above or below the layer as seen at a distance of 7.757 Å (*b* axis).

The *N*,*N*-diethyldithiocarbamate ion in its sodium salt is planar if the two terminal CH_3 groups are ignored (5). The mercuric ion is two-coordinated in methyl *N*,*N*-diethyldithiocarbamato mercury(II), with Hg—S and Hg—C distances of 2.418(7) and 2.04(3) Å respectively. The other sulfur of the dithiocarbamate group is weakly bonded to two mercuric ions with intramolecular and intermolecular Hg...S(1) distances of 2.964(7) and 3.147(7) Å respectively. These weak interactions and the fact that the two strong bonds centred on mercury are almost linear cause the molecule to be planar if the CH_3 of both ethyl groups are ignored. The angle S—Hg—C is 171.2(8)° which is less than 180° because the carbon, C(6), of the methyl group bends away from the weakly bonded sulfur atoms. Both terminal CH_3 of the ethyl groups in this molecule are bent toward one side of the plane, whereas, in the free *N*,*N*-diethyldithiocarbamate ion, in TETD (6), and in both α- and β-forms of bis(*N*,*N*-diethyldithiocarbamato)mercury(II), the terminal $-CH_3$ groups are bent toward different sides of the main plane. The corresponding zinc (7) and cadmium (8) complexes are isostructural with the α-form of the mercury(II) analog. The equations for the mean planes of the molecule and for certain fragments of the molecule are listed in Table 2. Plane 1 includes all the atoms except the CH_3 of the two ethyl groups. The carbon, C(6), which is bonded to Hg, deviates most from the plane (0.17 Å). The two methyl carbons of the ethyl groups deviate from the plane at approximately the same distance, 1.5 Å. Excluding C(6) and Hg consecutively from the least-squares plane gives planes 2 and 3. These two atoms are bent toward the same side as C(3) and C(5). The torsion angle between $\begin{matrix}S\\S\end{matrix}\!>\!C\!-\!N$, plane 4, and $C\!-\!N\!<\!\begin{matrix}C\\C\end{matrix}$, plane 5, is small (2.8°).

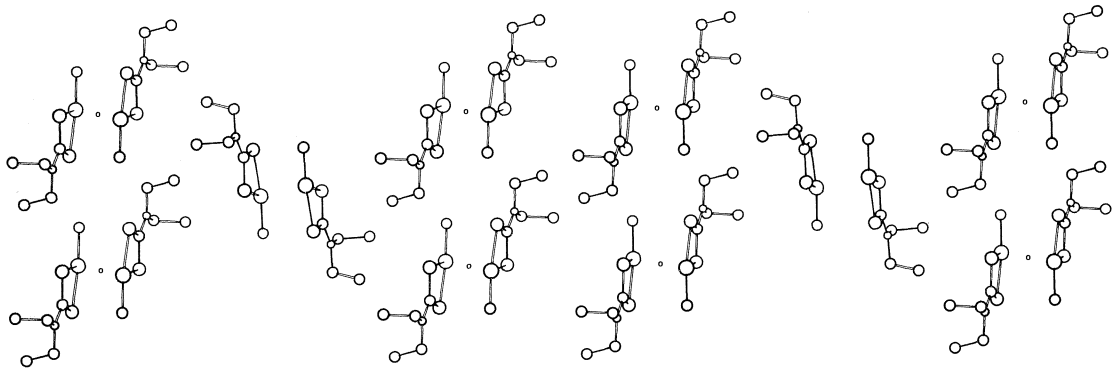

FIG. 2. The stereo pair of packing diagrams looking down from the *b* axis.

Can. J. Chem. Downloaded from www.nrcresearchpress.com by 210.87.254.5 on 09/05/12
For personal use only.

TABLE 2. Least-squares planes for the molecule in the form $lX + mY + nZ = p$ where X, Y, Z, are coordinates in Å, referred to orthogonal axes a, b, and c^*

Plane	Atom	l	m	n	p	Displacement (Å) Maximum		Other atoms	
1	All but ethyl CH_3 groups	−0.3086	−0.0765	0.9481	1.66	C(6) 0.17	C(3) 1.5	C(5) 1.6	
2	Same as 1 excluding C(6)	−0.3241	−0.1147	0.9390	1.55	S(2) −0.07	C(6) 0.4		
3	Same as 2 excluding Hg	−0.3374	−0.1258	0.9329	1.49	C(2) −0.04	Hg 0.12	C(6) 0.51	
4		−0.3557	−0.1164	0.9273	1.49	C(1) −0.02	Hg 0.15	C(6) 0.53	
5		−0.3195	−0.1485	0.9359	1.46	N 0.02	Hg 0.13	C(6) 0.55	

TABLE 3. Comparison of bond distances (Å) and angles (°)

(*a*) Dithiocarbamato complexes

Compound	Hg—S	S—C	Angle SCS	Ref.
$CH_3HgS_2CN(C_2H_5)_2$	2.418(7) 2.964(7)	1.79(3) 1.72(4)	117.5(3)	
α-$Hg[S_2CN(C_2H_5)_2]_2$	2.520(6) 2.663(6) 2.418(7) 2.698(6)	1.715(19) 1.735(20) 1.764(19) 1.698(21)	119.2(9) From two ligands	3
β-$Hg[S_2CN(C_2H_5)_2]_2$	2.398(4) 2.965(4)	1.782(12) 1.691(12)	119°(1)	3

(*b*) Methyl mercury with other S-containing ligands

Compound	CH_3—Hg	Hg—S	S—C	Angle CH_3—Hg—S	Ref.
CH_3—Hg—$S_2CN(C_2H_5)_2$	2.04(3)	2.418(7)	1.79(3)	171.2(8)	
CH_3—Hg—$SC(CH_3)_2CH(NH_3)COO.H_2O$	1.98(5)	2.376(8)	1.92(4)	176(1)	9
2nd molecule	1.82(5)	2.385(8)	1.80(4)	179(1)	
$CH_3Hg[S—C(CH_3)_2C(NH_2^+HgCH_3)COO^-$	1.885(7)	2.320(2)		176(1)	
CH_3Hg—S—CH_2CNH_3COO	2.10(4)	2.352(12)	1.81(3)	177(1)	10

Discussion

Methylmercury is bonded to one sulfur of the dithiocarbamate ion with some additional Hg---S close contact, which is in good agreement with the well-known affinity of mercury for sulfur donors. The Hg—S distances in mercuric *N*,*N*-diethyldithiocarbamate complexes are also comparable with this value (Table 3*a*). When comparing these distances in complexes in which S-containing amino acid is involved, Hg—S (dithiocarbamate) is long (Table 3*b*), probably due to the very close Hg---S contacts present in this compound. The chelating function of the ligand made the angle S—C—S, 117.5, smaller than the ideal value of 120° which was observed in free *N*,*N*-diethyldithiocarbamate (5).

According to the redox potential, *N*,*N*-diethyldithiocarbamate can be oxidized to TETD by Cl_2. It is well known that formation of complexes changes the redox potential of ligands. The presence of two products led us to speculate that CH_3Hg— attacks the S=C group followed by breakage of the S—S bond. It is difficult to rule out the attachment of CH_3Hg— on both S=C

Can. J. Chem. Downloaded from www.nrcresearchpress.com by 210.87.254.5 on 09/05/12
For personal use only.

groups, but attacking on one site is also very likely. There are many possible mechanisms, but a simplified scheme is presented here.

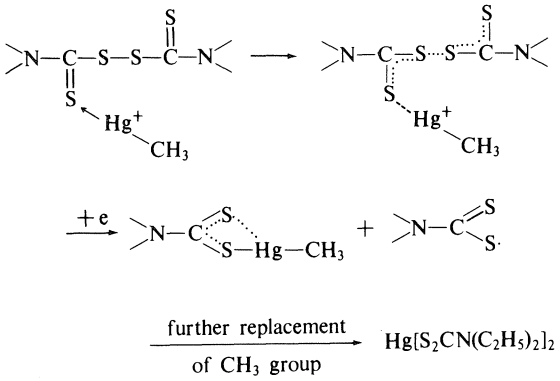

Further mechanistic studies on these reactions are underway. There are many questions unanswered concerning these redox reactions. Reports (11, 12) on these types of studies are not conclusive.

The infrared spectrum of TETD had been discussed by Shankaranarayana and Patel (13), who assigned some characteristic frequencies to a few functional groups. Coleman *et al.* (14) also have done a normal coordinate analysis of vibrational spectra of thiuram sulfides. The spectra are very difficult to interpret. In the present study, the main interest is the variation of vibration bands of *N*,*N*-diethyldithiocarbamate and disulfide in their interactions with mercury(II) as coordination ligands. The ir and

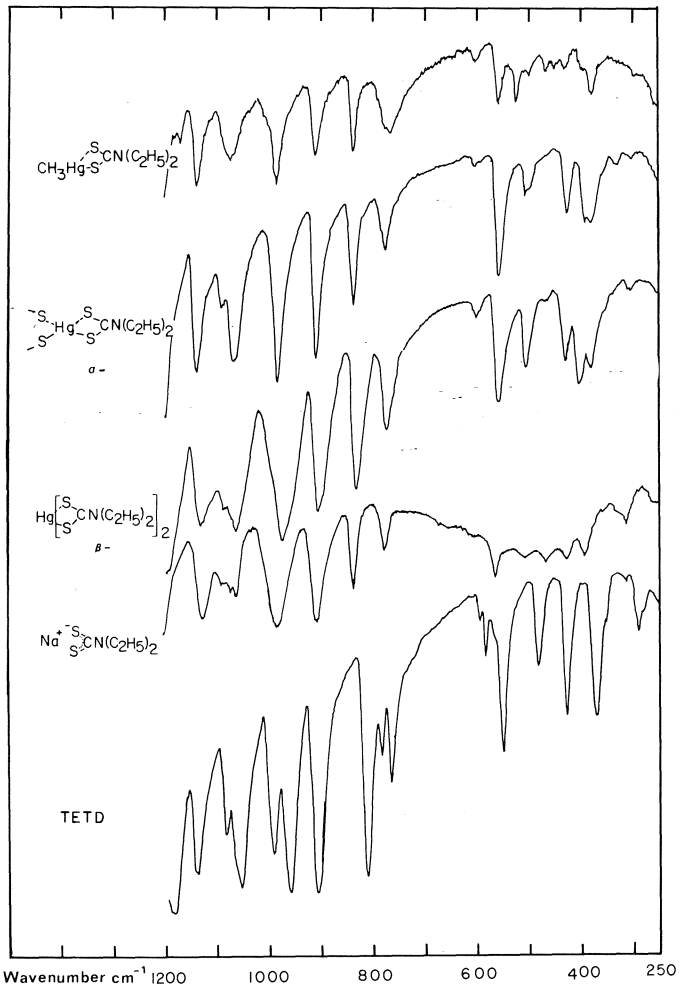

FIG. 3. The ir spectra of methyl *N*,*N*-diethyldithiocarbamato mercury(II) and related compounds.

Can. J. Chem. Downloaded from www.nrcresearchpress.com by 210.87.254.5 on 09/05/12
For personal use only.

Can. J. Chem. Downloaded from www.nrcresearchpress.com by 210.87.254.5 on 09/05/12
For personal use only.

TABLE 4. Vibration spectra of methyl *N*,*N*-diethyldithiocarbamato mercury(II) and related compounds

MeHg-$(S_2CN(C_2H_5)_2)$		α-Hg-$[S_2CN(C_2H_5)_2]_2$		β-Hg-$[S_2CN(C_2H_5)_2]_2$		$Na^+S_2^-CN(C_2H_5)_2$		TETD		Assignment and comments (Refs.)
Raman	Infrared	Raman	Infrared	Raman	Infrared	Raman	Infrared	Raman	Infrared	
1198s	1200s	1195w,br	1199s	1205w,br	1199s	1202w,br	1202m	1200w,br	1190s	
1139m	1139m	1140s	1139m	1145s	1135m	1144s	1127m	1150m	1145s	$\nu_{C-N} + \nu_{C=S} + \delta_{CNC}$ (14)
										Probably due to N—C_2H_5 (16)
1090w		1090vw,sd	1092sd	1098vw,sd		1090w	1090sd	1091w	1089m,sd	Present in O—C—NR_2, O—C—NHR (16)
1080w	1070m,br	1077m	1067m,br	1075m,br	1077w,sd	1071m	1072sd	1075m		but not OC—NH_2 (16)
1057w		1063w			1065w,br	1060w	1060w	1066m	1060s	
1000m	1000w,sd	982m	984s	1006m	1000sd	1007m	985s,br	1002vs	997s	
978m	984s	952m		975m	975s	990w		970s	965vs	$\nu_{C=S}$ (13–15)
918m	910m	901s	908s	907s	907s	908s	906m	903m	910vs	δ_{N-C-S} (13)
836vw	836m	844w	837m	838w	832s	840w	836m	822w	815vs	ν_{C-N} Symmetric of C—N—C moiety (15)
								788w	788w	Due to S—S present only in TETD
770w	765m,br	782w	775m	789w	774m	800w	776m	772w	769	ν_{C-N} (15)
605w	600w	601w,br	600w,br	604m	600w,br	608m		604w	595	
560m	568m	560s	558m	567s	559m	564vs	565m	568s,sd	585m 565sd	C—N in-plane deformation (15)
								556vs	550s	ν_{S-S} (13–15)
528vs	522m									ν_{Hg-CH_3}
		516w	506w	522w	505m			510w		
450m	448w					470w,br	466vw	487w	482m	$\nu_{S-S} + \delta_{S=C-S} + \delta_{CSS}$
431w	429w	436s	425w	436s	430m	436s	427vw	436s	430s	
				400m	400br	400vw	391w	370m	370s	$_{C=S}$ deformation (14)
380m	378	374m	390m,br	380m	390m,db	356m		351m	312w	
315w		336w		340m		312m	311w	300m	290m	
295w				300m	300w,br	228sd		264vw	280w	

NOTE: s = strong, w = weak, v = very, db = doublet, sd = shoulder, br = broad, m = medium.

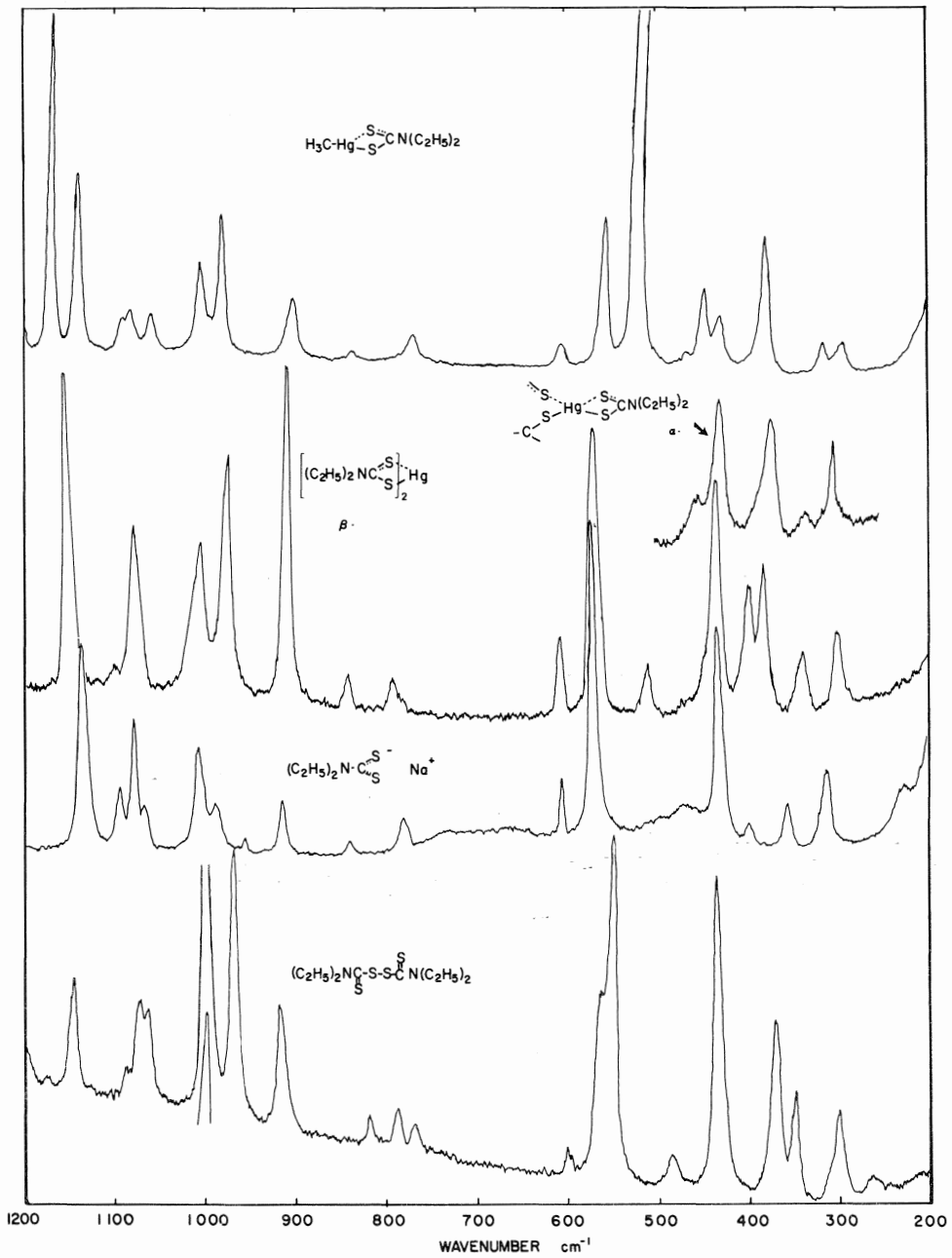

FIG. 4. The Raman spectra of methyl *N*,*N*-diethyldithiocarbamato mercury(II) and related compounds.

Raman spectra of methyl *N*,*N*-diethyldithiocarbamato mercury(II) and related compounds are shown in Figs. 3 and 4. A list of frequencies corresponding to these diagrams are given in Table 4. Some features are noted. (*i*) There are two strong bands at 1002 and 970 cm^{-1} (997 and 965 in ir) due to C=S in the spectra of TETD. These bands become medium intense in all complexes and weak in sodium *N*,*N*-diethyldithiocarbamate. However, the ir spectra show only one peak ($\sim$1000 cm^{-1}) in the complexes and sodium salt. This may be due to the delocal-

Can. J. Chem. Downloaded from www.nrcresearchpress.com by 210.87.254.5 on 09/05/12
For personal use only.

ization of the double, C=S, bond. These bands were also shown (14) to be due to a combination of ν_{C-N} and $\nu_{C=S}$, though the contribution from ν_{C-N} may be small. (*ii*) The assignment of δ_{N-C-S} to the band at $\sim 900\ cm^{-1}$ was given in ref. 13. Two weak Raman bands between 765 and 844 cm^{-1}, which become rather strong in the ir, can be assigned to ν_{C-N} of the C—N—C moiety (15), and the weak band at 788 cm^{-1}, which is absent in spectra other than TETD, is due to the S—S linkage. In addition, the strong band at 556 (550 in ir) is due to ν_{S-S}. (*iii*) A very strong band at 528 cm^{-1} in Raman and medium in ir is definitely ν_{Hg-CH_3}. Similar frequencies 538–550 cm^{-1} are also observed in methylmercury complexes with S-containing amino acids (17). (*iv*) The assignments in the range of 250–450 cm^{-1}, however, are very difficult. Coleman *et al.* gave all kinds of composite combinations for bands in these regions (14).

Acknowledgments

This work is supported by the National Research Council of Canada. We also want to thank Dr. S. Y. Tang for measuring the Raman spectra and for helpful discussions.

1. P. C. Jocelyn. Biochemistry of the SH group. Academic Press, New York. 1972.
2. N. J. Taylor, Y. S. Wong, P. C. Chieh, and A. J. Carty. J. Chem. Soc. Dalton Trans. 438 (1975).
3. H. Iwasaki. Acta Crystallogr. Sect. B, **29**, 2115 (1973).
4. International Tables for X-ray Crystallography. Vol. III. Kynoch Press, Birmingham. 1962. p. 201.
5. M. Colapietro, A. Domenicano, and A. Vaciago. J. Chem. Soc. Chem. Commun. 572 (1968).
6. I. L. Karle, J. A. Estlin, and K. Britts. Acta Crystallogr. **22**, 273 (1967).
7. M. Bonamico, G. Mazzone, A. Vaciago, and L. Zambonelli. Acta Crystallogr. **19**, 898 (1965).
8. M. Bonamico, L. Jorelli, A. Vaciago, and L. Zambonelli. J. Chem. Soc. A, 1351 (1968).
9. Y. S. Wong, P. C. Chieh, and A. J. Carty. Can. J. Chem. **51**, 2597 (1973).
10. Y. S. Wong, N. J. Taylor, P. C. Chieh, and A. J. Carty. J. Chem. Soc. Chem. Commun. 625 (1974).
11. V. Jamminen and E. Hjeh. Suom. Kemistil. B, **23**, 39 (1950).
12. R. M. Golding, C. M. Harris, K. J. Jessop, and W. C. Tennant. Aust. J. Chem. **25**, 2567 (1972).
13. M. L. Shankaranarayana and C. C. Patel. Spectrochim. Acta, **21**, 95 (1965).
14. M. M. Coleman, J. L. Koenig, J. K. Shelton. J. Polym. Sci. Polym. Phys. Ed. **12**, 1001 (1974).
15. F. R. Dollish, W. G. Fateley, and F. Bentley. Characteristic Raman frequencies of organic compounds. John Wiley and Sons, New York. 1974. p. 125.
16. C. N. R. Rao. Chemical application of infrared spectroscopy. Academic Press, New York. 1963.
17. Y. S. Wong. Ph.D. Thesis. University of Waterloo, Waterloo, Ontario. 1975.

Can. J. Chem. Downloaded from www.nrcresearchpress.com by 210.87.254.5 on 09/05/12
For personal use only.

Dielectric and nuclear magnetic resonance characterization of unstable clathrate hydrates of acetaldehyde and propionaldehyde[1]

D. W. DAVIDSON, S. R. GOUGH, AND J. A. RIPMEESTER
Division of Chemistry, National Research Council of Canada, Ottawa, Canada K1A 0R9

Received May 10, 1976

D. W. DAVIDSON, S. R. GOUGH, and J. A. RIPMEESTER. Can. J. Chem. **54**, 3085 (1976).

Sub-MHz dielectric absorption at low temperatures is used to demonstrate the formation by acetaldehyde and propionaldehyde of unstable clathrate hydrates, probably of type II. This result is supported by the proton nmr line shapes of propionaldehyde enclathrated in D_2O, which also show fast rotational tunnelling of the methyl group at 4 K.

D. W. DAVIDSON, S. R. GOUGH et J. A. RIPMEESTER. Can. J. Chem. **54**, 3085 (1976).

On utilise l'absorption diélectrique à des frequences inférieures de MHz, à des températures basses pour démontrer la formation par l'acétaldéhyde et le propionaldéhyde de clathrates instables d'hydrate probablement de type II. Ce résultat est suggéré par la forme des raies en résonance magnétique nucléaire du proton du propionaldéhyde sous forme de clathrate dans le D_2O qui montre aussi une rotation rapide par tunnel du groupe méthyle à 4 K.
[Traduit par le journal]

Can. J. Chem. Downloaded from www.nrcresearchpress.com by 210.87.254.105 on 09/05/12
For personal use only.

Following upon earlier work, Cohen and van der Horst observed (1) in 1938 that isotropic crystals believed to be a cubic form of ice were "almost always" formed when water was added to liquid acetaldehyde, acetone, or propionaldehyde which was cooled to below −20 °C. Acetone has since been found (2, 3) to form a stable cubic clathrate hydrate of von Stackelberg's structure II (4) (*Fd3m*, a = 17.16 Å at −38 °C), which decomposes incongruently at −19.8 °C (5). The question arises whether the "cubic ice" formed in the presence of the aldehydes, and found by Cohen and van der Horst to transform into hexagonal ice in a period of hours, may be attributed to the formation of unstable aldehyde clathrates. We have looked for the features characteristic of enclathrated aldehyde molecules in the dielectric relaxation and wide-line nmr behavior of aldehyde–water systems at low temperatures.

Dielectric measurements (6) were made at frequencies between 1 Hz and 1 MHz and at temperatures down to 4.2 K. Clathrate hydrates of polar molecules are known (7) to exhibit in this frequency range dielectric absorption at very low temperatures associated with reorientation of the guest molecules. Acetone hydrate, for example, shows a broad region of absorption which passes through a maximum at 10 kHz and 22 K (6). The presence of similar absorption in the aldehyde–water systems should provide an unequivocal indication of enclathration, since no other dielectric absorption process at such low temperatures appears to be possible in these systems.

Dielectric samples were prepared by a variety of methods, including that of Cohen and van der Horst (1). Generally, liquid aldehyde and water were cooled to 0 °C, mixed, and added to the precooled cell, which was then slowly cooled to a much lower temperature. Compositions ranged from about 1 to 20 moles of water per mole of aldehyde.

The absorption and dispersion curves given in Figs. 1 and 2 are typical of the results obtained at temperatures below 70 K. The magnitudes, but not the dependence on temperature and frequency, varied with the composition and thermal history of the sample. Although the ϵ' and ϵ'' values obtained are not numerically characteristic of the pure aldehyde hydrates, their frequency and temperature dependence are similar to those of other well-substantiated clathrate hydrates (6, 7) and clearly show the presence of substantial quantities of enclathrated aldehyde molecules in the heterogeneous samples studied. The temperature of maximum absorption at 10 kHz and the activation energy obtained from the temperature dependence of the frequency of maximum absorption for the

[1]NRCC No. 15450.

Can. J. Chem. Downloaded from www.nrcresearchpress.com by 210.87.254.105 on 09/05/12
For personal use only.

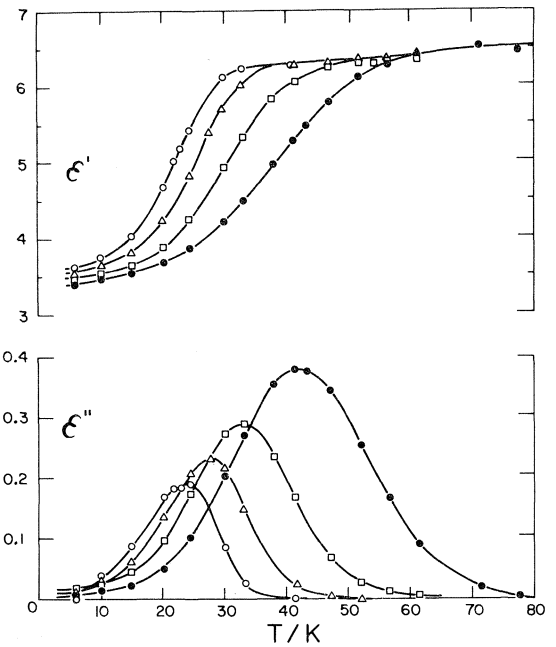

FIG. 1. Dielectric absorption and dispersion in an acetaldehyde–water sample prepared according to ref. 1 with crystals separated by filtration and pressed into a disc. Frequencies are ○ 1 Hz, △ 100 Hz, □ 10 kHz, ● 1 MHz.

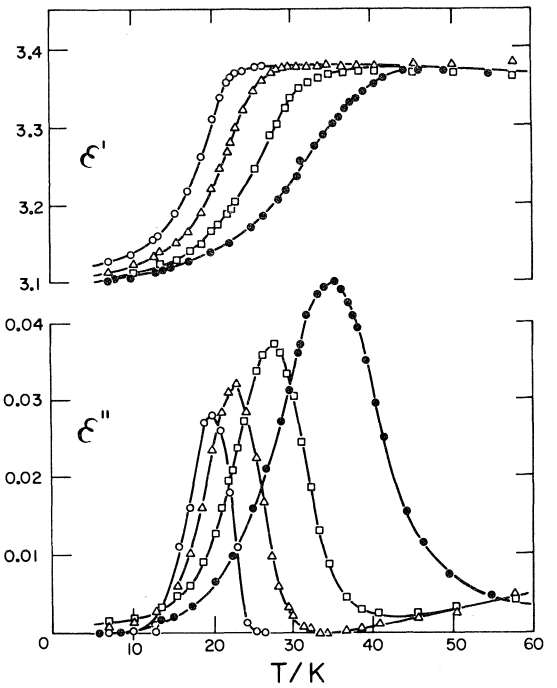

FIG. 2. Absorption and dispersion measured for a sample of overall composition $CH_3CH_2CHO \cdot 4H_2O$. Frequencies as in Fig. 1.

aldehyde hydrates are compared with corresponding values for other clathrate hydrates, all of structure II, in Table 1.

Derivative proton magnetic resonance line shapes were recorded (10) at temperatures between 4 and 240 K for a sample of composition $CH_3CH_2CHO \cdot 20D_2O$ prepared in a sealed tube from precooled freshly-distilled propionaldehyde and D_2O, alternately shaken with a Vortex mixer and cooled to about −30 °C, until the whole mass had solidified. The sample was conditioned for ~1 h and then stored under liquid nitrogen.

The nmr spectra obtained for this sample showed that practically all the propionaldehyde was incorporated in the D_2O clathrate.[2] Figure 3 shows the temperature dependence of the second moment of the proton absorption and derivative line shapes recorded at two temperatures. Below 20 K the experimental derivative curve has the shape expected for encaged propionaldehyde

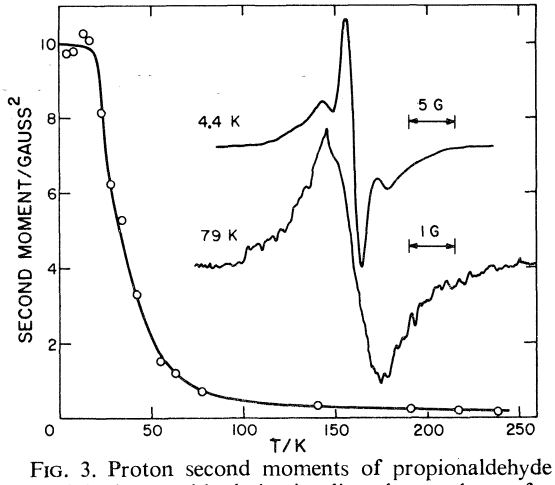

FIG. 3. Proton second moments of propionaldehyde deuteriohydrate, with derivative line shapes shown for two temperatures.

which contains a rotating (strictly, fast tunnelling) CH_3 group. To the extent that the six-proton spectrum of propionaldehyde may be described by a superposition of the individual polycrystalline spectra of CH_3, CH_2, and CHO group protons, each broadened by inter-group

[2]The amount of propionaldehyde giving rise to a very narrow liquid line near 200 K amounted to no more than a few percent.

TABLE 1. Dielectric absorption by encaged molecules

Compound	Temp. of max. abs. at 10 kHz (K)	Activation energy (kcal/mol)	Reference
Acetaldehyde	32.1	1.34	This work
Propionaldehyde	27.7	1.23	This work
Acetone	21.9	1.02	6
Trimethylene oxide	14.1	0.41	6
Tetrahydrofuran	24.2	0.91	6
Cyclobutanone	35.4	1.44	6
Isoxazole	23.9	1.25	8
p-Dioxane	39.7	1.72	9

and inter-molecular local fields, one expects a strong central line and derivative *extrema* near $\Delta H = \pm\alpha$, as observed. The latter correspond to peaks in the polycrystalline absorption, which extends from $-\alpha$ to 2α and -2α to α both for the two components of the rigid CH_2 spectrum (11) and for two of the three components of the rotating (12) or fast tunnelling (13) CH_3 spectrum. Here α is $3\mu/(2r^3)$, where μ is the proton magnetic moment and r is the intra-group proton separation, nearly the same for CH_2 and CH_3 protons (14). The central line is contributed by the third component of the CH_3 spectrum and by the CHO proton.

At low temperatures the experimental second moment of 10.0 G^2 agrees with the calculated value of 9.6 G^2, which includes a dominant intra-molecular contribution of 9.2 G^2 evaluated for the *cis* form of propionaldehyde (14), with rotation of the CH_3 group taken into account (15, 16). With increasing temperature the second moment (Fig. 3) falls to 5 G^2 at about 33 K and thereafter falls with increasing slowness over a wide temperature range, a characteristic common to many other clathrate hydrates (17). By 216 K the moment has reached 0.15 G^2, close to the value expected for isotropic reorientation of guest molecules in a cage whose symmetry has become effectively tetrahedral as a result of averaging over the sufficiently rapid reorientation of the D_2O molecules (10).

Nuclear magnetic resonance spectra of comparable quality were not obtained for acetaldehyde deuteriohydrate.

Both acetaldehyde (maximum van der Waals diameter 5.8 A) and the *cis* rotamer of propionaldehyde (6.5 Å) lie within the 5.5 to 6.6 Å size range of molecules which typically form clathrate hydrates of structure II (18). The larger *gauche* form of propionaldehyde (6.9 Å), which is less stable in the gas than the *cis* form by about 900 cal/mol (14), appears to be too large for normal enclathration.

Measurements of the time dependence of the magnitude of the low-temperature dielectric absorption and of the shape of the nmr spectrum showed, in confirmation of Cohen and van der Horst, the hydrates to be thermodynamically unstable. Thus, the absorption by encaged propionaldehyde fell by 60% after standing for 6 days at −80 °C, while acetaldehyde absorption fell by 12% after 6 days at −75 °C and by a further 60% after 4 days at −55 °C. On the other hand, the relatively small ratio of the number of protons present in the liquid and hydrate phases shown by the $CH_3CH_2CHO \cdot 20D_2O$ nmr sample increased by only ~85% after 7 days at −46 °C and the amount of deuteriohydrate present fell by only a few percent. These observations may be reasonably explained by the time-dependent conversion of free aldehyde into *gem*-diol: $RCHO + H_2O \rightarrow RCH(OH)_2$. This reaction has been extensively studied above 0 °C (19) and the equilibrium amount of free aldehyde found to drop sharply as the temperature falls. The rate of diol formation is strongly acid-catalyzed and is therefore much slower for freshly-distilled aldehyde (as in the nmr sample above) than for aldehyde containing acid resulting from oxidation by air.

We conclude that acetaldehyde and *cis*-propionaldehyde form structure II hydrates which are thermodynamically unstable with respect to *gem*-diol and ice, but which may be preserved indefinitely at liquid nitrogen temperature.

Can. J. Chem. Downloaded from www.nrcresearchpress.com by 210.87.254.105 on 09/05/12
For personal use only.

Acknowledgement

The assistance of R. E. Hawkins is gratefully acknowledged.

1. E. Cohen and C. J. F. van der Horst. Z. Phys. Chem. **B40**, 231 (1938).
2. A. S. Quist and H. S. Frank. J. Phys. Chem. **65**, 560 (1961).
3. G. J. Wilson and D. W. Davidson. Can. J. Chem. **41**, 264 (1963).
4. M. von Stackelberg and H. R. Müller. Z. Elektrochem. **58**, 25 (1954).
5. B. Morris and D. W. Davidson. Can. J. Chem. **49**, 1243 (1971).
6. S. R. Gough, R. E. Hawkins, B. Morris, and D. W. Davidson. J. Phys. Chem. **77**, 2969 (1973).
7. S. R. Gough and D. W. Davidson. *In* Physics and chemistry of ice. *Edited by* E. Whalley *et al.* Roy. Soc. Canada, Ottawa. 1973.
8. S. R. Gough, S. K. Garg, J. A. Ripmeester, and D. W. Davidson. Can. J. Chem. **52**, 3193 (1974).
9. S. R. Gough, J. A. Ripmeester, and D. W. Davidson. Can. J. Chem. **53**, 2215 (1975).
10. S. K. Garg, D. W. Davidson, and J. A. Ripmeester. J. Magn. Reson. **12**, 295 (1974).
11. G. E. Pake. J. Chem. Phys. **16**, 327 (1948).
12. E. R. Andrew and R. Bersohn. J. Chem. Phys. **18**, 159 (1950).
13. F. Apaydin and S. Clough. J. Phys. C, **1**, 932 (1968).
14. S. S. Butcher and E. B. Wilson, Jr. J. Chem. Phys. **40**, 1671 (1964).
15. H. S. Gutowsky and G. E. Pake. J. Chem. Phys. **18**, 162 (1950).
16. V. V. Moskalev. Sov. Phys. Solid State, **3**, 2218 (1962).
17. S. K. Garg and D. W. Davidson. *In* Physics and chemistry of ice. *Edited by* E. Whalley *et al.* Roc. Soc. Canada, Ottawa. 1973. p. 56.
18. D. W. Davidson. *In* Water: a comprehensive treatise. Vol. 2. *Edited by* F. Franks. Plenum Press, New York. 1973. p. 115.
19. R. P. Bell. Adv. Phys. Org. Chem. **4**, 1 (1966); R. P. Bell and J. C. Clunie. Trans. Faraday Soc. **48**, 439 (1952).

Can. J. Chem. Downloaded from www.nrcresearchpress.com by 210.87.254.105 on 09/05/12
For personal use only.

The photochemistry of 2-furaldehyde vapour. I. Photophysical processes: phosphorescence excited in the $\pi^* \leftarrow$ n transition[1]

A. GANDINI,[2] P. A. HACKETT,[3] AND R. A. BACK

Division of Chemistry, National Research Council of Canada, Ottawa, Canada K1A 0R6

Received March 31, 1976

A. GANDINI, P. A. HACKETT, and R. A. BACK. Can. J. Chem. **54**, 3089 (1976).

A search was made for emission from 2-furaldehyde, following excitation in the first two absorption bands. Only phosphorescence from the $^3n\pi^*$ state was observed. The pressure dependence of the lifetime and quantum yield of this emission was determined, as well as that of the quantum yield of intersystem crossing. A mechanism involving self-quenching of excited triplet 2-furaldehyde is proposed.

A. GANDINI, P. A. HACKETT et R. A. BACK. Can. J. Chem. **54**, 3089 (1976).

On a excité le 2-furfural dans ses deux premières bandes d'absorption afin d'étudier son émission. On a observé seulement de la phosphorescence de l'état $^3n\pi^*$. On a determiné l'influence de la pression sur le temps de vie et le rendement quantique de cette émission aussi bien que sur le rendement quantique du croisement intersystème. On propose un mécanisme qui considère l'auto-piégeage de l'état de triplet du 2-furfural.

Can. J. Chem. Downloaded from www.nrcresearchpress.com by 210.87.254.5 on 09/05/12
For personal use only.

Introduction

The photochemistry of furan derivatives has been the subject of several papers by Srinivasan and co-workers; 2-furaldehyde was among the compounds studied, but only from the point of view of its general behaviour in photodecomposition (1). There is no report in the literature dealing with the photophysics of 2-furaldehyde despite its interesting structure with mixed 'aromatic-dienic' properties, and the existence of two rotational isomers (2). The great ease with which this aldehyde suffers resinification reactions under a wide variety of conditions has probably discouraged such studies. However, furaldehyde is adequately stable if properly purified and handled, although its vapour pressure in the temperature range in which it can be used without the danger of thermal resinification is rather low.

This report deals with a thorough search for emission excited in both transitions known in the near ultraviolet spectrum of 2-furaldehyde and with a quantitative study of the only emission detected, *viz.* phosphorescence from its lowest triplet.

[1]NRCC No. 15459.

[2]Visiting Scientist from Centro Nacional de Investigaciones Científicas, Habana, Cuba, 1973. Present address as above.

[3]NRCC Postdoctoral Fellow, 1972–1974. Present address as above.

Experimental

Materials

Commercial 2-furaldehyde (BDH) was treated with activated charcoal and with sodium carbonate to remove some of the resinous and acidic impurities. It was then twice distilled under reduced pressure in a stream of nitrogen, generous head and tail portions being discarded in each fractionation. The final middle portion was collected over CaH_2 and transferred to the vacuum line where it was submitted to four bulb-to-bulb distillations. The final product was stored in the dark at room temperature, its purity was checked periodically by glc. No impurities were detected, confirming previous findings about the stability of 2-furaldehyde under these conditions (3). Pure hexafluoroacetone was available in these laboratories from previous studies. Biacetyl was purified as described (4). All other gases were best-grade commercial products free from quenching impurities.

Apparatus

A standard mercury-free vacuum line was used to transfer gases to the emission cell. Pressures were measured either with a quartz spiral gauge or an MKS Baratron capacitance manometer. 2-Furaldehyde is strongly adsorbed on glass and equilibration usually required about 1 h. The temperature of the cell was controlled by circulating water from a thermostat. The quartz cell (15 cm long) was provided with Suprasil windows of 4 cm diameter.

Phosphorescence decay curves were obtained using the apparatus shown in Fig. 1. Phosphorescence excited by a 2 mJ pulse of 337 nm radiation from a nitrogen laser (FWHM = 5 ns) was detected by an EMI 6256 photomultiplier which viewed the cell at right angles to the laser beam. A saturated solution of sodium nitrite was interposed between the photomultiplier and the cell to reduce scattered laser light. This solution was replaced by a Bausch and Lomb 33-86-07 monochromator in experi-

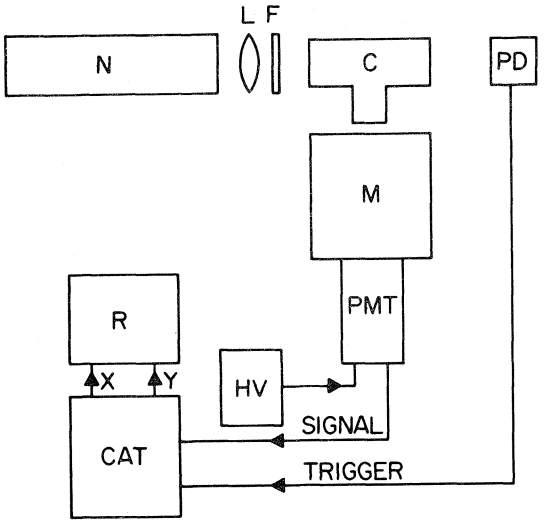

FIG. 1. Apparatus to measure phosphorescence decay curves: N, nitrogen laser; L, lens; F, glass filter; C, temperature controlled cell; PD, RCA 935 photodiode; M, monochromator; HV, Fluke 412 B High Voltage Power Supply; CAT, Hewlett Packard 5480A Memory Display; R, Hewlett Packard 7044A X, Y recorder.

ments in which the emission spectra were determined.

The photomultiplier dynode chain was wired for fast pulse response with capacitors on the last 5 dynodes; the load resistance was varied to give the system a time response of $\leq 1/10$ of the decay time of the emission being detected. The photo current was averaged over 128 laser pulses by a HP 5480A signal averager which was triggered by a pulse from an RCA 935 diode viewing the transmitted laser radiation. The averaged photocurrent-*vs.*-time curve was then printed on an *X–Y* recorder.

Relative quantum yields of emission were obtained using the steady state emission apparatus described previously (4). These were converted to absolute quantum yields by actinometry using the phosphorescence of hexafluoroacetone (4) and biacetyl (5) as standards.

The search for short-lived emission was carried out using a time-resolved single photon counting apparatus.

Results

Absorption Spectra

Several authors have studied the ultraviolet absorption spectrum of 2-furaldehyde and recently Zwarich and Rabinowitz (6) have given a thorough analysis of its first two major electronic transitions. Figure 2 shows the strong $\pi^* \leftarrow \pi$ transition recorded with low resolution. The weak $\pi^* \leftarrow$ n transition can also be observed in the gas phase (Fig. 3) and in non-polar solutions. In polar solutions and with ultrathin, liquid 2-furaldehyde, this band is shifted to shorter wavelengths and merges into the red end of the strong $\pi^* \leftarrow \pi$ absorption.

Observation of Emission

Excitation of the $\pi^* \leftarrow \pi$ transition produced no detectable emission even in the presence of as much as 1000 torr of C_4F_{10} or CO_2. The upper limit of the emission quantum yield for this system can be estimated as 10^{-5}. Excitation of the $\pi^* \leftarrow$ n transition produced long-lived emission which was totally quenched by 0.5 torr of butadiene or 2 torr of oxygen. No short-lived emission could be detected despite a most careful search involving a wide range of 2-furaldehyde pressures and addition of inert gases. The quantum yield of fluorescence from this system

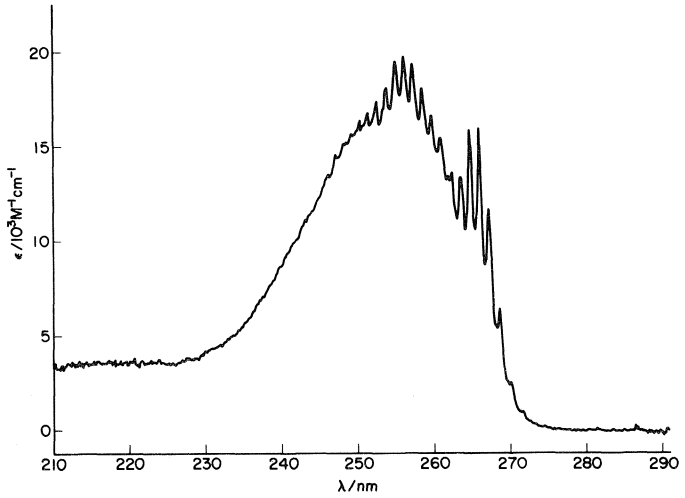

FIG. 2. $\pi^* \leftarrow \pi$ absorption band of 2-furaldehyde vapour taken with low resolution.

Can. J. Chem. Downloaded from www.nrcresearchpress.com by 210.87.254.5 on 09/05/12
For personal use only.

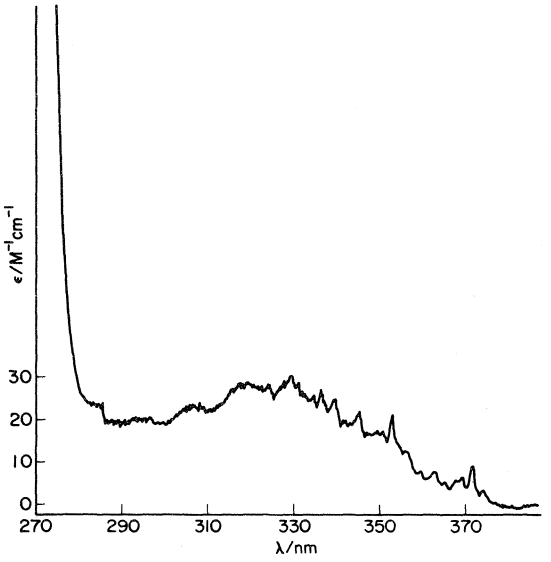

FIG. 3. $\pi^* \leftarrow$ n absorption band of 2-furaldehyde vapour taken with low resolution.

must be lower than 10^{-6}. The present study was thus limited to the only measurable emission, namely the phosphorescence excited in the $\pi^* \leftarrow$ n transition.

Phosphorescence Decay Curves

Phosphorescence decay curves of 2-furaldehyde showed two components, both exponential, a short-lived component whose lifetime was pressure dependent and a long-lived component whose lifetime was independent of pressure. The emission spectrum of each of the two components was obtained at a 2-furaldehyde pressure of 1.0 torr by analysing the semilogarithmic plots of the emission intensity against time. These plots were linear at longer times (2–10 ms after the pulse), always corresponding to a lifetime of 1.45 ms. The integrated intensity of the long-lived emission was calculated from the extrapolated values of the emission intensity at zero time. These plots were then used to correct the phosphorescence intensity in the time range 0–2 ms. Semilog plots of the corrected intensity of the short-lived emission then gave the lifetime of the decay, and extrapolation to zero time permitted the calculation of the integrated intensities.

This operation was repeated at 25 nm intervals in the range 400–600 nm, and the two spectra obtained are shown in Fig. 4. It was found that the relative intensity of the long-lived emission

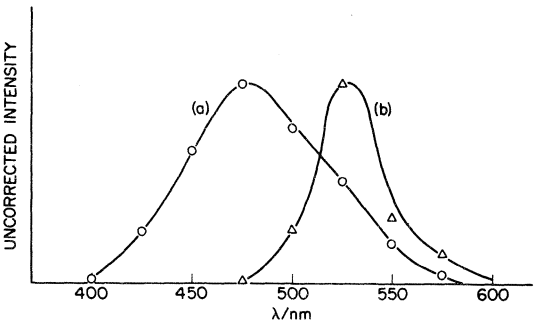

FIG. 4. Emission spectra of $^3n\pi^*$ 2-furaldehyde (*a*) and of quenching impurity (*b*). The intensity of (*b*) was the lower the purer the 2-furaldehyde used.

changed from sample to sample indicating that this emission was not intrinsic to 2-furaldehyde. Thus, crude, degassed 2-furaldehyde showed a large predominance of long-lived emission, whilst with purified 2-furaldehyde the short-lived emission predominated. Some clues to the origin of the long-lived emission can be seen in Fig. 5, which shows a series of decay curves taken at 525 nm, the maximum of the spectrum of the long-lived emission, at various pressure of *crude* 2-furaldehyde. There is an obvious pressure-dependent rise time to this emission indicating that this emitting species is formed from what gives short-lived, pressure-dependent emission. We interpret this behaviour as evidence for the presence of an impurity which efficiently quenches excited 2-furaldehyde to form an excited triplet state which phosphoresces with a high quantum yield.

Attempts to identify the impurity by glc and distillation failed, but pumping on purified 2-furaldehyde at room temperature reduced the contribution of the long-lived emission to less than 5% of the total emission intensity. Samples of 2-furaldehyde from three different sources[4] and samples of α-deutero-2-furaldehyde and 2-thiophene-carboxyaldehyde exhibited a similar impurity phosphorescence. A rough calculation shows that less than 1 part in 10^4 of an impurity capable of quenching furaldehyde triplet with a rate constant of 2×10^{10} M^{-1} s^{-1} and a triplet state emission yield of 0.2 would be sufficient to give an emission intensity equal to that from 2-furaldehyde itself, without contributing significantly to the observed 2-furaldehyde triplet decay rate.

[4]BDH, Merck and Fisher.

Can. J. Chem. Downloaded from www.nrcresearchpress.com by 210.87.254.5 on 09/05/12
For personal use only.

Can. J. Chem. Downloaded from www.nrcresearchpress.com by 210.87.254.5 on 09/05/12
For personal use only.

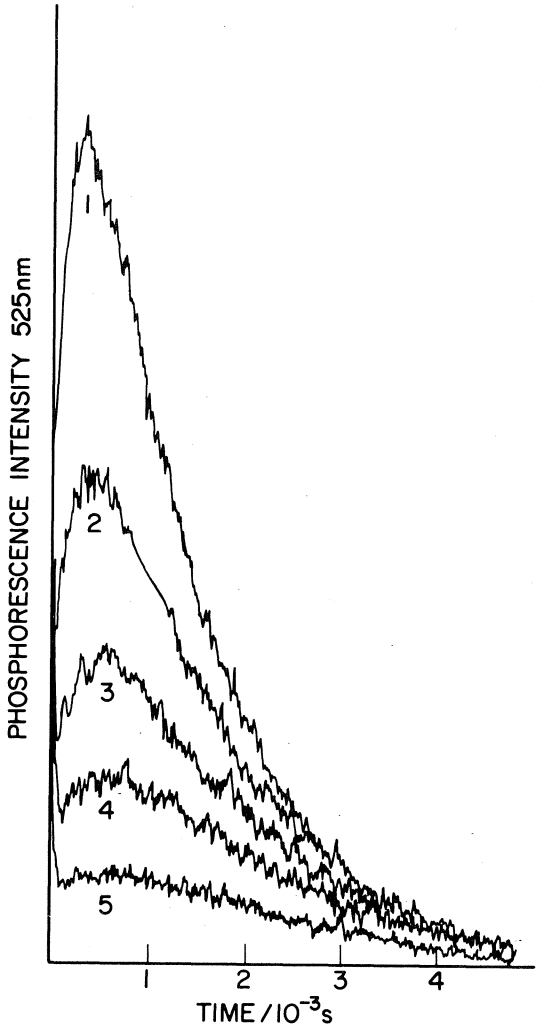

FIG. 5. Phosphorescence decay traces taken at 525 nm, as a function of 2-furaldehyde pressure: (*1*), 1.25 torr; (*2*), 0.89 torr; (*3*), 0.66 torr; (*4*), 0.47 torr; (*5*), 0.27 torr

In all the results and discussion which follow, we will be concerned only with the short-lived emission which is presumed to be from the $\pi^* \leftarrow$ n triplet state of 2-furaldehyde. The contribution of the long-lived emission was minimized to less than $\sim 1\%$ by careful purification of 2-furaldehyde and by monitoring the emission at 475 nm.

Phosphorescence Lifetimes

Figure 6 shows the pressure dependence of the phosphorescence decay time at 475 nm, measured at three different temperatures.

Quantum Yields of Phosphorescence

Figure 7 shows the variation of the quantum yield of phosphorescence as a function of 2-furaldehyde pressure at 22 °C. These data were measured at 475 nm. Experiments using steady state illumination showed that the quantum yield of phosphorescence was independent of excitation wavelength in the range 313–366 nm over the same pressure range.

Quantum Yields of Intersystem Crossing

The intensity of biacetyl phosphorescence sensitized by triplet 2-furaldehyde excited at 325 nm was compared with that of biacetyl phosphorescence induced by direct excitation at 420 nm. The quantum yields of intersystem crossing as a function of 2-furaldehyde pressure were calculated assuming completely efficient triplet energy transfer to biacetyl (4) and the results are given in Table 1.

Discussion

Excitation of the $\pi^* \leftarrow \pi$ Transition

The absence of emission excited in the $\pi^* \leftarrow \pi$ transition can be rationalized on the basis of a mechanism involving a rapid singlet $\rightarrow$ triplet $\rightarrow$ vibrationally excited ground-state path as discussed in the following paper (7). This double intersystem crossing must be very efficient both with 2-furaldehyde alone and in the presence of added inert gases. Obviously, molecules excited in this transition did not reach the $\pi^* \leftarrow$ n triplet state in these experiments, as there was no observable phosphorescence. Thus, there is no interaction between the two systems, in marked contrast with benzaldehyde (8).

Excitation of the $\pi^* \leftarrow n$ Transition

The fact that the quantum yield of intersystem crossing is close to unity down to about 0.3 torr (Table 1) coupled with the lack of observable fluorescence suggests a short lifetime (<2 ns) for the $\pi^* \leftarrow$ n singlet state. This fast and efficient intersystem crossing to the triplet manifold is also observed in benzaldehyde (8) and other aldehydes (9).

The recent assertion that a predissociation depletes the excited $n\pi^*$ singlet state of 2-furaldehyde at excitation energies greater than 31 000 cm^{-1} (6) (λ = 323 nm) can now be rejected on the basis of the following pieces of evidence: (*a*) the emission quantum yield is

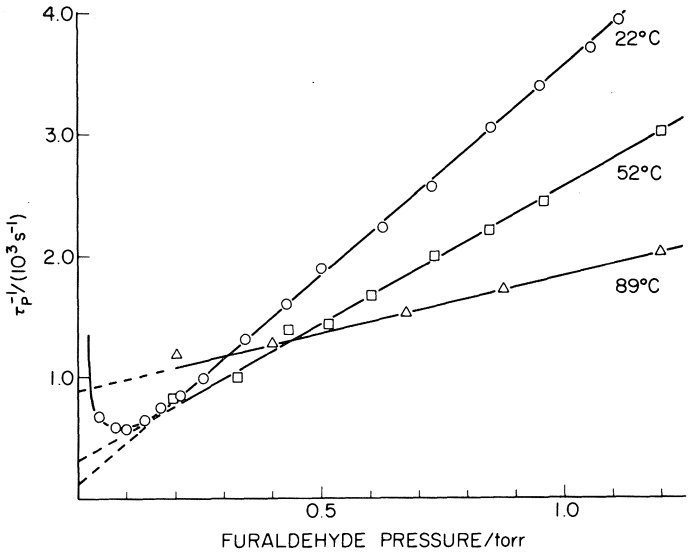

FIG. 6. Dependence of the phosphorescence lifetime on 2-furaldehyde pressure at various temperatures, using N_2 laser excitation (337 nm).

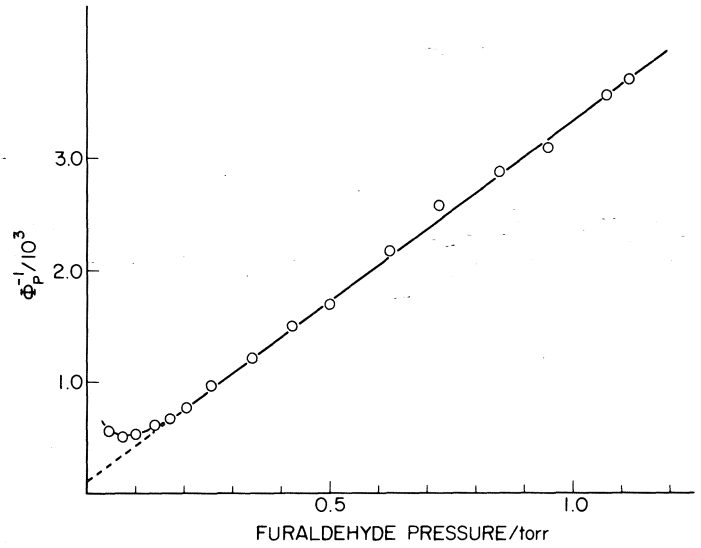

FIG. 7. Dependence of the quantum yield of phosphorescence on 2-furaldehyde pressure at 22 °C, using N_2 laser excitation (337 nm).

independent of excitation wavelength over the range 313 to 366 nm and (*b*) the quantum yield of 2-furaldehyde disappearance is less than 0.06 in the same wavelength range (7). The origin of the diffuseness of the absorption spectrum above 31 000 (6) could be due to an increase of the intersystem crossing rate constant or to crowding in the absorption spectra.

The triplet character of the state responsible for the observed emission is implied by the lifetime and by the sensitivity to oxygen and olefins. The pressure dependence of the emission can be rationalized in terms of the following mechanism:

[0] $$F + h\nu \rightarrow {}^1F \rightarrow {}^3F$$

[1] $$^3F \rightarrow F + h\nu p \qquad k_1$$

Can. J. Chem. Downloaded from www.nrcresearchpress.com by 210.87.254.5 on 09/05/12
For personal use only.

TABLE 1. Quantum yields of intersystem crossing for the $\pi^* \leftarrow$ n system[a]

2-Furaldehyde pressure (torr)	Φ_{ISC}
1.5	1.0
1.0	1.0
0.7	1.0
0.4	0.95
0.2	0.80
0.1	0.67

[a]The biacetyl pressure used was 0.30 torr.

[2] $^3F + F \rightarrow 2F$ k_2

[3] $^3F \rightarrow F$ k_3

Decomposition reactions have been omitted as the measured yield of carbon monoxide formation is only about 0.01 (7). Reaction 2 may include a reaction leading to the formation of the small yields of resin ($\phi \simeq 0.05$) (7) observed in this system.

Deviations from the expected linear Stern–Volmer plots (Figs. 6 and 7) occur below 0.2 torr. In the same pressure region the intersystem crossing quantum yields begin to fall below unity. This behaviour at low pressure could be accounted for by quenching of triplet 2-furaldehyde at the walls or by decomposition of vibrationally excited triplet 2-furaldehyde, initially formed by intersystem crossing, before collisional stabilization can occur. We are unable to distinguish between these two possibilities because determination of decomposition quantum yields at pressures below 0.2 torr is hampered by resin formation on the cell windows (7).

Table 2 lists the values of the rate constants (k_1, k_2, k_3) obtained from Figs. 6 and 7 on the basis of the proposed mechanism, together with the activation energies derived for reactions 2 and 3. Values for k_2 cannot be affected by the presence of the trace impurity responsible for the long-lived emission. Samples of both crude and highly purified 2-furaldehyde gave identical phosphorescence decay curves for the short-lived emission at 475 nm, indicating that quenching by the impurity did not contribute significantly to the observed decay rate of the 2-furaldehyde triplet.

The data obtained indicate that the $\pi^* \leftarrow$ n triplet state of 2-furaldehyde is deactivated

TABLE 2. Kinetic parameters for $^3n\pi^*$ 2-furaldehyde

T (°C)	Parameter	Value
22	k_1	$1.1\ s^{-1}$
	k_2	$6.3\times10^7\ l\ mol^{-1}\ s^{-1}$
	k_3	$1.19\times10^2\ s^{-1}$
52	k_2	$4.6\times10^7\ l\ mol^{-1}\ s^{-1}$
	k_3	$3.1\times10^2\ s^{-1}$ [a]
89	k_2	$2.1\times10^{-7}\ l\ mol^{-1}\ s^{-1}$
	k_3	$8.9\times10^2\ s^{-1}$ [a]
	E_2	-3.7 kcal mol^{-1}
	E_3	6.3 kcal mol^{-1}

[a]Neglecting small contribution from k_1.

efficiently to the ground state ($\phi > 90\%$). An interesting result is the negative activation energy for k_2. This suggests that the quenching reaction proceeds through a weakly-bound exciplex with an appreciable lifetime which decomposes reversibly as the temperature is increased:

[4] $$^3F + F \rightleftharpoons FF^* \begin{cases} \xrightarrow{5\%} \text{Resin} \\ \xrightarrow{95\%} F + F \end{cases}$$

The low collision efficiency of 10^{-4} which may be estimated from k_2 is in accord with such a mechanism.

Acknowledgements

We wish to thank Dr. J. Sarjeant of the Division of Physics, and Dr. D. Rayner of the Division of Biology for aid in the construction of the nitrogen laser.

1. H. HIRAOKA and R. SRINIVASAN. J. Chem. Phys. **48** 2185 (1968).
2. F. MOENNIG, H. DREIZLER, and H. D. RUDOLPH. Z. Naturforschg. **21***a*, 1633 (1966).
3. N. GALEGO and A. GANDINI. Revista CNIC (Cuba), **6**, 163 (1975).
4. A. GANDINI and K. O. KUTSCHKE. Proc. Roy. Soc. A**306**, 511 (1968).
5. G. M. ALMY and P. R. GILLETTE. J. Chem. Phys. **11**, 188 (1943).
6. R. ZWARICH and I. RABINOWITZ. J. Chem. Phys. **63**, 4565 (1975).
7. A. GANDINI, J. M. PARSONS, and R. A. BACK. Can. J. Chem. This issue.
8. M. BERGER, I. L. GOLDBLATT, and C. STEEL. J. Am. Chem. Soc. **95**, 1717 (1973).
9. J. C. DALTON, M. W. GEIGER, and J. J. SNYDER. J. Am. Chem. Soc. **98**, 398 (1976).

Can. J. Chem. Downloaded from www.nrcresearchpress.com by 210.87.254.5 on 09/05/12
For personal use only.

The photochemistry of 2-furaldehyde vapour. II. Photodecomposition: direct photolysis at 253.7 and 313 nm and Hg($^3P_1$)-sensitized decomposition[1]

A. GANDINI,[2] J. M. PARSONS, AND R. A. BACK
Division of Chemistry, National Research Council of Canada, Ottawa, Canada K1A 0R6

Received March 31, 1976

A. GANDINI, J. M. PARSONS, and R. A. BACK. Can. J. Chem. **54**, 3095 (1976).

The photolysis of furaldehyde vapour at 253.7 nm, 65 °C, and pressures from about 0.2 to 7 torr, produces CO, propyne, allene, furan, cyclopropene, CO_2, and C_2H_2. The quantum yield of CO approaches 2 at low pressure and decreases towards zero with increasing pressure of furaldehyde or added CO_2. Yields of the other products also decrease but show a more complex pressure dependence. A mechanism involving excited furaldehyde and excited C_4H_4O and C_3H_4 intermediates is suggested.

The Hg($^3P_1$)-photosensitized decomposition gives products very similar to those of the direct photolysis. Photolysis at 313 and 366 nm also leads to similar products but in much lower yields, with the major product, CO, having a quantum yield of about 0.01. Some photopolymerization was observed in all systems.

A. GANDINI, J. M. PARSONS et R. A. BACK. Can. J. Chem. **54**, 3095 (1976).

La photolyse du 2-furfural en phase vapeur à 253.7 nm et 65 °C dans le rang de pression 0.2–7 torr produit CO, propyne, allène, furanne, cyclopropène, CO_2 et C_2H_2. Le rendement quantique en CO tend à 2 aux faibles pressions et decroit vers zero quand on augmente la pression de furfural ou on ajoute CO_2. Les rendements des autres produits decroissent aussi mais leur comportement en fonction de la pression est plus complexe. On propose un mecanisme basé sur la formation d'intermédiares excités du furfural, du C_4H_4O et du C_3H_4.

La décomposition photosensibilizée au Hg($^3P_1$) montre un comportement très semblable à celui de la photolyse directe. La photolyse à 313 et 366 nm donne aussi les mêmes produits mais avec des rendements beaucoup plus faibles; le rendement du produit plus important, CO, est d'environ 0.01. Dans tous les systemes on observe de la photopolymerization.

Introduction

The photochemistry of 2-furaldehyde has been studied before only very briefly by Hiraoka and Srinivasan (1), who observed CO, furan, propyne, cyclopropene, and allene to be products. In the preceding paper (Part I) measurements of the phosphorescence of furaldehyde excited in the weak $\pi^* \leftarrow$ n absorption band (300–380 nm) have been reported (2). Careful experiments with excitation in the much stronger $\pi^* \leftarrow \pi$ absorption band (220–280 nm) showed no detectable light emission. The present photodecomposition studies in both absorption regions were undertaken to complement the photophysical measurements, and in particular to measure accurate quantum yields and to examine the pressure dependence of the photolysis. A brief study of the mercury-photosensitized decomposition was also made for comparison.

Experimental

Apparatus

The photolysis was studied in a cylindrical quartz cell, 5 cm in diameter and 30 cm long, fitted with plane quartz windows. Liquid furaldehyde, purified as previously described (2), was stored in a reservoir cooled by tapwater which could be warmed to give the desired vapour pressure as required. Pressure was measured with a quartz spiral gauge. These components were attached through metal valves to a small manifold and the entire assembly was enclosed in a heated air thermostat held at 65 °C. Pressures of 2-furaldehyde up to about 7 torr were used; higher pressures and temperatures above 65 °C led to excessive thermal decomposition and resin formation. From the heated manifold a valve led to a conventional vacuum line for evacuation, gas handling, and analysis.

Analysis

Gases noncondensable at −196 °C (CO, H_2, and CH_4) were removed through a U-trap cooled in liquid nitrogen, measured in a gas burette, and analysed by gas chromatography. In experiments with added CH_4, noncondensable gases were pumped away without measurement or analysis. Condensable products were removed through a trap held at −23 °C, which retained most of the furaldehyde, and were analysed by gas chromatography, using a 3-m column of 20% Ucon oil on Chromosorb-P held at 30 °C. In experiments with added CO_2, only the noncondensable gases were measured.

---

[1]NRCC No. 15460.

[2]Visiting Scientist from Centro Nacional de Investigaciones Científicas, Habana, Cuba, 1973. Present address as above.

Can. J. Chem. Downloaded from www.nrcresearchpress.com by 210.87.254.105 on 09/05/12
For personal use only.

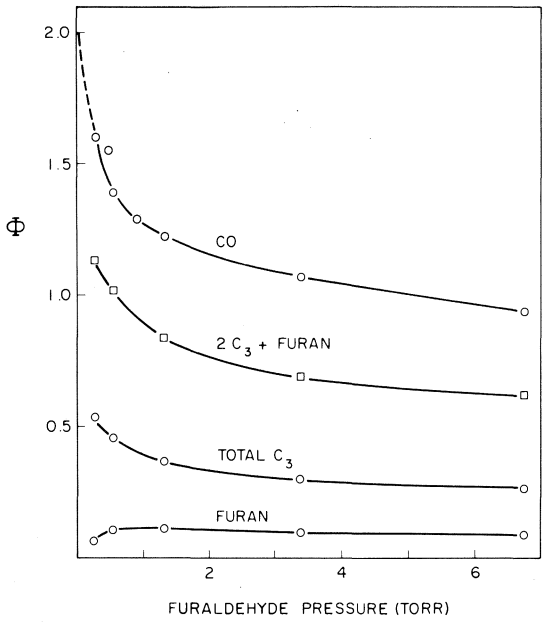

FIG. 1. Quantum yields of major products at 253.7 nm as a function of 2-furaldehyde pressure.

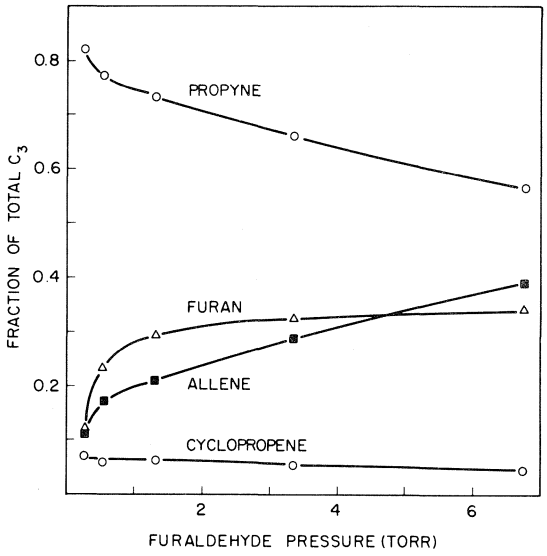

FIG. 2. Quantum yields of propyne, furan, allene, and cyclopropene, relative to total C_3-hydrocarbons, as a function of 2-furaldehyde pressure, at 253.7 nm.

Light Sources

A medium-pressure Hanovia S-500 mercury arc was used with appropriate filter solutions (3) to isolate 366, 313, and 253.7 (reversed) nm radiation. Light intensity incident on the reaction vessel was about 1×10^{-8}, 3×10^{-11}, and 5×10^{-10} einstein/s at 366, 313, and 253.7 nm, respectively. A Pen Ray lamp (Ultraviolet Products Inc.) was used as a source of 253.7 nm radiation in the mercury-photosensitized experiments. The light absorbed in each experiment was determined by measurements of transmitted light intensity by a photocell after examination with a 0.5 m grating monochromator had shown that the light sources were essentially monochromatic.

Results

Direct Photolysis at 253.7 nm

Products of the photolysis were CO, propyne, allene, furan, cyclopropene, CO_2, and acetylene, in approximately decreasing order of importance. Some resin was also formed and blank experiments showed H_2 was produced by photolysis of the resin; H_2 was definitely not a product of the photolysis of 2-furaldehyde vapour. Acetylene and CO_2 appeared to be genuine photolysis products, but very minor ones, with low and irregular quantum yields (about 0.02 and 0.01 respectively). Quantum yields of CO, total C_3-hydrocarbon, and furan are shown in Fig. 1 as a function of furaldehyde pressure, while Fig. 2 shows the relative yields of propyne, allene, cyclopropene, and furan from the same experiments, expressed as fractions of the total C_3-hydrocarbon. Quantum yield measurements were complicated by resin deposition on the vessel windows during the photolysis. The values shown are based on a number of careful measurements of CO yields, alternated with acetone actinometry (3) runs at closely matched optical densities, with relative light intensities monitored throughout with the photocell. 2-Furaldehyde pressure and photolysis time were kept low to minimize resin formation. Quantum yields of all other products were then measured relative to that of CO, or were related to CO yields through measurements of absorbed light intensity. Absolute quantum yields reported are probably accurate to $\pm 10\%$, while relative values are considerably less uncertain. All yields were observed to be approximately independent of photolysis time, and thus presumably are initial yields of primary products of the photolysis.

Figure 3 shows the effect of added CO_2 on the yields of CO, while Figs. 4 and 5 show the effect of added CH_4 on the yields of the condensable products.

The Mercury-photosensitized Decomposition

Products of the decomposition were the same

Can. J. Chem. Downloaded from www.nrcresearchpress.com by 210.87.254.105 on 09/05/12
For personal use only.

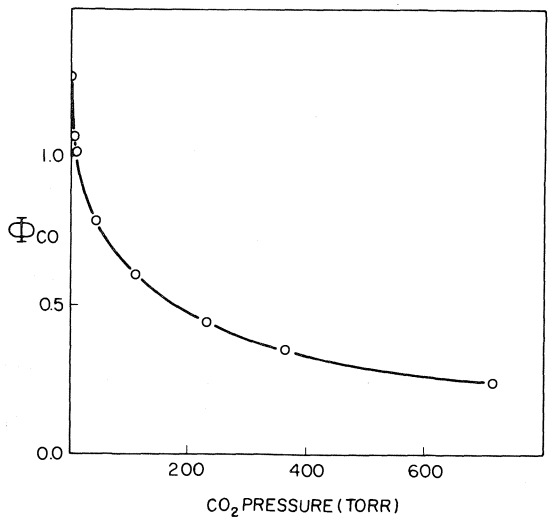

FIG. 3. Quantum yield of CO at 253,7 nm as a function of added CO_2. 2-Furaldehyde pressure 1.01 torr.

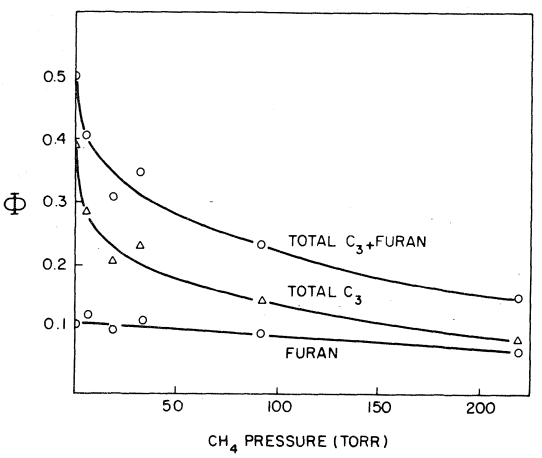

FIG. 4. Quantum yields of condensable products at 253.7 nm, as a function of added methane. 2-Furaldehyde pressure 1.01 torr.

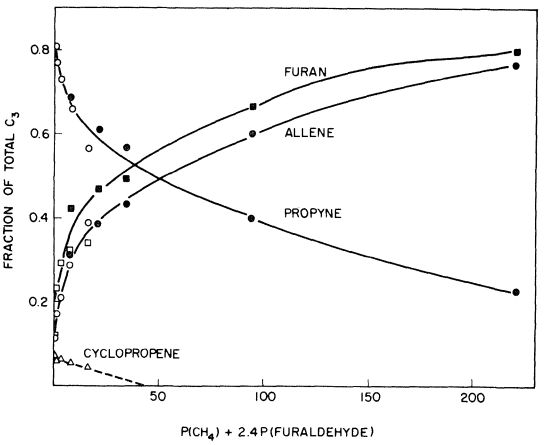

FIG. 5. Quantum yields of condensable products, relative to total C_3-hydrocarbons, as a function of added methane, at 253.7 nm. Open symbols: 2-furaldehyde alone; black symbols: 1.01 torr of 2-furaldehyde + methane.

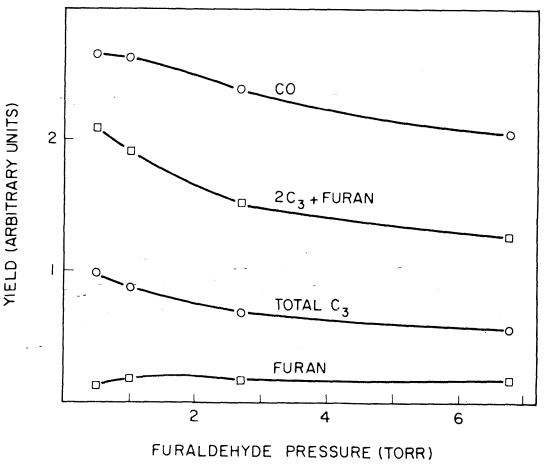

FIG. 6. Relative quantum yields of products of the $Hg(^3P_1)$-sensitized decomposition as a function of 2-furaldehyde pressure.

as those from the direct photolysis. Absolute quantum yields were not measured. Figure 6 shows relative yields of CO, total C_3-hydrocarbon, and furan as a function of 2-furaldehyde pressure. Figure 7 shows yields of propyne, allene, cyclopropene, and furan relative to the quantum yield of CO. The dashed lines show comparable data for yields of propyne and furan from the direct photolysis at 253.7 nm.

Direct Photolysis at 313 and 336 nm

Products of the photolysis were the same as those formed at 253.7 nm, but quantum yields were very much smaller. Low yields and weak absorption of light made long experiments necessary, and appreciable accumulation of resin on the windows made measurements difficult. A quantum yield of CO of about 0.01 at 313 nm with about 1 torr of 2-furaldehyde was estimated, using azomethane actinometry. Careful checks of the chromatic purity of the light source were made to ensure that the photolysis observed was indeed caused by 313 nm radiation and not by a minor component of shorter wavelength which would be much more strongly

Can. J. Chem. Downloaded from www.nrcresearchpress.com by 210.87.254.105 on 09/05/12
For personal use only.

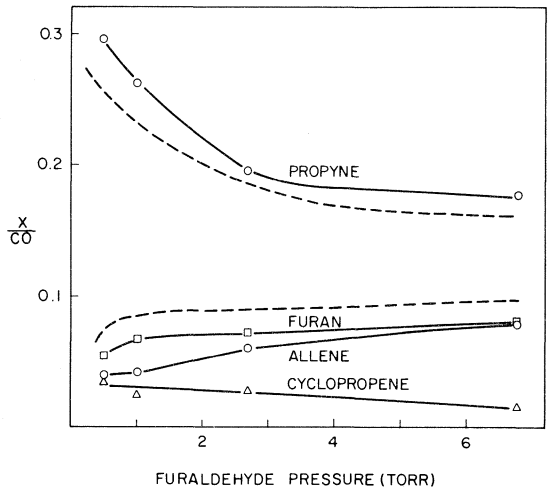

FIG. 7. Quantum yields of propyne, furan, allene, and cyclopropene, relative to the quantum yield of CO as a function of 2-furaldehyde pressure in the $Hg(^3P_1)$-sensitized decomposition. Dashed lines refer to data from photolysis at 253.7 nm.

absorbed and much more effective in causing photolysis. The CO produced was found to be proportional to the optical density at 313 nm, accurately measured with a narrow-band monochromator, and the reported quantum yield of CO of 0.01 thus appears to be genuine. The other products at 313 nm were formed in yields relative to CO approximately similar to those found at 253.7 nm, but the small amounts made accurate measurements impossible.

Brief measurements of CO yields at 366 nm showed that these were probably somewhat lower than at 313.

The quantum yield of furaldehyde consumption was measured using a broad excitation covering practically the whole of the $\pi^* \leftarrow n$ transition (310 to 370 nm). Benzaldehyde vapour was used as an actinometer (4) and the rate of disappearance of the two aldehydes was followed spectrophotometrically, monitoring the decrease in optical density of the $\pi^* \leftarrow \pi$ band. With 0.8 to 1.3 torr the value of Φ_{-F} obtained was 0.06 ± 0.01 in five determinations at 30 °C. Thus the quantum yield of resin formation must be about 0.05 in these conditions. The structure of the resin was studied briefly: its uv spectrum closely resembles that of furaldehyde; its ir spectrum shows strong absorptions corresponding to conjugated carbonyl groups, hydroxyl groups and bands typical of the furan ring. Prolonged photolysis of the resin gave CO, CO_2, and H_2 as products.

Discussion

Direct Photolysis at 253.7 nm

The products observed are similar to those found by Hiraoka and Srinivasan (1), but there are notable quantitative differences. Our value of $\Phi(CO)$ is 200 times larger than theirs measured in the same wavelength region, and cyclopropene is a much smaller fraction of the present hydrocarbon products than in the earlier work. The cause of the discrepancy in the CO yield is not clear, but the deposition of resin on the cell windows combined with the low pressure of 2-furaldehyde vapour could have led to an overestimate of the light absorbed in the gas phase in the earlier study. Another difference is the lack of carbon balance in the present data. This is seen in Fig. 1 where the sum of $2C_3$ + furan is between 65 and 75% of the CO; Hiraoka and Srinivasan found these quantities to be about equal in the direct photolysis, with a surplus of CO in the mercury-photosensitized decomposition.

The direct photolysis at 253.7 nm can be interpreted in terms of the following mechanism (where F = 2-furaldehyde)

[1] $F + h\nu \rightarrow F^* \rightarrow \cdots \rightarrow F^\#$

[2a] $F^\# \rightarrow C_4H_4O^* + CO$

[2b] $F^\# \rightarrow C_3H_4^* + 2CO$

[2c] $F^\# + M \rightarrow F + M$

[2d] $F^\# + F \rightarrow \text{Resin}$

[3a] $C_4H_4O^* \rightarrow C_3H_4^* + CO$

[3b] $C_4H_4O^* + M \rightarrow \text{Furan} + M$

[3c] $C_4H_4O^* + F \rightarrow \text{Resin}$

[4a] $C_3H_4^* \rightarrow \text{Propyne, cyclopropene}$

[4b] $C_3H_4^* + M \rightarrow \text{Allene} + M$

[4c] $C_3H_4^* + F \rightarrow \text{Resin}$

F^* in reaction 1 is the $\pi^* \leftarrow \pi$ singlet state, while $F^\#$ represents the excited state or states of 2-furaldehyde which decompose to yield the photolysis products. Some deductions may be drawn about the identity of $F^\#$. It is evident from Fig. 1 that appreciable collisional quenching of $F^\#$ occurs even at pressures below 1 torr of 2-furaldehyde, implying a relatively long lifetime,

Can. J. Chem. Downloaded from www.nrcresearchpress.com by 210.87.254.105 on 09/05/12
For personal use only.

Can. J. Chem. Downloaded from www.nrcresearchpress.com by 210.87.254.105 on 09/05/12
For personal use only.

yet no fluorescence was observed, even though the $\pi^* \leftarrow \pi$ transition is a strong one with $\epsilon_{max} \simeq$ 20 000. The diffuse character of the absorption spectrum (5), and the lack of fluorescence (2), both indicate a very short lifetime for F*, and it is clear that $F^{\#}$ cannot be the $\pi^* \leftarrow \pi$ singlet state. At high pressure the yield of CO tends towards zero (Fig. 3), which appears to rule out even a small fraction of fast decomposition of F*. The lack of light emission from the system also appears to eliminate the $\pi^* \leftarrow$ n singlet and triplet states, which might be populated by rapid intersystem crossing, as intermediates leading to decomposition, as formation of these species is known to lead to phosphorescence under approximately the same conditions as the present experiments (2). The short lifetime of F* is most plausibly accounted for by fast intersystem crossing to the $\pi^* \leftarrow \pi$ triplet state, and to investigate the role of the triplet state in the decomposition, photolyses were carried out with O_2 added at several pressures up to 37 torr. Yields of all products were reduced, but product ratios were almost unchanged and the reduction in yields was only about half that produced by an equivalent pressure of 2-furaldehyde. Oxygen thus lay between 2-furaldehyde and CO_2 in its efficiency in quenching the decomposition, and if $F^{\#}$ were a triplet state, much more efficient quenching might have been expected. On the other hand, the close similarity of the direct photolysis to the mercury-photosensitized decomposition, which very probably involves excitation of the triplet state, suggests a common precursor. The most reasonable explanation would appear to be that the direct photolysis does proceed through the $\pi^* \leftarrow \pi$ triplet state, but that this in turn crosses rapidly to the high vibrational levels of the ground state; in the mercury-photosensitized decomposition, the triplet state would be populated directly and would suffer a similar fate. Reaction 1 should then be written as

$$F + h\nu \xrightarrow{\text{fast}} {}^1F \xrightarrow{\text{fast}} {}^3F \xrightarrow{\text{fast}} F^{\#}$$

where ^1F and ^3F are the $\pi^* \leftarrow \pi$ singlet and triplet states respectively, and $F^{\#}$ is the vibrationally excited ground state from which decomposition occurs.

The quantum yield of CO appears to extrapolate to a value near 2 at zero pressure (Fig. 1),

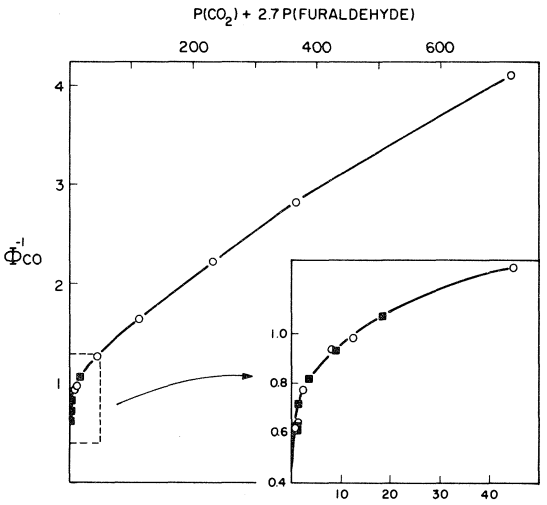

FIG. 8. Stern–Volmer plot for the quantum yield of CO at 253.7 nm. ■: 2-furaldehyde alone; ○: 1.01 torr of furaldehyde + CO_2.

suggesting that reaction 2*b* and the sequence [2*a*] + [3*a*] become quantitative as the 'deactivation' processes ([2*c*], [2*d*], [3*b*], [3*c*]) become negligible in the low-pressure limit. The CO yield falls steadily as total pressure is increased, reaching its lowest value of 0.25 at the highest pressure employed (Fig. 3). The deactivation reaction, 2*c*, must be invoked to account for most of this decrease; reaction 3*b* could only lead to a maximum decrease of about 0.1, the maximum yield of furan observed. The steady decrease in Φ(furan) and in the sum of Φ(furan) + Φ(total C_3) (Fig. 4), is further evidence for the importance of reaction 2*c*. A simple Stern–Volmer plot of Φ^{-1}(CO) *vs.* pressure, shown in Fig. 8, exhibits pronounced curvature, especially at low pressure. The inset shows the initial portion of the curve where the data for pure 2-furaldehyde overlap with those with added CO_2. The normalization factor 2.7 was found to give the best combined fit for the two sets of data, *i.e.*, 2-furaldehyde is 2.7 times more effective than CO_2 in reducing the yield of CO. The curvature in Fig. 8 again indicates that more than one deactivation step is involved in the supression of CO production.

The absolute yield of furan reaches a maximum value at quite a low pressure, about 1 torr of 2-furaldehyde. At this pressure it can be argued that the increase in furan due to stabilization of $C_4H_4O^*$ by reaction 3*b* is just balanced

Can. J. Chem. Downloaded from www.nrcresearchpress.com by 210.87.254.105 on 09/05/12
For personal use only.

by the decrease in formation of $C_4H_4O^*$ due to loss of its precursor, $F^\#$, in reactions 2*c* and 2*d*. The low value of the maximum quantum yield of furan, 0.1, implies that $F^\#$ is much more easily deactivated than $C_4H_4O^*$. It is seen from Fig. 5 that even at high pressure furan did not completely replace the C_3-hydrocarbons in the products, which implies that not all the C_4H_4O precursors of the C_3's can be deactivated to yield furan. For this reason reaction 2*b* is postulated, yielding C_3-hydrocarbons directly from $F^\#$ by a route which does not permit stabilization of a C_4H_4O intermediate to produce furan. Furan yields approached a high-pressure limit of about 80% of the total C_3, indicating that reaction 2*b* is 1.25 times faster than reaction 2*a*. It would seem reasonable to suggest that reaction 2*a* is a simple molecular elimination of CO (Norrish Type III), yielding furan in its ground state, but highly excited vibrationally. The $C_4H_4O^*$ which disappears in reactions 3*a*, 3*b*, and 3*c* could be the same excited furan, or alternatively could be an —O—CH=CH—CH=CH— biradical formed by ring opening. Reaction 3*b* would thus be either simple deactivation of excited furan, or ring closure following deactivation of the biradical. The decomposition reaction 3*a* would presumably proceed through the biradical in either case, with hydrogen migration and loss of CO. The mechanism of reaction 2*b* also deserves comment; one interesting possibility is the ring contraction suggested by Hiraoka and Srinivasan (1) by analogy with furan, followed by rapid successive elimination of two molecules of CO:

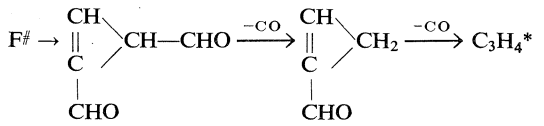

There is no positive evidence for a cyclopropene intermediate in the present system, and the relatively low yields of cyclopropene, *decreasing* with increasing pressure, perhaps weigh against it. The pressure dependence of the distribution of C_3H_4 hydrocarbons (Fig. 5) suggests that the $C_3H_4^*$ species formed in reactions 2*b* and 3*a* is an excited allene molecule, which at low pressure decomposes to propyne or cyclopropene and at high pressure is stabilized as allene.

If CO, furan, and C_3H_4 hydrocarbons were the only products of the photolysis, CO should

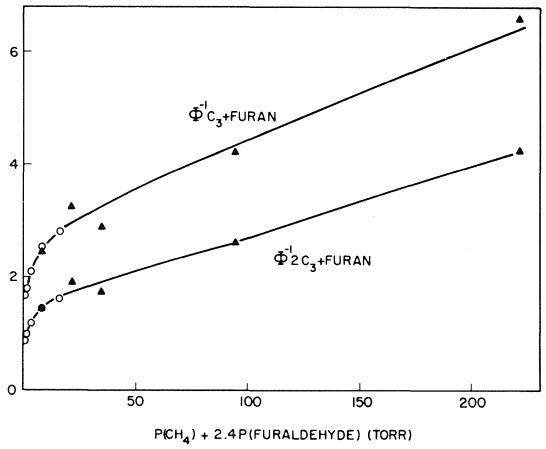

FIG. 9. Stern–Volmer plot for the quantum yield of condensable products at 253.7 nm. ○: 2-furaldehyde alone; ▲: 1.01 torr of 2-furaldehyde + methane.

be equal to furan + $2C_3H_4$. It is clear from Fig. 1 that this is not so; furan + $2C_3H_4$ varies from about 75% of the CO at the lowest pressure to about 65% at the highest. The observation of resin in the reaction cell suggests loss of furan or C_3H_4 by addition reactions of their precursors with 2-furaldehyde (reactions 3*c* and 4*c*) leading to higher products or resin. The results give no clue as to which of the two reactions is more important. Reaction 2*d* recognizes the possibility that reactions of excited 2-furaldehyde might also lead to resin formation; this is indistinguishable from reaction 2*c* in the present study. At sufficiently low pressure reactions 2*c*, 3*c*, and 4*c* should become negligible, and Φ(furan) + 2Φ(total C_3H_4) should approach 2. The data in Fig. 1 are compatible with such a limit.

A Stern–Volmer plot of Φ^{-1}(furan + $2C_3H_4$) in Fig. 9 shows marked curvature, similar to that for Φ^{-1}(CO) in Fig. 8. A similar plot of Φ^{-1}(furan + C_3H_4) in Fig. 9 is also curved; if $F^\#$ was always either deactivated by reaction 2*c* or decomposed to yield either furan or a C_3H_4 hydrocarbon, this plot should be linear; the curvature indicates that the system is more complex. A normalization of the data obtained with 2-furaldehyde alone with these from the experiments with added methane (Fig. 9) indicates that 2-furaldehyde is about 2.4 times more effective than methane in suppressing the formation of furan and C_3H_4. In considering the pressure dependence of the photolysis it may be noted that we are postulating three distinct deactivation reactions, 2*c*, 3*b*,

Can. J. Chem. Downloaded from www.nrcresearchpress.com by 210.87.254.105 on 09/05/12
For personal use only.

and 4*b* operating at three stages of the decomposition. In fact, these reactions may not be distinct, inasmuch as partial deactivation of $F^{\#}$ could lead to a less energetic $C_4H_4O^*$ and $C_3H_4^*$ species, and partial deactivation of $C_4H_4O^*$ could give $C_3H_4^*$ with less energy. These possible complications, together with the uncertainty about which reactions lead to resin formation, make it unprofitable to attempt a more quantitative treatment of the pressure dependence.

Finally, the minor products, CO_2 and C_2H_2, have been neglected in the discussion of mechanism. Their yields within a very large uncertainty were independent of pressure, suggesting a rapid but very minor decomposition of F^* directly to $CO_2 + 2C_2H_2$; this suggestion must be regarded as very tentative.

The Mercury-photosensitized Decomposition

As noted before, the products were similar to those of the direct photolysis (Figs. 6 and 7). At first sight the pressure dependence (Fig. 6) appears different; this is almost certainly due to incomplete quenching of $Hg(^3P_1)$ at the lower pressures, and when this is taken into account the pressure dependence is very similar to that of the direct photolysis. The only significant difference in the products is that slightly more propyne and slightly less furan were formed in the mercury-photosensitized reaction (Fig. 7). In discussing the mechanism of the direct photolysis, it was noted that the similarity of the two systems suggests that both proceed through the $\pi^* \leftarrow \pi$ triplet state which probably undergoes rapid internal conversion to a high vibrational level of the ground state from which decomposition occurs. The slight difference in the furan and propyne yields suggests that the decomposing 2-furaldehyde in the mercury-photosensitized system was somewhat more highly excited than that from the direct photolysis, perhaps because the latter has more opportunity for vibrational relaxation.

Direct Photolysis at 313 and 366 nm

Product yields were so low at these wavelengths that little can be deduced about the mechanism of the decomposition. There are severe difficulties in obtaining more quantitative results, chiefly because of resin formation and subsequent secondary photolysis of the resin and light loss at the windows. From the photophysical study it was concluded (2) that the $\pi^* \leftarrow$ n singlet state undergoes rapid intersystem crossing to the corresponding triplet state, which emits light, can be stabilized by collision (or resinify), or can cross to the ground state in a radiationless transition. All these processes are relatively slow, as the lifetime of the triplet state ranged from about 200 to 1500 μs. Decomposition of the triplet or the excited ground state must be extremely slow to account for its low quantum yield. The photochemistry of 2-furaldehyde in the $\pi^* \leftarrow$ n transition thus differs markedly from that in the $\pi^* \leftarrow \pi$. In both cases intersystem crossing to the corresponding triplet states is probably rapid. The $\pi^* \leftarrow \pi$ triplet is short-lived, no light is emitted, and decomposition, probably after crossing to the ground state, approaches an efficiency of unity at low pressure. The $\pi^* \leftarrow$ n triplet on the other hand phosphoresces with a quantum yield approaching 10^{-2} at low pressure, and undergoes little decomposition. The difference is probably due largely to the lower excitation energy of the $\pi^* \leftarrow$ n system.

Acknowledgements

The authors are grateful to Mr. D. Du Tremblay and to Miss. N. Galego who performed some of the photolysis experiments.

1. H. Hiraoka and R. Srinivasan. J. Chem. Phys. **48**, 2185 (1968).
2. A. Gandini, P. A. Hackett, and R. A. Back. Can. J. Chem. This issue.
3. J. G. Calvert and J. N. Pitts. Photochemistry. Wiley, New York. 1966.
4. M. Berger, I. L. Goldblatt, and C. Steel. J. Am. Chem. Soc. **95**, 1717 (1973).
5. R. Zwarich and I. Rabinowitz. J. Chem. Phys. **63**, 4565 (1975).

Activation entropy as a dominant factor in the oxidative addition of some group IV hydrides to an iridium(I) complex

J. P. FAWCETT AND J. F. HARROD

Department of Chemistry, McGill University, P.O. Box 6070, Station A, Montreal, P.Q., Canada H3C 3G1

Received April 26, 1976

J. P. FAWCETT and J. F. HARROD. Can. J. Chem. **54**, 3102 (1976).

The kinetics of the reactions

$$IrH(CO)(PPh_3)_3 + Ph_3MH \rightleftharpoons IrH_2(CO)(PPh_3)_2(MPh_3) + PPh_3$$

have been studied (M = Si, Ge, Sn). All three reactions proceed by predissociation of the iridium complex and concerted *cis* addition of Ph_3MH to the square-planar intermediate. The relative rate of addition of Ph_3MH increases in the order Si (1) < Ge (18) < Sn (70) and the difference in rate within experimental error is due entirely to change in ΔS^*. It is concluded that, for this particular series of oxidative addition reactions, solvation effects related to a change in polarity on passage to the transition state are more important than bond energies, or acid–base properties, in determining relative reaction energetics. The relevance of entropy barriers to the problem of paraffin activation is discussed.

J. P. FAWCETT et J. F. HARROD. Can. J. Chem. **54**, 3102 (1976).

La cinétique des réactions

$$IrH(CO)(PPh_3)_3 + Ph_3MH \rightleftharpoons IrH_2(CO)(PPh_3)_2(MPh_3) + PPh_3$$

ont été étudiées (M = Si, Ge, Sn). Les trois réactions procèdent selon une prédissociation du complexe de l'iridium et une addition *cis* concertée de Ph_3MH à l'intermédiaire plan-carré formé. La vitesse relative de l'addition de PhMH augmente selon l'ordre Si (1) < Ge (18) < Sn (70) et la différence de vitesse en tenant compte de l'erreur expérimentale est due entièrement à un changement dans la valeur de ΔS^*. Il est conclu que, pour cette série particulière de réactions d'addition oxydantes, les effets de solvatation reliés à un changement de polarité en passant à l'état de transition sont plus importants que les énergies des liens ou les propriétés acide–base, pour déterminer les énergies relatives de la réaction. L'importance des barrières d'entropie en rapport avec le problème de l'activation des paraffines est discutée.

[Traduit par le journal]

Can. J. Chem. Downloaded from www.nrcresearchpress.com by 210.87.254.40 on 09/05/12
For personal use only.

Introduction

A previous examination of the kinetics of the oxidative addition of a series of silicon hydrides to hydridocarbonyltris(triphenylphosphine)iridium(I), **1**, led to the conclusion that the activation energy for addition to the reactive intermediate, hydridocarbonylbis(triphenylphosphine)iridium(I), **2**, is little influenced by the nature of the addend (1). Since the energetics of all of the studied oxidative additions to **2** were closely similar to those for addition of triphenylphosphine to **2**, forming **1**, it was further concluded that the activation free energy for all of these processes was dominated by the free energy required for the displacement of the phosphine ligands of **2** towards the positions they occupy in the respective products (1). Such a concept has also been invoked in relation to other oxidative addition reactions (2–4).

The small differences in rate between the additions of phosphine and of the various silicon hydrides to **2** were found to be almost entirely due to differences in activation entropy (1).

The oxidative addition reactions of **1** are particularly useful since they can be studied for a wide range of rate constants by adjusting the amount of free phosphine in the medium. The reaction mechanism in the case of silicon hydrides was shown to be (5):

$$[1] \quad IrH(CO)(Ph_3P)_3 \underset{k_{+P}}{\overset{k_{-P}}{\rightleftharpoons}} IrH(CO)(Ph_3P)_2 + Ph_3P$$

$$[2] \quad IrH(CO)(Ph_3P)_2 + R_3SiH \underset{k_{-Si}}{\overset{k_{+Si}}{\rightleftharpoons}} IrH_2(CO)(Ph_3P)_2(R_3Si)$$

Under conditions of excess phosphine and a high enough concentration of R_3SiH to push

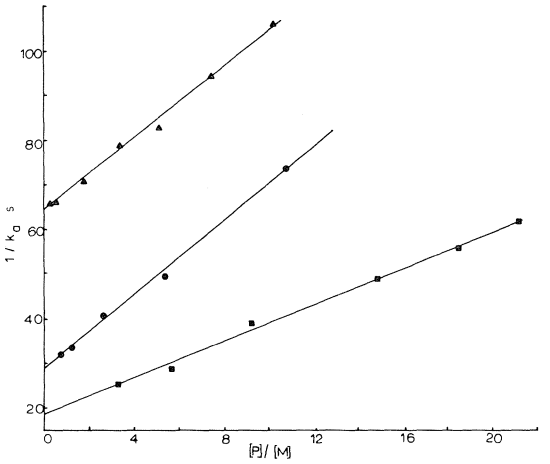

FIG. 1. Plots of $1/k_a$ vs. [P]/[M] for Ph_3GeH at 15.2° (▲), Ph_3SnH at 21.6° (●) and Ph_3SiH at 25.6° (■) (solvent toluene). The abscissa values for Ph_3SiH should be multiplied by 0.01 and those for Ph_3GeH by 0.1.

the reaction to completion, the rate law for these reactions is of the form:

$$[3] \qquad \frac{1}{k_a} = \frac{k_P}{k_{-P}k_{Si}} \cdot \frac{[P]}{[Si]} + \frac{1}{k_{-P}}$$

where k_a is the experimentally observed apparent first order rate constant. Appropriate use of this rate law yields a competition parameter, $K_+ = k_{+P}/k_{+Si}$ and the phosphine dissociation rate constant k_{-P}. The constancy of the latter provides an internal check that different reactions are proceeding by the same mechanism and allows an estimate of the reproducibility of reactions done by different workers with reagents from different sources.

One unfortunate feature of these reactions is that the individual rate constants cannot be separated and hence the activation parameters for several of the individual steps remain unknown.

We now wish to report detailed kinetic parameters for the oxidative addition of the isostructural series Ph_3MH (M = Si, Ge, and Sn) to the complex **1**. We have also measured the kinetic isotope effect for additions of Ph_3SiH and Ph_3SiD to **1**.

Results

The reaction conditions and measured values of k_a are listed in Tables 1–3 for Ph_3SiH (and Ph_3SiD), Ph_3GeH, and Ph_3SiH respectively. The derived values of k_{-P} and K_+ for each reaction and a few overall equilibrium constants, K, are listed in Table 4. In every case plots of $1/k_a$ *vs.* [P]/[M] showed high linearity and k_{-P} remained remarkably constant for a given temperature. It may therefore be safely concluded that the predissociative mechanism depicted in [1] and [2] was applicable in each case.

Some representative plots of $1/k_a$ *vs.* [P]/[M] for Si, Ge, and Sn are shown in Fig. 1. The activation parameters for the various reactions are listed in Table 5.

Discussion

The uniformity and simplicity of the rate law exhibited by the three rather different reagents used in the present work provide strong support for the previously suggested concerted oxidative addition mechanism (1). By 'concerted' we wish to imply a mechanism in which the cleavage of the MH bond and the attachment of the fragments to the Ir occurs by a process which, as far as kinetics is concerned, is a single step. Although this concept encompasses the possibility that M and H do not necessarily become attached to the Ir at the same instant in time, it excludes either homolytic, or heterolytic displacement reactions where Ph_3M or H are completely ejected from the transition complex.

Evidence has been cited to indicate that oxidative addition reactions may proceed by concerted (3, 4), by nucleophilic displacement (6), or by free radical mechanisms (7, 8). It would require an extraordinary set of coincidences for the reactions of Ph_3SiH, Ph_3GeH, and Ph_3SnH to react by a two, or more, step displacement reaction and yet so doggedly follow the rate law depicted in [3]. We shall therefore assume that these reactions are concerted.

A single remarkable fact stands out from the data listed in Tables 4 and 5, namely that the seventyfold increase in rate in going from silicon to tin is entirely due to an entropy effect. Within the framework of the previously proposed mechanism (1) this entropy effect may be accommodated by the hypothesis that the transition state dipole is more effectively dissipated by the more polarizable heavier atoms and the degree of solvent electrostriction is

Can. J. Chem. Downloaded from www.nrcresearchpress.com by 210.87.254.40 on 09/05/12
For personal use only.

TABLE 1. Reaction conditions and values of k_a for reactions of Ph_3SiH and Ph_3SiD[a]

Solvent	Temperature (°C)	$[PPh_3] \times 10^3$ M	$[Ph_3SiH] \times 10^3$ M	$k_a \times 10^4$ s^{-1}
Toluene	10.0	2.2	89	55
		5.5	104	44
		5.5	67	35
		5.4	35	27
		5.5	22	17
Toluene	15.2	2.1	78	118
		5.2	99	91
		5.2	64	83
		5.2	35	59
		5.2	21	42
Toluene	19.9	2.0	76.5	216[b]
		4.9	105	176[b]
		4.9	56	131[b]
		5.0	21	68[b]
		4.9	7	26[b]
Toluene	19.9	2.1	77	220
		5.2	98	180
		5.0	46	132
		5.2	21	76
Toluene	25.6	2.1	63	401
		5.2	91	347
		5.2	56	258
		5.2	35	205
		5.2	28	177
		5.2	24	161
Toluene	30.8	2.1	85	813
		2.2	56	747
		5.4	91	628
		5.4	56	518
		5.3	35	401
CH_2Cl_2	10.2	2.6	92	91
		5.6	107	68
		5.6	38	35
		5.6	23	24
		7.8	15	16
		7.8	7.6	9
CH_2Cl_2	20.6	2.2	85	325
		5.5	99	252
		5.5	35	123
		5.5	21	84
		7.7	14	46
		7.7	7.1	27
CH_2Cl_2	31.1	5.3	103	879
		5.3	37	517
		5.3	22	357
		7.4	15	198

[a]Concentration of $IrH(CO)(PPh_3)_3 = 7.5 \times 10^{-5}$ M.
[b]Data for Ph_3SiD.

Can. J. Chem. Downloaded from www.nrcresearchpress.com by 210.87.254.40 on 09/05/12
For personal use only.

TABLE 2. Reaction conditions and values of k_a for reactions of Ph_3GeH[a]

Solvent	Temperature (°C)	$[PPh_3] \times 10^3$ M	$[Ph_3GeH] \times 10^3$ M	$k_a \times 10^4$ s^{-1}
Toluene	10.0	2.1	86	69
		5.3	29	63
		7.4	22	58
		7.4	14	53
		7.4	7.2	43
Toluene	15.2	2.1	92	152
		5.2	99	151
		5.2	28	142
		7.3	21	127
		7.3	14	121
		5.2	7.0	106
		7.3	7.0	94
Toluene	19.9	5.1	102	266
		5.6	27	246
		7.1	22	234
		13	27	209
		7.1	7.3	173
Toluene	25.6	2.1	86	566
		6.5	100	542
		6.5	29	510
		7.5	21	468
		7.5	14	412
		6.5	7.1	364
		7.5	7.1	330
Toluene	30.8	5.4	94	1010
		5.4	27	967
		7.8	21	904
		7.6	13	768
		5.4	6.7	744
		7.8	6.9	628
CH_2Cl_2	10.2	5.1	98	111
		5.1	35	102
		5.1	21	96
		7.1	7.0	70
		7.1	3.0	52
CH_2Cl_2	20.6	5.3	98	446
		5.3	35	405
		5.3	21	381
		7.4	14	333
		7.4	7.0	267
		7.4	3.4	172
CH_2Cl_2	31.1	5.3	100	1460
		5.3	36	1330
		5.3	21	1260
		7.4	14	1090
		7.4	7.2	819
		7.4	3.4	574

[a]Concentration of $IrH(CO)(Ph_3P)_3 = 7.5 \times 10^{-5}$ M.

Can. J. Chem. Downloaded from www.nrcresearchpress.com by 210.87.254.40 on 09/05/12
For personal use only.

Can. J. Chem. Downloaded from www.nrcresearchpress.com by 210.87.254.40 on 09/05/12
For personal use only.

TABLE 3. Reaction conditions and values of k_a for reactions of Ph_3SnH[a]

Solvent	Temperature (°C)	$[PPh_3] \times 10^3$ M	$[Ph_3SnH] \times 10^3$ M	$k_a \times 10^4$ s^{-1}
Toluene	10.3	5.2	7.5	69
		5.2	4.5	67
		7.3	3.0	54
		7.3	1.5	42
		7.3	0.75	29
		14.6	0.75	16
Toluene	21.6	5.4	7.1	314
		5.4	4.2	300
		7.6	2.8	248
		7.6	1.4	203
		7.6	0.71	136
		15.2	0.71	87
Toluene	31.1	5.3	6.8	1010
		5.3	4.6	940
		7.4	3.1	892
		7.4	1.5	617
		7.4	0.77	408
		10.5	0.77	259
CH_2Cl_2	10.2	5.7	7.5	101
		5.7	4.5	100
		7.9	3.0	89
		7.9	1.5	65
		7.9	0.75	53
		15.9	0.75	32
CH_2Cl_2	20.1	5.4	7.1	384
		5.4	4.3	376
		7.6	2.8	328
		7.6	1.4	262
		7.6	0.71	190
		12	0.71	133
		15	0.71	118
CH_2Cl_2	31.2	6.7	3.4	1245
		7.8	2.7	1202
		7.8	1.3	941
		7.8	0.67	659
		12.2	0.67	490
		15.6	0.67	436

[a]Concentration of $IrH(CO)(PPh_3)_3 = 7.5 \times 10^{-5}$ M.

reduced.[1] It is perhaps worth noting that the isostructural character of the reactants in this series of reactions further pinpoints solvation entropy as the most likely origin of the entropy change differences.

The small positive isotope effect observed for the addition of Ph_3SiD is also consistent with a mechanism in which breaking of the Si—D bond has little influence on the free energy of activation. A similar conclusion was reported for the addition of D_2 to chlorocarbonylbis(triphenylphosphine)iridium(I) (6).

The equilibrium constant K for the overall reaction was too large to measure in the case of Ph_3SnH. That of Ph_3GeH could just be measured within the accessible temperature range of the instrument. Using an extrapolated value of K for Ph_3SiH at 70° of 0.4, it is evident that there is roughly a 1500-fold increase in K on going

[1]There is evidence that the bond moments for Si, Ge, and Sn bonded to transition metal carbonyl moieties increase slightly on descending the group, with a bond polarity $\overset{\delta^+}{M}—\overset{\delta^-}{M'}$ (M′ = Si, Ge or Sn). However, the polarizability increase is much greater (9).

TABLE 4. Derived rate and equlibrium constants

Reactant	Solvent	Temperature (°C)	$k_{-p} \times 10^2$ s^{-1}	$K_+ \times 10^2$	K
Ph_3SiH	Toluene	10.0	0.70	1180	
		15.2	1.48	1020	
		19.9	2.86	1100	6.3
		25.6	5.75	1220	
		30.8	10.4	1060	4.5
		40.0	—	—	2.5
Ph_3SiD	Toluene	19.9	2.94	1400	6.3
Ph_3SiH	CH_2Cl_2	10.2	1.1	1195	
		20.6	5.0	1850	
		31.1	14.5	3000	
Ph_3GeH	Toluene	10.0	0.70	62	
		15.2	1.56	62	
		19.9	2.75	60	
		25.6	5.76	68	
		30.8	10.60	58	
		70.0	—	—	625
Ph_3GeH	CH_2Cl_2	10.2	1.10	64	
		20.6	4.55	71	
		31.1	14.7	74	
Ph_3SnH	Toluene	10.3	0.78	18	
		21.6	3.5	14	
		31.1	11.5	18	
	CH_2Cl_2	10.2	1.1	11	
		20.1	4.4	13	
		31.2	15.6	11	

TABLE 5. Activation parameter differences for reactions of Ph_3MH with $IrH(CO)(Ph_3P)_3$

Reactant	Solvent	$\Delta H^*_P - \Delta H^*_M$ (kcal)	$\Delta S^*_P - \Delta S^*_M$ (eu)
Ph_3SiH	CH_2Cl_2	7 ± 2^a	29 ± 5^a
Ph_3SiH	Toluene	0	4.8^b
Ph_3GeH	CH_2Cl_2 / Toluene	0	-1.0^b
Ph_3SnH	CH_2Cl_2 / Toluene	0	-3.4^b

[a]From an Eyring plot of data in Table 4.
[b]Calculated assuming entire rate difference due to ΔS^*.

from Si to Ge at that temperature (see Table 4). Since the rate of the addition reaction only increases by a factor of 20 on going from Si to Ge, the elimination reaction for Ge must be 75 times slower than for Si. Although product solvation cannot be excluded as the source of the increased stability of the Ph_3GeH adduct ($\Delta G°$ decreased by *ca.* 3 kcal), it seems more likely to us that it is due to a stronger Ir—M bond.

An exception to the general constancy of K_+ for a given addend was found for the reaction of Ph_3SiH in CH_2Cl_2 (Table 4). The increase in K_+ with increasing temperature was much larger than could be accounted for on the basis of experimental error and corresponded to a decrease of ΔH^*_{Si} relative to ΔH^*_P of about 7 kcal. Since the values of K_+ at 10° were the same in CH_2Cl_2 and toluene, the reduction of ΔG^*_{Si} is evidently accompanied by a parallel

Can. J. Chem. Downloaded from www.nrcresearchpress.com by 210.87.254.40 on 09/05/12
For personal use only.

Can. J. Chem. Downloaded from www.nrcresearchpress.com by 210.87.254.40 on 09/05/12
For personal use only.

decrease in $\Delta S^{\ddagger}_{Si}$. The decrease in $\Delta S^{\ddagger}_{Si}$ relative to $\Delta S^{\ddagger}_{P}$ on going from toluene to dichloromethane, and the corresponding decrease in $\Delta H^{\ddagger}_{Si}$ relative to $\Delta H^{\ddagger}_{P}$, are in the opposite sense to that anticipated for an oxidative addition involving a very polar transition state.[2] If one accepts the hypothesis that the observed activation free energies for all of the other addition reactions are mainly a reflection of the energetics of deforming the iridium complex to its transition state geometry, the anomalous behavior of Ph_3SiH in CH_2Cl_2 must be a result of an anomalous solvation energy of the Ph_3SiH relative to Ph_3P, Ph_3GeH, and Ph_3SiH. There is no obvious reason why such an anomaly should occur, and an experimental determination of the relevant solvation energetics is presently under investigation in this laboratory.

Due to a variety of problems it was not possible to study these reactions in solvents of very high polarity. It is worth noting that, although the products remained the same, the kinetic behaviour in dimethylformamide and dimethylacetamide was very complicated and completely different from that in less polar solvents.

The results reported above highlight the dangers of making facile correlations between the reactivity of molecules in oxidative addition reactions and the bond energy of the addends. In particular, the assertion that the frequently observed greater reactivity of stannanes and germanes, relative to silanes, in oxidative addition is due to the differences in the M—H bond energy is clearly untenable in the absense of supporting kinetic evidence (10).

Although the present results offer no precise insights into the problem of activating C—H bonds, they do suggest that entropy factors and solvent effects are likely to be just as important as those of bond energy and the 'basicity' of the metal centre.

The useful activation of paraffins is unlikely to be achieved in organic solvents, or by catalysts containing organic ligands, since the active metal centre is more likely to react with the ligand, or solvent, than with a paraffin substrate. A natural approach to avoiding such problems would be to resort to the use of an inorganic catalyst in an aqueous medium. It is of interest that the only reported examples of catalytic activation of paraffins use such an approach (11, 12). In the case of hydrogen activation by halo-complexes of the group VIII metals in aqueous media, the reactions characteristically exhibit quite favorable entropies of activation, but prohibitive enthalpies (13). Such behaviour is also likely to be manifest in the activation of paraffins. An inherent advantage to this pattern of kinetic behaviour is that enthalpy barriers may, unlike entropy barriers, be countered by resort to higher temperature conditions.

A further manifestation of the effectiveness of reducing the entropy barrier to activation of C—H bonds is the frequent observation of reversible intramolecular oxidative addition of a C—H bond of a coordinated ligand (14). In some such reactions (15), the C—H bond is sufficiently remote from the coordinating centre that it may be assumed that the C—H bond energy is normal and the apparent enhanced reactivity arises mostly from the unimolecularity of the reaction. The saving in activation entropy for a unimolecular as opposed to a bimolecular process results in a reduction in $\Delta G^{\ddagger}$ of about 3 to 4 kcal and, since the molecularity of the reverse reaction remains unchanged, the same reduction in ΔG^{0} for a reversible process. In the case of intramolecular reactions, this reduction in entropy is purchased with the metal-to-ligand bond energy.

Experimental

Reagents

Carbonylhydridotris(triphenylphosphine)iridium(I) was prepared according to a literature procedure (16). The complex was normally freshly prepared and recrystallized prior to a series of measurements since samples several months old, although showing no evidence of decomposition, were found to give erratic results. A single recrystallization of old material restored its purity to a level where consistent kinetic results were obtained.

Triphenylsilane (PCR, Inc) was recrystallized twice from hexane before use and dried under high vacuum. Triphenylgermane, triphenylstannane, and triphenyldeuterosilane were all prepared by reduction of the chlorides with $LiAlH_4$ or $LiAlD_4$ in ether. Triphenylphosphine was recrystallized twice from ethanol and dried *in vacuo* in the molten state.

Toluene was usually distilled from CaH_2, although identical results were obtained with undistilled reagent grade toluene stored over molecular sieves. Dichloro-

[2]The values of $\Delta H^{\ddagger}$ and $\Delta S^{\ddagger}$ were both found to increase considerably for the addition of CH_3I to $Ir(CO)Cl(PPh_3)_2$, on going from benzene to dimethylformamide (6).

methane was distilled from $LiAlH_4$ and stored over molecular sieves.

Products

Since the products from the triphenylgermane and triphenylstannane reactions had not been previously prepared, samples were prepared by reaction of equimolar amounts of the iridium complex and the hydride in toluene and in dichloromethane. Both products had ir and proton nmr spectra almost identical to those of the Ph_3SiH adduct (17).

Kinetic Measurements

The reactions were followed spectrophotometrically by following the disappearance of the reactant iridium complex at 330 nm (ε = 18 500). Instrumentation and methods are described elsewhere (1).

Acknowledgment

Financial support for this work from the National Research Council of Canada is gratefully acknowledged.

1. J. F. HARROD, C. A. SMITH, and KHIN AYE THAN. J. Am. Chem. Soc. **94**, 8321 (1972).
2. R. UGO, A. PASINI, A. FUSI, and S. CENINI. J. Am. Chem. Soc. **94**, 7364 (1972).
3. J. F. HARROD and C. A. SMITH. J. Am. Chem. Soc. **92**, 2699 (1970).
4. L. VASKA. Acc. Chem. Res. **1**, 335 (1968).
5. J. F. HARROD and C. A. SMITH. Can. J. Chem. **48**, 870 (1970).
6. P. B. CHOCK and J. HALPERN. J. Am. Chem. Soc. **88**, 3511 (1966).
7. A. V. KRAMER, J. A. LABINGER, J. S. BRADLEY, and J. A. OSBORN. J. Am. Chem. Soc. **96**, 7145 (1974); A. V. KRAMER and J. A. OSBORN. J. Am. Chem. Soc. **96**, 7832 (1974).
8. M. F. LAPPERT and P. W. LEDNOR. Chem. Commun. 948 (1973).
9. R. UGO, S. CENINI, and F. BONATI. Inorg. Chim. Acta, **1**, 451 (1967); M. M. OLIVIER KAHN and M. BIGORGNE. C. R. Acad. Sci. Paris, (C) **263**, 973 (1966).
10. F. GLOCKLING and R. J. I. POLLOCK. J. Chem. Soc. Dalton Trans. 497 (1975).
11. J. R. SANDERS, D. E. WEBSTER, and P. B. WELLS. J. Chem. Soc. Dalton Trans. 1191 (1975).
12. R. J. HODGES, D. E. WEBSTER, and P. B. WELLS. Chem. Commun. 462 (1971).
13. J. F. HARROD, S. CICCONE, and J. HALPERN. Can. J. Chem. **39**, 1372 (1961).
14. G. W. PARSHALL. Acc. Chem. Res. **3**, 139 (1970).
15. P. A. KRAMER and C. MASTERS. J. Chem. Soc. Dalton Trans. 849 (1975).
16. G. YAGUPSKY and G. WILKINSON. J. Chem. Soc. A, 2325 (1971); Inorg. Synth. **13**, 127 (1972).
17. J. F. HARROD, D. F. R. GILSON, and R. CHARLES. Can. J. Chem. **47**, 2205 (1969).

Can. J. Chem. Downloaded from www.nrcresearchpress.com by 210.87.254.40 on 09/05/12
For personal use only.

Can. J. Chem. Downloaded from www.nrcresearchpress.com by 210.87.254.5 on 09/05/12
For personal use only.

Correlation of optical and electron spin resonance spectra for alkali metal solutions in ethylamine and tetrahydrofuran[1]

R. CATTERALL
Department of Chemistry, University of Salford, Salford M5 4WT, England

J. SLATER
Department of Chemistry, University of Leicester, Leicester LE1 7RH, England

AND

W. A. SEDDON AND J. W. FLETCHER
Chalk River Nuclear Laboratories, Atomic Energy of Canada Limited, Chalk River, Ont., Canada K0J 1J0

Received May 27, 1976

R. CATTERALL, J. SLATER, W. A. SEDDON, and J. W. FLETCHER. Can. J. Chem. **54**, 3110 (1976).

The band maxima of transient optical absorption spectra observed by pulse radiolysis in ethylamine (EA)/tetrahydrofuran (THF) mixtures containing sodium tetraphenylboron are correlated with electron spin resonance (esr) hyperfine splitting constants obtained in potassium/EA/THF solutions. The data suggest that the optical spectra can be attributed to the same 'monomeric' species as observed by esr in alkali metal solutions.

R. CATTERALL, J. SLATER, W. A. SEDDON et J. W. FLETCHER. Can. J. Chem. **54**, 3110 (1976).

On a établi une corrélation entre la bande maximale du spectre d'absorption optique de transition qui est observée lors de la radiolyse pulsée de mélanges éthylamine (EA)/tétrahydrofuranne (THF) contenant du tétraphénylbore sodium et les constantes de couplage hyperfines de résonance paramagnétique électronique (rpe) obtenues dans des solutions EA/THF de potassium. Les données indiquent que le spectre optique peut être attribué aux mêmes espèces "monomères" observés par rpe dans les solutions de métaux alcalins.

[Traduit par le journal]

Electron spin resonance (esr) spectra of most alkali metal solutions in amines and ethers consist of a singlet and a set of hyperfine lines assigned to solvated electrons, e_s^-, and a 'monomer' or solvated alkali atom species (1–11), respectively. Optical absorption spectra in these same solutions are, in general, composed of two bands attributed to metal-dependent and metal-independent species. The former or 'visible' band occurs in the region 10 000 – 15 000 cm^{-1} and has been assigned to the diamagnetic species M^- (11–16), whereas the latter band, which extends further into the infrared ($<7000\ cm^{-1}$), has generally been identified with solvated electrons, e_s^-, (11, 14, 15, 17–20). Ion-pair species, (M^+, e_s^-) (14, 15), have also been suggested as contributing to the infrared absorption.

More recently flash photolysis (13, 21–24) and pulse radiolysis (25–31) techniques have demonstrated the existence of distinct optical bands assigned to e_s^-, (M^+, e_s^-) and M^-. In ethylamine (EA) (25, 26) and tetrahydrofuran (THF) (27–30), the (M^+, e_s^-) band occurs at frequencies intermediate to that of e_s^- and M^- whereas in ethylenediamine (EDA) (20, 32–34) and methylamine (MA) (31, 35) little or no shift from the e_s^- band is observed.

Using EA/THF mixtures we now present evidence that the esr hyperfine structure and the new transient optical bands both arise from the same species.

For experimental reasons it was more convenient to monitor the optical absorption in the presence of sodium cations (sodium tetraphenyl boron, $NaB\phi_4$) (27, 29) and the esr spectra in potassium solutions. Details related to the pulse radiolysis and esr procedures have been described elsewhere (4, 26, 29, 31).

[1]AECL No. 5575.

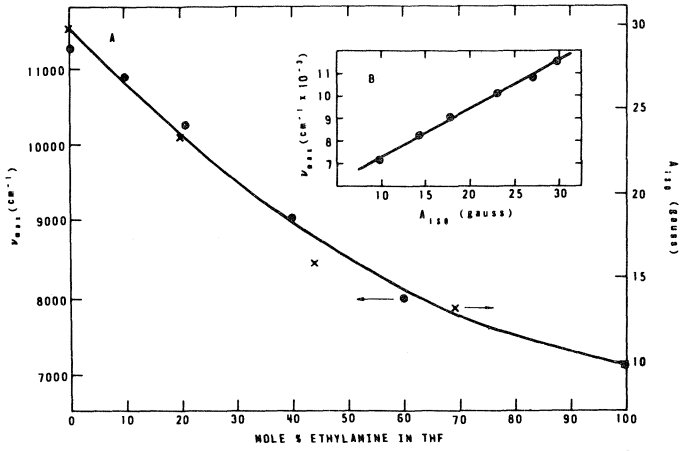

FIG. 1. (*A*) Variation in the optical absorption maximum (ν_{max}) and hyperfine splitting constant (A_{iso}) observed in THF/EA mixtures. ●, immediately after a 0.3 μs pulse in solutions containing 10^{-4} *M* sodium tetraphenylboron; X, right hand scale potassium solutions. (*B*) Correlation of ν_{max} and A_{iso} obtained from Fig. 1*A*.

Although optical transition and hyperfine interaction energies show marked changes with both the nature of the cation and the composition of the solvent, the available evidence suggests strongly that these effects are not interdependent. For example, the percentage decrease in the hyperfine interaction with additions of NH_3 to EA solutions is the same for Na and K (36) and Rb or Cs (37). Similarly, the shifts in the optical band for Na^+ and K^+ solutions when the solvent is changed from THF to isopropylamine are also closely similar (29, 38). In this paper we are concerned only with the effect of solvent dependence on the optical and esr parameters, and this can be considered independently of the metal.

Figure 1 shows the optical absorption band maxima ν_{max} (cm^{-1}) and the hyperfine coupling constant A_{iso} (G) as a function of solvent composition in EA/THF mixtures. Within experimental error the bandwidth remains constant at $\sim$7000 cm^{-1} but with increasing EA concentration a red shift of the absorption band is accompanied by a decrease in A_{iso}.

Qualitatively the shifts are very similar, and Fig. 1*b* shows a linear relation between ν_{max} and A_{iso} based on interpolation of separate smoothed curves through the data.

Of further interest is the symmetry of the deviation from ideal activity which we define by

$$\Delta_\nu = (\nu_{ideal} - \nu_{obs})/\nu_{ideal}$$

$$\Delta_A = (A_{ideal} - A_{obs})/A_{ideal}$$

where the subscripts refer to ideal and observed behaviour. The symmetry of the plots of Δ_ν and Δ_A (Fig. 2) indicate that both the optical transition and hyperfine energies are dependent upon the average solvent composition.

We suggest that the correlation established in Figs. 1 and 2 is strong support for our contention that both the esr and optical spectra arise from the 'same' species. The alternative that the

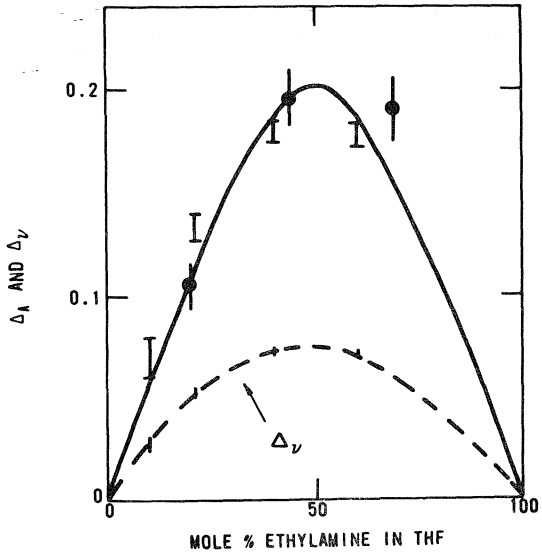

FIG. 2. Change in Δ_A and Δ_ν as a function of solvent composition. ● = Δ_A; - - - = Δ_ν; I = 2.5 Δ_ν (*i.e.* normalized to fit on the same curve as Δ_A).

Can. J. Chem. Downloaded from www.nrcresearchpress.com by 210.87.254.5 on 09/05/12
For personal use only.

optical and esr spectra do in fact represent different species of the same stoichiometry would require a coincidence in that their properties change in a parallel fashion. We believe this possibility is unlikely.

The monomeric species has been variously described as an expanded atom, solvated atom, ion-pair or some combination of all three (see refs. 1–11). Detailed interpretation of esr hyperfine interactions in $K/EA/NH_3$ mixtures requires a three state equilibrium model involving the solvated atom together with species having different proportions of EA and NH_3 in the vicinity of the metal nucleus (3). A similar conclusion has also been reached for metal-amine and ether solutions (40). Using this approach for THF/EA mixtures a simple model which involves the progressive replacement of THF molecules by EA can be considered as follows:

$$[1] \qquad M(THF)_n + EA \rightleftharpoons M(THF)_{n-1}EA + THF$$

$$[2] \qquad M(THF)_{n-1}EA + EA \rightleftharpoons M(THF)_{n-2}EA_2 + THF$$

If the hyperfine splittings observed in our work are compared with values for the free atom (10), then the atomic character ranges from 12% in EA to 36% in THF, indicating a significant contribution from solvated atoms to both the esr and optical spectra.

Alternatively, Szwarc (41) has rationalized the 'monomer' as a system involving the presence of solvated atoms in rapid equilibrium with tight and loose ion-pairs,

$$[3] \qquad M_s \rightleftharpoons (M^+, e_s^-)_{tight} \rightleftharpoons (M^+, e_s^-)_{loose}$$

An increase in solvent polarity from THF to EA would also be consistent with a shift of the equilibria to the right (41, 42).

1. K. D. Vos and J. L. Dye. J. Chem. Phys. **38**, 2033 (1963).
2. K. Bar-Eli and T. R. Tuttle, Jr. J. Chem. Phys. **40**, 2508 (1964).
3. L. R. Dalton, J. D. Rynbrandt, E. M. Hansen, and J. L. Dye. J. Chem. Phys. **44**, 3969 (1966); J. L. Dye and L. R. Dalton. J. Phys. Chem. **71**, 184 (1967).
4. R. Catterall, M. C. R. Symons, and J. W. Tipping. J. Chem. Soc. (A), 1529 (1966).
5. R. Catterall, I. Hurley, and M. C. R. Symons. J. Chem. Soc. Dalton Trans. 139 (1972).
6. R. Catterall, J. Slater, and M. C. R. Symons. J. Chem. Phys. **52**, 1003 (1970).
7. V. A. Nicely and J. L. Dye. J. Chem. Phys. **53**, 119 (1970).
8. R. Catterall, M. C. R. Symons, and J. W. Tipping. J. Chem. Soc. (A), 1234 (1967).
9. R. Catterall, M. C. R. Symons, and J. W. Tipping. Metal–ammonia solutions. I.U.P.A.C. Colloque Weyl II. *Edited by* J. J. Lagowski and M. J. Sienko. Butterworth and Co., London. 1970. p. 317.
10. R. Catterall, J. Slater, and M. C. R. Symons. Metal–ammonia solutions. I.U.P.A.C. Colloque Weyl II. *Edited by* J. J. Lagowski and M. J. Sienko. Butterworth and Co., London. 1970. p. 329.
11. J. L. Dye. Electrons in fluids. *Edited by* J. Jortner and N. R. Kestner, Springer-Verlag, West Berlin. 1973. p. 77.
12. S. Matalon, S. Golden, and M. Ottolenghi. J. Phys. Chem. **73**, 3098 (1969).
13. S. H. Glarum and J. H. Marshall. J. Chem. Phys. **52**, 5555 (1970).
14. I. Hurley, T. R. Tuttle, Jr., and S. Golden. Metal–ammonia solutions. I.U.P.A.C. Colloque Weyl II. *Edited by* J. J. Lagowski and M. J. Sienko. Butterworth and Co., London. 1970. p. 449.
15. M. T. Lok, F. J. Tehan, and J. L. Dye. J. Phys. Chem. **76**, 2975 (1972).
16. J. L. Dye, C. W. Andrews, and S. E. Mathews. Colloque Weyl IV. J. Phys. Chem. **79**, 3065 (1975).
17. H. Blades and J. W. Hodgins. Can. J. Chem. **33**, 411 (1955).
18. M. Ottolenghi, K. Bar-Eli, and H. Linschitz. J. Chem. Phys. **43**, 206 (1965).
19. J. L. Dye and R. R. Dewald. J. Phys. Chem. **68**, 135 (1964).
20. L. M. Dorfman, F. Y. Jou, and R. Wageman. Ber. Bunsenges. Phys. Chem. **75**, 681 (1971).
21. M. Fisher, G. Rämme, S. Claesson, and M. Szwarc. Chem. Phys. Lett. **9**, 309 (1971).
22. M. Fisher, G. Rämme, S. Claesson, and M. Szwarc. Proc. R. Soc. London A, **327**, 481 (1972).
23. L. J. Giling, J. G. Kloosterboer, R. P. H. Rettschnick, and J. D. W. van Voorst. Chem. Phys. Lett. **8**, 457 (1971).
24. J. G. Kloosterboer, L. J. Giling, R. P. H. Rettschnick, and J. D. W. van Voorst. Chem. Phys. Lett. **8**, 462 (1971).
25. J. W. Fletcher, W. A. Seddon, J. Jevcak, and F. C. Sopchyshyn. Chem. Phys. Lett. **18**, 592 (1973).
26. J. W. Fletcher, W. A. Seddon, and F. C. Sopchyshyn. Can. J. Chem. **51**, 2975 (1973).
27. B. Bockrath and L. M. Dorfman. J. Phys. Chem. **77**, 1002 (1973).
28. G. A. Salmon and W. A. Seddon. Chem. Phys. Lett. **24**, 366 (1974).
29. G. A. Salmon, W. A. Seddon, and J. W. Fletcher. Can. J. Chem. **52**, 3259 (1974).
30. B. Bockrath and L. M. Dorfman. J. Phys. Chem. **79**, 1509 (1975).
31. J. W. Fletcher and W. A. Seddon. Colloque Weyl IV. J. Phys. Chem. **79**, 3055 (1975).
32. R. R. Dewald and J. L. Dye. J. Phys. Chem. **68**, 128 (1964).
33. J. L. Dye, M. G. DeBacker, J. A. Eyre, and L. M. Dorfman. J. Phys. Chem. **76**, 839 (1972).
34. J. L. Dye, M. G. DeBacker, and L. M. Dorfman. J. Chem. Phys. **52**, 6251 (1970).

Can. J. Chem. Downloaded from www.nrcresearchpress.com by 210.87.254.5 on 09/05/12
For personal use only.

35. J. W. FLETCHER, W. A. SEDDON, J. J. JEVCAK, and F. C. SOPCHYSHYN. Can. J. Chem. **53**, 3571 (1975).
36. R. CATTERALL, M. C. R. SYMONS, and J. W. TIPPING. J. Chem. Soc. Faraday Trans. To be published.
37. L. R. DALTON. M.Sc. Thesis, Michigan State University, Michigan, 1966; J. L. DYE and L. R. DALTON. Unpublished work.
38. W. A. SEDDON, J. W. FLETCHER, and F. C. SOPCHYSHYN. Chem. Phys. In press.
39. R. CATTERALL, J. SLATER, and M. C. R. SYMONS. To be published.
40. R. CATTERALL and P. P. EDWARDS. Colloque Weyl IV; J. Phys. Chem. **79**, 3010 (1975).
41. M. SZWARC and J. J. GRODZINSKI. Ions and ion pairs in organic reactions. Vol. 2. *Edited by* M. Szwarc. J. Wiley and Sons, New York. 1974. p. 133.
42. M. SZWARC. Ions and ion pairs in organic reactions. Vol. 1. *Edited by* M. Szwarc, Wiley-Interscience, New York. 1972. p. 1.

Can. J. Chem. Downloaded from www.nrcresearchpress.com by 210.87.254.5 on 09/05/12
For personal use only.

Oxidative cleavage of tertiary cyclobutanols. A new synthetic approach to 1,4-ketols and 1,4-diketones

HSING-JANG LIU
Department of Chemistry. University of Alberta, Edmonton, Alta., Canada T6G 2G2

Received July 8, 1976

HSING-JANG LIU. Can. J. Chem. **54**, 3113 (1976).

The reaction of tertiary cyclobutanols with Jones reagent under mild conditions resulted in the oxidative cleavage of the cyclobutane ring to give, depending on the substitution pattern of the starting alcohol, a 1,4-ketol or a 1,4-diketone.

HSING-JANG LIU. Can. J. Chem. **54**, 3113 (1976).

La réaction de cyclobutanols tertiaires avec le réactif de Jones dans des conditions douces conduit à une coupure oxydante du noyau cyclobutanique pour donner, suivant la nature des substituants de l'alcool de départ, un cétol-1,4 ou une dicétone-1,4.

[Traduit par le journal]

In connection with our synthetic studies requiring cyclobutanones as key intermediates, a number of bicyclo[4.2.0]octan-7-ols (1) and bicyclo[3.2.0]heptan-6-ols (2) were subjected to Jones oxidation (3). Almost without exception, the oxidation reactions afforded, in addition to the expected ketones, variable amounts of lactones in minor products (Scheme 1). We were

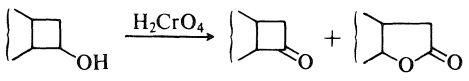

SCHEME 1

intrigued by the unusual lactone formation and further investigation on several of these reactions revealed that prolonged treatment did not cause any noticeable change in the composition of the product mixtures nor were lactones produced in any detectable quantity when the pure cyclobutanones were subsequently treated with Jones reagent (4). Clearly, the lactones and the cyclobutanones must have been produced independently from the corresponding starting alcohols via competitive reaction pathways.

These findings led to our present studies on the oxidation of tertiary cyclobutanols with Jones reagent. It was anticipated that, with the normal oxidation process to a ketone being precluded, a tertiary cyclobutanol would proceed exclusively by the oxidative cleavage of the cyclobutane ring to give, depending on its substitution pattern, 1,4-ketol **1** or 1,4-diketone **2** theoretically by the route outlined in Scheme 2.

Indeed, when alcohol **3** was treated with 8 *N* Jones reagent in acetone 0 °C for 1 h, it was smoothly oxidized to give an 82% yield of diketone **4**: ir (film) 1707 cm^{-1}; nmr (CCl_4) δ 0.94 (t, 3H, $J = 6$ Hz); mass spectrum M^+ 196.1463 (calcd. for $C_{12}H_{20}O_2$: 196.1464). Under the same condition, the oxidation of alcohol **5** afforded a 50% yield of ketol **6** (ir (film) 3430 and 1705 cm^{-1}; nmr (CCl_4) δ 0.91, 0.94, 1.06, and

35. J. W. FLETCHER, W. A. SEDDON, J. J. JEVCAK, and F. C. SOPCHYSHYN. Can. J. Chem. **53**, 3571 (1975).
36. R. CATTERALL, M. C. R. SYMONS, and J. W. TIPPING. J. Chem. Soc. Faraday Trans. To be published.
37. L. R. DALTON. M.Sc. Thesis, Michigan State University, Michigan, 1966; J. L. DYE and L. R. DALTON. Unpublished work.
38. W. A. SEDDON, J. W. FLETCHER, and F. C. SOPCHYSHYN. Chem. Phys. In press.
39. R. CATTERALL, J. SLATER, and M. C. R. SYMONS. To be published.
40. R. CATTERALL and P. P. EDWARDS. Colloque Weyl IV; J. Phys. Chem. **79**, 3010 (1975).
41. M. SZWARC and J. J. GRODZINSKI. Ions and ion pairs in organic reactions. Vol. 2. *Edited by* M. Szwarc. J. Wiley and Sons, New York. 1974. p. 133.
42. M. SZWARC. Ions and ion pairs in organic reactions. Vol. 1. *Edited by* M. Szwarc, Wiley-Interscience, New York. 1972. p. 1.

Can. J. Chem. Downloaded from www.nrcresearchpress.com by 210.87.254.6 on 09/05/12
For personal use only.

Oxidative cleavage of tertiary cyclobutanols. A new synthetic approach to 1,4-ketols and 1,4-diketones

HSING-JANG LIU
Department of Chemistry. University of Alberta, Edmonton, Alta., Canada T6G 2G2

Received July 8, 1976

HSING-JANG LIU. Can. J. Chem. **54**, 3113 (1976).

The reaction of tertiary cyclobutanols with Jones reagent under mild conditions resulted in the oxidative cleavage of the cyclobutane ring to give, depending on the substitution pattern of the starting alcohol, a 1,4-ketol or a 1,4-diketone.

HSING-JANG LIU. Can. J. Chem. **54**, 3113 (1976).

La réaction de cyclobutanols tertiaires avec le réactif de Jones dans des conditions douces conduit à une coupure oxydante du noyau cyclobutanique pour donner, suivant la nature des substituants de l'alcool de départ, un cétol-1,4 ou une dicétone-1,4.

[Traduit par le journal]

In connection with our synthetic studies requiring cyclobutanones as key intermediates, a number of bicyclo[4.2.0]octan-7-ols (1) and bicyclo[3.2.0]heptan-6-ols (2) were subjected to Jones oxidation (3). Almost without exception, the oxidation reactions afforded, in addition to the expected ketones, variable amounts of lactones in minor products (Scheme 1). We were

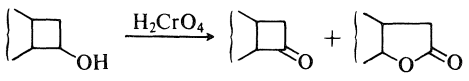

SCHEME 1

intrigued by the unusual lactone formation and further investigation on several of these reactions revealed that prolonged treatment did not cause any noticeable change in the composition of the product mixtures nor were lactones produced in any detectable quantity when the pure cyclobutanones were subsequently treated with Jones reagent (4). Clearly, the lactones and the cyclobutanones must have been produced independently from the corresponding starting alcohols via competitive reaction pathways.

These findings led to our present studies on the oxidation of tertiary cyclobutanols with Jones reagent. It was anticipated that, with the normal oxidation process to a ketone being precluded, a tertiary cyclobutanol would proceed exclusively by the oxidative cleavage of the cyclobutane ring to give, depending on its substitution pattern, 1,4-ketol **1** or 1,4-diketone **2** theoretically by the route outlined in Scheme 2.

Indeed, when alcohol **3** was treated with 8 *N* Jones reagent in acetone 0 °C for 1 h, it was smoothly oxidized to give an 82% yield of diketone **4**: ir (film) 1707 cm^{-1}; nmr (CCl_4) δ 0.94 (t, 3H, $J = 6$ Hz); mass spectrum M^+ 196.1463 (calcd. for $C_{12}H_{20}O_2$: 196.1464). Under the same condition, the oxidation of alcohol **5** afforded a 50% yield of ketol **6** (ir (film) 3430 and 1705 cm^{-1}; nmr (CCl_4) δ 0.91, 0.94, 1.06, and

TABLE 1. Oxidation of tertiary cyclobutanols with the Jones reagent

Alcohol[a]	Time	Product(s)[b]			
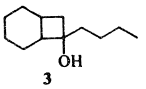 3	1 h	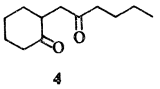 4	(82)		
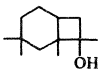 5	1 h	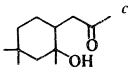 6 [c]	(50)	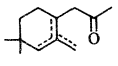 7	(21)
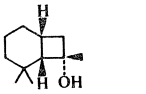	1 h	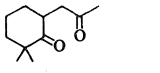	(80)		
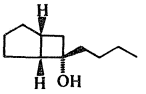	30 min	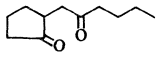	(42)		
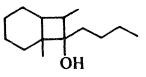	1 h	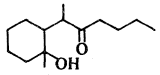 [d]	(48)	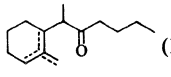	(10)
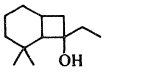	50 min	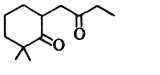	(78)		
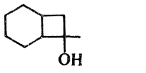	1 h	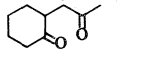	(85)		
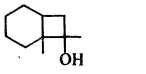	40 min	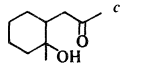 [c]	(66)		
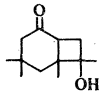 8	16 h	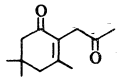 9	(62)		

[a]All the ring junctures are *cis*-fused. Where relative stereochemistry is not specified, a diastereomeric mixture was used.
[b]Percentage isolated yield in parentheses. Yields have not been optimized.
[c]A single isomer was obtained. Its stereochemistry remains to be ascertained.
[d]A mixture consisting of at least two isomers was obtained.

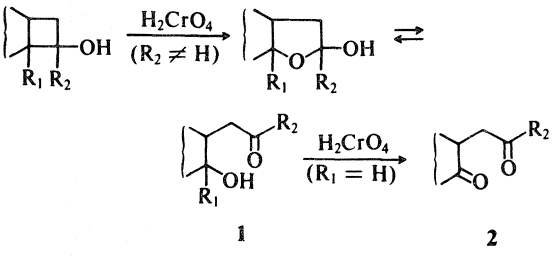

SCHEME 2

2.09 (all s, 3H each); mass spectrum M^+ 198.1625 (calcd. for $C_{12}H_{22}O_2$: 198.1620)) and a minor quantity of a mixture of enones **7**. The synthesis of 1,4-ketols and 1,4-diketones, compounds of broad synthetic utility,[1] by means of oxidative cleavage of tertiary cyclobutanols was thus shown to be feasible. The generality of the new method was further demonstrated by additional examples which are compiled in Table 1. By modifying the structure of the starting alcohol, this procedure could, in principle, be extended to the preparation of many other organic systems. The transformation of keto alcohol **8** to enedione **9** illustrates this point.

The cyclobutanols used in the present studies were readily prepared from appropriate cyclo-

[1]For a relevant discussion, see ref. 5.

Can. J. Chem. Downloaded from www.nrcresearchpress.com by 210.87.254.6 on 09/05/12
For personal use only.

alkenones by a photochemical approach. For instance, **8** was synthesized by irradiation of isophorone and isopropenyl acetate followed by hydrolysis (4 *N* NaOH–CH_3OH) of the resulting diastereomeric mixture of photoadducts (**8** with OAc replacing OH) (6). Alcohol **5** was obtained from **8** in two steps; thioketalization with 1,2-ethanedithiol and boron trifluoride etherate and desulfurization with W-2 Raney nickel. In cases where the required enol acetate, *e.g.*, 2-acetoxyl-1-hexene for **3**, could not be easily secured in desired quantity, it was found more convenient to carry out the synthesis via a suitable cyclobutanone intermediate. Thus, by the sequence used for the transformation of isophorone and isopropenyl acetate to **5**, bicyclo[4.2.0]octan-7-ol was readily prepared from 2-cyclohexenone and vinyl acetate. Oxidation with dimethyl sulfoxide and acetic anhydride (7) at 5 °C gave rise to the corresponding cyclobutanone which on treatment with *n*-butyllithium afforded **3**.

Acknowledgement

The author wishes to thank the National Research Council of Canada for financial support.

1. H. J. Liu and T. Ogino. Tetrahedron Lett. 4937 (1973).
2. J. A. Bulat. M.Sc. Thesis, University of Alberta, Edmonton, Alta. 1976.
3. K. Bowden, I. M. Heilbron, E. R. H. Jones, and B. C. L. Weedon. J. Chem. Soc. 39 (1946).
4. C. Djerassi, R. R. Engle, and A. Bowers. J. Org. Chem. **21**, 1547 (1956).
5. N. R. Hunter, G. A. MacAlpine, H. J. Liu, and Z. Valenta. Can. J. Chem. **48**, 1436 (1970).
6. Z. Valenta and H. J. Liu. Org. Synth. Submitted for publication.
7. J. D. Albright and L. Goldman. J. Am. Chem. Soc. **89**, 2416 (1967).

Can. J. Chem. Downloaded from www.nrcresearchpress.com by 210.87.254.6 on 09/05/12
For personal use only.

Canadian Journal of Chemistry

Published by
THE NATIONAL RESEARCH COUNCIL OF CANADA

Journal canadien de chimie

Publié par
LE CONSEIL NATIONAL DE RECHERCHES DU CANADA

Volume 54 Number 20 October 15, 1976 Volume 54 numéro 20 15 octobre 1976

Can. J. Chem. Downloaded from www.nrcresearchpress.com by 210.87.254.6 on 09/05/12
For personal use only.

Mercury photosensitization of 1-hexene and *cis*-2-octene vapor. Intramolecular hydrogen abstraction of vibrationally excited π,π^* triplet state[1]

YOSHIHISA INOUE,[2] SETSUO TAKAMUKU, AND HIROSHI SAKURAI
The Institute of Scientific and Industrial Research, Osaka University, Suita, Osaka 565, Japan

Received June 15, 1976

YOSHIHISA INOUE, SETSUO TAKAMUKU, and HIROSHI SAKURAI. Can. J. Chem. **54**, 3117 (1976).

Upon mercury photosensitization, the vibrationally excited triplet of the simple alkenes 1-hexene and *cis*-2-octene undergoes an olefinic type II reaction consisting of an intramolecular 1,5-hydrogen abstraction via a six-membered transition state and subsequent reaction of the resulting biradical, in sharp contrast to the well established allylic C—C and C—H bond cleavage of alkenes without a γ-hydrogen. The *cis–trans* photoisomerization of *cis*-2-octene and other intramolecular hydrogen abstractions of minor importance occurring through unfavorable transition states were also observed. The mercury photosensitization of various cyclic and acyclic alkenes so far reported are comparatively discussed.

YOSHIHISA INOUE, SETSUO TAKAMUKU et HIROSHI SAKURAI. Can. J. Chem. **54**, 3117 (1976).

Par photosensibilisation au mercure le triplet vibrationnellement excité des alcènes simples comme l'hexène-1 et l'octène-2 *cis* donne une réaction de type II oléfinique consistant en un arrachement d'hydrogène γ par un état de transition à six chaînons et réaction subséquente du biradical résultant. Ceci est en nette opposition avec le fait bien établi du clivage des liens allyliques C—C et C—H des alcènes qui ne possèdent pas un hydrogène en position γ. La photoisomérisation *cis–trans* de l'octène-2 *cis* et d'autres processus d'arrachement intramoléculaire d'atomes d'hydrogène se produisant selon des états de transition défavorables ont aussi été observés. La photosensibilisation au mercure de divers alcènes cycliques et acycliques déjà rapportés est discutée en comparaison avec les résultats du présent travail.

[Traduit par le journal]

Introduction

Extensive studies have been made on the photochemical behavior of alkyl-substituted ethylenes following triplet sensitization in the liquid phase. The *cis–trans* photoisomerization of acyclic alkenes via triplet state is one of the most studied photochemical reactions (1); with cycloalkenes, where *cis–trans* isomerization is geometrically difficult, cyclodimerization and polar addition take place (2). Regarding the photosensitization of simple alkenes in the vapor phase, on the other hand, it is generally accepted that triplet–triplet energy transfer from sensitizer generates a vibrationally excited triplet-state molecule of alkene, which exhibits some novel reactivities not observed in the liquid-phase photolysis. The best established reaction of such a vibrationally excited triplet alkene is allylic C—C and C—H bond cleavage followed by reactions of the resulting alkyl and allyl radicals (3–9). The vibrational activation in the triplet state of alkenes has also been reported to enhance an intramolecular 1,2-shift of allylic hydrogen,

[1]Preliminary report, ref. 25.
[2]To whom correspondence should be addressed.

Can. J. Chem. Downloaded from www.nrcresearchpress.com by 210.87.254.6 on 09/05/12
For personal use only.

providing cyclopropane derivatives (4, 10, 11).

A previous study of the photosensitization of *cis*-cyclooctene vapor showed that the vibrationally excited triplet of cyclooctene undergoes an efficient intramolecular γ-hydrogen abstraction through a cyclic, six-membered transition state, resulting in the formation of a cyclic 1,4-biradical (12). The 1,4-biradical thus formed undergoes competitive β-cleavage and cyclization, which provides an olefinic analog with the Norrish type II reaction of carbonyl compounds (13). Although the mechanism has not been fully clarified, the mercury sensitization of 1-pentene vapor also gives products which may be attributed to the intramolecular γ-hydrogen abstraction and the subsequent reaction of the resulting 1,4-biradical (14, 15). Consequently, it is suggested that the vibrationally excited π,π^* triplet of alkenes containing a γ-hydrogen atom shows an analogous reactivity with the type II photocleavage of carbonyl compounds, although the mechanism of vapor-phase photosensitization of alkenes has hitherto mainly involved the allylic C—C and C—H fission.

In the present study, we wish to discuss the detailed mechanism, generality, and importance of the intramolecular hydrogen abstraction reaction in the vapor-phase photosensitization of simple alkenes.

Experimental

Materials

*1-Hexene (**1**)*

Commercially available 1-hexene was purified by distillation through a spinning band column and preparative glc on polyethylene glycol-6000 (PEG) to a purity of >99.9%.

*1-Hexene-5,5-d_2 (**1***d*)*

The deuterium labelled hexene was prepared in a three step process starting from hex-5-en-2-one. The procedure consisted in $LiAlD_4$ reduction of the hexenone to hex-5-en-2-ol-5-*d*, followed by esterification with *p*-toluene-sulfonyl chloride to the tosylate and subsequent reduction with $LiAlD_4$ to give **1***d*. The product was purified by preparative glc to a purity of >99.9%. The nmr spectrum of **1***d* showed three vinyl protons at δ 5.7(t–q), 4.9(d), and 4.85(d), two allylic protons at 2.0(q), two methylene protons at 1.32(t), and three methyl protons at 0.88(s) in accord with the structure of **1***d*. The isotopic purity of **1***d* was determined to be 98.7% by nmr and mass spectrometry.

*cis-2-Octene (**2***c*)*

Commercially available *cis*-2-octene containing 5% *trans*-isomer was purified by preparative glc on PEG to a purity of 99.1%. The experimental sample contained a small amount (0.87%) of the *trans*-isomer (**2***t*) as an impurity. A correction was applied to all of the data for the presence of the impurity.

General Procedure

All the experiments were carried out at 25 ± 1 °C and under static conditions. The apparatus employed in the mercury sensitization was the same as described in the previous papers (9, 12). Control runs revealed that no detectable reaction occurred in the absence of uv irradiation. The quantum yields (Φ) for the mercury sensitization of **1**, **1***d*, and **2***c* were determined by propane actinometry at 300 torr, where $\Phi(H_2)$ was taken as unity (16). The absorption of the incident radiation was incomplete in the cell and appropriate corrections were made in the determination of the quantum yields.

After each run, products were trapped in a capillary at −196 °C; small amounts of the non-condensable products were discarded. The condensables were analyzed by glc on a 6 m column of 20% squalane at 50 °C for the products from 1-hexene, and on a 6 m column of 25% β,β'-oxydipropionitrile (ODPN) at 50 °C for those from 2-octene. The gas chromatographic analysis of the saturated compounds produced in the mercury sensitization of **2***c* was conducted with a 15 cm column of $HgSO_4$-scrubber, Absorite PM (Tokyo Kasei Co.), which absorbs only olefinic and aromatic compounds selectively (17), since some peaks of the saturated products were partially submerged in the peak of 2-octenes. All products, which can be separated from each other under these conditions, had retention times on glc and mass spectra identical with those of commercially obtained or independently synthesized authentic specimens. No searching attempt on glc was made for dimeric products.

Independent Synthesis of Authentic Specimens

The structures of the compounds synthesized were confirmed by means of nmr, ir, and mass spectrometry.

*cis- and trans-1,2-Dimethylcyclobutanes (**3***c* and **3***t*)*

The diethyl ester of *trans*-cyclobutane-1,2-dicarboxylic acid was converted to a mixture of *cis*- and *trans*-diesters by sodium-catalyzed epimerization in ethanol (18). The mixture (*cis*/*trans* = 0.15) of diesters was reduced to a mixture (*cis*/*trans* = 0.12) of *cis*- and *trans*-1,2-dimethylcyclobutanes in a three step process composed of $LiAlH_4$ reduction into *cis*- and *trans*-1,2-bis(hydroxymethyl)-cyclobutanes, esterification with *p*-toluene-sulfonyl chloride to the corresponding ditosylates, and in turn $LiAlH_4$ reduction of the ditosylates. Separation by preparative glc gave the pure specimens of **3***c* and **3***t*.

*cis- and trans-1,2-Diethylcyclobutanes (**6***c* and **6***t*)*

Photodimerization of 1,3-butadiene (19) was performed in the presence of Michler's ketone as a sensitizer to give a mixture of *cis*- and *trans*-1,2-divinylcyclobutanes and 4-vinylcyclohexene (13, 83, and 4%, respectively). Hydrogenation of the mixture over 5% Pd – charcoal gave a mixture of *cis*- and *trans*-1,2-diethylcyclobutanes and ethylcyclohexane, from which the pure specimens of **6***c* and **6***t* were separated by glc.

*cis- and trans-1-Methyl-2-ethylcyclopentanes (**7***c* and **7***t*)*

cis-Bicyclo[3.3.0]oct-2-ene, prepared by potassium-catalyzed cyclization of 1,3-cyclooctadiene (20), was converted to *cis*-1-hydroxymethyl-2-(2-hydroxyethyl)cyclopentane by ozonolysis at 0 °C and subsequent reductive

TABLE 1. Mercury photosensitization of 1-hexene (**1**) and 1-hexene-5,5-d_2 (**1***d*)

Compound	Pressure (torr)	Irradiation time (min)	Product Φ					
			Propene	**3***c*	**3***t*	**4**	**5**	*n*-Hexane
1	10	5	0.30	0.025	0.038	0.006	0.003	0.002
1 + NO[a]	10	5	0.30	0.023	0.034	0.005	0.003	[b]
1*d*	10	5	0.158	0.013	0.020	0.006	0.003	[c]
Φ_H/Φ_D	—	—	1.91	1.87	1.87	1.0	1.0	—

[a]Nitric oxide (1 torr) added.
[b]Not detected.
[c]Yield not determined.

cleavage of the ozonide with $NaBH_4$ according to a similar procedure described by Sousa and Bluhm (21). The *cis*-diol obtained was reduced to *cis*-1-methyl-2-ethylcyclopentane (**7***c*) by the same successive treatment employed in the synthesis of **3***c* and **3***t*. *trans*-Methylethylcyclopentane (**7***t*) was prepared by acetone-sensitized photoepimerization (22) of **7***c*.

Results

Mercury-sensitized Photolysis of 1-Hexene (1)

As major products, propene and *cis*- and *trans*-1,2-dimethylcyclobutanes (**3***c* and **3***t*) were obtained along with minor amounts of methylcyclopentane (**4**), cyclohexane (**5**), and *n*-hexane. The quantum yields of the products are shown in Table 1. Although trace amounts ($\Phi < 0.002$) of ethylene and 2-butenes were observed at substrate pressure ≤ 10 torr, any formation of these products was not detected in significant yield at higher pressure; no detectable propane was produced at any pressure employed.

The product distribution for a short reaction time (1 min) exactly accorded with the results shown in Table 1, thus indicating that these are the primary photoproducts.

A scavenging experiment was performed with a small amount of added nitric oxide to suppress free radical-induced reactions which is familiar to mercury photosensitization of hydrocarbons (23, 24). As shown in Table 1, the formation of *n*-hexane was completely suppressed by the addition of nitric oxide, while the yields of the other major products were virtually invariant.

The effect of the initial substrate pressure on the product yields was examined up to 51 torr. The results are shown in Fig. 1. The suppressing effect of the increasing pressure on the yields of propene, dimethylcyclobutanes (**3**), methylcyclopentane (**4**), and cyclohexane (**5**) is evident from the data.

Since the formation of the cyclobutanes **3** was considered to involve hydrogen abstraction at the 5-position of 1-hexene, 5,5-dideuterated 1-hexene **1***d* was synthesized and subjected to mercury sensitization in order to examine isotope effects on the reaction. The photolysis of the deuterated hexene **1***d* was carried out under comparable conditions to afford similar results but showed a remarkable decrease in the yields of propene and the cyclobutanes, as shown in Table 1. Any detectable decreases in deuterium content were not observed by mass spectrometric analysis of the products **3**–**5**. Mass spectrometric

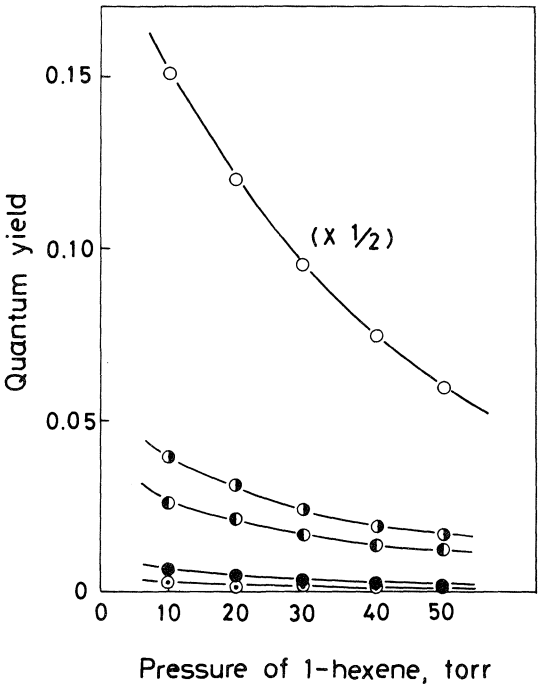

FIG. 1. Product yield as a function of 1-hexene pressure; irradiation time 5 min. ○, propene (×½); ◐, ◑, *cis*- and *trans*-dimethylcyclobutane (**3***c* and **3***t*); ●, methylcyclopentane (**4**); ⊙, cyclohexane (**5**).

Can. J. Chem. Downloaded from www.nrcresearchpress.com by 210.87.254.6 on 09/05/12
For personal use only.

TABLE 2. Mercury photosensitization of *cis*-2-octene (**2***c*)

Pressure (torr)		Irradiation	Product Φ							
2*c*	NO	time (min)	1-Butene	**6***t*	**6***c*+**8***t*[a]	**7***t*	**7***c*	**8***c*	**2***t*	*n*-Octane
10	0	5	0.084	0.008	0.010	0.002	0.003	0.003	0.44	0.005
10	1.0	5	0.088	0.008	0.010	0.002	0.002	0.003	0.44	[b]

[a]The combined yield of **6***c* and **8***t* is shown because of incomplete separation on glc.
[b]Not detected.

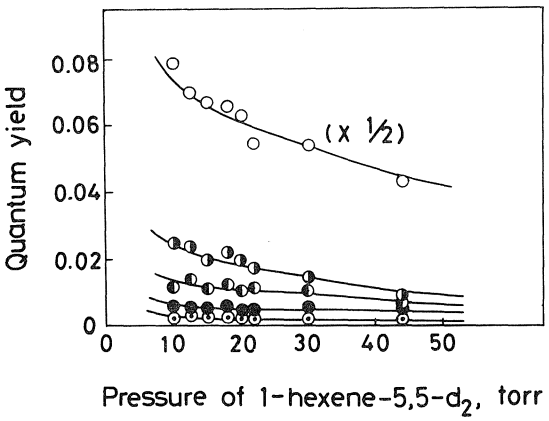

FIG. 2. Product yield as a function of 1-hexene-5,5-d_2 pressure; irradiation time 5 min. ○, propene-d_1 (×½); ◐, ◑, *cis*- and *trans*-dimethylcyclobutane-d_2; ●, methylcyclopentane-d_2; ⊙, cyclohexane-d_2.

analysis also revealed that more than 88% of the propene produced contains one deuterium atom, suggesting predominant transfer of a deuterium atom at the 5-position of **1***d*.

The pressure-dependence study was repeated for the mercury sensitization of the deuterated hexene under comparable conditions, since the deuteration at the 5-position of **1** is expected to affect the rate of hydrogen abstraction, as well as the quantum yields of propene and the cyclobutanes. As can be seen from Fig. 2, the product yields decreased with increasing pressure as in the case of **1** except for the greater reduction of the yields of propene and the cyclobutanes.

In other experiments, it was observed qualitatively that the vapor-phase photosensitization[3] of **1** (10 torr) at 2537 Å with benzene vapor (10 torr) as a sensitizer also gave the same major products, *i.e.* propene and the dimethylcyclobutanes in a molar ratio of about 20:1 while 65 h irradiation of benzene solution of **1** in a quartz tube by a 500 W high pressure mercury lamp produced no detectable yields of propene, **3**, **4**, and **5**.

[3]The benzene sensitization in the vapor phase was carried out in a mercury-free vacuum system using the same lamp and quartz reaction vessel.

Mercury-sensitized Photolysis of cis-2-Octene (**2***c*)

The major photolysis product was *trans*-2-octene (**2***t*), and additionally minor amounts of 1-butene, *cis*- and *trans*-1,2-diethylcyclobutanes (**6***c* and **6***t*), *cis*- and *trans*-1-methyl-2-ethylcyclopentanes (**7***c* and **7***t*), *cis*- and *trans*-1,2-dimethylcyclohexanes (**8***c* and **8***t*) were obtained. Although 1-octene was also produced (Φ = *ca.* 0.01 at 10 torr), accurate determination of the yield is difficult because of the incomplete separation on glc. The quantum yields are shown in Table 2. Any formation of *n*-butane and 2-butenes was not detected in significant amount. A short irradiation time (1 min) experiment gave the same distribution of products as shown in Table 2, indicating that these are the primary products.

The effect of added nitric oxide was examined and the results are shown in Table 2. The addition of the radical scavenger inhibited completely the formation of *n*-octane, while the yields of the other products were not practically affected.

The pressure-dependence study on the mercury sensitization of **2***c* was performed up to 350 torr by adding xenon as an inert gas, since the range available was limited by the low vapor pressure of the substrate at room temperature. The results are plotted in Fig. 3. In order to avoid complicated plots on the figure, the results for the yields of **6***c*, **7***c*, **7***t*, and **8***t* are omitted because of their similar pressure dependence. The yield of *n*-octane stayed constant over the entire pressure range employed, in accord with the nature of the well-known radical-induced reactions. The product yields except that of **2***t* decreased gradually

Can. J. Chem. Downloaded from www.nrcresearchpress.com by 210.87.254.6 on 09/05/12
For personal use only.

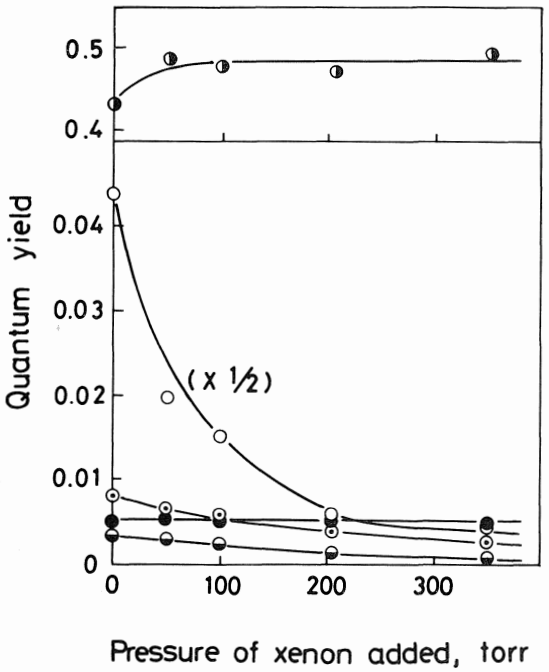

FIG. 3. Product yield as a function of xenon pressure in the mercury photosensitization of *cis*-2-octene (10 torr); irradiation time 5 min. ◑, *trans*-2-octene (**2***t*); ○, 1-butene (×½); ⊙, *trans*-1,2-diethylcyclobutane (**6***t*); ◒, *cis*-1,2-dimethylcyclohexane (**8***c*); ●, *n*-octane.

with increasing xenon pressure; the quantum yield of **2***t* contrarily increased to 0.49 and then remained constant at pressures $\geq$50 torr.

Discussion

The pressure dependence of the product yields and the lack of inhibition by nitric oxide indicate the intermediacy of the vibrationally excited triplet state of the alkenes, *i.e.* 1-hexene and *cis*-2-octene, consistent with the accepted view of the mercury photosensitization of alkenes (3–12). The formation of the cyclic compounds **3**–**5** in the photolysis of 1-hexene can be interpreted in terms of four intramolecular hydrogen abstraction processes followed by closure of the resulting biradicals (Scheme 1).

The mechanism which involves the familiar allylic C—C bond fission is ruled out for the formation of propene, since propane and 1,5-hexadiene which, if the allylic fission is operative, should be produced by the reaction of propyl and

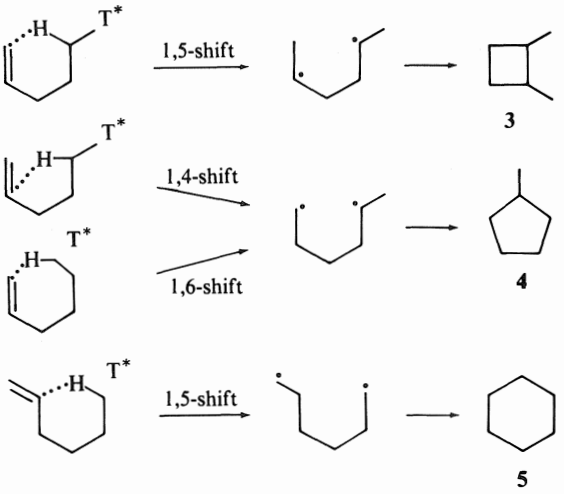

SCHEME 1

allyl radicals was not detected.[4] The negligible effect of the radical scavenger NO on the yield of propene also suggests the absence of any radical species as an intermediate. The formation of propene is interpreted in terms of competitive β-cleavage of the 1,4-biradical generated by the 1,5-hydrogen shift through a six-membered transition state as shown in Scheme 2.

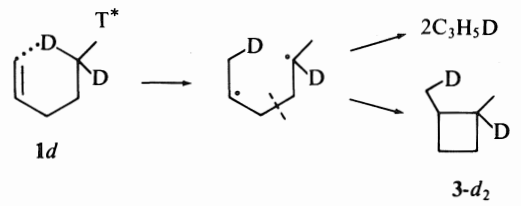

SCHEME 2

The above mechanism for propene formation is supported by the results of the deuterated experiment that (*1*) >88% of the propene produced in the mercury sensitization of **1***d* contained one deuterium, and (*2*) both yields of propene and the dimethylcyclobutanes decreased to a similar extent upon deuteration at the 5-position of 1-hexene (Φ_H/Φ_D in Table 1).

Intramolecular hydrogen abstraction in the six-membered transition state, followed by

[4] *n*-Hexane formation should be interpreted as a result of the hydrogen abstraction by excited mercury atoms which has been established in the mercury photosensitization of alkanes (23, 24).

Can. J. Chem. Downloaded from www.nrcresearchpress.com by 210.87.254.6 on 09/05/12
For personal use only.

Can. J. Chem. Downloaded from www.nrcresearchpress.com by 210.87.254.6 on 09/05/12
For personal use only.

competitive cyclization and β-cleavage of the resulting 1,4-biradical, may correspond to the Norrish type II reaction of carbonyl compounds (13). Other cyclic products also involve intramolecular hydrogen abstractions (Scheme 1); methylcyclopentane **4** is formed from a 1,4- and/or 1,6-shift via unfavorable five- and/or seven-membered transition states, and, because of the unfavorable primary 1,6-biradical intermediate, a small amount of cyclohexane is formed. Although this olefinic analog of the type II reaction does occur upon benzene sensitization of **1** in the vapor phase, no detectable product from these intramolecular hydrogen abstraction reactions was observed in the liquid-phase benzene sensitization of **1**. Therefore, the olefinic type II reaction, and the other intramolecular hydrogen abstractions as well, are characteristic of the vibrationally excited triplet generated in the vapor-phase photosensitization.

The pressure dependence study of the photolysis of **1** and **1***d* gives additional information on the lifetime of the excited triplet and the isotope effect on the rate of hydrogen transfer. The sequence [1]–[5] is proposed for the formation of propene and cyclobutanes **3**,

[1] $\mathbf{1} + Hg^* \rightarrow \mathbf{1}^* + Hg$

[2] $\mathbf{1}^* \rightarrow 2C_3H_6 + \mathbf{3}$

[3] $\rightarrow$ other products

[4] $\rightarrow \mathbf{1}$

[5] $\overset{1}{\rightarrow} \mathbf{1}$

where the asterisk represents the excited triplet state.

A steady-state treatment of the sequence [1]–[5] leads to the equation 6 for the reciprocal of the quantum yield of the type II reaction, *i.e.* the combined yield of propene $\times \frac{1}{2}$ and **3**.

$$[6] \qquad 1/\Phi_{\text{type II}} = \frac{k_2 + k_3 + k_4}{k_2} + \frac{k_5}{k_2}[\mathbf{1}]$$

In Fig. 4, the reciprocals of the combined yields of propene $\times \frac{1}{2}$ and **3** from the photolysis of **1** and **1***d* are plotted against the substrate pressure and good linear relations are obtained.

From the slopes and the intercepts, we obtained: $(k_2 + k_3 + k_4)/k_5 = 17.7$ and 24.5 torr in the photolysis of 1-hexene and 1-hexene-d_2, respectively. Assuming that the deactivation of

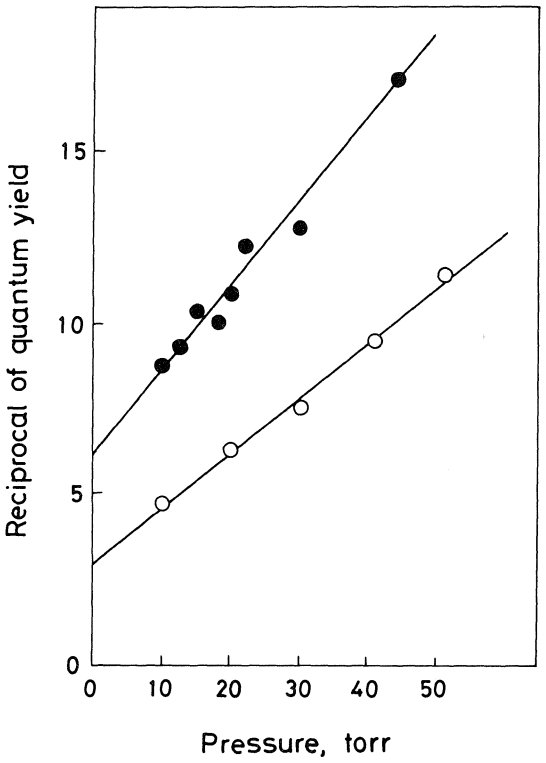

FIG. 4. Reciprocal of quantum yield of the olefinic type II reaction as a function of the substrate pressure in the mercury photosensitization of 1-hexene (○) and 1-hexene-5,5-d_2 (●).

triplet hexene occurs at each collision, *i.e.* $k_5 = 1.0 \times 10^{-10}$ cc/molecule s (4, 7), $k_2 + k_3 + k_4$ equals 0.56×10^8 s^{-1}. Thus, the 1-hexene triplet has a lifetime of 1.8×10^{-8} s. A similar calculation gives the lifetime of the deuterated 1-hexene triplet, 1.3×10^{-8} s.[5] These values are in fair agreement with the results of other alkene triplets, *e.g.* 6.3×10^{-9} s for 1-butene (4) and 5.0×10^{-9} s for cyclohexene (7). On the assumption that the cross sections of **1** and **1***d* do not differ too greatly, the isotope effect on the rate of process [2], denoted by k_H/k_D, is estimated from the slope of eq. 6. From Fig. 4, the value k_H/k_D for the olefinic type II reaction is calculated to be 1.5, and the isotope effect on the zero pressure extrapolated quantum yield, designated by $(\Phi_H/\Phi_D)_0$, is also calculated to be 2.1 from the intercepts. These are consistent with the mechanism in-

[5]Since the corrections for Lorentz broadening of mercury resonance line (7) were not made in the pressure dependence studies, the lifetimes may be somewhat longer than these calculated values.

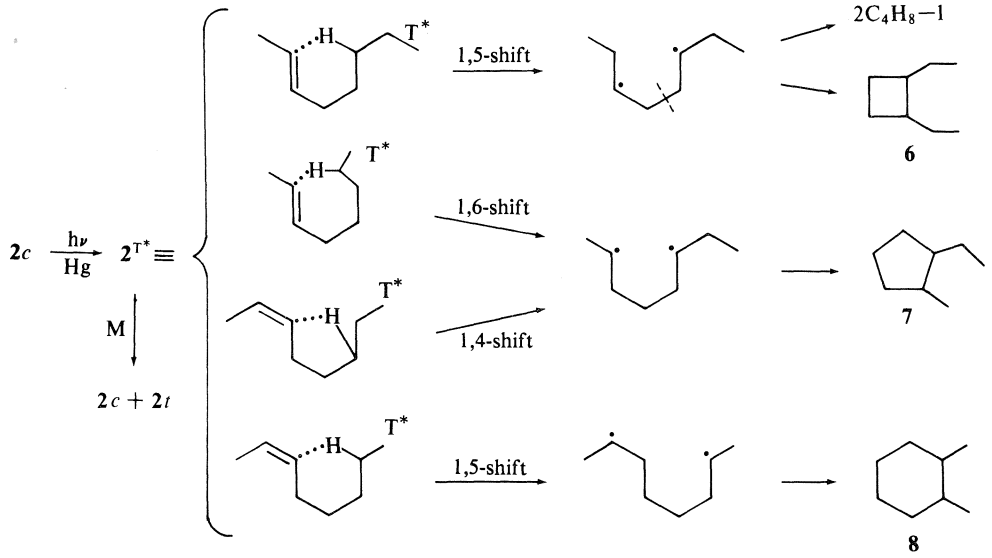

SCHEME 3

volving the intramolecular 1,5-hydrogen transfer process.

With the mercury photosensitization of *cis*-2-octene, where *cis–trans* isomerization can be observed, 1-butene and the *cis*- and *trans*-isomers of three cyclic products **6–8** were obtained along with *trans*-2-octene, **2***t*. Based on the observed suppressing effect of added xenon on the product yields and the lack of inhibition by nitric oxide, we propose intramolecular hydrogen abstraction of the hot triplet 2^{T*} for the formation of 1-butene and the cyclic products as shown in Scheme 3. Deactivation of the hot triplet by collision leads to the *cis* → *trans* isomerization as the major photoreaction.

The low yield for the intramolecular hydrogen

TABLE 3. Mercury photosensitization of some alkenes[a]

Alkene	Press (torr)	Allylic C—C fission	Olefinic type II reaction	Cyclo-propane formation	*cis–trans* Isomeri-zation	Other reactions	Reference
1-Butene	14.7	0.48[c]	—	0.04	—	<0.01	(4)
2-Butene	30	[e]	—	[e]	0.50	<0.01	[g]
1-Pentene[b]	15	5%	72%	[f]	—	22%	(14)
1-Hexene	10	[e]	0.21	[e]	—	0.02	This work
cis-2-Octene	10	[e]	0.06	[e]	0.44	0.01	This work
Cyclopentene	30	0.24	—	[e]	—	0.03[d]	(5)
1-Methylcyclopentene	10	0.20	—	[e]	—	0.01	(6)
Cyclohexene	10	0.20[c]	—	0.01[h]	—	0.01	(7)[h]
3-Methylcyclohexene	10	0.02	—	[e]	—	0.02	(8)
cis-4,5-Dimethylcyclohexene	9	0.008	—	[e]	—	0.03	(9)
trans-4,5-Dimethylcyclohexene	9	0.008	—	[e]	—	0.03	(9)
Cycloheptene	6	>0.05	>0.04[h]	[e]	—	<0.03	(10)[h]
cis-Cyclooctene	4.5	[e]	0.34	0.05	0.08	0.03	(18)
cis-Cyclononene[b]	1.0	[e]	43%	57%	[f]	[e]	(11)

[a]Shown in quantum yield reported, unless otherwise noted.
[b]Shown in % composition, since yields have been reported in μmol.
[c]Combined yield of allylic C—C and C—H bond fission.
[d]Dimeric products (Φ =0.43) were also obtained.
[e]Formation not reported.
[f]Yield not determined.
[g]References 26 and 27.
[h]Unpublished results of the authors.

Can. J. Chem. Downloaded from www.nrcresearchpress.com by 210.87.254.6 on 09/05/12
For personal use only.

abstraction reactions in this system may be attributable to the greater freedom in vibration and rotation than that of 1-hexene, since intramolecular relaxation of excess vibrational energy is considered to diminish the rate of the hydrogen abstractions.

The results of the mercury photosensitization studies of simple alkenes so far reported are summarized in Table 3. Reactions of the vibrationally excited triplet of alkenes may be classified according to the primary processes; (*1*) the allylic C—C and C—H bond fission, (*2*) the intramolecular hydrogen abstraction, mainly the olefinic type II reaction, (*3*) the 1,2-shift of allylic hydrogen providing cyclopropanes, and (*4*) the *cis–trans* isomerization as the result of collisional deactivation of the triplet. Other miscellaneous reactions reported are also listed. As shown in Table 3, the major photoreaction of the vibrationally excited triplet of open-chain alkenes without a γ-hydrogen is merely the allylic C—C and C—H bond cleavages in addition to the *cis–trans* isomerization. The alkenes carrying a γ-hydrogen atom contrarily undergo the olefinic type II reaction upon mercury photosensitization instead of the allylic fission. Regarding cycloalkenes, steric restrictions in cyclopentene and cyclohexene completely prevent intramolecular hydrogen abstraction and allylic fission is predominant, while the larger cyclic alkenes do undergo the type II reaction in high yield, especially in the photolysis of cyclooctene.

It is thus concluded that the vibrationally excited π,π^* triplet of simple alkenes with a γ-hydrogen mainly undergoes intramolecular hydrogen abstraction via a six-membered transition state, although the main course of the reaction of the triplet alkenes with vibrational activation had previously been believed to be the well-known allylic bond cleavage.

1. J. Saltiel, J. D'Agostino, E. D. Megarity, L. Metts, K. R. Neuberger, M. Wrighton, and O. C. Zafiriou. Org. Photochem. **3**, 1 (1973).
2. P. J. Kropp. J. Am. Chem. Soc. **91**, 5783 (1969).
3. J. G. Calvert and J. N. Pitts, Jr. Photochemistry. Wiley, New York. 1966. p. 98.
4. R. J. Cvetanović and L. C. Doyle. J. Chem. Phys. **37**, 543 (1962).
5. W. A. Gibbons, W. F. Allen, and H. E. Gunning. Can. J. Chem. **40**, 568 (1962).
6. G. R. De Maré, N. Aritheunis, J. Olbregts, and M. Termonia. J. Photochem. **4**, 299 (1975).
7. G. R. De Maré, O. P. Strausz, and H. E. Gunning. Can. J. Chem. **43**, 1329 (1965).
8. G. R. De Maré. Bull. Soc. Chim. Belges. **81**, 459 (1972).
9. Y. Inoue, S. Takamuku, and H. Sakurai. Bull. Chem. Soc. Jpn. **48**, 3101 (1975).
10. Y. Inoue, M. Kadohira, S. Takamuku, and H. Sakurai. Tetrahedron Lett. 459 (1974).
11. Y. Inoue, S. Takamuku, and H. Sakurai. Bull. Chem. Soc. Jpn. **49**, 1147 (1976).
12. Y. Inoue, K. Moritsugu, S. Takamuku, and H. Sakurai. J. Chem. Soc. Perkin II, 569 (1976).
13. P. J. Wagner. Acc. Chem. Res. **4**, 168 (1971).
14. J. R. Major, J. F. T. Pinkard, and J. C. Robb. Trans. Faraday Soc. **60**, 1247 (1964).
15. D. W. Placzek and B. S. Rabinovitch. Can. J. Chem. **43**, 820 (1965).
16. K. Yang. J. Am. Chem. Soc. **86**, 3941 (1964).
17. M. Hasegawa, H. Aoyama, and N. Yamaki. Jpn. Anal. **23**, 28 (1974).
18. J. Meinwald, J. J. Tufariello, and J. J. Hurst. J. Org. Chem. **29**, 2914 (1964).
19. G. S. Hammond, N. J. Turro, and R. S. H. Liu. J. Org. Chem. **28**, 3297 (1963).
20. P. R. Stapp and R. F. Kleinschmidt. J. Org. Chem. **30**, 3006 (1965).
21. J. A. Sousa and A. L. Bluhm. J. Org. Chem. **25**, 108 (1960).
22. R. G. Salomon and J. K. Kochi. Tetrahedron Lett. 4387 (1973).
23. J. G. Calvert and J. N. Pitts, Jr. Photochemistry. Wiley, New York. 1966. p. 93.
24. H. E. Gunning and O. P. Strausz. Adv. Photochem. **1**, 209 (1963).
25. Y. Inoue, S. Takamuku, and H. Sakurai. J. Chem. Soc. Chem. Commun. 896 (1975).
26. R. B. Cundall and T. F. Palmer. Trans. Faraday Soc. **56**, 1211 (1960).
27. M. Termonia and G. R. De Maré. Chem. Phys. Lett. **25**, 402 (1974).

Can. J. Chem. Downloaded from www.nrcresearchpress.com by 210.87.254.6 on 09/05/12
For personal use only.

Excess volume and viscosity of binary liquid acid–base mixtures

HORACIO N. SÓLIMO, ROQUE RIGGIO, JOSÉ A. ESPÍNDOLA, SILVIA DEL V. ALONSO, AND MIGUEL KATZ

Cátedra de Físico-Química, Facultad de Ciencias Exactas y Tecnología, Universidad Nacional de Tucumán, Tucumán, Argentina

Received April 1, 1976

Can. J. Chem. Downloaded from www.nrcresearchpress.com by 210.87.254.40 on 09/05/12
For personal use only.

HORACIO N. SÓLIMO, ROQUE RIGGIO, JOSÉ A. ESPÍNDOLA, SILVIA DEL V. ALONSO, and MIGUEL KATZ. Can. J. Chem. **54**, 3125 (1976).

Densities, viscosities, and refractive indices at 25 °C were determined for the systems: *o*-chlorophenol + *N*,*N*-dimethylaniline, *o*-chlorophenol + aniline, *o*-chlorophenol + *m*-toluidine, and *o*-chlorophenol + pyridine. From the experimental results the excess volume, excess viscosity, excess molar free energy of activation of flow, and the excess partial molar volume were calculated. There is evidence of complex formation between *o*-chlorophenol and the four bases.

HORACIO N. SÓLIMO, ROQUE RIGGIO, JOSÉ A. ESPÍNDOLA, SILVIA DEL V. ALONSO et MIGUEL KATZ. Can. J. Chem. **54**, 3125 (1976).

On a déterminé, à 25 °C, les densités, les viscosités et les indices de réfraction des systèmes *o*-chlorophénol + *N*,*N*-diméthylaniline, *o*-chlorophénol + aniline, *o*-chlorophénol + *m*-toluidine et *o*-chlorophénol + pyridine. A partir des résultats expérimentaux, on a calculé les volumes, les viscosités, les énergies libres molaires d'activation d'écoulement et les volumes molaires partiels apparents d'excès. On trouve des indications à l'effet qu'il y a formation de complexes entre *o*-chlorophénol et les quatre bases.

[Traduit par le journal]

Introduction

The present paper continues our investigation of the thermodynamic properties of binary liquid acid–base mixtures (1–3). Densities, viscosities, and refractive indices at different molar fraction were measured at 25 °C for the following systems: *o*-chlorophenol + *N*,*N*-dimethylaniline (CF + DMA), *o*-chlorophenol + aniline (CF + A), *o*-chlorophenol + *m*-toluidine (CF + T), and *o*-chlorophenol + pyridine (CF + P), where all species are polar and aniline, *m*-toluidine, and *o*-chlorophenol show hydrogen bonds in the pure state.

With the classification of Barker and Smith (4), our systems could be classified as 'associated solutions'.

The following thermodynamic functions were calculated from the experimental results: v^E (excess molar volume), η^E (excess viscosity), g^{*E} (excess molar free energy of activation of flow), and $v_i^{E,\infty}$ (excess molar partial volume at infinite dilution).

Experimental

The methods used in our laboratory for the densities, viscosities, and refractive indices measurements of binary liquid mixtures have been described previously (2).

Materials and Solutions

o-Chlorophenol, Merck p.a, was fractionally distilled over Zn powder, the middle fraction redistilled over BaO, and the middle colorless fraction collected. The purification of the other substances was previously described (2).

Mixtures were prepared by mixing weighed amounts of the pure liquids. Caution was taken to prevent evaporation.

Results

The experimental results for pure liquids are reported in Table 1 along with the values from the literature for comparison.

The experimental molar fractions, densities, viscosities, and refractive indices for all the systems[1] at 25 °C were used to calculate the excess thermodynamic functions with the following equations:

$$[1] \qquad \eta^E = \eta - (x_1\eta_1 + x_2\eta_2)$$

$$[2] \qquad v^E = v - (x_1v_1^0 + x_2v_2^0)$$

$$[3] \qquad g^{*E} = RT[\ln \eta v - (x_1 \ln \eta_1 v_1 + x_2 \ln \eta_2 v_2)]$$

$$[4] \qquad v_i^{E,\infty} = v_i^\infty - v_i^0$$

[1]Complete set of tabular data is available, at a nominal charge, from the Depository of Unpublished Data, CISTI, National Research Council of Canada, Ottawa, Canada K1A 0S2.

TABLE 1. Experimental values of density ρ (g cm^{-3}), viscosity η (cP), and refractive index at 25 °C

Component	ρ		η		n_D	
	Obs.	Lit.	Obs.	Lit.	Obs.	Lit.
CF	1.25750	1.2577(5)	3.31	—	1.55716	1.55676(5)
DMA	0.95232	0.95196(5)	1.228	1.285(9)	1.55661	1.55620(7)
A	1.01745	1.01750(7)	3.77	3.770(10)	1.58392	1.5840(7)
T	0.98444	0.98485(5)	3.25	3.31(8)	1.56578	1.56570(5)
P	0.97710	0.9772(6)	0.886	0.889(11)	1.50713	1.5067(10)

where η, η_1, and η_2 = viscosity of the mixture and of the pure components; v, v_1^0 and v_2^0 = molar volume of the mixture and of the pure components; x_1 = molar fraction of the *o*-chlorophenol; R = gas constant; T = absolute temperature; and v_i^∞ = partial molar volume of the i component at infinite dilution.

The molar volume v of the mixture is defined by

$$[5] \qquad v = \frac{x_1M_1 + x_2M_2}{\rho}$$

where M_1 and M_2 are the molecular weights of the components and ρ the density of the solution.

Each set of results was fitted with a Redlich–Kister (11) form of the type:

$$[6] \qquad X^E = x_1(1 - x_1)\sum_{j=1}^{n} a_j x_1^{j-1}$$

where X^E represents the excess property under consideration; a_j = polynomial coefficients; and n = polynomial degree.

The method of least-squares was used to determine the values of the coefficients a_j. In each case, the optimum number of coefficients was ascertained from an examination of the variation of the standard error of estimate with n,

$$[7] \qquad \sigma_x = [\sum(X_{obs}{}^E - X_{cal}{}^E)^2/(n_{obs} - n)]^{1/2}$$

where n_{obs} is the number of measurements.

The values adopted for the coefficients a_j (calculated with an IBM 1620 computer) and the standard error of the estimate σ associated with the use of [6] are summarized in Table 2.

Figures 1, 2, and 3 show experimental values of η^E, v^E, and g^{*E} as a function of the molar fraction of *o*-chlorophenol, respectively. The continuous curves were calculated from [6] using these values for the coefficients.

If at some point (Fig. 2) on the curve a tangent is drawn, it cuts the v^E axis ($x_1 = 0$) at a point corresponding to a $v_1{}^E$ value. Even though the coefficients a_2, a_3, ... from [6] have no physical significance, the first coefficient of this equation represents (12) the value of excess partial molar volume ($v_1{}^{E,\infty}$) at infinite dilution as long as this is the tangent where $x_1 = 0$.

The partial molar volumes at infinite dilution of the *o*-chlorophenol were calculated from [4] where $v_1{}^0$ = 102.235 cm^3 mol^{-1} and are included in Table 3 along with the excess partial molar volume at infinite dilution.

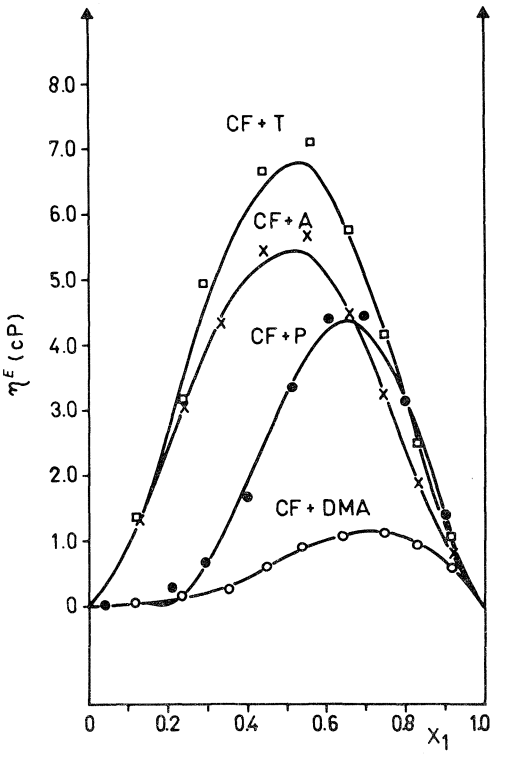

FIG. 1. Plot of η^E *vs.* x_1.

Can. J. Chem. Downloaded from www.nrcresearchpress.com by 210.87.254.40 on 09/05/12
For personal use only.

TABLE 2. Values of the coefficients for [5] determined by the method of least-squares[a]

System	Function	a_1	a_2	a_3	a_4	σ
CF + DMA	v^E	−1.638	0.391	−9.023	6.895	0.01
	η^E	1.069	−8.170	32.44	−17.02	0.05
	g^{*E}	9203	−1740	4714	−2198	7.90
CF + A	v^E	−2.636	−1.685	−9.011	11.53	0.03
	η^E	4.930	67.31	−67.11	—	0.18
	g^{*E}	1276	3766	−3617	—	7.81
CF + T	v^E	−3.683	−1.451	−5.580	6.487	0.01
	η^E	0.9976	98.68	−93.36	—	0.26
	g^{*E}	1347	4887	−4448	—	7.20
CF + P	v^E	−5.613	3.060	−23.39	21.55	0.02
	η^E	2.351	−50.40	233.0	−177.9	0.20
	g^{*E}	948.2	−1168	15680	−13330	10.38

[a]Units: v^E, cm³ mol⁻¹; η^E, cP; g^{*E}, cal mol⁻¹.

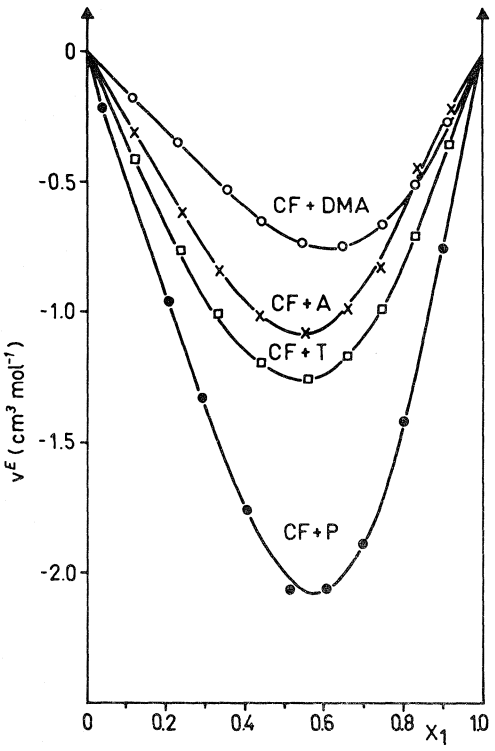

FIG. 2. Plot of v^E *vs.* x_1.

TABLE 3. Excess partial molar volume and partial molar volume at infinite dilution of component CF at 25 °C

System	$v_1^{E,\infty}$ (cm³ mol⁻¹)	v_1^{∞} (cm³ mol⁻¹)
CF + DMA	−1.638	100.597
CF + A	−2.636	99.599
CF + T	−3.683	98.552
CF + P	−5.613	96.622

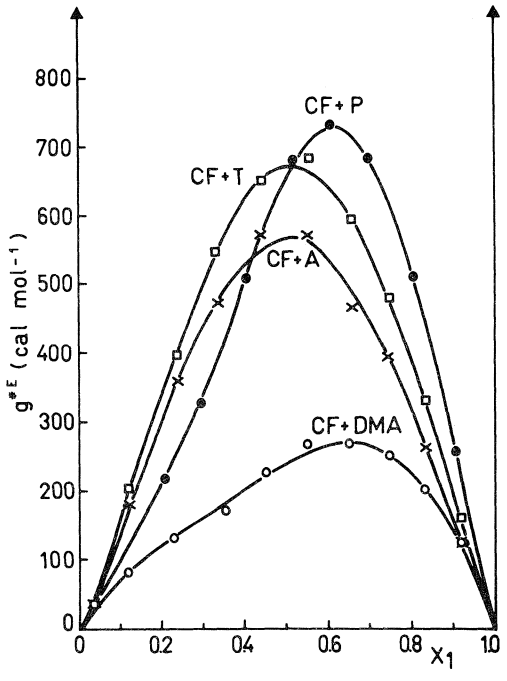

FIG. 3. Plot of g^{*E} *vs.* x_1.

Discussion

Figures 1 and 3 show well-marked maxima for the systems CF + A, CF + T, and CF + P, but for CF + DMA the maximum is not as well marked as the others.

Fialkov (13) and Fort and Moore (14) conclude that for the systems whose excess viscosity

Can. J. Chem. Downloaded from www.nrcresearchpress.com by 210.87.254.40 on 09/05/12
For personal use only.

Can. J. Chem. Downloaded from www.nrcresearchpress.com by 210.87.254.40 on 09/05/12
For personal use only.

show a similar behaviour as for the first three systems named before, the composition of the intermolecular complex formed can be fixed, at least to a first approximation, according to the molar relation indicated by the maxima. These complexes are more stable when the positive values of the maxima of η^E are bigger.

The stoichiometric relations of the formed complex can be obtained from Figs. 1 and 3; they are CF.T, CF.A, and 2CF.P. For the other system we cannot find a molar relation because the maximum is not well defined.

The symmetric curves of η^E and g^{*E} *vs.* x_1 for the systems CF + A and CF + T show that the necessary energy to break the hydrogen bonding in the mixing process for the pure liquids is similar for both components.

The other two systems show a shift of the maximum towards the higher mole fraction of *o*-chlorophenol, which indicates that the breaking energy of hydrogen bonding in *o*-chlorophenol, when mixing with pyridine, is not compensated by the weak N···H bonding of the base (15) and is not compensated at all when it is mixed with *N*,*N*-dimethylaniline, because of the absence of hydrogen bonding.

The *cis* isomer in *o*-chlorophenol presents an intramolecular hydrogen bond of the type O—H···Cl (16). This fact determines the impossibility of formation of hydrogen bonding with another molecule of the same kind. The ir spectrum (17) of *o*-chlorophenol shows O—H···O bonding between the *cis* and *trans* isomers with only 10% of the latter, approximately. The energy necessary to break the hydrogen bonding of the type O—H···O in *o*-chlorophenol is greater than the energy necessary to break the N—H···N one in aniline and *m*-toluidine (18); however, the little proportion of the *trans* isomer equilibrates this greater energy.

The behavior of these two systems is different from that containing propionic acid (2) and *m*-cresol (3) with the same bases.

The negative values of v^E in Fig. 2 for the four systems are explained by Prigogine (19) in terms of the different sizes of the molecules or the dipole–dipole interaction between them. The intermolecular association complex also contributes to these negative values.

In our case, all the chemical species are cyclic, so that little differences of size in the molecules are not important in the excess molar volume.

The minimum value of v^E for the system CF + P is explained by the great basic strength of pyridine (20) and the stability of the association complex (see Figs. 1 and 3). For the other systems the basic strength of the bases are similar; thus, the stability of the association complex accounts for the relative negative values.

Figure 3 shows for the CF + P system more positive g^{*E} values than the CF + T system. This situation is the reverse of that observed in Fig. 1 for η^E values. This could be explained considering that g^{*E} represents [3] the influence of η and v simultaneously (21). The greater contraction for the CF + P system is compensated with its lesser excess viscosity compared with the CF + T system. Nevertheless, the conclusions obtained with both excess functions are the same; thus the deformation of curves using g^{*E} in place of η^E is not important in this case.

From the analysis of the values in Table 3 we may conclude that the addition of 1 mol of *o*-chlorophenol in a large volume of the different bases produces a volume contraction in the order DMA < A < T < P.

The linear variation of the molar refraction for the four systems, calculated from the refractive indices by the Lorenz–Lorentz formula, in terms of the composition, is in agreement with the conclusion of Loiseleur (22) for a large number of ideal and nonideal systems. Neither the polar characteristics of the chemical species studied nor the existence of hydrogen bonding in the aniline, *m*-toluidine, and *o*-chlorophenol, and the intermolecular association complex seem to have any important effect on the linear dependence of this property on concentration.

Acknowledgments

This work was supported by a SECYT research grant. We are indebted to Mr. Eduardo Epstein for help in the computation programs.

1. H. N. Sólimo, R. Riggio, P. W. Lobo, and M. Katz. An. Asoc. Quim. Argent. **62**, 121 (1974).
2. H. N. Sólimo, R. Riggio, F. Davolio, and M. Katz. Can. J. Chem. **53**, 1258 (1975).
3. H. N. Sólimo and M. Katz. An. R. Soc. Esp. Fis. Quim. In press.
4. J. A. Barker and F. Smith. J. Chem. Phys. **22**, 375 (1954).
5. R. R. Dreisbach. Adv. Chem. Ser. **15** (1955).
6. W. Koglin. Kurzes Handbuch der Chemie. Vandenhoeck & Ruprecht, Göttingen. 1953. L–Z, p. 1449; A–Bix, p. 156.

7. J. TIMMERMANS. Physico-chemical constants of pure organic compounds. Elsevier Publishing Co., Inc., N.Y. 1950. p. 552, 553, and 556.
8. N. A. LANGE. Handbook of chemistry. 9th ed. McGraw Hill Handbook Publishers Inc., Sandusky, Ohio. 1956.
9. A. WEISSBERGER, E. S. PROSKAUER, J. A. RIDDIK, and E. E. TOOPS. Organic solvents. Vol. VII. 2nd ed. Interscience Publ. Inc., New York. 1959. pp. 235, 243.
10. International Critical Tables. McGraw Hill Book Co., Inc., New York and London. 1929. Vol. V, p. 36; Vol. VII, p. 218.
11. O. REDLICH and A. T. KISTER. Ind. Eng. Chem. **40**, 345 (1948).
12. J. P. GROLIER and A. VIALLARD. C. R. Acad. Sci. Ser. C, **265**, 953 (1967).
13. YU YA FIALKOV. Russ. J. Phys. Chem. **37**, 1051 (1963).
14. R. J. FORT and W. R. MOORE. Trans. Faraday Soc. **62**, 1112 (1966).
15. V. T. DESHPANDE and K. G. PATHKI. Trans. Faraday Soc. **58**, 2134 (1962).
16. L. PAULING. Uniones químicas. 3rd. ed. *Edited by* Kapelusz. 1965. p. 504.
17. J. ERRERA and P. MOLLET. J. Phys. Radium, **6**, 281 (1935).
18. A. L. MCCLELLAN and G. C. PIMENTEL. The hydrogen bond. W. H. Freeman & Co., San Francisco and London. 1960. p. 213.
19. I. PRIGOGINE. The molecular theory of solutions. North Holland Publ. Co., Amsterdam. 1957.
20. D. J. CRAM and G. S. HAMMOND. Organic chemistry. 2nd ed. McGraw Hill Book Co., New York. 1964.
21. R. MEYER, M. MEYER, J. METZGER, and A. PENELOUX. J. Chim. Phys. **68**, 406 (1971).
22. H. LOISELEUR. Thèse de doctorat-ès-Sciences, University of Lyon, Lyon. 1965. p. 80.

Can. J. Chem. Downloaded from www.nrcresearchpress.com by 210.87.254.40 on 09/05/12
For personal use only.

Crystal and molecular structure of *B*,*B*-bis(*p*-tolyl)boroxazolidine and the orthorhombic form of *B*,*B*-diphenylboroxazolidine

STEVEN J. RETTIG AND JAMES TROTTER

Department of Chemistry, University of British Columbia, 2075 Wesbrook Place, Vancouver, B.C., Canada V6T 1W5

Received April 6, 1976

STEVEN J. RETTIG and JAMES TROTTER. Can. J. Chem. **54**, 3130 (1976).

Crystals of *B*,*B*-bis(*p*-tolyl)boroxazolidine, **1***c*, are trigonal, $a = 25.1028(9)$, $c = 12.4184(7)$ Å, $Z = 18$, space group $R\bar{3}$. And crystals of *B*,*B*-diphenylboroxazolidine, **1***a*, are orthorhombic, $a = 17.6420(4)$, $b = 14.2527(3)$, $c = 10.205(1)$ Å, $Z = 8$, space group *Pbca*. Both structures were solved by direct methods and were refined by full-matrix least-squares procedures to final *R* values of 0.057 and 0.040 for 2230 and 1828 reflections with $I \geq 3\sigma(I)$ respectively. Both molecules have structures similar to related compounds and feature intermolecular N—H . . . O hydrogen bonds (N . . . O = 2.982(2) for **1***c* and 2.896(2) Å for **1***a*). Bond lengths are: for **1***c*; O—C, 1.413(3), O—B, 1.478(3), N—C, 1.488(3), N—B, 1.657(3), C(sp^3)—C(sp^3), 1.501(4), B—C, 1.616(3) and 1.623(3), mean C—C(ar), 1.395, N—H, 0.93(2) and 0.94(2), mean C(sp^3)—H, 1.00, and mean C(ar)—H, 1.00 Å; for **1***a*; O—C, 1.409(2), O—B, 1.476(2), N—C, 1.489(2), N—B, 1.655(2), C(sp^3)—C(sp^3), 1.507(3), B—C, 1.613(2) and 1.620(2), mean C—C(ar), 1.391, N—H, 0.93(2) and 0.92(2), mean C(sp^3)—H, 1.00, and mean C(ar)—H, 0.98 Å. A statistical analysis of the phenyl C—C distances in compounds **1***a*, **1***b*, and **1***c* has provided an example of statistically significant substituent-induced bond length variation in the phenyl rings.

STEVEN J. RETTIG et JAMES TROTTER. Can. J. Chem. **54**, 3130 (1976).

La structure cristalline de la bis(*p*-tolyl)-*B*,*B* boroxazolidine, **1***c*, est trigonale, $a = 25.1028(9)$, $c = 12.4184(7)$ Å, $Z = 18$, groupe d'espace $R\bar{3}$. Et la structure cristalline de la diphényl-*B*,*B* boroxazolidine, **1***a*, est orthorhombique, $a = 17.6420(4)$, $b = 14.2527(3)$, $c = 10.205(1)$ Å, $Z = 8$, groupe d'espace *Pbca*. Les deux structures ont été résolues par des méthodes directes et affinées par la méthode des moindres carrés (matrice complète) jusqu'à un facteur d'accord final *R* respectif de 0.057 et 0.040 pour 2230 et 1828 réflexions avec $I \geq 3\sigma(I)$. Les deux molécules ont des structures similaires aux composés parents et possèdent des liens hydrogènes intermoléculaires N—H . . . O (N . . . O = 2.982(2) pour **1***c* et 2.896(2) Å pour **1***a*). Les longueurs des liens sont: pour **1***c*: O—C, 1.413(3), O—B, 1.478(3), N—C, 1.488(3), N—B, 1.657(3), C(sp^3)—C(sp^3), 1.501(4), B—C, 1.616(3) et 1.623(3), la moyenne de C—C(ar), 1.395, N—H, 0.93(2) et 0.94(2), la moyenne de C(sp^3)—H, 1.00 et la moyenne de C(ar)—H, 1.00 Å; pour **1***a*; O—C, 1.409(2), O—B, 1.476(2), N—C, 1.489(2), N—B, 1.655(2), C(sp^3)—C(sp^3), 1.507(3), B—C, 1.613(2) et 1.620(2), la moyenne de C—C(ar), 1.391, N—H, 0.93(2) et 0.92(2), la moyenne de C(sp^3)—H, 1.00 et la moyenne de C(ar)—H, 0.98 Å. Une analyse statistique des distances des liens C—C dans le phényle des composés **1***a*, **1***b* et **1***c* a donné un exemple d'une variation statistiquement importante de la longueur des liens sous l'influence des substituants dans les noyaux phényles.

[Traduit par le journal]

Can. J. Chem. Downloaded from www.nrcresearchpress.com by 210.87.254.105 on 09/05/12
For personal use only.

Introduction

Recent structural investigations of boroxazolidines **1***a* (monoclinic form), **1***b*, and **2** (1–3) and the related compound **3** (4) have shown a reasonably consistent, but not entirely convincing, trend of bond length variation in the aromatic rings. The structural data (1–4) indicate that the tetrahedral boron substituent is electron releasing. When R is C_6H_5 as in **1***a*, **2**, and **3** the bonds in the phenyl rings should decrease in length with greater distance from the boron substituent since any electron density released must be accommodated in π^* antibonding orbitals. In the case of **1***b*, which has an electron withdrawing fluorine atom *para* to the boron, this effect should be amplified if the electronic effects of the substituents are localized. Such asymmetry has been noted in the four structures which have been determined but valid arguments can be raised that such bond length differences may be a result of thermal motion even though corrections have been applied in each case.

In order to establish that this variation of the phenyl ring bond distances is indeed an electronic effect and is not due to inadequate correction for thermal motion, the structures of *B*,*B*-bis(*p*-tolyl)boroxazolidine (**1***c*) and the orthorhombic form of *B*,*B*-diphenylboroxazolidine (**1***a*) are now

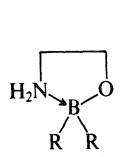

1

a R = C_6H_5
b R = *p*-FC_6H_4
c R = *p*-$CH_3C_6H_4$

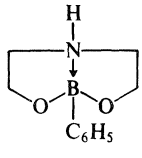

2

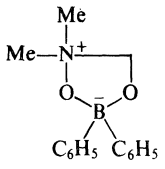

3

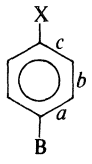

4

reported. Of special interest is the structure of **1***c* which has an electron releasing methyl group *para* to the boron. This should cause the 'outer' bonds in the phenyl rings to be longer than in the other compounds.

Experimental

B,B-Bis(p-tolyl)boroxazolidine

B,B-Bis(*p*-tolyl)boroxazolidine was prepared as previously described (5). Recrystallization from 100% ethanol gave crystals suitable for X-ray analysis. The crystal chosen for study was mounted with *c* parallel to the goniostat axis and had dimensions of *ca.* 0.3 × 0.3 × 0.5 mm. Unit-cell and space group data were obtained from film and diffractometer measurements. The unit-cell parameters were refined by a least-squares treatment of $\sin^2\theta$ values for 20 reflections measured on a diffractometer with Cu K_α radiation. Crystal data are:

$C_{16}H_{20}BNO$ f.w. = 253.2

Trigonal, a = 25.1028(9), c = 12.4184(7) Å, V = 6777.1(5) A^3, ρ_m = 1.12 (flotation in aqueous KI), Z = 18, ρ_c = 1.1165(1) g cm^{-3}, $F(000)$ = 2448 (23 °C, Cu K_α, λ = 1.5418 Å, μ = 5.3 cm^{-1}). Absent reflections: hkl, $-h + k + l \neq 3n$, space group $R\bar{3}$(C_{3i}^2, No. 148).

Intensities were measured on a Datex-automated General Electric XRD 6 diffractometer, with a scintillation counter, Cu K_α (nickel filter and pulse height analyser), and a θ–2θ scan at 2° min^{-1} over a range of (1.80 + 0.86 tan θ) deg in 2θ, with 10 s background counts being measured at each end of the scan. Data were measured to 2θ = 146° (minimum interplanar spacing 0.81 Å). The intensity of the check reflection, measured every 40 reflections, remained within ±5% of its mean value during the data collection. Lorentz and polarization corrections and check reflection scaling were applied, and the structure amplitudes were derived. No absorption correction was made in view of the low value of μ. Of the 3011 independent reflections measured, 747 had intensities less than $3\sigma(I)$ above background where $\sigma^2(I) = S + B + (0.06S)^2$ with S = scan count and B = time averaged background count. These reflections were given zero weight in the refinement but were included in the structure factor calculations.

The systematic absences allow space groups $R3$ or $R\bar{3}$, the latter being indicated by the E statistics. The structure was solved by direct methods using tangent formula refinement (6–8). Eight sets of signs for 249 reflections with normalized structure factor $|E| \geq 1.70$ were determined. The phase of 13 7 3 was fixed at 0 to define the origin and symbol phases were assigned to the reflections −6 19 5, 13 8 2, and 13 7 0. One set of signs was outstanding in that it had the lowest value of Rk (0.166) and the greatest number of phases determined (249) with 118 positive and 131 negative signs. An E-map calculated from this set clearly gave positions for the 19 non-hydrogen atoms.

Two cycles of isotropic followed by two cycles of anisotropic full-matrix least-squares refinement of the non-hydrogen atoms gave R = 0.101. A difference map at this point gave the positions of all 20 hydrogen atoms. The entire structure (including hydrogen atoms with isotropic thermal parameters) was refined for 6 cycles giving a final R of 0.057 and R_w of 0.075 for 2230 reflections with $I \geq 3\sigma(I)$ (34 reflections which had $|F_o| - |F_c| > 3\sigma(F)$ were removed from the data set in the final stages of refinement).

The least-squares refinement was based on the minimization of $\sum w[|F_o| - |F_c/(1 + gI)|]^2$ where g is the extinction parameter and I the uncorrected intensity. The final value of g was 5.73×10^{-8}. The scattering factors of ref. 9 were used for the non-hydrogen atoms and those of ref. 10 for the hydrogen atoms. Anomalous scattering factors from ref. 11 were used for the non-hydrogen atoms. The anisotropic thermal parameters employed in the refinement are U_{ij} in the expression:

$$f = f^0 \exp[-2\pi^2(U_{11}h^2a^{*2} + U_{22}k^2b^{*2} + U_{33}l^2c^{*2} + 2U_{12}hka^*b^* + 2U_{13}hla^*c^* + 2U_{23}klb^*c^*)]$$

where f^0 is the tabulated scattering factor and f is that corrected for thermal motion. The weighting scheme: $w = 1/\sigma^2(F)$ where $\sigma^2(F)$ is derived from the previously defined $\sigma^2(I)$ gave uniform average values of $w(|F_o| - |F_c|)^2$ over ranges of $|F_o|$ and was employed in the final stages of refinement. On the final cycle of refinement the mean parameter shift was 0.1σ and the largest shift, 1.1σ, was associated with the methyl hydrogen atom H(15*c*). The mean error in an observation of unit weight was 1.70.

B,B-Diphenylboroxazolidine

Crystals of the orthorhombic form of *B,B*-diphenylboroxazolidine were obtained by recrystallization of the monoclinic form (5) from 100% ethanol. Experimental details for **1***a* are the same as for **1***c* except where noted. The crystal used for data collection was mounted with *c* parallel to the goniostat axis and had dimensions of *ca.* 0.25 × 0.35 × 0.50 mm. A total of 22 reflections was used in the refinement of the unit-cell parameters. Crystal data are

$C_{14}H_{16}BNO$ f.w. = 225.1

Orthorhombic, a = 17.6420(4), b = 14.2527(3), c = 10.205(1) Å, V = 2566.0(4) $Å^3$, ρ_m = 1.17 (flotation in aqueous KI), Z = 8, ρ_c = 1.1653(2) g cm^{-3}, $F(000)$ = 960 (22 °C, Cu K_α, λ = 1.5418 Å, μ = 5.7 cm^{-1}). Absent

Can. J. Chem. Downloaded from www.nrcresearchpress.com by 210.87.254.105 on 09/05/12
For personal use only.

Can. J. Chem. Downloaded from www.nrcresearchpress.com by 210.87.254.105 on 09/05/12
For personal use only.

reflections: $0kl$, $k \neq 2n$, $h0l$, $l \neq 2n$, and $hk0$, $h \neq 2n$ define uniquely the space group $Pbca$ (D_{2h}^{15}, No. 61).

The intensity of the check reflection remained constant within ±4% during the data collection. Of 2567 independent reflections measured, 725 had intensities less than $3\sigma(I)$ above background.

The structure was solved by direct methods. Sixteen sets of signs for 361 reflections with normalized structure factor $|E| \geq 1.50$ were determined by a computer program which uses Sayre relationships in an iterative procedure (12). One set of signs was outstanding in that it converged in 5 cycles to a set having the highest consistency index (0.65) with 179 positive and 182 negative signs. The 17 non-hydrogen atoms accounted for the 17 highest peaks on an E-map calculated from this set.

Two cycles of isotropic followed by two cycles of anisotropic refinement of the non-hydrogen atoms gave $R = 0.124$. A difference map then gave the positions of the 16 hydrogen atoms. The entire structure (including hydrogen atoms with isotropic thermal parameters) was refined for 6 cycles giving a final R of 0.040 and R_w of 0.052 for 1828 reflections with $I \geq 3\sigma(I)$ (14 observed and 3 unobserved planes which had $(|F_o| - |F_c|) > 3\sigma(F)$ were given zero weight in the final stages of refinement). The mean error in an observation of unit weight was 1.10 and the final value of the extinction parameter g was 1.13×10^{-7}. The mean parameter shift on the final cycle was 0.26σ, the largest shift corresponding to 1.0σ.

The final positional parameters for both **1***c* and **1***a* are given in Table 1 and the thermal parameters in Table 2. Measured and calculated structure factors have been placed in the Depository of Unpublished Data.[1]

The thermal motions of both **1***c* and **1***a* have been analysed in terms of rigid-body modes of translation,

TABLE 1. Final positional parameters (fractional × 10^5, H × 10^3) with estimated standard deviations in parentheses

Atom	x	y	z
	$(p\text{-}CH_3C_6H_4)_2BOCH_2CH_2NH_2$		
O	28999(6)	35637(6)	23114(11)
N	27136(8)	33645(8)	42062(15)
C(1)	22907(10)	30781(12)	24615(21)
C(2)	22863(13)	28192(12)	35533(23)
C(3)	38327(8)	42119(8)	34792(15)
C(4)	40849(10)	38615(10)	38294(20)
C(5)	47107(10)	41002(12)	39445(21)
C(6)	51223(10)	47063(11)	37047(17)
C(7)	48823(11)	50596(11)	33263(21)
C(8)	42515(10)	48212(10)	32259(19)
C(9)	28662(8)	44126(9)	34430(16)
C(10)	27797(11)	46144(11)	44367(19)
C(11)	25928(12)	50493(12)	45283(23)
C(12)	24856(11)	53054(10)	36214(23)
C(13)	25802(11)	51182(11)	26386(22)
C(14)	27618(10)	46844(10)	25400(19)
C(15)	58046(12)	49684(20)	38579(29)
C(16)	22676(27)	57666(22)	37191(49)
B	31013(10)	39211(10)	33225(17)
H(*n*1)	250(1)	347(1)	469(2)
H(*n*2)	294(1)	324(1)	463(2)
H(1*a*)	199(1)	325(1)	246(2)
H(1*b*)	218(1)	273(1)	186(3)
H(2*a*)	190(2)	257(2)	392(3)
H(2*b*)	245(1)	252(2)	348(3)
H(4)	384(1)	344(1)	401(2)
H(5)	490(1)	385(1)	419(2)
H(7)	515(1)	548(1)	310(2)
H(8)	411(1)	511(1)	299(2)
H(10)	288(1)	445(1)	511(2)
H(11)	255(1)	519(1)	528(3)
H(13)	248(1)	528(1)	202(2)
H(14)	284(1)	455(1)	179(2)
H(15*a*)	599(3)	538(3)	385(5)
H(15*b*)	589(2)	469(2)	430(4)
H(15*c*)	604(2)	503(2)	310(3)
H(16*a*)	238(2)	596(2)	440(4)
H(16*b*)	185(4)	566(4)	360(6)
H(16*c*)	253(2)	613(3)	333(4)
	$(C_6H_5)_2BOCH_2CH_2NH_2$		
O	20127(6)	24456(7)	9778(8)
N	22689(8)	21673(9)	32273(11)
C(1)	13737(10)	19860(14)	15008(15)
C(2)	16286(15)	15654(17)	27824(19)
C(3)	32762(8)	31126(11)	17878(14)
C(4)	36650(10)	26077(13)	8284(17)
C(5)	44304(12)	27441(18)	5999(22)
C(6)	48300(12)	33817(21)	13282(26)
C(7)	44649(14)	38844(21)	22829(26)
C(8)	36992(11)	37601(15)	25030(19)
C(9)	19404(9)	39099(10)	24411(14)
C(10)	19332(10)	43197(11)	36854(15)
C(11)	15531(12)	51534(12)	39337(19)
C(12)	11720(12)	56119(13)	29459(21)
C(13)	11820(12)	52365(12)	17072(20)
C(14)	15548(10)	44027(12)	14660(16)
B	23863(10)	29574(11)	20570(13)
H(*n*1)	271(1)	181(1)	335(2)
H(*n*2)	217(1)	241(1)	404(2)
H(1*a*)	117(1)	150(1)	90(2)
H(1*b*)	94(1)	246(1)	167(2)
H(2*a*)	124(1)	147(2)	344(3)
H(2*b*)	180(2)	88(3)	273(4)
H(4)	339(1)	214(1)	34(2)
H(5)	468(1)	238(2)	−5(2)
H(6)	536(1)	354(2)	118(2)
H(7)	473(2)	430(2)	284(3)
H(8)	344(1)	420(2)	316(2)
H(10)	222(1)	400(1)	436(2)
H(11)	157(1)	541(2)	476(3)
H(12)	88(1)	620(2)	311(2)
H(13)	90(1)	557(1)	99(2)
H(14)	153(1)	409(1)	58(2)

[1]The structure factor table is available, at a nominal charge, from the Depository of Unpublished Data, CISTI, National Research Council of Canada, Ottawa, Canada K1A 0S2.

Can. J. Chem. Downloaded from www.nrcresearchpress.com by 210.87.254.105 on 09/05/12
For personal use only.

libration, and screw motion (13) using the computer program MGTLS. Rigid-body analyses were successful for the $CH_3C_6H_4B$ groups in **1***c* [rms σU_{ij} = 0.0013 Å^2, rms ΔU_{ij} = 0.0019 (C(3)–C(8)), and 0.0029 Å^2 (C(9)–C(14))] and for the C_6H_5B groups in **1***a* [rms σU_{ij} = 0.0010 Å^2, rms ΔU_{ij} = 0.0018 (C(3)–C(8)) and 0.0016 Å^2 (C(9)–C(14))]. The appropriate bond distances for both compounds have been corrected for libration (14, 15) and appear along with the uncorrected distances in Table 3.

Results and Discussion

The atom numbering schemes and 50% probability thermal ellipsoids for the two molecules are shown in Fig. 1. The structure of *B,B*-bis(*p*-tolyl)boroxazolidine (**1***c*) viewed into *c* is shown in Fig. 2 and that of *B,B*-diphenylboroxazolidine (**1***a*) viewed along *c* in Fig. 3. Bond angles are given in Table 4 and intra-annular torsion angles in the five-membered rings are listed in Table 5. Some weighted least squares mean planes are given in Table 6 and nonbonded contacts and details of the hydrogen bonding arrangements in Table 7.

The conformations of the five-membered boroxazolidine rings in compounds **1***a*, **1***b*, and **1***c* are significantly different from each other as shown in Table 5. Each of the four different conformations corresponds closely to one of the minimum strain energy conformations calculated for cyclopentane by Hendrickson (16). Since the four structures represent four different space

TABLE 2. Final thermal parameters and their estimated standard deviations
(*a*) Anisotropic thermal parameters ($U_{ij} \times 10^4$ Å^2)

Atom	U_{11}	U_{22}	U_{33}	U_{12}	U_{13}	U_{23}
			$(p\text{-}CH_3C_6H_4)_2BOCH_2CH_2NH_2$			
O	406(7)	478(8)	512(8)	148(6)	27(6)	−44(6)
N	418(9)	463(9)	556(11)	212(8)	69(8)	101(8)
C(1)	433(12)	591(13)	648(14)	139(11)	−13(10)	−53(11)
C(2)	562(14)	479(13)	801(17)	81(12)	−14(12)	99(12)
C(3)	406(10)	394(9)	425(9)	170(8)	17(8)	−12(7)
C(4)	431(11)	443(11)	738(15)	194(9)	43(10)	78(10)
C(5)	474(12)	649(14)	739(16)	291(11)	35(11)	73(12)
C(6)	407(11)	645(14)	491(11)	182(10)	3(8)	−88(10)
C(7)	458(12)	464(12)	697(14)	77(10)	62(10)	8(10)
C(8)	483(12)	440(11)	635(13)	188(9)	33(9)	66(9)
C(9)	374(9)	433(10)	490(11)	172(8)	28(8)	38(8)
C(10)	652(14)	581(13)	537(13)	341(11)	3(10)	5(10)
C(11)	768(16)	624(15)	693(16)	398(13)	31(12)	−103(12)
C(12)	547(13)	499(12)	853(17)	279(11)	−9(12)	−1(11)
C(13)	556(13)	559(13)	721(16)	293(11)	−27(11)	133(11)
C(14)	510(12)	551(12)	535(13)	272(10)	14(9)	57(9)
C(15)	427(13)	961(23)	804(20)	206(14)	−12(12)	−70(17)
C(16)	1193(34)	846(25)	1371(39)	748(26)	−29(29)	−59(26)
B	403(11)	422(11)	430(11)	188(9)	31(8)	39(9)
			$(C_6H_5)_2BOCH_2CH_2NH_2$			
O	496(6)	485(6)	211(5)	−21(5)	7(4)	−39(4)
N	480(7)	391(6)	237(5)	−16(6)	12(5)	11(5)
C(1)	507(9)	631(11)	342(8)	−108(8)	−5(7)	−95(7)
C(2)	850(15)	722(13)	472(10)	−377(12)	−149(10)	171(9)
C(3)	454(8)	455(8)	321(7)	−15(7)	1(6)	128(6)
C(4)	491(9)	558(10)	465(9)	73(8)	60(7)	118(8)
C(5)	542(11)	889(16)	653(12)	138(11)	171(10)	232(11)
C(6)	447(11)	1208(21)	880(16)	−106(13)	63(11)	363(15)
C(7)	606(13)	1108(19)	810(16)	−321(13)	−87(12)	66(14)
C(8)	573(10)	738(12)	525(10)	−175(9)	−13(9)	12(10)
C(9)	458(8)	386(7)	312(7)	−42(6)	38(6)	−2(6)
C(10)	658(10)	404(8)	338(7)	−60(8)	65(7)	−29(6)
C(11)	855(14)	434(10)	516(11)	−95(9)	201(9)	−120(8)
C(12)	695(12)	383(9)	801(13)	28(9)	176(10)	−25(9)
C(13)	692(12)	459(10)	660(12)	67(9)	−48(10)	57(8)
C(14)	620(10)	462(9)	413(9)	51(8)	−24(7)	26(7)
B	470(9)	384(8)	213(6)	−16(7)	−5(6)	21(6)

TABLE 2 *(Concluded)*

(*b*) Isotropic thermal parameters ($U \times 10^3$)

Atom	U (Å^2)	Atom	U (Å^2)
	$(p\text{-}CH_3C_6H_4)_2BOCH_2CH_2NH_2$		
H(*n*1)	67(7)	H(10)	80(8)
H(*n*2)	66(7)	H(11)	97(10)
H(1*a*)	61(7)	H(13)	82(9)
H(1*b*)	90(9)	H(14)	79(8)
H(2*a*)	99(10)	H(15*a*)	189(24)
H(2*b*)	94(10)	H(15*b*)	154(17)
H(4)	71(7)	H(15*c*)	110(11)
H(5)	87(9)	H(16*a*)	117(15)
H(7)	87(8)	H(16*b*)	224(34)
H(8)	59(6)	H(16*c*)	140(17)
	$(C_6H_5)_2BOCH_2CH_2NH_2$		
H(*n*1)	59(5)	H(6)	100(8)
H(*n*2)	67(6)	H(7)	123(10)
H(1*a*)	49(4)	H(8)	82(7)
H(1*b*)	62(6)	H(10)	51(5)
H(2*a*)	99(8)	H(11)	93(8)
H(2*b*)	166(15)	H(12)	74(6)
H(4)	61(5)	H(13)	75(6)
H(5)	85(7)	H(14)	70(6)

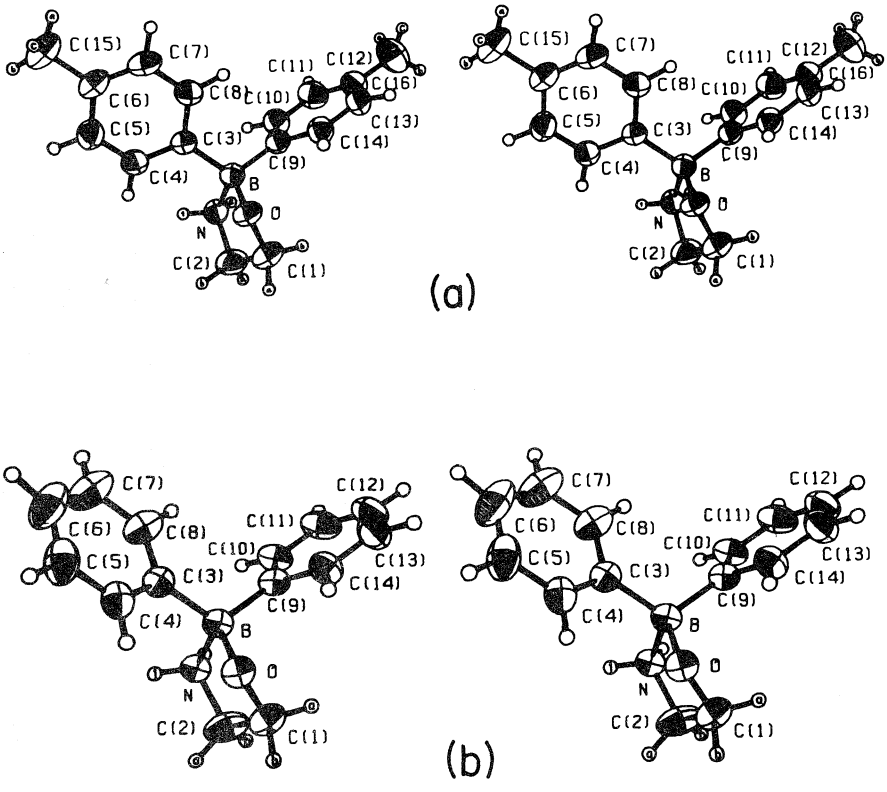

FIG. 1. Stereo views of *B*,*B*-bis(*p*-tolyl)boroxazolidine (*a*) and *B*,*B*-diphenylboroxazolidine (*b*); 50% ellipsoids are shown for the non-hydrogen atoms.

Can. J. Chem. Downloaded from www.nrcresearchpress.com by 210.87.254.105 on 09/05/12
For personal use only.

TABLE 3. Bond lengths (Å) with estimated standard deviations in parentheses

(*a*) Non-hydrogen atoms

Bond	Distance		Bond	Distance	
	Uncorrected	Corrected		Uncorrected	Corrected
$(p\text{-}CH_3C_6H_4)_2BOCH_2CH_2NH_2$			$(C_6H_5)_2BOCH_2CH_2NH_2$		
O—C(1)	1.413(3)		O—C(1)	1.409(2)	
O—B	1.478(3)		O—B	1.476(2)	
N—C(2)	1.488(3)		N—C(2)	1.489(2)	
N—B	1.657(3)		N—B	1.655(2)	
C(1)—C(2)	1.501(4)		C(1)—C(2)	1.507(3)	
C(3)—C(4)	1.386(3)	1.397	C(3)—C(4)	1.395(2)	1.404
C(3)—C(8)	1.391(3)	1.403	C(3)—C(8)	1.393(2)	1.403
C(3)—B	1.613(3)	1.616	C(3)—B	1.609(2)	1.613
C(4)—C(5)	1.381(3)	1.384	C(4)—C(5)	1.384(3)	1.390
C(5)—C(6)	1.378(3)	1.390	C(5)—C(6)	1.369(4)	1.380
C(6)—C(7)	1.380(4)	1.392	C(6)—C(7)	1.370(4)	1.378
C(6)—C(15)	1.509(3)	1.510			
C(7)—C(8)	1.390(3)	1.394	C(7)—C(8)	1.381(3)	1.389
C(9)—C(10)	1.392(3)	1.403	C(9)—C(10)	1.398(2)	1.406
C(9)—C(14)	1.404(3)	1.414	C(9)—C(14)	1.395(2)	1.402
C(9)—B	1.619(3)	1.623	C(9)—B	1.617(2)	1.620
C(10)—C(11)	1.392(3)	1.398	C(10)—C(11)	1.388(3)	1.391
C(11)—C(12)	1.388(4)	1.398	C(11)—C(12)	1.377(3)	1.384
C(12)—C(13)	1.371(4)	1.381	C(12)—C(13)	1.373(3)	1.381
C(12)—C(16)	1.513(4)	1.514			
C(13)—C(14)	1.380(3)	1.386	C(13)—C(14)	1.380(3)	1.384

(*b*) Bonds involving hydrogen atoms

Bond	Distance	Bond	Distance
$(p\text{-}CH_3C_6H_4)_2BOCH_2CH_2NH_2$		$(C_6H_5)_2BOCH_2CH_2NH_2$	
N —H(*n*1)	0.93(3)	N —H(*n*1)	0.93(2)
N —H(*n*2)	0.94(3)	N —H(*n*2)	0.92(2)
C(1) —H(1*a*)	1.07(3)	C(1) —H(1*a*)	1.04(2)
C(1) —H(1*b*)	1.03(3)	C(1) —H(1*b*)	0.99(2)
C(2) —H(2*a*)	0.96(4)	C(2) —H(2*a*)	1.02(4)
C(2) —H(2*b*)	1.03(3)	C(2) —H(2*b*)	0.96(3)
C(4) —H(4)	0.95(3)	C(4) —H(4)	0.97(2)
C(5) —H(5)	1.00(3)	C(5) —H(5)	0.96(2)
C(7) —H(7)	0.98(3)	C(6) —H(6)	0.97(3)
C(8) —H(8)	1.01(2)	C(7) —H(7)	0.94(3)
C(10)—H(10)	1.02(3)	C(8) —H(8)	1.02(2)
C(11)—H(11)	1.02(4)	C(10)—H(10)	0.97(2)
C(13)—H(13)	0.95(3)	C(11)—H(11)	0.92(3)
C(14)—H(14)	1.04(3)	C(12)—H(12)	0.99(2)
C(15)—H(15*a*)	0.89(6)	C(13)—H(13)	1.00(2)
C(15)—H(15*b*)	0.99(5)	C(14)—H(14)	1.00(2)
C(15)—H(15*c*)	1.08(4)		
C(16)—H(16*a*)	0.94(5)		
C(16)—H(16*b*)	0.95(9)		
C(16)—H(16*c*)	0.95(5)		

groups, packing considerations (in particular the N—H . . . O hydrogen bond common to all four structures) are believed to be responsible for the observed conformational differences.

The phenyl rings in both of the present structures are slightly, but significantly, nonplanar (see Table 6). As in related structures (**1***a*(monoclinic), **1***b*, **2**, and **3**) (1–4) the boron atoms are significantly displaced from the phenyl mean planes (0.039(2) and −0.007(2) Å from the

Can. J. Chem. Downloaded from www.nrcresearchpress.com by 210.87.254.105 on 09/05/12
For personal use only.

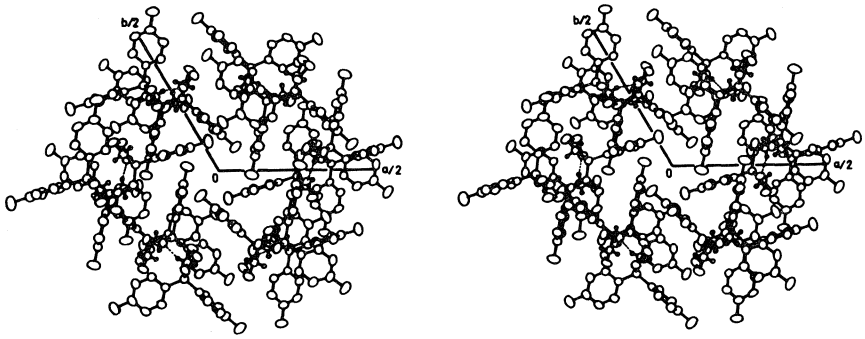

FIG. 2. The crystal structure of *B,B*-bis(*p*-tolyl)boroxazolidine viewed down *c*.

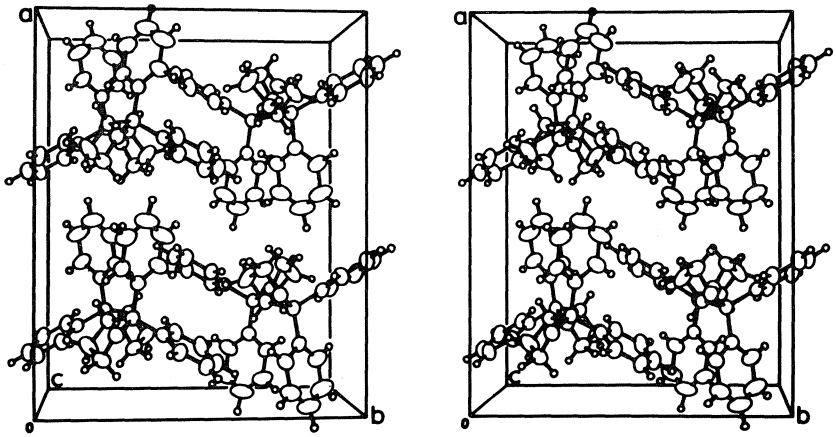

FIG. 3. The crystal structure of *B,B*-diphenylboroxazolidine viewed along *c*.

C(3)—C(8) planes and −0.041(2) and 0.042 Å from the C(9)—C(14) planes for **1***c* and **1***a* respectively). In the *p*-tolyl compound (**1***c*) the methyl carbon atoms C(15) and C(16) are displaced −0.053(4) and 0.046(6) Å from their respective mean planes. The dihedral angles defining the orientations of the phenyl rings (O[B—C(3)]C(4), N[B—C(3)]C(8), O[B—C(9)]C(14), and N[B—C(9)]C(10)) are 77.4(2), 150.7(2), 29.2(2), and −44.3(2)° for **1***c* and 15.6(2), 87.3(1), 32.0(2), and −42.8(2)° for **1***a*(orthorhombic).

The bond distances and angles in the five-membered rings and the B—C distances in the orthorhombic form of **1***a* and in **1***c* do not differ significantly from those found in the monoclinic form of **1***a* and in **1***b* (1, 2). The weighted mean bond distances for the four structures are: O—C, 1.412(2), O—B, 1.477(2), N—C, 1.488(1), N—B, 1.654(1), C—C, 1.503(3), and B—C, 1.618(1) Å. The geometry involving hydrogen atoms is as expected, mean bond lengths (rms deviations from the mean in parentheses) are: N—H, 0.935(5), C(sp^3)—H, 1.00(2), and C(ar)—H, 1.00(1) Å for **1***c* and N—H, 0.925(5), C(sp^3)—H, 1.00(2), and C(ar)—H, 0.98(1) Å for orthorhombic **1***a*.

A statistical analysis of the C—C bond lengths in compounds **1***a*, **1***b*, and **1***c* (values corrected for libration have been used in each case)[2] has provided an example of statistically significant substituent-induced bond length variation in the phenyl rings. This effect is expected but is usually not discernable for room temperature X-ray data (17, 18). Analysis of variance shows that the *a* and *b* bond lengths (see **4**) do not arise from the same population (at a confidence level of >99.999%) and further that both the *a* and *b* bond lengths are independent of the identity of

[2]Corrected bond lengths for monoclinic **1***a* (not given in ref. 1) have been placed in the Depository of Unpublished Data (see footnote 1).

Can. J. Chem. Downloaded from www.nrcresearchpress.com by 210.87.254.105 on 09/05/12
For personal use only.

the X substituent. The weighted mean *a* and *b* distances (rms deviations from the mean in parentheses) are 1.403(6) and 1.391(5) Å respectively. The length of the *c* bonds is found to depend on the identity of X, thus the substituent effect of X appears to be localized with respect to the bond lengths. The weighted mean *c* distances are 1.380(4), 1.377(3), and 1.390(7) Å respectively for **1***a* (X = H), **1***b* (X = F), and **1***c* (X = CH_3). The *c* bonds in **1***a* and **1***b* are not significantly different from one another but the *c* bonds in the *p*-tolyl derivative **1***c* are different from the *c* bonds in **1***a* and **1***b* at the 98% confidence level. All of the *c* bond lengths are significantly shorter than the *a* distances and the *c* bonds in **1***a* and **1***b* are shorter than the *b* bonds. The *c* distances in **1***c* are indistinguishable from *b* bond lengths.

The bond angles in the phenyl rings are known to be more sensitive to electronic differences than are the bond distances (17, 18). Mean angles in the phenyl rings at carbon atom bonded to **B** and at the *ortho*, *meta*, and *para* positions relative to B are 115.8(2), 122.2(2), 120.3(1), and 119.3(1)° for **1***a*: 116.0(1), 122.5(5), 118.6(4), and 121.9(1)° for **1***b*: and 115.6(2), 122.1(2), 121.5(2), and 117.2(1)° for **1***c*. The differences are significant at the *meta* and *para* positions while the other angles are nearly the same in all three compounds.

Figures 2 and 3 show the structures of *B,B*-bis(*p*-tolyl)boroxazolidine and *B,B*-diphenylboroxazolidine. Both structures consist of discrete molecular units each linked to two others by N—H . . . O hydrogen bonds (N . . . O = 2.982(2) Å for **1***c* and 2.896(2) Å for orthorhombic **1***a*) to form continuous spirals about the threefold screw axis in **1***c* and staggered arrays along the *c* glide plane in **1***a*. All other intermolecular nonbonded distances correspond to normal van der Waals interactions.

TABLE 4. Bond angles (deg) with estimated standard deviations in parentheses
(*a*) Non-hydrogen atoms

Bonds	Angle (deg)	Bonds	Angle (deg)
$(p\text{-}CH_3C_6H_4)_2BOCH_2CH_2NH_2$		$(C_6H_5)_2BOCH_2CH_2NH_2$	
C(1) —O —B	107.8(2)	C(1) —O —B	107.7(1)
C(2) —N —B	105.3(2)	C(2) —N —B	105.5(1)
O —C(1) —C(2)	105.3(2)	O —C(1) —C(2)	106.0(1)
C(1) —C(2) —N	104.4(2)	C(1) —C(2) —N	105.2(1)
C(4) —C(3) —C(8)	115.8(2)	C(4) —C(3) —C(8)	116.5(2)
C(4) —C(3) —B	121.9(2)	C(4) —C(3) —B	121.9(1)
C(8) —C(3) —B	122.3(2)	C(8) —C(3) —B	121.6(1)
C(3) —C(4) —C(5)	122.6(2)	C(3) —C(4) —C(5)	121.7(2)
C(4) —C(5) —C(6)	121.3(2)	C(4) —C(5) —C(6)	120.3(2)
C(5) —C(6) —C(7)	117.1(2)	C(5) —C(6) —C(7)	119.4(2)
C(5) —C(6) —C(15)	121.0(3)		
C(7) —C(6) —C(15)	121.9(3)		
C(6) —C(7) —C(8)	121.5(2)	C(6) —C(7) —C(8)	120.6(2)
C(3) —C(8) —C(7)	121.7(2)	C(3) —C(8) —C(7)	121.6(2)
C(10)—C(9) —C(14)	115.5(2)	C(10)—C(9) —C(14)	115.7(1)
C(10)—C(9) —B	122.8(2)	C(10)—C(9) —B	125.1(1)
C(14)—C(9) —B	121.6(2)	C(14)—C(9) —B	119.1(1)
C(9) —C(10)—C(11)	122.2(2)	C(9) —C(10)—C(11)	121.9(2)
C(10)—C(11)—C(12)	121.1(2)	C(10)—C(11)—C(12)	120.6(2)
C(11)—C(12)—C(13)	117.2(2)	C(11)—C(12)—C(13)	118.9(2)
C(11)—C(12)—C(16)	121.2(2)		
C(13)—C(12)—C(16)	121.7(3)		
C(12)—C(13)—C(14)	122.1(2)	C(12)—C(13)—C(14)	120.4(2)
C(9) —C(14)—C(16)	121.9(2)	C(9) —C(14)—C(13)	122.6(2)
O —B —N	99.9(1)	O —B —N	98.4(1)
O —B —C(3)	110.1(2)	O —B —C(3)	112.1(1)
O —B —C(9)	113.4(2)	O —B —C(9)	112.2(1)
N —B —C(3)	111.0(2)	N —B —C(3)	109.8(1)
N —B —C(9)	107.3(2)	N —B —C(9)	109.6(1)
C(3) —B —C(9)	114.2(2)	C(3) —B —C(9)	113.6(1)

Can. J. Chem. Downloaded from www.nrcresearchpress.com by 210.87.254.105 on 09/05/12
For personal use only.

TABLE 4 *(Concluded)*
(*b*) Angles involving hydrogen atoms

Bonds	Angle (deg)	Bonds	Angle (deg)
$(p\text{-}CH_3C_6H_4)_2BOCH_2CH_2NH_2$		$(C_6H_5)_2BOCH_2CH_2NH_2$	
C(2) —N —H(*n*1)	106(2)	C(2) —N —H(*n*1)	111(1)
C(2) —N —H(*n*2)	111(2)	C(2) —N —H(*n*2)	111(1)
B —N —H(*n*1)	117(2)	B —N —H(*n*1)	111(1)
B —N —H(*n*2)	112(2)	B —N —H(*n*2)	115(1)
H(*n*1) —N —H(*n*2)	106(2)	H(*n*1)—N —H(*n*2)	104(2)
O —C(1) —H(1*a*)	110(2)	O —C(1) —H(1*a*)	111(1)
O —C(1) —H(1*b*)	110(1)	O —C(1) —H(1*b*)	112(1)
C(2) —C(1) —H(1*a*)	110(2)	C(2) —C(1) —H(1*a*)	109(1)
C(2) —C(1) —H(1*b*)	110(1)	C(2) —C(1) —H(1*b*)	112(1)
H(1*a*) —C(1) —H(1*b*)	112(2)	H(1*a*)—C(1) —H(1*b*)	107(1)
N —C(2) —H(2*a*)	112(2)	N —C(2) —H(2*a*)	110(2)
N —C(2) —H(2*b*)	110(2)	N —C(2) —H(2*b*)	114(1)
C(1) —C(2) —H(2*a*)	119(2)	C(1) —C(2) —H(2*a*)	115(2)
C(1) —C(2) —H(2*b*)	109(2)	C(1) —C(2) —H(2*b*)	117(1)
H(2*a*) —C(2) —H(2*b*)	103(3)	H(2*a*)—C(2) —H(2*b*)	96(2)
C(3) —C(4) —H(4)	123(2)	C(3) —C(4) —H(4)	118(1)
C(5) —C(4) —H(4)	115(2)	C(5) —C(4) —H(4)	120(1)
C(4) —C(5) —H(5)	124(2)	C(4) —C(5) —H(5)	120(1)
C(6) —C(5) —H(5)	115(2)	C(6) —C(5) —H(5)	120(1)
C(6) —C(7) —H(7)	121(2)	C(5) —C(6) —H(6)	124(2)
C(8) —C(7) —H(7)	117(2)	C(7) —C(6) —H(6)	116(2)
C(3) —C(8) —H(8)	121(1)	C(6) —C(7) —H(7)	122(2)
C(7) —C(8) —H(8)	121(1)	C(8) —C(7) —H(7)	118(2)
C(9) —C(10)—H(10)	119(2)	C(3) —C(8) —H(8)	121(1)
C(11) —C(10)—H(10)	119(2)	C(7) —C(8) —H(8)	117(1)
C(10) —C(11)—H(11)	119(2)	C(9) —C(10)—H(10)	116(1)
C(12) —C(11)—H(11)	120(2)	C(11)—C(10)—H(10)	122(1)
C(12) —C(13)—H(13)	116(2)	C(10)—C(11)—H(11)	120(2)
C(14) —C(13)—H(13)	121(2)	C(12)—C(11)—H(11)	120(2)
C(9) —C(14)—H(14)	117(2)	C(11)—C(12)—H(12)	122(1)
C(13) —C(14)—H(14)	122(2)	C(13)—C(12)—H(12)	119(1)
C(6) —C(15)—H(15*a*)	109(4)	C(12)—C(13)—H(13)	119(1)
C(6) —C(15)—H(15*b*)	111(3)	C(14)—C(13)—H(13)	121(1)
C(6) —C(15)—H(15*c*)	112(2)	C(9) —C(14)—H(14)	116(1)
H(15*a*)—C(15)—H(15*b*)	131(5)	C(13)—C(14)—H(14)	121(1)
H(15*a*)—C(15)—H(15*c*)	84(4)		
H(15*b*)—C(15)—H(15*c*)	107(3)		
C(12) —C(16)—H(16*a*)	110(3)		
C(12) —C(16)—H(16*b*)	122(5)		
C(12) —C(16)—H(16*c*)	110(3)		
H(16*a*)—C(16)—H(16*b*)	106(5)		
H(16*a*)—C(16)—H(16*c*)	95(4)		
H(16*b*)—C(16)—H(16*c*)	110(6)		

TABLE 5. Intra-annular torsion angles (deg)

Bond	1*c*	1*a* (orthorhombic)	1*b*	1*a* (monoclinic)
B —O	32.1(2)	38.8(1)	32.9(3)	22.0(2)
O —C(1)	−44.2(2)	−43.2(1)	−42.1(3)	−39.6(2)
C(1)—C(2)	35.7(2)	26.4(2)	31.2(3)	39.3(2)
C(2)—N	−14.9(2)	−2.1(2)	−10.2(3)	−24.8(2)
N —B	−9.2(2)	−21.0(1)	−12.7(3)	3.1(2)

Can. J. Chem. Downloaded from www.nrcresearchpress.com by 210.87.254.105 on 09/05/12
For personal use only.

Can. J. Chem. Downloaded from www.nrcresearchpress.com by 210.87.254.105 on 09/05/12
For personal use only.

TABLE 6. Equations of weighted least-squares planes in the form $lX + mY + nZ = p$ where X, Y, and Z are orthogonal Å coordinates with respect to a, b^*, and c and deviations (Å) of atoms from the planes

Plane	χ^2	Equation	Deviations of atoms from plane							
			Atom	Deviation	Atom	Deviation	Atom	Deviation	Atom	Deviation
		$(p\text{-}CH_3C_6H_4)_2BOCH_2CH_2NH_2$								
1 C(3)–C(8)	65.7	$0.2078X - 0.2545Y - 0.9417Z = -5.5846$	C(C)	−0.006(2)	C(4)	0.009(3)	C(5)	0.001(3)	C(6)	−0.010(2)
			C(7)	0.012(3)	C(8)	−0.001(2)	B	0.039(2)	C(15)	−0.053(4)
			H(4)	0.02(3)	H(5)	0.01(3)	H(7)	0.07(3)	H(8)	−0.04(2)
2 C(9)–C(14)	24.5	$-0.6842X - 0.7292Y - 0.0104Z\ \%\ -8.1777$	C(9)	0.005(2)	C(10)	−0.006(3)	C(11)	−0.002(3)	C(12)	0.008(3)
			C(13)	−0.006(3)	C(14)	−0.002(3)	B	−0.041(2)	C(16)	0.046(6)
			H(10)	−0.06(3)	H(11)	−0.05(4)	H(13)	0.05(3)	H(14)	−0.02(3)
		$(C_6H^4)_2BOCH_2CH_2NH_2$ (orthogonal axes along a, b, c)								
1 C(3)–C(8)	16.7	$-0.2138X + 0.7100Y - 0.6709Z\ \%\ 0.6908$	C(3)	−0.001(2)	C(4)	−0.002(2)	C(5)	0.004(2)	C(6)	0.000(3)
			C(7)	−0.007(3)	C(8)	0.005(2)	B	−0.007(2)	H(4)	−0.04(2)
			H(5)	−0.02(2)	H(6)	0.06(3)	H(7)	−0.07(3)	H(8)	0.10(2)
2 C(9)–C(14)	60.0	$0.8325X + 0.5100Y - 0.2165Z = 5.1578$	C(9)	−0.006(2)	C(10)	0.007(2)	C(11)	0.000(2)	C(12)	−0.009(2)
			C(13)	0.007(2)	C(14)	0.002(2)	B	0.042(2)	H(10)	0.05(2)
			H(1)	0.02(2)	H(12)	−0.05(2)	H(13)	−0.01(2)	H(14)	−0.07(2)

Can. J. Chem. Downloaded from www.nrcresearchpress.com by 210.87.254.105 on 09/05/12
For personal use only.

TABLE 7

(*a*) Selected intermolecular contacts*

Atoms	Distance	Atoms	Distance
$(p\text{-}CH_3C_6H_4)_2BOCH_2CH_2NH_2$		$(C_6H_5)_2BOCH_2CH_2NH_2$	
O . . . O[1]	3.340(3)	O . . . C(10)[4]	3.438(2)
N . . . C(3)[2]	3.360(3)	O . . . H(10)[4]	2.67(2)
C(2) . . . O[2]	3.444(3)	C(11) . . . H(*n*1)[5]	2.76(2)
C(13) . . . H(2*a*)[3]	2.74(4)	C(12) . . . H(*n*1)[5]	2.65(2)
H(4) . . . H(1*a*)[2]	2.31(4)	H(2*b*) . . . H(14)[6]	2.39(3)

(*b*) Selected intramolecular contacts

Atoms	Distance	Atoms	Distance
$(p\text{-}CH_3C_6H_4)_2BOCH_2CH_2NH_2$		$(C_6H_5)_2BOCH_2CH_2NH_2$	
O . . . C(14)	3.015(3)	O . . . C(14)	2.946(2)
O . . . C(4)	3.277(3)	O . . . C(4)	2.928(2)
N . . . C(4)	3.055(3)	C(1) . . . C(9)	3.072(2)
N . . . C(10)	3.071(3)	C(9) . . . C(10)	3.111(3)
C(1) . . . C(9)	3.155(3)	O . . . H(14)	2.53(2)
C(9) . . . C(10)	3.107(3)	O . . . H(4)	2.55(2)
O . . . H(14)	2.63(3)	C(3) . . . H(*n*1)	2.65(2)
C(3) . . . H(*n*1)	2.75(3)	C(9) . . . H(*n*2)	2.72(2)
C(4) . . . H(*n*1)	2.68(3)	C(9) . . . H(8)	2.79(2)
C(5) . . . H(15*b*)	2.59(4)	C(10) . . . H(8)	2.73(2)
C(7) . . . H(15*a*)	2.56(6)	C(10) . . . H(*n*2)	2.77(2)
C(9) . . . H(*n*2)	2.59(3)	B . . . H(1*a*)	2.68(2)
C(9) . . . H(8)	2.76(2)	H(*n*1) . . . H(2*a*)	2.16(4)
C(10) . . . H(*n*2)	2.62(2)	H(*n*2) . . . H(2*b*)	2.20(3)
C(11) . . . H(16*a*)	2.60(4)	H(*n*2) . . . H(10)	2.29(3)
C(13) . . . H(16*c*)	2.74(5)	H(1*b*) . . . H(2*a*)	2.34(4)
H(*n*2) . . . H(2*a*)	2.20(4)	H(1*a*) . . . H(2*b*)	2.35(3)
H(*n*2) . . . H(10)	2.22(4)		
H(*n*1) . . . H(2*b*)	2.13(4)		
H(*n*1) . . . H(4)	2.20(4)		
H(1*a*) . . . H(2*b*)	2.29(4)		

(*c*) Hydrogen-bond data* (distances in Å and angles in deg)

D—H . . . A	H . . . A	D . . . A	∠DHA	∠XAH
		$(p\text{-}CH_3C_6H_4)_2BOCH_2CH_2NH_2$		
N—H(*n*1) . . . O[2]	2.09(3)	2.982(2)	158(2)	113(1), 135(1)
		$(C_6H_5)_2BOCH_2CH_2NH_2$		
N—H(*n*2) . . . O[6]	2.01(2)	2.896(2)	163(2)	122(1), 129(1)

*Superscripts refer to atoms at positions: [1] 2/3 − *x*, 2/3 − *y*, 1/3 − *z*; [2] 2/3 − *y*, 1/3 + *x* − *y*, 1/3 + *z*; [3] 1/3 − *x*, 2/3 − *y*, 2/3 − *z*; [4] *x*, 1/2 − *y*, *z* − 1/2; [5] 1/2 − *x*, 1/2 + *y*, *z*; [6] *x*, 1/2 − *y*, 1/2 + *z*.

Acknowledgements

We thank the National Research Council of Canada for financial support and the University of British Columbia Computing Centre for assistance.

1. S. J. RETTIG and J. TROTTER. Can. J. Chem. **51**, 1288 (1973).
2. S. J. RETTIG and J. TROTTER. Acta Crystallogr. **B30**, 2139 (1974).
3. S. J. RETTIG and J. TROTTER. Can. J. Chem. **53**, 1393 (1975).
4. S. J. RETTIG, J. TROTTER, and W. KLIEGEL. Can. J. Chem. **52**, 2531 (1974).
5. (*a*) R. L. LETSINGER and I. SKOOG. J. Am. Chem. Soc. **77**, 2491 (1955); (*b*) Y. RASIEL and S. RETTIG. Unpublished results.

6. J. KARLE and H. HAUPTMAN. Acta Crystallogr. **9**, 635 (1956).
7. J. KARLE and I. L. KARLE. Acta Crystallogr. **21**, 849 (1966).
8. (*a*) M. G. B. DREW. Private communication (1969). (*b*) M. G. B. DREW, D. H. TEMPLETON, and A. ZALKIN. Acta Crystallogr. B**25**, 261 (1969).
9. D. T. CROMER and J. B. MANN. Acta Crystallogr. A**24**, 321 (1968).
10. R. F. STEWART, E. R. DAVIDSON, and W. T. SIMPSON. J. Chem. Phys. **42**, 3175 (1965).
11. D. T. CROMER and D. LIBERMAN. J. Chem. Phys. **53**. 1891 (1970).
12. R. E. LONG. Ph.D. Thesis, University of California at Los Angeles, Los Angeles, California. 1965.
13. V. SCHOMAKER and K. N. TRUEBLOOD. Acta Crystallogr. B**24**, 63 (1969).
14. D. W. J. CRUICKSHANK. Acta Crystallogr. **9**, 747 (1956); **9**, 754 (1956).
15. D. W. J. CRUICKSHANK. Acta Crystallogr. **14**, 896 (1961).
16. J. B. HENDRICKSON. J. Am. Chem. Soc. **83**, 4537 (1961); **85**, 4059 (1963).
17. O. L. CARTER, A. T. MCPHAIL, and G. A. SIM. J. Chem. Soc. (A), 822 (1966).
18. A. DOMENICANO, A. VACIAGO, and C. A. COULSON. Acta Crystallogr. B**31**, 221 (1975); B**31**, 1630 (1975).

Can. J. Chem. Downloaded from www.nrcresearchpress.com by 210.87.254.105 on 09/05/12
For personal use only.

Crystal and molecular structure of 8,8-dimethyl-3,5-diphenyl-2,4,6-trioxa-1-azonia-3-bora-5-boranatabicyclo[3.3.0]octane

STEVEN J. RETTIG AND JAMES TROTTER

Department of Chemistry, University of British Columbia, 2075 Wesbrook Place, Vancouver, B.C., Canada V6T 1W5

AND

W. KLIEGEL AND H. BECKER

Institut für Pharmazeutische Chemie der Technischen Universität, 33 Braunschweig, Bundesrepublik Deutschland

Received April 6, 1976

STEVEN J. RETTIG, JAMES TROTTER, W. KLIEGEL, and H. BECKER. Can. J. Chem. **54**, 3142 (1976).

Crystals of 8,8-dimethyl-3,5-diphenyl-2,4,6-trioxa-1-azonia-3-bora-5-boranatabicyclo[3.3.0]-octane are monoclinic, $a = 22.323(1)$, $b = 9.555(1)$, $c = 16.0027(6)$ Å, $\beta = 109.055(4)°$, $Z = 8$, space group $C2/c$. The structure was solved by direct methods and was refined by full-matrix least-squares procedures to a final R of 0.048 and R_w of 0.066 for 2629 reflections with $I \geq 3\sigma(I)$. The central part of the molecule consists of two fused five-membered rings. One of them is a familiar BOCCN ring while the other is a novel and nearly planar BOBON ring containing one tetrahedral boron atom and one trigonal planar boron atom. Bond lengths are: O—B, 1.337(2)–1.467(2), N—B, 1.692(2), O—N, 1.440(2), O—C, 1.426(2), N—C, 1.513(2), B—C, 1.557(2) and 1.599(2), C(sp^3)—C(sp^3), 1.520(2)–1.530(2), C—C(ar), 1.372(4)–1.407(2), N—H, 0.89(2), mean C(ar)—H, 0.97(1), and mean C(sp^3)—H, 1.01(1) Å. The crystal structure consists of discrete molecules each linked to two others by N—H . . . O hydrogen bonds (N . . . O = 2.853(2) Å).

STEVEN J. RETTIG, JAMES TROTTER, W. KLIEGEL et H. BECKER. Can. J. Chem. **54**, 3142 (1976).

Les cristaux du diméthyl-8,8 diphényl-3,5 trioxa-2,4,6 azonia-1 bora-3 boranata-5 bicyclo-[3.3.0] octane sont monocliniques, $a = 22.323(1)$, $b = 9.555(1)$, $c = 16.0027(6)$ Å, $\beta = 109.055(4)°$, $Z = 8$; le groupe d'espace est $C2/c$. La structure a été démontrée par méthodes directes et a été affinée par la méthode des moindres carrés (matrice complète) jusqu'à une valeur finale de R de 0.048 et R_w de 0.066 pour 2629 réflexions avec $I \geq 3\sigma(I)$. La partie centrale de la molécule consiste en deux noyaux à cinq chaînons condensés. L'un des deux est un noyau BOCCN bien connu alors que l'autre est un nouveau noyau BOBON presque planaire contenant un atome de bore tétraédrique et un atome de bore trigonal plan. Les longueurs des liens sont: O—B, 1.337(2)–1.467(2), N—B, 1.692(2), O—N, 1.440(2), O—C, 1.426(2), N—C, 1.513(2), B—C, 1.557(2) et 1.599(2), C(sp^3)—C(sp^3), 1.520(2)–1.530(2), C—C(ar), 1.372(4)–1.407(2), N—H, 0.89(2), moyenne de C(ar)—H, 0.97(1) et la moyenne de C(sp^3)—H, 1.01(1) Å. La structure du cristal consiste en des molécules séparées qui sont liées à deux autres molécules par des liens hydrogène N—H . . . O (N . . . O = 2.853(2) Å).

[Traduit par le journal]

Introduction

Treatment of *N*-(2-hydroxyalkyl)nitrones **2** with diphenyl borinic anhydride (oxybisdiphenylborane) results in the formation of diphenylboron chelates **3** featuring a B,N-betaine structure (1). In some cases these reactions yield isolatable by-products, sometimes these by-products being the only substances isolated (2), which generally have the following properties: (*1*) The ir spectrum does not show the C=N stretching frequency at 1610–1670 cm^{-1} which characterizes the iminium salt structure **3** (1). (*2*) An absorption in the region of the NH/OH group vibrations is observed which also rules out chelate systems such as **3**. (*3*) Chemical and spectral data indicate the loss of the nitrone structure. (*4*) Instead of the diphenylboron grouping, only a monophenylboron system can be detected by the diphenyl carbazone reaction (3). (*5*) In addition to these findings the elemental analysis suggests a condensation product between 1 mol of *N*-(2-hydroxyalkyl)hydroxylamine **1** and 2 mol of benzeneboronic acid. Condensation reactions at this molar ratio give compounds identical to the above mentioned by-products (2).

Chemical properties and spectral data are consistent with several alternative structures **4***a–f*.

Can. J. Chem. Downloaded from www.nrcresearchpress.com by 210.87.254.40 on 09/05/12
For personal use only.

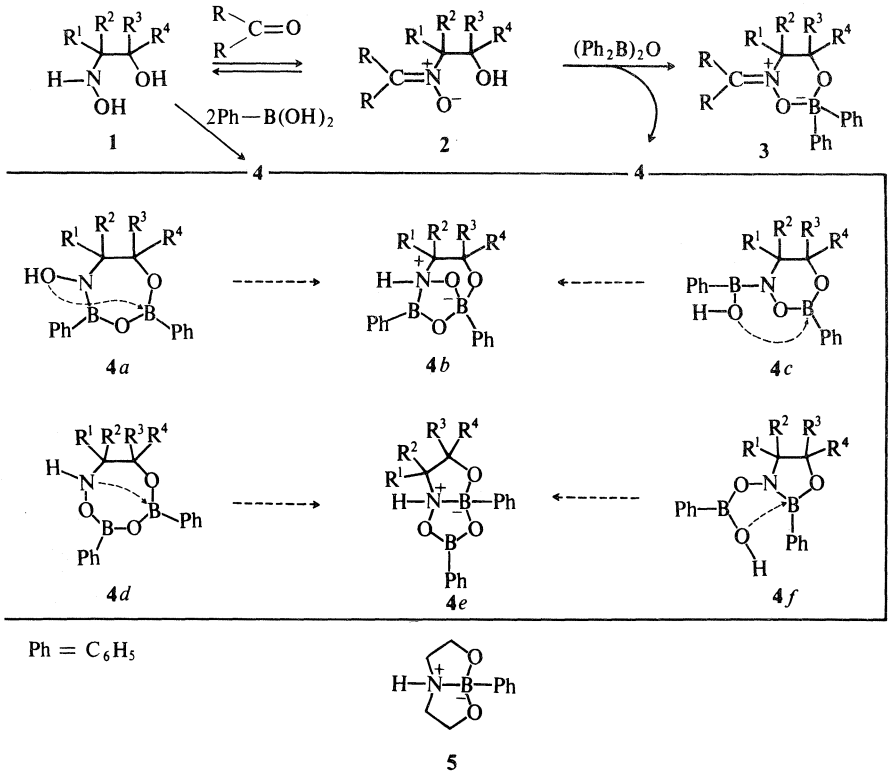

Seven-membered rings such as **4***a* containing a 'pyroboronic' structure within the ring system were described for the benzeneboronates of *vic*-diols (4–6) and *vic*-aminoalcohols (6) with *trans* grouping. A similar cyclic structure **4***d* with an eight-membered ring would also be conceivable. In forms **4***a* and **4***d*, as well as in the five- and six-membered ring condensates **4***f* and **4***c*, intramolecular complex formation is possible. O→B coordination in **4***a* and **4***c* would give the structure **4***b*, while **4***d* and **4***f* could exist in the form **4***e* by N→B and O→B coordination respectively.

Both **4***b* and **4***e* should display an ir low frequency shift of the N—H vibration as a result of quarternization of the nitrogen atom. Indeed, the registered absorptions at 3050–3150 cm^{-1} support this consideration. Similar absorptions at *ca.* 3100 cm^{-1} can be observed in the ir spectra of '*diptych*boroxazolidines' **5** (7), which are closely related to the structure **4***e* and have recently been shown to contain intramolecular N→B interactions (8). Since the investigation of a molecular model of **4***b* showed considerable strain, the structure **4***e* was favored but could not be unambiguously established. To this end an X-ray crystallographic analysis of the homologue **4** with $R^1 = R^2 = Me$ and $R^3 = R^4 = H$ has been undertaken.

Experimental

8,8-Dimethyl-3,5-diphenyl-2,4,6-trioxa-1-azonia-3-bora-5-boranatabicyclo[3.3.0]octane

A solution of 2-hydroxylamino-2-methylpropanol (**1**, $R^1 = R^2 = Me$, $R^3 = R^4 = H$), mp 66 °C (2), (1 mmol) and benzeneboronic acid (2 mmol) in 10 ml of ethanol was refluxed for 1 h. The ethanol was removed *in vacuo* and the remaining oil treated with ether and light petroleum ether until crystallization took place. Recrystallization from benzene–ethanol: mp 215–216 °C, yield: 90%.

Anal. calcd. for $C_{16}H_{19}B_2NO_3$ (f.w. 295.0): C 65.15, H 6.49, N 4.74. Found: C 65.15, H 6.46, N 4.73. ir (1:300, KBr): 3070 cm^{-1} (N—H). ^{1}H-nmr (60 MHz, DMSO-d_6/TMS) τ (ppm): 8.70 s (6, CH_3), 6.36 s (2, CH_2), 2.1–2.9 m (10, Ph). Mass spectrum (165 °C): m/e = 295 (M^+, 23%), 218 (M^+ − Ph, 46%).

X-Ray Crystallographic Analysis

Crystals suitable for X-ray analysis were obtained by recrystallization from acetone–chloroform. The crystal chosen for study was mounted with *b* parallel to the goniostat axis and had dimensions of *ca.* 0.35 × 0.45 × 0.35 mm. Unit-cell and space group data were obtained from film and diffractometer measurements. The unit-cell

Can. J. Chem. Downloaded from www.nrcresearchpress.com by 210.87.254.40 on 09/05/12
For personal use only.

Can. J. Chem. Downloaded from www.nrcresearchpress.com by 210.87.254.40 on 09/05/12
For personal use only.

parameters were refined by a least-squares treatment of $\sin^2\theta$ values for 23 reflections measured on a diffractometer with Cu K_α radiation. Crystal data are:

$C_{16}H_{19}B_2NO_3$ f.w. = 295.0

Monoclinic, a = 22.323(1), b = 9.555(1), c = 16.0027(6) Å, β = 109.055(4)°, V = 3226.5(4) Å^3, ρ_m = 1.20 (flotation in aqueous KI), Z = 8, ρ_c = 1.2144(1) g cm^{-3}, $F(000)$ = 1248 (22 °C, Cu K_α, λ = 1.5418 Å, μ = 6.6 cm^{-1}). Absent reflections: hkl, $h + k \neq 2n$, $h0l$, $l \neq 2n$, and $0k0$, $k \neq 2n$. Space group $C2/c$ (C_{2h}^6, No. 15).

Intensities were measured on a Datex-automated General Electric XRD 6 diffractometer, with a scintillation counter, Cu K_α (nickel filter and pulse height analyser), and a θ–2θ scan at 2° min^{-1} over a range of (1.80 + 0.86 tan θ) degrees in 2θ, with 10 s background counts being measured at each end of the scan. Data were measured to 2θ = 146° (minimum interplanar spacing 0.81 Å). The intensity of the check reflection, measured every 40 reflections throughout the data collection, remained constant to within ±5%. The final intensity of the check reflection was 0.975 times the initial value. Lorentz and polarization corrections and check reflection scaling were applied, and the structure amplitudes were derived. No absorption correction was made in view of the low value of μ. Of the 3220 independent reflections measured, 582 had intensities less than $3\sigma(I)$ above background where $\sigma^2(I) = S + B + (0.06S)^2$ with S = scan count and B = time averaged background count. These reflections were given zero weight in the refinement but were included in the structure factor calculations.

The systematic absences allow space groups Cc or $C2/c$. The centrosymmetric space group $C2/c$ was indicated by the E-statistics. The structure was solved by direct methods. Eight sets of signs were calculated for 402 reflections with normalized structure factor $|E| \geq 1.50$ by a computer program which uses Sayre relationships in an iterative procedure (9). One set of signs was outstanding in that it converged in 7 cycles to a set having the highest consistency index (9) (0.77) with 197 positive and 205 negative signs. The 22 non-hydrogen atoms accounted for the 22 highest peaks on an E-map calculated from this set of signs.

Two cycles of isotropic followed by two cycles of anisotropic full-matrix least-squares refinement of the non-hydrogen atoms gave R = 0.094. A difference map gave the positions of all 19 hydrogen atoms, which were included in all subsequent cycles of refinement with isotropic thermal parameters. The entire structure was refined for 4 cycles giving a final R of 0.048 and R_w of 0.066 for 2629 reflections with $I \geq 3\sigma(I)$ (9 reflections which had $|F_o| - |F_c| > 3\sigma(F)$ were removed from the data set in the final stages of refinement).

The least-squares refinement was based on the minimization of $\sum w[|F_o| - |F_c/(1 + gI)|]^2$ where g is the extinction parameter and I the uncorrected intensity. The final value of g was 2.0(1) × 10^{-7}. The scattering factors of ref. 10 were used for the non-hydrogen atoms and those of ref. 11 for the hydrogen atoms. Anomalous scattering factors from ref. 12 were used for the non-hydrogen atoms. The anisotropic thermal parameters employed in the refinement are U_{ij} in the expression:

$$f = f^0 \exp[-2\pi^2(U_{11}h^2a^{*2} + U_{22}k^2b^{*2} + U_{33}l^2c^{*2} + 2U_{12}hka^*b^* + 2U_{13}hla^*c^* + 2U_{23}klb^*c^*)]$$

where f^0 is the tabulated scattering factor and f is that corrected for thermal motion. The weighting scheme: $w = 1/\sigma^2(F)$ where $\sigma^2(F)$ is derived from the previously defined $\sigma^2(I)$ gave uniform average values of $w(|F_o| - |F_c|)^2$ over ranges of $|F_o|$ and was employed in the final stages of refinement.

On the final cycle of refinement the mean parameter shift was 0.04σ and no parameter shift was greater than 0.68σ. The mean error in an observation of unit weight was 1.637 and the final value of the scale factor k where $|F_o|$ (absolute scale) = $(1/k)\sqrt{(I/Lp)}$ was 3.171. The final positional and thermal parameters appear in Tables 1 and 2 respectively. Measured and calculated structure

TABLE 1. Final positional parameters (fractional × 10^5, H × 10^3) with estimated standard deviations in parentheses

Atom	x	y	z
O(1)	16736(5)	45897(11)	10961(7)
O(2)	14135(5)	27498(11)	18439(7)
O(3)	22807(5)	56456(10)	25214(7)
N	20298(6)	31817(13)	24081(8)
C(1)	20107(8)	37530(16)	32793(10)
C(2)	19027(8)	53073(16)	30577(12)
C(3)	26662(10)	34732(22)	39429(12)
C(4)	14941(12)	31131(23)	35821(15)
C(5)	28795(7)	43327(14)	16646(9)
C(6)	28665(8)	39279(17)	8192(11)
C(7)	34191(10)	37845(22)	6108(14)
C(8)	39978(9)	40264(21)	12344(14)
C(9)	40263(9)	44173(21)	20767(14)
C(10)	34731(8)	45772(18)	22818(12)
C(11)	6089(7)	33035(17)	3562(11)
C(12)	4539(8)	39891(20)	−4490(12)
C(13)	−1160(9)	37408(23)	−11099(14)
C(14)	−5436(10)	28082(24)	−9744(16)
C(15)	−3965(10)	21140(27)	−1875(19)
C(16)	1745(9)	23451(22)	4724(15)
B(1)	22378(8)	45383(16)	18851(10)
B(2)	12471(8)	36104(18)	10944(11)
H(n)	227(1)	242(2)	248(1)
H(2a)	143(1)	551(2)	273(1)
H(2b)	202(1)	587(2)	360(1)
H(3a)	276(1)	243(3)	405(2)
H(3b)	266(1)	388(3)	453(1)
H(3c)	301(1)	396(3)	374(1)
H(4a)	107(1)	325(2)	316(1)
H(4b)	153(1)	356(2)	419(1)
H(4c)	156(1)	209(3)	370(2)
H(6)	246(1)	381(2)	36(1)
H(7)	339(1)	355(3)	0(1)
H(8)	440(1)	392(3)	108(1)
H(9)	441(1)	458(2)	254(1)
H(10)	352(1)	484(2)	287(1)
H(12)	75(1)	464(2)	−55(1)
H(13)	−20(1)	422(3)	−169(2)
H(14)	−95(1)	269(3)	−147(2)
H(15)	−69(1)	138(3)	−10(2)
H(16)	26(1)	188(3)	104(2)

TABLE 2. Final thermal parameters and their estimated standard deviations

(*a*) Anisotropic thermal parameters ($U_{ij} \times 10^4$ Å^2)

Atom	U_{11}	U_{22}	U_{33}	U_{12}	U_{13}	U_{23}
O(1)	392(5)	277(6)	463(6)	19(4)	94(4)	50(4)
O(2)	408(6)	301(6)	486(6)	−57(4)	93(4)	17(4)
O(3)	493(6)	197(5)	535(6)	−24(4)	227(5)	−51(4)
N	382(6)	209(6)	397(6)	11(5)	118(5)	−18(5)
C(1)	570(9)	281(8)	422(8)	9(6)	215(7)	−35(6)
C(2)	582(10)	261(8)	543(9)	18(7)	281(8)	−67(7)
C(3)	756(13)	442(11)	413(9)	60(9)	103(8)	−28(7)
C(4)	836(14)	440(11)	679(12)	−43(10)	463(11)	3(9)
C(5)	423(7)	194(7)	450(8)	35(5)	166(6)	41(5)
C(6)	514(9)	364(9)	478(9)	28(7)	183(7)	−13(7)
C(7)	688(12)	525(11)	645(11)	94(9)	364(10)	−23(9)
C(8)	561(11)	485(11)	868(14)	140(8)	401(10)	66(9)
C(9)	396(9)	558(12)	780(13)	79(8)	162(8)	49(10)
C(10)	423(8)	407(9)	517(9)	54(7)	138(7)	−2(7)
C(11)	386(7)	346(8)	522(9)	49(6)	111(6)	−80(7)
C(12)	466(9)	435(10)	547(9)	74(7)	111(7)	−37(7)
C(13)	600(11)	578(13)	599(11)	178(10)	31(9)	−83(9)
C(14)	501(11)	579(13)	816(14)	20(9)	−79(10)	−204(11)
C(15)	524(11)	599(14)	1060(18)	−139(10)	77(11)	−82(13)
C(16)	517(10)	491(11)	736(13)	−89(8)	105(9)	14(9)
B(1)	404(8)	175(7)	425(8)	22(6)	133(7)	17(6)
B(2)	400(8)	282(8)	459(9)	42(7)	152(7)	−25(7)

(*b*) Isotropic thermal parameters ($U \times 10^3$)

Atom	U (Å^2)	Atom	U (Å^2)
H(*n*)	52(5)	H(7)	79(7)
H(2*a*)	55(5)	H(8)	85(7)
H(2*b*)	54(5)	H(9)	72(6)
H(3*a*)	90(8)	H(10)	53(5)
H(3*b*)	78(7)	H(12)	64(6)
H(3*c*)	82(7)	H(13)	84(7)
H(4*a*)	65(6)	H(14)	83(7)
H(4*b*)	70(6)	H(15)	107(9)
H(4*c*)	90(8)	H(16)	76(7)
H(6)	51(5)		

factors have been placed in the Depository of Unpublished Data.[1]

The ellipsoids of thermal motion for the non-hydrogen atoms are shown in Fig. 1. The thermal motion has been analysed in terms of the rigid-body modes of translation (**T**), libration (**L**), and screw (**S**) motion (13) using the computer program MGTLS. The rms standard error in the temperature factors σU_{ij} (derived from the least-squares analysis) is 0.0009 Å^2. Analyses were successful for the two phenyl groups: C(5)–C(10) and B(1) (rms ΔU_{ij} = 0.0013 Å^2) and C(11)–C(16) and B(2) (rms ΔU_{ij} = 0.0019 Å^2). Analysis of the 12 atom group O(1)–O(3), N, B(1), B(2), C(1)–C(5), and C(11) (rms ΔU_{ij} = 0.0034 Å^2) indicated significant independent motion within the rigid-body, in particular the methyl groups. Since an analysis of the same group without the methyl carbons gave a non-positive definite libration tensor, corrections to bonds within the fused ring system were made from the above mentioned analysis.

The appropriate bond distances and angles have been corrected for libration (14, 15), using shape parameters q^2 of 0.08 for all atoms involved. Appropriate bonds were corrected for independent motion based on the ΔU_{ij} (16, 17). Corrected bond distances appear in Table 3 along with the uncorrected values.

[1]The structure factor table is available, at a nominal charge, from the Depository of Unpublished Data, CISTI, National Research Council of Canada, Ottawa, Canada K1A 0S2.

Results and Discussion

Figure 1 shows a general view of the molecule with the crystallographic numbering scheme and

Can. J. Chem. Downloaded from www.nrcresearchpress.com by 210.87.254.40 on 09/05/12
For personal use only.

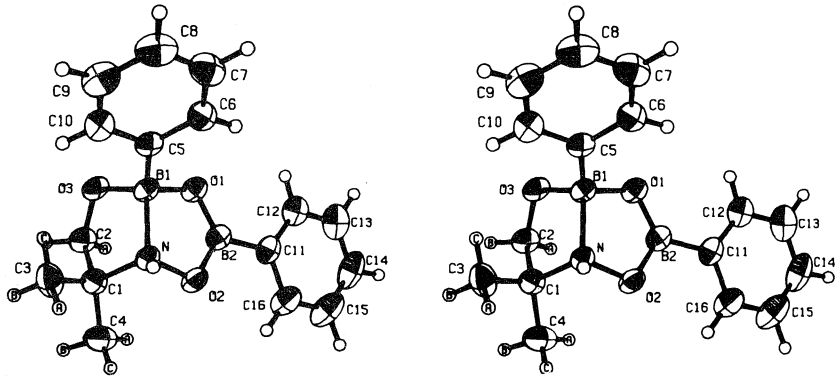

FIG. 1. A stereo view of the 8,8-dimethyl-3,5-diphenyl-2,4,6-trioxa-1-azonia-3-bora-5-boranata-bicyclo[3.3.0]octane molecule. 50% ellipsoids are shown for the nonhydrogen atoms.

TABLE 3. Bond lengths (Å) with estimated standard deviations in parentheses

(*a*) Non-hydrogen atoms

Bond	Distance		Bond	Distance	
	Uncorrected	Corrected		Uncorrected	Corrected
O(1)—B(1)	1.465(2)	1.467	C(5)—B(1)	1.595(2)	1.599
O(1)—B(2)	1.334(2)	1.337	C(6)—C(7)	1.386(2)	1.390
O(2)—N	1.438(2)	1.440	C(7)—C(8)	1.370(3)	1.378
O(2)—B(2)	1.401(2)	1.404	C(8)—C(9)	1.380(3)	1.387
O(3)—C(2)	1.423(2)	1.426	C(9)—C(10)	1.386(2)	1.390
O(3)—B(1)	1.450(2)	1.452	C(11)—C(12)	1.385(2)	1.393
N—C(1)	1.511(2)	1.513	C(11)—C(16)	1.390(3)	1.398
N—B(1)	1.688(2)	1.692	C(11)—B(2)	1.553(2)	1.557
C(1)—C(2)	1.528(2)	1.530	C(12)—C(13)	1.384(3)	1.387
C(1)—C(3)	1.525(3)	1.526	C(13)—C(14)	1.374(3)	1.383
C(1)—C(4)	1.518(2)	1.520	C(14)—C(15)	1.365(4)	1.372
C(5)—C(6)	1.398(2)	1.407	C(15)—C(16)	1.382(3)	1.385
C(5)—C(10)	1.390(2)	1.396			

(*b*) Bonds involving hydrogen atoms

Bond	Distance	Bond	Distance
N —H(*n*)	0.89(2)	C(7) —H(7)	0.98(2)
C(2)—H(2*a*)	1.03(2)	C(8) —H(8)	1.00(3)
C(2)—H(2*b*)	0.97(2)	C(9) —H(9)	0.94(2)
C(3)—H(3*a*)	1.02(3)	C(10)—H(10)	0.94(2)
C(3)—H(3*b*)	1.02(3)	C(12)—H(12)	0.95(2)
C(3)—H(3*c*)	1.03(3)	C(13)—H(13)	1.00(3)
C(4)—H(4*a*)	0.97(2)	C(14)—H(14)	1.00(2)
C(4)—H(4*b*)	1.04(2)	C(15)—H(15)	1.00(3)
C(4)—H(4*c*)	1.00(3)	C(16)—H(16)	0.97(2)
C(6)—H(6)	0.97(2)		

Fig. 2 shows the packing arrangement viewed into *b*. Bond angles are given in Table 4 and torsion angles defining the conformations of the five-membered rings in Table 5. Some weighted least squares mean planes are given in Table 6 and Table 7 lists nonbonded contacts and details of the hydrogen-bonding scheme.

The X-ray crystallographic analysis has shown the structure **4***e* to be correct. The five-membered BOCCN ring has a slightly distorted half-chair

Can. J. Chem. Downloaded from www.nrcresearchpress.com by 210.87.254.40 on 09/05/12
For personal use only.

Can. J. Chem. Downloaded from www.nrcresearchpress.com by 210.87.254.40 on 09/05/12
For personal use only.

TABLE 4. Bond angles (deg) with estimated standard deviations in parentheses

(*a*) Non-hydrogen atoms

Bonds	Angle (deg)	Bonds	Angle (deg)
B(1)—O(1)—B(2)	113.0(1)	C(8) —C(9) —C(10)	120.0(2)
N —O(2)—B(2)	107.5(1)	C(5) —C(10)—C(9)	122.0(2)
C(2)—O(3)—B(1)	110.0(1)	B(2) —C(11)—C(12)	120.5(2)
O(2)—N —C(1)	111.9(1)	B(2) —C(11)—C(16)	122.0(2)
O(2)—N —B(1)	105.7(1)	C(12)—C(11)—C(16)	117.6(2)
C(1)—N —B(1)	106.0(1)	C(11)—C(12)—C(13)	121.2(2)
N —C(1)—C(2)	100.8(1)	C(12)—C(13)—C(14)	120.2(2)
N —C(1)—C(3)	105.6(1)	C(13)—C(14)—C(15)	119.4(2)
N —C(1)—C(4)	113.7(1)	C(14)—C(15)—C(16)	120.7(2)
C(2)—C(1)—C(3)	112.0(1)	C(12)—C(16)—C(15)	120.9(2)
C(2)—C(1)—C(4)	112.8(1)	O(1) —B(1) —O(3)	115.0(1)
C(3)—C(1)—C(4)	111.3(1)	O(1) —B(1) —N	98.9(1)
O(3)—C(2)—C(1)	106.3(1)	O(1) —B(1) —C(5)	113.3(1)
B(1)—C(5)—C(6)	120.8(1)	O(3) —B(1) —N	100.2(1)
B(1)—C(5)—C(10)	122.6(1)	O(3) —B(1) —C(5)	112.8(1)
C(6)—C(5)—C(10)	116.6(1)	N —B(1) —C(5)	115.3(1)
C(5)—C(6)—C(7)	121.4(2)	O(1) —B(2) —O(2)	114.9(1)
C(6)—C(7)—C(8)	120.7(2)	O(1) —B(2) —C(11)	127.6(1)
C(7)—C(8)—C(9)	119.3(2)	O(2) —B(2) —C(11)	117.5(1)

(*b*) Angles involving hydrogen atoms

Bonds	Angle (deg)	Bonds	Angle (deg)
O(2) —N —H(*n*)	105(1)	C(5) —C(6) —H(6)	119(1)
C(1) —N —H(*n*)	112(1)	C(7) —C(6) —H(6)	120(1)
B(1) —N —H(*n*)	116(1)	C(6) —C(7) —H(7)	119(1)
O(3) —C(2)—H(2*a*)	111(1)	C(8) —C(7) —H(7)	121(1)
O(3) —C(2)—H(2*b*)	111(1)	C(7) —C(8) —H(8)	120(1)
C(1) —C(2)—H(2*a*)	111(1)	C(9) —C(8) —H(8)	120(1)
C(1) —C(2)—H(2*b*)	111(1)	C(8) —C(9) —H(9)	124(1)
H(2*a*)—C(2)—H(2*b*)	107(2)	C(10)—C(9) —H(9)	116(1)
C(1) —C(3)—H(3*a*)	113(1)	C(5) —C(10)—H(10)	122(1)
C(1) —C(3)—H(3*b*)	106(1)	C(9) —C(10)—H(10)	116(1)
C(1) —C(3)—H(3*c*)	110(1)	C(11)—C(12)—H(11)	119(1)
H(3*a*)—C(3)—H(3*b*)	107(2)	C(13)—C(12)—H(11)	119(1)
H(3*a*)—C(3)—H(3*c*)	111(2)	C(12)—C(13)—H(13)	119(1)
H(3*b*)—C(3)—H(3*c*)	110(2)	C(14)—C(13)—H(13)	121(1)
C(1) —C(4)—H(4*a*)	113(1)	C(13)—C(14)—H(14)	116(1)
C(1) —C(4)—H(4*b*)	107(1)	C(15)—C(14)—H(14)	124(1)
C(1) —C(4)—H(4*c*)	112(1)	C(14)—C(15)—H(15)	120(2)
H(4*a*)—C(4)—H(4*b*)	111(2)	C(16)—C(15)—H(15)	119(2)
H(4*a*)—C(4)—H(4*c*)	109(2)	C(11)—C(16)—H(16)	119(1)
H(4*b*)—C(4)—H(4*c*)	105(2)	C(15)—C(16)—H(16)	120(1)

TABLE 5. Observed intraannular torsion angles (deg)

Bond	Angle	Bond	Angle
B(1)—O(3)	−23.7(1)	B(1)—O(1)	−0.4(1)
O(3)—C(2)	41.7(1)	O(1)—B(2)	1.1(1)
C(2)—C(1)	−39.5(1)	B(2)—O(2)	−1.3(1)
C(1)—N	23.7(1)	O(2)—N	0.9(1)
N —B(1)	−1.8(1)	N —B(1)	−0.4(1)

Can. J. Chem. Downloaded from www.nrcresearchpress.com by 210.87.254.40 on 09/05/12
For personal use only.

TABLE 6. Equations of weighted least-squares planes in the form $lX + mY + nZ = p$ where X, Y, and Z are orthogonal Å coordinates with respect to a, b, and c^*. Deviations (Å) of atoms from the planes are also given

Plane	χ^2	Equation of plane	Deviation of atoms from plane							
			Atom	Deviation	Atom	Deviation	Atom	Deviation	Atom	Deviation
1	20.5	$0.0379X + 0.9603Y - 0.2764Z = 3.4907$	C(5)	0.000(1)	C(6)	−0.003(2)	C(7)	0.004(2)	C(8)	0.002(2)
C(5)–C(10)			C(9)	−0.006(2)	C(10)	0.004(2)	B(1)	0.038(2)	H(6)	0.05(2)
			H(7)	0.05(2)	H(8)	0.00(2)	H(9)	−0.03(2)	H(10)	−0.01(2)
2	40.7	$0.5756X - 0.7323Y - 0.3638Z = -1.8276$	C(11)	−0.005(2)	C(12)	0.001(2)	C(13)	0.005(2)	C(14)	−0.007(2)
C(11)–C(16)			C(15)	−0.002(2)	C(16)	0.009(2)	B(2)	−0.029(2)	H(12)	0.01(2)
			H(13)	0.06(3)	H(14)	−0.02(3)	H(15)	0.06(3)	H(16)	−0.03(2)
			O(1)	−0.167(1)	O(2)	0.150(1)				
3	55.9	$0.6159X - 0.6371Y - 0.4635Z\% - 1.6126$	B(1)	−0.002(2)	B(2)	0.010(2)	O(1)	−0.002(1)	O(2)	−0.004(1)
B(1), B(2), O(1), O(2), N			N	0.003(1)	C(11)	0.074(2)				

Dihedral angles between planes

Planes	Angle (deg)
1–2	125.5
1–3	117.4
2–3	8.2

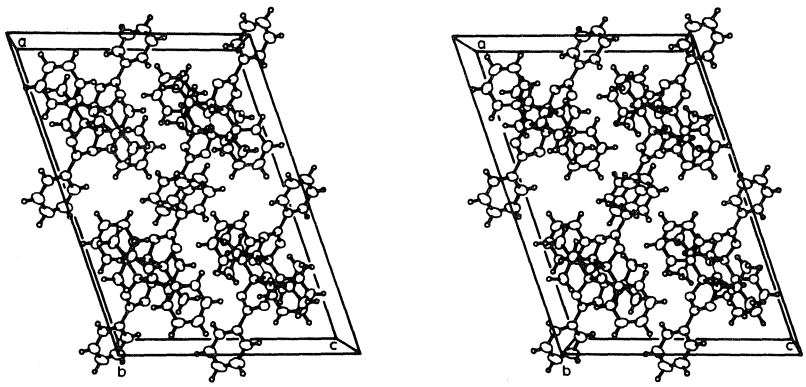

FIG. 2. The crystal structure viewed into *b*. Broken lines represent hydrogen bonds.

conformation with C(2) out of the rough plane defined by the other four atoms. Torsion angles in the ring correspond closely to those obtained from strain energy minimization calculations for cyclopentane with $\omega_1 = 25.0°$ (18). The novel B_2O_2N ring is nearly, but not rigorously, planar (see Table 6). All atoms lie within ± 0.01 Å of the mean plane. The nonplanarity of the B_2O_2N ring as well as that of the coordination group of trivalent B(2) (B(2) being displaced 0.012(2) Å from the O(1)O(2)C(11) plane) probably result from inter- and intramolecular steric forces.

Bond distances in the five-membered BOCCN ring differ significantly from those in the BOCCN

TABLE 7

(*a*) Selected intra- and intermolecular contacts

Intramolecular		Intermolecular*	
Atoms	Distance	Atoms	Distance
O(1)...C(12)	3.076(2)	O(2)...C(10)[1]	3.314(2)
O(1)...C(2)	3.088(2)	O(2)...O(3)[1]	3.411(2)
O(2)...C(16)	2.942(2)	C(11)...C(13)[2]	3.392(3)
O(2)...C(2)	3.091(2)	C(12)...C(12)[2]	3.436(3)
O(3)...C(10)	2.990(2)		
O(3)...C(3)	2.991(2)		
O(2)...H(16)	2.61(2)		
N...H(3*a*)	2.69(2)		
N...H(3*c*)	2.62(2)		
C(2)...H(3*c*)	2.68(2)		
C(3)...H(*n*)	2.43(2)		
C(3)...H(2*b*)	2.67(2)		
C(3)...H(4*b*)	2.69(2)		
C(3)...H(4*c*)	2.71(3)		
C(4)...H(2*a*)	2.64(2)		
C(4)...H(3*b*)	2.66(2)		
H(3*c*)...H(10)	2.24(3)		

(*b*) Hydrogen-bond data* (distances in Å and angles in deg)

D—H...A	H...A	D...A	∠DHA	∠XAH
N—H(*n*)...O(3)[1]	1.97(2)	2.853(2)	171(2)	126.7,123.0(5)
Intramolecular C—H...O interactions				
C(4)—H(4*a*)...O(2)	2.51(2)	2.750(2)	94(1)	122.6, 84.7(5)
C(6)—H(6)...O(1)	2.52(2)	2.908(2)	104(1)	113.3, 81.8(5)

*Superscripts refer to atoms at positions: [1] $1/2 - x, y - 1/2, 1/2 - z$; [2] $-x, 1 - y, -z$,

Can. J. Chem. Downloaded from www.nrcresearchpress.com by 210.87.254.40 on 09/05/12
For personal use only.

Can. J. Chem. Downloaded from www.nrcresearchpress.com by 210.87.254.40 on 09/05/12
For personal use only.

rings of the 2-aminoethyldiarylborinates (19–21) and *B*-phenyl*diptych*boroxazolidine, **5** (8). The O—B, O—C, C—C, C—N, and N—B distances are 1.452(2), 1.426(2), 1.530(2), 1.513(2), and 1.692(2) Å in the present structure; and weighted mean values (where appropriate) are 1.467(7), 1.415(4), 1.519(5), 1.486(1), and 1.666(3) Å for *B*-phenyl*diptych*boroxazolidine; and 1.477(2), 1.412(2), 1.503(3), 1.488(1), and 1.654(1) Å for the 2-aminoethyldiarylborinates.

Bond angles at tetrahedrally coordinated B(1) range from 98.9(1)° for O(1)—B(1)—N to 115.3(1)° for N—B(1)—C(5). The N—B bond is longer while both the O—B and C—B bonds are shorter than those in the related compounds mentioned above. The two B(1)—O bonds (B(1)—O(3), 1.452(2), and B(1)—O(1), 1.467(2) Å) are significantly different, indicative of the electronic differences between the two five-membered rings. The B(1)—C(5) distance of 1.599(2) A is significantly shorter than the values of 1.613(3) Å for *B*-phenyl*diptych*boroxazolidine (8), 1.618(1) Å (mean of four) for the 2-aminoethyldiarylborinates (19–21), and 1.631–1.648(8) Å for the tetraphenylborate anion (22).

Trivalent B(2) has distorted trigonal planar geometry. The angle at B(2) in the five-membered B_2O_2N ring (O(1)—B(2)—O(2)) is 114.9(1)° and the exocyclic angles are O(1)—B(2)—C(11), 127.6(1)° and O(2)—B(2)—C(11), 117.5(1)°, the greater angle being associated with the shorter B(2)—O bond. The difference between the two B(2)—O bonds (B(2)—O(1), 1.337(2) Å and B(2)—O(2), 1.404(2) Å) is highly significant. Trigonal B—O distances in other molecules range from 1.28 to 1.46 Å with a mean value of 1.36 Å (23) and the B—O distance in the related compound 2-phenyl-1,3,2-benzodioxaborol (24) is 1.394(3) Å. The B(2)—C(11) distance of 1.557(2) Å lies between the values of 1.537(6) Å for 2-phenyl-1,3,2-benzodioxaborol (24) and 1.571(3) and 1.589(5) Å for the crystallographically independent bonds in Ph_3B (25).

Both phenyl groups are slightly, but significantly, nonplanar (see Table 6). The torsion angles which define the orientation of the phenyl rings are O(1)[B(1)—C(5)]C(6), 13.6(2), O(3)[B(1)—C(5)]C(10), −31.9(2), O(1)[B(2)—C(11)]C(12), −6.7(2), and O(2)[B(2)—C(11)]C(16), −8.6(2)°. As can be seen in Fig. 1, the C(11)–C(16) ring lies roughly in the same plane as the B_2O_2N ring, the angle between normals to the mean planes being 8.2°. The C—C bond distances in the phenyl rings range from 1.372(4) to 1.407(2) Å with a mean value of 1.390 Å. As in related compounds (8, 19–21), bond distances in the phenyl ring decrease as they are removed from the boron substituent. The patterns of bond angles in both phenyl rings are consistent with those in related molecules (26).

The N—O(2) bond length of 1.440(2) Å lies at the long end of the 1.26–1.44 Å range of N—O single bond distances (23). The three C(sp^3)—C(sp^3) single bonds range from 1.520–1.530 Å with a mean value of 1.525 Å, slightly shorter than the usual 1.537 Å (23). The geometry involving hydrogen atoms is as expected, weighted mean C(ar)—H and C(sp^3)—H distances being 0.97(1) and 1.01(1) Å respectively.

The crystal structure consists of discrete molecules of 8,8-dimethyl-3,5-diphenyl-2,4,6-trioxa-1-azonia-3-bora-5-boranatabicyclo[3.3.0]octane, each linked to two others by N—H . . . O hydrogen bonds (N . . . O = 2.853(2) Å) to form continuous spirals about the 2_1 axes along *b* (see Fig. 2). All other intermolecular contacts correspond to normal van der Waals contacts. There are two short intramolecular O . . . H contacts listed in Table 7(*b*).

Acknowledgements

We thank the National Research Council of Canada for financial support and the University of British Columbia Computing Centre for assistance.

1. W. Kliegel. Tetrahedron Lett. 223 (1969).
2. W. Kliegel and H. Becker. In preparation.
3. R. Neu. Z. Anal. Chem. **176**, 343 (1960).
4. A. M. Yurkevich, S. G. Verenikina, E. G. Chauser, and N. A. Preobrazhenskii. Zh. Obsch. Khim. **36**, 1746 (1966).
5. D. S. Robinson, J. Eagles, and R. Self. Carbohydrate Res. **26**, 204 (1973).
6. I. R. McKinley, H. Weigel, C. B. Barlow, and R. D. Guthrie. Carbohydrate Res. **32**, 187 (1974).
7. O. C. Musgrave and T. O. Park. Chem. Ind. (London), **26**, 1552 (1955).
8. S. J. Rettig and J. Trotter. Can. J. Chem. **53**, 1393 (1975).
9. R. E. Long. Ph.D. Thesis, University of California at Los Angeles, Los Angeles, California. 1965.
10. D. T. Cromer and J. B. Mann. Acta Crystallogr. **A24**, 321 (1968).
11. R. F. Stewart, E. R. Davidson, and W. T. Simpson. J. Chem. Phys. **42**, 3175 (1965).
12. D. T. Cromer and D. Liberman. J. Chem. Phys. **53**, 1891 (1970).

13. V. SCHOMAKER and K. N. TRUEBLOOD. Acta Crystallogr. B**24**, 63 (1969).
14. D. W. J. CRUICKSHANK. Acta Crystallogr. **9**, 747 (1956); **9**, 754 (1956).
15. D. W. J. CRUICKSHANK. Acta Crystallogr. **14**, 896 (1961).
16. W. R. BUSING and H. A. LEVY. Acta Crystallogr. **17**, 142 (1964).
17. C. K. JOHNSON. *In* Crystallographic computing. Munksgaard, Copenhagen. 1970. pp. 207–226.
18. J. B. HENDRICKSON. J. Am. Chem. Soc. **83**, 4537 (1961); **85**, 4059 (1963).
19. S. J. RETTIG and J. TROTTER. Can. J. Chem. **51**, 1288 (1973).
20. S. J. RETTIG and J. TROTTER. Acta Crystallogr. B**30**, 2139 (1974).
21. S. J. RETTIG and J. TROTTER. Can. J. Chem. This issue.
22. R. J. SIME, R. P. DODGE, A. ZALKIN, and D. H. TEMPLETON. Inorg. Chem. **10**, 537 (1971).
23. L. E. Sutton (*Editor*). Chem Soc. Special Publ. No. 11, 1958, and No. 18, 1965.
24. F. ZETTLER, H. D. HAUSEN, and H. HESS. Acta Crystallogr. B**30**, 1876 (1974).
25. F. ZETTLER, H. D. HAUSEN, and H. HESS. J. Organomet. Chem. **72**, 157 (1974).
26. A. DOMENICANO, A. VACIAGO, and C. A. COULSON. Acta Crystallogr. B**31**, 1630 (1975).

Can. J. Chem. Downloaded from www.nrcresearchpress.com by 210.87.254.40 on 09/05/12
For personal use only.

Acid dissociation constants and rates as studied by ultrasonic absorption

LARRY W. GREEN,[1] PEETER KRUUS, AND M. JACQUELINE MCGUIRE
Department of Chemistry, Carleton University, Ottawa, Canada K1S 5B6

Received December 22, 1975

LARRY W. GREEN, PEETER KRUUS, and M. JACQUELINE MCGUIRE. Can. J. Chem. **54**, 3152 (1976).

Experimental ultrasonic absorption data on solutions of H_2SO_4 and H_3PO_4 are interpreted in terms of proton transfer equilibria. The acid dissociation constants obtained are compared with those obtained using other methods and are shown to be consistently lower. A model is proposed to explain this in terms of ΔV^θ and ΔH^θ involved in the steps leading to recombination of the proton with the anion. This model is supported by the values of the reaction distance parameters calculated from the value of the rate constant obtained for the recombination rate. The accuracy of this rate constant is dependent on the accuracy of the ΔV^θ value used for the equilibrium. Experimental density data are presented here as an aid in determining ΔV^θ. Problems involving activity coefficients in such solutions are discussed in the course of checking the values used for species present in sulfuric acid solutions.

LARRY W. GREEN, PEETER KRUUS et M. JACQUELINE MCGUIRE. Can. J. Chem. **54**, 3152 (1976).

Les résultats expérimentaux de l'absorption en ultrasons de solutions de H_2SO_4 et de H_3PO_4 sont interprétés en termes des équilibres de transferts de protons. Les constantes de dissociation des acides sont comparées avec celles obtenues en utilisant d'autres méthodes et il est montré qu'elles sont systématiquement plus basses. Un modèle est proposé pour expliquer ceci en termes du ΔV^θ et du ΔH^θ impliqués dans les étapes conduisant à la recombinaison du proton avec l'anion. Ce modèle est soutenu par les valeurs des paramètres de la distance de réaction calculées à partir de la valeur de la constante de vitesse obtenue pour le taux de recombinaison. La précision de cette constante de vitesse dépend de la précision de la valeur ΔV^θ utilisée pour l'équilibre. Des données expérimentales de densité sont présentées ici pour aider à la détermination du ΔV^θ. Des problèmes impliquant les coefficients d'activité dans de telles solutions sont discutés au cours de la vérification des valeurs utilisées pour les espèces présentes dans les solutions d'acide sulfurique.

[Traduit par le journal]

Can. J. Chem. Downloaded from www.nrcresearchpress.com by 210.87.254.5 on 09/05/12
For personal use only.

Introduction

Ultrasonic absorption due to proton-transfer equilibria in solutions of larger organic molecules has received considerable study recently (1–3). When the species concerned are quite large, then the relaxation time of a dissociation equilibrium

$$[1] \qquad H^+\cdot A^- + H_2O \underset{k_r}{\overset{k_d}{\rightleftharpoons}} H_3O^+ + A^-$$

is sufficiently long that the relaxation curve (α/f^2) *vs.* $\log f$ can be obtained completely by conventional ultrasonic absorption apparatus. In such a case, the rate constants k_d and k_r, and the ΔV of the equilibrium can be obtained (4). There is in such cases the possibility of other, *e.g.* conformational, equilibria contributing to the ultrasonic absorption.

In solutions of simple inorganic acids, it is unlikely that equilibria other than proton transfer contribute to the ultrasonic absorption. However, when the species HA, A^- are small, then the relaxation time is sufficiently short so that measurements in the GHz region are necessary in order to obtain τ directly from experiment. An analysis of the excess absorption at a single frequency as a function of concentration of acid leads, however, to a value of k_d/k_r (*i.e.* the equilibrium constant for [1]). Furthermore, if the ΔV^θ of [1] is known, the absolute values of k_d and k_r can also be determined (5).

Although there are a number of ways of determining proton transfer rates (*e.g.*, nmr, Raman spectroscopy, temperature and electric field jump, electrochemical with rotating elec-

[1]Present address: Division of Chemistry, National Research Council of Canada, Ottawa, Canada K1A 0R9.

Can. J. Chem. Downloaded from www.nrcresearchpress.com by 210.87.254.5 on 09/05/12
For personal use only.

trodes, neutron scattering, etc), this indirect method seems to be suitable and interesting for a number of equilibria. In ref. 5, the K, k_d, and k_r of a number of medium strong inorganic acids were obtained using such analysis. Here, a more complete analysis including the effect of activity coefficients is presented using more complete data.

On the basis of this analysis, a discussion is given of the relationship of acid dissociation constants as measured by ultrasonics to those measured by other means. Such data contributing to an elucidation of the species present in aqueous solutions seem to be important in developing a better understanding of marine and biological chemistry.

Experimental

The apparatus and procedure for ultrasonic absorption measurements are given in ref. 6. Measurements were made at the most convenient frequency, 31.6 MHz. Previous studies (5, 7) indicate no change in (α/f^2) with frequency for these solutions. The materials used to make up stock solutions were Fisher Certified ACS H_3PO_4 and $HClO_4$, and Baker Analyzed Reagent grade H_2SO_4. The concentrations of these solutions were obtained by titration with a standard NaOH solution using a pH meter. Solutions for the ultrasonic measurements were obtained by appropriate dilutions of samples of stock solutions. The accuracy of the concentrations was estimated to be better than 2%.

Density measurements were made on a Precision Density Meter DMA 02C similar to that described in ref. 8. Solutions for density measurements were made up by weight using freshly boiled distilled water and stock solutions of the above H_2SO_4 and H_3PO_4 and Fisher Certified ACS NaCl, Anachemia Reagent grade $NaH_2PO_4 \cdot H_2O$ and Baker Analyzed Reagent grade HCl. The densitometer was calibrated with three standard liquids obtained from the National Research Council of Canada.

Results

Theoretical Background for Interpretation of Ultrasonic Absorption

Derivations of the general equations for ultrasonic absorption due to an equilibrium such as [1] are given in ref. 4. When enthalpy effects can be neglected, as in the case of aqueous solutions, then the excess absorption is:

$$[2] \quad \alpha'/f^2 = \frac{2\pi^2\rho v \Delta V \Delta V^\theta}{RT} K_a \left(\frac{\partial\theta}{\partial K_a}\right)_T \frac{\tau}{1+\omega^2\tau^2}$$

Here ΔV, ΔV^θ refer to the reaction in [1]; they are usually assumed identical. ρ is the density, v the speed of the ultrasound, θ the degree of advancement or extent of reaction 1, ω the radial frequency, and τ the relaxation time. As in these cases $\omega \ll 1/\tau$ (5), $(1+\omega^2\tau^2)$ can be equated to unity.

In [2], K_a is the activity equilibrium constant,

$$[3] \quad K_a = K_\gamma K_c = \frac{\gamma_{H^+}\gamma_{A^-}}{\gamma_{HA}} \cdot \frac{C_{H^+} \cdot C_{A^-}}{C_{HA}}$$

The form of the derivative in [2] for phosphoric acid solutions is

$$[4] \quad \left(\frac{\partial\theta}{\partial K_a}\right)_T = \frac{1}{K_a}\left\{\frac{(2-\alpha)}{\alpha(1-\alpha)c} + \left(\frac{\partial \ln \gamma_{H^+}}{\partial\theta}\right)_T + \left(\frac{\partial \ln \gamma_{A^-}}{\partial\theta}\right)_T\right\}^{-1}$$

while for sulfuric acid solutions it is

$$[5] \quad \left(\frac{\partial\theta}{\partial K_a}\right)_T = \frac{1}{K_a}\left\{\frac{2-(1-\alpha)^2}{\alpha(1+\alpha)(1-\alpha)c} + \left(\frac{\partial \ln \gamma_{H^+}}{\partial\theta}\right)_T + \left(\frac{\partial \ln \gamma_{SO_4^{2-}}}{\partial\theta}\right)_T - \left(\frac{\partial \ln \gamma_{HSO_4^-}}{\partial\theta}\right)_T\right\}^{-1}$$

In [4] and [5], c is the stoichiometric concentration of the acid, while α is the degree of dissociation ($\alpha = C_{A^-}/c$). The relaxation time τ in [2] is given by

$$[6] \quad 1/\tau = k_r\left\{K_a\frac{\gamma_{HA}C_{HA}}{\gamma^*}\left[\frac{1}{C_{HA}} - \left(\frac{\partial \ln \gamma_{HA}}{\partial\theta}\right)_T + \left(\frac{\partial \ln \gamma^*}{\partial\theta}\right)_T\right] + \frac{\gamma_{H^+}\gamma_{A^-}C_{H^+}C_{A^-}}{\gamma^*}\left[\frac{1}{C_{H^+}} + \frac{1}{C_{A^-}} + \left(\frac{\partial \ln \gamma_{H^+}}{\partial\theta}\right)_T + \left(\frac{\partial \ln \gamma_{A^-}}{\partial\theta}\right)_T - \left(\frac{\partial \ln \gamma^*}{\partial\theta}\right)_T\right]\right\}$$

The activity coefficient γ^* of transition state $(H_3O^+ \ldots H_2PO_4^-)$ can be taken as unity for phosphoric acid solution, so that $(\partial \ln \gamma^*/\partial\theta)_T \simeq 0$. However, this is not the case for sulfuric acid solutions. The rate constant k_r in [6] is the limiting value as ionic strength $\mu \to 0$. Thus $k_d = K_a k_r$ in this limit.

When the activity coefficients γ_i are assumed

TABLE 1. Ion size parameters used in calculation of activity coefficients (9)

Ion	a_i/Å
H^+	9.0
SO_4^{2-}	4.0
HSO_4^-	4.5
$H_2PO_4^-$	4.5
$(H\text{---}SO_4)^{-*}$	6.5[a]
Mg^{2+}	8.0

[a]Estimate.

to follow the extended Debye–Hückel form,

$$[7] \qquad \log \gamma_i = \frac{-Az_i^2\sqrt{\mu}}{1 + Ba_i\sqrt{\mu}}$$

then the derivatives in [4], [5], and [6] are

$$[8] \qquad \left(\frac{\partial \ln \gamma_i}{\partial \theta}\right)_T = \frac{-2.303Az_i^2}{2\sqrt{\mu}(1 + Ba_i\sqrt{\mu})^2}$$

Here $A = 1.8246 \times 10^6/(\epsilon T)^{3/2}$, $B = 50.29 \times 10^8/(\epsilon T)^{1/2}$, a_i is the ionic size parameter (see Table 1), and ϵ the dielectric constant. The ionic strength $\mu = (1 + 2\alpha)c$ for sulfuric acid and $\mu = \alpha c$ for phosphoric acid solutions. In the case of sulfuric acid solutions, [8] must be multiplied by a factor of 2 as $\partial\mu/\partial\theta = 2$ in that case.

The experimental data were analyzed in various ways to test the sensitivity of different approximations. In general, the method was to assume a value of K_a. It was initially assumed that $K_c = K_a$, and from this estimate C_{H^+}, C_{A^-}, C_{HA}, and μ were calculated by solving a quadratic (5). Next the γ_i were calculated from [7], and a new value K_c was calculated through [3]. This iteration was repeated until K_c was constant to within 0.01%.

With values of K_a, C_i, γ_i known, a value of $k_r/(\Delta V^\theta)^2$ was obtained from [2] by setting $\partial(\sum[(\alpha'/f^2)_{exp} - (\alpha'/f^2)_{calc}]^2)/\partial k_r = 0$ and solving for k_r (5). A value of the standard deviation σ was also calculated. This whole calculation was repeated for a series of initial K_a values and the K_a giving the lowest σ was noted.

Interpretation of Density Data

There is considerable discrepancy in the ΔV^θ values quoted for the reactions concerned, especially that for $H_3PO_4 \rightleftharpoons H^+ + H_2PO_4^-$. It was therefore decided to obtain independent ΔV^θ values through density measurements. Density data at 25 °C for H_2SO_4 were obtained to test the apparatus and analysis against previously obtained data. These data, as well as other results which can be compared, are in good agreement with more precise data based on more extensive investigation (Fig. 1, Table 2). A more extensive density investigation is not warranted for this particular investigation, as several other sources of inaccuracies are present in the analysis of the ultrasonic results to obtain k_r values.

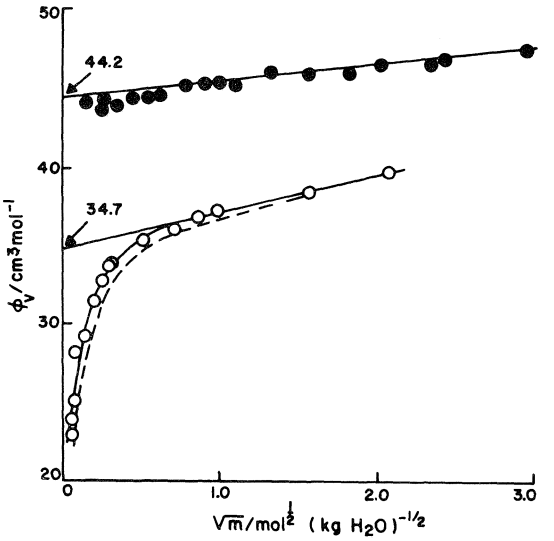

FIG. 1. ϕ_v data for H_3PO_4 and H_2SO_4: ● H_3PO_4, ○ H_2SO_4, experimental, --- refs. 13 and 12.

The density data were converted to apparent molal volume data by application of the relationship (10)

$$[9] \qquad \phi_v = \frac{1000(\rho - \rho^0)}{\rho\rho^0 m} + \frac{M}{\rho}$$

In [9], m is the molality and M the molecular weight of the solute. The standard partial molal volume of the solute, V^θ, can be obtained by extrapolating ϕ_v to $m = 0$. This extrapolation was made from plots of ϕ_v *vs.* $\sqrt{m}$, as to a first approximation, this results in a linear relationship for fully dissociated electrolytes. For more complete and accurate data, more sophisticated plots are warranted (11). There is difficulty in obtaining the ϕ_v^0 for species such as H_3PO_4, $H_2PO_4^-$, HSO_4^- as the degree of dissociation changes with m. Thus in some cases long extrapolations are necessary (Fig. 2).

Curves of ϕ_v *vs.* $\sqrt{m}$ were obtained for the systems shown in Table 2. The H_2SO_4 25 °C data

Can. J. Chem. Downloaded from www.nrcresearchpress.com by 210.87.254.5 on 09/05/12
For personal use only.

are shown in Fig. 1 together with corresponding data from the literature (12, 13) and the H_3PO_4 25 °C data. Figure 2 shows the full set of ϕ_v *vs.* $\sqrt{m}$ curves necessary to obtain ΔV^θ at 10 °C for $H_3PO_4 \rightleftharpoons H^+ + H_2PO_4^-$. The relatively large errors possible in some extrapolations, *e.g.* for NaH_2PO_4, introduce an uncertainty of up to ± 1.4 cm^3 mol^{-1} in the ΔV^θ value.

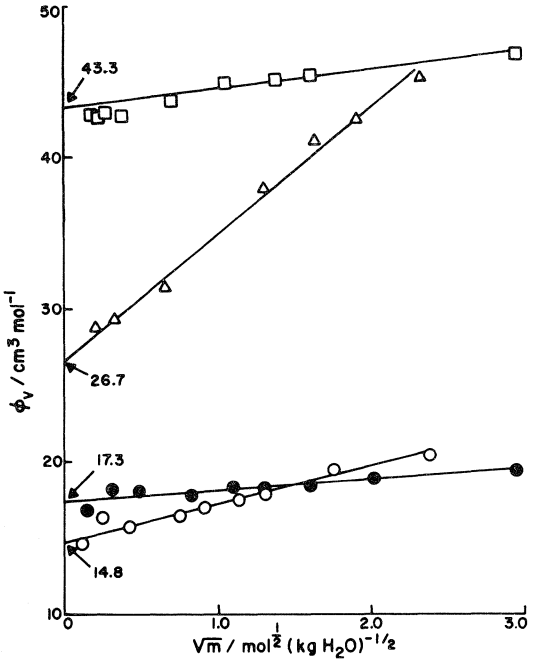

FIG. 2. ϕ_v data for determination of ΔV^θ of $H_3PO_4 \rightleftharpoons H^+ + H_2PO_4^-$ at 10.0 °C: ● HCl, ○ NaCl, △ NaH_2PO_4, □ H_3PO_4.

Table 3 shows a summary of the V_i^θ values for the species of interest. The ΔV^θ values for the two equilibria determined from these and other density determinations are listed in Table 4, together with values obtained by other methods. The differences can be due partly to the large uncertainties in the ΔV_θ values, but they can also reflect the differences in the actual species discerned by various methods of measurement.

Sensitivity of Results to Assumptions

The values of v, ρ, and ϵ used in the calculations were assumed constant with concentration of acid. This produces an error of less than 1% in the product ρv with c going from 0 to 0.26 mol l^{-1}, the extreme case. The excess absorption α'/f^2 was assumed to be $(\alpha/f^2)_{exp} - (\alpha/f^2)_{water}$. For a strong acid ($HClO_4$), $(\alpha/f^2)_{exp}$ was essentially constant with concentration up to 0.15 mol l^{-1} (Fig. 3). This is in agreement with previous data on nitric, hydrochloric, and perchloric acids (5). Two other possible curves for the variation of $(\alpha/f^2)_{exp}$ with perchloric acid concentration are sketched in Fig. 3. Rows 11 and 12 of Table 5 show the results of calculations using

TABLE 2. Experimental values of ϕ_v^0 with comparisons

Row	T/°C	System	ϕ_v^0/cm^3 mol^{-1}	Species	Comparisons
1	25.0	H_2SO_4	34.7±0.3	$H^+ + HSO_4^-$	35.1 (12); 35.7 (13, 10)
2	25.0	H_3PO_4	44.2±0.1	H_3PO_4	—
3	25.0	NaH_2PO_4	28.0±1.0	$Na^+ + H_2PO_4^-$	27.9 (10)
4	10.0	H_3PO_4	43.3±0.3	H_3PO_4	—
5	10.0	NaH_2PO_4	26.7±0.7	$Na^+ + H_2PO_4^-$	—
6	10.0	NaCl	14.8±0.2	$Na^+ + Cl^-$	16.6 at 25 °C; 13.0 at 0 °C (10)
7	10.0	HCl	17.3±0.2	$H^+ + Cl^-$	17.8 at 25 °C; 16.5 at 0 °C (10)

TABLE 3. Values of V_i^θ for species concerned

T/°C	Species	V_i^θ/cm^3 mol^{-1}	Source
25.0	H^+	0	By convention[a]
25.0	SO_4^{2-}	14.0;15.8	(10); (15)
25.0	HSO_4^-	35.7;31.1;34.7	(10); (15); Row 1, Table 2
25.0	$H_2PO_4^-$	27.9;27.8	(10); Row 3, Table 2 with $V_{Na^+}^\theta = -1.2$
25.0	H_3PO_4	44.2	Row 2, Table 2
10.0	H^+	0	By convention
10.0	$H_2PO_4^-$	29.2	Rows 5, 6, 7 of Table 2
10.0	H_3PO_4	43.3	Row 4, Table 2

[a]The convention $V_{H^+}^\theta = -5.4$ cm^3 mol^{-1} is used in ref. 14.

Can. J. Chem. Downloaded from www.nrcresearchpress.com by 210.87.254.5 on 09/05/12
For personal use only.

TABLE 4. Comparison of ΔV^θ values for $HA \rightleftharpoons H^+ + A^-$

Method	ΔV^θ	References
(*a*) $HSO_4^- \rightleftharpoons H^+ + SO_4^{2-}$ at 25.0 °C		
Density	−20.2, −21.6, −21.7, −15.3	12, 13, 10, 15
Conductivity	−16.4	16
Pressure Raman	−10 ± 3	17
(*b*) $H_3PO_4 \rightleftharpoons H^+ + H_2PO_4^-$ at 25.0 °C		
Density	−16.2, −16.4	18, Table 3
Conductivity	−15.5, −10.1 ± 0.5	19,[a]
Electromotive force	−14.9 ± 0.3	21
(*c*) $H_3PO_4 \rightleftharpoons H^+ + H_2PO_4^-$ at 10 °C		
Conductivity	−9.4 ± 1.0	[a]
Density	−14.1 ± 1.4	Table 3

[a]H. Chew, private communication.

these curves to test the sensitivity of the assumption of setting $(\alpha'/f^2) = (\alpha/f^2)_{exp} - (\alpha/f^2)_{water}$. The variation of the classical absorption (proportional to $\eta/\rho v^3$) was also neglected since in the extreme case ($c = 0.26$ mol l^{-1}), it differs by less than 3% from that of pure water.

Rows 1 to 4 of Table 5 show that the analysis gives consistent results up to 0.072 mol l^{-1} for H_2SO_4 solutions. An increase in the number of data points, with the additional points at higher concentrations, does not change the K_a value obtained from the analysis until the points are at $c > 0.072$ (Fig. 3).

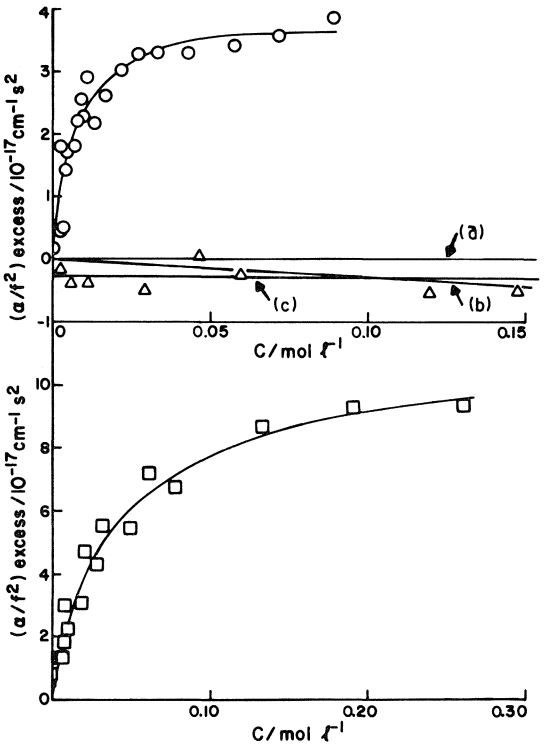

FIG. 3. Excess ultrasonic absorption as a function of concentration of acid: ○ H_2SO_4 at 25 °C, △ $HClO_4$ at 25 °C, □ H_2SO_4 at 0 °C.

Rows 5 to 9 of Table 5 show the effect of variation of the method of calculating activity coefficients. If μ is set equal to zero, then the γ_i are all unity and K_a is considerably larger. Rows 3, 6, and 7 indicate the sensitivity of the results to variation of the Debye–Hückel distance parameter. If the a_i are all set equal to zero (the limiting law) instead of the Table 1 values, then K_a decreases by 60%. If the a_i are set equal to some larger values, as suggested by analysis in Table 8 ($a_{H^+} = 10$, $a_{SO_4^{2-}} = 10$, $a_{HSO_4^{-*}} = 16$, $a_{HSO_4^-} = 13$ Å), then K_a increases by 40%. Rows 8 and 9 show the dependence of the results on the form of [7]. The results assuming the limiting law are already available in row 6. If a linear term $0.1 z_i \mu$ is added to [7], then K_a changes by only 12%. If next the a_i are all assumed to be 3.04 Å, the Davies form of the log γ_i equation is obtained (22). This changes K_a by 4%.

Row 10 shows that if K_a is constrained to have the value suggested by emf measurements, then the standard deviation of the experimental points from the best possible curve more than doubles. From rows 11 and 12 it can be seen that the assumption $(\alpha'/f^2) = (\alpha/f^2)_{exp} - (\alpha/f^2)_{water}$ can introduce an error of at most 20%. The changes in activity coefficients have a large effect on the value of k_r and k_d obtained by the analysis, with a maximum change of nearly a factor of 3.

Can. J. Chem. Downloaded from www.nrcresearchpress.com by 210.87.254.5 on 09/05/12
For personal use only.

TABLE 5. Results of analysis of H_2SO_4 25 °C ultrasonic data using various assumptions

Row	Conditions	Points	$\sigma/10^{-17}$	K_a	$k_r/10^{10}$ l mol^{-1} s^{-1}	$k_d/10^8$ s^{-1}
1	$c < 0.017$	13	0.34	0.0046	35.9	16.5
2	$c < 0.033$	16	0.30	0.0049	35.0	17.2
3	$c < 0.072$	19	0.28	0.0049	35.1	17.2
4	$c < 0.135$	21	0.33	0.0056	34.6	19.3
5	$\mu = 0$	19	0.34	0.0158	14.1	22.3
6	$a_i = 0$	19	0.45	0.0019	40.2	7.6
7	a_i large[a]	19	0.29	0.0068	29.2	19.8
8	Linear term to log γ_i	19	0.28	0.0058	33.2	19.2
9	Davies form of log γ_i[b]	19	0.28	0.0047	36.0	16.9
10	K_a fixed = 0.0105	19	0.67	0.0105	35.0	36.8
11	Assuming (*b*) in Fig. 3	19	0.29	0.0058	32.4	18.8
12	Assuming (*c*) in Fig. 3	19	0.30	0.0039	31.0	12.1

[a] $a_{H^+} = a_{SO_4^{2-}} = 10$; $a_{HSO_4^-} = 13$; $a_{HSO_4^{-*}} = 16$ A.
[b] $a_i = 3.04$ Å.

TABLE 6. Summary of results of ultrasonic absorption data analysis

T/°C	Data points	$\sigma/10^{-17}$	K_a	$k_r/10^{10}$ l mol^{-1} s^{-1}	$k_d/10^8$ s^{-1}
(*a*) HSO_4^-					
25.0	19	0.28	0.0049	35.1	17.1
18	11	0.32	0.0056	26.2	14.7
10	16	0.29	0.0065	25.1	16.3
0	11	0.44	0.0115	23.6	26.4
(*b*) H_3PO_4					
25.0	21	0.40	0.0029	13.2	3.8
18	10	0.40	0.0057	8.9	5.6
10	6	0.47	0.0059	7.6	3.6
5	5	0.79	0.0075	6.2	4.6
0	11	0.97	0.0069	5.3	3.6

The γ_i calculated for the species in H_2SO_4 solution cannot be checked directly with experimental results. However, they can be related to the $\gamma_\pm$ for H_2SO_4 which can be obtained from the emf values of appropriate cells (23). Such $\gamma_\pm$ are defined assuming H_2SO_4 to be a strong electolyte and do not involve $\gamma_{HSO_4^-}$. In terms of the γ_i used here

$$[10]\quad \gamma_\pm(H_2SO_4) = \left[\left(\gamma_{H^+}\left(\frac{1+\alpha}{2}\right)\right)^2 \cdot (\alpha\gamma_{SO_4^{2-}})\right]^{1/3}$$

The calculated $\gamma_\pm$ for H_2SO_4 assuming $K_a = 0.0102$ agree with the experimental (23) to within 6% even at 0.06 *m* concentrations, where $\gamma_\pm \simeq 0.3$.

The K_a and k_r for the Systems Studied

Table 6 summarizes the results of the analysis for the systems studied. The K_a shown are calculated by the initial method described. Only the curves for H_2SO_4 at 0.0 and 25.0 °C are displayed here (Fig. 3). Analogous experimental curves were obtained for other systems (see also ref. 5). Thus no experimental data except ultrasonic absorption have been utilized to obtain these K_a values. If the ionic strength were to be calculated from literature values of K_a, the K_a (ultrasonic) would decrease even further. If the a_i used in [7] were larger than those in Table 1, as suggested by results discussed later, then the K_a (ultrasonic) would become somewhat larger.

The values of k_r in Table 6 are calculated assuming $\Delta V \simeq \Delta V^\theta$ values of -21.6 cm^3 mol^{-1} for HSO_4^-, and -16.2 for H_3PO_4 at all temperatures (Table 4). The temperature variation in ΔV^θ is of the order of the uncertainty in the determination of ΔV^θ (Table 4). If a value -15.3 cm^3 mol^{-1} were used for HSO_4^-, then all HSO_4^- k_r values would be decreased by a factor of $(15.3/21.6)^2$ or 0.51, and k_d values decreased by this same factor.

Can. J. Chem. Downloaded from www.nrcresearchpress.com by 210.87.254.5 on 09/05/12
For personal use only.

Can. J. Chem. Downloaded from www.nrcresearchpress.com by 210.87.254.5 on 09/05/12
For personal use only.

TABLE 7. Comparison of the K_a for HSO_4^- at 25.0 °C

Method	K_a	References
Ultrasonic	0.0049	This work
Conductivity	0.0103	26
Electromotive force	0.0105	27
Volume	0.0103	13
Heat of solution	0.0103	25
Solubility	0.0103	28
Acid catalysis	0.010	29
Raman	0.040	30

TABLE 8. Distances defining the ion pair H^+-A^-

T/°C	K_1[a]	K_2[b]	a_2/Å
(*a*) HSO_4^-, a_1 = 5.17 Å (31)			
25	0.0105	0.04[c]	1.7[c]
25	0.0105	0.0049	26
18	0.0118	0.0056	24
10	0.0141	0.0065	24
0	0.0167	0.0115	14
(*b*) H_3PO_4, a_1 = 5.07 Å (31)			
25	0.00753	0.0029	38[d]
18	0.00805	0.0057	25
10	0.00851	0.0059	24
5	0.00877	0.0075	16
0	0.00897	0.0069	22

[a] K_a from ref. 25 (HSO_4^-) and ref. 18 (H_3PO_4).
[b] K_a (ultrasonic) from Table 4 except [c].
[c] Raman (30).
[d] This high value of a_2 may be due to an anomalously low K_a value due to experimental uncertainty. This possibility is supported by the high k_r value as seen in Fig. 5.

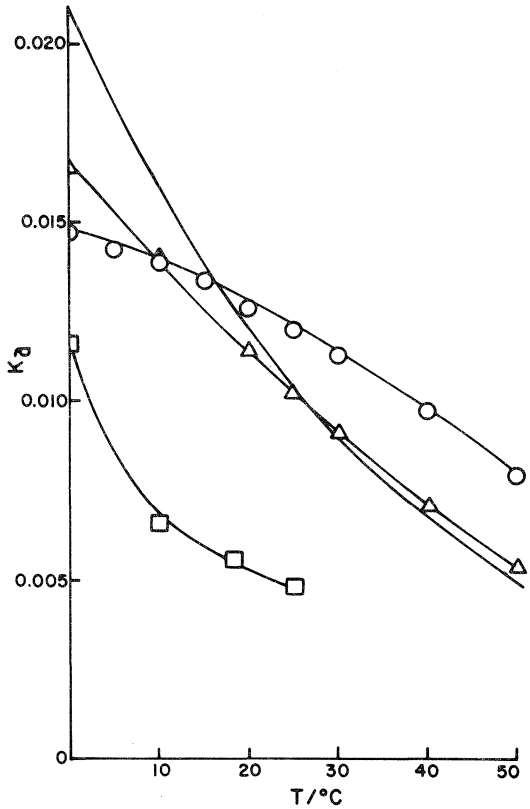

FIG. 4. Temperature dependence of K_a of HSO_4^-: ○ ref. 24, △ ref. 25, — from equation in ref. 22, p. 387, □ Table 6.

Discussion

Comparison of the K_a from Various Methods

The values of K_a (ultrasonic) as shown in Table 6 are in all cases smaller than those obtained using other experimental methods. This difference is readily seen in Tables 7, 8 and in Fig. 4. The values of K_a obtained here are determined primarily by the low concentration points. As α'/f^2 is small at low c, the error in α'/f^2 is large and the K_a (ultrasonic) values cannot be obtained to better than $\pm 20\%$ using any specific method of analysis. Independently obtained data in ref. 5 for 0 and 10 °C analyzed by the same methods gave K_a to within this limit. As indicated previously, concepts such as ionic radii and ionic strength are also not precisely defined in this context.

There have been a large number of investigations of the K_a for HSO_4^-. Reference 22 discusses these results in some detail. Table 7 shows a comparison of more recent determination of K_a for the HSO_4^- dissociation using various methods. As pointed out in ref. 31, the value of K_a obtained in analysis of experimental data is dependent on factors such as the ion size parameters used in the analysis.

The temperature dependence of the K_a of HSO_4^- is displayed in Fig. 4. There is considerable discrepancy in the value at 0.0 °C. The K_a values determined by ultrasonics are shown to be consistently below the values obtained by other means. Table 8 shows that this is also the case for H_3PO_4.

The K_a (ultrasonic) values are not dependent on the accuracy of the ΔV^θ values used. If ΔV varied considerably with concentration, then the K_a value would be affected. However, the results in ref. 12 show this to be unlikely.

The lower K_a obtained from ultrasonics can be explained by postulating that the $H^+ \cdot A^-$ which is the reactant in [1] is effectively an ion pair

TABLE 9. Reaction distance parameters calculated from eq. 2

T/°C	ϵ_r[a]	D_{H^+}[b]/10^{-5} cm^2 s^{-1}	D_{A^-}[b]/10^{-5} cm^2 s^{-1}	k_r/10^{10} l mol^{-1} s^{-1}	x/Å	a/Å[c]	a/Å[d]
(*a*) HSO_4^-							
25	78.3	9.32	2.14	35.1	−14.3	32	26
18	80.8	8.19	1.78	26.2	−14.2	30	24
10	83.8	6.95	1.42	25.1	−14.0	35	24
0	87.7	5.49	1.00	23.6	−13.9	40	14
(*b*) H_3PO_4							
25	78.3	9.32	1.60	13.2	−7.14	12	38
18	80.8	8.19	1.35	8.9	−7.08	9	25
10	83.8	6.95	1.09	7.6	−7.02	9	24
5	85.8	6.21	0.93	6.2	−6.98	9	16
0	87.7	5.49	0.78	5.3	−6.95	7	22

[a]From ref. 2, p. 457.
[b]Using $D_i = \Lambda_i RT/(F^2)$ with Λ_i the equivalent conductance, from ref. 22, p. 465.
[c]Using relation [12].
[d]Using relation [11], Table 8.

separated by several water molecules. Such a separation would have to be greater for ultrasonics than that effective in conductivity or electromotive force measurements. The K_a obtained from most recent Raman spectroscopy experiments is greater than that obtained from conductivity (30), although a value of 0.01 has been suggested in previous Raman work (32). Thus for the purpose of Raman measurements, the $H^+ \cdot A^-$ in [1] must be a contact ion pair or a covalent species (30).

A quantitative measure of the 'looseness' of the ion pair in [1] can be obtained on the basis of the Bjerrum model of ion pairing (31). Thus the assumptions of spherical ions with a continuous solvent with a macroscopic dielectric constant are present. As $c \rightarrow 0$, the number of H^+ ions at a distance between a_1 and a_2 of an A^- ion can be expressed in two ways:

$$[11] \quad 4\pi \int_{a_2}^{a_1} \exp[s/r] r^2 dr = \frac{1}{L\rho K_2} - \frac{1}{L\rho K_1}$$

Here $s = e^2/(\epsilon_r kT) = 7.15$ Å^{-1} at 25.0 °C for univalent A^-, and twice that for divalent $A^-(SO_4^{2-})$. L is Avogadros number and K_1, K_2 are the equilibrium constants defined with $H^+ \cdots A^-$ defined as pairs where the H^+ and A^- are within a_1 and a_2 of each other, respectively.

Table 8 shows the result of application of relationship [11] to the systems studied. A range of distances is shown for the ultrasonic results, corresponding to the range of uncertainty in the analysis. It should be noted that the sum of Debye radii from Table 1 for $H^+ + SO_4^{2-}$ is only 13 Å, but that this assumes a_{H^+} to be 9.0 Å, *i.e.* it is not for the bare H_3O^+ ion. A distance of about 11 Å corresponds to two water molecules between the bare H_3O^+ and the A^-, 14 Å to three, 17 Å to four etc. taking the diameter of the water molecule to be about 2.8 Å.

Analysis of k_r Values

Table 9 shows the results of the analysis of the k_r data from Table 6 in terms of diffusion-controlled rate theory which gives:

$$[12] \quad k_r = \frac{4\pi(D_+ + D_-)}{1000} Lx(\exp[x/a] - 1)^{-1}$$

where $x = z_+ z_- e^2/\epsilon_r kT$.

The values of k_r are determined primarily by the α'/f^2 values for higher c. These are more accurate than the low c values, but the accuracy of the k_r are dependent on the accuracy of the ΔV^θ measurements. These have considerable variation, as shown in Table 4. Rows 1 to 5 of Table 10 show for the 25 °C HSO_4^- case the sensitivity of the value of 'a' calculated from [12] to variations in k_r. Rows 2 and 3 use the extreme values from Table 5, row 4 the value if $\Delta V^\theta = -15.3$ cm^3 mol^{-1} and row 5 the value if $\Delta V^\theta \simeq -10$ cm^3 mol^{-1}. This last case, where $k_r = 7.5 \times 10^{10}$ l mol^{-1} s^{-1}, is in a region where [12] shows 'a' to be extremely sensitive to k_r.

The value of 'a' subsequently calculated from k_r is dependent on the validity of the diffusion-controlled rate theory. As pointed out in ref. 33, the actual rate k_r can be up to 60% smaller than that calculated through [12] if the hydrodynamic effects are included in the theory. The linear approximation form of this theory gives the result (33)

Can. J. Chem. Downloaded from www.nrcresearchpress.com by 210.87.254.5 on 09/05/12
For personal use only.

TABLE 10. Variation of distance parameters with assumptions[a]

Row	Conditions	$k_r/10^{10}$ l mol^{-1} s^{-1}	a/Å
1	Most probable value (HSO_4^- at 25 °C)	35.1	32
2	Minimum value from Table 5	14.1	8
3	Maximum value from Table 5	40.2	40
4	$\Delta V^\theta = -15.3$ cm^3 mol^{-1}	17.6	11
5	$\Delta V^\theta = -10$ cm^3 mol^{-1}	7.5	<3
6	$\beta = 0.64$ (eq. 13)	35.1	40
7	$\beta = 0.75$	35.1	42
8	H_3PO_4 at 25 °C, $\beta = 0$	13.2	12
9	$\beta = 0.64$	13.2	17
10	$\beta = 0.75$	13.2	19

[a]Sulfuric acid solutions at 25 °C (rows 1 to 7) and phosphoric acid at 25 °C (rows 8 to 10).

$$[13]\quad k_r = \frac{4\pi(D_+ + D_-)}{1000} Lx\{(\exp[x/a] - 1) + \beta((\exp[x/a])(1 - [a/x])^{-1} + [a/x])\}^{-1}$$

where $\beta = 3a_+a_-/a^2$. Rows 6 and 7 (sulfuric acid) and 8, 9, and 10 (phosphoric acid) show the results of application of this theory with $\beta = 0.64$ (a_+, a_- from Table 1), and $\beta = 0.75$, the maximum effect possible, when $a_+ = a_-$. Since much of the motion of the H^+ is not really 'hydrodynamic', but of the Grotthus type, this theory seems less suitable for reactions involving H^+ in water. This refinement still keeps the assumptions of hard-sphere ions and a solvent considered as a continuum with a dielectric constant ϵ_r obtained from macroscopic measurements.

An Arrhenius analysis of k_r (Fig. 5) gives activation energies of 22 kJ mol^{-1} for H_3PO_4 and 11 kJ mol^{-1} for HSO_4^-. The magnitudes of these activation energies are not dependent on the actual values of the ΔV^θ assumed. A change in ΔV^θ with temperature would cause an error to occur, but the ΔV^θ for such equilibria do not seem to be strongly temperature dependent (34). The uncertainties in these values are quite large, of the order of $\pm 40\%$. The values are of the order of magnitude expected of diffusion-controlled reactions involving H^+ ion, which has $E_{act} \simeq 14$ kJ mol^{-1} as obtained from the variation of D_{H^+} with temperature shown in Fig. 5.

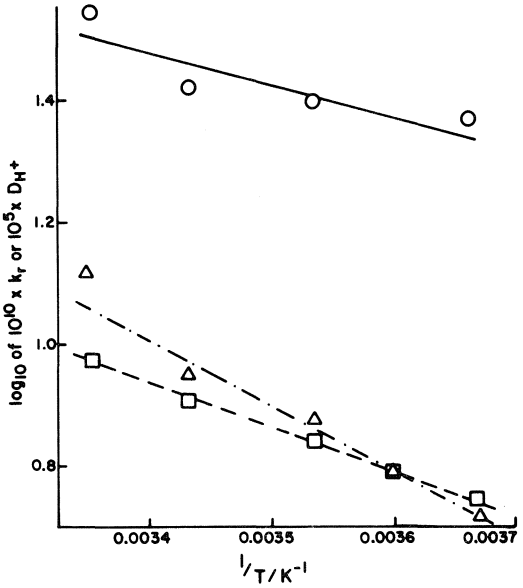

FIG. 5. Temperature dependence of the k_r and the diffusion coefficient of H^+, data from Table 9: ○ k_r for HSO_4^-, △ k_r for H_3PO_4, □ D_{H^+}.

Model for the Recombination Reaction

The distance 'a' at which, for the purposes of ultrasonic absorption, the reaction $H^+ + A^- \rightleftharpoons H^+ \cdot A^-$ is complete can be obtained from both the K_a and the k_r values. Although both methods for determination of values of 'a' give results which show a large amount of uncertainty, they both predict for both acids values of 'a' which allow several water molecules to be present between the H^+ and the A^- on formation of H^+A^-. This can be seen in the comparison in Table 9.

The lower values of a for phosphoric acid may be due to the neglect of any 'steric factor' in [12]. While there are four possible sites for the H^+ to go to in combining with SO_4^{2-}, there are only two in the case of $H_2PO_4^-$. For example, the value of 9 Å obtained for a for H_3PO_4 at three temperatures from the rates (Table 9) becomes 20 A if a steric factor 0.53 is introduced into the right hand side of [12].

Can. J. Chem. Downloaded from www.nrcresearchpress.com by 210.87.254.5 on 09/05/12
For personal use only.

This suggests that the process may occur somewhat as shown schematically in [14]. Here only the case of two water molecules between H_3O^+ and A^- is schematically shown for the sake of simplicity. This would correspond to an '*a*' of about 11 Å. The K_a data suggest more H_2O molecules to be present between the ions.

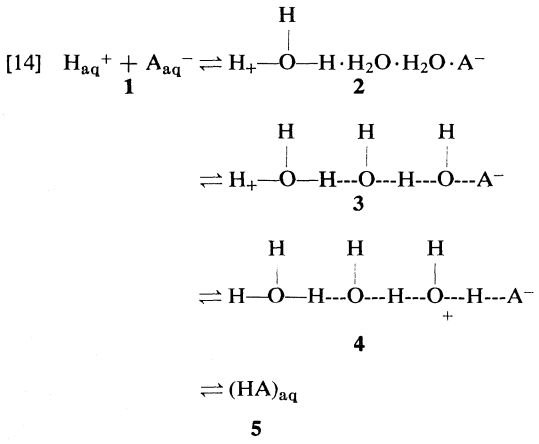

Equilibrium **2** $\rightleftharpoons$ **3** represents the orientation of the water molecules into a position so that the reaction can be completed by H-bond switching.

Raman spectroscopy might detect the equilibrium between the system in state **5** and the system in states **4**, **3**, **2**, **1**. Conductivity might detect the equilibrium **5**, **4** $\rightleftharpoons$ **3**, **2**, **1** and ultrasonics **5**, **4**, **3**, **2** $\rightleftharpoons$ **1**. Ultrasonics would actually be sensitive only to the **1** $\rightleftharpoons$ **2** equilibrium, as equilibria **2** $\rightleftharpoons$ **3**, **3** $\rightleftharpoons$ **4**, **4** $\rightleftharpoons$ **5** involve neither bimolecular steps nor hydrodynamic motion. Thus their relaxation times would be very short. They would not be likely to contribute noticeably to ultrasonic absorption as α'/f^2 is proportional to τ. Instead, a change in **2** would essentially automatically be reflected in **3**, **4**, and **5**. This is of course not the case of ion pairing in aqueous solutions of $Mg^{2+}SO_4^{2-}$, as hydrodynamic motion of the Mg^{2+} is necesary in the step analogous to **3** $\rightleftharpoons$ **4**, *e.g.* ref. 35. It would also not be the case for ion pairing involving protons in non-aqueous solvents such as dimethyl sulfoxide or dimethyl formamide (20).

Ultrasonic absorption is unique in methods for measuring K_a as in effect it measures directly the rate constants k_r and k_d, which are then combined to obtain K_a. Other methods measure the concentrations or activities of the species concerned. The value of K_a obtained from these approaches should of course be the same if the actual equilibrium detected is the same. Thus this aspect should not cause the differences seen in Table 7.

Ultrasonics would however detect an equilibrium different from *e.g.* conductivity as ultrasonics is in this case sensitive to a ΔV^θ while conductivity is sensitive to a ΔH^θ change. Other non-kinetic methods would be sensitive to a ΔG^θ change. On the Bjerrum model, the ΔH^θ for two singly charged ions in water 5.07 Å apart (Table 9) would be -3.4 kJ mol^{-1}, which is of the order of the energy of thermal motion ($RT \simeq 2.5$ kJ mol^{-1}). However, at a distance of 15 Å, $\Delta H^\theta \simeq -1.1$ kJ mol^{-1}. Thus when H^+ and A^- are this far apart, the interaction energy is small enough with respect to RT that the ions can be approximated to act independently in an electric field.

The value of the ΔV^θ used should be reexamined in the light of the above argument. The ΔV^θ change in **1** $\rightleftharpoons$ **2** is here assumed to be considerably larger than those of **2** $\rightleftharpoons$ **3**, **3** $\rightleftharpoons$ **4** or **4** $\rightleftharpoons$ **5**. Thus the ΔV^θ measured through density or conductivity measurements is taken to be a reasonable value for the ultrasonic absorption analysis. The K_a obtained by analysis of density data should in such a case be of the order of that obtained from ultrasonics. In ref. 13, it was shown that the H_2SO_4 density data could reasonably be fitted assuming a K_a of 0.0102, *i.e.* the conductivity value, when a number of assumptions are made. However, these assumptions and the limited accuracy of the ϕ_v *vs.* c curve may make it impossible to exclude a fit using the K_a (ultrasonic), 0.005. Nevertheless, data on $MgSO_4$ also suggest that it may not be valid to assume the ΔV^θ of **1** $\rightleftharpoons$ **2** to be the largest (35).

The actual value of ΔV^θ to be used for the ultrasonic analysis can be experimentally determined if k_r is obtained directly by extending the ultrasonic measurements to frequencies $> 1/\tau$. For this, reasonably accurate values of α'/f^2 must be obtained at $f > 300$ MHz as $\tau \simeq 10^{-9}$ s. Since the α'/f^2 is small and the systems are quite acidic, it is not likely that such measurements can be made with the necessary accuracy with instrumentation presently available.

Conclusions

The results presented show that ultrasonic absorption can be a useful method for obtaining

Can. J. Chem. Downloaded from www.nrcresearchpress.com by 210.87.254.5 on 09/05/12
For personal use only.

values of K_a and k_r for acids. The K_a values obtained from ultrasonics are consistently lower than those obtained by other methods for both HSO_4^- and H_3PO_4.

The analysis points out several problems involving the meaning of the sizes of aquated ions, ionic strength, and activity coefficients when results from several methods are used together. In the case of the H_2SO_4 solutions, the experimental $\gamma_\pm$ does not involve the HSO_4^- ion at all. Thus the $\gamma_\pm$ values obtained from emf measurements may not be proper to use in the calculation of colligative properties.

The temperature dependence of the recombination rates show an activation energy of the same order of magnitude as that for hydrogen ion diffusion, supporting the application of diffusion controlled rate theory for the analysis. Absolute values of the rate constants are dependent upon the accuracy and relevance of the ΔV^θ values assumed for the equilibrium concerned.

The results of analysis of the k_r and K_a values obtained both indicate however that the 'undissociated acid' as detected by ultrasonic absorption extends to a greater $H^+\cdots A^-$ distance than in the case of conductivity or electromotive force measurements. For HSO_4^- the distance is about 30 Å, and for H_3PO_4 about 10 Å, but there is a large amount of uncertainty in these values.

This type of information seems of importance in obtaining a more complete knowledge of the fundamental structure and dynamics in biological systems as well as in marine chemistry.

Acknowledgments

The authors acknowledge financial assistance from the Inland Waters Branch, Environment Canada (Contract 0SS3-0174), the National Research Council of Canada, and Carleton University. They wish to thank Dr. W. A. Adams and Environment Canada for use of their densitometer and Dr. G. C. Benson for supplying standard density liquids.

1. J. Lang, J. Sturm, and R. Zana. J. Phys. Chem. **77**, 2329 (1973); **78**, 80 (1974).
2. T. Sano and T. Yasunaga. J. Phys. Chem. **77**, 2031 (1973).
3. R. D. White and L. J. Slutsky. J. Phys. Chem. **76**, 1327 (1972).
4. J. Stuehr and E. Yeager. *In* Physical acoustics. Vol. II-A. *Edited by* W. P. Mason. Academic Press, New York. 1965. p. 351.
5. D. C. Hodgkin and P. Kruus. Can. J. Chem. **51**, 2297 (1973).
6. R. J. Fanning and P. Kruus. Can. J. Chem. **48**, 2052 (1970).
7. S. S. Yun, R. T. Beyer, and M. W. Dill. J. Chem. Phys. **36**, 2737 (1962).
8. W. A. Adams, R. Yank, R. O. Christie, and J. Kruus. Can. J. Chem. Eng. **52**, 121 (1974).
9. J. Kielland. J. Am. Chem. Soc. **59**, 1675 (1937).
10. F. J. Millero. Chem. Rev. **71**, 147 (1971).
11. G. Perron, J. E. Desnoyers, and F. J. Millero. Can. J. Chem. **53**, 1134 (1975).
12. I. M. Klotz and C. F. Eckert. J. Am. Chem. Soc. **64**, 1878 (1942).
13. R. E. Lindstrom and H. E. Wirth. J. Phys. Chem. **73**, 218 (1969).
14. H. L. Friedman and C. V. Krishnan. *In* Water: a comprehensive treatise. Vol. 3. *Edited by* F. Franks. Plenum, New York. 1973. p. 1.
15. P. Mukerjee. J. Phys. Chem. **65**, 740 (1961).
16. R. A. Horne, R. A. Courant, and G. R. Frysinger. J. Chem. Soc. 1515 (1964).
17. W. A. Adams and A. R. Davis. *In* Marine electrochemistry. *Edited by* J. Berkowitz. Electrochemical Society, Princeton, N.J. 1973. p. 53.
18. H. S. Harned and B. B. Owen. The physical chemistry of electrolytic solutions. 3rd ed. Reinhold, New York. 1958. p. 405.
19. A. J. Ellis and D. W. Anderson. J. Chem. Soc. 1765 (1961).
20. S. C. Chan and J. P. Valleau. Can. J. Chem. **46**, 853 (1968).
21. A. Distèche. J. Electrochem. Soc. **109**, 1084 (1962).
22. R. A. Robinson and R. H. Stokes. Electrolyte solutions. Revised edition. Butterworths, London. 1968.
23. H. S. Harned and W. J. Hamer. J. Am. Chem. Soc. **57**, 27 (1935).
24. W. J. Hamer. J. Am. Chem. Soc. **56**, 860 (1934).
25. J. M. Readnour and J. W. Cobble. Inorg. Chem. **8**, 2174 (1969).
26. H. S. Dunsmore and G. H. Nancollas. J. Phys. Chem. **68**, 1579 (1964).
27. C. E. Evans and C. B. Monk. Trans Faraday Soc. **67**, 2652 (1971).
28. W. L. Marshall and E. V. Jones. J. Phys. Chem. **70**, 4028 (1966).
29. H. M. Dawson, E. R. Pycock, and E. Spivey. J. Chem. Soc. 291 (1933).
30. D. J. Turner. J. Chem. Soc. Faraday Trans. I, **70**, 1346 (1974).
31. E. A. Guggenheim. Trans. Faraday Soc. **62**, 2750 (1966).
32. H. Chen and D. E. Irish. J. Phys. Chem. **75**, 2672 (1971).
33. J. M. Deutch and B. V. Felderhof. J. Chem. Phys. **59**, 1669 (1973).
34. G. K. Ward and F. J. Millero. J. Solution Chem. **3**, 417 (1974).
35. A. Bechtler, K. G. Breitschwerdt, and K. Tamm. J. Chem. Phys. **52**, 2975 (1970).

Can. J. Chem. Downloaded from www.nrcresearchpress.com by 210.87.254.5 on 09/05/12
For personal use only.

Heats of formation of some hydrates[1]

ALAN PHILLIPSON AND GORDON R. FINLAY
Department of Chemistry, Brock University, St. Catharines, Ont., Canada L2S 3A1

Received October 23, 1975[2]

ALAN PHILLIPSON and GORDON R. FINLAY. Can. J. Chem. **54**, 3163 (1976).

Heats of formation of hydrates may be measured by dissolving the hydrate and the corresponding anhydrate in water to attain the same final concentration and measure the difference in heats of solution.

Measurements were made at 0 °C in a modified Bunsen ice calorimeter, well insulated, and surrounded with an ice–water mixture.

The data obtained are a measure of the enthalpy involved in binding a mole of water into a crystal structure, to shed some light on the nature and mechanism of this binding. Several discrepancies are noted, in particular one involving $CdCl_2 \cdot \frac{5}{2}H_2O$. A method for adjusting calculations from 0 to 25 °C in the absence of heat capacity data is proposed.

The following hydrates have been studied: $LiCl \cdot H_2O$, $LiBr \cdot 2H_2O$, $CaCl_2 \cdot 2$ and $\cdot 6H_2O$, $MnCl_2 \cdot 1$ and $\cdot 2H_2O$, $CdCl_2 \cdot \frac{5}{2}H_2O$, $MnSO_4 \cdot 1$ and $\cdot 4H_2O$, $MgSO_4 \cdot 1$, $\cdot 4(?)$, and $\cdot 7H_2O$, and $K_2CO_3 \cdot \frac{3}{2}H_2O$.

Additionally, the heat of hydration of hydrazine to $N_2H_4 \cdot H_2O$ has been checked.

The formation of a coordinated hydrate, from liquid water, involves a heat effect which in the limit approaches 3 kcal mol^{-1}. The first mole of water added may be most strongly bonded (6–10 kcal), possibly since alternate sites in the coordination sphere may be available to it.

Values which differ markedly from these levels deserve a critical examination. Higher values may suggest the presence of OH^-, or other structural variations, errors in the published data or mistaken identification of the hydrate.

ALAN PHILLIPSON et GORDON R. FINLAY. Can. J. Chem. **54**, 3163 (1976).

Pour mesurer les chaleurs de formation des hydrates, on dissout ceux-ci et les produits correspondants non hydratés dans l'eau de façon à obtenir la même concentration et ainsi mesurer la différence dans les chaleurs de solution.

On a effectué des mesures à 0 °C dans un calorimètre à glace Bunsen, modifié, bien isolé et entouré d'un mélange glace–eau.

Les données obtenues sont une mesure de l'enthalpie impliquée lors de la fixation d'une molécule d'eau dans une structure cristalline; elles fournissent un peu de lumière sur la nature et le mécanisme de cette fixation. On note plusieurs anomalies; une en particulier implique le $CdCl_2 \cdot \frac{5}{2}H_2O$. On propose une méthode pour ajuster les calculs de 0 à 25 °C en l'absence de données des capacités calorifiques.

On a étudié les hydrates suivants: $LiCl \cdot H_2O$, $LiBr \cdot 2H_2O$, $CaCl_2 \cdot 2$ et $\cdot 6H_2O$, $MnCl_2 \cdot 1$ et $\cdot 2H_2O$, $CdCl_2 \cdot \frac{5}{2}H_2O$, $MnSO_4 \cdot 1$ et $\cdot 4H_2O$, $MgSO_4 \cdot 1$, $\cdot 4(?)$ et $\cdot 7H_2O$, et $K_2CO_3 \cdot \frac{3}{2}H_2O$.

De plus on a vérifié la chaleur de l'hydratation de l'hydrazine conduisant à $N_2H_4 \cdot H_2O$.

La formation, à partir de l'eau liquide, d'un hydrate coordonnée implique un effet de chaleur qui approche à la limite de 3 kcal/mol. La première molécule d'eau additionnée peut être associée très fortement (6–10 kcal); il est possible que l'implication de ce phénomène puisse être trouvé dans le fait que d'autres sites dans la sphère de coordination peuvent lui être disponible.

Les valeurs qui diffèrent d'une façon marquée de ces niveaux méritent un examen critique. Des valeurs plus élevées peuvent suggérer la présence de OH^- ou d'autres variations dans les structures, des erreurs dans les données publiées ou des identifications erronées des hydrates.

[Traduit par le journal]

Introduction

Solvates are a class of compounds formed by the association, usually in a crystal structure, of molecules of solute and solvent, which may exist separately from each other. The heat of solvation involved may be calculated from enthalpy of formation data or may be measured directly by measuring heats of solution for both solvate and ansolvate.

$$\text{Ansolvate} + \text{solvent} \rightarrow \text{Solvate in solution} + \Delta H_1$$

$$\text{Solvate} + \text{solvent} \rightarrow \text{Solvate in solution} + \Delta H_2$$

$$\Delta H_2 - \Delta H_1 = \Delta H_{\text{solvation}}$$

[1]Presented at 58th Canadian Chemical Conference of the Chemical Institute of Canada, Toronto, Ontario, May 1975.

[2]Revision received June 24, 1976.

Can. J. Chem. Downloaded from www.nrcresearchpress.com by 210.87.254.6 on 09/05/12
For personal use only.

TABLE 1. Thermochemical data on hydrates of copper sulfate

Parameter	Value		
	Monohydrate ($CuSO_4 \cdot H_2O$)	Trihydrate ($CuSO_4 \cdot 3H_2O$)	Pentahydrate ($CuSO_4 \cdot 5H_2O$)
ΔH (kcal mol^{-1} H_2O)	−6.845	−4.418	−3.79
ΔS (eu mol^{-1} H_2O)	−7.81	−7.75	−7.55
ΔC_p mol^{-1} H_2O (cal deg^{-1})	−9.9	−9.63	−9.35

For 130 cases of hydrates (highest hydrate reported), as listed in Bichowsky and Rossini (1)

$$\text{Anhydrate} + n(H_2O)(g) \rightarrow \text{Highest hydrate} + n(14.0)\ \text{kcal}$$
(Mean deviation ±1.2 kcal)

or

$$\text{Anhydrate} + n(H_2O)(l) \rightarrow \text{Highest hydrate} + n(3.5)\ \text{kcal}$$
(Mean deviation ±1.2 kcal)

For a typical ammoniate (*e.g.*, $SrCl_2 \cdot 8NH_3$) (2) the corresponding calculation shows:

$$\text{Ansolvate} + n(NH_3)(g) \rightarrow \text{Highest ammoniate} + n(10.1)\ \text{kcal}$$

or

$$\text{Ansolvate} + n(NH_3)(l) \rightarrow \text{Highest ammoniate} + n(5.35)\ \text{kcal}$$

The case of the hydrates of copper sulfate may be considered typical. Good data (2) is available and the system has been well studied. The values calculated from the thermodynamic data are as given in Table 1.

According to Wyckoff (3) the fifth water molecule is not coordinated about the cation but just 'tucked in' to the structure. This doesn't appear to affect the observed values seriously.

Experimental

The measurements of heats of solution were carried out in a Bunsen ice calorimeter, adapted from a design of Hieber and Mühlbauer (4). Such an instrument was used previously to determine heats of formation of BF_3 etherates and similar compounds (5). By careful insulation of the unit and surrounding it with an ice–water mixture the inward heat-leak, including the heat of stirring, was reduced to less than 0.1 cal min^{-1}. Results of duplicate runs could be held within ±0.25 cal (equivalent to ±4 mg of mercury weighed). By a drop method, the heat capacity of 10.00 ± 0.05 ml of H_2O was found to be 250 ± 2.0 cal. (Theoretical value, 250 ± 1.3.)

Whenever possible, we avoid the drop method by inserting the sample in a glass ampoule with or without a rubber bung closure and bringing the whole system to equilibrium temperature before commencing the reaction. By such means we are able to measure the heats of solution of quantities of solute ranging from 0.2 to 20 mmol using, in the case of water, approximately one mole of solvent, *i.e.*, concentrations ranging from 0.01 to 1 *M*. Most heat of formation data are listed at 25 °C (298.15 K). Our heats of solution are measured at 0 °C or 273.15 K. Where heat capacity data are available, these may be used to correct the heat of solution from 0 to 25 °C. If the heat capacity data are not available a rule of thumb correction may be made of 228 ± 12 cal mol^{-1} which will introduce no great error.

This correction may be justified as follows: (*a*) For nine cases of known hydrates, the decrease in heat capacity per mole of H_2O added averages 8.95 cal deg^{-1} or 224 cal over a 25 °C range. (*b*) For 31 cases of known hydrates the decrease in heat capacity per mole of H_2O added averages 9.26 cal deg^{-1} or 232 cal over 25 °C range. (*c*) Various authors, including Ladd and Lee (6), have suggested that the water in a crystalline hydrate may be considered as having a heat capacity like that of the vapour state. If we take the equation for the heat capacity of gaseous H_2O from Lewis and Randall (7) as:

$$C_p = 8.81 - 0.0019T + 2.22 \times 10^{-6}T^2$$

and solve at 298.15 °C; C_p = 8.44 cal mol^{-1} deg^{-1} and at 273.15 K, C_p = 8.46 cal mol^{-1} deg^{-1}. These values average to give a correction of 239 cal over 25 °C range. (*d*) The heat capacity of water in the solid state (*i.e.*, ice) at 0 °C is 8.87 cal mol^{-1} deg^{-1}. If we assume that the heat capacity of water of crystallization in a salt hydrate is similar to that of ice we can estimate the correction as 228 cal over the 25 °C range. (*e*) The formation of a crystalline hydrate from the corresponding ansolvate and liquid water involves a decrease in entropy which is commonly 7 to 8 units for each mole of water involved. This increase in organization may well be expected to decrease the heat capacity of the system by a roughly corresponding amount, which leads to a correction of about 230 cal over a 25 °C range. For example see the data listed above for copper sulfate.

Since the uncertainty of heat of formation data is seldom less than ±50 cal mol^{-1} and since here we are working by difference of two quantities, it is probably not worthwhile at present to worry over discrepancies less than 100 cal or ±0.1 kcal mol^{-1}.

Can. J. Chem. Downloaded from www.nrcresearchpress.com by 210.87.254.6 on 09/05/12
For personal use only.

TABLE 2. Heats of hydration of magnesium sulfate

Material	Moles H_2O	Measured heat of solvation in kcal mol^{-1} H_2O	Other solution values	Values calculated from ΔH formation
$MgSO_4$	1	−6.86	−6.99 (8)	−6.58 (1)
	4	−3.59	−3.84 (8)	−4.18 (10)
	7	−3.41	−3.55 (8)	−3.57 (10)
	1–4	−2.50	−2.79 (8)	−3.38 (10)
	1–7	−2.83	−2.97 (8)	−3.06 (10)
			−2.85 (9)	
	4–7	−3.16	−3.16 (8)	−2.75 (10)
	2			30.12 (10)
				30.12 (9)
	6		−3.59 (8)	−3.53 (10)
	4–6		−3.10 (8)	−2.23 (10)
	6–7		−3.27 (8)	−3.78 (10)

Materials

The chemicals studied here were purchased as analytical reagents where possible, or dehydrated from a higher hydrate to a constant weight at appropriate temperatures. Compositions were checked by thermogravimetric analysis and in most cases by titration with Karl Fischer reagent. Infrared spectra were also employed to confirm compositions for the sulfates and other compounds where feasible.

One sample labelled 'anhydrous' actually turned out to be well-crystallized tetrahydrate as we belatedly discovered after finding that its heat of solution was exactly the same as that of the tetrahydrate.

Results and Discussion

The results observed by us are reported in Tables 2 and 3 and are compared with data published elsewhere.

The values reported in Table 2 for the hydrates of magnesium sulfate are generally in good agreement with literature. Our measurements are in good agreement with other heat of solution values and are self-consistent. The notable exception is the heat of formation value reported for the dihydrate, which is very much out of line. Taken at face value, it would seem to indicate that the hydrate would be very unstable. Unfortunately we were not able to purchase nor produce a satisfactory sample of dihydrate.

The rate of solution of the monohydrate at 0 °C is rather slow, so only low concentrations were available for study here. Nonetheless our findings agree with those of others.

The seventh water molecule is reported to fit into a void in the crystal structure, the other six being coordinated octahedrally about the magnesium ion.

The results for $MnCl_2$ again seem reasonable and consistent. One older value for heat of formation of the dihydrate (−12.38) is obviously a mistake and should be rejected. The structure of the hydrates has been reported to involve hydroxyl group coordination between adjacent Mn atoms, and the dihydrate, at least, shows extensive hydrogen bonding. Neither of these considerations have much net effect on the observed enthalpy.

For $MnSO_4$ our results tend to be a little lower than those recorded in tables. Still lower are some results of heat of solution measurements reported by Jamieson *et al.* (13). These show values of −5.02 kcal mol^{-1} for the monohydrate, −2.27 for the tetrahydrate, −2.08 for the pentahydrate, and −1.87 for the heptahydrate. The values of Jamieson *et al.* are consistently some 500 cal mol^{-1} lower than ours. The reported value for the hexahydrate again appears to be a mistake of some sort, since it would imply an unstable compound.

For LiCl our results seem to check well and the other reported values are consistent. Lithium chloride has been widely used as a drying agent particularly for air-conditioning, but seems to conform to other hydrates insofar as the enthalpy considerations are concerned.

Similar results were found for both lithium bromide and lithium iodide, with the heat of solvation increasing in this series with increasing size of the anion, Cl < Br < I.

In the case of potassium carbonate, the heat of formation data are wildly discordant except for the relative values of the hemihydrate and the sesquihydrate which fall into line. Heat of solvation data from heats of solution (9) at

Can. J. Chem. Downloaded from www.nrcresearchpress.com by 210.87.254.6 on 09/05/12
For personal use only.

Can. J. Chem. Downloaded from www.nrcresearchpress.com by 210.87.254.6 on 09/05/12
For personal use only.

-4.42 kcal mol^{-1} for the hemihydrate and -4.58 for the sesquihydrate are at least within the range of our finding. This hydrate is reported to have extensive hydrogen bonding, but this again seems to have little effect on the net enthalpy. For our measurements, we guarded against contamination of the solution water with carbon dioxide by pre-boiling followed by rapid cooling.

The most interesting case of all was that of cadmium chloride. When the anhydrous salt is dissolved, heat is initially evolved, but then follows a competing process which absorbs heat. Whereas we had reached equilibrium in all other cases in less than 20 min, we had to extend the time to 40 min for this compound. This two-stage solution process is still not understood and deserves further investigation. We believe it may have contributed to the difficulties of others with this system.

Our values check moderately well with those reported by NBS (2). Lange's (9) values from heats of solution, -2.38 kcal mol^{-1} for the

TABLE 3. Heats of hydration of several salts*

Material	Moles H_2O	Measured heats of solvation in kcal mol^{-1} H_2O	Values calculated from ΔH formation kcal mol^{-1} H_2O†
$CaCl_2$	1		−6.78 (10)
	2	−3.48	−4.43 (10)
	4		−4.23 (10)
	6	−3.42	−3.62 (9)
			−3.82 (10)
	2–6	−3.39	
$MnCl_2$	1	−4.61	−5.45 (2)
			−4.88 (10)
	2	−4.51	−4.67 (2)
			−12.38 (10)
	1–2	−4.40	−3.88 (2)
	4		−3.75 (2)
			−4.60 (10)
$MnSO_4$	1	−5.58	−6.08 (2)
			−5.94 (10)
	4	−2.77	−2.96 (2)
	1–4	−1.83	−1.91 (2)
	5		−2.75 (10)
			−2.80 (2)
	6		+10.2 (1)
	7		−2.49 (2)
LiCl	1	−4.20	−4.29 (6)
			−4.16 (9)
			−4.41 (10)
	2		−3.69 (10)
	3		−3.65 (10)
LiBr	1		−6.11 (11)
			−6.15 (10)
	2	−4.69	−4.71 (11)
			−4.72 (10)
	3		−4.36 (10)
LiI	1	−8.18	−8.04 (11)
			−8.29 (10)
	2		−5.80 (11)
			−5.92 (10)
	3	−5.15	−5.17 (10)
			−5.09 (11)
	1–3	−3.64	−3.62 (11)
			−3.61 (10)
	½		−10.18 (10)

TABLE 3 (*Concluded*)

Material	Moles H_2O	Measured heats of solvation in kcal mol^{-1} H_2O	Values calculated from ΔH formation kcal mol^{-1} H_2O†
K_2CO_3	$\frac{1}{2}$		+195.32 (10)
	$1\frac{1}{2}$	−3.54	+62.01 (10)
	$\frac{1}{2}$–$1\frac{1}{2}$		−4.65 (10)
$CdCl_2$	1		−2.65 (2)
	$2\frac{1}{2}$	−1.81	−2.47 (2)
			+4.74 (12)
	4		−24.09 (1)

*We are grateful to the referee who questioned our calculations for K_2CO_3 and $CdCl_2$. We present them here in more detail.

$\Delta H_f°$ $K_2CO_3.\frac{3}{2}H_2O$ (9, 10)	−283.40
$\Delta H_f°$ K_2CO_3 (9, 14)	−273.93
$\Delta H_f°$ $\frac{3}{2}H_2O$ (9, 10, 14)	−102.48
$\Delta H_{solvation}$ (calculated)	+93.01
$\Delta H_{solvation}$ (mol^{-1} H_2O)	62.01
$\Delta H_f°$ $K_2CO_3.\frac{1}{2}H_2O$ (9, 10)	−210.43
$\Delta H_f°$ K_2CO_3 (9, 14)	−273.93
$\Delta H_f°$ $\frac{1}{2}H_2O$ (9, 10, 14)	−34.16
$\Delta H_{solvation}$ (calculated)	+97.66
$\Delta H_{solvation}$ (mol^{-1} H_2O)	+195.32

Obviously something is very wrong with one or more of these tabulated values. Quite possibly the K_2CO_3 value is incorrect. The calculation would seem to predict quite unstable hydrates.

For the $CdCl_2$ system, we calculate similarly:

	Ref. 12	Refs. 2, 9	This paper
$CdCl_2.2\frac{1}{2}H_2O$	−252.50	−270.54	
$CdCl_2$	−93.57	−93.57	
$\frac{5}{2}H_2O$	−170.79	−170.79	
$\Delta H_{solvation}$	+11.86	−6.18	
$\Delta H_{solvation}$ (mol^{-1} H_2O)	+4.74	−2.47	−1.81

†Reference numbers in parentheses.

monohydrate and −1.13 for the dihydrate (sic), are also at least in the neighbourhood. The remaining values are completely discordant. We are particularly puzzled by the value given by Patil and Secco (12). This is recent work and seems to have been carefully done, but would imply a very low stability for the hydrate $CdCl_2 \cdot 2\frac{1}{2}H_2O$.

No structure has yet been reported for this hydrate. Structures are known for $CdCl_2 \cdot 2NH_3$ in which the Cd is octahedrally coordinated to two Cl and four N. In $Cd(NO_3)_2 \cdot 2H_2O$ the Cd is coordinated to 7 oxygen (15), while the $Cd(NO_3)_2 \cdot 4H_2O$ crystal shows Cd with a coordination number of 8 (16). The $2\frac{1}{2}$ hydrate formula is apparently not like any of these, but seems to be well authenticated, and indeed the composition was found to be precisely $2\frac{1}{2}H_2O$ by both thermogravimetric methods and Karl Fischer analysis.

Some other systems in which discordant data are observed are those involving the hydrates of $Ca(NO_3)_2$, $CrCl_2$, KOH, NaOH, Hg_2NOH, $K_2Mg(SO_4)_2$, and Na_2Se.

Other solvate systems, amenable to this technique, are ammoniates, alcoholates, and numerous other compounds or complexes in which molecules may be combined.

As a check on the technique as applied to liquid hydrates, we determined the heat of hydration of hydrazine. This we found to be −1.79 kcal mol^{-1} in accord with a heat of solution of −1.82 (17) and with −1.79 (2) from the NBS Tables (derived from the original work of Hughes (18)). Incidentally our 'anhydrous' hydrazine was found to analyse 4.77% H_2O (Karl Fischer).

We submit that the technique described is sensitive and reproducible and recommend it (or analogous solution techniques) for the determination of heats of solvation and hence of heats of formation. As a practical matter, heats of formation of solvates seem to be approximately calculable by taking the heats of

Can. J. Chem. Downloaded from www.nrcresearchpress.com by 210.87.254.6 on 09/05/12
For personal use only.

formation of the ansolvate and the appropriate numbers of moles of solvating agent and adding an appropriate average value per mole. For H_2O, we would propose a nominal value of 6 kcal mol^{-1} for the first water molecule and 3 kcal for each subsequent mole of water.

1. F. BICHOWSKY and F. D. ROSSINI. Thermochemistry of chemical substances. Reinhold, New York. 1936.
2. D. D. WAGMAN, W. H. EVANS, V. B. PARKER, I. HALOW, S. M. BAILEY, and R. H. SCHUMM. Selected values of chemical thermodynamic properties. NBS. Tech. Notes 270-3 (1968); 270-4 (1969); 270-5 (1971); 270-6 (1971).
3. R. W. G. WYCKOFF. Crystal structures. 2nd ed. Vol. III. Interscience-Wiley, New York. 1965.
4. W. HIEBER and F. MUHLBAUER. Z. anorg. allgem. Chem. **186**, 97 (1930).
5. A. W. LAUBENGAYER and G. R. FINLAY. J. Am. Chem. Soc. **65**, 884 (1943).
6. M. L. C. LADD and W. H. LEE. J. Phys. Chem. **73**, 2033 (1969).
7. G. N. LEWIS and M. RANDALL. Thermodynamics. McGraw-Hill, New York. 1923.
8. J. W. S. JAMIESON and G. B. FROST. Can. J. Chem. **34**, 583 (1956).
9. J. A. DEAN. Lange's handbook of chemistry. 11th ed. McGraw-Hill, New York. 1973.
10. National Bureau of Standards. Circ. 500. Selected Values of Chemical Thermodynamic Properties. 1952.
11. R. C. WEAST (*Editor*). Handbook of chemistry and physics. 53rd ed. Chemical Rubber Co. Press. Cleveland 1972.
12. K. C. PATIL and E. A. SECCO. Can. J. Chem. **49**, 3831 (1971).
13. J. W. S. JAMIESON *et al.* Can. J. Chem. **43**, 2148 (1965).
14. D. R. STULL *et al.* J.A.N.A.F. Tables. Clearinghouse, Fed. Sci. Tech. Inform. U.S. Dept. of Commerce, N.B.S. Inst. Appl. Tech. 1968.
15. N. MILINSKI, B. RIBÁR, R. HERAK and S. DJURIĆ. Crystal Struct. Commun. **3**, 757 (1974).
16. B. MATKOVIĆ, B. RIBÁR, B. ZELENKO, and S. W. PETERSON. Acta Crystallogr. **21**, 719 (1966).
17. V. C. BUSHNELL, A. M. HUGHES, and E. C. GILBERT. J. Am. Chem. Soc. **59**, 2142 (1937).
18. A. M. HUGHES, R. J. CORRUCCINI, and E. C. GILBERT. J. Am. Chem. Soc. **61**, 2639 (1939).

Can. J. Chem. Downloaded from www.nrcresearchpress.com by 210.87.254.6 on 09/05/12
For personal use only.

Complexes of lanthanide iodides with 3-methylpyridine-1-oxide

LAKSHMINARAYANAN RAMAKRISHNAN AND SUNDARESA SOUNDARARAJAN
Department of Inorganic and Physical Chemistry, Indian Institute of Science, Bangalore-560012, India

Received June 6, 1975[1]

LAKSHMINARAYANAN RAMAKRISHNAN and SUNDARESA SOUNDARARAJAN. Can. J. Chem. **54**, 3169 (1976).

Complexes of lanthanide iodides with 3-methylpyridine-1-oxide of the formula $Ln(3\text{-}MePyO)_8I_3.xH_2O$ where $x = 0$ for Ln = La and Tb, $x = 1$ for Ln = Pr, and $x = 2$ for Ln = Nd, Sm, Dy, Yb, and Y have been prepared and characterized by chemical analyses, conductance, infrared, proton nmr, and DTA data. Infrared and proton nmr data have been interpreted in terms of the coordination of the ligand to the metal ion through the oxygen of the N—O group. Proton nmr spectrum of the Yb(III) complex is indicative of a restricted rotation of the pyridine ring about the N—O bond.

LAKSHMINARAYANAN RAMAKRISHNAN et SUNDARESA SOUNDARARAJAN. Can. J. Chem. **54**, 3169 (1976).

Des complexes des iodures de lanthanide avec l'oxyde-1 de méthyl-3 pyridine, de formule $Ln(3\text{-}MePyO)_8I_3.xH_2O$ où $x = 0$ pour Ln = La et Tb, $x = 1$ pour Ln = Pr et $x = 2$ pour Ln = Nd, Sm, Dy, Yb et Y, ont été préparés et caractérisés par analyses chimiques, conductance, infrarouge, rmn du proton et mesures de ATD. Les données d'infrarouge et de rmn du proton ont été interprétées en termes de la coordination du ligand à l'ion métallique par l'oxygène du groupement N—O. Le spectre rmn du proton du complexe Yb(III) indique que la rotation du noyau pyridine autour du lien N—O est restreinte.

[Traduit par le journal]

Introduction

Lanthanides are known to exhibit high coordination numbers in their complexes. The coordination number of a lanthanide complex is determined by (*a*) the size of the cation, (*b*) the size of the ligand, and (*c*) the nature of the anion. As the size of the cation drops as one goes from La(III) to Lu(III), a decrease in the coordination number has been observed in a few cases (1). Bulky ligands such as diphenylsulphoxide yield lanthanide complexes with relatively low coordination numbers (2). When the anion also competes with the organic ligand for coordination to the metal ion, the coordination number of the lanthanide complex is mainly decided by the nature of the anion. Complexes of dimethylsulphoxide (1, 3–7) with the lanthanides provide a good example of the effect of anion on the coordination number of the metal ion. Recently, we have started a programme of preparing cationic complexes of the lanthanides with ligands of different bulk and anions with various degrees of coordinating ability in order to study their effect on the coordination number of the metal ion. We have already reported (8, 9) the complexes of lanthanide perchlorates and iodides with pyridine-1-oxide (PyO). As a continuation, we have prepared and characterized complexes of a few lanthanide iodides with 3-methylpyridine-1-oxide (3-MePyO).

Experimental

Materials

Hydrated lanthanide iodides were prepared by dissolving the corresponding oxide (99.9% pure, obtained from the American Potash and Chemicals Corporation, U.S.A.) in hydriodic acid and evaporating the solution on a waterbath. The residue was washed several times with benzene till the washings were colourless and dried on a waterbath.

3-MePyO was obtained from Aldrich Chemical Co., U.S.A., and was used after distillation under reduced pressure (146 °C/15 mm Hg). All the solvents used were purified by standard methods.

Preparation of the Complexes

Preparation of Pr(III), Nd(III), Sm(III), Tb(III), Dy(III), Yb(III), and Y(III) Complexes

A 0.5 g sample of the hydrated lanthanide iodide was dissolved in 10 ml of acetone and 1.25 g of 3-MePyO in 10 ml of acetone was added to it with constant vigorous stirring. The complex precipitated immediately. The solid complex was filtered through a sintered crucible, washed well with ice cold acetone, and dried in a vacuum desiccator over phosphorus(V) oxide.

Preparation of the La(III) Complex

The La(III) complex could not be prepared by the above procedure. Hence the following procedure was

[1]Revision received June 1, 1976.

Can. J. Chem. Downloaded from www.nrcresearchpress.com by 210.87.254.105 on 09/05/12
For personal use only.

Can. J. Chem. Downloaded from www.nrcresearchpress.com by 210.87.254.105 on 09/05/12
For personal use only.

TABLE 1. Analytical and conductance data

Complex	Found %			Calculated %			Molar conductance (ohm^{-1} cm^2 mol^{-1}) in	
	Metal	Iodide	3-MePyO	Metal	Iodide	3-MePyO	Nitrobenzene	CH_3CN
$La(3\text{-}MePyO)_8I_3$	9.95	27.30	61.86	9.97	27.33	62.66	27.91	298.3
$Pr(3\text{-}MePyO)_8I_3.H_2O$	9.98	27.13	62.22	9.97	26.95	61.79	15.27	289.7
$Nd(3\text{-}MePyO)_8I_3.2H_2O$	10.05	26.67	61.24	10.07	26.56	60.88	30.26	310.6
$Sm(3\text{-}MePyO)_8I_3.2H_2O$	10.48	26.65	61.16	10.44	26.43	60.61	32.22	305.2
$Tb(3\text{-}MePyO)_8I_3$	11.24	26.79	61.24	11.25	26.95	61.79	30.21	311.6
$Dy(3\text{-}MePyO)_8I_3.2H_2O$	11.10	26.34	59.94	11.19	26.22	60.12	28.92	314.6
$Yb(3\text{-}MePyO)_8I_3.2H_2O$	11.78	25.80	59.14	11.82	26.07	59.67	31.61	309.5
$Y(3\text{-}MePyO)_8I_3.2H_2O$	6.39	27.80	62.46	6.45	27.61	63.30	28.52	305.6

TABLE 2. Some important ir bands (in cm^{-1}) and their assignment

3-MePyO*	La	Pr	Nd	Sm	Tb	Dy	Yb	Y	Assignment
1290vs	1269vs	1274vs	1275vs	1270vs	1272vs	1272vs	1275vs	1275vs	N—O stretching
1175vs	1160vs	1170vs	1170vs	1168vs	1173vs	1174vs	1172vs	1172vs	C—H in-plane vibration
1021vs	1026s	1028m	1029m	1025m	1025m	1025m	1029m	1029m	Ring breathing
952s	955s	951s	951s	951s	952m	951s	951s	951m	
883m	878w	883w	886w	888w	888w	885w	887w	885w	C—H out of plane vibration
853m	—	870w	870w	870w	870w	869w	870w	870w	
782vs	782m	782m	782m	782m	784s	782s	782s	784s	N—O bending
752s	750s	755s	755s	755s	758s	754s	757s	756s	C—H out of plane vibration
675vs	675vs	671s	671s	670s	673s	670s	674s	674s	Ring bending
555s	578vs	574vs	574s	574s	574s	574s	576s	576s	

*3-MePyO spectrum in CS_2 solution. Spectra of the complexes in Nujol mulls. Abbreviations: vs = very strong; s = strong; m = medium; w = weak.

Can. J. Chem. Downloaded from www.nrcresearchpress.com by 210.87.254.105 on 09/05/12
For personal use only.

adopted for its preparation. Hydrated lanthanum iodide (0.5 g) was dissolved in 10 ml of water and 1.25 g of 3-MePyO was added to this solution. The mixture was kept on a waterbath for the evaporation of the solvent. After evaporation was complete, the residue was washed several times with benzene and filtered through a sintered crucible. Drying of the complex obtained was effected by keeping it over phosphorus(V) oxide in a vacuum desiccator.

Analyses

The metal content of the complexes was estimated by EDTA titrations using xylenol orange as indicator. The iodide content was estimated by Volhard's method. The ligand content was estimated by spectrophotometry (at 256 nm) using the calibration curve method. The analytical data are presented in Table 1.

Physical Methods

Molar conductance data for all the complexes were obtained at room temperature (*ca.* 28 °C) in a Siemen's conductivity bridge using an immersion cell (type LTA) previously calibrated with standard KCl solutions. The concentrations of the solutions used were of the order of 0.001 *M*. The conductance data are presented in Table 1.

The infrared spectra of the ligand in CS_2 and of the complexes in Nujol mulls were recorded in a Carl Zeiss UR-10 infrared spectrophotometer. The principal ir bands and their assignments are presented in Table 2.

The proton nmr spectra were recorded on a Varian T-60 spectrometer (60 MHz) and for a few complexes on a Varian HA-100 spectrometer (100 MHz), using $CDCl_3$ as the solvent and TMS as the internal reference. The proton nmr spectra of the Yb(III) complex at different temperatures in the range 5–75 °C were recorded on a Varian HA-100 spectrometer using a Varian variable temperature controller. The solvent used in this study was CD_3CN and the internal reference was TMS.

Differential thermal analyses of two of the complexes were carried out in a manual type DTA instrument using a chromel–alumel thermocouple. The heating rate was adjusted to be 5 ± 1 °C/min. The sample used was a mixture of the complex and freshly ignited alumina in the ratio 1:1 by weight.

Results and Discussion

The analytical results show that the complexes have a general formula $Ln(3\text{-}MePyO)_8I_3 \cdot xH_2O$ where $x = 0$ for Ln = La and Tb, $x = 1$ for Ln = Pr, and $x = 2$ for Ln = Nd, Sm, Dy, Yb, and Y. The complexes are soluble in dimethylformamide, dimethylsulphoxide, nitrobenzene, and chloroform and insoluble in carbon tetrachloride and benzene. Their solubility in acetone is appreciable.

The thermal behaviour of two representative complexes, one containing water and the other free of water, was studied by the DTA technique. The Nd(III) complex gave an endothermic peak at 118 °C due to the elimination of water and another endothermic peak at 162 °C due to the melting of the complex. Three exothermic peaks were obtained at 265, 332, and 438 °C. The Tb(III) complex showed all the above exothermic peaks, but showed only one endothermic peak due to melting at 125 °C.

The ir spectra of the complexes do not show any significant dependence on the central metal ion. The N—O stretching vibration of the ligand (in CS_2) occurring at 1290 cm^{-1} is shifted to lower frequencies by about 15–20 cm^{-1} in the complexes, thus indicating the coordination of the ligand to the metal ion through the oxygen of the N—O group (11). The N—O bending vibration occurring at 782 cm^{-1} (in CS_2) and the C—H out of plane vibration occurring at 752 cm^{-1} (in CS_2) do not show any appreciable shift upon complexation. The shift in the N—O stretching frequency ($\Delta\nu_{N-O}$) of the ligand upon complexation is less in the present complexes than that observed for the corresponding 4-MePyO and PyO complexes of the lanthanide iodides (30–40 cm^{-1}).

Comparison of the ir spectra of the Tb(III) complex with those of the other complexes shows that there is no appreciable difference between them in the region 700–900 cm^{-1} where the rocking mode of the coordinated water is expected. This may indicate that the water molecules are not coordinated to the metal in the solid state. This conclusion is further supported by the small $\Delta\nu_{N-O}$ values observed in these complexes (11).

The conductance data for the complexes in nitrobenzene, a solvent of low donor properties, show that the complexes behave as 1:1 electrolytes in this solvent (10). But, the conductance data in acetonitrile, a solvent of appreciable donor properties, show that the complexes behave as 1:2 electrolytes in this solvent (10). Though this data suggest that at least one iodide may be coordinated to the metal ion in solution, in view of the small $\Delta\nu_{N-O}$ obtained in the ir spectra, the conductance data may be attributed to ion-pair formation in solution.

The proton nmr spectrum of the ligand (Table 3) shows a signal at 1.82 τ due to 2,6-H, a signal at 2.77 τ due to 4,5-H and a signal at 7.65 τ due to CH_3—. The assignments were made after comparing the spectrum of the ligand with the spectra of PyO, 4-MePyO, and 2-MePyO. Among the complexes, only La(III) and Y(III) complexes are

TABLE 3. Proton nmr spectral data* (τ, ppm)

Complex	2-H,6-H	4-H,5-H	CH_3—	H_2O
3-MePyO	1.82	2.77	7.65	—
$La(3\text{-}MePyO)_8I_3$	1.43	2.45	7.58	—
$Pr(3\text{-}MePyO)_8I_3.H_2O$	1.00	2.39	7.63	—
$Nd(3\text{-}MePyO)_8I_3.2H_2O$	1.37	2.45	7.68	—
$Sm(3\text{-}MePyO)_8I_3.2H_2O$†	—	2.53	7.57	—
$Yb(3\text{-}MePyO)_8I_3.2H_2O$	0.73 0.40	3.33 2.67	7.50	—
$Y(3\text{-}MePyO)_8I_3.2H_2O$	1.42	2.45	7.55	4.44

*60 MHz proton nmr data in $CDCl_3$ solutions.
†The 2-H signal of the Sm(III) complex could not be obtained in the available spectrometer.

diamagnetic and showed sharp signals; other complexes which are paramagnetic showed signals which are broadened to different extent. It has been observed (12) that the sign of the isotropic shift changes on going from Ce(III) to Yb(III). The change in sign of the isotropic shift has been attributed to either the change in the sign of $(g_L - 1)$ where g_L is the Lande g factor (13) or the changes in the structure of the complex species on going from Ce(III) to Yb(III) (14). The proton nmr spectra of the present complexes show a general down-field shift[2] of the 2,6-H signal. While the Pr(III) complex shows a down-field shift for 4,5-H signal, the Sm(III) and Yb-(III) complexes show an up-field shift of this signal. No shift is observed for the 4,5-H signal in the Nd(III) complex. The methyl signal is shifted to up-fields in the Pr(III) and Nd(III) complexes, while the Sm(III) and Yb(III) complexes showed a down-field shift of this signal.

Significant shifts in 2,6-H and 4,5-H signals (*ca.* 23 and 19 Hz respectively) in the diamagnetic complexes $La(3\text{-}MePyO)_8I_3$ and $Y(3\text{-}MPyO)_8I_3.2H_2O$ are indicative of the deshielding of the pyridine ring protons. This deshielding can be attributed to the drainage of electron density from the ligand to the metal due to coordination. All the other complexes studied are paramagnetic and contributions to the shift from both contact and pseudocontact (dipolar) interactions are possible in these complexes (15). While the Yb(III) complex gives separate signals for 2,6,4,5-H (Fig. 1), other paramagnetic complexes give only two signals for these protons. Broadening of the spectral lines has been observed due to relaxation effects in these complexes.

[2]Down-field and up-field shifts are referred to the diamagnetic complex $La(3\text{-}MePyO)_8I_3$.

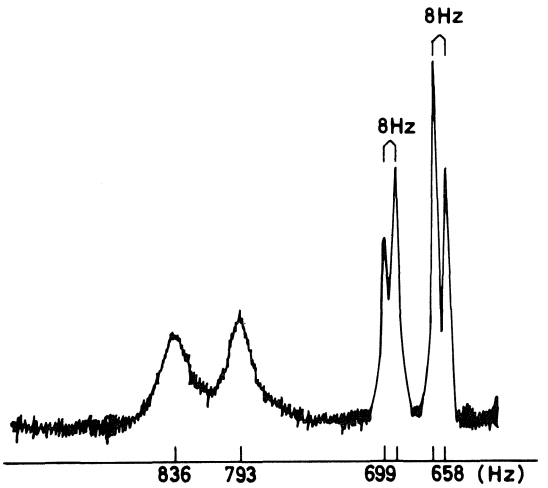

FIG. 1. Aromatic proton region of the proton nmr spectrum (100 MHz) of $Yb(3\text{-}MePyO)_8I_3.2H_2O$ in CD_3CN at 30 °C.

The signals of the Tb(III) and the Dy(III) complexes could not be observed due to excess broadening. In these cases even the TMS signal could not be identified. Signal due to water, which was expected in all the paramagnetic complexes (except the Tb(III) complex which does not contain water) could not be obtained. This may either be due to large shifts of the proton signals of water which could not be recorded in the available spectrometer or due to relaxation effects which broaden the signal, and may indicate that the water molecules might coordinate to the metal ion in solution.

Calculation of $\Delta H_i/g_L(g_L - 1)J(J + 1)$, where ΔH_i is the isotropic nmr shift of the ith proton and other symbols have their usual meaning, does not give a constant value for the various paramagnetic complexes studied. This indicates that contribution to the isotropic shift in the

Can. J. Chem. Downloaded from www.nrcresearchpress.com by 210.87.254.105 on 09/05/12
For personal use only.

Can. J. Chem. Downloaded from www.nrcresearchpress.com by 210.87.254.105 on 09/05/12
For personal use only.

present complexes is not predominantly contact in origin (16). A dominant pseudocontact contribution to the isotropic shift demands that the ratios of the shifts at different proton sites in various paramagnetic lanthanide complexes should be the same or nearly the same (17). As these ratios are not the same for the various paramagnetic complexes studied, we conclude that the pseudocontact contribution to the isotropic shift is also not predominant. Calculation of the geometric factor $(3\cos^2\theta - 1)r^{-3}$ at various proton sites for both eight coordinated dodecahedral and square antiprismatic geometries using standard bond angles and bond lengths and allowing for free and restricted rotation of the ligand about the N—O bond and comparison of ratios of the geometric factors at different sites have indicated that pseudocontact contribution is not the only contribution to the isotropic shift. Thus it may be suggested that both contact and pseudocontact interactions are responsible for the observed isotropic shifts in the present complexes.

It is interesting to note that four separate signals are obtained for the four aromatic protons of the ligand in the Yb(III) complex while the other complexes show only two signals. The 4-H,5-H portion of the Yb(III) complex spectrum resembles a classical AB pattern with $J_{AB} = 8$ Hz and $|\nu_A - \nu_B| = 32.01$ Hz at 30 °C. Probably, 6-H is not coupled to 5-H due to the fast relaxation it experiences as a result of its proximity to the paramagnetic centre as evidenced by the broadening of the 6-H signal (18). Temperature dependence of the aromatic proton signals of the Yb(III) complex has been studied in the temperature range 5–75 °C. The chemical shifts of the various protons do not show a linear dependence on temperature (Fig. 2). But the difference in chemical shifts between 2-H and 6-H, and 4-H and 5-H ($\Delta\nu$) shows a linear decrease with increasing temperature (Fig. 3).

The inequivalence of 2-H and 6-H, and 4-H and 5-H, in the Yb(III) complex, which was not observed in the other complexes, may be due to a restricted rotation of the ligand about the O—N bond. This will result in different dipolar interactions due to different $(3\cos^2\theta - 1)r^{-3}$ values for the four aromatic protons, making them inequivalent. As the temperature is increased, the rotation becomes less hindered and the 2-H and 6-H, and 4-H and 5-H signals tend to average out. Restricted rotation of the ligand can be possible in a situation as the present one where high coordination number and comparatively small ionic radius of the metal ion give a large steric hindrance for the rotation. Restricted

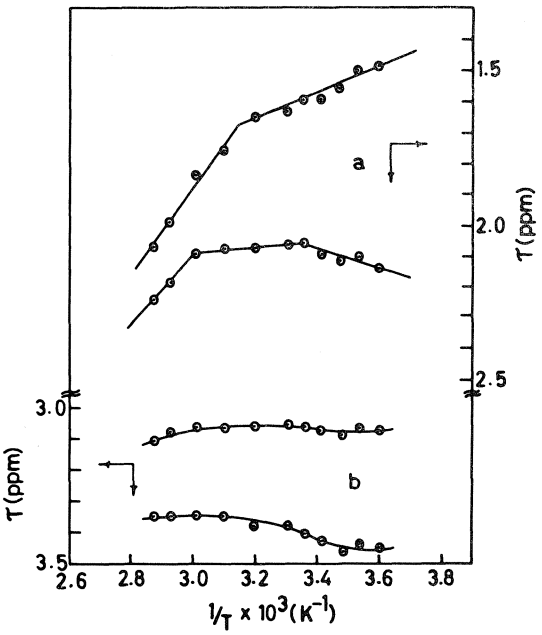

FIG. 2. Plot of chemical shifts of (*a*) 2-H and 6-H and (*b*) 4-H and 5-H resonances in the Yb(III) complex in CD_3CN *vs.* reciprocal temperature.

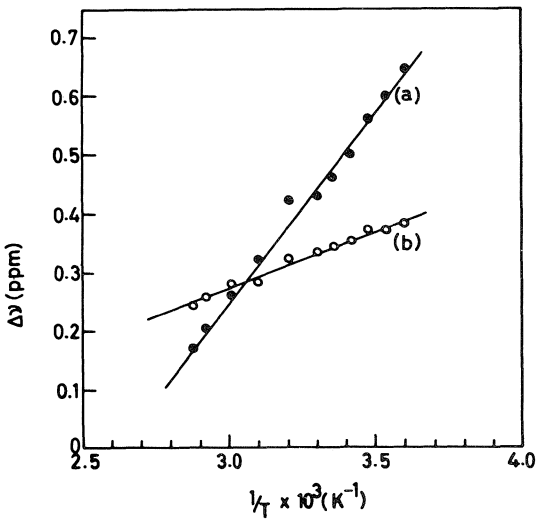

FIG. 3. Plot of the difference in chemical shifts of (*a*) 2-H and 6-H and (*b*) 4-H and 5-H resonances in the Yb(III) complex in CD_3CN *vs.* reciprocal temperature.

rotation of 3-MePyO in Co(II) complexes has been suggested by Kluiber and Horrocks (19) in order to explain the observed proton nmr spectra.

Acknowledgments

One of the authors (L.R.) thanks the authorities of the Indian Institute of Science, Bangalore, for a scholarship. The authors thank the referees of this paper for their valuable comments.

1. V. N. KRISHNAMURTHY and S. SOUNDARARAJAN. J. Inorg. Nucl. Chem. **29**, 517 (1967).
2. S. K. RAMALINGAM and S. SOUNDARARAJAN. Bull. Chem. Soc. Jpn. **41**, 106 (1968).
3. S. K. RAMALINGAM and S. SOUNDARARAJAN. Z. Anorg. Allg. Chem. **353**, 216 (1967).
4. S. K. RAMALINGAM and S. SOUNDARARAJAN. J. Inorg. Nucl. Chem. **29**, 1763 (1967).
5. M. KAWASHITA, O. A. SERRA, and V. K. LAKATOS OSORIO. J. Inorg. Nucl. Chem. **37**, 1998 (1975).
6. P. V. SIVAPULLAIAH and S. SOUNDARARAJAN. Curr. Sci. (India), **44**, 374 (1975).
7. D. K. KOPPIKAR and S. SOUNDARARAJAN. J. Inorg. Nucl. Chem. **38**, 174 (1976).
8. V. N. KRISHNAMURTHY and S. SOUNDARARAJAN. Can. J. Chem. **45**, 189 (1967).
9. L. RAMAKRISHNAN and S. SOUNDARARAJAN. Monatsh. Chem. **106**, 625 (1975).
10. W. J. GEARY. Coord. Chem. Rev. **7**, 81 (1971).
11. V. KAKIUTI, S. KIDA, and J. V. QUAGLIANO. Spectrochim. Acta, **19**, 201 (1963).
12. R. D. FISCHER. NMR of paramagnetic molecules. *Edited by* G. N. La Mar, W. Dew. Horrocks, Jr., and R. H. Holm. Academic Press, New York, N.Y. 1973, p. 534.
13. F. A. HART, J. E. NEWBERY, and D. SHAW. J. Inorg. Nucl. Chem. **32**, 3585 (1970).
14. T. H. SIDDALL, III, W. E. STEWART, and D. G. KARRAKER. Inorg. Nucl. Chem. Lett. **3**, 479 (1967).
15. E. R. BIRNBAUM and T. MOELLER. J. Am. Chem. Soc. **91**, 7274 (1969).
16. E. R. BIRNBAUM and S. STRATTON. Inorg. Chem. **12**, 379 (1973).
17. J. K. M. SANDERS, S. W. HANSON, and D. H. WILLIAMS. J. Am. Chem. Soc. **94**, 5325 (1972).
18. A. CARRINGTON and A. D. MCLACHLAN. Introduction to magnetic resonance. Harper and Row, New York and John Weatherhill, Tokyo. 1967. p. 210.
19. R. W. KLUIBER and W. Dew. HORROCKS. J. Am. Chem. Soc. **94**, 5325 (1972).

Can. J. Chem. Downloaded from www.nrcresearchpress.com by 210.87.254.105 on 09/05/12
For personal use only.

The thermal decomposition of methane. II. Secondary reactions, autocatalysis and carbon formation; non-Arrhenius behaviour in the reaction of CH_3 with ethane[1]

C.-J. CHEN AND M. H. BACK
Chemistry Department, University of Ottawa, Ottawa, Ont., Canada K1N 6N5
AND
R. A. BACK
Chemistry Division, National Research Council of Canada, Ottawa, Ont., Canada K1A 0R6

Received April 1, 1976

C.-J. CHEN, M. H. BACK, and R. A. BACK. Can. J. Chem. **54**, 3175 (1976).

In the thermal decomposition of methane at temperatures from 880 to 1103 K, hydrogen and ethane are the only primary products. The rate of formation of ethane falls rapidly towards zero as the reaction progresses until ethane reaches a steady-state concentration. This behaviour is interpreted in terms of a radical chain mechanism,

[4] $CH_3 + C_2H_6 \rightarrow CH_4 + C_2H_5$
[5] $C_2H_5 \rightarrow C_2H_4 + H$
[2] $H + CH_4 \rightarrow H_2 + CH_3$

Values of k_4 were obtained which confirm the non-Arrhenius behaviour of this reaction at these temperatures. Similar chain sequences propagated by addition or abstraction reactions of methyl radicals with ethylene, propylene, and acetylene can account for the formation and disappearance of these secondary products.

At a later stage in the pyrolysis a marked autocatalysis is observed and the yield of ethane increases sharply above its steady-state value. It is concluded that this autocatalysis is largely a homogeneous process and is not caused by or associated with carbon formation. Deposition of carbon on the surface was observed at a still later stage of the decomposition, and was quantitatively estimated by light absorption measurements. Possible mechanisms for the autocatalysis are discussed.

C.-J. CHEN, M. H. BACK et R. A. BACK. Can. J. Chem. **54**, 3175 (1976).

Lors de la décomposition thermique du méthane à des températures allant de 880 à 1103 K, l'hydrogène et l'éthane sont les seuls produits primaires. La vitesse de formation de l'éthane décroît rapidement vers zéro à mesure que la réaction progresse jusqu'à ce que l'éthane atteigne une concentration en état stationnaire. On interprète ce comportement en termes d'un mécanisme radicalaire en chaîne

[4] $CH_3 + C_2H_6 \rightarrow CH_4 + C_2H_5$
[5] $C_2H_5 \rightarrow C_2H_4 + H$
[2] $H + CH_4 \rightarrow H_2 + CH_3$

On a obtenu les valeurs de k_4 qui confirment, qu'à ces températures la réaction ne se comporte pas suivant la théorie d'Arrhénius. Une série de réactions en chaîne similaires propagées par les réactions d'addition et d'enlèvement des radicaux méthyles avec l'éthylène, le propylène et l'acétylène peuvent expliquer la formation et la disparition de ces produits secondaires.

Plus tard au cours de la pyrolyse, on observe une autocatalyse importante et le rendement d'éthane augmente considérablement au dessus de sa valeur à l'état stationnaire. On en conclut que cette autocatalyse est principalement un processus homogène et qu'il n'est pas causé ou associé avec la formation de carbone. On a observé la déposition de carbone à la surface plus tard au cours de la réaction de décomposition et on en a effectué une évaluation quantitative par des mesures d'absorption de lumière. On discute des mécanismes possibles pour l'autocatalyse.
[Traduit par le journal]

Introduction

In a previous paper (Part I) (1) it was shown that the initial products of the methane pyrolysis are solely ethane and hydrogen and that these are formed in a simple non-chain radical mechanism:

[1] $CH_4 \rightarrow CH_3 + H$
[2] $H + CH_4 \rightarrow CH_3 + H_2$
[3] $2CH_3 \rightarrow C_2H_6$

Values of k_1 were obtained over a range of temperature and pressure and it was concluded that reaction 1 was a homogeneous unimolecular

[1]NRCC No. 15438.

Can. J. Chem. Downloaded from www.nrcresearchpress.com by 210.87.254.105 on 09/05/12
For personal use only.

dissociation in its pressure-dependent region. It was also noted that the rate of formation of ethane decreased gradually from its initial value and that ethylene, then propylene, acetylene, and finally carbon, together with some other products, appeared successively with increasing time of reaction. An autocatalysis leading to sharply increased rates of formation of all products was also observed at a certain stage in the pyrolysis. The present paper deals with the mechanism of formation of the secondary and tertiary products. It will be seen that reactions of methyl radicals with ethane, ethylene, propylene, and acetylene can account for the products observed and quantitative information about some of the reaction rates can be obtained. The reaction of methyl radicals with ethane is of particular interest because it has been reported that its rate constant shows non-linear Arrhenius behaviour (2); the present study provides data at relatively high temperatures where the effect should be most pronounced.

Experimental

The apparatus and experimental procedure were described in Part I. The analysis procedure was modified to include quantitative analysis for propylene, acetylene, and allene, and qualitative analysis for butadiene and benzene by replacement of the second silica gel column with a 4 m column of Durapak operated at room temperature.

Carbon formation was studied by light absorption in a smaller cylindrical quartz vessel, 2.2 cm i.d. and 5.0 cm long, fitted with plane windows and mounted at the centre of a tubular furnace 50 cm long. Each end of the furnace was plugged with a similar cylindrical cell, 30 cm long and evacuated, to minimize heat loss, so that the reaction vessel including its plane windows was virtually free of temperature gradients. The vessel was connected to the vacuum line by small-bore tubing so that diffusion of particles or products into or out of the vessel should have been negligible. The carbon formation observed should thus be characteristic of the isothermal pyrolysis of methane at the vessel temperature. Deposition of carbon on the vessel windows during the course of the pyrolysis was measured by the absorption of light of 632.8 nm from a 2 mW He–Ne laser, using several traversals and measuring the transmitted light with a photodiode. In some experiments 4 additional quartz discs were mounted in the light path within the vessel to enhance the sensitivity of the measurement. In other experiments the laser beam was passed transversely through the reaction vessel through two small holes drilled in the tubular furnace, and the vessel was viewed from the end in an attempt to observe particle formation in the gas phase.

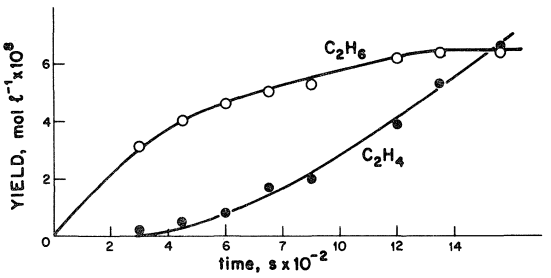

FIG. 1. Yield of ethane and ethylene as a function of time at 1038 K and 100 torr CH_4. ○ C_2H_6; ● C_2H_4.

Results and Discussion

Reaction of Methyl Radicals with Ethane

A typical yield–time plot for the formation of ethane and ethylene is shown in Fig. 1. Ethane was observed to reach a fairly well-defined steady-state plateau, except at the highest temperature, 1103 K. The only important loss process for ethane will be attack by methyl radicals, since these are the only radicals present in appreciable concentration (C_2H_5 and H, for example, disappear rapidly in reactions 5 and 2). The formation and disappearance of ethane may be accounted for by the following reactions:

[1] $$CH_4 \rightarrow CH_3 + H$$

[2] $$H + CH_4 \rightarrow H_2 + CH_3$$

[3] $$2CH_3 \rightleftarrows C_2H_6$$

[4] $$CH_3 + C_2H_6 \rightleftarrows CH_4 + C_2H_5$$

[5] $$C_2H_5 \rightarrow C_2H_4 + H$$

When the concentration of ethane has reached its steady-state value,

$$R_0 = \alpha k_4(CH_3)(C_2H_6)$$

where R_0 = initial rate of formation of ethane when reaction 4 is not important and $\alpha = k_5/(k_5 + k_{-4}(CH_4))$, the fraction of ethyl radicals formed in reaction 4 which decompose via reaction 5. Note that reaction −3 does not lead to a net consumption of ethane since the methyl radicals formed can only combine to reform ethane in the present system; the reaction sequence, 4, 5, and 2, and similar sequences with ethylene (see below) do not consume methyl radicals.

An estimate of α may be obtained from the relative rates of reactions 5 and 4. The value for k_5 may be calculated from the RRKM equation

Can. J. Chem. Downloaded from www.nrcresearchpress.com by 210.87.254.105 on 09/05/12
For personal use only.

TABLE 1. Kinetic and thermodynamic values used in calculations

Species	ΔH_f (298) [a] (kcal/mol)	S^0 (298) [b] (cal/deg mol)
CH_4	−17.9	44.5
C_2H_4	12.5	52.5
C_2H_6	−20.2	54.9
CH_3	34.0	46.1
C_2H_5	26.0	59.8
n-C_3H_7	20.7	67.2

Reaction	ΔH^0 (298) (kcal/mol)	ΔS^0 (298) (cal/deg mol)	$\overline{\Delta C_p}$ (1000–298) (cal/deg mol)
[4] $CH_3 + C_2H_6 \rightleftarrows CH_4 + C_2H_5$ $K_{995} = 66$	−5.7	+3.3	−1.4
[8] $CH_3 + C_2H_4 \rightleftarrows n$-$C_3H_7$ $K_{1038} = 4.2$ l/mol	−25.8	−31.7	+1.6
[9] $\log k^c = 13.8 - 38\,000/2.3RT$			
[−8] $\log k^c = 13.6 - 33\,100/2.3RT$			

[a] Values of ΔH_f, S^0, and C_p were taken from ref. 16.
[b] Standard state: atm of ideal gas.
[c] Values taken from ref. 17.

of Lin and Laidler (3). At 995 K and 100 torr CH_4, $k_5 = 3.26 \times 10^4\ s^{-1}$. A value of $k_{-4} = 9 \times 10^4\ M^{-1}\ s^{-1}$ can be calculated at 995 K, using the value of k_4 obtained in the present experiments together with the equilibrium constant. Thermodynamic quantities used in the calculation are given in Table 1. Thus at 995 K and 100 torr of CH_4, $R_5/R_{-4} = k_5/k_{-4}(CH_4) = 2.25 \times 10^2$, and $\alpha \approx 1$. This will also be true at higher temperatures, since $E_5 > E_{-4}$, and at the highest pressures of CH_4 employed, since the pressure-dependence of reaction 5 to some extent counteracts the dependence of R_{-4} on CH_4 pressure. Reaction −4 will therefore be ignored in all subsequent calculations.

The concentration of methyl radicals is given by $[CH_3] = [(R_0 + k_{-3}[C_2H_6])/k_3]^{1/2}$, and $k_4 = (R_0/[C_2H_6]_{ss})[(R_0 + k_{-3}[C_2H_6]_{ss})/k_3]^{-1/2}$ where $[C_2H_6]_{ss}$ is the ethane concentration in the steady-state plateau. Note that while reaction −3 did not enter directly into the ethane steady-state expression, it must be taken into account in calculating the steady-state methyl radical concentration.

The data from which k_4 were obtained are given in Table 2. Values for R_0 and $[C_2H_6]_{ss}$ were obtained from yield–time curves such as shown in Fig. 1. Values of k_{-3} were derived from RRKM calculations based on Model I described by Lin and Laidler (3) for the ethane decomposition. The rate constant for combination of methyl radicals, k_3, at 1000 K was taken as 4.0×10^{10} l mol^{-1} s^{-1}. While there is some discrepancy between these values for k_3 and k_{-3} (with respect to the equilibrium constant (4)) this choice for k_3 is justified in the present treatment because we wish to compare our results with other values of k_4 which were measured with respect to the same value of k_3. Values for αk_4 are given in the final column of Table 2; no variation with methane pressure was observed, supporting the previous conclusion that reaction −4 was negligible under our experimental conditions.

In a series of experiments at 880 K a small amount of ethane was added to the reactant methane and its consumption with time was measured. Dissociation of methane (reaction 1) can be neglected compared to reaction −3, and the methyl radical concentration will be given by $[CH_3] = (k_{-3}/k_3)^{1/2}\,[C_2H_6]^{1/2}$. The rate of disappearance of ethane may then be expressed as

$$-\mathrm{d}[C_2H_6]/\mathrm{d}t = k_4(k_{-3}/k_3)^{1/2}\,[C_6H_6]^{3/2}$$

Integrating from $[C_2H_6]_0$ to $[C_2H_6]_t$,

$$\frac{[C_2H_6]_0^{1/2} - [C_2H_6]_t^{1/2}}{[C_2H_6]_0^{1/2}\,[C_2H_6]_t^{1/2}} = \tfrac{1}{2}\,k_4\left(\frac{k_{-3}}{k_3}\right)^{1/2} t$$

A plot of the left-hand side of this equation against t is shown in Fig. 2. Using values for k_{-3}

Can. J. Chem. Downloaded from www.nrcresearchpress.com by 210.87.254.105 on 09/05/12
For personal use only.

TABLE 2. Values of k_4

P_{CH_4} (torr)	$[C_2H_6]_{ss}$ (mol/l $\times 10^8$)	R_0 (mol/l s $\times 10^{10}$)	k_{-3} ($s^{-1} \times 10^3$)	αk_4 (l/mol·s $\times 10^{-6}$)
T(K) = 995				
51	2.09	0.044	0.84	6.85
108	3.98	0.152	1.01	8.62
440	23.03	1.33	1.32	5.31
540	24.08	1.79	1.36	6.46
640	33.50	2.29	1.39	5.13
741	28.26	2.83	1.42	7.60
				Ave. 6±1
T(K) = 1038				
31.9	1.675	0.166	4.64	14.5
108	5.49	1.31	6.66	18.2
188	10.99	3.15	7.60	15.1
236	15.08	4.50	7.98	13.6
338	21.99	7.79	8.57	13.2
441	37.69	11.6	9.00	9.90
543	31.41	15.8	9.32	15.0
642	46.06	20.2	9.57	10.1
741	50.25	24.8	9.77	10.1
				Ave. 13±3
T(K) = 1068				
25.2	2.09	42.2	12.7	14.6
48.6	4.18	132.4	15.9	15.9
75.5	7.12	279	18.2	15.1
104	8.38	474	19.9	19.5
154	15.3	899	22.0	15.1
233	20.9	1720	24.3	17.6
339	36.9	3061	26.2	13.5
440	44.0	4529	27.6	15.1
600	67.0	7163	29.1	13.7
742	73.3	9743	30.1	14.6
				Ave. 15±2

and k_3 obtained as before, a value of $k_4 = 4.6 \times 10^6$ l mol^{-1} s^{-1} may be calculated from the slope of this line.

This value of k_4 together with the average values of k_4 from Table 2 are shown in an Arrhenius plot in Fig. 3, which also includes previous measurements of k_4. The values for k_4 below about 800 K were measured by standard photochemical or thermal techniques relative to the value of k_3 of 3.0×10^{10} l mol^{-1} s^{-1} at 298 K. The values measured by Pacey and Purnell (2) which are in close agreement with the present values, were obtained from a study of the pyrolysis of ethane in a flow system and were also calculated relative to this value for k_3. The results of Clark *et al.* (5) are direct measurements obtained by monitoring the radical concentration in shock tube experiments. In recent years there has been growing evidence that Arrhenius plots for some simple hydrogen abstraction reactions show marked upward curvature in the region 700–1500 K so that rate constants measured at these temperatures are considerably higher than predicted from the simple Arrhenius equation measured at lower temperatures. This behaviour has been discussed by Clark and Dove (6) who have shown that the observed increase in activation energy for reactions such as [2] and [4] may be accounted for within the framework of transition-state theory. The present results provide confirmation of this behaviour for the reaction of methyl radicals with ethane. The measurements of Yampolskii and Rybin (7) appear to indicate values for k_4 appreciably lower than the other data in Fig. 3. Their values, however, were measured relative to the rate constant for the reaction of methyl radicals with deuterium. If the temperature-dependence of the activation energy for the latter reaction was about the same as that for reaction 4, as it

Can. J. Chem. Downloaded from www.nrcresearchpress.com by 210.87.254.105 on 09/05/12
For personal use only.

Can. J. Chem. Downloaded from www.nrcresearchpress.com by 210.87.254.105 on 09/05/12
For personal use only.

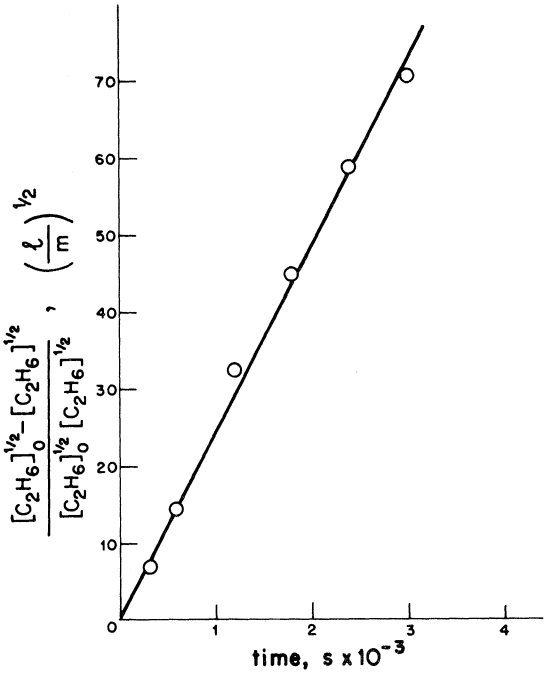

FIG. 2. Plot of $\frac{[C_2H_6]_0^{1/2} - [C_2H_6]_t^{1/2}}{[C_2H_6]_0^{1/2}[C_2H_6]_t^{1/2}}$ against t at 880 K.

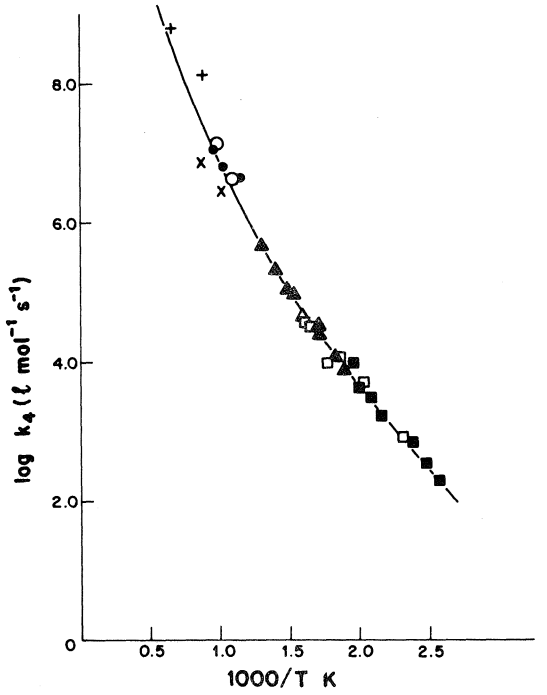

FIG. 3. Arrhenius plot of k_4. The line is a smooth curve through the points. +, ref. 5; ▲, ref. 18; □, ref. 19; ■, ref. 20; ○, ref. 2; ●, this work; ×, ref. 7.

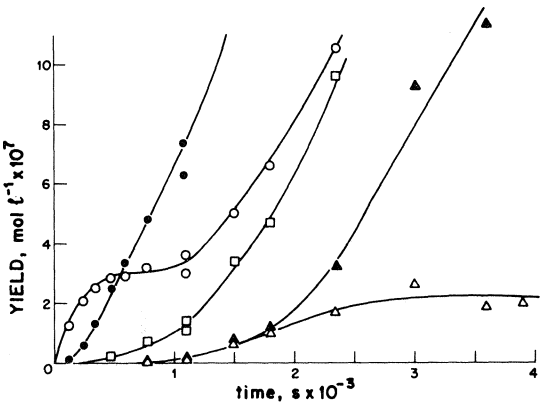

FIG. 4. Yield of products as a function of time at 1038 K and 443 torr methane. ○, C_2H_6; ●, C_2H_4; □, C_3H_6; ▲, C_2H_2; △, C_3H_4.

appears to be (6), then their ratio would show no upward curvature in the Arrhenius plot, and the low values reported for k_4 are explained.

Secondary Reactions of Ethylene

A yield–time plot for the formation of the main primary, secondary and tertiary products is shown in Fig. 4. The first secondary product is ethylene, followed by propylene, acetylene, and allene. Reaction of methyl radicals with ethylene will produce acetylene and propylene by abstraction and addition, respectively.

[6] $$CH_3 + C_2H_4 \rightarrow C_2H_3 + CH_4$$

[7] $$C_2H_3 \rightarrow C_2H_2 + H$$

[8] $$CH_3 + C_2H_4 \rightleftarrows n\text{-}C_3H_7$$

[9] $$n\text{-}C_3H_7 \rightarrow C_3H_6 + H$$

Dissociation of C_2H_3 and C_3H_7 radicals will be much faster than addition or abstraction at these temperatures and pressures, as shown previously for the ethyl radical. At temperatures of about 1000 K reaction −8 is about 10 times faster than reaction 9 (Table 1) and the concentration of n-C_3H_7 radicals will be given to a fair approximation by

$$[n\text{-}C_3H_7] = K_8[CH_3][C_2H_4]$$

where K_8 is the equilibrium constant for reaction 8. The ratio of the rates of formation of propylene and acetylene in the initial stages of their formation when reactions leading to their consumption are not important, should therefore be given by the expression,

$$\frac{R_{C_3H_6}}{R_{C_2H_2}} = \frac{k_9K_8}{k_6}$$

Can. J. Chem. Downloaded from www.nrcresearchpress.com by 210.87.254.105 on 09/05/12
For personal use only.

TABLE 3. Yield of product, mol/l $\times 10^8$, 1038 K, 443 torr CH_4

Interval (min)	Yield			
	C_2H_6	C_2H_4	C_2H_2	C_3H_6
6	28.8	18.0	0.184	0.85
6	28.2	16.8	0.276	0.80
6	28.1	16.6	0.203	0.69
6	28.1	16.3	0.184	0.78
6	28.2	17.3		0.64
6	28.2	16.4	0.230	0.69
6	28.2	16.1	0.230	0.62
6	28.4	17.1	0.230	0.70
12	35.1	51.0	1.48	7.65
12	35.0	51.4	1.42	7.35
12	34.7	51.0	1.41	7.45
12	34.5	50.2	1.48	7.05
24	56.2	131	7.78	36.8
24	58.4	138	7.62	38.0
24	57.5	133	7.50	35.8
24	57.7	135	8.05	37.6
36	121	376	35.1	112
36	123	393	37.8	117
36	124	397	38.3	118
36	123	393	33.9	115

Under these conditions the yield of propylene was about three times that of acetylene (Table 3), and using the values of K_8 and k_9 listed in Table 1 a value of $k_6 = 1 \times 10^6$ l mol^{-1} s^{-1} was obtained at 1038 K. This is in remarkably close agreement with a value of 1.5×10^6 obtained by a long extrapolation of the low-temperature data of Trotman-Dickenson and Steacie (8) using their Arrhenius parameters of $A = 2 \times 10^8$ M^{-1} s^{-1} and $E = 10$ kcal/mol. Thus it appears that reaction 6 does not show the deviation from the Arrhenius law observed in reaction 4 and other simple abstraction reactions. This observation, together with the activation energy, which seems rather low for abstraction of such a strongly bonded hydrogen ($D(C_2H_3—H) = 105$ kcal/mol), suggests that reaction 6 is not a simple abstraction, but perhaps proceeds through an addition complex that can lead to either addition or abstraction:

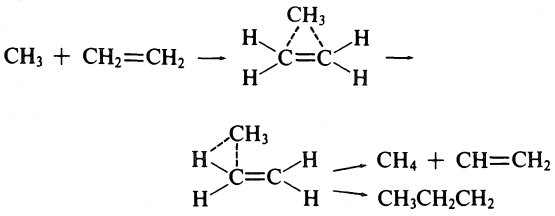

From the present data the addition reaction, [8], is about 30 times faster than the abstraction at 1038 K even though the former is almost certainly pressure dependent, well below its high-pressure limit.

Secondary Reactions of Propylene and Acetylene

Addition and abstraction chain reactions of methyl radicals should also be important loss processes for propylene and acetylene:

[10] $CH_3 + C_3H_6 \rightarrow CH_4 + C_3H_5$

[11] $C_3H_5 \rightarrow C_3H_4$ (allene) + H

[12] $CH_3 + C_3H_6 \rightleftarrows C_4H_9$

[13] $C_4H_9 \rightarrow C_4H_8 + H$

[14] $CH_3 + C_2H_2 \rightleftarrows CH_4 + C_2H$

[15] $CH_3 + C_2H_2 \rightleftarrows C_3H_5$

[16] $C_3H_5 \rightarrow C_3H_4$ (methyl acetylene) + H

Formation of butene was not observed even at high conversion, whereas allene was an important product. Thus in contrast to ethylene, it may be concluded that abstraction from propylene predominates over addition, reflecting the much lower C—H bond energy in propylene. Methyl acetylene, which could be formed through addition to acetylene, was also not observed, but the sensitivity for its detection was low in the analysis employed and it may have been present in appreciable yields. It is interesting that the methyl radical abstraction sequence with acetylene is blocked by the stability of the C_2H radical. The endothermicities[2] of the two possible dissociation reactions, $C_2H \rightarrow C_2 + H$ ($\Delta H = 139$ kcal/mol) and $C_2H \rightarrow C + CH$ ($\Delta H = 200$ kcal/mol), are too large to allow appreciable decomposition at the temperatures of the present study, and reaction 14 will simply be reversed by back reaction with CH_4. It must be concluded that dehydrogenation of acetylene is not the route to carbon formation in the pyrolysis of methane. Acetylene probably does play a part in carbon formation, but through condensation reactions rather than decomposition.

In the mechanism we are suggesting for the secondary reactions in the pyrolysis of methane, the methyl radical plays a dominant role. All other radicals decompose to yield hydrogen atoms which react with methane to regenerate

[2]Based on $D(HCC—H) = 112$ kcal/mol (9).

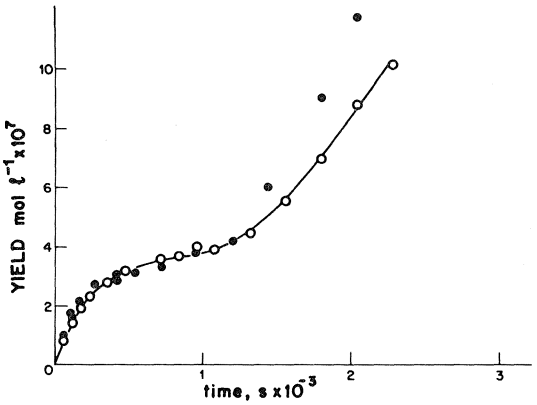

FIG. 5. Yield of ethane in packed and unpacked reaction vessel at 1038 K and 443 torr methane. ○, unpacked vessel; ●, packed vessel.

methyl radicals, resulting in efficient chain sequences which consume products without loss of methyl. The small number of products, and particularly the absence of higher alkanes, reflects the simplicity of this methyl-radical mechanism.

Autocatalysis, Carbon Formation, and Surface Effects

The autocatalysis, in which the yield of ethane begins to rise sharply again after the steady-state plateau (Fig. 4), is not predicted or explained by the reaction mechanism postulated above. Autocatalysis is most evident in the yield of ethane, but affects the other products as well, although it is less obvious because their yields are already rising sharply. Autocatalysis has frequently been reported in the decomposition of methane, and under various conditions of pressure, temperature, conversion or surface, may have a variety of causes (10–13). It has been attributed to reactions occurring on the surface of the vessel, possibly catalysed by a carbon film (14, 15).

The influence of surface on the decomposition was investigated in several ways. Experiments were performed in a vessel filled with quartz tubes which increased the surface/volume ratio by a factor of 10. Figure 5 shows the yield of ethane as a function of time in the packed and unpacked vessels. As noted earlier (1) the initial rate of formation of ethane was not changed in the packed vessel but some enhancement of the rate occurred in the autocatalytic region. A comparable increase in the yields of the secondary and tertiary products was also observed. The effect was relatively small, however, for a change in S/V ratio by a factor of 10, and the fraction of the reaction occurring on the surface in the autocatalytic region in the unpacked vessel was probably less than 10%.

The effect of carbon deposits in the present system was studied by two different approaches. Ordinarily, air was admitted to the reaction vessel after each experiment to oxidize any carbon that might be present, and the vessel was thoroughly pumped out; this procedure yielded reproducible results over long periods of time (1). In some experiments a carbon deposit was first laid down in the vessel by pyrolysing methane for a few hours. Subsequent pyrolyses in the presence of this carbon surface showed reaction rates faster than normal and somewhat erratic. There seems no doubt that a carbon-coated surface catalyses the reaction. It is not clear, however, at what stage of the reaction the carbon deposit begins to have a significant effect on the reaction. To test this point a series of experiments was performed in which the reactant and volatile products were removed and analysed at intervals, but any carbon or other nonvolatile deposit was retained, as the usual treatment with air was omitted. If a carbon deposit were formed on the surface during one pyrolysis interval, it should accumulate over the series of pyrolyses and the yields of products would be expected to increase if the deposit were catalytic. These experiments were done with intervals of 6, 12, 24, and 36 min at 1038 K and 443 torr methane. The results are summarized in Table 3. The time course of the reaction for continuous pyrolysis under the same conditions is shown in Fig. 4. In all of these experiments the yields of the products were reproducible within the error limits of the analysis and no change with successive experiments was observed. Even for the 36 min interval, which is well into the autocatalytic region, there was apparently no accumulation of carbon or other active substance on the walls of the vessel in sufficient quantity to affect the rate of formation of the products.

The second approach to the study of the carbon deposit was to measure its optical density. The optical density of the carbon film formed at 1109 K and 450 torr methane was measured as previously described and is shown as a function of time in Fig. 6. To calibrate the absorption measurements methane was pyrolysed to completion at 1200 K until an equilibrium

Can. J. Chem. Downloaded from www.nrcresearchpress.com by 210.87.254.105 on 09/05/12
For personal use only.

concentration of carbon was deposited on the surface. At this temperature the equilibrium constant for dissociation of methane into the elements is 62.5 atm (9), indicating that more than 98% of the methane is converted to carbon. The optical density of the film when this equilibrium has been attained is shown in Fig. 7 as a function of initial methane pressure. Using this calibration plot, the data in Fig. 6 may be converted to a rate of formation of carbon in the pyrolysis, and compared to the rate of formation of the volatile products; this is shown in Fig. 8.

It appears that carbon is not deposited until after the autocatalytic stage, a result which is in agreement with the 'interval' experiments and the lack of effect of surface on the reaction. To determine precisely the onset of carbon formation, the sensitivity of the optical density measurements must be examined. The detection limit of log I^0/I was estimated to be 0.004, which corresponds to a concentration of about 2×10^{-6} mol/l of carbon deposited from the gas phase. By introducing four additional quartz discs into the reaction vessel this limit was lowered to 1×10^{-6} mol l^{-1}. Below this level, the extent of the carbon deposit can only be estimated by extrapolation, indicated by the dotted line. The extent of the surface coverage at our limit of detection may be estimated by assuming a graphitic structure for the carbon film. The area of a graphite ring is 5.2×10^{-16} cm^2 and the area per atom therefore is 2.6×10^{-16} cm^2. In the reaction vessel in which the products were measured, this corresponds to 5.5×10^{-6} mol/l. Therefore the detection limit represents about 20% coverage of the surface with a monolayer, although the nature of the surface deposit in the early stages is of course not known. It is not certain what extent of surface coverage is necessary to produce a measurable effect on the reaction rate. Figure 8 shows that measurable carbon film formation follows the autocatalytic stage and is therefore not responsible for it, and the interval experiments (Table 3)

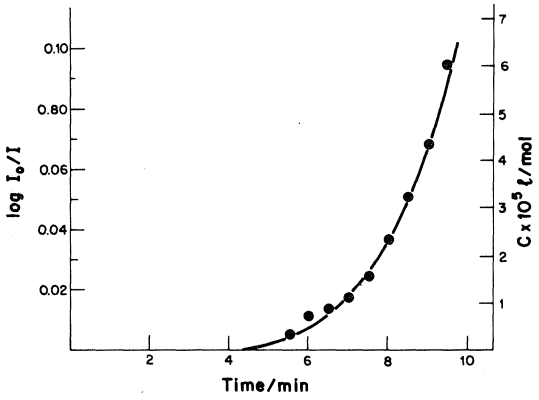

FIG. 6. log I_0/I as a function of time of the carbon film formed at 1109 K and 450 torr methane.

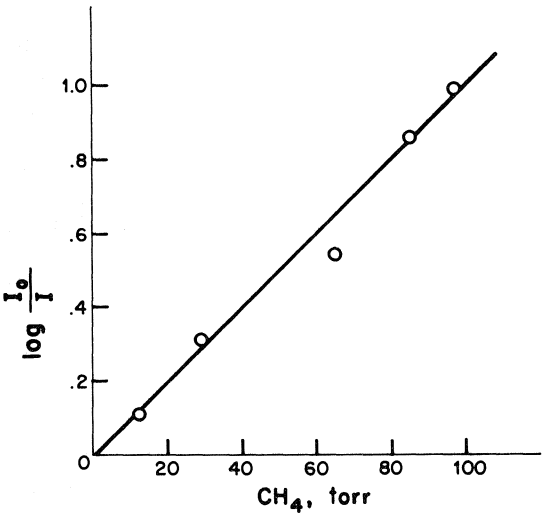

FIG. 7. A plot of log I_0/I as a function of the pressure of methane at 1200 K, measured under equilibrium conditions.

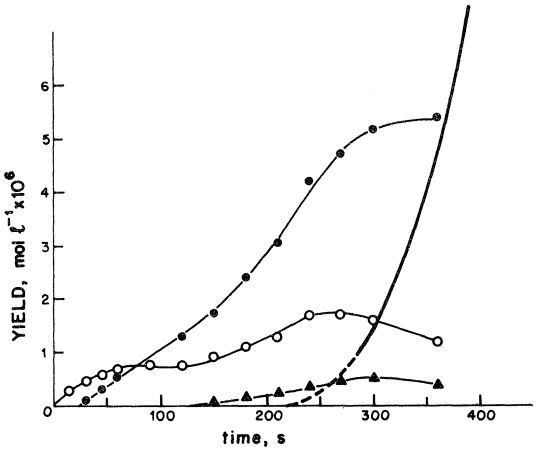

FIG. 8. Comparison of the formation of the carbon film on the surface with the formation of the main gaseous products at 1103 K. ○, C_2H_6; ●, C_2H_4; ▲, C_2H_2.

Can. J. Chem. Downloaded from www.nrcresearchpress.com by 210.87.254.105 on 09/05/12
For personal use only.

Can. J. Chem. Downloaded from www.nrcresearchpress.com by 210.87.254.105 on 09/05/12
For personal use only.

offer strong confirmation of this conclusion. Onset of carbon film formation is in fact accompanied by a decrease in the yields of ethane, ethylene, and acetylene, presumably corresponding to an efficient conversion of these products to carbon, but this occurs well after the autocatalytic stage.

It has been suggested that a fine smoke-like suspension of carbon particles rather than a surface deposit could act as a catalyst. These particles would have an enormous surface area and therefore would be much more effective than a surface deposit; the particles would also be swept out of the reaction vessel with the methane and volatile products, so that no cumulative effects would be observed in the interval experiments. To test this hypothesis, direct observation of carbon particles by light scattering was attempted. The laser beam was passed transversely through the vessel and viewed at right angles through the end windows. The beam was not visible in the vessel at any time during the reaction, including the autocatalysis and carbon deposition stages. It may be concluded that carbon particles of a size sufficient to cause appreciable scattering of visible light were not present in the gas phase.

The conclusion from all these experiments is that homogeneous rather than heterogeneous reactions must be responsible for the autocatalysis and that a new radical formation process must therefore become important in this region. Any process which increases the concentration of radicals in the system will lead to an increased rate of formation of ethane and a corresponding increase in all the products derived from it. Under the conditions of the experiments shown in Fig. 4, the unimolecular dissociation of propylene after 1800 s may be estimated to be about 10 times slower than the combined rates of formation of ethane and ethylene, using the value of the rate constant suggested by O'Neal and Benson (17), $\log k = 15.3 - 89\,200/2.3RT$. There is sufficient uncertainty in this value, however, that dissociation of propylene may not be ruled out as a significant secondary initiation.

Simple computer simulation of the reaction system shows which type of reaction might have the right properties for secondary initiation. Disproportionation reactions between olefins and methane such as $C_2H_4 + CH_4 \rightarrow C_2H_5 + CH_3$ appear not to cause a sharp enough rise in the reaction rate, and are probably too slow. Bimolecular reactions of olefins or acetylene such as $2C_2H_2 \rightarrow C_2H + C_2H_3$ are more promising in as much as they yield autocatalysis curves of the proper shape, but again the reaction rates are probably too slow. A bimolecular reaction of acetylene yielding a diradical which can initiate radical chains would also have the right kinetic properties. This type of reaction would have a lower activation energy than the bimolecular reaction giving two radicals (21) and could be fast enough to give the observed yields of products. Diradical formation has been postulated in the pyrolysis of acetylene itself (22) and seems to offer the most plausible mechanism for homogeneous autocatalysis in the present system, but these suggestions must be regarded as speculative.

Acknowledgment

The authors thank the National Research Council of Canada for financial support of this work.

1. C.-J. Chen, M. H. Back and R. A. Back. Can. J. Chem. **53**, 3580 (1975).
2. P. D. Pacey and J. H. Purnell. J. Chem. Soc. Faraday Trans. I, **68**, 1462 (1972).
3. M. C. Lin and K. J. Laidler. Trans. Faraday Soc. **64**, 79 (1968).
4. E. V. Waage and B. S. Rabinovitch. Int. J. Chem. Kinet. **3**, 105 (1971).
5. T. C. Clark, T. P. J. Izod, and G. B. Kistiakowsky. J. Chem. Phys. **54**, 1295 (1971).
6. T. C. Clark and J. E. Dove. Can. J. Chem. **51**, 2147 (1973).
7. Y. P. Yampolskii and V. M. Rybin. Reaction Kinet. Catal. Lett. **1**, 321 (1974).
8. A. F. Trotman-Dickenson and E. W. R. Steacie. J. Chem. Phys. **19**, 169 (1951); A. F. Trotman-Dickenson and G. S. Milne. Tables of Bimolecular Gas Reactions, NSRDS-NBS-9, 1967.
9. JANAF Thermochemical Tables, 2nd. ed. NSRDS-NBS-37 (1971).
10. I. A. Schneider and I. G. Murgulescu. Z. Phys. Chem. Leipzig, **237**, 81 (1968); **223**, 231 (1963); **218**, 338 (1961).
11. H. B. Palmer, J. Lahaye, and K. C. Hou. J. Phys. Chem. **72**, 348 (1968).
12. B. Eisenberg and H. Bliss. Chem. Eng. Prog. Sym. Ser. **63**, 3 (1967).
13. J. Tardieu de Maleissye et R. Delbourgo. Bull. Soc. Chim. Fr. 60 (1970); 1108 (1969).
14. M. L. Lieberman and G. T. Noles. Carbon, **12**, 689 (1974).

15. L. ODOCHIAN and I. A. SCHNEIDER. Rev. Roum. Chim. **15**, 1647 (1970); **16**, 1467 (1971); **17**, 441 (1972).
16. S. W. BENSON. Thermochemical kinetics, Wiley, New York. 1968.
17. H. E. O'NEAL and S. W. BENSON. Kinetic Data on Gas Phase Unimolecular Reactions, NSRDS-NBS-21, Washington, D.C. 1970.
18. J. R. MCNESBY. J. Am. Chem. Soc. **64**, 1671 (1960).
19. M. H. J. WIJNEN. J. Chem. Phys. **23**, 1357 (1955).
20. A. F. TROTMAN-DICKENSON, J. R. BIRCHARD, and E. W. R. STEACIE. J. Chem. Phys. **19**, 163 (1951).
21. L. M. QUICK, D. A. KNECHT, and M. H. BACK. Int. J. Chem. Kinet. **4**, 61 (1972).
22. P. C. STEHLING, J. D. FRAZEE, and R. C. ANDERSON. 8th Int. Symp. on Combust. Cal. Inst. Tech. 1960. p. 775.

Can. J. Chem. Downloaded from www.nrcresearchpress.com by 210.87.254.105 on 09/05/12
For personal use only.

Disubstituted derivatives of (L—L)$Fe_2(CO)_6$ (L—L = fluorocarbon bridged ligand)

LIAN SAI CHIA, WILLIAM R. CULLEN, JOHN R. SAMS, AND JAMES C. SCOTT
Chemistry Department, University of British Columbia, Vancouver, B.C., Canada V6T 1W5

Received April 20, 1976

LIAN SAI CHIA, WILLIAM R. CULLEN, JOHN R. SAMS, and JAMES C. SCOTT. Can. J. Chem. **54**, 3185 (1976).

The complexes (L—L)$Fe_2(CO)_6$ react with a range of bidentate ligands to give the complexes (L—L)′(L—L)$Fe_2(CO)_4$ ((L—L) = fluorocarbon-bridged ligand such as $f_4$fars, f_4AsP etc. (L—L)′ = fluorocarbon- and hydrocarbon-bridged ligands such as f_4AsP diars etc.). Spectroscopic studies, in particular magnetically perturbed Mössbauer measurements, indicate that (L—L)′ in most complexes is chelated to one iron atom, Fe^A. This leaves one CO group on Fe^A *cis* to the Fe^A—Fe^B bond and three on Fe^B. A smaller class of derivatives appear to have (L—L)′ bridging the two iron atoms *cis* to the Fe^A—Fe^B bond. The sign of V_{zz} is positive at both iron sites in the bridged derivatives. It is negative at Fe^A and positive at Fe^B in the other complexes.

LIAN SAI CHIA, WILLIAM R. CULLEN, JOHN R. SAMS et JAMES C. SCOTT. Can. J. Chem. **54**, 3185 (1976).

Les complexes (L—L)$Fe_2(CO)_6$ réagissent avec une variété de ligands bidentates pour donner des complexes (L—L)′(L—L)$Fe_2(CO)_4$ ((L—L) = ligands fluorocarbonés pontés tels que $f_4$fars, f_4AsP etc., (L—L)′ = ligands fluorocarbonés et hydrocarbonés pontés tels que f_4AsP, diars etc.). Des études spectroscopiques, en particulier des mesures Mössbauer, perturbées magnétiquements, indiquent que le ligand (L—L)′ dans la plupart des complexes est chélaté à un atome de fer, Fe^A. Ceci laisse un groupe CO sur le Fe^A *cis* au lien Fe^A—Fe^B et trois autres sur Fe^B. Une classe plus restreinte de dérivés semble avoir le ligand (L—L)′ reliant par un pont les deux atomes de fer *cis* au lien Fe^A—Fe^B. Le signe du V_{zz} est positif aux deux sites du fer dans les dérivés pontés. Il est négatif au Fe^A et positif au Fe^B dans les autres complexes.

[Traduit par le journal]

We have previously reported (1) that iron carbonyl complexes of the type $f_4$farsFe$_2$(CO)$_6$, **1**,[1]

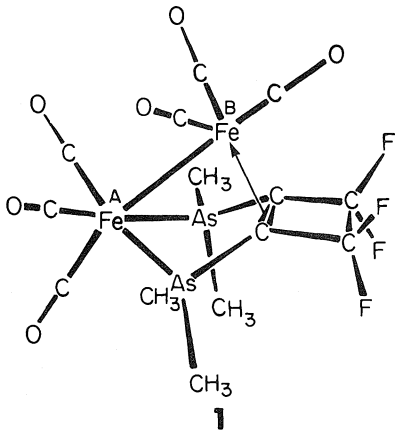

1

(2, 3) react with monodentate ligands and certain potentially bidentate ones affording monosubstituted derivatives of formula L(L—L)Fe$_2$(CO)$_5$ where the site of substitution is *trans* to the Fe^A—Fe^B bond and *cis* to the two group V atoms on Fe^A. Disubstitution by L seems to result in further displacement of CO from either Fe^A or Fe^B. The present investigation describes the reactions of (L—L)$Fe_2(CO)_6$ with a variety of bidentate ligands (L—L)′. The main product is (L—L)′(L—L)$Fe_2(CO)_4$ in which the ligand (L—L)′ is either chelating on Fe^A or bridging Fe^A and Fe^B. This investigation complements our studies on ligand substitution reactions of other derivatives of cobalt (4, 5) and iron carbonyls (6).

[1]See footnote* Table 1 for ligand abbreviations.

Experimental

All techniques and starting materials used in this investigation have been described previously (1).

Preparation of the Derivatives of (L—L)$Fe_2(CO)_6$

The general procedure was as follows, specific details are given in Table 1. The (L—L)$Fe_2(CO)_6$ complex (1.0 mmol), an equimolar amount of ligand (L—L)′, and acetone (15–20 ml) were sealed under vacuum in a Pyrex Carius tube and irradiated for several days with a 100 W ultraviolet lamp placed 10 cm away from the tube. The

Can. J. Chem. Downloaded from www.nrcresearchpress.com by 210.87.254.105 on 09/05/12
For personal use only.

Can. J. Chem. Downloaded from www.nrcresearchpress.com by 210.87.254.105 on 09/05/12
For personal use only.

TABLE 1. Analytical and preparative data for derivatives of $(L—L)Fe_2(CO)_6$*

Complex	Color†	Melting point (°C)	Reaction time (d)	Eluent‡	Yield (%)	Analyses(%) C Calcd.	C Found	H Calcd.	H Found	Molecular weight Calcd.	Molecular weight Found
$f_4AsP^cf_4AsPFe_2(CO)_4$	d.b.	190	7	C,D	25	45.7	45.9	3.2	3.5	1052	1040
$f_4fos^cf_4AsPFe_2(CO)_4$	d.b.	195	11	C,D	25	53.0	53.0	3.2	3.3	1132	1176
$f_6fars^cf_4AsPFe_2(CO)_4$	d.b.	190	11	C,D	22	36.4	36.3	2.8	2.7	1022	1051
$f_6AsP^cf_4AsPFe_2(CO)_4$	d.b.	215	8	C,D	18	44.6	44.2	2.9	2.8	1102	1085
$f_8fars^cf_4AsPFe_2(CO)_4$	d.b.	180	12.5	C,D	18	35.8	36.1	2.6	2.8		
$diars^cf_4AsPFe_2(CO)_4$	d.b.	213	10	C,D	15	41.6	41.4	3.1	3.3		
$dpam^bf_4AsPFe_2(CO)_4$	r.	160	10.5	B	26	50.8	51.3	3.5	3.9	1110	986
$dpae^bf_4AsPFe_2(CO)_4$	r.	155	31	B	12	49.1	50.8	3.6	3.6		
$arphos^bf_4AsPFe_2(CO)_4$	r.	161	31	B	10	53.3	52.7	3.7	4.1	1080	997
$dppp^bf_4AsPFe_2(CO)_4$	p.	172	10.5	B	20	56.0	55.7	4.0	4.3	1050	985
$f_4fars^bf_4AsPFe_2(CO)_4$	r.	190	20	B	15	37.0	37.2	2.9	2.9	972	998
$f_4AsP^bf_4AsPFe_2(CO)_4$	r.	205	4	B	8	45.6	45.6	3.2	3.2	1052	1101
$f_8fos^cf_4AsPFe_2(CO)_4$	d.b.	183	31	C,D	10	50.7	50.7	3.0	3.2	1232	1203
$dppm^cf_4AsPFe_2(CO)_4$	d.b.	215	16.5	C,D	15	55.2	55.2	3.8	4.2	1022	1068
$dpae^cf_4AsPFe_2(CO)_4$	d.b.	150	31	C,D	10	49.1	51.7	3.6	3.8		
$arphos^cf_4AsPFe_2(CO)_4$	d.b.	170	31	B,C	25	53.3	53.0	3.7	3.9	1080	1014
$dppe^cf_4AsPFe_2(CO)_4$	d.b.	150	7.5	C,D	50	55.6	56.4	3.9	4.3		
$f_6AsP^cf_6AsPFe_2(CO)_4$	d.b.	210	7	C,D	20	43.8	43.8	2.8	2.7	1152	1135
$f_4AsP^bf_6AsPFe_2(CO)_4$	r.	175	7	B	20	44.7	44.6	2.9	3.0	1102	1126
$f_4AsP^bf_4fosFe_2(CO)_4$	r.	220	7	B	30	53.0	53.0	3.2	3.2	1132	1102
$f_4fos^bf_4fosFe_2(CO)_4$	r.	215	20	B	10	59.4	59.0	3.3	3.4	1212	1124
$f_4AsP^cf_6farsFe_2(CO)_4$	d.b.	189	20	C,D	30	36.4	36.5	2.8	3.0	1022	978
$f_6fars^cf_6farsFe_2(CO)_4$	d.b.	200	8	B	10	26.6	26.2	2.4	2.5		
$f_4AsP^cf_8farsFe_2(CO)_4$	d.b.	171	9.5	B	15	35.8	35.8	2.6	2.8		
$f_8fars^cf_8farsFe_2(CO)_4$	d.b.	205	8.5	C,D	20	26.4	26.2	2.2	2.3	1092	1115
$diars^cf_4fosFe_2(CO)_4$	d.b.	194	10	C,D	40	50.2	50.6	3.6	3.9		

*In general a bidentate ligand (L—L)′ reacting with $(L—L)Fe_2(CO)_6$ gives monosubstituted $(L—L)'(L—L)Fe_2(CO)_5$ and disubstituted $(L—L)'(L—L)Fe_2(CO)_4$ derivatives. Only the latter class are described here. Details of the former have been given previously (1). The following abbreviations are used for the ligands (L—L): $f_n$fars = $(CH_3)_2AsC{=}CAs(CH_3)_2(CF_2)_{n/2}$; $f_n$fos = $(C_6H_5)_2PC{=}CP(C_6H_5)_2(CF_2)_{n/2}$; f_nAsP = $(C_6H_5)_2PC{=}CAs(CH_3)_2(CF_2)_{n/2}$; diars = 1,2-$[(CH_3)_2As]_2C_6H_4$; dpam = $[(C_6H_5)_2As]_2CH_2$; dpae = $[(C_6H_5)_2AsCH_2]_2$; dppm = $[(C_6H_3)_2P]_2CH_2$; dppe = $[(C_6H_5)_2PCH_2]_2$; dppp = $(C_6H_5)_2P(CH_2)_3P(C_6H_5)_2$; arphos = $(C_6H_5)_2PCH_2CH_2As(CH_3)_2$. $(L—L)^c$ is chelating on one Fe atom. $(L—L)^b$ bridges both Fe atoms. L is a monodentate ligand.

†d.b. = dark brown, r = red, p = purple.

‡Solvent key: A: 10–20% diethyl ether – 90–80% petroleum ether mixture; B: 20–50% diethyl ether – 80–50% petroleum ether mixture; C: CH_2Cl_2; D: acetone. The chromatographic column was eluted with the solvent in the following order: petroleum ether, A, B, C, and then D.

TABLE 2. Spectroscopic data for derivatives of $(L—L)Fe_2(CO)_6$ *

Complex	$\nu_{CO}(CH_2Cl_2)$ (cm^{-1})†				$\lambda_{max}(CH_2Cl_2)$ (nm) (ϵ_{molar})‡
diars^{c}f$_4$AsPFe$_2$(CO)$_4$	2002(10)	1942(8)		1902(7)	385(5267)
f$_4$AsP^{c}f$_4$AsPFe$_2$(CO)$_4$	2011(10)	1952(9)	1917(8)	1907(7)sh	403(8857)
f$_4$fos^{c}f$_4$AsPFe$_2$(CO)$_4$	2012(10)	1950(8)	1922(7)		412(8256)
f$_6$fars^{c}f$_4$AsPFe$_2$(CO)$_4$	2007(10)	1945(9)		1907(8)	392(9012)
f$_6$Asp^{c}f$_4$AsPFe$_2$(CO)$_4$	2011(10)	1951(7)		1906(6)	401(8816)
f$_8$fars^{c}f$_4$AsPFe$_2$(CO)$_4$	2010(10)	1950(9)		1907(7)	393(10205)
f$_8$fos^{c}f$_4$AsPFe$_2$(CO)$_4$	2012(10)	1951(9)		1908(6)	403(9486)
dppm^{c}f$_4$AsPFe$_2$(CO)$_4$	2004(10)	1942(9)		1904(8)	401(8657)
dpae^{c}f$_4$AsPFe$_2$(CO)$_4$	2004(10)	1939(8)	1913(7)		405(10116)
arphos^{c}f$_4$AsPFe$_2$(CO)$_4$	2004(10)	1939(9)	1916(8)		406(9144)
dppe^{c}f$_4$AsPFe$_2$(CO)$_4$	2007(10)	1944(9)	1921(8)		413(7675)
f$_6$AsP^{c}f$_6$AsPFe$_2$(CO)$_4$	2011(10)	1951(8)		1909(7)	393(8273)
f$_4$AsP^{c}f$_6$farsFe$_2$(CO)$_4$	2005(10)	1944(8)	1912(7)		403(10084)
f$_6$fars^{c}f$_6$farsFe$_2$(CO)$_4$	2006(10)	1945(9)	1910(8)		393(8432)
f$_4$AsP^{c}f$_8$farsFe$_2$(CO)$_4$	2002(10)	1945(9)	1912(8)		400(10124)
f$_8$fars^{c}f$_8$farsFe$_2$(CO)$_4$	2009(10)	1948(9)	1913(8)		392(8339)
diars^{c}f$_4$fosFe$_2$(CO)$_4$	2009(10)	1943(9)	1921(8)		372(5881)
f$_4$fars^{b}f$_4$AsPFe$_2$(CO)$_4$	1982(9)	1944(10)	1922(7)	1894(6)	431(5742)
f$_4$AsP^{b}f$_4$AsPFe$_2$(CO)$_4$	1988(9)	1947(10)	1922(6)	1901(5)	430(7013)
dpam^{b}f$_4$AsPFe$_2$(CO)$_4$	1983(8)	1946(10)	1918(4)	1898(3)	430(4052)
dpae^{b}f$_4$AsPFe$_2$(CO)$_4$	1981(9)	1939(10)	1915(6)	1890(4)	442(11662)
arphos^{b}f$_4$AsPFe$_2$(CO)$_4$	1982(9)	1944(10)	1918(7)	1902(6)	448(3279)
dppp^{b}f$_4$AsPFe$_2$(CO)$_4$	1982(9)	1932(10)	1914(6)	1870(3)	522(7070)
f$_4$AsP^{b}f$_6$AsPFe$_2$(CO)$_4$	1985(9)	1948(10)	1926(5)	1905(4)	416(8820)
f$_4$AsP^{b}f$_4$fosFe$_2$(CO)$_4$	1988(9)	1950(10)	1920(3)	1902(4)	406(1415)
f$_4$fos^{b}f$_4$fosFe$_2$(CO)$_4$	1994(9)	1954(10)	1928(6)	1910(8)	411(9532)
dppp^{b}f$_4$fosFe$_2$(CO)$_4$	1986(9)	1932(10)	1917(4,sh)	1881(3)	504(7985)

See footnote Table 1.
†Integers in parentheses refer to relative peak height.
‡ϵ_{molar} = molar extinction coefficient.

solute was isolated, dissolved in a small volume of dichloromethane, and chromatographed on Florisil as indicated in Table 1. Analytical and spectroscopic data for all new compounds are given in Tables 1 and 2.

Results and Discussion

Some potentially bidentate ligands react with $(L—L)Fe_2(CO)_6$ on ultraviolet irradiation to give complexes in which Fe^A is monosubstituted and the ligand has one 'dangling' end (1). The most common product, however, is that reported here. This is one in which two carbonyl groups have been displaced, the resulting complex having the formula $(L—L)'(L—L)Fe_2(CO)_4$, Table 1. The crystal structure of one such complex f$_4$AsP^{c}f$_4$AsPFe$_2$(CO)$_4$ has been determined (7) and the second ligand is chelated to Fe^A with the $(C_6H_5)_2P$ moiety *trans* to the $Fe^A—Fe^B$ bond.

The infrared spectra of the new complexes in the carbonyl region are listed in Table 2. The majority of the compounds have only three bands at ~2007, ~1946, and ~1912 cm^{-1}. In a few, including f$_4$AsP^{c}f$_4$AsPFe$_2$(CO)$_4$, the ~1912 cm^{-1} band is split into two at ~1919 and ~1907 cm^{-1}. Nevertheless the similarity of the spectra suggests that the second ligand is chelated to Fe^A as indicated in Fig. 1.

The ^{57}Fe Mössbauer spectra of these derivatives are quite distinctive, since for most of the complexes there are three component peaks with relative areas in the approximate ratio 1:1:2. A typical spectrum is illustrated in Fig. 1 for f$_4$AsP^{c}f$_6$farsFe$_2$(CO)$_4$. For some of the compounds the highest velocity line is broadened, and in one case [dppm^{c}f$_4$AsPFe$_2$(CO)$_4$] a clear, splitting of this line was resolved. There are two possible line assignments for spectra of this type, *viz.*: (*a*) lines 1 and 2 (reading from low to high velocity) to one iron atom and line 3 to the other, assuming line 3 to be a singlet or narrow doublet; (*b*) lines 1 and 3 to one iron atom and lines 2 and 3 to the other, if line 3 consists of two overlapping quadrupole-split components. As explained in detail elsewhere (8), magnetic-

Can. J. Chem. Downloaded from www.nrcresearchpress.com by 210.87.254.105 on 09/05/12
For personal use only.

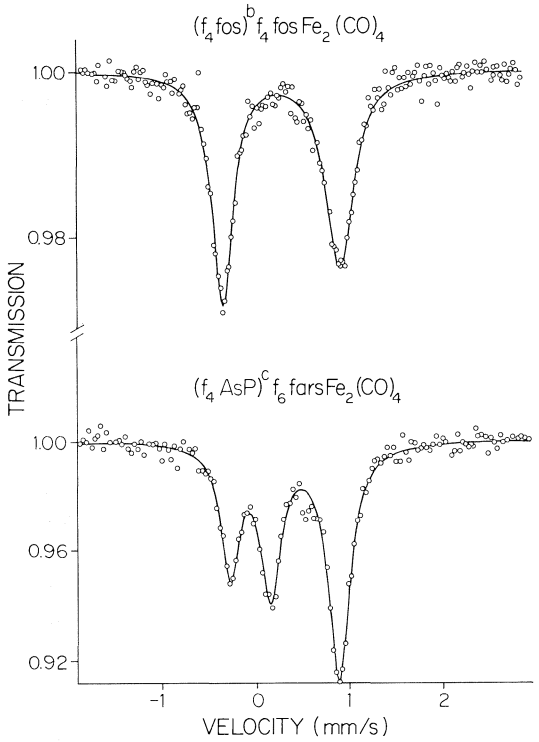

FIG. 1. ^{57}Fe Mössbauer spectra of $(f_4fos)^bf_4fosFe_2(CO)_4$ and $(f_4AsP)^cf_6farsFe_2(CO)_4$ at 80 K.

perturbation Mössbauer spectroscopy enables one to distinguish these two cases unambiguously, since the magnetically-split spectra will be very different in appearance. A spectrum of $f_4AsP^cf_4AsPFe_2(CO)_4$ recorded at 4.2 K in a longitudinal magnetic field of 50 kG showed that assignment (*a*) above could be rejected, and the Mössbauer parameters given in Table 3 have therefore been derived on the basis of assignment (*b*). This spectrum also showed that the sign of V_{zz}, the z component of the electric field gradient (efg), at the iron site giving the larger quadrupole splitting (site I) was positive, whilst that at the other iron site (II) was negative. Although it is difficult to obtain accurate estimates of the asymmetry parameters η from such spectra, best agreement between theoretically calculated spectra and the experimental one was achieved with $\eta = 0$ for site I. However, the computed spectra were quite insensitive to the η value assumed for site II and no reliable estimate of this parameter was obtained.

It remains to relate sites I and II specifically to the iron atoms Fe^A and Fe^B of Fig. 1. With our previous results for $(L—L)Fe_2(CO)_6$ (1, 2) and $L(L—L)Fe_2(CO)_5$ (1) complexes, this is a relatively easy task. Since in going from $(L—L)Fe_2(CO)_6$ to $(L—L)^c(L—L)Fe_2(CO)_4$ only the carbonyls on Fe^A are being replaced, we expect rather large changes in the Mössbauer parameters for this iron atom, particularly in the isomer shift, but only modest changes in isomer shift for Fe^B. The substitution of a carbonyl by a less effective π acceptor such as an arsine or phosphine invariably results in an increase in isomer shift, so it is clear that the larger isomer shift in the $(L—L)^c(L—L)Fe_2(CO)_4$ complexes must be attributed to Fe^A.

The quadrupole splittings for Fe^A in these compounds fall in the range $|\Delta E_Q| = 0.40$ to 0.67 mm/s, similar to values observed (1, 2) for this iron atom in $(L—L)Fe_2(CO)_6$ and $L(L—L)Fe_2(CO)_5$ derivatives, and the sign of V_{zz} at Fe^A is negative in all three types of complexes. It thus appears that there are no dramatic changes in the efg at Fe^A with substitution both *cis* and *trans* to the $Fe^A—Fe^B$ bond. The isomer shifts of Fe^A in the $(L—L)^c(L—L)Fe_2(CO)_4$ compounds span the rather narrow range $\delta =$ 0.46 to 0.53 mm/s, and are thus about 0.10 to 0.15 mm/s larger than those for the corresponding iron atom in $L(L—L)Fe_2(CO)_5$ derivatives. The insensitivity of δ to the nature of the chelating ligand is rather surprising since in most cases arsines give rise to larger isomer shifts than do phosphines. It seems likely that the large increase in δ on replacement of the penultimate carbonyl when going from $L(L—L)Fe_2(CO)_5$ to $(L—L)^c(L—L)Fe_2(CO)_4$ masks the more subtle differences in σ and π bonding characteristics of the ligands.

The isomer shifts at Fe^B in the $(L—L)^c(L—L)$-$Fe_2(CO)_4$ class of compounds are in general very similar to those observed previously (1, 2) for this iron atom in $(L—L)Fe_2(CO)_6$ and $L(L—L)$-$Fe_2(CO)_5$ complexes, showing that in every case substitution occurs only at Fe^A. On the other hand the Fe^B quadrupole splittings, which for the present compounds span the range $|\Delta E_Q| =$ 0.80 to 1.15 mm/s, are strongly lowered compared to the values found for the penta- and hexacarbonyl complexes.

Some of the red complexes $(L—L)'(L—L)Fe_2$-$(CO)_4$ have very different infrared spectra from the class described above. The ν(CO) bands are at $\sim$1985, $\sim$1947, $\sim$1921, and $\sim$1900 cm^{-1}.

Can. J. Chem. Downloaded from www.nrcresearchpress.com by 210.87.254.105 on 09/05/12
For personal use only.

TABLE 3. Mössbauer parameters at 80 K for (L—L)^c(L—L)$Fe_2(CO)_4$ complexes

(L—L)^c(L—L)*	δ (mm/s)†	ΔE_Q (mm/s)	Γ (mm/s)‡	Iron atom
(f_4AsP)^c(f_4AsP)§	0.50±0.01	−0.61±0.02	0.29, 0.30	*A*
	0.28±0.01	+1.05±0.02	0.30, 0.30	*B*
(f_6AsP)^c(f_4AsP)	0.49±0.01	0.67±0.01	0.27, 0.27	*A*
	0.29±0.01	1.07±0.01	0.27, 0.27	*B*
(f_6AsP)^c(f_6AsP)	0.47±0.01	0.59±0.01	0.27, 0.28	*A*
	0.29±0.01	0.96±0.01	0.23, 0.28	*B*
(f_4AsP)^c($f_6$fars)	0.52±0.02	0.73±0.02	0.26, 0.29	*A*
	0.30±0.02	1.15±0.02	0.24, 0.29	*B*
(f_4AsP)^c($f_8$fars)	0.46±0.02	0.64±0.02	0.24, 0.26	*A*
	0.30±0.02	1.01±0.02	0.23, 0.26	*B*
($f_6$fars)^c(f_4AsP)	0.53±0.02	0.40±0.03	0.26, 0.36	*A*
	0.27±0.02	0.91±0.03	0.31, 0.36	*B*
($f_8$fars)^c($f_8$fars)	0.49±0.02	0.65±0.02	0.22, 0.28	*A*
	0.32±0.02	0.99±0.02	0.25, 0.28	*B*
(diars)^c(f_4AsP)	0.50±0.02	0.45±0.02	0.32, 0.32	*A*
	0.28±0.02	0.86±0.02	0.29, 0.32	*B*
(dppm)^c(f_4AsP)	0.53±0.01	0.51±0.02	0.22, 0.22	*A*
	0.24±0.01	0.80±0.02	0.25, 0.30	*B*
(diphos)^c(f_4AsP)	0.51±0.03	0.59±0.04	0.36, 0.46	*A*
	0.27±0.03	1.08±0.04	0.34, 0.46	*B*
($f_8$fos)^c(f_4AsP)	0.49±0.02	0.64±0.02	0.27, 0.32	*A*
	0.28±0.02	1.06±0.02	0.24, 0.32	*B*
($f_4$fos)^c(f_4AsP)	0.49±0.02	0.62±0.03	0.24, 0.36	*A*
	0.25±0.02	1.10±0.03	0.26, 0.36	*B*

See footnote, Table 1.
†Isomer shifts are relative to sodium nitroprusside; subtract 0.27 mm/s to convert to iron foil standard.
‡Experimental undertainty ±0.02 mm/s.
§Signs of ΔE_Q determined with source and absorber at 4.2 K.

The highest ν(CO) band in the (L—L)$Fe_2(CO)_6$ parent molecules has been assigned to the CO groups on Fe^B (1). It seems that monosubstitution on Fe^A lowers $\nu(CO)_{max}$ by ~25 cm^{-1} and that chelation on Fe^A lowers it by ~54 cm^{-1}. The bands at ~1985 cm^{-1} in this new class of complexes are due to a lowering of ~74 cm^{-1} in $\nu(CO)_{max}$. This suggests that at least one CO group on Fe^B has been replaced by a group V donor.

The Mössbauer spectra of this class of complexes are also very different from those of the (L—L)^c(L—L)$Fe_2(CO)_4$ complexes. Most of the spectra consisted of two broadened lines (see Fig. 1) although in some cases three or four lines could be resolved. Details of the line assignments leading to the parameter values given in Table 4 will be discussed below.

Possible modes of ligation of the (L—L)′ moiety in these new complexes are intermolecular bridging, intramolecular bridging between Fe^A and Fe^B, or chelation at either Fe^A or Fe^B. Chelation at Fe^A would have to be at the two positions *cis* to the Fe—Fe bond since the other possible structure is adopted by (L—L)^c(L—L)-$Fe_2(CO)_4$ complexes. However, the isomer shift of Fe^A would still be expected to be about 0.50 mm/s, much larger than the values observed. For a similar reason chelation at Fe^B can also be ruled out. Although a dimeric structure involving intermolecular bridging of two (L—L)$Fe_2(CO)_4$ moieties is not inconsistent with the Mössbauer data, molecular weight determinations in dichloromethane indicate monomeric structures. The carbonyl infrared spectrum of (Ph_3As)$_2f_4$AsP$Fe_2(CO)_4$ (1) is very similar to those of the present (L—L)′(L—L)$Fe_2(CO)_4$ complexes, which tends to substantiate the absence of intermolecular bridging in the latter.

Thus, the most likely structures for these com-

Can. J. Chem. Downloaded from www.nrcresearchpress.com by 210.87.254.105 on 09/05/12
For personal use only.

TABLE 4. Mössbauer parameters at 80 K for (L—L)^b(L—L)$Fe_2(CO)_4$ complexes

(L—L)^b(L—L)*	δ (mm/s)†	ΔE_Q (mm/s)	Γ (mm/s)‡	Iron atom
(f_4AsP)^b(f_4AsP)§	0.30 ± 0.01	+1.26 ± 0.02	0.28, 0.29	*A*
	0.41 ± 0.01	+1.48 ± 0.02	0.28, 0.26	*B*
(f_4AsP)^b(f_6AsP)	0.35 ± 0.03	1.30 ± 0.04	0.34, 0.44	*A*
	0.35 ± 0.03	1.30 ± 0.04	0.34, 0.44	*B*
(f_4AsP)^b($f_4$fos)	0.32 ± 0.02	1.35 ± 0.03	0.29, 0.30	*A*
	0.39 ± 0.02	1.48 ± 0.03	0.29, 0.26	*B*
(dppp)^b(f_4AsP)	0.31 ± 0.01	1.28 ± 0.02	0.25, 0.25	*A*
	0.39 ± 0.01	1.84 ± 0.02	0.23, 0.24	*B*
(arphos)^b(f_4AsP)	0.30 ± 0.01	1.18 ± 0.02	0.24, 0.26	*A*
	0.43 ± 0.01	1.43 ± 0.02	0.24, 0.23	*B*
(dpam)^b(f_4AsP)	0.38 ± 0.04	1.22 ± 0.07	0.39, 0.33	*A*
	0.38 ± 0.04	1.22 ± 0.07	0.39, 0.33	*B*
($f_4$fars)^b(f_4AsP)	0.38 ± 0.02	1.09 ± 0.03	0.28, 0.31	*A*
	0.38 ± 0.02	1.09 ± 0.03	0.28, 0.31	*B*
(dppp)^b($f_4$fos)	0.29 ± 0.01	1.54 ± 0.02	0.25, 0.25	*A*
	0.42 ± 0.01	1.80 ± 0.02	0.25, 0.23	*B*
($f_4$fos)^b($f_4$fos)§	0.30 ± 0.01	+1.26 ± 0.02	0.26, 0.29	*A*
	0.38 ± 0.01	+1.35 ± 0.02	0.26, 0.29	*B*
($f_4$fos)^b($f_4$fos)‖	0.34 ± 0.03	1.31 ± 0.05	0.29, 0.38	*A*
	0.34 ± 0.03	1.31 ± 0.05	0.29, 0.38	*B*

See footnote, Table 1.
†Isomer shifts are relative to sodium nitroprusside; subtract 0.27 mm/s to convert to iron foil standard.
‡Experimental uncertainty ±0.02 mm/s.
§Signs of ΔE_Q determined with source and absorber at 4.2 K.
‖Fitted assuming equivalence of the two iron atoms. Standard deviation was 15% higher than for the two-site fit.

pounds are the ones in which the (L—L)′ ligand is bridging Fe^A and Fe^B intramolecularly. From molecular models constructed using the known bond angles and bond lengths of $f_4$fars$Fe_2(CO)_6$ (3) and f_4AsP$^c f_4$AsP$Fe_2(CO)_4$ (7) it is clear that there is no possibility of bridging from either apical (*i.e.*, *trans* to the Fe—Fe bond) position to any equatorial (*i.e.*, *cis* to the Fe—Fe bond) position on the other iron atom, nor from one apical position to another, as the distances to be spanned are too great. Thus, there remain only four possible bridging structures, those between the various equatorial positions, *viz.*: (*a*) 1–1′, (*b*) 2–2′, (*c*) 1–2′, (*d*) 2–1′. The latter two are less likely but cannot be discounted with certainty, and indirect methods cannot distinguish amongst these possible structures.

In those cases where only two lines could be resolved in the Mössbauer spectra there was usually considerable broadening of one or both lines, so that the δ and $|\Delta E_Q|$ values for the two iron atoms must be slightly different. The parameter values given in Table 4 therefore have correspondingly larger error limits for these complexes. Where three or four lines were resolved there was a choice as to which lines should be assigned to which iron atom. The assignments given were based on two facts which have been well established in our previous work on (L—L)$Fe_2(CO)_6$ and (L)(L—L)$Fe_2(CO)_5$ complexes (1, 2) and the data above for the (L—L)^c(L—L)$Fe_2(CO)_4$ compounds: (*a*) substitution of CO by a group V donor atom always increases the isomer shift of the substituted iron atom; (*b*) the increase in δ is larger for replacement of CO by an arsine than that for replacement of CO by a phosphine. Full details of the assignments may be found elsewhere (9). In the cases where (L—L)^b is a mixed ligand such as arphos or f_4AsP, these considerations also lead to the conclusion that the phosphorus atom is bonded to Fe^A and the arsenic atom to Fe^B.

Two of these derivatives, namely ($f_4$fos)^b-($f_4$fos)$Fe_2(CO)_4$ and (f_4AsP)^b(f_4AsP)$Fe_2(CO)_4$, were studied by magnetic-perturbation Mössbauer spectroscopy, and the spectrum of the

Can. J. Chem. Downloaded from www.nrcresearchpress.com by 210.87.254.105 on 09/05/12
For personal use only.

Can. J. Chem. Downloaded from www.nrcresearchpress.com by 210.87.254.105 on 09/05/12
For personal use only.

former complex at 4.2 K in a longitudinal magnetic field of 50 kG is shown in Fig. 2. In both cases V_{zz} was found to be positive at *both* iron sites, so that in going from (L—L)$Fe_2(CO)_6$ to (L—L)^b(L—L)$Fe_2(CO)_4$ there is a sign reversal in the quadrupole coupling constant for Fe^A. The magnitude of ΔE_Q is also substantially larger than in any of the other binuclear complexes we have studied (1, 2 and Table 3). These large changes in the efg at Fe^A are presumably due in part to the fact that substitution occurs *cis* to the Fe—Fe bond and there is no substitution *trans* to this bond. It should also be noted that ΔE_Q for Fe^B shows much more variation in magnitude than it does in related complexes (1, 2), a fact which is consistent with substitution at this iron atom.

Although the computed spectrum in Fig. 2 does not fit the experimental one particularly well, we should point out that attempts to fit the spectrum assuming only one iron site required unrealistic values for the linewidths ($\Gamma \gtrsim 0.4$ mm/s). Even so, agreement between theoretical and experimental spectra was less good (based on visual inspection) than the two-site fit shown.

The electronic spectra of all the derivatives have a strong band in the visible region. This is present in the parent (L—L)$Fe_2(CO)_6$ complexes and has been tentatively assigned (1) to a σ–σ^* transition involving the Fe—Fe bond. If this assignment is extended to the present complexes, the Fe—Fe bond strength apparently decreases as the degree of substitution increases in the order:

(L—L)$Fe_2(CO)_6$ > L(L—L)$Fe_2(CO)_5$ > (L—L)^c(L—L)$Fe_2(CO)_4$ ~ $L_2{}^A$(L—L)$Fe_2(CO)_4$ [2] > (L—L)^b(L—L)$Fe_2(CO)_4$ ~ $L_2{}^{AB}$(L—L)$Fe_2(CO)_4$ [2] > L_3(L—L)$Fe_2(CO)_3$

This is not unreasonable in view of the electronic and steric effects resulting from substitution.

The only anomalous complex is the supposed (dppp)^b(f_4AsP)$Fe_2(CO)_4$ which is purple and which has a typical infrared and visible spectra. This is also the only complex of the (L—L)^b-(L—L)$Fe_2(CO)_4$ class for which all four component lines could be resolved in the Mössbauer spectrum, and shows the largest difference in ΔE_Q values for the two sites.

[2]The complex contains the ligands L both on Fe^A ($L_2{}^A$) or one on Fe^A and Fe^B ($L_2{}^{AB}$).

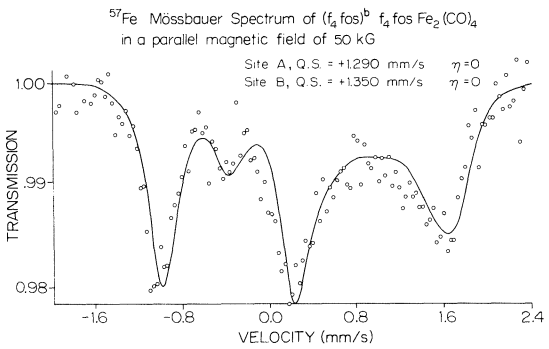

FIG. 2. Magnetically perturbed ^{57}Fe Mössbauer spectrum of ($f_4$fos)$^b f_4$fos$Fe_2(CO)_4$.

It has previously been noted that fluorocarbon-bridged ligands such as $f_4$fos have the ability to act either as chelating or bridging ligands. This gives rise to isomers of compounds such as ($f_4$fos)$_2Co_2(CO)_4$ (5) and $f_4$fos$Fe_2(SCH_3)_2(CO)_4$ (6). The present complexes afford further examples of this type of isomerism. Thus the compounds $f_4AsP^bf_4AsPFe_2(CO)_4$ and $f_4AsP^cf_4As$-$PFe_2(CO)_4$ have been isolated. An extension is seen in the pair of compounds $f_4AsP^bf_4fosFe_2$-$(CO)_4$ and $f_4fos^cf_4AsPFe_2(CO)_4$.

Acknowledgments

The authors are grateful to the National Research Council of Canada for financial support of this work. One of us (L.S.C.) wishes to thank the International Nickel Company of Canada for a Fellowship.

1. L. S. CHIA, W. R. CULLEN, J. R. SAMS, and J. C. SCOTT. Can. J. Chem. **53**, 2232 (1975).
2. W. R. CULLEN, D. A. HARBOURNE, B. V. LIENGME, and J. R. SAMS. Inorg. Chem. **8**, 95 (1969).
3. F. W. B. EINSTEIN and J. TROTTER. J. Chem. Soc. A, 824 (1967).
4. L. S. CHIA, W. R. CULLEN, M. FRANKLIN, and A. R. MANNING. Inorg. Chem. **14**, 2975 (1975).
5. L. S. CHIA and W. R. CULLEN. Inorg. Chem. **14**, 482 (1975).
6. J. P. CROW and W. R. CULLEN. Can. J. Chem. **49**, 2948 (1971).
7. F. W. B. EINSTEIN and R. D. G. JONES. Inorg. Chem. **12**, 255 (1973).
8. J. R. SAMS and J. C. SCOTT. J. Chem. Soc. Dalton Trans. 2265 (1974).
9. J. C. SCOTT. Ph.D. Thesis, University of British Columbia, Vancouver, B.C., Canada. 1973.

Kinetic and spectrophotometric studies of binding of iron(III) by glutathione[1]

TAHIR R. KHAN AND COOPER H. LANGFORD[2]
Department of Chemistry, Carleton University, Ottawa, Ont., Canada K1S 5B6

Received February 12, 1976

TAHIR R. KHAN and COOPER H. LANGFORD. Can. J. Chem. **54**, 3192 (1976).

In this report, determination of unbound aquo iron species is accomplished by a *kinetic method* involving reaction with sulfosalicylic acid (SSA) on a time scale which is very short with respect to reaction of SSA with the glutathione complexes of iron. The data are used to calculate conditional binding constants for Fe(III) to glutathione. Binding constants in 0.1 *M* ionic strength media were obtained between p*H* 1 and 2.4 by the kinetic method, and near p*H* = 3 by spectrophotometry *and* by examination of the ratio of rate of complex formation and dissociation. The conditional binding 'constant' *between* p*H* 1 and 3 is represented as $pK = -1.96 - 0.50pH$. This is consistent with the importance of reactions involving only very limited proton release. Spectrophotometric data show that the —OH group on $Fe(OH)^{2+}$ is lost on glutathione complexing. Kinetics of the complex formation reaction between aquo iron(III) species and glutathione are slower than rates of reaction of iron(III) with simple ligands.

The glutathione system is regarded as a model system important to natural water chemistry because it is a widely distributed biological sulfur-containing chelating agent.

TAHIR R. KHAN et COOPER H. LANGFORD. Can. J. Chem. **54**, 3192 (1976).

Dans ce travail, on rapporte la détermination des espèces aquo-ferriques non liées par *une méthode cinétique* impliquant la réaction de l'acide sulfosalicylique (SSA) à une échelle de temps qui est très courte par rapport à la réaction du SSA avec les complexes du glutathion avec le fer. On utilise ces données pour calculer les constantes de liaisons conditionnelles du Fe(III) avec le glutathion. On a obtenu ces constantes de liaison à une force ionique de 0.1 *M*, à des p*H* allant de 1 à 2.4 par la méthode cinétique et près de 3 par spectrophotométrie *et* par un examen des rapports des vitesses de formation et de dissociation des complexes. La constante de liaison conditionnelle *entre* des valeurs du p*H* 1 et 3 est représentée par $pK = -1.96 - 0.50pH$. Ceci est en accord avec l'importance des réactions impliquant un dégagement très faible de protons. Des données spectrophotométriques démontrent que le groupe OH du $Fe(OH)^{2+}$ est perdu lors de la complexation avec du glutathion. La cinétique de la réaction de formation du complexe entre les espèces aquo-ferriques et le glutathion sont plus faibles que les vitesses de réaction du fer(III) avec des ligands simples.

On considère que le système de glutathion est un système modèle important pour la chimie de l'eau naturelle parce que c'est un agent biologique chélatant contenant du soufre qui est distribué très largement.

[Traduit par le journal]

Introduction

Interest in kinetic methods of analysis using stopped flow spectrometers has developed recently (1–3). It is useful for identification of individual components of mixtures where components can react to give an easily detectable common product such that differential *rates* of reaction to that common product allow for distinction among components. In particular, the present report illustrates the use of kinetic analysis to study the position of equilibrium in an equilibrium mixture where *one component* of the equilibrated mixture reacts with a reagent giving an easily detectable product *faster* than the equilibration can respond to the perturbation. Our subject is the equilibrium between aquo-Fe(III) species and the widely distributed biological sulfur containing ligand system, glutathione. In the p*H* range from 1 to 3, the dissociation of glutathione from its complex with Fe(III) is relatively slow, as is the direct reaction of that complex with sulfosalicylic acid (SSA). Thus, it is possible to measure the uncomplexed aquo-Fe(III) species, $Fe(OH_2)_6^{3+}$ and $Fe(OH_2)_5OH^{2+}$, kinetically by their reaction with SSA before reaction occurs with iron glutathione.

[1]We acknowledge, with thanks, a research agreement with the Inland Waters Directorate, Environment Canada.

[2]Author to whom inquiries should be addressed.

Can. J. Chem. Downloaded from www.nrcresearchpress.com by 210.87.254.6 on 09/05/12
For personal use only.

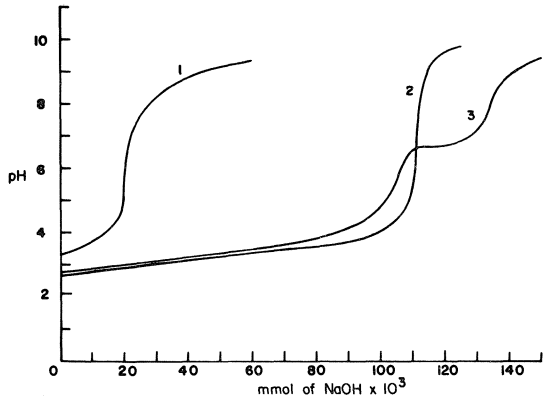

FIG. 1. Potentiometric titration of glutathione (20×10^{-3} mmol) curve *1*, Fe(III) (20×10^{-3} mmol) curve *2* and Fe–glutathione complex 1:1 (20×10^{-3} mmol) curve *3* against standard NaOH. $pK_{GSH} = 3.7$.

The kinetic method is especially useful for study of the iron(III)–glutathione system because of several special difficulties encountered by more conventional methods and the present study serves as a convenient method of comparison. The difficulties are as follows: potentiometric p*H* titration is of limited use because of the high acidity of $Fe(OH_2)_6^{3+}$ (see Fig. 1); direct spectrophotometry is of limited utility because *the only* large difference in spectra between free and complexed species is in the region of the hydroxyl to metal charge transfer transition of $Fe(OH_2)_5OH^{2+}$ which is not useful when $Fe(OH_2)_6^{3+}$ is the dominant species (*i.e.* spectrophotometry is useful only near p*H* = 3). It should be noted immediately that above p*H* = 3, precipitation is a problem.

The application of kinetic analysis must be distinguished from establishing an equilibrium *competition* between glutathione and SSA for Fe(III). In that case, the equilibrium between Fe(III) and SSA must be accurately known. In the present case, it is *only* necessary to establish *phenomenological* rate constants for reaction of SSA with Fe(III) in *each medium*. The treatment is developed according to the approach of Wills *et al.* (1). For two Fe(III) species reacting with SSA to form the strong red colour (λ_{max} 500 nm) the observed absorbance as a function of time, *P*, is written:

$$[1] \qquad P = A(1 - e^{-k_1 t}) + B(1 - e^{-k_2 t}) + X$$

where *A* and *B* are the initial concentrations of two components, k_1 and k_2 are the rate constants for the respective components, *t* is time, and *X* is a time independent term including background and any fast reacting component that has formed the product within mixing time. If, as in the present case, k_2 is small compared to k_1, [1] simplifies to the form:

$$[2] \qquad P = A(1 - e^{-k_1 t}) + X$$

where *A* is the desired concentration of aquo Fe(III) species and *X* is a small term indicative of fitting error (always $<1\%$). Our data, involving 200 to 500 points for *P* as a function of *t*, are fitted by a least-squares procedure to [2] with k_1 known from studies of Fe(III) in the absence of glutathione. The negligible values for *X* confirm the success of the fit. Note, especially, that *all* points (and *not* a somewhat arbitrarily chosen infinity for a system which is experiencing a slow reaction between the iron glutathione complex and SSA) contribute to fixing *A*. This is an advantage of the kinetic procedure.

Experimental

Stock solutions of Fe(III) were prepared by dissolving an accurately weighed amount of A.R. grade metal in minimum 1:15 nitric acid, evaporating excess acid without drying, then diluting to required volume. The solution was stored in aluminium foil wrapped flasks in the dark and care was taken to avoid exposure to light. Stock sulfosalicylic acid solutions were prepared by weighing accurately recrystallized Baker analysed material. Stock glutathione (GSH) solution was prepared by weighing directly glutathione (GSH) supplied by Aldrich Chemical Company. Standardized perchloric acid and sodium hydroxide were used to adjust the p*H* of working solutions whose Fe^{3+} concentration varied from 10^{-4} to 10^{-5} *M*. p*H* control is quite precise in consequence of the use of stoichiometric quantities of excess strong acid, not adjustment to 'meter' values. Finally, all working solutions were adjusted to an ionic strength of 0.100 with $NaClO_4$.

The kinetic data were obtained using a Durrum–Gibson stopped flow spectrophotometer interfaced to a PDP-11/10 computer using an AR-11 10 bit analog to digital converter. In earlier runs at p*H* above 2, the instrument output was stored with a Biomation 610 six bit digital storage device. Such spectra as were needed were recorded on a Cary 14 recording spectrophotometer. p*H* values (stoichiometrically fixed) were checked with a Beckman Expandomatic meter. Kinetic measurements, and all others where *T* is critical, were made at 25.0 °C. The p*H* range covered in present work ranges from 1.0 to 3.0. p*H* values of final solutions (Fe^{3+} or Fe–GSH solution mixed with SSA) were kept *constant* by maintaining hydrogen ion concentration in the SSA solution roughly *hundred fold excess* over iron. To ensure simple kinetics first order in Fe(III), SSA was always also in 100 fold excess.

Can. J. Chem. Downloaded from www.nrcresearchpress.com by 210.87.254.6 on 09/05/12
For personal use only.

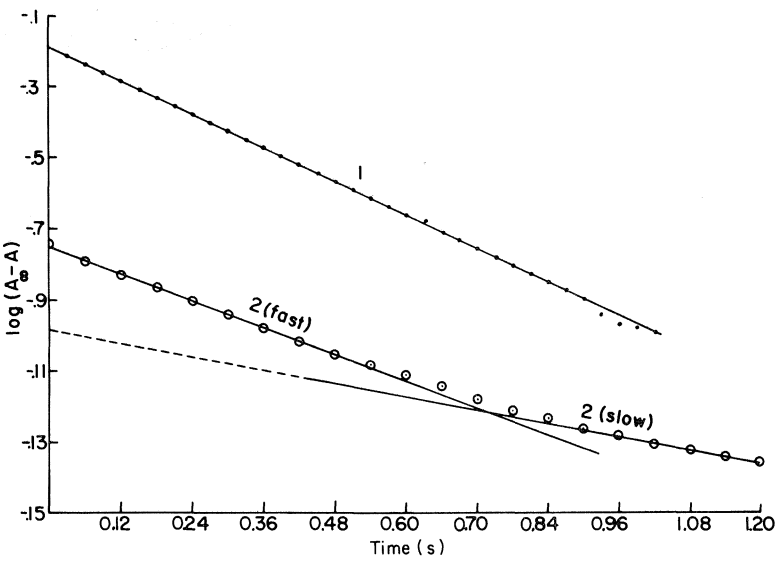

FIG. 2. Pseudo first-order plot for Fe and SSA, showing two components at pH above 2.4. Curve *1*, pH = 2.4; curve *2*, pH = 3.0.

In the present investigations, a quantitative appraisal of precision is very difficult. One of the two components in the analyte mixture is measured and the other is estimated by difference. Wills *et al.* (1) have made error analyses of the kinetic method using similar instruments and have shown an error function sensitive to rate constants. For this reason, an aquo iron reference was prepared for each Fe–GSH solution in a set of measurements at a given pH and rate constants were estimated for these references in conjunction with the corresponding analytes. The uncertainty in our rate constants leads to an error in free iron determination of the order of 4%, which multiplies by a factor of 5 in calculated values of equilibrium constants if it is assumed that no other errors arise in the presence of GSH. Equilibrium constants are therefore given to two significant figures.

The Fe concentrations were chosen to allow convenient kinetic determination. Larger values would lead to large infinity time absorbance in our instrument. Sensitivity is poor for smaller values. The GSH concentrations were limited to 1:1 ratios to Fe(III) at higher pH's to avoid higher complex formation.

Results

(a) Kinetic Evaluation of Binding

A basic requirement for the kinetic method is to establish characteristic rate constants for each component to be analysed. Pseudo first-order plots on references were constructed parallel to each analyte solution and analysed carefully covering the entire pH and concentration range. Representative plots of Fe(III) reference solutions appear in Fig. 2. Curve *1* in that figure indicates the precision of fit. Curve *2* shows that two components with similar rate constants may be easily resolved. But, in doing so, it also shows that a second component appears in Fe(III) solutions near pH = 3. Only one kinetically distinguishable Fe^{3+} species is present in solutions up to at least pH = 2.4. The complexity in kinetic plots might be attributed to the two species $Fe(OH_2)_6^{3+}$ and $Fe(OH_2)_5OH^{2+}$, but this is not possible since the transfer of a proton attached to oxygen in a solution buffered at an acidic pH will occur much too rapidly for these species to depart from an equilibrium distribution on the stopped flow time scale. The slower component is more likely a 'polymeric' species preceding the onset of hydrolytic precipitation. If so, this presents a very interesting problem in its own right. Kinetic study of species involved in hydrolytic polymerization is now under investigation in this laboratory. Kinetic analysis with SSA is used here up to pH = 2.4, but not beyond.

We now turn to a difficult feature of this presentation. If *both* aquo-Fe(III) (free) and Fe–GSH reacted on the stopped flow time scale with SSA in acid, we could clearly establish which species was responsible for which component in the kinetics. However, in the present case, where one component of the equilibrium mixture, namely Fe–GSH, appears to react with

Can. J. Chem. Downloaded from www.nrcresearchpress.com by 210.87.254.6 on 09/05/12
For personal use only.

TABLE 1. Tests of the assumption that only free Fe is kinetically important*

Reference			Fe–GSH solution		
Fe ($\times 10^4$ M)	Fitting error ($\times 10^6$ M)	k (s^{-1})	Fitting error ($\times 10^6$ M)	k (s^{-1})	Free Fe ($\times 10^4$ M)
2.19	0.5	1.21	1.8	1.21	1.71
1.93	0.4	1.14	1.2	1.13	1.55
1.67	0.4	1.09	1.1	1.08	1.37
1.40	0.2	1.03	0.1	1.05	1.17
1.14	0.2	0.96	0.0	0.98	0.98
0.88	0.1	0.86	0.1	0.90	0.77

*The reference solutions are Fe(III) solutions with no GSH added. The fitting error is defined by [2], and concentrations are estimated using [2]. The rate constants are separately obtained for reference solutions and *in this case* for Fe–GSH solutions from conventional log $(A - A_\infty)$ *vs.* t plots; pH = 1.00.

SSA only slowly, we face a difficult problem. Can we show that, indeed, *only* aquo-Fe(III) is reacting? There is the troublesome possibility that Fe–GSH also reacts, but at nearly the same rate as free iron. This unlikely and unhappy possibility may be ruled out only by a moderately elaborate demonstration depending on four successive points of successively increasingly compelling and convincing character. The four points are:

(*1*) If Fe–GSH reacts at a similar but slightly different rate with SSA than aquo-Fe(III), the fitting error parameter, X, in [2] would be larger in runs on the equilibrium mixtures of aquo-Fe(III) and Fe–GSH than in the calibration runs on aquo-Fe(III). This is not observed. This effect would *certainly* appear if rate constants differed by 50%. It would probably be resolvable for even smaller differences.

(*2*) Runs were carried out with excess GSH (10:1) for Fe(III) concentrations of 2.02×10^{-4} M at pH = 2.2, 2.4, and 2.7. In this case there was no reaction with SSA on the stopped flow time scale. Slow formation of FeSSA occurred on a time scale of hours with non-simple kinetics. This may involve higher complexes (*e.g.* $Fe(GSH)_2$), but it is clear that any remaining Fe–GSH does not react fast.

(*3*) For selected runs on equilibrium mixtures of aquo-Fe(III) and Fe–GSH, kinetic data were analyzed to give the rate constant best fitting the data without imposing a rate constant from calibration runs. As shown in Table 1, *such rate constants are in excellent agreement* with those from the calibration runs done in the absence of GSH.

(*4*) At pH = 3, it is possible to obtain a binding constant for GSH with Fe(III) by *entirely independent methods*, conventional spectrophotometry and the forward and reverse rates of the complex formation reaction between Fe(III) and GSH. As noted below, the independent value is entirely consistent with those obtained by the kinetic technique.

The length of the above four points may represent an operational definition of 'to labour the obvious', but it is important to be clear that not only intuitive plausibility but also the indications in points (*1*) and (*2*) and the confirmation in points (*3*) and (*4*) all conspire to establish that Fe–GSH reacts quite slowly with SSA in acid.

With these background results in hand, the data on binding may be presented. The *raw* experimental form of that data is *values of free* (unbound) *Fe(III) concentration* since this is the kinetically active component. Table 2 collects data for free Fe(III) as a function of the total Fe(III) introduced for conditions consistent with the limits mentioned at the end of the experimental section and covering all pH values examined. Calculated Fe(III) bound and GSH values are included. Table 2 and Fig. 3 show the best values estimated for the 'observed' constant defined by [3] as a function of pH.

$$[3] \qquad K_{obs} = \frac{[FeGSH]}{[Fe(III)]\,[GSH]}$$

Note that 'free' concentrations in [3] do not distinguish between $Fe(OH_2)_6^{3+}$ and $Fe(OH_2)_5OH^{2+}$ nor among GSH_2^+, GSH, or GS^-. All five of these are of significance in the pH range under study.

(b) Spectrophotometric Evaluation of Binding

The spectra of solutions with fixed Fe(III) and varying GSH concentrations at pH 3 gave a

Can. J. Chem. Downloaded from www.nrcresearchpress.com by 210.87.254.6 on 09/05/12
For personal use only.

Can. J. Chem. Downloaded from www.nrcresearchpress.com by 210.87.254.6 on 09/05/12
For personal use only.

TABLE 2. Results of kinetic analysis of Fe–GSH solutions

pH	Total Fe ($\times 10^4$ M)	Total GSH ($\times 10^4$ M)	Free Fe ($\times 10^4$ M)	Bound Fe ($\times 10^4$ M)
1.00	2.19	11.31	1.71	0.48
	1.93	9.77	1.55	0.38
	1.57	8.22	1.37	0.30
	1.40	6.68	1.17	0.23
	1.14	5.14	0.98	0.16
	0.88	3.60	0.77	0.11
		$K_{obs} = 285 \pm 19$ (pH = 1)		
1.50	2.11	6.34	1.64	0.47
	1.58	4.75	1.26	0.32
	1.05	3.17	0.92	0.13
	0.70	2.11	0.62	0.08
	0.35	1.06	0.31	0.04
*	0.18	0.53	0.17	0.01
		$K_{obs} = 546 \pm 60$ (pH = 1.5)		
2.03	2.00	2.20	1.81	0.19
	1.80	1.98	1.65	0.15
	1.60	1.76	1.43	0.17
	1.40	1.54	1.25	0.15
	1.20	1.32	1.08	0.12
	1.00	1.10	0.90	0.10
	0.80	0.88	0.75	0.05
	0.60	0.66	0.53	0.07
*	0.40	0.44	0.37	0.03
*	0.20	0.22	0.19	0.01
		$K_{obs} = 773 \pm 180$ (pH = 2.03)		
2.23	2.00	2.20	1.77	0.23
	1.80	1.98	1.59	0.21
	1.60	1.76	1.44	0.16
	1.40	1.54	1.24	0.16
	1.20	1.32	1.07	0.13
	1.00	1.10	0.90	0.10
	0.80	0.88	—	—
	0.60	0.66	0.53	0.07
*	0.40	0.44	0.35	0.05
*	0.20	0.22	—	—
		$K_{obs} = 850 \pm 170$ (pH = 2.23)		
2.40	2.00	2.20	1.58	0.42
	1.80	1.98	1.54	0.26
	1.60	1.76	1.45	0.15
	1.40	1.54	1.27	0.13
	1.20	1.32	1.08	0.12
	1.00	1.10	0.89	0.11
	0.80	0.88	0.70	0.10
	0.60	0.66	0.52	0.08
*	0.40	0.44	0.33	0.07
*	0.20	0.22	0.18	0.02
		$K_{obs} = 1121 \pm 250$ (pH = 2.40)		

*Difference between free and total Fe is near the sensitivity of our method. These values are therefore excluded from K calculations.

single isosbestic point (Fig. 4). This is assumed to represent the formation of FeGSH given the low concentrations. The ratio of free to complexed Fe(III) was calculated from data at 290 nm where there is a band due to Fe—OH and results are given in Table 3. The average

TABLE 3. Spectral determination of binding at pH 3*

Curve No. (Fig. 4)	Absorbance A	Total GSH ($\times 10^5$ mol dm^{-1})	Free GSH ($\times 10^5$ mol dm^{-1})	K
1	0.300	—	—	—
2	0.293	1.25	1.16	3280
3	0.293	2.00	—	—
4	0.287	2.40	2.24	3260
5	0.286	3.20	3.02	2650
6	0.280	4.00	3.75	3150
7	0.280	5.20	4.95	2380
8	0.254	10.0	9.42	3390

*$Fe_t = 2.40 \times 10^{-5}$; K (average) = 3020.

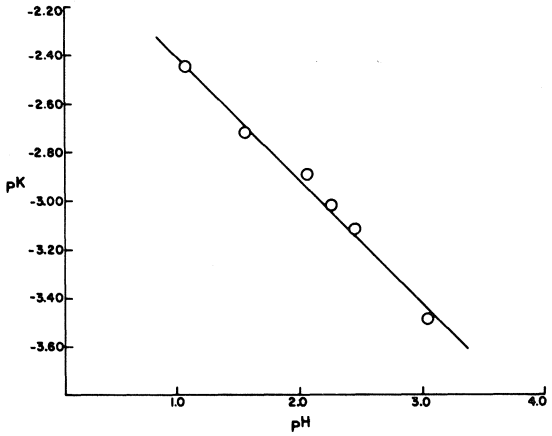

FIG. 3. Variation of pK with pH of the binding of glutathione to Fe(III).

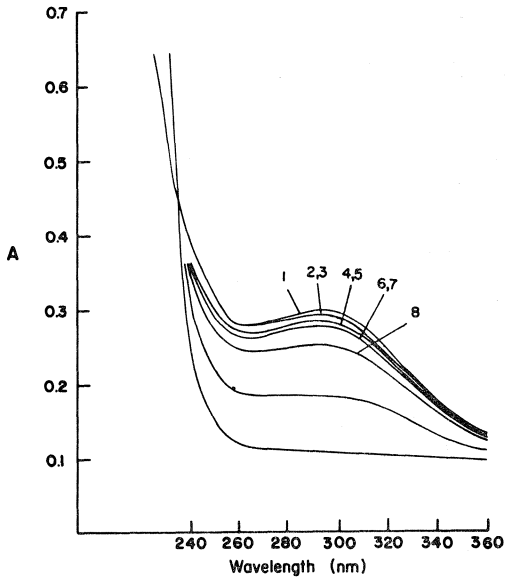

FIG. 4. Curves showing isosbestic point for Fe(III) and glutathione system, with Fe(III) concentration 2.4×10^{-5} M (top curve) and increasing concentrations of glutathione (lower curves).

value of $K = 3020$ is in good agreement with the value to be given below, which is based on a kinetic study of the reaction between Fe(III) and GSH. Note that the disappearance of the $\lambda = 290$ nm band on complexation suggests complexation replaces or leads to protonation of the bound —OH of $Fe(OH_2)_5OH^{2+}$.

(c) Evaluation of Binding from Complexation Kinetics

Using the band at 290 nm which makes possible spectrophotometric determination of binding, it is possible to carry out stopped flow measurements on the rate of reaction of glutathione with Fe(III) at pH 3. This study bears on the mechanism of the Fe(III)–glutathione interaction and is *separate* from the above kinetic analysis technique. However, the pseudo first-order rates of approach to equilibrium at pH = 3 as a function of excess glutathione shown in Fig. 5 is a straight line. The slope corresponds

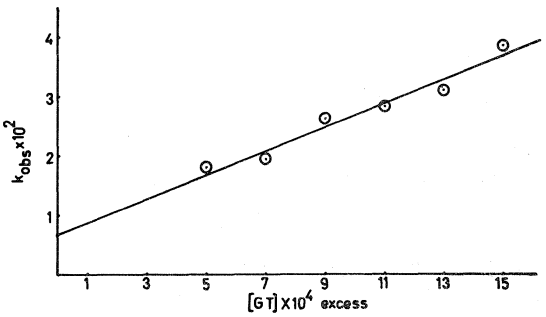

FIG. 5. Plot showing k_f and k_d for the reaction of Fe(III) (1.26×10^{-4} M) and glutathione at pH 3 and ionic strength 0.1.

Can. J. Chem. Downloaded from www.nrcresearchpress.com by 210.87.254.6 on 09/05/12
For personal use only.

Can. J. Chem. Downloaded from www.nrcresearchpress.com by 210.87.254.6 on 09/05/12
For personal use only.

to the second-order rate constant for complex formation (k_f) and the intercept corresponds to the first-order rate constant for dissociation of the complex (k_d). If the mechanism of complexation is not complicated, the binding constant (K) may be calculated as the ratio of k_f/k_d. Figure 5 gives k_f as 20.4 M^{-1} s^{-1} and k_d as 6.6×10^{-3} s^{-1}. The ratio of these two gives 3100 as an estimate for the value of the binding constant in good agreement with the value from equilibrium spectrophotometry.

(d) pH Dependence and Comparison of Methods

The dependence of the binding constants, determined as conditional constants at ionic strength of 0.100 M on pH, are shown in Fig. 3. Five values (pH = 1.0, 1.5, 2.0, 2.2, 2.4) are derived from kinetic analysis. The sixth (pH = 3.0) is derived from spectrophotometry and confirmed by mechanistic study. The inter method consistency is seen to be excellent, providing convincing support for the claims to success of the kinetic method. The pH dependence is represented as $pK = -1.96 - 0.50pH$.

Discussion

The present study merits some at least brief interpretive comment at three levels: (*a*) analytical implications, (*b*) equilibrium behaviour and its significance for natural water chemistry, and finally, (*c*) kinetics and mechanism of complex formation. We take these up in turn.

(a) Analytical Implications

A major intent of our present program is to develop analytical methods based on kinetics that allow the determination of specific labile components of mixtures which would be lumped into an uninformative quantity such as 'total iron' if advantage were not taken of the opportunity to measure rapid reaction processes. The present study gives a primitive example where the degree of success of the analysis is hard to specify unambiguously but is indicated to be promising *by the successful quantitative correlation with other better established methods for measuring conditional binding constants*. The *precision* in this study is similar to that discussed in the study of binding of Fe(III) to a fulvic acid reported earlier (3). We have here an advantage, with respect to asserting reasonable *accuracy*, flowing from the cross-check with other methods.

(b) Binding Equilibrium and Natural Water Chemistry

Glutathione is a widely distributed biological species with sulfur containing metal binding sites. Since the natural water chemistry of iron is thought to depend significantly on organic complexing using ligands of biological origin, the behaviour of glutathione is an interesting case. As indicated above, it is also difficult to study by the popular methods for measurement, titrimetry, and spectrophotometry.

Figure 3 suggests that binding of glutathione to Fe(III) is only weakly pH dependent. This pH dependence is not easily understood because of the complex acid–base behaviour of both GSH and Fe(III) (4, 5). In the pH range from 1 to 3, GSH_2^+, GSH, $Fe(OH_2)^{3+}$, and $Fe(OH_2)_5OH^{2+}$ are major species and GS^- is not entirely negligible. It is important to recognize that no great release of protons on binding of GSH to Fe(III) is allowed by a $\frac{1}{2}$ power $[H^+]$ dependence.[3] We can write down the following possible reactions (at least) for consideration:

$$[4] \qquad Fe^{3+} + GSH_2^+ \rightleftharpoons FeGSH^{3+} + H^+$$

$$[5] \qquad Fe^{3+} + GSH \rightleftharpoons FeGSH^{3+}$$

$$[6] \qquad Fe^{3+} + GSH \rightleftharpoons FeGS^{2+} + H^+$$

$$[7] \qquad Fe(OH)^{2+} + GSH \rightleftharpoons FeGS^{2+} + H_2O$$

If we assume that ligand deprotonation favours complex formation, as is usual, we must recognize that, in iron chemistry, hydrolysis resists complex formation. Alternatively, one recognizes that the coordinated hydroxyl group is 'reprotonated' on complex formation (a point directly demonstrated in the spectrophotometric experiments at pH = 3). It is important that the OH group on $FeOH^{2+}$ is 'displaced' by glutathione. This may either be a result of protonation of that —OH to give H_2O coordinated or to the displacement of that oxygen at Fe by a donor from glutathione. An attempt was made to distinguish the two by examining the decrease in broadening of the solvent nmr signal as the ligand reduces exchange of protons with paramagnetic sites in the iron coordination sphere. This was unsuccessful because even limited

[3]A half power $[H^+]$ dependence would become first power if binuclear iron complexes were formed requiring a second power dependence on free iron concentration. We have tested this possibility. It fails unambiguously. The iron dependence is first power.

binding of ligands at Fe(III) shortens the electronic relaxation times and alters nmr broadening (6). Nuclear magnetic resonance did not provide a probe of the number of water molecules remaining coordinated.

(c) Kinetics and Mechanism of Formation of Fe(III)–Glutathione Complex

At pH = 3, where the hydroxyl band in the iron spectrum vanishes on complex formation, stopped flow studies allowed measurement of the rate of approach to equilibrium as excess glutathione reacted with Fe(III). If complex formation is second order forward and complex dissociation is first order (the usual cases), the rate law for approach to equilibrium should be as shown in [8].

[8] Rate = $(k_f[\text{glutathione}] + k_d)[\text{Fe(III)}]$

The data fit this expression well (Fig. 5). That the mechanism is simple is indicated by the successful calculation of the binding constant as k_f/k_d. The value of k_d is small and typical for a chelating ligand. The value of k_f is significantly *less* than for the simple ligand SSA. This indicates that it is *not* the replacement of the first water molecule of Fe(III) by a ligand donor atom that is rate determining. Such a first step is ligand independent in Fe(III) chemistry (7). Apparently, some stage of ring closing of the chelate is rate determining in complex formation.

1. G. WILLS, W. H. WOODRUFF, J. R. FRYSINGER, D. W. MARGERUM, and H. L. PARDUE. Anal. Chem. **42**, 1350 (1970).
2. A. C. JAVIER, S. R. CROUCH, and H. V. MALMSTADT. Anal. Chem. **41**, 239 (1969).
3. C. H. LANGFORD and T. R. KHAN. Can. J. Chem. **53**, 2979 (1975).
4. N. W. PIRIE and K. G. PINHEY. J. Biol. Chem. **84**, 321 (1929).
5. R. M. MILBURN. J. Am. Chem. Soc. **79**, 537 (1957).
6. D. S. GAMBLE, C. H. LANGFORD, and J. P. K. TONG. Can. J. Chem. **54**, 1239 (1976).
7. C. H. LANGFORD and V. S. SASTRI. MTR international review of science. Inorganic chemistry, Series One. Vol. 9. 1972. p. 203.

Can. J. Chem. Downloaded from www.nrcresearchpress.com by 210.87.254.6 on 09/05/12
For personal use only.

On the use of the *n*-propylammonium and *n*-butylammonium salts of *d*-10-camphorsulfonic acid for the calibration of spectropolarimeters: the concentration and solvent dependency of the optical rotatory dispersion parameters[1]

YASUSHI NAKAGAWA
Department of Chemistry, University of Chicago, Chicago, IL., U.S.A. 60637
AND
MICHAEL F. GILLEN AND ROSS E. WILLIAMS[2]
Division of Biological Sciences, National Research Council of Canada, Ottawa, Ont., Canada K1A 0R6

Received June 15, 1976

YASUSHI NAKAGAWA, MICHAEL F. GILLEN, and ROSS E. WILLIAMS. Can. J. Chem. **54**, 3200 (1976).

The utility of the title ammonium salts for the calibration of ord spectropolarimeters has been investigated. The solvent and concentration dependency of the measured specific molar rotations at 306 and 270 nm suggest that they may be used for calibration purposes only under well-defined conditions. The results of the Kramers–Kronig transformation of their circular dichroic spectra are presented and compared with the measured ord spectra.

YASUSHI NAKAGAWA, MICHAEL F. GILLEN et ROSS E. WILLIAMS Can. J. Chem. **54**, 3200 (1976).

L'utilisation des deux sels ci-haut mentionés pour la calibration des spectropolarimètres dor a été étudiée. La rotation molaire spécifique à 306 nm et 270 nm dépendant du solvant ainsi que de la concentration, ces deux sels ne peuvent être utilisés à des fins de calibration que dans des conditions bien définies. Les résultats obtenus par la transformation de Kramers–Kronig des spectres de dichroïsme circulaire ont été comparés à ceux des spectres de dor.

Introduction

It has been previously suggested that amine salts of *d*-10-camphorsulfonic acid (CSA), in particular the *n*-propylammonium salt of camphorsulfonic acid (*n*-PrA-CSA) and the *n*-butylammonium salt of camphorsulfonic acid (*n*-BuA-CSA) might be of use for the calibration of circular dichromators (1). Unlike CSA, these salts are non-deliquescent, and are easily prepared, purified, and characterized. They also retain the desirable aqueous solubility and chiroptical properties of CSA itself. It is because of their apparent utility as circular dichroism (cd) standards that we have examined the optical rotatory dispersion (ord) spectra of these salts. In this communication the experimentally determined ord values are reported and compared with those of CSA.

Experimental

Sucrose used for ord calibration purposes was Ultra High Purity sucrose obtained from Baker Chemical Co. (lot no. UBC 805). The sucrose possessed the correct elemental analysis and was used without further purification. Hydrated CSA, *n*-PrA-CSA, and *n*-BuA-CSA were prepared as previously reported (1). Water used for all solutions was deionized before being distilled from glass.

Stock solutions of CSA and its salt derivatives were prepared for ord measurements in 50 ml volumetric flasks with solute concentrations of 100 ± 20 mg per 50 ml. Less concentrated solutions were obtained by diluting 2 ml of stock solution to 5 ml in a 5 ml volumetric flask. A stock solution of sucrose in water for calibration purposes was prepared in a 10 ml volumetric flask (2.6 g/10 ml).

Kramers–Kronig transformations were done on an IBM 360, model 67 computer using previously reported programs (2, 3). The programs were modified so that cd input data would be in terms of $[\theta]$, the specific molar ellipticity (deg cm^2/dmol) thus giving ord output values in terms of $[M]$, the specific molar rotation (deg cm^2/dmol). Circular dichroism data were inserted at 1.25 nm intervals. Circular dichroism data used to generate the ord output included only two cd bands: the 290 nm cd band and the 192 nm cd band which was assumed to be symmetrical and Gaussian. Data input included values from 330 to 150 nm. Data output included values from 400 to 100 nm.

Optical rotary dispersion measurements were made on a sucrose-calibrated Cary–Varian spectropolarimeter,

[1]NRCC No. 15461.
[2]Author to whom correspondence should be addressed.

Can. J. Chem. Downloaded from www.nrcresearchpress.com by 210.87.254.105 on 09/05/12
For personal use only.

TABLE 1. Measured ord parameters for CSA and its ammonium salt derivatives

Compound	Solvent	Concentration[a] (mg/ml)	Specific molar rotation, $[M]^b$ (deg cm² per dmol) 306 nm	270 nm
CSA(hydrate)	H_2O	1.51	$+4300 \pm 200^c$	-5300 ± 300^c
CSA(anhydrous)[d]	—	—	$+4600 \pm 200^c$	-5700 ± 300^c
n-PrA-CSA	H_2O	1.93	$+4520 \pm 50$	-5700 ± 50
		0.77	$+4320 \pm 70$	-5880 ± 50
	0.1 *N* HCl	2.06	$+4340 \pm 100$	-5740 ± 100
		0.82	$+4510 \pm 50$	-5790 ± 50
	0.1 *N* H_2SO_4	2.11	$+4550 \pm 50$	-5700 ± 50
		0.84	$+4550 \pm 50$	-5700 ± 50
n-BuA-CSA	H_2O	1.98	$+4510 \pm 50$	-5680 ± 50
		0.79	$+4510 \pm 50$	-5950 ± 50
	0.1 *N* HCl	1.92	$+4400 \pm 100$	-5660 ± 100
		0.77	$+4350 \pm 50$	-5980 ± 50
	0.1 *N* H_2SO_4	2.10	$+4490 \pm 50$	-5690 ± 50
		0.84	$+4480 \pm 50$	-5730 ± 60

[a]Samples were prepared by weighing 100 ± 20 mg into a 50.0 ml volumetric flask and diluting to the mark with solvent. Samples were diluted by removing 2.0 ml of the stock solution and diluting to 5.0 ml with solvent.

[b]All values given are the simple average of at least three measurements. Error limits given are the standard deviations obtained from the measured values.

[c]Optical rotatory dispersion literature values: at 306 nm: 4464 (6); 4654 (4); 4480 (7); 4120 (5); at 270 nm: −5586 (6); −5810 (4); −5700 (7); −5300 (5).

[d]The results of hydrated CSA have been corrected for water content (7.3% by weight) (6).

model 60. The specific rotation [α], for sucrose at 589 nm used for calibration was +66.5 (4). An instrument full range setting of 1° or 0.4° was used. All measurements were made using a quartz cell (1.0 cm path length) at a temperature of 20 ± 2 °C. For each sample, a base line was obtained before any sample measurements were made.

Results and Discussion

The spectropolarimeter being used for the ord measurements was first calibrated with a sucrose solution. So that the accuracy of the ord values being measured could be further checked and any variations due to instrumental response in the 250–350 nm region could be eliminated, the ord spectrum in water of a sample of hydrated CSA was also measured (Table 1). When the specific molar rotations at 306 and 270 nm were compared with those found in the literature, the determined values were lower than those previously reported, save for one set (5) with which the values were in good agreement. Correction of the measured values for a water content of 7.3% by weight (1, 6) gave a set of corrected values (Table 1) which were in good agreement with those determined on the anhydrous CSA samples (4, 6, 7). If the values reported by Cassim and Yang (5) were corrected by 7.3% their values agree with those determined on the anhydrous CSA samples as well. The ord parameters in water for the ammonium salt derivatives of CSA were then measured under the same conditions used to measure those of the CSA. The values obtained are reported in Table 1. As may be noted, when the concentration (by weight) of the ammonium salts in water was the same as CSA, the specific molar rotations measured were very similar to those of CSA (anhydrous). An improvement in the precision of the measurement was also noted. Although little or no effect (less than 0.6% change) was noted upon 25-fold dilution of the samples used for cd measurement (1), a 2.5-fold dilution of the ord samples in water produced a variable amount of change in the specific rotations depending on the compound and the wavelength at which the measurements were made. Thus, with *n*-PrA-CSA, the specific molar rotation, [*M*], at 306 nm decreased upon dilution whereas the [*M*] 306 nm of *n*-BuA-CSA remained unchanged. At 270 nm the [*M*] for both compounds increased upon dilution.

During the process of purification of the two ammonium salts it had previously been noted that the specific rotation, [α], at 589 nm was

Can. J. Chem. Downloaded from www.nrcresearchpress.com by 210.87.254.105 on 09/05/12
For personal use only.

Can. J. Chem. Downloaded from www.nrcresearchpress.com by 210.87.254.105 on 09/05/12
For personal use only.

concentration dependent when the measurements were made in water. In this case it was assumed that the position of an equilibrium between the sulfonic acid and alkylamine was being affected and that the effect could be overcome if a large excess of a competing acid were present to completely destroy any association between the two components of the salt mixture. Indeed, it was found that changing the solvent to 0.1 *N* HCl eliminated this concentration dependency at 589 nm. However, when the measurements of the specific molar rotations at 306 and 270 nm were made in 0.1 *N* HCl the concentration dependency persisted for both compounds (Table 1). Complete elimination of the concentration dependency could only be achieved by making the measurements in 0.1 *N* H_2SO_4 (Table 1). It will also be noted that when the concentration dependency was eliminated the specific molar rotations at 306 and 270 nm for both compounds were the same as the values obtained for CSA (anhydrous).

As an additional check of the measured ord results, we have transformed the previously measured cd spectra of the ammonium salts (1) into calculated ord spectra via the Kramers–Kronig transformation and compared the results with the measured data. By assuming that the 192 nm band was symmetrical and Gaussian, thereby extending the experimentally determined data into the far ultraviolet, a difference of $\pm 1.5\%$ between the measured ord and calculated ord amplitudes for CSA at 306 and 270 nm was obtained. Using the same ploy, transformation of the cd spectral data of the two ammonium salts of CSA resulted in the calculated ord amplitudes being larger than the measured at both wavelengths, *i.e.* $+2.4 \rightarrow 4.0\%$ at 306 nm and $+4.2 \rightarrow 5.6\%$ at 270 nm. Further improvement of the correspondence between data sets would require that the influence of any unmeasured bands be eliminated (2, 3). Unmeasured bands below 186 nm might arise from the sulfonic acid group's interaction with the amine and could be the source of the discrepancies. Until the size, sign, and location of such bands are determined further manipulation of the data seems unwarranted.

In conclusion, although the ammonium salts of CSA appeared to be useful for the calibration of circular dichrometers, their use as standards for the calibration of spectropolarimeters would depend on elimination of the dependency of their measured specific rotations at 306 and 270 nm on both concentration and solvent. If these latter two variables are adequately controlled and conditions defined for their use (*e.g.* 0.1 *N* H_2SO_4, 2.0 mg per ml) the ammonium salts of CSA might then be useful as standards for the calibration of optical rotatory dispersion spectropolarimeters.

Acknowledgement

The aid of J. P. Hawrenek and R. N. Jones, Division of Chemistry, N.R.C.C., in the set up and running of the programmes used for Kramers–Kronig transformation was very much appreciated.

1. M. F. Gillen and R. E. Williams. Can. J. Chem. **53**, 2351 (1975).
2. R. N. Jones. *In* Computers in chemistry and instrumentation. Vol. VII. *Edited by* J. S. Mattson, H. C. MacDonald, and H. B. Monk. Marcel Dekker Inc., New York, N.Y. In press.
3. J. P. Hawrenek and R. N. Jones. Spectrochim. Acta, Part A, **32**, 99 (1976).
4. D. F. DeTar. Anal. Chem. **41**, 1406 (1969).
5. J. Y. Cassim and J. T. Yang. Biochemistry, **8**, 1947 (1969).
6. W. C. Kruger and L. M. Pschigoda. Anal. Chem. **43**, 675 (1971).
7. A. J. Adler, N. J. Greenfield, and G. D. Fasman. *In* Methods in enzymology. Vol. XXVII. *Edited by* C. H. W. Hirs and S. N. Timasheff. Academic Press, New York, N.Y. 1973. p. 675.

Application of photoelectron spectroscopy to intramolecularly hydrogen-bonded systems. Part II. On the n–π* blue shift of carbonyl-containing molecules

R. S. BROWN

Department of Chemistry, University of Alberta, Edmonton, Alta., Canada T6G 2G2

Received February 11, 1976

R. S. BROWN. Can. J. Chem. **54**, 3203 (1976).

The photoelectron spectra of 2-hydroxycyclohexanone and 2-methoxycyclohexanone, show that the ionization assigned to removal of the carbonyl n-electron is 0.6 eV higher in the former, presumably due to the intramolecular hydrogen bond. The ultraviolet spectra of these molecules also exhibit a marked blue shift of the $n \rightarrow \pi^*$ transition in the former of roughly 0.5 eV. A discussion of the observations includes consideration of the effect of the intramolecular hydrogen bond on the ground and excited or ion state.

R. S. BROWN. Can. J. Chem. **54**, 3203 (1976).

Les spectres photoélectroniques de l'hydroxy-2 cyclohexanone et de la méthoxy-2 cyclohexanone montrent que l'ionisation attribuée à l'enlèvement de l'électron n du carbonyle est d'environ 0.6 eV plus élevée dans le premier cas; ce résultat est probablement dû à l'intervention d'un pont hydrogène intramoléculaire. Les spectres uv de ces molécules montrent aussi un effet ipsochrome marqué de la transition $n \rightarrow \pi^*$ du premier composé; l'ordre de grandeur est d'environ 0.5 eV. Une discussion de ces observations comprend les considérations de l'effet des liens hydrogène intramoléculaires sur les états fondamentaux et excités ou ioniques.

[Traduit par le journal]

Can. J. Chem. Downloaded from www.nrcresearchpress.com by 210.87.254.105 on 09/05/12
For personal use only.

The experimentally observed blue shift of the n–π* band of a carbonyl-containing molecule when placed in a hydrogen-bonding solvent was originally discussed by Brealy and Kasha (1) in terms of the stabilization of the carbonyl n-orbital upon hydrogen-bond (H-bond) formation with the solvent. Later Pimentel (2) refined this description by emphasizing the importance of solvation energies in both the ground and excited states and the Franck-Condon principle. Most recently Del Bene (3) has applied *ab initio* calculations with configuration interaction to the formaldehyde–water dimer (3*a*) and acetone–water dimer (3*b*) and concluded that the experimentally observed hypsochromic shift in these systems is due in part to the lowering of the n-orbital *and* the additional energy required to break the H-bond in the lowest excited singlet state of the dimer.

Our recent photoelectron spectroscopic (pes) investigations of intramolecularly H-bonded systems (4) have clearly demonstrated that the n-orbital involved in H-bond formation appears at higher ionization energy (IE) than its counterpart in a geometric isomer in which H-bonding is precluded. Presumably this would be observed for intramolecularly H-bonded hydroxy ketones as well, so it seemed of interest to study the n–π* blue shift in these systems (5) by both uv and pe spectroscopy. 2-Hydroxycyclohexanone (**1**) (6) and 2-methoxycyclohexanone (**2**) (7) were chosen as the most suitable candidates (8) for study under the assumption that the 2-OH and 2-OCH_3 groups should exhibit similar inductive effects, but that only the former can H-bond with the carbonyl n-orbital.

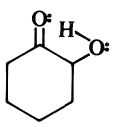

1

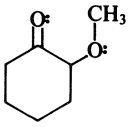

2

Results and Discussion

A comparison of the uv spectra of **1** (λ_{max} (cyclohexane) 272 nm (4.56 eV)) and **2** (λ_{max} (cyclohexane) 306 nm (4.05 eV)) shows a significant n–π* blue shift of roughly 0.5 eV in the former which is probably a result of the intramolecular H-bond (8) in this system. The pe spectra of **1** and **2** presented in Fig. 1 illustrate that the ionization energy of the highest occupied molecular orbital (homo) (assigned as pre-

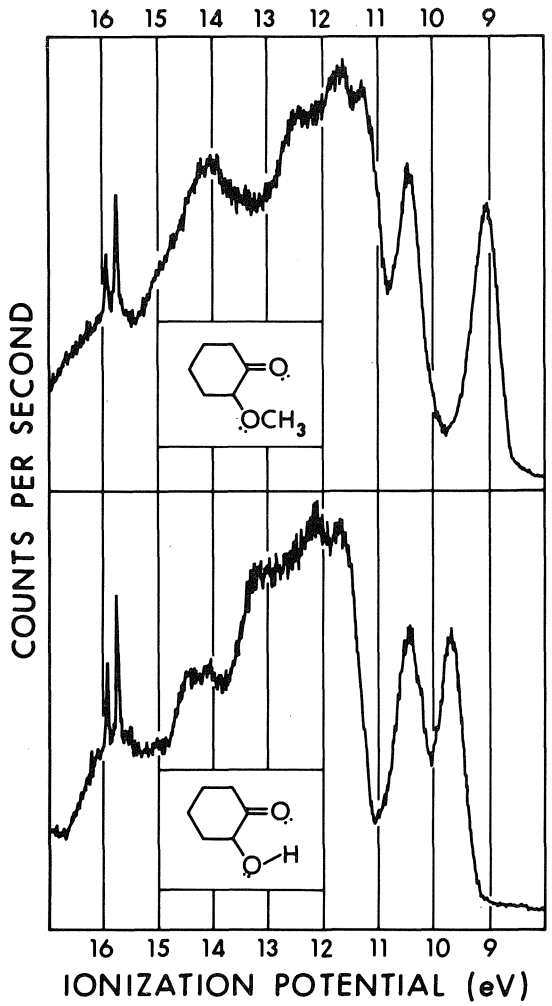

FIG. 1. The photoelectron spectra of 2-hydroxycyclohexanone (**1**) and 2-methoxycyclohexanone (**2**) using argon as an internal calibrating gas. Vertical ionization energies are as follows: (**1**) C=Ö, 9.70 eV; —Ö—H, 10.49 eV; (**2**) C=Ö, 9.06 eV; —Ö—CH_3, 10.46 eV.

dominantly the carbonyl n-orbital) is roughly 0.6 eV larger for **1** than **2**. Conformationally dependent pe spectral shifts have been observed in some systems (9), but such shifts are generally small (0.00 to 0.05 eV). Some evidence that the shifts between **1** and **2** do not totally result from axial–equatorial conformational differences at the α-carbon can be obtained from the nmr technique utilized by Garbisch (10). Comparing the chemical shift (δ 3.46, cyclohexane-d_{12}) of the conformationally mobile (*cf.* ref. 11) α-hydrogen of **2** with those of the relatively rigid equatorial and axial 2-methoxy-*cis*-1-decalones (12) indicates that in solution the ÖCH$_3$ group exists in an axial–equatorial ratio of 55:45. If these data are applicable to the gas phase, then the observed pe spectrum of **2** is a composite of both conformations. However, since the half-width (FWHM) of the $n_{C=O}$ ionization is the same for **2** (0.60 eV) and **1** (in which the α-hydroxy group is probably held equatorial by the H-bond (8)), it must be concluded that the $n_{C=O}$ IE for both conformations of **2** is identical. That this ionization is nearly the same as that found for cyclohexanone (IE^v $n_{C=O}$ = 9.14 eV (13)) suggests that substituent effects and/or O–O interactions are minimal or compensatory. We believe that the $n_{C=O}$ ionization energy difference between **1** and **2** must therefore be a direct consequence of the intramolecular H-bond present in **1** (8).

While it may be most tempting to suggest a correlation between the changing $n_{C=O}$ ionization energies and the n–π^* blue shift in passing from **2** to **1**, such correlations should be approached cautiously since they contain ambiguities concerning the π^* orbital energies and interelectronic repulsion terms involved in the n–π^* transition energies (14). However, if in the simplest analysis we were to assume the validity of Koopmans' theorem (15) and that the differences in the interelectronic repulsion terms involved in the n–π^* transitions for both molecules are similar, then the observation may suggest that the carbonyl n-orbital in **1** is stabilized by 0.6 eV relative to **2**. If this were so, then the observed n–π^* blue shift in passing from **2** to **1** is a result of the stabilization of the $n_{C=O}$ orbital in **1** due to intramolecular H-bonding in the ground state.

However, the experimental ionization energies are simply the differences in the total energy between the neutral molecule and the ion in a particular state (for example, *cf.* ref. 16). The pertinent question is how the presence of the hydrogen involved in the intramolecular H-bond in **1** will affect the total energy of the molecule in the ground state and ion state derived from ionization of a carbonyl n-electron. An extension of the ideas of Pimentel (2) to pe spectroscopy suggests that while the H-bond may be stabilizing in the ground state, such may not be the case in the ion state with its new electronic distribution. Since the Franck–Condon principle applies, and no nuclear reorganization occurs during

Can. J. Chem. Downloaded from www.nrcresearchpress.com by 210.87.254.105 on 09/05/12
For personal use only.

Can. J. Chem. Downloaded from www.nrcresearchpress.com by 210.87.254.105 on 09/05/12
For personal use only.

ionization, a change in the H-bond energetics would alter the separation of the two states.

Del Bene has examined the potential curve for the first excited singlet state of the formaldehyde–water dimer (*3a*) as a function of intermolecular distance and found it to be repulsive. Her results show that while the intermolecular H-bond lowers the overall energy of the ground state, it does not stabilize the excited singlet state of the same geometry compared to the separated dimer in which the H-bond is absent. The observed blue shift depends on both factors. Extrapolation of these results to the pe process, in which the fully charged ion states may well be more sensitive to the proximity of the hydrogen, indicates that ionization of the carbonyl n-electron which connects the ground and ion states may well reflect the stabilization of the former and destabilization of the latter. Hence the inference that the ionization energy difference between **1** and **2** results totally from a lowering of the n-orbital in **1** (Koopmans' theorem) cannot be established at this time without knowledge of the potential curves for the ground and ion states (*4b*).[1]

Experimental

Photoelectron spectra were obtained using a MacPherson 36 photoelectron spectrometer under conditions previously described (4). Ultraviolet spectra were obtained using a Pye Unicam SP1800 spectrophotometer on cyclohexane solutions. Spectra were run at various concentrations to ensure that concentration dependent shifts were absent. Compounds **1** and **2** were prepared by literature methods ((6) and (7) respectively) and spectra determined immediately after preparation. 2-Hydroxycyclohexanone (**1**) showed a rapid tendency to dimerize to a nonvolatile solid within hours of preparation as has been shown before (6).

[1]Note added in proof—In intermolecularly H-bonded dimers, although the n-orbital of the proton acceptor molecule is stabilized by hydrogen bonding, no quantitative relationship exists between the degree of n-orbital stabilization and the magnitude of the n–π^* blue shift. However, a comparison of the n-orbital energies of β-hydroxy acrolein in the non-H-bonded $C_s(t)$ form and H-bonded $C_s(c)$ form reveals a computed stabilization in the latter which is in quantitative agreement with the computed n–π^* blue shift. Whether this relationship is general for intramolecular H-bonds remains to be seen (J. E. Del Bene, private communication).

Acknowledgments

The author gratefully acknowledges the financial support of the University of Alberta and the National Research Council of Canada. We thank Prof. J. E. Del Bene for communicating her computational results prior to publication.

1. G. J. Brealy and M. Kasha. J. Am. Chem. Soc. **77**, 4462 (1965).
2. G. C. Pimentel. J. Am. Chem. Soc. **79**, 3323 (1957).
3. (*a*) J. Del Bene. J. Am. Chem. Soc. **95**, 6517 (1973); (*b*) J. Del Bene. J. Am. Chem. Soc. **96**, 5643 (1974).
4. (*a*) R. S. Brown. Can. J. Chem. **54**, 642 (1976); (*b*) R. S. Brown. Can. J. Chem. **54**, 1929 (1976).
5. R. C. Cookson and S. H. Dandegaonker. J. Chem. Soc. 353 (1954).
6. J. C. Sheehan, R. C. O'Neill, and M. A. White. J. Am. Chem. Soc. **72**, 3376 (1950).
7. M. Bergmann and M. Gierth. Ann. **448**, 64 (1966).
8. M. Oki, H. Iwamura, J. Aihara, and H. Iida. Bull. Chem. Soc. Jpn. **41**, 176 (1968); L. Joris and P. von R. Schleyer. J. Am. Chem. Soc. **90**, 4599 (1968).
9. Y. Gownelle, G. Menard, J. M. Pechine, D. Solgadi, F. Menes, and R. Botter. J. Electron. Spectrosc. Relat. Phenom. **7**, 247 (1975).
10. E. W. Garbisch. J. Am. Chem. Soc. **86**, 1780 (1964).
11. L. M. Jackman and S. Sternhall. Application of nuclear magnetic resonance spectroscopy in organic chemistry. Vol. 5. Pergamon Press, Braunschweig. 1969. p. 238.
12. H. O. House and H. W. Thompson. J. Org. Chem. **28**, 164 (1963).
13. D. Chadwick, D. C. Frost, and L. Weiler. Tetrahedron Lett. 4543 (1971).
14. H. Bock, K. Wittel, M. Veith, and N. Wiberg. J. Am. Chem. Soc. **98**, 109 (1976), and references therein.
15. T. Koopmans. Physica, **1**, 104 (1934).
16. J. H. D. Eland. Photoelectron spectroscopy. Butterworths, London. 1974. p. 83.

Application of photoelectron spectroscopy to intramolecularly hydrogen-bonded systems. Part IV. π-Systems; the photoelectron spectra of *syn*- and *anti*-7-norbornenol

R. S. BROWN

Department of Chemistry, University of Alberta, Edmonton, Alta., Canada T6G 2G2

Received February 16, 1976

R. S. BROWN. Can. J. Chem. **54**, 3206 (1976).

In an effort to determine the effect of an intramolecular hydrogen bond on the ionization energy of a simple π-system, the photoelectron spectra of *syn*- and *anti*-7-norbornenol have been determined. The difference in the ionization energy of the $\pi_{(C-C)}$ and $n_{\ddot{O}H}$ orbitals is 0.30 eV for the former, and 0.85 eV for the latter. The photoelectron spectrum of the *syn*-isomer shows that the $\pi_{(C-C)}$ bond is roughly 0.2 eV more difficult to ionize than its counterpart in the non-hydrogen bonded geometric isomer and has been interpreted as arising from hydrogen bond induced stabilization of the π-bond. That the spectral differences in the alcohols is not simply due to differing orbital interactions between the two isomers can be demonstrated by the photoelectron spectra of *syn*- and *anti*-7-methoxynorbornene. In these systems which allow no possibility of hydrogen bonding the $\pi_{(C-C)} - n_{\ddot{O}R}$ difference is the same for both isomers.

R. S. BROWN. Can. J. Chem. **54**, 3206 (1976).

Afin de pouvoir déterminer l'effet des ponts hydrogène intramoléculaires sur l'énergie d'ionisation d'un système π simple, on a déterminé les spectres photoélectroniques des norbornénols-7 *syn* et *anti*. La différence entre les énergies d'ionisation des orbitales $\pi_{(C-C)}$ et $n_{\ddot{O}H}$ est de 0.30 eV pour le premier et de 0.85 eV pour le dernier. Dans le spectre photoélectronique de l'isomère *syn* on observe que l'énergie nécessaire pour briser le lien $\pi_{(C-C)}$ est approximativement 0.2 eV plus grande que celle nécessaire pour briser le lien équivalent dans l'isomère géométrique ne possédant pas de pont hydrogène; on interprète ce résultat comme indiquant que le pont hydrogène induit une stabilisation du lien π. En faisant appel aux spectres photoélectroniques des méthoxy-7 norbornènes *syn* et *anti* on peut démontrer le fait que les différences spectrales dans les deux alcools ne sont pas dues uniquement à des interactions orbitalaires différentes entre les deux isomères. Dans ces systèmes, où il n'est pas possible d'effectuer des ponts hydrogènes, la différence $\pi_{(C-C)} - n_{\ddot{O}R}$ est la même pour les deux isomères.

[Traduit par le journal]

Intramolecular hydrogen bonding to π-systems, while not a common phenomenon, has been shown to occur in several organic molecules (1–6). Those molecules in which a π-bond acts as the electron donor terminus of the hydrogen bond (H-bond) generally exhibit an intramolecularly bonded O—H stretching frequency displaced from the fundamental by 11 to 55 cm^{-1} (3). While the sole criterion of the observation of two closely-spaced infrared (ir) O—H stretching frequencies as proof for the existence of H-bonds has been questioned (7), it seems generally accepted that one of the best examples of π-H-bonding can be found in *syn*-7-norbornenol (**1***a*). It has been reported that the intramolecularly H-bonded O—H stretching frequency of **1***a* occurs at 3574 cm^{-1} while that of the geometric isomer in which H-bonding is precluded is at 3630 cm^{-1} (5).

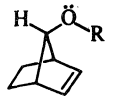

1*a* R = H
b R = CH_3

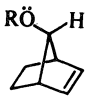

2*a* R = H
b R = CH_3

Our recent photoelectron spectroscopic (pes) studies on intramolecularly H-bonded systems (8) have conclusively demonstrated that the electron pair involved in H-bond formation exhibits higher ionization energy than its counterpart in a geometric isomer in which H-bonding is precluded. Since this can be demonstrated in a variety of systems, it seemed reasonable to expect that similar observations might be made in comparing the pe spectra of alcohols **1***a* and **1***b*. It is important to eliminate the possibility that any observed spectral differences are due to processes which involve mechanisms other than

Can. J. Chem. Downloaded from www.nrcresearchpress.com by 210.87.254.6 on 09/05/12
For personal use only.

Can. J. Chem. Downloaded from www.nrcresearchpress.com by 210.87.254.6 on 09/05/12
For personal use only.

H-bonding. To this end, the 7-methoxynorbornenes (**1***b* and **2***b*) were synthesized and their spectra determined as models for the alcohols which possess similar substituent effects but in which H-bonding is impossible. The following reveals our findings concerning these questions.

Results and Discussion

Conformationally induced changes in pe spectra have been demonstrated in various geometric isomers (9). Normally these spectral changes are quite small (0.00–0.15 eV), but it is important to demonstrate that any changes occurring in the pe spectra of isomers **1***a* and **2***a* are not simply attributable to differing orbital interactions between the two. A suitable probe for the 7-norbornenols would be the corresponding 7-methoxynorbornenes (**1***b* and **2***b*), and the pe spectra for these latter compounds are shown in Fig. 1. Perusal of the low energy regions of the spectra reveals that the observed splitting between the first two ionizations is 0.50 ± 0.02 eV for both **1***b* and **2***b*, although the absolute positions of the bands are roughly 0.15 eV higher for the *anti*-isomer **2***b*. The first band in both spectra is assigned to ionization from the π-system and is similar in value to that observed for norbornene (8.97 eV (10)) while the second is assigned to ionization of the electron pair predominantly located on oxygen. The important conclusion to be derived from the above observation is that the orbital interactions between the OCH_3 and $\pi_{(C=C)}$ groups as judged by pe spectroscopy do not appear to be different in the two isomers. Hence, those mechanisms which involve through space or through bond orbital interactions (11) cannot be contributing to the differences that are observed in the pe spectra of **1***a* and **2***a*.

With the question of orbital interactions in these systems clarified, one can now turn to a comparison of the pe spectra of the 7-norbornenols (**1***a* and **2***a*). Those spectra are displayed in Fig. 2 and the corresponding vertical ionization energies and assignments compiled in Table 1.

Figure 2 illustrates that the pe spectra of the *syn*- and *anti*-alcohols are quite different particularly in the low ionization energy regions. In both alcohols, the first ionization is assigned to removal of an electron from the π-bond, while the second arises from the $n_{\ddot{O}H}$ orbital. A comparison of the spectra shows that the $n_{\ddot{O}H} - \pi_{(C=C)}$ splitting in the *anti*-alcohol (**2***a*) is 0.50 eV larger than that in the *syn*-isomer (**1***a*). We feel that the differences between the first two bands in the pe spectra of **1***a* and **2***a* is a direct result of the intramolecular H-bond in the former. Previous ir investigations (5) have reported that

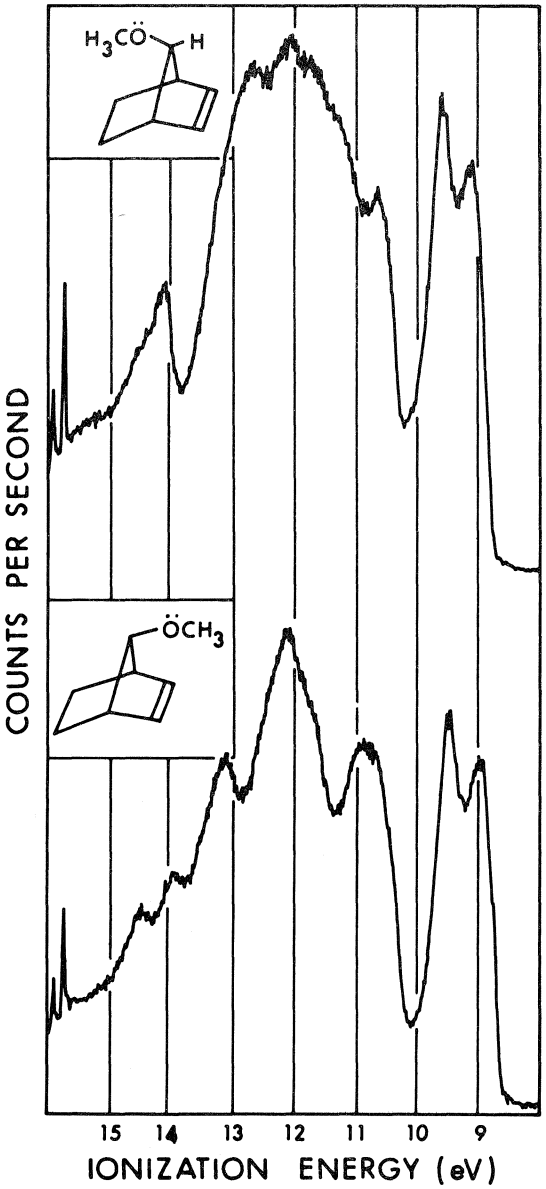

FIG. 1. The photoelectron spectra of *syn*- and *anti*-7-methoxynorbornene (**1***b* and **2***b* respectively) using argon as an internal calibrating gas.

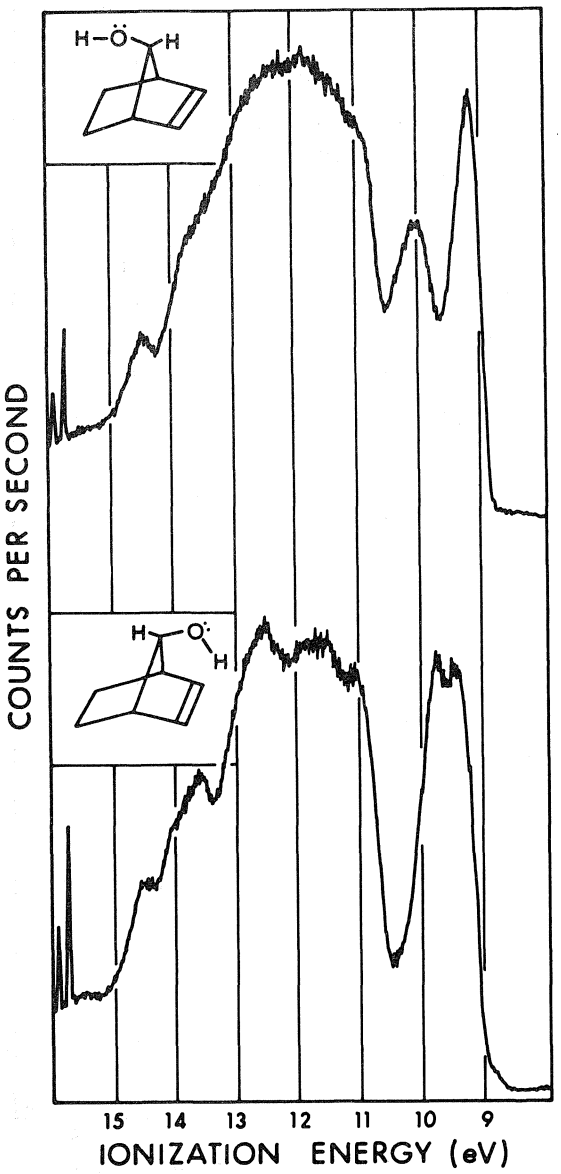

FIG. 2. The photoelectron spectra of *anti-* and *syn*-7-norbornenol (**2***a* and **1***a* respectively) using argon as an internal calibrating gas.

the *anti*-alcohol (**2***a*) shows a free Ö—H stretching frequency at 3630 cm^{-1}, while the *syn*-isomer shows a bonded Ö—H frequency at 3574 cm^{-1} as well as a free Ö—H band at 3624 cm^{-1}. Our present results on tetrachloroethylene solutions of the purified *syn*-isomer show only a bonded ÖH peak at 3575 cm^{-1} and no evidence for a free Ö—H band. By extrapolation, the ir data suggests that in the gas phase, the molecule may exist nearly entirely (>99%) in its hydrogen-bonded form. Our pe data provide corroboration for the intramolecularly H-bonded form, and suggest additional implications concerning the effect of the closely positioned hydrogen on the π-bond.

Few theoretical studies have addressed themselves to the question of H-bonding to π-systems (12). Of those that have, even those calculations of widely-differing sophistication seem to agree that there is a charge transfer of electron density from the π-system to the proton donor terminus of the H-bond which is symmetrically situated over the π-bond. Such would suggest that the π-system acquires some small (+)-charge from charge transfer to the proton donor, while the oxygen acquires excess (−)-charge. While this rationale is undoubtedly oversimplified (particularly with respect to charge–cloud repulsion and electrostatic and charge redistributions (13, 12*c*)) it is useful in predicting that the π-bond participating in the H-bond ought to become more difficult to ionize than in an isomer in which H-bonding is precluded. Similarly, the oxygen should become easier to ionize (than its counterpart in a non-H-bonding isomer) in full agreement with our observations and previous results in other intramolecularly H-bonded systems (8). Such spectral differences may not be totally due to electronic redistribution in the ground state, but undoubtedly arise from H-bond influences on the ground *and* ion states (8*b*, *c*). However, it is clear that pe spectroscopy can be used to detect ionization energy shifts in systems where π-orbitals serve as electron donors in H-bonds.

Experimental

Photoelectron spectra were determined at ambient temperature using a MacPherson Model 36ESCA photoelectron spectrometer under conditions previously described (8). Infrared (ir) spectra were recorded on a Perkin-Elmer 421 grating spectrophotometer in tetrachloroethylene solutions. Intramolecular could be distinguished from intermolecular H-bonding by observing the diminution of the bonded O—H stretching frequency attributable to the latter with increasing dilution.

*syn-7-Norbornenol (**1a**)*

This was prepared by the method of Baird (14) while the corresponding *anti*-isomer (**2***a*) was prepared by $LiAlH_4$ reduction of 7-norbornenone according to the procedure of Gassman and Pape (15). Recrystallization of the primary reaction product of the reduction from

Can. J. Chem. Downloaded from www.nrcresearchpress.com by 210.87.254.6 on 09/05/12
For personal use only.

TABLE 1. Vertical ionization energies IE^v in electron volts (eV) and assignments for some 7-substituted norbornenes

Compound	Vertical ionization energy (eV)		
	$\pi_{(C=C)}$	$n_{(\ddot{O}R)}$	$\Delta(n_{\ddot{O}R} - \pi_{(C=C)})$
Norbornene[a]	8.97		
anti-7-Methoxynorbornene (**2***b*)	9.11	9.59	0.48
syn-7-Methoxynorbornene (**1***b*)	8.95	9.45	0.50
anti-7-Norbornenol (**2***a*)	9.19	10.04	0.85
syn-7-Norbornenol (**1***a*)	9.41	9.71	0.30

[a]Reference 10.

hexane in our hands did not yield the pure *anti*-isomer (**2***a*) as reported (15) but rather a 1:6 mixture of **1***a*:**2***a*. Column chromatography of the mixture on Woelm neutral grade III alumina (30 × 2 cm/gm) using an eluent of 15:85 ether–hexane afforded the *anti*-isomer (**2***a*) in >95% purity (glpc, 20 in., 10% U.C.W.-982 on 80–100 mesh WAW-DCMS, 140 °C). The *syn*- and *anti*-isomers prepared as above had physical and spectral properties consistent with those reported.

*syn-7-Methoxynorbornene (**1***b*)

A methylation procedure formulated by Diner *et al.* (16) performed on 2.7 g (0.025 mol) *syn*-7-norbornenol with 7 g (0.05 mol) CH_3I and 1.1 g (0.027 mol) NaH suspension (57% in oil) yielded after work-up 2.5 g (80%) of the desired *syn*-ether: bp 100–102 °C/150 torr; nmr ($CDCl_3$) δ 6.03 (m, 2H), 3.42 (m, 1H), 3.23 (s, 3H), 2.87 (m, 2H), 1.83–1.52 (m, 2H), 1.13–0.75 (m, 2H); ir 3060, 2970, 2940, 2910, 2870, 2825, 1455, 1445, 1364, 1333, 1277, 1195, 1125, 1095 cm^{-1}; Raman (neat) 1558 cm^{-1} (C=C). *Exact Mass* calcd. for $C_8H_{12}O$: 124.08882; found: 124.08877.

*anti-7-Methoxynorbornene (**2***b*)

Methylation (16) of 1.2 g (0.011 mol) *anti*-7-norbornenol (**2***a*) using 3.0 g (0.022 mol) CH_3I in 60 ml anhydrous DME and 0.5 g (0.03 mol) NaH suspension (57% in oil) gave after work-up 1.0 g (73%) of the desired material (**2***b*): bp 83–87 °C/130 torr; nmr ($CDCl_3$) δ 5.98 (t, 2H), 3.24 (s, 3H), 3.12 (br s, 1H), 2.67 (m, 2H), 2.0–1.58 (m, 2H), 1.08–0.75 (m, 2H); ir 3130, 3060, 2975, 2935, 2890, 2830, 1457, 1450, 1435, 1340, 1327, 1297, 1252, 1191, 1158, 1090 (br) cm^{-1}; Raman (neat) 1555 cm^{-1}. *Exact Mass* calcd. for $C_8H_{12}O$: 124.08882; found: 124.08870.

Acknowledgments

The author gratefully acknowledges the financial assistance of the University of Alberta and the National Research Council of Canada. He is also grateful to Professor K. Kopecky for his generous gift of 7-norbornenone.

1. (*a*) M. D. JOESTEN and L. J. SCHAAD. Hydrogen bonding. Marcel Dekker, Inc., New York. 1974. p. 274; (*b*) S. N. VINOGRADOV. Hydrogen bonding. Van Nostrand Reinhold Co., New York. 1971. p. 134; (*c*) G. C. PIMENTEL and A. L. MCCLELLAN. The hydrogen bond. W. H. Freeman and Co., San Francisco. 1970. pp. 190, 202.
2. L. JORIS, P. VON R. SCHLEYER, and R. GLEITER. J. Am. Chem. Soc. **90**, 327 (1968).
3. P. VON R. SCHLEYER, D. S. TRIFAN, and R. BACSKAI. J. Am. Chem. Soc. **80**, 6691 (1958).
4. M. ŌKI and H. IWAMURA. Bull. Chem. Soc. Jpn. **32**, 567 (1959); M. ŌKI and H. IWAMURA. Bull. Chem. Soc. Jpn. **32**, 950 (1959); M. ŌKI and H. IWAMURA. Bull. Chem. Soc. Jpn. **32**, 955 (1959).
5. R. K. BLY and R. S. BLY. J. Org. Chem. **28**, 3165 (1965).
6. A. N. MURTY and R. F. CURL. J. Chem. Phys. **46**, 4176 (1967).
7. R. PICCOLINI and S. WINSTEIN. Tetrahedron Lett. 4 (1959).
8. (*a*) R. S. BROWN. Can. J. Chem. **54**, 0000 (1976); (*b*) R. S. BROWN. Can. J. Chem. **54**, 0000 (1976); (*c*) R. S. BROWN. Can. J. Chem. This issue.
9. R. BOTTER, F. MENES, Y. GOWNELLE, J. M. PECHINE, and D. SOLGADI. Int. J. Mass Spectrom. Ion Phys. **12**, 188 (1973); Y. GOWNELLE, C. MENARD, J. M. PECHINE, D. SOLGADI, F. MENES, and R. BOTTER. J. Electron Spectrosc. Relat. Phenom. **7**, 247 (1975).
10. P. BISCHOF, J. A. HASHMALL, E. HEILBRONNER, and V. HORNUNG. Helv. Chim. Acta, **54**, 783 (1971).
11. R. HOFFMANN. Acc. Chem. Res. **4**, 1 (1971); R. HOFFMANN, A. IWAMURA, and W. J. HEHRE. J. Am. Chem. Soc. **90**, 1499 (1968).
12. (*a*) W. JAKUBETZ and P. SCHUSTER. Tetrahedron, **27**, 101 (1971); (*b*) G. ALAGONA, R. CIMIRAGLIA, E. SCROCCO, and J. TOMASI. Theor. Chim. Acta, **25**, 103 (1972); (*c*) S.-I. YAMABE and K. MOROKUMA. J. Am. Chem. Soc. **97**, 4458 (1975).
13. (*a*) P. A. KOLLMAN and L. C. ALLEN. Chem. Rev. **72**, 283 (1972); (*b*) J. E. DEL BENE. J. Am. Chem. Soc. **95**, 5460 (1973).
14. W. C. BAIRD. J. Org. Chem. **31**, 2411 (1966).
15. P. G. GASSMAN and P. G. PAPE. J. Org. Chem. **29**, 160 (1964).
16. U. E. DINER, F. SWEET, and R. K. BROWN. Can. J. Chem. **44**, 1591 (1966).

Can. J. Chem. Downloaded from www.nrcresearchpress.com by 210.87.254.6 on 09/05/12
For personal use only.

A proton magnetic resonance determination of the rotational barrier in benzyl chloride and of the low energy conformations in benzyl bromide and iodide derivatives based on motionally averaged spin–spin interactions

TED SCHAEFER, LEONARD J. KRUCZYNSKI,[1] AND WILLIAM J. E. PARR[1]
Department of Chemistry, University of Manitoba, Winnipeg, Man., Canada R3T 2N2

Received May 3, 1976

TED SCHAEFER, LEONARD J. KRUCZYNSKI, and WILLIAM J. E. PARR. Can. J. Chem. **54**, 3210 (1976).

The long-range spin–spin coupling constants over six bonds between side-chain and ring protons in benzyl chloride derivatives are combined with solutions to the hindered rotor problem to demonstrate that the twofold barrier to internal rotation in benzyl chloride is 2.1 ± 0.4 kcal/mol. The low energy conformation is that in which the C—Cl bond lies in a plane perpendicular to the aromatic plane. Molecular orbital calculations at the MINDO/3 and STO-3G levels indicate that the conformation in which the C—Cl bond lies in a plane having an angle of 60° to the aromatic plane has a higher energy; comparable to kT at ambient temperatures. The geometry-optimized STO-3G results agree quantitatively with the derived barrier for benzyl chloride. A semiempirical relationship between the long-range couplings over four bonds and the internal barrier for a number of benzyl compounds indicates a barrier of 3.1 kcal/mol for benzyl bromide and of 3.6 kcal/mol for benzyl iodide, these values being lower limits. The observed coupling constants are only consistent with low-energy conformations analogous to that for benzyl chloride, so that they contrast with the low-energy conformation for benzyl fluoride in which the C—F bond lies in the aromatic plane. The present method for the determination of twofold barriers in benzyl derivatives is useful in the range from about 0.2 to 2 kcal/mol.

TED SCHAEFER, LEONARD J. KRUCZYNSKI et WILLIAM J. E. PARR. Can. J. Chem. **54**, 3210 (1976).

On combine les constantes de couplage spin–spin à longue distance à travers six liaisons entre les protons de la chaîne latérale et ceux de cycles des dérivés du chlorure de benzyle avec les solutions aux problèmes du rotor empêché pour démontrer que la barrière binaire à la rotation interne dans le chlorure de benzyle est de 2.1 ± 0.4 kcal/mol. La conformation de basse énergie est celle dans laquelle le lien C—Cl se trouve dans un plan perpendiculaire au plan aromatique. Des calculs d'orbitales moléculaires à des niveaux MINDO/3 et STO-3G indiquent que la conformation dans laquelle le lien C—Cl se trouve dans un plan ayant un angle de 60° par rapport au plan aromatique possède l'énergie la plus élevée; cette énergie est comparable à kT à des températures ambiantes. Les résultats STO-3G pour des géométries optimisées sont en bon accord quantitatif avec la barrière dérivée pour le chlorure de benzyle. Une relation semiempirique entre les constantes de couplage à longue distance à travers quatre liaisons et la barrière interne pour un certain nombre de composés benzyliques indique une barrière de 3.1 kcal/mol pour le bromure de benzyle et de 3.6 kcal/mol pour l'iodure de benzyle; ces valeurs sont des limites inférieures. Les constantes de couplage observées sont en accord uniquement avec des conformations de basse énergie analogues à celle du chlorure de benzyle; il n'est donc pas surprenant qu'elles soient en opposition avec la conformation de basse énergie du fluorure de benzyle dans lequel le lien C—F se trouve dans le plan aromatique. La méthode actuelle de déterminer les barrières binaires des dérivés benzyliques est utile dans l'écart de 0.2 à 2 kcal/mol.

[Traduit par le journal]

Introduction

In a recent study (1) of the high resolution nuclear magnetic resonance spectral parameters of benzyl fluoride derivatives, it was argued that the long-range spin–spin coupling constants over six bonds between fluorine nuclei and/or protons in the side chain and protons in the *para* position displayed a $\sin^2\theta$ dependence; θ being the angle defined in **1**. Solution of the hindered rotor problem, followed by the calculation of expectation values for $\sin^2\theta$, allowed the conclusion that **1** is the low-energy conformation

[1]Postdoctoral fellow, 1974–1975.

Can. J. Chem. Downloaded from www.nrcresearchpress.com by 210.87.254.42 on 09/05/12
For personal use only.

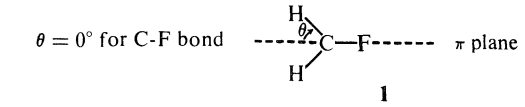

1

for benzyl fluoride and that the twofold barrier to internal rotation is 260 ± 50 cal/mol. This conclusion was in agreement with MINDO/3 and *ab initio* STO-3G molecular orbital calculations.

In this paper a similar study on benzyl chloride derivatives is reported. In addition, the low-energy conformations of benzyl bromide and of benzyl iodide are found. Previous work from this laboratory (2) suggested that the low-energy form of benzyl bromide is **2** and not **3**. This conclusion, although corroborated by the present

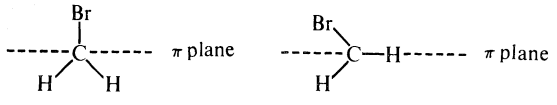

2 3

work, was based on an incorrect premise. Furthermore, an incorrect value for the barrier was deduced from that premise.

Experimental

The compounds were either obtained commercially or were prepared by standard methods. Solvents for spectral work were chosen so as to provide maximal spectral dispersion. Samples for pmr measurements were carefully degassed and contained internal tetramethylsilane. The pmr spectra were repeatedly calibrated at sweep rates of 0.02 or 0.01 Hz/s in the frequency sweep mode on an HA100 spectrometer at a probe temperature of 32 °C.

Molecular orbital calculations on benzyl chloride at the MINDO/3 level of approximation (3, 4) and in the *ab initio* STO-3G formulation (5, 6) were performed on an IBM 370/158 system. Standard geometries (7) were employed initially. Geometry optimization procedures were applied to the CH_2Cl moiety with results to be described below.

Results and Discussion

1. Spectral Analyses

These were relatively straightforward and were performed with the computer program LAME (8, 9). As an example, in Table 1 the spectral parameters for 4-nitrobenzyl iodide are given and correspond to an $AA'BB'X_2$ or $[AB]_2X_2$ spin system. Rather than tabulate all spectral parameters for the many other compounds, Table 2 shows the spectral parameters of immediate interest in this paper: the spin–spin coupling constants between side-chain protons and ring protons.

2. Barrier to Internal Rotation in 3,5-Dichlorobenzyl Chloride

(i) Unqualified Estimate

If a value of $^6J_p^{H,CH_2}$ at $\theta = 90°$ can be found, the observed value of -0.40 Hz for $^6J_p^{H,CH_2}$ in 3,5-dichlorobenzyl chloride will yield an average value of $\langle \sin^2 \theta \rangle$ and, via the procedure mentioned in the introduction and described in ref. 1, a barrier to internal rotation. In toluene, where $\langle \sin^2 \theta \rangle$ is 0.5, ^6J_p is -0.62 Hz (10) and is -0.60 Hz in 3,5-dichlorotoluene (Table 1), corresponding to $^6J_p = -1.22 \pm 0.02$ Hz when $\theta = 90°$. In 3,5-dichlorobenzyl fluoride $^6J_p = -1.02$ Hz when $\theta = 90°$ (1). Such a value is supported by INDO–MO calculations (1, 11), suggesting polarization of the adjacent C—H bonds by fluorine; thereby reducing the magnitude of ^6J_p. The electronegativity of chlorine lies midway between that of hydrogen and of fluorine. A linear dependence of ^6J_p on the

TABLE 1. Proton chemical shifts* and coupling constants† of 4-nitrobenzyl iodide as a 5 mol% solution in benzene-d_6

Parameter	Value‡	Parameter	Value‡
ν_{CH_2}	362.6	$^4J_o^{H,CH_2}$	−0.396(2)
ν_2	659.938(2)	$^5J_m^{H,CH_2}$	0.309(2)
ν_3	761.579(2)	rms deviation	0.0135 Hz
$^3J_o^{H,H}$	8.508(3)	Largest deviation	0.048 Hz
$^4J_m^{H_2,H_2}$	2.118(3)	Peaks observed	53
$^4J_m^{H_3,H_3}$	2.468(3)	Transitions calculated§	128
$^5J_p^{H,H}$	0.461(3)	Peaks assigned	126

*In Hz at 100 MHz to low field of internal TMS.
†In Hz.
‡The numbers in parentheses give the standard deviations in the last place.
§Above a relative intensity of 0.01 of the most intense peaks.

Can. J. Chem. Downloaded from www.nrcresearchpress.com by 210.87.254.42 on 09/05/12
For personal use only.

electronegativity of the halogen atom implies ${}^6J_p^{H,CH_2} = -1.14 \pm 0.02$ Hz when $\theta = 90°$. Then $\langle \sin^2 \theta \rangle = 0.40/1.14 = 0.35 \pm 0.02$. The reduced moment of inertia of 3,5-dichlorobenzyl chloride is 1.43×10^{-38} g cm^2 and the hindered rotor treatment yields the barrier to internal rotation as 2.1 ± 0.4 kcal/mol.

(ii) Qualifications

The treatment in (*i*) assumes that **4** is the low energy form and that the barrier to internal rotation is twofold, displaying a maximum in **5**.

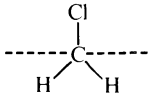

4

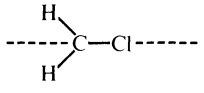

5

This assumption appears reasonable in view of the probable steric repulsion between the C—Cl bond and an *ortho* C—H bond of the aromatic ring in **5**.

An alternative approach, based on Raman depolarization (12) and Kerr constant data (13), assumes **6** as the low energy form[2]. If the barrier is high, say 3 kcal/mol or greater, then -0.40 Hz $= (0.75 + 0)/2 \times {}^6J_p$ $(\theta = 90°)$ and therefore

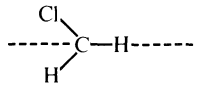

6

${}^6J_p$ $(\theta = 90°)$ is -1.07 Hz, a value which is not absurd. However, if the barrier is considerably smaller, the observed ${}^6J_p$ will tend towards $-1.07/2 = -0.53$ Hz. It follows that **6** is the low-energy form only if the barrier is large or if ${}^6J_p$ $(\theta = 90°)$ is considerably smaller in magnitude than -0.80 Hz, a value considered as unreasonable in view of the spectral and molecular orbital data for benzyl fluoride (1).

Similar remarks apply if **5** is the low-energy form.

(iii) Molecular Orbital Calculations

These were performed in order to confirm **4** as the correct ground state. The MINDO/3 computation on benzyl chloride, after optimization of the bond lengths and bond angles in the C—CH_2Cl fragment, gave the relative energies of **4**, **5**, and **6** as 0.00, 6.06, and 1.67 kcal/mol, respectively; in qualitative agreement with the deductions above.

The STO-3G calculations for a standard geometry yielded the relative energies as 0.00, 4.36, and 0.49 kcal/mol for **4**, **5**, and **6**. Optimization of the bond angles, but not of the bond lengths,[3] in the C—CH_2Cl group resulted in relative energies of 0.00, 2.22, and 0.37 kcal/mol. The predicted barrier of 2.2 kcal/mol happens to agree quantitatively with the barrier deduced from the coupling constants.

The calculated dipole moments of the three conformers differed by as little as 0.2 D, implying minimal solvation perturbations in the low dielectric constant medium.

It may be noted that **6**, suggested as the low-energy form on the basis of Raman depolarization data (12), is calculated to lie only 0.37 kcal/mol above **4**. Classically speaking, at 305 K the population of **6** is about half as large as that of **4**, perhaps accounting for the Raman phenomena. Of course, the energy difference is so small that a classical interpretation becomes ambiguous.

The STO-3G calculations indicate an increase in the C—C—Cl angle of 2° between **4** and **5**, suggesting steric repulsion between the C—Cl bond and the C—H bond of the ring as an important contribution to the barrier.

3. The Barriers in Benzyl Bromide and Iodide Derivatives

The ${}^6J_p^{H,CH_2}$ values of -0.32 and -0.31 Hz, respectively, for 3,5-dichlorobenzyl bromide and iodide are only consistent with a relatively large barrier to internal rotation, ≥ 3 kcal/mol; **2** and **7** being the low energy forms. For, if ${}^6J_p$ $(\theta = 90°)$ is not smaller in magnitude than 1.14 Hz,

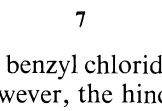

7

as argued for the benzyl chloride, this conclusion must follow. However, the hindered rotor treatment at 32 °C shows that $\langle \sin^2 \theta \rangle$ values become relatively insensitive to the barrier at such barrier values and an actual value cannot be ascertained.

[2]On the other hand, a more recent discussion of infrared and Raman spectra of 4-fluorobenzyl chloride (13*b*) appears to imply the presence of **4**, **5**, and **6**.

[3]The cpu time for one optimization was as large as 3 h, so that more extensive calculations become too expensive.

Can. J. Chem. Downloaded from www.nrcresearchpress.com by 210.87.254.42 on 09/05/12
For personal use only.

Can. J. Chem. Downloaded from www.nrcresearchpress.com by 210.87.254.42 on 09/05/12
For personal use only.

A semiempirical estimate can be made in a manner described below.

The previous estimate of the barrier in *p*-methylbenzyl bromide (2) was based on an incorrect value for $^6J_p^{H,CH_2}$ ($\theta = 90°$) of -0.84 Hz (see next section) and is unreasonably low. Note, however, that $^7J_7^{CH_2,CH_3}$ is $+0.34$ Hz in this compound, thereby confirming the σ–π electron mechanism (14) for $^6J_p^{H,CH_2}$ in a benzyl bromide and hence affirming the $\sin^2\theta$ dependence of the latter coupling.

4. The Anomalous $^6J_p^{H,CH_2}$ in 2,6-Dichloro Compounds

As discussed previously for benzyl fluoride, the low values of $^6J_p^{H,CH_2} \sim -0.2$ Hz for the

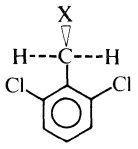

8

X = F, Cl, Br, I

conformations **8**, having a high barrier to internal rotation (15), most likely arise from a hyperconjugative interaction of the C—X bond with the π electron system in the aromatic ring (1). For the benzyl chloride, the MINDO/3 optimization procedures gave 91.7° for the C—C—Cl angle for the conformation analogous to **8**, suggesting a hyperconjugative stabilization of this small angle. As a result the methylene protons move towards the nodal plane of the π electrons, the C—C—H angle becoming 123.1° and reducing ^6J_p below the magnitude expected for tetrahedral bond angles at the methylene carbon atom. Photoelectron spectra (16), electron spin resonance data (17), as well as EHMO calculations (18), are consistent with such a hyperconjugative interaction in the benzyl halides.

Were the value of -0.21 Hz in 2,6-dichlorobenzyl bromide unmodified by such stabilization, $^6J_p^{H,CH_2}$ ($\theta = 90°$) would be -0.84 Hz. This assumption led to an underestimate of the barrier to internal rotation in *p*-methylbenzyl bromide (2).

On the other hand, the angle optimized STO-3G geometry for benzyl chloride yields 113° for the C—C—Cl angle and 110.6° for the C—C—H angle in **4**, in disagreement with the preceding explanation. However, an optimization of bond lengths *and* angles in **8** itself might well provide support for such an explanation. Thus, in **4** the hydrogen atoms in the C—H bonds of the CH_2Cl group carry a positive charge of 0.1 electron units and the chlorine atom a negative charge of 0.17 units. On the assumption that ring C—Cl bonds are similarly polarized in **8**, electrostatic attractions will tend to increase the C—C—H angle towards 120°.

TABLE 2. Long-range spin–spin coupling constants* between methylene protons and ring protons in some derivatives of toluene and benzyl chloride, bromide, and iodide

Derivative	$^4J_o^{H,CH_2}$	$^5J_m^{H,CH_2}$	$^6J_p^{H,CH_2}$
α,2,6-tri Cl (10 w/w% CS_2)	—	0.35	−0.20
α,3,5-tri Cl (5 mol% C_6D_6)	−0.52	—	−0.40
α,2,4-tri Cl (10 mol% C_6D_6)	−0.49	0.34 0.34	—
α,2,3-tri Cl (10 mol% CS_2)	−0.49	0.29	−0.35
α,3,4-tri Cl (10 mol% CS_2)	−0.53(H_2) −0.54(H_6)	0.28	—
α-Br-2,6-di Cl (10 mol% C_6D_6)	—	0.36	−0.21
α-Br-3,5-di Cl (10 mol% C_6D_6)	−0.44	—	−0.32
α-Br-4-NO_2 (8 mol% acetone)	−0.42	0.26	—
α-I-2,6-di Cl (10 mol% C_6D_6)	—	0.39	−0.24
α-I-3,5-di Cl (15 mol% C_6D_6)	−0.40	—	−0.31
CH_3; 2,6-di Cl (5 mol% CS_2)	—	0.38	−0.63
CH_3; 3,5-di Cl (3 mol% C_6D_6)	−0.72	—	−0.60

*In Hz, accurate to 0.02 Hz, sometimes to 0.01 Hz.

5. An Estimate of the Barrier in Benzyl Bromide and Iodide Based on $^4J_o^{H,CH_2}$

In Fig. 1, $^4J_o^{H,CH_2}$ in 3,5-dihalobenzyl-X compounds (Table 2) is plotted *vs.* the barrier to internal rotation obtained from the hindered rotor treatment. For X=F and CH_3 the data are taken from refs. 1 and 20. The barrier in toluene is 0.014 kcal/mol (21) and is taken as that in 3,5-dichlorotoluene. The arrows represent

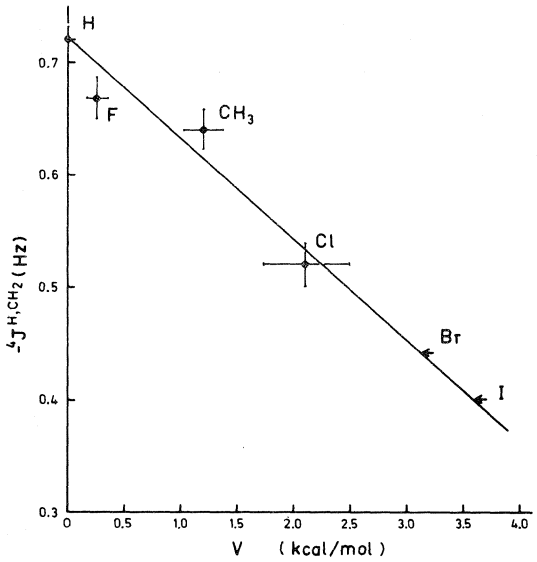

FIG. 1. The coupling constant over four bonds, ${}^4J_o^{H,CH_2}$, between side-chain protons and ring protons in a number of 3,5-dichlorobenzyl derivatives is plotted *vs.* the barrier to internal rotation, as determined by methods described in the text.

the barriers of 3.1 and 3.6 kcal/mol for benzyl bromide and benzyl iodide, respectively.

INDO–MO calculations of ${}^4J_o^{CH_3,H}$ in toluene (14) indicate a predominant σ–π contribution (depending on $\sin^2\theta$ in the manner of ${}^6J_p^{CH_3,H}$); modified, however, by a σ electron contribution which skews the angle dependence and, in particular, has substantial magnitudes at $\theta = 0°$ and 180° (C—H bond in aromatic plane). Consequently, although the rough relationship in Fig. 1 is plausible, the finite σ electron contribution to ${}^4J_o^{H,CH_2}$ entails unknown errors in any hindered rotor model applied to this coupling.

If the σ electron contribution were zero, then -0.72 Hz in the toluene would represent half of ${}^4J$ ($\theta = 90°$) because $\langle\sin^2\theta\rangle$ is one-half for a negligible barrier. Conformations **2** and **7** correspond to a $\langle\sin^2\theta\rangle$ of 0.25 for a large barrier and therefore the minimum value of ${}^4J$ would be $-1.44/4 = -0.38$ Hz, just smaller in magnitude than the observed value for benzyl iodide (iodine having a relatively low electronegativity). An average σ electron component could be subtracted, in which case the relationship observed in Fig. 1 is certainly less than absurd. Furthermore, note that the ${}^6J_p^{H,CH_2}$ values for benzyl bromide and iodide are entirely consistent with the barrier values indicated in Fig. 1.

6. Substituent Effects on Long-range Couplings

It is evident from the data in Tables 1 and 2 that substituents *meta* or *para* to the CH_2X group cause very minor changes in the long-range coupling constants of interest. For example, ${}^4J_o^{H,CH_2}$ is -0.40 Hz in both 4-nitro- and in 3,5-dichlorobenzyl iodide. The presence of substituents, other than those placed *ortho* to the CH_2X group, is an advantage because more precise spectral analyses are then possible. The accuracy of the small couplings is therefore higher.

Conclusions

The benzyl halides adopt low-energy conformations in which the C–halogen bond either lies in a plane perpendicular to the aromatic plane (Cl, Br, I) or in the aromatic plane (F). The conformation in which the C–halogen bond lies in a plane at 60° to the aromatic plane has an intermediate energy, comparable to kT at ambient temperatures. The twofold barrier to internal rotation rises from about 0.25 kcal/mol for benzyl fluoride to about 2.1 kcal/mol in benzyl chloride and is very likely greater than 3 kcal/mol in benzyl bromide and benzyl iodide.

The derivation of barrier heights in solution based on nuclear spin–spin couplings over six bonds is reasonably reliable for barriers lying between about 0.2 and 2 kcal/mol. The coupling over four bonds gives an indication of whether the internal barrier is very small or relatively large and may prove useful for compounds more complex than those considered here.

Acknowledgments

We are grateful to the National Research Council of Canada for financial support and to the Computer Center at the University of Manitoba for the provision of some computer time.

1. T. SCHAEFER, J. B. ROWBOTHAM, W. J. E. PARR, K. MARAT, and A. F. JANZEN. Can. J. Chem. **54**, 1322 (1976).
2. K. CHUM, J. B. ROWBOTHAM, and T. SCHAEFER. Can. J. Chem. **52**, 3489 (1974).
3. R. C. BINGHAM, M. J. S. DEWAR, and D. H. LO. J. Am. Chem. Soc. **97**, 1285 (1975).
4. Program #279. Q.C.P.E. University of Indiana, Bloomington, Indiana.

Can. J. Chem. Downloaded from www.nrcresearchpress.com by 210.87.254.42 on 09/05/12
For personal use only.

5. W. J. HEHRE, L. RADOM, and J. A. POPLE. J. Am. Chem. Soc. **94**, 1496 (1972).
6. Program #236. Q.C.P.E. University of Indiana, Bloomington, Indiana.
7. J. A. POPLE and M. S. GORDON. J. Am. Chem. Soc. **89**, 4253 (1967).
8. S. CASTELLANO and A. A. BOTHNER-BY. J. Chem. Phys. **41**, 3863 (1964).
9. C. W. HAIGH and J. M. WILLIAMS. J. Mol. Spectrosc. **32**, 398 (1969).
10. M. P. WILLIAMSON, R. J. KOSTELNIK, and S. M. CASTELLANO. J. Chem. Phys. **49**, 2218 (1968).
11. J. A. POPLE and D. L. BEVERIDGE. Approximate molecular orbital theory. McGraw-Hill Book Company, New York, N.Y. 1970.
12. L. VERDONCK and G. P. VAN DER KELEN. Spectrochim. Acta, Part A, **28**, 51 (1972); **28**, 55 (1972).
13. (*a*) K. E. CALDERBANK, R. J. W. LE FÈVRE, and R. K. PIERENS. J. Chem. Soc. B, 1463 (1970); (*b*) W. A. SETH-PAUL and H. SHINO. Spectrochim. Acta, Part A, **31**, 1605 (1975).
14. R. WASYLISHEN and T. SCHAEFER. Can. J. Chem. **50**, 1852 (1972).
15. J. PEELING, J. B. ROWBOTHAM. L. ERNEST, and T. SCHAEFER. Can. J. Chem. **52**, 2414 (1974).
16. H. SCHMIDT and A. SCHWEIG. Tetrahedron Lett. 981 (1973).
17. K. S. CHEN, P. J. KRUSIC, P. MEAKIN, and J. K. KOCHI. J. Phys. Chem. **78**, 2014 (1974).
18. I. BIDDLES and A. HUDSON. Chem. Phys. Lett. **18**, 45 (1973).
19. P. A. SCHERR, M. D. GLICK, J. H. SIEFERT, and R. D. BACH. J. Am. Chem. Soc. **97**, 1782 (1975).
20. T. SCHAEFER, W. NIEMCZURA, and L. KRUCZYNSKI. Chem. Phys. Lett. **38**, 498 (1976).
21. H. D. RUDOLPH, H. DREIZLER, A. JAESCHKE, and P. WENDLING. Z. Naturforsch. Teil A, **22**, 940 (1967).

Can. J. Chem. Downloaded from www.nrcresearchpress.com by 210.87.254.42 on 09/05/12
For personal use only.

A proton magnetic resonance and molecular orbital study of the conformational preferences of the vinylic fragment in some 2-vinylfurans and in 2-vinylthiophene

WILLIAM J. E. PARR,[1] RODERICK E. WASYLISHEN,[2] AND TED SCHAEFER

Department of Chemistry, University of Manitoba, Winnipeg, Man., Canada R3T 2N2

Received May 17, 1976

WILLIAM J. E. PARR, RODERICK E. WASYLISHEN, and TED SCHAEFER. Can. J. Chem. **54**, 3216 (1976).

The stereospecific spin–spin coupling constants over five bonds between the α-proton in the side chain and the protons in the heterocycle in 2-vinylfuran, in its β-nitro and β-aldehydic derivatives, and in 2-vinylthiophene are used to demonstrate the preponderance of the *s-trans* conformers in polar and nonpolar solutions. These conclusions are compared with predictions made by molecular orbital theory at the STO-3G, INDO, CNDO/2, and MINDO/3 levels. Long-range coupling constants between the protons in the side chain and protons in the heterocycle are calculated by CNDO/2 and INDO–MO–FPT and are compared with experiment. It is concluded that the five-bond couplings involving the α-proton are most sensitive to conformation and that they are transmitted mainly via a σ electron mechanism. The other long-range coupling constants are discussed in terms of σ and π electron mechanisms. The STO-3G calculations yield barriers to internal rotation of greater than 4.8 kcal/mol.

WILLIAM J. E. PARR, RODERICK E. WASYLISHEN et TED SCHAEFER. Can. J. Chem. **54**, 3216 (1976).

Afin de démontrer la prédominance des conformères *s-trans* dans des solvants polaires et non polaires, on fait appel aux constantes de couplage spin–spin stéréospécifiques à travers cinq liaisons entre les protons α de la chaîne latérale et les protons du vinyl-2 furanne et de ses dérivés β-nitro, β-aldéhydo, et du vinyl-2 thiophène. On compare ces conclusions avec les prédictions faites par des calculs théoriques d'orbitales moléculaires aux niveaux STO-3G, INDO, CNDO/2 et MINDO/3. On a calculé les constantes de couplage à longue distance entre les protons de la chaîne latérale et les protons des hétérocycles à l'aide des méthodes CNDO/2 et INDO–MO–FPT et on les a comparées avec les résultats expérimentaux. On en conclut que les couplages à travers cinq liaisons impliquant le proton α sont les plus sensibles aux effets de conformation et qu'ils sont transmis par l'intermédiaire d'un mécanisme électronique σ. On discute des autres constantes de couplage à longue distance en termes de mécanismes électroniques σ et π. Les calculs STO-3G prédisent des barrières à la rotation interne qui sont plus grandes que 4.8 kcal/mol.

[Traduit par le journal]

Introduction

The five bond spin–spin coupling constant, ^5J, between side-chain protons and ring protons in aromatic compounds is known to be highly stereospecific (1–7), and to be transmitted mainly via a σ electron mechanism (2, 8) when the bonds containing the protons lie in the aromatic plane. The coupling has been used to deduce the preferred conformation of side-chain substituents in benzaldehydes (2), phenols (7), styrenes (4), vinylpyridines (9), and in a number of furan derivatives substituted at the 2-position (1, 10–13). It has also been discussed for benzofurans and benzothiophenes (14–16).

In this paper, the stereospecificity of ^5J, together with the results of molecular orbital calculations at both the *ab initio* (STO-3G) and semiempirical (MINDO/3, CNDO/2, INDO) levels of molecular orbital theory is used to find the preferred conformation of the vinylic side chain in several 2-vinylfuran derivatives and in 2-vinylthiophene. In addition, the mechanisms by which the various long-range couplings in these compounds are transmitted are discussed in the light of a comparison of the experimental values with those predicted by finite-perturbation calculations at the INDO and CNDO/2 levels.

[1]Postdoctoral Fellow, 1974–1976.

[2]Present Address, Chemistry Department, University of Winnipeg, Winnipeg, Manitoba.

Can. J. Chem. Downloaded from www.nrcresearchpress.com by 210.87.254.5 on 09/05/12
For personal use only.

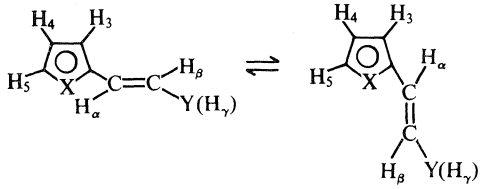

s-cis *s-trans*

1 **2**

X = O; Y = H_γ
Y = CHO
Y = NO_2
X = S; Y = H_γ

The numbering scheme is shown in **1** and **2**. A third conformer in which the X—C—C—H_α dihedral angle is 90° will be referred to as the *s*-90 conformer. If Y = CHO or NO_2, these fragments are taken as coplanar with the carbon–carbon double bond. The aldehydic proton in 2-furanacrolein is considered to be *cis* to H_α, in line with the available information on other *trans*-substituted acroleins (16*b*).

Experimental

2-Vinylthiophene and 2-vinylfuran were prepared according to the literature (16*c*), and the other compounds were of commercial origin. Samples containing a little tetramethylsilane (TMS) were made up to the required concentrations and were degassed by the freeze–pump–thaw technique.

Proton magnetic resonance spectra were obtained on a Varian HA-100D spectrometer operating in the frequency-sweep mode; sweep widths of 1 Hz/cm, together with sweep rates of 0.02 Hz/s were employed. Appropriate double irradiation experiments were used to obtain the relative signs of the long-range coupling constants. The probe temperature was 32 °C (305 K).

Molecular orbital calculations at the STO-3G (17), MINDO/3 (18), CNDO/2, and INDO–MO–FPT (19) levels were performed on an IBM 370/158 system. Ring geometries used in these calculations were taken from microwave data (20, 21), whilst standard geometries (22) were used for the vinylic fragments.

Results and Discussion

1. Spectral Analyses

All spectra were analysed with the aid of the computer program LAME (23). The final chemical shifts and coupling constants are listed in Tables 1 and 2.

The spectrum of 2-vinylthiophene was strongly second-order in nature and the experimental spectrum of this compound in benzene-d_6, together with the simulated spectrum, is illustrated in Fig. 1. The rms error for this simulation was 0.017 Hz and the largest standard deviation in a parameter set was 0.008 Hz. In the computer fit, only $J_{\alpha 3}$ was set negative. Because $J_{\beta 5}$ and/or $J_{\gamma 5}$ could possibly be negative also, simulations were performed with negative values for these couplings and are shown in Fig. 1. Inspection of the region at which H_5 resonates clearly shows that neither $J_{\beta 5}$ nor $J_{\gamma 5}$ can be negative, although the complex nature of the spectrum prevented further confirmation by suitable double resonance experiments. The sign of $J_{\beta 4}$ could not be determined.

The ring couplings and vinylic couplings in these compounds were assumed positive in all cases, and the relative signs of the long-range

TABLE 1. Spin–spin coupling constants in Hz* between olefinic and ring protons in furan and thiophene derivatives

	2-Vinylfuran		β-Nitrovinylfuran		2-Furanacrolein		2-Vinylthiophene	
Parameter	CS_2† (20%)	$(CD_3)_2C{=}O$ (20%)	CS_2 (2%)	$(CD_3)_2C{=}O$ (10%)	CS_2 (10%)	$(CD_3)_2C{=}O$ (24%)	C_6D_6 (20%)	$(CD_3)_2C{=}O$ (30%)
$^4J_{\alpha,3}$‡	−0.43	-0.43_5	−0.42	-0.40_5	−0.45	−0.40	−0.64	-0.61_5
$^5J_{\alpha,4}$	0.24	0.25	0.24	0.29	0.24	0.26	0.16	0.16
$^5J_{\alpha,5}$	0.44	0.43	0.54	0.53	0.46	0.48	0.73_5	0.72
$^5J_{\beta,3}$	0.50	0.54	0.58	0.58	0.49	0.50	0.42	0.44_5
$^5J_{\gamma,3}$	0.42	0.42	—	—	—	—	0.37	0.36
$^6J_{\beta,4}$	±0.02	±0.02	±0.06	±0.03	0.00	0.00	±0.05	±0.04
$^6J_{\beta,5}$	0.45	0.43	0.50	0.48	0.46	0.47	0.36	0.34
$^6J_{\gamma,4}$	0.15	0.14_5	—	—	0.00§	0.00§	0.24	0.25
$^6J_{\gamma,5}$	0.41	0.40	—	—	0.00§	0.00§	0.42	0.41

*Estimated accuracy is 0.02 Hz, standard errors normally lying below 0.01 Hz.
†Concentrations are given in mol%.
‡The labelling follows **1** and **2** in the text.
§These refer to coupling of the aldehydic proton.

Can. J. Chem. Downloaded from www.nrcresearchpress.com by 210.87.254.5 on 09/05/12
For personal use only.

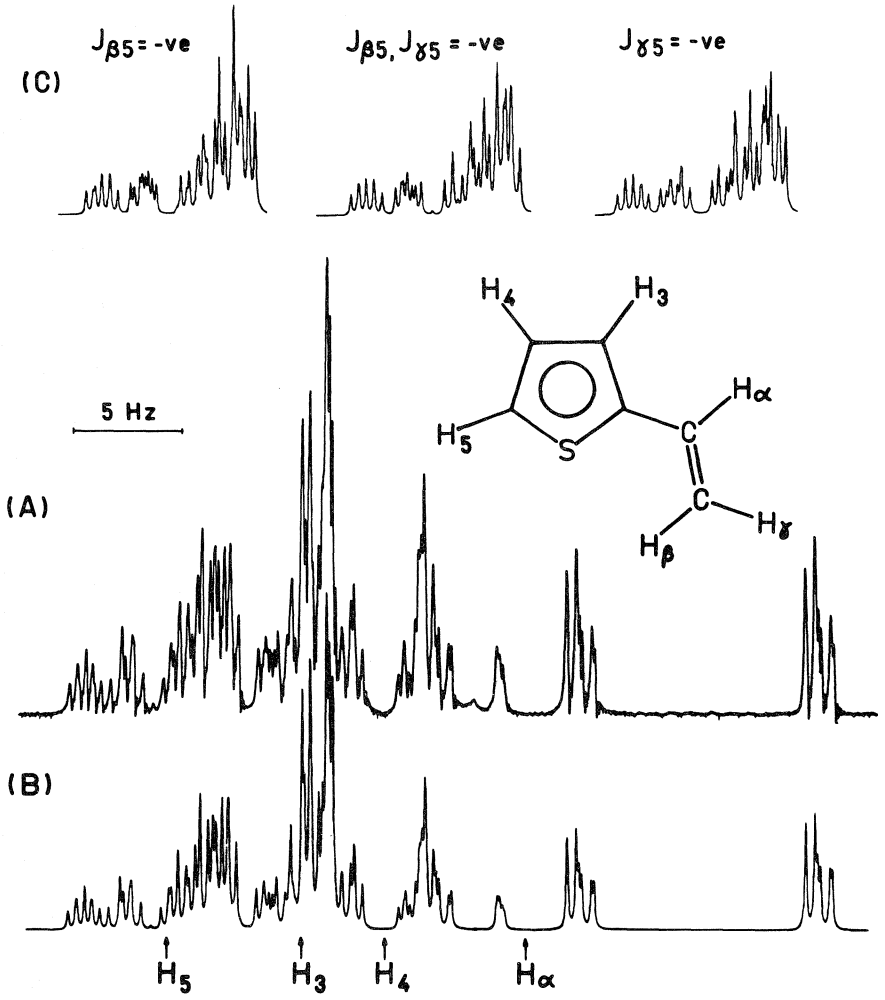

FIG. 1. The proton magnetic resonance spectrum at 100 MHz of a 20 mol% solution of 2-vinylthiophene in benzene-d_6, omitting the resonance peaks of two olefinic protons, is shown in *A*. In *B* the calculated spectrum is displayed for the signs of coupling constants given in Table 1. In *C* other possible sign combinations yield the calculated spectra in the region near the chemical shift of H_5.

couplings were extracted on this basis by suitable double resonance experiments on β-nitrovinylfuran and 2-vinylfuran. The vinylic protons in β-nitrovinylfuran gave spectral lines which were considerably broadened, presumably by incompletely relaxed coupling to the nitrogen quadrupole. The spectral parameters for the four compounds are given in Tables 1 and 2. The proton spectrum of β-nitrovinylfuran has been reported (24). The signs of the long-range couplings were not given but the magnitudes agree with the data in Table 1 except for $^4J_{\alpha 3}$.

2. Calculated Barriers to Rotation

For all four compounds, the STO-3G results in Table 3 indicate a substantial barrier to rotation about the carbon–carbon single bond, the *s*-90 conformation being less stable by 4.8 to 8.4 kcal/mol. The energy difference between the two planar conformations in a given compound, however, is predicted to be quite small (<1.0 kcal/mol), suggesting that both conformers are appreciably populated at 305 K. The *s-trans* conformation is calculated as more stable.

In styrene STO-3G gives the rotational barrier

Can. J. Chem. Downloaded from www.nrcresearchpress.com by 210.87.254.5 on 09/05/12
For personal use only.

TABLE 2. Other spectral parameters in furan and thiophene derivatives

	2-Vinylfuran		β-Nitrovinylfuran		2-Furanacrolein		2-Vinylthiophene	
Parameter	CS_2	$(CD_3)_2C{=}O$	CS_2	$(CD_3)_2C{=}O$	CS_2	$(CD_3)_2C{=}O$	C_6D_6	$(CD_3)_2C{=}O$
ν_α*	638.70	651.99	766.0	790.0	714.17	742.95	659.75	682.98
ν_β	557.02	560.58	736.69	756.58	643.81	651.12	547.59	552.56
ν_γ	504.76	510.12	—	—	952.96	964.93	491.33	508.69
ν_3	610.54	629.95	681.29	715.07	670.17	694.63	669.99	700.15
ν_4	622.90	636.74	653.44	667.02	646.42	661.47	666.19	694.34
ν_5	719.74	740.69	752.89	779.75	750.41	774.10	676.12	723.38
$^3J_{\alpha\beta}$	17.49	17.57	13.26	13.30	15.68	15.74	17.36	17.41
$^3J_{\alpha\gamma}$	11.28	11.32	—	—	−0.16†	−0.17†	10.85	10.89
$^2J_{\beta\gamma}$	1.47	1.52	—	—	7.70†	7.88†	0.80	0.85
$^3J_{34}$	3.29	3.32	3.48	3.55	3.46	3.47	3.54	3.53
$^3J_{45}$	1.82	1.87	1.82	1.83	1.80	1.83	5.09	5.11
$^4J_{35}$	0.80	0.78	0.72	0.72	0.74	0.72	1.18	1.19

*In Hz at 100 MHz to low field of internal TMS, concentrations as in Table 1.
†These are couplings to the aldehydic proton.

TABLE 3. Computed conformational energies and dipole moments

	STO-3G		INDO		CNDO/2		MINDO/3	
Compound	*E* (kcal/mol)	μ (D)	*E* (kcal/mol)	μ (D)	*E* (kcal/mol)	μ (D)	*E* (kcal/mol)	μ (D)
2-Vinylfuran								
s-trans	0.000	0.33	0.155	0.82	0.000	0.88	1.895	0.21
s-cis	0.617	0.39	0.000	0.64	0.171	0.69	0.397	0.40
s-90	6.139	0.42	3.237	0.66	2.915	0.70	0.000	0.40
β-Nitrovinylfuran								
s-trans	0.000	4.95	0.000	6.34	0.000	6.54	0.871	6.90
s-cis	0.950	4.82	0.315	6.15	0.375	6.34	0.000	6.83
s-90	8.402	4.10	5.91	5.39	—	—	1.059	5.99
2-Furanacrolein*								
s-trans	0.000	2.56	0.310	4.08	0.000	3.95	1.726	4.44
s-cis	0.557	2.09	0.000	3.23	0.047	3.03	0.000	4.10
s-90	7.281	1.86	5.146	3.10	—	—	0.615	3.74
2-Vinylthiophene								
s-trans	0.000	0.14	—	—	0.000	—	0.000	2.07
s-cis	0.338	0.24	—	—	2.904	—	2.835	2.13
s-90	4.85	0.30	—	—	2.458	—	0.726	2.09

*C=O *trans* to olefinic C=C, other conformations defined in **1** and **2** of the text.

as 1.9 kcal/mol, (25) in good agreement with a recent measurement (26), suggesting that calculations at the STO-3G level give reasonably reliable estimates of the rotational barriers in vinylic compounds. The relative energies of the two planar conformations are computed to be similar to those reported for vinylpyridines (9) and for substituted styrenes (4). STO-3G predicts the rotational barrier to increase in 2-vinylfuran derivatives as the electron-withdrawing power of substituent Y increases, understandable in terms of a corresponding increase in conjugation available in the planar conformations only.

INDO calculations predict that rotational barriers in the vinylfurans are rather smaller than those given at the *ab initio* level, but concur in finding only small energy differences between *s-cis* and *s-trans* conformations. Unfortunately, the *s-cis* conformers of 2-furanacrolein and β-nitrovinylfuran are predicted to be a little more stable than the *s-trans* conformers; not compatible with the observed stereospecific five-bond coupling constants (see below). This apparent

Can. J. Chem. Downloaded from www.nrcresearchpress.com by 210.87.254.5 on 09/05/12
For personal use only.

Can. J. Chem. Downloaded from www.nrcresearchpress.com by 210.87.254.5 on 09/05/12
For personal use only.

TABLE 4. Long-range proton spin–spin coupling constants calculated by CNDO/2 and INDO–MO–FPT

Parameter*	2-Vinylfuran			β-Nitrovinylfuran			2-Furanacrolein			2-Vinylthiophene		
	s-trans	*s-cis*	*s*-90	*s-trans*	*s-cis*	*s*-90	*s-trans*	*s-cis*	*s*-90	*s-trans*	*s-cis*	*s*-90
$^4J_{\alpha,3}$	I(C) −1.00(−0.25)	−0.91(−0.17)	−2.19(0.01)	I(C) −1.01(−0.23)	−0.94(−0.16)	−2.14	I(C) −1.07(−0.23)	−1.19(−0.16)	−2.22	C −0.59	−0.42	0.06
$^5J_{\alpha,4}$	I(C) 0.12(0.03)	0.99(0.52)	1.00(0.07)	I(C) 0.14(0.04)	0.93(0.49)	0.92	I(C) 0.11(0.02)	1.11(0.54)	1.04	C 0.00	0.57	0.09
$^5J_{\alpha,5}$	I(C) 0.76(0.55)	−0.20(0.08)	−1.17(0.06)	I(C) 0.67(0.56)	−0.22(0.09)	−1.11	I(C) 0.73(0.60)	−0.42(0.07)	−1.06	C 0.93	0.13	0.11
$^5J_{\beta,3}$	I(C) 0.65(0.02)	0.57(−0.06)	0.29(0.02)	I 0.62	0.41	0.23	I 0.65	0.78	0.33	C 0.01	−0.10	0.07
$^5J_{\gamma,3}$	I(C) 0.62(0.03)	0.57(−0.04)	0.00(0.04)	I —	—	—	I −0.44‡	−0.39‡	−0.11‡	C 0.04	−0.09	0.16
$^6J_{\beta,4}$	I(C) −0.21(0.06)	−0.25(0.01)	−0.12(0.03)	I −0.22	−0.10	−0.22	I −0.17	−0.32	−0.15	C 0.09	0.03	0.04
$^6J_{\beta,5}$	I(C) 0.39(−0.01)	0.44(0.04)	−0.01(0.03)	I 0.40	0.51	−0.03	I 0.37	0.60	−0.03	C −0.03	0.07	0.06
$^6J_{\gamma,4}$	I(C) 0.16(0.25)	−0.25(0.02)	0.09(−0.07)	I —	—	—	I 0.18‡	0.15‡	0.07‡	C 0.41	0.04	0.11
$^6J_{\gamma,5}$	I(C) 0.41(0.00)	0.80(0.21)	−0.07(0.08)	I —	—	—	I −0.30‡	−0.26‡	0.07‡	C 0.00	0.39	0.16

*In Hz, conformations defined in **1** and **2** of the text.
†I stands for INDO and C for CNDO/2.
‡Here γ stands for the aldehyde proton, implying an extra bond between the protons. Note that these couplings are not observed (Table 1).

TABLE 5. Calculated and estimated percentage of the *trans* form

Compound	STO-3G	INDO	CNDO/2	MINDO/3	Experimental A*	Experimental B†
2-Vinylfuran	73	44	57	3	65	57
β-Nitrovinylfuran	83	63	65	17	70	63
2-Furanacrolein	71	37	52	4	66	59
2-Vinylthiophene	64	—	80	76	80	77(74)‡

*Based on the magnitudes of $^5J_{\alpha 4}$ and $^5J_{\alpha 5}$ and on the assumption that $J_{\alpha 4}^2$ and $J_{\alpha 5}^1$ are zero and that $J_{\alpha 4}^1 = J_{\alpha 5}^2$. Superscripts refer to structures **1** and **2** in the text.
†Based on the assumptions above with the difference that $J_{\alpha 4}^1 = 0.75 J_{\alpha 5}^2$.
‡As before but $J_{\alpha 4}^1 = 0.61 J_{\alpha 5}^2$.

failure of the INDO method is similar to that reported for 2-pyridinealdehydes (27) and for 2-furanaldoximes (13).

The results of single geometry MINDO/3 calculations are not encouraging. Not only are the *s-cis* conformers of the 2-vinylfurans predicted as more stable than the *s-trans*, but the energy difference between the two planar forms is indicated as large while the overall barrier to rotation is computed as relatively low. The choice of the *s*-90 conformer of 2-vinylfuran (by MINDO/3) and that of the *s*-90 conformer of 2-vinylthiophene (by CNDO), as the most stable appears incorrect and is similar to other failures involving these methods (28), in which nonplanar forms have been favored in conjugated systems.

3. *Conformational Populations*

(a) Insensitivity to Solvent

The long-range couplings in Table 1 are insensitive to the polarity of the solvent, *e.g.*, $^5J_{\alpha 4}$ and $^5J_{\alpha 5}$ are the same in CS_2 and acetone solutions. These coupling constants are expected and calculated (Table 4) to be highly stereospecific. Apparently the populations of **1** and **2** are negligibly dependent on the dielectric constant of the medium, implying that the relative populations will be closely the same in the gas phase. In terms of Abraham's solvation theory (29), the dipole and electric quadrupole moments of the *s-cis* and *s-trans* conformers must therefore differ very little. The calculated dipole moments in Table 3 do indeed display a relatively small dependence on conformation, in general.[3] The insensitivity to solvent observed for the present compounds contrasts sharply with the behaviour of 2-furanaldehyde (11), which displays widely different conformational populations in solvents of different dielectric constant.

The insensitivity to solvent of the conformational populations indicates that a comparison of experimental deductions of the populations (based on the data in Table 1) with molecular orbital calculations on the isolated molecules is appropriate. The following discussion assumes the validity of such comparisons.

(b) Populations Based on $J_{\alpha 4}$ and $J_{\alpha 5}$

In view of the relatively large rotational barriers calculated by STO-3G, the population of the *s*-90 conformer is likely negligible at 305 K. Furthermore, the large barriers dictate small torsion amplitudes about the C—C bond connecting the fragments. Under these conditions the molecules approximate to two rapidly interconverting forms, **1** and **2**.

In styrene derivatives (4) $^5J_\alpha$ is highly stereospecific and calculations (31) of $^5J_\alpha$ by INDO and CNDO/2 methods show that the latter method is most reliable for this coupling constant. In Table 4, the CNDO/2 results suggest that $J_{\alpha 4}^2$ and $J_{\alpha 5}^1$ are effectively zero[4] and that $J_{\alpha 4}^1 = J_{\alpha 5}^2$. On that assumption, the observed sums of $J_{\alpha 4}$ and $J_{\alpha 5}$ in Table 1 yield the percentage of *trans* populations given in Table 5, where the MO predictions are also found. For example, in 2-vinylfuran $J_{\alpha 4} + J_{\alpha 5} = 0.68$ Hz and hence one has 0.44/0.68 or 65% *trans* form.

On the other hand, in 2-furanaldehyde, admittedly a different bonding situation, $J_{\alpha 4}^2$ and $J_{\alpha 5}^1$ evidently vanish (11) but $J_{\alpha 4}^1 = 0.75 J_{\alpha 5}^2$. If these conditions are taken as an extreme possibility for the vinyl compounds in Table 1, it follows that the percentage of *trans* =

[3]A prediction, based on dipole moment measurements, that β-nitrovinylfuran exists predominantly in the *s-trans* form (30) has only a tenuous basis in terms of the calculated dipole moments in Table 3.

[4]Superscripts refer to structures **1** and **2**.

Can. J. Chem. Downloaded from www.nrcresearchpress.com by 210.87.254.5 on 09/05/12
For personal use only.

$(75J_{\alpha5}/J_{\alpha4})/(1 + 0.75J_{\alpha5}/J_{\alpha4})$. In Table 5 it can then be seen that the *trans* form is still preponderant.

For 2-vinylthiophene the CNDO-2 calculations suggest $J_{\alpha4}{}^{1} = 0.61J_{\alpha4}{}^{2}$. In that event, the abundance of the *trans* form becomes 74%. On the other hand, in benzothiophene (16), the coupling analogous to $J_{\alpha5}{}^{1}$ is 0.03 ± 0.01 Hz while that analogous to $J_{\alpha4}{}^{1}$ is 0.84 ± 0.01 Hz. The sum of these two couplings is equal to the sum of $J_{\alpha4}$ and $J_{\alpha5}$ in Table 1, suggesting that the abundance of the *trans* form is nearer to 80% (see Table 5).

The mean value of the estimates in Table 5 can be compared with the theoretical predictions of the percentage of *trans* form. Both STO-3G and CNDO/2 are consistent in predicting the observed predominance of the *trans* form for the four compounds, the somewhat better agreement indicated for CNDO/2 being marred by the unlikely prediction that the *s*-90 form contributes substantially to the conformational equilibrium of 2-vinylthiophene.

The apparent success of MINDO/3 in predicting the amount of *trans* conformer for 2-vinylthiophene is vitiated by its prediction that the *s*-90 is the other abundant conformer (see Table 3), so that *s-cis* is negligibly populated at 305 K. Such a situation is intuitively unlikely and is contraindicated by the observed (Table 1) and calculated (Table 4) values of $^{5}J_{\alpha4}$ and $^{5}J_{\alpha5}$.

The dominance of the *trans* form for the sulfur compound is similar to that found for 2-thiophenealdehyde (33) which also exists predominantly in the *trans* form.

Finally, it may be noted that the predictions based on the MO theories, which calculate internal energies, can only be directly compared with the experimental estimates, which approximate to free energy differences, if the entropy and volume differences between the conformers are zero. In our opinion the uncertainties in theory and experiment are such that the latter differences can be ignored in the investigation described in this paper.

4. Other Long-range Couplings

As already indicated, the strongly stereospecific five-bond couplings, $J_{\alpha5}$ and $J_{\alpha4}$, are best reproduced by CNDO/2 calculations, implying (31) that they arise from a σ electron mechanism. The INDO parameterization includes one-centre exchange integrals and allows for π electron contributions to the couplings. However, as pointed out by Peat and Reynolds (31), the difference between the values calculated by the two methods does not necessarily represent the calculated π electron contributions, because INDO may well give a different magnitude for the σ electron effects than does CNDO/2. Furthermore, INDO may well overestimate the π electron contributions in systems of this kind (31). Accordingly, only a brief discussion is given of these coupling constants.

(a) The Four-bond Coupling, $J_{\alpha3}$

Both types of calculations indicate a small difference in the magnitudes for $^{4}J_{\alpha3}$ in the two planar forms and therefore suggest that $^{4}J_{\alpha3}$ is not a good measure of conformational populations.

(b) The Five-bond Couplings, $J_{\beta3}$ and $J_{\gamma3}$

CNDO/2 predicts near zero values for all conformations, whereas INDO predicts values only 0.1 Hz larger than observed. Furthermore, $^{5}J_{\beta3}$ is apparently insensitive to conformation. Similar remarks apply to $^{5}J_{\gamma3}$. In 1,3-butadiene derivatives, analogous couplings over five bonds are apparently also dominated by a π electron mechanism (32).

(c) $^{6}J_{\beta4}$ and $^{6}J_{\gamma4}$

$^{6}J_{\gamma4}$ is positive and, in the *s-trans* form, the coupled protons are situated at the ends of an all-*trans* arrangement of intervening bonds. Following an interpretation of an analogous coupling in a styrene derivative (4), $^{6}J_{\gamma4}$ is attributed to a σ electron mechanism. The CNDO/2 calculations, when weighted by the conformational populations estimated from $^{5}J_{\alpha4}$ and $^{5}J_{\alpha5}$, yield 0.16 Hz in 2-vinylfuran (observed value is 0.15 Hz) and 0.31 Hz in 2-vinylthiophene (observed value is 0.25 Hz). $^{6}J_{\beta4}$ is calculated as less than 0.1 Hz in all conformations by CNDO/2, in apparent agreement with experiment (see Tables 1 and 4).

(d) $^{6,7}J_{\beta5}$ and $^{6,7}J_{\gamma5}$

In 2-vinylfuran, comparison of the CNDO/2 and INDO predictions of $J_{\beta5}$ implies the absence of a σ electron mechanism and, because $J_{\beta5}$ is positive, that it is transmitted via a seven-bond route over the ring carbon skeleton and not via a six-bond route involving the oxygen atom. For $J_{\gamma5}$ an additional stereospecific σ electron contribution via an all-*trans* arrangement of

Can. J. Chem. Downloaded from www.nrcresearchpress.com by 210.87.254.5 on 05/05/12
For personal use only.

intervening bonds, including C—O bonds, is indicated by both types of calculation.

The somewhat larger value of $J_{\gamma 5}$ than of $J_{\beta 5}$ observed for 2-vinylthiophene, together with the dominance of the *s-trans* form, may imply that the sulfur atom is more efficient than the oxygen atom in transmitting spin state information for the all-*trans* arrangement of the intervening bonds in the *s-trans* form. The CNDO/2 values in Table 4 imply the same conclusion.

Acknowledgments

We are grateful to the National Research Council of Canada for financial support and to C. Pilger for the preparation of 2-vinylthiophene.

1. B. Roques and M. C. Fournie-Zaluski. Org. Magn. Reson. **3**, 305 (1971).
2. R. Wasylishen and T. Schaefer. Can. J. Chem. **49**, 3216 (1971).
3. H. M. Hutton, J. B. Rowbotham, B. H. Barber, and T. Schaefer. Can. J. Chem. **49**, 2033 (1971).
4. M. Barfield, C. J. Macdonald, I. R. Peat, and W. F. Reynolds. J. Am. Chem. Soc. **93**, 4195 (1971).
5. R. Wasylishen, J. B. Rowbotham, L. Ernst, and T. Schaefer. Can. J. Chem. **50**, 2575 (1972).
6. S. Forsén and R. A. Hoffman. J. Mol. Spectrosc. **20**, 168 (1966).
7. J. B. Rowbotham and T. Schaefer. Can. J. Chem. **52**, 3037 (1974).
8. S. Forsén, B. Åkermark, and T. Alm. Acta Chem. Scand. **18**, 2313 (1964).
9. J. B. Rowbotham and T. Schaefer. Can. J. Chem. **52**, 136 (1974).
10. B. Roques and S. Combrisson. Can. J. Chem. **51**, 573 (1973).
11. B. Larsen, F. Nicolaisen, and J. Nielsen. Acta Chem. Scand. **26**, 1736 (1972); R. J. Abraham and T. M. Siverns. Tetrahedron, **28**, 3015 (1972).
12. B. Roques, M. C. Fournie-Zaluski, and C. Chatain-Cathaud. Org. Magn. Reson. **7**, 167 (1975).
13. R. Wasylishen and T. Schaefer. Can. J. Chem. **50**, 274 (1972).
14. L. G. Alexakos and E. N. Givens. Tetrahedron Lett. 4345 (1969).
15. E. V. Blackburn, J. J. Cholerton, and C. J. Timmons. J. Chem. Soc. Perkin Trans. II, 101 (1972).
16. (*a*) F. Bolkau and M. L. Heffernan. Aust. J. Chem. **25**, 327 (1972); (*b*) P. Albriktsen and R. K. Harris. Acta Chem. Scand. **27**, 3993 (1973); (*c*) Organic synthesis. Coll. Vol. 4, J. Wiley and Sons. New York. 1963. p. 980; R. Paul and S. Tchelitcheff. Bull. Chem. Soc. Fr. 453 (1947).
17. W. J. Hehre, R. F. Stewart, and J. A. Pople. J. Chem. Phys. **51**, 2657 (1969); Program #236, Q.C.P.E. Indiana University, Bloomington, Indiana.
18. M. J. S. Dewar, D. H. Lo, and C. A. Ramsden. J. Am. Chem. Soc. **97**, 1311 (1975), and references therein; Program #279, Q.C.P.E., Indiana University, Bloomington, Indiana.
19. J. A. Pople and D. L. Beveridge. Approximate molecular orbital theory. McGraw-Hill Book Company, New York. 1970; Program #141, Q.C.P.E., Indiana University, Bloomington, Indiana.
20. B. Bak, D. Christensen, W. B. Dixon, L. Hansen-Nygaard, J. R. Anderson, and M. Schottländer. J. Mol. Spectrosc. **9**, 124 (1962).
21. B. Bak, D. Christensen, L. Hansen-Nygaard, and J. Rastrup-Andersen. J. Mol. Spectrosc. **7**, 58 (1961).
22. J. A. Pople and M. S. Gordon. J. Am. Chem. Soc. **89**, 4253 (1967).
23. S. Castellano and A. A. Bothner-By. J. Chem. Phys. **41**, 3863 (1964); C. W. Haigh and J. M. Williams. J. Mol. Spectrosc. **32**, 398 (1969).
24. T. N. Huckerby. Tetrahedron Lett. 353 (1971).
25. W. J. Hehre, L. Radom, and J. A. Pople. J. Am. Chem. Soc. **94**, 1496 (1972).
26. L. A. Carreira and T. G. Towns. J. Chem. Phys. **63**, 5283 (1975).
27. W. Danchura, T. Schaefer, J. B. Rowbotham, and D. J. Wood. Can. J. Chem. **52**, 2986 (1974).
28. H.-J. Hofmann and P. Birner. Chem. Phys. Lett. **37**, 608 (1976).
29. R. J. Abraham and E. Bretschneider. *In* Internal rotation in molecules. *Edited by* W. J. Orville-Thomas. J. Wiley and Sons, New York. 1974. Chapt. 13.
30. M. G. Gruntfest, Y. V. Kolodyashnyi, G. F. Potemkin, Z. N. Nazarova, and O. A. Osipov. J. Org. Chem. U.S.S.R. **7**, 1078 (1971), Engl. Trans.
31. I. R. Peat and W. F. Reynolds. Can. J. Chem. **52**, 2403 (1974).
32. M. Bacon and G. E. Maciel. Mol. Phys. **21**, 257 (1971).
33. L. Lunazzi and C. A. Veracini. J. Chem. Soc. Perkin Trans. II, 1739 (1973).

Can. J. Chem. Downloaded from www.nrcresearchpress.com by 210.87.254.5 on 09/05/12
For personal use only.

Reaction of dichlorobis(dimethylsulphoxide)platinum(II) with pyridine and isomerization of dichloro(dimethylsulphoxide)(pyridine)platinum(II)

PI-CHANG KONG, DANIEL IYAMUREMYE, AND F. D. ROCHON

Département de chimie, Université du Québec à Montréal, C.P. 8888, Montréal, Qué., Canada H3C 3P8

Received May 10, 1976

PI-CHANG KONG, DANIEL IYAMUREMYE, and F. D. ROCHON. Can J. Chem. **54**, 3224 (1976).

The reaction between *cis*-[Pt(DMSO)$_2$Cl$_2$] and pyridine, picoline, and lutidine has been studied by nmr techniques. The results obtained with 4-picoline are discussed. *trans*-[Pt(4-pic)-(DMSO)Cl$_2$] is first formed and then isomerizes to a mixture of *cis*- and *trans*-isomers.

cis-[Pt(DMSO)$_2$Cl$_2$] + 4-pic → *trans*-[Pt(DMSO)(4-pic)Cl$_2$] ⇄ *cis*-[Pt(DMSO)(4-pic)Cl$_2$]

An effective method to prepare *cis*-isomers has been derived from this study. The advantages of the new method are discussed.

PI-CHANG KONG, DANIEL IYAMUREMYE et F. D. ROCHON. Can. J. Chem. **54**, 3224 (1976).

La réaction entre *cis*-[Pt(DMSO)$_2$Cl$_2$] et la pyridine, picoline et lutidine, a été étudiée par résonance magnétique nucléaire. Les résultats obtenus avec la picoline-4 sont discutés. Le composé *trans*-[Pt(DMSO)(pic-4)Cl$_2$] est d'abord formé. Il y a ensuite isomérisation en un mélange d'isomères *cis* et *trans*.

cis-[Pt(DMSO)$_2$Cl$_2$] + pic-4 → *trans*-[Pt(DMSO)(pic-4)Cl$_2$] ⇄ *cis*-[Pt(DMSO)(pic-4)Cl$_2$]

Une méthode efficace pour préparer des isomères *cis* a été mise au point. Les avantages de cette nouvelle méthode sont discutés.

Introduction

Nucleosides (Nuc) can displace dimethylsulphoxide (DMSO) rather than the chlorine atoms, from *cis*-[Pt(DMSO)$_2$Cl$_2$] in DMSO solution to form first *trans*-[Pt(DMSO)(Nuc)Cl$_2$], which then isomerizes to the *cis*-compound (1). This lability of the DMSO group, which is coordinated to platinum through the sulphur atom, is quite surprising and led us to a parallel study of the reaction with pyridine derivatives. *Trans*- and *cis*-analogous compounds of pyridine derivatives have already been prepared (2, 5). The study of the reaction of *cis*-[Pt(DMSO)$_2$Cl$_2$] with these bases and of the *cis–trans* isomerization thus becomes straightforward. An effective method to prepare *cis*-isomers was derived from this study.

We have used nmr techniques to identify each compound formed in the system of *cis*-[Pt-(DMSO)$_2$Cl$_2$] and pyridines. Here we discuss the results of this study, and the advantages of the new method for preparing the *cis*-isomers.

Experimental Section

cis-[Pt(DMSO)$_2$Cl$_2$] was prepared according to the method described by Wayland and co-workers (6) and *cis*-[Pt(DMSO)$_2$Br$_2$] by the method described by Kukushkin *et al.* (3).

cis-[Pt(DMSO)(4-pic)Cl$_2$]: 0.047 g of 4-picoline was added to a 3 ml DMSO solution of *cis*-[Pt(DMSO)$_2$Cl$_2$] (0.211 g). The solution was left at room temperature for 2 days and then 1.5 ml of water was added. Needlelike white crystals appeared after 1 day. The crystals were filtered, washed first with water, then with methanol (15 ml, in 3 portions), and air-dried. Yield 75%, mp 178 °C (dec.). *Anal.* calcd: C 21.97, H 2.99, N 7.33; found: C 21.87, 21.75, H 2.90, 2.88, N 7.28.

All other complexes of the type *cis*-[Pt(DMSO)(Py)Cl$_2$] (Py = pyridine, picoline, and lutidine) were prepared in a similar way. *Anal.* calcd. for *cis*-[Pt(DMSO)(2-pic)Cl$_2$], mp 180 °C (dec.), (2-pic = 2-picoline): C 21.97, H 2.99, N 7.33. Found: C 22.15, H 2.73, N 7.49. Calcd. for *cis*-[Pt(DMSO)(2,6-Lu)Cl$_2$], mp 184 °C (dec.) (2,6-Lu = 2,6-lutidine): C 23.97, H 3.35, N 7.11; found: C 23.57, H 3.21, N 6.88. *Anal.* calcd. for *cis*-[Pt(DMSO)(2,6-Lu)-Br$_2$], mp 212 °C (dec.): C 20.00, H 2.78; found: C 20.39, H 2.91.

Results and Discussion

The reaction between *cis*-[Pt(DMSO)$_2$Cl$_2$] and pyridine, picoline or lutidine has been studied in DMSO solution by nmr techniques. The results obtained with 4-picoline are discussed below.

The nmr spectrum of 4-picoline (4-pic) in DMSO solution is shown on Fig. 1. The signals of the *ortho*-protons appear as a doublet at 8.37

Can. J. Chem. Downloaded from www.nrcresearchpress.com by 210.87.254.6 on 09/05/12
For personal use only.

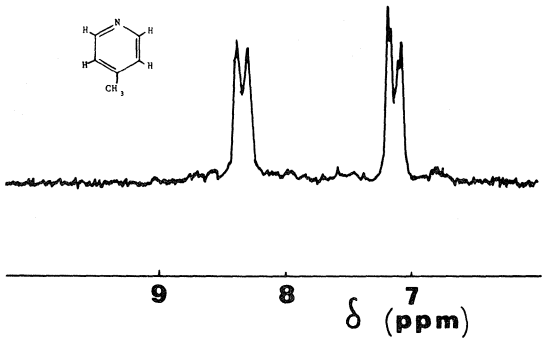

FIG. 1. Nuclear magnetic resonance spectrum of 4-picoline in DMSO solution.

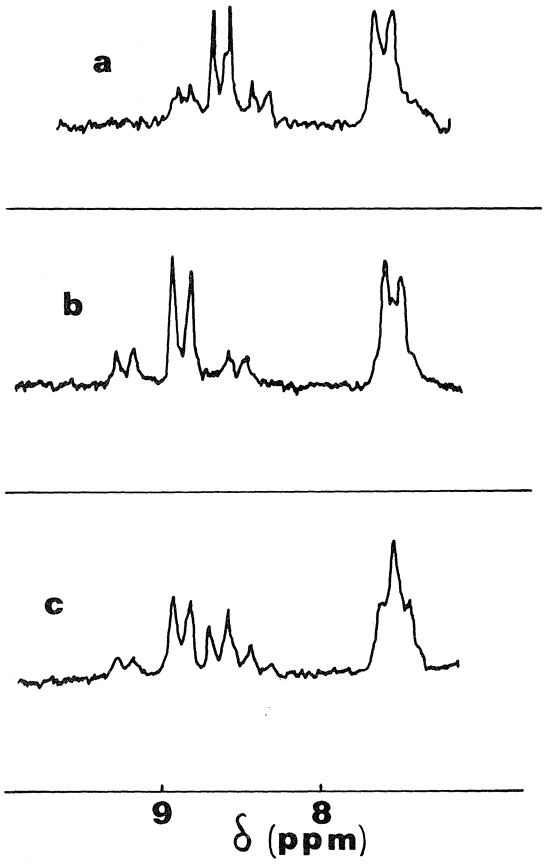

FIG. 2. Nuclear magnetic resonance spectrum of (*a*) *trans*-[Pt(DMSO)(4-pic)Cl_2] in fresh DMSO solution, (*b*) *cis*-[Pt(DMSO)(4-pic)Cl_2] in fresh DMSO solution, (*c*) equilibrium mixture of *cis* and *trans*-isomers.

ppm (δ) while the upfield doublet at 7.10 ppm is caused by the signals of the *meta*-protons. The signal of the methyl group at 2.30 ppm is not shown because of its low sensitivity on complexation.

The nmr spectra of *trans*- and *cis*-[Pt(DMSO)-(4-pic)Cl_2] in fresh DMSO solution are shown in Fig. 2 (*a*) and (*b*) respectively. The signals of the *ortho*-protons have shifted downfield from those of free picoline by 0.15 ppm for the *trans*-isomer and by 0.39 ppm for the *cis*-isomer. Both solutions gave, overnight, an identical equilibrium mixture of *cis* and *trans*-isomers in nearly equal amounts. The spectrum of the mixture is shown in Fig. 2(*c*).

cis-[Pt$(DMSO)_2Cl_2$] and 4-picoline were mixed in a 1:1 ratio in DMSO. The nmr spectrum recorded within 20 min was identical to the one shown in Fig. 2(*a*). The spectrum recorded the next day was the same as the one shown in Fig. 2(*c*). This indicated that a *trans*-compound is first formed. The complex then isomerizes to a mixture of both isomers. The reaction is therefore as follows.

$$\textit{cis}\text{-}[Pt(DMSO)_2Cl_2] + \text{4-pic} \rightarrow \textit{trans}\text{-}[Pt(DMSO)\text{-}(\text{4-pic})Cl_2] \rightleftarrows \textit{cis}\text{-}[Pt(DMSO)(\text{4-pic})Cl_2]$$

Upon addition of water to the mixture of isomers, the *cis*-compound cristallizes out and the above equilibrium is shifted to the right. The new method for synthesizing *cis*-compounds is based on this fact. Although the *trans*-isomer is first formed upon mixing *cis*-[Pt$(DMSO)_2Cl_2$] and pyridine in DMSO solution, it cannot be isolated pure, being contaminated with *cis*-[Pt$(DMSO)_2Cl_2$] or *cis*-[Pt(DMSO)(Py)Cl_2].

The advantages of the proposed method for preparing *cis*-[Pt(DMSO)(Py)Cl_2] are mainly that the starting compound *cis*-[Pt$(DMSO)_2Cl_2$] is easily prepared and very stable. The method can be used to prepare different compounds by using different pyridine derivatives. The final product is pure and no further purification is needed. At the moment, there are two ways to prepare *cis*-[Pt(DMSO)(Py)Cl_2] (Py = pyridine and picoline), *i.e.*, (*a*) the reaction of K[Pt(Py)Cl_3] with DMSO in water (3); and (*b*) the heating of *trans*-[Pt(DMSO)(Py)Cl_2] to its melting point (4, 5). K[Pt(Py)Cl_3] is not as easily prepared as *cis*-[Pt$(DMSO)_2Cl_2$] and it is not very stable in water. Heating *trans*-compounds often causes decomposition and the final products need further purification.

It is worth noting that nucleosides, even in excess, displace just one molecule of DMSO from

Can. J. Chem. Downloaded from www.nrcresearchpress.com by 210.87.254.6 on 09/05/12
For personal use only.

cis-[$Pt(DMSO)_2Cl_2$] and that the compound *trans*-[$Pt(DMSO)(Nuc)Cl_2$] isomerizes completely to the *cis*-isomer (1). But pyridine can displace the two DMSO molecules from *cis*-[$Pt(DMSO)_2Cl_2$] to form *cis*-[$Pt(Py)_2Cl_2$], and *trans*-[$Pt(DMSO)(Py)Cl_2$] isomerizes only partially to the *cis*-isomer.

cis-[$Pt(DMSO)(am)Cl_2$] (am = amine) can also be prepared by this method, by adding water to a DMSO solution of *trans*-[$Pt(DMSO)(am)Cl_2$].

Acknowledgements

Grateful acknowledgement is made to the National Research Council of Canada for financial support and to Johnson Matthey & Co. Limited for the loan of potassium chloroplatinite.

1. P. C. Kong, D. Iyamuremye and F. D. Rochon. Bioinorg. Chem. **6**, 83 (1976).
2. Yu. N. Kukushkin, Yu. E. Vyaz'menskii, and L. I. Zorina. Russ. J. Inorg. Chem. **13**, 1573 (1968).
3. Yu. N. Kukushkin, Yu. E. Vyaz'menskii, L. I. Zorina, and Yu. L. Pazukhina. Russ. J. Inorg. Chem. **13**, 835 (1968).
4. Yu. N. Kukushkin and E. D. Ageeva. Russ. J. Inorg. Chem. **17**, 767 (1972).
5. Yu. N. Kukushkin and Yu. E. Vyaz'menskii. Russ. J. Inorg. Chem. **15**, 248 (1970).
6. J. H. Price, A. N. Williamson, R. F. Shramm, and B. B. Wayland. Inorg. Chem. **11**, 1280 (1972).

Can. J. Chem. Downloaded from www.nrcresearchpress.com by 210.87.254.6 on 09/05/12
For personal use only.

Theoretical studies of some nonbenzenoid hydrocarbons. III. Acenaphthylene, fluoranthene, and related compounds

ARCHANA DASGUPTA AND NANDA K. DASGUPTA[1]

Department of Chemistry, The University of Alberta, Edmonton, Alta., Canada T6G 2G2

Received September 5, 1975[2]

ARCHANA DASGUPTA and NANDA K. DASGUPTA. Can. J. Chem. **54**, 3227 (1976).

The molecules acenaphthylene, pyracylene, fluoranthene, acefluoranthylene, and indeno-[1,2,3-*cd*]fluoranthene have been studied using the Pariser–Parr–Pople semi-empirical SCF MO method with the core resonance integral value developed by Lo and Whitehead and Dewar *et al.* It has been found that with this core resonance integral value developed for the prediction of ground state properties, $\pi^* \leftarrow \pi$ spectral transitions can also be predicted with reasonably good accuracy and the results are also compared with those calculated by using the core resonance integral value proposed by Yamaguchi *et al.* The resonance stabilization of acefluoranthylene and indeno[1,2,3-*cd*]fluoranthene has been studied. The attachment of a vinyl linkage at the 1,8 centres of naphthalene, or similar attachment to anthracene and phenanthrene, reduces the resonance energy below that of the parent compounds. The resonance stabilization has been predicted for aceanthrylene and acephenanthrylene.

All the molecules studied here have acenaphthylene moiety and it would be interesting to see whether there is any similarity in properties between acenaphthylene and other molecules or how the properties change with the introduction of benzene nucleus or ethylinic linkage or both in acenaphthylene moiety.

ARCHANA DASGUPTA et NANDA K. DASGUPTA. Can. J. Chem. **54**, 3227 (1976).

Les molécules acénaphtylène, pyracylène, fluoranthène, acéfluoranthylène et indéno [1,2,3-*cd*] fluoranthène ont été étudiées en utilisant la méthode semi-empirique SCF MO de Pariser, Parr et Pople avec la valeur de l'intégrale de résonance du noyau développée par Lo et Whitehead et Dewar *et al.* On a trouvé qu'avec cette valeur de l'intégrale de résonance du noyau développée pour la prédiction des propriétés de l'état fondamental, on peut aussi prédire les transitions spectrales $\pi^* \leftarrow \pi$ avec une assez bonne précision; les résultats sont aussi comparés à ceux calculés en utilisant la valeur de l'intégrale de résonance du noyau proposée par Yamaguchi *et al.* La stabilisation par résonance de l'acéfluoranthylène et l'indeno [1,2,3-*cd*] fluoranthène a été étudiée. Le rattachement d'un lien vinylique aux carbones-1,8 du naphtalène, ou un attachement similaire à l'anthracène ou au phénanthrène, réduit l'énergie de résonance en dessous de celle des composés parents. La stabilisation par résonance a été prédite pour l'acéanthrylène et l'acéphénanthrylène.

Toutes les molécules étudiées dans ce travail ont une partie acénaphtylène et il serait intéressant de voir s'il y a une similarité quelconque des propriétés entre l'acénaphtylène et d'autres molécules ou de voir comment changent les propriétés avec l'introduction d'un noyau benzénique ou d'un lien éthylénique ou des deux dans la partie acénaphtylène.

[Traduit par le journal]

Introduction

Recently we (1) published the results of calculations on some nonbenzenoid hydrocarbons utilizing the self-consistent field molecular orbital (SCF MO) method. The core resonance integral values used there were those of Lo and Whitehead (2) (designated as SCF(*a*) method), Chung and Dewar (3) (designated as SCF(*b*) method), and Dewar and Harget (4*a*) (designated as SCF(*c*) method). These core resonance integrals were proposed to predict the ground state properties of the conjugated systems. It was observed that using those values of resonance integrals not only the ground state properties but also the $\pi^* \leftarrow \pi$ spectral transitions could be predicted with good accuracy for some nonbenzenoid hydrocarbons (1). Here we would like to report the results of our calculations on some more nonbenzenoid hydrocarbons such as acenaphthylene **1**, pyracylene **2**, fluoranthene **3**, acefluoranthylene **4**, and indeno[1,2,3-*cd*]fluoranthene **5** (Fig. 1) in order to see how far the predicted spectral transitions could be correlated with the experimental ones using the resonance integral values suitable for the ground state

[1]Permanent address: Department of Chemistry, Visva-Bharati University, Santiniketan, West Bangal, India.

[2]Revision received May 25, 1976.

Can. J. Chem. Downloaded from www.nrcresearchpress.com by 210.87.254.40 on 09/05/12
For personal use only.

Can. J. Chem. Downloaded from www.nrcresearchpress.com by 210.87.254.40 on 09/05/12
For personal use only.

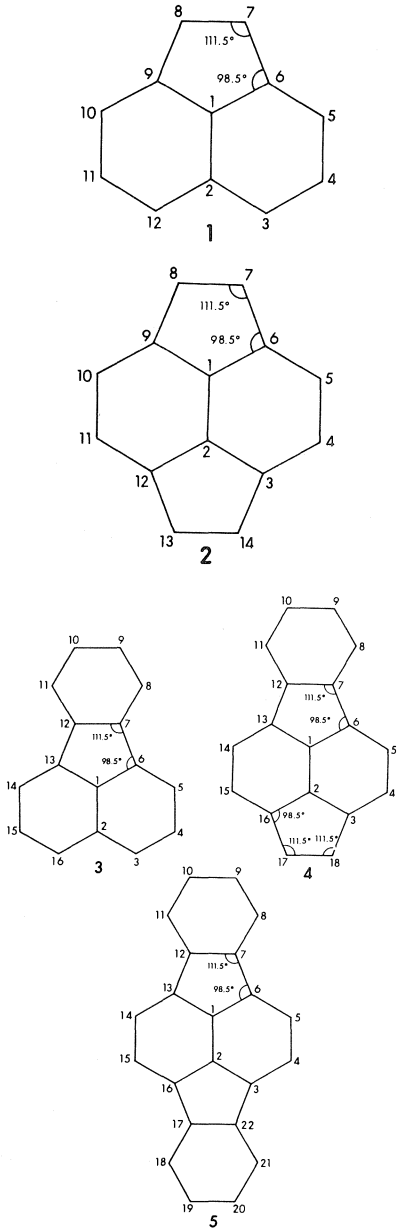

FIG. 1. Molecules: **1** acenaphthylene, **2** pyracylene, **3** fluoranthene, **4** acefluoranthylene, **5** indeno[1,2,3-*cd*]-fluoranthene. (All bonds equal to 1.40 Å and all angles in the hexagon are 120°.)

properties. For comparison we also performed calculations using the 'β-variable' technique of Yamaguchi *et al.* (5) (designated as SCF(*d*)) developed for the prediction of spectra.

All these molecules have been studied earlier using different sets of parameters. Acenaphthylene (6) and fluoranthene (6) were studied extensively. The molecule pyracylene is very interesting. It obeys Hückel's ($4n + 2$) rule and Craig's rule (7) of aromaticity. But it was observed by DasGupta and DasGupta (8) that the molecule is not aromatic and their observation is in good agreement with experiment (10*a*). Moreover, pyracylene might be treated as pentalenoid system (9), a perturbed [12] annulene with an internal vinyl cross link (10), or a naphthalene unit two vinyl bridges. The molecule has been synthesized and the properties have been reported by Trost *et al.* (10*a*). But according to Yamaguchi and Nakajima (10*b*) the molecule **2** is not pentalenoid. A search in literature has revealed that the molecule **4** has not yet been synthesized. The molecule **5** has been synthesized by Stubbs and Tucker (11) and studied theoretically by Ray and Sharma (12), Lo and Whitehead (13), and others (6*c*). The consistent treatment of all these molecules having acenaphthylene nucleus is the basis of the present article. In this paper we would like to report also the effect of ethylinic linkage in naphthalene unit on the resonance energy of the molecules.

Method and Parameter

The method used here is the Pariser and Parr (14) and Pople (15) semiempirical SCF-ASMO method. The method is well known and has been described elsewhere (16). The mode of evaluation of certain integrals and choice of parameters were also described in our previous paper (1*b*).

Results and Discussion

Spectra, Ionization Energy, and Electron Affinity

Table 1 contains experimental spectra of the molecules (**1**, **2**, **3**, and **5**) along with the calculated $\pi^* \leftarrow \pi$ singlet transitions with oscillator strengths of all the molecules. For comparison we have also included other theoretical results. The oscillator strengths were calculated using the relation (17)

$$f = 1.085 \times 10^{-5}\, \bar{\nu}\mu^2$$

with $\bar{\nu}$ is the transition energy in cm^{-1} and μ is the dipole length for the corresponding transition in Å.

From Table 1 it is clear that in all these cases the spectral transitions calculated by these

Can. J. Chem. Downloaded from www.nrcresearchpress.com by 210.87.254.40 on 09/05/12
For personal use only.

TABLE 1. $\pi^* \leftarrow \pi$ transitions and oscillator strengths (f)

		Experimental		Present work								Other work							
				SCF(*a*)		SCF(*b*)		SCF(*c*)		SCF(*d*)		Ref. 6*a*		Ref. 6*f*		Ref. 6*b*		Ref. 10*b*	
Molecule	Symmetry	eV	log ϵ	eV	f	eV	f	eV	f	eV	f	eV	f	eV	f	eV	f	eV	f
1	B_2	2.66	1.4	2.90	0.29	2.89	0.29					2.75	0.04	2.65	0.04	2.61	0.04	2.794‡	
	B_2	3.66	3.7	3.73	0.48	3.70	0.48	3.72	0.34	3.37	0.29	3.75	0.31	3.65	0.63	3.70	0.24	3.748‡	
	A_1	3.84	4.0	3.77	0.58	3.75	0.58	3.52	0.42	4.02	0.59	3.83	0.22	3.56	0.12	3.93	0.16	3.810‡	
	A_1	4.51	3.5	4.71	0.01	4.68	0.01	4.71	0.70	4.87	0	4.75	0	4.76	0.01	4.55	0.04	4.820‡	
														5.09	0.55				
	B_2	5.39	4.7	5.53	0	5.50	0	5.71	0.02	4.92	0.72	5.56	1.21	5.47	0	5.63	1.08	5.560‡	
				5.66	0.02	5.63	0.02												
2		2.90												2.77	0.49				
		3.04																	
	B_{2u}	3.06																3.23	0.048
	B_{3u}	3.22		3.27	0.09	3.25	0.09							3.15	0.15				
	B_{2u}	3.64		3.53	0.66	3.51	0.65	3.78	0.60	3.77	0.66								
	B_{3u}	3.73		3.71	0.86	3.69	0.85	3.84	0.78	3.69	0.81			3.64	0.24			3.75	0.33
	B_{2u}	3.80																4.09	0.18
	B_{2u}	5.23		5.31	0.44	5.28	0.44							5.04	0.37			5.41	0.008
	B_{3u}							5.37	0.62	5.25	0.63								
	B_{2u}	5.69		5.57	0.60	5.54	0.60	5.68	0.55	5.75	0.63			5.67	0.37			5.99	2.18
3	B_2	(~3.2)	(~2)	3.45	0.24	3.44	0.24					3.32	0.01	3.31	0.20	3.33	0.02		
	A_1	3.45	4.0	3.59	0.81	3.57	0.81	3.85	0.76	3.74	0.85	3.51	0.52	3.47	1.04	3.58	0.64		
	B_2	3.82	3.8	4.06	0.53	4.03	0.52	3.81	0.31	3.71	0.24	3.93	0.08	3.69	0.01	4.09	0.07		
	B_2							4.11	0.43	4.17	0.57								
	A_1	4.32	4.7									4.48	0.22	4.58	0.07				
	A_1	4.74	4.1	4.86	0.53	4.83	0.53	4.85	0.62	4.97	0.71	5.08	0.01	4.78	0.04	4.70	0.20		
	B_2	(4.96)	(4.2)	4.98	0	4.96	0	5.16	0.04	5.13	0.04	5.13	0.05	5.04	0.42	5.20	0.03		
	A_1			5.20	0.21	5.18	0.20	5.30	0.07	5.22	0.04	5.26	0.60						
	B_2	5.25	4.7	5.60	0.01	5.57	0.01	5.65	0.01	5.67	0.01	5.39	1.28	5.28	1.13	5.25	0		
4	B_2			2.06	0.01	2.05	0.01												
								2.68	0	2.50	0.01								
	A_1			3.36	0.89	3.35	0.88	3.65	0.80	3.46	0.89								
	B_2			3.92	0.85	3.90	0.84	4.04	0.81	3.85	0.82								
	A_1			4.66	0.02	4.63	0.02	4.96	0.11	4.73	0.05								
	B_2			5.06	0.47	5.03	0.46	5.03	0.62	5.10	0.37								
	A_1			5.22	0.52	5.20	0.51	5.14	0.43	5.02	0.54								
5	B_{2u}	3.02	4.55	3.25	1.01	3.24	1.08					3.06†		2.779	1.20				
	B_{2u}	3.38	3.98	3.55	0.98					3.31	1.12								
	B_{3u}	3.55	3.58	3.79	0	3.78	0							3.434	0.02				
	B_{3u}	4.24	5.10	4.22	0.90	4.20	0.89	4.30	0.85	4.07	0.86	3.98†		4.003	0.07				
	B_{3u}	4.72	4.53	4.89	0.62	4.86	0.62	4.88	0.57	4.85	0.55			4.645	0.32				
	B_{2u}	4.90	4.56	5.06	1.01	5.04	1.00	5.21	0.95	4.94	1.02	4.85†		4.825	0.16				

*Experimental value: Molecule 1, ref. 6(*a*); molecule 2, ref. 10(*a*), 10(*b*); molecule 3, ref. 6(*a*); molecule 5, ref. 11. Values in parentheses indicate shoulder.
†Reference 12.
‡Reference 6*d*.

TABLE 2. Ionization potential (eV) and electron affinity (eV)

		Value							
		Method				Experimental		Other work	
Parameter	Molecule	SCF(*a*)*	SCF(*b*)*	SCF(*c*)	SCF(*d*)*†	Value	Reference	Value	Reference
Ionization potential	**1**	8.41	8.40	10.01	8.28	8.02	22	8.71, 8.43	22
	2	8.05	8.05	9.70	7.91				
	3	8.16	8.15	9.66	7.99	7.80	22	8.36, 8.04	22
	4	8.11	8.11	9.69	7.95				
	5	8.05	8.04	9.54	7.92			8.94	12
Electron affinity	**1**	2.36	2.36	2.07	0.95	0.88‡	23	0.98	23
	2	2.99	2.99	2.58	1.43	1.55	10*a*		
	3	2.24	2.24	2.01	0.83	0.63, 0.82	6*e*, 23	0.92	23
	4	2.86	2.86	2.51	1.43				
	5	2.74	2.74	2.45	1.33	1.42§	24, 25		

*Corrected values of ionization potential are given for these cases.
†Corrected values of electron affinity are given for this case.
‡Data in the experimental column is relative electron affinity in T.H.F. and that in the last column is predicted electron affinity in gas phase.
§Predicted from the half wave reduction potential determined by Bergman (24). The half wave reduction potential of Bergman has been lowered by 0.52 V (25).

methods are in good agreement with the experiment, the SCF(*a*) and SCF(*b*) methods are better than SCF(*c*) and SCF(*d*) methods in which case there is no transition corresponding to the lowest experimental transition. The results are comparable to and in some cases better than other theoretical results shown in the table.

According to Koopman's theorem (18) the highest occupied orbital energy is equal to the ionization potential of the molecule. But ionization potential calculated in this way is 1 or 2 eV higher than the true value. For SCF(*a*) and SCF(*b*) methods where the β integrals remain constant we used Bloor's formula (19) for calculating the ionization potential (IP). For the SCF(*d*) method we used the relation of Kunii and Kuroda (20) for the calculation of ionization potential and electron affinity (EA).

Table 2 contains the corrected and uncorrected values of ionization potential and electron affinity of these molecules along with the experimental values where available and other theoretical results. Our results are in good agreement with experimental value. Specially with SCF(*d*) method the agreement with the experiment is very good.

Bond Length

Figure 2 displays the comparison of bond lengths calculated by the different methods. It is seen that the predicted bond length of C_6—C_7 bond and other similar bonds of all these molecules have single bond character and the value lies between 1.45 to 1.47 Å. An interesting feature is seen that when a bond is common to a five-membered and six-membered ring the bond is larger than an aromatic C—C bond if it is in naphthalene moiety and is equal to an aromatic C—C bond if it is not in naphthalene moiety. For the first type the bond length lies between 1.42 to 1.43 Å and examples are C_1—C_6 and C_1—C_9 bonds of acenaphthylene and similar bonds of other molecules. Examples of the second type are C_7—C_{12} bond of molecules **3**, **4**, **5**, and the C_{17}—C_{22} bond of the molecule **5**. The value of the bond length lies between 1.403 to 1.408 Å. But it is found that the same type of bond not attached to a six-membered ring (as for example C_7—C_8 of acenaphthylene, pyracylene and C_{17}—C_{18} bond of acefluoranthylene) has a double bond character. The predicted bond length lies between 1.351 to 1.358 Å.

Resonance Stabilization

Resonance stabilization for the molecules **1**, **2**, and **3** has been discussed in our previous papers (8). Calculated heats of atomization (ΔH_a), and π bond energies for the molecules **4** and **5** have been shown in Table 3 along with the resonance energy (E_R) calculated by the methods of Chung and Dewar (3), Lo and Whitehead (2), Dewar and de Llano (21), and Dewar and Harget (4*a*). An interesting thing is noticed that the vinyl linkage in 1,8 positions of naphthalene moiety reduces the resonance energy of the compound. Thus the resonance energy of

Can. J. Chem. Downloaded from www.nrcresearchpress.com by 210.87.254.40 on 09/05/12
For personal use only.

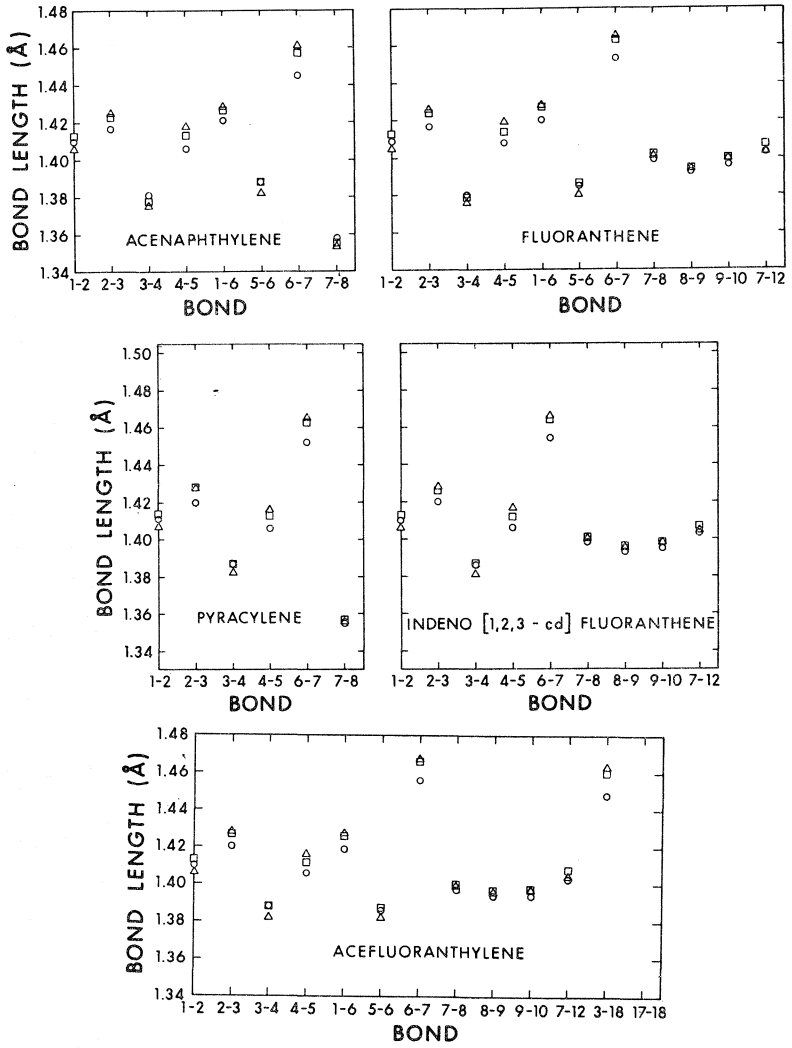

FIG. 2. Comparison of bond length: SCF(*a*) or SCF(*b*) ○, SCF(*c*) △, SCF(*d*) □.

TABLE 3. Heats of atomization (ΔH_a), π-bond energy ($E_{\pi b}$); and resonance energy, E_R

Molecule	ΔH_a (eV)		$E_{\pi b}$ (eV)	Resonance energy (eV)			
	Ref. 2*	Ref. 4†	Ref. 3‡	Ref. 2*	Ref. 3‡	Ref. 21§	Ref. 4†
4	152.438	152.893	27.036	6.783	6.818	1.674	2.317
5	186.310	186.764	33.621	8.839	8.892	2.545	3.226
Aceanthrylene	137.831					1.305	
Acephenanthrylene	138.144					1.617	

*Lo and Whitehead method (ref. 2).
†Dewar and Harget method (ref. 4).
‡Chung and Dewar method (ref. 3).
§Dewar and de Llano method (ref. 21).

Can. J. Chem. Downloaded from www.nrcresearchpress.com by 210.87.254.40 on 09/05/12
For personal use only.

Can. J. Chem. Downloaded from www.nrcresearchpress.com by 210.87.254.40 on 09/05/12
For personal use only.

acenaphthylene is less than that of naphthalene. Similarly acefluoranthylene has resonance energy less than that of fluoranthene. Moreover when there is more than one vinyl linkage in the naphthalene moiety there is further reduction of resonance energy. Thus the resonance energy of naphthalene, acenaphthylene, and pyracylene is in the order of naphthalene > acenaphthylene > pyracylene. From the difference in E_R values of naphthalene and acenaphthylene (0.242 eV) and fluoranthene and acefluoranthylene (0.247 eV), using the method of Dewar and de Llano, we find that the effect of vinyl linkage in naphthalene is to reduce the resonance energy by 0.245 eV. Thus the predicted resonance energy (0.836 eV) of pyracylene from acenaphthylene is in good agreement with the calculated value (0.767 eV). A similar situation is also seen in the case of aceanthrylene and acephenanthrylene whose resonance energy is less than those of anthracene and phenathrene, respectively. The predicted values of resonance energy for aceanthrylene and acephenanthrylene are 1.355 and 1.688 eV respectively and they are in good agreement with the theoretical results shown in Table 3.

From the value of resonance energy per C—C bond of acefluoranthylene it seems that the compound might be an aromatic one since the E_R/C—C is comparable to that of acenaphthylene (8).

The molecule **5** is an aromatic compound in agreement with its value of E_R and E_R/C—C. However, there is a difference in the value of E_R/C—C of the molecule calculated by us and that calculated by Lo and Whitehead (13). The difference in the value of E_R/C—C of the molecule **5** may be due to the difference in the assumption of initial geometry of the molecule.

One question is whether the molecule **5** can be treated as naphthalene and two benzene nuclei joined by single bonds or a fluoranthene moiety and a benzene ring joined by single bonds. The resonance energy calculated by Dewar *et al.* (21, 4*a*) suggests that the molecule **5** can be treated as fluoranthene and benzene nuclei joined by single bonds and the best result is obtained from an E_R value calculated by the Dewar and Harget (4*a*) method.

Conclusion

In the SCF(*a*) and SCF(*b*) methods the β integrals have been evaluated considering a hypothetical thermocycle. However, in the latter method all β integrals are of equal value whereas in the former they depend on the initial bond length. Since the fundamental intent of the SCF(*a*), SCF(*b*), and SCF(*c*) methods is to predict reasonably accurate heats of atomization, the charge densities, bond length, π-dipole moment, ionization potential, and electron affinity predicted by these methods are all consistent with one another, although the SCF(*c*) method differs from the other two in that the β and some γ integrals are recalculated at each iteration. It is interesting to note that a method (SCF(*a*) or SCF(*b*)) which has been parameterised for ground state properties should predict results better than a method (SCF(*d*)) which has been parameterised to predict spectral transitions.

Acknowledgements

The authors take the opportunity to express their sincere gratitude to Professor F. W. Birss for many comments, helpful discussions, and financial support. They are also thankful to the Computing Services, University of Alberta, for computational facilities.

1. (*a*) F. W. Birss and N. K. DasGupta. Can. J. Chem. **49**, 2840 (1971); (*b*) Archana DasGupta and Nanda K. DasGupta. Can. J. Chem. **52**, 155 (1974); **53**, 915 (1975); (*c*) Archana DasGupta and Nanda K. DasGupta. J. Mol. Struct. **27**, 113 (1975); Can. J. Chem. **53**, 3777 (1975).
2. D. H. Lo and M. A. Whitehead. Can. J. Chem. **46**, 2027 (1968).
3. A. L. H. Chung and M. J. S. Dewar. J. Chem. Phys. **42**, 756 (1965).
4. (*a*) M. J. S. Dewar and A. J. Harget. Proc. R. Soc. London, Ser. A, **315**, 443 (1970); (*b*) M. J. S. Dewar and G. J. Gleicher. J. Am. Chem. Soc. **87**, 685 (1965).
5. H. Yamaguchi, T. Nakajima, and T. L. Kunii. Theor. Chim. Acta, **12**, 349 (1968).
6. (*a*) E. Heilbronner, Jean-Pierre Weber, J. Michl, and R. Zahradnik. Theor. Chim. Acta, **6**, 141 (1966), (*b*) J. Koutecky, P. Hochmann, and J. Michl. J. Chem. Phys. **40**, 2439 (1964); (*c*) R. Zahradnik and J. Michl. Collect. Czech. Chem. Commun. **31**, 3442 (1966); J. Michl and R. Zahradnik. Collect. Czech. Chem. Commun. **31**, 3453 (1966); (*d*) P. Hochmann, R. Zahradnik, and V. Kavasnicka. Collect. Czech. Chem. Commun. **33**, 3478 (1968); (*e*) J. Michl. J. Mol. Spectrosc. **30**, 66 (1969); (*f*) G. Favini, A. Gamba, and M. Simonetta. Theor. Chim. Acta, **13**, 175 (1969); (*g*) A. Pullman, B. Pullman, E. D. Bergman, G. Berthier, E. Fischer, J. Hirschberg, and J. Pontis. J. Chim. Phys. **48**, 359 (1951); (*h*) N. K. DasGupta and Md. Asgar Ali. Indian J. Chem. **3**, 329 (1965).

7. D. P. CRAIG. Non benzenoid aromatic compounds. *Edited by* D. Ginsberg. Interscience Publishers, Inc., New York. 1959. Chapt. 1.
8. (*a*) A. DASGUPTA and N. K. DASGUPTA. Tetrahedron, **28**, 3587 (1972); (*b*) A. DASGUPTA and N. K. DASGUPTA. Theor. Chim. Acta, **33**, 177 (1974).
9. B. M. TROST and G. M. BRIGHT. J. Am. Chem. Soc. **89**, 4244 (1967).
10. (*a*) B. M. TROST, G. M. BRIGHT, C. FRIHART, and D. BRITELLI. J. Am. Chem. Soc. **93**, 737 (1971); (*b*) H. YAMAGUCHI and T. NAKAJIMA. Bull. Chem. Soc. Jpn. **44**, 682 (1971).
11. H. W. D. STUBBS and S. H. TUCKER. J. Chem. Soc. 2936 (1951).
12. N. K. RAY and K. K. SHARMA. Indian J. Chem. **10**, 668 (1972).
13. D. H. LO and M. A. WHITEHEAD. Chem. Commun. 771 (1968).
14. R. PARISER and R. G. PARR. J. Chem. Phys. **21**, 466 (1953); **21**, 767 (1953).
15. J. A. POPLE. Trans. Faraday Soc. **49**, 1375 (1953).
16. R. G. PARR. Quantum theory of molecular electron structure. Benjamin, New York. 1963.
17. L. SALEM. The molecular orbital theory of conjugated systems. W. A. Benjamin, Inc. N.Y. 1966. p. 358.
18. T. KOOPMAN. Physica, **1**, 104 (1934).
19. J. E. BLOOR. Can. J. Chem. **43**, 3026 (1965).
20. T. L. KUNII and H. KURODA. Theor. Chim. Acta, **11**, 97 (1968).
21. M. J. S. DEWAR and C. DE LLANO. J. Am. Chem. Soc. **91**, 789 (1969).
22. M. J. S. DEWAR, E. HASELBACH, and S. D. WORLEY. Proc. R. Soc. London, Ser. A, **315**, 431 (1970).
23. J. CHAUDHURI, J. JAGUR-GRODZINSKI, and M. SZWARE. J. Phys. Chem. **71**, 3063 (1967).
24. I. BERGMAN. Trans. Faraday Soc. **50**, 829 (1954).
25. G. J. HOIJTINK. Recl. Trav. Chim. **74**, 1525 (1955).

Can. J. Chem. Downloaded from www.nrcresearchpress.com by 210.87.254.40 on 09/05/12
For personal use only.

A Mössbauer study of organotellurium compounds. Part I

COLIN H. W. JONES AND ROBERT SCHULTZ

Department of Chemistry, Simon Fraser University, Burnaby, B.C., Canada V5A 1S6

AND

WILLIAM R. MCWHINNIE AND NIGEL S. DANCE

Department of Chemistry, University of Aston in Birmingham, Birmingham, England B4 7ET

Received March 16, 1976

Can. J. Chem. Downloaded from www.nrcresearchpress.com by 210.87.254.5 on 09/05/12
For personal use only.

COLIN H. W. JONES, ROBERT SCHULTZ, WILLIAM R. MCWHINNIE, and NIGEL S. DANCE. Can. J. Chem. **54**, 3234 (1976).

Mössbauer data for a wide range of organotellurium compounds are reported, including compounds of the type: R_2Te, Ar_2Te, Ar_2Te_2, R_2TeX_2, Ar_2TeX_2, and $ArTeX_3$; where R = alkyl, Ar = aryl, and X = Cl, Br, or I. The isomer shifts and quadrupole splittings are interpreted in terms of the relative populations of the tellurium 5*s* and 5*p* orbitals. The quadrupole splittings are rationalized in terms of a simple additive model, formulated within the framework of the Townes and Dailey theory.

COLIN H. W. JONES, ROBERT SCHULTZ, WILLIAM R. MCWHINNIE et NIGEL S. DANCE. Can. J. Chem. **54**, 3234 (1976).

On rapporte des données de Mössbauer pour une grande quantité de composés organotellurés incluant des composés du type R_2Te, Ar_2Te, Ar_2Te_2, R_2TeX_2, Ar_2TeX_2 et $ArTeX_3$ où R = alkyle, Ar = aryle et X = Cl, Br, ou I. On interprète les déplacements des isomères et les couplages quadrupolaires en termes des populations relatives des orbitales 5*s* et 5*p* du tellure. On rationalise les couplages quadrupolaires en termes d'un modèle additif simple formulé à l'intérieur de la théorie de Townes et Dailey.

[Traduit par le journal]

Introduction

While organotin and organo-antimony compounds have been extensively studied by the Mössbauer effect in the past, little attention has been paid to similar compounds of tellurium. Cheyne *et al.* (1) have studied complexes of tellurium(II) and (IV) with a number of organosulphur ligands and the present study extends that work to a wider range of organotellurium compounds. While the present work was in progress, Berry *et al.* (2) reported the Mössbauer data for 17 aryl tellurium(II) and (IV) compounds and Smith *et al.* (3) reported measurements for the dialkyl tellurium dihalides R_2TeX_2 (X = Cl, Br, I). Previously a measurement for α-Me_2TeI_2 made in our laboratory had been reported by Chan and Einstein (4). We report here the Mössbauer spectra of a number of diaryl and dialkyl tellurides, R_2Te, and diaryl ditellurides, R_2Te_2, diaryl and dialkyl dihalides, R_2TeX_2, and aryltrihalides, $RTeX_3$. The compounds $TeCl_4$(py), (p-$MeOC_6H_4$)$TeCl_3$(py), (p-$MeOC_6H_4$)$TeCl_3$(tmtu), and (p-$EtOC_6H_4$)TeOCl have also been studied, where py is pyridine and tmtu is tetramethylthiourea.

Of the classes of compounds studied here, crystal structures have been reported for (p-$(MeC_6H_4)_2Te$ (5), Ph_2Te_2 (6), (p-$ClC_6H_4)_2Te_2$ (7), Me_2TeCl_2 (8), α-Me_2TeI_2 (4), Ph_2TeBr_2 (9), and $ClCH_2CH_2TeCl_3$ (10). Infrared and Raman studies of the diaryl tellurium dihalides (11), and the aryl tellurium trihalides (12) and their hydrolysis products (13), have been reported by McWhinnie and co-workers, while the ir spectra of organotellurium trihalide complexes with tetramethylthiourea (14) and pyridine (15) have also been reported. The 1:1 and 1:2 adducts formed between $TeCl_4$ and pyridine have been investigated by Couch *et al.* (16) and Beattie *et al.* (17) respectively.

In the present paper Mössbauer data for the organotellurium compounds are interpreted in terms of the tellurium 5*s* and 5*p* orbital populations. It is shown that the quadrupole splittings for several of the compounds can be rationalized in terms of a simple additivity model based on the Townes and Dailey theory. This interpretation is consistent with the structures of the compounds where known or where proposed on the basis of ir and Raman data.

TABLE 1. ^{125}Te Mössbauer parameters

Compound	$\delta^*(\pm 0.08)$ I/Cu (mm s^{-1})	$\Delta(\pm 0.1)$ (mm s^{-1})	2Γ (mm s^{-1})	Reference†
Me_2Te	0.06	10.5	6.2	
Ph_2Te	0.18	10.5	5.9	
$(p\text{-}MeOC_6H_4)_2Te$	0.3	11.3		2
$(p\text{-}MeC_6H_4)_2Te$	0.7	10.1		2
Ph_2Te_2	0.37	10.7	6.1	
$(p\text{-}MeOC_6H_4)_2Te_2$	0.42	10.1	6.4	
	0.3	10.3		2
$(p\text{-}EtOC_6H_4)_2Te_2$	0.28	10.6	6.4	
$(p\text{-}PhOC_6H_4)_2Te_2$	0.32	10.0	6.7	
	0.3	10.3		2
$(p\text{-}MeC_6H_4)_2Te_2$	0.6	9.9		2
Me_2TeCl_2	0.58	9.4	5.8	
	0.64	9.97		3
Me_2TeBr_2	0.65	8.5	6.1	
	0.61	8.76		3
Me_2TeI_2	0.52	7.6	6.9	
	0.62	7.05		3
$(CH_2)_4TeBr_2$	0.54	7.1	5.8	
$(CH_2)_4TeI_2$	0.64	7.1	7.2	
Ph_2TeCl_2	0.5	9.2		2
$(p\text{-}MeOC_6H_4)_2TeCl_2$	0.68	9.1	5.9	
$(p\text{-}EtOC_6H_4)_2TeCl_2$	0.7	9.1		2
$(C_6H_4ClC{=}CH)_2TeCl_2$	0.57	8.0	5.5	
$(C_6H_4)_2OTeCl_2$	0.68	8.0	5.7	
Ph_2TeBr_2	0.60	7.9	5.9	
	0.5	8.1		2
$(p\text{-}EtOC_6H_4)_2TeBr_2$	0.52	7.6	6.9	
$(C_6F_5)_2TeBr_2$	0.73	5.3	5.7	
$(p\text{-}CH_3C_6H_4)_2TeI_2$	0.6	6.3		2
$(p\text{-}EtOC_6H_4)TeCl_3$	0.91	9.4	6.7	
	1.1	9.2		2
$(p\text{-}MeOC_6H_4)TeCl_3$	0.9	9.2		2
$(pyH)^+(p\text{-}EtOC_6H_4)TeCl_4)^-$	0.88	8.8	6.1	
$(p\text{-}EtOC_6H_4)TeOCl$	0.59	9.1	6.0	
$PhTeBr_3$	0.91	7.8	5.8	
$(p\text{-}EtOC_6H_4)TeBr_3$	1.0	8.0		2
$(p\text{-}EtOC_6H_4)TeI_3$	1.0	5.2		2
$(p\text{-}MeOC_6H_4)TeCl_3(py)$	0.73	7.6	6.1	
$(p\text{-}MeOC_6H_4)TeCl_3(tmtu)$	0.85	7.9	5.9	
$TeCl_4(py)$	0.86	4.5	6.4	

*δ with ^{125}Sb/Cu source at 80 K and absorber at 4.2 K. Conversion from ^{125}Sb/Cu to ^{125}I/Cu made by adding +0.15 mm s^{-1}.

†In data taken from ref. 2, the spectra were recorded with the source and absorbers at 4.2 K. The errors in both δ and Δ in ref. 2 were ± 0.1 mm s^{-1}. In data taken from ref. 3, the spectra were recorded with the source and absorber at 4.2 K. Errors quoted were, for Me_2TeCl_2 for example, δ (I/Cu) = 0.644(28) and Δ = 9.970(21). The δ values were converted from Te as standard by adding +0.60 mm s^{-1}.

Results and Discussion

The results of the present study, together with those of refs. 2 and 3, are presented in Table 1. A typical spectrum is shown in Fig. 1. Where comparisons can be made, the quadrupole splittings are in good agreement with those previously reported. A comparison of isomer shifts is less satisfactory. In ref. 2, two sources were used and there are some inconsistencies in the δ values reported in that work. Thus the difference in δ, reported relative to I/Cu, between $(p\text{-}MeC_6H_4)_2Te_2$ (0.6 mm s^{-1}) and $(p\text{-}MeOC_6H_4)_2Te_2$ (0.3 mm s^{-1}), and also between $(p\text{-}MeC_6H_4)_2Te$ (0.7 mm s^{-1}) and $(p\text{-}MeOC_6H_4)_2Te$ (0.3 mm s^{-1}), may well reflect difficulties in the isomer shift calibration rather than any real

Can. J. Chem. Downloaded from www.nrcresearchpress.com by 210.87.254.5 on 09/05/12
For personal use only.

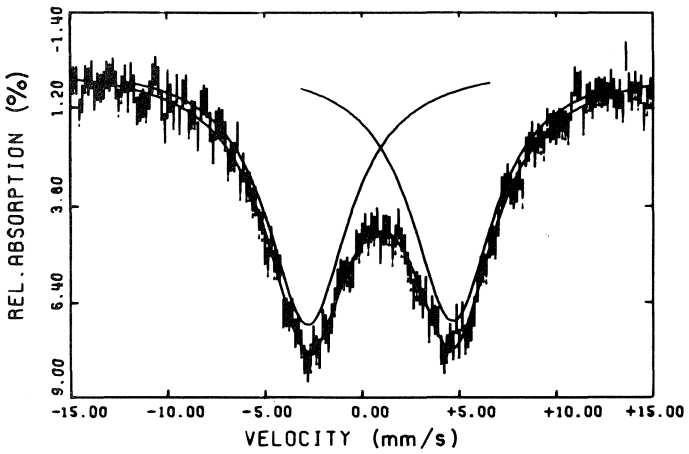

FIG. 1. A typical ^{125}Te Mössbauer spectrum for $(p\text{-}EtOC_6H_4)_2TeCl_2$.

difference between the ligands. The larger δ value for each of these pairs of compounds was obtained using an I/Cu source and the smaller value with a PbTe source.

In comparing the present results with those of Smith *et al.* (3), the δ and Δ values are in reasonable agreement, although the errors quoted in the present work are much greater than those quoted in ref. 3. It has been our experience that the errors arrived at through the computed fits to individual spectra are invariably much smaller than the errors associated with the reproducibility of independent measurements on the same compound.

Isomer Shifts

The nuclear radius term, $\Delta R/R$, is positive for the ^{125}Te transition (18) and thus δ becomes more positive as the *s*-electron density at the nucleus $|\psi_s(0)|^2$ increases. Removal of 5*p* electron density from tellurium will result in a deshielding of the *s*-electrons from the nucleus and an increase in $|\psi_s(0)|^2$, while removal of *s*-electrons will have a more marked effect in directly decreasing $|\psi_s(0)|^2$. There is evidence from iodine Mössbauer data that the effect on δ of the latter term is six times that of the former term for each electron removed (19).

The isomer shifts lie in the order:

$$\text{tellurides} \leq \text{ditellurides} < \text{dihalides} < \text{trihalides}$$

and this corresponds to an increasing *s*-electron density at the nucleus in that order. The bonding in the tellurides and ditellurides may be viewed as intermediate between pure *p* and sp^3, as suggested by the C—Te—C and C—Te—Te bond angles in $(p\text{-}MeC_6H_4)_2Te$ (101.0 ± 2.7°) (5), $(p\text{-}ClC_6H_4)_2Te_2$ (94.4°) (7), and Ph_2Te_2 (*ca.* 99°) (6). The incorporation of some tellurium 5*s* character in the Te—C and Te—Te bonds would tend to lower $|\psi_s(0)|^2$. The halogens, on the other hand, appear to remove predominantly 5*p* electron density from the tellurium, leading to an increased de-shielding of the 5*s* electrons from the nucleus and hence an increase in δ in passing from the dihalides to the trihalides.

Within the series of dihalides or trihalides, as the electronegativity of the halogen increases from I through Br to Cl, no measurable change in δ is observed, although the 5*p* electron density removed from the tellurium would be expected to increase in that order. This may be explained by the observation that δ increases by only *ca.* +0.4 mm s^{-1} on the removal of one tellurium 5*p* electron (1). This, together with the broad natural line-width of the ^{125}Te transition and hence the relatively large errors in δ, means that δ is not a particularly sensitive probe to small changes in the tellurium 5*p* orbital populations. In addition, the *s*–*p* hybrid character of the Te—C and Te—X bonds may vary as the electronegativity of X is changed. Such a change in hybrid character has been invoked to explain the constancy of the ^{119}Sn isomer shifts for the Sn(IV) organohalides (19).

Quadrupole Splittings

A number of models have been used in the past to rationalize nuclear quadrupole coupling data, including the point-charge model (19),

Can. J. Chem. Downloaded from www.nrcresearchpress.com by 210.87.254.5 on 09/05/12
For personal use only.

Can. J. Chem. Downloaded from www.nrcresearchpress.com by 210.87.254.5 on 09/05/12
For personal use only.

Townes and Dailey theory (19, 20), and a simple molecular orbital model, which in essence brings the other two theories together (19, 20). Given the presence of non-bonding pairs of electrons on tellurium in Te(II) and Te(IV) compounds, the Townes and Dailey theory would appear to provide the most satisfactory framework within which to discuss the ^{125}Te quadrupole splittings. The basic tenets of this theory, as it is generally applied, are that the electric field gradient derives predominantly from any imbalance in the tellurium 5*p* orbital populations, and that lattice terms, *d*-orbital contributions, and Sternheimer shielding and anti-shielding factors can all be ignored to a first approximation. The quadrupole coupling constants, e^2qQ, are then linearly related to the *p*-orbital imbalance, U_p, through the equation

$$\frac{e^2qQ}{e^2q_0Q} = -U_p$$

$$\Delta = \tfrac{1}{2}e^2qQ\left(1 + \frac{\eta^2}{3}\right)^{1/2}$$

where e^2q_0Q is the quadrupole coupling for one 5*p* electron on tellurium, which is assumed to remain constant with changes in oxidation state and has a value of *ca.* +24 mm s^{-1} (1); η is the asymmetry parameter. The sign of Δ was not determined in the present experiments, but may be inferred from a consideration of the bonding in the molecule. The *p*-orbital imbalance is defined as

$$U_p = -U_z + \frac{U_x + U_y}{2}$$

The *p*-orbital populations U_x, U_y, and U_z may be related to the bonding orbital populations through a consideration of the hybrid orbitals invoked to describe the bonding to the tellurium atom (19, 21). As will be illustrated below, a simple picture in which the bonding is assumed to occur predominantly through the tellurium 5*p* orbitals can be used to explain the general features of the quadrupole splitting data.

The tellurides and ditellurides have large quadrupole splittings, reflecting a considerable imbalance in the tellurium 5*p* orbital populations. As noted above, the bond angles, where known, and the Mössbauer isomer shifts suggest that the tellurium 5*s* electrons participate in the bonding and that the bonding may be viewed as intermediate between pure *p* and sp^3. For the tellurides, Townes and Dailey theory leads to the conclusion (20) that, assuming a suitable admixture of *s* and *p* orbitals to generate bond angles θ in the range $90° \leq \theta \leq 109.5°$

$$\frac{e^2qQ}{e^2q_0Q}(1 - \cos\theta) = 2 - U_C$$

$$\eta = 3\cos\theta$$

where θ is the C—Te—C bond angle and U_C is the Te—C bond orbital population. However it is often found that by ignoring small deviations from an idealized geometry a more consistent explanation for quadrupole splittings may be arrived at (19, 20). In the present case the simplest assumption that can be made is that the bonding is essentially pure *p* in character (*i.e.*, $\theta = 90°$). While the bond angles are known to be greater than 90° and the isomer shifts are relatively small, the assumption that the quadrupole splittings can be rationalized by ignoring the *s*-character in the bonds leads to a consistent explanation of the quadrupole splitting data as will be discussed below. The lone pairs on the tellurium would then be visualized as occupying the 5*s* orbital and the $5p_z$ orbital, the latter being directed out of the bonding plane. Since this would correspond to an excess of *p* electron density along the *z* axis, V_{zz} the principal component of the electric field gradient tensor would be taken as negative in sign, and the e^2qQ would then be positive, since *Q* the quadrupole moment of the $\frac{3}{2}$ state is negative in sign. For the tellurides Δ is the same, within the errors, for the different alkyl and aryl groups and the average value of 10.6 mm s^{-1} corresponds to an orbital population of *ca.* 1.1 for the Te—C bond. The ditellurides have very similar splittings to the tellurides, indicating a similar covalency of the Te—C and Te—Te bonds. Since the bond orbital population for the latter is presumably 1.0, this is quite consistent with a value of 1.1 for the Te—C bond noted above.

In the dialkyl (4, 8) and diaryl (9) tellurium dihalides the halogen ligands are found in *trans* axial positions, with the organic ligands occupying equatorial positions (Fig. 2). The stereochemically active lone-pair may be viewed as occupying the third equatorial position in a distorted trigonal bipyramid. Intermolecular bonding through distant bridging halogens is

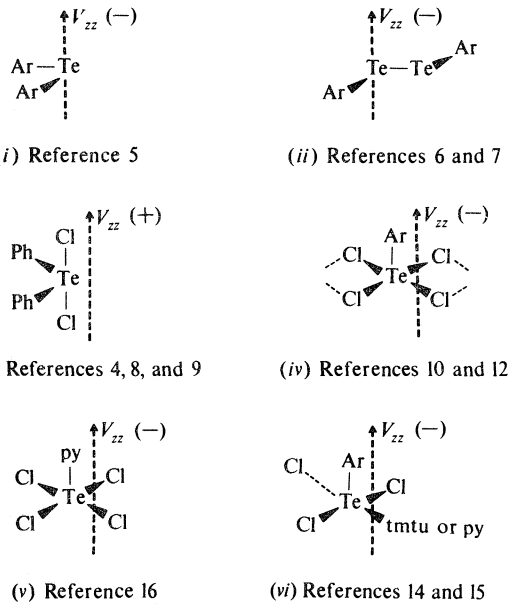

FIG. 2. Idealized structural types for the compounds studied, showing the assumed orientation and sign of V_{zz}.

also observed in the equatorial plane. The splittings for the compounds Me_2TeX_2 and Ph_2TeX_2 lie in the order Cl > Br > I. This trend may be readily understood if V_{zz} in these compounds lies along the X—Te—X bond axis, and that it is positive in sign. Thus, in the dichlorides the chlorine ligand may be viewed as removing considerable electron density from the tellurium $5p_z$ orbital, leading to an electron deficit along that axis compared with the *xy* (equatorial) plane. As the electronegativity of the halogen ligand decreases, the occupation of the tellurium $5p_z$ orbital would be expected to increase, and hence Δ to decrease, as is observed.

From Table 1, it can be seen that $(C_6H_4ClC{=}CH)_2TeCl_2$ and $(C_6H_4)_2OTeCl_2$ have smaller splittings than the other dichlorides, while the Δ's for the dibromides lie in the order:

$$Me_2TeBr_2 > Ph_2TeBr_2 \sim (p\text{-}EtOC_6H_4)_2TeBr_2 > (CH_2)_4TeBr_2 > (C_6F_5)_2TeBr_2$$

These differences in splittings may arise from differences in the donor characters of the organic ligands, changes in the *sp* hybrid character of the Te—C bonds or from variations in the degree of intermolecular bonding from one compound to another. Thus, C_6F_5 would be expected to be a poorer electron donor than Ph, and this would lead to a decrease in the 5*p* electron density in the *xy* plane, a smaller *p*-orbital imbalance and hence a smaller Δ in $(C_6F_5)_2TeBr_2$ than in Ph_2TeBr_2, as is observed. It is important to note that if V_{zz} lay through the lone-pair in the equatorial plane, a decrease in donor character of the organic ligand would lead to an increase, rather than a decrease, in Δ. In $(CH_2)_4TeBr_2$ the stereochemical requirements of accommodating the tellurium in the five-membered ring could lead to a significant change in the *sp* character of the Te—C bond.

While the quadrupole splittings of the dihalides span a wide range of values from 9.4 to 5.3 mm s^{-1}, the isomer shifts do not show any significant change. This reflects the fact that Δ is more sensitive to changes in the *p*-orbital populations (provided such changes give rise to a *p*-orbital imbalance) than is δ. Thus, Δ_0, the unit quadrupole splitting for one 5*p* electron, is *ca.* 12 mm s^{-1}, while removal of one 5*p* electron changes δ by only *ca.* +0.4 mm s^{-1} as noted above.

Considering the aryltellurium trihalides, it has been proposed by McWhinnie and Thavornyutikarn (12), on the basis of ir and Raman data, that these compounds are associated in the solid state and have the structure shown in Fig. 2(*iv*). The crystal structure of the compound $ClCH_2CH_2TeCl_3$ shows the tellurium to be present in a square-pyramidal arrangement, in which the $Cl\cdot CH_2CH_2$-ligand is in the axial position and each tellurium is bonded to two terminal and two bridging chlorines in a polymer chain (10). The ir and Raman spectra of the compound $(pyH)^+((p\text{-}EtOC_6H_4)TeCl_4)^-$ suggest the presence of a square-based pyramidal anion, in which the $p\text{-}EtOC_6H_4$ ligand occupies the axial position, and, as would be expected, the latter compound has very similar Mössbauer parameters to those of the aryltellurium trihalides.

The compounds $(p\text{-}MeOC_6H_4)TeCl_3$ and $(p\text{-}EtOC_6H_4)TeCl_3$ have larger isomer shifts, but the same quadrupole splittings, as the corresponding dichlorides. Similarly, $PhTeBr_3$ and $(p\text{-}EtOC_6H_4)TeBr_3$ have the same splittings as the corresponding dibromides, and $(p\text{-}CH_3C_6H_4)_2TeI_2$ and $(p\text{-}EtOC_6H_4)TeI_3$ also have similar splittings. These observations may be understood in terms of a simple additivity model for the quadrupole splittings.

In Townes and Dailey theory, considering the

Can. J. Chem. Downloaded from www.nrcresearchpress.com by 210.87.254.5 on 09/05/12
For personal use only.

Can. J. Chem. Downloaded from www.nrcresearchpress.com by 210.87.254.5 on 09/05/12
For personal use only.

dihalides to be trigonal bipyramidal with nominally sp^2 hybrids in the equatorial plane and axial pd hybrids defining the z-axis,

$$\frac{e^2qQ}{e^2q_0Q}\left(1 - \frac{\eta}{3}\right) = U_X - U_C$$

and

$$\frac{e^2qQ}{e^2q_0Q}\eta = \frac{3}{2}(U_C - U_2)(1 - \cot^2\gamma)$$

where U_X, U_C, and U_2 are the Te—X, Te—C, and non-bonding orbital populations respectively, η is the asymmetry parameter, and 2γ is the C—Te—C bond-angle (20). This formula will only hold if $(1 - \cot^2\gamma)$ is small, *i.e.*, if the lone-pair is predominantly 5*s* in character, which it appears to be in Me_2TeCl_2 ($2\gamma = 98°$), Ph_2TeBr_2 ($2\gamma = 94°$, and α-Me_2TeI_2 ($2\gamma = 91$ to 97°). For large values of 2γ, approaching 120°, for the U_X and U_C values observed in these compounds, V_{zz} would lie through the lone-pair. If the assumption is made that the bonding occurs only through tellurium 5*p* orbitals ($2\gamma = 90°$), then $\eta = 0$ and

$$\frac{e^2qQ}{e^2q_0Q} = -U_p = U_{X—Te—X} - U_C$$

i.e.,

$$U_p = U_C - U_{X—Te—X}$$

The X—Te—X linkage would be viewed as a 3*c*—4*e* bond.

If $2\gamma = 120°$ and V_{zz} lies through the lone-pair, it may be readily shown that:

$$U_p = -\frac{4}{3} + \frac{U_C}{6} + \frac{U_{X—Te—X}}{2}$$

$$\eta = \frac{3}{2}\frac{(U_X - U_C)}{U_p}$$

In the trihalides, assuming the structure in Fig. 2 and the presence of sp^3d^2 hybrids, Townes and Dailey theory predicts:

$$\frac{e^2qQ}{e^2q_0Q} = -U_X + \left(1 + \frac{U_C}{2}\right)$$

$$\eta = 0$$

If the bonding is assumed to be pure *p*, with the $5s^2$ electrons again present as a lone-pair,

$$U_p = U_{X—Te—X} - U_C$$

Thus, if the Te—C and X—Te—X bonds each have predominantly *p*-character and constant covalent character in the dihalides and the trihalides, then Δ should have the same magnitude but opposite signs in the two cases. Since it would be expected that $U_C > U_{X—Te—X}$, then Δ should be negative in the dihalides and positive in the trihalides. The present experiments confirm that the Δ values are the same in magnitude, but provide no information on the signs of Δ. The additive model as applied here obviously has limited validity, since within the dichlorides, for example, a range of quadrupole splittings is observed.

The above analysis suggests that, where the model is applicable, the X—Te—X bond has the same covalent character whether X is terminal or bridging, and it is interesting to note that in ICl_2^- and I_2Cl_6 $e^2q^{127}Q$ has the same magnitude in the two cases, the latter molecule containing two bridging chlorine atoms (19). The analysis also suggests that, in those instances where the dihalides and trihalides have the same magnitude for Δ, intermolecular bonding in the dihalides is not a major factor in determining Δ. The fact that (*p*-$EtOC_6H_4$)$TeCl_3$ and $(pyH)^+$-((*p*-$EtOC_6H_4$)$TeCl_4)^-$ have the same Δ, within the errors, supports the assumption that the field gradient derives from the valence shell orbital populations, and that lattice terms are not important.

Thus, for the compounds R_2Te, R_2TeX_2, and $RTeX_3$ the quadrupole splittings appear to be an additive property of the ligands.

The adducts of (*p*-$MeOC_6H_4$)$TeCl_3$ with pyridine and tetramethylthiourea, together with that of $TeCl_4$ with pyridine, are of interest, since they provide a further test of the additivity model for Δ briefly described above. The starting point in this analysis is the Te—C bond orbital population obtained from the tellurides. From Δ for the dichlorides, it is then possible to estimate $U_{Cl—Te—Cl}$, and, from Δ for $TeCl_4$(py), U_{py}. Previous data for the thiourea complexes provide an estimate of the orbital population of the Te—S bond, U_S (1). This analysis is shown in Table 2, and leads to the conclusion that $U_C = 1.11$, $U_{Cl—Te—Cl} = 0.35$ and $U_{py} = 0.73$, while $U_S = 0.70$ from ref. 1. The various *U* values then allow an estimate of Δ to be made for (*p*-$MeOC_6H_4$)$TeCl_3$(py) and (*p*-$MeOC_6H_4$)$TeCl_3$-(tmtu) and, assuming the structures shown in Fig. 2, the values of Δ shown in Table 3 are

TABLE 2. Orbital populations derived using Townes and Dailey theory

Compounds	Δ* (mm s^{-1})	U_p†	Orbital populations‡ U_x	U_y	U_z
Ar_2Te	(+)10.6 (average)	−0.89	1.11	1.11	[2.0]
$(p\text{-}MeOC_6H_4)_2TeCl_2$	(−) 9.1	+0.76	[1.11]	[1.11]	0.35
$(p\text{-}MeOC_6H_4)TeCl_3$	(+) 9.2	−0.76	0.35	0.35	[1.11]
$TeCl_4$.py	(+) 4.5	−0.38	[0.35]	[0.35]	0.73
Te(thiourea)$_2^{2+}$§	(+)15.6	−1.30	0.70	0.70	[2.0]

*The signs of Δ assumed are shown in parentheses.
†Where $U_p = -e^2qQ/e^2qQ_0$ and $e^2qQ = +24$ mm s^{-1}.
‡The values shown in square brackets were assumed in any one case.
§Taken from ref. 1.

TABLE 3. Predicted and observed quadrupole splittings

Compound	Δ (mm s^{-1}) Observed	Calculated*
$(p\text{-}MeOC_6H_4)TeCl_3$.py	7.6	(+)7.3
$(p\text{-}MeOC_6H_4)TeCl_3$.tmtu	7.9	(+)7.3

*Allowing for η.

TABLE 4. Bond orbital populations for different ligands

Estimator	Ligand U-values Parameter	Value
Ph_2TeCl_2	$U_{Cl-Te-Cl}$	0.4
Ph_2TeBr_2	$U_{Br-Te-Br}$	0.5
$(p\text{-}CH_3C_6H_4)TeI_2$	U_{I-Te-I}	0.6
$TeCl_4$(py)	U_{py}	0.7
Te(thiourea)$_2^{2+}$	U_S	0.7
$(C_6F_5)_2TeBr_2$	$U_{C_6F_5}$	0.8
Tellurides	U_C	1.1

arrived at. The agreement between the calculated and observed values of Δ is reasonable, given the many assumptions implicit in the analysis, and demonstrates that the Δ values are consistent with the proposed structures.

Table 4 gives the orbital populations for a number of ligands derived assuming p-bonding, together with the compound used for estimating the U value, taking U_C for the tellurides (1.11) as the standard reference point. Given the many assumptions implicit in the analysis of the Δ values and the fact that e^2q_0Q is not known accurately, the U values derived here have relative rather than absolute significance.

The compound $(p\text{-}EtOC_6H_4)TeOCl$ is of some interest, since here the quadrupole splitting is the same as that of the trichlorides, but the isomer shift is significantly smaller. On the basis of the ir and Raman data, it has been proposed that the tellurium in this compound is four co-ordinate, and a possible structure is that shown in Fig. 3. Such a structure would account for the observed complexity of the tellurium oxygen vibrations, the relatively high frequency of the tellurium halogen modes, and also the slight solubility of the compound (13). It is interesting that as the co-ordination number about the tellurium increases from four to five in going from the dihalides to trihalides the Mössbauer isomer shift increases. The relatively small isomer shift in $(p\text{-}EtOC_6H_4)TeOCl$ would appear to be more consistent with a co-ordination number of four, rather than five, and lends some support to the proposed structure for this compound.

Conclusion

The Mössbauer isomer shifts of the organotellurium compounds suggest the presence of a small amount of 5s character in the Te—C bond, and that halogen ligands remove predominantly 5p electron density from the tellurium. The quadrupole splittings may be rationalized assuming ideal geometries for the molecules and that the bonding occurs predominantly through the tellurium 5p orbitals. The Townes and Dailey

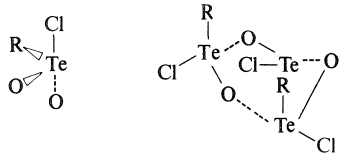

FIG. 3. Proposed environment of tellurium in RTe(O)X, and a possible ring structure (13).

Can. J. Chem. Downloaded from www.nrcresearchpress.com by 210.87.254.5 on 09/05/12
For personal use only.

theory then predicts that the organodihalides and the trihalides will have the same value for Δ, as is observed. The Δ values for $(p\text{-}MeOC_6H_4)TeCl_3$(py), $(p\text{-}MeOC_6H_4)TeCl_3$(tmtu), and $TeCl_4$(py) are consistent with the structures which have been proposed for those compounds. The isomer shift of $(p\text{-}EtOC_6H_4)Te(O)Cl$ is consistent with four- rather than five-co-ordination in this compound.

Experimental

The spectra were recorded using a 10 mCi $^{125}Sb/Cu$ source purchased from New England Nuclear. The characteristics of this source have been described by Boolchand (22). The moving source was maintained at *ca.* 80 K, using a cold-finger immersed in liquid nitrogen, while the absorbers of natural isotopic abundance were immersed in liquid helium in a Harwell Instruments Dewar. A Nuclear Science and Engineering Corporation AM-1 constant acceleration drive system was used. The absorber thicknesses were adjusted in each experiment to give *ca.* 5–10 mg cm^{-2} of ^{125}Te. Air- or moisture-sensitive compounds were mounted in absorber holders in a glove box, and cooled to 80 K before being transferred to the helium Dewar.

The 35.5 keV resonant γ-ray was monitored using a Xe/CO_2 (2 atm) Reuter-Stokes proportional detector with the window set on the 6 keV escape peak. A copper foil was interposed between the absorber and detector to reduce the background under the escape peak.

The spectra were recorded on a Nuclear Data 2200 series 1024 channel analyzer with a dual multi-scaler input. A room temperature ^{57}Fe iron foil standard spectrum was recorded on the reverse end of the drive system, using a $^{57}Co/Pd$ (New England Nuclear) source, with each ^{125}Te spectrum. Standard parameters were assumed for the iron foil spectra in calibrating the velocity scale and determining the zero velocity channel of the spectrometer. The 2×256 channel mirror image spectra, accumulated using the saw-tooth drive of the NSEC AM-1 system, were computer fitted to Lorentzians, using a programme first written by Stone (Appendix to ref. 23).

Many of the compounds studied here have previously been well-characterized and were synthesized using well established procedures (see ref. 24), and identified by chemical analysis and ir and Raman spectra where applicable. The compounds $(p\text{-}MeOC_6H_4)TeCl_3$(py) (12), $(p\text{-}MeOC_6H_4)TeCl_3$(tmtu) (11), and $TeCl_4$(py) (13) were synthesized using methods described in the respective references. The compounds $(pyH)^+((p\text{-}EtOC_6H_4)TeCl_4)^-$ and $(o\text{-}EtOC_6H_4)TeOCl$ were prepared and characterized as described in ref. 13.

1. R. M. Cheyne, C. H. W. Jones, and S. Husebye. Can. J. Chem. **53**, 1855 (1975) and references therein.
2. F. J. Berry, E. H. Kustan, and B. C. Smith. J. Chem. Soc. Dalton Trans. 1323 (1975).
3. K. V. Smith, J. S. Thayer, and R. J. Zabransky. Inorg. Nucl. Chem. Lett. **11**, 441 (1975).
4. L. Y. Y. Chan and F. W. B. Einstein. J. Chem. Soc. Dalton, 316 (1972).
5. W. R. Blackmore and S. C. Abrahams. Acta Crystallogr. **8**, 317 (1955).
6. G. Llabres, O. Dideberg, and L. Dupont. Acta Crystallogr. Sect. B, **28**, 2438 (1972).
7. F. H. Kruse, R. E. Marsh, and J. D. McCullough. Acta Crystallogr. **10**, 201 (1957).
8. G. D. Christofferson, R. A. Sparks, and J. D. McCullough. Acta Crystallogr. **11**, 782 (1958).
9. G. D. Christofferson and J. D. McCullough. Acta Crystallogr. **11**, 249 (1958).
10. D. Kobelt and E. F. Paulus. Angew. Chem. Int. Ed. Engl. **10**, 73 (1971).
11. W. R. McWhinnie and M. G. Patel. J. Chem. Soc. Dalton Trans. 199 (1972).
12. W. R. McWhinnie and P. Thavornyutikarn. J. Chem. Soc. Dalton Trans. 551 (1972).
13. P. Thavornyutikarn and W. R. McWhinnie. J. Organomet. Chem. **50**, 135 (1973).
14. K. J. Wynne and P. S. Pearson. Inorg. Chem. **10**, 2735 (1971).
15. K. J. Wynne, A. J. Clark, and M. Berg. J. Chem. Soc. Dalton Trans. 2370 (1972).
16. D. A. Couch, P. S. Elmes, J. E. Ferguson, M. L. Greenfield, and C. J. Wilkins. J. Chem. Soc. A, 1813 (1967).
17. I. R. Beattie, M. Milne, M. Webster, H. E. Blayden, P. J. Jones, R. C. G. Killean, and J. L. Lawrence. J. Chem. Soc. A, 482 (1969).
18. B. Martin and R. Schulé. Phys. Lett. B, **46**, 367 (1973).
19. G. M. Bancroft and R. H. Platt. *In* Inorg. Chem. Radiochem. **15**, 59 (1972).
20. E. A. C. Lucken. *In* Nuclear quadrupole coupling constants. Academic Press, London. 1969.
21. M. G. Clark, A. G. Maddock, and R. H. Platt. J. Chem. Soc. Dalton Trans. 281 (1972).
22. P. Boolchand. Nucl. Instrum. Methods, **114**, 159 (1974).
23. G. M. Bancroft, W. K. Ong, A. G. Maddock, R. H. Prince, and A. J. Stone. J. Chem. Soc. A, 1966 (1967).
24. W. C. Cooper (*Editor*). Tellurium. Van Norstrand, Reinhold Co., New York. 1971.

Can. J. Chem. Downloaded from www.nrcresearchpress.com by 210.87.254.5 on 09/05/12
For personal use only.

Convergence properties of the ω-β-variable method

EDUARDO ALBERTO CASTRO

Instituto de Investigaciones Fisicoquímicas Teóricas y Aplicadas, Sección Química Teórica, Diagonal 113 entre 63 y 64, 1900 La Plata, Argentina

Received April 7, 1976

EDUARDO ALBERTO CASTRO. Can. J. Chem. **54**, 3242 (1976).

The convergence properties of the ω-β-variable method are studied in order to extend some previous theoretical results about deviations of the electronic populations from the self-consistent final values. A linear correction for the whole effective Hückel Hamiltonian is employed and the inclusion of overlap integrals is discussed.

EDUARDO ALBERTO CASTRO. Can. J. Chem. **54**, 3242 (1976).

On a utilisé les propriétés de convergence de la méthode des variables β ω de façon à étendre quelques résultats théoriques antérieurs concernant les déviations des populations électroniques des valeurs autocohérentes finales. On utilise une correction linéaire pour l'hamiltonian de Hückel complet effectif et on discute de l'introduction des intégrales de recouvrements.

[Traduit par le journal]

Introduction

Different approaches have been introduced in order to improve the simple Hückel theory. In the ω-technique proposed by Streitwieser (1) the diagonal elements H_{ii} of the effective Hamiltonian H depend on the atomic orbital populations q_i

$$[1] \qquad H_{ii} = \alpha_0 + (1 - q_i)\omega\beta$$

where α_0 and β are energy parameters and ω is a positive constant. In the β-variable method (2) the non-diagonal elements H_{ij} of the effective Hamiltonian depend on the overlap population

$$[2] \qquad H_{ij} = \beta_0 \exp(ap_{ij} + b) \quad i \neq j$$

or (3)

$$[3] \qquad H_{ij} = \beta_0(Ap_{ij} + B) \quad i \neq j$$

where a, b, A, and B are constants and β_0 is a reference value for the coulombic integral. Equation 3 may be considered as an approximation of eq. 2.

In these methods, the dependence of the matrix elements H_{ij} on the density matrix necessitates the use of iterative techniques of calculation, which in turn have to be self-consistent. From the computational point of view, the principal problem to consider is that of convergence. When semiempirical methods are used, some arbitrary constants or approximations for integrals must be changed in order to avoid divergences. For example, it has been found (4) that the ω parameter must be arbitrarily changed to obtain convergence and that the inverse distance approximation for coulombic integrals in the Pariser–Parr–Pople method (P.P.P) is inconvenient in applications to polyenes with several heteroatoms. It is necessary to consider ways to overcome this kind of difficulty. Goodisman (5) made an analysis of the ω-technique and showed that, in general, with successive iterations, atomic populations should oscillate around self-consistent final values. This was found to be the case in earlier calculations (6).

This alternation around the exact values makes it possible to employ, in the n-iteration, the $n - 1$ and $n - 2$ iteration values of net populations in order to improve the convergence, as is done in several methods of calculation. In the present paper, we generalize the equations given by Goodisman, starting from a linear correction for Hamiltonian matrix elements, and show that the previous results represent a particular case. Furthermore, we discuss the introduction of overlap integrals, and show that this does more than simply complicate the equations without substantially changing the final results. Finally, we suggest that it is necessary to modify the original corrections for the Hamiltonian matrix elements, in order to introduce the overlap in a consistent way.

General Formulation

In the following we assume that overlap is

Can. J. Chem. Downloaded from www.nrcresearchpress.com by 210.87.254.105 on 09/05/12
For personal use only.

negligible. Then we point out in what way and under what conditions the inclusion of overlap integrals is valid.

The secular equation takes the form

$$[4] \quad \sum_{j=1}^{n} H_{ij}C_{jk} = E_k C_{ik} \quad i = 1, 2, \ldots, n$$

We assume that matrix elements H_{ij} change according to the following linear expression in p_{ij}

$$[5] \quad H_{ij} = Ap_{ij} + B \quad \forall\, i,j$$

where A and B are constants and p_{ij} is given by

$$[6] \quad p_{ij} = 2\sum_{k}^{(\mathrm{occ})} C_{ik}C_{jk} \equiv 2\sum_{k}{}' C_{ik}C_{jk}$$

for real coefficients. In order to simplify the equations, we assume that the occupation numbers are 2 or 0, so as to exclude those cases of molecules with an odd number of electrons or with excited states having singly occupied MO's. The MO's, as is usual in the LCAO approximation, are given in the form

$$[7] \quad \psi_k = \sum_{i=1}^{n} C_{ik}\phi_i \equiv \sum_{i} C_{ik}\phi_i$$

where the ϕ_i's are atomic orbitals. The orthonormalization requirement for AO's under the assumption of $S_{ij} = \delta_{ij}$ implies that

$$[8] \quad \sum_{i} C_{ik}C_{il} = \delta_{kl}$$

and the unitary condition implies that

$$[9] \quad \sum_{k} C_{ik}C_{jk} = \delta_{ij}$$

If we denote the exact or self-consistent values by bars, eq. 4 has the form

$$[10] \quad \sum_{j} \bar{H}_{ij}\bar{C}_{jk} = \bar{E}_k\bar{C}_{ik}$$

Following the procedure given in ref. 5, at some stage of the iterative process we have

$$[11] \quad C_{ik} = \bar{C}_{ik} + \delta C_{ik}$$

where δC_{ik} is the deviation of the coefficient C_{ik} from its final value before solving the secular equations.

We calculate the new Hamiltonian matrix elements H_{ij} in accord with eqs. 5 and 6, employing the coefficients given in eq. 11. The resolution of the secular equations produces new coefficients $\tilde{C}_{ik}$

$$[12] \quad \tilde{C}_{ik} = \bar{C}_{ik} + \delta' C_{ik}$$

where $\delta' C_{ik}$ indicates deviations of the coefficients from their final values after solving the secular equations.

Then we have the following equation to resolve

$$[13] \quad \sum_{j}(\bar{H}_{ij} + \delta H_{ij})(\bar{C}_{jk} + \delta' C_{jk}) = (\bar{E}_k + \delta' E_k)(\bar{C}_{ik} + \delta' C_{ik})$$

where $i = 1, 2, \ldots, n$ and $k = 1, 2, \ldots, n$.

Neglecting second-order terms, we obtain

$$[14] \quad \sum_{j}(\bar{H}_{ij}\delta' C_{jk} + \delta H_{ij}\bar{C}_{jk} + \bar{H}_{ij}\bar{C}_{jk}) = \bar{E}_k\bar{C}_{ik} + \bar{C}_{ik}\delta' E_k + \bar{E}_k\delta' C_{ik}$$

which is simplified by eq. 10 to

$$[15] \quad \sum_{j}(\bar{H}_{ij}\delta' C_{jk} + \delta H_{ij}\bar{C}_{jk}) = \bar{C}_{ik}\delta' E_k + \bar{E}_k\delta' C_{ik}$$

We multiply eq. 15 by $\bar{C}_{ik}$ and sum over i. Then, using eqs. 10, 8, and 5, we obtain

$$[16] \quad \delta' E_k = A\sum_{i}\sum_{j}\bar{C}_{jk}\bar{C}_{ik}\delta p_{ij}$$

for the change in energy in terms of self-consistent coefficients. Substituting eq. 16 in eq. 15 and rearranging, we get

$$[17] \quad \sum_{j}\bar{H}_{ij}\delta' C_{jk} - \bar{E}_k\delta' C_{ik} = A\left\{\bar{C}_{ik}\sum_{l}\sum_{j}\bar{C}_{jk}\bar{C}_{lk}\delta p_{lj} - \sum_{j}\bar{C}_{jk}\delta p_{ij}\right\}$$

If we express the deviations of bond orders after iteration in terms of quantities before iteration, and neglect second-order deviations, we obtain

$$[18] \quad \delta' p_{ij} = 2\sum_{k}{}'(\bar{C}_{ik}\delta' C_{jk} + \bar{C}_{jk}\delta' C_{ik})$$

We want to express $\delta' C_{rs}$ in terms of $\bar{C}_{rm}$'s, and so, without loss of generality, we can write

$$[19] \quad \delta' C_{ik} = \sum_{l} a_{lk}\bar{C}_{il}$$

In order to solve for a_{mk} we substitute eq. 19 in eq. 17, multiply by $\bar{C}_{im}$ $(m \neq k)$ and sum over i, and employ eqs. 8 and 10. The final result is

$$[20] \quad a_{mk} = -A(\bar{E}_m - \bar{E}_k)^{-1}\sum_{i}\sum_{j}\bar{C}_{im}\bar{C}_{jk}\delta p_{ij}$$

and

Can. J. Chem. Downloaded from www.nrcresearchpress.com by 210.87.254.105 on 09/05/12
For personal use only.

Can. J. Chem. Downloaded from www.nrcresearchpress.com by 210.87.254.105 on 09/05/12
For personal use only.

$$[21]\quad \delta' C_{qk} = -A\sum_l{}''(\bar{E}_l - \bar{E}_k)^{-1}\sum_s\sum_r \bar{C}_{sl}\bar{C}_{rk}\delta p_{sr}\bar{C}_{ql} \qquad q = i,j$$

where $\sum_l''$ denotes $\sum_l^{l\neq k}$.

Substituting eq. 21 in eq. 18, we obtain

$$[22]\quad \delta' p_{ij} = -2A\sum_k{}'\left\{\bar{C}_{ik}\sum_l{}''(\bar{E}_l - \bar{E}_k)^{-1}\sum_s\sum_r \bar{C}_{sl}\bar{C}_{rk}\delta p_{sr}\bar{C}_{jl} + \bar{C}_{jk}\sum_l{}''(\bar{E}_l - \bar{E}_k)^{-1}\sum_s\sum_r \bar{C}_{sl}\bar{C}_{rk}\delta p_{sr}\bar{C}_{il}\right\}$$

which may be written in a more compact form as

$$[23]\quad \delta' p_{ij} = -2A\left[\sum_s\sum_r \delta p_{rs}\sum_k{}'\sum_l{}'''(\bar{E}_l - \bar{E}_k)^{-1} \times \{\bar{C}_{sl}\bar{C}_{rk}(\bar{C}_{ik}\bar{C}_{jl} + \bar{C}_{jk}\bar{C}_{il})\}\right]$$

where $\sum_l'''$ means $\sum_l^{(\text{unocc})}$.

Equation 23 is the desired result. It gives the deviations of the overlap populations from their final values after an iteration in terms of their deviations before the iteration and contains eq. 18 of Goodisman as a special case (where $i = j$ and $A = -\beta\omega$).

The Closure Condition for $\delta' p_{ij}$

Diagonal elements of the density matrix are interpreted as partial electronic charges (when the overlap between atoms is neglected). The sum of these elements is equal to the total number of electrons considered, which is a constant. In such a case the following closure condition for $\delta' q_i$ is fulfilled

$$[24]\quad \sum_i \delta' q_i = 0$$

In the present more general case, a similar condition for $\delta' p_{ij}$ is not valid, *i.e.*

$$[25]\quad \sum_i\sum_j \delta' p_{ij} \neq 0$$

This may easily be seen from eq. 23, because if we ignore overlap, then we cannot interpret p_{ij} as a common charge between the i-atom and the j-atom. So the result, eq. 25, is consistent with the previous discussion.

If overlap integrals are introduced, the total electronic charge is expressed as

$$[26]\quad 2\sum_i{}'\sum_r\sum_s C_{ri}C_{si}S_{rs} = Q = \text{constant}$$

and condition eq. 24 must be changed to

$$[27]\quad \sum_s\sum_{r\leq s} \delta' p_{rs}S_{rs} = 0$$

Special Cases

(*A*) We now look for a relation between $\delta' p_{ij}$ and δp_{ij}. If we assume that the effect of δp_{rs} when $\forall r \neq i$, $s \neq j$ may be neglected in eq. 23, because of either the smallness of δp_{rs} or a cancellation between terms of different signs, then

$$[28]\quad \delta' p_{ij} = -2A\delta p_{ij}\sum_k{}'\sum_l{}'''(\bar{E}_l - \bar{E}_k)^{-1} \times \{\bar{C}_{ik}{}^2\bar{C}_{jl}{}^2 + \bar{C}_{ik}\bar{C}_{il}\bar{C}_{jk}\bar{C}_{jl}\}$$

In the very special case of cancellation of the terms within the second braces, or if their value is positive, then an alternation in the bond orders occurs after successive iterations.

(*B*) The remaining options analysed in ref. 5 cannot be treated here because they were based on the closure condition [24] and a similar condition does not exist in the present case. Thus the conclusions reached about alternation of signs with a linear correction will be valid only in the special case of a diagonal correction.

Inclusion of Overlap

Goodisman, in his analysis of the convergence in the ω-technique, pointed out that the inclusion of overlap integrals would probably not alter the final results, but merely complicate the equations (5). If overlap is introduced and the convergence is studied by a perturbation treatment similar to that previously given, it should necessarily be done in a consistent and coherent way. So we suggest that overlap integrals must be introduced into the secular equations as well as in the corresponding reactions for H_{ij}. A closure condition would then be reached and a study of the convergence for various special cases could be made. The possibilities mentioned could be fulfilled by employing other semiempirical methods which include overlap integrals into the matrix elements, such as the Extended Hückel Theory and P.P.P. methods.

Conclusions

We have shown that it is possible to extend the previous study on the ω-technique by employing a variation of the whole Hamiltonian matrix elements with the density matrix elements in a

linear form. This may be interpreted as a first-order approximation to the well-known exponential variation of the β-variable method. It is seen that the equations obtained reduced to the previous particular case of diagonal variation. The characteristics of the convergence (alternation around the final self-consistent values) are lost in the actual case, except under very special conditions. This is due to the loss of the closure condition for $\delta' p_{ij}$, which in turn is due to the neglect of overlap between atoms. This closure condition was essential in the analysis of the ω-technique for various special cases in order to produce alternations in sign for the deviations of net populations. It was pointed out in the preceding discussion that in order to make an analysis that is in better agreement with the physical interpretation of the chemical bond, it would be necessary to introduce overlap modifications to eq. 1 by taking into account integral S_{ij}. Perhaps a suitable approximation would be

$$[29] \qquad H_{ij} = A\sum_r\sum_s p_{ij}(S_{ir} + S_{js}) + B$$

where A, B are constants and S_{ij} is the overlap integral between atoms i and j. The sum could be extended over all the orbitals, or, more restrictively, over just the nearest neighbors.

For the particular case of the variation of diagonal elements in a modified ω-technique, relation 29 would be

$$[30] \qquad H_{ii} \equiv \alpha_i = A + B\sum_j S_{ij}q_i$$

or, in a more familiar expression,

$$[31] \qquad H_{ii} = \alpha_0 + \omega\beta\left(1 - \sum_j q_i S_{ij}\right)$$

1. A. STREITWIESER, JR. Molecular orbital theory for organic chemists. John Wiley, New York. 1961. p. 115.
2. G. V. BOYD and N. SINGER. Tetrahedron, **22**, 3383 (1966).
3. K. NISHIMOTO and L. S. FORSTER. Theoret. Chim. Acta, Berlin, **3**, 407 (1965).
4. E. A. CASTRO and O. M. SORARRAIN. J. Chim. Phys. **3**, 513 (1972).
5. J. GOODISMAN. Theoret. Chim. Acta, Berlin, **36**, 117 (1974).
6. R. ETTINGER. Tetrahedron, **20**, 2339 (1964).

Can. J. Chem. Downloaded from www.nrcresearchpress.com by 210.87.254.105 on 09/05/12
For personal use only.

Confidence in fluorescence lifetime determinations: a ratio correction for the photomultiplier time response variation with wavelength[1,2]

D. M. RAYNER,[3] A. E. MCKINNON,[3] AND A. G. SZABO[4]
Division of Biological Sciences, National Research Council of Canada, Ottawa, Canada K1A 0R6

AND

P. A. HACKETT
Division of Chemistry, National Research Council of Canada, Ottawa, Canada K1A 0R6

Received April 29, 1976

D. M. RAYNER, A. E. MCKINNON, A. G. SZABO, and P. A. HACKETT. Can. J. Chem. **54**, 3246 (1976).

The photomultipliers used in single photon counting fluorescence lifetime systems have a time response function which varies with wavelength. This variation results in a reduced confidence in the kinetic parameters obtained after deconvolution of the lamp intensity decay profile measured at the excitation wavelength from the sample emission decay profile measured at the emission wavelength. Moreover in the case of multi-component decays, inaccurate kinetic parameters are calculated because of this PMT variation. Using weighted residual plots, we demonstrate how one may make a satisfactory subjective appraisal of the adequacy of the deconvolution and the physical model of the decay processes. We have developed a ratio correction technique which accounts for the PMT time response variation with wavelength. This technique requires no *a priori* assumption of the nature of the PMT effect. Only when the data are corrected using the ratio correction technique can sufficient confidence in the accuracy of the singlet excited state parameters and the validity of the physical model be obtained.

D. M. RAYNER, A. E. MCKINNON, A. G. SZABO et P. A. HACKETT. Can. J. Chem. **54**, 3246 (1976).

Les photomultiplicateurs utilisés dans les systèmes de comptage des photons uniques pour déterminer le temps de vie de fluorescence ont une fonction de temps de réponse qui varie avec la longueur d'onde. Cette variation conduit à une confiance réduite dans les paramètres cinétiques obtenus après déconvolution du profil de décroissance de l'intensité de la lampe mesuré à la longueur d'onde d'excitation, à partir du profil de décroissance de l'émission de l'échantillon mesuré à la longueur d'onde d'émission. De plus dans le cas de décroissance à plusieurs composants, les paramètres cinétiques qui ne sont pas justes sont calculés à cause de cette variation PMT. Faisant appel à des courbes résiduelles pondérées, on démontre comment on peut faire une évaluation subjective satisfaisante de l'adéquation de la déconvolution et du modèle physique des processus de décroissance. On a développé une technique de correction par des rapports qui tient compte de la variation du temps de réponse PMT avec la longueur d'onde. Cette technique ne requiert aucune hypothèse à priori sur la nature de l'effet PMT. Ce n'est que lorsque les données sont corrigées en faisant appel à la technique de correction par des rapports que l'on peut obtenir une confiance suffisante dans l'exactitude des paramètres d'états excités singulets et dans de la validité du modèle physique.

[Traduit par le journal]

The increase in sophistication of the photophysical interpretation of excited state kinetics (1–4) and in the utilization of fluorescence lifetimes to study biological systems (5–10), where multi-component fluorescence decays are likely to be observed, demand a high degree of confidence in the experimental determination of the form of the fluorescence decay function.

In pulse fluorimeters the fluorescence decay of a sample excited at wavelength λ_{ex} is measured at wavelength λ_{em}. This decay profile, R^s_{em}, is a convolution[5] (11, 12) of the true fluorescence decay function of the sample emission, G^s_{em}, the

[1]NRCC 15449.

[2]Presented in part at the VIIIth International Conference on Photochemistry, Edmonton, Alberta, Aug. 1975.

[3]D.M.R. and A.E.M. are NRCC Postdoctoral Fellows 1973–1975. Present address of A.E.M. is Respiratory Laboratory, Princess Margaret Hospital, Private Bag, Christchurch, New Zealand.

[4]To whom correspondence should be addressed.

[5]$A \otimes B = \int_0^t A(\tau) \cdot B(t - \tau) d\tau$.

Can. J. Chem. Downloaded from www.nrcresearchpress.com by 84.22.46.98 on 09/08/12
For personal use only.

instrument response function, H_{em}, both at the emission wavelength, λ_{em}, and the intensity function of the excitation source, L_{ex}, at the wavelength of excitation, λ_{ex};

$$[1] \qquad R^{s}_{em} = G^{s}_{em} \otimes L_{ex} \otimes H_{em}$$

A scatter solution or a reflector is used to measure an experimental lamp decay profile, R^{l}_{ex}, which is a convolution of the lamp response function, L_{ex}, and an instrument response function, H_{ex}, at the excitation wavelength

$$[2] \qquad R^{l}_{ex} = L_{ex} \otimes H_{ex}$$

In most cases it is assumed that the instrument response functions, H_{ex} and H_{em}, are independent of wavelength and hence equal. Then, since the lamp response function, L_{ex}, is common to both eqs. 1 and 2, one makes the appropriate substitution of the measured lamp decay profile, R^{l}_{ex}, into eq. 1 and deconvolves (11–17) to obtain the true fluorescence decay function of the sample, G^{s}_{em}. In this way the known (11, 12, 18–20) time response variation with wavelength of the lamp is avoided. However it is also known (17, 18, 20) that the detecting photomultiplier tube (PMT) has a time response variation with wavelength. Therefore, if one desires a high degree of confidence in the adequacy of the physical model for the excited singlet state decay processes and the associated kinetic parameters which one obtains after the deconvolution of the measured data, this wavelength–time response variation of the PMT cannot be overlooked and H_{ex} cannot be considered to be equal to H_{em}.

Techniques for correcting or eliminating the PMT time response variation with wavelength have been recently described (17, 18, 20). In this paper we review these procedures and describe a ratio correction technique which overcomes some of the problems of the earlier procedures and satisfactorily corrects for the time response variation with wavelength of the PMT.

Confidence Criteria

We have chosen to deconvolute the measured decay profiles by the 'iterative convolution' method (12, 14), in which the parameters of an exponential model of the decay processes are estimated using weighted nonlinear least-squares. This decision was taken after an extensive study of several deconvolution methods (21). The iterative convolution method based on weighted nonlinear least-squares was the most successful in resolving multi-component luminescence decays which were of the same order as the decay of the excitation pulse. It is also mathematically rigorous and does not require any preliminary smoothing or extrapolation of the data.

It is essential to have a criterion for deciding whether the physical model which is assumed for the emission decay processes of the sample and the calculated kinetic parameters adequately describe the experimental observations. Direct comparison of the measured decay profile, R^{s}_{em}, with the 'best fit' decay profile obtained from the iterative convolution method is not sufficiently sensitive. Inspection of a weighted residual plot does, however, provide a satisfactory method of making this decision. The difference between the values of R^{s}_{em} and the 'best fit' decay profile for each channel is determined and weighted by the reciprocal of the number of counts accumulated in that channel. The reciprocal of the number of counts is the best estimate of the variance of the measured data (12–14) in that channel. The weighted residuals, when plotted against channel number, should appear to be randomly distributed about zero if the physical model and 'best fit' calculated decay processes for the emission decay processes are adequate.

Various tests are available which attempt to give a quantitative measure of the randomness of residuals (12, 14, 17, 22, 23). However, they can be used only as a guide for accepting or rejecting the calculated results. We have found that examination of the weighted residual plots allows one to make a satisfactory subjective judgement of the randomness of the residuals. A similar subjective judgement is used by others (14, 17) when they calculate and plot an auto-correlation function of the residuals.

Parameters such as the weighted sum of squares of residuals (WSSR) (21) and the root-mean-square (RMS) derivation (7) (which is the square root of the unweighted sum of squares of residuals divided by the number of channels) should not be used by themselves to assess the adequacy of the physical model.

Instrument Design Considerations

The single photon counting fluorescence lifetime system (Fig. 1) used in our experiments was

Can. J. Chem. Downloaded from www.nrcresearchpress.com by 84.22.46.98 on 09/08/12
For personal use only.

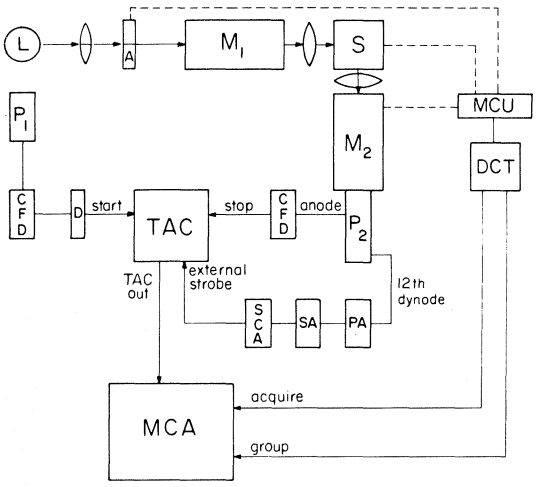

FIG. 1. Single photon fluorescence lifetime system; L, N_2 lamp; A, adjustable aperture; M_1, excitation monochromator, Bausch and Lomb #33-86-26-07 (f/3.5, 7.4 nm/mm); M_2 emission monochromator, Spex Micromate (f/2.5, 8 nm/mm); S, sample compartment; P_1, 'start' PMT, RCA 1P28; P_2, 'stop' PMT, RCA 8850; CFD, ORTEC Model 463, constant fraction discriminator; D, delay; PA, ORTEC Model 113 preamplifier; SA, ORTEC Model 440A, spectroscopy amplifier; SCA, ORTEC Model 420 single channel amplifier; TAC, ORTEC Model 457, time to amplitude converter; MCU, motor control unit; DCT, ORTEC Model 715, dual counter timer; MCA, Nuclear Data Model 4410, multichannel analyzer.

basically the same as that described by several other workers (11, 18, 19). However we have assembled our instrument using several design features which have not, to the best of our knowledge, previously been collectively incorporated in any one instrument. These features which will now be described and discussed were essential to avoid additional instrumental artifacts which could not be accounted for by the ratio correction technique developed in this paper. Failure to incorporate these design requirements significantly reduces the confidence one can have in the experimental results and in any correction technique.

In order to be able to correct rigorously for any wavelength effect it is necessary that the system include both excitation and emission monochromators. The use of two monochromators requires a high frequency nanosecond flash lamp of sufficient intensity to measure an emission decay in a reasonable period of time. A free running spark gap lamp was designed to meet these requirements. It operated under a high pressure of nitrogen and at a relatively high power which was controlled by the charging resistor. The charging resistor was immersed in oil and externally cooled to allow its use over its rated wattage. Because the lamp was coaxial in design no RF noise which interfered with the remainder of the system could be detected. Two methods by which the lamp decay profiles could be measured are the use of a glycogen suspension in water as a scatterer or a mirror as a reflector. These two different methods gave lamp decay profiles which were noticeably different. The use of the scatterer, with an optical density similar to that of the sample solution at the excitation wavelength, was favoured in agreement with Lewis *et al.* (18) because it was felt that it mimicked the geometry of a sample solution better than a mirror. It was also found that satisfactory deconvolutions could only be obtained when the scatterer solution was used.

Although two lamp profiles which were collected successively appeared to be superimposable on visual inspection, a statistical test of comparison (the variance test for the homogeneity of the binomial distribution was used (24)) showed a significant difference between the two profiles that could not be attributed to random noise. This problem of lamp drift has been discussed by Hazan *et al.* (25) and we have used an alternating technique similar in concept to theirs which satisfactorily deals with the problem. When the lamp decay profile was collected alternately for periods of 30 s each in two separate memory groups of the MCA over a total time of 24 h, there was no significant statistical difference between the profiles accumulated in each memory group. Thus the lamp decay profile change with time could be overcome by alternately measuring the lamp decay profile and sample emission profile for 30 s at a time until sufficient counts had accumulated in two separate memory groups of the MCA. The alternate collection of the lamp decay and sample emission profiles every 30 s required automated control of the sample selection, emission monochromator (M_2 in Fig. 1) wavelength and lamp intensity.

For the alternate collection of the lamp and sample emission decay profiles, the scatterer solution and sample of interest were contained in a sample compartment which was rotated by

Can. J. Chem. Downloaded from www.nrcresearchpress.com by 84.22.46.98 on 09/08/12
For personal use only.

Can. J. Chem. Downloaded from www.nrcresearchpress.com by 84.22.46.98 on 09/08/12
For personal use only.

a stepping motor. The wavelength of the emission monochromator was changed with another stepping motor depending on whether the lamp or sample emission profile was being measured.

Often it was found that the light intensity from the scatterer solution was greater than the emission intensity of the sample under investigation. Therefore in order to alternate the data acquisition in the manner described above, and maintain good counting statistics while performing the measurements in a reasonable period of time, an aperture (A in Fig. 1) was inserted into or removed from the light path between the lamp and the excitation monochromator (M_1 in Fig. 1). This location was selected so that the area of illumination of the sample remained constant.

The rotation of the sample compartment, changing of the emission monochromator wavelength and use of the excitation aperture were co-ordinated through a motor-control timing unit. This same unit also synchronized the change of the memory groups of the multichannel analyzer (MCA), and the data acquisition of the MCA with the operation of the various motors.

We preferred to use an RCA 8850, twelve stage PMT rather than a Phillips 56 DUVP fourteen stage PMT because of the distinct photoelectron energy resolution of the former tube (26, 27). The broad energy distribution of the single photon pulses of the 56 DUVP tube created an additional instrumental complication. The 'walk' specification of the constant fraction discriminator (CFD) is energy dependent resulting in timing errors when a broad energy range of pulses is received from the PMT. A variation of the technique described by others (26, 27) was used in order to ensure that only single photoelectron pulses were collected.

Experimental

Materials

2,5-Diphenyloxazole (PPO), 2,2′-*p*-phenylenebis(5-phenyloxazole) (POPOP), 2,5-bis(5′-*t*-butyl-2-benzoxazoyl)-thiophene (BBOT), and anthracene were scintillation grade reagents purchased from Eastman Kodak Co. and used without further purification. 9-Cyanoanthracene purchased from Aldrich Chemicals Co. was recrystallized three times from ethanol (mp 174–175 °C lit. (28) 170–172 °C). 2-Napthol purchased from British Drug Houses was recrystallized twice from ethanol–water (mp 122–123 °C lit. (10) 123 °C). 3,6-Diamino-2,7-dimethylacridine (acridine yellow) was synthesized as the free base according to the method described by Ullmann and Maric (29*a*) (mp 330 °C lit. (29*b*) 325 °C).

The solvent ethanol (95%) was purified according to the method outlined in Parker (30). Cyclohexane was MC/B Spectroquality Grade, purchased from Matheson, Coleman and Bell and used without further purification. All samples were degassed prior to measurement.

Instrumentation and Methods

Fluorescence spectra were measured on a Farrand MK-1 spectrofluorimeter. Absorption spectra were measured on a Cary 15 spectrophotometer.

The single photon counting fluorescence lifetime system is detailed in Fig. 1 and certain features are discussed in the text (Instrumental Design Considerations). The free running lamp (L) operated at 25 kV under 400 psi of nitrogen gas pressure. The 10 MΩ load resistor was immersed in oil and was externally cooled by water circulation. The lamp frequency, 15–30 kHz, was governed by the gap between the Pt electrodes, usually 1–2 mm.

The excitation monochromator (M_1) was a Bausch and Lomb Model #33-86-26-07, high intensity monochromator (f/3.5, reciprocal dispersion 7.4 nm/mm) whose slits were adjusted so that the excitation bandwidth was 7 nm. The emission monochromator (M_2) was a Spex Micromate monochromator (f/2.5, reciprocal dispersion 8 nm/mm) whose slits were set so that the emission bandwidth was 7 nm. Its wavelength could be changed as required with a stepping motor whose operation was controlled by the motor control unit (MCU).

The sample compartment (S) held up to four 10 × 10 mm fluorescence cells and could be rotated by another stepping motor. The geometry of the sample holder provided right angle detection of the emitted or scattered light.

The motor control unit which synchronized the operation of the aperture (A), sample compartment, and emission monochromator with the data acquisition by the Nuclear Data Model 4410 multichannel analyzer (MCA) used an ORTEC Model 715 Dual Counter-Timer (DCT) as the timing unit. The DCT provided a +3 V level signal at the 'interval out' connection when the timer was counting. The rise of this +3 V signal was used to begin data acquisition by the MCA. After starting, the data acquisition time period was controlled by the MCA and it was set (29 s) to be slightly less than the selected time interval (30 s) on the DCT. After the DCT time period elapsed the +3 V signal fell to 0 V. This falling edge was used by the NRC-built motor control unit to derive the signals which started the various stepping motors and changed the memory group of the MCA. The dwell time of the DCT was set so that further data acquisition did not begin until after all motor changes were completed.

The emission was detected using an RCA 8850, 12 stage PMT (P_2), whose base was wired according to the circuit recommended by RCA (31) for fast pulse response except that the voltage on the focussing electrode could be adjusted with a potentiometer. The applied voltage was kept as low as possible (1900 V) to minimize dark current. Singe photon derived pulses from this PMT were used as 'stop' pulses for the ORTEC Model 457 Biased Time to Amplitude Converter (TAC). The 'start' pulses for the TAC were obtained from an RCA 1P28 PMT (P_1), whose base was wired for fast response characteristics. The

'start' PMT detected the lamp pulses via a fibre optic which was attached to the lamp housing.

The following technique was used to ensure that only single photoelectron pulses were collected. The signal from the 12th dynode of the RCA 8850 PMT was amplified by an ORTEC Model 113 Preamplifier, shaped by an ORTEC Model 440A Spectroscopy Amplifier, and passed into an ORTEC Model 420 Single Channel Analyzer (SCA). The energy window on the SCA was set to provide an output pulse only when the signal from the 12th dynode corresponded to the energy distribution of single photoelectron pulses. The SCA output pulse was then used as an external strobe for the TAC. Thus an output from the TAC was obtained only when the stop pulse was due to a single photoelectron. The TAC output was connected to the Analog to Digital Converter of the MCA and the pulses were accumulated in the usual way.

In the initial setting up of the system the linearity of the TAC was checked and the 'walk' of the CFDs was adjusted to optimum conditions according to techniques described in the respective component manuals.

The time range of the TAC was set so that adequate decay profile definition was obtained in the MCA. In most cases 512 channels per memory group of the MCA were used.

The excitation and emission wavelengths for the sample under study were selected after comparison of the sample's absorption and emission spectrum with the emission spectrum of a calibration compound (see text). After this wavelength selection of the 'start' to 'stop' count ratio was adjusted to at least 30:1 for the lamp decay and sample emission profile in order to achieve good counting statistics and minimize pulse pile-up (11). The adjustable aperture (A) was used when it was necessary to attenuate the lamp intensity in order to obtain this ratio. The decay profiles were then alternately collected for periods of 29 s each. When approximately 10 000 counts had accumulated in both peak channels the data accumulation was terminated.

The calibration compound was excited at $\lambda_a < \lambda_{ex}$ and its emission decay profile was measured at λ_{ex} and λ_{em}.

To reduce the random noise in the profiles used to calculate the correction ratio a large number (>100 000) of counts were accumulated in the peak channel of these profiles. These profiles were usually measured overnight. The alternate collection of the decay profiles avoided any effects of lamp response changes over this period of time.

The decay profiles were transferred to the IBM 360-67, TSS computer via a remote terminal. This terminal could also be used to direct the computation involved in the correction technique and deconvolution. It consisted of an ASR 13 teletype, a G.E.C. TDM 114B13 Data Set acoustic coupler, an NRC-designed interface (32) and the NDP 812 minicomputer portion of the Nuclear Data Model 4410 MCA.

A correction ratio was calculated from the calibration compound's decay profiles (see text) using the fast Fourier Transform Algorithm (33). This ratio was applied to the appropriate Fourier transform of the sample's emission decay profile and then the inverse of the 'corrected' emission decay was calculated. The corrected emission decay profile and lamp decay profile were then deconvoluted by the weighted nonlinear least-squares iterative convolution technique[6] (21) to obtain the kinetic parameters of the sample's decay.

The Variation of Time Response of the PMT with Wavelength

Figure 2*a* shows the measured fluorescence decay profile at 415 nm (excitation at 355 nm) of the scintillator POPOP (1.5×10^{-5} *M*) in ethanol solution and the 'best fit' calculated fluorescence decay profile. The latter was obtained by deconvolution using the weighted nonlinear least-squares iterative convolution method. It was assumed that $H_{em} = H_{ex}$ in eqs. 1 and 2 and that a single exponential decay model described the fluorescence of POPOP. The agreement between the best fit ($\tau = 1.30$ ns) and the observed decay profiles particularly at the peak height is not satisfactory. The weighted residual plot (Fig. 2*b*) shows that the residuals were clearly non-random and emphasizes this lack of agreement. Non-random residuals imply either that the single exponential model for the fluorescence decay of POPOP was inappropriate or that the assumption that $H_{em} = H_{ex}$ was invalid. It is generally accepted (34) that a single exponential model for the fluorescence decay of dilute solutions of POPOP is correct. It is known, however, that the time response of the PMT varies with wavelength and hence it should not have been assumed that $H_{em} = H_{ex}$. Further comment on the legitimacy of a single exponential model for the fluorescence decay of POPOP cannot be made until a satisfactory correction for this instrumental artifact has been established.

The variation of the PMT time response with wavelength has been discussed and treated previously in the literature (17, 18, 20). Figure 3 shows the fluorescence decay profiles for PPO (1.5×10^{-5} *M*) in cyclohexane solution measured at 355 and 415 nm using for Fig 3*a* a Phillips 56 DUVP PMT and for Fig. 3*b* an RCA 8850 PMT. Excitation was at 290 nm for these measurements. The observed differences between the decay profiles measured at the two wavelengths for a particular tube, while small, cannot be neglected in any deconvolution in which the lamp decay profile, R^l_{ex}, and the sample decay profile, R^s_{em}, are measured at two different wavelengths. It is clear that the variation of the time

[6]Details of these programs are available from the authors on request.

Can. J. Chem. Downloaded from www.nrcresearchpress.com by 84.22.46.98 on 09/08/12
For personal use only.

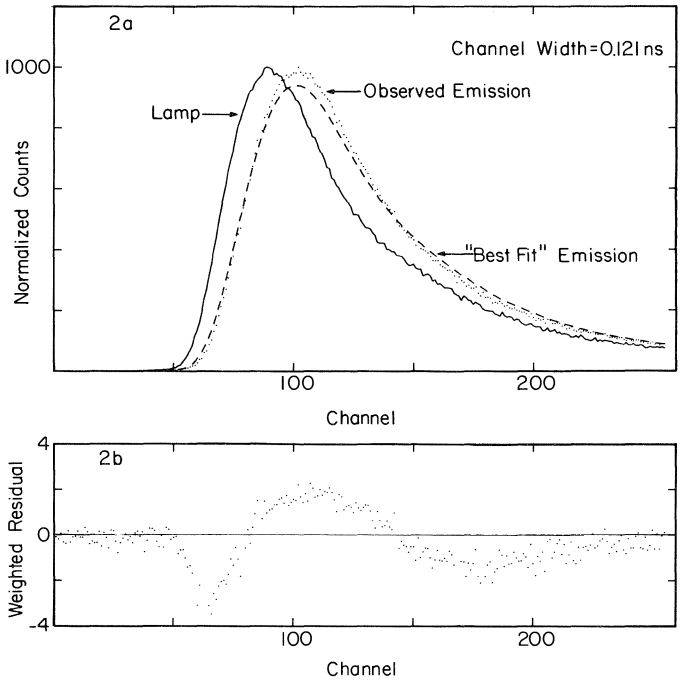

FIG. 2. (*a*) Measured lamp intensity profile —; measured emission decay profile · · ·; and calculated 'best fit' emission decay profile - - -; for the singlet lifetime determination of an ethanol solution of POPOP (1.5×10^{-5} *M*); Phillips 56 DUVP PMT; channel width 0.121 ns; λ_{ex} = 355 nm, λ_{em} = 415 nm. (*b*) Weighted residual plot for calculated 'best fit' decay profile in (*a*).

response of the PMT with wavelength is different for each tube. For the 56 DUVP PMT the decay profile measured at 415 nm was broadened when compared to that measured at 355 nm. While for the RCA 8850 tube the decay profile at 355 nm appeared to be shifted relative to that at 415 nm.

In their paper which described the Laplace transform deconvolution method in fuller detail, Gafni *et al.* (17) have represented the time response variation with wavelength of the PMT as a pure delay function. The residual plots which they obtained showed that the residuals were more randomly distributed when a delay function was included in the calculations. However for a Phillips 56 DUVP PMT such as that used to obtain the data in Fig. 3*a* the decay profile at one wavelength (415 nm) was broadened when compared to that at another wavelength (355 nm). The application of a delay function to correct for this variation is not a proper representation of the observed wavelength effect. We have found that the response differences observed at two wavelengths for the RCA 8850 PMT vary depending on the wavelength pairs used in the measurements. Allowing the deconvolution computations to fit, *a priori*, an arbitrary delay function in an attempt to account for the PMT effect and improve the fit of the calculated decay profiles reduces the confidence one can have in the calculated kinetic parameters. Any small variation of the physical model for the decay processes can be lost in the process.

Lewis *et al.* (18), using POPOP as a quantum counter, also demonstrated that the PMT time response variation with wavelength was significant. In their experiments a solution of the quantum counter and an appropriate filter was placed in front of the PMT. In this position the quantum counter acted as a wavelength shifter ensuring that the light incident on the photocathode had the same spectral characteristics irrespective of whether R^{l}_{ex} or R^{s}_{em} was being measured. They achieved a marked improvement in the agreement between the measured and calculated decay profiles using this technique. However, as they pointed out, the use of a quantum counter to correct for the PMT time response variation with wavelength was limited

Can. J. Chem. Downloaded from www.nrcresearchpress.com by 84.22.46.98 on 09/08/12
For personal use only.

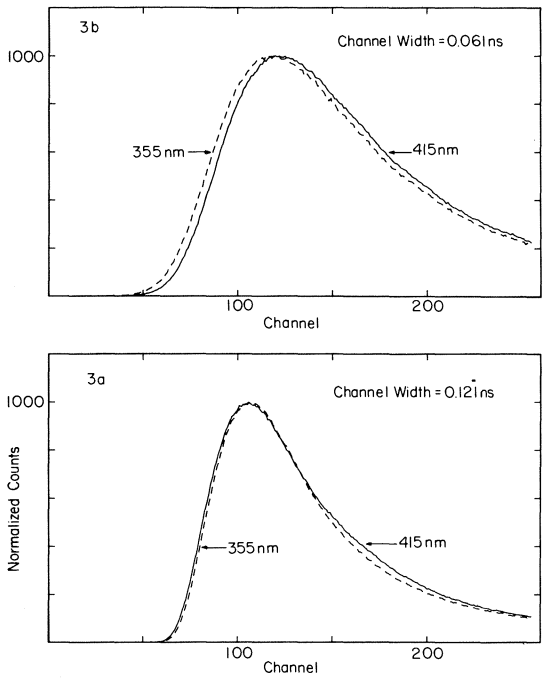

FIG. 3. Measured emission decay profile of a cyclohexane solution of PPO (1.5×10^{-5} *M*) at 355 nm, - - -; 415 nm, —; excitation at 290 nm; (*a*) Phillips 56 DUVP PMT, channel width 0.121 ns; (*b*) RCA 8850 PMT, channel width 0.061 ns.

to those determinations in which the sample fluoresced efficiently.

Wahl and co-workers (20) discussed the wavelength dependent instrument effects in greater detail. They suggested that the time response variation with wavelength of the PMT was most significant in the rising part of the measured decay profile while the time variation with wavelength in the tail of the decay profile could be attributed to the variation with wavelength of the lamp decay. The results in Fig. 3 where all measurements were obtained using the same excitation wavelength indicate that the PMT effect does not predominate in any single portion of the decay curves which is also consistent with the convolution theorem. Wahl presented a correction technique in which a reference compound was selected whose singlet decay processes were described by a single exponential function and whose fluorescence lifetime had been reasonably determined. Then using the same wavelength of excitation, λ_{ex}, the fluorescence decay profile of the reference compound R^r_{em}, and of the sample R^s_{em} were both measured at the sample's emission wavelength. R^r_{em} can be expressed in terms of the following convolution equation:

$$[3] \qquad R^r_{em} = L_{ex} \otimes G^r_{em} \otimes H_{em}$$

where G^r_{em} is the true fluorescence delay function for the reference compound. Since G^r_{em} has been assumed, deconvolution of eq. 3 would give $L_{ex} \otimes H_{em}$. Subsequent substitution into eq. 1 allows deconvolution of eq. 1 to obtain G^s_{em} avoiding the wavelength variation of H_{em} and H_{ex}. This correction technique, while mathematically sound and experimentally convenient, requires that one has a high degree of confidence in the physical model of the decay processes and

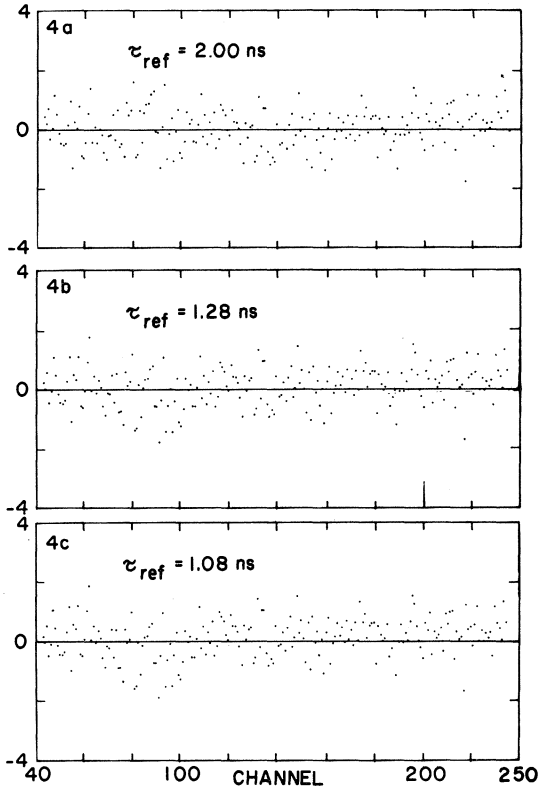

FIG. 4. Weighted residual plots for calculated 'best fit' emission decay profile for POPOP in ethanol (1.5×10^{-5} *M*) using the reference compound technique of Wahl *et al.* (20) to correct for the time response variation with wavelength of the PMT; reference compound was PPO (1.5×10^{-5} *M*) in cyclohexane solution; Phillips 56 DUVP PMT; λ_{ex} = 355 nm, λ_{em} = 415 nm for both the PPO and POPOP solutions; channel width 0.121 ns; (*a*) τ_{ref} = 2.00 ns; (*b*) τ_{ref} = 1.28 ns; (*c*) τ_{ref} = 1.08 ns.

Can. J. Chem. Downloaded from www.nrcresearchpress.com by 84.22.46.98 on 09/08/12
For personal use only.

Can. J. Chem. Downloaded from www.nrcresearchpress.com by 84.22.46.98 on 09/08/12
For personal use only.

the associated kinetic parameters of the reference compound.

The effect of any inaccuracy in the selection of the value for the fluorescence lifetime of the reference compound is illustrated in Fig. 4. In these experiments we measured the fluorescence decay profiles of POPOP and PPO where the latter was selected as the reference compound. λ_{em} was 415 nm and λ_{ex} was 355 nm. The residuals plotted in Fig. 4 all appear to be randomly distributed irrespective of the lifetime selected for the reference compound PPO. Thus assuming the singlet lifetime of PPO to be 1.08, 1.28, or 2.00 ns, values of 1.18, 1.38, or 2.13 ns were obtained for the singlet lifetime of POPOP in ethanol solution, respectively. Since sample purity, temperature, chemical stability, and degree of aeration can all affect the fluorescence lifetime of the reference compound, the confidence in the kinetic parameters calculated for the emission of the sample is reduced. More important, however, is the requirement that the reference compound's excited singlet decay processes must be understood. The selection of a single exponential model for the reference fluorescence decay, which in reality is the sum of two exponentials, prejudices the detection of multi-exponential processes in the sample's emission decay or distorts the analysis of a true single exponential decay in favour of a multi-exponential result.

Ratio Correction Technique

The assumptions required in the correction methods reviewed above reduce the confidence which one has in the deconvoluted kinetic parameters. We sought and developed a technique to correct for the time response variation with wavelength of the PMT which did not include any critical assumptions. The mathematical principles and experimental procedures involved in this technique are detailed below. The dramatic improvement in the randomness of residuals when this ratio technique was applied to measured experimental data of compounds and solutions whose singlet decay processes had previously been well studied not only verified the legitimacy of the correction but also gave us an exceptional degree of confidence in the kinetic parameters obtained.

A fluorescent compound, preferably one with a high fluorescence quantum yield and short fluorescence lifetime, is selected whose fluorescence spectrum spans λ_{ex} and λ_{em} used for the sample under investigation. This calibration compound is excited at a wavelength λ_a less than the excitation wavelength λ_{ex} used for the sample. The fluorescence decay profile of the calibration compound is then measured at λ_{ex} and λ_{em}. The fluorescence decay profiles of the calibration compound measured at λ_{ex} (R^c_{ex}) and at λ_{em} (R^c_{em}) are represented respectively by the following convolution equations

$$R^c_{ex} = L_a \otimes H_{ex} \otimes G^c_{ex} \quad [4]$$

$$R^c_{em} = L_a \otimes H_{em} \otimes G^c_{em} \quad [5]$$

where G^c_{ex} and G^c_{em} are the true fluorescence decay functions of the calibration compound at λ_{ex} and λ_{em}, respectively, and L_a is the lamp response function at λ_a. By appropriate substitution of eqs. 1, 2, 4, and 5 and the reasonable assumption that the fluorescence lifetime of the calibration compound is the same at the two wavelengths,[7]

$$G^c_{em} = G^c_{ex} \quad [6]$$

it can be shown that

$$R^s_{em} \otimes R^c_{ex} = G^s_{em} \otimes R^c_{em} \otimes R^l_{ex} \quad [7]$$

To use eq. 7 one would take the four measurements, R^s_{em}, R^c_{ex}, R^c_{em}, and R^l_{ex} and numerically convolve R^s_{em} with R^c_{ex} and R^c_{em} with R^l_{ex}. Deconvolution of $R^c_{em} \otimes R^l_{ex}$ from $R^s_{em} \otimes R^c_{ex}$ yields G^s_{em} from which the wavelength effects of the instrument (PMT) have been eliminated. However, this deconvolution cannot be carried out using nonlinear least-squares fitting procedures because the error in $R^s_{em} \otimes R^c_{ex}$ is no longer random. Equation 7 can be converted to a suitable form if we take its Fourier transform which converts the convolutions in eq. 7 to the products in eq. 8

$$r^s_{em} \cdot r^c_{ex} = g^s_{em} \cdot r^c_{em} \cdot r^l_{ex} \quad [8]$$

where r^s_{em}, r^c_{ex}, g^s_{em}, r^c_{em}, r^l_{ex} denote the Fourier transforms of R^s_{em}, R^c_{ex}, G^s_{em}, R^c_{em}, R^l_{ex} respectively. Equation 8 can be rearranged to give

[7] In most cases this is true except where exciplex or excimer kinetics are applicable. Therefore the selection of the calibration compound should be carefully considered avoiding conditions where such kinetics have been observed. Short singlet lifetimes and low concentrations of the compound will significantly reduce this possibility. Generally it is found that the compounds used in scintillation counting (34, 35) offer the best selection.

Can. J. Chem. Downloaded from www.nrcresearchpress.com by 84.22.46.98 on 09/08/12
For personal use only.

[9] $$r^{s}_{em} \cdot \frac{r^{c}_{ex}}{r^{c}_{em}} = g^{s}_{em} \cdot r_{ex}$$

where the inverse transform of $r^{s}_{em} \cdot r^{c}_{ex}/r^{c}_{em}$ is the 'corrected' emission decay function, $R^{s}_{em}(corr)$ and r^{c}_{ex}/r^{c}_{em} is the correction ratio. Taking the inverse transform of eq. 9 we obtain

[10] $$R^{s}_{em}(corr) = G^{s}_{em} \otimes R^{l}_{ex}$$

Deconvolution of eq. 10 then gives the kinetic parameters of the fluorescence decay G^{s}_{em}.

It was important to show that when the alternating data collection technique is used to account for the lamp intensity profile drift over the total accumulation time that the ratio correction procedure is mathematically sound. The mathematical treatment in the Appendix[8] confirmed the above and demonstrated that the correction procedure is invalid only in the case when the PMT time response function varied with wavelength, when the PMT is unstable and when the lamp intensity profile drifts, all at the same time.

The experimental procedure which is followed to effect this correction is straightforward. The four decay profiles R^{s}_{em}, R^{l}_{ex}, R^{c}_{em}, R^{c}_{ex} are measured and stored in the computer. The latter profiles can be stored and used for other experiments conducted at the same wavelength pair and instrument settings. To avoid any effects of data truncation on the Fourier calculations, the measurements R^{s}_{em}, R^{c}_{em}, and R^{c}_{ex} are extrapolated using a single exponential which is obtained by fitting a linear regression to the logarithm of the last 25% of the measured channels. The extrapolation is carried out until the tail of the curve is less than 0.1% of the peak. We have found using synthetic data sets that the use of a single exponential for extrapolation does not adversely affect the results. It is used only to remove the effects of sudden data truncation. Any smoothly decreasing function would do.

The Fourier transform of the extrapolated data may be efficiently calculated using the fast Fourier transform algorithm (33). The Fourier transform of the corrected measured emission decay is simply $r^{s}_{em} \cdot r^{c}_{ex}/r^{c}_{em}$ whose inverse transform when calculated gives $R^{s}_{em}(corr)$. Deconvolution of eq. 10 then proceeds using $R^{s}_{em}(corr)$ and R^{l}_{ex} in the usual manner to give the kinetic parameters of the fluorescence decay, G^{s}_{em}.

[8]Copies of the Appendix may be obtained, at a nominal charge, from the Depository of Unpublished Data, CISTI, National Research Council of Canada, Ottawa, Canada K1A 0S2.

Application of the Ratio Technique

The emission spectrum of PPO (35) spans the excitation (355 nm) and emission (415 nm) wavelengths used for the POPOP decay measurements and was therefore selected as a correction compound for this wavelength pair. The emission decay profiles of PPO in cyclohexane solution were measured at 355 and 415 nm using excitation at 290 nm. A Fourier correction ratio was then calculated and applied to the measured emission decay profile of POPOP in ethanol solution to give the corrected decay profile shown in Fig. 5. The corrected decay profile does not appear to be much different from the uncorrected decay profile. In fact the single exponential lifetime (τ = 1.28 ns) obtained after deconvolution of the corrected profile was not significantly different from that calculated from uncorrected data (τ = 1.30 ns). However, inspection of the residual plot (Fig. 6) which results from the deconvolution of the corrected data shows that the residuals now appear to be completely random in contrast to that obtained from the uncorrected data (Fig. 2*b*). In this latter case the non-random distribution of the residuals suggested that the physical model of a single exponential function for the emission decay of POPOP was inappropriate and that some other physical model may apply. The random distribution of residuals from the corrected data allows us to confidently state that the emission of POPOP obeys single exponential decay kinetics. It also indicates that the ratio correction procedure has successfully accounted for the major instrumental factor, which was the time response variation with wavelength of the PMT, that had resulted in a non-random distribution of residuals in the uncorrected data. The small differences noted in Fig. 3 have a significant effect on the level of confidence which one can have in the physical model and kinetic parameters for the emission decay. This was more dramatically illustrated in two component systems (*vide infra*).

We also measured the fluorescence lifetimes of several other compounds at the same excitation and emission wavelength pair as were used in the POPOP measurements, using PPO as the correc-

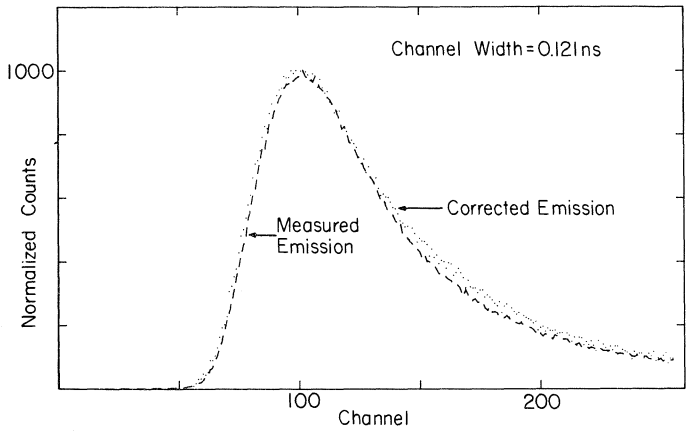

FIG. 5. Measured emission decay profile (same as Fig. 2*a*) - - -; corrected emission decay profile using the ratio correction procedure ··· for POPOP (1.5×10^{-5} *M*) in ethanol; λ_{ex} = 355 nm, λ_{em} = 415 nm; Phillips 56 DUVP PMT; PPO (1.5×10^{-5} *M*) in cyclohexane solution used as the correction compound to determine the correction ratio excited at λ_a = 290 nm; channel width 0.121 ns.

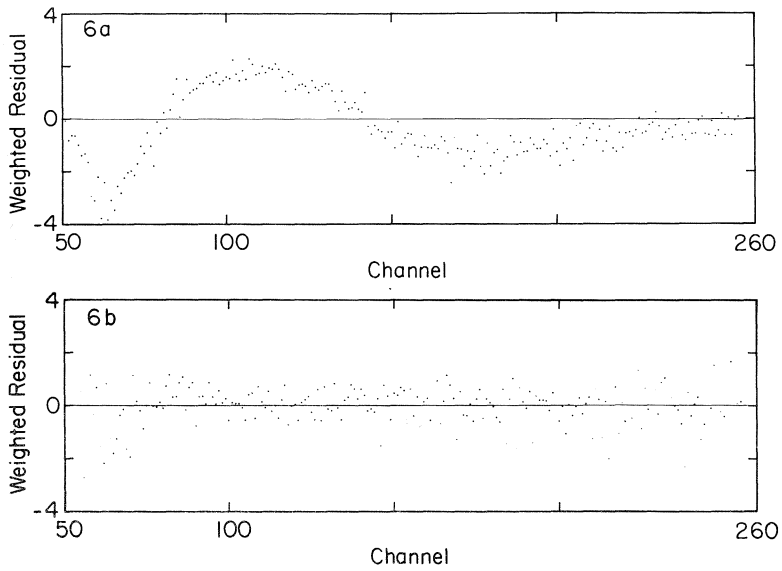

FIG. 6. Weighted residual plots for calculated 'best fit' emission decay profiles for POPOP in ethanol; (*a*) after deconvolution of uncorrected measured emission decay profile (Fig. 2*a*); (*b*) after deconvolution of corrected emission decay profile (Fig. 5) using the ratio correction procedure.

tion compound. In each case the residual plots obtained from corrected data indicated that the fluorescence decay could be described by single exponential functions. These results are listed in Table 1 where they are compared to previously reported lifetimes.

The measurement of the fluorescence decay profile of acridine yellow (AY) indicated that the ratio correction procedure was both required and valid at other wavelength pairs. The emission profile of AY (10^{-5} *M*) in ethanol solution was measured at 500 nm with excitation at 440 nm. For this wavelength pair BBOT was used as the correction compound. Again application of the ratio correction to the measured decay profile of AY and subsequent deconvolution provided a

Can. J. Chem. Downloaded from www.nrcresearchpress.com by 84.22.46.98 on 09/08/12
For personal use only.

TABLE 1. Fluorescence lifetimes obtained after application of ratio correction technique

Compound[b]	τ (ns) Uncorrected	With ratio correction[a]	Lit. value (ref.)
POPOP (ethanol)	1.30±0.03	1.28±0.02	[c]
POPOP	1.21±0.03	1.10±0.02	[c]
Anthracene (ethanol)	5.06±0.05	4.93±0.05	5.5 (34)
Anthracene	5.20±0.08	5.03±0.07	5.0 (34)
Anthracene[d]	4.17±0.04	3.99±0.03	—
BBOT	1.27±0.02	1.16±0.04	1.1 (35)
9-Cyanoanthracene	13.3 ±0.2	12.8 ±0.2	[c]
9-Cyanoanthracene[d]	10.7 ±0.4	10.5 ±0.3	10.3 (17)
2-Napthol (p*H* 9.5, water)	9.6 ±0.2	9.4 ±0.3	9.1 (36)

[a]PPO (1.5×10^{-5} *M*) in cyclohexane used as a correction compound: λ_{ex} = 355 nm, λ_{em} = 415 nm.
[b]All compounds in degassed cyclohexane solution unless otherwise noted.
[c]Not previously published.
[d]Not degassed.

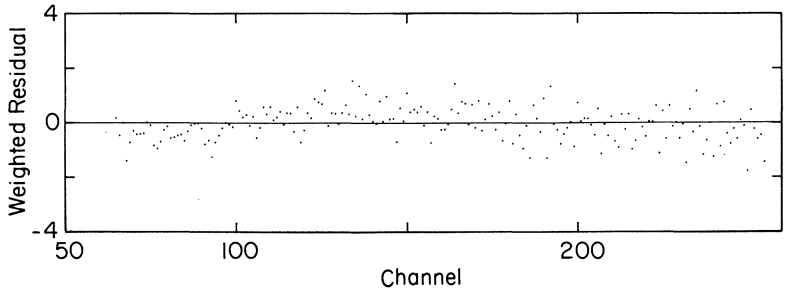

FIG. 7. Weighted residual plot for calculated 'best fit' emission decay profile for acridine yellow in ethanol after deconvolution of corrected emission decay profile using the ratio correction procedure.

random distribution of residuals (Fig. 7) with a singlet lifetime of 4.83 ns (lit. (35) 5.1 ns). If the data were not corrected a non-random distribution of residuals resulted.

Table 1 indicates that the lifetimes obtained were similar whether or not the ratio correction was applied to the measured decay of a given compound whose emission can be described by single exponential decay kinetics. This suggested that the correction technique was not really necessary to obtain the correct kinetic parameters except that it gave a greater confidence in the results obtained, since only then were the residuals randomly distributed. However, when the fluorescence decay of a sample whose emission is described by a multi component decay process was measured, the application of the ratio correction technique was essential to obtain accurate kinetic parameters.

The fluorescence decay profile (415 nm) of a

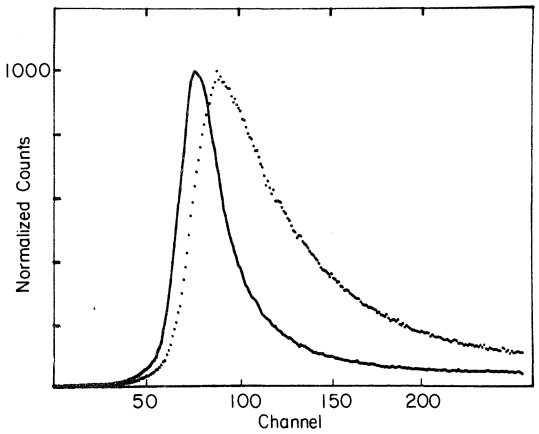

FIG. 8. Measured lamp intensity profile —; measured emission decay profile ···; of a cyclohexane solution of POPOP (5×10^{-6} *M*) and anthracene (2.1×10^{-5} *M*); λ_{ex} = 355 nm, λ_{em} = 415 nm; RCA 8850 PMT; channel width 0.1164 ns.

Can. J. Chem. Downloaded from www.nrcresearchpress.com by 84.22.46.98 on 09/08/12
For personal use only.

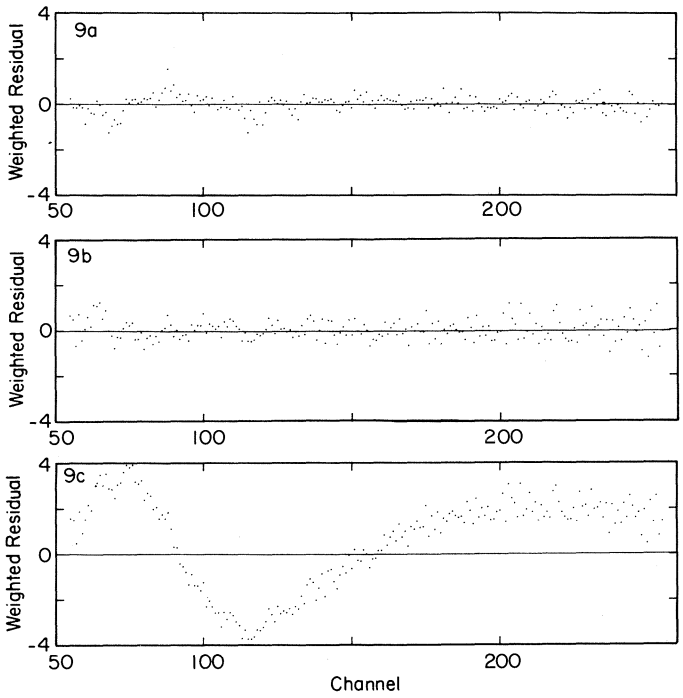

FIG. 9. Weighted residual plots for calculated 'best fit' emission decay profile for a cyclohexane solution of POPOP and anthracene (Fig. 8); (*a*) after deconvolution of uncorrected measured emission decay profile for two exponential decay components; (*b*) after deconvolution of corrected emission decay profile for two exponential decay components; (*c*) after deconvolution of corrected emission decay profile for only one exponential decay component.

TABLE 2. Fluorescence decay parameters for a solution[a] of POPOP and anthracene

Parameter	Value	
	Uncorrected	With ratio correction[b]
τ_1 (ns)	5.25 ±0.09	4.89 ±0.07
τ_2 (ns)	1.50 ±0.04	1.10 ±0.03
A_1[c]	0.023±0.03	0.027±0.02
A_2[c]	0.060±0.02	0.073±0.03

[a]Degassed cyclohexane solution of POPOP (5×10^{-6} *M*) and anthracene (2.1×10^{-5} *M*).
[b]PPO (1.5×10^{-5} *M*) in cyclohexane used as the correction compound: λ_{ex} = 355 nm, λ_{em} = 415 nm.
[c]A_1 and A_2 are the pre-exponential constants in the relationship; $G^s_{em} = A_1 e^{-t/\tau_1} + A_2 e^{-t/\tau_2}$.

cyclohexane solution of POPOP (5×10^{-6} *M*) and anthracene (2.1×10^{-5} *M*) was measured with excitation at 355 nm (Fig. 8). Deconvolution of the uncorrected decay data provided kinetic parameters for a two component exponential decay which were markedly different from those of the individual components themselves (Table 2). The non-random distribution of residuals (Fig. 9*a*) indicated the 'best fit' decay with these parameters did not satisfactorily represent the measured decay. Application of the ratio correction technique provided, however, kinetic parameters which were the same (Table 2) as those of the individual components. The random distribution of residuals (Fig. 9*b*) obtained after deconvolution of the corrected data for a two component exponential decay confirmed the legitimacy of the correction technique.

The above experiment was also an excellent example of the utility of inspecting residual plots for deciding on the physical model of the decay processes. The residual plot (Fig. 9*c*) for a single exponential 'best fit' of the corrected decay data indicated that this model was inappropriate. The random distribution of residuals for the two exponential component model (Fig. 9*b*) provided the necessary level of confidence to accept this model and kinetic results. This experiment demonstrated the importance of correcting for the time variation with wavelength of the PMT in the measured data. Otherwise one would be

Can. J. Chem. Downloaded from www.nrcresearchpress.com by 84.22.46.98 on 09/08/12
For personal use only.

Can. J. Chem. Downloaded from www.nrcresearchpress.com by 84.22.46.98 on 09/08/12
For personal use only.

uncertain whether a non-random distribution of residuals was due to the inappropriate choice of the kinetic model or to instrumental artifacts.

The correction ratio's stability depends on the stability of the PMT. Since it has been shown (*vide supra*) that the lamp intensity decay profile varies over the total time of an experiment, if the PMT is not stable over the entire acquisition period then it is impossible to solve rigorously the time response variation with wavelength effect of the PMT (see Appendix).[8] Fortunately we have found that a correction ratio for a given wavelength pair, which has been determined and stored in the computer, can be used for a considerable period of time (usually at least a week) provided that the instrument time settings and PMT voltages have not been changed. The stability of a correction function can be checked by measuring the emission decay of a standard compound and inspecting the residual plots for any deterioration of the randomness of residuals.

Once the kinetic behaviour and kinetic parameters have been accurately determined as we have now done for POPOP and BBOT, the correction technique described by Wahl *et al.* (20) for the PMT time response – wavelength effect can conveniently be employed. It is subject, however, to the effect of sample variability on the lifetime as discussed earlier.

The origin of the variation of the time response function with wavelength of the PMT has been discussed and treated by several workers (18, 20, 27). The initial kinetic energy and point of origin on the photocathode of the photoelectrons will determine their initial velocity and path to the first dynode which in turn affect the transit time of the electrons in the PMT.

Conclusions

It is paramount to have a high degree of confidence in the physical model of the fluorescence decay processes and in the accuracy of the kinetic parameters obtained from single photon counting fluorescence lifetime measurements. We have demonstrated how one may make a satisfactory subjective appraisal of the results obtained after deconvolution of the measured lamp intensity and sample emission decay profiles using weighted residual plots. Thus if the weighted residuals are not randomly distributed after a single exponential model has been used in the deconvolution computations further deconvolution using a double exponential model or other kinetic description is indicated. The inspection of the residual plots obtained from measurements on reference compounds reveals systematic or instrumental artifacts in the measured decays. In this work it was confirmed that the time response function of the PMT at the excitation and emission wavelengths was different and that this variation affected the degree of confidence which one could have in the deconvoluted results. More important, in the case of multicomponent decays inaccurate kinetic parameters were obtained if this variation were neglected in the calculations. We have developed and demonstrated the applicability of a ratio correction procedure which does not require any *a priori* assumptions of the nature of wavelength–time response variation of the PMT response function. Only when the ratio correction procedure was applied could we achieve a high degree of confidence in the accuracy of the kinetic parameters.

Acknowledgements

The authors wish to thank Mrs. L. Bramall for computational assistance and Mr. R. Athey and Mr. G. Charette for their technical assistance with the electronics.

1. W. R. Ware, D. Watt, and J. D. Holmes. J. Am. Chem. Soc. **96**, 7853 (1974).
2. W. R. Ware, J. D. Holmes, and D. R. Arnold. J. Am. Chem. Soc. **96**, 7861 (1974).
3. Abstracts of VIIIth International Conference on Photochemistry. Edmonton, Canada. Aug. 7–13, (1975).
4. K. Salisbury. *In* Photochemistry. Vol. 5. Specialist periodical report. *Edited by* D. Bryce-Smith. The Chemical Society, London. 1974. p. 119.
5. A. A. Thaer and M. Sernetz (*Editor*). Fluorescence techniques in cell biology. Springer-Verlag, Berlin. 1973.
6. A. Grinvald, J. Schlessinger, I. Pecht, and I. Z. Steinberg. Biochem. **14**, 1921 (1975).
7. E. Hass, M. Wilchek, E. Katchalski-Katzir, and I. Z. Steinberg. Proc. Nat. Acad. Sci. (U.S.), **72**, 1807 (1975).
8. B. Donzel, P. Gauduchon, and Ph. Wahl. J. Am. Chem. Soc. **96**, 801 (1974).
9. D. Genest, Ph. Wahl, and J. C. Auchet. Biophys. Chem. **1**, 266 (1974).
10. M. R. Loken, J. W. Hayes, J. R. Gohlke, and L. Brand. Biochem. **11**, 4779 (1972).
11. W. R. Ware. *In* Creation and detection of the excited state, Vol. 1A. *Edited by* A. A. Lamola. Marcel Dekker, New York. 1971.

12. A. E. W. KNIGHT and B. K. SELINGER. Spectrochim. Acta, **27A**, 1223 (1971).
13. W. R. WARE, L. J. DOEMENY, and T. L. NEMZEK. J. Phys. Chem. **77**, 2038 (1973).
14. A. GRINVALD and I. Z. STEINBERG. Anal. Biochem. **59**, 583 (1974).
15. B. VALEUR and J. MOIREZ. J. Chim. Phys. **70**, 500 (1973).
16. I. ISENBERG, R. D. DYSON, and R. HANSON. Biophys. J. **13**, 1090 (1973).
17. A. GAFNI, R. L. MODLIN, and L. BRAND. Biophys. J. **15**, 263 (1975).
18. C. LEWIS, W. R. WARE, L. J. DOEMENY, and T. L. NEMZEK. Rev. Sci. Instrum. **44**, 107 (1973).
19. A. E. W. KNIGHT and B. K. SELINGER. Aust. J. Chem. **26**, 1 (1973).
20. PH. WAHL, J. C. AUCHET, and B. DONZEL. Rev. Sci. Instrum. **45**, 28 (1974).
21. A. E. MCKINNON, D. MILLER, and A. G. SZABO. To be published.
22. N. R. DRAPER and H. SMITH. Applied regression analysis. Wiley, New York, N.Y. 1966. pp. 86–99.
23. J. DURBIN and G. S. WATSON. Biometrika, **58**, 1 (1971).
24. G. W. SNEDECOR and W. G. COCHRAN. Statistical methods. Iowa State University Press, Ames, Iowa. 1973. p. 240.
25. G. HAZAN, A. GRINVALD, M. MAYTAL, and I. Z. STEINBERG. Rev. Sci. Instrum. **45**, 1602 (1974).
26. R. SCHUYLER and I. ISENBERG. Rev. Sci. Instrum. **42**, 813 (1971).
27. J. A. MIEHE, G. KNISPEL. C. R. Acad. Sc. Paris, **273B**, 285 (1971).
28. P. KARRER and E. ZELLER. Helv. Chem. Acta, **2**, 482 (1919).
29. (*a*) F. ULLMANN and A. MARIC. Chem. Ber. **34**, 4308 (1901). (*b*) A. ALBERT. The acridines. 2nd ed. E. Arnold, London. 1966. pp. 112–113.
30. C. A. PARKER. Photoluminescence of solutions. Elsevier. London. 1968. p. 288.
31. RCA Electronic Components, Photomultiplier Tube, RCA-8850, #5-69.
32. R. J. ATHEY, A. E. MCKINNON, and D. RAYNER. To be published.
33. E. O. BRIGHAM and R. E. MORROW. IEEE Spectrum, 63 (1967).
34. J. B. BIRKS. Photophysics of aromatic molecules. Wiley-Interscience, London. 1970. p. 120.
35. I. B. BERLMAN. Handbook of fluorescence spectra of aromatic molecules. 2nd ed. Academic Press, New York. 1971.
36. M. R. LOKEN, J. W. HAYES, J. R. GOHLKE, and L. BRAND. Biochem. **25**, 4779 (1972).

Can. J. Chem. Downloaded from www.nrcresearchpress.com by 84.22.46.98 on 09/08/12
For personal use only.

Substituent effects on the ionization constants of phenylazobenzaldoximes

AHMAD S. SHAWALI[1] AND BAHEEGA M. ALTAHOU
Department of Chemistry, Faculty of Science, University of Kuwait, State of Kuwait

Received March 5, 1976

AHMAD S. SHAWALI and BAHEEGA M. ALTAHOU. Can. J. Chem. **54**, 3260 (1976).

Ionization constants, pK_a, for a set of 12 phenylazobenzaldoximes (**1**) have been determined in 50 vol% ethanol–water medium at 25 ± 0.1 °C and a μ of 0.1. Excellent linear correlations are obtained when pK_a values are plotted against the substituent constant, σ_X, and the polar substituent constant, $\sigma^*_{XC_6H_4}$, for substituted phenyl groups. The regression lines are: $pK_a = 9.905 - 0.737\sigma_X$; and $pK_a = 10.489 - 1.01\sigma^*_{XC_6H_4}$, respectively. The pK_a values have also been correlated with the extended Hammett equation. The correlation follows the equation: $pK_a = 9.897 - 0.713\sigma_{I,X} - 0.734\sigma_{R,X}$. It is concluded that *EE* and *ZE* forms of **1** exist in equilibrium in solution phase.

AHMAD S. SHAWALI et BAHEEGA M. ALTAHOU. Can. J. Chem. **54**, 3260 (1976).

On a déterminé, dans un milieu à 50% par volume d'éthanol–eau, à 25 ± 0.1 °C et à un μ de 0.1, les constantes d'ionisation, pK_a, d'une série de 12 phénylazobenzaldoximes (**1**). On a obtenu d'excellentes corrélations linéaires entre les valeurs de pK_a et les constantes de substituants σ_X et les constantes de substituants polaires $\sigma^*_{XC_6H_4}$ pour les groupes phényles substitués. Les lignes de regression sont $pK_a = 9.905 - 0.737\sigma_X$ et $pK_a = 10.489 - 1.01\sigma^*_{XC_6H_4}$. On a établi une corrélation entre les valeurs de pK_a et les valeurs de l'équation étendue d'Hammett. La corrélation suit l'équation suivante $pK_a = 9.897 - 0.713\sigma_{I,X} - 0.734\sigma_{R,X}$. On en conclut, qu'en solution, les formes *EE* et *ZE* de **1** existent en équilibre.

[Traduit par le journal]

Introduction

Although several reports (1–3) have been published concerning the synthesis and chelating properties of some arylazobenzaldoximes (**1**), no attempt has yet been made to study the acidities of these compounds. We wish now to report the preparation of a series of 12 of **1** and

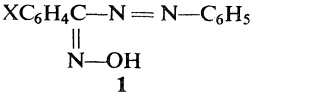

1

a, X = 4-MeO	*e*, X = 4-Br	*i*, X = 4-NO_2
b, X = 4-Me	*f*, X = 3-Cl	*j*, X = 3,4-O_2CH_2
c, X = H	*g*, X = 3-Br	*k*, X = 2-Cl
d, X = 4-Cl	*h*, X = 3-NO_2	*l*, X = 2-NO_2

the correlation of their ionization constants with the simple and extended Hammett equations [1] and [2] respectively.

$$[1] \qquad Q_X = \sigma_X + h$$

$$[2] \qquad Q_X = \alpha\sigma_{I,X} + \beta\sigma_{R,X} + h$$

Table 1 lists the compounds investigated, their mp's, and analytical and spectral data.

[1]Author to whom all inquiries should be addressed.

Results and Discussion

The ionization constants (pK_a's) of **1***a* to **1***l* were determined in 50 vol% ethanol–water medium at 25 ± 0.1 °C and a μ of 0.1 using a spectrophotometric method.

At $pH < 8$ each of the phenylazobenzaldoximes studied shows an intensive π–π^* absorption band near 305 nm. In alkaline media, the ambident anion, ArC(:NO^-)N:NPh ↔ ArC(N:O):-N$\bar{N}$Ph, shows an intensive π–π^* band in the region 325–400 nm. Spectra recorded at different *pH* values show an isosbestic point at 325 nm, Fig. 1. The absorbance of a freshly prepared solution measured at the wavelength of the absorption maximum of the anion plotted against *pH* shows a dependence in the shape of a dissociation curve of a monobasic acid, Fig. 2. From the *pH*–absorbance data, the pK_a values for **1***a* to **1***l* were calculated. The results are summarized in Table 2.

Inspection of the data in Table 2 reveals that the pK_a values of **1***a* to **1***l* are lower than those of the corresponding benzaldoximes ($pK_a = 10.695 - 0.857\sigma$, in water at 25 °C) (4*a*). The higher acidities of **1** as compared with those of benzal-

Can. J. Chem. Downloaded from www.nrcresearchpress.com by 210.87.254.40 on 09/05/12
For personal use only.

TABLE 1. Phenylazobenzaldoximes[a]

Compound	mp[b] (°C)	Ultraviolet maxima: Neutral form[c] λ nm (log *e*)	Ultraviolet maxima: Anion[d] λ nm (log *e*)
1*a*	148–149	430(2.55), 290(4.23)	354(4.38), 228(4.26)
1*b*	133–134	437(2.53), 300(4.21)	352(4.56), 240(4.25)
1*c*	137–138	436(2.55), 307(4.23)	350(4.40), 237(4.01)
1*d*	158–159	434(2.55), 307(4.24)	350(4.42), 275(3.90), 240(4.03)
1*e*	153–154	436(2.51), 305(4.24)	350(4.40), 275(3.91), 244(4.01)
1*f*	118–119	436(2.62), 307(4.36)	350(4.54), 275(3.95), 240(4.13)
1*g*	110–111	436(2.49), 307(4.23)	350(4.42), 275(3.81), 240(4.03)
1*h*	185–186	434(2.53), 307(4.32)	349(4.52), 270(4.17)
1*i*	186–187	435(2.54), 305(4.40)	349(4.48), 270(4.10)
1*j*	140–141	436(2.58), 302(4.32)	350(4.36), 290(4.00), 238(4.11)
1*k*	161–162	430(2.61), 310(4.46)	346(4.46), 275(3.67), 238(4.08)
1*l*	156–157	436(2.59), 310(4.72)	344(4.50), 265(4.06), 240(4.20)

[a]*Anal.* calcd. for $C_{13}H_{10}ClN_3O$ (**1***d*): N 16.18; found: N 16.22; calcd. for $C_{13}H_{10}BrN_3O$ (**1***e*): N 13.81; found: N 13.74; calcd. for $C_{13}H_{10}ClN_3O$ (**1***f*): N 16.18; found: N 16.15; calcd. for $C_{13}H_{10}BrN_3O$ (**1***g*): N 13.81; found: N 13.72; calcd. for $C_{13}H_{10}ClN_3O$ (**1***k*): N 16.18; found: N 16.09; calcd. for $C_{13}H_{10}N_4O_3$ (**1***l*): N 20.73; found: N 20.65.
[b]Literature mp (1–3, 16): **1***b* 133 °C, **1***c* 134 °C, **1***h* 183 °C, **1***i* 180 °C.
[c]In ethanol.
[d]In 50 vol% ethanol–water, p*H* 12.5.

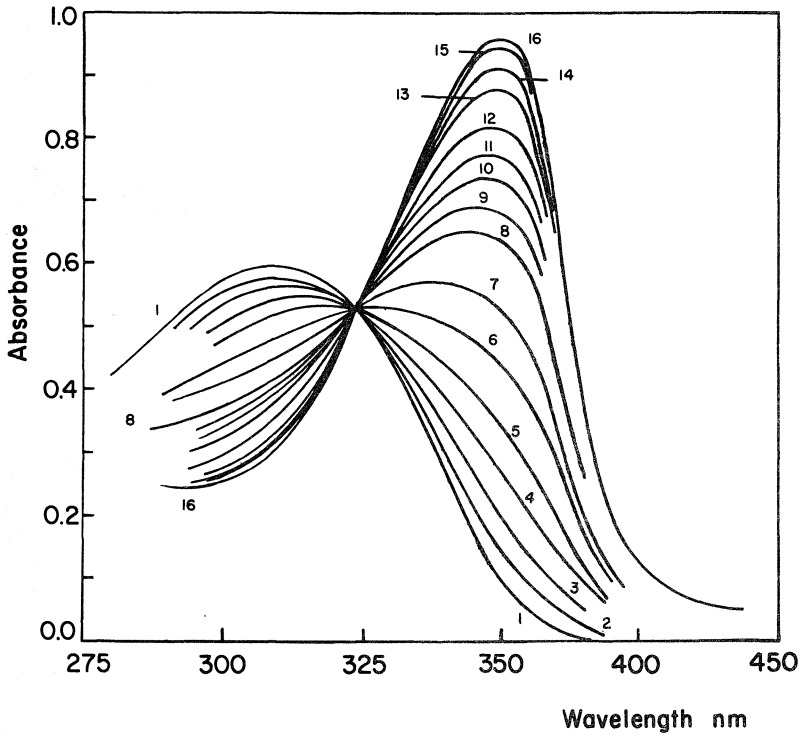

FIG. 1. Absorption spectra of phenylazo-*p*-bromobenzaldoxime (**1***e*) at different p*H* values. **1***e* 3.72×10^{-5} *M*; in 50 vol% ethanol–water, 25 °C. Run and p*H*: (1) 0.97; (2) 8.47; (3) 8.74; (4) 9.06; (5) 9.18; (6) 9.47; (7) 9.65; (8) 9.75; (9) 9.86; (10) 10.06; (11) 10.15; (12) 10.27; (13) 10.46; (14) 10.70; (15) 11.01; (16) 11.87.

Can. J. Chem. Downloaded from www.nrcresearchpress.com by 210.87.254.40 on 09/05/12
For personal use only.

TABLE 2. Ionization constants, pK_a, of substituted phenylazobenzaldoximes and substituent constants used in their correlation

Compound	pK_a[a]	σ_X	$\sigma_{I,X}$	$\sigma_{R,X}$	$\sigma^*_{XC_6H_4}$
1*a*	10.10	−0.27	0.27	−0.54	0.36
1*b*	10.02	−0.17	−0.04	−0.13	0.46
1*c*	9.89	0.00	0.00	0.00	0.58
1*d*	9.73	0.23	0.46	−0.23	0.75
1*e*	9.75	0.23	0.44	−0.21	0.74
1*f*	9.64	0.37	0.46	−0.09	0.85
1*g*	9.65	0.39	0.49	−0.10	0.86
1*h*	9.39	0.71	0.53	0.18	1.09
1*i*	8.95	1.27[b]	0.65	0.62	1.50
1*j*	10.00				
1*k*	9.61				
1*l*	9.41				

[a]Standard deviation ±0.01–0.03.
[b]For the *p*-nitro group it was necessary to use the enhanced sigma constant, σ^-. This need is undoubtedly caused by the direct conjugation of the negative charge on the reaction site with the substituent.

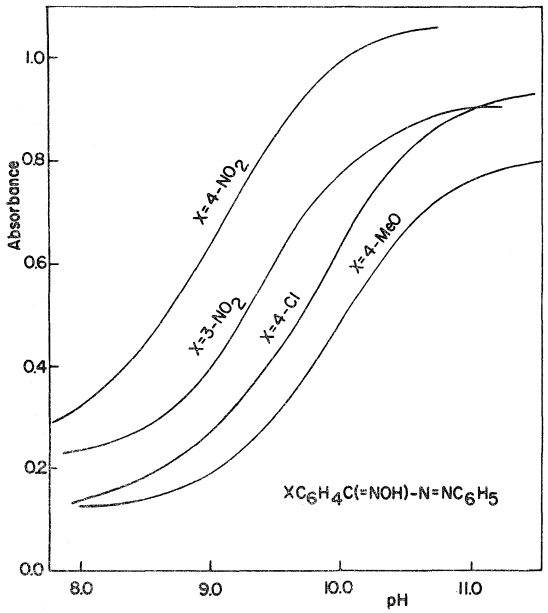

FIG. 2. Dependence of absorbance at 350 nm of some phenylazobenzaldoximes on p*H*.

doximes can be rationalized in terms of the electronic character of the α-phenylazo substituent, which has recently been reported to act as a –I–M group (5). Also, the data in Table 2 show clearly that both inductive and conjugative effects of the substituents examined are operative. For a deeper insight, the fit of the data to a free energy relationship was tested.

When examining the correlation of the dissociation constants of 1*a* to 1*l* with the Hammett equations [1] and [2], the nature (tautomeric and geometric) of the phenylazobenzaldoxime system must be considered. An earlier spectral study (3) of some of the compounds investigated has revealed that such compounds have the azo oxime structure (AO); no evidence for the tautomeric nitrosohydrazone form (NH) could be obtained. The spectral data of the compounds 1*a* to 1*l* agree with such a conclusion. Thus, the electronic absorption pattern of 1 in ethanol was characterized, in each case, by two bands: a weak n–π* band near 430 nm (log $e < 3$) and an intensive π–π* band near 300 nm (log $e > 4$), Table 1. Such a pattern is similar to that of *trans*-azobenzene: λ (log *e*) 445 nm (2.48), 319

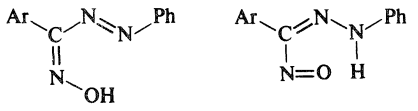

AO-form NH-form

(4.29) (3, 6). In addition, the absorption pattern of 1 in the uv region was found to be nearly independent of the nature of the solvent, Table 3, indicating the presence of only one tautomer in the solution phase. The relatively small differences observed are assumed to be caused by solute–solvent interactions (6).

Configurations of the C=N and N=N double bonds of a given compound in series 1 can lead to four possibilities: *EE*, *ZE*, *EZ*, and *ZZ*. From these only the last two structures are rejected *a priori* for steric reasons. The identity of the uv characteristics of 1 with those of

Can. J. Chem. Downloaded from www.nrcresearchpress.com by 210.87.254.40 on 09/05/12
For personal use only.

Can. J. Chem. Downloaded from www.nrcresearchpress.com by 210.87.254.40 on 09/05/12
For personal use only.

TABLE 3. Ultraviolet maxima of two phenylazobenzaldoximes in different solvents

Solvent	λ nm (log *e*)	
	1*b*	**1***c*
Ethanol	300(4.21)	307(4.23)
Cyclohexane	300(4.22)	305(4.27)
Dioxan	300(4.19)	302(4.21)
Dimethyl sulfoxide	305(4.20)	302(4.23)
Acetic acid	300(4.23)	310(4.19)
Chloroform	305(4.21)	310(4.24)
Dimethylformamide	300(4.25)	305(4.23)

trans-azo compounds supports this exclusion. Furthermore, it appears that the energy barrier between the *EE* and *ZE* isomers is relatively low so that they exist in equilibrium in the solution phase of **1**. Lower barriers are usually found when the double bond in question is involved in resonance (7). In agreement with this conclusion, the vibration spectra of **1***a* to **1***l* in the solid state and in solution as well, show the $\bar{\nu}_{N-O}$ band at higher frequencies (1030 cm^{-1}) than that in hydroxylamine ($\bar{\nu}_{N-O}$ 912 cm^{-1}) and its *N*-alkyl derivatives ($\bar{\nu}_{N-O}$ 950 cm^{-1}) (8). This can be attributed to resonance contribution from structures of type **2**, which can, in turn, permit rotation of oxime group. The equilibrium mixture of *EE* and *ZE* isomers in the solution of **1** is also indicated by the pmr spectra of **1***a* and **1***b* in $CDCl_3$. Thus, the resonances of protons of the *p*-methoxyl group in **1***a* appear as a doublet at δ 3.88 and 3.85 ppm. Also, the spectrum of **1***b* contains a doublet at δ 2.45 and 2.41 ppm assignable to the *p*-methyl group protons. The magnitude of separation (in Hz) of the peaks of each of such doublets was found to be directly proportional to the applied field strength. An earlier report (3) has further revealed that the relative areas under the peaks of the doublet of **1***b* are solvent and concentration dependent. Other nmr evidence for the existence of *cis–trans* isomers has also been demonstrated for the isomeric *p*-tolylazobenzaldoxime (3). Unsymmetrical ketoximes were reported to exhibit similar solution equilibria of isomers which can be identified by their nmr spectra (9).

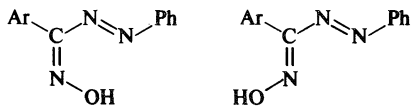

EE (*trans-trans*) *ZE* (*cis-trans*)

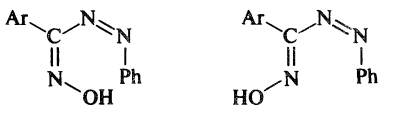

EZ (*trans-cis*) *ZZ* (*cis-cis*)

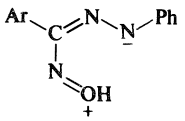

2

In view of the nature of the phenylazobenzaldoxime system, the spectrophotometric acid dissociation constant, pK_a, thus obtained, corresponds to the overall acid–base reaction in Scheme 1.

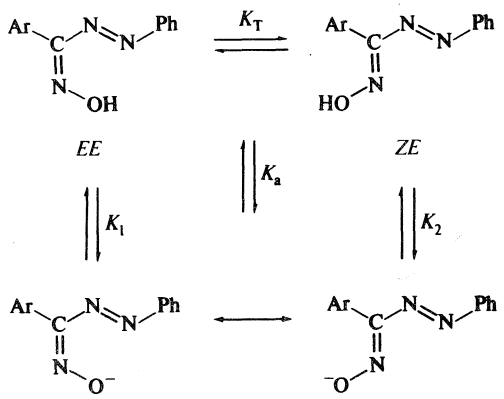

SCHEME 1

In such cases, the value of the overall constant, K_a, is related to the dissociation constants K_1 and K_2 of the *EE* and *ZE* isomers, respectively, by the equations:

[3] $$\log K_a = \log K_1 - \log (1 + K_T)$$

[4] $$\log K_a = \log K_2 - \log (1 + (1/K_T))$$

where $K_T = [ZE]/[EE]$.

Analytically, the value of $\log K_a$ can be expressed by [5] derived by adding [3] and [4] and substituting $(\rho_i\sigma_X + h_i)$ for the $\log K_i$ term.

[5] $$\log K_a = \tfrac{1}{2}(\rho_1 + \rho_2)\sigma_X + \tfrac{1}{2}(h_1 + h_2 - \log Y)$$

where

$$Y = (2 + ((K_T^2 + 1)/K_T))$$

TABLE 4. Substituent constants

Substituent	$\sigma^*_{XC_6H_4}$	Substituent	σ_X[a]	σ_X[b] (ref.)
3,4-$O_2CH_2C_6H_3$	0.48	3,4-O_2CH_2	−0.14	−0.16 (17)
2-ClC_6H_4	0.86	2-Cl	0.40	0.50 (18)
2-$O_2NC_6H_4$	1.07	2-O_2N	0.68	0.80 (19)

[a]This work.
[b]Literature value.

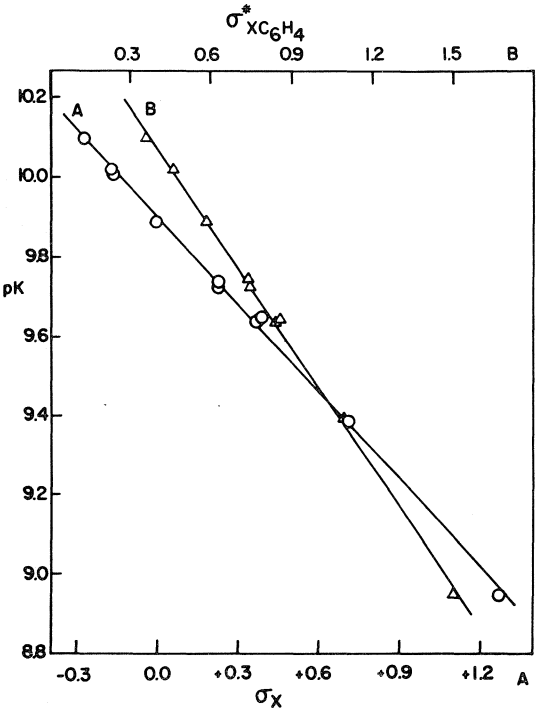

FIG. 3. Correlations of acid dissociation constants (pK_a) of phenylazobenzaldoximes with the substituent constants, σ_X (*A*) and $\sigma^*_{XC_6H_4}$ (*B*).

Equation 5 is equivalent to [1] with $\rho = \frac{1}{2}(\rho_1 + \rho_2)$, and $h = \frac{1}{2}(h_1 + h_2 - \log Y)$. In deriving [5], it is assumed that the value of the equilibrium constant, K_T, which is included in the Y term, exhibits insignificant variation, if any, with the electrical properties of the substituent. This is supported by the closeness of the pK_a values of **1***d*, **1***f*, and **1***k* to that for the unsubstituted compound **1***c*. Also, the linearity observed between pK_a values and σ_X constant confirmed *a posteriori* the correctness of our assumption.

Two ways were followed in correlating the pK_a values of series **1** with the simple Hammett equation [1]. In the first case, the pK_a values were plotted *vs.* the Hammett substituent constant σ_X of the X-substituent, Fig. 3. In the second case, we included the phenyl group with the substituent, and plotted the pK_a values against the polar substituent constant, $\sigma^*_{XC_6H_4}$ for substituted phenyl groups (10), Fig. 3. As shown, excellent linear relations were obtained in both cases when the data of compounds **1***a* to **1***i* were utilized. The regression lines expressing such correlations follow [6] and [7] respectively.

$$[6] \qquad pK_a = 9.905 - 0.737\sigma_X \qquad r = 0.997$$

$$[7] \qquad pK_a = 10.487 - 1.01\sigma^*_{XC_6H_4} \qquad r = 0.986$$

Equation 7 was utilized to calculate the $\sigma^*_{XC_6H_4}$ for the 3,4-$O_2CH_2C_6H_3$, 2-ClC_6H_4, and 2-$O_2NC_6H_4$ groups using the corresponding pK_a values of **1***j* to **1***l* respectively. The calculated values of such constants are listed in Table 4. From the latter values of σ^*, thus obtained, the σ_X constants of the substituents: 3,4-O_2CH_2, 2-Cl, and 2-O_2N were further calculated (10); they are also collected, together with the literature values, in Table 4.

Next, the ionization constants for **1** were correlated with the extended Hammett equation [2] by multiple regression analysis (11). The correlation of pK_a values with [2] may be justified in a similar manner as above. The data used in the correlation are given in Table 2. For the *para* substituents, the $\sigma_{I,X}$ were taken from the collection of Taft and co-workers (12); the $\sigma_{R,X}$ constants were obtained from the relation:

$$\sigma_{R,X} = \sigma_{p,X} - \sigma_{I,X}$$

For the *meta*-substituents, the $\sigma_{R,X}$ constants were estimated by the method of Charton (13), using the relation:

$$\sigma_{R,X} = 0.25\sigma_{m,X}$$

The $\sigma_{p,X}$ and $\sigma_{m,X}$ constants were from the compilation of Ritchie and Sager (14). The results of the correlation with [2] are presented in Table 5. The value of the multiple correlation

Can. J. Chem. Downloaded from www.nrcresearchpress.com by 210.87.254.40 on 09/05/12
For personal use only.

TABLE 5. Results of correlation with [2]

Parameter	Value	Parameter	Value
$-\alpha$	0.713	S_α[b]	0.03
$-\beta$	0.734	S_β[b]	0.10
h	9.897	S_h[b]	0.01
R[a]	0.999	n[c]	9

[a]Multiple correlation coefficient.
[b]Standard errors of the estimates: α, β, and h respectively.
[c]Number of points.

coefficient of 0.999 indicates an excellent correlation. The values of α and β, thus obtained, indicate that for series **1** the composition of the electrical effect, E, defined as the ratio β/α has a value of 1.03.

For oximes in which the substituent X has the *anti* configuration, **3**, (for example, *syn*-aldoximes and *syn*-phenylketoximes) E values of 1.18 and 1.27 were observed (4*b*, 13). On the other hand, oximes such as *anti*-aldoximes and *anti*-phenylketoximes, in which the substituent X has the *syn* configuration **4**, have E values of 0.27 and 0.43 respectively (4*b*, 13). A comparison of these E values with that of 1.03 observed for phenylazobenzaldoximes suggests that both the *EE* and *ZE* forms of **1** exist in equilibrium in solution phase, in accord with the spectroscopic evidence presented above.

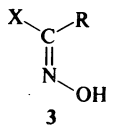

3

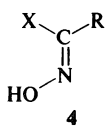

4

Experimental

Melting points are uncorrected. Infrared spectra were taken on a Pye-Unicam SP1000 spectrophotometer. Electronic absorption spectra were measured on a Pye-Unicam SP8000 spectrophotometer. Nuclear magnetic resonance spectra were done on a Varian T-60A spectrometer using TMS as internal standard. Microanalyses were performed by Alfred Bernhardt, Microanalytisches Laboratorium, West Germany.

Phenylazobenzaldoximes **1***a* to **1***l* were prepared by following the procedure of Bamberger and Pemsel (1). Of the compounds prepared, **1***a* to **1***c* and **1***h* to **1***i* have been reported (1–3). The characterization data and the uv maxima of the compounds prepared are summarized in Table 1. All compounds **1***a* to **1***l* in $CDCl_3$ show, in their pmr spectra, multiplet signals for aromatic protons in the region 7–8 ppm, and a broad NOH signal in the range 9–12 ppm. The latter signal disappears upon shaking the solution of **1** with D_2O and a new signal due to DOH resonance appears near 4.6 ppm. In addition, compound **1***j* exhibits a singlet at δ 6.08 (2H, 3,4-O_2CH_2) ppm. Infrared spectra of all compounds in KBr show the following characteristic bands: a broad band in the region 3200–2800 cm^{-1} due to a bonded OH stretch, and a sharp one near 1030 cm^{-1} assignable to an N—O stretch. The solution phase in $CHCl_3$ or CCl_4 shows an additional sharp band near 3585 cm^{-1} assignable to a non-bonded OH group.

A radiometer pH meter type 63 fitted with a combined glass electrode type GK2301C was employed for determination of pH. The instrument was accurate to ± 0.01 pH unit. It was calibrated using two standard Beckman buffer solutions at pH 4.01 and 7.00. The pH meter readings (B) recorded in ethanol–water solutions were converted to hydrogen ion concentration [H^+] by means of the widely used relation of Van Uitert and Haas (15), namely

$$-\log H^+ = B + \log U_H$$

where $\log U_H$ is the correction factor for the solvent composition and ionic strength for which B is read. For this purpose, readings were made on a series of solutions containing known amounts of hydrochloric acid and sodium chloride such that the ionic strength was equal to 0.1 in 50 vol% ethanol–water at 25 $\pm$ 0.1 °C. The value of $\log U_H$ was found to be -0.25.

The acid dissociation constants of **1***a* to **1***l* were evaluated spectrophotometrically. An aliquot of a stock solution of the appropriate phenylazobenzaldoxime in ethanol was diluted with aqueous hydrochloric acid and ethanol so that the final solution was 5×10^{-5} M in the azo oxime, 0.1 M in HCl, and contained 50% by volume ethanol. The test solution (50 ml) was then transferred to a water-jacketed thermostatted cell. The pH of the solution was measured and the spectrum was recorded using either the ionic medium or the corresponding aqueous ethanol as a blank. In both cases identical absorbance values in the wavelength range employed were obtained. The pH of the test solution was increased by addition of small volume of concentrated carbonate free sodium hydroxide made up from the same solvent. Since the total change in volume did not exceed 1.0%, no correction was made for dilution. After each spectral measurement, the pH was checked, and in all cases, the two values before and after the spectral measurement were found to be the same within the limits of the accuracy of the pH meter. Figure 1 shows the collected spectra of **1***e*, taken as a typical example at different pH values. In each run 10–15 pH readings were taken and the value of pK_a was calculated from each reading using the equation: $pK_a = pH_i + \log (A_b - A_i)/(A_i - A_a)$; where A_i is the absorbance of the solution at pH_i and A_a and A_b are the absorbance values of the strongly acid and alkaline solutions of **1** respectively. Each compound was subjected to three pK_a determinations, and the average values, given in Table 2 are within ± 0.01–0.03 pK_a units.

1. E. BAMBERGER and W. PEMSEL. Ber. **36**, 85 (1903).
2. A. CHAKRAVORTY and K. C. KALIA. Inorg. Nucl. Chem. Lett. **3**, 319 (1967); Inorg. Chem. **7**, 2016 (1968); Inorg. Chem. **8**, 2586 (1969).
3. A. CHAKRAVORTY and K. C. KALIA. J. Org. Chem. **35**, 2231 (1970).
4. (*a*) H. H. JAFFE. Chem. Rev. **53**, 191 (1953); (*b*) M.

Can. J. Chem. Downloaded from www.nrcresearchpress.com by 210.87.254.40 on 09/05/12
For personal use only.

CHARTON and B. I. CHARTON. J. Org. Chem. **34**, 1871 (1969).
5. T. H. FISHER and A. W. MEIERHOEFER. Tetrahedron, **31**, 2019 (1975).
6. A. E. GILLAM and E. S. STERN. Electronic absorption spectroscopy. Edward Arnold, London. 1960. p. 271.
7. E. L. ELIEL. Stereochemistry of carbon compounds. McGraw-Hill Book Co. Inc. N.Y. 1962. p. 341.
8. M. DAVIES and N. A. SPIERS. J. Chem. Soc. 3971 (1959).
9. E. LUSTIG. J. Phys. Chem. **65**, 491 (1961).
10. Y. NAGAI, H. MATSUMOTO, J. NAKANO, and H. WATANBE. Bull. Chem. Soc. Jpn. **45**, 2560 (1972).
11. M. R. SPIEGEL. Theory and problems of statistics. Schaum Publishing Co. N.Y. 1961. p. 269.
12. S. EHRENSON, R. T. C. BROWNLEE, and R. W. TAFT. *In* Progress in physical organic chemistry. Vol. 10. *Edited by* A. Streitwiesser, Jr. and R. W. Taft. Interscience Publishers, John Wiley and Sons. 1973. Chapt. 1.
13. M. CHARTON. *In* Progress in physical organic chemistry. Vol. 10. *Edited by* A. Streitwiesser, Jr. and R. W. Taft. Interscience Publishers, John Wiley and Sons. 1973. Chapt. 2.
14. C. D. RITCHIE and W. F. SAGER. *In* Progress in physical organic chemistry. Vol. 2. *Edited by* A. Streitwiesser, Jr. and R. W. Taft. Interscience Publishers, John Wiley and Sons. 1964.
15. L. G. VAN UITERT and C. G. HAAS. J. Am. Chem. Soc. **75**, 451 (1953).
16. L. HUNTER and C. B. ROBERTZ. J. Chem. Soc. 823 (1941).
17. H. H. JAFFE and H. L. JONES. Adv. Heterocycl. Chem. **3**, 209 (1964).
18. M. T. TRIBBLE and J. G. TRAYNHAM. J. Am. Chem. Soc. **91**, 379 (1969).
19. R. W. TAFT. Steric effects in organic chemistry. *Edited by* M. S. Newman. John Wiley and Sons, N.Y. 1956.

Can. J. Chem. Downloaded from www.nrcresearchpress.com by 210.87.254.40 on 09/05/12
For personal use only.

^{13}C nuclear magnetic resonance studies. 61.[1] The effect of solute–solvent association on internal rotation in substituted benzaldehydes

R. E. KLINCK[2] AND J. B. STOTHERS

Department of Chemistry, University of Western Ontario, London, Ont., Canada N6A 5B7

Received May 7, 1976

R. E. KLINCK and J. B. STOTHERS. Can. J. Chem. **54**, 3267 (1976).

Complete lineshape analyses of the ^{13}C nmr signals of the *ortho* and *meta* carbons have been carried out for two *p*-substituted benzaldehydes in methylene chloride-d_2 and toluene-d_8 solutions over a wide temperature range. The activation parameters have been determined for the formyl group rotation and large negative values are found for $\Delta S^{\ddagger}$ when the latter solvent is used. These results suggest that solute–solvent association has a steric effect on the transition state.

R. E. KLINCK et J. B. STOTHERS. Can. J. Chem. **54**, 3267 (1976).

On a effectué une analyse complète de la forme des bandes des signaux rmn de ^{13}C des carbones *ortho* et *méta* de deux benzaldéhydes substitués en *para*; ces études ont été effectuées en solutions dans le chlorure de méthylène d_2 et le toluène d_8 à plusieurs températures différentes. On a déterminé les paramètres d'activation à la rotation du groupe formyle et on a trouvé de grandes valeurs négatives pour le $\Delta S^{\ddagger}$ avec le dernier solvant. Ces résultats suggèrent que l'association soluté–solvant a un effet stérique sur l'état de transition.

[Traduit par le journal]

Introduction

Rotational barriers about σ-bonds possessing some π-character have been investigated extensively (1, 2) and several such studies of substituted benzaldehydes have been reported (3–13). It has been shown that complexation with BF_3 (5–8) or protonation in superacids (9–12) increases the barrier to rotation relative to that of the free aldehyde. The utility of ^{13}C nmr spectroscopy has recently been illustrated with the free aldehydes (13). The much larger chemical shift differences for the non-equivalent *ortho* and *meta* carbons compared with those for the non-equivalent *ortho* and *meta* protons greatly improve the analysis. Most studies have been conducted in 'inert' solvents such as methylene chloride, vinyl chloride, or mixtures of freons. Since our earlier proton study (4) indicated a significant solvent effect in toluene solutions, we decided to reinvestigate this system using ^{13}C nmr and complete lineshape analysis (2) to determine if the entropy effect found in the earlier study is indeed important.

Experimental

The *p*-methoxy- and *p*-dimethylaminobenzaldehydes used in this study are commercially available and were purified by distillation and recrystallization, respectively, before use. Methylene chloride-d_2 and toluene-d_8 were obtained from Merck, Sharp and Dohme, Canada, and used without further purification. Solution concentrations of 2–3 mol% were examined. Spectra were obtained with a Varian XL-100-15 spectrometer, equipped with variable temperature accessories and operating in the FT mode. The solvent signals were used for the ^2H lock. The probe temperature was monitored before and after the collection of each spectrum with a thermocouple placed in a sample tube containing toluene. Temperatures should be reliable to within ± 1 °C. Initially, spectral widths of 4000 Hz were used to obtain spectra from +30 °C to −110 °C at 20 °C intervals. These revealed the variations of the *ortho* and *meta* carbon linewidths with temperature and indicated approximate coalescence temperatures. For the complete lineshape analysis, spectral widths of 800 Hz were used for the *ortho* and *meta* carbon region and 500 Hz for the methyl carbon region. The latter spectra were obtained for the purpose of evaluating the effective transverse relaxation time, T_2^*. These spectra were obtained from +30 °C to −100 °C at approximately 10 °C intervals, with 5 °C intervals being used near the coalescence temperatures.

Treatment of Experimental Data

Complete lineshape analysis was used to determine the rate constant for the exchange. The Eyring rate equation was used to evaluate the activation parameters $\Delta H^{\ddagger}$, $\Delta S^{\ddagger}$, and $\Delta G^{\ddagger}$. Two compounds, *p*-dimethylaminobenzaldehyde and *p*-methoxybenzaldehyde were each studied in CD_2Cl_2 and in $C_6D_5CD_3$ solutions. The former

[1]For part 60, see ref. 20; part 59, see ref. 21; part 58, see ref. 22.

[2]Permanent Address: Adirondack Community College, Shens Falls, N.Y. U.S.A. 12801.

Can. J. Chem. Downloaded from www.nrcresearchpress.com by 210.87.254.42 on 09/05/12
For personal use only.

Can. J. Chem. Downloaded from www.nrcresearchpress.com by 210.87.254.42 on 09/05/12
For personal use only.

solvent was used to allow comparison of the results with those of earlier determinations. In addition the $\Delta S^{\ddagger}$ values obtained provide an assessment of the uncertainties involved in the method of analysis.

Complete Lineshape Analysis

The complete lineshape analysis was carried out using a modification of the computer program EXCHG.[3] Input includes the zero-exchange chemical shifts of the two sites (ν_A and ν_B) and T_2*. Initial estimates of the exchange time, τ, are iterated to provide the best theoretical fit to the experimental data as indicated by a minimum standard deviation. Plots are then provided to illustrate the quality of the fit. Since the free induction decays were stored, any phasing errors could be corrected through subsequent Fourier transformations of the original data.

Determination of ν_A and ν_B

At sufficiently low temperatures, the rotation of the formyl group is essentially 'frozen' and distinct signals appear for each *ortho* and *meta* carbon. The maximum separations of the *ortho* signals and the *meta* signals at low temperature were initially taken as the zero-exchange separations, $\Delta\nu$. The appropriate separation and the center of the observed spectral pattern were used to obtain values for ν_A and ν_B at each temperature.

In some cases, once the zero-exchange temperature is reached, $\Delta\nu$ remains constant upon further decreases in temperature. In other cases $\Delta\nu$ continued to vary indicating that the zero-exchange separation is temperature dependent Consequently, plots of the separations below the zero-exchange temperature were extrapolated over the entire temperature range to provide better estimates of the $\Delta\nu$ for each temperature.

In toluene-d_8, one of the slow exchange *ortho* signals was masked by solvent signals. To obtain the zero-exchange separation, a plot of the temperature dependence of the chemical shift of the *ortho* signal above coalescence was extrapolated to lower temperatures. Using this value and the chemical shift of the signal observed, the zero-exchange separation could be estimated.

[3]Program EXCHG was written by Dr. Nancy K. Wilson of the Environmental Protection Agency, Research Triangle Park, N.C., and provides a simplified lineshape analysis for completely decoupled spin systems.

Determination of T_2 Values*

The effective transverse relaxation time, T_2*, can be obtained from the zero-exchange linewidth, ω_0 as follows:

$$[1] \qquad T_2^* = \frac{1}{\pi\omega_0}$$

Because the linewidths of signals from non-exchanging carbons vary with the conditions under which a given spectrum is run, the methyl carbon linewidth was used to determine T_2*. Above 0 °C, it was found that the *ortho* and *meta* carbon linewidths do not change appreciably relative to those of the other carbons. Therefore, it can be assumed that the exchange rate at room temperature is too rapid to cause detectable broadening and that the differences in linewidths between the *ortho*, *meta*, and methyl carbons reflect the differences in T_2* for these carbons. Using these differences and the observed methyl linewidths, values of ω_0 for the *ortho* and *meta* carbons can be determined for each temperature studied. For example, for *p*-methoxybenzaldehyde in CD_2Cl_2 at 28 °C, $\omega(ortho)$ = 0.84 Hz, $\omega(meta)$ = 0.76 Hz, and ω(methyl) = 0.63 Hz. Therefore

$$[2] \qquad \omega_0(ortho) = \omega(\text{methyl}) + 0.21$$

$$[3] \qquad \omega_0(meta) = \omega(\text{methyl}) + 0.13$$

These relations were used to obtain ω_0 values for the *ortho* and *meta* carbons of *p*-methoxybenzaldehyde in CD_2Cl_2 at the other temperatures. Similar expressions were obtained for the other solutions studied. Equation 1 was then used to calculate the T_2* value for the complete lineshape analysis. It should be noted that T_2* values are not particularly critical except in cases of extremely fast or extremely slow exchange rates. Calculations showed that variations of 10–20% in T_2* give rise to variations of $<1\%$ in log kh/k_BT values used for the Eyring plots. This method of determination ensures that T_2* values are well within the above limits.

Results and Discussion

The zero-exchange chemical shift differences, $\Delta\nu$, for the *ortho* and *meta* carbons at -100 °C are listed in Table 1. In methylene chloride-d_2 solution $\Delta\nu$ was found to be temperature dependent for both carbons of *p*-methoxybenzaldehyde and for the *ortho* carbons of *p*-dimethyl-

TABLE 1. Zero-exchange separations and coalescence temperatures for the *ortho* and *meta* carbon signals of *p*-substituted benzaldehydes

		meta Carbons		*ortho* Carbons	
Solvent	Substituent	$\Delta\nu$ (Hz)	t_c (°C)	$\Delta\nu$ (Hz)	t_c (°C)
CD_2Cl_2	OMe	67	−87	222	−75
	NMe_2	44	−58	224	−41
$C_6D_5CD_3$	OMe	76	−100	~200	−74
	NMe_2	53	−70	~200	−40

TABLE 2. Activation parameters for formyl group rotation of *p*-substituted benzaldehydes in CD_2Cl_2[a]

Substituent	Carbons	$\Delta H^{\ddagger}$ (kcal/mol)	$\Delta S^{\ddagger}$ (eu)	$\Delta G^{\ddagger}_{298}$ (kcal/mol)	$\Delta G^{\ddagger}_c$ (kcal/mol)
OMe	*ortho*	9.1±0.2	0.6±1.0	8.9±0.5	9.0±0.4
	meta	9.3±0.2	2.1±0.8	8.6±0.4	8.9±0.3
	Combined[b]	9.1±0.2	1.2±0.9	8.8±0.4	
NMe_2	*ortho*	10.8±0.3	1.3±1.4	10.5±0.7	10.6±0.6
	meta	10.0±0.2	−2.4±1.1	10.7±0.6	10.5±0.5
	Combined[b]	10.3±0.3	−0.8±1.2	10.6±0.6	

[a]Errors shown are standard deviations obtained from the least-squares analysis.
[b]Obtained from a single least-squares analysis of both *ortho* and *meta* data.

aminobenzaldehyde. In toluene-d_8 solution, the temperature dependence of $\Delta\nu$ could not be determined for the *ortho* carbons because one signal was masked by the solvent. For the *meta* carbons, the coalescence temperature is sufficiently low that the temperature dependence of $\Delta\nu$ could not be adequately determined. In a given solvent the *meta* separation varies with substituent whereas the *ortho* separation is reasonably constant. This is to be anticipated since the *meta* carbons are closer to the substituent. Coalescence temperatures for the *ortho* carbon signals were the same in the two solvents, but those for the *meta* carbons differ. The solute–solvent association in toluene solutions proposed earlier (14–16) could be responsible. Solvent molecules associate with the more electron deficient region of the solute. Therefore a greater solvent effect was found for those carbons nearest the methoxyl and dimethylamino substituents.

The activation parameters obtained from the analysis of the *ortho* and *meta* carbon signals of the two solutes in CD_2Cl_2 solution are listed in Table 2. For each solute, the results obtained from the *ortho* and *meta* carbons are in excellent agreement. A least-squares analysis using the combined data provides as good a fit as the separate analyses. The results obtained compare favorably with those found previously (13). Within experimental error the entropies of activation are found to be close to zero. These results indicate the feasibility of the method employed and confirm the assumption of a negligible entropy of activation in rotations of this type.

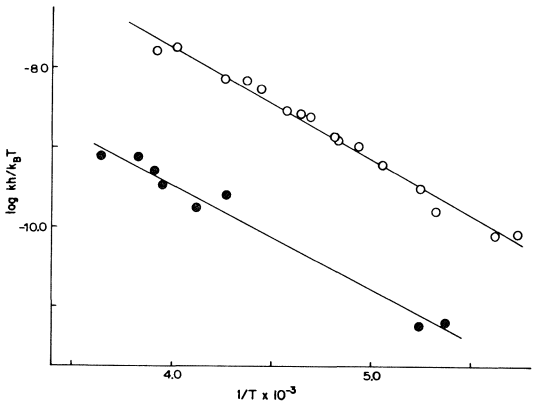

FIG. 1. Eyring plots for the data from the *meta* carbons of *p*-methoxybenzaldehyde (○) and *p*-dimethylaminobenzaldehyde (●) in toluene-d_8 solution.

Figure 1 illustrates the Eyring plots obtained for the *meta* carbon signals of the two solutes in

Can. J. Chem. Downloaded from www.nrcresearchpress.com by 210.87.254.42 on 09/05/12
For personal use only.

TABLE 3. Activation parameters for formyl group rotation of *p*-substituted benzaldehydes in $C_6D_5CD_3$[a]

Substituent	Carbons	$\Delta H^{\ddagger}$ (kcal/mol)	$\Delta S^{\ddagger}$ (eu)	$\Delta G^{\ddagger}_{298}$ (kcal/mol)	$\Delta G^{\ddagger}_{c}$ (kcal/mol)
OMe	*ortho*	7.5±0.5	−6.7±2.1	9.4±1.1	9.1±0.9
	meta	6.5±0.2	−9.4±1.0	9.3±0.5	8.2±0.4
NMe_2	*ortho*	7.8±0.7	−10.7±2.9	10.9±1.6	10.7±1.4
	meta	6.0±0.4	−19.2±1.7	11.8±0.9	9.9±0.7

[a]Errors shown are standard deviations obtained from the least-squares analysis.

$C_6D_5CD_3$ solution. The activation parameters obtained from both carbon signals are listed in Table 3. Because of the difficulty in assigning $\Delta\nu$ values for the *ortho* carbons, the agreement between the results obtained from the two carbons is not as good as that observed in the CD_2Cl_2 solutions. In addition, data for the *ortho* carbons are limited to temperatures above coalescence. For these reasons, the results from the *ortho* carbon signals are not as reliable as those for the *meta* carbon signals, and a least-squares analysis of the combined results is not justified. However, the results obtained from the *meta* carbons can be considered to be as reliable as those obtained from the CD_2Cl_2 solutions. Therefore, we conclude that the large negative values for $\Delta S^{\ddagger}$ in toluene-d_8 are real, and the aromatic solvent is actively involved in the rotation process such that the transition state is highly ordered, and therefore less probable than the transition state which occurs in methylene chloride solution.

Large negative entropies of activation have been found for a number of ring inversions in six-membered heterocyclic compounds (for a general review see ref. 17). While theoretical considerations indicate that some of these processes should have negative $\Delta S^{\ddagger}$ values, in many cases the experimental values are considerably larger. This appears to occur in situations where steric effects may be important. In a study of hindered rotations of substituted biphenyls, Cagel and Eyring (18) suggest that as the size of the *ortho* substituents increases, the formation of activated complex becomes less probable, thereby leading to large negative entropies. A similar interpretation has been given by Gschwend (19) to account for the large negative entropy found for ring inversion of 1-oxo[2.2]metacyclophane relative to that for the 1-hydroxyl derivative. For the former a highly rigid transition state having the carbonyl and phenyl groups coplanar appears to be required. The present data indicate that solvation forces can also exert a steric effect on the rotation process and, for the formyl group at least, the activation parameters for the process should be determined to establish the entropic contribution.

Acknowledgements

We are grateful to the National Research Council of Canada for financial support of this study and to Dr. N. K. Wilson for kindly providing the EXCHG program for the line-shape analysis. We thank Inara Grikis and Marlene Brown for technical assistance.

1. H. KESSLER and K. O. KALINOWSKI. *In* Topics in stereochemistry. Vol. 7. *Edited by* N. L. Allinger and E. L. Eliel. Interscience, New York. 1972.
2. I. O. SUTHERLAND. *In* Annual reports on NMR spectroscopy. Vol. 4. *Edited by* E. F. Mooney. Academic Press, New York. 1971.
3. F. A. L. ANET and M. AHMAD. J. Am. Chem. Soc. **86**, 119 (1964).
4. R. E. KLINCK, D. H. MARR, and J. B. STOTHERS. J. Chem. Soc. Chem. Comm. 409 (1967).
5. A. GREENVALD and M. RABINOVITZ. J. Chem. Soc. Chem. Comm. 642 (1969).
6. M. RABINOVITZ and A. GRINVALD. J. Am. Chem. Soc. **94**, 2724 (1972).
7. A. GRINVALD and M. RABINOVITZ. J. Chem. Soc. Perkin Trans. II, 94 (1974).
8. V. S. RAO and P. M. NAIR. Indian J. Chem. 82 (1973).
9. R. JOST, P. RIMMELIN, and J. M. SOMMER. J. Chem. Soc. Chem. Comm. 879 (1971).
10. A. ELLENCWEIG and M. RABINOVITZ. Tetrahedron Lett. 4439 (1971).
11. D. M. WONG. Ph.D. Thesis, University of California, Los Angeles. 1972.
12. T. DRAKENBERG, S. FORSÉN, and J. M. SOMMER. J. Chem. Soc. Perkin Trans. II, 520 (1974).
13. T. DRAKENBERG, R. JOST, and J. SOMMER. J. Chem. Soc. Chem. Comm. 1011 (1974); J. Chem. Soc. Perkin Trans. II, 1682 (1976).
14. R. E. KLINCK and J. B. STOTHERS. Can. J. Chem. **40**, 2329 (1962).

Can. J. Chem. Downloaded from www.nrcresearchpress.com by 210.87.254.42 on 09/05/12
For personal use only.

15. R. E. KLINCK and J. B. STOTHERS. Can. J. Chem. **44**, 37 (1966).
16. R. E. KLINCK. Can. J. Chem. **51**, 787 (1973).
17. V. M. GITTINS, E. WYN-JONES, and R. F. M. WHITE. *In* Internal rotation in molecules. *Edited by* W. J. Orville-Thomas. John Wiley and Sons, New York. 1974.
18. F. W. CAGLE, JR., and H. EYRING. J. Am. Chem. Soc. **73**, 5628 (1951).
19. H. W. GSCHWEND. J. Am. Chem. Soc. **94**, 8430 (1972).
20. A. STOESSL, J. B. STOTHERS, and E. W. B. WARD. Phytochem. **15**, 855 (1976).
21. G. I. BIRNBAUM, C. P. HUBER, M. L. POST, J. B. STOTHERS, J. R. ROBINSON, A. STOESSL, and E. W. B. WARD. J. Chem. Soc. Chem. Commun. 330 (1976).
22. J. B. STOTHERS and C. T. TAN. Can. J. Chem. **54**, 917 (1976).

Downloaded from www.nrcresearchpress.com by 210.87.254.42 on 09/05/12
For personal use only.

Concerning stereochemical assignments from ^{13}C spectra of systems experiencing γ substituent effects. Deshielding antiperiplanar interactions can mislead the unwary[1]

W. A. AYER, L. M. BROWNE, AND S. FUNG
Department of Chemistry, University of Alberta, Edmonton, Alta., Canada T6G 2G2
AND
J. B. STOTHERS
Department of Chemistry, University of Western Ontario, London, Ont., Canada N6A 5B7

Received May 25, 1976

W. A. AYER, L. M. BROWNE, S. FUNG, and J. B. STOTHERS. Can. J. Chem. **54**, 3272 (1976).

A variety of substituents bonded to quaternary carbons exert marked deshielding effects at antiperiplanar γ carbons. The shifts produced by methyl groups are *ca.* 2 ppm, while hydroxyl groups cause shifts as large as 6 ppm. These shifts are particularly clearly demonstrated by the C-19 shieldings in 5α-substituted steroids. For 9,10-disubstituted decalins, the effect is such that *cis* and *trans* isomers are not easily distinguished from their ^{13}C spectra. These shifts contrast sharply with the corresponding effects found for substituents bonded to less highly substituted carbon skeletons.

W. A. AYER, L. M. BROWNE, S. FUNG et J. B. STOTHERS. Can. J. Chem. **54**, 3272 (1976).

Un grand nombre de substituants liés à des carbones quaternaires excercent des effets importants de déblindage sur les carbones γ antipériplanaires. Les déplacements produits par les groupes méthyles sont d'environ 2 ppm alors que les groupes hydroxyles provoquent des déplacements qui peuvent aller jusqu'à 6 ppm. On démontre particulièrement clairement ces déplacements avec les blindages causés par le C-19 dans les stéroïdes substitués en 5α. Dans le cas des décalines substituées en 9,10, l'effet est tel que les isomères *cis* et *trans* ne peuvent pas être distingués facilement grâce à leur spectre ^{13}C. Ces déplacements sont en opposition importante avec les effets correspondants trouvés pour les substituants liés à des carbones moins substitués du squelette carboné.

[Traduit par le journal]

In the course of the structural elucidation of cybullol (1), a fungal metabolite of *Cyathus bulleri* Brodie, its ^{13}C nmr spectrum was determined to obtain further support for its formulation as the dimethyldihydroxydecalin **1**, the structure proposed from chemical and other physical data. The principal point of interest centred on the stereochemistry of the ring junction and, initially, it seemed reasonable to expect that the shielding of the angular methyl carbon could settle this point directly. We had earlier obtained the ^{13}C shielding data for eight of the nine 10-methyl-*trans*-decalols (2) and, although the desired model, 10-methyl-*trans*-decal-5-ol, had not been available, it was assumed that the angular methyl carbon shielding would not be appreciably affected by the antiperiplanar hydroxyl at C-5. This assumption followed from the finding that although antiperiplanar carbons γ to oxygen tend to exhibit marked upfield shifts for compounds in which oxygen is bonded to secondary or tertiary carbons (3), when oxygen is bonded to quaternary carbon the antiperiplanar γ carbons are slightly deshielded as indicated by the results for 1-substituted bicyclo[2.2.2]octanes and adamantanes (4). Data were also available for seemingly better models, two steroidal 5α,6-diols (5), for which the 5α hydroxyl group appeared to deshield C-19 by 1–2 ppm. On this basis, an angular methyl shielding near 18 ppm was anticipated for structure **1** with a *trans* ring

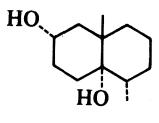

1

junction since there was good evidence that the other substituents were equatorial. On the other

[1]Part 62 in the series ^{13}C NMR studies, for part 61 see ref. 15.

Can. J. Chem. Downloaded from www.nrcresearchpress.com by 210.87.254.6 on 09/05/12
For personal use only.

Can. J. Chem. Downloaded from www.nrcresearchpress.com by 210.87.254.6 on 09/05/12
For personal use only.

hand, a *cis* ring junction for **1** would be expected to shift the angular methyl carbon to *ca.* 22 ppm since in this case the γ *gauche* hydroxyl at C-5 could be expected to shield the methyl carbon by *ca.* 6 ppm relative to its absorption position in 10-methyl-*cis*-decalin (6). The predicted difference for the two geometries, therefore, was expected to allow a clear cut assignment. Upon examination, the angular methyl shielding in **1** was found to be 21.1 ppm which strongly favored the *cis* assignment for the ring junction but, in fact, **1** has the *trans* stereochemistry as proven by its conversion to the known metabolite, geosmin, whose structure had been established by stereoselective synthesis (7). In view of the relatively low-field position of the angular methyl shielding of **1**, several model compounds were prepared to examine the variation of the angular methyl shielding in closely related systems. These data establish that the antiperiplanar γ effects of a variety of substituents are deshielding if the effect is transmitted via quaternary carbons, a result *directly opposite* to that found for systems with less highly substituted interconnecting carbons.

From the finding that hydroxyl substitution at the ring junction, antiperiplanar to the angular methyl carbon in the methyldecalin system, caused a marked downfield shift of the latter, some simpler systems were examined to establish that the shift was indeed due to the hydroxyl group. It had been assumed that equatorial methyl or hydroxyl substitution at the 2- and 6-positions would cause little perturbation at the angular methyl. This was found to be valid as the data in Table 1 attest. Introduction of the 5α hydroxyl group in the *trans*-decalins causes a downfield shift of *ca.* 4.5 ppm. It is interesting that this effect is markedly attenuated if a second hydroxyl is vicinal to the 5α group; this is exactly analogous to the result cited above for the steroid models. Some 10-methyl-*cis*-decalins were also examined and the angular methyl shieldings accord well with expectation since these carbons absorb near 22 ppm or 6 ppm upfield from the shielding of the parent system. One example having an antiperiplanar methyl group is also included in Table 1 from which it can be seen that the 10-methyl carbon suffers a 2.4 ppm downfield shift.

As this study was in progress, the results from a systematic investigation of hydroxysteroids

TABLE 1. Angular methyl shieldings in some 10-methyl decalins

	trans[a]		*cis*[a]	
Substitution	δ_c (C-10)	$\Delta\delta$	δ_c (C-10)	$\Delta\delta$
Nil	15.7		28.2[b]	
5-OH	20.4	+4.7	22.4	−5.8
4α-Me-5-OH	20.3	+4.6	22.3[c]	−5.9
2α-OH	16.6			
2α,5-(OH)$_2$	21.0	+4.4		
2α,5-(OH)$_2$-6-Me	21.1	+4.5		
3-Oxo	14.9			
3-Oxo-4α-Me-5-OH	20.8	+5.9		
3-Oxo-5-OH			21.5	−6.7
4β-OH	19.1			
4β,5-(OH)$_2$	20.6	+1.5		
4α,5-(OH)$_2$			22.3	−5.9
3α,5-(OH)$_2$			21.5	−6.7
2β-OH	9.8			
2β-OH-2α-Me	12.2	+2.4		

[a]Stereochemistry of the ring junction.
[b]From ref. 6.
[c]This compound was kindly provided by Prof. J. A. Marshall.

were reported (8) and included the data for 5α-cholestanol for which the C-19 signal is shifted to 3.9 ppm downfield from its position in the cholestane spectrum. Earlier, downfield shifts of 5.4 and 6.0 ppm had been reported for C-19 in the 5α-amino and 5α-azido derivatives of cholestane (9). To extend our examination of these antiperiplanar effects to other steroids, seven additional examples were included[2] and these results are collected in Table 2. As has been suggested (5), the introduction of the 5α hydroxyl group may tend to increase the ring flattening in the vicinity of the substituent thereby reducing the γ *gauche* effects of the methylene groups at the angular methyl group and decreasing its shielding. However, the tabulated data indicate that this is a minor influence since the larger downfield shifts are found for the less space demanding groups. For example, the cyano group causes a shift of 8 ppm and the azido group 6.0 ppm while the hydroxyl group exerts a more pronounced effect than methyl. It seems, therefore, that the antiperiplanar influence of these substituents arises from electronic interactions rather than from steric perturbations but

[2]We are indebted to Professor J. Levisalles for kindly providing samples of the 5α-substituted cholestan-3-ones and to Professor E. W. Warnhoff and Wayne Yerhoff for preparing the 5α-halo-6-oxocholestanyl acetates for our use in this study.

TABLE 2. Antiperiplanar γ effects in some steroids

Parent system	Substituent	δ_c (C-19)	$\Delta\delta_c$	Reference
Cholestanes	Nil	12.2		
	5α-OH	16.1	3.9	8
	5α-N_3	18.2	6.0	9
	5α-NH_2	17.6	5.4	9
Cholestan-3-ones	Nil	11.5		This work
	5α-OH	15.8	4.3	This work
	5α-OMe	16.1	4.6	This work
	5α-Me	14.2	2.7	This work
	5α-F	15.9	4.4	This work
	5α-CN	19.5	8.0	This work
6-Oxocholestan-3-yl acetates	Nil	13.0		This work
	5α-Br	14.5	1.5	This work
	5α-Cl	15.0	2.0	This work

the sign reversal relative to that for corresponding interactions through less highly substituted carbons (3) is puzzling. While Eliel *et al.* (3) proposed a hyperconjugative interaction of the electron pairs on the heteroatom with the C_α—C_β bond with subsequent alternation of the electron density at the γ antiperiplanar carbon to account for the observations in the less highly substituted systems, this seems to be less likely in light of the present results. In contrast to the tendencies in less highly substituted systems, significant shifts are not restricted to the first-row elements but are also apparent for chlorine and bromine.

With the finding of an appreciable shift produced by methyl substitution it was of interest to check for corresponding effects in other carbon skeletons. From the data for a variety of norbornane (10, 11) and bicyclo[2.2.2]octane derivatives (12), it is apparent that similar shifts occur in these systems. One way in which this can be illustrated is to compare the observed shieldings for a suitably disubstituted derivative with the shieldings predicted by simple additivity of the shielding effects of the two substituents. On this basis, differences of 3.3 and 1.6 ppm are found for the C-6 shielding of the 2,2-dimethyl derivatives of norbornane and bicyclo-

2

a X = OH, δ_c(C-6) 20.0
b X = Me, δ_c(C-6) 22.4

3

a X = OH, δ_c(C-6) 22.0
b X = Me, δ_c(C-6) 25.0

octane, respectively, *i.e.*, with the observed signal at lower field than predicted. Alternatively, one can examine the shielding effect produced by the introduction of an antiperiplanar methyl group into a monosubstituted derivative. For example, the effect on the C-6 shielding caused by the following substitutions: *endo*-norbornan-2-ol (**2***a*) → *exo*-2-methyl-*endo*-norbornan-2-ol (**3***a*); *endo*-2-methylnorbornane (**2***b*) → 2,2-dimethylnorbornane (**3***b*) (10) and 2-methylbicyclo[2.2.2]octane → the 2,2-dimethyl derivative. For these cases, downfield shifts of 2.0, 2.6, and 3.0 ppm, respectively, are found. It has been recognized for several years that simple additivity of substituent effects breaks down in highly substituted systems and that additional parameters are required to correlate shielding data in such systems (13). Initially, however, the corrections for the more branched systems were restricted to the α and β positions but in a recent compilation of substituent parameters (14), a factor of 2 ppm to account for the downfield shift of C-3 in, for example, 1,1-dimethylcyclohexane was included which could be ascribed to the antiperiplanar interaction illustrated by the results in this report.

From the foregoing it is apparent that the shielding of a γ carbon antiperiplanar to a nucleus other than hydrogen can experience a pronounced perturbation either upfield or downfield depending on the degree of substitution of the intervening carbons. Recognition of this phenomenon is essential for the successful interpretation of the ^{13}C spectra of a wide variety of compounds and the trends offer an interesting challenge for theoretical description. As illustrated in this report, an oversimplified approach

Can. J. Chem. Downloaded from www.nrcresearchpress.com by 210.87.254.6 on 09/05/12
For personal use only.

to the estimation of ^{13}C shieldings can be misleading for seemingly straightforward stereochemical assignments.

Experimental

The ^{13}C spectra were obtained with a Varian XL-100-15 system operating in the Fourier transform mode. All compounds were examined as 5–10% (w/v) solutions in deuteriochloroform using tetramethylsilane as an internal reference. Carbon types, *i.e.* methyl, methylene, methine, and quaternary, were identified by off-resonance decoupling and the methyl signals for compounds containing both tertiary and secondary methyl groups were differentiated by selective decoupling at low irradiating power. The precision of the shielding data is judged to be ± 0.05 ppm.

Acknowledgements

We wish to thank the National Research Council of Canada for financial assistance, Prof. J. Levisalles, Prof. J. A. Marshall, Prof. E. W. Warnhoff, and Wayne Yerhoff for providing some model compounds, and Marlene Brown for technical assistance.

1. W. A. Ayer and M. G. Paice. Can. J. Chem. **54**, 910 (1976).
2. S. H. Grover and J. B. Stothers. Can. J. Chem. **52**, 876 (1974).
3. E. L. Eliel, W. F. Bailey, L. D. Kopp, R. L. Willer, D. M. Grant, R. Bertrand, K. A. Christensen, D. K. Dalling, M. W. Duch, E. Wenkert, F. D. Schell, and D. W. Cochran. J. Am. Chem. Soc. **97**, 322 (1975).
4. T. Pehk, E. Lippmaa, V. V. Sevostjanova, M. M. Krayuschkne, and A. I. Tarasova. Org. Magn. Reson. **3**, 783 (1971); G. E. Maciel and H. C. Dorn. J. Am. Chem. Soc. **93**, 1268 (1971); G. E. Maciel, H. C. Dorn, R. L. Green, W. A. Kleschick, M. R. Peterson, and G. U. Wahl. Org. Magn. Reson. **6**, 178 (1974).
5. S. Lang, D. N. Lincoln, and V. Wray. J. Chem. Soc. Perkin Trans. II, 344 (1975).
6. D. K. Dalling, D. M. Grant, and E. G. Paul. J. Am. Chem. Soc. **95**, 3718 (1973).
7. J. A. Marshall and A. R. Hochsteller. J. Org. Chem. **33**, 2593 (1968).
8. H. Eggert, C. L. Van Antwerp, N. S. Bhacca, and C. Djerassi. J. Org. Chem. **41**, 71 (1976).
9. Q. Khuong-Huu, G. Lukacs, A. Pancrazi, and R. Goutarel. Tetrahedron Lett. 3579 (1972).
10. J. B. Grutzner, M. Jautelat, J. B. Dence, R. A. Smith, and J. D. Roberts. J. Am. Chem. Soc. **92**, 7107 (1970).
11. J. B. Stothers, C. T. Tan, and K. C. Teo. Can. J. Chem. **54**, 1211 (1976).
12. J. B. Stothers and C. T. Tan. Can. J. Chem. **54**, 917 (1976).
13. D. M. Grant and E. G. Paul. J. Am. Chem. Soc. **86**, 2984 (1964); D. K. Dalling and D. M. Grant. J. Am. Chem. Soc. **89**, 6612 (1967).
14. D. K. Dalling and D. M. Grant. J. Am. Chem. Soc. **94**, 5318 (1972).
15. R. E. Klinck and J. B. Stothers. Can. J. Chem. This issue.

Can. J. Chem. Downloaded from www.nrcresearchpress.com by 210.87.254.6 on 09/05/12
For personal use only.

Metabolites of bird's nest fungi. Part 6.[1] The synthesis of (±)-cybullol and a new synthesis of (±)-geosmin

WILLIAM A. AYER, LOIS M. BROWNE, AND STEVEN FUNG
Department of Chemistry, University of Alberta, Edmonton, Alta., Canada T6G 2G2

Received June 7, 1976

WILLIAM A. AYER, LOIS M. BROWNE, and STEVEN FUNG. Can. J. Chem. **54**, 3276 (1976).

The stereoselective transformation of 6,10-dimethyl-4-octal-3-one (**8**) to racemic cybullol (**1**), a metabolite of *Cyathus bulleri* Brodie, is reported. The transformation 4,10-dimethyl-4-octal-3-one to (±)-geosmin (**15**) is described. The results of the photosensitized [4 + 2] cycloaddition of oxygen to a number of 10-methyl-2,4-hexalins are discussed.

WILLIAM A. AYER, LOIS M. BROWNE et STEVEN FUNG. Can. J. Chem. **54**, 3276 (1976).

On rapporte la transformation stéréosélective de la diméthyl-6,10 octal-4 one-3 (**8**) en cybullol racémique (**1**), un métabolite du *Cyathus bulleri* Brodie. On décrit la transformation de la diméthyl-4,10 octal-4 one-3 en (±)-géosmine (**15**). On discute des résultats obtenus lors de la cycloaddition photosensibilisée [4 + 2] de l'oxygène à un certain nombre de méthyl-10 hexalines-2,4.

[Traduit par le journal]

Examination of the metabolites of some of the small gastromycetous fungi known as Bird's Nest fungi (Nidulariaceae) in these laboratories has led to the isolation of a variety of terpenoid (*e.g.*, *Cyathus helenae* Brodie (1), *Cyathus bulleri* Brodie (2)) and non-terpenoid (*e.g.*, *Cyathus intermedius* (3)) constituents. We now wish to report the stereoselective synthesis of racemic cybullol (**1**), a degraded eudesmane-type sesquiterpene produced by *C. bulleri* (2). At the same time we report a new, high yield, synthesis of the related fungal metabolite, geosmin (4).

Cybullol, **1**, is a dimethyldecalindiol in which the two hydroxyl groups bear a *cis*-1,4-relationship in a *trans*-fused system. A facile synthetic approach to a *cis*-1,4-cyclohexanediol system involves the [4 + 2] cycloaddition of a 1,3-cyclohexadiene with molecular oxygen to give a cyclic peroxide, followed by reduction, as outlined in Scheme 1.

It is well documented that the photooxygenation of steroidal conjugated dienes is sensitive to steric effects (oxygen as a dienophile, ref. 5*a*; sensitized photooxygenation of olefins, ref. 5*b*) and that the *endo*-peroxide produced is usually on the side opposite to nearby angular methyl groups. However, relatively few examples of photooxygenation of hexalin dienes have been reported (6). In order to further investigate the stereochemistry of photooxygenation of hexalin systems as well as to provide a model compound for a ^{13}C nuclear magnetic resonance (cmr) study reported elsewhere (7), we examined initially the photooxygenation of 10-methyl-2,4-hexalin, **4** (Scheme 2).

The diene **4** was prepared from 10-methyl-4-octal-3-one (8) by the method of Dauben *et al.* (9). Photosensitized oxygenation (5, 6) in the presence of eosin Y yielded the *endo*-peroxide **5** and the γ-hydroxyenone **6**. Catalytic hydrogenation of the *endo*-peroxide gave a crystalline diol, which was assigned the relative stereo-

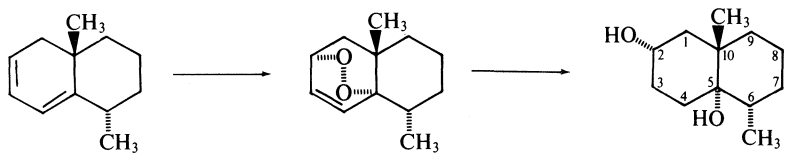

2 3 1

SCHEME 1

[1]For part 5 see ref. 3.

Can. J. Chem. Downloaded from www.nrcresearchpress.com by 210.87.254.105 on 09/05/12
For personal use only.

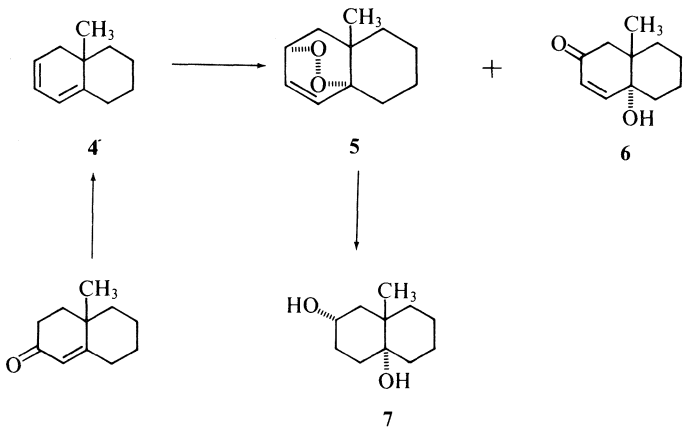

SCHEME 2

chemistry shown in **7** on the basis of pyridine induced shifts (relative to chloroform) of the methyl protons in the proton magnetic resonance (pmr) spectrum (2, 10). For diol **7**, the pyridine shift is −0.04 for the C-10 methyl. Since the equatorial secondary hydroxyl at C-2 should not influence these induced shifts (10), these data indicate that the tertiary hydroxyl is antiperiplanar to the tertiary methyl, *i.e.*, the diol obtained has the relative stereochemistry shown in **7**. It follows that the *endo*-peroxide has structure **5** and that oxygenation occurred on the side opposite to the angular methyl. Interestingly the cmr spectrum of diol **7** shows the tertiary methyl signal at low field (δ 21.0) similar to that observed in cybullol (δ 21.1) and other *trans*-10-methyl-5-decalols (2). This unusual deshielding (11) by antiperiplanar hydroxyl is discussed in detail elsewhere (7).

The octalone required for the synthesis of cybullol, **1** (Scheme 3) is *trans*-6,10-dimethyl-4-octal-3-one, **8**. Compound **8** is not readily accessible by applying the usual annelation procedures to 2,6-dimethylcyclohexanone (ref. 12, and references cited therein). In most cases low yields of **8** are obtained, or the predominant product formed is 1,2,5-trimethylbicyclo[3.3.1]-non-2-en-9-one (**9**). Several modified annelation procedures for the preparation of **8** have been reported (12, 13). In our hands, the method of Hooz and Benderley (13*a*) and that of Caine and Tuller (13*b*) were most convenient for large scale preparation. Octalone **8** was transformed to the conjugated diene **2** by treatment of the tosylhydrazone of **8** with *n*-butyllithium (9). Purification by chromatography over silica gel gave compound **2** in 50% yield. Subsequently it was found that compound **2** could be prepared in high purity and in greater than 80% yield from **8** by lithium aluminum hydride reduction to the allylic alcohol **10** followed by pyrolysis (6*b*, 14).

Photooxygenation of **2** did not yield the cyclic peroxide as readily as had been anticipated from the model studies. The products from the photooxygenation experiments varied depending on the conditions. For example, photooxygenation of a methanol–benzene solution of **2** in the presence of eosin Y at room temperature overnight gave a mixture of several compounds (thin layer chromatogram, tlc) from which *endo*-peroxide **3** could be isolated in low yield. Low temperature (−78 °C) photooxygenation of **2** in the presence of eosin Y was complete after 8 h (disappearance of diene). Chromatographic separation of the reaction mixture gave traces of *endo*-peroxide **3** along with the γ-hydroxyenone **11** (13%) and the diepoxide **12** (13%). Presumably compound **12** arises by photochemical rearrangement of **3** since it is known that this type of rearrangement occurs under both photochemical and thermal conditions (15). Low temperature photooxygenation of a methanol–ether solution of **2** in the presence of eosin Y and rose bengal was complete in 2 h. The photolysis mixture consisted mainly of compound **3** together with small amounts of compound **12** (tlc). Chromatographic separation of the components led to isolation of *endo*-peroxide **3** in 20% yield. Catalytic hydrogenation of **3** over platinum oxide provided in 49% yield, crystalline

Can. J. Chem. Downloaded from www.nrcresearchpress.com by 210.87.254.105 on 09/05/12
For personal use only.

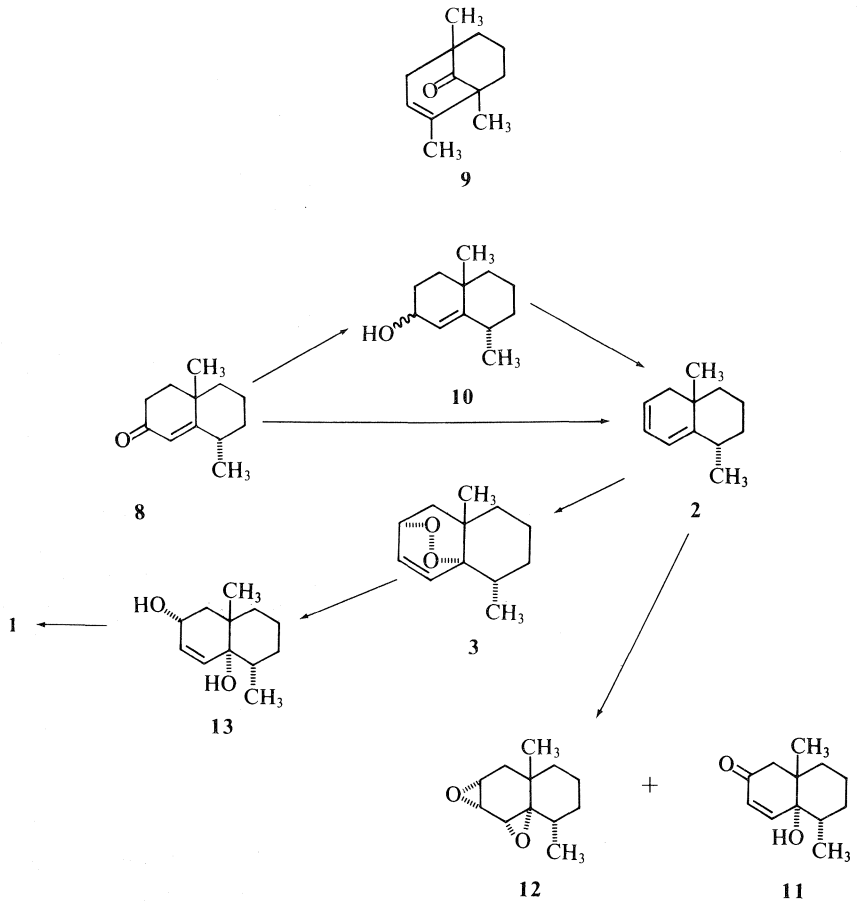

SCHEME 3

(±)-cybullol, identical with an authentic sample (2).

In an effort to improve the overall yield in the sequence **2** to **1**, several other synthetic routes were explored. Two chemical methods (16, 17) for generating the reactive oxygen species were investigated but neither method led to improved yields of compound **3**. Attempted transformation of diene **2** to *endo*-peroxide **3** by treatment with a large excess of sodium hypochlorite–hydrogen peroxide (16) gave unreacted starting material. Treatment of **2** with the triphenylphosphite–ozone complex (17) gave *endo*-peroxide **3** in only 15% yield. Attempted conversion of the initially formed cyclic peroxide *in situ* to the more stable allylic diol **13** by photooxygenation in the presence of thiourea (18) was unsuccessful. The crude photolysis product contained the same mixture of compounds (tlc) as the product obtained in the absence of thiourea. We also explored the use of **11** and **12** as precursors to cybullol. Lithium aluminum hydride reduction of γ-hydroxyenone **11** gave a 1:2 mixture of allylic diol **13** and its C-2 epimer, whereas lithium aluminum hydride reduction of diepoxide **12** gave a 1:3 mixture of cybullol and an unidentified compound. An improved overall yield of **1** was obtained when it was found that a change of solvent (ether–methanol (1:1) to methylene chloride) in the photooxygenation reaction gave increased yields of compound **3**. Thus low temperature photooxygenation of a methylene chloride solution of **2** in the presence of rose bengal led to *endo*-peroxide **3** in 46% overall yield from **10**. It was also found that a two step transformation of **3** to **1** proceeded

Can. J. Chem. Downloaded from www.nrcresearchpress.com by 210.87.254.105 on 09/05/12
For personal use only.

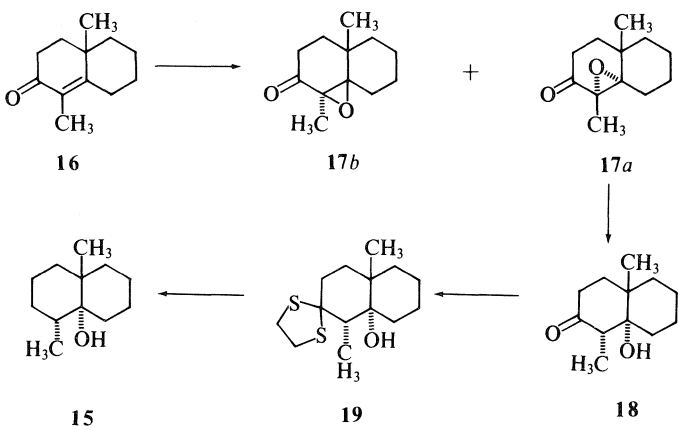

SCHEME 4

more efficiently than direct catalytic hydrogenation. Treatment of **3** with aluminum amalgam (19) yielded the crystalline allylic diol **13** in 77% yield. Catalytic hydrogenation of **13** then gave cybullol (**1**) in quantitative yield.

Geosmin, **15**, a degradation product of cybullol, is the fungal metabolite responsible for the 'earthy' aroma of freshly plowed soil (20) and beetroot (21), and the muddy taste in surface water supplies (22) and trout (23). The constitution of geosmin was first suggested by Gerber (24) and the structure and relative stereochemistry proven by Marshall's stereoselective synthesis (4) of the racemic form. Herein we report another stereoselective synthesis of racemic geosmin in 24% overall yield from the dimethyloctalone **16** (Scheme 4).

Oxidation of dimethyloctalone **16** (25) with alkaline hydrogen peroxide gave an 85% yield of a 6:5 mixture of α- and β-epoxy ketones, **17***a* and **17***b* (26). The epimeric mixture **17** was not separated but was reduced directly with lithium in ammonia. The product obtained was a viscous oil which partially solidified on standing. Isolation of the solid material by crystallization gave in 53% yield a single crystalline ketol; the mother liquors contained mainly unreacted epoxy ketone **17***b*. The ketol so obtained was assigned the relative stereochemistry shown in **18** on the basis of pyridine induced shifts of the C-10 methyl ($\Delta\delta$ +0.04) in the pmr spectrum (2, 10, 27). Removal of the carbonyl in **18** was effected in over 95% yield by thio ketal formation followed by desulfurization with Raney nickel. The crystalline product obtained was identical in ir, pmr, mass spectrum, and tlc behavior with (−)-geosmin (2, 28). Geosmin has not previously been obtained in crystalline form. It is interesting to note that the crystalline material has the characteristic penetrating odor of natural geosmin.

Experimental

Mass spectra were recorded on an A.E.I. model MS-9 or MS-12 mass spectrometer and are reported as *m/e* (relative intensity). Unless diagnostically significant only peaks at least 20% as intense as the base peak are reported. Infrared spectra were recorded on a Unicam SP1000 or a Perkin Elmer Model 421 dual grating spectrophotometer. Proton magnetic resonance spectra were measured using a Varian HA-100 spectrophotometer with tetramethylsilane as internal standard. Melting points were recorded on a Fisher–Johns melting point apparatus and are uncorrected.

Silica gel tlc plates were 0.5 mm silica gel G (E. Merck, Darmstadt) containing 1% electronic phosphor (General Electric, Cleveland); materials were detected by spraying with 30% sulfuric acid and charring. Silica gel (Woelm, less than 0.08 mm) was used for elution chromatography.

General Procedure for Photooxygenation

A solution of diene and sensitizer was irradiated through a pyrex filter with a Hanovia 250 W medium pressure mercury dispersion lamp while oxygen was bubbled through the reaction mixture. The reaction was monitored by the disappearance of diene (tlc). When all diene had been consumed, the photolysis mixture was concentrated and either separated or used as such in subsequent reactions as described below.

10β-Methyl-2α,5α-epidioxy-3-octalin, **5**

Photooxygenation of 10-methyl-2,4-hexalin (**4**) (8) (0.58 g) was carried out in benzene–methanol (1:1, 200 ml) containing eosin Y (5 mg) for 12 h. Thin layer chromatography (pentane–ether, 4:1) showed the presence of two components (R_f 0.41, 0.12). Elution chromatography with pentane–ether (9:1) gave *endo*-peroxide **5**

Can. J. Chem. Downloaded from www.nrcresearchpress.com by 210.87.254.105 on 09/05/12
For personal use only.

Can. J. Chem. Downloaded from www.nrcresearchpress.com by 210.87.254.105 on 09/05/12
For personal use only.

as an oil (0.30 g, 43%, R_f 0.41); pmr ($CDCl_3$) δ 0.96 (s, 3, C-10 CH_3), 1.32 (d of d, 1, J = 2.2, 13 Hz, H-1α), 1.86 (d of d, 1, J = 4, 13 Hz, H-1β), 4.53 (octet, 1, J = 1.5, 2.2, 4, 5.7 Hz, H-2β), 6.23 (d of d, 1, J = 1.5, 8 Hz, H-3), 6.54 (d of d, 1, J = 5.7, 8 Hz, H-4); double irradiation at 4.53 collapses 1.32, 1.86, 6.23, 6.54 to doublets; ms m/e calcd. for $C_{11}H_{16}O_2$: 180.1150, found: 180.1157 (6), 148(52), 133(27), 105(29), 97(23), 95(54), 93(25), 91(34), 83(30), 82(55), 81(38), 79(26), 69(33), 67(58), 56(25), 55(99), 53(27), 43(36), 41(100). Further elution gave 5α-hydroxy-10β-methyl-3-octal-2-one, **6** (R_f 0.12); ir ($CHCl_3$) 1660 (C=O), 1620 (C=C) cm^{-1}; pmr ($CDCl_3$) δ 1.24 (s, 3, C-10 CH_3), 6.10 (br s, 1, OH), 6.20 (d of d, 1, J = 2, 10 Hz, H-4), 6.77 (d, 1, J = 10 Hz, H-3); ms m/e calcd. for $C_{11}H_{16}O_2$: 180.1151, found: 180.1158 (2), 162(100), 147(28), 134(25), 119(48), 106(33), 105(37), 91(78).

10β-Methyl-2α,5α-decalin Diol, **7**

A solution of *endo*-peroxide **5** (0.13 g) in ether (20 ml) was hydrogenated over palladium–charcoal (5%, 10 mg) at 40 psi hydrogen for 1 h. The product was filtered, concentrated, and purified by preparative tlc (ether) to give crystalline diol **7** (0.07 g, 49%); mp 167–169 °C; ir ($CHCl_3$) 3600, 3450 (OH) cm^{-1}; pmr ($CDCl_3$) δ 1.02 (s, 3, C-10 CH_3), 3.98 (septet, 1, J = 5 Hz, H-2a); pmr (pyridine-d_5) δ 1.06 (s, 3, C-10 CH_3); ms m/e calcd. for $C_{11}H_{20}O_2$: 184.1463, found: 184.1466 (46), 176(73), 151(61), 148(28), 138(35), 137(41), 128(39), 127(76), 123(26), 122(26), 112(100), 111(43), 110(28), 109(63), 108(48), 97(35), 95(39), 93(30), 85(73), 84(35), 83(50), 82(68), 81(46), 73(52), 71(33), 69(40), 68(41), 67(46), 57(39), 55(63), 43(65), 41(65). *Anal.* calcd. for $C_{11}H_{20}O_2$: C 71.70, H 10.94; found: C 71.21, 71.09, H 10.86, 10.90.

6α,10β-Dimethyl-2,4-hexalin, **2**

(a) Via Tosylhydrazone of **8**

6α,10β-Dimethyl-4-octal-3-one, **8** (12*a*, *b*) (1.0 g), tosylhydrazine (1.1 g), and acetyl chloride (20 μl) in anhydrous tetrahydrofuran (30 ml) were heated under reflux for 3.5 h. Anhydrous benzene (50 ml) was added and the solvents removed by distillation until a boiling point of 80 °C was reached. The reaction flask was cooled (5 °C) and *n*-butyllithium (8 ml, 1.9 *M*) was added. After stirring overnight, the reaction mixture was diluted with water and sodium chloride added to saturate the solution which was then extracted with ether. The ether extract was dried ($MgSO_4$) and concentrated. Elution chromatography of the product (pentane) gave diene **2** (0.45 g, 50%) as a yellow oil.

(b) Via Pyrolysis of Allylic Alcohol **10**

A solution of octalone **8** (3.7 g) in ether (70 ml) was added dropwise to a cooled (0 °C) solution of lithium aluminum hydride in ether (70 ml, 0.5 *M*). The reaction mixture was allowed to stir at room temperature for 1 h, then excess hydride was destroyed and the product isolated in the usual way. 6α,10β-Dimethyl-4-octal-3-ol (3.6 g, 97%) was isolated as an oil; ir (neat) 3350 (OH), 1655 (C=C) cm^{-1}; pmr ($CDCl_3$) 0.99 (d, 3, J = 7 Hz, C-6 CH_3), 1.11 (s, 3, C-10 CH_3), 4.2 (br s, 1, H-3), 5.4 (br s, 1, H-4); ms m/e calcd. for $C_{12}H_{20}O$: 180.15142, found: 180.15149 (1), 162(60), 147(100), 119(27), 105(45), 91(51).

Allylic alcohol **10** (0.5 g) was impregnated on pyridine treated alumina (5 g, Woelm neutral grade activity I, mixed with 2% w/v anhydrous pyridine) and loosely packed in a glass gas chromatography column (5 ft × $\frac{1}{4}$ in.). The column was placed in a gas chromatograph oven with one end connected to the injector and the other connected directly to the collector. The flow rate of carrier gas was set ~150 ml/min, then the oven was heated to 250 °C, and maintained at that temperature for 2 h. The pyrolysis product (collected in a U-shaped tube immersed in a dry ice – acetone bath) was obtained as a colorless oil (0.36 g, 80%); λ_{max} (EtOH) 248, 254, 266, 274 nm; ir (neat) 3020, 1640, 1585 (C=C) cm^{-1}; pmr ($CDCl_3$) δ 0.98 (s, 3, C-10 CH_3), 1.17 (d, 3, J = 8 Hz, C-6 CH_3), 5.58 (m, 3, H-2, H-3, H-4); ms m/e calcd. for $C_{12}H_{18}$: 162.14085, found: 162.14071 (63), 147(83), 119(34), 106(35), 105(75), 93(22), 91(100), 79(24), 77(25), 55(24), 41(46).

Diene **2** was characterized further as its Diels–Alder adduct with 4-phenyl-1,2,4-triazoline-3,5-dione (27); mp 128–130 °C (from ether). *Anal.* calcd. for $C_{20}H_{23}N_3O_2$: C 71.19, H 6.87, N 12.45; found: C 71.23, 71.17, H 6.78 6.76, N 12.67 12.72.

Photooxygenation of Diene **2**

Photooxygenation of diene **2** (0.35 g) in methanol–benzene (4:1) containing eosin Y (5 mg) overnight gave a crude reaction mixture which contained at least six components (tlc silica gel, pentane–ether, 1:1). Separation of the mixture by preparative tlc (pentane–ether, 1:1) led to the isolation of *endo*-peroxide **3** (0.05 g, 13%) as an oil.

Photooxygenation of diene **2** (0.47 g) in methanol–ether (1:1) containing eosin Y (~10 mg) at −78 °C for 8 h gave a crude reaction mixture which contained at least six components (tlc). Elution chromatography of a portion of the product (pentane–ether, 4:1) led to the isolation of traces of *endo*-peroxide **3**, (0.009 g, 4%) γ-hydroxyenone **11** (0.03 g, 13%) and diepoxide **12** (0.03 g, 13%).

Photooxygenation of diene **2** (0.55 g) in ether–methanol (1:1) containing eosin Y (0.005 g) and rose bengal (0.005 g) at −78 °C was complete in 2 h. The concentrated photolysis mixture was divided into two equal portions. One portion was purified by elution chromatography (pentane–ether, 9:1) to yield *endo*-peroxide **3** (0.06 g, 20%) as an oil. The remaining portion was dissolved in ether–methanol (1:1, 20 ml) and hydrogenated over platinum oxide at 40 psi hydrogen for 1 h. The solution was filtered and concentrated. Elution chromatography gave cybullol, **1** (0.06 g, 20%).

Photooxygenation of diene **2** (obtained by pyrolysis of allylic alcohol **10** (0.50 g)) in methylene chloride at −78 °C containing rose bengal (0.01 g) was complete in 2 h. The crude extract showed the presence of mainly 2 components (tlc). Elution chromatography (pentane–ether 9:1) yielded *endo*-peroxide **3** (0.26 g, 46% overall from **10**) as an oil.

6α,10β-Dimethyl-2α,5α-epidioxy-3-octalin, **3**

Endo-peroxide **3** was isolated as an oil (R_f 0.8, pentane–ether 1:1); ir (neat) 3140, 1455, 1440, 1370, 1010, 970, 960, 920, 885, 870, 765, 690, 670 cm^{-1}; pmr ($CDCl_3$) δ 0.94 (s, 3, C-10 CH_3), 1.00 (d, 3, J = 7 Hz, C-6 CH_3), 1.32 (d of d, 1, J = 3, 13 Hz, H-1α), 1.88 (d of d, 1, J = 4,

Can. J. Chem. Downloaded from www.nrcresearchpress.com by 210.87.254.105 on 09/05/12
For personal use only.

13 Hz, H-1β), 4.52 (octet, 1, J = 1.5, 3, 4, 6 Hz, H-2β), 6.44 (d of d, 1, J = 1.5, 8 Hz, H-4), 6.58 (d of d, 1, J = 6, 8 Hz, H-3); ms m/e calcd. for $C_{12}H_{18}O_2$: 194.1307, found: 194.1313 (2), 162(100), 147(36), 119(20), 106(38), 105(48), 92(20), 91(68), 79(20).

6α,10β-Dimethyl-2α,3α,4α,5α-diepoxydecalin, ***12***

Diepoxide **12** was isolated as an oil. (R_f 0.5, pentane–ether 1:1); ir (neat) 1460, 1375, 960, 950, 930, 900, 870, 815, 740, 720 cm^{-1}; nmr ($CDCl_3$) δ 0.72 (d, 3, J = 7 Hz, C-6 CH_3), 1.06 (s, 3, C-10 CH_3), 2.92 (q, 1, J = 5 Hz, H-2β), 3.20 (d of t, 1, J = 3, 5 Hz, H-3β), 3.31 (d, 1, J = 3 Hz, H-4β); ms m/e calcd. for $C_{12}H_{18}O_2$: 194.1306, found: 194.1302 (5), 161(23), 126(92), 123(22), 109(52), 107(36), 105(46), 97(28), 96(32), 95(100), 93(60), 91(53). 84(45), 81(80), 80(25), 79(46), 77(33), 73(26).

6α,10β-Dimethyl-5α-hydroxy-3-octal-2-one, ***11***

γ-Hydroxyoctalone **11** was crystalline, mp 99–102 °C (R_f 0.48 pentane–ether 4:1); ir ($CHCl_3$) 3600, 3500 (OH), 1680 (C=O), 1620 (sh, w, C=C) cm^{-1}; nmr ($CDCl_3$) δ 0.99 (d, 3, J = 6 Hz, C-6 CH_3), 1.06 (s, 3, C-10 CH_3), 2.00 (d of d, 1, J = 1, 16 Hz, H-1α), 2.67 (d of d, 1, J = 1, 16 Hz, H-1β), 5.95 (d of d, 1, J = 2, 10 Hz, H-3), 6.96 (d, 1, J = 10 Hz, H-4); ms m/e calcd. for $C_{12}H_{18}O_2$: 194.1307, found: 194.1305 (33), 111(72), 110(31), 93(47), 91(29), 82(26), 81(24), 79(23), 77(23), 69(24), 67(26), 55(44), 53(23), 51(100).

Oxygenation using Triphenylphosphite–Ozone (15)

Methylene chloride (35 ml) was added to a 100 ml 3-necked flask equipped with a dropping funnel, a gas inlet tube, and a drying tube. This was cooled to −78 °C and ozone (generated from oxygen using a Welsbach Laboratory ozonator) was bubbled through the solution. Triphenylphosphite (2.8 g) in methylene chloride (20 ml) was added dropwise at such a rate that the solution remained blue at all times (~1.5 h). When addition was complete, the blue solution was flushed with dry oxygen-free nitrogen to remove the remaining ozone.

Diene **8** (prepared by pyrolysis of allylic alcohol **10** (0.5 g)) in cold methylene chloride (10 ml) was added to the cold (−78 °C) triphenylphosphite–ozone solution. The reaction mixture was allowed to warm to room temperature, then concentrated. Elution chromatography led to the isolation of *endo*-peroxide **3** (0.08 g, 15% from **10**).

6α,10β-Dimethyl-3-octal-2α,5α-diol. ***13***

endo-Peroxide **3** (0.032 g) in ether (5 ml) was added to freshly prepared aluminum amalgam (0.2 g) (19). After 0.5 h, the reaction mixture was filtered, the aluminum turnings washed with ether, and the combined ether extracts concentrated. Allylic diol **13** (0.026 g, 77%) was obtained as colorless crystals, mp 109–111 °C; ir ($CHCl_3$) 3600, 3440 (OH) cm^{-1}; pmr ($CDCl_3$) δ 0.91 (d, 3, J = 6 Hz, C-6 CH_3), 0.98 (s, 3, C-10 CH_3), 4.31 (t of t, 1, J = 1.5, 2.5, 7 Hz, H-2β), 5.78 (t of d, 1, J = 1.5, 2.5, 10 Hz, H-3), 6.00 (d of d, 1, J = 1.5, 10 Hz, H-4); pmr (pyridine-d_5) δ 1.06 (d, 3, J = 6 Hz, C-6 CH_3), 1.10 (s, 3, C-10 CH_3); ms m/e calcd. for $C_{12}H_{20}O_2$: 196.1463, found: 196.1460 (7), 178(100), 163(63), 136(35), 135(37), 126(45), 122(22), 121(37), 109(39), 108(26), 107(72), 105(21), 97(28), 95(44), 94(75), 91(36), 84(20), 82(33), 81(85), 80(68), 79(60), 77(35), 71(33), 69(40), 67(50), 57(26), 55(85), 53(33).

6α,10β-Dimethyldecalin-2α,5α-diol, (($\pm$)-Cybullol), ***1***

Allylic diol **13** (0.020 g) in ether (20 ml) was hydrogenated over platinum oxide at 40 psi hydrogen for 1 h. The solution was filtered and concentrated to give ($\pm$)-cybullol, **1** (0.021 g, quantitative) which was recrystallized from ether, mp 145–147 °C (mp for (−)-cybullol (2) 125–126 °C). The ir, pmr, and mass spectra were identical with authentic cybullol (2). *Anal.* calcd. for $C_{12}H_{22}O_2$: C 72.68, H 11.18; found: C 72.61, H 11.15.

4,10β-Dimethyl-4,5-epoxyoctal-3-one, ***17*** *(26)*

Hydrogen peroxide (30%, 24.0 ml) and sodium hydroxide (4 *N*, 11.6 ml) were added dropwise, and simultaneously to a cooled (0 °C), rapidly stirred solution of dimethyloctalone **16** (25) (13.3 g) in methanol (300 ml). The reaction mixture was allowed to stand at 0 °C for 1 day, then at room temperature for 3 days. The mixture was diluted with water and extracted with ether. The ether extract was washed with water, dried ($MgSO_4$), and concentrated to give **17** (12.3 g, 85%) as an oil which was purified by distillation (bp 90–93 °C/0.1 torr): ir (neat): 1720 cm^{-1}; pmr ($CDCl_3$) δ 1.06 (3, s), 1.20 (3, s), 1.37 (3, s), 1.42 (3, s); ms m/e calcd. for $C_{12}H_{18}O_2$: 194.1307, found: 194.1306 (7), 176(18), 151(20), 109(100), 81(25), 67(37), 55(27), 43(57), 41(35). *Anal.* calcd. for $C_{12}H_{18}O_2$: C 74.19, H 9.34; found: C 73.87, H 9.15.

4α,10β-Dimethyl-5-hydroxydecal-3-one, ***18***

Liquid ammonia (70 ml) was distilled through a tube containing sodium hydroxide into a dry flask containing epoxy ketones **17** (1.14 g). Lithium (0.2 g) was added in small pieces to the stirred solution. After 6 h excess ammonium chloride was added and the ammonia allowed to evaporate. Water was added to the residue and the resulting mixture was extracted with ether. The ether extract was washed with water, dried ($MgSO_4$), and concentrated to a viscous oil (1.06 g) which partially solidified on standing. The crude solid was crystallized from Skellysolve B to give ketol **18** (0.33 g, 53% from **17***a*), mp 109–110 °C; ir ($CHCl_3$) 3600, 1720 cm^{-1}; pmr ($CDCl_3$) δ 0.99 (d, 3, J = 6 Hz, C-4 CH_3), 1.28 (s, 3, C-10 CH_3); pmr (pyridine-d_5) 1.26 (d, 3, J = 6 Hz, C-4 CH_3), 1.24 (s, 3, C-10 CH_3); ms m/e 196(19), 112(100), 97(22), 55(27), 41(20). *Anal.* calcd. for $C_{12}H_{20}O_2$: C 73.43, H 10.27; found: C 73.72, H 10.44.

($\pm$)-Geosmin, ***15***

Ketol **18** (0.215 g) in glacial acetic acid (15 ml) was treated with ethanedithiol (1 ml) and boron trifluoride etherate (0.1 ml). The resulting solution was allowed to stand at room temperature for 15 min then quickly worked-up by dilution with brine and extraction with ether. The ether extract was washed with 4 *N* sodium hydroxide, then water, then dried ($MgSO_4$) and concentrated to give thio ketal **19** (0.287 g, 96%). An analytical sample was obtained by recrystallization from Skellysolve B, mp 95–96 °C; ir ($CHCl_3$) 3600 cm^{-1}; pmr ($CDCl_3$) δ 1.07 (s, 3, C-10 CH_3), 1.12 (d, 3, J = 6 Hz, C-4 CH$_3$), 3.17 (m, 4); ms m/e calcd. for $C_{14}H_{24}OS_2$: 272.1268, found: 272.1268 (59), 254(56), 225(49), 133(39), 132(58), 112(100), 55(45). *Anal.* calcd. for $C_{14}H_{24}OS_2$: C 61.71, H 8.88; found: C 61.71, H 8.78.

Thio ketal **19** (0.92 g), Raney nickel (W-2, 2 g), and absolute ethanol (10 ml) were stirred at room temperature for 1.5 h then heated under reflux for 2 h. Additional

Raney nickel (1 g) was added and heating continued an additional 2 h. The mixture was cooled, filtered, diluted with water, and extracted with pentane. The pentane extract was washed with brine, dried ($MgSO_4$), and solvents removed by distillation to give (±)-geosmin **15** (0.62 g, quantitative) as a colorless oil. On standing at 0 °C liquid geosmin crystallized, mp 78–82 °C. The spectroscopic data obtained for synthetic geosmin is identical in all respects with an authentic sample (2); ir (CCl_4) 3630 (OH) cm^{-1}; pmr ($CDCl_3$) δ 0.77 (d, 3, J = 6 Hz, C-4 CH_3), 1.03 (s, 3, C-10 CH_3); pmr (pyridine-d_5) 0.93 (d, 3, J = 6 Hz, C-4 CH_3), 1.04 (s, 3, C-10 CH_3); ms m/e calcd. for $C_{12}H_{22}O$: 182.1670, found: 182.1677 (10), 149(18), 112(100).

Acknowledgements

We wish to thank the National Research Council of Canada for financial support and Prof. J. Hooz and Dr. A. Benderley for helpful discussions and for a sample of compound **8**.

1. W. A. Ayer and H. Taube. Can. J. Chem. **51**, 3842 (1973); W. A. Ayer and L. L. Carstens. Can. J. Chem. **51**, 3157 (1973).
2. W. A. Ayer and M. G. Paice. Can. J. Chem. **54**, 910 (1976).
3. W. A. Ayer and D. R. Taylor. Can. J. Chem. **54**, 1703 (1976).
4. J. A. Marshall and A. R. Hochsteller. J. Org. Chem. **33**, 2593 (1968).
5. (*a*) K. Gollnick and G. O. Schenck. *In* 1,4[One, Four]cycloaddition reactions. *Edited by* J. Hamer. Academic Press, New York. 1967. pp. 255. (*b*) R. W. Denney and A. Nickon. Org. React. **20**, 133 (1973); (*c*) C. K. Gollnick. Adv. Photochem. **6**, 1 (1968).
6. (*a*) T. G. Halsall, W. J. Rodewald, and D. Willis. Proc. Chem. Soc. 231 (1958); (*b*) H. C. Barrett and G. Buchi. J. Am. Chem. Soc. **89**, 5665 (1967); (*c*) J. W. Huffman. J. Org. Chem. **37**, 2736 (1972); (*d*) I. Sasson and J. Labovitz. J. Org. Chem. **40**, 3670 (1975).
7. W. A. Ayer, L. M. Browne, S. Fung, and J. B. Stothers. Can. J. Chem. This issue.
8. C. Heathcock, J. E. Ellis, J. E. McMurry, and A. Coppolino. Tetrahedron Lett. 4995 (1971).
9. W. G. Dauben, M. E. Lorber, N. D. Vietmeyer, R. H. Shapiro, J. H. Duncan, and K. Tomer. J. Am. Chem. Soc. **90**, 4763 (1968).
10. P. V. Demarco, E. Farkas, D. Doddrell, B. L. Mylari, and E. Wenkert. J. Am. Chem. Soc. **90**, 5480 (1968).
11. (*a*) S. H. Grover and J. B. Stothers. Can. J. Chem. **52**, 870 (1974); (*b*) E. L. Eliel, W. F. Bailey, L. D. Kopp, R. L. Willer, D. M. Grant, R. Bertrand, K. A. Christensen, D. K. Dalling, M. W. Duch, E. Wenkert, F. M. Schell, and D. W. Cochran. J. Am. Chem. Soc. **97**, 322 (1975).
12. J. A. Marshall and D. J. Schaeffer. J. Org. Chem. **30**, 3642 (1965).
13. (*a*) A. Benderley. Ph.D. Thesis, University of Alberta, Edmonton, Alberta. 1975. p. 39; (*b*) D. Caine and F. N. Tuller. J. Org. Chem. **34**, 222 (1969).
14. E. von Rudloff. Can. J. Chem. **39**, 1860 (1961).
15. K. K. Maheshwari, P. DeMayo, and D. Wiegand. Can. J. Chem. **48**, 3265 (1970).
16. C. S. Foote and S. Wexler. J. Am. Chem. Soc. **86**, 3879 (1964).
17. R. W. Murray and M. L. Kaplan. J. Am. Chem. Soc. **91**, 5358 (1969).
18. G. Kaneko, A. Sugimoto, and S. Tanaka. Synthesis, 876 (1974).
19. H. Wislicenus and L. Kaufmann. Ber. **28**, 1323 (1895).
20. N. N. Gerber and H. A. Lechevalier. Appl. Microbiol. **13**, 935 (1965).
21. (*a*) K. E. Murray and P. A. Bannister. Chem. Ind. 973 (1975); (*b*) T. E. Acru, C. Y. Lee, R. M. Butts, and J. Barnard. J. Agric. Food Chem. **24**, 430 (1976).
22. L. L. Medsker, D. Jenkins, and J. F. Thomas. Env. Sci. Tech. **2**, 461 (1968).
23. M. Yurkowski and J. A. L. Tabachek. J. Fish. Res. Board Can. **31**, 1851 (1974).
24. N. N. Gerber. Tetrahedron Lett. 2971 (1968).
25. P. A. Zoretic, B. Branchaud, and T. Maestrone. Tetrahedron Lett. 527 (1975).
26. M. E. Kuehne and J. A. Nelson. J. Org. Chem. **35**, 161 (1970).
27. D. H. Williams. Tetrahedron Lett. 2305 (1965).
28. L. L. Medsker, D. Jenkins, and J. F. Thomas. Env. Sci. Tech. **2**, 461 (1968).
29. L. F. Fieser and M. Fieser. *In* Reagents for organic synthesis. No. 1. John Wiley and Sons, London. 1967. p. 849.

Can. J. Chem. Downloaded from www.nrcresearchpress.com by 210.87.254.105 on 09/05/12
For personal use only.

A characteristic vector analysis of solvent effects for thermodynamic data

W. Ronald Fawcett and T. Marek Krygowski[1]

Guelph Waterloo Centre for Graduate Work in Chemistry, (Guelph Campus), Department of Chemistry, University of Guelph, Guelph, Ontario, Canada N1G 2W1

Received March 18, 1976

W. Ronald Fawcett and T. Marek Krygowski. Can. J. Chem. **54**, 3283 (1976).

Characteristic vector analysis has been performed on six sets of thermodynamic data relating to the solvation of electrolytes, polar molecules, and single ions in pure solvents. The analysis shows that variation in a given thermodynamic property with nature of the solvent can be accounted for with two characteristic vectors and that these vectors are linearly related to empirical measures of solvent basicity and acidity. The results confirm that an empirical relation proposed earlier by the present authors can be used to describe solvation effects with the limitation that the basicity of strongly structured protic solvents is difficult to describe quantitatively.

W. Ronald Fawcett et T. Marek Krygowski. Can. J. Chem. **54**, 3283 (1976).

L'analyse du vecteur caractéristique a été effectuée sur six séries de données thermodynamiques en relation avec la solvatation des électrolytes, des molécules polaires et des ions isolés dans des solvants purs. L'analyse montre que les variations dans une propriété thermodynamique donnée avec la nature du solvant pouvent être expliquées à l'aide de deux vecteurs caractéristiques et que ces vecteurs sont linéairement reliés à des mesures empiriques de basicité et d'acidité du solvant. Les résultats confirment que la relation empirique déjà proposée par les présents auteurs peut être utilisée pour décrire les effets de solvatation avec la restriction que la basicité des solvants protiques fortement structurés est difficile à décrire quantitativement.

[Traduit par le journal]

Can. J. Chem. Downloaded from www.nrcresearchpress.com by 210.87.254.6 on 09/05/12
For personal use only.

Introduction

The description of solvent effects on physico-chemical properties may be classified with respect to two extreme viewpoints (1). On one hand the solvent is regarded as a continuum and solute–solvent interactions are considered to be non-specific. A well-known model in this category is that due to Born for calculating the free energy of ionic solvation (2). At the opposite extreme, solute–solvent interactions are considered to be discrete and are often discussed with respect to the donating and accepting properties of the solvent (1). Koppel and Palm (1) have argued that a complete description of solvent effects must consider both non-specific and specific effects; they proposed a general correlation equation which relates the variation of a given physico-chemical parameter Q with solvent to two specific and two non-specific properties of the solvent:

$$[1] \qquad Q = Q_0 + \alpha A + \beta B + \eta Y + \pi P$$

A and B are parameters measuring the Lewis acidity or acceptor properties and Lewis basicity or donator properties of the solvent, respectively. The non-specific parameters Y and P measure solvent polarity and polarisability; according to dielectric theory (2), they may be related to the bulk dielectric constant ε and refractive index of the solvent n by the equations

$$[2] \qquad Y = \frac{\varepsilon - 1}{\varepsilon + 2}$$

and

$$[3] \qquad P = \frac{n^2 - 1}{n^2 + 2}$$

Several experimentally determined quantities have been proposed as measures of solvent acceptor and donor properties (3, 4). The most popular parameters for solvent acidity are the Dimroth–Reichardt parameter E_T (5) and the parameter Z introduced by Kosower (6). Both of these parameters are based on the energy associated with exciting an electron in model compounds with a strongly dipolar ground state to an excited state for which the dipole moment is negligibly small (4). More recently, Mayer *et al.* (7) have introduced a new acidity parameter called the acceptor number (AN)

[1]Present address: Institute for Fundamental Problems in Chemistry, University of Warsaw, Warsaw, Poland.

Can. J. Chem. Downloaded from www.nrcresearchpress.com by 210.87.254.6 on 09/05/12
For personal use only.

which is derived from the ^{31}P nmr shifts produced in triethylphosphine oxide by electrophilic solvent interactions which lower the electron densities at the phosphorus atom due to the inductive effect. Solvent basicity is often measured using the donor number (DN) of Gutmann and Schmid (8) or the parameter B introduced by Gordy and Stanford (36), and recently by Koppel and co-workers (1, 9) and by Kagiya *et al.* (37). In this case there seems to be some difficulty in assigning basicity parameters to strongly associated solvents (4).

Koppel and Palm (1) have used [1] to analyze a collection of kinetic and spectroscopic data obtained in a wide variety of pure solvents. However, they were able to obtain statistically reliable values of the four regression coefficients α, β, η, and π in only a few cases. An alternative empirical approach was proposed by the present authors (3, 4) in which it is assumed that only specific solute–solvent interactions need be considered. The parameters chosen to describe solvent acidity and basicity were E_T and DN, respectively and the solvent effect on property Q was written as follows:

$$[4] \qquad Q = Q_0 + \alpha E_T + \beta \mathrm{DN}$$

This equation was tested with a large collection of data in which solute–solvent interactions were of both ion–dipole and dipole–dipole nature, the correlation being successful in 75% of the cases considered (3, 4).

Since the above approaches to describing solvent effects are empirical in nature, it was of interest to determine independently the factors which result in variation in a given physicochemical quantity with solvent. In this regard, the method of characteristic vector analysis is ideal when a large collection of data for a given quantity is available. Since this statistical technique is not familiar to many chemists, its principle features are outlined in the following section.

The Method of Characteristic Vector Analysis

The method of characteristic vector analysis or factor analysis has been applied to the analysis of spectroscopic data (10–12), linear free energy relationships (13, 38), solvent effects on chemical shifts in nmr spectroscopy (14, 15), and to the prediction of non-electrolyte activity coefficients (16). In all cases the observed quantity was assumed to be linearly dependent on several independent variables. In the following discussion, its application to thermodynamic data relating to solvation will be outlined.

It is assumed that a thermodynamic parameter Q, for example, the heat of solution, is measured for m solutes in each of n pure solvents. These data are arranged in a matrix of m rows and n columns where $m \geq n$. The method of characteristic vector analysis determines the number p and form of a set of characteristic vectors $V_k (k = 1, 2, \ldots, p)$ which, in linear combination, account for the variation in Q with solvent. Having found a set of scalar multiples γ_{ik} characteristic of a given solute i one can then reproduce the original data matrix using linear relationships of the form

$$[5] \qquad Q_{ij} = \bar{Q}_{ij} + \sum_{k=1}^{p} \gamma_{ik} V_{jk}$$

where $\bar{Q}_j$ is the average value of the thermodynamic property in solvent j for m solutes, and V_{jk} the component of vector V_k corresponding to solvent j. In order to determine the magnitude of the characteristic vectors V_k

$$\left(V_k^2 = \sum_{j=1}^{n} V_{jk}^2 \right)$$

a mean corrected data matrix is calculated by subtracting the mean row $\bar{Q}_j$ from each row in Q. The resulting matrix $X (X_{ij} = Q_{ij} - \bar{Q}_j)$ is premultiplied by its transpose X^T to obtain $P = X^T X$, a square matrix of order n, which is directly related to the variance–covariance matrix. The characteristic vectors are obtained by diagonalizing matrix P. When the data contain no error, the number of characteristic vectors is equal to the number of non-zero diagonal elements. Otherwise, the number of significant characteristic vectors can be obtained by analysis of the experimental error in the original data (17). An important property of these vectors is that they are orthogonal, that is, they represent statistically independent types of variability. A second important point is that the derivation of the vectors ensures that the first vector (first diagonal element) accounts for the largest amount of variation in the data, the second vector, the second largest amount, and so forth. Finally, the scalar multiples γ_{ik} can be determined from each characteristic

Can. J. Chem. Downloaded from www.nrcresearchpress.com by 210.87.254.6 on 09/05/12
For personal use only.

TABLE 1. A summary of solvent parameters*

Solvent	Symbol	ε	n	DN	B	E_T	Z	AN
Acetic anhydride	AA	22.45_{20}	1.3878_{20}	10.5	100	43.9		
Acetone	A	20.7	1.3561	17.0	224	42.2	65.7	12.5
Acetonitrile	AN	37.5	1.3416	14.1	160	46.0	71.3	18.9
Benzene	B	2.30	1.4979	0.1	48	34.5	54.0	8.2
Benzonitrile	BN	25.2	1.5272	11.9	155	42.0	65.0	15.5
Diethyl ether	DEE	4.265	1.3527	19.2	280	34.6		3.9
Dimethylacetamide	DMA	37.8	1.4351	27.8	343	43.7	66.9	13.6
Dimethylformamide	DMF	36.7	1.4269	26.6	291	43.8	68.5	16.0
Dimethylsulphoxide	DMSO	46.6	1.4742_{30}	29.8	362	45.0	71.1	19.3
Ethanol	E	24.3	1.3594		235	51.9	79.6	37.1
				(31.5)				
Ethylacetate	EA	6.0	1.3698	17.1	174	38.1		
Formamide	F	109.6	1.4468		270	56.6	83.3	39.8
				(24.7)				
Hexamethylphosphoramide	HMPA	29.6	1.4570	38.8	471	40.9	62.8	10.6
Methanol	M	32.6	1.3266	19.0	218	55.5	83.6	41.3
				(25.7)				
N-methylacetamide	NMA	178.9_{30}	1.4301_{30}			52.1	22.9	
N-methylformamide	NMF	182.4	1.4300		287	54.1		32.1
N-methyl-2-pyrrolidone	NMP	32.0	1.4680	27.3		42.2		13.3
Nitrobenzene	NB	34.8	1.5506	4.4	67	42.0		14.8
Nitromethane	NM	38.6	1.3795	2.7	65	46.3	71.2	20.5
Propionitrile	PN	27.2_{20}	1.3635_{20}	16.1	162	43.7		
Propylene carbonate	PC	65.1	1.4195	15.1		46.6		18.3
Pyridine	PY	12.3	1.5067	33.1	472	40.2	64.0	14.2
Sulfolane	S	43.3_{30}	1.4817_{30}	14.8	157	44.0	77.5	
Tetrahydrofuran	THF	7.39	1.4036	20.0	287	37.4	58.8	8.0
Water	W	78.3	1.3325	18.0	156	63.1	94.6	54.8
				(33.0)				

*The dielectric constant ε and refractive index n were taken from the compilations of Mann (18) and Fialkov *et al.* (19). The parameters DN, B, E_T, and AN were taken from compilations by the original authors (5–9). The values of DN in parentheses for protic solvents were calculated from $^{23}Na^+$ nmr chemical shifts measured by Popov and co-workers (20).

vector using the relation

$$[6] \qquad \gamma_{ik} = \frac{1}{V_k^2} \sum_{j=1}^{n} V_{jk} X_{ij}$$

Simonds (10) has outlined a procedure for obtaining the characteristic vectors and scalar multiples which avoids matrix diagonalization. This procedure which is easily adapted to the digital computer cannot be used when the number of significant characteristic vectors is large but is ideal when they number one, two, or three. Otherwise, one can use a standard matrix diagonalization package, the characteristic vectors and scalar multiples being obtained from the eigenvalues and eigenvectors respectively. Simonds' procedure was used to obtain the results discussed below.[2] It should be emphasized that the accuracy of the derived vectors depends on the relative number of rows and columns in the data matrix. The minimum number of rows (solutes) is equal to the number of columns (solvents); as the number of rows (solutes) increases, the accuracy of the vectors describing the characteristics of the solvents also increases. Unfortunately, it is often the case that only one datum is missing in a given potential data matrix. In order to use the data matrix, one must remove either the row or column containing the missing point, thereby reducing either the accuracy of the derived vectors or the number of solvents considered.

Finally, since the purpose of the present study was to determine the number of characteristic vectors in the data matrices considered and to test whether they are related to common empirical parameters used to describe solvation, no attempt was made to normalize the resultant vectors to a common scale (14). Thus, the magnitude of a given vector common to two data matrices depends on the nature of the solutes in each matrix; in the absence of error, the components of the vector obtained from one matrix are linearly related to those obtained from the second so that a common scale for the vector can be defined by a change in coordinates. A procedure for carrying out the normalization has been described by Weiner *et al.* (14).

[2]A copy of the computer programme used is available from the authors on request.

Results and Discussion

The solvent parameters considered in the following analysis are summarized in Table 1 for common solvents of higher dielectric constant. As expected, good linear correlations are obtained between the two basicity parameters DN and B, and among the three acidity parameters E_T, Z, and AN (4). On the other hand, the basicity, acidity, polarity, and polarizability parameters are all linearly independent of one another. Thus, the four parameters chosen by Koppel and Palm (1) to describe solvent effects have one of the required properties of characteristic vectors. The question remains whether the experimental quantities chosen empirically to describe solvent acidity and basicity are the best possible. The relative importance of the four parameters must also be determined.

The method of characteristic vector analysis was successfully applied to the analysis of six data matrices of physico-chemical quantities determined for a set of solutes in a given number of pure solvents. In all cases, more than 90% of the observed variation in property Q could be accounted for using two characteristic vectors. In almost all cases, addition of a third vector resulted in explanation of the remaining variation; it was assumed that this vector could be assigned to experimental error in the data. The first two vectors were tested to determine whether they could be correlated with the solvent parameters discussed above. In no case could either of these vectors be correlated with the parameters P and Y. In all cases, one of the vectors could be successfully correlated with either of the parameters E_T or DN (correlation coefficient $r \geq 0.85$), the correlation with the second vector sometimes being less successful. The less successful correlation was usually with the parameter DN. It should be noted that three of the data matrices in Table 2 involve properties of single ions which have been calculated from thermodynamic data after having made an extra-thermodynamic assumption (22, 24).

The correlations with vectors obtained from the analysis of data for the mutual heats of solution of solvent A (as solute) in solvent B (as solvent) (21) are illustrated in Figs. 1 and 2. The data were analyzed in this case to obtain vectors characteristic of the solute, that is, the

Can. J. Chem. Downloaded from www.nrcresearchpress.com by 210.87.254.6 on 09/05/12
For personal use only.

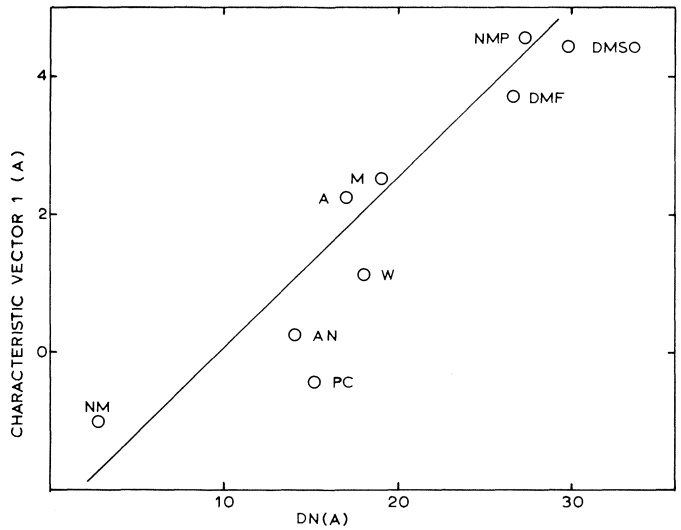

FIG. 1. The components of the first characteristic vector for nine solvents as solutes determined from the mutual heats of solution of a given solvent A in nine other pure solvents (21) plotted against the donor number of the solute, DN according to Gutmann and Schmid (8).

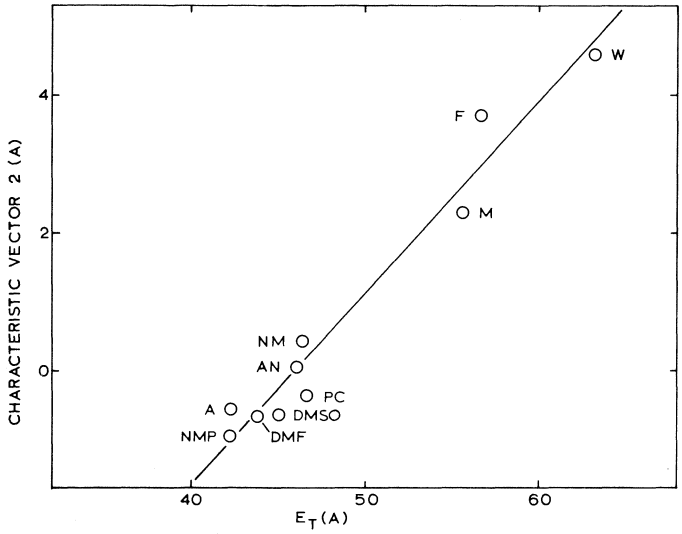

FIG. 2. The components of the second characteristic vector for 10 solvents as solutes determined from the mutual heats of solution of a given solvent A in nine other pure solvents (21) plotted against the acidity of solute A as estimated by the Dimroth–Reichardt parameter, E_T (5).

component whose mole fraction is small. For this reason, the values of DN chosen for protic solvents were those characteristic of the isolated solvent molecule as measured by Gutmann and Schmid in dilute 1,2-dichlorethane solutions (8). It is apparent from the figures that excellent correlations hold between the first characteristic vector and the basicity parameter DN, and between the second vector and the acidity parameter E_T. By interchanging rows and columns in the original data matrix the analysis was performed to obtain the vectors characteristic of the solvent. In this case the first vector correlates weekly with E_T whereas a good correlation holds between the second vector and DN. In the latter correlation, the

Can. J. Chem. Downloaded from www.nrcresearchpress.com by 210.87.254.6 on 09/05/12
For personal use only.

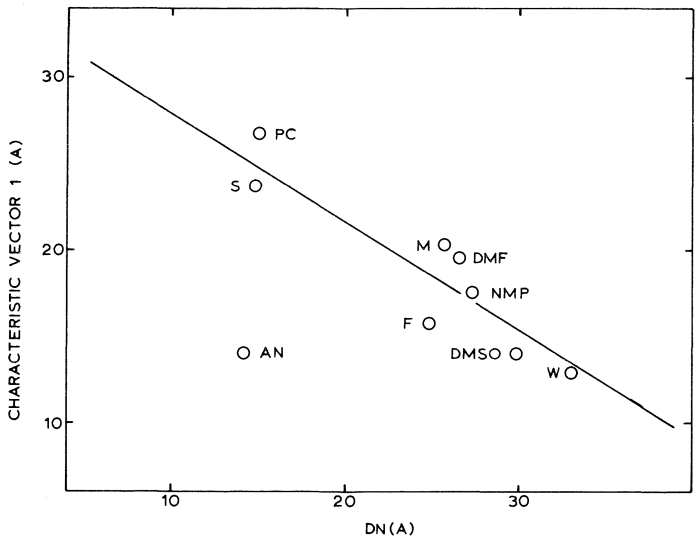

FIG. 3. The components of the first characteristic vector for nine solvents determined from data for the free energy of solution of nine 1–1 electrolytes in a given pure solvent A (22) plotted against the donor number of the solvent, DN according to Gutmann and Schmid (8).

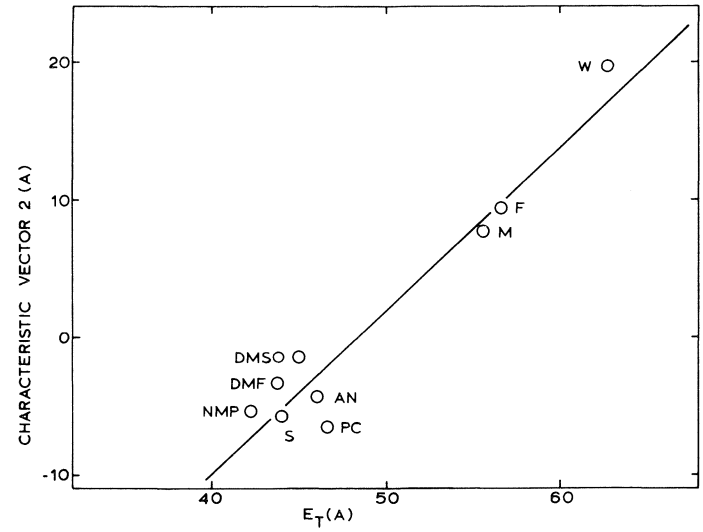

FIG. 4. The components of the second characteristic vector for nine solvents determined from data for the free energy of solution of nine 1–1 electrolytes in a given pure solvent A (22) plotted against the acidity of solvent A as estimated by the Dimroth–Reichardt parameter, E_T (5).

values of DN for protic solvents were those for the bulk solvent as determined by Popov *et al.* The poor correlation with E_T is due to large scatter of the points for acetonitrile, nitromethane, and propylene carbonate from the regression line. These solvents have very low mutual heats of solution with aprotic solutes so that one might expect large errors in the corresponding components of the characteristic vectors.

The vectors obtained from analysis of data for the free energy of solution of nine 1–1 electrolytes (AgCl, AgBr, AgI, AgN_3, AgSCN, $AgPh_4B$, NaCl, Ph_4AsPh_4B, and Ph_4AsI where Ph = phenyl) in nine different solvents (22) are shown in Figs. 3 and 4. In this case the first

Can. J. Chem. Downloaded from www.nrcresearchpress.com by 210.87.254.6 on 09/05/12
For personal use only.

Can. J. Chem. Downloaded from www.nrcresearchpress.com by 210.87.254.6 on 09/05/12
For personal use only.

TABLE 2. A summary of results of the characteristic vector analysis

Data matrix	Number of		Vector 1			Vector 2		
	Solutes	Solvents	Percent of trace	Correlates with	Correlation coefficient	Percent of trace	Correlates with	Correlation coefficient
Heats of solution of solvent A (as solute) in solvent B (as solvent) (21)								
A. Vectors for solute	10	10	56.6	DN	0.932	35.4	E_T	0.978
B. Vectors for solvent	10	10	68.6	E_T	0.772	27.8	DN	0.931
Free energies of solution for 1–1 electrolytes (22)	9	9	78.9	DN	0.890	17.5	E_T	0.957
Heats of solution for 1–1 and 2–1 electrolytes (22, 23)	9	6	96.6	DN	0.872	2.8	E_T	0.921
Heats of solution for monovalent ions (24)*	9	6	78.2	E_T	0.975	21.8	DN	0.996
Heats of transfer for monovalent ions (22)	7	7	90.4	E_T	0.909	8.7	DN	0.773
Free energies of transfer for monovalent ions (22)	10	6	92.4	E_T	0.981	5.5	DN	0.764

*Division of experimental enthalpies of solvation into components for the individual ions was based on the Born–Bjerrum equation (24).

Can. J. Chem. Downloaded from www.nrcresearchpress.com by 210.87.254.6 on 09/05/12
For personal use only.

characteristic vector is predominant, accounting for 78.9% of the trace. If one excludes the component for acetonitrile an acceptable correlation is obtained with the basicity parameter DN, the parameters chosen for protic solvents being those for the bulk solvent. The departure of the point for acetonitrile can be attributed to the fact that six of the nine salts for which data are available are silver salts. Specific interaction between Ag^+ and acetonitrile is possible via the metal ion's *d*-electrons and the π-orbitals of the CN-group in the solvent; this interaction undoubtedly increases the effective donor number of acetonitrile for interaction with transition metal ions. An excellent correlation holds between the second vector and the acidity parameter E_T (Fig. 4). Similar results were obtained with data for the heats of solution of 1–1 and 2–1 electrolytes in six different solvents (22, 23). The first vector which correlates well with solvent basicity accounts for 96.6% of the trace. However, in order to achieve a good correlation, the parameters for protic solvents were those for the isolated molecules rather than those characteristic of bulk solvent. This result may be a reflection of the fact that some of the salts contain divalent cations which interact more strongly with solvent molecules in their immediate vicinity. In the Frank and Wen model of water structure surrounding ions (25), one distinguishes three types of water: 'A' water which is strongly bound to the ion by ion–dipole interactions, 'B' water in which the normal structure is broken and neither ion–dipole or dipole–dipole interactions predominate, and 'C' water in which the normal structure is maintained through dipole–dipole interactions and hydrogen bonding. Ions with high charge to radius ratios such as Li^+, the alkaline earth cations, and di- and trivalent transition metals ions are surrounded immediately with 'A' water with a layer of 'B' water beyond the tightly bound dipoles. Cs^+ Rb^+, K^+, Cl^-, Br^-, and I^- do not have any ordering effect and thus are surrounded by a B region only. Since the donicity of water and other protic solvents depends on the degree of structure of the solvent, the corresponding components of the characteristic vector will depend on the choice of solutes in the data matrix. A similar problem exists in defining the donicity of structured aprotic solvents such as dimethyl sulfoxide. Thus, Erlich *et al.* (26) have observed that dimethyl sulfoxide is a better base in pyridine solutions than as a pure solvent. However, the magnitude of the structure effect is probably less than that for protic solvents.

Due to the lack of complete data matrices the above analysis could not be carried out for other thermodynamic data relating to solvation in pure solvents. However, it was applied to several thermodynamic parameters derived for single ions on the basis of various extra thermodynamic assumptions. Somsen and Weeda (24) have considered the division of ionic enthalpics of solvation into components due to the cation and anion using both the continuum model based on the Born–Bjerrum equation and the discontinuous model for solvation developed by Buckingham (27). The data were obtained chiefly in protic solvents, namely, water, methanol, ammonia, and four amide solvents, the only aprotic solvent being dimethyl formamide; the ions considered were all monoatomic (Li^+, Na^+, K^+, Rb^+, Cs^+, F^-, Cl^-, Br^-, and I^-). The present analysis was successful for both sets of single ionic enthalpies, the first vector correlating with E_T and the second with DN; in the case of data obtained on the basis of the continuum model the first vector accounted for 78.2% of the trace whereas in the second, it accounted for 95.8%. The predominant influence of solvent acidity can be attributed to the fact that the solvents considered were chiefly strongly structured protic solvents. As has been noted previously (3), changes in solvent structure which accompany ion solvation follow the corresponding change in solvent acidity. Single ion free energies, enthalpies, and entropies of transfer from water as a reference solvent to another solvent have been tabulated by Cox and co-workers (22). In this case the extra-thermodynamic assumption is that the free energy, enthalpy, and entropy of transfer of the tetraphenylarsonium cation are each equal to the corresponding quantity for the tetraphenylborate anion. The variation in these quantities with solvent was accounted for using two characteristic vectors (Table 2). The first vector which is linearly related to E_T accounts for the majority of the variation. As pointed out above the relative contributions of the two vectors depend on the choice of solutes. In the

Can. J. Chem. Downloaded from www.nrcresearchpress.com by 210.87.254.6 on 09/05/12
For personal use only.

case of the free energies of transfer, the ions considered were Na^+, K^+, Rb^+, Cs^+, Ag^+, Ph_4As^+, Cl^-, Br^-, I^-, and Ph_4B^-. It can be argued that the predominance of the acidity vector in explaining the observed variation in the free energy of transfer is a reflection of the importance of structural effects, the majority of the ions being large structure breakers. Although insufficient data are available at present, careful comparison of the results of these analyses could be useful in assessing the validity of the extra-thermodynamic assumptions made in deriving the above quantities.

Solvent effects observed for the chemical shifts of specific nuclei in nmr spectroscopy have received considerable attention in the literature (28, 29). Buckingham *et al.* (30) have argued that the solvent effect on proton chemical shifts can be expressed as a linear combination of four terms, two magnetic terms accounting for bulk susceptibility of the solvent and anisotropy in solvent susceptibility, and two electrostatic terms due to van der Waals forces and the solvent reaction field. Detailed models have been developed for the electrostatic terms; accordingly the reaction field term depends on the dielectric constant and refractive index of the solvent in a complex manner (29, 30). By choosing a suitable reference compound such that only the electrostatic terms affect the observed chemical shifts, Weiner and Malinowski (31) have shown that the proposed electrostatic terms do not successfully account for the proton shifts of polar solutes in a variety of solvents. They have argued that one cannot use the bulk dielectric constant in estimating the reaction field term and have proposed a fifth term to account for permanent dipole interactions. Solvent effects on the chemical shifts of ^{13}C and ^{19}F nuclei have also been studied (32–34). In the case of ^{13}C chemical shifts for the methyl groups in methyl iodide and acetonitrile (32), the usual model for the reaction field (30) could not account for the observed solvent effect. Emsley and Phillips (33) concluded that the reaction field effect observed for the ^{19}F chemical shifts of a variety of fluorinated aromatic compounds was directly related to solvent polarity [2]; however, the correlations between these quantities were often weak, this result being attributed to specific interactions of the reference compound, hexafluorobenzene with aromatic solvents. Taft *et al.* (34) attributed the solvent effect observed for the ^{19}F chemical shifts of *m*-substituted fluorobenzenes relative to fluorobenzene to donor–acceptor solvent–substituent interactions. However, the chemical shifts observed for a given substituent in different solvents are not described by [4]. In conclusion, it is clear that a workable model for the electrostatic contributions to solvent effects in chemical shifts has not yet been developed. Certainly, the model proposed here is not expected to be generally valid when the effect of solute–solvent interactions pertains to a specific atom in the solute molecule and thus, is not necessarily a manifestation of the macroscopic effect of the interactions. Of course, carefully selected solutes will exhibit chemical shifts which can be related to the acid–base properties of the solvent; an example is the ^{31}P chemical shift in triethyl phosphine which is used by Mayer *et al.* (7) to define the acidity parameter AN.

Finally, it should be noted that replacing the acidity parameter E_T by AN or Z, or the basicity parameter DN by B does not result in improved correlations with the characteristic vectors for the thermodynamic data discussed above. The chief reason for using E_T at present is that it has been measured for a larger collection of solvents. Mayer *et al.* (7) have argued that the acidity parameters E_T and Z give a low estimate of solvent acidity for solvents with dielectric constants less than 10 because the solvation of the polar ground state of the reference compounds used to define these parameters contains a contribution from solvent polarizability. This discrepancy would not have been detected in the present analysis since most solvents considered have higher dielectric constants. As pointed out above and earlier (4), there is a problem in defining a quantitative measure of basicity for protic solvents. The basicity parameter B of Koppel and Palm (35), modified recently by Koppel and Paju (9), is based on the difference in stretching frequencies of free phenol and phenol hydrogen-bonded to a given base in carbon tetrachloride solution. The parameter B always was more poorly correlated with the appropriate characteristic vector than the parameter DN. However, further elucidation of the problem of defining acidity and basicity parameters must await the

collection of further experimental data. In conclusion, it is emphasized that the above analysis demonstrates clearly that only two independent parameters are needed to account for the observed variation in thermodynamic data with solvent. If solvent polarity and polarizability are truly components of the total solvent effect, then their contributions cannot be identified at present. The suggestion made previously (3, 4) that a structural factor should be added as a third parameter also cannot be justified by the present results. The failure of [4] to account for solvent effects in some cases must be attributed to the difficulty in accounting for the structural contribution to the basicity parameter DN.

Acknowledgments

We are indebted to Professor J. T. Edward and Dr. S. C. Wong of McGill University, Montreal, Que., for bringing method of characteristic vector analysis to our attention and for providing their computer programme. The financial assistance of the National Research Council of Canada is gratefully acknowledged.

1. I. A. KOPPEL and V. A. PALM. *In* Advances in linear free energy relationships. *Edited by* N. B. Chapman and J. Shorter. Plenum Publishing Co., New York, N.Y. 1972. Chapt. 5.
2. M. BORN. Z. Physik. **1**, 45 (1920).
3. T. M. KRYGOWSKI and W. R. FAWCETT. J. Am. Chem. Soc. **97**, 2143 (1975).
4. W. R. FAWCETT and T. M. KRYGOWSKI. Aust. J. Chem. **28**, 2115 (1975).
5. C. REICHARDT. Lösungsmittel effekte in der organische chemie. Verlag Chemie, Weinheim/Bergstr., Germany. 1973.
6. E. M. KOSOWER. J. Am. Chem. Soc. **80**, 3253 (1958); **80**, 3261 (1958); **80**, 3267 (1958).
7. U. MAYER, V. GUTMANN, and W. GERGER. Monatshefte Chem. **106**, 1235 (1975).
8. V. GUTMANN and R. SCHMID. Coord. Chem. Rev. **12**, 263 (1974).
9. I. A. KOPPEL and A. I. PAJU. Reakts. Sposobn. Organ. Soedin. **11**, 121 (1974).
10. J. L. SIMONDS. J. Opt. Soc. Am. **53**, 968 (1963).
11. R. L. REEVES. J. Am. Chem. Soc. **88**, 2240 (1966).
12. J. J. KANKARE. Anal. Chem. **42**, 1322 (1970).
13. P. H. WEINER. J. Am. Chem. Soc. **95**, 5845 (1973).
14. P. H. WEINER, E. R. MALINOWSKI, and A. R. LEVINSTONE. J. Phys. Chem. **74**, 4537 (1970).
15. P. H. WEINER and E. R. MALINOWSKI. J. Phys. Chem. **75**, 1207 (1971).
16. P. T. FUNKE, E. R. MALINOWSKI, D. E. MARTINE, and L. Z. POLLARA. Separ. Sci. **1**, 661 (1967).
17. J. T. BULMER and H. F. SHURVELL. J. Phys. Chem. **77**, 256 (1973).
18. C. K. MANN. Electroanal. Chem. **3**, 57 (1969).
19. YU. YA. FIALKOV, A. N. ZHITOMIRSKY, and YU. A. TARASENKO. The physical chemistry of non-aqueous solutions. Khimia, Leningrad. 1973.
20. M. S. GREENBERG, R. L. BOCHNER, and A. I. POPOV. J. Phys. Chem. **77**, 2449 (1973).
21. B. G. COX, A. J. PARKER, and W. E. WAGHORNE. J. Am. Chem. Soc. **95**, 1010 (1973).
22. B. G. COX, G. R. HEDWIG, A. J. PARKER, and D. W. WATTS. Aust. J. Chem. **27**, 477 (1974).
23. G. R. HEDWIG and A. J. PARKER. J. Am. Chem. Soc. **96**, 6589 (1974).
24. G. SOMSEN and L. WEEDA. J. Electroanal. Chem. **29**, 375 (1971).
25. H. S. FRANK and W. Y. WEN. Discuss. Faraday Soc. **24**, 133 (1957).
26. R. H. ERLICH, M. S. GREENBERG, and A. I. POPOV. Spectrochim. Acta, A, **29**, 543 (1973).
27. A. D. BUCKINGHAM. Discuss. Faraday Soc. **24**, 151 (1957).
28. P. LASZLO. Prog. N.M.R. Spectrosc. **3**, 231 (1966).
29. J. W. EMSLEY and L. PHILLIPS. Prog. N.M.R. Spectrosc. **7**, 1 (1971).
30. A. D. BUCKINGHAM, T. SCHAEFER, and W. G. SCHNEIDER. J. Chem. Phys. **32**, 1227 (1960).
31. P. H. WEINER and E. R. MALINOWSKI. J. Phys. Chem. **75**, 3971 (1971).
32. J. K. BECCONSALL and P. HAMPSON. Mol. Phys. **10**, 21 (1965).
33. J. W. EMSLEY and L. PHILLIPS. Mol. Phys. **11**, 437 (1966).
34. R. W. TAFT, E. PRICE, I. R. FOX, I. C. LEWIS, K. K. ANDERSON, and G. T. DAVIS. J. Am. Chem. Soc. **85**, 709 (1963).
35. I. A. KOPPEL and V. A. PALM. Reakts. Sposobn. Organ. Soedin. **8**, 291 (1971).
36. W. GORDY and S. C. STANFORD. J. Chem. Phys. **8**, 170 (1940); **9**, 204 (1941).
37. T. KAGIYA, Y. SUMIDA, and T. INOUE. Bull. Chem. Soc. Jpn. **41**, 767 (1968).
38. S. WOLD. Chem. Scripta, **5**, 97 (1974).

Can. J. Chem. Downloaded from www.nrcresearchpress.com by 210.87.254.6 on 09/05/12
For personal use only.

Vibrational spectra of crystalline malononitrile

R. SAVOIE, R. BROUSSEAU, AND C. NOLIN

Département de Chimie, Université Laval, Québec, (Qué), Canada G1K 7P4

Received April 13, 1976

R. SAVOIE, R. BROUSSEAU, and C. NOLIN. Can. J. Chem. **54**, 3293 (1976).

The infrared and Raman spectra of the four solid phases of malononitrile have been recorded. The crystal structures of these solids are now relatively well established from the present results and from previous X-ray and nuclear quadrupole resonance data. Phase I belongs to the $P2_1/n$ space group of the monoclinic system, with four molecules per unit cell. In phase II, the molecules occupy two sets of general positions in a crystal of $P2_1$ symmetry. The molecular site symmetry is C_s in phase III which is highly symmetric. The structure of the low-temperature metastable phase IV appears to be very similar to that of phase I.

R. SAVOIE, R. BROUSSEAU et C. NOLIN. Can. J. Chem. **54**, 3293 (1976).

Nous avons enregistré les spectres infrarouges et Raman des quatre phases solides de la malononitrile. Nos résultats, ajoutés à ceux déjà obtenus par diffraction des rayons-X et par résonance quadrupolaire, permettent de spécifier assez bien les structures cristallines de ces solides. La phase I appartient au groupe $P2_1/n$ du système monoclinique, avec quatre molécules par maille élémentaire. Dans la phase II, les molécules occupent deux ensembles de positions générales dans un crystal de symétrie $P2_1$. La symétrie des sites moléculaires est C_s dans la phase III qui est hautement symétrique. La structure de la phase métastable de basse température (IV) semble très voisine de celle de la phase I.

Can. J. Chem. Downloaded from www.nrcresearchpress.com by 210.87.254.105 on 09/05/12
For personal use only.

Introduction

The molecular parameters and symmetry (C_{2v}) of the malononitrile ($CH_2(CN)_2$) molecule are well established from microwave data (1). The fundamental vibrational frequencies of this molecule are also well known, following various Raman (2, 3) and infrared (3–5) investigations complemented by force constant calculations (3, 4, 6).

Solid malononitrile has been shown by a ^{14}N pure nuclear quadrupole resonance (pnqr) study (7) to exist in four different forms (see Fig. 1), although only one of the three solid–solid phase transitions (that from phase II to phase III) shows a normal specific-heat anomaly (8). According to X-ray diffraction data (9), the room-temperature (phase I) crystal belongs to the $P2_1/n$ (C_{2h}^5) space group of the monoclinic system, with four molecules located on general positions in the unit cell. These findings are consistent with the results of the pnqr study which show that the nitrogen atoms occupy two different sets of sites in this solid. Furthermore, the recent infrared and Raman measurements of Castellucci and Manzelli (10) have been easily interpreted on the basis of this reported crystal structure. Phase II of malononitrile is also monoclinic, but it has not been definitely established whether the crystal belongs to the $P2_1/m$ (C_{2h}^2) or to the $P2_1(C_2^2)$ space group (9). Little is known of the remaining two solid phases, except for the number of different sets of sites occupied by the nitrogen atoms, as obtained from the nuclear quadrupole resonance experiments. The present study was undertaken in an effort to learn more about the structures of the various solid phases of malononitrile.

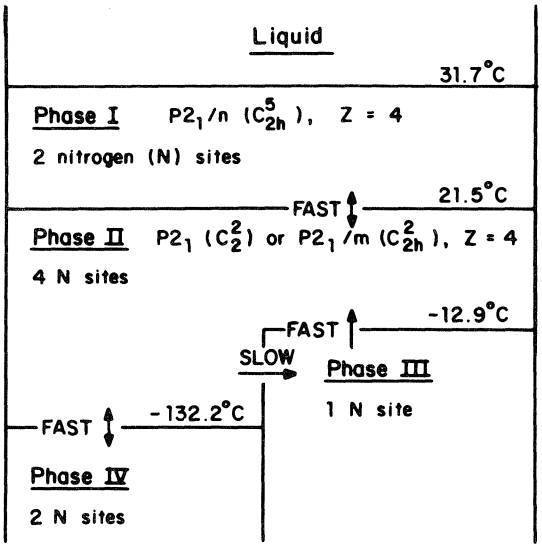

FIG. 1. The solid phases of $CH_2(CN)_2$.

TABLE 1. Atomic and molecular sites in crystalline malononitrile

Structure*	Molecular sites†	Number of nonequivalent atomic sites: Nitrogen Calc.	Nitrogen Exp.‡	Hydrogen Calc.	Hydrogen Exp.§
Phase I					
$P2_1/n$ (C_{2h}^5)	4 C_1	2	2	2	2
Phase II					
$P2_1/m$ (C_{2h}^2)	4 C_1	2	4	2	3
	2 C_s(N) + 2 C_s(N)	4	4	2	3
	2 C_s(H) + 2C_s(H)	2	4	4	3
	2 C_s(N) + 2 C_s(H)	3	4	3	3
$P2_1$(C_2^2)	2 C_1 + 2 C_1	4	4	4	3
Phase III		—	1	—	2
Phase IV		—	2	—	2

*From X-ray diffraction data, ref. 9.
†4 C_1 = four molecules per unit cell on one set of sites of C_1 symmetry. 2 C_s(N) = 2 molecules per unit cell located on one set of sites of C_s symmetry, the nitrogen atoms being located in the planes of symmetry.
‡From the ^{14}N pure nuclear quadrupole resonance study, ref. 7.
§From the present results with $CHD(CN)_2$ isolated in $CH_2(CN)_2$.

Experimental

The malononitrile used in our experiments was obtained commercially (Aldrich Chemicals) and purified by sublimation at reduced pressure. Partly deuterated samples (3%at. D) were prepared by mixing the normal product and the required amount of D_2O made slightly alkaline by the addition of a small amount of Na_2CO_3. The deuterated malononitrile was then purified by sublimation after evaporation of the water in the mixture.

The infrared spectra were obtained from samples prepared by slow crystallization of the liquid between two infrared windows, which were subsequently mounted in a conventional liquid nitrogen cryostat. In the 300–4000 cm^{-1} region, AgCl, Irtran-4, and Si windows separated by aluminum spacers 6–18 μm thick were used. Much thicker samples, held by crystalline quartz or silicon windows separated by 250 μm thick Teflon spacers, were needed in the far-infrared (20–400 cm^{-1}). The spectra were recorded on a Perkin-Elmer Model 621 spectrophotometer calibrated with an indene calibration solution (11) in the 200–400 cm^{-1} region, and with a RIIC Model FS-720 interferometer in the far-infrared.

The Raman spectra were obtained with the polycrystalline samples contained in a 6 mm diameter Pyrex cell placed inside a glass Dewar with flat windows at the end. The low-temperature measurements were made with the samples cooled by a flow of cold nitrogen gas. As the transition from phase II to phase III normally resulted in breakage of the sample cell, the latter had to be first heated superficially so as to obtain after sublimation of some of the product a sample slightly smaller than the cell itself, to allow for the expansion of the crystal at the transition. The spectra were recorded with a Spex Model 1400 spectrometer, using the 488 and 514.5 nm exciting lines from a Spectra Physics Model 165 argon laser. The instrument was calibrated with a neon discharge lamp. The Raman spectra, as well as the infrared measurements, were recorded with a spectral resolution of 1 cm^{-1} in most regions and the frequencies reported below are believed to be accurate to better than ± 2 cm^{-1} for sharp peaks.

Results and Discussion

A. Atomic and Molecular Sites

The ^{14}N pure quadrupole nuclear resonance study of Zussman and Alexander (7) has led to the determination of the number of sets of sites occupied by the nitrogen atoms in the various solid phases of malononitrile (see Fig. 1 and Table 1). Equivalent results are obtainable spectroscopically for the hydrogen atoms by using dilute solid solutions of isotopically substituted species. In the case of malononitrile deuterated to a small extent only, the D atoms are found almost exclusively in the mixed $CHD(CN)_2$ species, which are relatively well isolated from each other in the solid $CH_2(CN)_2$ matrix. In these conditions the C—D oscillations are essentially free from intermolecular vibrational coupling and their frequencies depend, among other factors, on the local environment of the deuterium atoms in the crystal. The vibrational motions of the D atoms can therefore be split in the solid, the predicted number of components being equal to the number of

Can. J. Chem. Downloaded from www.nrcresearchpress.com by 210.87.254.105 on 09/05/12
For personal use only.

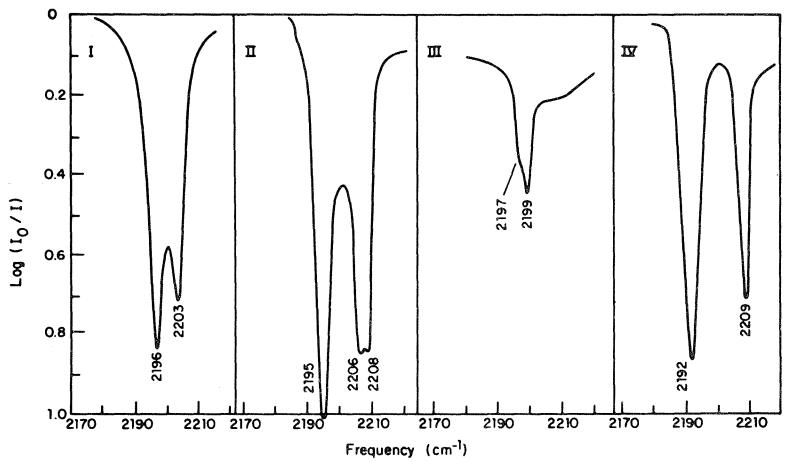

FIG. 2. Infrared spectra in the C—D stretching region of $CHD(CN)_2$ molecules isolated in a solid $CH_2(CN)_2$ matrix.

nonequivalent D (or H) atoms in the unit cell of the crystal. Such site splitting is clearly observed in the C—D stretching region of the infrared spectrum of a 150 μm thick sample of $CH_2(CN)_2$ containing 3% $CHD(CN)_2$ (see Fig. 2). As indicated in Table 1, the results show that there are at least two different types of hydrogen atoms in phases I, III, and IV and at least three different types in phase II.

The number of different sets of sites occupied by the N and H atoms in crystalline malononitrile is obviously related to the molecular site symmetry. This relation is unambiguous in the case of phase I where the molecules occupy one set of general positions in the unit cell. The molecular site symmetry is then C_1, and although the positions of the four molecules in the unit cell can be interchanged by operations generated by the symmetry element of the space group, it is impossible to interchange the two nitrogen (and also the two hydrogen) atoms within any given molecule. Thus, there are two different types of such atoms in phase I, as confirmed by the pnqr measurements and the present results, which also show the situation to be exactly the same in phase IV.

The problem is more complex in phase II which, according to X-ray diffraction data, belongs either to the $P2_1/m$ (C_{2h}^2) or to the $P2_1(C_2^2)$ space group. In the centrosymmetric structure, the four molecules in the unit cell can occupy general positions, or they can be located on two different sets of sites of C_s symmetry. As indicated in Table 1, none of these possibilities can account for both the pnqr and spectroscopic results. The non-centrosymmetric $P2_1$ structure is therefore the correct one, even though only three of the four predicted components have been detected in the infrared spectrum.

Although the crystal structure of phase III is not known, the pnqr measurements have shown that all the nitrogens are equivalent in this modification of the solid. This implies that all the molecules are equivalent in the crystal; that is to say, the molecules occupy only one set of sites in the unit cell, and the molecular site symmetry is other than C_1, as the nitrogen atoms within the same molecule would be nonequivalent if general positions were occupied. Only the C_{2v}, C_2, and C_s molecular site symmetries are therefore compatible with the nuclear quadrupole resonance results. Furthermore, the doublet associated with the C—D stretching vibration of isolated $CHD(CN)_2$ molecules in phase III of $CH_2(CN)_2$ (Fig. 2) indicates that the H atoms within a same molecule are not related through a C_2 symmetry axis in this phase. The molecular site symmetry is therefore C_s, with further restriction that the CH_2 molecular groups rest in the planes of symmetry of the crystal, with the CN groups being symmetrically oriented on each side of these planes.

B. Spectra of Phase I

The infrared and Raman spectra of single crystals of malononitrile at room temperature

Can. J. Chem. Downloaded from www.nrcresearchpress.com by 210.87.254.105 on 09/05/12
For personal use only.

Can. J. Chem. Downloaded from www.nrcresearchpress.com by 210.87.254.105 on 09/05/12
For personal use only.

Table 2

Vibrational frequencies (in cm^{-1}) of crystalline malononitrile.

Phase I (25°C)		Phase II (-70°C)		Phase III (-190°C)		Phase IV (-190°C)		Assignments
Infrared	Raman	Infrared	Raman	Infrared	Raman	Infrared	Raman	
-	-	-	25?	-	-	-	23?	Lattice vibrations
-	55	-	50	-	50	-	55	
-	58sh	-	61	-	52?	-	62	
65?	-	68	-	68	-	69	-	
-	-	75	-	77	-	74	77?	
-	-	-	-	-	-	79	-	
-	-	-	83sh	-	-	86?sh	-	
-	87	-	91	-	90	-	95	
-	-	-	-	100	-	-	102sh	
-	-	-	-	-	-	107	105	
-	-	-	-	-	115	123sh	121	
-	-	-	-	-	126	126	127	
-	-	140	136	138	142	-	-	
-	-	-	-	146	-	-	-	
165sh	156	-	156	154	162	-	161	
170	-	170	-	182	-	172	-	CCN bend, ν_6 (A_1)
-	182	184	182	192	179	184	186	
339	-	338	341	347sh	-	343sh	-	CCN bend, ν_{15} (B_2)
342sh	346	345	346	350	350	345	347	
357	-	-	-	355sh	-	-	-	?
-	-	-	364	-	-	-	-	CCN bend, ν_{12} (B_1)
366	365	367	365	368?	373?sh	368	366	
-	369	-	371	-	-	-	372	CCN bend, ν_8 (A_2)
372	373	373	374	373	375	375	375	
		-	574	-	575	-	-	^{13}C (ν_5)
-	580	580sh	-	584sh	-	581sh	581	CCC bend, ν_5 (A_1)
582	-	582	582	586	585	582	-	
-	-	-	891sh	892sh	-	887sh	-	^{13}C (ν_4)
890	-	889	-	893sh	-	889	-	C-C stretch, ν_4 (A_1)
893sh	895	892	896	895	897	892	895	
908	-	906	-	-	-	-	-	$\nu_5 + \nu_{15}$
-	-	913	-	912	-	913	-	
-	-	926	-	940	-	926	-	^{13}C (ν_{14})
930	933	931	-	-	-	931	-	CH_2 rock, ν_{14} (B_2)
938	938	937	939	947	949	938	939	

Can. J. Chem. Downloaded from www.nrcresearchpress.com by 210.87.254.105 on 09/05/12
For personal use only.

Table 2 (concluded)

Phase I (25°C)		Phase II (-70°C)		Phase III (-190°C)		Phase IV (-190°C)		Assignments
Infrared	Raman	Infrared	Raman	Infrared	Raman	Infrared	Raman	
-	-	-	-	-	-	939sh	-	$\nu_5 + \nu_{12}$?
-	-	972	-	-	-	973	-	^{13}C (ν_{11})
985	984	982	983	-	-	982	982	C-C stretch, ν_{11} (B_1)
995sh	-	987	986	987	986	990sh	985	
-	-	992	-	-	990	994	-	
-	-	1213	1213	-	1216	1210	-	Torsion, ν_7 (A_2)
1215	1216	-	1217	1228	1228	-	1215	
1244	-	-	-	1245	-	1240	-	$\nu_4 + \nu_{15}$
-	-	-	-	-	-	1247	-	
1259	-	-	-	1268	-	1259	-	$\nu_4 + \nu_{12}$
1275	-	-	-	-	-	1273	-	$\nu_{14} + \nu_{15}$
1278	-	-	-	1282	-	-	-	
1308	-	1308	-	1308	-	-	-	$\nu_4 + (\nu_{12}$ or $\nu_8)$
-	1311	1320sh	1312	-	-	-	1310	CH_2 wag, ν_{10} (B_1)
1321	-	1322	-	1321	1324	1321	-	
-	1376	-	-	1374sh	1373	-	-	^{13}C (ν_3)
-	-	1386	-	1387	-	1385	1384	CH_2 bend, ν_3 (A_1)
1387	-	1389sh	1389	1389sh	1388	1389?sh	-	$\nu_7 + \nu_6$
1395sh	1392	1393	1397	-	-	1391	1397	
2221	-	2222	-	2223	-	2220/30	-	?
-	-	-	-	-	-	-	2262sh	C-N stretch, ν_2 (A_1)
2269	2263	2268	2265	2265	2262	2265	2265	C-N stretch, ν_9 (B_1)
-	-	-	-	2274	2274	2273sh	-	$\nu_3 + \nu_4$
2273sh	2273	2275	2273	2277	2278	2275	2275	
2288sh	2285	2282sh	-	2283	-	2289	-	
2296sh	-	2293	2292	2294	-	-	-	
-	-	-	-	-	2913/17	2926sh	-	^{13}C (ν_1) ?
-	-	-	-	2920?	-	-	-	C-H stretch, ν_1 (A_1)
2933	2932	2932	2931	2930	2928	2931	2929	
-	-	2961	-	-	-	2963sh	-	^{13}C (ν_{13})?
-	-	-	-	2957?sh	-	-	-	C-H stretch, ν_{13} (B_2)
2969	2968	2971	2969	2962	2964	2973	2971	

sh=shoulder

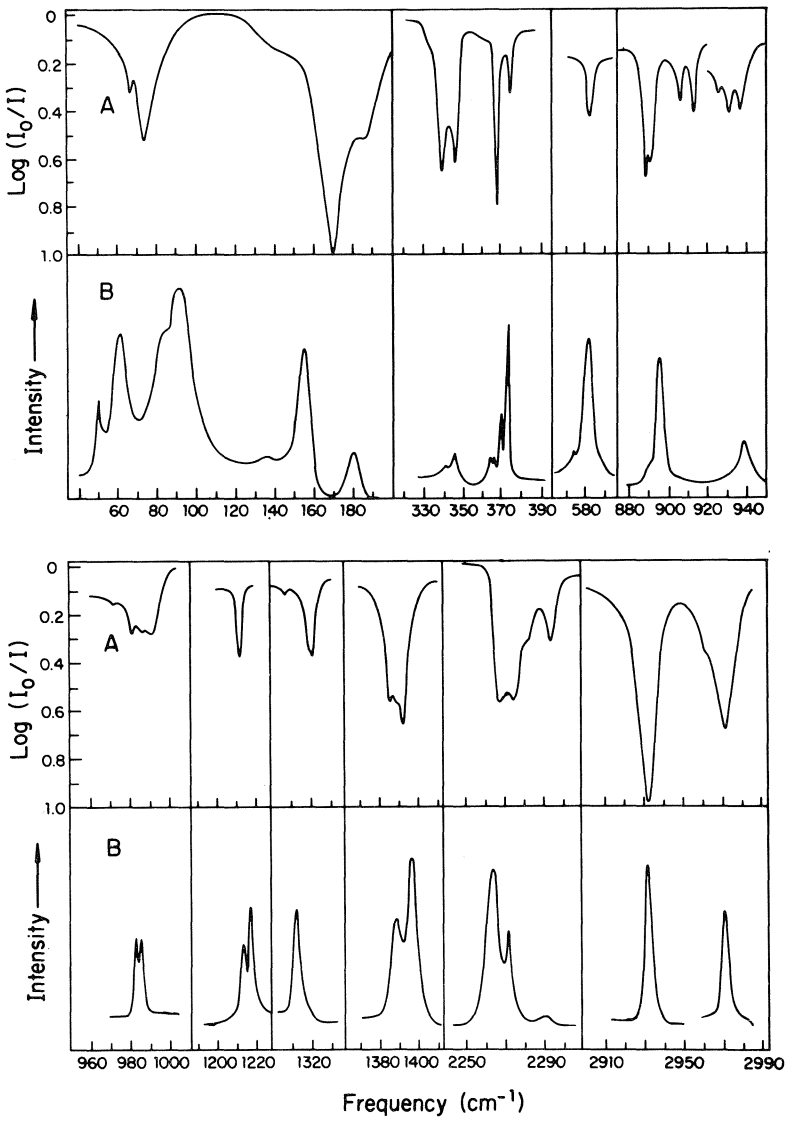

FIG. 3. (*A*) Infrared and (*B*) Raman spectra of crystalline malononitrile in phase II at −70 °C.

have been carefully recorded and analyzed by Castelluci and Manzelli (10). Their polarization measurements have made possible the observation of most of the vibrational components predicted on the basis of the reported crystal structure of the solid. Our own spectra, although less detailed, are in good agreement with those already published and will therefore not be reported here. However, the frequencies given in Table 2 are from our own work, to allow for a more meaningful comparison with the corresponding results on the other solid phases of $CH_2(CN)_2$.

C. Spectra of Phase II

As discussed in section A, phase II of malononitrile belongs to the $P2_1(C_2^2)$ space group of the monoclinic system, with four molecules per unit cell. Since a general position in this space group has multiplicity two (12), there are two sets of sites of C_1 symmetry occupied in this case. The vibrational correlation diagram (13),

Can. J. Chem. Downloaded from www.nrcresearchpress.com by 210.87.254.105 on 09/05/12
For personal use only.

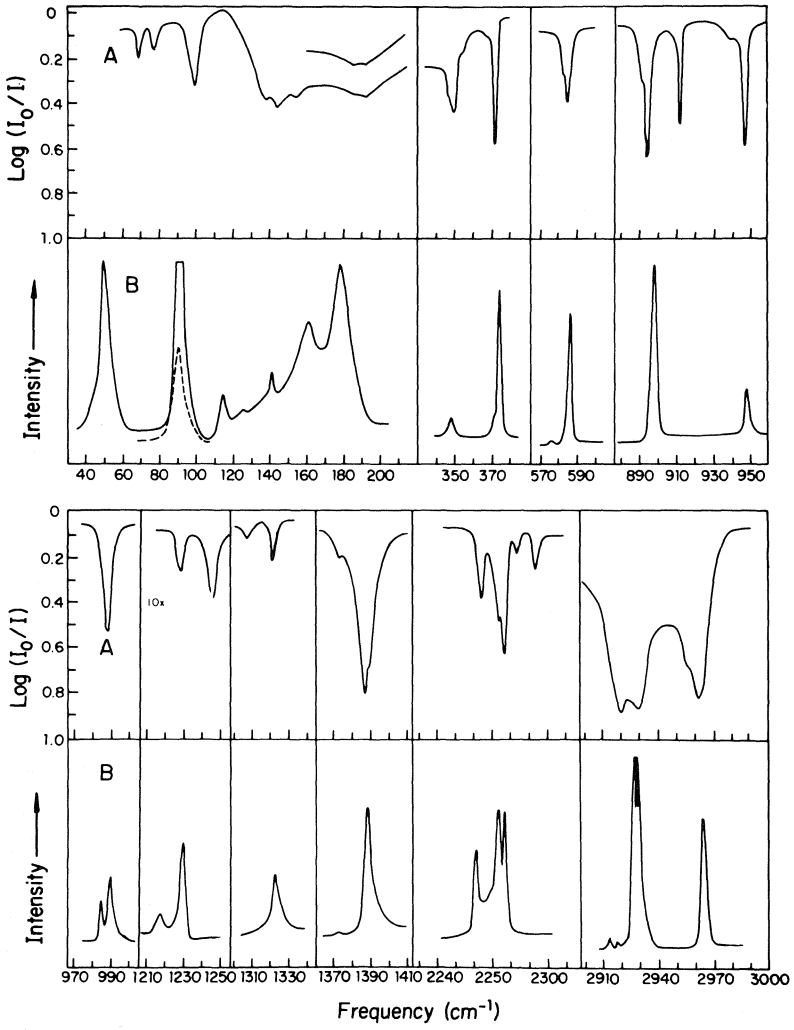

FIG. 4. (*A*) Infrared and (*B*) Raman spectra of crystalline malononitrile in phase III at −190 °C.

TABLE 3. Correlation diagram for each set of sites in phase II of $CH_2(CN)_2$

Free molecule C_{2v}	Molecular site C_1	Crystal C_2	Activity
A_1			
A_2	A	A	R, ir
B_1		B	R, ir
B_2			

shown in Table 3, indicates that for each set the fundamental vibrations of the free molecule should give doublets in the solid-phase spectra. A total of four coincident infrared and Raman components are therefore expected for each fundamental.

Four infrared and four Raman components are not clearly visible for each gas phase fundamental. As shown in Fig. 3 (see also Table 2), most fundamentals are split into two components in one type of spectrum or the other. However, some of the fundamentals ($\nu_3(A_1)$, $\nu_{10}(B_1)$, $\nu_{11}(B_1)$) occur as triplets in the infrared spectrum. Note that this is not compatible with a centrosymmetric $P2_1/m$ structure, which should be characterized by non-coincident infrared and Raman doublets, independently of the site symmetry.

Can. J. Chem. Downloaded from www.nrcresearchpress.com by 210.87.254.105 on 09/05/12
For personal use only.

Can. J. Chem. Downloaded from www.nrcresearchpress.com by 210.87.254.105 on 09/05/12
For personal use only.

The vibrational spectra of phase II of $CH_2(CN)_2$ are more easily interpreted by comparing the crystal structure of this solid with that of phase I. In the latter, the molecular structure departs significantly from that of the free molecule. For example, the C—N internuclear distances of the two CN groups within the same molecule in the solid differ by approximately 3%, as shown by X-ray diffraction (9). As mentioned previously, the molecules in the unit cell are all equivalent in phase I, but the nitrogen (and hydrogen) atoms within any given molecule are different. Furthermore, in phase I, the symmetry elements of the $P2_1/n$ space group (12) are such that the four molecules in the unit cell are related by pairs of two through a center of inversion. All that is needed for the transition to phase II to take place is a small reorientation or displacement of one pair of molecules relative to the other, so as to destroy the centrosymmetric nature of the crystal. The present results suggest that there is very little change at the molecular level when this occurs. For example, the frequencies of the C—D vibrations of $CHD(CN)_2$ molecules isolated in a $CH_2(CN)_2$ matrix (Fig. 2), which indirectly measure the nonequivalence of the H atoms within the same molecule, are 2196/2203 cm^{-1} in phase I as compared to 2195/2207 cm^{-1} on the average in phase II. In the latter phase, only three peaks are observed in this region although four components are predicted for the $P2_1$ structure. It thus seems logical to assume that two components are hidden in the 2195 cm^{-1} band, whose intensity is approximately equal to that of the 2206/2208 cm^{-1} doublet. By comparison with the results in phase I, the doublets at 2195/2206 cm^{-1} and 2195/2208 cm^{-1} can be associated to the two different types of molecules in the unit cell of the crystal, which indicates that these differ little even if they occupy two nonequivalent sets of sites. The relative simplicity of the vibrational spectra of $CH_2(CN)_2$ is therefore explainable by the near equivalence of the molecules in the unit cell.

D. Spectra of Phase III

The transition from phase II to phase III in malononitrile is characterized by considerable changes in the vibrational spectra. The fine structure in the ν_3, ν_7, and ν_8 regions of the Raman spectrum disappears and remarkable intensity changes occur in the region of the C—N stretching fundamentals. Simplification of the infrared spectrum also takes place, in particular in the ν_3 and ν_{11} regions. The vibrational spectra of phase III are for the most part less complicated than those of phase II, and the very slow transition to phase III can be easily followed from the progressive disappearance of the triplet at 926/931/937 cm^{-1}, which is replaced by a single band at 947 cm^{-1} in the infrared spectrum.

As discussed above (Section *A*), the infrared spectrum of isolated $CHD(CN)_2$ and the pnqr results on phase III of malononitrile are compatible with a C_s molecular site symmetry only. The vibrational spectra of phase III of $CH_2(CN)_2$ (see Fig. 4 and Table 2) also allow the elimination of the C_{2v} and C_2 molecular site symmetries in this modification of the solid. The vibrational correlation diagrams for any factor group chosen show that, for both site symmetries, the fundamentals of A_1 symmetry in the free molecule should give only one infrared-active component in the solid, whereas doublets are experimentally observed in all cases. The splitting of these fundamentals is also incompatible with the space groups of the monoclinic system, the triclinic system being excluded as it cannot accommodate sites of C_s symmetry.

The small splitting of the C—D stretching vibrational frequency of $CHD(CN)_2$ molecules isolated in $CH_2(CN)_2$ in phase III (2 cm^{-1}) compared to that in the other three phases (12 cm^{-1} on the average) indicates that the two hydrogen atoms within the same molecule are much more equivalent in phase III. This suggests that the molecules in this phase are considerably less distorted than in the three other solid phases. The increase in the symmetry of the crystal at the phase II to phase III transition seems to be directly related to the appreciable entropy change (-4.81 J/(mol K)) associated with this phase change (8). The expansion of the solid at the transition, which often resulted in a broken sample cell in our Raman experiments, also points to an important rearrangement of the crystal in this process. The very sluggish transition from phase II to phase III is clearly quite different from the spontaneous transition from phase I to phase II, which involves only minor modifications of the crystal structure

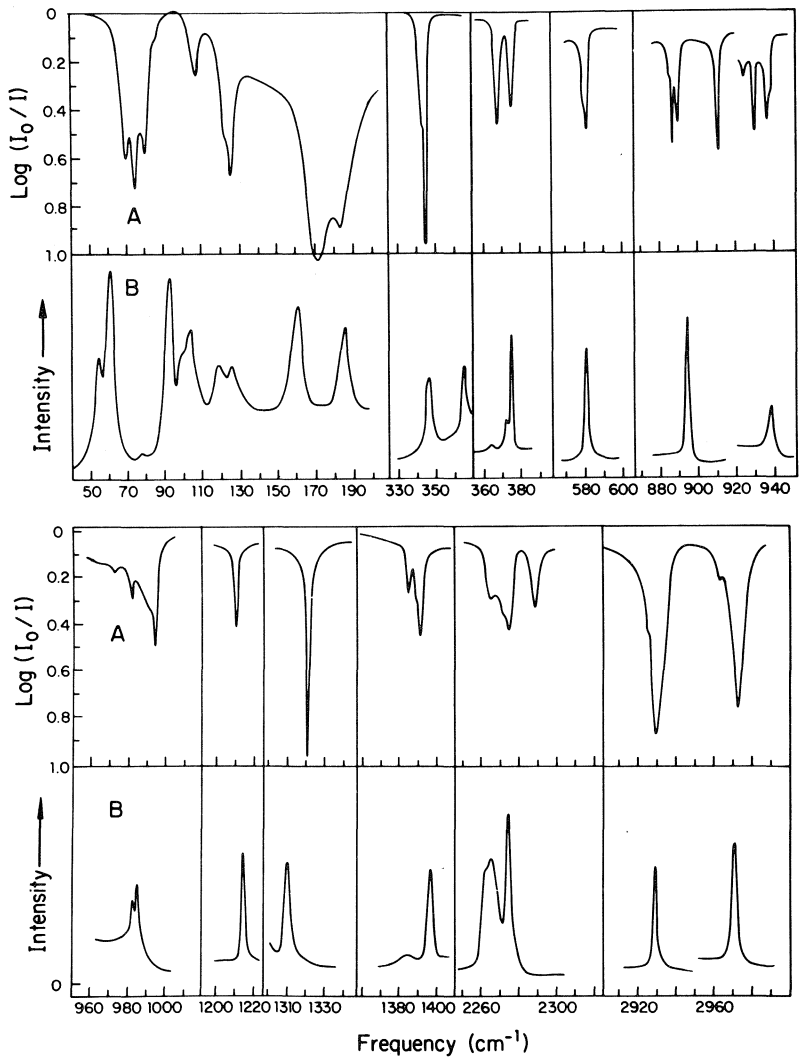

FIG. 5. (*A*) Infrared and (*B*) Raman spectra of crystalline malononitrile in phase IV at −190 °C.

and does not give a detectable anomaly in the heat capacity curve of the solid.

E. Spectra of Phase IV

The vibrational spectra of the low-temperature metastable phase (phase IV) of malononitrile (see Fig. 5 and Table 2) are slightly less complicated than those of phase II, except for an increased number of lattice modes in the spectra of phase IV.

The infrared spectrum of $CHD(CN)_2$ molecules isolated in $CH_2(CN)_2$ in phase IV (Fig. 2) and the ^{14}N pnqr measurements indicate that the molecular site symmetry in this solid is C_1, with only one set of molecular sites being occupied in the unit cell. The absence of any appreciable anomaly in the heat capacity curve at the transition temperature (8) suggests that the structure differs little from that of phase II. The monoclinic system is therefore indicated, and it is conceivable that the crystal structure of phase IV is identical to that of phase I. Whatever the case may be, a combination of C_1 site symmetry and C_2, C_s, or C_{2h} factor group shows that each fundamental should give two infrared and two Raman-active components in the spectra of the crystal. The experimental results can be reasonably interpreted on this

Can. J. Chem. Downloaded from www.nrcresearchpress.com by 210.87.254.105 on 09/05/12
For personal use only.

basis, especially in the case of the infrared spectrum where many fundamentals occur as doublets. The predicted splitting is generally not observed in the Raman spectrum, but this could be due to the fact that one of the two components is much stronger than the other one. This could mean that the structure of phase IV is centrosymmetric, as a similar situation was encountered in phase I. In the latter, only one band (due to the A_g component) was in general detected in our Raman spectrum of polycrystalline samples, whereas the much weaker B_g component was clearly resolved in the polarized Raman spectrum (10) of a single crystal.

Acknowledgment

The authors gratefully acknowledge financial support of this work by the National Research Council of Canada.

1. E. HIROTA and Y. MORINO. Bull. Chem. Soc. Jpn. **33**, 158, 705 (1960).
2. K. W. F. KOHLRAUSCH and G. P. YPSILANTI. Z. Phys. Chem. B-**29**, 274 (1934).
3. T. FUJIYAMA and T. SHIMANOUCHI. Spectrochim. Acta, **20**, 829 (1964).
4. F. HALVERSON and R. FRANCEL. J. Chem. Phys. **17**, 694 (1949).
5. L. L. AMES, D. WHITE, and D. E. MANN. J. Chem. Phys. **38**, 910 (1963).
6. B. J. VAN DER VEKEN and H. O. DESSEYN. J. Mol. Struct. **23**, 427 (1974).
7. A. ZUSSMAN and S. ALEXANDER. Solid State Comm. **5**, 259 (1967); J. Chem. Phys. **49**, 3792 (1968).
8. H. L. GIRDHAR, E. F. WESTRUM, Jr., and C. A. WULFF. J. Chem. Eng. Data, **13**, 239 (1968).
9. N. NAKAMURA, S. TANISAKI, and K. OBATAKE. Phys. Lett. A, **34**, 372 (1971). K. OBATAKE and S. TANISAKI. Phys. Lett. A, **44**, 341 (1973).
10. E. CASTELLUCI and P. MANZELLI. Chem. Phys. **9**, 135 (1975).
11. R. N. JONES and A. NADEAU. Spectrochim. Acta, **20**, 1175 (1964).
12. N. F. M. HENRY and K. LONSDALE (*Editors*). International tables for X-ray crystallography, Vol. I. Kynoch Press, Birmingham, England. 1952.
13. W. G. FATELEY, F. R. DOLLISH, N. T. MCDEVITT, and F. F. BENTLEY. Infrared and Raman selection rules for molecular and lattice vibrations: The correlation method. Wiley-Interscience, New York. 1972.

Can. J. Chem. Downloaded from www.nrcresearchpress.com by 210.87.254.105 on 09/05/12
For personal use only.

Erratum: L'étude de l'adsorption des halogenures d'ammonium quaternaire à l'interface mercure–solution

HUGUES MÉNARD ET FRANK M. KIMMERLE
Département de chimie, Université de Sherbrooke, Sherbrooke (Qué.), Canada J1K 2R1

Reçu le 22 mai 1976
(Ref.: Can. J. Chem. **54**, 2488 (1976))

A la suite d'une erreur lors de la mise en photo, la fig. 12 devrait être remplacée par celle-ci.

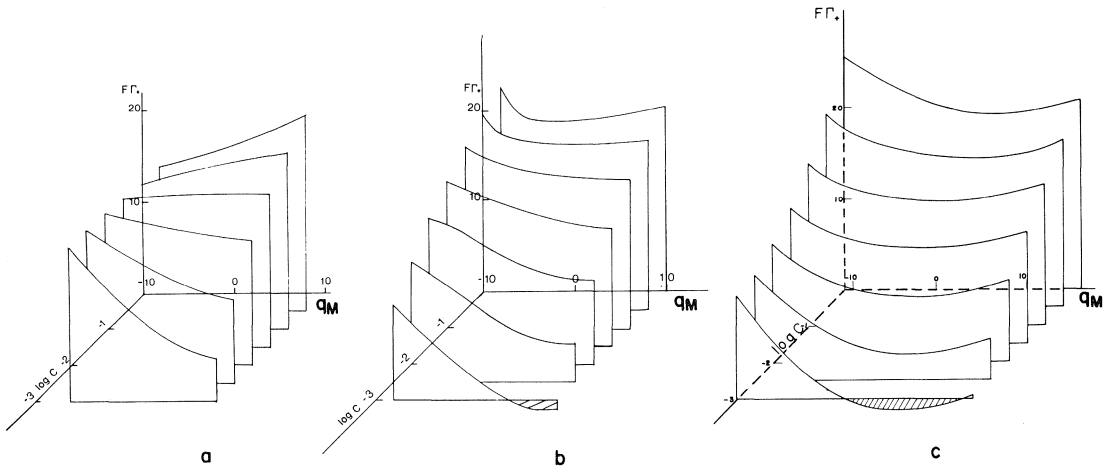

FIG. 12. Excès ionique de surface; coordonnées identiques à celles de la fig. 8: (*a*) Bu_4NBr, (*b*) Pr_4NBr, (*c*) Et_4NBr.

Erratum: The reaction of catechol and derivatives with potassium superoxide

E. LEE-RUFF AND A. B. P. LEVER
Department of Chemistry, York University, Toronto, Ont., Canada M3J 1P3
AND
J. RIGAUDY
Laboratoire de Recherches Organiques de l'E.S.P.C.I., 10, rue Vauquelin, Paris, France

Received July 7, 1976
(Ref.: Can. J. Chem. **54**, 1837 (1976))

The authors wish to acknowledge Dr. G. P. Khare (York University) as a co-author of this paper.

Can. J. Chem. Downloaded from www.nrcresearchpress.com by 210.87.254.105 on 09/05/12
For personal use only.

COMMUNICATIONS

Catalysed Diels–Alder reactions. The realization of orientation control with a bifunctional aliphatic dienophile

MASATOSHI KAKUSHIMA, JESÚS ESPINOSA, AND ZDENEK VALENTA
Department of Chemistry, University of New Brunswick, Fredericton, N.B., Canada E3B 5A3

Received July 30, 1976

MASATOSHI KAKUSHIMA, JESÚS ESPINOSA, and ZDENEK VALENTA. Can. J. Chem. **54**, 3304 (1976).

The Lewis acid catalysed addition of methyl *trans*-4-oxobutenoate (**7**) to *trans*-piperylene (**8**) gives selectively product **9**. $SnCl_4$ is a particularly efficient catalyst. A postulate of the preferential formation of a complex with the formyl group is used to explain the *regio-* and *stereo*-specificity of the reaction. Synthetic implications of this finding are discussed.

MASATOSHI KAKUSHIMA, JESÚS ESPINOSA et ZDENEK VALENTA. Can. J. Chem. **54**, 3304 (1976).

L'addition, catalysée par les acides de Lewis, de l'oxo-4 butanoate de méthyle *trans* (**7**) au pipérylène *trans* (**8**) conduit d'une façon sélective au produit **9**. Le $SnCl_4$ est un catalyseur particulièrement efficace. On utilise une hypothèse impliquant la formation préférentielle d'un complexe avec le groupe formyle afin d'expliquer la *régio-* et la *stéréo*-spécificité de la réaction. On discute des implications en synthèse de ces résultats.

[Traduit par le journal]

We have recently reported an orientation reversal in additions of unsymmetrically substituted 1,3-butadienes to 2,6-dimethyl-1,4-benzoquinone and 1,4-toluquinone (1). For example, thermal addition of 1-substituted dienes proceeded exclusively by orientation **1** (R = CH_3 or CH_3COO) while an addition catalysed by BF_3 or $AlCl_3$ went quantitatively in the opposite sense (**2**). An extension of this 'guidance-by-catalysis' to simple aliphatic dienophiles would have much wider synthetic utility. Presently, compounds of type **6** are not readily available synthetically because both thermal (2) and catalysed (3) additions **3** + **4** lead predominantly to **5**. Synthetic versatility using 2-substituted dienes (predominance of '*para*' products in thermal as well as catalysed additions) and 1,2-disubstituted dienes is similarly limited.

We now wish to report a simple method using the formyl group as a directing Lewis base which opens a way to compounds **6**. *trans*-4-Oxobutenoate (**7**) was chosen as a dienophile because (*i*) it can be prepared in one step from methyl crotonate (4) and (*ii*) many methods exist to convert the formyl group in the adducts into H, CH_3, or other desired substituents. Results using **7** and *trans*-piperylene **8** are summarized in Table 1. While thermal addition produces the expected complex mixture[1] (reaction 1), an addition catalysed by $SnCl_4$ (5) gives adduct **9**,[2] mp 35–38 °C, as the only product (reactions 4 and 5). The desired regio- and stereospecificity has thus been achieved. A similar, but less efficient, guidance was observed with $AlCl_3$ (reaction 2) and with BF_3 etherate (reaction 3).

The exclusive formation of **9** (out of four possible C=C adducts) indicates reaction geometry **11** and is readily explained by the postulate that, in the dienophile, the formyl group complexes preferentially[3] (or that only the formyl

[1]Dehydrogenation (10% Pd–C, 200 °C) gave a 2:3 mixture of *o-* and *m*-toluic acid methyl esters (glc).

[2]Dehydrogenation (10% Pd–C, 200 °C) gives *m*-toluic acid methyl ester. The coupling values in the 220 MHz spectrum of **9** ($\delta(CDCl_3)$ 0.94 (CH_3, d, J = 7 Hz), 2.90 (C_1—H, ddd, J = 10.5, 10.5, 6 Hz), 3.07 (C_2—H, ddd, J = 10.5, 5.5, <0.5 Hz), 9.75 (—C*H*O, J = <0.5 Hz)) establish its stereochemistry, confirmed by spectra of the hydrogenation product of **9**, mp 50–57 °C, and of the corresponding acid, mp 102–104 °C (C=C reduced, CHO replaced by COOH.)

[3]$SnCl_4$ forms stable bidentate complexes (7). The exact nature and geometry of the Lewis acid attachment in **11** cannot be specified at present.

Can. J. Chem. Downloaded from www.nrcresearchpress.com by 210.87.254.105 on 09/05/12
For personal use only.

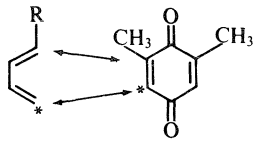

1

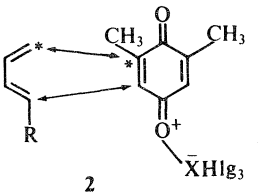

2

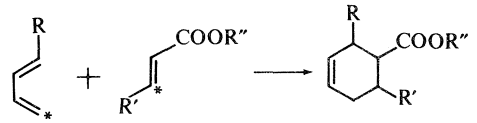

3 (R = alkyl, aryl, acetoxy) 4 (R′ = H or alkyl) 5 (R′ = H or alkyl)

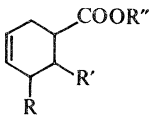

6 (R = alkyl, aryl, or acetoxy; R′ = H or alkyl)

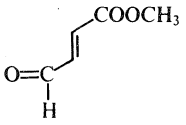

7

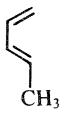

8

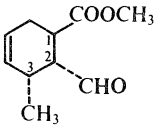

9

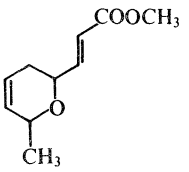

10

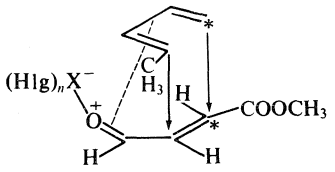

11

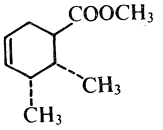

12

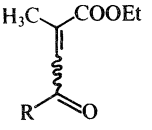

13

complex reacts) and that the charged formyl group determines the orientation (regiospecificity) and the more favourable *endo* state (stereospecificity).[4] These results with **8** as model diene indicate a general method for the synthesis of many substituted cyclohexenes. Based on present knowledge (1, 2, 3), 1-alkyl-, 1-aryl-, 1-acyloxy-,[5] and 1,2-dialkylated 1,3-butadienes (1) can all be expected to add in the same sense as **8**. Furthermore, it can be predicted that a catalysed addition of 2-substituted butadienes[5] to **7** will lead selectively to products with a 1,4-arrangement of the diene substituent and the formyl group.

To show one example of the synthesis of 'unnatural' compounds **6**, **9** was converted into **12** [$(CH_2SH)_2$, $BF_3 \cdot Et_2O$; deactivated RaNi], not accessible in useful quantities by a thermal or catalysed addition of **8** to *trans*-crotonate.

The method works equally well with ketones (*e.g.*, $COCH_3$ instead of CHO in **7**) and work presently underway in our laboratory indicates that the formyl and keto groups even 'win out' in catalysed additions to dienophiles of type **13** (*E* or *Z*; R = H or CH_3). This constitutes a true violation of the normal directivity rules of addition (2, 3).

[4]The *cis,cis*-stereoisomer of **9** should thus become available by using the *cis*-isomer of **7** as the dienophile.

[5]Alkolydienes polymerize too rapidly to be useful.

Acknowledgments

The support of this work by the National Research Council of Canada is grateful acknowledged. We wish to thank Professor J. D. White, Oregon State University, for his experimental procedure using $SnCl_4 \cdot 5H_2O$ and for bringing the possible advantages of this catalyst to our attention. Mr. Robert Forbes, a senior

Can. J. Chem. Downloaded from www.nrcresearchpress.com by 210.87.254.105 on 09/05/12
For personal use only.

TABLE 1. Diels–Alder additions of **7** to **8** in methylene chloride

Reaction	Molar ratio **7**:**8**:catalyst	Catalyst	T (°C)	Time	Product(s); yield	Remarks
1	1:2.5:0	—	40	35 h	Mixture of 3 adducts containing a —CHO group; no **10** formed. Ratio 5:3:1 (nmr). Major adduct is **9**	Diene polymer removed by chromatography
2	1:1.01:1.01	$AlCl_3$ (freshly sublimed in HCl stream)	0	1 h	40% of **9** + 30% of **10**	Diene additions to activated carbonyl groups are known (6)
3	1:1.03:0.85	$BF_3 \cdot Et_2O$ (distilled)	40	10 min	55% of **9** + 5% of **10** + 5% of C_2-epimer of **9**	2-Epi-**9** is an artefact; treatment of **9** with $BF_3 \cdot Et_2O$ in boiling CH_2Cl_2 for 1 h gives a 1:1 mixture of **9** and 2-epi-**9**
4	1:1.15:1	$SnCl_4$* (anhydrous)	0	<5 min	75% of **9**	Yield of recrystallized product is given; reaction essentially quantitative
5	1:1.1:0.1	$SnCl_4$* (anhydrous)	0	30 min	75% of **9**	Yield of recrystallized product

*Obtained neat and as a 1 M solution in CH_2Cl_2 from Alpha Products, Beverly, Mass., U.S.A.

student in this department, has made an experimental contribution.

1. Ž. STOJANAC, R. A. DICKINSON, N. STOJANAC, R. J. WOZNOW, and Z. VALENTA. Can. J. Chem. **53**, 616 (1975).
2. YU. A. TITOV. USSR Chem. Rev. **31**, 267 (1962); A. S. ONISHCHENKO. Diene synthesis. Israel Program of Scientific Translations, Jerusalem. 1964; J. SAUER. Angew. Chem. Int. Ed. Engl. 6, 16 (1967).
3. P. YATES and P. EATON. J. Am. Chem. Soc. **82**, 4436 (1960); T. INUKAI and T. KOJIMA. J. Org. Chem. **32**, 869 (1967); A. W. MCCULLOCH and A. G. MCINNES. Can. J. Chem. **49**, 3152 (1971); K. N. HOUK and R. W. STROZIER. J. Am. Chem. Soc. **95**, 4094 (1973).
4. F. BOHLMANN and E. INHOFFEN. Chem. Ber. **89**, 1276 (1956).
5. G. I. FRAY and R. ROBINSON. J. Am. Chem. Soc. **83**, 249 (1961); E. F. LUTZ and G. M. BAILEY. J. Am. Chem. Soc. **86**, 3899 (1964); W. KREISER, W. HAUMESSER, and A. F. THOMAS. Helv. Chim. Acta, **57**, 164 (1974); J. N. MARX and L. R. NORMAN. J. Org. Chem. **40**, 1602 (1975).
6. S. B. NEEDLEMAN and M. C. CHANG KUO. Chem. Rev. **62**, 405 (1962); A. KONOWAL, J. JURCZAK, and A. ZAMOJSKI. Rocz. Chem. **42**, 2045 (1968); R. A. RUDEN and R. BONJOUKLIAN. J. Am. Chem. Soc. **97**, 6892 (1975).
7. J. J. MYHER and K. E. RUSSELL. Can. J. Chem. **42**, 1555 (1964).

Can. J. Chem. Downloaded from www.nrcresearchpress.com by 210.87.254.105 on 09/05/12
For personal use only.

The construction of the substituted denudatine system by diene addition

K. WIESNER, T. Y. R. TSAI, G. I. DMITRIENKO, AND K. P. NAMBIAR

Natural Products Research Center, University of New Brunswick, P.O. Box 4400, Fredericton, N.B., Canada E3B 5A3

Received July 30, 1976

K. WIESNER, T. Y. R. TSAI, G. I. DMITRIENKO, and K. P. NAMBIAR. Can. J. Chem. **54**, 3307 (1976).

A simple stereospecific synthesis of the denudatine model **20** is described.

K. WIESNER, T. Y. R. TSAI, G. I. DMITRIENKO et K. P. NAMBIAR. Can. J. Chem. **54**, 3307 (1976).

On décrit une synthèse stéréospécifique simple du modèle **20** de la dénudatine.

[Traduit par le journal]

Can. J. Chem. Downloaded from www.nrcresearchpress.com by 210.87.254.6 on 09/05/12
For personal use only.

We have shown recently (1) that the diene **1** added maleic anhydride stereospecifically and gave exclusively the *exo* adduct **2**. We now wish to report a highly efficient and simple method for the synthesis of denudatine and substituted denudatine derivatives based on this finding. We have synthesized small quantities of the aromatic intermediates **3** and **4** by methods which we have previously reported in detail (2). However, with the substitution pattern of the aromatic ring in **3** and **4** these methods are laborious and a far more efficient route based on the addition of *p*-quinone and cyclopentadiene carboxylic ester is being worked out at present. In the meantime we report the construction of the denudatine C–D ring system on the model compound **5** prepared from an intermediate in the synthesis of **3** and **4** (Scheme 1).

Compound **5** was alkylated with bromomethyl acetate and potassium carbonate in acetone (3).

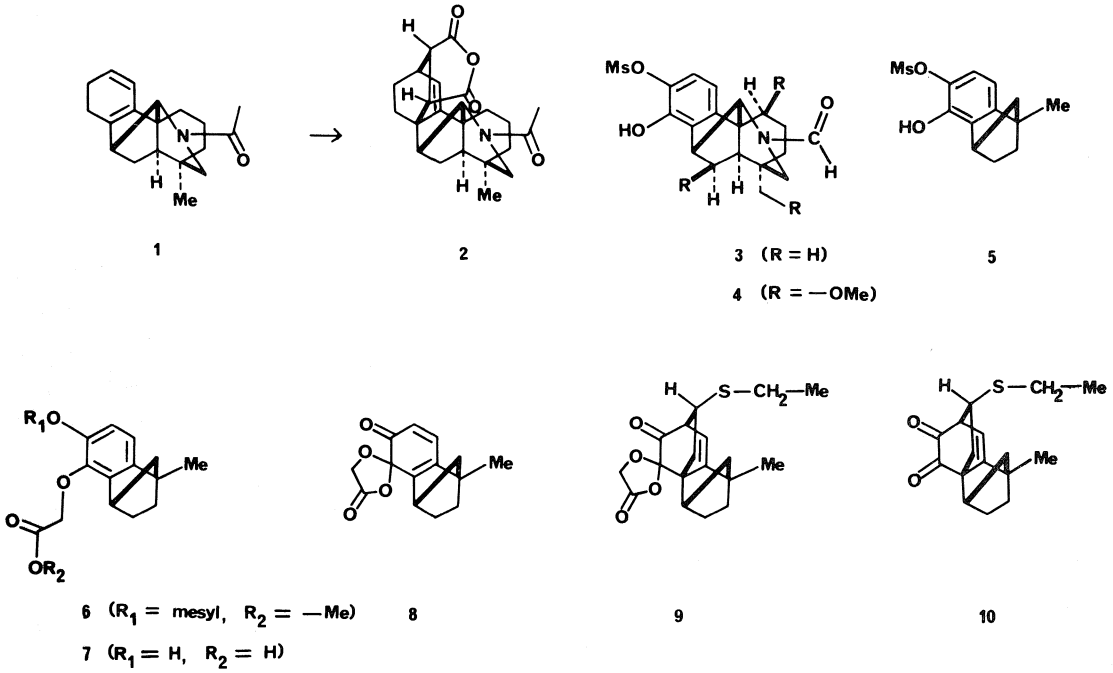

1 **2** **3** (R = H) **4** (R = —OMe) **5**

6 (R_1 = mesyl, R_2 = —Me) **7** (R_1 = H, R_2 = H) **8** **9** **10**

SCHEME 1

Can. J. Chem. Downloaded from www.nrcresearchpress.com by 210.87.254.6 on 09/05/12
For personal use only.

The product **6** obtained in a yield of 95% was used without purification.[1] Hydrolysis of **6** with 3 *N* potassium hydroxide yielded the crude acid **7**. This material was dissolved in dichloromethane and the solution was stirred with an aqueous solution of sodium acetate at 0–5 °C while a solution of *N*-bromosuccinimide in aqueous sodium acetate was added (3).

The dichloromethane solution of the masked quinone **8** obtained in this manner was dried, evaporated to dryness, and immediately treated with an excess of ethyl vinyl sulfide in ether. The product **9** which is a mixture of the two epimers at the spiro carbon was purified by recrystallization (mp 120–121 °C) and was obtained in a yield of 85% from **6**. Hydrolysis of **9** in aqueous methanolic potassium carbonate yielded 92% of the diketone **10** (mp 92–93 °C; ir ($CHCl_3$) 1743, 1733 cm^{-1} (diketone); nmr ($CDCl_3$) τ 8.74 (t, 3H, J = 7, S—CH_2—CH_3), 4.16 (d, 1H, J = 6, vinylic H)).

The diketone **10** was treated with an excess of trimethylsilylmethyl magnesium chloride in tetrahydrofuran (THF) (4). The product **11** was obtained in a yield of 75% after recrystallization (mp 116–117 °C; ir 1720 cm^{-1} (ketone); nmr τ 9.88 (s, 9H, —$Si(CH_3)_3$), 8.74 (t, 3H, J = 7, —S—CH_2—CH_3), 4.2 (*d*, 1H, J = 6, vinylic H)). Desulphurization of **11** with Ra–Ni in ethanol under reflux gave **12** (mp 138–139 °C, ir 1718 cm^{-1} (ketone); nmr (similar to **11** but —S—CH_2—CH_3 missing)) in a quantitative yield.

Treatment of compound **12** with 70% perchloric acid in THF at 45 °C for 2 h yielded 90% of the oily α,β-unsaturated ketone **13** (4) (ir 1705, 1632 cm^{-1} (ketone, exocyclic double bond); nmr τ 8.75 (s, 3H, C—CH_3), 4.97, 4.32 (d, J = 2, 1H, for each exocyclic vinylic proton), 4.15 (d, J = 6, 1H, vinylic proton)).

Compound **13** was treated with an excess of methanethiol in a mixture of water, THF, and sodium borate. The pure oily product **14** was obtained in a yield of 90% (ir 1715 cm^{-1} (ketone); nmr τ 7.89 (s, 3H, —S—CH_3)). Hydroboration, followed by hydrogen peroxide treatment (5) of compound **14** proceeded stereospecifically with respect to the double bond and yielded two products **15***a* and **15***b* epimeric at the R_2 asymmetric center, in a total yield of 85%.

15*a* (mp 179–180 °C; nmr τ 8.75 (s, 3H, —C—CH_3), 7.82 (s, 3H, —S—CH_3), 6.39 (d, 1H, J = 7, *CH*—OH), 6.23 (d, 1H, J = 10, C*H*—OH)).

15*b* (oily, the spectral data were similar to those of **15***a*, the mass spectra of **15***a* and **15***b* were identical).

Both **15***a* and **15***b* were transformed separately into the identical intermediate **18**. In order to conserve space we describe only the sequence with compound **15***a*. This material was acetylated with acetic anhydride and pyridine to the diacetate **16***a* (mp 106–107 °C) in a yield of 90%. Partial hydrolysis of **16***a* in an aqueous methanolic solution of potassium carbonate (p*H* 9.5) yielded 80% of the oily monoacetate **17***a* which was separated from some starting material **16***a* and diol **15***a* by chromatography on silica gel.

The monoacetate **17***a* was oxidized with dimethylsulfoxide and dicyclohexyl carbodiimide to the oily ketoacetate **18** in a yield of 80% and this material was saponified quantitatively to the oily ketoalcohol **19** in a mixture of THF and aqueous potassium hydroxide.

Compound **19** was heated under reflux with methyl iodide and the ternary sulfonium iodide which resulted was stirred at room temperature with aqueous potassium carbonate.

The crystalline hydroxyketone **20** (mp 115–116 °C) was obtained in a yield of 86% (ir (CCl_4) 1722, 1634 cm^{-1} (ketone, exocyclic double bond); nmr τ 8.72 (s, 3H, C—CH_3), 6.04 (d, 1H, J = 10, C*H*OH), 4.74, 3.95 (d, J = 2, 1H for each vinylic proton)).

Reduction of the ketone **20** with sodium borohydride yielded a mixture of oily epimeric alcohols one of which must have been analogous in configuration to the alkaloid denudatine **22**. These compounds were not investigated in detail. Instead the hydroxyketone **20** was converted to the crystalline (mp 153–154 °C) *p*-bromobenzoyl derivative **21** and this material was submitted to Dr. J. F. Blount, Hoffmann-La Roche, Nutley, New Jersey for X-ray structure determination. The result of the analysis confirmed the structure and configuration portrayed in the formula **21**. We believe that the method reported in this article represents not only a route to denudatine, but more important a very simple route to polysubstituted denudatine de-

[1]All crystalline compounds gave correct elemental analyses. Mass, nmr, and ir spectra of all compounds were recorded and were consistent with the structures assigned. Only specially significant values are reported to conserve space.

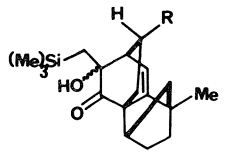

11 (R = $-S-CH_2-Me$)

12 (R = H)

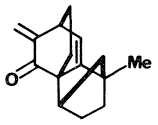

13

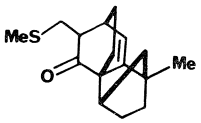

14

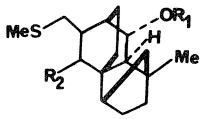

15a, 15b (R_1=H, R_2=~OH)

16a (R_1=Ac, R_2=~OAc)

17a (R_1=Ac, R_2=~OH)

18 (R_1=Ac, R_2=O)

19 (R_1=H, R_2=O)

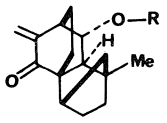

20 (R=H)

21 (R=p-bromobenzoyl)

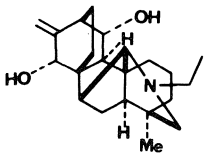

22

rivatives, which as we have already shown may be rearranged to alkaloids of the delphinine type (6).

Acknowledgments

We wish to thank Dr. J. F. Blount for the excellent and rapid structure determination of our final product and the National Research Council of Canada, Ottawa and Hoffmann-La Roche, Vaudreuil, Quebec, for financial support for these studies.

1. K. Wiesner, P. T. Ho, and S. Oida. Can. J. Chem. **52**, 1042 (1974).
2. K. Wiesner, P. T. Ho, D. Chang, Y. K. Lam, C. S. J. Pan, and W. Y. Ren. Can. J. Chem. **51**, 3975 (1973); S. F. Lee, G. M. Sathe, W. W. Sy, P. T. Ho, and K. Wiesner. Can. J. Chem. **54**, 1039 (1976).
3. D. Berney and P. Deslongchamps. Can. J. Chem. **47**, 515 (1969).
4. F. C. Whitmore, L. H. Sommer, J. Gold, and R. E. Van Strien. J. Am. Chem. Soc. **69**, 1551 (1947); R. A. Ruden and B. L. Gaffney. Synth. Commun. **5**, 15 (1975).
5. H. C. Brown and G. Zweifel. J. Am. Chem. Soc. **83**, 2544 (1961).
6. K. Wiesner, P. T. Ho, W. C. Liu, and M. N. Shanbhag. Can. J. Chem. **53**, 2140 (1975).

Can. J. Chem. Downloaded from www.nrcresearchpress.com by 210.87.254.6 on 09/05/12
For personal use only.

A new method of quaternizing amines and its use in amino acid and peptide chemistry[1]

FRANCIS C. M. CHEN AND N. LEO BENOITON
Department of Biochemistry, University of Ottawa, Ottawa, Canada K1N 9A9

Received July 8, 1976

FRANCIS C. M. CHEN and N. LEO BENOITON. Can. J. Chem. **54**, 3310 (1976).

Methyl iodide and potassium bicarbonate in methanol is presented as a mild, efficient, and selective reagent for the quaternization of amino groups. It does not attack hydroxyl groups. Its use with amino acids, derivatives of lysine, and small peptides is described.

FRANCIS C. M. CHEN et N. LEO BENOITON. Can. J. Chem. **54**, 3310 (1976).

On propose l'iodure de méthyle et le bicarbonate de potassium dans le méthanol comme réactif doux, efficace et sélectif pour la quaternisation des groupes aminés. Il ne réagit pas avec les groupes hydroxyles. On décrit son utilisation avec les acides aminés, des dérivés de la lysine et de petits peptides.

[Traduit par le journal]

Methods used for quaternizing primary or secondary amines involve alkylating agents and a strong inorganic base to bind the acid which is generated, and often prolonged reaction times and heat, which are conducive to undesirable side-reactions (1).[2,3] Compounds of biological interest such as carnitine (4) and $N^{\epsilon},N^{\epsilon},N^{\epsilon}$-trimethyllysine (5–7) have been prepared in this manner. Diazomethane in aqueous solution has also been used to prepare the latter (3), but the reaction is very slow. Our realization of the deficiency in these methods prompted a search for a better one.

We found the use of methyl iodide and the highly basic, sterically hindered and weakly nucleophilic amine 1,2,2,6,6-pentamethylpiperidine as hydrohalide acceptor (8) to be quite satisfactory for the quaternization of protected derivatives such as Bz-Lys-NHPh, Bz-Phe-Lys-OMe, and Boc-Ala-Lys-OMe; however, we were unable to separate the product from the hydroiodide of the base in the latter case. Furthermore, application of this method to zwitter-ionic compounds was impractical, since the reaction was incomplete and some quaternized base was also formed.

We wish to report the efficient quaternization of primary, secondary, and tertiary amines, using methyl iodide and potassium bicarbonate in methanol.[4] The reaction is carried out by stirring 1 ml of methyl iodide, 1 g of $KHCO_3$ and 1 mmol of substrate in 20 ml of methanol at room temperature, usually for 24 h. The method is mild,[5] reasonably selective, and of general applicability. Examples studied include various amino acids, peptides and their derivatives, derivatives and peptides containing a dimethylamino acid, and a benzylamino acid and histidine.[6] Only the tritylamino group and *p*-nitroaniline resisted, and were completely inert to the reagent.

The reagent does not attack a primary, secondary, or phenolic hydroxyl group, a primary or secondary amide, an ethyl ester, or an amino group protected by a benzyloxycarbonyl, *tert*-butyloxycarbonyl, or *p*-toluenesulfonyl radical.[7]

[1]Presented at the 14th European Peptide Symposium, Wépion, Belgium, April 11–17, 1976. Supported by a grant from the Medical Research Council of Canada. N.L.B. is an Associate of the M.R.C.C.

[2]Abbreviations are in compliance with IUPAC–IUB recommendations (2). Amino acid symbols represent the L-isomer. Boc = *tert*-butyloxycarbonyl, Bz = benzoyl, Bzl = benzyl, Z = benzyloxycarbonyl.

[3]For example, the formation of 10% of Bz-MeGly-Lys(Me_3^+)-O^- during the methylation of Bz-Gly-Lys-OH with dimethyl sulfate (3).

[4]Quaternization also occurred in 95% methanol, or using sodium bicarbonate, but did not using ethyl iodide in single experiments.

[5]Boc-Ser(Bzl)-OH which is susceptible to β-elimination was completely stable to the reagent.

[6]Ac-His-OH gave three Ac-His(Me_2)-OH positional isomers.

[7]Anomalous results were obtained with β-hydroxy, α-amino acids when the carboxyl group was an ester. H-Ser-OMe also underwent *O*-methylation to give Me_3^+Ser(Me)-OMe·I^- (75%, mp 98–101 °C), and the side-chain of H-Thr-OMe was cleaved. Carnitine remained inert to the reagent.

Can. J. Chem. Downloaded from www.nrcresearchpress.com by 210.87.254.105 on 09/05/12
For personal use only.

Can. J. Chem. Downloaded from www.nrcresearchpress.com by 210.87.254.105 on 09/05/12
For personal use only.

It also attacks sulfides and disulfides, and esterifies carboxyl groups to a small extent depending on their nature. The extent of esterification is exemplified by the following: leucine, γ-aminobutyric acid, serine, tyrosine, H-Gly-Gly-Gly-OH (0–3%); and Z-Ser-OH, Boc-Lys-OH, H-Gly-Gly-OH (8%).

For preparative purposes, the reaction mixture is evaporated to dryness, and the residue is left in chloroform on a mechanical shaker for 30 min. Evaporation of the extract gives the salt-free quaternary ammonium compounds if they do not contain a free carboxyl group. Zwitterionic compounds remain in the residue, but are freed of undesired ester by the extraction. Neutralization of the residue with aqueous hydrochloric acid, followed by evaporation and extraction with anhydrous acetone, gives the salt-free betaines. Compounds[8] prepared in this manner, from the corresponding unmethylated derivative, are Boc-Ala-Lys(Me_3^+)-OMe·I^- (from chloroform – ethyl acetate, 90%, mp 65–75 °C, $[\alpha]_D^{23}$ −30.7°, C, H, N), Me_3^+Ser-OH·I^- (48 h reaction time, from acetone – ethyl acetate, 90%, mp 77–79 °C, $[\alpha]_D^{23}$ −4.6°, C, H, N), Me_3^+Leu-OH·I^- (96%, mp 182–183 °C, C, H, N), Me_3^+-Thr-OH·I^- (85%, mp 145–147 °C), Me_3^+Phe-OEt·I^- (70%, mp 224–225 °C), Me_3^+Gly-Gly-O^- (80%), Me_3^+Gly-Gly-Gly-O^- (90%), Me_3^+-Ala-Gly-OMe·I^- (80%, mp 123–125 °C), Me_3^+Gly-Gly-Leu-OMe·I^- (97%), Z-Lys(Me_3^+)-O^-·H_2O (from acetone containing 1 drop methanol – ethyl acetate, 75%, mp 199–201 °C, $[\alpha]_D^{23}$ −4°, C, H, N), Boc-Lys(Me_3^+)-O^- (80%), and Boc-Orn(Me_3^+)-O^- (80%). The Z-derivative was labile to evaporation of its aqueous solution containing iodide, so was isolated by adsorption onto a cationic ion-exchange resin followed by elution with aqueous ammonia. The Boc-amino acid betaines, which were sensitive also to the resin treatment, were extracted into ethanol after removal of any ester. Final traces of inorganic salt were removed by extracting into cold ethanol again after evaporation of the mixture. Fine powders (hygroscopic) were obtained.

It is hoped that this method will prove useful in this and other areas of natural product chemistry.[9]

[8]All compounds had satisfactory nmr spectra. Optical rotations are for $c = 2$ in water.

1. J. Goerdeler. *In* Houben-Weyl, Methoden der organischen Chemie, Stickstoffverbindungen II/III. Vol. XI/2. *Edited by* E. Muller. Georg Thieme Verlag, Stuttgart, BRD. 1958. pp. 587–640.
2. IUPAC–IUB Commission on Biochemical Nomenclature. J. Biol. Chem. **247**, 977 (1972).
3. G. J. Moore and N. L. Benoiton. Can. J. Biochem. **53**, 1145 (1975).
4. F. Mazzetti and R. M. Lemmon. J. Org. Chem. **22**, 228 (1957).
5. T. Takemoto, K. Daigo, and N. Takagi. Yakugaku Zasshi, **84**, 1180 (1964).
6. B. Goffinet and G. Amiard. Fr. Patent No. 1, 176,-117 (1959); Chem. Abstr. **55**, 19865 (1961).
7. J. H. Seely and N. L. Benoiton. Can. J. Biochem. **48**, 1122 (1970).
8. H. Z. Sommer, H. I. Lipp, and L. L. Jackson. J. Org. Chem. **36**, 824 (1971).

[9]Dr. M. Kates of this department has found in a single experiment using tlc for analysis of products, that the reagent converted a phosphatidyl ethanolamine completely to the phosphatidyl choline, but with a small amount of lysophosphatidyl choline also appearing. The latter could be minimized or possibly eliminated by shortening the reaction time. Further investigation is contemplated.

Studies in solvolysis. Part IX. Some comments on anion–cation combination reactions

KENNETH HILLIER, JOHN MARSHALL WILLIAM SCOTT, DOUGLAS JAMES BARNES, AND FREDRICK JOSEPH PETER STEELE

Faculty of Medicine and Chemistry Department, Memorial University, St. John's, Nfld., Canada A1C 5S7

Received July 5, 1976

KENNETH HILLIER, JOHN MARSHALL WILLIAM SCOTT, DOUGLAS JAMES BARNES, and FREDRICK JOSEPH PETER STEELE. Can. J. Chem. **54**, 3312 (1976).

The general validity of the Ritchie equation $\log (k_n/k_0) = N^+$ is evaluated on the basis of the bimolecular rate constants for various nucleophiles attacking crystal violet, malachite green, and the tris-*p*-anisylmethyl carbonium ion. A more general form of the Ritchie equation is required to accommodate the data *viz.* $\log (k_n/k_0) = S^+N^+$ (S^+ = constant) for the most reactive carbonium ion. The latter modified form of the Ritchie equation is analogous to the Swain–Scott equation $\log (k_0/k_n) = sn$ and the new form follows the usual relationship between reactivity and selectivity, *i.e.* the value of S^+ for the tris-*p*-anisylmethyl carbonium ion is less than unity.

KENNETH HILLIER, JOHN MARSHALL WILLIAM SCOTT, DOUGLAS JAMES BARNES, et FREDRICK JOSEPH PETER STEELE. Can. J. Chem. **54**, 3312 (1976).

On évalue la validité générale de l'équation de Ritchie, $\log (k_n/k_0) = N^+$, en se basant sur les constantes de vitesses de réactions bimoléculaires de divers nucléophiles s'attaquant au cristal violet, au vert de malachite et à l'ion tris-*p*-anisylméthylcarbonium. On doit faire appel à une forme plus généralisée de l'équation de Ritchie pour tenir compte de toutes les données; par exemple on peut utiliser $\log (k_n/k_0) = S^+N^+$ (S^+ = constante) pour le carbocation le plus réactif. Cette dernière forme modifiée de l'équation de Ritchie est analogue à l'équation de Swain–Scott, $\log (k_0/k_n) = sn$, et la nouvelle forme suit la relation habituelle entre réactivité et sélectivité; par exemple la valeur de S^+ pour l'ion tris-*p*-anisylméthylcarbonium est plus faible que un.

[Traduit par le journal]

If nucleophilic substitution reactions are considered to take place via the Winstein (for a list of important references and explanation of symbols, see ref. 1) mechanism

[1]
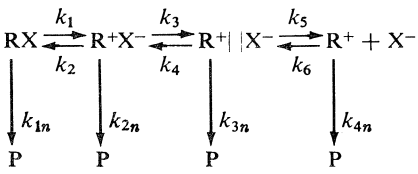

then a comparison of reactivities of nucleophiles reacting *via* the k_{1n} (or k_{2n}) and the k_{4n} steps is of interest. The problem so posed might be tackled by attempting to generate linear free energy relationships (LFER) between the k_{1n} (or k_{2n}) and k_{4n} rate constants if suitable rate constants are available. Since k_{1n} (or k_{2n}) values are available predominantly for primary centers and k_{4n} values are only known for tertiary centers, a LFER between such kinetic quantities would be likely to demonstrate stereochemical limitations.

To date two distinct and separate LFER's have been proposed in relation to the k_{1n} and k_{4n} rate constants. Primary centers (k_{1n}) have been considered via the Swain–Scott (2) LFER

[2] $$\log k/k_0 = sn$$

for which the standard nucleophile is water and the standard substrate is methyl bromide. The empirical s values are structure-sensitive (1) CH_3F (0.65 ± 0.07); CH_3Cl (0.95 ± 0.01); CH_3Br (1.00); CH_3I (1.12 ± 0.03) and significantly do *not* follow the reactivity of these substances with any particular nucleophile ($CH_3F < CH_3Cl < CH_3I < CH_3Br$). The deviation from the anticipated selectivity-reactivity sequence has been interpreted in terms of the Sneen (3, 4) intimate ion-pair mechanism (involving k_1, k_2, and k_{2n}) with the condition $k_2 > k_{2n}$. This provides an adequate rationalization of the poor correlation between reactivity and selectivity for the methyl halides.

In contrast to nucleophilic displacements at a primary center, anion–cation combination reac-

Can. J. Chem. Downloaded from www.nrcresearchpress.com by 210.87.254.5 on 09/05/12
For personal use only.

TABLE 1. Rate constants for the reactions of nucleophiles with crystal violet, malachite green and tri-*p*-anisylmethyl cation (25 °C)

	Crystal violet[a]		Malachite green[a]		Tri-*p*-anisylmethyl[a]	
Nucleophile	k_n, M^{-1} s^{-1}	log k_n	k_n, M^{-1} s^{-1}	log k_n	k_n, M^{-1} s^{-1}	log k_n
Water	2.00×10^{-7}	−6.70	—	—	2.2×10^{-1}	−0.66
	$(3.51\times10^{-7})^b$	−6.46	3.80×10^{-6}[c]	−5.42	$(2.2\times10^{-1})^{d,e}$	−0.66
Dabco	—	—	—	—	—	—
	—	—	2.6×10^{-3}[f]	−2.59	$6.2\pm0.3\times10^{1}$[g]	1.79
Triethylamine	—	—	—	—	—	—
	—	—	3.0×10^{-2}[f]	−1.52	$2.60\pm0.13\times10^{2}$[g]	2.42
Ammonia	$3.49\pm0.08\times10^{-2}$	−1.46	$3.03\pm0.06\times10^{-1}$	−0.52	$1.91\pm0.12\times10^{3}$	3.28
	—	—	—	—	$(1.6\times10^{3})^h$	—
Cyanide	$6.10\pm0.08\times10^{-2}$	−1.22	$4.90\pm0.05\times10^{-1}$	−0.31	—	—
	$(8.8\times10^{-2})^c$	−1.06	$(6.9\times10^{-1})^c$	−0.16	2.7×10^{3}[i]	3.43
Methoxylamine	$1.10\pm0.03\times10^{-1}$	−0.96	$9.6\pm0.2\times10^{-1}$	−0.02	$6.21\pm0.29\times10^{3}$	3.79
	—	—	$(9.1\times10^{-1})^j$	—	—	—
Hydroxide	$2.00\pm0.05\times10^{-1}$	−0.70	$1.60\pm0.06\times10^{0}$	0.20	$9.19\pm0.56\times10^{3}$	3.96
	$(2.05\times10^{-1})^c$	−0.69	$(2.18\times10^{0})^c$	0.34	$(8.2\times10^{3})^d$	3.91
Hydroxylamine	$6.32\pm0.73\times10^{-1}$[k]	−0.20	$4.34\pm0.08\times10^{0}$	0.64	$1.83\pm0.10\times10^{4}$	4.26
	—	—	$(9.0\times10^{0})^j$	—	—	—
Hydrazine	$6.03\pm0.04\times10^{0}$	0.78	$4.23\pm0.37\times10^{1}$	1.63	$9.43\pm0.53\times10^{4}$	4.98
	—	—	$(4.0\times10^{1})^j$	—	$(3.2\times10^{5})^h$	5.51
Sulfite	$3.58\pm0.03\times10^{2}$	2.55	$4.47\pm0.08\times10^{3}$	3.65	$5.10\pm0.40\times10^{6}$	6.71
	$(4.7\times10^{2})^j$	—	$(4.0\times10^{3})^j$	—	—	—
Hydrazine H^+	$6.14\pm0.22\times10^{-3}$	−2.21	$2.56\pm0.09\times10^{-2}$	−1.59	—	—
	—	—	—	—	—	—
Hypochlorite	$9.49\pm0.09\times10^{1}$	1.98	$1.40\pm0.05\times10^{3}$	3.15	—	—
	—	—	—	—	—	—

[a]Ionic strength ranged between 10^{-3} to 10^{-1} *M* when not indicated for crystal violet and malachite green and the rates for the tri-*p*-anisylmethyl cation are in the presence of 0.05 *M* NaCl: see refs. 9 and 10.
[b]Reference 6.
[c]Reference 7.
[d]Reference 8.
[e]Reference 11.
[f]Reference 12.
[g]Reference 13.
[h]Reference 14. We do not at present understand the source of the discrepancy between these measurements.
[i]Reference 14.
[j]Data obtained at 23 °C; see ref. 15.
[k]Data obtained at μ = 0.60 and 1.20 *M*.
[l]Data obtained at 30 °C; see ref. 16.

tions (k_{4n}) involving tertiary centers show no change in selectivity with change of substrate. Thus on the basis of an extensive series of measurements using water as the standard nucleophile and 4-nitromalachite green (or malachite green) as the standard substrate Ritchie (Part XIII, see ref. 5; for further references see Parts I to XII.) proposes the equation

$$[3] \qquad \log k/k_0 = N^+$$

which accommodates this unusual and interesting situation. The purpose of the present communication is to establish an important exception to eq. 3. In Table 1 we have collected and report second order rate constants for the attack of a wide range of charged and neutral nucleophiles on the triarylmethyl carbonium ions, crystal violet (C.V.), malachite green (M.G.), and the tri-*p*-anisylmethyl cation (T-*p*-AMC). The LFER between M.G. and C.V. (Fig. 1) is excellent and has a slope of 1.01 ± 0.02 which is in agreement with eq. 3. However, the equally excellent LFER involving M.G. and the T-*p*-AMC (Fig. 2) gives a slope which is significantly less than unity (0.81 ± 0.01) and thus requires a modified version of eq. 3 which is logically

$$[4] \qquad \log k/k_0 = S^+N^+$$

In the case of the tertiary centers the quantity S^+ appears to be a much slower changing function of reactivity than for the primary compounds. The relationship of the *n* and N^+ scales remains an interesting problem as does the significance of eq. 4 with respect to the mechanism of these

Can. J. Chem. Downloaded from www.nrcresearchpress.com by 210.87.254.5 on 09/05/12
For personal use only.

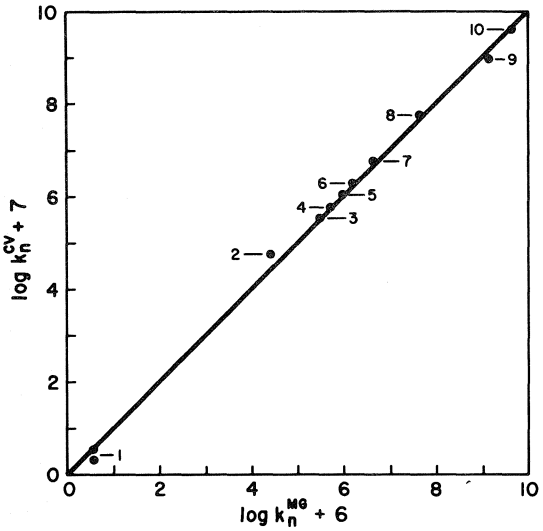

FIG. 1. Rates of reactions of nucleophiles with malachite green *vs.* the rates of reactions of nucleophiles with crystal violet. Points are identified as follows: (*1*) water; (*2*) hydrazine H^+; (*3*) ammonia; (*4*) cyanide; (*5*) methoxylamine; (*6*) hydroxide; (*7*) hydroxylamine; (*8*) hydrazine; (*9*) hypochlorite; (*10*) sulfite.

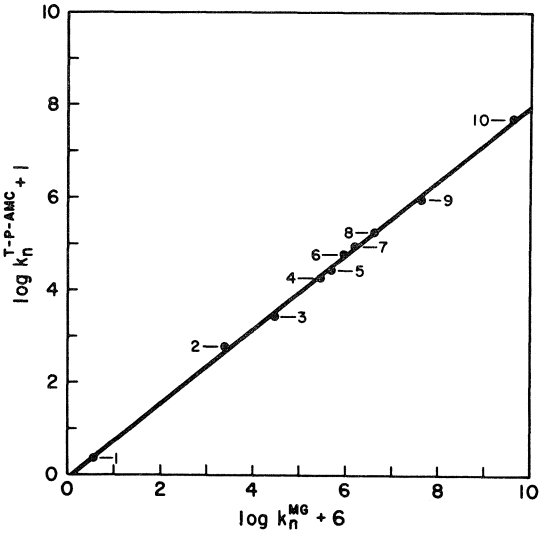

FIG. 2. Rates of reactions of nucleophiles with malachite green *vs.* the rates of reactions of nucleophiles with tri-*p*-anisylmethyl cation. Points are identified as follows: (*1*) water; (*2*) DABCO; (*3*) triethylamine; (*4*) ammonia; (*5*) cyanide; (*6*) methoxylamine; (*7*) hydroxide; (*8*) hydroxylamine; (*9*) hydrazine; (*10*) sulfite.

reactions. Fuller discussions of this aspect of our work will appear elsewhere.

Acknowledgement

The authors wish to thank the National Research Council of Canada for support of this work.

1. J. M. W. SCOTT. Can. J. Chem. **48**, 3807 (1970).
2. C. G. SWAIN and C. B. SCOTT. J. Am. Chem. Soc. **75**, 141 (1953).
3. R. SNEEN and J. W. LARSEN. J. Am. Chem. Soc. **91**, 362 (1969).
4. R. SNEEN. Acc. Chem. Res. **6**, 46 (1973).
5. C. D. RITCHIE. J. Am. Chem. Soc. **97**, 1170 (1975).
6. C. D. RITCHIE *et al.* J. Am. Chem. Soc. **97**, 1163 (1975).
7. C. D. RITCHIE, G. A. SKINNER, and V. G. BADDING. J. Am. Chem. Soc. **89**, 2063 (1967).
8. C. A. BUNTON and S. K. HUANG. J. Am. Chem. Soc. **94**, 3536 (1972).
9. D. J. BARNES, K. HILLIER, and J. M. W. SCOTT. In press.
10. K. HILLIER, F. J. P. STEELE, and J. M. W. SCOTT. Can. J. Chem. To be published.
11. E. A. HILL and W. J. MUELLER. Tetrahedron Lett. 2565 (1968).
12. C. D. RITCHIE. J. Am. Chem. Soc. **94**, 3275 (1972).
13. J. N. RIDE, P. A. H. WYATT, and Z. M. ZOCHOWSKI. J. C. S. Perkin II, 1188 (1974).
14. C. A. BUNTON and S. K. HUANG. J. Am. Chem. Soc. **95**, 2701 (1973).
15. C. D. RITCHIE and P. O. I. VIRTANEN. J. Am. Chem. Soc. **95**, 1882 (1973).
16. J. E. DIXON and T. C. BRUICE. J. Am. Chem. Soc. **93**, 6592 (1971).

Can. J. Chem. Downloaded from www.nrcresearchpress.com by 210.87.254.5 on 09/05/12
For personal use only.

Can. J. Chem. Downloaded from www.nrcresearchpress.com by 210.87.254.105 on 09/05/12
For personal use only.

Canadian Journal of Chemistry

Published by
THE NATIONAL RESEARCH COUNCIL OF CANADA

Journal canadien de chimie

Publié par
LE CONSEIL NATIONAL DE RECHERCHES DU CANADA

Volume 54 Number 21 November 1, 1976 Volume 54 numéro 21 1 novembre 1976

Heat capacities of aqueous electrolytes: eight 1:1 electrolytes and ΔC_p^0 for ionization of water at 298 K

PREM PAUL SINGH,[1] EARL M. WOOLLEY,[2] KEITH G. MCCURDY, AND LOREN G. HEPLER
Department of Chemistry, University of Lethbridge, Lethbridge, Alta., Canada T1K 3M4

Received April 29, 1976

PREM PAUL SINGH, EARL M. WOOLLEY, KEITH G. MCCURDY, and LOREN G. HEPLER. Can. J. Chem. **54,** 3315 (1976).

We have made measurements with a flow calorimeter leading to apparent molal heat capacities of aqueous solutions of NaCl, HCl, KBr, KCl, KOH, NaBr, HBr, and NaOH at 298 K. Results have been used to derive apparent molal heat capacities of these electrolytes at infinite dilution and thence $\Delta C_p^0 = -215.2 \pm 4$ J K^{-1} mol^{-1} for ionization of H_2O(liq) at 298 K.

PREM PAUL SINGH, EARL M. WOOLLEY, KEITH G. MCCURDY et LOREN G. HEPLER. Can. J. Chem. **54,** 3315 (1976).

On a fait des mesures, à l'aide d'un calorimètre à écoulement, qui permettent de déterminer les capacités calorifiques molales partielles apparentes de solutions aqueuses de NaCl, HCl, KBr, KCl, KOH, NaBr, HBr et NaOH à 298 K. On a utilisé ces résultats pour en dériver les capacités calorifiques molales apparentes de ces électrolytes à dilution infinie d'où on a tiré que $\Delta C_p^0 = -215.2 \pm 4$ J k^{-1} mol^{-1} pour l'ionisation de H_2O(liquide) à 298 K.

[Traduit par le journal]

Introduction

It has been known since 1858 when Kirchhoff (1) derived

$$[1] \qquad (\partial \Delta H/\partial T)_p = \Delta C_p$$

that heat capacities are useful for classical thermodynamic calculations. Following Einstein's (2) application of quantum theory and statistical thermodynamics to the theory of the temperature dependence of the heat capacities of simple solids, there have been many instances in which heat capacities have been used in obtaining information about the microscopic properties of various systems. Although generalizations concerning the usefulness of heat capacities are about equally valid for solids, liquids, gases, and solutions, difficulties in making the appropriate measurements on solutions have severely inhibited such investigations.

Recent developments in calorimetry have diminished some of the experimental difficulties previously associated with measurement of heat capacities of dilute solutions. Nearly simultaneous increased interest in the properties of aqueous solutions at temperatures other than ~298 K has provided new incentive for applying calorimetry to investigation of heat capacities of aqueous solutions with a view toward providing thermodynamic properties that will be useful for calculations leading to knowledge of aqueous systems at various temperatures.

In this paper we report the results of our heat

[1]On leave from Department of Chemistry and Biochemistry, Punjab Agricultural University, Ludhiana, India.

[2]On leave from Department of Chemistry, Brigham Young University, Provo, Utah, U.S.A.

TABLE 1. Apparent molal heat capacities of aqueous electrolytes at 298 K*

Solute	ϕ_C^0 (J K^{-1} mol^{-1})	B (eq. 2)	Concentration range (m)	Number of concentrations investigated
NaCl	−84.6±0.4	13.4±1.3	0.08–0.50	11
HCl	−127.2±0.2	−6.9±0.8	0.07–0.57	15
KCl	−114.1±0.2	6.7±0.7	0.05–0.72	12
KBr	−119.1±0.1_4	3.3±0.5	0.05–0.60	11
KOH	−127.0±0.2	9.9±0.9	0.05–0.44	12
NaOH	−96.2±0.2	28.0±0.5	0.10–0.73	11
NaBr	−88.4±0.2	13.5±0.8	0.04–0.46	13
HBr	−132.6±0.2	4.6±1.3	0.05–0.31	20

*We use ± values here to indicate standard deviations. Limits on systematic uncertainties are discussed in the text.

capacity measurements on dilute aqueous solutions of eight important 1:1 electrolytes (NaCl, HCl, KBr, KCl, KOH, NaBr, HBr, and NaOH) at 298 K. Part of the motivation behind these measurements was simply to determine apparent and partial molal heat capacities of these electrolytes for subsequent thermodynamic calculations. More immediately, we are concerned with combination of the results of this investigation to obtain ΔC_p^0 for ionization of water.

Experimental

Most of our heat capacity measurements have been made with a Picker flow calorimeter that has been described in several publications (3–7) from the Université de Sherbrooke. Because the flow calorimeter measures volumetric specific heats, we have also measured densities of all of our solutions as previously described (8). Calorimetrically measured volumetric heat capacities have been combined with our densities and known compositions of solutions to obtain apparent molal heat capacities (ϕ_C) as described previously (3, 4) and subsequently modified (7).

Most of our calorimetric measurements were made with flow rate about 0.6 cc/min. Heating rates were generally set at 100 mW. Measurements on solutions with concentrations less than ~0.15 mol/kg were made relative to water. Some measurements on more concentrated solutions were also made relative to water, but most were made relative to more dilute solutions.

A few heat capacity measurements on relatively concentrated solutions were made with the 100 ml glass calorimeter of the LKB 8700 system.

Solutions of NaCl, NaBr, KCl, and KBr were prepared by weight from Fisher certified analytical reagents and freshly degassed distilled water.

Five different stock solutions of NaOH (B.D.H. Analar) were prepared at different times. Carbonate was removed as described by Vogel (9). The resulting carbonate-free solutions were standardized against potassium acid phthalate. All dilutions of these stock solutions were made with degassed water.

One stock solution of NaOH was freed from carbonate by careful addition of $Ba(OH)_2$ solution to precipitate barium carbonate. Five different stock solutions of KOH (B.D.H. Analar) were also prepared in this way. All of these solutions were then standardized by titration as described above.

Five HCl (ACS reagent grade) solutions were standardized against NaOH solutions prepared as above, while one HCl solution was standardized against HgO as described by Kolthoff *et al.* (10). Stock solutions of HBr were prepared and standardized similarly; all such solutions were stored in brown bottles and handled in a partially darkened laboratory.

Results and Discussion

Our experimental results (compositions of solutions, thermal data from calorimetric measurements, and densities of solutions) have been combined as previously described (3–7) to obtain apparent molal heat capacities (ϕ_C).[3] The ϕ_C values so obtained are accurately represented by equations of the form

$$[2] \qquad \phi_C = \phi_C^0 + 28.95m^{1/2} + Bm$$

in which ϕ_C^0 represents the apparent molal heat capacity at infinite dilution. The coefficient of $m^{1/2}$ is derived from the Debye–Hückel theory and B is an adjustable parameter for each solute. We list ϕ_C^0 and B values for each electrolyte in Table 1, along with the concentration ranges of solutions and statistical measures of the accuracy of fit of [2].

Although our principal interest in this investigation has been the measurements on relatively dilute solutions in order to obtain ϕ_C^0 values, we

[3]Complete set of the actual experimental data is available, at a nominal charge, from the Depository of Unpublished Data, CISTI, National Research Council of Canada, Ottawa, Canada K1A 0S2.

Can. J. Chem. Downloaded from www.nrcresearchpress.com by 210.87.254.105 on 09/05/12
For personal use only.

Can. J. Chem. Downloaded from www.nrcresearchpress.com by 210.87.254.105 on 09/05/12
For personal use only.

have made a few measurements on more concentrated solutions in order to obtain some independent checks on the accuracy of the flow calorimeter. To this end we have used the LKB (non-flow) 8700 calorimetric system for measurements leading to apparent molal heat capacities of 1.0 and 3.2 *m* NaCl solutions. Details of the method and results will be reported later; for now it is sufficient to state that results of these measurements and our measurements with the flow calorimeter (with calculations done as described recently (7)) are in good agreement. Further, these results for concentrated solutions are also in good agreement with heat capacities measured by Cerutti (11). Thus we have confidence in the accuracy as well as the sensitivity of the flow calorimeter.

We now turn to several comparisons of our ϕ_C^0 values with those reported by earlier investigators.

Parker (12) has reviewed earlier heat capacity measurements on aqueous NaCl and selected $\phi_C^0 = -90.0$ J K^{-1} mol^{-1} as the "best" value. Measurements of enthalpies of solution at different temperatures have led Criss and Cobble (13) to $\phi_C^0 = -79.1$ J K^{-1} mol^{-1}. Flow calorimetric measurements have led Picker *et al.* (3) to $\phi_C^0 = -82.4$ J K^{-1} mol^{-1} and Desnoyers and co-workers (4, 7) to $\phi_C^0 = -84.4$ J K^{-1} mol^{-1}. Our $\phi_C^0 = -84.6$ J K^{-1} mol^{-1} is in good agreement with the latter two values and in fair agreement with the value obtained by Criss and Cobble (13).

Parker (12) has selected $\phi_C^0 = -136.4$ J K^{-1} mol^{-1} for aqueous HCl. Enthalpy of solution measurements have led Ahluwalia and Cobble (14) to $\phi_C^0 = -127.6$, while flow calorimetric measurements have led Desnoyers and co-workers (4, 7) to $\phi_C^0 = -124.1$ J K^{-1} mol^{-1}. Our $\phi_C^0 = -127.2$ J K^{-1} mol^{-1} for aqueous HCl is in especially good agreement with one of these values and fair agreement with another.

For aqueous KCl we have $\phi_C^0 = -114.6$ J K^{-1} mol^{-1} from Parker (12) and -114.2 J K^{-1} mol^{-1} from Desnoyers and co-workers (4, 7), in excellent agreement with our -114.1 J K^{-1} mol^{-1}. There is similar excellent agreement between $\phi_C^0 = -120.1$, -118.3, and -119.1 J K^{-1} mol^{-1} for aqueous KBr from Parker (12), Desnoyers and co-workers (4, 7), and from our work, respectively.

Our $\phi_C^0 = -127.0$ J K^{-1} mol^{-1} for aqueous KOH is in agreement with $\phi_C^0 = -126.8$ J K^{-1} mol^{-1} selected by Parker (12). For aqueous NaOH we have $\phi_C^0 = -102.1$, -94.6, and -96.2 J K^{-1} mol^{-1} from Parker (12), Desnoyers and co-workers (7, 15), and from our work, respectively.

Parker (12) has selected $\phi_C^0 = -95.4$ J K^{-1} mol^{-1} for aqueous NaBr. Desnoyers and co-workers (4, 7) have reported $\phi_C^0 = -88.1$ J K^{-1} mol^{-1}, in good agreement with our -88.4 J K^{-1} mol^{-1}.

For aqueous HBr Parker (12) has selected $\phi_C^0 = -141.8$ J K^{-1} mol^{-1}, while our measurements have led us to $\phi_C^0 = -132.6$ J K^{-1} mol^{-1}.

One of the principal purposes of this research has been to obtain quantities that would permit calculation of ΔC_p^0 for ionization of water that we represent by

$$[3] \qquad H_2O(liq) = H^+(aq) + OH^-(aq)$$

Because $\phi_C^0 \equiv \bar{C}_p^0$ for a solute at infinite dilution, we can combine our results from Table 1 as follows to obtain the desired ΔC_p^0 of ionization of water:

$$[4] \quad \Delta C_p^0 = \phi_C^0(MOH) + \phi_C^0(HX) - \phi_C^0(MX) - C_p^0(H_2O)$$

Using our results from Table 1 with $C_p^0(H_2O) = 75.29$ J K^{-1} mol^{-1} (16), we obtain the four semi-independent ΔC_p^0 values that are listed in Table 2. On the basis of all these results, we choose $\Delta C_p^0 = -215.2 \pm 0.8$ J K^{-1} mol^{-1} as the best value to be derived from our work. Here we have used $\pm$ to indicate the standard deviation; limits on systematic uncertainties are discussed below.

Our assessment of uncertainties in the various measured quantities and subsequent calculations leading to ϕ_C and ϕ_C^0 values suggests that the *total* uncertainty in each of these latter quantities

TABLE 2. ΔC_p^0 values for ionization of H_2O(liq) at 298 K*

M^+, X^-	ΔC_p^0 (J K^{-1} mol^{-1})
K^+, Cl^-	-215.4 ± 0.4
K^+, Br^-	-215.8 ± 0.3
Na^+, Cl^-	-214.1 ± 0.5
Na^+, Br^-	-215.7 ± 0.3

*We use $\pm$ values here to indicate standard deviations. Limits on systematic uncertainties are discussed in the text.

as listed in our Table 1 is about ± 3 J K^{-1} mol^{-1}. This estimate of *total* uncertainty is consistent with agreement of some of our results with related results of some other investigators already cited. Because all of our measurements and calculations leading to $\phi_C{}^0$ values have been carried out similarly, relative accuracies of our results are better than indicated by the above *total* uncertainties; we estimate that *total* uncertainties in differences between any two of our $\phi_C{}^0$ values are about ± 1 J K^{-1} mol^{-1}. We therefore estimate that the *total* uncertainty in our $\Delta C_p{}^0$ for ionization of water is ± 4 J K^{-1} mol^{-1}.

Various previous investigations have led to $\Delta C_p{}^0$ values for ionization of water at 298 K ranging from -195 to -225 J K^{-1} mol^{-1}, as recently reviewed and calculated (17, 18). Largely on the basis of results from Parker (12), values at the negative end of this range were selected (17, 18) as the "best" ones then available. We now suggest that these earlier values should be replaced by our new $\Delta C_p{}^0 = -215.2$ J K^{-1} mol^{-1} (estimated ± 4 J K^{-1} mol^{-1}).

Acknowledgments

We thank the National Research Council of Canada for support of this research and Brigham Young University for sabbatical leave support to E.M.W. We also thank Professor J. E. Desnoyers for sending us a manuscript copy of his paper that is cited as ref. 7.

NOTE ADDED IN PROOF:

G. Olofsson and I. Olofsson (University of Lund, Sweden) have recently informed us that they have completed calorimetric measurements leading to the standard enthalpy of ionization of water at six temperatures from 0 to 50 °C. They have analyzed their results to obtain $\Delta C_p{}^0 = -214 \pm 5$ J K^{-1} mol^{-1} for ionization of water at 298 K, in excellent agreement with the new value we have reported here.

1. G. KIRCHHOFF. Ann. Phys. (2)**103**, 177 (1858).
2. A. EINSTEIN. Ann. Phys. **22**, 180 (1907).
3. P. PICKER, P.-A. LEDUC, P. R. PHILIP, and J. E. DESNOYERS. J. Chem. Thermodyn. **3**, 631 (1971).
4. J.-L. FORTIER, P.-A. LEDUC, and J. E. DESNOYERS. J. Solution Chem. **3**, 323 (1974).
5. P. PICKER. Can. Res. Dev. 11 (1974).
6. G. PERRON, J.-L. FORTIER, and J. E. DESNOYERS. J. Chem. Thermodyn. **7**, 1177 (1975).
7. J. E. DESNOYERS, C. DE VISSER, G. PERRON, and P. PICKER. J. Solution Chem. In press.
8. P. PICKER, E. TREMBLAY, and C. JOLICOEUR. J. Solution Chem. **3**, 377 (1974).
9. A. I. VOGEL. A text-book of quantitative inorganic analysis. Longmans Canada, Ltd., Toronto. 1962.
10. I. M. KOLTHOFF, E. B. SANDELL, E. J. MEEHAN, and S. BRUCKENSTEIN. Quantitative chemical analysis. 4th ed. McMillan, New York. 1971.
11. P. J. CERUTTI. Ph.D. Thesis, University of South Carolina, 1975.
12. V. B. PARKER. Thermal properties of aqueous uni-univalent electrolytes. National Standard Reference Data Series, National Bureau of Standards 2, Washington, D.C. 1965.
13. C. M. CRISS and J. W. COBBLE. J. Am. Chem. Soc. **83**, 3223 (1961).
14. J. C. AHLUWALIA and J. W. COBBLE. J. Am. Chem. Soc. **86**, 5381 (1964).
15. G. PERRON, J. E. DESNOYERS, and F. J. MILLERO. Can. J. Chem. **53**, 1134 (1975).
16. D. D. WAGMAN, W. H. EVANS, V. B. PARKER, I. HALOW, S. M. BAILEY, and R. H. SCHUMM. National Bureau of Standards Technical Note 270-3. Washington, D.C. 1968.
17. L. G. HEPLER and E. M. WOOLLEY. *In* Water: a comprehensive treatise. Vol. 3. *Edited by* F. Franks. Plenum Press, New York. 1973.
18. G. OLOFSSON and L. G. HEPLER. J. Solution Chem. **4**, 127 (1975).

Can. J. Chem. Downloaded from www.nrcresearchpress.com by 210.87.254.105 on 09/05/12
For personal use only.

Crystal structure of $CaK_2As_2O_7$ and $CdK_2P_2O_7$

ROMOLO FAGGIANI AND CRISPIN CALVO
Institute for Materials Research, McMaster University, Hamilton, Ont., Canada L8S 4M1

Received December 11, 1975[1]

ROMOLO FAGGIANI and CRISPIN CALVO. Can. J. Chem. **54**, 3319 (1976).

Crystals of $CaK_2As_2O_7$ and $CdK_2P_2O_7$, both grown from the melt, are monoclinic with $Z = 4$. The lattice parameters are $a = 9.222(6)$, $b = 5.835(3)$, $c = 14.698(10)$ Å, $\beta = 105.84(5)°$ with space group $P2_1/c$ for the diarsenate and $a = 9.737(2)$, $b = 5.548(1)$, $c = 12.766(2)$ Å, $\beta = 106.50(2)°$ with space group $C2/c$ for the diphosphate. The structures were refined by full-matrix least-squares methods utilizing 2070 reflections ($R = 0.056$) for the diarsenate and 1145 reflections ($R = 0.067$) for the diphosphate. Both structures contain pseudo-hexagonally packed anions, in staggered configurations, forming layers with the divalent cations in six coordinate sites between the layers. The average M—O bond lengths are 2.342 and 2.290 Å for M = Ca and Cd respectively. The K ion has nine oxygen atoms with mean K—O bond lengths of 2.943 and 3.020 Å in the diarsenate in the coordination sphere. The mean of the ten shortest K—O is 2.939 Å in the diphosphate.

ROMOLO FAGGIANI et CRISPIN CALVO. Can. J. Chem. **54**, 3319 (1976).

Les cristaux du $CaK_2As_2O_7$ et du $CdK_2P_2O_7$, ont été obtenus tous les deux à partir de l'état fondu et sont monocliniques avec $Z = 4$. Les paramètres de la maille sont $a = 9.222(6)$, $b = 5.835(3)$, $c = 14.698(10)$ Å, $\beta = 105.84(5)°$ avec un groupe d'espace $P2_1/c$ pour le diarsenate et $a = 9.737(2)$, $b = 5.548(1)$, $c = 12.766(2)$ Å, $\beta = 106.50(2)°$ avec un groupe d'espace $C2/c$ pour le diphosphate. On a affiné les structures par la méthode des moindres carrés (matrice complète) utilisant 2070 réflexions ($R = 0.056$) pour le diarsenate et 1145 réflexions ($R = 0.067$) pour le diphosphate. Chacune des structures contient des ions placés dans des positions pseudo hexagonales, dans des configurations décalées, formant des couches avec les cations divalents placés dans des sites hexacoordonnés entre les couches. Les longueurs moyennes des liaisons M—O sont respectivement de 2.342 et de 2.290 Å pour M = Ca et Cd. L'ion K est lié à six atomes d'oxygène; les valeurs moyennes des liaisons K—O sont de 2.943 et de 3.020 Å dans la sphère de coordination du diarsenate. Dans le diphosphate, la valeur moyenne des dix distances K—O les plus courtes est de 2.939 Å.

[Traduit par le journal]

Introduction

At present the known structure types with diortho ions, X_2O_7, and stoichiometry $M_3X_2O_7$ are limited. $Pb_3Si_2O_7$, lead barysilite, is rhombohedral with space group $R\bar{3}c$ (1). A large number of compounds are found to crystallize in the akermanite structure type (2). Akermanite itself has the composition $Ca_2MgSi_2O_7$, while the isostructural melite (3) and hardystonite (4) have compositions corresponding to $Ba_2FeSi_2O_7$ and $Ca_2ZnSi_2O_7$ respectively. These structures are tetragonal with a near 8 Å and c near 5 Å.

The structure type changes when all the cations have radii near or greater than 1 Å. The structures become monoclinic, as in the present cases and in $K_2ZrSi_2O_7$ (5) and $CaK_2P_2O_7$ (6), or triclinic as in $Na_2ZrSi_2O_7$ (7). The unit cell parameters of the two diphosphates and diarsenates are closely related although the space groups differ. On the other hand, the parameters of $CaK_2P_2O_7$, transformed to space group $P2_1/c$, are $a = 9.79$, $b = 5.69$, $c = 13.57$ Å, with $\beta = 112° 11'$ (6) as compared with those of $K_2ZrSi_2O_7$ where $a = 9.54$, $b = 5.60$, $c = 14.26$ Å, and $\beta = 116.51°$. This suggests that these structures might be isostructural.

Experimental

$CaK_2As_2O_7$

Crystals of $CaK_2As_2O_7$ were prepared by thoroughly mixing K_2CO_3, CaO, and As_2O_5 in the molar ratios of 1:1:1 and heating the mix in a platinum crucible held at 700 °C for 4 h. The crucible and sample were then cooled to 500 °C at 3°/h and quenched to room temperature. Clear, colorless, mildly hygroscopic crystals were obtained. One of these, of cylindrical shape and a radius of 0.075 mm and length of 0.25 mm, was selected and sealed in a capillary tube. Precession photographs showed the space group to be $P2_1/c$ ($0k0$, k odd and $h0l$, l odd reflections were absent). Accurate lattice parameters were obtained by least-square fit to 15 well-centred reflections with 2θ near 25°. Graphite monochromatized MoKα

[1]Revision received July 21, 1976.

Can. J. Chem. Downloaded from www.nrcresearchpress.com by 210.87.254.42 on 09/05/12
For personal use only.

TABLE 1. Atomic and thermal parameters for $CaK_2As_2O_7$ with standard deviations in parentheses*

Atom	x	y	z	U_{11}	U_{22}	U_{33}	U_{12}	U_{13}	U_{23}
Ca	0.7341(1)	0.2726(2)	0.13742(9)	11.1(6)	10.5(6)	11.9(5)	−0.2(5)	3.7(5)	−0.6(5)
K(1)	0.5337(2)	0.2318(3)	0.3348(1)	17.6(7)	16.5(7)	24.4(7)	−1.8(7)	4.7(6)	−2.1(7)
K(2)	0.9669(2)	0.2558(3)	0.3879(1)	26.5(9)	28.5(8)	16.5(8)	8.8(7)	5.7(7)	3.9(8)
As(1)	0.31519(8)	0.2065(1)	0.02852(5)	13.3(3)	8.7(3)	10.5(3)	0.1(3)	4.2(2)	0.6(2)
As(2)	0.17478(7)	0.2603(1)	0.19770(4)	9.9(3)	8.2(3)	12.6(3)	0.5(3)	4.4(2)	−0.2(3)
O(C)	0.1654(5)	0.3006(8)	0.0749(3)	16(2)	29(3)	17(2)	9(2)	6(2)	4(2)
O(1)	0.2609(5)	0.0097(7)	0.2285(3)	15(3)	9(2)	19(2)	0(2)	4(2)	0(2)
O(2)	−0.0066(5)	0.2615(9)	0.1929(4)	12(2)	32(3)	25(3)	3(2)	6(2)	0(2)
O(3)	0.2687(5)	0.4881(8)	0.2501(3)	18(3)	10(2)	21(3)	−5(2)	6(2)	−6(2)
O(4)	0.2743(6)	−0.0681(8)	0.0017(4)	41(3)	15(2)	19(3)	−4(2)	9(3)	−5(2)
O(5)	0.4728(5)	0.2504(9)	0.1127(3)	17(3)	29(3)	23(2)	−4(2)	2(2)	−5(2)
O(6)	0.2867(6)	0.3680(4)	−0.0681(3)	38(3)	20(3)	20(3)	5(2)	14(2)	8(2)

*Thermal parameters appear in the thermal factor through exp $-2\pi^2 \times 10^{-3}(h^2b_1^2U_{11} + \ldots + 2hkb_1b_2U_{12} + \ldots)$ with the b_i's as reciprocal lattice vectors. All U's in Å².

(0.71069 Å) at 21 °C gave the following crystal data:
$CaK_2As_2O_7$ fw = 292.24
Monoclinic: a = 9.222(6), b = 5.835(3), c = 14.698(10) Å, β = 105.84(5)° V = 758.30 Å³, Z = 4, D_m = 3.31 ± 2 g/cm³, D_{calcd} = 3.340 g/cm³. The density was measured by pycnometry with isopropyl alcohol as the displacement liquid.

A total of 2070 symmetry independent reflections were collected within a sphere with $2\theta_{max} = 60°$ on a Syntex $P\bar{1}$ diffractometer. A total of 1681 was considered observed ($I > 3\sigma$ with σ based upon counting statistics for the peak and background). The data set was corrected for Lorentz, polarization effects, and absorptions (μR = 0.82 cm⁻¹). A trial structure was obtained by direct methods which determined the signs of the 81 reflections with highest E values. The atomic parameters for the heavier scatterers were obtained from the E map. The peak heights from this map were not proportional to the scattering power of the atoms and therefore Ca, K, and As were not distinguished in the initial model. Subsequent difference syntheses led to the correct cationic identification and location of the oxygen atoms. The refinement proceeded by minimizing $\sum\omega(|F_o| - |F_c|)^2$ using the full-matrix least-squares program written by J. S. Stephens for the CDC 6400. Scattering curves for Ca^{2+}, K^+, As, and O, corrected for dispersion (8) were taken from Cromer and Waber (9). Weights were chosen as

$$\omega = \left[1000\,\frac{\sigma(F_o^2)}{F_o^2} + 0.01F_o^2\right]^{-1}$$

with coefficients determined so that $\omega[|F_o| - |F_c|]^2$ would not vary with $|F_o|$. The final parameters are in Table 1 and the observed and calculated structure factors have been tabulated.[2] R = 0.056 and

$$R_\omega = \left\{\frac{\sum\omega(|F_o| - |F_c|)^2}{\sum\omega|F_o|^2}\right\}^{1/2} = 0.043$$

[2]Photocopies of this table are available upon request, at a nominal charge, from the Depository of Unpublished Data, CISTI, National Research Council of Canada, Ottawa, Canada K1A 0S2.

In the final cycle of refinement all the calculated shifts were less than ⅓ of the estimated standard deviations.

$CdK_2P_2O_7$

Crystals of $CdK_2P_2O_7$ were grown by reacting stoichiometric portions of $CdCO_3$, K_2SO_4, and $(NH_4)_2HPO_4$. The sample was thoroughly mixed, heated in a Pt crucible to 900 °C, and slowly cooled, at 3°/h, to below 600 °C. Suitable crystals were extracted from the sample.

A crystal was ground into a cylinder, whose radius was 0.025 mm and height was 0.1 mm. Unit cell parameters were determined from fifteen 2θ values lying between 20 and 25°, using MoKα_1 radiation (0.70926 Å) and a graphite monochromater in conjunction with a Syntex $P\bar{1}$ diffractometer. The crystal data at 22 °C are as follows:
$CdK_2P_2O_7$ fw = 364.55
Monoclinic: a = 9.737(2), b = 5.548(1), c = 12.766(2) Å, β = 106.50(2)°, V = 661.06 Å³, Z = 4, D_{calcd} = 3.66 g/cm³, D_m = 3.69 g/cm³ (3). Space group $C2/c$, extinctions hkl with $h + k$ odd, $h0l$ with l odd.

The intensities of the reflections were examined in the angular range within 2θ = 65°. Those reflections whose intensity measure were negative after correcting for background were discarded. Those in excess of 3σ, with σ derived from the intensity statistics, were treated as observed. The entire data set was corrected for Lorentz, polarization, and absorption. The intensity of a total of 1145 unique symmetry independent reflections were determined.

The structure was solved from the Patterson function after positioning the Cd ions on centers of symmetry and noting that the anion contained a crystallographic two-fold axis. The structure was refined by full-matrix least-squares methods using atomic scattering factors for Ca^{2+}, K^+, P, and O from Cromer and Waber (9). These were corrected for dispersion (8). Weights were taken as $\omega = [86.4 - 1.96F_o + 0.012F_o^2]^{-1}$ with the coefficients determined so that $\omega(F_o - F_c)^2 \approx 1$. When the shifts in the parameters between cycles of refinement ceased to be significant the anisotropic components of the thermal parameters were allowed to vary. The R value was 0.067 when all shifts were less than ¼ of the estimated standard deviation, and the refinement was terminated. The value of R_ω = 0.066. The atomic parameters are in Table 2.

Can. J. Chem. Downloaded from www.nrcresearchpress.com by 210.87.254.42 on 09/05/12
For personal use only.

TABLE 2. Atomic parameter for $CdK_2P_2O_7$ with estimated standard deviations in parentheses*

Atom	Site	x	y	z	U_{11}	U_{22}	U_{33}	U_{12}	U_{13}	U_{23}
Cd	4*c*	1/4	1/4	0	7.1(3)	7.4(3)	7.2(3)	—	1.8(2)	—
K	8*f*	0.3505(2)	0.2919(3)	0.3309(2)	12.3(7)	9.0(6)	23.0(8)	1.0(5)	5.5(6)	0.0(5)
P	8*f*	−0.0281(2)	0.2833(3)	0.1298(1)	5.3(6)	6.0(7)	7.4(7)	0.0(5)	1.6(5)	0.0(5)
O(C)	4*e*	0	0.1558(14)	1/4	26(4)	10(3)	5(3)	—	5(3)	—
O(1)	8*f*	0.8776(6)	0.3209(11)	0.3793(5)	8(2)	14(2)	17(2)	1(2)	6(2)	1(2)
O(2)	8*f*	−0.1060(6)	0.5182(10)	0.1341(4)	13(2)	8(2)	12(2)	4(2)	1(2)	1(2)
O(3)	8*f*	−0.1140(6)	0.0951(11)	0.0553(5)	13(2)	13(2)	14(2)	−6(2)	−1(2)	−5(2)

*Thermal parameters appear in the structure factor expression as $T = \exp -2\pi^2 10^{-3}(U_{11}h^2b_1^2 + \ldots + 2U_{12}hkb_1b_2 + \ldots)$ with the b_i's as reciprocal lattice vectors. All U's in Å^2.

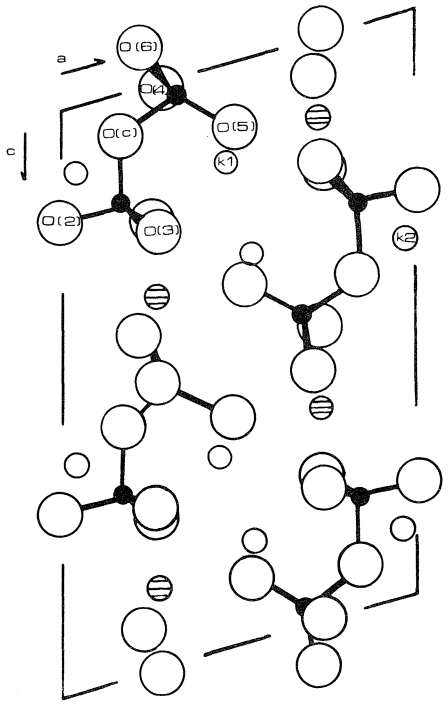

FIG. 1. Structure of $CaK_2As_2O_7$ projected onto the *ac* plane. The large circles are oxygen atoms, the small filled circles are As atoms, the medium sized open circles are K^+ ions, and the lined circles are Ca^{2+}.

Description of the Structures

$CaK_2As_2O_7$

The structure of $CaK_2As_2O_7$ is seen in Fig. 1. The anions are near the levels $y = \pm 1/4$ and in a hexagonal layer arrangement defined by $(\bar{1}02)$. Calcium ions lie between adjacent layers sharing terminal oxygen atoms with six separate anions. Within a layer the anions are in chains parallel to *b* related alternately by two-fold screw axes and a center of symmetry. The potassium ions lie between adjacent anions within the layers. K(1) ions lie between the anions related by the screw axes and K(2) ions between those related by centers of symmetry. Both K(1) and K(2) also lie near $y = \pm 1/4$ and are each coordinated to nine oxygen atoms. The K(1)—O bond lengths range from 2.819 to 3.160 Å while those of K(2)—O range from 2.751 to 3.256 Å (Table 3). K(1) shares three terminal oxygen atoms with each of two diarsenate ions bridging across the ends of these two anions. It shares an edge, O(4)*a*—O(5)*a*, with another diarsenate and a corner with a fourth anion.

The environment of K(2) is quite different. It shares oxygen atoms with four separate diarsenate ions. Two terminal oxygens, O(2) and O(4), and a bridging oxygen are shared with one diarsenate ion and an edge, consisting of O(2) and O(C), is shared with the diarsenate ion translated by one *b* axis length. Three terminal

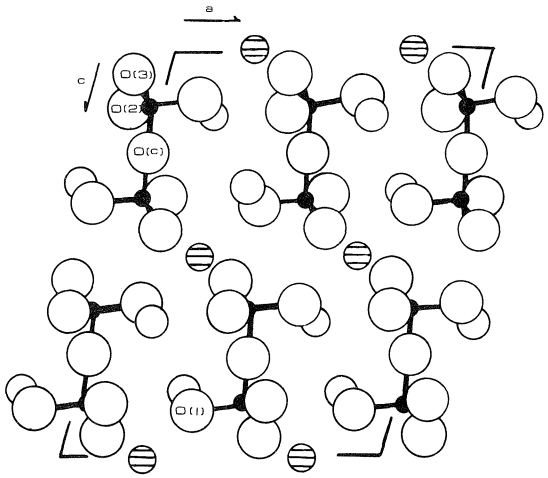

FIG. 2. The structure of $CdK_2P_2O_7$ projected onto the *ac* plane. The large circles are oxygen atoms and the small filled circles are P. The medium sized open circles are K^+ and the lined ones Cd^{2+} ions. The layers lie between planes normal to (100).

Can. J. Chem. Downloaded from www.nrcresearchpress.com by 210.87.254.42 on 09/05/12
For personal use only.

TABLE 3. Bond lengths and angles in $CaK_2As_2O_7$ with estimated standard deviations in parentheses*

Bond	Length (Å)	Bonds	Angle (deg)	Bonds	Angle (deg)
As(1)—O(C)	1.786(5)	O(C)—As(1)—O(4)	103.7(3)	O(4)—As(1)—O(5)	114.9(2)
—O(4)	1.668(5)	—O(5)	106.3(3)	—O(6)	111.7(2)
—O(5)	1.651(5)	—O(6)	101.2(3)	O(5)—As(1)—O(6)	117.0(3)
—O(6)	1.665(5)				
As(2)—O(C)	1.798(5)	O(C)—As(2)—O(1)	106.0(2)	O(1)—As(2)—O(2)	114.6(2)
—O(1)	1.666(4)	—O(2)	100.7(2)	—O(3)	115.3(2)
—O(2)	1.655(5)	—O(3)	103.7(2)	O(2)—As(2)—O(3)	114.2(3)
—O(3)	1.657(4)	As(1)—O(C)—As(2)	120.9(2)		
Ca—O(5)	2.341(5)	O(5)—Ca—O(2)	167.7(2)	O(2)—Ca—O(3)*a*	86.6(2)
—O(2)	2.307(5)	—O(3)*a*	82.0(2)	—O(4)*b*	94.5(2)
—O(3)*a*	2.348(5)	—O(4)*b*	92.8(2)	—O(1)*a*	86.6(2)
—O(4)*b*	2.351(5)	—O(1)*a*	87.0(2)	—O(6)*b*	97.7(2)
—O(1)*a*	2.398(5)	—O(6)*b*	91.4(2)	O(3)*a*—Ca—O(4)*b*	104.4(2)
—O(6)*b*	2.316(5)	O(4)*b*—Ca—O(1)*a*	175.3(2)	—O(1)*a*	80.2(2)
		—O(6)*b*	95.6(2)	—O(6)*b*	159.1(2)
<Ca—O>	2.342	O(1)*a*—Ca—O(6)*b*	79.6(2)		
K(1)—O(1)	2.882(4)	K(2)—O(C)*a*	3.034(5)		
—O(3)	2.846(4)	—O(2)	2.943(6)		
—O(5)	3.160(6)	—O(2)*a*	3.178(5)		
—O(6)*c*	3.055(6)	—O(3)*a*	2.978(4)		
—O(3)*a*	2.853(5)	—O(4)*a*	3.256(6)		
—O(4)*a*	2.819(5)	—O(6)*c*	2.932(6)		
—O(5)*a*	2.919(5)	—O(C)*c*	2.875(5)		
—O(1)*a*	2.836(5)	—O(1)*a*	2.751(4)		
—O(5)*a*	3.125(5)	—O(2)*a*	3.238(5)		
<K(1)—O>	2.943	<K(2)—O>	3.020		

*Symmetry transformations exclusive of lattice translations $a = \bar{x}, \bar{y}, \bar{z}$; $b = x, \frac{1}{2} + y$; $c = \frac{1}{2} - z$; $d = x, \frac{1}{2} - y, \frac{1}{2} + z$.

oxygen atoms, O(1), O(2), and O(3), are shared with a third anion and the ninth oxygen atom, O(6), is shared with a fourth anion.

The calcium ions lie between layers and are bonded to six oxygen atoms whose configuration is that of a distorted trigonal antiprism. These are all terminal oxygen atoms and arise from six separate anions. The geometry of the oxygen atoms around these cations is substantially distorted from octahedral.

The diarsenate ion consists of two irregular tetrahedra sharing a common corner oxygen. The average As—O(—As) bond length is 1.792 Å and the mean terminal As—O bond length is 1.660 Å. The individual bridging and terminal As—O bond lengths are not significantly different although the differences between the bridging and terminal As—O bond lengths are. All the O(C)—As—O bond angles are less than ideal suggesting that the primary distortion involves a motion of the As from the center of the tetrahedron towards the terminal face. The anion has nearly staggered configuration with an As—O—As angle of 120.9°.

$CdK_2P_2O_7$

In $CdK_2P_2O_7$ the anion also has a staggered configuration but lies on crystallographic two-fold axes (Fig. 2). The anion form layers parallel to (001) with adjacent anions in the layer related by the two-fold screw axis. The layers propagate through the *c* glide plane with the Cd ions lying on centers of symmetry and sharing one terminal oxygen atom with each of six separate anions.

The potassium ions are bonded to ten oxygen atoms within a sphere of 3.25 Å. These cations lie near $y = \pm 1/4$, are within the layer, and are bonded to each of the terminal oxygen atoms of three half anions and to one briding oxygen atom. This bonding, in part, strengthens the interlayer interaction.

The diphosphate anion consists of two phosphate groups distorted from regularity by the displacement of the phosphorus atom towards

Can. J. Chem. Downloaded from www.nrcresearchpress.com by 210.87.254.42 on 09/05/12
For personal use only.

TABLE 4. Bond lengths and angles in $CdK_2P_2O_7$ with estimated standard deviations in parentheses*

Bond	Length (Å)	Bonds	Angle (deg)	Bonds	Angle (deg)
P—O(C) (2×)	1.640(4)	O(C)—P—O(1)*a*	102.9(2)	O(1)*a*—P—O(2)	112.9(3)
—O(1)*a*	1.517(4)	—O(2)	106.8(3)	—O(3)	115.1(4)
—O(2)	1.516(6)	—O(3)	102.0(3)	O(2)—P—O(3)	115.3(3)
—O(3)	1.497(6)				
		P—O(C)—P	128.9(5)		
Cd—O(1)*a,g*	2.272(7)	O(1)*a*—Cd—O(2)*b*	94.2(2)	O(2)*b*—Cd—O(3)*b*	93.5(2)
—O(2)*b,a*	2.278(5)	—O(3)*b*	91.5(2)	—O(2)*d*	180
—O(3)*b,d*	2.321(6)	—O(1)*g*	180	O(3)*b*—Cd—O(3)*d*	180
<Cd—O>	2.290				
K—O(1)*a*	2.962(5)				
—O(1)*a*	2.680(6)				
—O(2)*d*	3.065(6)				
—O(3)*a*	3.241(7)				
—O(3)*g*	2.856(6)				
—O(C)*d*	2.848(6)				
—O(1)*d*	2.995(6)				
—O(2)*a*	2.837(6)				
—O(2)*e*	2.839(6)				
—O(3)*e*	3.067(6)				
<K—O>	2.939				

*Symmetry transformations exclusive of lattice translations, $a = -x, y, \frac{1}{2} - z$; $b = -x, -y, -z$; $c = x, -y, \frac{1}{2} + z$; $d = \frac{1}{2} + x, \frac{1}{2} + y, z$; $e = \frac{1}{2} - x, \frac{1}{2} + y, \frac{1}{2} - z$; $f = \frac{1}{2} - x, \frac{1}{2} - y, -z$; $g = \frac{1}{2} + x, \frac{1}{2} - y, \frac{1}{2} + z$.

the face composed of terminal oxygen atoms. The bond angles involving the bridging oxygen atom lie between 102.0 and 106.8° and those involving only terminal oxygen atoms lie between 112.9 and 115.3°. The shorter P—O(3) bond, compared to that involving O(1) and O(2), is to be expected from the fact that the K—O(3) interactions are in general weaker than those involving either O(1) or O(2). The P—O—P angle is 128.9 Å (Table 4).

Discussion

The structures of these two compounds bear comparison with that of $ZrK_2Si_2O_7$ (6) not only because the stoichiometries are the same but also because it might correspond to the structure of $CaK_2P_2O_7$. Its structure, Fig. 3, also has layers of diortho groups which nearly parallel the layer direction. These layers are normal to (001) and the anions in the layers are generated by centers of symmetry. Again adjacent layers are related by the *c* glide plane. All three structures have anions with a staggered configuration with the smaller cation in the same type of site. The potassium ions lie within layers and are coordinated with eight oxygen atoms.

Layers of anions are also found in the $Na_4P_2O_7$ (10) and $Na_4As_2O_7$ (11) structures. In the former case the anions within a layer are generated by two-fold screw axes and a centering operation in the latter case. The separation between layers is of the order of 6 to 7 Å as in the present cases but the symmetry operation relating layers is a *c*

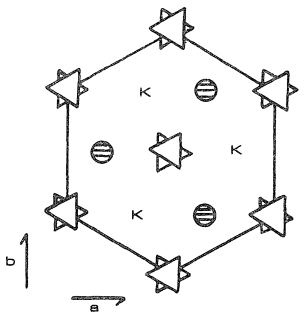

FIG. 3. An idealized view of $CdK_2As_2O_7$, $CdK_2P_2O_7$, and $ZrK_2Si_2O_7$ normal to the layer. The X_2O_7 groups are shown as superimposed triangles whose corner represent the terminal oxygen atoms (not to scale). The cross hatched circles indicate either Ca, Cd, or Zr. Only the potassium ions, depicted by K, near the top of the layer are shown. Adjacent layers in $CaK_2As_2O_7$ and $ZrK_2Si_2O_7$ are related by centers of symmetry and by *c*-glide plane in $CdK_2P_2O_7$.

Can. J. Chem. Downloaded from www.nrcresearchpress.com by 210.87.254.42 on 09/05/12
For personal use only.

glide plane in the diarsenate and two-fold screw axes and centers of symmetry in the diphosphate. The cationic bonding differs in these sodium structures. It is possible that the detail of the potassium ion bonding determines the packing in the three separate structures discussed above.

These structure types are possibly interconvertible or could invert to a similar disordered structure. The layers in $CdK_2P_2O_7$ and $ZrK_2Si_2O_7$ are polar with the polarity determined by the component of the X—O—X vector along with the *b* axis. These changes would require a substantial redistribution in the bonding of the potassium ions.

Differential thermal analysis studies show that $CaK_2As_2O_7$ and $CdK_2P_2O_7$ each manifest two phase transformations. These occur near 375 and 410 °C in the former compound and near 580 and 680 °C in the latter. The nature of these transformations is not known.

The geometry of the $P_2O_7^{4-}$ anion is very similar to that in $Na_2P_2O_7$ (10) although the latter has a nearly eclipsed configuration. The bridging angles differ by less than 2°. The average bridging P—O bond is 1.636 Å in $Na_4P_2O_7$ compared with 1.640 Å in $CdK_2P_2O_7$. The average terminal bond length is 1.513 Å in $Na_4P_2O_7$ and 1.510 Å in $CdK_2P_2O_7$. The diarsenate configuration also compares very well in the present compound and in $Na_4As_2O_7$ (11). It is nearly staggered in both compounds with the bridging angle differing by about 3°. The average bridging and terminal As—O bond lengths are 1.782 and 1.660 Å in $Na_4As_2O_7$, respectively. These values are essentially the same as in $CaK_2As_2O_7$.

Acknowledgement

This research was supported by a grant from the National Research Council of Canada.

1. W. Petter, A. B. Harnik, and U. Keppler. Z. Kristallogr. **133**, 445 (1971).
2. C. B. Finch, G. W. Clark, L. A. Harris, and C. S. Just. J. Crystal Growth, **23**, 295 (1974).
3. J. V. Smith. Am. Mineral. **38**, 643 (1953).
4. S. J. Louisnathan. Z. Kristallogr. **130**, 427 (1969).
5. A. N. Cernov, B. A. Maksimov, V. V. Iljukhin, and N. V. Belov. Dokl. Akad. Nauk. SSSR, **193**, 1293 (1970).
6. A. A. Voronkov, N. G. Sumjackaja, and Ju. A. Pjatenko. Z. Strukt. Khim. **11**, 932 (1970).
7. J. R. Lehr, L. H. Brown, A. W. Frazier, J. P. Smith, and R. D. Thrasher. Chemical Engineering Bulletin No. 6, Tennessee Valley Authority, National Fertilizer Development Center, Muscle Shoals, Alabama. 1967.
8. International Tables for X-ray Crystallography Vol. III, Birmingham: Kynoch Press. 1962.
9. D. T. Cromer and J. T. Waber. Acta Crystallogr. **18**, 104 (1965).
10. K. Y. Leung and C. Calvo. Can. J. Chem. **50**, 2519 (1972).
11. K. Y. Leung and C. Calvo. Can. J. Chem. **51**, 2082 (1973).

Can. J. Chem. Downloaded from www.nrcresearchpress.com by 210.87.254.42 on 09/05/12
For personal use only.

The polymerization of oxetane with hexafluorophosphate salts[1]

P. E. BLACK AND D. J. WORSFOLD
Division of Chemistry, National Research Council of Canada, Ottawa, Canada K1A 0R9

Received June 15, 1976

P. E. BLACK and D. J. WORSFOLD. Can. J. Chem. **54**, 3325 (1976).

Oxetane has been polymerized using both triethyloxonium hexafluorophosphate and triphenylmethyl hexafluorophosphate as initiators at −30 °C. The former gives a slow polymerization with a slow initiation process. The latter gives a rapid initiation and rapid initial polymerization which may slow down to rates similar to those found for the former initiator. The results are interpreted in terms of the formation of two types of tertiary oxonium ions. One type incorporates the oxetane molecule and is suggested to have a very rapid reaction with more oxetane. The second type does not involve the oxetane molecule but an ether linkage, such as in the polymer chain, and reacts only slowly with oxetane.

P. E. BLACK et D. J. WORSFOLD. Can. J. Chem. **54**, 3325 (1976).

On a polymérisé de l'oxétanne utilisant l'hexafluorophosphate de triéthyloxonium et l'hexafluorophosphate de triphénylméthyle comme initiateurs à −30 °C. Le premier conduit à une polymérisation lente avec un processus d'initiation lent. Le dernier conduit à une initiation rapide et une polymérisation initiale rapide qui peut ralentir jusqu'à des taux semblable à ceux trouvés pour le premier initiateur. On interprète les résultats en termes de la formation de deux types d'ions oxonium tertiaires. L'un incorpore la molécule d'oxétanne et on suggère qu'il réagit d'une façon très rapide avec d'autres oxétannes. Le second type n'implique pas de molécules d'oxétanne mais plutôt un lien éther similaire à celui de la chaîne polymérique; il ne réagit que lentement avec l'oxétanne.

[Traduit par le journal]

A detailed kinetic analysis of the polymerization of oxetane by boron trifluoride based catalysts by Rose (1) was interpreted in terms of initiation, propagation, and termination reactions, with the propagating species being a tertiary oxonium ion. A subsequent study was made by Saegusa *et al.* (2) who determined the concentration of the tertiary oxonium ions present and suggested that initiation was rapid and that the system was typical of a living polymerization such as that proposed for tetrahydrofuran. Unlike THF, however, this reaction is essentially non-reversible because of the high heat of reaction. Later Dreyfuss and Dreyfuss (3) studied the concurrent formation of cyclic trimers and tetramers, but this reaction only occurred at higher temperatures.

Such a system, if the interpretation of Saegusa and co-workers was correct, would seem a suitable one in which to study the equilibrium between the free ion and ion pair forms of the propagating chain end and to determine the propagation rate constants of the two species, as has been done for THF (4). Because the tetrafluoroborate ion has been shown not to be the most stable (5), it was thought preferable to use hexafluorophosphate as the counter ion. Triethyloxonium hexafluorophosphate (TOH) was chosen to be the initiator, as a one-to-one correspondence between initiator and active chain ends could be expected. On closer investigation there appeared to be a number of difficulties with this simple mechanism. Later triphenylmethyl hexafluorophosphate (TMH) was also used as an initiator and this confirmed the non-applicability of the straightforward reaction scheme for these initiators.

Experimental

All manipulations of reagents were performed in glass vacuum apparatus. The initiators were prepared by standard methods, purified under vacuum, and subdivided in solution into fragile bulbs or tubes fitted with breakseals. The solvent was always methylene chloride.

The reactions initiated by TOH with half-lives of hours were followed by vacuum dilatometry. The faster reactions initiated by TMH, with half-life times of less than a minute, were followed by the temperature rise method used by Plesch (6, 7).

Molecular weights and distributions were found by gpc using the universal calibration method (8).

[1]NRCC No. 15492.

Can. J. Chem. Downloaded from www.nrcresearchpress.com by 210.87.254.42 on 09/05/12
For personal use only.

Can. J. Chem. Downloaded from www.nrcresearchpress.com by 210.87.254.42 on 09/05/12
For personal use only.

Results

The rate of polymerization of oxetane in methylene chloride initiated by TOH was studied as a function of initiator concentration at −30 °C. After the initial 10% of reaction, which was disturbed by filling the dilatometer and temperature equilibration, the disappearance of monomer followed a first-order law for the first half-lifetime. Some tailing off of the rate was found after this period. The half-life times were several hours. The rate constant found, assuming a first-order dependence on monomer concentration (0.566 M) and initiator, was $(2.56 \times 10^{-2}) \pm (3.3 \times 10^{-3})$ M^{-1} s^{-1}, and it showed no trend with initiator concentration over the range $(5 \times 10^{-4}) - (2 \times 10^{-3})$ M. Rates were also measured in the presence of the salt, tetrabutylammonium hexafluorophosphate, with the intention to repress any free-ion propagation reaction. The mean rate constant was $(3.12 \times 10^{-2}) \pm (2.3 \times 10^{-3})$ M^{-1} s^{-1}, which is marginally higher than that in the absence of salt, with a tendency to higher rates at higher salt concentrations. As this behaviour was different from that found for tetrahydrofuran, a closer look was taken at the mechanism.

The polymers produced in some of these reactions were isolated and studied by gpc, Table 1. The polymer molecular weights are largely independent of [M]/[C], and the distributions were wider than the Poisson distribution expected from the simple reaction scheme.

To ascertain whether the initiation was as rapid as anticipated, the tertiary oxonium ion concentration was analysed by the method of Saegusa and Matsumoto (9), involving reaction with sodium phenolate and separating the high molecular weight portion by distillation (10). For reactions at 0, −20, and −30 °C with 10^{-2} M initiator, the total trialkyloxonium ion was about 80% of the added TOH and was nearly constant for 24 h. This compared with 99% in a comparable reaction of THF at 0 °C. After a reaction time of 5 h, the trialkyloxonium ions of higher molecular weight were 62, 24, and 15% of the total, respectively at the three temperatures above, compared with 100% for THF at 0 °C. After 24 h at −20 °C the yield of high molecular weight oxonium ions had increased to 51%. Hence even though oxetane is highly basic (11), the initiation reaction appears to be slow, and although the number of polymer trialkyloxonium ions was increasing throughout the reaction, the rate of disappearance of monomer did not increase after the first 10% of reaction. The first 10% was not followed because of the time taken for temperature equilibration, etc.

TABLE 1. Polymers from the reaction of oxetane and TOH at −30 °C

[TOH] $\times 10^3$	[Oxetane]	M_n	M_w/M_n
0.544	0.513	26 400	1.88
1.37	0.513	18 900	1.63
1.73	0.513	21 400	1.83
1.87	0.513	22 800	1.67

TABLE 2. Reaction of TMH and oxetane

Temp. (°C)	[TMH] $\times 10^2$	[Oxetane]	Yield of tertiary oxonium ions (%)*
0	1.83	0.54	49
−30	1.73	0.65	36
−40	1.68	0.30	34
−40	1.73	1.20	45
−90	1.85	0.62	13
−40	0.114	0.49	100
−40	0.097	0.49	100

*After 30 min.

In order to circumvent the slow initiation with TOH, triphenylmethyl hexafluorophosphate (TMH) was used as an initiator. To determine whether initiation was indeed rapid, on the assumption that the propagation was slow, the tertiary oxonium ion concentration was determined after TMH had reacted with oxetane for 30 min. The results are in Table 2, from which it is evident that not all the TMH had formed oxonium ions at that time under all conditions. Only under the conditions of the last two entries was initiation complete as was confirmed by the disappearance of the uv absorption band of the triphenylmethyl cation.

As initiation appeared complete at 10^{-3} M initiator, attempts were made to measure the rates of polymerization at this concentration by dilatometry at −30 °C, but it was found that the reaction was more or less complete before the dilatometer was filled. Analysis of the reaction mixture at this point gave polymer yields of over 70%. Reactions performed in sealed tubes at −78 °C were found to be complete in 10 min.

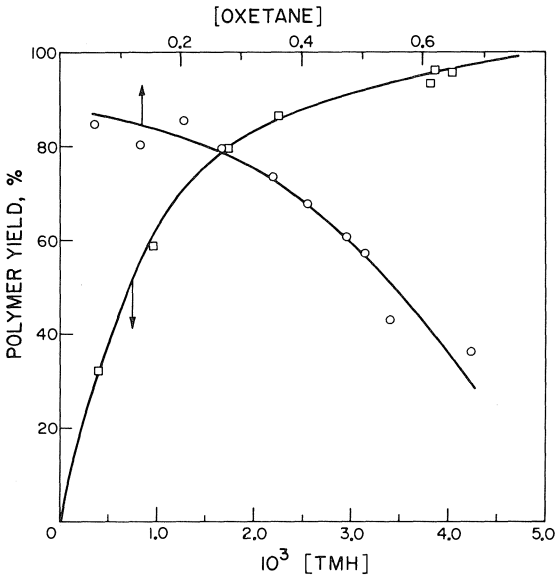

FIG. 1. Polyoxetane yield at the end of the fast reaction with triphenylmethyl hexafluorophosphate as a function of: ○ oxetane concentration, □ TMH concentration.

Rate measurements were then made by the temperature rise method at −30 °C.

It was found that when the initiator bulb was broken into the oxetane solution there was an immediate rapid reaction, but, except at higher initiator concentrations, the reaction appeared to stop before the monomer was exhausted. The results are shown in Fig. 1. The yield at this point was found from the temperature rise, the weight of polymer, and the residual monomer concentration. But it was also found that although the reaction appeared completed by the temperature rise method, if the reaction mixture was left many hours the yield of polymer increased and the reaction would go to completion. Hence, there was an initial rapid reaction followed by a slow reaction, the latter with the same time scale as the reaction initiated with TOH. The initial rates, although rather scattered, appeared close to first order in monomer and initiator, with a bimolecular rate constant $9.3 \pm 2.6\ M^{-1}\ s^{-1}$.

Polymers isolated from the reaction mixtures after the fast part of the reaction were examined by gpc to determine the molecular weights and distributions, and by uv spectroscopy to determine whether there was one initiator fragment per chain. The results are collected in Table 3. Two polymers were analyzed for phenolate groups after termination by sodium phenolate after long reaction times. The last entry in this table was the polymer obtained from an experiment when the monomer was added in two batches in the temperature rise apparatus. Both additions gave a temperature rise, and the mixture was left 16 h before analysis.

Although there is good agreement between the molecular weights from the gpc and uv measurements, there is poor agreement with that calculated from the [M]/[C] ratio. The agreement is better at higher molecular weights, so the discrepancy elsewhere may in part be caused by loss of very low molecular weight polymer when the polymer is precipitated to free it from any triphenylmethane formed.

Discussion

When TMH was used as an initiator the propagation reaction was seen to be rapid with a half-life of 10–20 s. From the results it is seen that at high initiator concentrations (above

TABLE 3. Polymers from reaction of TMH and oxetane at −30 °C

[TMH] ×10³	[Oxetane]	M_n (calcd.)*	M_n (gpc)	M_n (uv)	M_w/M_n
1.85	0.068	1 800	3 900	4 000	4.2
3.81	0.272	3 900	6 500	6 000	2.6
1.72	0.272	7 270	12 500	11 800	2.0
1.55	0.544	8 800	19 200	18 600	2.0
1.37	0.476	12 000	20 500	22 000	2.0
1.35‡	0.601	26 000	32 600	27 000	1.5
0.99‡	0.459	27 000	34 700	29 000	1.5
1.54†	0.535	18 000	16 200		2.0

*Calculated from ratio [Monomer consumed]/[TMH], at end of fast reaction.
†Polymer from reaction with two additions of oxetane.
‡Polymers terminated with NaOPh, M_n (uv) calculated from OPh absorption.

Can. J. Chem. Downloaded from www.nrcresearchpress.com by 210.87.254.42 on 09/05/12
For personal use only.

Can. J. Chem. Downloaded from www.nrcresearchpress.com by 210.87.254.42 on 09/05/12
For personal use only.

10^{-2} *M*) not all the initiator was consumed to form oxonium ions whilst the monomer was completely polymerized, whereas at lower initiator concentrations, all the initiator formed monomer or polymer oxonium ions although not all monomer was consumed in the fast reaction. From this it may be concluded that the rate of initiation was comparable to that of the fast polymerization. Moreover, as each polymer chain appeared to contain one triphenylmethyl group, the initiation reaction appeared to be a straightforward ring-opening addition of oxetane to TMH to form a tertiary oxonium ion with a second oxetane molecule as shown below. It is then presumably this tertiary oxonium ion which propagated, because if the reaction was terminated with sodium phenoxide, a phenoxide group was found for nearly all chains.

It is also seen that although initially the polymerization was rapid, there was dramatic reduction in speed soon after all the initiator was consumed. After this point the propagation continued slowly, and would go to completion if left long enough with apparently most of the oxonium ions still present. Moreover, even though the initiation continued throughout this rapid stage and the number of chain ends was increasing, no rate acceleration was observed except during the first 2–3 s, which was the lag of mixing and temperature measurement in this particular temperature rise apparatus.

The system behaves as if an initially very active chain end is formed which after a short period of very rapid propagation becomes quiescent. At high [M]/[C] ratios where much monomer remains after the rapid reaction, the M_w/M_n ratio at this point would be determined by the process that reduces the chain activity. The M_w/M_n ratio would not be large, but not 1 as in a Poisson distribution in a normal living polymerization. At low [M]/[C] ratios the distribution would be broader because some of the chains are initiated when the monomer is depleted. The variation in M_w/M_n in Table 2 does follow such a trend.

When TOH was used as an initiator the monomer consumption was hundreds of times slower, as was also the initiation reaction. Although there was an increase in growing polymer chains throughout the reaction, the rate of reaction did not seem to increase. It is possible to apply a similar scheme to that shown above to this initiator system also. If the freshly initiated chain were to have a very high activity, and then become more or less dormant the rate of disappearance of monomer would then be dependent on the slow initiation reaction. Moreover, the molecular weight of the polymer would tend to be independent of the initiator concentration as found. The polymer would also have a broader distribution. In addition in such long term polymerization systems several side reactions of ether exchange can cause modifications and even cyclic polymer formation. The scheme proposed is Scheme 1.

That the propagation is rapid is shown by the rapidity of the initial polymerization with TMH. The reaction of TOH with oxetane has been shown to be slow, hence it could be expected that if the dormant species **2** formed it would have a similarly slow reaction with oxetane to reform the rapidly propagating oxonium ion **1**. The exchange reaction between species **1** and **2** is the common ether exchange between oxonium salts and ether commonly postulated to occur in cyclic ether polymerization.

The chain length of the polymers formed in the initial rapid stage when TMH is the initiator is an indication of the chain length of the spurt of propagation when the active species **1** is formed or reformed, if account is taken of the depletion of monomer in these reactions.

The overall rates of polymerization found with TOH as initiator are three times faster than those found by Saegusa *et al.* (2) using a BF_3-based initiator. It seems possible that a similar mechanism might apply in this system. Saegusa only reported the total oxonium ion concentration and a polymerization rate 55 min after the reaction was initiated to support this mechanism. Any early rapid reaction would have been lost under these circumstances, and because of his high monomer concentration (3 *M*) from Fig. 1 this portion of the reaction would have been relatively minor. If this is the case the propagation rate constants he found would not be the simple ones he thought they were, but a complex one involving the true propagation constant and the reinitiation step. The proposed scheme has more in common with the original scheme presented by Rose, except the latent species is the tertiary oxonium ion involving the chain ether linkage. In Rose's study, his rates were also measured after a substantial part (over 50%) of

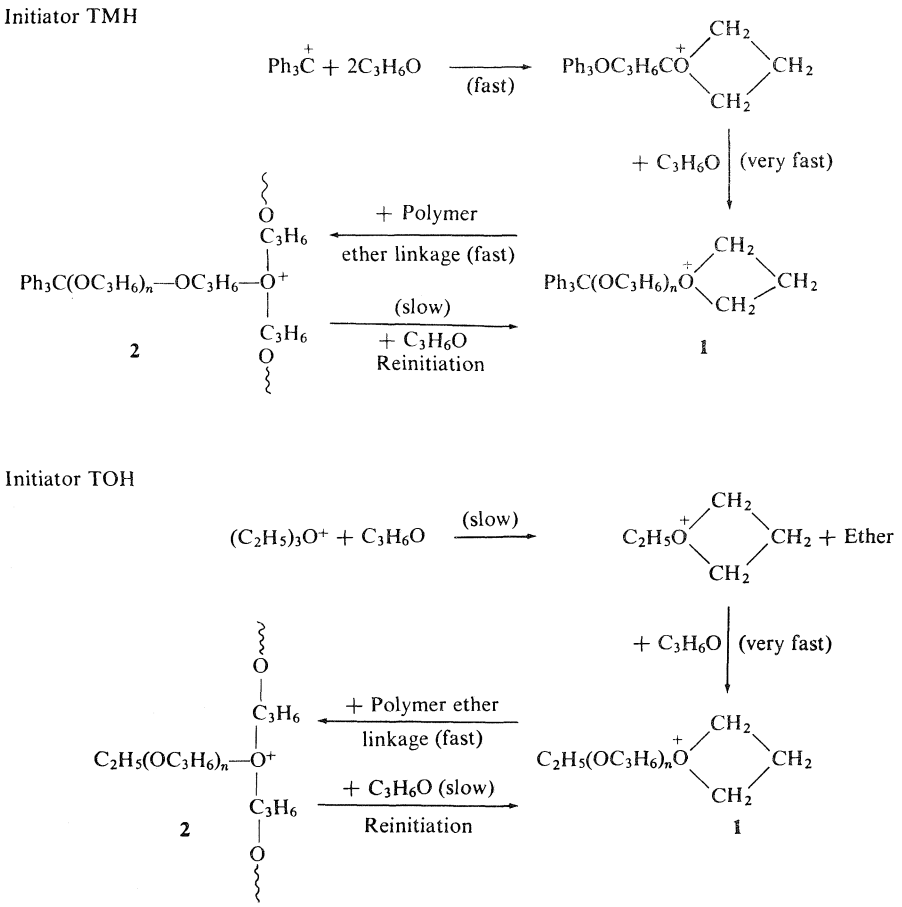

SCHEME 1. Polymerization scheme. PF_6^- counter ions have been omitted for clarity.

the reaction had occurred, and he could very well have missed any early rapid reaction. In fact, it might well be he was forced to miss the first 50% because of the rapid reaction; his half-life times were of the order of minutes.

1. J. B. ROSE. J. Chem. Soc. 542 (1956); 546 (1956).
2. T. SAEGUSA, Y. HASHIMOTO, and S. MATSUMOTO. Macromolecules, **4**, 1 (1971).
3. P. DREYFUSS and M. P. DREYFUSS. Polym. J. **8**, 81 (1976).
4. P. BOURDAUDUCQ and D. J. WORSFOLD. Macromolecules, **8**, 562 (1975).
5. F. R. JONES and P. H. PLESCH. J. Chem. Soc., Chem. Commun. 1231 (1969).
6. R. H. BIDDULPH and P. H. PLESCH. Chem. Ind. **37**, 1482 (1959).
7. R. P. BELL and J. C. CLUNIE. Proc. R. Soc. **212**, 16 (1952).
8. Z. GRUBISIC-GALLOT, P. REMPP, and H. BENOIT. J. Polym. Sci. Part B, **5**, 753 (1967).
9. T. SAEGUSA and S. MATSUMOTO. J. Polym. Sci. Part A, **6**, 1559 (1968).
10. T. SAEGUSA and S. MATSUMOTO. J. Macromol. Sci. Part A, **4**, 873 (1970).
11. S. IWATSUKI, N. TAKIKAWA, M. OKADA, Y. YAMASHITA, and Y. ISHII. Kogyo Kagaku Zasshi, **67**, 1236 (1964).

Can. J. Chem. Downloaded from www.nrcresearchpress.com by 210.87.254.42 on 09/05/12
For personal use only.

The application of iterative optimization techniques to chemical kinetic data of large random error

GEORGE H. SCHMID, VALERIA M. CSIZMADIA, PAUL G. MEZEY AND IMRE G. CSIZMADIA
Lash Miller Chemical Laboratories, Department of Chemistry, University of Toronto, Toronto, Ont., Canada M5S 1A1

Received November 24, 1975[1]

GEORGE H. SCHMID, VALERIA M. CSIZMADIA, PAUL G. MEZEY, and IMRE G. CSIZMADIA. Can. J. Chem. **54**, 3330 (1976).

The possibilities of improving the computational processing of chemical rate measurements, in the frame of linear and non-linear least-square fit methods, are investigated. A simple scaling technique to avoid the distortion of the fitted parameters, inherent in the logarithmic transformation of the rate equation, is tested on several examples, and an iterative discarding method for the selection of accurate data points is recommended.

GEORGE H. SCHMID, VALERIA M. CSIZMADIA, PAUL G. MEZEY et IMRE G. CSIZMADIA. Can. J. Chem. **54**, 3330 (1976).

On a étudié les possibilités d'utilisation, par ordinateur, des mesures de vitesse réaction à l'intérieur de méthodes de concordance linéaire et non-linéaire par la méthode des moindre carrés. On vérifie sur plusieurs exemples une méthode simple d'echellement qui évite la distorsion des paramètres entrant en concordance qui est inhérente à la transformation logarithmique de l'équation de vitesse; on recommande aussi une méthode itérative d'élimination permettant de choisir les points les plus corrects des données.

[Traduit par le journal]

Introduction

There are many physical methods that may be used to follow the rate of a chemical reaction. Some of these are very precise (*e.g.* uv spectroscopy) but do not have universal applicability, while others are not so precise but enjoy a much broader applicability.

For example, nuclear magnetic resonance (nmr) measurements are relatively easy to carry out and could represent an ideal method to monitor the rate of a reaction where alternative methods are not readily applicable. Under very special circumstances one might be satisfied with the measurement of peak heights (1) but usually it becomes necessary to measure the area under the absorption curve by integration. Nuclear magnetic resonance integrations are known to be notoriously imprecise. This lack of precision counterbalances the practical aspect of nmr spectroscopy in rate measurements.

Though it is well known that imprecise integration may lead to considerable error in the calculated rate constants, in the majority of kinetic studies based on nmr measurements little or no computational effort has been made to minimize these distorting effects. The rate constant k for a first order kinetic process

$$[1] \qquad M \xrightarrow{k} \text{Product}$$

is usually calculated from the integrated rate equation

$$[2] \qquad [M] = f(k, t)$$

simply by unweighted linear least-square fitting. In eq. 2 concentration [M] is a function of time t and the rate constant k is a parameter to be determined by the fitting.

Since the computational work involved in a least-square curve fitting is predetermined by the functional dependence in [2], it is usual to transform the more complicated function of [2] into one in which only linear dependence occurs. For example, in the case of a first order reaction shown in [1] the explicit form of [2] is

$$[3] \qquad [M] = [M]_0 e^{-kt}$$

This exponential functional dependence [3] is usually transformed into a linear form

$$[4] \qquad \ln [M] = -kt + \ln [M]_0$$

before the least-square fit is attempted.

The actual curve fitting is carried out in the log concentration – time space instead of the con-

[1]Revision received May 28, 1976.

Can. J. Chem. Downloaded from www.nrcresearchpress.com by 210.87.254.5 on 09/05/12
For personal use only.

centration–time space. For precise measurements the result of the least-square fit to eq. 4 is equivalent (in practical terms) to that to eq. 3. However, for less precise measurements the difference between the two methods becomes noticeable. Linear fitting methods for the direct determination of exponential factors (see *e.g.* refs. 2, 3) are equally burdened by the imprecision of the experimental data.

The purpose of the present study is to analyse the limits of the computational processing of nmr data in the hope that the optimum information is in fact extracted from such rate measurements through a systematic mathematical optimization of least-square fits.

Method

Experimental

In the present study[2] we investigated a reaction of molecular rearrangement converting a Markovnikov adduct (M) of ArSCl to $PhCH{=}CHCH_3$ to the corresponding anti-Markovnikov adduct (aM):

Threo

[5a] 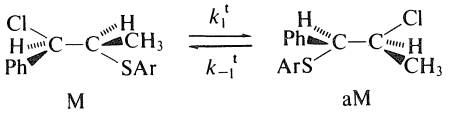

M aM

Erythreo

[5b] 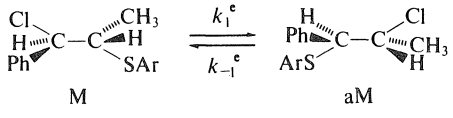

M aM

The reaction conditions (solvent, initial concentration, and temperature) were selected in such a way that the equilibrium was never reached in less than 30 h. This relative slowness of the reaction is important in minimizing the errors.

In the present case d_4 acetic acid was used as solvent, the reaction was carried out at two different temperatures, 37.9 and 45.1 °C. The temperatures were maintained to the accuracy of ±0.15 °C. In order to aid further the accuracy of nmr measurements the initial concentrations were chosen to be as high as 1 *M* or in its vicinity.

The actual reactions were carried out in small flasks containing 10 ml reacting solutions. Samples amounting to 0.5 ml were drawn from time to time and transferred quickly to an nmr tube. The tube was stoppered and cooled immediately in Dry Ice – acetone. The time measurement was taken at the moment the nmr tube was inserted in the Dry Ice bath. Since only that section of the spectrum which contained the two tertiary hydrogens was recorded it was possible to carry out 5 to 10 integrations in a period of 5 min. During this time a warming up occurred from the Dry Ice – acetone temperature (−70 °C) to the probe temperature (+30 °C). The consequence of this warming up may be assigned as an error in the time value associated with the sample point. Thus the individual measurements truly belong to different reaction times, but it is impossible to assign a correct time value to the actual measurements. For this reason all the integrals recorded are assumed to have the nominal time associated with the freezing of the reaction. The error of the nominal time is considerably less than 5 min as illustrated in Fig. 1.

The measured concentration for the above reaction may conveniently be expressed in %

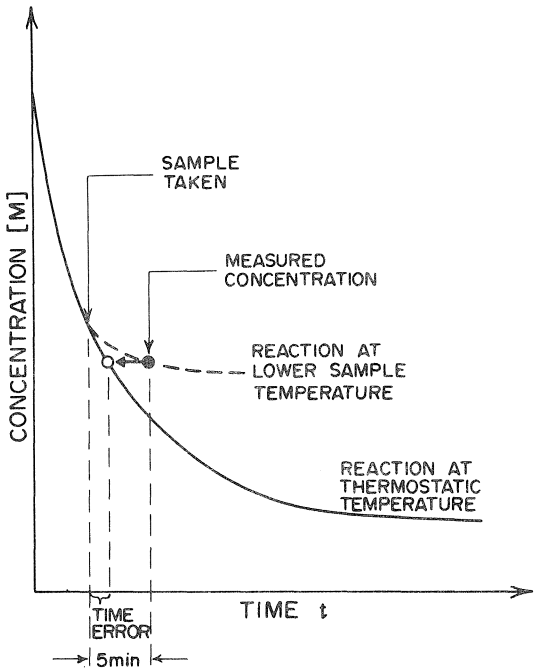

FIG. 1. The time error associated with a measured point, as resulted from the warming up of the sample.

[2]In a subsequent paper (4) the chemical aspects of these reactions will be discussed in a more detailed form.

Can. J. Chem. Downloaded from www.nrcresearchpress.com by 210.87.254.5 on 09/05/12
For personal use only.

Can. J. Chem. Downloaded from www.nrcresearchpress.com by 210.87.254.5 on 09/05/12
For personal use only.

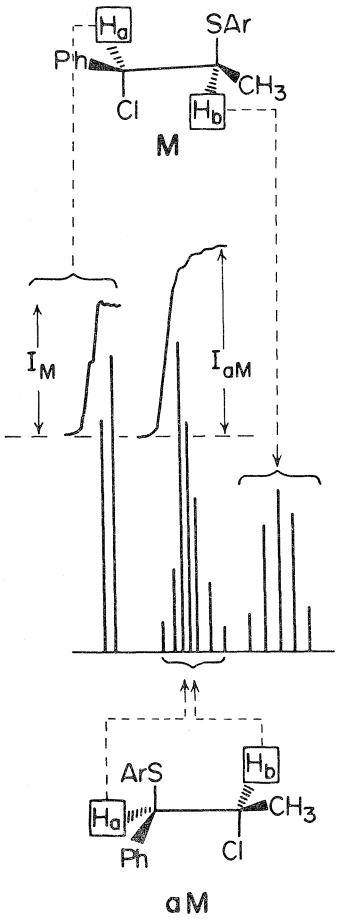

FIG. 2. Interpretation of the nmr spectra of M and aM isomers.

concentration, and a % peak area is used to replace % concentration. Since the reaction is of first order such a transformation in the concentration unit has no effect on the numerical value of the computed rate constant. As illustrated in Fig. 2 the peaks of the two tertiary protons in the aM isomer (product) are considerably overlapped. The peak of the tertiary proton near the CH_3 group in the M isomer (reactant) is frequently disturbed by the side band of the solvent peak. For these reasons the integral (I_M^{benzylic}) of the benzylic proton in M is taken twice in order to have a measure equivalent to the integral (I_{aM}) of the two protons in the aM isomer. Thus the % M concentration was calculated according to eq. 6 (for further details see Fig. 2).

$$[6] \qquad [M]\% = \frac{2I_M^{\text{benzylic}}}{(2I_M^{\text{benzylic}} + I_{aM})} \times 100$$

All measurements were taken on a Varian H60 NMR spectrometer. Particular attention was given to instrumental setting in order to avoid saturation of the upper spin state.

Theoretical

(a) A Linear Scaled Least-Square Fit Method

The rearrangement specified by [5*a*] and [5*b*] can be summarized by the following kinetic equation:

$$[7] \qquad M \underset{k_{-1}}{\overset{k_1}{\rightleftharpoons}} aM$$

The initial concentrations are labelled by $[M]_0$ and $[aM]_0$, and the final (*i.e.* equilibrium) concentrations are specified by $[M]_\infty$ and $[aM]_\infty$, respectively. The integrated first order rate equation thus has the following form:

$$[8] \qquad \{[M] - [M]_\infty\} = \{[M]_0 - [M]_\infty\}e^{-kt},$$

where $k = k_1 + k_{-1}$. A concentration profile illustrating the above notations is shown schematically in Fig. 3*a*.

For every measured time t there is an observed concentration [M] that deviates from the concentration [M]* that falls on the ideal concentration–time profile. This deviation for the ith point is labelled by D_i,

$$[9] \qquad D_i^2 = ([M]_i^* - [M]_i)^2$$

Due to the simplicity of the linear least-square fit methods the experimentally observed points are seldom fitted to the exponential type integrated rate eq. 8 directly (5). Instead, a logarithmic transformation is usually applied,

$$[10] \qquad \ln \{[M] - [M]_\infty\} = -(k_1 + k_{-1})t + \ln \{[M]_0 - [M]_\infty\}$$

and the actual least-square fit is carried out on eq. 10. A typical log concentration – time profile is shown in Fig. 3*b*. The deviation of actual points from the ideal logarithmic profile is labelled by d_i and it represents the difference in log relative concentrations defined by eq. 11.

$$[11] \qquad d_i^2 = (\ln \{[M]_i^* - [M]_\infty\} - \ln \{[M]_i - [M]_\infty\})^2$$

Though it is well known that transformation of

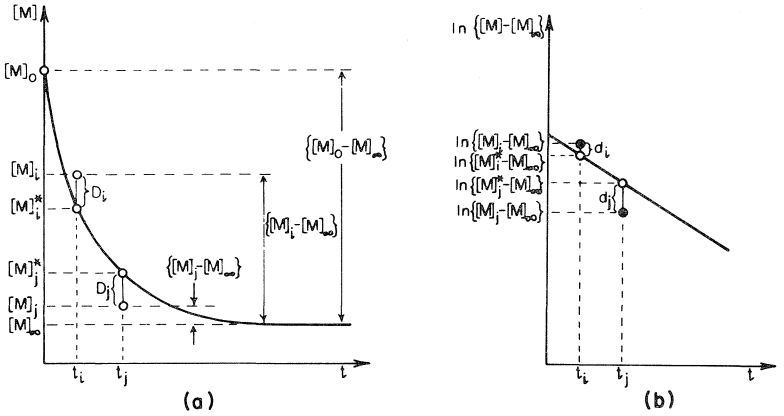

FIG. 3. (*a*) A schematic representation of the concentration profile of a reversible first order reaction. [M], [M]*, and D stand for the measured concentration, 'ideal' concentration, and the deviation of those two, respectively. (*b*) A schematic representation of the log relative concentration profile of a reversible first order reaction. [M], [M]*, and d stand for the measured concentration, 'ideal' concentration, and the deviation, respectively.

the variable, such as in eq. 10, may result in considerable distortion of the fit results (6, 7), in most kinetic studies these distortions are usually ignored.

It should perhaps be pointed out that considering a pair of equal deviations D_i and D_j belonging to different t_i and t_j times in the exponential plot (*cf.* Fig. 3*a*), the corresponding pair of deviations d_i and d_j in the linear plot (*cf.* Fig. 3*b*) are not equal. In fact there is a relative shrinkage of deviations for early measurements (such as the point represented by t_i) and a relative expansion for late measurements (such as the point represented by t_j). This is a consequence of the non-linearity of the transformation of eq. 8 into eq. 10. Consequently, in any of the cases of uneven fluctuations of the data points, the results of a least-square fit in the log concentration – time space will be distorted (yielding different rate constants and standard deviations) with respect to the results of a least-square fit in the original concentration – time space. In order to counterbalance such a distortion a simple scaling procedure is recommended as outlined below.

Deviation d_i can be expressed as

$$[12] \qquad d_i = \ln \{[M]_i^* - [M]_\infty\} - \ln \{[M]_i - [M]_\infty\} = \ln \frac{[M]_i^* - [M]_\infty}{[M]_i - [M]_\infty}$$

consequently

$$[13] \qquad e^{d_i} = \frac{[M]_i^* - [M]_\infty}{[M]_i - [M]_\infty}$$

and

$$[14] \qquad \{[M]_i^* - [M]_i\} = \{[M]_i - [M]_\infty\}(e^{d_i} - 1)$$

Since d_i is small, from a limited expansion of e^{d_i} we get

$$[15] \qquad e^{d_i} \approx 1 + d_i$$

Comparing [14] and [15] we obtain

$$[16] \qquad \{[M]_i^* - [M]_i\} \approx \{[M]_i - [M]_\infty\} d_i$$

that is

$$[17] \qquad D_i \approx \{[M]_i - [M]_\infty\} d_i$$

This result is equivalent to the one we may obtain by approximating the ratio of deviations with the corresponding derivative of the logarithmic transformation:

$$[18] \qquad \frac{d_i}{D_i} \equiv \frac{\Delta \ln \{[M]_i - [M]_\infty\}}{\Delta\{[M]_i - [M]_\infty\}} \approx \frac{d\,(\ln \{[M]_i - [M]_\infty\})}{d\{[M]_i - [M]_\infty\}} = \frac{1}{\{[M]_i - [M]_\infty\}}$$

Equation 17 gives an approximative relation between d_i and D_i.

Can. J. Chem. Downloaded from www.nrcresearchpress.com by 210.87.254.5 on 09/05/12
For personal use only.

If the actual least-square fit is carried out in the log concentration – time space on a linear function one needs to minimize the corresponding sum of squares of deviations:

$$[19] \qquad d^2 = \frac{1}{n}\sum d_i^2$$

where n is the number of measurements.

In order to simulate an exponential least-square fit in the concentration–time space (*cf.* eq. 8), one should weight each of the d_i deviations by the factor $\{[M]_i - [M]_\infty\}$. This in fact leads to the approximate relation for the sum of squares of concentration deviations,

$$[20] \quad D^2 = \frac{1}{n}\sum D_i^2 = \frac{1}{n}\sum\{[M]_i - [M]_\infty\}^2 d_i^2$$

that has to be minimized in the course of the fitting procedure.

There is, however, another potential source of distortion. It is necessary to assign a fixed value to $[M]_\infty$ *before* the linear fitting is attempted to eq. 10. It is clear from this equation that due to the logarithmic representation only those data points can be considered for which $[M]_i > [M]_\infty$. This inequality certainly holds for the true concentrations, however, a considerable percentage of the data for the late measurements may fall under the true $[M]_\infty$ value due to experimental errors. Since all those data points for which $[M]_i \leq [M]_\infty$ holds must be discarded *before* the fitting, the error distribution of data points retained for the late measurements may become considerably asymmetrical. This asymmetry results in a positive error in the calculated concentrations, *i.e.* an upward 'shift' in the concentration profile, provided the *true* $[M]_\infty$ value is assumed. This particular error may be reduced by taking a lower value for $[M]_\infty$ than its true value, thus discarding fewer or no data points before the fitting is carried out. In fact, it is a common practice to take the lowest measured [M] value or a value close to it as $[M]_\infty$. It should be pointed out, however, that the entire concentration profile obtained with a linear fitting strongly depends on the $[M]_\infty$ value assumed, and any deviation from its true value necessarily leads to incorrect results. In practical terms, whenever the experimental errors are large enough to allow some measured $[M]_i$ values to fall under the true $[M]_\infty$ value the linear least-square fitting is necessarily distorted for any assumed value of $[M]_\infty$. In addition, if the measured concentration values are subject to systematic errors (*e.g.* slow side reaction) as well as to random errors, it is likely that $[M]_\infty$ deviates the most from the ideal reaction profile. In fact, there is a considerable uncertainty in the assumed $[M]_\infty$ value itself, since it is chosen or extrapolated from the more inaccurate late measurements.

For these reasons a direct fitting to eq. 8 *without* applying the logarithmic transformation may appear to be more attractive, particularly if $[M]_\infty$ is also treated as a parameter to be determined in the course of the fitting, just as is the rate constant k itself.

(b) A Non-linear Fit Applying the Method of Conjugate Gradients

Although the method discussed in the previous section was designed to simulate the least-square fit to the integrated rate equation in its original, exponential form in the concentration–time space, one may undoubtedly expect the most accurate results from a direct non-linear fit to eq. 8. For this reason we carried out non-linear least-square fit calculations using the method of conjugate gradients (8, 9). The function F to be minimized is given in the form

$$[21] \qquad F = D = \left(\sum_i \frac{D_i^2}{n}\right)^{1/2}$$

where the square deviations D_i^2 are defined by eq. 9. In these calculations the initial concentration $[M]_0$, the final concentration $[M]_\infty$, and the rate constant k were regarded as parameters (*cf.* eq. 8), and function F was optimized in all three parameters:

$$[22] \qquad F = F([M]_0, [M]_\infty, k)$$

From the explicit formula for D_i^2 (*cf.* eqs. 9 and 21) expressions for the components of the gradient vector

$$[23] \quad \boldsymbol{G} = \left\{\left(\frac{\partial F}{\partial [M]_0}\right), \left(\frac{\partial F}{\partial [M]_\infty}\right), \left(\frac{\partial F}{\partial k}\right)\right\}$$

are readily available. The gradients evaluated at a series of points, approaching the optimum, were used in a standard conjugate gradients minimization procedure (8, 9) to locate the minimum of F, where $\boldsymbol{G} = \boldsymbol{O}$.

The present formulation of the three-param-

Can. J. Chem. Downloaded from www.nrcresearchpress.com by 210.87.254.5 on 05/05/12
For personal use only.

Can. J. Chem. Downloaded from www.nrcresearchpress.com by 210.87.254.5 on 09/05/12
For personal use only.

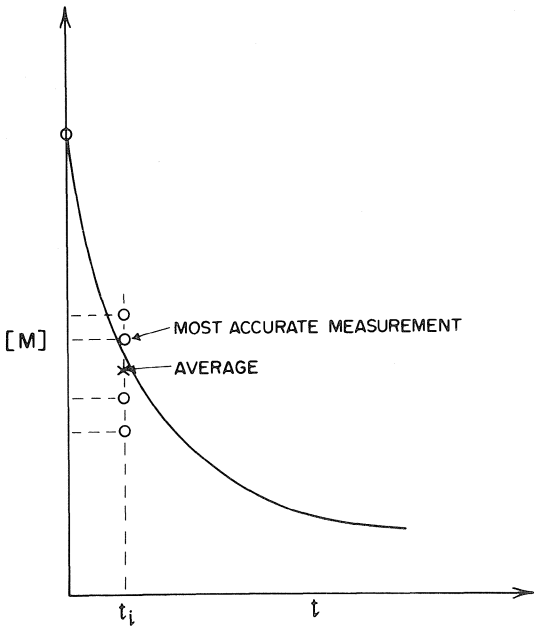

FIG. 4. Relationship of individual measurements and their average to the concentration–time profile.

eter, non-linear fitting problem is equivalent to the one proposed by Moore (10). The actual optimisation of the parameters $[M]_0$, $[M]_\infty$, and k in the present method is, however, carried out with the powerful technique of conjugate gradients, that is superior to the least-square shift method applied by Moore.

(c) Iterative Selection of Points of Small Error

It is a customary technique in kinetic studies to average parallel concentration measurements associated with a given time. This method is quite acceptable if the concentration measurements are accurate, such as those obtained by usual titrimetric or spectrophotometric experiments. However, if nmr is used to monitor the change in concentration, one obtains a scatter of points hardly acceptable by normal standards. The simple averaging of such concentration values virtually guarantees that the most accurate measurement at a given time is lost in the sense that the average will almost certainly deviate from it. This suggests that parallel measurements should be treated on equal footing in the least-square fit (*cf.* Fig. 4).

If the average deviation (*cf.* eq. 21) for the original set of points $\{([M]_i, t_i]\}^{(0)}$ is $D^{(0)}$, some points may deviate from the 'ideal' concentration value calculated from the fitted equation by more than $mD^{(0)}$ where m is a chosen parameter. The jth point may be discarded if $D_j^{(0)} > mD^{(0)}$. Using this technique we may select a subset $\{([M]_i, t_i)\}^{(1)}$ of the original set of points $\{([M]_i, t_i)\}^{(0)}$. With the new set $\{([M]_i, t_i)\}^{(1)}$ a new least-square fit is carried out resulting in a new value $k^{(1)}$ for the rate constant and new $D_i^{(1)}$ deviations. For some points j of the set $\{([M]_i, t_i)\}^{(1)}$, the inequality $D_j^{(1)} > mD^{(0)}$ may hold, because to the new subset $\{([M]_i, t_i)\}^{(1)}$ the fit is different. These points may be discarded resulting in a further subset $\{([M]_i, t_i)\}^{(2)}$. The full fitting and discarding process can be repeated until no further points are to be omitted, *i.e.* $\{([M]_i, t_i)\}^{(p)} = \{([M]_i, t_i)\}^{(p+1)}$, for a given parameter m. With properly chosen parameter m this method ensures that the most accurate points are retained in the final (pth) least-square fit. In the present study a range of $1.0 \leq m \leq 3.5$ was examined in some detail.

Results and Discussion

The rearrangement reaction of the threo [5*a*] and erythro [5*b*] Markovnikov adducts were investigated at two different temperatures, 37.9 and 45.1 °C. The % concentrations $[M]_i$, as derived from % peak areas of the nmr spectra at time t_i are listed in Table 1.

The results of a conventional least-square fit of the data points to eq. 10 and those of a least-square fit scaled according to eq. 20 are compared for all four sets of measurements in Table 2. In Table 2 n designates the number of points, $k = k_1 + k_{-1}$ is the overall rate constant of the reaction, Δk is the standard deviation of k and r is the correlation coefficient.

The scaling process does not improve the quality of fit significantly for relatively accurate measurements. However, for the less accurate measurements the largest change in the rate constant is accompanied by a considerable improvement in the quality of fit, as shown by the corresponding correlation coefficients.

Besides the results of a conventional linear least-square fit and the scaled linear least-square fit, the results obtained by the combined method of scaling and iterative discarding are also shown in Table 2 for a set of selected values of parameter m.

Taking relatively large m values, such as 3.5 or

Can. J. Chem. Downloaded from www.nrcresearchpress.com by 210.87.254.5 on 09/05/12
For personal use only.

3.0 only very few if any of the points are omitted and the discarding process terminates after few iterations. The remaining points result in essentially the same fitted parameters as the original set of points. Smaller values for m ($m < 2.5$), however, result in a significant improvement in the fit as is demonstrated by the improved correlation coefficients. One has to avoid, however, an excessive discarding of data points using too low values for m, that could result in excellent correlation coefficients but at the cost of losing information that is represented by points of intermediate deviations D_i. Previous pilot calculations using $m < 1.0$ revealed that a more dramatic discarding of points may considerably distort the fitted parameters. Assuming that the measurements are subject to random errors only, the integration of the function of standard normal distribution between $-m$ and m yields a relation between m and the percentage of the points omitted. For example the value $m = 1.5$ corresponds to 13.4% while $m = 2.0$ to 4.6%. As retaining approximately 90% of the original points seems to be essential, it is suggested that the parameter range $1.5 \leq m \leq 2.0$ represents the optimum compromise.

In Table 3 the results obtained by the non-linear least-square fit method are summarized. The results of the linear fitting were taken as initial parameters for the non-linear least-square

TABLE 1. Results of concentration measurements (t in s, [M] in % concentration)

(*a*) Temperature = 37.9 °C

Erythro				Threo			
t	[M]	t	[M]	t	[M]	t	[M]
3840	90.9, 89.9	27540	55.7, 55.3	1800	91.5, 91.8	34740	59.3, 58.1
	89.1, 89.3		55.7, 55.3		91.4, 91.8		58.1, 59.1
	90.2, 89.7		55.5, 55.2		91.8		59.1, 59.1
5400	86.8, 87.0	30660	51.0, 51.3	3840	88.7, 89.7		58.8, 59.0
	87.1, 86.2		51.3, 51.3		89.2, 88.8	34860	57.6, 57.4
	86.2, 86.9		51.4		88.7, 89.7		57.4, 57.1
	86.5	34740	47.7, 47.7	5400	87.5, 87.2		57.4, 57.9
8340	80.4, 80.0		48.4, 48.0		87.2, 87.5	42000	54.2, 54.4
	80.0, 80.4		48.7, 48.3		87.2, 87.4		54.5, 53.9
	80.4, 81.1	37860	50.0, 50.7		87.9		55.3, 54.6
10260	76.4, 76.0		49.6, 50.3	8340	81.5, 81.1	45060	53.2, 52.7
	76.7, 77.2		50.5, 50.5		81.7, 82.4		52.2, 51.9
	76.5, 76.4	42000	45.1, 44.8		82.2, 81.8		52.6, 53.3
	76.5		44.4, 44.7		82.4		53.2
13140	70.5, 71.4		44.4	10260	80.0, 79.7	49680	50.0, 50.7
	72.3, 70.9	45060	44.2, 43.1		80.3, 80.3		51.2, 51.2
	71.5, 70.2		43.7, 43.7		79.8, 80.0		51.9, 51.4
16260	67.7, 68.0		43.3		79.7	52680	48.5, 49.1
	68.0, 66.7	49200	42.1, 42.1	13140	77.3, 78.3		47.8, 48.8
20340	61.7, 61.1		43.0, 43.9		77.9, 77.6		48.4, 47.5
	61.1, 60.4		42.3, 43.2		78.1, 77.5		48.5
	60.5, 61.4	52260	40.0, 40.0		78.3, 78.3	57240	47.1, 46.5
	61.5, 62.1		40.4, 40.0	16260	75.5, 75.9		47.4, 47.5
23460	58.4, 57.6		40.0, 39.8		75.7, 75.4		45.9, 47.7
	58.0, 57.6	56400	38.2, 38.4		75.2, 75.1	60360	45.7, 46.1
	57.4, 57.7		38.4, 38.4		75.6, 75.5		46.1, 47.0
	57.5		38.4, 39.0	27540	66.4, 66.4		46.9, 46.1
					66.4, 67.2		46.9, 46.7
					67.4	72360	43.6, 44.8
				30660	62.5, 62.3		43.7, 44.0
					62.9, 62.3		43.1, 43.7
					62.3, 62.6		43.5, 43.6
						455760	25.4, 24.2
							23.8, 25.0
							24.9, 23.9
							22.4

TABLE 1 (*Concluded*)
(*b*) Temperature = 45.1 °C

Erythro				Threo			
t	[M]	*t*	[M]	*t*	[M]	*t*	[M]
1020	93.1, 94.0	17760	44.2, 44.5	900	94.3, 94.2	16080	57.6, 57.6
	92.8, 92.7		44.8, 44.9		94.3, 94.1		57.1, 57.4
	92.2, 92.2		44.2, 44.1		94.7, 95.2		57.1, 58.5
	92.3		43.3		94.1, 95.2		57.6, 59.0
2820	86.0, 84.6	21420	38.8, 37.2		95.0, 95.2	18780	54.5, 55.4
	85.2, 84.8		37.3, 38.4	2160	90.2, 90.9		55.1, 55.1
	84.6, 85.4		37.1, 37.1		89.2, 90.5		57.0, 56.3
	86.0, 85.2	23220	37.6, 37.3		90.5, 90.5		57.3, 55.7
	86.0		39.6, 38.5		90.0	21180	50.5, 49.5
4200	77.6, 78.0		36.5, 37.9	3660	86.7, 85.7		50.0, 49.5
	77.1, 76.6	26820	38.6, 36.0		86.0, 86.0		50.0, 48.5
	76.4, 77.8		38.6, 36.8		85.2, 87.1		50.0, 49.0
	77.1		35.3, 37.2		85.5, 86.0		50.0
4800	73.3, 74.2		35.7	5460	78.9, 79.6	24540	43.5, 45.2
	72.4, 74.2	28620	35.4, 36.4		79.6, 78.6		45.2, 45.2
	72.9, 73.9		36.6, 35.6		78.6, 78.3		46.3, 44.1
	73.6, 72.5		36.8, 37.3		79.3, 78.9		43.5
	73.3		37.3		78.9, 78.2	31740	36.8, 35.6
7200	64.6, 64.3	32280	32.6, 33.7	7380	75.0, 76.5		37.4, 36.8
	64.6, 64.6		33.7, 33.3		74.0, 75.2		36.8, 36.8
	64.6, 64.6		32.3		75.2, 75.0		37.8
	63.9, 64.6	34080	32.0, 34.0		74.5, 74.5	37200	35.4, 36.4
	63.9		35.1, 32.8		75.0, 74.7		39.1, 35.6
8160	61.7, 61.0		31.9	9180	69.6, 69.2		34.1, 36.0
	61.5, 61.3	37680	32.7, 33.3		68.6, 69.9		36.0
	61.9, 62.3		32.5, 33.3		69.2, 70.1	42600	29.2, 31.9
	63.2, 63.0		34.9, 34.0		68.6, 68.6		32.6, 33.3
10560	55.6, 55.6		32.4	11580	65.9, 65.8		31.5, 31.5
	56.5, 56.6	39480	32.3, 31.3		65.1, 65.9		32.3, 31.5
	56.0, 55.6		32.7, 33.5		67.5, 65.9	47400	29.1, 31.3
	55.8, 55.0		32.8, 32.4		64.2, 65.9		30.8, 30.9
11760	52.3, 53.5		32.2		65.9		28.2, 27.5
	52.9, 51.8	40320	32.0, 30.3	13860	60.2, 60.7	52800	29.1, 29.8
	52.3, 54.0		32.8, 33.5		60.7, 61.5		29.7, 29.2
	53.4, 51.7		33.8, 33.8		61.4, 61.5		28.7, 30.0
	52.9		31.1		62.2, 61.5		
14160	48.2, 46.9	47280	30.9, 32.3		62.2		
	47.9, 48.5		33.3, 31.2				
	48.5, 48.2		34.2, 34.2				
	47.6, 47.5		32.9, 33.3				
15960	46.6, 46.5		32.9				
	44.8, 45.0						
	46.3, 45.6						
	45.5						

fit. Test calculations revealed that the final results of the non-linear fit are insensitive to the initial guess of parameters $[M]_0$, $[M]_\infty$, and k. The iterative discarding technique brings about a similar improvement in the fit to that occurred in the case of scaled linear fits. The parameter range $1.5 \leq m \leq 2.0$ seems to represent the optimum compromise between the opposing requirements of data quality and quantity.

There is a relatively large difference between the experimental $[M]_\infty$ value (27%) and the non-linear least-square adjusted value (33%) in the case of the erythro isomer at 37.9 °C. This suggests that in addition to random errors this set of measurements is probably subject to systematic errors as well. This 6% deviation indicates the possibility of a slow side reaction.

It is interesting to compare the rate constants

Can. J. Chem. Downloaded from www.nrcresearchpress.com by 210.87.254.5 on 09/05/12
For personal use only.

Can. J. Chem. Downloaded from www.nrcresearchpress.com by 210.87.254.5 on 09/05/12
For personal use only.

TABLE 2. Comparison of results obtained with conventional and scaled linear least-square fit techniques

T (°C)	Compound	Parameter	Value								
			Conventional	Scaled	Scaling with discarding						
					$m = 3.5$	$m = 3.0$	$m = 2.5$	$m = 2.0$	$m = 1.5$	$m = 1.25$	$m = 1.0$
37.9	Erythro-M.A.	n	102	102	102	102	97	94	89	81	69
		$[M]_\infty$	27%	27%	27%	27%	27%	27%	27%	27%	27%
		k	3.13996E-5	3.26562E-5	3.26562E-5	3.26562E-5	3.32635E-5	3.35939E-5	3.35542E-5	3.33187E-5	3.30571E-5
		Δk	5.92953E-6	2.34952E-7	2.34952E-7	2.34952E-7	2.46613E-7	2.54266E-7	2.61130E-7	2.67137E-7	2.92367E-7
		r	−0.994943	−0.994905	−0.994905	−0.994905	−0.996380	−0.997041	−0.997594	−0.998117	−0.998611
	Threo-M.A.	n	128	128	123	122	122	122	122	121	120
		$[M]_\infty$	21%	21%	21%	21%	21%	21%	21%	21%	21%
		k	6.63716E-6	1.58103E-5	1.74256E-5	1.76281E-5	1.76281E-5	1.76281E-5	1.76281E-5	1.76693E-5	1.77385E-5
		Δk	8.96499E-7	1.03562E-7	1.11755E-7	1.12805E-7	1.12805E-7	1.12805E-7	1.12805E-7	1.13055E-7	1.14275E-7
		r	−0.937166	−0.961317	−0.991842	−0.995372	−0.995372	−0.995372	−0.995372	−0.995978	−0.996278
45.1	Erythro-M.A.	n	154	154	152	152	150	144	133	123	102
		$[M]_\infty$	28%	28%	28%	28%	28%	28%	28%	28%	28%
		k	6.38277E-5	7.91436E-5	8.02600E-5	8.02600E-5	8.10268E-5	8.27465E-5	8.42071E-5	8.49668E-5	8.43515E-5
		Δk	5.73413E-6	4.95227E-7	5.03673E-7	5.03673E-7	5.10115E-7	5.27248E-7	5.60909E-7	5.94076E-7	6.48368E-7
		r	−0.967464	−0.983589	−0.986275	−0.986275	−0.987904	−0.990911	−0.993463	−0.994946	−0.996431
	Threo-M.A.	n	137	137	137	134	133	131	119	108	94
		$[M]_\infty$	22%	22%	22%	22%	22%	22%	22%	22%	22%
		k	4.67813E-5	4.67264E-5	4.67264E-5	4.71705E-5	4.72802E-5	4.72916E-5	4.68385E-5	4.70959E-5	4.70309E-5
		Δk	5.61282E-6	2.73808E-7	2.73808E-7	2.80090E-7	2.81857E-7	2.84891E-7	2.98931E-7	3.13602E-7	3.25523E-7
		r	−0.993123	−0.995803	−0.995803	−0.996686	−0.996873	−0.997101	−0.997868	−0.99849	−0.999093

Can. J. Chem. Downloaded from www.nrcresearchpress.com by 210.87.254.5 on 09/05/12
For personal use only.

TABLE 3. Comparison of results obtained with non-linear least-square fit techniques

T (°C)	Compound	Parameter	Value: Without discarding	With iterative discarding: $m = 3.5$	$m = 3.0$	$m = 2.5$	$m = 2.0$	$m = 1.5$	$m = 1.25$	$m = 1.0$
37.9	Erythro-M.A.	n	102	102	98	96	95	95	87	72
		$[M]_0$	99.4898%	99.4898%	99.7411%	99.8524%	99.8145%	99.4898%	99.8274%	99.9786%
		$[M]_\infty$	33.0562%	33.0562%	32.9166%	32.8513%	32.6518%	33.0562%	32.3834%	32.9431%
		k	4.10449E-5	4.10449E-5	4.13885E-5	4.15374E-5	4.13077E-5	4.15515E-5	4.102980E-5	4.19633E-5
		Δk	1.84407E-6	1.84407E-6	1.43991E-6	1.25270E-6	1.17469E-6	1.23155E-6	9.73842E-7	7.42473E-7
	Threo-M.A.	n	128	128	128	127	117	109	98	85
		$[M]_0$	93.4769%	93.4769%	93.4769%	93.5124%	93.69 2%	93.7837%	93.9225%	94.0157%
		$[M]_\infty$	24.8120%	24.8120%	24.8120%	24.7377%	24.7633%	24.6485%	24.6631%	24.5798%
		k	1.95779E-5	1.95779E-5	1.95779E-5	1.95921E-5	1.98593E-5	1.97498E-5	1.97715E-5	1.97957E-5
		Δk	9.23300E-7	9.23300E-7	9.23300E-7	8.92940E-7	7.34890E-7	6.35160E-7	3.70916E-6	2.96374E-6
45.1	Erythro-M.A.	n	154	154	154	154	144	131	121	102
		$[M]_0$	99.9506%	99.9506%	99.9506%	99.9506%	99.9734%	99.6700%	99.4095%	99.5288%
		$[M]_\infty$	31.3447%	31.3447%	31.3447%	31.3447%	31.5185%	31.4270%	31.5439%	31.2748%
		k	9.85998E-5	9.85998E-5	9.85998E-5	9.85998E-5	9.92038E-5	9.84900E-5	9.86872E-5	9.81682E-5
		Δk	7.25075E-6	7.25075E-6	7.25075E-6	7.25075E-6	6.29054E-6	5.23763E-6	4.66728E-6	3.83497E-6
	Threo-M.A.	n	137	137	134	133	128	115	110	98
		$[M]_0$	97.3639%	97.3639%	97.4839%	97.5315%	97.6249%	97.6085%	97.6857%	97.6987%
		$[M]_\infty$	22.3562%	22.3562%	22.4103%	22.5019%	23.1249%	23.5110%	23.5793%	23.4535%
		k	4.76697E-5	4.76697E-5	4.81129E-5	4.83505E-5	4.91782E-5	4.93348E-5	4.95686E-5	4.92453E-5
		Δk	2.37848E-6	2.37848E-6	2.15381E-6	2.10524E-6	1.93116E-6	1.56241E-6	1.42659E-6	1.18192E-6

TABLE 4. Comparison of rate constants* obtained using various optimization techniques

		Rate constant				
		Linear least-square fit			Non-linear least-square fit	
T (°C)	Compound	Conventional	Scaling	Scaling + discarding $m = 1.5$	Without discarding	With discarding $m = 1.5$
37.9	Erythro-M.A.	3.13996	3.26562	3.35542	4.10449	4.15515
	Threo-M.A.	0.663716	1.58103	1.76281	1.95779	1.97498
45.1	Erythro-M.A.	6.38277	7.91436	8.42071	9.85998	9.84900
	Threo-M.A.	4.67813	4.67264	4.68385	4.76697	4.93348

*$k = k_1 + k_{-1}$ in s^{-1}, 10^5 k values are listed.

TABLE 5. Percent deviations of calculated rate constants from the 'most precise values'

	% deviation			
	37.9 °C		45.1 °C	
Method	Erythro	Threo	Erythro	Threo
Non-linear with discard	0	0	0	0
Non-linear without discard	1.2	0.9	0.1	3.4
Linear with scaling and discard	19.3	10.7	14.5	5.0
Linear with scaling	21.4	19.9	19.6	5.3
Linear without scaling	24.4	66.4	35.2	5.2

obtained by the five different methods of calculation, as shown in Table 4. Though the scaled linear fit method combined with iterative discarding yields better results than the conventional fit, in some cases the results are still considerably different from the rate constants obtained by the non-linear fitting techniques. Clearly, the non-linear technique, optimizing all three parameters $[M]_0$, $[M]_\infty$, k, is expected to be superior to the linear fitting that optimizes one parameter, k, only. Assuming that the results obtained with non-linear fitting and discarding are the most precise, we can restate the results for rate constants in terms of percent deviation from this 'most precise value', as is shown in Table 5. It is clear that in three of the four cases considered the differences between linear and non-linear fitting are significant, and more important than the differences between the types of linear fitting in one case. This suggests that the improvement by scaling the deviations in the linear least-square framework may be satisfactory for rate measurements of average inaccuracy, but the use of non-linear fitting techniques, combined with iterative discarding is recommended whenever larger inaccuracy is suspected, as is the case for the majority of nmr measurements.

Though the combination of any of the scaled linear or non-linear least-square fit methods and the iterative discarding method brings about a considerable improvement of the fitted results, it should be emphasized that both modifications presuppose *a priori* knowledge of the order of the reaction, *i.e.* the general form of the rate equation. The improvement is possible because the functional form of the rate equation represents a relatively rigid restriction for the fit, on the basis of which it is possible to decide which data points are more 'erroneous' and which are precise. Consequently, the data processing of nmr rate measurements by the iterative scaled least-square fit methods is recommended only if the 'error' of the measured points originates from the imprecision of the measuring technique alone, and there are no inherent deviations from the assumed functional form of the integrated rate equation or side reactions to be concerned with.

Acknowledgement

The continued financial support of the National Research Council of Canada is gratefully acknowledged.

Can. J. Chem. Downloaded from www.nrcresearchpress.com by 210.87.254.5 on 09/05/12
For personal use only.

1. A. G. BROOK *et al.* Unpublished results.
2. E. S. SWINBOURNE. J. Chem. Soc. 2371 (1960).
3. E. S. SWINBOURNE. Aust. J. Chem. **16**, 170 (1963).
4. G. H. SCHMID and V. M. CSIZMADIA. To be published.
5. Y. BARD. Nonlinear parameter estimation. Academic Press, 1974. p. 56.
6. E. M. PUGH and G. H. WINSLOW. The analysis of physical measurements. Addison-Wesley. 1966.
7. D. MARGERISON. The treatment of experimental data. *In* Comprehensive chemical kinetics. Vol. 1. *Edited by* C. H. Bamford and C. F. H. Tipper. Elsevier, 1969.
8. R. FLETCHER and M. J. D. POWELL. Comput. J. **6**, 163 (1963).
9. W. C. DAVIDON. Variable metric method for minimization. A.E.C. Research and Development Report ANL-5990 (Rev.) 1959.
10. P. MOORE. J. Chem. Soc. Faraday I, **68**, 1890 (1972).

Can. J. Chem. Downloaded from www.nrcresearchpress.com by 210.87.254.5 on 09/05/12
For personal use only.

Some thermodynamic properties of K_3AlF_6–$KAlF_4$ melts

WILLIAM T. THOMPSON[1] AND DAVID G. W. GOAD
Research Centre, Aluminum Company of Canada, Ltd., Kingston, Ont., Canada K7L 4Z4

Received June 2, 1976

WILLIAM T. THOMPSON and DAVID G. W. GOAD. Can. J. Chem. **54**, 3342 (1976).

The partial pressure of $KAlF_4$ over K_3AlF_6–$KAlF_4$ melts at temperatures as high as 815 °C was measured by thermogravimetry. Melt activities were calculated from the measurements. The results are discussed with reference to the use of this salt mixture as a flux for aluminum alloys.

WILLIAM T. THOMPSON et DAVID G. W. GOAD. Can. J. Chem. **54**, 3342 (1976).

On a mesuré, par thermogravimétrie, la pression partielle de $KAlF_4$ au-dessus de K_3AlF_6–$KAlF_4$ à l'état fondu à des températures allant jusqu'à 815 °C. A partir de ces mesures, on a calculé les activités du sel fondu. On discute de ces résultats en termes de l'utilisation de ce mélange de sel comme flux pour les alliages d'aluminium.

[Traduit par le journal]

Introduction

The properties of molten fluorides and mixtures thereof are of considerable importance to the metallurgy of aluminum. These melts are employed not only as electrolytes in the Hall-Héroult reduction cell but also as protective phases or fluxes which prevent excessive oxidation of metal during manufacturing operations in which aluminum or its alloys are molten.

Molten mixtures of potassium fluoride and aluminum fluoride possess properties required of a suitable flux. In particular these melts are non-reactive with respect to metallic aluminum and, as the phase diagram in Fig. 1 indicates, mixtures with a composition near the K_3AlF_6–$KAlF_4$ eutectic have the necessary low melting temperature (1).

One of the difficulties, however, with the use of this flux is its volatility; although potassium fluoride and aluminum fluoride have negligible vapour pressure (2) at temperatures as high as 700 °C, the compound $KAlF_4$ has a significant one which is important in some applications (3). In addition there is a tendency for AlF_3 dissolved in the melt to react with atmospheric water vapour to form aluminum oxide and hydrogen fluoride vapour. The latter constituent, even in low concentrations, presents a potential hazard.

In order to understand more fully evaporation and hydrolysis of this flux the present experimental thermodynamic study was undertaken in which the equilibrium partial $KAlF_4$ pressure over K_3AlF_6–$KAlF_4$ melts was determined. These measurements in addition to providing pertinent thermodynamic information necessary in evaporation rate calculations make possible the determination of the AlF_3 activity required for thermodynamic calculations related to the hydrolysis equilibrium.

Experiments

Partial pressures were determined by the entrainment method (4). This technique involves determining the mass of fluoride vapour transported from the vicinity of the condensed material in a flowing inert carrier gas. Although this method is a dynamic one in that true thermodynamic equilibrium is not permitted to develop, the procedure nevertheless allows quite precise determination of partial pressures when certain conditions are satisfied.

The essential features of the apparatus are depicted in Fig. 2. The main features of the experimental design are: the use of graphite to prevent volatile fluorides from attacking the vycor in the vicinity of the crucible; the small entrance and exit hole areas relative to the surface area of the flux (less than 1%); a fired asbestos paper gasket to force all of the flowing argon to pass over the crucible; a recording electrobalance to record weight changes in the crucible contents.

With reference to Fig. 2, suppose the gas emitted from the lower hole in the graphite cylinder were representative of the composition of the equilibrium vapour. The mole fraction of fluoride ($KAlF_4$) in the escaping gases, X_F, is given by

$$X_F = \frac{\dot{n}_F}{\dot{n}_A + \dot{n}_F} \qquad [1]$$

[1]Associate Professor, Department of Mining & Metallurgical Engineering, McGill University, Montreal, Quebec.

Can. J. Chem. Downloaded from www.nrcresearchpress.com by 210.87.254.42 on 09/05/12
For personal use only.

Can. J. Chem. Downloaded from www.nrcresearchpress.com by 210.87.254.42 on 09/05/12
For personal use only.

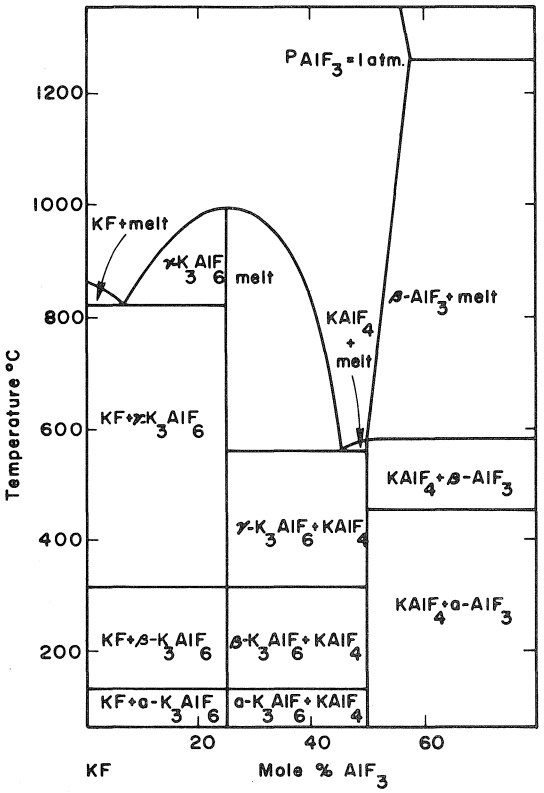

FIG. 1. KF–AlF_3 phase diagram (ref. 1).

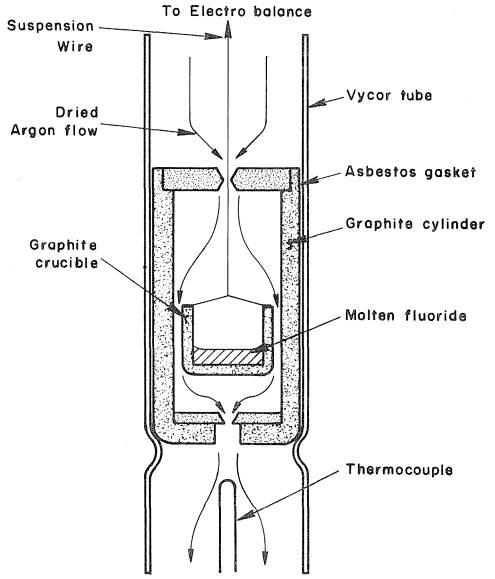

FIG. 2. Detail of furnace chamber.

where $\dot{n}_A$ and $\dot{n}_F$ are the mol/min of argon and fluoride escaping from the lower hole. Equivalently $\dot{n}_F$ may be regarded as the loss in moles of fluoride from the crucible per minute when loss by diffusion through the upper hole is negligible.

Regarding the gas mixture as ideal, the partial pressure of fluoride, P_F, in the vapour is

$$[2] \qquad P_F = \left(\frac{\dot{n}_F}{\dot{n}_A + \dot{n}_F}\right) P_t$$

where P_t is the total gas pressure. It follows therefore that

$$[3] \qquad P_F = \frac{(\dot{w}_F/MW_F)}{(\dot{w}_F/MW_F) + (\dot{V}_A/22414)} P_t$$

where $\dot{w}_F$ is the weight loss of the crucible contents in g/min, MW_F is the molecular weight of the escaping fluoride vapour, and $\dot{V}_A$ is the flow of argon in ml/min at standard temperature and pressure.

The experiment, accordingly, involved the measurement of $\dot{w}_F$, $\dot{V}_A$, and P_t for various temperatures and melt compositions.

Potassium fluoride – aluminum fluoride fluxes were prepared by weighing the pure anhydrous fluorides in air. Anhydrous potassium fluoride was prepared by heating chemically pure $KF.2H_2O$ at 400 °C in air for several days. During this period, the caked salt was occasionally crushed and pulverized in a mortar. The salt was cooled in an evacuated desiccator for about 1 h prior to use. Sublimed aluminum fluoride was oven dried at 100 °C for a few hours to remove any absorbed water.

In a typical experiment a graphite crucible was equipped with a fixed length of Nichrome suspension wire, lowered into the furnace chamber and heated to about 800 °C for several hours in a flowing argon atmosphere until there was no detectable weight loss. The argon was research grade, 99.9995% pure. After cooling, the crucible was charged with a mixture of AlF_3 and KF powders. Since potassium fluoride is quite hygroscopic, the time required to weigh accurately, to mix and add the salts to the crucible was kept to a minimum.

With the loaded crucible resuspended in the furnace, the entire apparatus was evacuated and then filled with dry argon. The balance was tared and the evacuation and argon purging procedure repeated. Prior to precise weight loss determinations, the suspension wire was carefully aligned so as not to rub on the edge of the hole in the top of the graphite chamber.

For all of the measurements the electrobalance was set to permit determination of weight changes over a 2 g interval. Depending on the sample temperature, relative weight changes were observed on 40, 100, or 200 mg full recorder scale settings. It was generally observed that ½ h elapsed after each change in furnace temperature prior to the rate of weight loss becoming constant. In order to reduce error in determining the rate of weight loss by graphically determining the slope of the recorder trace, the time each temperature was maintained generally exceeded 1 h. The flowing gases contribute an aerodynamic force to the crucible weight; however, since only rate of

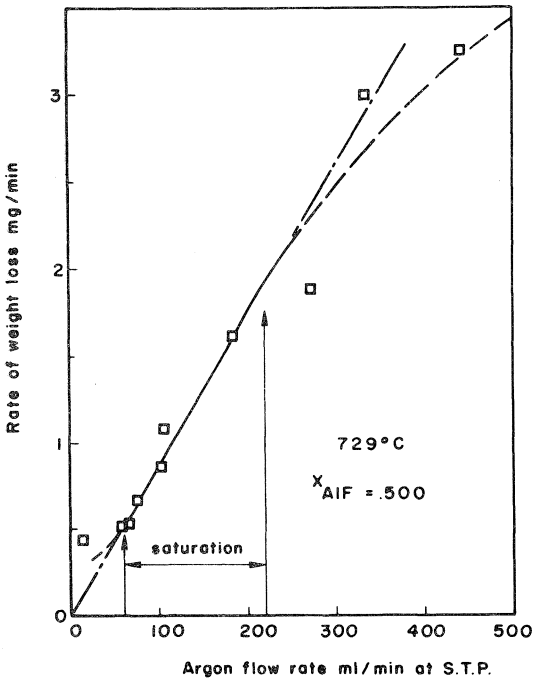

FIG. 3. Test of saturation.

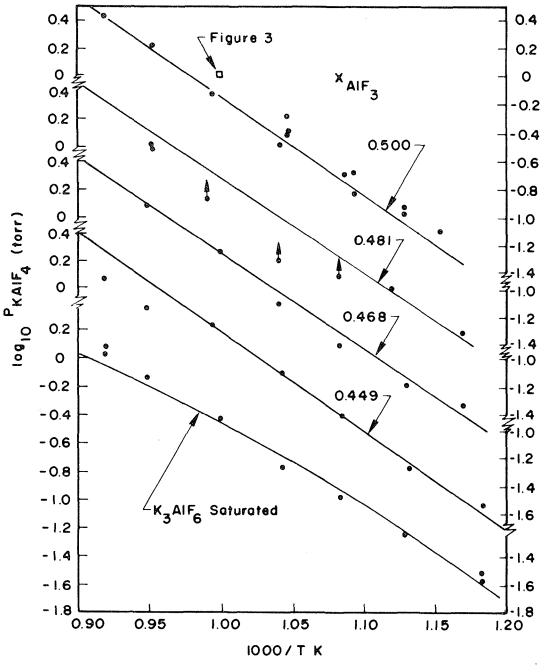

FIG. 4. Partial pressure measurements.

weight change was significant in the present investigation, this effect was unimportant when the flow rate was kept constant. Based upon the ability to hold a constant flow, the noise on the recorder trace and the duration of each determination, it is estimated that the precision of an individual weight loss determination in Table 1 is about 1%.

Results

The use of eq. 3 to calculate equilibrium partial pressures requires that the argon flowing through the sample chamber becomes saturated with fluoride vapour. The usual test for this condition is to show that the rate of weight loss is proportional to the rate of passage of the carrier gas. The experimental results shown in Fig. 3 indicate that over the flow range from about 60 to 220 ml/min at STP, the argon carrier gas is saturated, $(\dot{V}_A/\dot{W}_F)$ is constant and the implication is, by the rearrangement of eq. 3, that the calculated partial pressure of fluoride vapour species F is independent of the flow rate.

Partial pressures calculated using eq. 3 assuming the vapour escaping from the melt to be $KAlF_4$ monomer only are listed in Table 1. These data are displayed in Fig. 4 on conventional log $P - 1/T$ plots. Excluded are measurements made on solid phase mixtures and $KAlF_4$ solid saturated melts. To isolate the different compositions studied more effectively, the log P scale is appropriately broken. The lines represent traces of a mathematical 'best fit' surface obtained by multiple regression analysis, the details and implications of which appear in the next section.

Two items in Fig. 4 merit attention: the magnitude of the partial pressures and the lack of systematic deviation from linearity of the plots pertaining to one phase melts (melts of fixed composition). The magnitude of the partial $KAlF_4$ pressure over pure $KAlF_4$) ($X_{AlF_3} = 0.5$) at 584 °C (the melting point or peritectic) is 0.049 torr compared with independent mass spectrometric measurements extrapolated to that temperature = 0.045 torr (3). Linearity of the plots pertaining to melts of fixed composition is usually observed for systems having only one vapour species. Thus although the plots cannot substantiate the case for mainly monomeric vapour, the data are not inconsistent with this interpretation.

Can. J. Chem. Downloaded from www.nrcresearchpress.com by 210.87.254.42 on 09/05/12
For personal use only.

TABLE 1. Experimental results

Argon flow (ml/min at STP)	Rate of weight loss (mg/min)	Sample T (°C)	Total pressure (torr)	X_{AlF_3}	P_{KAlF_4} (torr)
136	1.429	815	755	0.400*	1.25
129	1.176	815	761	0.400*	1.09
134	0.829	782	761	0.412*	0.742
136	0.429	736	761	0.424*	0.379
139	0.200	686	759	0.434*	0.172
139	0.119	649	758	0.440*	0.102
138	0.0661	612	757	0.445*	0.0572
138	0.0351	572	758	0.449*	0.0304
116	0.0267	572	758	0.449*	0.0275
152	0.0364	572	765	0.450	0.0289
157	0.0667	611	766	0.450	0.0513
152	0.158	649	766	0.450	0.126
146	0.296	686	765	0.450	0.245
145	0.645	732	765	0.449	0.537
141	0.822	781	766	0.448	0.704
147	1.40	815	763	0.448	1.14
115	1.12	782	769	0.469	1.18
120	0.538	736	769	0.468	0.544
122	0.240	689	769	0.468	0.239
124	0.125	651	770	0.468	0.122
124	0.0672	612	768	0.468	0.0657
118	0.0333	573	767	0.468	0.0341
110	0.905	778	774	0.482	1.00
122	0.415	737	775	0.482	0.416
124	0.159	689	774	0.481	0.157
79	0.0784	651	770	0.481	0.121
65	0.0509	620	772	0.481	0.0954
77	0.0302	583	769	0.481	0.0476
117	0.915	777	771	0.481	0.950
124	0.0563	575	775	0.500	0.0555
120	0.114	613	777	0.500	0.116
117	0.194	648	780	0.500	0.204
117	0.321	687	780	0.500	0.338
116	0.703	733	781	0.500	0.746
115	1.52	779	783	0.500	1.63
130	2.70	815	774	0.500	2.53
135	0.0121	534	774	0.500	0.0109
107	1.08	730	759	0.500	1.21
334	2.99	730	759	0.500	—
101	0.857	730	757	0.500	1.01
75	0.668	728	757	0.500	1.06
59	0.524	729	759	0.500	1.06
853	2.21	729	758	0.500	—
62	0.530	729	758	0.500	1.02
13	0.450	729	758	0.500	—
182	1.60	728	758	0.500	1.05
421	3.23	728	758	0.500	—
286	1.88	729	758	0.500	—
233	0.289	641	758	0.500	0.148
104	0.175	641	758	0.500	0.201
115	0.0794	592	757	0.500	0.0824
116	0.102	613	757	0.500	0.105
113	0.485	682	756	0.500	0.512
116	0.0405	572	755	0.500	0.0416
136	0.465	632	754	0.500	0.407
199	0.664	682	754	0.500	0.397
204	6.83	815	754	0.500	3.96

*K_3AlF_6 saturated; composition from liquidus (ref. 1).

Can. J. Chem. Downloaded from www.nrcresearchpress.com by 210.87.254.42 on 09/05/12
For personal use only.

Can. J. Chem. Downloaded from www.nrcresearchpress.com by 210.87.254.42 on 09/05/12
For personal use only.

Thermodynamic Analysis

The following equilibrium exists between the arbitrarily selected components of the melt, KF and AlF_3, and $KAlF_4$ in the vapour phase.

[4] $$KF_{(solid)} + AlF_{3\,(solid\,\beta)} \rightleftharpoons KAlF_{4\,(gas,1\,atm)}$$

The subscripts refer to the standard states that will be employed. At constant temperature, it follows that

[5] $$d \ln P_{KAlF_4} = d \ln a_{KF} + d \ln a_{AlF_3}$$

Further, the activities of KF and AlF_3 are related at constant temperature by the Gibbs–Duhem equation

[6] $$X_{KF}\, d \ln a_{KF} + X_{AlF_3}\, d \ln a_{AlF_3} = 0$$

Thus P_{KAlF_4} is related to the activity of AlF_3 in the melt by

[7] $$d \ln P_{KAlF_4} = \frac{1 - 2X_{AlF_3}}{1 - X_{AlF_3}}\, d \ln a_{AlF_3}$$

When liquid standard states are used for melt components of a binary solution, following the convention of Margules, the isothermal partial excess free energy $\bar{G}_1^{E}$ may be represented by the empirical series

[8] $$\bar{G}_1^{E} = \sum_{i=0}^{n} \beta_i X_2^{i+2}$$

where n is a small number. In the present case owing to the narrow composition range available for study and the limited precision of the $KAlF_4$ partial pressure determinations, it is necessary to assume that $\bar{G}_{AlF_3}^{E}$ may be adequately represented by the expression

[9] $$\bar{G}_{AlF_3}^{E} = RT \ln \gamma^*_{AlF_3} = \beta X_{KF}^2$$

where γ^* is the activity coefficient when the liquid standard state is employed.

The coefficient β is usually a linear function of absolute temperature; however, in this analysis, to minimize the number of adjustable parameters, it will be taken as a constant, the implication being that all the excess partial free energy is lumped into the partial enthalpy.

Since it is impractical to employ the liquid standard state of AlF_3, the free energy of fusion at temperature T may be put into the eq. 9, to yield the activity coefficient relative to solid β-AlF_3. Accordingly

[10] $$\ln a_{AlF_3} = \ln X_{AlF_3} + \frac{\beta}{RT} X_{KF}^2 + \frac{\Delta G_f}{RT}$$

where ΔG_f is essentially a linear function of T.

Differentiation of eq. 10 and substitution into eq. 7 gives

[11] $$d \ln P_{KAlF_4} = \left(\frac{1 - 2X_{AlF_3}}{X_{AlF_3} - X_{AlF_3}^2}\right) d\, X_{AlF_3} - 2\left(\frac{\beta}{RT}\right)(1 - 2X_{AlF_3})\, d\, X_{AlF_3}$$

Integration of this equation results in

[12] $$\ln P_{KAlF_4} = \ln (X_{AlF_3} X_{KF}) - 2\left(\frac{\beta}{RT}\right) X_{AlF_3} + 2\left(\frac{\beta}{RT}\right) X_{AlF_3}^2 + I$$

where I is an integration constant that depends on temperature. This constant may be determined by realizing that eq. 12 must become

[13] $$\ln P_{KAlF_4} = \frac{-\Delta H_v^0}{RT} + \frac{\Delta S_v^0}{R}$$

where ΔH_v^0 and ΔS_v^0 are the standard enthalpy and entropy of vaporization of $KAlF_4$ liquid when X_{AlF_3} is 0.5. It follows that

[14] $$I = \frac{-\Delta H_v^0 + \beta/2}{RT} + \frac{\Delta S_v^0 + R \ln 4}{R}$$

Substituting eq. 14 into eq. 12, changing to base ten logarithms, and expressing P_{KAlF_4} in torr, we have

[15] $$\log \frac{P_{KAlF_4}}{X_{KF}X_{AlF_3}} = \left\{\frac{\beta - 2\Delta H_v^0}{9.150}\right\}\frac{1}{T} + \left\{\frac{-\beta}{2.288}\right\}\frac{X_{KF}X_{AlF_3}}{T} + \left\{\frac{\Delta S_v^0}{4.575} + 3.483\right\}$$

The terms in braces were determined by performing a multiple linear regression analysis (Dataline Mulreg) on the experimental points shown in Fig. 4, and listed in Table 1 with the result that

[16] $$\frac{\beta - 2\Delta H_v^0}{9.15} = -1.92 \times 10^4$$

[17] $$\frac{-\beta}{2.288} = 4.95 \times 10^4$$

[18] $$\frac{\Delta S_v^0}{4.575} + 3.483 = 7.25$$

The standard error of estimate of $\log (P_{KAlF_4}/X_{KF}X_{AlF_3})$ is 0.13. The result of the regression analysis makes possible the construction of the best fit lines drawn through the points in Fig. 4. Although there is considerable imprecision in establishing the coefficients in eq. 15 these yield the following information for the transformation of liquid $KAlF_4$ to vapour at standard atmospheric pressure

[19] $$\Delta H_v^0 = 31.3 \text{ kcal/g-mol}$$

[20] $$\Delta S_v^0 = 17.2 \text{ cal/K g-mol}$$

The entropy of vaporization is somewhat lower than the Trouton value. Nevertheless these values are about what might be expected and imply a normal boiling point of $KAlF_4$ in the vicinity of 1550 °C. From the value of β it follows from eq. 10 that at 600 °C, since a_{AlF_3} is unity at $X_{AlF_3} = 0.502$ (1),

[21] $$\log a_{AlF_3} = \log X_{AlF_3} - 28.3X_{KF}^2 + 7.33$$

This activity isotherm appears in Fig. 5. The activity isotherm of $KAlF_4$ with respect to pure liquid is also shown. The equation for this line is based on

[22] $$a_{KAlF_4} = \frac{P_{KAlF_4}}{P_{KAlF_4}^0}$$

hence

[23] $$\log a_{KAlF_4} = \log (X_{AlF_3}X_{KF}) + 49500\frac{X_{AlF_3}X_{KF}}{T} - \frac{12400}{T} + 0.602$$

It is possible to determine activity isotherms for KF and K_3AlF_6 consistent with those given by eqs. 21 and 23. These are represented in Fig. 5 but the values of a_{KF} are so small that they cannot be distinguished from the lower horizontal axis.

Can. J. Chem. Downloaded from www.nrcresearchpress.com by 210.87.254.42 on 09/05/12
For personal use only.

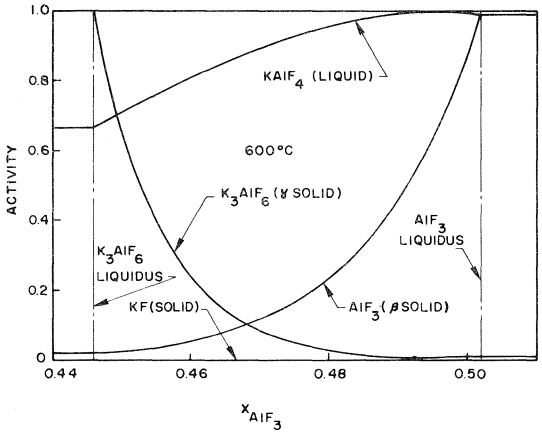

FIG. 5. Activity isotherms at 600 °C.

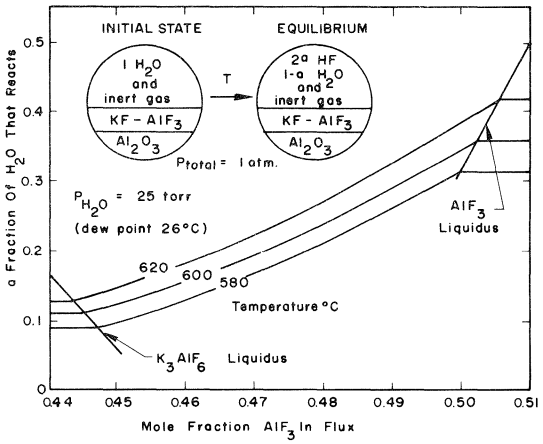

FIG. 7. Thermodynamics of flux hydrolysis.

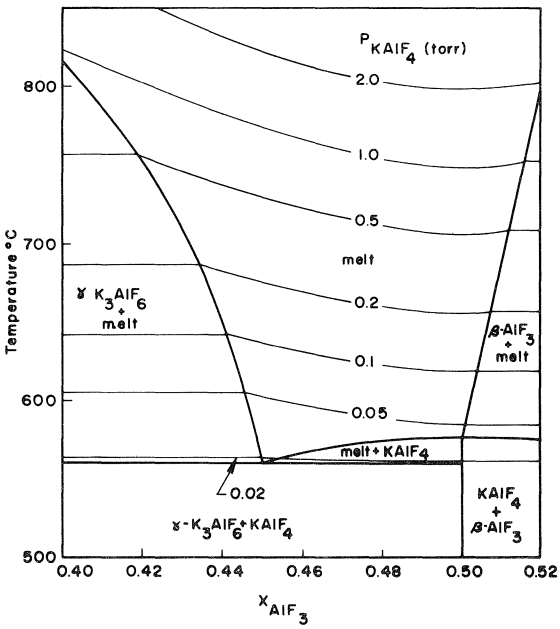

FIG. 6. $KAlF_4$ partial pressure isobars.

Discussion

Using the results of the regressions, it is possible to construct partial $KAlF_4$ isobars on the $KF–AlF_3$ phase diagram. These are shown in Fig. 6. Since $KAlF_4$ is essentially the only contributor to the vapour phase, these isobars may also be regarded as total equilibrium pressure isobars. All of the curves pass through a minimum at the composition associated with pure $KAlF_4(0.5X_{AlF_3})$ and, as a result of certain thermodynamic assumptions detailed in the preceding section, are symmetrical about this composition. In the two phase regions, the isobars are, in keeping with the phase rule, horizontal. The nature of the $KAlF_4$ melting feature is deliberately drawn as shown since it is not clear whether this compound melts congruently or incongruently (1).

In a practical application, a principal factor in determining loss of flux by evaporation is the equilibrium partial pressure. Figure 7 therefore is useful in understanding the effects of altering the temperature and composition. For example, it shows that decreasing the temperature only 35 °C, from 600 °C to 565 °C (with other factors constant) decreases evaporation rate by about 60%. Changing the composition from $X_{AlF_3} = 0.5$ to 0.4 at 600 °C also decreases evaporation rate but less drastically.

Melts containing AlF_3 are susceptible to hydrolysis as a result of the reaction

$$[24]\quad 2AlF_{3(solid)} + 3H_2O_{(gas,1\,atm)} \rightarrow 6HF_{(gas,1\,atm)} + Al_2O_{3(solid)}$$

For the standard states indicated, the standard free energy change at 600 °C (2) is 18.9 kcal/g-mol Al_2O_3.

This information, together with the previously calculated AlF_3 activity, permits a calculation of the extent to which water vapour can react with the molten flux.

Consider the idealized system depicted in the upper portion of Fig. 7. A quantity of inert gas, n g-mol, and 1 g-mol of water vapour is in

Can. J. Chem. Downloaded from www.nrcresearchpress.com by 210.87.254.42 on 09/05/12
For personal use only.

Can. J. Chem. Downloaded from www.nrcresearchpress.com by 210.87.254.42 on 09/05/12
For personal use only.

contact with a relatively large quantity of molten flux. The system is closed to the surroundings with respect to mass transfer; temperature and pressure are held constant (by change in volume if necessary) while equilibrium is developing. In the initial state,

$$[25] \qquad P_{H_2O} = \left(\frac{1}{1+n}\right)P_{total}$$

Let α be the fraction of H_2O that reacts with AlF_3. When equilibrium is established

$$[26] \qquad (P_{H_2O})_{eq} = \left(\frac{1-\alpha}{1+\alpha+n}\right)P_{total}$$

$$[27] \qquad (P_{HF})_{eq} = \left(\frac{2\alpha}{1+\alpha+n}\right)P_{total}$$

Since the flux is regarded as saturated with sparingly soluble Al_2O_3 (5), the activity of Al_2O_3 is one and the equilibrium H_2O and HF partial pressure are related by

$$[28] \quad \log P_{HF} = (-4.72 + 2\log a_{AlF_3} + 3\log P_{H_2O})/6$$

Assuming the properties of Al_2O_3-saturated fluoride melts are similar to the pure binary fluoride solutions, the AlF_3 activity is given by eq. 21. It follows that for an arbitrary initial H_2O partial pressure such as 25 torr (n is 29.4), α may be evaluated for any particular melt composition and total pressure by the substitution of eqs. 26 and 27 into eq. 28 and the solution of the resulting quadratic equation for α. The results of such calculations are depicted in Fig. 7 where it is clear that there is a decided advantage, from the point of view of minimizing hydrolysis, in using fluxes with the minimum AlF_3 content.

The positive standard entropy change for the hydrolysis reaction results in ΔG^0 becoming more positive as the temperature is decreased. The constant in eq. 28 becomes therefore increasingly negative and the resulting fraction of H_2O that reacts becomes significantly less. The temperature effect is illustrated in Fig. 7.

Acknowledgments

The authors wish to thank Dr. E. G. Torrible and Mr. J. A. Hirschfield for many helpful discussions and the Aluminum Company of Canada for permission to publish this work.

1. B. Jensen. Phase and structure determination for new complex alkali aluminum fluorides. Institute of Inorganic Chemistry, Norwegian Technical University, Trontheim, 1969.
2. JANAF Thermochemical Tables, The Dow Chemical Company Ltd., 1965–1967.
3. E. N. Kolosov, L. N. Sidorov, and G. F. Voronin. Russ. J. Phys. Chem. **45**, 11 (1971).
4. O. Kubaschewski, E. Ll. Evans, and C. B. Alcock. Metallurgical thermochemistry. Pergamon Press Ltd., London. 1967.
5. E. W. Dewing. Private communication.

Electrochimie de composés organométalliques. I. Electrosynthèse de cyclopentadiène cyclopentadiényl cobalt substitués[1]

NABIL EL MURR ET ETIENNE LAVIRON

Laboratoire de Polarographie Organique associé au C.N.R.S. (L.A. 33), Faculté des Sciences, 6 Boulevard Gabriel, 21000 Dijon, France

Reçu le 3 mai 1976

NABIL EL MURR et ETIENNE LAVIRON. Can. J. Chem. **54**, 3350 (1976).

Des anions cobaltocène ont été générés électrochimiquement dans le diméthylformamide. Par réaction avec divers électrophiles, on obtient avec des rendements quantitatifs des cyclopentadiène cyclopentadiényl cobalt substitués, dont certains sont inaccessibles par les méthodes usuelles.

Des cyclopentadiène cyclopentadiényl cobalt substitués ont également été obtenus avec d'excellents rendements, par réaction du cobaltocène généré électrochimiquement et d'halogénures organiques.

NABIL EL MURR and ETIENNE LAVIRON. Can. J. Chem. **54**, 3350 (1976).

Cobaltocene anions have been prepared electrochemically in dimethylformamide. Their reaction with various electrophiles gives, in quantitative yields, substituted cyclopentadiene cobalt cyclopentadienyls, some of which cannot be prepared by usual methods.

Substituted cyclopentadiene cobalt cyclopentadienyls are also obtained in excellent yield, by reaction of electrochemically generated cobaltocene with organic halides.

Introduction

La chimie du ferrocène et celle de son analogue l'ion cobalticinium n'ont pas connu le même développement. Le premier a été longuement étudié et un très grand nombre de ses dérivés ont été synthétisés, alors que très peu d'études ont été consacrées à l'ion cobalticinium.

Cette différence peut s'expliquer par le comportement différent des deux métallocènes vis-à-vis de la substitution. Le ferrocène peut être considéré comme une molécule aromatique électroniquement riche analogue à l'anisol (1): il donne lieu à la réaction de Friedel et Craft (2), il réagit avec les agents électrophiles pour conduire à différents dérivés substitués et avec les organolithiens il forme le ferrocényl lithium (3). La préparation de dérivés substitués du ferrocène est donc très facile, ce qui explique le développement de la chimie de ce métallocène.

Dans le cas de l'ion cobalticinium au contraire, il est très difficile d'obtenir des dérivés substitués: cet ion peut être comparé à l'ion pyridinium (4); l'existence de la charge positive exclut la possibilité de toute attaque électrophile. L'action d'agents électrophiles sur le cobaltocène ne permet pas non plus la préparation de dérivés substitués, car le cobaltocène est oxydé en ion cobalticinium dans les conditions de ces réactions. L'action des réactifs de Grignard, des organolithiens et des ions hydrures sur les sels de cobalticinium conduit à des dérivés d'addition (5–7) (réaction 1). L'action d'halogénures organiques sur le cobaltocène conduit au même résultat (8–10) (réaction 2).

[1]

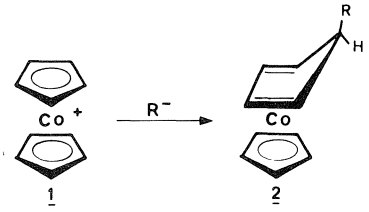

1 2

[2]

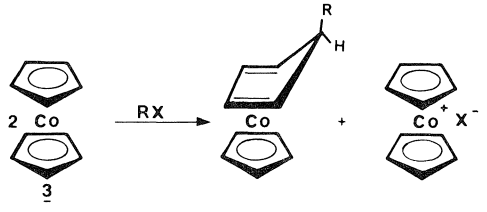

3

Les dérivés substitués de l'ion cobalticinium ont été obtenus jusqu'ici soit en condensant directement des ions cyclopentadiényles substitués sur un sel de cobalt, soit en transformant à l'aide de réactions classiques les substituants

[1]Ce travail a été réalisé en partie dans le cadre de la R.C.P. "Electrochimie organique et organométallique séléctive .

Can. J. Chem. Downloaded from www.nrcresearchpress.com by 210.87.254.105 on 09/05/12
For personal use only.

Can. J. Chem. Downloaded from www.nrcresearchpress.com by 210.87.254.105 on 09/05/12
For personal use only.

déjà présents sur le squelette métallocénique (11–13). Dans les deux cas les techniques opératoires sont laborieuses et le nombre de dérivés ainsi obtenus est resté très restreint. Cette difficulté de préparation des dérivés substitués du cobalticinium explique en partie le peu de développement de sa chimie.

Au cours d'une étude électrochimique des sels de cobalticinium (14–15), nous avons pu mettre en évidence, outre le stade de réduction de l'ion cobalticinium en cobaltocène, qui était déjà connu (16–18), une seconde étape de réduction. Comme nous l'avions proposé (15), et comme nous avons pu le confirmer par la suite (19), cette seconde étape correspond à la formation de l'anion cobaltocène (réaction 3).

[3] 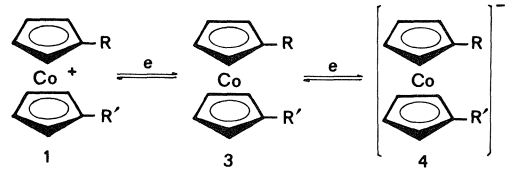

Résultats et discussion

Nous avons pu montrer en étudiant un grand nombre de dérivés substitués du cobalticinium que la formation de l'anion est générale. Dans le tableau 1, nous indiquons les potentiels de demi-vague correspondant aux deux étapes de réduction de quelques dérivés. Une étude par voltammétrie cyclique montre que ces deux étapes sont réversibles, en milieu aqueux ou non aqueux, même pour des vitesses de balayages inférieures à 0.1 V s^{-1}.

Dans ce qui suit, nous montrerons comment la préparation électrochimique du cobaltocène ou celle de son anion peut être mise à profit pour la préparation de dérivés d'addition du cobaltocène. Dans un article suivant, nous étudierons le problème du passage par oxydation de ces dérivés d'addition aux sels de cobalticinium correspondants.

I-Préparation des cyclopentadiène cyclopentadiényl cobalt à partir du cobaltocène généré électrochimiquement

Différents travaux ont montré qu'une réaction d'addition pouvait avoir lieu en mettant en contact le cobaltocène et un halogénure organique (8–10) (réaction 2). A partir de deux molécules de cobaltocène, on obtient une molécule de cyclopentadiène cyclopentadiényl cobalt *exo* substitué et une molécule de sel de cobalticinium. Nous avons réalisé cette réaction en utilisant du cobaltocène généré électrochimiquement à partir de l'ion cobalticinium (schéma 1).

TABLEAU 1. Potentiels de demi-vague, en volt (e.c.s.), des deux vagues de réduction des hexafluorophosphates de cobalticinium mono- et disubstitués: $[(C_5H_4R)\text{-}Co(C_5H_4R')]^+ PF_6^-$. $C = 5 \times 10^{-4}$; solutions dans le DMF; sel de fond $(C_4H_9)_4N^+ClO_4^-$; Electrode à goutte de mercure; temps de chute = 0.5 s

(*a*) Dérivés disubstitués

R = R′	$-E_{1/2}$	$-E_{1/2}'$
H*	0.87	1.82
CH_3	0.99	1.99
$CH(CH_3)_2$	0.93	1.93
$C(OH)(CH_3)_2$	0.96	1.84
$CH(CH_3)(C_2H_5)$	0.96	1.94
$C(OH)(CH_3)(C_2H_5)$	0.94	1.82
$CH(CH_3)(C_6H_5)$	0.92	1.90
CO_2H	0.43	1.35
CO_2CH_3	0.36	1.30
NH_2	1.34	2.21

(*b*) Dérivés monosubstitués (R′ = H)

R	$-E_{1/2}$	$-E_{1/2}'$
$CH(C_6H_5)_2$	0.84	1.80
$C(OH)(C_6H_5)_2$	0.83	1.69
CO_2H	0.62	1.58
CO_2CH_3	0.59	1.55
$CONH_2$	0.68	1.63
NH_2	1.13	2.00

*A la suite d'une erreur, les valeurs de −0.77 et −1.73 ont été indiquées dans la réf. 19.

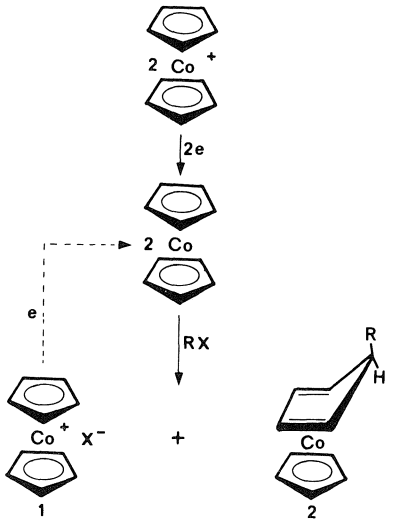

SCHÉMA 1

TABLEAU 2. Caractéristiques comparées de la préparation chimique et électrochimique des cyclopentadiène cyclopentadiényl cobalt

Dérivé	Réaction					
	Chimique			Electrochimique		
	T (°C)	Temps (h)	Rdt. (%)	T (°C)	Temps (h)	Rdt. (%)
2*a* R = $CH_2C_6H_5$	20	0.33	47.5 (8)	20	2	95
2*b* R = $CHClC_6H_5$	40	50	44 (9)	20	7	96
2*c* R = CCl_3	20	1	45 (6)	20	1	98
2*d* R = CH_2Br	40	5	45 (10)	20	5	90

La préparation électrochimique de solutions de cobaltocène présente les deux avantages suivants.

(*a*) Le cobaltocène est difficile à obtenir chimiquement du fait de son instabilité; électrochimiquement, il est extrêmement facile de l'obtenir à partir du sel de cobalticinium correspondant qui est très stable, facile à préparer (20), et d'un prix de revient moins élevé que le cobaltocène.

(*b*) Lors de la réaction de dérivés halogénés sur le cobaltocène (réaction 2), le rendement est nécessairement limité à 50% par rapport à ce dernier. Electrochimiquement (schéma 1), on peut avoir un rendement de 100% puisque le cobaltocène est régénéré au fur et à mesure de la réaction.

Nous avons préparé divers cyclopentadiène cyclopentadiényl cobalt par réduction d'un sel de cobalticinium en présence d'un composé halogéné RX (tableau 2). Les rendements sont excellents. Un autre avantage est dans certains cas la rapidité de la réaction qui est peut être plus grande parce que la concentration en cobaltocène diminue moins rapidement par suite de sa régénération électrochimique.

II-Préparation des cyclopentadiène cyclopentadiényl cobalt à partir des anions cobaltocènes

(a) Réaction avec l'anhydride carbonique

Les solutions de l'anion cobaltocène ne sont pas très stables ni en milieu hydroalcoolique ni dans le diméthylformamide, par suite d'une réaction avec l'eau ou avec les sels supports (tétraalkylammonium). Nous avons donc généré l'anion en présence d'un réactif approprié pour que la réaction envisagée ait lieu *in situ* avant la disparition de l'anion. Nous avons d'abord généré l'anion cobaltocène en présence de CO_2 (schéma 2); l'étude électrochimique montre qu'on obtient avec un rendement pratiquement quantitatif le sel de carboxycyclopentadiène cyclopentadiényl cobalt **5**.

Le dérivé **5** présente des caractéristiques électrochimiques analogues à celles du cyclopentadiène cyclopentadiényl cobalt (tableau 3), c'est-à-dire une vague anodique irréversible à 2 Faraday et une autre cathodique également irréversible à 2 Faraday; ces caractéristiques permettent de suivre très facilement la réaction d'addition du nucléophile sur l'anion cobaltocène.

L'addition d'ions H^+ à la solution du dérivé **5** conduit à l'acide **6**. Cet acide a été mis en évidence grâce à son polarogramme (tableau 3). Nous avons tenté de l'isoler mais sa très grande solubilité dans le DMF et dans l'eau ainsi que

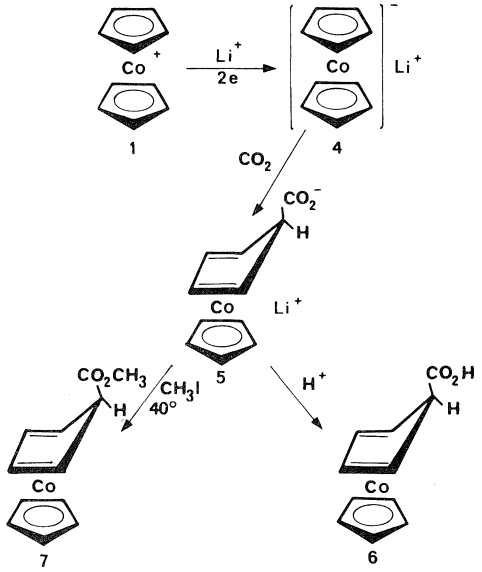

SCHÉMA 2

Can. J. Chem. Downloaded from www.nrcresearchpress.com by 210.87.254.105 on 09/05/12
For personal use only.

Can. J. Chem. Downloaded from www.nrcresearchpress.com by 210.87.254.105 on 09/05/12
For personal use only.

TABLEAU 3. Potentiels de demi-vague, en volt (e.c.s.), de la vague d'oxydation et de la vague de réduction des cyclopentadiène cyclopentadiényl cobalt (RC_5H_5)-$Co(C_5H_5)$. Polarogrammes enregistrés dans le DMF: sel de fond $(C_4H_9)_4N^+ClO_4^-$; électrode à goutte de mercure; temps de chute = 0.5 s

R	$E_{1/2}$ Anodique*	$E_{1/2}$ Cathodique†
H	−0.08	−2.40
C_6H_5	0.16	−2.33
$CH_2C_6H_5$	0.11	−2.41
$CH(CH_3)_2$	0.06	−2.44
C_2H_5	0.06	−2.40
CO_2^-	−0.58	−2.61
CO_2H	−0.22	—‡
CO_2CH_3	0.43	−2.42

*Vague anodique irréversible à 2 Faraday.
†Vague cathodique irréversible à 2 Faraday.
‡La vague cathodique, pour ce dérivé, est masquée par la décharge des ions H^+ que nous avons ajoutés dans le milieu pour transformer CO_2^- en CO_2H.

son instabilité nous ont incités à faire réagir l'anion **5** *in situ* avec CH_3I; on obtient ainsi avec un rendement quantitatif l'ester correspondant **7**.

Différents travaux ont été consacrés à l'étude de la structure des dérivés du cyclopentadiène cyclopentadiényl cobalt (6, 21, 22); la position *exo* ou *endo* des substituants a été longuement discutée. Actuellement et après des études de structure par rayons X, il est admis que le spectre infrarouge de ces dérivés est révélateur de leur structure; si dans le spectre ir d'un dérivé substitué sur le cyclopentadiène la bande intense aux environs de 2760 cm^{-1} n'apparaît pas, ceci veut dire que le substituant occupe la position *exo*; dans le cas où un atome d'hydrogène occupe cette position *exo* le spectre présente alors une bande intense entre 2740 et 2780 cm^{-1} (22).

Les bandes les plus intenses dans le spectre ir du dérivé **7** sont situées respectivement à: 2958, 1736, 1432, 1299, 1205, 1190, 1167, 1111, 1072 et 1000 cm^{-1}. Aucune bande n'est visible dans la région de 2760 cm^{-1}; ceci montre que dans **7** le groupement CO_2CH_3 occupe la position *exo*. Ce résultat semble indiquer *a priori* que dans l'anion cobaltocène la charge négative formelle est localisée sur le cycle; cette conclusion mérite une étude plus approfondie et nous tentons actuellement la préparation de solutions stables de cet anion pour les analyser par rmn.

Jusqu'ici la synthèse des dérivés du cyclopentadiène cyclopentadiényl cobalt a été effectuée à partir du cobaltocène ou de l'ion cobalticinium non substitué, avec la conséquence que seuls des dérivés monosubstitués sur le cyclopentadiène ont été obtenus. Possédant une technique opératoire facile il nous a semblé intéressant de généraliser les résultats à des dérivés substitués du cobalticinium en vue d'obtenir des cyclopentadiène cyclopentadiényl cobalt disubstitués sur le cyclopentadiène.

Une solution d'hexafluorophosphate de diméthyl-1,1′ cobalticinium présente, dans le diméthylformamide, un polarogramme similaire à celui du sel de cobalticinium non substitué ($E_{1/2} = -0.99$, $E_{1/2}' = -1.99$ V e.c.s.).

L'électrolyse d'une telle solution au niveau de la deuxième vague ($E = -2.1$ V e.c.s.) en présence d'anhydride carbonique conduit à une solution rouge foncée caractéristique des dérivés du cyclopentadiène cyclopentadiényl cobalt. Comme dans le cas précédent nous sommes passés directement à l'ester, par traitement *in situ* par l'iodure de méthyle (schéma 3). En fin de réaction, nous avons isolé une huile rouge **11** très sensible à l'oxydation.

Dans le cas des dérivés symétriquement disubstitués en 1 et 1′ tel que **8**, trois isomères **12**, **13**, **14** du dérivé **11** peuvent être théoriquement obtenus (fig. 1): le groupement ester peut occuper soit le sommet porteur du groupement CH_3 (**12**) soit les sommets α (**13**) ou β (**14**).

L'analyse par chromatographie en couche mince (gel de silice; éther–hexane) du mélange

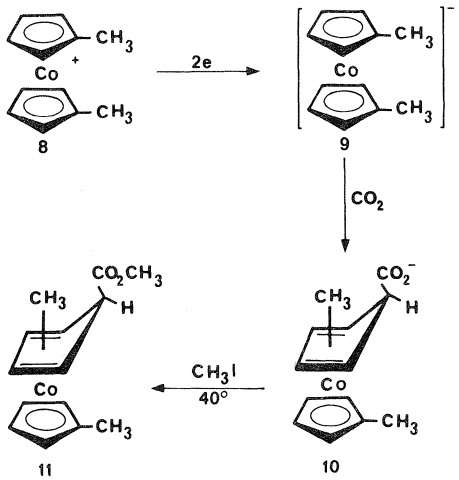

SCHÉMA 3

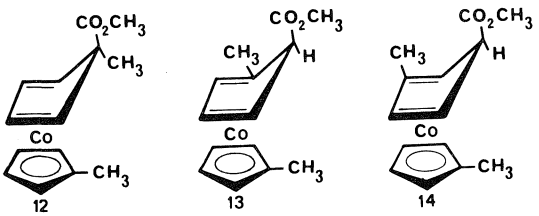

FIG. 1. Isomères de **11**.

11, bien que délicate à cause de la destruction de la molécule, nous a permis néanmoins de distinguer deux produits dont les R_f sont très proches. L'étude du spectre de rmn d'un mélange fraîchement préparé s'est révélée plus concluante (fig. 2). Dans ce spectre on note l'existence des deux isomères **13** et **14**; l'isomère **12**, s'il existe, serait à l'état de traces (on ne trouve dans le spectre aucun signal correspondant à un méthyl fortement déblindé du fait de la position *endo* et de l'effet du groupement ester porté par le même carbone).

L'intégration, dans la région de résonance des groupements méthyle, des spectres enregistrés à partir de différents échantillons préparés dans les mêmes conditions opératoires, montre que **13** est majoritaire et constitue environ 60% du mélange. Nos tentatives de séparation de ces deux isomères par différentes techniques classiques ont échoué et ont abouti à la destruction de la molécule.

Ce mélange d'isomères constitue à notre connaissance le premier exemple de dérivés hétérotrisubstitués dans la série du cyclopentadiène cyclopentadiényl cobalt. Dans le spectre ir de ce mélange on note, comme pour **7**, l'absence de bande intense aux environs de 2760 cm^{-1}; ceci montre que dans **13** et **14** le groupement ester occupe la position *exo*.

(*b*) *Réactions avec les halogénures organiques RX*

L'anion cobaltocène réagit également avec les halogénures organiques RX. La technique opératoire consiste à générer électrochimiquement l'anion cobaltocène en présence de RX.

Comme le cobaltocène peut se former, tant qu'il reste du sel de cobalticinium en solution, par réaction entre l'anion et le sel de cobalticinium (réaction inverse de la dismutation), une possibilité de réaction entre le cobaltocène et RX peut exister (réaction 2); pour éliminer ce type de

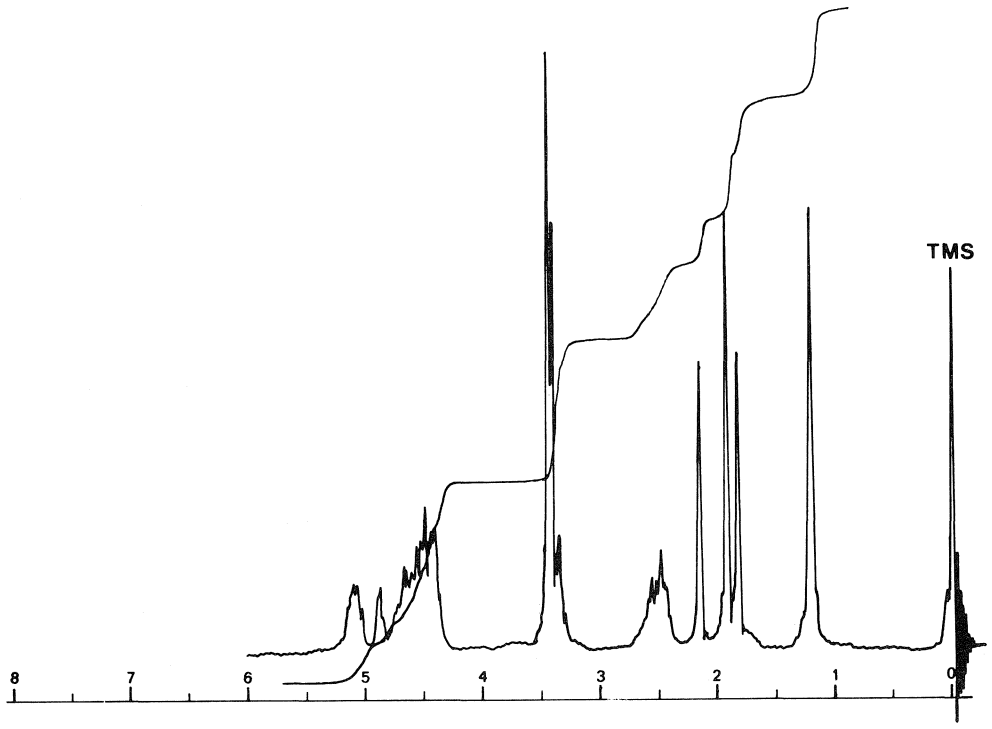

FIG. 2. Spectre rmn de **13** + **14** ($CDCl_3$).

Can. J. Chem. Downloaded from www.nrcresearchpress.com by 210.87.254.105 on 09/05/12
For personal use only.

réaction, nous avons choisi des halogénures organiques connus pour être inactifs vis-à-vis du cobaltocène ou réagissant avec une vitesse très faible. Dans tous les cas étudiés la réaction est très rapide (environ $\frac{1}{2}$ h) et les rendements quantitatifs (réaction 4).

[4] 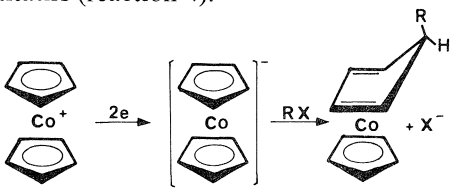

Nous avons effectué trois réactions à partir de l'anion cobaltocène non substitué et avons obtenu les trois cyclopentadiène cyclopentadiényl cobalt **15**, **16** et **17** (**15** R = C_6H_5; **16** R = C_2H_5; **17** R = $CH(CH_3)_2$); seul **15** a été isolé et identifié à un échantillon obtenu par voie chimique. **16** et **17** très instables, ont été étudiés électrochimiquement et leurs caractéristiques sont données dans le tableau 3.

Nous avons également réalisé un exemple de réaction d'halogénure organique sur l'anion du diméthyl-1,1′ cobaltocène (réaction 5).

[5] 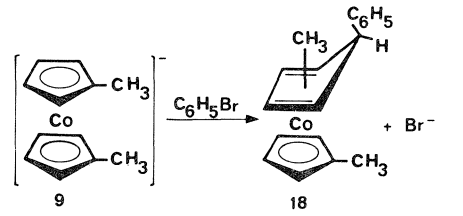

9 18

Le spectre rmn de **18** montre que l'on obtient un mélange d'isomères 1-2 et 1-3 disubstitués sur le cyclopentadiène. Ces isomères sont en proportions égales dans le mélange et leur séparation a également échoué parce qu'ils sont très sensibles aux oxydants et en particulier à l'oxygène de l'air.

Conclusion

En résumé, nos résultats concernant la synthèse des dérivés du cyclopentadiène cyclopentadiényl cobalt montrent l'étendue des services que peuvent apporter, dans la série des organométalliques, les différentes techniques électrochimiques.

Les synthèses effectuées après réduction (soit à 1 Faraday soit à 2 Faraday) de l'ion cobalticinium non substitué sont réalisées avec des rendements presque quantitatifs alors que par les méthodes classiques les rendements sont au plus égaux à 50%.

L'action de l'anhydride carbonique sur l'anion cobaltocène nous a permis d'obtenir des dérivés (acide et ester) dont la synthèse n'est pas envisageable par les techniques connues jusqu'à présent. Le carbomethoxycyclopentadiène cyclopentadiényl cobalt a été obtenu sous forme de mono cristal et l'étude de sa structure par rayons X[2] nous permettra sans doute de comprendre le mécanisme d'attaque du CO_2 et de préciser la nature de l'anion cobaltocène; de plus elle pourra présenter un complément d'information concernant la substitution *endo* ou *exo* dans la série.

Enfin, l'action de l'anhydride carbonique ou du bromobenzène sur l'anion du diméthyl-1,1′ cobaltocène, nous a permis de préparer sous forme d'un mélange les premiers exemples d'une nouvelle série de dérivés trisubstitués du cyclopentadiène cyclopentadiényl cobalt. Comme nous le montrerons dans l'article suivant de cette série, la séparation peut se faire à un stade ultérieur; elle nous a permis d'obtenir, pour la première fois, des isomères 1,2,1′ et 1,3,1′ trisubstitués dans la série de l'ion cobalticinium.

Partie expérimentale

Polarographie et électrolyses

Tous les polarogrammes ont été enregistrés à l'aide d'un polarographe Tacussel "Tipol" à trois électrodes. Le temps de chute de l'électrode à goutte de mercure était régulé à 0.5 s au moyen d'un marteau.

Les potentiels sont donnés par rapport à une électrode au calomel saturée aqueuse. Le diméthylformamide est de qualité H.P.; il est utilisé sans purification préalable. Le sel de fond est le perchlorate de tétrabutyl ammonium (préparé par G. Frederick Smith Chemical Company) à une concentration de 0.1 *M*. La cellule polarographique est une cellule "Metrohm" thermostatée à 20 °C.

Le produit à étudier est dissous à une concentration de 10^{-3} *M* et la solution est dégazée à l'aide d'un courant d'argon.

Les électrolyses à potentiel contrôlé ont été effectuées sur nappe de mercure en utilisant un potentiostat "Tacussel ASA 100-1C" et un intégrateur "Tacussel I G 5". Nous avons étudié les réactions, soit dans une petite cellule en suivant leur évolution par polarographie, soit dans une cellule d'un litre pour les électrolyses préparatives. Dans ce dernier cas les quantités de substance électrolysée vont de 0.5 à 5 g.

Synthèse des composés ***2a***, ***2b***, ***2c*** *et* ***2d***

L'hexafluorophosphate de cobalticinium (1 g) est dis-

[2]N. El Murr et E. Laviron, travail en cours.

Can. J. Chem. Downloaded from www.nrcresearchpress.com by 210.87.254.105 on 09/05/12
For personal use only.

Can. J. Chem. Downloaded from www.nrcresearchpress.com by 210.87.254.105 on 09/05/12
For personal use only.

sous dans 100 ml de DMF (électrolyte support LiCl à 1 *M*). On ajoute un excès d'halogénure organique (environ 4 mol de RX pour 1 mol de $(C_5H_5)_2CoPF_6$). Le potentiel imposé est de -1.1 V (e.c.s.) sauf dans le cas de **2***c* où il est de -0.85 V (e.c.s.) à cause du potentiel de réduction de CCl_4 qui se situe vers -0.8 V; dans ce cas il faut ajouter au cours de l'électrolyse quelques millilitres de CCl_4.

Comme l'un des rapporteurs l'a suggéré, on ne peut totalement exclure la suite de réactions:

$$CCl_4 + 2e \rightarrow CCl_3^- + Cl^-$$
$$Cp_2Co^+ + CCl_3^- \rightarrow \mathbf{2}c,$$

bien que l'action de CCl_4 sur le cobaltocène conduise à **2***c* (voir réf. 6).

Lorsque l'électrolyse est terminée, on ajoute à la solution de DMF contenant le cyclopentadiène cyclopentadiényl cobalt une grande quantité d'eau (1.5 l) et on extrait à l'éther. La phase organique est séparée puis lavée successivement deux fois à l'eau, deux fois avec une solution de carbonate de potassium et enfin plusieurs autres fois à l'eau jusqu'à p*H* neutre. La phase éthérée est alors séchée sur $MgSO_4$ puis évaporée. Les dérivés **2***a*, **2***b*, **2***c* et **2***d* sont purifiés et identifiés comme indiqué dans la littérature (6, 8, 9, 10).

Méthoxycarbonyl cyclopentadiène cyclopentadiényl cobalt ***7***

Une solution de 1.7 g d'hexafluorophosphate de cobalticinium et de 8.5 g de LiCl dans 200 ml de DMF est placée dans la cellule d électrolyse.

Après désoxygénation on fait passer un courant de gaz carbonique et on impose un potentiel de -2 V. Après environ 1 h, l'intensité du courant tend vers zéro, on arrête alors l'électrolyse. On adapte à la cellule un réfrigérant, une entrée d'argon et une ampoule à brome à l'aide de laquelle on ajoute 20 ml d'iodure de méthyle. La température est amenée à 40 °C et l'agitation magnétique maintenue pendant 4 h. Le méthoxycarbonyl cyclopentadiène cyclopentadiényl cobalt est ensuite extrait comme dans le cas des composés **2***a*–**2***d*.

On obtient 1.2 g de substance (rendement 96%). Le produit brut est chromatographié sur alumine (Al_2O_3 "Merck" activité II–III) avec l'éther comme éluant. La solution éthérée rouge est évaporée et on recristallise dans un mélange d'éther et d'éther de pétrole. On obtient des aiguilles rouges pf 90–92 °C; spectre ir (CCl_4) bande C=O à 1736 cm^{-1}; spectre rmn ($CDCl_3$) 5.31 (t, protons β du cyclopentadiène), 4.81 (s, 5H, cyclopentadiényl), 3.43 (s, 3H, CO_2CH_3, le signal masque le multiplet correspondant à l'hydrogène *endo*) et 2.80 ppm (protons α du cyclopentadiène). *Anal.* calc. pour $C_{12}H_{13}O_2Co$: C 58.08, H 5.28; trouvé: C 57.95, H 5.27

Méthoxycarbonyl-1 méthyl-2 et méthoxycarbonyl-1 méthyl-3 cyclopentadiène méthylcyclopentadiényl cobalt ***11***

Cette synthèse est effectuée dans des conditions opératoires très proches de la précédente.

A partir de 2 g d'hexafluorophosphate de diméthyl-1,1′ cobalticinium **8**, on a obtenu 1.4 g du mélange **11** (rendement 96%). Le potentiel imposé dans ce cas est de -2.2 V (e.c.s.), et l'intensité du courant de réduction ne tend pas vers zéro même après 2 à 3 h d'électrolyse car à ce potentiel l'anhydride carbonique et les ions Li^+ sont réduits. Bien que le mécanisme de la réaction puisse être compliqué du fait de la décharge simultanée de CO_2, Li^+ et **8**, on obtient **11** avec un excellent rendement.

Pour s'assurer de la fin de la réaction, des prélèvements sont effectués et analysés par polarographie. Une fois la réaction terminée (1½–2 h), on traite par CH_3I à 40 °C et on extrait et purifie **11** comme précédemment. Le spectre ir de **11** (dans CCl_4) présente des bandes intenses à 2958, 2915, 1724, 1428, 1370, 1364, 1342, 1300, 1160, 1087, 1015, 943, 926, 920 et 909 cm^{-1}.

Phényl cyclopentadiène cyclopentadiényl cobalt ***15***

L'électrolyse est effectuée comme précédemment à -1.95 V (e.c.s), en présence de C_6H_5Br pendant environ 30 min. Après extraction, le bromobenzène restant est éliminé sous vide; on obtient 0.78 g de produit rouge (rendement 98%), qui, après sublimation et recristallisation dans le pentane donne des cristaux rouges pf 129–131 °C (litt. (4) pf 128–129.5 °C).

1. M. Rosenblum. Chemistry of the iron group metallocenes. John Wiley and Sons, New York. 1965.
2. R. B. Woodward, M. Rosenblum et M. C. Whiting. J. Am. Chem. Soc. **74**, 3458 (1952).
3. M. D. Rausch et D. J. Ciappenelli. J. Organomet. Chem. **10**, 127 (1967).
4. E. O. Fischer et G. E. Herberich. Chem. Ber. **94**, 1517 (1961).
5. C. Furlani et I. Collamati. Chem. Ber. **95**, 2928 (1962).
6. M. L. H. Green, L. Pratt et G. Wilkinson. J. Chem. Soc. 3753 (1959).
7. M. Rosenblum, B. North, D. Wells et W. P. Giering. J. Am. Chem. Soc. **94**, 1239 (1972).
8 G. H. Herberich et E. Bauer. J. Organomet. Chem. **16**, 301 (1969).
9 G. E. Herberich, G. Greis et H. F. Heil. J. Organomet. Chem. **22**, 723 (1970).
10. G. E. Herberich, E. Bauer et J. Schwarzer. J. Organomet. Chem. **17**, 445 (1969).
11. N. El Murr et R. Dabard. J. Organomet. Chem. **39**, C82 (1972).
12. J. E. Sheats et M. D. Rausch. J. Org. Chem. **35**, 3245 (1970).
13. N. El Murr. J. Organomet. Chem. **112**, 177 (1976).
14. N. El Murr et R. Dabard. C. R. Acad. Sc. Paris, **272**, 1989 (1971).
15. N. El Murr, R. Dabard et E. Laviron. J. Organomet. Chem. **47**, C13 (1973).
16. J. A. Page et G. Wilkinson. J. Am. Chem. Soc. **74**, 6149 (1952).
17. H.-S. Hsiung et G. H. Brown. J. Electrochem. Soc. **110**, 1085 (1963).
18. A. A. Vlcek. Coll. Czech. Chem. Commun. **30**, 952 (1965).
19. N. El Murr et E. Laviron. Tetrahedron Lett. 875 (1975).
20. J. E. Sheats et T. Kirsch. Synth. Inorg. Met.-Org. Chem. **3**, 59 (1973).
21. M. R. Churchill et R. Mason. Proc. R. Soc. London, Ser. A, **279**, 191 (1964).
22. P. H. Bird et M. R. Churchill. Chem. Commun. 777 (1967).

Electrochimie de composés organométalliques. II. Nouvelle voie d'accès aux sels de cobalticinium substitués[1]

NABIL EL MURR ET ETIENNE LAVIRON

Laboratoire de Polarographie Organique associé au C.N.R.S. (L.A. 33), Faculté des Sciences, 6 Boulevard Gabriel, 21000 Dijon, France

Reçu le 3 mai 1976

NABIL EL MURR et ETIENNE LAVIRON. Can. J. Chem. **54**, 3357 (1976).

L'oxydation par voie électrochimique, par l'air, par les ions hydrogène et par le tétrafluoroborate de triphénylméthane de divers cyclopentadiène cyclopentadiényl cobalt substitués a été étudiée. Les dérivés possédant un hydrogène *exo* par rapport au métal conduisent aux sels de cobalticinium correspondants. Lorsque le substituant *exo* est CH_3 ou C_6H_5, il y a dégradation de la molécule. Quand le substituant *exo* est CO_2CH_3, l'oxydation par le tétrafluoroborate de triphénylméthane s'effectue avec élimination de l'hydrogène *endo* pour conduire au sel de cobalticinium substitué avec un rendement quantitatif.

NABIL EL MURR and ETIENNE LAVIRON. Can. J. Chem. **54**, 3357 (1976).

The oxidation of several substituted cyclopentadiene cobalt cyclopentadienyls electrochemically, by air, by hydrogen ions, and by triphenylmethyl tetrafluoroborate has been studied. The derivatives with an *exo* hydrogen yield the corresponding cobalticinium salts. When the *exo* substituent is CH_3 or C_6H_5, a degradation occurs. If the *exo* substituent is CO_2CH_3, oxidation by triphenylmethyl tetrafluoroborate takes place with *endo* hydrogen elimination, leading to the substituted cobalticinium salt in quantitative yield.

Introduction

Dans un article précédent (1), nous avons décrit une méthode de synthèse des dérivés du cyclopentadiène cyclopentadiényl cobalt à partir des cobaltocènes **3**[2] ou des anions cobaltocènes **4** et **9** générés électrochimiquement par électrolyse à potentiel imposé des solutions de sels de cobalticinium.

Cette technique électrochimique nous a permis de préparer avec des rendements pratiquement quantitatifs certains cyclopentadiène cyclopentadiényl cobalt $(RR'C_5H_4)Co(R''C_5H_4)$ déjà signalés dans la littérature (**2***a*–**2***d*: R′ = R″ = H et R = $CH_2C_6H_5$, $CHClC_6H_5$, CCl_3, CH_2Br) et d'autres jamais obtenus par des voies classiques, en particulier ceux résultant de l'action de l'anhydride carbonique sur les anions **4** et **9** (**6**: R′ = R″ = H, R = CO_2H; **7**: R′ = R″ = H, R = CO_2CH_3; **11**: R′ = R″ = CH_3, R = CO_2CH_3; **18**: R′ = R″ = CH_3, R = C_6H_5).

Nous étudions dans cet article la possibilité d'obtenir des dérivés substitués du cobalticinium par oxydation des cyclopentadiène cyclopentadiényl cobalt; comme nous l'avions souligné dans des articles précédents (1–3), les voies d'accès à des ions cobalticinium substitués sont limitées et laborieuses et les rendements sont généralement faibles.

Bien que quelques travaux (4–6) semblent montrer que l'oxydation d'un cyclopentadiène cyclopentadiényl cobalt substitué par attaque nucléophile sur l'ion cobalticinium (7) ou radicalaire sur le cobaltocène (8) ne permette pas de conserver le substituant, il nous a semblé intéressant de réexaminer cette question.

Nous exposerons dans cet article les résultats de cette étude et nous décrirons une nouvelle voie d'accès à des dérivés substitués du cobalticinium.

Résultats et discussion

I-Oxydation des cyclopentadiène cyclopentadiényl cobalt

Pour mieux comprendre le comportement des cyclopentadiène cyclopentadiényl cobalt substitués $(RR'C_5H_4)Co(R''C_5H_4)$, nous avons procédé à une étude de leur oxydation au moyen de divers agents oxydants. Nous avons étudié en premier lieu des dérivés déjà signalés dans la littérature; les dérivés **2***e*: R = R′ = R″ = H;

[1]Ce travail a été réalisé en partie dans le cadre de la R.C.P. "Electrochimie organique et organométallique sélective".

[2]Par souci de simplification, nous avons attribué les mêmes numéros pour désigner les mêmes produits mentionnés dans cet article et dans l'article précédent (1).

Can. J. Chem. Downloaded from www.nrcresearchpress.com by 210.87.254.6 on 09/05/12
For personal use only.

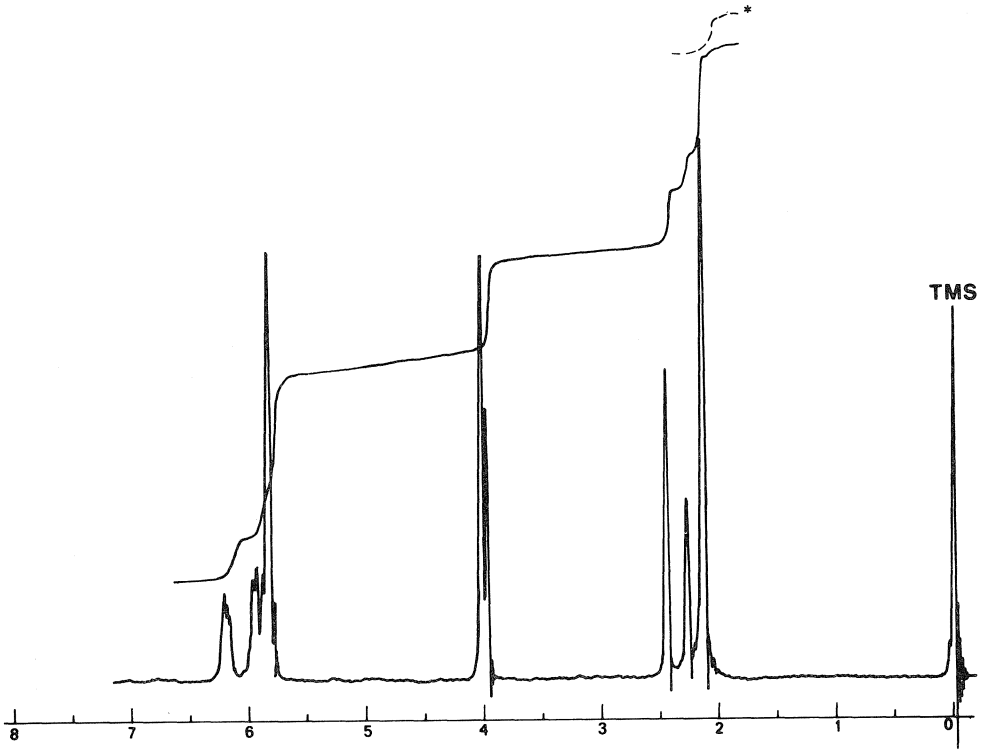

FIG. 1. Spectre rmn de **21** + **22** (acétone-d_6):* --- ^1H du solvant.

2*f*: R = H, R′ = R″ = CH_3; **2***g*: R = H, R′ = R″ = CO_2CH_3 sont obtenus par réduction par $NaBH_4$ des sels de cobalticinium correspondants, et le dérivé **2***h*: R = CH_3, R′ = R″ = H est obtenu par réduction de l'ion cobalticinium par CH_3Li.

Les spectres ir de **2***e*, **2***f* et **2***g* présentent dans la région 2740–2780 cm^{-1} une bande intense caractéristique d'un hydrogène en position *exo* dans le cyclopentadiène; l'absence de cette bande dans le spectre ir de **2***h* semble montrer que pour ce dérivé, c'est le groupement méthyle qui occupe la position *exo*, l'hydrogène se trouvant en *endo* (9).

Les quatre composés présentent, en milieu hydroalcoolique, une vague anodique dans le domaine de potentiel de l'électrode à goutte de mercure. Cette vague est toutefois très proche du courant de décharge anodique dans le cas de **2***g* en milieu acide et n'est pas visible en milieu basique pour **2***g* et **2***h*. Nous avons donc procédé à une étude en utilisant une électrode de carbone vitreux tournante (tableau 1).

Dans le but de déterminer le nombre d'électrons qui entrent en jeu lors de l'oxydation électrochimique des cyclopentadiène cyclopentadiényl cobalt, nous avons réalisé une coulométrie à potentiel contrôlé pour les dérivés les plus stables **2***e* et **2***g*. Dans les deux cas, cette oxydation se fait à 2 Faraday. Ce résultat a été également vérifié par comparaison des hauteurs des vagues anodiques à celle de la première vague de

TABLEAU 1. Potentiels de demi-vague, en volt (e.c.s.) de la vague d'oxydation des cyclopentadiène cyclopentadiényl cobalt. Solutions hydroalcooliques à 40% d'éthanol; p*H* mesurés à l'électrode de verre. Tampon Britton–Robinson; sel de fond NaCl 0.1 *M*

	Electrode de mercure		Electrode de carbone vitreux	
Produit	p*H* = 4.1	p*H* = 9.7	p*H* = 4.1	p*H* = 9.7
2*e*	−0.35	−0.42	−0.31	−0.43
2*f*	−0.47	−0.51	−0.41	−0.50
2*g**	+0.20	—	+0.22	+0.12
2*h*	−0.12	—	−0.21	−0.25

*Electrolyte support H_2SO_4 0.1 *N*. Pour **2***g* en milieu basique, il y a hydrolyse des fonctions esters. Les solutions de **2***h* se dégradent assez rapidement à des p*H* > 9.

Can. J. Chem. Downloaded from www.nrcresearchpress.com by 210.87.254.6 on 09/05/12
For personal use only.

Can. J. Chem. Downloaded from www.nrcresearchpress.com by 210.87.254.6 on 09/05/12
For personal use only.

réduction des ions cobalticinium (1 Faraday): pour une même concentration, le rapport est de deux.

L'oxydation des cyclopentadiène cyclopentadiényl cobalt peut être effectuée de plusieurs manières; nous en avons considéré trois: l'oxydation par l'oxygène de l'air, l'oxydation par les ions H^+ et l'oxydation électrochimique.

Oxydation par O_2

Les solutions hydroalcooliques des dérivés **2***e*, **2***f*, **2***g* et **2***h* abandonnées à l'action de l'oxygène de l'air ne présentent plus de vague anodique. Pour **2***e*, **2***f* et **2***g*, cette vague disparaît au profit de la vague de réduction de l'ion cobalticinium correspondant. L'oxydation du dérivé **2***g* est plus lente que celle de **2***e* et **2***f* mais nous n'avons pas fait d'étude cinétique précise du phénomène.

Après passage d'oxygène à travers les solutions de **2***h*, on n'observe pas de vague cathodique dans le domaine de l'électrode à goutte. En solution **2***h* n'est pas transformé en sel de méthylcobalticinium par l'oxygène de l'air mais subit probablement une dégradation totale.

Oxydation électrochimique

De même que l'oxydation par l'oxygène de l'air, l'oxydation électrochimique de **2***e*, **2***f* et **2***g* conduit presque quantitativement aux ions cobalticinium correspondants; ces derniers ont été isolés à l'état de sels d'hexafluorophosphate après électrolyse complète des cyclopentadiène cyclopentadiényl cobalt sur électrode de graphite à +0.4 V; ces sels ont été identifiés grâce à leurs polarogrammes et à leurs spectres de rmn

La réaction d'oxydation peut s'écrire:

[1] $(RC_5H_5)Co(RC_5H_4) \rightarrow (RC_5H_4)_2Co^+ + H^+ + 2e^-$

L'oxydation électrochimique de **2***h* ne conduit pas au sel de méthylcobalticinium; après électrolyse, nous avons mis en évidence la présence de cyclopentadiène et de méthylcyclopentadiène. Il y a donc décomposition de l'*exo*-méthylcyclopentadiène cyclopentadiényl cobalt au cours de l'électrolyse.

Oxydation par H^+

La transformation du cyclopentadiène cyclopentadiényl cobalt **2***e* en ion cobalticinium par action des ions H^+ a été déjà signalée par Green *et al.* (10), mais aucune étude quantitative n'a été effectuée. Nous avons repris cette réaction et l'avons étudiée en détail pour les divers dérivés préparés. En milieu tamponné acide (pH = 2.7 à 4.5), la cinétique de cette réaction a été suivie en enregistrant la diminution de la hauteur de la vague d'oxydation de **2***e*, **2***f* et **2***h* (électrode de carbone vitreux tournante) en fonction du temps, à différents pH. Cette étude montre que la réaction est du premier ordre par rapport aux cyclopentadiène cyclopentadiényl cobalt pour **2***e*, **2***f* et **2***h*; elle est également du premier ordre par rapport à H^+ dans le cas de **2***e* et **2***f* ($\log k = \log k_0 - pH$); dans le cas de **2***h* l'ordre n'est pas défini par rapport à H^+.

Le dérivé **2***g* ne subit aucune transformation en milieu acide; (on ne note aucune évolution dans les solutions d'acide perchlorique 5 *N*). La valeur de $E_{1/2} = +0.22$ V de la vague d'oxydation de **2***g* montre d'ailleurs que ce dernier est plus stable que les trois autres vis-à-vis de l'oxydation.

Après réaction de **2***e* et **2***f* avec H^+, nous avons isolé les sels de cobalticinium correspondants. Cette réaction peut s'écrire de la façon suivante:

[2] $(RC_5H_5)Co(RC_5H_4) + H^+ \xrightarrow{k} (RC_5H_4)Co^+ + H_2$

Dans le cas de **2***h*, nous n'obtenons pas de sel de cobalticinium, mais comme lors de l'électrolyse, nous observons le décomposition en cyclopentadiène et méthylcyclopentadiène.

Nous avons regroupé dans le tableau 2, pour deux pH, les valeurs de la constante de vitesse k.

Les résultats de notre travail montrent que **2***h* a toujours un comportement anormal. Des quatre produits étudiés, seul **2***h* subit une dégradation totale quel que soit le mode d'oxydation utilisé et est instable en milieu alcalin. La différence fondamentale entre **2***e*, **2***f* et **2***g* d'une part et **2***h* d'autre part est que seul le ligand cyclopentadiénique de **2***h* possède un groupement, autre que H, en position *exo* par rapport au métal. Cette différence est probablement à l'origine du comportement singulier de l'*exo*-

TABLEAU 2. Constante de vitesse, k en s^{-1}, de la réaction d'attaque des cyclopentadiène cyclopentadiényl cobalt par les ions H^+; étude effectuée en milieu tamponné hydroalcoolique, pH mesuré à l'électrode de verre

	Dérivé			
pH	**2***e*	**2***f*	**2***g*	**2***h*
2.72	4.52×10^{-3}	8.05×10^{-3}	$\simeq 0$	2.93×10^{-3}
3.30	1.2×10^{-3}	2.00×10^{-3}	$\simeq 0$	9.00×10^{-4}

Can. J. Chem. Downloaded from www.nrcresearchpress.com by 210.87.254.6 on 09/05/12
For personal use only.

méthylcyclopentadiène cyclopentadiényl cobalt.

Cette première étude de l'oxydation des cyclopentadiène cyclopentadiényl cobalt nous a permis de confirmer que comme pour l'oxydation chimique, l'oxydation électrochimique ne permettait pas, tout au moins dans le cas des dérivés *exo* substitués par des groupements alkyles, leur transformation en sels de cobalticinium substitués. Toutefois, possédant des dérivés **7** et **11** ayant un groupement *exo* (CO_2CH_3) (1), il nous a semblé intéressant d'étudier leur oxydation électrochimique.

Dans un milieu hydroalcoolique, l'oxydation sur toile de carbone de l'*exo* méthoxycarbonylcyclopentadiène cyclopentadiényl cobalt **7** nous a permis de mettre en évidence la formation du sel de méthoxycarbonyl cobalticinium; ce dernier a été identifié par comparaison de son polarogramme à celui d'un échantillon préparé selon la méthode décrite par Sheats et Rausch (11). Bien que le rendement de cette réaction ($\simeq$10%) soit trop faible pour être exploité pour la synthèse, cette oxydation est importante puisqu'elle est le premier exemple de transformation d'un dérivé *exo* substitué du cyclopentadiène cyclopentadiényl cobalt en sel de cobalticinium substitué.

II-Synthèse de sels de cobalticinium substitués

Pour améliorer les rendements de l'oxydation du dérivé **7**, nous avons étudié son comportement vis-à-vis des oxydants chimiques tel que le tétrafluoroborate de triphénylméthane (réaction 3).

[3] 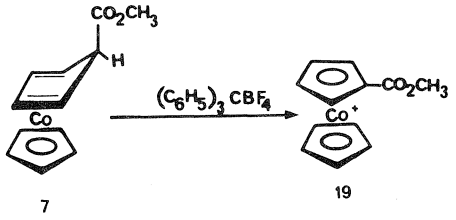

7 19

Par cette réaction, on obtient **19** de façon quantitative; ceci montre que le cation triphényl méthane arrache dans ce cas sélectivement les ions hydrures en position *endo*; un tel exemple de sélectivité a déjà été signalé par Khand *et al.* (12) dans la série du cyclopentadiène cyclohexadiényl fer.

Un traitement analogue appliqué à l'*exo* phénylcyclopentadiène cyclopentadiényl cobalt **15** ne conduit pas au sel de phénylcobalticinium **20**. Dans ce cas, c'est le groupement *exo* qui se détache (schéma 1) et l'ion cobalticinium non substitué est isolé avec de faibles rendements; une dégradation importante de **15** se produit au cours de la réaction.

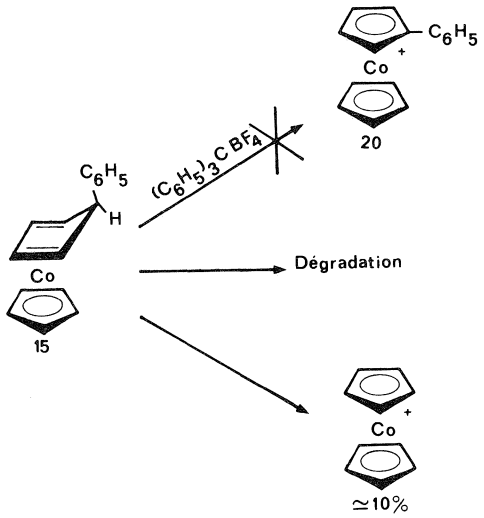

SCHÉMA 1

Appliquée aux produits obtenus par réaction de l'anhydride carbonique avec l'anion du diméthyl-1,1′ cobalticinium (1), l'oxydation par le tetrafluoroborate de triphénylméthane conduit à un mélange de sels de cobalticinium 1,2,1′ et 1,3,1′ trisubstitués (schéma 2).

Les rendements des réactions du schéma 2 sont quantitatifs et les proportions des isomères dans le mélange sont conservées; d'après le spectre de rmn (fig. 1) du mélange on constate en effet que **21** constitue environ 60 à 65% du mélange.

Dans un but de synthèse de nouvelles séries de dérivés trisubstitués du cobalticinium, il était important de séparer les isomères **21** et **22**. La séparation au niveau des dérivés **13** et **14** ayant échoué (1), nous l'avons tentée sur les sels **21** et **22**. Les tentatives de séparation par les méthodes classiques (recristallisation ou chromatographie) se sont avérées infructueuses; nous avons alors essayé cette séparation par voie indirecte.

Rosenblum *et al.* (13) ont montré que le sel de diméthoxycarbonyl-1,1′ cobalticinium traité par $NaBH_4$ conduit à un seul dérivé réduit dans lequel le carbone sp^3 est en α de la fonction ester (réaction 4).

[4] $(CO_2CH_3—C_5H_4)_2Co^+ \xrightarrow{NaBH_4} \mathbf{2}g$

Can. J. Chem. Downloaded from www.nrcresearchpress.com by 210.87.254.6 on 09/05/12
For personal use only.

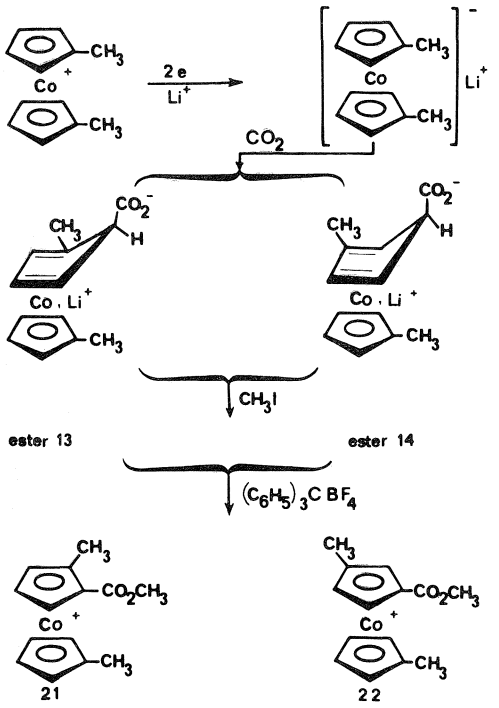

SCHÉMA 2

Nous avons soumis le mélange de sels **21** et **22** à l'action des ions hydrures dans le tétrahydrofurane; d'après les résultats de Rosenblum *et al.* qui s'expliquent par la déficience électronique, dans l'ion cobalticinium, des sommets α par effet attracteur du groupement ester, nous pouvions envisager la formation des isomères **23**, **24**, **25** et **26** (schéma 3).

Le mélange de dérivés obtenus est très sensible à l'oxydation; sa stabilité est très faible et ne se compare pas à celle du dérivé **2***g*. Cette instabilité est probablement due à l'effet donneur des groupements méthyle: une solution du mélange laissée quelques minutes à l'air redonne les sels de cobalticinium de départ. La chromatographie sur couche mince de gel de silice (éluant: éther 30%, hexane 70%) montre la présence de trois produits dont les R_f respectifs sont: 0.53, 0.67 et 0.74; les deux premiers sont en quantité plus importante que le troisième.

Les taches des dérivés réduits sont de couleur rouge, mais après quelques instants sur la plaque de chromatographie, l'oxydation en sel de cobalticinium se manifeste par le changement de couleur du rouge au jaune. La chromatographie préparative est très délicate, du fait de cette oxydation rapide et les deux produits migrant en tête sont très mal séparés et au point de départ une grande partie du mélange s'adsorbe sur le gel de silice à l'état d'ion cobalticinium (mélange de **21** et **22**). Malgré ces difficultés, nous avons pu récupérer deux fractions (à l'état de sel de cobalticinium), l'une formée du mélange des deux fractions migrant en tête (R_f = 0.67 et 0.74) et l'autre du dérivé dont le R_f = 0.53. Nous avons effectué la désorption de ces sels de cobalticinium à l'aide de l'acétone additionnée de quelques gouttes d'acide chlorhydrique. Après traitement adéquat, nous avons précipité les sels de cobalticinium à l'état d'hexafluorophosphate ou de tétraphenylborate.

Les spectres de rmn montrent que les deux fractions obtenues sont pures; la première (R_f = 0.67 et 0.74) est identifiée au dérivé **21**, la seconde présente les caractéristiques du sel 1,3,1′ trisubstitué **22**. D'après cette séparation, il semble raisonnable d'admettre que dans les conditions opératoires du schéma 3, si **23** et **24** se sont formés, ils possèdent pratiquement le même R_f = 0.53, alors que **25** et **26** se différencient; ces produits étant instables, nous n'avons pas pu

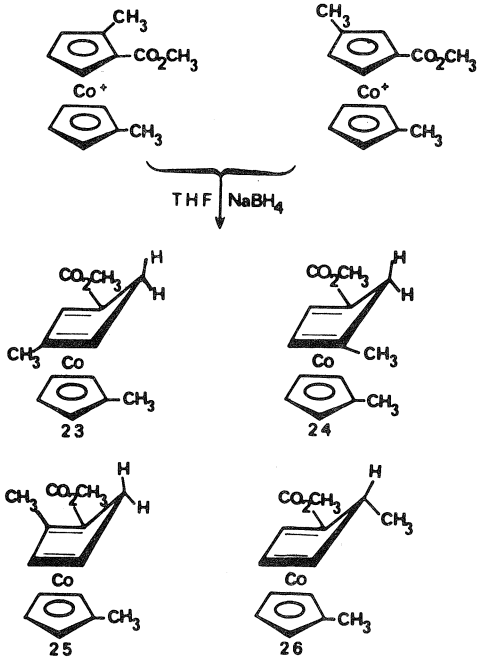

SCHÉMA 3

effectuer une étude structurale pour attribuer à **25** et **26** les R_f correspondants.

Bien que délicate à cause de la très grande oxydabilité des dérivés réduits, cette technique nous a permis de séparer des isomères de position dans la série du cobalticinium; c'est la première fois qu'une telle séparation est effectuée et les sels **21** et **22** sont les premiers exemples de dérivés trisubstitués dans la série de l'ion cobalticinium.

Ces dérivés trisubstitués possèdent une fonction ester facilement hydrolysable, ainsi que des groupements méthyle oxydables, par $KMnO_4$/NaOH, en fonctions acides. Au départ de tels triacides et à l'aide de réactions chimiques classiques (3), de nombreux dérivés du cobalticinium peuvent être obtenus et feront l'objet de prochaines publications.

Conclusion

Les cyclopentadiène cyclopentadiényl cobalt étudiés dans cet article peuvent se rattacher à deux types.

(*a*) Ceux ayant un hydrogène *exo* par rapport au métal (**2***e*, **2***f*, **2***g*, **23**–**26**). Nous avons pu confirmer que pour ces composés l'oxydation conduit aux sels de cobalticinium correspondants.

(*b*) Ceux ayant un substituant en position *exo* (**2***h*, **7**, **13**, **14**, **15**). Lorsque le substituant est CH_3 ou C_6H_5, l'oxydation s'accompagne d'une destruction de la molécule (une destruction de la molécule a également été signalée pour CCl_3 et C_6H_5CO(4)). Au contraire, si le groupement est CO_2CH_3 (**7**, **13**, **14**), l'oxydation s'effectue avec départ de l'hydrogène *endo*, pour conduire au sel de cobalticinium substitué avec un rendement de 100%.

Il est difficile à l'heure actuelle d'interpréter cette influence de la nature du substituant. Deux types de réoxydation différant suivant la nature du substituant ont été observés récemment dans la série des cyclohexadiényl cyclopentadiényl fer *exo* substitués mais n'ont pu être expliqués (6).

Bien qu'actuellement, la réoxydation des *exo* methoxycarbonyl cyclopentadiène cyclopentadiényl cobalt en sels de cobalticinium substitués ne soit qu'un cas particulier, elle présente un grand intérêt pour la synthèse dans la série des sels de cobalticinium. Elle nous a permis de préparer les premiers sels de cobalticinium trisubstitués, qui ne peuvent être à l'heure actuelle obtenus par d'autres méthodes; les sels que nous avons obtenus possèdent des fonctions facilement transformables à l'aide de réactions chimiques classiques pour donner une large gamme de dérivés trisubstitués.

Partie expérimentale

Oxydation électrochimique

L'étude polarographique et l'électrolyse de divers produits est effectuée à l aide de l'appareillage et selon les techniques déjà décrites dans notre article précédent (1).

Les courbes $i = f(E)$ ont été tracées sur électrode tournante de carbone vitreux et les électrolyses préparatives ont été effectuées sur une toile de carbone.

Les solutions de sels de cobalticinium obtenus après électrolyse de **2***e*, **2***f* et **2***g* sont concentrées, filtrées et les sels précipités par addition d'une solution saturée d'hexafluorophosphate de sodium. Ces sels sont identifiés par comparaison à des échantillons obtenus par voie chimique (3).

Au cours de l'électrolyse des solutions de l'*exo* méthylcyclopentadiène cyclopentadiényl cobalt, un courant d'azote entraine les substances volatiles formées dans un piège contenant de l'éthanol. La comparaison du spectre uv de cette solution éthanolique à celui d'un mélange de cyclopentadiène et de méthylcyclopentadiène dans l'éthanol montre qu'au cours de l'oxydation l'*exo* méthylcyclopentadiène cyclopentadiényl cobalt se dégrade; un dépôt métallique de cobalt est également observé dans la cellule d'électrolyse.

Oxydation par O_2

Dans des solutions hydroalcoolique à 40% d'éthanol, on fait passer pendant quelques minutes un courant d'air; après dégazage de la solution, les polarogrammes sont tracés et l'évolution est notée par comparaison des hauteurs des vagues d'oxydation et par l'apparition des vagues de réduction des ions cobalticinium pour les dérivés **2***e*, **2***f* et **2***g*. Les solutions du dérivé **2***h* subissent une dégradation lorsqu'elles sont oxydées par l'oxygène de l'air.

L'étude cinétique de l'attaque des ions H^+ est réalisée en mesurant à un pH constant et à un potentiel fixe (sur le palier de la vague d'oxydation) l'évolution du courant de diffusion en fonction du temps $i = f(t)$.

Les solutions à 40% d'éthanol sont tamponnées et les produits s'y trouvent à une concentration de 5×10^{-4} M. Pour un même produit, les courbes $i = f(t)$ sont tracées à différents pH, compris entre 2.7 et 4.5; au-delà de cette dernière valeur, l'évolution est très lente et le temps de demi-réaction est trop important.

Synthèses

Méthoxycarbonyl cobalticinium ***19***

A une solution de 130 mg (5×10^{-4} M) de méthoxycarbonyl cyclopentadiène cyclopentadiényl cobalt **7** dans 40 ml de CH_2Cl_2 anhydre, on ajoute 350 mg (10^{-3} M) de tétrafluoroborate de triphényl méthane.

Après agitation pendant 5 min, on extrait à l'eau (40 ml) la phase aqueuse jaune est lavée deux fois à l'éther et

Can. J. Chem. Downloaded from www.nrcresearchpress.com by 210.87.254.6 on 09/05/12
For personal use only.

traitée au noir animal. La solution aqueuse est filtrée et le méthoxycarbonyl cobalticinium est précipité en sel d'hexafluorophosphate par addition d'une solution de $NaPF_6$. Après filtration du précipité jaune (125 mg) le reste de méthoxycarbonyl cobalticinium est précipité à l'état de sel de tétraphényl borate (100 mg). Le rendement global est de 95%. Les deux sels obtenus sont recristallisés et identifiés par comparaison avec des échantillons préparés selon une méthode déjà décrite dans la littérature (11).

Méthoxycarbonyl-1 diméthyl-2,1' et méthoxycarbonyl-1 diméthyl-3,1' cobalticinium ***21*** *et* ***22***

L'oxydation du mélange de **13** et **14** est effectuée dans CH_2Cl_2 anhydre, par le tétrafluoroborate de triphényl méthane comme dans le cas précédent; les rendements de cette oxydation sont de 95%.

A 0.6 g du mélange de **21** et **22** dans 70 ml de THF on ajoute un large excès de $NaBH_4$ (0.3 g). Après 20 min d'agitation, la couleur de la solution tourne du jaune au rouge foncé, on y ajoute de l'eau et on extrait à l'éther. La phase éthérée est lavée à l'eau jusqu'à p*H* neutre, séchée sur $MgSO_4$ et filtrée. Après évaporation de l'éther, on obtient 0.39 g d'une huile rouge (mélange des composés **23**, **24**, **25** et **26**) très sensible à l'air (rendement 100%).

Le mélange des cyclopentadiène cyclopentadiényl cobalt ainsi obtenu est dissous dans 20 ml d'éther anhydre puis chromatographié sur plaque de gel de silice (éluant éther–hexane 3:7); le mélange doit être étendu et élué sur la plaque très rapidement, sinon une importante oxydation a lieu. En fin de chromatographie deux bandes rouges se détachent nettement, elles deviennent jaunes dès qu'on sort la plaque du bac de chromatographie: les deux produits ainsi séparés s'oxydent en sel de cobalticinium. On note également une bande jaune qui n'a pas migré. Après désorption de ces dérivés, (désorbant acétone + HCl) on évapore le solvant et les résidus sont dissous dans très peu d'eau puis précipités à l'état d'hexafluorophosphate ou de tétraphénylborate. Les deux bandes qui ont migré correspondent après oxydation aux dérivés **21** et **22**; celle qui n'a pas migré est constituée du mélange de ces deux composés, elle est dans une proportion d'environ 60% et elle résulte de l'oxydation du mélange de **23**, **24**, **25** et **26** lors de son étalement sur la plaque chromatographique. Ce mélange de **21** et **22** ainsi récupéré est de nouveau réduit par $NaBH_4$ puis chromatographié; l'opération est répétée jusqu'à séparation totale des deux isomères **21** et **22** qui sont recristallisés dans l'eau.

Hexafluorophosphate de méthoxycarbonyl-1 diméthyl-2,1' cobalticinium **21** pf 95–97 °C. *Anal.* calc. pour $C_{14}H_{16}O_2CoPF_6$: C 40.02, H 3.84; trouvé: C 39.89, H 3.81.

Hexafluorophosphate de méthoxycarbonyl-1 diméthyl-3,1' cobalticinium **22** pf 132–134 °C. *Anal.* calc. pour $C_{14}H_{16}O_2CoPF_6$: C 40.02, H 3.84; trouvé: C 40.00, H 3.82.

1. N. El Murr et E. Laviron. Can. J. Chem. Cette édition.
2. N. El Murr et R. Dabard. J. Organomet. Chem. **39**, C82 (1972).
3. N. El Murr. J. Organomet. Chem. **112**, 177 (1976).
4. E. O. Fischer et G. H. Herberich. Chem. Ber. **94**, 1517 (1961).
5. C. Furlani et I. Collamati. Chem. Ber. **95**, 2928 (1962).
6. A. N. Nesmeyanov, N. A. Vol'kenau, L. S. Shilovtseva et V. A. Petrakova. J. Organomet. Chem. **85**, 365 (1975).
7. R. Mason et G. Wilkinson. Experientia Suppl. **9**, 233 (1964).
8. G. H. Herberich et J. Schwartzer. Angew. Chem. Int. Ed. Engl. **9**, 897 (1970).
9. P. H. Bird et M. R. Churchill. Chem. Commun. 777 (1967).
10. M. L. H. Green, L. Pratt et G. Wilkinson. J. Chem. Soc. 3753 (1959).
11. J. E. Sheats et M. D. Rausch. J. Org. Chem. **35**, 3245 (1970).
12. I. U. Khand, P. L. Pauson et W. E. Watts. J. Chem. Soc. C, 2024 (1969).
13. M. Rosenblum, B. North, D. Wells et W. P. Giering. J. Am. Chem. Soc. **94**, 1239 (1972).

Can. J. Chem. Downloaded from www.nrcresearchpress.com by 210.87.254.6 on 09/05/12
For personal use only.

The thermally induced rearrangements of 2-vinyloxirane

ROBERT J. CRAWFORD, STUART B. LUTENER, AND ROBERT D. COCKCROFT
Department of Chemistry, The University of Alberta, Edmonton, Alta., Canada T6G 2G2

Received May 17, 1976

ROBERT J. CRAWFORD, STUART B. LUTENER, and ROBERT D. COCKCROFT. Can. J. Chem. **54**, 3364 (1976).

The kinetics of the gas phase thermolysis of 2-vinyloxirane (**4**) have been studied over the temperature range 270–310 °C. The racemization of chiral **4** occurs six times faster than the structural isomerization to 2,3-dihydrofuran, (*E*)- and (*Z*)-2-butenal, and 3-butenal. The butenals undergo a slow thermolysis to propene and carbon monoxide. *cis*-Deuterio- and *trans*-3-deuterio-vinyloxirane have been synthesized and their interconversion is slow. Deuterium kinetic isotope effects on *mono*- and *dideuterio*-**4** suggest that for the formation of the butenals the rate determining step involves rupture of the oxirane C—O bond. The dihydrofuran is produced by thermolysis of the oxirane C—C bond. The preferred mechanistic interpretation is that a carbon–oxygen diradical serves as an intermediate for butenal formation, and that a carbonyl-ylide is involved in the formation of the dihydrofuran.

The relative rates, at 307.4 °C, of *cis–trans*-isomerization:dihydrofuran formation:racemization:butenal formation for 3-*deuterio*-2-vinyloxirane are 1.0:0.88:40.2:5.94, respectively.

ROBERT J. CRAWFORD, STUART B. LUTENER et ROBERT D. COCKCROFT. Can. J. Chem. **54**, 3364 (1976).

On a étudié, à des températures allant de 270–310 °C, la cinétique de la thermolyse en phase gazeuse du vinyl-2 oxiranne (**4**). La racémisation du composé **4** chiral se produit 6 fois plus rapidement que l'isomérisation de structure en dihydro-2,3 furanne, en butène-2 als (*E*) et (*Z*) et en butène-3 al. Les butènals subissent une thermolyse lente conduisant au propène et au monoxyde de carbone. On a aussi synthétisé les deutério-3 vinyloxirannes *cis* et *trans* et leur interconversion est lente. Les effets isotopiques cinétiques du deutérium sur les *mono*- et *dideutério* **4** suggèrent que, pour la formation des butènals, l'étape déterminant la vitesse de la réaction implique la rupture du lien C—O de l'oxiranne. Le dihydrofuranne se produit par thermolyse du lien C—C de l'oxiranne. L'interprétation mécanistique préférée implique qu'il y a formation d'un diradical carbone–oxygène comme intermédiaire pour la formation des butènals et qu'un carbonyl-ylide est impliqué dans la formation de la dihydrofuranne.

Les vitesses relatives, à 307.4 °C, pour l'isomérisation *cis–trans*: la formation de dihydrofuranne: la racémisation: la formation de butènal à partir du deutério-3 vinyl-2 oxiranne sont respectivement de 1.0:0.88:40.2:5.94.

[Traduit par le journal]

Introduction

Thermal isomerizations of strained cyclic systems have been extensively studied in an effort to elucidate the mechanistic details of bond-cleavage processes (for reviews see ref. 1). The thermolysis of cyclopropane and its substituted derivatives has been the focus of considerable attention and has resulted in the identification of structural, geometrical, and optical isomerization processes (2). The trimethylene diradical, first proposed as an intermediate by Chambers and Kistiakowsky (3), has frequently been the subject of experimental tests (2, 4), and of extensive theoretical studies (5). Hoffmann (5*a*) has suggested that an analogous biradical-like species exists for the oxirane system and that this intermediate would be stabilized by virtue of resonance interactions with the non-bonded electron pair on oxygen. These calculations suggested that the most stable intermediate is that formed by carbon–carbon bond cleavage of the oxirane ring of **1** to give the carbonyl-ylide **2** and that the preferred mode of ring opening is conrotatory. Experimentally oxiranes have been the subject of frequent studies (6) and when resonance stabiliz-

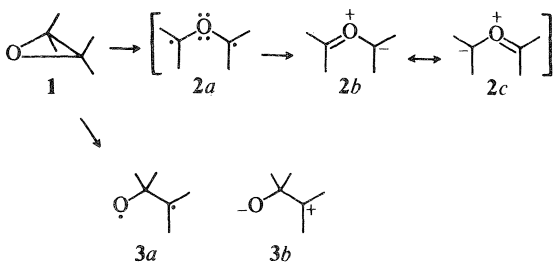

Can. J. Chem. Downloaded from www.nrcresearchpress.com by 210.87.254.6 on 09/05/12
For personal use only.

Can. J. Chem. Downloaded from www.nrcresearchpress.com by 210.87.254.6 on 09/05/12
For personal use only.

ing groups are placed on the ring the carbonyl-ylide has been observed directly as an intermediate of both thermal (7) and photochemical processes (8). The preferred mode of ring opening has been observed to be conrotatory in thermal processes (9). The oxiranes which do not have groups capable of stabilizing the carbonyl-ylide generally show an alternative mode of ring opening, that of carbon–oxygen bond cleavage. While this mode has been necessary to rationalize many of the products it is not clear that a carbon–oxygen diradical **3***a* similar to the trimethylene diradical is produced as a discrete intermediate, and whether **3***b* is a possible contributing structure. This same question has been posed by Yankee and Cram (10) with respect to the homolytic and/or heterolytic opening of cyclopropanes. Evidence from their work indicates the zwitterion and the diradical are species which behave in a different manner from one another. In only a few of the systems studied (6) has this thermal carbon–oxygen cleavage appeared to be competitive with that of carbon–carbon cleavage. Flowers and co-workers have evaluated the role of these two modes of ring opening for 2,2,3,3-tetramethyloxirane (6*a*) and *cis*- and *trans*-2,3-dimethyloxirane (6*b*). Our earlier studies with 2,3-divinyloxirane (11) demonstrate that product studies alone are not an adequate means of assessing the rate of carbon–carbon ring cleavage because of the facile reversible ring-closure from the carbonyl-ylide intermediate **2**. Oxirane racemization studies give a better appraisal of the true case of carbon–carbon bond cleavage.

To study the ring-opening of oxiranes with carbon–carbon bond cleavage competitive with that of carbon–oxygen bond cleavage we have chosen to examine the rates of racemization and structural isomerization of 2-vinyloxirane along with some of its deuterated isomers.

Results

(i) Synthesis

Chiral 2-vinyloxirane (**4**), optically pure and of known absolute configuration, was synthesized from the isopropylidene derivative of D-glyceraldehyde, which was prepared from commercially available D-mannitol (12), as outlined in Scheme 1. The synthesis of 2-vinyloxirane-3,3-d_2 (**5**) from methyl-2-hydroxy-3-butenoate by lithium aluminum deuteride reduction is outlined in Scheme 2. The preparation of *cis*- and *trans*-3-deuterio-2-vinyloxirane (**6** and **7**) was achieved by the methods outlined in Scheme 3. The oxiranes were purified by preparative gas chromatography and their rotations and proton magnetic resonance spectra are recorded in the experimental section.

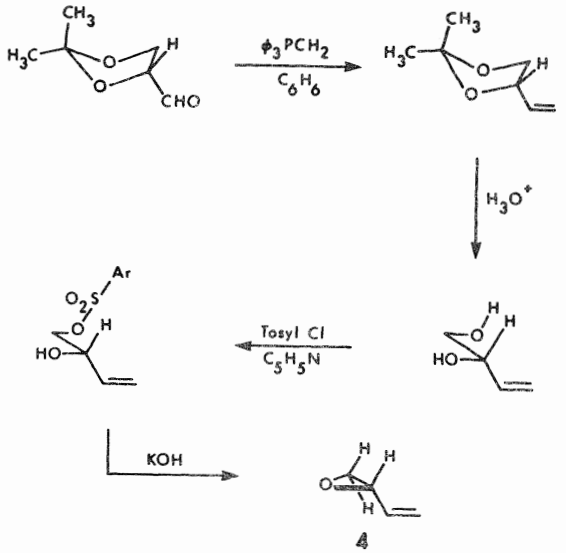

SCHEME 1

(ii) Thermolysis-product Studies

Preliminary product studies were carried out using sealed, degassed, ampoules. A non-condensable product (−196 °C) was quantitatively measured and identified as carbon monoxide by the use of high resolution mass spectrometry. The quantity produced varied from 2 to 14% from samples heated in apparently identical tubes at 299 °C for 100 min (25% thermolysis of **4**). In the same manner propene (not condensable at −78 °C) was isolated and identified. The

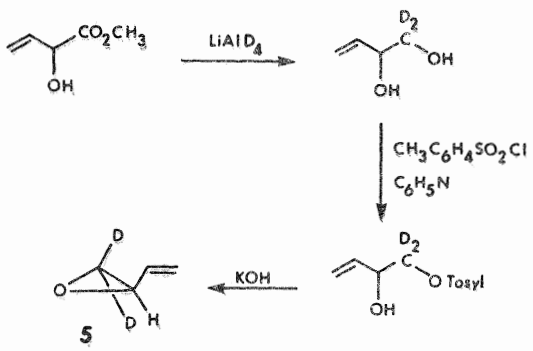

SCHEME 2

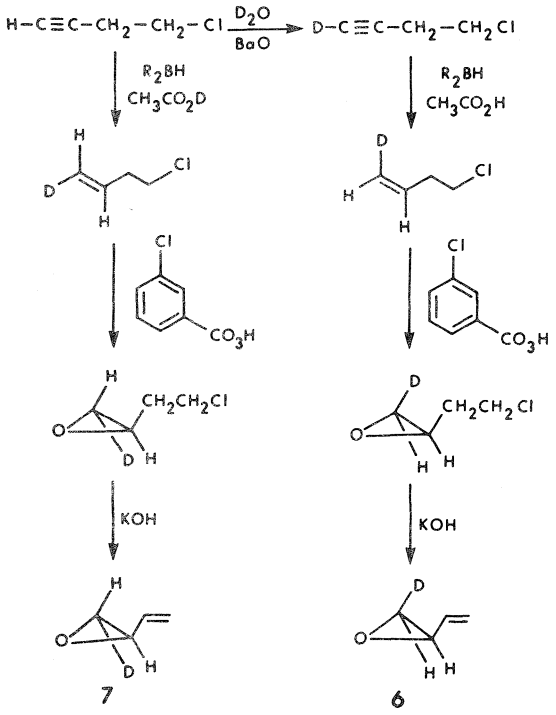

SCHEME 3

condensable products were isolated and purified by preparative gas chromatography (gc). They were characterized by comparison of their spectral properties and gc retention times with those of authentic compounds. Thus the thermolysis of vinyloxirante (**4**) was shown to produce

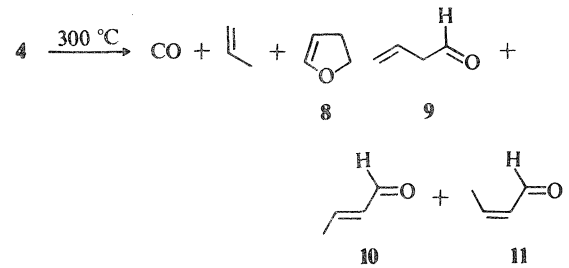

2,3-dihydrofuran (**8**), 3-butenal (**9**), (*E*)-2-butenal (**10**), and (*Z*)-2-butenal (**11**) along with the aforementioned non-condensable gases. The latter materials were cleanly separated by gc on a 10 ft × 1/8 in. i.d. 10% β,β′-oxydipropionitrile column on 80–100 mesh high-performance Chromosorb WAW/DMCS support. This appears to be the first time that the nmr spectra, of relatively high purity, of **9** and **11** have been obtained. Careful examinations of the gc retention times and thermal stabilities of such materials as 2,5-dihydrofuran and cyclopropanecarboxyaldehyde (possible isomerization products) allow us to say that, if produced, they are but minor products (<0.1%).

Quantitative experiments were conducted in a 1 litre static pyrex vessel at 307 °C. The vessel needed to be conditioned to obtain reproducible kinetic data. On conditioning the product proportions changed; whereas upon admission of air to the system erratic kinetic data were again produced. The proportions of the thermodynamically less stable 3-butenal and (*Z*)-2-butenal were greater than those of (*E*)-2-butenal in the non-conditioned vessel, the opposite is true of the conditioned vessel (see Figs. 1 and 2). Surface catalysis of oxirane thermolysis has been noted by several other workers (6). The surprising feature here is that what appears to be the kinetically generated product proportions are being observed under conditions which render erratic and catalyzed rate data, whereas when our kinetic data are highly reproducible the

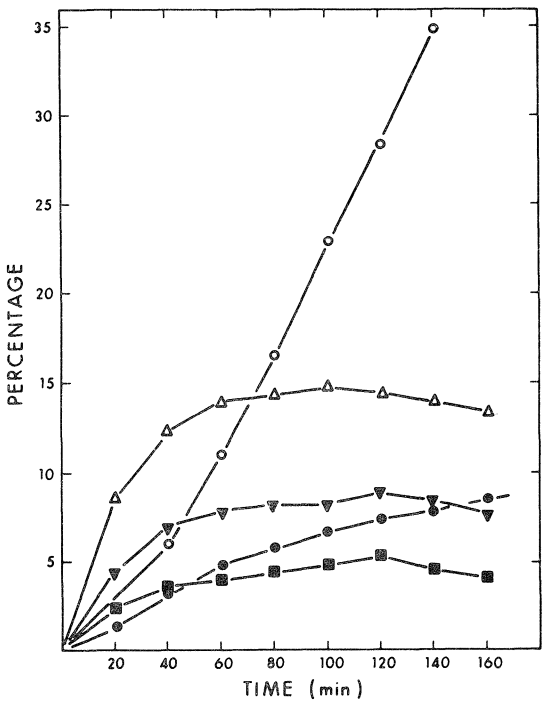

FIG. 1. Product distribution for the thermolysis, at 307.4 °C, of vinyloxirane (**4**) in a well conditioned vessel: △ (*E*)-2-butenal, ○ propene + carbon monoxide, ▼ (*Z*)-2-butenal, ■ 3-butenal, and ● 2,3-dihydrofuran.

Can. J. Chem. Downloaded from www.nrcresearchpress.com by 210.87.254.6 on 09/05/12
For personal use only.

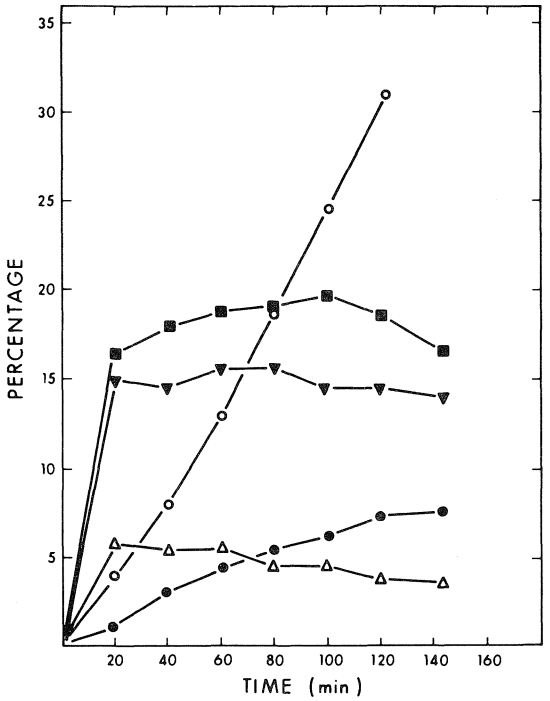

FIG. 2. Product distribution for the thermolysis, at 307.4 °C, of vinyloxirane with a trace of air added. For key see Fig. 1.

product proportions more closely resemble those of thermodynamic control. Only the product proportions change, the same products being obtained from both the conditioned and unconditioned vessels.

After thermolysis of the 2-vinyloxirane-3,3-d_2 (**5**) the products were separated by preparative gc and their 100 MHz ^{1}H nmr spectra obtained. Inspection of the nmr spectrum obtained from the 2,3-dihydrofuran produced by thermolysis of **5** reveals the absence of the C-2 triplet at δ 4.2 and the simplification of the C-3 multiplet (δ 2.6), which is consistent with the location of both deuterium atoms at C-2. The spectrum of the 3-butenal produced indicates the absence of the C-1 aldehyde signal (δ 9.8) and a considerable decrease in the C-2 methylene signals intensity, consistent with a deuterium migration to C-2. The two vinyl signals at δ 5.2 and 5.9 are in the approximate intensity ratio of 1:2 suggesting that deuterium is not present at C-3 and C-4. These conclusions were confirmed by inspection of the corresponding 13.81 MHz deuterium magnetic resonance (^{2}H nmr) spectrum which displayed only two distinct deuterium signals 2.3 ppm downfield (C-1-*D*) and 4.2 ppm upfield (C-2-*D*), from the reference deuteriochloroform, in the ratio 57:43.

A comparison of the nmr spectra of deuterated **10** and **11** from **4** indicates that only deuterium is located at the C-1 aldehyde position, as evidenced by the absence of the aldehyde signals at δ 9.42 and 10.04. A reduction in intensity of both the C-2 olefinic and C-4 methyl signals is apparent suggesting deuterium at both positions. These conclusions were confirmed by an examination of the ^{2}H nmr spectra which display three distinct signals for each 2-butenal isomer. The 100 MHz ^{1}H nmr spectrum of recovered 2-vinyloxirane was unchanged from that of the starting material. Thus the deuterium distribution in the products may be summarized as:

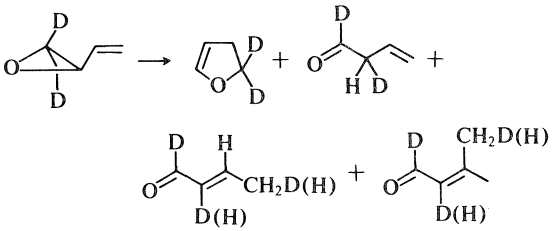

A significant feature discernable from the ^{1}H nmr spectra is the fact that some deuterium has been lost from the 2 position of the 3-butenal produced from **5**, *i.e.*, the ratio of deuterium at C-1 to that at C-2 is 1.00 to 0.73. The feasibility of a surface catalyzed exchange process was established by a control experiment. When 2-vinyloxirane was allowed to undergo thermolysis in a reaction vessel, which had been pretreated with D_2O, a small amount (approximately 3%), as detected by high resolution mass spectrometry, of deuterium was incorporated into the 2-butenals produced. The reactant recovered had no deuterium incorporated. It seems probable that a slow tautomerism is occurring on the vessel's surface.

The similarity of the deuterium distribution in the 2-butenals and 3-butenal produced from **6** and **7** (see Table 1) suggests that there is no stereochemical preference for the mode of hydrogen migration. The butenal analyses were obtained on the products of runs carried to two half-lives at 307.4 °C. Inspection of the proton nmr of the recovered 2-vinyloxirane indicated 9% *cis-trans* isomerization. Thus the interconversion of **6** and **7** is too slow to account for

Can. J. Chem. Downloaded from www.nrcresearchpress.com by 210.87.254.6 on 09/05/12
For personal use only.

TABLE 1. The fraction of deuterium label observed, by ^1H and ^2H nmr, at each position of the butenals produced from the thermolysis of **5**, **6**, and **7** at 307.4 °C (190 min)

Reactant	Product	Mole fraction of molecules having D at C_1	C_2	C_3	C_4
5	3-Butenal	1.0[a]	0.72	0	0
	(*E*)-2-Butenal	1.0	0.52	0	0.42
	(*Z*)-2-Butenal	1.0	0.51	0	0.45
6[b]	3-Butenal	0.69	0.31	0	0
	(*E*)-2-Butenal	0.73	0.10	0	0.10
7[b]	3-Butenal	0.69	0.32	0	0
	(*E*)-2-Butenal	0.68	0.18	0	0.14

[a]The absence of a pmr signal at δ 9.62 suggests only D at Cl.
[b]Samples of (*Z*)-2-butenal had isomerized to, and were identical with, (*E*)-2-butenal upon standing in the nmr tube.

the comparable product distribution, and we conclude that the isomerization of hydrogen, or deuterium, is essentially independent of its original stereochemistry at C-3. Due to the subsequent thermolysis of the butenals to carbon monoxide and propene we are not able to accurately determine isotope effects for the migration step.

(iii) Kinetic Data

Kinetic data for the thermolysis processes were obtained from a well conditioned Pyrex vessel (1 litre) over the range 292 to 312 °C with the temperature controlled to better than ±0.1 °C. Dimethoxyethane was chosen as an internal standard as it has a convenient gc retention time between that of 3-butenal and the 2-butenal and is thermally stable under the conditions of the reaction. Reactant samples were prepared by degassing a mixture of 2-vinyloxirane (140 mg) and freshly purified anhydrous 1,2-dimethoxyethane (130 mg) in a breakseal. The samples were warmed to 100 °C and expanded into the reaction vessel through the inlet system. The thermolysis was followed by periodically expanding an aliquot onto the vacuum line and analyzing the product on a gc system that was connected directly to the vacuum line. The product composition was determined by electronic integration of the thermal conductivity detector response. Reproducible data were obtained only after the reaction vessel had been 'aged' by treatment with light hydrocarbon (Skelly B) at 350 °C followed by two treatments with hexamethyldisilazane at 300 °C. Traces of oxygen rapidly destroyed the surface condition as has been noted by others (6).

The rate constants for the disappearance of 2-vinyloxirane along with the probable errors (13) and activation parameters are listed in Table 2.

The results of the product composition studies indicated that the 2,3-dihydrofuran warranted further investigation. For a compound reacting by simultaneous first-order processes we can write:

$$A \xrightarrow{k_1} B$$

$$A \xrightarrow{k_2} C$$

$$A \xrightarrow{k_i} I$$

$$\frac{d[B]}{dt} = k_1[A]$$

$$\frac{d[C]}{dt} = k_2[A] \ldots\ldots \frac{d[I]}{dt} = k_i[A]$$

and

$$-\frac{d[A]}{dt} = k_1[A] + k_2[A] + \ldots\ldots k_i[A]$$

$$= k_n[A]$$

where

$$k_n = \sum_{i=1}^{n} k_i$$

and thus

$$\frac{d[B]}{dt} \Big/ -\frac{d[A]}{dt} = k_1[A]/k_n[A] = k_1/k_n$$

Can. J. Chem. Downloaded from www.nrcresearchpress.com by 210.87.254.6 on 09/05/12
For personal use only.

TABLE 2. Kinetic data for the rate of thermolysis of 2-vinyloxirane at 0.15 atm initial pressure

Temperature (°C)	No. of runs	$k_t \times 10^5$ (s^{-1})	Activation parameters
292.70	4	4.18±0.13	E_a = 47.8±1.1 kcal mol^{-1}
297.52	7	6.15±0.21	log A = 14.1±0.8
302.16	6	8.38±0.26	$\Delta H^{\ddagger}$ = 46.7±1.1 kcal mol^{-1}
307.40	8	12.42±0.15	$\Delta S^{\ddagger}_{573}$ = +4.7±3 eu
312.50	9	17.7 ±0.3	

TABLE 3. Kinetic data for the rate of formation of 2,3-dihydrofuran (**8**) at 0.15 atm from 2-vinyloxirane

Temperature (°C)	No. of runs	$k_8 \times 10^5$ (s^{-1})	Activation parameters
292.70	4	0.60±0.03	E_a = 50.6±1.2 kcal mol^{-1}
297.52	5	0.95±0.03	log A = 14.3±0.9
302.16	5	1.32±0.10	$\Delta H^{\ddagger}$ = 49.5±1.2 kcal mol^{-1}
307.40	5	1.88±0.05	$\Delta S^{\ddagger}_{300}$ = +6.2±3 eu
312.50	5	2.82±0.12	

TABLE 4. Kinetic data for the observed deuterium isotope effects on the thermolysis of 2-vinyloxiranes (**4**, **5**, **6**, and **7**) at 307.40 °C

Oxirane	No. of runs	$k_{obs} \times 10^4$ (s^{-1})	k_H/k_D[c]	$\delta\Delta G^{\ddagger}/n$[d] (cal mol^{-1})
4	8	1.25±0.01[b]		
5	3	0.98±0.01[a]	1.28±0.02	+141±15
6	3	1.06±0.01[a]	1.17±0.03	+219±19
7	3	1.07±0.01	1.20±0.02	+185±25

[a]Not corrected for isotopic purity (see experimental section).
[b]Error at the 90% confidence level.
[c]Corrected isotopic purity using the expression $k_{obs} = f_0k_0 + f_1k_1 + f_2k_2$ where f_0, f_1, and f_2 are the mole fractions of d_0, d_1, and d_2 compounds present and k_0, k_1, and k_2 are the respective rate constants.
[d]Where n is the number of deuteriums present in **5**, **6**, and **7**.

A plot of [B] *vs.* [A] should therefore be linear and the slope given by k_1/k_n. Since an internal standard was present in the kinetic runs we can equally well construct a plot of I_8/I_{DME} *vs.* I_A/I_{DME}, where I_8 represents the gc integration count for 2,3-dihydrofuran (**8**) and I_{DME} is the integration count for the internal standard dimethoxyethane. The slope was determined by least-squares analysis of the data and the values of the rate constants for the formation of **8** are given in Table 3.

The deuterated oxiranes **5**, **6**, and **7** were also subjected to thermolysis at 307.4 °C and their rate constants and isotope effects are given in Table 4. After correction for isotopic purity the isotope effects for **6** and **7** are indistinguishable at the 90% confidence level.

To further delineate the mechanism of thermal isomerization of 2-vinyloxirane a study of the racemization of chiral **4** was undertaken. A preliminary experiment was conducted at 292.7 °C in the static system by carrying thermolysis to one half-life and then recovering unreacted vinyloxirane by preparative gc. The vinyloxirane was found to be completely racemic. The racemization process was then studied over the temperature range 255 to 275 °C. Aliquots were periodically removed from the reaction system and the optical rotation determined in 2-propanol in a thermostated 1.00 dm cell. The specific rotations were calculated with a correction applied for the percentage thermal decomposition that had occurred. Preparative gc on the sample indicated that the only chiral

Can. J. Chem. Downloaded from www.nrcresearchpress.com by 210.87.254.6 on 09/05/12
For personal use only.

TABLE 5. Kinetic data for the rate of racemization of (+)-(*S*)-2-vinyloxirane at 0.5 atm pressure

Temperature (°C)	$k_a \times 10^5$ (s^{-1})	Activation parameters
255.0	1.77±0.02	E_a = 44.2±0.7 kcal mol^{-1} log A = 13.53±0.3
265.1	3.96±0.05 3.92±0.05	$\Delta H^{\ddagger}$ = 43.1±0.7 kcal mol^{-1} $\Delta S^{\ddagger}_{300}$ = +2.1±1 eu
275.0	8.22±0.06	

material present was the oxirane. The first-order rate constants and activation parameters for the racemization process are listed in Table 5.

The *cis-trans* isomerization of **6** and **7** was measured at 307.4 °C only. After heating a sample of **6** to 307.4 °C for 190 min (two half-lives for the thermolysis process) the recovered oxirane was purified by preparative gc and examined by nmr. Integration of the signals at δ 2.63 and 2.95 gave a quantitative measure of the ratio of **7** and **6** respectively. The rate constant $k_{6,7} = k_{7,6}$, was evaluated by the experiment $2tk_{6,7} = \ln (C_a/C_c - C_t)$. The rate constant $k_{6,7}$ was found to be 1.7×10^{-5} s^{-1} at 307.4 °C and starting from **7** a value of $k_{7,6}$ was found to be 1.8×10^{-5} s^{-1}. Because of the extensive thermolysis of the oxirane it was not feasible to carry out the **6** ⇄ **7** isomerization study over a range of temperatures. The comparative rate data, at 307.4 °C, for each of the isomerization processes examined are listed in Table 6.

Experimental

All boiling points are uncorrected. Purifications by preparative gc were carried out on a Nester Faust model 850 'Prepkromatic'. The columns used were 6 ft biwall tubing packed with 20% β,β′-oxydipropionitrile (ODPN) or 20% Carbowax 1500 on Chromosorb W 30–60 mesh. The carrier gas was helium at a flow rate of 500 ml min^{-1}. The purity of materials was checked using a Varian model 1200 gas chromatograph with 6 ft columns of ⅛ in. i.d. packed with 10% ODPN or 10% Carbowax 1500 on high performance Chromosorb WAW/DMCS 80–100 mesh.

TABLE 6. Relative rate data, at 307.4 °C, for the reactions of *cis*-3-deuterio-2-vinyloxirane (**6**)

Reaction	$k \times 10^5$ (s^{-1})	Relative rate
Thermolysis (k_t)	10.7	5.94
Dihydrofuran formation (k_8)	1.58	0.88
Racemization (k_a)	72.4[a]	40.2
cis ⇄ *trans* isomerization (k_t)	1.80	1.0

[a]Extrapolated from lower temperatures using the data from Table 5, for **4** and assuming the isotope effect on racemization to be small since a sample of chiral **5**, gave a k_H/k_D value of 1.01 ± 0.03.

The nuclear magnetic resonance (nmr) spectra were obtained using a Varian A60 or HA100 spectrometer. The proton decoupled deuterium magnetic resonance spectra were obtained using a Bruker HFX 100 spectrometer.

Gas chromatography/mass spectrum analysis was performed on a Varian 1200 gas chromatograph coupled to an A.E.I. MS 9, and an MS-50. Optical rotations were determined using a Perkin-Elmer model 241 polarimeter.

Microanalyses were performed by the Microanalytical Laboratory of the Department of Chemistry, University of Alberta.

Thermolysis Kinetics

Quantitative rate experiments were conducted in the static Pyrex vacuum system constructed as shown in the schematic diagram in Fig. 3. The system was equipped throughout with Hoke stainless steel diaphragm and bellows valves. The reaction vessel consisted of a Pyrex flask (1 litre) situated in a well-insulated air bath with fast air circulation provided by a high-speed fan located at the bottom of the bath. Main heaters controlled by a Variac were used to bring the temperature to about 20 °C below the desired temperature, and secondary heaters controlled by a Melabs model CTCIA proportional temperature controller were used to maintain the desired oven temperature. The temperature was measured by a five-junction iron–constantan thermocouple which had been calibrated against a Hewlett-Packard (HP) model 2801A quartz thermometer. The temperature stability of the system was monitored by coupling the output of the HP model 3420B digital voltmeter to a HP model 7100BM strip chart recorder. The long-term stability was better than ±0.1 °C and was typically ±0.06 °C.

The Hoke model 4213Q6Y high temperature valves (V1, V2) attached to the reaction vessel were located inside the oven to eliminate any dead-space effects during the sampling procedure. The vacuum manifold valves (H1, H2, H3, H4) were Hoke model 4251N6Y stainless-steel bellows valves. The valves utilized for the gc sample injection system were quick-action Hoke model C415K knife-edge stainless-steel bellows valves. Heating tape was applied to the oven inlet system from H3 to V1 and maintained at 100 °C. Heating tape was applied to the oven outlet system and gc injector system and maintained at 75 °C.

Sample analysis was performed on a 6 ft column (⅛ in. i.d.) of 10% ODPN on high-performance 80–100 mesh Chromosorb WAS/DMCS with a helium gas flow rate of

Can. J. Chem. Downloaded from www.nrcresearchpress.com by 210.87.254.6 on 09/05/12
For personal use only.

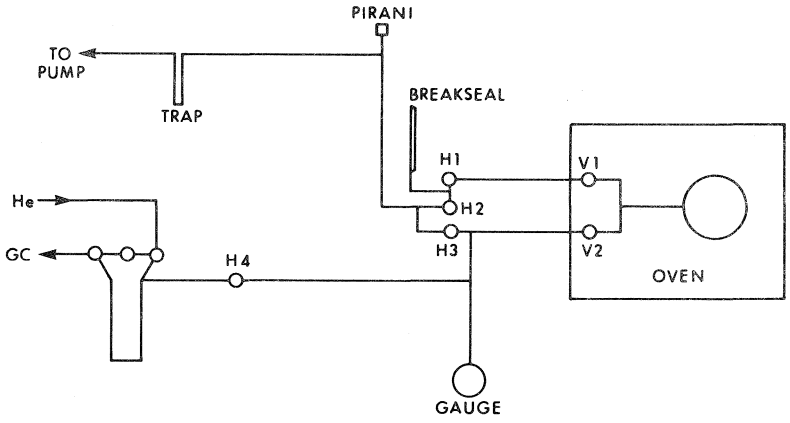

FIG. 3. Schematic diagram of the static Pyrex vacuum system used in these experiments.

25 ml min^{-1} coupled to a Gowmac model TR11B thermal conductivity detector. Gas chromatographic integration was performed with a HP model 3370A electronic integrator.

All samples for the kinetic runs were prepared from materials dried by distillation from calcium hydride, and were degassed and transferred to breakseals by standard procedures.

Kinetics of Racemization of 2-Vinyloxirane

A degassed sample (1 g) was introduced into the 1 litre reaction vessel from a heated inlet system. Recovery of residual sample showed that 0.8 g had been introduced to give an initial pressure of approximately 0.5 atm. Aliquots (~70 mg) were recovered periodically, analyzed by gc, and the optical rotation determined in a solution of 2-propanol using a thermostated 1 dm cell. The specific rotations were calculated with a correction applied from the gc analysis. The rate constant (k_z) was determined using the equation $k_z t = \ln([\alpha]_t - [\alpha]_\infty)/[\alpha]_0 - [\alpha]_\infty)$. Since $[\alpha]_\infty$ was observed to be zero a plot of $\ln([\alpha]_t/[\alpha]_0)$ *vs.* time gave a straight line.

4-Chloro-1-butyne-1-d

4-Chloro-1-butyne (60 g), prepared by the method of Roberts and Mazur (14), was dissolved in methylene chloride (200 ml) and repeated exchanges with deuterium oxide (50 ml) and barium oxide (50 mg) effected by vigorous magnetic stirring for 24 h. Deuterium incorporation was monitored by nmr integration of an aliquot from the methylene chloride layer. After five exchanges the alkyne proton was no longer observable in the spectrum. The methylene chloride layer was dried over 4 Å molecular sieves and the solvent removed by spinning-band distillation. Distillation of the residual liquid gave 52.7 g (87.8%) bp 83–84 °C; ^{1}H nmr δ TMS ($CDCl_3$) 2.67 (t, 2H), 3.62 (t, 2H) and the absence of the alkyne proton resonance observed at δ 2.00 in the reactant.

(Z)-4-Chloro-1-butene-1-d

The procedure was adapted from that of Zweifel and Brown (15). Diglyme and boron trifluoride etherate were freshly purified before use. A mixture of diglyme (150 ml), sodium borohydride (6.8 g 0.18 mol) and 2-methyl-2-butene (33.6 g, 0.48 mol) was stirred and cooled below 5 °C in an ice–salt bath. Boron trifluoride etherate (34.1 g, 0.24 mol) was added over a period of 2 h at a rate such that the reaction temperature was maintained below 10 °C. The reaction mixture initially became homogeneous and then a thick white precipitate of the organoborane was produced. After stirring for an additional 3.5 h the mixture was cooled to 0 °C and a solution of 4-chloro-1-butyne-1-*d* (17.7 g 0.2 mol) in diglyme (20 ml) was added as rapidly as possible while controlling the reaction temperature below 5 °C. The reaction mixture was stirred overnight and allowed to warm to room temperature. After cooling to 0 °C glacial acetic acid (100 ml) was added at a rate such that the reaction mixture was maintained below 5 °C. After stirring an additional 5 h at room temperature the mixture was added to ice-cold water (1500 ml) and extracted with methylene chloride (4 × 200 ml). The combined extracts were washed with cold sodium hydroxide solution then with saturated sodium chloride solution until neutral and dried over calcium sulfate. The methylene chloride was removed by spinning-band distillation and the residual liquid fractionated to give 6.7 g (36.6%) bp 69–70 °C/700 torr; ^{1}H nmr δ TMS ($CDCl_3$) 2.5 (q, 2H), 3.56 (t, 2H), 6.0 (m, 1H) and 5.05 (d, 1H).

cis-2-β-Chloroethyl-3-deuterio-oxirane

(*Z*)-4-Chloro-1-butene-1-*d* (6.3 g 0.069 mol) was dissolved in methylene chloride (180 ml) and *meta*-chloroperbenzoic acid (22 g, 0.127 mol) was added in portions over a period of 0.5 h at room temperature. After stirring overnight the mixture was filtered to remove the precipitated *meta*-chlorobenzoic acid and then distilled at room temperature under reduced pressure. The distillate was fractionated through a Vigreaux column to remove the bulk of the methylene chloride and the residual liquid fractionated to give 6.14 g (89.5%) bp 56–58 °C/28 torr; ^{1}H nmr δ TMS ($CDCl_3$) 1.82 (q, 2H), 2.58 (d, 1H), 2.88 (q, 1H) and 3.57 (t, 2H).

cis-3-Deuterio-2-vinyloxirane (6)

The procedure was essentially that devised by Reppe (29). A mixture of *cis*-2-β-chloroethyl-3-deuteriooxirane

Can. J. Chem. Downloaded from www.nrcresearchpress.com by 210.87.254.6 on 09/05/12
For personal use only.

Can. J. Chem. Downloaded from www.nrcresearchpress.com by 210.87.254.6 on 09/05/12
For personal use only.

(2.13 g, 0.02 mol) and finely powdered potassium hydroxide (5.6 g, 0.1 mol) was gradually heated to 100 °C and the distillate collected in a cooled receiver (1.49 g, 100%). Final purification was accomplished by preparative gc on 20% β,β′-oxydipropionitrile (ODPN) on Chromosorb W at 40 °C; ^{1}H nmr δ TMS ($CDCl_3$): 2.81 (d, 1H), 3.20 (q, 1H) and the vinyl group resonance as a multiplet 5.05–5.7 (3H). Careful integration of the spectrum indicated 3.2% protium at the labelled position.

(+)-(S)-Isopropylidene-3-buten-1,2-diol

A solution of methylene triphenylphosphorane in benzene was prepared using the method of Schlosser *et al.* (16). A solution of isopropylidene D-glyceraldehyde (18.3 g, 0.14 mol) prepared by the method of Baer and Fischer (12) was dissolved in benzene (50 ml) and added dropwise over 1 h. The reaction temperature was held below 10 °C by external cooling. After a further 1 h the excess ylide was destroyed by the addition of a solution of acetone in benzene until the reaction mixture was essentially colourless. The reaction mixture was filtered and the benzene removed by distillation through a Vigreaux column. The residual oil was diluted with hexane (1000 ml), stirred vigorously, and then filtered to remove the precipitated triphenylphosphine oxide. The filtrate was washed with water and dried over 4 Å molecular sieves. The solution was distilled through a Vigreaux column to remove benzene and hexane and the residue distilled under reduced pressure to give 10.5 g (59.5%) bp 50–52 °C/50 torr. An analytical sample was purified by preparative gc on ODPN. *Anal.* calcd. for $C_7H_{12}O_2$: C 65.57, H 9.44; found: C 65.39, H 9.67. $[\alpha]_{589}^{24}$ + 30.96; $[\alpha]_{365}^{24}$ +105.7; (9.8 g/100 ml, 2-propanol); ^{1}H nmr δ TMS ($CDCl_3$) 1.57 (s, 3H), 1.60 (s, 2H), 3.58 (t, 1H), 4.1 (q, 1H), 4.5 (q, 1H), 5.1–6.2 (m, 3H).

(−)-(S)-3-Buten-1,2-diol

The procedure was analogous to that of Meric and Vigneron (17). Dilute hydrochloric acid (3 *N*, 25 ml) was added to a solution of isopropylidene-3-buten-1,2-diol (10.0 g) in 98% ethanol (115 ml), and the mixture refluxed for 1 h. It was then cooled and the excess acid neutralized by careful addition of solid sodium bicarbonate. The mixture was filtered and the precipitate washed with fresh ethanol (200 ml). The filtrate was evaporated under reduced pressure to give a viscous oil together with some inorganic salts. This product was dissolved in methanol (50 ml), and ether (250 ml) gradually added with vigorous stirring. The mixture was filtered to remove the precipitated inorganic salts and the filtrate was evaporated to give a clear, pale yellow oil. Residual water was removed by azeotropic distillation with benzene. The combined yield of diol from four of the above runs was 21 g. Distillation under reduced pressure gave 20.4 g, bp 58–60 °C/2 torr: $[\alpha]_{589}^{22}$ −43.6; $[\alpha]_{365}^{22}$ −152.8; (4.62 g/100 ml, 2-propanol).

To check for any racemization during the cleavage of the isopropylidene group, a sample of the diol was reconverted to the isopropylidene derivative by treatment with 2,2-dimethoxypropane in the presence of a catalytic quantity of *p*-toluenesulfonic acid. The product was purified by preparative gc on ODPN and the rotation measured: $[\alpha]_{589}^{22}$ +29.65; $[\alpha]_{365}^{22}$ +100.80; (6.32 g/100 ml, 2-propanol). It was thus concluded that less than 5% racemization had occurred during the cleavage of the isopropylidene group.

(+)-(S)-2-Vinyloxirane (4)

A solution of (*S*)-3-buten-1,2-diol (2.20 g, 0.025 mol, $[\alpha]_{589}^{22}$ −43.6) in dry pyridine (25 ml) was stirred and cooled below 5 °C. Freshly recrystallized *p*-toluenesulfonyl chloride (5.25 g, 0.028 mol) was added over 10 min and the mixture stirred 18 h at 5 °C. The reaction mixture was poured into ice-cold water (125 ml) and extracted with several portions of ether. The combined ether extracts were washed with ice-cold hydrochloric acid (3 *N*) until the washes remained acidic. The ether extracts were then washed with saturated sodium bicarbonate solution, followed by a saturated sodium chloride solution and dried over anhydrous sodium sulfate. Evaporation of the ether at room temperature gave a colourless oil 5.72 g (96%) which rapidly crystallized. Finely powdered potassium hydroxide (8 g) was added to the monotosylate thus prepared and the mixture gradually warmed in an oil bath to 100–110 °C. The distillate was collected in a cooled receiver. From several runs, the yield averaged 1–1.5 g of 2-vinyloxirane containing a small amount of ether and water. The 2-vinyloxirane was further purified by preparative gc on ODPN at 40 °C: $[\alpha]_{589}^{25}$ +8.306; $[\alpha]_{365}^{25}$ +45.883; (6.959 g/100 ml, 2-propanol).

3-Buten-1,2-diol-1,1-d_2

Lithium aluminum deuteride (5.0 g, 0.12 mol, Ventron 98.5%) was added to freshly dried ether (350 ml) under a nitrogen atmosphere, and the mixture cooled in ice. A solution of methyl 2-hydroxy-3-butenoate (17.5 g 0.15 mol) in dry ether (50 ml) was added dropwise over 1 h, and the reaction mixture stirred an additional 40 h at room temperature. Ether (100 ml, saturated with water) was then added dropwise, followed by a saturated solution of sodium potassium tartrate in water. The ether layer was separated and the aqueous layer subjected to continuous extraction with ether for 3 days. The combined ether extracts were evaporated and the residual oil azeotroped with benzene to remove any residual water. The residual oil was then distilled under reduced pressure to give 9.9 g (73%) bp 65–68 °C/2 torr.

2-Vinyloxirane-3,3-d_2

The procedure was that described above for the conversion of (−)-(*S*)-3-buten-1,2-diol to (+)-(*S*)-2-vinyloxirane. The nmr δ TMS ($CDCl_3$) 3.35 (t, 1H), 5.2–5.8 (m, 3H). The deuterium incorporation was found to have 1.5% protium at C-3 by nmr.

(E)-4-Chloro-1-butene-1-d

The procedure was essentially that previously described for the conversion of 4-chloro-1-butyne-1-*d* to (*Z*)-4-chloro-1-butene-1-*d*. 4-Chloro-1-butyne was treated with diisoamylborane followed by protonolysis with deuterioacetic acid. The deuterioacetic acid was prepared by treatment of acetic anhydride with deuterium oxide according to the procedure of Roberts and Mazur (14). The product was purified by spinning-band distillation to give a 47.5% yield of (*E*)-4-chloro-1-butene-1-*d*; ^{1}H nmr δ TMS ($CDCl_3$) 2.5 (q, 2H), 3.56 (t, 2H), 5.5–6.2 (m, 1H) and 5.1 (d, 1H).

Can. J. Chem. Downloaded from www.nrcresearchpress.com by 210.87.254.6 on 09/05/12
For personal use only.

trans-2-β-Chloroethyl-3-deuterio-oxirane

The synthetic procedure was the same as that previously described for the epoxidation of (*Z*)-4-chloro-1-butene-1-*d*. The product was distilled under reduced pressure to give a 58% yield of *trans*-2-β-chloroethyl-3-deuterio-oxirane; ^{1}H nmr δ TMS ($CDCl_3$) 2.0 (q, 2H), 3.65 (t, 2H), 2.53 (d, 1H) and 3.05 (m, 1H).

trans-3-Deuterio-2-vinyloxirane (7)

The synthetic procedure was that previously described for the conversion of *cis*-2-β-chloroethyl-3-deuterio-oxirane to *cis*-3-deuterio-2-vinyloxirane. The product (91%) was purified by preparative gc on ODPN at 40 °C; ^{1}H nmr δ TMS ($CDCl_3$) 2.50 (d with fine splitting, 1H), 3.20 (m, 1H), and the vinyl group resonance as a multiplet 5.05–5.7 (3H). The quartet centered δ 2.81 was attributed to the presence of undeuterated 2-vinyloxirane. Careful integration of the ^{1}H nmr spectrum indicated that the product was a mixture of *trans*-3-deuterio-2-vinyloxirane (81.4%) and non-deuterated 2-vinyloxirane (18.6%).

(−)-(R)-2-Vinyloxirane

This oxirane was prepared by partial asymmetric destruction of 2-vinyloxirane with di-3-pinanylborane by adaption of the procedure of Brown and Zweifel (18). A mixture of sodium borohydride (0.165 g, 0.0044 mol), (+)-α-pinene (1.36 g, 0.01 mol; Aldrich, α_D +43.5°, neat), and diglyme (10 ml) was stirred and cooled under a nitrogen atmosphere in an ice bath. Boron trifluoride etherate (0.71 g, 0.005 mol) was added dropwise over 0.5 h at such a rate that the reaction temperature was maintained below 5 °C. After stirring for 4 h (below −5 °C) the resulting white suspension was cooled to −30 °C and vinyloxirane (0.70, 0.01 mol) was added rapidly. The mixture was maintained at −10 °C for 1.5 h and then water (0.5 ml) added to quench the reaction. It was then distilled at 0 °C under reduced pressure into a cooled receiver (acetone–CO_2), and the water layer separated from the distillate. The oxirane was purified by preparative gc on a 6 ft Carbowax 1500 column at 40 °C to give 0.246 g (34%) of (−)-(*R*)-2-vinyloxirane: $[\alpha]_{589}^{25}$ −0.675, $[\alpha]_{365}^{25}$ −5.040 (4.444 g/100 ml, 2-propanol). The optical purity was estimated to be about 9% based on the (+)-(*S*)-2-vinyloxirane obtained by synthesis from D-mannitol.

(−)-(R)-2-Vinyloxirane-3,3-d_2

This compound was prepared by the partial asymmetric destruction of 2-vinyloxirane-3,3-d_2 by the procedure previously described above for 2-vinyloxirane. Purification by preparative gc on Carbowax 1500 at 40 °C gave 0.313 g (43.5%) of (−)-(*R*)-2-vinyloxirane-3,3-d_2: $[\alpha]_{589}^{25}$ −0.977, $[\alpha]_{365}^{25}$ −5.752 (3.686 g/100 ml, 2-propanol).

Discussion

Thermolysis of the Oxirane CC Bond

The most facile reaction of 2-vinyloxirane is the racemization process observed when chiral oxirane is used. The fact that this proceeds 72 times faster than the interconversion of **6** to **7** indicates that the process involves enantiomerization and not diastereomerization. This is best rationalized in terms of the formation of a carbonyl-ylide, *e.g.*, **12**, and reclosure. It is suggested that this proceeds in a conrotatory fashion (9), however, all that is required in this case is that the same mode of synchronous rotation is used for the reclosing as for the opening. The data from Table 5 indicate that the activation enthalpy for this process (k_α) $\Delta H^{\ddagger}$ is +43.1 ± 0.7 kcal mol^{-1}, the small value for $\Delta S^{\ddagger}$, +2.1 eu, is reasonable since the activation process involves not only the breaking of the C-2 to C-3 bond, a process expected to give a positive $\Delta S^{\ddagger}$ term, but involves the loss of rotation about the C-2—vinyl bond for the allylic resonance. This type of cleavage for oxiranes has been observed before and is well documented (7–11).

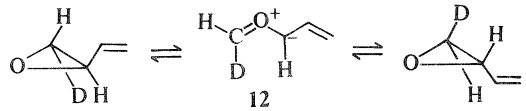

12

Thermolysis of the Oxirane C—O Bond

It is clear that products such as **9**, **10**, and **11** result from the cleavage of the O—C-2 bond. That a diradical such as **13** may be implicated comes from a consideration of the deuterium distribution in the products of thermolysis of **6** and **7**. Table 1 indicates that the deuterium

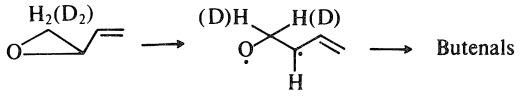

13

distribution in the products is the same for both the *cis*- and *trans*-deuterated oxirane, an observation which is best accommodated by a stage along the reaction coordinate wherein the two reactants converge, and cannot be readily accounted for by a shift of H or D concerted with ring opening, *e.g.*,

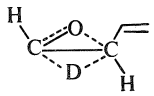

The observed deuterium kinetic isotope effects on the formation of butenals (Table 4) are small when considered in terms of the traditional primary deuterium kinetic isotope effects wherein a C—H stretching mode is part of the reaction coordinate (19). It has been suggested (20) that a reduced value of the isotope effect would be

TABLE 7. Isotope effects for reactions having non-linear activated complexes[a]

Reaction	k_H/k_D	T (°C)	$\delta\Delta G^{\ddagger}$ (cal mol^{-1})
$Ph_2C(OH)-CH(D)Ph \rightarrow Ph_2CH(D)-C(=O)-Ph$	3.3	43.3	750
$(CH_3)_2C(OH)-CH(D)CH_3 \rightarrow (CH_3)_2CH(D)C(=O)-CH_3$	1.68	60	340
$(CH_3)_2CH(OTs)-CH(D)CH_3 \rightarrow (CH_3)_2CCH_2CH_3(OCOCH_3)$	2.1	25	440
2-Vinyloxirane $\rightarrow$ Butenals[b]	1.27	307	278

[a]Taken from ref. 20.
[b]This work.

TABLE 8. Infrared frequencies used to calculate the isotope effects for oxirane ring opening and hydrogen (deuterium) migration

Mode	C_2H_4O(22)	C_2D_4O(22)	$C_6H_{12}N_4$(23)	$C_6D_{12}N_4$(23)
CH stretch (A)	3079	2317	2955	2288
CH stretch (S)	3019	2174	2990	2110
CH_2 deformation	1490	1013	1455	1120
F_2 wag	1420	970	1370	1075
E twist	1143	896	1325	1000
F_2 rock	821	577	850	670

expected for a reaction proceeding via a non-linear activated complex, such as that for hydrogen migration in a pinacol rearrangement. The free energy change for the 2-vinyloxirane–butenal interconversion is given in Table 7 along with those of other hydrogen migration processes. While the value of $\delta\Delta G^{\ddagger}$ is small it is in fact larger than that normally observed for secondary deuterium isotope effects (21). A possible unique source of secondary deuterium isotope effects is that which would be observed by the changes in vibrational frequencies for the methylene group on going from the strained oxirane ring system to that of the putative diradical **13**. An estimation of the magnitude of this effect was made by using the infrared vibrational frequencies of ethylene oxide and ethylene oxide-d_4 (22) and comparing them with the methylene group of hexamethylenetetramine and hexamethylenetetramine-d_{12} (23). The latter was chosen because the methylene group is located between atoms of electronegativity greater than tetrahedral carbon. The relevant frequencies are given in Table 8. If we consider the sum $\delta\Delta W$ given by:

$$\delta\Delta W = [\sum W(C_2H_4O) - \sum W(C_2D_4O)] - [\sum W(C_6H_{12}N_4) - \sum W(C_6D_{12}N_4)]$$

for the respective methylene groups we obtain a value of 93 cm^{-1}. This gives a free energy difference of 133 cal mol^{-1} such that $k_Hk_D = 1.12$ for the initial ring opening at 307 °C.

If the rate determining transition state is the migration of a hydrogen, or deuterium, in a manner analogous to a twisting of the methylene, as in **14**, then the reaction coordinate corresponds to the E twist mode and $\delta\Delta W = 325$ cm^{-1} giving a free energy difference of 465 cal mol^{-1} and a value of $k_H/k_D = 1.50$ for butenal formation at 307 °C.

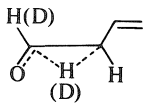

14

The mechanism for butenal formation must fit the following mechanistic constraints: (*a*) *cis–trans* isomerization of the deuterated oxiranes is slower than butenal formation; (*b*) a kinetic deuterium isotope effect, bigger than that of a secondary nature, is observed for the formation of butenals; (*c*) that both **6** and **7** give rise to comparable deuterium labelling patterns in the butenal products such as to imply the stereo-

Can. J. Chem. Downloaded from www.nrcresearchpress.com by 210.87.254.6 on 09/05/12
For personal use only.

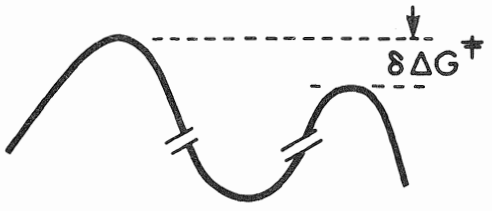

FIG. 4. Reaction coordinate wherein a C,O-diradical is a post transition state intermediate which displays an isotope effect for H *vs.* D migration.

chemical equivalence of the methylene hydrogens (deuteriums) along the reaction coordinate.

These constraints can be accommodated by a reaction scheme involving the putative diradical **13** as a post-transition state intermediate on the reaction coordinate as depicted in Fig. 4. It can be shown that a deuterium isotope effect in the second step of the reaction would be observed in the overall kinetics. If we consider the data for the thermolysis of **6** then we can obtain an estimate of the difference in height of the free-energy barriers ($\delta\Delta G^{\ddagger}$, Fig. 4) for the forward and reverse processes. If the reverse reaction is responsible for the *cis–trans* isomerization ($k_i = 1.80 \times 10^{-5}$ s^{-1}, at 307.4 °C, see Table 6) and it is compared with the value for the rate of butenal formation ($k_t - k_s = 9.12 \times 10^{-5}$ s^{-1})[1] then $\delta\Delta G^{\ddagger}$ of Fig. 4 may be calculated as RT ln $[(9.12 \times 10^{-5})/(2 \times 1.8 \times 10^{-5})]$ or 1.07 kcal mol^{-1}. The factor of two is included since the molecules returning from **13** → **6** have an equal probability of becoming **7**. Thus for every 10^3 molecules of **6** per unit time being converted to **13** we have 715 proceeding to product and 285 reverting to **6** + **7**. Upon going to the dideuterio oxirane **5** we would expect the rate of production of **13** to drop slightly, because of the ring opening isotope effect, *i.e.*, to 949 molecules of **6** per unit time, and the number reaching the product stage to decrease by 1.17/1.28 to 653. For the non-deuterated oxirane **4** the initial barrier would decrease in such a manner as to produce 1063 molecules of **13** per unit time and the number reaching the product stage would similarly increase by 1.17/1.00 times that of **6** or 836 molecules per unit time. Such a scheme is completely compatible with the rate data of Table 6 and the kinetic isotope effect data of Table 4.

The experimental results presented are best interpreted in terms of a carbon–oxygen diradical intermediate, but the *cis–trans* isomerization of the 3-deuterio-2-vinyloxiranes could equally well be occurring from a carbonyl-ylide, *e.g.*, **12**, and not upon the reaction coordinate to butenal formation. If such is the case then the rate-determining transition state would be the same as suggested in our reaction model, but it is difficult to understand why *cis–trans* isomerization is not faster than observed. For these reasons we prefer the diradical **13** as an intermediate in the formation of butenals.

*The Thermochemistry of Formation of **12** and **13***

The heats of formation of the reactant **4** (+2.6 kcal mol^{-1}) and the intermediates **12** (+42.9 kcal mol^{-1}) and **13** (+46.5 kcal mol^{-1}) can be estimated by group additivities (24). The heats of formation of the transition states leading to these species are +45.7 and +49.1 kcal mol^{-1} respectively (estimated error ±2 kcal mol^{-1}). It can be seen that the group additivities give a reasonable estimate for the heat of formation of the putative diradical **13**. The data used to estimate the heat of formation of **12** make use of the heat of formation of $CH_3OCH_2\cdot$ from O'Neal and Benson (25), and do not allow for the resonance contributions **2***b* and **2***c* described in the Introduction, which would be expected to deepen the energy well for this type of intermediate. Probably the most significant thermochemical conclusion we can generate is that it is 3.7 kcal mol^{-1} more difficult to break the C—O bond, in vinyloxirane, than it is to break the C—C.

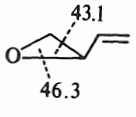

Butenal Products

None of our data allow us to state with any assurance how the butenals are produced. It is possible that the diradical **13** produces 3-butenal directly by a 1,2-hydrogen shift, or that a shift to oxygen produces 1,3-butadien-1-ol which tautomerizes by a thermochemically allowed 1,5-hydrogen shift to (*Z*)-2-butenal. It is clear from the product studies that the thermodynamically unstable 3-butenal slowly isomerizes into (*E*) and

[1]The secondary deuterium kinetic isotope effects for dihydrofuran formation from **5** and **6** were observed to be 1.30 and 1.18 respectively.

Can. J. Chem. Downloaded from www.nrcresearchpress.com by 210.87.254.6 on 09/05/12
For personal use only.

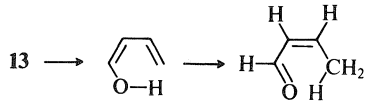

possibly (*Z*)-2-butenal. It is also possible that the slow conversion of these products to propene and carbon monoxide occurs from 3-butenal via a concerted H transfer, *e.g.*,

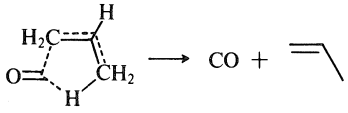

This latter process is under active investigation. The small incorporation of deuterium into the thermolysis product of **4** suggests that surfact catalysis is playing a role in the final structures. Further studies of surface effects are required to elucidate this component of the reaction.

Acknowledgements

The authors wish to thank the National Research Council of Canada for financial aid and Dr. A. Hogg for technical assistance with the mass spectrometry.

1. (*a*) R. G. Bergman. *In* Free radicals. Vol. I. *Edited by* J. Kochi. Wiley-Interscience, New York, N.Y. 1973. p. 991; (*b*) H. M. Frey. Adv. Phys. Org. Chem. **4**, 147 (1966); (*c*) H. M. Frey and R. Walsh. Chem. Rev. **69**, 103 (1969); (*d*) M. R. Willcott, R. L. Cargill, and A. B. Sears. Prog. Phys. Org. Chem. **9**, 25 (1972).
2. J. A. Berson, L. D. Pedersen, and B. K. Carpenter. J. Am. Chem. Soc. **98**, 122 (1976).
3. T. S. Chambers and G. B. Kistiakowsky. J. Am. Chem. Soc. **56**, 399 (1934).
4. (*a*) R. G. Bergman and W. Carter. J. Am. Chem. Soc. **91**, 7411 (1969); (*b*) R. J. Crawford and T. R. Lynch. Can. J. Chem. **46**, 1457 (1968); (*c*) J. A. Berson and J. M. Belquist. J. Am. Chem. Soc. **90**, 7343 (1968).
5. (*a*) R. Hoffmann. J. Am. Chem. Soc. **90**, 1475 (1968); (*b*) J. A. Horsley *et al.* J. Am. Chem. Soc. **94**, 279 (1972); (*c*) A. K. Q. Siu, W. M. St. John, and E. F. Hayes. J. Am. Chem. Soc. **92**, 7249 (1970); (*d*) L. Salem. Acc. Chem. Res. **4**, 422 (1971).
6. (*a*) M. C. Flowers, R. M. Parker, and M. A. Voisey. J. Chem. Soc. B, 239 (1970); (*b*) M. C. Flowers and R. M. Parker. J. Chem. Soc. 1980 (1971); (*c*) S. W. Benson. J. Chem. Phys. **40**, 105 (1964); (*d*) M. L. Neufeld and A. T. Blades. Can. J. Chem. **41**, 2956 (1963).
7. (*a*) D. R. Arnold and L. A. Karnischky. J. Am. Chem. Soc. **92**, 1404 (1970); (*b*) W. J. Linn. J. Am. Chem. Soc. **87**, 3665 (1965).
8. (*a*) T. Do-Minh, A. M. Trozzolo, and G. W. Griffin. J. Am. Chem. Soc. **92**, 1402 (1970); (*b*) D. R. Paulsen, F. Y. N. Tang, and R. B. Sloan. J. Org. Chem. **38**, 3967 (1973).
9. (*a*) H. Hamberger and R. Huisgen. Chem. Commun. 1190 (1971); (*b*) A. Dalmen, H. Hamberger, R. Huisgen, and V. Markowski. Chem. Commun. 1192 (1972); (*c*) H. J. H. MacDonald and R. J. Crawford. Can. J. Chem. **50**, 428 (1972).
10. E. W. Yankee and D. J. Cram. J. Am. Chem. Soc. **92**, 6328 (1970); **92**, 6331 (1970); **92**, 6333 (1970).
11. (*a*) A. Robert, J. J. Pomeret, and A. Foucaud. C. R. Acad. Sci. Paris, Ser. C, **270**, 1739 (1970); (*b*) J. C. Paladini and J. Chuche. Tetrahedron Lett. **46**, 4383 (1971); (*c*) R. J. Crawford, V. Vukov, and H. Tokunaga. Can. J. Chem. **51**, 3718 (1973).
12. E. Baer and H. O. L. Fischer. J. Biol. Chem. **128**, 463 (1939).
13. A. J. Gordon and R. A. Ford. The chemist's companion. Wiley-Interscience, New York, N.Y. 1972. p. 491.
14. J. D. Roberts and R. H. Mazur. J. Am. Chem. Soc. **73**, 2509 (1951).
15. G. Zweifel and H. C. Brown. Org. React. **13**, 1 (1963).
16. M. Schlosser, G. Muller, and K. F. Christmann. Angew. Chem. Int. Ed. Engl. **5**, 667 (1968).
17. R. Meric and J.-P. Vigneron. Bull. Soc. Chim. Fr. 327 (1973).
18. H. C. Brown and G. Zweifel. J. Am. Chem. Soc. **83**, 486 (1961).
19. W. A. Van Hook. *In* Isotope effects in chemical reactions. *Edited by* C. J. Collins and N. S. Bowman. Am. Chem. Soc. Monograph 167. 1971. Chapt. 1.
20. K. B. Wiberg. Physical organic chemistry. John Wiley and Sons, Inc., New York, N.Y. 1964. p. 362.
21. E. A. Halevi. Prog. Phys. Org. Chem. **1**, 109 (1963).
22. J. E. Bertie and D. A. Othen. Can. J. Chem. **51**, 1155 (1973).
23. J. E. Bertie and M. Solinas. J. Chem. Phys. **61**, 1666 (1974).
24. S. W. Benson. Thermochemical kinetics. John Wiley and Sons, Inc., New York, N.Y. 1968.
25. H. E. O'Neal and S. W. Benson. *In* Free radicals. Vol. II. *Edited by* J. Kochi. Wiley–Interscience, New York, N.Y. 1973. p. 275.

Can. J. Chem. Downloaded from www.nrcresearchpress.com by 210.87.254.6 on 09/05/12
For personal use only.

Synthesis of some 4-pyranones and 4-pyridones structurally related to isoproterenol

HAYDN W. R. WILLIAMS
Medicinal Chemistry Department, Merck Frosst Laboratories, P.O. Box 1005, Pointe Claire/Dorval, P.Q., Canada H9R 4P8

Received May 25, 1976

HAYDN W. R. WILLIAMS. Can. J. Chem. **54**, 3377 (1976).

The syntheses of 2-isopropylamino-1-(5-hydroxy-4*H*-pyran-4-on-2-yl)ethanol and the corresponding 4-pyridone and 1-methyl-4-pyridone analogues are described. The selective reduction of an aliphatic nitro group in the presence of a benzyl ether linkage was a key step in the reaction sequence.

HAYDN W. R. WILLIAMS. Can. J. Chem. **54**, 3377 (1976).

On décrit les synthèses de l'isopropylamino-2 (hydroxy-5 4*H*-pyrannone-4 yl-2)-1 éthanol et des pyridone-4 et méthyl-1 pyridone-4 analogues correspondantes. La réduction sélective d'un groupe nitro aliphatique en présence d'un lien éther benzylique s'est avérée une étape clé dans la séquence de réaction.

[Traduit par le journal]

A number of examples exist in the literature of compounds which influence catecholamine biosynthesis or metabolism by virtue of the presence in the molecules of cyclic chelating moieties. These chelating groups presumably confer on the compounds affinity for the enzymes involved in the metabolism of sympathomimetic amines by interaction with the catechol-binding sites in the enzymes. Thus Belleau showed in 1961 that 4-methyltropolone had catechol-*O*-methyltransferase (COMT) inhibitory activity (1). Isosteres of dihydroxyphenylalanine (DOPA) containing 3-hydroxypyran-4-one (**1**) or 3-hydroxypyrid-4-one (**2**) ring systems also show COMT inhibitory activity (2); while the latter compound has also been shown to be a substrate for DOPA decarboxylase (3) it is interesting to note that the isomeric natural product mimosine (**3**) (leucenol) is not (4). Other 3-hydroxy-4-pyranones, 3-hydroxy-2-pyridones, and 3-hydroxy-4-pyridones have been examined as COMT inhibitors (5).

This structural feature might also be expected to confer on a molecule affinity for adrenergic receptors and the compound would then show sympathomimetic or sympatholytic activity depending upon the overall molecule–receptor interaction. The tetronic acid derivatives **4***a* and **4***b* related to noradrenaline and α-methylnoradrenaline were synthesized, probably on the basis of such considerations (6).

This paper describes the syntheses of isosteres of isoproterenol containing the hydroxypyranone (**5**) and hydroxypyridone (**6**) ring systems which were made with the aim of obtaining β-sympathomimetic compounds, preferably with specificity for β_2-adrenergic receptors (for a review of this topic see ref. 7). A similar rationale must have been the motivation for the preparation of the isostere of salbutamol[1] (**7**) which is claimed to be a bronchial dilator with little cardiac effect (8).

The starting material for the syntheses was the benzyl ether of comenaldehyde (**9**) which has been described by Thomas (9). Initially, oxidation of the benzyl ether of kojic acid (**8**) with manganese dioxide in benzene gave acceptable yields (*ca.* 66%) of **9** but this oxidation proved to be very dependent on the activity of the batch of oxidant and, as the method of Thomas (who percolated a solution of the alcohol down a column of manganese dioxide) did not seem to lend itself to large scale preparations, an alternative method was sought. It was found that the alcohol could be oxidized to the aldehyde in consistent yields of about 65% under conventional Pfitzner–Moffatt oxidation conditions (10). None of the dimeric products encountered when 5-benzyloxy-2-benzenesulphonyloxymethyl-4-pyrone (**10**) was oxidized with dimethyl sulphoxide (9) were observed under Pfitzner–

[1] 2-*tert*-Butylamino-1-(4-hydroxy-3-hydroxymethylphenyl)ethanol, a selective β-stimulant. See ref. 7 for more information.

Can. J. Chem. Downloaded from www.nrcresearchpress.com by 210.87.254.42 on 09/05/12
For personal use only.

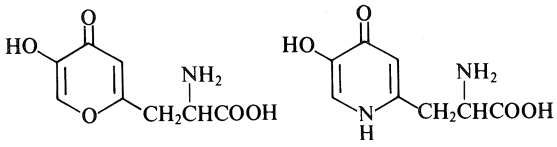

1 2

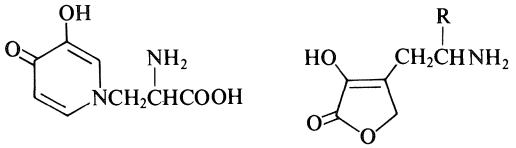

3 4 *a*, R = H
b, R = CH_3

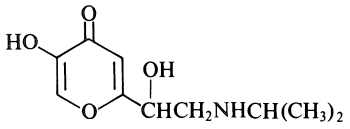

5

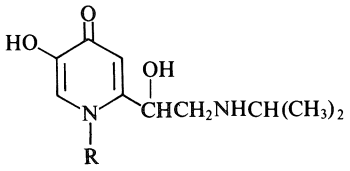

6 *a*, R = H
b, R = CH_3

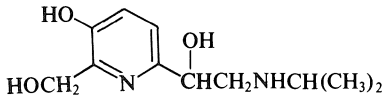

7

SCHEME 1

Moffatt conditions. Base-catalyzed (Et_3N) condensation of **9** with 1 equiv. of nitromethane in tetrahydrofuran gave the bis-compound **11**[2] as the only isolated product; but by using excess nitromethane as solvent, the yield of **11** could be kept to a minimum and the desired nitroethanol **12***a* was obtained in 57% yield. The nitro group was reduced without concomitant loss of the benzyl group by reduction with hydrogen and Raney nickel. The blocking group was readily removed by hydrogenation in the presence of palladium-on-charcoal as illustrated by the conversion of **13***a* to **14***a*. In a single experiment, condensation of **9** with nitroethane (in excess) afforded **12***b* in moderate yield and no bis-condensation product corresponding to **11** was observed. The same sequence of hydrogenations on **12***b* gave **14***b*.

Introduction of the isopropyl group on the nitrogen atom was effected by reductive alkylation with acetone and sodium borohydride. Such reductive alkylations had served us well in making secondary amines in the dihydrobenzodioxepin series (11) but the procedure was not entirely satisfactory here (see Experimental) and it is likely that the newer reagent, sodium cyanoborohydride, which has been described since this work was done, would be more effective. Reaction of **15** with either ammonia or methylamine gave the corresponding pyridones **16***a* and **16***b*, and the three compounds **15**, **16***a*, and **16***b* were debenzylated to **5**, **6***a*, and **6***b* by hydrogenolysis over palladium-on-charcoal.

In the event, while **5** showed potent activity as a β-adrenergic stimulant, it did not show the desired specificity that is required in a modern bronchial dilator drug. The pyridones **6***a* and **6***b* had a much lower order of activity.[3]

Experimental

Melting points (uncorrected) were determined in a Thomas Hoover capillary melting point apparatus. The ir spectra were recorded with a Perkin-Elmer 157 spectrometer and are for potassium bromide wafers. The nmr spectra were recorded using a Varian A60A spectrometer with TMS as internal standard in organic solvents, or DSS in D_2O. Microanalyses were performed by Organic Microanalyses Laboratories (Dr. C. Daessle) and mass spectra were provided by Morgan Schaffer Corporation, both of Montreal.

5-Benzyloxy-2-formyl-4H-pyran-4-one **9**

(*a*) A mixture of 5-benzyloxy-2-hydroxymethyl-4*H*-pyran-4-one (12) (30.0 g, 0.129 mol), active manganese dioxide[4] (90 g), and benzene (1.44 l) was heated under reflux for 1 h and then filtered. The filter cake was extracted with chloroform (200 ml) and the combined solution was evaporated to give 19.6 g (66%) of **9**, mp 120–121 °C; ir ν_{max} 3100, 2855, 1720, 1655, 1210, 940. This crystalline variety of **9** was obtained from the first

[2]Compound **11** was probably the racemic stereoisomer. See the experimental part.

[3]H. M. Guirgis, R. A. Hall, and N. N. Share, unpublished results.

[4]Prepared by the method of Attenburrow *et al.*, J. Chem. Soc. 1094 (1952).

Can. J. Chem. Downloaded from www.nrcresearchpress.com by 210.87.254.42 on 09/05/12
For personal use only.

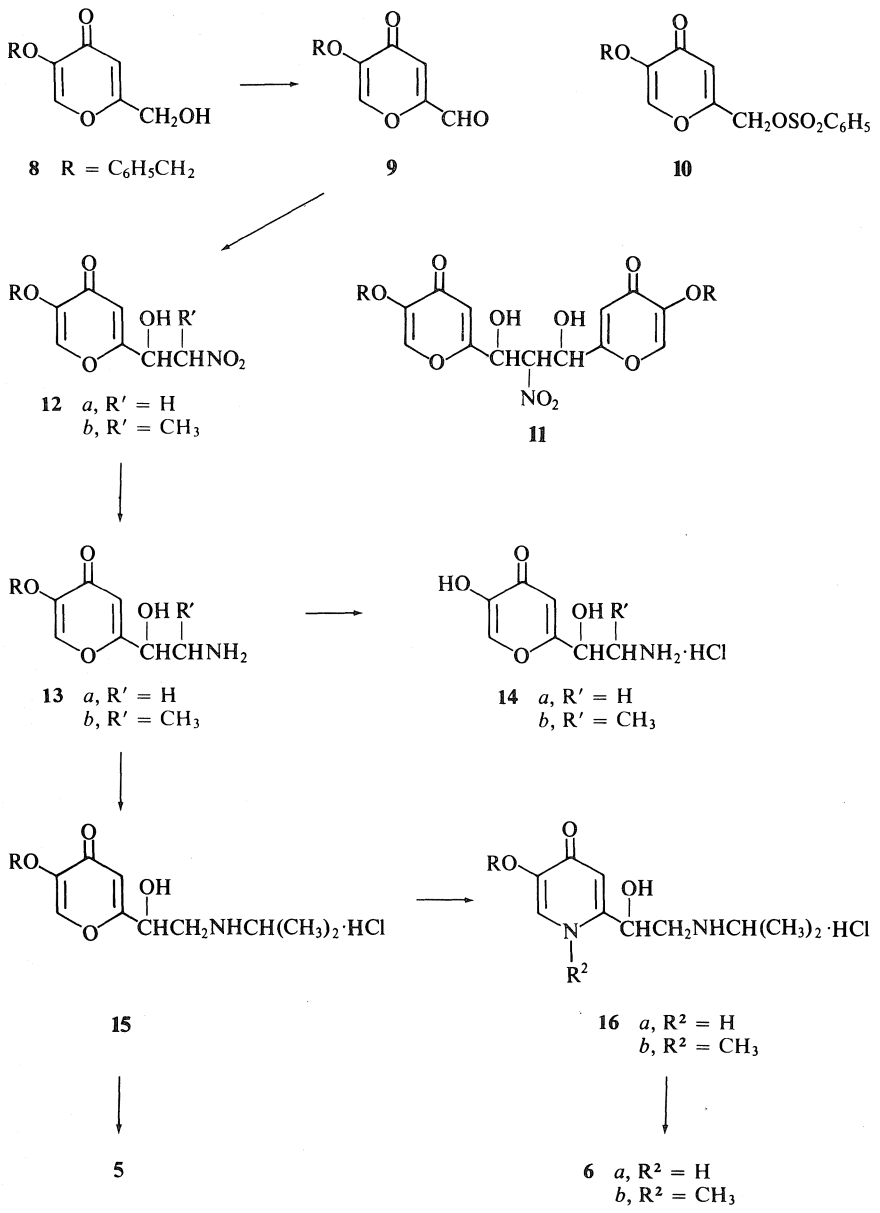

SCHEME 2

few preparations of this compound but later a second crystalline form, mp 137–138 °C, (from EtOAc) was obtained from this reaction, and also from the Pfitzner–Moffatt oxidation procedure.[5]

(*b*) To a stirred mixture of **8** (46.4 g, 0.20 mol), pyridine (15.8 g, 0.20 mol), trifluoroacetic acid (11.4 g, 0.1 mol), and dry dimethyl sulphoxide (600 ml) was added a solution of dicyclohexylcarbodiimide (123.6 g, 0.6 mol) in dimethyl sulphoxide (50 ml) slowly during 1 h. The mixture was stirred for 1 h and left at room temperature overnight. Methylene chloride (1 litre) was added, and then a solution of oxalic acid dihydrate (75.6 g, 0.6 mol) in methanol (320 ml) was added dropwise with stirring. When gas evolution had abated the mixture was filtered and the filter cake was washed with methylene chloride (500 ml). The combined filtrate was washed in succession

[5]Literature mp 141 °C, ref. 9.

Can. J. Chem. Downloaded from www.nrcresearchpress.com by 210.87.254.42 on 09/05/12
For personal use only.

Can. J. Chem. Downloaded from www.nrcresearchpress.com by 210.87.254.42 on 09/05/12
For personal use only.

with water (300 ml), 5% hydrochloric acid (200 ml), water (300 ml), 5% sodium carbonate solution (100 ml), and again with water (2 × 100 ml). Dicyclohexyl urea was filtered off as necessary to facilitate these separations. After drying ($MgSO_4$) the solution, it was evaporated to *ca.* 300 ml in a rotary evaporator, and then diluted with ethyl acetate (250 ml) before further evaporation at atmospheric pressure to *ca.* 250 ml which yielded 17.00 g (37%) of **9**, mp 134.5–136.5 °C. A second crop of 13.90 g (30%), mp 133–135 °C, was obtained by evaporating the mother liquor to *ca.* 70 ml; ir ν_{max} 3080, 2920, 1719, 1640, 1615, 1205, 970, 934, 922, 778. The ir spectrum differed considerably from that of the low melting form in the 1000–700 cm^{-1} region.

1-(5-Benzyloxy-4H-pyran-4-on-2-yl)-2-nitroethanol ***12a***

The aldehyde **9** (13.30 g, 57.8 mmol) was suspended in nitromethane (10 ml) and triethylamine (0.3 ml) was added with stirring. The solid dissolved almost completely before product began to crystallize. The mixture was stirred at room temperature for 2 h and the solid was collected, washed with a little nitromethane, and dried at 35 °C *in vacuo*. Crude **12***a* (10.5 g, 62%), mp 161–163 °C (dec.), was obtained. The crude product was dissolved in boiling acetonitrile (80 ml) and the solution was filtered to remove any bis-compound **11**. On cooling 9.61 g (57%) of **12***a*, mp 163–164 °C (dec.), was obtained. Pure **12***a* has mp 167–168 °C (dec.); ir ν_{max} 3210 (br), 1639, 1605, 1550, 1377, 1210; nmr δ (DMSO-d_6) 8.02 (s, 1H, 6-H), 7.29 (s, 5H, aryl-H), 6.53 (d, 1H, J = 5 Hz, OH), 6.45 (s, 1H, 3-H), 4.89 (s superimposed on m, 5H, CH_2O, CH(OH) and CH_2NO_2); *m/e* 291. *Anal.* calcd. for $C_{14}H_{13}NO_6$: C 57.73, H 4.50, N 4.81; found: C 57.75, H 4.78, N 5.01.

Even slight departures from the above procedure gave rise to appreciable amounts of **11** which was the only isolated product of the procedure described below.

1,3-Bis(5-benzyloxy-4H-pyran-4-on-2-yl)-2-nitropropane-1,3-diol Monohydrate ***11***

To a stirred suspension of **9** (1.15 g, 5 mmol) in a mixture of nitromethane (305 mg, 5 mmol) and tetrahydrofuran (10 ml) was added triethylamine (505 mg, 5 mmol). A clear yellow solution soon formed and on seeding a solid crystallized, 620 mg (48%), mp 173–175 °C (dec.). The compound can be recrystallized from acetic acid and its crystallization is markedly speeded up by the addition of a little water because it crystallizes as a hydrate. Recovery is 70–75%, mp 200–201 °C (dec.); ir ν_{max} 3240 (br), 1645, 1615, 1560, 1365, 1210; nmr δ (DMSO-d_6) 8.27 and 8.18 (2s, 2 × 1H, 6-H and 6′-H), 7.40 (2s, 2 × 5H, aryl-H's), ~6.88 (br s, 2H, 2 × OH), 6.52 and 6.42 (2s, 2 × 1H, 3-H and 3′-H), 4.95 and 4.91 (2s Superimposed on m, 7H, 2 × CH_2O, 2 × CH(OH) and $CHNO_2$). The non-equivalence of the protons in the benzyloxy pyranone moieties is suggested as evidence that the compound (which is homogeneous by tlc) is a racemic compound and not one of the two possible meso-compounds. Increase of the temperature in the nmr probe does tend to make the signals of corresponding protons move towards one another, but even at 127 °C, when decomposition is beginning to take place, the signals for the 3- and 6-protons of the pyranone rings are still separated and sharp: hence restriction of rotation in the molecule is unlikely to be a cause of the non-equivalence.[6] Mass spectrum *m/e* 456 ($M^+ - (HNO_2 + H_2O)$), 365 (456 − C_7H_7). *Anal.* calcd. for $C_{27}H_{23}NO_{10}\cdot H_2O$: C 60.11, H 4.67, N 2.59; found: C 60.17, H 4.84, N 2.36.

1-(5-Benzyloxy-4H-pyran-4-on-2-yl)-2-nitropropan-1-ol ***12b***

Condensation of **9** with excess nitroethane in place of nitromethane gave 61% of crude **12***b*, mp 140–145 °C. Recrystallization of the compound twice from acetonitrile afforded **12***b* of mp 164.5–166 °C; ir ν_{max} 3260 (br), 1637, 1610, 1554, 1250, 1203; nmr δ (DMSO-d_6) 8.34 (s, 1H, 6-H), 7.54 (s, 5H, aryl-H), 6.80 (d, 1H, J = 5 Hz, OH), 6.65 (s, 1H, 3-H), 5.56 (s, 2H, CH_2O), ~5 (m, 2H, CH(OH) and $CHNO_2$), 1.46 (d, 3H, J = 6.5 Hz, CH_3). *Anal.* calcd. for $C_{15}H_{15}NO_6$: C 59.01, H 4.95, N 4.59; found: C 58.82, H 5.03, N 4.88.

The stereochemistry of the side chain in **12***b* (also **13***b* and **14***b*) was not determined.)

1-(5-Benzyloxy-4H-pyran-4-on-2-yl)-2-aminoethanol Hydrochloride ***13a***

A suspension of **12***a* (14.3 g, 49.2 mmol) and Raney nickel (*ca.* 8 g) in a mixture of ethanol (150 ml) and acetic acid (10 ml) was hydrogenated at an initial pressure of 50 psi and at room temperature. The drop in pressure (11.2 psi from 4.34 l) was almost theoretical (11.5 psi). The filtered reaction mixture was acidified with a slight excess of 5 *N* ethanolic hydrogen chloride solution and evaporated to a syrup. The latter was dissolved in hot ethanol (45 ml) and the solution on dilution with 2-propanol (45 ml) afforded a solid, 12.11 g (83%), mp 181–182 °C (dec.). Pure **13***a*, crystallized from ethanol, has mp 186–187 °C (dec.); ir ν_{max} 3500–2600 (very br), 1650, 1595, 1210, 1199; nmr δ (DMSO-d_6) 8.24 (s, 1H, 6-H), 7.39 (s, 5H, aryl-H), 6.48 (s, 1H, 3-H), 4.99 (s, 2H, CH_2O), ~4.8 (m, 1H, CH(OH)), ~3.1 (m, 2H, CH_2N) and 4 exchangeable H from 6.7–9 ppm. *Anal.* calcd. for $C_{14}H_{15}NO_4\cdot HCl$: C 56.48, H 5.42, Cl 4.70, N 11.91; found: C 56.51, H 5.00, Cl 4.61, N 11.58.

2-Amino-1-(5-benzyloxy-4H-pyran-4-on-2-yl)propanol Hydrochloride ***13b***

Similarly, reduction of **12***b* yielded **13***b* in 78% yield, mp 214–215 °C (dec.) after recrystallization from methanol–ether; ir ν_{max} 1658, 1625, 1220, 989; nmr δ (D_2O) 8.13 (s, 1H, 6-H), 7.50 (s, 5H, aryl-H), 6.77 (s, 1H, 3-H), 5.07 (s, 2H, CH_2O), ~3.6 (m, 1H, CHN), 1.31 (d, 3H, J = 6.5 Hz, CH_3). The CH(OH) signal appeared to be under that for HDO at 4.6 ppm. *Anal.* calcd. for $C_{15}H_{17}NO_4\cdot HCl$: C 57.79, H 5.82, N 4.49; found: C 57.15, H 5.75, N 4.37.

1-(5-Hydroxy-4H-pyran-4-on-2-yl)-2-aminoethanol Hydrochloride ***14a***

A suspension of **13***a* (2.98 g, 10 mmol) and 10% palladium-on-charcoal (300 mg) in methanol (30 ml) was hydrogenated at atmospheric pressure and room temperature until 256 ml of hydrogen had been absorbed. The

[6]Thanks are due to Mr. Scott Williamson for his interest in doing the temperature variation nmr studies.

Can. J. Chem. Downloaded from www.nrcresearchpress.com by 210.87.254.42 on 09/05/12
For personal use only.

reactant dissolved and some product crystallized during the course of the reaction. The solid mixture of catalyst and product was filtered, boiled with methanol (100 ml), and the catalyst then removed by filtration. Evaporation of the combined methanol solutions to *ca.* 15 ml induced crystallization of **14***a*, 1.40 g, mp 203–204 °C (dec.) and a further 350 mg of product, mp ~195–197 °C (dec.), was obtained by further evaporation and dilution with 2-propanol. Crude yield 84%. The salt can be recrystallized from methanol–ether, mp 203–204 °C; ir ν_{max} 3240–2980 (br bands), 1638, 1605, 1590, 1572, 1208; nmr δ (DMSO-d_6) ~8.3 (br s, ~5H, exchangeable H), 8.24 (s, 1H, 6-H), 6.59 (s, 1H, 3-H), 4.87 (d of d, 1H, J_{AB} = 3 Hz, J_{AC} = 8 Hz, CH(OH)), 3.2 (m, 3H, CH_2NCH), 1.18 (d, 6H, J = 6.5 Hz, 2 × CH_3). *Anal.* calcd. for $C_7H_9NO_4 \cdot HCl$: C 40.50, H 4.86, Cl 17.08, N 6.75; found: C 40.21, H 4.93, Cl 17.09, N 7.04.

2-Amino-1-(5-hydroxy-4H-pyran-4-on-2-yl)propanol Hydrochloride ***14b***

Hydrogenolysis of **13***b* gave **14***b* in 62% yield, mp 226–227 °C (dec.) after recrystallization from 95% alcohol–ether; ir ν_{max} 3320, 1657, 1622, 1261, 1212; nmr (D_2O) 8.20 (s, 1H, 6-H), 6.75 (s, 1H, 3-H), 3.77 (m, 1H, CHN), 1.32 (d, 3H, J = 6.5 Hz, CH_3). The signal for CH(OH) was obscured by that for HDO at *ca.* 4.65 ppm. *Anal.* calcd. for $C_8H_{11}NO_4 \cdot HCl$: C 43.35, H 5.46, N 6.32; found: C 43.20, H 5.26, N 6.26.

1-(5-Benzyloxy-4H-pyran-4-on-2-yl)-2-isopropylamino-ethanol Hydrochloride ***15***

A suspension of **13***a* (2.98 g, 10 mmol) and anhydrous sodium carbonate (1.06 g, 10 mmol) in 2-propanol (60 ml) was stirred at room temperature for 30 min. Acetone (638 mg, 11 mmol) was added and stirring was continued for 1 h. Then sodium borohydride (760 mg, 20 mmol) was added portionwise during 15 min and the reaction mixture was stirred for 45 min. Reaction was found by tlc (silica gel with 1:50 ammonium hydroxide – 2-propanol) to be incomplete.[7] More acetone (464 mg, 8 mmol) was added and after 30 min, sodium borohydride (380 mg, 10 mmol) was added in one portion. After stirring the mixture for 1 h no starting material was detected. The suspension was acidified carefully with ~5 *N* ethanolic hydrogen chloride, and the mixture was evaporated to dryness under vacuum. Extraction of the solid residue with boiling ethanol (3 × 30 ml) acidified with a little ethanolic hydrogen chloride (~1 ml in total) gave crude **15**, 1.632 g (48%), mp 199–202 °C (dec.). An analytical specimen of **15** crystallized from ethanol in colourless plates, mp 204.5–205 °C (dec.), ir ν_{max} 1638, 1612, 1591, 1585, 1230, 1220; nmr δ (DMSO-d_6) 8.37 (s, 1H, 6-H), 7.56 (s, 5H, aryl-H), 6.61 (s, 1H, 3-H), 5.08 (s on m, 3H, CH_2O and CH(OH)), 3.28 (m, 2H, CH_2N). *Anal.* calcd. for $C_{17}H_{21}NO_4 \cdot HCl$: C 60.09, H 6.53, Cl 10.43, N 4.12; found: C 60.27, H 6.56, Cl 10.70, N 4.08.

1-(5-Hydroxy-4H-pyran-4-on-2-yl)-2-isopropylamino-ethanol Hydrochloride ***5***

A solution of **15** (1.50 g, 4.42 mmol) in methanol (30 ml) was hydrogenated at room temperature and pressure in the presence of 10% palladium-on-charcoal (50 mg) until 115 ml of hydrogen had been absorbed. (Theoretical absorption was 108 ml at 25 °C.) The filtered solution was evaporated to a syrup, and a 1:1 mixture of ethanol and 2-propanol (10 ml) was added. The mixture was evaporated again and the residue triturated with 2-propanol (10 ml) until solid. This crude product is apparently solvated, 1.13 g, mp 93–95 °C, with gas evolution. It was dissolved in boiling ethanol (20 ml) and the filtered solution was evaporated to ~5 ml, then diluted with 2-propanol (2 ml), and chilled at ~5 °C overnight. The yield of **5** was 764 mg (69%), mp 175–177 °C (dec.); ir ν_{max} 3445, 1615, 1593, 1577, 1560, 1210; nmr δ (DMSO-d_6/D_2O) 8.14 (s, 1H, 6-H), 6.57 (s, 1H, 3-H), 4.83 (d of d, 1H, J_{AB} = 3 Hz, J_{AC} = 8 Hz, CH(OH)), 3.5–3.0 (m, 3H, CH_2NCH), 1.18 (d, 6H, J = 6.5 Hz, 2 × CH_3). *Anal.* calcd. for $C_{10}H_{15}NO_4 \cdot HCl$: C 48.10, H 6.46, Cl 14.20, N 5.61; found: C 47.82, H 6.49, Cl 14.59, N 5.82.

1-(5-Benzyloxy-1H-pyrid-4-on-2-yl)-2-isopropylamino-ethanol Hydrochloride ***16a***

A mixture of **15** (1.03 g, 3.03 mmol), concentrated ammonium hydroxide (15 ml), and tetrahydrofuran (15 ml) was heated in a steel bomb at 100 °C for 3½ h. The solution was evaporated to dryness in a rotary evaporator and the residue was treated with three portions of 2-propanol (25 ml plus 2 × 15 ml) and evaporated to dryness. The solid was collected with the aid of 1:1 methanol – 2-propanol (10 ml) giving 958 mg (93%) of crude **16***a*, mp 227–229 °C (dec.). The greyish-tan solid was dissolved in hot methanol (22 ml) and the solution was treated with charcoal and filtered. Dilution of the filtrate with 2-propanol (22 ml) induced the crystallization of rosettes of needles, 771 mg (75%), mp 233–234 °C (dec.); ir ν_{max} 1617, 1585, 1490, 1240; nmr δ (DMSO-d_6) 7.95 (s, 1H, 6-H), 7.57 (s, 5H, aryl-H), 6.92 (s, 1H, 3-H), 5.2 (s, 2H, CH_2O), ~5.0 (m, 1H, CH(OH)), ~3.22 (m, 3H, CH_2NCH), 1.32 (d, 6H, J = 6.5 Hz, 2 × CH_3). Two exchangeable H were located in the region 6.5–8.3, one near 5.1 and one near 3.2 ppm. *Anal.* calcd. for $C_{17}H_{22}N_2O_3 \cdot HCl$: C 60.27, H 6.84, Cl 10.46, N 8.27; found: C 60.12, H 6.93, Cl 10.30, N 8.16.

1-(5-Hydroxy-1H-pyrid-4-on-2-yl)-2-isopropylamino-ethanol Hydrochloride ***6a***

A mixture of **16***a* (442 mg, 1.3 mmol), 10% palladium-on-charcoal (50 mg), and methanol (10 ml) was stirred with hydrogen at room temperature and pressure. Hydrogen uptake was 31 ml; theoretical 33.4 ml at 27 °C. The filtered solution was evaporated to a gum which was triturated with acetone (10 ml) containing water (0.05 ml).[8] The gum became semisolid during this treatment, and became completely solid on further trituration with 1:1 acetone–tetrahydrofuran (10 ml). The yield of **6***a* was 217 mg (63%), mp 108–111 °C; ir ν_{max} 1645, 1630, 1612(m), 1597, 1495, 1247; nmr δ (DMSO-d_6/D_2O) 7.72 (s, 1H, 6-H), 6.70 (s, 1H, 3-H), 4.97 (m, 1H, CH(OH)), ~3.2 (m, 3H, CH_2NCH), 1.30 (d, 6H, J = 6 Hz, 2 × CH_3). *Anal.* calcd. for $C_{10}H_{16}N_2O_3 \cdot$

[7]On one occasion the reaction did not start until some methanol was added to the mixture: it then proceeded as described here.

[8]Solid isolated by anhydrous work-up deliquesces in air and later resolidifies.

$HCl \cdot H_2O$: C 45.03, H 7.18, Cl 13.29, N 10.50; found: C 45.16, H 7.01, Cl 13.11, N 10.37.

1-(5-Benzyloxy-1-methyl-1H-pyrid-4-on-2-yl)-2-isopropylaminoethanol Hydrochloride ***16b***

A mixture of **15** (2.04 g, 6.02 mmol), methylamine (4.1 g), and *tert*-butanol (17.5 ml) was heated in a Carius tube at 100 °C for 4 h. The solution was evaporated to dryness and the residue was treated with two portions of ethanol (2 × 25 ml) and evaporated to dryness after each. The solid was dissolved in hot ethanol (25 ml) and the solution was treated with charcoal and filtered. Dilution of the filtrate with acetone (50 ml), and seeding, brought about the crystallization of **16***b*, 1.08 g (51%), mp 220–221 °C (dec.). An analytical sample of **16***b* crystallized from ethanol–ether had the same melting point; ir ν_{max} 1619, 1560, 1292, 1237; nmr δ (CD_3OD) 7.85 (s, 1H, 6-H), 7.61 (m, 5H, aryl-H), 6.93 (s, 1H, 3-H), 5.26 (s on m, 3H, CH_2O and CH(OH)), 4.91 (s, 3H, HOD), 3.97 (s, 3H, 1-CH_3), ~3.2–3.7 (m, 3H, CH_2NCH), 1.46 (d, 6H, J = 6.5 Hz, 2 × CH_3). *Anal.* calcd. for $C_{18}H_{24}N_2O_3 \cdot HCl$: C 61.27, H 7.14, Cl 10.05, N 7.94; found: C 61.14, H 7.06, Cl 10.39, N 7.87.

1-(5-Hydroxy-1-methyl-1H-pyrid-4-on-2-yl)-2-isopropylaminoethanol Hydrochloride Monomethanolate ***6b***

A mixture of **15***b* (1.089 g, 3.09 mmol), methanol (25 ml), and 10% palladium-on-charcoal (50 mg) was stirred with hydrogen at room temperature and pressure. Hydrogen uptake was 71 ml: theoretical 74.4 ml at 21 °C. The catalyst was filtered off and the solution was evaporated to dryness yielding a solid which was collected with the aid of 2-propanol (3 ml); 816 mg, mp 224–226 °C (dec.). Recrystallization of the crude product from solution in boiling methanol (21 ml) by dilution with acetone (30 ml) afforded **6***b*, 683 mg (75%), mp 231–232 °C; ir ν_{max} 3300, 1632, 1565, 1527, 1495, 1265; nmr δ (D_2O) 7.84 (s, 1H, 6-H), 6.97 (s, 1H, 3-H), 5.35 (d of d, 1H, J_{AB} = 4 Hz, J_{AC} = 8.5 Hz, CH(OH)), 3.93 (s, 3H, 1-CH_3), 3.41 (s superimposed on m, 6H, CH_3O, CH_2-NCH), 1.42 (d, 6H, J = 6.5 Hz, 2 × CH_3). *Anal.* calcd. for $C_{11}H_{18}N_2O_3 \cdot HCl \cdot CH_3OH$: C 48.90, H 7.86, Cl 12.02, N 9.50; found: C 48.70, H 7.88, Cl 11.82, N 9.36.

Acknowledgments

The author would like to express thanks to Dr. J. G. Atkinson for discussions and to Dr. C. S. Rooney for his advice and encouragement. Mr. S. C. Ho and his colleagues provided the nmr spectra.

1. B. Belleau and J. Burba. Biochim. Biophys. Acta, **54**, 195 (1961).
2. H. W. R. Williams. Brit. Patent No. 980 417; Chem. Abstr. **62**, 7864d (1965).
3. S. J. Norton and E. Sanders. J. Med. Chem. **10**, 961 (1967).
4. W. J. Hartman, R. I. Akawie, and W. G. Clark. J. Biol. Chem. **216**, 507 (1955).
5. R. T. Borchardt. J. Med. Chem. **16**, 581 (1973).
6. E. Galantay, C. Hoffman, and N. Paolella. J. Org. Chem. **35**, 4277 (1970).
7. R. T. Brittain, D. Jack, and A. C. Ritchie. Adv. Drug. Res. **5**, 243 (1970).
8. W. E. Barth. Ger. Patent No. 2 204 195; Chem. Abstr. **77**, 151 968n (1972).
9. A. F. Thomas. J. Chem. Soc. 439 (1962).
10. K. E. Pfitzner and J. G. Moffatt. J. Am. Chem. Soc. **87**, 5661 (1965); **87**, 5670 (1965).
11. C. S. Rooney, R. S. Stuart, B. K. Wasson, and H. W. R. Williams. Can. J. Chem. **53**, 2279 (1975).
12. A. F. Thomas and A. Marxer. Helv. Chim. Acta, **43**, 469 (1960).

Can. J. Chem. Downloaded from www.nrcresearchpress.com by 210.87.254.42 on 09/05/12
For personal use only.

Chromyl chloride oxidations. IV. The oxidations of cyclohexene and 1-methylcyclohexene[1,2]

FRANK WILLIAM BACHELOR AND UKKEN OUSEPH CHERIYAN
Department of Chemistry, The University of Calgary, Calgary, Alta., Canada T2N 1N4

Received February 5, 1976

FRANK WILLIAM BACHELOR and UKKEN OUSEPH CHERIYAN. Can. J. Chem. **54**, 3383 (1976).

The chromyl chloride oxidations of cyclohexene and 1-methylcyclohexene have been reexamined. The products from cyclohexene were found to be cyclohexanone, *cis*- and *trans*-2-chlorocyclohexanols, 2-chlorocyclohexanone, cyclohex-2-enol, cyclohex-2-enone, and cyclohexene oxide. Treatment of cyclohexene oxide with chromyl chloride produced only *trans*-2-chlorocyclohexanol and 2-chlorocyclohexanone. The products from 1-methylcyclohexene were 2-methylcyclohexanone, 1-methylcyclopentyladehyde, *cis*- and *trans*-2-methyl-2-chlorocyclohexanol, 2-methyl-2-chlorocyclohexanone, 2-methylcyclohex-2-enone, and 4-methylcyclohex-2-enone. Treatment of 2-methylcyclohexene oxide with chromyl chloride yielded only 2-methylcyclohexanone and 1-methylcyclopentylaldehyde. The origin of the various products and possible mechanisms for their formation is discussed. A 1,3-cyclic addition reaction is proposed for the formation of the *cis*-chlorohydrins.

FRANK WILLIAM BACHELOR et UKKEN OUSEPH CHERIYAN. Can. J. Chem. **54**, 3383 (1976).

On a étudié les réactions d'oxydation, par le chlorure de chromyle, du cyclohexène et du méthyl-1 cyclohexène. On a trouvé que les produits formés à partir du cyclohexène sont la cyclohexanone, les chloro-2 cyclohexanols-*cis* et -*trans*, la chloro-2 cyclohexanone le cyclohexène-2 ol, la cyclohexène-2 one et l'oxyde de cyclohexène. La réaction entre l'oxyde de cyclohexène et le chlorure de chromyle ne conduit qu'au chloro-2 cyclohexanol-*trans* et à la chloro-2 cyclohexanone. Les produits obtenus à partir du méthyl-1 cyclohexène sont la méthyl-2 cyclohexanone, le méthyl-1 cyclopentanecarboxaldéhyde, les méthyl-2 chloro-2 cyclohexanols-*cis* et -*trans*, la méthyl-2 chloro-2 cyclohexanone, la méthyl-2 cyclohexène-2 one et la méthyl-4 cyclohexène-2 one. La réaction de l'oxyde du méthyl-2 cyclohexène avec le chlorure de chromyle conduit uniquement à la méthyl-2 cyclohexanone et au méthyl-2 cyclopentanecarboxaldéhyde. On discute de l'origine des divers produits et des divers mécanismes pouvant expliquer leur formation. On propose une réaction de cycloaddition-1,3 pour expliquer la formation des chlorohydrines *cis*.

[Traduit par le journal]

The results of our recent work (1) on the oxidation of α-pinene with chromyl chloride have encouraged us to examine the scope and mechanism of this reaction further. The oxidation of α-pinene with chromyl chloride demonstrated that at least three different types of reactions are occurring: acid-catalyzed rearrangements, direct oxidation, and allylic oxidation. Further examination of this reaction suggests that a simpler system less prone to rearrangement be selected. For this purpose we have selected cyclohexene and 1-methylcyclohexene as the olefins. Both of these cycloalkenes have been examined before (2–4) in this reaction, but we have isolated several new products from each oxidation, some of which are quite important in any attempt to interpret the mechanistic implications.

[1]Taken in part from the thesis of U.O.C. for the Ph.D. degree, December 1973.

[2]For part III, see ref. 12.

Table 1 lists the products found when cyclohexene was oxidized with chromyl chloride in methylene chloride. This oxidation was carried out both at -5 and -80 °C. The results are significantly different in yields of the various products. Two changes in particular stand out. First, there is essentially no polymeric material produced in the low temperature oxidation, whereas at -5 °C approximately 20% of the material remains as high boiling pot residue. This difference at low temperature is made up by increases in the chlorohydrin yields, particularly of *trans*-2-chlorocyclohexanol, and a small increase in the amount of cyclohexene oxide to a total of about 2%.

We have isolated three products which were not previously reported by Stairs *et al.* (3) in this oxidation: 2-chlorocyclohexanone **8**, 2-cyclohexenol **7**, and the elusive cyclohexene oxide **2** (5). Although Stairs *et al.* (3) had isolated 2-chlorocyclopentanone from the oxidation of

Can. J. Chem. Downloaded from www.nrcresearchpress.com by 210.87.254.105 on 09/05/12
For personal use only.

Can. J. Chem. Downloaded from www.nrcresearchpress.com by 210.87.254.105 on 09/05/12
For personal use only.

TABLE 1. Oxidation products and yields from cyclohexene and chromyl chloride

Product	Yield (%)		
	−5 °C	−80 °C	Ref. 3
Cyclohexene oxide (**2**)	<1	2	—
trans-2-Chlorocyclohexanol (**3**)	24	42	21
cis-2-Chlorocyclohexanol (**4**)	16	21	14
Cyclohexanone (**5**)	4	3	5.5
Cyclohex-2-enone (**6**)	8	8	17
Cyclohex-2-enol (**7**)	4	4	—
2-Chlorocyclohexanone (**8**)	6	6	—
Polymeric material	20	—	21.5
Cyclohexene (recovered)	18	14	21

cyclopentene with chromyl chloride, they failed to find the corresponding product in the cyclohexene series. We found that the mixture of chlorohydrins obtained by fractional distillation contained a carbonyl component.[3]

We suspected that the carbonyl compound might be the α-chloro ketone and an authentic specimen was prepared. The relative retention time of the chloro ketone coincided with that of the *cis*-chlorohydrin, but we subsequently found that they could be effectively separated on a Poropak P-S column. The appearance of the unsaturated alcohol **7** is no surprise considering that we had found two examples of unsaturated alcohols in the oxidation of α-pinene (1).

It was particularly gratifying to find cyclohexene oxide, **2**, as one of the products of this reaction. Epoxides have long been suspected of being intermediates in the chromyl chloride oxidation of olefins (6, 7) and with the exception of a personal communication reference in a review article by Freeman (8) this appears to be the only report of the isolation of an epoxide in this reaction. Epoxides have been found in oxidations by chromic anhydride (9) and chromyl acetate (2, 10).

Many of the products from chromyl chloride oxidations can be rationalized by postulating an epoxide intermediate. In order to examine further the role of the epoxide as an intermediate we first wished to prove that the epoxide is not an artifact. The presence of the *trans*-chlorohydrin and the basic work-up procedure might lead one to suspect that perhaps some epoxide might be formed during the isolation of the products, but treatment of *trans*-2-chlorocyclohexanol with 5% aqueous sodium bicarbonate failed to produce any detectable amount of epoxide. Therefore the cyclohexene oxide is a direct oxidation product from cyclohexene.

The secondary products from cyclohexene oxide were examined by oxidizing a 10:1 mixture of 1-pentene and cyclohexene oxide with chromyl chloride. 1-Pentene was chosen as none of the products of its oxidation coincided with any of the products from cyclohexene on gas chromatographic analysis. The only products detected which originated from cyclohexene oxide were α-chlorocyclohexanone, *trans*-2-chlorocyclohexanol, and a higher boiling polymeric residue. Oxidation of cyclohexene oxide with chromyl chloride and no added olefin led to exactly the same products. No cyclohexene oxide was recovered in either of the oxidations. One would have anticipated the formation of cyclohexanone in these reactions as the Lewis acid catalyzed rearrangements of epoxides to ketones is a well-known transformation (11). However, none was found. This strongly suggests that ketone formation proceeds through some other intermediate. Since no unsaturated alcohols or ketones were found in the epoxide rearrangements these also must proceed via another intermediate and are undoubtedly allylic oxidations on the olefin.

The sources of the oxygen atom and the halogen in the chlorohydrins were examined independently. A chromyl chloride oxidation of cyclohexene was decomposed with anhydrous sodium carbonate dissolved in ^{18}O enriched H_2O. The mixture of chlorohydrins was isolated and examined by mass spectrometry. No enrichment of ^{18}O was found in the chlorohydrin. Therefore the oxygen atom in the chlorohydrins must come from the chromyl chloride.

In a second reaction, the oxidation mixture was decomposed by adding it to an ice cold saturated aqueous sodium bromide solution. No products containing bromine were found. Therefore the formation of the *cis*-chlorohydrin and

[3]In analyzing the chlorohydrins we found that although both pure isomers were stable on our analytical instrument (a Hewlett Packard model 402 biomedical gas chromatograph all glass system), isomerization of the *cis*-2-chlorocyclohexanol occurred readily on our preparative instrument (a Varian Autoprep model 705, metal injection port). This isomerization occurred on both Carbowax and SE-30 columns. Pure *trans*-2-chlorocyclohexanol was recovered unisomerized from the same system. We believe that this isomerization occurs at the injection port and not on the column.

Can. J. Chem. Downloaded from www.nrcresearchpress.com by 210.87.254.105 on 09/05/12
For personal use only.

TABLE 2. Oxidation products and yields from 1-methylcyclohexene and chromyl chloride

Product	Yield (%)	
	−5 °C	Ref. 4
2-Methylcyclohexanone (**10**)	26	52.5
1-Methylcyclopentancarbaldehyde (**11**)	22	38.5
2-Chloro-2-methylcyclohexanone (**12**)	4	9.3
cis-2-Chloro-2-methylcyclohexanol (**13**)	12	—
2-Methyl-2-cyclohexenone (**14**)	3	—
3-Methyl-2-cyclohexenone (**15**)	3	—
trans-2-Chloro-2-methylcyclohexanol (**16**)	<1	—
Polymeric material	18	?
1-Methylcyclohexene (recovered)	10	?

the opening of the epoxide must occur by direct attack of chromyl chloride or one of its reduction products prior to the addition of water. Since a considerable amount of hydrogen chloride must be generated in this reaction this could easily explain the epoxide opening to the *trans*-chlorohydrin. We will say more about the formation of the *cis* isomer later in this paper.

The oxidation products of 1-methylcyclohexene are listed in Table 2. Although Nenitzescu and co-workers (4) reported only three oxidation products from this reaction we have identified seven. There is also a considerable amount of high boiling residue (approximately 18%) generated in this reaction at −5 °C. Again, three types of products are recognizable; products of direct oxidation (**12**, **13**), products of oxidative rearrangement (**10**, **11**, **16**), and products of allylic oxidation (**14**, **15**). No epoxide could be detected in this oxidation.

The fate of a possible epoxide intermediate from 2-methylcyclohexene in this reaction was examined by an experiment similar to the cyclohexene case. 1-Methylcyclohexene oxide was oxidized with 1 equiv. of chromyl chloride in the presence of a 10-fold excess of 1-pentene. Two products derived from the epoxide were found. These were 2-methylcyclohexanone, **10**, and 1-methylcyclopentylaldehyde, **11**. A non-distillable residue accounted for approximately 35% of the epoxide. No epoxide remained and no chlorinated products were formed.

Very little *trans*-chlorohydrin is formed in the oxidation of 1-methylcyclohexene (<1%) whereas the amount of *cis*-chlorohydrin is roughly the same as that produced in the oxidation of cyclohexene. This again implies that the two chlorohydrins are formed by decidedly different mechanisms, provided that one of the chlorohydrins is not selectively removed during the course of the reaction. Both chlorohydrins were subjected to the reaction conditions in the presence of 1-pentene. Both chlorohydrins yielded about 9% of 2-methyl-2-chlorocyclohexanone, **12**, and the remainder was recovered unreacted. This means that the chlorohydrins are relatively stable compounds yielding only the products of over-oxidation, the chloro ketones. In addition, neither isomer seems to be particularly more reactive than the other in this oxidation. This suggests that the ratio of the *cis*- and *trans*-chlorohydrins found is meaningful and that very little *trans*-chlorohydrin is produced initially in the oxidation of 1-methylcyclohexene.

The pronounced difference in the products from oxidation of cyclohexene and 1-methylcyclohexene is undoubtedly due to the tertiary carbonium ion which is produced at the tertiary end of the double bond in 1-methylcyclohexene either by opening of an epoxide or by electrophilic attack of a chromium species on the double bond. This ion would tend to undergo more S_N1 type reactions, as is demonstrated by rearrangement products. In the case of cyclohexene, the carbonium ion would be secondary and the tendency here would be to resemble more S_N2 type products, as shown by the production of the *trans*-chlorohydrin.

The question of how the *cis*-chlorohydrins are formed remains to be answered. Stairs *et al.* (3) were unable to choose between three possibilities, an intermediate open carbonium ion which should lead to an equilibrium mixture of chlorohydrins, a concerted attack by chromyl chloride similar to a 1,3-dipolar addition, or a cyclic oxonium ion. The open carbonium ion can be discarded because the equilibration of the chlorohydrins seems to favor strongly the *trans* isomer. This can be seen from the thermal equilibration data from the gas chromatography results. Even if all of the α-chloroketone were derived from the *trans* isomer the ratio would still be much too high for the amount of *cis* isomer present. The formation of approximately 12% of the *cis*-chlorohydrin and very little of the *trans* isomer in the methylcyclohexene oxidation also strongly militates against a carbonium ion intermediate. Since both chlorohydrins seem to be stable to rearrangement, it is likely that the rearrangement

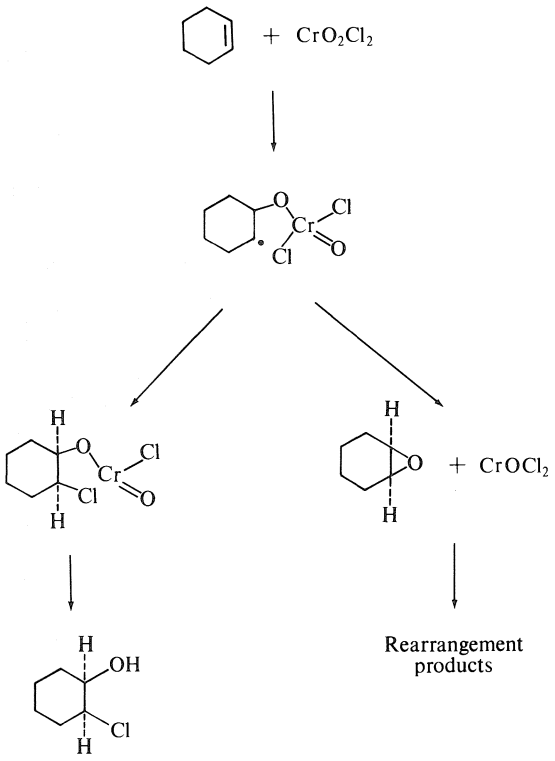

SCHEME 1

products come from a carbonium ion or carbonium ion-like intermediate and this should not favor one chlorohydrin over the other, at least not to the extent observed here. The cyclic oxonium ion would not lead to the *cis*-chlorohydrin since it should react similarly to an epoxide and would lead to *trans* products.

We therefore favor a 1,3-addition mechanism for the formation of the *cis*-chlorohydrin. Whether it be a stepwise or concerted addition we cannot say, but it would appear to involve attack of an electrophilic or radical oxygen atom of chromyl chloride, which can then cyclize either to an epoxide or to a chlorohydrin as outlined in Scheme 1. Evidence from reactions with norbornenes (12) seems to favor a radical mechanism. This will be described in detail in a subsequent paper. Many of the secondary products from this oxidation are then derived from the epoxide. However, the *cis*-chlorohydrins are stable and lead only to the overoxidation product, the α-chloro ketone.

Experimental

Methods and Measurements

Unless otherwise stated a 6 ft glass column ($\frac{1}{4}$ in. diameter) packed with 20% Carbowax 20M on Chromosorb W was used for analytical glc. Preparative glc was carried out on an 8 ft column ($\frac{3}{8}$ in. diameter) packed with 20 or 30% Carbowax 20M on Chromosorb W; carrier gas helium, flow rate 50 ml/min unless otherwise stated. A flame ionization detector was used for both applications.

Quantitative estimations are based on analytical glc data. The area enclosed by each peak was taken as a measure of the amount of the corresponding compound present, with no corrections for relative sensitivities.

Oxidation of Cyclohexene with Chromyl Chloride

(*A*) Cyclohexene (41 g, 0.5 mol) was dissolved in 700 ml of dry methylene chloride and cooled in an ice–salt bath to 0 to −5 °C. Chromyl chloride (78 g, 0.5 mol) dissolved in 250 ml of dry methylene chloride was added to this solution dropwise with stirring during a period of 2 h. The mixture was then added with stirring to 13 g of sodium bisulphite dissolved in 250 ml of water and containing 250 g of crushed ice. The mixture was then extracted with ether. The lower aqueous layer was separated, saturated with sodium chloride, and extracted exhaustively with ether. The ether extracts were combined, washed with water, and dried over anhydrous magnesium sulphate and the solvents removed by slow distillation through a 30 cm fractionating column. The crude products thus obtained weighed 42 g.

Further distillation of the crude products through the same fractionating column over a steam bath yielded 8.2 g of unreacted cyclohexene. The residue was distilled under vacuum (15 torr) through a 15 cm fractionating column and everything boiling under 100 °C was collected in a receiver cooled in a dry ice – acetone bath. This yielded 24 g of distillate (*A*) and left approximately 9 g of high boiling material in the pot. The distillate was further fractionated at reduced pressure (15 torr) and three fractions were collected: *A*-1 (2.1 g), bp 60–70 °C; *A*-2 (2.9 g), bp 70–80 °C; and *A*-3 (17.2 g), bp 80–90 °C.

Isolation of Cyclohexanone, 2-Cyclohexenol, and 2-Cyclohexenone

Analysis of fraction *A*-1 by glc showed one major peak, with relative retention time (rrt) (relative to cyclohexene) 6.5 and a minor peak containing two partially resolved components with relative retention times 16.6 and 19 (column temperature 70 °C) respectively. The major component was subsequently separated by preparative glc using a 20% Carbowax column (column temperature 140 °C) and found to be cyclohexanone (ir, nmr).

Fraction *A*-2 was found to contain mainly two compounds with relative retention times 16.6 and 19 (column temperature 70 °C) respectively. Purification by preparative glc (column, 20% Carbowax; temperature 140 °C) yielded a mixture of two compounds which had the following absorptions in the infrared spectrum (CCl_4): 3680 (sharp), 3490 (broad), 3040, and 1690 cm^{-1}. The 2,4-dinitrophenylhydrazone was prepared. Recrystallization of the solid from chloroform–methanol gave red-

Can. J. Chem. Downloaded from www.nrcresearchpress.com by 210.87.254.105 on 09/05/12
For personal use only.

Can. J. Chem. Downloaded from www.nrcresearchpress.com by 210.87.254.105 on 09/05/12
For personal use only.

orange needles; mp 166–167 °C undepressed on admixture with an authentic specimen from 2-cyclohexenone, mp 167 °C. Infrared spectra of both the solids in KBr were identical.

An α-naphthylurethane derivative was prepared from the mixture and the solid was recrystallized three times from hexane, mp 153–154 °C. The 1-naphthylurethane of 2-cyclohexenol prepared similarly melted at the same range and a mixture melting point with the former showed no depression. The infrared spectra of both compounds in KBr were superimposable. Comparison of the relative retention times of 2-cyclohexenol and 2-cyclohexenone showed that the compound with rrt 16.6 was 2-cyclohexenone and the one with rrt 19 was 2-cyclohexenol.

Identification of α-Chlorocyclohexanone and cis- and trans-2-Chlorocyclohexanols

Fraction *A*-3 on analytical glc showed one major peak containing two partially resolved components (column temperature 70 °C) with relative retention times (relative to cyclohexene) 48.2 and 52.8 respectively. This mixture was purified further by fractional distillation at 15 torr and the fractions boiling between 85–95 °C collected. The infrared spectrum (neat) of the mixture showed the following absorptions: 3450 (broad) and 1740 cm^{-1} (weak). Mass spectrum *m/e* ions at 136, 134, and 132.

An α-naphthylurethane derivative was prepared and recrystallized three times from hexane, mp 163–164 °C. The α-naphthylurethane derivative of *trans*-2-chlorocyclohexanol was similarly prepared; the pure crystalline derivative obtained melted at the same range. A mixture melting point with the former showed no depression. The infrared spectra in KBr of both the compounds were identical.

In another experiment 2 g of the mixture were shaken with 100 ml of 2% aqueous sodium hydroxide solution and the mixture was extracted exhaustively with ether. The extracts were combined, solvent removed, and the residue fractionally distilled under reduced pressure (20 torr) over a steam bath to remove the epoxide. Further distillation of the residue at 15 torr gave a fairly pure compound (bp 87–88 °C at 15 torr, rrt 48.2), whose α-naphthylurethane derivative, after two recrystallizations from hexane, melted at 93–94 °C. The 1-naphthylurethane derivative of *cis*-2-chlorocyclohexanol prepared similarly melted at the same range. A mixture melting point of the two compounds showed no depression. The infrared spectra of both the derivatives in KBr were identical.

Comparison of the rrt of *cis*-2-chlorocyclohexanol and *trans*-2-chlorocyclohexanol with the mixture *A*-3 showed that the component with rrt 48.2 was the *cis*-chlorohydrin and the one with rrt 52.8 was the *trans*-chlorohydrin.

The relative retention time of α-chlorocyclohexanone and the mixture *A*-3 was compared on the same column under identical conditions (6 ft, 20% Carbowax column; $\frac{1}{4}$ in. diameter; column temperature 70 °C). The chloro ketone and *cis*-chlorohydrin had the relative retention times 48.1 and 48.2 respectively. Therefore, the mixture was analyzed at 180 °C on a 4 ft, $\frac{1}{4}$ in. diameter, glass column packed with Poropak P-S. It showed two clearly separable peaks with relative retention times (relative to cyclohexene) 30 and 35. Under the same conditions *cis*- and *trans*-2-chlorocyclohexanols had the same relative retention time of 30 (relative to cyclohexene) and α-chlorocyclohexanone 35.

To about 500 mg of *A*-3 three drops of α-chlorocyclohexanone were added and the infrared spectrum of the liquid mixture measured. The spectrum was found to be identical to that of the original mixture (*A*-3) except that a number of absorptions, particularly that at 1740 cm^{-1}, were much stronger.

The high boiling material from the above reaction distilled between 100 and 120 °C at 0.4 torr. Analysis by glc (column temperature 150 °C) showed it contained several compounds: ir (CCl_4) 3045, 1725 (strong), 1690 (weak), and 1080 cm^{-1} (strong); mass spectrum *m/e* ions at 220, 205, 200, 198, and 178. The 200 and 198 peaks were in the ratio 1:3.

The relative amount of each constituent in the distillate *A* was estimated by analytical glc. The area enclosed by each peak was taken as being proportional to the amount of the respective compound. The yield of each component was then calculated on the basis of initial cyclohexene: unreacted cyclohexene 20%, cyclohexanone 4%, 2-cyclohexenol 4%, 2-cyclohexenone 8%, α-chlorocyclohexanone 6%, *cis*-2-chlorocyclohexanol 16.4%, *trans*-2-chlorocyclohexanol 24.8%.

Oxidation of Cyclohexene with Chromyl Chloride

(*B*) Cyclohexene (20.5 g, 0.25 mol) dissolved in 300 ml of methylene chloride was oxidized with 39 g (0.25 mol) of chromyl chloride dissolved in the same solvent at 0 to −5 °C. The reaction mixture was decomposed by adding to 300 ml of ice cold water. The reaction mixture was then worked up, and the ratio of the oxidation products determined as described above: cyclohexanone 4.2%, 2-cyclohexenol 4.1%, 2-cyclohexenone 8.1%, α-chlorocyclohexanone 6%, *cis*-2-chlorocyclohexanol 16.6%, *trans*-2-chlorocyclohexanol 24.3%, and unidentified high boiling material 21.3% (yields based on initial cyclohexene). About 20% of the cyclohexene was recovered unreacted.

Synthesis of trans-2-Chlorocyclohexanol

This compound was synthesized from cyclohexene by the method described in "Organic Synthesis" (13). Forty grams of cyclohexene yielded approximately 25 g of *trans*-chlorohydrin.

Synthesis of α-Chlorocyclohexanone and cis-2-Chlorocyclohexanol

α-Chlorocyclohexanone was prepared by the chlorination of cyclohexanone (14). Reduction of the chloro ketone with aluminum isopropoxide yielded a mixture of *cis*- and *trans*-chlorohydrins (15). From this, pure *cis*-chlorohydrin was separated by treatment with aqueous sodium hydroxide followed by fractional distillation. Twelve grams of α-chlorocyclohexanone thus gave approximately 4 g of *cis*-chlorohydrin.

Isomerization of cis-2-Chlorocyclohexanol

Pure *cis*-2-chlorocyclohexanol was injected on a 30% Carbowax preparative column (column temperature 160 °C) and the sample collected and analyzed by analytical glc. It was found to contain 23.5% *trans*-

Can. J. Chem. Downloaded from www.nrcresearchpress.com by 210.87.254.105 on 09/05/12
For personal use only.

chlorohydrin and 76.5% *cis*-chlorohydrin. When the mixture collected was injected into the preparative system again the amount of *trans*-chlorohydrin was found to increase to about 48%.

Pure *cis*-2-chlorocyclohexanol was injected on an SE-30 column (30% SE-30 on Chromosorb W, length 12 ft, diameter $\frac{3}{8}$ in., column temperature 140 °C) and the compound collected. Analysis of this compound by glc showed that it contained approximately 40% *trans*-chlorohydrin. When the latter mixture was reinjected the amount of the *trans*-chlorohydrin increased to about 60%.

Pure *trans*-2-chlorocyclohexanol was collected completely unisomerized when subjected to the same treatment.

Isolation of Cyclohexene Epoxide from the Products of Cyclohexene Oxidation

(*A*) Cyclohexene (82 g, 1 mol), dissolved in 1400 ml of methylene chloride, was cooled in an ice–salt bath to 0 to −5 °C and oxidized with 155 g (1 mol) of chromyl chloride dissolved in 500 ml of the same solvent. The reaction mixture was then added with stirring to 2 l of 5% aqueous sodium bicarbonate containing 500 g of crushed ice and the mixture worked up as described. About 80 g of crude products were collected which on analytical glc (column temperature 70 °C) showed a minor peak with rrt 3 (relative to cyclohexene) in addition to the peaks due to the compounds already identified. It was found that cyclohexene epoxide had the same rrt as the above compound. The crude product was slowly distilled through a 60 cm spinning band column. After most of the unreacted cyclohexene was removed, the temperature of the pot was raised slowly. About 1 ml of the distillate was collected before the compounds in the pot started darkening. The distillation was immediately stopped. This distillate was found to be a mixture of cyclohexene and the new compound. The latter was separated in a pure state by preparative glc using a 30% Carbowax column (column temperature 120 °C). Comparison of the infrared and nmr spectra of this compound with those of authentic cyclohexene epoxide confirmed its identity with the latter.

The residue from the above distillation was distilled at reduced pressure (15 torr) through a 15 cm fractionating column and the yield of each constituent in the combined distillates was estimated by glc: unreacted cyclohexene about 18%, cyclohexene epoxide ~0.5%, cyclohexanone 4%, 2-cyclohexenol 4%, 2-cyclohexenone 8%, α-chlorocyclohexanone 6%, *cis*-2-chlorocyclohexanol 16%, *trans*-2-chlorocyclohexanol 24%, and unidentified high boiling material 20%.

(*B*) Cyclohexene (8.2 g, 0.1 mol) dissolved in 140 ml of methylene chloride was cooled to 0 to −5 °C in an ice–salt bath and to this 3.1 g (0.02 mol) of chromyl chloride dissolved in 40 ml of methylene chloride were added with stirring all at once. The mixture was immediately added with stirring to 100 ml of 5% aqueous sodium bicarbonate containing 25 g of crushed ice. The whole operation lasted less than a minute. The crude products obtained after work-up were distilled through a 60 cm spinning band column to remove the unreacted cyclohexene. The residue amounted to approximately 1.6 g and the unreacted cyclohexene, 6.6 g. The residue was distilled in a microdistillation apparatus at 15 torr pressure and the distillate collected in a receiver cooled in liquid nitrogen. The ratio of the constituents in the distillate was estimated by glc. The yield of each constituent based on reacted cyclohexene was as follows: cyclohexene epoxide ~0.6%, cyclohexanone 4%, 2-cyclohexenol 4%, 2-cyclohexenone 7%, α-chlorocyclohexanone 5%, *cis*-2-chlorocyclohexanol 17%, *trans*-2-chlorocyclohexanol 25%, and high boiling material 20%.

Oxidation of Cyclohexene with Chromyl Chloride at Low Temperature

Cyclohexene (20.5 g, 0.25 mol) dissolved in 200 ml of methylene chloride was cooled to −80 to −85 °C in a dry ice – acetone bath. To this 39 g (0.25 mol) of chromyl chloride in 100 ml of methylene chloride were added with stirring during the course of 3 h. After the addition was complete the reaction mixture was decomposed by adding it to 300 ml of 10% aqueous sodium bicarbonate. The mixture was then extracted with ether and the solvents were removed by distillation as usual. The crude product, thus obtained, was distilled below 100 °C at 15 torr without leaving any significant amount of residue. The yield of each product was as follows: cyclohexene epoxide 2%, cyclohexene 14%, cyclohexanone 3%, 2-cyclohexen-1-ol 4%, 2-cyclohexen-1-one 8%, α-chlorocyclohexanone 6%, *cis*-2-chlorocyclohexanol 21%, and *trans*-2-chlorocyclohexanol 42%.

Action of Sodium Bicarbonate on trans-2-Chlorocyclohexanol

Pure *trans*-2-chlorocyclohexanol (500 mg) was shaken with 8 ml of 5% aqueous sodium bicarbonate containing 5 g of crushed ice for 1 h. The mixture was then exhaustively extracted with ether and the solvent removed. Analysis of the product by glc showed that the *trans*-chlorohydrin was completely unchanged.

Studies on Anion Incorporation

Cyclohexene (21 g, 0.25 mol) was oxidized with 39 g (0.25 mol) of chromyl chloride at 0 to −5 °C as already described and the complex was decomposed by adding to 300 ml of ice cold saturated aqueous sodium bromide solution with stirring. The products were worked up and fractionally distilled at reduced pressure (15 torr). Analysis of the distillate failed to show any bromohydrins. Unreacted cyclohexene 19%, cyclohexanone 4%, 2-cyclohexenol 4%, 2-cyclohexenone 9%, α-chlorocyclohexanone 6%, *cis*-2-chlorocyclohexanone 17%, *trans*-2-chlorocyclohexanol 24%, and unidentified high boiling material 21%.

Studies on ^{18}O Incorporation into the Chlorohydrins

Cyclohexene (21 g, ~0.25 mol) dissolved in 100 ml of methylene chloride was cooled to 0 to −5 °C and oxidized with 39 g (0.25 mol) of chromyl chloride dissolved in 100 ml of the same solvent. After the addition of chromyl chloride was complete the reaction mixture was added with stirring to 50 ml of 1.645% ^{18}O enriched water at ice bath temperature containing 8 g of anhydrous sodium carbonate, and the products worked up as usual. The crude product was fractionally distilled at 15 torr and the fraction boiling between 80–90 °C was collected. This was refractionated two times under reduced pressure

Can. J. Chem. Downloaded from www.nrcresearchpress.com by 210.87.254.105 on 09/05/12
For personal use only.

TABLE 3. Peak heights (mm) for normal chlorohydrin*

	137	138	138/137
1	160.5	10.0	0.0623
2	163	10.5	0.0644
3	164.5	10.0	0.0608
4	160	10.0	0.0625
			Avg. 0.0625 ± 0.002

*Calculated $(M+2)^+/(M+1)^+$ for $C_6H_{11}O^{37}Cl$ = 0.0633.

TABLE 4. Peak heights (mm) for chlorohydrin from $H_2{}^{18}O$ reaction

	137	138	138/137
1	262	16.0	0.0611
2	266	16.5	0.0620
3	268	17.0	0.0634
4	268	17.0	0.0634
			Avg. 0.0625 ± 0.001

(15 torr) to yield a mixture containing only the *cis*- and *trans*-chlorohydrins.

The heights of the 137 and 138 peaks of authentic *trans*-2-chlorocyclohexanol were measured from a mass spectrum under the following conditions for the mass spectrometer: 70 eV, ~250 μA emission, Faraday coupling, pressure ≅2 × 10^{-5} torr. Four measurements were taken. The ions at masses 137 and 138, which are the $(M+1)^+$ and $(M+2)^+$ peaks of the ^{37}Cl isotope molecular ion were chosen because it was easiest to measure these peaks without interference from other isotopes, namely the ^{37}Cl isotope.

The ratio of $(M+2)^+$ to $(M+1)^+$ (Tables 3 and 4) for the natural abundance of ^{18}O in the chlorohydrin can be calculated from the following formula (16):

$$\frac{(M+2)^+}{(M+1)^+} = \frac{\frac{1}{200}(1.1 \times N_C)^2 + (0.20 \times N_O)}{1.1 \times N_C}$$

Where N_C is the number of C atoms and N_O the number of O atoms.

Oxidation of 1-Pentene

1-Pentene (17.5 g, 0.25 mol) was dissolved in 150 ml of methylene chloride and cooled to 0 to −5 °C. To this 39 g of chromyl chloride (0.25 mol) dissolved in 100 ml of the same solvent was added drop by drop during a period of about 2 h. After the addition was complete the reaction mixture was added with stirring to 200 ml of 10% aqueous sodium bicarbonate solution. The reaction products were extracted with ether and the solvent removed by slow distillation through a 60 cm spinning band column. The crude product obtained (~12 g) distilled completely below 70 °C at 20 torr. The distillate was analyzed by glc (column temperature 70 °C) and gave peaks with the following retention times relative to cyclohexene, 1.8, 2.8, 10.5, and 11.

Rearrangement of Cyclohexene Epoxide

(*A*) 1-Pentene (175 g, 2.5 mol) and cyclohexene epoxide (24.5 g, 0.25 mol) were dissolved in 300 ml of methylene chloride and cooled to 0 to −5 °C in an ice–salt bath. To this 39 g of chromyl chloride (0.25 mol) dissolved in 100 ml of the same solvent were added with stirring drop by drop during a period of 2 h. The reaction mixture was then added to 10% aqueous sodium bicarbonate and the products extracted with ether. The solvents were removed by distillation slowly through a 60 cm spinning band column and the crude products analyzed by glc (column temperature 70 °C). In addition to the peaks due to the products of 1-pentene oxidation two peaks with relative retention times 48.1 and 52.8 were seen. The crude products were fractionally distilled at 15 torr and the fraction boiling between 80–95 °C collected (13.8 g). The distillate contained two compounds with relative retention times 48.1 and 52.8 in the ratio 1:4 which corresponded to the relative retention times of α-chlorocyclohexanone and *trans*-2-chlorocyclohexanol, respectively. An infrared spectrum (neat) of the mixture showed peaks at 3450 and 1740 cm^{-1}; mass spectrum, *m/e* ions at 136, 134, and 132. To about 1 g of the distillate six drops of α-chlorocyclohexanone were added and the infrared spectrum measured. It was identical to that of the original distillate except that a number of absorptions, particularly the one at 1740 cm^{-1}, were much stronger. The 1-naphthylurethane derivative of the alcohol in the mixture was prepared, mp 163–164 °C.

(*B*) 1-Pentene (88 g, 1.25 mol) and 12.3 g (0.125 mol) cyclohexene epoxide dissolved in 200 ml of methylene chloride were oxidized at −5 °C with 19.5 g (0.125 mol) of chromyl chloride dissolved in 50 ml of the same solvent. The reaction mixture was decomposed by adding it to 200 ml of 10% ice cold aqueous sodium bisulphite and the products isolated and analyzed as described above. These amounted to 7.6 g of α-chlorocyclohexanone and *trans*-2-chlorocyclohexanol in the ratio of 1:4; the nondistillable residue amounted to 6.1 g.

Action of Chromyl Chloride on Cyclohexene Epoxide

To cyclohexene epoxide (9.8 g, 0.1 mol) dissolved in 150 ml of methylene chloride and cooled to 0 to −5 °C was added 15.6 g of chromyl chloride (0.1 mol) in 50 ml of the same solvent during the course of 1 h. The reaction mixture was decomposed by adding to 250 ml of 10% ice cold aqueous sodium bicarbonate. The reaction products were then extracted with ether and the solvents removed by distillation through a 60 cm spinning band column. The crude mixture when analyzed by glc (column temperature 70 °C) was found to contain only two compounds with relative retention times 48.1 and 52.8. This was fractionally distilled at 15 torr. The distillate weighed 5.3 g and was found to contain α-chlorocyclohexanone and *trans*-2-chlorocyclohexanol approximately in the ratio of 1:4 by weight. The pot residue (4.6 g) had the same infrared and mass spectra as the nondistillable material obtained when the epoxide was treated with chromyl chloride in the presence of 1-pentene.

Oxidation of 1-Methylcyclohexene with Chromyl Chloride

1-Methylcyclohexene (24 g, 0.25 mol) was dissolved in 200 ml of methylene chloride and cooled to 0 to −5 °C. This was oxidized with 39 g (0.25 mol) of chromyl chloride

Can. J. Chem. Downloaded from www.nrcresearchpress.com by 210.87.254.105 on 09/05/12
For personal use only.

dissolved in 100 ml of the same solvent. The reaction mixture was then added to 300 ml of ice cold 10% aqueous sodium bicarbonate and worked up as usual. The crude product obtained weighed 22.4 g. This was fractionally distilled at atmospheric pressure to remove the unreacted alkene. Further distillation under reduced pressure (15 torr) yielded four fractions: (1) bp 40–50 °C; (2) bp 50–65 °C; (3) bp 65–75 °C; and (4) bp 75–95 °C.

When analyzed by glc, fraction 1 (column temperature 90 °C) was found to contain mainly two compounds with relative retention times 1 and 2.8. These were separated by preparative glc using a 20% Carbowax column (column temperature 140 °C). The compound with rrt 1 had the following spectral properties: infrared (liquid film) 2810, 2710, and 1740 cm^{-1} (strong); nmr (CCl_4) τ 0.62 (1H, s) and 8.88 (3H, s); mass spectrum, molecular ion at m/e 112. These data correspond to those of 1-methylcyclopentylaldehyde as previously reported (4). All relative retention times in this oxidation are related to this compound. The infrared and nmr spectra of the compound with rrt 2.8 were found to be identical to those of 2-methylcyclohexanone.

Analysis of fraction 2 showed mainly two components with relative retention times 3.8 and 4.9 in addition to two minor peaks with relative retention times 5.2 and 6. These were separated by preparative glc using a 30% Carbowax column (column temperature 160 °C). The major components collected were purified further by the same method. The infrared and nmr spectra of the compound with rrt 3.8 were found to be identical to those of authentic 2-methylcyclohex-2-enone. The other component with rrt 4.9 had the following physical properties: mass spectrum, molecular ion at m/e 110; infrared spectrum (CCl_4) 3020, 1685, and 950 cm^{-1}; nmr spectrum (CCl_4) τ 4.23 (1H, m, $J < 1$ Hz) and 8.28 (3H, m). These data fit the structure of 3-methylcyclohex-2-enone.

Fraction 3 contained one major component with rrt 6 and two minor components with relative retention times 7.2 and 8. The major component was separated by preparative glc on a 30% Carbowax column (column temperature 160 °C). The infrared and nmr spectra of this compound were found to be identical to those of 2-chloro-2-methylcyclohexanone.

Fraction 4 was refractionated at 15 torr and the distillate boiling between 80–90 °C collected. Analysis by glc showed that it contained one major component with rrt 9.7 (column temperature 90 °C) and a few minor components one of which had an rrt of 15.8. When the separation of the components was attempted by preparative glc they were found to decompose on the column. Therefore, the mixture was distilled again at reduced pressure through a fractionating column to yield a 95% pure sample which had an rrt of 9.7. The infrared and nmr spectra and rrt of this compound were found to be similar to those of authentic (*Z*)-2-chloro-2-methylcyclohexanol. The minor component that was present as the main impurity had the same rrt (15.8) as (*E*)-2-chloro-2-methylcyclohexanol.

The yield of each compound obtained in the above oxidation was found to be as follows: unreacted 1-methylcyclohexene 10%, 2-methylcyclohexanone 26%, 1-methylcyclopentylaldehyde 21%, (*Z*)-2-chloro-2-methylcyclohexanol 12%, 2-chloro-2-methylcyclohexanone 5%, 2-methylcyclohex-2-enone 3%, 3-methylcyclohex-2-enone 3%, the compound that was suspected to be (*E*)-2-chloro-2-methylcyclohexanol less than 1%, unidentified volatile material 10%, and pot residue about 10%. The yields are based on reacted 1-methylcyclohexene and were calculated from the analytical gas chromatogram of the crude product.

Synthesis of 2-Chloro-2-methylcyclohexanone and 2-Methylcyclohex-2-enone

2-Chloro-2-methylcyclohexanone and 2-methylcyclohexenone were prepared according to the method of Warnhoff and Johnson (17).

Synthesis of (Z)-2-Chloro-2-methylcyclohexanol

This was prepared by reducing 2-chloro-2-methylcyclohexanone with lithium aluminum hydride by a modification of the method of Bodot *et al.* (18). Lithium aluminum hydride (3 g) was dissolved in 150 ml of dry ether and filtered under nitrogen. The filtrate was added with stirring to 15.8 g of 2-chloro-2-methylcyclohexanone dissolved in 150 ml of dry ether and cooled in an ice bath under a dry atmosphere during the course of 1.5 h. The complex formed was decomposed with moist ether and filtered. The residue was washed with ether and the washings and filtrate combined. The ether solutions on evaporation yielded 14.6 g of crude product. This was fractionally distilled at 15 mm to yield chlorohydrin approximately 97% pure.

Synthesis of 1-Methylcyclohexene Epoxide

This compound was prepared by the oxidation of 1-methylcyclohexene with *meta*-chloroperbenzoic acid according to the method of Crandall and Lin (19). Thirty grams of olefin yielded 28 g of epoxide boiling at 132–134 °C.

Synthesis of (E)-2-Chloro-2-methylcyclohexanol

This was synthesized from 1-methylcyclohexene epoxide by treating an etherial solution of the latter with etherial HCl in the cold as reported in the literature (18). Twelve grams of epoxide yielded about 13.2 g of chlorohydrin.

Rearrangement of 1-Methylcyclohexene Epoxide

1-Pentene (70 g, 1 mol) and 11.2 g (0.1 mol) of 1-methylcyclohexene epoxide were dissolved in 200 ml of methylene chloride and cooled in an ice–salt bath to 0 to −5 °C. To this were added 16 g (0.1 mol) of chromyl chloride in 100 ml of the same solvent during the course of 2 h. The reaction mixture was then added to 200 ml of 10% ice cold aqueous sodium bicarbonate and worked up as usual. The crude product was found to contain two substances with relative retention times 1 and 2.8 (column temperature 90 °C) in addition to the products of 1-pentene oxidation. The crude mixture was fractionally distilled at 15 torr and the fraction boiling between 40–60 °C was collected in a receiver cooled in a dry ice – acetone bath. This contained all of the above two compounds with relative retention times 1 and 2.8. These were separated on a 20% Carbowax column (column temperature 140 °C). The two compounds were found to be 1-methylcyclopentylaldehyde and 2-methylcyclohexanone respectively. The amount of these substances in the distillate was estimated by glc. This was found to be about 6.7 g in the ratio 3:2 (aldehyde:ketone). The non-

distillable material accounted for approximately 35% of the epoxide.

Rearrangement of (Z)-2-Chloro-2-methylcyclohexanol

(*Z*)-2-Chloro-2-methylcyclohexanol (11.8 g, ~0.08 mol) and 1-pentene (56 g, 0.8 mol) were dissolved in methylene chloride (300 ml) and cooled to 0 to −5 °C. Chromyl chloride (13 g, ~0.08 mol) dissolved in methylene chloride (75 ml) was added to this mixture with stirring during the course of 1 h. The reaction mixture was then added to 200 ml of 20% ice cold aqueous sodium bisulphite solution and the products extracted with ether and worked up as usual. The crude product was analyzed by glc. In addition to the products of 1-pentene oxidation a minor peak with rrt 6 and a major peak with rrt 9.7 were found. The mixture was fractionally distilled at 15 torr and the fraction boiling between 65–90 °C collected. This contained all of the above two components. Further fractionation of the distillate under the same conditions yielded a fraction boiling between 72–76 °C which was purified by glc (30% Carbowax column, 160 °C) to yield pure 2-chloro-2-methylcyclohexanone. The residue in the flask was found to be (*Z*)-2-chloro-2-methylcyclohexanol. The amount of the chloro ketone and the chlorohydrin was estimated by glc. The yield of chloro ketone based on the amount of the chlorohydrin reacted was 8%. About 90% of the chlorohydrin was recovered unchanged.

Rearrangement of (E)-2-Chloro-2-methylcyclohexanol

(*E*)-2-Chloro-2-methylcyclohexanol (12 g, ~0.09 mol) and 57 g of 1-pentene (~0.8 mol) were treated in the same manner as described above with 13 g of chromyl chloride (~0.08 mol) and worked up. This yielded 9% of chloro ketone (yield based on chlorohydrin used). About 89% of the chlorohydrin was recovered unreacted.

Acknowledgments

We wish to thank the University of Calgary for support which enabled us to carry out this project. Mr. Cheriyan held a University of Calgary Dissertation Fellowship during the last year of his tenure as a graduate student.

1. F. W. Bachelor and U. O. Cheriyan. Can. J. Chem. **50**, 4022 (1972).
2. S. J. Cristol and K. R. Eilar. J. Am. Chem. Soc. **72**, 4353 (1950).
3. R. A. Stairs, D. G. M. Diaper, and A. L. Gatzke. Can. J. Chem. **41**, 1059 (1963).
4. C. N. Rentea, I. Necsoiu, M. Rentea, A. Ghenciulescu, and C. D. Nenitzescu. Tetrahedron, **22**, 3501 (1966).
5. F. W. Bachelor and U. O. Cheriyan. Chem. Commun. 195 (1973).
6. C. D. Nenitzescu. Bull. Soc. Chim. Fr. 1349 (1958).
7. R. C. Paul, P. Singh, and S. L. Chadha. Indian J. Chem. **7**, 625 (1964).
8. F. Freeman. Rev. React. Species Chem. React. **1**, 37 (1973).
9. (*a*) H. E. Stavely and G. N. Bollenback. J. Am. Chem. Soc. **65**, 1290 (1943); **65**; 1600 (1943). (*b*) J. Roček and J. C. Drozo. J. Am. Chem. Soc. **92**, 6668 (1970).
10. W. J. Hickinbottom, D. Peters, and D. G. M. Wood. J. Chem. Soc. 1360 (1955).
11. H. O. House. Modern synthetic methods. 2nd ed. W. A. Benjamin, Inc., New York. 1972. pp. 318–320.
12. F. W. Bachelor and U. O. Cheriyan. Tetrahedron Lett. No. 35, 3291 (1973).
13. G. H. Coleman and H. F. Johnstone. Organic synthesis. Coll. Vol. I. 2nd ed. John Wiley and Sons, New York. 1948. p. 158.
14. M. S. Newman, M. D. Farbman, and H. Hiper. Organic synthesis. Coll. Vol. III. 2nd ed. John Wiley and Sons, New York. 1955. p. 188.
15. H. C. Stevens and O. Crummitt. J. Am. Chem. Soc. **74**, 4876 (1952).
16. F. W. McLafferty. Interpretation of mass spectra. W. A. Benjamin, Inc., New York. 1966. Table II.
17. E. W. Warnhoff and W. S. Johnson. J. Am. Chem. Soc. **75**, 494 (1953).
18. H. Bodot, J. Julien, and M. Mousseron. Bull. Chim. Soc. 1097 (1958).
19. J. K. Crandall and Luan-Ho C. Lin. J. Org. Chem. **33**, 2375 (1968).

Can. J. Chem. Downloaded from www.nrcresearchpress.com by 210.87.254.105 on 09/05/12
For personal use only.

Nuclear magnetic resonance studies of the acid–base chemistry of amino acids and peptides. III. Determination of the microscopic and macroscopic acid dissociation constants of α,ω-diaminocarboxylic acids

THOMAS L. SAYER AND DALLAS L. RABENSTEIN

Department of Chemistry, University of Alberta, Edmonton, Alta., Canada T6G 2G2

Received May 3, 1976

THOMAS L. SAYER and DALLAS L. RABENSTEIN. Can. J. Chem. **54**, 3392 (1976).

The acid–base chemistry of 2,3-diaminopropionic acid (dap), 2,4-diaminobutyric acid (dab), ornithine (orn), and lysine (lys) has been studied by ^{13}C and proton nmr spectroscopy. Macroscopic acid dissociation constants for titration of the two ammonium groups of each molecule have been calculated from the ^{13}C chemical shift titration curves for the alkyl carbon atoms by nonlinear least squares curve fitting methods. Microscopic acid dissociation constants for the simultaneous titration of the two ammonium groups of protonated orn and lys have been obtained from their proton chemical shift titration curves and from the ^{13}C titration curves for orn and dap. The results indicate that the α-ammonium group of each of these α,ω-diaminocarboxylic acids is more acidic than its ω-ammonium group, but that the difference decreases as the number of carbons separating the ammonium groups decreases so that the acidities of the two ammonium groups of dap are almost identical. Results of pmr studies of the acid–base chemistry of glycyl-L-lysine and L-lysylglycine also are reported.

THOMAS L. SAYER et DALLAS L. RABENSTEIN. Can. J. Chem. **54**, 3392 (1976).

On a étudié, à l'aide de la spectroscopie rmn du proton et du ^{13}C, la chimie acide–base de l'acide diamino-2,3 propionique (dap), de l'acide diamino-2,4 butyrique (dab), de l'ornithine (orn) et de la lysine (lys). On a calculé les constantes macroscopiques de dissociation acide pour la titration des deux groupes ammonium de chaque molécule à partir des courbes de titration des déplacements chimiques du ^{13}C des atomes de carbone alkylés en faisant appel à des méthodes non linéaires d'ajustement des courbes par la méthode des moindres carrés. Les constantes microscopiques de dissociation acide pour la titration simultanée des deux groupes ammonium de l'ornithine et de la lysine protonées ont pu être obtenues à partir de leur courbe de titration des déplacements chimiques des protons et des courbes de titration du ^{13}C pour l'ornithine et le dap. Les résultats indiquent que le groupe ammonium α de chacun des acides α,ω-diaminocarboxyliques est plus acide que le groupe ω-ammonium; toutefois la différence diminue à mesure que le nombre d'atomes de carbone séparant les groupes ammonium diminue; ceci implique que les acidités des deux groupes ammonium du dap sont presque identiques. On rapporte aussi les résultats d'études rmp de la chimie acide–base de la glycyl-L-lysine et de la L-lysylglycine.

[Traduit par le journal]

Introduction

The acid–base chemistry of amino acids is usually characterized in terms of macroscopic acid dissociation constants obtained from p*H* titration data. If the amino acid contains two or more functional groups of comparable acidity, the p*H* ranges for titration of the two groups overlap and titration can occur by two independent pathways. In such cases, the macroscopic constants are composites of the microscopic constants which describe the acid–base chemistry at the molecular level.

Microscopic acid dissociation constants can be determined for such molecules if the extent of titration of at least one of the two acid groups can be measured as a function of p*H*. Thus, the microconstants of cysteine, tyrosine, and related molecules containing a sulfhydryl or a phenolic group have been determined by selectively monitoring the titration of the sulfhydryl or the phenolic group by uv spectroscopy (1–5). However, the microscopic acid–base chemistry of amino acids containing two acidic groups of the same type is not amenable to study by absorption spectroscopy, and thus the only microconstants which have been reported for amino acids such as lysine and glutamic acid are those which have been estimated from their potentiometrically determined macroconstants and those of related molecules (6, 7).

Can. J. Chem. Downloaded from www.nrcresearchpress.com by 210.87.254.105 on 09/05/12
For personal use only.

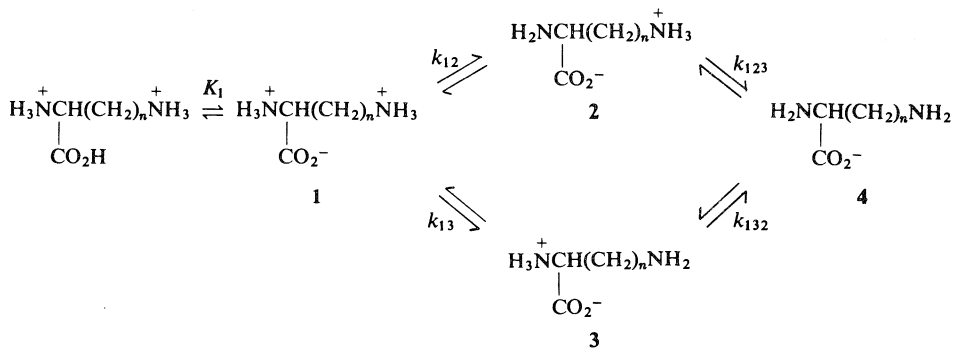

FIG. 1. Microscopic acid dissociation scheme for α,ω-diaminocarboxylic acids.

Recently, we described methods for determining microscopic acid dissociation constants by nmr (8). In this paper, we report the results of proton and ^{13}C nmr studies of the acid–base chemistry of the α,ω-diaminocarboxylic acids lysine, ornithine, 2,4-diaminobutyric acid, and 2,3-diaminopropionic acid. The results of pmr studies of the acid–base chemistry of two lysine dipeptides are also presented.

Experimental

The amino acids and peptides were commercial products and were used as received. 2,3-Diaminopropionic acid, ornithine, lysine, glycyl-L-lysine, and L-lysylglycine were obtained as their monohydrochloride salts. The 2,4-diaminobutyric acid was obtained as its dihydrochloride salt. No impurities were detectable in the nmr spectra of the amino acids and peptides. A stock solution of tetramethylammonium (TMA) nitrate was prepared by titration of a 25% aqueous solution of TMA hydroxide (Eastman Organic Chemicals) with HNO_3 to p*H* 7.

The p*H* measurements were made as described previously (8). ^1H nmr spectra were obtained on Varian A60-D or HA-100 high resolution spectrometers at 25 ± 1 °C. ^1H chemical shifts were measured relative to the central resonance of the TMA triplet, but are reported relative to the methyl proton resonance of sodium 2,2-dimethyl-2-silapentane-5-sulfonate (DSS). The central resonance of the TMA triplet is 3.175 ppm downfield from the methyl resonance of DSS. Positive chemical shifts indicate protons less shielded than the methyl protons of DSS. ^{13}C nmr spectra were obtained on a Bruker HFX-90 spectrometer operating at a frequency of 22.63 MHz and equipped with a Nicolet 1085 computer. The pulsed Fourier transform mode was used with proton decoupling. The ^{19}F resonance from C_6F_6 in a coaxial capillary was used for the lock signal. ^{13}C chemical shifts were measured relative to internal dioxane, with positive shifts corresponding to less shielding than at the carbon nuclei of dioxane. The ^{13}C nuclei of internal dioxane are 67.73 ppm less shielded than those of external TMS.

Solutions were prepared in distilled water and contained appropriate amounts of the chemical shift reference compound (0.005 *M* TMA or 0.1 *M* dioxane). Samples were prepared at closely spaced p*H* intervals within the p*H* range over which the two ammonium groups are titrated by adjusting the p*H* of appropriate solutions. The p*H* was adjusted with concentrated HNO_3 or KOH to minimize dilution. At the amino acid and peptide concentrations used, it was not practical to control the ionic strength with inert electrolyte. To minimize variations in ionic strength, samples were prepared by initially adjusting the p*H* with HNO_3 or KOH to one end of the p*H* region to be studied; samples were then taken as the p*H* was adjusted through the p*H* region of interest.

Acid dissociation constants were evaluated both as mixed activity–concentration constants (activity of hydrogen ion – concentration of acid and its conjugate base) and as concentration constants. Hydrogen ion concentrations were obtained from p*H* meter readings using activity coefficients calculated with the Davies equation (9). (The term p*H* is used in this paper to represent $-\log a_{H^+}$.) The acid dissociation constants reported in the tables are mixed constants; factors for conversion to concentration constants are given in the footnotes to the tables. The weighted nonlinear least squares curve fitting program KINET was used to evaluate the macroscopic and microscopic acid dissociation constants from the chemical shift data (10).

Results

α,ω-Diaminocarboxylic Acids

The microscopic acid–base equilibria for the two ammonium groups of a protonated α,ω-diaminocarboxylic acid are shown in Fig. 1. The equilibrium to which a given microconstant refers is indicated by its subscript; the last number in the subscript denotes the group involved in the equilibrium to which the constant refers while the preceding numbers indicate groups which deprotonated in preceding steps. The carboxyl, α-ammonium, and ω-ammonium groups are labeled 1, 2, and 3 respectively. The

Can. J. Chem. Downloaded from www.nrcresearchpress.com by 210.87.254.105 on 09/05/12
For personal use only.

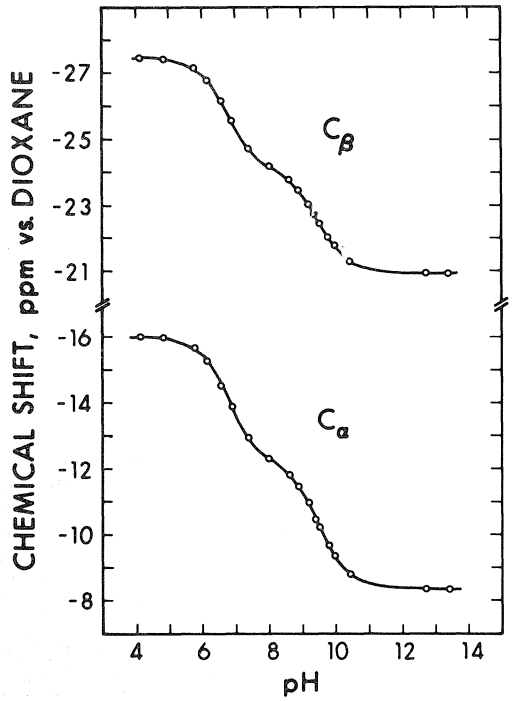

FIG. 2. pH dependence of the chemical shifts of the alkyl carbons of 2,3-diaminopropionic acid. 0.185 M solution, 25 °C.

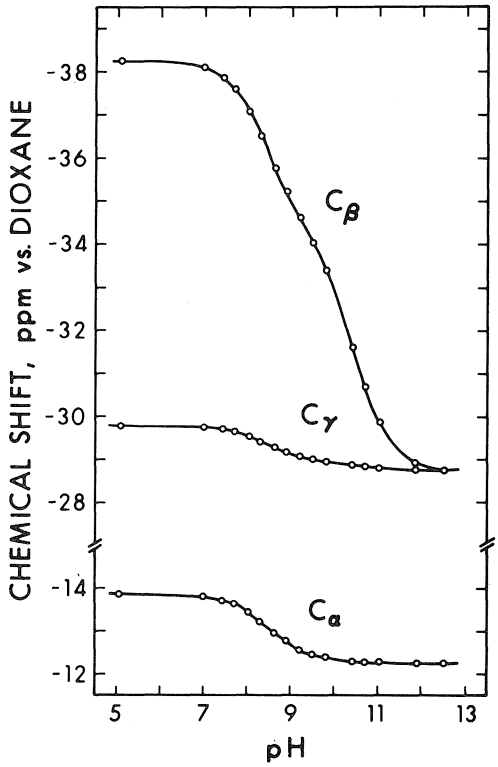

FIG. 3. pH dependence of the chemical shifts of the alkyl carbons of 2,4-diaminobutyric acid. 0.185 M solution, 25 °C.

carboxylic acid group is completely dissociated at the pH values where the ammonium groups deprotonate. Equations 1 and 2 relate the macroscopic constants to the microscopic constants.

$$[1] \qquad K_2 = k_{12} + k_{13}$$

$$[2] \qquad K_3 = \frac{k_{123}k_{132}}{k_{123} + k_{132}}$$

Titration of the two ammonium groups of 2,3-diaminopropionic acid (dap), 2,4-diaminobutyric acid (dab), ornithine (orn), and lysine (lys) was studied by ^{13}C nmr; the ^{13}C data is presented in the form of ^{13}C chemical shift titration curves in Figs. 2–5. Titration of the two ammonium groups of orn and of lys also was monitored by observing the resonance patterns for the nonlabile protons on the α-methine and ω-methylene carbon atoms. The chemical shift titration curves for the protons on the α and δ carbons of orn are presented in Fig. 6; those for the protons on the α and ϵ carbons of lys have been presented previously (8).

Macroscopic constants were estimated from each of the ^{13}C chemical shift titration curves in Figs. 2–5 by nonlinear least squares curve fitting to [3].

$$[3] \qquad \delta_{obs} = \frac{a_{H^+}{}^2\delta_{H_2A} + K_1a_{H^+}\delta_{HA} + K_1K_2\delta_A}{a_{H^+}{}^2 + K_1a_{H^+} + K_1K_2}$$

where δ_{obs} is the observed chemical shift and δ_{H_2A}, δ_{HA}, and δ_A are the chemical shifts of the particular carbon atom for the three macroscopic protonation states (8). Equation 3 is applicable to chemical shift titration curves of nuclei whose chemical shifts are affected by deprotonation of both acidic groups of a diprotic acid. ^{13}C chemical shift studies of amines, carboxylic acids, and aminocarboxylic acids indicate that the chemical shift of carbons up to five bonds removed from the amino group is dependent on the protonation state of the amino group (11). δ_{H_2A} and δ_A were obtained from the limiting shifts at the low and high pH ends of the titration

Can. J. Chem. Downloaded from www.nrcresearchpress.com by 210.87.254.105 on 09/05/12
For personal use only.

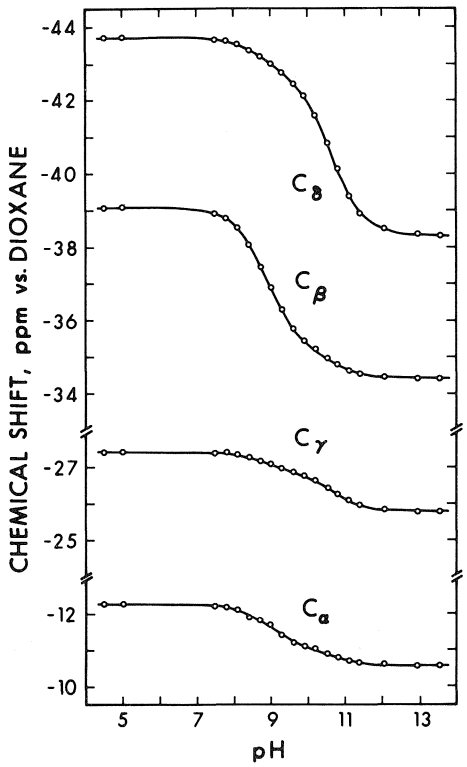

FIG. 4. pH dependence of the chemical shifts of the alkyl carbons of ornithine. 0.185 M solution, 25 °C.

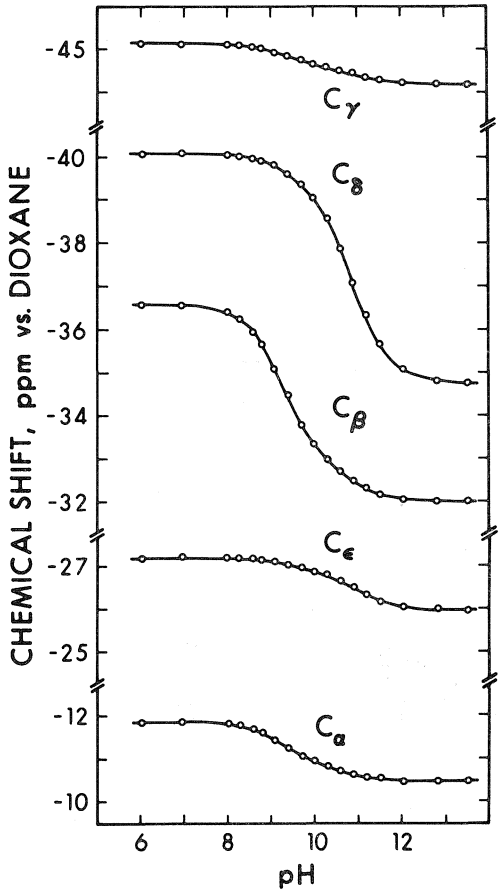

FIG. 5. pH dependence of the chemical shifts of the alkyl carbons of lysine. 0.185 M solution, 25 °C.

curves. δ_{HA} cannot be measured directly and thus was obtained simultaneously with K_1 and K_2 from the nonlinear least squares curve fitting. The results obtained from the individual titration curves are presented in Table 1. Also presented in Table 1 are the averages of the individual values for each molecule, each value weighted inversely by its standard deviation.

Microscopic constants were calculated from the ^{13}C chemical shift titration curves for dap and orn and from the pmr titration curves for orn and lys. The calculation procedure involved first calculating from the chemical shift data the fractional deprotonation of each group as a function of pH with [4] and [5]. In [4],

$$[4] \qquad f_{2,d} = \frac{\delta_{i,obs} - \delta_{i,p} - f_{3,d}\Delta_\omega}{\delta_{i,d} - \delta_{i,p} - \Delta_\omega}$$

$f_{2,d}$ and $f_{3,d}$ are the fractional deprotonations of the α- and ω-ammonium groups, $\delta_{i,obs}$ is the chemical shift observed for the ith carbon or proton at the particular pH, $\delta_{i,p}$ and $\delta_{i,d}$ are the chemical shifts of the ith carbon or proton in the fully protonated and deprotonated forms of the molecule and Δ_ω is the total change in the chemical shift of the ith carbon due to deprotonation of the ω-ammonium group. In [5] $\delta_{j,obs}$, $\delta_{j,p}$,

$$[5] \qquad f_{3,d} = \frac{\delta_{j,obs} - \delta_{j,p} - f_{2,d}\Delta_\alpha}{\delta_{j,d} - \delta_{j,p} - \Delta_\alpha}$$

and $\delta_{j,d}$ are defined as above for the jth carbon or proton and Δ_α is the total change in the chemical shift of the jth carbon or proton due to deprotonation of the α-ammonium group. $f_{2,d}$ and $f_{3,d}$ were obtained simultaneously from the chemical shift data for the ith and jth carbons or protons either by first setting Δ_ω and Δ_α to zero to obtain initial estimates of $f_{2,d}$ and $f_{3,d}$ and then iteratively refining these values or by direct calculation with equations obtained by substi-

Can. J. Chem. Downloaded from www.nrcresearchpress.com by 210.87.254.105 on 09/05/12
For personal use only.

TABLE 1. Macroscopic acid dissociation constants calculated from ^{13}C chemical shifts[a,b,c]

	2,3-Diaminopropionic acid			2,4-Diaminobutyric acid		
	pK_2	pK_3	δ_{HA}[d]	pK_2	pK_3	δ_{HA}
C_α	6.79±0.02	9.53±0.01	−12.20±0.03	[e]	[e]	
C_β	6.77±0.02	9.53±0.01	−24.07±0.02	8.40±0.02	10.42±0.01	−34.36±0.04
C_γ				8.42±0.04	10.51±0.18	−28.98±0.02
C_δ						
C_ϵ						
Average	6.78	9.53		8.41	10.42	
Literature[f]	6.77	9.53		8.24	10.35	

	Ornithine			Lysine		
	pK_2	pK_3	δ_{HA}	pK_2	pK_3	δ_{HA}
C_α	8.92±0.07	10.65±0.18	−11.09±0.07	9.26±0.05	10.79±0.15	−10.86±0.05
C_β	8.86±0.01	10.58±0.04	−35.36±0.03	9.29±0.01	10.89±0.04	−32.88±0.03
C_γ	8.74±0.07	10.65±0.01	−42.70±0.05	9.34±0.08	10.99±0.10	−44.63±0.04
C_δ	8.88±0.07	10.69±0.03	−26.86±0.03	9.41±0.07	10.91±0.01	−39.31±0.06
C_ϵ				9.50±0.20	11.03±0.06	−26.88±0.05
Average	8.86	10.65		9.31	10.91	
Literature[f]	8.83	10.68		9.21	10.81	

[a]Mixed activity–concentration constants. To convert to approximate concentration constants, subtract 0.09 from each pK.
[b]The uncertainty reported with each constant is a linear estimate of the standard deviation (10).
[c]Concentration of each amino acid: 0.185 M. μ = 0.2–0.4 M for 2,3-diaminopropionic acid, ornithine, and lysine. μ = 0.4–0.55 M for 2,4-diaminobutyric acid.
[d]ppm *vs.* internal dioxane.
[e]The standard error of the fitted constants was greater than the constants.
[f]Mixed constants calculated from the thermodynamic constants of ref. 13 for μ = 0.3 M for 2,3-diaminopropionic acid, ornithine, and lysine and μ = 0.45 M for 2,4-diaminobutyric acid. Activity coefficients calculated with the Davies equation (9).

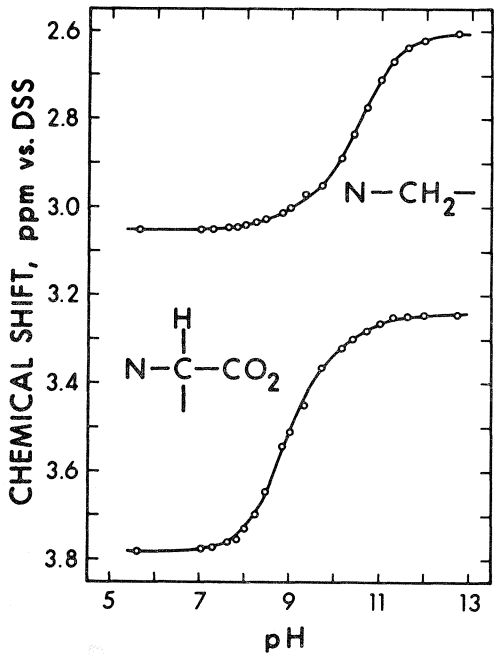

FIG. 6. pH dependence of chemical shifts of the protons on the alpha and delta carbons of ornithine in a 0.10 M solution. 25 °C.

tution of [5] into [4] and [4] into [5]. The microconstants were then determined by nonlinear least squares curve fitting the fractional deprotonation values to [6] and [7] (8). The results

$$[6] \qquad f_{2,d} = \frac{k_{12}a_{H^+} + k_{12}k_{123}}{a_{H^+}^2 + K_2a_{H^+} + K_2K_3}$$

$$[7] \qquad f_{3,d} = \frac{k_{13}a_{H^+} + k_{13}k_{132}}{a_{H^+}^2 + K_2a_{H^+} + K_2K_3}$$

obtained from the proton chemical shift titration curves for orn and lys and from the ^{13}C titration curves for dap are given in Table 2. Within the standard deviation of the estimates, the values obtained for pk_{12} and pk_{123} for orn from its ^{13}C chemical shift titration curves are identical to those given in Table 2 whereas pk_{13} and pk_{132} both differ by 0.14 of a pk unit.

In fitting the fractional deprotonation data to [6] and [7], the macroscopic constants were set equal to those obtained by combining the fractional deprotonation data to obtain the average number of acidic protons per molecule, $\bar{p}$

$$[8] \qquad \bar{p} = 2 - f_{2,d} - f_{3,d}$$

Can. J. Chem. Downloaded from www.nrcresearchpress.com by 210.87.254.105 on 09/05/12
For personal use only.

TABLE 2. Macroscopic and microscopic acid dissociation constants[a,b,c]

	Lysine[d]	Ornithine[d]	2,3-Diamino-propionic acid[d]	Glycyllysine	Lysylglycine
pK_2	9.27	8.85	6.78	8.13	7.75
pK_3	10.82	10.61	9.53	10.57	10.72
pk_{12}	9.31	8.91	7.07	8.13	7.75
pk_{13}	10.30	9.79	7.10		
pk_{123}	10.78	10.55	9.25	10.57	10.72
pk_{132}	9.79	9.68	9.21		

[a]Mixed activity–concentration constants. To convert to approximate concentration constants, subtract 0.10 from each pk or pK.
[b]The linear estimate of the standard deviation (10) of each pk or pK is ≤ 0.02.
[c]0.19 M lysine, 0.185 M 2,3-diaminopropionic acid, μ = 0.2–0.4 M; 0.10 M ornithine, 0.099 M glylys, and 0.11 M lysgly, μ = 0.1–0.2 M.
[d]For lysine, $\Delta_\alpha = \Delta_\omega$ = 0.017 ppm; for ornithine, $\Delta_\alpha = \Delta_\omega$ = 0.030 ppm; for 2,3-diaminopropionic acid, Δ_α = 5.23 ppm, Δ_β = 6.53 ppm.

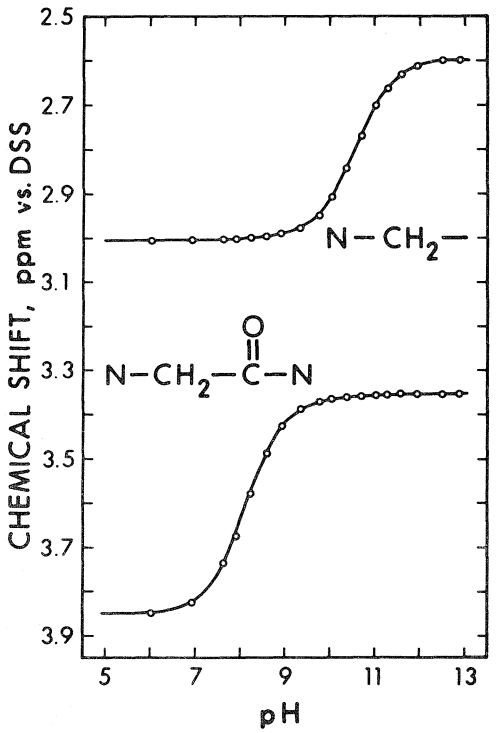

FIG. 7. pH dependence of the protons on the alpha carbon of glycine and the epsilon carbon of lysine in glycyllysine. 0.099 M, 25 °C.

and then curve fitting the $\bar{p}$ *vs.* pH data to [9] (8).

$$[9] \qquad \bar{p} = \frac{2a_{H^+}{}^2 + K_2 a_{H^+}}{a_{H^+}{}^2 + K_2 a_{H^+} + K_2 K_3}$$

The values used for Δ_α and Δ_ω in the calculation of fractional deprotonations were obtained from chemical shift data for model compounds and are given in the footnotes to Table 2.[1]

Reliable values for the microconstants could not be obtained from the ^{13}C data for lysine due to the sensitivity of pk_{13} and pk_{132} to uncertainties in Δ_α and Δ_ω. Microconstants could not be obtained from the ^{13}C data for dab because its ^{13}C data is inconsistent with model compound data.

Lysine Dipeptides

Chemical shift titration curves for the protons on the carbons bonded to the ammonium nitrogens of glycyllysine (glylys) and lysylglycine (lysgly) are shown in Figs. 7 and 8. The carboxylic acid, α-ammonium, and ϵ-ammonium groups of both dipeptides are labeled 1, 2, and 3 respectively. Due to the number of bonds separating the ammonium groups, each of the titration curves reflects almost entirely the titration of a single ammonium group. Examination of the titration curves for glylys indicates that first the glycyl ammonium group is titrated and then the ϵ-ammonium group of the lysyl residue, with very little overlap of the pH ranges over which titration occurs. Thus, titration of glylys occurs almost entirely via the monoprotonated tautomer $H_2NCH_2CONHCH(CH_2CH_2CH_2CH_2NH_3^+)CO_2^-$ and macroconstants K_2 and K_3 are essentially equal to k_{12} and k_{123}. Similarly, there is almost complete titration of the α-ammonium group of lysgly before titration of

[1]The values reported previously (8) for pk_{12} and pk_{123} for lys are identical to those given in Table 2. The values for pk_{13} and pk_{132} differ by 0.10 pk unit because Δ_α and Δ_ω had previously been assumed to be zero for lys.

Can. J. Chem. Downloaded from www.nrcresearchpress.com by 210.87.254.105 on 09/05/12
For personal use only.

Can. J. Chem. Downloaded from www.nrcresearchpress.com by 210.87.254.105 on 09/05/12
For personal use only.

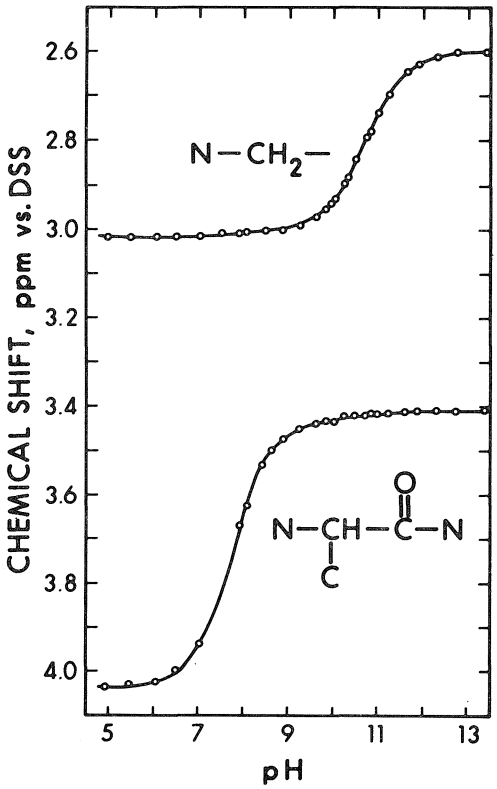

FIG. 8. pH dependence of the protons on the alpha and epsilon carbons of the lysyl residue of lysylglycine. 0.11 M, 25 °C.

the ϵ-ammonium group. The macroconstants obtained from the nmr data in Figs. 7 and 8 are reported in Table 2. These values are also given in Table 2 as the microconstants for the predominant titration pathway at the molecular level.

Discussion

α,ω-Diaminocarboxylic Acids

As noted in the introduction, the acid–base chemistry of lysine and other amino acids containing two ammonium groups has not been characterized at the molecular level. Edsall and Blanchard estimated values of 9.8 and 10.54 for pk_{132} and pk_{123} for lysine using relationships derived from the macroconstants of model compounds related to lysine (6). Lysine and *N*-methylated lysine model compounds have been studied by pmr by Bradbury and Brown (12). These authors noted a slight inflection in the lysine chemical shift titration curves which they correctly attributed to a mutual interaction of the two lysine ammonium groups. However, they chose to ignore the protonation tautomer $H_2N(CH_2)_4CH(NH_3^+)CO_2^-$ and calculated a single pK value for each of the ammonium groups from the chemical shift titration data. The pH dependence of pM_2 and pM_3 for lysine, where pM_2 and pM_3 are apparent acid dissociation constants defined as

$$pM_2 = -\log \frac{a_{H^+} f_{2,d}}{1 - f_{2,d}}$$

and

$$pM_3 = -\log \frac{a_{H^+} f_{3,d}}{1 - f_{3,d}}$$

indicate that the chemical shift titration data is more correctly analyzed in terms of the microscheme in Fig. 1. Other authors have assumed, in studies of the aqueous solution chemistry of the α,ω-diaminocarboxylic acids studied in this work, that titration of the two ammonium groups proceeds exclusively by the sequence **1** → **2** → **4** (Fig. 1) (13). The results obtained in this work clearly indicate that some deprotonation occurs via the tautomer $H_2N(CH_2)_nCH(NH_3^+)CO_2^-$, with the relative importance of this pathway increasing as n decreases.

The results in Table 2 for the α,ω-diaminocarboxylic acids indicate the ammonium groups of these molecules to be generally more acidic than those of typical alkylamines. For comparison, the pK of ethylamine is 10.81. The greater acidity of the ammonium groups of the α,ω-diaminocarboxylic acids has been attributed to the combined inductive effects of the CO_2^-, NH_3^+, and NH_2 substituents (13–15). The effects of the NH_3^+ and NH_2 substituents on the acidity of an NH_3^+ group can be predicted from the microscopic constants of symmetrical diamines, and defined according to the scheme shown below, and the pK values of monoalkylamines. For example, the difference between the pK of

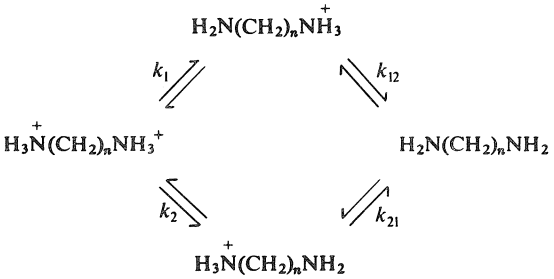

TABLE 3. Acid dissociation constants for symmetrical diamines

	Ethylenediamine	1,3-Diaminopropane	1,4-Diaminobutane	1,5-Diaminopentane
pK_1[a]	7.22	8.88	9.61	10.02
pK_2	10.03	10.64	10.82	10.96
pk_1[b]	7.52	9.18	9.91	10.32
pk_{12}	9.73	10.34	10.52	10.66
NH_3^+ substituent effect[c]	−3.29	−1.63	−0.90	−0.49
NH_2 substituent effect[d]	−1.08	−0.47	−0.29	−0.15

[a]Macroconstants from Schwarzenbach, Massen, and Ackermann (16).
[b]Calculated from macroconstants; see text.
[c]Defined as equal to $pk_1 - 10.81$ where 10.81 = pK of ethylamine.
[d]Defined as equal to $pk_{12} - 10.81$.

TABLE 4. Predicted microscopic and macroscopic constants for α,ω-diaminocarboxylic acids

	2,3-Diaminopropionic acid	2,4-Diaminobutyric acid	Ornithine	Lysine
pk_{12}	6.49	8.03	8.80	9.27
pk_{13}	6.96	8.85	9.91	10.35
pk_{123}	9.17	10.01	10.52	10.69
pk_{132}	8.70	9.19	9.41	9.61
pK_2	6.36	7.97	8.77	9.24
pK_3	9.30	10.07	10.55	10.72

ethylamine and pk_1 of $H_3\overset{+}{N}(CH_2)_nNH_3^+$ gives the increase in the acidity of an NH_3^+ group due to an NH_3^+ substituent n carbons removed, while the difference between the pK and pk_{12} gives the effect of an NH_2 group n carbons removed. The values calculated in this way for NH_2 and NH_3^+ substituent effects are listed in Table 3. The microconstants from which the substituent effects were obtained are listed in Table 3; the microconstants were calculated from the macroconstants with the relations $k_1 = K_1/2$ and $k_{12} = 2K_2$.

To the extent that the effect of substituents on the acidity of the NH_3^+ group is additive, the microconstants for the NH_3^+ groups of the α,ω-diaminocarboxylic acids can be predicted from the substituent effects in Table 3 and the pK values for the appropriate aminocarboxylic acids. For example, pk_{12} and pk_{132} of ornithine can be predicted from the pK_2 of 2-aminovaleric acid and the substituent effects in Table 3 for NH_3^+ and NH_2 substituents four carbons removed. pk_{13} and pk^{123} can be predicted in a similar way from the pK_2 of 5-aminovaleric acid. The microconstants estimated in this way for dap, dab, orn, and lys are given in Table 4.

With the exception of the values predicted for pk_{132}, the predicted microconstants for orn and lys are within 0.1 pk units of those observed. The predicted values for pk_{12} and pk_{132} for dap are significantly less than observed. These differences are probably due in part to ionic strength effects. However, the substituent effects may not be completely additive, possibly because of disubstitution at the alpha carbon; it has been observed that the chemical shift of the alpha carbon of alpha amino acids is anomalous with respect to the additivity of chemical shift substituent parameters derived from the ^{13}C chemical shifts of amines, carboxylic acids, and aminocarboxylic acids (11).

Lysine Dipeptides

The results in Table 2 indicate that conversion of the CO_2^- group of lysine to $CONHCH_2CO_2^-$ increases the acidity of the lysine α-ammonium group by 1.56 pk units. The greater acidity of the α-ammonium group of lysine as compared to monoalkylamines is due partly to the inductive effect of the CO_2^- group (14, 15). When the CO_2^- is converted to $CONHCH_2CO_2^-$, its acid strengthening effect is even greater because of the increased inductive effect of the peptide bond and a decreased electrostatic effect due to the increased separation of the alpha NH_3^+ and the CO_2^-. The acidity of the glycine ammonium group is increased by an almost identical amount by conversion of glycine to glylys (the pK_2 of

Can. J. Chem. Downloaded from www.nrcresearchpress.com by 210.87.254.105 on 09/05/12
For personal use only.

glycine is 9.70). The acidity of the ϵ-ammonium group is not significantly affected by incorporation of the alpha ammonium group or the carboxylate group of lysine into peptide bonds. If the polar side chains of lysyl residues in proteins are at the protein surface and interact with the surrounding water, it might be expected that their acidity would be similar to that of the ϵ-ammonium groups of glylys and lysgly. For comparison, Bradbury and Brown report pK values ranging from 10.1 to 10.7 for the ϵ-ammonium groups of the six lysyl residues of lysozyme (12).

Acknowledgments

This research was supported in part by the National Research Council of Canada and by the University of Alberta. Financial support to T.L.S. by a National Research Council of Canada Scholarship and by an I.W. Killam Fellowship is gratefully acknowledged.

The authors are indebted to T. Nakashima and G.Bigam for assistance in obtaining the ^{13}C nmr spectra.

1. R. E. Benesch and R. Benesch. J. Am. Chem. Soc. **77**, 5877 (1955).
2. J. T. Edsall, R. B. Martin, and B. R. Hollingworth. Proc. Natl. Acad. Sci. USA, **44**, 505 (1958).
3. E. Coates, C. G. Marsden, and B. Rigg. Trans. Faraday Soc. **65**, 3032 (1969).
4. R. B. Martin. J. Phys. Chem. **75**, 2657 (1971).
5. P. J. Niebergall, R. L. Schnaare, and E. T. Sugita. J. Pharm. Sci. **61**, 232 (1972).
6. J. T. Edsall and M. H. Blanchard. J. Am. Chem. Soc. **55**, 2337 (1933).
7. J. T. Edsall and J. Wyman. Biological chemistry. Academic Press, New York, N.Y. 1958. p. 496.
8. D. L. Rabenstein and T. L. Sayer. Anal. Chem. In Press.
9. L. Meites. Handbook of analytical chemistry. McGraw-Hill, New York, N.Y. 1963. pp. 1–8.
10. J. L. Dye and V. A. Nicely. J. Chem. Educ. **48**, 443 (1971).
11. D. L. Rabenstein and T. L. Sayer. J. Magn. Reson. In Press.
12. J. H. Bradbury and L. R. Brown. Eur. J. Biochem. **40**, 565 (1973).
13. R. W. Hay and P. J. Morris. J. Chem. Soc. Perkin Trans. II, 1021 (1972).
14. J. Clark and D. D. Perrin. Q. Rev. **18**, 295 (1964).
15. M. Charton. J. Org. Chem. **29**, 1222 (1964).
16. G. Schwarzenbach, B. Massen, and H. Ackermann. Helv. Chim. Acta, **35**, 2333 (1952).

Can. J. Chem. Downloaded from www.nrcresearchpress.com by 210.87.254.105 on 09/05/12
For personal use only.

Kinetics of oxidation of nitrite by hypochlorite ions in aqueous basic solution

J. M. CACHAZA, J. CASADO, A. CASTRO, AND M. A. LÓPEZ QUINTELA

Departamento de Química Física, Centro Coordinado del C.S.I.C., Universidad de Santiago, España

Received May 14, 1976

J. M. CACHAZA, J. CASADO, A. CASTRO, and M. A. LÓPEZ QUINTELA. Can. J. Chem. **54**, 3401 (1976).

The kinetics of oxidation of nitrite to nitrate by hypochlorite ions in aqueous basic solution ($pH \simeq 11$) have been studied using a dynamic spectrophotometric technique. The rate law is

$$-d[ClO^-]/dt = ([ClO^-][NO_2^-]/[OH^-]^2) \times (d + e[NO_2^-])$$

At 298.0 K and ionic strength 0.40 *M*, $d = (3.4 \pm 0.2) \times 10^{-8}$ mol l^{-1} s^{-1} and $e = (2.8 \pm 0.2) \times 10^{-6}$ s^{-1}. The associated activation energies are 56 ± 3 and 61 ± 3 kJ mol^{-1} respectively. A mechanism is proposed involving the reversible initial step:

$$NO_2^- + HOCl \leftrightharpoons NO_2Cl + OH^-$$

with the NO_2Cl undergoing two parallel subsequent reactions, one a unimolecular decomposition and the other an attack by NO_2^- on NO_2Cl.

J. M. CACHAZA, J. CASADO, A. CASTRO, et M. A. LÓPEZ QUINTELA. Can. J. Chem. **54**, 3401 (1976).

On a étudié la cinétique de l'oxydation des nitrites en nitrates par les ions ClO^- en solution aqueuse alcaline ($pH \simeq 11$) en utilisant une technique spectrophotométrique dynamique. L'équation de vitesse obtenue est:

$$-d[ClO^-]/dt = ([ClO^-][NO_2^-]/[OH^-]^2) \times (d + e[NO_2^-])$$

A 298.0 K et force ionique 0.40 *M*; $d = (3.4 \pm 0.2) \times 10^{-8}$ mol l^{-1} s^{-1} et $e = (2.8 \pm 0.2) \times 10^{-6}$ s^{-1}. Les énergies d'activation associées sont de 56 ± 3 et 61 ± 3 kJ mol^{-1} respectivement. On a proposé un mécanisme qui permet d'interpréter avec satisfaction l'équation de vitesse et qui implique la formation de chlorure de nitrile par l'étape réversible initiale:

$$NO_2^- + ClOH \leftrightharpoons ClNO_2 + OH^-$$

avec deux réactions subséquentes parallèles du $ClNO_2$: l'une, sa décomposition unimoléculaire et l'autre une nouvelle attaque de l'espèce NO_2^- sur le $ClNO_2$.

Introduction

The kinetic study of the reactions of nitrite ions has been of increasing interest due to their biological and chemical implications. Nitrite ions are common contaminants in natural waters, which subsequently are chlorinated for various uses. For this reason the kinetic study of reactions which take place when nitrite and hypochlorite ions exist in water is of some importance. Although a kinetic study of the reaction of chlorine with nitrite ions was done several years ago (1, 2), it was not until the study by Lister and Rosenblum (3) and, more recently, by Pendlebury and Smith (4) that it was examined systematically. The former group carried out their research in strongly basic solution in which the reaction takes place slowly, whereas the latter worked in strongly acid solution where the reaction is relatively rapid, thus requiring relaxation techniques for its study. In the work of Pendlebury and Smith, a mechanism compatible with those that can be postulated for the reactions of other halogens with nitrite ions was proposed. As will be shown in this work, a mechanism similar to that suggested by those authors satisfactorily interprets the experimental rate law in basic solution.

Experimental

A dynamic spectrophotometric technique has been employed. Absorbance was measured at 292 nm where there is a maximum in the absorption spectrum of hypochlorite ions. Although nitrate and nitrite ions absorb at the same wave length this does not introduce great difficulties because (*1*) their extinction coefficients are

Can. J. Chem. Downloaded from www.nrcresearchpress.com by 210.87.254.42 on 09/05/12
For personal use only.

Can. J. Chem. Downloaded from www.nrcresearchpress.com by 210.87.254.42 on 09/05/12
For personal use only.

lower than those of the hypochlorite ion, (*2*) in the working conditions employed the absorbance of nitrite ions may be considered either constant (high nitrite concentration) or negligible (low nitrite concentration), and (*3*) the nitrate ion concentration is always irrelevant.

All kinetic measurements were performed in triplicate with rate constants agreeing to within 7%. The ionic strength was maintained constant at 0.40 *M* by adding sodium chloride or sodium nitrate and no change in the p*H* was observed during a particular experiment. The initial p*H* was measured by preparing a mixture identical to the reaction mixture except that no nitrite was present.

Kinetic measurements were performed in 1 cm pathlength rectangular quartz cells of a Pye Unicam SP 1700 spectrophotometer with an AR 25 linear recorder and an SP 874 constant temperature cell holder.

Hypochlorite solutions were prepared by saturating a sodium hydroxide solution with gaseous chlorine, followed by standardization and dilution immediately prior to kinetic experiments. All chemicals were Merck p.a. and standard analytical procedures were used for their estimation. The known extinction coefficients (5, 6) for the various anions at 292 nm were checked on separate samples, and the following values were used in the calculations:

Ion	ϵ_{292} (M^{-1} cm^{-1})
ClO^-	360
NO_2^-	8.8
NO_3^-	6.4

All the kinetic data were analyzed by the method of least squares arranging the data in a linear form of $y = ax + b$. The least-squares analyses were performed on an IBM 1130.

Results[1]

The accepted stoichiometry for the reaction is given by the equation

$$[1] \qquad ClO^- + NO_2^- \rightarrow NO_3^- + Cl^-$$

Generally, nitrite and chloride were present in large excess over hypochlorite and the p*H* was constant in any particular experiment. Under these conditions ln *A*, where *A* is the absorbance of hypochlorite ions at time *t*, was linear with the time for at least 80% of the reaction (Fig. 1). For each experiment a pseudo first-order rate constant, k_p, was calculated from

$$[2] \qquad k_p = -\mathrm{d} \ln A/\mathrm{d}t$$

Since *A* is proportional to the concentration of hypochlorite ions, it follows that the rate law is

$$[3] \qquad -\mathrm{d}[ClO^-]/\mathrm{d}t = k_p[ClO^-]$$

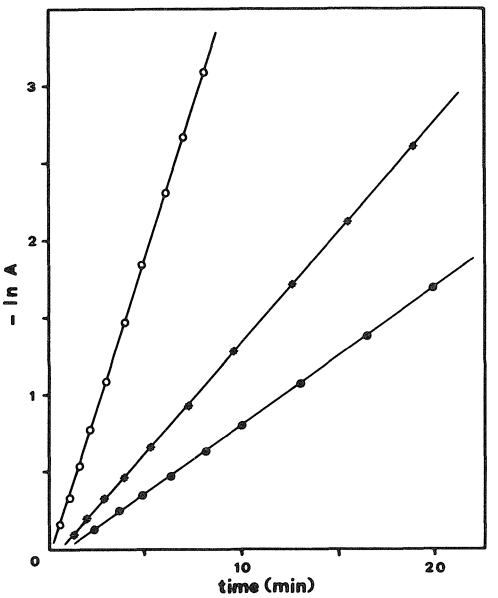

FIG. 1. Typical pseudo first-order rate plots for the oxidation of nitrites by hypochlorite ion at 298.0 K and $[NaClO]_0 = 3.0 \times 10^{-3}$ *M*: (○) [NaOH] = 3.0×10^{-3} *M*, $[NaNO_2] = 0.1400$ *M*, $\mu = 0.40$; (*) [NaOH] = 3.0×10^{-3} *M*, $[NaNO_2] = 0.0820$ *M*, $\mu = 0.18$; (●) [NaOH] = 1.8×10^{-3} *M*, $[NaNO_2] = 0.0359$ *M*, $\mu = 0.40$.

Confirmation that the reaction was genuinely first order in hypochlorite ions was obtained by finding that k_p was independent of initial hypochlorite ion concentration in the range $(8.0–31.2) \times 10^{-4}$ *M* (at constant $[NO_2^-]$, $[Cl^-]$, p*H*). At constant $[NO_2^-]$ and p*H*, k_p was (Fig. 2): (*1*) independent of chloride concentration (up to 0.3 *M*), (*2*) independent of nitrate concentration (up to 0.2 *M*), (*3*) independent of ionic strength in the range 0.15–0.40 *M*. k_p was measured when the nitrite ion concentration was varied in the range 0.0329–0.1520 *M* (at constant p*H*), and it was found (Fig. 3) that

$$[4] \qquad k_p = a[NO_2^-] + b[NO_2^-]^2$$

For the conditions shown in Fig. 3*b*, $a = (5.0 \pm 0.4) \times 10^{-3}$ l mol^{-1} s^{-1} and $b = (0.36 \pm 0.03)$ l^2 mol^{-2} s^{-1}.

At constant $[NO_2^-]$, k_p was inversely proportional to the square of the hydroxide con-

[1]Tables of data, upon which the figures are based, are available, at a nominal charge, from the Depository of Unpublished Data, CISTI, National Research Council of Canada, Ottawa, Canada K1A 0S2.

Can. J. Chem. Downloaded from www.nrcresearchpress.com by 210.87.254.42 on 09/05/12
For personal use only.

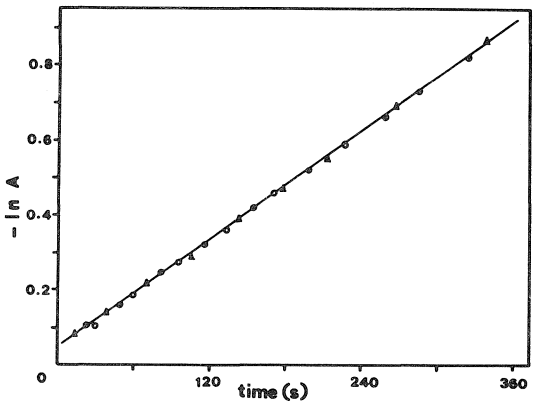

FIG. 2. Rate of oxidation of nitrites by hypochlorite ion at 298.0 K: [NaOH] = 3.0×10^{-3} *M*, [$NaNO_2$] = 0.0820 *M* and $[NaClO]_0 = 2.7 \times 10^{-3}$ *M*; (▲) [NaCl] = 2.7×10^{-3} *M*, [$NaNO_3$] = 0.3217 *M*, μ = 0.40; (○) [NaCl] = 0.3225 *M*, μ = 0.40; (●) [NaCl] = 0.1725 *M*, μ = 0.15.

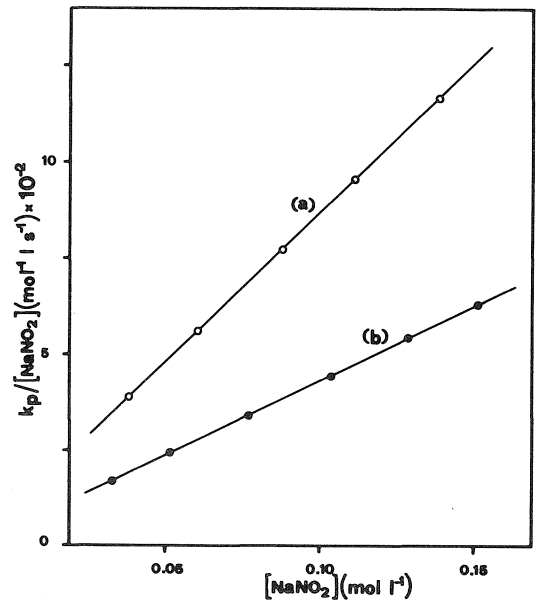

FIG. 3. Relation between the rate constant and nitrite ion concentration in the oxidation of nitrites at 298.0 K and μ = 0.40: (*a*) [NaOH] = 1.9×10^{-3} *M*; (*b*) [NaOH] = 2.7×10^{-3} *M*.

centration when the p*H* was varied from 10.93 up to 11.56 (Fig. 4):

$$[5] \qquad k_p = c/[OH^-]^2$$

For these conditions $c = (1.7 \pm 0.1) \times 10^{-8}$ mol^2 l^{-2} s^{-1}.

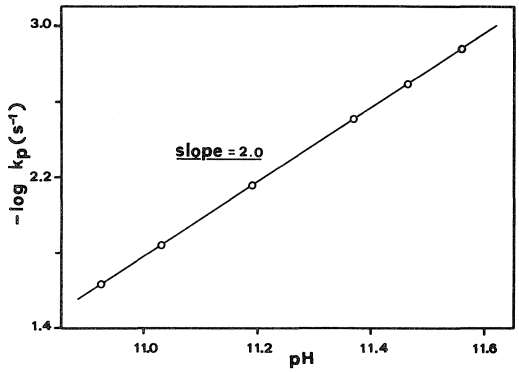

FIG. 4. Effect of p*H* on the rate of oxidation of nitrites at 298.0 K, [$NaNO_2$] = 0.0715 *M*, μ = 0.40.

Combination of [4] and [5] gives

$$[6] \qquad k_p = d[NO_2^-]/[OH^-]^2 + e[NO_2^-]^2/[OH^-]^2$$

so that the overall rate is

$$[7] \qquad -d[ClO^-]/dt = ([ClO^-][NO_2^-]/[OH^-]^2)(d + e[NO_2^-])$$

Although the values of *a*, *b*, and *c* were used to obtain those of *d* and *e* by [6], and although these turned out to be fairly constant, it was considered that this procedure did not give equal weight to each of the experiments performed. A computer program was therefore written to refine the values of *d* and *e*. It was considered that the *best* values of *d* and *e* would be those which, when substituted in [6], yielded values of the calculated rate constant, k_p (calcd), in *closest agreement* with the 19 experiments involved. *Closest agreement* was defined as meaning the minimum value of the average of the square of the fractional deviation, *E*, where *E* is defined by

$$[8] \qquad E = (1/n) \sum[(k_p(\text{calcd}) - k_p)/k_p]^2$$

n being the number of experiments involved. The values thus obtained at 298.0 K are:

$$d = (3.4 \pm 0.2) \times 10^{-8} \text{ mol l}^{-1} \text{ s}^{-1}$$

$$e = (2.8 \pm 0.2) \times 10^{-6} \text{ s}^{-1}$$

for which $E = 4 \times 10^{-2}$. Equation 7 is therefore an adequate description of the results.

To test rate equation 7 at lower nitrite concentrations, experiments were performed with [NO_2^-] equal to [ClO^-] using initial concentrations in the range (0.8–2.7) $\times 10^{-3}$ *M*. Integrat-

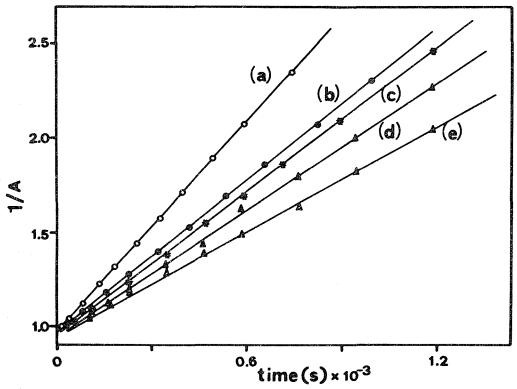

FIG. 5. Pseudo second-order rate plots for the oxidation of nitrites with $[NaNO_2]_0 = [NaClO]_0 = 2.7 \times 10^{-3}$ *M* at various temperatures, [NaOH] = 2.6×10^{-3} *M*, $\mu = 0.40$: (*a*) ○ 301 K; (*b*) ● 298 K; (*c*) * 297 K; (*d*) ▲ 294 K; (*e*) △ 292 K.

ing, for these conditions, the rate equation 7 gives

$$[9] \quad 1/A - (e/\epsilon d) \times \ln\{(\epsilon d + eA)/A[OH^-]^2\} = (d/\epsilon[OH^-]^2) \times t + I$$

ϵ being the molar absorptivity of hypochlorite ions and *I* the integration constant.

In these working conditions it was observed that the second term of the left side of [9] is constant, thus a linear relationship should exist between the values of $1/A$ and t whose slope should be $d/\epsilon[OH^-]^2 = (1.4 \pm 0.1) \times 10^{-3}$ s^{-1} (for $d = 3.4 \times 10^{-8}$ mol l^{-1} s^{-1} and $[OH^-] = 2.6 \times 10^{-4}$ *M*). Figure 5*b* shows that these expectations are fulfilled and that the value of this slope (1.5×10^{-3} s^{-1}) agrees with the predicted value. Therefore, the rate equation is valid for both high ($[NO_2^-]/[ClO^-] \simeq 20$) and low nitrite concentrations ($[NO_2^-]/[ClO^-] = 1$).

Some experiments were carried out at different temperatures to evaluate the activation parameters.

The activation energy (Fig. 6*c*), $E^{\neq} = 60 \pm 3$ kJ mol^{-1}, was obtained from a satisfactorily linear Arrhenius plot. Since, for these experimental conditions, both terms of the rate equation are comparable, the activation energy found belongs to the overall process.

Experiments were carried out at low nitrite concentration ($[NO_2^-]$ equal to $[ClO^-]$) and at different temperatures, and the parameter *d* was then obtained from [9]. From the linear Arrhenius plot, as shown in Fig. 6*a*, it results that $E_d^{\neq} = 56 \pm 3$ kJ mol^{-1}.

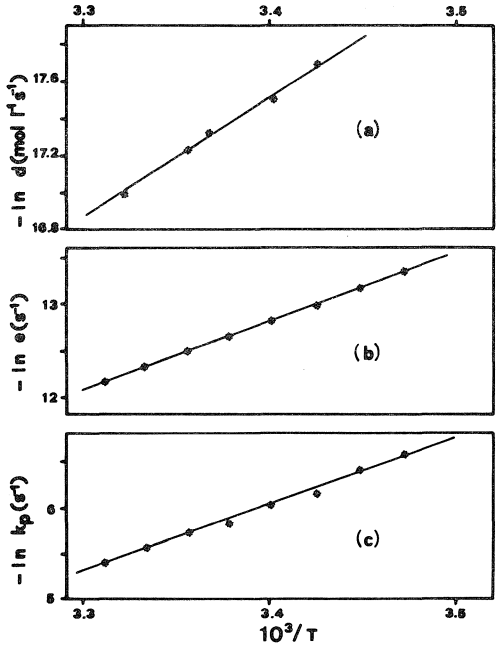

FIG. 6. Plots of ln k_p ($[NaNO_2] = 0.0715$ *M*, [NaOH] = 2.6×10^{-3} *M* and $\mu = 0.40$) ln *d* ($[NaClO]_0 = [NaNO_2]_0 = 2.7 \times 10^{-3}$ *M*, [NaOH] = 2.6×10^{-3} *M* and $\mu = 0.40$) and ln *e* (calculated from [6]) *vs.* $10^3/T$ (K).

Knowing the values of k_p and *d* at different temperatures, the values of the parameter *e* can be obtained from [6]. The parameter *e* also fulfils the Arrhenius law (Fig. 6*b*), with an activation energy $E_e^{\neq} = 61 \pm 3$ kJ mol^{-1}.[2]

Discussion

The mechanism of Pendlebury and Smith (4*a*, 4*b*) for the oxidation of nitrite ions by aqueous chlorine and bromine interprets the experimental rate in a satisfactory manner:

$$[10] \quad ClO^- + H_2O \leftrightharpoons ClOH + OH^- \qquad (K_h) \text{ very fast}$$

$$[11] \quad NO_2^- + ClOH \leftrightharpoons NO_2Cl + OH^- \qquad (k_1, k_{-1})$$

$$[12] \quad NO_2Cl + NO_2^- \leftrightharpoons N_2O_4 + Cl^- \qquad (k_2, k_{-2})$$

$$[13] \quad N_2O_4 + OH^- \rightarrow NO_3^- + NO_2^- + H^+ \qquad (k_3)$$

$$[14] \quad NO_2Cl \leftrightharpoons NO_2^+ + Cl^- \qquad (k_4, k_{-4})$$

$$[15] \quad NO_2^+ + OH^- \rightarrow NO_3^- + H^+ \qquad (k_5)$$

[2]The value of $E_e^{\neq}$ has been proved experimentally by another method. Full details can be obtained by correspondence with the authors.

Can. J. Chem. Downloaded from www.nrcresearchpress.com by 210.87.254.42 on 09/05/12
For personal use only.

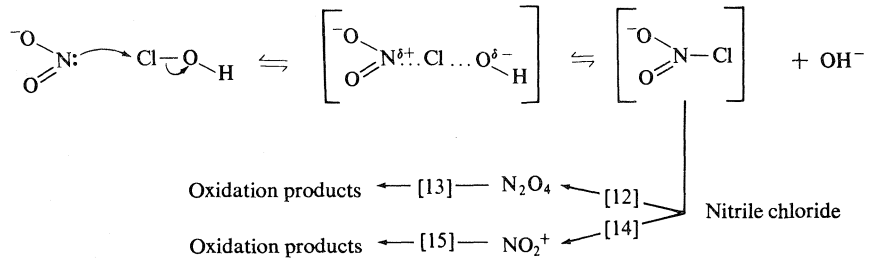

SCHEME 1

The rate law can be expressed as follows,

[16] $$\text{Rate} = d[NO_3^-]/dt = k_3[N_2O_4][OH^-] + k_5[NO_2^+][OH^-]$$

Application of the steady state approximation to NO_2^+, N_2O_4, and NO_2Cl, leads to

[17] $$\text{Rate} = \left(\frac{k_2k_3[NO_2^-][OH^-]}{k_{-2}[Cl^-] + k_3[OH^-]} + \frac{k_4k_5[OH^-]}{k_{-4}[Cl^-] + k_5[OH^-]}\right) \times \left(\frac{k_1[NO_2^-][ClOH]}{k_{-1}[OH^-] + k_2[NO_2^-]\left[1 - \frac{k_{-2}[Cl^-]}{k_{-2}[Cl^-] + k_3[OH^-]}\right] + k_4\left[1 - \frac{k_{-4}[Cl^-]}{k_{-4}[Cl^-] + k_5[OH^-]}\right]}\right)$$

Although this expression of the rate equation is rather complex, some of the experimental facts which have been mentioned allow for the introduction of several simplifications. It is shown in this paper that large changes in the concentration of chloride ion have no influence on the rate of reaction. This can be only explained if $k_3[OH^-] \gg k_{-2}[Cl^-]$, and $k_5[OH^-] \gg k_{-4}[Cl^-]$.

Therefore, the rate law is reduced to

[18] $$\text{Rate} = \left(\frac{K_h k_1[ClO^-][NO_2^-]}{k_{-1}[OH^-]^2 + (k_2[NO_2^-] + k_4)[OH^-]}\right) \times (k_4 + k_2[NO_2^-])$$

where $K_h = [ClOH][OH^-]/[ClO^-]$.

In a similar way, taking into account [5] and Fig. 4 which show a linear correlation between the values of k_p and $1/[OH^-]^2$ ($r_{xy} = 0.9998$), it follows that $k_{-1}[OH^-] \gg k_4 + k_2[NO_2^-]$. Hence, the rate equation can be finally written as

[19] $$d[NO_3^-]/dt = -d[ClO^-]/dt = ([ClO^-][NO_2^-]/[OH^-]^2) \times (\alpha + \beta[NO_2^-])$$

where $\alpha = K_h k_1 k_4/k_{-1}$ and $\beta = K_h k_1 k_2/k_{-1}$, this equation is identical in form to that found experimentally [7].

The above inequalities which require that the hydroxide ion is more nucleophilic than chloride or nitrite agree with the results given by other authors working with different systems (7, 8), and are in line with the hypothesis proposed in similar articles (4).

One of the main steps of this mechanism is the formation of NO_2Cl [11]. This step can be understood as a migration of the nitrogen lone pair to the chlorine atom, breaking the bond between chlorine and oxygen atoms, as is shown in Scheme 1.

The rate equation obtained in this paper is different from that of Lister and Rosenblum (rate = $k[ClO^-][NO_2^-]/[OH^-]$) for the same reaction in strongly basic solution. Nevertheless, this equation can be interpreted in the light of the mechanism given here. If it is assumed that when the pH is increased the rate of formation of NO_2Cl becomes significantly slower than the other steps of the mechanism, the rate of the reaction will be determined by this step, and the rate law should become that found by Lister and Rosenblum, above. Moreover, if the respective

Can. J. Chem. Downloaded from www.nrcresearchpress.com by 210.87.254.42 on 09/05/12
For personal use only.

constants are compared:

$k_1 \gg 100$ mol l^{-1} s^{-1} (25 °C, p$H \simeq$ 11) see footnote 3

$k = 27$ mol l^{-1} s^{-1} (60 °C, p$H \simeq$ 13) see ref. 3

the assumption above is verified. Thus, the fact that the rate law differs in weakly and strongly basic solutions can be explained. There is not, however, an obvious rationalization of why the rate of formation of NO_2Cl should be slower when the pH is increased.

[3]Taking for K_h the value of 3.1×10^{-7} (3), from [7] and [19] it follows that

[20] $$k_1 k_4 = 0.1 k_{-1}$$

Since $k_{-1}[OH^-] \gg k_4$, the equation 20 gives

[21] $$k_1 \gg 1/10[OH^-]$$

and taking the average value of the hydroxide ions concentration employed in the experiments performed ($\simeq 10^{-3}$ M), leads to

[22] $$k_1 \gg 100 \text{ mol l}^{-1} \text{ s}^{-1}$$

Acknowledgment

We wish to thank Ldo. E. Patiño for his revision of the English version of the manuscript.

1. N. M. Vaksberg. J. Appl. Chem. **13**, 1504 (1940).
2. E. A. Shilov. J. Appl. Chem. **34**, 465 (1956).
3. M. W. Lister and P. Rosenblum. Can. J. Chem. **39**, 1645 (1961).
4. (*a*) J. N. Pendlebury and R. H. Smith. Aust. J. Chem. **26**, 1847 (1973); (*b*) **26**, 1857 (1973).
5. M. I. Valente Soares, P. G. Santos Pereira, and A. M. Antunes. Rev. Port. Quim. **13**, 151 (1971).
6. A. Hussain, P. Trudell, and A. J. Repta. J. Pharm. Sci. **59**, 8 (1970); **59** 1168 (1970).
7. M. S. Newman. Steric effects in organic chemistry. John Wiley and Sons, Inc. U.S.A. 1963.
8. J. O. Edwards and R. G. Pearson. J. Am. Chem. Soc. **84**, 16 (1962).

Can. J. Chem. Downloaded from www.nrcresearchpress.com by 210.87.254.42 on 09/05/12
For personal use only.

A kinetic study of the reaction of adamantanethione with 2-adamantanethiol[1]

J. C. SCAIANO,[2] J. P.-A. TREMBLAY,[3] AND K. U. INGOLD
Division of Chemistry, National Research Council of Canada, Ottawa, Ont., Canada K1A 0R9

Received April 8, 1976

J. C. SCAIANO, J. P.-A. TREMBLAY, and K. U. INGOLD. Can. J. Chem. **54**, 3407 (1976).

The title reaction is a free radical chain process which yields di(2-adamantyl)disulfide(2). The kinetics of this reaction have been studied in benzene solution at 50 °C using both thermal and photochemical initiation. Thermal initiators which yield resonance stabilized carbon-centered radicals were surprisingly inefficient at starting the reaction. The kinetics indicate that the rate controlling propagation step is hydrogen abstraction from the thiol, AdHSH, by the carbon-centered radical, AdHSSAd•. Rotating sector studies gave a rate constant for this step, $k_2 = 4 \times 10^4\ M^{-1}\ s^{-1}$. There is some kinetically first order chain termination, but the predominant termination process involves the diffusion-controlled bimolecular self-reactions of AdHSSAd• radicals, $2k_t = 1.8 \times 10^{10}\ M^{-1}\ s^{-1}$.

J. C. SCAIANO, J. P.-A. TREMBLAY et K. U. INGOLD. Can. J. Chem. **54**, 3407 (1976).

La réaction indiquée dans le titre est un processus radicalaire à chaîne qui conduit au disulfure de di(adamantyl-2) (2). La cinétique de cette réaction a été étudiée en solution dans le benzène à 50 °C en utilisant les modes d'initiation thermique et photochimique. Les initiateurs thermiques qui conduisent à des radicaux carbonés stabilisés par résonance sont étonnamment inefficaces pour initier la réaction. La cinétique indique que la propagation qui est l'étape lente de la réaction se fait par abstraction de l'hydrogène du thiol, AdHSH, par le radical carboné AdHS-SAd•. Des études de secteur tournant ont donné pour cet étape une constante de vitesse $k_2 = 4 \times 10^4\ M^{-1}\ s^{-1}$. Il y a dans cette réaction un processus de terminaison de chaîne de premier ordre mais le processus prédominant de terminaison implique des réactions bimoléculaires d'annihilation des radicaux AdHSSAd•, contrôlées par la diffusion, selon $2k_t = 1.8 \times 10^{10}\ M^{-1}\ s^{-1}$.

[Traduit par le journal]

A variety of free radicals have been shown to add to carbon–sulfur double bonds (1–4), but there is little quantitative information about the rates of such reactions. De Mayo and co-workers (2) have recently shown that the photoreduction of adamantanethione by 2-adamantanethiol is a two-step chain process in which the thiyl radical adds to the C=S double bond in step one and the resultant carbon-centered radical abstracts hydrogen from the S—H bond in step two, *i.e.*,

[1] 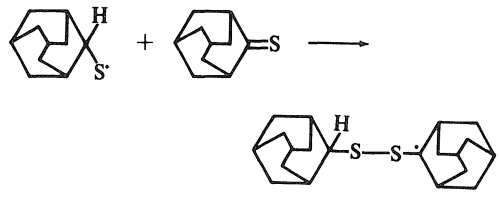

[2] 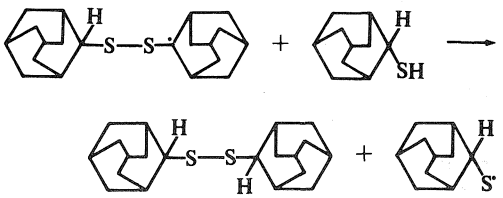

We decided to examine the kinetics of this reaction and determine the rate constants for chain propagation and for chain termination by the photochemical 'rotating-sector' technique (5). Our hope was that reaction 1 would prove to be rate-controlling. This reaction is of interest both because of the paucity of rate data on additions to C=S double bonds and because it may be related to the surprisingly rapid (often diffusion-controlled) self-quenching of thioketones in their triplet state (2, 6–9). Unfortunately, reaction 2 turned out to be rate-controlling which means that we have only been able to put a lower limit on the rate constant for

[1]NRCC No. 15399.
[2]NRCC Visiting Research Officer, 1975.
[3]NRCC summer student, 1975.

Can. J. Chem. Downloaded from www.nrcresearchpress.com by 210.87.254.6 on 09/05/12
For personal use only.

reaction 1. The overall chain process shows a number of interesting features, particularly with regard to the efficiency of thermal initiation.

Experimental

Materials

Adamantanethione and 2-adamantanethiol were prepared and purified by the methods of Greidanus (10). They were stored at low temperature under argon and the thiol was carefully sublimed before each experiment.

Di-*tert*-butyl hyponitrite was prepared by the method of Kiefer and Traylor (11) and azocumene by the method of Nelsen and Bartlett (12). 2,2,3,3,-Tetraphenylbutane was very kindly presented to us by Dr. L. R. Mahoney. Azo(bis)isobutyronitrile and azo(bis)cyclohexylnitrile were commercial materials.

Procedure

A reaction vessel was designed which allowed the thione and thiol to be degassed as solids while, in a separate compartment, a benzene solution of the initiator was degassed by several freeze–thaw cycles. The thione and thiol could then be dissolved in the initiator solution under oxygen-free conditions.[4] All rates were measured at 50 °C and cyclopropane was used as an inert gas above the solution in order to prevent the benzene from boiling.

The actual reaction cell had a square cross section and was made from four 1 cm × 4 cm optical quartz windows. It was mounted in a brass block, the body of which had been drilled so as to produce a number of interconnecting channels through which water from a heated reservoir (50 °C) was circulated. This maintained the reactants at a constant temperature.

The reaction was monitored continuously by following the disappearance of the thione spectrophotometrically. For this purpose, the light from a 6 V flashlight bulb, powered by a LAMBDA regulated power supply, was passed first through a Corning 3387 filter, then through the reaction cell, through a second Corning 3387 filter, and on to an RCA 935 phototube (with S-5 response) connected to a 67 V battery. The output signal from the phototube was zeroed against a 1.5 V mercury battery before each run and the resultant signal was amplified (× 100) and fed to a strip-chart recorder (1 mV full scale). This experimental arrangement allowed reaction rates to be measured easily for conversions well below 1%. In addition, it allowed several measurements to be made on each sample. The noise level, expressed in terms of thione concentration, never exceeded 6×10^{-5} *M*. Blank experiments showed that the monitoring light beam was of sufficiently low intensity that it did not induce any detectable reaction.

Reactions were initiated either thermally (with di-*tert*-butyl hyponitrite, azocumene, tetraphenylbutane, or azo(bis)isobutyronitrile) or photochemically using azo(bis)cyclohexylnitrile as the photo-initiator. For the latter, the reaction vessel was irradiated through a 1 cm × 4 cm window in the brass block in a direction perpendicular to the monitoring light beam. The initiating light came from a 250 W high-pressure mercury lamp. The optical system consisted of two quartz lenses which brought the light to a focus and a third quartz lens which produced a parallel beam which was passed through a 5 mm Corning 7-51 optical filter[5] and onto the window in the brass block. For the rotating sector experiments, a 10.5 in. diameter wheel having two diagonally opposed 45° sectors removed was used to chop the initiating light beam at its focus. This wheel, which has a dark:light ratio, r, equal to 3, was powered by a synchronous motor which was connected by a gear train so as to obtain a variety of precisely known chopping speeds.

Rates of nitrogen evolution from some of the initiators were measured using the apparatus described previously (13).

Results and Discussion

The results of experiments with four thermal initiators are summarized in Table 1. Tetraphenylbutane was chosen for the initial kinetic measurements because it is generally found to be a highly efficient initiator (14, 15). The overall rate with this initiator can be represented by

$$\frac{-\mathrm{d[Thione]}}{\mathrm{d}t} = k'[\mathrm{Initiator}]^{0.58\pm0.04}[\mathrm{Thiol}]^{0.96\pm0.07} \times [\mathrm{Thione}]^{0.05\pm0.03}$$

The same kinetic expression is obeyed by reactions initiated with di-*tert*-butylhyponitrite, azo(bis)isobutyronitrile, and azocumene. The numerical value of k' is, of course, a characteristic of the initiator employed and the temperature of the reaction.

The following simple reaction sequence, in which Ad represents the 2-adamantylidene group, gives a rate expression in good agreement with experiment:

(i) $\mathrm{Initiator} \xrightarrow{k_1} 2\mathrm{R}^{\bullet}$

(i_1) $\mathrm{R}^{\bullet} + \mathrm{Ad{=}S} \rightarrow \mathrm{RSAd}^{\bullet}$

or

(i_2) $\mathrm{R}^{\bullet} + \mathrm{AdHSH} \rightarrow \mathrm{RH} + \mathrm{AdHS}^{\bullet}$

[1] $\mathrm{AdHS}^{\bullet} + \mathrm{Ad{=}S} \rightarrow \mathrm{AdHSSAd}^{\bullet}$

[2] $\mathrm{AdHSSAd}^{\bullet} + \mathrm{AdHSH} \xrightarrow{k_2} \mathrm{AdHSSHAd} + \mathrm{AdHS}^{\bullet}$

[3] $2\mathrm{AdHSSAd}^{\bullet} \xrightarrow{2k_t} \text{Non-radical products}$

[4]Unless this procedure was followed, the rate measurements were irreproducible, an effect previously observed by de Mayo and co-workers (2).

[5]The transmission spectra of the filters used for initiating and monitoring the reaction were chosen so they did not overlap.

Can. J. Chem. Downloaded from www.nrcresearchpress.com by 210.87.254.6 on 09/05/12
For personal use only.

TABLE 1. Kinetic data for the thermally initiated reaction of adamantanethione with 2-adamantanethiol in benzene at 50 °C

[Initiator]/M	[Thione]/M	[Thiol]/M	$\frac{-\mathrm{d[Thione]}}{\mathrm{d}t} \times 10^6$ [a]	$k' \times 10^4$ [a]
Tetraphenylbutane				
0.001	0.06	0.06	1.01	9.3
0.003	0.06	0.06	1.75	8.5
0.008	0.06	0.06	3.42	9.5
0.002	0.06	0.03	0.88	10.7
0.002	0.06	0.06	1.51	9.3
0.002	0.06	0.12	3.34	10.3
0.002	0.06	0.18	3.79	7.7
0.002	0.06	0.23	6.75	10.7
0.002	0.12	0.06	1.58	9.6
0.002	0.09	0.06	1.51	9.3
tert-Butyl hyponitrite				
0.011	0.05	0.07	18.4	36
0.021	0.10	0.14	54.8	37
0.010	0.10	0.05	11.0	31
0.010	0.10	0.09	18.4	30
0.010	0.10	0.14	34.1	36
Azo(bis)isobutyronitrile				
0.144	0.10	0.10	7.55	2.3
Azocumene				
0.001	0.06	0.06	2.0	19

[a] In M s units.

The overall rate can be represented by

$$\frac{-\mathrm{d[Ad{=}S]}}{\mathrm{d}t} = k_2\left(\frac{2fk_i}{2k_t}\right)^{1/2}[\mathrm{Initiator}]^{0.5}[\mathrm{AdHSH}]$$

where f is the overall efficiency of chain initiation. This expression is in agreement with the experimental kinetic equation *except* for the order in initiator concentration (see below). The rate-controlling step in the chain progagation is hydrogen abstraction from the thiol (reaction 2), and chain termination occurs predominantly by the bimolecular self-reaction of two carbon-centered AdHSSAd$^\bullet$ radicals.

The data in Table 1 suggests that the hyponitrite is considerably more efficient at initiating this reaction than are the other three thermal initiators. That is, if we assume that the hyponitrite has its usual 96% efficiency in chain starting, *i.e.*, $f = 0.96$ (11) (which is not unreasonable since *tert*-butoxy radicals will enter into reaction i_2 rapidly and irreversibly), then the efficiencies for the other initiators can be calculated from the relation

$$\left(\frac{f}{0.96}\right)^{0.58} = \frac{k'}{k'_{(\mathrm{Me_3CON})_2}}\left(\frac{k_{i(\mathrm{Me_3CON})_2}}{k_i}\right)^{0.58}$$

Values of f are given in Table 2. The f values for the three initiators that give carbon-centered, R$^\bullet$ radicals are significantly lower than the values normally found for these compounds. Of course, this conclusion is based on the assumption that *tert*-butyl hyponitrite decomposes at the same rate in this medium as in other media. This appeared probable as the hyponitrite is not often subject to induced decomposition (11), and was confirmed by measuring the rate of nitrogen evolution from 0.013 M hyponitrite in *tert*-butylbenzene containing 0.1 M thione and 0.1 M thiol at 50 °C. The rate at which nitrogen was evolved was identical to the rate in the absence of the two sulfur compounds and was in agreement with literature data (11). We therefore believe that this initiator starts chains at its usual rate in our reaction system. The low initiating efficiencies of the other initiators is probably connected with the fact that they all produce resonance stabilized (16) R$^\bullet$ radicals. Presumably such radicals are inefficient in their abstraction from the thiol (reaction i_2) and in their addition to the thione (reaction i_1, which might even be reversible).

The results of the rotating sector experiments

Can. J. Chem. Downloaded from www.nrcresearchpress.com by 210.87.254.6 on 09/05/12
For personal use only.

TABLE 2. Efficiencies of thermal initiators at 50 °C

Initiator	k_i/s^{-1} at 50°	$k' \times 10^3$ [a]	f
tert-Butyl hyponitrite	5.5×10^{-5} [b]	3.4	(0.96)[c]
Tetraphenylbutane	3.9×10^{-5} [d]	0.95	0.15
Azo(bis)isobutyronitrile	2.4×10^{-6} [e]	0.23	0.21
Azocumene	4.3×10^{-5} [f]	1.9	0.45

[a]In M s units.
[b]Reference 11.
[c]Assumed.
[d]Reference 14.
[e]Reference 19*a*.
[f]Reference 12.

are represented in Fig. 1. In this figure, the ratio of the reaction rate, R, at a flash duration, λ, to the rate under steady illumination, R_0, is plotted against λ (5). The sectored disc used in these experiments had a dark:light ratio, r, equal to 3.0, and since there was no reaction in the absence of illumination the rate ratio, R/R_0, tends to 0.25 at large values of λ, *i.e.* for slow rotation. For fast rotations, R/R_0 tends to a limiting value of 0.44. This corresponds to a kinetic order in initiation of 0.59, which is in good agreement with the value found for the thermally initiated reactions. The fact that this order is not 0.50 must be interpreted in terms of

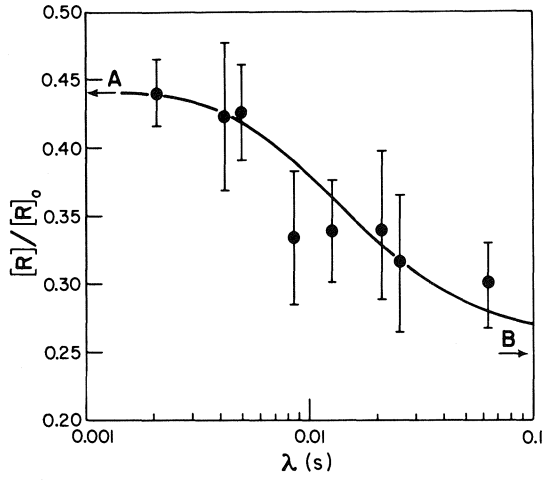

FIG. 1. Rotating sector data for the reaction of 0.1 M adamantanethione with 0.1 M 2-adamantanethiol in benzene at 50 °C. At full light intensity, the reaction rate, R_0, is 3.1×10^{-5} M s^{-1} and the rate of chain initiation is 1.36×10^{-6} M s^{-1}. The chain length is therefore about 23. Arrow A indicates the limiting value of R/R_0 (0.44) at fast rotation and arrow B the limiting value (0.25) at slow rotation. Following Burnett and Melville's nomenclature (5) this rotating sector plot yields $\gamma = 0.12$ and $m = 2.5$ s for $\lambda = 0.16$ s.

a kinetically first order termination process (reaction 4) which occurs concurrently with the second order process (reaction 3) (5).

$$\text{[4]} \qquad \text{AdHSSAd}^{\bullet}\ (+\ \text{X?}) \xrightarrow{k_4} \text{Non-radical products}$$

Analysis of the rotating sector data in the usual manner (5) yields the following rate constants:

$$k_2 = 4.0 \times 10^4\ M^{-1}\ \text{s}^{-1}$$
$$2k_t = 1.8 \times 10^{10}\ M^{-1}\ \text{s}^{-1}$$
$$k_4 = 38\ \text{s}^{-1}$$

The second order chain terminating process, *i.e.*, the bimolecular self-reaction of the AdHSSAd$^{\bullet}$ radicals, occurs at the diffusion-controlled limit, which is somewhat surprising for two large radicals (17). That is, according to the modified Debye equation (18), the rate constant for a diffusion-controlled reaction can be represented by

$$k_{\text{diff}} = 8RT/3000\eta\ M^{-1}\ \text{s}^{-1}$$

For benzene at 50 °C, η is 0.442 cP, and k_{diff} is calculated to be 1.6×10^{10} M^{-1} s^{-1}.

Chain termination processes that are kinetically first order are quite frequently encountered in radical chain processes (5, 19), but the precise nature of the chemical reaction which is involved is usually impossible to assess.

We are aware of only one rate constant for hydrogen abstraction from an alkylthiol by a non-stabilized alkyl radical. This is a value of 1.4×10^6 M^{-1} s^{-1}, due to Sivertz and co-workers (20), for abstraction from *n*-butylthiol by the *sec*-alkyl radical formed in the addition of *n*-butylthiyl radicals to 1-pentene at 25 °C. The rate constant for reaction 2 is significantly smaller than this value, which presumably reflects the decreased reactivity of AdHSSAd$^{\bullet}$ radicals which result both from steric factors and

Can. J. Chem. Downloaded from www.nrcresearchpress.com by 210.87.254.6 on 09/05/12
For personal use only.

from stabilization (16) of the radical by the adjacent sulfur atom.

Reaction 2 was rate controlling under all conditions. If we assume that AdHS· radicals, like other thiyl radicals (21, 22), undergo their bimolecular self-reaction at the diffusion-controlled limit, then reaction 1 must have a rate constant that is at least ten times greater than that for reaction 2, *i.e.*, $k_1 \geq 4 \times 10^5\ M^{-1}\ s^{-1}$. For comparison, the rate constant for self-quenching of adamantanethione triplets, which might involve formation of an intermediate S—S coupled biradical, is diffusion-controlled (7).

Comparison of our results with the overall quantum yields reported by de Mayo and co-workers (2) suggests that the quantum yield for initiation by direct excitation of the thione was *ca.* 3×10^{-4} and that their chain lengths were *ca.* 3000.[6]

Acknowledgement

We should like to thank Professor Paul de Mayo for initiating our interest in thione chemistry and for many valuable discussions during the course of this work.

1. J. C. Scaiano and K. U. Ingold. J. Am. Chem. Soc. **98**, 4727 (1976).
2. J. R. Bolton, K. S. Chen, A. H. Lawrence, and P. de Mayo. J. Am. Chem. Soc. **97**, 1832 (1975).
3. W. H. Sharkey. Adv. Polymer Sci. **17**, 73 (1975) and references cited.
4. D. H. R. Barton and S. W. McCombie. J. Chem. Soc. Perkin Trans. I, 1574 (1975).
5. G. M. Burnett and H. W. Melville. Investigation of rates and mechanisms of reactions. *In* Technique of organic chemistry, Vol. VIII, Part II. *Edited by* S. L. Friess, E. S. Lewis, and A. Weissberger. Interscience, New York. 1963. Chapt. 20.
6. D. R. Kemp and P. de Mayo. Chem. Commun. 233 (1972).
7. A. H. Lawrence, P. de Mayo, R. Bonneau, and J. Joussot-Doubien. Mol. Photochem. **5**, 361 (1973).
8. A. H. Lawrence, C. C. Liao, P. de Mayo, and V. Ramamurthy. J. Am. Chem. Soc. **98**, 2219 (1976).
9. A. Cox, D. R. Kemp, R. Lapouyade, P. de Mayo, J. Joussot-Dubien, and R. Bonneau. Can. J. Chem. **53**, 2386 (1975).
10. J. W. Greidanus. Can. J. Chem. **48**, 3530 (1970); **48**, 3593 (1970).
11. H. Kiefer and T. G. Traylor. Tetrahedron Lett. 6163 (1966).
12. S. F. Nelsen and P. D. Bartlett. J. Am. Chem. Soc. **88**, 137 (1966).
13. J. A. Howard and K. U. Ingold. Can. J. Chem. **47**, 3809 (1969).
14. K. Zeigler. Ann. **551**, 150 (1942).
15. L. R. Mahoney. J. Am. Chem. Soc. **88**, 3035 (1966).
16. D. Griller and K. U. Ingold. Acc. Chem. Res. **9**, 13 (1976).
17. G. B. Watts and K. U. Ingold. J. Am. Chem. Soc. **94**, 491 (1972).
18. P. Debye. Trans. Electrochem. Soc. **82**, 265 (1942).
19. J. A. Howard and K. U. Ingold. Can. J. Chem. (*a*) **40**, 1851 (1962); (*b*) **43**, 2729 (1965); (*c*) **43**, 2737 (1965); (*d*) **44**, 1113 (1966).
20. R. Back, G. Trick, C. McDonald, and C. Silvertz. Can. J. Chem. **32**, 1078 (1954); M. Onyszchuk and C. Sivertz. Can. J. Chem. **33**, 1034 (1955); C. Sivertz. J. Phys. Chem. **63**, 34 (1959).
21. D. M. Graham, R. L. Mieville, R. H. Pallen, and C. Sivertz. Can. J. Chem. **42**, 2250 (1964).
22. J. W. Purdie, H. A. Gillis, and N. V. Klassen. Chem. Commun. 1163 (1971).

[6]This comparison refers to data obtained at room temperature on an optical bench, see ref. 2, *i.e.* the temperature difference between the two sets of experiments has been ignored.

Can. J. Chem. Downloaded from www.nrcresearchpress.com by 210.87.254.6 on 09/05/12
For personal use only.

Medium-sized cyclophanes. XX. ^{13}C nuclear magnetic resonance of cyclophanes: *p*-orbital compression shift and orbital deformation[1]

TETSUO TAKEMURA[2] AND TAKEO SATO[3]

Department of Chemistry, Tokyo Metropolitan University, Setagaya-ku, Tokyo, 158 Japan

Received May 3, 1976

TETSUO TAKEMURA and TAKEO SATO. Can. J. Chem. **54**, 3412 (1976).

The ^{13}C nmr spectra of [2.2]meta-, metapara-, and paracyclophanes were determined. By comparing the chemical shifts with those of acyclic models two types of anomalies were revealed.

(*1*) Bridging methylene carbon resonances for [2.2]metacyclophanes having an alkyl group *ortho* to the bridge were shifted upfield as a result of van der Waals' compression. The upfield shift is much larger (5–12 ppm) for cyclophanes than for models (2–4 ppm) reflecting the rigid nature of the molecular geometry of the former.

(*2*) Interestingly, inner aryl carbon resonances in [2.2]metacyclophanes and protonated aryl carbon resonances in [2.2]paracyclophanes were shifted downfield by 6–7 ppm. The complementary upfield shift of uncompressed atoms, hydrogen or carbon, connected to those carbons was also noticed. The downfield shift of compressed sp^2 carbon results from interaction between two *p*-orbitals along the same orbital axis, *p*-orbital compression, and is attributable to decreased electron density.

TETSUO TAKEMURA et TAKEO SATO. Can. J. Chem. **54**, 3412 (1976).

On a déterminé le spectre rmn du ^{13}C des [2.2.]méta-, métapara- et paracyclophanes. Une comparaison des déplacements chimiques de ces composés avec ceux de modèles acycliques révèle la présence de deux types d'anomalies.

(*1*) La résonance du carbone méthylénique effectuant le pont des [2.2]métacyclophanes possédant un groupe alkyle en *ortho* par rapport au pont est déplacée vers les hauts champs due à une compression de van der Waals. Ce déplacement vers les hauts champs est beaucoup plus grand (5–12 ppm) pour les cyclophanes que pour les modèles (2–4 ppm) et ces différences reflètent la nature rigide de la géométrie moléculaire des premiers.

(*2*) Il est intéressant de noter toutefois que les résonances des carbones intérieurs du noyau aromatique des [2.2]métacyclophanes et les résonances des carbones aromatiques protonées des [2.2]paracyclophanes sont déplacées vers les bas champs par 6–7 ppm. On a aussi noté un déplacement complémentaire vers les hauts champs des atomes non comprimés d'hydrogène ou de carbone attachés à ces atomes de carbones. Le déplacement vers les bas champs des carbones sp^2 comprimés provient d'une interaction entre les deux orbitales *p* le long du même axe orbitalaire, une compression d'orbitale *p*, qui est attribuée à une diminution de la densité électronique.

[Traduit par le journal]

Introduction

The potential of ^{13}C nmr for elucidation of conformational and proximity effects has been well established (3). It is also well known that there is a good correlation between electron density and ^{13}C shieldings (3, 4). We determined the carbon resonances for a series of [2.2]cyclophanes **1–14** together with several model compounds, **15–19**. We found a new spectral parameter termed *p*-orbital compression shift, a paramagnetic shift of compressed aromatic carbon resonances. We discuss it in terms of geometrical features associated with bridged aromatic systems and *p*-orbital deformation.

Basic Geometry

The unusual geometry and the resulting strain of cyclophanes have been studied by X-ray crystallography, proton nmr, and heats of combustion (5). The crystal structure of [2.2]metacyclophane (**1**) revealed a distorted benzene ring in a shallow boat form (6). The closest benzene carbons are only 2.69 Å apart, which is the shortest distance between non-bonded atoms in cyclophanes. With [2.2]paracyclophane (**3**) two benzene rings are held in a face-to-face geometry (7) in which various anomalies exist, including stretch of benzyl–benzyl bond, bent benzene, and

---

[1]For part XIX, see ref. 1. A preliminary account of this work appeared in ref. 2.

[2]Present address: Department of Chemistry, Science University of Tokyo, Shinjuku-ku, Tokyo, 162 Japan.

[3]Author to whom correspondence should be addressed.

Can. J. Chem. Downloaded from www.nrcresearchpress.com by 210.87.254.6 on 09/05/12
For personal use only.

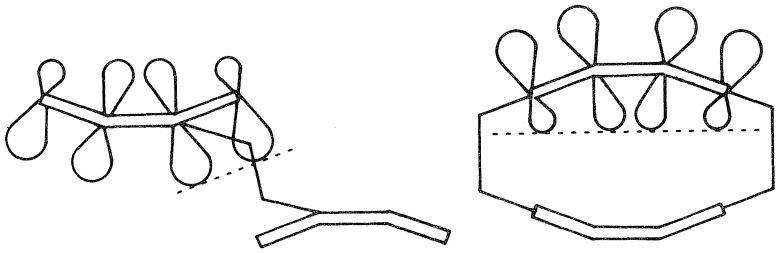

FIG. 1. Deformation of *p*-orbital lobes on bent benzene carbons.

bond angle deformation. The shortest distance between facing aryl carbons is 2.78 Å.

The *p*-orbital lobes on a bent benzene carbon are assumed to be deformed in a less symmetrical shape as the results of π–π repulsion and rehybridization (Fig. 1). Aromatic hydrogens in **3** and related cases, for example, are unexpectedly bent toward the inside (8). This causes rehybridization on the sp^2 carbon resulting in an increased electron density on the outside face of benzene rings. Aromatic carbons carrying the bridge are also severely distorted (angle distortion viewed from cross section is 11.2° (8)), and we expect the *p*-lobe to be smaller inside and larger outside.

With **1**, however, hydrogens on C-8,16 positions are pushed away from the facing benzene plane as the result of extensive steric repulsion. This causes an increased *p*-lobe toward the inside. A severe π–π repulsion is expected at C-8,16 (Fig. 1). A similar argument is possible for [2.2]metaparacyclophane (**2**) (5).

These repulsive and angle strains are reflected in large strain energies (9), which are 12, 23, and 31 kcal/mol, respectively, for **1**, **2**, and **3**. Electronic interaction between aryl rings in cyclophanes has been studied by uv spectra with the aid of charge-transfer complexation technique. While π–π interaction is insignificant in **1** (10*a*) the π-basicity of **3** is strongly enhanced as compared with models (10*b*). The uv spectra of **3** and multi-layered analogs have been extensively studied (11). The esr studies of anion radicals (12) and photoelectron spectra (13) of these compounds were also examined.

Results

[2.2]Cyclophanes (Fig. 2)

Chemical shifts for **1**–**3** were assigned as shown in Fig. 2.

The proton noise decoupled spectra were determined by the PFT method using a Varian XL-100 or a Jeol FX-60 spectrometer using internal TMS as the reference, on solutions dissolved in $CDCl_3$ (0.2–0.3 *M*). Compound **1** showed five resonances. The methylene carbon absorbs at 41.4 ppm. Of the four aryl carbon resonances, the non-protonated carbon at 138.6 ppm was assigned to C-3. Among the three protonated carbons one at 125.1 ppm appeared as a double intensity peak and was assignable to C-4.

Resonances at 128.6 and 136.3 ppm were assigned to C-5 and C-8, respectively, based on the following evidence. In proton nmr, aryl protons at the C-8,16 positions shift to upfield by about 3 ppm more than outer aryl protons such as C-4,5H. Two carbon resonances can be differentiated by comparing residual coupling constants in the off-resonance spectra. Also, the resonance for C-5 is sharper than that of C-8 since $J_{^{13}C-H} > J_{^{13}CCCH} > J_{^{13}CCH}$. (14) Similarly, the resonance for C-5 in **2** appeared as a sharp doublet at 126.8 ppm in the off-resonance spectrum. With these results, the peak at 133.0

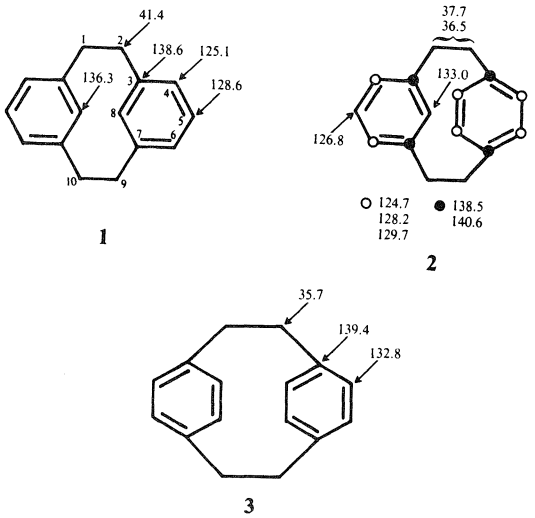

1 2 3

FIG. 2. Chemical shifts for **1**-**3**.

Can. J. Chem. Downloaded from www.nrcresearchpress.com by 210.87.254.6 on 09/05/12
For personal use only.

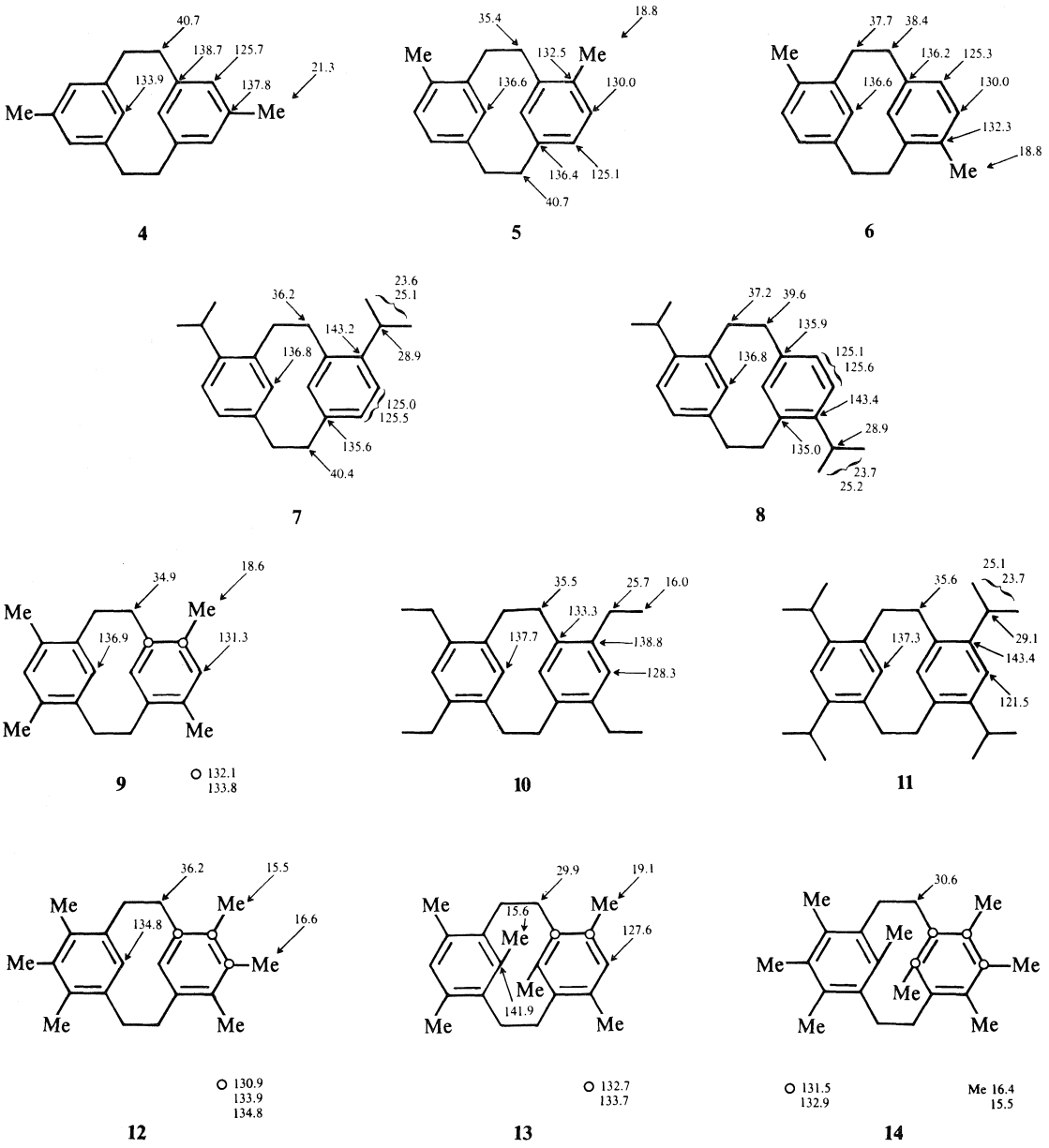

FIG. 3. Chemical shifts for alkyl derivatives of [2.2]metacyclophanes.

ppm is assigned to C-8. Other protonated carbons showed three absorptions at 124.7, 128.2, and 129.7 as double intensity peaks. The assignment is straightforward with **3**.

Alkyl Derivatives of [2.2]Metacyclophanes (Fig. 3) and Models (Fig. 4)

Based on the chemical shifts found for **1**, the resonances for alkyl derivatives were assigned. These include dimethyl **4**–**6**, diisopropyl **7** and **8**, tetramethyl **9**, tetraethyl **10**, tetraisopropyl **11**, hexamethyl **12** and **13**, and octamethyl derivatives **14**. The preparations of the materials were reported elsewhere (15).

Calculation using additivity parameters (16) was helpful for the assignment. For example,

Can. J. Chem. Downloaded from www.nrcresearchpress.com by 210.87.254.6 on 09/05/12
For personal use only.

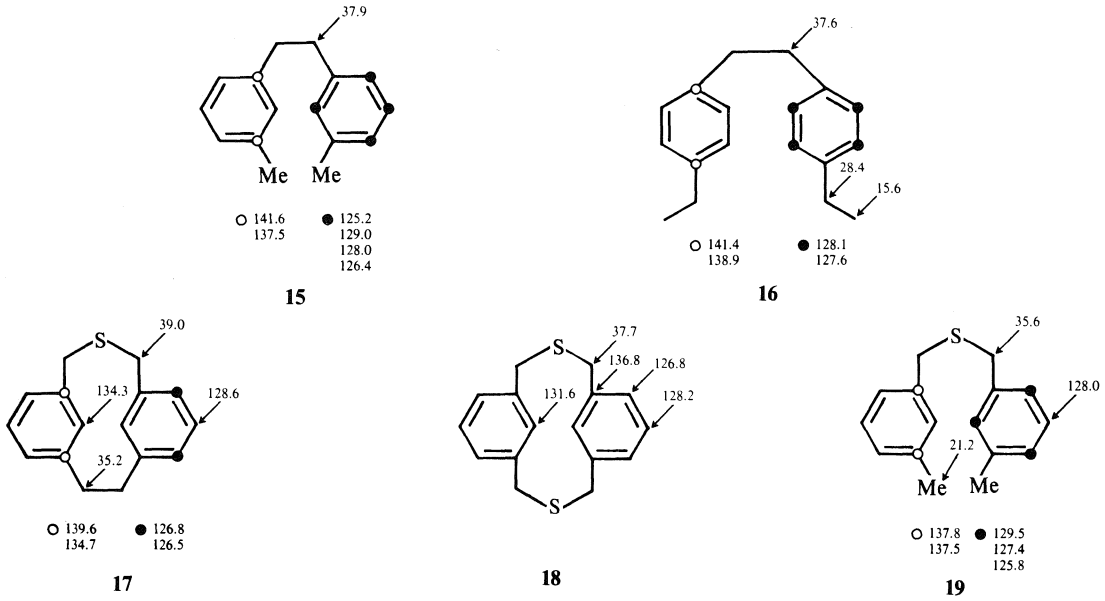

FIG. 4. Chemical shifts for model compounds of [2.2]metacyclophane derivatives.

calculated shifts for the dimethyl compound **4** were within 0.2 ppm of observed values (Table 1). Differentiation of otherwise difficult *cis* and *trans* isomers, **5**/**6** and **7**/**8**, is possible as reported elsewhere (15).

Resonances for acyclic models are shown in Fig. 4. For larger-ring analogs **17** and **18** (17) the lowest-field protonated carbon signal was assigned to the inner aryl carbon based on the same method differentiating between C-5 and C-8 in **1**.

Discussion

Two types of steric compression shifts were noticed for [2.2]metacyclophanes. These are the usual upfield shift of compressed methylene carbons and a downfield shift caused by direct *p*-orbital compression between non-bonded sp^2 carbons.

Table 2 summarizes the chemical shifts of bridging methylene carbons for *o*-alkyl derivatives and shift differences from unsubstituted **1**. An upfield shift is the result of van der Waals' compression (18). This is caused by compression between *s*-orbitals of interacting hydrogens which induce polarization along a C—H bond (hereafter *s*-orbital compression). The shift difference reaches 11.5 ppm with the hexamethyl derivative **13** indicating highly overcrowded molecular geometry. For unsymmetrically substituted **5** two types of methylene carbons are clearly recognized (C-1,2 −6.0 ppm; C-9,10 −0.7 ppm). The mag-

TABLE 1. Comparison of calculated and observed chemical shifts for **4**

Carbon	Shift (ppm) Observed	Calculated*	Δ (ppm)
C-3	138.7	138.6	+0.1
C-4	125.7	125.9	−0.2
C-5	137.8	137.8	0.0
C-8	133.9	133.8	+0.1

*Reference 16.

TABLE 2. Chemical shifts and van der Waals' shifts for bridging methylene carbons (ppm)

Compound	C-1,2 (9, 10)	Δ_{MCP}*
1	41.4	0.0
5	35.4	−6.0
	(40.7)	(−0.7)
9	34.9	−6.5
10	35.5	−5.9
11	35.6	−5.8
12	36.2	−5.2
13	29.9	−11.5
14	30.6	−10.8

*MCP; [2.2]metacyclophane **1**.

Can. J. Chem. Downloaded from www.nrcresearchpress.com by 210.87.254.6 on 09/05/12
For personal use only.

Can. J. Chem. Downloaded from www.nrcresearchpress.com by 210.87.254.6 on 09/05/12
For personal use only.

nitude of the shift is not dependent on alkyl groups for **9**, **10**, and **11** ($-5.8 \sim 6.5$ ppm), suggesting that the shift is caused mainly by the γ-effect. The shift, however, is larger than the usual γ-shift such as that observed for the *o*-xylene–toluene pair (-2.0 ppm) (18) or dibenzyl models; methylene carbons in 2,2′,5,5′-tetramethyldibenzyl shift to upfield by 3.6 ppm compared with those of 3,3′-dimethyldibenzyl (**15**).

Grant and Cheney (18) have computed expected highfield shifts for various conformers of *o*-xylene based on an empirical correlation between non-bonded repulsive energy and chemical shifts. The upfield shift for a geared conformer of *o*-xylene in which one of the hydrogen atoms of the methyl group lies in a benzene plane is computed to be -4.4 ppm. With **9** the upfield shift amounts to 6.5 ppm. Since the equatorial hydrogens in **9** are fixed in a benzene plane a severe in-plane interaction is possible between methyl hydrogens, which causes an additional shift (-2.1 ppm).

The inner aryl carbon resonance of **1** is shifted to downfield from *m*-xylene by 6.2 ppm or from the acyclic model **15** by at least 7.3 ppm. A similar downfield shift was observed for alkyl derivatives (Table 3). No such anomalous shift is obtained for larger ring-sized compounds, such as **18** or acyclic model **19**.

With compound **3**, C-4,5,7,8 resonances are shifted to downfield by at least 4.7 ppm compared with **16**. The resonance for the C-3 carbon was found to be only slightly affected. With compound **2** the C-8 carbon resonance is shifted downfield by at least 4.0 ppm compared with **15**.

The origin of the downfield shift can be attributed to the following factors: (*1*) magnetic anisotropy of bridging methylene, (*2*) diamagnetic ring current effect, (*3*) rehybridization due to excessive strain, and (*4*) direct *p*-orbital compression.

TABLE 3. *p*-Orbital compression shifts of inner aryl carbon resonances relative to the corresponding arenes (ppm)

Compound	Alkyl benzenes	Δ
1	*m*-Xylene	+6.2
4	Mesitylene	+6.5
5	Pseudocumene	+6.1
9	Durene	+5.7
12	Pentamethylbenzene	+3.3
13	Pentamethylbenzene	+7.4

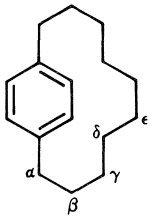

20

Of these the anisotropy effect can be neglected (19). Roberts and co-workers (20) compared the carbon resonances of cyclopentadecane and [12]-paracyclophane (**20**) and assigned the highest field methylene carbon resonance, which was shifted upfield by 0.7 ppm compared with that fo the saturated model, to the ring current effect. Whether this is really the case is, however, questionable since Kaneda, Inoue, and Misumi[4] found through extensive selective decoupling studies that the highest field methylene signal for **20**, as well as for other related systems, is due to a γ-carbon. The ring current effect is not large in carbon resonances and probably operates in an opposite direction.

Rehybridization will play an important role in severely distorted cases such as [2.2]paracyclophanes, multi-layered analogs, and cyclic diacetylene such as **24**. For protonated carbons of **1**, however, $J_{^{13}C-H}$ hybridization indices (21) are only slightly affected (Table 4).

The major cause of the downfield shift of the compressed aryl carbon resonances, especially those protonated carbon resonances, in strained molecules, can be attributed to a decrease in electron density due to *p*-orbital compression. It is caused by a direct non-bonded interaction between two *p*-orbitals, and is maximized when these are brought together along the same orbital axis. Electron density increases where such strain is absent. A localized π-electron system is formed by π-electron dislocation. With **1**, a marked downfield shift ($+6 \sim 7$ ppm, compared with **15** or *m*-xylene) occurs at C-8,16. In turn, upfield shifts are observed for connected atoms; C-3,7,11,15 (-3 ppm) and inner aryl protons C-8,16H (-3 ppm in pmr). The upfield shift of the inner aryl proton has been attributed to ring current effect (5) but a part of it may be caused by the increased shielding of the proton by induced polarization.

[4]T. Kaneda, T. Inoue, and S. Misumi, Abstracts, 8th Symposium for Structural Organic Chemistry, Kyoto, 1975.

Can. J. Chem. Downloaded from www.nrcresearchpress.com by 210.87.254.6 on 09/05/12
For personal use only.

TABLE 4. Coupling constants and hybridization indices for **1**

Carbon	$J_{^{13}C-H}$ (Hz)	λ^{2*}
C-4	154	2.2
C-5	158	2.2
C-8	160	2.1

*λ, the mixing coefficient which determines the *p*-character of the hybrid ($s + \lambda p$) atomic orbital bonding to carbon.

Unlike **1**, the two benzene rings in **3** are nearly completely overlapped and no π-electron localization is possible within a carbon framework. With protonated carbons polarization along the C—H bond causes a downfield shift of carbon and an upfield shift of proton resonances. For alkylated aryl carbons, however, no efficient way exists to release the *p*-orbital compression. In fact, those carbons carrying the bridge are shown to be unchanged. This may be due to rehybridization effects which outweigh the deshielding terms.

Misumi and co-workers observed a protonated aryl carbon resonance pseudo-geminal to the alkyl substituent in [2.2]paracyclophane such that the marked carbon in **21** is shifted downfield only slightly ($CDCl_3$). This can be understood by

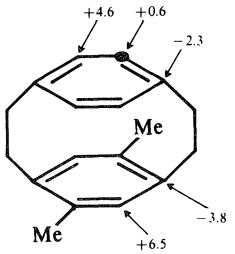

21

(shift changes from 2,5-diethyl-*p*-xylene)

the inhibition of polarization along the C_{Ar}—H bond by the presence of the pseudo-geminal methyl group. They also found the downfield shift of protonated aryl carbon resonances in a sandwiched benzene ring in three-decked cyclophanes[5]. The comparison of bridging methylene carbon resonances of **1**, **2**, and **3** with those of models revealed the shifts of +3.5, −1.4, and −1.9 ppm, respectively. The upfield shifts found for **2** and **3** are due to an eclipsed conformation of the ethylene bridge.

Related Cases

A similar downfield shift of inner aryl carbon resonance was observed in *trans*-[2.2]-2,7-naphthalenophane (**22**) compared with 7,7′-dimethyl-2,2′dinaphthylethane (**23**) (+3.6 ppm). The *cis*

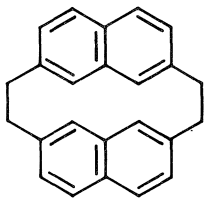

22

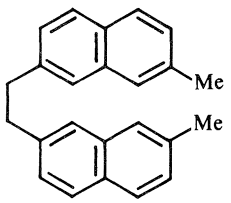

23

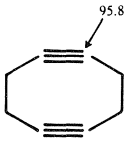

24

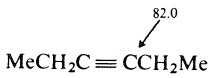

25

isomer had normal aryl carbon resonances (1) since two interacting *p*-orbitals are nearly perpendicular. Compared with an acyclic model (**25**) (22), 1,5-cyclooctadiyne (**24**) (23) (C_6D_6) showed a marked downfield shift of the acetylenic carbon resonance, while a higher homolog 1,8-tetradecadiyne showed a normal acetylenic carbon resonance at 81.0 ppm (24). Recently, downfield shifts of sp^3 carbon resonances in overcrowded molecules have been reported. (δ or ϵ shift) in addition to an anomalous upfield shift (25). These include the downfield shift of the methyl resonance in 1,8-dimethyl naphthalene compared with 1-methylnaphthalene (26). The deshielding δ effect was also observed with *o*-alkyl anisoles (27) and sulfur analogs (28). A downfield shift, 6.6 ppm, was observed for 7,12-dimethylbenz[*a*]anthracene compared with 7-methylbenz[*a*]anthracene (29). Those involving perturbation in sp^3 carbons appear to be more or less conformational in origin as observed for anomalous shielding in the equatorial 5-methyl group in 1,3-dioxane (30).

Experimental

The compounds used in this study were obtained by the method described previously (5, 15, 17). The proton noise

[5]H. Horita, H. Tatemitsu, T. Otsubo, Y. Sakata, S. Misumi, M. Mishima, and Y. Tsuno, Abstracts, 32nd Annual Meeting of the Chemical Society of Japan, Tokyo, 1975.

decoupled spectra were determined using a Varian XL-100 or Jeol FX-60 spectrometer operating in the FT mode. All shieldings were measured relative to internal TMS with 0.2–0.3 *M* solutions in $CDCl_3$ using 10 mm sample tubes.

1. T. SATO, H. MATSUI, and R. KOMAKI. J. Chem. Soc. Perkin Trans. I. In press.
2. T. SATO, T. TAKEMURA, and M. KAINOSHO. Chem. Commun. 97 (1974).
3. N. K. WILSON and J. B. STOTHERS. Topics in stereochemistry. Vol 8. *Edited by* E. L. Eliel and N. L. Allinger. An Interscience Publication, John Wiley and Sons. 1974. p. 1.
4. M. KARPLUS and J. A. POPLE. J. Chem. Phys. **38**, 2803 (1963).
5. R. W. GRIFFIN, JR. Chem. Rev. **63**, 45 (1963); T. SATO. Nippon Kagaku Zasshi, **92**, 277 (1971); D. J. CRAM and J. M. CRAM. Acc. Chem. Res. **4**, 204 (1971); F. VÖGTLE and P. NEUMANN. Angew. Chem. Int. Ed. Engl. **11**, 73 (1972).
6. C. J. BROWN. J. Chem. Soc. 3278 (1953).
7. C. J. BROWN. J. Chem. Soc. 3265 (1953).
8. C. L. COULTER and K. N. TRUEBLOOD. Acta Crystallogr. **16**, 667 (1963).
9. R. H. BOYD. Tetrahedron, **22**, 119 (1966); C. SHIEH, D. C. MCNALLY, and R. H. BOYD. Tetrahedron, **25**, 3653 (1969).
10. (*a*) E. LANGER and H. LEHNER. Tetrahedron, **29**, 375 (1973); (*b*) D. J. CRAM and R. H. BAUER. J. Am. Chem. Soc. **81**, 5971 (1959); L. A. SINGER and D. J. CRAM. J. Am. Chem. Soc. **85**, 1080 (1963).
11. S. IWATA, K. FUKE, M. SASAKI, S. NAGAKURA, T. OTSUBO, and S. MISUMI. J. Mol. Spectrosc. **46**, 1 (1973).
12. F. GERSON and W. B. MARTIN, JR. J. Am. Chem. Soc. **91**, 188 (1969); D. J. WILLIAMS, J. M. PEARSON, and M. LEVY. J. Am. Chem. Soc. **93**, 5483 (1971).
13. R. BOSCHI and W. SCHMIDT. Angew. Chem. Int. Ed. Engl. **12**, 402 (1973).
14. F. J. WEIGHT and J. D. ROBERTS. J. Am. Chem. Soc. **89**, 2967 (1967); G. J. KARABATSOS, J. D. GRAHAM, and F. M. VANE. J. Am. Chem. Soc. **84**, 37 (1962).
15. T. SATO and T. TAKEMURA. J. Chem. Soc. Perkin Trans II. In press.
16. J. B. STOTHERS. Carbon-13 nmr spectroscopy. Academic Press, New York. 1972. p. 96.
17. T. SATO, M. WAKABAYASHI, K. HATA, and M. KAINOSHO. Tetrahedron, **27**, 2737 (1971).
18. D. M. GRANT and B. V. CHENEY. J. Am. Chem. Soc. **89**, 5315 (1967); W. R. WOOLFENDEN and D. M. GRANT. J. Am. Chem. Soc. **88**, 1496 (1966); T. SCHAEFER, W. F. REYNOLDS, and T. YONEMOTO. Can. J. Chem. **41**, 2969 (1963).
19. J. A. POPLE. Mol. Phys. **7**, 301 (1964).
20. R. H. LEVIN and J. D. ROBERTS. Tetrahedron Lett. 137 (1973).
21. C. JUAN and H. S. GUTOWSKY. J. Chem. Phys. **37**, 2198 (1962); K. MISLOW. Tetrahedron Lett. **22**, 1415 (1964).
22. G. C. LEVY and G. L. NELSON. Carbon-13 nuclear magnetic resonance for organic chemists. John Wiley and Sons Inc., 1972. p. 71.
23. E. KLOSTER-JENSEN and JAKOB WIRZ. Angew. Chem. Int. Ed. Engl. **12**, 671 (1973).
24. C. CHARRIER, D. E. DORMAN, and J. D. ROBERTS. J. Org. Chem. **38**, 2644 (1973).
25. R. B. JONES and L. PHILLIPS. Annual Reports of the Chemical Society, Organic Chemistry, 1974. p. 26.
26. A. J. JONES, T. D. ALGER, D. M. GRANT, and W. M. LITCHMAN. J. Am. Chem. Soc. **92**, 2386 (1970).
27. G. W. BUCHANAN, G. MONTAUDO, and P. FINOCCHIARO. Can. J. Chem. **52**, 767 (1974).
28. G. W. BUCHANAN, C. REYES-ZAMARA, and D. E. CLARKE. Can. J. Chem. **52**, 3895 (1974).
29. R. S. OZUBKO, G. W. BUCHANAN, and I. C. P. SMITH. Can. J. Chem. **52**, 2493 (1974).
30. R. BERTRAND, K. A. CHRISTENSEN, D. K. DALLING, M. W. DUCH, E. WENKERT, F. M. SCHELL, and D. W. COCHRAN. J. Am. Chem. Soc. **97**, 322 (1975).

Can. J. Chem. Downloaded from www.nrcresearchpress.com by 210.87.254.6 on 09/05/12
For personal use only.

Synthesis of *d,l*-epiramulosin and the configuration of ramulosin[1]

JOHN A. FINDLAY, JOHN M. MATSOUKAS, AND JIRI KREPINSKY
Chemistry Department, University of New Brunswick, Fredericton, N.B., Canada E3B 5A3

Received May 25, 1976

JOHN A. FINDLAY, JOHN M. MATSOUKAS, and JIRI KREPINSKY. Can. J. Chem. **54**, 3419 (1976).

The synthesis of epiramulosin **1***b*, the epimer of ramulosin, a metabolite of *Pestolatia ramulosa*, has been achieved via a seven step sequence from butadiene and $\Delta^{\alpha,\beta}$-hexenolactone and the assignment of the relative and absolute configurations of ramulosin is achieved.

JOHN A. FINDLAY, JOHN M. MATSOUKAS et JIRI KREPINSKY. Can. J. Chem. **54**, 3419 (1976).

On a effectué la synthèse de l'épiramulosine **1***b*, l'épimère de la ramulosine, un métabolite du *Pestolatia ramulosa*, par l'intermédiaire d'une séquence en sept étapes à partir du butadiène et de la $\Delta^{\alpha,\beta}$-hexènolactone; on a fait les attributions de configurations relative et absolue de la ramulosine.

[Traduit par le journal]

The structure **1***a*, devoid of stereochemical detail, was proposed by Stodola *et al.* (1) in 1964 for ramulosin, an optically active metabolite of the fungus *Pestolatia ramulosa*. We now report the synthesis of epiramulosin **1***b* providing corroboration of structure and allowing assignment of relative configuration to the metabolite ramulosin.

The key starting material *d,l*-δ-$\Delta^{\alpha,\beta}$-hexenolactone **2** was prepared from commercially available hexa-2,4-dienoic acid (sorbic acid) by treatment with 7 equiv. of hydrobromic acid to furnish

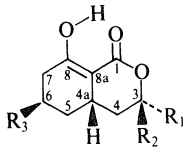

1*a* R_1 = Me, R_2, R_3 = H
1*b* R_1, R_3 = H, R_2 = Me
1*c* R_1 = Me, R_2 = H, R_3 = OH

crystalline 3,5-dibromocaproic acid which was treated directly with hot water to provide **2** in 41% overall yield. This constitutes a substantial improvement of the method of Kuhn and Jerchel (2) (22% overall yield) for the preparation of the lactone **2**.

Attempts to effect a Diels–Alder type cycloaddition reaction of the δ-hexenolactone **2** with 1-methoxybutadiene and 1-acetoxybutadiene under a broad variety of conditions were unsuccessful. Thus no product was formed when a 4:1 molar ratio of diene to dienophile **2** was used in methylene chloride, benzene, or toluene at temperatures between −40 and 190 °C under nitrogen atmosphere. Only starting material was recovered when similar attempts were made in systems using catalysts such as boron trifluoride etherate, aluminum trichloride, nickel acetylacetonate (3), and stannic chloride.

Study of the system butadiene – δ-hexenolactone **2** revealed that no reaction takes place much below 195 °C but at that temperature a major Diels–Alder adduct (40%) is formed sometimes accompanied by a minor adduct (<2%). The spectral characteristics of the major product are consistent with its assigned structure **3***b* and the relative stereochemistry (hydrogens at C-3 and C-4a *trans*) is dictated by Diels–Alder rules. Thus the minor adduct **3***a* results from the less

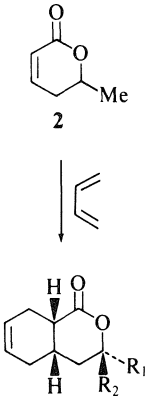

3*a* R_1 = Me, R_2 = H
3*b* R_1 = H, R_2 = Me

[1]This work is incorporated in the Ph.D. Thesis of John M. Matsoukas (U.N.B.), 1976.

Can. J. Chem. Downloaded from www.nrcresearchpress.com by 210.87.254.42 on 09/05/12
For personal use only.

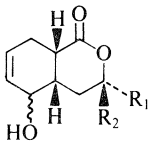

4

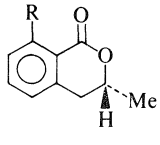

5*a* R = H
5*b* R = OH

sterically favoured approach of diene and dienophile.

Attempted allylic oxidation at C-8 of the ene lactone **3***b* was unsuccessful; thus treatment with selenium dioxide in aqueous dioxane gave predominantly **4** accompanied by minor amounts of the aromatization product **5***a* and the diene lactone **6**. The crystalline alcohol **4** could be converted into the α,β-unsaturated ketone **7** upon treatment with Collins' reagent thus confirming that C-5 was the preferred site for the allylic oxidation. Treatment of **3***b* with selenium dioxide under anhydrous conditions gave the aromatic lactone **5***a* as major product.

Quantitative conversion of the ene lactone **3***b* to the dihydro derivative **8** could be accomplished by hydrogenation with either Adams' catalyst or 10% palladium-on-charcoal using ethanol as solvent.

Functionalization at C-8a was achieved by bromination of **8** with pyridinium hydrobromic perbromide in dioxane at 85–90 °C which furnished a single oily monobromination product in 56% yield. Assuming that the bromination proceeds via the enol form of the lactone **8** the sterically preferred side for the bromonium ion formation would be α, hence this product is assigned structure **9***a*. This is in agreement with the finding that the C-3 proton appears at lower field (δ 4.8) in the bromide **9***a* than in the lactone **8** (δ 4.5) indicative of deshielding via a *cis* relationship of bromine and the C-3 proton. In addition dehydrobromination of **9***a* with 1,5-diazabicyclo[4.3.0]non-5-ene (DBN) in toluene at 95 °C gave both **10** (45%) and **11** (20%). In view of the usual *trans* diaxial stereoelectronic requirement for facile base catalysed eliminations the bromine in **9** should be *trans* diaxial to

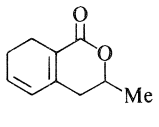

6

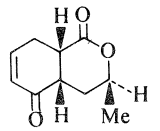

7

protons at C-4a and C-8 consistent only with an α bromine at C-8a. This is corroborated by the finding that treatment of **9***a* with either collidine or dimethylaniline gave almost exclusively **11**.

The structurally related α-chlorolactone **9***b* was prepared by treatment of **8** with sulfuryl chloride in carbon tetrachloride at 80 °C for 24 h under nitrogen. The C-3 proton in the nmr spectrum of **9***b* is also found at lower field (δ 4.75) than in the lactone **8**.

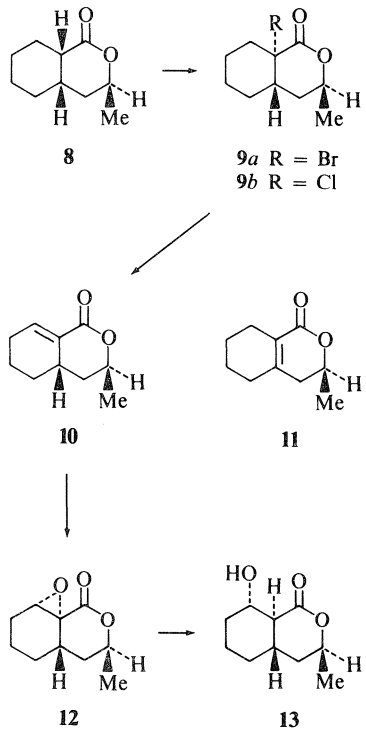

8

9*a* R = Br
9*b* R = Cl

10

11

12

13

1*b*

The structure of the α,β-unsaturated lactone **10** was fully supported by spectral data. Thus the infrared spectrum ($CHCl_3$) displays a strong carbonyl maximum at 1705 cm^{-1} while the ultraviolet spectrum (ethanol) shows λ_{max} = 225 nm (ϵ 4200) in agreement with the calculated value (λ_{max} = 230 ± 5 nm). The nmr spectrum ($CDCl_3$) shows a signal at δ 7.05 (1H, complex m) due to the C-8 vinylic hydrogen while the C-3 hydrogen is located at δ 4.6 (1H, complex m) and the three allylic protons give rise to an unresolved pattern between δ 2.2–2.5.

Hydration of **10** with mercuric acetate using Brown's method (4) failed to yield any hydration product. Starting material was recovered and no

Can. J. Chem. Downloaded from www.nrcresearchpress.com by 210.87.254.42 on 09/05/12
For personal use only.

Can. J. Chem. Downloaded from www.nrcresearchpress.com by 210.87.254.42 on 09/05/12
For personal use only.

decolorization of the solution (Brown's test) was noted.

Successful oxygenation of **10** was achieved by *m*-chloroperbenzoic acid in dichloroethane and furnished the oily epoxide **12** in 94% yield. The structural assignment is consistent with the nmr spectrum ($CDCl_3$) which shows the C-8 hydrogen at δ 3.35 (1H, br s) and the α configuration of the epoxide in **12** is designated in view of the preferred approach of peracids from the less hindered side in electrophilic attack on similar substrates (5).

The β-hydroxylactone **13** was obtained by treatment of the oxirane lactone **12** with chromous chloride in a two phase (ether–water) system. The α,β-unsaturated lactone **11** was also obtained in this reaction and this course of events is not unprecedented (6). Similar reactions using a one phase system were unsuccessful.

Oxidation of the β-hydroxylactone **13** with Collins' reagent in methylene chloride at room temperature afforded a 90% yield of a crystalline product (mp 64–65 °C) after chromatography which proved to be closely similar but non-identical with natural ramulosin (mp 120–121 °C). Thus the nmr spectrum ($CDCl_3$) of the synthetic compound displayed the C-3 methine proton signal at δ 4.8 (apparent sextuplet) while in ramulosin the corresponding signal is centred at δ 4.45 and is more broadly split. A minor difference ($\Delta\delta$ 0.02) is also noted in the location of the methyl signals in the spectra of the two epimers. Epiramulosin and ramulosin show identical ultraviolet chromophores and both show strong infrared absorption bands at 1650 cm^{-1}. Minor differences in R_f can be noted by careful thin layer chromatographic study.

Thus ramulosin can now be assigned the relative configuration portrayed in **1***a* which is in accord with the nmr based assignment **1***c* by Tanenbaum and Agarwal (7) to 6-hydroxy ramulosin a *Pestolatia ramulosa* metabolite not yet chemically correlated with ramulosin. These authors have obtained (−)mellein **5***b* both by dehydrogenation of 6-hydroxyramulosin **1***c* and from shake cultures of *P. ramulosa*. Since the absolute configuration **5***b* of (−)mellein has been established (8) then the absolute configuration of 6-hydroxyramulosin must be as in **1***c*. This strongly suggests absolute configuration **1***a* for ramulosin in view of the common biogenetic origin of the three metabolites **1***a*, **1***c*, and **5***b*.

Preliminary experiments indicate that the methyldihydro isocoumarin **5***a* inhibits the growth of *Ceratosystus ulmi* (causal fungus of Dutch Elm disease) in plate culture.

Experimental

Melting points were determined on a Kofler hot stage apparatus and are uncorrected. Mass spectra were obtained with an Hitachi–Perkin-Elmer RMU-6D spectrometer. The nmr spectra were recorded in $CDCl_3$ with a Varian T-60 instrument employing tetramethylsilane as internal standard. Line positions are reported in ppm from this standard. The ir spectra were recorded with a Perkin-Elmer 457 grating infrared spectrophotometer.

3,5-Dibromohexanoic Acid from 2,4-Hexadienoic Acid

A two-necked 1 litre round-bottomed flask was partially filled with water (160 ml) and cooled in an ice bath. Anhydrous hydrobromic acid (100 g) was introduced through one neck within a period of 30 min while the solution was stirred vigorously. 2,4-Hexadienoic acid (sorbic acid) (60 g) was added through the second neck in small portions, followed by anhydrous hydrobromic acid (200 g) over a period of 45 min until the sorbic acid was completely dissolved and the solution became yellow and transparent. Stirring was continued at room temperature and a few hours later the solution started to become cloudy and changed color. An oily liquid phase separated in the bottom of the flask. After 36 h the cloudy solution was cooled in an ice bath (or seeded with a crystal from a previous preparation), whereupon large white crystals separated. Filtration under vacuum afforded 3,5-dibromohexanoic acid (137 g, quantitative yield), mp 45–52 °C. Mass spectrum *m/e* 194, 192 (M − HBr), 112, 94. The nmr spectrum δ_{TMS} ($CDCl_3$) 1.8 (d, $J \simeq 7$ Hz, 3H, CH_3—), 2.1–2.6 (complex m, —γ-CH_2—), 3.05 (d, $J \simeq 7$ Hz, 2H, —CH_2—COOH), 4.1–4.8 (complex m, 2H, 2 × —CHBr—), 11.3 (s, 1H, —COOH).

δ-$\Delta^{\alpha,\beta}$-Hexenolactone (2) from 3,5-Dibromohexanoic Acid

A solution of 3,5-dibromohexanoic acid (137 g) in water (1200 ml) in a 2 l flask equipped with a condenser was refluxed for almost 2 h until an oily mass which was formed finally dissolved. The flask was cooled and the solution was extracted with portions of chloroform (3.5 l total). The chloroform solution was concentrated to 500 ml and was washed with 2 N Na_2CO_3 solution (3 × 150 ml). The aqueous phase was extracted with chloroform (2 × 200 ml) and combined with the first chloroform extract. The chloroform solution was dried over anhydrous magnesium sulphate and evaporated. The remaining dark liquid was filtered through a 3 in. column of silica gel (400 g, benzene as eluant) which removed colored impurities and gave hexenolactone (23 g, 41% yield) as a colorless liquid, homogeneous on tlc. Mass spectrum *m/e* 112 (M^+), 97, 68. The nmr spectrum δ_{TMS} ($CDCl_3$) 1.45 (d, $J \simeq 7$ Hz, 3H, CH_3—CHO—), 2.2–2.5 (complex m, 2H, —CH_2—), 4.3–4.9 (m, 1H, —CHO—), 6.0 (t's of a d, $J = 10$ and $J \simeq 1.5$ Hz, 1H, =CH—COO—), 6.8–7.15 (complex m, 1H, β =CH—). The ir spectrum ν_{max} ($CHCl_3$) 1740 cm^{-1} (unsaturated lactone).

Can. J. Chem. Downloaded from www.nrcresearchpress.com by 210.87.254.42 on 09/05/12
For personal use only.

*Diels–Alder Adduct **3b** from δ-$\Delta^{\alpha,\beta}$-Hexenolactone and Butadiene*

In a Pyrex tube was placed hydroquinone (10 mg) and hexenolactone **2** (4.5 g, 4×10^{-2} mol). The tube was cooled in a dry ice – acetone bath and butadiene (15 ml = 9 g = 16.6×10^{-2} mol) and then dried thiophene-free benzene (2 ml) was added. The solvent and reactants occupied $\frac{1}{3}$ of the tube space. The sealed tube was put in an autoclave at 195 °C for 10 h. After evaporation of solvent and excess butadiene, the residue was purified via a silica gel column (150 g packed with chloroform) yielding adduct **3b** (2.5 g, 39%), mp 63–64 °C, eluted with chloroform (some fractions contained the minor adduct **3a** in admixture). *Anal.* calcd. for $C_{10}H_{14}O_2$: C 72.26, H 8.49, O 19.25; found: C 71.98, H 8.40, O 19.42. Mass spectrum *m/e* 166 (M^+), 136, 121. The nmr spectrum δ_{TMS} ($CDCl_3$) 1.40 (d, J = 6 Hz, 3H, CH_3—), 1.7–2.5(complex poorly resolved signals, 8H, $2\times$ >CH— and $3 \times$ —CH_2—), 4.6 (br unresolved m, —CHO—), 5.7 (br s, 2H, —CH=CH—). The ir spectrum ν_{max} ($CHCl_3$) 1740 cm^{-1} (δ lactone).

*Hydrogenation of Adduct **3b***

A mixture of adduct (**3b**) (498 mg, 3 mmol) and Adam's catalyst PtO_2 (50 mg, 0.021 mmol) in ethyl alcohol (15 ml) was subjected to hydrogenation. The solution was stirred for 3 h at room temperature and normal pressure. Then it was filtered and the solvent evaporated yielding a pure oily material **8** (502 mg, quantitative), homogeneous to thin layer chromatography. Mass spectrum *m/e* 168 (M), 153, 124. The nmr spectrum δ_{TMS} ($CDCl_3$) 1.35 (d, J = 6 Hz, 3H, CH_3—), 1.3–2.2 (br unresolved signals, 12H), 4.5 (complex m, 1H, —CHO—). The ir spectrum ν_{max} ($CHCl_3$) 1730 cm^{-1} (lactone).

*Bromolactone **9a** from Lactone **8***

A mixture of dihydro adduct **8** (502 mg, 3 mmol) and pyridinium hydrobromic perbromide (1.0 g, 3.1 mmol) in dried, distilled dioxane (15 ml) was stirred at 90 °C. After 3 h, white particles appeared in the red solution and after a further 30 min, the solvent was evaporated and the residue was treated with water (15 ml) and extracted with chloroform (3×20 ml). The material obtained by evaporation of the chloroform was purified by chromatography with a column of silica gel (150 g, packed in $CHCl_3$) using benzene as eluant. The oily compound **9a**, homogeneous to thin layer chromatography, (420 mg, 56% yield) was obtained. The mass spectrum *m/e* 204 ($M - CO_2$), 166 (M – HBr). *Anal.* calcd. for $C_{10}H_{15}BrO_2$: C 51.94, H 6.54; found: C 51.79, H 6.49. The nmr spectrum δ_{TMS} ($CDCl_3$) 1.45 (d, 3H, J = 6 Hz), 1.4–3.3 (complex m, 11H), 4.8 (sextuplet, $J \simeq 6$ Hz, 1H, —CHO—). The ir spectrum ν_{max} 1760 cm^{-1} (lactone).

*α,β-Unsaturated Lactones **10** and **11** from Bromolactone **9a***

A mixture of bromolactone **9a** (370 mg, 1.5 mmol) and 1,5-diazabicyclo[4.3.0]non-5-ene (DBN) (500 mg, 4 mmol) in toluene (8 ml) was stirred at 95 °C for 24 h under nitrogen atmosphere. The solvent was then evaporated and the residue washed with dilute acetic acid (2.5 ml in 17.5 ml H_2O) to remove excess DBN and extracted with chloroform (3×20 ml). After evaporation of the solvent, the residue was chromatographed on a column of silica gel (100 g packed in $CHCl_3$) using benzene–ether (90:10) as eluant. The oily compound **11** (50 mg, 20% yield) was recovered in early benzene–ether (90:10) fractions. The mass spectrum *m/e* 166 (M^+). The nmr spectrum δ_{TMS} ($CDCl_3$) 1.35 (d, J = 6 Hz, 3H, CH_3—), 1.4–2.3 (complex m's, 10H), 4.5 (complex m, 1H, —CHO—). The ir spectrum ν_{max} ($CHCl_3$) 1710 (α,β-unsaturated lactone). The crystalline product **10** (112 mg, 45% yield), mp 35–40 °C, was obtained in later benzene–ether (90:10) fractions. The mass spectrum *m/e* 166 (M^+), 151, 148, 137. The nmr spectrum δ_{TMS} ($CDCl_3$) 1.4 (d, J = 7 Hz, 3H, CH_3—), 1.4–2.1 (complex m's, 6H), 2.2–2.5 (poorly resolved m's, 3H, allylic), 4.6 (complex m, 1H, —CHO—), 7.05 (m, 1H, —CH=C). The ir spectrum ν_{max} ($CHCl_3$) 1705, 1650 (α,β-unsaturated lactone).

*Epoxylactone **12** from α,β-Unsaturated Lactone **10***

The α,β-unsaturated lactone **10** (112 mg, 0.66 mmol) in dichloroethane (10 ml) was treated with *m*-chloroperbenzoic acid (205 mg, 1.2 mmol) at room temperature for 24 h under nitrogen atmosphere. The peracid was purified by washing with phosphate buffer (pH = 7.5). The solvent was evaporated and the residue was washed with a saturated solution of $NaHCO_3$ to remove excess acid and extracted with methylene chloride. After evaporation of solvent and purification by layer chromatography (benzene–ether 50:50), an oily material **12** (115 mg, 94% yield) homogeneous to thin layer chromatography was obtained. *Anal.* calcd. for $C_{10}H_{14}O_3$: C 65.91, H 7.74, O 26.34; found: C 65.82, H 7.70, O 26.63. The mass spectrum *m/e* 182 (M^+), 156, 154, 139. The nmr spectrum δ_{TMS} ($CDCl_3$) 1.4 (d, J = 6 Hz, 3H, CH_3), 1.4–2.4 (complex m's, 9H), 3.35 (br s, 1H, oxirane), 4.4–4.8 (complex m, 1H, —CHO—). The ir spectrum ν_{max} 1755 cm^{-1} (lactone).

*Hydroxylactone **13** from Epoxylactone **12***

To a solution of chromous chloride (5 ml) made as described by Hirschmann and Hirschmann (10) disodium phosphate (500 mg) was added. Epoxylactone **12** (122 mg, 0.67 mmol) was dissolved in ether (30 ml) and the two solutions were mixed under carbon dioxide atmosphere. The two-phased mixture was stirred for 3 h at room temperature. The ether phase was evaporated and the residue was purified by thin layer chromatography (benzene–ether, 50:50), yielding α,β-unsaturated lactone **10** (60 mg, 60%) and the oily compound **13**, homogeneous on thin layer chromatography. *Anal.* calcd. for $C_{10}H_{16}O_3$: C 65.19, H 8.75, O 26.05; found: C 64.87, H 8.69, O 26.21. The mass spectrum *m/e* 184 (M^+), 166 ($M - H_2O$). The nmr spectrum δ_{TMS} ($CDCl_3 + D_2O$) 1.35 (d, $J \simeq 6$ Hz, 3H, CH_3—), 1.5–2.6 (complex m's, 9H), 4.4–4.9 (complex m, 2H, —CHOH—, —CHO—). The ir spectrum ν_{max} ($CHCl_3$) 1725 cm^{-1} (lactone), 3500 cm^{-1} br (hydroxyl).

*Epiramulosin **1b** from Hydroxylactone **13***

A mixture of hydroxylactone **13** (45 mg, 0.24 mmol) and chromium oxide pyridine complex (300 mg, 1.6 mmol) in methylene dichloride (10 ml) was stirred at room temperature for 1 h under nitrogen atmosphere. The solution was filtered and the solvent evaporated to give a residue which, after purification with thin layer

chromatography (benzene–ether 50:50), afforded crystalline epiramulosin **1***b* (40 mg, 90% yield), mp 64–65 °C. *Anal.* calcd. for $C_{10}H_{14}O_3$: C 65.91, H 7.74, O 26.34; found: C 65.83, H 7.70, O 26.41. The mass spectrum *m/e* 182 (M^+), 167, 163, 154. The nmr spectrum δ_{TMS} ($CDCl_3$) 1.4 (d, $J \simeq 7$ Hz, 3H, CH_3—), 1.4–2.0 (complex m's, 6H), 2.3–2.6 (m's, 3H, allylic), 4.8 (apparent sextuplet, 1H, —CHO—). The ir spectrum ν_{max} 1650, 1615 cm^{-1} (enol lactone), 3000–3500 cm^{-1} br (bonded OH). The uv spectrum λ_{max} (95% ethanol) 265 nm (ϵ 10 000).

This compound proved to be similar but non-identical with an authentic sample of natural ramulosin (mp 120–121 °C) in nmr, ir, and tlc behaviour.

Allylic Oxidation of Adduct 3b

A solution of selenium dioxide (55 mg, 0.5 mmol) in dioxane–water (2 ml – 0.5 ml) was added dropwise over a 2 h period to a magnetically stirred refluxing solution of adduct **3***b* (166 mg, 1 mmol) in dioxane (2 ml). The solution rapidly yellowed and the color intensified to orange and then red as selenium was deposited on the walls of the flask. After 24 h, the solution was diluted with 20 ml water and the organic material extracted with chloroform (3 × 20 ml). The chloroform phase was dried over anhydrous magnesium sulphate. The solvent was evaporated and the residue was purified by layer chromatography (benzene–ether 75:25) yielding a major crystalline compound (73 mg, 80% yield), mp 90–96 °C. The mass spectrum *m/e* 164 ($M - H_2O$), 149 ($M - H_2O - CH_3$). The nmr spectrum δ_{TMS} ($CDCl_3$) 1.4 (d, $J \simeq 6$ Hz, 3H, CH_3—), 1.4–2.8 (complex m's, 6H), 4.1 (br s, 1H, —CHOH—), 4.5 (complex m, 1H, —CHO—), 5.9 (br split s, 2H, —CH=CH—). The ir spectrum ν_{max} ($CHCl_3$) 3400–3550 cm^{-1} (hydroxyl), 1730 cm^{-1} (δ lactone).

Chlorolactone 9b from Lactone 8

A mixture of lactone **8** (168 mg, 1 mmol) and sulfuryl chloride (395 mg, 3 mmol) in carbon tetrachloride (5 ml) was stirred at 80 °C for 24 h under a nitrogen atmosphere. The solvent was evaporated and the residue was purified by short column chromatography (benzene–ether 95:5). An oily compound, homogeneous to thin layer chromatography, was obtained (40 mg, 20% yield) and in later fractions, starting material **8** was recovered. The mass spectrum *m/e* 164 (M – HCl), 149 (M – HCl – CH_3). The nmr spectrum δ_{TMS} ($CDCl_3$) 1.45 (d, $J \simeq 6$ Hz, 3H, CH_3—), 1.4–3.0 (complex m's, 11H), 4.75 (sextuplet, $J \simeq 6$ Hz, 1H, —CHO—). The ir spectrum ν_{max} ($CHCl_3$) 1730 cm^{-1} (δ lactone).

Acknowledgments

Financial assistance from the National Research Council of Canada is gratefully acknowledged and thanks are accorded to M. A. Stilwell, Maritimes Forest Research Centre, Fredericton, New Brunswick, for conducting the bioassays with *Ceratocystus ulmi*. Thanks are due also to C. W. Hesseltine, Northern Regional Research Laboratory, Peoria, Illinois for providing a sample of natural ramulosin.

1. F. Stodola, C. Cabot, and C. Benjamin. Biochem. J. **93**, 92 (1964).
2. R. Kuhn and J. Jerchel. Ber. **76**, 413 (1943).
3. P. Garratt and M. Wyott. Chem. Commun. 251 (1974).
4. H. Brown and P. Geoghegan. J. Org. Chem. **35**, 1844 (1970).
5. B. Rickborn and S. Luo. J. Org. Chem. **30**, 2212 (1965); R. Carlson and N. Behn. J. Org. Chem. **32**, 1363 (1967).
6. C. Robinson and R. Henderson. J. Org. Chem. **37**, 567 (1972).
7. S. Tanenbaum and S. Agarwal. Tetrahedron Lett. 2377 (1970).
9. W. Klyne and J. Buckingham. Atlas of stereochemistry. Oxford University Press. London. 1974. p. 180.
10. H. Hirschmann, F. Hirschmann, and J. Corcoran. J. Org. Chem. **20**, 572 (1955).

Can. J. Chem. Downloaded from www.nrcresearchpress.com by 210.87.254.42 on 09/05/12
For personal use only.

Monomeric di-oxygen adducts of high spin cobalt(II) complexes

G. P. KHARE, E. LEE-RUFF, AND A. B. P. LEVER[1]

Department of Chemistry, York University, 4700 Keele St., Downsview, Ont., Canada M3J 1P3

Received May 17, 1976

G. P. KHARE, E. LEE-RUFF, and A. B. P. LEVER. Can. J. Chem. **54**, 3424 (1976).

The complexes Co(*s*-R_2en)$_2X_2$ where R is Me, Et, and X is Cl, Br, I, NCS, or NO_3, are shown to reversibly bind di-oxygen in polar solvents. Electron spin resonance and spectrophotometric measurements reveal the formation of 1:1 adducts which are fairly stable towards further reaction. Thermodynamic binding constants are determined and are found to be larger than hitherto reported for such Co(II)–O_2 systems. This is ascribed to the high basicity of the amines employed. Conductivity measurements reveal extensive hydrogen bonding for these adducts in butyronitrile.

G. P. KHARE, E. LEE-RUFF et A. B. P. LEVER. Can. J. Chem. **54**, 3424 (1976).

On démontre que les complexes Co(*s*-R_2en)$_2X_2$, où R = Me, Et et X = Cl, Br, I, NCS ou NO_3 se lient d'une façon réversible à l'oxygène moléculaire dans des solvants polaires. Des mesures spectrophotométriques et de rpe révèlent la formation d'adduits 1:1 qui sont relativement stables vis à vis d'autres réactions. Les constantes thermodynamiques de liaison ont été déterminées et on a trouvé qu'elles sont plus larges que celles rapportées antérieurement pour des systèmes tels que Co(II)–O_2. Ce résultat est attribué à la grande basicité des amines utilisées. Des mesures de conductivité révèlent l'existence d'importantes liaisons hydrogène pour ces adduits dans le butyronitrile.

[Traduit par le journal]

Introduction

Cobalt(II) complexes carrying molecular oxygen have been known since 1938 (1). Since this time intensive effort has been made to understand the structure, mode of metal–di-oxygen binding, and ligand requirements necessary to confer good carrying properties. The field has recently been reviewed (2). In recent times interest has increased because of the role played by analogous iron compounds in living systems. In particular these carriers mimic the transport proteins where oxygen is stabilized by binding to iron in a porphyrin environment. Indeed coboglobin, the cobalt analog of hemoglobin, has been prepared (3) and shown to have activity fairly similar to that of the iron species. In addition to transporting oxygen, some iron proteins will also catalyze the oxygenation of various substrates (4). Cobalt analogs are not known in nature but synthetic cobalt compounds, by analogy with coboglobin, might be anticipated to have some comparable activity.

It is surprising to note that there are only a few reports dealing with the oxidase and oxygenase activity exhibited by *model* complexes of either iron or cobalt. Ternary complexes of the type S-CoL(O_2) or S-CoL(O_2)CoL, where S is a substrate and L are various ligands (5–7), have been claimed as intermediates. However, the exact mechanisms for action of the enzymes or of model compounds are far from understood.

We have discovered a series of cobalt oxygen-carrying complexes which mimic the enzymes and will form ternary complexes, which are currently under investigation. In this paper we report details of the reaction of these complexes with molecular oxygen. The complexes are derivatives of the general type Co(*s*-R_2en)$_2X_2$ (*s*-R_2en is an *N*,*N'* symmetrically disubstituted alkyl ethylenediamine and, X is Cl^-, Br^-, I^-, NO_3^-, and NCS^-), whose preparation of characterization have been previously reported (8). These compounds bind molecular oxygen reversibly in polar organic solvents yielding 1:1 adducts in solution. They are stable in the solid state in dry air, and will dissolve in many non-polar organic solvents to yield solutions of the cobalt(II) species which will *not* absorb molecular oxygen at room temperature, though there is some evidence for marginal adduct formation at low temperatures. If various organic substrates, such as ethyl *p*-hydroxybenzoate are added to these non-polar solutions, then oxygen uptake does take place to form complexes in which model complex, substrate, and di-oxygen, are simultaneously bound (ternary complex). Details of

Can. J. Chem. Downloaded from www.nrcresearchpress.com by 210.87.254.40 on 09/05/12
For personal use only.

these derivatives will be presented in due course (9).

In this fashion these model complexes mimic many oxygenase enzyme systems in that reaction with di-oxygen only takes place *after* the substrate has been added to the system (4, 10). Thermodynamic data reported here reveal that this series of complexes form the most stable 1:1 adducts with di-oxygen yet reported for cobalt(II).

Experimental Section

Materials

Cobalt(II) salts were obtained commercially and used without further purification. *N,N'*-Diethylethylenediamine (*s*-Et_2en) and *N,N'*-dimethylethylenediamine (*s*-Me_2en) were obtained commercially (Koch-Light Laboratories Ltd., U.K.), but were distilled prior to use. *N*-Butyronitrile (Aldrich Chemical Co.) was refluxed and distilled from CaH_2 prior to use.

Preparation of Co(s-R_2en)$_2X_2$ Complexes

All preparations and manipulations of the cobalt complexes were carried out under an atmosphere of prepurified nitrogen. The procedures followed were the same as previously described (8). Prior to thermodynamic measurements, the complexes were recrystallized to analytical purity using acetonitrile under a nitrogen atmosphere.

Isolation of Oxygen Adducts

This isolation was achieved only for the complex Co(*s*-Me_2en)$_2Cl_2$. Pink solutions of Co(Me_2en)$_2Cl_2$ in ethanol, at room temperature, were exposed to dry oxygen gas for 10 min in the presence of excess *s*-Me_2en. To the red–brown solutions thus obtained was added a saturated solution of either $NaClO_4$, or NH_4PF_6 in ethanol. The oxygen adducts precipitate out as dark brown solids which were filtered and washed with ethanol and diethyl ether and dried *in vacuo*. The compounds cannot be recrystallized without decomposition and are difficult to obtain analytically pure (see text). *Anal.* calcd. for [Co(*s*-Me_2en)$_2$(Cl)O_2]ClO_4: Co 14.67, found: Co 13.66; calcd. for [Co(*s*-Me_2en)$_2$(Cl)O_2]PF_6: Co 13.08, found: Co 12.69. The dry samples decomposed slowly at room temperature. Electron paramagnetic resonance of solid samples were essentially identical to the spectra of other reported monomeric oxygen adducts in frozen solution.

Instruments

Electron paramagnetic resonance spectra were recorded on a Varian Associates E-4 Spectrometer. The *g* values were determined by calibration with DPPH powder (2.0037).

Conductivity measurements were made on a Wayne-Kerr Conductivity universal bridge model B221A.

A Beckman Model DU Spectrometer was used for spectroscopic measurements, using a cell thermostated with a Precision Scientific Lo-Temptrol circulating bath.

Equilibrium Measurements

The equilibrium constants *K* for the reaction

$$[1]\quad \text{Co}(s\text{-Et}_2\text{en})_2\text{Cl}_2 + \text{O}_2 \overset{K}{\rightleftharpoons} [\text{Co}(s\text{-Et}_2\text{en})_2\text{Cl}(\text{O}_2)]^+ + \text{Cl}^-$$

were measured at 20 °C (±0.1 °C) in butyronitrile using visible spectroscopy. In a typical measurement, 5.0×10^{-5} *M* of Co(*s*-Et_2en)$_2X_2$ complex was weighed into a reaction flask (specially designed and equipped with a quartz cell, 1 cm pathlength so that spectra could be recorded at various stages of the experiment). The flask was then evacuated and filled with nitrogen gas. Freshly distilled and degassed butyronitrile (30 ml) was then introduced in the flask using a syringe. Stringent precautions were taken to exclude oxygen from the system at this stage. Amine ligand *s*-Et_2en (5.0×10^{-1} *M*) was added to the reaction flask with the help of a calibrated syringe and the electronic spectrum of the pink cobalt(II) complex recorded. The reaction flask after connection to the vacuum line was cooled in liquid nitrogen to freeze the solvent, and then evacuated to approximately 10^{-5} torr. Subsequently, after temperature equilibration, the contents of the flask were exposed to varying amounts of air at known pressures. The pink solution on exposure to di-oxygen turns brown immediately. Whilst the reaction with di-oxygen seems essentially instantaneous, the contents of the flask were stirred for ½ h, in the presence of the known pressure of air, to ensure complete equilibration, prior to the absorbance of the solution being measured. The oxygen complex, but not the cobalt(II) precursor, has strongly rising absorption below 450 nm. Equilibrium constants were calculated from the change in absorption at a specific wavelength in the range λ = 350–450 nm. Values of *K* were found to be independent of the wavelength used.

Results and Discussion

(i) Octahedral–Tetrahedral Equilibrium

Previous studies (8) have revealed that the complexes under discussion, Co(*s*-R_2en)$_2X_2$, are octahedral and believed to be *trans* in all cases.

In the absence of air, these complexes dissolve freely in most donor organic solvents yielding blue or pink solutions depending upon R and X. In general an octahedral–tetrahedral equilibrium is set up:

$$[2]\quad \text{Co}(s\text{-R}_2\text{en})_2\text{X}_2 \rightleftharpoons \text{Co}(s\text{-R}_2\text{en})\text{X}_2 + s\text{-R}_2\text{en}$$

The blue solutions have electronic spectra in the visible region typical of tetrahedral cobalt(II) species (11). Cooling of the solution or addition of excess amine reverses the equilibrium regenerating the pink octahedral species solution. In some solvents solvolysis of X^- may also occur to a limited extent. Addition of excess X^- to such solutions does not restore the octahedral species implying that loss of amine, rather than loss of X^- is the principal mechanism for formation of the

Can. J. Chem. Downloaded from www.nrcresearchpress.com by 210.87.254.40 on 09/05/12
For personal use only.

TABLE 1. Equilibrium constants for $Co(Et_2en)_2X_2 + O_2 \rightleftharpoons [Co(Et_2en)_2X(O_2)]^+ + X^-$ reaction at 20 °C

Complex ~5.0×10^{-5} mol	Solvent	[Added amine] (mol)	log K aq[a] (mm^{-1})	$P_{O_{2(1/2)}}$[b]	n[c]
$Co(s\text{-}Et_2en)_2Cl_2$	Butyronitrile	5.0×10^{-3}	−1.26(4)	17.4	1.01
	Benzonitrile	5.0×10^{-3}	−1.28(1)	16.4	1.06
$Co(s\text{-}Et_2en)_2(NCS)_2$	Butyronitrile	5.0×10^{-3}	−1.50(3)	30.8	1.11
$Co(s\text{-}Et_2en)_2(NO_3)_2$	Butyronitrile	5.0×10^{-3}	−0.59(11)	3.4	1.01
$Co(s\text{-}Et_2en)_2Br_2$	Butyronitrile	5.0×10^{-3}	−0.39(6)	2.4	1.00
$Co(s\text{-}Et_2en)_2I_2$	Butyronitrile	5.0×10^{-3}	—	~1	1.00

[a]Numbers in parentheses are estimated standard deviations in the least significant figure.
[b]Because of very small amount of O_2 involved for this measurement the values for log K could not be obtained and $P_{O_{2(1/2)}}$ is only roughly estimated number.
[c]n is the slope of the plot of log $(A - A_0)/(A_\infty - A)$ *vs.* log p_{O_2} (13).

tetrahedral species. This equilibrium was studied only in sufficient depth to provide a means of ensuring that our thermodynamic measurements were carried out in solutions containing essentially 100% of the octahedral species. The tetrahedral species does not react with molecular oxygen.

Using the intensity of the tetrahedral absorption spectra as a guide, equilibrium [2] was demonstrated qualitatively to lie more to the right in the sequence:

[3] $$X = NO_3^- < NCS^- \lesssim I^- < Br^- < Cl^-$$

In the case of the nitrate complex, solutions in solvents such as acetonitrile and ethanol (and probably other solvents) contain essentially 100% of the octahedral species as would be anticipated. The tetrahedral species predominates when $X = Cl^-$. Experiments revealed that addition of a 50-fold excess of amine (s-Et_2en) was sufficient to move equilibrium [2] completely to the left, in the case of $X = Cl^-$, and hence for all counter-ions.

(ii) Reaction with Molecular Oxygen

Addition of molecular oxygen to a solution of one of the above complexes in the presence of excess amine in a polar solvent such as methanol, ethanol, acetonitrile, pyridine, butyronitrile, etc., results in an immediate colour change from pink to brown. In the case of the nitrate and thiocyanate complexes, excess amine is unnecessary for oxygen uptake to occur since these complexes are already predominantly octahedral in solution. Similarly, cooled solutions of the halides will absorb oxygen. However, even in these cases, the presence of excess amine increases the affinity for di-oxygen, by a mechanism which is not yet understood.

Solutions of the oxygen adduct are moderately stable towards further reaction. However, over prolonged periods of time (days), they either produce brown insoluble precipitates or auto-oxidize, forming red solutions containing Co(III) amine species. Generally speaking, 1:1 adducts usually react further to yield dimeric oxygen bridged derivatives (2). There is no evidence that this happens with these species, thereby allowing for a thermodynamic study of the 1:1 adducts. Reproducible results may be obtained over the time period of the experiment (hours).

(iii) Thermodynamic Measurements

Measurement of the absorption of the oxygen adduct, at fixed wavelength, as a function of oxygen pressure provides a means both of determining the nature of the adduct (from the stoichiometry of the reaction) and of its stability (from the equilibrium constant) (*e.g.* ref. 12). An appropriate log plot (see Table 1) of a function of the observed absorbance versus the partial oxygen pressure yielded a slope of 1 for all the complexes studied indicating a 1:1 stoichiometry for reaction 1. Electron spin resonance spectra (see below) of oxygenated solutions containing either the s-Me_2en or s-Et_2en complexes confirmed the presence of these 1:1 adducts, although poor solubility has so far prevented any thermodynamic measurements with the former amine.

The equilibrium constants, and calculated $P_{1/2}$ values, were obtained under identical conditions of excess amine for all the complexes investigated. We cannot be sure that these repre-

Can. J. Chem. Downloaded from www.nrcresearchpress.com by 210.87.254.40 on 09/05/12
For personal use only.

TABLE 2. Molar conductivity of $Co(s\text{-}Et_2en)_2X_2$ complexes

Complex	Solvent	Λ Under N_2[a]	Λ Under N_2 + amine[b]	Λ Under O_2 + amine[c]
$Co(s\text{-}Et_2en)_2Cl_2$	Butyronitrile	—[d]	4.5[e]	8.1[e]
	Acetonitrile	63	73	93
$Co(s\text{-}Et_2en)_2Br_2$	Butyronitrile	—	11	16
	Acetonitrile	55	66	76
$Co(s\text{-}Et_2en)_2(NCS)_2$	Butyronitrile	—	13	24
	Acetonitrile	94	136	189
$Co(s\text{-}Et_2en)_2(NO_3)_2$	Butyronitrile	—	26	36
	Acetonitrile	271	283	305
$Co(s\text{-}Et_2en)_2I_2$	Butyronitrile	—	43	61
	Acetonitrile	—	—	—
$((C_2H_5)_4N)Cl$	Butyronitrile	65	—	—
	Acetonitrile	146	—	—

[a]Measurement of degree of solvolysis of X in [2].
[b]Measurement of degree of solvolysis of X in [5].
[c]Measurement of degree of ionization in [6].
[d]Not measured.
[e]Reactions were measured at a 5×10^{-5} *M* concentration of complex with a 100-fold molar excess of sym-Et_2en as indicated. Units of conductivity are mho mol^{-1} cm^{-2}.

sent limiting values since further addition of amine tends to lead to precipitation over the time period of the experiment.

The ability to bind oxygen increases in the sequence:

[4] $$SCN^- < Cl^- < NO_3^- \sim Br^- < I^-$$

The ability of cobalt(II) to bind oxygen, in the presence of nitrogen donor ligands, is known to be dependent upon the amount of electron density transmitted to the cobalt(II) ion and hence on to the coordinated di-oxygen molecule (13). The esr data reported below confirm that these complexes should be regarded in the usual fashion as derivatives of Co(III) containing a coordinated superoxide ion (O_2^-). The log *K* values reported in Table 1 imply that these amine complexes bind di-oxygen more strongly than in any other 1:1 adduct of cobalt(II). Certainly this is consistent with the fact that these are probably more strongly basic amines than those hitherto investigated. The sequence [4] also reflects increasing binding of oxygen as the counter-ion ligand donates more charge, although the position of the nitrate group seems anomalous.

(iv) Conductivity Measurements

In order to understand the role played by the solvent in the oxygenation of the metal complex, the conductivity of the solution was followed as the reaction proceeded.

In acetonitrile, in the absence of excess amine, the halogen complexes disassociate according to [2], yielding tetrahedral species whose conductivity is low under a nitrogen atmosphere, due to some solvolysis of the halide ions (Table 2). When excess amine is added, the conductivity increases slightly due to some solvolysis of the octahedral species as indicated in [5]. This equilibrium lies incompletely to the right. When oxygen is admitted the conductivity rises but reaches a limiting value within the range expected for a 1:1 electrolyte (15). This observation is consistent with [6].

[5] $$Co(s\text{-}R_2en)_2X_2 + CH_3CN \rightleftharpoons Co(s\text{-}R_2en)_2(CH_3CN)X^+ + X^-$$

[6] $$Co(s\text{-}R_2en)_2(CH_3CN)X^+ + O_2 \rightarrow Co(s\text{-}R_2en)_2(O_2)X^+ + CH_3CN$$

In the case of $X = NO_3^-$, additional solvolysis occurs in acetonitrile with some dissociation of the remaining coordinated nitrate group in [2], [5], and [6]. It seems probable that reaction 1 is driven, in part, by the solvolysis of X^- creating a site for molecular oxygen to bind. Thus the oxygenation reaction takes place in donor, and necessarily polar, solvents, but not in non-donor, non-polar, solvents. It will take place in propyl-

Can. J. Chem. Downloaded from www.nrcresearchpress.com by 210.87.254.40 on 09/05/12
For personal use only.

TABLE 3. Electron paramagnetic resonance parameters[a] for O_2^- adducts of Co(*s*-R_2en)$_2X_2$

Compound	Solvent	g_{iso}	$g_{\parallel}$	$g_{\perp}$	A_{iso}^{Co}	$A_{\parallel}^{Co}$	$A_{\perp}^{Co}$
Co(*s*-Et_2en)$_2Cl_2$	EtOH	2.029	2.094_5	1.996	14.4	27.4	7.9
Co(*s*-Et_2en)$_2Br_2$	EtOH	2.017	2.079	1.986	12.6	28.2_5	4.8
	BuCN	2.028	2.076_5	2.003	14.6	28.0	7.9
Co(*s*-Et_2en)$_2I_2$	EtOH	2.019	2.074	1.987	12.1[b]	27.0	4.7
	BuCN	2.029	2.081	2.002	14.9	27.5	8.5_5
Co(*s*-Et_2en)$_2$(NO_3)$_2$	EtOH	2.023[c]	2.068_5	2.001	13.5[c]	28.4	6.0
	BuCN		2.078	1.97[d]		27.5	
Co(*s*-Et_2en)$_2$(NCS)$_2$	EtOH	2.024	2.072	2.000	14.4	24.0	9.6
Co(*s*-Me_2en)$_2Cl_2$	EtOH	2.030[c]	2.073	2.008	14.2_5[c]	26.4	8.2

[a]Isotropic data collected at ~ -50 °C except where indicated. Anisotropic data collected at liquid nitrogen temperature. The $g_{\perp}$ values were calculated from g_{iso} and the well resolved $g_{\parallel}$ spectrum. Hyperfine coupling constants in G.
[b]Eight-line spectrum poorly resolved.
[c]Measured in ethanol at 25 °C.
[d]Estimated from frozen spectrum.

ene carbonate, which is a polar, but non-donor, solvent. This observation provides compelling evidence that solvolysis of X^-, rather than coordination of the solvent to the cobalt(II) ion, is important.

When conductivity measurements were carried out in butyronitrile, it was initially disturbing to note the very low conductivities produced (Table 2). For the complexes in butyronitrile, under a nitrogen atmosphere, and containing excess amine, the conductivities were, for most ions, much less than anticipated for a 1:1 electrolyte (Table 2) (14). Addition of di-oxygen caused a small increase, but with the exception of the iodide, the conductivities were still markedly low. In the chloride complex, for example, the solution even after oxygenation was almost non-conducting. The logical explanation is that ion-pairing is occurring, even though butyronitrile is sufficiently polar to separate ion pairs at the low concentrations employed. The sequence of conductivities:

[7] $$Cl^- < Br^- < SCN^- < NO_3^- < I^-$$

parallels the abilities of these ions to hydrogen bond. It seems probable, therefore, that the counter-ion X is indeed being ionized, as in [6], but remains hydrogen bonded to the amine hydrogen atoms, in this solvent.

(v) Electron Spin Resonance Data

The oxygen adducts exhibit a fluid esr spec-

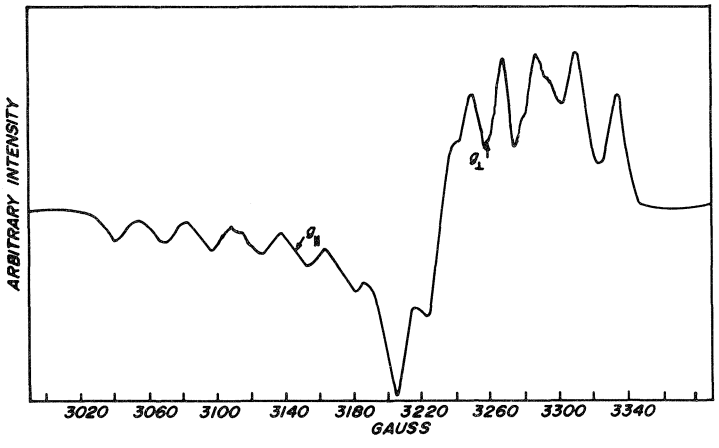

FIG. 1. The electron spin resonance spectrum of Co(*s*-Et_2en)$_2Br_2$ dissolved in ethanol at liquid nitrogen temperature. (Modulation amplitude 0.8×10^0 G; gain 5×10^3; field 9.150 GHz).

Can. J. Chem. Downloaded from www.nrcresearchpress.com by 210.87.254.40 on 09/05/12
For personal use only.

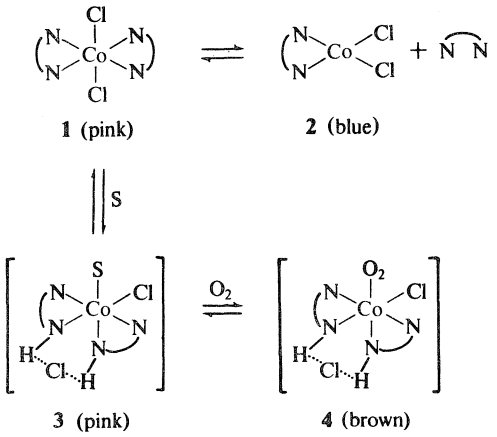

trum in solution, at near ambient temperatures, typical of cobalt di-oxygen ($Co(III)–O_2^-$) 1:1 adducts, *i.e.* an 8-line hyperfine spectrum, due to $I = 7/2$ of ^{59}Co, with a g value near 2.0 (13, 15). The magnitude of the isotropic coupling constant is also comparable to those previously described. Frozen or solid state samples show the expected anistropic, near axial, spectra (Fig. 1, Table 3).

The parameter values are comparable with those previously reported, except in one respect. They are atypical in that the various parameters are much less dependent upon the nature of X^- than would be anticipated (13). This could be explained if a *cis* structure for the complexes (Fig. 2) is postulated. Under such circumstances the unpaired electron density, lying primarily on the di-oxygen molecule, should be less sensitive to the nature of X. The spectra are rhombically distorted which would be consistent with a *cis* formulation. However, the *trans* isomer should also exhibit rhombic distortion since it can have at most D_{2h} symmetry. Further work is necessary to clarify this conclusion. Because of the additional solvation factors involved, the sensitivity of $P_{1/2}$ to X is not vitiated by the above argument.

We note in conclusion that solutions of the cobalt complexes in solvents such as dichloromethane (a non-polar solvent) show no signals in their esr spectra at room temperature since oxygenation does not occur to any measurable degree. If an organic substrate, such as ethyl *p*-hydroxybenzoate, is added to such a solution, in the presence of di-oxygen, a strong 8-line signal is rapidly generated, showing formation of a 1:1 adduct necessarily containing the substrate. Over a period of time, this collapses and is replaced by a 15-line signal, indicative of a bridging superoxy species. Details of these reactions will be published in due course (9).

Acknowledgements

We are indebted to Geraldine O'Brien and Ernest Quan for experimental assistance, and to the National Research Council of Canada and York University for financial assistance.

1. T. TSUMAKI. Bull. Chem. Soc. Jpn. **13**, 252 (1938).
2. J. S. VALENTINE. Chem. Rev. **73**, 235 (1973); G. MCLENDON and A. E. MARTELL. Coord. Chem. Rev. **19**, 1 (1976).
3. B. M. HOFFMAN and D. H. PETERING. Proc. Nat. Acad. Sci. **67**, 637 (1970).
4. T. E. King, H. S. Mason, and M. Morrison (*Editors*). Oxidases and related redox systems. Vols. 1 and 2. University Park Press, Baltimore. 1973.
5. D. WAGNEROVA, E. SCHWERTNEROVA, and I. VPREK SISKA. Coll. Czech. Chem. Commun. **38**, 756 (1973).
6. A. NISHINAGA, T. TOGO, and T. MATSUURA. Chem. Commun. 896 (1974).
7. A. NISHINAGA, K. WATANBE, and T. MATSUURA. Tetrahedron Lett. 1291 (1974).
8. A. B. P. LEVER and E. MANTOVANI. Can. J. Chem. **51**, 1567 (1973).
9. G. P. KHARE, E. LEE-RUFF, and A. B. P. LEVER. Unpublished results.
10. Y. ISHIMURA, V. ULLRICH, and J. A. PETERSON. Biochem. Biophys. Res. Commun. **42**, 140 (1971).
11. A. B. P. LEVER. Inorganic electronic spectroscopy. Elsevier Publ. Co., Amsterdam. 1968.
12. J. A. IBERS, D. V. STYNES, H. C. STYNES, and B. R. JAMES. J. Am. Chem. Soc. **96**, 1358 (1974).
13. B. M. HOFFMAN, D. L. DIEMENTE, and F. BASOLO. J. Am. Chem. Soc. **92**, 61 (1970).
14. W. J. GEARY. Coord. Chem. Rev. **7**, 81 (1972).
15. F. A. WALKER. J. Am. Chem. Soc. **92**, 4235 (1970).

Can. J. Chem. Downloaded from www.nrcresearchpress.com by 210.87.254.40 on 09/05/12
For personal use only.

Synthesis and vibrational spectra of some lead(II) halide adducts with O-, S-, and N-donor atom ligands

IVOR WHARF,[1] THOR GRAMSTAD,[2] RAMESH MAKHIJA, AND MARIO ONYSZCHUK
Department of Chemistry, McGill University, Montreal, P.Q., Canada H3C 3G1

Received March 10, 1976

IVOR WHARF, THOR GRAMSTAD, RAMESH MAKHIJA, and MARIO ONYSZCHUK. Can. J. Chem. **54**, 3430 (1976).

Lead(II) halides (PbX_2 where X = Cl, Br, and I) formed five types of adducts with monodentate (L) and bidentate (LL) ligands: $PbX_2 \cdot L$, $PbX_2 \cdot 2L$, $2PbX_2 \cdot L$, $PbX_2 \cdot LL$, and $PbX_2 \cdot 2LL$, but not all halides and ligands produced each type. Monodentate ligands were dimethylsulphoxide, *N*,*N*-dimethylacetamide, *N*,*N*-dimethylthioacetamide, thioacetamide, 2,6-dimethyl-γ-pyrone, *N*-methyl-2-pyridone, *N*-methyl-2-pyrollidinone, thiourea, pyridine, piperidine, and aniline, while bidentate ligands were ethylenediamine, tetramethylethylenediamine, 1,10-phenanthroline, and 2,2′-bipyridine. Infrared and Raman spectra are reported together with ligand vibrational frequencies shifted by coordination. Under similar experimental conditions qualitative trends in acceptor and donor abilities appeared to be $PbI_2 > PbBr_2 > PbCl_2$ and S-donors > O-donors, respectively.

IVOR WHARF, THOR GRAMSTAD, RAMESH MAKHIJA et MARIO ONYSZCHUK. Can. J. Chem. **54**, 3430 (1976).

Les halogénures de plomb(II) (PbX_2 où X = Cl, Br et I) forment cinq types d'adduits avec des ligands monodentates (L) et bidentates (LL): $PbX_2 \cdot L$, $PbX_2 \cdot 2L$, $2PbX_2 \cdot L$, $PbX_2 \cdot LL$ et $PbX_2 \cdot 2LL$; toutefois tous les halogénures et tous les ligands ne produisent pas chaque type d'adduit. Les ligands monodentates sont le diméthylsulfoxyde, la *N*,*N*-diméthylacétamide, la *N*,*N*-diméthylthioacétamide, la thioacétamide, la diméthyl-2,6 γ-pyrone, la *N*-méthylpyridone-2, la *N*-méthylpyrollidinone-2, la thiourée, la pyridine, la pipéridine et l'aniline; les ligands bidentates sont l'éthylènediamine, la tétraméthyléthylènediamine, la phénanthroline-1,10 et la bipyridine-2,2′. On rapporte les spectres infrarouges et Raman de même que les fréquences vibrationnelles des ligands qui sont déplacées par coordination. Dans des conditions expérimentales semblables, les tendances qualitatives dans les capacités comme accepteur ou comme donneur semblent être respectivement $PbI_2 > PbBr_2 > PbCl_2$ et les S-donneurs > les O-donneurs.

[Traduit par le journal]

Introduction

In contrast to the large number of tin(II) halide complexes which have been prepared and characterized, little is known about adducts of lead(II) halides. Except for earlier studies on lead(II) halide adducts with thiourea (1), pyridine (2), aniline (3), and ammonia (4), most of the work to date (5–11) has dealt with lead(II) halide adducts only in a cursory way and little vibrational data is available. Only the lead(II) halide – thiourea system has received detailed study (12, 13), with a crystal structure (14) and a partial infrared assignment (15) of the thiourea (tu) adduct $PbCl_2 \cdot 2tu$ having been published. In this work, the reactions of lead(II) halides with various oxygen-, sulphur-, and nitrogen-donor ligands were surveyed to determine adduct stoichiometries and qualitative trends in adduct formation. Infrared and Raman data were obtained in the ligand region to ascertain the coordinating atom of the ligand.

Experimental

Lead(II) chloride and all ligands were of reagent grade and were used as obtained from commercial suppliers.

Lead(II) bromide and iodide were prepared by mixing aqueous solutions of lead nitrate with aqueous solutions of potassium bromide and iodide respectively. Liquid oxygen- and sulphur-donor ligands and solvents such as benzene and carbon tetrachloride were stored over molecular sieves, but absolute ethanol and anhydrous ether were used as received. Most liquid amines were stored over NaOH, while pyridine and aniline were used freshly distilled from NaOH. When necessary, liquid aliphatic amines and benzene were dried prior to use by distillation from CaH_2 under nitrogen.

Carbon, hydrogen, and nitrogen analyses were done by

[1]Present address: Dawson College (Selby Campus), Westmount, Quebec.

[2]On sabbatical leave from the University of Bergen, Norway, 1973–1974.

Chemalytics Inc., Arizona. Lead was determined gravimetrically as lead sulphate. Melting points were measured in sealed glass capillaries using a Gallenkamp apparatus and are uncorrected. Infrared spectra of samples as Nujol mulls between KBr plates were measured using a Perkin-Elmer 521 spectrometer, and Raman spectra of powder samples in glass capillaries were recorded on a Jarell-Ash 25-300 instrument using Kr^+ (647.1 nm) and Ar^+ (514.5 nm) laser excitation. For sharp bands of moderate to strong intensity, infrared and Raman frequencies are accurate to $\pm 2\,cm^{-1}$.

Preparations

A. Adducts with Liquid Amides and Dimethylsulphoxide

Lead(II) halide (2 to 6 g) was dissolved in excess liquid ligand (20 to 40 ml) with warming if necessary. Addition of carbon tetrachloride or benzene to the filtered solution gave the product which was filtered and dried in a vacuum. Prepared in this manner were: *Lead(II) bromide – N,N-dimethylacetamide*, with CCl_4, 52% yield, white, decomp. >200 °C (Found: C, 10.8; H, 1.9; N, 1.8; Pb, 45.5. $PbBr_2 \cdot C_4H_9NO$ requires C, 10.6; H, 2.0; N, 3.1; Pb, 45.6). *Lead(II) iodide – N,N-dimethylacetamide*, with CCl_4, 87%, light-yellow, decomp. >200 °C (Found: C, 8.8; H, 1.7; N, 2.1; Pb, 37.3. $PbI_2 \cdot C_4H_9NO$ requires C, 8.8; H, 1.7; N, 2.6; Pb, 37.8). *Lead(II) bromide – N-methylpyrollidinone*, with CCl_4, 85%, white, decomp. >180 °C (Found: C, 12.9; H, 1.9; N, 2.7; Pb, 44.1. $PbBr_2 \cdot C_5H_9NO$ requires C, 12.9; H, 1.95; N, 3.0; Pb, 44.4). *Lead(II) iodide – N-methylpyrollidinone*, with CCl_4, 86%, light-yellow, decomp. >180 °C (Found: C, 10.9; H, 1.4; N, 1.7; Pb, 36.0. $PbI_2 \cdot C_5H_9NO$ requires C, 10.7; H, 1.6; N, 2.5; Pb, 36.5). *Lead(II) iodide – bis(N-methyl-2-pyridone)*, with C_6H_6, 100%, off-white, decomp. >235 °C (Found: C, 22.3; H, 2.2; N, 4.2; Pb, 29.7. $PbI_2 \cdot 2C_6H_7NO$ requires C, 21.2; H, 2.1; N, 4.1; Pb, 30.5). *Lead(II) bromide – bis(dimethylsulphoxide)*, with CCl_4, 65%, white needles, m.p. (decomp.) ~100 °C (Found: C, 9.3; H, 2.3; Pb, 38.5. $PbBr_2 \cdot 2C_2H_6OS$ requires C, 9.2; H, 2.3; Pb, 39.6). *Lead(II) iodide – bis(dimethylsulphoxide)*, with CCl_4, 58%, cream needles, m.p. (decomp.) ~135 °C (Found: C, 8.1; H, 2.2; Pb, 32.45. $PbI_2 \cdot 2C_2H_6OS$ requires C, 7.8; H, 2.0; Pb, 33.6).

Lead(II) iodide – dimethylsulphoxide. Lead(II) iodide (3.2 g) was dissolved in hot dimethylsulphoxide (30 ml) and ethanol (80 ml) was added to the filtered solution to give a flocculent cream precipitate which, after filtration and washing with ethanol (3 × 25 ml), yielded the *yellow mono-adduct*, 97% yield, decomp. 173–178 °C (Found: C, 4.1; H, 0.95; Pb, 38.4. $PbI_2 \cdot C_2H_6OS$ requires C, 4.5; H, 1.1; Pb, 38.4).

B. Adducts with Liquid Amines

Lead(II) halide (3 to 4 g) was stirred with 100 ml of a solution of amine (10 to 30 ml) in benzene or ethanol for a sufficient time (2 to 4 days) to ensure complete reaction. The solid product was filtered and dried in a vacuum. Obtained this way were: *Lead(II) iodide – piperidine*, from C_6H_6, 68%, yellow, decomp. >230 °C (Found: C, 10.3; H, 2.0; N, 2.5; Pb, 37.7. $PbI_2 \cdot C_5H_{11}N$ requires C, 11.0; H, 2.0; N, 2.6; Pb, 38.0). *Lead(II) chloride – aniline*, from C_6H_6, 96%, white plates, decomp. >90 °C (Found: C, 18.6; H, 1.8; N, 3.7; Pb, 56.4. $PbCl_2 \cdot C_6H_7N$ requires C, 19.4; H, 1.9; N, 3.8; Pb, 55.8). *Lead(II) iodide – aniline*, from C_6H_6, 98%, yellow, decomp. >130 °C (Found: C, 12.9; H, 1.0; N, 2.45; Pb, 37.4. $PbI_2 \cdot C_6H_7N$ requires C, 13.0; H, 1.3; N, 2.5; Pb, 37.4). *Tris(Lead(II) bromide) – bis(aniline)*, from benzene, 85%, cream-yellow, decomp. >123 °C (Found: C, 10.6; H, 0.8; N, 2.05; Pb, 48.1. $3PbBr_2 \cdot 2C_6H_7N$ requires C, 11.2; H, 1.1; N, 2.2; Pb, 48.3). *Lead(II) chloride – bis(pyridine)*, from C_6H_6, 91%, white (Found: Pb, 48.4. $PbCl_2 \cdot 2C_5H_5N$ requires Pb, 47.5). *Lead(II) bromide – pyridine*, from C_2H_5OH, 97%, white, decomp. >190 °C (Found: C, 12.7; H, 1.0; N, 2.4; Pb, 46.8. $PbBr_2 \cdot C_5H_5N$ requires C, 13.5; H, 1.1; N, 3.1; Pb, 46.4). *Lead(II) bromide – bis(pyridine)*, from C_6H_6, 96%, white (Found: Pb, 39.6. $PbBr_2 \cdot 2C_5H_5N$ requires Pb, 39.45). *Lead(II) iodide – pyridine*, from C_2H_5OH, 94%, light-yellow, decomp. >200 °C (Found: C, 11.6; H, 0.7; N, 2.5; Pb, 38.15. $PbI_2 \cdot C_5H_5N$ requires C, 11.5; H, 0.9; N, 2.6; Pb, 38.4). *Lead(II) iodide – bis(pyridine)*, from C_6H_6, 96%, cream-yellow, decomp. >95 °C (Found: C, 19.0; H, 1.2; N, 4.3; Pb, 33.4. $PbI_2 \cdot 2C_5H_5N$ requires C, 19.4; H, 1.6; N, 4.5; Pb, 35.5). *Lead(II) chloride – bis(ethylenediamine)*, from C_6H_6, 96%, white, decomp. >215 °C (Found: C, 12.3; H, 3.95; N, 13.0; Pb, 51.5. $PbCl_2 \cdot 2C_2H_8N_2$ requires C, 12.05; H, 4.05; N, 14.1; Pb, 52.0). *Lead(II) bromide – bis(ethylenediamine)*, from C_6H_6, 96%, white, decomp. >205 °C (Found: C, 10.3; H, 3.3; N, 10.1; Pb, 42.1. $PbBr_2 \cdot 2C_2H_8N_2$ requires C, 9.9; H, 3.3; N, 11.5; Pb, 42.6). *Lead(II) iodide – bis(ethylenediamine)*, from C_6H_6, 90%, white, decomp. >180 °C (Found: C, 8.6; H, 2.5; N, 9.5; Pb, 35.4. $PbI_2 \cdot 2C_2H_8N_2$ requires C, 8.3; H, 2.8; N, 9.6; Pb, 35.7). *Lead(II) chloride – N,N,N′,N′-tetramethylethylenediamine*, from C_2H_5OH, 94%, white, decomp. >273 °C (Found: C, 18.1; H, 3.9; N, 6.2; Pb, 52.8. $PbCl_2 \cdot C_6H_{16}N_2$ requires C, 18.3; H, 4.1; N, 7.1; Pb, 52.6). *Lead(II) bromide – N,N,N′,N′-tetramethylethylenediamine*, from C_2H_5OH, 95%, white, decomp. >230 °C (Found: C, 14.7; H, 3.2; N, 5.1; Pb, 42.8. $PbBr_2 \cdot C_6H_{16}N_2$ requires C, 14.9; H, 3.3; N, 5.8; Pb, 42.9). *Lead(II) iodide – N,N,N′,N′-tetramethylethylenediamine*, from C_2H_5OH, 97%, yellow, decomp. >195 °C (Found: C, 12.4; H, 2.8; N, 4.35; Pb, 35.8. $PbI_2 \cdot C_6H_{16}N_2$ requires C, 12.5; H, 2.8; N, 4.85; Pb, 35.9).

C. Adducts with Solid Ligands

Lead(II) halide (2 to 4 g) was stirred with a solution (50 to 100 ml) of ligand (2- to 20-fold excess) dissolved in benzene or ethanol for a sufficient time (2 to 5 days) to ensure complete reaction. The solid product was filtered and dried in a vacuum. Adducts obtained in this manner were: *Lead(II) iodide – thioacetamide*, in C_2H_5OH, 98%, yellow, decomp. >200 °C (Found: C, 4.4; H, 0.7; N, 3.0; Pb, 38.3. $PbI_2 \cdot C_2H_5NS$ requires C, 4.5; H, 0.9; N, 2.6; Pb, 38.65). *Lead(II) bromide – N,N-dimethylthioacetamide*, in C_2H_5OH, 98%, white, decomp. >212 °C (Found: C, 9.6; H, 1.75; N, 2.9; Pb, 44.6. $PbBr_2 \cdot C_4H_9NS$ requires C, 10.2; H, 1.9; N, 3.0; Pb, 44.1). *Lead(II) iodide – N,N-dimethylthioacetamide*, in C_2H_5OH, 99%, yellow, decomp. >218 °C (Found: C, 8.4; H, 1.3; N, 2.2; Pb, 36.5. $PbI_2 \cdot C_4H_9NS$ requires C, 8.5; H, 1.6; N, 2.5; Pb, 36.7). *Bis(lead(II) bromide) – 2,6-dimethyl-γ-pyrone*, in C_6H_6, 97%, white, decomp. >290 °C (Found: C, 9.6; H, 0.8; Pb, 48.3. $2PbBr_2 \cdot C_7H_8O_2$ requires C, 9.8; H, 0.9; Pb, 48.3). *Bis(lead(II) iodide) – 2,6-dimethyl-γ-pyrone*, in C_6H_6, 96%, yellow, decomp. 240 °C (Found: C, 8.1; H,

0.8; Pb 39.2. $2PbI_2 \cdot C_7H_8O_2$ requires C, 8.0; H, 0.8; Pb, 39.6). *Lead(II) chloride – 1,10-phenanthroline*, in C_6H_6, 94%, white, decomp. >340 °C (Found: C, 31.55; H, 1.7; N, 5.9; Pb, 44.4. $PbCl_2 \cdot C_{12}H_8N_2$ requires C, 31.45; H, 1.8; N, 6.1; Pb, 45.2). *Lead(II) bromide – bis(1,10-phenanthroline)*, in C_6H_6, 95%, cream-yellow, decomp. 235 °C (Found: C, 39.4; H, 2.1; N, 6.6; Pb, 28.7. $PbBr_2 \cdot 2C_{12}H_8N_2$ requires C, 39.6; H, 2.2; N, 7.7; Pb, 28.5). *Lead(II) iodide – bis(1,10-phenanthroline)*, in C_6H_6, 95%, decomp. >290 °C (Found: C, 34.85; H, 1.8; N, 6.6; Pb, 26.1. $PbI_2 \cdot 2C_{12}H_8N_2$ requires C, 35.1; H, 1.95; N, 6.8; Pb, 25.2). *Lead(II) chloride – 2,2'-bipyridine*, in C_2H_5OH, 91%, white, decomp. >300 °C (Found: C, 27.4; H, 1.9; N, 5.6; Pb, 46.7. $PbCl_2 \cdot C_{10}H_8N_2$ requires C, 27.7; H, 1.9; N, 6.45; Pb, 47.7). *Lead(II) bromide – 2,2'-bipyridine*, in C_2H_5OH, 96%, cream, decomp. >300 °C (Found: C, 22.4; H, 1.6; N, 5.3; Pb, 39.4. $PbBr_2 \cdot C_{10}H_8N_2$ requires C, 23.0; H, 1.5; N, 5.35; Pb, 39.6). *Lead(II) iodide – 2,2'-bipyridine*, in C_2H_5OH, 90%, yellow, decomp. >300 °C (Found: C, 19.6; H, 1.25; N, 4.0; Pb, 33.1. $PbI_2 \cdot C_{10}H_8N_2$ requires C, 19.45; H, 1.3; N, 4.5; Pb, 33.6).

D. Thiourea Adducts

Lead(II) iodide – thiourea. Lead(II) iodide (2.3 g) was stirred with a boiling solution of thiourea (7.6 g) in water (300 ml) for 2 h. After evaporation to 150 ml, the hot mixture was filtered. The filtrate on cooling gave the *yellow mono-adduct* which was filtered, washed with a *small* amount of ethanol (10 ml) and ether (10 ml) and dried in a vacuum. Yield 48%, mp 200–205 °C (decomp.). (Found: C, 2.2; H, 0.6; N, 5.1; Pb, 38.1. $PbI_2 \cdot CH_4N_2S$ requires C, 2.2; H, 0.75; N, 5.2; Pb, 38.6).

Lead(II) bromide – thiourea. Lead(II) bromide (3.7 g) was dissolved in a boiling solution of thiourea (3.0 g) in water (150 ml). Filtration of the boiling solution followed by *rapid* cooling of the filtrate to room temperature gave *fine cream needles* of the *mono-adduct* which were filtered, washed with ethanol and ether, and air-dried. Yield 55%, mp 193–197 °C (decomp.). (Found: C, 2.4; H, 0.7; N, 6.3; Pb, 46.6. $PbBr_2 \cdot CH_4N_2S$ requires C, 2.7; H, 0.9; N, 6.3; Pb, 46.8).

Filtration of the solution obtained by dissolving lead(II) bromide (2.2 g) in a boiling solution of thiourea (3.8 g) in water (100 ml) followed by *slow* cooling of the hot filtrate gave *yellow needles* of *lead(II) bromide – bis(thiourea)* which was dried as for the mono-adduct. Yield 81%, mp 181–184 °C (Found: Pb, 39.9. $PbBr_2 \cdot 2CH_4N_2S$ requires Pb, 39.6). Lead(II) chloride (2.8 g) treated in the same way with thiourea (3.1 g) in water (150 ml) gave *white needles* of *lead(II) chloride – bis(thiourea)*. Yield 78%, mp 187–189 °C (Found: Pb, 48.3. $PbCl_2 \cdot 2CH_4N_2S$ requires Pb, 48.15).

Results and Discussion

Stoichiometric lead(II) halide adducts were successfully prepared in high yields by the direct reaction of donor ligands with crystalline lead(II) halides using two procedures. Neat liquid ligands having high donor abilities, such as pyridine and dimethylsulphoxide, dissolve lead(II) halides to give clear solutions from which adducts of 1:1 and 1:2 ratios can be precipitated by the addition of benzene or carbon tetrachloride,

$$[1] \quad PbX_2\,(s) \xrightarrow[\text{solvent (L)}]{\text{donor}} PbX_2 \cdot xL\,(\text{soln}) \xrightarrow[\text{or } C_6H_6]{CCl_4} PbX_2 \cdot nL\,(s) \quad (n = 1,2)$$

Solid ligands, taken in large excess dissolved in benzene or ethanol, combine with lead(II) halides in an apparently heterogeneous reaction,

$$[2] \quad PbX_2\,(s) + L\,(\text{soln}) \xrightarrow[C_2H_5OH]{C_6H_6 \text{ or}} PbX_2 \cdot nL\,(s) \quad (n = 1,2)$$

This reaction must be allowed to occur with rapid stirring for a sufficiently long time, usually 2 to 5 days, to ensure completion as determined by the constant composition of the product. Lead(II) halides probably dissolve slightly under these conditions to form adducts of such low solubility that they precipitate.

The results of the two preparative schemes are summarized in Table 1 which also includes combinations of reactants which did not produce stable stoichiometric adducts. Adducts were judged to be stable if they could be stored for several days at ambient temperatures without loss of ligand (16). All stable adducts are insoluble in common organic solvents except the parent ligand, if liquid. Most adducts with monodentate ligands lose ligand easily when washed with ordinary organic solvents, the most effective being ethanol. Microanalytical data could not be obtained for $PbX_2 \cdot 2py$ (X = Cl, Br) because these adducts lost ligand when stored at room temperature for 2 to 3 weeks.

Infrared spectra[3] of all adducts were measured in the range 1700–400 cm^{-1} except for $PbX_2 \cdot 2mpd$ (X = Br, I) when the range was 1700–1300 cm^{-1} and for $2PbX_2 \cdot dmp$ (X = Br, I) when the range was 1700–1100 cm^{-1}. Raman spectra[3] were recorded in the same ranges for all adducts with O- and S-donor ligands except $PbX_2 \cdot mpld$ (X = Br, I), $PbX_2 \cdot 2mpd$ (X = Br, I), and $2PbI_2 \cdot dmp$ which gave excessive background fluorescence. Ligand frequencies

[3]Tables of complete infrared and Raman data together with proposed assignments are on deposit and may be obtained at a nominal charge from the Depository of Unpublished Data, CISTI, National Research Council of Canada, Ottawa, Canada, K1A 0S2.

TABLE 1. Results of reactions of lead(II) halides with various O-, S-, and N-donor ligands[a]

Ligand	$PbCl_2$	$PbBr_2$	PbI_2
O-Donor Ligands			
Dimethylsulphoxide (dmso)	1:2[c]	1:2[b]	1:2[b]
	—	—	1:1
N,N-Dimethylacetamide (dma)	1:1[c]	1:1[b]	1:1[b]
N-Methyl-2-pyrrolidinone (mpld)	N.I.	1:1[b]	1:1[b]
N-Methyl-2-pyridone (mpd)	—	1:2[c]	1:2[b]
2,6-Dimethyl-γ-pyrone (dmp)	N.I.	2:1[b]	2:1[b]
Acetamide	—	N.I.	N.I.
Urea	N.I.	—	N.I.
S-Donor Ligands			
Thiourea (tu)	1:2	1:2	—
	—	1:1	1:1[b]
N,N-Dimethylthioacetamide (dmta)	N.I.	1:1[b]	1:1
Thioacetamide (tam)	N.I.	N.I.	1:1[b]
N-Donor Ligands			
Ethylenediamine (en)	1:2	1:2	1:2
Tetramethylethylenediamine (tmen)	1:1	1:1	1:1
2,2'-Bipyridine (bipy)	1:1	1:1	1:1
1,10-Phenanthroline (phen)	—	1:2	1:2
	1:1	—	—
Pyridine (py)	1:2[b]	1:2[b]	1:2
	—	1:1	1:1
Piperidine (pip)	—	N.I.	1:1
Aniline (an)	1:1	3:2	1:1
Pyrrolidine	—	N.I.	N.I.
Diethylamine	—	—	N.I.
N-Methylpyrrolidine	—	—	N.I.
n-Propylamine	—	—	N.I.

[a]Ratios (*m*:*n*) give the stoichiometries of reproducible adducts $mPbX_2 \cdot nL$. N.I. means adducts could not be isolated.
[b]Adduct which lost volatile ligand on storage or when washed with ethanol or benzene.
[c]Adduct of irreproducible composition.

which showed characteristic shifts on coordination are given in Tables 2 and 3. These results confirm that each ligand is coordinated rather than merely incorporated in the crystal lattice of the lead halide adduct. When the ligands are potentially bifunctional, frequency shifts indicate coordination through the chalcogen atom for amides, thioamides, and thiourea, and through the carbonyl oxygen for 2,6-dimethyl-γ-pyrone.

The parent lead(II) halides have structures of mainly ionic character based on close-packing of the halide ions (17). In $PbCl_2$ and $PbBr_2$ which are isomorphous, lead is nine-coordinate, while PbI_2 has six-coordinate lead in a structure based on the CdI_2 layer lattice. Since lead(II) normally has a coordination of six or more in complexes (18), it is reasonable to consider the lead halide adducts reported here, noting their very low solubilities in many solvents and their tendency to decompose rather than melt when heated, as having polymeric structures with halogen and sometimes also ligand donor atom bridges to enable each lead atom to achieve a coordination of six or more. The adducts whose structures have been determined by X-ray methods, $PbCl_2 \cdot 2tu$ (14) and $PbBr_2 \cdot 2dmso$ (19), are both polymeric with lead seven- and six-coordinate respectively. The only other lead halide adduct whose structure has been reported, $3PbBr_2 \cdot 2H_2O$ (unstable at room temperature) (20), has water molecules lodged in a distorted lead(II) bromide lattice with each lead atom eight-coordinate.

Vibrational data for $PbCl_2 \cdot 2tu$ and $PbBr_2 \cdot 2dmso$ are consistent with the published structures of these compounds. Thus for $PbCl_2 \cdot 2tu$, the coincidence of infrared and Raman frequencies (within experimental error) agrees with the $C_{2v}^9(Pna2_1)$ space group of this compound. Moreover, the main skeletal vibrations of thiourea are split in both infrared and Raman

TABLE 2. Coordination sensitive ligand frequencies (cm^{-1}) for lead(II) halide adducts with chalcogen donor ligands[f]

dma IR	$PbBr_2 \cdot dma$ IR	$PbBr_2 \cdot dma$ R	$PbI_2 \cdot dma$ IR	$PbI_2 \cdot dma$ R	Assignment[a]
1645vs	1598s	1586w	1597s	1584m	ν(C=O)
1500m	1509m	1506w	1506m	1504wm	ν(C—NC_2)

mpld IR	$PbBr_2 \cdot mpld$ IR	$PbI_2 \cdot mpld$ IR	Assignment[b]
1692vs	1625vs	1629vs	ν(C=O)

mpd IR	$PbBr_2 \cdot 2mpd$ IR	$PbI_2 \cdot 2mpd$ IR	Assignment[c]
1661vs	1659sh 1649vs 1632sh	1657vs 1644vs 1614sh	ν(C=C)
1600sh 1585vs	1567 1559 1546 } vs	1575sh 1557sh 1547vs	ν(C=O)

dmso IR	$PbI_2 \cdot dmso$ IR	$PbI_2 \cdot dmso$ R	$PbI_2 \cdot 2dmso$ IR	$PbI_2 \cdot 2dmso$ R	$PbBr_2 \cdot 2dmso$ IR	$PbBr_2 \cdot 2dmso$ R	Assignment[d]
1057s 1027sh	1022m	1021w	1014m	1005s	1017sh 1012s	1009w	ν(S=O) + $\rho(CH_3)$
954wm	979vs	980w	992vs 954s	949m	979vs	976m 951sh	
698wm	714m	715m	708w	712sm	712w	714vs	$\nu_{as}(SC_2)$
668w	—	678vs	—	678vs	—	679vs	$\nu_s(SC_2)$

dmp IR	$2PbBr_2 \cdot dmp$ IR	$2PbBr_2 \cdot dmp$ R	$2PbI_2 \cdot dmp$ IR	Assignment[e]
1683sh 1667vs	1663 1656 } vs	1662wm 1655m	1657sh 1650vs	ν(C=C)
1609vs 1597vs	1591m 1580sh 1569m 1538vs	1590w 1579m 1571w 1541m	1579wm 1573m 1562w 1533vs	ν(C=O)

tam IR	$PbI_2 \cdot tam$ IR	$PbI_2 \cdot tam$ R	Assignment[f]
1650vs	1625s	1623w	$\delta(NH_2)$
719sm	703s	700s	ν(C=S)
708m	721m	—	$\tau(NH_2)$

dmta IR	$PbBr_2 \cdot dmta$ IR	$PbBr_2 \cdot dmta$ R	$PbI_2 \cdot dmta$ IR	$PbI_2 \cdot dmta$ R	Assignment[g]
1532vs	1561 1556 } s	1558w	1556sh 1553m	1559 1552 } m	ν(C—NC_2)
862wm	852m	—	851m	—	ν(C=S)

TABLE 2 (*Concluded*)

tu IR	$PbCl_2 \cdot 2tu$ IR	$PbCl_2 \cdot 2tu$ R	$PbBr_2 \cdot 2tu$ IR	$PbBr_2 \cdot 2tu$ R	Assignment[h]
1609vs	1621, 1612 s	1618mw	1621, 1611 vs	1615w	$\delta(NH_2)$
1458s	1509, 1503 w	1509, 1504	1496, 1489 w	1500wm, 1492sh	$\nu_{as}(CN_2)$
1413s	1435sh, 1425m	1435sh, 1427m	1427m	—	$\nu_s(CN_2)$
728s,sp	713m, 710s	713vs, 709s	716w, 705m	712sh, 709vs	ν(C=S)

tu IR	$PbBr_2 \cdot tu$ IR	$PbBr_2 \cdot tu$ R	$PbI_2 \cdot tu$ IR	$PbI_2 \cdot tu$ R	Assignment
1609vs	1628m, 1597vs	—, —	1621sh, 1613s	1623w, 1615w	$\delta(NH_2)$
1458s	1502m	1500w	1485wm	1490w	$\nu_{as}(CN_2)$
1413s	—	1421w	1428m	1426w	$\nu_s(CN_2)$
728s,sp	709m, 699m	712s, 701s	712s,sp	710vs,sp	ν(C=S)

[a]References 5, 6, and 24.
[b]Reference 25.
[c]Reference 26.
[d]Reference 27.
[e]Reference 28.
[f]Reference 29.
[g]Reference 30.
[h]References 15 and 31.
[i]Only the principal contribution is given in assignments.

spectra, consistent with an interaction between the two crystallographically distinct thiourea molecules in the asymmetric unit of this crystal. Similarities in the vibrational spectra of $PbCl_2 \cdot 2tu$ and $PbBr_2 \cdot 2tu$, together with their similar needle-like crystal forms and physical properties, suggest that $PbBr_2 \cdot 2tu$ has a polymeric crystal structure like that of $PbCl_2 \cdot 2tu$. For $PbBr_2 \cdot tu$, ν(C=S) is also split, implying that coupling occurs between at least two thiourea molecules, perhaps acting as bridges, in a structure related to that of $PbCl_2 \cdot 2tu$. A polymeric structure would also account for the high melting point and insolubility of $PbBr_2 \cdot tu$ in a range of organic solvents. In $PbBr_2 \cdot 2dmso$ and $PbI_2 \cdot 2dmso$, the extensive splitting of ligand bands in the S=O stretching region is consistent with vibrational coupling of two dmso molecules coordinated to the same lead atom, as found for $PbBr_2 \cdot 2dmso$. The adducts $PbX_2 \cdot 2mpd$ (X = Br, I) and $PbX_2 \cdot 2py$ (X = Cl, Br, I) may also have similar structures with two ligand molecules coordinated to each lead atom since several nondegenerate ligand modes are split in the infrared spectra of these adducts. For the remaining adducts in this work, no structural conclusions can be drawn from their vibrational spectra.

Some tentative and qualitative trends in Lewis acidities and basicities are indicated by the range of monodentate ligand adducts isolated and their properties. For example, in the case of lead(II) halide reactions with ethanol solutions of *N*,*N*-dimethylthioacetamide, $PbCl_2$ did not form an adduct, $PbBr_2 \cdot dmta$ decomposed when washed with ethanol, while $PbI_2 \cdot dmta$ was resistant to this treatment. These observations and similar ones on pyridine adducts suggest an apparent order of Lewis acidity of $PbI_2 > PbBr_2 > PbCl_2$, although the possibility of the observations being due to solubility and/or crystal lattice effects cannot be excluded. Changes in ligand ν(C=O), ν(C=S), and ν(S=O) frequencies due to coordination are not significantly different in each series of PbX_2 adducts (Table

TABLE 3. Coordination sensitive ligand frequencies (cm^{-1}) for lead halide – amine adducts[h]

Infrared				
en	$PbCl_2 \cdot 2en$	$PbBr_2 \cdot 2en$	$PbI_2 \cdot 2en$	Assignment[a]
~1590s,br	1602s 1579s	1594vs 1575s	1580s 1567s	$\delta(NH_2)$
1311m	1285w 1273w 1256w	1281w 1268w 1254w	1265wbr	CH_2 twist
1093m	1116m 1064m	1113m 1058m	1109m 1052m	ν(C—C) + ν(C—N)
1050m	1020 1000 vs	1020 996 vs	1010vs	

Infrared				
tmen	$PbCl_2 \cdot tmen$	$PbBr_2 \cdot tmen$	$PbI_2 \cdot tmen$	Assignment[b,i]
1097wm	1065m	1069m	1073m	n.a.
1033vs	1030vs 1009s	1027m 1007m	1026m 1010m	
933m	952s 923m	950s 920w	949s 923m	
834m	785vs	783s	784s	
829m	767s	765m	767m	

Infrared				
dipy	$PbCl_2 \cdot dipy$	$PbBr_2 \cdot dipy$	$PbI_2 \cdot dipy$	Assignment[c]
398m	410m	409m	408m	ring tors
753vs	773vs	773vs	770vs	δ(CH) out-of-plane
991m	1006m 1011vs	1008vs 1010vs	1006s 1011vs	ring breathing

Infrared				
phen H_2O	$PbCl_2 \cdot phen$	$PbBr_2 \cdot 2phen$	$PbI_2 \cdot 2phen$	Assignment[d,i]
1508vs	1519vs	1513vs	1514vs	n.a
738vs	727vs	726vs	725vs	
730vs 705vs	722vs	720 718 vs	719vs	
626s	639s	635vs	634vs	
411s	419m	429w 420m	426w 417m	

py IR	$PbI_2 \cdot 2py$ IR	$PbI_2 \cdot 2py$ R	$PbBr_2 \cdot 2py$ IR	Assignment[e,j]
406m	410wm	409w	412m	16*b*
605m	618 623 m	623m	618 625 sm	6*a*
990s	1000s		1000	1
	1003vs	1002m	1005 vs	
1583vs	1593 1596 s	1592m	1593 1598 s	8*a*

TABLE 3 (*Concluded*)

Infrared				
py	$PbCl_2 \cdot 2py$	$PbBr_2 \cdot py$	$PbI_2 \cdot py$	Assignment[e,j]
406m	406m 415w	415m	414m	16*b*
605m	619s 629w	629s	625m	6*a*
990s	999s 1010wm	1007s	1005vs	1
1583vs	1594sm	1602s	1598s	8*a*

Infrared		
pip	$PbI_2 \cdot pip$	Assignment[f]
548m	583m	skel. def.
742s	739w	ρ(NH)
820w	806s	skel. def.
1006w	1016s	$\rho(CH_2)$

Infrared				
an	$PbCl_2 \cdot an$	$3PbBr_2 \cdot 2an$	$PbI_2 \cdot an$	Assignment[g]
505sm 529w	489m 515sm 536m	514m 539s	510m 526w 535wm	X-sens.
		564m		?
808w	798 803 } m	800s	800s	X-sens.
1052w	1064m	1068w	1066w	$\tau(NH_2)$
1276s	1256 1248 } m	1241w 1227m	1242w 1224m	X-sens.

[a]Reference 32.
[b]Reference 33.
[c]Reference 34.
[d]Reference 35.
[e]Reference 36.
[f]Reference 37.
[g]Reference 38.
[h]Only principal contribution is given in assignment.
[i]n.a. = no assignment available.
[j]Nomenclature for pyridine modes as given in ref. 39

2); nor are such shifts reliable indicators of donor–acceptor strengths (21), especially when only solid state infrared data are available. Unfortunately, because of their insolubility, we were unable to make any other physical measurements on the adducts which would reflect relative acceptor powers on a quantitative basis. Therefore, it must be emphasized that the criteria used in this work, isolation of an adduct and its ability to be stored for a period of time (16), at best provide only a rough qualitative basis for proposing trends in Lewis acid–base strength.

A qualitative comparison of adducts formed by ligands which differ only in the coordinating atom can also be made by examining the behaviour of $PbCl_2$ with urea and thiourea, or of PbI_2 with acetamide and thioacetamide. In both cases, under comparable experimental conditions, only adducts with the sulphur donors were isolated. This implies, but does not prove, that donor abilities are in the order S-donors > O-donors toward $PbCl_2$ and PbI_2. This order is not unexpected considering that Pb(II) is classified as borderline soft in the hard and soft acid–base

concept of Pearson (22), and therefore should bind more strongly with soft S-donors than with hard O-donors. Support for the borderline soft behaviour of Pb(II) is also provided by our observation that lead(II) halides form adducts with the softer ligands, aniline and pyridine, but not with the harder aliphatic amines. Lead(II) is probably made even softer by symbiosis (23) with the surrounding halogen atoms, an effect which should decrease in the order $I > Br > Cl$, and hence acceptor powers should decrease in the order $PbI_2 > PbBr_2 > PbCl_2$. Bearing in mind the qualitative nature of our observations on the formation and stability of lead(II) halide adducts, a more detailed analysis of Lewis acid–base trends is premature at this stage.

Acknowledgements

The technical assistance of Mr. A. D. Baranyi and Mr. R. Zamboni was very much appreciated. The financial support of the National Research Council of Canada and of Le Ministère de l'Education, Gouvernement du Québec is gratefully acknowledged.

1. A. Rosenheim and V. J. Meyer. Z. anorg. Chem. **49**, 17 (1906).
2. G. W. Heise. J. Phys. Chem. **16**, 373 (1912).
3. H. Mandal. Chem. Ber. **54**, 703 (1921).
4. W. Biltz and W. Fischer. Z. anorg. Chem. **124**, 230 (1922).
5. M. A. J. Jungbauer and C. Curran. Nature, **202**, 290 (1964).
6. W. E. Bull, S. K. Madan, and J. E. Willis. Inorg. Chem. **2**, 303 (1963).
7. J. Selbin, W. E. Bull, and L. H. Holmes, Jr. J. Inorg. Nucl. Chem. **16**, 219 (1961).
8. P. Boldrini. Can. J. Chem. **49**, 1564 (1971).
9. M. Schafer and C. Curran. Inorg. Chem. **5**, 265 (1966).
10. I. M. Cheremisina, E. V. Khlystunova, and V. L. Varand. Bull. Acad. Sci. (USSR) (Div. Chem.), **21**, 2064 (1972).
11. D. M. Czakis-Sulikowska, J. Radwanska-Doozckalska, and A. Gorecka. Roczniki Chem. **47**, 2345 (1973).
12. A. K. Orlanskaya, G. N. Katseva, N. L. Strelets, and E. A. Gyunner. Russ. J. Inorg. Chem. **14**, 199 (1969).
13. Ya. D. Fridman, S. D. Gorokhov, and T. V. Fokina. Russ. J. Inorg. Chem. **19**, 1140 (1974).
14. M. Nardelli and G. Fava. Acta Crystallogr. **12**, 727 (1959).
15. K. Swaminathan and H. M. N. H. Irving. J. Inorg. Nucl. Chem. **26**, 1291 (1964).
16. S. F. A. Kettle. Coordination compounds. Thomas Nelson and Sons, Ltd., London, 1969. pp. 41 to 54.
17. R. W. G. Wyckoff. Crystal structures. Vol. 1. 2nd ed. John Wiley and Sons, Inc., New York. 1963. pp. 276, 298.
18. F. A. Cotton and G. Wilkinson. Advanced inorganic chemistry. 3rd ed. John Wiley and Sons, Inc., New York. 1972. p. 332; I. Goldberg and F. H. Herbstein, Acta Crystallogr. B**29**, 246 (1973); S. L. Lawton and G. T. Kokotailo. Inorg. Chem. **11**, 363 (1972).
19. A. D. Baranyi, M. Onyszchuk, S. Fortier, and G. Donnay. J. Chem. Soc. Dalton. In press.
20. J. Anderson and G. Lundgren. Acta Chem. Scand. **24**, 2670 (1970).
21. R. S. Drago and N. A. Matwiyoff. Acids and bases. D. C. Heath and Co., Lexington, Mass. 1968. p. 71.
22. R. G. Pearson. J. Am. Chem. Soc. **85**, 3533 (1963); Surv. Prog. Chem. **5**, 1 (1969).
23. C. K. Jörgensen. Inorg. Chem. **3**, 1201 (1964).
24. G. Durgaprasad, D. N. Sathyanarayana, C. C. Patel, H. S. Randhawa, and C. N. R. Rao. Spectrochim. Acta, **28A**, 2311 (1972).
25. K. Kurosaki. Nippon Kagaku Zasshi, **82**, 1691 (1961); S. K. Madan. Inorg. Chem. **6**, 421 (1967).
26. R. A. Coburn and G. O. Dudek. J. Phys. Chem. **72**, 1177 (1968); D. Cook. Can. J. Chem. **43**, 741 (1965).
27. M. Tranquille, P. Labarbe, M. Fouassier, and M.-T. Forel. J. Mol. Struct. **8**, 273 (1971); F. A. Cotton, R. Francis, and W. D. Horrocks, Jr. J. Phys. Chem. **64**, 1534 (1960).
28. D. Cook. Can. J. Chem. **39**, 1184 (1961); T. Gramstad. Spectrochim. Acta, **19**, 1698 (1963).
29. I. Suzuki. Bull. Chem. Soc. Jpn. **35**, 1449 (1962); C. D. Flint and M. Goodgame. J. Chem. Soc. (A), 750 (1968).
30. A. Ray and D. N. Sathyanarayana. Bull. Chem. Soc. Jpn. **45**, 2712 (1972).
31. G. B. Aitken, J. L. Duncan, and G. P. McQuillan. J. Chem. Soc. (A), 2695 (1971).
32. H. Brusset, Nguyen Quy Dao, and M. Jouan. Adv. Raman Spectrosc. **1**, 226 (1972); K. Krishnan and R. A. Plane. Inorg. Chem. **5**, 852 (1966).
33. G. B. Deacon and J. C. Parrott. Aust. J. Chem. **25**, 1169 (1972); S. C. Jain and R. Rivest. Inorg. Chim. Acta, **3**, 552 (1969).
34. J. S. Strukl and J. L. Walter. Spectrochim. Acta, **27A**, 233 (1971).
35. K. Krishnan and R. A. Plane. Spectrochim. Acta, **25**, 83 (1969).
36. N. S. Gill, R. H. Nuttall, D. E. Scaife, and D. W. A. Sharp. J. Inorg. Nucl. Chem. **18**, 79 (1961).
37. E. R. Razumova, V. T. Aleksanyan, and G. V. Sorokin. Bull. Acad. Sci. (USSR) (Div. Chem. Sci.), **23**, 515 (1974).
38. J. C. Evans. Spectrochim. Acta, **16**, 428 (1960).
39. C. H. Kline, Jr., and J. Turkevich. J. Chem. Phys. **12**, 300 (1944).

Structural and energetics effects in the chemical ionization of halogen-substituted benzenes and toluenes

HEI-WUN LEUNG AND ALEX G. HARRISON
Department of Chemistry, University of Toronto, Toronto, Ont., Canada M5S 1A1

Received June 3, 1976

HEI-WUN LEUNG and ALEX G. HARRISON. Can. J. Chem. **54**, 3439 (1976).

The H_2, D_2, CH_4, and CD_4 chemical ionization (CI) mass spectra of XC_6H_5, $C_6H_5CH_2X$, and $XC_6H_4CH_3$ (X = Cl, Br, and I) have been determined. For the benzyl halides the dominant ion observed in all CI spectra is the m/q 91 (benzyl) ion formed by loss of HX(DX) from the protonated (deuteronated) molecule. The CI spectra of the isomeric halotoluenes differ substantially from the spectra of the benzyl halides indicating that isomerization to a common (tropylium-like) structure does not occur in CI. In the H_2 CI of XC_6H_4Y (Y = H or CH_3) the major fragment ions observed are $YC_6H_5 \cdot H^+$, $YC_6H_5^{+\cdot}$, and $YC_6H_4^+$, with the relative yields depending strongly on the halogen substituent. Neither the $YC_6H_5 \cdot H^+$ ion, resulting from HX loss from the $H_3^+ \cdot XC_6H_4Y$ complex, nor the $YC_6H_4^+$ ion, resulting from HX loss from $XC_6H_4Y \cdot H^+$, are observed when X = I. On the other hand $YC_6H_5^{+\cdot}$, resulting from elimination of X· from $XC_6H_4Y \cdot H^+$, is observed only for X = Br and I. In the CH_4 CI of XC_6H_4Y, in addition to $XC_6H_4Y \cdot H^+$ ions, $CH_3C_6H_4Y \cdot H^+$ ions (HX loss from the $CH_5^+ \cdot XC_6H_4Y$ complex) are observed for X = F and Cl, while $YC_6H_5^{+\cdot}$ ions (loss of X· from $XC_6H_4Y \cdot H^+$) are observed only when X = I. In addition, displacement of I· by $C_2H_5^+$, and by $C_3H_5^+$, is observed in the CH_4 CI of the iodo-substituted compounds. The dependency of the products observed and their relative yields on the identity of the halogen substituent is discussed in relation to the reaction energetics.

HEI-WUN LEUNG et ALEX G. HARRISON. Can. J. Chem. **54**, 3439 (1976).

On a déterminé les spectres de masse par ionisation chimique (IC) à l'aide de H_2, D_2, CH_4 et CD_4 des XC_6H_5, $C_6H_5CH_2X$ et $XC_6H_4CH_3$ (X = Cl, Br et I). Dans le cas des halogénures de benzyle, l'ion le plus important observé dans tous les spectres IC est l'ion de m/q 91 (benzyle) formé par la perte de HX(DX) à partir de la molécule protonée (deutérée). Les spectres IC des divers halogénures isomères de toluène diffèrent d'une façon importante des spectres des halogénures de benzyle; ce résultat indique qu'une isomérisation vers une structure commune (ressemblant à l'ion tropylium) ne se produit pas dans le IC. Dans le cas de l'ionisation chimique par le H_2 des XC_6H_4Y (Y = H ou CH_3) les ions les plus importants observés lors des fragmentations sont les $YC_6H_5 \cdot H^+$, $YC_6H_5^{+\cdot}$ et $YC_6H_4^+$ et les rendements relatifs dépendent fortement de la nature de l'halogène. On n'observe l'ion $YC_6H_5 \cdot H^+$, résultant de la perte de HX à partir de $H_3^+ \cdot XC_6H_4Y$ et l'ion $YC_6H_4^+$ résultant de la perte de HX à partir de $XC_6H_4Y \cdot H^+$, lorsque X = I. Par ailleurs on n'observe l'ion radical $YC_6H_5^{+\cdot}$, résultant de l'élimination de X à partir de $XC_6H_4Y \cdot H^+$, que pour X = Br et I. Dans le cas de l'ionisation chimique par CH_4 du XC_6H_4Y, on observe, (pour X = F et Cl) en plus des ions $XC_6H_4Y \cdot H^+$, des ions de formules $CH_3C_6H_4Y \cdot H^+$ (résultant de la perte de HX à partir du complexe $CH_5^+ \cdot XC_6H_4Y$) par ailleurs on n'observe les ions $YC_6H_5^{+\cdot}$ (provenant de la perte de X· à partir de $XC_6H_4Y \cdot H^+$) que lorsque X = I. De plus, lors de l'IC par CH_4, on observe le déplacement de I· par $C_2H_5^+$ et par $C_3H_5^+$ des composés substitués par de l'iode. On discute en termes des énergies de réaction, de la dépendance qui existe entre la nature de l'halogène substituant et la nature et les rendements relatifs des produits observés.

[Traduit par le journal]

Introduction

A recent communication from this laboratory (1) reported the hydrogen and methane chemical ionization (CI) mass spectra of fluorobenzene, benzyl fluoride, and the isomeric fluorotoluenes. It was observed that benzyl fluoride and the fluorotoluenes showed substantially different mass spectra in both the H_2 and CH_4 CI providing strong evidence that ring expansion to a tropylium-type structure did not occur prior to fragmentation of the protonated molecule. Thus, the behaviour of these toluene derivatives under CI conditions is quite different from their behaviour under electron impact (EI) conditions, where the mass spectra are essentially identical, in agreement with the substantial evidence (1–3) that ring expansion to a symmetrical tropylium structure occurs under EI conditions prior to

Can. J. Chem. Downloaded from www.nrcresearchpress.com by 84.22.46.98 on 09/08/12
For personal use only.

fragmentation of the molecular ion.[1]

The CI mass spectra of fluorobenzene and the fluorotoluenes (but not benzyl fluoride) showed an unexpected reaction of H_3^+ and CH_5^+ with the neutral molecule (reaction 1, X = F)

[1] $$RH_2^+ + XC_6H_4Y \rightarrow RC_6H_4Y \cdot H^+ + HX$$

(where Y = H, CH_3, R = H, CH_3) resulting in elimination of HF from the collision complex formed between H_3^+ or CH_5^+ and the neutral molecule, with formation of product ions most simply represented as the appropriate protonated benzene, toluene, or xylene depending on the identity of R and Y.

As an extension of this study we have determined the H_2 and CH_4 CI mass spectra of the chloro-, bromo-, and iodo-substituted benzenes and toluenes and the isomeric benzyl halides. Both D_2 and CD_4 also have been used as reagent gases to aid in elucidating reaction mechanisms. The results show interesting structural and energetics effects on the product distributions obtained and provide further evidence that ring expansion to a symmetrical structure does not occur in the chemical ionization of these halogen-substituted toluenes. The evidence concerning the possible role of ring expansion in the EI fragmentation of these halogen-substituted toluenes is conflicting and has been reviewed recently (4).

Experimental

The chemical ionization mass spectra were obtained using a Dupont 21-490 mass spectrometer equipped with a high-pressure chemical ionization source. The source temperature was ~150 °C while the samples were introduced through a heated inlet system at ~100 °C. Reagent gas pressures were in the range 0.3–0.5 mm. Under these conditions electron impact ionization of the sample was negligible.

The compounds used were commercially available samples and showed no impurities in their EI mass spectra. Reagent grade CH_4 and H_2 were obtained from Matheson and Co. and were used without further purification, as was the CD_4 which was obtained from Merck, Sharp and Dohme, Montreal. The D_2 (Matheson and Co.) was passed through a heated palladium thimble prior to use to remove a low-level impurity of mass 28 (probably N_2).

[1]In the work reported in ref. 3 small differences were observed in the relative abundances of metastable ions for fragmentation of the isomeric fluorotoluene molecular ions. This was taken as evidence that the fragmentation did not occur entirely through a symmetrical tropylium structure, however, the small differences noted could arise from differences in internal energy distribution rather than differences in structure.

Results and Discussion

Chemical Ionization of Chloro-substituted Compounds

The H_2 and D_2 CI mass spectra of chlorobenzene, benzyl chloride, and the three isomeric chlorotoluenes are shown in Fig. 1. The H_2 CI spectrum obtained for benzyl chloride is similar to that of benzyl fluoride (1), showing a very low-intensity peak for the protonated molecule, MH^+, with the major part of the ionization in both cases being found at m/q 91, corresponding to formation of the benzyl cation by the facile loss of neutral hydrogen halide from MH^+. As was observed in the case of benzyl fluoride, when D_2 is used as the reagent gas there is significant deuterium incorporation in the fragment ion (resulting in formation of $C_7H_6D^+$, m/q 92), indicating some mixing of H and D in the MD^+ ion prior to fragmentation. However, for both benzyl halides, the $C_7H_6D^+$ ion signal is much lower than that predicted for complete H/D equilibration in MD^+ prior to fragmentation.

The H_2 CI mass spectrum of chlorobenzene is similar to the spectrum of fluorobenzene in that $C_6H_5^+$, m/q 77 ($MH^+ - HX$), and m/q 79 ($C_6H_7^+$) are the major fragment ions observed; the latter ion is the product of reaction 1 for X = Cl, R = Y = H. However, the spectra differ in showing a much-reduced MH^+ intensity for chlorobenzene compared to fluorobenzene, where MH^+ was the base peak in the spectrum. Similarly, the chlorotoluenes show a much-reduced MH^+ ion intensity compared to the fluorotoluenes. A further difference is that the major fragment ion for the chlorotoluenes is $C_7H_7^+$ (m/q 91, $MH^+ - HCl$) while $C_7H_6F^+$ ($MH^+ - H_2$) is the major fragment ion in the H_2 CI mass spectra of the fluorotoluenes. The m/q 93 ($C_7H_9^+$) ion, corresponding to the product ion from reaction 1 (X = Cl, R = H, Y = CH_3) is ~35% of the $C_7H_7^+$ base peak in the H_2 CI of the chlorotoluenes.

Further differences between the fluoro- and chloro-substituted compounds are apparent when the D_2 CI spectra are compared. In the D_2 CI mass spectra of fluorobenzene and the fluorotoluenes the ions, m/q 77 and m/q 91, corresponding to loss of hydrogen fluoride from MH^+, showed essentially no shift, indicating that in the

Can. J. Chem. Downloaded from www.nrcresearchpress.com by 84.22.46.98 on 09/08/12
For personal use only.

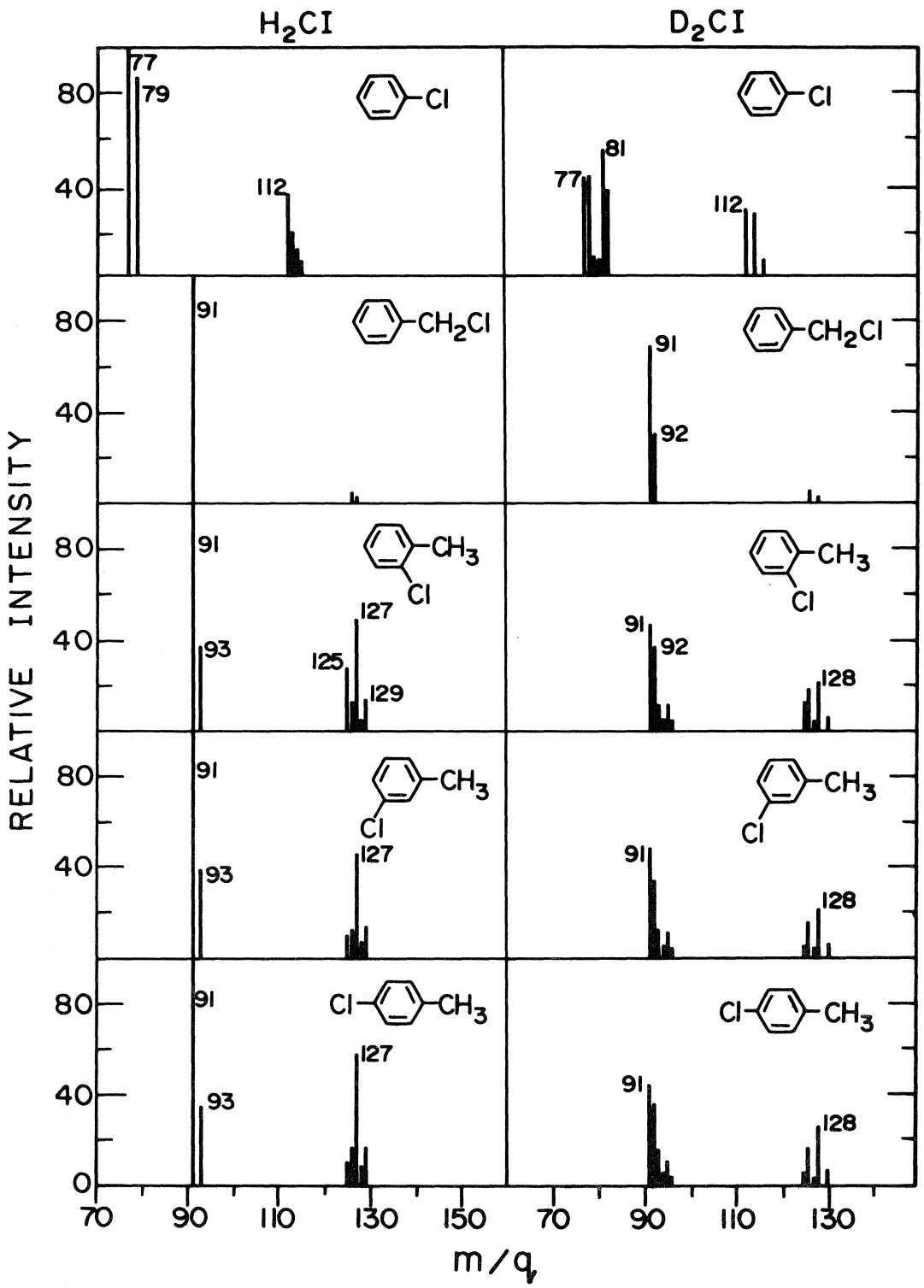

FIG. 1. H_2 and D_2 CI of chloro-substituted compounds.

Can. J. Chem. Downloaded from www.nrcresearchpress.com by 84.22.46.98 on 09/08/12
For personal use only.

Can. J. Chem. Downloaded from www.nrcresearchpress.com by 84.22.46.98 on 09/08/12
For personal use only.

D_2 CI the added deuteron was specifically lost as DF from the MD^+ ion. By contrast, in the D_2 CI of chlorobenzene and the chlorotoluenes the $MD^+ - HCl$ (m/q 78 and m/q 92) ion signals, in each case, are approximately equal to the $MD^+ - DCl$ (m/q 77 and m/q 91) ion signals, indicating essentially equal probabilities for loss of DCl and HCl in the fragmentation of MD^+. The reasons for this difference between the fluoro and chloro compounds are not clear. It should be noted, however, that complete equilibration of H/D in the MD^+ ion in the chlorobenzene system would lead to loss of HX being favoured over loss of DX by a factor of 5:1. A further difference in the D_2 CI spectra of the fluoro and chloro compounds concerns the product of reaction 1. For fluorobenzene and the fluorotoluenes the product ions from reaction 1 with D_3^+ as reactant showed specific retention of two deuterium atoms in the product ions indicating specific elimination of DF from the $D_3^+ \cdot XC_6H_4Y$ collision complex. This is not the case for the chloro compounds, as is particularly evident from the D_2 CI spectrum of chlorobenzene where m/q 82 ($C_6H_4D_3^+$) is almost equal in intensity to m/q 81 ($C_6H_5D_2^+$), indicating that in reaction 1 for the chloro compounds there are almost equal probabilities for HCl and DCl elimination from the $D_3^+ \cdot M$ complex. This also appears to be true for the chlorotoluenes, although in the D_2 CI the sums of the relevant ion intensities (m/q 95 and m/q 96) are, in all cases, considerably lower than the m/q 93 intensities in the H_2 CI spectra, indicating that the importance of reaction 1 is reduced with D_3^+ as the reactant ion. It should be noted that the apparent non-specificity of the reactions for the chloro compounds cannot be due to specific loss of DCl from the MD^+ and $D_3^+ \cdot M$ species followed by reaction of the fragment ions with the large excess of D_2 present since such reactions were not observed for the same ions produced in the D_2 CI of the analogous fluoro compounds under the same conditions (1).

The CH_4 and CD_4 CI mass spectra of the chloro-substituted compounds studied are shown in Fig. 2. The CH_4 CI mass spectrum of benzyl chloride, like the spectrum of benzyl fluoride, shows only a low abundance of the MH^+ ion, the dominant ion in the spectrum being the benzyl ion (m/q 91) formed by loss of HCl from MH^+. However, in contrast to the benzyl fluoride system, the benzyl ion formed in the CD_4 CI of benzyl chloride shows ~12% deuterium incorporation leading to m/q 92 ($C_7H_6D^+$), indicating partial isotopic mixing in MD^+ prior to fragmentation by loss of DCl (HCl). The CH_4 CI spectrum benzyl chloride also shows an ion signal at m/q 119 (shifting to m/q 124 in the CD_4 CI) which is 8% of the m/q 91 base peak. This ion does not contain chlorine and we postulate reaction 2 to explain the formation of this product. The reaction is not observed in the CH_4 CI of benzyl fluoride

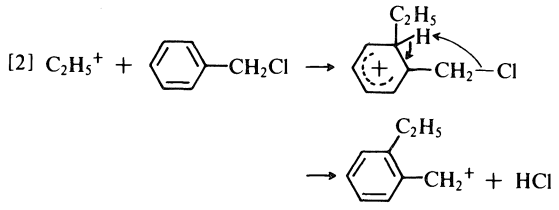

In contrast to the CH_4 CI spectrum of benzyl chloride, the CH_4 CI mass spectra of the isomeric chlorotoluenes show MH^+ as the base peak with only minor loss of HCl from MH^+ to form m/q 91 ($C_7H_7^+$), in agreement with the spectra of fluorotoluenes. It is obvious that rearrangement to a common (tropylium-like) structure does not occur prior to fragmentation in the CH_4 CI of the isomeric benzyl chloride and chlorotoluenes. The CH_4 CI mass spectrum of chlorobenzene shows a low-intensity peak at m/q 93, while the spectra of the chlorotoluenes show low-intensity peaks at m/q 107 (in all cases shifting upwards by four mass units in the CD_4 CI) corresponding to the $RC_6H_4Y \cdot H^+$ ion formed in reaction 1 (R = CH_3, X = Cl). The importance of this reaction is much reduced compared to the analogous fluoro compounds (1).

Chemical Ionization of Bromo-substituted Compounds

The H_2 and D_2 CI mass spectra of the bromo-substituted compounds are shown in Fig. 3. The spectrum of benzyl bromide is characteristic of benzyl halides in that essentially no MH^+ ions are observed, the only significant ion in the spectrum being the benzyl cation (m/q 91) formed by loss of HBr from MH^+. In the D_2 CI spectrum approximately 25% of the signal for the benzyl ion moves to m/q 92 indicating incorporation of a deuterium in the ion and thus loss of HBr from MD^+. This is similar to the

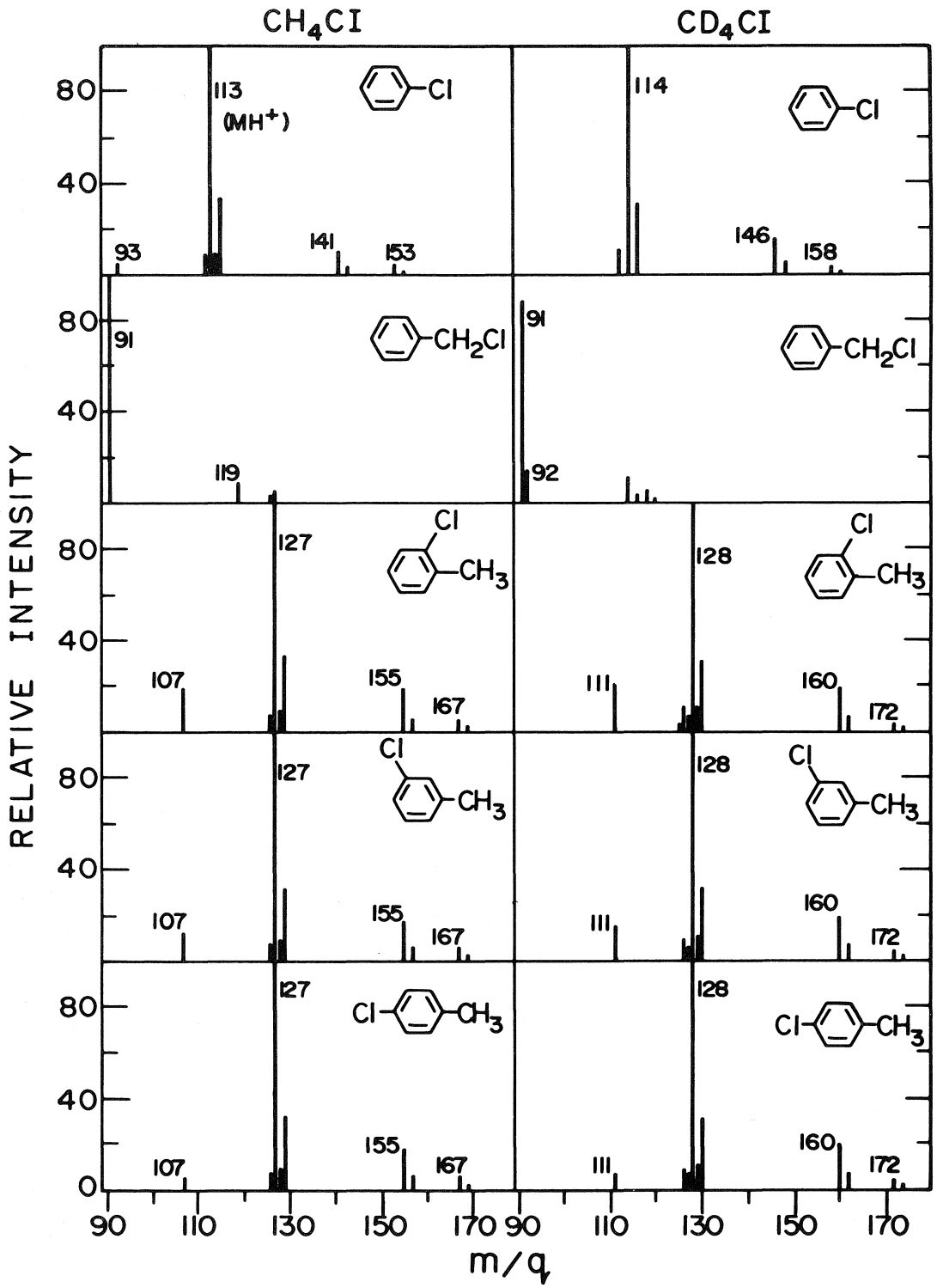

FIG. 2. CH_4 and CD_4 CI of chloro-substituted compounds.

Can. J. Chem. Downloaded from www.nrcresearchpress.com by 84.22.46.98 on 09/08/12
For personal use only.

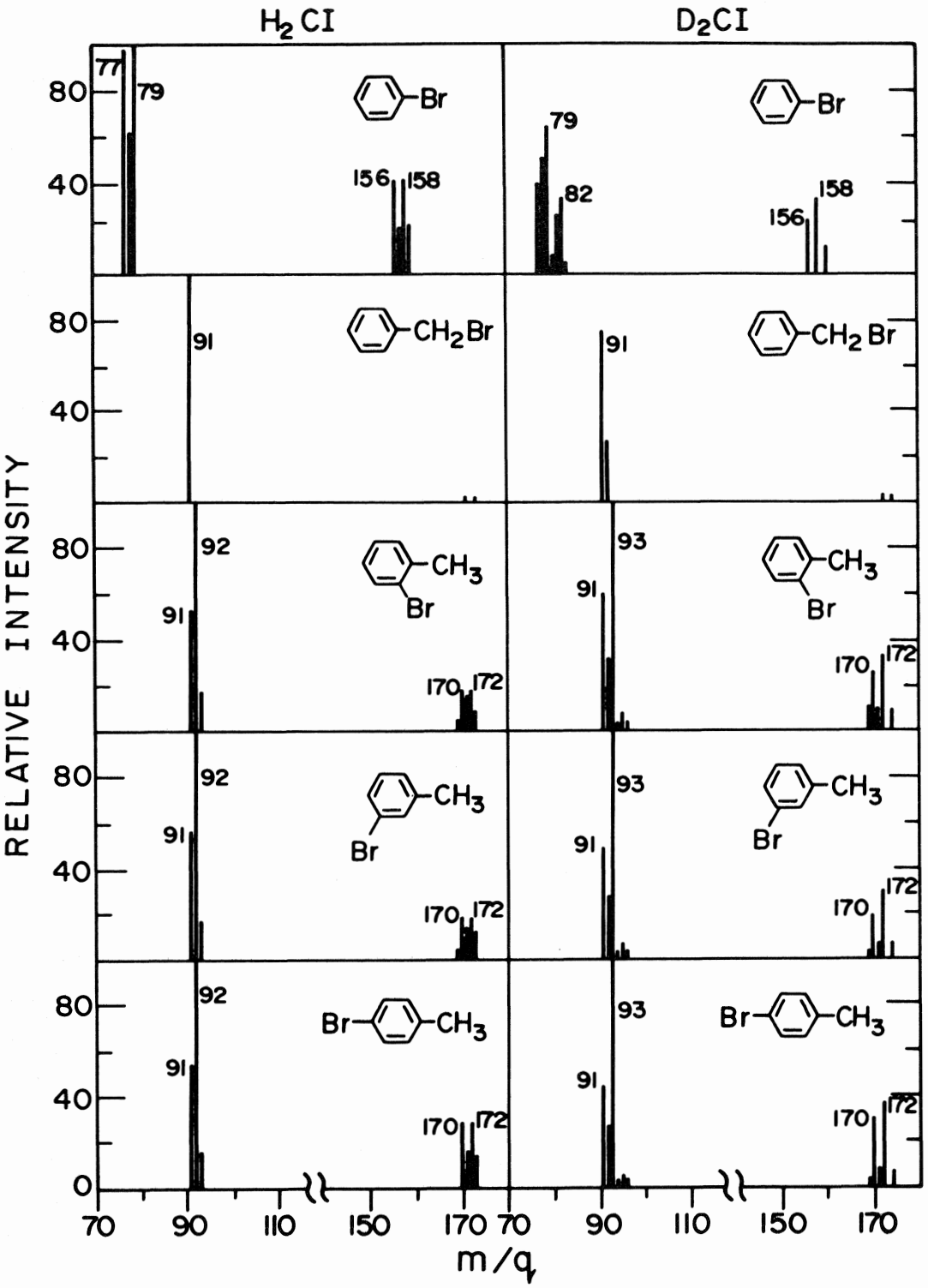

FIG. 3. H_2 and D_2 CI of bromo-substituted compounds.

Can. J. Chem. Downloaded from www.nrcresearchpress.com by 84.22.46.98 on 09/08/12
For personal use only.

results obtained for benzyl fluoride and benzyl chloride.

The H_2 CI mass spectra of bromobenzene and the bromotoluenes show only weak signals for MH^+ with the $M^{+\cdot}$ ion, formed by charge transfer from H_3^+, being more abundant. For bromobenzene the $C_6H_7^+$ (m/q 79) ion formed by reaction 1 (R = H, X = Br) is the base peak in the spectrum, while an abundant $C_6H_5^+$ (m/q 77) ion is observed, corresponding to loss of HBr from MH^+. An unexpected reaction product, not observed in the H_2 CI of fluorobenzene or chlorobenzene, is the abundant m/q 78 ($C_6H_6^{+\cdot}$) ion formed by reaction 3, involving loss of a bromine atom from MH^+

$$[3] \quad H_3^+ + BrC_6H_4Y \rightarrow H_2 + BrC_6H_4Y \cdot H^+ \rightarrow Br + C_6H_5Y^{+\cdot}$$

In the H_2 CI of the bromotoluenes (Y = CH_3) the ion resulting from reaction 3 (m/q 92) constitutes the base peak in the spectra, while the product of reaction 1, m/q 93 ($C_7H_9^+$), is of only minor importance and the $C_7H_7^+$ (m/q 91) ion, resulting from HBr elimination from MH^+, is the second most intense ion in the mass spectra.

The D_2 CI mass spectra of bromobenzene and the bromotoluenes cannot be interpreted quantitatively because of overlap of peaks. However, it is apparent that the $YC_6H_5 \cdot H^+$ product of reaction 1 incorporates in part two deuterium atoms and in part three deuterium atoms, as was found for the chloro compounds, and is of reduced importance compared to the H_2 CI spectra (as was also observed for the chloro compounds). The product ions resulting from HBr loss from MH^+ show significant deuterium incorporation in the D_2 CI spectra, again in agreement with the results for chloro analogues. The $YC_6H_5^{+\cdot}$ product of reaction 3 shows essentially a quantitative shift to $YC_6H_4D^{+\cdot}$ (m/q 79 and m/q 93) as expected from the proposed mechanism. This specific incorporation of deuterium also is observed in the analogous reaction of the iodo compounds (see below). These results rule out the alternative mechanism involving loss of H(D) from the $YC_6H_5 \cdot H^+$ ion produced in reaction 1 since in the D_2 CI this route would lead to significant incorporation of two and three deuterium atoms in the product ion.

The CH_4 and CD_4 CI mass spectra of the bromo compounds are shown in Fig. 4. Again the spectrum of benzyl bromide is characteristic of benzyl halides in showing the benzyl ion (m/q 91) as the major peak in the mass spectrum. By contrast the MH^+ ion forms the base peak in the spectra of the bromotoluenes and there is only minor loss of HBr to form $C_7H_7^+$ (m/q 91). The CI spectrum of benzyl bromide shows a low intensity peak at m/q 119 (shifting to m/q 124 in the CD_4 CI) resulting from reaction 4, analogous to reaction 2 in benzyl chloride

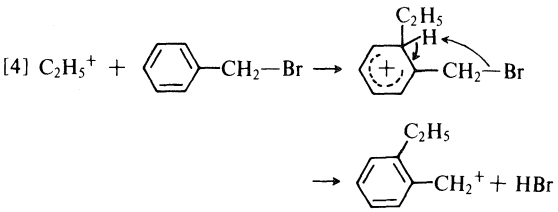

By contrast, the CI spectra of the bromotoluenes all show low intensity ion signals at m/q 120 (shifting to m/q 125 in the CD_4 CI) which must result from reaction 5 (illustrated for the *para* isomer)

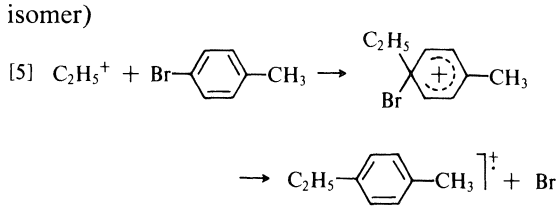

In addition, the CI spectrum of bromobenzene shows a weak peak at m/q 93 while the CI spectra of the bromotoluenes show weak peaks at m/q 107 (in all cases shifting upwards by 4 mass units in the CD_4 CI) resulting from reaction 1 (R = CH_3, X = Br, Y = H or CH_3).

Chemical Ionization of Iodo-substituted Compounds

The H_2 and D_2 CI mass spectra of the five iodo-substituted compounds studied are shown in Fig. 5. The H_2 CI mass spectrum of benzyl iodide is characteristic of benzyl compounds in showing $C_6H_5CH_2^+$ (m/q 91) as the only significant ion. As was found for the other benzyl halides there is a partial shift to m/q 92 ($C_7H_6D^+$) in the D_2 CI spectrum. By contrast, the H_2 CI of the iodotoluenes, although showing no MH^+ ion signal, exhibit only minor fragmentation to form $C_7H_7^+$, m/q 91 ($MH^+ - HI$). The major fragmentation route for both the iodotoluenes and iodobenzene is reaction 6 involving loss of an

Downloaded from www.nrcresearchpress.com by 84.22.46.98 on 09/08/12
For personal use only.

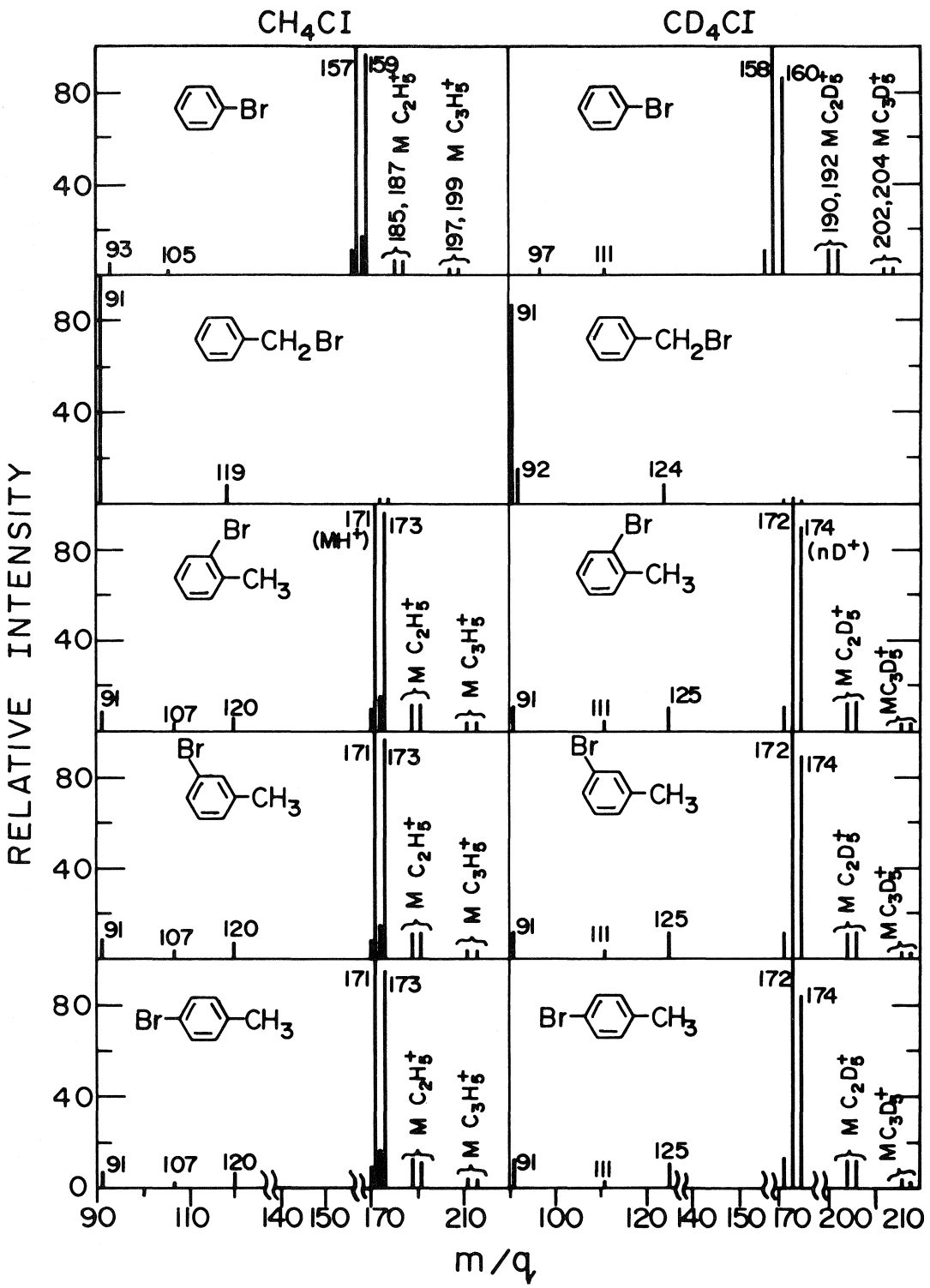

FIG. 4. CH_4 and CD_4 CI of bromo-substituted compounds.

Can. J. Chem. Downloaded from www.nrcresearchpress.com by 84.22.46.98 on 09/08/12
For personal use only.

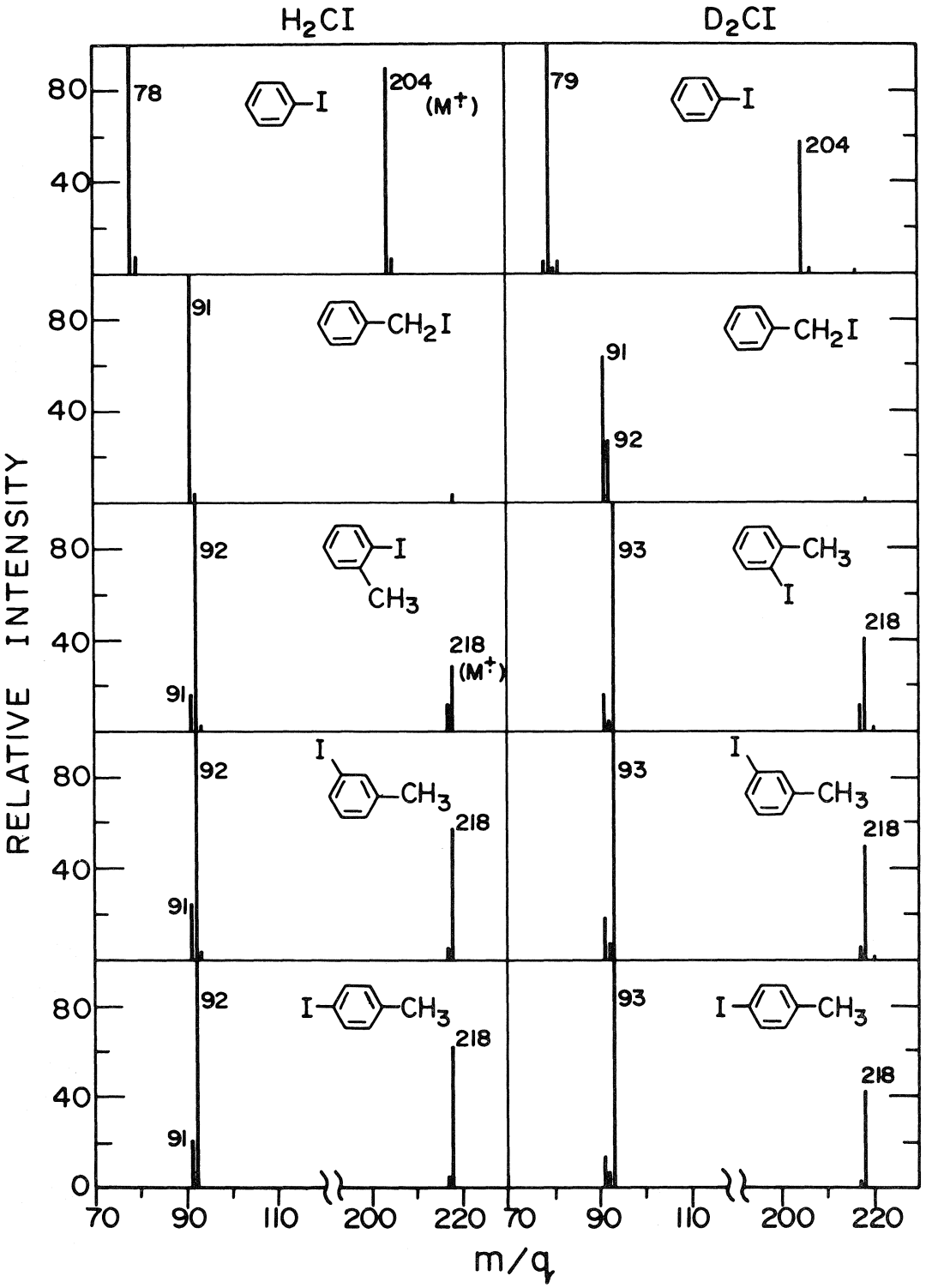

FIG. 5. H_2 and D_2 CI of iodo-substituted compounds.

Can. J. Chem. Downloaded from www.nrcresearchpress.com by 84.22.46.98 on 09/08/12
For personal use only.

Can. J. Chem. Downloaded from www.nrcresearchpress.com by 84.22.46.98 on 09/08/12
For personal use only.

iodine atom from MH^+ giving m/q 78

[6] $H_3^+ + IC_6H_4Y \rightarrow H_2 + C_6H_4Y \cdot H^+ \rightarrow I + C_6H_6Y^{+\cdot}$

(Y = H) for iodobenzene and m/q 92 (Y = CH_3) for the iodotoluenes. In the D_2 CI mass spectra the ions resulting from reaction 6 move upwards by one mass unit indicating, as expected, a specific incorporation of one deuterium atom from the reactant ion in the product species. Abundant $M^{+\cdot}$ ion signals are observed in the H_2 and D_2 CI spectra of iodobenzene and the iodotoluenes resulting from charge transfer from H_3^+ (D_3^+).

The CH_4 and CD_4 CI mass spectra of the iodo compounds are shown in Fig. 6. The CH_4 CI mass spectrum of benzyl iodide again is characteristic of benzyl compounds, showing the benzyl ion (m/q 91) as the major ion in the mass spectrum, with ~16% D incorporation in the CD_4 CI spectrum. A low-intensity ion is observed at m/q 119 (m/q 124 in the CD_4 CI spectrum) corresponding to ethyl ion addition with loss of HI, analogous to reactions 2 and 4 in benzyl chloride and benzyl bromide.

The CH_4 CI mass spectra of the ring-substituted iodotoluenes differ from the CH_4 CI mass spectrum of benzyl iodide in showing an abundant MH^+ ion signal, a moderately intense $M^{+\cdot}$ ion signal, with the major fragmentation of MH^+ leading to elimination of I· rather than HI, resulting in formation of $C_7H_8^{+\cdot}$ (m/q 92) as the base peak in the mass spectrum. The ion (m/q 120) resulting from displacement of an iodine atom by $C_2H_5^+$ is much more intense in the CI of the iodotoluenes than the corresponding ion in the CH_4 CI of the bromotoluenes, and is accompanied by significant ion signals at m/q 132 (shifting to m/q 137 in the CD_4 CI spectra) corresponding to the displacement of I· by $C_3H_5^+$. The general reaction is shown in [7] for the *para* substituted compound.

[7] $R^+ +$ 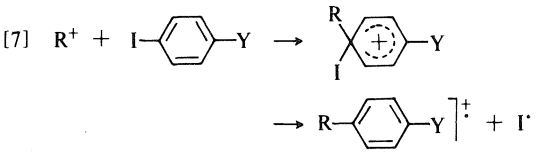 $\rightarrow$

The CH_4 and CD_4 CI spectra of iodobenzene show the same features as the spectra of the iodotoluenes. A significant feature of the CH_4 CI mass spectra of the ring-substituted iodo compounds is the absence of the product of reaction 1 (m/q 93 for iodobenzene, m/q 107 for the iodotoluenes) which is a prominent reaction product for the fluoro compounds but decreases in importance as one proceeds through the halogen series.

Structural and Energetics Effects in Chemical Ionization Spectra

In both the H_2 and CH_4 chemical ionization, the mass spectra of the benzyl halides differ markedly from the mass spectra of the ring-substituted halotoluenes. This provides strong evidence that in chemical ionization, in contrast to electron impact ionization, rearrangement to a common symmetrical tropylium-type structure does not occur prior to fragmentation. Although the CI mass spectra of the benzyl halides are all very similar, showing the benzyl ion (m/q 91) as the only significant ion in the spectra, both the H_2 and CH_4 CI mass spectra of the ring-substituted halobenzenes and halotoluenes show pronounced changes as one proceeds through the series from the fluoro-substituted compounds to the iodo-substituted compounds.

The reactions of H_3^+ with the halobenzenes lead to the protonated molecule, MH^+, and three possible fragment ions, $C_6H_7^+$, $C_6H_6^{+\cdot}$, and $C_6H_5^+$, as summarized by reactions 8 to 11.

[8] $H_3^+ + C_6H_5X \rightarrow C_6H_5X \cdot H^+ + H_2$

[9] $\rightarrow C_6H_7^+ + HX$

[10] $\rightarrow C_6H_6^{+\cdot} + H_2 + X\cdot$

[11] $\rightarrow C_6H_5^+ + H_2 + HX$

For the four halobenzenes studied the observed intensities of the product ions from these reactions (expressed as percent total ionization, neglecting the $M^{+\cdot}$ formed by charge transfer) are summarized in Table 1. Also included in Table 1 are the calculated reaction enthalpies. These have been calculated using $\Delta H_f(H_3^+)$ = 266 kcal mol^{-1} ($PA(H_2)$ = 100 kcal mol^{-1} (5)), $\Delta H_f(C_6H_7^+)$ = 200 kcal mol^{-1} ($PA(C_6H_6)$ = 183 kcal mol^{-1} (6)), and $\Delta H_f(C_6H_5X \cdot H^+)$ derived from the proton affinities $PA(C_6H_5F)$ = 182 kcal mol^{-1} (6) and $PA(C_6H_5Cl)$ = 182 kcal mol^{-1} (6) and assuming the same proton affinities for bromobenzene and iodobenzene. The remaining thermochemical data were taken from ref. 7 except for $\Delta H_f(C_6H_5^+)$ for which the value of 266 kcal mol^{-1} (8) was used.

Although reaction 9 is, overall, the most

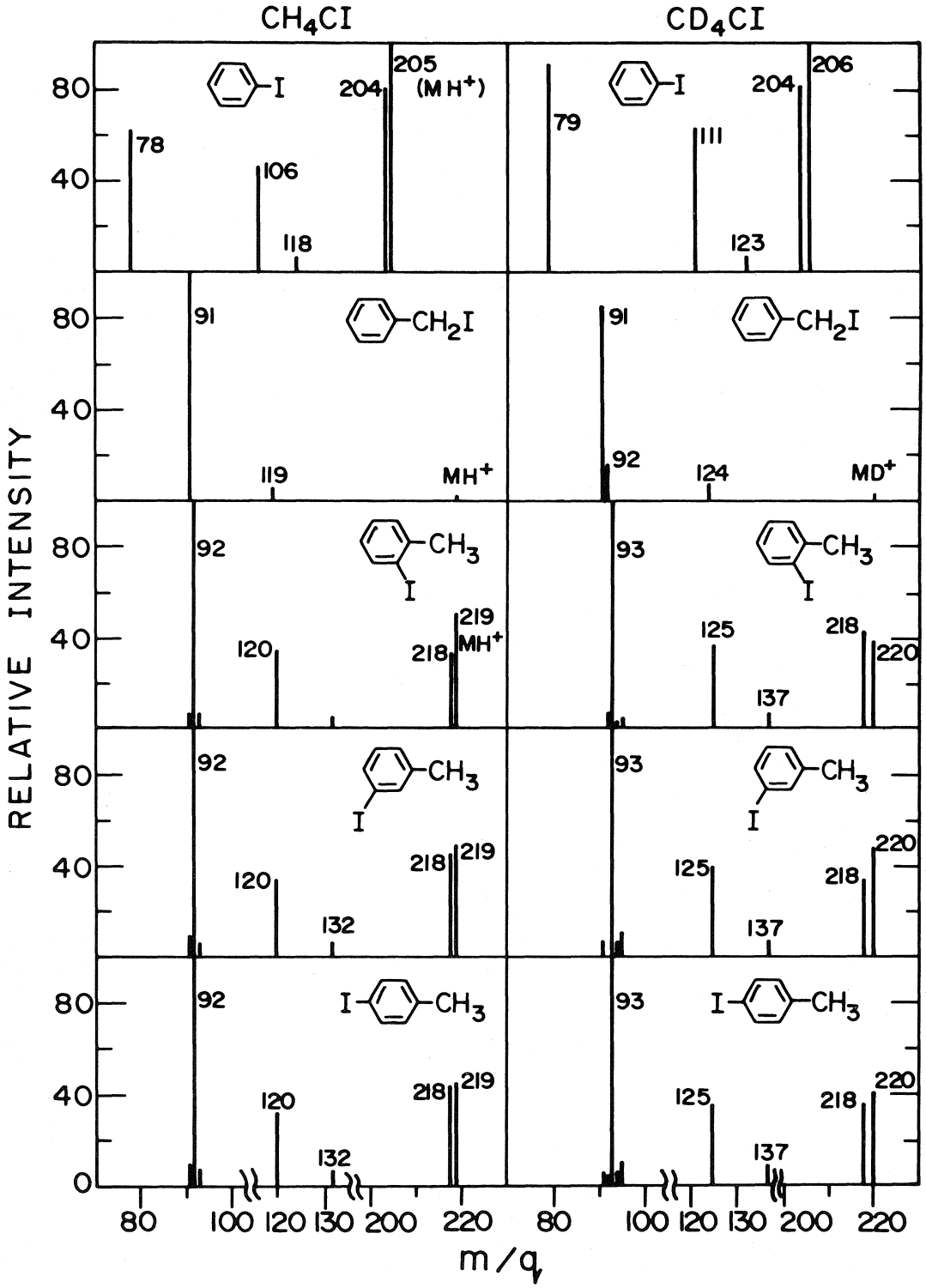

FIG. 6. CH_4 and CD_4 CI of iodo-substituted compounds.

Can. J. Chem. Downloaded from www.nrcresearchpress.com by 84.22.46.98 on 09/08/12
For personal use only.

TABLE 1. Fractional yields and reaction thermochemistry for reaction of H_3^+ with phenyl halides (C_6H_5X)

	Reaction 8		Reaction 9		Reaction 10		Reaction 11	
X	$C_6H_5X \cdot H^+$	ΔH^*	$C_6H_7^+$	ΔH^*	$C_6H_6^{+\cdot}$	ΔH^*	$C_6H_5^+$	ΔH^*
F	0.54	−82	0.27	−101	0	+12	0.19	−38
Cl	0.12	−82	0.41	−98	0	−17	0.47	−35
Br	0.13	−82	0.33	−96	0.20	−30	0.33	−33
I	0	−82	0	−94	1.00	−45	0	−31

*ΔH in kcal mol^{-1}.

exothermic reaction of H_3^+ with the halobenzenes, its importance initially increases as we proceed from fluorobenzene to chlorobenzene, decreases in importance for bromobenzene, and is not observed for iodobenzene. In the halotoluenes the analogous reaction 1 (H_3^+ reactant) decreases rapidly in importance as one proceeds through the halotoluene series. It is not clear whether this variation in the importance of reaction 9 is a structural effect or is related to reaction competition influenced by reaction energetics. The reaction obviously requires formation of a complex between H_3^+ and the neutral molecule and it is possible that complex formation is in competition with simple proton transfer, which leads to formation of MH^+ (reaction 8) and, by fragmentation, to the other products $C_6H_6^{+\cdot}$ and $C_6H_5^+$. The thermochemical data in Table 1 show that, as we proceed from fluorobenzene to iodobenzene, the difference in reaction exothermicity favouring reaction 9 over the simple proton transfer reaction 8 decreases, and this may be the explanation for the decreasing importance of reaction 9 through the halobenzene series. A similar rationalization can be advanced for the decrease in importance of formation of the $CH_3C_6H_5 \cdot H^{+\cdot}$ ion in the H_2 CI of the halotoluenes as one proceeds from the fluoro- to the iodo-substituted compounds; however, quantitative calculations are not possible since the proton affinities of the halotoluenes are not known.

Although the results in Table 1 indicate that the yield of $C_6H_5^+$ parallels the yield of $C_6H_7^+$, suggesting the possibility that $C_6H_5^+$ may originate by loss of H_2 from $C_6H_7^+$, the results obtained with D_3^+ as reactant ion appear to preclude this route as a major route for formation of $C_6H_5^+$. In the D_2 CI of fluorobenzene $C_6H_5D_2^+$ is formed by the reaction analogous to [9], however, no deuterium incorporation is observed in the phenyl ion product as might be expected if $C_6H_5^+$ originated by fragmentation of $C_6H_7^+$. In the D_2 CI of chlorobenzene and bromobenzene both $C_6H_5D_2^+$ and $C_6H_4D_3^+$ are observed, however, the phenyl ion product incorporates either zero or one deuterium atom (with roughly equal probability) again inconsistent with a major route to $C_6H_5^+$ being by fragmentation of $C_6H_7^+$. Further, it should be noted that protonation of benzene directly by H_3^+ does not lead to formation of $C_6H_5^+$. Thus we conclude that $C_6H_5^+$ probably originates by loss of HX from $C_6H_5X \cdot H^+$ (reaction 12). Similarly, the label retention results (incorporation of one D in the D_2 CI) indicate that $C_6H_6^{+\cdot}$ originates by loss of X$^\cdot$ from $C_6H_5X \cdot H^+$ (reaction 13)

[12] $$C_6H_5X \cdot H^+ \rightarrow C_6H_5^+ + HX$$

[13] $$C_6H_5X \cdot H^+ \rightarrow C_6H_6^{+\cdot} + X$$

The energy requirements for these fragmentation reactions for ground state $C_6H_5X \cdot H^+$ are given by $\Delta H_{12} = \Delta H_{11} - \Delta H_8$ and $\Delta H_{13} = \Delta H_{10} - \Delta H_8$. From the thermochemical data in Table 1 it is seen that only reaction 12 (reaction 11 overall) is thermochemically possible for the fluorobenzene system. The observation of a significant yield of $C_6H_5^+$ in the H_2 CI of fluorobenzene must mean that an appreciable fraction of the $C_6H_5F \cdot H^+$ ions formed in reaction 8 have >44 kcal mol^{-1} ($\Delta H_{11} - \Delta H_8$) excitation energy, or greater than 50% of the reaction exothermicity. Both reactions 12 and 13 are thermochemically permitted in the chlorobenzene system, however, reaction 12 is strongly favoured energetically and is the only reaction observed. At the internal energy of MH^+ necessary for reaction 13 to occur (>65 kcal mol^{-1}) reaction 12 would be much more rapid. For protonated bromobenzene reactions 12 and 13 have approximately equal energy requirements and both

Can. J. Chem. Downloaded from www.nrcresearchpress.com by 84.22.46.98 on 09/08/12
For personal use only.

fragmentation reactions are observed, however, for protonated iodobenzene reaction 13 is strongly favoured thermochemically and is the only reaction observed. No $C_6H_5I \cdot H^+$ ion signal is observed in the H_2 CI of iodobenzene and this implies that all of the protonated molecules have >37 kcal mol^{-1} ($\Delta H_{10} - \Delta H_8$) excitation energy.

Although quantitative calculations are not possible, similar thermochemical arguments can be advanced to explain the shift from $C_7H_7^+$ as the major fragment ion in the H_2 CI of the fluoro- and chlorotoluenes to $C_7H_8^{+\cdot}$ as the major fragment ion in the H_2 CI of the bromo- and iodotoluenes. However, these arguments apply *only* if one assumes that the $C_7H_7^+$ ions formed in the H_2 CI of the halotoluenes have the methyl-substituted phenyl structure. If rearrangement to a benzyl or tropylium structure occurs in the fragmentation reaction 14 for X = Br or I,

[14] $$CH_3C_6H_4X \cdot H^+ \rightarrow C_7H_7^+ + HX$$

this reaction should be strongly favoured energetically over formation of $C_7H_8^{+\cdot}$, even for the iodotoluenes. The fact that very little $C_7H_7^+$ is observed in the H_2 CI of the iodotoluenes and that formation of $C_7H_8^{+\cdot}$ competes favourably with formation of $C_7H_7^+$ in the H_2 CI of the bromotoluenes, provides further evidence that rearrangement of the molecular framework to a benzyl or tropylium structure does not occur prior to fragmentation in the H_2 CI of the halotoluenes.

The CH_4 CI mass spectra of the halobenzenes and the halotoluenes also show large changes through the series from the fluoro compounds to the iodo compounds. An unexpected reaction of $C_2H_5^+$ (reaction 15) results in the formation of

[15] $$C_2H_5^+ + XC_6H_4Y \rightarrow C_2H_5C_6H_4Y^{+\cdot} + X^\cdot$$

$C_2H_5C_6H_4Y^{+\cdot}$ (Y = H or CH_3) as an abundant product ion in the CH_4 CI of the iodo-substituted compounds and as a minor product in the CH_4 CI of the bromo-substituted compounds. Thermochemical calculations show that reaction 15 is 29 kcal mol^{-1} exothermic for iodobenzene, 14 kcal mol^{-1} exothermic for bromobenzene, approximately thermoneutral for chlorobenzene, and 28 kcal mol^{-1} endothermic for fluorobenzene. By contrast, the simple proton transfer reaction 16 is $\sim$22 kcal mol^{-1} exothermic throughout the series. Thus, reaction 15 is favoured energetically over proton transfer for X = I and competes successfully. However, reaction 16, along with formation of the collisionally-stabilized complex, $C_2H_5 \cdot C_6H_5X^+$, are the major reaction channels for $C_2H_5^+$ with the other halobenzenes and halotoluenes.

[16] $$C_2H_5^+ + C_6H_5X \rightarrow C_6H_5X \cdot H^+ + C_2H_4$$

The reaction of CH_5^+ with C_6H_5X and $CH_3C_6H_4X$ proceeds by two major routes, reaction 17, involving simple proton transfer, and reaction 18, involving complex formation with elimination of HX.

[17] $$CH_5^+ + XC_6H_4Y \rightarrow XC_6H_4Y \cdot H^+ + CH_4$$

[18] $$\rightarrow CH_3C_6H_4Y \cdot H^+ + HX$$

Reaction 18 is important for X = F where the product ion accounts for $\sim$35% of the total ionization, is a minor reaction channel (2–5% of the total ionization) for X = Cl and Br, and is not observed for X = I. Thermochemical calculations show that reaction 18 is $\sim$71 kcal mol^{-1} exothermic for fluorobenzene, with the exothermicity decreasing to $\sim$63 kcal mol^{-1} for iodobenzene, while reaction 17 is $\sim$52 kcal mol^{-1} exothermic for all halobenzenes. Thus, this may be another example of the effect of differences in reaction exothermicity on the competition between complex formation and simple proton transfer.

For iodobenzene and the iodotoluenes fragmentation of MH^+ to yield $C_6H_5Y^{+\cdot}$ is observed. We calculate that the overall reaction

[19] $$CH_5^+ + C_6H_5X \rightarrow CH_4 + C_6H_5X \cdot H^+ \rightarrow C_6H_6^{+\cdot} + X^\cdot$$

is 18 kcal mol^{-1} exothermic for iodobenzene, 4 kcal mol^{-1} exothermic for bromobenzene but endothermic for chlorobenzene ($\Delta H = +9$ kcal mol^{-1}) and fluorobenzene ($\Delta H = +38$ kcal mol^{-1}). The observation of reaction 19 in the iodobenzene system clearly establishes that a significant fraction of the $C_6H_5X \cdot H^+$ ions have internal excitations ≥ 34 kcal mol^{-1} ($\Delta H_{19} - \Delta H_{17}$), or $>65\%$ of the exothermicity of reaction 17. The failure to observe reaction 19 for bromobenzene indicates that no $C_6H_5X \cdot H^+$ ions have excitation energies as large as 48 kcal mol^{-1} ($\Delta H_{19} - \Delta H_{17}$ for bromobenzene).

Loss of HX from the protonated molecule formed in the CH_4 CI is endothermic for all halobenzenes and, also, for all halotoluenes if,

Can. J. Chem. Downloaded from www.nrcresearchpress.com by 84.22.46.98 on 09/08/12
For personal use only.

for the latter, one assumes a methyl-substituted phenyl structure for the product ion. However, if rearrangement to a benzyl or tropylium structure occurred, loss of HX from the protonated molecule would be very exothermic for all halotoluenes. The absence of significant yields of $C_7H_7^+$ in the CH_4 CI of the halotoluenes provides further evidence that rearrangement of the molecular framework does not occur in the chemical ionization of these compounds.

Acknowledgement

The authors are indebted to the National Research Council of Canada for financial support.

1. A. G. HARRISON and P.-H. LIN. Can. J. Chem. **53**, 1314 (1975).
2. J. M. S. TAIT, T. W. SHANNON, and A. G. HARRISON. J. Am. Chem. Soc. **84**, 4 (1962).
3. S. SAFE, W. D. JAMIESON, and D. J. EMBREE. Can. J. Chem. **52**, 867 (1974).
4. J. T. BURSEY, M. M. BURSEY, and D. G. I. KINGSTON. Chem. Rev. **73**, 191 (1973).
5. J. L. BEAUCHAMP. *In* Interactions between ions and molecules. *Edited by* P. Ausloos. Plenum Press, N.Y. 1975.
6. R. YAMDAGNI and P. KEBARLE. J. Am. Chem. Soc. **98**, 1320 (1976).
7. Ionization potentials, appearance potentials, and heats of formation of gaseous positive ions. NSRDS-NBS26, 1969.
8. H. M. ROSENSTOCK, J. T. LARKINS, and J. A. WALKER. Int. J. Mass. Spectrom. Ion Phys. **11**, 309 (1973).

Can. J. Chem. Downloaded from www.nrcresearchpress.com by 84.22.46.98 on 09/08/12
For personal use only.

Molecular motion, phase transitions, and disorder in the pyridinium halides[1]

JOHN A. RIPMEESTER
Division of Chemistry, National Research Council of Canada, Ottawa, Canada K1A 0R9

Received March 23, 1976

JOHN A. RIPMEESTER. Can. J. Chem. **54**, 3453 (1976).

The solid pyridinium chloride, bromide, and iodide salts were studied using ^1H nuclear magnetic resonance and differential scanning calorimetry. Phase transitions were observed at 345 K for the chloride, 269 K for the bromide, and 247 K for the iodide. Well below each transition, the pyridinium ions are held rigidly in the crystal lattice, whereas above each transition the ions reorientate rapidly about an axis at right angles to the ring planes. From the temperature dependence of the spin–lattice relaxation times the high temperature phase reorientational activation energies were determined to be 1.55, 2.30, and 4.20 kcal/mol for the chloride, bromide, and iodide, respectively.

JOHN A. RIPMEESTER. Can. J. Chem. **54**, 3453 (1976).

Les sels solides: chlorure, bromure et d'iodure de pyridinium ont été étudiés en utilisant la résonance magnétique nucléaire ^1H et la calorimétrie à balayage différentiel. Des transitions de phase ont été observées à 345 K pour le chlorure, 269 K pour le bromure et 247 K pour l'iodure. Bien au-dessous de chaque transition, les ions pyridinium sont tenus rigidement dans le réseau cristallin tandis qu'au dessus de chaque transition les ions se réorientent rapidement autour d'un axe perpendiculaire aux plans des cycles. A partir de la variation des temps de relaxation spin–réseau avec la température, les énergies d'activation pour la réorientation de phase à haute température ont été déterminées comme étant 1.55, 2.30 et 4.20 kcal/mol pour le chlorure, le bromure et l'iodure respectivement.

[Traduit par le journal]

Introduction

Pyridine forms salts with many organic as well as inorganic acids. However, relatively little is known about the motional properties of the pyridinium ion in the solid state. Studies of motions in solids containing this ion should be of interest for several reasons. Even though the pyridinium ion is essentially planar it does not have the regular sixfold symmetry of benzene. The appearance of even an in-plane motion should in principle give rise to a phase transition (1, 2). Also it is known that hydrogen bonding between the pyridine nitrogen proton and the anion may profoundly affect the motional properties of the ring (3).

Various other publications have dealt with structure and bonding in pyridinium salts. Variations in the N—H stretching and bending frequencies as measured for various salts by infrared techniques (4–7) have been interpreted in terms of differing degrees of hydrogen bonding. Single crystal X-ray results for pyridinium chloride (8) and nitrate (9) have been interpreted in terms of static, ordered structures, with significant hydrogen bonding between anion and cation. On the other hand, X-ray studies on some of the hexafluoro group-V anion salts of pyridine (10) and pyridinium iodide (11) favor a sixfold disordered ring, with hydrogen bonding absent.

In this work we report the results of broadline nmr as well as spin–lattice relaxation time measurements on the pyridinium halides. As in all three of the compounds studied evidence was found for a phase transition, differential scanning calorimetry was used to measure the transition temperatures and heats of transition for the salts.

Experimental Section

(a) *Materials*

The materials used in the preparation of the salts were reagent grade chemicals. Pyridinium chloride and bromide were prepared by passing the dry hydrogen halides through acetone solutions of pyridine. The iodide was prepared by mixing pyridine with an aqueous HI solution. The salts were dried over P_2O_5 after recrystallization from absolute or aqueous ethanol. The samples for CW nmr were sealed in Pyrex tubes after heating to 100 °C under vacuum. The samples for the relaxation time and DSC studies were further purified by vacuum sublimation.

[1]NRCC No. 15415.

Can. J. Chem. Downloaded from www.nrcresearchpress.com by 210.87.254.6 on 09/05/12
For personal use only.

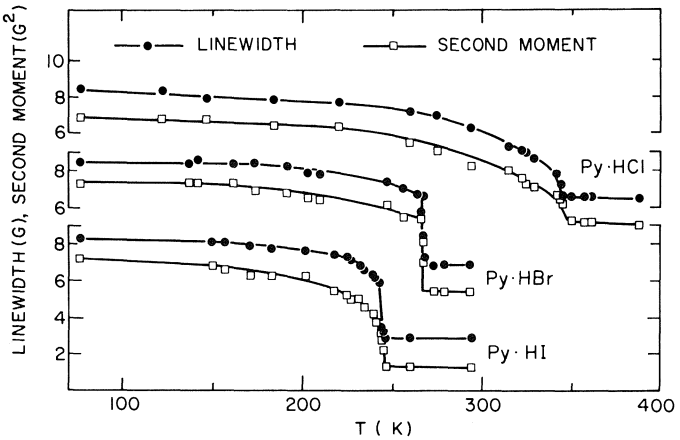

FIG. 1. Proton linewidths and second moments for the pyridinium halides; the vertical scale for the bromide and chloride have been offset by 4 units and 8 units respectively.

Melting points for the chloride and bromide salts were (literature values (4) in parentheses) 141 °C (142 °C) and 218 °C (214 °C) respectively.

Analyses for C, H, and N were carried out for the iodide, which decomposed on heating. *Anal.* calcd. for Py.HI: C 29.0, H 2.9, N 6.8. Found: C 28.6, H 2.9, N 6.5.

(*b*) *Equipment and Experimental Techniques*

The broadline nmr spectra were obtained using a Varian crossed-coil spectrometer operating at a frequency of 16 MHz. Pulsed nmr measurements were made using a Bruker SXP nmr spectrometer operating at a frequency of 16 MHz. Spin–lattice relaxation times (T_1) were measured using 90°–τ–90° pulse sequences.

Methods of temperature measurement and control, as well as methods of data treatment have been described previously (12, 13).

Transition temperatures and heats of transition were measured using a Perkin-Elmer DSC 1-B Differential Scanning Calorimeter. Sample sizes ranged from 10 to 50 mg and scanning rates used were 5 and 10 deg/min. Heats of transition were measured by comparing the transitional peak areas with the melting peak area for indium metal.

Results and Analysis

(*a*) *CW Nuclear Magnetic Resonance Results*

Spectra recorded for the pyridinium halides generally were smooth, featureless curves. The limiting high and low temperature second moments of 1.2 ± 0.1 and 6.8 ± 0.5 G² are in good agreement with those reported previously (3). The near-discontinuous behaviour of the pyridinium chloride linewidths and second moments (see Fig. 1) near 350 K is suggestive of a phase transition.

The linewidth and second moment *vs.* temperature curves for the bromide and iodide salts resemble to some extent those observed for the chloride (see Fig. 1). Some preliminary narrowing was evident before the resonances narrowed suddenly at 246 K for the iodide and 269 K for the bromide. Second moments for the bromide and iodide were 7.2 ± 0.4 G² and 7.0 ± 0.3 G² at 77 K, and 1.35 ± 0.08 G² and 1.30 ± 0.06 G² at room temperature, respectively. It is probable that the sudden line narrowing observed for these two compounds accompanies phase transitions.

The room temperature crystal structure for pyridinium chloride is known (8) and may be used for second moment calculations. In agreement with a previous calculation, a rigid lattice second moment of 6.73 G² is found taking the N—H and C—H bond-lengths to be 1.08 Å, and assuming the protons to lie on an extension of the vector joining ring atoms *para* to each other.

Rigid lattice second moments were calculated taking into account contributions from all abundant magnetic nuclei within a 6 Å sphere. Contributions from outside this sphere were estimated by an integral. The chlorine and nitrogen nuclei were assumed to be Zeeman quantized for the second moment calculations. Theoretical second moments were calculated also for the case where the pyridinium ion performed reorientations about the axis at right angles to the ring plane. For this second situation it was necessary to assume that the crystal structure in the high temperature phase was identical to the one found at room temperature. Reduced

Can. J. Chem. Downloaded from www.nrcresearchpress.com by 210.87.254.6 on 09/05/12
For personal use only.

Can. J. Chem. Downloaded from www.nrcresearchpress.com by 210.87.254.6 on 09/05/12
For personal use only.

TABLE 1. Summary of second moment results

Compound	Type of motion[a]	^{1}H second moment (G^2) Calculated	Experimental
Py·HCl	RL	6.73	6.8 ±0.5 (77 K)
	RR	1.45	1.2 ±0.1 (360 K)
Py·HBr	RL	—	7.2 ±0.4 (77 K)
	RR	—	1.35±0.08 (296 K)
Py·HI	RL	—	7.0 ±0.3 (77 K)
	RR	—	1.30±0.06 (296 K)

[a]RL = rigid lattice, RR = ring reorientation.

second moments due to motions were found under the assumption that these motions take place as a jumping between allowed sites. The approach to the problem was similar to that used by Miller and Gutowsky (14). The complete expression for motionally reduced second moments has been tabulated by Rigny *et al.* (15). The value calculated in this manner is 1.45 G^2 in agreement with a value of 1.26 G^2 previously calculated for random in-plane rotation of the pyridinium ion (3). The second moment data have been summarized in Table 1. It is evident that the values calculated for pyridinium chloride apply equally well to the bromide and iodide cases.

(b) Spin–Lattice Relaxation Times

Spin–lattice relaxation times (T_1) were measured for the three salts between the respective phase transition temperatures and ~400 K. T_1 changes discontinuously at the phase transition, and increases monotonically with temperature (Fig. 2).

For the fast motion case, where τ_c, the correlation time for the in-plane reorientations of the pyridinium ions, is much shorter than the inverse radio frequency ($\tau_c \ll \omega_0^{-1}$), the expression for T_1 becomes [2] (16)

$$[1] \qquad T_1^{-1} = 10\gamma^2 \Delta SM \tau_c/3$$

Here it is assumed that the spin–lattice relaxation time is determined entirely by fluctuations of the interproton dipolar interactions due to

[2]The use of eq. 1 as taken from ref. 16 is based on an adjustment of the B.P.P. equation to allow for both anisotropic motions and intermolecular interactions. Derivations based on Woessner's equation (17) for anisotropic motions, or Anderson's treatment (18) of the six site in-plane rotor yield the identical equation.

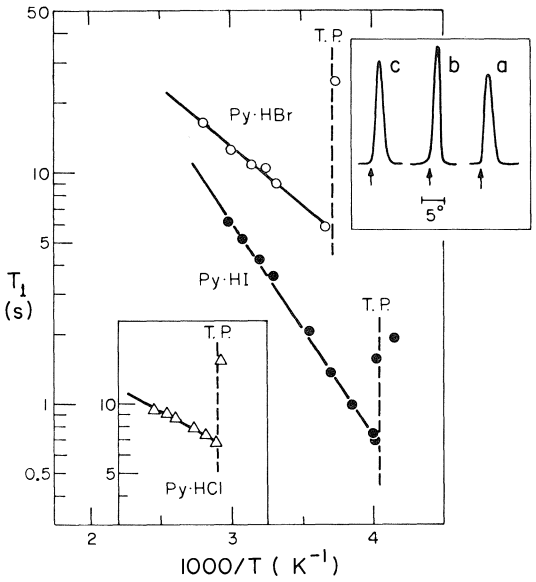

FIG. 2. Proton spin–lattice relaxation times for pyridinium chloride, bromide and iodide as a function of inverse temperature. T.P. marks the transition temperatures. Upper insert shows DSC peaks: (*a*) Py·HCl, (*b*) Py·HBr, (*c*) Py·HI. Arrows mark transition temperatures given in Table 2. Heating rate: 5°/min.

molecular reorientations. ΔSM is then the change in the observable second moment produced by these reorientations. For an activated process, τ_c is written in terms of an inverse frequency factor τ_0, and an activation energy E_a

$$[2] \qquad \tau_c = \tau_0 \exp(E_a/RT)$$

In the fast motion limit, the activation energy can be derived directly from a log T_1 *vs.* inverse temperature plot, and values of 4.22, 2.30, and 1.55 kcal/mol are found for the iodide, bromide, and chloride respectively. Motional correlation times for these salts can be estimated using eq. 1 taking ΔSM to be 5.7 G^2 (see Table 1). For the iodide, $\tau_c \simeq 1.0 \times 10^{-10}$ s at 250 K, for the bromide $\tau_c \simeq 1.3 \times 10^{-11}$ s at 270 K, and for the chloride $\tau_c \simeq 2.1 \times 10^{-12}$ at 346 K, so that evidently the ring reorientations become extremely fast right above the phase transitions.

(c) Differential Scanning Calorimetry Studies

For each of the three halide salts a peak was observed in the DSC traces (see insert, Fig. 2), and the transition temperatures derived (see Table 2) agree well with those found from the nmr results. The transition enthalpies are 538,

TABLE 2. Summary of phase transition data, N—H stretch frequencies, and activation energies

Compound	N—H stretch frequency (cm^{-1})	Transition temperature (K)	Transition enthalpy (cal/mol)	Transition entropy (cal/mol deg)	Activation energy (kcal/mol)
Py·HCl	2430[a]	345 ±1	538	1.56	1.55±0.1
Py·HBr	2800[a]	269.0±0.5	586	2.18	2.30±0.2
Py·HI	2990[a]	246.8±0.5	460	1.86	4.20±0.2

[a]Reference 6.

586, and 460 cal/mol for the chloride, bromide, and iodide salts respectively, and these lead to transition entropies of 1.56, 2.18, and 1.86 cal/mol deg. The uncertainty in the above results, as judged by the scatter obtained for a number of runs on different samples of the same material is ~5%.

Discussion

For pyridinium chloride, one short ring atom – chloride ion distance was assigned to be a N—H---Cl hydrogen bond in a room temperature X-ray study (8), and we can take this as evidence that the low temperature phases for the salts are ordered. Recently a room temperature X-ray study on pyridinium iodide (11) showed the pyridinium ion to be disordered. Although there are discrete sites for each ring atom, no distinction between carbon and nitrogen atoms could be made. In the previous sections it was shown that the pyridinium halides undergo phase transitions from a low temperature phase with static pyridinium ions to a high temperature phase where the pyridinium rings reorient rapidly about an axis at right angles to the ring plane. As molecular motion of the pyridinium rings sets in, the associated disorder requires the presence of a phase transition (1, 2). It is of interest to attempt an interpretation of the experimental transition entropies in terms of a change in the configurational entropy, $R \ln N_I/N_{II}$. Here N_I and N_{II} are the number of distinguishable allowed orientations in the high and low temperature phases respectively. If the low temperature phase is fully ordered, and the high temperature phase six-fold disordered as suggested in the iodide X-ray study (11), $N_I/N_{II} = 6$ which leads to a ΔS value of 3.56 cal/mol deg. The experimental transition entropies lead to N_I/N_{II} ratios between 2 and 3 if indeed the total transition entropies can be assigned to configurational changes. These relatively small ratios require there to be some disorder below, or else some residual order above the transition temperature. The latter case is not unreasonable in the sense that mutual interaction of the dipole moments and positive charges on the reorientating pyridinium rings may lead to correlated motions and/or domain structures.

It is interesting to note the effect of hydrogen bond strength between anion and cation on the phase transitions and molecular motion. A direct measure of the N—H—halide hydrogen bond strength is the lowering of the infrared active N—H stretching frequency from the free N—H value, approximately 3300 cm^{-1} (4). From Table 2 it can be seen that as the hydrogen bond strength decreases on going from the chloride to the iodide, the transition temperature decreases as well.

In contrast with the transition temperature dependence on the hydrogen bond strength, the pyridinium ion reorientational activation energies decrease as the N—H---X bond strength increases. This suggests that localized hydrogen bonding does not contribute directly to the pyridinium ion reorientational barriers, and is similar to behaviour usually attributed to molecular crystals where van der Waals rather than electrostatic interactions determine the potential barriers. The trend in reorientational activation energies observed here may be understood in terms of relatively strong repulsive interactions between the large positively charged pyridinium ions which could cause rather less efficiently packed structure for the salts with the smaller anions where cation–cation contacts are more likely to occur.

From the results presented here it is evident that the pyridinium ring disordering process is

Can. J. Chem. Downloaded from www.nrcresearchpress.com by 210.87.254.6 on 09/05/12
For personal use only.

not simple or easily described by Darmon and Brot's "all or nothing" theory (1). Additional understanding of the ring disordering process requires more experimental information, especially on the structural properties of the pyridinium salts.

Acknowledgment

The author thanks Professor B. A. Dunell for the use of the broadline nmr apparatus.

1. I. Darmon and C. Brot. Mol. Cryst. **2**, 301 (1967).
2. C. Brot and I. Darmon. J. Chem. Phys. **53**, 2271 (1970).
3. C. H. Matthews and D. F. R. Gilson. Can. J. Chem. **48**, 2625 (1970).
4. D. Cook. Can. J. Chem. **39**, 2009 (1961).
5. S. R. Johnson and K. A. Rumon. J. Phys. Chem. **69**, 74 (1965).
6. R. Foglizzo and A. Novak. J. Chim. Phys. **66**, 1539 (1969).
7. R. Foglizzo and A. Novak. J. Chem. Phys. **50**, 5366 (1969).
8. C. Rerat. Acta Crystallogr. **15**, 427 (1962).
9. A. J. Serewicz, B. K. Robertson, and E. A. Meyers. J. Phys. Chem. **69**, 1915 (1965).
10. R. F. Copeland, S. H. Conner, and E. A. Meyers. J. Phys. Chem. **70**, 1288 (1966).
11. H. Hartl. Acta Crystallogr. B**31**, 1781 (1975).
12. B. A. Dunell, C. A. Fyfe, C. A. McDowell, and J. Ripmeester. Trans. Faraday Soc. **65**, 1153 (1969).
13. S. K. Garg, D. W. Davidson, and J. A. Ripmeester. J. Mag. Reson. **15**, 295 (1974).
14. G. R. Miller and H. S. Gutowsky. J. Chem. Phys. **39**, 1983 (1963).
15. J. Michel, M. Drifford, and P. Rigny. J. Chim. Phys. **67**, 31 (1970).
16. S. Albert, H. S. Gutowsky, and J. A. Ripmeester. J. Chem. Phys. **56**, 2844 (1972).
17. D. E. Woessner. J. Chem. Phys. **36**, 1 (1962).
18. J. E. Anderson. J. Chem. Phys. **43**, 3575 (1965).

Can. J. Chem. Downloaded from www.nrcresearchpress.com by 210.87.254.6 on 09/05/12
For personal use only.

Vapour phase catalytic transformations of terpene hydrocarbons in the $C_{10}H_{16}$ series. III. Dehydrogenation of Δ^3-carene over modified chromia and chromia–alumina catalysts[1]

V. KRISHNASAMY[2] AND (late) L. M. YEDDANAPALLI
Department of Chemistry, Loyola College, Madras-34, India

Received April 5, 1976

V. KRISHNASAMY and L. M. YEDDANAPALLI. Can. J. Chem. **54**, 3458 (1976).

The vapour phase dehydrogenation of 3-carene has been studied over chromia, chromia–alumina, chromia doped with potassium, and chromia–alumina doped with potassium and fluoride ions. Addition of potassium to chromia and chromia–alumina up to 1% by weight does not significantly affect the overall conversion of 3-carene whereas it increases its dehydrogenation to *p*- and *m*-cymenes. Potassium ions above 1% lower both the total conversion and dehydrogenation of 3-carene to cymenes. The ratio of *p*- to *m*-cymene over chromia–alumina is enhanced by added potassium ions up to 2%, but over chromia it remains unaffected. Addition of potassium to chromia decreases the formation of menthanes and menthadienes but its addition to chromia–alumina reduces the formation of menthanes and increases that of menthadienes. Impregnation of chromia–alumina with hydrofluoric acid suppresses the formation of menthadienes and increases that of menthanes. All these are explained in terms of the effect of added potassium and fluoride ions on the acidity of the catalysts.

V. KRISHNASAMY et L. M. YEDDANAPALLI. Can. J. Chem. **54**, 3458 (1976).

On a étudié la déshydrogénation en phase vapeur du Δ^3-carène sur du chrome, du chrome–alumine, du chrome dopé avec du potassium et du chrome-alumine dopé avec du potassium et des ions fluorures. Si l'on additionne jusqu'à 1% par poids de potassium au chrome ou au chrome–alumine, il n'y a pas d'effet significatif sur la conversion globale du carène-3 alors qu'il y a une augmentation de sa déshydrogénation en *p*- et *m*-cymènes. Les ions potassium, au dessus de 1%, abaissent à la fois la conversion et la déshydrogénation du carène-3 en cymènes. Le rapport *p*/*m*-cymènes sur du chrome–alumine est augmenté par l'addition de potassium jusqu'à 2% mais sur le chrome ce rapport reste constant. L'addition de potassium au chrome abaisse la formation des menthanes et des menthadiènes mais son addition au chrome-alumine réduit la formation du menthane alors qu'elle augmente celle des menthadiènes. L'imprégnation du chrome-alumine avec de l'acide fluorhydriqué supprime la formation des menthadiènes et augmente celle des menthanes. On explique tous ces résultats en termes de l'effet des ions additionnés de potassium et fluorure sur l'acidité du catalyseur.

[Traduit par le journal]

Introduction

Chromia gel and chromia–alumina have been widely used in the dehydrogenation of alkanes and naphthenes (1). It has been shown by MacIver and co-workers (2), working on cyclohexane, that the activity and selectivity of these catalysts are improved by the presence of potassium ions. Using chromia–alumina catalysts, Yeddanapalli and Desikan (3) have investigated the dehydrogenation of 3-carene with regard to the influence of chromium content of the chromia–alumina catalyst on the relative proportions of *p*- and *m*-cymenes in the product. The mechanism and the nature of the active centres involved in the dehydrogenation of 3-carene over chromia and chromia–alumina have been discussed by Yeddanapalli, Krishnasamy, and Ratnasamy (4). In the present investigation a detailed study of the effects of potassium and fluoride ions on the activity and selectivity of chromia and chromia–alumina in the dehydrogenation of 3-carene to *p*- and *m*-cymenes in the vapour phase is reported.

Experimental

(1) Materials

3-Carene was obtained by fractionation of first quality turpentine oil (supplied by the Government Turpentine and Rosin Co., Ltd., Bareily, India) using a 152 cm

[1]This paper is dedicated to the Memory of Rev. Father, Prof. L. M. Yeddanapalli, who died on June 6, 1970.

[2]Present address: Reader in Chemistry, A.C. College of Technology, University of Madras, Madras 600 025.

Can. J. Chem. Downloaded from www.nrcresearchpress.com by 210.87.254.105 on 09/05/12
For personal use only.

Can. J. Chem. Downloaded from www.nrcresearchpress.com by 210.87.254.105 on 09/05/12
For personal use only.

fractionating column packed with stainless steel helices containing 22 theoretical plates at reduced pressures and was analysed by gas chromatographic method for its purity.

Chromia A (*i.e.*, chromia gel without dope, surface area 14 m^2/gm by BET method) was prepared by the usual 'gel by jelly' method as reported by Turkevich *et al* (5). Chromia B and chromia C (*i.e.*, the doped varities) were prepared by doping chromia A with appropriate amounts of potassium nitrate to give respectively 1 and 2% by weight of potassium.

Chromia–alumina D (5.78% Cr, surface area 116 m^2/gm by BET method) was prepared by the method adopted by Eischens and Selwood (6) and Yeddanapalli and Desikan (3). The alumina for the above was obtained from aluminium isopropoxide by hydrolysing with water. Chromia–alumina catalysts E, F, G, H, I, and J were prepared by impregnating chromia–alumina D with the requisite amounts of potassium nitrate to give respectively, 0.5, 1.0, 1.5, 2.0, 3.3, and 4.7% by weight of potassium ions. Chromia–alumina K was obtained by impregnating chromia–alumina D with hydrofluoric acid (40% E. Merck) so as to give 2% by weight of the hydrofluoric acid added. Prior to each run the catalyst was activated by heating in a current of air for 12 h at 500 °C and then reduced by passing pure dry hydrogen for 6 h at the same temperature.

(2) Apparatus and Procedure

The dehydrogenation reactions were carried out in a fixed bed flow type reactor at atmospheric pressure. Five grams of catalyst (4 × 4 mm cylindrical pellets) were placed in a Pyrex reaction tube of 25 cm long and 3 cm internal diameter. Above the catalyst bed Pyrex glass beads (4 mm diameter) were placed to a height of 5 cm. The tube was inserted into the furnace (a cylindrical steel tube of internal diameter 4 cm, coated with a thin layer of asbestos and wound uniformly with nichrome wire) and heated electrically to the requisite temperature.

3-Carene was passed over the catalyst using a constant feed-rate syringe pump that could be operated at different feed rates. The liquid products collected for the first 15 min of each run (each run of one hour's duration) were discarded, and analysis was made only of the products collected after this time. This was to ensure the attainment of a steady state for the reaction over the catalyst.

The liquid products of dehydrogenation were identified and estimated using a Perkin-Elmer Infracord Model 137 and a Perkin-Elmer Vapour Fractometer Model 154-D. Products other than cymenes were quantitatively estimated by a Perkin-Elmer Column K, consisting of a 2 m column of carbowax on chromosorb. The column temperature for the best resolution within a reasonable time was found to be 115 °C with the hydrogen inlet pressure of 15 psi. *p*- and *m*-Cymenes were separated and estimated in a specially prepared 2 m column filled with 40–60 mesh acid-washed Kiesulguhr, coated with the stationary liquid, consisting by weight of 9% Bentone-34 and 4% Apiezon-L, heated at 108 °C with hydrogen passed at a pressure of 28 psi.

Scheme 1 shows the reaction sequence pertaining to the dehydrogenation of 3-carene over chromia and chromia–alumina catalysts.

Scheme 2 indicates possible transformations following the isomerisation of 3-carene over chromia and chromia–alumina catalysts.

The total acidity of chromia and chromia–alumina was estimated by *n*-butylamine titration following the method of Hirschler and Schneider (7) and the results are given in Table 1. The carbon deposited in any form on the surface of the catalyst during the dehydrogenation of 3-carene has been determined from the amount of carbon dioxide obtained on regeneration of the catalyst by air and passing the gaseous products through a heated platinised asbestos column at about 500 °C. The carbon dioxide formed was estimated by absorption in excess alkali of known concentration and back titration. The results are given in Table 2.

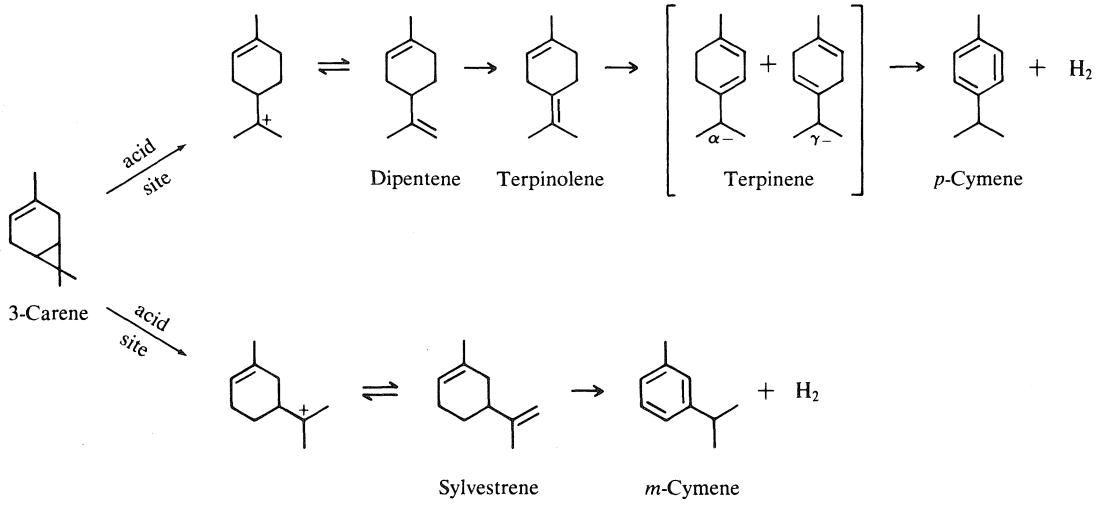

SCHEME 1

Can. J. Chem. Downloaded from www.nrcresearchpress.com by 210.87.254.105 on 09/05/12
For personal use only.

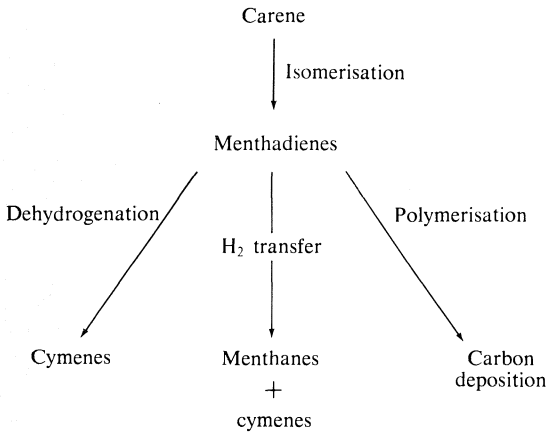

SCHEME 2

TABLE 1. Total acidity of chromia and chromia–alumina

Catalyst	Total acidity (*n*-butylamine mequiv./g)
Chromia gel (fresh)	0.14
Chromia–alumina (fresh)	0.64
Chromia–alumina (used)	0.50

TABLE 2. Estimation of carbon over chromia and chromia–alumina (feed, 3-carene; LHSV = 2)

Catalyst	Potassium (wt.%)	Reaction temperature (°C)	Carbon (wt.%)
Chromia–alumina	0.0	400	4.6
Chromia–alumina	0.5	400	4.1
Chromia–alumina	1.0	400	3.4
Chromia–alumina	2.0	400	3.0
Chromia gel	0.0	400	2.5

Results and Discussion

Dehydrogenation of 3-Carene

Figure 1 illustrates the variations in the overall activity of chromia gel with 1 and 2% potassium content at 400 °C. Figure 2 shows the effect of potassium on the rate and reaction products of 3-carene over chromia–alumina at 360 °C. The data obtained using chromia–alumina impregnated with 2% hydrofluoric acid at temperatures ranging from 360 to 425 °C are summarised in Table 3. The results obtained at 450 °C over chromia gel catalyst (A) poisoned by carbon monoxide are presented in Table 4. The influence of aging the catalyst (chromia–alumina) and impregnating it with potassium on the ratio of *p*-cymene to *m*-cymene (*p*/*m*) at 400 °C is

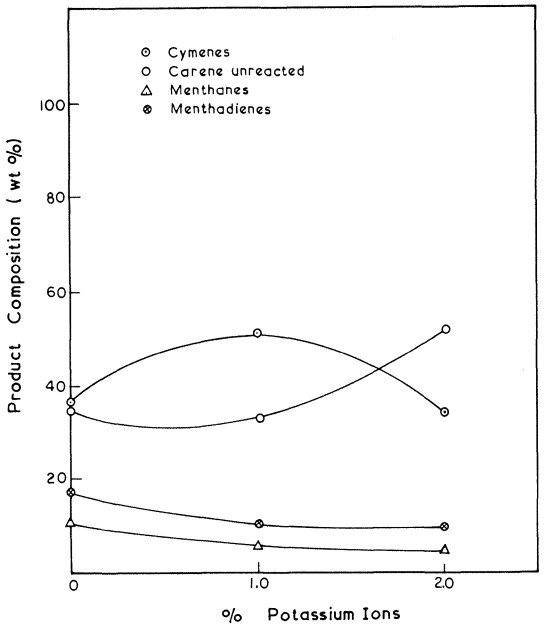

FIG. 1. Dehydrogenation of 3-carene over chromia-gel, effect of potassium ions, temperature 400 °C, LHSV = 2.

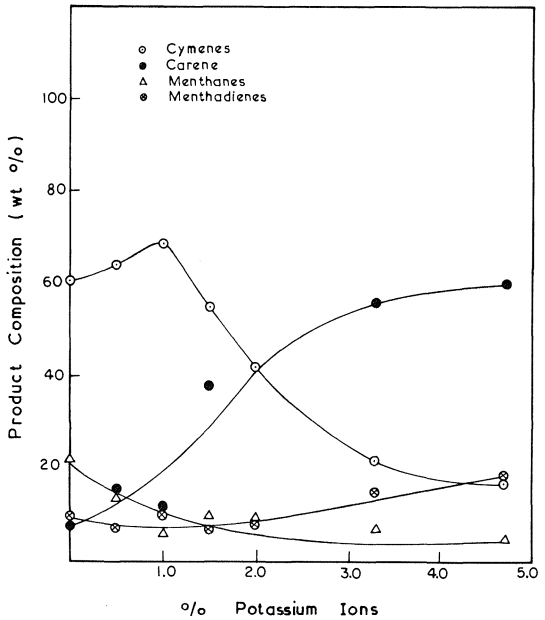

FIG. 2. Dehydrogenation of 3-carene over chromia–alumina (5.78% Cr), effect of potassium ions, temperature 360 °C, LHSV = 2.

TABLE 3. Dehydrogenation of 3-carene over reduced chromia–alumina, effect of hydrogen fluoride (2% HF) (LHSV = 2)

Temperature (°C)	Liquid products (wt.%)					
	3-Carene reacted	Menthadienes	Menthanes	Total cymenes	*p*-Cymene	*m*-Cymene
360	94	0	33	61	31	30
380	96	0	32	64	31	33
400	98	0	31	67	34	33
425	98	0	28	70	35	35

TABLE 4. Dehydrogenation of 3-carene over reduced chromia gel, effect of carbon monoxide (temperature = 450 °C, LHSV = 2)

Mode of poisoning	Liquid products (wt.%)					
	3-Carene reacted	Menthadienes	Menthanes	Total cymenes	*p*-Cymene	*m*-Cymene
Prepoisoning	36	7	11	18	10	8
Simultaneous poisoning	28	10	10	8	4	4
Without poisoning	75	14	9	52	32	20

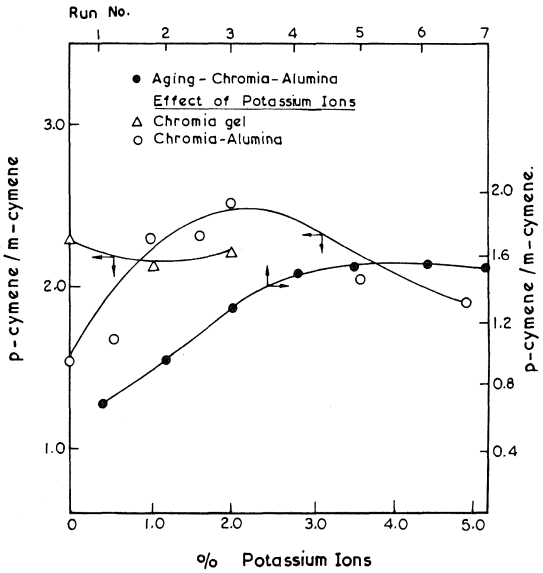

FIG. 3. The effect of aging of the catalyst and the effect of impregnation with potassium ions on the ratio of cymenes (*p*/*m*), temperature 400 °C.

illustrated in Fig. 3. In the same figure is also represented the effect of doped potassium ions over chromia on the *p*/*m* selectivity. The effect of aging on *p*/*m* ratio was not observed in the case of chromia catalyst.

Pines and Chen (8) have reported that chromia by itself can act as a dehydrogenation and isomerisation catalyst. Alumina enhances the isomerisation step, though according to MacIver and co-workers (2) a sizeable portion of chromia-alumina is similar in chemical properties to pure chromia. Impregnation of chromia–alumina with potassium has been reported (1) to decrease its isomerisation and cracking activity without affecting its dehydrogenation ability. The decrease in the isomerisation and cracking activity is interpreted as due to the interaction between the acidic centres and added potassium ions. Weller and Voltz (9) have also observed a similar effect of potassium ions in chromia and chromia–alumina catalysts.

The determination of acidity of pure alumina (alumina D) by *n*-butylamine titration in a separate experiment not shown here indicates that it contains a spectrum of strong and weak acid sites. Treatment of pure alumina with lithium[3] removes all strong acid sites and increases the weak acid sites, whereas treatment of the same with HF increases the strong acid sites without affecting the weak sites. This would seem to suggest that addition of potassium and

[3]V. Krishnasamy, unpublished results.

Can. J. Chem. Downloaded from www.nrcresearchpress.com by 210.87.254.105 on 09/05/12
For personal use only.

Can. J. Chem. Downloaded from www.nrcresearchpress.com by 210.87.254.105 on 09/05/12
For personal use only.

fluoride ions to chromia and chromia–alumina would have the same effect as the addition of lithium and fluoride ions to alumina itself.

The total acidity of fresh chromia–alumina (catalyst D) and chromia gel (catalyst A) are found to be 0.64 mequiv./g and 0.14 mequiv./g (*cf.* Table 1) of *n*-butylamine respectively. The total acidity may be due to strong as well as weak acid sites at least over chromia–alumina since the alumina used in the preparation of chromia–alumina is found to contain different acid sites as mentioned earlier. Over the strong acid sites, the menthadienes formed from 3-carene may polymerize or become menthanes by hydrogen transfer or get transformed into cymenes as indicated in Scheme 2.

Addition of potassium in small quantities to chromia–alumina increases the formation of cymenes by poisoning the strong acid sites which would otherwise tend to polymerise the menthadienes. This is supported by the data on carbon estimation given in Table 2. It may also be noted from Fig. 2 that potassium brings down the formation of menthanes which may be formed by hydrogen transfer as indicated in Scheme 2. This also would contribute to the increase of cymene formation. Although the acid sites on chromia are less numerous than on chromia–alumina (*vide* Table 1) they still cause polymerization. By neutralisation of these sites by potassium, the dehydrogenation activity of chromia also increases (*cf.* Fig. 1). Addition of potassium ions decreases the formation of menthadienes over chromia, but increases their formation over chromia–alumina. This may be accounted for by the fact that potassium ions poison all the acid sites over chromia (may be of one type) but leave unaffected the weak acid sites over chromia–alumina, which can still isomerise 3-carene to menthadienes. These menthadienes cannot be dehydrogenated to cymenes since the dehydrogenation centres are blocked by successive addition of potassium ions (*cf.* Fig. 2). Similar results have been obtained in the presence of pyridine (10).

The decreased activity of chromia and chromia–alumina by a larger amount of potassium ions, above 1%, may be due to reduction in the number of isomerising and dehydrogenating sites either by chemical combination or by physical blocking by potassium ions as suggested by MacIver and co-workers (2).

The decrease in the activity of chromia by carbon monoxide may be due to two factors (*i*) the effect of partial pressure of carbon monoxide and (*ii*) the coordination of carbon monoxide with Cr(II) ions. It may be noted that the presence of Cr(II) ions has been reported by Van Reijen *et al.* (11) based on electron spin resonance and magnetic susceptibility measurements on chromia–alumina and chromia–silica catalysts.

The ratio of *p*-cymene to *m*-cymene, when 3-carene is dehydrogenated over a fresh chromia–alumina, is 0.66 (Fig. 3) its total acidity is 0.64 mequiv./g of *n*-butylamine (Table 1). On stabilising the catalyst by alternate dehydrogenation of 3-carene for 1 h and regeneration with air for 6 h, the acidity decreases to 0.5 mequiv./g and the p/m attains a constant value of 1.5. This increase in p/m ratio with a corresponding decrease in the acidity of the catalyst seems to suggest that strong acid sites are responsible for the formation of *m*-isomer, assuming that the strong acid centres get deactivated easily during the reaction.

The effect of potassium addition is to bring about a decrease of strong acid centres and hence a decrease of *m*-cymene and a consequent increase in the p/m ratio. For instance it can be seen from Fig. 3 that the p/m value increases from 1.5 to 2.6 on addition of 2% potassium to chromia–alumina D. On the other hand, hydrofluoric acid increases the strong acid sites and enhances the formation of *m*-cymene, decreasing the p/m value (*cf.* Table 3).

Referring to Fig. 3 again and to Table 2 the p/m value of 2.3 for pure chromia does not change on addition of potassium and is not too different from 2.6 for chromia–alumina impregnated with 2% potassium. This observation is to be correlated with the carbon deposit of 2.5% over pure chromia and the 4.6% over chromia–alumina and 3.0% over chromia–alumina impregnated with 2% potassium.

When chromia was poisoned by carbon monoxide the ratio of p/m goes down (*cf.* Table 4) unlike the case of potassium where it remains unaltered. Carbon monoxide which can coordinate with chromium ions on the surface of the catalyst can give rise to carboxylate ions and these ions will increase the acidity of the catalyst and decrease the value of p/m. Clark *et al.* (12) have also reported an increase in the polymer-

isation activity of supported chromium oxide catalyst in the presence of carbon monoxide which was attributed by them as due to the coordination of carbon monoxide with chromium. It would therefore appear that the formation of *m*-cymene from 3-carene requires stronger acid sites on the catalyst surface.

Acknowledgements

This work was supported by the Ministry of Education, Government of India and the Council of Scientific and Industrial Research, New Delhi under the Research Unit "Chemisorption and Catalysis". V.K. thanks the Ministry of Education and the CSIR for Junior Research Fellowships. He is also grateful to Dr. K. Chandrasekharan, Professor of Chemical Engineering, A.C. College of Technology for his valuable help in revising the paper.

1. F. G. CIAPETTA, R. M. DOBRES, and R. W. BAKER. *In* Catalysis. *Edited by* P. H. Emmett. Reinhold, New York. 1958. p. 495.
2. J. M. BRIDGES, G. T. RYMER, and D. S. MACIVER. J. Phys. Chem. **66**, 871 (1962).
3. L. M. YEDDANAPALLI and P. DESIKAN. J. Sci. Ind. Res. Sect. B, **21**, 116 (1962).
4. L. M. YEDDANAPALLI, V. KRISHNASAMY, and P. RATNASAMY. Indian J. Chem. **9**, 131 (1971).
5. J. TURKEVICH, H. FEHRER, and H. S. TAYLOR. J. Am. Chem. Soc. **63**, 1129 (1941).
6. R. P. EISCHENS and P. W. SELWOOD. J. Am. Chem. Soc. **69**, 1590 (1947).
7. A. E. HIRSCHLER and A. SCHNEIDER. J. Chem. Eng. Data, **6**, 313 (1961).
8. H. PINES and C. T. CHEN. J. Am. Chem. Soc. **82**, 3562 (1960).
9. S. W. WELLER and S. E. VOLTZ. J. Phys. Chem. **59**, 569 (1959).
10. V. KRISHNASAMY. Ph. D. Thesis, Madras University, Madras, India. 1968.
11. L. L. VAN REIJEN, W. M. H. SACHTLER, P. COSSEE, and D. M. BROUWER. Proceedings of Third International Congress on Catalysis, Amsterdam. 1964. p. 829.
12. A. CLARK, J. N. FINCH, and B. H. ASHE. Proceedings of Third International Congress on Catalysis, Amsterdam. 1964. p. 1010.

Can. J. Chem. Downloaded from www.nrcresearchpress.com by 210.87.254.105 on 09/05/12
For personal use only.

The basicity of aliphatic carboxylic acids

DONALD G. LEE AND M. H. SADAR[1]

Department of Chemistry, The University of Regina, Regina, Sask., Canada S4S 0A2

Received April 13, 1976

DONALD G. LEE and M. H. SADAR. Can. J. Chem. **54**, 3464 (1976).

The basicities of four aliphatic carboxylic acids (propionic, isovaleric, 3-chloropropionic, and 3-fluoropropionic) have been investigated using nmr chemical shift data. The results indicate that the protonation behaviour of the unsubstituted and the halogen substituted compounds are not defined by the same acidity function.

DONALD G. LEE et M. H. SADAR. Can. J. Chem. **54**, 3464 (1976).

On a étudié, à l'aide de données de déplacements chimiques en rmn, les basicités de quatre acides carboxyliques aliphatiques (les acides propionique, isovalérique, chloro-3 propionique et fluoro-3 propionique). Les résultats indiquent que, vis à vis la protonation, les comportements des composés non substitués et des dérivés halogénés ne sont pas définis par la même fonction d'acidité.

[Traduit par le journal]

Introduction

The quantitative measurement of basicity is a problem of continuing importance because of the numerous reactions in organic and biochemistry that are subject to acid catalysis of the type summarized by reactions 1 and 2 (1).

[1] $$BH^+ \underset{}{\overset{K_{BH^+}}{\rightleftharpoons}} B + H^+$$

[2] $$BH^+ + C \rightarrow \text{Products}$$

In order to understand such reactions completely it is essential to have a reliable measure of the basicity constant; however, the problem of obtaining accurate estimates for these constants is complicated because although the standard state is dilute aqueous solutions, the bases themselves are appreciably protonated only in concentrated acid. Consequently, any method which might be devised now or in the future for basicity constant measurements will necessarily involve extrapolations. Other authors (2–5) have addressed themselves to this problem and it is unnecessary to repeat these discussions here, save to remind ourselves that all reported pK_{BH^+} values for weak organic bases contain uncertainties due to possible errors in extrapolation.

In previous publications we have described in detail how nmr chemical shift data can be used to estimate basicity constants for aliphatic alcohols (6), ethers (7), ketones (8), and esters (9). In this paper we wish to report results which have been obtained from a similar study of the basicity of aliphatic carboxylic acids and to compare these results with those which have been obtained for other classes of aliphatic compounds.

Carboxylic acids are suitable substrates for such a study because their conjugate acids are involved as intermediates in several important reactions including esterification (10). The basicities of several aromatic carboxylic acids have been determined using ultraviolet–visible spectroscopy (11, 12); however, attempts to use similar techniques for aliphatic carboxylic acids have been less successful (13–15), presumably because the results are highly dependent on the wavelength at which the measurements are made (16).

One of the earliest attempts to investigate the protonation of carboxylic acids using nmr spectroscopy was that of Deno, Pitman, and Wisotsky (17). They used chemical shift differences in order to study the equilibrium between the protonated acids and their respective acyl cations. Siigur, Pehk, Haldna, and Lippmaa (18) used a ^{13}C nuclear magnetic double resonance method to measure the ionization ratios of acetic acid in aqueous sulfuric acid and concluded that the protonation behavior of this compound did not follow a sigmoidal curve when plotted against H_0 or H_A. Olah and White (19) studied the nmr spectra of protonated acetic, propionic, and benzoic acids in a FSO_3H–SbF_5 medium and

[1]Present address: Faculty of Engineering, Middle East Technical University, Gaziantep Extension Campus, Gaziantep, Turkey.

Can. J. Chem. Downloaded from www.nrcresearchpress.com by 210.87.254.40 on 09/05/12
For personal use only.

found that the acids were completely protonated and produced alkyloxocarbonium ions under nonequilibrium conditions.

There has been a great deal of interest in the structure of cations obtained by the protonation of carboxylic acids. Several investigations (11, 15, 20, 21) have indicated that carbonyl protonation takes place and nmr studies of carboxylic acids in superacid media at low temperature revealed that the positive charge was delocalized over both the oxygens (22, 23).

To date, no attempt has been made to develop an acidity function for carboxylic acids.

Experimental Section

The carboxylic acids were obtained commercially and purified by vacuum distillation. Sulfuric acid solutions up to 95% were prepared by diluting reagent grade acid with doubly distilled water. Acid solutions of higher concentrations were obtained by addition of fuming sulfuric acid (20% SO_3). Standardization was accomplished by titrating weighed amounts of each sulfuric acid solution with standardized sodium hydroxide solutions. The H_0 values up to 98% H_2SO_4 are those reported by Jorgenson and Hartter (24) and beyond 98% H_2SO_4 those of Gillespie, Peel, and Robinson (25).

All spectra were obtained using a Varian A-60A spectrophotometer. Each measurement was made by adding 0.10 ml of the base to 5.0 ml of standardized acid in a volumetric flask. After inverting the flask several times to ensure homogeneity, a small portion was transferred to an nmr tube and the spectrum recorded at 37 ± 1 °C. Since only the difference in the chemical shift is required, no internal standard was used. The instrument was carefully tuned using TMS and chloroform as standards and a frequent sweep width calibration was done using a signal generator.

The protonation of four carboxylic acids (propionic, isovaleric, 3-chloropropionic, and 3-fluoropropionic) was investigated in this way. 2-Chloro- and 2-fluoropropionic acid could not be studied because they were not fully protonated under attainable conditions. Butanoic acid was avoided because of its bad odor and valeric acid was found to give very weak signals because of its low solubility in aqueous sulfuric acid.

The data obtained are summarized in Table 1. It was observed that the chemical shift differences were reproducible to within 0.5 Hz with somewhat better resolution being obtained in the region of 60–90% H_2SO_4. Since I is a ratio, $[BH^+]/[B] = (\Delta - \Delta_B)/(\Delta_{BH^+} - \Delta)$ where Δ_B is the chemical shift difference between two selected sets of hydrogens of the unprotonated carboxylic acid, Δ_{BH^+} is the difference between the chemical shifts of the same hydrogens in the completely protonated carboxylic acid, and Δ the corresponding value when the carboxylic acid is partially protonated, it is necessary to assume a possible error of ±0.5 Hz in both the numerator and the denominator and the error limits reported in this paper are all based on the possibility of errors of this magnitude in the values of I.

Results and Discussion

Because it is known from the work of Yates and McClelland (26) that the protonation behaviour of a wide variety of compounds can be defined, to a good approximation, by [3] plots of log I *vs.* H_0 were prepared for all four sets of data

$$\log I = -mH_0 + pK_{BH^+} \qquad [3]$$

in Table 1. A summary of a least-squares analysis of the plots obtained is given in Table 2.[2] It is significant to note that the results obtained for propionic and isovaleric acid are very similar, but that both 3-chloro- and 3-fluoropropionic acid are less basic and have lower m values. The lower basicity of these compounds (as evidenced by the lower intercepts reported in Table 2) is related to a decrease in electron density caused by introduction of electron withdrawing groups near the site of protonation. The change in slopes is a consequence of the fact that an increase in the acidity of a solution is always accompanied by a decrease in the amount of water available for solvation of the species involved. Compounds which on protonation form conjugate acids that have high solvation requirements exhibit lower m values (6). Consequently, one may conclude that the conjugate acids of the halogenated compounds have greater solvation requirements, presumably because the positive charge is more highly localized.

It is apparent that protonation of the unsubstituted and the halogenated carboxylic acids define two different acidity functions. In other words the Hammett postulate (4) that activity coefficients can be neglected if one is dealing with similar compounds does not hold for all carboxylic acids. Apparently, it is possible to define an acidity function which would be applicable to unsubstituted carboxylic acids, but the same function could not be used for halogenated carboxylic acids.

Before such an acidity function can be calculated, however, it is necessary to arrive at the best possible value for the pK_{BH^+} of the compound on which the acidity function will be

[2]During the preparation of these plots it was noted that linearity was maintained only up to an acidity of $H_0 = -8.4$ (85% H_2SO_4). Apparently [3] does not hold for these compounds in very concentrated sulfuric acid solutions. A probable reason for this may be the almost complete lack of water available for solvation above 85% H_2SO_4 (27).

Can. J. Chem. Downloaded from www.nrcresearchpress.com by 210.87.254.40 on 09/05/12
For personal use only.

TABLE 1. Chemical shift data

	Propionic acid		Isovaleric acid		3-Chloropropionic acid		3-Fluoropropionic acid	
H_2SO_4 (%)	Δ (Hz)	log *I*	Δ (Hz)	log *I*	Δ (Hz)	log *I*	Δ (Hz)	log *I*
0			77.3					
8.5	79.5		77.5					
19.2	80.0		78.5					
32.8	80.0							
34.6	80.9		79.3					
35.8			80.0		54.0			
41.8	81.5							
44.6	81.8		80.3		54.0		115.0	
47.6	81.8		80.5		53.5		114.5	
48.9			80.3				114.5	
49.1	81.9							
51.7	82.0		80.8		54.0		115.0	
53.3			81.0	−1.10	53.0		114.5	
53.4	82.4	−1.18						
55.9	82.5	−1.13						
57.2					52.5	−1.13		
57.3			81.3	−1.02			113.5	
57.9	82.8	−1.01	81.5	−0.97				
60.2	83.0	−0.94						
62.0			82.5	−0.77	51.5	−0.89	113.0	
62.3	83.3	−0.85						
63.7			82.8	−0.72			113.0	
66.4	83.8	−0.72	83.5	−0.62	51.0	−0.80	113.0	−0.97
67.7	85.0	−0.50	84.0	−0.55			112.5	−0.86
70.5			84.5	−0.49			112.0	−0.77
70.6	85.5	−0.42			49.0	−0.53		
73.7	86.8	−0.24	86.5	−0.29			111.5	−0.69
74.7	86.5	−0.28			48.5	−0.48	111.0	−0.62
75.3	87.0	−0.21	88.0	−0.15			110.5	−0.55
77.4	88.5	−0.03	89.0	−0.06	47.0	−0.33	110.0	−0.49
80.9	88.5	−0.03						
82.8	91.5	0.35	93.0	0.29	45.0	−0.16	108.0	−0.29
85.4	93.8	0.75	95.5	0.55	43.0	0.00	106.5	−0.15
86.7	94.8							
87.7	95.0		96.5	0.69	40.0	0.24	105.5	−0.06
88.3	95.5		98.0				103.0	0.15
89.5	95.5		98.8		36.0	0.65	101.0	0.33
92.6	96.0				34.0			
93.7	96.0		99.3		33.0		99.0	0.55
95.1			99.5		33.0		98.0	0.69
95.9			99.5					
96.6	96.0				32.0			
97.6			100.0				96.5	
98.6			100.0				96.0	
101.0			100.3		32.0		94.5	
102.5			100.3				94.5	
103.7							94.5	

based. This may be accomplished by use of a Bunnett–Olson plot (2) (Fig. 1). The results obtained from an analysis of the Bunnett–Olson plots for propionic and isovaleric acid were identical within the limits of experimental error ($pK_{BH^+} = -2.85 \pm 0.34$ and slope $= 0.72 \pm 0.06$).

An alternative method of obtaining pK_{BH^+} values has been suggested by Marziano, Cimino, and Passerini (29). Through utilization of [4],

Can. J. Chem. Downloaded from www.nrcresearchpress.com by 210.87.254.40 on 09/05/12
For personal use only.

TABLE 2. Statistical analysis for plots of log I *vs.* $-H_0$

Compound	Slope, m	Intercept*	pK_{BH^+}†	r‡	n§
Propionic acid	0.37 ± 0.08	-6.99 ± 0.15	-2.60 ± 0.40	0.918	14
Isovaleric acid	0.35 ± 0.03	-7.03 ± 0.15	-2.46 ± 0.23	0.968	14
3-Chloropropionic acid	0.25 ± 0.02	-8.30 ± 0.17	-2.06 ± 0.19	0.985	10
3-Fluoropropionic acid	0.26 ± 0.02	-8.82 ± 0.12	-2.30 ± 0.20	0.992	10

*H_0 value at which the compound is one-half protonated.
†pK_{BH^+} = slope × intercept.
‡Correlation coefficient.
§Number of points.

TABLE 3. Results obtained by use of Marziano–Cimino–Passerini plots*

Compound	Slope, n_B	pK_{BH^+}	r†	n‡
Propionic acid	2.14 ± 0.07	-3.26 ± 0.40	0.987	15
Isovaleric acid	1.59 ± 0.03	-2.83 ± 0.20	0.994	14
3-Chloropropionic acid	1.09 ± 0.09	-2.61 ± 0.20	0.958	9
3-Fluoropropionic acid	1.21 ± 0.07	-2.87 ± 0.20	0.973	11

*Equation 4 where A is ethanol and B is a carboxylic acid.
†Correlation coefficient.
‡Number of points.

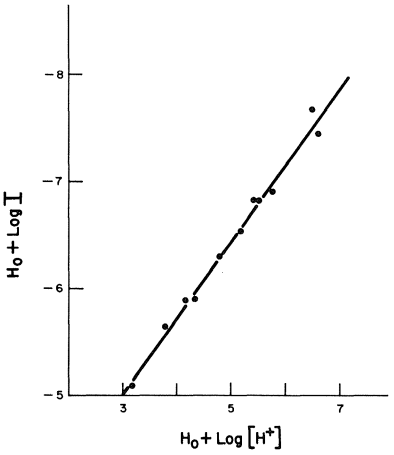

FIG. 1. Bunnett–Olson plot for propionic acid.

where A is a base of known basicity, it is possible to calculate the pK_{BH^+} of the base, B, under

[4] $\log I_B - \log [H^+] =$

$m_B (\log I_A - \log [H^+] - pK_{AH^+}) + pK_{BH^+}$

consideration. In order to use this equation effectively, there must be a substantial range of acidities over which A and B are partly protonated. Consequently, an attempt was made to use this procedure by comparing the carboxylic acids with ethanol, a base whose protonation behaviour has previously been studied (6). The results obtained by use of this procedure, as summarized in Table 3, are consistent within the limits of experimental uncertainty with those obtained by the Bunnett–Olson method and by use of [3]. Consequently, it would appear that all of the available approaches to the problem of carboxylic acid basicities lead to similar conclusions and that the pK_{BH^+} values are about -3. It is unfortunate, however, that at the present time rather large error limits must be applied to these values. Development of methods whereby these uncertainties can be substantially reduced remains as an area of research that merits further consideration.

If the value of -2.85 is accepted as the pK_{BH^+} of propionic acid, an acidity function, H_{CA}, can be generated by application of [5] to the data in

TABLE 4. Carboxylic acid acidity functions

H_2SO_4 (%)	H_{CA}	H_{CA}'
55	-1.72	
60	-1.90	-1.15
65	-2.10	-1.32
70	-2.35	-1.50
75	-2.65	-1.68
80	-2.99	-1.89
85	-3.38	-2.10
90		-2.34

Can. J. Chem. Downloaded from www.nrcresearchpress.com by 210.87.254.40 on 09/05/12
For personal use only.

Can. J. Chem. Downloaded from www.nrcresearchpress.com by 210.87.254.40 on 09/05/12
For personal use only.

Table 1. The results obtained by drawing a smooth curve through a plot of the calculated values of H_{CA} against $\%H_2SO_4$ are summarized in Table 4.

$$[5] \qquad H_{CA} = -\log I + pK_{BH^+}$$

In a similar way, it is possible to develop an acidity function, H_{CA}', that describes the mode of protonation of halogenated carboxylic acids such as 3-fluoro- and 3-chloropropionic acid. Since, for these two compounds, it is impossible to prepare Bunnett–Olson plots because they are not extensively protonated below 85% H_2SO_4 (2), the pK_{BH^+} values reported in Table 2 were used. Numerical values for the H_{CA}' function are also included in Table 4.

It should be noted here that if the pK_{BH^+} values obtained by the methods of Marziano, Cimino, and Passerini were used the H_{CA} and H_{CA}' values would all be reduced by about 0.5 units.

It seems apparent from these and a large number of other results (6, 9, 28) that there is no universal acidity function applicable to all compounds as had once been envisaged. Each class of compounds responds in a different way to changes in acidity and thus generates its own acidity function. In fact, as this work shows, even compounds of the same general class are found to generate unique acidity functions. Consequently, each compound may have to be subjected to an individual investigation if one wishes to exactly understand its basicity.

On the other hand, it appears that within the limits of available experimental precision the protonation of most nonsubstituted aliphatic compounds may be described by a relatively few acidity functions which are dependent only on the nature of the functional group. Six such functions are compared in Fig. 2. The dashed lines represent extrapolations which were made by assuming that all of these functions were approximately proportional to the H_0 acidity function and that they must all be equal when $H_0 = 0$. In other words, smooth curves were drawn from the end of the experimentally determined functions in such a way that they all became equal to pH in dilute solutions.

The differences in these plots are most likely a consequence of the fact that each protonation reaction has different solvation requirements. As the concentration of H_2SO_4 is increased the acidity increases, but the amount of water available for solvation of the various species involved is decreased. Hence, if the conjugate acid has high solvation requirements as compared to the unprotonated base, the corresponding acidity function will rise less steeply. It follows then that the conjugate acids of alcohols (ROH_2^+) have high solvation requirements, presumably because of the extensive possibilities for hydrogen bonding available to these ions. Ethers have slightly lower solvation requirements because the positive charge can be delocalized inductively. Carboxylic acids have even lower solvation requirements because the positive charge can be delocalized over three atoms $\left(R{-}C\begin{matrix}\diagup O{-}H \\ + \\ \diagdown O{-}H\end{matrix}\right)$. For the same reason that

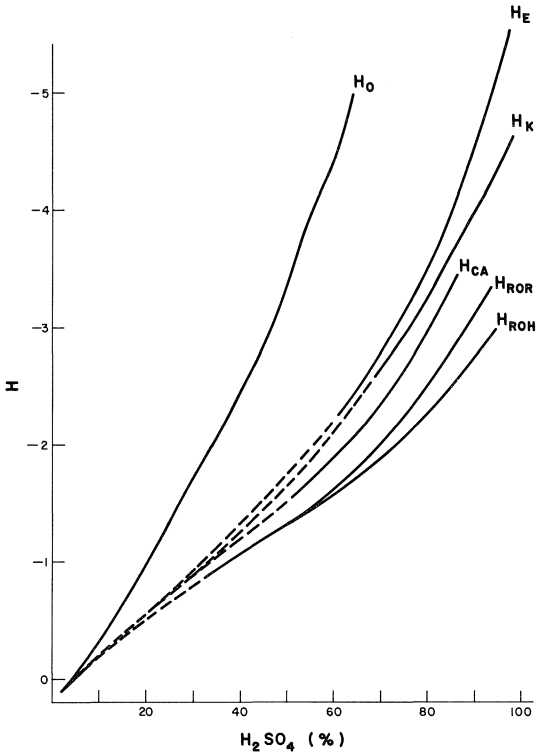

FIG. 2. Acidity functions. H_0 is the Hammett acidity function (4). H_E is an acidity function for esters (9). H_K is an acidity function for ketones (8). H_{CA} is an acidity function for carboxylic acids as described in this work. H_{ROR} is an acidity function for ethers (7). H_{ROH} is an acidity function for alcohols (6).

the ether function is steeper than the alcohol function, the ester function is steeper than the carboxylic acid function. In the case of ketones, the positive charge can be shared by an oxygen and a carbon atom ($H—\overset{+}{O}=CR_2 \leftrightarrow H—O—\overset{+}{C}R_2$). Since it is known from other studies that carbonium ions are not stabilized extensively by hydration (30) the involvement of the second resonance structure explains why these compounds define an acidity function that is steep compared to the other mono-oxygen compounds.

Acknowledgments

The authors are pleased to acknowledge the financial assistance of the Saskatchewan Research Council and the National Research Council of Canada.

1. M. L. Bender. Mechanisms of homogeneous catalysis from protons to proteins. Part One. Wiley-Interscience, Toronto, Ontario. 1971. pp. 19–144.
2. J. F. Bunnett and F. P. Olsen. Can. J. Chem. **44**, 1899 (1966); **44**, 1917 (1966).
3. E. M. Arnett. Prog. Phys. Org. Chem. **1**, 223 (1963).
4. L. P. Hammett. Physical organic chemistry. 2nd ed. McGraw-Hill, London. 1970. Chapt. 9. pp. 263–313.
5. M. Liler. Reaction mechanisms in sulphuric acid. Academic Press, London. 1971. Chapt. 3. pp. 59–144.
6. D. G. Lee and R. Cameron. J. Am. Chem. Soc. **93**, 4724 (1971).
7. D. G. Lee and R. Cameron. Can. J. Chem. **50**, 445 (1972).
8. D. G. Lee. Can. J. Chem. **48**, 1919 (1970).
9. D. G. Lee and M. H. Sadar. J. Am. Chem. Soc. **96**, 2862 (1974).
10. C. K. Ingold. Structure and mechanism in organic chemistry. 2nd ed. G. Bell and Sons, London. 1969. pp.1144–1153.
11. R. Stewart and K. Yates. J. Am. Chem. Soc. **82**, 4059 (1960).
12. K. Yates and H. Wai. Can. J. Chem. **43**, 2131 (1965).
13. J. T. Edward and I. C. Wang. Can. J. Chem. **40**, 966 (1962).
14. A. R. Goldfarb, A. Mele, and N. Gutstein. J. Am. Chem. Soc. **77**, 6194 (1955).
15. S. Hoshino, H. Hosoya, and S. Nagakura. Can. J. Chem. **44**, 1961 (1966).
16. J. Siigur and U. Haldna. Org. React. **7**, 197 (1970).
17. N. C. Deno, C. U. Pitman, and M. J. Wisotsky. J. Am. Chem. Soc. **86**, 4370 (1964).
18. J. Siigur, T. Pehk, U. Haldna, and E. Lippmaa. Org. React. **7**, 179 (1970).
19. G. A. Olah and A. M. White. J. Am. Chem. Soc. **89**, 3591 (1967).
20. H. Hosoya and S. Nagakura. Spectrochim. Acta, Part A, **17**, 324 (1961).
21. A. Casadevall, G. Cauquil, and R. Corriu. Bull. Soc. Chim. Fr. 187 (1964); 204 (1964).
22. T. Birchall and R. J. Gillespie. Can. J. Chem. **43**, 1045 (1965).
23. H. Hogeveen, A. F. Bickle, C. W. Hilbers, E. L. Mackor, and C. MacLean. Chem. Commun. 898 (1966).
24. M. J. Jorgenson and D. R. Hartter. J. Am. Chem. Soc. **85**, 878 (1963).
25. R. J. Gillespie, T. E. Peel, and E. A. Robinson. J. Am. Chem. Soc. **93**, 5083 (1971).
26. K. Yates and R. A. McClelland. J. Am. Chem. Soc. **89**, 2686 (1967).
27. R. A. Cox. J. Am. Chem. Soc. **96**, 1059 (1974).
28. P. Bonvicini, A. Levi, V. Lucchini, G. Modena, and G. Scorrano. J. Am. Chem. Soc. **95**, 5960 (1973); G. Scorrano. Acc. Chem. Res. **6**, 132 (1973); P. Haake, R. D. Cook, and G. H. Hurst. J. Am. Chem. Soc. **89**, 2650 (1967); C. C. Greig and C. D. Johnson. J. Am. Chem. Soc. **90**, 6453 (1968); K. Yates, J. B. Stevens, and A. R. Katritzky. Can. J. Chem. **42**, 1957 (1964); R. I. Zalewski and G. E. Dunn. Can. J. Chem. **47**, 2263 (1969); **48**, 2538 (1970); T. G. Bonner and J. Phillips. J. Chem. Soc. B, 650 (1966).
29. N. C. Marziano, G. M. Cimino, and R. C. Passerini. J. Chem. Soc. Perkin Trans. II, 1915 (1973).
30. N. C. Deno, J. J. Jaruzelski, and A. Schriesheim. J. Am. Chem. Soc. **77**, 3044 (1955); E. M. Arnett and R. D. Bushick. J. Am. Chem. Soc. **86**, 1564 (1964); M. T. Reagan. J. Am. Chem. Soc. **91**, 5506 (1969).

Can. J. Chem. Downloaded from www.nrcresearchpress.com by 210.87.254.40 on 09/05/12
For personal use only.

Photolyse du chloro-2 propane gazeux à $\lambda = 147$ et 123.6–116.5 nm

PIERRE GAGNON ET JAN A. HERMAN

Groupe de Dynamique moléculaire, Département de Chimie, Université Laval, Québec, (Qué.), Canada G1K 7P4

Reçu le 17 octobre 1975[1]

PIERRE GAGNON et JAN A. HERMAN. Can. J. Chem. **54**, 3470 (1976).

La réaction de décomposition de loin la plus importante (~70%) dans la photolyse du chloro-2 propane gazeux à $\lambda = 147$ et 123.6–116.5 nm est celle donnant du propène et du chlorure d'hydrogène (ou du chlore et hydrogène atomiques). L'allène, le propyne et partiellement l'acétylène et l'éthylène proviennent de la décomposition secondaire du propène excité. L'emploi de capteurs de radicaux a permis d'identifier certains d'entre eux: CH_2:, CH_3·, C_2H_5·, iso-C_3H_7·, C_3H_4Cl· et C_4H_9·.

PIERRE GAGNON and JAN A. HERMAN. Can. J. Chem. **54**, 3470 (1976).

In the photolysis at $\lambda = 147$ nm and 123.5–116.5 nm of gaseous 2-chloropropane the preponderant decomposition process (~70%) gives propene and HCl (or H + Cl). Allene, propyne, and a fraction of the ethylene and acetylene are formed in the secondary decomposition of excited propene. The use of scavengers allowed the identification of the following free radicals: CH_2:, CH_3·, C_2H_5·, iso-C_3H_7·, C_3H_4Cl· and C_4H_9·.

Introduction

Ce travail s'inscrit dans le programme de recherche de ce laboratoire sur la photolyse dans l'ultraviolet à vide des chloroalcanes. A notre connaissance la photolyse dans l'ultraviolet à vide du chloro-2 propane gazeux n'a pas été entreprise. Les études les plus proches sont celles de radiolyse du chloropropane liquide (1, 2). Dans ce dernier cas, la rupture de la liaison C—Cl domine le schéma de la décomposition des chloropropanes liquides.

Dans cette étude, nous nous sommes penchés sur les mécanismes primaires de décomposition du $CH_3CHClCH_3$ gazeux aux rayonnements de 8.4 eV ($\lambda = 147.0$ nm) et 10.0 eV ($\lambda = 123.6$ nm). A ces longueurs d'onde la molécule n'est pas ionisée.

Procédure expérimentale

Les sources de lumière ultraviolette sont des lampes à rayonnement de résonance du krypton, $\lambda = 123.6$ (~85%) et 116.5 nm (~15%), et du xénon, $\lambda = 147$ nm (~98%), construites suivant la description de Ausloos et coll. (3). Ces lampes sont munies de fenêtres en fluorure de lithium. Elles sont fixées par un joint étanche à des cellules d'irradiation d'environ 300 ml.

L'actinométrie est réalisée pour le rayonnement de résonance du krypton par la mesure du courant d'ionisation dans les cellules d'irradiation contenant de l'oxyde nitrique ou de l'isobutylène dont les rendements quantiques de photoionisation sont connus (4–6). Pour le rayonnement de résonance du xénon, le débit des photons est déterminé en réalisant la photolyse de l'isobutylène gazeux, dont les rendements quantiques des produits de décomposition sont donnés dans la littérature (5).

Les produits organiques de photolyse sont analysés par chromatographie en phase gazeuse dans des instruments équipés de détecteurs à ionisation de flamme. Les produits sont séparés sur une colonne de squalane (hydrocarbures C_1 à C_4 et certains produits chlorés), tandis que le dichlorométhane l'est sur une colonne de Porapak Q. Toutes les irradiations sont faites à la température ambiante soit 23 ± 3 °C.

Le chloro-2 propane provient de chez Eastman Co. Avant son emploi, il est purifié soit par chromatographie à gaz préparative (pureté obtenue >99.999%), soit par barbotage de l'hélium dans le réactif refroidi à −77 °C (pureté >99.99%). L'oxyde nitrique, l'hydrogène sulfuré et l'iodure d'hydrogène proviennent de chez Matheson Co., et ils sont purifiés par des méthodes standards avant leur emploi.

Résultats

Les résultats sont exprimés sous la forme de rendements quantiques ils sont présentés au tableau 1. L'acide chlorhydrique qui est un produit majeur de la photolyse n'a pu être analysé en raison de difficultés analytiques (7). De même les produits de condensation polyhalogénés n'ont pas été analysés. Ainsi, il ne faut pas s'attendre à ce que le bilan massique soit retrouvé. Cependant, nous avons identifié, mais pas mesuré quantitativement, le dichlorométhane: sa production augmente avec l'énergie des photons incidents et son rendement semble être voisin à celui du chloropropène dans l'irradiation du C_3H_7Cl pur.

[1]Revision reçue le 1 avril 1976.

Can. J. Chem. Downloaded from www.nrcresearchpress.com by 210.87.254.42 on 09/05/12
For personal use only.

Can. J. Chem. Downloaded from www.nrcresearchpress.com by 210.87.254.42 on 09/05/12
For personal use only.

TABLEAU 1. Rendements quantiques de la photolyse du chloro-2 propane à 5 torr (dose absorbée $\sim 8 \times 10^{16}$ photons)

λ (nm)	Additif	CH_4	C_2H_2	C_2H_4	C_2H_6	C_3H_6	C_3H_8	C_3H_4[a]	CH_3Cl	C_2H_3Cl	i-C_4H_{10}	C_4H_8[b]	n-C_4H_{10}	2-C_4H_8[c]	C_2H_5Cl	C_3H_5Cl
123.6–115.6	—	0.023	0.032	0.076	0.011	0.76	0.008	0.041	0.014	0.035	0.004	0.011	0	0	0	0.12
	NO(5%)	0.017	0.038	0.076	0	0.72	0	0.046	0.010	0.033	0	0	0	0	0	0.033
	H_2S(10%)	0.092	0.042	0.073	0.011	0.59	0.035	0.039	0.006	0.032	0.006	0.015	0.008	0.027	0.006	0.041
	HI(5%)	0.092	0.11	0.070	0.12	0.53	0.064	0.040	0.014	0.032	0.006	0.010	0.022	0.029	0.014	0.034
147.0	—	0.065	0.008	0.06	0.006	0.67	0.083	0.011	0.009	0.026	0.015	0.009	0	0	0.003	0.13
	NO(5%)	0.01	0.01	0.06	0.002	0.71	0	0.013	0.01	0.031	0	0.002	0	0	0.003	0.04
	H_2S(10%)	0.08	0.01	0.06	0.005	0.68	0.19	0.011	0.01	0.033	0.025	0.005	0.003	0.010	0.007	0.09
	HI(5%)	0.063	0.025	0.06	0.009	0.72	0.16	0.014	0.011	0.034	0.01	0.002	0.002	0.006	0.023	0.045

[a]Allène + propyne.
[b]Iso-C_4H_8 + 1-C_4H_8.
[c]*trans* + *cis* 2-C_4H_8.

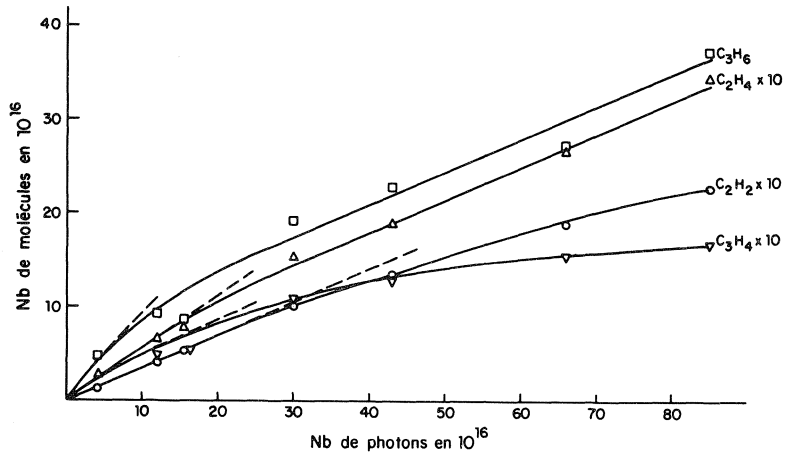

FIG. 1. Photolyse du réactif pur; effet de dose à λ = 123.6–116.5 nm: (□) C_3H_6, (△) C_2H_4, (○) C_2H_2 et (▽) C_3H_4.

Pour les irradiations à λ = 123.6 nm l'effet de dose n'est pas perceptible jusqu'à conversion d'environ 0.05% du chloropropane, mais au-delà, il devient bien visible pour les produits insaturés (fig. 1). Les rendements de ces derniers diminuent au fur et à mesure de l'accumulation de ces produits. Une tendance similaire se retrouve pour les irradiations à λ = 147 nm.

Entre 1 et 20 torr il n'y a pas d'effet de pression marqué pour la majorité des produits formés pendant l'irradiation à λ = 123.6 nm. Entre 1 et 5 torr, le rendement du chloro-2 propène augmente, tandis que celui du chlorure de méthyle diminue (fig. 2). Le rendement en C_2H_2 diminue rapidement aux basses pressions (<2 torr et ensuite plus lentement avec l'augmentation de la pression (fig. 2). Le rendement en C_2H_4 aux basses pressions (<1 torr) n'est pas très bien caractérisé, mais il semble augmenter pour ensuite quelque peu diminuer avec l'augmentation de la pression (fig. 2). Dans le cas des irradiations à λ = 147 nm les effets de pression entre 0.5 et 20 torr sont encore moins marqués que pour la photolyse à plus haute énergie. Seul

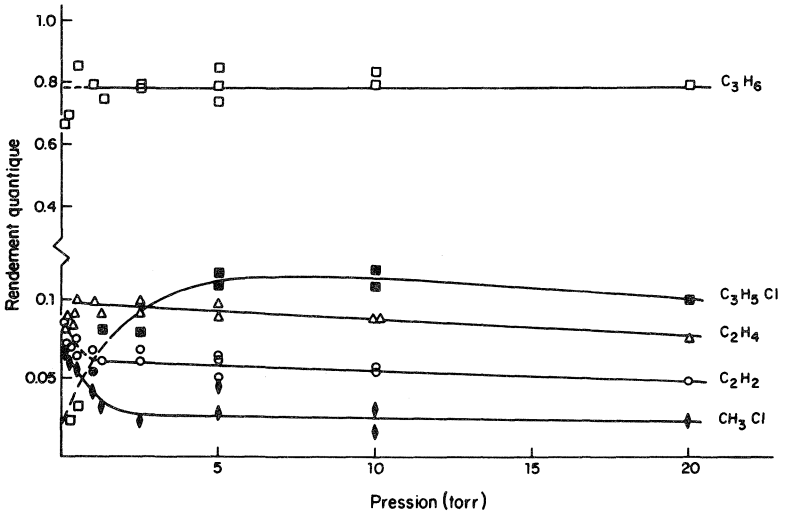

FIG. 2. Photolyse du réactif pur; effet de pression à λ = 123.6–116.5 nm: (□) C_3H_6, (△) C_2H_4, (○) C_2H_2, (◆) CH_3Cl et (■) C_3H_5Cl.

Can. J. Chem. Downloaded from www.nrcresearchpress.com by 210.87.254.42 on 09/05/12
For personal use only.

Can. J. Chem. Downloaded from www.nrcresearchpress.com by 210.87.254.42 on 09/05/12
For personal use only.

le rendement du CH_4 diminue d'environ 50% entre 0.2 et 2 torr.

Les effets des additifs HI, H_2S et NO sont présentés au tableau 1. On peut remarquer un rendement plus faible en propène en présence du H_2S et du HI aux irradiations à $\lambda = 123.6$ nm. Nous reviendrons sur cet effet dans la discussion.

Discussion

Les résultats obtenus sont trop fragmentaires pour permettre une interprétation détaillée des processus intervenant dans la photolyse du chloro-2 propane. A ce stade de l'étude nous pouvons tirer que quelques conclusions partielles.

Le spectre d'absorption dans l'ultraviolet à vide du iso-C_3H_7Cl est cité par Robin (8). A $\lambda = 147$ nm (68 027 cm^{-1}) l'absorption se fait dans le continuum D résultant des transitions d'orbitales de l'atome d'halogène ayant peu de recouvrement avec les orbitales des groupements CH_3. A $\lambda = 123.6$ nm (80 906 cm^{-1}) l'absorption est située dans un large continuum attribué au moins en partie au groupe alkyl du chloro-2 propane.

L'énergie de dissociation de la liaison C—Cl du chloro-2 propane est 73.3 ± 2.3 kcal/mol et même si les auteurs de cette détermination considèrent cette valeur comme possiblement trop faible (9) elle est inférieure d'au moins 15 kcal à l'énergie de liaison H—SH (90 kcal/mol) (10). Cela implique que dans le système étudié l'emploi du H_2S comme intercepteur de radicaux libres peut s'avérer beaucoup moins efficace que dans des systèmes hydrocarbonés purs de même nombres d'atomes de carbone. Dans le cas du HI, dont l'énergie de liaison est 70.4 ± 0.2 kcal/mol (11), on peut espérer que la réaction 1 concurrence efficacement le processus d'interception des radicaux par la molécule parente (processus 2)

[1] $$R^{\cdot} + HI \rightarrow RH + I^{\cdot}$$

[2] $$R^{\cdot} + \text{iso-}C_3H_7Cl \rightarrow RCl + C_3H_7^{\cdot}$$

Dans le cas présent il est probable que même 5% de HI ne soit suffisant pour intercepter tous les radicaux libres (tableau 1); signalons à titre de comparaison que moins de 1% de HI suffit pour capter tous les radicaux formés lors de la photolyse à 8.4 et 10.0 eV du propane (12). La photolyse en présence de fortes concentrations de HI mène aussi à des complications cinétiques. Signalons en juste une, celle de l'augmentation de l'acétylène qui demeure inexpliquée. Pour ces raisons les rendements quantiques en présence d'intercepteurs de radicaux présentés au tableau 1 reflètent un espect plutôt qualitatif que quantitatif des processus issus de la photolyse.

(a) Le propène

Ce produit est de loin le plus important dans la photolyse du chloro-2 propane. Il est formé avec un rendement quantique élevé: $\Phi(C_3H_6) = 0.67$ à $\lambda = 147$ nm et $\Phi(C_3H_6) = 0.76$ à $\lambda = 123.6$–116.5 nm. Dans les limites des erreurs des techniques expérimentales le rendement du propène ne change pas avec l'emploi des capteurs de radicaux, donc il proviendrait de le décomposition monomoléculaire:

[3] $$\text{iso-}C_3H_7Cl \xrightarrow{h\nu} C_3H_6 + HCl\ (H + Cl)$$
$$\Delta H_3 = 15.7\ (\sim 120)\ \text{kcal/mol}$$

Comme on peut s'attendre le rendement plus élevé en propène correspond à l'absorption de photons plus énergetiques. Par ailleurs aux deux longueurs d'onde il y a suffisamment d'énergie pour que le propène formé soit excité et qu'il puisse se décomposer à son tour en fragments ou produits stables. A $\lambda = 123.6$ nm le rendement plus bas en propène en présence du HI ou du H_2S (tableau 1) peut être du à une réaction d'addition de l'iode atomique ou du $HS^{\cdot}$ selon la cas sur la double liaison du C_3H_6.

(b) Le chloro-2 propène

Les rendements moléculaires du chloro-2 propène aux deux longueurs d'onde de photolyse sont ceux trouvés pour le système iso-C_3H_7Cl + NO. Il existe qu'une seule possibilité pour expliquer ce produit moléculaire:

[4] $$\text{iso-}C_3H_7Cl \xrightarrow{h\nu} C_3H_5Cl^{*} + H_2$$
$$\Delta H_4 \approx 34\ \text{kcal/mol}$$

[4a] $$\longrightarrow C_3H_5Cl + H^{\cdot} + H^{\cdot}$$
$$\Delta H_{4a} \approx 140\ \text{kcal/mol}$$

L'énergie accumulée dans le chloropropène issus de la réaction 4 est suffisante pour entrainer la décomposition de ce dernier suivant les processus:

[5] $$C_3H_5Cl^{*} \rightarrow C_2H_2 + CH_3Cl$$
$$\Delta H_5 \approx 32\ \text{kcal/mol}$$

[6] $$\rightarrow \text{Autres produits}$$

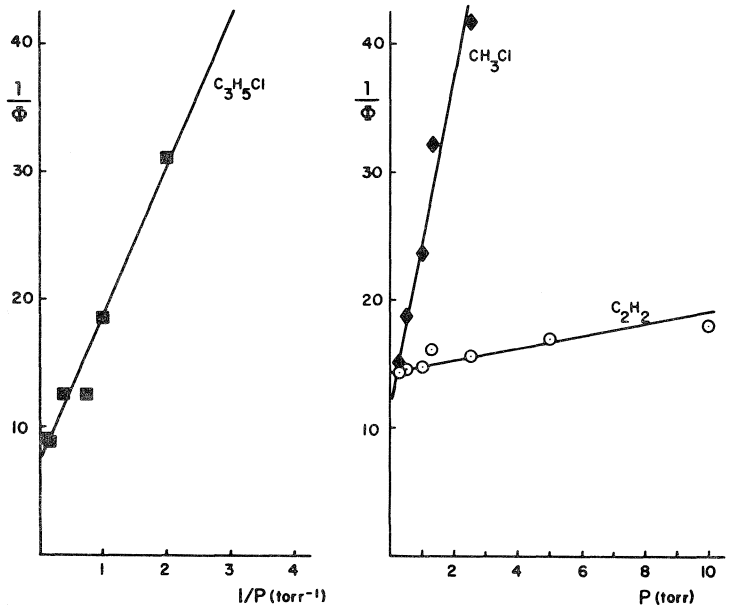

FIG. 3. L'inverse des rendements quantiques du chloro-2 propène en fonction de l'inverse de la pression (partie gauche) et inverse des rendements de l'acétylène et du chlorure de méthyl en fonction de la pression (partie droite).

La molécule excitée, $C_3H_5Cl^*$, peut cependant être stabilisée par collision et cet effet se fera d'autant plus sentir que la pression est plus élevée:

$$[7] \qquad C_3H_5Cl^* \xrightarrow{[M]} C_3H_5Cl$$

comme le témoigne la fig. 2. A partir des réactions 4, 5, 6 et 7 on peut établir des expressions cinétiques reliant les rendements quantiques $\Phi(C_3H_5Cl)$, $\Phi(C_2H_2)$ et $\Phi(CH_3Cl)$ avec la pression:

$$[8] \qquad \frac{1}{\Phi(C_3H_5Cl)} = \frac{1}{\Phi^{\infty}(C_3H_5Cl)}\left(1 + \frac{k_5 + k_6}{k_7}\frac{1}{P}\right)$$

$$[9] \qquad \frac{\Phi^0(C_2H_2)}{\Phi(C_2H_2)} = \frac{\Phi^0(CH_3Cl)}{\Phi(CH_3Cl)} = 1 + \frac{k_7}{k_5 + k_6}P$$

où $\Phi^{\infty}(C_3H_5Cl)$ indique le rendement extrapolé à pression très élevée, tandis que $\Phi^0(C_2H_2, CH_3Cl)$ sont les rendements extrapolé à pression nulle.

Suivant ce mécanisme on devrait s'attendre à ce que le rapport des constantes de vitesse, $k_7/(k_5 + k_6)$, soit le même pour les deux expressions [8] et [9], de même que les rendements extrapolés Φ^0 de l'acétylène et du chlorure de méthyl soient égaux entre eux. La fig. 3, à laquelle on a porté Φ^{-1} en fonction de P^{-1} pour le C_3H_5Cl (partie gauche) et en fonction de P pour les C_2H_2 et CH_3Cl (partie droite), montre que même si des relations linéaires existent le rapport $k_7/(k_5 + k_6)$ n'a pas la même valeur pour les trois droites. En fait, il varie de deux ordres de grandeur. Il en va de même pour Φ^0 qui est différent pour C_2H_2 et CH_3Cl. Ces résultats négatifs peuvent être interprétés de deux manières, soit que le mécanisme proposé n'est pas valide, soit que le traitement est incomplet et ne tient pas compte de la possibilité de formation des produits en question par d'autres voies que celle indiquée plus haut. Le tableau 1 montre d'ailleurs qu'une partie du C_3H_5Cl est d'origine radicalaire ($\sim$0.03 à λ = 123.6 nm et 0.09 à λ = 147 nm) provenant probablement d'une réaction de dismutation:

$$[10] \qquad R^{\cdot} + C_3H_6Cl^{\cdot} \rightarrow RH + C_3H_5Cl$$

En effet, on peut espérer avoir une assez grande quantité du radical $C_3H_6Cl^{\cdot}$ provenant des réactions:

$$[11] \qquad H^{\cdot} + \text{iso-}C_3H_7Cl \rightarrow H_2 + C_3H_6Cl^{\cdot}$$

$$[12] \qquad Cl^{\cdot} + \text{iso-}C_3H_7Cl \rightarrow HCl + C_3H_6Cl^{\cdot}$$

L'acétylène peut aussi être formé dans d'autres processus de décomposition de fragments excités,

Can. J. Chem. Downloaded from www.nrcresearchpress.com by 210.87.254.42 on 09/05/12
For personal use only.

Can. J. Chem. Downloaded from www.nrcresearchpress.com by 210.87.254.42 on 09/05/12
For personal use only.

ce qui expliquerait un rendement quantique initial différent d'avec celui du chlorure de méthyl.

(c) L'allène, le propyne, l'éthylène et l'acétylène

Les rendements quantiques de l'allène et du propyne dépendent faiblement de la présence des capteurs de radicaux. Pour les deux lampes d'émission employées le rendement est plus élevé en présence de NO, qu'en absence de capteurs de radicaux. Nous supposons que la vraie valeur est celle en présence du NO parce que dans ce cas la majorité des radicaux libres sont interceptés et ne réagissent plus avec les C_3H_4 formés. En présence du H_2S ou du HI il y a possibilité de réaction du radical HS· ou I· avec les C_3H_4, réactions semblables à celles observées par Collin et Perrin (13) dans le cas des HS· + oléfines. La réaction suivante peut être à l'origine de l'allène et du propyne:

[13] $$C_3H_6^* \rightarrow C_3H_4 + H_2 \text{ (ou } 2H\cdot)$$

Le processus 13 a été proposé par Varachek et Koob (14) dans la photolyse du propane. Ces réactions de décomposition doivent être très rapides, puisque dans les deux cas le rendement en C_3H_4 ne dépend pas de la pression, du moins dans l'intervalle des pressions étudiées. A $\lambda =$ 123.6 nm, il y a plus d'énergie disponible qu'à 147 nm, environ 37 kcal/mol, donc décomposition plus importante, ce qui est corroboré par les résultats expérimentaux (tableau 1).

A la pression de 5 torr le rendement quantique de l'éthylène ne dépend pas de la présence de capteurs de radicaux, donc il est d'origine moléculaire. A $\lambda = 147$ nm $\Phi(C_2H_4)$ dépend de la pression et il est légèrement inférieur au rendement de l'éthylène calculé à $\lambda =$ 123.6–116.5 nm. Dans les deux cas il est probable que c'est le même processus qui mène à la formation du C_2H_4, bien qu'à $\lambda =$ 123.6–116.5 nm l'espèce qui se décompose possède plus d'énergie: la réaction de décomposition est donc plus rapide et n'est pas influencée par la pression. Une première possibilité de décomposition primaire est:

[14] $$\text{iso-}C_3H_7Cl \xrightarrow{h\nu} C_2H_4 + CH_3Cl \qquad \Delta H_{14} = 24.8 \text{ kcal/mol}$$

Les produits provenant du processus 14 possèdent beaucoup d'énergie et il est possible que l'un d'eux se décompose encore. Par ailleurs $\Phi(C_2H_4)_{123.6} > \Phi(C_2H_4)_{147}$, ce qui laisse supposer que le processus 14 n'est pas la principale source du C_2H_4 car une énergie supérieure à $\lambda =$ 123.6 nm devrait être en faveur d'une décomposition secondaire du C_2H_4. Une autre voie possible de formation de l'éthylène est la décomposition des radicaux excités iso-C_3H_7* et C_2H_4Cl*:

[15] $$\text{iso-}C_3H_7Cl \xrightarrow{h\nu} \text{iso-}C_3H_7^* + Cl\cdot \qquad \Delta H_{15} = 79 \text{ kcal/mol}$$
$$\rightarrow C_2H_4 + CH_3\cdot$$

[16] $$\text{iso-}C_3H_7Cl \xrightarrow{h\nu} C_2H_4Cl^* + CH_3\cdot \qquad \Delta H_{16} = 83.5 \text{ kcal/mol}$$
$$\rightarrow C_2H_4 + Cl\cdot$$

La décomposition secondaire du C_3H_7· est proposée dans la photolyse du propane comme source du C_2H_4 et des radicaux CH_3· (15). Si les réactions 15 et 16 ont lieu nous devrions trouver $\Phi(CH_3\cdot) = \Phi(C_2H_4)$. Le rendement du radical methyl peut être calculé en faisant la différence des rendements du CH_4 dans les deux systèmes: iso-C_3H_7Cl + HI et iso-C_2H_7Cl + NO. Aux deux longueurs d'onde on trouve $\Phi(CH_3\cdot) \simeq$ 0.07. A $\lambda =$ 123.6–116.5 nm cela coincide bien avec le rendement quantique du C_2H_4, tandis qu'à $\lambda = 147$ nm $\Phi(CH_3\cdot)$ est plus élevé d'environ 17%, mais cet écart est dans les limites des erreurs expérimentales. De plus les expériences en présence du HI (ou du H_2S) mettent en évidence l'existence du radical C_2H_4Cl·, puisqu'on trouve un rendement quantique plus élevé du C_2H_5Cl en présence du HI. Ceci indique que dans ce système une certaine quantité de radicaux C_2H_4Cl· sont thermalisés à la pression à laquelle les expériences ont été effectuées.

En raison de son caractère insaturé l'acétylène peut agir aussi comme capteur de radicaux libres; nous supposons donc que les valeurs des rendements quantiques de formation du C_2H_2 sont celles trouvées pour le système iso-C_3H_7Cl + NO. La formation de l'acétylène peut résulter de trois voies, processus 5, 17 et 18:

[17] $$C_3H_6^* \rightarrow C_2H_2 + CH_4$$

[18] $$C_2H_4^* \rightarrow C_2H_2 + H_2$$

A $\lambda =$ 123.6 nm $\Phi(C_2H_2)$ est plus élevé que le rendement moléculaire du méthane; la réaction 17 n'est pas la seule à donner l'acétylène.

(d) Le chlorure de vinyle

Aux erreurs d'expérience près, la présence des capteurs de radicaux n'affecte pas les rendements quantiques du chlorure de vinyle; il est donc de provenance moléculaire. Il peut être formé par deux voies possibles:

$$[19]\quad \text{iso-}C_3H_7Cl \xrightarrow{h\nu} C_2H_3Cl + CH_4 \text{ (ou } C_2H_3Cl + CH_3^{\bullet} + H^{\bullet}\text{)} \qquad \Delta H_{19} \simeq 24 \text{ kcal/mol}$$

$$[20]\quad \longrightarrow C_2H_5Cl^{*} + CH_2^{\bullet} \qquad \Delta H_{20} \simeq 72 \text{ kcal/mol}$$
$$\hookrightarrow C_2H_3Cl + H_2$$

Le processus 19 ne peut être la seule voie de production parce que $\Phi(C_2H_3Cl) > \Phi(CH_4)$, de même que la faible valeur du $\Phi(CH_3^{\bullet}) \simeq 0.07$ ne peut expliquer à la fois la production du C_2H_3Cl et du CH_4 (réactions 15 et 16). Le processus de décomposition du chlorure d'éthyle [20] en chlorure de vinyle a été observé (7). L'absence du C_2H_5Cl à $\lambda = 123.6$ nm et un faible rendement quantique ($\Phi(C_2H_5Cl) = 0.003$) à $\lambda = 147$ nm plaident en faveur des processus de décomposition 20.

(e) Les butanes et les butènes

La formation des butanes et de butènes résulte de l'insertion du $CH_2^{\bullet}$ dans la molécule parent. L'existence de ce radical est clairement démontrée à $\lambda = 147$ nm par la présence du C_2H_5Cl moléculaire. Par analogie avec les hydrocarbures on peut espérer des réactions du radical $CH_2^{\bullet}$ avec le chloropropane:

$$[21]\quad CH_2^{\bullet} + \text{iso-}C_3H_7Cl \rightarrow C_4H_9Cl^{*} \rightarrow C_4H_9^{\bullet} + Cl$$
$$[22]\quad \hookrightarrow C_4H_8 + HCl$$

conduisant à un chlorobutane excité qui se décompose en radical butyl et chlore atomique, ou directement en butène et HCl. La preuve du processus 21 est faite dans les expériences en présence du HI ou du H_2S qui réagissent avec le radical $C_4H_9^{\bullet}$ donnant l'iso- et le *n*-butane, lesquels ne se forment pas en présence d'oxyde nitrique.

Conclusion

La photolyse du chloro-2 propane aux longueurs d'onde de 123.6–116.5 nm et 147 nm indique que le processus de décomposition primaire de loin le plus important est celui donné par l'expression 3. Une décomposition secondaire du propène et du chloropropène excités formés lors de la rupture primaire conduit (au moins en partie) à une série de composés insaturés en C_2. L'emploi de capteurs de radicaux a permis de mettre en évidence quelques radicaux issus de différents processus de décomposition de molécules excitées. Ces radicaux sont les suivants: $CH_2^{\bullet}$, $CH_3^{\bullet}$, $C_2H_5^{\bullet}$, iso-$C_3H_7^{\bullet}$, $C_3H_4Cl^{\bullet}$ et $C_4H_9^{\bullet}$.

Remerciements

Nous remercions le Dr. J. Gawlowski pour les discussions stimulantes relatives à l'interprétation de ces expériences. Nos remerciements vont aussi au Conseil national de recherches du Canada pour l'aide financière qui a permis de conduire ces travaux à terme.

1. R. H. Wiley, C. H. Jarboe, Jr., J. P. Harrell et D. J. Parish. (*a*) Proc. Chem. Soc. London, 347 (1957); (*b*) Radiat. Res. **13**, 479 (1960).
2. (*a*) M. A. Sweeney. Ph.D. Thesis, University of California, Berkeley. 1962; (*b*) D. DeYonge et J. Ceulemans. Bull. Soc. Chim. Belg. **84**, 871 (1975).
3. R. Gorden, Jr., R. E. Rebbert et P. Ausloos. Natl. Bur. Stand. Tech. Note, No. 496 (1969).
4. K. Watanabe, R. M. Matsunaga et H. Sakai. J. Appl. Opt. **6**, 391 (1967).
5. J. A. Herman, K. Herman et P. Ausloos. J. Chem. Phys. **52**, 28 (1970).
6. A. A. Siddiqi, C. T. Chen, G. G. Meisels et R. Gorden, Jr. J. Chem. Phys. **57**, 4506 (1972).
7. L. Cremieux et J. A. Herman. Can. J. Chem. **52**, 3098 (1974).
8. M. B. Robin. Higher excited states of polyatomic molecules. Vol. 1. Academic Press, New York. 1974. pp. 155–172.
9. J. B. Farmer et F. P. Lossing. Can. J. Chem. **33**, 861 (1955).
10. J. A. Kerr. Chem. Rev. **66**, 465 (1966).
11. B. de B. Darwent. Bond dissociation energies of simple molecules. Natl. Bur. Stand. Ref. Data Ser. Natl. Bur. Stand. (U.S.), **31** (1970).
12. P. Ausloos, R. E. Rebbert et S. Lias. J. Photochem. **2**, 267 (1973/74).
13. G. J. Collin et P. M. Perrin. Can. J. Chem. **50**, 2400 (1972); **52**, 2337 (1974).
14. J. H. Varachek et R. D. Koob. Can. J. Chem. **51**, 344 (1973).
15. J. Gawlowski, J. A. Herman et P. Gagnon. Can. J. Chem. **53**, 1348 (1975).

Can. J. Chem. Downloaded from www.nrcresearchpress.com by 210.87.254.42 on 09/05/12
For personal use only.

H_3O^+ ions in aqueous acid solutions. The infrared spectra revisited

PAUL A. GIGUÈRE AND SYLVIA TURRELL
Département de chimie, Université Laval, Québec, (Qué.) Canada G1K 7P4

Received August 6, 1976

PAUL A. GIGUÈRE and SYLVIA TURRELL. Can. J. Chem. **54**, 3477 (1976).

We have re-examined the infrared absorption between 4000 and 800 cm^{-1} of aqueous solutions of the four hydrogen halides at concentrations up to saturation, and under better experimental conditions than heretofore. The new spectra confirm definitely our previous assignment of the three broad bands around 2900, 1730, and 1200 cm^{-1} to fundamental vibrations of the H_3O^+ ion. Other proposed interpretations are shown to be untenable; in particular that of Ackermann, based on alleged similarities in the spectra of strong acids and bases. In hydrofluoric acid, hydrogen-bonded ion pairs are responsible for the shifts of the H_3O^+ frequencies. There is no evidence in the spectra for higher species, such as $H_5O_2^+$. We conclude that the H_3O^+ ion has an appreciably longer lifetime in concentrated aqueous acids than in water. It also forms much stronger hydrogen bonds than H_2O because of its ionic charge.

PAUL A. GIGUÈRE et SYLVIA TURRELL. Can. J. Chem. **54**, 3477 (1976).

Nous avons repris, dans des conditions expérimentales améliorées, l'étude des spectres infrarouges de solutions aqueuses des quatre halogénures d'hydrogène à diverses concentrations jusqu'à saturation. Les nouveaux résultats confirment définitivement notre première attribution des trois bandes larges vers 2900, 1730 et 1200 cm^{-1} à des vibrations de l'ion H_3O^+. Par ailleurs, les spectres de bases fortes en solutions concentrées sont nettement différents de ceux des acides, contrairement à la conclusion d'Ackermann. Dans l'acide fluorhydrique la formation de paires d'ions par liaison hydrogène très forte, $F^- \cdots H_3O^+$, conduit à des décalages importants des vibrations de l'ion H_3O^+. D'autre part, nous n'avons pas relevé d'indices d'espèces plus complexes, comme $H_5O_2^+$. L'ion H_3O^+ doit donc avoir une vie moyenne sensiblement plus longue dans les acides concentrés que dans l'eau pure. De plus, à cause de sa charge ionique il forme des liaisons hydrogène beaucoup plus fortes que H_2O.

Can. J. Chem. Downloaded from www.nrcresearchpress.com by 210.87.254.5 on 09/05/12
For personal use only.

About twenty years ago we reported the first spectra of aqueous solutions of strong acids interpreted in terms of individual H_3O^+ ions (1). At first our interpretation was acknowledged as essentially correct (2), but since then it has been challenged on various grounds, both theoretical and experimental. Prominent among these was the argument of Ackermann (3) stressing the similarity of the absorption spectra of strong bases (NaOH) and strong acids (HCl). From this he concluded that the spectra merely reflected a perturbation of the water structure by the solute. It was also argued that the H_3O^+ ion in solution is too short-lived to have a recognizable vibrational spectrum. Actually, our lowest observed frequency for H_3O^+ (1200 cm^{-1}) implies an average lifetime of at least 0.3 picoseconds (ps), definitely longer than that derived from the proton mobility in water, 0.2 ps (4, 5). The same conclusion was reached from a vibrational analysis of the H_3O^+ ion in aqueous acids (6) which yielded frequencies much lower than our experimental values. On the other hand, an extensive investigation of the infrared optical constants of strong acids and bases (7) has led to conclusions essentially in agreement with ours. As a result, our assignment of the infrared absorption spectra of H_3O^+ ions is still a controversial question (5, 8). So much so, that in a recent 'comprehensive treatise' (9) the H_3O^+ ion is barely mentioned! In an effort to clear up the situation we decided to re-examine the spectra of the hydrogen halides solutions, the simplest of the strong acids, using the latest improvements in materials and techniques.

The New Spectra

In the new spectra (Fig. 1) the characteristic bands of the H_3O^+ ion at about 1730 and 1200 cm^{-1} stand out much clearer than in our previous ones (1). This was achieved by using an expanded ordinate scale (5×) for enhanced intensity, and a slower attenuator response (10 s, full scale deflection) for lower noise level. The grating spectrometer (Perkin-Elmer, Model 621) was used in both single and double beam operation. Capillary films of the aqueous acids were prepared simply by pressing between a pair of

Can. J. Chem. Downloaded from www.nrcresearchpress.com by 210.87.254.5 on 09/05/12
For personal use only.

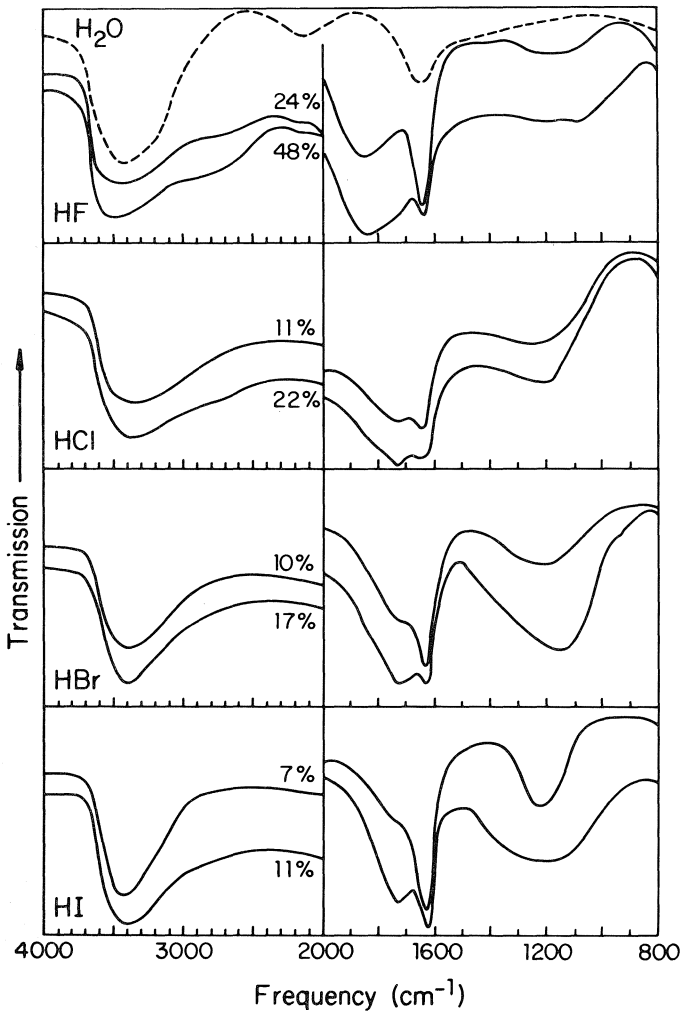

FIG. 1. Infrared absorption spectra of capillary films of aqueous solutions of the four hydrohalic acids (concentrations in mol%). Expanded ordinate scale (5×) below 2000 cm^{-1}.

optical flats a tiny droplet of the liquid of roughly constant size. Due to the strong absorbancy of the solutions, spacers, no matter how thin, could not be used. Optical CaF_2 is the most suitable window material up to its transmission limit, near 8 μ. In the lower frequency range, AgCl was used for hydrofluoric and hydrochloric acids, and KRS-5 with the other two acids. Commerical "reagent grade" solutions of the four acids were sufficiently pure, except for hydrochloric acid which sometimes contains traces of HBr. This causes a slight corrosion of the AgCl windows, as noted before (1). All concentrations are in mol%, a more appropriate unit than normality or weight composition. For all four acids the highest concentration is that of so-called saturated solutions (under atmospheric pressure): namely, some 37 wt. % for HCl, and nearly 50% for the other three.

Because the O—H stretching bands of the ion are largely overlapped by those of water, they are hardly distinguishable in the single-beam spectra, even of the most concentrated solutions. In the differential spectra with water in the reference beam, the antisymmetric stretching $\nu_3(E)$ appears as a broad absorption region centered around 2900 cm^{-1}. Much better characterized are the two bending modes, $\nu_4(E)$ at 1730 $\pm$ 10 cm^{-1}, and $\nu_2(A)$ at 1200 $\pm$ 50 cm^{-1}. The wide uncertainty on the latter frequency reflects some slight

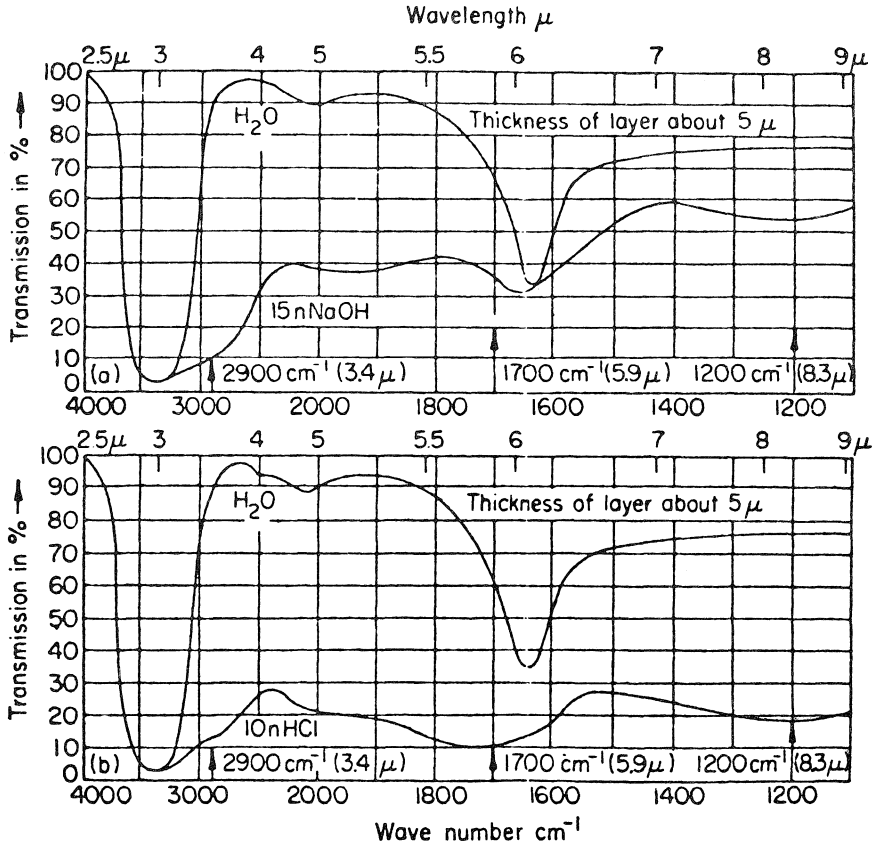

FIG. 2. Infrared spectra of Ackermann (3) reproduced from ref. 17.

shifts with the nature and concentration of the acids. The 1200 cm^{-1} band is certainly the most characteristic of H_3O^+, located as it is in a 'window' of the water spectrum. This is also true of the deuterated spectra where, in addition, the ν_2 band of D_3O^+ at 900 $\pm$ 10 cm^{-1} always appears more clearly than the ν_4 band at 1350 $\pm$ 30 cm^{-1} (1). As may be gathered from Fig. 1, hydrofluoric acid is markedly different from the other hydrohalic acids in its infrared spectra (10–12), as well as in its electro-chemical properties (13). For instance, the H_3O^+ bands are strongly shifted: ν_3, down to about 2770 cm^{-1}, and more surprisingly, ν_4, up to 1830 $\pm$ 10 cm^{-1}. As for ν_2, its contour changes considerably with acid concentration.[1] As explained elsewhere (12) these particularities can be rationalized in terms of ion pairs of hydroxonium fluoride, $H_3O^+ \cdots F^-$, linked by a very strong and short hydrogen bond. Such ion pairs can also account, among others, for the remarkable weakness of hydrofluoric acid.

The Spectra of Ackermann

By comparison, the spectra of Ackermann (3) now appear to be rather limited in their scope and relevance to the problem at hand. First, the use of CaF_2 windows with cut-off at 9 μ impaired observation of the entire 1200 cm^{-1} band, and precluded confirmation of the isotope shift in deuterated compounds (14). More important, the published spectra are of rather thick samples, some 5 μ (Fig. 2), with total absorption of the order of 80% or more in the regions of interest. Still, the two maxima around 1730 and 1200 cm^{-1} are clearly visible. However, they have unaccountably disappeared in the plots of calculated

[1]An error in drawing the spectra of hydrofluoric acid for the preceding paper (12) has escaped notice. The minimum of absorption shown in the 1400 cm^{-1} region was very much exaggerated, specially for the most concentrated solution.

Can. J. Chem. Downloaded from www.nrcresearchpress.com by 210.87.254.5 on 09/05/12
For personal use only.

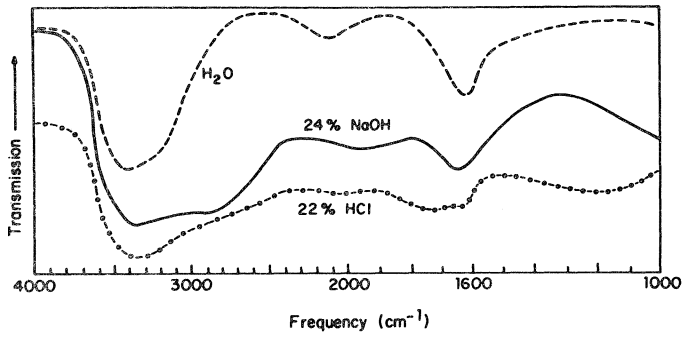

FIG. 3. Infrared absorption of concentrated solutions of sodium hydroxide and hydrochloric acid.

extinction coefficients: compare Figs. 5 and 8 in ref. 3. But the most puzzling results are found in the spectrum of a strong NaOH solution, which shows an absorption band at 1200 cm^{-1}, as in the acid solutions, and a broadening on the high-frequency side of the 1640 cm^{-1} band of water. We have not been able to detect such features in the absorption of NaOH solutions of approximately the same concentration (Fig. 3). Likewise, there is no trace of them in the normal-incidence reflectance spectra reported by Williams and co-workers (7). On the contrary, their spectra, like ours, show a minimum of the absorption coefficient near 1200 cm^{-1}. As for the ν_2 band of water, it is shifted, if at all, to *lower* frequency in solutions of electrolytes (15). Whatever the origin of these extraneous features, the conclusion derived from them is obviously unfounded.

The $H_5O_2^+$ Group

Another peculiarity to which Ackermann has drawn attention is the continuum, or increased background, between the various absorption bands in solutions of acids and bases. This phenomenon, first noticed long ago in the Raman spectrum of aqueous nitric acid (16), has not yet received a satisfactory explanation. Zundel (17), who has studied it extensively, ascribes it to so-called "$H_5O_2^+$ groupings". This new species, not to be confused with the $H_5O_2^+$ ion present in some crystalline acid dihydrates (18, 19), is said to be due to "the excess proton tunneling along the hydrogen bond between two water molecules" (17). Because the latter are believed to retain their individuality as vibrating groups, Zundel rejects our assignments of the H_3O^+ bands in favor of the following: the bands at 2900 and 1730 cm^{-1} would be the OH stretching and bending respectively of peripheral water molecules in hypothetical $H_9O_4^+$ groups; the 1200 cm^{-1} band could be the overtone of the libration band of water. First, there is no experimental evidence whatsoever for distinct $H_9O_4^+$ groups in aqueous acids. *A priori*, there is no reason why such a complex species, as well as the above mentioned $H_5O_2^+$ groupings with which it conflicts, should be longer-lived, and better characterized than H_3O^+ ions. Furthermore, a frequency of 1730 cm^{-1} is far too high for the bending mode of water molecules. As for the 1200 cm^{-1} band, assignment to an overtone is ruled out by the following observations: (*a*) its intensity is too high, and it *increases* with *decreasing* water concentration; (*b*) its frequency at the maximum is often appreciably higher than twice the libration frequency of H_2O in acid solutions (1, 7). At any rate, the existence of discrete $H_5O_2^+$ groups in aqueous acids now appears very doubtful in the light of recent findings, both theoretical and experimental. (*a*) Extended *ab initio* calculations (20) have established the absence of a symmetric double-well potential for the central proton in such a hypothetical species. (*b*) An extensive study of aqueous hydrochloric acid by X-ray and neutron diffraction (21) has confirmed that the H_3O^+ ions are hydrogen bonded to four H_2O molecules with the same average O···O distance of 2.52 Å.

As for the argument based on the lifetime of the H_3O^+ ion, it was no doubt taken too literally. Calculations of the proton mobility from conductivity data necessarily involve some approximations. For instance, the inter-oxygen distance of 2.45 Å used by Conway, Bockris, and Linton

Can. J. Chem. Downloaded from www.nrcresearchpress.com by 210.87.254.5 on 09/05/12
For personal use only.

Can. J. Chem. Downloaded from www.nrcresearchpress.com by 210.87.254.5 on 09/05/12
For personal use only.

(4) for their quantum mechanical analysis is now known to be too short. The proton potential is particularly sensitive to that parameter. Then, a symmetric double-minimum potential was obtained by superposition of two Morse curves. Recent calculations (20, 22) lead instead to a rather flat potential for the migrating proton. More importantly, however, Conway, Bockris, and Linton (4) had shown previously that the rate-determining step in proton transfer is the rotation of adjacent water molecules to present a favorable orientation. Now, simply from chemical intuition it is clear that the effective lifetime of the H_3O^+ ion must increase appreciably with acid concentration. Each molecule of acid added to water increases the number of protons waiting to jump, and decreases the number of proton-acceptor sites. A quantitative analysis of that effect would be useful. It is noteworthy that in our spectra (Fig. 1) H_3O^+ ions can be detected through their ν_4 band in a solution of hydriodic acid of only 7 mol%; that is with twelve molecules of water available on the average for the hydration of each pair of ions.

Hydrogen Bonds

Another question on which the infrared spectra provide interesting information is that of hydrogen bonding in aqueous acids. From casual observation alone it is clear that the H_3O^+ ion forms much stronger hydrogen bonds than H_2O. For instance, the O—H stretching frequency of the ion is about 500 cm^{-1} lower, and the bending frequency ν_4, about 85 cm^{-1} higher than the corresponding vibrations in liquid water. Likewise, the half-width of the H_3O^+ band at 1730 cm^{-1} is three to four times that of the ν_2 band of water. As explained before (23, 24) this large effect must be ascribed to the positive charge on the hydrogen atoms which makes H_3O^+ a much better proton donor, and a poorer proton acceptor, than H_2O. The reverse is true of the OH^- anion. Newton and Ehrenson (20) arrived at the same conclusion from their molecular orbital calculations. A striking demonstration of the role of ionic charges may be seen in the case of liquid sulfur dioxide solutions. In that solvent water is essentially monomeric (25), but the H_3O^+ ion is strongly hydrogen bonded, not only to the counterion (Cl^- or Br^-), but also to SO_2 (24, 26). The diffraction study of Triolo and Narten (21) has shown an average inter-oxygen distance, $H_2O\cdots H_3O^+$, of 2.52 Å in aqueous hydrochloric acid, as compared with 2.76 Å in liquid water and ice. Such a short distance would correspond to an energy of the order of 10–12 kcal mol^{-1} according to the one-dimensional model of Lippincott and Schroeder (27). Although rather short, these hydrogen bonds are not symmetric; nor are those, even shorter (~1.4 Å?), of the ion pairs in hydrofluoric acid, because the end-atoms are different.

Incidentally, these hydrogen-bonded ion pairs are of a different nature from the 'contact ion pairs' usually encountered in electrolytic solutions. Whereas the latter are of a purely electrostatic origin, the former possess a definite covalent, *i.e.* directional character. Conceivably, all strong acids contain very small equilibrium concentrations of these $H_3O^+\cdots X^-$ pairs, depending on the proton acceptor power of the anion. For instance, this could explain the relative strength of the four hydrohalic acids. Indeed, their dissociation constants, *viz.* pK = 3.2 for HF, −7.4 for HCl, −9.5 for HBr, and −10 for HI (13) seem proportional to the expected hydrogen-bond strengths.

In conclusion, there now exists a sufficient body of direct experimental evidence to dispel any doubt about the reality of the H_3O^+ ion as a dominant species in aqueous acids. Quantum theory shows that the proton spends only about 1% of its time in tunneling (4). Important as it is, that process must not detract from the existence of discrete H_3O^+ ions. Accordingly, the use of such notations as H^+ or $H^+(H_2O)$, and names like proton hydrate should be discontinued because they are erroneous and misleading. Conventionally, the term hydrate refers to an ion or a molecule surrounded by an indefinite number of hydrogen-bonded water molecules. In forming an H_3O^+ ion the water molecule loses its identity. The three O—H bonds of the ion are even stronger than those in H_2O, and become equivalent by resonance. This is reflected in the so-called enthalpy of hydration of the proton, a quantity larger by a factor of two to three, than that of all other univalent ions, including OH^- (8).

Acknowledgement

This investigation, like the original one (1), was made possible through the continuing financial support of the National Research Council of Canada.

1. M. FALK and P. A. GIGUÈRE. Can. J. Chem. **35**, 1195 (1957).
2. R. P. BELL. The proton in chemistry. 1st ed. Cornell University Press, New York. 1959. p. 22.
3. T. ACKERMANN. Z. Phys. Chem. Frankfurt, **27**, 253 (1961).
4. B. E. CONWAY, J. O'M. BOCKRIS, and H. LINTON. J. Chem. Phys. **24**, 834 (1956).
5. R. P. BELL. The proton in chemistry. 2nd ed. Cornell University Press, New York. 1973. p. 21.
6. R. MORE O'FERRALL, G. W. KOEPPL, and A. J. KRESGE. J. Am. Chem. Soc. **93**, 1 (1971).
7. P. RHINE, D. WILLIAMS, G. M. HALE, and M. R. QUERRY. J. Phys. Chem. **78**, 1405 (1974).
8. G. PIMENTEL and A. L. MCCLELLAN. Ann. Rev. Phys. Chem. **22**, 357 (1971).
9. F. FRANKS (*Editor*). Water. A comprehensive treatise. Vol. 3. Aqueous solutions of simple electrolytes. Plenum Press, New York. 1973.
10. L. H. JONES and T. A. PENNEMAN. J. Chem. Phys. **22**, 781 (1954).
11. N. ZENGIN. Commun. Fac. Sci. Univ. Ankara, Ser. A**11**, 1 (1961): *In* Chem. Abs. **57**, 16008 (1962).
12. P. A. GIGUÈRE. Chem. Phys. Lett. **41**, 598 (1976).
13. F. A. COTTON and G. WILKINSON. Advanced inorganic chemistry. 2nd ed. Interscience Publishers, New York. 1966. p. 223.
14. T. ACKERMANN. Z. Phys. Chem. Frankfurt, **41**, 113 (1964).
15. P. RHINE, D. WILLIAMS, G. M. HALE, and M. R. QUERRY. J. Phys. Chem. **78**, 238 (1974).
16. L. GIOTTO. Nuovo Cimento, **15**, 273 (1938).
17. G. ZUNDEL. Hydration and intermolecular interaction. Academic Press, New York. 1969. pp. 169–172.
18. J. O. LUNDGREN and I. OLOVSSON. Acta Crystallogr. **23**, 966 (1967); **23**, 971 (1967).
19. J. M. WILLIAMS. Inorg. Nucl. Chem. Lett. **3**, 297 (1967).
20. M. D. NEWTON and S. EHRENSON. J. Am. Chem. Soc. **93**, 4971 (1971).
21. R. TRIOLO and A. H. NARTEN. J. Chem. Phys. **63**, 3624 (1975).
22. W. P. KRAEMER and G. H. F. DIERCKSEN. Chem. Phys. Lett. **5**, 463 (1970).
23. P. A. GIGUÈRE. Rev. Chim. Min. **3**, 627 (1966).
24. M. SCHNEIDER and P. A. GIGUÈRE. Compt. Rend. B**267**, 551 (1968).
25. H. HOYER. Z. Elektrochem. **64**, 631 (1960).
26. P. A. GIGUÈRE and C. MADEC. Chem. Phys. Lett. **37**, 569 (1976).
27. E. R. LIPPINCOTT and R. SCHROEDER. J. Chem. Phys. **23**, 1099 (1955).

Can. J. Chem. Downloaded from www.nrcresearchpress.com by 210.87.254.5 on 09/05/12
For personal use only.

Canadian Journal of Chemistry

Published by
THE NATIONAL RESEARCH COUNCIL OF CANADA

Journal canadien de chimie

Publié par
LE CONSEIL NATIONAL DE RECHERCHES DU CANADA

Volume 54 Number 22 November 15, 1976 Volume 54 numéro 22 15 novembre 1976

A wide-line nuclear magnetic resonance study of molecular motions in piperidinium salts

MARIE-CLAUDE BERNARD,[1] CHRISTOPHER ORVIG, AND D. F. R. GILSON[2]

Department of Chemistry, McGill University, P.O. Box 6070, Station A, Montreal, P.Q., Canada H3C 3G1

Received June 16, 1976

MARIE-CLAUDE BERNARD, CHRISTOPHER ORVIG, and D. F. R. GILSON. Can. J. Chem. **54**, 3483 (1976).

Wide line nmr and differential scanning calorimetric studies confirm the existence of crystal phase transitions in piperidinium iodide. The highest temperature phase involves isotropic rotation of the piperidinium ion. No crystal structure transitions occur in the chloride, bromide, or hexafluorophosphate salts although these compounds undergo second moment transitions indicating probable rotation of the piperidinium ion about the N—C_3 axis.

MARIE-CLAUDE BERNARD, CHRISTOPHER ORVIG et D. F. R. GILSON. Can. J. Chem. **54**, 3483 (1976).

Des études par rmn (raies larges) et par balayage calorimétrique différentiel confirment l'existence de transitions de phase cristalline pour l'iodure de pipéridinium. La phase à température la plus élevée implique une rotation isotrope de l'ion pipéridinium. Il n'y a pas de transitions de structure cristalline du chlorure, du bromure ou de l'hexafluorophosphate toutefois ces composés subissent des transitions du moment second indiquant, selon toute probabilité, qu'il y a une rotation de l'ion pipéridinium autour de l'axe N—C_3.

[Traduit par le journal]

Introduction

The infrared spectra of solid piperidinium halides have been studied by Cabana and Sandorfy (1). The spectra of the chloride and bromide showed little change between room temperature and −190 °C but the marked differences in the spectra of the iodide led Cabana and Sandorfy to suggest that a phase change occurred in the latter compound. Room temperature crystal structure studies of the chloride, bromide, and sulphide salts showed that these compounds are isostructural (2–5) with the piperidinium ring in the chair form. However, the high values for the temperature factors reported in these X-ray studies indicate that some ring atoms undergo large amplitude thermal motions. The piperidinium ion is an analogue of cyclohexane and phase transitions and molecular motions in this compound have been studied by Andrew and Eades (6). The possibility that phase changes involving molecular reorientations occur in the piperidinium salts appeared worth examining and this paper reports the results of wide line nmr studies of piperidinium chloride, bromide, iodide, and hexafluorophosphate. The halide series represents a trend in which decreasing hydrogen bonding between the piperidinium ion and the anion occurs and the hexafluorophosphate anion was included in the study since this

[1]NRCC Post-doctoral fellow 1972–1973.
[2]To whom correspondence should be addressed.

Can. J. Chem. Downloaded from www.nrcresearchpress.com by 210.87.254.5 on 09/05/12
For personal use only.

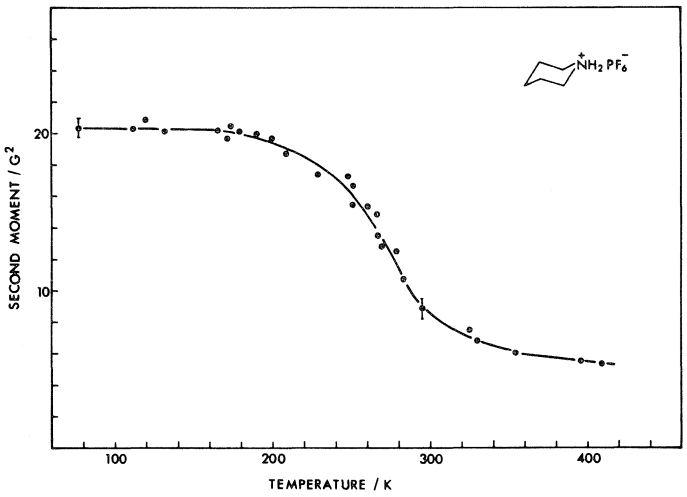

FIG. 1. Temperature dependence of the second moment for piperidinium hexafluorophosphate. (Error bars indicate standard deviation.)

ion showed the weakest interactions in a study of pyridinium salts (7).

Experimental

The compounds were prepared by addition of the appropriate acid to piperidine followed by recrystallization. The nmr spectra were obtained using a spectrometer constructed from Varian units operating at 60 MHz for proton resonance. Variation of the sample temperature was achieved by regulating the flow of heated or cooled nitrogen gas and the temperature measured with copper–constantan thermocouples placed up- and downstream from the sample. Differential scanning calorimetric experiments were performed with a Perkin-Elmer DSC-1B.

Results

The behaviour of the second moment with temperature was similar for piperidinium chloride, bromide, and hexafluorophosphate with extremely broad and gradual transitions covering the temperature ranges; chloride 350–460 K; bromide 240–380 K; and hexafluorophosphate 190–360 K. The second moment dependence is shown in Fig. 1 for piperidinium hexafluorophosphate. In contrast the iodide, Fig. 2, showed two sharp transitions at 305–325 and 384 K. Experimental second moment values at various temperatures are given in Table 1. The dsc results are given in Table 2. Apart from melting, no thermal transitions occurred for the chloride and bromide whereas the iodide exhibited three separate transitions.

TABLE 1. Experimental second moment values of piperidinium salts at various temperatures

Compound	Second moment (G^2)	Temperature (K)
Chloride	19.4±0.8	77
	16.2	350
	8.2	460
Bromide	19.0±0.7	77
	17.8	240
	8.1	380
Iodide	22.9±0.7	77
	17.7	305
	8.5	325
	4.2	384
	0.5	386
Hexafluorophosphate	20.4±0.6	77
	20.0	190
	5.9	360

TABLE 2. Differential scanning colorimetric transition temperatures and enthalpies in piperidinium halides

Compound	Temperature (K)	Enthalpy (kcal/mol)
Chloride	521 (decomp.)	—
Bromide	466 (mp)	1.73
Iodide	315	1.27
	361	1.46
	372	0.09
	465 (mp)	1.74

Can. J. Chem. Downloaded from www.nrcresearchpress.com by 210.87.254.5 on 09/05/12
For personal use only.

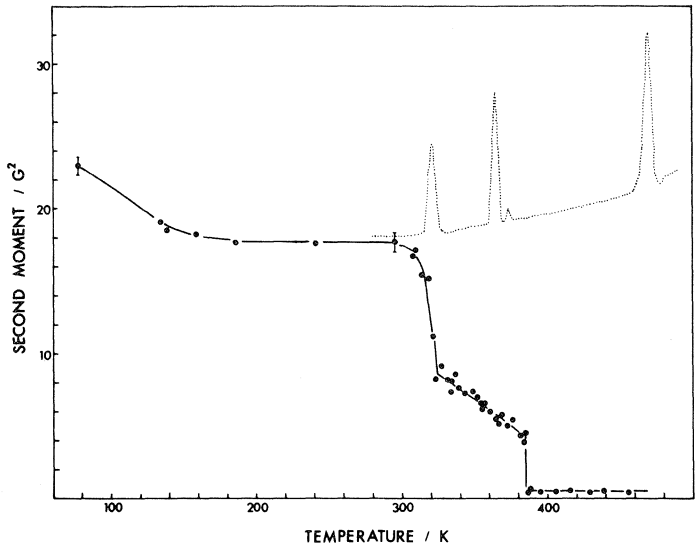

FIG. 2. Temperature dependence of the second moment and dsc trace for piperidinium iodide. (Error bars indicate standard deviation.)

Discussion

Several different molecular reorientational motions of the piperidinium ion can be considered: (*i*) rotation about the axis through the nitrogen atom and the opposite carbon atom C_3, an S_2 rotation, (*ii*) rotation about the axis perpendicular to the ring which, if the NH_2 group is considered to be equivalent to the CH_2 groups, would be a C_3 rotation for the rigid chair form, (*iii*) rotation about the axis through the midpoints of the C_1—C_2 and C_4—C_5 carbon–carbon bonds, a C_2 rotation, (*iv*) the ring-puckering motion (which is the chair–chair interconversion in a six membered ring), and (*v*) isotropic rotation about the centre of gravity of the ion. Motions (*ii*) and (*v*) occur in cyclohexane (6) and the other possibilities reflect the difference in symmetry of the piperidinium ion *vs.* cyclohexane.

The results of the theoretical second moment calculations are given in Table 3. These calculations were based upon the X-ray crystal structure reported by Rérat (2) for piperidinium chloride with the assumed bond lengths C—H = 1.096 Å and N—H = 1.050 Å. In comparing these values with the experimental results it should be noted that the chloride and bromide are known to be isostructural and thus should have similar second moment values but the structures of the iodide and hexafluorophosphate salts are unknown. Thus there is some uncertainty in the intermolecular second moment contribution for these compounds. The theoretical second moments for the ring puckering case were calculated using the factor $(1 - \frac{3}{4}\sin^2 2\gamma_{ij})$ given by Andrew and Brookeman (8), where γ_{ij} is the angle between the directions of the vector r_{ij} in the two possible conformations.

TABLE 3. Calculated second moment values for piperidinium chloride

Species	Second moment (G^2)		
	Intramolecular	Intermolecular	Total
Rigid	19.0	4.6	23.6
(*i*) S_2 rotation	2.9	4.4	7.3
(*ii*) C_3 rotation	4.3	1.3	5.5
(*iii*) C_2 rotation	3.1	1.9	5.0
(*iv*) Ring puckering	14.1	4.6	18.7
(*v*) Isotropic	0	1.5	1.5

Can. J. Chem. Downloaded from www.nrcresearchpress.com by 210.87.254.5 on 09/05/12
For personal use only.

Can. J. Chem. Downloaded from www.nrcresearchpress.com by 210.87.254.5 on 09/05/12
For personal use only.

At the lowest temperature studied, 77 K, only the piperidinium iodide second moment approaches the rigid lattice value and for the other three salts the agreement between experimental and calculated second moments favours the ring puckering motion. The same holds for the iodide salt over the temperature range 175–300 K. However, in the X-ray crystal structure study of piperidinium hexathiotetraarsenate (9) it was specifically noted that there was no evidence of conformational disorder, which might be expected if the chair–chair interconversion process occurred in the solid state. Furthermore, the temperatures at which this process normally occurs in solution are much higher than 77 K although the potential barrier in the solid might be different. It appears more probable that the reduced second moment values at low temperatures result from the anisotropic oscillations of the rigid molecule. This is supported by the X-ray evidence for all these compounds of large thermal parameters for the carbon atoms furthest from the nitrogen atom which also have rather long interatomic contact distances.

At temperatures close to the melting points, the experimental and theoretical second moments for the chloride and bromide are in best agreement for the S_2 rotation. Since the nitrogen and C_3 atoms lie on mirror planes in the unit cell this motion does not introduce disorder. For the hexafluorophosphate a more extensive motion may occur, most probably the C_3 rotation, since hydrogen bonding in this salt is weaker than in the chloride or bromide. The temperature ranges over which the transitions occur follow the expected trend of hydrogen bond strengths.

The conclusion that a phase transition occurs in piperidinium iodide is supported by both the wide-line nmr and the dsc results (Fig. 2). In fact, three solid phase transitions occur, one of them with a very small transition enthalpy. The second moment values suggest that the first transition involves an S_2 reorientation of the piperidinium ion, and, from the sharpness of the transition, a change in crystal structure must also occur. Additional motions of the piperidinium ion follow and at 384 K a second crystal transition occurs to a structure in which the ion is capable of isotropic rotation. The low value of the second moment above 384 K indicates that the intramolecular contribution must be zero. The total second moment, however, is non-zero and therefore lattice diffusion does not occur. The transition temperatures observed by the nmr and dsc methods agree quite well but Cabana and Sandorfy (1) reported that the infrared spectra changed suddenly between -10 and -20 °C, *i.e.* about 40° below the lowest temperature transition observed in the present study.

The high degree of rotational motion in piperidinium iodide should be reflected in the entropy of fusion. From the dsc measurements, however, the entropies of fusion for the iodide and bromide were 3.6 and 3.7 cal deg^{-1} mol^{-1}, respectively, values which are close to the 3 cal deg^{-1} mol^{-1} expected for positional disordering alone and higher than the entropies observed for plastic crystals in which lattice diffusion occurs. The low value for piperidinium bromide is surprising since the rotational motions in this compound are less extensive than in the iodide.

Acknowledgment

This work was supported by grants from the National Research Council of Canada.

1. A. Cabana and C. Sandorfy. Can. J. Chem. **40**, 615 (1962).
2. C. Rèrat. Acta. Crystallogr. **13**, 72 (1960).
3. C. Escobar, H. Cid-Dresner, D. Boys, and M. Prèndez. Bull. Soc. Fr. Mineral. Cristallogr. **96**, 215 (1973).
4. E. J. Smail and G. M. Sheldrick. Acta Crystallogr. B**29**, 2027 (1973).
5. J. K. Dattagupta. Acta Crystallogr. B**30**, 552 (1974).
6. E. R. Andrew and R. G. Eades. Proc. R. Soc. A**216**, 398 (1953).
7. C. H. Matthews and D. F. R. Gilson. Can. J. Chem. **48**, 2625 (1970).
8. E. R. Andrew and J. R. Brookeman. J. Magn. Reson. **2**, 259 (1970).
9. E. J. Porter and G. M. Sheldrick. J. Chem. Soc. A, 3130 (1971).

Enthalpies of solution and single ion enthalpies of transfer from water to dioxane–water mixtures

OM N. BHATNAGAR
Department of Chemistry, University of Manitoba, Winnipeg, Man., Canada R3T 2N2

Received April 29, 1976

OM N. BHATNAGAR. Can. J. Chem. **54**, 3487 (1976).

Standard enthalpies of solutions of sodium bromide, potassium bromide, tetrabutyl phosphonium bromide, tetraphenyl phosphonium bromide, and sodium tetraphenyl boron have been measured in 20%, 44.5%, and 64.5% dioxane–water mixture. On the extra thermodynamic assumption $\Delta\Delta H_s(Ph_4P^+) = \Delta\Delta H_s(^-BPh_4)$ single ion enthalpies of transfer from water to dioxane–water mixtures have been calculated for various ions.

OM N. BHATNAGAR. Can. J. Chem. **54**, 3487 (1976).

On a mesuré les enthalpies standards de solution du bromure de sodium, du bromure de potassium, du bromure de tétrabutylphosphonium, du bromure de tétraphénylphosphonium et du tétraphénylbore sodium dans des mélanges dioxanne–eau à 20%, 44.5% et 64.5%. En faisant l'hypothèse thermodynamique supplémentaire que $\Delta\Delta H_s(Ph_4P^+) = \Delta\Delta H_s(^-BPh_4)$, on a calculé, pour divers ions, les enthalpies de transfert d'ions uniques de l'eau à des mélanges dioxanne–eau.

[Traduit par le journal]

Can. J. Chem. Downloaded from www.nrcresearchpress.com by 210.87.254.5 on 09/05/12
For personal use only.

Introduction

I have been interested in the study of thermodynamic properties of electrolyte solutions in dioxane–water mixtures for some time (1–3). The solvation enthalpies of some tetraalkyl ammonium bromides in dioxane–water mixtures were reported in a recent paper (3). It was shown that the behaviour of these electrolytes was quite similar to their behaviour in water and that the structure-making capacity of tetraalkyl ammonium ions increases with the increase in the size of the ion. Thus from the study in dioxane–water mixtures Bu_4N^+ ion was found to be the most active in structure promotion. It was thought to be of interest to see how this behaviour would change (*i*) by changing the central atom from nitrogen to phosphorus, (*ii*) by changing the nature of tetraalkyl ion from aliphatic ($[C_4H_9]_4^-$) to aromatic ($[C_6H_5]_4^-$), (*iii*) by changing the small Br^- ion to a bulky $^-BPh_4$ ion.

In this paper the standard enthalpies of solution, ΔH_s^0, of sodium bromide, potassium bromide, tetrabutyl phosphonium bromide (Bu_4PBr), tetraphenyl phosphonium bromide ($[C_6H_5]_4PBr$) and sodium tetraphenyl boron ($NaBPh_4$) in 20%, 44.5%, and 64.5% dioxane–water mixtures are reported. In addition, an attempt has been made to divide the standard enthalpies of transfer $\Delta\Delta H_s$ from water to dioxane–water mixtures into the single ion enthalpies of transfer using certain extra thermodynamic assumptions.

Experimental

Purification of Dioxane

The dioxane was purified according to the procedure given in the literature (4). The dioxane–water mixtures were made by weighing.

Purification of Salts

NaBr and KBr were Fisher certified grade and were used without further purification. These salts were dried at 120 °C for 24 h before using.

Bu_4PBr was twice recrystallized from acetone–ether mixture and dried at 65 °C under vacuum.

Ph_4PBr was dissolved in a 9:1 (v/v) acetone – 2-propanol mixture and reprecipitated by the addition of an equal volume of benzene and dried under vacuum at 100 °C.

$NaBPh_4$ was recrystallized by the procedure given in the literature (5).

The samples were made in a dry box.

Apparatus and Procedure

The measurements were made at 25 ± 0.002 °C in a submarine type solution calorimeter, the details of calorimeter design, temperature measuring system, and operating procedure are given elsewhere (6).

Results and Discussion

The enthalpies of solution (ΔH_s) for various electrolytes were measured as a function of concentration in the concentration range of 1×10^{-4}

Can. J. Chem. Downloaded from www.nrcresearchpress.com by 210.87.254.5 on 09/05/12
For personal use only.

to 1×10^{-2} *M*. All data are extrapolated to infinite dilutions using the extended Debye–Hückel equation (3). The advantage of using this equation is discussed in detail by Criss and Cobble (7). The standard enthalpies of solution (ΔH_s^0) of the electrolytes from this study as well as from previous studies are summarized in Table 1. The ΔH_s^0 for NaBr and KBr become less endothermic in passing from water to 64.5% dioxane – water mixtures. Similar behaviour was observed for other alkali metal halides such as LiCl, NaCl, and NaI in dioxane–water mixtures (3, 8). The ΔH_s^0 for Bu_4PBr become more endothermic in passing from water to 64.5% dioxane – water mixtures; a similar trend was observed for tetraalkylammonium bromides like Et_4NBr, Pr_4NBr, Bu_4NBr (3), and Am_4NBr (9). The ΔH_s^0 values for Ph_4PBr and $NaBPh_4$ pass through an extrema around 20% dioxane – water mixture. The ΔH_s^0 of $NaBPh_4$ reported by Mohanty *et al.* (10) in 20% dioxane – water mixture is lower than that reported in this paper, but the ΔH_s^0 of $NaBPh_4$ reported by Arnett (11) in dioxane–water mixtures are closer to the values obtained in this study (Table 1), and show an extrema around 20% dioxane – water mixture. ΔH_s^0 for Me_4NBr in dioxane–water mixtures also show an extrema but the position of the extrema is shifted towards higher dioxane content. ΔH_s^0 composition profiles for $NaBPh_4$ in various aqueous binary mixtures (11) show the existence of the extrema but the position of the extrema varies from solvent to solvent. Fuchs and Hagan (12) recently reported the extrema in the ΔH_s^0 composition profile of DMSO–water mixtures for Bu_4NCl, Bu_4NBr, Bu_4NI, Ph_4PBr, and $NaBPh_4$; these extrema were attributed to the desolvation of ions. In dioxane–water mixtures no extrema was observed for Bu_4NBr and Bu_4PBr up to 64.5% dioxane – water mixtures ($X_{\text{Dioxane}} = 0.27$). Mohanty *et al.* (10) did not observe any extrema in ΔH_s^0 of Bu_4NBr in dioxane–water mixture up to 0.3 mole fraction of dioxane. DeVisser and Somsen (13) reported the extrema for Bu_4NBr in the ΔH_s^0 composition profile of *N*,*N*-dimethylformamide (DMF) – water mixture at approximately 0.3 mol fractions of DMF but did not find any extrema in ΔH_s^0 for formamide (F) – water and *N*-methylformamide (NMF) – water mixtures, but there was a sharp decrease in enthalpy of solution when the mole fraction of F or NMF was ≈ 0.3.

Maxima or minima in ΔH_s^0 composition profiles are generally attributed to the changes in solvent properties and solvation or desolvation of the ions. It is well known that the addition of a small quantity of non-electrolyte to pure water frequently leads to profound changes in solvent properties (14). Often the maxima observed in water-rich region of the aqueous binary mixtures are interpreted as due to an increase in water structure on the addition of non-electrolytes. A number of studies in alcohol–water mixtures (14, 15), DMSO–water (12), acetone–water (16) supports this view and suggests that at higher concentrations of non-electrolyte a progressive 'destructurization' of the solvent takes place. The nature of the dioxane–water interactions in the water-rich region is still controversial. While there is ample evidence from nmr (17), self diffusion (18), proton spin lattice relaxation (19), heat capacity (20), and other studies (21) that in water-rich region dioxane actually enhances the water structure, there are other workers who disagree with these conclusions (10, 22, 23). In face of these controversies in dioxane–water mixtures it is difficult to draw any straightforward conclusions for the extrema found in ΔH_s^0 composition profile in the case of Me_4NBr, Ph_4PBr, and $NaBPh_4$.

It is well known that in aqueous solutions alkali metal and halide ions in general disrupt the water structure (24–29) and R_4N^+ ions in general promote it (30–35). In water the enthalpy of solution of simple electrolytes (36) and Me_4NBr (37) (which are known to disrupt water structure) decreases with increasing temperature, while the enthalpy of solution of Bu_4NBr (37), Am_4NBr (38), salts with large complex ions (45), and neutral organic molecules (39, 40) (which are known to promote the water structure) becomes more positive with increasing temperature. By increasing the water temperature hydrogen bonding and dielectric constant decrease, the introduction of dioxane in water in large quantity at constant temperature has an effect similar to that of raising the temperature of water. Since the variation of ΔH_s^0 of simple electrolytes and tetraalkylammonium salts (with the exception of Ph_4PBr and $NaBPh_4$) in dioxane–water mixtures is similar to the variation of ΔH_s^0 of these electrolytes in water with increasing temperatures one can conclude by implication that salts like Et_4N^+, Pr_4N^+, Bu_4N^+, Bu_4P^+, and Am_4N^+ pro-

Can. J. Chem. Downloaded from www.nrcresearchpress.com by 210.87.254.5 on 09/05/12
For personal use only.

mote the water structure in dioxane–water mixtures, while alkali halides disrupt the water structure in dioxane–water mixtures. From nmr studies of a number of inorganic salts in 50% dioxane – water mixtures, Fratiello and Douglass (50) conclude that "there is selective solvation by water molecules of cations in these binary mixtures, with no indication of interaction between dioxane and either ionic species. Although the shift data indicate water solvation only of small, highly charged cations, one must consider that the observed shift is actually the resultant of both structure breaking and solvation processes. Thus even in systems in which a structure breaking process predominates, such as alkali halide solutions, solvations of cations by water must be occurring."

Ph_4P^+ and BPh_4^- ions are believed to disrupt the water structure (41–44, 51), although these conclusions are questioned by some workers (45). Since at present there is no clear-cut way to classify solutes as structure makers or breakers, different approaches often lead to different conclusions. It is not surprising that there is disagreement among various workers whether $NaBPh_4$ and other solutes containing aromatic hydrocarbons are structure makers or breakers. It has been suggested that the interaction of the π orbitals from the phenyl group with water molecules leads to the structure breaking action by aromatic hydrocarbons. In order to explain the extrema in ΔH_s^0 composition profile of Ph_4PBr and $NaBPh_4$, if it is assumed that Ph_4P^+ and BPh_4^- disrupt the water structure, then a decrease in exothermicity of these compounds in passing from water to 20% dioxane – water mixture would indicate that the structure breaking effect of phenyl group is less than the structure promotion effect of dioxane (in small quantity) and as a result a net structure promotion is observed. On increasing the dioxane content from 20% to 64.5% the progressive 'destructurization' of the solvent mixture takes place. This, in combination with the structure breaking effect of the phenyl group, give rise to an overall structure breaking effect in the form of an increase in exothermicity in ΔH_s^0 values.

Ionic Enthalpies of Transfer from Water to Dioxane–Water Mixtures

Recently Parker and co-workers (46, 47) have discussed the essential equivalence of four types of extrathermodynamic assumptions used in the determination of free energies and enthalpies of transfer of ions from solvent to solvent. I have chosen the assumption that $\Delta\Delta H_s(Ph_4P^+) = \Delta\Delta H_s(BPh_4^-)$.

The main reason for choosing this system is that the enthalpy of solution, ΔH_s^0, of Ph_4PBr is concentration independent in water and dioxane–water mixtures. A good discussion of the reason for choosing Ph_4PBr, $NaBPh_4$, and NaBr for evaluating single ion enthalpies is given by Fuchs and Hagan (12). The single ion enthalpies of transfer were determined from the following scheme:

$$\Delta\Delta H_s(Ph_4P^+) = \Delta\Delta H_s(BPh_4^-)$$
$$= \tfrac{1}{2}[\Delta\Delta H_s(Ph_4PBr) + \Delta\Delta H_s(NaBPh_4) - \Delta\Delta H_s(NaBr)]$$
$$\Delta\Delta H_s(Br^-) = \Delta\Delta H_s(Ph_4PBr) - \Delta\Delta H_s(Ph_4P^+)$$
$$\Delta\Delta H_s(Na^+) = \Delta\Delta H_s(NaBPh_4) - \Delta\Delta H_s(BPh_4^-)$$

Using the above relationships the single ion enthalpies of transfer from water to dioxane–water mixtures were evaluated. Table 1 gives a summary of ΔH_s^0 of various electrolytes in H_2O, 20%, 44.5%, and 64.5% dioxane – water mixtures as well as the enthalpies of transfer ($\Delta\Delta H_s$) from water to dioxane–water mixtures. Table 2 gives the single ion enthalpies of transfer from water to dioxane–water mixtures. Single ion enthalpies of transfer for most ions become more exothermic in passing from 20% to 64.5% dioxane – water mixtures with few exceptions like halide ions which show a completely opposite behaviour from the alkali ions. Grunwald and co-workers (48) calculated the single ion free energies of transfer of some alkali and halide ions from water to 50% dioxane – water mixtures. The deviations in $\Delta\Delta H_s$ for the halide ions from the alkali ions is also reported by Grunwald *et al.* from their studies. For certain other ions such as Bu_4N^+, Am_4N^+, and Bu_4P^+ ionic enthalpies of transfer pass through a maximum at 44.5% dioxane content. From Table 2 it is clear that with the increase in ionic radii of cation, the ionic enthalpies of transfer become more endothermic in 20%, 44.5%, and 64.5% dioxane – water mixtures, with the exception of Ph_4P^+ ion. The anions show an opposite behaviour to that of the cations with the exception of BPh_4^- which also does not fit into a pattern.

TABLE 1.[a] Standard enthalpies of solution (ΔH_s^0 cal/mol) in water and dioxane–water mixtures and enthalpies of transfer ($\Delta\Delta H_s$) from water to dioxane–water mixtures for various electrolytes at 25 °C

		ΔH_s^0			$\Delta\Delta H_s$		
Salts	H_2O	20% D	44.5% D	64.5% D	W→20% D	W→44.5% D	W→64.5% D
LiCl	−8 850[b]	−9 140	−10 160	−11 150	−290	−1 310	−2 300
NaCl	928[b]	600	170	−280	−328	−758	−1 208
NaBr[c]	−144[b]	−895	−1 255	−2 506	−751	−1 111	−2 362
NaI	−1 800[b]	−3 220[d]	−4 950[d]	−6 350[d]	−1 420	−3 150	−4 550
KBr[c]	4 750[b]	4 025	2 300	1 030	−725	−2 450	−3 720
Me_4NBr	5 745[e]	5 860	6 070	5 100	115	325	−645
Et_4NBr	1 430[e]	1 870	2 065	2 395	440	635	965
Pr_4NBr	−1 055[e]	902	2 610	3 295	1 957	3 665	4 350
Bu_4NBr	−2 050[e]	1 075	4 680	5 540	3 125	6 730	7 590
Am_4NBr	796[e]	6 800[e]	9 400[e]	10 250[e]	6 004	8 604	9 454
Bu_4PBr[c]	−3 160[f]	933	4 370	4 800	4 093	7 530	7 960
Ph_4PBr[c]	1 900[f]	5 055	4 185	3 110	3 155	2 285	1 210
$NaBPh_4$[c]	−4 805[g]	−2 200	−7 400	−13 460	2 605	−2 595	−8 655
		−2 300[h]	−7 250[h]	−13 000[h]			
		−1 949[e]					

[a]Photocopies of the numerical results may be obtained, at a nominal charge, from the Depository of Unpublished Data, CISTI, National Research Council of Canada, Ottawa, Canada K1A 0S2. All data from ref. 3 except where indicated otherwise.
[b]Data taken from ref. 49.
[c]Data from the present work. (Claimed accuracy of the data on the average ±8 cal/mol^{-1}.)
[d]Data taken from ref. 8.
[e]Data taken from refs. 9, 10.
[f]Data taken from ref. 12.
[g]Data taken from ref. 45.
[h]Data taken from ref. 11.

TABLE 2. Single ion enthalpies of transfer (in cal/mol) from water to dioxane–water mixture

Ions	20% Dioxane	44.5% Dioxane	64.5% Dioxane
Li^+	−612	−3547	−7205
Na^+	−650	−2995	−6113
K^+	−624	−4334	−7471
Me_4N^+	215	−1559	−4396
Et_4N^+	540	−1249	−2786
Pr_4N^+	2057	1780	598
Bu_4N^+	3225	4845	3838
Am_4N^+	6104	6719	5702
Bu_4P^+	4193	5645	4208
Ph_4P^+	3255	400	−2541
BPh_4^-	3255	400	−2541
Cl^-	322	2237	4905
Br^-	−100	1884	3751
I^-	−770	−154	1563

Acknowledgements

I would like to thank Dr. A. N. Campbell for interest in this work and the National Research Council of Canada for financial support through a grant to Dr. A. N. Campbell.

1. A. N. CAMPBELL and O. N. BHATNAGAR. Can. J. Chem. **49**, 217 (1971).
2. A. N. CAMPBELL and O. N. BHATNAGAR. Can. J. Chem. **50**, 1627 (1972).
3. O. N. BHATNAGAR and A. N. CAMPBELL. Can. J. Chem. **52**, 203 (1974).
4. A. N. CAMPBELL and B. G. OLIVER. Can. J. Chem. **47**, 2671 (1969).
5. J. F. SKINNER and R. M. FUOSS. J. Phys. Chem. **68**, 1882 (1964).
6. O. N. BHATNAGAR and A. N. CAMPBELL. Chem. Instrum. **4**, 179 (1973).
7. C. M. CRISS and J. W. COBBLE. J. Am. Chem. Soc. **83**, 3223 (1961).
8. D. K. P. MISHCHENKO and S. V. SHADSKII. Teor i Eksperim Khim Akad. Nauk. Ukr. SSR, **1**, 60 (1965).
9. R. K. MOHANTY and J. C. AHLUWALIA. J. Chem. Thermodyn. **4**, 53 (1972).
10. R. K. MOHANTY, T. S. SARMA, S. SUBRAMANIAN, and J. C. AHLUWALIA. Trans. Faraday Soc. **65**, 2333 (1969).
11. E. M. ARNETT. Physico-chemical processes in mixed aqueous solvents. *Edited by* F. Franks. Elsevier Publishing Comp. Inc., N.Y. 1967. p. 105.
12. R. FUCHS and C. PATRICK HAGAN. J. Phys. Chem. **77**, 1797 (1973).
13. C. DE VISSER and G. SOMSEN. J. Solution Chem. **3**, 847 (1974).
14. F. FRANKS and D. J. G. IVES. Q. Rev. **20**, 1 (1966).
15. L. AVEDIKIAN, G. PERRON, and J. E. DESNOYERS. J. Solution Chem. **4**, 331 (1975).
16. D. N. GLEW, H. D. MAK, and N. S. RATH. Chem. Commun. 264 (1968).

Can. J. Chem. Downloaded from www.nrcresearchpress.com by 210.87.254.5 on 09/05/12
For personal use only.

17. C. J. CLEMETT. J. Chem. Soc. (A), 455 (1969).
18. C. J. CLEMETT. J. Chem. Soc. (A), 458 (1969).
19. C. J. CLEMETT. J. Chem. Soc. (A), 761 (1969).
20. O. KIYOHARA, G. PERRON, and J. E. DESNOYERS. Can. J. Chem. **53**, 2591 (1975).
21. H. P. BENNETTO and D. FEAKINS. Hydrogen-bonded solvent systems. *Edited by* A. K. Covington and P. Jones. Taylor and Francis Ltd., London. 1968. p. 239.
22. A. FRATIELLO and D. C. DOUGLASS. J. Mol. Spectrosc. **11**, 465 (1963).
23. A. BEN-NAIM and G. MORAN. Trans. Faraday Soc. **61**, 821 (1965).
24. M. KAMINSKY. Discuss. Faraday Soc. **24**, 171 (1957).
25. H. S. FRANK and M. G. EVANS. J. Chem. Phys. **13**, 507 (1945).
26. A. J. ELLIS. J. Chem. Soc. (A), 660 (1966); 1579 (1966).
27. L. A. DUNN. Trans. Faraday Soc. **64**, 2591 (1968).
28. L. G. HEPLER. Can. J. Chem. **47**, 4613 (1969).
29. F. J. MILLERO. Water and aqueous solutions. *Edited by* R. A. Horne, Wiley-Interscience, New York. 1972. p. 519.
30. H. S. FRANK and W. Y. WEN. Discuss. Faraday Soc. **24**, 133 (1957).
31. G. H. HAGGIS, J. B. HASTEEL, and T. J. BUCHANAN. J. Chem. Phys. **20**, 1452 (1952).
32. W. G. HERTZ and M. O. ZEIDLER. Ber. Bunsenges. Physik. Chem. **68**, 821 (1964).
33. S. LINDENBAUM. J. Phys. Chem. **70**, 814 (1966).
34. Y. C. WU and H. L. FRIEDMAN. J. Phys. Chem. **70**, 2030 (1966).
35. C. DE VISSER and G. SOMSEN. J. Chem. Soc. Faraday Trans. I, **69**, 1440 (1973).
36. J. C. AHLUWALIA and J. W. COBBLE. J. Am. Chem. Soc. **86**, 5377 (1964).
37. M. J. MASTROIANNI and C. M. CRISS. J. Chem. Thermodyn. **4**, 321 (1972).
38. R. K. MOHANTY, S. SUNDER, and J. C. AHLUWALIA. J. Phys. Chem. **76**, 2577 (1972).
39. E. M. ARNETT, W. B. KOVER, and J. V. CARTER. J. Am. Chem. Soc. **91**, 4028 (1969).
40. D. M. ALEXANDER and D. J. T. HILL. Aust. J. Chem. **22**, 347 (1969).
41. M. TAMRES. J. Am. Chem. Soc. **74**, 3375 (1952).
42. I. M. GOLDMEN and R. O. CRISLER. J. Org. Chem. **23**, 751 (1958).
43. G. KALFOGLEN and L. H. BOWEN. J. Phys. Chem. **73**, 2729 (1969).
44. P. R. PHILIP and C. JOLICOEUR. J. Phys. Chem. **77**, 3071 (1973).
45. S. SUBRAMANIAN and J. C. AHLUWALIA. J. Phys. Chem. **72**, 2525 (1968).
46. R. ALEXANDER, A. J. PARKER, J. H. SHARPE, and W. E. WAG-HORNE. J. Am. Chem. Soc. **94**, 1148 (1972).
47. B. G. COX and A. J. PARKER. J. Am. Chem. Soc. **95**, 402 (1973).
48. E. GRUNWALD, G. BOUGHMAN, and G. KOHNSTAM. J. Am. Chem. Soc. **82**, 5801 (1960).
49. V. B. PARKER. Thermal properties of aqueous uni-univalent electrolytes, NSRDS-NBS 2, National Bureau of Standards, Washington, D.C. 1965.
50. A. FRATIELLO and D. C. DOUGLASS. J. Chem. Phys. **39**, 2017 (1963).
51. F. J. MILLERO. J. Chem. Eng. Data, **15**, 562 (1970).

Can. J. Chem. Downloaded from www.nrcresearchpress.com by 210.87.254.5 on 09/05/12
For personal use only.

Nuclear magnetic resonance study of electrolytes in 1,3-dimethylethyleneurea

JOSEPH ROSENFARB AND JOSEPH A. CARUSO
Department of Chemistry, University of Cincinnati, Cincinnati, Ohio 45221

Received May 11, 1976

JOSEPH ROSENFARB and JOSEPH A. CARUSO. Can. J. Chem. **54**, 3492 (1976).

A series of lithium, sodium, potassium, and ammonium salts were investigated by proton magnetic resonance spectroscopy in 1,3-dimethylethyleneurea, a relatively new non-aqueous solvent of high polarity and moderately high dielectric constant. The salts were found to shift the solvent proton peaks linearly as a function of salt concentration. Thiosulfate, perchlorate, and iodide salts shifted the solvent peaks downfield while tetraphenylborate salts uniquely shifted the peaks upfield indicating an unusual type of solvation behavior for the tetraphenylborates in this solvent.

JOSEPH ROSENFARB et JOSEPH A. CARUSO. Can. J. Chem. **54**, 3492 (1976).

On a étudié par rmn du proton dans la diméthyl-1,3 éthylène urée un solvant non aqueux relativement nouveau de haute polarité et de constante diélectrique modérée, une série de sels de lithium, de sodium, de potassium et d'ammonium. On a trouvé que les sels déplacent les signaux des protons du solvant d'une façon linéaire en fonction de la concentration du sel. Les sels du thiosulfate, du perchlorate et de l'iodure déplacent les pics du solvant vers les bas champs alors que les sels du tétraphénylborate sont les seuls à déplacer les pics vers les hauts champs; ces résultats indiquent un type particulier de comportement desolvatation des tétraphénylborates dans ce solvant.

[Traduit par le journal]

Proton magnetic resonance which has been used to investigate the solvation behavior of ions in aqueous solutions (1–4) has been extended to non-aqueous media as well (5). Recently 1,3-dimethylethyleneurea (DMEU) has been investigated with regard to some of its fundamental properties (6) and to the behavior of electrolytes therein (7, 8). It was found that DMEU is a solvent of high polarity (4.09 in dioxane) (9), moderately high dielectric constant (37.6 at 1 MHz) (6), and possesses good dissociative power towards electrolytes, comparable to that of *N*-methyl-2-pyrrolidone and methanol. Particularly interesting was the property that sodium and potassium salts were isoconducting in DMEU (7). Therefore further study into the nature of solvation in DMEU was indicated.

Experimental

Salts and Solvent

Lithium and ammonium perchlorate (G. Frederick Smith) were used without further purification. Sodium perchlorate (Fisher), ammonium thiocyanate (Baker Analyzed Reagent), sodium and potassium thiocyanate (Merck), sodium and ammonium iodide (Baker Analyzed Reagent), were recrystallized from acetone with ether. Potassium and ammonium tetraphenylborate were synthesized from aqueous solutions equimolar in sodium tetraphenylborate and the appropriate iodide. The precipitates were thoroughly washed with deionized water, dried, and recrystallized from acetone with water portions. All salts were finely ground and dried in the appropriate manner (5, 7, 10).

DMEU was freshly prepared as previously described (6) and had a specific conductance of about 5×10^{-8} ohm^{-1} cm^{-1}.

Measurements

Chemical shift data were obtained using a Varian A-60 nmr spectrometer. Tetramethylsilane (5%) was used as an internal reference from which peak shifts were calculated. Since an internal reference was used, no bulk diamagnetic corrections were applied (11). Shift data were reproducible to ± 0.3 Hz or 0.005 ppm.

Results and Discussion

A number of alkali halides, tetraalkylammonium salts, and multivalent salts have been investigated in aqueous solution (1, 12). It was observed that a downfield (negative) shift of the water peak could be associated with a polarization of the oxygen atom which withdrew electron density (deshielded) from the hydrogens. The opposite occurred when electron density was increased around the hydrogens causing an upfield (positive) shift. Small ions (therefore greater charge density) for example had a more polarizing effect on the oxygen as did multivalent cations; or in a decreasing order of positive

Can. J. Chem. Downloaded from www.nrcresearchpress.com by 210.87.254.40 on 09/05/12
For personal use only.

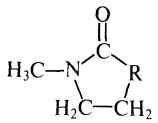

R	*Name*
O	3Me2Ox
N—CH_3	DMEU

FIG. 1. Structures of 3-methyl-2-oxazolidone and 1,3-dimethylethyleneurea.

shifts: LiI > NaI > KI. Similarly, the effect of anions of smaller size can be seen by the following order of positive shifts of the water peak: NaCl > NaI. The shift in water was said to be due to (*a*) the breaking of hydrogen bonds for ion solvation which would increase electron density around the protons and, (*b*) polarization of the oxygen atom, which deshields the protons but also allows these now 'more positive' protons to more strongly interact with the anion. What is observed then, is an overall effect on the chemical shift (1, 12), as the shift draws contributions from ion–solvent interaction as well as changes in solvent structure (13, 14).

Non-aqueous media, such as the *N*-substituted-2-oxazolidones previously studied (5) and DMEU, often do not have hydrogen bonding to any significant extent, but ions do have to break dipole–dipole interactions in order to be solvated. DMEU and 3-methyl-2-oxazolidone (3Me2Ox) have available two and three sites, respectively, for ionic interactions. DMEU can interact through the carbonyl and nitrogens while 3Me2Ox possibly could interact through the etherial oxygen as well (Fig. 1).

The chemical shift data for the salts studied in DMEU are summarized in Table 1. A comparison of shifts (5) for a given salt in DMEU and 3Me2Ox indicates that the shifts, whether negative or positive, are generally greater in 3Me2Ox. The trend for both solvents is that the *N*-methyl protons are shifted to a lesser extent than are the 4 and 5 position methylene protons.

For a given anion, the shifts in DMEU appear to remain relatively the same, that is, to within about 0.01 ppm. For example; sodium, potassium, and ammonium tetraphenylborates have approximately the same shifts. This same trend also is noted for 3Me2Ox (5). Perchlorate and thiocyanate salts for a given cation also are generally the same, a result not seen for 3Me2Ox.

The sodium iodide shifts were found to be the most different with respect to the corresponding perchlorate and thiocyanate salts in both DMEU and in 3Me2Ox. It was observed that iodide solutions immediately yellowed in DMEU as they do in tetramethylurea and tetraethylurea (7, 10, 15). Iodides do not discolor 3Me2Ox solutions to any extent. The processes whereby this discoloration proceeds still need to be investigated, and may offer some explanation as to the difference in solutions noted for the iodide salts.

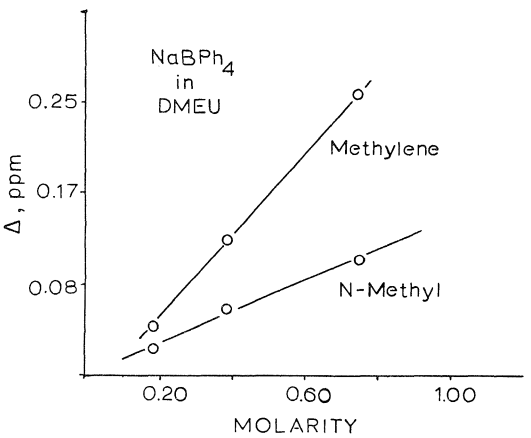

FIG. 2. Plot of the change in chemical shift (ppm, δ) *vs.* concentration of tetraphenylborate in DMEU.

As seen for the liquid oxazolidones (5), the tetraphenylborates cause an upfield (positive) shift of the DMEU peaks suggesting that the tetraphenylborate anion causes unusual solvation effects resulting in increased shielding of the solvent protons. A complete explanation of this behavior will require further study. These shifts are comparable to those seen for 3Me2Ox (5).

Previous authors have pointed out that peak shift should be a linear function of concentration until the solvent molecule is shared by more than one ion (5, 16). A linear plot of the change in peak shift *vs.* concentration of salt as seen in Fig. 2 is typical of salts studied in DMEU at the concentrations used in this study.

Conclusion

It appears likely that in DMEU the electrolytes investigated are either completely dissociated or form solvent separated ion pairs as suggested by conductance measurements (7, 8). Clearly, the tetraphenylborate anion shows a

Can. J. Chem. Downloaded from www.nrcresearchpress.com by 210.87.254.40 on 09/05/12
For personal use only.

Can. J. Chem. Downloaded from www.nrcresearchpress.com by 210.87.254.40 on 09/05/12
For personal use only.

TABLE 1. Proton magnetic resonance (^1H) shift data for salts in DMEU*

Concentration (M)	(N—CH_3)		—$(CH_2)_2$—	
	δ (ppm)	$\Delta\delta$ (ppm)	δ (ppm)	$\Delta\delta$ (ppm)
		$NaBPh_4$		
0.75	2.593	+0.105	2.997	+0.257
0.38	2.638	+0.060	3.130	+0.123
0.19	2.675	+0.023	3.207	+0.047
		$KBPh_4$		
0.75	2.590	+0.098	2.982	+0.258
0.38	2.648	+0.040	3.130	+0.110
0.19	2.678	+0.010	3.190	+0.050
		NH_4BPh_4		
0.75	2.593	+0.095	3.000	+0.240
0.38	2.650	+0.038	3.135	+0.105
0.19	2.680	+0.008	3.197	+0.043
		NaSCN		
0.75	2.715	−0.017	3.295	−0.042
0.38	2.705	−0.007	3.267	−0.013
0.19	2.693	−0.005	3.252	−0.002
		KSCN		
0.75	2.708	−0.017	3.277	−0.033
0.38	2.703	−0.012	3.263	−0.020
0.19	2.690	−0.002	3.253	−0.010
		NH_4SCN		
0.75	2.715	−0.023	3.298	−0.062
0.38	2.703	−0.012	3.268	−0.032
0.19	2.690	−0.002	3.250	−0.013
		$LiClO_4$		
0.75	2.720	−0.032	3.287	−0.047
0.38	2.708	−0.008	3.270	−0.030
0.19	2.697	−0.008	3.250	−0.010
		$NaClO_4$		
0.75	2.713	−0.022	3.280	−0.037
0.38	2.705	−0.013	3.263	−0.020
0.19	2.698	−0.007	3.255	−0.012
		NH_4ClO_4		
0.75	2.708	−0.020	3.287	−0.047
0.38	2.702	−0.013	3.268	−0.028
0.19	2.700	−0.012	3.257	−0.017
		NaI		
0.75	2.723	−0.032	3.318	−0.082
0.38	2.705	−0.013	3.285	−0.048
0.19	2.693	−0.002	3.260	−0.023
		NH_4I		
0.75	2.718	−0.027	3.302	−0.065
0.38	2.705	−0.013	3.277	−0.040
0.19	2.692	0.000	3.255	−0.018

*Shifts are given with respect to tetramethylsilane as the reference and ppm are reported using the δ scale. + indicates shift towards TMS. − indicates shift away from TMS.

distinctly different solvation behavior than do the other anions studied. The iodides, which go through a possible charge-transfer process (10), discolor the solution and may solvate in a more complex fashion. Linear plots for concentration of salt *vs.* change in peak shift for all salts

indicate that in DMEU, as with 3Me2Ox, the solvent molecule is not shared by more than one ion for the concentration range considered. Chemical shift results compare closely to those seen for 3Me2Ox. A smaller effect for the *N*-methyl shifts compared to larger shifts for the 4 and 5 methylene groups may be due in part to the methyl groups which may partially block direct interaction of the cation with the nitrogens. Finally, DMEU, a moderately high dielectric solvent (37.6) (6), has shown similar solvation behavior to 3Me2Ox, a comparatively high dielectric (77.5) (17) non-aqueous solvent.

1. J. N. Shoolery and B. J. Alder. J. Chem. Phys. **23**, 805 (1955).
2. V. A. Shcherbakov. Zh. Strukt. Khim. **2**, 484 (1961).
3. M. S. Berquist and E. Forslind. Acta Chem. Scand. **16**, 2069 (1962).
4. J. C. Hindman. J. Chem. Phys. **36**, 1000 (1962).
5. (*a*) T. L. Buxton and J. A. Caruso. J. Phys. Chem. **77**, 1882 (1973); (*b*) T. L. Buxton and J. A. Caruso. J. Am. Chem. Soc. **96**, 6033 (1974).
6. J. Rosenfarb, H. L. Huffman, Jr., and J. A. Caruso. J. Chem. Eng. Data, **21**, 150 (1976).
7. J. Rosenfarb and J. A. Caruso. J. Solution Chem. **5**, 345 (1976).
8. J. Rosenfarb and J. A. Caruso. J. Solution Chem. **5**, 355 (1976).
9. E. J. Lien and W. D. Kumler. J. Med. Chem. **11**, 214 (1968).
10. B. J. Barker and J. A. Caruso. J. Am. Chem. Soc. **93**, 1341 (1971).
11. H. G. Hertz and W. Spalthoff. Z. Electrochem. **63**, 1096 (1959).
12. J. F. Hinton and E. S. Amis. Chem. Rev. **67**, 367 (1967).
13. J. Davies, S. Ormondroyd, and M. C. R. Symons. Trans. Faraday Soc. 3465 (1971).
14. G. W. Stockton and J. S. Martin. J. Am. Chem. Soc. **94**, 6921 (1972).
15. B. J. Barker, J. Rosenfarb, and E. Z. Riesen. J. Solution Chem. **4**, 571 (1975).
16. B. P. Fabricand and S. Goldberg. J. Chem. Phys. **34**, 1624 (1961).
17. H. L. Huffman, Jr. and P. G. Sears. J. Solution Chem. **1**, 187 (1972).

Can. J. Chem. Downloaded from www.nrcresearchpress.com by 210.87.254.40 on 09/05/12
For personal use only.

Surface and kinetic effects in gas chromatographic studies of polystyrene

GREGORY J. COURVAL[1] AND DEREK G. GRAY

Pulp and Paper Research Institute of Canada and the Department of Chemistry, McGill University, P.O. Box 6070, Station A, Montreal, P.Q., Canada H3C 3G1

Received May 25, 1976

GREGORY J. COURVAL and DEREK G. GRAY. Can. J. Chem. **54**, 3496 (1976).

Considerable variation in the measurement of polymer–solvent interactions using gc retention data may occur due to kinetic factors, surface excess concentrations of probe vapour, and non-linear partition isotherms. The kinetic factors, which appear as a flow rate dependence of the retention volume, are analysed in terms of a previously reported theoretical model for retention on polymeric stationary phases passing through the glass transition. The predicted linear extrapolations to zero flow rate are obtained for the retention of *n*-tetradecane on polystyrene. The variation of this flow rate dependence with temperature and with the thickness of the stationary phase are also in qualitative agreement with the theory. A simplified model for the effect of loading on the retention diagram is presented. Non-linear absorption and bulk sorption isotherms result in a dependence of retention volume on sample size, necessitating an extrapolation of the measured retention volumes to zero peak height. The temperature variation of the flow rate dependence, the effect of loading, and the effect of sample size on retention volume are all further complicated by uneven distribution of polymer on support. From scanning electron micrographs of the beads it is evident that 'beading up' of the polystyrene on the glass surface may occur at low loadings, resulting in a non-uniform coating with large areas of the beads uncoated. It is concluded that in order to obtain reliable data on polymer–solvent interactions using gas chromatography, all of the above-mentioned factors must be considered.

GREGORY J. COURVAL et DEREK G. GRAY. Can. J. Chem. **54**, 3496 (1976).

Il peut se produire de grandes variations dans les mesures des interactions polymère–solvant en se basant sur des données de rétention en cpg; ces variations proviennent de facteurs cinétiques, de concentrations d'excès au niveau de la surfaces et d'isothermes de partition non-linéaires. On analyse les facteurs cinétiques, qui apparaissent par une dépendance des volumes de rétention sur les vitesses d'écoulement, en termes du modèle théorique rapporté antérieurement pour la rétention sur des phases stationnaires sous forme de polymère passant à travers une transition de verre. Comme prévu, on obtient des extrapolations linéaires sur une vitesse d'écoulement de zéro pour la rétention de *n*-tétradécane sur du polystyrène. La variation de la vitesse d'écoulement avec la température et avec l'épaisseur de la phase stationnaire est aussi en accord qualitatif avec la théorie. On présente un modèle simplifié de l'effet du chargement sur le diagramme de rétention. Les isothermes nonlinéaires d'absorption et de sorbtion de masse conduisent à une dépendance du volume de rétention sur la grosseur de l'échantillon et ceci nécessite une extrapolation des volumes de retention mesurés vers une valeur nulle pour la hauteur des pics. De plus la variation avec la température de la dépendance de la vitesse d'écoulement ainsi que l'effet du chargement et l'effet de la grosseur de l'échantillon sur le volume de rétention sont compliqués par une distribution non uniforme du polymère sur le support. A partir de micrographes obtenus par balayage électronique, on peut en conclure qu'il peut y avoir "perlage" du polystyrène à la surface du verre à des chargements faibles et ceci conduit à des recouvrements non uniformes laissant de vastes portions des billes sans recouvrement. On en conclut que pour obtenir des données fiables concernant les interactions polymère–solvant en faisant appel à la cpg, on doit considéré tous les facteurs mentionnés plus haut.

[Traduit par le journal]

Introduction

The use of gas chromatography as a means of studying polymeric materials is now well established (1). Briefly, the experiment consists of using the polymer under study as the stationary phase in the gas chromatographic column and measuring the time required to elute a low molecular weight vapour. The resulting retention volume is a measure of the polymer–vapour interaction and various thermodynamic parameters may be calculated from this quantity. Most of the work in this area has dealt with the interaction at effectively infinite dilution of various vapours with homopolymers well above their melting points or glass transition temperatures

[1]Present address: The Glidden Company of Canada, Toronto, Ontario.

Can. J. Chem. Downloaded from www.nrcresearchpress.com by 210.87.254.6 on 09/05/12
For personal use only.

Can. J. Chem. Downloaded from www.nrcresearchpress.com by 210.87.254.6 on 09/05/12
For personal use only.

(2–9). Conder and Purnell (10–13) extended the gc method so that thermodynamic information at finite concentrations of the vapour phase in the polymer could be determined. Their technique has been used by Brockmeier *et al.* (14, 15) to measure solubility isotherms of several hydrocarbons in amorphous and semicrystalline polymers. The most recent development (16, 17) has been the extension of the gas chromatographic method to three component systems, where the stationary phase consists of a blend of polymers or a polymer–plasticizer mixture, in order to determine the interaction parameters between the two components of the stationary phase. In addition to the thermodynamic parameters derived from gas chromatography, the method has also been used to measure glass transition temperatures of polymers (2, 18), degrees of crystallinity (19), and crystallization kinetics (20) of polyethylene, diffusion coefficients (21), and various surface properties (22, 23) of polymers.

The calculation of thermodynamic interaction parameters from gas chromatography requires that equilibrium between the bulk stationary phase and the vapour phase be established rapidly, and that all retention mechanisms other than solution in the polymer should be either negligibly small or corrected for when determining the true bulk retention volume. For example, it has recently been shown (24) that the adsorption of polar vapours onto the surface of polar polymeric stationary phases may in fact contribute quite significantly to the measured retention volume. An extrapolation procedure using columns with different surface-to-volume ratios of polymer was used in order to separate the bulk and surface components of the retention volume. When the establishment of equilibrium between the vapour and stationary phases is not instantaneous, kinetic factors which alter the retention volume may occur. Slow diffusion of a hydrocarbon probe through an amorphous polystyrene stationary phase has been shown (25) to result in skewed, broad peaks and retention volumes which are lower than the true thermodynamically controlled values. This is particularly true in the region of the glass transition, where diffusion through the bulk of the polymer is extremely slow. Below the glass transition, where the probe vapour cannot penetrate the stationary phase, it has been proposed (2) that the retention in the column is due solely to adsorption onto the polymer surface. Thus in order to derive meaningful thermodynamic information on the bulk polymer–vapour interaction, it is necessary to work well above the glass transition temperature of the polymer. However, even above the glass transition temperature, there may be an excess concentration of the vapour adsorbed at the polymer/vapour interface. This surface effect would be expected to increase as the surface-to-volume ratio of the polymer is increased, *i.e.* as the loading of stationary phase on the gc support is decreased. In a recent paper from this laboratory (26) it was shown how peak shapes and some of the kinetic phenomena associated with polymeric stationary phases may be predicted, at least qualitatively, both above and below the glass transition temperature by including a term accounting for surface adsorption in the basic conservation equation of gas chromatography. The purpose of the present work then is to examine in greater detail how surface effects and kinetic factors may give rise to retention volumes which are not a true measure of the thermodynamic interaction between the probe vapour and the polymeric stationary phase, using as an illustration the retention behaviour of *n*-tetradecane on polystyrene.

Experimental

The atactic polystyrene (Polysciences Inc., mw 110,000) was coated onto 80–100 mesh glass beads from toluene solution by allowing the solvent to slowly evaporate, with constant stirring. The loading on each sample was determined by soxhlet extraction with toluene of a carefully weighed quantity of the coated beads. The columns consisted of 0.25 in. o.d. copper tubing and were approximately 5 ft in length. A summary of the column characteristics is given in Table 1. The average thickness of the coating was calculated from the geometric surface area of the glass beads, assuming even coverage of the polymer over the entire bead. Retention times for *n*-tetradecane (Quantkits, Polyscience Corp.) were measured on a Hewlett-Packard Model 5711 gas chromatograph equipped with dual flame ionization detectors, using nitrogen as the carrier gas. Peak retention volumes were corrected conventionally for column dead volume and pressure drop (27). After each injection, the column was heated to approximately 190 °C in order to rid the polystyrene of any last traces of tetradecane from the previous injection.

Scanning electron micrographs of the coated beads were taken on a Stereoscan Mark 2A (Cambridge Instruments Co.) microscope. Samples were coated with a thin (approximately 20 nm) layer of a gold–palladium alloy prior to their being placed into the microscope chamber.

TABLE 1. Characteristics of polystyrene columns

Weight of glass beads (g)	Weight of polystyrene (g)	% loading	Average stationary phase thickness (μm)
49.692	0.079	0.16	0.09
42.358	0.256	0.59	0.33
16.168	0.164	1.01	0.56
25.618	0.721	2.74	1.52
23.169	1.154	4.75	2.63

Results and Discussion

A qualitative comparison may be made between the effects of flow rate, injection size, and column loading on the observed retention behaviour of tetradecane on polystyrene and the predictions of the simplified peak shape equation derived in the previous paper (26). For convenience, we will outline the basis of the equation before dealing with its practical implications. Briefly, it is assumed that a gas phase concentration of probe vapour c (mol/ml) may be related to a bulk concentration q (mol/g of stationary phase) and a surface excess concentration Γ (mol/cm^2 of stationary phase surface) by

$$[1] \qquad \frac{dq}{dt} = K(\beta . c - q)$$

$$\Gamma = \beta_s . c$$

where β and β_s are appropriate partition coefficients for the bulk equilibrium and the instantaneously achieved surface equilibrium, and K is a rate constant for the approach to bulk equilibrium. Using these relationships in the basic mass balance equation of chromatography, along with suitable boundary conditions, the vapour phase concentration (per mole of probe initially injected) may be derived as a function of the volume V of carrier gas passed through the column. At the column outlet this defines the shape of the chromatographic peak.

$$[2] \quad C(V, l) = \frac{K}{\dot{V}}\left[\frac{V_b}{V - V_m - V_s}\right]^{1/2} \times I_1\left[\frac{2K}{\dot{V}}[V_b(V - V_m - V_s)]^{1/2}\right] \times \exp\left[-\frac{K}{\dot{V}}(V + V_b - V_m - V_s)\right] + \exp\left(-\frac{V_b K}{\dot{V}}\right) \times \delta(V - V_m - V_s)$$

Here $V_m = a.l$, $V_b = m.l.\beta$, $V_s = s.l.\beta_s$, and $\dot{V}$ is the carrier gas column flow rate where a is the gas phase volume per unit column length, l is the length of the column, m is the mass of polymer per unit column length, and s is the surface area of the polymer per unit column length. I_1 is the first order modified Bessel function and δ is the Dirac delta function. Thus the peak shape is expressed in terms of V_m, which corresponds to the gc column hold-up volume, a retention volume V_b which characterizes the bulk interaction, and a retention volume V_s which characterizes the surface adsorption. For given values of these retention volumes, the chromatographic peak shape depends upon the value of the kinetic parameter $K/\dot{V}$. If the only slow process is the rate of equilibration of vapour in the bulk polymer, then according to the simplest theory of chromatographic rate processes (28)

$$[3] \qquad K = \frac{\pi^2}{4} \cdot \frac{D}{y^2}$$

where D is the diffusion coefficient of the probe vapour through the polymer and y is the layer thickness of the polymeric stationary phase.

As the rate of bulk sorption tends to zero, *i.e.*, $K \simeq 0$, the above model predicts gc peak shapes which are characteristic of adsorption of the vapour probe onto glassy polymer surfaces. The peaks should have a sharp front and a sloping tail because of the kinetic effects of flow diffusion into the bulk polymer, and should be eluted with a retention volume independent of flow rate, at

$$[4] \qquad V^* = V_m + V_s$$

In Fig. 1, peaks for *n*-tetradecane on polystyrene at 77 °C are found to correspond to this model. Both peaks, at 4.76% (A) and 1.01% loadings (B), are essentially identical in shape and show the same degree of peak spreading. (Peak spreading in this case may be adequately

Can. J. Chem. Downloaded from www.nrcresearchpress.com by 210.87.254.6 on 09/05/12
For personal use only.

Can. J. Chem. Downloaded from www.nrcresearchpress.com by 210.87.254.6 on 09/05/12
For personal use only.

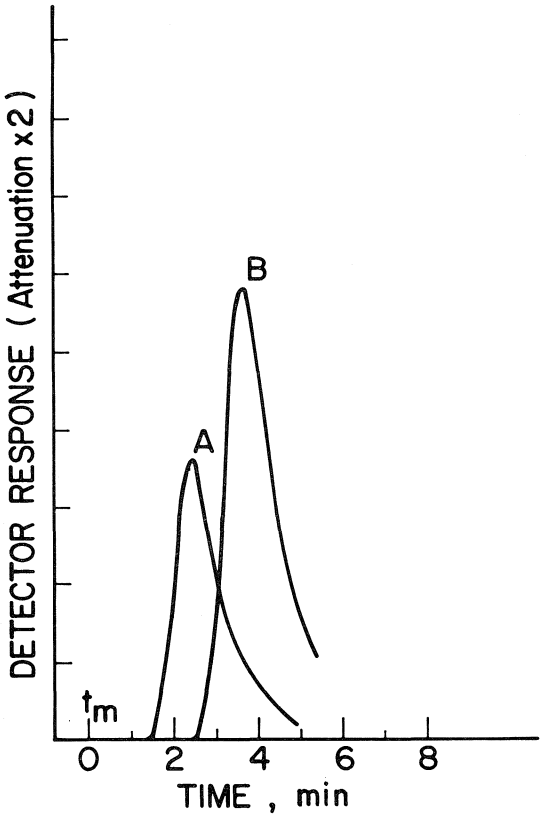

FIG. 1. Experimental peak shapes at 77 °C for *n*-tetradecane on polystyrene for the 4.76% (*A*) and the 1.01% (*B*) loadings. The flow rate was 20 ml/min.

defined as the peak width at half height divided by the total retention time.) Thus the effect of loading on peak shape and spreading is seen to be negligible below the polystyrene glass transition temperature, as would be expected if surface adsorption is the only retention mechanism operating in this temperature region.

For sufficiently large values of $K/\dot{V}$ it has been shown that [1] reduces to a Gaussian shaped curve with a peak maximum at

$$[5] \qquad V^* = V_m + V_b + V_s$$

Thus for thin layers of polymer, where diffusion of the probe through the polymer is rapid, no flow rate dependence of the retention volume is predicted. The effect of flow rate becomes important as the value of K decreases from that which gives a Gaussian peak. When the kinetic effects are not too severe, [2] may be rewritten as

$$[6] \quad C(V) = \frac{K^{1/2}}{(4\pi\dot{V})^{1/2}} \frac{(V_b)^{1/4}}{(V - V_m - V_s)^{3/4}} \times \exp\left\{ -\frac{K}{\dot{V}}(\sqrt{V_b} - \sqrt{V - V_m - V_s})^2 \right\}$$

The position of the peak maximum, $V = V^*$, may be obtained by differentiating this expression with respect to V and setting $\partial C(V)/\partial V = 0$. If we then write $E = V^* - (V_m + V_b + V_s)$, where E thus gives the deviation of the peak maximum from its equilibrium value, then it may be shown that for $E \ll V_b$

$$[7] \qquad E \simeq -\frac{3}{2}\dot{V}/K$$

or, substituting from [3]

$$[8] \qquad E \propto -\dot{V}y^2/D$$

Effect of Flow Rate on Retention Volume

The measured retention volume is thus predicted to be less than the equilibrium value by an amount which depends linearly on the flow rate. The effect of flow rate on specific retention volume is illustrated in Fig. 2 for the 1.01, 2.74, and 4.75% loadings at 157 °C. These results and those reported in other work (4, 29) show a linear flow rate dependence and extrapolation to

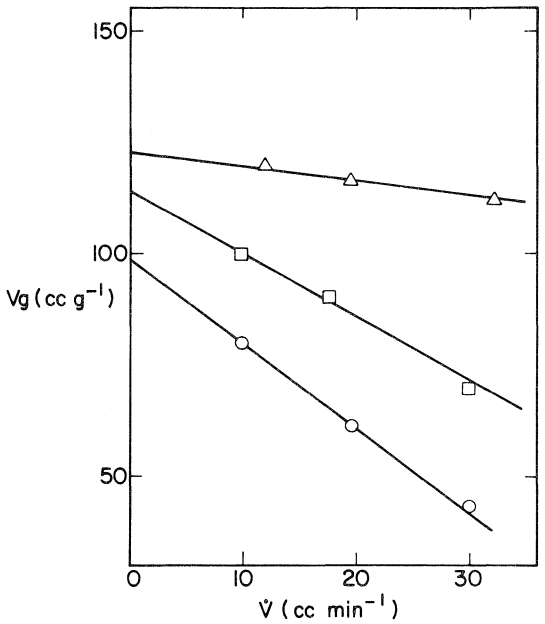

FIG. 2. Specific retention volume *vs.* flow rate for the 1.01 (△), 2.74 (□), and 4.75 (○) loadings at 157 °C.

Can. J. Chem. Downloaded from www.nrcresearchpress.com by 210.87.254.6 on 09/05/12
For personal use only.

zero flow rate thus should give the equilibrium retention volume. Although the flow rate dependence is linear over the range of flow rates investigated, a more complex relationship between retention volume and flow rate may exist at very low flow rates (8), possibly due to peak spreading mechanisms other than slow diffusion in the stationary phase (26). Nevertheless the very low flow rate dependence for the 1.01% loading suggests that the specific retention volume at zero flow rate should be an accurate measure of the bulk polymer–vapour interaction.

Equation 8 also predicts that the slope of the line relating retention volume to flow rate should increase as the square of the layer thickness. From Fig. 2 it is evident that the slopes do increase with layer thickness but calculations show that they increase as $(y)^{1.3}$ rather than $(y)^2$. This discrepancy is probably due to the fact that [3] was derived for a uniform coating of even thickness whereas, as will be shown from the scanning electron micrographs, the real coating is far from uniform.

The effect of flow rate on retention volume will also be temperature dependent, since the rate of diffusion of the vapour through the polymer increases with increasing temperature. This effect is illustrated in Fig. 3, where the specific retention volume is shown as a function of flow rate for the 2.74% loading. Below T_g, the tetradecane is adsorbed onto the surface of the polystyrene, a process which is assumed to achieve instantaneous equilibrium, resulting in a retention volume which is almost independent of flow rate. The effect of flow rate is seen to be greater at 139.7 °C, where diffusion through the polystyrene is very slow. At 184.9 °C the diffusion rate has increased to the point where the effect of flow rate is again small. From [8] it is evident that E, the deviation from equilibrium retention volume, should vary inversely with the diffusion coefficient D. An attempt has previously been made to measure diffusion coefficients in polymers using the flow rate dependence of the peak width (21). However the dependence of E on D suggests an alternative method of measuring D by gas chromatography, that is, from the slope of the lines relating retention volume to flow rate.

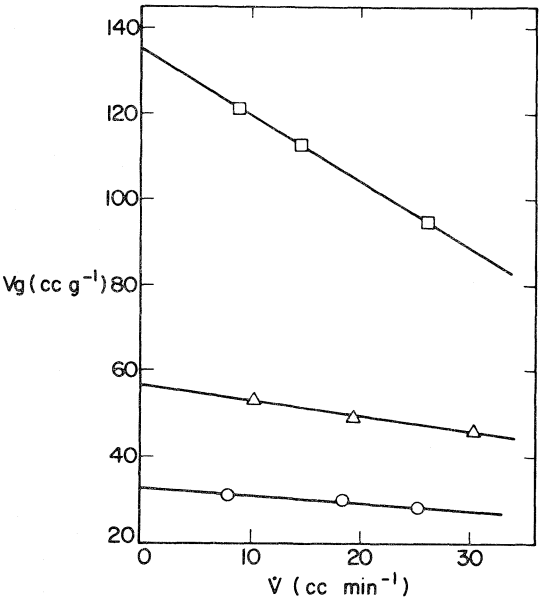

FIG. 3. Specific retention volume *vs.* flow rate at 139.7 (□), 184.9 (△), and 88.8 °C (○) for the 2.74% loading.

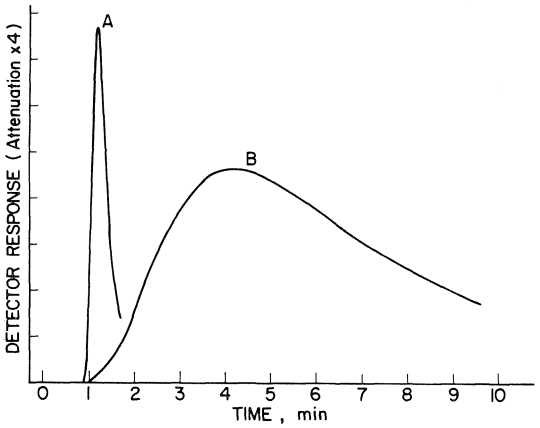

FIG. 4. Experimental peak shapes at 157 °C for the 1.01% (*A*) and 4.75% (*B*) loadings. The flow rate was 20 ml/min.

The rate of approach to bulk equilibrium will also affect peak shapes as well as retention volumes. In contrast to the peaks obtained at 77 °C shown in Fig. 1, are those obtained at 157 °C shown in Fig. 4. The peak for the 1.01% loading (peak A) is very sharp and narrow, indicating a rapid equilibration between the polystyrene stationary phase and the tetradecane vapour. On the other hand the peak for the 4.75% loading is seen to be very much broader and skewed, with a long tail. This behaviour, suggestive of non-equilibrium partitioning of the

Can. J. Chem. Downloaded from www.nrcresearchpress.com by 210.87.254.6 on 09/05/12
For personal use only.

tetradecane, is undoubtedly due to the thicker coating of polystyrene on the beads with the higher loading. The peak shapes obtained experimentally will not correspond exactly to the proposed model (26) for two reasons. Firstly, it was assumed when developing the theory that peak spreading was due solely to bulk interactions of the vapour with the stationary phase. It is well known however that other peak spreading mechanisms, such as longitudinal diffusion in the column, can increase the width of the peak. Secondly, from an experimental point of view, working at extremely low attenuations on the gas chromatograph results in background noise from the detector and in baseline drift which perturbs the shape of the peaks.

Effect of Loading on Retention Volume

Changing the loading of polymer on a given weight of support affects two parameters in [4]. Firstly, the value of K increases with decreasing thickness, with the attendant changes in peak shape and peak retention volume discussed in the previous paragraph. Secondly, by altering the surface-to-volume ratio of the polymer stationary phase, the relative magnitude of V_s and V_b will be changed. Thus for a given weight of polymer, doubling the weight of support on which it is coated will approximately double the surface area (30) and hence V_s will also approximately double while V_b remains unchanged. The effect of altering the surface-to-volume ratio of the stationary phase is illustrated schematically in Fig. 5. If there is no adsorption of the tetradecane onto the polystyrene surface, then $V_s = 0$ and the retention volume will quickly drop to zero as the temperature decreases towards T_g. This effect is indicated by the dashed-and-dotted line. As the value of V_s increases, the total retention volume (solid line) will change as shown in curves I to IV, which represent increasing surface-to-volume ratios of stationary phase. It is evident that the discontinuity at T_g decreases as the surface retention (dashed line) accounts for a relatively greater proportion of the total retention volume. In the limit of retention due to surface adsorption alone, *i.e.*, $V_b = 0$, the discontinuity of T_g would disappear completely, as would the change in slope of the retention diagram on going through the glass transition. Decreasing the surface-to-volume ratio also results in the maxima in the retention

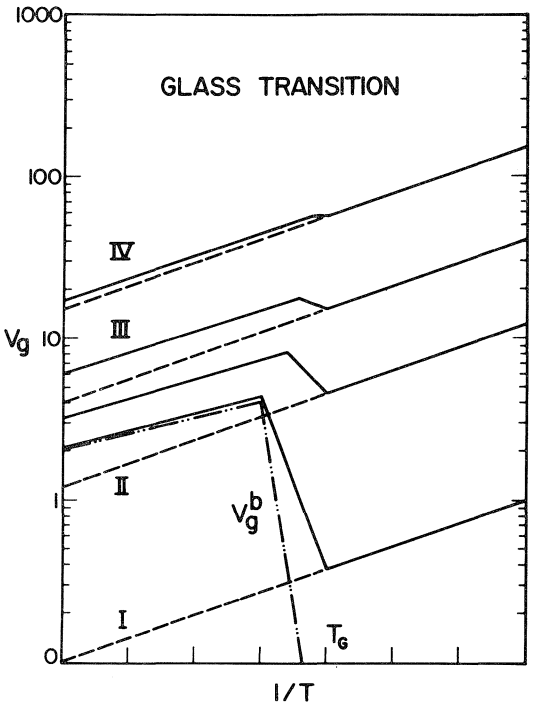

FIG. 5. Model of specific retention volume *vs.* reciprocal temperature for the polymer glass transition. Solid line: total retention volume; dashed line: surface retention volume; dashed-and-dotted line: bulk retention volume.

diagrams being shifted to higher temperatures, since thinner layers of polymer should allow bulk equilibrium to be achieved at lower temperatures.

It is assumed here that the heat of adsorption of the vapour on the polymer surface is the same both above and below T_g. Although there is no experimental justification for this, with weakly interacting probes and polymers the heats should be very close to the heat of vapourization of the pure liquid probe. A difference in the heats would appear as a discontinuity in the slope of the surface retention diagram at T_g. If the heats are the same above and below T_g, the value of the surface component of the retention volume above T_g may be determined by extrapolation from the region below T_g, where $V^* = V_m + V_s$. By altering the loadings and extrapolating to infinite loading, the bulk contribution should also be determinable (24). In the non-equilibrium region near T_g, it should be noted that for a given weight of stationary phase, a decrease in

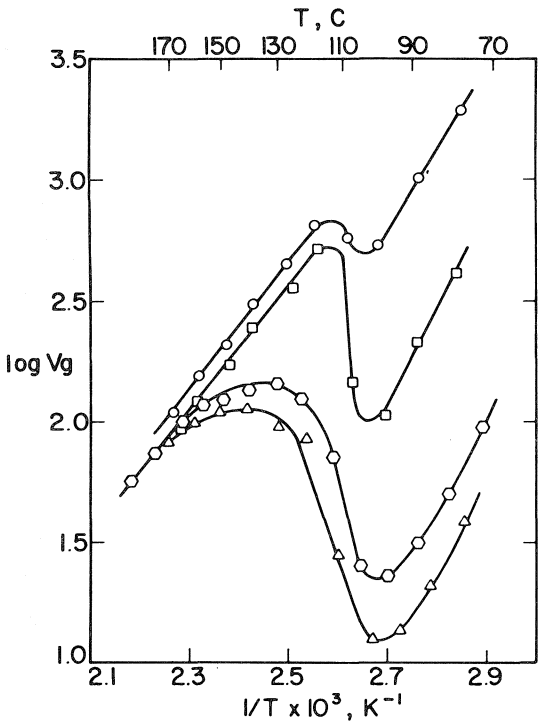

FIG. 6. Specific retention volume *vs.* reciprocal temperature for *n*-tetradecane on polystyrene at loadings of 0.59 (○), 1.01 (□), 2.74 (○), and 4.75% (△). All retention volumes extrapolated to infinite dilution and zero flow rate.

the layer thickness will produce an increase in V^* through the effects on both V_s and K.

The effect of loading on the specific retention volume of tetradecane on polystyrene, after all extrapolations to infinite dilution and zero flow rate have been made, is shown in Fig. 6. The discontinuity at T_g is seen to diminish as the surface-to-volume ratio of the polystyrene stationary phase increases, in agreement with the model presented above. The predicted shift to lower temperatures of the maxima in the retention diagrams as the loading is decreased is also clear. In contrast with the 1.01% loading, which shows a sharp increase in retention volume at T_g, the higher loadings exhibit only a very gradual increase over a much wider temperature interval until about 170 °C. Above this temperature these three retention diagrams coincide. It is clear then that as the loading increases, the measured retention volumes are controlled more by the kinetics of transfer of the probe vapour between the stationary and mobile phases than by thermodynamic interactions. It is only well above T_g, where the peak retention volume is unaffected by kinetic factors, that $V^* = V_m + V_b + V_s$ and the linear combination model illustrated in Fig. 5 should be operative. The temperature at which this occurs will of course depend upon the nature of the probe liquid as well as the polymer, as alkanes with a lower molecular weight than tetradecane will be able to diffuse more rapidly through the polystyrene. In spite of these kinetic effects, a value of 51 ± 5 kJ/mol for the infinite dilution heat of solution of *n*-tetradecane in polystyrene was calculated from the linear portions of the 0.59 and 1.01% loading data above T_g. This value is in reasonably good agreement with other recently determined data (31).

Although the retention diagrams for the 1.01, 2.74, and 4.75% loadings all coincide at temperatures greater than 170 °C, that of the 0.59% loading occurs at retention volumes well above the others. It would appear then that in this case surface adsorption must be contributing a significant percentage of the total retention volume. By extrapolating the linear portion of the retention diagram below T_g to higher temperatures, 26% of the retention volume was attributable to surface adsorption for the 0.59% loading at 135 °C, compared to less than 4% for the 1.01% loading. Thus the effects of loading on retention, as predicted in Fig. 5, are found to be obeyed qualitatively. Very recently, Braun and Guillet (32) reported extensive experimental results for the retention of hexadecane on polystyrene coated onto Chromosorb, which also agree well with this model for the effect of layer thickness on retention close to T_g.

Effects of Isotherm Curvature

A quantitative estimation of the surface and bulk contributions is rendered difficult, however, for two reasons. Firstly, the surface area of the polystyrene and its variation with loading are not well defined, as shown by the electron micrographs to be discussed shortly, and as shown from the discussion of Conder *et al.* (30) on the effects of loading. Secondly, the model for retention behaviour is derived for linear partition isotherms (eq. 1), which implies that the retention volumes are independent of the size of the injected vapour sample. This condition is satisfied for infinitely dilute solutions of vapour in the stationary phase. Since of course a finite amount

Can. J. Chem. Downloaded from www.nrcresearchpress.com by 210.87.254.6 on 09/05/12
For personal use only.

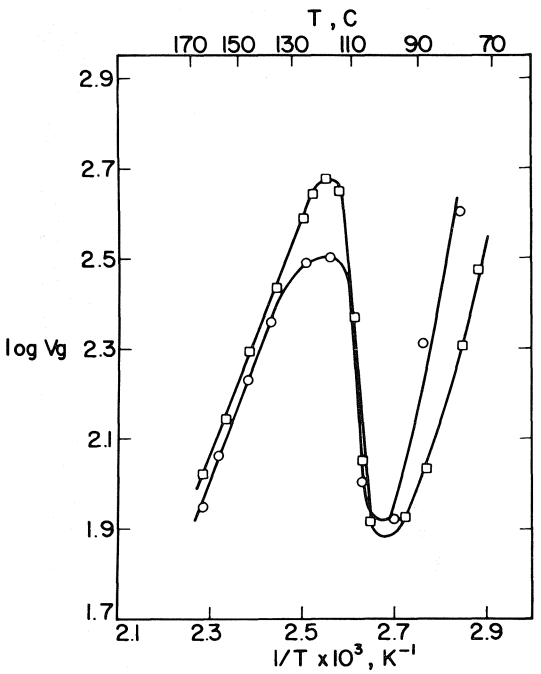

FIG. 7. Specific volume *vs.* reciprocal temperature for the 1.01% loading at finite injection size (□) and for retention volumes that have been extrapolated to infinite dilution (○). Flow rate was 20 ml/min.

of vapour is introduced into the column at each injection, the effect of injection size on the measured retention volume requires consideration. In these experiments, several retention volumes were measured for different injection sizes at each temperature and flow rate, and extrapolated to infinite dilution. A comparison of the specific retention volumes extrapolated to infinite dilution and those obtained at finite injection size is shown in Fig. 7 for the 1.01% loading. It is clear that the effect is much greater below the glass transition temperature than above and that the infinite dilution retention volumes are less than the finite concentration values above T_g, but greater below T_g. The size of the injection may alter the measured retention volume for a variety of reasons (27), of which the most important for the polystyrene system are non-linearity of the partition isotherms (with β or β_s no longer independent of c) and adsorption effects on uncoated support. The small but significant increase in retention volume with increasing injection size above T_g may be due to a curved isotherm which is anti-Langmuir in form (concave away from the vapour pressure axis when sorbed vapour is plotted against vapour pressure) as has been observed for ethylbenzene on polystyrene (14). The more pronounced effect below T_g, where injection size causes a decrease in retention volume, implies that the adsorption isotherm is of the often-observed Langmuir type. This behaviour has previously been observed for *n*-decane on both polystyrene coated glass beads and on solid poly(styrene-co-divinyl benzene) beads (23). When kinetic effects are absent, the dependence of peak shapes and retention volumes on the amount of injected probe has been used to determine adsorption isotherms on polymer surfaces (22, 23, 33).

If the isotherm curvature is not too severe over the range of vapour concentrations used, then an empirical linear extrapolation to zero peak height may be used, as in the results presented here. Alternatively, measurement of retention volumes for a constant vapour phase concentration, or preferably for a constant surface coverage (3), may be made. However, in the current study, where K has finite values, the shape of the peaks is determined both by K and $\beta_s(c)$, a complex situation not covered by [6].

Distribution of Polymer on Support

If a portion of the glass bead is uncovered, a further complication arises in that a second adsorption isotherm should hold for the glass surface. Although it is generally assumed that the stationary phase forms an even and complete coating on the support, in practice such a coating does not exist. As the amount of polymer on a given weight of support decreases, 'beading up' of the polymer can occur, resulting in areas of uncoated glass beads being exposed to the probe vapour. Although no specific interaction would be expected between tetradecane and the hydrophilic glass surface, adsorption onto the glass may obscure the shape of the peak or alter the apparent retention volume. This may explain the anomalous behaviour illustrated in Fig. 8 by the retention diagrams for the 0.16 and 1.01% loadings. In contrast to the other higher loadings, the minimum in the 0.16% retention diagram occurs at about 120 °C, *i.e.* roughly 20° higher than the other loadings. The first deviation of the retention diagram from linearity on increasing the temperature has been shown to correspond

Can. J. Chem. Downloaded from www.nrcresearchpress.com by 210.87.254.6 on 09/05/12
For personal use only.

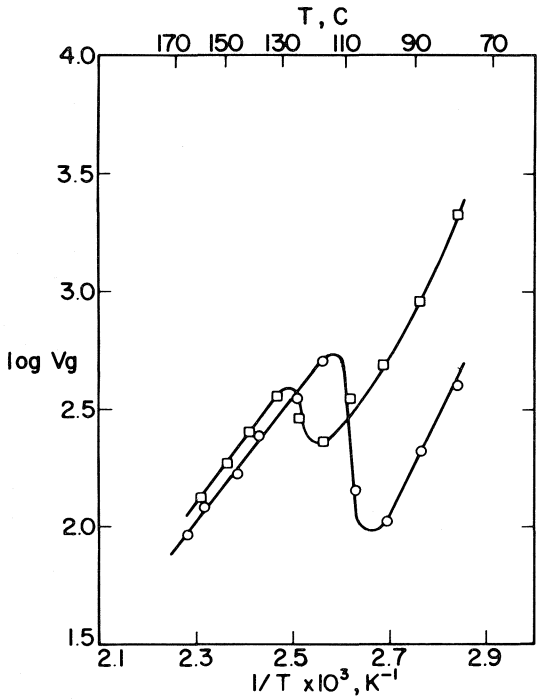

FIG. 8. Specific retention volume *vs.* reciprocal temperature for the 0.16% (□) and 1.01% (○) loadings.

quite closely with the glass transition temperature of the polymer. Since it is not likely that the glass transition temperature of the polystyrene should change for the 0.16% loading, this discrepancy must be due to either adsorption onto the uncoated areas of the glass beads, resulting in a relatively higher contribution from V_s to the total retention volume, or to 'beading up' of the polystyrene on the glass beads, resulting in an effectively lower value of the kinetic parameter K, which would also decrease the retention volume. It may be noted that even when completely covered, the solid support may still exert an effect on the retention behaviour of the probe due to adsorption of the probe vapour onto active sites on the support surface. This will lead to a dependence of retention volumes on sample size, in this case the larger errors are for the smallest injections (27). Obviously this situation should be avoided.

In order to determine the degree of coverage of the glass bead support by the polystyrene, scanning electron micrographs of the glass beads with different loadings of polymer were taken. A comparison of the 0.16, 0.59, and 4.75% loadings is shown in Fig. 9. The beads with the 0.16% loading are for the most part uncoated, with only small 'patches' of polystyrene on each bead. This 'beading up' effect may account for

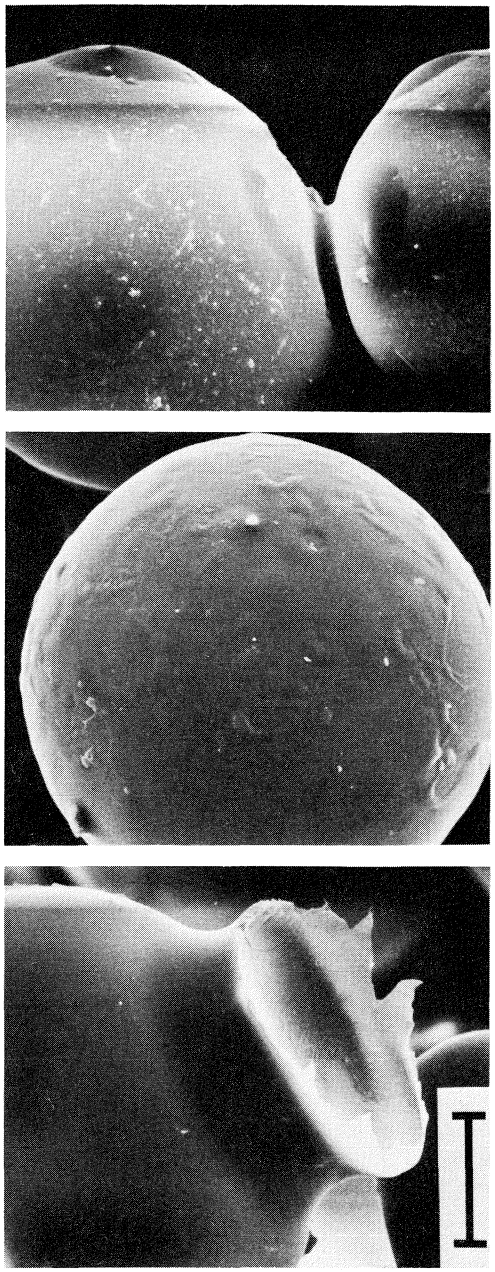

FIG. 9. Scanning electron micrographs of polystyrene-coated glass beads. Top photograph, 0.16% loading; middle photograph, 0.59% loading; bottom photograph, 4.75% loading. The scale bar represents 40 μm.

Can. J. Chem. Downloaded from www.nrcresearchpress.com by 210.87.254.6 on 09/05/12
For personal use only.

Can. J. Chem. Downloaded from www.nrcresearchpress.com by 210.87.254.6 on 09/05/12
For personal use only.

the discrepancy in the 0.16% retention diagram, due to slow diffusion of tetradecane through the relative thick 'patches' of polystyrene. By increasing the loading to 0.59%, the coating has become more or less uniform, although some areas of the bead remain uncoated. The bead with the 4.75% loading is completely covered with a relatively thick, but nonuniform layer of polystyrene. This last micrograph clearly shows where this bead was at one point attached by the polystyrene to another bead. Although the corresponding area on the other bead would be uncoated, one can conclude that at this loading most beads are completely covered with polymer. Altogether, it is clear from Fig. 9 that the coating of polymeric stationary phases on glass bead supports may be far from complete and uniform. If this is the case with a low surface area support like glass beads, the coating should be even less uniform on higher surface area supports such as Chromosorb.

That the apparent discrepancy in Fig. 8 is due to incomplete coverage of the support by the polymer is also indicated by the peak spreading data shown in Fig. 10. In this diagram, the spreading of the peaks (measured by dividing the peak width at half height by the retention time) for the 1.01 and 0.16% column loadings is given as a function of reciprocal temperature. In both cases the greatest peak spreading occurs at the maxima in the retention diagrams, as expected. More importantly, it is clear that the temperature at which peak spreading starts rising (*i.e.* approximately 97 °C) occurs at the same point for both loadings, even though the measured peak retention volumes for the 0.16% loading are still decreasing at this temperature. Thus not only do these results agree with the explanation for the apparent discrepancy in the 0.16% loading data but they also support the contention (26) that it is the onset of peak spreading, not the minimum in the retention diagram or the first deviation from linearity, that signals the beginning of the glass transition in polymers as determined by gas chromatography.

An interesting comparison between these results and the recent work of Lipatov and Nesterov (34) can be made at this point. In their experiments on the retention of hydrocarbons on polystyrene, an increase in retention volume above T_g with decreasing loading was found when the coating of stationary phase on a glass

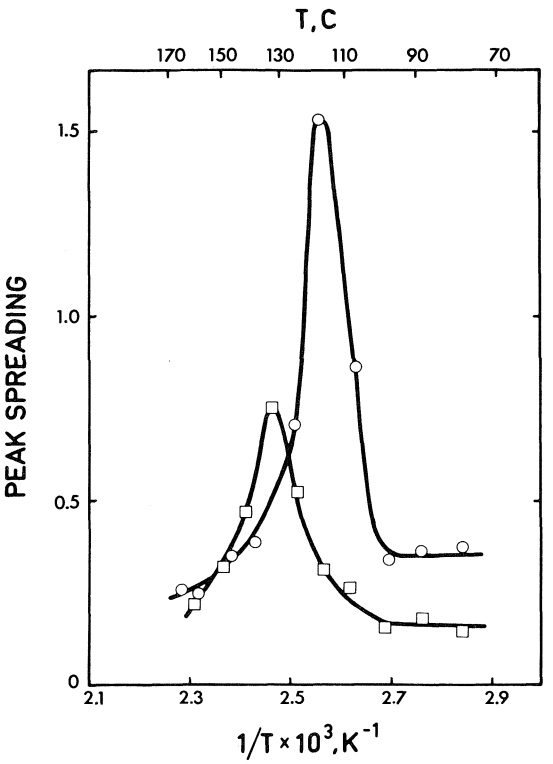

FIG. 10. Peak spreading as a function of reciprocal temperature for the 1.01 (○) and 0.161 (□) loadings.

bead support was less than 0.57 μm in thickness (calculated assuming even coverage). This result is in excellent agreement with our data. Lipatov and Nesterov also found an increase in the glass transition temperature when the layer thickness was less than 0.28 μm. These increases in T_g and retention volume are attributed by these authors to a structuring effect of the polymer molecules in contact with the support surface, rather than to adsorption of the probe vapour onto uncoated areas of the support surface. This leads to an apparent contradiction in their explanation for these two effects. The glass transition temperature is said to increase with decreasing layer thickness because a proportionately greater number of polymer molecules are in contact with the glass surface. These molecules require more energy to be set in motion than those away from the surface, resulting in a higher T_g. However their explanation for the increase in V_g with decreasing layer thickness is that the adsorbed layer has a looser structure than the bulk polymer, resulting in a higher solubility of the probe

Can. J. Chem. Downloaded from www.nrcresearchpress.com by 210.87.254.6 on 09/05/12
For personal use only.

vapour. It would seem that the two explanations for these effects cannot both be correct. Nonetheless it is reasonable that the structure of the polymer on the support should have some effect on gas chromatographic measurements. Indeed, it has recently been shown (35) that retention on poly(methyl methacrylate) is dependent upon the type of solvent used to deposit the polymer onto the support. The essential problem remains as how to differentiate between adsorption of the vapour at the polymer – mobile phase interface, the polymer–support interface, uncoated support – mobile phase interface, and the effect of polymer structure for very thin layers of stationary phase. These four factors are also critically dependent on the distribution of the coating on the support. In this work we have emphasized the effects of adsorption at the polymer–mobile phase interface. It is clear that all adsorption effects must be accounted for before results can be interpreted in terms of altered bulk polymer structure in thin layers. A method of preparing very thin, even coatings of stationary phase on support is required and may be the basis for future work.

Summary and Conclusions

Non-equilibrium partitioning of the probe vapour, isotherm curvature and adsorption onto the stationary phase support have been shown to influence the measured retention volume. We may summarize each of these effects as follows:

Flow Rate Effect

Retention volume decreases linearly with increasing flow rate in accordance with [7]. An extrapolation to zero flow rate is required at all temperatures, but the effect is most pronounced in the glass transition region. The effect of flow rate decreases with the decreasing loading in qualitative agreement with [8]. It is only at temperatures greater than 170 °C that the kinetic parameter K became sufficiently large to allow bulk equilibrium to be attained for the highest loadings used in these experiments.

Effect of Loading

When kinetic effects are not too severe, the effect of changing the amount of stationary phase on a given weight of support is seen to conform qualitatively to the model presented in Fig. 5. At very low loadings, adsorption onto the uncoated glass bead support or 'beading up' of the polystyrene on the support may lead to retention volumes which are uncharacteristic of the polymer–vapour interaction, particularly in the glass transition region.

Effect of Injection Size

Due to isotherm curvature, it is necessary to extrapolate several peaks of different size to zero peak height in order to obtain retention volumes at infinite dilution of probe in the stationary phase. This effect is much more critical below T_g than above. The exact dependence of retention volume on injection size is determined by the curvature of the solubility and adsorption isotherms.

In brief, when using gas chromatography as a means of studying polymer–solvent interactions, it is necessary to determine the extent to which all of the above factors influence the retention volume, and not to rely on a single series of measurements. It is clear that in any system there is always a balance between using high loadings, where kinetic effects are large but surface effects minimal, and low loadings where the opposite is true. The present system was chosen in order to emphasize some of the problems involved in using this method. By altering the experimental conditions, information on the nature of adsorption isotherms and the fundamental properties of ultra-thin layers of polymers as well as bulk polymer–solvent interactions may be obtained using gas chromatography. It is clear however that other techniques are required in order to fully understand these phenomena.

NOTE ADDED IN PROOF: In a recent paper, Braun and Guillet (36) also discuss the gas chromatographic behaviour of polymers through the glass transition. They present a model in which the bulk retention is divided into active and inactive fractions, whose magnitude depends on the rate of diffusion of the probe through the polymer. If a distribution of polymer layer thicknesses is assumed, then their model gives retention data generally in agreement with this work. However, their model offers no interpretation of the changes in peak shape which occur at the glass transition.

Acknowledgment

G.J.C. thanks the National Research Council of Canada for a Graduate Studentship.

1. J. E. GUILLET. New developments in gas chromatography. *Edited by* J. H. Purnell. Wiley-Interscience, New York. 1973. p. 187.
2. O. SMIDSROD and J. E. GUILLET. Macromolecules, **2**, 272 (1969).
3. D. PATTERSON, Y. B. TEWARI, H. P. SCHREIBER, and J. E. GUILLET. Macromolecules, **4**, 356 (1971).
4. R. D. NEWMAN and J. M. PRAUSNITZ. J. Phys. Chem. **76**, 1492 (1972).
5. F. H. COVITZ and J. W. KING. J. Polym. Sci. A-1, **10**, 689 (1972).
6. W. R. SUMMERS, Y. B. TEWARI, and H. P. SCHREIBER. Macromolecules, **5**, 12 (1972).
7. H. P. SCHREIBER, Y. B. TEWARI, and D. PATTERSON. J. Polym. Sci. A-2, **11**, 15 (1973).
8. R. N. LICHTENTHALER, D. D. LIU, and J. M. PRAUSNITZ. Macromolecules, **7**, 565 (1974).
9. Y. K. LEUNG and B. E. EICHINGER. J. Phys. Chem. **78**, 60 (1974).
10. J. R. CONDER and J. H. PURNELL. Trans. Faraday Soc. **64**, 1505 (1968).
11. J. R. CONDER and J. H. PURNELL. Trans. Faraday Soc. **64**, 3100 (1968).
12. J. R. CONDER and J. H. PURNELL. Trans. Faraday Soc. **65**, 824 (1969).
13. J. R. CONDER and J. H. PURNELL. Trans. Faraday Soc. **65**, 839 (1969).
14. N. F. BROCKMEIER, R. W. MCCOY, and J. A. MEYER. Macromolecules, **5**, 464 (1972).
15. N. F. BROCKMEIER, R. W. MCCOY, and J. A. MEYER. Macromolecules, **6**, 176 (1973).
16. D. D. DESHPANDE, D. PATTERSON, H. P. SCHREIBER, and R. S. SU. Macromolecules, **7**, 530 (1974).
17. O. OLABISI. Macromolecules, **8**, 316 (1975).
18. J.-M. BRAUN, A. LAVOIE, and J. E. GUILLET. Macromolecules, **8**, 311 (1975).
19. A. N. STEIN and J. E. GUILLET. Macromolecules, **3**, 102 (1970).
20. D. G. GRAY and J. E. GUILLET. Macromolecules, **4**, 129 (1971).
21. D. G. GRAY and J. E. GUILLET. Macromolecules, **6**, 223 (1973).
22. B. CHABERT, J.-P. SOULIER, and G. EDEL. Ann. Chim. **5**, 193 (1970).
23. D. G. GRAY and J. E. GUILLET. Macromolecules, **5**, 316 (1972).
24. G. COURVAL and D. G. GRAY. Macromolecules, **8**, 326 (1975).
25. D. G. GRAY and J. E. GUILLET. Macromolecules, **7**, 244 (1974).
26. G. J. COURVAL and D. G. GRAY. Macromolecules, **8**, 916 (1975).
27. A. B. LITTLEWOOD. Gas chromatography. 2nd ed. Academic Press, New York. 1970. Chapt. 2.
28. J. J. VAN DEEMTER, F. J. ZUIDERWEG, and A. KLINKENBERG. Chem. Sci. **5**, 271 (1956).
29. W. E. HAMMERS and C. L. DELIGNY. Recl. Trav. Chim. Pays Bas, **90**, 912 (1971).
30. J. R. CONDOR, D. C. LOCKE, and J. H. PURNELL. J. Phys. Chem. **73**, 700 (1969).
31. A. LAVOIE. M.Sc. Thesis, University of Toronto, Toronto, Ont., Canada. 1971.
32. J.-M. BRAUN and J. E. GUILLET. Macromolecules, **8**, 882 (1975).
33. P. R. TREMAINE and D. G. GRAY. J. Chem. Soc. Faraday Trans. I, **71**, 2170 (1975).
34. YU. S. LIPATOV and A. E. NESTEROV. Macromolecules, **8**, 889 (1975).
35. M. CROUCHER. Ph.D. Thesis, McGill University, Montreal, P.Q., Canada. 1976.
36. J. M. BRAUN and J. E. GUILLET. Macromolecules, **9**, 617 (1976).

Can. J. Chem. Downloaded from www.nrcresearchpress.com by 210.87.254.6 on 09/05/12
For personal use only.

The reaction of steroid 2,4-dienes with acetylenes

PETER YATES AND FRANÇOISE M. WALLISER
Lash Miller Chemical Laboratories, University of Toronto, Toronto, Ont., Canada M5S 1A1

Received July 12, 1976

PETER YATES AND FRANÇOISE M. WALLISER. Can. J. Chem. **54**, 3508 (1976).

Reaction of 2,4-cholestadiene, 2,4-androstadien-17-one, or 3-trimethylsiloxy-2,4-cholestadiene with dimethyl acetylenedicarboxylate or methyl propiolate in boiling xylene results in the cleavage of rings A and B and the formation of 4-(2-arylethyl)-5-isopropenyl-7a-methyltetrahydroindane derivatives. They are considered to be formed via Diels–Alder addition of the acetylene to the steroid diene followed by a retro-Diels–Alder cleavage of the resulting bicyclo[2.2.2]octadiene system. Attempts to isolate the Diels–Alder adducts by carrying out the additions at lower temperature were unsuccessful, since no reaction occurred. However, when 2,4-androstadien-17-one was treated with dicyanoacetylene in boiling benzene, it was possible to isolate a mixture of two stereoisomeric Diels–Alder adducts containing the bicyclo[2.2.2]-octadiene system in ring A; this was converted in boiling xylene to a retro-Diels–Alder product analogous to the products obtained with the other acetylenic dienophiles.

PETER YATES et FRANÇOISE M. WALLISER. Can. J. Chem. **54**, 3508 (1976).

La réaction du cholestadiène-2,4, de l'androstadiène-2,4 one-17 et du triméthylsiloxy-3 cholestadiène-2,4 avec l'acétylènedicarboxylate de méthyle ou le propiolate de méthyle dans le xylène bouillant conduit à une rupture des cycles A et B et à la formation de dérivés (aryl-2 éthyl)-4 isopropényl-5 méthyl-7a tétrahydroindanes. On considère que ces composés sont formés par une addition de Diels–Alder de l'acétylène au diène stéroïdal, l'addition suivie par une coupure du type rétro-Diels–Alder du système bicyclo[2.2.2]octadiène. Des essais en vue d'isoler les adduits de Diels–Alder, en effectuant des réactions d'addition à des températures plus basses, n'ont pas fourni les résultats attendus puisqu'il ne se produit aucune réaction. Toutefois, lorsque l'on a traité l'androstadiène-2,4 one-17 avec le dicyanoacétylène dans le benzène bouillant, on a pu isoler un mélange de deux adduits stéréoisomères de Diels–Alder contenant le système bicyclo[2.2.2]octadiène du cycle A; celui-ci peut être transformé dans le xylène bouillant en un produit du type rétro-Diels–Alder qui est analogue aux produits obtenus avec les autres diénophiles acétyléniques.

[Traduit par le journal]

Solo and his co-workers (1, and earlier papers in this series) have made extensive investigations of the chemistry of bridged ring D steroids, which they prepared by Diels–Alder addition of dienophiles to steroid 14,16-dienes. By contrast, steroids with carbon-bridged rings other than ring D have not been studied systematically, although a number have been prepared. Nagata and co-workers (2) obtained 2,5-ethano derivatives by ring closure of a steroid with a two-carbon unit at C.5, and Kocor and Kroszczynski have prepared a related derivative from a steroid with a two-carbon unit at C.2 (3). However, the method of synthesis most frequently employed has again been the Diels–Alder reaction; cases of the application of this method to give carbon-bridged steroids are given in Table 1. It may be noted that the yields of adducts are often low, except when the 1,3-diene forms part of a 1,3,5-triene system; this reflects the circumstance that there is frequently severe competition from ene-reactions, unless steric retardation of the Diels–Alder reaction is ameliorated by the presence of an additional conjugated ethylenic bond (11). Thus, ergosteryl acetate (**1**) gives with maleic anhydride the Diels–Alder adduct **2** (16%) and in addition three ene-products of type **3** (7). In some cases the ene-reactions occur to the exclusion of the Diels–Alder reaction; for example, **1** and dicyanoacetylene give only ene-products related to **3** (11). We now report on an investigation of the applicability of the reactions of steroid 2,4-dienes with acetylenic dienophiles to the synthesis of steroids incorporating a bicyclo[2.2.2]octadiene system in ring A.

2,4-Cholestadiene (**4**) failed to react with dimethyl acetylenedicarboxylate in boiling benzene or toluene, but gave a 1:1 adduct in boiling xylene. The spectra of this product (Table 2) showed that it was not a Diels–Alder adduct of type **5**, but demonstrated that it was **6**, derived by a retro-Diels–Alder cleavage of the bicyclo-

Can. J. Chem. Downloaded from www.nrcresearchpress.com by 210.87.254.5 on 09/05/12
For personal use only.

TABLE 1. Diels–Alder adducts from steroid dienes[a]

Diene	Dienophile	Yield (%)[b]	Ref.
Ring A			
2,4-Cholestadiene	Maleic anhydride	43[c]	4
	Benzyne	6.5	5
		1.5(β)	
	Tetrafluorobenzyne	15	5
1,3,5-Cholestatrien-7-one	Maleic anhydride	59	6
Ring B			
Ergosteryl acetate	Maleic anhydride	16	7
7-Dehydrocholesteryl methyl ether	Tetrafluorobenzyne	22	5
7-Dehydrocholesteryl acetate	Methyl acrylate	64	8
	Acrolein	42	8
Lumisteryl acetate	Maleic anhydride	35	9
9(11)-Dehydroergosteryl acetate	Maleic anhydride	—	10
	Dicyanoacetylene	65	11
		2(β)	
5,7,9(11)-Cholestatrienyl acetate	Maleic anhydride	77	12
	Dimethyl acetylenedicarboxylate	35	12
	Tetrafluorobenzyne	3	5
		9(β)	
Ring C			
6,8(14),9(11),22-Ergostatetraen-3β-yl acetate	Maleic anhydride	71	13

[a]See ref. 1 for ring D adducts.
[b]α-Adduct, unless otherwise indicated.
[c]Purity and stereochemistry of product not established.

[2.2.2]octadiene system of **5**. Its infrared (ir) and ultraviolet (uv) spectra showed the presence of the phthalate ester moiety (*cf.* dimethyl phthalate (14); λ_{max} 5.81 μm; λ_{max} 225 (ε 8300), 274 nm (ε 1250)), and its proton magnetic resonance (pmr) spectrum showed that this moiety was substituted at a position adjacent to one of the carbomethoxy groups. The presence of the isopropenyl group was shown by the bands at 6.05 and 11.15 μm in its ir spectrum and the signals at δ 1.68 and 4.80 in its pmr spectrum (*cf.* 2,3-dimethyl-1-butene: δ 1.68 and 4.77 (15)). The stereochemistry depicted in **6** is assigned on the basis of the expectation that the configuration at all centers in **1**, other than C.10, will be retained in the product.

The formation of benzenoid systems by the retro-Diels–Alder cleavage of bicyclo[2.2.2]octadienes has ample precedent, and, indeed, Eckhard *et al.* (5) have previously observed the formation of the related compounds **9** and **10** upon pyrolysis at 250 °C of the Diels–Alder adducts, **7** and **8**, of **4** with benzyne and tetrafluorobenzyne, respectively. The failure to isolate the Diels–Alder adduct **5** in the present case is attributable to both the lower dienophilicity of dimethyl

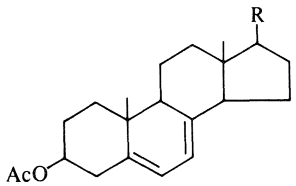

1

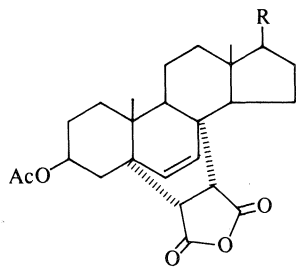

2

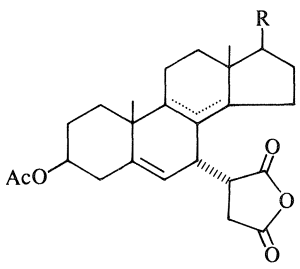

3

R = —CHCH=CHCHCH(CH$_3$)$_2$
CH$_3$ CH$_3$

Can. J. Chem. Downloaded from www.nrcresearchpress.com by 210.87.254.5 on 09/05/12
For personal use only.

Can. J. Chem. Downloaded from www.nrcresearchpress.com by 210.87.254.5 on 09/05/12
For personal use only.

TABLE 2. Spectra of retro-Diels–Alder products **6** and **13** and Diels–Alder adducts **21**

Spectrum	6	13	21
$\lambda_{max}(CHCl_3)$, μm			4.50(w)
	5.76	5.76	5.75
	6.05(w)	6.07(w)	6.21(w)
	6.25(w)	6.23(w)	6.27(w)
	11.15(m)	11.15(w)	
λ_{max}, nm(ϵ)[a]	232(8200)	232(8100)	213(6800)
	281(1800)	280(1800)	243(7500)
	290(1600)	286–289(1600)	
$^H\delta(CDCl_3)$	0.73(s, 3H)	0.95(s, 3H)	0.88(s, 3H)
	0.84(s, 3H)	1.75(s[b])	1.00(s, 3H)
	1.68(s, 3H)	3.90(s, 3H)	3.7–4.0(m, 1H)
	3.90(s, 3H)	3.93(s, 3H)	6.1–6.7(m, 2H)
	3.93(s, 3H)	4.83(s, 2H)	
	4.80(br s, 2H)	7.2–7.5(m, 2H)	
	7.2–7.5(m, 2H)	7.7–7.9(m, 1H)	
	7.7–8.0(m, 1H)		

[a]Solvents: **6** hexane; **13** MeOH; **21** EtOH.
[b]Superimposed on multiplet.

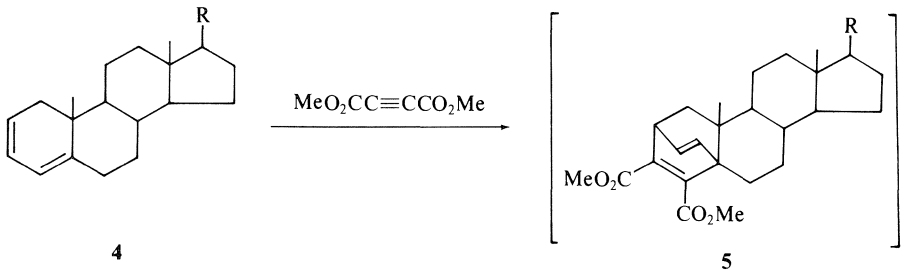

4 **5**

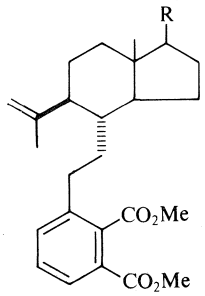

6

R = $-\underset{\underset{CH_3}{|}}{CH}CH_2CH_2CH_2CH(CH_3)_2$

acetylenedicarboxylate relative to the benzynes and the greater facility of the retro-Diels–Alder cleavage of **5**, relative to that of **7** and **8**.

2,4-Androstadien-17-one (**12**), prepared by dehydration of dehydroisoandrosterone (**11**) with alumina,[1] was found to have the same reactivity

[1]In this case, unlike that of the dehydration of cholesterol, no 3,5-diene was formed.

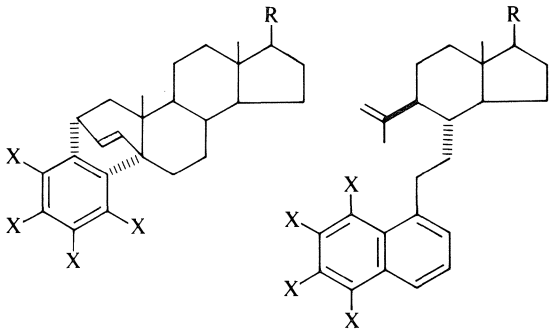

7 X = H
8 X = F

9 X = H
10 X = F

R = $-\underset{\underset{CH_3}{|}}{CH}CH_2CH_2CH_2CH(CH_3)_2$

towards dimethyl acetylenedicarboxylate as 2,4-cholestadiene: it failed to react in boiling benzene or toluene, while in boiling xylene it gave a 1:1 adduct, **13**, analogous to **6**. The structure **13** was again assigned on spectroscopic grounds (see Table 2) and was corroborated in this case by ozonolysis of the adduct to give the methyl ketone **14** (λ_{max} 5.78, 5.85(sh) μm; δ 2.21 (s, 3H)).

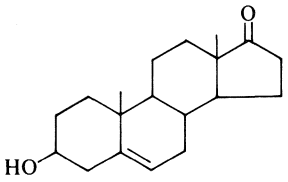

11

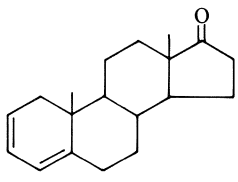

12

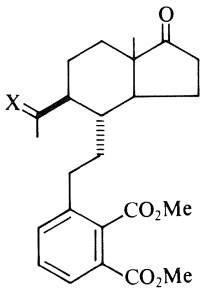

13 X = CH_2
14 X = O

In the cases of the reactions of both **4** and **12** with dimethyl acetylenedicarboxylate, all attempts to isolate, or even detect, the Diels–Alder adducts that are considered to be the intermediates in the formation of **6** and **13**, respectively, were unsuccessful. In an attempt to facilitate the initial Diels–Alder reaction so that it might be carried out at a temperature below that which brings about the cleavage of the adduct, the reaction of dimethyl acetylenedicarboxylate with **15**, the 3-trimethylsiloxy derivative of **4**, was investigated.[2] However, it was again necessary to heat the reactants in boiling xylene in order for reaction to occur, and the product, isolated after hydrolysis of the reaction mixture, was **16**, an analogue of **6** and **13**.

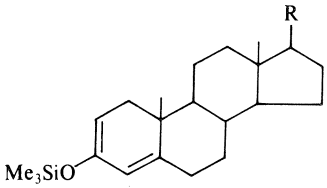

15

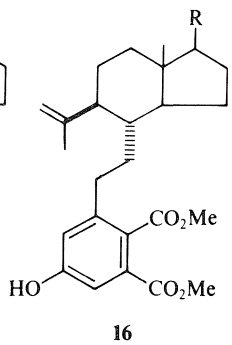

16

R = $-\underset{\underset{CH_3}{|}}{CH}CH_2CH_2CH_2CH(CH_3)_2$

We then turned to two other dienophiles. One was methyl propiolate; although electronic factors make it a less reactive dienophile than dimethyl acetylenedicarboxylate, it was hoped that its reduced steric requirements might serve to compensate for this. In the event, reaction of methyl propiolate with **12** again had to be effected in boiling xylene and a 7:3 mixture of the two retro-Diels–Alder products **17** and **18** was formed. These showed analogous spectroscopic properties to those of **13**, and were readily distinguished from one another in that the pmr spectrum of **17** showed two 2-proton multiplets at δ 7.35 and 7.85, while that of **18** showed a 3-proton multiplet at δ 7.35 and a 1-proton multiplet at δ 7.85. The ratio of these products is determined by the ratio of the inter-

[2]With a similar aim, **12** was treated with dimethyl acetylenedicarboxylate in the presence of aluminum chloride at room temperature (16) but only isomerization of **12** to its 3,5-isomer occurred.

Can. J. Chem. Downloaded from www.nrcresearchpress.com by 210.87.254.5 on 09/05/12
For personal use only.

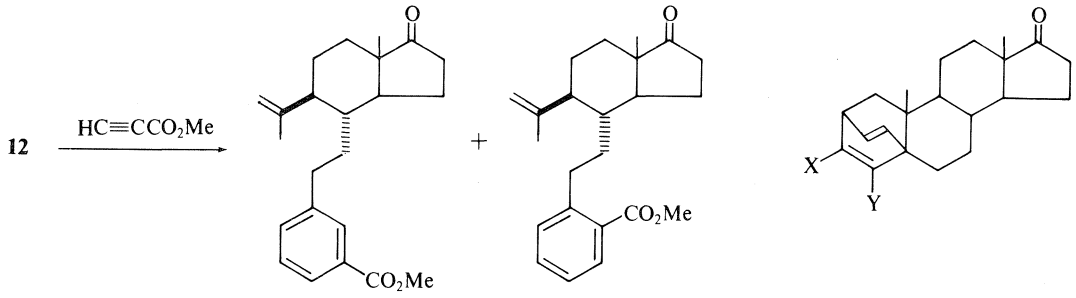

17 **18** **19** X = CO_2Me, Y = H; **20** X = H, Y = CO_2Me

mediate Diels–Alder adducts; the predominant formation of **17**, derived from the *meta* adduct **19**, rather than **18**, derived from the *ortho* adduct **20**, is attributable to the paramount influence of steric factors in determining the orientation in the Diels–Alder reaction (17).

The third dienophile investigated was dicyanoacetylene, whose reactivity was expected to be high on both electronic and steric grounds (11). Reaction of dicyanoacetylene with **12** could in fact be effected in boiling benzene to give a product whose elemental composition showed it to correspond to a 1:1 adduct and whose spectra (Table 2) were not analogous to those of the products obtained with the other dienophiles, but were in good accord with its formulation as the Diels–Alder adducts **21**α and/or **21**β. Its uv spectrum was very similar to that of the Diels–Alder adduct, **22**, of dicyanoacetylene with 9(11)-dehydroergosteryl acetate (λ_{max} 214 (ϵ 9900), 244 nm (ϵ 6875) (11)) and differed from that to be expected for the ene-reaction products **23** and **24** (*cf.* **25** and **26** (11): λ_{max} 227 nm (ϵ 13 100) and 227 nm (ϵ 15 400), respectively) or for a phthalonitrile derivative formed by a retro-Diels–Alder cleavage of **21** (*cf.* phthalonitrile (18): λ_{max} 237 (ϵ 10 500), 276 (ϵ 1120), 280.5 (ϵ 1660), 290 nm (ϵ 1700)). Its pmr spectrum confirmed the absence of a phthalonitrile moiety, and showed in the δ 4–7 region only a 2-proton multiplet at δ 6.05–6.65, assigned to the vinyl protons of **21** (*cf.* **22** (11): δ 6.06 and 6.44 (AB system, J = 7 Hz, 2H)); this spectrum also contraindicated structures **23** and **24**, which would be expected to show signals corresponding to four vinyl protons in the δ 5–6 region. A 1-proton multiplet at δ 3.85 is assigned to the bridgehead proton in **21**, and the two 3-proton singlets at δ 0.88 and 1.00 are assigned to the C.19 and C.18 methyl groups, respectively, the former being shielded relative to the C.19 methyl group in **12** (δ 0.95) by a bridging ethylenic double bond.

Although the recrystallized adduct **21** was sharp melting and could not be separated into the individual stereoisomers **21**α and **21**β, the complexity of the vinyl signal in its pmr spectrum suggested that it might be a mixture of **21**α and **21**β. That this in fact was the case was demonstrated by hydrogenation of **21** over platinum at atmospheric pressure, which led to a dihydro product **27**. As in the case of **22** (11), reduction occurred at the disubstituted ethylenic bond, as demonstrated by the absence of a vinylic proton signal in the pmr spectrum of **27**. The upfield region of this spectrum showed three singlets at δ 0.86, 0.91, and 1.11, clearly indicating that it

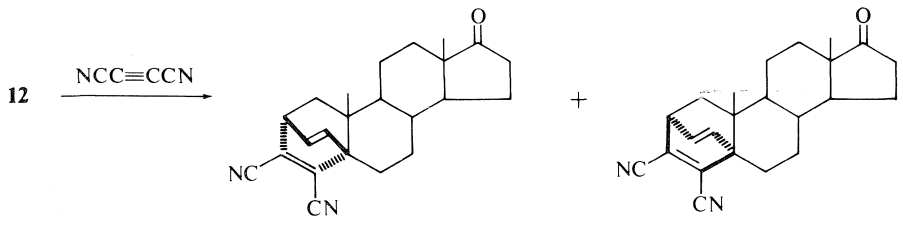

21α **21**β

Can. J. Chem. Downloaded from www.nrcresearchpress.com by 210.87.254.5 on 09/05/12
For personal use only.

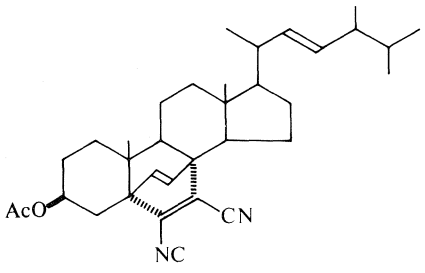

22

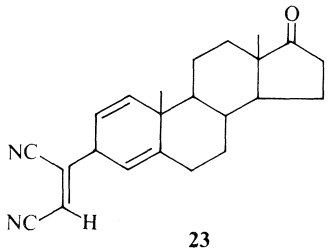

23

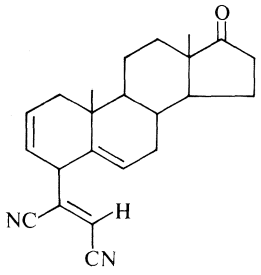

24

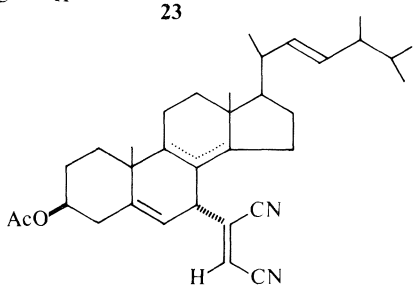

25 $\Delta^{8(9)}$
26 $\Delta^{8(14)}$

was a mixture of stereoisomers, **27**α and **27**β, and that the original adduct was a mixture of the stereoisomers **21**α and **21**β. The dihydro product could be separated by crystallization into the individual isomers. The preponderant isomer showed methyl proton signals at δ 0.86 and 1.11, while the other isomer showed corresponding signals at δ 0.86 and 0.91, and each showed a 1-proton multiplet at δ 2.9, attributed to the bridgehead proton in **27**. The latter isomer can be assigned structure **27**β since one of its methyl signals is shifted significantly to higher field relative to the methyl signals of the other isomer, indicating that the residual ethylenic bridge is shielding the C.19 methyl group and thus has the β orientation. The preponderant isomer is then **27**α, and the preponderant isomer of the adduct itself is **21**α, in accord with previous observations that preferential attack by dienophiles usually occurs from the α side of ring A and B steroid 1,3-dienes (Table 1).

Further evidence for the assignment of structure **21** to the mixture of adducts was provided by the observation that when this mixture was heated in boiling xylene it was converted to a product whose spectra showed it to be the retro-Diels–Alder product **28**, the analogue of **13**. The same product was formed when **12** and dicyanoacetylene were heated together in boiling xylene.

Thus the Diels–Alder reactions of steroid 2,4-dienes with acetylenes are not complicated by the occurrence of ene-reactions as in the case of

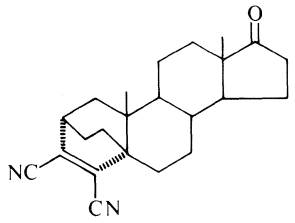

27α

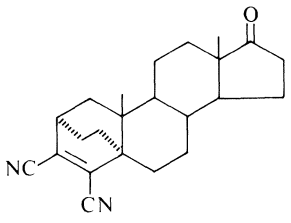

27β

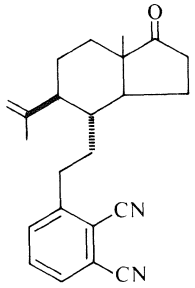

28

Can. J. Chem. Downloaded from www.nrcresearchpress.com by 210.87.254.5 on 09/05/12
For personal use only.

steroid 5,7-dienes,[3] but suffer from another hazard, rapid retro-Diels–Alder reaction of the adduct under the conditions required for its formation. This drawback can be surmounted by the use of a sufficiently activated and sterically unencumbered acetylenic dienophile. Finally, it may be noted that the retro-Diels–Alder reaction of the adducts provides a simple method for the joint cleavage of rings A and B of steroids.

Experimental

Melting points were determined on a Fisher–Johns apparatus and are uncorrected. Infrared spectra were recorded with chloroform as solvent unless otherwise specified. Proton magnetic resonance spectra were recorded with deuterochloroform as solvent. Organic solutions were dried over anhydrous magnesium sulfate; solvents were evaporated with a Büchi 'Rotovapor R'. Unless otherwise specified, chromatographic columns were prepared with silica gel (N.R. Grace, Davison Chemical Division, 100–200 mesh, ASTM D1319-61T, Grade 923) as solid phase. Preparative thin layer chromatography was performed on Quanta/Gram precoated 20×20 cm^2 silica gel plates (thickness 2 mm), activated for 15 min at 130 °C.

*2,4-Cholestadiene (**4**)*

(i) Dehydration of Cholesterol (cf. refs. 5, 20)

A stirred mixture of cholesterol (20.0 g, 0.052 mol), freshly activated alumina (40 g, 0.40 mol, BDH Chemical, heated for 24 h at 600 °C), and distilled *p*-cymene (300 ml) was heated under reflux in a Dean–Stark apparatus for 16 h. The cold mixture was filtered and the crude product obtained by evaporation of the solvent was crystallized from acetone to give a mixture (12.0 g, 63%) of 2,4-cholestadiene (**4**) and 3,5-cholestadiene. These were separated by chromatography on a silver nitrate impregnated silica gel column, prepared as follows. Silica gel (100 g) was added to an aqueous solution (180 ml) of silver nitrate (25 g) and the slurry was stirred for 10 min in the dark; the water was evaporated, first with a water aspirator, then in an oven at 60 °C for 14 h; the silica gel was activated at 130 °C for 4 h and a column (diameter 2.2 cm, height 35 cm) wrapped in aluminum foil was filled with this w/w 4:1 silica gel – silver nitrate mixture. The mixture of dienes (864 mg) was placed on the column in petroleum ether (bp 60–70 °C) and the column was eluted with this solvent (300 ml), giving a void first fraction. Elution with petroleum ether – benzene (99:1 v/v; 300 ml) gave 3,5-cholestadiene (258 mg). The third fraction obtained by elution with petroleum ether – benzene 98:2 v/v; 600 ml), contained a mixture of unidentified products (33 mg). Elution with petroleum ether – benzene (97:3 v/v; 600 ml, and 95:5 v/v; 100 ml) gave 2,4-cholestadiene (**4**) (567 mg, 41%). Crystallization from acetone yielded **4** (450 mg), mp 65–66 °C (lit. (5) mp 66–68 °C); λ_{max}(hexane) 266 (ϵ 6000), 275 nm (ϵ 5800) (lit. (5) λ_{max}(hexane) 266, 275 nm (ϵ 6100)); λ_{max} 6.10 (w), 6.33 (w) μm; $^{H}\delta$ 0.63 (s, 3H), 0.83 (s, 3H), 5.2–5.95 (m, 3H).

(ii) Via Cholest-4-en-3-one (cf. ref. 21)

In a 100 ml three-necked flask fitted with a condenser and a magnetic stirring bar were placed cholest-4-en-3-one (22) (10 g, 0.026 mol), *p*-toluenesulfonylhydrazine (4.85 g, 0.026 mol), tetrahydrofuran (40 ml), and concentrated hydrochloric acid (3 drops). The solution was boiled under reflux for 6 h, dry benzene (25 ml) was then added, and tetrahydrofuran was distilled at atmospheric pressure (bp 66–67 °C). The vapor temperature then rose to 70 °C and the benzene–water azeotrope was allowed to distil; the distillation was continued until the vapor temperature was *ca* 80 °C. The tosylhydrazone, which was not isolated was identified by its ir spectrum (λ_{max} 6.13 (w), 7.30, 8.55 μm). The solution was cooled in an ice bath and methyllithium in ether (1.82 *M*; 33 ml, 0.06 mol) was added dropwise with stirring over a 30 min period. The ice bath was removed and water (30 ml) was slowly added. The mixture was extracted with ether and the extract was dried and stripped of solvent to yield **4** (5.2 g, 63%), which was crystallized from acetone, to give material, mp 64–66 °C.

*Reaction of 4 with Dimethyl Acetylenedicarboxylate. Formation of **6***

A solution of **4** (100 mg, 0.27 mmol) and dimethyl acetylenedicarboxylate (200 mg, 1.4 mmol) in xylene (3 ml) was boiled under reflux for 20 h. After evaporation of the solvent and the remaining dienophile (0.5 torr; 80 °C) a yellow oil was obtained, which was purified on preparative tlc plates eluted twice with benzene. The product was recovered with ether. The solution was dried and the solvent was removed to yield **6** (52 mg, 40%), which was crystallized from methanol; mp 66–67 °C; λ_{max}(hexane) 232 (ϵ 8200), 281 (ϵ 1800), 290 nm (ϵ 1600); λ_{max} 5.76, 6.05 (w), 6.25 (w), 11.15 μm; $^{H}\delta$ 0.73 (s, 3H), 0.84 (s, 3H), 1.68 (s, 3H), 3.90 (s, 3H), 3.93 (s, 3H), 4.80 (s, 2H), 7.2–7.5 (m, 2H), 7.7–8.0 (m, 1H); *m/e* 510 (6), 478 (49). *Anal.* calcd. for $C_{33}H_{50}O_4$: C 77.60, H 9.87; found: C 77.46, H 9.76.

*2,4-Androstadien-17-one (**12**)*

The diene **12** was prepared from dehydroisoandrosterone (**11**) following the same procedure as for 2,4-cholestadiene (method *i*); **12** was purified by chromatography on neutral alumina (Woelm–Grade II) using chloroform as eluent. The diene was recrystallized from chloroform–pentane (v/v 3:2) (yield: 51%); mp 129–130 °C (lit. (23) mp 134–136 °C); λ_{max}($CHCl_3$) 267 nm (ϵ 6000) with a shoulder at 272–279 nm (lit. (23) λ_{max} 266 nm (ϵ 6200) with a shoulder at 271–275 nm); λ_{max} 5.75, 6.3 (br w) μm; $^{H}\delta$ 0.95 (s, 3H), 1.00 (s, 3H), 5.4–6.0 (m, 3H); *m/e* 270 (100).

*Reaction of **12** with Dimethyl Acetylenedicarboxylate. Formation of **13***

A solution of **12** (270 mg, 1.00 mmol) and dimethyl acetylenedicarboxylate (464 mg, 5 mmol) in xylene (5 ml) was boiled under reflux for 20 h. After evaporation of the solvent and the remaining dienophile (0.5 torr; 80 °C) a yellow oil was obtained, which was chromatographed

[3]It may be noted, however, that 2,4-cholestadiene (**4**) gives with dimethyl azodicarboxylate both a Diels–Alder adduct (20%) and ene-reaction products (16%) (19).

Can. J. Chem. Downloaded from www.nrcresearchpress.com by 210.87.254.5 on 09/05/12
For personal use only.

Can. J. Chem. Downloaded from www.nrcresearchpress.com by 210.87.254.5 on 09/05/12
For personal use only.

on a silica gel column with elution with ether; further purification on preparative plates eluted twice with chloroform gave **13** (73 mg, 30%), which crystallized from methanol as white needles, mp 54–55 °C; λ_{max}(MeOH) 232 (ϵ 8100), 280 (ϵ 1800), 286–289 nm (ϵ 1600); λ_{max} 5.76, 6.07 (w), 6.23 (w), 11.15 μm; $^{H}\delta$ 0.95 (s, 3H), 1.75 (s), 3.90 (s, 3H), 3.93 (s, 3H), 4.83 (s, 2H), 7.2–7.5 (m, 2H), 7.7–7.9 (m, 1H). The electron impact ionization mass spectrum of **13** did not show a molecular ion (M 412); the chemical ionization mass spectrum gave the following results: (*i*) with methane: *m/e* 441 (20, $M + 29$), 427 (5, $M + 15$), 413 (9, $M + 1$), 395 (30, $M - 17 \equiv M + 15 - 32$), 381 (100, $M - 31 \equiv M + 1 - 32$), (*ii*) with hydrogen: 413 (20, $M + 1$), 381 (80, $M + 1 - 32$), 380 (100, $M - 32$).

*Ozonolysis of **13**. Formation of **14***

Ozone was bubbled through a solution of **13** (200 mg, 0.49 mmol) in methanol (50 ml) at −78 °C until a blue coloration of the solution was detected. The passage of ozone was then stopped and a stream of oxygen was passed through the solution until the blue color disappeared. Aqueous sodium iodide (0.5 *M*; 4 ml) and acetic acid (2 drops) were then added to the solution. The stirred solution was left at room temperature for 14 h and heated at 45 °C for 1 h. The iodine was destroyed with aqueous sodium bisulfite (0.5 *M*; 3 ml), the solution was neutralized by sodium carbonate, the methanol was evaporated, and the product was extracted with ether. The extract was dried and after evaporation of the solvent **14** (160 mg, 80%) was isolated and crystallized from methanol as white needles, mp 126–127 °C; λ_{max}(MeOH) 232 (ϵ 8100), 280 (ϵ 1800), 286–289 nm (ϵ 1600); λ_{max} 5.78, 5.85 (sh) 6.24 (w) μm; $^{H}\delta$ 0.97 (s, 3H), 2.21 (s, 3H), 3.90 (s, 3H), 3.93 (s, 3H), 7.25–7.5 (m, 2H), 7.7–7.9 (m, 1H), *m/e* 414 (9). *Anal.* calcd. for $C_{24}H_{30}O_6$: C 69.54, H 7.30; found: C 69.27, H 7.34.

*3-Trimethylsiloxy-2,4-cholestadiene (**15**) (cf. ref. 24)*

Tetrahydrofuran (15 ml) dried over lithium aluminum hydride was distilled under nitrogen into a 50 ml, three-necked flask fitted with a thermometer and a magnetic stirring bar containing dry diisopropylamine (1.45 ml, 0.010 mol). The solution was cooled to 0 °C. Methyllithium (0.012 mol) in ether (1.82 *M*; 6.5 ml) was slowly added with stirring, so that the temperature did not exceed 0 °C. To this solution of lithium diisopropylamide was added, dropwise and with stirring over a 10 min period, a solution of cholest-4-en-3-one (3.84 g, 0.0100 mol) in tetrahydrofuran–ether (5:2 v/v; 15 ml). Dry trimethylchlorosilane (2.5 ml, 0.022 mol) was rapidly added with stirring to the solution kept at 0 °C. After the addition was complete a white solid (LiCl) began to separate. The resulting mixture was stirred at room temperature for 30 min. Tetrahydrofuran and ether were then evaporated, the residue was treated with dry hexane (40 ml), and the mixture was filtered. The filtrate was rapidly washed with a cold aqueous 5% sodium bicarbonate solution and with water, and dried. The solvent was evaporated to yield **15** (4.56 g, 93%). The silyl ether **15** was very sensitive to moisture and had to be kept in a dry atmosphere; mp 91–92 °C; λ_{max} 6.06 (m) μm; $^{H}\delta$ 0.2 (s, 9H), 0.66 (s, 3H), 4.3–4.8 (m, 1H), 5.2–5.4 (m, 1H); *m/e* 456 (65).

*Reaction of **15** with Dimethyl Acetylenedicarboxylate. Formation of **16***

A solution of **15** (0.98 g, 2.13 mmol) and dimethyl acetylenedicarboxylate (1.51 g, 8 mmol) in dry xylene (25 ml) was boiled under reflux under nitrogen for 16 h. Evaporation of the solvent and the remaining dienophile (0.5 torr; 80 °C) yielded a yellow oil, which was dissolved in methanol (15 ml). Concentrated hydrochloric acid (8 drops) was added to the solution, which was stirred at room temperature for 2 h. The methanol was evaporated and the residue was extracted with ether. The extract was dried and the solvent was evaporated to yield crude **16**. This was purified by chromatography on a silica gel column eluted first with chloroform, then with chloroform – ethyl acetate (99:1 v/v and 98:2 v/v) to yield **16** (450 mg; 40%), which was crystallized from methanol; mp 65–66 °C; $\lambda_{max}(CS_2)$ 3.0 (w), 5.78, 6.05 (w), 6.21 (w) μm; $^{H}\delta$ 0.73 (s, 3H), 0.84 (s, 3H), 1.68 (s, 3H), 3.90 (s, 3H), 3.93 (s, 3H), 4.80 (s, 2H), 6.8–6.9 (m, 1H), 7.1–7.2 (m, 1H); *m/e* 526 (11), 494 (92).

*Reaction of **12** with Methyl Propiolate. Formation of **17** and **18***

A solution of **12** (135 mg, 0.50 mmol) and methyl propiolate (210 mg, 2.5 mmol) in xylene was heated at 140 °C in a sealed tube for 72 h. The solvent and the remaining dienophile were evaporated *in vacuo*. The residual oil was submitted to chromatography on silica gel preparative plates eluted twice with chloroform. A mixture of adducts **17** and **18** was isolated (65.6 mg, 30%); λ_{max} 5.79, 6.08 (w), 6.22 (w), 6.30 (w), 11.2 (m) μm. The approximate composition of the mixture, determined by pmr spectroscopy, was 7:3 of **17** and **18**. Fractional crystallization of the mixture from methanol led to pure **17** and to **18** containing **17** as an impurity. Compound **17** had mp 66–67 °C; λ_{max}(MeOH) 232 (ϵ 10 600), 279 (ϵ 1800), 284–287 nm (ϵ 1700); $\lambda_{max}(CS_2)$ 5.73, 5.78, 11.20 (m) μm, $^{H}\delta$ 0.93 (s, 3H), 1.68 (s, 3H), 3.93 (s, 3H), 4.83 (s, 2H), 7.2–7.5 (m, 2H), 7.85 (m, 2H). Compound **18** had mp 96–99 °C; $\lambda_{max}(CS_2)$ 5.75, 5.79, 11.22 (m) μm; $^{H}\delta$ 0.93 (s, 3H), 1.68 (s, 3H), 3.90 (s, 3H), 7.2–7.5 (m, 3H), 7.85 (m, 1H) (the spectra also show weak signals due to the presence of **17**); *m/e* 354 (19). *Anal.* (on mixture of **17** and **18**) calcd. for $C_{23}H_{30}O_4$: C 77.93, H 8.53; found: C 77.72, H 8.49.

*Reaction of **12** with Dicyanoacetylene*

*(i) In Boiling Benzene; Formation of **21***

A solution of dicyanoacetylene (5.20 mmol) in anhydrous benzene (8 ml of a 0.65 *M* solution) (25) was added to a solution of **12** (1.00 g, 3.60 mmol) in anhydrous benzene (12 ml). The mixture was boiled under reflux under nitrogen for 14 h. After evaporation of the solvent and of the remaining dicyanoacetylene a red oil was obtained. This was chromatographed on a silica gel column with chloroform – ethyl acetate (95:5 v/v) as eluent. A colorless oil was obtained (652 mg, 51%), which was crystallized from methanol to give **21**; mp 158–159 °C; λ_{max}(EtOH) 213 (ϵ 6800), 243 nm (ϵ 7500); λ_{max} 4.50 (w), 5.75, 6.21 (w), 6.27 (w) μm; $^{H}\delta$ 0.88 (s, 3H), 1.00 (s, 3H), 3.7–4.0 (m, 1H), 6.1–6.7 (m, 2H). *Anal.* calcd. for $C_{23}H_{26}ON_2$: C 79.73, H 7.56, N 8.09, mw 346.2045; found: C 79.35, H 7.47, N 8.15, *m/e* 346.2045.

(ii) In Boiling Xylene; Formation of ***28***

A solution of dicyanoacetylene (1.88 mmol) in anhydrous benzene (1.5 ml of a 1.25 *M* solution) was added to a solution of **12** (325 mg, 1.20 mmol) in anhydrous xylene (3 ml). The mixture was boiled under reflux under nitrogen for 16 h. After evaporation of the solvent, a dark brown oil was obtained, which was purified by chromatography on a silica gel preparative plate with elution with chloroform to give **28** (150 mg) as an oil; λ_{max} 4.60 (w), 5.80, 6.21 (w), 6.42 (w), 11.20 (m) μm; $^{H}\delta$ 0.96 (s, 3H), 4.82 (s, 2H), 7.4–7.8 (m, 3H); *m/e* 346.

Compound **28** was also formed in quantitative yield when a solution of **21** in xylene was boiled under reflux for 13 h.

Hydrogenation of ***21****. Formation of* ***27****α and* ***27****β*

The adducts **21** (275 mg, 0.80 mmol) in ethyl acetate (50 ml) were hydrogenated at atmospheric pressure over platinum (100 mg) until 1 equiv. of hydrogen had been absorbed (22 h). After filtration of the catalyst and removal of the solvent, the dihydro product **27** was obtained as a colorless oil (230 mg, 83%). Fractional crystallization of this from methanol gave the less soluble β-adduct (**27**β) and the more soluble α-adduct (**27**α) in a *ca.* 1:3 ratio. Compound **27**β had mp 238–240 °C; λ_{max} (EtOH) 242 nm (ϵ 8000); λ_{max} 5.75, 6.23 (w) μm; $^{H}\delta$ 0.86 (s, 3H), 0.91 (s, 3H), 2.90 (m, 1H). Compound **27**α had mp 226–227 °C; λ_{max}(EtOH) 242 nm (ϵ 8700); λ_{max} 5.75, 6.23 (w) μm; $^{H}\delta$ 0.86 (s, 3H), 1.11 (s, 3H), 2.9 (m, 1H). *Anal.* calcd. for $C_{23}H_{28}ON_2$: C 79.27, H 8.10, N 8.04, mw 348.2202; found: C 78.58, H 7.95, N 7.94, *m/e* 348.2202.

Acknowledgements

We thank the National Research Council of Canada for support of this work. One of us (F.M.W.) thanks the Canada Council for an Award.

1. A. J. Solo, S. Eng, and B. Singh. J. Pharm. Sci. **62**, 1474 (1973).
2. W. Nagata, M. Narisada, T. Sugasawa, and T. Wakabayashi. Chem. Pharm. Bull. **16**, 885 (1968).
3. M. Kocor and W. Kroszczynski. Tetrahedron Lett. 5143 (1970).
4. H. E. Stavely and W. Bergmann. J. Org. Chem. **1**, 575 (1936).
5. I. F. Eckhard, H. Heaney, and B. A. Marples. J. Chem. Soc. C, 2098 (1969).
6. S. Akagi and Y. Okada. Chem. Pharm. Bull. **9**, 476 (1961).
7. D. N. Jones, P. F. Greenhalgh, and I. Thomas. Tetrahedron, **24**, 297 (1968).
8. K. Tsuda and S. Nozoe. Chem. Pharm. Bull. **8**, 1128 (1960).
9. K. D. Bingham, G. D. Meakins, and J. Wicha. J. Chem. Soc. C, 671 (1969).
10. H. Honigmann. Ann. **508**, 89 (1934).
11. A. Abramovitch and P. W. Le Quesne. J. Org. Chem. **39**, 2197 (1974).
12. A. van der Gen, W. A. Zunnebeld, U. K. Pandit, and H. O. Huisman. Tetrahedron, **21**, 3651 (1965).
13. G. D. Laubach, E. C. Schreiber, E. J. Agnello, and K. J. Brunings. J. Am. Chem. Soc. **78**, 4743 (1956).
14. L. Keller, C. Tamm, and T. Reichstein. Helv. Chim. Acta, **41**, 1633 (1958).
15. O. L. Chapman and C. W. Borden. J. Org. Chem. **26**, 4193 (1961).
16. P. Yates and P. Eaton. J. Am. Chem. Soc. **82**, 4436 (1960).
17. Y. A. Titov. Russ. Chem. Rev. **31**, 267 (1962).
18. UV atlas of organic compounds. Vol. 1. Butterworths, London, 1966. Spectrum No. D9/1.
19. M. Tomoeda, R. Kikuchi, M. Urata, and T. Futamura. Chem. Pharm. Bull. **18**, 542 (1970).
20. E. L. Skau and W. Bergmann. J. Org. Chem. **3**, 166 (1938); J. Am. Chem. Soc. **60**, 986 (1938).
21. W. G. Dauben, M. E. Lorber, N. D. Vietmeyer, R. H. Shapiro, J. H. Duncan, and K. Tomer. J. Am. Chem. Soc. **90**, 4762 (1968).
22. J. F. Eastham and R. Teranishi. Org. Synth. **4**, 192 (1963).
23. B. Berkoz, A. D. Cross, M. E. Adame, H. Carpio, and A. Bowers. J. Org. Chem. **28**, 1976 (1963).
24. H. O. House, L. J. Czuba, M. Gall, and H. D. Olmstead. J. Org. Chem. **34**, 2324 (1969); C. Girard and J. M. Conia. Tetrahedron Lett. 3327 (1974).
25. C. Moreu and J. C. Bongrand. Ann. Chim. (Paris), [9] **14**, 5 (1920); A. T. Blomquist and E. C. Winslow. J. Org. Chem. **10**, 149 (1945).

Can. J. Chem. Downloaded from www.nrcresearchpress.com by 210.87.254.5 on 09/05/12
For personal use only.

Chemistry of amido radicals: Stereochemical controls in Π radical reactions[1]

T. C. JOSEPH, JOSIAH N. S. TAM, MASAYUKI KITADANI, AND YUAN L. CHOW
Department of Chemistry, Simon Fraser University, Burnaby, B.C., Canada V5A 1S6

Received January 26, 1976[2]

T. C. JOSEPH, JOSIAH N. S. TAM, MASAYUKI KITADANI, and YUAN L. CHOW. Can. J. Chem. **54**, 3517 (1976).

The acyclic amido radicals generated from the corresponding *N*-bromo-*N*-*tert*-alkylamides reacted like *N*-radicals, rather than *O*-radicals, and preferentially abstracted a δ-hydrogen of the alkyl chain, rather than a γ-hydrogen of the acyl chain. On the basis that, in these amido radicals, the conformation of the transition state of the hydrogen transfer is a five-membered ring and the stereoelectronic requirement for the transfer demands a colinear arrangement of the radical containing orbital and the C—H bond, the results are satisfactorily rationalized by the Π electron configuration of the amido radicals. It is also established that the chain length of these *N*-bromoamide photodecompositions increases as the intramolecular hydrogen transfer of the corresponding amido radicals becomes easier; the hydrogen abstraction step must be the rate determining step in the chain reaction. The spontaneous formations of γ-iminolactones from γ-bromoamides indicate that the intramolecular nucleophilic displacement by the *O*-center of the amido group is facilitated since its transition state conformation readily accommodates the stereoelectronic requirements for the nucleophilic substitution. A colinear approach of the *p*-orbital of the more nucleophilic *N*-center to the rear side of the γ-C—Br bond is shown to be prohibitively strained.

T. C. JOSEPH, JOSIAH N. S. TAM, MASAYUKI KITADANI et YUAN L. CHOW. Can. J. Chem. **54**, 3517 (1976).

Les radicaux amido acycliques, générés à partir des *N*-bromo *N*-*tert* alkylamides correspondantes, réagissent comme les radicaux *N*-alkyles plutôt que comme des radicaux *O*-alkyles; ils réagissent préférentiellement pour enlever un hydrogène en δ de la chaîne alkylée plutôt qu'un hydrogène en γ de la chaîne acylée. En faisant l'hypothèse que, dans ces radicaux amido, la conformation de l'état de transition du transfert d'hydrogène est un cycle à cinq membres et que les conditions stéréoélectroniques pour le transfert demandent un arrangement colinéaire de l'orbitale contenant le radical et du lien C—H, on peut rationaliser d'une façon satisfaisante les résultats par la configuration électronique Π des radicaux amido. On a aussi établi que la longueur de la chaîne de ces photodécompositions de *N*-bromoamides augmente à mesure que le transfert d'hydrogène intramoléculaire des radicaux amido correspondants devient plus facile; l'étape de l'enlèvement de l'hydrogène doit être l'étape déterminante dans la réaction en chaîne. Les réactions spontanées de formation de γ-iminolactones à partir de γ-bromoamides indiquent que le déplacement nucléophile intramoléculaire par l'intermédiaire du centre oxygéné du groupe amido est facilité puisque la conformation de son état de transition accommode facilement les demandes stéréoélectroniques de la substitution nucléophile. La tension provoquée par une approche colinéaire de l'orbitale *p* du centre azoté, qui est plus nucléophile, vers la face arrière du lien γ-C—Br est prohibitive.

[Traduit par le journal]

In recent years, the existence of amido radicals[3] (RCONR′) as transient reactive intermediates has been demonstrated by esr spectroscopy (2–6), flash photolysis (7), ^{13}C-CIDNP studies (8), and reaction patterns (9–13). These results have stimulated considerable interest in the chemistry of nitrogen-centered radicals (14, 15), which had previously not attracted as much attention as oxygen- and sulfur-centered radicals (16, 17). From the molecular orbital point of view,[4] amido radicals are unique in that the unpaired electron can be accommodated either in

[1]Part of this work was reported in a preliminary communication (see ref. 1).

[2]Revision received June 22, 1976.

[3]As INDO calculations show, the nature of the R and R′ groups may modify the electronic configuration of amido radicals (4, 5). The present discussion will be limited to those acyclic amido radicals in which R and R′ are alkyl groups.

[4]The ground state geometry of the NH_2 radical has been shown to be similar to the singlet CH_2 and has Π electronic configuration (17*b*).

Can. J. Chem. Downloaded from www.nrcresearchpress.com by 210.87.254.105 on 09/05/12
For personal use only.

Can. J. Chem. Downloaded from www.nrcresearchpress.com by 210.87.254.105 on 09/05/12
For personal use only.

the *p*-orbital or in the sp^2-orbital of the nitrogen center, giving rise to Π (**1**) and Σ (**2**) electronic configurations respectively (2–6). *A priori*, the ordering of the energy levels of these two configurations is not readily predicted since the energy resulting from promotion of one sp^2 electron (in Π radicals) to the *p*-orbital (to form Σ radicals) and those from the delocalization of the unpaired electron and the pair of electrons in the *p*-orbital of amido radicals are not readily estimated. While the Σ and Π electronic configurations in the ground state of amido radicals are ultimately related to the reactivity of amido radicals generated by various methods, scarcity and uncertainty of published data do not permit a generalization at the present stage. Hydrogen abstraction, both intramolecular and intermolecular, is probably the best established reaction pathway among the amido radical reactions (7–13). Addition of *N*-alkylamido radicals to olefins has been reported only recently (18, 19).

The ground state electronic configuration of amido radicals has been a controversial question. The recent esr work by Danen and Gellert (2) is generally accepted as a definitive evidence in favor of a Π radical configuration for *N*-alkylamido radicals. This has led us to speculate that a Π amido radical may react as an *N*-centered radical (**1**) as well as an *O*-centered radical (**3**), whereas a Σ radical will react predominantly as an *N*-centered species (**2** and **4**). In view of the well recognized fact that intramolecular hydrogen abstraction generally occurs at the fifth position from the radical center (20–22), an amido radical may functionalize the alkyl side chain at the β- or δ-position depending on the *O*- or *N*-radical character. It is also desirable to establish the preference of hydrogen abstraction from the acyl and the alkyl side chains in amido radicals since this information may shed light on the electronic configuration of the ground state of amido radicals. We have studied the photodecomposition of *N*-bromo-*N*-alkylamides in an attempt to clarify the reactivities of amido radicals.

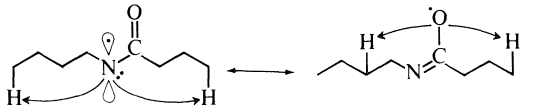

1(π) **3**

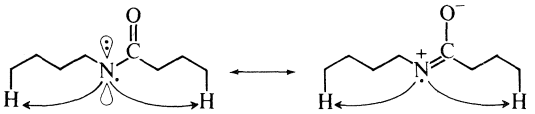

2(Σ) **4**

Results

As the possible precursors for the generation of amido radicals, we had chosen *N*-bromo derivatives of *N*-alkylamides as the model compounds rather than the *N*-chloro and *N*-nitroso analogues, on account of the relatively mild reactivity of the bromine atom, the resulting counter radical generated in the photolysis. The other two classes of compounds are less satisfactory; atomic chlorine is an aggressive hydrogen abstractor (23), and nitric oxide leads to an undesirable mixture containing $\cdot NO_2$ and $\cdot NO_3$ (9). The desired bromoamides were prepared by reacting *tert*-butylhypobromite with the parent *N*-alkylamides. The light yellow benzene solutions of the crude bromoamides were irradiated in a Pyrex flask with a medium-pressure Hanovia mercury lamp at room temperature. All photolyses were complete in less than an hour as indicated by a negative KI test and the disappearance of the yellow color. In general the photolysate was evaporated and the crude product was examined by ir and nmr spectroscopy and was worked up accordingly.

As an exploratory step, *N*-bromo and *N*-chloro derivatives of *N*-alkylvaleramide were used as model compounds to study the modes of photodecomposition. The results are similar to those published by Neale *et al.* (13), who have concluded that the presence of an *N*-*tert*-butyl group markedly improves the chance of the intramolecular halogen–hydrogen atom exchange reaction. We also observed that photodecomposition of the corresponding *N*-chloramides in a Pyrex apparatus required an induction period, while in a quartz apparatus equipped with a Corex filter the reaction proceeded immediately and rapidly.

Our general strategy was to generate an amido radical having comparable numbers and types of C—H bonds at suitable positions so that competitive intramolecular hydrogen abstraction among these positions could be observed. For this purpose, photolyses of bromoamides **5**, **9**, and **13** were carried out in benzene. The chemical

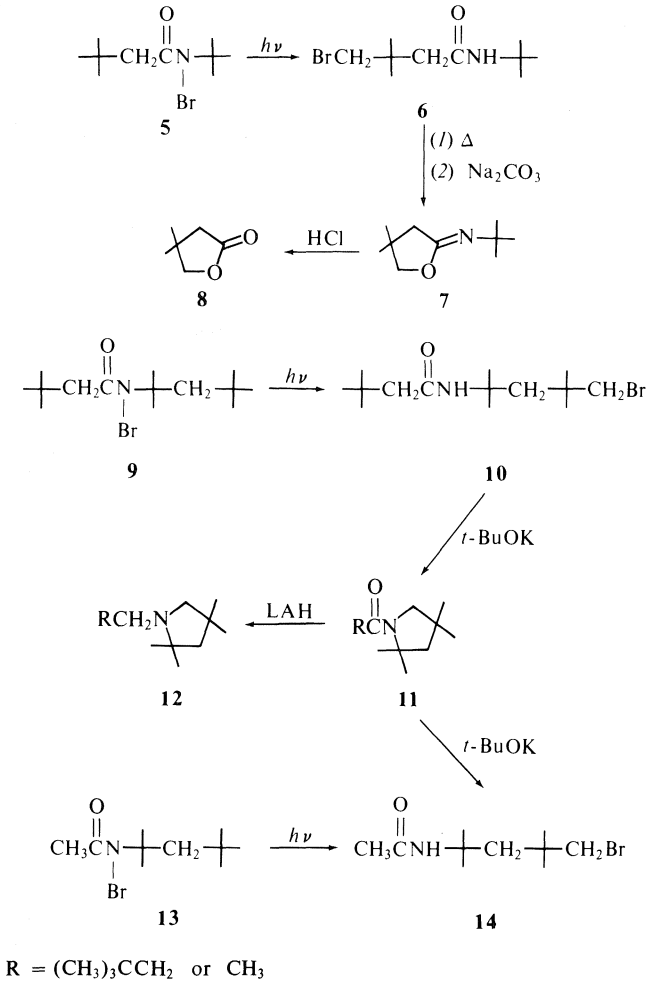

SCHEME 1

transformations are summarized in Scheme 1. Identification of the primary rearrangement products was greatly facilitated by the clean nmr spectra of the bromo compounds **6**, **10**, and **14**, which exhibited a two proton singlet at τ 6.4 region for —CH_2Br. While bromides **10** and **14** could be recrystallized, bromide **6** cyclized readily to the HBr salt of iminolactone **7** on heating in benzene. Judging from the clean nmr and ir spectra, the yields of the bromides were essentially quantitative. As a comparison, the *N*-chloro analogue of **9** was also photolysed but gave only 12% of **10** (Br = Cl) and a large quantity of the parent amide. It is pertinent to mention that owing to the presence of neighboring quaternary carbon centers, hydrolysis of amide **11** was unsuccessful, and that of **7** required prolonged heating in 4 *N* aqueous HCl solution.

Although there are two suitably placed sets of hydrogens for abstraction by the *N*-centered radical and two by the *O*-centered radical in the amido radical generated from **9**, the results clearly showed that the hydrogens in the alkyl terminal were abstracted in preference to those in other positions. No trace of lactone **8** was obtained when the photolysate from **9** was treated with concentrated H_2SO_4. In all cases studied, there was no indication that an *O*-radical was also abstracting the β-hydrogen atom of the alkyl chain. Should such an abstraction mode be operative, the resulting β-

Can. J. Chem. Downloaded from www.nrcresearchpress.com by 210.87.254.105 on 09/05/12
For personal use only.

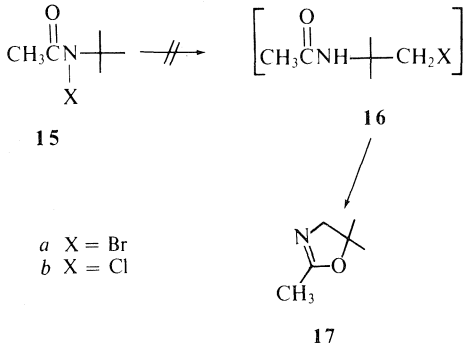

bromides would generate complex nmr patterns that would be readily recognizable.

The lack of *O*-radical reactivity was further supported by failure to detect formation of oxazoline **17** (or bromide **16**, X = Br) in the photolysis of bromoamide **15**, where no abstractable hydrogen other than the β-hydrogens was available for 1,5-transfer. From this photolysis a nearly quantitative yield of *N-tert*-butylacetamide was isolated. In view of the reported formation of oxazoline **17** in 37% yield in the photolysis of chloramide **15** (X = Cl) (13), this photolysis was repeated under comparable conditions. In our experiments, the parent amide was isolated in >90% yield and oxazoline **17** was detected by the nmr signal (13) at τ 6.2 in <10% yield. It is most likely that chloride **16** (X = Cl) is formed via an intermolecular hydrogen abstraction by chlorine atom, but not by a genuine intramolecular pathway. In such an intermolecular hydrogen abstraction, it is reasonable to expect that the *tert*-butyl hydrogens are abstracted by the electronegative chlorine atom in preference to the methyl hydrogens (23).

The photoinduced intramolecular bromine–hydrogen exchange reaction is obviously a free radical chain process, as shown by the high quantum yields of the photolyses (Table 1). The quantum yields were determined as described in the Experimental section, and corresponded to the averaged minimum chain length. While the degassed solutions of *N*-bromoamides decomposed smoothly, undegassed solutions were slow to decompose, owing presumably to inhibition by oxygen. Clearly the chain length was longer where there was a facile hydrogen abstraction pathway, *e.g.*, an intramolecular δ-hydrogen atom transfer from the alkyl chain. This observation suggests that the intramolecular hydrogen abstraction process is the rate determining step in the bromoamide decomposition.

TABLE 1. Quantum yield determination

N-Bromoamide	Concentration ($\times 10^2$ mol/l in benzene)	Φ^a	Relative Φ
5	1.74	33.9	3.5
13	1.40	131	13.5
15(X = Br)	1.44	9.7	1.0

[a]The averaged minimum quantum yields.

An application of this 1,5-hydrogen transfer reaction during *N-tert*-butyl-*N*-bromoamide photolysis was demonstrated in the synthesis of iminolactone **19** starting from 3β-hydroxy-5-androsten-17-carboxylic acid (**18**) in 25% overall yield. The percentage yield of **19** was improved to better than 60% starting from the correspond-

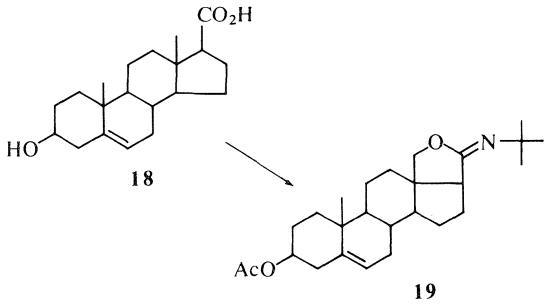

ing *N-tert*-butylcarboxamide. The reaction sequence is described in the Experimental section and consists of, in addition to the standard processes described above, the steps of bromination to protect the $\Delta^{5,6}$-olefinic bond and zinc debromination to regenerate the same double bond. Since the C-18 methyl and the C-17 carboxamido groups are oriented nearly coplanar, both hydrogen transfer as well as the subsequent iminolactone cyclization process must be very efficient.

Discussion

The experimental results described above establish two salient points, namely, (*i*) that the *N*-alkylamido radicals studied so far do not react as *O*-radicals in intramolecular hydrogen abstractions, and (*ii*) that a δ-hydrogen of the alkyl side-chain, rather than a γ-hydrogen of the acyl side chain, is preferentially transferred to the *N*-radical center. The lack of *O*-radical reactions

Can. J. Chem. Downloaded from www.nrcresearchpress.com by 210.87.254.105 on 09/05/12
For personal use only.

Can. J. Chem. Downloaded from www.nrcresearchpress.com by 210.87.254.105 on 09/05/12
For personal use only.

does not prove that the electronic ground state of an amido radical has the Σ configuration,[5] since spin densities and relative reactivities of the *N*- and *O*-radicals in the Π configuration are yet unknown. Since only one set of nmr signals is observed for each bromoamide, and, in addition, Corey–Pauling scale models predict considerable steric hindrance between the two alkyl groups, one would expect that these groups would have a *trans* configuration around the amido linkage. This would lead to a Σ configuration for the 'nascent' state of the amido radical, assuming that the molecular geometry of bromoamides is not altered drastically during the decomposition. Since electronic reorganization can generally take place in much shorter times than bond formation or bond breaking, it is not mandatory that the amido radicals maintain this Σ radical configuration during the course of the reaction. If the corresponding Π electronic configuration corresponds to the lower-energy species, then rapid relaxation to this form would precede the chemical transformation.

From their esr studies, Danen and Gellert (2) have concluded that the unpaired electron in the Π amido radical configuration is not extensively delocalized to the *O*-center of the carbonyl group. It is therefore reasonable to assume that these alkylamido radicals, while possessing a Π configuration, must exhibit only weak *O*-radical character. A Π configuration for the amido radicals is also suggested by the INDO calculations[6] (4, 5) and the ^{13}C-CIDNP experiments (8). Further, INDO calculations show that the energy level of an *O*-amido radical configuration is higher than that of the corresponding *N*-radical by 10–20 kcal/mol (4, 5).

The observed preferential 1,5-hydrogen transfer from the alkyl side chains is no doubt a result of a favored transition state geometry of the hydrogen abstraction process in these amido radicals. For the completely flexible acyclic amido radicals under consideration, the transition state model of 1,5-hydrogen transfer as proposed for aminium radical (20) and alkoxy radical (21) reactions will be adapted. This transition state model assumes that the six participating nuclei can freely rotate around the C—C bonds to give a favorable transition state conformation in which the radical containing orbital and the C—H bond to be broken are oriented coplanar to one another and at the same time as close to colinear as the conformational variations allow. In other words, it is believed that the orientation of the reacting orbitals for a maximum overlap (*cf.* 26, 27) is as important a controlling factor as the close proximity of the reacting centers. In the absence of any other contrary evidence, it is also assumed that the amido radicals maintain the Π electronic configuration, but the delocalization energy of the unpaired electron in the nitrogen *p*-orbital is very small as discussed previously.

Based on these assumptions, the geometries of intramolecular hydrogen transfers from the acyl and alkyl chains in amido radicals are depicted in **20** and **21**. By using Dreiding stereomodels, it

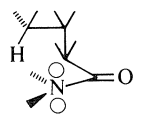

20

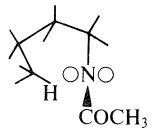

21

can be shown that in radical **21** the C—N bond of the alkyl side chain can rotate freely to gain a near colinearity of the *p*-orbital at the *N*-center and a C—H bond at the δ-carbon and, therefore, can achieve a maximum overlap of the *p*- and *s*-orbitals. On the contrary, just to assume a coplanar conformation of the γ-C—H bond of the acyl side chain and of the *p*-orbital at the *N*-center requires the rotation of the aliphatic chain around the C—CO bond for nearly 90° as shown in **20**; in this geometry the three reacting centers are much too far apart to effect the hydrogen transfer. A probable alternative is the rotation of the N—CO bond by breaking the Π amido radical overlap that should bring the reacting centers closer and into a near colinear

[5]In a previous paper describing photoreaction of *N*-nitrosamides (24), we proposed transition states embracing the principle of a Σ electronic configuration for ground state amido radicals. This has led others (25) to interpret our subsequent publications (1, 9) on amido radicals in a similar sense. We wish to state that our earlier proposal of Σ radical transition states (24) was in error.

[6]In the recent 59th conference of the Chemical Institute of Canada held in London, Ontario (June 7–9, 1976), Professor N. C. Baird has reported that by *ab initio* calculations the ground state of the HCONH radical has a Π electronic configuration. These studies show that the Π configuration possesses a lower energy than the Σ electronic configuration by 11 kcal/mol.

Can. J. Chem. Downloaded from www.nrcresearchpress.com by 210.87.254.105 on 09/05/12
For personal use only.

arrangement. The energy barrier to disrupt the Π radical overlap is probably very small, but an amount of 2–3 kcal/mol is sufficient to retard the γ-hydrogen transfer of the acyl chain to the extent that the δ-hydrogen transfer of the alkyl chain is the only process observed. These arguments are further supported by failure to functionalize the acyl side chain in the photolysis (9, 12, 13) of *N*-nitroso-*N*-methylcaproamide, and *N*-nitroso and *N*-bromo derivatives of *N*-methylvaleramide.[7] The corresponding amido radicals undergo a bimolecular elimination reaction to form the C=N bond, which is obviously a lower energy pathway than the intramolecular hydrogen transfer (7, 9, 13).

This interpretation is also consistent with the increased functionalization of the γ-position in the acyl chain in *N*-halovaleramide photolysis when the *N*-methyl group is substituted with an *N*-*tert*-butyl group (13). No doubt, inability of elimination to form the C=N bond in the latter case is a part of the reason for the increase. In addition, the severe steric repulsion between the *N*-*tert*-butyl and the carbonyl oxygen causes twisting of the *tert*-butyl group out of coplanarity. This distortion from the Π electronic configuration helps the amido radical to attain a proper transition state geometry and further facilitates the hydrogen transfer as discussed above.

While the observed amido radical reactions have been rationalized by the Π electronic configuration, it is also necessary to examine applicability of the alternative Σ radical model in which the unpaired electron is localized in the sp^2-orbital, instead of in the *p*-orbital. As can be seen from Dreiding models, the transition state conformations for the 1,5-hydrogen transfers to the Σ amido radical center do not show any significant difference whether it involves a γ-hydrogen of the acyl side chain or a δ-hydrogen of the alkyl chain. A Σ amido radical therefore is not expected to generate the discrepancies observed in the 1,5-hydrogen transfers.

Finally, the facile cyclization of bromide **6** to the hydrobromide of iminolactone **7** and other allied cases (13, 22, 28) requires a comment. Mechanistically, intramolecular nucleophilic substitutions are commonly recognized to require a colinear overlap of the attacking orbital and the σ* antibonding orbital of the breaking bond in the transition state. In the present case the amide group intramolecularly displaces the bromide group from the *O*-center rather than from the more nucleophilic *N*-center of the amide group. As the electron pair of the *N*-center is located in the *p*-orbital for delocalization with the carbonyl group, a close approach in a near colinear alignment of the pair with the σ* antibonding orbital of the γ-C—Br bond must experience considerable strain in the transition state. This stereochemical constraint can be seen easily from the model **20** since the stereoelectronic situations are very similar to those of the Π radical hydrogen transfer but a much closer approach of the reacting centers is necessary in the nucleophilic substitution. In contrast the oxygen center of the amido radical can use an electron pair in the sp^2-orbital as the nucleophile which can assume a geometry that can satisfy the stereoelectronic requirements readily to displace the C—Br bond. The conformation of this transition state is essentially the same as that of a Σ amido radical abstraction of a γ-hydrogen of the acyl chain.

[7]The corresponding *N*-chloro derivatives appear to undergo 1,5-chlorine–hydrogen exchange reaction; the yields are, however, low (13).

Experimental

Melting points, determined with Fisher-Jones hot stage, were uncorrected. Unless specified otherwise, nmr spectra were obtained in $CDCl_3$ solution with TMS internal standard with a Varian A56/60, and ir spectra in films or Nujol mulls with a Perkin-Elmer 457 spectrophotometer, and mass spectra with a Perkin-Elmer RMU-6E mass spectrometer at the chamber voltage of 80 eV. Elemental analyses were performed by Dr. A. Bernhardt, Mikroanalytisches Laboratorium, West Germany. Unless specified otherwise, nmr signals are singlet with the number of the equivalent proton given in the bracket.

Material

The parent amides were prepared by the reaction of *tert*-butylamine or *tert*-octylamine with the necessary acylchlorides and were purified by distillation. The sodium hypobromite solution was prepared according to the procedure provided by Professor C. Walling.[8] To a cold (0 °C) solution of sodium hypochlorite (800 ml, 0.5 mol) containing sodium bromide (51.5 g), *tert*-butyl alcohol (48 ml, 0.5 mol) and acetic acid (30 ml) were added to 0 °C. After shaking for 5 min at 0 °C, the product was extracted with CCl_4 (30 ml × 3). The combined CCl_4 solutions were washed with water (20 ml) and were dried over Na_2SO_4 to yield a 0.85 *M* *tert*-hypobromite solution (110 ml) as determined by iodimetry.

[8]We are grateful to Professor Walling for the information.

Can. J. Chem. Downloaded from www.nrcresearchpress.com by 210.87.254.105 on 09/05/12
For personal use only.

TABLE 2. Infrared and nmr data of haloamides

Haloamide	Infrared (cm^{-1})	Nuclear magnetic resonance (τ value)[a]
	N-Bromoamide	
5	1655	8.98(9), 8.57(9) 7.55(2)
9	1620	9.01(9), 8.98(9) 8.50(6), 8.05(2)
13	1640	9.01(9), 8.50(6) 8.05(2), 7.77(3)
15(X = Br)[c]	1666[b]	8.55(9), 7.73(3)
	N-Chloroamide	
13	1670	9.01(9), 8.49(6) 8.08(2), 7.87(3)
15	1688[b]	8.57(9), 7.87(3)

[a]All signals are singlet and the numbers of protons from integrations are given in parentheses.
[b]Spectra taken in CCl_4.
[c]Solid at 0 °C.

N-Chloro- and N-Bromo-N-alkylamides

An amide (*ca.* 1 g) and the required volume of the above hypobromite solution were agitated in a shaker for 2 h at room temperature. Carbon tetrachloride was removed under vacuum to give a yellow solid of the bromoamide. If the solid showed absorption at 3300 and 1550 cm^{-1} regions the procedure was repeated. The ir and nmr data of the bromoamide are given in Table 2. The solid without purification was used in photolyses.

According to the published method, *tert*-butylhypochlorite was prepared. An amide (1 g), *tert*-butylhypochlorite (100% excess), and Na_2CO_3 (10 mg) in CCl_4 (5 ml) were refluxed for 2 h. The CCl_4 filtrate was evaporated under vacuum to give a colorless liquid showing no ir absorption at 3300 and 1550 cm^{-1}. The ir and nmr data of the chloramides are given in Table 2.

Photolysis of the Haloamides

An *N*-bromoamide (~1–3 g) in benzene (100 ml) was irradiated in a Pyrex apparatus under nitrogen with an Hanovia medium pressure mercury lamp at room temperature. The progress of the photolysis was monitored by the disappearance of the yellow color of bromoamide and with a KI–AcOH solution test. The photolysis was generally over in less than 1 h. The solution was evaporated to give the *C*-bromo compound.

A quartz apparatus equipped with a Corex filter was used for *N*-chloramide photolysis which was carried out in a similar manner.

Reaction of N-Bromo-N-tert-butyl-3,3-dimethylbutanoamide (5)

Bromoamide **5** (2.10 g) was photolysed in 1 h to give a crude product of *C*-bromo compound **6** (2.1 g); ir 3310 and 1640 cm^{-1}; nmr τ 8.78 (6), 8.58 (9), 7.90 (2), and 6.33 (2).

The crude **6** (1.6 g) was boiled briefly in benzene and the residue was recrystallized from a $CHCl_3$–acetone (1:3) mixture twice to give the hydrobromide of iminolactone **7** (1.3 g); mp 196–198 °C; ir 1675 and 1530 cm^{-1}; nmr τ 8.78 (6), 8.30(9), 6.60(2), and 5.43 (2). *Anal.* calcd. for $C_{10}H_{20}NOBr$: C 48.00, H 8.06, N 5.60; found: C 48.07, H 7.75, N 5.74.

Free iminolactone **7** was liberated by a treatment of the HBr salt with Na_2CO_3 solution and was extracted with CH_2Cl_2. The residue was distilled at 120 °C/15 torr to give colorless liquid: ir 1708, 1145, 1040, and 1015 cm^{-1}; nmr τ 8.81(6), 8.75(9), 7.83(2), and 5.97(2); ms *m/e* 169 (M^+), 168, 155, 154 (100%), 114, 84, 57, 56, 43, 41.

Iminolactone **7** (600 mg) was refluxed in 4 *N* aqueous HCl (5 ml) solution for 24 h. The aqueous solution was diluted with water (15 ml) and was extracted with ether to give a residue (170 mg). The aqueous layer was further basified and extracted to afford the recovered iminolactone **7**. The neutral residue was chromatographed on a silicic acid column (1.6 × 6 cm) in which elution with $CHCl_3$ gave a colorless oil. This oil was distilled at 110–112.5 °C/14 torr to give lactone **8** (113 mg): ir (CCl_4) 1785, 1465, 1418, 1282, 1155, 1035, and 1020 cm^{-1}; nmr τ 8.58(6), 7.48(2), and 5.87(2); ms *m/e* 114 (M^+), 70, 56, 55.

Reaction of N-Bromoamide (9)

The parent amide, *N*-(1′,1′,3′,3′-tetramethylbutyl)-3,3-dimethylbutanoamide, was prepared from 3,3-dimethylbutanoyl chloride and *tert*-octylamine to give a white solid; ir 3330, 1640, and 1545 cm^{-1}; nmr τ 9.01(9), 9.00(9), 8.58(6), 8.25(2), and 8.05(2). The amide (2.02 g) was brominated to give bromoamide **9** (2.95 g). Bromoamide **9** (2.65 g) was photolysed in 20 min to give a solid (2.63 g) which showed a clean nmr spectra indicating the presence of <5% of the parent amide. The analytical sample of **10** was prepared by percolating a $CHCl_3$ solution of the solid through a silicic acid column and was recrystallized from acetone – petroleum ether mixture (1:5) to afford a white solid; mp 75–76 °C; ir 3360, 1640, and 1545 cm^{-1}; nmr τ 9.10(9), 8.89(6), 8.61(6), 8.13(2), 8.07(2), 6.63(2); ms *m/e* 307 (M^+) 305, 225, 194, 192, 169, 154, 112, 72, 58 (100%). *Anal.* calcd. for $C_{14}H_{28}NOBr$: C 54.89, H 9.21, N 4.57, Br 26.09; found: C 54.76, H 9.01, N 4.71, Br 26.31.

Bromide **10** (454 mg) and *t*-BuOK (256 mg) in *tert*-butyl alcohol were refluxed for 2 h. The residue (335 mg) isolated by a usual working up was chromatographed on a silicic acid column to afford pyrrolidine **11** (R = $(CH_3)_3CCH_2$—, 232 mg) as a colorless liquid; ir 1650 and 1410 cm^{-1}; nmr τ 9.00(9), 8.90(6), 8.55(6), 8.34(2), 8.00(2), and 7.20(2); ms *m/e* 225 (M^+), 210, 169, 154, 126, 112, 71, 57, 55. *Anal.* calcd. for $C_{14}H_{27}NO$: C 74.61, H 12.08, N 6.21; found: C 74.77, H 11.80, N 6.29.

Pyrrolidine **11** was heated with 70% H_2SO_4 at 160 °C for 3 h. The usual work-up procedure gave a black tar and an 'acidic fraction' but no basic extract. The acidic fraction was shown to be pure 3,3-dimethylbutanoic acid as compared with the ir spectrum of an authentic sample.

The pyrrolidine **11** (430 mg) in ether (30 ml) was reduced with $LiAlH_4$ for 24 h at room temperature. The product was distilled at 12 mm to give a colorless oil of **12** (R = $(CH_3)_3CCH_2$—, 270 mg): ir 2770, 2810, 2865, and 1362 cm^{-1}; nmr τ 9.02(9), 8.89(6), 8.83(6), 8.67(m, 2), 8.37(2), 7.60(m,2), and 7.29(2). The picrate of **12** was recrystallized from aqueous methanol: mp 142–143 °C. *Anal.* calcd. for $C_{20}H_{32}N_4O_7$: C 54.53, H 7.16, N 12.87; found: C 54.63, H 7.32, N 12.72.

Reaction of N-Bromoamide 13

The yellow solid of bromoamide **13** (2.4 g) was photo-

lysed for 1 h to give a crude product, the nmr spectrum of which was shown to contain <10% of the parent amide. Recrystallization of the crude product from acetone–petroleum ether (1:9) mixture twice gave white crystals of *C*-bromide **14**: mp 83–83.5 °C; ir 3300, 3080, 1640, 1560, 1365, and 1300 cm^{-1}; nmr τ 8.90(6), 8.61(6), 8.10(2), 8.13(3), and 6.67(2); ms *m/e* 249 (M^+), 234, 232, 192, 190, 169, 154, 126, 114, 112, 100, 98, 72, 58. *Anal.* calcd. for $C_{10}H_{20}NOBr$: C 48.01, H 8.05, N 5.60; found: C 50.71, H 7.97, N 5.34.

C-Bromide **14** (518 mg), and *t*-BuOK (235 mg) in *tert*-butyl alcohol were refluxed for 2 h. After usual work-up, it afforded a colorless liquid (370 mg) which was chromatographed on a silicic acid column. The product obtained from $CHCl_3$ elution was distilled at 110 °C/10 torr to give pyrrolidine **11** as a liquid (R = CH_3, 146 mg); ir 1630 and 1400 cm^{-1}; nmr τ 8.88(6), 8.58(6), 8.30(2), 8.12(3), and 6.79(2); ms *m/e* 169 (M^+) 154, 112, 70, 55. Treatment of **11** (R = CH_3) with 80% H_2SO_4 in a water bath gave no other isolable product than the pyrrolidine **11** (35%) and a hard tar.

Pyrrolidine **11** (R = CH_3, 440 mg) in ether (35 ml) was reduced with $LiAlH_4$ for 24 h at room temperature. Upon usual work-up, it afforded a colorless liquid of **12** (R = CH_3, 317 mg): ir 1450, 1380, 1365, 1295, 1230, 1177, 1160, and 1035 cm^{-1}; nmr τ 9.02(6), 8.93(6), 8.93 (t, J = 7 Hz, 3), 8.48(2), 7.70 (q, J = 7 Hz, 2). The picrate of **12** (R = CH_3) was recrystallized from aqueous methanol; mp 128–130 °C. *Anal.* calcd. for $C_{16}H_{24}N_4O_7$: C 50.00 H 6.29, N 14.28; found: C 50.14, H 6.24, N 14.62.

*Photolysis of N-Chloro-N-tert-octylacetamide (**13**, Br = Cl)*

The chloramide in benzene (50 ml) was photolysed to give a crude product which was shown by its nmr spectrum to be a mixture of *C*-chloride **14** (Br = Cl) and the parent amide in the ratio of 1:7. The *C*-chloride showed nmr singlets at τ 8.93(6), 8.28(2), 9.20(3), and 6.62(2).

*Photolysis of N-Halo-tert-butylacetamide (**15**)*

A degassed solution and undegassed solution of *N*-bromoamide **15** (124 mg) in benzene (6 ml) was irradiated simultaneously for 1 h. Titration with $Na_2S_2O_3$ solution showed that the degassed one was completely decomposed while only 10% of the undegassed one was decomposed under the same conditions. The degassed solution was distilled on a water bath to give a residue which showed an nmr spectrum identical with the parent amide.

A benzene solution (10 ml) of *N*-chloroamide **15** (136 mg) was irradiated through a Vycor filter to give a residue which showed the nmr peaks of the parent amide and a weak peak at τ 6.20. The intensity of τ 6.20 peaks is about 5% of that of the methyl peak of the parent amide at τ 8.13.

Synthesis of Iminolactone (**19**)

Acetylation of 3β-hydroxy-5-androsten-17-carboxylic acid (0.9 g) was followed by treatments with $SOCl_2$ and then *tert*-butylamine. The crude amide was recrystallized from a petroleum ether – CH_2Cl_2 mixture to give the *N-tert*-butylamide (490 mg): mp 225–226 °C; ir 3420, 1720, 1660, 1250; nmr τ 4.67 (m, 1H), 5.42 (m, 1H), 7.98 (s, 3H), 8.65 (s, 9H), 8.98 (s, 3H), 9.30 (s, 3H). *Anal.* calcd. for $C_{26}H_{41}NO_3$: C 75.14, H 9.94, N 3.37; found: C 75.01, H 9.74, N 3.49.

The amide was treated with bromine (190 mg) in $CHCl_3$ (5 ml) for 1 h at room temperature. The recovered solid was reacted with *tert*-butylhypobromide in CCl_4 to give a yellow solid (756 mg). The solid in benzene (45 ml) was irradiated under nitrogen at room temperature for 1 h and the solution was briefly heated over a water bath. The solvent was removed and the residue was heated with zinc powder (500 mg) in AcOH for 1 h. The crude product was taken up in CH_2Cl_2 (40 ml) and was washed with $NaHCO_3$ solution. The crude product exhibited ir absorption at 1720, 1700, 1670 cm^{-1} and two *tert*-butyl signals at τ 8.7 and 8.9 in a ratio of 1:3. Silicic acid chromatography of this oil gave the *N-tert*-butylamide (125 mg) and iminolactone **19** (304 mg): mp 198–202 °C; ir 1725, 1705, 1240 cm^{-1}; nmr τ 4.97 (m, 1H), 5.53 (m, 1H), 6.17 (AB quartet, J = 9 Hz), 8.05 (s, 3H), 8.87 (s, 9H), 9.05 (s, 3H).

Quantum Yield Determination

Benzene solution (5 ml) of *N*-bromoamides (approximately 0.01 *M*) were pipetted into photolysis tubes and degassed. For actinometry potassium ferric oxalate solution (0.006 *M*) was also placed in a tube (29). The tubes were placed in a rotating platform and irradiated with a G.E. black light lamp (FC8T9/BL) for 10 min. The consumption of bromoamide was determined with a 1/1000 *N* sodium thiosulfate solution titration. The actinometric solution was treated as reported and the light energy input was calculated to be 6.9×10^{-10} einstein s^{-1} $tube^{-1}$. The quantum yield is given in Table 1.

1. Y. L. Chow and T. C. Joseph. J. Chem. Soc. Chem. Commun. 490 (1969).
2. W. C. Danen and R. W. Gellert. J. Am. Chem. Soc. **94**, 6853 (1972).
3. E. Hedaya, R. L. Hinman, U. Schomaker, S. Theodoropulas, and L. M. Kyle. J. Am. Chem. Soc. **89**, 4875 (1967).
4. (*a*) T. Koenig, J. A. Hoobler, and N. R. Mabey. J. Am. Chem. Soc. **94**, 2514 (1972); (*b*) T. Koenig, J. A. Hoobler, C. E. Klopfenstein, F. Sunderman, G. Hedden, and B. R. Russel. J. Am. Chem. Soc. **96**, 4573 (1974).
5. T. Mojelsky. Ph.D. Thesis, Simon Fraser University, Burnaby, B.C. 1975.
6. H. Bower, J. McRae, and M. C. R. Symons. J. Chem. Soc. A, 2400 (1971).
7. J. N. S. Tam, R. W. Yip, and Y. L. Chow. J. Am. Chem. Soc. **96**, 4543 (1974).
8. C. Brown and A. J. Lawson. Tetrahedron Lett. 191 (1975).
9. Y. L. Chow, J. N. S. Tam, and A. C. H. Lee. Can. J. Chem. **47**, 2441 (1969); Y. L. Chow and J. N. S. Tam. J. Chem. Soc. C, 1138 (1970).
10. Y. L. Chow, J. N. S. Tam, C. J. Colon, and K. S. Pillay. Can. J. Chem. **51**, 2469 (1973).
11. O. E. Edwards and R. S. Rosich. Can. J. Chem. **45**, 1287 (1965).
12. L. P. Kuhn, G. G. Kleinspehn, and A. C. Duckworth. J. Am. Chem. Soc. **89**, 3858 (1967).
13. R. S. Neale, N. L. Marcus, and R. G. Schepers. J. Am. Chem. Soc. **88**, 3051 (1966).
14. S. F. Nelson. *In* Free radicals. Vol. 2. *Edited by* J. K.

Can. J. Chem. Downloaded from www.nrcresearchpress.com by 210.87.254.105 on 09/05/12
For personal use only.

Kochi. John Wiley and Sons, New York, N.Y. 1973. p. 527.
15. A. R. FORRESTER. *In* Free radical reactions. *Edited by* W. A. Waters. University Park Press, Baltimore, Maryland. 1973. p. 139.
16. R. M. KELLOG. *In* Methods in free-radical chemistry. *Edited by* E. S. Huyser. Marcel Dekker, Inc., New York. 1972. p. 1.
17. (*a*) J. A. HOWARD. Adv. Free-Radical Chem. **4**, 49 (1970); (*b*) G. HERZBERG. The spectra and structures of simple free radicals. Cornell University Press, Ithaca, N.Y. 1970. pp. 128–143.
18. (*a*) D. TOUCHARD and J. LESSARD. Tetrahedron Lett. 4425 (1971); (*b*) D. TOUCHARD and J. LESSARD. Tetrahedron Lett. 3827 (1973).
19. Y. L. CHOW and R. A. PERRY. Tetrahedron Lett. 531 (1972).
20. E. J. COREY and W. R. HERTLER. J. Am. Chem. Soc. **82**, 1657 (1960).
21. C. WALLING and A. PADWA. J. Am. Chem. Soc. **85**, 1597 (1963).
22. D. H. R. BARTON, A. L. J. BECKWITH, and A. GOOSEN. J. Chem. Soc. 181 (1965).
23. W. A. PRYOR. Free radicals. McGraw-Hill Book Co., New York, 1966. Chapt. 12.
24. Y. L. CHOW and A. C. H. LEE. Chem. Ind. 827 (1967).
25. B. DANIELI, P. MANITTO, and G. RUSSO. Chem. Ind. 329 (1969); 203 (1971).
26. R. KH. FREIDLINA. Adv. Free-Radical Chem. **1**, 271 (1965).
27. S. GLASSTONE, K. J. LAIDLER, and H. EYRING. The theory of rate processes. McGraw-Hill, New York. 1941. p. 88.
28 J. N. S. TAM, T. MOJELSKY, K. HANAYA, and Y. L. CHOW. Tetrahedron, **31**, 1123 (1975).
29. C. G. HATCHARD and C. A. PARKER. Proc. Roy. Soc. London, Ser. A, **235**, 518 (1956).

Can. J. Chem. Downloaded from www.nrcresearchpress.com by 210.87.254.105 on 09/05/12
For personal use only.

A pulse Fourier transform equivalent of the homonuclear (proton–proton) INDOR experiment[1]

KLAUS BOCK,[2] ROLAND BURTON, AND LAURANCE D. HALL
Department of Chemistry, University of British Columbia, Vancouver, B.C., Canada V6T 1W5

Received May 25, 1976

KLAUS BOCK, ROLAND BURTON, and LAURANCE D. HALL. Can. J. Chem. **54**, 3526 (1976).

A simple, selective pulse sequence has been developed whereby the equivalent of a continuous wave INDOR nmr experiment, can be performed in the pulse Fourier transform mode of operation. The advantages and limitations of this approach for proton nmr studies are demonstrated with four samples, uridine (**1**), cytidine (**2**), vinyl acetate (**3**), and 2,3,4,-tri-*O*-acetyl-1,6-anhydro-β-D-mannopyranose (**4**). The observed responses depend upon the flip angle of the monitoring pulse. A small flip angle (20–30°) detects responses only for those transitions having an energy level in common with the perturbed transition, whereas a 90°-flip angle also results in responses from those transitions which have an indirect connectivity relationship.

KLAUS BOCK, ROLAND BURTON et LAURANCE D. HALL. Can. J. Chem. **54**, 3526 (1976).

On a développé une séquence simple à pulsation sélective par laquelle on peut effectuer l'équivalant d'une expérience rmn INDOR en onde continue dans le mode d'opération de transformation pulsée de Fourier. On a démontré les avantages et les limitations de cette approche par des études rmn du proton avec quatre exemples soit l'uridine (**1**), la cytidine (**2**), l'acétate de vinyle (**3**) et le tri-*O*-acétyl-2,3,4 anhydro-1,6 β-D-mannopyranose (**4**). Les réponses observées dépendent de l'angle de "rupture" de la pulsation examinée. Avec un petit angle de "rupture" (20–30°) on détecte des réponses uniquement pour les transitions ayant un niveau d'énergie en commun avec la transition perturbée; un angle de "rupture" de 90° permet toutefois d'obtenir aussi des réponses pour les transitions qui ont une relation de connection indirecte.

[Traduit par le journal]

Introduction

Multiple resonance nmr experiments have long provided (1) an invaluable aid to continuous-wave (c.w.) proton nmr spectroscopy and there is now a pressing need for the development of equivalent experiments which are compatible with the detection of resonances in the pulse Fourier transform (F.t.) mode. We now describe a simple pulse nmr experiment which is equivalent in many respects to the c.w., proton–proton INDOR experiments (ref. 2*a* and for review articles, ref. 2*b*). This study differs significantly from previous experiments with heteronuclear systems (3) since, as predicted by Ernst and co-workers (4) and by Meakin and Jesson (5), both the number and the intensity of the observed responses depend on the intensity of the monitoring pulse.

We are aware of only three previous attempts to perform proton–proton INDOR experiments in the F.t. mode. Feeney and Partington (6) described a hybrid experiment in which a c.w. perturbing pulse was used and its effect monitored with a pulse of unstated duration in the F.t. mode. More recently, Kushida *et al.* (7) have described a pulse experiment more similar to that described in this study. Unfortunately both reports were only in the form of 'preliminary communications', giving no experimental details. We shall not refer to either paper here. Since this manuscript was written, a further preliminary communication has been published (8) in which INDOR-like responses were detected in the F.t. mode, *using small flip angles only*. The general conclusions of those workers parallel those given in this paper for small flip angles, but do not include the extra details concerning 90°-flip angles which we describe.

In a c.w. INDOR experiment, a weak, 'observing', radiofrequency field (ω_1) is used to monitor the intensity of a single transition and

[1]Part 9 of a series, "Applications of pulsed N.M.R. spectroscopy". For part 8 see ref. 12. A full account of this study was presented at the Canadian Chemical Conference of the Chemical Institute of Canada, Toronto, May 25–28, 1975.

[2]Visiting Associate Professor at U.B.C., 1974–1975. Permanent address, Department of Organic Chemistry, The Technical University of Denmark, DK-2800, Lyngby, Denmark.

Can. J. Chem. Downloaded from www.nrcresearchpress.com by 210.87.254.6 on 09/05/12
For personal use only.

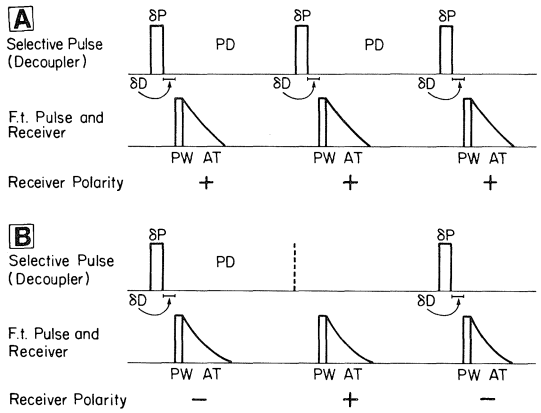

FIG. 1. Flow sheet depicting the pulse sequences used to elicit responses. The sequence in A gives the entire nmr spectrum and the transitions which have been selectively perturbed appear as a negative going peak. The sequence shown in B is the difference mode of operation in which only those transitions whose intensities have been changed by the selective pulse are observed; all others are effectively cancelled. It is necessary in this mode of operation to specify an even set of acquisitions and under these conditions the transitions being selectively perturbed give positive going peaks. δP = width of selective pulse; δD = delay between selective pulse and F.t. pulse; PW = width of F.t. (monitoring) pulse; AT = acquisition time for F.I.D.; PD = Pulse delay (four times T_1 value).

then a second radiofrequency field (ω_2) is slowly scanned through the appropriate frequency range. A response is produced each time this frequency impinges on a transition which has an energy level in common[3] with that transition being monitored.

In the equivalent Fourier transform experiment, the transition to be 'monitored' is irradiated with a 180° pulse[4] provided in the form of a weak pulse of rather long duration (commonly 0.1–1.0 s). This pulse inverts the spin population of the energy levels associated with that transition and the effects of this perturbation on the transition probabilities and hence on the intensities of the observed transitions, are monitored by a non-selective pulse in the usual F.t. manner, as summarized in Fig. 1. It has been predicted (4, 5) that for strongly spin-coupled homonuclear systems the observed responses depend upon the intensity (flip angle) of the non-selective, monitoring pulse. For small flip angles (*ca.* 20°) the intensities of the observed transitions should correspond closely to those which would be obtained from a slow-passage c.w. experiment; for a 90°-flip angle the relative observed intensities may differ appreciably from those of the c.w. experiment.

In this paper we shall discuss a series of experiments which illustrate the scope of the above phenomenon in the context of proton nmr spectra of organic molecules in solution. We shall also discuss the choice of a suitably selective 180° pulse and the effects of changing the delay time (δD) between the 180° pulse and the monitoring pulse. Our approach has been deliberately directed towards practical aspects and no attempts have been made to quantitatively document our findings.[5]

Results and Discussion

In order to minimize any confusion arising from possible off-resonance effects of the perturbing 180° pulse, a series of calibration experiments were performed with uridine (**1**);

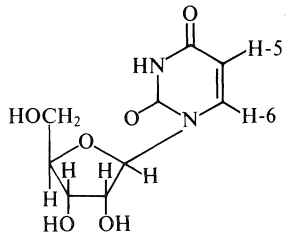

1

the normal 100 MHz nmr spectrum is shown in Fig. 2*A*. Three different combinations of the duration (δP) and intensity of the selective perturbing pulse were chosen such that in each

[3]The so-called 'connectivity' relationship defined by R. Freeman and W. A. Anderson (13).

[4]The total power of a pulse can be defined in terms of the number of degrees (or radians) through which it will tip the magnetisation vector (the flip angle); this is the product of the field strength ($\gamma H/2\pi$ Hz) times the duration of the pulse (τ). The longer the pulse used to produce a particular flip angle, the more selective will be the effects of that pulse.

[5]A referee expressed concern that the 'leakage' model given later in this paper has no theoretical basis and commented that it "may prove inadequate if it is applied to spin systems that are more tightly coupled than those discussed in the present paper". We concur completely with both these reservations and emphasize that our model is not proffered as a substitute for a quantitative theory; nevertheless we have found that it provides a convenient rationale and we present it as such.

Can. J. Chem. Downloaded from www.nrcresearchpress.com by 210.87.254.6 on 09/05/12
For personal use only.

Can. J. Chem. Downloaded from www.nrcresearchpress.com by 210.87.254.6 on 09/05/12
For personal use only.

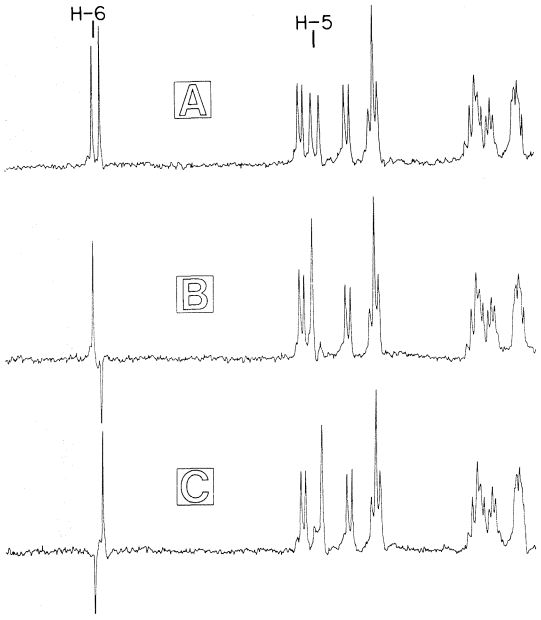

FIG. 2. Proton nmr spectra of uridine in dimethyl sulphoxide-d_6 (0.1 M) measured in the F.t. mode using 10 transients and a sensitivity enhancement factor of 1.5. A shows the normal spectrum monitored with a non-selective 25° pulse. The spectrum in B shows the effect of selectively inverting the high field transition of H-6 with a 180° pulse (δP = 0.1 s, 94 dB) and then monitoring the effect of this perturbation using a non-selective 25° pulse (δD = 10 ms). In C the selective pulse has been positioned on the lower field transition of H-6. Note the changes in the intensities of the H-5 transitions.

case a 180° pulse was produced. The frequency at which this pulse was applied was varied in 1 Hz increments through the region of the H-6 resonance and its effects on the intensity of the transitions of H-5 were monitored with a non-selective 90° pulse. The data obtained from these experiments are plotted in Fig. 3. It can be seen that even for a pulse of 0.10 s duration there is discrimination between the responses elicited by separately irradiating each of the two transitions of H-6. However, increasing the pulse length to 0.3 s provides a better discrimination, with a plateau of *ca.* 3 Hz between the responses of the two transitions ($J_{5,6}$ = 8.3 Hz). There is a steady decrease in the percentage enhancement produced as the duration of the selective pulse is increased such that the highest frequency selectivity used (Fig. 3*D*) results in only a 20% enhancement compared to the 55% obtained by the shorter, less selective pulse (Fig. 3*A*). This is almost certainly due to relaxation during the

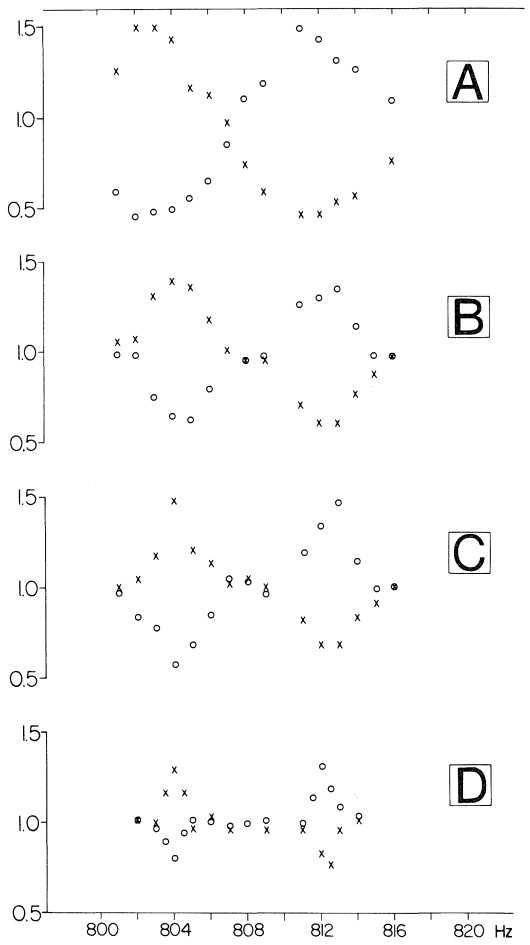

FIG. 3. Plot of the normalized intensity of the two transitions of the H-5 resonance of uridine (**1**), measured as a function of the frequency of a selective 180° pulse located near to the H-6 resonance. The data for experiments A, B, and D were monitored using a 90° pulse whereas a 25° pulse was used for C. The duration of the selective 180° pulse was as follows: A, 0.1 s (94 dB); B, 0.3 s (84 dB); C, 0.3 s (84 dB); D, 1.0 s (75 dB).

pulse, since the *selective*[6] T_1 value of H-6 is only 0.85 s (*vide infra*). Thus the selective T_1 values of the resonances of a molecule provide an important practical limitation to the frequency selectivity with which an individual experiment can be performed.

The above experiments were repeated using a

[6]If a resonance is relaxing exclusively via the dipole–dipole mechanism then the T_1 value measured by a selective inversion experiment will be 1.5 times the T_1 value obtained by a conventional non-selective T_1 measurement (9).

Can. J. Chem. Downloaded from www.nrcresearchpress.com by 210.87.254.6 on 09/05/12
For personal use only.

25° monitoring pulse and the results from one of that series is shown in Fig. 3*C*; the frequency selectivity was found to be essentially the same as that of the 90°-pulse experiments. This is hardly surprising since we are only dealing here with a two-spin system.

Typical spectra from the above series of experiments, using a 25° monitoring pulse are shown in Fig. 2*B* and 2*C*. Although the changes in intensity of the H-5 resonance are easily recognized by visual comparison of the normal and selectively perturbed spectra, there are some advantages (*vide infra*) in using a 'difference' mode of display. The pulse sequence used for this purpose is summarized in Fig. 1*B* and in essence it simply normalizes the final display by subtracting a selectively disturbed spectrum from a normal spectrum. In principle, the only responses in such a difference spectrum should arise from resonances that have been perturbed in intensity; the spectra of cytidine (**2**) which has

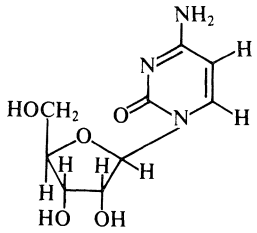

2

some overlap of the H-1′ and H-5 resonances (Fig. 4) show that this can almost be realized in practice, but that some small additional peaks also appear due to some errors in the cancellation. We find that the efficiency with which any two spectra can be subtracted from one another varies somewhat, and we do not believe that the reasons for this are yet known. We have often found it advantageous to increase the delay period (δD) between the selective and the monitoring pulse, but this is not invariably the case.

Attention was next directed to vinyl acetate (**3**), which gives a well resolved ABX spectrum, as indicated in Fig. 5*A* and which has the added advantage that now the proton T_1 values are

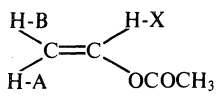

3

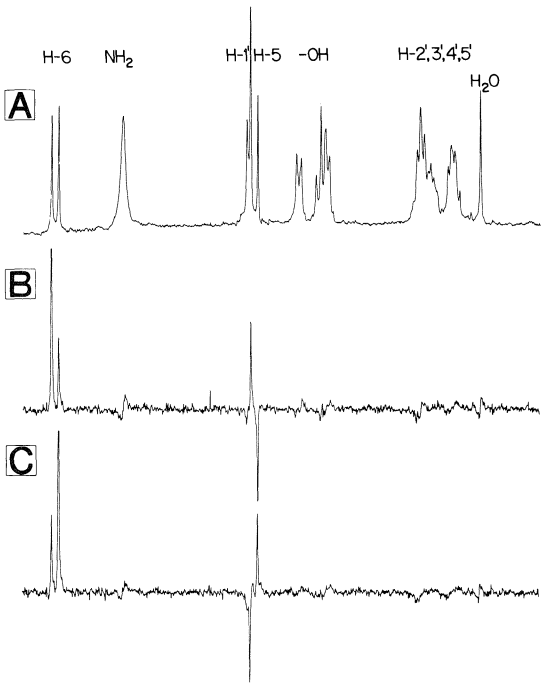

FIG. 4. The 100 MHz proton nmr spectra of cytidine in dimethyl sulphoxide-d_6 (0.1 *M*). A shows the normal spectrum measured with five transients (90°) and a sensitivity enhancement of 1.5. The spectra in B and C were each measured in the difference mode (Fig. 1*B*) using 20 transients (90°) and a resolution enhancement of 1.5 and δD = 100 ms. In B a selective 180° pulse (0.3 s, 84 dB) had been previously applied to the low field transition of H-6. In C, the high field transition of H-6 had been inverted by the same 180° pulse.

substantially longer than the length of even the most selective pulse. Several, completely separate series of experiments were performed.

The series of experiments shown in Fig. 5, and summarized in Table 1, all involved the application of a selective, 180° pulse to the upfield transition of H-X (X4) but the duration of the monitoring pulse was varied from 72° to 18° (the effect of a 90° pulse is shown in Fig. 6*B*). Several important points deserve comment. First, we note that a 90° (or 72°) monitoring pulse (Figs. 6*B* and 5*B*) elicits intensity changes from all of the H-A and H-B transitions, whereas a pulse of flip angle 36° or less (Figs. 5*D* and 5*E*) only detects responses from those transitions having a direct connectivity relationship with X4. This is directly in accord with predictions (4, 5). It is interesting that the responses detected by the 18° pulse approximate very closely to the theoretical

TABLE 1. Normalized intensities of the H-A and H-B transitions of vinyl acetate (3) produced by a selective 180° pulse (0.3 s, 84 dB) applied to the high field transition of the X part of the spectrum (X4) followed by sampling of the entire proton spectrum with a non-selective pulse of different flip angle (θ)

Flip angle (θ)	A					B				
	1	2	3	4	$\frac{1}{4}\sum I/I_0$	1	2	3	4	$\frac{1}{4}\sum I/I_0$
18°	1.83	1.00	0	1.07	0.97	1.93	1.13	0	1.00	1.02
36°	1.76	1.05	0	1.04	0.96	1.61	1.13	0	0.93	0.92
54°	1.74	1.05	0.30	0.97	1.02	1.60	1.16	0.43	1.01	1.05
72°	1.51	1.03	0.33	1.01	0.97	1.36	1.21	0.23	0.83	0.91
90°	1.77	1.28	0.42	0.96	1.11	1.33	1.18	0.51	0.87	1.02

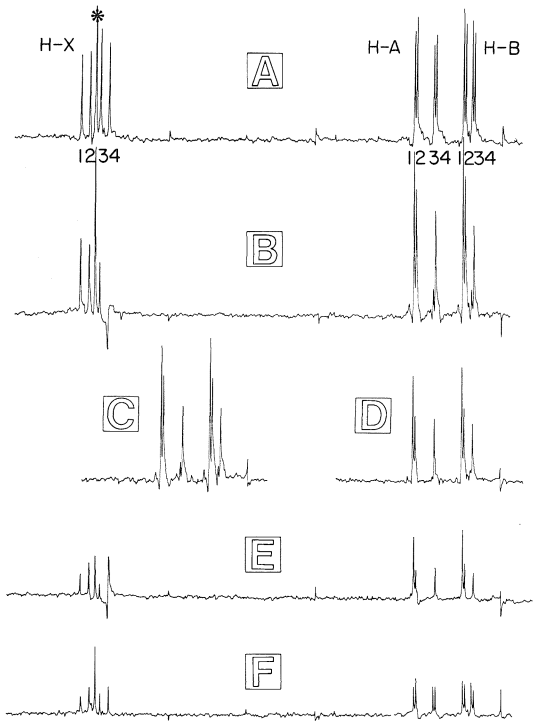

FIG. 5. Partial 100 MHz proton nmr spectra of vinyl acetate in chloroform-*d* solution (0.1 *M*); each spectrum was measured using a single transient and a sensitivity enhancement of 1.5. A shows the normal spectrum measured with a 72° pulse and F shows the normal spectrum measured with a 18° pulse. The remaining spectra illustrate the effect on the H-A and H-B transitions of a selective 180° pulse (0.3 s, 84 dB) applied to transition X4. B was monitored with a 72° pulse; C with a 54° pulse; D with a 36° pulse; and E with a 18° pulse. The normalized intensities are shown in Table 1. The peak marked * is the proton resonance of residual $CHCl_3$ in $CDCl_3$.

threshold with two transitions A1, B1 having their intensity doubled whilst two others, A3 and B3, have decreased to zero intensity. This finding has important practical implications since this is now the maximum intensity perturbation which is theoretically attainable and is clearly the most efficient way of eliciting INDOR-like responses.

However, the practical situation is complicated by the fact that any spectrum excited by a 20° monitoring pulse automatically has a lower intrinsic signal-to-noise ratio than one excited by a 90° pulse. If this were a normal F.t. experiment, this loss of signal could be regained with no loss of time because it would be possible to decrease the pulse delay period (*PD*) and thereby to acquire more transients in a fixed period of time. However, the rate limiting step of the experiments described here is the recovery rate of the transition which has been selectively inverted, which still requires at least four times the selective (10) T_1 period for full relaxation, regardless of the flip angle of the monitoring pulse. That factor, coupled with the fact that one would have to perform two experiments equivalent to that illustrated in Fig. 5*E* in order to obtain information concerning all eight of the H-A and H-B transitions, compared with a single experiment such as that shown in Fig. 6*B*, provides two reasons why one might deliberately choose to monitor intensity changes, and hence INDOR responses, with a 90° pulse. One then has to contend with the fact that the observed intensity changes are not quantitative (*i.e.* double or zero), but that is of little moment if one is predominantly interested in determining transition *frequencies* and, as we discuss below, even the intensity changes appear to show some degree of consistency.

In the second series of experiments each of the X transitions was individually inverted in turn and the effects monitored with a 90° pulse. Typical spectra are shown in Fig. 6. In marked contrast to the results obtained using the *ca.* 20° monitoring pulse, we now note that in every case

Can. J. Chem. Downloaded from www.nrcresearchpress.com by 210.87.254.6 on 09/05/12
For personal use only.

Can. J. Chem. Downloaded from www.nrcresearchpress.com by 210.87.254.6 on 09/05/12
For personal use only.

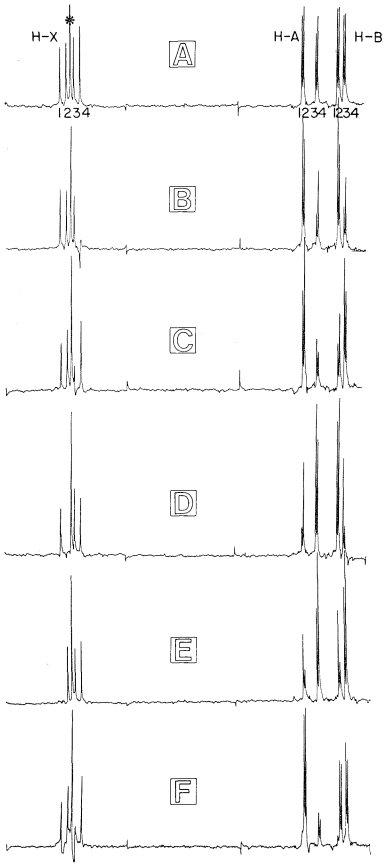

FIG. 6. Partial proton resonance spectra of vinyl acetate measured using a single, non-selective 90° pulse and a resolution enhancement of 1.5. The normal spectrum is shown in A. The selective 180° pulse (0.3 s, 84 dB) was followed by a pulse delay of 10 ms. The spectra in B to E show the effect of selectively inverting with a 180° pulse (0.3 s, 84 dB), in sequence, X4, X3, X2, or X1. The spectrum in F gives the result of simultaneously inverting X3 and X4 with a 180° pulse (0.1 s, 94 dB). The peak marked * is the proton resonance of residual $CHCl_3$ in $CDCl_3$.

all the transitions of H-A and H-B give responses, and not only those having a direct connectivity relationship with the perturbed X transition. The experimental data are summarized in Table 2 where it will be noted that the induced intensity changes appear to follow a regular, internally consistent pattern; although the intensity of individual transitions varies from one experiment to another, the normalized sum of the intensities of each proton closely approximate to unity.

The explicit theory for the intensity changes observed in the above experiments involves the density matrix treatment (4, 5) and is beyond the scope of the present study. However, the internal consistency and symmetry of these changes (Table 2) were sufficient to prompt us to invoke a simplistic rationale. We must emphasize that we do not imply that this rationale has any mechanistic significance.

The intensity changes summarized in Table 2 are consistent with a model that starts with the inversion of the spin-states of one transition. This should lead to intensity changes only for these transitions which have a direct connectivity relationship; $\Delta F_z = 2$, the progressive-, and $\Delta F_z = 0$ the regressive-relationship. If, however, some secondary rearrangement of spin-populations could occur as a result of 'leakage' from, or to, the initially perturbed energy levels, then all of the transition intensities would be changed, including those corresponding to $\Delta F_z = 1$. In Table 2 those secondary changes are represented by 'δ'; '2δ' is a symbolism for those transitions which have secondary changes for both energy levels. We do not intend to imply any precise, quantitative function associated with this symbolism and just intend it to be used as a convenient short-hand to indicate the sense of some secondary perturbation.

Consider, for example, the effect of inverting the populations of the two energy levels associated with X4 on transitions A2, A4. Leakage of spins $(-\delta)$ from the now depleted lower spin state should result in an increase in the transition intensity of A2 with a concomitant decrease in

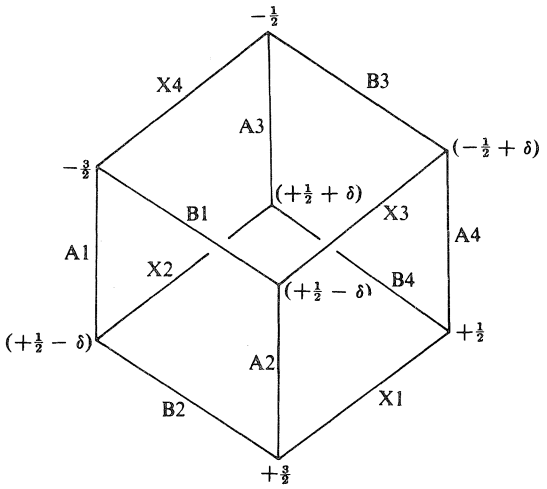

TABLE 2. Spin state diagram for vinyl acetate assuming J_{AX} and J_{BX} positive and J_{AB} negative. Table shows normalized intensities (average for two experiments) provided by a selective 180° pulse (0.3 s, 84 dB) to the X transitions, X1, X2, X3, X4. The lower line shows the normalized intensities produced by a selective 180° pulse (0.1 s, 94 dB) applied simultaneously to the X3 and X4 transitions. The table also shows the ΔF_z values, including secondary population leakage (δ), which is expected from these selective inversion experiments (see text). The total intensity of a given proton signal $(\sum I/I_0)/(\sum \Delta F_z)$ in the horizontal direction shows the experimental error whereas the same value in the vertical direction shows how regularly these secondary changes are produced

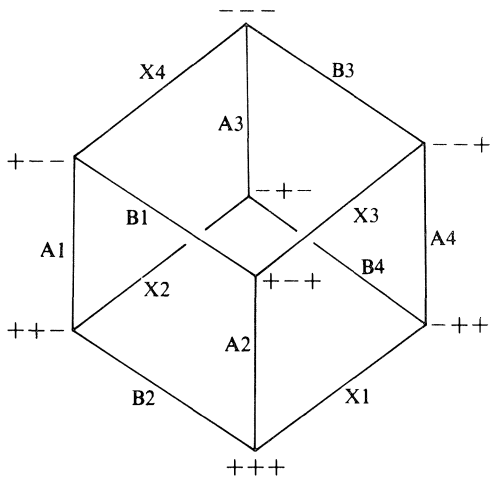

		X				A					B				
		1	2	3	4	1	2	3	4	$\frac{\sum I/I_0}{\sum \Delta F_z}$	1	2	3	4	$\frac{\sum I/I_0}{\sum \Delta F_z}$
	X					+	+	−	−		+	+	−	−	
	A	+	+	−	−						−	+	−	+	
	B	+	−	+	−	−	+	−	+						
X4	I/I_0	1.00	0.90	0.76	*	1.77	1.28	0.42	0.96	1.11	1.53	1.18	0.51	0.87	1.02
	ΔF_z	1	$1-2\delta$	$1-2\delta$		$2-\delta$	$1+\delta$	$1-\delta$	$1-\delta$		$2-\delta$	$1+\delta$	δ	$1-\delta$	
X3	I/I_0	0.71	1.02	*	0.90	1.32	1.75	0.88	0.45	1.10	0.49	0.81	1.62	1.22	1.04
	ΔF_z	$1-2\delta$	1		$1-2\delta$	$1+\delta$	$2-\delta$	$1-\delta$	δ		δ	$1-\delta$	$2-\delta$	$1+\delta$	
X2	I/I_0	0.80	*	1.00	0.75	0.34	0.89	1.83	1.33	1.10	1.25	1.60	1.00	0.40	1.06
	ΔF_z	$1-2\delta$		1	$1-2\delta$	δ	$1-\delta$	$2-\delta$	$1+\delta$		$1+\delta$	$2-\delta$	$1-\delta$	δ	
X1	I/I_0	*	0.90	0.82	0.80	0.80	0.33	1.20	1.77	1.03	0.92	0.41	1.22	1.71	1.07
	ΔF_z		$1-2\delta$	$1-2\delta$	1	$1-\delta$	δ	$1+\delta$	$2-\delta$		$1-\delta$	δ	$1-\delta$	$2-\delta$	
	$\frac{\sum I/I_0}{\sum \Delta F_z}$					1.05	1.06	1.08	1.13		1.05	1.00	1.09	1.05	
X3	I/I_0	0.79	0.90	*	*	1.48	1.42	0.44	0.31	0.91	0.90	0.86	1.13	0.96	0.96
X4	ΔF_z	$1-2\delta$	$1-2\delta$			2	2	0	0		1	1	1	1	

the intensity of A4 arising from the increase ($+\delta$) of the population of the upper spin-state. At this stage we can return again to the intensities of the $\Delta F_z = 0$ and $\Delta F_z = 2$ lines, and note that these too show an additional symmetry; for example the B1 transition increases more than A1, and A3 decreases more than B3.

Naive as it is, the above model offers a systematic rationalisation for all of the experiments we have monitored using a 90° pulse. It has the additional advantage of being at variance with fortuitous off-resonance effects and hence provides some circumstantial evidence against the occurrence of those effects. Consider for example, the effect which a selective 180° pulse applied to X3 has on the intensities of the other X transitions. Transitions X1 and X4 decrease in intensity more than X2; this accords with the

Can. J. Chem. Downloaded from www.nrcresearchpress.com by 210.87.254.6 on 09/05/12
For personal use only.

Can. J. Chem. Downloaded from www.nrcresearchpress.com by 210.87.254.6 on 09/05/12
For personal use only.

population leakage model but is inconsistent with an off-resonance effect, which should induce a maximal change in the transitions nearer to the 180° pulse, namely X1 and X3.

An illustration of the utility of this model comes from some selective, double-inversion experiments. Simultaneous inversion of transitions X3, X4 gave the spectra shown in Fig. 6*F* in which the intensities of transitions A1, A2 are identically increased, A3, A4 are identically decreased, and transitions B1, B2, B3, B4 are essentially unchanged in intensity from their normal values. Inspection of the energy level diagram immediately following inversion of X3 and X4 shows that these changes are exactly as they should be; note that $\Delta F_z = 1$ for all the B transitions. Note too that even the secondary

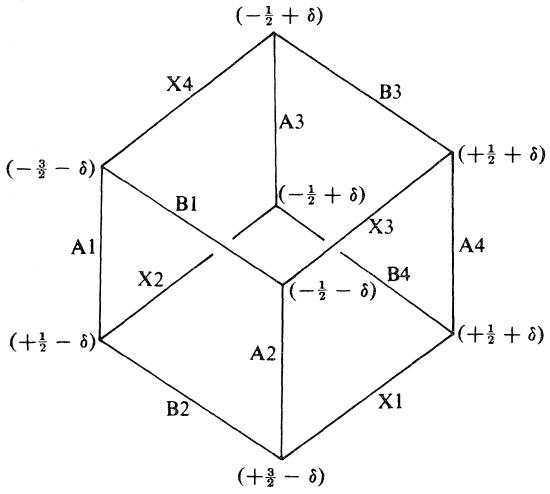

population changes (δ) are now such that the pairs of transitions A1, A2 and A3, A4 should have identical intensities, and should not exhibit the type of differential which was observed to accompany inversion of a single X transition.

The long, proton spin–lattice relaxation times for vinyl acetate enabled us to evaluate the effects of relaxation during the selective pulse itself (δP) and during the delay period (δD), on the intensity of the observed transitions; this was most readily studied by observing the changes in intensity of the A and B transitions produced by a 180° pulse applied to X4, as a function of the delay time (δD). Monitoring by a 90° pulse showed that increases in δD from 0.1 to 30 s resulted in a progressive decrease in the induced changes; importantly, however, there appeared to be no clearly defined differential between the responses of transitions having $\Delta F_z = 2$ or 0 and those with $\Delta F_z = 1$. As expected, a 20° monitoring pulse showed a steady decrease in the response intensity with increase in δD, but no 'leakage' into the $\Delta F_z = 1$ transitions was observed.

In the last section of this paper we shall discuss some experiments which were performed in order to see how the experiments described above fared in the context of an organic molecule of a more typical complexity. The normal proton spectrum of 2,3,4-tri-*O*-acetyl-1,6-anhydro-β-D-mannopyranose (**4**) is shown in Fig. 7*A*. Two,

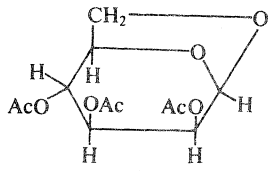

4

selective inversion experiments were monitored with 90° pulse; selective inversion of either B1 (Fig. 7*B*) or B4 (Fig. 7*C*) produced substantial changes in the H-5 and H-6 resonances. Without giving the full details here, these responses were completely consistent with the model discussed earlier; from the practical viewpoint, the changes seen in the H-5 resonance are more readily interpreted than those of the experiment monitored with a 20° pulse, in which fewer transitions were affected.

The experiment shown in Fig. 7*D* shows the clarity with which the different mode of operation can be used to detect resonances and the special advantage of a double inversion experiment; here irradiation of both of the low field transitions of H-2 has induced responses in *all* of the transitions of H-3. Note that H-1 does not produce a well defined response; this is as it should be since, as demonstrated for vinyl acetate, double inversion experiments have a special level of control. This point is further illustrated in Fig. 7*E* where simultaneous irradiation of transitions A3, A4 and sampling with a 25° pulse only induces responses from all of the B transitions and causes no change at all in the H-5 resonance. The experiment shown in the insert involves the same double inversion, but now using a 90° monitoring pulse, with display in the difference mode; the general resemblance to a c.w. INDOR spectrum is now remarkable.

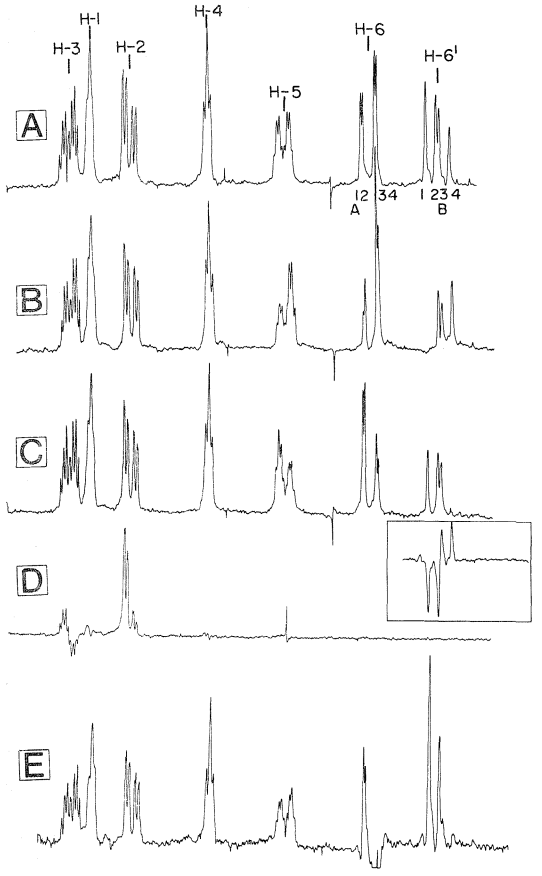

FIG. 7. Partial 100 MHz proton nmr spectra of 2,3,4-tri-*O*-acetyl-1,6-anhydro-β-D-mannopyranose (**4**) in benzene-d_6 solution (0.2 *M*) measured with a single transient and a sensitivity enhancement factor of 1.5. A shows the normal spectrum. B shows the effect of inverting transition B1 with a selective 180° pulse (0.1 s, 93 dB), as monitored by a 90° pulse. C is the same experiment, but with selective inversion of B4. The spectrum in D was obtained by selectively irradiating the two low field transitions of H-2 (0.1 s, 93 dB) and sampling the result with 10 transients (90° pulse) in the difference mode. In E, transitions A3, A4 were simultaneously inverted (0.1 s, 94 dB) and the effect monitored with two transients (25° pulse). The insert shows the same experiment measured with four transients (90° pulse) in the difference mode.

Conclusions

The Fourier transform experiment described here should provide a powerful tool for structural studies of organic substances by F.t. nmr spectroscopy. The selective excitation using a 180° pulse ensures an optimal INDOR[7] response from the nuclei being studied and the fact that the entire experiment is computer controlled ensures that it can be applied with equal ease to dilute solutions where repeated time-averaging is required. In this regard it is noteworthy that the ease with which frequencies[8] and pulse widths can be selected is also very high, and further that the accuracy with which the 180° pulse is positioned is not too critical. It is possible to monitor the effect of the perturbing pulse in either of two distinctive ways, each of which has some advantages. If a small flip angle is used, less than 30° say, then only transitions having a direct connectivity relationship will be detected, and it is necessary to perform several separate experiments in order to determine all of the transition frequencies; however, the intensities of the observed transitions measured under these conditions are well defined. Alternatively, a 90°-flip angle can be used for the monitoring pulse and in this case all the transitions of any spin-coupled proton may be detected, at least in a three-spin system, which is a great advantage; although the observed intensities do not have a simple relationship, a *qualitative* assignment can be based on a simple model invoking the equivalent of secondary rearrangements of spin populations. In practice the experiment using a 90°-flip angle can result in a substantial saving of time since more responses are detected for each selective inversion experiment, and their signal-to-noise ratio is also higher.

Responses detected by either pulse-length can be displayed in a 'difference' mode in which the spectrum which is actually plotted is normalized with respect to the unperturbed spectrum. This form of display is equivalent to that of a c.w. INDOR spectrum in the sense that a spin coupling is used as a type of 'nuclear filter' to remove all resonance signals except those which are spin coupled to the resonance being monitored. Although the residual peaks remaining in the difference spectra shown in Figs. 4 and 7 indicate that this normalization procedure is not yet perfect, there is never any ambiguity as to which are the systematic responses.

The advantages of this Fourier transform experiment over the c.w. INDOR experiment are numerous and varied. Besides the obvious ease with which these F.t. experiments can be performed and time averaged, the fact that the

[7]Another referee suggested the term 'INDOR' only be applied to those pulse experiments which are displayed in the 'difference' mode and again we concur with that suggestion.

[8]A noteworthy development in this regard is that of tailored excitation (10).

Can. J. Chem. Downloaded from www.nrcresearchpress.com by 210.87.254.6 on 09/05/12
For personal use only.

intensity changes are excited with potentially 100% efficiency ensures that these experiments have intrinsically high sensitivity. A further useful experiment which has no general c.w. counterpart, is the double (or multiplet) inversion experiment; here advantage can be taken both of controlling the bandwidth of a 180° pulse by varying the duration (δP) of that pulse, and also of applying several such pulses to completely separate regions of the nmr spectrum. The experiments which we have performed are in complete qualitative agreement with the predictions of Ernst and co-workers (4) and Meakin and Jesson (5); we have made no attempt to quantitate our findings and feel that any such attempts would require considerably more time-averaging than that required for our experiments.

Experimental

All nmr experiments were performed with a Varian XL-100 (15″) instrument fitted with a Varian 620 L (16K) computer and a Linc Tape (model CO600). Modifications were made to the Varian Fourier transform programme (994100-D/X-2) to enable the computer to gate the Varian Gyrocode decoupler to provide the 180° pulse, rather than the conventional radiofrequency transmitter; these changes are summarized in Fig. 1, and full details are available on request.

The samples were studied as 0.1 *M* solutions, which were degassed by six freeze–pump–thaw cycles: Uridine (**1**) (Terra Marine) in dimethyl sulphoxide-d_6 (99.5%, Merck, Sharpe and Dohme), cytidine (**2**) (Terra Marine) in dimethyl sulphoxide-d_6 (99.5%, Merck, Sharpe and Dohme), vinyl acetate (**3**) (Aldrich Chemical Co.) in chloroform-*d* (99.8%, Norell Chemical Co.), and 2,3,4-tri-*O*-acetyl-1,6-anhydro-β-D-mannopyranose (**4**) (11) in benzene-d_6 (99.5%, Merck, Sharpe and Dohme; this sample was made 0.2 *M*).

The operation of the spectrometer for these experiments is almost identical with the standard Varian option. The normal nmr spectrum is measured and the frequencies of the transitions to be selectively irradiated are counted. The gyrocode decoupler is then set to irradiate at the required frequency, with the appropriate attenuation. An option is selected to enable either the 'direct' or 'difference' mode of display to be used (Fig. 1*A* or *B*). Thereafter all the standard Varian software instructions are used. It is important to choose an even number of transients if the difference mode of display is to be used (Fig. 1*B*).

Acknowledgments

It is a pleasure to thank Dr. Howard D. W. Hill of Varian Associates for stimulating discussions and the National Research Council of Canada for their financial support of this work via operating grant A 1905 (to L.D.H.). One of us (K.B.) wishes to thank the Technical University of Denmark, the Otto Moensted Foundation, and N.A.T.O. for funds for a sabbatical leave.

1. (*a*) J. D. BALDESCHWIELER and E. W. RANDALL. Chem. Rev. **63**, 81 (1963); (*b*) R. A. HOFFMAN and S. FORSEN. Progr. Nucl. Magn. Reson. Spectrosc. **1**, 15 (1966); (*c*) W. VON PHILIPSBORN. Angew. Chem. Int. Ed. Engl. **10**, 472 (1971).
2. (*a*) E. B. BAKER. J. Chem. Phys. **37**, 911 (1962); (*b*) W. MCFARLANE. Ann. Rev. N.M.R. Spectrosc. **1**, 135 (1968); V. J. KOWALEWSKI. Progr. Nucl. Magn. Reson. Spectrosc. **5**, 1 (1969).
3. (*a*) K. G. R. PACHLER and P. L. WESSELS. J. Magn. Reson. **12**, 337 (1973); (*b*) A. A. CHALMERS, K. G. R. PACHLER, and P. L. WESSELS. Org. Magn. Reson. **14**, 243 (1974); (*c*) H. J. JACOBSEN, S. AA. LINDE, and S. SØRENSEN. J. Magn. Reson. **15**, 385 (1974).
4. S. SCHAUBLIN, A. HOHENER, and R. R. ERNST. J. Magn. Reson. **13**, 196 (1974).
5. P. MEAKIN and J. P. JESSON. J. Magn. Reson. **11**, 182 (1973); **13**, 354 (1974).
6. J. FEENEY and P. PARTINGTON. Chem. Commun. 611 (1973).
7. K. KUSHIDA, K. AOKI, and S. SATOH. J. Am. Chem. Soc. **97**, 443 (1975).
8. K. G. R. PACHLER and P. L. WESSELS. Chem. Commun. 1038 (1974).
9. R. FREEMAN, H. D. W. HILL, B. L. TOMLINSON, and L. D. HALL. J. Chem. Phys. **61**, 4466 (1974); H. D. W. HILL and L. D. HALL. J Am. Chem. Soc. **98**, 1269 (1976).
10. B. L. TOMLINSON and H. D. W. HILL. J. Chem. Phys. **59**, 1775 (1973).
11. K. BOCK and C. PEDERSEN. Acta Chem. Scand. **27**, 2701 (1973).
12. K. BOCK and L. D. HALL. J. Carbohydr. Nucleosides Nucleotides. In press.
13. R. FREEMAN and W. A. ANDERSON. J. Chem. Phys. **37**, 2053 (1962).

Can. J. Chem. Downloaded from www.nrcresearchpress.com by 210.87.254.6 on 09/05/12
For personal use only.

Estimation of the stereoselectivity of reduction of 3,3,5,5-tetramethylcyclohexanone by sodium borohydride

DONALD C. WIGFIELD, GERALD W. BUCHANAN, CATHERINE A. ASHLEY, AND STEVE FEINER
Department of Chemistry, Carleton University, Ottawa, Ont., Canada K1S 5B6

Received May 17, 1976

DONALD C. WIGFIELD, GERALD W. BUCHANAN, CATHERINE A. ASHLEY, and STEVE FEINER. Can. J. Chem. **54**, 3536 (1976).

4-(1-Hydroxyethyl)-3,3,5,5-tetramethylcyclohexanone has been prepared to serve as a model for 3,3,5,5-tetramethylcyclohexanone on which the reduction stereochemical product ratio may be experimentally determined. Reduction with sodium borohydride in 2-propanol gives two epimers in a 95.5:4.5 ratio. The major isomer is shown to be the less stable by equilibration over Raney nickel. Proton and ^{13}C nmr spectra confirm that this major epimer is *cis*-4-(1-hydroxyethyl)-3,3,5,5-tetramethylcyclohexanol and show that this compound exists predominantly in the conformation with an axial hydroxyethyl group and an equatorial hydroxyl group. It is concluded that reduction of this model compound proceeds at least 95.5% by equatorial attack.

DONALD C. WIGFIELD, GERALD W. BUCHANAN, CATHERINE A. ASHLEY, et STEVE FEINER. Can. J. Chem. **54**, 3536 (1976).

On a préparé (l'hydroxy-1 éthyl)-4 tétraméthyl-3,3,5,5 cyclohexanone pour servir de modèle pour la tétraméthyl-3,3,5,5 cyclohexanone; avec ce composé le rapport stéréochimique des produits de réduction peut être déterminé expérimentalement. La réduction avec le borohydrure de sodium dans le propanol-2 donne deux épimères dans le rapport 95.5:4.5. Faisant appel à l'équilibration sur du nickel de Raney, on montre que l'isomère prépondérant est le moins stable. Les spectres rmn du proton et du ^{13}C confirment que l'épimère formé d'une façon prépondérante est (l'hydroxy-1 éthyl)-4 tétraméthyl-3,3,5,5 cyclohexanol *cis* et on montre que ce composé existe d'une façon préférentielle dans la conformation avec un groupe hydroxyéthyle en position axiale et un groupe hydroxyle en position équatoriale. On conclut que la réduction de ce composé modèle se produit avec au moins 95% d'attaque équatoriale.

[Traduit par le journal]

Reduction of cyclohexanones with sodium borohydride is a reaction that displays well-known and interesting stereoselectivity. In 1953 Barton was able to make the qualitative generalization that unhindered cyclohexanones yield primarily the equatorial alcohol, but that hindered cyclohexanones show the opposite stereoselectivity, yielding primarily the axial alcohol (1). This generalization has since been amply confirmed, but in spite of the synthetic and mechanistic activity in this area, the origin of the stereoselectivity still remains in doubt. Among simple cyclohexanones, the ketone at the hindered extreme of the spectrum has been 3,3,5,5-tetramethylcyclohexanone, and it has frequently been an irritating point that, because of the symmetry of this molecule, its stereoselectivity remains unknown. Estimates, in fact, have varied from 0.5% to 30% equatorial alcohol (for a discussion of these estimates, see ref. 2). In this paper we report the use of a closely related model compound to obtain an experimental value for the stereoselectivity of reduction of 3,3,5,5-tetramethylcyclohexanone by sodium borohydride in 2-propanol.

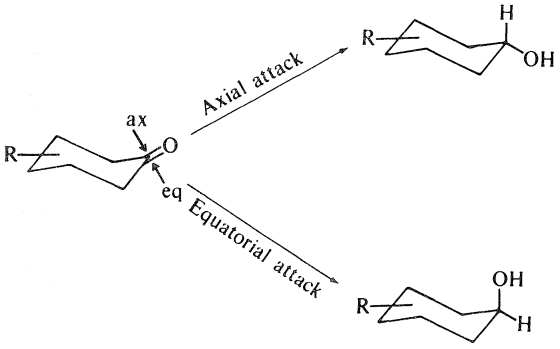

FIG. 1. Axial and equatorial hydride attack on cyclohexanones.

The criterion in the selection of a model compound was clearly the introduction of a substituent to break the symmetry of 3,3,5,5-tetramethylcyclohexanone, but one which would have the minimum perturbation on the stereochemical outcome. Substituents at the 2-position

Can. J. Chem. Downloaded from www.nrcresearchpress.com by 210.87.254.105 on 09/05/12
For personal use only.

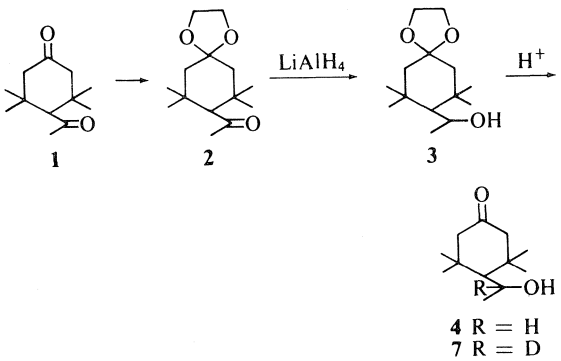

1 2 3

FIG. 2. Synthetic route to model compounds.

markedly affect the stereoselectivity (3); the 3-positions are already full, and thus a 4-substituent is dictated. Equatorial substituents at C-4 have a minimal effect on the stereoselectivity; indeed, the product ratio from 4-methylcyclohexanone and 4-*tert*-butylcyclohexanone are essentially indistinguishable (4). An available[1] compound of this type is 4-acetyl-3,3,5,5-tetramethylcyclohexanone (**1**), but although a

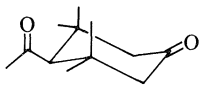

1

stereochemical product ratio can be obtained from reduction of this compound, its significance is questionable because of the possibility of epimerization at C-4. A number of attempts to modify the acetyl group were unsuccessful owing to its very hindered environment: indeed all such reactions failed with the exception of reduction by lithium aluminum hydride. However, this differential reactivity between the two ketone groups of **1** allowed the route to a suitable model compound (**4**) to be performed as shown in Fig. 2.

Compound **4**, 4-(1-hydroxyethyl)-3,3,5,5-tetramethylcyclohexanone, clearly possesses the required structural features for the stereochemical analysis.

Stereochemistry of Reduction

Mixtures of epimeric cyclohexanols from reduction of cyclohexanones are most conveniently analysed by glc; a number of columns have been used for this purpose and it is generally observed that the axial alcohol of an axial–equatorial pair has a shorter retention time (3, 5). The system with a 50 ft SCOT TCEP column previously used in our work has proved to be an especially powerful tool in this regard, giving base-line separation of all epimeric pairs of cyclohexanols we have examined (3, 4). The reduction under present investigation, however, has some unusual ambiguity; while axial attack (the expected minor pathway) to give *trans*-4-(1-hydroxyethyl)-3,3,5,5-tetramethylcyclohexanol (**5**) is straightforward, the *cis* isomer (**6**), arising from equatorial attack of hydride (the expected major pathway), offers possible conformational complexity (see Fig. 3). The conformation **6***a* possesses a severe 1,3,5 triaxial interaction between the hydroxyl group and two methyl groups, and relief of this interaction by ring flip to conformation **6***b* may more than offset the conformational energy of the hydroxyethyl group which must simultaneously change from an equatorial to an axial configuration. Thus it is possible that the epimeric separation could be between two equatorial alcohols rather than, as usual, an axial–equatorial pair.

The result of reduction of ketol **4** by sodium borohydride in 2-propanol was the production of two products in a 95.5:4.5 ratio; the evidence discussed below demonstrates these products to be the epimeric alcohols **6** and **5** respectively.

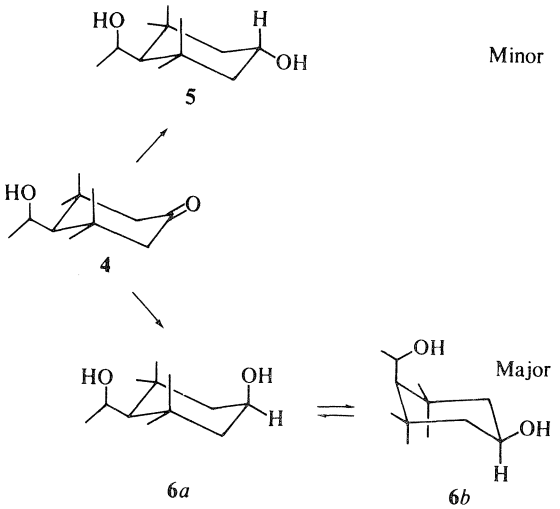

6*a* **6***b*

FIG. 3. Epimeric reduction products.

[1]We are very grateful to Roure Bertrand Fils et Justin Dupont for a generous sample of **1**.

Can. J. Chem. Downloaded from www.nrcresearchpress.com by 210.87.254.105 on 09/05/12
For personal use only.

Can. J. Chem. Downloaded from www.nrcresearchpress.com by 210.87.254.105 on 09/05/12
For personal use only.

Epimer Equilibration

Treatment with Raney nickel is known to cause epimerization of the hydroxyl group in cyclohexanols (6); application of this treatment to the two products from reduction of ketol **4** resulted in a steady increase of the minor component at the expense of the major. This result not only showed that the two products were interconvertible, but also provided a 99% pure sample of the *minor* component, to complement the 95.5% sample of the major component for subsequent spectroscopic examination.

Re-oxidation

Oxidation of both major and minor components by Jones oxidation gave diketone **1** as a single product. The combination of this evidence with the epimer equilibration evidence establishes that the two components are indeed the epimers **5** and **6** leaving only the question of which is which. In this regard, the epimer equilibrations establish that the major component is the thermodynamically less stable epimer and presumably is the *cis* epimer **6**. Spectroscopic confirmation of this assignment and conformational clarification are outlined below.

Proton Nuclear Magnetic Resonance

Nuclear magnetic resonance analysis of the methine proton adjacent to hydroxyl has been a very useful method for determining the axial/equatorial nature of the hydroxyl group in cyclohexanols (7). Examination of the methine signals in **5** and **6**, however, were not directly observable because of the interference of the corresponding proton in the hydroxyethyl group. Accordingly, the appropriately deuterated ketol analogue **7** (see Fig. 2) was prepared by replacing $LiAlH_4$ in the synthetic sequence by $LiAlD_4$. Deuterated ketol **7** was then reduced with $NaBH_4$ in 2-propanol, and epimer equilibration as described above again gave 95.5% and 99% purity samples of the less and of the more stable epimers respectively for nmr investigation.

Methine signals for equatorial alcohols are generally at δ 3.2–3.7 and of half-width 22 Hz, whereas those for axial alcohols are δ 3.6–4.2 with a half-width of 7 Hz (7). The methine signals of the major and minor components of reduction of **7** were remarkably similar; δ 4.1 with half-width 15 Hz for the major component, and δ 4.4 with half-width 16 Hz for the minor component. Although the signals are at lower field than usual and of narrower half-width, the similarity between them (and particularly the *higher* field signal of the major component) makes it very improbable that there is a configurational difference at C-1, consistent with the idea presented above that conformation **6***b* is prevalent and that both components are equatorial alcohols.

^{13}C Nuclear Magnetic Resonance

From the proton nmr data discussed above it appears that the two epimers have structures **5** and **6***b*, and therefore differ by virtue of being epimeric at C-4 rather than at C-1. It is well known that an axial substituent in a cyclohexane ring offers substantial shielding to the γ carbons (the *gauche* effect) (8), and thus ^{13}C nmr spectroscopy provides a means for stereochemical distinction between epimers **5** and **6***b*. In this case the γ carbons are C2,6 and, these being the only methylene carbons in the epimers, it is possible to make rapid and positive identification of these signals. In the minor component C2,6 give signals at δ 52.4 and δ 54.7 (two peaks due to asymmetry of the hydroxyethyl group), very close to the signal position of C2,6 in 3,3,5,5-tetramethylcyclohexanone itself, δ 53.8 (9). In the major component C2,6 give signals at δ 48.6 and δ 50.2. This upfield shift of 4.2 ppm is clearly in accord with the presence of an axial substituent at C-4 in the major component. In addition, consistent with the idea of **6***b* being the predominant conformation over **6***a*, the shifts of C3,5 (γ to C-1) between the two epimers are much closer (1.6 ppm).

The above data indicates that the major component of reduction of ketol **4** by sodium borohydride is *cis*-4-(1-hydroxyethyl)-3,3,5,5-tetramethylcyclohexanol which exists predominantly as conformation **6***b*. Reduction of compound **4**, a model for 3,3,5,5-tetramethylcyclohexanone, therefore proceeds by at least 95.5% equatorial attack.[2]

[2]The conclusion that the stereoselectivity is *exactly*, rather than *at least*, 95.5% would require the assumption that reduction occurs exclusively through the ketone conformation with the hydroxyethyl group equatorial. Reduction through the conformation with this group axial would be expected to give predominantly alcohol **5**, and thus it is extremely improbable that this conformation plays any significant role. Additionally, the ^{13}C nmr spectrum of the ketone **4** shows no evidence of this conformation, particularly in the complete absence of any *gauche* effect to C-2 and C-6 with respect to 3,3,5,5-tetramethylcyclohexanone itself. The ketone spectrum was unchanged at −90 °C.

Can. J. Chem. Downloaded from www.nrcresearchpress.com by 210.87.254.105 on 09/05/12
For personal use only.

Experimental

Melting points were determined on a Fisher-Johns block and are uncorrected. Infrared spectra were obtained on a Perkin-Elmer 257 spectrophotometer and proton nmr spectra in $CDCl_3$, with TMS as internal standard, on a Varian T-60 or XL100 instrument. ^{13}C nmr spectra (natural abundance) were obtained on a Varian XL-100-12 nmr spectrometer equipped with a Nicolet Technology Corporation Fourier transform data system. Microanalyses were performed by Spang Microanalytical Laboratories, Ann Arbor, Michigan. Gas–liquid chromatography was performed on a Hewlett-Packard F and M Model 402 gas chromatograph, unless otherwise stated.

Samples of *4-acetyl-3,3,5,5-tetramethylcyclohexanone* **1** and its mono *ethylene ketal* **2** were obtained through the generosity of Roure Bertrand Fils et Justin Dupont.

4-(1-Hydroxyethyl)-3,3,5,5-tetramethylcyclohexanone, , Ethylene Ketal **3**

Lithium aluminum hydride (0.6 g, 1.6×10^{-2} mol) was added cautiously with stirring (magnetic bar) to anhydrous ether (100 ml) in a 250 ml round-bottom flask. To the stirred suspension was added ethylene ketal **2** (2.4 g, 1.0×10^{-2} mol). The flask was fitted with a condenser and $CaCl_2$ drying tube, and the reaction stirred at room temperature for $12\frac{1}{2}$ days. The reaction mixture was then cooled to ~ -10 °C in an ice–acetone bath, and water (0.6 ml), 15% sodium hydroxide solution (0.6 ml), and water (1.8 ml) added in that order in a dropwise manner (10). The resulting white granular precipitate was gravity filtered, and washed with ether (2×20 ml). The ether solutions were combined, washed with water (2×20 ml), dried (Na_2SO_4), and evaporated to give a clear colourless liquid (2.25 g, 93%). Chromatographic (6 ft QF-1 column, 195 °C, retention time 8.4 min) and spectral ($\nu_{max}(CHCl_3)$ 3680, 3620 (OH), 2960, 2900 (CH), 1470, 1360, 890 cm^{-1}; δ 3.6–4.4 (5H, m, H adjacent to O) and 1.0–1.6 (21 H, m, all other H with CH_3's at 1.00 (s), 1.13 (s), 1.22 (s), 1.33 (s), and 1.48 (d, $J = 5$ Hz))) analysis indicated the material to be suitable for direct acid hydrolysis to **4** without further purification. *4-(1-Hydroxyethyl-1-d_1)-3,3,5,5-tetramethylcyclohexanone, ethylene ketal* was prepared as described above replacing $LiAlH_4$ by $LiAlD_4$.

4-(1-Hydroxyethyl)-3,3,5,5-tetramethylcyclohexanone **4**

A solution of ketal **3** (1.0 g, 4.1×10^{-3} mol) in 1.0 *N* hydrochloric acid (50 ml) and methanol (150 ml) in a 500 ml stoppered round-bottom flask was stirred (magnetic bar) at room temperature for 24 h. The mixture was then cooled (ice–water bath) and solid sodium bicarbonate added until the solution was neutralized (p*H* > 7.0, p*H* paper). The neutralized solution was evaporated (rotary evaporator) to remove methanol; water (25 ml) was added and the solution extracted with ether (3×10 ml). The ether extracts were combined, dried (Na_2SO_4), and evaporated to give a white crystalline solid (0.81 g, 100%), which after three crystallizations from petroleum ether (bp 30–60 °C) had mp 101–102 °C; $\nu_{max}(CHCl_3)$ 3690, 3610 (OH), 2960, 2890 (CH), 1700 (C=O) cm^{-1}; δ 4.2–4.5 (1H, m, CH—O), 2.20 (4H, br s, $2 \times CH_2$), and 1.0–1.6 (17H, m, all other H with CH_3 signals at 1.07 (s), 1.10 (s), 1.20 (s), 1.27 (s), 1.45 (d, $J = 5$ Hz)); glc (6 ft QF-1, 180 °C) retention time 18.5 min. *Anal.* calcd. for $C_{12}H_{22}O_2$: C 72.68, H 11.18; found: C 72.74, H 11.32. The monodeuterio ketal **7** was prepared in an analogous manner from the monodeuterio ketal.

Sodium Borohydride Reduction of Ketol **4**, *and Raney Nickel Equilibration of the Resulting Alcohols*

Ketol **4** was reduced by sodium borohydride in 2-propanol at 25 °C using the procedures of reduction, work-up, and analysis previously described (11). Gas–liquid chromatographic analysis on a CW6000 column, and also on the TCEP SCOT column system (3, 5) showed the epimeric alcohol mixture to be in the ratio 95.5:4.5. Mass analysis of the epimeric alcohol mixture gave *m/e* 200.1756 (calcd. for $C_{12}H_{24}O_2$: 200.1776). Raney nickel for alcohol equilibration was prepared by repeated washing with water of the commercial (W. R. Grace) product until the washings were neutral to litmus, followed by an additional 10 washings (a total of ~35 washings). The nickel was then washed three times with 95% ethanol, three times with absolute ethanol, and stored under ethanol. For alcohol equilibrations, 5 g of this nickel were transferred to a 100 ml three-neck flask and rinsed three times with anhydrous 2-propanol which had been freshly distilled from CaO after heating under reflux for 3 h. The epimeric alcohols (95.5:4.5) (1 g) in anhydrous 2-propanol (25 ml) were added and the mixture heated under reflux under a N_2 stream for 144 h. Gas–liquid chromatographic analysis of the alcohol mixture showed a progressive increase of the minor epimer at the expense of the major epimer during this period. The mixture was then filtered through a fine sintered glass funnel and the nickel rinsed with 2-propanol before being carefully destroyed with concentrated hydrochloric acid. The 2-propanol filtrate and washings were evaporated, water (20 ml) was added, and the aqueous solution extracted with ether (3×5 ml). The combined ether extracts were dried (Na_2SO_4) and evaporated to give a residue in which the major epimer had been almost completely converted to the minor epimer. Despite the equilibration being conducted under a nitrogen atmosphere, some oxidation to ketone **4** invariably occurred. Purification of the epimeric alcohols from the ketone **4** was achieved by preparative layer chromatography (alumina F-254; ether–benzene (60:40), R_f 0.34). Proton nmr of both monodeuterated epimers (from reduction of **7**) showed a large envelope at δ 1–2 (22H) and the 1H signal of the methine proton at C-1; in epimer **5** this signal was at δ 4.4 (half-width 16 Hz); in epimer **6** at δ 4.1 (half-width 15 Hz). ^{13}C nmr of epimer **5**; δ 23.4, 24.5 (equatorial CH_3), 27.6 (CH_3—CH(OH)), 34.0, 34.6 (axial CH_3), 36.6, 36.8 (C-3, C-5), 52.4, 54.7 (C-2, C-6), 59.9 (C-4), 65.0, 68.3 (C-OH): epimer **6**; δ 26.3, 26.5 (equatorial CH_3), 27.7 (CH_3—CH(OH)), 34.0, 34.8 (axial CH_3), 35.0, 35.1 (C-3, C-5), 48.6, 50.2 (C-2, C-6), 58.6 (C-4), 67.5, 69.0 (C—OH). *Reoxidation of epimers* **5** *and* **6** was achieved by treating a solution of the alcohol (100 mg) in a mixture of acetone (3 ml) and water (3 ml) with Jones reagent (prepared by dissolving chromium trioxide (33.5 g) in water (63 ml), adding concentrated H_2SO_4 (29 ml) and then the minimum amount of water to achieve clear solution) (0.12 ml) for 20 min at room temperature. The green salts were filtered from the reaction mixture and washed with acetone. The filtrate and washings were combined and excess oxidant destroyed by dropwise addition of 2-propanol. Solid sodium

bicarbonate was added until the solution was neutral. The suspension was filtered and the combined filtrate and washings concentrated and extracted with ether. The combined ether extracts were dried (Na_2SO_4) and evaporated to give a pure sample of a compound shown to be identical in all respects (spectral, chromatographic) with 4-acetyl-3,3,5,5-tetramethylcyclohexanone **1**.

Acknowledgments

The financial support of the National Research Council of Canada is gratefully acknowledged.

1. D. H. R. Barton. J. Chem. Soc. 1027 (1953).
2. D. J. Phelps. Ph.D. Thesis. Carleton University, Ottawa, Canada. 1973.
3. D. C. Wigfield and D. J. Phelps. J. Am. Chem. Soc. **96**, 543 (1974) and references therein.
4. D. C. Wigfield and D. J. Phelps. J. Org. Chem. **41**, 2396 (1976).
5. D. C. Ayres, D. N. Kirk, and R. Sawdaye. J. Chem. Soc. B, 505 (1970).
6. E. L. Eliel and S. H. Schroeter. J. Am. Chem. Soc. **87**, 5031 (1965).
7. R. U. Lemieux, R. K. Kullnig, H. J. Bernstein, and W. G. Schneider. J. Am. Chem. Soc. **80**, 6098 (1958); E. L. Eliel, M. H. Gianni, Th. H. Williams, and J. B. Stothers. Tetrahedron Lett. 741 (1962); D. H. Williams and N. S. Bhacca. J. Am. Chem. Soc. **86**, 2742 (1964).
8. J. B. Stothers. Carbon-13 nmr spectroscopy. Academic Press, New York, 1972. pp. 112–118, 404–414.
9. J. B. Stothers and C. T. Tan. Can. J. Chem. **52**, 308 (1974).
10. V. M. Mićović and M. L. Mihailović. J. Org. Chem. **18**, 1190 (1953).
11. D. C. Wigfield and D. J. Phelps. Can. J. Chem. **50**, 388 (1972).

Can. J. Chem. Downloaded from www.nrcresearchpress.com by 210.87.254.105 on 09/05/12
For personal use only.

Metals intercalated in graphite. V. A concentration cell with intercalated bromine

JEAN-MARC LALANCETTE AND ROGER ROUSSEL
Département de chimie, Université de Sherbrooke, Sherbrooke (Qué.), Canada J1K 2R1

Received May 31, 1976

JEAN-MARC LALANCETTE and ROGER ROUSSEL. Can. J. Chem. **54**, 3541 (1976).

Bromine intercalates can be used as electrodes in concentration cells. Voltages of the order of 50 mV can be obtained with thermal gradients of 60–75 °C, in the range 0–100 °C. The cell can be operated on a continuous basis by allowing the high activity electrode to distill bromine to the low activity electrode.

JEAN-MARC LALANCETTE et ROGER ROUSSEL. Can. J. Chem. **54**, 3541 (1976).

Les composés d'insertion du brome dans le graphite peuvent jouer le rôle d'électrodes dans une pile à concentration. Des voltages de l'ordre de 50 mV sont observés en appliquant un gradiant de 60–75 °C se situant dans la région 0–100 °C. La cellule peut opérer en continue si l'on permet la distillation du brome de l'électrode à haut niveau d'activité vers l'électrode à bas niveau d'activité.

Can. J. Chem. Downloaded from www.nrcresearchpress.com by 210.87.254.105 on 09/05/12
For personal use only.

Bromine can be intercalated in graphite. This intercalation is spontaneous when bromine is in contact with graphite at room temperature, the intercalation being accompanied by an important expansion of the volume of graphite which then assumes a typical blue color. Rudorff (1) has shown, by X-ray diffraction studies, that the compound C_8Br corresponding to the saturation of the lattice of graphite with bromine is, in fact, a stack of alternating layers of bromine and carbon, two layers of bromine (7.05 Å) alternating with two layers of carbon (3.38 Å).

The bromine intercalates are not stable and will decompose spontaneously if not left in equilibrium with bromine vapor. The isotherms of fixation of bromine by graphite have been reported and Hooley (2) has shown the important influence of the size of graphite particles on such isotherms. The intercalation of bromine in graphite is not entirely reversible, however. Depending on the source of graphite (3) variable amounts of bromine in the range of 5–10% remain strongly held by the lattice and can be removed only by strong heating, with the formation of volatile derivatives of carbon incorporating bromine.

The electronic state of intercalated bromine has been examined by several authors. According to Ubbelohde and co-workers (4), at low concentrations of bromine in graphite there must be a complete ionization of bromine. At higher concentrations of bromine, only a part of the bromine would exist in the ionic form. For Hennig (5), in the case of C_8Br one bromine atom exists in the ionic form for every seven bromine atoms. The residual bromine remaining in graphite would also be present in the form of partly dissociated and partly molecular entities.

This paper, as part of a study of the chemistry of graphite intercalates (6), reports the use of bromine–graphite intercalates as electrodes in a concentration cell.

The characteristics of a concentration cell are the following. The anode and the cathode call upon the same reversible system and the net energy withdrawn from the cell comes from the reaction of the system used to a difference in the activity of a common ion at the anode and at the cathode. The polarity of the concentration cell is such as to remove the difference of concentration existing initially between each electrode by discharge or removal of appropriate entities at each electrode and diffusion of ions through the bridge between the electrodes.

We have noted that bromine–graphite intercalates held at different temperatures could give rise to a concentration cell. Each electrode then represents a similar system involving the same species whose activities are related to their temperature. The overall situation is illustrated by [1].

[1]

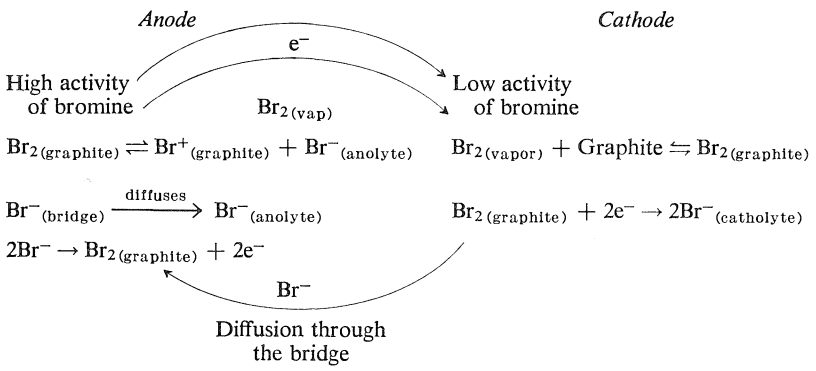

In the case of such a concentration cell it can be assumed that the intercalated bromine behaves as a gas held within graphite and having an activity related to its pressure. If a temperature difference exists between the electrodes, the warmer electrode will become the anode while the cooler electrode behaves as a cathode. Providing that there exists an appropriate bridge between the graphite electrodes, a concentration cell will exist. Such a cell has been operated and is illustrated in Fig. 1. The pressure–temperature relation for bromine is known for pure bromine (7).

From the existing literature cited above, bromine intercalated in graphite can be assumed to be a solution of bromine in a solid matrix of graphite. As indicated by Ubbelohde and Hennig, the intercalated bromine is partly dissociated within the lattice of graphite. The percentage of dissociation is related to the actual concentration of bromine in graphite and must also be influenced by temperature. Consequently, the factors influencing the activity of the intercalated bromine at an electrode are numerous and complex. We have noted that the observed potential can be related in a first approximation to the difference of temperature between the electrodes by assuming an activity coefficient of one for the intercalated bromine. From [2] it can

$$[2]\quad \Delta E = \frac{RT_{\text{anode}}}{2F} \ln \left(\frac{[Br_2]_{\text{anode}}}{[Br^-]_{\text{anode}}}\right) - \frac{RT_{\text{cathode}}}{2F} \ln \left(\frac{[Br_2]_{\text{cathode}}}{[Br^-]_{\text{cathode}}}\right)$$

be noted that $\Delta E = 43$ mV if the vapor pressures of pure bromine at 0 °C (65 torr) and 50 °C (689 torr) are used. The variations in the dissociation of bromine resulting from the differences in the temperature and concentrations lead to a calculated value of ΔE of 43 mV. This is in acceptable agreement with the observed value (35 mV) when it is noted that the variation in the activity of the bromide ion at a concentration of 10%, as occurs in the bridge, is not known for the temperature range involved.

If the temperature gradient of the cell is inverted, the cathode becomes the anode and the cell is thus reversed. This inversion of the temperature gradient gives an inversion of the sign of the voltage. When the warm electrode is operated at a temperature not higher than 50 °C there is little distillation of bromine from the anode to the cathode. If, however, the temperature is raised to 100 °C then an appreciable amount of bromine is transferred to the cathode. A situation is reached where bromine vapor

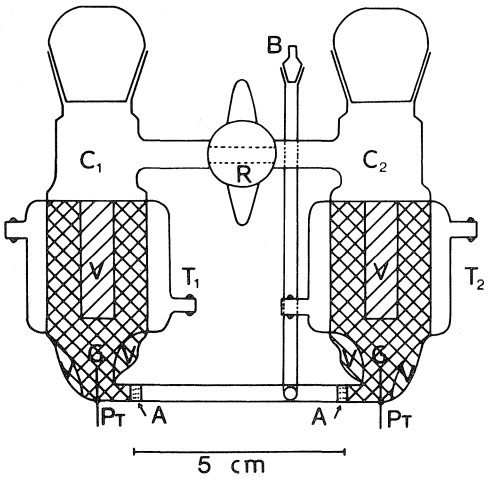

FIG. 1. Concentration cell of bromine–graphite intercalates.

Can. J. Chem. Downloaded from www.nrcresearchpress.com by 210.87.254.105 on 09/05/12
For personal use only.

Can. J. Chem. Downloaded from www.nrcresearchpress.com by 210.87.254.105 on 09/05/12
For personal use only.

diffusion compensates for the bromine loss at the cathode due to diffusion of the bromide ion to the anode via the bridge. This then leads to a closed circuit for the bromine, the different steps involved being diffusion of the bromide ion through the bridge, oxidation of the bromide ion to bromine at the anode, distillation of bromine as bromine vapor to the cathode, and reduction of bromine to bromide at the cathode. As long as an appropriate difference of temperature is maintained between the electrodes, the system will operate.

The bromine graphite intercalates have an electrical conductivity which is in the metallic range. Consequently, the limiting factor for current density will probably be the transference properties of the bridge. As far as the diffusion of bromine vapor is concerned, this occurs at a significant level when the temperature of the anode reaches the boiling point of bromine, around 60 °C. The work to be done in order to achieve this transfer of bromine involves the heat of desorption of bromine from graphite and the latent heat of evaporation of bromine. The process being activated by heat transfer, its efficiency must be governed by the second law of thermodynamics, as is that of any thermal process. Nevertheless, it certainly offers interesting possibilities for the recovery of 'waste heat' energy, or solar heat, because of the small difference of temperatures required to activate the system and the low temperature of operation. With electrodes of large area having good chemical resistance to moist bromine, such a cell could sustain a large current with very low internal resistance. This would allow an arrangement of several cells in series to achieve practical voltages without undue losses by internal ohmic resistance.

Other systems using intercalated mixed halogen, namely ICl_3, ICl, and IBr have been examined. A somewhat similar result was observed, the potential being in the range of those observed for bromine intercalates. However, the reversible character of the electrodes is lost since thermal treatment induces some irreversible changes in the mixed halogen structures. Consequently these systems are of lesser interest.

Experimental

Concentration Cells with Bromine

The cell used is illustrated in Fig. 1. A graphite–bromine intercalate (G) of composition $C_{18}Br$ and prepared from graphite (spectroscopic grade, finer than 20 mesh) and bromine (reagent grade) was introduced in each cell (C_1, C_2, Pyrex). Each of the electrodes was in a jacket kept at a constant temperature (±2 °C) by circulation of water from thermostated baths. The bridge solution (10% KBr solution in water and saturated with bromine (≃3% by weight of bromine)) was introduced between the cells at B and allowed to diffuse to the electrodes through a sintered glass ring A of porosity M (Corning). Initially the cells were at atmospheric pressure and the valve (R) could be opened or closed to allow or prevent diffusion of bromine vapor between the two electrodes. A cylindrical core made of Vycor glass wool (V) was placed at the center of the electrodes to assist the bromine diffusion, between the electrodes. A collar made of the same material was placed at the bottom of the electrodes to prevent heat loss. Platinum electrodes (Pt) were used as electrical outlets at each of the electrodes. $C_{18}Br$ (25 g) was placed in each electrode.

Two sets of experimental conditions have been studied. In the first series of experiment, the anode was kept at 50 °C and the cathode at 0 °C. The equilibrium voltage, measured with a Syntron Donner digital voltmeter (model no. 900-4A), was +35 mV and this value was reached after 100 min following the application of the temperature gradient. After 180 min the circulation of the warm and cold water was inverted and the constant difference of potential was measured as −35 mV. Under such experimental conditions, a minimal amount of bromine was exchanged between the electrodes. In a particular experiment, with the gradient 0–50 °C, it was noted that 0.19 g of bromine was exchanged between two flasks containing 20 g of $C_{18}Br$ and joined by a 10 mm tube, under a vacuum of 1 torr.

In the second set of experiments, the arrangement was as above except that the anode was kept at 101 °C and the cathode at 8 °C. The observed voltage was +69 mV after 1 h and was not as stable as in the previous experiment, the voltage increasing slowly as bromine distilled to the cold electrode. In a separate experiment, with two flasks each containing 10 g of graphite and 4 g of bromine and connected under vacuum by a 10 mm tube, it was noted that if a flask was kept at 90 °C and the other at 25 °C, 2.0 (±0.3 g) of bromine was transferred before a new equilibrium was reached.

Concentration Cells with Mixed Halogens

The preparative method used for the formation of mixed halogens was from Brauer (8). Using the experimental technique described above, the following results have been observed: with 20% ICl_3 in graphite, +11 mV for electrodes at 60 and 5 °C respectively; with 33.3% ICl in graphite, +35 mV for electrodes at 60 and 5 °C respectively; 34.8% IBr in graphite, +35 mV for electrodes at 60 and 5 °C respectively. The following systems were used as bridges. For ICl: 2.0 g of ICl in 100 ml of THF; for ICl_3: 2.3 g of ICl_3 in 100 ml of THF; and for IBr: 3.0 g IBr in 100 ml of THF containing 0.2 ml 40% HBr.

Acknowledgment

The authors thank the National Research Council of Canada for financial assistance.

1. W. RUDORFF. Z. Anorg. Chem. **245**, 383 (1941).
2. J. G. HOOLEY. Can. J. Chem. **40**, 745 (1962).
3. A. HÉROLD. Bull. Soc. Chim. Fr. 999 (1955).
4. L. C. F. BLACKMAN, J. F. MATHEWS, and A. R. UBBELOHDE. Proc. R. Soc. London, Ser. A, **256**, 15 (1960).
5. (*a*) G. R. HENNIG. J. Chem. Phys. **19**, 922 (1951); (*b*) G. R. HENNIG. J. Chem. Phys. **20**, 1443 (1952).
6. (*a*) J.-M. LALANCETTE and R. ROUSSEL. Can. J. Chem. **54**, 2110 (1976). (*b*) J.-M. LALANCETTE, L. ROY, and J. LAFONTAINE. Can. J. Chem. **54**, 2505 (1976).
7. P. PASCAL. Nouveau traité de chimie minérale. Vol. XVI. Masson et Cie, Paris. 1960. p. 346.
8. G. BRAUER. Handbook of preparative inorganic chemistry. Academic Press, New York. 1965. p. 291.

Can. J. Chem. Downloaded from www.nrcresearchpress.com by 210.87.254.105 on 09/05/12
For personal use only.

Evaluation of a spin-labeled inhibitor of acetylcholinesterase

CATHERINE KAVANAGH-CARON, MARCEL CARON, NORMAND BRISSON, AND HERMANN DUGAS[1]
Département de Chimie, Université de Montréal, Montréal (Qué.), Canada H3C 3V1

Received June 2, 1976

CATHERINE KAVANAGH-CARON, MARCEL CARON, NORMAND BRISSON, and HERMANN DUGAS. Can. J. Chem. **54**, 3545 (1976).

This paper describes the synthesis of **1**, a spin-labeled analog of *N,N*-dimethyl-2-phenylaziridinium chloride **2**. The compound is formed *in situ* from **3***b* and acts as a poor competitive inhibitor of bovine erythrocyte acetylcholinesterase with a K_i value of 2.1×10^{-3} *M*.

CATHERINE KAVANAGH-CARON, MARCEL CARON, NORMAND BRISSON et HERMANN DUGAS. Can. J. Chem. **54**, 3545 (1976).

Cet article décrit la synthèse de **1**, un marqueur de spin analogue du chlorure de *N,N*-diméthyl phényl-2 aziridinium **2**. Le composé est formé *in situ* à partir de **3***b* et agit comme un faible inhibiteur compétitif de l'acétylcholinesterase d'érythrocytes de boeuf. La valeur du K_i est de 2.1×10^{-3} *M*.

In recent years, the spin-label method has been applied to a wide spectrum of problems and has been especially successful in biochemical and biological applications (1–3). For example, new spin-labeled drugs have been synthesized to study the mechanism of drug action at a molecular level and the topography of specific binding sites in receptor macromolecules (4–8).

Acetylcholinesterase is known to possess at least two important sites for substrate binding (9). There is an esteratic site which cleaves the ester bond of acetylcholine and there is also an anionic site nearby which recognizes the polar part of the substrate. Chignell and co-workers (5, 7) have synthesized spin-labeled choline esters as probes for the active site of the enzyme. On the other hand, no spin-labeled derivatives specific for the anionic site are known to date. We would like to report here the synthesis of **1**, a compound that could have such a property.

The work of Belleau *et al.* (10–12) has shown that *N,N*-dimethyl-2-phenylaziridinium chloride (DPA) **2** is a potent anionic-site-directed irreversible inhibitor of acetylcholinesterase. Therefore, we decided to synthesize **3***b*, the precursor of **1** *in situ*. This compound is a labeled analog of DPA that could be used as a suitable probe to monitor the enzyme structure and geometry at the anionic site.

m-Aminostyrene **4** and 3-carboxy-2,2,5,5-tetramethyl-1-pyrrolidinyloxyl **5**, prepared from 3-carbamoyl-2,2,5,5-tetramethylpyrrolidine (Frinton Lab.) according to the procedure of Rozantsev and Krinitzkaya (13), were used as starting materials. Both compounds were coupled using a water-soluble carbodiimide to give the amide **6** in 71% yield. This compound was epoxidized to **7** and then treated with dimethylamine to give only **3***a* as the ring-opening product in 80% yield. The presence of a peak at *m/e* 58 for the

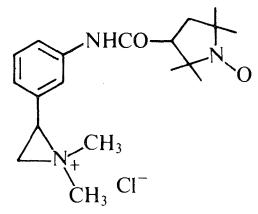

1

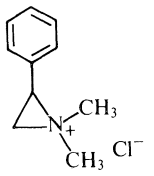

2

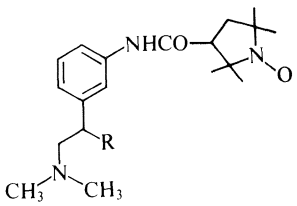

3
a R = OH
b R = OMs

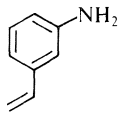

4

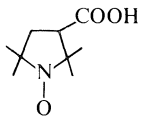

5

[1]Author to whom correspondence should be addressed.

Can. J. Chem. Downloaded from www.nrcresearchpress.com by 210.87.254.6 on 09/05/12
For personal use only.

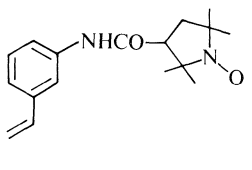

6

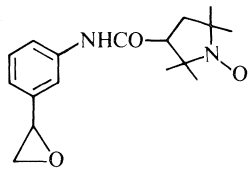

7

fragment ($CH_2N(CH_3)_2$) in the mass spectrum confirms the direction of opening of the epoxide ring. This result agrees with the work of Chapman and Triggle (14) for the synthesis of phenylethylamine derivatives. Treatment of **3***a* with mesyl chloride in dry $CHCl_3$ gave the expected hydrochloride salt of the mesyl amine **3***b* with a yield of 75%. This compound gives a typical three line epr signal with $a_0 = 15.0$ G in water. Analogous sulfonic acid esters (15) have been shown to be active towards acetylcholinesterase and a compound such as **3***b* is expected to cyclize instantaneously to the aziridinium chloride salt **1** in aqueous buffer above p*H* 7.0 (10).

Kinetic measurements at p*H* 7.4 using the procedure of Belleau and Tani (10) showed that **3***b* acts only as a poor competitive inhibitor of bovine erythrocyte acetylcholinesterase (Sigma). An inhibition constant K_i of 2.1×10^{-3} *M* was calculated from Lineweaver–Burk plots. Similar results were obtained by Belleau and Tani (10) using 3′- and 4′-OCH_3 derivatives of **2**.

Although this paper reports an efficient synthesis of a spin-labeled inhibitor of acetylcholinesterase, the compound will have limited value as a reporter group because of its low inhibition capacity.

Experimental

Melting points were determined on a Bûchi type S apparatus and are uncorrected. Microanalyses were performed by H. Seguin of the National Research Council of Canada, Ottawa. High resolution mass spectra were measured with a Varian MS9 instrument by A. S. Blair and P. Coulombe at the University of Montreal. For tlc, commercial plates of silica gel (Eastman) were used. Nitroxide groups give white spots on a blue background with the Zinzadze reagent (16–17).

N-(3-Carboxy-2,2,5,5-tetramethyl-1-pyrrolidinyloxyl)-3-aminostyrene, **6**

To a solution of the acid **5** (6.51 g, 35 mmol) in 75 ml of dry $CHCl_3$ at 0 °C was added 1-cyclohexyl-3-(2-morpholinoethyl)carbodiimide metho-*p*-toluenesulfonate (Aldrich) (14.93 g, 35 mmol). The solution was stirred for 10 min at 0 °C, then *m*-amino-styrene **4** (4.16 g, 35 mmol) was added. After 2 h, the solution was left at room temperature for 20 h. The solution was washed with water, dried (Na_2SO_4), and evaporated to dryness to give a crude red oil. The material was chromatographed on silica gel and compound **6** was eluted with Et_2O and recrystallized in the same solvent. The yellow crystals (7.1 g, 71%) were judged pure by tlc; mp 139.5–140 °C; uv, λ_{max}(EtOH) 242 nm (88 400); ms, *m/e* 287.

N-(3-Carboxy-2,2,5,5-tetramethyl-1-pyrrolidinyloxyl)-3-ethylepoxyaniline, **7**

Compound **6** (5.74 g, 20 mmol) was added to a solution of *m*-chloroperbenzoic acid 85% (5.06 g, 25 mmol) in 125 ml of dry $CHCl_3$ at 0 °C. After stirring vigorously for 1 h, the solution was left aside at 4 °C for 24 h. The solution was washed twice with 10% NaOH and then with water until neutrality. The $CHCl_3$ solution was dried (Na_2SO_4), then evaporated to dryness to give a crude yellow oil which showed two spots on tlc using Zinzadze reagent (16). The latter oily material was crystallized in ether (4.87 g, 80%) and was used as such for the next reaction: uv λ_{max}(EtOH) 240 nm (7200); ms *m/e* 303.1707 ($C_{17}H_{23}N_2O_3$, 303.1708).

N-(3-Carboxy-2,2,5,5-tetramethyl-1-pyrrolidinyloxyl)-3-(2-hydroxy-N,N-dimethylethyl)aniline, **3***a*

At 0 °C, a solution of **7** (4.54 g) in 100 ml of dry C_6H_6 was treated with a large excess of anhydrous dimethylamine. After 4 days at room temperature, the solution was filtered and evaporated. The red oil obtained was chromatographed on silica gel. The fraction eluted with $CHCl_3$–MeOH (8:2) contained 3.3 g of **3***a* and was crystallized with a mixture of C_6H_6–Et_2O, mp 153–154 °C; ms *m/e* 348.2286 ($C_{19}H_{30}N_3O_3$, 348.2285). The presence of the fragment *m/e* 58 ($CH_2N(CH_3)_2$) indicated clearly that the epoxide ring opened only in the direction anticipated. *Anal.* calcd. for $C_{19}H_{30}N_3O_3$: C 65.49, H 8.68, N 12.07; found: C 65.38, H 8.49, N 12.22.

N-(3-Carboxy-2,2,5,5-tetramethyl-1-pyrrolidinyloxyl)-3-(2-mesyl-N,N-dimethylethyl)aniline Hydrochloride, **3***b*

The amino-alcohol **3***a* (1.2 g) in 9 ml of dry C_6H_6 was added dropwise to a solution of mesyl chloride (0.39 g) in 7 ml of dry C_6H_6 at 20 °C. The solution was stirred and kept at room temperature for 2 h, then the yellow precipitate formed was collected by filtration (1.17 g, 75%). Recrystallization from MeOH and anhydrous Et_2O afforded pale orange crystals of pure **3***b* in the hydrochloride form, mp 237 °C (dec.). The compound is very hygroscopic and should be manipulated under nitrogen atmosphere. *Anal.* calcd. for $C_{20}H_{33}N_3O_5ClS$: C 51.91, H 7.13, N 9.08, Cl 7.66, S 6.93; found: C 52.14, H 7.25, N 9.17, Cl 7.42, S 6.79.

Acknowledgements

We are grateful to the Département d'Hygiène du Milieu, Université de Montréal, for their assistance in measuring the inhibition of acetylcholinesterase. The financial support from the Defense Research Board, Ottawa, is also acknowledged.

1. H. M. McConnel and B. G. McFarland. Q. Rev. Biophys. **3**, 91 (1970).

Can. J. Chem. Downloaded from www.nrcresearchpress.com by 210.87.254.6 on 09/05/12
For personal use only.

2. O. H. GRIFFITH and P. JOST. Methods in pharmacology. Vol. 2. *Edited by* C. F. Chignell. Appleton-Century Crafts, New York, N.Y. 1972. p. 223.
3. I. C. P. SMITH. Biological applications of electron spin resonance. *Edited by* H. M. Swartz, J. R. Bolton, and D. C. Borg. Wiley-Interscience, New York, N.Y. 1972. p. 483.
4. J. D. MORRISETT, C. A. BROOMFIELD, and B. E. HACKLEY, JR. J. Biol. Chem. **244**, 5758 (1969).
5. C. F. CHIGNELL, D. K. STARKWEATHER, and R. H. ERLICH. J. Med. Chem. **15**, 876 (1972).
6. R. J. GARGIULO, G. J. GIOTTA, and H. H. WANG. J. Med. Chem. **16**, 707 (1973).
7. R. H. ERLICH, D. K. STARKWEATHER, and C. F. CHIGNELL. Mol. Pharmacol. **9**, 61 (1973).
8. B. K. SINHA and C. F. CHIGNELL. J. Med. Chem. **18**, 669 (1975).
9. D. J. TRIGGLE. Chemical aspects of the autonomic nervous system. Academic Press, New York. 1965.
10. B. BELLEAU and H. TANI. Mol. Pharmacol. **2**, 411 (1966).
11. B. BELLEAU and H. TANI. Can J. Pharm. Sci. **4**, 14 (1969).
12. B. BELLEAU and V. DITULLIO. Can. J. Biochem. **49**, 1131 (1971).
13. E. G. ROZANTSEV and L. A. KRINITZKAYA. Tetrahedron, **21**, 491 (1965).
14. N. B. CHAPMAN and D. J. TRIGGLE. J. Chem. Soc. 1385 (1963).
15. G. E. ULLYOT and J. F. KERWIN. Medicinal chemistry. Vol. 2. *Edited by* F. F. Blicke and C. M. Suter. Wiley and Sons, New York, N.Y. 1956. p. 234.
16. C. ZINZADZE. Ind. Eng. Chem. **7**, 227 (1935).
17. R. ANEJA and A. D. DAVIS. Chem. Phys. Lipids, **4**, 60 (1970).

Can. J. Chem. Downloaded from www.nrcresearchpress.com by 210.87.254.6 on 09/05/12
For personal use only.

Synthesis of 5,10,11,12,17,22,23,24-octahydrotetrabenzo[*a,d,i,l*]cyclohexadecene derivatives[1]

ROGER N. RENAUD AND JOHN W. BOVENKAMP

Division of Chemistry, National Research Council of Canada, Ottawa, Canada K1A 0R6

Received August 6, 1976

ROGER N. RENAUD and JOHN W. BOVENKAMP. Can. J. Chem. **54**, 3548 (1976).

The reaction between 2,2′-bis(bromomethyl)diphenylmethane and diethyl sodiomalonate gives mainly 11,11,23,23-tetracarboethoxy-5,10,11,12,17,22,23,24-octahydrotetrabenzo[*a,d,i,l*]-cyclohexadecene together with some polymeric compounds. No eight-membered ring products were detected. Starting from the tetracarboethoxy compound described above, the syntheses of a series of di- and tetrasubstituted tetrabenzo[*a,d,i,l*]cyclohexadecenes are described.

ROGER N. RENAUD et JOHN W. BOVENKAMP. Can. J. Chem. **54**, 3548 (1976).

Le bis(bromométhyl)-2,2′ diphénylméthane en présence du sodiomalonate d'éthyle donne le tétracarboéthoxy-11,11,23,23 octahydro-5,10,11,12,17,22,23,24 tétrabenzo[*a,d,i,l*]cyclohexadécène. Une certaine quantité de composés polymériques est aussi formée mais aucune trace de composés monomériques n'a été décelée. Une série de composés di- et tétrasubstitués fut synthétisée à partir du nouveau cyclohexadécène ainsi formé.

Introduction

During our synthetic work on eight-membered ring compounds (1) needed for conformational studies by nmr spectroscopy (2, 3), we discovered a method whereby the novel sixteen-membered ring system, namely the 5,10,11,12,-17,22,23,24-octahydrotetrabenzo[*a,d,i,l*]cyclohexadecene **1***a*, could be prepared. It was observed that **2***b* in the presence of diethyl sodiomalonate (see Scheme 1) gives as the major product **1***a*. No eight-membered ring compounds could be detected; however, some unidentified substances of higher molecular weight were formed. Since this is an entirely new ring system a number of octahydrotetrabenzo[*a,d,i,l*]cyclohexadecenes were prepared starting from **1***a*.

Bergmann and Pelchowicz (4) have reported the synthesis of the isomeric tetrabenzocyclo-

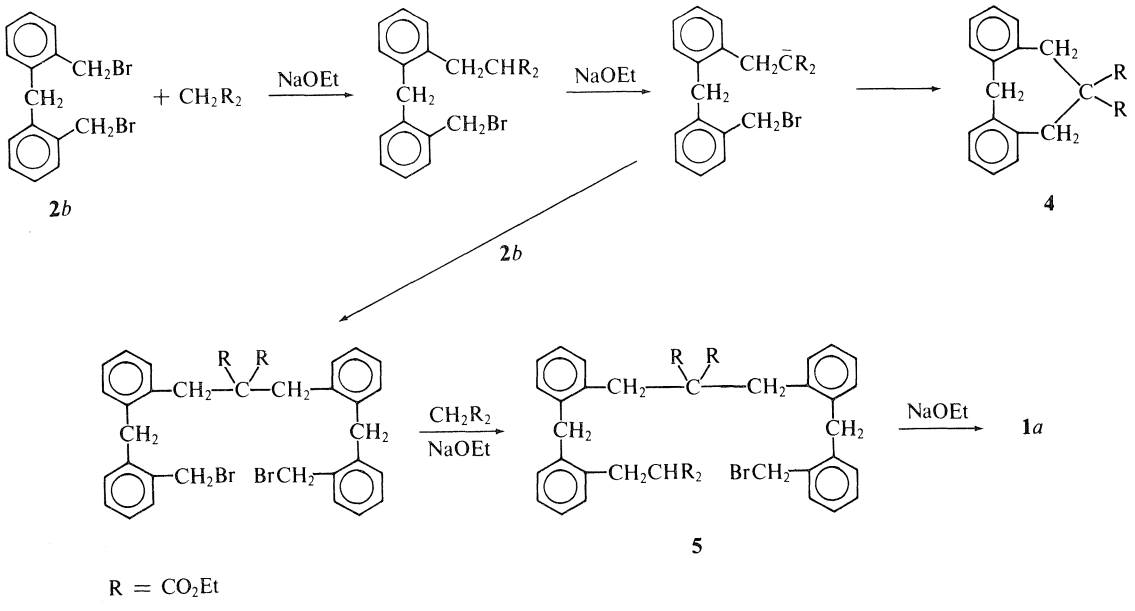

SCHEME 1

[1]NRCC No. 15489.

Can. J. Chem. Downloaded from www.nrcresearchpress.com by 210.87.254.6 on 09/05/12
For personal use only.

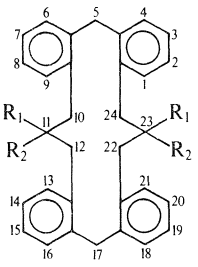

1

	R_1*	R_2*
a	CO_2Et	CO_2Et
b	CO_2H	H
c	CO_2Me	H
d	CH_2OH	H
e	CH_2OTs	H
f	CH_3	H
g	CH_2OH	CH_2OH
h	CH_2OTs	CH_2OTs
i	CH_3	CH_2OH

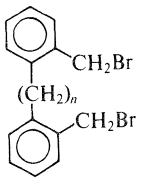

2

a $n = 0$
b $n = 1$
c $n = 2$

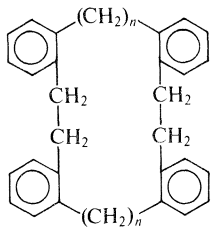

3

a $n = 0$
b $n = 1$
c $n = 2$

*When $R_1 \neq R_2$, a mixture of *cis* and *trans* isomers is present.

hexadecene **3***c* by the reaction of **2***c* with phenyllithium. Interestingly, it was found by these authors that only **2***a* undergoes an intramolecular cyclization to form a six-membered ring compound (dihydrophenanthrene) while **2***b* and **2***c* undergo bimolecular cyclization to form the fourteen (**3***b*) and the sixteen (**3***c*) membered rings respectively. An improved method of preparation for **3***c* was reported by Griffin *et al.* (5). The general method of preparation was the application of the Wittig reaction starting from *o*-xylylene dibromide. Another isomeric tetrabenzocyclohexadecene was obtained by the electrochemical dimerization of 1-(3,4-dimethoxyphenyl)-4-(4-methoxyphenyl)butane (6). The approaches described by these authors were not appropriate for the synthesis of **1**.

Having obtained the tetraester **1***a* in good yield from **2***b* and ethyl sodiomalonate, it was found necessary to apply drastic conditions in order to hydrolyze it. In refluxing ethylene glycol, in the presence of base, only the diacid **1***b* was obtained upon acidification. We were not successful in hydrolyzing **1***a* without decarboxylation. The diacid was successively converted to the diester **1***c*, the diol **1***d*, the ditosylate **1***e*, and, finally, to the dimethyl derivative **1***f*.

A series of tetrasubstituted derivatives of **1** was also prepared. The tetraester **1***a* was reduced to the tetraol **1***g* and then to the tetratosylate **1***h*. On reduction with lithium aluminum hydride, the tetratosylate **1***h* gave the diol **1***i*. The structure given for the diol[2] was based on nmr and infrared spectroscopic data and also on the fact that it formed a ditosylate which was subsequently reduced back to the original diol. Thus, as has been observed in other sterically hindered tosylates (7), the S—O bonds are broken in **1***h*. That is, at C-11 and C-23, one C—O bond and one S—O bond are broken.

Experimental

All melting points are uncorrected. The ir spectra were obtained on a Perkin-Elmer grating spectrophotometer and only the characteristic bands are reported. Nuclear magnetic resonance spectra were measured using a Varian EM-360 spectrometer and a Varian HA-100 spectrometer. All chemical shifts are reported on the δ scale. Molecular weight determinations were carried out either by obtaining the molecular peak with a Hitachi–Perkin-Elmer RMU-6D mass spectrometer or by a Mechrolab vapour pressure osmometer apparatus.

2,2′-Bis(bromomethyl)diphenylmethane (2b)

This compound was synthesized from 5*H*-dibenzo-[*a*,*d*]cyclohepten-5-one as described by one of us (2).

Preparation of 1a

The general procedure described by Ford and Newcomb (8) was modified.

To a stirred solution of sodium ethoxide in absolute ethanol (1.67 g of sodium (0.0726 mol) in 24 ml of absolute ethanol) under nitrogen was added diethylmalonate (5.8 g, 0.0362 mol) in 87 ml of anhydrous ether. To this solution was added 2,2′-bis(bromomethyl)di-

[2]The structure with both methyl groups on C-11 and both hydroxymethyl groups on C-23 is also consistent with the data; however, this possibility is regarded as unlikely.

Can. J. Chem. Downloaded from www.nrcresearchpress.com by 210.87.254.6 on 09/05/12
For personal use only.

Can. J. Chem. Downloaded from www.nrcresearchpress.com by 210.87.254.6 on 09/05/12
For personal use only.

phenylmethane (10.0 g, 0.0282 mol) in 110 ml of ether. The mixture was refluxed for 11 h and then allowed to cool to room temperature. The precipitated solid was collected by filtration, washed with a small amount of ether, stirred with water (400 ml), filtered, and finally dissolved in chloroform. The chloroform solution was filtered from the insoluble fibrous material and upon removal of the solvent, 4.45 g of a white solid melting at 233–236 °C were obtained. A further 0.57 g of product (mp 237–239 °C) was obtained by treating the original solution with saturated aqueous sodium chloride, extracting with ether, and precipitating the product by reducing the volume of the ether extract to 50 ml and cooling to 5 °C for 1 h. The total yield of the combined ester was 50%. An analytical sample (mp 239–240 °C) was prepared by recrystallization from benzene.

The molecular weight was calculated to be 704 and was found to be 697 using benzene as the solvent; nmr ($CDCl_3$) 6.63–7.40 (16H, m, aromatic), 4.07 (8H, q, methylenes of the ethyl groups), 3.83 (4H, s, methylenes at C-5 and C-17), 3.44 (8H, s, methylenes at C-10, C-12, C-22, and C-24), 1.18 (6H, t, two methyls); ir ($CHCl_3$) 1722 cm^{-1} (ester C=O). *Anal.* calcd. for $C_{44}H_{48}O_8$: C 74.97, H 6.86; found: C 75.05, H 6.72.

Preparation of ***1c***

To a solution of sodium hydroxide (4 g) dissolved in warm ethylene glycol (80 ml) was added the tetraester **1***a* (4.45 g, 6.3 mmol). The mixture was refluxed for 2 h and then allowed to cool to room temperature. The solution was diluted with water and then neutralized with hydrochloric acid. On filtration, followed by washing with water and drying, a white powder **1***b* melting at 370–374 °C was obtained in 86% yield (2.75 g).

The diacid **1***b* (1.35 g, 2.7 mmol) was converted to the diester **1***c* by treatment with an ethereal solution of diazomethane in excess. On removal of the ether, a white solid was obtained in 86% yield (1.23 g) melting at 276–280 °C. An analytical sample was prepared by recrystallization from benzene (mp 282–283.5 °C). The solvent was so strongly retained by this compound that it was necessary to grind it up and to keep it overnight at 100 °C under vacuum in order to obtain a suitable elemental analysis: nmr ($CDCl_3$) 6.63–7.43 (16H, m, aromatic), 3.78 (4H, s, methylenes at C-5 and C-17), 3.53 and 3.46 (6H, two s's, methyl peaks, 2.84 (10H, br s, methylenes at C-10, C-12, C-22, and C-24, and methines at C-11 and C-23); ir ($CHCl_3$) 1730 cm^{-1} (ester C=O). *Anal.* calcd. for $C_{36}H_{36}O_4$: C 81.17, H 6.81; found: C 81.40, H 6.97.

Preparation of 11,23-Dideuterio Derivative of ***1c***

The same procedure as described for the preparation of **1***c* was followed except that sodium deuteroxide in ethylene glycol-d_2 was used for the hydrolysis and 12 *N* deuterium chloride in D_2O was used for the neutralization of the dibasic acid. The nmr spectrum of the deuterated compound showed that the singlet at 2.84 ppm now integrated for two less hydrogens and this singlet had sharpened appreciably due to removal of coupling.

Preparation of the 5,5,11,17,17,23-Hexadeuterio Derivative of ***1c***

Deuteration of the diacid **1***b* (1.14 g) was achieved by the procedure of Atkinson *et al.* (10). The deuterio diacid was converted to the diester **1***c* with an excess of ethereal diazomethane. It was shown by nmr that the methine protons at C-11 and C-23, and the methylene protons at C-5 and C-17 had exchanged while the methylene protons at C-10, C-12, C-22, and C-24 had not.

Preparation of ***1d***

The diester **1***c* (1.25 g, 2.35 mmol) in anhydrous ether (10 ml) was added slowly to a suspension of lithium aluminum hydride (0.42 g, 11 mmol) in anhydrous ether (20 ml) and heated to reflux for 24 h. The excess hydride was then destroyed with water and the ether was removed on the flash evaporator. The solid was washed with hydrochloric acid and then with water. The remaining solid was continuously extracted with ether for 3 days to give 1.05 g (94%) of a white powder melting at 289–291 °C.

Preparation of ***1e***

The diol **1***d* (1.01 g, 2.12 mmol) was dissolved in dry pyridine (14 ml) and the solution was cooled to 0 °C. *p*-Toluenesulphonyl chloride (1.00 g, 5.25 mmol) was added and the temperature was slowly allowed to rise to that of the room. After stirring overnight, the solution was poured into cold dilute sulphuric acid and the resultant white precipitate, after being washed with water and dried, weighed 1.60 g (96%) (mp 168–185 °C). This material was purified by precipitation from a solution in methanol by addition of water. The white powder obtained in 49% yield (0.82 g) melted at 184–188 °C. *Anal.* calcd. for $C_{48}H_{48}O_6S_2$: C 73.44, H 6.16; found: C 73.26, H 6.24.

Preparation of ***1f***

The ditosylate **1***e* (0.70 g, 0.90 mmol), dissolved in dry tetrahydrofuran (10 ml), was added to a suspension of lithium aluminum hydride (0.10 g, 2.6 mmol) in 10 ml of dry tetrahydrofuran. After the mixture was refluxed overnight, the excess hydride was destroyed with 5% aqueous sodium hydroxide solution and the solid was removed by filtration. The crude solid (0.36 g) obtained on removal of the solvent was purified by column chromatography using silica gel and chloroform as the eluent. The first 20 ml of solvent eluted contained 0.22 g (55%) of a white solid melting at 229–231 °C. On recrystallization from ethanol, the melting point rose to 233.5–235.5 °C. Mol. Wt. calcd. for $C_{34}H_{36}$: 444; found (in benzene): 460; ms *m/e* 444 (M^+); nmr ($CDCl_3$): 6.60–7.30 (16H, m, aromatic), 3.71 (4H, s, methylenes at C-5 and C-17), 2.11–2.98 (8H, two m's, methylenes at C-10, C-12, C-22, and C-24), 1.78 (2H, br m, methines at C-11 and C-23), 0.88 (6H, d, J = 6.5 Hz, methyl). *Anal.* calcd. for $C_{34}H_{36}$: C 91.84, H 8.16; found: C 91.23, H 8.28.[3]

[3]This compound very strongly retained solvents. An elemental analysis on the solid gave a percent carbon of 89.38. Another recrystallization from ethanol gave the same melting point and elemental analysis. It was found necessary to grind the solid with a mortar and a pestle and to dry it at 100 °C under high vacuum. One application of this procedure improved the percent of carbon to 90.32 and a second application with a longer grinding period gave the results shown. Under the circumstances, these were accepted.

Can. J. Chem. Downloaded from www.nrcresearchpress.com by 210.87.254.6 on 09/05/12
For personal use only.

Preparation of **1***g*

A procedure described by Ripoll (9) was modified. A suspension of the tetraester **1***a* (0.50 g, 0.71 mmol) in anhydrous ether (2 ml) was added in portions to lithium aluminum hydride (0.25 g, 6.6 mmol) in anhydrous ether (13 ml). After a 72 h reflux, ethyl acetate (1 ml), water (0.5 ml), and enough hydrochloric acid (6 *N*) to obtain a p*H* of 1, were successively added to the reaction flask. The mixture was filtered from the small amount of solid present. The ether layer was separated and the aqueous layer was extracted twice with ether. The ether extracts were combined and dried over anhydrous $MgSO_4$. The solvent was removed leaving a white solid as residue. This product was purified by precipitation from chloroform (4 ml). The product which was initially soluble nearly all precipitated out in 5 to 7 min to give a white powder (0.34 g, 89%) mp 241–242 °C; nmr (DMSO-d_6): 6.83–7.60 (16H, m, aromatic), 4.62 (4H, br s, four OH; elimination of 4H by exchange with D_2O), 4.27 (4H, s, methylenes at C-5 and C-17), 3.38 (8H, s, methylenes of the CH_2OH groups), 2.72 (8H, s, methylenes at C-10, C-12, C-22, and C-24; ir ($CHCl_3$), 3620 (free OH), 3419 (bonded OH). *Anal.* calcd. for $C_{36}H_{40}O_4$: C 80.56, H 7.51; found: C 80.41, H 7.39.

Preparation of **1***h*

To a solution of the tetrahydroxymethyl **1***g* (0.12 g, 0.22 mmol) in dry pyridine (2 ml) was added purified *p*-toluenesulphonyl chloride (0.22 g, 1.16 mmol) and the resultant solution was refluxed for 4 h. The reaction mixture was cooled and poured into cold dilute sulphuric acid. After filtration and drying, the resulting solid weighed 0.23 g (89%). An analytical sample was prepared by dissolution in a boiling mixture of methanol–benzene followed by addition of water until saturation was reached. The product came down as an oil which slowly solidified to a white solid melting at 162–165 °C. *Anal.* calcd. for $C_{64}H_{64}O_{12}S_4$: C 66.65, H 5.59; found, C 66.83, H 5.68.

Preparation of **1***i*

The tetratosylate **1***h* (0.24 g, 0.20 mmol) was treated with lithium aluminum hydride (0.10 g, 2.6 mmol) as in the preparation of **1***f*. On removal of the solvent, an oily product (0.14 g) was obtained which was heated to 105 °C/0.01 torr in a Späth bulb. The oil that distilled over was shown by nmr to contain no aromatic protons. The solid remaining (0.11 g) was recrystallized from a methanol–water mixture to give a tan coloured solid (0.056 g, 54%) melting at 120–130 °C to a very viscous oil; nmr ($CDCl_3$) 6.90–7.60 (16H, m, aromatic), 2.2–4.4 (16H, a series of peaks representing all the methylenes), 1.77 (2H, br s, OH; elimination of 2H by exchange with D_2O), 0.80, and 0.95 (6H, methyl peaks); ir ($CHCl_3$) 3622 cm^{-1} (free OH), 3430 cm^{-1} (bonded OH). *Anal.* calcd. for $C_{36}H_{40}O_2$: C 85.67, H 7.99; found: C 85.89, H 8.31.

Discussion

There is sufficient evidence to establish the structure of the sixteen-membered ring skeleton of the compounds which have been synthesized. The elemental analysis and the nmr spectral data of the compounds **1***a* to **1***i* as well as molecular weight determinations on **1***a* and **1***f* are all in agreement with the assigned structures. Further evidence was obtained by partial deuteration of **1***c*. Undeuterated **1***c* has a broad singlet at 3.78 ppm (4H) and a broad singlet at 2.84 ppm (10H). On replacing the methine protons at C-11 and C-23 with deuterium[4], the peak at 3.78 ppm is unchanged while the broad singlet at 2.84 ppm now represents 8H and has sharpened appreciably due to removal of coupling. This result is in agreement with the $-CH_2\underset{\displaystyle COOCH_3}{\underset{|}{CH}}CH_2-$ units in **1***c*.

In another experiment, the methine protons at C-11 and C-23 in **1***c* were exchanged according to the procedure of Atkinson *et al.* (10).[4] The nmr spectrum of this compound showed no peak at 3.78 ppm and a singlet at 2.84 ppm (8H), Therefore, under these conditions, the methylene protons at C-5 and C-17, which are activated by two benzene rings (11), also exchange, while the methylene protons at C-10, C-12, C-22, and C-24 do not. Thus, these results along with the chemical, spectral, and analytical data all confirm the assignment of the sixteen-membered ring skeleton **1**.

The relatively high yield of the sixteen-membered ring compound **1***a* from **2***b* and diethyl sodiomalonate was surprising.[5] It is known that eight-membered ring compounds are formed when **2***b* reacts with primary amines (even with *tert*-butylamine) to give alkylated dibenzoazocines (2, 3). However, attempts to obtain **4** (R = CO_2Et) (Scheme 1) either by high dilution or by addition of two successive 1 equiv. quantities of diethyl sodiomalonate were unsuccessful. It is felt that the failure of the eight-membered ring to form in this case is due to the steric effect of the two large ester groups during cyclization. Evidence for this was obtained with the smaller malononitrile which gives a high yield of the eight-membered ring **4** where R = CN (1).

[4]See Experimental.

[5]The reaction mixture does contain some higher molecular weight compounds. Three spots with higher R_f values than **1***a* were observed in the crude reaction mixture with the use of thin layer chromatography. A molecular weight determination of the reaction product after nearly all of **1***a* had been removed gave a value of 1029.

As stated under the structural diagram of **1**, all substances in which $R_1 \neq R_2$ can exist as either the *cis* or the *trans* isomer or more likely as stereoisomeric mixtures. There is no reason to believe that the formation of **1***b* from **1***a* would be stereospecific. This is clearly seen in the nmr spectrum of **1***c* where two sharp methyl ester peaks are observed (separated by 4 Hz). In the crude, one methyl ester peak predominates somewhat over the other while, after one recrystallization, the size of the two methyl ester peaks are approximately equal. Even after a number of recrystallizations a sizeable amount of both isomers is still present. It is the sample with approximately equal methyl ester peaks which was used to prepare **1***f*. In **1***f*, only one methyl doublet (due to coupling with the adjacent methine proton) appears in the proton nmr and thus either the chemical shifts of the methyl peaks of the two isomers overlap or only one isomer is present. The C^{13} nmr spectrum also shows only one methyl peak for **1***f* but the aromatic region has more than the number of peaks which would be expected for only one isomer. This would indicate that the chemical manipulations from **1***c* to **1***f* have not selectively removed one isomer and that **1***f* (and hence **1***d* and **1***e*) is also a mixture.

Acknowledgement

We are grateful to Dr. R. R. Fraser of the University of Ottawa for helpful discussions and to Mr. H. Séguin for the elemental analyses and the mass spectral determinations.

1. R. N. Renaud and J. W. Bovenkamp. In press.
2. R. N. Renaud, R. B. Layton, and R. R. Fraser. Can. J. Chem. **51**, 3380 (1973).
3. R. R. Fraser, M. A. Raza, R. N. Renaud, and R. B. Layton. Can. J. Chem. **53**, 167 (1975).
4. E. D. Bergmann and Z. Pelchowicz. J. Am. Chem. Soc. **75**, 4281 (1953).
5. C. E. Griffin, K. R. Martin, and B. E. Douglas. J. Org. Chem. **27**, 1627 (1962).
6. V. D. Parker and A. Ronlán. J. Am. Chem. Soc. **97**, 4714 (1975).
7. L. J. Dolly and D. R. Rosencrantz. J. Org. Chem. **28**, 1888 (1963); A. S. Hussey, H. P. Liao, and R. H. Baker. J. Am. Chem. Soc. **75**, 4727 (1953).
8. W. T. Ford and M. Newcomb. J. Am. Chem. Soc. **95**, 6277 (1973).
9. J.-L. Ripoll. Bull. Soc. Chim. Fr. 2567 (1974).
10. J. G. Atkinson, J. J. Csakvary, G. T. Herbert, and R. S. Stuart. J. Am. Chem. Soc. **90**, 498 (1968).
11. A. F. Thomas. Deuterium labeling in organic chemistry. Appleton - Century - Crofts, New York. 1971. p. 27.

Can. J. Chem. Downloaded from www.nrcresearchpress.com by 210.87.254.6 on 09/05/12
For personal use only.

The ionization constant of heavy water (D_2O) in the temperature range 298 to 523 K

DAVID WILLIAM SHOESMITH AND WOON LEE

Research Chemistry Branch, Whiteshell Nuclear Research Establishment, Pinawa, Man., Canada R0E 1L0

Received June 7, 1976

DAVID WILLIAM SHOESMITH and WOON LEE. Can. J. Chem. **54**, 3553 (1976).

The ionization constant of liquid D_2O has been measured over the temperature range 298 to 523 K using an aqueous electrolyte concentration cell. Values for the standard free energy, enthalpy, entropy, and heat capacity of ionization have been calculated. The results are compared to similar results for liquid H_2O.

DAVID WILLIAM SHOESMITH et WOON LEE. Can. J. Chem. **54**, 3553 (1976).

On a mesuré la constante d'ionisation du D_2O liquide à des températures allant de 298 à 523 K utilisant une cellule à concentration d'électrolyte aqueux. On a calculé les valeurs pour les énergies libres, les enthalpies, les entropies et les capacités calorifiques standards. On compare ces résultats avec des résultats similaires obtenus pour l'eau liquide.

[Traduit par le journal]

Can. J. Chem. Downloaded from www.nrcresearchpress.com by 210.87.254.40 on 09/05/12
For personal use only.

Introduction

In the CANDU–PHW[1] nuclear reactor, D_2O is used both as a moderator and a coolant. In the coolant circuit the D_2O is maintained at temperatures between 523 and 573 K. To minimise corrosion and the spread of radioactive corrosion products in the coolant circuit, strict control of the chemical conditions is necessary. At present a large amount of the required chemical information is obtained from experiments performed with light water systems under similar conditions. To establish a firmer basis for the calculation of the most favourable chemical conditions for reactor operation it is necessary to obtain an accurate knowledge of the physical chemical properties of D_2O and how they differ from those of H_2O at temperatures up to 573 K.

One essential parameter is the ionization constant. This has been extensively measured for H_2O (1–13) up to 1000 °C. The accuracy of these measurements has been assessed recently by Hepler and Wooley (14) and by Sweeton *et al.* (11). The ionization constant for D_2O has been measured a number of times at 298 K (15–20) but only two studies (16, 19) have investigated the temperature dependence of pK_{D_2O} and then only over a narrow temperature range.

The present work employs the high temperature aqueous electrolyte concentration cell,

$$Pt/D_2,DCl(m_1),KCl(m_2)//KCl(m_2),NaOD(m_1),D_2/Pt$$

to obtain the ionization constant of D_2O, along the saturation vapour pressure curve, up to 523 K.

[1]Canadian Deuterium Uranium – Pressurized Heavy Water.

Experimental

Equipment

The electrolyte concentration cell used in this study was the same as described previously by MacDonald, Butler, and Owen (10). The cell temperature was controlled by immersion in an oil bath. The temperature was followed in both cell compartments and in the bulk of the oil fluid, using chromel–alumel type K thermal couples and a multi-point Leeds and Northrup Speedomax Recorder precalibrated for temperature measurement. The recorder calibration allowed resolution to ±0.5 K. Resolution to ±0.1 K was achieved using a potentiometer.

All potential measurements were made with a Dana Model 5330 Digital Voltmeter capable of 1 μV resolution. Potentials were recorded after they had become constant to within 0.1 mV for at least 15 min.

Chemicals

The D_2O was supplied by AECL Commercial Products and was 99.78 ± 0.05% D_2O. Its specific conductance was 0.57 ohm^{-1} cm^{-1} at 23 °C. NaOD (40% in D_2O) and DCl (38% in D_2O) were supplied by ICN Pharmaceuticals. The KCl was supplied by Fisher (Certified ACS).

Procedure

The experimental procedure was essentially the same as previously reported (10).

The DCl and NaOD solutions were made up by volume and the exact concentration determined by titration against standard HCl or NaOH solution. The concentration used in the calculations was based on a large number of titrations with an overall reproducibility of approximately 0.1%.

To estimate the degree of mixing of solutions from the two compartments after experiments at elevated temperatures, the contents of each compartment were titrated

Can. J. Chem. Downloaded from www.nrcresearchpress.com by 210.87.254.40 on 09/05/12
For personal use only.

after each run. The concentrations were between 5 and 20% different from the original values. However, most of this mixing occurred on cooling which was uncontrolled and consequently fairly rapid between 523 and 373 K. The potential became erratic on cooling and the porous Teflon junction began to leak. Usually the titration was not performed until ~16 h after completion of the experiment, allowing plenty of time for mixing through the faulty junction. That leakage was not occurring during the actual experiment was indicated by the stability of the measured potential at elevated temperatures, and its reproducibility over a series of separate experiments. Above 473 K leaky junctions could be detected by a rapid drift in the measured potential. Potential values were used only if this drift was less than 0.1 to 0.3 mV over the 15 min period during which values were recorded. To minimize this effect no more than two values were recorded at temperatures >473 K during any individual run.

Results

The potential difference between the electrodes in the two compartments is related to activities by

$$[1] \qquad E = 2.303\frac{RT}{F}\log\frac{(a_{D^+})_2}{(a_{D^+})_1} + E_j$$

where E = cell potential, a_i = activity of species i, T = temperature in K, and subscripts 1 and 2 refer to the outer (DCl) and the inner (NaOD) compartments, respectively. E_j is the junction potential. Hence the following expression can be written for pK_{D_2O},

$$[2] \quad pK_{D_2O} = -\frac{F(E - E_j)}{2.303RT} - \log[(m_{D^+})_1(m_{OD^-})_2] - \log\frac{\gamma_{D^+}\gamma_{OD^-}}{a_{D_2O}}$$

where γ_i are activity coefficients. The molalities m_{D^+} and m_{OD^-} are calculated from the molar concentrations at 298 K using the published densities for KCl solutions in D_2O (21). In the experiments performed here, KCl is always present in concentrations in excess of the acid and base concentrations and, consequently, will be the major factor in determining the solution ionic strength. Values for concentrations of KCl outside the published range (0.05 to 0.3 mol l^{-1}) are obtained by linear extrapolation. Such an extrapolation is justified on the basis of the linear variation of density with concentration for KCl in H_2O over the concentration range 0.067 to 1.276 mol l^{-1} (22).

The liquid junction potential can be estimated by means of the Henderson equation in the approximate form applicable to solutions of nearly constant composition (6), *i.e.*

$$[3] \qquad E_j = \frac{RT|Z_i|}{Z_iF}\frac{\sum[(m_i)_2 - (m_i)_1]\lambda_i}{\sum|Z_i|m_i\lambda_i}$$

where Z_i = ionic charge. The equivalent conductances, λ_i, for K^+, Na^+, Cl^-, D^+, and OD^- in D_2O are known only at 298 K (23, 30). Values for higher temperatures are generated by two different methods. In the first method the known λ_i (equivalent conductance) values in H_2O for the above ions are fitted to expressions of the type

$$[4] \quad \lambda_i = (\lambda_i)_{T=273} + a(T - 273) + b(T - 273)^2 + c(T - 273)^3$$

The values of the coefficients a, b, and c derived for the H_2O system and the measured equivalent conductances at 298 K for the ions in D_2O are then used to generate a series of values of λ_i for each ion in D_2O as a function of temperature.

In the second method, λ_i values are generated from viscosities (η) using the relationship

$$[5] \qquad \log\lambda_i^0 = a'\log\eta + b'$$

The coefficients a' and b' are taken from the light water data of Smolyakov and Veselova (25) and applied to values for the viscosity of D_2O as a function of temperature (28). The values derived by the two methods differed by 5% at 298 K and 7% at 523 K. The values from eq. 4 are used in calculating E_j. Since there are no criteria by which to compare the above two methods, the choice is arbitrary.

The approximate nature of this calculation has only a small effect on the derived values of pK_{D_2O} since the liquid junction potential represents only a minor correction to the measured potential in all cases except for the solution of lowest ionic strength ($\bar{I} = 0.0285$). The calculated effect on pK_{D_2O} of a $\pm 10\%$ change in λ_i values is small and shows that the change is negligible compared to other errors in the experiments. For $\bar{I} = 0.0285$ the liquid junction potential rises as high as 3 mV. For all other solutions the value of E_j never exceeds 1.3 mV and rarely rises above 0.8 mV.

The activity coefficient term in eq. 2 is calculated using the expression

$$[6] \quad \log\frac{\gamma_{D^+}\gamma_{OD^-}}{a_{D_2O}} = \frac{-2S\bar{I}^{1/2}}{1 + AI^{-1/2}} + B\bar{I} + C\bar{I}^{3/2}$$

Can. J. Chem. Downloaded from www.nrcresearchpress.com by 210.87.254.40 on 09/05/12
For personal use only.

given by Harned and Cook (26) and used by Mesmer and co-workers (6, 11) and MacDonald *et al.* (10). The coefficients in eq. 6 are given by

[7] $S = 1.8246 \times 10^6 \rho_{D_2O}{}^{1/2}/(\epsilon_{D_2O}T)^{3/2}$

[8] $A = 50.29 \times 10^8 a^0 \rho_{D_2O}{}^{1/2}/(\epsilon_{D_2O}T)^{1/2}$

where ϵ = dielectric constant and ρ = density.

[9] $B = 0.266 + 5.2 \times 10^{-4}(T - 273)$

[10] $C = -0.035 - 4.88 \times 10^{-4}(T - 273)$

In eq. 8, a^0 is the ion size parameter and is assumed to be independent of temperature. A value of 3.6×10^{-8} cm is used in the present work. Since the dielectric constants for H_2O and D_2O differ only slightly (<1%) between 298 and 373 K, the expression

[11] $\epsilon = 5321T^{-1} + 233.76 - 0.9297T + 0.001417T^2 - 0.068292T^3$

based on the experimental data for H_2O, measured by Akerlof and Oshry (27), is used to evaluate ϵ_{D_2O}. The densities of D_2O are taken from the tables prepared by Elliott (28).

The cell voltage, as a function of temperature, was recorded for four different concentrations of KCl, and pK values calculated as outlined above.[2] Data were also recorded for $\bar{I} = 0.0285$, but the pK_{D_2O} values obtained were erratic. The relatively large value of E_j previously mentioned and the errors incorporated in its calculation lead to large uncertainties in the value of pK_{D_2O}. Consequently the values for $\bar{I} = 0.0285$ are not used subsequently.

Interpolated values for 25 deg intervals are plotted as a function of ionic strength in Fig. 1. These plots are extrapolated to $\bar{I} = 0$ and the pK_{D_2O} values obtained at zero ionic strength are listed in Table 1 and plotted in Fig. 2. Also listed in Table 1 are the values obtained by Covington *et al.* (19), and the values for pK_{D_2O} reported by Sweeton *et al.* (11).

The data of Table 1 were fitted to the expression

[12] $pK_{D_2O} = p_1T^{-1} + p_2 \ln T + p_3T + p_4T^{-2} + p_5$

[2]Complete set of the actual experimental data is available, at a nominal charge, from the Depository of Unpublished Data, CISTI, National Research Council of Canada, Ottawa, Canada K1A 0S2.

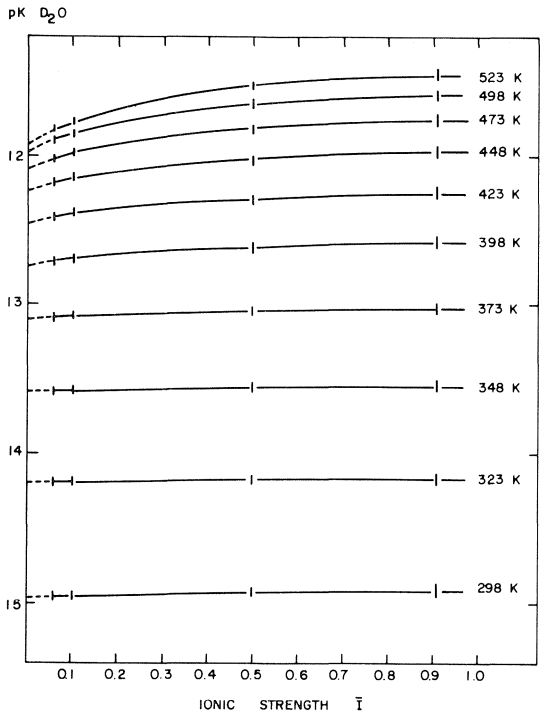

FIG. 1. Variation of pK_{D_2O} with ionic strength as a function of temperature.

TABLE 1. Ionization constant in molal units for D_2O extrapolated to zero ionic strength

T (K)	$pK_{D_2O}{}^a$	$pK_{D_2O}{}^b$	$pK_{D_2O}{}^c$	$pK_{H_2O}{}^d$
298	14.957	14.958	14.955	13.993
323	14.184	14.178	14.182	13.272
348	13.571	13.579		12.709
373	13.115	13.111		12.264
398	12.746	12.744		11.914
423	12.459	12.460		11.642
448	12.246	12.246		11.441
473	12.096	12.096		11.302
498	12.004	12.004		11.222
523	11.968	11.967		11.196

[a]Experimental values.
[b]Values calculated from eq. 12.
[c]Values from ref. 19.
[d]Values from ref. 11.

The values of the coefficients p_1 to p_5 are listed in Table 2 along with the values derived for H_2O by Sweeton *et al.* (11). Equation 12 fits the data with a standard deviation of 0.0012, and values calculated using this expression are also tabulated in Table 1. The difference

[13] $\Delta pK = pK_{D_2O} - pK_{H_2O}$

is plotted as a function of temperature in Fig. 3.

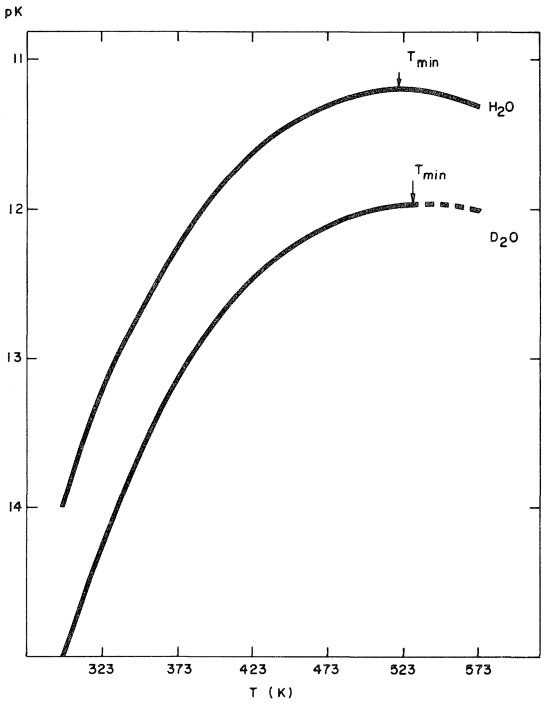

FIG. 2. Variation of pK with temperature. The data for H_2O is from ref. 11. T_{min} indicates the temperature at which pK passes through a minimum. --- indicates extrapolated values calculated from eq. 12.

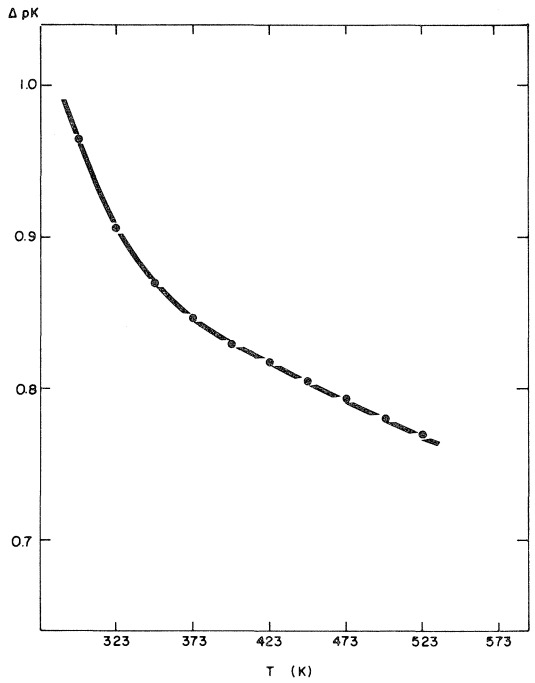

FIG. 3. Difference in the pK values for D_2O and H_2O (from the data of Fig. 2) plotted as a function of temperature.

TABLE 2. Values of the coefficients derived for a fit to eq. 12

Coefficient	Value	
	This work	For H_2O from ref. 11
p_1	−36 319	−34 691.6
p_2	−104.37	−105.15
p_3	0.10287	0.10757
p_4	2.612×10^6	2.358×10^6
p_5	671.35	670.86

Discussion

The data are fitted to eq. 12 rather than to an equation of the form

[14] $$pK = p_6T^{-1} + p_7 + p_8T$$

used by Covington *et al.* (19) because eq. 12 is found to reproduce more accurately the high temperature thermodynamic data for ionization reactions (29). Also a fit to eq. 12 allows the data for H_2O to be extrapolated more accurately to higher temperatures (29) and allows a comparison of the thermodynamic parameters for D_2O ionization with the corresponding values for H_2O (11).

Comparison of our pK_{D_2O} values with those reported by Covington *et al.* (19) using the cell

[15] Pt/D_2, NaOD, NaCl in D_2O, AgCl/Ag

shows excellent agreement for the temperature range in which the data are duplicated (Table 1). Some idea of the uncertainties associated with pK_{D_2O} can be gained using the maximum accuracy in the measured parameters. Thus the effects, on pK_{D_2O}, of (*i*) a ±0.1 mV in E; (*ii*) a 0.1% change in m_i; and (*iii*) a 10% variation in the estimated ionic equivalent conductances were computed. On the basis of such estimates the uncertainties in pK_{D_2O} may be given as ±0.009 at 298 K, rising to ±0.014 at 423 K and 0.023 at 523 K.

Expressions for the thermodynamic parameters for D_2O ionization are obtained from eq. 12 by the application of standard thermodynamic relationships. Thus the standard free energy, enthalpy, entropy and heat capacity of ionization can be calculated from the following expressions

Can. J. Chem. Downloaded from www.nrcresearchpress.com by 210.87.254.40 on 09/05/12
For personal use only.

TABLE 3. Thermodynamic quantities for the ionization of D_2O and H_2O at 298 K

Parameter	Value			
	D_2O			H_2O
	This work	Ref. 19	Ref. 30	(Ref. 11)
$-\Delta G^0$ (kJ mol^{-1})	85.23	85.37		79.87
ΔH^0 (kJ mol^{-1})	60.87	59.88	60.62	55.82
ΔS^0 (kJ K^{-1} mol^{-1})	−0.8175	−0.8548	−0.8301[a]	−0.8067
ΔC_p^0 (J K^{-1} mol^{-1})	−301.9	−229.3		−231.4
$pK_{D_2O\ min}$	11.943	12.356		11.203
T_{min}	528.5	494		518

[a]Calculated from the ΔH^0 of ref. 30 and the ΔG^0 of ref. 19.

[16] $$\Delta G^0 = 2.303R\{p_1 + p_2T\ln T + p_3T^2 + p_4T^{-1} + p_5T\}$$

[17] $$\Delta H^0 = -2.303R\{-p_1 + p_2T + p_3T^2 - 2p_4T^{-1}\}$$

[18] $$T\Delta S^0 = \Delta H^0 - \Delta G^0$$

[19] $$\Delta C_p^0 = -2.303R\{p_2 + 2p_3T + 2p_4T^{-2}\}$$

The values for ΔG^0, ΔH^0, and $-T\Delta S^0$ are compared to similar values in H_2O in Fig. 4. The values calculated from the data of Covington *et al.* (19) are also included for comparison. Some discrepancy exists between our results and those of Covington *et al.* around the lowest temperature (298 K) used in the present work. To facilitate this comparison the values for 298 K are tabulated in Table 3 and compared to the calorimetric results of Goldberg and Hepler (30). Our value for ΔH^0 agrees within experimental error with the calorimetric value but differs by between 1 and 2% from that of Covington *et al.* We refitted our data to eq. 14 and obtained $\Delta H_{298}{}^0 = 59.31$ kJ mol^{-1} in close agreement with Covington. As expected, the enthalpy value obtained is dependent on the equation chosen to fit the data. Consequently, our value of $\Delta H^0 = 60.87$ cannot be used to rule out the value of Covington. Since eq. 12 has been shown to be the most reliable fit to such data (24) and produces better agreement with the calorimetric value our value would appear to be more reliable.

Figure 4 shows that the variation with temperature for each thermodynamic parameter changes only slightly on going from H_2O to D_2O. The divergence of the $T\Delta S^0$ terms as the temperature increases over the range 273 to 373 K, and the simultaneous convergence of the ΔH^0 terms suggests that the variations in these parameters account for the change in pK in this temperature range (see Fig. 3)). $\Delta\Delta S^0$ is changing more rapidly with temperature than $\Delta\Delta H^0$ suggesting that the major influence on ΔpK in this region is the change in entropy of ionization. This may be due mainly to changes in solute–solvent

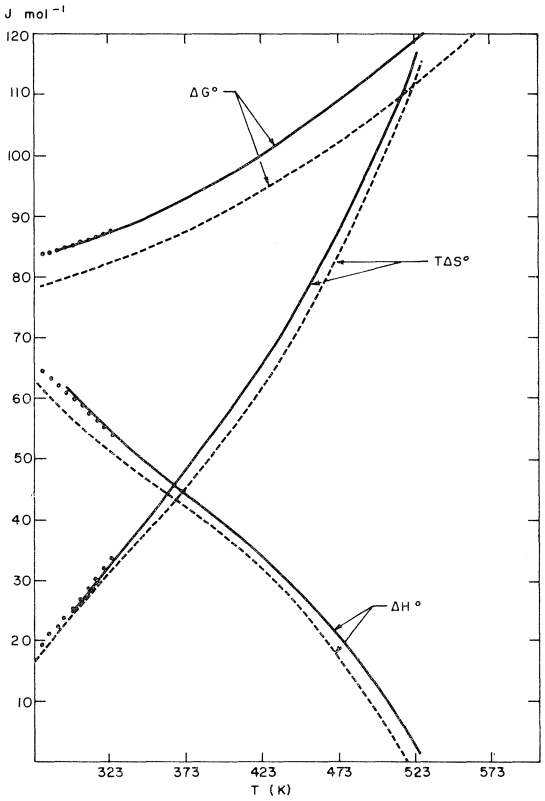

FIG. 4. Variations in the free energy (ΔG^0), enthalpy (ΔH^0) and entropy ($-T\Delta S^0$) of ionization with temperature; — D_2O (this work); --- H_2O (from the data of ref. 11); ● D_2O (from the data of ref. 19).

Can. J. Chem. Downloaded from www.nrcresearchpress.com by 210.87.254.40 on 09/05/12
For personal use only.

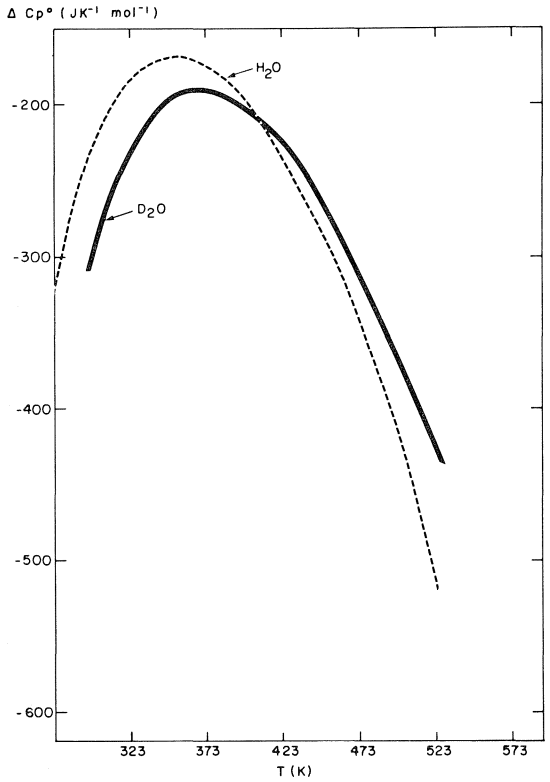

FIG. 5. Variation in the heat capacity (ΔC_p^0) with temperature; — D_2O; ---H_2O (from the data of ref. 11).

interactions with increasing temperature, D_2O being a more structured liquid at low temperatures than H_2O. This effect has been discussed in detail by Larson and Hepler (31) and to a lesser extent by Laughton and Robertson (32).

The heat capacity passes through a maximum at ~370 K, Fig. 5. The variation with temperature is very similar to that of H_2O. The heat capacity is more negative for D_2O than H_2O at the lower temperatures (27) as expected.

To assess the reliability of these C_p^0 values, confirmation is required from independent measurements. Hopefully this will be forthcoming from calorimetric experiments now in progress.[3]

Also included in Table 3 are estimates from eq. 12 of the minimum pK_{D_2O} value attainable and the temperature at which it is attained. The value of T_{min} is 7.5° greater than the value in H_2O, and ($pK_{D_2O\ min}$) is greater than ($pK_{H_2O\ min}$) by 0.74.

1. A. A. NOYES, Y. KATO, and R. B. SOSMAN. J. Am. Chem. Soc. **32**, 159 (1910).

[3]L. G. Hepler, private communication.

2. T. ACKERMANN. Z. Electrochem. **62**, 411 (1958).
3. E. U. FRANCK. Z. Phys. Chem. Frankfurt am Main, **8**, 92, (1956); **8**, 107 (1956); **8**, 192 (1956).
4. V. D. PERKOVETS and P. A. KRYUKOV. Izv. Sib. Otd. Akad. Nauk SSSR, Ser. Khim. Nauk, **3**, 9 (1969).
5. W. B. HOLZAPFEL. J. Chem. Phys. **50**, 4424 (1969).
6. R. E. MESMER, C. F. BAES, JR., and F. H. SWEETON. J. Phys. Chem. **74**, 1937 (1970).
7. J. V. DOBSON and H. R. THIRSK. Electrochim. Acta, **16**, 315 (1971).
8. J. R. FISHER and H. L. BARNES. J. Phys. Chem. **76**, 90 (1972).
9. G. J. BIGNOLD, A. D. BREWER, and B. HEARN. Trans. Faraday Soc. **67**, 2419 (1971).
10. D. D. MACDONALD, P. BUTLER, and D. OWEN. Can. J. Chem. **51**, 2590 (1973).
11. F. H. SWEETON, R. E. MESMER, and C. F. BAES, JR. J. Solution Chem. **3**, 191 (1974).
12. H. S. HARNED and B. B. OWEN. The physical chemistry of electrolyte solutions. 3rd ed. Reinhold, N.Y. 1958.
13. E. A. GUGGENHEIM and J. C. TURGEON. Trans. Faraday Soc. **51**, 747 (1955).
14. L. G. HEPLER and E. M. WOOLLEY. *In* Water; a comprehensive treatise. Vol. 3. *Edited by* F. Franks. Plenum, New York. 1973. Chapt. 3.
15. E. ABEL, E. BRATU, and O. REDLICH. Z. Phys. Chem. Abt. A, **173**, 353 (1935).
16. W. F. K. WYNNE-JONES. Trans. Faraday Soc. **32**, 1397 (1936).
17. R. W. KINGERLEY and V. K. LAMER. J. Am. Chem. Soc. **63**, 3256 (1941).
18. P. K. GLASOE and F. A. LONG. J. Phys. Chem. **64**, 188 (1960).
19. A. K. COVINGTON, R. A. ROBINSON, and R. G. BATES. J. Phys. Chem. **70**, 3820 (1966).
20. L. PENTZ and E. R. THORNTON. J. Am. Chem. Soc. **89**, 6931 (1967).
21. O. YA. SAMOILOV, I. B. RABINOVICH, Z. V. VOLOKHOVA, and A. F. BORINA. Zh. Strukt. Khim. **11**, 207 (1970).
22. Handbook of Chemistry and Physics, 53rd ed. CRC Press, Cleveland, Ohio. 1972–1973, D202.
23. L. G. LONGSWORTH and D. A. MACINNES. J. Am. Chem. Soc. **59**, 1666 (1937).
24. C. G. SWAIN and D. F. EVANS. J. Am. Chem. Soc. **88**, 383 (1966).
25. B. S. SMOLYAKOV and G. A. VESELOVA. Elektrokhimiya, **10**, 896 (1974); **11**, 700 (1975).
26. H. S. HARNED and M. A. COOK. J. Am. Chem. Soc. **59**, 2304 (1937).
27. G. C. AKERLOF and H. I. OSHRY. J. Am. Chem. Soc. **72**, 2844 (1950).
28. J. N. ELLIOTT. Tables of the thermodynamic properties of heavy water. AECL-1673. 1963.
29. G. OLOFSSON and L. G. HEPLER. J. Solution Chem. **4**, 127 (1975).
30. R. N. GOLDBERG and L. G. HEPLER. J. Phys. Chem. **72**, 4654 (1968).
31. J. W. LARSON and L. G. HEPLER. *In* Solute–solvent interactions. *Edited by* J. F. Coetzee and C. D. Ritchie. Marcel Dekker, New York. 1969. Chapt. 1.
32. P. M. LAUGHTON and R. E. ROBERTSON. *In* Solute–solvent interactions. *Edited by* J. F. Coetzee and C. D. Ritchie. Marcel Dekker, New York. 1969. Chapt. 7.

Can. J. Chem. Downloaded from www.nrcresearchpress.com by 210.87.254.40 on 09/05/12
For personal use only.

Excess energy–volume and cohesive energy density coefficients for binary systems. Comparison with constant pressure functions

DIGBY D. MACDONALD
Department of Chemistry, University of Calgary, Calgary, Alta., Canada T2N 1N4

Received March 15, 1976

DIGBY D. MACDONALD. Can. J. Chem. **54**, 3559 (1976).

Excess energy–volume and cohesive energy density coefficients have been calculated for the hexane + perfluoro-hexane, water + DMSO, water + *tert*-butanol, water + methanol, water + acetonitrile, and methanol + DMSO systems. These parameters are compared with other constant pressure excess functions of mixing for these binary systems, and it is proposed that they represent additional criteria for the classification of liquid mixtures.

DIGBY D. MACDONALD. Can. J. Chem. **54**, 3559 (1976).

On a calculé les énergie–volume d'excès et les coefficients de densité d'énergie de cohision pour les systèmes hexane + perfluoro-hexane, eau + DMSO, eau + *tert*-butanol, eau + méthanol, eau + acétonitrile et méthanol + DMSO. On a comparé ces paramètres avec d'autres fonctions d'excès à pression constante pour le mélange de ces systèmes binaires et on suggère qu'ils représentent des critères additionnels pour les classifications des mélanges liquides.

[Traduit par le journal]

Can. J. Chem. Downloaded from www.nrcresearchpress.com by 210.87.254.42 on 09/05/12
For personal use only.

Introduction

The thermal–pressure coefficient, $(\partial p/\partial T)_V$, and the related energy–volume coefficient (eq. 1),

$$[1] \qquad (\partial U/\partial V)_T = T(\partial p/\partial T)_V - p$$

are being used increasingly in the study of binary liquid systems (1–10). These parameters have proven useful in the investigation of structural changes in binary systems as a function of composition, in addition to their important application for the derivation of excess functions of mixing at constant volume (11).

Real liquid mixtures are never ideal, and the deviation from ideality may be classified according to the signs and values of the various excess functions of mixing. The excess functions are normally defined for the molar Gibbs energy (G), enthalpy (H), entropy (S), and volume (V), although there is no *a priori* reason why equally valid excess functions cannot be defined for other properties so long as the ideal parameter conforms to the definition of the thermodynamically ideal mixture.

In this paper we define the intensive thermal–pressure, energy–volume, and cohesive energy density coefficients for an ideal binary liquid mixture. The corresponding excess functions for six binary liquid systems are calculated from data in the literature, and are compared with the behaviour of other constant pressure excess thermodynamic functions of mixing.

Ideal Mixtures

The Thermal–Pressure Coefficient

The molar volume of an ideal mixture containing x_1 mole fraction of component 1 and x_2 mole fraction of component 2 is given by

$$[2] \qquad V_m^{id} = x_1 V_1^0 + x_2 V_2^0$$

where V_i^0 is the molar volume of pure component i. The molar volume of the ideal mixture is a function of both temperature and pressure. Therefore, the isobaric coefficient of thermal expansion and the isothermal compressibility for the ideal mixture may be defined as follows

$$[3] \qquad \alpha^{id} = (\partial V_m^{id}/\partial T)_p/V_m^{id}$$

$$[4] \qquad \kappa^{id} = -(\partial V_m^{id}/\partial p)_T/V_m^{id}$$

Substitution of eq. 2 into eqs. 3 and 4 yields the following expressions for α^{id} and κ^{id} in terms of the properties of the pure components,

$$[5] \quad \alpha^{id} = (x_1\alpha_1^0 V_1^0 + x_2\alpha_2^0 V_2^0)/(x_1 V_1^0 + x_2 V_2^0)$$

$$[6] \quad \kappa^{id} = (x_1\kappa_1^0 V_1^0 + x_2\kappa_2^0 V_2^0)/(x_1 V_1^0 + x_2 V_2^0)$$

where α_i^0 and κ_i^0 are the isobaric coefficient of thermal expansion and the isothermal compressibility, respectively, of the ith pure component.

Can. J. Chem. Downloaded from www.nrcresearchpress.com by 210.87.254.42 on 09/05/12
For personal use only.

The thermal–pressure coefficient for the ideal mixture is, therefore, given by

[7] $$\beta^{id} = \alpha^{id}/\kappa^{id}$$

which, upon substitution of eqs. 5 and 6, yields

[8] $$\beta^{id} = (x_1\alpha_1^0V_1^0 + x_2\alpha_2^0V_2^0)/(x_1\kappa_1^0V_1^0 + x_2\kappa_2^0V_2^0)$$

The form of eq. 8 for the thermal–pressure coefficient for an ideal system may be compared with that assumed by Dunlap and Scott (8), *viz.* $\beta^{id} = x_1\beta_1^0 + x_2\beta_2^0$, where β_1^0 and β_2^0 are the thermal–pressure coefficient for the pure components. Since $\beta = (\partial S/\partial V)_T$, then the definition of Dunlap and Scott could only be valid if the entropy of an ideal system were given by the mole fraction average of the entropies of the components (*i.e.* $x_1S_1^0 + x_2S_2^0$). This is, of course, incorrect (12).

The Energy–Volume Coefficient and Cohesive Energy Density

The energy–volume coefficient for an ideal system is defined as

[9] $$(\partial U/\partial V)^{id} = T\beta^{id} - p$$

where β^{id} is given by eq. 8.

By definition, ideal mixing occurs with no change in the enthalpy of the system. Thus, the energy of vaporisation for an ideal mixture is given by the following equation

[10] $$\Delta U_V^{id} = x_1\Delta H_{V,1} + x_2\Delta H_{V,2} - RT + pV_m^{id}$$

where $\Delta H_{V,1}$ and $\Delta H_{V,2}$ are the enthalpies of vaporisation of components 1 and 2, respectively, to the ideal gas state. Division of ΔU_V^{id} by the volume of the ideal mixture yields the cohesive energy density of the ideal system. For a real mixture the appropriate expression for the energy of vaporisation becomes[1]

[11] $$\Delta U_V = x_1\Delta H_{V,1} + x_2\Delta H_{V,2} - H_p^E - RT + pV_m$$

which, upon division by V_m yields the cohesive energy density for the real binary system.

It has been suggested by a number of authors (1–3, 5, 10) that the ratio of the energy–volume coefficient to the cohesive energy density is a useful indication of the extent of intermolecular interaction in a liquid. Accordingly, the ratio for an ideal system is defined as

[12] $$n_{id} = (\partial U/\partial V)^{id}/(\Delta U_V^{id}/V_m^{id})$$

where $(\partial U/\partial V)^{id}$ and ΔU_V^{id} are given by eqs. 9 and 10, respectively.

Discussion

The deviation in behaviour of a real mixture from the ideal case is normally expressed in terms of the excess functions, γ^E, defined as follows

[13] $$\gamma^E = \gamma - \gamma^{id}$$

Excess energy–volume coefficients, cohesive energy densities and parameter n for the hexane + perfluoro-hexane (8), water + DMSO (1), water + *tert*-butanol (2), water + methanol (2), water + acetonitrile (5, 19), and methanol + DMSO (4, 20) systems were calculated using eqs. 9, 10, 11, 12, and 13, and are plotted in Figs. 1 to 3.

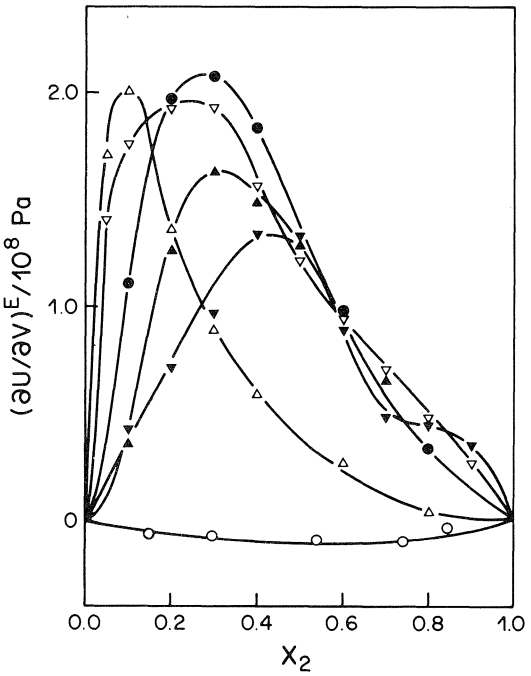

FIG. 1. Plot of the excess energy–volume coefficient, $(\partial U/\partial V)^E$, *vs.* mole fraction of the second component for the hexane + perfluoro-hexane (○), water + DMSO (●), water + *tert*-butanol (△), water + methanol (▲), water + acetonitrile (▽), and methanol + DMSO (▼) systems at 298.15 K.

[1]The last term has been omitted in previous publications (1, 2, 4, 5) since it is less than 1% of the value of RT for most liquids at atmospheric pressure and at T = 298 K. It is included here for completeness.

Can. J. Chem. Downloaded from www.nrcresearchpress.com by 210.87.254.42 on 09/05/12
For personal use only.

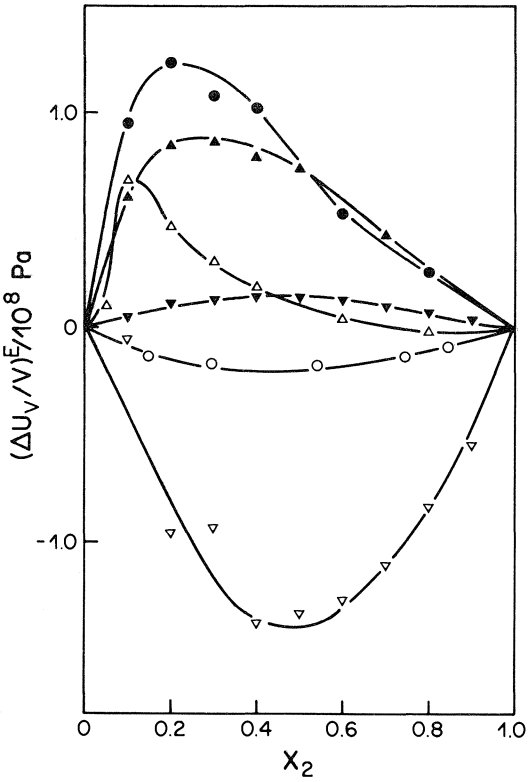

FIG. 2. Plot of the excess cohesive energy density, $(\Delta U_V/V)^E$, *vs.* mole fraction of the second component for various binary systems at 298.15 K. System identification as in Fig. 1.

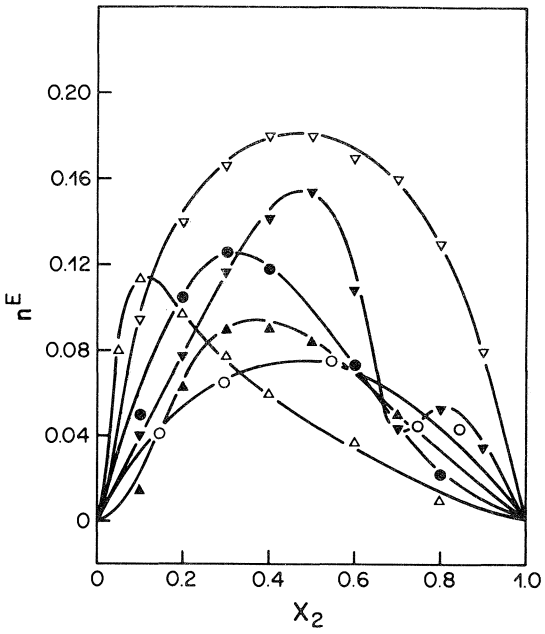

FIG. 3. Plot of the excess parameter n^E *vs.* mole fraction of the second component for various binary systems at 298.15 K. System identification as in Fig. 1.

The positions and magnitudes of the extrema in the above excess functions are summarized in Table 1, together with corresponding data taken from the literature for other constant pressure excess functions of mixing.

The essential features of the data given in Table 1 may be summarized as follows: (*i*) in all cases $(\partial U/\partial V)^E$ and V^E are opposite in sign, (*ii*) $(\Delta U_V/V)^E$ and H^E are also opposite in sign, (*iii*) n^E is positive, and (*iv*) the two systems which exhibit critical demixing (UCST) at atmospheric pressure and at temperatures not far from 298 K have negative excess cohesive energy densities.

The relationship between $(\partial U/\partial V)^E$ and V^E may be rationalised on the basis of the effect of distance on attractive intermolecular interaction (1, 2). Thus, for a positive V^E the average intermolecular distance in the mixture will be greater than in the unmixed system, and hence $(\partial U/\partial V)$ will tend to be less, *i.e.* $(\partial U/\partial V)^E$ is negative. Furthermore, given that insufficient data are available to permit location of the extremum in the excess volume coefficient to better than ± 0.05 mole fraction, there is reasonable agreement between the extremum compositions for both excess functions. It is interesting to note that the greatest deviation between the extremum positions occurs for the two aqueous systems. It is possible that this is a manifestation of the unique structural properties of these systems which have been discussed at length by Franks and Ives (24).

The opposite signs for $(\Delta U_V/V)^E$ and H^E can be explained by dividing eqs. 10 and 11 by V_m^{id} and V_m, respectively, followed by substitution into eq. 13 to yield

$$[14] \quad (\Delta U_V/V)^E = -(x_1\Delta H_{V,1} + x_2\Delta H_{V,2} - RT)(V^E/V_m V_m^{id}) - H_p^E/V_m$$

Thus, for H_2O + DMSO, H_2O + TBA, H_2O + MeOH, and MeOH + DMSO the excess volumes and enthalpies are negative, so that the two terms on the right hand side of eq. 14 are positive (note that RT is small compared with the enthalpies of vaporisation). Accordingly, these systems exhibit positive cohesive energy densities. Similarly, both H_p^E and V^E are posi-

Can. J. Chem. Downloaded from www.nrcresearchpress.com by 210.87.254.42 on 09/05/12
For personal use only.

TABLE 1. Compositions and magnitudes of extrema in the excess functions of mixing for various binary systems*

System		$\left(\frac{\partial U}{\partial V}\right)^{E}$ /10^5 Pa	$\left(\frac{\Delta U_V}{V}\right)^{E}$ /10^5 Pa	n^E	V^E /10^{-6} m_3 mol^{-1}	$G_p{}^E$ /J mol^{-1}	$H_p{}^E$ /J mol^{-1}	$S_p{}^E$ /J K^{-1} mol^{-1}	CT§ /K
C_6H_{14}/C_6F_{14}	{	0.5–0.7†	0.55	0.5	0.5_2 (8)	0.48 (8)	0.50 (8)	0.50 (8)	0.3–0.5 (8)
	{	−90‡	−180	+0.076	+5.37	+1338	+2195	+2.78	295.8
H_2O/DMSO	{	0.3	0.25	0.3	0.40 (13, 14)	0.40 (13)	0.35 (13)	0.35 (13)	—
	{	+2100	+1200	+0.126	−0.98	−1318	−2554	−5.6	—
H_2O/TBA	{	0.1	0.1	0.1	0.30 (15)	0.45 (15)	0.1 (15)	0.28 (15)	—
	{	+2000	+700	+0.114	−0.93	+1054	−627	−4.39	—
H_2O/MeOH	{	0.3	0.3	0.3_5	0.4 (16)	0.5 (23)	0.3 (23)	0.40 (23)	—
	{	+1650	+880	+0.094	−0.98	+307	−878	−3.8	—
H_2O/CH_3CN	{	0.25	0.4–0.5	0.45	0.35–0.45 (18, 19)	0.55 (17)	0.65 (17)	0.4 (17)	0.38 (18)
	{	+1960	−1400	+0.180	−0.57	+1100	+1075	−0.30	272.1
MeOH/DMSO	{	0.45	0.45	0.45	0.5	0.5 (21, 22)	0.5 (21, 22)	0.4 (21, 22)	—
	{	+1340	+160	+0.154	−0.56	−800	−390	+1.44	—

*Reference numbers in parentheses.
†Mole fraction of second component.
‡Magnitude of excess function at the extremum.
§UCST.

Can. J. Chem. Downloaded from www.nrcresearchpress.com by 210.87.254.42 on 09/05/12
For personal use only.

tive for $C_6H_{14} + C_6F_{14}$, so that $(\Delta U_V/V)^E$ is negative. However, in the case of $H_2O + CH_3CN$, H_p^E is positive but V^E is negative. The negative excess cohesive energy density exhibited by this system therefore arises from the dominance of the second term on the right hand side of eq. 14, *i.e.* the extra enthalpy gained by the system upon mixing more than offsets the contribution from a reduction in volume. One other combination of terms is possible, *viz.* a positive V^E but negative H_p^E. However, none of the systems examined so far fall into this class.

An interesting feature of the n^E values plotted in Fig. 3 is that they are positive for all systems. While the physical meaning of n has not yet been firmly established, the extensive compilations of this parameter by Allen, Gee, and Wilson (25) and Hildebrand (26) show that for weakly interacting fluids $n \approx 1$. On the other hand, liquids which are characterised by strong intermolecular interaction exhibit n values which are less than unity, particularly if the system is extensively hydrogen bonded. Positive n^E values, therefore, suggest that there is an overall decrease upon mixing in the extent of *those types of interaction* which contribute principally to the determination of n. It is stressed, however, that this interpretation is tentative, and more detailed information is required as to the nature of intermolecular interactions in these systems before the exact physical meaning of n, and hence n^E, can be established.

Finally, it is of interest to note that complete correlation does not exist between $(\partial U/\partial V)_T^E$, $(\Delta U_V/V)^E$ and n^E and the traditional constant pressure excess functions of mixing for the systems considered in this work (see Table 1). Accordingly, any models which are proposed to account for the behaviour of a mixture must explain these new excess functions *as well as* the traditional ones. In this respect, the excess functions which are defined in this paper represent additional criteria for the classification of real liquid mixtures.

1. D. D. MACDONALD and J. B. HYNE. Can. J. Chem. **49**, 611 (1971).
2. D. D. MACDONALD and J. B. HYNE. Can. J. Chem. **49**, 2636 (1971).
3. D. D. MACDONALD, J. B. HYNE, and F. L. SWINTON. J. Am. Chem. Soc. **92**, 6355 (1970).
4. K. M. CHAPMAN and D. D. MACDONALD. J. Chem. Thermodyn **8**, 675 (1976).
5. D. F. GRANT-TAYLOR and D. D. MACDONALD. Can. J. Chem. **54**, 2813 (1976).
6. R. E. GIBSON and O. H. LOEFFLER. J. Am. Chem. Soc. **61**, 2515 (1939).
7. R. E. GIBSON and O. H. LOEFFLER. J. Am. Chem. Soc. **63**, 898 (1941).
8. R. D. DUNLAP and R. L. SCOTT. J. Phys. Chem. **66**, 631 (1962).
9. M. R. J. DACK. Chem. Soc. Rev. **4**, 211 (1975).
10. A. F. M. BARTON. J. Chem. Ed. **48**, 156 (1971).
11. R. L. SCOTT. J. Phys. Chem. **64**, 1241 (1960).
12. J. S. ROWLINSON. Liquids and liquid mixtures. 2nd ed. Butterworths, London. 1969.
13. J. J. LINDBERG and J. KENTTAMAA. Suomen Kemistilehti, **B33**, 104 (1960).
14. C. F. LAU, P. T. WILSON, and D. V. FENBY. Aust. J. Chem. **23**, 1143 (1970).
15. J. KENTTAMAA, E. TOMMILA, and M. MARTTI. Ann. Acad. Sci. Fen. **A93**, 1 (1959).
16. C. CARR and J. A. RIDDICK. Ind. Eng. Chem. **43**, 692 (1951).
17. A. L. VIERK. Z. Anorg. Chem. **261**, 283 (1950).
18. D. A. ARMITAGE, M. J. BLANDAMER, M. J. FOSTER, N. J. HIDDEN, K. W. MORCOM, M. C. R. SYMONS, and M. J. WOOTTEN. Trans. Faraday Soc. **64**, 1193 (1968).
19. D. F. GRANT-TAYLOR. M.Sc. Thesis, Victoria University of Wellington, New Zealand. 1975.
20. K. M. CHAPMAN. M.Sc. Thesis, Victoria University of Wellington, New Zealand. 1975.
21. K. QUITZSCH, H. ULBRECHT, and G. GEISELER. Z. Phys. Chem. **234**, 33 (1967).
22. K. QUITZSCH, H. PRINZ, K. SUEHNEL, PHAM VAN SUN, and G. GEISELER. Z. Phys. Chem. **241**, 273 (1969).
23. R. F. LAMA and B. C-Y. LU. J. Chem. Eng. Data, **10**, 217 (1965).
24. F. FRANKS and D. J. G. IVES. Q. Rev. Chem. Soc. **20**, 1 (1966).
25. G. ALLEN, G. GEE, and G. J. WILSON. Polymer, **1**, 456 (1960).
26. J. H. HILDEBRAND. Phys. Rev. **34**, 984 (1929).

Through-space or proximate $^{19}F,^{19}F$ and $^{19}F,^{1}H$ spin–spin coupling constants in some benzenesulfonyl fluoride derivatives

WILLIAM J. E. PARR[1] AND TED SCHAEFER

Department of Chemistry, University of Manitoba, Winnipeg, Man., Canada R3T 2N2

Received June 7, 1976

WILLIAM J. E. PARR and TED SCHAEFER. Can. J. Chem. **54**, 3564 (1976).

The analysis of the fluorine and proton magnetic resonance spectra of 2,4,6-trimethylbenzenesulfonyl fluoride and of 2,5-difluorobenzenesulfonyl fluoride yields the signs and magnitudes of the spin–spin coupling constants containing a through-space component. The coupling between the fluorine nucleus and the methyl protons over five bonds is +1.9 Hz, opposite in sign to the −3.1 Hz observed for the corresponding coupling in 2,6-dimethylbenzoyl fluoride. The difference of 5 Hz is possibly a consequence of the different conformational preferences of the SO_2F and COF substituents. The coupling over four bonds between the fluorine nucleus on the side chain and that on the ring is +11.6 Hz in 2,5-difluorobenzenesulfonyl fluoride. It is argued that this value indicates a preference of the S—F bond for a plane lying, on average, nearly perpendicular to the benzene ring. Similar indications are noted for pentafluorobenzenesulfonyl fluoride and for pentafluorobenzenesulfinyl fluoride.

WILLIAM J. E. PARR et TED SCHAEFER. Can. J. Chem. **54**, 3564 (1976).

L'analyse des spectres rmn du proton et du fluor des fluorures de tétraméthyl-2,4,6 benzènesulfonyle et de difluoro-2,5 benzènesulfonyle conduit aux signes et aux amplitudes des constantes de couplage spin–spin contenant une composante à travers l'espace. La constante entre le noyau de fluor et les protons du groupe méthyle à travers cinq liaisons est de +1.9 Hz, d'un signe opposé au −3.1 Hz observé pour le couplage correspondant dans le fluorure de diméthyl-2,6 benzoyle. La différence de 5 Hz est probablement une conséquence de préférences conformationnelles différentes pour les substituants SO_2F et COF. Le couplage à travers quatre liaisons entre le noyau de fluor de la chaîne latérale et celui du noyau est de +11.6 Hz dans le fluorure de difluoro-2,5 benzènesulfonyle. On suggère que cette valeur indique que le lien S—F préfère se trouver, en moyenne, dans un plan presque perpendiculaire à celui du noyau benzénique. Des indications semblables sont notées pour les fluorures de pentafluorobenzènesulfonyle et de pentafluorobenzènesulfinyle.

[Traduit par le journal]

Introduction

It is probable (1–8) that all large $^{19}F,^{19}F$ nuclear spin–spin coupling constants, $^{n}J^{F,F}$ (where n is the formal number of intervening bonds), attributable to a close proximity of the atoms or bonds containing the coupled nuclei, are positive. Thus, in derivatives of **1**, $^{4}J^{F,F}$ for the indicated conformation lies near +75 Hz (3),

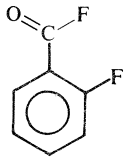

1

while in *o*-fluorobenzotrifluoride derivatives it appears (9–13) that (see **2** and **3**) the through-space contributions to $^{4}J^{F,F}$ are $^{4}J_{0}{}^{F,F} \sim 80$ Hz,

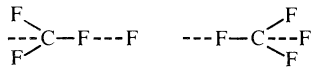

0°, 120° 60°, 180°

2 **3**

$^{4}J_{60}{}^{F,F} \sim 20$ Hz, $^{4}J_{120}{}^{F,F} \sim 7.4$ Hz, $^{4}J_{180}{}^{F,F} \sim 0$ Hz. The actual observed couplings are averages over the various conformations, whose populations are dependent on the size and nature of the second substituent *ortho* to the CF_3 group. It should be noted that a σ–π mechanism (14–16), operating via the intervening π electron system, and other indirect (17) mechanisms, could contribute as much as 2 Hz to the observed coupling constants.

With one exception (18, 19), the available semiempirical theories (7) and a molecular orbital model (6) suggest a positive sign for a through-space $^{n}J^{F,F}$. For the corresponding $^{n}J^{H,F}$ values a negative sign is calculated (19–23) and

[1]Postdoctoral fellow, 1974–1976.

Can. J. Chem. Downloaded from www.nrcresearchpress.com by 210.87.254.40 on 09/05/12
For personal use only.

Can. J. Chem. Downloaded from www.nrcresearchpress.com by 210.87.254.40 on 09/05/12
For personal use only.

measured (20–23) when the hydrogen and fluorine nuclei lie within a distance comparable to the sum of the van der Waals radii of the hydrogen and fluorine atoms. More generally (24) INDO–MO–FPT calculations indicate large negative or positive values for $^{n}J^{H,F}$, depending on the relative orientation of the proximate bonds containing the nuclei. For example, in **4**, $^{5}J^{H_7,F}$ is computed as +26 Hz when the C—F

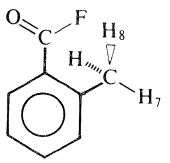

4

and C—H_7 bonds are situated in the aromatic plane (22) while $^{5}J^{H_8,F} \sim 1$ Hz. As the carbonyl group moves out of plane, and the ^{19}F approaches H_8, this coupling becomes large and negative. It follows that the signs of the observed $^{5}J^{H,F}$ will depend on the relative magnitudes of positive and negative contributions, which, in turn, are determined by a delicate balance of the non-bonded interactions determining the molecular geometry.

In this paper the signs and magnitudes of $^{4}J_o^{F,SO_2F}$ in 2,5-difluorobenzenesulfonyl fluoride, and of $^{5}J_o^{F,CH_3}$ in 2,4,6-trimethylbenzenesulfonyl fluoride, are measured and discussed in terms of through-space mechanisms. Deductions about the conformational preferences of the sulfonyl fluoride fragment are presented.

Experimental

The trimethyl derivative was of commercial origin while the 2,5-difluoro derivative was prepared from *p*-difluorobenzene via chlorosulfonation, followed by treatment with aqueous KF.

The proton magnetic resonance spectra of degassed 5 mol% solutions in $CDCl_3$ were calibrated in the frequency-sweep mode on an HA 100 spectrometer at 32 °C at sweep rates of 0.02 Hz/s. The ^{19}F magnetic resonance spectra were calibrated at 56.4 MHz on a DA60-I spectrometer at 29 °C. Double resonance experiments designed to determine relative signs of coupling constants were performed in the usual manner (25, 26).

Results and Discussion

(1) Spectral Analyses

The spectral parameters, determined in the accepted manner by the use of the computer programs LAME (28, 29) and NUMAR (29), are given in Table 1. A conservative estimate of the errors in the spectral parameters is 0.04 Hz, the rms deviations between calculated and observed transition frequencies being as large as 0.027 Hz. The largest standard deviations in the LAME analyses, as high as 0.014 Hz, occurred for the ^{19}F spectra.

The two *ortho* methyl groups in the trimethyl derivative are not magnetically equivalent because $^{4}J_o^{H,CH_3} \neq {}^{6}J_p^{H,CH_3}$. However, these couplings will not differ by appreciably more than 0.1 Hz (30) so that the spectrum is insensitive to $^{4}J^{H_3,H_5}$ and sensitive only to $(^{4}J_o^{H,CH_3} + {}^{6}J_p^{H,CH_3})/2$. The latter parameter may contain a somewhat larger error than 0.04 Hz. In any event, $^{5}J_o^{H,CH_3}$ is of interest and is no doubt accurate to at least 0.1 Hz.

The signs of the coupling constants are given on the basis of $^{3}J_o^{H,F} > 0$ (31, 32), $^{3}J_o^{H,H} > 0$ (33), and $^{5}J_p^{F,F} > 0$ (34).

(2) The Sign and Magnitude of $^{7}J^{F,CH_3}$

The σ–π mechanism no doubt dominates this coupling over seven bonds, has zero magnitude when the S—F bond lies in the benzene plane, and very likely increases as $\sin^2\theta$, where θ is the angle by which the S—F bond twists out-of-plane. It is not known what the maximum value of $^{7}J^{F,CH_3}$ is, *i.e.*, when $\theta = 90°$, but the substantial magnitude of +0.68 Hz (compare $^{7}J^{CH_3,CH_3} = +0.62$ Hz in *p*-xylene (35, 36)) suggests an out-of-plane orientation of the S—F bond.

(3) Sign and Magnitude of $^{5}J_o^{F,CH_3}$

In 2,4,6-trimethylbenzenesulfonyl fluoride $^{5}J_o^{F,CH_3}$ is +1.9 Hz, in sharp contrast to the −3.1 Hz measured in 2,6-dimethylbenzoyl fluoride. In benzoyl fluoride the COF group prefers an in-plane arrangement by about 5 kcal/mol (37). As shown previously (22), the presence of two *ortho* methyl groups constrains the COF group to an out-of-plane arrangement. The concomitant close approach of the fluorine atom to the hydrogen atoms of the methyl groups ensures that the negative through-space contributions dominate $^{5}J_o^{F,CH_3}$.

INDO–MO–FPT calculations (38), based on the parameterization of Galasso (39), were performed on 2-methylbenzenesulfonyl fluoride for a number of possible conformations. A standard geometry (40) was assumed for all but the SO_2F

TABLE 1. Chemical shift* and spin–spin coupling parameters

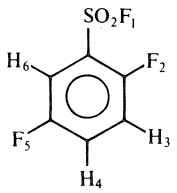

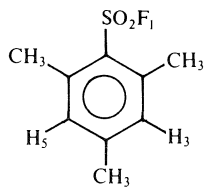

Parameter	Value	Parameter	Value	Parameter	Value
ν_1	3594.35†	$^4J_m^{H_6F_2}$	5.018	ν_1	3823.40†
ν_2	1738.904‡	$^4J_m^{H_3F_5}$	3.892	ν_2	262.46
ν_5	1833.238	$^4J_m^{H_4H_6}$	3.202	ν_4	233.12
ν_3	733.771	$^4J_o^{H_6F_1}$	−0.225	$\nu_{3,5}$	701.51
ν_4	747.495	$^4J_o^{F_1F_2}$	11.594	$^4J_o^{H_3,CH_3(4)}$	−0.64
ν_6	767.067	$^5J_m^{F_1F_5}$	1.690	$(^4J_o^{H_3,CH_3(2)}+{}^6J_p^{H_5,CH_3(2)})/2$	−0.63
$^3J_o^{H_3F_2}$	8.746	$^5J_p^{F_2F_5}$	17.569	$^5J_o^{F,CH_3}$	1.90
$^3J_o^{H_4F_5}$	7.198	$^5J_m^{H_3F_1}$	0.781	$^5J_m^{H,F}$	0.96
$^3J_o^{H_6F_5}$	6.988	$^5J_p^{H_3H_6}$	0.331	$^5J_m^{CH_3,CH_3}$	−0.19
$^3J_o^{H_3H}$	9.199	$^6J_p^{H_4F_1}$	−0.583	$^7J_p^{F,CH_3}$	0.68
$^4J_m^{H_4F_2}$	3.699				

*Proton shifts and coupling constants in Hz for 5 mol% solutions in $CDCl_3$; shifts to low field from internal tetramethylsilane at 100 MHz.
†In Hz at 56.443 MHz to low field of internal $CFCl_3$ for 10 mol% solutions in $CHCl_3$.
‡In Hz at 56.443 MHz to high field of internal CF_3CCl_3 for 10 mol% solutions in $CHCl_3$.

group, whose geometry was approximated as follows. The bond angles and lengths of the chlorosulfonyl group in CH_3SO_2Cl and $C_6H_5SO_2Cl$ are the same to within experimental error (41). By analogy, the geometry of the SO_2F group in the benzenesulfonyl fluoride derivatives was taken as that in CH_3SO_2F (42), *viz.*, S—F (1.56 Å), C—S (1.76 Å), S—O (1.41 Å), ∠CSF (98.1°), ∠CSO (110.4°).

The results of the calculations are not given here.[2] However, it may be noted that they showed a conformational dependence similar to that for 2,6-dimethylbenzoyl fluoride (22) and that they were consistent with a preference for an out-of-plane conformation of the S—F bond.

(4) The Sign and Magnitude of $^4J_o^{F,SO_2F} \equiv {}^4J^{F,F}$

(i) F,F Distance Dependence of $^4J^{F,F}$

Over a narrow range of F,F distances, r_{FF}, the through-space $J^{F,F}$ is very sensitive (1, 7, 13) to r_{FF}. Hilton and Sutcliffe (13) suggest the empirical equation 1

$$[1] \quad J^{F,F}\,(\text{Hz}) = 6800 \exp[-1.99 r_{FF}\,(\text{Å})]$$

[2]A referee objected strongly to the use of these numbers. The interested reader may obtain them from the authors.

for r_{FF} values between 2.2 and 4.0 Å. This equation roughly holds for 2-fluorobenzotrifluoride derivatives, yielding numbers about 10% too low at small r_{FF} (and large $^4J^{FF}$) values and numbers within a few Hz of observed (deduced) $^4J^{FF}$ values at intermediate F,F distances.

An indication of the rough general validity of [1] is given by the observed $^4J^{F,COF}$ of 38.8 Hz in pentafluorobenzoylfluoride (3). If, in the *trans* arrangement of the ring C—F and (O=)C—F bonds, $^4J^{F,F}$ is no larger than 1.5 Hz (43), the through-space contribution to $^4J^{F,COF}$ is roughly 75 Hz. The same COF geometry as was used for the calculations on 2,6-dimethylbenzoylfluoride (22) yields r_{FF} = 2.30 Å for a rigid, planar conformation having a *cis* arrangement of the two C—F bonds. Equation 1 predicts $^4J^{F,F}$ as 69.6 Hz, the agreement between the observed (deduced) through-space contribution and the calculated value being as good as for the 2-fluorobenzotrifluoride derivatives.

Of course, [1] is based on rigid conformations of the latter compounds and, apart from its empirical nature, already contains the averages over the torsional motions undergone by the

Can. J. Chem. Downloaded from www.nrcresearchpress.com by 210.87.254.40 on 09/05/12
For personal use only.

CF_3 group in its various stable conformations. The application to the benzoyl fluoride derivative above is therefore consistent with the derivation of [1], as is the discussion of $^4J^{F,SO_2F}$ below.

(ii) Conformational Deductions Based on $^4J^{F,SO_2F}$

Using the geometry of SO_2F described in the previous section and a C—F bond length of 1.33 Å, one has possibilities described by **5** to **8** for 2,5-difluorobenzenesulfonyl fluoride. A conformation in which the two X—F bonds are situated *trans* to each other has an F,F distance too large for a significant contribution from [1]. On the other hand, an indirect contribution of perhaps a few Hz to $^4J^{F,F}$ is presumably possible for this conformation, as well as for **5** to **8**. Therefore the following deductions are perforce of an approximate nature.

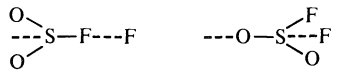

5

r_{FF} = 2.17$_5$ Å
^4J = 89.7 Hz

6

r_{FF} = 2.90 Å
^4J = 21.4 Hz

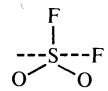

7

r_{FF} = 3.47 Å
^4J = 6.8 Hz

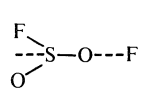

8

r_{FF} = 3.96 Å
^4J = 2.6 Hz

The observed 11.6 Hz for $^4J^{F,F}$ in 2,5-difluorobenzenesulfonyl fluoride is compatible with equal populations of **6** and **8**, having an average $^4J^{F,F}$ of 12.0 Hz, and being about 2 kcal/mol more stable at 305 K than any other conformation. On the other hand, it appears unlikely that **8** is equal in energy to **6** because it brings two negatively charged atoms rather close to each other; the S^+—O^- and C^+—F^- are polarized in the indicated manner. A more likely situation involves a ground state intermediate between **6** and **7**, having an angle of twist of the S—F bond of about 75° from the in-plane form **5**.[3]

In any event, it is clear that **5** is not an important conformation and that, on average, the S—F bond is twisted out of the aromatic plane by a value nearer 90° than 0°. Such an average allows the polar C—F bond in the ring and the polar bonds in the SO_2F a reasonable interbond distance and may be compared with the data below in (*iv*).

(iii) Conformational Indications From $^6J_p^{H,SO_2F}$

In benzoylfluoride $^6J_p^{H,COF}$ is insensibly different from zero (16), as it is in 2,6-difluorobenzoyl fluoride (3). If this coupling is dominated by a σ–π mechanism the zero magnitudes are reasonable. $^6J_p^{H,SO_2F}$ in the 2,5-difluorobenzenesulfonyl fluoride is −0.58 Hz, consistent with an out-of-plane conformation for the S—F group on the assumption that the coupling is dominated by a σ–π mechanism. In the trimethyl derivative $^7J_p^{F,CH_3}$ is +0.68 Hz, consistent with a σ–π mechanism for $^6J_p^{H,SO_2F}$; particularly if in the latter compound the S—F bond spends more time in the perpendicular plane than it does in the 2,5-difluoro derivative. Consequently, $^6J_p^{H,SO_2F}$ is consistent with the deductions based on $^4J_o^{F,SO_2F}$.

(iv) Comparison with $^4J^{F,SO_2F}$ *and* $^4J^{F,SOF}$ *in the Pentafluorobenzenesulfonyl and Pentafluorosulfinyl Fluorides*

In $C_6F_5SO_2F$, $^4J^{F,SO_2F}$ is ±15.5 Hz (44). Taking the positive sign because of the data in Table 1, one may again draw the inference that conformations analogous to **5** are not appreciably populated. Rather, if a conformation analogous to **7** is taken as that of low energy, then averages of calculations based on [1] at intervals of a few degrees in the angle of twist of the S—F bond indicate a large amplitude of oscillation about the C—S bond; perhaps as large as 40°. This depiction of the conformational behaviour in $C_6F_5SO_2F$ is consistent with the apparent failure to freeze out (44) one conformation at temperatures as low as −130 °C because, of course, the ^{19}F magnetic resonance spectrum of **7** will be qualitatively similar to the spectrum at room temperature; particularly if the barrier to rotation is very low, as suggested by the large amplitude of oscillation in **7**.

In C_6F_5SOF, $^4J^{F,SOF}$ is ±6.9 Hz (44). If the positive sign is correct, it is interesting to note that [1] predicts this value for a conformation analogous to **7**; assuming that r_{FF} is similar in the two molecules. Certainly a large angle of twist from the all-planar conformation is indicated by the magnitude of $^4J^{F,SOF}$, which con-

[3]In the gas phase the angle of twist of the S—Cl bond in benzenesulfonyl chloride (41) lies near 75° but, of course, the chlorine atom is relatively large and the preferred conformation may arise from steric repulsions between the S—Cl bond and the ring C—H bonds.

Can. J. Chem. Downloaded from www.nrcresearchpress.com by 210.87.254.40 on 09/05/12
For personal use only.

trasts markedly with the $^4J^{F,COF}$ value in C_6F_5COF. Furthermore, the coupling of ± 2.7 Hz to the *para* fluorine nucleus, $^6J^{F,SOF}$, suggests considerable nonplanarity. Perhaps a conformation analogous to **7** is indeed the low energy form, in which case the spectral behaviour (44) at -130 °C is rational. There is also the implication of rather weaker conjugation for the SOF group or perhaps of a conjugation which is not strongly decreased as a function of rotational angle. The latter situation is compatible with partially filled *d* orbitals on sulfur.

Acknowledgment

We are grateful to the National Research Council of Canada for financial assistance.

1. J. Hilton and L. H. Sutcliffe. Prog. Nucl. Magn. Reson. Spectrosc. **10**, 27 (1975).
2. C. W. Haigh, J. Hilton, L. H. Sutcliffe, and G. J. T. Tiddy. J. Magn. Reson. **18**, 241 (1975).
3. T. Schaefer, W. Niemczura, and K. Marat. J. Chem. Soc. Faraday Trans. II, **71**, 1526 (1975).
4. J. Hilton and L. H. Sutcliffe. J. Chem. Soc. Faraday Trans. II, **71**, 1395 (1975).
5. J. Hilton and L. H. Sutcliffe. J. Magn. Reson. **14**, 241 (1974).
6. F. B. Mallory. J. Am. Chem. Soc. **95**, 7747 (1973).
7. A. D. Buckingham and J. E. Cordle. J. Chem. Soc. Faraday Trans. II, **70**, 994 (1974).
8. C. Schumann and F. Cavagna. J. Magn. Reson. **18**, 172 (1975).
9. H. S. Gutowsky and V. D. Mochel. J. Chem. Phys. **39**, 1195 (1963).
10. J. Jonas and H. S. Gutowsky. J. Chem. Phys. **42**, 140 (1965).
11. J. Jonas, L. Borowski, and H. S. Gutowsky. J. Chem. Phys. **47**, 2441 (1967).
12. R. E. Richards and T. Schaefer. Trans. Faraday Soc. **54**, 1447 (1958).
13. J. Hilton and L. H. Sutcliffe. Spectrochim. Acta, Part A, **32**, 201 (1976).
14. H. M. McConnell. J. Mol. Spectrosc. **1**, 11 (1957).
15. D. J. Blears, S. S. Danyluk, and T. Schaefer. J. Chem. Phys. **47**, 5037 (1967).
16. R. J. Kostelnik, M. P. Williamson, D. E. Wisnosky, and S. M. Castellano. Can. J. Chem. **47**, 3313 (1969).
17. M. Barfield and M. Karplus. J. Am. Chem. Soc. **91**, 1 (1969).
18. K. Hirao, H. Nakatsuji, H. Kato, and T. Yonezawa. J. Am. Chem. Soc. **94**, 4078 (1972).
19. K. Hirao, H. Nakatsuji, and H. Kato. J. Am. Chem. Soc. **95**, 31 (1973).
20. T. Schaefer and J. B. Rowbotham. Chem. Phys. Lett. **29**, 633 (1974).
21. J. B. Rowbotham, M. Smith, and T. Schaefer. Can. J. Chem. **53**, 986 (1975).
22. T. Schaefer, K. Chum, K. Marat, and R. E. Wasylishen. Can. J. Chem. **54**, 800 (1976).
23. H. Fritz, T. Winkler, and W. Kung. Helv. Chim. Acta, **58**, 1822 (1975).
24. R. E. Wasylishen and M. Barfield. J. Am. Chem. Soc. **97**, 4545 (1975).
25. J. P. Maher and D. F. Evans. Proc. Chem. Soc. 208 (1961).
26. R. Freeman and W. A. Anderson. J. Chem. Phys. **37**, 2053 (1962).
27. S. Castellano and A. A. Bothner-By. Mellon Institute Publication, Pittsburgh, Pa. 1967.
28. C. W. Haigh and J. M. Williams. J. Mol. Spectrosc. **32**, 398 (1969).
29. A. R. Quirt and J. S. Martin. J. Magn. Reson. **5**, 318 (1971); Private communication.
30. M. P. Williamson, R. Kostelnik, and S. M. Castellano. J. Chem. Phys. **49**, 2218 (1968).
31. P. Diehl and I. Gränacher. J. Chem. Phys. **34**, 1846 (1961).
32. A. Saupe. Z. Naturforsch. Teil A, **19**, 161 (1964); Z. Naturforsch. **20**, 572 (1965).
33. R. Freeman. J. Chem. Phys. **43**, 3087 (1965).
34. G. J. den Otter, W. Heijser, and C. Maclean. J. Magn. Reson. **13**, 11 (1974).
35. C. J. Macdonald and W. F. Reynolds. Can. J. Chem. **48**, 1002 (1970).
36. J. B. Rowbotham and T. Schaefer. Can. J. Chem. **52**, 489 (1974).
37. R. K. Kakar. J. Chem. Phys. **56**, 1189 (1972).
38. J. A. Pople, J. W. McIver, Jr., and N. S. Ostlund. J. Chem. Phys. **49**, 2960 (1968); **49**, 2965 (1968).
39. V. Galasso. Theor. Chim. Acta, **34**, 137 (1974).
40. J. A. Pople and M. Gordon. J. Am. Chem. Soc. **89**, 4253(1967).
41. J. Brunvoll and I. Hargittai. J. Mol. Struct. **30**, 361 (1976).
42. I. Hargittai and M. Hargittai. J. Mol. Struct. **15**, 399 (1973).
43. S. Ng and C. H. Sederholm. J. Chem. Phys. **40**, 2090 (1964).
44. P. Meakin, D. W. Ovenall, W. A. Sheppard, and J. P. Jesson. J. Am. Chem. Soc. **97**, 522 (1975).

Can. J. Chem. Downloaded from www.nrcresearchpress.com by 210.87.254.40 on 09/05/12
For personal use only.

Synthesis of bridged azabicyclic ketones. Solvolysis of enol ether and ethylene ketal *N*-chloramines in acidic medium

ROLAND FURSTOSS, RAHIM TADAYONI, GILBERT ESPOSITO, JEAN LACRAMPE, ANDREAS HEUMANN, AND BERNARD WAEGELL

Laboratoire de Stéréochimie associé au CNRS, Université d'Aix-Marseille III, Faculté des Sciences et Techniques de Saint-Jérôme, rue Henri Poincaré, 13397 – Marseille Cedex 4 – France

Received March 18, 1975[1]

ROLAND FURSTOSS, RAHIM TADAYONI, GILBERT ESPOSITO, JEAN LACRAMPE, ANDREAS HEUMANN, and BERNARD WAEGELL. Can. J. Chem. **54**, 3569 (1976).

The syntheses of 2-azabicyclo[2.2.2]octanes, 2-azabicyclo[3.2.1]octanes and 2-azabicyclo-[3.3.1]nonanes, by means of intramolecular cyclizations of *N*-chloramines under acidic solvolytic conditions, are described. The cyclization is regioselective for the enol ethers and dioxolanes. The latter reacts in an unsaturated open form. The experimental data lead us to conclude that the reaction mechanism involves an electrophilic chlorination of the enol ether double bond.

ROLAND FURSTOSS, RAHIM TADAYONI, GILBERT ESPOSITO, JEAN LACRAMPE, ANDREAS HEUMANN et BERNARD WAEGELL. Can. J. Chem. **54**, 3569 (1976).

Nous décrivons les synthèses d'aza-2 bicyclo[2.2.2] et d'aza-2 bicyclo[3.2.1]octanes ainsi que d'aza-2 bicyclo[3.3.1]nonanes, réalisées par cyclisation intramoléculaire de *N*-chloramines en milieu acide. Ces cyclisations sont rendues régiosélectives par l'utilisation d'éthers d'énol et de dioxolanes, ces derniers réagissant sous une forme "ouverte" insaturée. Les résultats expérimentaux nous conduisent à conclure que le mécanisme de la réaction implique une chloration électrophile de la double liaison de l'éther d'énol.

Introduction

N-Chloramines are versatile synthetic intermediates in organic synthesis. Depending on the reaction conditions they form chloronium ions (1–3), nitrogen centered radicals (4–11), nitrenes (12), or nitrenium ions (13), although intervention of the latter species in certain solvolytic reactions of *N*-chloramines has been called in question (10, 11). In the presence of various reagents, *N*-chloramines react with double bonds (1–8), aromatic rings (4, 14–17), or unactivated hydrogens (10, 18) if conveniently located within the molecular framework.

The present paper describes the intramolecular interaction of *N*-chloramines with enol ethers and ethylene ketals in acidic medium. Using this route bridged azabicyclic ketones bearing the nitrogen adjacent to the bridgehead carbon have been efficiently synthesized. The availability of this rapid synthetic method is attractive, since such amino ketones are building blocks of numerous alkaloids (19–21) as well as of derivatives with potential pharmacological properties. This process is complementary to other reactions yielding functionalized azabicyclic derivatives such as aqueous silver catalyzed solvolysis of ethylenic *N*-chloramines (22), photochemical cyclizations of *N*-nitroso derivatives (23), and intramolecular nucleophilic opening of epoxides by amides (26, 27). However, the method proposed here is often more unequivocal, straightforward, and efficient, since it avoids the difficulties involved in the oxidation of amino alcohols (28) or hydrolysis of oximes. In the reaction described, the enol ether or the ethylene ketal is the precursor of the keto group in the azabicyclic derivative. These groups simultaneously protect the carbonyl group and insure regiospecificity in the chlorination reaction which is essentially electrophilic in nature.

It is noteworthy that this process, which is currently considered as an undesirable side reaction in radical reactions, has not been used extensively for synthetic purposes. In fact, we show that in the case of the enol ether and ethylene ketal *N*-chloramines, it provides an excellent route to bridged bicyclic amino ketones.

Synthesis of Enol Ethers and Ethylene Glycol Ketals

All *N*-chloramines used in this investigation have been prepared by treating the correspond-

[1]Revision received July 6, 1976.

Can. J. Chem. Downloaded from www.nrcresearchpress.com by 210.87.254.5 on 09/05/12
For personal use only.

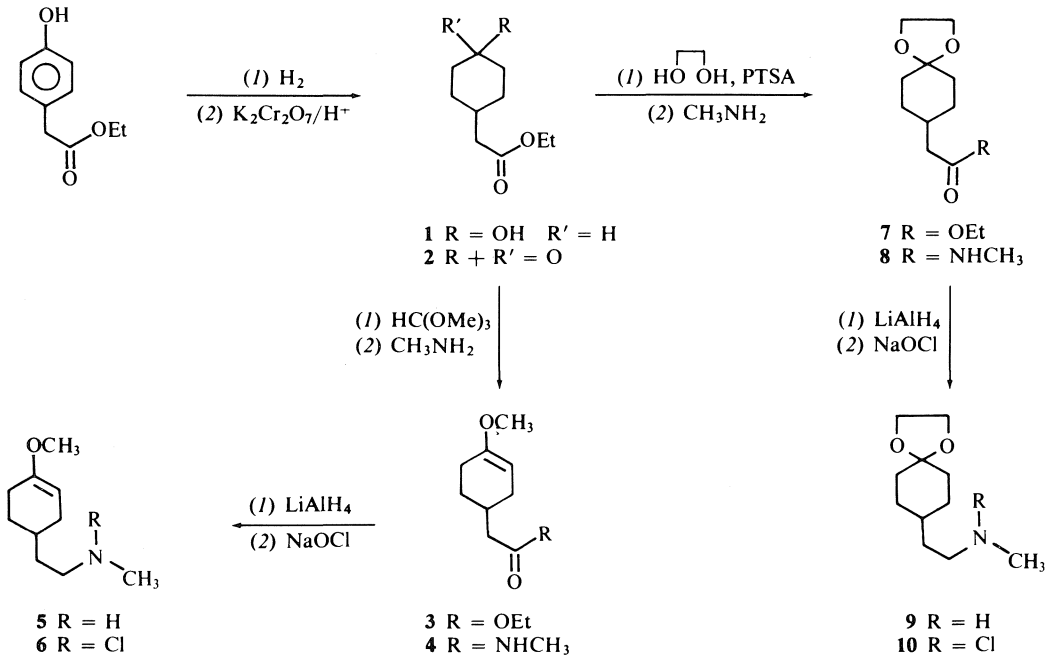

SCHEME 1

ing amines with 1 *M* sodium hypochlorite solution. A general route has been developed, which allows the synthesis of enol ether chloramines **6**, **11**, and **14** and ethylene ketal chloramines **10**, **13**, **16**, **18**, and **19** (see Scheme 2) using suitable substituted phenol derivatives[2] as starting material. The synthesis of chloramines **6** (enol ether) and **10** (dioxolane), shown in Scheme 1, illustrates this synthetic pathway.

Catalytic hydrogenation of ethyl-4-hydroxyphenyl acetate yields the *cis* and *trans* alcohols **1** which give ketone **2** by potassium dichromate oxidation. Reaction of **2** with trimethyl orthoformate in presence of potassium hydrogen sulfate affords enol ether **3**. Treatment of the latter with a methanolic solution of methylamine gives amide **4**, which is reduced by lithium aluminium hydride to amine **5**.

The corresponding dioxolane derivative **9** is easily obtained by treatment of ketone **2** with ethylene glycol in the presence of *p*-toluenesulfonic acid, followed by treatment with methylamine to yield **8** and lithium aluminium hydride reduction, yielding the amine **9**.

[2]In the case of the *ortho*-chloramine **18** the synthesis may start with commercially available 2-carbethoxycyclohexanone.

The preparation of *N*-chloramines **11** and **13** have been described elsewhere (29, 30).

Cyclization of Enol Ethers

(1) Cyclization in Pure Trifluoroacetic Acid

In contrast to a genuine Hofmann–Loeffler–Freytag reaction, in which an *N*-chloramine is irradiated by uv light in order to initiate a radical reaction, we found that solvolysis of *N*-chloramines **6**, **11**, and **14** in pure trifluoroacetic acid leads respectively to bicyclic amino ketones **20**, **12**, and **15** without irradiation[3] (respective yields 77, 15, and 75%). See Scheme 2 and Table 1. In the case of chloramine **6**, enol ether **21** is additionally obtained as a cyclization product (19%). The additional products obtained by solvolysis of **11** have been described previously (30).

(2) In Methanol

The striking difference arising from the use of methanol as a solvent (instead of pure CF_3COOH), is the formation in high yields of epimeric chloro ketals **17** and **22**. These can be

[3]All experiments described were carried out without irradiation.

Can. J. Chem. Downloaded from www.nrcresearchpress.com by 210.87.254.5 on 09/05/12
For personal use only.

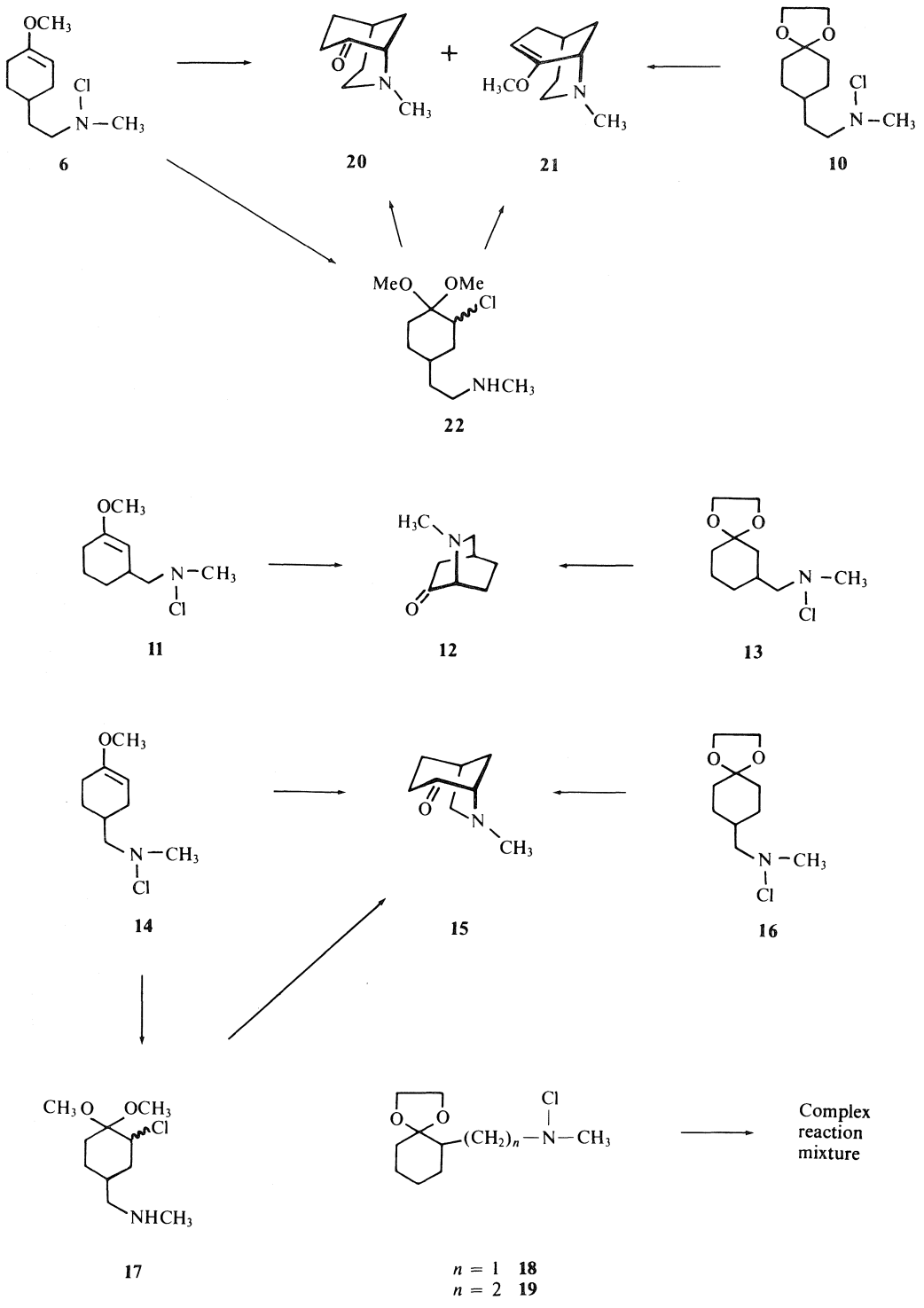

SCHEME 2

Can. J. Chem. Downloaded from www.nrcresearchpress.com by 210.87.254.5 on 09/05/12
For personal use only.

TABLE 1. Cyclization of enol ethers and ethylene ketals

Starting material	Reaction conditions*	Reaction products	Yields (%)
6	A	**20** + **21**	77/19
	C	**20** + **21**	20/50
	D	**21** + **22**	8/85
10	A	**20**	10
	B	**20** + **21**	50/30
11	A	**12** + other compounds (30)	15
13	A	**12**	5
	B	**12**	60
14	A	**15**	75
	B	**15** + **17**	10/90
16	A	**15**	26
	B	**15**	50
18	A	Complex reaction mixture	
	B		
19	A	Complex reaction mixture	
	B		

*A = CF_3COOH (pure); B = CF_3COOH–MeOH; C = MeOH (with acidic treatment before isolation); D = MeOH (without acidic treatment before isolation).

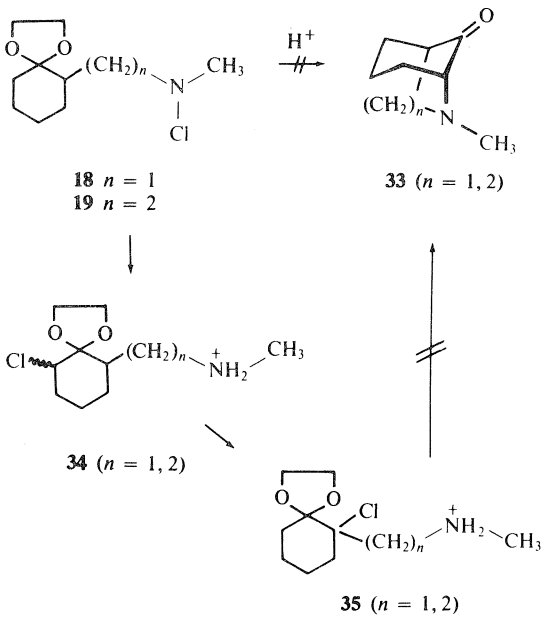

SCHEME 3

cyclized by acidic hydrolysis followed by base treatment, to ketones **15** and **20** respectively. A similar result has been obtained by Dygos for solvolysis of **14** in pure methanol (31). However, in the case of chloro ketal **22**, this treatment predominantly affords the elimination–cyclization product **21**.

Interestingly, solvolysis of chloramine **14** in an anhydrous mixture of MeOH–CF_3COOH (7:3), leads to the same chloro ketals **17** (90% of the product), but the reaction time is dramatically shortened compared to the non-acidic conditions (5 min instead of 15 h).

These results clearly emphasize the important role of the nucleophilic character of the solvent, as well as the influence of its acidity on the reaction rate.

Obviously the enol ether provides an activation of the α position of the carbonyl group from which it was generated, as well as protection of this group. Based on these considerations we were led to a study of another protecting group, namely the ethylene ketal (in **10**, **13**, and **16**).

Cyclization of Ethylene Ketals

(1) In Pure CF_3CO_2H

Solvolysis of *N*-chloramines **10**, **13**, and **16** in pure trifluoroacetic acid gives ring closure products **20** (10%), **12** (5%), and **15** (26%) in low yields accompanied by polymeric products and tars. In the case of **10**, four detectable compounds were formed beside **20**. Analysis by glc coupled with mass spectra, shows that no bridged amino ketones such as **23** were formed (Scheme 4).

(2) In Trifluoroacetic Acid – Methanol

In addition to these results obtained with pure CF_3COOH, solvolysis of *N*-chloramines **10**, **13**, and **16**, in an anhydrous trifluoroacetic acid – methanol solution leads to amino ketones **20**, **12**, and **15** with comparatively higher yields and better selectivity. (Respective yields of 50, 60, and 50% compared to 10, 5, and 26%.) The fact that enol ether **21** is obtained as a reaction product (10–30%) in the solvolysis of *N*-chloramine **10** gives an important clue concerning the reaction mechanism (see Discussion).

Surprisingly enough, solvolysis of *N*-chloramines **18** and **19**, does not lead to the expected amino ketones **33**. This can be rationalized in terms of steric arguments as will be discussed later.

Discussion of Mechanisms

As a result of the nature of the N—Cl bond,

Can. J. Chem. Downloaded from www.nrcresearchpress.com by 210.87.254.5 on 09/05/12
For personal use only.

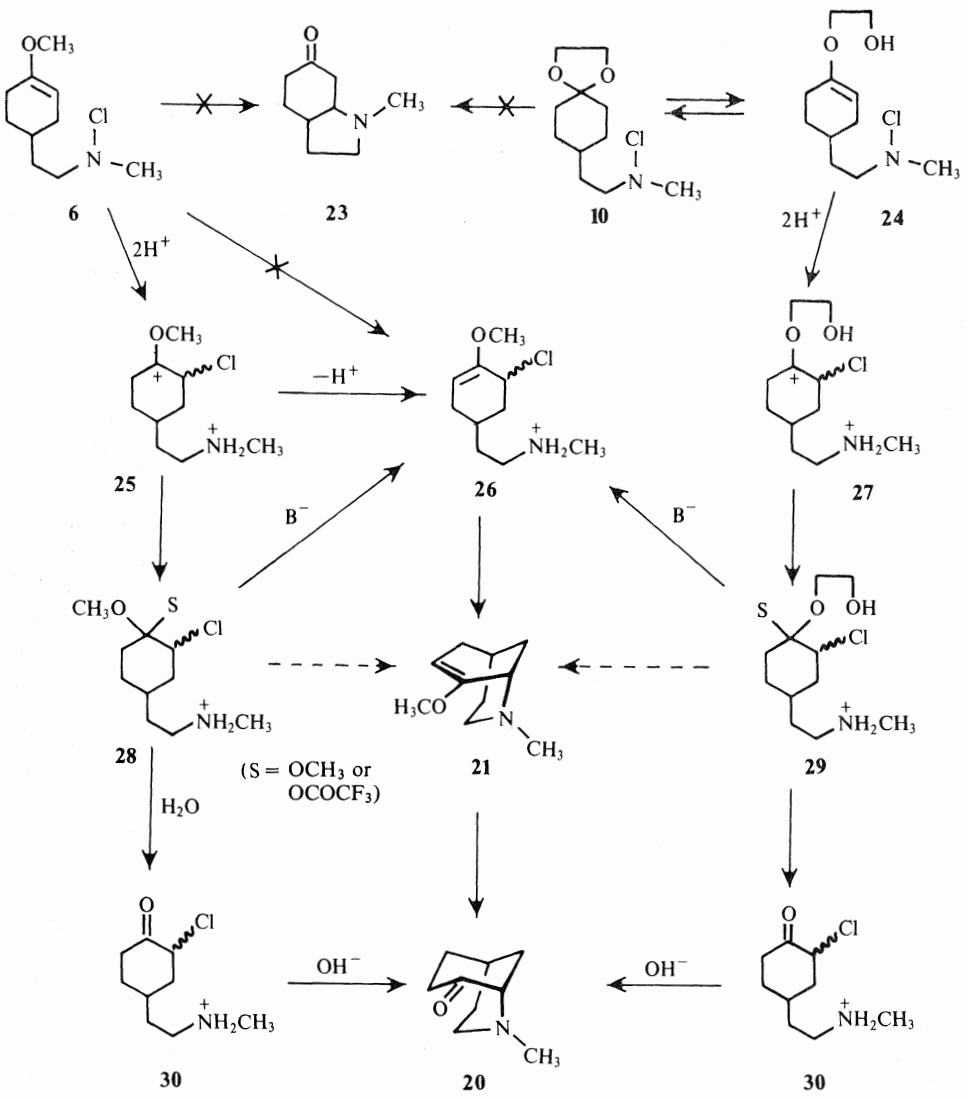

SCHEME 4

N-chloramine decomposition may follow various mechanistic pathways. In acidic medium it is possible to consider: (*i*) radical reactions involving either addition of an aminium radical ($R_2\dot{N}H^+$) to a double bond (4, 5) or hydrogen abstraction from a saturated carbon atom, *i.e.*, the Hofmann–Loeffler–Freytag reaction (18); (*ii*) ionic reactions such as electrophilic chlorination (1, 3) or possibly nitrenium ion additions (13).

The cyclization mechanism of **6** and **10** will be discussed extensively since it is representative for the mechanism occurring in the case of **11**, **13**, **14**, and **16** (Scheme 4).

(1) Cyclization of Enol Ether N-Chloramines

A highly exothermic reaction is observed when *N*-chloramine **6** (as well as **11** and **14**) is dissolved in trifluoroacetic acid: this might be taken as an argument in favour of a thermally initiated aminium radical formation.

This radical could then give rise: (*i*) to a

Can. J. Chem. Downloaded from www.nrcresearchpress.com by 210.87.254.5 on 09/05/12
For personal use only.

Can. J. Chem. Downloaded from www.nrcresearchpress.com by 210.87.254.5 on 09/05/12
For personal use only.

Hofmann–Loeffler–Freytag reaction or (*ii*) to an addition reaction to the enol ether double bond.

However, the experimental conditions, *i.e.*, presence of oxygen, short reaction time, immediate disappearance of the *N*-chloramine proven by iodometric analysis, are not in favour of the implication of such a radical. This is confirmed by the fact that the cyclization definitely does not occur in δ position relative to the nitrogen, (which is the normal course of the Hofmann–Loeffler–Freytag reaction) to give **23**.[4] This δ position is particularly suitable in this case, as it is thermodynamically favoured (allylic position).

We have verified that such a skeleton is by no means difficult to form, as **31** readily cyclizes to **32**, interestingly with a *cis* ring junction (32).[5]

In addition, the fact that we observe a strong solvent effect, as evidenced in going from pure trifluoroacetic acid to a mixture of CF_3CO_2H–MeOH, supports an ionic process rather than a radical pathway.

Finally, the possible radical processes are excluded by the formation of high yields of the chloro ketals **22** in the presence of methanol. This actually also excludes the implication of nitrenium ions in these solvolyses.

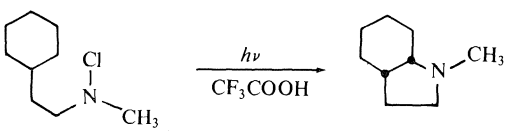

31 **32**

The mechanism we propose involves chloronium ion addition to the enol ether double bond of *N*-chloramine **6** to form the methoxy stabilized carbonium ion **25** (Scheme 4). The latter can either undergo elimination to **26** or be attacked by the solvent to give an intermediate of type **28**. The direct pathway from **25** to **26** does not look too reasonable as it involves the elimination of the less acidic hydrogen. Accordingly, **26** is much more likely to be formed via **28** followed by a kinetically controlled base elimination.[6] Intermediate **28** (S = OCH_3) can be isolated in good yield when the solvent contains a good nucleophile such as methanol.[7] The latter derivative can then undergo: (*i*) a base initiated elimination leading to **26** which cannot be isolated as it immediately undergoes a base induced cyclization to the bicyclic derivative **21**; (*ii*) a hydrolysis to **30** which could not be isolated as it cyclizes very easily to **20** in basic medium.

All these data, and especially the fact that **28** (S = OMe) could be isolated and characterized as the free amine **22** (Scheme 2), are strongly in favour of the process involving the electrophilic chlorination of the enol ether double bond. It is interesting to note that the ratios of cyclized products **20** (ketone) and **21** (enol ether) are inverted, in going from solvolysis of enol ether *N*-chloramine **6** in pure CF_3COOH (**20**/**21** = 80:20), to basic cyclization of the intermediate **22** (**20**/**21** = 20:80). This is probably due to different reactivities of compounds **28** S = OCH_3 and S = $OCOCF_3$. In the case of the dimethyl ketal **28** (S = OCH_3) elimination of MeOH is favored, giving higher quantities of enol ether **21**, whereas the use of pure CF_3COOH in the solvolytic mixture results in predominant formation of **20** after hydrolysis of the more stable trifluoroacetoxy intermediate **28** (S = $OCOCF_3$).

Similar cyclization processes will occur for **11** and **14**.

(2) Cyclizations of Ethylene Ketal N-Chloramines

In contrast to the case of enol ether chloramines, ethylene ketal chloramines dissolve in trifluoroacetic acid non-exothermically. However, as shown by the reaction products (Scheme 2 and Table 1), the behaviour of *N*-chloramines **10**, **13**, and **16** is rather similar to that of the corresponding enol ethers **6**, **11**, and **14**, especially when the reaction is carried out in a trifluoroacetic acid – methanol mixture. No compounds which could arise from a Hofmann–Loeffler–Freytag process have ever been observed (29, 33).

This leads us to postulate open forms of the corresponding dioxolanes as intermediates in the reaction, although we have not been able to isolate them. In fact, it is known that, in acidic medium, dioxolanes are in equilibrium with

[4]It should be noted that in chloramine **11** the double bond can isomerize. The δ position relative to the nitrogen then becomes allylic. However in this case as well as (30), the cyclization does not occur at this carbon and the formation of 6-azabicyclo[3.2.1]octan-3-one was never observed.

[5]We thank Professor Mokotoff (University of Pittsburg U.S.A.) for the physical data relative to **32**.

[6]We thank one of the referees for this suggestion.

[7]When the solvent is pure trifluoroacetic acid, it can be understood that the reaction proceeds less satisfactorily because of the poor nucleophilic character of the acid.

Can. J. Chem. Downloaded from www.nrcresearchpress.com by 210.87.254.5 on 09/05/12
For personal use only.

open forms such as **24**. These forms are actually postulated as intermediates in α bromination reactions of dioxolanes (34), and have been used as key intermediates in alkaloid synthesis by Wenkert (35) or in transannular aminations by Johnson (36).

Accordingly, the same mechanism involving electrophilic chlorination (see Scheme 4) of the thus formed double bonds would apply to these derivatives and explain the observed products.

Furthermore, formation of 30% of **21** by solvolysis of **10** in a trifluoroacetic acid – methanol mixture, definitely shows that methanol must be involved in an intermediate such as **29** (S = OMe) (Scheme 4).

As noted earlier, *N*-chloramines **18** and **19** (Schemes 2 and 3) do not cyclize to the expected azabicyclic ketones **33**. This can be easily understood on the basis of the mechanism proposed. In fact, Gaudry and Marquet (34) have shown that, in the presence of methanol, bromination of ethylene ketals always occurs at the less substituted carbon. However, in acidic medium, the bromide rearranges to the more substituted carbon. Accordingly, **34** which would result from the initial chlorination of the enol ether structure, should rearrange to **35**.

These derivatives could not cyclize because of the strain involved in the three or four membered spiro systems which would be formed.

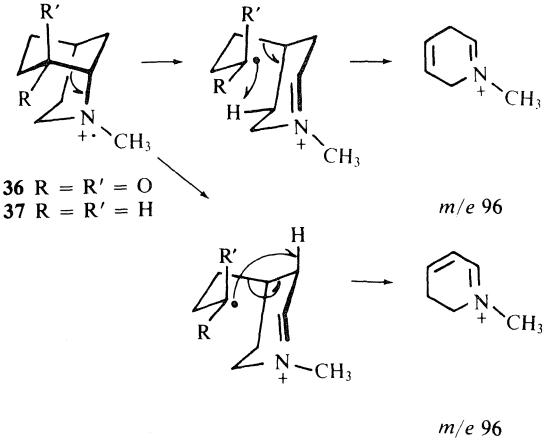

Structure Determination and Spectroscopic Data

All new structures described above have been determined on the basis of their spectroscopic data (ir, nmr, mass) reported in the experimental section or in previous papers. Some points of interest will be discussed below.

(1) Mass Spectroscopy

Fragmentation processes in mass spectroscopy are particularly characteristic of the various bicyclic structures, as was shown earlier in the azabicyclo[3.2.1]octane series (39). In the case of compounds **36** and **37**, for instance, the base peak (100%) is located at *m/e* 96, a feature which is in perfect agreement with the proposed structures. It should be pointed out, however, that such fragments also appear, but not as base peaks, in the mass spectra of different bridged azabicyclic derivatives (10).

(2) Infrared Spectroscopy

As shown by Leonard and co-workers (40, 41) in medium ring amino ketones such as **38**, the interaction of a nitrogen with a carbonyl group lowers the stretching frequency of the carbonyl (to 1681 cm^{-1} in **38**). The carbonyl frequencies observed in our molecules ranging from 1707 to 1720 cm^{-1} (for **12**, **15**, **20**, and **39**) indicate that there is no marked interaction between the nitrogen and the carbonyl group ($\nu_{C=O}$ is about 1710 cm^{-1} for the parent ketones).

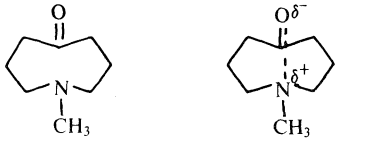

38 $\nu_{C=O}$ = 1681 cm^{-1}

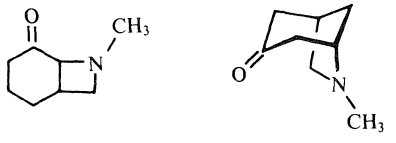

39 (30) **40**

(3) Ultraviolet Spectroscopy

Heteroatoms such as Cl or N can induce bathochromic and hyperchromic effects in the $n \rightarrow \pi^*$ band of carbonyls and, in some cases, a new band can appear at 220 nm (42–44).

Shifting toward longer wavelength (bathochromic effect) would be due to coupling of the carbonyl π and π^* energy levels with the free σ and σ^* energy levels of the C—N bond (45).

In the case of bicyclic α and β amino ketones it is possible to obtain stereochemical information

TABLE 2. Ultraviolet data

	12	15	20	39	40
λ_{max} (nm)	320	318	322	310	280
ϵ_{max}	490	395	318	80	80

from these data (45, 46). Bathochromic and hyperchromic effects can be observed in α-amino ketones if the nitrogen lone pair is *trans* antiparallel relative to the C_α—CO bond. In such a configuration, the non-bonding part of the lone pair can overlap with the *p*-orbital of the carbonyl carbon (W configuration).

The molecules which we have studied (**12**, **15**, **20**, **39**, and **40**) definitely exhibit noticeable effects (see Table 2) especially for **12**, **15**, and **20**.

Although it is difficult, on this basis, to define which conformation is the most favourable, it is clear that the nitrogen lone pair does rapidly invert, so that both conformations are populated.

Conclusion

The work which we have described shows that ionic intramolecular electrophilic chlorination of activated double bonds or ethylene ketals provides an interesting synthetic pathway toward bridged azabicyclic ketones.

Experimental

Infrared spectra were recorded on a Perkin-Elmer Model 257 using CCl_4 or $CHCl_3$ as a solvent, nmr spectra were obtained on a Varian A-60-A (60 MHz Hmr); all chemical shifts are reported in ppm downfield from internal TMS. Mass spectra were recorded on a Varian MAT CH5 at 70 eV. Product ratios were determined by glc analysis on Aerograph 90 P 4 or Intersmat IGC 12 MB using hydrogen as a carrier gas. The following (packed) columns (2–4 m) have been employed: (*a*) Carbowax 20M (10–30%) on Chromosorb P (washed with 5% KOH–MeOH); (*b*) SE-30 (10–30%) on Chromosorb P (washed with 5% KOH–MeOH).

The picrates have been prepared by adding the amine (50 mg) to a saturated solution (10 ml) of picric acid in ethanol. The precipitate was filtered and recrystallized twice from ethanol.

I. Preparation of 1-Methoxy-4-(N-chloro-N-methylaminoethyl)cyclohexene ***6*** *(38)*

(1) Ethyl-4-hydroxyphenyl Acetate (47)

A solution of 4-hydroxyphenylacetic acid (50 g, 0.328 mol) and concentrated sulfuric acid (3 ml) in ethanol (150 ml) was refluxed for 3 h. The cooled solution was evaporated, and the residue combined with water (200 ml) and extracted with ether. The ethereal extracts were washed with sodium bicarbonate solution, dried ($MgSO_4$), and concentrated. Distillation of the crude reaction product yielded the liquid ester (54.5 g, 92%) bp 138 °C/0.5 torr (lit. (47) bp 156–157 °C/1.5 torr); ir (CCl_4) 3600, 3400 (OH), 1700–1740 (ester), 1100 cm^{-1} (C—O); nmr (CCl_4) δ 1.16 (t, 3H), 3.41 (s, 2H), 4.06 (q, 2H), 6.55–8.05 ppm (m, 5H); ms M^+ 180 ($C_{10}H_{12}O_3$).

(2) Ethyl-4-hydroxycyclohexyl Acetate ***1*** *(48)*

A slurry of ethyl-4-hydroxyphenyl acetate (50 g, 0.31 mol) sodium ethoxide (3 g), Raney Nickel (4–5 g), and dry ethanol (170 ml) were placed in an autoclave with agitation and hydrogenated at 150–160 °C, 125–140 kg pressure overnight. The cooled solution was filtered, concentrated, and the residue taken up in ether and washed with a small amount of brine. The dried ethereal solution was evaporated and distilled to yield **1** (34 g, 64%): bp 106 °C/0.3 torr (lit. (48) bp 115–116 °C/0.4 torr); ir (CCl_4) 3610, 3390 (OH), 1730 cm^{-1} (ester); nmr (CCl_4) δ 1.21 (t, 3H), 1.41–2.3 (m, 12H), 3.0 (s, 1H), 4.48 ppm (q, 2H); ms M^+ 186 ($C_{10}H_{18}O_3$), base peak *m/e* 98.

(3) Ethyl-4-oxocyclohexyl Acetate ***2***

A solution of potassium dichromate (18 g) in water (90 ml) and concentrated sulfuric acid (13.5 ml) was added slowly to ethyl-4-hydroxycyclohexyl acetate **1** (31 g, 0.16 mol) dissolved in ether (80 ml) at a rate such that gentle refluxing of the reaction mixture was maintained. Refluxing was continued for 15 h. The two phases were separated and the aqueous layer extracted with ether. The combined ethereal layers were washed with sodium bicarbonate solution and brine, dried over $MgSO_4$, and the solvent evaporated. Distillation of the crude reaction product yielded ketone **2** (27 g, 88%): bp 110–115 °C/1 torr; ir (CCl_4) 1710–1740 cm^{-1} (C=O); nmr (CCl_4) δ 1.23 (t, 3H), 1.52–2.5 (m, 11H), 4.1 ppm (q, 2H); ms M^+ 184 ($C_{10}H_{16}O_3$), base peak *m/e* 96.

(4) Ethyl-4-methoxy-3-cyclohexenyl Acetate ***3***

A solution of ethyl-4-oxocyclohexyl acetate **2** (30 g, 0.16 mol) and *p*-toluenesulfonic acid (200 mg) in dry methanol (27 ml) was placed in a distillation apparatus equipped with an addition funnel. After dropwise addition of trimethyl orthoformate (21 g, 0.198 mol) the reaction flask was heated in order to distill the methanol at atmospheric pressure, followed by reduced pressure distillation. Yield of **3** 25 g (77%); bp 84–85 °C/0.5 torr; ir (CCl_4) 1730 (CO), 1665 (C=C), 1210 cm^{-1} (O—CH_3); nmr (CCl_4) δ 1.21 (t, 3H), 1.53–2.4 (m, 9H), 3.41 (s, 3H), 4.1 (q, 2H), 4.4 ppm (m, 1H); ms M^+ 198 ($C_{11}H_{18}O_3$).

(5) N-Methyl-4-methoxy-3-cyclohexenyl Acetoxamide ***4***

About 30 g (~1 mol) of methylamine was condensed into a 500 ml flask, fitted with a dry ice condenser, which contained methanol (100 ml), sodium methoxide (4 g), and ethyl-4-methoxy-3-cyclohexenyl acetate **3** (15 g, 0.075 mol). The flask was stoppered and stirred magnetically for 72 h, at room temperature. Methanol and remaining methylamine were evaporated and the white, solid residue dissolved in CH_2Cl_2 (100 ml) containing a small amount of water. The two layers were separated and the CH_2Cl_2 phase was washed with a small volume of brine. The aqueous layers were extracted with CH_2Cl_2 and the combined organic layers dried and evaporated. The residue **4** (13 g, 92%) was recrystallized from cyclohexane: mp 105–105.5 °C; ir ($CHCl_3$) 3450, 3320 (N—H), 1660 (C=O, C=C), 1170 cm^{-1} (OCH_3); nmr ($CDCl_3$) δ 1.2–2.4 (m, 9H), 2.8 (d, 3H), 3.5 (s, 3H), 4.6 (m, 1H), 6.1 ppm (br s, 1H).

Can. J. Chem. Downloaded from www.nrcresearchpress.com by 210.87.254.5 on 09/05/12
For personal use only.

Can. J. Chem. Downloaded from www.nrcresearchpress.com by 210.87.254.5 on 09/05/12
For personal use only.

(6) 1-Methoxy-4-(N-methylaminoethyl)cyclohexene ***5***

N-Methyl-4-methoxy-3-cyclohexenyl acetoxamide **4** (12 g, 0.069 mol) dissolved in dry THF (100 ml) was added slowly to a rapidly stirred slurry of $LiAlH_4$ (4 g, 0.1 mol) in THF (135 ml). Stirring was continued and the mixture heated to reflux for 10 h. After cooling in an ice bath the mixture was carefully hydrolyzed by adding dropwise: water (4 ml), NaOH solution (15%, 4 ml), and water (12 ml) followed by further rapid stirring for 15 min. The solution was filtered and the remaining residue carefully washed with ether. The combined organic layers were dried ($MgSO_4$) and evaporated, and the residue (10 g, 85%) distilled in 3 g portions in order to avoid excessive polymerization. Yield of **5** 7.2 g (60%); bp 60–61 °C/0.1 torr; ir (CCl_4) 1668 (C=C), 1210 cm^{-1} (O—Me); nmr (CCl_4) δ 1.05–2.3 (m, 9H), 1.15 (s, 1H), 2.35 (s, 3H), 2.56 (t, 2H), 3.43 (s, 3H), 4.48 ppm (m, 1H). ms M^+ 169 ($C_{10}H_{19}NO$), base peak *m/e* 44.

(7) 1-Methoxy-4-(N-chloro-N-methylaminoethyl)-cyclohexene ***6***

Yield 93%; ir (CCl_4) 1665 (C=C) 1210 cm^{-1} (O—CH_3); nmr (CCl_4) δ 1.2–2.3 (m, 9H), 2.9 (s, 3H and m, 2H), 3.4 (s, 3H), 4.5 ppm (m, 1H).

II. Preparation of Dioxolane N-Chloramine ***10***

(1) 1,4-Dioxaspiro[4.5]decane-8-ethyl Acetate ***7***

Ethyl-4-oxocyclohexyl acetate **2** (27 g, 0.146 mol), ethyleneglycol (14 g, 0.226 mol), benzene (100 ml), and *p*-toluenesulfonic acid (50 mg) were dehydrated by means of azeotropic distillation in a Dean–Stark trap over a period of 10 h. The cooled solution was washed with sodium carbonate solution and brine, dried ($MgSO_4$), and evaporated. Distillation gave pure **7** (28 g, 83%): bp 95–98 °C/0.3 torr; ir (CCl_4) 1730 (C=O), 1100 cm^{-1} (C—O); nmr (CCl_4) δ 1.23 (t, 3H), 1.4–2.3 (m, 11H), 3.81 (s, 4H), 4.08 ppm (q, 2H); ms M^+ 228 ($C_{12}H_{20}O_4$) base peak *m/e* 99.

(2) 1,4-Dioxaspiro[4.5]decane-8-(N-methyl) Acetoxamide ***8***

1,4-Dioxaspiro[4.5]decane-8-ethyl acetate **7** (25 g, 0.109 mol), methylamine (40 g, 1.3 mol) dissolved in methanol (200 ml), and sodium methoxide (0.5 g) were transformed to **8** (22 g, 94%) in the same manner as described for the enol ether amide **4**: mp 102 °C; ir ($CHCl_3$) 3480 (N—H), 1660 (C=O), 1100 cm^{-1} (C—O); nmr ($CDCl_3$) δ 1.46–2.18 (m, 12H), 2.80 (d, 3H), 3.91 ppm (s, 4H).

(3) 1,4-Dioxaspiro[4.5]-8-(N-methylaminoethyl)-decane ***9***

1,4-Dioxaspiro[4.5]decane-8-(*N*-methyl) acetoxamide **8** (20 g, 0.098 mol) was reduced by means of $LiAlH_4$ (4 g, ~0.1 mol) in THF (100 ml) in the same manner as described for amine **5** to yield **9** (15 g, 75%) (this product does not tend to polymerize during distillation): bp 94–98 °C/0.3 torr; ir (CCl_4) 1100 cm^{-1} (C—O); nmr (CCl_4) δ 1.10–1.86 (m, 11H), 1.23 (s, 1H), 2.35 (s, 3H), 2.40–2.72 (t, 2H), 3.81 ppm (s, 4H); ms M^+ 199 ($C_{11}H_{21}NO_2$), base peak *m/e* 44.

(4) 1,4-Dioxaspiro[4.5]-8-(N-chloro-N-methylamino-ethyl)decane ***10***

Yield 93%; nmr (CCl_4) δ 1.16–1.61 (m, 11H), 2.86 (s, 3H), 2.68–3.0 (t, 2H), 3.82 ppm (s, 4H). The preparation procedures for the *N*-chloramines **11**, **14**, **13**, **16**, **18**, and **19** as well as for the corresponding amines, are identical to those described for **6** and **10**.

III. 1-Methoxy-3-(N-chloro-N-methylaminomethyl)cyclo-hexene ***11***

The synthesis of **11** is described elsewhere (30, 49).

IV. 1-Methoxy-4-(N-chloro-N-methylaminomethyl)cyclo-hexene ***14*** *(31)*

Compound **14** was synthesized by identical procedures to those described for **6**. The physical data for the synthetic intermediates are the following.

(1) Ethyl-4-hydroxycyclohexyl Carboxylate

Yield 85%; bp 100 °C/0.5 torr (lit. (32) bp 142–145 °C/15 torr); ir (CCl_4) 3620 and 3450 (OH), 1730 cm^{-1} (C=O); nmr (CCl_4) δ 1.25 (t, 3H), 1.4–2.5 (m, 10H), 3.7 (s, 1H), 4.12 ppm (q, 2H).

(2) Ethyl-4-oxocyclohexyl Carboxylate

Yield 90%; bp 118 °C/5 torr; ir (CCl_4) 1710–1730 cm^{-1} (C=O); nmr (CCl_4) δ 1.26 (t, 3H), 1.5–3.0 (m, 9H), 4.16 ppm (q, 2H).

(3) Ethyl-4-methoxy-3-cyclohexene Carboxylate

Yield 85%; bp 73 °C/0.45 torr; ir (CCl_4) 1730 (CO), 1670 (C=C), 1200 cm^{-1} (OMe); nmr (CCl_4) δ 1.3 (t, 3H), 1.7–2.5 (m, 7H), 3.45 (s, 3H), 4.1 (q, 2H), 4.5 ppm (large t, 1H).

(4) N-Methyl-4-methoxy-3-cyclohexene Carboxamide

Yield 97%; mp 98–99 °C (recrystallized from cyclohexane); ir ($CHCl_3$) 3460, 3350 (NH), 1660 (C=C), 1170 cm^{-1} (OMe); nmr ($CDCl_3$) δ 1.7–2.5 (m, 7H), 2.85 (d, 3H), 3.55 (s, 3H), 4.6 (m, 1H), 5.8 ppm (m, 1H).

(5) 1-Methoxy-4-(N-methylaminomethyl)cyclohexene

Yield 70%; bp 47 °C/0.3 torr; ir (CCl_4) 1660 cm^{-1} (C=C); nmr (CCl_4) δ 0.8 (s, 1H), 1.2–2.2 (m, 7H), 2.4–2.6 (m, 2H), 2.35 (s, 3H), 3.45 (s, 3H), 4.5 ppm (m, 1H).

(6) 1-Methoxy-4-(N-chloro-N-methylaminomethyl)-cyclohexene ***14*** *(31)*

Yield 93%.

V. 1,4-Dioxaspiro[4.5]-7-(N-chloro-N-methylamino-methyl)decane ***13*** *(29)*

The physical data for the synthetic intermediates leading to **13** have been described elsewhere (29). Yield 94%; nmr ($CDCl_3$) δ 1.15–2.1 (m, 9H), 2.75 (d, J = 10 Hz, 2H), 2.93 (s, 3H), 4.0 ppm (s, 4H).

VI. 1,4-Dioxaspiro[4.5]-8-(N-chloro-N-methylamino-methyl)decane ***16*** *(33)*

The physical data of the synthetic intermediates leading to **16** have been described elsewhere (33). Yield 91%; nmr (CCl_4) δ 1.0–2.0 (m, 9H), 2.68 (d, J = 6 Hz, 2H), 2.89 (s, 3H), 3.86 ppm (s, 4H).

VII. Synthesis and Cyclization of N-Chloro-N-methyl-cyclohexylethylamine

(1) N-Methylcyclohexyl Acetoxamide

Ethylcyclohexylacetic acid (Fluka) was treated with methylamine in methanol to give *N*-methylcyclohexyl acetoxamide. Yield 79%; mp 94–96 °C; ir ($CHCl_3$) 3460 (N—H), 1650 cm^{-1} (C=O); nmr ($CDCl_3$) δ 0.4–2.8 (m, 13H), 2.81 (d, 3H), 5.5 ppm (br s, 1H).

(2) N-Methylcyclohexylethylamine

Yield 86%; nmr (CCl_4) δ 0.91 (s, 1H), 1–2 (m, 13H), 2.4–2.73 (m, 2H), 2.39 ppm (s, 3H).

Can. J. Chem. Downloaded from www.nrcresearchpress.com by 210.87.254.5 on 09/05/12
For personal use only.

(3) N-Methyloctahydroindole ***32*** *(cis-N-Methyl-7-azabicyclo[4.3.0]nonane* ***32****)*

N-Chloro-*N*-methylcyclohexylethylamine **31** (4.7 g, 0.026 mol) in CF_3COOH (80 ml) was irradiated by means of a Hanovia lamp (150 W) for 4 h. The reaction was continued and the product isolated as was described for the solvolysis of enol ether *N*-chloramines in trifluoroacetic acid. Yield 2.4 g (64%); bp 52 °C/5 torr; nmr (CCl_4) δ 1–2.6 (m, 13H), 2.15 (s, 3H), 3.12 ppm (m, 1H); ms M^+ 139, base peak *m/e* 96; mp of the picrate 195–212 °C (dec.).

VIII. Preparation of N-Chloramines (General Procedure)

A heterogeneous mixture of amine (0.006 mol), CH_2Cl_2 (4 ml) and 1 *M* sodium hypochlorite solution (12 ml, 0.012 mol) was vigorously stirred for 90 min at room temperature in the absence of light. The two phases were separated and the aqueous layer was extracted with CH_2Cl_2. The combined dichloromethane solutions were washed with brine, dried ($MgSO_4$), and evaporated without heat and light. Yield 90–95% crude reaction product. The chloramines were subjected to cyclization conditions without further purification, the purity being monitored by nmr spectroscopy (N—CH_3).

IX. Solvolysis of Enol Ether N-Chloramines (General Procedures)

(1) In Pure CF_3COOH

The enol ether *N*-chloramine (5–10 mmol) was added dropwise to a ten fold quantity (10–20 ml) of cooled (0 °C) and stirred anhydrous CF_3COOH. Iodometric titration revealed, that the *N*-chloramines, had disappeared immediately. The mixture was warmed to room temperature and the acid evaporated *in vacuo*. The brown residue was dissolved in methanol (10–20 ml) and solid potassium bicarbonate (1–2 g) was added portionwise to p*H* 10. After refluxing for 1 h the methanol was evaporated without heating, and a small portion of water was added and the mixture was extracted with methylene chloride (3–4 times). The combined organic layers were dried ($MgSO_4$), the solvent evaporated, and the residue distilled *in vacuo* or simply filtered on alumina by means of a short chromatographic column to remove polymeric products before being analyzed by glc.

(2) In CF_3COOH–MeOH

The enol ether *N*-chloramine (5 mmol) in dry methanol (10 ml) was added dropwise to a stirred anhydrous CF_3COOH (5 ml) (distilled over P_2O_5) at 0 °C. The solution was warmed to room temperature and neutralization was accomplished by refluxing the reaction mixture with powdered potassium carbonate for 30 min. Methanol was evaporated, the residue taken in a small portion of water and extracted with ether. Evaporation of the combined and dried ($MgSO_4$) ethereal solution yielded the products which were subjected to glc analysis.

(3) In Methanol

A solution of the *N*-chloramine (5 mmol) in absolute methanol (50 ml) was refluxed until no more N—Cl was detectable by iodometric titration (15–20 h). Methanol was evaporated and the residue treated with dilute HCl (5%, 20 ml) by stirring rapidly for 1 h. The aqueous solution was made basic with 50% sodium hydroxide and extracted with ether, the combined ether layers were dried ($MgSO_4$) and the solvent evaporated.

X. Solvolysis of Dioxolane N-Chloramines (General Procedures)

(1) In Pure CF_3COOH

The same procedure was applied as was described for the reaction of enol ether *N*-chloramines in pure CF_3COOH (IX–1). The lower reactivity of dioxolanes requires a reaction time of about 2 h after the addition of the *N*-chloramine to trifluoroacetic acid had been completed.

(2) In CF_3COOH–MeOH

A solution of the dioxolane *N*-chloramine (20 mmol) in methanol (40 ml) was added dropwise to rapidly stirred CF_3COOH (7 ml) at 0 °C. The reaction mixture was warmed and refluxed until all N—Cl had disappeared (iodometric test) (~90 min). After cooling, potassium carbonate (10–12 g) was added and refluxing was continued for ½ h in order to neutralize the acid and to achieve cyclization. Methanol was evaporated, the residue taken up in a small quantity of water, and the products isolated by ether extraction in the usual manner.

XI. Reaction Products

(1) N-Methyl-2-azabicyclo[2.2.2]octan-6-one ***12***

The physical data of **12** have been described elsewhere (30, 49, 50).

(2) N-Methyl-6-azabicyclo[3.2.1]octan-4-one ***15***

The physical data of **15** have been described elsewhere (38).

(3) 8-Methoxy-N-methyl-2-azabicyclo[3.3.1]non-7-ene ***21*** *(38)*

Infrared (CCl_4) 1660 cm^{-1} (C=C) 1210 cm^{-1} (OMe); nmr (CCl_4) δ 1.10–2.64 (m, 9H), 2.11 (s, 3H), 2.95 (br t, 1H), 3.43 (s, 3H), 4.70 ppm (br t, 1H); ms M^+ 167 ($C_{10}H_{17}NO$), base peak *m/e* 110.

21 is easily hydrolyzed to **20**. The product mixture (80% **21** and 20% **20**) (400 mg) and hydrochloric acid (5%, 10 ml) were rapidly stirred and heated to 40 °C for 20 h. The mixture was neutralized with KOH (50%), the product extracted with ether, and the ether solutions dried and evaporated. Yield 350 mg (95%) of **20**.

(4) N-Methyl-2-azabicyclo[3.3.1]nonan-8-one ***20*** *(38, 52)*

Infrared (CCl_4) 1707 cm^{-1} (CO); nmr (CCl_4) δ 1.5–3.0 (m, with a br s at 1.95, 12H), 2.18 ppm (s, 3H); ms M^+ 153 ($C_9H_{15}NO$) base peak *m/e* 96; picrate mp 212–214 °C (dec.) (lit. mp (52) 218–219 °C).

20 can be hydrogenolyzed (30) to the parent hydrocarbon *N*-methyl-2-azabicyclo[3.3.1]nonane (80%): nmr (CCl_4) 1.4–2.0 (m, 11H), 2.3 (s, 3H), 2.7 ppm (m, 3H); ms M^+ 139 ($C_9H_{17}N$), base peak *m/e* 96.

XII. Isolation of the Dichloro Ketal Intermediate ***22*** *(4,4-Dimethoxy-3-chloro-(N-methylaminoethyl)-cyclohexane) by Solvolyzing* ***6*** *in Methanol Without Acidic Treatment*

(1) Preparation of ***21*** *and* ***22***

1-Methoxy-4-(*N*-chloro-*N*-methylaminoethyl)cyclohexene **6** (0.9 g, 4.5 mmol) in methanol (50 ml) was refluxed for 15 h (negative iodometric test). Methanol was evaporated, the residue was taken up with water and extracted with ether, the ethereal solutions dried, and the solvent evaporated. Yield 94%; glc (1.1 g (99%) mixture of **22** (90%) and **21** (10%). **22** (two isomers with the same mass in a ratio of 1:4): nmr (CCl_4) δ 1.0 (s, 1H, NH_2),

1.1–2 (m, 9H), 2.36 (s, 3H, N—CH_3), 2.55 (t, J = 7 Hz, 2H, N—CH_2), 3.14 and 3.17 (2s, 6H, OMe), 4.1 ppm (br s, 1H, Cl—C—H); ms m/e 44 (100), 137 (20), 168 (44), 220 (12), 222 (4) (M—CH_3).

(2) Cyclization of 4,4-Dimethoxy-3-chloro-(N-methylaminoethyl)cyclohexane ***22***

The mixture containing **22** (90%) and **21** (10%) (800 mg, 3.4 mmol) was stirred in presence of HCl (5%, 20 ml) for 1 h. The mixture was neutralized with NaOH (50%) and the products extracted with ether. Yield 600 mg (73%): **20** (20%) and **21** (80%). The products thus obtained were identical to those generated by solvolysis of *N*-chloramines **6** and **10**.

(3) Isolation of 4,4-Dimethoxy-3-chloro-(N-methylaminomethyl)cyclohexane ***17*** *(31)*

1-Methoxy-4-(*N*-chloro-*N*-methylaminomethyl)cyclohexene **14** was solvolyzed in rigorously dried methanol and CF_3COOH (procedure IX–2) to give a mixture of epimers **17** (90%) and **15** (7–10%). **17**: nmr (CCl_4) δ 1–2.2 (m, 10H), 2.35 (s, 3H, N—CH_3), 3.16 and 3.18 (2s, 6H, OCH_3), 4.14 ppm (br s, 1H, CH—Cl). **17** was identical in all respects to the product described by Dygos (31).

Acknowledgments

We thank Professor R. Moriarty, University of Chicago, for helpful discussions and the following organizations for financial support: C.N.R.S. (R. Furstoss), D.F.G. (A. Heumann), D.G.R.S.T. (J. Lacrampe), D.R.M.E. (G. Esposito) and Roussel Uclaf, Romainville (R. Tadayoni and A. Heumann).

1. R. S. Neale and N. L. Hinman. J. Am. Chem. Soc. **85**, 2666 (1963).
2. R. S. Neale. J. Am. Chem. Soc. **86**, 5340 (1964).
3. R. S. Neale. J. Org. Chem. **32**, 3263 (1967).
4. F. Minisci. Synthesis, 1 (1973).
5. R. S. Neale. Synthesis, 1 (1971).
6. J. M. Surzur, L. Stella, and P. Tordo. Bull. Soc. Chim. Fr. 111 (1970); 115 (1970).
7. J. M. Surzur, L. Stella, and R. Nougier. Tetrahedron Lett. 903 (1971).
8. Y. Ogata, Y. Izawa, and H. Tomioka. Tetrahedron, **23**, 1509 (1967).
9. K. Heusler. Tetrahedron Lett. 97 (1970).
10. O. E. Edwards, G. Bernath, J. Dixon, J. M. Paton, and D. Vocelle. Can. J. Chem. **52**, 2123 (1974).
11. J. W. Bastable, J. D. Hobson, and W. D. Riddell. J. Chem. Soc. 2205 (1972).
12. C. A. Wilke and D. R. Dimmel. J. Am. Chem. Soc. **94**, 8600 (1972).
13. P. G. Gassman. Acc. Chem. Res. **3**, 26 (1970).
14. H. Bock and K. L. Kompa. Chem. Ber. **99**, 1347 (1966); **99**, 1357 (1966); **99**, 1361 (1966).
15. L. Stella. Thèse de Doctorat ès Sciences physiques. 1972. No CNRS A O 6273 (France).
16. P. Kovacic, M. K. Lowery, and K. W. Field. Chem. Rev. **70**, 639 (1970).
17. J. W. Strand and P. Kovacic. J. Am. Chem. Soc. **95**, 2977 (1973).
18. M. E. Wolff. Chem. Rev. **63**, 55 (1963).
19. M. Gates and G. Tschudi. J. Am. Chem. Soc. **78**, 1380 (1956).
20. G. Buchi, D. L. Coffen, K. Kocsis, P. E. Sonnet, and F. E. Ziegler. J. Am. Chem. Soc. **88**, 3099 (1966).
21. E. Hardegger and H. Ott. Helv. Chim. Acta, **38**, 312 (1955).
22. P. G. Gassman and J. H. Dygos. Tetrahedron Lett. 4745 (1970).
23. Y. L. Chow, R. A. Perry, and B. C. Menon. Tetrahedron Lett. 1549 (1971).
24. E. L. May and J. G. Murphy. J. Org. Chem. **20**, 1197 (1955).
25. E. L. May and J. G. Murphy. J. Org. Chem. **21**, 223 (1956).
26. R. J. Schultz, W. H. Staas, and L. A. Spurlock. J. Org. Chem. **38**, 3091 (1973).
27. J. W. Huffman, C. B. S. Rao, and T. Kamiya. J. Org. Chem. **32**, 697 (1967).
28. L. D. Dolby and S. J. Nelson. J. Org. Chem. **38**, 2882 (1973).
29. G. Esposito, R. Furstoss, and B. Waegell. Tetrahedron Lett. 895 (1971).
30. R. Furstoss, G. Esposito, P. Teissier, and B. Waegell. Bull. Soc. Chim. Fr. 2485 (1974).
31. J. H. Dygos. Diss. Abstr. **97**, 3913B (1970).
32. M. Mokotoff. J. Heterocycl. Chem. **10**, 1063 (1973).
33. G. Esposito, R. Furstoss, and B. Waegell. Tetrahedron Lett. 899 (1971).
34. M. Gaudry and A. Marquet. Bull. Soc. Chim. Fr. 4169 (1969).
35. E. Wenkert, K. J. Dave, and R. V. Stevens. J. Am. Chem. Soc. **90**, 6197 (1968).
36. R. A. Johnson. J. Org. Chem. **37**, 312 (1972).
37. A. Heumann, R. Furstoss, and B. Waegell. Tetrahedron Lett. 993 (1972).
38. R. Tadayoni, A. Heumann, R. Furstoss, and B. Waegell. Tetrahedron Lett. 2879 (1973).
39. R. Furstoss, A. Heumann, B. Waegell, and J. Gore. Org. Mass Spectrosc. **6**, 1207 (1972).
40. N. J. Leonard, M. Oki, and S. Chiavarelli. J. Am. Chem. Soc. **77**, 6234 (1955).
41. N. J. Leonard and M. Oki. J. Am. Chem. Soc. **77**, 6241 (1955).
42. R. C. Cookson. J. Chem. Soc. 282 (1954); 352 (1955).
43. C. B. Clarke and A. R. Pinder. J. Chem. Soc. 1967 (1958).
44. R. C. Cookson, J. Henstock, and J. Hudec. J. Am. Chem. Soc. **88**, 1060 (1966).
45. J. Hudec. Chem. Commun. 829 (1970).
46. M. T. Hugues and J. Hudec. Chem. Commun. 831 (1970).
47. K. Tomita and H. A. Lardy. J. Biol. Chem. **235**, 3294 (1960).
48. E. M. Protiva, J. O. Jilek, V. Hach, E. Adlerova, and V. Mychajlyszyn. Chem. Listy, **51**, 2109 (1957); Chem. Abstr. **52**, 6370*a* (1958).
49. R. Furstoss, P. Teissier, and B. Waegell. Tetrahedron Lett. 1263 (1970).
50. M. P. Cava, C. K. Wilkins, Jr., D. R. Dalton, and K. Bessho. J. Org. Chem. **30**, 3772 (1965).
51. W. A. M. Davies, A. R. Pinder, and I. G. Morris. Tetrahedron, **18**, 405 (1962).
52. P. G. Gassman and J. H. Dygos. Tetrahedron Lett. 4749 (1970).

Can. J. Chem. Downloaded from www.nrcresearchpress.com by 210.87.254.5 on 09/05/12
For personal use only.

Hydrogen forming reactions of thermal electrons in hydrogen halides: kinetics and thermodynamics

SURJIT S. NAGRA AND DAVID ANTHONY ARMSTRONG
Department of Chemistry, University of Calgary, Calgary, Alta., Canada T2N 1N4

Received May 14, 1976

SURJIT S. NAGRA and DAVID ANTHONY ARMSTRONG. Can. J. Chem. **54**, 3580 (1976).

New competition kinetic studies of electron reactions in HCl and HBr in the 10^{18} to 10^{20} molecule cm^{-3} concentration region are reported and shown to support the findings of earlier investigations. The capture of thermal electrons by $(HX)_2$ dimers is examined from a kinetic and thermodynamic point of view. The $(HX)_2^{-*}$ intermediate previously proposed by several groups is considered to be involved in both systems. Differences in the magnitudes and concentration dependences of the rates can be explained, if reaction *5b* is fast ($k_{5b} \simeq 10^{13}$ s^{-1}) in

[5*b*] $$(HX)_2^{-*} \rightarrow H + XHX^-$$

HBr but relatively slow in HCl $\lesssim 2 \times 10^9$ s^{-1}, where [6*a*] and [6*b*] are the major product-forming reactions. Thermochemical data show [5*b*] to be strongly favoured energetically in

[6*a*] $$(HX)_2^{-*} + HX \rightarrow (HX)_2^- + HX$$

[6*b*] $$(HX)_2^{-*} + HX \rightarrow H + X.^-2HX$$

HBr, and close to thermoneutral in HCl. Reaction *6b* is energetically favourable in HCl. The present data require an autoionisation life-time of $\sim 10^{-12}$ s for $(HX)_2^{-*}$. From other considerations that of HX^{-*} is expected to be $\lesssim 10^{-13}$ s. This means that formation of $(HX)_2^{-*}$ must take place by collisions of electrons with HX molecules which are in effect already interacting. Production of stabilised HX^- from $(HX)_2^{-*}$ does not appear to contribute in HCl, but

[5*c*] $$(HX)_2^{-*} \rightarrow HX + HX^-$$

may occur in other HX systems. The general implications of the mechanism for electron capture in HF and HX mixtures with other polar vapours are mentioned.

SURJIT S. NAGRA et DAVID ANTHONY ARMSTRONG. Can. J. Chem. **54**, 3580 (1976).

On rapporte de nouvelles études cinétiques par des réactions de compétition d'électrons dans HCl et HBr dans l'écart de concentration de 10^{18} à 10^{20} molécules par cm^{-3}; on montre que ces études sont en accord avec les résultats obtenus antérieurement. On examine la réaction de capture d'électrons thermiques par des dimères $(HX)_2$ à partir de point de vue cinétique et thermodynamique. On considère que l'intermédiare $(HX)_2^{-*}$, qui avait été proposé antérieurement par plusieurs groupes, est impliqué dans chacun des systèmes. On peut expliquer les amplitudes et les dépendances des vitesses sur la concentration si la réaction [5*b*] est rapide

[5*b*] $$(HX)_2^{-*} \rightarrow H + XHX^-$$

($k_{5b} \simeq 10^{13}$ s^{-1}) dans HBr mais relativement lente dans HCl $\lesssim 2 \times 10^9$ s^{-1}, où [6*a*] et [6*b*] sont les réactions majeures conduisant à des produits.

[6*a*] $$(HX)_2^{-*} + HX \rightarrow (HX)_2^- + HX$$

[6*b*] $$(HX)_2^{-*} + HX \rightarrow H + X.^-2HX$$

Les données thermodynamiques montrent que [5*b*] est particulièrement favorisé du point de vue énergétique dans le cas de HBr et pratiquement thermoneutre dans HCl. Au point de vue énergétique, la réaction [6*b*] est favorable dans le cas de HCl. Les données actuelles imposent un temps d'autoionisation de $\sim 10^{-12}$ s pour $(HX)_2^{-*}$. A partir d'autres considérations, on croit que celui de HX^{-*} est $\lesssim 10^{-13}$ s. Ceci signifie que la formation de $(HX)_2^{-*}$ doit se produire par des collisions d'électrons avec des molécules HX qui sont en fait déjà en interaction. Il ne semble pas que la production de HX^- stabilisé à partir de $(HX)_2^{-*}$ contribue dans HCl; toutefois il peut se produire dans d'autres systèmes. On mentionne les implications générales du

[5*a*] $$(HX)_2^{-*} \rightarrow HX + HX^-$$

mécanisme pour la capture d'électrons dans les mélanges de HF et de HX avec d'autres vapeurs polaires.

[Traduit par le journal]

Can. J. Chem. Downloaded from www.nrcresearchpress.com by 210.87.254.42 on 09/05/12
For personal use only.

Can. J. Chem. Downloaded from www.nrcresearchpress.com by 210.87.254.42 on 09/05/12
For personal use only.

Introduction

Electron capture reactions in gaseous hydrogen halides have been studied by physical (1, 2) and chemical (3–7) methods. In HI dissociative capture

[1] $e^- + HX \rightarrow H + X^-$ (X = F, Cl, Br, I)

has a large cross section (1) and zero energy threshold, which means that it is undoubtedly the main reaction of low energy electrons in this gas (8). As one proceeds to the halides of lower molecular weight the threshold energy of [1] becomes progressively larger (see comparative data on $\Delta E^0_{298,[1]}$ in Fig. 1*a*) and the cross sections smaller (1), making it a less and less likely process for electrons of thermal energies. In fact from previous radiation chemistry studies (3–8) with the competition kinetic technique this reaction appears to be relatively unimportant in HBr and HCl. However, in the 0.1 to 4 atm pressure region there is evidence for a different thermal electron capture mechanism with a rate which is second order in hydrogen halide concentration. In general terms it can be described by one or a combination of the three overall processes [2*a*], [2*b*], and [2*c*].

[2*a*] $e^- + 2HX \rightleftarrows H_2 + X_2^-$

[2*b*] $e^- + 2HX \rightleftarrows H + XHX^-$

[2*c*] $e^- + 2HX \rightleftarrows HX + HX^-$

The rate in HBr is much larger than in HCl, where it is also sensitive to total gas pressure (6, 8). However, careful consideration[1] of the results and conclusions in refs. 1, 3, 4, 5, 6, and 7 has led us to propose a common mechanism for capture in the two gases. This is based on reactions 3 through 7.

[3] $2HX \overset{K}{\rightleftharpoons} (HX)_2$

[4] $e^- + (HX)_2 \underset{k_a}{\overset{k_c}{\rightleftharpoons}} (HX)_2^{-*}$

[5] $(HX)_2^{-*} \xrightarrow{[5a]} H_2 + X_2^-$; $\xrightarrow{[5b]} H + XHX^-$; $\xrightarrow{[5c]} HX + HX^-$

$$k_r = k_{5a} + k_{5b} + k_{5c}$$

[6] $(HX)_2^{-*} + HX \xrightarrow{[6a]} (HX)_2^- + HX$; $\xrightarrow{[6b]} H + X^-.2HX$

$$k_s = k_{6a} + k_{6b}$$

[7] $(HX)_2^{-*} + M \xrightarrow{k_sM} (HX)_2^- + M$

The present publication begins by exploring the feasibility of the above mechanism. Subsequently we reexamine the conclusions of the earlier competition kinetic studies in the light of new results from similar experiments and of recent work (9) on electron thermalisation rates. The mechanism is then shown to be capable of explaining the results of the earlier studies and those reported here, provided k_r is much larger for HBr than for HCl. Finally the general implications of these findings are discussed.

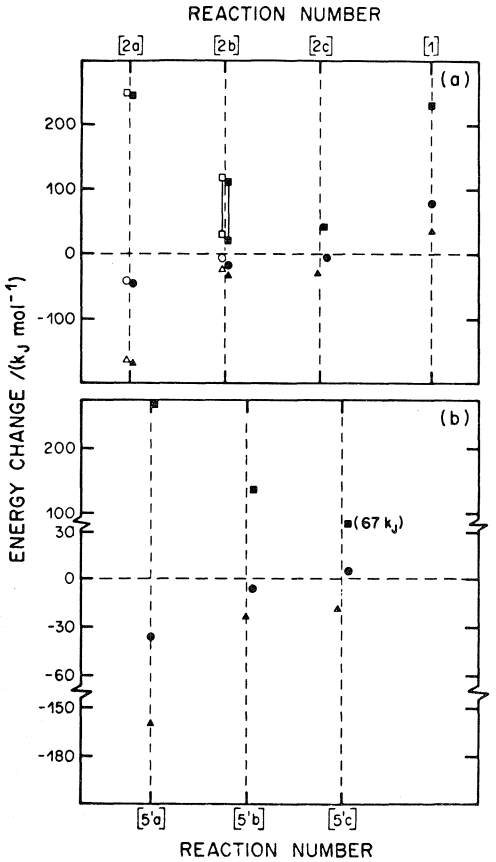

FIG. 1. Energy changes calculated for various electron capture reactions in hydrogen halides. □ HF, ○ HCl, △ HBr; filled points are ΔE^0_{298}, open ones ΔG^0_{298}; reaction numbers are given on the abscissa.

[1]This research was supported by NRCC Grant No. A3571. A preliminary report was given at Colloque Weyl IV. See J. Phys. Chem. **79**, 2875 (1975).

Can. J. Chem. Downloaded from www.nrcresearchpress.com by 210.87.254.42 on 09/05/12
For personal use only.

Experimental

Materials

Hydrogen chloride (electronic grade), hydrogen bromide (99.8%), carbon dioxide (99.6%), and sulphur hexafluoride (99.99%) were all obtained from the Matheson Company. Propane (research grade) was obtained from the Phillips Petroleum Company. Hydrogen chloride was purified by γ-irradiation as a liquid at Dry Ice temperature and several distillations through copper turnings and a trap (ethanol–nitrogen slush) at 170 K. Hydrogen bromide was purified by irradiating the gas at room temperature with X-ray followed by distillation through copper turnings and a trap at 170 K. Purified HBr and HCl were stored at liquid nitrogen temperature. All other gases were purified in the vacuum line by trap-to-trap distillation from 170 to 70 K. Middle fractions were stored in bulbs attached to the mercury-free preparation line.

Apparatus and Procedure

The radiation source, cell, and preparation procedures were essentially as described in ref. 7. The low temperature experiments with HBr were carried out by placing the cell in an insulated vessel containing Dry Ice (for 200 K), and ethanol–water (56:44 by volume for 243 K) freezing mixtures. For high temperature radiolysis the reaction cell containing HBr was heated in an aluminium container wrapped with an electrothermal heating tape and placed in a well insulated fibre glass container. The temperature as measured with an iron–constantan thermocouple was maintained constant within ± 1 deg during irradiation (30 min) by regulating the variac power supply. Mixtures of HCl and buffer gases were irradiated at room temperature only.

Product analysis was as previously reported (7).

Dose Rate Determinations

Ionization measurements have been previously discussed in detail (7). The dose rate D_m in eV[2] per hour for each mixture was calculated from the sum of the dose rates of all the components each taken as $(3600 I^s W/e)$ where I^s is the saturation ionization current for the required partial pressure of that component, e is the electron charge, and W, the energy in eV required to create an ion pair in the pure component. For two gases 1 and 2, the W values, ionization currents per unit pressure (or J values) and $\bar{\rho}_1^2$, the weighed mean stopping power ratio for the spectrum of energies of the electrons traversing the Pyrex chamber, are related by the expression

$$W_2 = W_1 \times \bar{\rho}_1^2 \times J_1/J_2$$

Using our measured J values and stopping power ratios given in the tables of Huyton and Woodward (10) we calculated W values of HCl and SF_6 as 25.5 and 34.97 eV, respectively.[2] These are in good agreement with the literature values of 25.0 (11) and 34.9 (12) for HCl and SF_6 respectively. The magnitude of W for propane (23.45 eV) was taken from ref. 11. All others were as used in ref. 7.

[2]One eV $= 1.60 \times 10^{-19}$ J and one eV per molecule $=$ 96.49 kJ mol^{-1}.

Results and Discussion

(1) Production of $(HX)_2^{-*}$

Although the existence of HX^- ions does not appear to have been confirmed by experiment, calculations by a variety of methods (13–15) suggest that some HX molecules may have a positive electron affinity. For this reason we included reaction 5*c* in the mechanism. Further, some theoretical studies (*cf.* ref. 15, curve D in Fig. 2 of ref. 16, and the potential energy (PE) curves in Fig. 1 of ref. 14 imply that in these instances a large part of the potential energy curve of HX^- may lie below the zero point vibrational level of HX in the Frank Condon region, making transitions of the type:

$$[8] \quad HX\ (^1\Sigma^+,\ v = 0) + e^-(KE \sim 0.04\ eV) \underset{k_{-8}}{\overset{k_8}{\rightleftharpoons}} HX^{-*}(^2\Sigma^+,\ v > 0)$$

highly probable. As originally recognized by Chen and Armstrong (3) one must therefore consider the possibility of the $(HX)_2^{-*}$ intermediate being formed in reactions 8 and 9 as an alternative to [3] and [4].

$$[9] \quad HX^{-*} + HX \rightleftharpoons (HX)_2^{-*}$$

We now examine evidence relating to the magnitude of k_{-8}, which appears in the expression for the rate of formation of the intermediate via [8] and [9], *viz*: $d[(HX)_2^{-*}]/dt = k_9 k_8 k_{-8}^{-1}[HX]^2[e^-]$. This rate constant can be identified as the reciprocal of τ_a, the autoionisation lifetime for $HX^-\ ^2\Sigma^+$ ions in vibrational levels correlating with $HX\ ^1\Sigma^+$ ($v = 0$) and electrons of thermal energy ($\sim$0.04 eV). The magnitude of τ_a will be equal to $\hbar\Gamma_{HX}^{-1}$, where Γ_{HX} is the entry width for the capture reaction in Breit–Wigner formalism (17, 18). Since the HX orbital into which the extra electron goes is a σ orbital, its coupling with *s*-wave electrons is not forbidden by symmetry (16). Thus, as previously pointed out (14, 16), Γ_{HX} is expected to be large and τ_a relatively small, smaller for example than 2×10^{-12} s observed (19) for $O_2^{-*}(^2\Pi_g) \rightarrow O_2(^3\Sigma) + e^-$ where *d*-wave electrons are involved and the angular momentum barrier has an appreciable effect (16, 17).

Estimates of τ_a for electrons of kinetic energy near ΔE_0^0 for reaction 1 are accessible from experimental data. For example the fact that the reverse reaction for HCl (20) has a cross section

Can. J. Chem. Downloaded from www.nrcresearchpress.com by 210.87.254.42 on 09/05/12
For personal use only.

close to the Langevin value means that autoionisation must occur in a period much shorter than the time a rebounding H and X^- pair would spend in the potential well of HX, $\lesssim 4 \times 10^{-14}$ s. This observation agrees with the fact that Christophorou, Compton, and Dickson (1) reported $\tau_a \sim 4 \times 10^{-15}$ s from their study of dissociative attachment in HCl and HBr. An even shorter τ_a ($< 10^{-15}$ s) is obtained from $\Gamma_{HX} = 1.8$ eV, which was used by Fiquet-Fayard to obtain a theoretical fit to structure in the energy dependence of the dissociative capture cross section for HCl (16). For electrons of thermal energy τ_a should be larger than the above estimates, because Γ usually decreases with decreasing energy.[3] If we assume a half power dependence on KE, which seems reasonable for an *s*-wave electron (18), and take $\Delta E^0_{298} = 0.82$ eV for HCl and 0.39 eV for HBr then, it follows that τ_a for thermal energy electrons ($\sim$0.04 eV) should be $\leq 10^{-13}$ s.

The average velocity of HCl molecules at 298 K is $\sim 4 \times 10^4$ cm s^{-1} and that of HBr is less. Thus the distance between an HX^{-*} ion and an HX molecule could only change by about 4×10^{-9} cm or about one-tenth of the HX collision diameter (21) during the average lifetime of HX^{-*}. Since HX molecules with that separation would already be interacting with each other (r_e in the intermolecular potential is 3.7×10^{-8} cm (22)) and because the de Broglie wavelength λ of a 0.04 eV electron is 68×10^{-8} cm, the concept of [8] and [9] occurring as separate processes is somewhat unreasonable. The production of the $(HX)_2^{-*}$ intermediate via [3] and [4] is therefore to be preferred over [8] and [9]. This is of course equally true if the potential energy curve of HX^- lies above the zero point level of HX and reaction 8 is unfavourable.

(2) Thermodynamic Considerations

The $(HX)_2$ dimer molecules formed in reaction 3 are assumed to be bound by relatively weak hydrogen bonding or dispersion forces. As such they belong to the general class of weakly bound dimers known as van der Waals molecules (22). The equilibrium constants estimated for HCl and HBr from PVT data (23) using methods given in ref. 24 are both in the range 2.5 to 3.0×10^{-22} cm^3 $molecule^{-1}$ at 298 K. (An identical value was derived for HCl on substituting the magnitudes of r_e and ϵ/k from ref. 22 in the statistical mechanics equation and plot in Fig. 8.2 of ref. 24).) For the nonpolar molecular gases in which dimer molecules have been studied in some detail the equilibrium constants from such calculations are in reasonable agreement with experimental dimer populations found in mass spectrometric studies (22, 25). For HX molecules one must recognize that the intermolecular potential will not be isotropic and hydrogen bonding interactions will lead to preferred orientations. In the case of HF spectroscopic studies (26) and several different theoretical calculations (27, 28 and references therein) agree on a linear F—H···F arrangement with the second F—H bond at an angle of about 160° to this axis as being the most stable configuration. $\Delta E_{[3]}$ for the HF dimer lies in the range -21 to -29 kJ mol^{-1} (27, 28). Discrete lines in the infrared spectrum of HCl have also been attributed to a hydrogen bonded dimer (29, 30) and from the temperature dependence of the integrated absorption intensities $\Delta E_{[3]}$ was estimated to be 9.0 kJ mol^{-1}.[4] A slightly higher value of 11.3 kJ mol^{-1} was obtained in a CNDO calculation for a linear dimer (31). We found no published values of $\Delta E_{[3]}$ for HBr, but one would expect it to become progressively smaller in the series HF, HCl, HBr due to the decrease in polarity.

The average of the two $\Delta E_{[3]}$ values for HCl is -10 ± 1.3 mol^{-1} giving $\Delta H^0_{298,[3]} = -12.6$ kJ mol^{-1}. If one combines the values of ΔG^0_{298} calculated from *K* for HCl at 298 K with this, then $\Delta S^0_{298,[3]} = -83$ J K^{-1} mol^{-1}. Noting that earlier estimates of standard entropies of dimerisation are near -109 J K^{-1} mol^{-1} for H_2O (32) and HF (33), where $\Delta E_{[3]} \sim -20$ kJ mol^{-1} (34), and change toward -80 for more weakly bonded dimers with ΔE near -12 kJ mol^{-1}, the above result for HCl is entirely reasonable. For HBr the decrease in entropy may be smaller, since $(HBr)_2$ is likely to be less tightly bound. However, subsequently we use the same parameters for reaction 3 in HBr as in HCl. We also use a published (33) value of $\Delta S^0_{298,[3]} = -108$ J K^{-1} mol^{-1} in HF, and do not consider the

[3]See ref. 67 for evidence of this in more complex molecular systems.

[4]Actually this was interpreted as the value of $\Delta H_{[3]}$. However since the experiments were run at constant density we interpret it as a $\Delta E_{[3]}$. Also because of the $\sim \pm 10\%$ uncertainty we make no distinction between $\Delta E^0_{0,[3]}$ and $\Delta E_{298,[3]}$ here or for HF.

TABLE 1. Spectroscopic parameters for X_2^- and XHX^- ions

Parameter	Value					
	Br_2^-	$BrHBr^-$	Cl_2^-	$ClHCl^-$	F_2^-	FHF^-
r_e of X—X/10^{-8} cm	2.66[a]	3.35[b]	2.65[c] (2.6)[a]	3.14[b]	1.91[c]	2.26[b]
$I/10^{-38}$ cm^2 g^{-1} (calcd.)	4.70	7.35	1.77	2.87	0.560	0.806
ν_1/cm^{-1}	170[a]	170[d]	240[e]	260[d,f]	510[c]	600[g]
ν_2/cm^{-1}		~580[d]		~600[d,f]		1220[g]
ν_3/cm^{-1}		670[d]		700[d,f]		1450[g]
EA of X_2^-/kJ mol^{-1}	242[h]		230[h]		297[h]	
D_{298,XHX^-}/kJ mol^{-1}		75[i]		99[i]		126[i] 213[j]
g_e = 2 for X_2^- and 1 for XHX^-						

[a]Reference 36.
[b]Reference 37.
[c]Reference 38.
[d]References 39–41.
[e]Mean of 220 (36) and 260 (38).
[f]Reference 42.
[g]Reference 43.
[h]Reference 44.
[i]Reference 45.
[j]Reference 46.

higher polymers, which are known to exist (27).

When reaction 4 is taken in sequence with each of [5*a*], [5*b*], and [5*c*], the reactions 5′*a*, 5′*b*, and 5′*c*

[5′*a*] $e^- + (HX)_2 \rightleftharpoons H_2 + X_2^-$

[5′*b*] $e^- + (HX)_2 \rightleftharpoons H + XHX^-$

[5′c] $e^- + (HX)_2 \rightleftharpoons HX + HX^-$

are derived. Likewise combination with [3] *and* [4] leads to the overall capture reactions 2*a*, 2*b*, and 2*c* given in the Introduction. We begin our analysis of the thermodynamic feasibility of the mechanism by calculating ΔG^0_{298}, ΔS^0_{298}, and ΔH^0_{298} for these overall processes.

The magnitudes of ΔG^0_{298} were calculated from ΔH^0_{298} and ΔS^0_{298}. The electron affinities of the X atoms used in calculating ΔH^0_{298} and thence ΔE^0_{298} were the ones recommended by Christophorou (11). The bond dissociation energies of H_2, HX, and X_2 molecules were from ref. 35. The HX electron affinities were from ref. 13 (see comment on HF in section 7). The magnitudes and sources of corresponding parameters for the X_2^- and XHX^- ions are given in Table 1. Expressions for ΔS^0 were obtained from $\partial(RT \ln Q)/\partial T$, where $RT \ln Q$ is defined via the standard expressions $\Delta G^0 = -RT \ln K = \Delta E_0^0 - RT \ln Q$ (24, 47). The statistical weights, vibrational frequencies, and moments of inertia used for the atomic species and HX and H_2 molecules in the partition functions for deriving Q were taken from refs. 48 and 49. Those for the XHX^- and X_2^- ions are listed in Table 1 along with their sources. The X_2^- ions were considered to be in their $^2\Sigma_{u^+}$ ground states (38). The contributions of vibrational modes with frequency ≥ 500 cm^{-1} to vibrational partition functions at 298 K were taken as unity. The partition function for the free electron was based on Boltzman statistics, which are appropriate for our very low electron density ($\lesssim 10^4$). ΔS^0_{298} was found from $\partial(RT \ln Q)/\partial T$ on substituting T = 298 K. Due to its low mass the entropy loss on removal of the electron is relatively small (12 J K^{-1} electron^{-1}; see Sackur Tetrode equation (24)). Thus the net entropy losses which arise from the effect of this and of changes in the rotational partition functions are not large, for example, −26, −44, and −12 J K^{-1} mol^{-1} in HBr for [2*a*], [2*b*], and [2*c*] respectively. For HCl and HF they are smaller and we have not reported ΔS *per se*. However, the calculated values of ΔG^0_{298} and ΔE^0_{298}, which are subject to an uncertainty of ±25 kJ mol^{-1}, are presented in Fig. 1*a*.

When allowance is made for the loss in entropy due to removal of e^- reaction 2*c* has a negative ΔG^0_{298} for any HX with an electron affinity

Can. J. Chem. Downloaded from www.nrcresearchpress.com by 210.87.254.42 on 09/05/12
For personal use only.

Can. J. Chem. Downloaded from www.nrcresearchpress.com by 210.87.254.42 on 09/05/12
For personal use only.

greater than 1.3 kJ mol^{-1}.[5] Reaction 2*a* is seen to be strongly endothermic in HF. Reaction 2*b* would be close to thermoneutral (see the lower points of joined pairs) if the large (~213 kJ mol^{-1}) theoretical and experimental (46) values of $D_{298,X^-—HX}$ were correct. However, from their systematic studies of gas phase ion binding Yamdagni and Kebarle (45) state that the bond energy should be close to 125 kJ mol^{-1}, in which case [2*b*] is strongly endothermic. Thus present data in Fig. 1*a* show no favourable channels for HF. The thermodynamic feasibility of thermal electron reactions other than [2*c*] in HBr is confirmed by the fact that [2*a*] and [2*b*] are exothermic and exhibit negative ΔG^0_{298} values. In HCl [2*a*] is energetically favourable and [2*b*] close to thermoneutral.

The above findings for HBr and HCl are highly significant to the present investigation, but we are also particularly interested in the thermochemistry of reactions 5*a*, 5*b*, and 5*c*. Since the total internal energy of the $(HX)_2^{-*}$ complex is unaltered between its formation in reaction 4 and the instant at which one of [5*a*], [5*b*], or [5*c*] occurs, the ΔE^0_{298} values for the latter reactions will be the same as for [5′*a*], [5′*b*], and [5′*c*] respectively. The magnitudes of ΔE^0_{298} for these three reactions were obtained from those of [2*a*], [2*b*], and [2*c*] by subtracting the $\Delta E^0_{298,[3]}$ values given above. They are presented in Fig. 1*b*, where a more expanded scale is used than in Fig. 1*a*. These results are considered further in section 7.

(3) Hydrogen Formation and Competition Kinetics

The irradiation of gases with ^{60}Co γ-rays or other ionising radiation leads to the formation of electrons, positive ions, and neutral excited species. The reactions of ions and neutral excited species in hydrogen halide systems have been discussed elsewhere (8, 50), and here we shall concentrate entirely on hydrogen forming reactions of electrons.

Previous radiation chemical studies (4–6, 51) have shown that electron scavengers reduce hydrogen formation in irradiated HCl by an amount, which correlates with the yield of electrons from ionisation measurements. A similar correlation exists for HBr when allowance is made for the small but significant proportion of electrons captured in [1] during thermalisation (3, 7). From the similarity of results with different electron scavengers (HBr with CCl_4 (52)[6] and SF_6 (3, 7), and HCl with SF_6, CCl_4, and C_7F_{14} (6)) and the known fact that SF_6 cannot compete for H atoms undergoing reaction 10 in HCl and HBr (8, 50), it appears that they do not interfere

$$H + HX \rightarrow H_2 + X \qquad [10]$$

with hydrogen forming reactions other than electron capture by HX. When the hydrogen halides are added to gases whose molecules are unreactive to thermal electrons the yield of hydrogen is usually enhanced and, more importantly, G_s, which is the maximum reduction in $G(H_2)$ on the addition of other electron scavengers, generally corresponds closely to the electron yield calculated from $G_{ionisation}$ ($= 100/W$) for the system. The values of the total hydrogen yield and G_s from present experiments with HCl–propane mixtures, which are plotted as a function of stopping power fraction of HCl (Z_{HCl})[7] in Fig. 2, serve to illustrate this point. G_s rises with Z_{HCl} and is within 10% of $G_{ionisation}$ for $Z_{HCl} = 0.2$, which corresponds to 30 mol% of HCl. Similar results were obtained in the present study for mixtures of HCl with CO_2 and C_2F_6 and have been reported previously for HBr with CO_2, C_2F_6, and Xe (7), and with H_2S (53). With HBr the scavenging of thermal electrons is usually complete at much lower [HX] (*e.g.*: <10 mol% in CO_2 (7)).

The foregoing observations lead to the conclusion that one molecule of hydrogen is produced for every electron reacting with HCl or HBr. This requires that each H atom from [5*b*] and [6*b*] undergoes [10]. Also each $(HX)_2^-$ produced in [6*a*] and [7] must form a molecule of hydrogen. This would probably occur, after further clustering by HCl (4), through [11]

[5]This was calculated from the loss in translational entropy of e^-, and S^0_{298} was assumed to be the same for HX^- and HX. The result is a maximum loss in entropy, since the entropy of HX^- is likely to be greater than that of HX due to: (*a*) a gain in rotational entropy arising from the probably larger value of r_e, and (*b*) a larger vibrational contribution due to lower vibrational frequencies.

[6]In this system the $CHCl_3$ yield from $e^- + CCl_4 \rightarrow Cl^- + CCl_3\cdot$ and $CCl_3\cdot + HBr \rightarrow CHCl_3 + Br\cdot$ was also observed and found to be equal to the reduction in $G(H_2)$.

[7]As defined in ref. 7 $Z = (1 + \overline{\rho^2 HX} P_2/P_{HBr})^{-1}$, where $\overline{\rho^2 HX}$ is the weighted mean stopping power ratio.

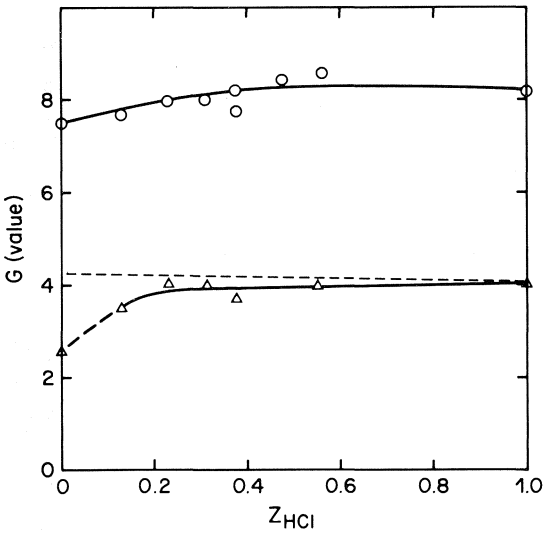

FIG. 2. Ionization yields and hydrogen yields plotted as a function of stopping power fraction Z for mixtures of HCl and propane at 298 K. ○, total hydrogen yields; △, hydrogen yields due to electron reactions. The dashed line shows $G_{ionization}$. Dose rates varied from 2.23×10^{18} to 3.0×10^{18} eV g^{-1} h^{-1} for mixtures with total pressure 8.00×10^4 to 26.67×10^4 N m^{-2}.

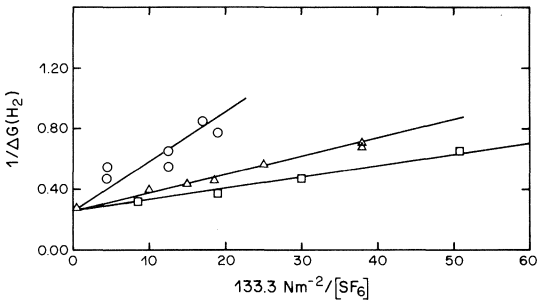

FIG. 3. Typical plots of reciprocal of the reductions of hydrogen yield *vs.* the reciprocal of the pressure of SF_6 for mixtures of HCl and propane at 298 K. □, pressure of HCl; 5.33×10^4 N m^{-2}, total dose rate = 2.23×10^{18} eV g^{-1} h^{-1}; △, pressure of HCl and propane each equal to 5.33×10^4 N m^{-2}, total dose rate = 2.71×10^{18} eV g^{-1} h^{-1}; ○, pressure of HCl and propane equal to 5.33×10^4 N m^{-2} and 21.33×10^4 N m^{-2} respectively, total dose rate = 2.99×10^{18} eV g^{-1} h^{-1}.

followed by [10]. Similar reactions must occur for HX^- if it is formed in [5*c*].

[11] $$HX + (HX)_x^- \rightarrow H + X^-.xHX$$

When HX is made to compete with known concentrations of an added electron scavenger, S, the results may be plotted in accord with expression 12 (7). The rate of electron capture per unit concentration of electrons (=(rate of electron capture by HX)$[e^-]^{-1}$)

[12] $$\{\Delta G(H)_2\}^{-1} = G_s^{-1}\left\{1 + \frac{(\text{rate of e capture by HX})}{k_{13}[e^-]} \times \frac{1}{[S]}\right\}$$

can then be obtained from the product of the rate constant k_{13} and the slope over intercept for this plot. The remainder of the present discussion is

[13] $$e + S \rightarrow S^-$$

confined to results for S = SF_6, which by virtue of its high vapour pressure can be used over a wide range of temperatures. Also information concerning secondary reactions of the SF_6^- and SF_5^- ions formed by electron capture is available from ion cyclotron resonance experiments, which have shown that these ions are rapidly converted to XHX^- in reactions with HCl and HBr (54). Since XHX^- ions are probably the main long-lived negative ion species in the absence of SF_6 (see below), the use of this scavenger should have the advantage of not affecting ion recombination reactions. This conclusion is supported by the fact that the recombination coefficient in HCl is unaffected by SF_6 (55). It may be noted that rates of HX capture calculated from previous results with CCl_4 and C_7F_{14} (4, 6) are within a factor of two of those for SF_6. In the present study k_{13} was taken as 2×10^{-7} cm^3 $molecule^{-1}$ s^{-1} independent of the gas mixture (56). Figure 3 shows examples of results from the present study plotted in accord with expression 12.

It can be shown that rates of capture from experiments where HX fails to completely suppress electron–ion recombination and electron–product reactions will be high by a fraction approximately equal to $(G_{ionisation} - G_s)/G_s$. Since this correction is somewhat uncertain we have avoided experiments where it exceeds 10%. The usual uncertainty in the measured rates as judged by the standard deviations of points from plots like those in Fig. 3 was ±10%.

(4) Rates of Electron Capture and Thermalisation

Figure 4 shows a comparison on a log–log scale of the hydrogen halide concentration dependences of the capture rates for HBr and HCl (see the upper and lower solid lines respectively).

Can. J. Chem. Downloaded from www.nrcresearchpress.com by 210.87.254.42 on 09/05/12
For personal use only.

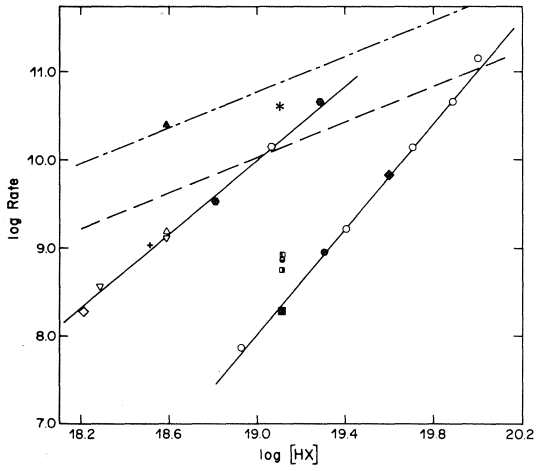

FIG. 4. Electron reaction and thermalisation rates as a function of HX concentration in molecules cm^{-3}. Lower solid line: Electron capture rate s^{-1} in HCl. Pure HCl: ○ ref. 6, ◆ ref. 8; ● ref. 4; ■ present data; mixtures of $5.3_3 \times 10^4$ N m^{-2} of HCl with $10.6_7 \times 10^4$ N m^{-2} of: ◧ C_3H_8, ◒ C_2F_6, ◨ CO_2. Upper solid line: electron capture rate s^{-1} in HBr. Pure HBr: ○ ref. 7, ● ref. 3; mixtures: with C_2F_6, CO_2, and Xe, ◇ and △ from ref. 7, 1.33×10^4 N m^{-2} HBr with $25.3_3 \times 10^4$ N m^{-2} CO_2 this study +. Electron thermalization rate for HX with $K_u = 3.6 \times 10^{-8}$, -----. Electron thermalization rate for HX with $K_u = 6 \times 10^{-9}$, ---. The points ▲ and * are total thermalization rates for 7.20×10^4 N m^{-2} CO_2 + 1.60×10^4 N m^{-2} HBr and 10.67×10^4 N m^{-2} CO_2 + 5.33×10^4 N m^{-2} HCl respectively.

Warman and Sauer (9) have recently given rate coefficients for the thermalisation of electrons (K_u) in a number of gases. Where comparisons can be made (*e.g.* for CO_2, C_2H_4, and certain hydrocarbons) their results give experimental thermalisation times which tend to be shorter, but generally agree within a factor of two with those calculated by Christophorou, Gant, and Baird (57) from the data of drift experiments. The lower dashed line in Fig. 4 is the rate of thermalisation due to hydrogen halide calculated by the method of Warman and Sauer and assuming a rate coefficient for HX equal to that of CO_2 ($K_u = 6 \times 10^{-9}$ cm^3 $molecule^{-1}$ s^{-1}). We regard this as a lower limit to the thermalisation rate, since we have evidence (7) that HBr is about six times better than CO_2 as an electron moderator in the 0.15 to 0.7 eV range. The uppermost dashed line was obtained on that basis *i.e.* K_u for HX = 3.6×10^{-8} cm^3 $molecule^{-1}$ s^{-1}. Some thermalisation rates for specific buffer gas – HX mixtures were calculated with the contribution of the buffer gas included and these are also shown. Except at the very highest HX concentrations with no buffer the thermalisation rates exceed the observed rates of capture by a large factor and it is evident that the electrons are reacting at energies in the thermal range near 0.04 eV.

(5) Analysis of the HCl Data

Application of the steady-state approximation to reactions 3 through 7 and 13 leads to [14],

$$[14] \qquad \{\Delta G(H_2)\}^{-1} = g_e^{-1}\left[1 + \frac{\{k_r + k_s[HX] + k_s^M[M]\}Kk_c[HX]^2}{\{k_a + k_r + k_s[HX] + k_s^M[M]\}k_{13}} \times \frac{1}{[S]}\right]$$

which is equivalent to expression 12 with g_e, the yield of scavengable electrons in the system, replacing G_s and with:

$$[15] \qquad \text{(Rate of e capture by HX)[e]}^{-1} = \frac{\{k_r + k_s[HX] + k_s^M[M]\}Kk_c[HX]^2}{\{k_a + k_r + k_s[HX] + k_s^M[M]\}}$$

On imposing the conditions $k_a \gg k_s^M[M] \simeq k_s[HX] > k_r$ [15] becomes:

$$[16] \qquad \text{(Rate of e capture by HX)[e]}^{-1} = \{k_s + k_s^M[M]/[HX]\}Kk_ck_a^{-1}[HX]^3$$

The experimental rates from the various studies of HCl which fall on the lower solid line in Fig. 4 were all obtained in the absence of buffer gas *i.e.* for [M] = 0. In agreement with [16] and the conclusions of refs. 5 and 6 the slope of the line through them is 3. When divided by $[HCl]^3$ these rates, except for the highest [HCl] which may involve some non-thermal electrons and was not included, lead to $k_sKk_ck_a^{-1} = 10.4 \pm 0.7 \times 10^{-50}$ cm^9 $molecule^{-1}$ s^{-1}. The excellent agreement of the data from the two laboratories involved is demonstrated by the fact that this average is the same as the value given by the original data of Johnson and Redpath alone (6) and reported as their k_7.

As shown by the points for added C_3H_8,

Can. J. Chem. Downloaded from www.nrcresearchpress.com by 210.87.254.42 on 09/05/12
For personal use only.

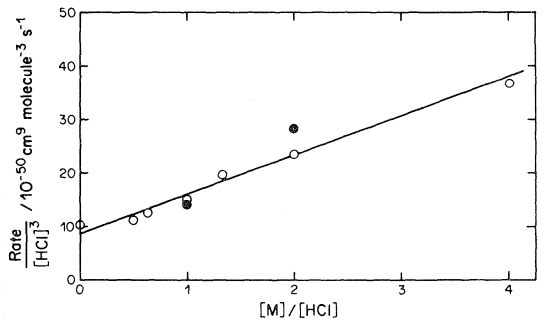

FIG. 5. Rate/[HCl]^3 *vs.* [M]/[HCl] at 298 K for mixtures of varying composition: ○, HCl and propane; ●, HCl and CO_2. Pressure of HCl was varied between 2.67×10^4 to 16.0×10^4 N m^{-2} and that of the buffer gas between 2.67×10^4 to 21.33×10^4 N m^{-2}.

C_2F_6, and CO_2 in Fig. 4 the addition of buffer gases enhances the rate of capture in HCl, a feature which is in accord with the k_s^M[M]/[HX] term on the right side of [16]. In their study Johnson and Redpath investigated the dependence of the electron capture rate on [HCl] in the presence of *excess* propane. They used N_2O as an electron scavenger and showed that the order in HCl was reduced to two, which agrees with [16] for [M] $\gg$ [HX]. However, because the N_2O capture is a three body process and the rate coefficient for N_2O as a third body was unknown, the rate coefficient for HCl under these conditions could not be obtained. We have determined rates of electron capture in HCl–propane mixtures of several compositions with SF_6 as scavenger. From the linearity of the plot in Fig. 5 these are seen to conform to expression 17, which is a simple rearrangement of [16].

$$[17] \quad (\text{Rate of e capture by HX})[e]^{-1}[HX]^{-3} = \left\{k_s + k_s^M \frac{[M]}{[HX]}\right\}\frac{Kk_c}{k_a}$$

The ratio of the slope over intercept gives $k_s^{C_3H_8}/k_s = 0.8_9$. The similar but less extensive data for CO_2 were also in accord with [17] and showed that $k_s^{CO_2}/k_s = 0.9_0$.

The use of ion–molecule reaction rate theory (58) leads to values of 1.2×10^{-9}, 1.1×10^{-9}, and 0.8×10^{-9} cm^3 molecule^{-1} s^{-1} for k_s, $k_s^{C_3H_8}$, and $k_s^{CO_2}$ respectively. From these we find $k_s^{C_3H_8}/k_s = 0.9_1$ and $k_s^{CO_2}/k_s = 0.67$, in reasonable agreement with the experimental ratios. Accepting $k_s \simeq 10^{-9}$ cm^3 molecule^{-1} s^{-1} and $K = 3 \times 10^{-22}$ cm^3 molecule^{-1}, then from $k_s K k_c k_a^{-1} = 10.4 \times 10^{-50}$ cm^9 molecule^{-3} s^{-1} one obtains $k_c k_a^{-1} = 3.5 \times 10^{-19}$ cm^3 molecule^{-1}. As stated in Section 1 a large entry width is expected for reaction 8. The entry width for capture of electrons by the $(HX)_2$ dimer should therefore also be large (17) and the cross section for reaction 4 close to the theoretical maximum value of $\lambda^2(4\pi)^{-1}$ (1, 59). Taking $k_c = \bar{v} \times \lambda^2(4\pi)^{-1}$, where $\bar{v}$ is the relative velocity of the electrons and $(HX)_2$ dimers, its magnitude is found to be $\simeq 3 \times 10^{-7}$ cm^3 molecule^{-1} s^{-1} at 298 K. Hence, $k_a \simeq k_c/3.5 \times 10^{-19} \simeq 10^{12}$ s^{-1}, and τ_a for the $(HX)_2^{-*}$ ion is about 10^{-12} s. The enhancement over τ_a for the monomer HX^{-*} ($\lesssim 10^{-13}$ s, see above) is in keeping with the fact that autoionisation lifetimes increase with the number of internal degrees of freedom in structurally related molecules (59).

The fact that the HCl results conform to expression 17 indicates that reactions 5*a*, 5*b*, and 5*c* are negligibly slow. The sum of their rate constants k_r must be less than $\sim 20\%$ of the lowest k_s[HX] value used here, which is 2×10^9 s^{-1}. Once this condition is accepted then, as the above discussion shows, the observed rates can be accounted for by individual rate coefficients with reasonable magnitudes.

(6) Analysis of the HBr Data

The [HBr] dependence of the rate of electron capture (see upper solid line in Fig. 4) differs from that for HCl in that the rate in the concentration range studied is: (*a*) much larger, (*b*) depends on the square rather than the cube of [HX], and (*c*) the points obtained with and without buffer gases lie on the same line, indicating no significant effect of buffer gas on capture rates. As previously shown the kinetics can be represented by expression 18. With $K = 3 \times 10^{-22}$ cm^3 molecule^{-1}, the value of $Kk_c = 1.0 \times 10^{-28}$ cm^6 molecule^{-2} s^{-1} calculated

$$[18] \quad (\text{Rate of e capture by HX})[e]^{-1} = Kk_c[HX]^2$$

from the results in Fig. 4 for a temperature of 298 K requires $k_c \simeq 3 \times 10^{-7}$ cm^3 molecule^{-1} s^{-1}. This is the same as used in the above discussion for the HCl system. Also, if $k_a \simeq 10^{12}$ s^{-1} as estimated for HCl, then the condition for the overall rate expression 15 to become simplified to [18] is $k_r \gg k_a > k_s$[HX] + k_s^M[M]. In other words either one of reactions 5*a* through 5*c* or a combination of them is now faster than the autoionisation of $(HX)_2^{-*}$.

Can. J. Chem. Downloaded from www.nrcresearchpress.com by 210.87.254.42 on 05/05/12
For personal use only.

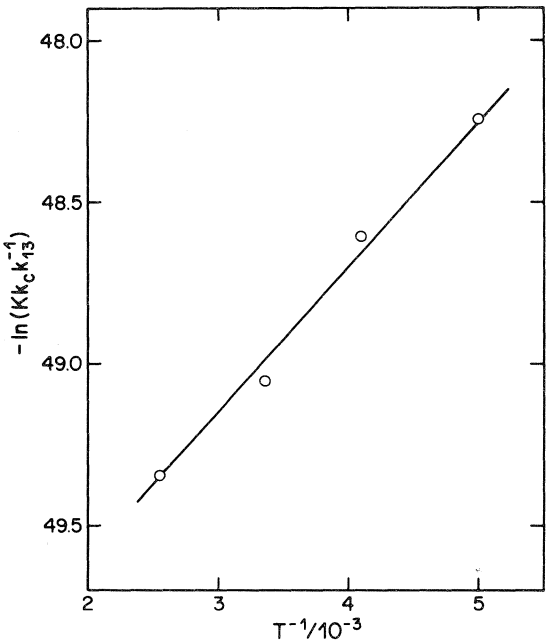

FIG. 6. Arrhenius plot for $(Kk_c k_{13}^{-1})$ for the thermal electron capture in HBr system in the temperature range 200–393 K.

When applied to [14] the same condition leads to:

$$[19] \quad \{\Delta G(H_2)\}^{-1} = g_e^{-1}\left\{1 + \frac{Kk_c}{k_{13}} \times \frac{[HX]^2}{[S]}\right\}$$

By studying the magnitudes of (slope)(intercept)$^{-1}$ from plots of eq. 19 for data at different temperatures we obtained the temperature dependence of $Kk_c k_{13}^{-1}$. The results are presented as an Arrhenius plot in Fig. 6. The slope of the solid line (least mean squares fit) corresponds to $E_c - E_{[13]} + \Delta E_{[3]} = -3.74$ kJ mol^{-1}.

From work elsewhere (60) the temperature dependence of k_{13} in the range used here appears to be small, though one might expect a small negative dependence on T due to the inverse dependence of the capture cross section on mean electron energy, which has been observed in drift experiments (11). Actually this type of energy dependence (*i.e.* energy exponent near -1) of cross sections is frequently observed for molecules with capture cross sections approaching the maximum of $\lambda^2(4\pi)^{-1}$ (11). Since the magnitude of Kk_c can only be explained for σ_c near $\lambda^2(4\pi)^{-1}$ (see above) one must assume that the temperature dependence of k_c would be similar to that of k_{13} and therefore $\Delta E_{[3]}$ must be near to -3.7 kJ mol^{-1}. This is somewhat less than the average of the literature values for HCl (-10 kJ mol^{-1}), as would have been expected.

A further point of interest derived from the experiments at different temperatures was that $G(H_2)$ from HBr in the absence of scavenger was within experimental error (± 0.2 molecules per 100 eV) the same over the range 200 to 394 K. This agrees with the fact that $G(H_2)$ from HCl has previously been shown to be the same at 200 and 298 K (4). Unfortunately the greater complexity of the capture mechanism and the fact that minute traces of chlorine scavenge $(HX)_x^-$ (4) make determinations of $E_c - E_{[13]} + E_{[3]}$ impractical in that system.

(7) Comparisons of Different HX Systems

The discussion in the preceding sections has shown that the mechanism based on reactions 3 through 7 is able to account for the capture rates observed at 298 K over the concentration ranges 10^{18} to 2×10^{19} molecules cm^{-3} in HBr and 10^{19} to 10^{20} molecules cm^{-1} in HCl. It also holds over the temperature range 200 to 394 K in HBr. The change in the magnitude of k_r from $\leq 2 \times 10^9$ s^{-1} in HCl to $> 10^{12}$ s^{-1} (*i.e.* $> k_a$) in HBr is the only alteration in the kinetic parameters required to explain the difference in behaviour for the two gases. The small value of k_r in HCl indicates that even the clearly exothermic reaction 5*a* does not proceed readily. Since it requires the two H atoms *and* the two X atoms to approach each other, its slowness may be explained by their electrostatic repulsions, which would mitigate against this geometry in the dimer and lead to the preferred linear hydrogen bonding interaction. The absence of reaction 5*c* in HCl may be due to the fact that dissociation of $(HCl)_2^{-*}$ does not give stabilised HCl^-. Therefore it cannot be taken as direct evidence against the existence of this species. The uncertainties in our calculations are such that $\Delta E^0_{298,[5b]}$ may be slightly positive in HCl. Alternatively the slowness of [5*b*] in this system may be due to a small activation energy barrier. The present results and those of ref. 6 support reactions 6*a* and 6*b* as the rate controlling processes in HCl, while other work (4, 61) implies that $k_{6a}/k_{6b} \simeq 1.7$ in HCl and $\simeq 3.4$ in DCl. If reaction 20 is taken in sequence with [5′*b*] one obtains [6′*b*].

$$[20] \quad XHX^- + HX \rightleftharpoons X^-.2HX$$

$$[6'b] \quad e^- + (HX)_2 + HX \rightleftharpoons H + X^-.2HX$$

Can. J. Chem. Downloaded from www.nrcresearchpress.com by 210.87.254.42 on 09/05/12
For personal use only.

Can. J. Chem. Downloaded from www.nrcresearchpress.com by 210.87.254.42 on 09/05/12
For personal use only.

This would have the same ΔE^0_{298} as [6*b*]. Using Yamdagni and Kebarle's thermochemical data for $X^-.2HX$ (45), we find ΔE^0_{298} [6*b*] $= -52$ kJ mol^{-1} for HCl. Given that exothermic ion–molecule reactions normally have low activation energy and are rapid, there is therefore a reasonable probability of [6*b*] competing with the stabilisation process [6*a*] and proceeding with k_{6b} near 10^{-9} cm^3 molecule^{-1} s^{-1}.

The evidence for production of clustered $(HX)_x^-$ via [6*a*] was based on the effects of chlorine (4). The assumption that chlorine did not compete with HCl for thermal electrons was based on mass spectrometric observations (4). It is borne out by a recently reported rate coefficient for thermal electron capture by chlorine (62). The small value of 3×10^{-10} cm^3 molecule^{-1} s^{-1} means that for the conditions where scavenging of $(HX)_x^-$ was observed in refs. 4 and 61 ([HCl] $= 2 \times 10^{19}$ and $[Cl_2] \lesssim 10^{17}$ molecules cm^{-3}) the rate of electron capture by chlorine would have been $\gtrsim 3 \times 10^7$ s^{-1}, which is an order of magnitude less than that by HCl (see Fig. 4). The experiments of ref. 62 also showed that the effective two body rate coefficient for capture of electrons by HCl is $< 2 \times 10^{-13}$ cm^3 s^{-1} in a flow system at a total concentration of $\sim 10^{16}$ molecule cm^{-3} and with [HCl] $\sim 2 \times 10^{15}$ molecule cm^{-3}. If we neglect $(k_s[HX] + k_s^M[M])$ and assume $k_r \sim 2 \times 10^9$ s^{-1} and $k_c K k_a^{-1} = 10^{-40}$ cm^6 molecule^{-2} from section 5, the present mechanism predicts an effective two body coefficient of $< 10^{-15}$ cm^3 molecule^{-1} s^{-1}. Values above this would imply the occurrence of processes not detected in our pressure regime, and may indicate that stable ions can be formed through capture of electrons by interacting HCl – buffer gas molecules in the flow system.

On grounds similar to those stated above for HCl, the geometry of the dimer species is also likely to favour [5*b*] over [5*a*] in HBr. Given that [5*b*] is exothermic (see Fig. 1*b*), the dissociation of $(HBr)_2^{-*}$ to H and $BrHBr^-$ resembles the dissociation of HI^{-*} to H and I^-. The fact that the latter process competes favourably with autoionisation ($\sigma_{[1]}$ in HI $\simeq \lambda^2(4\pi)^{-1}$ (1)) provides a rationalisation for the large value of $k_{5b} \simeq 10^{13}$ s^{-1}, which is required to accommodate the HBr results. The data in Fig. 1*b* suggest that reaction 5*c* may also occur, but as stated above stable HBr^- ions have not been observed and this reaction is less certain than [5*b*].

As shown in Fig. 1*b* the product channels for $(HF)_2^{-*}$ are much less favourable than are those for HCl.[8] Thus if electron capture occurs via the dimer mechanism one must expect it to proceed through reactions 6*a* and 7 as in HCl, and lead to clustered $(HF)_x^-$. The situation is complicated by the fact that in this system hexamers and other polymeric species may take part in electron capture. However, pulse radiolysis investigations would be useful for determining whether clustered negative ions with significant lifetimes were formed, and whether their structure was similar to that of the solvated electron in dense ammonia and water vapour (63).

In closing we wish to point out that a modified form of the present mechanism should apply to mixtures of the hydrogen halides with water (64) or hydrogen sulfide (53, 65). Thus Huyton and Woodward (65) attributed electron capture in HCl–H_2S mixtures to reaction 21 and a more rapid capture was observed in HBr–H_2S mixtures

[21] $\qquad e + HCl + H_2S \rightarrow$ Products

(53). We suggest that HX---H_2Y complexes are involved in these systems. Furthermore we would point out that formation of linear dimers and higher polymers of polar molecules, which do not individually possess a positive electron affinity, will lead to dipole moments greater than those of the monomers. This should strongly increase the interactions with electrons (see discussions of the effect of dipole moment in ref. 66 and earlier references cited in ref. 11), and may provide a nucleus for initial electron localisation, which could be followed by clustering and permanent solvation.

1. L. G. Christophorou, R. N. Compton, and H. W. Dickson. J. Chem. Phys. **48**, 1949 (1968) and references cited therein.
2. R. Azria, L. Roussier, R. Paineau, and M. Tronc. Revué due Physiqué Appliqueé Paris, **9**, 375 (1975).
3. J. D. Chen and D. A. Armstrong. J. Chem. Phys. **48**, 2310 (1968).
4. R. S. Davidow and D. A. Armstrong. J. Chem. Phys. **48**, 1235 (1968).
5. G. R. A. Johnson and J. L. Redpath. J. Phys. Chem. **72**, 765 (1968).

[8]One should note that the points in Fig. 1 (*a*) and (*b*) for reactions [2*C*] and [5^1*C*] in HF are based on E.A. $\simeq -42$ kJ mol^{-1} from ref. 13. This value is supported by theoretical calculations carried out subsequent to those of ref. 15 and considered to be more reliable (K. D. Jordan, private communication).

Can. J. Chem. Downloaded from www.nrcresearchpress.com by 210.87.254.42 on 09/05/12
For personal use only.

6. G. R. A. JOHNSON and J. L. REDPATH. Trans. Faraday Soc. **66**, 861 (1970).
7. S. S. NAGRA and D. A. ARMSTRONG. Can. J. Chem. **53**, 3305 (1975).
8. D. E. WILSON and D. A. ARMSTRONG. Radiat. Res. Rev. **2**, 297 (1970).
9. J. M. WARMAN and M. C. SAUER. J. Chem. Phys. **62**, 1971 (1975).
10. D. W. HUYTON and T. W. WOODWARD. Radiat. Res. Rev. **2**, 205 (1970).
11. L. G. CHRISTOPHOROU. *In* Atomic and molecular radiation physics. Wiley, New York. 1971.
12. R. S. DAVIDOW and D. A. ARMSTRONG. Radiat. Res. **28**, 143 (1966).
13. G. R. FREEMAN. Radiat. Res. Rev. **1**, 1 (1968).
14. O. H. CRAWFORD and B. J. D. KOCH. J. Chem. Phys. **60**, 4512 (1974).
15. K. M. GRIFFING, J. KENNEY, J. SIMONS, and K. D. JORDAN. J. Chem. Phys. **63**, 4073 (1975).
16. F. FIQUET-FAYARD. J. Phys. B, **7**, 810 (1974).
17. A. HERZENBERG. J. Chem. Phys. **51**, 4942 (1969).
18. J. M. BLATT and V. F. WEISSKOPF. Theoretical nuclear physics. Wiley, New York. 1952.
19. R. E. GOANS and L. G. CHRISTOPHOROU. J. Chem. Phys. **60**, 1036 (1974).
20. F. C. FEHSENFELD, C. J. HOWARD, and E. E. FERGUSON. J. Chem. Phys. **58**, 5841 (1973).
21. E. A. MOELWYN-HUGHES. Physical chemistry. Pergamon Press, New York. 1957. p. 597.
22. G. E. EWING. Angew. Chem. Int. Ed. Engl. **11**, 486 (1972).
23. Handbook of Chemistry and Physics. 53rd ed., CRC Press, D-146. 1973.
24. O. K. RICE. Statistical mechanics, thermodynamics and kinetics. W. H. Freeman and Co., San Francisco, California. 1967.
25. R. E. LECKENBY and E. J. ROBBINS. Proc. R. Soc. London, Ser. A, **291**, 389 (1966).
26. T. R. DYKE, B. J. HOWARD, and W. KLEMPERER. J. Chem. Phys. **56**, 2442 (1972).
27. J. E. DELBENE and J. A. POPLE. J. Chem. Phys. **55**, 2296 (1971).
28. H. K. SHIN. J. Chem. Phys. **63**, 2901 (1975).
29. D. H. RANK, P. SITARAM, W. A. GLICKMAN, and T. A. WIGGINS. J. Chem. Phys. **39**, 2673 (1963).
30. D. H. RANK, W. A. GLICKMAN, and T. A. WIGGINS. J. Chem. Phys. **43**, 1304 (1965).
31. H. ITOH and H. HINAZUMI. J. Phys. B, **6**, L294 (1973).
32. J. D. LAMBERT. Discuss. Faraday Soc. **15**, 226 (1953).
33. F. MEYER. Z. Electrochem. **63**, 577 (1959).
34. H. A. GEBBIE, W. J. BURROUGHS, J. CHAMBERLAIN, J. E. HARRIES, and R. G. JONES. Nature, **221**, 143 (1969).
35. United States Department of Commerce, JANAF Thermochemical Tables, 2nd ed. NSRDS-NBS 37. U.S. Printing Office, Washington. 1971.
36. W. B. PERSON. J. Chem. Phys. **38**, 109 (1963).
37. L. W. SCHROEDER and J. A. IBERS. Inorg. Chem. **7**, 594 (1968).
38. T. L. GILBERT and A. C. WAHL. **55**, 5247 (1971).
39. J. C. EVANS and G. Y.-S. LO. J. Phys. Chem. **70**, 11 (1966); **70**, 20 (1966); **71**, 3942 (1967).
40. D. E. MILLIGAN and M. E. JACOX. J. Chem. Phys. **55**, 2550 (1971).
41. J. W. NIBLER and G. C. PIMENTAL. J. Chem. Phys. **47**, 710 (1967).
42. B. S. AULT and L. ANDREWS. J. Chem. Phys. **63**, 2466 (1975).
43. J. A. IBERS. J. Chem. Phys. **41**, 25 (1964).
44. W. A. CHUPKA and J. BERKOWITZ. J. Chem. Phys. **55**, 2724 (1971).
45. R. YAMDAGNI and P. KEBARLE. J. Am. Chem. Soc. **93**, 7139 (1971); Can. J. Chem. **52**, 2449 (1974).
46. G. J. JIANG and G. R. ANDERSON. J. Phys. Chem. **77**, 1764 (1973).
47. P. J. ROBINSON and K. A. HOLBROOK. Unimolecular reactions, Wiley, N.Y. 1971.
48. G. HERZBERG. Atomic spectra and atomic structure. Dover Publications, N.Y. 1944.
49. G. HERZBERG. Molecular spectra and molecular structure, Vol. 1, Spectra of diatomic molecules, 2nd ed. Van Nostrand Co. Inc., Toronto, Ontario. 1965.
50. D. A. ARMSTRONG and C. WILLIS. Int. J. Radiat. Phys. Chem. **8**, 221 (1976).
51. C. WILLIS, A. W. BOYD, and D. A. ARMSTRONG. Can. J. Chem. **47**, 3783 (1969).
52. D. R. MCCRACKEN and D. A. ARMSTRONG. J. Chem. Phys. **55**, 982 (1971).
53. M. FORYS and K. WOJCIECHOWSKI. Radiochem. Radioanal. Lett. **10**, 277 (1972).
54. M. S. FOSTER and J. L. BEAUCHAMP. Chem. Phys. Lett. **31**, 479 (1975).
55. D. E. WILSON and D. A. ARMSTRONG. Can. J. Chem. **48**, 600 (1970) and unpublished results.
56. F. J. DAVIS and B. R. NELSON. Chem. Phys. Lett. **6**, 277 (1970).
57. L. G. CHRISTOPHOROU, K. S. GANT, and J. K. BAIRD. Chem. Phys. Lett. **30**, 104 (1975).
58. T. SU and M. T. BOWERS. Int. J. Mass. Spectrom. Ion Phys. **12**, 347 (1973) and references cited therein.
59. R. N. COMPTON and R. H. HUEBNER. Advances in radiation chemistry. Vol. 2. *Edited by* M. Burton and J. L. Magee. Wiley, N.Y. 1970. p. 281.
60. H. MASSEY. Negative ions. 3rd ed. Cambridge University Press, London. 1976. p. 372.
61. D. K. JARDINE, D. A. ARMSTRONG, A. W. BOYD, and C. WILLIS. Can. J. Chem. **49**, 187 (1971).
62. A. A. CHRISTODOULIDES, R. SCHUMACHER, and R. N. SCHINDLER. J. Phys. Chem. **79**, 1904 (1975).
63. A. GAATHON, G. CZAPSKI, and J. JORTNER. J. Chem. Phys. **58**, 2648 (1973).
64. A. W. BOYD, C. WILLIS, and D. A. MILLER. Can. J. Chem. **51**, 4048 (1973).
65. D. W. HUYTON and T. W. WOODWARD. J. Chem. Soc. Faraday Trans. I, **69**, 1049 (1973).
66. O. H. CRAWFORD. Mol. Phys. **20**, 585 (1971).
67. L. G. CHRISTOPHOROU, A. HADJIANTONIOU, and J. G. CARTER. J. Chem. Soc. Faraday Trans. II, **69**, 1713 (1973).

The xenon sensitised radiolysis of HBr[1]

SURJIT S. NAGRA AND DAVID ANTHONY ARMSTRONG
Department of Chemistry, University of Calgary, Calgary, Alta., Canada T2N 1N4

Received June 15, 1976

SURJIT S. NAGRA and DAVID ANTHONY ARMSTRONG. Can. J. Chem. **54**, 3592 (1976).

The ^{60}Co γ-radiolysis of mixtures of HBr with Xe has been investigated at room temperature. Ionisation measurements and hydrogen yields provide strong evidence for energy transfers between the two components. The small but significant decrease in ionisation yields at low HBr:Xe is independent of total pressure and consistent with a competition between HBr and Xe for the Hornbeck–Molnar states of Xe. The increase in ionisation yields at higher HBr:Xe (Z above 0.2) is probably due to collisionally-induced ionisation or chemi-ionisation reactions of highly excited states of HBr.

As in previously reported experiments with H_2S the hydrogen yields from HBr are strongly enhanced in the presence of Xe. The maximum sensitisation of 4 molecules of H_2 per 100 eV can be explained by energy transfer from excited states of Xe ($G \sim 2.5$) and subexcitation electrons having energy between 4.3–8.3 eV ($G \sim 1.5$) in Xe. The results obtained from thermal electron scavenging with SF_6 confirm previous findings that inert gases are inefficient at moderating electrons to thermal energies. At high $[SF_6]/[HBr]$, SF_6 interferes with hydrogen-forming reactions other than those of electrons.

SURJIT S. NAGRA et DAVID ANTHONY ARMSTRONG. Can. J. Chem. **54**, 3592 (1976).

On a étudié, à température de la pièce, la radiolyse γ par le ^{60}Co de mélanges de HBr avec du Xe. Les mesures d'ionisation et les rendements hydrogène fournissent de bons arguments en faveur d'un transfert d'énergie entre les deux composants. La diminution faible mais significative dans le rendement d'ionisation à des rapports faibles de HBr:Xe est indépendante de la pression totale et en accord avec les compétitions entre HBr et Xe pour les états Hornbeck–Molnar du Xe. L'augmentation des rendements d'ionisation à des rapports plus élevés de HBr:Xe (Z au-dessus de 0.2) est probablement due à des ionizations induites par des collisions ou des réactions de chemi-ionisation des états hautement excités du HBr.

Comme dans les cas rapportés antérieurement avec H_2S, les rendements en hydrogène à partir de HBr sont grandement augmentés par la présence de Xe. On peut expliquer la sensibilisation maximum de quatre molécules de H_2 par 100 eV par un transfert d'énergie à partir des états excités du Xe ($G \sim 2.5$) et par des électrons subexcités ayant des énergies entre 4.3–8.3 eV ($G \sim 1.5$) dans le Xe. Les résultats obtenus à partir du piégeage des électrons thermiques par SF_6 confirment les résultats obtenus antérieurement à l'effet que les gaz inertes sont inefficaces pour modérer des électrons aux énergies thermiques. A des rapports de concentration de $[SF_6]/[HBr]$ élevés, SF_6 interfère avec des réactions produisant de l'hydrogène mais n'impliquant pas des électrons.

[Traduit par le journal]

Introduction

A recent publication from this laboratory (1) reported on electron capture and hydrogen-forming reactions of HBr irradiated in mixtures with a number of gases. With C_2F_6 and CO_2 the ionisation and product yields were linear functions of the stopping power fractions of HBr and the added gas. However, for HBr–Xe mixtures there was a departure from this relatively straightforward behaviour and evidence for energy transfer between excited species of the two components was obtained. Here we present and discuss the results for the xenon mixtures in detail.

[1]Research supported by NRCC 3571.

Experimental

Xenon research grade (99.995% purity) was obtained from the Matheson Company. It was further purified in the vacuum line by trap-to-trap distillation from 170 to 70 K. Purified gas was stored in a bulb attached to the mercury-free preparation line. Details of other materials used, purification methods, irradiation procedures and equipment, ion current measurements, hydrogen analysis and dosimetry determinations were essentially the same as described previously (1).

Results

Ionisation Yields

The yields of ions per 100 eV of radiation energy absorbed in the HBr–Xe mixtures, G_m^i, are plotted in Fig. 1 as a function of Z, the stopping power fraction of HBr. As used in

Can. J. Chem. Downloaded from www.nrcresearchpress.com by 210.87.254.5 on 09/05/12
For personal use only.

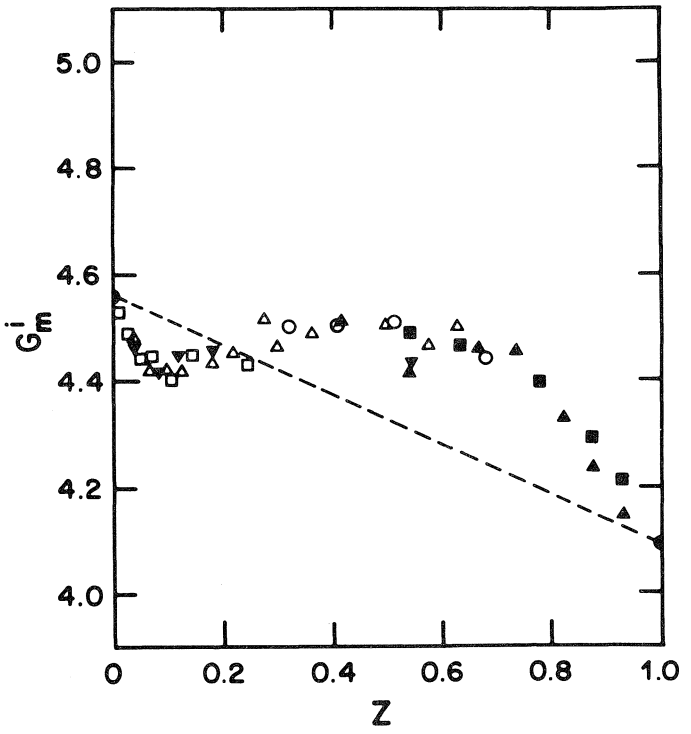

FIG. 1. Ionization yields, G_m^i in Xe–HBr mixtures plotted as a function of Z, the stopping power fraction of HBr: □, Xe 550 torr and HBr 10–550 torr; ▼, Xe 400 torr and HBr 25–675 torr; △, Xe 200 torr and HBr 10–480 torr; ○, Xe 100–450 torr and HBr 300 torr; ■, Xe 25–200 torr and HBr 500 torr; ▲, Xe 10–500 torr and HBr 200 torr; ●, pure components.

ref. 1 and previously defined (2) this quantity is equal to $(1 + \overline{\rho_{HBr}^{Xe}} P_{Xe}/P_{HBr})^{-1}$. Here $\overline{\rho_{HBr}^{Xe}}$ is the ratio of the weighted mean stopping powers of xenon and HBr taken from ref. 2, while the quantities P_{Xe} and P_{HBr} are the partial pressures of xenon and HBr in the mixture.

The complex variation of G_m^i with increasing Z in Fig. 1 is in marked contrast to the linear dependence on Z, which was observed for G_m^i in HBr–CO_2 and HBr–C_2F_6 mixtures with the same apparatus (1). Its interpretation in terms of interactions between highly excited states of xenon and HBr is given in the Discussion section.

Hydrogen Yields

The points on line A in Fig. 2 are total hydrogen yields plotted against Z. Since every electron produced by ionisation forms a molecule of hydrogen (3), one can obtain the yields of hydrogen from species other than e by subtracting the values of G_m^i in Fig. 1 from the total hydrogen yields for the same Z. These yields are shown by the points on line B in Fig. 2. The significance of the other lines is explained later.

Effects of SF_6

As shown in ref. 1 the rate controlling step in the mechanism through which thermal electrons form hydrogen is second order in HBr. It can be represented by [1],

[1] $$e + 2HBr \rightarrow H + BrHBr^-$$

since hydrogen atoms react stoichiometrically with HBr to form H_2 and Br. The contribution $G(H_2)_{e,t}$ of thermal electrons to hydrogen production in the presence of an electron scavenger S, like SF_6, is given by expression [2]

[2] $$G(H_2)_{e,t} = G_m^s\{1 + k_3[S]/k_1[HBr]^2\}^{-1}$$

where G_m^s is the yield of thermal electrons in the mixture and k_3 the rate constant of reaction 3.

[3] $$e + S \rightarrow S^-$$

Due to this competition $G(H_2)$ from HBr–Xe mixtures is suppressed to a plateau for $[SF_6]$/

Can. J. Chem. Downloaded from www.nrcresearchpress.com by 210.87.254.5 on 09/05/12
For personal use only.

TABLE 1. Hydrogen yields from reactions of hot and thermal electrons in mixtures of HBr with xenon

[HBr] (molecules cm^{-3})	[Xe]/[HBr]	H_2 molecules per 100 eV from: Hot ([4] e+HBr→)	Thermal ($=G_m^s$)[a] ([1] e+2HBr→)	Total ($=G_m^i$)[b]	Fraction of subexcitation electrons thermalised ($=G_m^s/G_m^i$)
6 to 22×10^{18}	0	1.1	3.0	4.0_9	0.7_3
6×10^{18}	0.6	1.8	2.7	4.5_0	0.6_1
3.9×10^{18}	0.8	1.5	3.0	4.4_7	0.6_7
1.6×10^{18}	4	1.6	2.8	4.4_3	0.6_3

[a]Determined from scavenging experiments with $[SF_6]/[HBr]$ in the range 0 to 5×10^{-2}. Uncertainties are ±0.2 per 100 eV.
[b]Uncertainties are $\pm0.0_2$ per 100 eV.

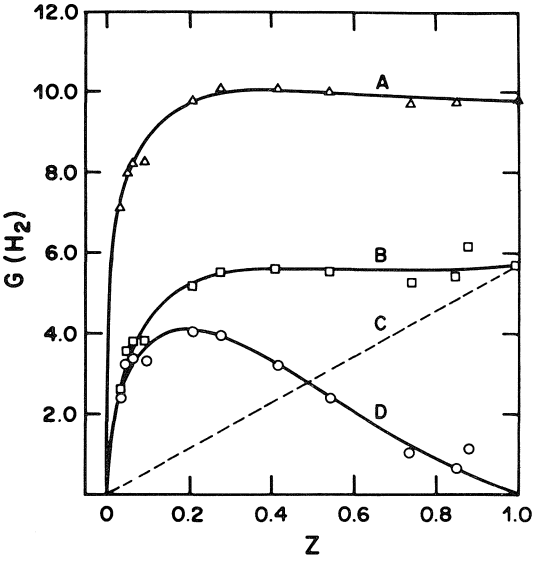

FIG. 2. Hydrogen yields, $G(H_2)$ in Xe–HBr mixtures plotted as a function of Z, the stopping power fraction of HBr: A, total H_2 yield; B, total $H_2 - G_m^i$; C, H_2 yield in HBr alone from processes other than electron capture; D, net H_2 yield from sensitisation by Xe, obtained by subtracting C from B.

[HBr] = 0 to 0.01 as exemplified in Fig. 3(*a*), the data for which are taken from ref. 1 for [HBr] and [Xe] = $1.6_2\times10^{18}$ and 6.48×10^{18} molecules cm^{-3}, respectively. The net reduction is less than the total yield of electrons given by G_m^i, because the cross section for reaction 4 is large enough that about 30% of the subexcitation electrons with initial kinetic energy above the reaction threshold are captured before they cool to thermal energy (~0.04 eV at 298 K). In this study we investigated the effect of [Xe]/[HBr] on this fraction. G_m^s was determined from experiments with SF_6, corrections being made for the removal of hot electrons by this scavenger (1). The results are presented in Table 1.

[4] $\quad e + HBr \rightarrow H + Br^-$

As shown by the data in Fig. 3(*a*) SF_6 scavenges essentially all thermal electrons for $[SF_6]/[HBr]$ about 0.02 and thereafter $G(H_2)$ decreases only slowly up to $[SF_6]/[HBr] = 0.05$. In this study higher $[SF_6]/[HBr]$ ratios were used to determine whether reaction 4 could be suppressed as well as [1]. The results for a mixture with [HBr] and [Xe] equal to 1.3×10^{18} and 1.78×10^{19} molecules cm^{-3} respectively are shown in Fig. 3(*b*). The upper dashed line at a $G(H_2)$ value of 5.3 molecules per 100 eV is the yield expected for complete scavenging of thermal electrons. The lower dashed line shows the yield calculated by subtracting G_m^i from the total $G(H_2)$ and is the residual hydrogen when reactions 1 and 4 are both suppressed. It is seen that SF_6 was able to reduce $G(H_2)$ below 5.3 molecules per 100 eV, which implies that it does compete with [4]. However, the points for $[SF_6]/[HBr] \geq 0.48$ lie substantially below the lower dashed line, indicating that hydrogen forming processes other than [1] and [4] are also effected at these large SF_6 concentrations. We shall return to this point later.

Discussion

Ionisation Processes

Ionisation in the inert gases arises mainly from transitions of the monatomic species to ionic or auto-ionising states (4, 5). For xenon representative equations are

[5] $\quad Xe \rightsquigarrow Xe^+ + e$

[6] $\quad Xe \rightsquigarrow Xe^a$

Can. J. Chem. Downloaded from www.nrcresearchpress.com by 210.87.254.5 on 09/05/12
For personal use only.

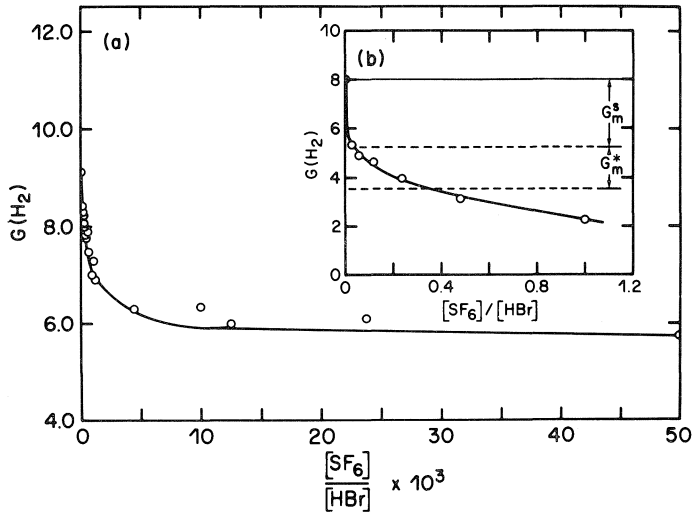

FIG. 3. Effect of SF_6 on hydrogen yields for mixtures of Xe and HBr: $G(H_2)$ *vs.* $[SF_6]/[HBr]$ for: (*a*) 200 torr Xe and 50 torr HBr, dose rate = 2.4×10^{18} eV g^{-1} h^{-1}, and (*b*) 40 torr HBr and 550 torr Xe at higher SF_6 concentrations.

[7] $$Xe^a \longrightarrow Xe^+ + e$$

where Xe^a symbolises an auto-ionising state. Dimer ions can be formed in three body reactions

[8] $$Xe^+ + 2Xe \rightarrow Xe_2^+ + Xe$$

for which $k_8 = 3 \times 10^{-31}$ cm^6 $molecule^{-1}$ s^{-1} in xenon (6). However, some dimer species are also produced by the Hornbeck–Molnar mechanism, involving reactions 9 and 10 (7).

[9] $$Xe \text{-}\wedge\!\!\wedge\!\!\rightarrow Xe^{**}$$

[10] $$Xe^{**} + Xe \longrightarrow Xe_2^+ + e$$

For xenon [9] has a threshold of 11.16 eV (4). The cross section for Xe** production by electron impact peaks sharply about 2 eV above this and then falls, until above 60 eV it decreases only slowly with electron energy (8). The magnitude of k_{10} from mass spectrometric measurements (8) is $9 \times 10^{-14}/\alpha$ for 70 eV impacting electrons and $9 \times 10^{-13}/\alpha$ for 13 eV impacting electrons.[2] Here α is $\sigma_9/(\sigma_5 + \sigma_6)$. If one assumes $\alpha \simeq 0.003$ and $\simeq 0.03$ for 70 eV and E maximum respectively as in argon (8) then $k_{10} \simeq 3 \times 10^{-11}$ cm^3 $molecule^{-1}$ s^{-1}.

[2]Photoionisation studies indicate a large number of Hornbeck–Molnar states with varying magnitudes of k_{10} (7) and excitation cross sections. The values from electron impact excitation would be weighted mean values and are more appropriate to radiation chemistry.

In the presence of HBr electrons will be captured in reactions 1 and 4 and HBr^+ ions will be produced both directly and by auto-ionisation processes (9). The HBr^+ ions may also be expected from the charge transfer reaction 11, since the ionisation potentials of xenon and HBr are

[11] $$Xe^+ + HBr \rightarrow Xe + HBr^+$$

respectively 12.1_3 (4) and 11.6_2 eV (10). Since the ionisation potential of Xe_2^+ ($\simeq$ 11.2 eV (4)) is too small for charge transfer to HBr, these ions probably become clustered. However, if k_{11} is of the order of a typical ion molecule rate constant and greater than 10^{-10} cm^3 $molecule^{-1}$ s^{-1}, it can be shown that reaction 11 would dominate over [8] for all the mixtures used here. Because of this and the fact that the Hornbeck–Molnar states are quenched by HBr (see below), the ions undergoing recombination in the presence of xenon under our conditions should be the same as those in pure HBr except that clustering would be less extensive.

We turn now to the quenching of the Hornbeck–Molnar states and other processes which may affect the total yields of ions in the system. Previous observations of decreases in G_m^i for the other rare gases in the presence of molecular gases at low stopping power fraction have been attributed to quenching of the Hornbeck–Molnar states (11). Following Klots' treatment the cor-

Can. J. Chem. Downloaded from www.nrcresearchpress.com by 210.87.254.5 on 09/05/12
For personal use only.

responding reactions in the xenon–HBr system are

[12] $Xe^{**} + HBr \rightarrow$ Ion pairs

[13] $Xe^{**} + HBr \rightarrow$ Neutral products

with k_{13} obviously finite. Also the magnitude of G^i_m should be given by expression [14]

$$[14]\quad G^i_m = G^i_{Xe}\epsilon_{Xe} + G^i_{HBr}\epsilon_{HBr} - g(Xe^{**})\epsilon_{Xe}\left[\frac{k_{13}[HBr]}{k_{10}[Xe] + (k_{12} + k_{13})[HBr]}\right]$$

which can be rearranged to [15] with G^{ic}_m replacing $(G^i_{Xe}\epsilon_{Xe} + G^i_{HBr}\epsilon_{HBr})$.

$$[15]\quad \frac{\epsilon_{Xe}}{G^{ic}_m - G^i_m} = \frac{1}{g(Xe^{**})}\left\{\frac{k_{12} + k_{13}}{k_{13}} + \frac{k_{10}[Xe]}{k_{13}[HBr]}\right\}$$

Application of [15] to the results for $Z < 0.1$ in Fig. 1 necessitates the calculation of the effective electron fractions ϵ_{Xe} and ϵ_{HBr}. Klots used a "fitting procedure" to obtain the best values of these functions, $g(Xe^{**})k_{13}(k_{12} + k_{13})^{-1}$ and $k_{10}(k_{12} + k_{13})^{-1}$ from his observations, but the behaviour of G^i_m above $Z = 0.2$ is too complex for that procedure to be effective here. Two different approaches were therefore used: (*a*) ϵ_{Xe} was taken as unity and ϵ_{HBr} as zero, which is not a serious approximation, since Z is ≤ 0.11 for the [Xe]/[HBr] range used, and (*b*) ϵ_{Xe} and ϵ_{HBr} were assumed to be equal to the stopping power fractions $(1 - Z)$ and Z respectively. Figure 4 presents the results plotted in accord with the first approach. The fact that the data for the three pressures are accommodated on the same line is consistent with a competition between HBr and xenon for the excited Xe** species. If for example HBr were competing against reaction 7 for Xe^a, pressure independent plots would not be expected.

The intercept in Fig. 4 leads to $g(Xe^{**})k_{13} \times (k_{12} + k_{13})^{-1} = 0.2_8$, while that from the plot using the second approach was 0.2_0. Thus, given that $k_{13}(k_{12} + k_{13})^{-1} \leq 1$, $g(Xe^{**})$ is ≥ 0.20. Since the value of α is expected to be small we may assume it to be equal to $g(Xe^{**})/G^i_{Xe}$, which in fact gives the weighted mean value for the electron energy distribution in the present radiolysis. Thus from the present data $\alpha \geq 0.2 \times 4.6^{-1}$ or ≥ 0.04, which may be compared with $\alpha \geq 0.27$, ≥ 0.04, and ≥ 0.11 reported by Klots

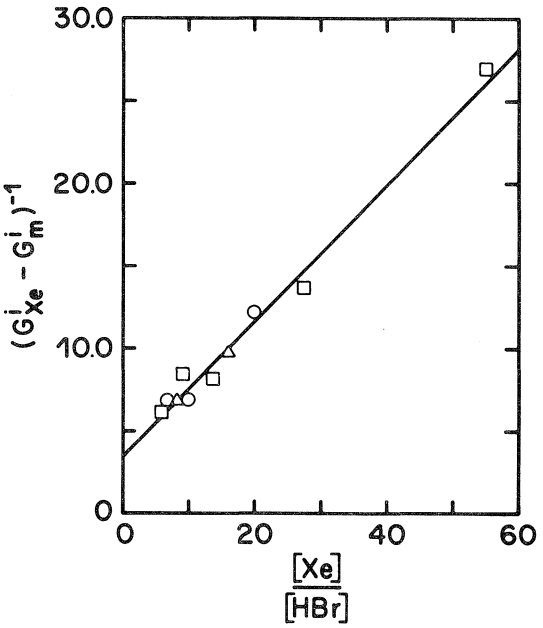

FIG. 4. Reciprocal of $(G^i_{Xe} - G^i_m)$ *vs.* [Xe]/[HBr] for mixtures of Xe and HBr with different pressures of Xe; □, 550 torr; △, 400 torr; ○, 200 torr.

for neon, argon, and krypton respectively. From the ratios of the slopes to the intercepts in Fig. 4, $k_{10}(k_{12} + k_{13})^{-1}$ was 0.1 and approach (*b*) gave the same value. This ratio lies in the same range (0.06 to 0.7) as those reported for quenching of the corresponding states of the other rare gases (11). Also, if one assumes $k_{10} \simeq 3 \times 10^{-11}$ cm^3 $molecule^{-1}$ s^{-1} as estimated above, then $(k_{12} + k_{13}) \simeq 3 \times 10^{-10}$ cm^3 $molecule^{-1}$ s^{-1}, which is similar to 6×10^{-10} cm^3 $molecule^{-1}$ s^{-1} for quenching of the $Xe^*(^3P_2)$ metastable by HBr (12).

The broad maximum in G^i_m occurring near $Z = 0.5$ is more difficult to interpret than the decrease in ionisation for Z in the range 0 to 0.1. Taken at face value it suggests that a highly excited state of HBr with a yield of about 0.2 per 100 eV produces neutral products, but is capable of forming ions in the presence of xenon. This could involve either a chemi-ionisation reaction with xenon or collisionally induced ionisation of the HBr excited state. The present data do not permit further conclusions, but an investigation of the ion yields by the more precise method of total absorption of α or β particles (see, for example, ref. 11) might reveal further details relating to these processes. Also a

Can. J. Chem. Downloaded from www.nrcresearchpress.com by 210.87.254.5 on 09/05/12
For personal use only.

Can. J. Chem. Downloaded from www.nrcresearchpress.com by 210.87.254.5 on 09/05/12
For personal use only.

mass spectrometric search for chemi-ionisation would be of interest.

Hydrogen Yields from Electron Capture Reactions

As stated in the Results section some subexcitation electrons form hydrogen via reaction 4 while cooling through the 0.8 to 0.15 eV range where the cross section for resonance capture is significant. The remainder are captured in [1] after thermalisation. As seen from Table 1 the fraction of electrons G_m^s/G_m^i reacting at thermal energies does not increase with addition of xenon as it did for addition of CO_2, where (G_m^s/G_m^i) rose from 0.7_3 for pure HBr to 0.8_0 for $[CO_2]/[HBr] = 4$ (1). This was attributed to the additional moderating effect of CO_2. The lack of evidence for a moderating effect by xenon is in keeping with the large mass and absence of degrees of freedom which the electron could excite. It is also consistent with the almost negligible electron thermalisation rates observed (13) in the heavy inert gases.

At this point it is important to recognize that E_0, the energy of the lowest excited state, lies at 8.3_1 eV in xenon (4) while in HBr it is at about 4.3 eV (14). Thus the energy spectrum of the subexcitation electrons is expected to be different in the two gases. For example, using the approximate formula $\overline{S\epsilon} \simeq E_0\{2 + E_0/I\}^{-1}$ (15), where I is the ionisation potential, one finds average subexcitation energies of $\overline{S\epsilon} = 2.5$ eV in HBr and 3.1 eV in xenon. The shift toward higher energy in xenon should lead to a small increase in the yield per 100 eV of subexcitation electrons with energy above the 0.3 eV maximum of the cross section for reaction 4, and this is probably the reason for the fact that G_m^s/G_m^i in Table 1 in fact shows a slight tendency to *decrease* with [Xe]/[HBr].

Hydrogen Yields from Subexcitation Electrons with Initial Kinetic Energy between 4.3 and 8.3 eV and from Xenon Excited States

Line C in Fig. 2 is the yield of hydrogen expected from processes other than electron capture occurring in HBr calculated on the assumption that the energy absorbed by the HBr molecules in the mixture is a linear function of Z. These other processes are mainly dissociations of excited species (9). Curve B is the yield actually observed in the mixtures. The difference, which is shown by curve D, is the net extent of sensitisation by xenon.

Because the energy dependence of excitation cross sections may be complex and because of the significant roles of secondary and tertiary electrons, the partitioning of energy in a two component mixture need not necessarily be linear in Z calculated for the initial electron energy spectrum as for line C.[3] However, the extent of sensitisation observed here is too large to be due simply to a failure of Z to describe the energy partitioning. In our view it must be attributed primarily to energy transfer to HBr from neutral xenon excited states and to the excitation of HBr by electrons which are below E_0 for xenon but above it for HBr. Using the experimental points from Fig. 6 of Opal, Peterson, and Beaty (16) it was estimated that roughly 25% of the electrons formed by ionisation of xenon with 500 eV electrons would have energies in that range. This percentage corresponds to a yield per 100 eV of 1.2. A higher yield of electrons in the 4.3 to 8.3 eV region may occur in the radiolysis due to the presence of lower energy secondary and tertiary electrons in the degradation spectrum (see, for example, the discussion of the importance of excitations by slow electrons in ref. 15). However, it seems very unlikely that this would exceed 2 per 100 eV. These electrons would be expected to possess relatively large cross sections (*cf.* data for HCl (17)) for exciting the low lying Q $^3\Pi_1$, $^1\Pi$ and $^3\Pi_{0^+}$ states of HBr (18–20),

[16] $\quad e(\text{energy} > 4.3\text{ eV}) + HBr \rightarrow e + HBr^*\ Q(^1\Pi,^3\Pi)$

which dissociate (18) and produce hydrogen through reaction 18 (9).

[17] $\quad HBr^* \rightarrow H + Br$

[18] $\quad H + HBr \rightarrow H_2 + Br$

A yield of 1 to 2 molecules per 100 eV may therefore result from [16] through [18].

A rudimentary estimate of the total number of xenon excited states formed per 100 eV may be gained from the energy balance (15). Thus, taking $G_{Xe}^i = 4.56_6$, the average energy of transitions to ionic states (including those via [6]–[7] and [9]–[10] as 13.4 eV and $\overline{S\epsilon} = 3.1$, the energy consumed in ionisations in pure xenon is 75 eV ($= 4.56_6 \times (13.4 + 3.1)$), per total energy expenditure of 100 eV. Since the mean energy per

[3]See ref. 11 and references cited therein for discussions of energy deposition in mixtures.

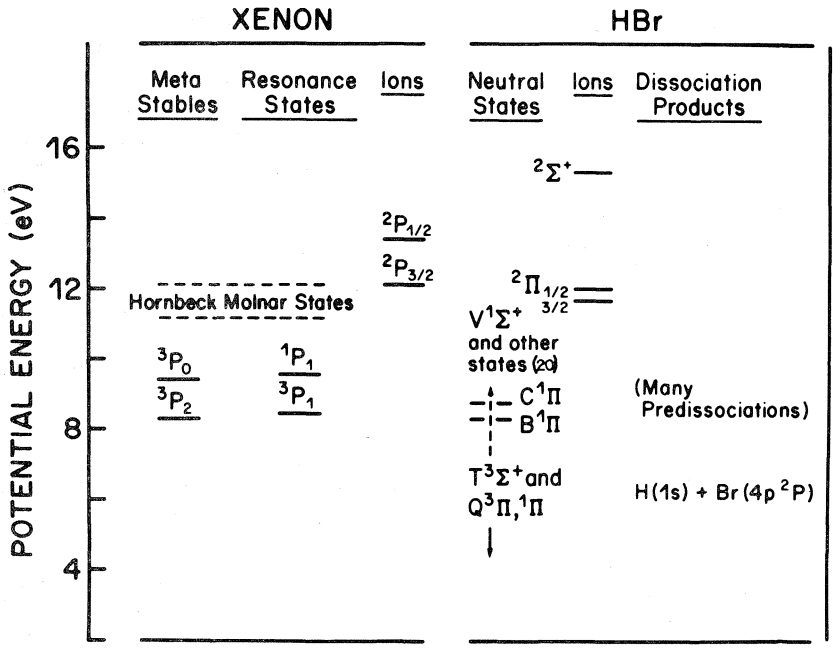

FIG. 5. Energies of xenon and HBr. Data for xenon from ref. 4 and for HBr from refs. 9, 14, and 18 to 20.

excitation must be near 9 eV the total number of excited states should be about 2.7 per 100 eV. This is much lower than ~5.0 assumed in ref. 21, but in better agreement with 1.9 per 100 eV (g(singlets) $\simeq$ 1.5 and g(triplets) $\simeq$ 0.4) estimated by Sato, Okazaki, and Ohno using binary encounter theory (22). As shown in Fig. 5 the energies of all the neutral excited states are large enough to cause dissociation of HBr and hydrogen formation. The maximum sensitisation of 4 molecules of hydrogen per 100 eV seen in Fig. 2 can therefore be explained by g(singlet) + g(triplet) ~ 2.5 and g^e_{subex} (4.3 to 8.3 eV) $\simeq$ 1.5 per 100 eV in xenon, provided the energy transfers from Xe* to HBr are sufficiently rapid. If the transfer cross sections for all xenon states are similar to 6×10^{-10} cm^3 molecule^{-1} s^{-1} measured for Xe $^3P_0$ quenching by HBr (12), then the xenon excited state lifetimes at [HBr] = 3×10^{18} molecules cm^{-3} would be ~0.6 ns, which is about one fifth of the radiative lifetimes of the singlet states (~3.5 ns (4, 23)). On these grounds energy transfer *is* therefore likely to be by far the most important mechanism of Xe* loss. It will be made more efficient by radiation trapping (4, 24).

Beyond the maximum, curve D in Fig. 2 runs linearly down to $G(H_2) = 0$ at $Z = 1$, which indicates the decreasing contribution of xenon states to the radiolysis. The overall behaviour of curve D in Fig. 2 bears a strong resemblance to that of the H_2S–Xe system, where the maximum $G(H_2)$ from energy transfer is near 5 for both γ (21, 25, 26) and α radiolysis (27). The tendency for a slightly higher value than in HBr may be due to a contribution from reaction 19

[19] $$H_2S + Xe^* \rightarrow 2H + S + Xe$$

which is energetically feasible (25) and would lead to two molecules of hydrogen per Xe* (27). However, the general similarities of the H_2S– and HBr–Xe systems imply [g(Xe*) + g^e_{subex} (4.3 to 8.3 eV)] = 4 to 5 per 100 eV.

As pointed out in the Results section the values of $G(H_2)$ for $[SF_6]/[HBr] \geq 0.48$ show that SF_6 is interfering with hydrogen-forming reactions other than [1] and [4]. Thus when it is used as an electron scavenger in the inert gas systems its concentration must be low relative to HBr (or other substrate molecules), and not just low relative to [Xe]. The present experiments do not show whether SF_6 is competing with HBr for Xe* states or for electrons in the 4.3 to 8.3 eV range. More information on their quench-

Can. J. Chem. Downloaded from www.nrcresearchpress.com by 210.87.254.5 on 09/05/12
For personal use only.

ing cross sections for Xe* states (the quenching cross section of HBr is about twice that of SF_6 for $Xe^*(^3P_2)$ (12)) and electron impact spectra near threshold should help to resolve this point. Competitions between H_2S and SF_6 for Xe* have already been considered in the H_2S–SF_6–Xe system (25).

1. S. S. NAGRA and D. A. ARMSTRONG. Can. J. Chem. **53**, 3305 (1975).
2. D. W. HUYTON and T. W. WOODWARD. Rad. Res. Rev. **2**, 205 (1970).
3. S. S. NAGRA and D. A. ARMSTRONG. Can. J. Chem. This issue.
4. B. BROCKLEHURST. Rad. Res. Rev. **1**, 223 (1968).
5. C. E. KLOTS. Fundamental processes in radiation chemistry. *Edited by* P. Ausloos, John Wiley, N.Y. 1968.
6. D. C. LORENTS, D. J. ECKSTROM, and D. HUESTIS. Stanford Research Institute Report SRI MP 73-2 Menlopark, California. 1973.
7. R. E. HUFFMAN and D. H. KATAYAMA. J. Chem. Phys. **45**, 138 (1966).
8. F. H. FIELD and J. L. FRANKLIN. J. Am. Chem. Soc. **83**, 4509 (1961); J. L. FRANKLIN. Adv. Chem. **72**, 1, (1968).
9. D. A. ARMSTRONG and C. WILLIS. Int. J. Radiat. Phys. Chem. **8**, 221 (1976).
10. K. WATANABE, T. NAKAYAMA, and J. R. MOTTL. J. Quant. Spectrosc. Radiat. Transfer, **2**, 369 (1962).
11. C. E. KLOTS. J. Chem. Phys. **46**, 3468 (1967).
12. J. E. VELAZCO and D. W. SETSER. Chem. Phys. Lett. **25**, 197 (1974).
13. J. M. WARMAN and M. C. SAUER, JR. J. Chem. Phys. **62**, 1971 (1975).
14. G. HERZBERG. Molecular spectra and molecular structure. I. Spectra of diatomic molecules. D. Van Nostrand. N.Y. 1950.
15. I. SANTAR and J. BEDNAR. Czech. Chem. Commun. **34**, 1 (1969).
16. C. B. OPAL, W. K. PETERSON, and E. C. BEATY. J. Chem. Phys. **55**, 4100 (1971).
17. R. N. COMPTON, R. H. HUEBNER, P. W. REINHARDT, and L. G. CHRISTOPHOROU. J. Chem. Phys. **48**, 901 (1968).
18. R. S. MULLIKEN. Phys. Rev. **51**, 310 (1937).
19. R. F. BARROW and J. G. STAMPER. Proc. Roy. Soc. A, **263**, 277 (1961).
20. M. L. GINTER and S. G. TILFORD. J. Mol. Spectrosc. **37**, 159 (1971); **34**, 206 (1970).
21. M. AHMAD, D. W. HUYTON, and T. W. WOODWARD. J. Chem. Soc. Faraday Trans. I, **68**, 1857 (1972).
22. S. SATO, K. OKAZAKI, and S. OHNO. Bull. Chem. Soc. Jpn. **47**, 2174 (1974).
23. P. G. WILKINSON. Can. J. Phys. **45**, 1715 (1967).
24. A. GEDANKEN, J. JORTNER, B. RAZ, and A. SZOKE. J. Chem. Phys. **57**, 3456 (1972).
25. M. FORYS. Radiation Eff. **25**, 111 (1975).
26. M. FORYS, A. JOWKO, and I. SZAMREJ. J. Phys. Chem. **80**, 1035 (1976).
27. K. JEZIERSKA. Nukleonika, **16**, 213 (1971).

Can. J. Chem. Downloaded from www.nrcresearchpress.com by 210.87.254.5 on 09/05/12
For personal use only.

Thermodynamics of basic ionization of some aminoethers in water

SHEILA TERESA LOBO[1] AND ROSS ELMORE ROBERTSON
Department of Chemistry, University of Calgary, Calgary, Alta., Canada T2N 1N4

Received March 15, 1976

SHEILA TERESA LOBO and ROSS ELMORE ROBERTSON. Can. J. Chem. **54**, 3600 (1976).

Basic ionization constants (K_b) of 2-methoxyethylamine, 3-methoxypropylamine, and bis-2-methoxyethylamine in water have been measured as a function of temperature between 5 and 45 °C, thus enabling values of ΔG_b^0, ΔH_b^0, ΔS_b^0, and ΔC_{pb}^0 to be calculated. The results conform with the ability of the ether function to destroy hydrophobicity in water.

SHEILA TERESA LOBO et ROSS ELMORE ROBERTSON. Can. J. Chem. **54**, 3600 (1976).

On a mesuré, en fonction de la température entre 5 et 45 °C, les constantes d'ionization basiques (K_b) de la méthoxy-2 éthylamine, de la méthoxy-3 propylamine et de la bis-méthoxy-2 éthylamine dans l'eau; on a donc pu calculer les ΔG_b^0, ΔH_b^0, ΔS_b^0 et ΔC_{pb}^0. Les résultats sont en accord avec l'habilité de la fonction éther de détruire l'hydrophobicité de l'eau.

[Traduit par le journal]

Introduction

Some time ago Rossall and Robertson (1) reported that the substitution of a *p*-MeO group in benzenesulfonyl chloride resulted in a more positive temperature coefficient of the enthalpy of activation ($\Delta C_p^{\neq}$) of the solvolysis reaction in water than would be expected from other data (2). This positive shift in $\Delta C_p^{\neq}$ was attributed to a temperature dependent solvation effect, a rationalization supported by reference to corresponding effects found for ΔC_{pa}^0 for the aqueous ionization of anisic acid (3, 4). Further support for this view is apparent in the hydrolysis of 3-methoxybenzyl nitrate (5).

We were unable to find corresponding evidence for the ionization of aminoethers, although there had been an extensive investigation of the amino acids because of their obvious relation to biological processes (3, 6). Beyond the latter, and certain simple alkyl amines, careful investigations of the thermodynamics of ionization of substituted amines in water appear to be limited to certain diamines and amino-alcohols. Values of ΔG_a^0, ΔH_a^0, and ΔS_a^0 have been reported for 1,2-, 1,3-, 1,4-, 1,5-, and 1,6-diaminoalkanes by Paoletti and co-workers (7). Everett, Landsman, and Pinsent (8) determined the thermodynamic parameters for the ionization of 1,2- and 1,6-diaminohexane in water, while a similar study of amino-alcohols has been made by Bates and co-workers (9–12) and by Timimi and Everett (13). The latter found ΔC_{pa}^0 values to be less positive for amino-alcohols than the corresponding alkylamines, a result which was consistent with the expected antagonism of the hydroxyl group to hydrophobic hydration (14). However, some amino-alcohols gave unexpectedly large negative ΔC_{pa}^0 values which were not explained. Intramolecular hydrogen bonding has been suggested, without proof, as a possibility for the reduced value of ΔC_{pa}^0 for 2-hydroxyethylamine compared to ethylamine. In view of the proposed temperature dependent solvation effect on the MeO-group observed in our kinetic studies noted above and in the ionization of substituted benzoic acids (3), the temperature dependence of the ionization of three aminoethers, *i.e.* 2-methoxyethylamine, 3-methoxypropylamine, and bis-2-methoxyethylamine, were studied to determine the corresponding value of ΔC_{pa}^0 in water. In the kinetic examples and in the substituted benzoic acid equilibria the MeO-group was attached directly to a mobile system and changes in the interaction between water and the methoxy group with temperature were transmitted more directly to the seat of reaction than in the present series. The consequence of this structural difference on ΔC_{pa}^0 was not foreseen.

We report here the results of the determination of pK_b for the noted aminoethers and the derived thermodynamic parameters ΔG_b^0, ΔH_b^0, ΔS_b^0, and ΔC_{pb}^0 between 5 and 45 °C.

Experimental

Details of the apparatus and technique of the con-

[1]Present address: Istituto di Chimica Fisica, Università di Pisa, 56100 Pisa, Italia.

Can. J. Chem. Downloaded from www.nrcresearchpress.com by 210.87.254.40 on 09/05/12
For personal use only.

Can. J. Chem. Downloaded from www.nrcresearchpress.com by 210.87.254.40 on 09/05/12
For personal use only.

ductance–dilution method used have been described elsewhere (15, 16).

The aminoethers used were commercially available (Chemicals Procurement Laboratories Inc.) and were purified by standard methods before use. This involved refluxing over calcium hydride for 48 h, distilling under a nitrogen atmosphere, and redistilling the middle fraction under nitrogen. The purity of the amines was checked by gc using three different types of columns: (*a*) 6 ft × ¼ in. Chromosorb 103 (specifically useful for amine analysis), 80/100 mesh, (*b*) 6 ft × ¼ in. 20% Triton-x/305 on High Performance Chromosorb W, 80/100 mesh, (*c*) 6 ft × ¼ in. UCW98 on High Performance Chromosorb W, 80/100 mesh. Mass spectral and nmr analyses were also carried out and compared with literature values where possible. In no case were significant impurities found.

The determination of K_b involves the use of limiting equivalent conductances, Λ_0, for the aminoether hydrochlorides. The hydrochlorides were prepared by passing dry hydrogen chloride gas (Matheson of Canada Ltd.) through an ethereal solution of the pure amine. Since the salts were very deliquescent, they were transferred to a rotary evaporator to remove most of the ether. The last traces of ether and water were removed by short path distillation under high vacuum. In the case of the salt of bis-2-methoxyethylamine, recrystallization was attempted from a toluene–ethanol mixture under anhydrous conditions. Large needles were obtained. A special apparatus was used for filtration under anhydrous conditions. The last traces of toluene were removed by high vacuum. Mass spectral, gc, and nmr analyses of the hydrochlorides showed no traces of impurities.

Results and Discussion

In Table 1 we report[2] K_b as a function of temperature for 2-methoxyethylamine as a typical data set. Although K_b values were determined on the molar scale, they were converted to the molal scale (17). The % difference reported in column 3 is

$$[1] \quad \{[K_b(\text{obsd.}) - K_b(\text{calcd.})]/K_b(\text{obsd.})\} \times 100$$

where K_b(calcd.) is obtained by fitting the experimentally determined K_b values and temperatures to an equation of the type

$$[2] \quad \log K_b = A + B/T + C \log T$$

using the method of Clarke and Glew (18). The method of evaluation of K_b from the Shedlovsky–Kay equation (19) has been given elsewhere (15–17). In Table 2 are reported the values of the constants of [2]. The thermodynamic parameters ΔG_b^0, ΔH_b^0, ΔS_b^0, and ΔC_{pb}^0, derived by use of [2] for 2-methoxyethylamine, bis-2-methoxyethylamine, and 3-methoxypropylamine are reported in Table 3. Except for pK_a values for 2-methoxyethylamine and 3-methoxypropylamine, no thermodynamic parameters were available in the literature for comparison. It was of interest to compare the parameters of the aminoethers with related substituted amines, *e.g.* 2-OH-ethylamine and ethylenediamine as well as simple aliphatic amines. The relevant data are reported in Table 4. As most of the data reported in the literature are for the acid ionization process it was necessary to convert the data obtained by us to that for the corresponding acid ionization process

$$[3] \quad BH^+(aq) \rightleftharpoons B(aq) + H^+(aq)$$

by combining thermodynamic parameters for the dissociation of water with those for the basic ionization process. The values used for water were from a critical assessment of data by Olofsson and Hepler (20). The temperature chosen for comparison is 25 °C, because most data have been measured at this temperature. We are aware of inversion of acidities of carboxylic acids with increase in temperature (21) and of triethylamine compared with cyclohexyl-, hexyl-, and di-*n*-propylamines (22), but in lieu of a better alternative, 25 °C seems to be the best

TABLE 1. Ionization constants for 2-methoxyethylamine for a series of temperatures in water by a conductance method

T (°C)	K_b(obsd.)×10^5 (molal)	% difference	Λ_0 (cm^2 Ω^{-1} mol^{-1})
4.999	1.991	+0.17	157.10
5.001	1.985	−0.14	157.11
10.011	2.116	−0.47	176.88
10.014	2.123	−0.14	176.89
15.003	2.253	+0.08	197.01
20.001	2.362	−0.02	217.45
20.002	2.364	+0.06	217.45
25.010	2.462	+0.14	238.32
25.011	2.457	−0.06	238.32
30.005	2.543	+0.21	259.47
30.007	2.537	−0.03	259.48
35.000	2.594	−0.23	280.94
35.001	2.596	−0.16	280.94
39.984	2.649	+0.14	302.65
40.016	2.642	−0.14	302.79
44.870	2.675	+0.06	324.21
45.019	2.676	+0.07	324.86

[2]Corresponding data for the ionization of bis-2-methoxyethylamine and 3-methoxypropylamine are available, at a nominal charge, from the Depository of Unpublished Data, CISTI, National Research Council of Canada, Ottawa, Canada K1A 0S2.

TABLE 2. Empirical constants* for interpolation of basic ionization constants

Amine	A	B	C
2-Methoxyethylamine	66.36874	−3394.104	−24.08398
Bis-2-methoxyethylamine	82.45507	−4518.317	−29.37656
3-Methoxypropylamine	72.49270	−3497.024	−26.16898

*For the equation $\log_{10} K_b = A + B/T + C \log_{10} T$ where T is in K and between 5 and 45 °C. See footnote, Table 2 of ref. 17.

TABLE 3. Thermodynamic parameters for the basic ionization of aminoethers in water as a function of temperature

Amine	T (°C)	ΔG_b^0 (cal mol^{-1})	ΔH_b^0 (cal mol^{-1})	ΔS_b^0 (cal mol^{-1} deg^{-1})	ΔC_{pb}^0 (cal mol^{-1} deg^{-1})
2-Methoxyethylamine	5	5983.9 ± 0.5	2218 ± 17	−13.54 ± 0.06	
	25	6288.3 ± 0.3	1261 ± 5	−16.86 ± 0.02	−47.9 ± 0.8
	45	6656.9 ± 0.5	304 ± 18	−19.97 ± 0.06	
Bis-2-methoxyethylamine	10	7170.0 ± 0.7	4145 ± 32	−10.68 ± 0.11	
	25	7353.0 ± 0.5	3269 ± 9	−13.70 ± 0.03	−58.3 ± 2.1
	40	7580.2 ± 0.7	2394 ± 34	−16.56 ± 0.11	
3-Methoxypropylamine	5	5146.9 ± 0.6	1537 ± 23	−12.98 ± 0.08	
	25	5443.1 ± 0.4	492 ± 6	−16.59 ± 0.02	−52.0 ± 1.2
	45	5809.0 ± 0.7	−543 ± 26	−19.97 ± 0.08	

TABLE 4. A comparison of thermodynamic parameters for the acidic ionization of certain amines in water at 25 °C

Amine	pK_a*	ΔG_a^{0*} (cal mol^{-1})	ΔH_a^0 (cal mol^{-1})	ΔS_a^{0*} (cal mol^{-1} deg^{-1})	ΔC_{pa}^0 (cal mol^{-1} deg^{-1})	Reference
Ethylamine	11.155	15 219	13 710	−5.06	7.4	26
2-Methoxyethylamine	9.867	13 461	12 079	−4.64	−5.8	This work
Ethylenediamine	10.404	14 194	11 940	−7.56	9.4	26
Ethanolamine	9.975	13 608	12 080	−5.13	−1.2	9
Propylamine	11.046	15 069	13 840	−4.12	7.6	26
3-Methoxypropylamine	10.486	14 305	12 843	−4.90	−1.7	This work
Propanolamine	10.434	14 234	12 698	−5.15	17.5	26
Diethylamine	11.316	15 438	12 730	−9.08	15.1	26
Bis-2-methoxyethylamine	8.910	12 155	10 071	−6.99	4.6	This work
Diethanolamine	9.180	12 523	10 010	−8.43	12.1	26
Piperidine	11.429	15 592	12 642	−9.89	18.0	27
Morpholine	8.793	11 995	9 331	−8.93	11.5	26

*Corrected for symmetry.

compromise. This should be noted when examining small fluctuations in thermodynamic parameters. Another point worth mentioning before further discussion is the statistical or symmetry factor (23), because the higher the number of equivalent protons in the ammonium ion, the greater the probability of losing one. This correction only applies to pK_a, ΔG_a^0, and ΔS_a^0 values and with its inclusion only the intrinsic properties of the molecules and ions and their interaction with water are reflected in the ionization process.

Comparison of pK_a values of the aminoethers with related unsubstituted compounds (refer to Table 4) shows that the methoxy group has a weakening effect on basicity, as might be expected (24), and this effect is reduced with increasing separation from the amino group. However, a comparison with the effect of the hydroxy group on the amine is not as predicted

Can. J. Chem. Downloaded from www.nrcresearchpress.com by 210.87.254.40 on 09/05/12
For personal use only.

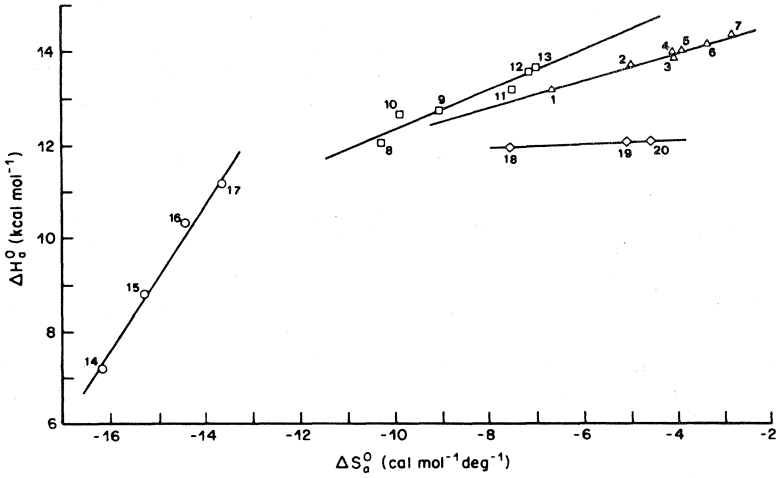

FIG 1. Plot of ΔH_a^0 *vs.* ΔS_a^0 for selected amines. (△) Primary amines (*1*, methylamine; *2*, ethylamine; *3*, propylamine; *4*, isopropylamine; *5*, *n*-butylamine; *6*, cyclohexylamine; *7*, *tert*-butylamine). (□) Secondary amines (*8*, dimethylamine; *9*, diethylamine; *10*, piperidine; *11*, di-*n*-propylamine; *12*, diisopropylamine; *13*, di-*n*-butylamine). (○) Tertiary amines (*14*, triethylenediamine; *15*, trimethylamine; *16*, triethylamine; *17*, quinuclidine). (◇) Substituted ethylamines (*18*, ethylenediamine; *19*, ethanolamine; *20*, 2-methoxyethylamine).

by the inductive effect. Although, on the basis of σ_I values (24), the 2-OH-ethylammonium ion is expected to be a stronger acid than the 2-MeO-ethylammonium ion, this was not found (pK_a 9.975 *vs.* 9.867). The difference is admittedly small and could be caused by the better solvation of the OH group, a suggestion consistent with solvent-sensitive substituent effects (25).

Since ΔG_a^0, ΔH_a^0, ΔS_a^0, and ΔC_{pa}^0 values for several aliphatic amines have been critically assessed by Jones and Arnett (26), an attempt (16) was made to correlate these parameters for simple aliphatic amines, some cyclic amines studied by us (27), and related substituted amines, after making corrections for symmetry. The latter was necessary because without it no distinct correlations have previously been made for the aqueous ionization of substituted anilinium ions (28), of substituted benzoic acids (29, 4), of phenols (3), of carboxylic acids (30), of thiols (31), or of amines (6), for ΔG_a^0 *vs.* ΔH_a^0, ΔG_a^0 *vs.* ΔS_a^0, and ΔH_a^0 *vs.* ΔS_a^0. No significant correlation was found for seven primary alkylamines or for six secondary amines for a ΔG_a^0 *vs.* ΔH_a^0 plot. However, an excellent correlation was obtained for five tertiary amines (correlation coefficient $r = 0.998$) and for three related substituted ethyl amines (—OMe, —OH, and —NH_2) with $r = 0.98$. The amines correlated are cited in the caption below Fig. 1 which is a plot of ΔH_a^0 *vs.* ΔS_a^0. The values of the thermodynamic parameters of the amines have been taken from the review article by Jones and Arnett (26), except for ethanolamine (9) and the cyclic amines (27), and have been corrected for symmetry where relevant. The lack of correlation in the primary alkylamines with respect to ΔG_a^0 *vs.* ΔH_a^0 is mainly due to ΔS_a^0 differences arising possibly from chain-stiffening (32). This usually gives rise to compensating changes in ΔH^0 and ΔS^0, a trend revealed in a plot of ΔH_a^0 *vs.* ΔS_a^0, for primary, secondary, and tertiary amines and substituted ethylamines (Fig. 1). Only in the case of the primary amines is there almost complete compensation which is evident from the slope of the plot (292 K). In contrast to the primary alkylamines which give no correlation for ΔG_a^0 *vs.* ΔH_a^0, the substituted ethylamines give good correlations for both ΔG_a^0 *vs.* ΔH_a^0 and ΔG_a^0 *vs.* ΔS_a^0 in spite of large ΔS_a^0 differences. Interestingly, the slope of the ΔG_a^0 *vs.* ΔS_a^0 plot is −248 K, which is close to −218 K, a value predicted by the Bjerrum electrostatic model (33) for proton ionization processes in water. This has not been found for substituted anilinium ions by Liotta and co-workers (28) who obtained a value of 1087 K, or by Christensen *et al.* (6) who obtained a value of −41 K for the

Can. J. Chem. Downloaded from www.nrcresearchpress.com by 210.87.254.40 on 09/05/12
For personal use only.

Can. J. Chem. Downloaded from www.nrcresearchpress.com by 210.87.254.40 on 09/05/12
For personal use only.

ionization of a variety of different primary ammonium ions, both values being nowhere close to the predicted value of −218 K. The failure of the Bjerrum model has been attributed (6) to a very small contribution from electrostatic effects and more important ones from specific solvation effects in the case of the ammonium ions. Since, in the dissociation of ammonium ions, the electrostatic contribution is primarily a result of charge–dipole interaction between the dissociating proton and the electric dipole of the neutral species, the presence of substituents should affect this interaction considerably and probably be a more dominant factor than specific solvation effects. This is evident for the substituted ethylamines from the good agreement with the prediction based on Bjerrum's model. The relationship of these amines to the unsubstituted primary amines and other aliphatic amines is illustrated in Fig. 1. From this figure and Table 4 a decrease in ΔH_a^0 is noted on progressing from the primary to the secondary to the tertiary amine, both for the substituted and unsubstituted amines, a trend in agreement with the inductive effect. The inductive effect of the methoxy and hydroxy groups is also evident in a comparison of the substituted amines with corresponding unsubstituted amines.

If, according to evidence cited by Timimi and Everett (13), solvent effects cause entropy to vary in an opposite sense to heat capacity, examination of ΔC_{pa}^0 in Table 4 should lead us to expect large increments in ΔS_a^0 compared to the unsubstituted compounds for the aminoethers, diamines, and amino-alcohols. Ethylenediamine and propanolamine definitely do not conform with this idea. As for the hydroxylamines, the results have been rationalized by Everett *et al.* The entropy value of morpholine compared to piperidine can also be explained. However, the methoxy group in 2-methoxyethylamine shows an unusually large negative value of −5.8 cal mol^{-1} deg^{-1} compared to the small positive increment in ΔS_a^0 of 0.42 cal mol^{-1} deg^{-1} found for ethylamine. It is apparent from the ΔC_{pa}^0 values that whereas ethylammonium ion becomes a weaker acid with increasing temperature, the 2-methoxyethylammonium ion becomes a stronger acid with respect to ΔH_a^0. In the work of Rossall and Robertson (1) which prompted this investigation, the effect of the methoxy group on the rate of hydrolysis of *p*-methoxybenzenesulfonyl chloride decreased with temperature: in the ammonium ion ionization the corresponding effect is increased with temperature.

Before attempting to rationalize the opposed effects of temperature on ΔH_a^0 and $\Delta H^{\ddagger}$ it will be useful to examine the corresponding effect in the case of the *meta*- and *para*-methoxy substituted benzoic acids. Relative to the parent compound, the *meta*-methoxy acid is a stronger acid, with a ΔC_{pa}^0 value of −23 cal mol^{-1} deg^{-1}, and becomes increasingly so with a rise in temperature. The ΔC_{pa}^0 value for the unsubstituted benzoic acid is −38 cal mol^{-1} deg^{-1} (3). The *meta*-methoxy group introduces some factor which increases the ΔC_{pa}^0 value. Rossall and Robertson have suggested that such a factor was a logical consequence of the effect of temperature on water structure and the reasonable assumption that the methyl group would tend to interfere with the interaction of water with the unshared electrons on the methoxy oxygen atom (35, 36). It is generally accepted that as the temperature increases, there is a gradual breakdown in water structure, with an increase in the number of unbonded water molecules (36). Accordingly, the methyl group in —OMe will offer less steric hindrance to the solvation of the oxygen atom in —OMe with an increase in temperature. Hence the interaction of —OMe with water will increase with temperature, and the effect of the group on the ionization process will decrease. This will result in the enhanced acid strength of the *meta*-methoxy benzoic acid relative to benzoic acid in the lower temperature range, this difference being reduced with a rise in temperature. In the case of the *p*-methoxy benzoic acid, the same change in the solvation effect with rising temperature will reduce the electromeric supply of electrons to the carboxylic acid group via the phenyl ring, hence a more negative ΔC_{pa}^0 would be expected. This is found.

If an attempt is made to apply this special temperature dependent solvation effect of —OMe to the ionization of 2-methoxyethylammonium ion, the weakening of the inductive effect of the methoxy group with increasing temperature would be expected to bring about just the opposite effect on ΔC_{pa}^0 to that observed above (*i.e.* ΔC_{pa}^0 value should be more positive for 2-methoxyethylammonium ion than that for the

Can. J. Chem. Downloaded from www.nrcresearchpress.com by 210.87.254.40 on 09/05/12
For personal use only.

ethylammonium ion). This result pointed to a factor overlooked in our initial consideration.

While a part of the difference can be attributed to the more effective operation of the methoxy group on an aromatic system, with amines, the predominant effect of —OMe on ΔC_{pa}^0 appears to arise from the structure-breaking effect of —OMe on the hydrophobic bonding about the neutral amine. This conclusion is based on the following consideration. In the ionization of the substituted ammonium ions, hydrophobic bonding makes an exothermic contribution to the overall value of ΔH_a^0. If the extent of hydrophobic bonding about the neutral amine is reduced, for example, by the presence of an interacting group such as —OMe, then the effect of temperature on the hydrophobic solvation will be reduced and the observed ΔC_{pa}^0 will be less positive than otherwise. This effect will be expected to be greater when the methoxy group is closer to the nitrogen atom since this is the volume most influenced by charge. Thus for 2-methoxyethylamine, $\Delta C_{pa}^0 = 5.8$ cal mol^{-1} deg^{-1}, whereas for 3-methoxypropylamine, $\Delta C_{pa}^0 = -1.7$ cal mol^{-1} deg^{-1}. Bis-2-methoxyethylamine showed a similar reduction ($\Delta C_{pa}^0 = 4.6$ cal mol^{-1} deg^{-1}) relative to the unsubstituted amine, diethylamine ($\Delta C_{pa}^0 = 15.1$ cal mol^{-1} deg^{-1}). The ether function reduces the ΔC_{pa}^0 value in cyclic systems, as well. Thus, morpholine, with a ΔC_{pa}^0 value of 11.5 cal mol^{-1} deg^{-1} (refer to Table 4) shows a reduction in ΔC_{pa}^0 relative to the unsubstituted cyclic amine, piperidine ($\Delta C_{pa}^0 = 18.0$ cal mol^{-1} deg^{-1}). These reduced ΔC_{pa}^0 values, due to the presence of the ether function, support evidence cited for the structure-breaking effect of this group (37–40). A similar but reduced effect is shown by the —OH group, consistent with the ability of this group to fit into water structure. Further support for believing the special solvation effect is not important here may be seen in the good agreement of the slope of the ΔG_a^0 *vs.* ΔS_a^0 plot with predictions based on the simple Bjerrum model.

These results may be summarized by noting that in the amino ethers the dominant effect of the MeO-group on ΔC_{pa}^0 appears to be on the hydrophobic hydration shell. This effect is undoubtedly present in the kinetic examples cited in the Introduction and for anisic acid as well, but in these latter cases the internal transmission of electronic effects is more effective and in these cases is dominant.

Acknowledgment

We wish to acknowledge the assistance and advice given by Professor L. G. Hepler during this investigation.

1. B. Rossall and R. E. Robertson. Can. J. Chem. **49**, 1441 (1971).
2. R. E. Robertson. Prog. Phys. Org. Chem. **4**, 213 (1967).
3. J. W. Larson and L. G. Hepler. Solute solvent interactions. *Edited by* J. F. Coetzee and C. D. Ritchie. Marcel Dekker, New York. 1969. Chapt. 1.
4. P. D. Bolton, K. A. Fleming, and F. M. Hall. J. Am. Chem. Soc. **94**, 1033 (1972).
5. K. M. Koshy and R. E. Robertson. Can. J. Chem. **52**, 2485 (1974).
6. J. J. Christensen, R. M. Izatt, D. P. Wrathall, and L. D. Hansen. J. Chem. Soc. A, 1212 (1969).
7. R. Barbucci, P. Paoletti, and A. Vacca. J. Chem. Soc. A, 2202 (1970).
8. D. H. Everett, D. A. Landsman, and B. R. W. Pinsent. Proc. R. Soc. Ser. A, **215**, 416 (1952).
9. R. G. Bates and G. D. Pinching. J. Res. Natl. Bur. Stand. **46**, 349 (1951).
10. R. G. Bates and H. B. Hetzer. J. Phys. Chem. **65**, 308 (1961).
11. H. B. Hetzer and R. G. Bates. J. Phys. Chem. **66**, 308 (1962).
12. R. G. Bates and G. G. Allen. J. Res. Natl. Bur. Stand. Sect. A, **64**, 343 (1960).
13. B. A. Timimi and D. H. Everett. J. Chem. Soc. B, 1380 (1968).
14. F. Franks and D. J. G. Ives. Q. Rev. Chem. Soc. **20**, 1 (1966).
15. W. Van der Linde, D. Northcott, W. Redmond, and R. E. Robertson. Can. J. Chem. **47**, 279 (1969).
16. S. T. Lobo. Ph.D. Thesis. University of Calgary, Calgary, Alberta. 1975.
17. S. T. Lobo, T. Murty, and R. E. Robertson. Can. J. Chem. This issue.
18. E. C. W. Clarke and D. N. Glew. Trans. Faraday Soc. **62**, 539 (1966).
19. T. Shedlovsky and R. L. Kay. J. Phys. Chem. **60**, 151 (1956).
20. G. Olofsson and L. G. Hepler. J. Solution Chem. **4**, 127 (1975).
21. E. J. King. Acid–base equilibria. Pergamon Press, Oxford. 1965.
22. S. Bergström and G. Olofsson. J. Solution Chem. **4**, 535 (1975).
23. S. W. Benson. J. Am. Chem. Soc. **80**, 5151 (1958).
24. R. W. Taft, N. C. Deno, and P. S. Skell. Ann. Rev. Phys. Chem. **9**, 287 (1958).
25. L. G. Hepler. J. Am. Chem. Soc. **85**, 3089 (1963).
26. F. M. Jones, III and E. M. Arnett. Prog. Phys. Org. Chem. **11**, 263 (1974).
27. S. T. Lobo, T. S. S. R. Murty, and R. E. Robertson. Submitted for publication.

28. C. L. LIOTTA, E. M. PURDUE, and H. P. HOPKINS, JR. J. Am. Chem. Soc. **95**, 2439 (1973).
29. T. MATSUI, H. C. KO, and L. G. HEPLER. Can. J. Chem. **52**, 2906 (1974).
30. J. J. CHRISTENSEN, R. M. IZATT, and L. D. HANSEN. J. Am. Chem. Soc. **89**, 213 (1967).
31. R. J. IRVING, L. NELANDER, and I. WADSÖ. Acta Chem. Scand. **18**, 769 (1964).
32. A. G. EVANS and S. D. HAMANN. Trans. Faraday Soc. **47**, 34 (1951).
33. E. J. KING. Acid–base equilibria. Pergamon Press, Oxford. 1965. Chapts. 7, 8.
34. L. N. FERGUSON. J. Am. Chem. Soc. **77**, 5288 (1955).
35. J. C. MARTIN and P. D. BARTLETT. J. Am. Chem. Soc. **79**, 2533 (1957).
36. G. NEMETHY and H. A. SCHERAGA. J. Chem. Phys. **36**, 3382 (1962).
37. K. KUSANO, J. SUURKUUSK, and I. WADSÖ. J. Chem. Thermodyn. **5**, 757 (1973).
38. S. CABANI, G. CONTI, and L. LEPORI. Trans. Faraday Soc. **67**, 1943 (1971).
39. S. CABANI, G. CONTI, A. MARTINELLI, and E. MATTEOLI. J. Chem. Soc. Faraday Trans. I, **69**, 2112 (1973).
40. S. CABANI, G. CONTI, E. MATTEOLI. To be published.

Can. J. Chem. Downloaded from www.nrcresearchpress.com by 210.87.254.40 on 09/05/12
For personal use only.

Thermodynamic parameters for the basic ionization of some cyclic amines in water

SHEILA TERESA LOBO,[1] TANIKELLA S. S. R. MURTY,[2] AND ROSS ELMORE ROBERTSON
Department of Chemistry, University of Calgary, Calgary, Alta., Canada T2N 1N4

Received March 15, 1976

SHEILA TERESA LOBO, TANIKELLA S. S. R. MURTY, and ROSS ELMORE ROBERTSON. Can. J. Chem. **54**, 3607 (1976).

The thermodynamic parameters defining the basic dissociation in water of diethylamine, cyclohexylamine, piperidine, and quinuclidine have been determined by a dilution method based on conductance measurements. The values of ΔS_a^0 and ΔC_{pa}^0 for the acid ionization of the corresponding ammonium ions at 25 °C are ΔS_a^0 −8.08, −1.24, −8.51, −13.65 cal deg^{-1} mol^{-1} and ΔC_{pa}^0 13.9, −2.7, 18.0, 4.2 cal deg^{-1} mol^{-1}. The relation between these derived values and solvation changes are discussed, the apparent anomalous values of ΔC_{pa}^0 for cyclohexylamine and quinuclidine being noted, but not rationalized.

SHEILA TERESA LOBO, TANIKELLA S. S. R. MURTY et ROSS ELMORE ROBERTSON. Can. J. Chem. **54**, 3607 (1976).

Les paramètres thermodynamiques définissant la dissociation basique, dans l'eau, de la diéthylamine, de la cyclohexylamine, de la pipéridine et de la quinuclidine ont été déterminés par une méthode de dilution basée sur des mesures de conductivités. A 25 °C, les valeurs de ΔS_a^0 et de ΔC_{pa}^0 pour l'ionisation acide des ions ammonium correspondants sont ΔS_a^0 −8.08, −1.24, −8.51, −13.65 cal deg^{-1} mol^{-1} et ΔC_{pa}^0 13.9, −2.7, 18.0, 4.2 cal deg^{-1} mol^{-1}. On discute de la relation entre ces valeurs dérivées et les changements dans la solvation; on note les valeurs apparemment anormales du ΔC_{pa}^0 de la cyclohexylamine et de la quinuclidine mais on ne peut les rationaliser.

[Traduit par le journal]

Introduction

In this paper we report the thermodynamic quantities defining the ionization of certain cyclic amines in water and note the relationship between these quantities and structure.

The search for structure–reactivity relationships for the ionization of amines in water has a long history (1–8). The simple approach, based on a comparison of pK_a values, led to the well-known amine anomaly (9, 10) where $R_2NH > R_3N > RNH_2$, an order contrary to normal expectations based on inductive effects. It was subsequently found that the expected order was followed in the gas phase (11–14) and hence the anomaly could not be attributed to steric effects (15, 16) or to other internal factors (17) but rather was associated with solvation.

The clue to the anomaly was recognized by Everett and Wynne-Jones when they determined ΔS_a^0 and ΔC_{pa}^0 for the methylamines in water (18), following their classic study of the ionization of carboxylic acids (19). They found that in such equilibria the solvation of the neutral species and solvent–solvent interaction were not small compared to the contribution arising from ion–solvent interaction with respect to these parameters. It was also evident that ΔS_a^0 and ΔC_{pa}^0 were better indicators of solvent reorganization than pK_a but the experimental requirements were more stringent. For the latter reason it may not be surprising that the notable publications in this area are limited. Of course ΔH_a^0 and ΔC_{pa}^0 can be determined now more directly by modern precision calorimetry and more data in this area are becoming available through this approach.

The importance of the solvation of the neutral amine in determining the value of ΔC_{pa}^0 is generally recognized to depend on the unique propensity of water to form three-dimensional dynamic structures, a phenomenon frequently referred to as hydrophobic hydration (20). The nature of this structural solvation is not singular and this characteristic necessarily introduces uncertainties in attempts to interpret solvation

[1]Present address: Istituto di Chimica Fisica, Università di Pisa, 56100 Pisa, Italia.

[2]Present address: Carothers Research Laboratory, E. I. Dupont de Nemours & Company, Wilmington, Delaware, U.S.A. 19898.

Can. J. Chem. Downloaded from www.nrcresearchpress.com by 210.87.254.42 on 09/05/12
For personal use only.

Can. J. Chem. Downloaded from www.nrcresearchpress.com by 210.87.254.42 on 09/05/12
For personal use only.

changes reflected in ΔS_a^0 and ΔC_{pa}^0. The first step in achieving a better understanding of such solvation changes is to obtain reliable data for a range of amines with differing but related structural features. This need prompted an extension of our earlier work to an examination of the ionization of cyclic amines. The latter structural feature was expected to provide a predictable change in surface area which might then be expected to provide recognizable differences in the corresponding values of ΔS_a^0 and ΔC_{pa}^0, granted the above hypotheses applied. Diethylamine was studied for comparison with piperidine.

Well after this study was in progress, certain thermodynamic results obtained by other methods were published (Table 4). It is gratifying, if not surprising, to note good agreement between our results and those obtained by alternative techniques.

The work reported here exploits a convenient dilution technique in conjunction with the conductance method described earlier (21) to obtain pK_a, ΔG_a^0, ΔH_a^0, ΔS_a^0, and ΔC_{pa}^0.

The ability to determine conductances at a series of concentrations for a given temperature without opening the system has a particular advantage in studies of the ionization of amines, where the introduction of traces of CO_2 must be avoided.

Experimental

The conductance method, used for the determination of ionization constants, dictated stringent experimental conditions with respect to purity of materials, quality of water, temperature control, accuracy of conductance–concentration measurements, and exclusion of carbon dioxide from solutions. Details of the experimental set-up and technique have been described elsewhere (21).

All amines used were commercially available samples. The purity of the amines was checked by glc using three different types of columns: (*a*) 6 ft × ¼ in. Chromosorb 103 (specifically useful for analysis of amines), 80/100 mesh; (*b*) 6 ft × ¼ in. 20% Triton – x/305 on High Performance Chromosorb W, 80/100 mesh; (*c*) 6 ft × ¼ in. UCW98 on High Performance Chromosorb W, 80/100 mesh. Mass spectral and nmr analyses were also carried out and the spectra compared with those in the literature. In no case were significant impurities found.

With the exception of quinuclidine, which is a solid, all the amines were refluxed over calcium hydride and the middle fraction obtained on distillation was redistilled under a nitrogen atmosphere. Piperidine was checked for pyridine impurity by uv. It showed no band at 260 nm. Quinuclidine was obtained from the commercially available quinuclidine hydrochloride (Eastman White Label) which was recrystallized from absolute ethanol. The free amine was prepared by the method used by Brown and Eldred (22).

In order to measure the dissociation constant, K_b, the limiting equivalent conductance, Λ_0, for the amine hydrochloride is essential. The hydrochlorides of the amines were prepared by passing dry hydrogen chloride gas (Matheson of Canada Ltd.) through an ethereal solution of the pure amine. After washing the hydrochloride with ether, the salt was dried in a rotary evaporator under vacuum and subsequently in a vacuum desiccator over silica gel. The purity of the salt was checked by mass spectral analysis and also by reconverting the hydrochloride to the amine and rechecking the purity of the amine as noted above. Quinuclidine hydrochloride was a commercially available sample, recrystallized from absolute ethanol and dried under vacuum.

Potassium chloride used for the determination of cell constants was of analytical grade, recrystallized from conductivity water twice and fused in a platinum boat in an electric furnace (23).

K_b was determined at 5 deg intervals and Λ_0 at 10 deg intervals between 5 and 45 °C.

Results and Discussion

The concentration–conductance data obtained were fitted to the Shedlovsky–Kay equation (24):

$$[1] \qquad \frac{1}{\Lambda S(z)} = \frac{1}{\Lambda_0} + \frac{C\Lambda S(z) f^2}{K_b \Lambda_0^2}$$

where

$$S(z) = 1 + z + (z^2/2) + \ldots$$

and

$$z = \left(\frac{\alpha\Lambda_0 + \beta}{\Lambda_0^{3/2}}\right)(\Lambda C)^{1/2}$$

$$\alpha = 8.203 \times 10^5/(DT)^{3/2}$$

$$\beta = 82.43/\eta(DT)^{1/2}$$

$$-\log f^2 = a(cx)^{1/2}$$

$$a = \frac{3.649 \times 10^6}{(DT)^{3/2}}$$

$$x = \frac{\Lambda S(z)}{\Lambda_0}$$

Since the equilibrium of interest is

$$[2] \qquad B(aq) \rightleftharpoons BH^+(aq) + OH^-(aq)$$

$\Lambda_0(BH^+\ OH^-)$ values used in [1] are obtained as follows: the value of $\Lambda_0(BH^+\ Cl^-)$ for each amine is determined experimentally, and by using $\Lambda_0(OH^-)$ and $\Lambda_0(Cl^-)$ values from the literature in the Kohlrausch equation (25)

Can. J. Chem. Downloaded from www.nrcresearchpress.com by 210.87.254.42 on 09/05/12
For personal use only.

TABLE 1. Ionization constants for diethylamine for a series of temperatures in water by a conductance method

T (°C)	K_b(obsd.)$\times 10^4$ (molal)	% difference	$\Lambda_0(BH^+OH^-)$ ($cm^2\ \Omega^{-1}\ mol^{-1}$)
5.079	8.817	+0.13	155.5
5.117	8.786	−0.27	155.6
10.706	9.444	+0.28	177.3
10.750	9.436	+0.15	177.6
14.997*	9.742	−0.68	194.6
15.045*	9.870	+0.59	194.8
19.897	10.13	−0.36	215.4
20.278	10.15	−0.40	216.9
24.913	10.45	+0.16	235.5
24.914	10.46	+0.26	235.5
29.976	10.64	+0.41	256.0
29.977*	10.69	+0.87	256.0
30.080	10.57	−0.27	256.4
33.916*	10.56	−0.87	273.2
33.990	10.64	−0.13	273.4
40.061	10.62	−0.01	300.2
40.079	10.64	+0.18	300.3
44.923	10.52	+0.18	322.4
44.928	10.47	−0.29	322.4

*These values were not included in the evaluation of the constants in [9].

[3] $\Lambda_0(BH^+\ OH^-) = \Lambda_0(BH^+\ Cl^-) + \Lambda_0(OH^-) - \Lambda_0(Cl^-)$

we obtain $\Lambda_0(BH^+\ OH^-)$, the quantity to be used in [1]. A linear least-squares analysis of the concentration–conductance data in [1] gives a straight line, from the slope of which K_b can be calculated. The values of K_b so determined for a series of temperatures are reported in Table 1 for diethylamine.[3] The Λ_0 values reported, at the temperatures at which K_b were determined, are for the amine hydroxides and are interpolated from large-scale plots of Λ_0 *vs.* temperature.

[3]Corresponding data for cyclohexylamine, piperidine, and quinuclidine are available, at a nominal charge, from the Depository of Unpublished Data, CISTI, National Research Council of Canada, Ottawa, Canada K1A 0S2.

The % differences reported in these tables are

[4] $\{K_b(\text{obsd.}) - K_b(\text{calcd.})/K_b(\text{obsd.})\} \times 100$

where K_b(calcd.) is obtained from fitting K_b(obsd.)–temperature data to an equation of the type

[5] $\log K_b = A + B/T + C \log T \ldots \quad (T = \text{K})$

using the method of Clarke and Glew (26) in order to obtain the thermodynamic parameters ΔG_b^0, ΔH_b^0, ΔS_b^0, and ΔC_{pb}^0. Although the experimentally measured K_b values are on the molar scale, they have been converted to the molal scale by the relation

[6] $pK_b(c) = pK_b(m) - \log d_0$

where (c) and (m) designate molarity and molality respectively and d_0 is the density of water, values of which were obtained from tabulations by Kell (27).

The empirical constants of [5] for the amines are reported in Table 2. These are useful in the interpolation of K_b values at any desired temperature between 5 and 45 °C. The thermodynamic parameters ΔG_b^0, ΔH_b^0, ΔS_b^0, and ΔC_{pb}^0 are listed at 5, 25, and 45 °C in Table 3 along with the standard errors.

Thermodynamic parameters for the ionization of amines are frequently reported for the following equilibrium:

[7] $BH^+(aq) \rightleftharpoons B(aq) + H^+(aq)$

In order to facilitate comparison of the values obtained in this work with those available in the literature, the thermodynamic parameters for the ionization of water are required. Subtraction of the values of the parameters for the basic ionization process from those corresponding to the ionization of water lead to the thermodynamic parameters for acidic ionization represented by [7]. The values chosen for pK_w, ΔG_w^0, ΔH_w^0,

TABLE 2. Empirical constants* for interpolation of basic ionization constants

Amine	A	B	C
Diethylamine	96.52296	−4562.903	−34.02811
Cyclohexylamine	70.63409	−3153.478	−25.64113
Piperidine	102.5219	−4821.366	−36.05758
Quinuclidine	83.46892	−4250.075	−29.12139

*For [5] between 278–315 K. The constants in this table are empirical and when used we are left with 5 figure logarithms, which admittedly contain a guard figure.

TABLE 3. Thermodynamic parameters for the basic ionization of amines in water as a function of temperature

	T (°C)	ΔG_b^0 (cal mol^{-1})	ΔH_b^0 (cal mol^{-1})	ΔS_b^0 (cal mol^{-1} deg^{-1})	ΔC_{pb}^0 (cal mol^{-1} deg^{-1})
Diethylamine	5	3889.1 ± 1.0	2070 ± 33	−6.54 ± 0.12	
	25	4067.4 ± 0.7	717 ± 10	−11.24 ± 0.03	−67.6 ± 1.7
	45	4336.5 ± 1.1	−635 ± 36	−15.62 ± 0.12	
Cyclohexylamine	5	4298.4 ± 1.9	256 ± 60	−14.53 ± 0.21	
	25	4624.8 ± 0.7	−763 ± 14	−18.07 ± 0.05	−51.0 ± 2.7
	45	5019.6 ± 1.2	−1782 ± 51	−21.38 ± 0.16	
Piperidine	5	3750.2 ± 0.7	2489 ± 34	−4.52 ± 0.12	
	25	3917.0 ± 0.7	698 ± 9	−10.80 ± 0.03	−71.7 ± 1.4
	45	4180.0 ± 1.0	−735 ± 33	−15.45 ± 0.10	
Quinuclidine	5	3807.6 ± 2.3	3351 ± 72	−1.64 ± 0.25	
	25	3881.1 ± 1.5	2193 ± 21	−5.66 ± 0.07	−57.9 ± 3.2
	45	4032.3 ± 1.8	746 ± 79	−9.42 ± 0.20	

TABLE 4. Comparison of thermodynamic parameters for the acidic ionization of amines in water at 25 °C

Amine	pK_a	ΔG_a^0 (cal mol^{-1})	ΔH_a^0 (cal mol^{-1})	ΔS_a^0 (cal mol^{-1} deg^{-1})	ΔC_{pa}^0 (cal mol^{-1} deg^{-1})	Reference
Diethylamine	11.018	15 031	12 623	−8.08	13.9	This work
			12 730			28
			12 608		13.4	29
	10.98					30
					19.1	31
Cyclohexylamine	10.609	14 473	14 103	−1.24	−2.7	This work
	10.58	14 429				32
	10.62	14 494				1
			14 380	−0.16		28
			14 259		5.7	33
Piperidine	11.128	15 181	12 642	−8.51	18.0	This work
	11.1236	15 175	12 770	−8.08	20.8	34
	11.06	15 083				35
	11.18	15 252				36
	11.00	15 006				37
			12 657			46
			12 610			38
					15.8	31
Quinuclidine	11.154	15 217	11 147	−13.65	4.2	This work
	10.95	14 938				1
	10.74	14 652				39

ΔS_w^0, ΔC_{pw}^0 for the ionization of water are based on a recent critical evaluation of the available data by Olofsson and Hepler (40). In Table 3 the thermodynamic parameters for acidic ionization in water at 25 °C are reported on the molality scale for the amines studied in this investigation. Also a comparison of the thermodynamic parameters with literature values is made for the same amines. Where comparison was possible all values of the thermodynamic parameters measured in this work are in good agreement with those in the literature (Table 4), except for the value of ΔC_{pa}^0 for cyclohexylamine.[4]

In the interpretation of the thermodynamic results reported in Table 3 it is obvious that these quantities include both internal and external effects; the former include polar, inductive, and where present resonance effects of both the ion

[4]After completion of this work, we received a preprint from Dr. L. G. Olofsson, University of Lund, Sweden, reporting a ΔC_{pa}^0 value for cyclohexylamine of 5.7 cal deg^{-1} mol^{-1} (33).

Can. J. Chem. Downloaded from www.nrcresearchpress.com by 210.87.254.42 on 09/05/12
For personal use only.

Can. J. Chem. Downloaded from www.nrcresearchpress.com by 210.87.254.42 on 09/05/12
For personal use only.

and the neutral amine and the latter the difference of the interaction of these species with water. We assume that the external effects of charge development are reflected in changes in the solvation shell and are larger than internal effects. As noted above, the aqueous solution of the weakly polar alkyl group will have that special character associated with the term 'hydrophobic'. It would now seem that this term must include a range of structural features (as yet undefined) depending on the nature of the adjacent solute surface. Thus Friedman and Krishnan (41) make a distinction between this type of solvation when adjacent to an alkyl group and when adjacent to a rare gas molecule, though both types of solvation share the common feature in gas → aqueous solution equilibria of producing large positive heat capacity differences which are presumed to reflect temperature effects on adjacent water structure. A further complication can be recognized in that the amines have the possibility of hydrogen bonding to water in the neutral state, a factor which will alter through primary, secondary, and tertiary types (42). There will be differences also in the substituted ammonium ions arising from structural interference with solvation in the inner sphere (43) and corresponding modification of the second-sphere disruption, again modified by the presence or absence of adjacent groups.

These potential complexities obstructing interpretation should be reduced by examining changes in ΔS_a^0 or ΔC_{pa}^0 for related structures. This is the approach used by Cox, Everett, Landsman, and Munn (44). That alkyl and cyclic amines can be expected to be solvated to a certain extent hydrophobically is supported by such physical evidence as ΔC_{p2}^0 values, *i.e.* partial molal heat capacities at infinite dilution for alkylamines (31, 45), the increasingly negative values for entropies of hydration (46), the temperature of maximum density shifts for secondary amines (47), and the ultrasonic effects on dilute solutions of diamines (48). However, the dispersal of hydrophobic bonding by charge development accompanying ionization is not sufficient to account for observed differences in the parameters defining ionization. It is reasonable to expect that the transfer of a proton to nitrogen will break down the hydrophobic structure in the immediate neighbourhood, and bind nearest neighbour solvent molecules, while disrupting outer layer structures. If water is already hydrogen bonded to the nitrogen (42), the entropy and heat capacity change at the nitrogen atom due to addition of a proton need not be large compared to the disruptive effects of the charge. Since the effect of charge falls off as the square of the distance, the hydrophobic solvation shell about larger amine molecules will be altered only partially by ionization and may not be altered at all beyond three carbon atoms. This would suggest predictable changes in ΔC_{pa}^0 where we compare cyclic and straight chain alkyl amines.

An examination of ΔS_a^0 for the cyclic amines (Table 4) shows that cyclohexylamine has the least negative value and quinuclidine the largest negative value of ΔS_a^0, consistent with the view of Trotman-Dickenson (49) for solvation in the ionization of the methyl substituted amines. In considering such differences we must bear in mind that the effect of charge on the hydrogen bonding ability of the nitrogen atom (49) may be more important than hydrophobic solvation in determining ΔS_a^0. The value of ΔS_a^0 for piperidine is more negative than that for diethylamine but here the minor variation may be due to an extra CH_2 group *vs.* the possible effect of chain stiffening (50), a factor not important in the cyclic amine. However, if the latter effect is important, it is not reflected in a comparison of triethylamine with quinuclidine where the ΔS_a^0 values are -14.43 and -13.65 cal mol^{-1} deg^{-1}. The chain-stiffening effect should be absent in quinuclidine; hence in the absence of some compensating effect this positive contribution to ΔS_a^0 is small.

That the ΔC_{pa}^0 values are generally positive and larger for tertiary amines than secondary amines and these in turn more positive than primary alkyl amines in the simple aliphatic series is recognized (9). In this investigation we found a value of -2.7 cal mol^{-1} deg^{-1} for cyclohexylamine, a value in disagreement with the above generalization. However, there appears to be a difference outside experimental limits between this value and that reported by Bergström and Olofsson (33) (5.7 cal mol^{-1} deg^{-1}), although there does not appear to be a large discrepancy with respect to ΔH_a^0 values (Table 4) at 25 °C. The value of ΔC_{pa}^0 for piperidine reported here is in fair agreement with that of Bates and Bower obtained by an emf method

Can. J. Chem. Downloaded from www.nrcresearchpress.com by 210.87.254.42 on 09/05/12
For personal use only.

(34). Cabani and co-workers (31) report a more recent value of 15.8 cal mol^{-1} deg^{-1} and these authors choose a value for ΔC_{pa}^0 of 18 ± 2 cal mol^{-1} deg^{-1} as normal for the secondary amines, which includes the ΔC_{pa}^0 value obtained here.

That the ΔC_{pa}^0 value of piperidine (18 cal mol^{-1} deg^{-1}) is higher than that of the open chain analogue, diethylamine (13.9 cal mol^{-1} deg^{-1}), is surprising. Evidence (31, 51) exists in the literature to support the view that the open chain compounds have a higher structure promoting ability than their cyclic analogues, a consequence of the larger hydrocarbon surface than the former exposed to the solvent through less restricted motion. Thus $\Phi C_p(CH_2) = 22 + 2$ cal mol^{-1} deg^{-1} for open chain compounds but 18 ± 2 cal deg^{-1} mol^{-1} for cyclic compounds (31). Also, the restricted rotation in the cyclic molecule could afford a more exposed positive charge in the ion to the water structure which could compete with hydrophobic hydration and thus increase ΔC_{pa}^0 for the cyclic molecule over the value for the open chain compound. Since the ionization of the amine consists of contributions due to the neutral and charged species, it is difficult to say which factor is the more important, the disruption of water structure by the positive charge or the formation of structure by the neutral species. An objection may be raised to this comparison in that diethylamine and piperidine are not strictly analogous because of the extra methylene group in the latter. However, using pyrrolidine as a strictly analogous molecule, the value of ΔC_{pa}^0 is higher for the cyclic molecule (16.6 cal deg^{-1} mol^{-1} (9)).

We may contrast the above comparison with the value of ΔC_{pa}^0 found for triethylamine and for quinuclidine. The value of ΔC_{pa}^0 for triethylamine is approximately 40 cal mol^{-1} deg^{-1}. Everett and co-workers report a value of 44.7 cal mol^{-1} deg^{-1} (44); Bergström and Olofsson 36.1 cal mol^{-1} deg^{-1} (33), Jones (29) 38.4 cal mol^{-1} deg^{-1}. Whatever the true value, there can be no doubt that it is widely different from the value of 4.2 cal mol^{-1} deg^{-1} reported here for quinuclidine. This barrel shaped molecule could be compared to the similar shaped triethylenediamine (NEt_3N) molecule. Wen *et al.* (52) have measured limiting partial molal volumes, $\bar{V}_2^0$, and viscosities of aqueous solutions of NEt_3N at two different pH values to obtain the effect of the neutral (NEt_3N) and charged species (NEt_3NH^+) on water structure. On the basis of viscosity β coefficients, dB/dT, and $\bar{V}_2^0$ values for the two species, these authors conclude that NEt_3N is a strong structure-maker in water and that NEt_3NH^+ is either a very weak structure-maker or has no net effect on water structure. This would lead to the prediction of a small ΔC_{pa}^0 value for NEt_3N, much smaller than that for triethylamine because in NEt_3N the three hydrocarbon chains are pinned back and so hydrophobic structure formation should be less. Quinuclidine, with one less hydrophilic centre than NEt_3N, should be a better structure-promoter in water and hence have a larger ΔC_{pa}^0 than NEt_3N but smaller than that for triethylamine. Preliminary results (53) for the first ionization step of NEt_3N indicate a ΔC_{pa}^0 value of 14 ± 3 cal mol^{-1} deg^{-1} at 25 °C, a value definitely lower than that for other tertiary amines, but, surprisingly, higher than the value of 4.7 cal mol^{-1} deg^{-1} for quinuclidine. A similar trend is noted for ethylenediamine with respect to the unsubstituted parent compound ethylamine (9.4 cal mol^{-1} deg^{-1} compared to 7.4 cal mol^{-1} deg^{-1} (9)). However, the cyclic molecule piperazine when compared to piperidine does not follow this trend (ΔC_{pa}^0 = 20.2 cal mol^{-1} deg^{-1} compared to 17.9 cal mol^{-1} deg^{-1} (9) or 7 cal mol^{-1} deg^{-1} (54)). It is of interest that the ΔS_a^0 values for the pairs of compounds cited above are more negative for the nitrogen analogues. Thus for quinuclidine and NEt_3N, ΔS_a^0 is −13.65 cal mol^{-1} deg^{-1} and −16.17 cal mol^{-1} deg^{-1} (9); for ethylamine and ethylenediamine the values are −2.88 and −5.38 cal mol^{-1} deg^{-1} (9); for piperidine and piperazine −8.51 and −10.15 cal mol^{-1} deg^{-1} (9). If there is a general rationale which will encompass the difference in ΔC_{pa}^0 and ΔS_a^0 for these pairs of compounds we have been unable to find it.

Acknowledgments

We wish to acknowledge the assistance given by Professor L. G. Hepler of the University of Lethbridge at several stages of this investigation. The work was supported in part by a grant from the National Research Council of Canada.

1. N. F. Hall and M. R. Sprinkle. J. Am. Chem. Soc. **54**, 3469 (1932).
2. H. K. Hall, Jr. J. Am. Chem. Soc. **79**, 5441 (1957).
3. R. P. Bell and A. F. Trotman-Dickenson. J. Chem. Soc. 1288 (1949).

Can. J. Chem. Downloaded from www.nrcresearchpress.com by 210.87.254.42 on 09/05/12
For personal use only.

4. F. E. CONDON. J. Am. Chem. Soc. **87**, 4481 (1965).
5. F. E. CONDON. J. Am. Chem. Soc. **87**, 4485 (1965).
6. F. E. CONDON. J. Am. Chem. Soc. **87**, 4491 (1965).
7. F. E. CONDON. J. Am. Chem. Soc. **87**, 4494 (1965).
8. E. FOLKERS and O. RUNQUIST. J. Org. Chem. **29**, 830 (1964).
9. F. M. JONES, III and É. M. ARNETT. Prog. Phys. Org. Chem. **11**, 263 (1974).
10. E. M. ARNETT, F. M. JONES, III, M. TAAGEPERA, W. G. HENDERSON, J. L. BEAUCHAMP, D. HOLTZ, and R. W. TAFT. J. Am. Chem. Soc. **94**, 4724 (1972).
11. M. S. B. MUNSON. J. Am. Chem. Soc. **87**, 2332 (1965).
12. J. I. BRAUMAN and L. K. BLAIR. J. Am. Chem. Soc. **90**, 6561 (1968).
13. J. I. BRAUMAN and L. K. BLAIR. J. Am. Chem. Soc. **91**, 2126 (1969).
14. J. I. BRAUMAN and L. K. BLAIR. J. Am. Chem. Soc. **93**, 4315 (1971).
15. H. C. BROWN, H. I. SCHLESINGER, and S. Z. CARDON. J. Am. Chem. Soc. **64**, 325 (1942).
16. H. C. BROWN, H. BARTHOLOMAY, JR., and M. D. TAYLOR. J. Am. Chem. Soc. **66**, 435 (1944).
17. S. R. PALIT. J. Phys. Colloid Chem. **51**, 1028 (1947).
18. D. H. EVERETT and W. F. K. WYNNE-JONES. Proc. R. Soc. London, Ser. A, **177**, 499 (1941).
19. D. H. EVERETT and W. F. K. WYNNE-JONES. Trans. Faraday Soc. **35**, 1380 (1939).
20. H. S. FRANK and M. W. EVANS. J. Chem. Phys. **13**, 507 (1945).
21. W. VAN DER LINDE, D. NORTHCOTT, W. REDMOND, and R. E. ROBERTSON. Can. J. Chem. **47**, 279 (1969).
22. H. C. BROWN and N. R. ELDRED. J. Am. Chem. Soc. **71**, 445 (1949).
23. T. SHEDLOVSKY. J. Am. Chem. Soc. **54**, 1411 (1932).
24. T. SHEDLOVSKY and R. L. KAY. J. Phys. Chem. **60**, 151 (1956).
25. H. S. HARNED and B. B. OWEN. The physical chemistry of electrolytic solutions. 3rd ed. Reinhold Publishing Co., New York. 1958. p. 233.
26. E. C. W. CLARKE and D. N. GLEW. Trans. Faraday Soc. **62**, 539 (1966).
27. G. S. KELL. J. Chem. Eng. Data, **12**, 66 (1967).
28. J. J. CHRISTENSEN, R. M. IZATT, D. P. WRATHALL, and L. D. HANSEN. J. Chem. Soc. A, 1212 (1969).
29. F. M. JONES, III. Ph.D. Thesis. University of Pittsburgh, Pittsburgh, Pa. 1971.
30. W. S. FYFE. J. Chem. Soc. 1347 (1955).
31. S. CABANI, G. CONTI, A. MARTINELLI, and E. MATTEOLI. J. Chem. Soc. Faraday Trans. I, **69**, 2112 (1973).
32. G. GIRAULT-VEXLEARSCHI. Bull. Soc. Chim. Fr. 589 (1956).
33. S. BERGSTRÖM and G. OLOFSSON. J. Solution Chem. **4**, 535 (1975).
34. R. G. BATES and V. E. BOWER. J. Res. Natl. Bur. Stand. **57**, 153 (1956).
35. W. F. K. WYNNE-JONES and G. SALOMON. Trans. Faraday Soc. **34**, 1321 (1938).
36. J. P. HOROWITZ and C. C. RILA. J. Am. Chem. Soc. **80**, 431 (1958).
37. L. W. PICKETT, M. E. CORNING, G. M. WIEDER, D. A. SEMENOW, and J. M. BUCKLEY. J. Am. Chem. Soc. **75**, 1618 (1953).
38. L. SACCONI, P. PAOLETTI, and M. CIAMPOLINI. J. Am. Chem. Soc. **82**, 3831 (1960).
39. R. G. PEARSON and F. V. WILLIAMS. J. Am. Chem. Soc. **76**, 258 (1954).
40. G. OLOFSSON and L. G. HEPLER. J. Solution Chem. **4**, 127 (1975).
41. H. L. FRIEDMAN and C. V. KRISHNAN. *In* Water, a comprehensive treatise. Vol. 3. *Edited by* F. Franks. Plenum Press, New York. 1973. Chapt. 1.
42. K. K. KUNDU, P. K. CHATTOPADHYAY, and M. N. DAS. J. Chem. Soc. A, 2034 (1970).
43. H. S. FRANK and W. Y. WEN. Discuss. Faraday Soc. **24**, 133 (1957).
44. M. C. COX, D. H. EVERETT, D. A. LANDSMAN, and R. J. MUNN. J. Chem. Soc. B, 1373 (1968).
45. J. KONICEK and I. WADSÖ. Acta Chem. Scand. **25**, 1541 (1971).
46. S. CABANI, G. CONTI, and L. LEPORI. Trans Faraday Soc. **67**, 1933 (1971).
47. F. FRANKS and B. WATSON. Trans. Faraday Soc. **63**, 329 (1967).
48. K. SASAKI and K. ARAKAWA. Bull. Chem. Soc. Jpn. **45**, 3287 (1972).
49. A. F. TROTMAN-DICKENSON. J. Chem. Soc. 1293 (1949).
50. A. G. EVANS and S. D. HAMANN. Trans. Faraday Soc. **47**, 34 (1951).
51. S. CABANI, G. CONTI, and L. LEPORI. Trans. Faraday Soc. **67**, 1943 (1971).
52. W. Y. WEN, N. TAKEGUCHI, and D. P. WILSON. J. Solution Chem. **3**, 103 (1974).
53. S. CABANI, G. CONTI and E. MATTEOLI. Private communication.
54. S. CABANI, G. CONTI, E. MATTEOLI, and P. GIANNI. Gazzetta. In press.

The hydrolysis of substituted benzyl nitrates in water. II. Effect of *ortho*-substitution

KALAVELIL MATTHEW KOSHY,[1] ROSS ELMORE ROBERTSON,[2] GEORGE STANLEY DYSON, AND SURENDRA SINGH[3]

Department of Chemistry, University of Calgary, Calgary, Alta., Canada T2N 1N4

Received May 10, 1976

KALAVELIL MATTHEW KOSHY, ROSS ELMORE ROBERTSON, GEORGE STANLEY DYSON, and SURENDRA SINGH. Can. J. Chem. **54**, 3614 (1976).

The relative effects of methyl substitution on the rates of hydrolysis of benzyl nitrates in water showed but small differences from earlier reports involving the displacement of Cl^- in mixed solvents. The values of the α-deuterium isotope effects for the hydrolysis of the 2,4- and 2,6-dimethyl homologs were similar to that for the *p*-methylbenzyl nitrate suggesting an approach to limiting hybridization in each case. In spite of this similarity, there was a large negative shift in the value of $\Delta C_p^{\neq}$ for the hydrolysis of the 2,6-dimethylbenzyl nitrate compared to the values for the 2-methyl and 4-methyl members of the series. The value of $\Delta C_p^{\neq}$ for the 3-methyl was about the same as for the unsubstituted member. The mechanistic implications of these results while in agreement with the Swain–Thornton reaction rule emphasize the importance of external as well as internal factors in the determination of charge development and separation at the transition state. Steric hindrance or charge dispersal in the cation, or both, in limiting the rate of product formation, delay the attainment of the transition state and hence favor more negative values of $\Delta C_p^{\neq}$.

KALAVELIL MATTHEW KOSHY, ROSS ELMORE ROBERTSON, GEORGE STANLEY DYSON et SURENDRA SINGH. Can. J. Chem. **54**, 3614 (1976).

Les effets relatifs de substitution par des groupes méthyles sur les vitesses d'hydrolyse de nitrates de benzyle dans l'eau ne montrent que des différences faibles par rapport aux données rapportées antérieurement et impliquant le déplacement de Cl^- dans des solvants mixtes. Les valeurs des effets isotopiques du deutérium en α sur l'hydrolyse des homologes diméthyl-2,4 et 2,6 sont semblables à ceux observés pour le nitrate de *p*-méthylbenzyle et ceci suggère une approche à l'hybridisation limitante dans chaque cas. Malgré cette similitude, on a observé un très grand déplacement négatif dans la valeur de $\Delta C_p^{\neq}$ pour l'hydrolyse du nitrate de diméthyl-2,6 benzyle comparé aux valeurs des dérivés méthyl-2 et méthyl-4 de cette série. La valeur de $\Delta C_p^{\neq}$ pour le méthyl-3 est approximativement la même que celle du dérivé non-substitué. Les impliquations mécanistiques de ces résultats, même si elles sont en accord avec les règles de Swain–Thornton pour ces réactions, mettent en relief l'importance de facteurs externes aussi bien qu'internes dans la détermination du développement et de la séparation de la charge dans l'état de transition. Des effets stériques ou de dispersion de charge sur le cation, ou les deux, dans l'étape déterminante de la formation du produit ralentissent l'atteinte de l'état de transition et favorisent donc des valeurs plus négatives du $\Delta C_p^{\neq}$.

[Traduit par le journal]

In solvolytic reactions, the degree of charge development and separation at the transition state depends on several factors including the structure of the particular reactant and the ionizing and nucleophilic properties of the solvent (1). Such postulates as those of Hammond (2) and of Swain and Thornton (3) represent attempts to find underlying principles with predictive value for characterizing the transition state. In this connection the temperature coefficient of the $\Delta H^{\neq}$ ($\Delta C_p^{\neq}$) for ionogenic reactions of the S_N type in water has been found to be a useful guide to the degree of charge development or more precisely, a measure of the external effects of charge development. Indications derived from $\Delta C_p^{\neq}$ values for the hydrolysis of a series of substituted benzyl nitrates (4) show that this series tends to follow the Swain–Thornton reaction rule rather than that of Hammond. Since the values of $\Delta C_p^{\neq}$ in such a series depend on the

[1]Present address: Department of Chemistry, Scarborough College, University of Toronto, Toronto, Ontario.

[2]Author to whom all correspondence should be addressed.

[3]Present address: Department of Chemical Engineering, McMaster University, Hamilton, Ontario.

Can. J. Chem. Downloaded from www.nrcresearchpress.com by 210.87.254.6 on 09/05/12
For personal use only.

TABLE 1. Empirical constants for the interpolation of rates*

Compound	A_1	$-A_2$	$-A_3$
o-Methylbenzyl nitrate	138.1437	11 214.991	42.2431
m-Methylbenzyl nitrate	149.8946	12 119.904	46.1540
2,6-Dimethylbenzyl nitrate	208.8562	13 925.92	66.5687
2,4-Dimethylbenzyl nitrate	576.419	29 334.66	194.008

*For the equation $\log_{10} k = A_1 + A_2/K + A_3 \log_{10} K$.

Can. J. Chem. Downloaded from www.nrcresearchpress.com by 210.87.254.6 on 09/05/12
For personal use only.

external effects of charge, it was of interest to examine the question of why the product-forming step is delayed in the more reactive homologs.

Koshy and Robertson (4) showed that the value of $\Delta C_p^{\ddagger}$ obtained for the hydrolysis of a series of substituted benzyl nitrates varied in a systematic fashion from a minimal value of about -30 cal mol^{-1} deg^{-1} for the 4-nitro- and 4-trifluoromethyl substituted benzyl nitrates to -101 cal mol^{-1} deg^{-1} for the 4-methylbenzyl nitrate. The range of values began at about -30 cal deg^{-1} mol^{-1} for the corresponding chlorides (5) but was significantly less negative for the 4-methylbenzyl chloride (-80 cal mol^{-1} deg^{-1}). The latter differences could arise from the property of the nitrate ion to be a more effective structure breaker than the chloride ion as claimed by Kay (6). Alternately there was the possibility that other factors could be responsible, such as reaching the transition state at a different degree of charge development (7, 8) or a different tendency of the partially solvated ion-pair to return to the initial state and thus make varying anomalous contributions to $\Delta C_p^{\ddagger}$ (9, 10). We consider these alternatives unlikely. Here the relative values of $\Delta C_p^{\ddagger}$ are used as a basis for examining the probable effect of methyl substitution on the degree of charge separation at the transition state and how this charge development relates to the overall rate of hydrolysis.

Specific rate constants were determined by the same conductance method used in previous studies (11) and the same precautions were observed with respect to supersaturation, temperature measurement and control. The rate data obtained over the range of temperature in necessarily dilute solutions ($<1 \times 10^{-4}\ M$) in all cases conform to strict first-order requirements. These specific rate constants were fitted by an LMS program to the empirical equation $\log k_1 = A_1 + A_2/T + A_3 \log T$. The coefficients so derived are given in Table 1 and provide a method for calculation of rate constants at temperatures within the noted range and estimation outside that range. If the conventional assumptions are accepted regarding the equilibrium condition of the transition state, corresponding values of the apparent $\Delta H^{\ddagger}$, $\Delta S^{\ddagger}$, and $\Delta C_p^{\ddagger}$ may be derived from these constants (11) (Table 2). It is worth noting that the significance of such terms depends very much on these assumptions. The further assumption that $d\Delta H/dT$ is invariant with temperature to 0 K is surely arbitrary but this fact in itself need not vitiate the potential value of this coefficient as a probe for characterizing certain properties of the transition state not otherwise available. The rates of hydrolysis at 40 °C and relative rates compared to that for benzyl nitrate are given in Table 3. The effect of methyl substitution in this system is found to be different from results found by earlier workers for displacement of the Cl^- ion in mixed solvent but the differences are not remarkable (12, 13). Here the summed effect of the 2- and 4-methyl substitution is greater than the combined effect by a factor of less than 2, while Charlton and Hughes reported (12) that for solvolysis of the corresponding chlorides in 50/50 ethanol/water, the combined effect of these substituents is greater by about the same factor. The k_o/k_p ratio for the nitrates is 0.21 while the ratio for the chlorides in the noted solvent mix is 0.54, a difference which might be taken as an indication of a greater degree of steric hindrance in the former (14) even though ionizing conditions were better. The accelerating effect of the 2-methyl is less than that of the 4-methyl by a factor of about 4.8 and the 2,6-dimethyl less effective than 2,4-dimethyl by a factor of about 2. While there may be some small steric acceleration in these reactions (which on the basis of α-deuterium isotope effects (Table 4) approach limiting mechanism (21, 22)) steric hindrance to 'nucleophilic attack' appears to be a significant source of difference in reactivity of

Can. J. Chem. Downloaded from www.nrcresearchpress.com by 210.87.254.6 on 09/05/12
For personal use only.

TABLE 2. Derived quasi-thermodynamic values for the hydrolysis of a series of substituted benzyl nitrates in water*

Nitrate	$\Delta S^{\ddagger}$ (cal mol^{-1} deg^{-1})	$\Delta H^{\ddagger}$ (cal mol^{-1})	$\Delta C_p^{\ddagger}$ (cal mol^{-1} deg^{-1})	k_1 (T °C) (s^{-1})	Reference
Benzyl	1.11 ±0.12 (50)	24 960 ± 40	−58 ±3	1.55×10^{-4} (50)	4
	−3.2 ±0.13 (75)	23 500 ± 50		2.52×10^{-3} (75)	
4-Methylbenzyl	11.7 ±0.1 (25)	25 460 ± 30	−101 ±5	4.84×10^{-4} (25)	4
	3.52±0.3 (50)	22 920 ±100		1.24×10^{-2} (50)	
3-Methylbenzyl	2.57±0.14 (50)	24 870 ± 50	−54 ±5	3.72×10^{-4} (50)	This work
	−1.3 ±0.2 (75)	23 500 ± 80		6.0 ×10^{-3} (75)	
2-Methylbenzyl	8.8 ±0.2 (25)	25 660 ± 50	−86 ±8	1.00×10^{-4} (25)	This work
	1.84±0.50 (50)	23 510 ± 75		2.71×10^{-3} (50)	
2,6-Dimethylbenzyl	1.61±0.1 (10)	25 700 ± 28	−134 ±4	2.80×10^{-4} (10)	This work
	9.14±0.15 (25)	23 690 ± 45		2.70×10^{-3} (25)	
2,4-Dimethylbenzyl	21.8 ±0.3 (5)	26 440 ±100	—	5.58×10^{-4} (5)	This work

*The numbers in parentheses indicate °C.

TABLE 3. Relative rates for the solvolysis of substituted benzyl nitrates in water at 40 °C

Compound	k (s^{-1} × 10^4)	Relative rate
Benzyl nitrate	0.4339	1
2-Methylbenzyl nitrate	8.019	18
3-Methylbenzyl nitrate	1.011	2.3
4-Methylbenzyl nitrate	37.53	86
2,6-Dimethylbenzyl nitrate	178.0	410
2,4-Dimethylbenzyl nitrate	361.6	833

TABLE 4. Kinetic α-deuterium isotope effects for the solvolysis of benzyl nitrates in water

Compound	k_H/k_D (per two deuterium atoms)	Temperature (°C)
Benzyl nitrate	1.249±0.003	50
2-Methylbenzyl nitrate	1.324±0.003	40
4-Methylbenzyl nitrate	1.392±0.003	25
2,6-Dimethylbenzyl nitrate	1.366±0.003	25

the corresponding pairs. The addition of a second *ortho*-methyl is seen to increase the rate somewhat more than the first ($k_{2,6\text{-diMe}}/k_H$:$(k_{2\text{-Me}}/k_H)^2$ = 1.27:1) suggesting the presence of a small degree of steric acceleration (15–17) but this factor would not be expected to account for the large negative shift in $\Delta C_p^{\ddagger}$ found for the 2,6-dimethyl homolog. This negative shift in $\Delta C_p^{\ddagger}$ can be explained by a delay in the product forming step, the most evident cause being a relatively larger steric effect to the nucleophile than in the case of the 2-methyl but one which does not cancel out the possibility of steric acceleration. Obviously this explanation is not unique.

Considering the traditional view that solvation changes tend to bring about compensating changes in $\Delta H^{\ddagger}$ and $\Delta S^{\ddagger}$ (18, 19) and the large negative values of $\Delta C_p^{\ddagger}$ (Table 2) which may be taken as evidence of considerable changes occurring in solute–solvent interaction in the activation process, it is perhaps surprising that no correlation was found between $\Delta H^{\ddagger}$ and $\Delta S^{\ddagger}$. A non-linear correlation was found between log k_{sub}/k_H and $\Delta\Delta H^{\ddagger}$ and between $\Delta C_p^{\ddagger}$ and $\Delta\Delta H^{\ddagger}$ for the methyl substituted benzyl nitrates (Fig. 1). That internal stabilization of the cation

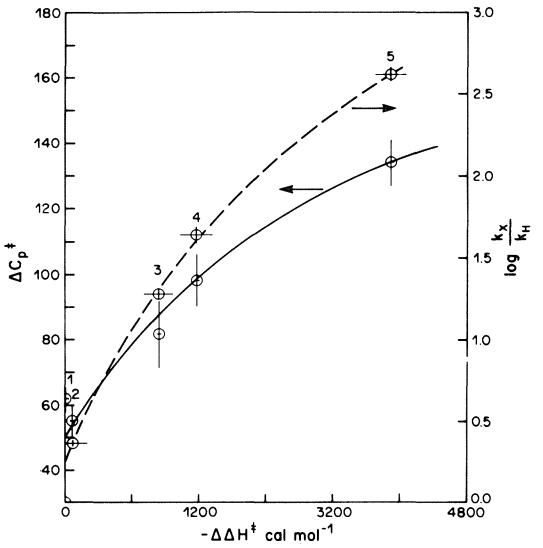

FIG. 1. log k_X/k_H *vs.* $\Delta\Delta H^{\ddagger}$ ---, $\Delta C_p^{\ddagger}$ *vs.* $\Delta\Delta H^{\ddagger}$ —: (*1*) benzyl nitrate, (*2*) 3-methylbenzyl nitrate, (*3*) 2-methylbenzyl nitrate, (*4*) 4-methylbenzyl nitrate, (*5*) 2,6-dimethylbenzyl nitrate.

Can. J. Chem. Downloaded from www.nrcresearchpress.com by 210.87.254.6 on 09/05/12
For personal use only.

should lower the activation enthalpy is to be expected and that internal dispersion of the positive charge on the cation should enhance the external effects of the forming anion is logical, if, in addition, it is recognized that such dispersion tends to postpone the product forming step. The conclusion that the more reactive the solute, the greater the charge on the anion and the later the transition state along the reaction coordinate seems to be supported by the experimental facts in this series. A similar delay could be obtained through steric hindrance to nucleophilic attack or through the equivalent anchimeric interaction. These results are seen to be in accord with the "reacting-bond rule" proposed by Swain and Thornton (3), though it does not follow that that particular rule is a necessary rationalization for the present system.[4] The trends evident in Table 2 and Fig. 1 show that with increasing electron release, more negative values of $\Delta C_p^{\neq}$ are obtained, as was also found by Koshy and Robertson (4), and this result is consistent with greater charge on the NO_3^- group at the transition state and presumably a longer C···O bond. If we ask why the transition state should be delayed in the very cases where bond breaking was made more favourable, then it seems reasonable to conclude that the reason is related to the product forming step which in these cases is related to delocalization of the positive charge. While this conclusion is not inconsistent with the Swain–Thornton rule it shifts the emphasis to the decreasing probability of nucleophilic interaction. An obvious corollary is that the longer the reacting bond, the greater the solvent interaction with the developing anion, hence a reduction in the internal electrostatic interaction as a consequence of the dispersal of the positive charge. The latter fact provides further indirect support for the claim that in the hydrolysis of halides and nitrates, the interaction of solvent with the anion is the main contributor to $\Delta C_p^{\neq}$ (20). This of course is consistent with a large body of observations with respect to the relative effect of solvent polarity and reaction rates (1, 21). This again is consistent with the claim (20) that those reactants which hydrolyse with a $\Delta C_p^{\neq}$ of about -30 cal mol^{-1} deg^{-1} do not appreciably disturb water structure adjacent to the quasi-anion at the transition state. This may be the consequence of charge dispersal in the anion (the sulfonates (11)) or internal cancellation (20) or simply a low degree of charge development on the anion at the transiton state. It is to be regretted that the experimental temperature range available does not permit a determination of $\Delta C_p^{\neq}$ for the hydrolysis of the 2,4-dimethyl homolog, thus permitting a distinction between the possible importance of steric and electronic influence on $\Delta C_p^{\neq}$ in the case of the 2,6-homolog. The possibility of introducing an electron withdrawing substituent in the 2,4-dimethylbenzyl nitrate was considered, but while this approach would permit $\Delta C_p^{\neq}$ to be determined, the change in electron distribution would also alter $\Delta C_p^{\neq}$ (4).

A consideration of the α-deuterium isotope effects for the hydrolysis of methyl-substituted benzyl nitrates (Table 4) shows that while small differences in k_H/k_D are apparent, there is no evidence of important differences in hybridization at the transition state between the 2-, the 4-, and the 2,6-substituted homologs. This evidence may be taken as support for the conclusion that the differences in the values of $\Delta C_p^{\neq}$ (Table 2) arise from external effects of the displaced anion. The mere addition of a methyl group (3-methyl), while increasing the bulk of the forming cation, is known to have little effect on the electron distribution. It is wholly consistent with the interpretation presented here that no appreciable change would be expected in charge development at the transition state and, since steric effects are unlikely, hence no change in the value of $\Delta C_p^{\neq}$.[5]

The $\Delta C_p^{\neq}$ values found for the hydrolysis of substituted benzyl nitrates here and in our previous paper (4) are seen to bear a relationship to the conceived electron distribution in the cationic moiety (Fig. 1) and to the consequent probability of nucleophilic attack on the α-carbon, *i.e.* on the delocalization of a positive charge and on steric considerations (*e.g.* $k_{4\text{-Me}}:k_{2\text{-Me}}:k_{2,6\text{-diMe}}$, Table 2). This conclusion provides support for the claim of Sneen and Larsen (24) that "all nucleophilic substitutions

[4]According to this rule, "the greater the electron density, the longer the bond should be when the free energy for bond breaking is reached". The alternative explanation given above is based on a quite different argument.

[5]The value of $\Delta C^{\neq}$ for 3-trifluoromethylbenzylnitrate is -54 ± 16 cal mol^{-1} deg^{-1} about the same as found for the 3-methylbenzylnitrate and suggesting about the same degree of charge development at the transition state. The rate, relative to benzyl nitrate at 40 °C (=1), is 0.035.

Can. J. Chem. Downloaded from www.nrcresearchpress.com by 210.87.254.6 on 09/05/12
For personal use only.

at a saturated carbon atom proceed via an ion-pair" and would seem to counter the classical concept of the S_N1 mechanism (24) in which the rate of the product forming step was neglected. Of course the gradation of mechanism recognized by Sneen and Larsen was already implicit in modifications of the original (1) and further developed and made explicit by Winstein and co-workers (26). Our results support the concept of the ion-pair intermediate but further require that the rate of product formation is still a significant factor even where by other tests the mechanism might be expected to conform to S_N1 characteristics.[6] The variety of evidence for the ionic intermediates postulated by Winstein and co-workers (26) was obtained in acetic acid, which is a poor nucleophile; in water which is a fair nucleophile and a very good solvent, the existence of ions beyond the tight-ion-pair seems less likely. Finally we would disagree with the suggestion of Sneen and Larsen that the classical mechanistic distinction is without utility (24). Notwithstanding recognized simplifications, the S_N1–S_N2 dichotomy still provides a useful if rough guide in postulating probable pathways.

Experimental Detail

o-Methylbenzyl Nitrate

o-Methylbenzoic acid was converted to the chloride (using thionyl chloride) before reduction with $LiAlH_4$. The resulting *o*-methylbenzyl alcohol was converted to *o*-methylbenzyl chloride using thionyl chloride which in turn was converted to the nitrate by dissolving 10 g (0.07 mol) of the chloride in dry ether with 23.8 g (0.14 mol) of powdered silver nitrate and stirring together for 48 h at room temperature. The precipitated silver chloride was removed by filtration and the filtrate was poured into 250 ml of ice cold water. Organic and aqueous layers were separated. The aqueous layer was extracted with 25 ml of ether and the combined organic layer was dried over anhydrous Na_2SO_4. The product on fractional distillation under reduced pressure gave 6.1 g of *o*-methylbenzyl nitrate, which was further purified by distillation on a micro spinning band column, bp 70–71 °C/3–4 mm; nmr_{TMS} (CCl_4) δ 7.25 (s, 4H, aryl), 5.43 (s, 2H, —CH_2—), 2.40 (s, 3H, —CH_3); ms parent peak at *m/e* 167, base peak at *m/e* 91, and significant fragments at *m/e* 120, 119, 104, 77, 65, 39.

o-Methylbenzyl Nitrate (α-D_2)

The reaction sequence was exactly as described above except that the $LiAlH_4$ was replaced by $LiAlD_4$, product bp 45 °C/4 mm; nmr_{TMS} (CCl_4) δ 7.27 (s, 4H, aryl), 2.39 (s, 3H, —CH_3); ms parent peak at *m/e* 169, base peak at *m/e* 91, and significant fragments at *m/e* 121, 119, 107, 106, 92, 65.

m-Methylbenzyl Nitrate

Reduction with $LiAlH_4$ was done on *m*-methylbenzoyl chloride, which in turn was obtained from *m*-toluic acid (99% Aldrich), using $SOCl_2$. The resulting *m*-methylbenzyl alcohol was then converted to the chloride using $SOCl_2$. The heterogeneous method was used to prepare the nitrate from the chloride, as described in case of *o*-methylbenzyl nitrate, bp 90 °C/4–5 mm; nmr_{TMS} (CCl_4) δ 7.22 (s, 4H, aryl), 5.37 (s, 2H, —CH_2—), 2.40 (s, 3H, —CH_3); ms parent peak at *m/e* 167, base peak at *m/e* 91, significant fragments at *m/e* 120, 119, 105, 77, 65, 39.

2,6-Dimethylbenzyl Nitrate

2,6-Dimethylbenzoic acid (Frinton Laboratories) was reduced to 2,6-dimethylbenzyl alcohol by reacting 5 g (0.033 mol) of the acid with 1 g (0.026 mol) of lithium aluminium hydride in ether (50 ml) at room temperature for 4 h followed by treatment with 30 ml of 10% sulphuric acid. The alcohol was recovered from the organic layer by evaporating off the solvent, after drying with anhydrous $MgSO_4$; yield 3.5 g, mp 82 °C. The alcohol was converted to the chloride using the method of Swain and Langsdorf (27). Distillation of the product in a semi-micro spinning band column under reduced pressure gave 2 g of 2,6-dimethylbenzyl chloride; bp 65 °C (0.8 mm). The nitrate was obtained from the chloride by treating 2 g (0.013 mol) dissolved in dry ether with 4 g (0.024) of powdered silver nitrate for 24 h at room temperature. The product was recovered as described earlier; bp 60 °C/0.1 mm; nmr_{TMS} (CCl_4) δ 7.1 (m, 3, aryl), 5.6 (s, 2, methylene), 2.35 (s, 6, methyl).

2,4-Dimethylbenzyl Nitrate

2,4-Dimethylbenzoic acid was prepared from 2,4-dimethylacetophenone (28). 2,4-Dimethylbenzyl nitrate was prepared in a normal procedure described for 2,6-dimethylbenzyl nitrate: 2,4-dimethylbenzoic acid bp 125 °C, 2,4-dimethylbenzyl alcohol bp 120 °C/55 mm, 2,4-dimethylbenzyl nitrate bp 70 °C/2 mm; nmr of 2,4-dimethylbenzyl nitrate: nmr_{TMS} (CCl_4) δ 6.76–7.12 (m, 3H, aryl), 5.20 (s, 2H, —CH_2—), 2.22 (s, 6H, —CH_3); ms parent peak at *m/e* 181, base peak at *m/e* 105, and significant fragments at *m/e* 135, 134, 133, 119, 91, 79.

[6]The exceptional cases for hydrolysis in water will be those which because of steric hindrance (*e.g.* 2,6-dimethylbenzyl nitrate or 1-adamantyl structure or possibly some form of neighboring group participation) the rate of front side displacement of the anion exceeds the rate of the product forming step.

1. C. K. Ingold. Structure and mechanism in organic chemistry. Cornell University Press, Ithaca, 2nd ed. New York, N.Y. 1969.
2. G. Hammond. J. Am. Chem. Soc. **77**, 334 (1955).
3. C. G. Swain and E. R. Thornton. J. Am. Chem. Soc. **84**, 817 (1962).
4. K. M. Koshy and R. E. Robertson. Can. J. Chem. **52**, 2485 (1974).
5. K. M. Koshy, R. E. Robertson, and W. M. J. Strachan. Can. J. Chem. **51**, 2958 (1973).
6. R. L. Kay. Adv. Chem. Ser. **73**, 1 (1968).
7. T. T. Tidwell. J. Org. Chem. **39**, 3533 (1974).
8. S. G. Smith and D. J. W. Goon. J. Org. Chem. **34**, 3127 (1969).

9. W. J. ALBERY and B. H. ROBINSON. Trans. Faraday Soc. **65**, 980 (1969).
10. J. M. W. SCOTT and R. E. ROBERTSON. Can. J. Chem. **50**, 167 (1972).
11. R. E. ROBERTSON. Prog. Phys. Org. Chem. **4**, 213 (1967).
12. J. C. CHARLTON and E. D. HUGHES. J. Chem. Soc. 850 (1956).
13. R. W. TAFT, JR. *In* Steric effects in organic chemistry. *Edited by* M. S. Newman. John Wiley Co., New York, N.Y. Chapt. 13.
14. R. W. TAFT, JR., M. S. NEWMAN, and F. H. VERHOEK. J. Am. Chem. Soc. **72**, 4511 (1950).
15. G. BADDELEY. Nature, **144**, 144 (1939).
16. H. C. BROWN. Boranes in organic chemistry. Cornell University Press, Ithaca, N.Y. 1972. Chapt. 8.
17. L. C. R. BARCLAY, H. R. SONAWANE, and J. C. HUDSON. Can. J. Chem. **50**, 2318 (1972).
18. J. E. LEFFLER and E. GRUNWALD. Rates and equilibria of organic reactions. John Wiley & Sons Inc., New York, N.Y. 1963. Chapt. 13.
19. J. G. IVES and P. D. MARSDEN. J. Chem. Soc. 649 (1965).
20. S. SINGH and R. E. ROBERTSON. In press.
21. S. WINSTEIN, E. GRUNWALD, and H. W. JONES. J. Am. Chem. Soc. **73**, 2700 (1951).
22. V. J. SHINER, JR. *In* Isotope effects in chemical reactions. *Edited by* C. J. Collins and N. S. Bowman. Van Nostrand and Reinhold Co., New York, 1970. Chapt. 2.
23. K. M. KOSHY and R. E. ROBERTSON. J. Am. Chem. Soc. **96**, 914 (1974).
24. R. A. SNEEN and J. W. LARSEN. J. Am. Chem. Soc. **91**, 362 (1969).
25. E. D. HUGHES. Discuss. Faraday Soc. 185 (1937).
26. S. WINSTEIN, B. APPEL, R. BAKER, and A. DIAZ. Chem. Soc. Spec. Publ. **19**, 109 (1965).
27. C. G. SWAIN and W. P. LANGSDORF, JR. J. Am. Chem. Soc. **73**, 2813 (1951).
28. W. A. PERKINS, JR. and J. F. S. STONE. J. Chem. Soc. **127**, 2275 (1925).

Can. J. Chem. Downloaded from www.nrcresearchpress.com by 210.87.254.6 on 09/05/12
For personal use only.

Hydrazine derivatives. III. A study of alkylation of guanazole

JOSÉ J. FUENTES AND JACQUES A. LENOIR[1]

Department of Chemistry, Sir George Williams Campus, Concordia University, Montreal, P.Q., Canada H3G 1M8

Received June 21, 1976

JOSÉ J. FUENTES and JACQUES A. LENOIR. Can. J. Chem. **54**, 3620 (1976).

Spectroscopic results from mono- and dibenzylidene derivatives of 1-alkylguanazoles establish that alkylation of 3,5-diamino-1,2,4-triazole (guanazole) with alkyl halides in basic non-aqueous media occurs at position N-1.

JOSÉ J. FUENTES et JACQUES A. LENOIR. Can. J. Chem. **54**, 3620 (1976).

L'examen spectroscopique de dérivés mono- et dibenzylidéniques des alcoyl-1 guanazoles démontrent que l'alcoylation du diamino-3,5 triazole-1,2,4 (guanazole) par l'intermédiaire d'halogénures d'alcoyles en milieu basique et non-aqueux s'effectue à la position N-1.

Can. J. Chem. Downloaded from www.nrcresearchpress.com by 210.87.254.6 on 09/05/12
For personal use only.

In view of the promising future of guanazole (3,5-diamino-1,2,4-triazole) and its derivatives (1), a study of the base-catalyzed alkylation in non-aqueous medium of guanazole itself was undertaken. However, a mixture of ethyl chloroacetate in ethanol–water solution and sodium hydroxide reacted with guanazole at both its exocyclic nitrogens by ammonolysis of the ester to form a diamide (2). Monosubstitution occurs only at position N-1 with various alkyl halides in absolute methanol in the presence of sodium methoxide. Even using ethyl monobromoacetate as the alkyl derivative the corresponding N-1 acetate derivative of guanazole is obtained. Mass spectrometry was used to establish the structure of the above compound as (3,5-diamino-1,2,4-triazolyl-1)acetic acid formed by the base-catalyzed alkylation of guanazole with ethyl bromoacetate in non-aqueous solution and hydrolyzed to the corresponding acid (Table 1). The fragmentation pattern has been rationalized from previously reported mass spectra of 1,2,4-triazoles (6, 7) (Scheme 1).

Evidence for monosubstitution at N-1 is afforded through the dibenzylidene derivatives of 1-alkyl substituted guanazoles by proton magnetic resonance and elemental analysis (Tables 2–5).

The report (4) that 3,5-diamino-4-phenylmethylol-1,2,4-triazole (**1**) forms with 3,5-diamino-1,2,4-triazole and benzaldehyde in boiling ethanol has not been verified by the present authors, even after many experimental variations. Evidence for the hydroxyl group was never observed. Instead, the condensation always gave benzylidene derivatives involving the exocyclic amino groups.

TABLE 1. Isotopic analysis for (3,5-diamino-1,2,4-triazolyl-1)acetic acid

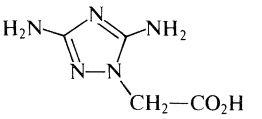

m/e	Found	$C_4H_7N_5O_2$ (theor.)
157	100	100
158	6.29	6.42
159	0.75	0.58

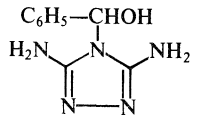

1

The mono- and dibenzylidene derivatives of guanazole and N-1 alkylated guanazoles are unstable in the presence of small amounts of mineral acids even at room temperature (3). These benzylidene derivatives are formed with basic catalysts such as sodium acetate and in more difficult cases, piperidine. Stability of the dibenzylidene derivatives towards alkaline reagents as reported (3) was verified but some decomposition was observed after 24 h, and in the case of 1-*n*-propylguanazole 10 days at room temperature were required for complete decomposition of its mono- and dibenzylidene derivatives.

[1]Author to whom correspondence should be addressed.

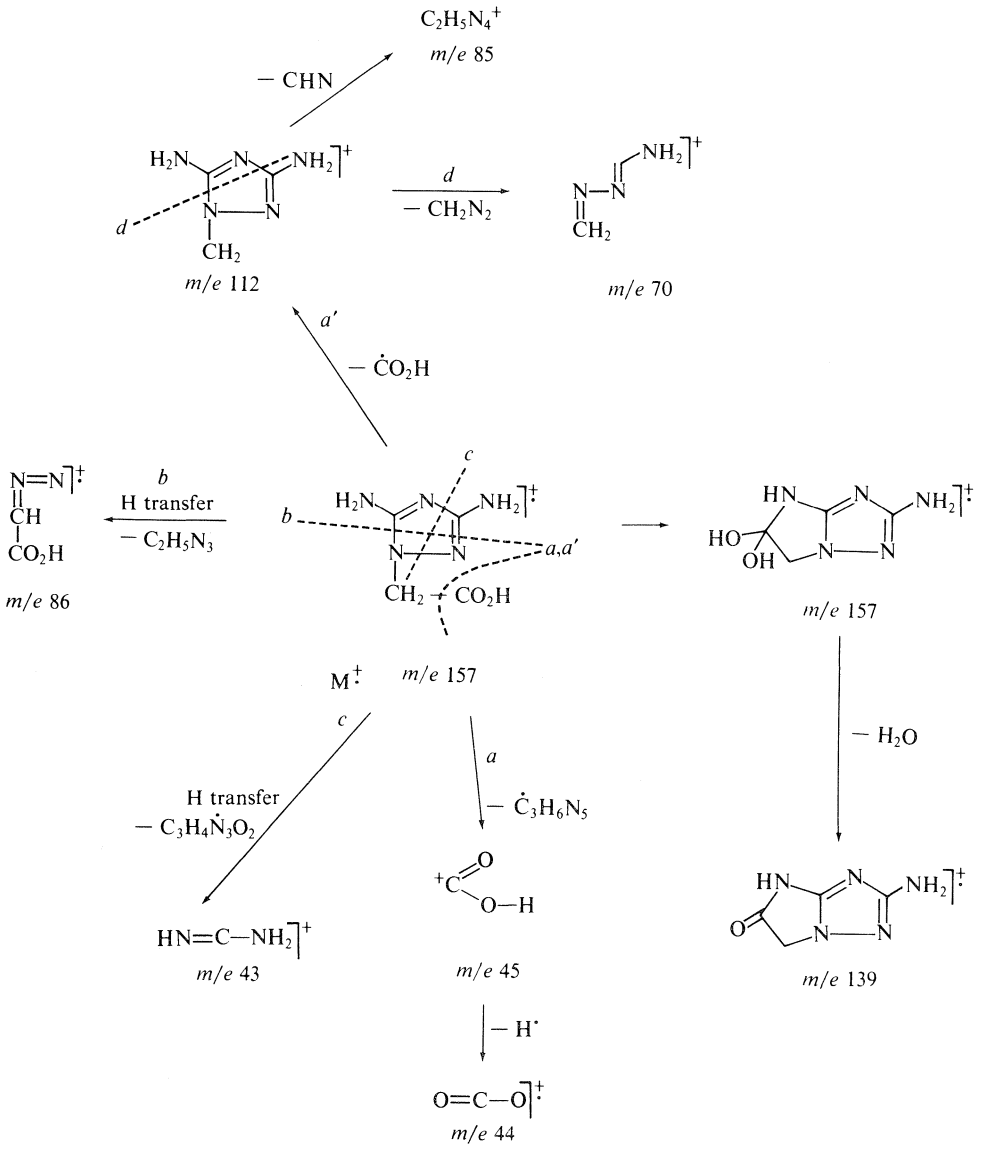

SCHEME 1

Tables 4 and 5, respectively, contain the complete chemical shift values for the benzylidene protons of the mono- and dibenzylidene derivatives of the alkylation products; the values in Table 5 indicate that alkylation occurred at N-1.

Although two isomeric monobenzylidene derivatives are possible, only one isomer was isolated. This could be explained by the difference in reactivity of the two primary amino groups in the original 1-substituted guanazoles. A similar behavior has been observed in the reaction of monoamino-1,2,4-triazoles in which only the 3-amino derivatives reacted with an excess of diformylhydrazide; the 5-amino derivatives failed to give the reaction under the same conditions (5). The difference in chemical shifts, albeit small, in the dibenzylidene protons shows a non-equivalence only in 1-substituted guanazoles.

Can. J. Chem. Downloaded from www.nrcresearchpress.com by 210.87.254.6 on 09/05/12
For personal use only.

TABLE 2. Monobenzylidene derivatives of substituted guanazoles

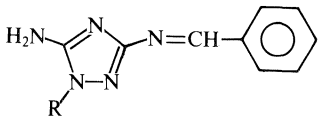

R	Melting point (°C)	R_f[a]	Formula	N (%) Calcd.	N (%) Found
H[b]	235–237[c]	0.21	—	—	—
CH_3[d]	130–132	0.21	$C_{10}H_{11}N_5$	34.80	34.74
$CH_2CH_2CH_3$[b]	205–207	0.40	$C_{12}H_{15}N_5$	30.54	30.46
C_6H_5[b]	230[e]	0.57	$C_{15}H_{13}N_5$	26.14	26.59
$CH_2C_6H_5$[b]	135–139	0.46	$C_{16}H_{15}N_5$	25.25	24.85
$CH_2CO_2CH_3$[b]	168–169	0.38	$C_{12}H_{13}N_5O_2$	27.02	26.23

[a]Silica gel tlc plates, solvent: ethyl acetate.
[b]Recrystallized from the reaction mixture.
[c]Melting point 228–233 °C, ref. 3; mp 234 °C, ref. 10.
[d]Recrystallized from ethyl acetate: hexane.
[e]Melting point 228 °C, ref. 11.

TABLE 3. Dibenzylidene derivatives of substituted guanazoles

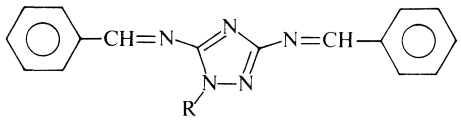

R	Melting point (°C)	R_f[a]	Formula	N (%) Calcd.	N (%) Found
H[b]	207–210[c]	0.63	—	—	—
CH_3[d]	145–147	0.75	$C_{17}H_{15}N_5$	24.20	24.46
$CH_2CH_2CH_3$[e]	*ca.* 70	0.73	$C_{19}H_{19}N_5$	22.06	22.55
C_6H_5[f]	132	0.85	$C_{22}H_{17}N_5$	19.92	19.31
$CH_2C_6H_5$[g]	142–143	0.83	$C_{23}H_{19}N_5$	19.16	18.97
$CH_2CO_2CH_3$[h]	83	0.83	$C_{19}H_{17}N_5O_2$	20.11	18.82

[a]Silica gel tlc plates, solvent: ethyl acetate.
[b]Recrystallized from the reaction mixture.
[c]Melting point 206–209 °C, ref. 3.
[d]Recrystallized from hexane.
[e]Oil that crystallized on standing; rinsed with cold hexane.
[f]Recrystallized from ether – petroleum ether.
[g]Purified from the monobenzylidene derivative by silica gel dry column; solvent: ethyl acetate.
[h]Recrystallized from ether–hexane.

Experimental

The infrared spectra were taken on a Perkin-Elmer Model 257 grating infrared spectrophotometer. The samples were prepared in the form of discs with dry potassium bromide.[2] The proton magnetic resonance spectra were obtained on an EM 360 nmr Varian Anaspect spectrometer. The samples were dissolved in DMSO-d_6, unless otherwise specified, using TMS as internal standard. The chemical shift values were expressed in ppm units from the TMS peak. The ultraviolet spectra were taken on a Perkin-Elmer Model 202 ultraviolet–visible spectrophotometer. The samples were dissolved in absolute ethanol. The mass spectrum was performed by Morgan Schaffer Corporation, Montreal, Quebec. The elemental analyses were carried out by Galbraith Laboratories, Inc., Knoxville, Tenn. Thin layer chromatography was performed on Eastman Kodak silica gel fluorescent-indicator plates. The eluting solvents used were: (A) ethyl acetate: ethanol (1:2, v/v); (B) methanol:chloroform:concentrated ammonium hydroxide (4:4:1, v/v/v); (C) ethyl acetate. The plates were developed in the appropriate solvent. The solvent was removed by hot air and the plates were placed in an atmosphere of iodine vapors. Guanazole and the substituted guanazoles gave brown spots. The benzylidene derivatives were visible under the ultraviolet light. Authentic samples of guanazole, 1-methylguanazole, and 1-phenylguanazole were prepared according to Kaiser and Roemer (8).

[2]Infrared spectra are available upon request to J.A.L.

Can. J. Chem. Downloaded from www.nrcresearchpress.com by 210.87.254.6 on 09/05/12
For personal use only.

TABLE 4. Monobenzylidene derivatives of substituted guanazoles. Proton nuclear magnetic resonance spectra

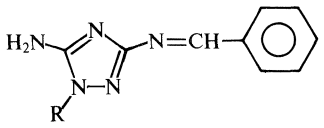

R	Chemical shifts (ppm)[a]	
H	7.20–8.40 (m, 5)	6.20 (s, 2 exch.)
	9.20 (s, 1)	12.23 (br, 1 exch.)
CH_3	3.60 (s, 3)	6.40 (s, 2 exch.)
	7.30–8.40 (m, 5)	
	9.13 (s, 1)	
$CH_2CH_2CH_3$	0.90 (t, 3)	6.43 (s, 2 exch.)
	1.78 (sextet, 2)	
	3.93 (t, 2)	
	7.33–8.40 (m, 5)	
	9.13 (s, 1)	
C_6H_5	7.26–8.30 (m, 10)	6.70 (s, 2 exch.)
	9.26 (s, 1)	
$CH_2C_6H_5$	5.28 (s, 2)	6.66 (s, 2 exch.)
	7.50(s) + 7.60–8.03(m)(10)	
	9.20 (s, 1)	
$CH_2CO_2CH_3$	3.76 (s, 3)	6.55 (s, 2 exch.)
	4.91 (s, 2)	
	7.35–8.25 (m, 5)	
	9.13 (s, 1)	

[a]Solvent: DMSO-d_6, TMS as internal standard. Abbreviations: s = singlet; br = broad; t = triplet; m = multiplet; exch. = exchangeable.

Alkylation Reactions of Guanazole

A typical procedure is illustrated with methyl iodide. Sodium methoxide (0.6 g, 0.011 mol) was added to a stirred solution of guanazole (1 g, *ca.* 0.01 mol) in methanol (100 ml). The solution thus obtained was heated under reflux and a solution of methyl iodide (1.72 g, 0.012 mol) in methanol (15 ml) was added dropwise over a period of 30 min. The reaction mixture was refluxed for an additional 20 min. The reaction mixture was then cooled and sodium methoxide (0.6 g, 0.011 mol) was added followed by the addition of a solution of methyl iodide (1.72 g, 0.012 mol) in methanol (15 ml). This new mixture was then refluxed for 3 h. The methanolic solution was evaporated. Ethanol was added to the semi-solid residue which was then neutralized with 2 *N* hydrochloric acid. A solution of picric acid (3.4 g) in a minimum amount of hot ethanol was added to the neutralized ethanolic solution. Upon cooling, the picrate (2.35 g, 68.7%) of the product melting at 253–258 °C was obtained. Two recrystallizations of a sample of the crude picrate raised the melting point to 266–267.5 °C (lit. (9) mp 273–274 °C). The compound was identified as 1-methylguanazole. The infrared spectrum was identical to that of the picrate of the product prepared from cyanoguanidine and methylhydrazine dihydrochloride: pmr 3.43 (s, 3), 7.75 (s, exch.), 8.65 (s, aromatic protons of picric acid). The picrate was dissolved in hot water and absorbed on AG-1, X-8, 100–200 mesh, anion exchange resin column in the acetate ion form, which retained the picric acid. The column was rinsed with water and the effluent was evaporated. The oily residue from the evaporation was dissolved in benzene and this solution was then evaporated to dryness. This process was repeated three times with the result that traces of water were eliminated. This final residue was crystallized from methanol – diethyl ether to give the free base corresponding to 1-methylguanazole (0.75 g, 66.3%) melting at 145 °C (lit. (9) mp 157–159 °C). The infrared spectrum of this product was identical to an authentic sample of 1-methylguanazole prepared from cyanoguanidine and methylhydrazine dihydrochloride. Proton magnetic resonance, ultraviolet, and infrared spectroscopies, and thin-layer chromatography confirmed the above results.

The following guanazole derivatives were similarly prepared.

(*a*) 1-*n*-Propylguanazole, 30% yield; picrate, mp 194–195 °C; free base, mp 110–112 °C (from ethanol–ether); uv (λ in nm, log ϵ) (213, 3.8); R_f 0.35 (solvent A); pmr 0.80 (t, 3), 1.56 (sextet, 2), 3.60 (t, 2), 4.66 (br, 2 exch.), 5.86 (s, 2 exch.). *Anal.* calcd. for $C_5H_{11}N_5$: N 49.65; found: N 49.04.

(*b*) 1-Benzylguanazole, 40% yield; picrate, mp 212–215 °C; free base, mp 169–170 °C (from benzene); uv (λ in nm, log ϵ) (210, 4.1); R_f 0.43 (solvent A); pmr 4.90 (s, 2), 7.30 (s, 5), 4.76 (br, 2 exch.), 6.08 (s, 2 exch.) *Anal.* calcd. for $C_9H_{11}N_5$: N 37.38; found: N 37.38.

Can. J. Chem. Downloaded from www.nrcresearchpress.com by 210.87.254.6 on 09/05/12
For personal use only.

TABLE 5. Dibenzylidene derivatives of substituted guanazoles. Proton nuclear magnetic resonance spectra

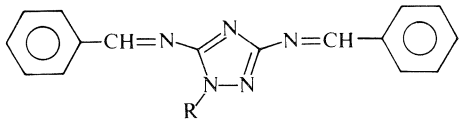

R	Chemical shifts (ppm)[a]	
H	7.25–8.53 (m, 10)	9.50 (s, 2)
CH_3	4.01 (s, 3)	9.36 (s, 1)
	7.40–8.46 (m, 10)	9.40 (s, 1)
$CH_2CH_2CH_3$	0.93 (t, 3)	9.40 (s, 1)
	1.90 (sextet, 2)	9.45 (s, 1)
	4.40 (t, 2)	
	7.30–8.35 (m, 10)	
$CH_2CH_2CH_3$[b]	1.00 (t, 3)	9.40 (s, 1)
	2.05 (sextet, 2)	9.46 (s, 1)
	4.42 (t, 2)	
	7.23–8.50 (m, 10)	
$CH_2CH_2CH_3$[c]	0.98 (t, 3)	9.26 (s, 1)
	1.98 (sextet, 2)	9.30 (s, 1)
	4.31 (t, 2)	
	6.98–8.61 (m, 10)	
C_6H_5	7.36–8.36 (m, 15)	9.45 (s, 1)
		9.52 (s, 1)
C_6H_5[b]	7.26–8.36 (m, 15)	9.46 (s, 1)
		9.53 (s, 1)
$CH_2C_6H_5$	5.66 (s, 2)	9.40 (s, 1)
	7.46(s) + 7.60–8.55(m)(15)	9.50 (s, 1)
$CH_2CO_2CH_2CH_3$	1.26 (t, 3)	9.42 (s, 1)
	4.30 (q, 2)	9.48 (s, 1)
	5.40 (s, 2)	
	7.32–8.47 (m, 10)	

[a]Solvent: DMSO-d_6, TMS as internal standard unless otherwise specified. Abbreviations: s = singlet; d = doublet; t = triplet; q = quartet; m = multiplet.
[b]Solvent: $CDCl_3$, TMS as internal standard.
[c]Solvent: CD_2Cl_2, TMS as internal standard.

(*c*) Methyl (3,5-diamino-1,2,4-triazolyl-1)acetate, 35% yield; picrate, mp 235–237 °C; free base, mp 179–181 °C; uv (λ in nm, log ε) (215, 3.8); R_f 0.35 (solvent A); pmr 3.71 (s, 3), 4.58 (s, 2), 4.81 (br, 2 exch.), 6.06 (br, 2 exch.). *Anal.* calcd. for $C_5H_9N_5O_2$: N 40.92; found: N 40.44.

(*d*) (3,5-Diamino-1,2,4-triazolyl-1)acetic acid, from alkaline hydrolysis of (*c*); 100% yield; mp 295 °C; uv (λ in nm, log ε) (215, 1.4); R_f 0.21 (solvent B); pmr 4.81 (s, 2) (solvent DMSO-d_6 + DCl/D_2O). *Anal.* calcd. for $C_4H_7N_5O_2 \cdot \frac{1}{2}H_2O$: C 30.57, H 5.13, N 42.15; found: C 31.07, H 5.68, N 42.80.

Preparation of the Monobenzylidene Derivatives of Guanazole and 1-Substituted Guanazoles

Equimolar amounts of guanazoles (where R = H, CH_3, $CH_2CH_2CH_3$, C_6H_5, $CH_2C_6H_5$, $CH_2CO_2CH_3$ at position 1) and benzaldehyde were stirred in ethanol for several hours at room temperature in the presence of sodium acetate. In most cases, the product crystallized from the reaction mixture. Alternatively, the reaction mixture was evaporated to dryness. The residue thus obtained was partitioned between chloroform and water. The organic layer was rinsed with water and dried over anhydrous sodium sulfate. The dried solution was filtered and the filtrate was evaporated to dryness. The crude monobenzylidene derivatives were recrystallized from the appropriate solvents as shown in Table 5.

Preparation of the Dibenzylidene Derivatives of Guanazole and 1-Substituted Guanazoles

The guanazoles and excess benzaldehyde in absolute ethanol were refluxed for several hours (when R = H, the reaction was completed in 1 h as shown by thin layer chromatography) in the presence of anhydrous sodium acetate, piperidine, or both basic catalysts. The resulting yellow solution was evaporated and the residue was partitioned between chloroform and water (in the case of guanazole itself, the dibenzylidene derivative crystallized from the reaction mixture). The chloroform layer was rinsed with water and dried over anhydrous sodium

Can. J. Chem. Downloaded from www.nrcresearchpress.com by 210.87.254.6 on 09/05/12
For personal use only.

sulfate. The dried solution was filtered and the filtrate was evaporated to dryness. The dibenzylidene derivative was obtained by recrystallization of the residue from the appropriate solvent as shown in Table 3.

1. (*a*) F. H. S. CURD, D. G. DAVEY, D. N. RICHARDSON, and R. B. ASHWORTH. J. Chem. Soc. 1739 (1949); (*b*) W. ZERWECK and K. KELLER. U.S. Patent No. 2 218 077 (October, 1940); (*c*) G. F. D'ALELIO and J. W. UNDERWOOD. U.S. Patent Nos. 2 295 566 (September, 1942); 2 312 320 (March 1943); 2 389 896 (November, 1945); (*d*) A. BAYLEY. U.S. Patent Nos. 2 395 776 (February, 1946); 2 406 654 (August, 1946); (*e*) J. K. SIMONS. U.S. Patent No. 2 456 090 (December, 1948); (*f*) G. W. KIDDER, C. DEWEY, R. E. PARKS, and G. L. WOODSIDE. Science, **109**, 511 (1949); (*g*) L. G. NICKELL, P. GREENFIELD, and P. R. BURKHOLDER. Bot. Gaz., **112**, 42 (1950); (*h*) H. C. KIRKPATRICK and R. C. LINDNER. Phytopathology, **44**, 529 (1954); (*i*) R. W. BROCKMAN, S. SHADDIX, W. R. LASTER, JR., and F. M. SCHABEL, JR. Cancer Res. **30**, 2358 (1970); (*j*) M. A. HAHN and R. H. ADAMSON. J. Natl. Cancer Inst. **48**, 783 (1972); (*k*) R. L. FYE and G. C. LABRECQUE. J. Econ. Entomol. **64**, 756 (1971); (*l*) L. H. CHANCE, J. P. MOREAU, and G. L. DRAKE, JR. J. Coated Fibrous Mat. **2**, 161 (1973); (*m*) C. DAVE and L. CABALLES. J. Pharm. Sci. **63**, 347 (1974).
2. A. KREUTZBERGER and B. MEYER. Arch. Pharm. **307**, 281 (1974).
3. P. PAPINI and S. CHECCHI. Gazz. Chim. Ital. **82**, 735 (1952).
4. V. V. MOZOLIS and S. P. JOKUBAITYTE. Liet. TSR Mokslu Akad. Darb. Ser. B, **5**, 95 (1973).
5. N. K. BERESNEVA, V. A. LOPYREV, and K. L. KRUPIN. Khim. Geterotsikl. Soedin. **5**, 848 (1969).
6. B. T. HEITKE and C. G. MCCARTY. Can. J. Chem. **52**, 2861 (1974).
7. K. T. POTTS, R. ARMBRUSTER, and E. HOUGHTON. J. Heterocycl. Chem. **8**, 773 (1971).
8. D. W. KAISER and J. J. ROMER, U.S. Patent Nos. 2 648 670 (August, 1953); 2 648 671 (August 1953).
9. W. P. NORRIS and R. A. HENRY. J. Org. Chem. **29**, 650 (1964).
10. R. STOLLÉ and W. DIETRICH. J. Prakt. Chem. **139**, 193 (1934).
11. G. PELLIZZARI and C. RONCAGLIOLO. Gazz. Chim. Ital. **31**, 477 (1901).

Can. J. Chem. Downloaded from www.nrcresearchpress.com by 210.87.254.6 on 09/05/12
For personal use only.

Etude du mécanisme de la formation de phosphates d'énols à partir de composés carbonyles α-halogénés et de trialcoylphosphites

EMILE M. GAYDOU

Institut Universitaire de Technologie de Marseille, rue des Géraniums, 13337 Marseille Cedex 3, France

ET

JEAN-PIERRE BIANCHINI

Ecole Supérieure de Chimie de Marseille, rue Henri Poincaré, 13397 Marseille Cedex 4, France

Reçu le 13 janvier 1976

EMILE M. GAYDOU et JEAN-PIERRE BIANCHINI. Can. J. Chem. **54**, 3626 (1976).

Des études cinétiques de ω-chloro- et ω-bromoacétophénones *méta*- et *para*-substituées sur divers trialcoylphosphites ont été effectuées en vue d'élucider le mécanisme de la formation des phosphates d'énols correspondants. Les valeurs pour les énergies d'activation, les entropies d'activation, ainsi que les constantes ρ de Hammett ont été déterminées. Le mécanisme de la réaction est discuté en tenant compte par ailleurs de la stéréochimie des produits obtenus dans le cas d'aldéhydes et de méthylcétones α-halogénées diversement substitués.

EMILE M. GAYDOU and JEAN-PIERRE BIANCHINI. Can. J. Chem. **54**, 3626 (1976).

Kinetic studies of the reactions of *meta*- and *para*- substituted ω-chloro- and ω-bromoacetophenones with various trialkylphosphites were done in order to elucidate the mechanism for the formation of the corresponding enols. Values were determined for the energies and entropies of activation as well as for the Hammett ρ constants. The mechanism of the reaction is discussed taking into account also the stereochemistry of the products obtained in the case of aldehydes and of variously substituted α-halogenated methylketones.

[Journal translation]

Les réactions faisant intervenir un phosphore trivalent sur un composé carbonylé α-halogéné, ont fait l'objet de nombreux travaux (1–4). L'action d'un trialcoylphosphite sur une cétone α-halogénée peut conduire à un mélange de phosphates d'énols (réaction de Perkow) et de β-cétophosphonates (réaction d'Arbuzov) suivant la nature du phosphite, de l'halogène, du composé carbonylé et des conditions opératoires.

Nos études cinétiques (7) ainsi que celles effectuées par d'autres chercheurs (5, 6, 8) sont en faveur d'une attaque préférentielle sur le carbone de la fonction carbonyle. Toutefois, il paraît difficile, à l'aide de ces seules données cinétiques de discuter de la nature de l'état de transition.

La stéréosélectivité de la réaction de Perkow (15, 16) apparait comme une méthode élégante pour aborder le problème de son mécanisme. En effet, il est possible dans certains cas d'obtenir les deux isomères géométriques *E* et *Z*:

L'influence de X (chlore ou brome) sur le rapport *E*/*Z* (15) nous a conduit à effectuer de nouvelles études cinétiques sur des ω-chloro- et des ω-bromoacétophénones diversement substituées, bien que cette étude ait déjà été partiellement abordée par Arcoria et Fisichella (5) dans le cas d'ω-chloroacétophénones *para*-substituées.

Nous avons rassemblé dans les tableaux 1 et 2 les différents composés carbonylés α-halogénés et les différents phosphites utilisés.

Résultats

Etude cinétique

Nous nous sommes proposés d'étudier la cinétique de la formation des phosphates d'énols à partir d'une série d'ω-haloacétophénones diversement substituées. Dans le cas où l'halogène est un atome de chlore il ne se forme que le phosphate d'énol. Lorsque l'halogène est un

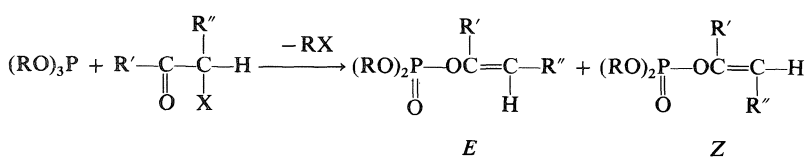

Can. J. Chem. Downloaded from www.nrcresearchpress.com by 210.87.254.6 on 09/05/12
For personal use only.

atome de brome, il est possible d'isoler un mélange de cétophosphonate *A* et de phosphate d'énol *P*.

Dans toutes les réactions de cinétiques ou de compétitions envisagées, nous avons vérifié que la formation du mélange vinylphosphate–céto-

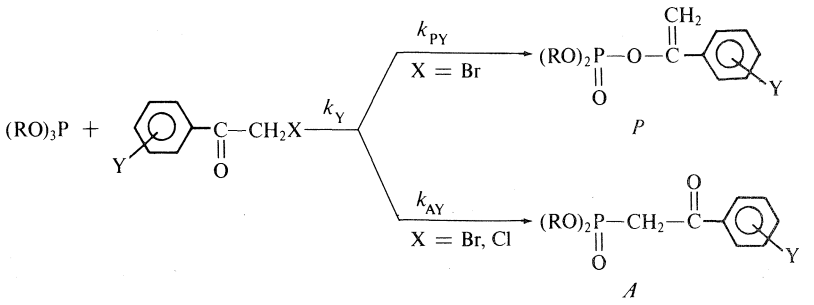

TABLEAU 1. Composés carbonylés α-halogénés utilisés

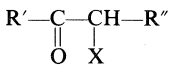

Composé[a]	X	R′	R″
1*a*	Cl	H	CH_3
1*b*	Br		
2*b*	Br	H	C_6H_5
3*a*	Cl	H	Cl
4*b*	Br	H	Br
5*a*	Cl	CH_3	CH_3
5*b*	Br		
6*a*	Cl	CH_3	C_6H_5
6*b*	Br		
7*a*	Cl	CH_3	CO_2CH_3
7*b*	Br		
8*b*	Br	CH_3	Br
9*a*	Cl	*p*-$CH_3OC_6H_4$	H
9*b*	Br		
10*b*	Br	*p*-$CH_3C_6H_4$	H
11*a*	Cl	C_6H_5	H
11*b*	Br		
12*b*	Br	*p*-FC_6H_4	H
13*a*	Cl	*p*-ClC_6H_4	H
13*b*	Br		
14*a*	Cl	*m*-BrC_6H_4	H
15*b*	Br	*p*-BrC_6H_4	H
16*a*	Cl	*m*-$NO_2C_6H_4$	H
17*b*	Br	*p*-$NO_2C_6H_4$	H

[a]Indice *a* pour les dérivés chlorés, *b* pour les dérivés bromés.

phosphonate dépasse 90–95%. La détermination du rapport [vinylphosphate]/[cétophosphonate] a été effectuée à l'aide de la chromatographie en phase gazeuse. L'identification des produits formés est aisée en résonance magnétique nucléaire (10–12). En effet, les protons vinyliques des phosphates d'énols apparaissent vers 5 à 6 ppm, alors que le méthylène du cétophosphonate se situe vers 3.2–3.6 ppm.

Les cinétiques dans le cas des halogénures de phénacyle **11***a* et **11***b* sur les trialcoylphosphites ont été déterminées en résonance magnétique nucléaire.

Nous avons vérifié que la réaction de Perkow est du premier ordre par rapport à la cétone α-halogénée et au phosphite. La vitesse de la réaction est donnée par la relation:

$$v = k[\text{trialcoylphosphite}][\text{cétone } \alpha\text{-halogénée}]$$

(A) Influence du solvant

L'influence du solvant ayant été étudiée dans le cas des cétones α-chlorées (7) nous ne l'avons abordée que dans le cas particulier du bromure de phénacyle **12***b* sur le triéthylphosphite **19** (tableau 3). On peut observer que la vitesse de la réaction de Perkow est peu modifiée lorsque l'on change la polarité du solvant. Elle passe en

TABLEAU 2. Phosphites utilisés: $(RO)_2P—OR'$

Composé	R	R′
18	CH_3	CH_3
19	C_2H_5	C_2H_5
20	*i*-C_3H_7	*i*-C_3H_7
21	*n*-C_4H_9	*n*-C_4H_9
22	*p*-$CH_3C_6H_4$	CH_3

Can. J. Chem. Downloaded from www.nrcresearchpress.com by 210.87.254.6 on 09/05/12
For personal use only.

TABLEAU 3. Influence du solvant sur la réaction du triéthylphosphite **19** sur le bromure de phénacyle **11***b*[a]

Solvant	Constante diélectrique (25)	k_P/k_A	$10^5 \times k_P$ ($l\ mol^{-1}\ s^{-1}$)
Benzène	2.3	1.032	10.15±0.03
Chlorobenzène	5.6	1.182	14.53±0.08
Acétonitrile	37.5	0.583	20.0 ±0.1

[a]Concentration initiale: $[(C_2H_5O)_3P] = 0.102\ mol\ l^{-1}$; $[C_6H_5COCH_2Br] = 0.155\ mol\ l^{-1}$. Température: 40.1 °C. k_P = constante de vitesse de la réaction de Perkow; k_A = constante de vitesse de la réaction de Arbuzov.

TABLEAU 4. Influence du groupement R du phosphite sur la réaction $(RO)_3P$ + halogénure de phénacyle dans le benzène[a]

Composé	R	X	$10^5 \times k$ ($M^{-1}s^{-1}$)	σ^* (22)	E_s (20)	k_{Cl}/k_{Br}	k(Et)/k(*i*-Pr)
18	CH_3	Cl	5.5	−0.000	0.00		
19	C_2H_5	Cl Br	7.4 10.15	−0.100	−0.07	0.73	0.42 1.35
20	$(CH_3)_2CH$	Cl Br	17.5 7.5	−0.190	−0.47	2.34	

[a]Concentration initiale: 0.1 *M* pour chaque constituant. Température: 40.1 °C.

effet de 10.15 dans le benzène à 20.0 dans l'acétonitrile. La vitesse de la réaction d'Arbuzov est beaucoup plus sensible à cette variation (23) ce qui se traduit par un changement important du rapport des constantes de vitesses de Perkow et d'Arbuzov k_P/k_A qui passe ainsi de 1.03 dans le benzène à 0.58 dans l'acétonitrile.

(B) Influence des groupements R du phosphite

Les mesures ont été faites avec les phosphites **18**, **19** et **20**, et les cétones **11***a* et **11***b* (tableau 4). On peut remarquer que la vitesse augmente, dans le cas du chlorure de phénacyle **11***a* en même temps que la constante σ^* (22). Ce phénomène avait déjà été observé par l'un de nous (7). Par contre la vitesse de la réaction diminue dans le cas du bromure de phénacyle **11***b*. Un résultat analogue a été signalé avec des isobutyrophénones α-bromées par Borowitz *et al.* (6). Il s'en suit que le rapport k_{Cl}/k_{Br} est très sensible à la nature des groupements R du phosphite.

(C) Influence de la température

Les mesures ont été effectuées avec des triéthyl et triisopropyl phosphites **19** et **20** sur le bromure de phénacyle **11***b* et à trois températures (tableau 5). Nous avons calculé les paramètres d'activation correspondants. Les énergies d'activation sont faibles et sont de l'ordre de grandeur de celles déjà connues pour la réaction de Perkow (6, 7). Les entropies d'activation sont fortement négatives (−44.5 et 49.0 ue).

(D) Influence des groupements substitués de la cétone

(a) Cas des cétones α-bromées—Cette étude a été réalisée dans le benzène à 40 °C à des concentrations de 0.1 mol l^{-1} en phosphite et en cétone. La détermination des produits résultant des réactions de Perkow et d'Arbuzov nous a permis de calculer le rapport des constantes de vitesse k_{PY}/k_{AY} de ces deux réactions pour chaque constituant Y et les trois phosphites **18**, **19** et **20**. Nous avons effectué des réactions de compétition entre une ω-bromoacétophénone *para*-substituée et le bromure de phénacyle pour un phosphite donné. Dans ces conditions, il est possible de calculer le rapport des constantes de vitesses globales k_Y/k_H. Une partie de ces résultats ayant été publiée (17, 23) dans le cas de la réaction d'Arbuzov, nous n'avons rassemblé dans les tableaux 6, 7 et 8

Can. J. Chem. Downloaded from www.nrcresearchpress.com by 210.87.254.6 on 09/05/12
For personal use only.

TABLEAU 5. Influence de la température et paramètres d'activation pour la réaction de Perkow relative à l'action des trialcoylphosphites **19** et **20** sur le bromure de phénacyle **11***b* dans le benzène[a]

R	Température (°C)	k_P/k_A	$10^5 \times k_P$ (l mol^{-1} s^{-1})	Paramètres d'activation de la réaction de Perkow E_a (kcal mol^{-1})	ΔH^{+b} (kcal mol^{-1})	ΔS^{+c} (ue)
C_2H_5	29.9	1.110	5.80±0.02			
19	40.4	1.032	10.15±0.03	10.7	10.05	−44.5
	50.0	0.930	17.30±0.04			
$(CH_3)_2CH$	29.9	0.815	4.50±0.02			
20	40.1	0.740	7.50±0.04	9.32	8.71	−49.0
	50.0	0.664	11.70±0.06			

[a]Concentration initiale: $[(RO)_3P] = 1.02$ mol l^{-1}; $[C_6H_5COCH_2Br] = 1.55$ mol l^{-1}.
[b]Déterminées par la méthode des moindres carrés ±1.0 kcal.
[c]Déterminées par la méthode des moindres carrés ±4 ue.

TABLEAU 6. Action du triméthylphosphite **18** sur les ω-bromoacétophénones *para*-substituées. Détermination du rapport des constantes de vitesse relatives à la réaction de Perkow k_{PY}/k_{PH}

Composé	Y	k_Y/k_H	k_{PY}/k_{AY}	k_{PY}/k_{PH}	log (k_{PY}/k_{PH})	σ (21)	σ^+ (20)
9*b*	CH_3O	0.715	0.22	0.214	−0.668	−0.268	−0.778
10*b*	CH_3	0.700	0.55	0.413	−0.384	−0.17	−0.311
11*b*	H	1.00	1.51	1.009	0.00	0.00	0.00
12*b*	F	1.07	1.87	1.16	0.064	0.062	−0.073
13*b*	Cl	1.41	4.00	1.87	0.273	0.227	0.114
15*b*	Br	1.63	4.54	2.22	0.346	0.232	0.150
17*b*	NO_2	6.34	52	10.3	1.015	0.778	0.790

TABLEAU 7. Action du triéthylphosphite **19** sur les ω-bromoacétophénones *para*-substituées. Détermination du rapport des constantes de vitesse relatives à la réaction de Perkow k_{PY}/k_{PH}

Composé	Y	k_Y/k_H	k_{PY}/k_{AY}	k_{PY}/k_{PH}	log (k_{PY}/k_{PH})
9*b*	CH_3O	0.630	0.173	0.183	−0.737
10*b*	CH_3	0.738	0.43	0.437	−0.359
11*b*	H	1.00	1.03	1.00	0.000
12*b*	F	1.05	1.24	1.156	0.063
13*b*	Cl	1.54	2.54	2.17	0.336
15*b*	Br	1.50	2.53	2.12	0.326
17*b*	NO_2	9.48	29	18.1	1.257

que les résultats qui permettront de déterminer les rapports des constantes de vitesses relatives à la réaction de Perkow pour le triméthyl, triéthyl et triisopropylphosphite **18**, **19** et **20**.

(b) Cas des cétones α-chlorées—Les réactions de compétition ont été effectuées dans le benzène à 40.0 °C à des concentrations de 0.1 mol l^{-1} en phosphite et en cétone. Dans tous les cas envisagés il ne se forme que le produit résultant de la réaction de Perkow. Nous avons rassemblé dans le tableau 9 les rapports des constantes de vitesses pour les phosphites **18**, **19** et **20**.

(c) Essai de corrélation—Si l'on porte sur un graphique log (k_{PY}/k_{PH}) en fonction des constantes $\sigma > 0$ (21), on obtient une bonne corrélation pour chacun des trois phosphites (tableau 10). Un traitement statistique nous a permis de déterminer les valeurs des constantes ρ de Hammett ainsi que les coefficients de cor-

Can. J. Chem. Downloaded from www.nrcresearchpress.com by 210.87.254.6 on 09/05/12
For personal use only.

Can. J. Chem. Downloaded from www.nrcresearchpress.com by 210.87.254.6 on 09/05/12
For personal use only.

TABLEAU 8. Action du triisopropylphosphite **20** sur les ω-bromoacétophénones *para*-substituées. Détermination du rapport des constantes de vitesse relatives à la réaction de Perkow k_{PY}/k_{PH}

Composé	Y	k_Y/k_H	k_{PY}/k_{AY}	k_{PY}/k_{PH}	$\log (k_{PY}/k_{PH})$
9*b*	CH_3O	0.552	0.14	0.159	−0.797
10*b*	CH_3	0.660	0.33	0.389	−0.409
11*b*	H	1.00	0.74	1.00	0.000
12*b*	F	1.20	0.94	1.36	0.134
13*b*	Cl	1.82	1.65	2.66	0.425
15*b*	Br	2.02	1.81	3.06	0.485
17*b*	NO_2	12.4	13.5	27.1	1.434

TABLEAU 9. Action des trialcoylphosphites **18**, **19** et **20** sur les ω-chloroacétophénones diversement substituées. Détermination du rapport des constantes de vitesse relatives à la réaction de Perkow k_Y/k_H

				18 R = CH_3		**19** R = C_2H_5		**20** R = $(CH_3)_2CH$	
Composé	Y	σ (21)	σ^+ (20)	k_Y/k_H	$\log (k_Y/k_H)$	k_Y/k_H	$\log (k_Y/k_H)$	k_Y/k_H	$\log (k_Y/k_H)$
9*a*	*p*-OCH_3	−0.268	−0.778	0.0457	−1.34	0.776	−1.11	0.10	−1.00
11*a*	*p*-H	0.00	0.00	1.00	0.00	1.00	0.00	1.00	0.00
13*a*	*p*-Cl	0.227	0.114	2.09	0.32	2.24	0.35	2.51	0.40
14*a*	*m*-Br	0.391	0.405	4.17	0.62	5.49	0.74	6.60	0.82
16*a*	*m*-NO_2	0.710	0.674	10.5	1.02	20.4	1.31	33.1	1.52

TABLEAU 10. Action des trialcoylphosphites $(RO)_3P$ **18**, **19** et **20** sur les halogénures de phénacyle $C_6H_5COCH_2X$. Détermination des constantes ρ de Hammett et des coefficients de corrélation r

			σ (21)		$\sigma > 0$ (21)		σ^+ (20)	
X	Composé	R	ρ	r	ρ	r	ρ	r
Cl	**18**	CH_3	2.280	0.943	1.452	0.998	1.635	0.995
Cl	**19**	CH_3CH_2	2.381	0.979	1.876	0.998	1.646	0.996
Cl	**20**	$(CH_3)_2CH$	2.501	0.991	2.171	0.998	1.693	0.987
Br	**18**	CH_3	1.552	0.984	1.312	0.998	1.120	0.986
Br	**19**	CH_3CH_2	1.817	0.992	1.641	0.999	1.303	0.987
Br	**20**	$(CH_3)_2CH$	2.058	0.990	1.827	0.999	1.473	0.984

TABLEAU 11. Réaction de

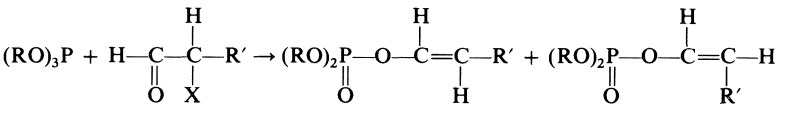

E *Z*

Essai n°	Phosphite	Aldéhyde	Phosphate R′	*E* (%)	*Z* (%)
1	**18**	**1***a*	CH_3	75	25
2	**19**	**1***a*	CH_3	75	25
3	**21**	**1***a*	CH_3	80	20
4	**22**	**1***a*	CH_3	90	10
5	**18**	**1***b*	CH_3	>95	<5
6	**18**	**2***b*	C_6H_5	100	0
7	**18**	**3***a*	Cl	80	20
8	**18**	**4***b*	Br	95	5
9	**21**	**4***b*	Br	>95	<5

rélation *r*. La valeur de ρ varie de 1.45 à 2.17 lorsque l'on passe du triméthyl au triisopropylphosphite, dans le cas de cétones α-chlorées. Il est à noter que la valeur de ρ que nous obtenons pour le triéthylphosphite (1.88) est très proche de celle obtenue par Arcoria et Fisichella (5) puisqu'ils trouvent 1.89. Dans le cas des cétones bromées, les valeurs de ρ sont plus faibles et sont comprises entre 1.31 et 1.83. Si l'on tient compte de l'ensemble des valeurs de σ (positives et négatives) les coefficients de corrélation sont d'une façon générale plus faibles.

On peut remarquer que ce coefficient de corrélation s'améliore lorsque l'on passe d'une part du triméthyl au triisopropylphosphite et d'autre part des cétones α-chlorées aux cétones α-bromées. Une meilleure corrélation est obtenue en utilisant les constantes σ^+ (20), mais en revanche *r* devient moins bon lorsque l'effet donneur d'électrons des groupements alcoyle du phosphite augmente et lorsque l'on passe des cétones α-chlorées aux cétones α-bromées. D'une façon générale on observe une bonne corrélation avec σ^+ dans le cas des cétones α-chlorées avec le triméthyl ou le triéthylphosphite et une bonne corrélation avec σ dans le cas des cétones α-bromées avec le triéthyl ou le triisopropylphosphite.

Stéréosélectivité de la réaction de Perkow

Nous avons abordé la stéréosélectivité de la réaction de Perkow en faisant intervenir d'une part l'encombrement stérique au niveau des composés carbonylés α-halogénés, d'autre part en envisageant l'influence de la nature de l'halogène (chlore ou brome) et l'encombrement stérique au niveau du phosphite. Lorsque l'on fait varier ces différents facteurs, il est possible d'observer la formation de phosphates d'énols *Z* et *E*. Les proportions des différents produits

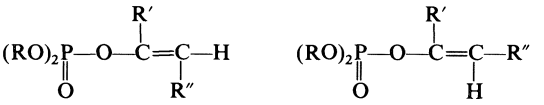

Z *E*

ont été déterminées par rmn ou par cpg (10), l'analyse en spectrométrie de masse se révélant assez délicate pour identifier les deux isomères géométriques (14).

(A) Cas des aldéhydes α-halogénés

Dans tous les cas envisagés, le phosphate d'énol *E* est prépondérant (tableau 11). On peut constater, par ailleurs, que le rapport *E*/*Z* varie très peu suivant la nature du phosphite et de l'halogène. La température et le solvant n'ont que très peu d'influence sur ce rapport aux erreurs d'expérience près.

(B) Cas des méthylcétones α-halogénées

Lorsque l'halogène est un atome de chlore, on constate la formation prépondérante du dérivé *E* (tableau 12). La variation du substituant R′ de la cétone (CH_3, C_6H_5, $CO_2C_2H_5$)

Can. J. Chem. Downloaded from www.nrcresearchpress.com by 210.87.254.6 on 09/05/12
For personal use only.

TABLEAU 12. Réaction

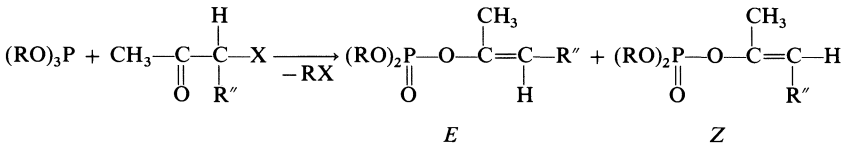

E *Z*

Essai n°	Phosphite	Cétone	Phosphate R″	*E* (%)	*Z* (%)
10	**18**	**5***a*	CH_3	75	25
11	**18**	**5***b*	CH_3	35	65
12	**18**	**6***a*	C_6H_5	62	38
13	**18**	**6***b*	C_6H_5	25	75
14	**19**	**6***a*	C_6H_5	65	35
15	**19**	**6***b*	C_6H_5	20	80
16	**18**	**7***a*	CO_2CH_3	70	30
17	**18**	**7***b*	CO_2CH_3	20	80
18	**18**	**8***b*	Br	>95	<5

TABLEAU 13. Influence de R sur la réaction

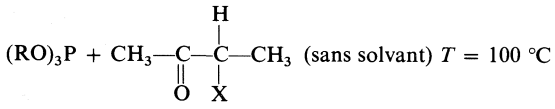

Essai n°	R	X	Phosphates (%) *E*	*Z*
10	CH_3	Cl	75	25
11		Br	35	65
19	C_2H_5	Cl	80	20
20		Br	29	71
21	n-C_4H_9	Cl	85	15
22		Br	25	75

TABLEAU 14. Influence du solvant sur la réaction

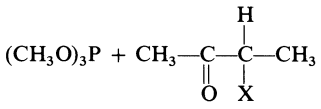

Essai n°	Solvant	X	Phosphates (%) *E*	*Z*
10	Sans	Cl	75	25
11	(T = 100 °C)	Br	35	65
23	Dioxanne	Cl	72	28
24	à reflux	Br	35	65
25	Acétonitrile	Cl	75	25
26	à reflux	Br	36	64

n'affecte que très peu le rapport E/Z, pas plus que la nature du phosphite (tableau 13), que la réaction ait lieu avec ou sans solvant (tableau 14). Dans le cas des cétones α-bromées, c'est le dérivé *Z* qui est prépondérant, excepté pour l'α,α-dibromoacétone **8***b* (essai 18). En effet, dans le cas de composé carbonylé fortement encombré, la formation du phosphate d'énol correspondant résulterait d'une attaque du phosphite sur l'halogène (16). Dans le cas des phénylcétones, le phosphate d'énol *Z* est généralement prépondérant (11*b*, 15) cependant on peut remarquer que le rapport E/Z est très sensible à la nature du phosphore trivalent (tableau 15).

TABLEAU 15. Influence des groupements R et R′ du phosphore trivalent sur la réaction (11*b*):

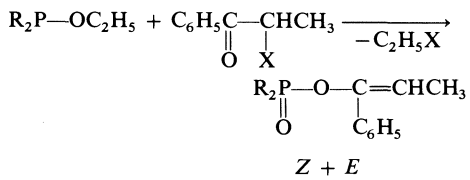

Z + *E*

X	R	*E* (%)	*Z* (%)
Cl	C_6H_5	40	60
Cl	OC_2H_5	61	39
Br	C_6H_5	50	50
Br	OC_2H_5	70	30

Can. J. Chem. Downloaded from www.nrcresearchpress.com by 210.87.254.6 on 09/05/12
For personal use only.

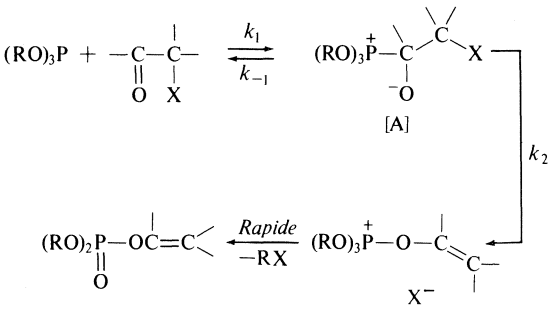

SCHÉMA 1

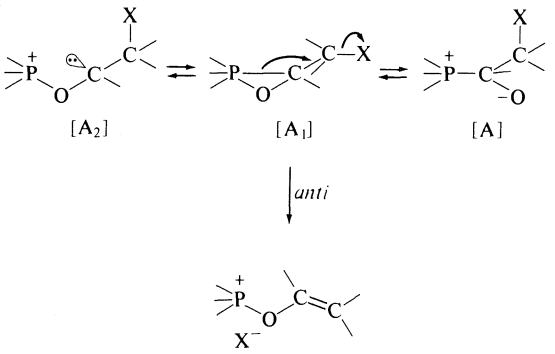

SCHÉMA 2

Discussion des résultats

Il est admis que la réaction d'addition d'un nucléophile sur un groupement carbonylé est réversible (19, 31). Le phosphite peut donc s'additionner sur le carbone du carbonyle suivant une réaction d'addition réversible dont la constante de vitesse apparente est k_1. L'intermédiaire [A] formé se décompose ensuite suivant une réaction, dont la constante de vitesse est k_2, pour donner le sel d'énol phosphonium (schéma 1). Dans ces conditions, il est possible d'envisager un état de transition situé entre les réactifs et le composé [A] et un autre, entre ce dernier et le sel d'énolphosphonium. De ces deux états de transition celui qui déterminera la stéréochimie de la réaction, dépendra de la valeur du rapport k_1/k_2.

Dans le cas où $k_2 > k_{-1}$, la première étape de la réaction ne sera pas réversible, la structure de l'état de transition sera proche des réactifs (32).

Dans le cas où $k_2 < k_{-1}$, la première étape de la réaction sera réversible et la nature des produits formés dépendra de la structure de [A] dans l'état de transition (30). Il est difficile d'émettre

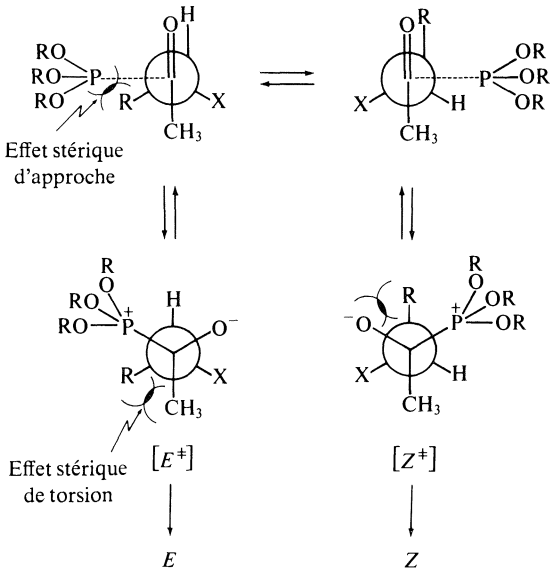

SCHÉMA 3

une hypothèse en ce qui concerne la structure de [A]. On peut envisager un hétérocycle à trois atomes de type oxaphosphoriranne [A_1], faisant intervenir un atome de phosphore pentacoordiné. Il est possible d'envisager aussi un dérivé oxanionique [A] ou carbanionique [A_2]. Ces trois intermédiaires pouvant conduire, par une réaction d'élimination *anti*-périplanaire au sel d'énolphosphonium (schéma 2).

En effet, bien que les réactions d'élimination *syn*-périplanaires soient possible (33, 34) nous avons constaté que ce type d'élimination ne se produit pas en étudiant la réactivité des phosphites sur des cétones bicycliques α-halogénées dont les conformations bloquées sont déterminées sans ambiguité (18).

La littérature est assez riche en ce qui concerne l'analyse conformationnelle des aldéhydes et des cétones α-halogénées (24). Il s'en suit que l'on peut envisager deux attaques du phosphite sur le composé carbonylé α-halogéné (schéma 3).

Les résultats consignés dans les tableaux 11 à 14 montrent que la formation du phosphate d'énol *E* est prépondérante dans le cas des aldéhydes α-halogénés et des méthylcétones α-chlorées. La formation des phosphates d'énol *Z* est prépondérante dans le cas des méthylcétones α-bromées et des phénylcétones α-halogénées. Il semble donc possible d'envisager

Can. J. Chem. Downloaded from www.nrcresearchpress.com by 210.87.254.6 on 09/05/12
For personal use only.

deux états de transition $[E^{\pm}]$ et $[Z^{\pm}]$ (schéma 3). Quelle que soit la structure exacte de l'état de transition, il apparait clairement que les contraintes stériques d'approche et de torsion seront plus importantes dans $[E^{\pm}]$ que $[Z^{\pm}]$ (15). L'effet stérique d'approche dans le cas des méthylcétones α-chlorées, sera compensé par l'effet inducteur de l'atome de chlore. Dans le cas des méthylcétones α-bromées l'intermédiaire $[Z^{\pm}]$ sera prépondérant car l'effet inductif de l'atome de brome est insuffisant bien que l'attaque ait lieu sur la conformation prépondérante (24).

Les énergies d'activation que nous obtenons (10.7 et 9.32 kcal mol^{-1} pour les triéthyl et triisopropylphosphites) sont plus faibles que celles obtenues pour la réaction d'Arbuzov (23). Les entropies d'activation sont fortement négatives et on peut supposer que ceci est dû à l'encombrement du phosphite. En effet, ΔS passe de -38.2 ue (7) dans le cas de la réaction du triméthylphosphite sur le chlorure de phénacyle à -49.0 ue (tableau 5) dans le cas du triisopropylphosphite sur le bromure de phénacyle. On peut penser que l'angle des liaisons O—P—O augmente lorsque le transfert de charge s'effectue au niveau de l'atome de phosphore (23) et que l'état de transition $[E^{\pm}]$ est assez avancé, proche d'un carbone sp^3 (15) ou d'un intermédiaire de type carbanionique ce qui expliquerait la participation des électrons du cycle aromatique et une meilleure corrélation avec σ^+.

L'état de transition $[Z^{\pm}]$ (cas des phénylcétones et des méthylcétones α-bromées) sera plus proche des produits de départ ce qui explique que la participation des électrons du noyau aromatique dans le cas des acétophénones α-bromées est difficile à mettre en évidence puisque l'on observe une meilleure corrélation avec σ. Ceci peut s'expliquer aussi par le fait que le départ d'un atome de brome est beaucoup plus rapide que celui d'un atome de chlore.

Partie expérimentale

I. Produits

Composés carbonylés α-halogénés

Les préparations des composés **1***a*, **4***b*, **5***a*, **6***a*, **9***b* et **10***b* ont été décrites précédemment (13*a*, 13*b* et 23). Les composés **1***b* (25), **2***b* (26), **5***b* (27), **6***b* (29), **7***b* (28) ont été obtenus par bromation directe des aldéhydes, cétones ou esters correspondants. Les autres produits sont commerciaux. Les ω-bromoacétophénones commerciales ont été recristallisées plusieurs fois dans l'éthanol à 95% jusqu'à ce que l'on obtienne un seul spot en ccm.

Phosphites

La préparation du composé **22** a été décrite précédemment (13*a*). Les autres trialcoylphosphites utilisés sont commerciaux. Ils ont été débarrassés des dialcoylphosphites correspondants par action du sodium en solution étherée. Après plusieurs distillations on obtient des produits purs.

II. Cinétiques

Les cinétiques ont été effectuées à l'aide de cellules comportant deux compartiments dont l'un contient la cétone bromée et l'autre le phosphite. L'ensemble est maintenu sous atmosphère d'azote. Après mise en température, le mélange est réalisé par agitation. Les concentrations utilisées sont indiquées dans les tableaux.

(a) Cinétiques par résonance magnétique nucléaire

Cette technique a été utilisée dans le cas des halogénures de phénacyle **11***a* et **11***b* sur les phosphites **18**, **19** et **20**. Les prélèvements sont effectués à intervalles réguliers à l'aide d'une seringue. Pour chaque détermination de constante de vitesse 10 à 12 prélèvements ont été effectués dans la zone correspondant à la formation de 20 à 70% de produits. La référence interne est le *p*-xylène pour tous les solvants utilisés, sauf dans le cas de l'acétonitrile où nous avons choisi le triphénylméthane. La détermination du degré d'avancement de la réaction est effectuée en comparant les rapports d'intégration des protons vinyliques et de la référence. Chaque prélèvement est dilué (ce qui a pour effet de stopper la réaction) puis enregistré deux fois sans TMS et on effectue quatre intégrations de plus grande amplitude possible.

Dans le cas de la cétone bromée **11***b*, la détermination du rapport [énolphosphate]/[cétophosphonate] à l'aide de la chromatographie en phase gazeuse nous permet de calculer d'une part les constantes de vitesse globale et d'autre part les constantes de vitesse relatives aux réactions de Perkow et d'Arbuzov. Les calculs ont été effectués par voie statistique (7). La précision des résultats obtenus est indiquée dans chaque tableau.

(b) Réactions de compétition

Ces réactions ont été étudiées à l'aide de la chromatographie en phase gazeuse. Les surfaces des pics ont été corrigées à l'aide de coefficients de réponse déterminés par étalonnage avec des produits purs. L'appareil utilisé est un Intersmat I.G.C. 12, détecteur à ionisation de flamme, colonne $\frac{1}{8}$ in. × 2 m phase silicone S.E. 30 à 5%, support Chromosorb WAW D.M.C.S. 80/100 mesh; gaz vecteur azote U, débit 20 cm^3/min; température du four 180 à 240 °C suivant les produits; intégrateur: Autolab.

Dans tous les cas envisagés, lorsqu'il se forme un phosphonate (cas des acétophénones α-bromées), le temps de rétention de ce dernier est supérieur à celui du phosphate d'énol correspondant. On utilise la relation (31):

$$\frac{k_Y}{k_H} = \frac{\log([Y]_i/[Y]_f)}{\log([H]_i/[H]_f)} = \frac{k_{YP} + k_{YA}}{k_{HP} + k_{HA}}$$

Par ailleurs, la détermination des rapports $k_{PY}/k_{AY} = \alpha'$ et $k_{PH}/k_{AH} = \alpha$ nous permet de calculer la valeur des rapports:

$$\frac{k_{YP}}{k_{HP}} = \frac{k_Y}{k_H}\frac{1 + 1/\alpha}{1 + 1/\alpha'}$$

Can. J. Chem. Downloaded from www.nrcresearchpress.com by 210.87.254.6 on 09/05/12
For personal use only.

Can. J. Chem. Downloaded from www.nrcresearchpress.com by 210.87.254.6 on 09/05/12
For personal use only.

Chaque réaction de compétition a été effectuée au minimum deux fois, et l'analyse du milieu réactionnel quatre fois. La reproductibilité des mesures est de l'ordre de 2%. Les calculs et la détermination des constantes ρ de Hammett ont été effectuées par voie statistique (7). Les valeurs des constantes σ utilisées sont indiquées dans les tableaux.

III. Détermination des pourcentages E et Z des produits de réaction

Elle a été effectuée par chromatographie en phase gazeuse. Les conditions, l'appareil utilisé ainsi que la reproductibilité des mesures sont celles décrites au paragraphe II-*b*. Un bon accord est obtenu avec le dosage des protons de l'enchaînement vinylique par résonance magnétique nucléaire (appareil Varian A60). L'identification des composés *E* et *Z* a été effectuée par résonance magnétique nucléaire du ^1H (10 à 12). Divers essais d'isomérisation $E \rightleftarrows Z$ ont été effectués sur quelques échantillons à l'état pur ou sur le mélange réactionnel. L'isomérisation thermique est extrêmement lente et ne se produit pas dans l'appareil de cpg.

Mode opératoire utilisé

Les produits sont fraîchement distillés ou recristallisés avant la manipulation. Les solvants utilisés sont rigoureusement anhydres et les manipulations sont effectuées sous atmosphère d'azote purifié.

(a) Sans solvant—Le phosphite (0.05 mol) et le composé carbonylé α-halogéné (0.05 mol) sont mélangés, sans solvant et portés à une température de 100 à 150 °C (13) pendant 0.1 à 0.5 h. Le mélange résiduel est ensuite analysé. L'identification est effectuée à l'aide de produits de références préalablement synthétisés.

(b) Avec solvant—A 15 cm^3 de solvant, on ajoute la cétone (0.05 mol) et le phosphite (0.05 mol). On porte à reflux pendant 1 à 2 h. Le mélange est ensuite analysé après avoir chassé le solvant.

1. F. W. Lichtenthaller. Chem. Rev. **61**, 607 (1961).
2. R. F. Hudson. Structure and mechanism in organophosphorus chemistry. Academic Press, New York. 1965. pp. 135–153.
3. B. Miller. Top. Phosphorus Chem. **2**, 178 (1965).
4. A. J. Kirby et S. G. Warren. The organic chemistry of phosphorus. Elsevier, New York. 1967. pp. 37–123.
5. A. Arcoria et S. Fisichella. Tetrahedron Lett. 3347 (1971).
6. I. J. Borowitz, S. Firstenberg, G. B. Borowitz et D. Schuessler. J. Am. Chem. Soc. **94**, 1623 (1972).
7. E. M. Gaydou, G. Buono et R. Freze. Bull. Soc. Chim. Fr. 2284 (1972).
8. J. Konecny, R. Dousse et J. Rosales. Helv. Chim. Acta, **55**, 3048 (1972).
9. D. B. Denney et F. A. Wagner, Jr. Phosphorus, **3**, 27 (1973).
10. (*a*) E. M. Gaydou, J. R. Llinas, G. Peiffer et A. Guillemonat. Ann. Fac. Sci. Marseille, **43**, 83 (1970); (*b*) E. M. Gaydou. Tetrahedron Lett. 4469 (1972); (*c*) E. M. Gaydou et J. R. Llinas. Org. Magn. Reson. **6**, 23 (1974); (*d*) E. M. Gaydou. Can. J. Chem. **51**, 3412 (1973).
11. (*a*) I. J. Borowitz, S. Firstenberg, E. W. R. Casper et R. K. Crouch. J. Org. Chem. **36**, 3282 (1971); (*b*) I. J. Borowitz, K. C. Yee et R. K. Crouch. J. Org. Chem. **38**, 1713 (1973).
12. C. B. C. Boyce, S. B. Webb, L. Phillips et P. A. Worthington. J. Chem. Soc. Perkin Trans. I, 2881 (1973).
13. (*a*) E. M. Gaydou. Bull. Soc. Chim. Fr. 2275 (1973); (*b*) E. M. Gaydou, R. Freze et G. Buono. Bull. Soc. Chim. Fr. 2279 (1973).
14. (*a*) E. M. Gaydou, G. Peiffer et M. Etienne. Org. Mass Spectrom. **9**, 157 (1974); (*b*) E. M. Gaydou et G. Peiffer. Org. Mass. Spectrom. **9**, 514 (1974).
15. E. M. Gaydou. Tetrahedron Lett. 4473 (1972).
16. I. J. Borowitz et R. K. Crouch. Phosphorus, **2**, 209 (1973).
17. E. M. Gaydou et J. P. Bianchini. Chem. Commun. 541 (1975).
18. E. M. Gaydou. Travaux non publiés.
19. (*a*) Y. Ogata et M. Yamashita. J. Am. Chem. Soc. **90**, 4670 (1970); (*b*) Y. Ogata et M. Yamashita. Tetrahedron, **27**, 2725 (1971); (*c*) Y. Ogata et M. Yamashita. Tetrahedron, **27**, 3395 (1971); (*d*) Y. Ogata et M. Yamashita. J. Org. Chem. **36**, 2584 (1971).
20. P. R. Wells. Chem. Rev. **63**, 171 (1963).
21. H. H. Jaffe. Chem. Rev. **53**, 191 (1953).
22. R. W. Taft, Jr. J. Am. Chem. Soc. **75**, 4231 (1953).
23. E. M. Gaydou et J. P. Bianchini. Bull. Soc. Chim. Fr. 2643 (1975).
24. E. M. Gaydou. Thèse, Marseille, N° C.N.R.S. A.O. 7802. 1972.
25. (*a*) M. Poite. Thèse, Marseille. 1961; (*b*) J. J. Riehl. C. R. Acad. Sci. **245**, 1321 (1957); (*c*) M. Chanon et J. Metzger. Bull. Soc. Chim. Fr. 2842 (1968).
26. J. J. Riehl. C. R. Acad. Sci. **245**, 1321 (1957).
27. J. R. Catch et D. F. Elliott. J. Chem. Soc. 1278 (1948).
28. (*a*) Epprecht. Ann. **278**, 79 (1894); (*b*) A. T. Blomquist et F. H. Balowin. J. Am. Chem. Soc. **70**, 29 (1948).
29. (*a*) M. Gaudry et A. Marquet. Bull. Soc. Chim. Fr. 4169 (1969); (*b*) M. Gaudry et A. Marquet. Tetrahedron, **26**, 5611 (1970); **26**, 5617 (1970).
30. E. L. Eliel. Stereochemistry of carbon compounds. McGraw-Hill, New York. 1962. p. 149.
31. S. Patai. The chemistry of the carbonyl group. John Wiley, New York. 1966. Chapt. 12.
32. (*a*) S. Winstein et N. J. Holness. J. Am. Chem. Soc. **77**, 5562 (1955); (*b*) E. L. Eliel et R. S. Ro. Chem. Ind. (London), 251 (1956); (*c*) E. L. Eliel et C. A. Lukach. J. Am. Chem. Soc. **79**, 5986 (1957); (*d*) E. L. Eliel, N. L. Allinger, S. J. Angyal et G. A. Morrison. Conformational analysis. Interscience Publishers, New York. 1966. p. 48.
33. (*a*) J. Sicher, J. Zavada et J. Krupicka. Tetrahedron Lett. 1619 (1966); (*b*) J. Sicher, J. Zavada et M. Pankova. Chem. Commun. 1147 (1968); (*c*) J. Sicher. Angew. Chem. Int. Ed. Engl. **11**, 200 (1972).
34. (*a*) D. S. Bailey et W. H. Saunders, Jr. J. Am. Chem. Soc. **92**, 6904 (1970); (*b*) D. S. Bailey, F. C. Montgomery, G. W. Chodak et W. H. Saunders, Jr. J. Am. Chem. Soc. **92**, 6911 (1970).

Canadian Journal of Chemistry

Published by
THE NATIONAL RESEARCH COUNCIL OF CANADA

Journal canadien de chimie

Publié par
LE CONSEIL NATIONAL DE RECHERCHES DU CANADA

Volume 54 Number 23 December 1, 1976 Volume 54 numéro 23 1 decembre 1976

Can. J. Chem. Downloaded from www.nrcresearchpress.com by 210.87.254.40 on 09/05/12
For personal use only.

The *cis–trans* isomerization of the radical anion of biacetyl

A. John Elliot and Jeffrey K. S. Wan
Department of Chemistry, Queen's University, Kingston, Ont., Canada K7L 3N6

Received July 19, 1976

A. John Elliot and Jeffrey K. S. Wan. Can. J. Chem. **54**, 3637 (1976).

The equilibrium between the *cis* and the *trans* isomers of the biacetyl radical anion has been studied by esr spectroscopy. The dependence of this equilibrium on the solvent composition and temperature was followed.

A. John Elliot et Jeffrey K. S. Wan. Can. J. Chem. **54**, 3637 (1976).

On a étudié, grâce à la rpe, l'équilibre entre les isomères *cis* et *trans* du radical anion du biacétyle. On a établi la relation entre cet équilibre et la composition du solvant ainsi que la température.

[Traduit par le journal]

Introduction

The ketyl radicals which are formed when biacetyl is photoreduced in alcoholic solvents have their electron spin states abnormally populated so that the esr spectrum shows emissive initial (triplet mechanism) polarization in addition to the expected emissive–absorptive (radical-pair mechanism) polarization (1). The presence of the initial polarization is surprising because the slow rate of hydrogen abstraction by the triplet biacetyl from alcohols should have permitted any non-thermal population distribution within the triplet manifold, the origin of this polarization (2), to have disappeared. To probe this anomaly, we have been looking into the photoreduction of biacetyl in the presence of triethylamine (TEA) which is considered (3) to be a more effective quencher. However, because TEA is a base, the semidione radical anion of biacetyl is formed in these experiments rather than the ketyl radical. Furthermore, it has been reported (4, 5) that this radical anion can exist in both the *cis* and *trans* configuration:

[1] 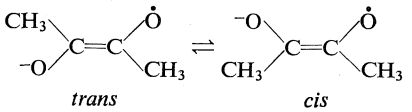

trans *cis*

Our preliminary experiments confirmed the existence of these isomers and we found that the ratio of *cis* to *trans* isomer changed depending on the solvent used, the temperature, and the TEA concentration. Before any CIDEP studies could be undertaken, we have had to characterize this *cis–trans* isomerization of the semidione radical anion of biacetyl.

Russell and co-workers (4) studied the isomers in DMSO at 25 °C. They considered the isomers to be in equilibrium with a constant $K = [cis]/[trans] \approx 5 \times 10^{-2}$. However, they reported that the equilibrium was shifted towards the *cis* form when sodium or lithium ions were added to the solution due to the formation of chelating ion pairs.

Norman and Pritchett (5) have studied the isomers in aqueous solutions at p$H \approx 7$. When the radical anion was generated by reduction of biacetyl with $\dot{C}H_2OH$, the ratio of *cis* to *trans* form was $\sim 5 \times 10^{-2}$. However, when the radical anion was formed by the reaction of hydroxyl radicals with acetoin, the ratio was unity. As one or both of these systems appeared not to be in thermodynamic equilibrium, they suggested (5) that the approach to equilibrium was kinetically controlled and it had not been reached under

Can. J. Chem. Downloaded from www.nrcresearchpress.com by 210.87.254.40 on 09/05/12
For personal use only.

their experimental conditions in which the radicals resided in the cavity for only about 0.1 s.

Experimental

The radicals were generated photolytically in the cavity of a Varian E-3 esr spectrometer with light from a 200 W high pressure mercury lamp. The temperature was varied by flowing thermostated nitrogen past the sample. In those experiments where the temperature was changed, the solutions were photolyzed in Pyrex cells and were not flowed. In these static samples, the biacetyl concentration (1.8 mol dm^{-3}) was sufficiently high to ensure depletion did not occur during the experiments. A lower biacetyl concentration (0.2 mol dm^{-3}) was used in those experiments where the solution was photolyzed as it flowed through a flat quartz cell in the cavity. All solutions were deoxygenated by bubbling with nitrogen.

In some experiments the biacetyl radical anion ($B\dot{A}^-$) was generated by photolyzing biacetyl (BA) dissolved in an alcohol in the presence of TEA. The TEA concentration was always sufficient to ensure the triplet state of biacetyl (BA*) was quenched by the amine and not the solvent (3):

[2] $$BA + h\nu \wavy BA^*$$

[3] $$BA^* \xrightarrow{TEA} B\dot{A}^-$$

The anion was also produced by photolyzing a slowly flowing phosphate buffered (p*H* 7) aqueous solution containing 0.2 mol dm^{-3} biacetyl and 1 mol dm^{-3} 2-propanol. Here the triplet biacetyl was quenched by the 2-propanol

[4] $$BA^* \xrightarrow{\text{2-propanol}} B\dot{A}^-$$

There were probably two mechanisms for the formation of the biacetyl radical anion when phosphate buffered (p*H* 7) aqueous solutions contain 2 vol% hydrogen peroxide and 0.2 mol dm^{-3} acetoin were photolyzed:

[5] $$H_2O_2 + h\nu \rightarrow 2\dot{O}H$$

[6] $$\dot{O}H + CH_3CHOHCOCH_3 \rightarrow B\dot{A}^-$$

and

[7] $$CH_3CHOHCOCH_3 + h\nu \rightarrow (CH_3CHOHCOCH_3)^*$$

[8] $$(CH_3CHOHCOCH_3)^* + CH_3CHOHCOCH_3 \rightarrow B\dot{A}^- + CH_3CHOH\dot{C}(OH)CH_3$$

The second radical formed in reaction 8, $CH_3CHOH\dot{C}(OH)CH_3$, is not normally seen when acetoin is photolyzed (6).

Although all organic chemicals were distilled before used, it was conceivable that when the biacetyl radical anion was generated from acetoin, we were actually photolyzing biacetyl as an impurity (6). To check this possibility a Pyrex filter was inserted into the light beam to prevent light with $\lambda < 300$ nm from entering the cavity. The esr signal disappeared completely confirming reactions 5–7. When the Pyrex filter is placed into the light beam in the biacetyl experiment, the signal intensity is only reduced by half since biacetyl has a photoactive absorption near 400 nm.

The two forms of the radical anion of biacetyl have different hyperfine coupling constants. By comparison to the earlier publications (4, 5) we have assigned the larger coupling constant to the *cis* form of the anion. In the three alcoholic solvents we used (methanol, ethanol, and 2-propanol) the proton coupling constants were 0.79 mT for the *cis* form and 0.68 mT for the *trans* form. The splitting constants did not vary over the temperature range −30 to +20 °C. Our values for the splitting constants in aqueous solutions of $a_{cis}^{H} = 0.82$ mT and $a_{trans}^{H} = 0.71$ mT are in good agreement with those of Norman and Pritchett (5).

To determine the ratio of the *cis* to the *trans* form, the ratio of the peak heights were used as the spectral linewidth of both forms were equal at any given temperature.

Results and Discussion

When biacetyl was photolyzed in alcoholic solutions containing TEA, both the *cis* and the *trans* isomer of the radical anion were observed (Fig. 1). However, the ratio of the two forms varied with the concentration of TEA, the solvent and the temperature. For a given alcohol, the ratio of the *cis* to the *trans* form increases as the amine concentration is increased. For a given amine concentration and temperature, the *cis–trans* ratio increases in going from methanol, ethanol to 2-propanol (Fig. 1). Furthermore, for any solution, the *cis–trans* ratio (K) decreases as the temperature is lowered. In all cases ln K was found to be a linear function of reciprocal absolute temperature as shown in Fig. 2. This suggests both isomers may be in equilibrium with each other.

Because Norman and Pritchett found a non-equilibrium situation when they generated the anions in a flow system (5), we decided to photolyze an ethanol solution containing 0.2 mol dm^{-3} biacetyl and 0.2 mol dm^{-3} TEA as it flowed through the cavity and measure K as a function of flow rate. For all flow rates up to that which gave a cavity residence time of 2 s (the fastest flow studied), K was found to be constant, which does suggest we are dealing with an equilibrium under our conditions.

From the linear relationship between ln K and T^{-1} we can estimate ΔH^0 for reaction 1. For all solutions studied ΔH^0 fell in the range 9.2 to 12.5 kJ mol^{-1}. ΔH^0 increased slightly as the concentration of TEA was increased, *e.g.* with ethanol ΔH^0 rose from 10.0 to 12.1 kJ mol^{-1} when the TEA concentration was increased from 0.23 to 3.0 mol dm^{-3}. From these results and those shown in Table 1 it is obvious that the major contribution to shifts in K is the change in the entropy rather than the enthalpy term.

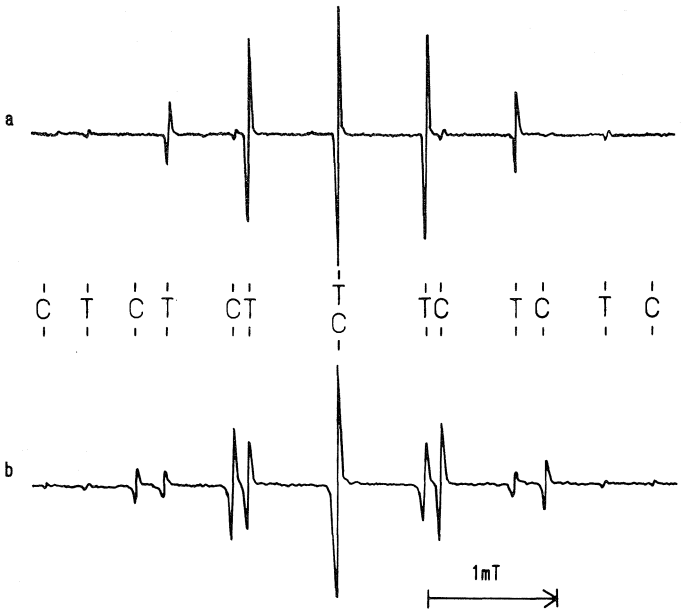

FIG. 1. The esr spectra showing the *cis* (C) and *trans* (T) conformers of the biacetyl radical anion formed when solutions of (*a*) methanol and (*b*) 2-propanol each containing 1.8 mol dm^{-3} biacetyl and 0.23 mol dm^{-3} TEA are photolyzed at −12 °C.

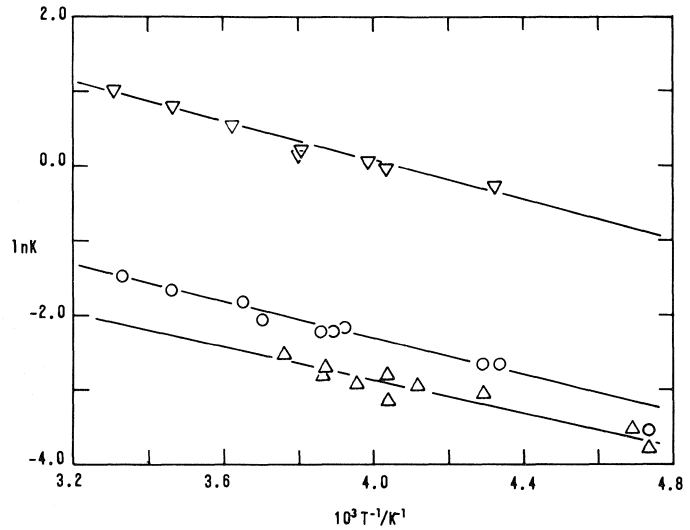

FIG. 2. The plot of ln *K* against reciprocal temperature for 2-propanol (▽), ethanol (○), and methanol (△). The biacetyl concentration was 1.8 and the TEA concentration was 0.23 mol dm^{-3}.

The photolysis of aqueous solutions containing biacetyl and TEA could not be undertaken as the two solutes reacted with each other. These reactions, presumably base catalyzed condensations, also occurred to a much lesser extent in the alcoholic solutions. However, these reactions which proceeded more rapidly in methanol than in 2-propanol, were slowed down by lowering the temperature of the sample.

To study the radical anion in an aqueous solution, a phosphate buffer (p*H* 7) was used to keep the p*H* above the pK_A (=4.4) of the radical anion (5, 7). The radical anion was generated from biacetyl and from acetoin as described in

Can. J. Chem. Downloaded from www.nrcresearchpress.com by 210.87.254.40 on 09/05/12
For personal use only.

TABLE 1. ΔH^0, ΔS^0, and K for reaction 1 during the photolysis of alcoholic solutions containing 1.8 mol dm^{-3} biacetyl and 0.23 mol dm^{-3} TEA

Alcohol	ΔH^0 (kJ mol^{-1})	ΔS^0 (J mol^{-1})	K (261 K)
2-Propanol	10.9	44.3	1.35
Ethanol	10.0	20.5	0.12
Methanol	9.2	12.9	0.07

the Experimental section. Regardless of which method was used, a value of $K \approx 4 \times 10^{-2}$ was always obtained. Changing the buffer concentration from 5×10^{-2} to 2.5×10^{-3} mol dm^{-3} also did not change K. These results again support our premise that we are studying an equilibrium.

The most probable reason why the systems of Norman and Pritchett (5) did not have the same *cis*-to-*trans* ratio is that one of the reagents or products in the Ti(III) system interacted with the anion as to shift the position of the equilibrium or to slow down its dynamics. This is not unreasonable since Russell and co-workers (4) found the position of the equilibrium is influenced by the presence of the metal ions. In our work, we have considered the possibility that we might be photolyzing the radical anion which has a $\lambda_{max} \approx 310$ nm and a $\epsilon_{310} = 3 \times 10^3$ mol^{-1} cm^{-1} (7). The observed equilibrium could then be brought about by the rapid photoisomerization if the radical anion is initially formed preferentially in one form. To test this possibility we photolyzed a solution of 2-propanol containing 1.8 mol dm^{-3} biacetyl and 0.55 mol dm^{-3} TEA at -15 °C with and without a glass filter which cut off light with $\lambda < 450$ nm. With the filter in place, only the biacetyl will be photolyzed. The value of K with and without the filter was the same although in the latter case the spectral intensity was reduced about twenty-five times.

Regardless of what the mechanism of the interconversion between the two isomers is, the process has to be 'slow' compared to the hyperfine coupling constant (expressed in s^{-1}) of the radicals since both forms are observed. The large enthalpy factor excludes any efficient thermal activation. Electron transfer from the anion to a neutral molecule could be the mechanism (4) but the fact that biacetyl appears to exist in the *trans* configuration in solution (5, 8) seems to mitigate against this mechanism. A more promising mechanism is one involving the ketyl radical as an intermediate:

[9] 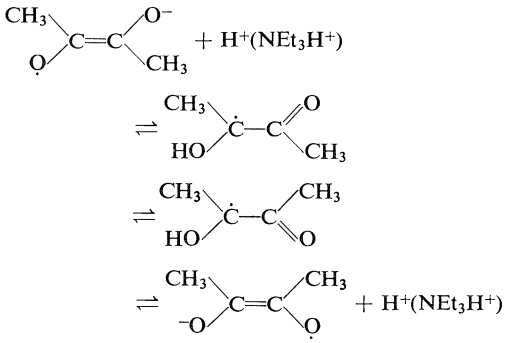

It is not unreasonable to expect the ketyl radical to have a lower barrier to isomerization (*i.e.* less double bond character) than the anion since the hyperfine coupling indicates the methyl groups are quite inequivalent (5). Most probably the rate limiting step for the interconversion is the protonation of the anion. For those experiments where the proton source was NEt_3H^+ we are unable to estimate this rate. However, for the aqueous solutions we can attempt an estimate. If we assume the protonation is diffusion controlled ($k_D \approx 10^9$ mol^{-1} dm^3 s^{-1}), then with a hydrogen ion concentration of 10^{-7} mol dm^{-3} (*i.e.* pH = 7) the psuedo first order rate constant ($k_D[H^+]$) will be 10^2 s^{-1}. This implies a half life about 10^{-2} s which is rapid enough to set up an equilibrium under our conditions where the radical anions are very long lived.

Acknowledgment

This research is supported by the National Research Council of Canada.

1. P. B. AYSCOUGH, G. LAMBERT, and A. J. ELLIOT. J. Chem. Soc. Faraday I, **72**, 1770 (1976).
2. J. K. S. WAN, S. K. WONG, and D. A. HUTCHINSON. Acc. Chem. Res. **7**, 58 (1974).
3. N. J. TURRO and R. ENGEL. J. Am. Chem. Soc. **91**, 7113 (1969).
4. G. A. RUSSELL and R. D. STEPHENS. J. Phys. Chem. **70**, 1320 (1966); G. A. RUSSELL, J. L. GERLOCK, and D. F. LAWSON. J. Am. Chem. Soc. **93**, 4088 (1971); G. A. RUSSELL, D. F. LAWSON, H. L. MALKUS, and P. R. WHITTLE. J. Chem. Phys. **54**, 2164 (1971).
5. R. O. C. NORMAN and R. J. PRITCHETT. J. Chem. Soc. B, 3119 (1967).
6. H. ZELDES and R. LIVINGSTON. J. Chem. Phys. **47**, 1465 (1967).
7. J. LILLIE, G. BECK, and A. HENGLEIN. Ber. Bungsen. Phys. Chem. **72**, 529 (1968).
8. P. H. CLURETON, C. G. LEFEVRE, and R. J. W. LEFEVRE. J. Chem. Soc. 3625 (1964).

Can. J. Chem. Downloaded from www.nrcresearchpress.com by 210.87.254.40 on 09/05/12
For personal use only.

The Raman spectra of tricoordinate CdX_2Y^- halogenocadmate(II) anions in the solid state

J. GUILLERMO CONTRERAS
Instituto de Quimica, Universidad de Concepciòn, Casilla 3-C, Concepciòn, Chile

AND

DENNIS G. TUCK
Department of Chemistry, University of Windsor, Windsor, Ont., Canada N9B 3P4

Received March 18, 1976

J. GUILLERMO CONTRERAS and DENNIS G. TUCK. Can. J. Chem. **54**, 3641 (1976).

Anionic complexes of cadmium, of the type $[CdX_2Y]^-$, where X and Y are chlorine, bromine or iodine, have been prepared as the tetra-*n*-propylammonium salts. Raman spectra have been recorded, and serve to establish that these anions have C_{2v} symmetry in the solid state. Force constants calculated on the Urey–Bradley approximation are correlated with previously reported results for CdX_3^- species.

J. GUILLERMO CONTRERAS et DENNIS G. TUCK. Can. J. Chem. **54**, 3641 (1976).

On a préparé, sous forme de sels de tétra-*n*-propyl ammonium, des complexes anioniques du cadmium du type $[CdX_2Y]^-$, où X et Y peuvent être égal à Cl, Br et I. On a enregistré les spectres Raman de ces anions; ces données ont permis d'attribuer à ces entités une symétrie C_{2v} à l'état solide. On a effectué une corrélation entre les constantes de force calculées d'après l'approximation de Urey–Bradley et les résultats rapportés antérieurement pour les espèces CdX_3^-.

[Traduit par le journal]

Introduction

Anionic halide complexes of cadmium are known to extend over a range of coordination numbers and stereochemistries (1–5). The tricoordinate halide complexes have been the subject of a number of studies involving vibrational spectroscopy. Davies and Long (5) assigned the Raman spectra of aqueous and non-aqueous solutions in terms of planar (D_{3h}) CdX_3^- anions. Sanyal and Singh (6) later carried out force constant calculations based on these results.

In a previous paper (7), we reported the preparation of the tetra-*n*-propylammonium salts of the trihalogenocadmate(II) anions CdX_3^- (X = Cl, Br, I) and showed that the Raman spectra of these salts imply the presence of discrete anions of C_{2v} symmetry. Force constant calculations supported the assignments. The distortion from the expected D_{3h} symmetry, ascribed to lattice effects, was most pronounced for $CdCl_3^-$, with CdI_3^- being closest to the D_{3h} situation.

In view of this conclusion, it seemed worthwhile to investigate the properties of mixed halide complexes of the type CdX_2Y^-. Each of the six possible anions with $X \neq Y$ = Cl, Br, I has now been prepared, again as the tetra-*n*-propylammonium salts. The Raman spectra of the solids, and force constant calculations, can be interpreted in terms of anions of C_{2v} symmetry, and the values of the force constants compared with those reported earlier for CdX_3^- species (7).

Experimental

General

The Raman spectra were recorded on a Laser He/Ne Cary 81 spectrometer. Cadmium analyses were by atomic absorption.

Preparative

The general preparative method used throughout this work was similar to that described earlier (7). Cadmium dihalides were either dissolved or suspended in anhydrous methanol, a stoichiometric quantity of the appropriate tetrapropylammonium halide added, and the solution stirred for 3–4 h at room temperature. The solvent was pumped off and the resulting solid dissolved in a 1:1 mixture of either acetone/acetonitrile or methanol/acetonitrile. Slow evaporation yielded colorless crystals which were recrystallised twice from the same solvent mixtures.

Analytical results, and molar conductivities which show that the compounds are 1:1 electrolytes in acetonitrile, are given in Table 1.

Calculations

The calculations were carried out as described previously (7). Since no experimentally determined molecular

Can. J. Chem. Downloaded from www.nrcresearchpress.com by 210.87.254.6 on 09/05/12
For personal use only.

TABLE 1. Analytical results and conductivity measurements for the salts n-$Pr_4N[CdX_2Y]$

Anion	Λ_m^{25} [a]	Observed (%)				Calculated (%)			
		C	H	N	Cd	C	H	N	Cd
CdI_2Cl	103	24.9	4.3	2.1	19.4	24.5	4.8	2.4	19.1
CdI_2Br	129	22.5	4.3	2.3	17.8	22.8	4.4	2.2	17.8
$CdBr_2Cl$	120	29.2	5.7	2.8	22.3	29.2	5.7	2.8	22.8
$CdBr_2I$	126	24.7	4.9	2.3	19.0	24.6	4.8	2.4	19.2
$CdCl_2Br$	117	32.9	6.4	3.0	25.4	32.1	6.2	3.1	25.0
$CdCl_2I$	129	29.8	5.9	2.9	22.9	29.0	5.6	2.8	22.6

[a]Molar conductivity in acetonitrile, for approximately mM solutions.

TABLE 2. The Raman spectra of crystalline n-$Pr_4N[CdX_2Y]$ salts[a]

Frequency			
$(C_3H_7)_4NCdCl_3$[b]	$(C_3H_7)_4NCdCl_2Br$	$(C_3H_7)_4NCdCl_2I$	Assignment[c]
252ms	202ms	126s	ν_1 (A_1)
294s	292s	286w	ν_2 (A_1)
98mw	107w	103w	ν_3 (A_1)
314ms	313m	310mw	ν_4 (B_2)
76mw	79mw	76w	ν_5 (B_2)
184vw	[d]	162vw	ν_6 (B_1)

Frequency			
$(C_3H_7)_4NCdBr_2Cl$	$(C_3H_7)_4NCdBr_3$[b]	$(C_3H_7)_4NCdBr_2I$	Assignment[c]
314m	164s	126s	ν_1 (A_1)
166s	187m	173w	ν_2 (A_1)
75m	77mw	74mw	ν_3 (A_1)
197s	201ms	192m	ν_4 (B_2)
62w	58w	66w	ν_5 (B_2)
135mw	143vw	[d]	ν_6 (B_1)

Frequency			
$(C_3H_7)_4NCdI_2Cl$	$(C_3H_7)_4NCdI_2Br$	$(C_3H_7)_4NCdI_3$[b]	Assignment[c]
319m	197mw	118s	ν_1 (A_1)
128s	126s	162ms	ν_2 (A_1)
79w	76w	74w	ν_3 (A_1)
169m	174mw	171ms	ν_4 (B_2)
62vw	58vw	55w	ν_5 (B_2)
98vw	123mw	105vw	ν_6 (B_1)

[a]Frequencies in cm^{-1}.
[b]Spectra from ref. 7
[c]Assignment based on C_{2v} molecular symmetry.
[d]Not observed.

structure parameters are available for these anions, bond lengths were taken from the literature (7, 8). Values of 230, 240, and 258 pm were used for the Cd—Cl, Cd—Br and Cd—I respectively; all X—Cd—Y and X—Cd—X angles were assumed to be 120°, as required by the C_{2v} symmetry assignment (see below).

Results and Discussion

The Raman spectra of the tetra-n-propylammonium salts of $[CdX_2Y]^-$ are given in Table 2, together with previous results for the CdX_3^- species for comparison. Figure 1 shows a typical spectrum, that for $[CdCl_2I]^-$. The first implication of these data is that the $[CdX_2Y]^-$ anions are indeed present, since the spectrum of (say) $[CdCl_2Br]^-$ is not simply the appropriate sum of the spectra of $CdCl_3^-$ and $CdBr_3^-$. The Raman spectra of these CdX_3^- salts lead us to conclude that the anions are present as discrete

Can. J. Chem. Downloaded from www.nrcresearchpress.com by 210.87.254.6 on 09/05/12
For personal use only.

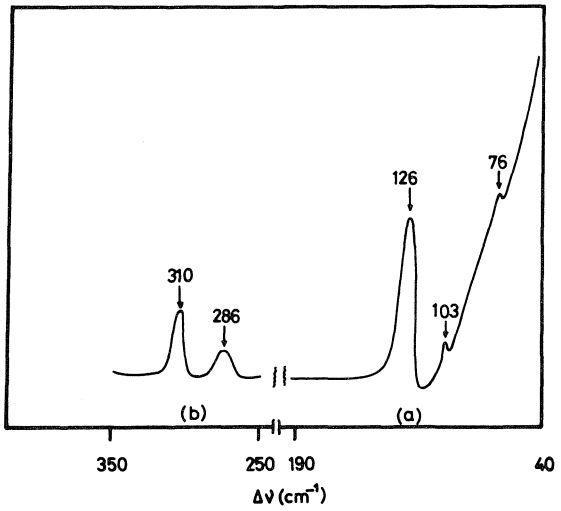

FIG. 1. The Raman spectrum of (n-Pr_4N)[$CdCl_2I$] between 350 and 40 cm^{-1} (conditions: region (a) slit width 5, slit length 5, sensitivity 100, period control 5; region (b) slit width 8, slit length 10, sensitivity 300, period control 15).

units in the crystalline lattice rather than the chain structure identified in $MCdCl_3$ (M = K, Rb, NH_4) salts (8, 9). A similar conclusion as to the nature of the lattice, stemming from the presence of the large Pr_4N^+ cation, appears valid in the present case. Preliminary assignment of the spectra were therefore in terms of C_{2v} symmetry for discrete CdX_2Y^- anions; it should be emphasized that C_{2v} cannot be distinguished from C_s on the basis of these spectra, although the former is intuitively the more appealing.

Certain systematic variations can be seen in the values in Table 2. In the $CdCl_2Y^-$ species, there is an appreciable decrease in ν_1, the Cd—Y stretching mode, with the increasing mass of Y. There is a very small monotonic decrease in ν_2, the ν_s ($CdCl_2$) stretch, but the frequencies of the other modes are almost independent of Y. A different situation holds for the $CdBr_2Y^-$ anions, with ν_1 decreasing in the order Cl > Br > I, but ν_2 showing the sequence Cl < Br > I. For CdI_2Y^-, the decrease in ν_1 parallels that for the other two groups of anions, whereas ν_2, the $\nu(CdI_2)$ stretch, is reduced by approximately 40 cm^{-1} when either chloride or bromide is substituted for iodide. In no case is there any dramatic change in the frequency of the bending modes on substitution.

All the compounds studied show low frequency bands in the range 55–80 cm^{-1}. These are evidently not associated with the Pr_4N^+ cation, and are assigned as ν_5 (Table 2).

Force Constant Calculations

The potential function for the force constant calculations was assumed to be of the form

$$2V = \sum_{i=1}^{3}[2K_i'r_i\Delta r_i + K_i(\Delta r_i)^2] + \sum_{i<j}[2H_{ij}'r^2\Delta_{ij} + H_{ij}(r_0\Delta_i)^2] + \sum_{i<j}[2F_{ij}'q_{ij}\Delta q_{ij} + F_{ij}(\Delta q_{ij})^2]$$

where Δr_i and Δ_{ij} are the valence bond stretches and angle bends respectively, and Δq_{ij} denotes the changes in nonbonded interatomic distances. The scaling bond lengths r_0 were taken as $r_{Cd—X}$ for all angles. The out-of-plane deformation mode belongs to a different class and has not been included in the calculation; in any case, the results in Table 2 show that we were not able to observe this rather weak emission from each anion.

The potential function contains eight force constants, but all of these cannot be determined from only five vibrational frequencies. By following the usual assumption that $F' = -0.1F$, the number of parameters to be determined is reduced to six, and if a value is assumed for any one of these, the remaining five can then be evaluated. We have explored the consequences of transferring values of either F_{II} or H_{II} from previous calculations on CdX_3^- species (6, 7). The choice of F_{II} yielded unrealistic values in the calculations, and the final calculations were made after including H_{II} (H_{XMX}) values for the CdX_3^- anions. Table 3 gives the calculated force constants for the five in-plane normal modes of the CdX_2Y^- anions, and the potential energy distributions amongst these force constants are shown in Tables 4–6. The results are in agreement with the presumed C_{2v} symmetry of the anions.

The calculated eigenvectors, and the potential energy distribution amongst the force constants, show that $\nu_1(A_1)$ is essentially the pure ν(Cd—Y) stretching mode in each case, except in the case of CdI_2Br^-. A comparison of the values in Table 6 with those published previously reveals that the contribution of K_{II} to ν_1 decreases from

Can. J. Chem. Downloaded from www.nrcresearchpress.com by 210.87.254.6 on 09/05/12
For personal use only.

TABLE 3. Urey–Bradley force constants for CdX_2Y^- complexes (X ≠ Y = Cl, Br, I) (values in 10^5 dyn cm^{-1})

Symbol[a]	Description	Value					
		$CdCl_2Br^-$	$CdCl_2I^-$	$CdBr_2Cl^-$	$CdBr_2I^-$	CdI_2Cl^-	CdI_2Br^-
K_I	K(Cd—Y)	1.024	0.435	1.439	0.474	1.515	0.902
K_{II}	K(Cd—X)	1.308	1.284	0.836	0.792	0.728	0.764
H_I	H(X—Cd—Y)	0.004	0.005	−0.003	0.005	0.013	0.016
H_{II}[b]	H(X—Cd—X)	0.023	0.023	0.010	0.010	0.057	0.057
F_I	F(X···Y)	0.134	0.132	0.121	0.155	0.091	0.081
F_{II}	F(X···X)	0.139	0.130	0.083	0.148	0.032	0.127

[a]K = stretching; H = bending; F = repulsive force constants. The subscripts I and II distinguish Cd—X and Cd—Y modes (*c.f.* column 2).
[b]Force constants transferred from ref. 7.

TABLE 4. The vibrational spectra and potential energy distribution (%) amongst force constants for the $CdCl_2Y^-$ (Y = Br, I) anions

Anion		Frequency (cm^{-1})							
		Observed	Calculated	K_I	K_{II}	H_I	H_{II}	F_I	F_{II}
$CdCl_2Br^-$	ν_1	202	202	85	—	—	1	12	2
	ν_2	292	294	3	82	—	—	4	11
	ν_3	107	105	—	—	2	26	28	44
	ν_4	313	311	—	97	—	—	4	—
	ν_5	79	81	—	1	8	—	91	—
$CdCl_2I^-$	ν_1	126	127	70	—	—	7	12	9
	ν_2	286	288	—	84	—	—	5	11
	ν_3	103	101	5	—	2	22	37	34
	ν_4	310	309	—	97	—	—	4	—
	ν_5	76	77	—	1	11	—	88	—

TABLE 5. The vibrational spectra and potential energy distribution (%) amongst force constants for the $CdBr_2Y^-$ (Y = Cl, I) anions

Anion		Frequency (cm^{-1})							
		Observed	Calculated	K_I	K_{II}	H_I	H_{II}	F_I	F_{II}
$CdBr_2Cl^-$	ν_1	314	314	92	2	—	—	6	—
	ν_2	166	168	—	79	—	—	13	8
	ν_3	75	75	—	—	−8	—	105	—
	ν_4	197	196	—	97	—	—	4	—
	ν_5	62	61	—	—	−3	18	32	52
$CdBrI^-$	ν_1	126	127	69	1	—	—	23	6
	ν_2	173	171	8	74	—	—	4	14
	ν_3	74	72	—	—	3	11	36	50
	ν_4	192	194	—	95	—	—	5	—
	ν_5	66	67	—	—	9	—	91	—

29% in CdI_3^-, through 12% for CdI_2Br^- to 1% in CdI_2Cl^-, so that the extent of coupling depends sharply on the species Y in CdI_2Y^-. For the $CdBr_2Y^-$ system, the only significant coupling is in the symmetrical $CdBr_3^-$ (9% contribution), while in the $CdCl_2Y^-$ series, the contribution of K_{II} to ν_1 is always less than 4%. A similar situation is found on examining the contribution of K_I to the symmetric CdX stretching mode (ν_2) of CdX_2Y^-; only for the two iodobromo species is there any significant coupling (~10%). The antisymmetric Cd—X stretching mode (ν_4) is a pure vibration in every case, involving no contribution from K_I; the potential energy distribution shows that the K_{II} makes a contribution of over 95% throughout. In general, then, we conclude that there is relatively little coupling between the stretching

Can. J. Chem. Downloaded from www.nrcresearchpress.com by 210.87.254.6 on 09/05/12
For personal use only.

TABLE 6. The vibrational spectra and potential energy distribution (%) amongst force constants for the CdI_2Y^- (Y = Cl, Br) anions

Anion		Frequency (cm^{-1}) Observed	Calculated	K_I	K_{II}	H_I	H_{II}	F_I	F_{II}
CdI_2Cl^-	ν_1	319	319	94	1	—	—	4	—
	ν_2	128	130	—	76	—	6	15	3
	ν_3	79	79	—	—	28	—	71	—
	ν_4	169	168	—	95	2	—	3	—
	ν_5	62	64	—	10	6	60	10	15
CdI_2Br^-	ν_1	197	197	81	12	—	4	2	1
	ν_2	126	128	9	64	—	1	14	13
	ν_3	76	74	1	1	6	46	12	34
	ν_4	174	173	—	96	2	—	2	—
	ν_5	58	60	—	—	35	—	64	—

vibrations in CdX_2Y^-, in contrast to the situation with the symmetrical CdX_3^- anions of the same symmetry.

Finally we note that the assignment of the low frequency bands as ν_5 yields a sensible set of force constants, thus supporting the assignment to internal modes of the CdX_2Y^- anion rather than to lattice vibrations.

Bond Character in CdX_2Y^-

The results of force constant calculations have been used to establish the ionic character of the bonding in halide complexes of cadmium (7), indium (10), and tin (11). In particular, the dependence of the stretching force constants upon electronegativity differences ($\chi_{halogen} - \chi_{metal}$) and charge distribution have supported such arguments.

The present results are qualitatively in agreement with an ionic bonding model for CdX_2Y^-. We note firstly that the average values for K_{II} are close to those in the CdX_3^- anions. From the results for $CdCl_2Br^-$ and $CdCl_2I^-$, $\bar{K}_{II}$, the average force constant for the Cd—Cl stretch, is 1.30 (the mean of 1.308 and 1.284); the analogous values for Cd—Br and Cd—I are 0.81 and 0.75. The values for K_{II} in the CdX_3^- anions are 1.35, 0.88, and 0.77, and it seems reasonable to deduce that the bonding character is very similar in both groups of anions.

A more detailed consideration of the dependence of both K_I and K_{II} on ligand electronegativity in related pairs of anions leads to some interesting relationships. For example, the small decrease in K_{II} in the CdI_2X^- anions with respect to the value for CdI_3^- can be rationalized as a weakening of the Cd—I bond due to the substitution of one iodine by a more electronegative bromine or chlorine. In agreement with this, there is a concomitant increase in K_I for the same anions. Such a trend is not, however, shown by the dibromo and dichloro complexes. Simplified calculations based on Sanderson's approach (12, 13) show an almost linear relationship between K_{II} and the partial charge on the cadmium atom for the dichloro and diiodo anions, but for the dibromo species a plot of K_{II} against the calculated cadmium charge has a maximum at $CdBr_3^-$. Such calculations therefore lend qualitative support to the similarity in ionic character in CdX_3^- and CdX_2Y^- anions, but more sophisticated charge calculations, and other experimental data, are required for further exploration of this problem.

1. G. BERGERHOFF and O. SCHMITZ-DUMONT. Z. Anorg. Chem. **284**, 10 (1956).
2. T. V. LONG, A. W. HERLINGER, E. F. EPSTEIN, and I. BERNAL. Inorg. Chem. **9**, 459 (1970).
3. R. A. ROLFE, D. E. SHEPPARD, and L. A. WOODWARD. Trans. Faraday Soc. **50**, 1275 (1954).
4. D. M. ADAMS, J. CHATT, J. M. DAVIDSON, and J. GERRATT. J. Chem. Soc. 2189 (1963).
5. J. E. D. DAVIES and D. A. LONG. J. Chem. Soc. A, 2054 (1968).
6. N. K. SANYAL and B. P. SINGH. J. Pure Appl. Phys. 758 (1971).
7. J. G. CONTRERAS and D. G. TUCK. Can. J. Chem. **53**, 3487 (1975).
8. D. M. ADAMS and D. C. NEWTON. J. Chem. Soc. A, 3499 (1971).
9. C. H. MACGILLAVRY, H. NIJUELD, S. DIERDORP, and K. KARSTEN. Rec. Trav. Chem. **58**, 193 (1939).
10. J. G. CONTRERAS and D. G. TUCK. Inorg. Chem. **11**, 2967 (1972).
11. I. WHARF and D. F. SHRIVER. Inorg. Chem. **8**, 914 (1969).
12. R. T. SANDERSON. Inorganic Chemistry, Reinhold Publ. Co., New York. 1967.
13. H. J. STOKLOSA. J. Chem. Educ. **50**, 290 (1973).

Can. J. Chem. Downloaded from www.nrcresearchpress.com by 210.87.254.6 on 09/05/12
For personal use only.

Reduction of sulfates by hydrogen

FATHI HABASHI, SHAHEER A. MIKHAIL, AND KIM VO VAN
Department of Mining and Metallurgy, Laval University, Quebec, P.Q., Canada G1K 7P4

Received March 12, 1976

FATHI HABASHI, SHAHEER A. MIKHAIL, and KIM VO VAN. Can. J. Chem. **54**, 3646 (1976).

The initial stage of reduction of anhydrous sulfates by H_2 may lead to the formation of any of the following: (1) sulfates at lower valency, *e.g.*, reduction of $CuSO_4$, $HgSO_4$, $Fe_2(SO_4)_3$; (2) metals, *e.g.*, Cu_2SO_4, Ag_2SO_4; (3) sulfides, *e.g.*, $NiSO_4$, $CoSO_4$, $CdSO_4$, $CaSO_4$, $SrSO_4$, $BaSO_4$, and alkaline metal sulfates; (4) oxides, *e.g.*, $Al_2(SO_4)_3$, $MgSO_4$, $BeSO_4$; (5) a mixture of oxide and sulfide, *e.g.*, $FeSO_4$, $MnSO_4$, $ZnSO_4$, $PbSO_4$. While $CuSO_4$, Ag_2SO_4, and $PbSO_4$ are the only sulfates that yield metals on reduction, $CuSO_4$ is the most interesting because it yields the metal at 350 °C. $PbSO_4$ is reduced to metal at about 800 °C, and Ag_2SO_4 already yields the metal by thermal decomposition above 800 °C.

FATHI HABASHI, SHAHEER A. MIKHAIL et KIM VO VAN. Can. J. Chem. **54**, 3646 (1976).

La première étape de la réduction des sulfates anhydres par H_2 peut conduire à la formation de n'importe lequel des composés suivants: (1) des sulfates à un état de valence inférieur, *e.g.* réduction du $CuSO_4$, $HgSO_4$, $Fe_2(SO_4)_3$; (2) des métaux, *e.g.*, Cu_2SO_4, Ag_2SO_4; (3) des sulfures, *e.g.* $NiSO_4$, $CoSO_4$, $CdSO_4$, $CaSO_4$, $SrSO_4$, $BaSO_4$ et les sulfates de métaux alcalins; (4) des oxydes, *e.g.*, $Al_2(SO_4)_3$, $MgSO_4$, $BeSO_4$; (5) un mélange d'oxyde et de sulfure, *e.g.*, $FeSO_4$, $MnSO_4$, $ZnSO_4$, $PbSO_4$. Alors que $CuSO_4$, Ag_2SO_4 et $PbSO_4$ sont les seuls sulfates qui conduisent à des métaux par réduction, $CuSO_4$ est le plus intéressant parce qu'il conduit au métal à 350 °C. $PbSO_4$ est réduit en métal à environ 800 °C et Ag_2SO_4 conduit déjà au métal par décomposition thermique au dessus de 800 °C.

[Traduit par le journal]

Introduction

The reduction of $CuSO_4$ by H_2 is of potential technical importance because the sulfate is reduced to metal at a fairly moderate temperature (350–400 °C) (1, 2). Also, it was shown that Cu_2SO_4 was formed as an intermediate product during reduction and SO_2 and H_2O are the only gaseous products (2, 4):

$$2CuSO_4 + 2H_2 \rightarrow Cu_2SO_4 + SO_2 + 2H_2O$$

$$Cu_2SO_4 + 2H_2 \rightarrow 2Cu + SO_2 + 2H_2O$$

To follow up this work, it would be interesting to know the behavior of other sulfates on reduction, a topic on which little is written. Thus, in Gmelin (5) there is some information on the reduction of alkaline metal and alkaline earth sulfates but nothing worthwhile on the other sulfates. For these reasons, the present study was undertaken to examine the reduction of a number of metallurgically important sulfates, and to know whether other sulfates are also reduced to metal like the case of $CuSO_4$.

Experimental

Studies were conducted using thermogravimetric analysis (TGA) and X-ray diffraction. Two TGA instruments were available. A Fisher 10-560-100 assembly with a Cahn RG electrobalance; the heating system consisted of a vertical tube furnace connected to the model 360 linear temperature programmer which provided a linear heating rate. A heating rate of 10 °C/min was used. An *X–Y* recorder Honeywell Electronik 19 was connected to the system. The sample was about 20 mg. The other instrument was a Stanton model in which the weight of sample was about 200 mg. The Fisher instrument was suitable for conducting dynamic tests, *i.e.*, increasing the temperature at a constant rate and getting a continuous plot of the change in weight while the Stanton was suitable for conducting tests in which the heating could be interrupted and the residue could be collected and analyzed by X-ray diffraction. For the X-ray analysis, a Norelco X-ray diffractometer with CuK_α radiation was used. It consisted of Diffraction Unit type 12045-12046, Wide range Goniometer type 42201-42202, Electronic Circuit Panel type 12048-12049, and AMR Focusing Monochromator Model 3-202 with a graphite crystal. Finely ground reagent grade sulfates were used in all tests.

Results and Discussion

TGA plots of the reduction of various sulfates by H_2 are given in Fig. 1. The intermediate and final products of reduction are also shown on these diagrams. The arrows indicate the temperature at which the reaction was interrupted and the products were identified by X-ray diffraction. The products are indicated in their

Can. J. Chem. Downloaded from www.nrcresearchpress.com by 210.87.254.5 on 09/05/12
For personal use only.

Can. J. Chem. Downloaded from www.nrcresearchpress.com by 210.87.254.5 on 09/05/12
For personal use only.

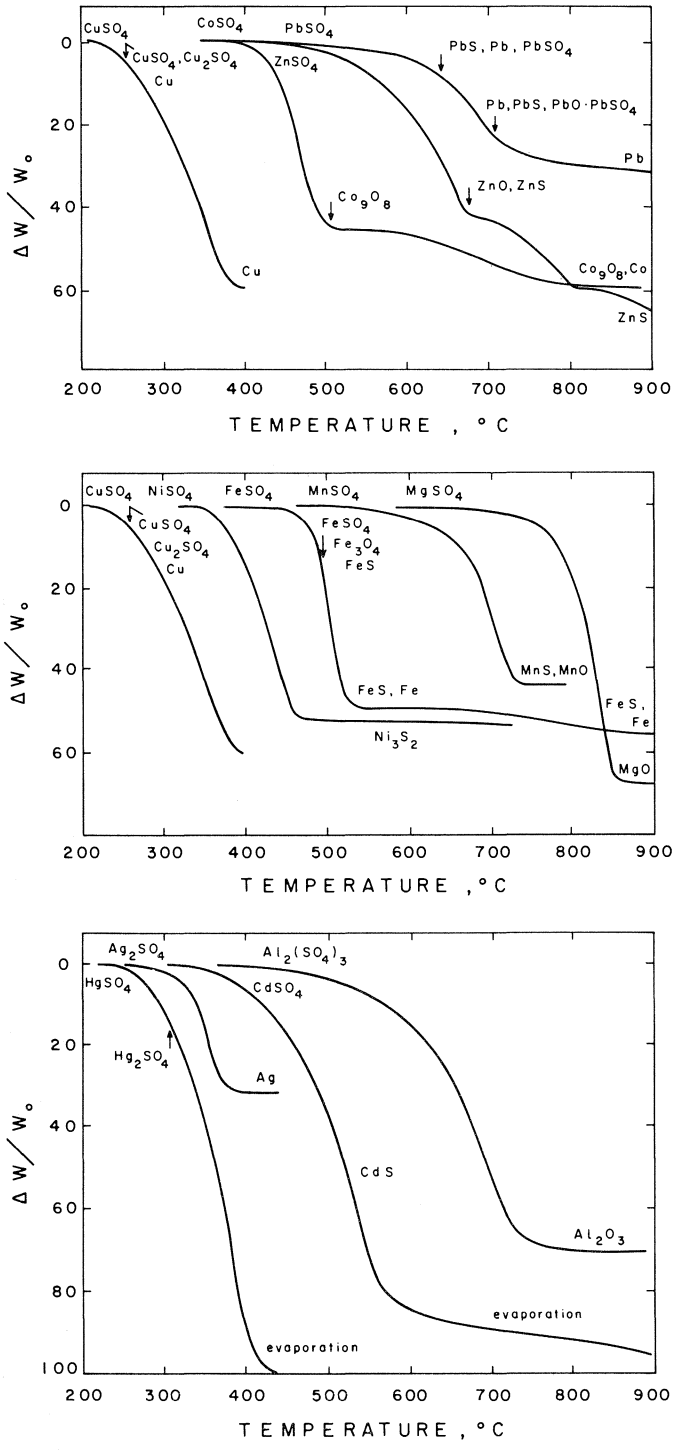

FIG. 1. Reduction of sulfates by H_2 using TGA. The arrows indicate the temperature at which the reaction was interrupted and the products identified by X-ray diffraction analysis.

TABLE 1. Starting temperature of reduction of different sulfates by H_2 as determined by TGA, and products of reduction at higher temperatures as determined by X-ray

Sulfate	Starting temperature of reduction (°C)	Reduction products at higher temperatures			
		T (°C)	Major	Intermediate	Minor
Cu_2SO_4 (ref. 3)	120	300	Cu	—	—
$CuSO_4$	230	270	$CuSO_4$	Cu_2SO_4	Cu
		400	—	—	Cu
$HgSO_4$	240	300	Hg_2SO_4	—	—
		430	—	—	—*
Ag_2SO_4	260	425	Ag	—	—
$NiSO_4$	340	550	Ni_3S_2	—	—
		750	Ni_3S_2	—	—
$CdSO_4$	340	530	CdS	—	—
		900	—	—	—*
$CoSO_4$	400	510	Co_9O_8	—	—
		900	Co_9O_8	—	Co
$ZnSO_4$	400	680	ZnO	ZnS	—
		900	(Zn)*	—	ZnS
$Fe_2(SO_4)_3$†	400	450	$Fe_2(SO_4)_3$	$FeSO_4$	—
		500	$FeSO_4$	$Fe_2(SO_4)_3$	(Fe_3O_4)
$PbSO_4$	420	650	PbS	Pb	$PbSO_4$
		710	Pb	PbS	$PbO.PbSO_4$
		900	Pb	—	—
$Al_2(SO_4)_3$	430	900	Al_2O_3	—	—
$FeSO_4$	440	500	$FeSO_4$	Fe_3O_4	FeS
		600	Fe	FeS	—
		900	Fe	FeS	—
$MnSO_4$	540	800	MnS	MnO	—
$MgSO_4$	670	900	MgO	—	—
Na_2SO_4 (ref. 5)	700	900	Na_2S	—	—

*Evaporation
†Reduction conducted in a boat heated in a tube furnace.

order of increased occurrence. Table 1 shows all this information together with the temperature at which reduction starts. From these data the initial stage of reduction can therefore be summarized as follows:

(1) Reduction to lower valency

$CuSO_4$, $HgSO_4$, and $Fe(SO_4)_3$ are reduced to Cu_2SO_4, Hg_2SO_4, and $FeSO_4$ respectively. Hg_2SO_4 volatilizes during reduction while the reduction of $Fe_2(SO_4)_3$ is only partial and it turns black.

(2) Reduction to metal

Beside the reduction of Cu_2SO_4 to Cu, it was also found that Ag_2SO_4 is reduced to Ag.

(3) Reduction to sulfide

Nickel, Co, and Cd sulfates are reduced to sulfides according to:

$$3NiSO_4 + 10H_2 \rightarrow Ni_3S_2 + SO_2 + 10H_2O$$

$$9CoSO_4 + 34H_2 \rightarrow Co_9S_8 + SO_2 + 34H_2O$$

$$CdSO_4 + 4H_2 \rightarrow CdS + 4H_2O$$

At high temperature a small amount of metallic Co is formed in the case of $CoSO_4$ while CdS volatilized.

(4) Reduction to oxide

Aluminium and Mg sulfates are reduced to oxides according to:

$$Al_2(SO_4)_3 + 3H_2 \rightarrow Al_2O_3 + 3SO_2 + H_2O$$

$$MgSO_4 + H_2 \rightarrow MgO + SO_2 + H_2O$$

(5) Reduction to oxide and sulfide

Manganese, Zn, Pb, and Fe(II) sulfates are reduced to a mixture of oxides and sulfides according to the equations:

$$2MnSO_4 + 5H_2 \rightarrow MnO + MnS + SO_2 + 5H_2O$$

$$2ZnSO_4 + 5H_2 \rightarrow ZnO + ZnS + SO_2 + 5H_2O$$

$$2PbSO_4 + 5H_2 \rightarrow PbO + PbS + SO_2 + 5H_2O$$

$$4FeSO_4 + 6H_2 \rightarrow Fe_3O_4 + FeS + 3SO_2 + 6H_2O$$

In the case of $ZnSO_4$, ZnO is reduced further to

Can. J. Chem. Downloaded from www.nrcresearchpress.com by 210.87.254.5 on 09/05/12
For personal use only.

TABLE 2. Reduction of $FeSO_4$ by H_2 at 500 °C. Products identified by X-ray diffraction analysis

Time (min)	Reduction products			Color
	Major	Intermediate	Minor	
5	$FeSO_4$, Fe_3O_4	FeS		Black, white
8	FeO, FeS	Fe		Black
10	Fe, FeS	FeO		Black
20	Fe, FeS		FeO	Black
30	Fe, FeS			Black
120	Fe, FeS			Black

TABLE 3. Thermal decomposition of anhydrous sulfates in air. All sulfates behave similarly in an inert atmosphere except Cu_2SO_4 and $FeSO_4$, for this see Table 4

Sulfate	Starting temperature of decomposition (°C)	Temperature of energetic decomposition (°C)	Products	Reference
Cu_2SO_4	120	200	CuO, $CuSO_4$	3
		600	$CuO.CuSO_4$	
		750	CuO	
$CuSO_4$	650	670	$CuO.CuSO_4$	6–10, 12
		710	CuO	
$HgSO_4$	450	500	$HgO.HgSO_4$	7, 8, 10
		>500	$2HgO.HgSO_4$	
Ag_2SO_4	800	900	Ag	7, 8, 11, 12
$NiSO_4$	700	765	NiO	6–12
$CdSO_4$	825	850	$2CdO.CdSO_4$	7–12
		890	CdO	
$CoSO_4$	720	770	Co_3O_4	6–12
$ZnSO_4$	700	720	$2ZnO.ZnSO_4$	6–10, 12
		760	ZnO	
$PbSO_4$	640	700	$PbO.PbSO_4$, $2PbO.PbSO_4$, $4PbO.PbSO_4$	6–9, 12
		960	PbO	
$Al_2(SO_4)_3$	590	640	Al_2O_3	7–8, 10
$FeSO_4$	500	535	$Fe_2O(SO_4)_2$*	7–9, 12
		650	Fe_2O_3	
$MnSO_4$	700	800	Mn_3O_4	7–9, 11, 12
$MgSO_4$	890	970	MgO	7-10, 12
Na_2SO_4	1200	—	No decomposition	5–8

*Formed as a result of oxidation: $2FeSO_4 + \frac{1}{2}O_2 \rightarrow Fe_2O(SO_4)_2$.

metal while ZnS remains unchanged. The reduction of $PbSO_4$ leads to PbS and apparently PbO which is rapidly reduced to Pb. At about 720 °C an oxysulfate phase, $PbO.PbSO_4$, appears together with Pb and PbS. Finally, above 800 °C only metallic lead remains.

The reduction of $FeSO_4$ was studied in some detail by heating a sample in a boat at 500 °C in H_2 atmosphere for different periods of time and examining the products by X-ray diffraction and wet chemical analysis and also analyzing the exit gases. The results showed that SO_2 was the only gaseous product during the initial stage of reduction and was followed later by a small amount of H_2S. Magnetite and FeS were the initial solid reaction products; Fe_3O_4 was subsequently reduced to FeO and then to Fe (Table 2). The molar ratio Fe/FeS at the end of reaction was about 2.5 as determined by wet methods, thus indicating that the overall reaction is approximately:

$$4FeSO_4 + 10H_2 \rightarrow 3Fe + FeS + 3SO_2 + 10H_2O$$

Can. J. Chem. Downloaded from www.nrcresearchpress.com by 210.87.254.5 on 09/05/12
For personal use only.

TABLE 4. Thermal decomposition of Cu_2SO_4 and $FeSO_4$ in an inert atmosphere

Sulfate	Starting temperature of decomposition (°C)	Temperature of energetic decomposition (°C)	Products	Reference
Cu_2SO_4	220	300	Cu, $CuSO_4$	3
		650	$CuO.CuSO_4$, Cu_2O	
		800	CuO	
$FeSO_4$	475	575	$Fe_2O_2SO_4$	13
		675	Fe_2O_3	

The reduction of $FeSO_4$ represents a unique case in which a part of the metal ion undergoes an increase in valency, *i.e.*, oxidation during the initial stages of reduction. However, this is not surprising since during its thermal decomposition in an inert atmosphere, $FeSO_4$ yields Fe_2O_3 (Table 4).

It is interesting to mention that data in the literature (5) reveal that $BeSO_4$ and $MgSO_4$ behave differently from the other alkaline earth sulfates; they are reduced to oxides while $SrSO_4$ and $BaSO_4$ are reduced to sulfides. $CaSO_4$ is partially reduced at 700 °C to CaS and above 900 °C to CaO. It is believed that at high temperature an interaction between CaS and $CaSO_4$ takes place leading to the formation of CaO as follows:

$$CaS + 3CaSO_4 \rightarrow 4CaO + 4SO_2$$

On the other hand, alkali metal sulfates are all reduced to sulfides according to:

$$M_2SO_4 + 4H_2 \rightarrow M_2S + 4H_2O$$

where M is an alkali metal. The reduction of Na_2SO_4 is of historical interest since it was a major step in the manufacture of Na_2CO_3 by LeBlanc Process.

It is evident from the present work that $CuSO_4$, $PbSO_4$, and Ag_2SO_4 are the only sulfates that yield metals on reduction. Silver sulfate, however, decomposes to metal by heating above 790 °C (Table 3) and $PbSO_4$ is reduced to Pb above 800 °C. For comparative purposes, data on the thermal decomposition of some sulfates compiled from different sources (5–12) are given in Tables 3 and 4.

Conclusion

Various products can be obtained on the reduction of metal sulfates; these can be sulfates at lower valency, metals, sulfides, oxides, or a mixture of oxide and sulfide. Of these, the reduction of $CuSO_4$ is of significant technical importance since it yields metallic Cu at a moderate temperature of 350–400 °C.

Acknowledgement

The financial aid of the National Research Council of Canada is greatly appreciated.

1. F. HABASHI and R. DUGDALE. Met. Trans. **4** (5), 1429 (1973).
2. K. VO VAN and F. HABASHI. Can. J. Chem. Eng. **52**, 369 (1974).
3. K. VO VAN and F. HABASHI. Can. J. Chem. **50**, 3872 (1972).
4. M. NAGAMORI and F. HABASHI. Met. Trans. **5** (2), 523 (1974).
5. Gmelins Handbuch der Anorganischen Chemie. Verlag Chemie. Weinheim.
6. G. A. KOLTA and M. H. ASKAR. Thermochim. Acta, **11** (1), 65 (1975).
7. K. H. STERN and E. L. WEISE. Bull. no. 7, Nat. Bur. Stand. Washington, D.C. 1966.
8. H. H. KELLOGG. Trans. Met. Soc. AIME, **230**, 1622 (1964).
9. A. G. OSTROFF and R. T. SANDERSON. J. Inorg. Nucl. Chem. **9**, 45 (1959).
10. H. H. WILLARD and R. D. FOWLER. J. Am. Chem. Soc. **54**, 496 (1932).
11. G. MARCHAL. J. Chim. Phys. **22**, 559 (1925).
12. H. O. HOFMAN and W. WANJUKOW. Trans. AIME, **43**, 523 (1912).
13. D. W. JOHNSON and P. K. GALLAGHER. Thermochim. Acta, **5**, 455 (1973).

Can. J. Chem. Downloaded from www.nrcresearchpress.com by 210.87.254.5 on 09/05/12
For personal use only.

Reduction of binary sulfate mixtures containing $CuSO_4$ by H_2

FATHI HABASHI AND SHAHEER A. MIKHAIL
Department of Mining and Metallurgy, Laval University, Quebec, P.Q., Canada G1K 7P4

Received March 12, 1976

FATHI HABASHI and SHAHEER A. MIKHAIL. Can. J. Chem. **54**, 3651 (1976).

The reduction of a binary sulfate mixture cannot be predicted from the behavior of the individual components. Thus, while $CuSO_4$ is reduced to Cu at 400 °C and $NiSO_4$ is reduced to Ni_3S_2, the sulfate mixture yields Cu, Ni_3S_2, and Cu_2S. Also while $FeSO_4$ is completely stable in H_2 at 400 °C, (Cu,Fe) SO_4 yields Cu and Cu_5FeS_4. The formation of Cu_2S in the first case and Cu_5FeS_4 in the second was unexpected. On the other hand, (Cu,Mn)SO_4 is stable in H_2 up to 550 °C although pure $CuSO_4$ is completely reduced at 400 °C. $CoSO_4$ also interferes when reduced in presence of $CuSO_4$, while Na_2SO_4, $MgSO_4$, $Al_2(SO_4)_3$, $ZnSO_4$, $CdSO_4$ do not interfere within limited temperature range. Of these only Na_2SO_4 forms a complex sulfate with $CuSO_4$. No Cu_2SO_4 was identified when $CuSO_4$ was reduced in presence of other sulfates although it is an intermediate product during the reduction of pure $CuSO_4$.

FATHI HABASHI et SHAHEER A. MIKHAIL. Can. J. Chem. **54**, 3651 (1976).

Le cours de la réduction d'un mélange binaire de sulfates ne peut pas être prédit à partir du comportement des composés individuels. Par exemple, alors que le $CuSO_4$ est réduit en Cu à 400 °C et le $NiSO_4$ est réduit à Ni_3S_2, le mélange de sulfates conduit à du Cu, du Ni_3S_2 et du Cu_2S. Aussi alors que le $FeSO_4$ est complètement stable vis-à-vis du H_2 à 400 °C, (Cu,Fe)SO_4 conduit à du Cu et du Cu_5FeS_4. La formation du Cu_2S dans le premier cas et du Cu_5FeS_4 dans le second était inattendue. Par ailleurs (Cu,Mn)SO_4 est stable vis-à-vis du H_2 jusqu'à 550 °C même si le $CuSO_4$ pur est complètement réduit à 400 °C. Le $CoSO_4$ interfère aussi lorsqu'il est réduit en présence de $CuSO_4$, alors que Na_2SO_4, $MgSO_4$, $Al_2(SO_4)_3$, $ZnSO_4$, $CdSO_4$ n'interfèrent pas à l'intérieur des limites de température. Parmi ces composés, il n'y a que le Na_2SO_4 qui forme un sulfate complexe avec le $CuSO_4$. On n'a pas pu identifier de Cu_2SO_4 quand le $CuSO_4$ a été réduit en présence d'autres sulfates quoiqu'il soit un produit intermédiaire lors de la réduction du $CuSO_4$ pur.

[Traduit par le journal]

Introduction

Studies on the reduction of $CuSO_4$ were undertaken in connection with a proposed method for copper recovery which would compete with other methods, *e.g.*, electrolysis or precipitation by H_2 under pressure (1, 2). In this process, $CuSO_4.nH_2O$ is crystallized from solution, dehydrated, then reduced by H_2 at 350–380 °C or by CO at about 500 °C to yield metallic copper according to the overall equations:

$$CuSO_4 + 2H_2 \rightarrow Cu + SO_2 + 2H_2O$$

$$CuSO_4 + 2CO \rightarrow Cu + SO_2 + 2CO_2$$

Solutions containing copper may be obtained by leaching low-grade oxide ore, sulfide concentrates, or scrap metal. It is evident that the purity of the copper produced will depend on the behavior of impurities in solution during crystallization and reduction. Sulfates that are insoluble in $CuSO_4$ solution such as $CaSO_4$, $BaSO_4$, $PbSO_4$, and Ag_2SO_4, or those that undergo hydrolysis, *e.g.*, $Ti(SO_4)_2$ and $SnSO_4$, will not interfere during the crystallization process and therefore can be eliminated.

It is also expected that the sulfates that accompany $CuSO_4$, but are reduced at a much higher temperature such as $MgSO_4$ and Na_2SO_4 (starting reduction temperature 670 and 700 °C respectively (3)) would not cause contamination problems. However, it is not certain whether the formation of solid solutions or complex sulfates will influence the reduction process. Also, it is not known what would be the product of reduction of $CuSO_4$ containing impurities such as $NiSO_4$, $CdSO_4$, $CoSO_4$, $ZnSO_4$, $Al_2(SO_4)_3$, $FeSO_4$, and $MnSO_4$ whose starting temperature of reduction is in the range 340–540 °C (3); can the products of reduction be predicted from the behavior of the individual sulfate?

Solubility data of binary sulfates containing $CuSO_4$ as one component are available in literature (4) and from these data it can be concluded that during crystallization the following cases

Can. J. Chem. Downloaded from www.nrcresearchpress.com by 210.87.254.42 on 09/05/12
For personal use only.

Can. J. Chem. Downloaded from www.nrcresearchpress.com by 210.87.254.42 on 09/05/12
For personal use only.

will arise for the hydrated crystals: (*1*) Sulfates that form complex salts with $CuSO_4$: Na_2SO_4, K_2SO_4, Rb_2SO_4, $(NH_4)_2SO_4$, and Tl_2SO_4. (*2*) Sulfates that form solid solutions with $CuSO_4$: $MgSO_4$, $ZnSO_4$, $MnSO_4$, $NiSO_4$, $CaSO_4$, and $FeSO_4$. (*3*) Sulfates that do not form complex salts or solid solutions with $CuSO_4$: Li_2SO_4, $BeSO_4$, $Al_2(SO_4)_3$, and $CdSO_4$. On dehydration, it is not certain that the above classification will still be valid since the complex sulfates may decompose, and the solid solutions may interact or breakdown due to a difference in structure in the anhydrous form.

The present work was therefore undertaken to study the role of metal sulfates during the crystallization of an aqueous solution of $CuSO_4$ and their effect on its dehydration and reduction.

Experimental

Finely ground reagent grade sulfates were used in all the tests. Aluminum sulfate was chosen as a representative of the group of sulfates that do not form complex salts or solid solution, Na_2SO_4 as a representative of the group of sulfates that form complex salts, and finally all sulfates that form solid solutions with $CuSO_4$ were studied.

The general procedure for preparing a sample was as follows. A solution nearly saturated with respect to $CuSO_4$ was prepared, then crystals of the other sulfate added to it portionwise with continuous stirring until the solution became saturated with respect to the added sulfate. Dissolution was usually conducted while heating, and the crystals were obtained on cooling to room temperature. In the case of $CuSO_4$–$FeSO_4$ special precautions had to be taken to prevent the reaction:

$$Cu^{2+} + Fe^{2+} \rightarrow Cu^{+} Fe^{3+}$$

The sulfate mixture was prepared at room temperature[1] and was deaerated and kept under inert atmosphere to prevent oxidation of Fe^{2+} ion; also few drops of H_2SO_4 were added to prevent its hydrolysis. Crystallization took place by cooling the solution in an ice bath. The crystals were collected, dried between tissue paper, and kept in desiccator. They were later dehydrated by heating in inert atmosphere then examined by X-ray diffraction method. Reduction by H_2 was performed at different temperatures and the products were examined by X-ray diffraction.

A Norelco X-ray diffractometer with CuK_α radiation was used. It consisted of: Diffraction Unit type 12045-12046, Wide Range Goniometer type 42201-42202, Electronic Circuit Panel type 12048-12049, and AMR Focusing Monochromator Model 3-202 with a graphite crystal. The diffraction patterns of reaction products obtained were compared with those in the ASTM card index and their contents were classified qualitatively as major, intermediate, and minor depending on the height of the major peaks.

[1]Oxidation of Fe^{2+} by Cu^{2+} takes place to a minor extent on boiling.

Thermogravimetric analysis (TGA) and differential thermal analysis (DTA) were also used. The TGA instrument was a Fisher 10-560-100 assembly with a Cahn RG electrobalance. The heating system consisted of a vertical tube furnace connected to the model 360 linear temperature programmer which provides a linear heating rate. A heating rate of 10 °C/min was used. An *X–Y* recorder Honeywell Electronik 19 was connected to the system. The sample was about 20 mg. The DTA instrument was a Stanton model 6-25 with a non-magnetic stainless steel sample holder, and platinum–rhodium crucibles with control base recess. Calcined Al_2O_3 was the reference material.

Results and Discussion

Crystallization and Dehydration of Binary Sulfates

When the binary sulfates were crystallized from solution, hydrated crystals were obtained, which in most cases were homogeneous on microscopic examination but sometimes had colors different from the mechanical mixture of the individual hydrated components. For example crystals obtained from the $CuSO_4$–$FeSO_4$–H_2O system were very pale blue although $CuSO_4.5H_2O$ is dark blue and $FeSO_4.7H_2O$ is pale green. Further, in some cases when the hydrated crystals were heated in inert atmosphere at 300 °C to remove the water, the color of the anhydrous mixture was unrelated to the color of the individual anhydrous salts. Thus anhydrous $CuSO_4$ and $FeSO_4$ are white, but the anhydrous mixture obtained by dehydrating the mixture obtained from solution was violet.[2] This intense coloration can be an indication of a partial valence change during heating, probably to Cu^{+} and Fe^{3+}. No attempt at present is made to identify these species; this will be the subject of a future study. More data on the color of the sulfate systems studied is given in Table 1.

When the anhydrous sulfate mixture was examined by X-ray diffraction method, there was a difficulty in identifying mixed crystals because most of the anhydrous sulfates studied showed nearly similar X-ray diffraction patterns. The following statement, however, can be made: (*1*) An anhydrous complex sulfate was confirmed in the case of $CuSO_4$–Na_2SO_4. (*2*) The presence of anhydrous solid solution was positive in the

[2]The same violet color was obtained when chalcopyrite, $CuFeS_2$, was oxidized by concentrated H_2SO_4 at 200 °C to form anhydrous sulfates, a process once seriously considered by the Anaconda Company in Tucson, Arizona and Treadwell Corporation for recovering copper from concentrates.

TABLE 1. Color of the individual sulfates and their binary mixtures with $CuSO_4$

Sulfate	Color of the anhydrous sulfate	Color of the hydrated sulfate	Color of the binary hydrated mixture with $CuSO_4$	Color of the binary anhydrous mixture with $CuSO_4$
$CuSO_4$	White	($5H_2O$) dark blue ($2H_2O$) pale blue		
$FeSO_4$	White	($7H_2O$) pale green	(nH_2O) pale blue ($2H_2O$) beige	Violet
$MnSO_4$	Pink	(H_2O) pink	Very pale blue	Canary yellow
$CoSO_4$	Dark blue	($7H_2O$) red	Purple	Purple
$NiSO_4$	Yellow	($6H_2O$) green	Very pale green	White
$ZnSO_4$	White	($7H_2O$) white	Very pale blue	White
$MgSO_4$	White	($7H_2O$) white	Very pale blue	White
Na_2SO_4	White	($10H_2O$) white	Turquoise	White
$CdSO_4$	White	($7H_2O$) white	White + blue*	White
$Al_2(SO_4)_3$	White	($19H_2O$) white	Pale blue	White

*Heterogeneous mixture as revealed by microscopic examination.

case of $CuSO_4$–$FeSO_4$ and $CuSO_4$–$MnSO_4$.[3] (*3*) The presence of anhydrous solid solution was doubtful in case of $CuSO_4$–$CoSO_4$, $CuSO_4$–$NiSO_4$, $CuSO_4$–$ZnSO_4$, and $CuSO_4$–$MgSO_4$. (*4*) No anhydrous solid solutions were present in the systems $CuSO_4$–$Al_2(SO_4)_3$ and $CuSO_4$–$CdSO_4$.

Reduction of Binary Sulfates

The simplest systems in which no complex sulfates or solid solutions are formed were studied first; these are $CuSO_4$–$Al_2(SO_4)_3$ and $CuSO_4$–$CdSO_4$. It was found that $Al_2(SO_4)_3$ had no effect on the reduction of $CuSO_4$ up to 400 °C, and $CdSO_4$ had no effect up to 320 °C but traces of CdS were formed at 400 °C. In both cases metallic Cu was obtained together with the unreacted sulfate which could be removed by leaching with water.

The effect of formation of complex sulfates was studied next; this is the case of $CuSO_4.Na_2SO_4$. It was found that $CuSO_4$ was reduced selectively at 300–400 °C, *i.e.*, Na_2SO_4 had no effect on the reduction and the complex sulfate behaved as if it were a mechanical mixture of $CuSO_4$ and Na_2SO_4. This is contrary to expectation since the formation of a complex sulfate was thought to influence the reduction because a new crystal structure was formed. The salt $CuSO_4.Na_2SO_4$ is stable in inert atmosphere up to 470 °C.

The effect of formation of solid solutions was studied in two systems in which solid solutions with $CuSO_4$ were positively identified. These were $CuSO_4$–$FeSO_4$ and $CuSO_4$–$MnSO_4$.

$CuSO_4$–$FeSO_4$

Crystals obtained from a solution saturated with $CuSO_4$ and $FeSO_4$ gave a distinctive X-ray diffraction pattern. This material is identified here as $(Cu,Fe)SO_4.nH_2O$. When heated in argon, another crystalline form was obtained at 200 °C, having the composition $(Cu,Fe)SO_4.mH_2O$. The amount of water of crystallization was determined experimentally and m was found to be equal to 2. The latter material was beige in color with a slight orange tint. Since its X-ray diffraction pattern is not indexed by the ASTM system, it is given here in Table 2. When heated further to 300 °C, it lost its water of crystallization to form $(Cu,Fe)SO_4$ which has a violet color.

The results of the thermal decomposition of $(Cu,Fe)SO_4.nH_2O$ are summarized in Table 3. It can be seen that the anhydrous material is stable in inert atmosphere up to 500 °C. Above this temperature, there is a gradual decomposition to give $CuSO_4$ and Fe_2O_3. In the region 600 to 700 °C, $CuSO_4$ gradually decomposes to CuO while Fe_2O_3 is partially converted to Fe_3O_4. No DTA peaks were observed in the temperature range 500 to 700 °C but rather a gradual endothermic effect (Fig. 1). Also it is remarkable that no oxysulfate, $CuO.CuSO_4$, is formed as is the case when pure $CuSO_4$ is decomposed. TGA curve for heating the crystals in argon is shown in Fig. 2.

When heated in H_2 atmosphere, $(Cu,Fe)SO_4.2H_2O$ was stable up to 210 °C (Table 4 and

[3]Although $CuSO_4$ and $FeSO_4$ are not isostructural and are therefore not expected to form a solid solution over the whole range, yet, apparently there is a limited solubility of one in the other.

Can. J. Chem. Downloaded from www.nrcresearchpress.com by 210.87.254.42 on 09/05/12
For personal use only.

Can. J. Chem. Downloaded from www.nrcresearchpress.com by 210.87.254.42 on 09/05/12
For personal use only.

TABLE 2. X-Ray diffraction pattern of $(Cu,Fe)SO_4.2H_2O$ ($Cu\ K_\alpha$ radiation)

d(Å)	I/I_0	d(Å)	I/I_0
4.96	33	2.26	20
4.86	47	2.10	14
3.75	10	2.00	14
3.52	100	1.85	7
3.41	24	1.79	5
3.31	26	1.74	5
3.13	57	1.68	17
2.60	15	1.61	10
2.54	46	1.59	6
2.40	7	1.51	6
2.32	11		

Fig. 1). Above this temperature, however, the following observations were made: (*1*) At 210 °C the crystals lost their water of hydration to form $(Cu,Fe)SO_4$ as indicated by the X-ray pattern. No Cu_2SO_4 was identified at 230 °C as in the case when pure $CuSO_4$ was reduced. (*2*) At 300 °C the individual diffraction patterns of $CuSO_4$ and $FeSO_4$ appeared as well as that of Cu. Under the microscope Cu appeared as whiskers. The material was soluble in water leaving Cu metal. (*3*) Bornite, Cu_5FeS_4, appeared at 350 °C among the reduction products. (*4*) The sulfates disappeared completely at 425 °C and two new phases appeared, namely, Fe_3O_4 and $CuFeS_2$ in addition to bornite and Cu although the temperature at which pure $FeSO_4$ starts to be influenced by H_2 is 440 °C and the products of reduction are Fe_3O_4 and FeS. (*5*) At 500 °C, $CuFeS_2$ decomposed and the reduction products were: Fe, Cu_5FeS_4, Cu, and FeS.

For comparative purposes, three sets of experiments were conducted on a mechanical mixture of $CuSO_4$ and $FeSO_4$. The first set consisted of the reduction of different $CuSO_4$:$FeSO_4$ ratios by H_2 at 500 °C. Different samples were prepared with molar ratios ranging between pure $CuSO_4$ and pure $FeSO_4$. It was found that in addition to Cu and Fe, bornite formation was evident in all experiments. Equimolar mixture of $CuSO_4$ and $FeSO_4$ was chosen to carry out the

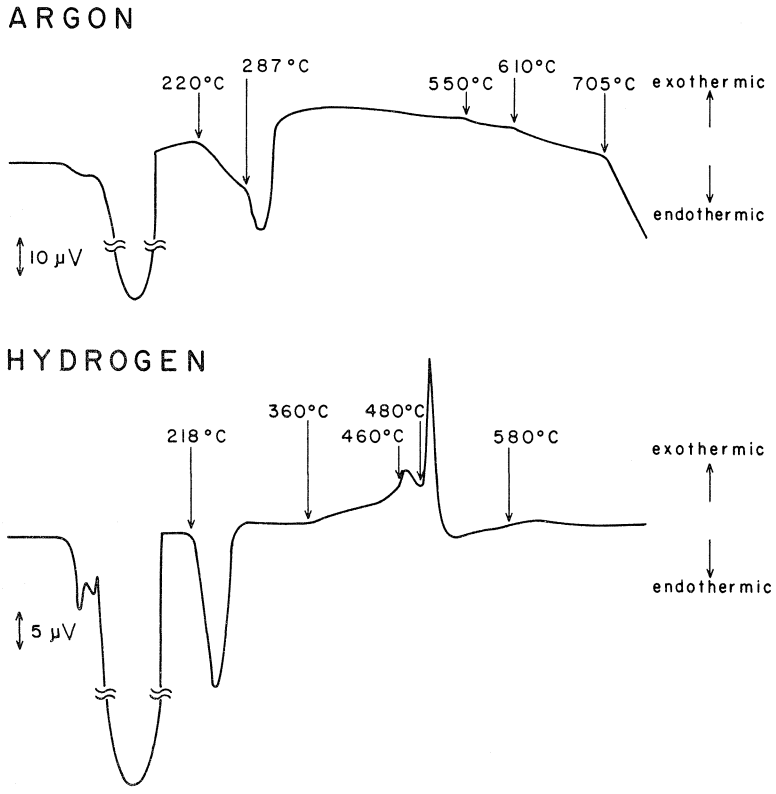

FIG. 1. Differential thermal analysis curves of $(Cu,Fe)SO_4.nH_2O$ crystals in argon and in H_2.

TABLE 3. Thermal decomposition of $(Cu,Fe)SO_4.nH_2O$ in argon*

Temperature (°C)	Reaction products			Color
	Major	Intermediate	Minor	
200	$(Cu,Fe)SO_4.2H_2O$			Beige
300	$(Cu,Fe)SO_4$			Violet
500	$(Cu,Fe)SO_4$			Violet
600	$CuSO_4$	Fe_2O_3		Red-brown
700	Fe_3O_4, CuO		Fe_2O_3	Red-black

*Heating in a boat for 1 h. Products identified by X-ray diffraction analysis.

TABLE 4. Reduction of $(Cu,Fe)SO_4.nH_2O$ by H_2 in a boat for 1 h*

Temperature (°C)	Reduction products			Color
	Major	Intermediate	Minor	
180	$(Cu,Fe)SO_4.2H_2O$		$CuSO_4$	Beige
210	$(Cu,Fe)SO_4$		Cu	Beige
230	$(Cu,Fe)SO_4$		Cu	Beige
300	Cu	$FeSO_4$, $CuSO_4$		Black
350	Cu	$FeSO_4$, $CuSO_4$	Cu_5FeS_4	Black
400	Cu	$FeSO_4$	$CuSO_4$, Cu_5FeS_4	Black
425	Fe_3O_4, $CuFeS_2$	Cu_5FeS_4	Cu	Black
450	Fe_3O_4	$CuFeS_2$, Cu_5FeS_4	Cu	Black
500	Fe, Cu_5FeS_4	Cu, FeS		Black

*Products identified by X-ray diffraction analysis.

second set of experiments to study the kinetics of the reduction at 500 °C. It was found that bornite formation was evident in case of the mechanical mixture as well. The third set of experiments was carried out to study the effect of reduction temperature. The results showed that up to 400 °C the mixture behaved in an additive way; thus Cu_2SO_4 was identified when reduction took place at 280 °C, the product was white in color and showed X-ray diffraction patterns due to $CuSO_4$ and $FeSO_4$. At 500 °C, however, bornite formation was evident.

It seems that it is not a question of presence of solid solution because a mechanical mixture of $CuSO_4$ and $FeSO_4$ behaves similarly to the solid solution with the exception that a slightly higher temperature is needed for the bornite phase to appear. This shows that in this case the solid solutions are less stable than the individual sulfates. Probably the proposed reaction in the solid state between Cu^{2+} and Fe^{2+} leading to the partial formation of Cu^+ and Fe^{3+} is responsible for the early appearance of metallic Cu during heating in H_2, because of the ease of reduction of Cu^+ to Cu.

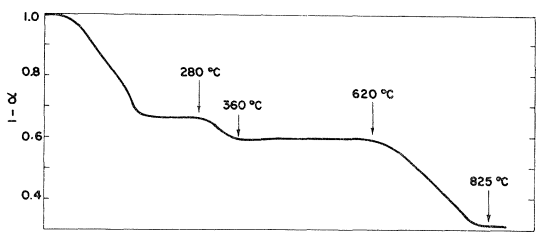

FIG. 2. Thermogravimetric analysis curve for the thermal decomposition of $(Cu,Fe)SO_4.nH_2O$ in argon.

Since not much information is available on the crystals $(Cu,Fe)SO_4.nH_2O$, DTA curves are presented in Fig. 3 for their decomposition in air. It can be seen that decomposition starts at 595 °C, but there are two small changes in the heating curve at 222 and 520 °C which were reproducible and could not be explained, as well as a small endotherm starting at 290 °C, which is apparently due to the loss of the last molecule of H_2O. In this respect the behavior of this material is different from the component sulfates. Thus, the exothermic peak that starts at 475 °C due to the formation of ferric oxysulfate, $Fe_2O(SO_4)_2$ (Fig. 3), is absent, and decomposition goes directly to Fe_2O_3 at about 600 °C while $CuSO_4$ remains unreacted.

Can. J. Chem. Downloaded from www.nrcresearchpress.com by 210.87.254.42 on 09/05/12
For personal use only.

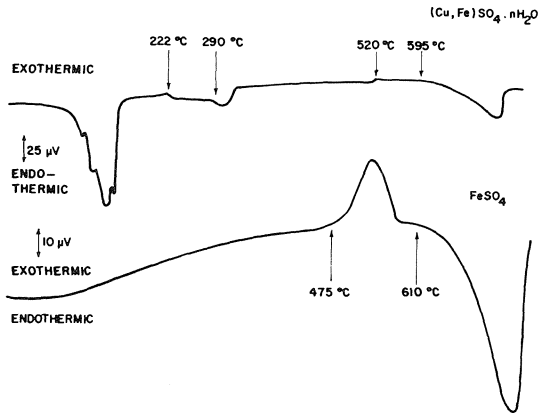

FIG. 3. Differential thermal analysis curve for heating $(Cu,Fe)SO_4.nH_2O$ and $FeSO_4$ in air.

$CuSO_4$–$MnSO_4$

The reduction of pure $MnSO_4$ is noticeable at 540 °C. When the solid solution was heated in H_2 at 400 °C, excess $CuSO_4$ in the mixture was reduced to Cu while excess $MnSO_4$ remained unchanged together with the solid solution. At 500 °C, the reduction products were the same except traces of $Cu_{1.96}S$ appeared. At 550 °C the solid solution was still present. It is evident, therefore, that $CuSO_4$ bound with $MnSO_4$ in the solid solution is resistant to reduction. Contrary to the previous case, this example shows that solid solutions can be more stable than at least one of the individual sulfates.

Other Systems

It was not possible to ascertain on basis of X-ray diffraction whether or not solid solutions existed in the following systems: $CuSO_4$–$CoSO_4$, $CuSO_4$–$NiSO_4$, $CuSO_4$–$ZnSO_4$, and $CuSO_4$–$MgSO_4$ because of the similarity of the patterns of the individual sulfates. For this reason, they are presented together.

While pure $CoSO_4$ is reduced to Co_9S_8 at 400 °C, the binary mixture $CuSO_4$–$CoSO_4$ is already reduced at 380 °C, *i.e.*, the reduction temperature of $CoSO_4$ is lowered by at least 20 °C in the presence of $CuSO_4$. Similar observation was found for the reduction of the binary mixture $CuSO_4$–$NiSO_4$ with the difference that beside the expected products Cu and Ni_3S_2, some Cu_2S was also formed. On the other hand, when the binary mixtures $CuSO_4$–$ZnSO_4$ and $CuSO_4$–$MgSO_4$ were reacted with H_2 at 380 °C, only $CuSO_4$ was reduced, *i.e.*, $ZnSO_4$ and $MgSO_4$ do not interfere.

Since the systems $CuSO_4$–$NiSO_4$ and $CuSO_4$–$FeSO_4$ proved to be the most complex with reduction products and the reduction temperatures different from those of the individual sulfates, it was decided to search for another system that might lead to similar reduction behavior. The system $FeSO_4$–$NiSO_4$ was chosen since it is known that hydrated solid solutions are formed in this system. It was found that there was a similarity in the X-ray diffraction patterns between the crystals obtained by crystallizing then dehydrating a $FeSO_4$–$NiSO_4$ mixture and the individual anhydrous sulfates and it could not be ascertained whether or not anhydrous solid solutions existed. The results of reducing these crystals are shown in Table 5, from which it can be seen that the reduction temperature of $FeSO_4$ is decreased by at least 40 °C in presence of $NiSO_4$ and that the complex sulfide pentlandite, $(Fe,Ni)_9S_8$, was formed and no FeS could be detected although the latter is a major reduction product of $FeSO_4$.

Conclusions

(*1*) The X-ray diffraction patterns of anhydrous Fe^{II}, Co, Ni, Mn, Zn, and Cd sulfates resemble to a great extent that of $CuSO_4$ and in most cases it was not possible to decide whether

TABLE 5. Reduction of $FeSO_4$-$NiSO_4$ (mixed) crystals in H_2*

Temperature (°C)	Reduction products			Color
	Major	Intermediate	Minor	
300	$FeSO_4$, $NiSO_4$	—	—	Green
400	Ni_3S_2	$FeSO_4$	$(Fe,Ni)_9S_8$	Black
500	Ni_3S_2 $(Fe,Ni)_9S_8$	—	Fe	Brass

*Products identified by X-ray diffraction analysis.

Can. J. Chem. Downloaded from www.nrcresearchpress.com by 210.87.254.42 on 09/05/12
For personal use only.

anhydrous solid solutions were formed or not when $CuSO_4$ and another sulfate were crystallized from solution, then dehydrated. Anhydrous solid solutions were only positively identified in the systems $CuSO_4$–$FeSO_4$ and $CuSO_4$–$MnSO_4$ while an anhydrous complex sulfate was identified in the case of $CuSO_4$–Na_2SO_4.

(*2*) The reduction of a sulfate mixture prepared by crystallization from aqueous solution then dehydrated may be different from that of the individual anhydrous sulfates. When $CuSO_4$ is reduced at 380 °C in presence of another sulfate it was found that the following sulfates do not influence the reduction: Na_2SO_4, $MgSO_4$, $Al_2(SO_4)_3$, $ZnSO_4$, and $CdSO_4$. On the other hand $CoSO_4$, $NiSO_4$, $FeSO_4$, $MnSO_4$ interfere in the following manner: $CoSO_4$ and $NiSO_4$ are reduced at a lower temperature than expected and in the latter case a Cu_2S phase appears. $FeSO_4$ is also reduced at a lower temperature than expected and a complex sulfide phase, Cu_5FeS_4, is formed. $MnSO_4$ forms a stable solid solution with $CuSO_4$ which is reduced at a temperature higher than that expected.

(*3*) The formation of a complex sulfide phase during the reduction of a sulfate mixture was also observed during the reduction of $FeSO_4$–$NiSO_4$. In this case pentlandite $(Fe,Ni)_9S_8$ was observed.

(*4*) No Cu_2SO_4 was formed as intermediate product during the reduction of $CuSO_4$ in admixture with another sulfate although it was identified during the reduction of pure $CuSO_4$.

(*5*) The formation of solid solutions or complex salts might be expected to alter conditions; it does in some cases but not in every case. Thus, $CuSO_4$ and Na_2SO_4 form a complex salt but the presence of one sulfate does not influence the other during reduction. On the other hand, when solid solutions are formed the reduction products may be different from that of the individual components as indicated earlier.

(*6*) There are indications that the anhydrous solid solution $(Cu^{II},Fe^{II})SO_4$ may be partly transformed into $(Cu^{I},Fe^{III})SO_4$; this is based on the color change, X-ray diffraction, behaviour during oxidation, reduction, and thermal decomposition.

(*7*) To get pure metallic Cu by reduction of $CuSO_4$, the impurities Fe, Co, and Ni must be absent from the solution before obtaining the sulfate crystals. Other sulfates such as Na_2SO_4, $MgSO_4$, $Al_2(SO_4)_3$, $ZnSO_4$, $CdSO_4$, and $MnSO_4$ may be tolerated and would be removed from metallic Cu by leaching with water, provided the reduction temperature does not exceed 380 °C.

Acknowledgements

The financial aid of the National Research Council of Canada is greatly appreciated. A discussion with Professor F. Claisse was very useful.

1. F. Habashi and R. Dugdale. Met. Trans. **4** (5), 1429 (1973).
2. K. Vo Van and F. Habashi. Can. J. Chem. Eng. **52**, 369 (1974).
3. F. Habashi, S. A. Mikhail, and K. Vo Van. Can. J. Chem. This issue.
4. Gmelins Handbuch der Anorganischen Chemie, Volume 60, Kupfer, Part B3, Verlag Chemie, Weinheim, 1965.

Can. J. Chem. Downloaded from www.nrcresearchpress.com by 210.87.254.42 on 09/05/12
For personal use only.

Cinetique chimique en milieu micellaire. Relation entre vitesse de réaction et structure du milieu[1]

GENEVIÈVE ROUX ET ANDRÉ VIALLARD

Laboratoire de Thermodynamique et Cinétique Chimique, Groupe de Chimie Physique, U.E.R. des Sciences Exactes et Naturelles, B.P. 45, 63170 Aubière, France et Ecole Nationale Supérieure de Chimie, Boulevard Côte-Blatin, 63000, Clermont-Ferrand, France

Reçu le 3 mai 1976

GENEVIÈVE ROUX et ANDRÉ VIALLARD. Can. J. Chem. **54**, 3658 (1976).

Une réaction a été réalisée entre deux réactifs dont l'un, ionique, est dissous dans une phase aqueuse, l'autre, le solubilisat, est réparti entre la phase aqueuse et une phase micellaire. L'étude cinétique de cette réaction a permis la mise en évidence de différents régimes de réaction.

Suivant les conditions expérimentales, on peut avoir, soit un équilibre du solubilisat entre phase aqueuse et phase micellaire, soit une limitation de la vitesse de réaction par la vitesse de diffusion de ce réactif de la phase micellaire à la phase aqueuse.

On montre alors que de telles études cinétiques permettent de déterminer quantitativement la répartition du solubilisat entre les différentes phases et à l'intérieur même des micelles.

GENEVIÈVE ROUX and ANDRÉ VIALLARD. Can J. Chem. **54**, 3658 (1976).

A reaction has been studied between two reactants where one, ionic, is dissolved in the aqueous phase and the other, nonionic, is distributed between the aqueous phase and a micellar phase. The kinetic study of this reaction has helped to elucidate the mechanism of the reaction.

Depending on the experimental conditions, it is possible to have either an equilibrium of the nonionic solute between the aqueous and micellar phases, or a reaction rate limited by the rate of diffusion of this reactant from the micellar phase to the aqueous phase. It will be shown that such kinetic studies can be used to determine quantitatively the distribution of the solute between the various phases and even inside the micelles.

[Journal translation]

Introduction

Depuis une dizaine d'années, la chimie des tensio-actifs et ses applications, diverses et nombreuses, connaissent un essor important. Lorsqu'on dissout un tensio-actif dans un solvant tel que l'eau, ses solutions peuvent présenter des structures très particulières suivant la concentration. Corrélativement, elles peuvent être le siège de phénomènes assez inattendus. Aussi, industriels et chercheurs, chimistes et biochimistes s'intéressent-ils de plus en plus à ces milieux.

Lorsque la concentration en tensio-actif est faible, ces solutions sont dites micellaires. Bien que d'aspect homogène, elles sont hétérogènes à l'échelle submicroscopique. En effet, les molécules de tensio-actifs se regroupent spontanément en agrégats appelés micelles. Ces micelles sont formées d'un "coeur" composé des parties organiques et du "manteau" qui entoure le "coeur". Ce manteau contient les parties hydrophiles, il est de ce fait responsable de la solubilité des micelles dans l'eau.

Ces micelles ont la propriété de solubiliser des molécules qui sans elles seraient insolubles, permettant ainsi le déroulement de certaines réactions chimiques. Elles peuvent avoir des effets catalytiques, mais aussi bloquer certaines réactions et, au total, donc en permettre le contrôle, à condition de parvenir à une entière maîtrise de cette technique.

Actuellement, les physico-chimistes s'intéressent d'un point de vue plus fondamental au rôle catalytique des micelles. Une synthèse de nombreux travaux déjà effectués est déjà publiée (1–3). Les micelles ioniques ont fait l'objet des premières études, car avec elles, les méthodes de mesure sont plus facilement mises en oeuvre. Maintenant, l'intérêt se porte vers les réactions se déroulant dans des milieux contenant des molécules tensio-actives non ioniques. L'étude de processus chimiques se déroulant dans ces milieux entre un composé solubilisé dans les micelles et un autre dissous dans la phase con-

[1]Ce travail constitue une partie de la thèse de doctorat de G. Roux à l'Université de Clermont-Ferrand, France.

Can. J. Chem. Downloaded from www.nrcresearchpress.com by 210.87.254.40 on 09/05/12
For personal use only.

Can. J. Chem. Downloaded from www.nrcresearchpress.com by 210.87.254.40 on 09/05/12
For personal use only.

tinue nous a paru devoir être particulièrement intéressante.

Nous nous sommes intéressés à ce type de réaction dans le cas particulier de l'hydrolyse alcaline d'esters peu solubles dans l'eau. On a là une réaction entre des espèces chimiques relativement simples, de plus, cette réaction est bien connue en milieu homogène en l'absence de tensio-actifs.

Dans un tel système, l'ester est partiellement solubilisé dans les micelles, la soude est dans la phase aqueuse. On peut admettre que la réaction se déroule au sein de celle-ci. L'ester, pour être hydrolysé, devra donc diffuser à l'intérieur des micelles et des micelles vers la phase aqueuse. On peut donc penser qu'il devrait être possible, selon les conditions expérimentales, de mettre en évidence une limitation de la réaction chimique par la diffusion.

Les vitesses de diffusion seront conditionnées par les interactions solubilisat/tensio-actif. Selon la nature de l'ester utilisé, la nature et la structure du tensio-actif, ces interactions seront plus ou moins importantes. La localisation de l'ester à l'intérieur des micelles sera elle aussi fonction de leur nature et de leur intensité. On peut donc penser pouvoir ainsi, grâce à des études cinétiques dans ces milieux, acquérir un certain nombre de données dans ce domaine.

Partie expérimentale

Une méthode conductométrique a permis de suivre l'évolution de la réaction. Sa description et celle du dispositif expérimental utilisé ont été faites dans un travail antérieur (4).

(1) Conditions expérimentales

L'ester choisi est le benzoate de méthyle purifié par chromatographie en phase vapeur sur Carbowax 20 M.

Les tensio-actifs non ioniques utilisés sont des condensats d'alkyls phénols (nonyl phénol) sur un nombre variable de molécules d'oxyde d'éthylène. Ce sont des produits commerciaux "Sinnova", de pureté 99%, nous les avons donc utilisés tels quels.

Leur formule générale est

$$CH_3—(CH_2)_8—C_6H_4—(O—CH_2—CH_2)_n—OH$$

On les représentera à l'aide du symbole NP*n*.

Les hydrolyses sont réalisées à 25 °C en présence de soude de concentration initiale de l'ordre de 0.01 *M* en général, avec un excès d'ester. La concentration en tensio-actif est relativement faible, variant de 10^{-3} à 10^{-2} *M*. Elle est très supérieure à la concentration critique micellaire qui est de l'ordre de 10^{-4} *M*. Un certain nombre de paramètres sont variables: structure et concentration du tensio-actif, volume initial de l'ester introduit, concentration initiale en soude.

Remarque

Lorsque nous nous sommes intéressés à la structure du tensio-actif, nous avons fait varier uniquement la longueur de la chaîne éthoxylée. En présence de tensio-actif, la solubilité de l'ester est augmentée; elle dépend de la nature et de la concentration du tensio-actif. Ceci permet de travailler dans un plus large domaine de variation de la quantité d'ester introduit qu'en milieu homogène, sans tensio-actif.

(2) Résultats expérimentaux

Les vitesses instantanées de réaction sont déterminées à partir des concentrations à l'aide de la méthode différentielle de Broche et Gibert (5). Les concentrations des réactifs, elles, sont calculées à partir des valeurs expérimentales de la conductibilité électrique du milieu. On utilise pour celà, une loi linéaire pour la variation de la conductivité en fonction de l'avancement de la réaction. Une telle loi est suffisante ici pour une étude comparative. On peut alors traduire l'évolution de la réaction par des graphiques en coordonnées $(v/x, x)$ où v est la vitesse de réaction $-dx/dt$, x étant la concentration instantanée en soude.

Sur les figs 1 et 2, nous avons donné quelques exemples de courbes obtenues en faisant varier les différents paramètres envisagés. Il faut noter que la réaction d'hydrolyse de l'ester en milieu homogène, sans tensio-actif, est du second ordre, représentée par une droite dont la pente est égale à la constante de vitesse et dont l'ordonnée à l'origine est proportionnelle à la concentration finale de l'ester en excès.

Figure 1, on verra l'influence de la nature et de la concentration du tensio-actif. Pour une concentration constante en tensio-actif (2×10^{-3} *M*), une concentration initiale en soude identique de l'ordre de 0.01 *M* et pour une concentration initiale en ester de 12.5×10^{-3} *M*, les courbes *a'*, *b'* et *c'* sont représentatives respectivement des hydrolyses réalisées en présence des tensio-actifs NP 12, NP 15 et NP 30 et de même pour une concentration initiale en ester de 22.5×10^{-3} *M*, les courbes *a*, *b*, *c* représentent respectivement l'influence des tensio-actifs NP 12, NP 15, NP 30. Les courbes *a* et *d* pour le NP 12 et *b* et *e* pour le NP 15 traduisent, elles, l'influence de la concentration du tensio-actif pour des concentrations initiales en soude et ester identiques. On notera la position de la droite (courbe *s'*) représentative de la réaction d'ordre deux, en milieu homogène, en l'absence de tensio-actif, lorsque la concentration initiale en ester est de 12.5×10^{-3} *M*, celle en soude de 0.01 *M*. La solubilité de l'ester dans l'eau pure est de l'ordre de 15×10^{-3} *M*. La courbe *s* représente la réaction d'hydrolyse pour une concentration initiale en ester de 22.5×10^{-3} *M* en l'absence de tensio-actif. Pour des concentrations en ester supérieures à sa solubilité, la réaction est du premier ordre (6), v/x reste constant. Au-dessous de la valeur de la solubilité de l'ester dans l'eau, la réaction est du second ordre et v/x varie linéairement avec x.

La fig. 2 traduit l'influence de la concentration initiale en ester (courbes *a*, *b*, *c*) et de la concentration initiale en soude (courbes *c* et *d*) pour le tensio-actif NP 12 pris à la concentration de 2×10^{-3} *M*.

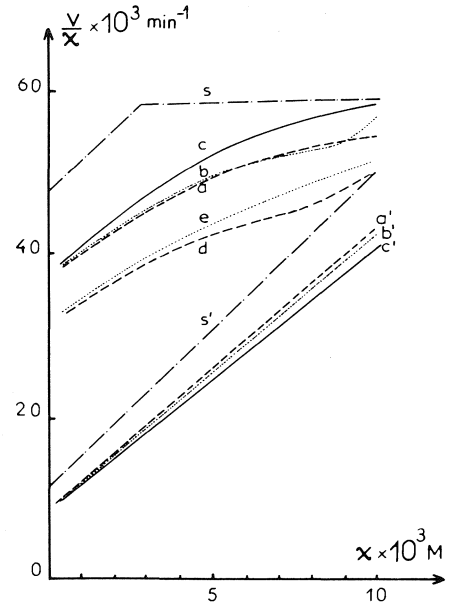

FIG. 1. Influence de la nature et de la concentration du tensio-actif sur la vitesse d'hydrolyse du benzoate de méthyle:

Courbe		[Ester] (M)	[Soude] (M)
a′	NP 12*	0.0125	0.01
b′	NP 15*	0.0125	0.01
c′	NP 30*	0.0125	0.01
a	NP 12*	0.0225	0.01
b	NP 15*	0.0225	0.01
c	NP 30*	0.0225	0.01
d	NP 12†	0.0225	0.01
e	NP 15‡	0.0225	0.01

*[NPn] = 2×10^{-3} M.
†[NP 12] = 4.6×10^{-3} M.
‡[NP 15] = 3.9×10^{-3} M.

L'examen de cet ensemble de courbes montre que systématiquement la vitesse de réaction est ralentie par la présence du tensio-actif. Dans la représentation choisie, les courbes $v/x = f(x)$ ne sont plus des droites, la réaction n'est donc plus globalement du second ordre. La vitesse dépend de tous les paramètres étudiés.

Si la concentration initiale en ester est faible (léger excès par rapport à la soude), le rapport v/x diminue lorsque la chaîne hydrophile de la molécule de tensio-actif s'allonge; par contre, si l'excès d'ester est important, la concentration initiale en ester étant telle que les micelles sont proches de la saturation, le rapport v/x augmente avec l'allongement de la chaîne.

Si on augmente la concentration du tensio-actif, la valeur du rapport v/x diminue. Des résultats analogues ont été obtenus par Mitchell, dans le cas de l'hydrolyse du benzoate de propyle (7).

Lorsque la quantité d'ester introduit augmente, le

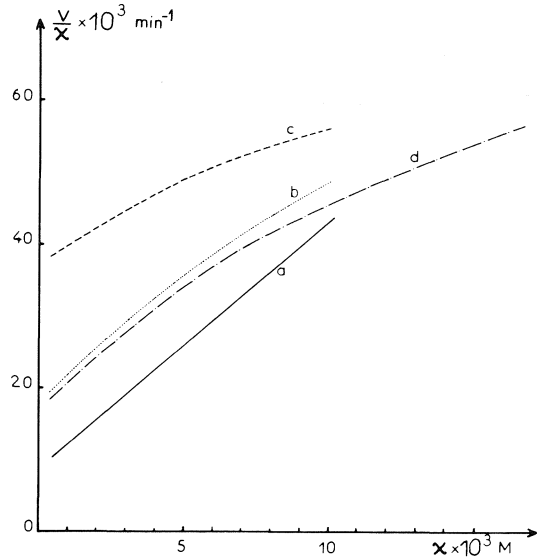

FIG. 2. Influence des concentrations initiales en ester et en soude sur la vitesse d'hydrolyse du benzoate de méthyle ([NP 12] = 2×10^{-3} M):

Courbe		[Ester] (M)	[Soude] (M)
a	NP 12	0.0125	0.01
b	NP 12	0.0158	0.01
c	NP 12	0.0225	0.01
d	NP 12	0.0225	0.0165

rapport v/x croît aussi, et la forme des courbes $v/x = f(x)$ dépend de la quantité introduite. v/x diminue aussi si la concentration initiale en soude croît.

Si v/x représente effectivement la concentration de l'ester dans la phase aqueuse, il apparaît donc que, en présence de tensio-actif, cette concentration est toujours inférieure à ce qu'elle serait en son absence.

En particulier, en fin de réaction, la concentration de l'ester en excès dans la phase aqueuse, libre de réagir avec les dernières traces de soude, est inférieure à celle que devrait donner l'excès total d'ester dans le milieu.

On peut donc penser que l'ester est piégé dans les structures micellaires formées par le tensio-actif que, de ce fait, il n'est pas libre de réagir avec la soude et qu'il doit, pour y parvenir, diffuser des micelles vers la phase aqueuse. L'exploitation des courbes $v/x = f(x)$ devrait permettre de mettre en évidence ces phénomènes de diffusion.

(3) Exploitation des résultats

Nous utiliserons le modèle suivant. La réaction d'hydrolyse est une réaction du second ordre se déroulant dans la phase aqueuse avec une constante de vitesse k_2. L'ester est réparti entre micelles et phase aqueuse et diffuse des micelles vers la phase aqueuse. Dans ce cas, la concentration y_{aq} de l'ester en phase aqueuse s'obtient aisément à partir de la vitesse de réaction v et de la

Can. J. Chem. Downloaded from www.nrcresearchpress.com by 210.87.254.40 on 09/05/12
For personal use only.

Can. J. Chem. Downloaded from www.nrcresearchpress.com by 210.87.254.40 on 09/05/12
For personal use only.

concentration en soude x. On a $y_{aq} = k_2^{-1}(v/x)$. On peut donc déterminer l'évolution des quantités d'ester n_{aq} et n_m (nombres de moles) présentes respectivement en phase aqueuse et dans les micelles tout au long de la réaction, en fonction de la quantité totale d'ester n_t.

Les couples de valeurs (n_{aq}, n_t et n_m, n_t) déterminées pour chaque hydrolyse sont alors représentatives de l'évolution de la composition des phases aqueuse et micellaire au cours des réactions.

On constate alors, qu'à la précision expérimentale près, pour un même tensio-actif à concentration donnée, l'ensemble des valeurs n_{aq} et n_m correspondant à des hydrolyses réalisées, soit avec des volumes initiaux d'ester différents, soit avec des concentrations initiales en soude différentes, se place sensiblement sur deux courbes $n_{aq} = f(n_t)$ et $n_m = g(n_t)$. Ceci signifie que, dans les cas étudiés, les fonctions f et g représentatives des lois d'évolution des quantités d'ester réparties en phase aqueuse et dans les micelles sont spécifiques en première approximation de la nature et de la concentration du tensio-actif.

Les courbes $f(n_t)$ et $g(n_t)$ obtenues pour les tensio-actifs NP 12, NP 15 et NP 30 sont tracées sur les figs 3 et 4, soit pour les trois tensio-actifs à concentration constante (2×10^{-3} M), soit pour NP 12 pris à deux concentrations

L'allure de ces courbes est comparable; elle est représentée fig. 5.

Il semble exister deux domaines.

Dans le domaine I, lorsque la quantité totale d'ester présente dans le milieu est grande (proche de la saturation des micelles) la quantité d'ester dans la phase aqueuse varie peu au cours de l'hydrolyse, alors que celle contenue dans les micelles décroît rapidement.

Ensuite, avec l'avancement de la réaction, lorsque la quantité totale d'ester dans la phase aqueuse atteint une certaine valeur, les valeurs n_{aq} et n_m décroissent de façon sensiblement linéaire avec la quantité totale d'ester présente; c'est le domaine II.

Considérons le rapport $C_r = n_m/n_{aq}$. C_r est le coefficient de répartition de l'ester à un instant donné entre les phases micellaire et aqueuse. On constate que, dans le domaine I, ce rapport varie de façon sensiblement linéaire avec la quantité d'ester présente dans le milieu, alors que, dans le domaine II, il reste sensiblement constant.

Interprétation des résultats – discussion

Les résultats présentés ci-dessus permettent de constater que, selon la quantité totale d'ester présent (domaine I ou II) les quantités d'ester dans chaque phase varient de façon différente.

Nous avons interprété ces résultats de la façon suivante. Etant donné la plus grande solubilité de l'ester dans les hydrocarbures que dans l'eau (miscibilité totale dans un cas, très faible dans l'autre), on peut penser que l'ester est préférentiellement solubilisé dans le "coeur" organique micellaire. Cependant, le caractère polaire de son groupement hydrophile lui donne une certaine solubilité dans le "manteau" qui est la phase "aqueuse" de la micelle. Si donc la réaction a lieu en phase aqueuse vraie, les molécules d'ester doivent diffuser, les unes du "manteau" vers la phase aqueuse, les autres depuis le "coeur" vers le "manteau" puis vers la phase aqueuse.

Les interactions ester – partie hydrophobe, ester – partie hydrophile du tensio-actif sont d'importance inégale. Il semble donc raisonnable de penser que les vitesses de diffusion des molécules d'ester seront différentes selon leur localisation dans les micelles.

(1) Mise en évidence des vitesses de diffusion

Etant donné qu'il existe deux régions différentes de variation des quantités d'ester solubilisé dans les micelles et en phase aqueuse, il doit donc y avoir deux régimes différents de "réaction".

(*a*) Dans le domaine I, la quantité d'ester en phase aqueuse varie lentement en dépit de la réaction chimique. On en déduit que si elle varie peu, c'est que la vitesse de diffusion de l'ester ne limite pas la réaction chimique (4). L'équilibre des concentrations en ester entre phases est alors le facteur responsable de la vitesse globale d'évolution de la réaction; la légère variation de la quantité de l'ester en phase aqueuse est due au déplacement de l'équilibre par suite de la réaction. Par contre, la quantité d'ester contenue dans les micelles diminue rapidement, de façon à compenser sensiblement celle disparue par réaction dans la phase aqueuse: c'est bien dire que, dans ce domaine, la vitesse de diffusion ne limite pas la réaction chimique. On pourrait alors définir un coefficient de partage de l'ester entre phases:

$$K^c = \frac{y_m}{y_{aq}} = C_r \times \frac{v_{aq}}{v_m}$$

où y_m et y_{aq} sont les concentrations de l'ester dans les phases micellaire et aqueuse de volumes respectifs v_{aq} et v_m.

Malheureusement, le volume de la phase micellaire est difficilement accessible. Lorsqu'on tente de telles estimations, soit à partir de modèles de structure, soit à partir de résultats de mesures par diverses méthodes, l'expérience montre que les résultats sont très divers, donc très incertains.

(*b*) Dans le domaine II, les quantités d'ester dans les micelles et en phase aqueuse décroissent

Can. J. Chem. Downloaded from www.nrcresearchpress.com by 210.87.254.40 on 09/05/12
For personal use only.

linéairement en fonction de la quantité totale d'ester. Celle-ci, et de ce fait celle dans les micelles, est plus faible, il y a alors changement de régime. Il n'y a plus équilibre de l'ester entre les phases, la quantité d'ester contenue dans la phase aqueuse diminuant rapidement. On peut donc penser que, dans ce cas, la vitesse de diffusion de l'ester des micelles vers la phase aqueuse limite celle de la réaction chimique.

Puisque le coefficient de répartition C_r reste sensiblement constant, on aura pour le débit de matière dû à la diffusion:

$$\frac{dn_{aq}}{dt} = \frac{1}{C_r} \times \frac{dn_m}{dt}$$

La variation de la quantité d'ester en phase aqueuse étant due à la réaction et à la diffusion, on a:

$$v_{aq}dy_{aq} = v_{aq}(dy)_r - dn_m$$

On désigne par dy_{aq} la variation de concentration de l'ester en phase aqueuse et par $(dy)_r$ la contribution de la réaction chimique à cette variation.

Si l'on pose $V_r = (dy)_r/dt$, on en déduit que:

$$\frac{dn_m}{dt} = \frac{C_r}{C_r + 1} v_{aq} V_r$$

Dans ce domaine, le débit de diffusion de l'ester est donc proportionnel au débit de l'ester consommé par réaction chimique en phase aqueuse.

Le coefficient de proportionnalité dépend du coefficient de répartition de l'ester, donc de la nature et de l'intensité des interactions ester–tensio-actif et, par conséquent, de la nature et de la concentration du tensio-actif.

Ce changement de régime au cours de l'avancement de la réaction, selon la quantité totale d'ester peut s'interpréter à l'aide de considérations sur la structure du milieu.

Lorsque les micelles sont proches de la saturation (n_t grand) l'ester est réparti entre "coeur" et "manteau". La structure du "coeur" est dense, l'ester y est fortement retenu; par contre, la structure du "manteau" est beaucoup plus lâche et l'ester est peu lié. Les molécules d'ester, peu retenues dans l'enchevêtrement des chaînes hydrophiles vont pouvoir en sortir facilement pour remplacer celles qui disparaissent par réaction chimique en phase aqueuse; le "manteau" s'appauvrit donc en ester. Cet appauvrissement déclenche alors le processus de diffusion de l'ester du "coeur" vers le "manteau"; l'ester étant plus retenu dans le coeur, cette vitesse est beaucoup plus lente, et lorsqu'il n'y aura plus d'ester dans le manteau, cette vitesse limitera alors la réaction chimique. La phase aqueuse s'appauvrira à son tour en ester et il n'y aura plus équilibre.

(2) Répartition de l'ester dans les micelles

Si l'on admet ce processus de diffusion, lente du "coeur" vers le "manteau" et rapide du "manteau" vers la phase aqueuse, la courbe représentant l'évolution de la quantité d'ester dans les micelles permet alors de prévoir la répartition de l'ester à l'intérieur des micelles entre "coeur" et "manteau". Son étude apporte donc des informations sur l'intensité des interactions ester–tensio-actif, interactions qui dépendent de la nature du tensio-actif.

Soit $n_m(c)$ la quantité d'ester solubilisé dans le coeur et $n_m(m)$ celle dans le manteau. Si le domaine II correspond à la diffusion lente de l'ester du "coeur" vers la phase aqueuse, la quantité d'ester n_m s'identifie à $n_m(c)$.

Dans le domaine I, où il y a simultanément diffusion rapide et diffusion lente, n_m est égale à la somme $n_m(c) + n_m(m)$. Si la quantité d'ester $n_m(c)$, dans ce domaine, varie toujours linéairement avec n_t, $n_m(m)$ est alors représentée par la différence entre la courbe d'évolution de n_m et la droite représentative de celle de $n_m(c)$.

Pour une quantité totale d'ester donnée, il est donc possible d'estimer la répartition de l'ester dans le milieu: d'une part entre la phase aqueuse et les micelles, d'autre part à l'intérieur des micelles. Pour un ester donné, cette répartition dépend de la nature et de la concentration du tensio-actif.

(a) Nature du tensio-actif

Nous nous sommes intéressés plus particulièrement aux tensio-actifs NP 12, NP 15 et NP 30, pour lesquels la chaîne hydrophile est suffisamment longue pour permettre une bonne solubilisation de l'ester et offrir un domaine micellaire assez large pour qu'il soit possible d'y réaliser des hydrolyses.

Sur la fig. 3, on trouvera les courbes $n_{aq} = f(n_t)$ et $n_m = g(n_t)$ pour ces trois tensio-actifs à même concentration (2×10^{-3} *M*). Bien que leur allure soit comparable, l'évolution de n_{aq} et n_m présente des différences selon la nature du

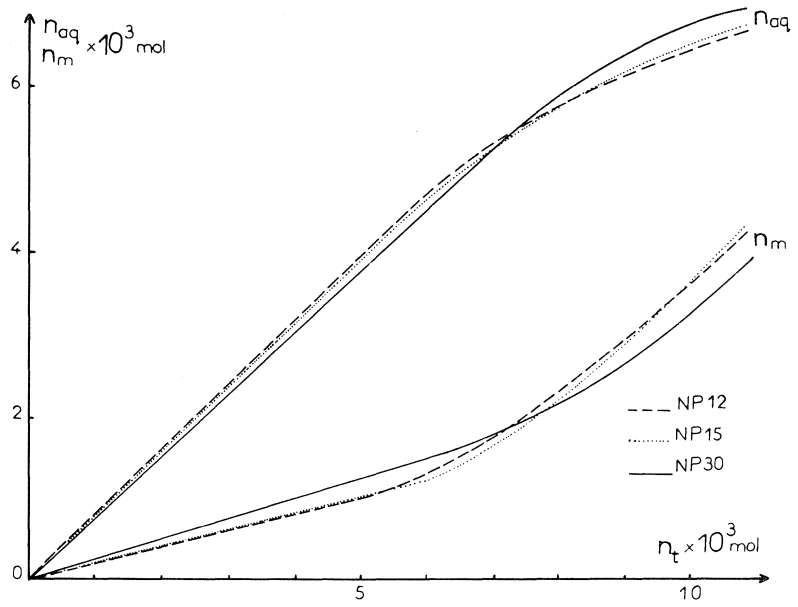

FIG. 3. Variation des quantités d'ester n_{aq} et n_m en fonction du nombre total de moles d'ester présent n_t dans 500 cm^3 de solution obtenue avec les tensio-actifs NP 12, NP 15 et NP 30 à la concentration de 2×10^{-3} *M*.

tensio-actif et selon le domaine de variation de ces grandeurs.

Tout d'abord, on observe que la quantité totale d'ester susceptible d'être "solubilisé" augmente lorsque la longueur de la chaîne hydrophile diminue. Par exemple, pour une concentration en tensio-actif de 2×10^{-3} *M*, les concentrations de l'ester à saturation sont respectivement de 27.4×10^{-3} *M*, 26×10^{-3} *M* et 23×10^{-3} *M* pour les tensio-actifs NP 12, NP 15 et NP 30. En l'absence de tensio-actif, la solubilité est de 15×10^{-3} *M*.

Dans le domaine I, pour une même quantité totale d'ester, n_{aq} augmente de NP 12 à NP 30 et corrélativement n_m diminue.

Par contre, dans le domaine II, pour n_t donné, l'allongement de la chaîne provoque une diminution de la quantité d'ester en phase aqueuse et une augmentation dans les micelles. C_r, qui dans ce domaine reste constant, augmente donc quand on passe de NP 12 à NP 30. Les valeurs sont respectivement de 0.2, 0.21 et 0.28 pour les NP 12, NP 15 et NP 30.

On peut donc penser que, si la précision expérimentale autorise que l'on attribue une signification à la position relative de ces différentes courbes, l'allongement de la chaîne hydrophile modifie la répartition de l'ester dans les phases et à l'intérieur des micelles. Mais, au total, elle se traduit toujours par un accroissement de la quantité d'ester piégé dans le coeur micellaire.

Dans le domaine I, il y a un appauvrissement en ester des micelles au profit de la phase aqueuse et, dans les micelles, un appauvrissement du manteau au profit du coeur, tandis que, dans le domaine II, il y a appauvrissement de la phase aqueuse par rapport aux micelles, au bénéfice du coeur.

Il semble que l'examen de la structure des solutions micellaires de ces différents tensio-actifs permette de donner une interprétation de ces phénomènes.

En effet, d'après Schick *et al.* (8), pour une série de tensio-actifs de même reste hydrophobe, mais de longueur de chaîne éthoxylée croissante, le nombre d'agrégation (nombre de monomères par micelles) diminuerait; il passerait de 100 pour le NP 12 à 44 pour le NP 30; le volume du "coeur" serait peu modifié, la taille des micelles varierait peu, ce qui semble indiquer une structure moins étirée des chaînes lorsque diminue le nombre d'agrégation.

Considérons donc deux solutions des tensio-

Can. J. Chem. Downloaded from www.nrcresearchpress.com by 210.87.254.40 on 09/05/12
For personal use only.

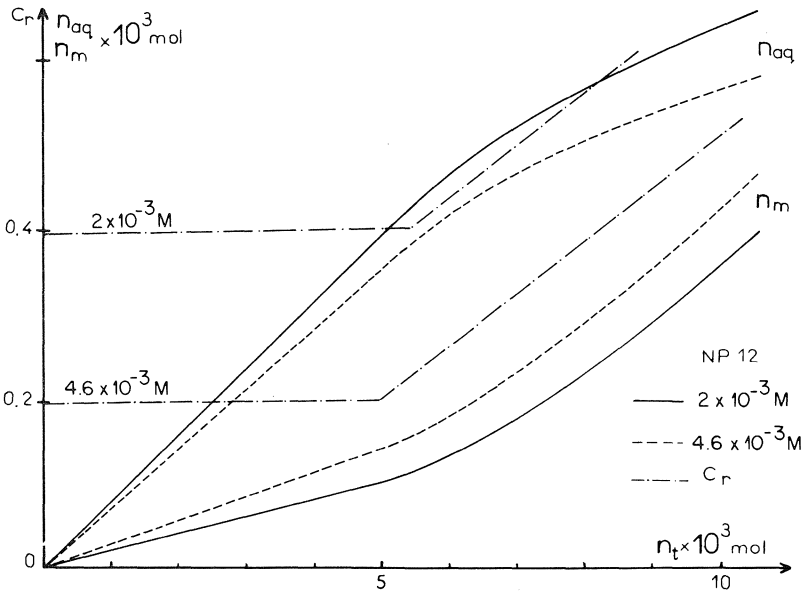

FIG. 4. Variation de n_{aq}, n_m et C_r en fonction du nombre total de moles d'ester présent n_t dans 500 cm^3 de solution obtenue avec le tensio-actif NP 12 pris à plusieurs concentrations.

actifs (*1*) et (*2*): si n_i est le nombre de molécules du tensio-actif i, N_i le nombre de micelles et a_i le nombre d'agrégation, on a pour (*1*) $n_1 = a_1N_1$ et pour (*2*) $n_2 = a_2N_2$.

Soit v_{ci} le volume du coeur dans une micelle de i et V_{ci} celui total des "coeurs" dans la solution de i. On aura:

$$V_{c1} = v_{c1} \times N_1 = v_{c1} \times \frac{n_1}{a_1}$$

$$V_{c2} = v_{c2} \times N_2 = v_{c2} \times \frac{n_2}{a_2}$$

avec $n_1 = n_2 = n$ si les concentrations des tensio-actifs sont identiques et $v_{c1} = v_{c2}$ si le volume du coeur est peu affecté par le nombre de molécules par micelle. Soit:

$$\frac{V_{c1}}{V_{c2}} = \frac{a_2}{a_1}$$

$$V_{c2} = \frac{a_1}{a_2}V_{c1}$$

Les volumes des "coeurs" micellaires varieraient donc comme l'inverse des nombres d'agrégation.

Si donc le nombre d'agrégation diminue lorsque s'allonge la chaîne éthoxylée ($a_2 < a_1$), le volume de la phase "coeur" doit augmenter.

A cet accroissement de volume de la phase "coeur" s'ajoute une diminution de sa "densité". Il doit en résulter une plus grande capacité de cette phase à dissoudre le soluté (ester). Les systèmes eau/ester/hexane dans lesquels nous avons fait des études cinétiques (4) peuvent à cet égard être considérés comme des modèles de ces systèmes eau/ester/"coeurs" micellaires. Nous avons vu au cours du travail cité ci-dessus que l'accroissement du volume de phase organique se traduit, pour une quantité donnée de soluté, par un accroissement de la quantité solubilisée dans cette phase (c'est le phénomène utilisé dans l'extraction).

(b) Concentration du tensio-actif

Nous avons aussi étudié l'influence de la concentration du tensio-actif sur le déroulement de l'hydrolyse et sur la répartition de l'ester entre les différentes phases. Le tensio-actif étudié est le NP 12. On trouvera fig. 4 les courbes traduisant l'évolution de n_{aq} et n_m en fonction de la quantité totale d'ester pour deux concentrations différentes du tensio-actif.

Un examen de cette figure montre que la quantité d'ester solubilisé dans les micelles augmente et que cette augmentation est due à celle de la quantité solubilisée dans les coeurs, au détriment du manteau et de la phase aqueuse pure.

Or, lorsque la concentration en tensio-actif augmente, la composition d'une micelle est peu

Can. J. Chem. Downloaded from www.nrcresearchpress.com by 210.87.254.40 on 09/05/12
For personal use only.

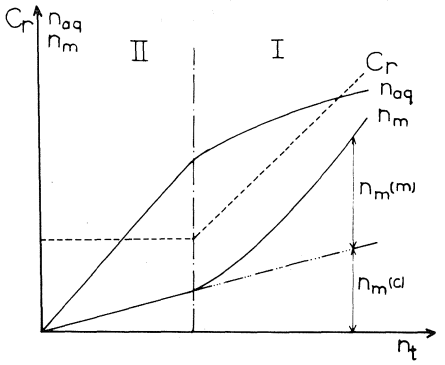

FIG. 5. Allure de variation des courbes $n_{aq} = f(n_t)$, $n_m = g(n_t)$ et $C_r = h(n_t)$.

modifiée, c'est le nombre de micelles dans la solution qui augmente (9). Comme nous l'avons vu ci-dessus, le volume total des "coeurs" augmente avec le nombre de micelles et corrélativement avec lui, la quantité d'ester solubilisé dans les "coeurs" pour une quantité totale d'ester donnée.

Remarque

Les raisonnements développés ici ne s'appliquent qu'à des solutions diluées de tensio-actifs. En effet, si la concentration en tensio-actif augmente beaucoup, la structure des micelles est modifiée et on ne peut plus supposer un volume "coeur" micellaire constant. Alors, le volume total des "coeurs" ne variera plus proportionnellement à la concentration du tensio-actif.

Conclusion

Il ressort de cette étude cinétique de l'hydrolyse alcaline des esters en milieu micellaire, que dans certaines conditions expérimentales, la vitesse globale de cette réaction peut résulter d'une limitation de la réaction chimique par des phénomènes de diffusion.

Pour un ester donné, les facteurs susceptibles de modifier la vitesse globale de la réaction sont avant tout la structure moléculaire et la concentration du tensio-actif. Ces facteurs déterminent aussi la répartition de l'ester entre les différentes phases et à l'intérieur des micelles, entre les différentes parties de celles-ci. On notera le rôle fondamental que les interprétations avancées conduisent à donner au coeur micellaire qui constitue ainsi la phase organique du milieu. La phase aqueuse micellaire (manteau) jouerait un rôle intermédiaire entre phases organique et aqueuse, mais assez secondaire, puisque son volume ne semble pas être un paramètre qu'il soit nécessaire d'introduire. On peut donc penser que cette phase est riche en eau au point de différer assez peu de la phase aqueuse pure.

Quand bien même toutes ces conclusions ne seraient que provisoires, des études cinétiques sont susceptibles d'apporter des données sur les interactions entre le solubilisat (l'ester ici) et les différentes parties de la molécule de tensio-actif à l'intérieur des micelles.

1. M. G. GOL'DFEL'D et R. M. DAVYDOV. Russ. J. Phys. Chem. **46**, 943 (1972).
2. E. CORDES (*Editor*). Reaction kinetics in micelles. Plenum Press, New York. 1973.
3. J. H. FENDLER et E. J. FENDLER. Catalysis in micellar and macromolecular systems. Academic Press, New York. 1975.
4. G. ROUX et A. VIALLARD. J. Chim. Phys. **73**, 189 (1976).
5. A. BROCHE et R. GIBERT. Bull. Soc. Chim. 131 (1955).
6. A. VIALLARD. Chem. Eng. Sci. **14**, 183 (1961).
7. A. G. MITCHELL. J. Pharm. Pharmacol. **15**, 761 (1963).
8. M. J. SCHICK, S. M. ATLAS et F. R. EIRICH. J. Phys. Chem. **66**, 1326 (1962).
9. S. IKEDA et K. KARIUCHI. J. Colloid Interface Sci. **23**, 134 (1967).

Can. J. Chem. Downloaded from www.nrcresearchpress.com by 210.87.254.40 on 09/05/12
For personal use only.

The proton magnetic resonance spectra of phenol in the absence of intermolecular proton exchange

TED SCHAEFER, J. B. ROWBOTHAM,[1] AND KALVIN CHUM
Department of Chemistry, University of Manitoba, Winnipeg, Man., Canada R3T 2N2

Received June 21, 1976

TED SCHAEFER, J. B. ROWBOTHAM, and KALVIN CHUM. Can. J. Chem. **54**, 3666 (1976).

The proton magnetic resonance spectra in the absence of intermolecular proton exchange for 0.27, 0.59, and 0.79 *M* solutions of phenol in CCl_4 are analyzed. The long-range coupling over five bonds between the hydroxyl and ring protons is estimated as 0.33 Hz in the monomer and as 0.20 Hz in the trimer of a monomer–trimer model. Support for the decrease in the coupling on trimerization is found in CNDO/2 and INDO MO FPT calculations. The long-range coupling over six bonds is unobservable, consistent with conformations of the trimer in which the phenol molecules remain planar. Water catalyzes the intermolecular proton exchange and, in its absence, the transfer of hydroxyl protons from molecule to molecule within the associated species is inefficient.

TED SCHAEFER, J. B. ROWBOTHAM et KALVIN CHUM. Can. J. Chem. **54**, 3666 (1976).

On a analysé les spectres de résonance magnétique nucléaire du proton en l'absence d'échange protonique intermoléculaire pour des solutions 0.27, 0.59 et 0.79 *M* de phénol dans CCl_4. On a estimé que les couplages à longue distance à travers cinq liaisons entre l'hydroxyle et les protons du cycle est de 0.33 Hz dans le monomère et de 0.20 Hz dans le trimère d'un modèle monomère-trimère. On trouve un support pour la diminution de la constante de couplage lors de la trimérisation dans des calculs CNDO/2 et INDO MO FPT. On n'a pu observer de couplage à longue distance à travers six liens; ce résultat est en accord avec les conformations du trimère dans lequel les molécules de phénol restent dans un plan. L'eau catalyse l'échange protonique intermoléculaire et en son absence le transfert de protons hydroxyliques d'une molécule à l'autre à l'intérieure des espèces associées est inefficace.

[Traduit par le journal]

Introduction

The ring proton resonance spectrum of phenol dissolved in CCl_4 was first analyzed precisely by Castellano *et al.* (1). Long-range spin–spin couplings between the hydroxyl proton and the ring protons were not observed, no doubt because of relatively rapid intermolecular proton exchange. Such coupling constants are easily observed when strong intramolecular hydrogen bonding to carbonyl or nitro groups exists (2–4). More recently, stereospecific long-range couplings involving the hydroxyl proton have been used to deduce the relative strengths of intramolecular hydrogen bonds to halogen substituents (4–6).

In this paper experiments are described which succeed in reducing the rate of intermolecular hydroxyl proton exchange in CCl_4 solutions of phenol to the extent that long-range couplings to the ring protons become observable. Self association of phenol in CCl_4 has been extensively investigated (7–11), so that the present coupling data throw some light on the conformation of the phenol molecule in the associated state and on the perturbation of the couplings caused by self association. Some inferences about the mechanism of proton exchange in nonaqueous solutions are also made.

Experimental

The assumption that water catalyzes the intermolecular proton exchange in CCl_4 solution dictated the method of sample preparation. Zone refined phenol from Aldrich Chemical Co., rated at 99.9(+)% purity, with an mp of 40.68 °C, and CCl_4 from Fisher, containing 0.02% of water (certified A.C.S.), were used in the following procedure.

Sample tubes, stopcock attachments for purposes of degassing by the freeze–pump–thaw technique, pipettes containing small wads of white Kleenex tissue, and 5 ml vials containing molecular sieve, were kept in beakers on a hot plate in a dry box. The temperature at the bottom of the beaker ranged from 180 to 210 °C. After 3 days under these conditions, solutions of phenol in CCl_4, containing a little tetramethylsilane and prepared on a balance outside the dry box, were added to the vials containing the molecular sieve. These vials were stoppered and left for a day in the dry box, well away from the hot plate. The solution was then transferred (in the dry box)

[1]Research associate, summer 1975.

Can. J. Chem. Downloaded from www.nrcresearchpress.com by 210.87.254.6 on 09/05/12
For personal use only.

TABLE 1. Proton chemical shifts* and coupling constants† for a 0.79 *M* solution of phenol in CCl_4

Parameter	Value	Parameter	Value
ν_{OH}	616.10	$^5J_p^{H,H}$	0.442(6)
$\nu_{2,6}$	673.301(4)‡	$\|^4J_o^{H,OH}\|$	0.07 ± 0.02
$\nu_{3,5}$	710.430(4)	$^5J_m^{H,OH}$	0.257(6)
ν_4	682.006(5)	$\|^6J_p^{H,OH}\|$	≤0.03
$^3J_o^{H_2,H_3}$	8.178(6)	rms deviation	0.023
$^3J_o^{H_3,H_4}$	7.419(5)	Largest deviation	0.054§
$^4J_m^{H_2,H_6}$	2.694(6)	Peaks observed	66
$^4J_m^{H_2,H_4}$	1.043(5)	Transitions calculated	152
$^4J_m^{H_3,H_5}$	1.744	Peaks assigned	123

*In Hz at 100 MHz to low field of internal tetramethylsilane at 32 °C.
†In Hz.
‡Numbers in parentheses give standard deviations in the last number.
§A low intensity peak.

to the sample tube in such a manner as to filter it through a wad of tissue, a stopcock assembly was attached to the sample tube, and the final assembly was removed from the dry box to a vacuum rack for degassing. The sample tube contained a few pellets of molecular sieve. The flame-sealed sample tube was left for a few days before spectral work began.

These precautions ensured that *some* samples gave proton magnetic resonance spectra displaying long-range coupling to the ring protons. The concentrations of phenol are not exactly known but can be deduced from the hydroxyl proton shifts. Of course, concentrations were such that reliable spectral analyses could be performed.

The proton magnetic resonance spectra were calibrated on a HA100 spectrometer in the frequency sweep mode at a temperature of 305 K. MO calculations were performed on an IBM 370/158 system.

Results and Discussion

Sample Concentrations

Loss of solvent during the elaborate sample preparation procedure introduced an uncertainty into the concentrations. However, these may be deduced from previous work (8, 9, 11) on the chemical shift of the hydroxyl proton in CCl_4 at temperatures between 20 and 50 °C. The three solutions which yielded proton magnetic resonance spectra of analytical quality had concentrations of 0.27 ± 0.01, 0.59 ± 0.02, and 0.79 ± 0.02 *M*. These numbers are deduced from an infinite dilution hydroxyl proton shift in CCl_4 of 4.25 ppm at 32 °C and a shift for the completely trimerized phenol of 7.96 ppm, relative to internal tetramethylsilane.

Spectral Analyses

These were performed with the computer program LAME (12, 13). The results for the 0.79 *M* solution are given in Table 1, the ring proton coupling parameters comparing well with those obtained for 10% w/w solutions in CCl_4 and in C_6D_6 (1). Decoupling of the hydroxyl proton showed that $^6J_p^{H,OH} \leq 0.03$ Hz and repeated simulations of the hydroxyl and ring proton spectra in the absence and presence of decoupling showed that $^4J_o^{H,OH}$ was $\pm 0.07 \pm 0.02$ Hz, where the negative sign is probably the correct one.

Repeated measurements of the splittings due to $^5J_m^{H,OH}$ in the *meta* proton spectral region, which is well-separated from the *ortho* and *para* proton regions, indicate that $^5J_m^{H,OH}$ is known to an accuracy of 0.01 Hz. The standard deviation in the LAME analysis was 0.006 Hz and should presumably be multiplied by about 3. However, the standard deviation is that found in conjunction with the values given for all the other parameters in Table 1. Figure 1 displays an isolated doublet in the *meta* proton region, illustrating the method of calibration.

Degree of Association in Solution

In Table 2 the concentrations, hydroxyl proton chemical shifts, and the extent of association are tabulated for the three solutions in CCl_4 which gave reliable spectra. From the work of Dale and Gramstad (11) at 20, 35, and 50 °C, and from the relatively close agreement of this work with that of other workers (7, 8, 10), it can be concluded that K_3 for the monomer–trimer equilibrium for phenol in CCl_4 is 2.7 l^2 mol^{-2} at 32 °C. Furthermore, at this temperature, the shift of the monomer is 4.25 ppm and the shift of the trimer is 7.96 ppm relative to internal tetra-

Can. J. Chem. Downloaded from www.nrcresearchpress.com by 210.87.254.6 on 09/05/12
For personal use only.

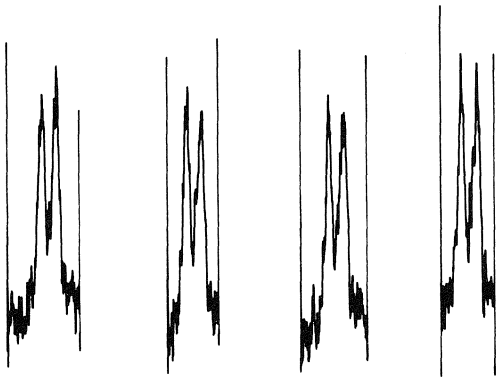

FIG. 1. A doublet of the *meta* proton resonance centered at 719.05 Hz from internal tetramethylsilane for a 0.29 *M* solution in CCl_4, illustrating the method of calibration. The four values for the splittings are 0.30_2, 0.30_2, 0.29_2, and 0.29_7 Hz, having a mean value of 0.29_8 Hz. Similar calibrations of other isolated doublets yielded, finally, an average value of 0.29_4 Hz with a standard deviation of less than 0.01 Hz.

methylsilane. The concentrations and the extent of association then follow as in Table 2.

Conformational Indications from $^6J_p^{H,OH}$

The magnitude of $^6J_p^{H,OH}$ is less than or equal to 0.03 Hz. If, as for $^6J_p^{H,CH}$ in toluene (14), this coupling follows a $\sin^2\theta$ relationship where θ is the angle by which the O—H bond twists out of the aromatic plane, one may write

$$[1] \qquad {}^6J_p^{H,OH} = {}^6J_{90}\langle\sin^2\theta\rangle$$

In [1], $^6J_{90}$ is the maximum magnitude of $^6J_p^{H,OH}$. The observed value depends on the average value of $\sin^2\theta$ which, in turn, depends on the temperature, the reduced moment of inertia, and on the magnitude of the two-fold potential hindering the internal rotation of hydroxyl group about the C—O bond (15).

TABLE 2. Hydroxyl proton chemical shifts,* coupling constants,† and degree of association for some phenol solutions in CCl_4 at 32 °C

Concentration‡ (*M*)	ν_{OH}	$^5J_m^{H,OH}$	Associated‡ (%)
0.27±0.01	5.16	0.294	26
0.59±0.02	5.89	0.268	47
0.79±0.02	6.16	0.257	54

*In ppm relative to internal tetramethylsilane.
†In Hz to an accuracy of 0.01 Hz.
‡On the basis of 4.25 ppm for the monomer, 7.96 ppm for the trimer, and a self association constant of 2.7 l^2/mol^2 (11).

The magnitude of $^6J_{90}$ can be approximated from the value of 38 G (16) for the hyperconjugative interaction constant, Q^H_{COH}, in radicals of phenol derivatives. Q^H_{CCH} is 52 G (17), so that (18)

$$^6J_{90}^{H,OH} = {}^6J_{90}^{H,CH}Q^H_{COH}/Q^H_{CCH} = -1.24 \times 38/52 = -0.91 \text{ Hz}$$

It follows[2] that $\langle\sin^2\theta\rangle$ is about 0.033 and the procedure described recently (15) then yields a two-fold barrier of greater than 3 kcal/mol. In the gas phase (22–24) the internal barrier is 3.4 ± 0.2 kcal/mol. It appears reasonable that in the trimer the energy of hydrogen bonding will increase the effective barrier to internal rotation, the enthalpy per hydrogen bond being near 3 kcal/mol (11). It has been suggested (11) that phenol forms a hydrogen bond to CCl_4 whose enthalpy of formation is −2.3 kcal/mol, although in our opinion this includes general dispersion forces (25).

It appears that the very small magnitude of $^6J_p^{H,OH}$ is consistent with all these data. In particular, it indicates that hydrogen bond formation does not cause a large (say 20° or more) out-of-plane twist of the hydroxyl group in the associated state. If the trimer is cyclic and, furthermore, if the hydrogen bonds are largely electrostatic in nature, an in-plane conformation is entirely reasonable.

Conformational Indications from $^5J_m^{H,OH}$

In Fig. 2 are shown plots of $^5J_m^{H,OH}$ *vs.* the hydroxyl proton shift, ν_{OH}, and *vs.* the fraction of associated phenol molecules. Extrapolation to monomer shift and to zero concentration yields $^5J_m^{H,OH}$ as 0.33 ± 0.01 Hz for a phenol molecule surrounded by CCl_4 molecules at 32 °C. Extrapolation to the trimer shift yields $^5J_m^{H,OH}$ as 0.20 ± 0.01 Hz. The extrapolations are somewhat lengthy but are believed to be reliable.

Partial support for these variations in $^5J_m^{H,OH}$ comes from CNDO/2 and INDO MO FPT (26)

[2]It might have been argued that a decrease in θ implies an increase in the conjugation of the oxygen atom with the π system of the ring. A π electron mechanism operating via the partially double C⋯O bond would then enhance the magnitude of $^6J_p^{H,OH}$ at $\theta = 0°$. However, the opposite occurs in aniline, benzaldehyde, benzoyl fluoride, and in their derivatives; $^6J_p^{H,NH}$, $^6J_p^{H,CHO}$, and $^6J_p^{H,CFO}$ being nonzero only for conformations in which the N—H, C—H(O), and C—F(O) bonds do not lie in the aromatic plane (19–21).

Can. J. Chem. Downloaded from www.nrcresearchpress.com by 210.87.254.6 on 09/05/12
For personal use only.

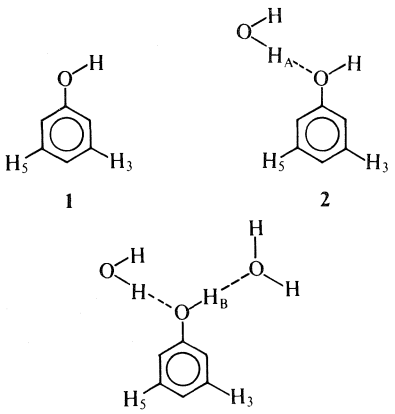

1 2 3

calculations on the structures **1**, **2**, and **3**. A standard geometry (27) was assumed for the phenyl group. The C—O bond length was taken as 1.375 Å (23) and the O—H bond length was 0.944 Å (23). The CCO angle has been estimated to have values of *ca.* 120° (24), 122.5° (22), and 125.2° (23), while the COH angle has been given as 109° (22) and as 114.5° (23).

The angle dependence of the calculated long-range coupling constants for a planar conformation **1** was small. Thus, CNDO/2 gave ${}^5J_m{}^{H,OH} \equiv ({}^5J_3{}^{H,OH} + {}^5J_5{}^{H,OH})/2$ as 0.360 Hz at 120°, 108°; and gave 0.379 Hz at 125.2°, 114.45°. The corresponding INDO values were 0.433 Hz and 0.471 Hz. Theory indicates an insensitivity of ${}^5J_m{}^{H,OH}$ to the two bond angles.

In the absence of other sharp criteria, the INDO conformation of lowest energy, corresponding to a CCO angle of 122.5° and a COH angle of 112° (CNDO/2 gave 110°) was used in the calculations on **2** and **3**, where the water molecules have an HOH angle of 104.5°.

In **2** the projection of one of the O—H bonds of the water molecule, intended as a simulation of intermolecular hydrogen bonding in phenol, bisects the COH angle. The intermolecular H,O distance was varied between 1.3 and 2.0 Å, with the result that the CNDO/2 energy minimum occurred at 1.6 Å corresponding to a ${}^5J_m{}^{H,OH}$ of 0.368 Hz and comparing to 0.371 Hz for **1** in this geometry. Accordingly, ${}^5J_m{}^{H,OH}$ is predicted as insensitive to the association represented by **2**.

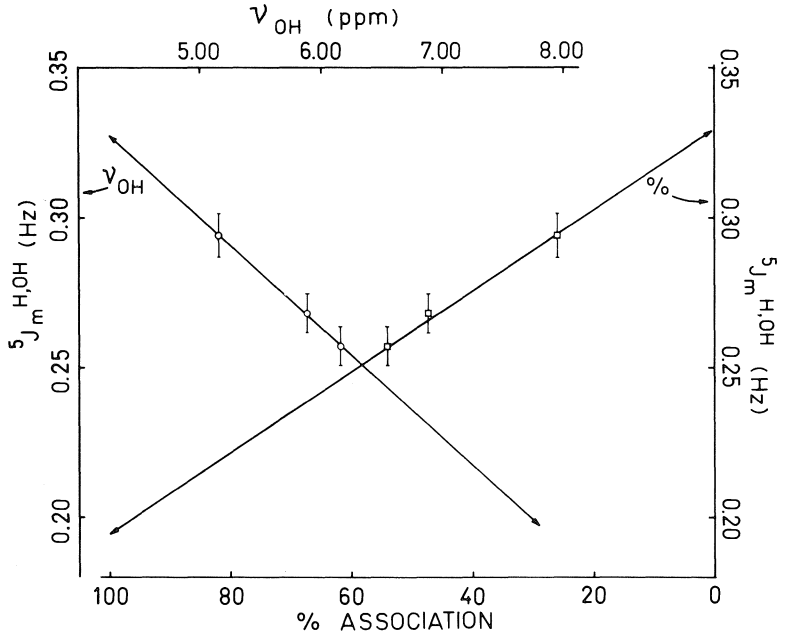

FIG. 2. The coupling over five bonds between the hydroxyl proton and the ring protons is plotted *vs.* the shift of the hydroxyl proton (○) and *vs.* the percentage association of the phenol (□); the coupling scale for the latter plot being on the right. Extrapolations of both plots agree that for the monomer in CCl_4 at 32 °C the coupling is 0.33 ± 0.01 Hz and is 0.20 ± 0.01 Hz for the trimer. See text.

Can. J. Chem. Downloaded from www.nrcresearchpress.com by 210.87.254.6 on 09/05/12
For personal use only.

Can. J. Chem. Downloaded from www.nrcresearchpress.com by 210.87.254.6 on 09/05/12
For personal use only.

The distance of 1.6 Å in **2** was then fixed for **3** and the distance between the phenol proton and the oxygen atom of a second water molecule was varied between 1.3 and 1.9 Å. CNDO/2 gave 1.6 Å at the minimum energy and $^5J_m^{H,OH}$ as 0.315 Hz, whereas INDO found a minimum energy of **3** at 1.5 Å and a $^5J_m^{H,OH}$ of 0.329 Hz.

In other words, INDO predicts a decrease of 0.124 Hz for $^5J_m^{H,OH}$ between **1** and **3**, CNDO/2 giving a decrease of 0.056 Hz. The extrapolated experimental decrease of 0.13 Hz between the 0.33 Hz of the monomer and the 0.20 Hz of the trimer is in qualitative agreement with the calculations. Of course, the monomer in solution is surrounded by CCl_4 molecules with which it may associate (11, 25), but presumably not as strongly as with other phenol molecules, so that the calculations are only a partial simulation of the actual situation.

Parenthetically, it may be noted that $^6J_p^{H,OH}$ was calculated as less than 0.03 Hz for **1**, **2**, and **3**, *i.e.*, for planar conformations, and INDO gave $^4J_o^{H,OH} \equiv (^4J_2^{H,OH} + {}^4J_6^{H,OH})/2$ as -0.043 Hz at the minimum energy of **3** and as -0.118 Hz for the minimum energy of **1**, consistent with an observed value of $\pm 0.07 \pm 0.02$ Hz.

Intermolecular Exchange

The exchange of hydroxyl protons between phenol molecules is catalyzed by water. The observation of long-range coupling constants to the hydroxyl proton in the presence of phenol-trimers means that the exchange is very slow within the complex, because a mean preexchange lifetime of much less than approximately 1 s would entail the absence of observable couplings. However, the trimerization causes a decrease of 0.13 Hz in the observable long-range coupling. In principle such a decrease is compatible with a very slow rate of exchange within the trimer, any broadening of spectral peaks being hardly noticeable under such conditions. However, the MO calculations suggest that the decrease arises from electronic perturbations caused by self association and we prefer this explanation.

Caveat

The extrapolation to infinite dilution of the $^5J,\nu_{OH}$ plot in Fig. 2 is independent of the association model and, if the extrapolation is valid, the value for $^5J_m^{H,OH}$ of 0.33 ± 0.01 Hz in the monomer is also independent of the association model. Although its magnitude must clearly be less than in the monomer, the value of $^5J_m^{H,OH}$ for the associated species depends on the association model in that the model determines the value of ν_{OH} for complete association.

The number of parameters in the equations relating an observable to the equilibrium constants and to the concentrations of the various species in a multispecies equilibrium is too large for a unique solution. It is known, however, that a monomer–trimer model gives a good fit to the observed shifts over a large concentration range (8), whereas monomer–dimer and monomer–tetramer models do not. However, dimerization constants between 0.7 and 1.5 *l*/mol have been reported (28, 29) at concentrations between 0 and 0.25 *M*. The chemical shift for the lowest concentration in Table 2, combined with the shift-concentration data in ref. 9, yields a dimer shift of 6.94 to 8.37 ppm depending on which of the dimerization constants is employed. From Fig. 2 it then follows that $^5J_m^{H,OH}$ is 0.20 ± 0.03 Hz for the dimer in a monomer–dimer model.

Nevertheless, we favor the monomer–trimer model because the monomer–dimer model gives a poor fit to the observed shifts at low phenol concentrations (8) and, perhaps, because the INDO calculations of $^5J_m^{H,OH}$ are consistent with the monomer–trimer model.

Conclusions

The long-range coupling constants between the hydroxyl and ring protons in phenol indicate that self association in CCl_4 solution does not produce conformations in which the hydroxyl group is twisted substantially out of the plane of the aromatic ring. Both experiment and theory suggest that self association of phenols causes a noticeable decrease in the coupling over five bonds and that in the monomer its magnitude is very similar to that observed for the analogous couplings in benzaldehyde (30), aniline (19), and in toluene derivatives (31) in solution.

Acknowledgment

We are grateful to the National Research Council of Canada for financial assistance.

1. S. Castellano, C. Sun, and R. Kostelnik. Tetrahedron Lett. 5205 (1967).
2. S. Forsen and R. A. Hoffman. J. Mol. Spectrosc. **20**, 168 (1966).

3. T. SCHAEFER and G. KOTOWYCZ. Can. J. Chem. **46**, 2865 (1968).
4. J. B. ROWBOTHAM, M. SMITH, and T. SCHAEFER. Can. J. Chem. **53**, 986 (1975).
5. J. B. ROWBOTHAM and T. SCHAEFER. Can. J. Chem. **52**, 3037 (1974).
6. T. SCHAEFER and J. B. ROWBOTHAM. Can. J. Chem. **54**, 2243 (1976).
7. J. R. JOHNSON, S. D. CHRISTIAN, and H. E. AFFSPRUNG. J. Chem. Soc. A, 764 (1967).
8. M. SAUNDERS and J. B. HYNE. J. Chem. Phys. **29**, 1319 (1958).
9. T. GRAMSTAD and E. D. BECKER. J. Mol. Struct. **5**, 253 (1970).
10. J. AHLF and D. PLATTHAUS. Ber. Bunsenges. Phys. Chem. **74**, 204 (1970).
11. A. J. DALE and T. GRAMSTAD. Spectrochim. Acta, Part A, **28**, 639 (1972).
12. S. CASTELLANO and A. A. BOTHNER-BY. Mellon Institute Publication, Pittsburgh, Pa. 1967.
13. C. W. HAIGH and J. M. WILLIAMS. J. Mol. Spectrosc. **32**, 398 (1969).
14. R. WASYLISHEN and T. SCHAEFER. Can. J. Chem. **50**, 1852 (1972).
15. T. SCHAEFER, J. B. ROWBOTHAM, W. J. E. PARR, K. MARAT, and A. F. JANZEN. Can. J. Chem. **54**, 1322 (1976).
16. A. T. BULLOCK. J. Magn. Reson. **15**, 580 (1974).
17. C. CHACHATY, A. FORCHIONI, J. VIRLET, and J. C. RONFARD-HARET. Chem. Phys. Lett. **29**, 436 (1974).
18. R. WASYLISHEN and T. SCHAEFER. Can. J. Chem. **49**, 94 (1971).
19. R. WASYLISHEN, J. B. ROWBOTHAM, L. ERNST, and T. SCHAEFER. Can. J. Chem. **50**, 2575 (1972).
20. C. L. BELL, S. S. DANYLUK, and T. SCHAEFER. Can. J. Chem. **47**, 3529 (1969).
21. T. SCHAEFER, K. CHUM, K. MARAT, and R. E. WASYLISHEN. Can. J. Chem. **54**, 800 (1976).
22. C. R. QUADE. J. Chem. Phys. **48**, 5490 (1968).
23. H. D. BIST, J. C. D. BRAND, and D. R. WILLIAMS. J. Mol. Spectrosc. **24**, 402 (1967).
24. E. MATHIER, D. WELTI, A. BAUDER, and Hs. H. GUNTHARD. J. Mol. Spectrosc. **37**, 63 (1971).
25. G. KOTOWYCZ and T. SCHAEFER. Can. J. Chem. **46**, 3110 (1968).
26. J. A. POPLE, J. W. MCIVER, JR., and N. S. OSTLUND. J. Chem. Phys. **49**, 2960 (1968), **49**, 2965 (1968).
27. J. A. POPLE and M. S. GORDON. J. Am. Chem. Soc. **89**, 4253 (1967).
28. M. M. MAGUIRE and R. WEST. Spectrochim. Acta, **17**, 369 (1961).
29. H. SEIDEL, C. RITTER, J. FRUWERT, and G. GEISELER. Spectrochim. Acta, Ser. A, **32**, 705 (1976).
30. R. J. KOSTELNIK, M. P. WILLIAMSON, D. E. WISNOSKY, and S. M. CASTELLANO. Can. J. Chem. **47**, 3313 (1969).
31. H. M. HUTTON, J. B. ROWBOTHAM, B. H. BARBER, and T. SCHAEFER. Can. J. Chem. **49**, 2033 (1971).

Can. J. Chem. Downloaded from www.nrcresearchpress.com by 210.87.254.6 on 09/05/12
For personal use only.

Pulse radiolytic formation of Na^- from alkali metal – sodium ion solutions in ethylamine[1]

WILLIAM ARTHUR SEDDON, JOHN WALLACE FLETCHER, AND FRED CHARLES SOPCHYSHYN
Physical Chemistry Branch, Atomic Energy of Canada Limited, Chalk River Nuclear Laboratories, Chalk River, Ont., Canada K0J 1J0

Received June 4, 1976

WILLIAM ARTHUR SEDDON, JOHN WALLACE FLETCHER, and FRED CHARLES SOPCHYSHYN. Can. J. Chem. **54**, 3672 (1976).

The formation of Na^- from K, Rb, Cs, or Li ethylamide solutions containing small amounts of Na^+ has been observed by pulse radiolysis. In K, Rb, or Cs solutions evidence is presented which shows that the production of Na^- occurs via the corresponding alkali anions K^-, Rb^-, or Cs^-. However solutions containing Li behave much differently and indicate that Na^+ is 'complexed' or associated with Li^+ ions. Probable reaction mechanisms are discussed.

WILLIAM ARTHUR SEDDON, JOHN WALLACE FLETCHER et FRED CHARLES SOPCHYSHYN. Can. J. Chem. **54**, 3672 (1976).

On a observé, par radiolyse pulsée, la formation de Na^- à partir de solutions d'éthylènamide de K, Rb, Cs ou Li contenant de petites quantités de Na^+. Dans le cas des solutions de K, Rb ou Cs, on présente des données qui montrent que les Na^- se produisent par l'intermédiaire des anions alcalins correspondants K^-, Rb^- ou Cs^-. Toutefois les solutions contenant du Li se comportent d'une facon très différente; il semble que le Na^+ est complexé ou associé avec les ions Li^+. On discute des mécanismes probables pour ces réactions.

[Traduit par le journal]

Introduction

Extensive investigations on the optical, magnetic, and conductance properties of alkali metal solutions in amines and ethers (refs. 1–3 and references therein) have demonstrated that in general three species: the solvated electron e_s^-, ion-pairs (M^+, e_s^-) or 'monomers' M^0, and alkali anions M^-, coexist in equilibrium.

[1] $$e_s^- + M^+ \rightleftharpoons (M^+, e_s^-) \text{ or } M^0$$

[2] $$M^0 + e_s^- \rightleftharpoons M^-$$

With the exception of Li solutions, which do not appear to form Li^- (3), the equilibria in ethylamine are predominantly in favour of M^- with Na^- being the least dissociated of the series (4). More recently, pulse radiolysis studies (5–7) have also indicated the importance of reaction 3

[3] $$M^0 + M^0 \rightleftharpoons M^+ + M^-$$

Using a variety of solvents, Hurley *et al.* (8, 9) were the first to demonstrate that regardless of the alkali metal in solution the presence of trace amounts of Na^+ from the Pyrex reaction vessels also resulted in the formation of Na^-. This leaching process is sufficiently rapid that, for K solutions in ethylenediamine (10), contact for as little as 10 s is sufficient to produce Na^-. Because of such contamination earlier flash photolysis studies in ethers (11), and ethylamine (12), need reinterpretation.

In this paper we describe our observations on the processes leading to the formation of Na^- in K, Rb, Cs, and Li ethylamide solutions containing added Na^+. Correlations with flash photolysis studies are also discussed.

Experimental

Detailed descriptions of the experimental techniques and facilities have been given previously (4, 13–15). Briefly, solutions were irradiated with 0.3 μs pulses from a 2.5 MeV Van de Graaff electron accelerator and transient signals recorded using fast infrared detectors (16). Alkali metal ethylamide solutions were prepared from the pure metals with Na^+ present either in the form of the ethylamide or as NaI. The effect of Na^+ was monitored by observing the formation and decay of e_s^- and 'monomer' species, (M^+, e_s^-) or M^0, at 1400–1500 nm and the growth of Na^- at 700 nm. The formation and decay of K^-, Rb^-, or Cs^- were also observed at 890, 950, and 1100 nm, respectively.

Results

For a detailed description of the results obtained in solutions containing the pure alkali

[1]AECL No. 5582.

Can. J. Chem. Downloaded from www.nrcresearchpress.com by 210.87.254.105 on 09/05/12
For personal use only.

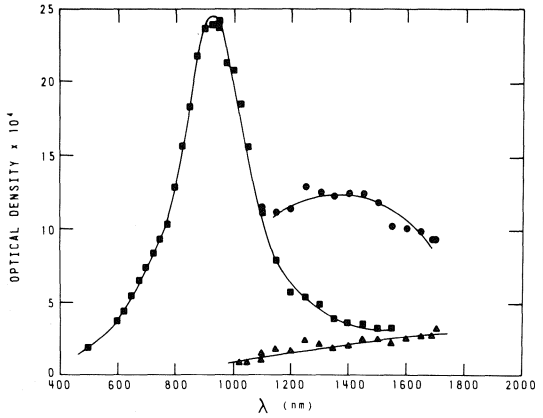

FIG. 1. Optical absorption spectra observed in $\sim 2.5 \times 10^{-4}$ *M* RbNHEt solutions, ▲ immediately after the pulse; ● after ~ 5 μs; ■ after 400 μs. Dose/pulse $\sim 3.7 \times 10^{19}$ eV l^{-1}. Optical densities are normalised to a dose of 2.4×10^{18} eV l^{-1} in a 1 cm cell.

metal ethylamides (Li, Na, K, and Cs) the reader should refer to our earlier paper (4). In the present study we chose initial concentrations of K, Rb, or Cs such that the formation of the parent alkali metal 'monomer' was essentially complete within 1–10 μs after the pulse (4, 6, 7). The effect of $[Na^+]$ was then followed with reference to such solutions.

Potassium

Solutions containing $\sim 5 \times 10^{-3}$ *M* potassium ethylamide (KNHEt) were investigated as a function of NaNHEt or NaI with such concentrations ranging from $\sim 10^{-5}$ to 2×10^{-3} or 10^{-3} to 10^{-1} *M*, respectively. In all cases the decay of the 1400 nm ('monomer') band was second order and, within experimental error, independent of $[Na^+]$. As noted previously (4), the absorbance at 1400 nm decays to a finite value the magnitude of which decreases progressively with increasing $[Na^+]$.

Concomitant with the 1400 nm decay a build up of the K^- band is observed at 890 nm. This in turn is followed by a mixed first and second order decay, with the subsequent formation of Na^-. The rate of decay of K^- increases with $[Na^+]$.

Rubidium

Figure 1 shows the optical spectra obtained as a function of time in $\leq 10^{-3}$ *M* RbNHEt solutions. In common with the other alkali metal ethylamides (4), the spectrum observed immediately after the pulse is relatively weak with $\lambda_{max} > 1800$ nm. During the next 5–10 μs the intensity increases producing a strong absorption with $\lambda_{max} = 1400$ nm. This absorption then subsequently decays to form a long-lived species with a characteristic band peaking at 930–950 nm (9, 12) now assigned to the species Rb^-.

The addition of 10^{-4} *M* NaI produces an effect very similar to that observed in KNHEt solutions. The rate of decay of the infrared band remains unaffected whereas the Rb^- now decays rapidly and is accompanied by a corresponding growth in the Na^- absorption.

Cesium

Solutions containing $\leq 3 \times 10^{-3}$ *M* CsNHEt were investigated as a function of $[Na^+]$ from 10^{-4} to 10^{-2} NaI. Again the predominant effect is that the otherwise 'stable' Cs^- band (7) decays with the concomitant formation of Na^-. Both the rate of formation of Na^- and the rate of decay of Cs^- increase with $[Na^+]$.

Lithium

Solutions containing 0.1 *M* LiNHEt were investigated in the presence of 10^{-4} to 10^{-1} *M* NaI. These mixtures do not exhibit the features common to the K, Rb, or Cs systems.

In pure LiNHEt solutions a slow growth producing a long-lived absorption with a maximum at ~ 1600 nm is observed on a ms time scale (4, 6). The addition of Na^+ enhances both the rate of formation and the ultimate intensity of this absorption band (4). The band eventually decays producing, at the same time, a growth in Na^-. It is significant, however, that the rate of formation of Na^- is much slower than is observed for comparable Na^+ concentrations present either in NaNHEt solutions or in mixtures containing K, Rb, or Cs ethylamides. Both the decay of the infrared band and the formation of Na^- appear to be second order.

Discussion

Qualitatively a considerable degree of agreement is evident between our work and earlier flash photolysis studies of alkali metal solutions in ethylamine (12), provided that the latter study is reinterpreted in terms of current knowledge regarding the nature of the species in solution. In both series of experiments it is clear that K,

Can. J. Chem. Downloaded from www.nrcresearchpress.com by 210.87.254.105 on 09/05/12
For personal use only.

Can. J. Chem. Downloaded from www.nrcresearchpress.com by 210.87.254.105 on 09/05/12
For personal use only.

Rb, or Cs/Na mixtures behave similarly whereas Li/Na mixtures are completely different.

Quantitative comparisons are more difficult. For example, the flash photolysis studies were restricted to wavelengths ≤ 1000 nm and, to minimize solution decomposition, were mainly conducted at -80 °C. The initial solutions also contained a significant concentration of Na^- in equilibrium with e_s^- and 'monomer' species. Furthermore it was not recognized until recently that both e_s^- and the 'monomer' species absorb in the infrared but with a significant difference in λ_{max} (4).

In general the kinetic analysis of these systems is very complex. This is particularly evident concerning M^- where concurrent build up and decay processes, coupled with extensive spectral overlap, make detailed analysis impractical. Observations on the decay of the infrared band and the build up of the Na^- band are the most clear cut. However, even at these wavelengths the final absorption represents an equilibrium condition which must be taken into account in order to deduce the appropriate rate constant. Care must also be taken to minimize the dose effect which otherwise leads to competing radical processes (4, 17).

Potassium, Rubidium, Cesium/Sodium Solutions

In K, Rb, or Cs/Na solutions it is evident that the formation of Na^- occurs predominantly via the corresponding M^- species with M^- being formed initially from the 'monomer' species (4). This observation agrees with the conclusion reached from photolysis studies (12) that the regeneration of Na^- (formerly described as the V band) occurred predominantly via the corresponding K^-, Rb^-, or Cs^- (R band) species.

In some cases an equally good fit for the formation of Na^- can be obtained with either a first or second order plot. However, decreasing the dose/pulse and progressing down the series $K^- \rightarrow Rb^- \rightarrow Cs^-$ improves the second order quality and self consistency of the second order 'rate constant'. Kinetically, then, the formation of Na^- appears as a mixed order process with the relative contributions from first and second order components dependent on the dose/pulse and the nature of the mixed metal system.

A mechanism composed of reactions 1 to 3 and 4 to 8 is compatible with our observations.

[4] $e_s^- + Na^+ \rightleftharpoons Na^0$

[5] $M^- + Na^+ \rightleftharpoons Na^0 + M^0$

[6] $Na^0 + e_s^- \rightleftharpoons Na^-$

[7] $Na^0 + Na^0 \rightleftharpoons Na^- + Na^+$

[8] $Na^0 + M^0 \rightleftharpoons Na^- + M^+$

If $k_1[M^+] \gg k_4[Na^+]$ and equilibria 2 and 3 lie well to the right then reaction 5f is the rate controlling process and the Na^- formation will appear pseudo first order. At lower dose rates the equilibrium concentrations of e_s^- and M^0 become more significant. Assuming reactions 3 and 6–8 occur concurrently then an increase in the second order component would be expected. Likewise, if equilibria 2 and 3 shift more to the left with a change in the nature of M^-, then a further increase in second order character would be anticipated. This latter type of behaviour is observed (see later) and is consistent with the increased dissociation of M^- in the order $Na^- < K^- < Rb^- < Cs^-$.

Based on the above reaction sequence we have utilized the computer program WR 20 (18) to simulate the results obtained in K/Na solutions. Rate constants were first estimated from the experimental data and then varied to obtain the best fit. Corrections for spectral overlap were included in the calculations. The concentrations of the mixture were such that the equilibrium position of reactions 1 and 4 lie well to the right and hence reactions 2 and 6 are of little importance under our experimental conditions. From the kinetic treatment we deduce that $k_{-3} \ll k_5$, $k_{-5} \ll k_8$, $k_{-7} \ll k_{-8}$, k_3, k_7, and $k_8 \sim 2 \times 10^{10}\ M^{-1}\ s^{-1}$, $k_5 \sim 1 \times 10^9\ M^{-1}\ s^{-1}$, and the equilibrium constant $K_8 \sim 2 \times 10^4$. On this basis calculated rates of decay for K and K^- and formation for K^- and Na^- are consistent with experiment. In general, however, the systems are too complex to justify extensive curve fitting procedures of this type.

For purposes of comparison Table 1 summarizes the observed rate constants expressed as a 'second order' constant, k_{Na^-}, consistent with the overall process $e_s^- + e_s^- \overset{Na^+}{\rightleftharpoons} Na^-$, together with the second order constant $k_{(-M^0)}$ for the decay of M^0 in the same system. The rate constants were calculated as in our previous paper (4) assuming ϵ_{Na^-} and ϵ_{M^0} to be 8.5×10^4 and $2.7 \times 10^4\ M^{-1}\ cm^{-1}$, respectively (6). It should be noted that k_{Na^-} for K/Na mixtures is less than the values of k_3, k_7, or k_8 required in

Can. J. Chem. Downloaded from www.nrcresearchpress.com by 210.87.254.105 on 09/05/12
For personal use only.

TABLE 1. 'Second order' rate constants for the formation of Na^- and decay of M^0 in mixed-metal ethylamide solutions containing 2×10^{-4} *M* NaNHEt and/or NaI. See text for details

Second metal	Concentration (*M*)	$k_{(Na^-)} \times 10^{-10}$ (M^{-1} s^{-1})	$k_{(-M^0)} \times 10^{-10}$ (M^{-1} s^{-1})
Nil		0.8	0.8
K	5×10^{-3}	~0.8	0.8
Rb	2×10^{-4}	~0.8	0.8
Cs	3×10^{-3}	0.2_5	0.3_4
	3×10^{-4}	0.6_6	0.7
Li	1×10^{-1}	~0.1	~0.1

the computer calculations. This is simply a consequence of the slower rate controlling reaction 5. Nevertheless the experimental values calculated as 'second order' do give a measure of the relative differences between the various mixed-metal systems.

Flash photolysis studies (12) are also entirely consistent with this mechanism. For example, reinterpretation of the spectrum observed in potassium/ethylamine solutions shows that Na^-, with λ_{max} at 675 nm, is the predominant species but with K^- (910 nm) present as a minor component. Photolysis at 660 nm bleaches the Na^- band in accordance with reaction 9 (19).

$$[9] \qquad Na^- \overset{h\nu}{\rightleftharpoons} Na^0 + e_s^-$$

The subsequent growth of an absorption in the 'infrared' (monitored at $\leq$1000 nm) is then explicable by reaction 1 (where $M^+ = K^+$) with the K^0 species becoming the precursor (formerly postulated as species X) of K^- via reactions 2 and 3. The decay of K^- and concomitant formation of Na^- as shown in Figs. 3 and 4 of reference 12 can then occur as discussed above. A similar sequence is evident from an analysis of the cesium/ethylamine solutions but is more difficult to establish because of the extensive spectral overlap at the wavelengths investigated.

Lithium/Sodium Solutions

In these solutions the conversion process to form Na^- is very much different than the features common to K, Rb, and Cs. It is significant that the rate of formation of Na^- is, in all cases, much slower than would be anticipated for a similar Na^+ concentration in either pure NaNHEt solutions or in mixtures with K, Rb, or Cs. In the latter cases the observed 'second order' rate constant for Na^- formation, k_{Na^-} is proportional to [total Na]$^{1/2}$ and hence consistent with the dissociation of NaNHEt or NaI in the mixture. However, in Li/Na mixtures k_{Na^-} is proportional to [total Na]$^{1/3}$. It appears therefore, in the Li/Na mixtures that the NaNHEt is associated or complexed with the excess Li ethylamide. In this way the effective $[Na^+]$ is significantly reduced, with the Na^- then being formed at a rate dependent on the e_s^-–M^0 equilibrium characteristics of the overall system and the dissociation constant of the aggregate or complex.

For example, in pure lithium solutions equilibrium 1 lies predominantly to the right. However, in the presence of Na^+ the rate of formation of the 1400–1600 nm 'monomer' band is noticeably greater than in pure lithium solutions, but much less than in pure sodium solutions (4). Since both Li and Na 'monomers' absorb at about the same wavelength this suggests the formation of Na^0 from the equilibrium mixture via reaction 4 rather than via a subsequent step such as reaction 10.

$$[10] \qquad Li^0 + Na^+ \rightarrow Na^0 + Li^+$$

The Na^- formation then presumably occurs via reactions 6–8, with the overall intensity gradually increasing with $[Na^+]$ to that observed in NaNHEt solutions or in mixtures containing K, Rb, or Cs.

Effect of [Na$^+$] on the Overall Equilibria

Table 2 summarizes the effect of $[Na^+]$ on the equilibrium ratios of M, M^-, and Na^- in mixtures containing Li, K, Rb, or Cs. Equilibrium concentrations were estimated from the plateau optical densities (OD), measured ~1 ms after the pulse, for M, M^-, and Na^-. For comparative purposes these values are expressed in terms of $K_A = (OD_{M^-}/OD_{Na^-})Y^{1/2}$ and $K_B = (OD_{M^0}/OD_{Na^-})Y^{1/2}$ where $Y = [Na^+]/[M^+]$ is used to normalize the ratios for differing Na^+ and M^+

TABLE 2. Effect of Na^+ concentration on the overall equilibria in Li, K, Rb, and Cs solutions

Second metal	Concentration (*M*)	K_A	K_B
Li	1×10^{-1}		9.5×10^{-4}
K	5×10^{-3}	0.09	1.4×10^{-2}
Rb	2×10^{-4}	<0.09	$\approx 5 \times 10^{-2}$
Cs	3×10^{-3}	$\ll$0.09*	5.5×10^{-2}

*Assuming Cs^-/Cs^0 is the same as in pure CsNHEt solutions (7).

concentrations. Because of spectral overlap K_A can only be estimated for Rb and Cs/Na mixtures.

The significant feature to note is that the final equilibrium favours Na^- in all cases but to a progressively smaller extent in progressing down the series Li, K, Rb, and Cs. For all the species under consideration the trend in stability increases in the order $e_s^- < Li^0 < Na^0 < K^0 < Rb^0 < Cs^0 < Cs^- < Rb^- < K^- < Na^-$. These observations are in general, consistent with the qualitative trends noted by Dye *et al.* (20), that K_1 decreases in the order Cs, Rb, K, Na (Li), whereas for K_2 the reverse is true.

Summary

In K, Rb, or Cs solutions containing Na^+, the formation of Na^- occurs via a rapid mixed order process via the corresponding K^-, Rb^-, or Cs^- species. With Li solutions the Na^+ appears to be associated or complexed with the Li^+ ions thereby effectively restricting the competition for the parent e_s^- and subsequent conversion to Na^-.

1. J. J. Lagowski and M. J. Sienko (*Editors*). Metal ammonia solutions. Colloque Weyl II, Int. Union Pure and Appl. Chem., Butterworth and Co., London. 1970.
2. M. T. Lok, F. J. Tehan, and J. L. Dye. J. Phys. Chem. **76**, 2975 (1972).
3. J. L. Dye. Electrons in fluids. *Edited by* J. Jortner and L. R. Kestner. Springer-Verlag, West Berlin. 1973. p. 77.
4. J. W. Fletcher, W. A. Seddon, and F. C. Sopchyshyn. Can. J. Chem. **51**, 2975 (1973).
5. G. A. Salmon, W. A. Seddon, and J. W. Fletcher. Can. J. Chem. **52**, 3259 (1974).
6. J. W. Fletcher and W. A. Seddon. Colloque Weyl IV. J. Phys. Chem. **79**, 3055 (1975).
7. J. W. Fletcher, W. A. Seddon, J. J. Jevcak, and F. C. Sopchyshyn. Can. J. Chem. **53**, 3571 (1975).
8. I. Hurley, T. R. Tuttle, Jr., and S. Golden. J. Chem. Phys. **48**, 2818 (1968).
9. I. Hurley, T. R. Tuttle, Jr., and S. Golden. Metal ammonia solutions. Colloque Weyl II, Int. Union Pure and Appl. Chem., Butterworth and Co., London. 1970. p. 449.
10. M. G. DeBacker and J. L. Dye. J. Phys. Chem. **75**, 3092 (1971).
11. J. Eloranta and H. Linschitz. J. Chem. Phys. **38**, 2214 (1963).
12. M. Ottolenghi, K. Bar-Eli, and H. Linschitz. J. Chem. Phys. **43**, 206 (1965).
13. W. A. Seddon, C. Willis, M. J. Young, and E. B. Selkirk. Atomic Energy of Canada Ltd. report AECL-3853.
14. W. A. Seddon, J. W. Fletcher, and F. C. Sopchyshyn. Can. J. Chem. **51**, 1123 (1973).
15. E. B. Selkirk and W. A. Seddon. Atomic Energy of Canada Limited report AECL-4134.
16. W. A. Seddon, E. B. Selkirk, and J. W. Fletcher. Int. J. Radiat. Phys. Chem. **5**, 323 (1973).
17. G. A. Salmon, W. A. Seddon, and J. W. Fletcher. Can. J. Chem. **52**, 3259 (1974).
18. K. H. Schmidt. Argonne National Laboratory Report ANL-7693.
19. D. Huppert and K. H. Bar-Eli. J. Phys. Chem. **74**, 3285 (1970).
20. J. L. Dye, C. W. Andrews, and S. E. Mathews. Colloque Weyl IV. J. Phys. Chem. **79**, 3065 (1975).

Can. J. Chem. Downloaded from www.nrcresearchpress.com by 210.87.254.105 on 09/05/12
For personal use only.

Proton and deuteron nuclear magnetic resonance study of host and guest motions in ethylene oxide-d_4 clathrate hydrate[1]

JOHN A. RIPMEESTER

Division of Chemistry, National Research Council of Canada, Ottawa, Ont., Canada K1A 0R9

Received June 28, 1976

JOHN A. RIPMEESTER. Can. J. Chem. **54**, 3677 (1976).

The motions of water molecules in ethylene oxide-d_4 clathrate hydrate have been studied between 200 and 280 K using continuous wave and pulsed ^{1}H nmr methods. The ^{1}H second moment and rotating frame relaxation time variation with temperature show that reorientation and diffusion of water molecules occur as two distinct processes. From the relaxation time data, activation energies of 8.15 and 12.0 kcal/mol are found for reorientation and diffusion, respectively.

From the non-zero guest molecule D quadrupole coupling constant observed between ~100 and 280 K, it is evident that there is some net orientation of the guest molecules in the hydrate cages at all temperatures. Also, there is a slow motional averaging superimposed on the rapid guest molecule reorientation which can be described approximately by the same parameters as the water molecule reorientation.

JOHN A. RIPMEESTER. Can. J. Chem. **54**, 3677 (1976).

On a étudié, entre 200 et 280 K, et faisant appel aux méthodes rmn du proton en ondes continue ou pulsée, les mouvements des molécules d'eau dans un hydrate clathrate d'oxyde d'éthylène-d_4. Les variations avec la température du moment second du proton et du temps de relaxation du cadre tournant montrent que la réorientation et la diffusion des molécules d'eau se produisent par deux processus distincts. A partir des données de temps de relaxation, on a trouvé que les énergies d'activation pour la réorientation et la diffusion sont respectivement de 8.15 et 12.0 kcal/mol.

En se basant sur les constantes de couplage quadrupolaire de ^{2}H, qui sont differentes de zero, pour les molécules hôtes entre ~100 et 280 K, il est évident qu'il y a une réorientation nette des molécules hôtes dans les cages d'hydrate à toutes les températures. De plus il s'établit lentement une moyenne des mouvements qui est superposée à la réorientation rapide des molécules hôtes et que l'on peut décrire approximativement par les mêmes paramètres que la réorientation des molécules d'eau.

[Traduit par le journal]

Introduction

In a previous publication (1) evidence was presented that in the tetrahydrofuran (THF) clathrate hydrate the reorientation of the water molecule rate is somewhat faster than the translational diffusion rate, a result opposite to that found for ice itself. The clear resolution of the change of proton second moment and of the rotating frame relaxation times observed for THF-d_8 hydrate into distinct reorientation and diffusion contributions was limited by the relative closeness of the reorientational and diffusional correlation times; these differed by a factor of ~10 at 253 K.

Dielectric relaxation measurements (2) show that the water reorientation rate in ethylene oxide hydrate is faster than in THF hydrate. The greater difference between reorientational and diffusional correlation times expected in EO hydrate should help to resolve the contributions to the motional reduction of the second moment and to the rotating frame relaxation time.

Ethylene oxide (oxirane) forms a structure I clathrate (3) of composition $EO \cdot 6.9H_2O$ (4). The dielectric properties of EO hydrate and the CW nmr spectra of the guest molecules in the D_2O hydrate have been studied between 2 and 270 K (2). Recently, guest molecule spin–lattice relaxation times (T_1) of EO deuteriohydrate have been reported between 77 and 280 K (5).

^{1}H second moments, spin–lattice relaxation times (T_1), and rotating frame relaxation times ($T_{1\rho}$) were measured for a clathrate of composition of EO-$d_4 \cdot 7H_2O$ to elucidate the motions of the water molecules. In addition, deuteron nmr measurements revealed some significant features of the motion of the guest molecules.

[1]NRCC No. 15503.

Can. J. Chem. Downloaded from www.nrcresearchpress.com by 210.87.254.40 on 09/05/12
For personal use only.

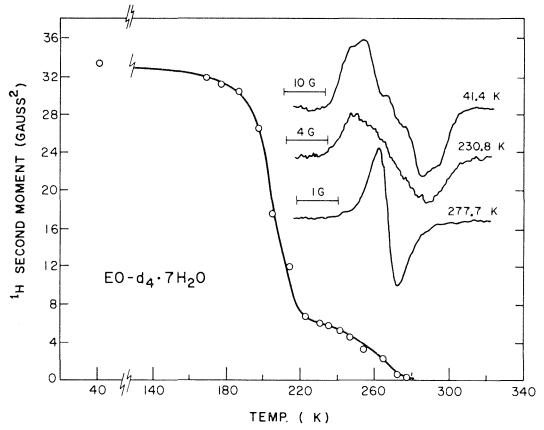

FIG. 1. Second moment *vs.* temperature for EO-d_4·7H$_2$O. Inset shows typical spectral lineshapes at various temperatures.

Experimental Methods

The hydrate of EO-d_4 was prepared by sealing in glass tubes quantities of EO-d_4 and conductivity water to give a composition of EO-d_4·7H$_2$O. The samples used for relaxation time measurements were degassed thoroughly by means of freeze–pump–thaw cycles. To ensure good thermal contact between the sample and the glass tube walls, a low pressure of helium gas was admitted to each tube before sealing. After quenching in liquid nitrogen, the samples were annealed at ~5 °C for several days.

The marginal oscillator used to obtain the ^{1}H CW spectra, the means of temperature measurement and control, and the methods of second moment calculation have been described previously (2). A Bruker SXP spectrometer operating at a frequency of 9.2 MHz was used for the pulsed nmr measurements. ^{1}H and D T_1 measurements were made using 90°–τ–90° pulse sequences; ^{1}H $T_{1\rho}$'s were measured by means of a 90° pulse followed by a variable length pulse shifted in phase by 90° with respect to the first. ^{1}H T_2 values were found by fitting an exponential curve to the initial portion of the free induction decays. Since the ^{1}H line shape becomes Lorentzian only above ~250 K, these T_2 values are only approximate and are meant to illustrate the changes of T_2 with temperature. D quadrupole echoes were generated using 90°–τ–90°$_{90°}$ pulse sequences. The parameters used to describe the shape and decay of the echo are discussed in a later section.

A Digital Equipment Corporation PDP-8L computer and peripheral equipment were used to enhance signal-to-noise ratios by means of time averaging and to calculate time constants from magnetization recovery curves and free induction decays.

Results and Discussion

^{1}H Lineshapes and Second Moments

Figure 1 shows a plot of the EO-d_4·7.0H$_2$O proton second moments *vs.* temperature. At ~40 K the second moment has a value of 33.3 ± 0.6 G^2, and at this temperature both the second moment and lineshape (see inset, Fig. 1) resemble the corresponding properties observed for THF-d_8·17H$_2$O (1) and ice I$_h$ (6, 7) at low temperatures. Saturation problems such as encountered for various ices (6, 8) at low temperatures were not encountered for this hydrate. (Near ~40 K the D spin–lattice relaxation time is quite short, and the water proton magnetization can relax via the proton–deuteron dipolar cross-relaxation mechanism.)

There are two distinct regions of motional narrowing, centered at ~210 and ~250 K (Fig. 1). Although there is some overlap of the two regions, a distinct plateau occurs at ~225 K at a second moment value of 6.5 G^2. From the dielectric relaxation study of EO hydrate (2), and by analogy with the nmr study of THF hydrates (1), the low temperature line narrowing region corresponds to random reorientation of water molecules, a motion which reduces the theoretical observable second moment to ~7 G^2 (1).

The second motional narrowing region then corresponds to centre-of-mass diffusion of the water molecules. The predicted observable second moment drops to zero for this motion, a value approached above ~0 °C. The lineshape is essentially Lorentzian at this temperature, as expected in the extreme motional narrowing limit.

^{1}H Relaxation Times

The entire proton T_1 curve (Fig. 2) can be attributed to water molecule reorientation. The straight line portion of the log T_1–inverse temperature plot gives an activation energy of 7.7 kcal/mol, a value identical to the one derived for dielectric relaxation of the water molecules (2).

Quantitative interpretation of the relaxation time data is complicated by the presence of a distribution in reorientational correlation times of the water molecules. The water dielectric relaxation in EO hydrate could be roughly described (2) by a Cole–Cole distribution with the width parameter α varying from 0.07 at −40 °C to 0.14 at −130 °C, although the experimental results indicated that the distributions were more sharply cut-off than the Cole–Cole distribution.

The low temperature $T_{1\rho}$ minimum (Fig. 2),

Can. J. Chem. Downloaded from www.nrcresearchpress.com by 210.87.254.40 on 09/05/12
For personal use only.

Can. J. Chem. Downloaded from www.nrcresearchpress.com by 210.87.254.40 on 09/05/12
For personal use only.

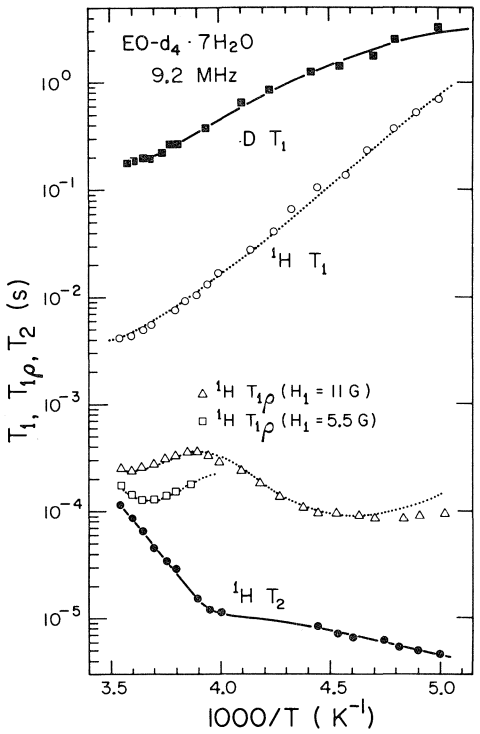

FIG. 2. ^{1}H static and rotating frame spin–lattice relaxation times (T_1, $T_{1\rho}$), spin–spin relaxation time (T_2), and D spin–lattice relaxation times shown as a function of inverse temperature for EO-d_4·7H_2O.

clearly assignable to reorientation of water molecules, is too shallow to be interpreted in terms of the BPP equation with a single correlation time. Several functions, including the Cole–Cole and the Fröhlich, or rectangular, distributions were incorporated in the BPP expression (9) and fitted to the T_1 and $T_{1\rho}$ data by assuming a simple temperature dependence of the distribution width parameter. Although neither of these functions describes the data accurately, the rectangular distribution appears to be somewhat better over the temperature range in question.

Incorporation of this distribution in the T_1 expression gives

$$[1]\quad T_1^{-1} = 2\Delta M_2[f(\omega_0,b,a) + 4f(2\omega_0,b,a)]/3\ln(b/a)$$

where $f(\omega,b,a) = (\tan^{-1}\omega b - \tan^{-1}\omega a)/\omega$, ΔM_2 is the second moment averaged by the water reorientation, and the cut-off times a and b are related to τ, the center of the rectangular distribution by $\tau = \sqrt{ab}$ with $b > \tau > a$.

In order to account for the temperature dependence of the $T_{1\rho}$ data, diffusion of the water molecules must also be taken into account. It is assumed that two mechanisms contribute to $T_{1\rho}$ according to

$$[2]\quad T_{1\rho}^{-1} = T_{1\rho}^{-1}\text{(reorientation)} + T_{1\rho}^{-1}\text{(diffusion)}$$

where the diffusional contribution is treated as before (1). The reorientational contribution in the weak collision limit is

$$[3]\quad T_{1\rho}^{-1} = 2\Delta M_2[2.5f(\omega_0,b,a) + f(2\omega_0,b,a) + 1.5f(2\omega_1,b,a)]/3\ln(b/a)$$

The dotted line in Fig. 2 was calculated using eqs. 1 to 3 and

$$\Delta M_2(\text{reorientation}) = 23.4\ \text{G}^2$$
$$\tau = 9.40 \times 10^{-15}\exp(4102/RT)$$
$$\Delta M_2(\text{diffusion}) = 6.5\ \text{G}^2$$

and

$$\tau = 1.35 \times 10^{-15}\exp(6040/RT)$$

The width parameter, b/a, was assumed to vary inversely with temperature from a value of 4 at 280 K to a value of 24 at 200 K. This choice of parameters, although not unique, yields a reasonable reproduction of the T_1 data and the $T_{1\rho}$ data above about 215 K.

The proton T_2 temperature dependence (Fig. 2) reflects the line narrowing which accompanies the reorientational and diffusive motions. Near the hydrate decomposition temperature T_2 approaches $T_{1\rho}$, again as expected in the extreme motional narrowing limit.

Water molecule motional parameters for THF-d_8·17H_2O, EO-d_4·7H_2O, and ice I_h are summarized in Tables 1 and 2. The marked increase in reorientational mobility of the clathrate water molecules compared with those in ice I_h stands out, as does the corresponding decrease in reorientational activation energies. On the other hand, the diffusion process appears to be much the same for the three "ices" considered here. The results summarized in Table 1 support the contention that reorientation and diffusion of water molecules are distinct and independent processes (10, 11).

Water molecule reorientation in ices is usually assumed to accompany the diffusion of Bjerrum defects. The low activation energy for water

TABLE 1. Water molecule motional parameters

Compound	Motion	τ_0 (s)	E_a (kcal/mol)
$EO \cdot 7H_2O$[a]	Reorientation	9.40×10^{-15}	8.15 (7.7)[d]
	Diffusion	1.35×10^{-15}	12.0
$THF \cdot 17H_2O$[b]	Reorientation	1.93×10^{-13}	7.2 (7.4)[d]
	Diffusion	1.41×10^{-16}	12.0
Ice I_h[c]	Reorientation	5.3×10^{-16}	12.25
	Diffusion	2.0×10^{-17}	13.9

[a]This work.
[b]Reference 1.
[c]References 23, 24.
[d]Values derived from dielectric relaxation measurements, refs. 2, 25.

TABLE 2. Motional correlation times at 0 °C

Compound	Motion	τ_c (s)
EO hydrate[a]	Reorientation	3.5×10^{-8} (2.8×10^{-8})[g]
	Diffusion	5.4×10^{-6}
THF hydrate[b]	Reorientation	1.1×10^{-7} (1.0×10^{-7})[g]
	Diffusion	5.6×10^{-7}
Ice I_h[c]	Reorientation	2.1×10^{-5}
	Diffusion	2.6×10^{-6}
Water on charcoal[d]		5.9×10^{-12}
Water on zeolite 13X[e]		4.2×10^{-10}
Water on cell walls[f]		3.0×10^{-10}

[a]This work.
[b]Reference 1.
[c]References 23, 24.
[d]Reference 13.
[e]Reference 14.
[f]Reference 15.
[g]Values derived from dielectric relaxation measurements, refs. 2, 25.

reorientation in EO and THF hydrates as well as several other clathrates (11, 12), which was shown to depend on the degree of polarity of the guest molecule, and possibly also on the occurrence of oxygen atoms in the guest, must then reflect the facile formation of such defects.

Finally, for THF and EO hydrates there is excellent agreement between results obtained from nmr and dielectric relaxation for the water molecule reorientational parameters (Tables 1 and 2).

In Table 2, clathrate hydrate water molecule motional parameters at 0 °C are compared with motional jump times for water molecules adsorbed on various substances (13–16). These latter jump times are assumed to characterize both reorientation and diffusion, as no distinction between the two processes can be made. In all cases the mean motional jump times for sorbed water molecules are faster than either the reorientational or diffusive correlation times for the ices. It may well be that the presence of unique reorientation and diffusion processes is a primary difference between the true ices and sorbed water, where the absence of water molecules with 'ice-like' mobility reflects the lack of a 3 dimensional H-bonded lattice.

In light of the results reported here, the usual assumption that rotational and translational lifetimes for water molecules in both ice and water are about equal (17) should be treated with caution.

Deuteron T_1 Nuclear Magnetic Resonance Studies

Deuteron spin–lattice relaxation times of the guest molecules are shown in Figs. 2 and 3. At temperatures below the T_1 maximum at 184 K the log T_1 *vs.* inverse temperature plot is linear and an activation energy of 0.89 kcal/mol can be derived from the slope. The relevant relaxation process here is the rapid fluctuation ($\omega\tau_c \ll 1$) of the electric field gradients (efg) at the deuteron sites brought about by the fast guest molecule

Can. J. Chem. Downloaded from www.nrcresearchpress.com by 210.87.254.40 on 09/05/12
For personal use only.

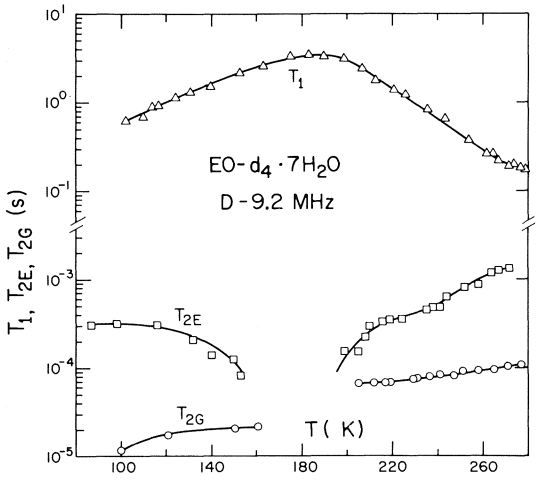

FIG. 3. D spin–lattice relaxation times (T_1), linewidth parameter (T_{2G}) and spin echo decay time (T_{2E}) plotted as a function of temperature.

reorientation. The activation energy is in good agreement with the value of 0.9 kcal/mol found by Hayward and Packer (5) from proton spin–lattice relaxation times on EO·7D_2O (4), but is appreciably lower than the dielectric relaxation value of 1.4 kcal/mol (2). The lower nmr activation energy possibly reflects reorientations about the EO polar axis which the dielectric method does not detect.

Above 184 K the D T_1's decrease with increasing temperature and become nearly parallel to the proton T_1's (Fig. 2). Therefore, it is tempting to attribute these two time constants to the same motional mechanism. Just as the proton T_1's are governed by water molecule reorientation, the deuteron spins can be relaxed by fluctuations in the D–^{1}H nuclear dipolar interactions. In the slow motion limit ($(\omega_H\tau_c)^2$, $(\omega_D\tau_c)^2 \gg 1$) and with $\omega_H \gg \omega_D$, the appropriate expression for T_1 is (ref. 18, p. 295).

$$[4] \quad T_1^{-1} = \tfrac{1}{2}\gamma_D^2 \Delta SM(D - {}^1H) \times 3/\omega_D^2\tau_c$$

At 250 K τ_c for water molecule reorientation is 1.26×10^{-7} s. The change in the proton contribution to the deuteron second moment due to water molecule reorientation, $\Delta SM(D - {}^1H)$, is calculated to be 0.48 G^2 for isotropic guest molecule reorientation. From the ^{1}H second moment studies of EO·7D_2O (4) $\Delta SM(D - {}^1H)$ probably should be about twice as large as this calculated value, presumably because of less than isotropic reorientation of the guest molecules. The T_1 value calculated from eq. 4 is then 17.3 s, about 40 times larger than the experimental value.

The relatively short D T_1's above 200 K must then be due to a quadrupolar mechanism, which may, or may not, be related to water molecule reorientation. This implies that at slightly lower temperatures there is a non-zero D quadrupole coupling constant which is at least partially averaged when the appropriate motion becomes fast enough. The magnitude of the fluctuating component of the electric field gradient can be estimated from $(e^2qQ/h)_{eff}$, the effective quadrupole coupling constant in the T_1 expression (ref. 18, p. 313).

$$[5] \quad T_1^{-1} = \frac{3\pi^2}{10}\left[\frac{e^2qQ}{h}\right]^2_{eff} \times 2/\omega_D^2\tau_c$$

If again use is made of the water reorientational correlation time for τ_c and the experimental T_1 value at 250 K, $(e^2qQ/h)_{eff}$ = 12.5 kHz.

Deuteron Quadrupole Echo Studies

Significant information should also be contained in the D nmr lineshapes. In the study of anisotropic motion in molecular solids, complicating intermolecular interactions are much less important in D nmr, where the lineshape determining interaction is between the nuclear electric quadrupole moment and the electric field gradient at the nucleus, than in ^{1}H nmr, where many internuclear dipolar interactions must be accounted for.

For a D nucleus in a molecular C—D bond, the quadrupole coupling constant e^2qQ/h gives the magnitude of the quadrupole coupling tensor principal component. The asymmetry parameter η measures the departure from cylindrical symmetry of the efg tensor. For C—D bonds η is usually small (< 0.1) and here will be taken to be zero.

In powdered samples, the variation of crystallite orientation in the magnetic field gives rise to the familiar spin 1 powder doublet with a characteristic doublet splitting

$$[6] \quad a = \tfrac{3}{4}(e^2qQ/h) \times \tfrac{1}{2}(3\cos^2\theta - 1)$$

Here, θ is the angle between the principal axis of the efg tensor and any molecular axis about which reorientation is sufficiently rapid. In pulsed nmr experiments, the fine structure

Can. J. Chem. Downloaded from www.nrcresearchpress.com by 210.87.254.40 on 09/05/12
For personal use only.

Can. J. Chem. Downloaded from www.nrcresearchpress.com by 210.87.254.40 on 09/05/12
For personal use only.

manifests itself as a modulation of the free induction decay (fid) at the frequency a. When the fid decays in a time of the same order as the instrument recovery time, the line shape information can be obtained from the quadrupole echo generated by an appropriate pair of pulses (19). For a D nucleus the expression for the quadrupole echo following a $90°–\tau–90°_{90°}$ pulse sequence is

$$[7] \qquad S(t) = \int_{-\infty}^{\infty} f(a) \cos \{a(t - 2\tau)\} da$$

where $f(a)$ is the distribution function for the quadrupole frequency a.

In the case of EO-d_4·$7H_2O$, well defined modulation of the quadrupole echo can be observed below ~25 K.[2] The modulation frequency of ~120 kHz leads to a quadrupole coupling constant of ~160 kHz and can be assigned to EO-d_4 guest molecules held rigidly in their cages.

Above ~70 K, the guest molecule motions are quite rapid ($\tau_c \ll 10^{-8}$ s), but far from random, and, as judged from the absence of well-defined quadrupole frequencies, the quadrupole echo should be interpreted in terms of a distribution of such frequencies. In turn this suggests that the axes of preferred reorientation of the guest molecules vary from cage to cage.

For EO-d_4·$7H_2O$, the quadrupole echo shape could be analyzed in terms of a Gaussian function according to

$$[8] \qquad S(t) = S(2\tau) \exp [- (t - 2\tau)^2/2T_{2G}^2]$$

A typical plot of $S(t)$ *vs.* $(t - 2\tau)^2$ is shown in Fig. 4*A* for $t \geq 2\tau$. Alternatively T_{2G} could be obtained from $t_{1/2}$, the echo half width at half maximum, from

$$[9] \qquad T_{2G} = (2 \ln 2)^{-1/2} t_{1/2}$$

T_{2G} values derived from EO-d_4·$7H_2O$ are plotted as a function of temperature in Fig. 3. The rms quadrupole frequency $\langle \bar{a}^2 \rangle^{1/2}$ (in Hz), as obtained from

$$[10] \qquad \langle \bar{a}^2 \rangle^{1/2} = (2\pi T_{2G})^{-1}$$

was found to be 13.9, 2.34, and 1.46 kHz respectively at 100, 210, and 270 K (see Fig. 5). These values should be compared with the quadrupole frequency for an EO-d_4 molecule held rigidly in the clathrate cages, namely 120 kHz, as found for $T < 25$ K.[2]

Between ~160 and 209 K a quadrupole echo cannot be observed for times τ significantly

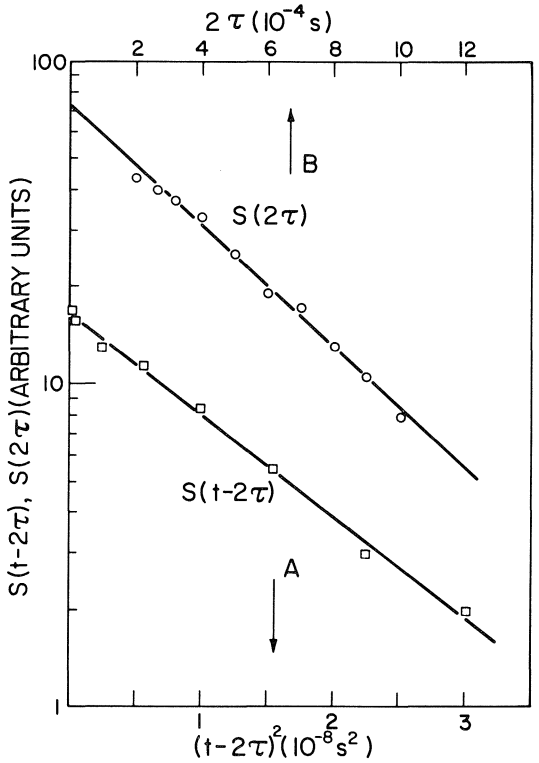

FIG. 4. Typical plot of spin echo amplitude $S(t - 2\tau)$ as a function of $(t - 2\tau)^2$ (*A*) and spin echo maximum $S(2\tau)$ as a function of pulse spacing 2τ (*B*) (T = 241 K).

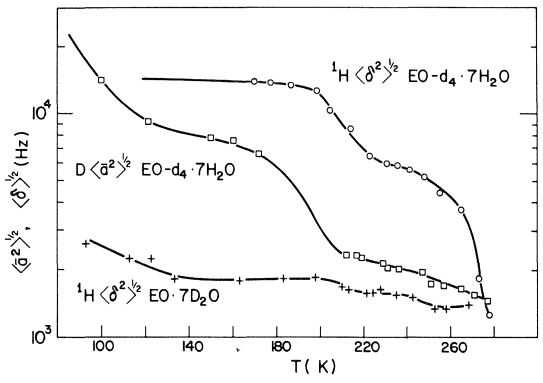

FIG. 5. ^{1}H rms linewidths $\langle \delta^2 \rangle^{1/2}$ for EO-d_4·$7H_2O$ and EO·$7D_2O$ and D rms quadrupole frequency $\langle a^2 \rangle^{1/2}$ for EO-d_4·$7H_2O$ plotted as a function of temperature.

[2]Unpublished results.

Can. J. Chem. Downloaded from www.nrcresearchpress.com by 210.87.254.40 on 09/05/12
For personal use only.

greater than $\sim T_{2G}$. In this temperature region there is a relatively slow motional averaging of the guest molecule residual orientation which causes $\langle \bar{a}^2 \rangle^{1/2}$ to be decreased from ~7.5 kHz at 160 K to 2.34 kHz at 210 K.

The effective fluctuating quadrupole coupling constant of 12.5 kHz (see eq. 5) can be identified approximately with the change in width at half height of the D lineshape function on going from 160 to 210 K; this change in width is given by $(8 \ln 2)^{1/2} \Delta \langle \bar{a}^2 \rangle^{1/2}$ and has a value of 12.2 kHz.

The decrease in echo amplitude with increasing pulse spacing τ in the $90°-\tau-\beta_{90°}$ pulse sequence is due to spin–spin relaxation. In general, the time constant for the echo amplitude decay depends on the turning angle β of the second pulse (20). For EO-d_4·$7H_2O$ the turning angle was always 90° and the decays were approximately exponential according to

$$[11] \qquad S(2\tau) \propto \exp(-2\tau/T_{2E})$$

A typical plot is shown in Fig. 4*B*. The T_{2E} obtained in this manner are shown in Fig. 3 as a function of temperature. Note that T_{2E} drops between ~140 and 210 K and for a temperature range centered at 180 K an echo with $T_{2E} > T_{2G}$ cannot be observed. This effect is analogous to the line broadening and fade out observed in CW D nmr studies (21) when τ_c, the correlation time for the motion is about equal to $(2\pi|\nu_1 - \nu_2|)^{-1}$. Here ν_1 and ν_2 are the quadrupole transition frequencies for a stationary deuteron. In absence of well defined frequencies ν_1 and ν_2, we can identify $|\nu_1 - \nu_2|$ with the rms width of the D resonance line just below the fade out temperature at 160 K, about 7.5 kHz, and this leads to a correlation time

$$\tau_c \sim (2\pi \langle \bar{a}^2 \rangle^{1/2})^{-1} = 2.1 \times 10^{-5} \text{ s}$$

From dielectric relaxation measurements (22) the mean water molecule reorientational correlation time is 2.5×10^{-5} s at 177 K, a temperature well within the fade out region. This again illustrates that the efg fluctuations and water molecule reorientations have similar correlation times.

We can also attempt to interpret the T_{2E} values observed well away from the region where motional effects occur in terms of nuclear dipole–dipole interactions. Below ~140 K the main interaction of this type will be between rigidly held water molecule protons and guest deuterons. The second moment calculated for this interaction with isotropically rotating guest molecules is 1.7 G^2. By comparing experimental proton second moments with calculated values for EO·$7D_2O$ (2), it is evident that the 1.7 G^2 should be doubled to take into account nonrandom reorientation. Assumption of gaussian lineshape and a second moment of 3.4 G^2 leads to a T_2 value of 1.65×10^{-4} s, close to the experimental T_{2E} value of 3.1×10^{-4} s derived for a Lorentzian lineshape. Both the longer time constant and the lineshape for EO-d_4·$7H_2O$ may be understood in terms of an averaging of the proton local field at the deuteron sites (ref. 18, p. 123). A quasi-Lorentzian lineshape with a half-maximum width much less than the rms width is expected for heteronuclear dipolar broadening of a set of I spins by a set of S spins if $(\gamma_S/\gamma_I)^2$ is a large number.

The increase in T_{2E} with increase of temperature above ~220 K is mainly due to an averaging of water proton – guest deuteron nuclear dipolar interactions as the water molecules start to diffuse through the lattice. The limiting high temperature value for the deuteron dipolar second moment will be determined by inter-guest D–D interactions, as all ^{1}H–D dipolar interactions are averaged by the sufficiently rapid water molecule reorientation and diffusion. For randomly reorientating guest molecules the D second moment will be 1.1×10^{-2} G^2. This leads to a T_2 value of 2.0×10^{-3} s for a Gaussian lineshape. The experimental value, derived from an exponential decay, is $\sim 1.35 \times 10^{-3}$ s, still somewhat short of the calculated value. The difference could again be accounted for by a less than random guest molecule reorientation.

The D echo decay times T_{2E} prove to be a useful parameter to monitor low frequency ($\tau_c \sim 10^{-5}$ s^{-1}) guest molecule motions. Temperature regions where low frequency efg fluctuations take place are easily distinguished from those where only nuclear dipole–dipole interactions are averaged.

The D nmr studies demonstrate that reorientation of most EO-d_4 molecules is nonrandom in the structure I cages at all temperatures. The small degree of residual orientation, and any change therein, is much better defined by D than ^{1}H measurements. This is illustrated in Fig. 5 which shows ^{1}H rms linewidths $\langle \delta^2 \rangle^{1/2}$, defined by $\langle \delta^2 \rangle^{1/2} = \gamma H_L/2\pi$ where H_L is the

proton local field (ref. 18, p. 547) for EO-d_4·$7H_2O$ and EO·$7D_2O$ and also $\langle \bar{a}^2 \rangle^{1/2}$, the rms quadrupole frequency for EO-d_4·$7H_2O$.

Above ~0 °C relatively rapid reorientation and diffusion of the host water molecules takes place, so that the residual orientation of the guest molecules in the hydrate cages probably reflects the aspherical nature of the van der Waals interactions between the cage walls and the guest molecules. This is consistent with the average symmetry of the large structure I hydrate cages, ($\bar{4}2m$), which, according to the composition EO·6.8_9H_2O (4), contain up to 90% of the EO molecules. These symmetries are attained only when rapid water molecule reorientation causes the different cage configurations resulting from the disordered hydrogen bonding scheme to be averaged over the reorientational motion of the water molecules. When water molecule reorientations slow down, the many possible cage configurations freeze in and the sites available to the guest molecules become energetically different, thus restricting the guest motional freedom. In this sense the high temperature guest molecule motion and the water molecule reorientation are intimately connected.

At high temperatures, where the structure I hydrate cages have well-defined average symmetries, one might expect that EO molecules in the large and small cages have different residual orientations. In this study we did not see separate signals for the guest molecules in the large and small cages. However, direct observation of the D free induction decay, or quadrupole echo, is not the best way of looking for fine structure. Experiments to obtain detailed D nmr lineshapes in the high temperature region are in progress.

It should be possible to correlate any net orientation effects observed by D nmr at high temperatures with those suggested in the X-ray structural study (3), and also with calculations of the potential energy as a function of orientation for an EO molecule in the structure I large cage (2).

Acknowledgments

The author acknowledges helpful discussion with D. W. Davidson and S. K. Garg, and the technical assistance of R. E. Hawkins.

1. S. K. Garg, D. W. Davidson, and J. A. Ripmeester. J. Magn. Reson. **15**, 295 (1974).
2. S. K. Garg, B. Morris, and D. W. Davidson. J. Chem. Soc. Faraday II, **68**, 481 (1972).
3. M. von Stackelberg and B. Meuthen. Z. Elektrochem. **62**, 130 (1958); R. K. McMullan and G. A. Jeffrey. J. Chem. Phys. **42**, 2725 (1965).
4. D. N. Glew and N. S. Rath. J. Chem. Phys. **44**, 1710 (1966).
5. R. J. Hayward and K. J. Packer. Mol. Phys. **25**, 1443 (1973).
6. K. Kume. J. Phys. Soc. Jpn. **15**, 1493 (1960).
7. D. E. Barnaal and I. J. Lowe. J. Chem. Phys. **46**, 4800 (1967).
8. S. W. Rabideau, E. D. Finch, and A. B. Denison. J. Chem. Phys. **49**, 4660 (1968).
9. T. M. Connor. Trans. Faraday Soc. **60**, 1574 (1964).
10. L. Onsager and L. K. Runnels. J. Chem. Phys. **50**, 1089 (1969).
11. D. W. Davidson. *In* Water — a comprehensive treatise. Vol. 2. *Edited by* F. Franks. Plenum Press, New York, N.Y. 1973. p. 195.
12. B. Morris and D. W. Davidson. Can. J. Chem. **49**, 1243 (1971).
13. H. A. Resing, J. K. Thompson, and J. J. Krebs. J. Phys. Chem. **68**, 1621 (1964).
14. H. A. Resing and J. K. Thompson. Adv. Chem. Ser. **101**, 473 (1971).
15. H. A. Resing and R. A. Neihof. J. Colloid Interface Sci. **34**, 480 (1970).
16. H. A. Resing. Adv. Mol. Relaxation Processes, **3**, 199 (1972).
17. H. J. C. Berendson. *In* Water — a comprehensive treatise. Vol. 5. *Edited by* F. Franks. Plenum Press, New York, N.Y. 1973. p. 319.
18. A. Abragam. The principles of nuclear magnetism. Oxford University Press, Oxford. 1961.
19. I. Solomon. Phys. Rev. **110**, 61 (1958).
20. H. Abe, H. Yasuoka, and A. Hirai. J. Phys. Soc. Jpn. **21**, 77 (1966).
21. T. Chiba. J. Chem. Phys. **39**, 947 (1963).
22. D. W. Davidson and G. J. Wilson. Can. J. Chem. **41**, 1424 (1963).
23. R. P. Auty and R. H. Cole. J. Chem. Phys. **20**, 1309 (1952).
24. M. Weithase, F. Noack, and J. von Schutz. Z. Phys. **246**, 91 (1971).
25. R. E. Hawkins and D. W. Davidson. J. Phys. Chem. **70**, 1889 (1966).

Can. J. Chem. Downloaded from www.nrcresearchpress.com by 210.87.254.40 on 09/05/12
For personal use only.

Kinetics and mechanism of substitution reactions of (dimethylsulfoxide)pentaamminecobalt(III) ion in dimethylsulfoxide solvent: complications due to redox and conjugate base processes

S. T. Danny Lo, Evelyn M. Oudeman, Jean C. Hansen, and Thomas W. Swaddle[1]

Department of Chemistry, The University of Calgary, Calgary, Alta., Canada T2N 1N4

Received June 17, 1976

S. T. Danny Lo, Evelyn M. Oudeman, Jean C. Hansen, and Thomas W. Swaddle. Can. J. Chem. **54**, 3685 (1976).

Simple anation and solvent exchange reactions of $Co(NH_3)_5DMSO^{3+}$ in DMSO are accompanied by reactions in which the conjugate base of this complex undergoes either internal redox to cobalt(II) or relatively rapid substitution. These conjugate base reactions are eliminated by addition of H^+, although a minor redox pathway persists within ion pairs of $Co(NH_3)_5DMSO^{3+}$ with chloride or bromide. The latter pathway is evidently not mechanistically related to the solvent exchange or anation reactions, which proceed by dissociative interchange (I_d) according to the activation parameters (volume of activation = $+10\ cm^3\ mol^{-1}$ for DMSO exchange; enthalpy of activation = 123, 121, and $\sim$126 kJ mol^{-1} for DMSO exchange and bromide and chloride anation respectively). Enthalpies of activation for solvent exchange and for the limiting anation rate are shown to be better criteria of mechanism than the corresponding rate coefficients.

S. T. Danny Lo, Evelyn M. Oudeman, Jean C. Hansen et Thomas W. Swaddle. Can. J. Chem. **54**, 3685 (1976).

Les réactions d'anation simple et d'échange de solvant du $Co(NH_3)_5DMSO^{3+}$ dans le DMSO sont accompagnées par des réactions dans lesquelles la base conjuguée de ce complexe subit soit une réaction rédox interne conduisant à du cobalt(II) ou des réactions de substitution relativement rapide. On élimine ces réactions des bases conjuguées par addition de H^+; toutefois un chemin mineur de réduction persiste à l'intérieur des paires d'ions du $Co(NH_3)_5DMSO^{3+}$ avec le chlorure ou le bromure. Il est évident que cette dernière voie n'est pas reliée d'une façon mécanistique avec l'échange de solvant ou les réactions d'anation qui procèdent par un échange dissociatif (I_d) si l'on se fie aux paramètres d'activation (volume d'activation = $+10\ cm^3\ mol^{-1}$ pour l'échange DMSO; l'enthalpie d'activation = 123, 121 et $\sim$126 kJ mol^{-1} pour les échanges avec le DMSO et d'anation du chlorure et du bromure). On montre que les enthalpies d'activation pour l'échange du solvant et pour la vitesse limite l'étape déterminante de l'anation sont des meilleurs critères pour établir le mécanisme que les coefficients correspondants de vitesse.

[Traduit par le journal]

Introduction

We recently summarized (1) the evidence which indicates that, when water is the solvent, simple substitution reactions of cobalt(III) ammines

$$[1]\quad Co(NH_3)_5(solvent)^{3+} + Y^{n-} \underset{}{\overset{K_{IP}}{\rightleftharpoons}} \{Co(NH_3)_5(solvent)^{3+}, Y^{n-}\} \xrightarrow{k_i} Co(NH_3)_5Y^{(3-n)+} + solvent$$

proceed by a dissociative interchange (I_d) mechanism (2), that is, one in which Co–solvent bond breaking within the ion pair or encounter complex $\{Co(NH_3)_5(solvent)^{3+}, Y^{n-}\}$ is the rate determining process. We also pointed out, however, that cobalt(III) complexes may be anomalous in this respect, since the evidence collected to date suggests that, in general, octahedral cationic complexes of other trivalent transition metals M(III) undergo simple ligand substitution by an associative interchange (I_a) mechanism, in which bond making by Y^{n-} within the encounter complex is involved in the rate determining process (1).

We now report on our attempts to extend the data available for reaction 1 to include dimethylsulfoxide (DMSO) as the solvent. This solvent was chosen, partly because of the considerable recent interest (3–10) in the complex $Co(NH_3)_5DMSO^{3+}$ in itself, but mainly because the lower dielectric constant of DMSO relative to water

[1]Author to whom correspondence should be addressed.

Can. J. Chem. Downloaded from www.nrcresearchpress.com by 210.87.254.105 on 09/05/12
For personal use only.

Can. J. Chem. Downloaded from www.nrcresearchpress.com by 210.87.254.105 on 09/05/12
For personal use only.

was expected to allow ion pairing to proceed essentially to completion at practical concentrations of Y^{n-} and so permit the limiting first order rate coefficients k_i to be measured directly, this being impossible in water for mononegative Y^-. Moreover, complexes of the type $M(NH_3)_5Y^{(3-n)+}$ are known for a wide variety of M(III), and it was intended that the present study would form the basis of an extended comparative study of ligand substitution mechanisms in nonaqueous solvents in relation to the nature of M. In addition, there was the possibility that the predominant mechanism of reaction 1 might change on changing the solvent.

Finally, the relatively large size and bulky shape of the DMSO molecule raise the possibility that the need for a refinement of the Langford–Muir criterion of an I_d mechanism (11) might become apparent for reaction 1 when DMSO is the solvent (footnote 3 of ref. 12). Where the solvent molecules (*e.g.* water) are small, movements to and from the reaction site are relatively free, and Co–solvent bond breaking will generally lead either to net exchange with the ubiquitous solvent molecules or to unselective scavenging of Y^{n-} within the encounter complex. One may therefore expect, with Langford and Muir (11), that k_i will be about the same for all Y^{n-} in a given solvent, and less than (or, at most, equal to) the first order rate coefficient k_{ex} for solvent exchange in free $Co(NH_3)_5(solvent)^{3+}$, in the absence of some general labilization of the complex on forming an ion pair. These expectations may not, however, be realized if the bulkiness of the solvent molecules resulted in a high probability of recombination with the *same* solvent molecule, rather than a *different* one, after cobalt–solvent bond fission, so that the measured value of k_{ex} would be considerably lower than the true bond breaking rate coefficient. Similarly, access to the reaction site would be easier for small than for large Y^{n-}. Thus, k_i could vary somewhat with the nature of Y^{n-} and could exceed k_{ex}, especially when Y^{n-} is small, even though the mechanism remained strictly I_d. These complications are seen to be essentially statistical, *i.e.*, entropic, in origin, and serve to emphasize that *the general kinetic characteristic of an I_d mechanism is the constancy of the enthalpy of activation associated with the rate coefficients k_i and k_{ex}* throughout a series of reactions such as reaction 1 in which Y^{n-} is varied. This is because the enthalpic part of the free energy of activation is always that required to break the same metal–solvent bond, within a given I_d series; clearly, no such constancy of enthalpies of activation would be expected for an I_a process, and indeed the latter behavior characterizes I_a substitution at chromium(III) centers (12).

We present here evidence that the mechanism of reaction 1 does remain I_d on going from water to DMSO as solvent, and that refinement of the Langford–Muir criterion in terms of enthalpies of activation does appear to be necessary for DMSO. Unfortunately, our experiments were complicated by unexpected conjugate base reaction pathways and redox phenomena, but these are of interest in themselves and are of importance in considering past and future studies in this field.

Experimental

Materials

Tetraethylammonium chloride and bromide (Baker Chem. Co.) were recrystallized from hot dimethylformamide (DMF) by adding ether, and were dried under high vacuum. Analytical reagent grade *p*-toluenesulfonic acid hydrate (Fisher Scientific Company) was used without further recrystallization. Dimethylsulfoxide (ACS grade, Fisher Chemical Corp.) and DMSO-d_6 (Merck, Sharp and Dohme Canada Ltd.) were purified by a method analogous to the purification of DMF as described elsewhere (13).

$[Co(NH_3)_5DMSO](ClO_4)_3 \cdot 2H_2O$ was prepared and recrystallized by the method of Mac-Coll and Beyer (10). $[Co(NH_3)_5Cl](ClO_4)_2$ and $[Co(NH_3)_5Br](ClO_4)_2$ were prepared as described previously (14). The purity of these complexes was checked by microanalysis.

Kinetic Measurements

The progress of the exchange reaction between the coordinated DMSO-h_6 in $[Co(NH_3)_5DMSO]^{3+}$ with DMSO-d_6 solvent was followed by removing samples at appropriate intervals from thermostatted solutions of the perchlorate salt, freezing them until required, and recording the pmr spectra of the thawed samples with a Varian A-60 spectrometer at room temperature. The height of the coordinated DMSO-h_6 peak (τ = 7.27 ppm) was measured relative to that of the NH_3 resonance (τ = 6.07). The pressure dependence of the reaction rate was similarly measured by removing samples from a prepressurized syringe, as described previously (14).

The progress of the anation reactions was followed spectrophotometrically using a Cary Model 17H spectrophotometer as described elsewhere (12). The relevant molar absorptivity (ϵ) data are recorded in Table 1.

Cobalt(II) Analyses

The concentration of cobalt(II) in the reaction mixtures was determined spectroscopically as either $CoCl_4^{2-}$

TABLE 1. Molar absorptivities (in $dm^3\ mol^{-1}\ cm^{-1}$) of perchlorate salts of pentaamminecobalt(III) complexes in DMSO

Complex	Molar absorptivity at wavelength (nm)						
	312	419[a]	505[a]	544[a]	423[b]	544[b]	580[b]
$Co(NH_3)_5DMSO^{2+}$	200	11.3	46.4	55.6	14.7	58.1	22.9
$Co(NH_3)_5Cl^{2+}$		11.3	57.4	55.6			
$Co(NH_3)_5Br^{2+}$					14.7	58.1	48.5
$Co(NH_3)_5NCS^{2+}$	1700						

[a][complex] = [*p*-toluenesulfonic acid] = (1 to 2) $\times 10^{-3}$ mol dm^{-3}; $[Cl^-] \sim 3$[complex].
[b][complex] = [*p*-toluenesulfonic acid] = (1 to 2) $\times 10^{-3}$ mol dm^{-3}; $[Br^-] \sim 3$[complex].

(absorption maximum in DMSO at 683 nm with $\epsilon = 304$ $dm^3\ mol^{-1}\ cm^{-1}$) or $CoBr_4^{2-}$ (maximum in DMSO at 703 nm with $\epsilon = 108.9$ $dm^3\ mol^{-1}\ cm^{-1}$). In some cases, the cobalt(II) content was determined gravimetrically as dithiocyanatotetrapyridinecobalt(II) (15).

Results

In preliminary experiments, the anation reaction (reaction 1, with $Y^{n-} = Cl^-$, Br^-, NCS^-; solvent = DMSO) was followed spectrophotometrically (at 340, 580, and 312 nm, respectively) at 45 °C, using only $[Co(NH_3)_5DMSO](ClO_4)_3$ and excess $(C_2H_5)_4NCl$, $(C_2H_5)_4NBr$, or KNCS as solutes. In no case was the expected first order dependence on $[Co(NH_3)_5DMSO^{3+}]$ observed beyond a few percent reaction; rather, the reaction appeared to be autocatalytic (see, for example, Fig. 1), most notably when Y^{n-} was NCS^-, and also was slightly accelerated by exposure to the room lights at least when Y^{n-} was Br^-. Nevertheless, the initial rates of the reactions in the dark suggested approximate values of the limiting first order rate coefficient k_i of (1.6, 1.0, and 1.2) $\times 10^{-4}\ s^{-1}$ at 45 °C for $Y^{n-} = Cl^-$, Br^-, and NCS^-.

Closer examination of the products of reaction 1 after completion at 45 °C, however, revealed the presence of 9% and 7% cobalt(II) along with $Co(NH_3)_5Y^{(3-n)+}$ for $Y^{n-} = Cl^-$ and Br^- respectively, while, over the same time but in the absence of other solutes, $Co(NH_3)_5DMSO^{3+}$ and $Co(NH_3)_5Br^{2+}$ perchlorates yielded 11% and 4% cobalt(II) respectively in DMSO at 45 °C. Great care was taken to free the starting materials of cobalt(II) by recrystallization, and it was established that the reaction rates were independent of the mode of purification of the solvent and of the presence or absence of added water or $[Co(DMSO)_6](ClO_4)_2$. Thus, neither cobalt(II) alone nor trace contaminants were responsible for the autocatalytic substitution and redox decomposition phenomena. The addition of hydrogen ion (as the poorly complexing *p*-toluenesulfonic or trifluoromethanesulfonic acids), however, eliminated cobalt(II) formation, except where chloride or bromide ions were present, in which cases reduction of the cobalt center was still greatly diminished. The relative amount of cobalt(II) present in these latter cases at the end of the substitution reactions increased with increasing halide ion concentration, but

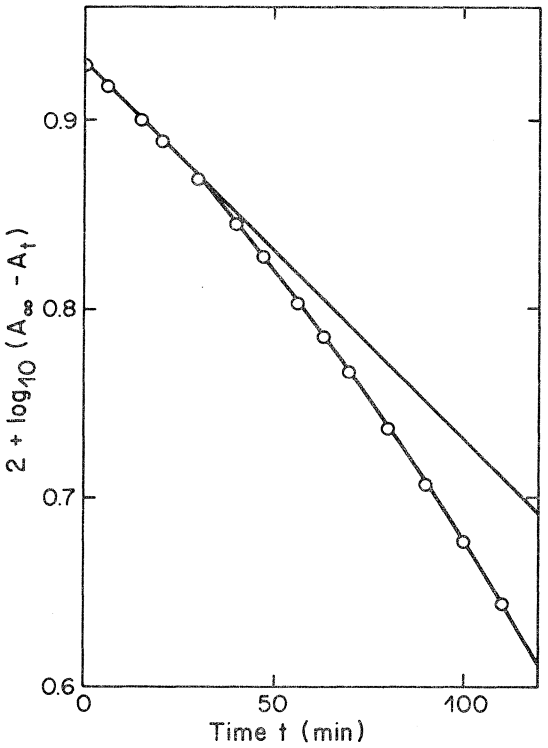

FIG 1. Reaction of $Co(NH_3)_5DMSO^{3+}$ (2.0 mmol dm^{-3}) with Br^- (15.0 mmol dm^{-3}) in DMSO at 45.0 °C without added acid. Optical absorbances A_t measured at 580 nm.

Can. J. Chem. Downloaded from www.nrcresearchpress.com by 210.87.254.105 on 09/05/12
For personal use only.

TABLE 2. Relative amounts of $Co(II)$, $Co(NH_3)_5DMSO^{3+}$, and $Co(NH_3)_5Y^{(3-n)+}$ present at the completion of reaction 1 in DMSO solvent at 50.7 °C

Y^{n-}	Initial $[Co(NH_3)_5DMSO^{3+}]$[a] (mmol dm^{-3})	Initial $[CH_3C_6H_4SO_3H]$ (mmol dm^{-3})	Initial $[(C_2H_5)_4NY]$ (mmol dm^{-3})	Final $[Co^{2+}]$[b] (%)	Final $[Co(NH_3)_5DMSO^{3+}]$ (%)	Final $[Co(NH_3)_5Y^{2+}]$ (%)
Cl^-	0.975	0.904	2.75	0.74	0	99
	0[c]	0.904	0	0	0	100
	0.975	0.904	4.93	0.80	0	99
			8.09	0.91	0	99
			15.68	1.0	0	99
			25.7	1.2	0	99
		2.70	25.7	1.1	0	99
		0.904	50.0	3.1	0	97[d]
Br^-	0.978	1.05	9.24	0.49	18	81
	0[c]	1.05	0	0	26	74
	0.978		19.0	0.76	20	80
			29.7	1.14	17	82
			57.5	1.52	10	88
			85.9	1.7	6	92
			117.9	1.7	5	93
		3.10	117.9	1.6	5	93
		1.05	117.9	0	64	36[e]

[a] As perchlorate salt.
[b] Determined spectrophotometrically as CoY_4^{2-}; uncertainty, ± 10%.
[c] Using $[Co(NH_3)_5Y](ClO_4)_2$ as starting material, 1.0 mmol dm^{-3}.
[d] $[Co(NH_3)_5Cl]Cl_2$, which was precipitated on completion of the reaction, was removed by filtration before determination of Co(II).
[e] At 80.0 °C.

was independent of $[H^+]$ so long as this was on the order of the initial [Co(III)], and did not increase further after the end of the substitution reaction; it was shown separately that $Co(NH_3)_5Cl^{2+}$ and $Co(NH_3)_5Br^{2+}$ did not undergo reduction under these experimental conditions. These observations, which were quantitatively reproducible, are summarized in Table 2, and indicate that reduction of cobalt(III) takes place primarily through a conjugate base species, presumably $Co(NH_3)_4(NH_2)DMSO^{2+}$, which can be expected also to undergo substitution relatively rapidly (1, 2, 16).

[2] $Co(NH_3)_5DMSO^{3+} \rightleftharpoons Co(NH_3)_4(NH_2)DMSO^{2+} + H^+$

Reduction to cobalt(II) results in labilization of the cobalt center leading to ammonia release

[3] $Co(NH_3)_4(NH_2)DMSO^{2+} \rightarrow Co^{2+} + 5NH_3 +$ oxidized DMSO

which forces reaction 2 to the right and so is autocatalytic. The persistence of a small degree of cobalt(II) formation under acidic conditions when Cl^- or Br^- were present was significant only at the lower reaction temperatures, and it was shown that the presence of small amounts of cobalt(II) did not affect the rate of reaction 1.

In the light of these findings, all further rate measurements were carried out with the addition of acid. For the anation reactions (reaction 1, $Y^{n-} = Cl^-$ or Br^-, solvent = DMSO), plots of $\ln (A_\infty - A_t)$ *vs.* time t, where A_t is the optical absorbance at time t, were then linear over the first 50% reaction for $Y^{n-} = Br^-$ (later, A_t changed slightly *less* rapidly than the first order rate law required), and over the first 65–80% for $Y^{n-} = Cl^-$. Exposure to the room lighting did not affect the reaction rates. The anation reaction proceeded effectively to completion for $Y^{n-} = Cl^-$, so that the observed pseudo-first order rate coefficient k_{obs} equalled the anation rate coefficient k_{an}, but for $Y^{n-} = Br^-$, anation was not quite complete (*cf.* Table 1), and k_{obs} was the sum of k_{an} (which was directly estimable from the initial reaction rate, on the assumption of eventual complete reaction) and the reverse (solvolysis) rate coefficient, k_{sol}. These data are collected in Tables 3 and 4.

The values of k_{an} indicate limiting values k_i at 45 °C of approximately 1.4×10^{-4} s^{-1} for $Y^{n-} = Cl^-$ and, by interpolation, 4.2×10^{-5} s^{-1} for $Y^{n-} = Br^-$. The latter value is less than half that observed in the absence of added acid, which

Can. J. Chem. Downloaded from www.nrcresearchpress.com by 210.87.254.105 on 09/05/12
For personal use only.

TABLE 3. Pseudo-first order rate coefficients k_{obs}, k_{an}, and k_{sol} the formation of $Co(NH_3)_5Br^{2+}$ from $Co(NH_3)_5DMSO^{2+}$ and Br^- in DMSO

$[Co(NH_3)_5DMSO^{3+}]^a$ (mmol dm^{-3})	$[CH_3C_6H_4SO_3H]$ (mmol dm^{-3})	$[(C_2H_5)_4NBr]$ (mmol dm^{-3})	Temperature (°C)	$10^5k_{obs}{}^b$ (s^{-1})	$10^5(k_{an}+k_{sol})^c$ (s^{-1})	$10^5k_{sol}{}^d$ (s^{-1})
1.015	1.053	117.9	55.7	19.0 ±0.2		
				18.5 ±0.2		
			60.8	37.5 ±0.7		
			40.0	1.95±0.03		
			50.7	10 ±1.0		
		85.9		10.1 ±0.2	11.2±0.2	1.1
		57.6		9.01±0.2	10.3±0.2	1.3
		29.7		7.5 ±0.2	9.3±0.2	1.8
		19.0		5.6 ±0.1	7.4±0.2	1.8
		9.2		4.3±0.08	5.4±0.1	1.1

[a]As the perchlorate salt.
[b]From initial reaction rate, assuming 100% $Co(NH_3)_5Br^{2+}$ at infinite time.
[c]From plots of ln $(A_\infty - A_t)$ *vs.* t, using experimental A_∞; represents sum of forward (k_{an}) and back (k_{sol}) reaction rate coefficients.
[d]By difference.

TABLE 4. Pseudo-first order rate coefficients k_{obs} for the formation of $Co(NH_3)_5Cl^{2+}$ from $Co(NH_3)_5DMSO^{3+}$ and Cl^- in DMSO

$[Co(NH_3)_5DMSO^{3+}]^a$ (mmol dm^{-3})	$[CH_3C_6H_4SO_3H]$ (mmol dm^{-3})	Temperature (°C)	$[(C_2H_5)_4NCl]$ (mmol dm^{-3})	$10^5k_{obs}{}^b$ (s^{-1})
0.975	0.904	50.7	25.7	22.3
			20.0	23.8
		45.0	20.0	12.0
		39.2	20.0	4.1
		50.7	15.7	23.3
			11.6	18.0
			8.09	17.5
			4.93	10.9
2.50	2.51	45.1	49.9	13.9
	2.50		25.0	12.9
2.51			17.5	8.95
2.50	2.57		12.9	8.44
	2.50		12.5	7.89
			10.0	5.77
			7.50	4.56

[a]As the perchlorate salt.
[b]Experimental uncertainty ±2%.

indicates that a major portion of the bromide anation reaction proceeds via the conjugate base species of reaction 2 when no acid is added. The value of k_i for chloride anation is also slightly less than in the absence of added acid. The k_i data for $Y^{n-} = Br^-$ gave a linear Arrhenius plot with activation energy $E_a \sim 123$ kJ mol^{-1} (corresponding to $\Delta H_i^* = 121 \pm 3$ kJ mol^{-1}, $\Delta S_i^* = +51 \pm 9$ J K^{-1} mol^{-1}); the corresponding data for $Y^{n-} = Cl^-$ are not available because of the poor solubility of $[Co(NH_3)_5Cl]Cl_2$ at high $[Cl^-]$, but the temperature dependence of k_{obs} over a limited (10 °C) range at $[Cl^-] = 0.02$ mol dm^{-3} indicates $\Delta H_i^* \sim 126$ kJ mol^{-1}.

The solvent exchange reaction (Y^{n-} = solvent = DMSO in reaction 1) proceeded according to first order kinetics over 60–80% reaction, in the presence of added *p*-toluenesulfonic acid, and no cobalt(II) could be detected even after 10 half-lives of the exchange reaction. The values of the rate coefficients k_{ex} listed in Table 5 were obtained from the first order rate equation with a standard deviation of about 4% on the average, but reproducibility was about ±9%. Plots of ln k_{ex} against $1/T$ and against pressure P were linear within the experimental uncertainty; the relevant parameters and their standard errors are $\Delta H_{ex}^* = 123 \pm 2$ kJ mol^{-1}, $\Delta S_{ex}^* = 61 \pm 6$

Can. J. Chem. Downloaded from www.nrcresearchpress.com by 210.87.254.105 on 09/05/12
For personal use only.

Can. J. Chem. Downloaded from www.nrcresearchpress.com by 210.87.254.105 on 09/05/12
For personal use only.

TABLE 5. Pseudo-first order rate coefficients for the exchange of DMSO-d_6 between $Co(NH_3)_5DMSO\text{-}d_6^{3+}$[a] and DMSO-$h_6$ solvent in the presence of *p*-toluenesulfonic acid[b]

Temperature (°C)	Pressure (MPa)[c]	$10^5 k_{ex}$[d] (s^{-1})
55.7	0.1	$29._1$
50.7		$14._8$
45.0		6.3_5
35.0		1.3_8
45.0	50.7	5.1_4
	101.3	4.3_8
	202.7	2.9_3

[a]Concentration 0.39 ± 0.01 mol dm^{-3}.
[b]Concentration 0.41 ± 0.01 mol dm^{-3}.
[c]0.1 MPa = 1 bar = 0.9869 atm.
[d]Standard deviations typically ±4%; reproducibility, ±9%.

J K^{-1} mol^{-1}, and $\Delta V_{ex}^* = +10.0 \pm 1.2$ cm^3 mol^{-1}. The value of k_{ex} at 45 °C and 0.1 MPa is less than one-fifth of that reported by Reynolds *et al.* (8) for the same conditions but without added acid. This discrepancy is attributable to the incursion of the conjugate base pathway in Reynolds' experiments. The data of Table 2 indicate that it is $Co(NH_3)_5DMSO^{3+}$, and not $Co(NH_3)_5Cl^{2+}$ or $Co(NH_3)_5Br^{2+}$, which is susceptible to redox decomposition; accordingly, 'autocatalysis' of solvent exchange can be expected to be even more marked than that of anation, and it may be significant that Reynolds *et al.* (8) quote an unusually large experimental uncertainty (>20%) in k_{ex}.

Discussion

The strongly positive value of ΔV_{ex}^* leaves little doubt that Co—DMSO bond breaking is the rate determining process in the solvent exchange reaction (1), and hence consideration of the generalized reaction 1 in the light of the principle of microscopic reversibility, together with experience with other systems (12), leads to the expectation that the anation reactions will also proceed via an I_d mechanism in DMSO just as in water in the absence of interfering effects (see below). This inference receives strong support from the fact that ΔH_i^* for anation by bromide and (with less certainty) chloride, and ΔH_{ex}^* for the solvent exchange reaction, are the same within the experimental error, whereas they differ markedly for the analogous reactions of $Cr(DMF)_6^{3+}$ in DMF solvent, a system in which substitution evidently proceeds by an I_a mechanism (12). It would also seem that the reservations expressed in the Introduction and elsewhere (12), regarding the relative values of k_{ex} and the various k_i in an I_d mechanism in a solvent such as DMSO, are justified, since, at 45 °C, k_i for chloride anation exceeds k_{ex} for solvent exchange by a factor of 2.2 and the interpolated k_i for the larger anion, bromide (4.2×10^{-5} s^{-1}), by a factor of 3.3. Similar studies of reaction 1 with DMF as solvent, which we will report later, confirm that equality of ΔH_i^* and ΔH_{ex}^*, rather than a close interrelationship of k_i and k_{ex}, is characteristic of an I_d process.

The foregoing conclusions refer to reaction 1 in DMSO solvent to which acid has been added, and appear to answer the questions originally posed. Unfortunately, the fact that conjugate base and redox reactions can be important, while of interest in itself, obliges us to reexamine those simplistic conclusions.

Dimethylsulfoxide is somewhat more basic towards H^+ than is water, but much less acidic (17, 18), and accordingly its autoprotolysis constant is about 10^{-32} to 10^{-33} (18–21).[2] It is difficult to generalize about the strengths of electrically neutral acid molecules in DMSO, but it appears that the intrinsic basicity of the solvent, favoring ionization, is offset by the relatively low dielectric constant, so that most inorganic acids and organic oxyacids are somewhat less dissociated in DMSO than in water (20–24). Protonic cations such as $Co(NH_3)_5DMSO^{3+}$, however, should be more acidic in DMSO than in water, since the lower dielectric constant should *favor* proton release on the basis of electrostatics. In retrospect, therefore, it is not surprising that cobalt(III) ammine conjugate base formation (reaction 2) makes significant contributions to the kinetics of the anation and solvent exchange reactions in 'neutral' DMSO. These effects are absent from the $Cr(DMSO)_6^{3+}/DMSO/Y^{n-}$ system (25, 26), and, while recognizing that cobalt(III) is more susceptible to conjugate base effects than is chromium(III), one may reasonably suppose that the conjugate base of $Co(NH_3)_5DMSO^{3+}$ forms by deprotonation of an NH_3 ligand, rather than the DMSO, but an ambiguity does exist.

[2]The value of 5×10^{-18}, given by Kolthoff and Reddy (17), seems to be anomalous.

Can. J. Chem. Downloaded from www.nrcresearchpress.com by 210.87.254.105 on 09/05/12
For personal use only.

It is also clear from the data of Table 2 that the conjugate base species provides the main redox pathway, although reduction of the cobalt(III) center occurs to a minor extent in the presence of excess bromide or chloride ions. Neither $Co(NH_3)_5Cl^{2+}$ nor $Co(NH_3)_5Br^{2+}$ yielded cobalt(II), however; this shows that the reduction of the cobalt(III) center is effected by *coordinated* DMSO, although it was not possible to determine the ultimate fate of the DMSO ligand. Furthermore, the minor degrees of reduction of $Co(NH_3)_5DMSO^{3+}$ observed in the presence of free Cl^- or Br^- are not attributable to direct reduction of cobalt(III) by these halide anions. This latter possibility may also be discounted on the grounds that chloride is thermodynamically a poorer reductant than bromide, yet is at least as effective in promoting reduction of cobalt(III) ammines in DMSO.[3]

The reduction of cobalt(III) ammines by DMSO in the presence of Cl^- or Br^- is reminiscent of the catalysis by mildly reducing anions of topological changes in cobalt(III) complexes containing quadridentate or bidentate arsine ligands reported by Bosnich *et al.* (27, 28), who attribute this catalysis to the formation of a labile, transient, but undetected cobalt(II) intermediate. Similarly, catalysis of the aquation of cobalt(III) ammines through reduction to cobalt(II) by hydroxide ion has been invoked by Gillard (29) as an alternative to the now generally-accepted conjugate base mechanism (16). We have argued previously (30) against Gillard's proposal, partly on the basis of the complete lack of correlation of the catalytic power of various anions with their thermodynamic reducing power (as above), and indeed Gillard *et al.* have recently reported failure to detect any cobalt(II) intermediates in the base hydrolysis of $Co(NH_3)_5Cl^{2+}$ (31). Thus, although redox catalysis by halide ions of simple cobalt(III) substitutions has been suggested previously, there is no direct evidence that it actually occurs, and, conversely, where some reduction of cobalt(III) accompanies substitution, as in the present case, it does not follow that the substitution mechanism involves redox processes in any way. Indeed, the fact that k_i for $Y^{n-} = Cl^-$ is more than three times that for the stronger reductant Br^- in reaction 1 in DMSO is clear evidence against redox catalysis of substitution in these systems.

The observations that conjugate base formation (reaction 2) provides the most favorable pathway for redox (reaction 3), and that a numerical connection seems to exist between redox rates relative to anation within the different ion pairs,[3] suggest that halide ion catalysis of redox may operate through an *internal* conjugate base process within the ion pairs, since neither HBr nor HCl is completely dissociated in DMSO (22, 23). This process, a proton transfer from $Co(NH_3)_5DMSO^{3+}$ to the halide ion, would be similar in essence to that believed to occur in reactions of anions of weak acids with complex ions in water (1). It could also explain (16) why k_i for $\{Co(NH_3)_5DMSO^{3+}, Cl^-\}$ is more than twice k_{ex} for the free complex ion, and more than three times k_i for the bromide analog (HCl is at least 10 times weaker than HBr in DMSO (22)). The close similarity between ΔH_i^* for Cl^- and Br^- anation and ΔH_{ex}^* for solvent exchange, however, would seem to rule out this attractive alternative to the simple I_d mechanism, since ΔH^* values associated with internal conjugate base processes are much higher than for simple interchange processes, at least for water as solvent (1). Thus, the function of Cl^- and Br^- in promoting the redox reaction may involve nucleophilic attack of halide on the coordinated (and therefore polarized) DMSO molecule, much as the attack of iodide on doubly-protonated DMSO in acidic aqueous DMSO initiates redox processes (32).

In summary, although conjugate base phenomena and redox processes complicate the observation and interpretation of the kinetics of reaction 1, where the solvent is DMSO and Y^{n-} is Cl^-, Br^-, NCS^-, or DMSO itself, the substitution processes observed in the presence of

[3]At the same stoichiometric halide concentrations, chloride produces more cobalt(II) than does bromide (Table 2), but the yields of cobalt(II) are equal for the same extents of ion pairing of $Co(NH_3)_5DMSO^{3+}$ by Cl^- and Br^-. The data of Tables 3 and 4 relate to various ionic strengths, so that constant K_{IP} values (eq. 1) cannot be obtained from them, but we can say that ion pairing is (for example) 50% complete when $k_{obs} = 0.50k_i$. This occurs (at 50.7 °C) when $[Cl^-] \sim 5$ mmol dm^{-3}, or when $[Br^-] \sim 17$ mmol dm^{-3}, and Table 2 shows that the yields of cobalt(II) at these concentrations are the same (0.7–0.8%) within the experimental uncertainty. Anation within the ion pairs, however, is 3.3 times faster for Cl^- than Br^-, so that redox must be correspondingly faster in the chloride ion pair, since it ceases on completion of the anation reaction.

Can. J. Chem. Downloaded from www.nrcresearchpress.com by 210.87.254.105 on 09/05/12
For personal use only.

p-toluenesulfonic acid are evidently of the simple I_d type. The strongly positive ΔV_{ex}^* value, and the apparent equality of ΔH_{ex}^* with ΔH_i^*, support this.

Finally, in view of the large effect of conjugate base pathways on the rates of reaction 1 in DMSO, a check was made on the effect of added acid on the DMSO exchange rates reported by Lantzke and Watts (33) for *cis*-$Co(en)_2Cl(DMSO)^{2+}$. It was found that the exchange rates were virtually unaffected by the addition of acid in that case; the reasons for this contrast with solvent exchange between $Co(NH_3)_5DMSO^{3+}$ and DMSO may lie simply in a markedly lower acidity of the dipositive chelate complex relative to the tripositive ammine. In any event, it appears that our present findings do not detract from the usefulness of the extensive contributions of Watts' school (13, 33–37) and others (*e.g.*, 11) in this field, but future work should include routine checks for conjugate base and redox pathways.

Acknowledgment

We thank the National Research Council of Canada for financial support.

1. T. W. Swaddle. Coord. Chem. Rev. **14**, 217 (1974).
2. C. H. Langford and H. B. Gray. Ligand substitution processes. W. A. Benjamin, New York, N.Y. 1966.
3. L. A. De Oliveira, H. E. Toma, and E. Giesbrecht. Inorg. Nucl. Chem. Lett. **12**, 195 (1976).
4. W. L. Reynolds. Inorg. Chem. **14**, 680 (1975).
5. J. MacB. Harrowfield, A. M. Sargeson, B. Singh, and J. C. Sullivan. Inorg. Chem. **14**, 2864 (1975).
6. N. Rodriguez, E. Kremer, C. R. Piriz Mac-Coll, and L. Beyer. Z. Anorg. Allg. Chem. **412**, 59 (1975).
7. D. A. Buckingham, W. Marty, and A. M. Sargeson. Inorg. Chem. **13**, 2165 (1974).
8. W. L. Reynolds, E. S. Barber, and R. Crandell. Int. J. Chem. Kinet. **6**, 51 (1974).
9. W. L. Reynolds, M. Biruš, and S. Ašperger. J. Chem. Soc. Dalton Trans. 716 (1974); J. Chem. Soc. Chem. Commun. 822 (1973).
10. C. R. Piriz Mac-Coll and L. Beyer. Inorg. Chem. **12**, 7 (1973).
11. C. H. Langford and W. R. Muir. J. Am. Chem. Soc. **89**, 3141 (1967); Inorg. Chem. **7**, 1032 (1968).
12. S. T. D. Lo and T. W. Swaddle. Inorg. Chem. **15**, 1881 (1976).
13. I. R. Lantzke and D. W. Watts. Aust. J. Chem. **19**, 949 (1966).
14. W. E. Jones, L. R. Carey and T. W. Swaddle. Can. J. Chem. **50**, 2739 (1972).
15. A. I. Vogel. A textbook of quantitative inorganic analysis. 3rd. ed. Longmans, London. 1961.
16. F. Basolo and R. G. Pearson. Mechanisms of inorganic reactions. 2nd ed. J. Wiley and Sons, New York, N.Y. 1967. pp. 177–193.
17. I. M. Kolthoff and T. B. Reddy. Inorg. Chem. **1**, 189 (1962).
18. W. S. MacGregor. Ann. N. Y. Acad. Sci. **141**, 3 (1967).
19. L. N. Bykova and S. I. Petrov. Zh. Anal. Khim. **27**, 1076 (1972).
20. J. Courtot-Coupez and M. Le Demezet. C. R. Acad. Sci. Ser. C, **266**, 1438 (1968).
21. R. Stewart and J. R. Jones. J. Am. Chem. Soc. **89**, 5069 (1967).
22. C. McCallum and A. D. Pethybridge. Electrochim. Acta, **20**, 815 (1975).
23. R. L. Benoit and C. Buisson. Electrochim. Acta, **18**, 105 (1973).
24. C. D. Ritchie and R. E. Uschold. J. Am. Chem. Soc. **89**, 2752 (1967).
25. D. L. Carle and T. W. Swaddle. Can. J. Chem. **51**, 3795 (1973).
26. S. T. D. Lo and D. W. Watts. Aust. J. Chem. **51**, 491, 501 (1975).
27. B. Bosnich, W. G. Jackson, and S. B. Wild. Inorg. Chem. **13**, 1121 (1974).
28. B. Bosnich, W. G. Jackson, and J. W. McLaren. Inorg. Chem. **13**, 1133 (1974).
29. R. D. Gillard. J. Chem. Soc. A, 917 (1967).
30. W. E. Jones, R. B. Jordan, and T. W. Swaddle. Inorg. Chem. **8**, 2504 (1969).
31. I. G. Browning, R. D. Gillard, J. R. Lyons, and P. R. Mitchell. J. Chem. Soc. Dalton Trans. 373 (1974).
32. J. H. Krueger. Inorg. Chem. **5**, 132 (1966).
33. I. R. Lantzke and D. W. Watts. J. Am. Chem. Soc. **89**, 815 (1967); Aust. J. Chem. **20**, 35 (1967); **20**, 2623 (1967).
34. L. F. Chin, W. A. Millen, and D. W. Watts. Aust. J. Chem. **18**, 453 (1965).
35. W. R. Fitzgerald and D. W. Watts. Aust. J. Chem. **19**, 1411 (1966); J. Am. Chem. Soc. **90**, 1734 (1968).
36. W. R. Fitzgerald, A. J. Parker, and D. W. Watts. J. Am. Chem. Soc. **90**, 5744 (1968).
37. M. L. Tobe and D. W. Watts. J. Chem. Soc. 4614 (1962).

Optical spectra of electrons solvated in liquid ethers: temperature effects[1]

FANG-YUAN JOU AND GORDON R. FREEMAN
Chemistry Department, University of Alberta, Edmonton, Alta., Canada T6G 2G2

Received March 16, 1976

FANG-YUAN JOU and GORDON R. FREEMAN. Can. J. Chem. **54**, 3693 (1976).

The optical absorption band of electrons solvated in ethers has an approximately Gaussian shape on the low energy side of the absorption maximum. The high energy side is wider and has an approximately Lorentzian shape down to $A/A_{max} \approx 0.3$, then extends into a long tail to high energies. The energy at the absorption maximum E_{Amax} and the Gaussian and Lorentzian dispersion parameters g and l are reported as functions of temperature for electrons in diethyl ether (DEE), di-*n*-propyl ether (DPE), di-*n*-butyl ether (DBE), and tetrahydrofuran (THF). The values in eV of the parameters at 180 K are: $E_{Amax} = 0.76$ in THF, 0.67 in DEE, 0.65 in DPE and DBE; $l = 0.32$ in THF, DEE, and DPE, 0.39 in DBE; $g = 0.19$ in all the ethers. The temperature coefficients of E_{Amax} are $\sim -2 \times 10^{-3}$ eV/K, those of l are $-(1 \pm 1)10^{-4}$ eV/K, and those of g are $+4 \times 10^{-4}$ eV/K. The band becomes less asymmetrical as the temperature increases. To make progress in the theoretical treatment of solvated electron spectra attention should be focussed on the separate values of g and l and their temperature dependences; the width at half height $W_{1/2}$ thereby loses theoretical significance. The decadic molar absorbancy ϵ_{max} (M^{-1} cm^{-1}) is 2.9×10^4 in DEE and DPE, 2.6×10^4 in DBE, and 2.1×10^4 in THF. The oscillator strengths f are 0.7 in the *n*-alkyl ethers and 0.6 in THF. The value of E_{Amax} in *p*-dioxane is 0.1 eV greater than that in THF and about 0.2 eV greater than those in the open chain ethers. This agrees with a prediction based upon the relative mobilities of electrons in the ethers.

FANG-YUAN JOU et GORDON R. FREEMAN. Can. J. Chem. **54**, 3693 (1976).

La bande d'absorption optique des électrons solvatés dans l'éther possède une forme qui est approximativement Guassienne dans la région d'énergy au dessous le maximum d'absorption. Dans la région d'énergie au dessus le maximum d'absorption, la bande est plus large et possède approximativement une forme Lorentzienne jusqu'à $A/A_{max} \approx 0.3$ alors qu'elle se poursuit vers les fortes énergies sous forme de longue queue. On rapporte, en fonction de la température, l'énergie d'absorption maximum E_{Amax} et les paramètres de dispersion Gaussien et Lorentzien, g et l, des électrons dans l'éther éthylique (EDE), l'éther propylique (EDP), l'éther *n*-butylique (EDB) et le tétrahydrofuranne (THF). A 180 K, les valeurs des paramètres exprimées en eV sont: $E_{Amax} = 0.76$ dans le THF, 0.67 dans le EDE, 0.65 dans le EDP et EDB; $l = 0.32$ dans THF, EDE et EDP et 0.39 dans EDB; $g = 0.19$ dans tous les éthers. Les coefficients de température de E_{Amax}, l et g sont respectivement de $\sim -2 \times 10^{-3}$ eV/K, $-(1 \pm 1) \times 10^{-4}$ eV/K et $+4 \times 10^4$ eV/K. La bande devient moins asymétrique à mesure que la température augmente. Afin de faire des progrès dans le traitement théorique des spectres d'électron solvaté, on doit porter une attention particulière aux valeurs respectives de g et l ainsi qu'à leurs relations avec la température; la largeur à demi hauteur, $W_{1/2}$, perd alors de son importance théorique. L'absorbance molaire décadique, ϵ_{max} (M^{-1} cm^{-1}) est de 2.9×10^4 dans EDE et EDP, 2.6×10^4 dans EDB et de 2.1×10^4 dans le THF. Les forces de l'oscillateur f sont de 0.7 dans les éthers linéaires et de 0.6 dans le THF. La valeur de E_{Amax} dans le *p*-dioxane est de 0.1 eV plus grande que celle dans le THF et environ 0.2 eV plus grande que celles des éthers linéaires. Les résultats sont en accord avec la prédiction qui peut être faite en se basant sur les mobilités relatives des électrons dans les éthers.

[Traduit par le journal]

Introduction

It has recently been noted that there is a similarity between the thermal activation energy for electron migration in diethyl ether and the optical absorption energy of solvated electrons in that liquid (1). It therefore became desirable to measure the temperature dependence of the position and shape of the optical spectra of electrons in a number of ethers in which the mobilities had been determined. That was the main purpose of the present work.

The relatively low mobility of electrons in *p*-dioxane led to the prediction that the optical absorption energy of electrons in *p*-dioxane would be greater than that in diethyl ether (1).

[1]Assisted financially by the National Research Council of Canada.

Can. J. Chem. Downloaded from www.nrcresearchpress.com by 210.87.254.42 on 09/05/12
For personal use only.

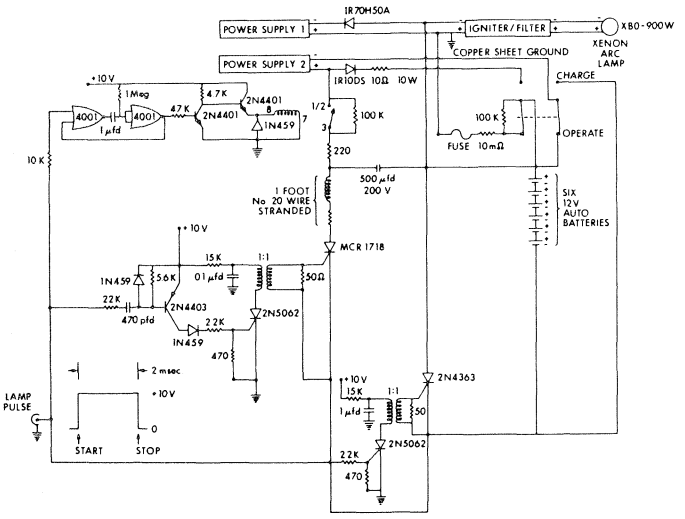

FIG. 1. Lamp power supply and pulser. Power supply 1 = Sorenson SRL-40-50, 40 V, 50 A. Power supply 2 = Power Designs Inc. model 105TA, 80–100 V; it is used in the silicon controlled rectifier turn-off circuit and to trickle charge the batteries. The fuse is four strands taken from #20 stranded wire, 10 cm long.

This is opposite to the relative values that would be expected on the basis of the dielectric constants of the liquids, which are respectively 2.2 and 4.4 at 293 K. The prediction has been fulfilled.

Experimental

Materials

The diethyl ether (DEE) was Mallinckrodt anhydrous analytical reagent grade; di-*n*-propyl ether (DPE) was Aldrich gold label (99+%); di-*n*-butyl ether (DBE) and tetrahydrofuran (THF) were BDH reagent grade; *p*-dioxane (PD) was Baker analyzed reagent (99.9%).

Lithium aluminum hydride powder was obtained from Ventron Corp. The potassium thiocyanate was Fisher certified reagent.

BDH dry sodium (99.8%) was cut into lumps and stored in Fisher certified grade *n*-hexane (99%). BDH potassium was removed from the liquid paraffin in which it was purchased, washed with *n*-hexane, placed in fresh *n*-hexane and the surface cut off, then placed in fresh *n*-hexane for 1 week. It was then placed in fresh hexane for another week before use.

Each ether was refluxed for at least 2 h over lithium aluminum hydride, under an atmosphere of ultrapure argon (Linde). The ether was then distilled under vacuum and the middle portion collected over freshly prepared sodium–potassium (~1:3 by volume) alloy. After magnetic stirring for 1 day with the alloy the ether was degassed by pumping for about 2 min on the liquid without previously cooling it. The required amount of ether was further degassed by distillation into a trap at 77 K, the exit side of which was continuously open to the high vacuum line. The sample was then distilled into a bulb at 77 K attached to the optical cell. Finally, the bulb was sealed with a flame after the gas pressure in the system had been reduced to 10^{-6} torr.

To minimize contamination of the system, glass blowing was done with nitrogen rather than with breath.

Apparatus and Technique

Pulses of 1.8 MeV electrons at a current of about 80 mA were obtained from a van de Graaff accelerator. The absorption band shapes were measured with 1.0 μs pulses, while 30 ns, 100 ns, and 1.0 μs pulses were used for $G\epsilon$ determination; G is the solvated electron yield (e^-_{solv}/100 eV) and ϵ is the decadic molar absorbancy (M^{-1} cm^{-1}).

Each pulse was measured by a secondary emission monitor connected to an integrator. The monitor was calibrated against dose received in the optical cell, using aqueous 5 mM KCNS saturated with oxygen as a dosimeter. It was assumed that $G((CNS)_2^-) = 2.8$ and ϵ_{480} nm = 7500 M^{-1} cm^{-1} (2–4). The dosimetry was corrected for the electron density of the samples.

The light source was a Xe arc (Osram XB0 900W) in an Oriel Optics Corp. model C-60-50 lamp housing. A Pyrex filter preceded the quartz collimating lens to remove light with $\lambda < 320$ nm. This prevented ozone formation in the room. The lamp was run at 650 W and pulsed to 15 kW for 2 ms when an absorption measurement was desired. The pulsing circuit is shown in Fig. 1.

Two Bausch and Lomb monochromator housings of type 33-86-25 were used with three different gratings, types 33-86-02 (400–800 nm), -03 (700–1200 nm), and -78 (1100–2300 nm). The light beam could be switched from one monochromator to the other by a moveable mirror. The gratings were calibrated with a He–Ne laser using $\lambda = n \times 632.8$ nm, n = 1, 2, 3, and the Xe lamp spectrum (peaks from 450 to 2100 nm). The light intensity reaching the detector was controlled by adjusting the

Can. J. Chem. Downloaded from www.nrcresearchpress.com by 210.87.254.42 on 09/05/12
For personal use only.

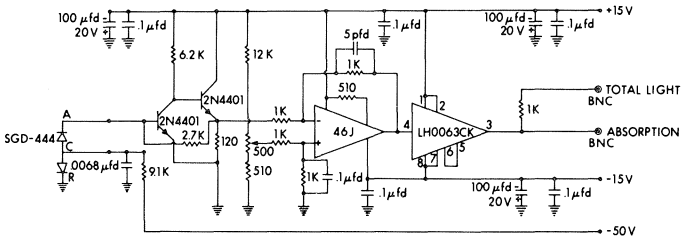

FIG. 2. Amplifier circuit for the visible light detector.

slits on the monochromator. The bandpass was 4 ± 1 nm for -02 and -03 gratings and 40 ± 10 nm for -78.

Appropriate filters were used to eliminate second order diffraction and stray light. For infrared measurements a Corning CS7-56 was always placed between the lamp and the cell. The filter placed in front of the monochromator was 7-56 for 1000–1500 nm, 7-56 plus 4-67 for 1500–1800 nm, 7-56 plus 4-71 for 1800–1900 nm, 7-56 plus 4-97 for 1900–2000 nm and 7-56 plus 4-72 for 2000–2250 nm. For visible light a filter was always placed in front of the monochromator, and in front of the lamp only for the lower temperature samples; CS 4-97 for 400–500 nm, 3-72 for 480–700 nm, and 2-64 for 700–1100 nm.

The infrared photocell was a Barnes Engineering A-10D/D10S InSb diode. It was cooled to 77 K in a Dewar having side view sapphire windows. The detector was used over the wavelength range 800–2300 nm. The amplifier had a gain of 2700 ohm/V, with a 40 ns rise time (10–90%) and a linear dynamic output range from 0 to 10 V. At each wavelength setting the incident light intensity was offset by a Tektronix 7A13 plug-in so that the output signal could be displayed on a Tektronix 7623 oscilloscope. The combined cell and amplifier rise time for 3 to 97% response was measured by Čerenkov emission from *n*-pentane to be 600 ns, independent of wavelength.

The silicon visible light detector covered the wavelength range 400–1100 nm. The system was the same as that described earlier (3), with a modification of the amplifier (Fig. 2) to accommodate the rapid increase of incident light from the pulsed lamp. The overall rise and fall times for 3 to 97% response of the detector, amplifier, and 7623 oscilloscope was 90 ns with 5 MHz band-width in the 7A13 plug-in.

Sample photographs of signals obtained with the two detector systems are shown in Fig. 3. The linearity of these systems was evaluated by measuring the I_0 dependence of the absorption of $(CNS)_2^-$ at 480 nm in a KCNS solution at 298 K, of e^-_{solv} at 1000 nm in pure water at 298 K, and of e^-_{solv} at 1600 nm in diethyl ether at 155 K. They were linear within the 2% average error of the light input, from 0.1 to 5.0 V for the visible detector and from 0.1 to 2.5 V for the ir detector.

The optical cell holder and low temperature bath were similar to those described earlier (3) with the following modifications. The Styrofoam walls were 5 cm thick. The 'window' for the entrance of the electron beam was a 3 cm deep pit in the outside of one of the walls. Warmed air was blown on the outsides of the electron and optical windows to keep them frost free. The copper–constantan thermocouples were calibrated using liquid nitrogen (77 K), "pasty slushes (5)" of *n*-pentane (142 K), toluene (178 K), and *n*-octane (117 K), as well as ice/water (273 K) and boiling water (372.6) K.

The optical slit in the cell holder was adjusted so that the transmitted beam excluded light that had penetrated the irradiated front face of the cell.

The sample cells were made of Spectrosil. The optical path lengths used were 15 mm for $400 < \lambda < 1650$ nm and 3 mm for $800 < \lambda < 2300$ nm.

Physical Properties of the Liquids

The densities d (6) and dielectric constants D_s (1, 7) of the liquids were taken from the references indicated. The normal melting point of THF is approximately 165 K, in agreement with that reported in ref. 8; the value 208 K recorded in refs. 6 and 9 is wrong.

Results

Spectrum Shape, Temperature Dependence

Optical absorption maxima could only be measured with confidence when they fell at wavelengths $\leq 2.1\ \mu m$ ($E_{Amax} \geq 0.6$ eV). In all the ethers this occurred only at temperatures below room temperature. The optical spectra of

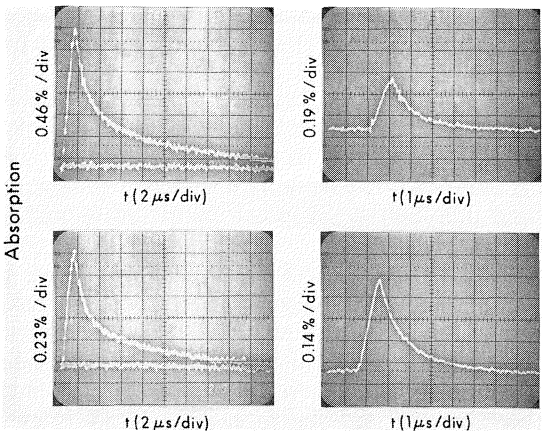

FIG. 3. Examples of absorption signals obtained with the ir (*a*, *c*) and visible light (*b*, *d*) detectors. Di-*n*-butyl ether at 177 K: (*a*) λ = 1950 nm; (*b*) λ = 995 nm. Di-*n*-propyl ether at 298 K: (*c*) λ = 1003 nm; (*d*) λ = 1000 nm.

Can. J. Chem. Downloaded from www.nrcresearchpress.com by 210.87.254.42 on 09/05/12
For personal use only.

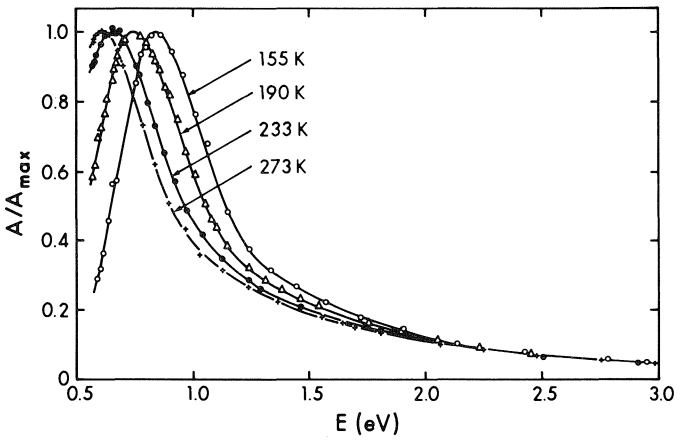

FIG. 4. Effect of temperature on the optical absorption spectrum of liquid THF after a 1.0 μs pulse of 1.8 MeV electrons. Normal melting point = 165 K.

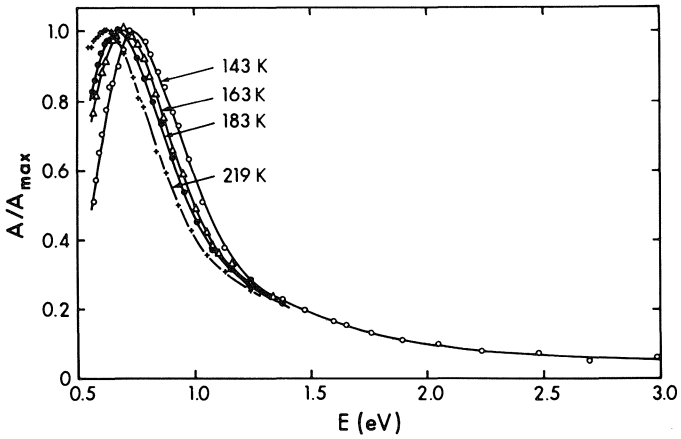

FIG. 5. Effect of temperature on the optical absorption spectrum of liquid DEE after a 1.0 μs pulse of 1.8 MeV electrons. Normal melting point = 157 K.

solvated electrons were therefore measured at the temperatures ranging from that at which $\lambda_{Amax} \approx 2.1$ μm down to the supercooled liquid. When the sample froze light was not transmitted, and this limited the lowest temperature studied for each ether.

Spectra obtained for solvated electrons in THF are shown in Fig. 4. The absorption maximum falls at 0.61 eV at 273 K and shifts to 0.84 eV in the supercooled liquid at 154 K. The main body of the band is moderately skewed towards high energy and the high energy tail is even longer than one would expect from the skew of the peak.

The spectra of solvated electrons in the liquids DEE, DPE, and DBE (Figs. 5–7) are similar to that in THF. The energies at the absorption maxima at a given temperature occur at lower energies than in THF.

At the higher temperatures where the observed decay was first order, the absorption A_{obs} at the end of a pulse was corrected for decay during the pulse using [1].

$$[1] \qquad A_c = A_{obs} k t_p / [1 - \exp(-k t_p)]$$

where A_c is the corrected absorbance, t_p is the pulse duration time, and $k = (0.69/t_{1/2})$ is the decay constant. The correction was negligible for $t_p = 100$ ns and was normally $<20\%$ for $t_p = 1.0$ μs.

At absorption energies >1.7 eV ($\lambda < 700$ nm) the signal half-life increased with increasing

Can. J. Chem. Downloaded from www.nrcresearchpress.com by 210.87.254.42 on 09/05/12
For personal use only.

Can. J. Chem. Downloaded from www.nrcresearchpress.com by 210.87.254.42 on 09/05/12
For personal use only.

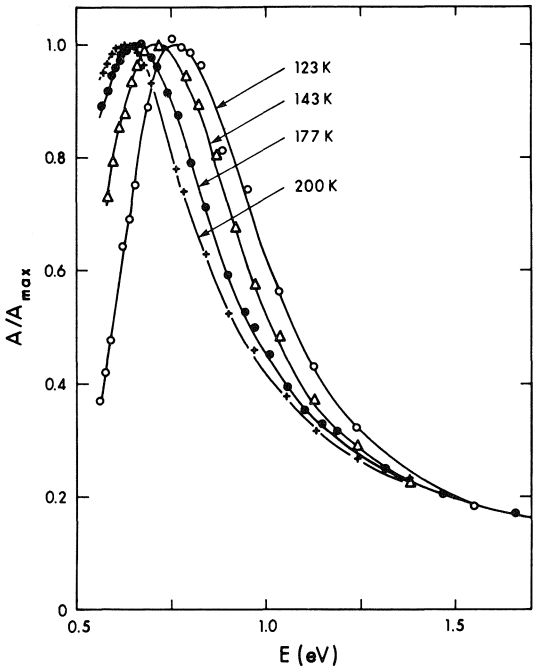

FIG. 6. Effect of temperature on the optical absorption spectrum of liquid DPE after a 1.0 μs pulse of 1.8 MeV electrons. Normal melting point = 151 K.

energy (Fig. 8). This indicates that other species such as radicals or ions contribute to the absorption at high energies. It was assumed that the solvated electron absorption decays at the same rate at all wavelengths under the present conditions of temperature and time scale. The absorbance at high energies due to solvated electrons was calculated from [2]:

$$[2] \qquad A^{\lambda}(e^{-}_{solv}) = 2(A^{\lambda}_{obs} - A^{\lambda}_{1/2})$$

where $A^{\lambda}_{1/2}$ is the absorbance at wavelength λ at a time equal to the half-life at $\lambda = 1.0\,\mu$m ($E = 1.24$ eV). Figure 9 illustrates the shape of [2] for THF at 174 K.

The energy at the band maximum E_{Amax} and the width at half height $W_{1/2}$ were determined from a least-squares fit of Lorentzian and Gaussian shape equations to the measured absorbance A (10). Convenient forms of these equations for curve fitting are [3] and [4].

Lorentzian,

$$[3] \quad A/A_{max} = \{1 + [(E - E_{Amax})/l]^2\}^{-1} \qquad E > E_{Amax}$$

Gaussian,

$$[4] \quad \ln (A/A_{max}) = -[(E - E_{Amax})/g]^2 \ln 2 \qquad E < E_{Amax}$$

where A_{max} is the maximum absorbance and l and g are the portions of the width at half-height on the Lorentzian and Gaussian sides, respectively. In curve fitting, [3] and [4] were treated separately, using A_{max}, l, and g as variables and E_{Amax} as an adjustable parameter. The degree to which [3] and [4] fit the spectra is illustrated in Fig. 9. The main peak portion is satisfactory, but the high energy tail is longer than predicted by the Lorentzian. In determining l, only experimental values $(A/A_{max}) > 1/3$ were used.

The temperature dependences of E_{Amax}, l, g,

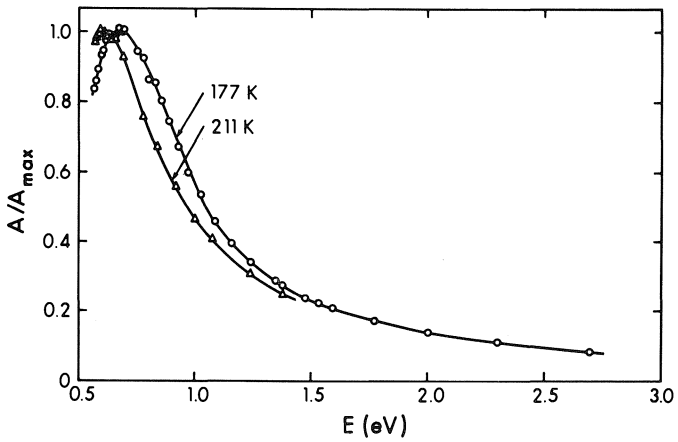

FIG. 7. Effect of temperature on the optical absorption spectrum of liquid DBE after a 1.0 μs pulse of 1.8 MeV electrons. Normal melting point = 178 K.

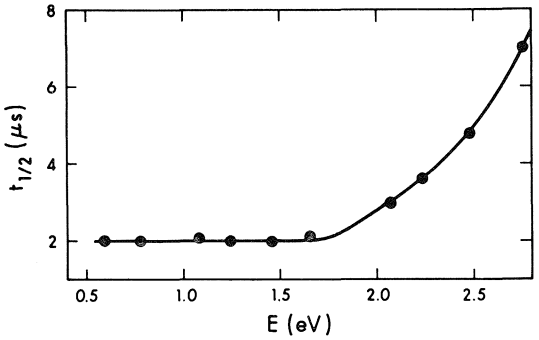

FIG. 8. Decay half life of optical absorption signal in THF at 174 K, as a function of photon energy.

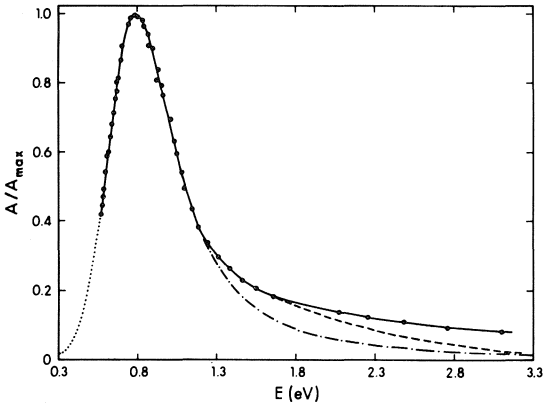

FIG. 9. Normalized optical absorption spectrum of liquid THF at 174 K after a 1.0 μs pulse of 1.8 MeV electrons. ○, experimental; --- eq. 2; -·-·-, eq. 3; ··· eq. 4.

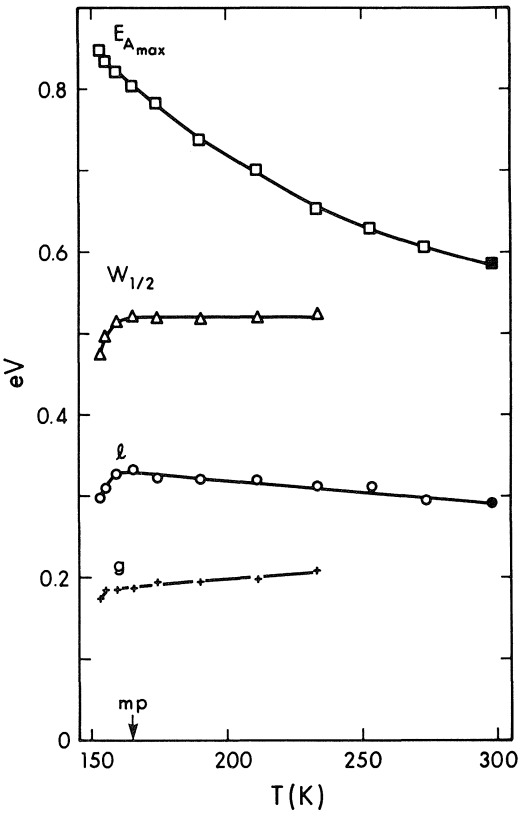

FIG. 10. Variation of E_{Amax}, $W_{1/2} = (l + g)$, l and g with temperature in THF. The filled points are data from ref. 10.

and $W_{1/2} = (l + g)$ in THF are shown in Fig. 10. The values of E_{Amax} and l from ref. 9 are included. The value of E_{Amax} increases somewhat more than linearly with decreasing temperature; the average rate over the range is -1.8×10^{-3} eV/deg. The value of l in the normal liquid increases slightly with decreasing temperature, while g decreases at about the same rate. The temperature independence of $W_{1/2}$ therefore appears to be accidental. The decrease of l, and hence of $W_{1/2}$, in the supercooled liquid might be due to glass formation.

The temperature dependences of the solvated electron spectrum parameters in the open chain ethers were similar to those in THF (Fig. 11). The values of g in all the liquid ethers at a given temperature are the same within ± 0.01 eV (Figs. 11 and 12). The values of l are nearly equal in THF, DEE, and DPE, but are 0.06 eV larger in DBE. The spectra were remeasured in DBE and the large l is real. The values of E_{Amax} in THF are about 0.1 eV greater than those in DEE; the latter are 0.02 eV larger than those in DPE and DBE.

The change in the temperature dependence of l in DPE at $T \leq 120$ K (Fig. 11) might be due to glass formation. Curiously, the change is in the opposite direction to that in THF.

$G\epsilon_{max}$, Time Dependence

The value of $G\epsilon_{max}$ was estimated indirectly. The absorption maximum of electrons solvated in ethers lies in the ir. The response time of the ir detector circuit was 600 ns, whereas that of the visible light detector circuit was 90 ns. The ir detector response characteristics and the electron decay times were independent of wavelength over the time and wavelength regions concerned. The ratio $A_{max}/A_{1.0\,\mu m}$ was measured over as

Can. J. Chem. Downloaded from www.nrcresearchpress.com by 210.87.254.42 on 09/05/12
For personal use only.

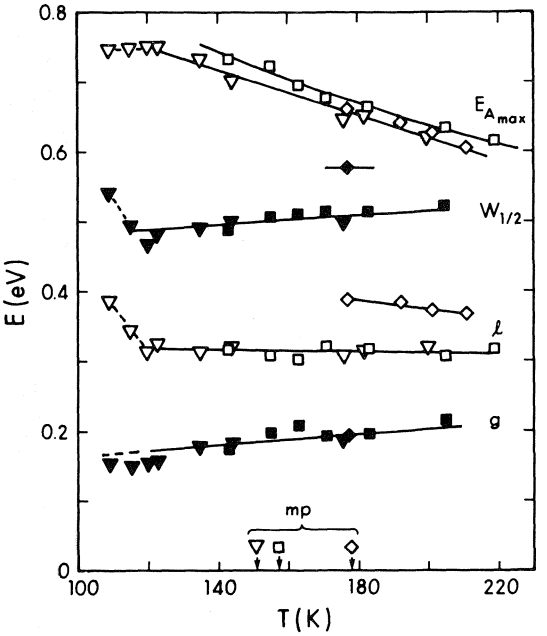

FIG. 11. Variation of E_{Amax}, $W_{1/2} = (l + g)$, l and g with temperature in DEE (□), DPE (▽), and DBE (◇).

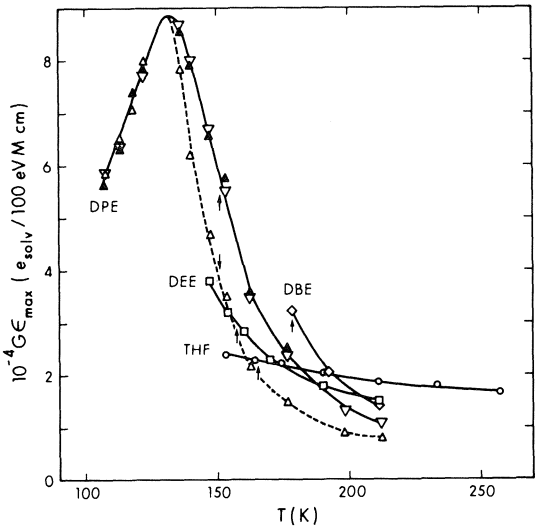

FIG. 12. Temperature dependence of $G\epsilon_{max}$ for solvated electrons in liquid ethers. For DPE 30 ns (▲), 100 ns (▽), and 1.0 μs (△) radiation pulses were used, while for the other ethers the pulse length was 100 ns. At low temperatures where ϵ increased with time, the maximum value of ϵ was chosen. The arrows mark the normal melting points. It was not possible to supercool DBE.

wide a temperature range as possible in each ether. The value of $G\epsilon_{1.0\ \mu m}$ at the end of the 100 ns pulse was then measured with the visible light detector and multiplied by $A_{max}/A_{1.0\ \mu m}$ to obtain $G\epsilon_{max}$. The value of $G\epsilon_{max}$ increases with decreasing temperature in each ether, but goes through a maximum in supercooled DPE (Fig. 12). The maximum might indicate glass formation at the lowest temperatures.

Values of $G\epsilon_{max}$ in DPE were similarly determined for 30 ns and 1.0 μs pulses. The former were essentially the same as those at 100 ns, due to the 90 ns response time of the visible light detector circuit. The 1.0 μs pulses gave lower values of $G\epsilon_{max}$ at $T > 130$ K; at $T < 130$ K the values were the same (Fig. 12), which further indicates a solvent structural change with greatly increased viscosity at about 130 K.

The difference between the 100 ns and 1.0 μs curves in Fig. 12 reflects the amount of geminate neutralization that occurred during the 900 ns time interval (11). The relative amounts of decay that occur on a microsecond timescale after a 100 ns pulse in DPE at different temperatures are shown in Fig. 13. First order plots (log A against t) of these traces and of others taken at slower sweep speeds were similar to those in ref. 11. A relatively rapid initial decay portion corresponds to geminate neutralization of solvated electrons, and the longer, first order tail of the decay represents reaction of the 'free ion' solvated electrons (11). An initial rapid decay was barely discernable in DPE at 298 K, so geminate neutralization was nearly complete in 100 ns. The portion of geminate electrons observable at 100 ns increased with decreasing temperature and dominated the measurements at $T < 212$ K; in Fig. 13 the free ion portion corresponds to $A \leq 5 \times 10^{-4}$ at $t = 0$ at all temperatures. The rate of geminate neutralization decreases with temperature due to the decreasing mobilities of the ions and electrons (1).

Spectrum Shift with Time

The rounding of the left shoulders of the traces for $T < 150$ K in Fig. 13 signifies a shift of the absorption spectrum with time. Spectra measured in DPE at 109 K at different times after 1.0 μs pulses are shown in Fig. 14. The absorbance grows at $E > 0.62$ eV and diminishes at lower photon energies. The spectrum parameters are listed in Table 1.

When no optical filter was placed in front of the cell, absorption on the low energy side of

Can. J. Chem. Downloaded from www.nrcresearchpress.com by 210.87.254.42 on 09/05/12
For personal use only.

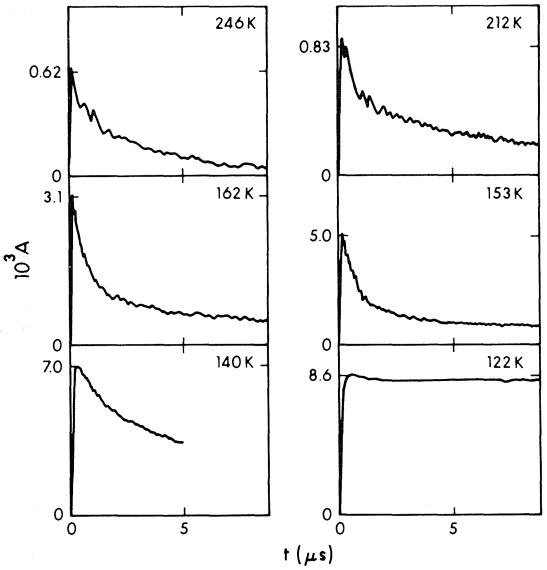

FIG. 13. Oscilloscope traces of optical absorbance of electrons solvated in DPE during and after a 100 ns pulse of 1.8 MeV electrons (1.5×10^{16} eV/g). Wavelength = 1.0 μm; visible light detector; optical path length = 1.5 cm.

the spectrum was larger than that shown in Fig. 14; electrons were being photoexcited out of deeper traps and relocalized in shallower traps.

Shifting of the spectrum in DPE took place during 20 μs at 123 K and 150 μs at 115 and 108 K, although nearly all of the shift occurred during the first 30% of the stated period.

Para-dioxane

It was not possible to measure the optical spectrum of solvated electrons in pure liquid PD, because the freezing point is high (12 °C) and the free ion yield is low (0.08 (1)). Therefore, PD was added to THF and the spectrum shift was measured relative to the spectrum in THF; PD shifted the spectrum to higher energy. A plot of E_{Amax} against volume % of PD is shown in Fig. 15. Although extrapolation to pure PD might not give accurate results, a similar plot for electrons in ethylenediamine/hexamethylphosphoric triamide solutions was linear (12). Thus the optical absorption energy of electrons in PD is 0.1 eV greater than that in THF, which is in turn greater than those in the open chain ethers. These results agree with the prediction based upon the relative mobilities of electrons in the ethers (1).

Discussion

Spectrum Shape, Temperature Dependence

The skew of the absorption band towards high energies is reasonably interpreted by bound-continuum transitions (13–15). Lugo and Delahay (14) proposed the relation 5 for the high energy tail, based upon a hydrogen-like model of photoionization.

$$[5] \qquad A/A_{\text{max}} \propto E^{-8/3}$$

Figure 16 displays plots of A/A_{max} against $E^{-8/3}$

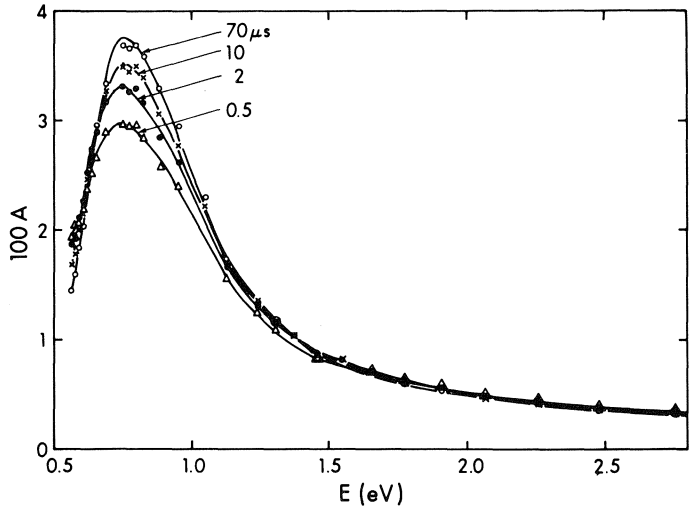

FIG. 14. Optical absorption spectra of localized electrons in DPE at 109 K at different times after 1.0 μs pulses of 1.8 MeV electrons (1.3×10^{17} eV/g). Absorbance normalized to 0.3 cm optical path length.

Can. J. Chem. Downloaded from www.nrcresearchpress.com by 210.87.254.42 on 09/05/12
For personal use only.

Can. J. Chem. Downloaded from www.nrcresearchpress.com by 210.87.254.42 on 09/05/12
For personal use only.

TABLE 1. Change of e^-_{solv} optical spectrum parameters with time in DPE at 109 K after a 1.0 μs generative pulse

t (μs)	E_{Amax} (eV)	$W_{1/2}$ (eV)	l (eV)	g (eV)*	l/g
0.5	0.74	0.64	0.42	0.22	1.9
2	0.74	0.59	0.40	0.18	2.2
10	0.74	0.56	0.39	0.17	2.3
70	0.75	0.52	0.37	0.15	2.4

*Several forms of Gaussian function are in frequent use. The form [4] is convenient in the discussion of Gaussian–Lorentzian band shapes because the sum of g and l equals the band width at half height. More frequently used forms in other areas are (17, 18):

$$\ln F = -[(E - E_0)/\sigma_1]^2$$

and

$$\ln F = -[(E - E_0)^2/2\sigma_2^2]$$

The relationship between the dispersion parameters are $\sigma_1 = 1.41\sigma_2 = 1.20g$.

for electrons solvated in DEE at three temperatures. The behavior is distinctly nonlinear at 143 K, but the extent of deviation from linearity decreases with increasing temperature. The same trend occurred in the other ethers. The significance of the change in band shape with temperature is not known. The decrease of the average slope with increasing temperature is due to the shift of E_{Amax}.

We do not take the lack of linearity in Fig. 16 to support the suggestion (16) that excitation to higher states beyond $2p$ is unlikely. It would have been surprising if structures as complex as solvated electrons had been accurately described by a hydrogen-like model.

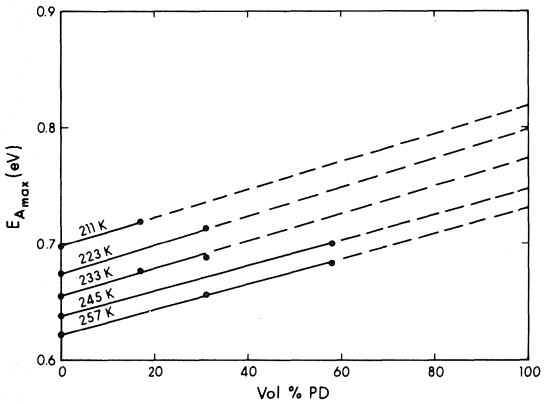

FIG. 15. Energies of optical absorption maxima for solvated electrons in liquid THF–PD solutions at different temperatures. The maximum concentration of PD attainable at a given temperature was limited by the freezing of the solution.

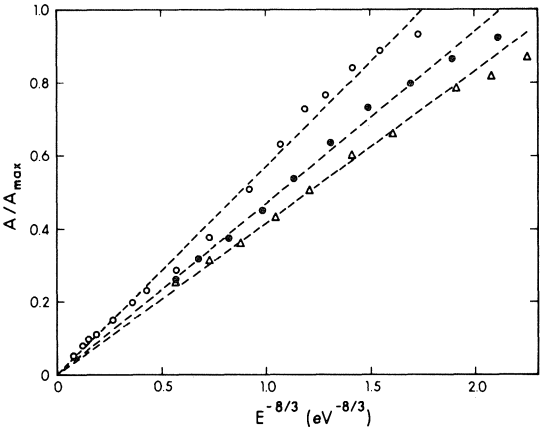

FIG. 16. Plot of A/A_{max} against $E^{-8/3}$ for the high energy side of the absorption spectrum of electrons solvated in DEE. Temperature: ○, 143 K; ●, 183 K; △, 219 K. The long-lived contribution to the absorbance at high energies ($E^{-8/3} < 0.3$) was removed using [2].

The Gaussian shape of the low energy side of the absorption band might reflect a random distribution of trap depths. The full width of the Gaussian distribution at half height is $2g$, which represents about two thirds of $W_{1/2}$ (Figs. 10 and 11). The distribution of trap depths could therefore account for the main portion of the band width. The values of g in all the liquid ethers are satisfactorily represented by [6].

$$[6] \qquad g = 0.12 + 4 \times 10^{-4}T \text{ eV}$$

The increase of g with temperature is attributed to thermal agitation of the ground and excited energy levels of solvated electrons, changes in the ground levels being the greater. The temperature coefficient in [6] corresponds to about four times Boltzmann's constant.

The magnitude of g is similar to that of the thermal energy fluctuations (17, 18) in systems comprised of several molecules in the liquid at 100–300 K. However, the two quantities are not the same. Thermal fluctuations extrapolate to zero at $T = 0$, whereas g does not (eq. 6). The constant term on the right hand side of [6] may be attributed to an irreducible structure.

The temperature dependence of l tends to be of the opposite sign to that of g, and smaller. The values of l in the liquids DEE, DPE, and THF are described by [7].

$$[7] \qquad l = (0.34 \pm 0.02) - (1 \pm 1)10^{-4}T \text{ eV}$$

The larger values of l in DBE may be due to a

Can. J. Chem. Downloaded from www.nrcresearchpress.com by 210.87.254.42 on 09/05/12
For personal use only.

structure effect caused by the large butyl groups. This type of effect will be sought in other systems.

The changes in g and l mean that the band becomes less asymmetrical as the temperature increases.

By focussing attention on the separate values of g and l, that of $W_{1/2}$ loses theoretical significance. Attempts to theoretically interpret $W_{1/2}$ as a unit have been unsatisfactory and should be abandoned. We encourage theoreticians to try to explain the values of g and then l.

The variation of E_{Amax} with temperature is nonlinear when the temperature range is great enough. The values for electrons in THF (Fig. 10) correspond to [8].

$$[8] \quad E_{\text{Amax}} = 1.51 - 5.7 \times 10^{-3}T + 8.7 \times 10^{-6}T^2 \text{ eV}$$

For DEE (Fig. 11) one has

$$[9] \quad E_{\text{Amax}} = 1.10 - 3.2 \times 10^{-3}T + 4.5 \times 10^{-6}T^2 \text{ eV}$$

which is quite well represented by the linear equation [9′] (19) over the experimental temperature range.

$$[9'] \quad E_{\text{Amax}} \approx 0.96 - 1.6 \times 10^{-3}T \text{ eV}$$

For the liquids DPE and DBE the results in Fig. 11 follow [10].

$$[10] \quad E_{\text{Amax}} = 0.94 - 1.6 \times 10^{-3}T \text{ eV}$$

Current theoretical models for the interpretation of E_{Amax} (20) are sufficiently crude and flexible that they agree readily with experiment. Further work should await satisfactory explanation of the values of g and l.

Solvated electrons in radiolysis systems are formed by the localization of de-energized electrons. After the initial localization of an electron in a potential fluctuation in the liquid, molecular polarization and rearrangement occur about the charge center. These processes alter the energy levels of the electron, hence its optical absorption spectrum. In low temperature alcohols (21), spectra generated by 10 ns pulses of radiation decay rapidly in the infrared and grow in the blue. Although the present equipment had a time resolution of only 90–600 ns, spectral shifts were observed for electrons in low temperature ethers (Fig. 14 and Table 1). Both l and g decrease as the spectrum approaches its equilibrium position. The decrease of g represents deepening of the shallower traps by the polarization processes. Although g decreases more than l, the decrease in l and the constancy of E_{Amax} (Table 1) are not understood. The narrowing of the band indicates that the environment of the electrons becomes more uniform.

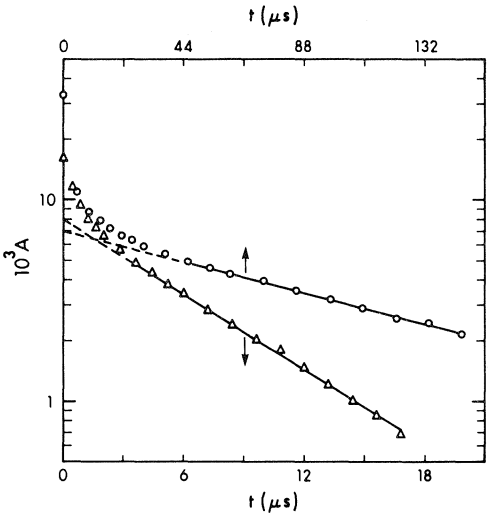

FIG. 17. First order plots of optical absorbance decay at 1.0 μm in DPE at 153 K (○) and 176 K (△). The linear tails were extrapolated to zero time to obtain absorbances equivalent to the free ion yields. Time was measured from the end of the 1.0 μs radiation pulse.

$G\epsilon_{max}$ and ϵ_{max}

Optical measurements give values of $G\epsilon$. An independent value of G is needed to obtain ϵ. To this end the contributions of the 'free ion' and 'geminate' solvated electrons were distinguished kinetically.

The solvated electrons react with geminate cations and with impurities. The geminate reaction does not follow a simple order (22), but when it is complete what remains is a pseudo first order reaction between 'free ion' solvated electrons and impurities (Fig. 17). The first order portion was extrapolated to zero time to obtain the absorbance equivalent to the free ion yield. Values of $G_{\text{fi}}\epsilon_{\text{max}}$ so obtained are listed in Table 2. The free ion yields have previously been measured by the charge clearing method (1), so the molar absorbancy ϵ_{max} of e^-_{solv} in the ethers can be determined. Values lie in the region 2–3 $\times$ 10^4 M^{-1} cm^{-1}, which is between those for electrons in ammonia (23) and water (24, 25). The data are summarized in Table 2.

Values of ϵ_{max} for electrons in a number of

TABLE 2. Optical absorbancy ϵ_{max} and oscillator strength f of e^-_{solv} in liquid ethers

Ether	T (K)	$G_{fi}\epsilon_{max}$	G_{fi}*	ϵ_{max} (10^3 M^{-1} cm^{-1})	f
DEE	160	15 700	0.58	27	0.71
	170	14 500	0.57	27	
	190	17 500	0.54	30	
	211	16 100	0.51	32	
				Ave. 29 ± 2	
DPE	140	6 300	0.21	29	0.70
	153	7 200	0.22	33	
	176	7 400	0.23	32	
	212	6 300	0.26	24	
				Ave. 29 ± 3	
DBE	178	5 800	0.21	28	0.70
	192	5 300	0.21	25	
	211	5 500	0.22	25	
				Ave. 26 ± 1	
THF	174	15 200	0.68	22	0.60
	190	14 700	0.68	22	0.59
	211	13 800	0.72	19	0.56
				Ave. 21 ± 1	
NH_3†	203–240			48 ± 2	0.66 ± 0.03
H_2O‡§	269–363			19 ± 1	0.75 ± 0.02
CH_3OH§	176–423			10	0.47
C_2H_5OH§	161–418			9	0.49

*Reference 1.
†Reference 23.
‡Values for $G_{fi}\epsilon_{max}$ are from ref. 24 and of $G_{fi} = G(F^-)/6$ in 1 mM SF_6 from ref. 25.
§Reference 3. We have removed the correction for the internal field of the solvent, because its true value is uncertain (30).

ethers at room temperature were reported earlier (10), but the value used for G_{fi} was only given for THF. A meaningful comparison can therefore only be made for that ether. The value of $G_{fi}\epsilon_{max}$ in THF was 15 600 M^{-1} cm^{-1} (10), similar to that found in the present work (Table 2). The authors (10) chose the value $G_{fi} = 0.39$, estimated by applying the Schuler equation to the optical absorption of the pyrenide ion in pulse irradiated pyrene solutions. They disfavored $G_{fi} = 0.69$ obtained from the nitrogen yields in nitrous oxide solutions (26). The charge clearing method (1) favors the latter value, which would have given $\epsilon_{max} = 2.3 \times 10^4$ M^{-1} cm^{-1} in agreement with that in Table 2. It appears that the molar extinction coefficients (absorbancies) and oscillator strengths listed in Table 1 of ref. 10 are too high.

The oscillator strength f can be estimated from [11] (27).

$$[11] \qquad f = 3.5 \times 10^{-5} \int \epsilon_E dE$$

where ϵ_E (M^{-1} cm^{-1}) is the decadic molar absorbancy at photon energy E (eV). The previously applied (3) correction for the internal field due to polarization of the solvent molecules surrounding the absorber (28) is apparently not adequate (27, 29, 30). Equation 11 is recommended when an accurate empirical equation is not available (30). However, values of f estimated from [11] may be wrong by 20–30% (29, 30), which reduces their usefulness as quantities for comparison with theoretical calculations.

Curves similar to those in Figs. 5–8 were extrapolated to zero absorbance by using the Gaussian equation on the low energy side and by linear extrapolation to $A = 0$ at $E = 4.0$ eV on the high energy side. Integration under the curves, then multiplying the results by 3.5×10^{-5} ϵ_{max} gave $f = 0.7$ for the open chain ethers and 0.6 for THF. The values are similar to those obtained in other polar solvents (Table 2).

The maximum yield of solvated electrons observed was that in DPE at 135 K; it reached $G(e^-_{solv}) = 3.0$. The decrease in yield at $T < 135$ K was probably due to geminate neutralization occurring before solvation. Similar observations have been made in 1-propanol (31). It would be valuable to know whether, with a much shorter resolution time, higher values of $G(e^-_{solv})$ than 3.0 could be observed at $T > 135$ K.

Can. J. Chem. Downloaded from www.nrcresearchpress.com by 210.87.254.42 on 09/05/12
For personal use only.

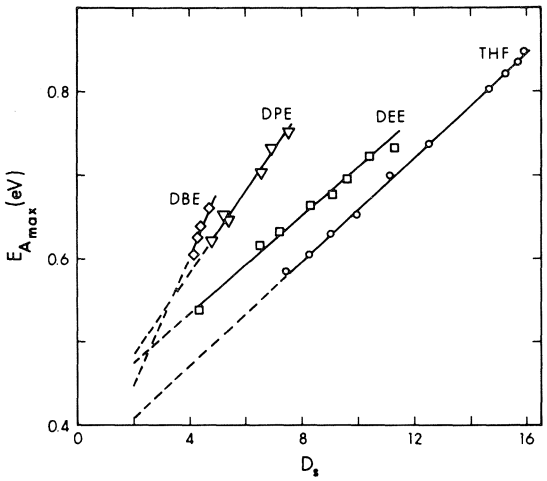

FIG. 18. Plots of E_{Amax} against the static dielectric constant D_s. The dielectric constant of each ether was changed by changing the temperature.

Variation of E_{Amax} with Static Dielectric Constant D_s

As the temperature of each ether decreases its dielectric constant increases. Plots of E_{Amax} against D_s are shown in Fig. 18. The optical transition energy increases roughly linearly with D_s in each ether, but the lines do not coincide. For a given D_s the value of E_{Amax} increases in the order THF < DEE < DPE < DBE. This reflects the influence of solvent structure upon solvated electron energy levels (32).

The dielectric constants of *n*-alkanes are about 2. Extrapolation of the ether curves to $D_s = 2$ (Fig. 18) indicates that electron excitation energies in *n*-alkanes should be 0.1–0.2 eV smaller than those in the ethers. This agrees with deductions based upon the relative mobilities of electrons in the liquids (18).

PD is anomalous because it contains internally cancelling dipoles. Assuming that the oxygen atom is the negative end of a dipole in ether, the CH_2 groups in PD will be more positive than the C_2H_5 groups in DEE. One can therefore imagine a deeper trap in liquid PD than in DEE.

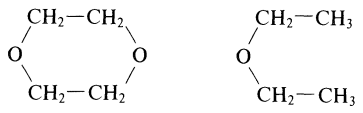

PD DEE

Acknowledgement

We are grateful to the personnel of the Radiation Research Center for aid with the electronics.

1. J.-P. DODELET and G. R. FREEMAN. Can. J. Chem. **53**, 1263 (1975).
2. J. H. BAXENDALE, P. L. T. BEVAN, and D. A. STOTT. Trans. Faraday Soc. **64**, 2389 (1968).
3. K. N. JHA, G. L. BOLTON, and G. R. FREEMAN. J. Phys. Chem. **76**, 3876 (1972).
4. G. L. BOLTON, K. N. JHA, and G. R. FREEMAN. Can. J. Chem. **54**, 1497 (1976).
5. R. E. RONDEAU. J. Chem. Eng. Data, **11**, 124 (1966).
6. R. W. GALLANT. Physical properties of hydrocarbons. Vol. 2. Gulf Publishing Co., Houston, Texas. 1970.
7. M. SZWARC. Carbanions, living polymers and electron transfer processes. Interscience, New York. 1968. pp. 161–162.
8. R. T. MORRISON and R. N. BOYD. Organic chemistry. 2nd ed. Allyn and Bacon, Inc., New York. 1966. p. 1075.
9. R. C. Weast (*Editor*). Handbook of chemistry and physics. Vol. 50. Chemical Rubber Co., Cleveland, Ohio. 1969.
10. F.-Y. JOU and L. M. DORFMAN. J. Chem. Phys. **58**, 4715 (1973).
11. R. A. VERMEER and G. R. FREEMAN. Can. J. Chem. **52**, 1181 (1974).
12. E. A. SHAEDE, L. M. DORFMAN, G. J. FLYNN, and D. C. WALKER. Can. J. Chem. **51**, 3905 (1973).
13. T. KAJIWARA, K. FUNABASHI, and C. NALEWAY. Phys. Rev. A, **6**, 808 (1972).
14. R. LUGO and P. DELAHAY. J. Chem. Phys. **57**, 2122 (1972).
15. K. FUEKI, D.-F. FENG, and L. KEVAN. J. Chem. Phys. **59**, 6201 (1973).
16. N. R. KESTNER and J. JORTNER. J. Phys. Chem. **77**, 1040 (1973).
17. R. SCHILLER, SZ. VASS, and J. MANDICS. Int. J. Radiat. Phys. Chem. **5**, 491 (1973).
18. J.-P. DODELET, K. SHINSAKA, and G. R. FREEMAN. Can. J. Chem. **54**, 744 (1976).
19. J.-P. DODELET, F.-Y. JOU, and G. R. FREEMAN. J. Phys. Chem. **79**, 2876 (1975).
20. L. KEVAN. Adv. Radiat. Chem. **4**, 181 (1974).
21. J. H. BAXENDALE and P. WARDMAN. J. Chem. Soc. Faraday Trans. I, **69**, 584 (1973).
22. G. R. FREEMAN. J. Chem. Phys. **43**, 93 (1965); **46**, 2822 (1967).
23. R. K. QUINN and J. J. LAGOWSKI. J. Phys. Chem. **73**, 2326 (1969).
24. B. D. MICHAEL, E. J. HART, and K. H. SCHMIDT. J. Phys. Chem. **75**, 2798 (1971).
25. K. N. JHA, T. G. RYAN, and G. R. FREEMAN. J. Phys. Chem. **79**, 868 (1975).
26. K. N. RAO, G. C. GOYAL, and G. RAMANAN. Radiat. Eff. **14**, 101 (1972).
27. A. MACCOLL. Q. Rev. Chem. Soc. London, **1**, 16 (1947).
28. W. KAUZMANN. Quantum chemistry. Academic Press, New York. 1957. p. 581.
29. N. Q. CHAKO. J. Chem. Phys. **2**, 644 (1934).
30. R. S. MULLIKEN and C. A. RIEKE. Rep. Prog. Phys. **8**, 231 (1941).
31. R. S. DIXON and V. J. LOPATA. J. Chem. Phys. **62**, 4573 (1975); **63**, 3679 (1975).
32. G. R. FREEMAN. J. Phys. Chem. **77**, 7 (1973).

Can. J. Chem. Downloaded from www.nrcresearchpress.com by 210.87.254.42 on 09/05/12
For personal use only.

Charge-transfer interaction of bithienyls and some thiophene derivatives with electron acceptors

RAFIE ABU-EITTAH AND FAKHREIA AL-SUGEIR
Department of Chemistry, Faculty of Science, University of Kuwait, Kuwait

Received February 3, 1976

RAFIE ABU-EITTAH and FAKHREIA AL-SUGEIR. Can. J. Chem. **54**, 3705 (1976).

The charge transfer complexes of 2,2′-bithienyl, 5,5′-dimethyl-2,2′-bithienyl, and some thiophene derivatives as donors with tetracyanoethylene as an acceptor have been studied spectrophotometrically. In addition, complexes of the first donor with chloranil and iodine have been studied. The formation constants and extinction coefficients of the molecular complexes formed have been determined by graphical as well as iterative methods. From measurements at different temperatures, the thermodynamic functions of the complex formation have been calculated. The ionization potentials of the donors have been obtained from the energies of the charge transfer transitions.

RAFIE ABU-EITTAH et FAKHREIA AL-SUGEIR. Can. J. Chem. **54**, 3705 (1976).

On a étudié spectrophotométriquement les complexes de transfert de charge du bithiényl-2,2′, du diméthyl-5,5′ bithiéthyl-2,2′ et de quelques dérivés thiophéniques comme donneurs et du tétracyanoéthylène comme accepteur. De plus on a étudié les complexes du premier donneur avec du chloranil et l'iode. On a déterminé, par des méthodes graphiques ainsi que par des méthodes itératives, les constantes de formation et les coefficients d'extinction des complexes moléculaires formés. A partir de mesures à diverses températures, on a calculé les fonctions thermodynamiques pour la formation des complexes. Les potentiels d'ionisation des donneurs ont été obtenus à partir des énergies de transition des transferts de charge.

[Traduit par le journal]

Can. J. Chem. Downloaded from www.nrcresearchpress.com by 210.87.254.42 on 09/05/12
For personal use only.

Introduction

Thiophenes as well as bithienyls can give n as well as π charge transfer complexes when mixed with electron acceptors. It has been shown that thiophene and some of its polynuclear derivatives give 1:1 charge transfer π–σ^* and π–π^* complexes when they interact with iodine and tetracyanoethylene (1–4). Electron-impact studies have shown that the highest occupied orbital in sulphur-containing hetero-aromatics is a π orbital (5). On the other hand, pyridines are predominantly n donors (6). Charge transfer complexes of substituted phenyl sulphides and thiophenol with iodine have been examined (7, 8), and the donor site is concluded to be the sulphur atom; the ionization potential of the donors have been calculated (9). The formation constant, K_{ct}, of cyclopentadithiophene complexes with 1,3,5-trinitrobenzene are much higher than the corresponding constants when bithienyls are the donors (10). This increase is accounted for as arising from the inductive effect of the CH_2-group.

The formation constant, K_{ct}, and the molar extinction coefficient, ϵ_{ct}, for a given donor–acceptor system are usually determined graphically. The results obtained often show an apparent dependence of K_{ct} on the donor and acceptor concentrations (11) or the wavelength of measurement (12). These anomalies have been mainly attributed either to deviation of Beer's law (13), solvation of the complex, or to concentration requirements that have to exist in order to minimize the error in the calculated ϵ_{ct} or K_{ct} (14). Iterative procedures are not widely used for evaluation of such parameters; Farrel and Ngo (15) used such procedure to compute the formation constants of the "anilines–tetracyanoethylene" charge-transfer complexes. The nature of bonding in the charge transfer complexes has recently been discussed (16).

In this work the complex formation of 2,2′-bithienyls and some thiophenes with iodine, chloranil, and tetracyanoethylene are investigated. Numerical values of K_{ct} and ϵ_{ct} are computed graphically and using Rosenbrock and Storcy (17) iterative techniques. From measurements at different temperatures, some thermodynamic functions are computed. The ionization potentials of the donors are calculated from energy of the ct transitions.

TABLE 1. Charge-transfer absorption maximum, nm, of the studied compounds with TCNE, CHL, and I_2 at 25 °C

Donor	Absorption		
	TCNE	CHL	I_2
2,2′-Bithienyl	650	565	390
5,5-Dimethyl-2,2′-bithienyl	750		
2-Methylthiophene	410, 500		
2-Bromothiophene	370, 474		
2-Chlorothiophene	465, 365		
2-Iodothiophene	500		
Tetrahydrothiophene	510		

Experimental

Materials

Tetracyanoethylene (TCNE Fluka AG purum grade) was recrystallized from chlorobenzene. Chloranil (CHL) Merck reagent grade was recrystallized from benzene whereas iodine (May and Baker resublimed grade) was purified by sublimation. Chloroform (B.D.H. Analytical reagent) was used without further purification. Bithienyls were prepared as in previous work (18) whereas the studied thiophenes (Koch-light) were purified by vacuum distillation.

Measurements

Absorption spectra were determined using a Unicam SP 700 spectrophotometer with thermostated cell compartment and 1.0 cm fused silica cells. The spectra were scanned in the region needed to include the whole ct band.

Results and Discussion

Band Maximum of the Charge-transfer Complexes

The absorption spectra of the ct complexes of 2,2′-bithienyl, 5,5′-dimethyl-2,2′-bithienyl, some halothiophenes, 2-methylthiophene, and tetrahydrothiophene with various electron acceptors (TCNE, CHL, and I_2) are given in Table 1.

In the region 330–800 nm, some of the observed complexes exhibit a single ct transition while the others show two ct bands. If the two bands correspond to two different complexes (*e.g.* one n the other π complex) we would expect a 1:2 donor:acceptor complex. This was not the case as observed from the linearity of the modified Benesi–Hildebrand plots for a wide range of the donor concentrations. Thus, the two bands of the ct complex are two ct transitions for one molecular complex.

Equilibrium Studies

The interaction between the electron donor and acceptor is represented by the equilibrium

$$A + D \underset{}{\overset{K_{ct}}{\rightleftharpoons}} AD$$

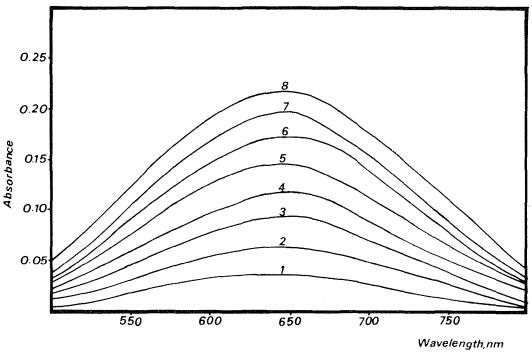

FIG. 1. Absorption spectra of pure TCNE $A = 0.0021$ M and 2,2′-bithienyl $D = 0.0643$ M and their mixed solutions at 17 °C. The concentrations of 2,2′-bithienyl are (*1*) 0.0081 M, (*2*) 0.0161 M, (*3*) 0.0242 M, (*4*) 0.0322 M, (*5*) 0.0402 M, (*6*) 0.0482 M, (*7*) 0.0564 M, (*8*) 0.0643 M. Pure A and D show no absorbance. TCNE = 0.0021 M in all solutions.

where A, D, and AD are, respectively, the acceptor, the donor, and the 1:1 charge transfer complex. The spectroscopic determinations of K_{ct} and ϵ_{ct} are usually carried out with the donor concentration $[D]_0 > [A]_0$ or with equimolar concentrations. If only the complex, AD, absorbs at the wavelength of measurement and Beer's law is obeyed, an alternative of the original Benesi–Hildebrand (19) equation will then be (20)

$$[1] \quad \frac{[A]_0[D]_0}{OD} = \frac{1}{K_{ct}\epsilon_{ct}} + \frac{[A]_0 + [D]_0}{\epsilon_{ct}} - \frac{X}{\epsilon_{ct}}$$

where X is the concentration of 1:1 ct complex. Neglecting the last term, a plot of $[A]_0[D]_0/OD$ *vs.* $[A]_0 + [D]_0$ gives a straight line, if $[A]_0 = [D]_0$ and against $[D]_0$ gives a straight line if $[D]_0 > [A]_0$. In this work, depending on the system under study, both alternatives were used.

The spectra of series of solutions containing excess varying donor (2,2′-bithienyl) concentration ($6.5 \times 10^{-2} - 0.8 \times 10^{-2}$) and a constant small acceptor (TCNE) concentration (21×10^{-4}) were scanned against the solvent (chloroform) as a blank.

Molecular Complexes of 2,2′-Bithienyl

The spectra of the ct complexes of 2,2′-bithienyl and TCNE are shown in Fig. 1 and application of eq. 1 to the results is shown in Fig. 2. From the slope and intercept of the straight lines of Fig. 2, the numerical values of K_{ct} and ϵ_{ct} are calculated. The same procedure is

Can. J. Chem. Downloaded from www.nrcresearchpress.com by 210.87.254.42 on 09/05/12
For personal use only.

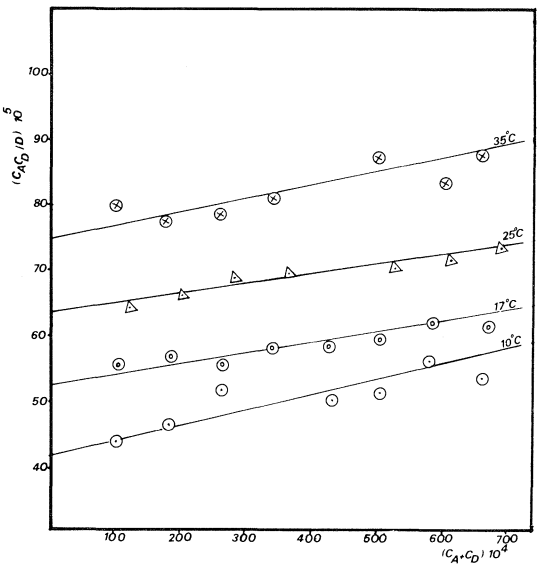

FIG. 2. Relation between $C_A C_D/OD$ and $C_A + C_D$ for 2,2′-bithienyl–TCNE system.

repeated at different temperatures and using the other acceptors, chloranil and iodine. The properties of the complex formed are expected to vary according to the type of the acceptors orbital π^* or σ^*.

The values of K_{ct} and ϵ_{ct} determined graphically are approximate and may show some discrepancies *i.e.* either be dependent on the donor concentration or the wavelength at which computations are carried out (the computations are carried out at λ_{max} of the ct band). To get reliable values, iterative procedures (Rosenbrook optimization method) were used to compute K_{ct} and ϵ_{ct}. This procedure depends on minimizing the sum of the squares of the differences between OD observed and OD calculated as outlined. Since the absorbance, OD, is only due to the formed complex, eq. 1 can be rearranged as

$$[2]\quad \frac{OD}{\epsilon_{ct}} - \left([A]_0 + [D]_0 + \frac{1}{K_{ct}}\right) + \frac{\epsilon_{ct}[A]_0[D]_0}{OD} = 0$$

Equation 2 is second order in OD and can be solved by the usual procedure if K_{ct} and ϵ_{ct} are known. The function $Y(K_{ct},\epsilon_{ct})$ is defined such that

$$[3]\quad Y(K_{ct},\epsilon_{ct}) = \sum_{i=1}^{n} [OD_{observed} - OD_{calculated}]^2$$

where n is the number of experimental data. The values of K_{ct} and ϵ_{ct} which give the minimum value of the function Y are the most likely formation constant and molar extinction coefficient of the formed charge transfer complex. An extended precession program is used to solve eq. 2 iteratively to get values of K_{ct} and ϵ_{ct} which minimize the function Y. The entry values of K_{ct} and ϵ_{ct} are the ones obtained from the graphical method. The results of computation are given in Table 2 and the iteratively computed values are considered more reliable than the graphical ones. In the derivation of the Y function (eqs. 2 and 3) the concentration of the charge transfer complex was not neglected. Accuracy of the iterative procedure is indicated by the resulting value of the minimum function Y.

The reproducibility of the results, as given in Table 2, seems to be quite satisfactory. This is seen from the variation of K_{ct} and the product $K_{ct} \cdot \epsilon_{ct}$ with temperature.

The stability of the molecular complex formed between 2,2′-bithienyl and the used acceptors (as judged by the value of K_{ct}) is in the order TCNE > I_2 > CHL. In complexes with CHL and TCNE the acceptor orbital is π^* but with I_2 it is the σ^* one. Molecular complexes of σ type are expected to be more stable than those of the π type. However, the nature of both the donor orbitals, n or π, and the acceptor orbitals seems to affect significantly the stability of the molecular complex (21, 22). Hexamethylbenzene (pure π donor) gives a molecular complex with TCNE whose K_{ct} is 148 whereas its complex with I_2 has a K_{ct} value of 1.35. The order is reversed with pure n donor (pyridine), K_{ct} with TCNE is 0.77 and with I_2 is 151. Referring to Table 2, the values of K_{ct} for the molecular complex of bithienyl + TCNE and bithienyl + I_2 makes it hard to decide whether the donating orbital is an n or π orbital. As a result we suggest that the donating orbital has both n and π properties. The n character comes from the contribution of the sulphur p orbital in the donating molecular orbital of bithienyl. This means that the p electrons (unshared) of sulphur atom are not completely delocalized in forming the π system of bithienyl but they still possess an apparent n character. The mixed n and π character of the formed ct complex was also suggested when Aloisi *et al.* investigated the molecular complexes of some sulphides (9). The greater electron

Can. J. Chem. Downloaded from www.nrcresearchpress.com by 210.87.254.42 on 09/05/12
For personal use only.

TABLE 2. Values of K_{ct} and ϵ_{ct} obtained from both graphical and iterative methods for the 2,2′-bithienyl and some electron acceptors

Acceptor	Method[a]	$K_{ct} \cdot \epsilon_{ct}$	K_{ct} (M^{-1})	ϵ_{ct} (M^{-1} cm^{-1})	$\sum(OD_{obs} - OD_{calc})^2 \times 10^4$	Temperature (°C)
TCNE	Gr	2070	4.6	450		
	I	2310	3.61	640	6.2	10.0
	Gr	1845	3.0	615		
	I	1960	3.31	592	0.43	17.0
	Gr	1564	2.31	680		
	I	1577	2.39	660	0.47	25.0
	Gr	1333	2.24	595		
	I	1292	1.7	760	0.7	36.0
CHL	Gr	800	1.0	800		
	I	799	0.96	832	3.75	9.5
	Gr	699	0.67	1043		
	I	698	0.67	1042	0.63	16.0
	Gr	514	0.55	935		
	I	586	0.56	1046	1.23	25.0
	Gr	505	0.39	1296		
	I	535	0.38	1406	0.48	34.0
I_2	Gr	1725	1.68	1027		
	I	1782	1.83	963	4.20	9.5
	Gr	1643	1.54	1067		
	I	1641	1.47	1116	1.87	16.5
	Gr	1346	0.85	1583		
	I	1352	0.71	1904	1.52	25.0
	Gr	1103	0.66	1671		
	I	1096	0.68	1612	0.31	32.5

[a]Gr, graphical; I, iterative.

affinity of TCNE than that of chloranil accounts for the higher stability of the 'bithienyl + TCNE' complex.

For a given donor, the ct maximum follow the order expected from the equation

[4] $$(h\nu_{ct})_1 - (h\nu_{ct})_2 = (EA)_2 - (EA)_1$$

which relates the energies of the ct of complexes between the same donor electron affinities of two acceptor. Using the results of Table 1 and substituting in eq. 4 a value of 0.28 eV is computed for the difference between the electron affinities of TCNE and CHL. Using a value of 1.37 eV for electron affinity of CHL (23), one gets 1.65 eV for the electron affinity of TCNE. This compares satisfactory with the value previously reported (23, 24).

The values of the iteratively computed K_{ct} were used to compute ΔH^0 and ΔS^0 of the molecular complexes formed from a plot of $R \ln K_{ct}$ *vs.* $1/T$ (Fig. 3), results are given in Table 3. It is interesting to find that the reaction of bithienyl with I_2 is more exothermic than its reaction with TCNE. Also, ΔS^0 for the first reaction is more negative than that for the second.

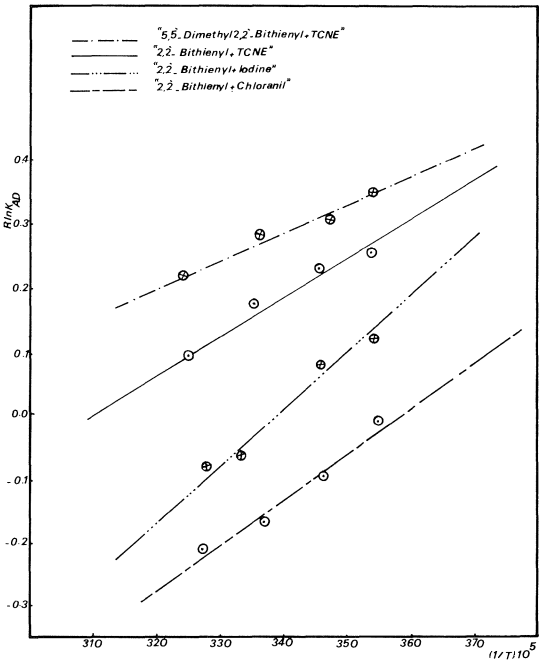

FIG. 3. The relation between $R \ln K_{AD}$ and $1/T$ for some charge transfer complexes.

Can. J. Chem. Downloaded from www.nrcresearchpress.com by 210.87.254.42 on 09/05/12
For personal use only.

TABLE 3. Thermodynamic parameter of the studied molecular complexes

Donor	Acceptor					
	TCNE		I_2		CHL	
	$-\Delta H^0$	$-\Delta S^0$	$-\Delta H^0$	$-\Delta S^0$	$-\Delta H^0$	$-\Delta S^0$
2,2′-Bithienyl	5.9±0.1	18.5±1.3	8.8±0.6	27.7±2.1	7.2±0.6	25.4±2.1
5,5′-Dimethyl-2,2′-bithienyl	4.4±0.3	11.9±0.8				
2-Methylthiophene	7.3±0.4	24.8±1.4				
2-Iodothiophene	3.7±0.4	13.3±1.6				
2-Bromothiophene	5.8±0.4	21.1±1.4				
2-Chlorothiophene	4.6±0.4	17.6±1.2				
Tetrahydrothiophene	3.4±0.3	12.3±1.1				

Complexes of 5,5′-Dimethyl-2,2′-bithienyl and Some α-Substituted Thiophenes with TCNE

To confirm the results obtained with 2,2-bithienyl the molecular complex of 5,5′-dimethyl-2,2′-bithienyl with TCNE was investigated by the same procedures; results are given in Table 4. The complex formed proved to be more stable than that of the bithienyl complex. The equilibrium constant, K_{ct}, for the complex of 5,5′-dimethyl-2,2′-bithienyl with TCNE is almost twice as large as that of the 2,2′-bithienyl with the same acceptor. This increase results from the inductive effect of the methyl groups.

It seemed useful to extend the investigation to the complexes of some α-substituted thiophenes. Comparison of the results of this series of compounds with those of 2,2′-bithienyl will give a deeper insight on: the effect of conjugation of the sulphur *p* electrons of the compound on the complex formed and the possibility of getting more stable complexes with bithienyl than with substituted thiophenes. The same procedure was followed and the results are given in Table 4, the only acceptor used was TNCE. The trend of the variation of the product $K_{ct} \cdot \epsilon_{ct}$ as given in Table 4 seems to be in the right direction. The values of the minimum function of eq. 3 suggest that the computed K_{ct} and ϵ_{ct} are reliable. It is interesting to compare the value of K_{ct} and ϵ_{ct} of 'bithienyl + TCNE' complex with that of '2-methylthiophene + TCNE' complex. It is seen that K_{ct} for the bithienyl complex is at all temperatures larger than that of the 2-methylthiophene complex. This is in accord with the variation of K_{ct} of benzene + TCNE and biphenyl + TCNE (2). The value of K_{ct} for 2-methylthiophene molecular complex is about twice that of thiophene and this has been interpreted to be due to the inductive effect of CH_2-group. Therefore, conjugation of the two thiophene rings in 2,2′-bithienyl increases the basicity of the donor more than the inductive effect of the CH_2-group. The values of K_{ct} for 'α-halothiophenes + TCNE' are dependent on the inductive effect of the halogen. That of the 2-iodocomplex is the highest and that of the 2-chloro-complex is the lowest.

The complexes of tetrahydrothiophene + TCNE have been investigated hoping that the formed n complex will have significantly different K_{ct} from the other complexes, this was not the case and as a result the nature of the formed molecular complexes of bithienyl + TCNE and thiophenes + TCNE cannot be assigned as pure n or pure π complexes. However, intensity of ct transition when tetrahydrothiophene is the donor is significantly higher than when the donor is any of the studied hetero-aromatics.

Ionization Potential of the Donor

The empirical relations derived by Aloisi and Pignataro (4)

$$(A)\quad \text{IP (eV)} = 2.9 + 1.89 \times 10^{-4}\bar{\nu}_{I_2}\ (\text{cm}^{-1})$$
$$(B)\quad \text{IP (eV)} = 5.00 + 1.53 \times 10^{-4}\bar{\nu}_{CHL}\ (\text{cm}^{-1})$$
$$(C)\quad \text{IP (eV)} = 5.21 + 1.65 \times 10^{-4}\bar{\nu}_{TCNE}\ (\text{cm}^{-1})$$

were used to estimate the ionization potential of the donors used. The results are given in Table 5 and seem to be satisfactory as compared with the experimental ones. Though the above equations were applicable for complexes of simple thiophene derivatives yet their application to complexes of bithienyls and tetrahydrothiophene appears to be reliable, though the latter is an n donor. No data is available in the literature for the IP of 2-iodothiophene, tetrahydrothiophene,

Can. J. Chem. Downloaded from www.nrcresearchpress.com by 210.87.254.42 on 09/05/12
For personal use only.

TABLE 4. Numerical values of K_{ct} and ϵ_{ct} obtained from different methods for some of the studied donors with TCNE

Donor	Method	$K_{ct} \cdot \epsilon_{ct}$	K_{ct} (M^{-1})	ϵ_{ct} (M^{-1} cm^{-1})	$\sum(OD_{obs} - OD_{calc})^2 \times 10^4$	Temperature (°C)
5,5′-Dimethyl-	Gr	10530	5.85	1800		
2,2′-bithienyl	I	10536	5.77	1826	0.23	10.0
	Gr	10000	5.0	2000		
	I	10159	4.98	2040	0.72	15.0
	Gr	9757	4.62	2112		
	I	8056	4.39	1835	0.3	25.0
	Gr	6850	3.33	2057		
	I	5633	2.94	1916	7.3	35.0
2-Methyl-	Gr	1850	1.85	1000		
thiophene	I	1844	1.78	1036	13.8	6.0
	Gr	1981	1.67	1059		
	I	1755	1.48	1186	8.4	10.0
	Gr	1759	1.43	1107		
	I	1587	1.29	1230	1.9	14.8
	Gr	1384	1.12	1113		
	I	1273	1.03	1236	6.5	25.4
2-Chloro-	Gr	308	0.67	450		
thiophene	I	308	0.51	605	0.03	9.5
	Gr	278	0.44	631		
	I	279	0.42	664	0.01	19.5
	Gr	266	0.36	704		
	I	252	0.31	818	0.02	30.0
	Gr	173	0.32	782		
	I	238	0.27	880	0.24	35.0
2-Bromo-	Gr	286	0.87	329		
thiophene	I	279	0.73	382	0.06	9.0
	Gr	289	0.68	425		
	I	286	0.53	539	0.17	16.5
	Gr	255	0.5	529		
	I	261	0.42	622	0.04	25.0
	Gr	216	0.32	675		
	I	210	0.29	723	0.11	35.0
2-Iodothiophene	Gr	419	1.15	364		
	I	416	0.96	433	0.62	10.0
	Gr	500	1.11	450		
	I	400	0.82	465	0.16	16.5
	Gr	334	0.73	458		
	I	325	0.61	533	0.41	32.0
Tetrahydro-	Gr	1600	0.80	2000		
thiophene	I	1574	0.77	2044	1.06	10.5
	Gr	1516	0.71	2117		
	I	1485	0.68	2184	1.57	15.5
	Gr	1372	0.61	2250		
	I	1348	0.57	2364	0.87	24.5
	Gr	1234	0.48	2560		
	I	1224	0.48	2550	0.38	35.0

2,2′-bithienyl, or its 5,5′-dimethyl derivative yet our values determined from ct studies seem to be consistent. The molecular complexes of 2-methyl, 2-bromo, and 2-chlorothiophene show two ct bands corresponding to two electronic transitions. Ionization potentials calculated from ct data and given in Table 5 were those corresponding to the lower energy transition. The double peak bands have been observed for ct complexes of TCNE with thiophene (4), with thiophenols and related compounds (25). This has been interpreted as due to transitions from two orbitals of the donors to the same orbital of the acceptor. This appears to be a reasonable as-

Can. J. Chem. Downloaded from www.nrcresearchpress.com by 210.87.254.42 on 09/05/12
For personal use only.

TABLE 5. Ionization potentials of the studied donors from transition energies of the charge transfer complexes and from electron impact method

Donor	First ionization potential (eV) of donor			
	I_2	CHL	TCNE	Electron impact[a]
2,2′-Bithienyl	7.75	7.71	7.75	—[b]
5,5′-Dimethyl-2,2′-bithienyl			7.41	—
2-Methylthiophene			8.51	8.63
2-Iodothiophene			8.51	—
2-Bromothiophene			8.72	8.93
2-Chlorothiophene			8.80	9.06
Tetrahydrothiophene			8.45	—
Thiophene			8.89	9.12

[a]Reference 5.
[b]Not reported in literature.

Can. J. Chem. Downloaded from www.nrcresearchpress.com by 210.87.254.42 on 09/05/12
For personal use only.

sumption for TCNE, since an energy difference of 2.07 eV is calculated between the lowest and second lowest empty molecular orbitals (26). The difference between the two ionization potentials, as computed from the two ct bands (Table 1), is 0.72, 0.95, and 0.93 eV for 2-bromothiophene and 2-chlorothiophene respectively. For thiophene the two ionization potentials, as determined from the two photoelectron bands, differ by 0.62 eV (27) which compares well with the difference between the energies of its two ct transitions.

The appearance of two ct bands in the spectra of complexes having substituted benzenes as donors has been associated with the formation of two isomeric complex configurations (28, 29). Even with this rationalization, the two ct transitions are suggested to originate from the E_1 level of benzene after removing its degeneracy by substitution. The formation of at least two definite molecular configurations, in which the C_2 axes of TCNE and thiophene are parallel or perpendicular, is quite feasible and the appearance of two ct bands may be attributed to their formation. However, it is found that the energy differences between the two highest occupied MO's of some heterocycles (thiophene, furan, and pyrrole) correlate well with the energy differences between the two ct bands in the spectra of their complexes (30). This favours the suggestion that the appearance of two ct bands in the spectra of some of the molecular complexes under investigation is due to transitions from the two highest occupied MO's of the donor to the same vacant MO of the acceptor.

1. R. P. LANG. J. Am. Chem. Soc. **84**, 4438 (1962).
2. A. R. COOPER, C. W. P. CROWNC, and P. G. FARRELL. Trans. Faraday Soc. **62**, 18 (1966).
3. T. K. NUKHERJEE. J. Phys. Chem. **73**, 3442 (1969).
4. G. GAETANO ALOISI and S. PIGNATARO. J. Chem. Soc. Faraday Trans. I, **69**, 534 (1972).
5. S. PIGNATARO, P. LINDA, and G. MARINO. J. Chem. Soc. B, 1585 (1971).
6. G. G. ALOISI, G. BEGGIATO, and U. MAZZUCATO. Trans. Faraday Soc. **66**, 3075 (1970).
7. S. SANTINI, G. REICHENBACH, and U. MAZZUCATO. J. Chem. Soc. Perkin Trans. II, 494 (1974).
8. G. REICHENBACH, S. SUNTINI, and U. MAZZUCATO. J. Chem. Soc. Faraday Trans. I, **69**, 143 (1973).
9. G. GAETANO ALOISI, S. SANTINI, and S. SORRISO. J. Chem. Soc. Faraday Trans. I, **70**, 1908 (1974).
10. A. KRAAK and H. WYNBERG. Tetrahedron, **24**, 3911 (1968).
11. S. D. ROSS and M. M. LABES. J. Am. Chem. Soc. **79**, 76 (1957).
12. T. NATSNO and O. HIGUCHI. Bull. Chem. Soc. Jpn. **41**, 518 (1968).
13. R. FOSTER and J. HORMAN. J. Chem. Soc. B, 171 (1966).
14. D. A. DERANLEAN. J. Am. Chem. Soc. **91**, 4044 (1969).
15. P. G. FARRELL and PHI-NAGO NGO. J. Phys. Chem. **77**, 2545 (1973).
16. M. S. SAMBHI. J. Phys. Chem. **77**, 2290 (1973).
17. H. H. ROSENBROCK and C. STORCY. Computational techniques for chemical engineers. Pergamon Press, London. 1066.
18. W. STEIN KOPF, R. LEITSMANN, and K. H. HOFMANN. Ann. **546**, 180 (1941).
19. H. A. BENESI and I. H. HILDEBRAND. J. Am. Chem. Soc. **71**, 2703 (1949).
20. R. ABU-EITTAH and A. EL-KOURASHY. J. Phys. Chem. **76**, 2405 (1972).
21. R. FOSTER. Organic charge transfer complexes. Academic Press, London. 1969.
22. W. J. MCKINNEY and A. I. POPOV. J. Am. Chem. Soc. **91**, 5215 (1969).

23. G. BRIEGLEB. Angew. Chem. Int. Ed. **3**, 617 (1964).
24. R. D. SRIVASTAVA and G. PRASAD. Bull. Chem. Soc. Jpn. **43**, 1611 (1970).
25. H. BOCK, G. WAGNER, and J. KRONER. Tetrahedron Lett. 3713 (1971).
26. B. R. PENFOLD and W. N. LIPSCOMB. Acta Crystallogr. **4**, 589 (1961).
27. J. H. D. ELAND. Int. J. Mass Spectrosc. Ion Phys. **2**, 471 (1969).
28. L. E. ORGEL. J. Chem. Phys. **23**, 1352 (1955).
29. R. S. MULLIKEN. Recl. Trav. Chim. Pays-Bas, **75**, 845 (1956).
30. Z. YOSHIDA and T. KOBAYASHI. Tetrahedron, **26**, 267 (1970).

Can. J. Chem. Downloaded from www.nrcresearchpress.com by 210.87.254.42 on 09/05/12
For personal use only.

Studies in the usnic acid series. II.[1] The condensation of (+)-usnic acid with hydroxylamine

JAMES P. KUTNEY, IGNACIO H. SANCHEZ, AND TREVOR YEE

Department of Chemistry, University of British Columbia, 2075 Wesbrook Place, Vancouver, B.C., Canada V6T 1W5

Received July 2, 1976

JAMES P. KUTNEY, IGNACIO H. SANCHEZ, and TREVOR YEE. Can. J. Chem. **54**, 3713 (1976).

The results of the reaction of usnic acid (**1**) with hydroxylamine are presented. Four products, two isomeric isoxazoles (**2** and **4**), a novel oxazocine structure (**3**), and $\Delta^{2,11}$-enaminousnic acid (**5**) were isolated and characterized. These data clarify the earlier published results in this area.

JAMES P. KUTNEY, IGNACIO H. SANCHEZ et TREVOR YEE. Can. J. Chem. **54**, 3713 (1976).

On présente les résultats de réaction de l'acide usnique (**1**) avec l'hydroxylamine. On a isolé et caractérisé quatre produits: deux isoxazoles isomères (**2** et **4**), une nouvelle structure oxazocine (**3**) et l'acide $\Delta^{2,11}$ ènaminousnique (**5**). Ces données permettent de clarifier des résultats publiés antérieurement dans ce domaine.

[Traduit par le journal]

Can. J. Chem. Downloaded from www.nrcresearchpress.com by 210.87.254.40 on 09/05/12
For personal use only.

During our synthetic approaches towards the laboratory preparation of usnic acid biodegradation products, it became essential to prepare derivatives in which the sensitive β-triketone system in ring C of (+)-usnic acid (**1**) was fully protected towards a variety of experimental conditions. Having previously determined (21) that in the reaction of **1** with a series of amines, attack of the amino group occurs preferentially at the C-2 acetyl side chain in ring C, it was of interest to study further the formation of stable heterocyclic systems, such as isoxazoles, as possible protecting groups for the ketone system in the usnic acid series.

The facile synthesis of 1,2-isoxazoles from a variety of starting materials is a well documented process (1–6). Furthermore the reductive cleavage of the N—O bond in the isoxazole ring to provide the vinylogous amides (β-ketoenamines) and thereby facile regeneration of the original 1,3-dicarbonyl system prompted us to study in detail the synthesis of such materials.

Earlier workers (7–9) reported the formation of the so-called "usnic acid oxime anhydride", mp 230 °C, molecular formula $C_{18}H_{15}O_6N$, in the reaction of racemic usnic acid with hydroxylamine acetate in alcoholic solution. To our surprise, we found that (+)-usnic acid (**1**) does not react with hydroxylamine hydrochloride in 95% ethyl alcohol, and it was therefore decided to attempt first the formation of the corresponding oxime by standard techniques followed by its thermal cyclization to the desired heterocyclic system.

Thus, when **1** was reacted with hydroxylamine hydrochloride (1.5 equiv.) in dry pyridine at room temperature, complete conversion to the desired "oxime" was promptly observed. However, its thermal cyclization (absolute ethyl alcohol, reflux) led to the formation of not one but four different products (Fig. 1).

The least polar product, **2**, isolated as bright yellow prisms (or needles), mp 230–231 °C, possessed the molecular formula $C_{18}H_{15}O_6N$, as determined by elemental analysis and high resolution mass spectrometry, thereby corresponding to the material originally isolated by Widman (7). Its ultraviolet spectrum (λ_{max} 374, 329, 281, and 219 nm) showed maxima corresponding to a substituted 4-ketoisoxazole, a system known to absorb in the 210–230 nm region (10) while in its infrared spectrum only those absorptions corresponding to the C-1 carbonyl group (1680 cm^{-1}) and the chelated aromatic methyl ketone (1625 cm^{-1}) were observed. Its pmr spectrum (Table 1) was most informative and showed that while all other signals remained approximately constant, as compared to those of (+)-usnic acid **1** (11), the C-11 methyl group (the isoxazole ring methyl group) and the olefinic proton at C-4 appeared shifted to δ 2.51 and 6.45 ppm, respectively. Moreover, the characteristic signal for the chelated enolic hydroxyl function at C-3 (usual range δ 18–19 ppm) was not observed.

Compound **3**, of intermediate polarity, was

[1]For part I, see ref. 21.

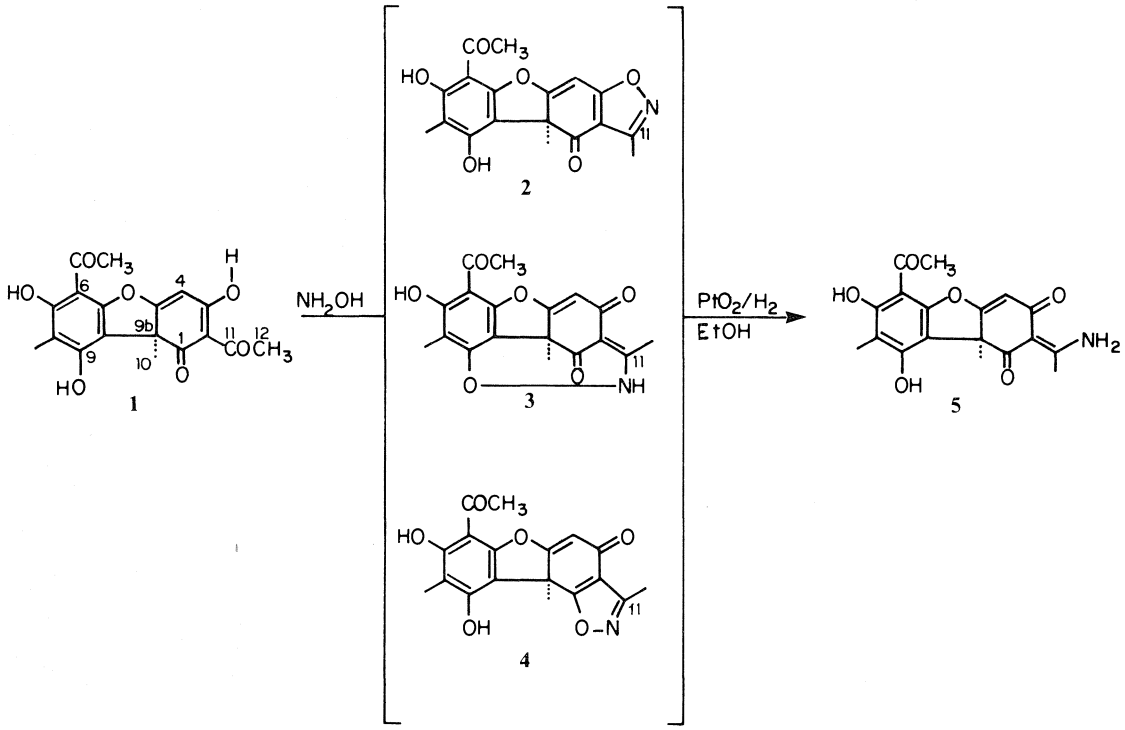

FIG. 1. The condensation products of (+)-usnic acid (**1**) with hydroxylamine and their reductive cleavage.

isolated as colourless needles, mp 260–261 °C, $[\alpha]_D^{26}$ (CH_3CN) +244°, and also possessed the molecular formula $C_{18}H_{15}O_6N$. While its ultraviolet (λ_{max} 326, 281, and 233 nm) and infrared (1660, 1620, 1580 cm^{-1}) spectra proved quite similar to those of other usnic acid – amine monocondensation products (21), its pmr spectrum (Table 1) yielded definitive evidence as to the type of oxygen–nitrogen bond which was involved. Thus in addition to a new broad one-proton signal at δ 4.38 ppm, a resonance well within the range for unsaturated hydroxylamines (12), a higher field signal for the C-11 methyl group (δ 2.48 ppm) was observed. Moreover, the lack of the characteristic signal for the C-9 phenolic hydroxyl group (usual range δ 10–11 ppm), indicates that it is this oxygen atom that is involved in the intramolecular cyclization, thus producing a novel 8-membered ring heterocyclic system, the oxazocine **3**. This postulate is in agreement with our previous observations (21) that reaction occurs primarily at the C-2 acetyl grouping and that the initial condensation products (imines) suffer rapid tautomerization to the more stable enamine system.

Compound **4**, yellow crystals, mp 178–179 °C, $[\alpha]_D^{26}$ +851°, molecular formula $C_{18}H_{15}O_6N$, proved to be the third product obtained in this reaction. Its ultraviolet (λ_{max} 390, 336, 282, 258, and 222 nm) and infrared (1675, 1620 cm^{-1}) spectra were quite similar to those of the isoxazole **2**, with the small differences arising mainly from a change in substitution pattern, a situation often observed in the isoxazole series (10). The difference in the substitution pattern was also observed in the pmr spectrum of this product which showed the C-11 methyl group (isoxazole methyl group) resonance and the C-4 olefinic proton at δ 2.60 and 6.36 ppm, respectively (Table 1).

The complex mass spectra of isoxazoles **2** and **4** (*m/e* 341, 326, 313, 312, 298, 285, 273, 272, 260, 257, 244, 232, 217 and 341, 326, 313, 298, 272, 256, 244, 217 respectively) are indicative of the electron impact-induced isoxazole → azirine → oxazole rearrangements postulated for the series (13–15) and are reminiscent of their photochemical behaviour (16). A similar pattern

Can. J. Chem. Downloaded from www.nrcresearchpress.com by 210.87.254.40 on 09/05/12
For personal use only.

TABLE 1. The proton magnetic resonance data of the usnic acid – hydroxylamine condensation products

Compound	Functionality							
	C_{9b}-CH_3	C_8-CH_3	C_{11}-CH_3	C_6-$COCH_3$	C_4-H	C_9-OH	C_3-OH	N-H
1	1.76	2.10	2.70	2.70	5.96	11.01	18.93	—
2	1.80	2.08	2.51	2.70	6.45	10.55	—	—
3	1.87	2.12	2.48	2.74	6.13	—	—	4.38
4	1.80	2.10	2.60	2.68	6.36	10.89	—	—
5	1.66	2.00	2.59	2.65	5.75	11.72	—	9.56 12.05

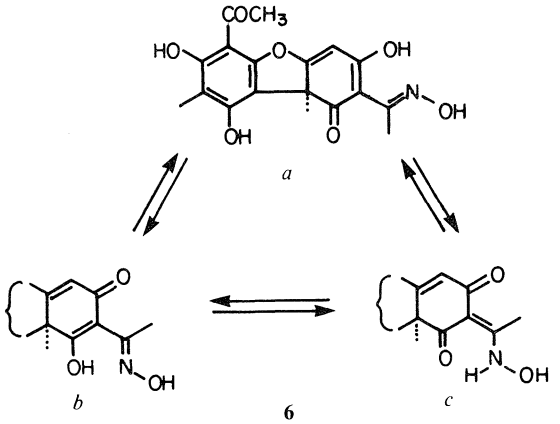

FIG. 2. The postulated equilibration of (+)-usnic acid oxime (**6**).

was observed for the oxazocine **3** (*m/e* 341, 326, 308, 298, 280, 260, 232, 217). Although the behaviour of oxazocines in the mass spectrometer has not yet been studied, we feel that ring opening and recyclization to isoxazole derivatives are important characteristics in the present series.

The fourth and final component to be isolated was shown to be identical in all respects with (−)-$\Delta^{2,11}$-enaminousnic acid (**5**), the product resulting from the condensation of (+)-usnic acid (**1**) with aqueous ammonia (21). Its formation is probably due to traces of ammonia present as an impurity in the hydroxylamine hydrochloride.

Under the described conditions, the formation of such materials can be rationalized as arising from the *syn*-methyl oxime **6***a* (Fig. 2), the initial condensation product, which subsequently equilibrates with the isomeric *syn*-methyl oxime **6***b* and with the unsaturated hydroxylamine derivative **6***c*. Thermal cyclization of such intermediates would then produce the isolated products. It is interesting to mention that thin layer chromatographic investigation of the crude "oxime" reaction mixture prior to any attempts to perform the cyclization revealed variable amounts of the final products, thus indicating an inherently facile cyclization process.

Based on this postulate we have also studied the modification of relative yields and product distribution caused by changes in the parameters governing the thermal cyclization of intermediate **6**. The results are summarized in Table 2. Thus, if cyclization is carried out in a basic solvent (Experiment I), without isolation of **6**, the main product is the oxazocine **3**, suggesting that under such conditions **6***c* must be the predominant species. However, if protonation of the intermediate occurs (Experiments II and III), regardless of solvent and temperature, the isomeric isoxazole **4** is the main product. Experiments II and III indicate the importance of the C-9 phenolate anion on the formation of **3**.

It should also be mentioned that all attempts to further increase the yield of the isoxazole **2** by the use of protected species such as the diacetate **7** were unsuccessful, resulting only in partial deacetylation to (+)-usnic acid monoacetate (**8**).

Further structural proof for the proposed

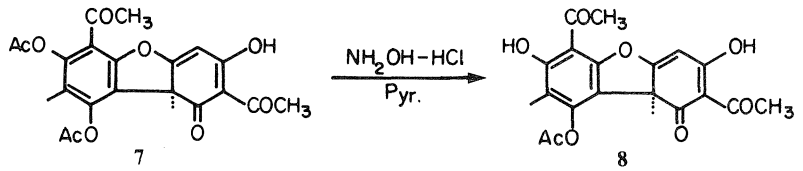

Can. J. Chem. Downloaded from www.nrcresearchpress.com by 210.87.254.40 on 09/05/12
For personal use only.

TABLE 2. The thermal cyclization of (+)-usnic acid oxime (6)

Experiment	Conditions*	Yields of isolated materials (%) 2	3	4	Total yield (%)
I	*a*, *c*	21	60.5	5.5	87
II	*a*, *b*, *c*	20	2	56.5	79
III	*a*, *b*, *d*	16	21	58	95
IV	*e*	30.5	†	†	†

**a*, oxime formation in pyridine (1 h, rt); *b*, work-up and isolation of the "oxime"; *c*, thermal cyclization in absolute ethyl alcohol (1 h, 90 °C); *d*, thermal cyclization in anhydrous pyridine (1 h, 110 °C); *e*, oxime formation – thermal cyclization (one-step reaction) in 1:1 dry pyridine – absolute ethyl alcohol (1.5 h, 80 °C).

†Not determined.

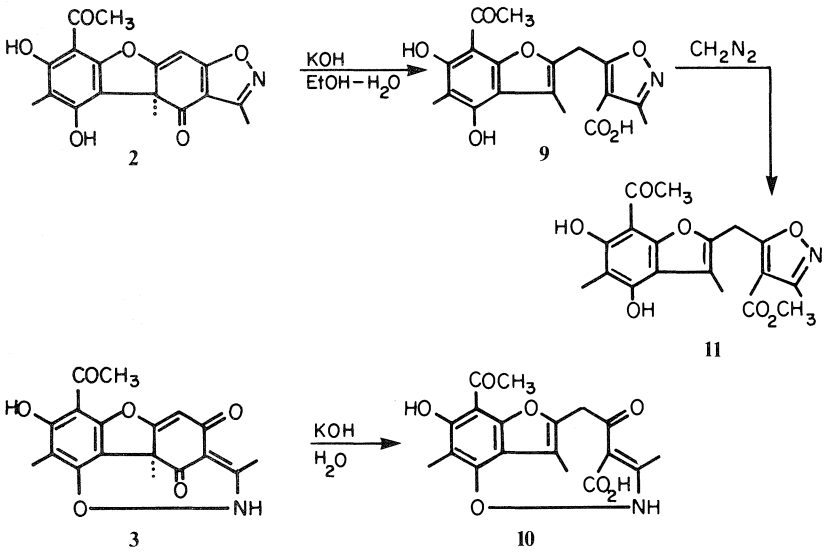

FIG. 3. The reactions of isoxazole **2** and oxazocine **3** with strong base.

structures **2**–**4** was obtained from experiments involving their reductive cleavage (H_2/PtO_2) (1–3, 17, 18) to **5** (21) (Fig. 1). The latter substance, behaving as a vinylogous amide, was easily hydrolyzed to the parent ketone **1** under both alkaline (1.2 *N* NaOH) and acidic (80% HOAc) (7) conditions. Although the former conditions were applied successfully to several members of the series, with complete retention of optical activity (21), the latter system resulted in racemization (7, 19). Strong alkaline treatment (20% KOH) (20) of **2** and **3** produced the carboxylic acids **9** and **10** (36 and 28% yield respectively) corresponding to nucleophilic cleavage at the nonenolizable C-1 carbonyl group in these compounds (Fig. 3). The acid **9** was further characterized as its methyl ester **11**.

In conclusion these studies have clarified the results previously reported with usnic acid (**1**) and hydroxylamine. The significance of these results as they pertain to biodegradation studies in the usnic acid series, will be presented in future publications.

Experimental

Melting points were determined on a Kofler block and are uncorrected.

Ultraviolet (uv) spectra were recorded on a Cary 14 spectrophotometer in methanol solution (unless otherwise noted) and the absorption maxima are reported in nm.

Infrared (ir) spectra were measured in chloroform solution on Perkin-Elmer model 710 or 457 spectrophotometers and the absorption maxima are quoted in wave numbers (cm^{-1}).

Can. J. Chem. Downloaded from www.nrcresearchpress.com by 210.87.254.40 on 09/05/12
For personal use only.

Can. J. Chem. Downloaded from www.nrcresearchpress.com by 210.87.254.40 on 09/05/12
For personal use only.

Proton magnetic resonance (pmr) spectra were measured in deuterochloroform ($CDCl_3$) solution (unless otherwise indicated) at room temperature. Routine spectra were recorded at 60 MHz on a Varian T-60 spectrometer, and analytical or comparison spectra at 100 MHz on either a Varian HA-100 or a Varian XL-100 spectrometer. Line positions are given in the δ (ppm) scale using tetramethylsilane (TMS) as internal standard. The integrated peak areas, multiplicity, and proton assignments are indicated in parentheses.

Low resolution mass (ms) spectra were determined at 70 eV on either an AEI-902 or an Atlas CH-4B mass spectrometer, while high resolution mass spectra were recorded exclusively on an AEI-MS-902 mass spectrometer.

Circular dichroism (cd) spectra were obtained on a Jasco model J-20 spectropolarimeter in methanol solution (unless otherwise indicated). The wavelength of the absorption maxima is reported in nm. The differential molar extinction coefficient ($\Delta\epsilon$) and the sign of the observed Cotton effect are indicated in parentheses.

Optical rotations ($[\alpha]_D$) were measured on a Perkin-Elmer model 141 polarimeter at the sodium D line in chloroform solution (unless otherwise noted) using cells with a 0.1 dm path.

Microanalyses were performed by Mr. P. Borda of the Microanalytical Laboratory, University of British Columbia.

Merck silica gel G (acc. to Stahl) impregnated with oxalic acid (2%) and with 2% fluorescent indicator added, was used as adsorbent for thin layer chromatography (tlc), unless otherwise noted. The tlc plates were activated in an oven at 90 °C for 4 h before use. For qualitative chromatography layers of 0.3 mm thickness were used and the spots were visualized by viewing under ultraviolet (uv) light or spraying with a 1% ethanolic ferric chloride solution. For preparative (plc) chromatography large (20 × 20 and 20 × 60 cm) plates with a thicker layer (0.7 mm) were used. The developing systems were *A*, petroleum ether (30–60 °C) – acetone (4:1), and *B*, chloroform – ethyl acetate (3:2), unless otherwise indicated.

Column chromatography was performed on either Mackerey-Nagel (0.2–0.5 mm grain size) or Merck 60 (0.063–0.2 mm grain size) silica gel.

The usnic acid utilized throughout the course of this study was obtained from Koch-Light Laboratories, England, as the optically active dextrorotatory isomer, (+)-usnic acid, isolated from ichen sources (*Usnea barbata*).

In order to present in a coherent manner the characteristic spectroscopic data for those compounds that are formally derived from usnic acid and retain its basic skeletal features, we have decided to maintain through the course of this work the numbering system recommended for the parent molecule (*i.e.* the approved dibenzofuran numbering (22)) instead of using those arising from the corresponding systematic names. In all other instances the latter numbering systems will be used.

*Condensation of (+)-Usnic Acid (**1**) with Hydroxylamine Hydrochloride – Experiment I*

A solution of (+)-usnic acid (**1**) (10.0 g, 29.069 mmol) in dry pyridine (30 ml) was treated with hydroxylamine hydrochloride (3.0 g, 43.165 mmol) and stirred at room temperature under a nitrogen atmosphere for 1 h. The reaction mixture was then diluted with absolute ethyl alcohol (200 ml) and heated to reflux under nitrogen for 1 h. The resulting dark brown solution was then concentrated under reduced pressure to a thick syrup, acidified with 1 *N* hydrochloric acid, and thoroughly extracted with ethyl acetate (3 × 150 ml). The combined extracts were washed with water, dried over anhydrous sodium sulfate, and evaporated under reduced pressure to produce a crude crystalline product (11.8 g), which was purified by column chromatography on Macherey-Nagel silica gel (500 g) to afford the following pure components.

*Fraction I. (+)-Isoxazol[4,5-b]usnic Acid (**2**) (Usnic Acid Oxime Anhydride) (10-Acetyl-6,6a-dihydro-7,9-dihydroxy-5,6aα,8-trimethyl-6-oxoisoxazolo[4,5-b]-dibenzofuran)*

Bright yellow needles from ethyl acetate (2.10 g, 6.158 mmol; 21%); mp 230–231 °C (lit. (7) mp 230 °C); $[\alpha]_D^{27}$ +669° (*c* 0.060); uv λ_{max} (log ϵ) 374 (2.66), 329 (3.69), 281 (3.76), 219 (4.63); ir ν_{max} 3600–2600 (OH, chelated), 1680 (C=O, enone system), 1625 (C=O, chelated aromatic acetyl; C=C, enol ether), 1600 (C=C, aromatic ring); pmr ($CDCl_3$–DMSO-d_6) δ 1.80 (3H, s, C_{9b}-CH_3), 2.08 (3H, s, C_8-CH_3), 2.51 (3H, s, C_{11}-CH_3), 2.70 (3H, s, C_6-$COCH_3$), 6.45 (1H, s, C_4-H), 10.55 (1H, s, C_9-OH), 13.30 ppm (1H, s, C_7-OH); ms *m/e* 341 (M^+, base peak), 326 (*M* − 15), 313, 312, 298, 285, 273, 272, 260, 257, 244, 232, 217. *Anal.* calcd. for $C_{18}H_{15}O_6N$: C 63.34, H 4.43, N 4.10; found: C 63.42, H 4.51, N 3.95. High resolution molecular weight determination: calcd.: 341.090; found: 341.090; cd λ_{max} ($\Delta\epsilon$) 373 (+6.88), 334 (+13.23), 285 (+9.26), 255 (−11.41), 229 (−15.77).

*Fraction II. (+)-2H-[1,2]Oxazocinousnic Acid (**3**) (1-Acetyl-8-hydroxy-3a,4,10b,11-tetrahydro-3,9,10bα-trimethyl-4,11-dioxo-2H-4,5-dihydro[1,2]oxazocino-[4,5,6,7,8-a,m,l,k]dibenzofuran)*

Colorless needles from ethyl acetate (6.00 g, 17.595 mmol; 60.5%), mp 260–261 °C; $[\alpha]_D^{26}$ (CH_3CN) +244° (*c* 0.5725); uv λ_{max} (log ϵ) 326 (3.83), 281 (4.24), 233 (4.45); ir (Nujol) ν_{max} 3200–2900 (OH, chelated), 1660 (C=O, diketoenamine system), 1620 (C=O, chelated aromatic acetyl grouping; C=C, enol ether, aromatic ring), 1580 (C=O, chelated ketoenamine system); pmr (CD_3COCD_3–DMSO-d_6) δ 1.87 (3H, s, C_{9b}-CH_3), 2.12 (3H, s, C_8-CH_3), 2.48 (3H, s, C_{11}-CH_3), 2.74 (3H, s, C_6-$COCH_3$), 4.38 (1H, br, N-H), 6.13 (1H, s, C_4-H), 13.61 ppm (1H, s, C_7-OH); ms *m/e* 341 (M^+), 326 (*M* − 15, base peak), 308, 298, 280, 260, 232, 217. *Anal.* calcd. for $C_{18}H_{15}O_6N$: C 63.34, H 4.43, N 4.10; found: C 63.49, H 4.29, N 3.91. High resolution molecular weight determination: calcd.: 341.090; found: 341.093. cd λ_{max} ($\Delta\epsilon$) 345 (+9.20), 332 (+9.40), 320 (+9.60), 268 (−7.44), 235 (−5.09), 222 (−11.75).

*Fraction III. (+)-Isoxazolo[5,4-a]usnic Acid (**4**) (7-Acetyl-4,10b-dihydro-8,10-dihydroxy-3,9,10bα-trimethyl-4-oxoisoxazolo[5,4-a]dibenzofuran)*

Yellow crystals from ethyl acetate (0.55 g, 1.612 mmol; 5.5%), mp 178–179 °C; $[\alpha]_D^{27}$ +851° (*c* 0.1315); uv λ_{max} (log ϵ) 390 (3.34), 336 (3.73), 282 (4.23), 258 (4.11), 226 (4.48); ir ν_{max} 3400–2900 (OH, chelated), 1675 (C=O, enone system), 1620 (C=O, chelated aromatic acetyl grouping; C=C, enol ether, aromatic ring); pmr δ 1.80

Can. J. Chem. Downloaded from www.nrcresearchpress.com by 210.87.254.40 on 09/05/12
For personal use only.

(3H, s, C_{9b}-CH_3), 2.10 (3H, s, C_8-CH_3), 2.60 (3H, s, C_{11}-CH_3), 2.68 (3H, s, C_6-$COCH_3$), 6.36 (1H, s, C_4-H), 10.89 (1H, s, C_9-OH), 13.40 ppm (1H, s, C_7-OH); ms *m/e* 341 (M^+, base peak), 326, 313, 298, 272, 256, 244, 217. *Anal.* calcd. for $C_{18}H_{15}O_6N$: C 61.34, H 4.43, N 4.10; found: C 63.31, H 4.50, N 3.92. High resolution molecular weight determination: calcd.: 341.090; found: 341.089.

*Fraction IV. (−)-$\Delta^{2,11}$-Enaminousnic Acid (**5**) (6-Acetyl-7,9-dihydroxy-8,9bα-dimethyl-2-ethylid-2,11-ene-11-amino-1,9b,2,3-tetrahydro-1,3-dioxodibenzofuran)*

Pale yellow prisms from ethyl acetate or chloroform (82.5 mg, 0.240 mmol; 0.82%), mp 253–254 °C; mixed up with (−)-$\Delta^{2,11}$-enaminousnic acid 252–254 °C; $[\alpha]_D^{27}$ −224° (*c* 0.087); chromatographic (silica gel – oxalic acid plates, solvent systems *A* and *B*) and spectroscopic (uv, ir, pmr) properties were identical with those of pure (−)-$\Delta^{2,11}$-enaminousnic acid (**5**) obtained previously (21).

*Condensation of (+)-Usnic Acid (**1**) with Hydroxylamine Hydrochloride – Experiment II*

A solution of (+)-usnic acid (**1**) (5.0 g, 14.534 mmol) and hydroxylamine hydrochloride (1.5 g, 21.582 mmol) in dry pyridine (20 ml) was stirred at room temperature under a nitrogen atmosphere for 0.5 h. The reaction mixture was cooled in an ice bath, acidified with 1 *N* hydrochloric acid, and extracted with ethyl acetate (3 × 70 ml). The combined organic extracts were thoroughly washed with water, dried over anhydrous sodium sulfate, and evaporated under reduced pressure. The crude oxime (5.413 g) was then dissolved in absolute ethyl alcohol (150 ml) and heated to reflux under nitrogen for 1 h. The solvent was eliminated by evaporation under reduced pressure, and the residue (5.320 g) purified by column chromatography on Woelm silica gel (200 g, activity I) to afford **2** (20%), **3** (2%), and **4** (56.5%).

*Condensation of (+)-Usnic Acid (**1**) with Hydroxylamine Hydrochloride – Experiment III*

A solution of (+)-usnic acid (**1**) (5.0 g, 14.534 mmol) and hydroxylamine hydrochloride (1.50 g, 21.582 mmol) in dry pyridine (20 ml) was stirred at room temperature under a nitrogen atmosphere for 0.5 h. After cooling in an ice bath the reaction mixture was acidified with 1 *N* hydrochloric acid and extracted with ethyl acetate (3 × 70 ml). The combined extracts were washed with water, dried over anhydrous sodium sulfate, and evaporated under reduced pressure. The crude oxime (5.432 g) was dissolved in dry pyridine (150 ml) and heated to 110 °C (oil bath temperature) under nitrogen atmosphere for 2 h. The cold reaction mixture was acidified with 1 *N* hydrochloric acid, extracted with ethyl acetate (3 × 80 ml), and the combined extracts washed with water, dried over anhydrous sodium sulfate, and evaporated under reduced pressure. The residue (5.852 g) was purified by column chromatography on Macherey-Nagel silica gel (300 g) to afford **2** (16%), **3** (21%), and **4** (58%).

*Condensation of (+)-Usnic Acid (**1**) with Hydroxylamine Hydrochloride – Experiment IV*

A suspension of (+)-usnic acid (**1**) (25.0 g, 72.674 mmol) in dry pyridine (50 ml) and absolute ethyl alcohol (50 ml) was treated with hydroxylamine hydrochloride (5.6 g, 80.57 mmol) and heated at 80 °C (oil bath temperature) under a nitrogen atmosphere for 1.5 h. Upon cooling a deep yellow crystalline product formed and the reaction mixture was diluted with cold distilled water (200 ml), acidified with 1 *N* hydrochloric acid, and extracted with ethyl acetate (3 × 200 ml). The combined extracts were thoroughly washed with water, dried over anhydrous magnesium sulfate, and evaporated under reduced pressure. The crystalline residue (25.820 g) was purified by column chromatography on Merck silica gel (400 g) eluting with benzene – ethyl acetate (5%) to produce **2** in 30.5% yield. The other components isolated during the chromatographic purification were not investigated further.

*Acid Catalyzed Hydrolysis of (−)-$\Delta^{2,11}$-Enaminousnic Acid (**5**). Formation of (±)-Usnic Acid (**1**)*

A suspension of (−)-$\Delta^{2,11}$-enaminousnic acid (**5**) (20 mg, 0.058 mmol) in 80% acetic acid (0.5 ml) was heated to reflux under a nitrogen atmosphere for 8 h. The brown solution was then diluted with distilled water (10 ml) and extracted with benzene (3 × 5 ml). The combined organic extracts were washed with water, dried over anhydrous sodium sulfate, and evaporated under reduced pressure. The residue (18.9 mg) was crystallized from benzene – ethyl alcohol to produce (±)-usnic acid (**1**) (15.0 mg, 0.043 mmol; 75%), yellow needles mp 195–197 °C (lit. (8) mp 193–194 °C); mixed mp with authentic (±)-usnic acid 194–196 °C; $[\alpha]_D^{26}$ 0° (*c* 0.081). The chromatographic and spectroscopic properties of this sample were identical to those of (±)-usnic acid (commercially available).

*Base Catalyzed Hydrolysis of (−)-$\Delta^{2,11}$-Enaminousnic Acid (**5**). Formation of (+)-Usnic Acid (**1**)*

A solution of (−)-$\Delta^{2,11}$-enaminousnic acid (**5**) (50 mg, 0.145 mmol) in freshly prepared 1.2 *N* sodium hydroxide (10 ml) was stirred at room temperature under nitrogen atmosphere for 0.5 h. After acidification with 1 *N* hydrochloric acid, the reaction mixture was extracted with ethyl acetate (3 × 8 ml), and the combined extracts washed with water, dried over anhydrous sodium sulfate, and evaporated under reduced pressure. Crystallization of the residue from chloroform–methanol produced pure (+)-usnic acid (**1**) (42 mg, 0.122 mmol; 84%), bright yellow needles, mp 202–204 °C; mixed mp with authentic (+)-usnic acid 202–204 °C; $[\alpha]_D^{26}$ +490° (*c* 0.095). All the spectroscopic characteristics of this sample showed identity with those of pure (+)-usnic acid (**1**).

*Reductive Cleavage of (+)-Isoxazolo[4,5-b]usnic Acid (**2**). Formation of (−)-$\Delta^{2,11}$-Enaminousnic Acid (**5**)*

A suspension of (+)-isoxazolo[4,5-*b*]usnic acid (**2**) (130 mg, 0.381 mmol) in 95% ethyl alcohol (9 ml) was hydrogenated over Adam's catalyst (PtO_2, 30 mg) at atmospheric pressure. After the uptake of 1 mol equiv. of hydrogen (9.31 ml at 25 °C) the reaction mixture was filtered through Celite and the solvent evaporated under reduced pressure to afford a colorless residue (135 mg) which was purified by preparative layer chromatography (silica gel plates, ethyl acetate) to give pure (−)-$\Delta^{2,11}$-enaminousnic acid (**5**) (125 mg, 0.364 mmol; 96%), pale yellow plates from chloroform, mp 252–253 °C; mixed mp with authentic sample of (−)-$\Delta^{2,11}$-enaminousnic acid, 252–254 °C; $[\alpha]_D^{27}$ −233° (*c* 0.095). This material was identical in all respects (chromatography, spectroscopy) with (−)-$\Delta^{2,11}$-enaminousnic acid (**5**), the condensation product of (+)-usnic acid (**1**) with aqueous ammonia (21).

Can. J. Chem. Downloaded from www.nrcresearchpress.com by 210.87.254.40 on 09/05/12
For personal use only.

Reductive Cleavage of (+)-2H-[1,2]Oxazocinousnic Acid (3). Formation of (−)-$\Delta^{2,11}$-Enaminousnic Acid (5)

A solution of (+)-2*H*-[1,2]oxazocinousnic acid (**3**) (158 mg, 0.463 mmol) in ethyl acetate (20 ml) and absolute ethyl alcohol (5 ml) was hydrogenated over Adam's catalyst (PtO_2, 50 mg) at atmospheric pressure. After 1 mol equiv. of hydrogen (11.3 ml at 25 °C) had been taken up the reaction mixture was filtered through Celite and the solvent evaporated under reduced pressure. The residue was crystallized from chloroform to produce colorless plates of (−)-$\Delta^{2,11}$-enaminousnic acid (**5**) (142 mg, 0.404 mmol; 87%).

Reductive Cleavage of (+)-Isoxazolo[5,4-a]usnic acid (4). Formation of (−)-$\Delta^{2,11}$-Enaminousnic Acid (5)

A solution of (+)-isoxazolo[5,4-*a*]usnic acid (**4**) (100 mg, 0.293 mmol) in ethyl acetate (15 ml) and absolute ethyl alcohol (5 ml) was hydrogenated over Adam's catalyst (PtO_2, 35 mg) at atmospheric pressure. After the uptake of 1 mol equiv. of hydrogen (7.16 ml at 25 °C) the reaction mixture was filtered through Celite and the solvent evaporated under reduced pressure. The residue was recrystallized from ethyl acetate to produce colorless plates of (−)-$\Delta^{2,11}$-enaminousnic acid (**5**) (97 mg, 0.282 mmol; 96.5%).

Cleavage of (+)-Isoxazolo[4,5-b]usnic Acid (2) under Basic Conditions

A suspension of (+)-isoxazolo[4,5-*b*]usnic acid (**2**) (4.0 g, 11.73 mmol) in ethyl alcohol (20 ml), and distilled water (60 ml) was treated with a solution of potassium hydroxide (40 g) in distilled water (120 ml) and heated at 70 °C (oil bath temperature) under a nitrogen atmosphere for 25 min. The resulting dark brown solution was diluted with cold distilled water (200 ml), acidified with 1 *N* hydrochloric acid, and extracted with ethyl acetate (3 × 20 ml). The combined extracts were washed with water (2 × 100 ml), dried over anhydrous sodium sulfate, and evaporated under reduced pressure. The brown foam (4.090 g) obtained was purified by column chromatography on silica gel Merck (400 g) to provide 2-(7-acetyl-4,6-dihydroxy-3,5-dimethylbenzofuranyl)-5′-(4′-carboxy-3′-methylisoxazolyl)methane (**9**), long fluffy needles from methanol (1.520 g, 4.2333 mmol; 36%), mp 258–259 °C; $[\alpha]_D$ (CH_3OH) 0° (*c* 0.205); uv λ_{max} (log ϵ) 350 (3.33), 302 (3.85), 242 (4.02); ir (Nujol) ν_{max} 3500–3000 (OH, COOH), 1720 (C=O, isoxazole carboxylic acid), 1610, 1600 (C=C, aromatic ring, isoxazole); pmr ($CDCl_3$–DMSO-d_6) δ 2.08 (3H, s, C_5-CH_3), 2.35 (3H, s, C_3–CH_3), 2.40 (3H, s, $C_{3'}$-CH_3), 2.66 (3H, s, C_7-$COCH_3$), 4.50 (2H, s, —CH_2—), 8.92 (2H, br, C_4-OH, $C_{4'}$-COOH), 13.72 ppm (1H, s, C_6-OH); ms *m/e* 359 (M^+, base peak), 313, 298, 286, 272, 257, 233, 217, 215, 161, 126, 91, 83, 43. *Anal.* calcd. for $C_{18}H_{17}O_7N$: C 60.16, H 4.77, N 3.90; found: C 60.20, H 4.78, N 3.88. High resolution molecular weight determination: calcd.: 359.100; found: 359.103.

Reaction of the Isoxazole-4′-carboxylic Acid 9 with Diazomethane. Preparation of 2-(7-Acetyl-4,6-dihydroxy-3,5-dimethylbenzofuranyl)-5′-(4′-carboxymethyl-3′-methylisoxazolyl)methane (11)

To a solution of the isoxazole-4′-carboxylic acid (**9**) (100 mg, 0.278 mmol) in dry methanol (25 ml) was added dropwise a freshly prepared ethereal solution of diazomethane until a pale yellow solution resulted. The reaction mixture was stirred at room temperature for 20 min and the solvent evaporated under reduced pressure. The residue upon recrystallization from methanol afforded the desired methyl ester (**11**) (95 mg, 0.254 mmol; 91%), silky needles, mp 217–218 °C; $[\alpha]_D$ (CH_3OH) 0° (*c* 0.0795), uv λ_{max} (log ϵ) 349 (3.35), 303 (3.85), 242 (4.04); ir (Nujol) ν_{max} 3500–3100 (OH, COOH, chelated), 1720 (C=O, isoxazole carboxylic ester), 1615 (C=C, aromatic ring); pmr ($CDCl_3$–DMSO-d_6) δ 2.11 (3H, s, C_5-CH_3), 2.40 (3H, s, C_3-CH_3), 2.42 (3H, s, $C_{3'}$-CH_3), 2.69 (3H, s, C_9-$COCH_3$), 3.90 (3H, s, $C_{4'}$-$COOCH_3$), 4.54 (2H, s, —CH_2—), 9.12 (1H, s, C_4-OH), 13.72 ppm (1H, s, C_6-OH); ms *m/e* 373 (M^+, base peak), 341, 313, 285, 270, 238, 232, 217, 215, 142, 91, 83. *Anal.* calcd. for $C_{19}H_{19}O_7N$: C 61.12, H 5.13, N 3.95; found: C 61.12, H 4.94, N 3.65. High resolution molecular weight determination: calcd.: 373.160; found: 373.120.

Base Cleavage of (+)-2H-[1,2]Oxazocinousnic Acid (3)

A solution of (+)-2*H*-[1,2]oxazocinousnic acid (**3**) (3.973 g, 11.651 mmol) in freshly prepared 20% aqueous potassium hydroxide (200 ml) was stirred at room temperature under a nitrogen atmosphere for 1.5 h. The dark brown reaction mixture was diluted with cold distilled water (200 ml), acidified with 1 *N* hydrochloric acid, and extracted with ethyl acetate (3 × 120 ml). The combined extracts were washed with water, dried over anhydrous sodium sulfate, and evaporated under reduced pressure to afford a pale yellow foam (4.508 g). Purification by column chromatography on Macherey-Nagel silica gel (160 g) yielded 8-acetyl-4-carboxy-9-hydroxy-3,10,12-trimethyl-5-oxo-2*H*-5,6-dihydro[1,2]oxazocino-[7,8,9,10-6,*c*,*d*]dibenzofuran (**10**), fluffy pale yellow needles from methanol (1.190 g, 3.314 mmol; 28%), mp 210–212 °C; $[\alpha]_D$ (CH_3OH) 0° (*c* 0.1235); uv λ_{max} (log ϵ) 356 (3.07), 287 (3.83), 237 (3.84); ir (Nujol) ν_{max} 3500–2400 (OH, NH), 1685 (C=O, carboxylic acid), 1640 (C=O, chelated aromatic acetyl), 1620 (C=O, enone system), 1590 (C=C); pmr ($CDCl_3$–DMSO-d_6) δ 2.11 (3H, s, C_{10}-CH_3), 2.33 (3H, s, C_{12}-CH_3), 2.46 (3H, s, C_3-CH_3), 2.73 (3H, s, C_8-$COCH_3$), 4.28 (2H, s, C_6-H_2), 6.36 (2H, br, C_4-COOH and C_3-NH), 13.71 ppm (1H, s, C_9-OH); ms *m/e* 359 (M^+), 317, 233, 215, 84, 44 (base peak), 43. *Anal.* calcd. for $C_{18}H_{17}O_7N$: C 59.43, H 4.85, N 3.85; found: C 59.56, H 4.72, N 3.69. High resolution molecular weight determination: calcd. for $C_{18}H_{17}O_7N$: 359.100; found: 359.098.

Acknowledgements

Financial aid from the National Research Council of Canada is gratefully acknowledged. One of us (I.H.S.) wishes to thank N.R.C.C. for a scholarship during the period of this study. We would also like to acknowledge the efforts of Ms. I. B. Krizsan in preparing the illustrations.

1. N. K. Kotchetkov and S. D. Sokolov. Adv. Heterocycl. Chem. **2**, 365 (1962).
2. A. Quilico. Heterocyclic compounds. Vol. 17. *Edited by* A. Weissberger. Interscience Publishers, New York, N.Y. 1962. p. 5.
3. R. P. Barnes. Heterocyclic compounds. Vol. 5.

Edited by R. C. Elderfield. John Wiley and Sons Inc., New York, N.Y. 1952. Chapt. 7.
4. C. F. Bean, M. C. D. Dyer, R. A. Schwarz, and C. R. Hauser. J. Org. Chem. **35**, 1806 (1970).
5. J. F. W. McOmie. Advances in organic chemistry; methods and results. Vol. 3. Interscience Publishers, New York, N.Y. 1963. p. 191.
6. G. Buchi and J. Vederas. J. Am. Chem. Soc. **94**, 9128 (1972).
7. O. Widman. Ann. **310**, 230 (1900); **324**, 139 (1902).
8. C. Schopf and K. Heuck. Ann. **459**, 263 (1927).
9. C. Schopf and F. Ross. Ann. **546**, 1 (1941).
10. G. Speroni. Heterocyclic compounds. Vol. 17. *Edited by* R. H. Wiley. Interscience Publishers, New York, N.Y. 1962. Chapt. 5.
11. S. Forsen, M. Nilsson, and C. A. Wachtmeister. Acta Chem. Scand. **16**, 583 (1962).
12. The Sadtler standard nuclear magnetic resonance spectra catalog. Sadtler Research Laboratories, Philadelphia, Pa. Spectrum No. 4402.
13. T. Nishkiwaki. Org. Mass Spectrom. **5**, 123 (1971).
14. D. C. Nonhebel. Org. Mass Spectrom. **3**, 1519 (1970).
15. R. K. M. R. Kallury and R. G. Cooks. Aust. J. Chem. **22**, 563 (1969).
16. B. Singh and E. F. Ullman. J. Am. Chem. Soc. **89**, 6911 (1967).
17. E. C. Taylor and E. E. Garcia. J. Org. Chem. **29**, 2116 (1964).
18. A. C. Cope and N. A. Lebel. J. Am. Chem. Soc. **82**, 4656 (1960).
19. S. MacKenzie. J. Am. Chem. Soc. **77**, 2214 (1955).
20. D. H. R. Barton and T. Bruun. J. Chem. Soc. 603 (1952).
21. J. P. Kutney and I. H. Sanchez. Can. J. Chem. **54**, 2795 (1976).
22. A. M. Patterson, L. T. Capell, and D. F. Walker. The ring index. 2nd ed. American Chemical Society, Washington, D.C. 1960. p. 388.

Can. J. Chem. Downloaded from www.nrcresearchpress.com by 210.87.254.40 on 09/05/12
For personal use only.

Studies in the usnic acid series. III.[1] The base catalyzed usnic acid – isousnic acid rearrangement. The synthesis of (+)-isousnic acid

JAMES P. KUTNEY, IGNACIO H. SANCHEZ, AND TREVOR YEE

Department of Chemistry, University of British Columbia, 2075 Wesbrook Place, Vancouver, B.C., Canada V6T 1W5

Received July 2, 1976

JAMES P. KUTNEY, IGNACIO H. SANCHEZ, and TREVOR YEE. Can. J. Chem. **54**, 3721 (1976).

Investigations concerning the alkaline cleavage of (+)-isoxazolo[4,5-*b*]usnic acid (**8**) are described. During these studies a novel rearrangement from the 'normal' (usnic acid) to the 'iso' (isousnic) series was revealed. The rearrangement process was then utilized in the synthesis of (+)-isousnic acid (**3**).

JAMES P. KUTNEY, IGNACIO H. SANCHEZ et TREVOR YEE. Can. J. Chem. **54**, 3721 (1976).

On décrit des études concernant la coupure alcaline de l'acide (+) isoxazolo[4,5-*b*] usnique (**8**). Au cours de ces études, on a découvert un nouveau réarrangement permettant de passer de la série normale (acide usnique) à la série iso (isousnique). On a utilisé ce réarrangement dans la synthèse de l'acide (+) isousnique (**3**).

[Traduit par le journal]

Can. J. Chem. Downloaded from www.nrcresearchpress.com by 210.87.254.42 on 09/05/12
For personal use only.

During our synthetic investigations leading towards the synthesis of (+)-6-desacetylusnic acid (**2***a*), a biodegradation product of (+)-usnic acid,[2] we have discovered a novel base-catalyzed usnic acid – isousnic acid rearrangement which eventually led to the preparation of optically active (+)-isousnic acid (**3**) (2–5), the natural isomer of **1**. The results of these investigations are discussed and, in addition, some clarification of previously published chemistry in the usnic acid area is provided.

Barton and Bruun (6) first studied the behaviour of (+)-usnic acid anhydrophenylhydrazone (**4**) (7) with methanolic potassium hydroxide and were able to isolate a material, mp 206–207 °C, having the molecular formula $C_{23}H_{22}O_5N_2$ for which the structure **5** (referred to as the 'normal' series in this present discussion) was postulated. Moreover, under more vigorous conditions (aqueous or ethanolic potassium hydroxide) the high melting, optically inactive pyrazole-4-carboxylic acid (**6**) was obtained. More recently, compound **5** has been similarly prepared by Takahashi *et al.* (8) via (−)-usnic acid isomethoxide monoacetate (**7**) (9).

Although the preparation of **5** according to the Barton conditions (6) could be readily achieved in our laboratory, the regeneration of the β-triketone system characteristic of **1** from the *N*-phenyl pyrazole moiety proved troublesome and could not be achieved to any satisfactory degree. In our search for suitable compounds that would allow such a regeneration at appropriate stages in the synthetic pathway, we prepared the alkali-stable isoxazole derivative **8** (1) (Fig. 1). While the original cleavage conditions (6) employed with **8** resulted in severe decomposition and less than 5% of the desired deacylated material, the required reaction was successfully carried out in a water – ethyl alcohol mixture at 70 °C for a short period of time. From the complex reaction mixture, three different types of products were isolated: type I, those resulting from solvent addition to the C_4—C_{4a} double bond (**9** and **10**); type II, those obtained from solvent addition, removal of the aromatic acetyl group and rearrangement to the 'iso' series (**11** and **12**), and type III, representing cleavage of the C-ring in the present skeleton (**13**).

The recognition of the interesting base-catalyzed rearrangement from the 'normal' to the 'iso' series (**8** → **11** and **12**) was made possible from an extensive analysis of spectroscopic data which were not available to the earlier workers (6, 8) in this area. In particular, nuclear magnetic resonance (nmr) and circular dichroism (cd) data could be effectively utilized for this purpose and some specific comments concerning these results are appropriate.

The postulated structures for the compounds in the normal series (type I, **9** and **10**; type III, **13**) are based, in part, on previous observations by Asahina and Okazaki (10), Dean and Robert-

[1]For part II, see ref. 1.

[2]J. P. Kutney, I. H. Sanchez, and T. Yee, manuscript in preparation.

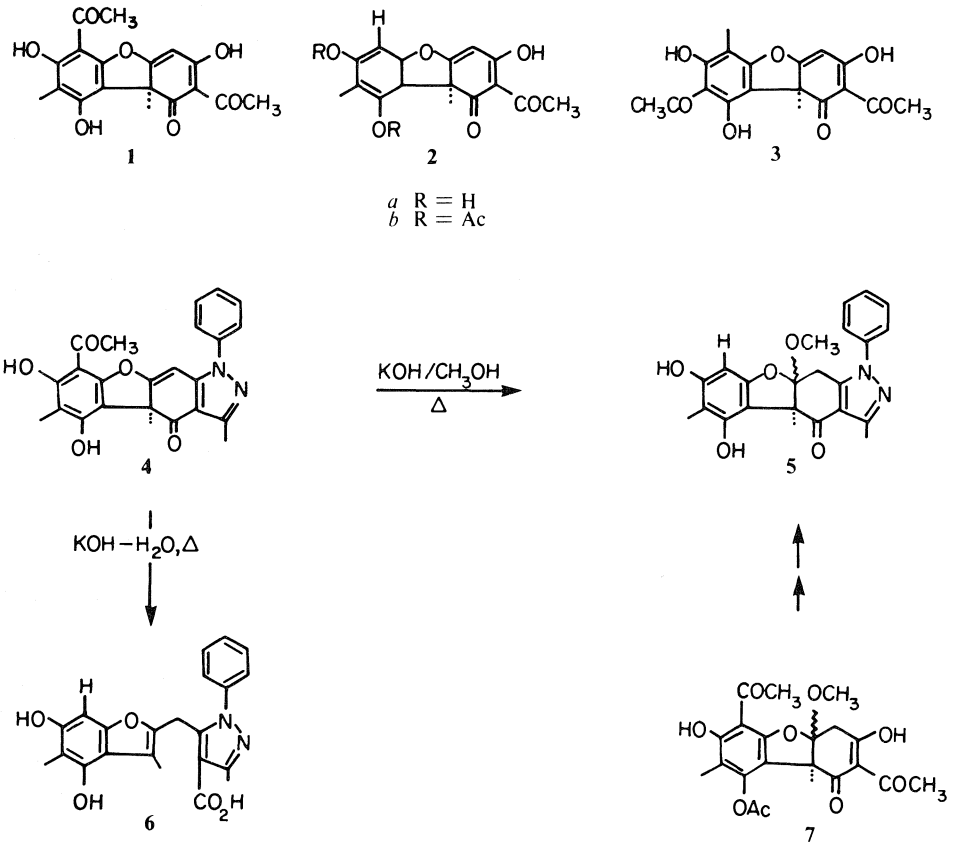

son (11), and Shibata and co-workers (12, 13), but primarily on a careful analysis of the typical chemical shifts observed in the nmr spectra of the normal and iso series (Tables 1 and 2) and the cd data (Table 3).

Table 1 illustrates the characteristic chemical shift for the ring A acetyl group which, independent of any modification in ring C, always occurs at lower field ($\Delta\delta$ 0.05–0.16 ppm) for the compounds in the iso series.

Furthermore, the chemical shifts observed for the C_4-methylene protons in the C_{4a}-α- (com-

TABLE 1. The observed chemical shifts for the acetyl groups in the usnic (normal) and isousnic acid (iso) series

Compound	Chemical shift, ppm (δ units)			
	C_6-$COCH_3$	C_8-$COCH_3$	C_2-$COCH_3$	C_{11}-CH_3
Normal series				
(+)-Usnic acid (**1**)	2.70		2.70	—
(+)-Isoxazolo[4,5-*b*]usnic acid (**8**)	2.70		—	2.51
(−)-Dihydrousnic acid (**21**)	2.64		2.60	—
(+)-Usnic acid anhydrophenylhydrazone (**4**)	2.63		—	2.60
Cleavage product (**10**)	2.55		—	2.42
Cleavage product (**13**)	2.66		—	2.40
Iso series				
(+)-Isousnic acid (**3**)		2.77	2.68	—
(+)-Isodihydrousnic acid (**22**) (5)		2.69	2.58	—
(+)-Isousnic acid anhydrophenylhydrazone (**23**) (5)		2.79	—	2.60
(−)-Placodiolic acid (**14**) (15)		2.76	2.69	—

Can. J. Chem. Downloaded from www.nrcresearchpress.com by 210.87.254.42 on 09/05/12
For personal use only.

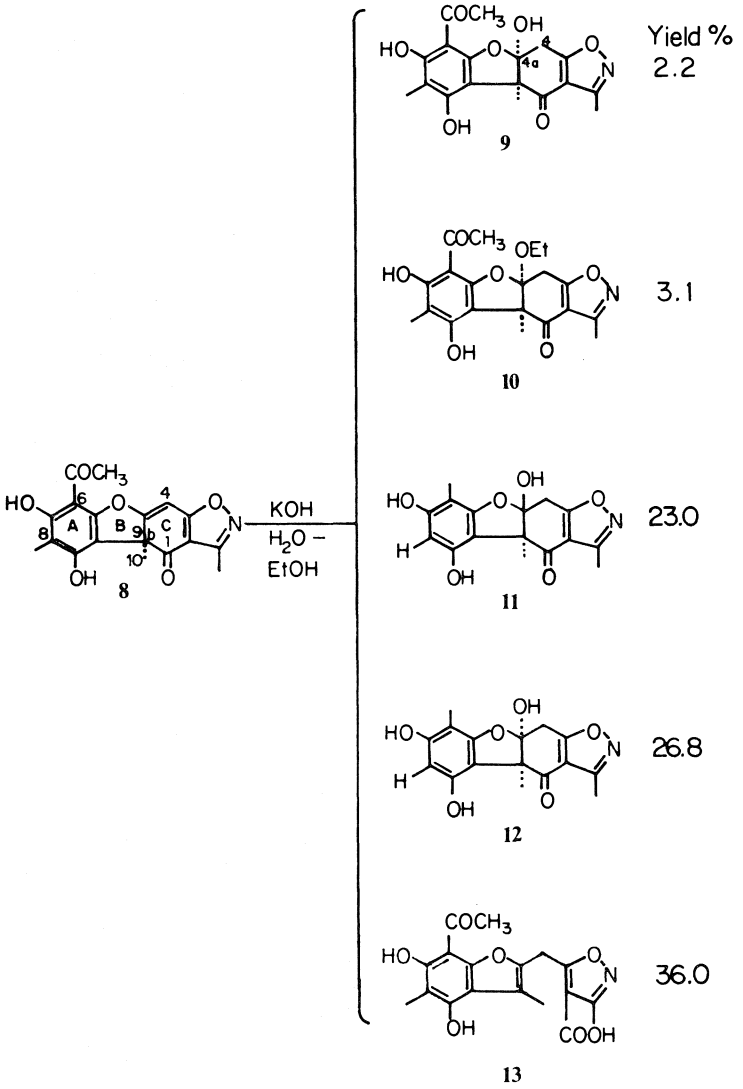

FIG. 1. The alkaline cleavage of (+)-isoxazolo[4,5-*b*]usnic acid (**8**).

pounds **10**, **12** and **21**) and β-series (compound **11**) can be used as characteristic in assigning the configuration of the C_{4a}-substituent, since we have noted that for the α-series they consistently occur at a higher field than those for the β-series (Table 2). These assignments were made only after careful examination of molecular models which revealed that only in the C_{4a}-α-series is the β-hydrogen of the C_4-methylene group seen to be directly above the plane of the aromatic ring A, thus experiencing an anisotropic shielding (14). From entry 5 in Table 2, showing the reported data for (−)-placodiolic acid (**14**) (15), we were able to extend our observations to the enantiomeric series derived from (−)-usnic acid (**15**) (3) and show that in this case the opposite reasoning applies.

Finally, the angular methyl group (C_{9b}-methyl) is also responsive to the change in conformation brought about by the introduction of a substituent at the C_{4a}-position, occurring at lower field for the α-series (*cis*-B/C junction, for example **10** and **12**) than for the β-series (*trans*-B/C junction, for example, **11**) in both the

Can. J. Chem. Downloaded from www.nrcresearchpress.com by 210.87.254.42 on 09/05/12
For personal use only.

TABLE 2. The observed chemical shifts for the C_4-methylene protons and the C_{9b}-methyl group in the normal and iso series

Compound	Chemical shift, ppm (δ units)	
	C_{4a}-Methylene group	C_{9b}-Methyl group
(−)-Dihydrousnic acid (**21**)	3.10	1.70
Cleavage product (**10**) (α-OEt)	3.17	1.94
Cleavage product (**12**) (α-OH)	3.08	1.88
Cleavage product (**11**) (β-OH)	3.53	1.68
(−)-Placodiolic acid (**14**) (15)	3.37	1.46
(+)-Isodihydrousnic acid (**22**) (5)	3.10	1.70

TABLE 3. The circular dichroism properties of the cleavage products of (+)-isoxazolo[4,5-*b*]usnic acid (**8**)

Compound	Circular dichroism properties, λ_{max} ($\Delta\epsilon$)		
9 (C_{4a}-αOH)	280(+6.08)	251(+8.42)	225(−14.51)
10 (C_{4a}-αOEt)	279(+11.11)	250(+14.10)	226(−26.87)
11 (C_{4a}-βOH)	330(+2.64)	276(−0.61)	236(+11.89)
12 (C_{4a}-αOH)	295(+4.21)	267(+9.92)	239(−1.97)

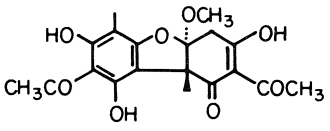

14

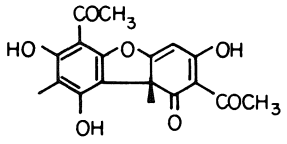

15

normal (entries 1 and 2 in Table 2) and iso compounds (entries 3, 4, and 6) as well as the enantiomeric family (entry 5).

Similar differentiation between the normal and iso series can be made from analysis of the cd characteristics of the various compounds (Table 3).

The next step in our synthetic scheme (Fig. 2) was the dehydration of the C_{4a}-hydroxy derivatives **11** and **12** and, although a variety of dehydrating agents were studied, the best experimental conditions were those employed by Barton and co-workers (6) in their synthesis of (±)-usnic acid, namely a 0.5% (v/v) solution of concentrated sulfuric acid in acetic anhydride at 50 °C under a nitrogen atmosphere. In this manner the desired unsaturated diacetate **14** was obtained in over 90% yield. In the nmr spectrum of **14**, the aromatic proton was seen as a singlet at δ 6.72. The lack of correspondence with the normal series, suggestive of a rearrangement, was first noted at this point since the aromatic proton in (+)-6-desacetylusnic acid diacetate (*2b*) (1), a normal series derivative, resonates at δ 6.81. Additional evidence for this rearrangement was obtained through saponification (1 *N* NaOH) to the diphenol **15**, which showed, in its nmr spectrum, the aromatic proton at δ 6.31. This proton signal is usually observed at δ 6.20 in the normal series (for example, in diphenol *2a*). Treatment of **15** with acetyl chloride – boron trifluoride etherate in dichloromethane (17) regenerated **14** in 87% yield thereby excluding any possibility of rearrangement during this conversion.

Regeneration of the protected β-triketone system was carried out by hydrogenolysis (1) (H_2-PtO_2/EtOH) of the isoxazole O—N bond in **14** to produce, in 95% yield, the expected diacetate **16**. Alkaline treatment (1 *N* NaOH) of **16** furnished, in 75% yield, (+)-8-desacetylisousnic acid (**17**), the synthetic isomer of the biodegradation metabolite (*2a*). Significant differences between these two materials (*i.e.* normal *vs.* iso-series) were observed in both their nmr (Table 4) and cd spectra (Table 5).

In order to complete the synthesis of (+)-isousnic acid (**3**) from the synthetic intermediate **17**, it is necessary only to introduce an acetyl group at the 8-position. Although the base-

Can. J. Chem. Downloaded from www.nrcresearchpress.com by 210.87.254.42 on 09/05/12
For personal use only.

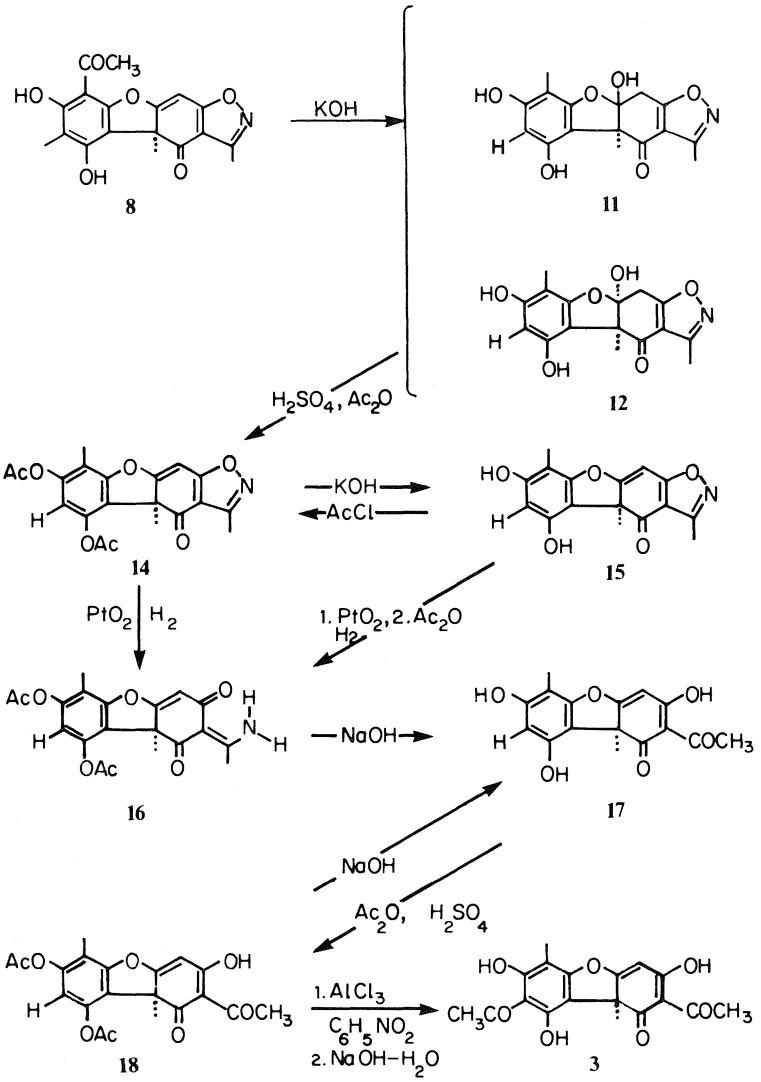

FIG. 2. The synthesis of (+)-isousnic acid (**3**).

catalyzed acetylation (pyridine–Ac_2O) of the diphenol **17** produces the desired diacetate **18** in only 35% yield, it was observed, and this is a general characteristic of the usnic acid series (2), that acidic conditions (H_2SO_4–Ac_2O) greatly increased the yield of the diacetate (87%). Finally, the diacetate **18** was treated under the Fries rearrangement conditions (18) (anhydrous aluminum trichloride in anhydrous nitrobenzene) to produce, in 62% yield, synthetic (+)-isousnic acid identical in all respects with an authentic sample kindly provided by Professor S. Shibata. Table 6 presents a comparison of the nmr data of (+)-usnic acid (1) and (+)-isousnic acid (**3**).

The final point of interest was then to determine whether the rearrangement has indeed occurred during the base-catalyzed aromatic deacylation (*i.e.* **8** → **11** and **12**). In consideration of our synthetic scheme (Figs. 1 and 2), we decided to look into the other possible conversion where rearrangement could have occurred, namely the acid-catalyzed dehydration of the hemiacetals **11** and **12** (*i.e.* **11** and **12** → **14**). Thus a sample of **12** was acetylated (Pyr–Ac_2O) at

Can. J. Chem. Downloaded from www.nrcresearchpress.com by 210.87.254.42 on 09/05/12
For personal use only.

Can. J. Chem. Downloaded from www.nrcresearchpress.com by 210.87.254.42 on 09/05/12
For personal use only.

TABLE 4. Proton magnetic resonance data of (+)-8-desacetylisousnic acid (**17**) and (+)-6-desacetylusnic acid (**2***a*) and their corresponding diacetates (in ppm, δ scale)

Functionality	**17** $CDCl_3$	**17** C_6D_6–$CDCl_3$	**2***a* $CDCl_3$	**18** $CDCl_3$	**2***b* $CDCl_3$
C_{9b}-CH_3	1.70	1.72	1.70	1.80	1.78
C_6-CH_3	2.07	2.13	—	2.13	—
C_8-CH_3	—	—	2.11	—	1.97
C_7-$OCOCH_3$	—	—	—	2.31	2.31
C_9-$OCOCH_3$	—	—	—	2.40	2.43
C_2-$COCH_3$	2.59	2.65	2.61	2.54	2.52
C_4-H	5.80	5.89	5.62	5.87	5.81
C_6-H	—	—	6.26	—	6.81
C_8-H	6.23	6.22	—	6.69	—
C_7-OH	8.85	5.90	5.67	—	—
C_9-OH	9.71	9.95	10.23	—	—
C_3-OH	18.71	18.65	18.64	18.25	18.41

TABLE 5. Circular dichroism data for (+)-6-desacetylusnic acid (**2***a*) and (+)-8-desacetylusnic acid (**17**): λ_{max} ($\Delta\epsilon$)

2*a*		**17**	
CH_3OH	CH_3OH + KOH	CH_3OH	CH_3OH + KOH
328(+9.99)	345(+8.11)	325(+9.43)	342(+7.81)
284(−6.66)	310(+6.86)	282(−6.73)	309(+6.20)
262(−3.53)	285(+1.66)	264(−5.66)	285(−1.61)
241(+13.11)	264(−12.90)	238(+12.40)	266(−13.74)
	236(+10.19)		

TABLE 6. Proton magnetic resonance data of (+)-usnic acid (**1**) and (+)-isousnic acid (**3**)

Functionality	(+)-Usnic acid (**1**)	(+)-Isousnic acid (**3**)
C_{9b}-CH_3	1.76	1.85
C_6-CH_3	—	2.10
C_8-CH_3	2.10	—
C_2-$COCH_3$	2.70	2.68
C_6-$COCH_3$	2.70	—
C_8-$COCH_3$	—	2.77
C_4-H	5.96	5.96
C_9-OH	11.01	11.28
C_7-OH	13.31	14.35
C_3-OH	18.83	18.81

room temperature to produce **19**, for which the retention of configuration of the C_{4a}-substituent was deduced from its nmr spectrum (C_4-methylene protons occurring at δ 3.38 as an AB quartet, J = 18 Hz). This material, when reacted under dehydration conditions (16) identical to those employed earlier produced, in 70% yield, the diacetate **14**, suggesting that the epimeric hemiacetals **11** and **12** must already exist as rearranged species. Moreover, if the rearrangement was to occur at this stage, polyacetylated compounds derived from the ring-opened intermediates should also be present in the reaction mixture, as has been demonstrated (19) in a similar series of compounds. However, since even after careful analysis of the reaction products no such materials have been found, we postulate that the rearrangement occurs during the alkaline treatment. On this basis, we propose the corrected structure **20** (*i.e.* iso series) for compound **5**, obtained during the methanolic potassium hydroxide treatment (6) of (+)-usnic acid anhydrophenylhydrazone (**4**).

It must be mentioned here that the only other case in which such an interconversion has been reported (12, 13, 20) involves the pyrolytic transformation of (−)-dihydrousnic acid (**21**) into (+)-isodihydrousnic acid (**22**), which, as expected, reverts to the normal series **21** even during recrystallization.

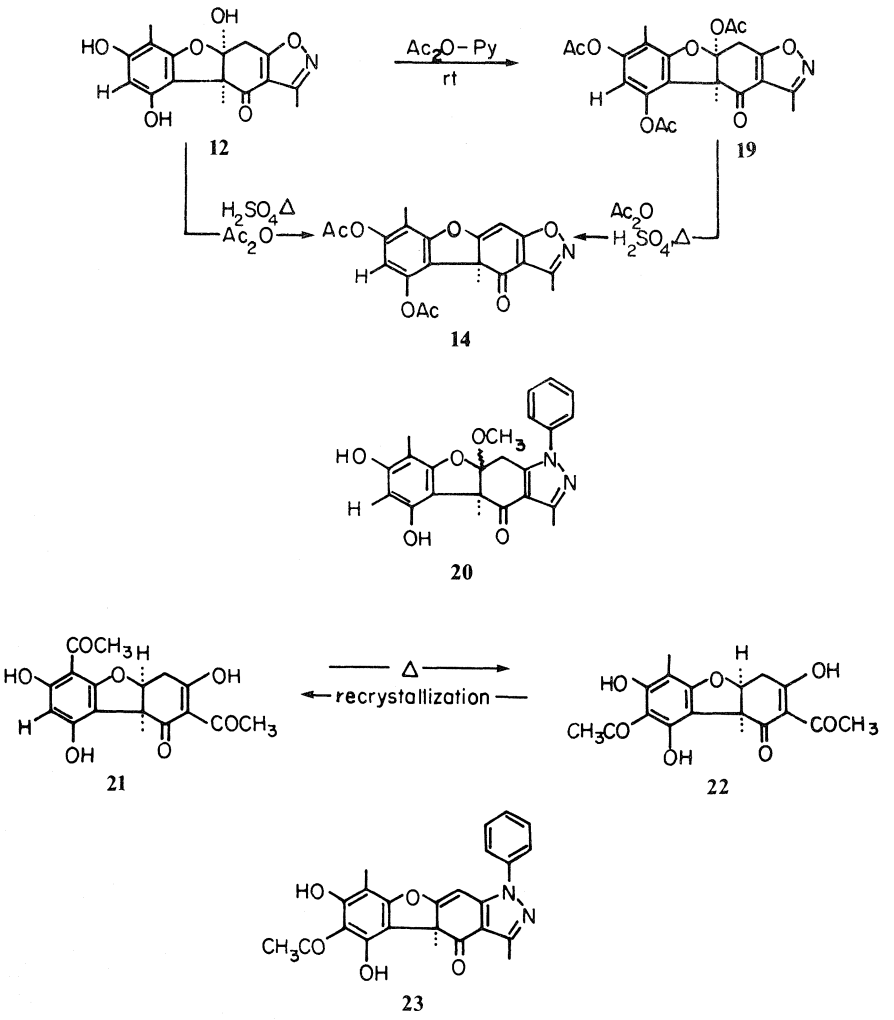

In conclusion, these studies have clarified some of the interesting chemistry inherent in the usnic acid series and have provided evidence for a novel rearrangement process. The results of these investigations and their relevance to biodegradation studies in this area will form the subject of future publications.

Experimental

All details concerning spectral measurements, chromatographic separations, etc. are provided in the accompanying publication (1). The numbering system employed is that approved for the dibenzofuran series (21).

*Base Cleavage of (+)-Isoxazolo[4,5-b]usnic Acid (**8**) – Experiment I*

To a suspension of (+)-isoxazolo[4,5-*b*]usnic acid (**8**) (50 mg, 0.146 mmol) in dry methanol (10 ml) was added powdered potassium hydroxide (500 mg) and the reaction mixture refluxed under a nitrogen atmosphere for 3 h. Examination by thin layer chromatography (silica gel – oxalic acid, solvent system *B*) revealed mostly dark brown decomposition products. Therefore, the reaction mixture was not investigated further.

*Base Cleavage of (+)-Isoxazolo[4,5-b]usnic Acid (**8**) – Experiment II*

A suspension of (+)-isoxazolo[4,5-*b*]usnic acid (**8**) (4.0 g, 11.73 mmol) in ethyl alcohol (20 ml), and distilled water (60 ml) was treated with a solution of potassium hydroxide (40 g) in distilled water (120 ml) and heated at 70 °C (oil bath temperature) under a nitrogen atmosphere for 25 min. The resulting dark brown solution was diluted with cold distilled water (200 ml), acidified with 1 *N* hydrochloric acid, and extracted with ethyl acetate (3 × 20 ml). The combined extracts were washed with water (2 × 100 ml), dried over anhydrous sodium sulfate,

Can. J. Chem. Downloaded from www.nrcresearchpress.com by 210.87.254.42 on 09/05/12
For personal use only.

Can. J. Chem. Downloaded from www.nrcresearchpress.com by 210.87.254.42 on 09/05/12
For personal use only.

and evaporated under reduced pressure. The brown foam (4.090 g) obtained was purified by column chromatography on silica gel Merck (400 g). The following products were obtained.

Fraction I. (+)-α-Hydroxyisoxazolo[4,5-b]usnic Acid ***(9)*** *(10-Acetyl-1a,2,6,6a-tetrahydro-1aα,7,9-trihydroxy-5,6aα,8-trimethyl-6-oxoisoxazolo[4,5-b]dibenzofuran*

Colorless prisms from chloroform–ether, mp 202–204 °C; (0.100 g, 0.2780 mmol; 2.2%); $[\alpha]_D^{25}$ (CH_3OH) +435° (*c* 0.092); uv λ_{max} (log ε) 330 (3.27), 286 (3.79), 223 (3.91); ir (KBr) ν_{max} 3600–3100 (OH, chelated), 1680 (C=O, enone system), 1620 (C=O, chelated aromatic acetyl; C=C, aromatic ring); ms *m/e* 359 (M^+), 302, 236, 85, 83 (base peak). *Anal.* calcd. for $C_{18}H_{17}O_7N$: C 60.17, H 4.77, N 3.90; found: C 60.22, H 4.69, N 3.91. High resolution molecular weight determination: calcd.: 359.100; found: 359.104. cd λ_{max} (Δε) 280 (+6.08), 251 (+8.42), 225 (−14.51).

Fraction II. (+)-α-Ethoxyisoxazolo[4,5-b]usnic Acid ***(10)*** *(10-Acetyl-1aα-ethoxy-7,9-dihydroxy-1a,2,6,6a-tetrahydro-5,6aα-8-trimethyl-6-oxoisoxazolo[4,5-b]-dibenzofuran)*

Colorless hexagonal prisms from benzene (0.145 g, 0.374 mmol; 3.1%), mp 219–220 °C; $[\alpha]_D^{26}$ (CH_3CN) +218° (*c* 0.1235); uv λ_{max} (log ε) 330 (3.54), 285 (3.93), 223 (4.00); ir ν_{max} 3500–3200 (OH, chelated), 1695 (C=O, enone system), 1620 (C=O, chelated aromatic acetyl), 1595 (C=C, aromatic ring); pmr δ 1.18 (3H, t, *J* = 7 Hz, C_{4a}-αOCH$_2$CH$_3$), 1.94 (3H, s, C_{9b}-CH$_3$), 2.04 (3H, s, C_8-CH$_3$), 2.42 (3H, s, C_{11}-CH$_3$), 2.55 (3H, s, C_6-COCH$_3$), 3.17 (2H, AB q, *J* = 18 Hz, C_4-H$_2$), 3.74 (2H, q, *J* = 7 Hz, C_{4a}-OCH$_2$CH$_3$), 6.58 (1H, br, C_9-OH), 13.46 (1H, s, C_7-OH); ms *m/e* 387 (M^+, base peak), 372, 235, 233, 217, 154, 82. *Anal.* calcd. for $C_{20}H_{21}O_7N$: C 62.01, H 5.46, N 3.62; found: C 62.10, H 5.44, N 3.69. High resolution molecular weight determination: calcd.: 387.132; found: 387.1315. cd λ_{max} (Δε) 279 (+11.11), 250 (+14.10), 226 (−26.87).

Fraction III. (+)-β-Hydroxydesacetylisoxazolo[4,5-b]-isousnic Acid ***(11)*** *(1a,2,6,6a-Tetrahydro-1aβ,7,9-trihydroxy-5,6aα,10-trimethyl-6-oxoisoxazolo[4,5-b]-dibenzofuran)*

Colorless prisms from benzene containing traces of ethyl acetate (0.856 g, 2.7 mmol; 23%), mp 176.5–177.5 °C; $[\alpha]_D^{26}$ (CH_3CN) +193° (*c* 0.031); uv λ_{max} (log ε) 329 (2.35), 260 (2.30), 223 (4.06); ir (KBr) ν_{max} 3600–3200 (OH, chelated), 1665 (C=O, enone system), 1620 (C=C, aromatic ring); pmr ($CDCl_3$–DMSO-d_6) δ 1.68 (3H, s, C_{9b}-CH$_3$), 1.91 (3H, s, C_6-CH$_3$), 2.39 (3H, s, C_{11}-CH$_3$), 3.53 (2H, AB q, *J* = 18 Hz, C_4-H$_2$), 6.06 (1H, s, C_8-H), 7.10 (1H, br, C_{4a}-βOH), 7.72 (1H, br, C_7-OH), 8.49 ppm (1H, br, C_9-OH); ms *m/e* 317 (M^+, base peak), 194, 193, 178, 124, 79, 52. *Anal.* calcd. for $C_{16}H_{15}O_6N$: C 60.56, H 4.77, N 4.41; found: C 60.50, H 4.69, N 4.39. High resolution molecular weight determination: calcd.: 317.090; found: 317.088. cd λ_{max} (Δε) 330 (+2.64), 276 (−0.61), 236 (+11.89).

Fraction IV. (+)-α-Hydroxydesacetylisoxazolo[4,5-b]-isousnic Acid ***(12)*** *(1a,2,6,6a-Tetrahydro-1aα,7,9-trihydroxy-5,6aα,10-trimethyl-6-oxoisoxazolo[4,5-b]-dibenzofuran)*

Colorless prisms from chloroform – petroleum ether (30–60 °C) (0.997 g, 3.145 mmol; 27%), mp 224–226 °C; $[\alpha]_D^{26}$ (CH_3CN) +307° (*c* 0.0325); uv λ_{max} (log ε) 286 (3.08), 262 (3.20), 221 (3.84); ir ν_{max} 3600–3100 (OH, chelated), 1690 (C=O, enone system), 1640, 1600 (C=C); pmr ($CDCl_3$–DMSO-d_6) δ 1.88 (6H, s, C_{9b}- and C_6-CH$_3$), 2.37 (3H, s, C_{11}-CH$_3$), 3.08 (2H, AB q, *J* = 18 Hz, C_4-H$_2$), 5.94 (1H, br, C_{4a}-αOH), 6.00 (1H, s, C_8-H), 7.64 (1H, br, C_7-OH), 8.00 ppm (1H, br, C_9-OH); ms *m/e* 317 (M^+, base peak), 275, 260, 246, 219, 194, 178. *Anal.* calcd. for $C_{16}H_{15}O_6N$: C 60.56, H 4.77, N 4.41; found: C 60.47, H 4.72, N 4.45. High resolution molecular weight determination: calcd.: 317.090; found: 317.087. cd λ_{max} (Δε) 295 (+4.21), 267 (+9.92), 239 (−1.97).

Fraction V. 2-(7-Acetyl-4,6-dihydroxy-3,5-dimethylbenzofuranyl)-5′-(4′-carboxy-3′-methylisoxazolyl)-methane ***(13)***

Long fluffy needles from methanol (1.520 g, 4.2333 mmol; 36%), mp 258–259 °C; $[\alpha]_D^{26}$ (CH_3OH) 0° C (*c* 0.205); uv λ_{max} (log ε) 350 (3.33), 302 (3.85), 242 (4.02); ir (Nujol) ν_{max} 3500–3000 (OH, COOH), 1720 (C=O, isoxazole carboxylic acid) 1610, 1600 (C=C, aromatic ring, isoxazole); pmr ($CDCl_3$–DMSO-d_6) δ 2.08 (3H, s, C_5-CH$_3$), 2.35 (3H, s, C_3-CH$_3$), 2.40 (3H, s, $C_{3'}$-CH$_3$), 2.66 (3H, s, C_7-COCH$_3$), 4.50 (3H, s, —CH$_2$), 8.92 (2H, br, C_4-OH, $C_{4'}$-COOH), 13.72 ppm (1H, s, C_6-OH); ms *m/e* 359 (M^+, base peak), 313, 298, 286, 272, 257, 233, 217, 215, 161, 126, 91, 83, 43. *Anal.* calcd. for $C_{18}H_{17}O_7N$: C 60.16, H 4.77, N 3.90; found: C 60.20, H 4.78, N 3.88. High resolution molecular weight determination: calcd.: 359.100; found: 359.103.

Acid Catalyzed Dehydration of (+)-α-Hydroxydesacetylisoxazolo[4,5-b]isousnic Acid ***(12)****. Formation of (+)-Desacetylisoxazolo[4,5-b]isousnic Acid Diacetate* ***(14)*** *(7,9-Diacetoxy-6,6a-dihydro-5,6aα,10-trimethyl-6-oxoisoxazolo[4,5-b]dibenzofuran)*

A solution of (+)-α-hydroxydesacetylisoxazolo[4,5-*b*]-isousnic acid (**12**) (411 mg, 1.296 mmol) in a mixture of concentrated sulfuric acid in acetic anhydride (0.5%, 4 ml) was heated at 50 °C (oil bath temperature) under a nitrogen atmosphere for 1 h. The resulting light brown solution was poured onto crushed ice (15 g), stirred at room temperature for 1 h, and then extracted with ethyl acetate (2 × 20 ml). The combined extracts were washed with water, dried over anhydrous sodium sulfate, and evaporated under reduced pressure to afford a colorless foam (530 mg), which was purified by column chromatography on Macherey-Nagel silica gel (25 g) to yield pure (+)-desacetylisoxazolo[4,5-*b*]isousnic acid diacetate (**14**) (458.5 mg, 1.195 mmol; 93%); colorless prisms from chloroform–methanol or ethyl alcohol, mp 148.5–149.5 °C; $[\alpha]_D^{26}$ (CH_3CN) +250° (*c* 0.024); uv λ_{max} (log ε) 300 (3.41), 245 (3.75), 216 (4.21); ir ν_{max} 1770 (C=O, acetates), 1675 (C=O, enone system), 1620–1600 (C=C); pmr δ 1.83 (3H, s, C_{9b}-CH$_3$), 2.16 (3H, s, C_6-CH$_3$), 2.32 (3H, s, C_7-OCOCH$_3$), 2.49 (3H, s, C_9-OCOCH$_3$), 2.53 (3H, s, C_{11}-CH$_3$), 6.00 (1H, s, C_4-H), 6.72 ppm (1H, s, C_8-H); ms *m/e* 386 (M^+, base peak), 344, 302, 260, 218, 217, 190, 135, 44. *Anal.* calcd. for $C_{20}H_{17}O_7N$: C 62.22, H 4.47, N 3.65; found: C 62.72, H 4.50, N 3.57. High resolution molecular weight determination: calcd.: 386.100; found: 386.099. cd λ_{max} (Δε) 330 (+18.45), 265 (−5.88), 225 (−15.73).

Can. J. Chem. Downloaded from www.nrcresearchpress.com by 210.87.254.42 on 09/05/12
For personal use only.

*Acid Catalyzed Dehydration of (+)-β-Hydroxydesacetylisoxazolo[4,5-b]isousnic Acid (**11**). Formation of (+)-Desacetylisoxazolo[4,5-b]isousnic Acid Diacetate (**14**)*

A solution of (+)-β-hydroxydesacetylisoxazolo[4,5-*b*]-isousnic acid (**11**) (200 mg, 0.630 mmol) in a mixture of concentrated sulfuric acid in acetic anhydride (0.5%; 2 ml) was heated at 50 °C (oil bath temperature) under a nitrogen atmosphere for 1 h. The reaction mixture was poured over cracked ice (10 g) and extracted with ethyl acetate (3 × 10 ml). The combined extracts were washed with water (4 × 5 ml), dried over anhydrous sodium sulfate, and evaporated under reduced pressure to afford a colorless foam (278 mg) which was purified by column chromatography on Macherey-Nagel silica gel (10 g) to produce pure (+)-desacetylisoxazolo[4,5-*b*]isousnic acid diacetate (**14**) (232 mg, 0.605 mmol; 96%), colorless prisms from ethyl alcohol, mp 148–149 °C; mixed mp with authentic (+)-desacetylisoxazolo[4,5-*b*]isousnic acid diacetate, 148–150 °C. Both samples showed identical spectroscopic properties.

*Acid Catalyzed Dehydration of a Mixture of (+)-α- and (+)-β-Hydroxydesacetylisoxazolo[4,5-b]isousnic Acid (**12** and **11**)*

A mixture of α-hydroxydesacetyl (**12**) (224 mg, 0.706 mmol) and β-hydroxydesacetylisoxazolo[4,5-*b*]isousnic acid (**11**) (216 mg, 0.681 mmol) was dissolved in a solution of concentrated sulfuric acid in acetic anhydride (0.5%, 4 ml) and heated at 50 °C (oil bath temperature) under a nitrogen atmosphere for 1 h. The resulting solution was poured onto cracked ice (25 g) and extracted with ethyl acetate (3 × 30 ml). The combined extracts were thoroughly washed with water, dried over anhydrous sodium sulfate, and evaporated under reduced pressure. The residual foam (417 mg) was purified by column chromatography on Macherey-Nagel silica gel (20 g) to afford pure (+)-desacetylisoxazolo[4,5-*b*]isousnic acid diacetate (**14**) (387.5 mg, 1.011 mmol; 73%), colorless prisms from ethyl alcohol, mp 147–149 °C; mixed mp with an authentic sample from previous experiments, 147–149 °C.

*Basic Hydrolysis of (+)-Desacetylisoxazolo[4,5-b]isousnic Acid Diacetate (**14**). Preparation of (+)-Desacetylisoxazolo[4,5-b]isousnic Acid (**15**) (6,6a-Dihydro-7,9-dihydroxy-5,6aα,10-trimethyl-6-oxoisoxazolo-[4,5-b]dibenzofuran)*

A solution of (+)-desacetylisoxazolo[4,5-*b*]isousnic acid diacetate (**14**) (320 mg, 0.535 mmol) in freshly prepared 1 *N* sodium hydroxide (4 ml) and tetrahydrofuran (1 ml) was stirred at room temperature under a nitrogen atmosphere for 1 h. The reaction mixture was diluted with cold distilled water (5 ml), acidified with 1 *N* hydrochloric acid, and extracted with ethyl acetate (3 × 10 ml). The combined extracts were washed with water, dried over anhydrous sodium sulfate, and evaporated under reduced pressure to afford a colorless foam (272 mg). Purification by column chromatography on Macherey-Nagel silica gel (30 g) produced (+)-desacetylisoxazolo-[4,5-*b*]isousnic acid (**15**) (214 mg, 0.715 mmol; 86%), colorless needles from chloroform–benzene, mp 140–142 °C; $[\alpha]_D^{26}$ (CH_3CN) +255° (*c* 0.0235); uv (CH_3CN) λ_{max} (log ε) 301 (3.40), 222 (4.18); ir (Nujol) ν_{max} 3500 (OH), 3450–3100 (OH, chelated), 1660 (C=O, enone system), 1630 (C=C, aromatic ring); pmr ($CDCl_3$–DMSO-d_6) δ 1.80 (3H, s, C_{9b}-CH_3), 2.14 (3H, s, C_6-CH_3), 2.46 (3H, s, C_{11}-CH_3), 5.95 (1H, s, C_4-H), 6.31 (1H, s, C_8-H), 8.59 ppm (2H, br, C_7-OH and C_9-OH); ms *m/e* 299 (M^+), 284, 256, 243, 231, 218, 202, 190, 184, 43 (base peak). *Anal.* calcd. for $C_{16}H_{13}O_5N \cdot \frac{1}{2}H_2O$: C 62.33, H 4.57, N 4.54; found: C 62.41, H 4.40, N 4.44. High resolution molecular weight determination: calcd.: 299.079; found: 299.079.

*Attempted C-Acylation of (+)-Desacetylisoxazolo[4,5-b]-isousnic Acid (**15**)*

A solution of (+)-desacetylisoxazolo[4,5-*b*]isousnic acid (**15**) (100 mg, 0.334 mmol) in freshly distilled acetyl chloride (3 ml) was treated with boron trifluoride etherate (0.05 ml) and heated to reflux under a nitrogen atmosphere for 3.5 h. Excess acetyl chloride was removed by evaporation under reduced pressure to give a brown glass (135 mg) purified by preparative layer chromatography (silica gel – oxalic acid plates, solvent system *A*) to afford pure (+)-desacetylisoxazolo[4,5-*b*]isousnic acid diacetate (**14**) (112 mg, 0.292 mmol; 87%), colorless prisms from ethyl alcohol, mp 145–146 °C; mixed mp with the authentic diacetate, 144–146 °C. All other spectroscopic properties proved identical as well.

*Reductive Isoxazole Ring Opening of (+)-Desacetylisoxazolo[4,5-b]isousnic Acid Diacetate (**14**). Formation of (+)-Desacetyl-$\Delta^{2,11}$-enaminoisousnic Acid Diacetate (**16**) (7,9-Diacetoxy-6,6bα-dimethyl-2-ethylid-2,11-ene-11-amino-1,9b,2,3-tetrahydro-1,3-dioxodibenzofuran)*

(+)-Desacetylisoxazolo[4,5-*b*]isousnic acid diacetate (**14**) (212 mg, 0.554 mmol) in absolute ethyl alcohol (20 ml) was hydrogenated over Adam's catalyst (PtO_2, 20 mg) at atmospheric pressure. After the uptake of 1 mol equiv. of hydrogen (13.5 ml at 25 °C) the reaction mixture was filtered through Celite and the filtrate evaporated under reduced pressure to afford a pale brown glassy material (238 mg), purified by preparative layer chromatography (silica gel plates, solvent system *B*) to produce pure (+)-desacetyl-$\Delta^{2,11}$-enaminoisousnic acid diacetate (**16**) (203 mg, 0.527 mmol; 95%) as a colorless glass that could not be induced to crystallize. $[\alpha]_D^{26}$ (CH_3CN) +243° (*c* 0.0205); uv λ_{max} (log ε) 328 (3.42), 284 (3.85), 268 (3.95), 204 (4.16); ir ν_{max} 3500 (N—H), 3400–3200 (N—H, chelated), 1770 (C=O, acetates), 1700 (C=O, ketoenamine system), 1630 (C=C), 1580 (C=O, chelated ketoenamine system); pmr δ 1.71 (3H, s, C_{9b}-CH_3), 2.08 (3H, s, C_6-CH_3), 2.28 (3H, s, C_7-$OCOCH_3$), 2.35 (6H, s, C_{11}-CH_3 and C_9-$OCOCH_3$), 5.65 (1H, s, C_4-H), 6.40 (1H, br, N-H), 6.57 (1H, s, C_8-H), 10.56 ppm (1H, br, N-H); ms *m/e* 385 (M^+), 302, 260, 218, 190, 119, 85, 83 (base peak), 43. *Anal.* calcd. for $C_{20}H_{19}O_7N$: C 62.33, H 4.97, N 3.63; found: C 62.52, H 5.01, N 3.65. High resolution molecular weight determination: calcd.: 385.116; found: 385.114. cd λ_{max} (Δε) 330 (+7.5), 290 (−3.03), 270 (−1.36), 244 (+5.19).

*Hydrolysis of (+)-Desacetyl-$\Delta^{2,11}$-enaminoisousnic Acid Diacetate (**16**). Formation of (+)-8-Desacetylisousnic Acid (**17**) (2-Acetyl-1,9b-dihydro-6,9bα-dimethyl-3,7,9-trihydroxy-1-oxodibenzofuran)*

A solution of (+)-desacetyl-$\Delta^{2,11}$-enaminoisousnic acid

Can. J. Chem. Downloaded from www.nrcresearchpress.com by 210.87.254.42 on 09/05/12
For personal use only.

diacetate (**16**) (180 mg, 0.467 mmol) in tetrahydrofuran (1 ml) was treated with freshly prepared 1 *N* sodium hydroxide solution (10 ml) and stirred at room temperature under a nitrogen atmosphere for 1 h. The reaction mixture was then acidified with 1 *N* hydrochloric acid and extracted with ethyl acetate (3 × 10 ml); the combined extracts were washed with water, dried over anhydrous sodium sulfate and evaporated under reduced pressure to produce a yellow glassy material (155 mg). This product was purified by column chromatography on Merck silica gel (15 g) to yield pure (+)-8-desacetylisousnic acid (**17**) (106 mg, 0.350 mmol; 75%), bright yellow small needles from chloroform – light petroleum ether, mp 210–211 °C (melts partially at 183–184 °C with change of crystalline form to thick prismatic needles); $[\alpha]_D^{26}$ +605° (*c* 0.06525); uv λ_{max} (log ϵ) 325 (3.22), 267 (3.82), 231 (4.04); uv (CH_3OH + NaOH) λ_{max} (log ϵ) 330 (3.32), 268 (3.82), 244 (4.04); ir ν_{max} 3600–2700 (OH, chelated), 1680 (C=O, enone system), 1640, 1620 (C=C, enol ether, aromatic ring), 1540 (C=O, chelated tricarbonyl system); pmr ($CDCl_3$–DMSO-d_6) δ 1.70 (3H, s, C_{9b}-CH_3), 2.07 (3H, s, C_6-CH_3), 2.59 (3H, s, C_2-$COCH_3$), 5.80 (1H, s, C_4-H), 6.23 (1H, s, C_8-H), 8.85 (1H, s, C_7-OH), 9.71 (1H, s, C_9-OH), 18.71 ppm (1H, s, C_3-OH); pmr ($CDCl_3$–C_6D_6) δ 1.72 (3H, s, C_{9b}-CH_3), 2.13 (3H, s, C_6-CH_3), 2.65 (3H, s, C_2-$COCH_3$), 5.89 (1H, s, C_4-H), 5.90 (1H, br, C_7-OH), 6.22 (1H, s, C_8-H), 9.95 (1H, s, C_9-OH), 18.65 ppm (1H, s, C_3-OH); ms *m/e* 302 (M^+) 218, 206, 191, 105 (base peak), 78, 43. *Anal.* calcd. for $C_{16}H_{14}O_6$: C 63.57, H 4.66; found: C 63.55, H 4.69. High resolution molecular weight determination: calcd.: 302.079; found: 302.072. cd λ_{max} ($\Delta\epsilon$) 325 (+9.43), 282 (−6.73), 264 (−5.66), 238 (+12.40); cd (CH_3OH + KOH) λ_{max} ($\Delta\epsilon$) 342 (+7.81), 309 (+6.20), 285 (−1.61), 266 (−13.74), 237 (+5.93).

*Acetylation of (+)-8-Desacetylisousnic Acid (**17**). Formation of (+)-8-Desacetylisousnic Acid Diacetate (**18**) (2-Acetyl-7,9-diacetoxy-1,9b-dihydro-6,9bα-dimethyl-3-hydroxy-1-oxodibenzofuran) – Experiment I*

A solution of (+)-8-desacetylisousnic acid (**17**) (50 mg, 0.166 mmol) in 1:1 mixture of acetic anhydride – pyridine (1 ml) was allowed to stand at room temperature overnight. The resulting dark red solution was poured onto crushed ice (5 g) and extracted with ethyl acetate (3 × 10 ml). The combined extracts were thoroughly washed with water, dried over anhydrous sodium sulfate, and evaporated under reduced pressure to yield a dark orange glassy material (65.5 mg) which upon purification by preparative layer chromatography (silica gel – oxalic acid plates, solvent system *A*) yielded the pure (+)-8-desacetylisousnic acid diacetate (**18**) (35.3 mg, 0.091 mmol; 55%), pale yellow crystalline product from ethyl alcohol, mp 150–152 °C; $[\alpha]_D^{26}$ +275° (*c* 0.02); uv λ_{max} (log ϵ) 325 (3.39), 280 (3.75), 259 (3.93), 219 (4.11); ir ν_{max} 3300–3000 (OH, chelated), 1770 (C=O, acetates), 1690 (C=O, enone system), 1630 (C=C, enol ether, aromatic ring), 1540 (C=O, chelated triketone system); pmr δ 1.80 (3H, s, C_{9b}-CH_3), 2.13 (3H, s, C_6-CH_3), 2.31 (3H, s, C_7-$OCOCH_3$), 2.40 (3H, s, C_9-$OCOCH_3$), 2.54 (3H, s, C_2-$COCH_3$), 5.87 (1H, s, C_4-H), 6.69 (1H, s, C_8-H), 18.25 ppm (1H, s, C_3-OH); ms *m/e* 386 (M^+, base peak), 344, 302, 260, 233, 218, 191. *Anal.* calcd. for $C_{20}H_{18}O_8$: C 62.17, H 4.69; found: C 62.20, H 4.69. High resolution molecular weight determination: calcd.: 386.100; found: 386.099.

*Acetylation of (+)-8-Desacetylisousnic Acid (**17**). Formation of (+)-8-Desacetylisousnic Acid Diacetate (**18**) – Experiment II*

(+)-8-Desacetylisousnic acid (**17**) (18 mg, 0.0597 mmol) was dissolved in a solution of concentrated sulfuric acid in acetic anhydride (0.5%, 2 ml) and allowed to stand at room temperature overnight. The reaction mixture was poured onto crushed ice (5 g), extracted with ethyl acetate (3 × 5 ml), and the combined extracts washed with water, dried over anhydrous sodium sulfate, and evaporated under reduced pressure to afford a pale yellow residue (25.2 mg). Purification by preparative layer chromatography (silica gel – oxalic acid plates, solvent system *A*) afforded the pure (+)-8-desacetylisousnic acid diacetate (**18**) (20.2 mg, 0.052 mmol; 87%), pale yellow crystals from ethyl alcohol, mp 150–152 °C; mixed mp with an authentic sample from previous experiments, 151–152 °C.

*Fries Rearrangement on (+)-8-Desacetylisousnic Acid Diacetate (**18**). Isolation of (+)-Isousnic Acid (**3**) (2,8-Diacetyl-1,9b-dihydro-6,9bα-dimethyl-3,7,9-trihydroxy-1-oxodibenzofuran)*

A solution of (+)-8-desacetylisousnic acid diacetate (**18**) (25 mg, 0.065 mmol) and anhydrous aluminum trichloride (34.42 mg, 0.26 mmol) in dry nitrobenzene (0.5 ml, distilled from calcium hydride) was heated at 60 °C (oil bath temperature) under a nitrogen atmosphere for 1 h. The cold reaction mixture was diluted with chloroform (3 ml), treated with a freshly prepared sodium hydroxide solution (2%, 1 ml) and stirred at room temperature for 1 h. The hydrolysis mixture was transferred to a separatory funnel, the aqueous layer removed, and the organic layer washed twice with 1 *N* sodium hydroxide solution (2 × 2 ml). The combined aqueous fractions were acidified with 1 *N* hydrochloric acid, extracted with ethyl acetate (3 × 5 ml), and the combined extracts washed with water, dried over anhydrous sodium sulfate, and evaporated under reduced pressure. The residue was immediately purified by preparative layer chromatography (silica gel – oxalic acid plates, solvent system *A*) to afford pure (+)-isousnic acid (**3**) (13.8 mg, 0.040 mmol; 62%), yellow prisms from chloroform–methanol, mp 152–153 °C (lit. (3, 4) mp 152–153 °C); mixed mp with authentic (+)-isousnic acid (**3**), 152–153 °C; $[\alpha]_D^{26}$ +505° (*c* 0.02275) (lit. (3, 4) $[\alpha]_D^{25}$ +500°); uv λ_{max} (log ϵ) 336 (3.65), 285 (4.21), 232 (4.17); ir ν_{max} 3400–2400 (OH, chelated), 1690 (C=O, enone system), 1630 (C=O, chelated aromatic acetyl; C=C, enol ether, aromatic ring), 1540 (C=O, chelated triketone system); pmr δ 1.85 (3H, s, C_{9b}-CH_3), 2.10 (3H, s, C_6-CH_3), 2.68 (3H, s, C_2-$COCH_3$), 2.77 (3H, s, C_8-$COCH_3$), 5.96 (1H, s, C_4-H), 11.28 (1H, s, C_9-OH), 14.35 (1H, s, C_7-OH), 18.81 ppm (1H, s, C_3-OH); ms *m/e* 344 (M^+), 260 (base peak), 233, 217. *Anal.* calcd. for $C_{18}H_{16}O_7$: C 62.78, H 4.69; found: C 62.75, H 4.73. High resolution molecular weight determination: calcd.: 344.089; found: 344.090. cd λ_{max} ($\Delta\epsilon$) 355 (+5.60), 293 (+14.29), 266 (−15.18), 244 (+9.58).

*Base Hydrolysis of (+)-8-Desacetylisousnic Acid Diacetate (**18**). Preparation of (+)-8-Desacetylisousnic Acid (**17**)*

A solution of (+)-8-desacetylisousnic acid diacetate

Can. J. Chem. Downloaded from www.nrcresearchpress.com by 210.87.254.42 on 09/05/12
For personal use only.

(**18**) (30 mg, 0.0776 mmol) in tetrahydrofuran (1 ml) was treated with freshly prepared 1% sodium hydroxide solution (8 ml) and stirred at room temperature under a nitrogen atmosphere for 1 h. The cold reaction mixture was acidified with 1 *N* hydrochloric acid, extracted with ethyl acetate (2 × 20 ml), and the combined extracts washed with water, dried over anhydrous sodium sulfate, and evaporated under reduced pressure to produce a yellowish glassy material (35.4 mg). Purification by preparative layer chromatography (silica gel – oxalic acid, solvent system *A*) yielded pure (+)-8-desacetylisousnic acid (**17**) (21.9 mg, 0.0725 mmol; 93.5%), bright yellow microneedles from chloroform – petroleum ether, mp 209–210 °C (melts partially at 183–184 °C); mixed mp with a pure sample of (+)-8-desacetylisousnic acid, 209–211 °C. All spectroscopic properties of these substances were identical as well.

*Acetylation of (+)-α-Hydroxydesacetylisoxazolo[4,5-b]-isousnic Acid (**12**). Preparation of (+)-α-Acetoxy-desacetylisoxazolo[4,5-b]isousnic Acid Diacetate (**19**) (1a,2,6,6a-Tetrahydro-1aα,7,9-triacetoxy-5,6aα,10-trimethyl-6-oxoisoxazolo[4,5-b]dibenzofuran)*

A solution of the (+)-α-hydroxy-isomer (**12**) (85 mg, 0.268 mmol) in a 1:1 mixture of acetic anhydride–pyridine (1 ml) was allowed to stand at room temperature overnight. Usual work-up and purification of the residue by preparative layer chromatography (silica gel – oxalic acid, solvent *A*) produced (+)-α-acetoxydesacetylisoxazolo[4,5-*b*]isousnic acid diacetate (**19**) (70 mg, 0.158 mmol; 59%), colorless plates from ethyl alcohol, mp 169–171 °C; $[\alpha]_D^{26}$ (CH_3CN) +116° (*c* 0.0345); uv (CH_3CN) λ_{max} (log ϵ) 276 (2.96), 238 (3.67), 220 (3.88); ir ν_{max} 1775 (C=O, acetates), 1770 (C=O, enone system), 1605 (C=C, aromatic ring); pmr δ 1.95 (3H, s, C_{9b}-CH_3), 1.98 (3H, s, C_6-CH_3), 2.11 (3H, s, C_{4a}-αOCOCH_3), 2.30 (3H, s, C_7-OCOCH_3), 2.43 (3H, s, C_9-OCOCH_3), 2.46 (3H, s, C_{11}-CH_3), 3.38 (2H, AB q, J = 18 Hz, C_4-H_2), 6.75 ppm (1H, s, C_8-H); ms *m/e* 443 (M^+), 401, 359, 317 (base peak), 299, 284, 43. *Anal.* calcd. for $C_{22}H_{21}O_9N$: C 59.59, H 4.77, N 3.16; found: C 59.43, H 4.83, N 3.10. High resolution molecular weight determination: calcd.: 443.122; found: 443.124.

*Acid Catalyzed Dehydration of (+)-α-Acetoxydesacetyl-isoxazolo[4,5-b]isousnic Acid Diacetate (**19**). Isolation of (+)-Desacetylisoxazolo[4,5-b]isousnic Acid Diacetate (**14**)*

The (+)-triacetate (**19**) (50 mg, 0.112 mmol) was dissolved in a mixture of concentrated sulfuric acid in acetic anhydride (0.5%, 2 ml) and heated at 50 °C (oil bath temperature) under a nitrogen atmosphere for 1 h. The reaction mixture was hydrolyzed by pouring into crushed ice and extracting with ethyl acetate (3 × 5 ml). The combined extracts were washed with water, dried over anhydrous sodium sulfate, and evaporated under reduced pressure. The residue (35 mg) was purified by preparative layer chromatography (silica gel – oxalic acid plates, solvent *A*) to produce pure (+)-desacetylisoxazolo-[4,5-*b*]isousnic acid diacetate (**14**) (30 mg, 0.0782 mmol; 70%), colorless needles from ethyl alcohol, mp 144.5–146 °C; mixed mp with authentic diacetate, 145–147 °C. Identity was also demonstrated by all other spectroscopic properties.

Acknowledgements

Financial aid from the National Research Council of Canada is gratefully acknowledged. One of us (I.H.S.) wishes to thank N.R.C.C. for a scholarship during the period of this study. We would also like to acknowledge the efforts of Ms. I. B. Krizsan in preparing the illustrations.

We would like to thank Professor S. Shibata, Faculty of Pharmaceutical Sciences, University of Tokyo, for the generous gift of a sample of (+)-isousnic acid (**3**).

1. J. P. Kutney, I. H. Sanchez, and T. Yee. This issue.
2. Y. Asahina and S. Shibata. Chemistry of lichen substances. Japan Society for the Promotion of Science, Tokyo, Japan. 1954. p. 171.
3. C. F. Culberson. Chemical and botanical guide to lichen products. The University of North Carolina Press, Chapel Hill, North Carolina. 1969. p. 171.
4. C. F. Culberson. The Bryologist, **73**, 201 (1970).
5. H. Taguchi and S. Shibata. Tetrahedron Lett. 4867 (1967).
6. D. H. R. Barton and T. Bruun. J. Chem. Soc. 603 (1952).
7. Y. Asahina and M. Yanagita. Chem. Ber. **71**, 2260 (1938); **72**, 1140 (1939).
8. K. Takahashi, Y. Honda, and S. Miyashita. Chem. Pharm. Bull. (Tokyo), **11**, 1229 (1963).
9. K. Takahashi. Chem. Pharm. Bull. (Tokyo), **1**, 36 (1953).
10. Y. Asahina and K. Okazaki. J. Pharm. Soc. Jpn. **63**, 626 (1943).
11. F. Dean and A. Robertson. J. Chem. Soc. 2166 (1955).
12. S. Shibata, J. Shoji, N. Tokutake, Y. Kaneko, H. Shimizu, and H. Chiang. Chem. Pharm. Bull. (Tokyo), **10**, 477 (1962).
13. H. Taguchi and S. Shibata. Chem. Pharm. Bull. (Tokyo), **18**, 374 (1970).
14. R. M. Silverstein and G. C. Bassler. Spectrometric identification of organic compounds. John Wiley and Sons Inc., New York, N.Y. 1967. Chapt. 4.
15. S. Huneck. Tetrahedron, **28**, 4011 (1972).
16. D. H. R. Barton, A. M. Deflorin, and O. E. Edwards. J. Chem. Soc. 530 (1956).
17. E. Kurosawa. Bull. Chem. Soc. Jpn. **34**, 300 (1961).
18. A. H. Blatt. Org. React. **1**, 342 (1942).
19. J. A. Elix and D. Tronson. Aust. J. Chem. **26**, 1093 (1973).
20. J. Shoji. Chem. Pharm. Bull. (Tokyo), **10**, 483 (1962).
21. A. M. Patterson, L. T. Capell, and D. F. Walker. The ring index. 2nd ed. American Chemical Society, Washington, D.C. 1960. p. 388.

The conductances and viscosities of aqueous solutions of indium tribromide, indium nitrate, and aluminum bromide at 25 °C

ALAN N. CAMPBELL

Department of Chemistry, University of Manitoba, Winnipeg, Man., Canada R3T 2N2

Received April 23, 1976

Can. J. Chem. Downloaded from www.nrcresearchpress.com by 210.87.254.40 on 09/05/12
For personal use only.

ALAN N. CAMPBELL. Can. J. Chem. **54**, 3732 (1976).

The specific and equivalent conductances of aqueous solutions of indium tribromide, aluminum tribromide, and indium nitrate at 25 °C have been determined at concentrations ranging from 4.771 to 0.00577 *N*. The results for indium tribromide are in good agreement with those of Heydweiller (for 18 °C), the only previous figures, and which are limited to the relatively concentrated range. Below a concentration of 0.005 *N*, results for indium tribromide are valueless, because the conductance increases with time, owing to progressive hydrolysis. It is therefore not possible to determine the limiting conductance of indium tribromide experimentally. Although the aluminum trichloride results are independent of time, there is probably also a certain amount of hydrolysis at extreme dilution.

The transport number of In^{3+} in $InBr_3$ was determined at different concentrations, using the Hittorf method. The limiting value of the transport number, obtained by extrapolation to zero concentration, was 0.454. This leads to values of 62.1 mhos for $\frac{1}{3}In^{3+}$ and 140.5 mhos for Λ^0 for $\frac{1}{3}InBr_3$. These values are very different from those previously obtained (1), which were founded on an assumption which now appears to be untenable.

The viscosities of aqueous solutions have also been determined and the results for the dilute region fitted to the Jones and Dole rule.

ALAN N. CAMPBELL. Can. J. Chem. **54**, 3732 (1976).

Les conductivités spécifiques et équivalentes de solutions aqueuses de tribromure d'indium, de tribromure d'aluminium et de nitrate d'indium, à 25 °C, ont été déterminées à des concentrations allant de 4.771 à 0.00577 *N*. Les résultats obtenus avec le tribromure d'indium sont en accord avec ceux de Heydweiller (à 18 °C) qui étaient les seules valeurs rapportées antérieurement et qui étaient limitées à des écarts de concentration relativement faibles. A des concentrations plus basses que 0.005 *N*, les résultats pour le tribromure d'indium sont sans valeur dû au fait que la conductivité augmente avec le temps à cause d'une hydrolyse progressive. Il n'est donc pas possible de déterminer expérimentalement la conductivité limite du tribromure d'indium. Quoique les résultats obtenus avec le trichlorure d'aluminium soient indépendants du temps, il y a probablement aussi une certaine quantité d'hydrolyse à dilution extrême.

Le nombre de transport de In^{3+} dans $InBr_3$ a été déterminé à diverses concentrations utilisant la méthode de Hittorf. La valeur limite du nombre de transport, obtenue par extrapolation à concentration zéro, est de 0.454. Ceci conduit à des valeurs de 62.1 mhos pour $\frac{1}{3}In^{3+}$ et 140.5 mhos pour Λ^0 de $\frac{1}{3}InBr_3$. Ces valeurs diffèrents de celles rapportées antérieurement (1) qui avaient été établies en faisant une hypothèse qui semble aujourd'hui intenable.

On a aussi déterminé les viscosités des solutions aqueuses et les résultats obtenus dans la région diluée sont en accord avec la règle de Jones et Dole.

[Traduit par le journal]

Introduction

In a series of papers (1–4), the author has dealt with the chemistry of indium trichloride. It was thought that it would be interesting and of value to repeat these observations on indium bromide. Despite the similarity between the halide salts of the same metal, the properties of indium chloride and of indium bromide are not identical.

The principal work reported in this paper deals with the conductance (specific and equivalent) of indium bromide solutions from a concentration of 4.771 *N* down to 0.005 *N*, below which concentration the readings become uncertain because of hydrolysis. As a standard of comparison the conductance of aluminum tribromide was also determined, over the same concentration range, the assumption being that aluminum bromide behaves 'normally'. If it is assumed that all trivalent electrolytes ionise in stages, then the difference between 'normal' and 'abnormal' electrolyes should consist in the 'normal' electrolytes existing principally as M^{3+} at all concentrations, while the 'abnormal' ones would give appreciable amounts of the complex ions, MCl_2^+ and

Can. J. Chem. Downloaded from www.nrcresearchpress.com by 210.87.254.40 on 09/05/12
For personal use only.

MCl^{2+}, at all concentrations except high dilution.

The fact that, in the dilute region, the conductance of indium bromide solutions increases with time means that any attempt to determine the limiting conductance, Λ^0, of indium tribromide (or, for that matter, of indium trichloride) by extrapolation, graphical or algebraic, must be abandoned. The remaining method of determining Λ^0 is through the transport number. Since the author is himself sceptical of a method which he previously used to obtain Λ^0 and which, even at the time, he described as "one which may be open to criticism", he was led in the present work to redetermine the transport number at different concentrations.

Experimental

Materials

The starting materials were metallic indium (99.99%) for which I am indebted to the generosity of Cominco, of Trail, B.C., and reagent grade hydrobromic acid. Indium tribromide was prepared by refluxing metallic indium with excess hydrobromic acid until the metal dissolved completely. The product was evaporated to dryness on the steam bath. The solid product contains 10% water, despite the fact indium tribromide is anhydrous (5). The solid was redissolved in water, when the solution was found to be quite acidic (about 1 *N*). Air was then bubbled through the solution over-night. The solution was then concentrated by boiling down in presence of a fragment of metallic indium: bubbles of hydrogen were given off from the indium in this process. Finally the product was brought to solidification on the steam bath. This process was repeated several times. The final product was greyish in colour but dissolved to a colourless solution having a p*H* of 5. This 'dirty' colour has been observed by other workers and seems to be characteristic of the compound. Purification by recrystallization is practically impossible because of the high solubility (85%) of the salt. Indium nitrate is prepared very readily by solution of metallic indium in excess nitric acid (50%), followed by evaporation to dryness and recrystallization from water.

Procedures

The experimental procedures have been described previously (1–4). In the conductance measurements, every solution was analyzed gravimetrically by precipitation as silver bromide, down to a concentration of 0.01 *N*. Concentrations below this were, of necessity, obtained by weight dilution with conductance water. Indium nitrate solutions were also analyzed down to 0.01 *N* concentration, using as method of analysis precipitation of indium as $In(OH)_3$, followed by ignition to In_2O_3.

The Hittorf method was used for the determination of transport numbers. The method is well known and therefore need not be described, but the cell was modified as shown in Fig. 1, which gives the main dimensions. These dimensions were chosen so as to allow relatively large concentration changes at the anode and cathode, without danger of change occurring in the centre compartment. The centre compartment was always analyzed but no change in concentration was ever detected. Current was obtained from a constant current apparatus built by the Department of Electrical Engineering of the National Research Council of Canada. In different experiments, the current was varied between 0.002 and 0.015 amp. The two glass spoons in the anode and cathode compartments have platinum wires sealed into them. They were filled with molten indium and allowed to cool. In this way good contact between indium and platinum was obtained; it is not easy to machine a rod of indium or to obtain good electrical contact with it.

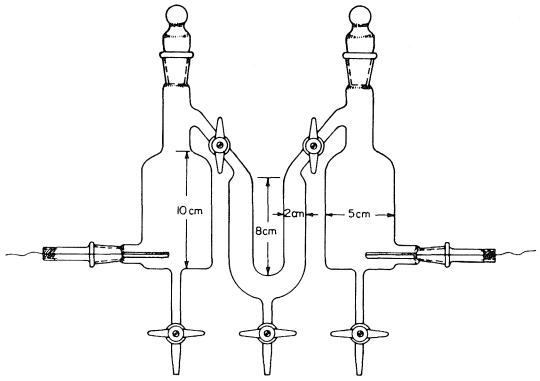

FIG. 1. Apparatus for transport number determination.

The results obtained were not always consistent, nor did the anode result always agree perfectly with the cathode result. The reasons for this are not obvious. Passivity and over-voltage to indium deposition are practically absent. The results were plotted and the best curve drawn.

Results and Discussion

If the three conductance curves of aluminum tribromide, indium tribromide, and indium nitrate are compared, the differences are striking. In the more concentrated regions, the conductance of $AlBr_3$ is from two to three times as great as that of $InBr_3$, while that of $In(NO)_3$ lies between the two.

In a previous paper (4) the author succeeded in calculating the ionisation constant for the first stage of the ionisation of $InCl_3$, assuming it to be

$$InCl_3 \rightleftharpoons InCl_2^+ + Cl^-$$

The existence of the $InCl_2^+$ ion has been demonstrated by Ferri (5) and by Jarv (6). If the figure for Λ^0 for $InBr_3$ of 143.2, or any other figure for that matter, is accepted, a similar calculation applied to the present figure gives

Molarity (M)	$\alpha = \frac{\Lambda\eta}{\Lambda^0}$	$K = \frac{\alpha^2 M}{(1-\alpha)}$
1.59	0.146	3.969×10^{-2}
1.356	0.1655	4.45×10^{-2}
1.353	0.1615	4.20×10^{-2}
0.984	0.1924	4.51×10^{-2}
0.953	0.1924	4.51×10^{-2}
0.402	0.2085	5.23×10^{-2}
0.152	0.3108	2.12×10^{-2}
0.0328	0.491	1.605×10^{-2}

It appears that the tendency for indium nitrate to form complex ions of the $In(NO_3)_2^+$ and $In(NO_3)^{2+}$ types is distinctly less than that of $InCl_3$ and $InBr_3$ to form the corresponding complexes.

Very fair constancy exists between 1.59 and 0.953 M (4.77 and 2.859 N), followed by a rapid decrease in the value of K, with further dilution, as with $InCl_3$. Considering that the above calculations are founded on the impossible assumption that the only ionisation present in these solutions is first stage, the results are surprising.

TABLE 1. Temperature coefficients of conductance

$\sqrt{c}$	$\frac{\Lambda_{25\,°C}}{\Lambda_{18\,°C}}$
2	1.096
1.946	1.180
1.414	1.165
1.002	1.172
0.7065	1.167
0.447	1.093
0.3167	1.170

Since it is impossible to determine Λ^0 for the indium tribromide by conductance measurements, the transport number remains the only practical solution to the problem. Using the apparatus previously described the following results were obtained by interpolation

N	$\sqrt{N}$	Transport No. of $\frac{1}{3}In^{3+}$
0.16	0.4	0.499
0.116	0.34	0.490
0.102	0.32	0.488
0.084	0.29	0.483
0.0484	0.22	0.473
0.04	0.2	0.470
0.0256	0.16	0.465
0.0196	0.14	0.462
0.0144	0.12	0.460
0.01	0.10	0.460

When the values of the transport number are plotted against $\sqrt{N}$, the extrapolated value for $\sqrt{N} = 0$ is 0.454. This leads to values of 65.0 mhos for λ^0 for $\frac{1}{3}In^{3+}$ and 143.2 for Λ^0 for $InBr_3$. The curve of transport number *vs.* square root of concentration is unusual in two ways: (*1*) the transport number decreases numerically with dilution; (*2*) the change with concentration is unusually great. Both effects, however, are to be expected as the necessary result of the shift in the equilibria among the complex ions with dilution.

The only previous work on the conductance of indium bromide is that of Heydweiller (7) carried out at 18 °C. These results, together with those of the present paper, are expressed graphically in Fig. 2. For comparable concentrations, the temperature coefficients are given in Table 1, my

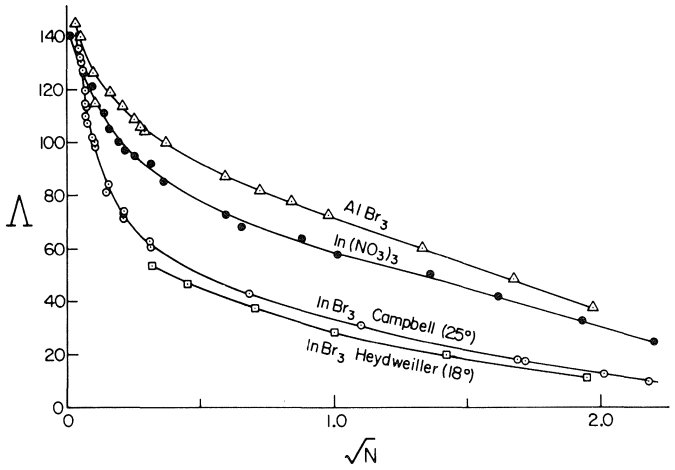

FIG. 2. Equivalent conductance *vs.* square root of equivalent concentration.

Can. J. Chem. Downloaded from www.nrcresearchpress.com by 210.87.254.40 on 09/05/12
For personal use only.

TABLE 2. Some physical properties of $InBr_3$, $AlBr_3$, $In(NO_3)_3$

Concentration (equiv. l^{-1}) c	$\sqrt{c}$	Specific conductance, κ (mho cm^{-1})	Equivalent conductance Λ	Density (g/cc)	Relative viscosity (H_2O = 1)
		$InBr_3$			
4.771	2.184	0.04485	9.40	1.458	2.218
4.069	2.017	0.04981	12.24	1.406	1.937
4.059	2.015	0.04843	11.93	1.386	1.937
2.952	1.718	0.05011	16.97	1.302	1.660
2.859	1.619	0.04992	17.46	1.115	1.213
1.207	1.099	0.03713	30.75	1.040	1.071
0.455	0.6715	0.02002	43.86	1.007	1.015
0.0984	0.3137	0.005791	60.96	1.001	1.000
0.0448	0.2117	0.003239	72.27	1.000	1.000
0.02157	0.1466	0.001960	82.20	—	—
0.01142	0.1069	0.001138	99.68	—	—
0.00585	0.0765	0.000664	113.5		
0.00510	0.07142	0.000606	118.9		
0.00323	0.0568	0.000423	131.4		
0.00468	0.0684	0.000535	114.0		
0.09615	0.316	0.006113	63.45		
0.0459	0.214	0.003429	74.86		
0.0225	0.1509	0.001929	84.23		
0.0138	0.1175	0.0013544	98.15		
		$AlBr_3$			
3.868	1.967	0.1444	37.34	1.2967	2.358
2.797	1.672	0.1357	48.5	1.2152	1.724
1.773	1.332	0.1069	60.28	1.1342	1.293
0.9644	0.982	0.06961	72.18	1.0731	1.066
0.6932	0.8326	0.05374	77.53	1.0512	1.005
0.5181	0.720	0.04201	81.08	1.0381	—
0.350	0.591	0.03009	85.96	1.0248	—
0.1341	0.366	0.01329	99.14	1.0079	—
0.0782	0.2796	0.008259	105.6	1.0030	—
0.06235	0.250	0.006757	108.4	1.0023	—
0.04260	0.2064	0.0048303	113.4	1.0006	—
0.01027	0.1013	0.001173	114.2	—	—
0.08528	0.292	0.0099245	103.5	—	—
0.008555	0.09249	0.001076	125.8	—	—
0.007222	0.08498	0.0009170	127.0	—	—
0.006032	0.07766	0.0007797	129.3	—	—
		$In(NO_3)_3$			
7.829	2.798	0.097638	12.47	—	—
6.242	2.498	0.1008699	16.16	—	—
5.970	2.443	0.10725	17.96	1.4390	4.440
4.826	2.197	0.11808	24.47	1.3540	3.117
3.731	1.932	0.1202	32.22	1.2743	2.309
2.610	1.616	0.10964	42.01	1.1928	1.764
1.855	1.362	0.092386	49.80	1.1357	1.492
1.033	1.016	0.059960	58.03	1.0699	1.265
0.785	0.886	0.050248	64.05	1.0549	1.185
0.570	0.755	0.038949	68.30	1.0478	1.1468
0.357	0.597	0.026088	73.18	1.0225	1.0891
0.133	0.365	0.0113787	85.43	1.0053	1.0524
0.0980	0.313	0.0090899	92.57	1.0032	1.0465
0.0640	0.253	0.006095	95.70	0.999	1.032
0.0520	0.228	0.005097	97.64	—	—
0.0400	0.200	0.004074	100.88	—	—
0.0297	0.172	0.003115	104.74	—	—
0.0220	0.148	0.002454	111.7	—	—
0.00996	0.0998	0.0013458	140.5	—	—

Can. J. Chem. Downloaded from www.nrcresearchpress.com by 210.87.254.40 on 09/05/12
For personal use only.

results being interpolated to Heydweiller's concentrations. On the supposition that the variation is largely due to the uncertainty of graphical interpolation, it is permissible to take the mean of the ratios $\Lambda_{25°C}/\Lambda_{18°C}$ as 1.149. The temperature coefficient of fluidity of water, between 18 and 25 °C, is 111.91/94.71 = 1.182, fairly good confirmation, if any were needed, of Heydweiller's results and my own. Below a concentration of 0.005 *N*, results are valueless, because the conductance increases with time; for example, the resistance of a 0.0047 *N* solution of $InBr_3$ fell from 14 041 to 11 392 ohms in 20 h. After 24 h, a white deposit appeared. Obviously, hydrolysis is taking place. At higher concentrations, the conductance is constant although hydrolysis must still take place. If, however, the equilibrium concentration of $In(OH)_3$ (or other hydrolysis product) is calculated from the hydrolysis constant given in a previous paper (4) and compared with the concentration given by the solubility product of indium hydroxide the former will be seen to be less than the latter, in other words, hydrolysis equilibrium is established. Similar considerations apply to the hydrolysis of aluminum bromide. Since the conductance is constant with time at all concentrations, however small, hydrolysis equilibrium must always be established. According to Parsons (8) the limiting conductance of $\frac{1}{3}Al^{3+}$ is 63 at 25 °C, but he gives no reference. If this figure is correct, the limiting conductance of $\frac{1}{3}AlBr_3$ should be 141.2, at 25 °C. If the results of this work are plotted on a fine scale, as Λ *vs.* $\sqrt{N}$, it is seen that the curve becomes a straight line at concentrations less than $\sqrt{N} = 0.06$ ($N = 0.0036$) but the intercept for $\sqrt{N} = 0$, gives $\lambda^0 = 153$ (approx.). The value of λ^0 for $\frac{1}{3}Al^{3+}$, *viz.* 72, seems rather high. The average of trivalent ions given in Robinson and Stokes (9) is 67.57 ± 2. It seems more probable that hydrolysis accounts for some of the increase in conductivity at very high dilutions.

Viscosity

The viscosity of the more concentrated solutions are given in Table 2 but because of the interest in the rule of Jones and Dole (10), according to which

$$\eta(H_2O = 1) = 1 + A\sqrt{c} + Bc$$

where A and B are constants, it was necessary to determine viscosities of dilute solutions of indium bromide and for this purpose a Cannon and Fenske viscometer with a water run-time of 465.2 s was used. The results were

Concentration (mol l^{-1})	$\sqrt{M}$	$(\eta - 1)/\sqrt{M}$
0.0908	0.3013	0.1975
0.0649	0.2548	0.1700
0.0259	0.1611	0.137
0.00634	0.0796	0.073

When these figures are plotted in the form of $(\eta - 1)/\sqrt{M}$ *vs.* $\sqrt{M}$, they are found to lie on a straight line with intercept $A = 300 \times 10^{-4}$ and slope $B = 0.556$. The figures do not differ greatly from those of Jones and Stauffer (11) for lanthanum chloride, as indeed, according to theory, they should not; electrolytes of similar type should have closely similar, though not identical, A and B values.

1. A. N. Campbell. Can. J. Chem. **51**, 3006 (1973).
2. A. N. Campbell, E. M. Kartzmark, and O. N. Bhatnagar. Can. J. Chem. **52**, 1954 (1974).
3. A. N. Campbell. Can. J. Chem. **52**, 3769 (1974).
4. A. N. Campbell. Can. J. Chem. **53**, 1761 (1975).
5. D. Ferri. Acta Chem. Scand. **26**, 733 (1972).
6. T. Jarv. M.Sc. Thesis, University of Waterloo, Waterloo, Ontario. 1975.
7. A. Heydweiller. Z. Anorg. Chem. **88**, 104 (1914).
8. R. Parsons. Handbook of electrochemical constants. Butterworth's Scientific Publications. London. 1959.
9. R. A. Robinson and R. H. Stokes. Electrolyte solutions. 2nd ed. Butterworth Sci. Publ. London, 1959. p. 463.
10. G. Jones and M. Dole. J. Am. Chem. Soc. **51**, 2950 (1929).
11. G. Jones and R. E. Schauffer. J. Am. Chem. Soc. **62**, 335 (1940).

Can. J. Chem. Downloaded from www.nrcresearchpress.com by 210.87.254.40 on 09/05/12
For personal use only.

A Mössbauer study of organotellurium compounds. Part II. Halides, acetates, and benzoates

FRANK J. BERRY[1] AND COLIN H. W. JONES
Department of Chemistry, Simon Fraser University, Burnaby, B.C., Canada V5A 1S6

Received July 9, 1976

FRANK J. BERRY and COLIN H. W. JONES. Can. J. Chem. **54**, 3737 (1976).

^{125}Te Mössbauer data, measured at 4.2 K, are reported for a number of organotellurium(IV) compounds, including Ar_2TeF_2, $ArTeF_3$, $Ar_2Te(OCOCH_3)_2$, $Ar_2Te\ OCOC_6H_5)_2$, where Ar = Ph, *p*-$EtOC_6H_4$, *p*-$MeOC_6H_4$, *p*-C_7H_7, and the compounds $Ph_2(CH_3)TeI$ and $Ph(CH_3)_2TeI$. Evidence is presented that while the difluorides appear to be similar in structure to the other dihalides (X = Cl, Br, I), in the trifluorides the co-ordination about the tellurium is significantly different to that found in the other trihalides (X = Cl, Br, I). The iodides studied have parameters consistent with their formulation as $Ph_2(CH_3)Te^+I^-$ and $Ph(CH_3)_2Te^+I^-$. The dicarboxylates have parameters similar to those of the dihalides, although the diphenyl tellurium diacetate and dibenzoate have relatively small Δ's in comparison with those of the other derivatives studied and it would appear that subtle changes in the co-ordination about tellurium occur with changes in the aryl ligand.

FRANK J. BERRY et COLIN H. W. JONES. Can. J. Chem. **54**, 3737 (1976).

On rapporte des données de Mössbauer ^{125}Te, mesurées à 4.2 K, pour un certain nombre de composés organotellurés(IV) incluant Ar_2TeF_2, $ArTeF_3$, $Ar_2Te(OCOCH_3)_2$, $Ar_2Te(OCOC_6H_5)_2$ où Ar = Ph, *p*-$EtOC_6H_4$, *p*-$MeOC_6H_4$, *p*-C_7H_7 et les composés $Ph_2(CH_3)TeI$ et $Ph(CH_3)_2TeI$. On présente des données indiquant que les dérivés difluorés semblent avoir des structures semblables aux autres dérivés dihalogénés (X = Cl, Br, I); par ailleurs la coordination autour du tellure dans les dérivés trifluorés serait très différente de celle trouvée dans les autres dérivés trihalogénés (X = Cl, Br, I). Les dérivés iodés étudiés ont des paramètres qui sont en accord avec des formules telles que $Ph_2(CH_3)Te^+I^-$ et $Ph(CH_3)_2Te^+I^-$. Les dicarboxylates ont des paramètres semblables à ceux des dérivés dihalogénés; toutefois le diacétate et le dibenzoate de diphényltellure ont des Δ qui sont relativement faibles si on les compare à ceux des autres dérivés étudiés et il semble que des changements subtils dans la coordination autour du tellure se produisent avec des changements dans le ligand aromatique.

[Traduit par le journal]

Introduction

A number of studies have recently been made of the ^{125}Te Mössbauer spectra of organotellurium compounds (1–3). The present paper extends the previous investigations of organotellurium(IV) halides to include the difluorides and trifluorides. A simple additivity model has been used to interpret the quadrupole splittings in the other dihalides and trihalides (3) and it was of interest to determine whether or not the splittings for the fluorides would be consistent with that model.

The iodides $PhMeTeI_2$, Ph_2MeTeI, and $PhMe_2TeI$ have also been studied. The latter two compounds were of particular interest, since they presumably contain three co-ordinate tellurium in the R_3Te^+ cation (4).

The aryl tellurium diacetates and dibenzoates have previously been investigated by ir spectroscopy (5). The compound $Ph_2Te(OCOCH_3)_2$ was found to have a relatively simple ir spectrum whereas (*p*-$EtOC_6H_4$)$Te(OCOCH_3)_2$ and $Ph_2Te(OCOPh)_2$ gave more complex spectra, which were interpreted as evidence for either the coupling of vibrations of different carboxylate groups in the same molecule or the presence of both uni- and bidentate carboxylate groups. It was felt that the Mössbauer data, and in particular the quadrupole splittings, might provide further information about the environment of the tellurium atom in these compounds.

Results

The ^{125}Te Mössbauer parameters for the compounds investigated in this work are given in Table 1. A number of diaryltellurium(IV) dihalides (X = Cl, Br, I) have been studied pre-

[1]Present address: The University Chemical Laboratory, Lensfield Road, Cambridge, England.

Can. J. Chem. Downloaded from www.nrcresearchpress.com by 210.87.254.105 on 09/05/12
For personal use only.

Can. J. Chem. Downloaded from www.nrcresearchpress.com by 210.87.254.105 on 09/05/12
For personal use only.

TABLE 1. ^{125}Te Mössbauer parameters

Compound	δ* (mm s^{-1})	Δ (mm s^{-1})	Γ (mm s^{-1})
Ph_2TeF_2	0.52±0.06	10.4±0.1	6.1
$(p\text{-}EtOC_6H_4)_2TeF_2$	0.36±0.11	10.1±0.2	5.2
$(p\text{-}MeOC_6H_4)_2TeF_2$	0.54±0.08	10.0±0.1	5.2
$(p\text{-}MeOC_6H_4)_2TeCl_2$	0.61±0.03	9.2±0.1	6.2
$(p\text{-}MeOC_6H_4)_2TeBr_2$	0.72±0.08	7.8±0.2	5.6
$(p\text{-}MeOC_6H_4)_2TeI_2$	0.51±0.12	6.1±0.2	5.5
$(p\text{-}MeOC_6H_4)TeF_3$	0.56±0.05	8.6±0.1	6.3
$(p\text{-}EtOC_6H_4)TeF_3$	0.60±0.03	8.6±0.1	5.9
$Ph_2(CH_3)TeI$	0.38±0.09	5.6±0.2	7.0
$Ph(CH_3)_2TeI$	0.32±0.06	5.4±0.1	5.7
$Ph(CH_3)TeI_2$	0.56±0.07	6.4±0.1	5.8
$Ph_2Te(OCOCH_3)_2$	0.59±0.04	8.0±0.1	6.1
$(p\text{-}MeOC_6H_4)_2Te(OCOCH_3)_2$	0.50±0.07	9.3±0.1	6.4
$(p\text{-}C_7H_7)_2Te(OCOCH_3)_2$	0.60±0.04	9.5±0.1	6.1
$Ph_2Te(OCOPh)_2$	0.76±0.09	8.2±0.2	7.1
$(p\text{-}MeOC_6H_4)_2Te(OCOPh)_2$	0.52±0.04	9.5±0.1	5.8
$(p\text{-}EtOC_6H_4)_2Te(OCOPh)_2$	0.56±0.04	9.4±0.1	6.1

*δ with respect to ^{125}I/Cu. The conversion from ^{125}Sb/Cu was made by adding +0.15 mm s^{-1}. Absorbers were at 4.2 K and the source at 80 K.

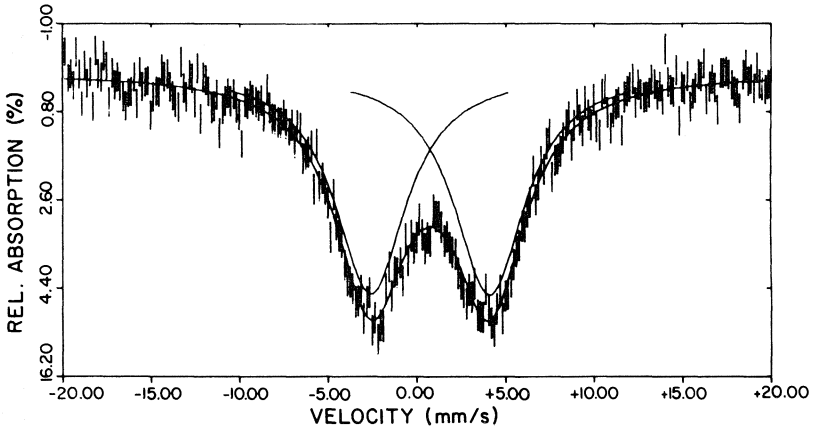

FIG. 1. The spectrum for $Ph_2Te(OCOCH_3)_2$.

viously (1, 3). The compounds $(p\text{-}MeOC_6H_4)_2TeX_2$ (X = Cl, Br, I), which were not previously studied, were included here to provide internal standards and were found to have parameters in excellent agreement with those of other simple diaryltellurium dihalides. A sample spectrum is shown in Fig. 1.

Discussion

The Aryltellurium(IV) Fluorides

The three difluorides studied have similar isomer shifts and quadrupole splittings, consistent with the previous observation that the Ph, p-$MeOC_6H_4$, and p-$EtOC_6H_4$ ligands have essentially the same influence on the tellurium orbital populations (3). The quadrupole splittings for the dihalides are observed to lie in the order F > Cl > Br > I. Thus with increasing electronegativity of the halogen there is an increasing p-orbital imbalance on the tellurium as measured by Δ. The structures of the diorganotellurium dihalides (X = Cl, Br, I) may be viewed as ψ-trigonal bipyramidal (Fig. 2) with the lone-pair occupying the fifth co-ordinate position in the equatorial plane (6, 7). However, the relatively small C—Te—C bond angles for the dihalides, ranging from 91 to 98°, and the positive Möss-

TABLE 2. Average Mössbauer parameters for the dihalides and trihalides

	F		Cl		Br		I	
Compound*	δ	Δ	δ	Δ	δ	Δ	δ	Δ
Ar_2TeX_2	0.47	10.2	0.62	9.2	0.61	7.9	0.55	6.3
$ArTeX_3$	0.58	8.6	0.97	9.3	1.0	7.9	1.0	5.2

*Average δ and Δ values, in mm s^{-1}, for the diaryltellurium dihalides and aryltellurium trihalides, taken from this work and refs. 1 and 3.

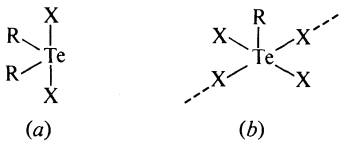

FIG. 2. Co-ordination about the tellurium in the dihalides and trihalides (X = Cl, Br, I).

bauer isomer shifts suggest that the lone-pair has predominantly $5s^2$ character. The bonding to tellurium in these molecules may therefore be considered to be predominantly $5p$ in character and V_{zz}, the principal component of the electric field gradient, would then lie along the X—Te—X bond axis and would be positive in sign, the halogens removing more $5p$ electron density from the tellurium than the Te—C bond. The increase in Δ with the electronegativity of X is consistent with an increased removal of p-electron density along the z axis. The difluorides clearly follow this trend and the Mössbauer data are consistent with the difluorides having a similar structure to that of the other dihalides.

The difluorides have the largest Δ of the dihalides, suggesting that fluorine is very effective in removing $5p$-electron density from the tellurium. Since removal of $5p$ electrons should lead to a deshielding of tellurium $5s^2$ electrons, and hence an increase in the s-electron density at the nucleus, the difluorides might be expected to have the most positive of the isomer shifts of the dihalides, $\Delta R/R$ being positive for ^{125}Te (8). However, ^{125}Te isomer shifts are small in comparison with the broad natural linewidth and δ is not very sensitive to small changes in the p-orbital populations. The dihalides are all observed to have similar isomer shifts and the difluorides appear to have δ's which fall at the lower end of the velocity range observed (Table 2). This suggests a marginally greater stereochemical activity of the $5s$ electrons in the difluorides than in the other dihalides.

It may be noted that for the Te(IV) tetrahalides, TeX_4, the isomer shifts for X = Cl, Br, I are all comparable (9) and for the antimony(III) trihalides, SbX_3, the s-electron densities at the nucleus lie in the order $SbI_3 > SbBr_3 \sim SbCl_3 \sim SbF_3$ (10). The range of isomer shifts observed for ^{121}Sb is of course generally much greater than that for ^{125}Te, as a result of a much larger $\Delta R/R$. The relative constancy of $|\psi_s(0)|^2$ within each series for SbX_3, TeX_4, and R_2TeX_2 suggests that the stereochemical activity of the lone-pair in each case changes in a complex way with changes in the electronegativity of the halogen and possible changes in co-ordination number about the antimony or tellurium.

The trifluorides have isomer shifts comparable to those of the difluorides and smaller quadrupole splittings. This contrasts with the behaviour of the other trihalides (X = Cl, Br, I), for which δ was found to be greater than that of the corresponding dihalides while the quadrupole splittings were the same in magnitude for Cl and Br (see Table 2). The structure which has been proposed (11, 12) for the trihalides is shown in Fig. 2*b*. On the basis of the structures shown in Fig. 2, and noting that the halogens remove predominantly p-electron density from the tellurium, it would be expected that the trihalides would have more positive isomer shifts than the dihalides. Moreover a simple additivity model would suggest that, assuming predominantly p-bonding, for any one halogen the dihalide and trihalide would have the same magnitude for Δ, although they would differ in sign (3). These trends are followed for the chlorides and bromides if not for the iodides.

However, the Mössbauer parameters of the trifluorides are clearly quite different from those of the other trihalides. The relatively small isomer shifts of the trifluorides could be explained by a greater participation of the $5s$ electrons in bonding, *i.e.*, a greater p-character

Can. J. Chem. Downloaded from www.nrcresearchpress.com by 210.87.254.105 on 09/05/12
For personal use only.

Can. J. Chem. Downloaded from www.nrcresearchpress.com by 210.87.254.105 on 09/05/12
For personal use only.

for the lone pair. However, with reference to Fig. 2*b* this would imply a greater Δ than that of the difluorides, rather than the smaller Δ which is observed. Thus it appears that the co-ordination about the tellurium in the trifluorides must be significantly different from that in the other trihalides. This is not unexpected since TeF_4 (13) has a structure which is significantly different from that of $TeCl_4$ (14) or TeI_4 (15), while SbF_3 (16) also differs in structure, and in its Mössbauer parameters, from that of the other antimony(III) trihalides.

Arylalkyltellurium Iodides

The compound $Ph(CH_3)TeI_2$ has precisely the same Mössbauer parameters as $(p\text{-}CH_3OC_6H_4)_2TeI_2$, although a somewhat smaller Δ than $\alpha\text{-}Me_2TeI_2$ (7.1–7.6 mm s^{-1}) (2, 3). Thus the presence of both alkyl and aryl substituents on the tellurium atom does not lead to any unusual or unexpected results and, as previously observed, the alkyl and aryl ligands have very similar properties.

The compounds $Ph(CH_3)_2TeI$ and $Ph_2(CH_3)TeI$ in all probability contain the $Ph(CH_3)_2Te^+$ and $Ph_2(CH_3)Te^+$ cations. There is X-ray structural evidence that Ph_3SeCl contains the Ph_3Se^+ cation (4) and the ir spectrum of $(CH_3)_3Se^+$ has been interpreted as evidence for $(CH_3)_3Se^+$ (17). Conductance measurements in a variety of solvents on the compounds R_3TeX (R = Me, Ph; X = Cl, Br, I) including the compound $Ph_2(CH_3)TeI$, also support their formulation as $R_3Te^+X^-$ in solution (18–20).

As would be expected, $Ph(CH_3)_2TeI$ and $Ph_2(CH_3)TeI$ have the same Mössbauer parameters. The small isomer shifts of these compounds are quite consistent with the presence of R_3Te^+ cations, since the co-ordination of I to the tellurium would have been expected to lead to a more positive δ. The isomer shifts of $Ph(CH_3)_2TeI$ and $Ph_2(CH_3)TeI$ are more positive than those of the organotellurides R_2Te, for which $\delta \approx 0.2$ mm s^{-1} (1, 3). It is clear that the covalent Te—C bond must have significant *s*-character but that the removal of *s* and *p* electron density is such as to lead to a small net increase in $|\psi_s(0)|^2$ through deshielding of the remaining 5*s* electrons at the nucleus. The small quadrupole splittings of these compounds are also consistent with *s*-character in the Te—C bonds, since this necessarily implies some *p*-character of the lone-pair. Other possible contributions to the electric field gradient at the tellurium could arise from inequalities in the Te—C bonds in the Ph_2MeTe^+ and $Ph(CH_3)_2Te^+$ cations or from lattice terms, although the lone-pair will in all probability be the main contributor.

It is interesting to note that the quadrupole splittings of *ca.* 5.5 mm s^{-1} for $Ph_2(CH_3)TeI$ and $Ph(CH_3)_2TeI$ correspond to a coupling constant of 350 MHz, assuming $\eta = 0$, while the coupling constant for Ph_3Sb is 530 MHz (10). Taking the ratio of the principal components of the field gradient tensor per 5*p* electron for antimony and tellurium to be 0.87 (21), the ratio of the coupling constants corresponds to a ratio of $Q_{gnd}(^{121}Sb)/Q_{ex}(^{125}Te)$ of 1.7, which is not inconsistent with previous estimates of the magnitude of the quadrupole moments of these two states (10, 22). Thus the magnitudes of the quadrupole splitting for $Ph_2(CH_3)TeI$ and $Ph(CH_3)_2TeI$ are consistent with those compounds containing pyramidal $Ph_2(CH_3)Te^+$ and $Ph(CH_3)_2Te^+$ cations which are iso-electronic and iso-structural with Ph_3Sb.

Diacetates and Dibenzoates

The ir spectra of the dicarboxylates have been interpreted as evidence for a ψ-trigonal bipyramidal geometry for these molecules, the carboxylate ligands occupying *trans* axial positions (5). The Mössbauer data for these compounds are generally consistent with that structure, exhibiting isomer shifts and quadrupole splittings generally comparable with those of the dichlorides. However, it is clear that the phenyl compounds exhibit much smaller quadrupole splittings than the other derivatives. The ir spectrum of $(p\text{-}EtOC_6H_4)_2Te(OCOCH_3)_2$ was found to be more complex than that of $Ph_2Te(OCOCH_3)_2$, suggesting the possible presence of both uni- and bidentate carboxylate ligands in the former case and only unidentate in the latter. The different quadrupole splittings of $(p\text{-}MeOC_6H_4)_2Te(OCOCH_3)_2$ and $Ph_2Te(OCOCH_3)_2$ are certainly consistent with a different environment about the tellurium in those two compounds.

The compound $Ph_2Te(OCOPh)_2$ was found to have a complex ir spectrum similar to that of $(p\text{-}EtOC_6H_4)_2Te(OCOCH_3)_2$ rather than that of the diphenyl diacetate. However, the Mössbauer data suggest that the tellurium environments in

TABLE 3. Bond orbital populations, U_L, for different ligands

Estimator	U_L	U_L value	Reference
Organotellurides	U_C	1.1	3
Ph_2TeCl_2	$U_{Cl-Te-Cl}$	0.4	3
Ph_2TeBr_2	$U_{Br-Te-Br}$	0.5	3
$(p\text{-}CH_3C_6H_4)TeI_2$	U_{I-Te-I}	0.6	3
Ph_2TeF_2	U_{F-Te-F}	0.2	This work
$(p\text{-}MeOC_6H_4)TeF_3$	U_{F-Te-F}	0.4	This work
$Ph_2Te(OCOCH_3)_2$	U_{O-Te-O}	0.4	This work
$(p\text{-}MeOPh)_2Te(OCOCH_3)_2$	U_{O-Te-O}	0.3	This work
$Ph_2Te(OCOPh)_2$	U_{O-Te-O}	0.4	This work
$(p\text{-}MeOPh)_2Te(OCOPh)_2$	U_{O-Te-O}	0.3	This work

the diphenyl diacetate and dibenzoate are very similar. Thus the ir and Mössbauer data are not wholly consistent, but both suggest that the structures of the diacetates and dibenzoates may show subtle differences with changes in the aryl ligands. A more full interpretation of the Mössbauer data must await structural studies on the carboxylates.

The Additivity Model

It has previously been shown (3) that a simple additivity model, based on Townes and Dailey theory, works surprisingly well in accounting for the main features of the quadrupole splitting data for the compounds R_2Te, R_2TeX_2, and $RTeX_3$ (X = Cl, Br) and the compounds $TeCl_4 \cdot$ py, $RTeX_3 \cdot$ tmtu, and $RTeX_3 \cdot$ py. The model was used to estimate the tellurium *p*-orbital population in the bond to the ligand concerned, U_L. Thus for R_2Te, assuming as an approximation that the lone-pairs have $5s^2$ and $5p_{z^2}$ character, where the *z*-orbital is directed out of the bonding (*xy*) plane, Townes and Dailey theory allows a simple estimate of U_C, the tellurium *p*-orbital population in the Te—C bond. This then allows estimates of the other tellurium-ligand *p*-orbital populations to be made. Using this same approach, ligand *U* values may be arrived at for the compounds studied here and representative values are given in Table 3. The difference in the $U_{F—Te—F}$ value for Ph_2TeF_2 and $(p\text{-}MeOC_6H_4)TeF_3$, for example, is simply a restatement of the failure of the additivity model, the probable reasons for this having been discussed above.

Experimental

The compounds studied were prepared as described in the literature (23–27) and characterized by melting points, analytical data, and proton nmr spectra.

The Mössbauer spectra were recorded on samples of natural isotopic abundance at 4.2 K using an $^{125}Sb/Cu$ source at *ca.* 80 K as previously described (3). The absorbers contained 5–10 mg cm^{-2} ^{125}Te. Mirror image 256 channel spectra were recorded and average values of δ, Δ, and 2Γ were calculated. In all cases the spectra were found to give statistically acceptable fits with X^2/N values lying within the 5% confidence limit.

Conclusions

The present study has extended the range of organotellurium compounds studied using the Mössbauer effect and has identified a number of compounds, namely the organotellurium trifluorides and the diphenyltellurium-diacetate and dibenzoate, where the simple additivity model breaks down. In these compounds the coordination about the tellurium would appear to differ significantly from that in the other organotellurium trihalides, or the other dicarboxylates, respectively. The Mössbauer parameters for the mono-iodides support their formulation as $R_2R'Te^+I^-$.

Acknowledgements

One of the authors (C.H.W.J.) wishes to thank the National Research Council of Canada for a grant supporting this research. F.J.B. wishes to thank Dr. B. C. Smith, Birkbeck College, for his interest and encouragement in this work.

1. F. J. BERRY, E. H. KUSTAN, and B. C. SMITH. J. Chem. Soc. Dalton Trans. 1323 (1975).
2. K. V. SMITH, J. S. THAYER, and B. J. ZABRANSKY. Inorg. Nucl. Chem. Lett. **11**, 441 (1975).
3. C. H. W. JONES, R. SCHULTZ, W. R. MCWHINNIE, and N. S. DANCE. Can. J. Chem. To be published.
4. J. D. MCCULLOUGH and P. F. MARSH. J. Am. Chem. Soc. **72**, 4556 (1950).
5. B. C. PANT, W. R. MCWHINNIE, and N. S. DANCE. J. Organomet. Chem. **63**, 305 (1973).

Can. J. Chem. Downloaded from www.nrcresearchpress.com by 210.87.254.105 on 09/05/12
For personal use only.

6. L. Y. Y. CHAN and F. W. B. EINSTEIN. J. Chem. Soc. Dalton Trans. 316 (1972).
7. W. R. MCWHINNIE and M. G. PATEL. J. Chem. Soc. Dalton Trans. 199 (1972).
8. B. MARTIN and R. SCHULE. Phys. Lett. B, **46**, 367 (1973).
9. J. J. JOHNSTONE, C. H. W. JONES, and P. VASUDEV. Can. J. Chem. **50**, 3037 (1972).
10. L. H. BOWEN. *In* Mössbauer effect data index for 1972. *Edited by* J. G. Stevens and V. E. Stevens. Plenum, New York. 1973. p. 71.
11. D. KOBELT and E. F. PAULUS. Angew. Chem. Int. Ed. Engl. **10**, 73 (1971).
12. W. R. MCWHINNIE and P. THAVORNYUTIKARN. J. Chem. Soc. Dalton Trans. 551 (1972).
13. A. J. EDWARDS and M. A. MOUTY. J. Chem. Soc. A, 703 (1969).
14. B. BUSS and B. KREBS. Inorg. Chem. **10**, 2795 (1971).
15. V. PAULAT and B. KREBS. Angew. Chem. **88**, 28 (1976).
16. L. H. BOWEN, J. G. STEVENS, and G. G. LONG. J. Chem. Phys. **51**, 2010 (1969).
17. K. J. WYNNE and J. W. GEORGE. J. Am. Chem. Soc. **91**, 1649 (1969).
18. D. A. COUCH, P. S. ELMES, J. E. FERGUSON, M. L. GREENFIELD, and C. J. WILKENS. J. Chem. Soc. A, 1813 (1967).
19. M. T. CHEN and J. W. GEORGE. J. Am. Chem. Soc. **90**, 4580 (1968).
20. K. J. WYNNE and P. S. PEARSON. Inorg. Chem. **9**, 106 (1970).
21. R. G. BARNES and W. V. SMITH. Phys. Rev. **93**, 95 (1954).
22. B. M. CHEYNE, C. H. W. JONES, and P. VASUDEV. Can. J. Chem. **50**, 3677 (1972).
23. R. E. LYONS and G. S. BUSH. J. Am. Chem. Soc. **30**, 831 (1908).
24. K. LEDERER. Ber. **49**, 1076 (1916).
25. G. T. MORGAN and R. E. KELLETT. J. Chem. Soc. 1080 (1926).
26. B. C. PANT. J. Organometal. Chem. **65**, 51 (1974).
27. F. J. BERRY, E. H. KUSTAN, M. ROSHANI, and B. C. SMITH. J. Organomet. Chem. **99**, 115 (1975).

Can. J. Chem. Downloaded from www.nrcresearchpress.com by 210.87.254.105 on 09/05/12
For personal use only.

Cinétique de l'interaction des complexes Cu(II)–oxine, Cu(II)–biuret et Cu(II) – acide salicylique avec l'EDTA

ELISABETH MALLARET-GOUT ET MIKLOS ZADOR
Département de Chimie, Université de Montréal, C.P. 6210, Montréal, (Qué.), Canada

Reçu le 23 décembre 1975[1]

ELISABETH MALLARET-GOUT et MIKLOS ZADOR. Can. J. Chem. **54**, 3743 (1976).

La cinétique de l'interaction des complexes Cu(II)–biuret, Cu(II)–oxine et Cu(II) – acide salicylique avec l'EDTA a été étudiée. Le mécanisme de la réaction implique un transfert de protons lent suivi de la réaction rapide du complexe protoné avec l'EDTA. La constante de vitesse comprend la contribution de diverses espèces de l'EDTA en solution ainsi que de H_2O et de H_3O^+. L'importance relative des divers termes varie toutefois d'un système à l'autre.

ELISABETH MALLARET-GOUT and MIKLOS ZADOR. Can. J. Chem. **54**, 3743 (1976).

The kinetics of the interaction of the complexes Cu(II)–biuret, Cu(II)–oxine, and Cu(II) – salicyclic acid with EDTA has been studied. The mechanism of the reaction involves a slow transfer of a proton followed by the rapid reaction of the protonated complex with EDTA. The rate constant contains contributions from the various forms of EDTA in solution as well as those from H_2O and H_3O^+. However, the relative importance of the various terms varies from one system to another.

[Journal translation]

Introduction

Le mécanisme de dissociation de divers complexes du Cu(II) peut être étudié en faisant réagir ceux-ci avec l'EDTA. Ce dernier forme avec le Cu(II) un complexe très stable ($K = 10^{18.7}$ (1)). Un grand nombre de complexes se décomposent d'après l'équation globale 1:

[1] $$CuL_n + EDTA \rightarrow CuEDTA + nL$$

Le mécanisme de cette réaction peut être assez complexe, comme l'indiquent les études antérieures. En particulier, il a été montré par Margerum et coll. que la forme protonée, H_2EDTA^{2-}, agit comme agent de transfert de proton à l'azote peptidique, ce qui entraîne la dissociation et un réarrangement du lien cuivre–triglycine (2). L'EDTA a également été utilisé pour déterminer la constante de dissociation des complexes Cu(II)–adénine (3) et Cu(II)–adénosine (4).

Ce travail est consacré à l'étude de l'interaction de l'EDTA avec trois complexes, soit Cu(II)–biuret, Cu(II)–oxine et Cu(II) – acide salicylique.

Partie expérimentale

Réactifs

Le biuret (J. T. Baker, "Baker Grade") et l'oxine, (hydroxy-8 quinoléine, B.D.H. "Analar") ont été utilisés tels quels. L'acide salicylique (Eastman) a été recristallisé d'un mélange eau–éthanol. La solution de perchlorate cuivrique a été obtenue en dissolvant l'oxyde dans l'acide perchlorique. L'EDTA utilisé est de Fisher Scientific Co.

La force ionique des solutions a été maintenue constante (0.5 *M*) en utilisant le perchlorate de lithium (Alfa Inorganics); la contribution des diverses espèces de l'EDTA à la force ionique a été calculée en tenant compte des équilibres acide–base aux p*H* considérés en utilisant les constantes de la littérature (1).

Méthodes cinétiques

La cinétique des réactions a été étudiée en utilisant un système à flux stoppé Durrum–Gibson, de la compagnie Durrum Instrument Co.; l'appareil a été thermostaté à 25.0 ± 0.1 °C.

Une des seringues de l'appareil contient la solution du Cu(II) et du ligand dans des conditions de concentration et de p*H* où le complexe a une concentration appréciable. L'autre seringue contient l'EDTA. Dans les cas où la vitesse de réaction ne peut être mesurée dans le domaine de p*H* où le complexe domine, le p*H* des deux solutions est différent; le p*H* de l'expérience est celui obtenu après mélange.

La réaction s'accompagne d'une variation de l'absorbance ce qui donne un signal au photomultiplicateur. Ce signal est introduit dans une mémoire reliée par une interface à une calculatrice programmable Tektronix 31. Le système de mémoire permet d'accumuler 256 données à intervalle de temps choisi. A la fin de chaque expérience, ces données sont directement interprétées en utilisant un programme de régression approprié. La valeur de la constante de vitesse est la moyenne de six expériences. La description détaillée du système mémoire–interface que nous avons mis au point, fera l'objet d'une publication ultérieure.

Les longueurs d'onde choisies varient d'un système à

[1]Revision reçue le 28 mai 1976.

Can. J. Chem. Downloaded from www.nrcresearchpress.com by 210.87.254.6 on 09/05/12
For personal use only.

Can. J. Chem. Downloaded from www.nrcresearchpress.com by 210.87.254.6 on 09/05/12
For personal use only.

l'autre. On a choici, respectivement: $\lambda = 510$ nm pour Cu(II)–biuret, $\lambda = 360$ nm pour Cu(II)–oxine et $\lambda = 400$ nm pour Cu(II) – acide salicylique. La concentration des solutions en complexes est de 3×10^{-4} à 4×10^{-3} *M* de façon à obtenir des absorbances raisonnables. La concentration en EDTA varie de 5×10^{-3} à 5×10^{-2} *M*. Dans tous les cas la disparition du complexe entraîne la diminution de l'absorbance. Dans les cas des systèmes Cu(II)–oxine et Cu(II)–biuret, l'apparition du complexe Cu(II)–EDTA a également pu être observée, à la longueur d'onde de 720 nm. Dans chaque cas l'EDTA était pris en grand excès par rapport au complexe et on obtenait des cinétiques d'ordre un.

Résultats

1. Système Cu(II)–biuret

Le biuret ($NH_2CONHCONH_2$ ou BH_2) forme deux complexes avec le Cu(II). Ces complexes ne se forment qu'en milieu très basique, étant donné qu'ils impliquent des groupes $—NH_2$ dissociés. D'après les données de la littérature (5) on a les réactions suivantes:

$$Cu^{2+} + BH_2 + nH_2O \rightleftharpoons [CuB(OH)_n]^{n-} + (n + 2)H^+$$

$$Cu^{2+} + 2BH_2 \rightleftharpoons CuB_2^{2-} + 4H^+$$

Le dernier complexe, CuB_2^{2-}, est l'espèce dominante en présence d'un grand excès de ligand en milieu très basique (pH = 12.8, B/Cu = 20).

L'interaction du complexe CuB_2^{2-} avec l'EDTA n'a pu être étudiée qu'à des p$H \geq 9$. En effet, à des pH plus acides la réaction est trop rapide pour être étudiée par le "flux stoppé". L'étude a été effectuée à six pH différents (entre pH = 9 et pH = 12.8) et à quatre concentrations de l'EDTA. Les résultats ont été obtenus en mélangeant la solution de CuB_2^{2-} (pH = 12.8) avec la solution de l'EDTA de pH plus faible pour donner le pH requis après mélange.

Le complexe CuB_2^{2-} se dissocie d'une part à cause du saut de pH et, d'autre part, à cause de la réaction d'échange avec l'EDTA. Le produit de la réaction est le complexe $CuEDTA^{2-}$ en équilibre avec $CuEDTAOH^{3-}$, en proportion variable d'après le pH final ($[CuEDTAOH^{3-}]/[CuEDTA^{2-}][OH^-] = 10^{2.4}$ (1)).

Le fait que la dissociation du complexe CuB_2^{2-} ($\lambda = 510$ nm) se fait avec la même vitesse que l'apparition de CuEDTA ($\lambda = 720$ nm) indique que les deux processus ont la même étape déterminante.

La constante de vitesse d'ordre un, k_{exp}, de la réaction (*i*) augmente linéairement avec la concentration en EDTA à pH constant et, (*ii*) l'augmentation de la concentration en H^+ entraîne aussi l'augmentation de k_{exp} comme le montre la fig. 1. Ces résultats indiquent clairement que la dissociation de CuB_2^{2-} implique une catalyse acide.

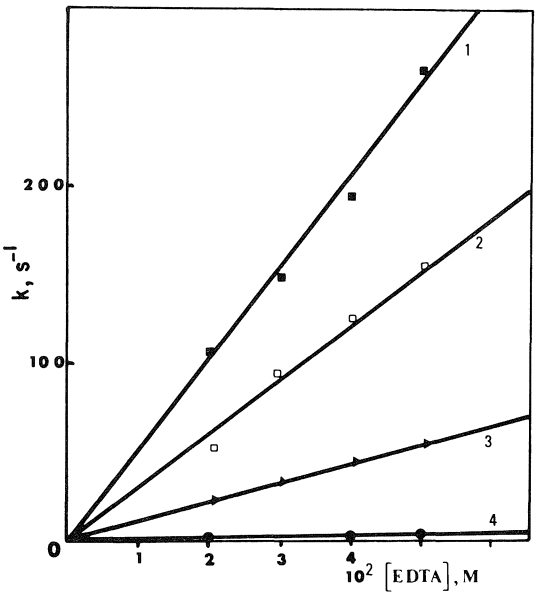

FIG. 1. Variation de la constante de vitesse du système CuB_2^{2-}–EDTA avec la concentration en EDTA à divers pH. T = 25 °C; force ionique = 0.5 *M*; [Cu(II)] = 1.0×10^{-3} *M*, [biuret] = 2.0×10^{-2} *M*; (*1*) pH = 9.0; (*2*) pH = 9.5; (*3*) pH = 10.3; (*4*) pH = 12.4.

L'interprétation des résultats est basée sur l'expression de vitesse [2] qui implique une catalyse acide générale telle qu'observée par Pagenkopf et Margerum pour la dissociation du complexe Cu(II)–triglycine (2).

$$[2] \quad k_{exp} = k_0 + k_{H^+}[H^+] + \sum k_{H_nEDTA^{4-n}}[H_nEDTA^{4-n}]$$

Ce type d'équation est suggéré par le fait que d'autres acides faibles catalysent également la transformation. Ainsi, à pH constant, la constante de vitesse expérimentale varie linéairement avec la concentration en H_3BO_3 et en NH_4^+, ce qui a permis de déterminer les constantes catalytiques pour ces acides: $k_{H_3BO_3} = 4 \times 10^3\ M^{-1}\ s^{-1}$; $k_{NH_4^+} = 1.3 \times 10^4\ M^{-1}\ s^{-1}$ à 25 °C.

Les paramètres de l'éq. 2 ont été déterminés par une méthode de régression multiple pondérée. A chaque pH on calcule d'abord la concentration de diverses espèces de l'EDTA en solution en utilisant les valeurs des constantes

Can. J. Chem. Downloaded from www.nrcresearchpress.com by 210.87.254.6 on 09/05/12
For personal use only.

d'acidité de la littérature (1) et on les introduit dans l'éq. 2. Seuls les termes dont la contribution à la vitesse est significative sont retenus.

Il ressort de l'analyse, qu'aux pH très basiques (p$H \sim 12.4$, courbe 4, fig. 1) seule $EDTA^{4-}$ contribue, en plus de k_0, à la réaction d'échange. La diminution de pH augmente la contribution de $HEDTA^{3-}$, qui devient prépondérante à p$H = 11.4$. Il est à souligner que de p$H = 9.5$ à p$H = 9$, la concentration de $HEDTA^{3-}$ ne change pratiquement pas et malgré tout on observe une augmentation importante de k_{exp} (courbes 2 et 1, fig. 1); ce fait est attribué à H_2EDTA^{2-}, dont la contribution devient prépondérante à p$H = 9$.

En termes quantitatifs, l'interprétation des résultats conduit à l'éq. 3.

$$[3]\quad k_{exp}\,(s^{-1}) = 0.53 + 2.2 \times 10^6[H_2EDTA^{2-}] + 2.2 \times 10^3[HEDTA^{3-}] + 37[EDTA^{4-}]$$

La contribution d'un terme, $k_{H^+}[H^+]$ n'est pas significative aux pH étudiés (p$H \geq 9$), ce qui implique que la valeur de k_{H^+} ne dépasse pas $\sim 10^9\ M^{-1}\ s^{-1}$.

2. Système Cu(II)–oxine

L'hydroxy-8 quinoléine (ou oxine) forme deux complexes avec le Cu(II), d'après les équilibres suivants (6):

$$Cu^{2+} + OxH \underset{}{\overset{K_1}{\rightleftharpoons}} CuOx^+ + H^+$$
$$K_1 = 10^{12.6}$$

$$CuOx^+ + OxH \rightleftharpoons CuOx_2 + H^+$$

Le complexe 1:2 est très peu soluble ($K_{ps} = 10^{-29.6}$ (7) et précipite dans les conditions de pH ou il prédomine. En effet, dû à la dissociation de l'oxine d'après l'équilibre

$$OxH \underset{}{\overset{K_{a1}}{\rightleftharpoons}} Ox^- + H^+$$
$$pK_a = 3.8$$

on peut voir qu'à des concentrations en Cu(II) et en oxine de l'ordre de $10^{-3}\ M$, la précipitation a lieu à des p$H > 5$.

En milieu plus acide, par contre, il y a protonation du ligand libre:

$$OxH + H^+ \rightleftharpoons OxH_2^+$$

et à des p$H < 2$ ceci cause la dissociation des complexes.

Le complexe 1:1, $CuOx^+$, domine vers p$H =$ 3–3.5 en présence d'un excès de Cu(II) (Cu/Ox =

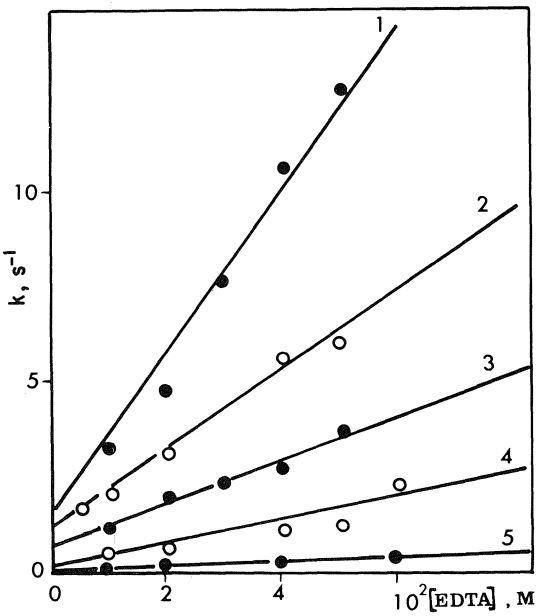

FIG. 2. Variation de la constante de vitesse du système $CuOx^+$–EDTA avec la concentration en EDTA à divers pH. $T = 25$ °C; force ionique = 0.5 M; [Cu(II)] = $6.0 \times 10^{-4}\ M$; [oxine] = $3.0 \times 10^{-4}\ M$; (*1*) p$H = 5.9$; (*2*) p$H = 6.2$; (*3*) p$H = 6.5$; (*4*) p$H = 7.0$; (*5*) p$H = 8.0$.

2). Sa réaction avec l'EDTA a pu être étudiée entre p$H = 5.9$ et 8. A p$H < 5.9$, elle est trop rapide tandis qu'à p$H > 8$ elle est très lente et le signal devient trop faible pour conduire à des résultats fiables.

La précipitation de $CuOx_2$ n'a pas lieu à ces pH, due à la réaction rapide de $CuOx^+$ avec l'EDTA, après le saut très rapide de pH lors du mélange des solutions. Le saut du pH pourrait par ailleurs entraîner la formation transitoire de complexes hydroxylés mixtes bien qu'en général ils ne soient formés qu'à des pH élevés. Aucune évidence directe n'est disponible à ce sujet, ce qui est dû au fait que l'espèce le plus stable à ces pH est $CuOx_2$.

L'ensemble des résultats est illustré par la fig. 2. On constate que k_{exp} augmente (*i*) avec la concentration en EDTA et (*ii*) avec l'acidité de milieu, donc on a affaire à une catalyse acide. L'interprétation des résultats a été faite de manière analogue au cas décrit plus haut; elle conduit à l'éq. 4.

$$[4]\quad k_{exp}\,(s^{-1}) = 1.3 \times 10^6[H^+] + 1.6 \times 10^5[H_3EDTA^-] + 2.1 \times 10^2[H_2EDTA^{2-}]$$

Can. J. Chem. Downloaded from www.nrcresearchpress.com by 210.87.254.6 on 09/05/12
For personal use only.

Le terme indépendant de l'EDTA (ordonnée à l'origine de la fig. 2) est dû à H^+; le terme k_0 n'est pas significatif aux pH étudiés. Parmi les termes dépendant de l'EDTA la contribution la plus importante est de H_2EDTA^{2-}; celle de H_3EDTA^- devient significative aux pH les plus faibles (~25% à pH = 5.9).

La catalyse par d'autres acides faibles a été vérifiée à l'aide de l'acide maléique (MaH_2, $k_{MaH^-} = 3.4 \times 10^2\ M^{-1}\ s^{-1}$) et l'$\alpha$-picoline H^+ ($k_{\alpha\text{-}pH^+} = 40\ M^{-1}\ s^{-1}$). Comme pour le système précédent, la disparition de $CuOx^+$ (λ = 360 nm) correspond à l'apparition de $CuEDTA^{2-}$, donc il y a une même étape déterminante pour ces processus.

3. Système Cu(II) – acide salicylique

L'acide salicylique (SH_2) forme un complexe 1:1 avec le Cu^{2+}:

$$Cu^{2+} + SH_2 \rightleftharpoons CuS + 2H^+$$

La constante de stabilité du complexe est donnée par la relation (8):

$$K = [CuS]/[Cu^{2+}][S^{2-}] = 10^{10.6}$$

Ce complexe est stable entre pH = 5 à 7. A pH > 7 il y a précipitation de $Cu(OH)_2$, tandis qu'à des pH < 5 il n'y a pas suffisamment de complexe. La cinétique d'intéraction avec l'EDTA a pu être étudiée entre pH = 9 à 13, en mélangeant la solution du complexe (pH ~ 5–7) avec une solution d'EDTA de pH plus élevé. Il est à noter que le saut de pH est très important dans ce cas. Au pH de l'expérience il est probable que des composés hydroxylés, tels $CuSOH^-$ ou $CuS(OH)_2^{2-}$ existent et soient au moins en partie responsables des cinétiques observées. Ceci rend donc l'extrapolation des résultats aux pH où le complexe CuS est stable (pH = 5 à 7) peu certain.

La constante de vitesse est indépendante de la concentration en EDTA pour toutes les expériences; elle augmente linéairement avec la concentration en H^+. On obtient donc une relation simple pour la constante de vitesse.

$$[5] \qquad k_{exp}\,(s^{-1}) = 78 + 8.5 \times 10^{10}[H^+]$$

A des pH < 9 la vitesse de réaction est trop grande pour être étudiée, dû à la valeur très élevée, $8.5 \times 10^{10}\ M^{-1}\ s^{-1}$ de la constante k_{H^+}.

Discussion

Les résultats obtenus dans ce travail doivent être comparés à ceux obtenus par Margerum et coll. qui ont étudié le mécanisme de transfert de proton dans le système Cu(II)–triglycine–EDTA (2):

$$CuH_{-2}L + HX \rightarrow CuH_{-1}L + X^-$$

Ils ont observé une catalyse acide générale, avec une constante de vitesse du type $k = \sum k_{HX}[HX]$; la constante de vitesse est constituée de la contribution de tous les acides (HX) dans le milieu. Ceci a conduit à la conclusion que le transfert de proton est l'étape lente de la réaction. Ils ont montré que, dans le cas de l'EDTA, seule l'espèce H_2EDTA^{2-} est réactive, même dans les conditions où $HEDTA^{3-}$ domine.

Donc l'EDTA ne réagit pas avec Cu(II)–triglycine en tant que nucléophile, mais plutôt comme agent de transfert de proton.

La dissociation des complexes CuB_2^{2-} et $CuOX^+$ semble s'effectuer par un mécanisme du même type. Cependant, dans notre cas plusieurs espèces de l'EDTA et d'autres acides faibles contribuent aux constantes de vitesse. La nature et le nombre de termes apparaissant dans l'équation de vitesse dépendent et du système considéré et de la gamme de pH étudiée.

Le cas du complexe CuS semble être différent étant donné que la réaction est indépendante de l'EDTA. Ce système est de plus affecté d'incertitudes, quant à la nature exacte des espèces à pH élevé où des complexes hydroxylés peuvent exister. Dans les cas de CuB_2^{2-} et de $CuOx^+$ les résultats suggèrent un mécanisme avec transfert de proton lent:

$$[6]^2 \qquad CuL + HX \overset{\text{lent}}{\rightleftharpoons} CuLH^+ + X^-$$

$$[7]^2 \qquad CuLH^+ + EDTA \xrightarrow{\text{rapide}} CuEDTA + L + H^+$$

Le transfert de proton lent implique la rupture simultanée d'un lien Cu—N (ou possiblement Cu—O dans le cas de $CuOx^+$). La forme ainsi obtenue réagit ensuite avec l'EDTA. L'étape 7 peut aussi s'effectuer en deux étapes: dissociation préalable de $CuLH^+$, suivie de la réaction connue comme très rapide (9), de l'EDTA avec le Cu(II) libéré.

Un autre mécanisme est cependant compatible avec les résultats. Celui-ci implique également l'affaiblissement ou la rupture du lien de coordi-

[2]Pour fins de simplicité la charge exacte des complexes est omise.

nation entre le Cu(II) et le ligand par fixation rapide d'un proton sur le ligand (éq. 8). Le complexe protoné réagit ensuite avec les diverses espèces de l'EDTA en solution (éq. 9).

$$[8] \qquad CuL + H^+ \underset{}{\overset{\text{rapide}}{\rightleftharpoons}} CuLH^+$$
$$K = [CuLH^+]/[CuL][H^+]$$

$$[9] \quad CuLH^+ + H_nEDTA^{4-n} \xrightarrow[\text{lent}]{k_n} CuEDTA + L + nH^+$$

Ce type de mécanisme a été proposé par Margerum et coll. pour l'interaction du complexe Cu(II) – glycyl glycyl-L-histidine avec divers ligands (10).

Ce mécanisme conduit, en ce qui concerne les termes dépendant de l'EDTA, à l'équation:

$$[10] \quad d[CuEDTA]/dt = \sum_n k_n K[CuL][H^+][H_nEDTA^{4-n}]$$

A cause de l'équilibre de protonation:

$$[H_{n+1}EDTA^{3-n}] = K_a^{-1}[H^+][H_nEDTA^{4-n}]$$

l'éq. 10 ne peut pas être distinguée cinétiquement de la catalyse acide générale (éqs 6 et 7) qui conduit à l'éq. 11.

$$[11] \quad d[CuEDTA]/dt = \sum_n k_n'[CuL][H_nEDTA^{4-}]$$

Le choix entre ces deux mécanismes est évidement assez difficile à faire. Il diffèrent par le choix de l'étape déterminante mais sont en accord sur le fait que la protonation du complexe est indispensable. Il n'y a pas encore suffisamment de données dans la littérature pour un appui massif pour l'un ou pour l'autre.

Dans nos cas l'effet catalytique des acides faibles autres que dérivant de l'EDTA milite en faveur de la catalyse acide générale sans toutefois écarter catégoriquement la contribution de l'autre mécanisme.

Dans le cas de CuB_2^{2-} des valeurs très élevées de constantes catalytiques sont obtenues qui sont inhabituelles pour un transfert de proton "lent". La valeur de $k_{H_2EDTA^{2-}}$ 2.2×10^6 M^{-1} s^{-1} est cependant d'un facteur de 10^2 plus faible que les constantes de vitesse de transfert de proton d'un acide de force comparable, tel le *p*-nitrophénol, à des bases faibles telle l'imidazole (11).

Ce résultat est donc en accord avec deux hypothèses: (*i*) basicité élevée de l'azote terminal du biuret sur lequel le proton se fixe et en plus (*ii*) grande facilité de rupture du lien Cu—N, par rapport aux systèmes similaires étudiés.

Le même raisonnement s'applique à $HEDTA^{3-}$ ($k = 2.2 \times 10^3$ M^{-1} s^{-1}) qui est un acide encore plus faible ainsi qu'à l'acide borique et l'ion ammonium ($k_{H_3BO_3} = 4 \times 10^3$ M^{-1} s^{-1}; $k_{NH_4^+} = 1.3 \times 10^4$ M^{-1} s^{-1}).

L'augmentation des constantes avec la force des acides est en accord qualitatif avec une relation de type Brönsted ou, avec la théorie de transfert de proton de Eigen (11); l'interprétation quantitative ne serait cependant pas significative due à la complexité du système et le nombre restreint d'acides étudiés.

L'interprétation des résultats d'après l'éq. 10 conduit également à des constantes élevées. Pour le terme $[H^+][HEDTA^{3-}]$ on aurait une valeur maximum de $kK = 3.1 \times 10^{12}$ M^{-2} s^{-1}, et pour $[H^+][EDTA^{4-}]$ $kK = 3.6 \times 10^{13}$ M^{-2} s^{-1}. Des valeurs de cet ordre de grandeur ne donnent des constantes, k, de la réaction 9 raisonnables que si K est très élevé. Ceci implique une basicité relativement grande du complexe, hypothèse identique à celle qui permet de rationaliser la catalyse acide générale.

Les valeurs élevées dans les deux cas sont la conséquence logique de deux faits simples: (*i*) vitesses de réaction élevées et (*ii*) catalyse acide à des concentrations en H^+ de 10^{-9} à 10^{-12} M (où seuls les acides très faibles existent en concentrations appréciables).

Le complexe CuB_2^{2-} réagit aussi directement avec $EDTA^{4-}$, probablement par un mécanisme SN_2. Cette réaction n'intervient cependant qu'aux pH les plus élevés. La constante relativement faible (37 M^{-1} s^{-1}) est une indication du fait que l'EDTA, à cause de l'encombrement stérique est un nucléophile médiocre. Ce point a été souligné par Margerum et coll. (10) qui, dans le cas de Cu(II)–triglycine ont obtenu une constante de 600 M^{-1} s^{-1} pour l'EDTA, ce qui est très faible par rapport à celle du trien (1.1×10^7 M^{-1} s^{-1}) qui est un bon nucléophile.

La discussion précédente concernant la catalyse acide s'applique aussi au cas de $CuOx^+$, mais il y a néanmoins certaines particularités à souligner.

D'abord dans ce cas les termes impliquant $EDTA^{4-}$ et $HEDTA^{3-}$ ne sont pas significatifs, dû à la gamme de pH plus acide où ces espèces

Can. J. Chem. Downloaded from www.nrcresearchpress.com by 210.87.254.6 on 09/05/12
For personal use only.

sont pratiquement absentes. Les diverses constantes de vitesse augmentent également avec la force de l'acide, en accord qualitatif avec les connaissances acquises en catalyse acide générale.

Dans ce cas, le terme $k_{H^+}[H^+]$ a une contribution significative; il y a donc une voie réactionnelle indépendante de l'EDTA, ce qui suggère évidemment que l'étape lente précède la réaction avec l'EDTA. Dans le mécanisme suggéré, ceci correspond à la protonation "lente" de $CuOx^+$, avec rupture d'un lien de coordination Cu—N ou Cu—O.

Toutefois même dans ce cas-ci, il reste une alternative, notamment protonation rapide de $CuOx^+$ suivie de la rupture lente d'un ou de deux liens Cu(II)–oxine, conduisant à une espèce pouvant réagir rapidement avec l'EDTA.

Dans le cas de $CuOx^+$ le ligand n'occupe que deux sites de coordination du Cu(II) laissant les autres libres à l'attaque par l'EDTA. Il est très significatif que la protonation du ligand sortant soit nécessaire pour la rupture des liens Cu(II)–oxine et pour que la réaction d'échange soit complète. Ceci est cependant dû au fait que l'$EDTA^{4-}$ est un nucléophile médiocre, ce qui est encore plus vrai pour H_2EDTA^{2-} qui est l'espèce dominante vers p$H \sim 6$.

La constante de vitesse de dissociation de $CuOx^+$, k_d, peut être estimée à partir de la relation $k_f/k_d = K = 10^{12.6}$. Il est à toute fin pratique certain, vu l'ensemble des connaissances acquises sur l'intéraction du Cu^{2+}, avec divers ligands, que la constante de vitesse de formation de $CuOx^+$ à partir de Cu^{2+} et de Ox^-, ne dépasse pas une valeur maximum de $k_{f_{max}} \sim 10^9\ M^{-1}\ s^{-1}$. La limite supérieure de k_d est donc $\sim 10^{-3.6}\ s^{-1}$. Cette valeur est de loin inférieure aux constantes k_{exp} mesurées dans toute la gamme étudiée. Ceci implique que la dissociation "non-catalytique" de $CuOx^+$, qui pourrait être suivie d'une réaction très rapide de Cu^{2+} avec l'EDTA, est négligeable par rapport aux processus catalysés.

Remerciements

Les auteurs remercient le Ministère de l'Education du Québec pour l'octroi qui a rendu possible la réalisation de ce travail. Le Conseil des Arts du Canada est remercié pour la bourse d'études accordée (E.M.-G.).

1. L.G. Sillén et A. E. Martell. Stability constants of metal–ion complexes. The Chemical Society, London. 1964. p. 634.
2. G. K. Pagenkopf et D. W. Margerum. J. Am. Chem. Soc. **90**, 501 (1968); **90**, 6963 (1968).
3. G. Boivin et M. Zador. Can. J. Chem. **51**, 3322 (1973).
4. G. Boivin et M. Zador. Can. J. Chem. **50**, 3117 (1972).
5. M. Kato. Z. Anorg. Allg. Chem. **300**, 84 (1959); M. Kato. Z. Phys. Chem. N.F. **23**, 375 (1960).
6. P. Näsänen et V. Penttinen. Acta Chim. Scand. **6**, 837 (1952).
7. G. Charlot. Les méthodes de la chimie analytique. Masson et Cie, Paris. 1961. p. 70.
8. D. D. Perrin. Nature, **182**, 741 (1958).
9. D. C. Olson et D. W. Margerum. J. Am. Chem. Soc. **85**, 297 (1963); N. Tanaka, H. Osawa et M. Kanaka. Bull. Chem. Soc. Jpn. **36**, 530 (1963).
10. J. C. Cooper, L. F. Wong, D. L. Venezky et D. W. Margerum. J. Am. Chem. Soc. **96**, 7560 (1974).
11. M. Eigen. Angew. Chem. **75**, 489 (1963).

Can. J. Chem. Downloaded from www.nrcresearchpress.com by 210.87.254.6 on 09/05/12
For personal use only.

Flash thermolysis: multiple sigmatropic rearrangements in *ortho*-substituted aromatic compounds[1]

PIERRE DE CHAMPLAIN,[2] JEAN-LOUIS LUCHE,[3] ROBERT A. MARTY,[4] AND PAUL DE MAYO
Department of Chemistry, University of Western Ontario, London, Ont., Canada N6A 5B7

Received July 7, 1976

PIERRE DE CHAMPLAIN, JEAN-LOUIS LUCHE, ROBERT A. MARTY, and PAUL DE MAYO. Can. J. Chem. **54**, 3749 (1976).

A number of *o*-disubstituted benzenoid substances on flash thermolysis undergo 1,4-elimination of water or alcohols to yield *o*-quinonoid derivatives. Those products possessing a pentadienyl hydrogen subsequently undergo a 1,5-sigmatropic rearrangement: in many cases the rearrangement product undergoes yet further transformations, such as addition or hydrolysis, and such reactions have been used for their characterization. Included are: the conversion of *N*-methyl anthranilate esters to *o*-aminobenzaldehyde; *o*-(*N*-methyl)benzyl alcohol and methyl ether to *o*-toluidine; *o*-methoxymethylformanilide to *o*-tolyl isocyanate; and *o*-carboxymethylformanilide to *o*-aminobenzaldehyde.

PIERRE DE CHAMPLAIN, JEAN-LOUIS LUCHE, ROBERT A. MARTY et PAUL DE MAYO. Can. J. Chem. **54**, 3749 (1976).

Sous l'influence de la thermolyse éclair, un certain nombre de dérivés benzéniques *o*-disubstitués perdent de l'eau ou des alcools, par éliminations-1,4, pour conduire à des dérivés *o*-quinonoïdes. Les produits possédant un hydrogène pentadiènyle subissent un réarrangement sigmatropique-1,5; dans plusieurs cas, le produit de réarrangement subit des transformations subséquentes, comme des réactions d'addition ou d'hydrolyse, et on a utilisé ces réactions pour fins de caractérisation. On a étudié les conversions: des esters du *N*-méthyl anthranilate en *o*-aminobenzaldéhyde; de l'alcool *o*-(*N*-méthyl)benzilique ou de son éther méthylique en *o*-toluidine; de l'*o*-méthoxyméthylformanilide en isocyanate d'*o*-tolyle; et de l'*o*-carboxyméthylformanilide en *o*-aminobenzaldéhyde.

[Traduit par le journal]

Can. J. Chem. Downloaded from www.nrcresearchpress.com by 210.87.254.40 on 09/05/12
For personal use only.

Some time ago (1) we reported that the flash thermolysis of *o*-nitroanisole yielded benzaldehyde, together with, in smaller amount, salicylaldehyde. The route to these products was shown to be that indicated in Scheme 1 by the generation of the various radical intermediates (**a**, **b**) by alternative pathways. The results were those to be expected from Scheme 1 and, in addition, substitution of deuterium in the methoxyl group of 4-methylnitroanisole gave the deuterated tolualdehyde expected.

A natural extension of this work was the study of the nitrogen equivalent of the substance **2**; that is, the ester **3**, which might be expected to give benzaldehyde as the product. In fact, a different pathway was followed during the thermolysis which it is the purpose of the present paper to describe.

Thermolysis at 770 °C gave a new product tentatively assigned the structure **4**. Hydrolysis gave *o*-aminobenzaldehyde in ~60% yield. It was characterized as the phenylhydrazone. Repetition using the methyl ester gave the same result, and this substance, **5**, was used in all subsequent experiments.

The spectroscopic evidence for the structure of **4** is as follows: the pmr spectrum showed a singlet at δ 9.9 and a broad peak at ~8.9 ppm (exchangeable in D_2O) assigned to the amine. Absorption at 4.8 ppm was assigned to the methylene group.

Thermolysis and collection of the product on a cryostat on a sodium chloride plate (the apparatus has been described elsewhere (2)) permitted the recording of the infrared spectrum at liquid nitrogen temperature. Bands at 1680 and 1660 cm^{-1} were observed. The former vanished by the time the temperature −115 °C was attained and the spectrum then resembled that obtained at room temperature. An additional intermediate of high reactivity was therefore required and is believed to be the imine **6**. With traces of water and partial hydrolysis the aminal could be easily

[1]Flash thermolysis, part 12.

[2]Present address: Department of Chemistry, Algonquin College, Ottawa, Ont., Canada K1S 0C5.

[3]Present address: CERMO, Université Scientifique et Medicale de Grenoble, 39041 Grenoble, France.

[4]Present address: The School of Mines and Industries, Ballarat, Mt. Helen 3350, Victoria, Australia.

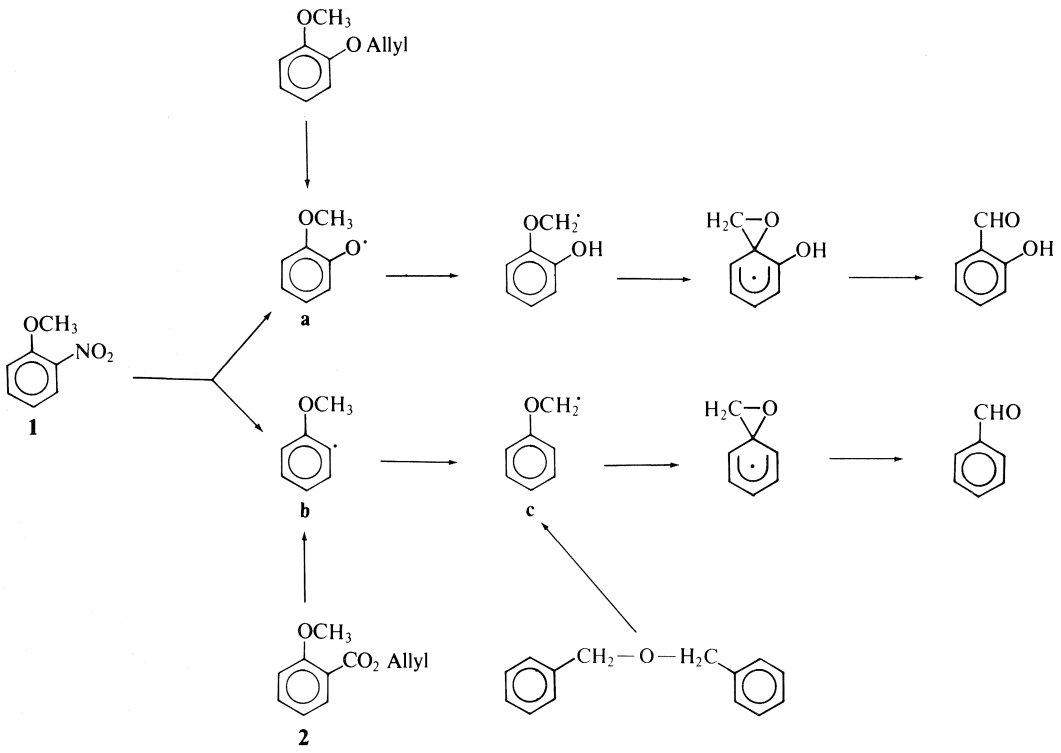

SCHEME 1

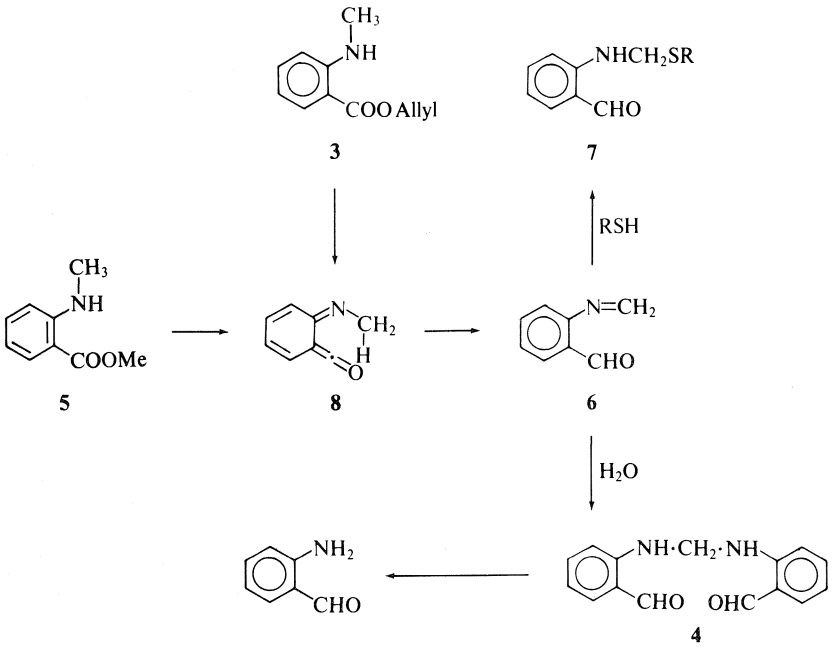

Can. J. Chem. Downloaded from www.nrcresearchpress.com by 210.87.254.40 on 09/05/12
For personal use only.

Can. J. Chem. Downloaded from www.nrcresearchpress.com by 210.87.254.40 on 09/05/12
For personal use only.

obtained. Under these circumstances the provision of a better nucleophile should result in preferential trapping of the imine. Co-depositions of thiophenol and of thioglycollic ester, during the thermolysis, were successful in trapping the intermediate, and the products **7**, R = Ph, and R = CH_2COOEt, were obtained.

The mechanism indicated is reasonable and has an analogy for its sequential individual steps. Thermal 1,4- elimination of alcohols is not uncommon, and there are other routes to the so-obtained *o*-methylene quinones (for examples, for instance, see ref. 3). The ketene **8** does not, apparently, survive the thermolytic condition since a ketene band was not observed in the cryostat. However, 1,5-sigmatropic hydrogen shifts are notoriously facile and there is close analogy for the conversion of **8** to **6** in that of **9** → **10** (4) and **11** → **12** (5).

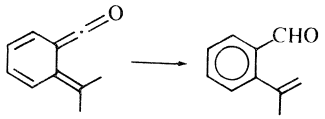

9 **10**

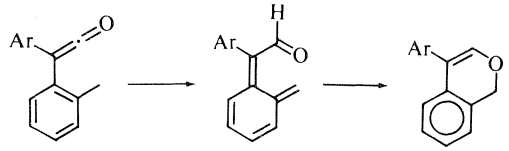

11 **12**

In the absence of the *N*-methyl group **8** evidently could not undergo a sigmatropic hydrogen shift. On the other hand, the elimination to give the equivalent of **8** should occur and its characterization would provide further evidence for the overall scheme. As in the previous case, the ketene **13** could not be expected to be isolable under normal conditions. Two experiments were performed which indicated its transient existence.

Thermolysis of **14** at 840 °C with the simultaneous introduction of ethanol between the furnace and the cold finger gave in low yield a mixture of anthranilate esters shown to be a 7:1 ratio of ethyl to methyl derivatives. The formation of the starting material is possibly due to the co-deposition of the eliminated methanol in the proximity of the ketene, or may simply be unthermolyzed starting material. Co-deposition of thiophenol gave a 29% yield of **15**. Analysis of the thermolysate (875 °C) in the absence of additional trapping agent at liquid nitrogen temperature in the cryostat gave an infrared spectrum showing bands at 2220, 2080, 1825, 1790, and 1710 cm^{-1}. Gradual warming resulted in the early disappearance of the bands at 2080 and 1710 cm^{-1} (−150 °C). The bands at 1825 and 1790 cm^{-1} disappeared near −40 °C. We assign the first set to the ketene and imine (6, 7). The second set is probably to be attributed to the β-lactam **16**. For the same substance Ziegler and Sterk (7) report 1810 cm^{-1} (gas phase). The equivalent thiolactone (**17**) is also unstable at −40 °C (6).

The band at 2220 cm^{-1} is associated with a comparatively stable entity since it survived at room temperature, although it gradually decreased with time. Careful examination of the material obtained using thiophenol as the trapping agent allowed the isolation of a new substance which was identified as **18** (see Experimental). This is evidently a product of the addition of thiophenol to cyclopentadienyl nitrile, the latter being the species responsible for the band at 2220 cm^{-1} in the cryostat. This nitrile is the known rearrangement product of pyridyl carbene and phenyl nitrene, a transformation first reported by Crow and Wentrup (8) and since extensively studied (9). The route from **13** to the surface containing pyridyl carbene and phenyl

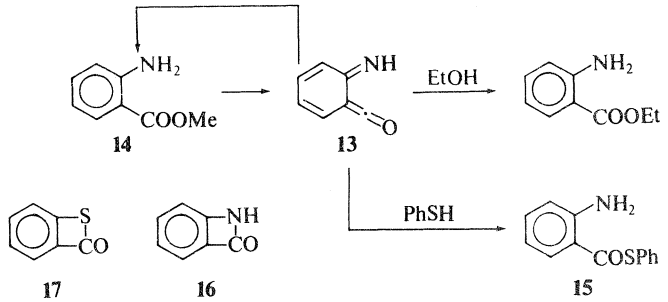

14 **13** **15** **17** **16**

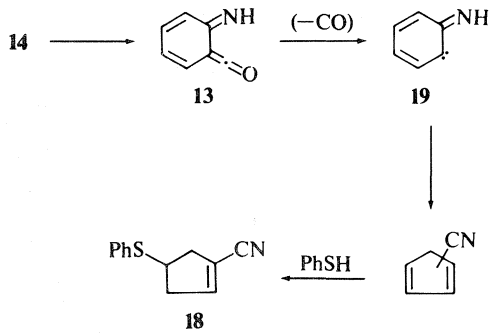

nitrene may be rationalized by postulating the loss of CO followed by rearrangement of **19**, the derived carbene.

In the scheme shown for the elimination of methanol to give **13** the carbonyl group did not play an obvious function. The question then arose as to whether the replacement of this by sp^3 carbon would affect the cause of the reaction. Accordingly the ether **20** was thermolyzed in the presence of thiophenol. The thioether **21** was obtained in yields of over 50% and its properties and those of its benzoyl derivative corresponded with those in the literature (10). The role of the azetidine **22**, if any, in this sequence is unknown. The sp^2 carbon is therefore, as expected, not required for the elimination. It remained to be seen whether, in this system, the ketene was required for the subsequent sigmatropic shift in those molecules where it was possible. Both the ether **23** and the alcohol **24** were accordingly prepared. The alcohol was thermolyzed at 800 °C. In the absence of added trapping agent the pmr spectrum showed peaks at 4.30 and 2.2 ppm consistent with structure **25**. It could not be obtained pure, but on steam distillation gave 65% of *o*-toluidine. In the presence of thiophenol as trapping agent an adduct was obtained having all the spectroscopic properties expected of **26**, but attempts to obtain it in pure form were unsuccessful. That it was most probably **26** was shown by acid hydrolysis to formaldehyde, this being identified as the 2,4-dinitrophenylhydrazone (80%). In addition, desulphurization with Raney nickel gave *N*-methyl-*o*-toluidine. With this evidence we feel confident of the correctness of our interpretation. Thermolysis of **23** also led to **25** in an estimated yield (pmr) of 70%.

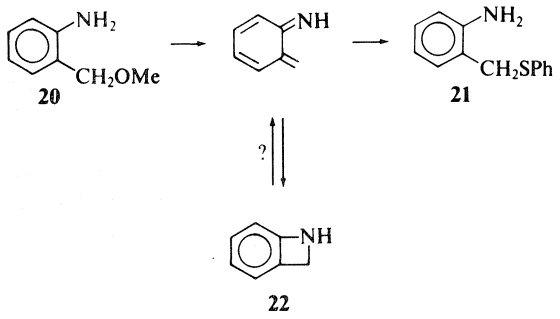

Thus far the only requirement for this elimination–rearrangement sequence is the presence of a leaving group in the benzylic position adjacent to the amine. It was presumed that the amine itself was necessary to increase the acidity of the departing hydrogen, but no acidity was required for the subsequent sigmatropic shift. Hence hydrogen sources other than methyl groups could be envisaged. One such was the formanilide, **27**,

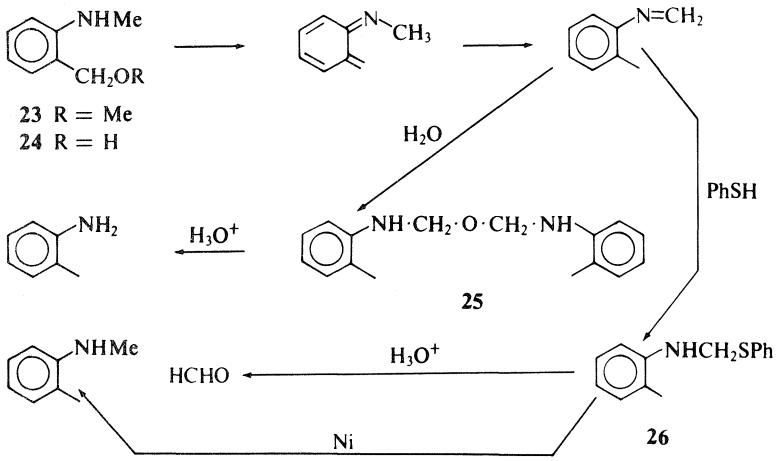

Can. J. Chem. Downloaded from www.nrcresearchpress.com by 210.87.254.40 on 09/05/12
For personal use only.

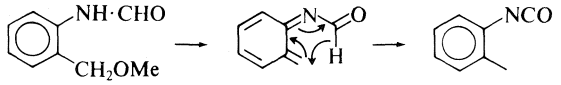

27

where the predicted product of such a sequence would be *o*-tolyl isocyanate. Thermolysis (800 °C) gave material in which the expected band in the infrared spectrum was readily visible (2260 cm^{-1}). Warming with methanol gave the urethane, but better yields of the urethane were obtained by co-deposition of the thermolysate with methanol (89%) or ethanol. In another experiment the thermolysate was distilled, after deposition, at −45 °C (chlorobenzene – liquid nitrogen slurry) which removed the methanol (identified spectroscopically), and which left the isocyanate. This was also identified spectroscopically.

We were thus encouraged by this success to attempt the thermolysis of the ester **28**. Following a similar sequence the presently unknown *o*-formyl isocyanate **29** would be expected in the

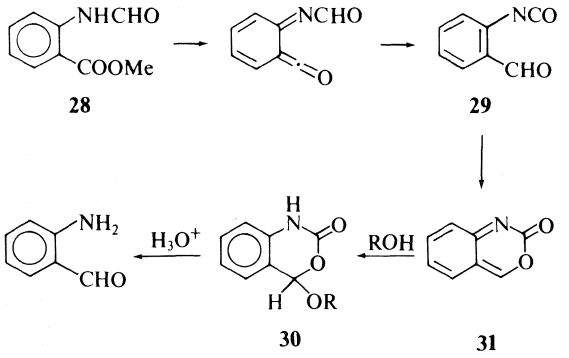

28 29 30 31

thermolysate. The product of thermolysis however did not contain an isocyanate band and its mass spectrum showed it to be isomeric with the starting material. A methoxyl group (3.64 ppm) was present, and a single proton singlet at 6.06 ppm. An NH broad singlet appeared at 9.76 ppm and was exchangeable with D_2O. However, prolonged treatment with D_2O led to decomposition, and from the product *o*-aminobenzaldehyde could be isolated.

On this basis we are led to assign the structure **30**, R = Me, to the thermolysis product, and its formation may be a consequence of a further pericyclic transformation in the isocyanate to give **31** which would be expected to react rapidly with alcohols. Alternatively, **30** may be formed directly from the hemiacetal of **29**. Other mechanisms are conceivable, as, for instance the point of attachment of the alkoxyl group is the same in the starting material and the product, it can be argued that the C—O linkage is never broken. Such a process is indicated in Scheme 2.

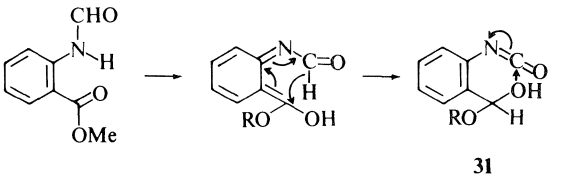

31

SCHEME 2

A rigid decision is not possible on the available evidence. Co-deposition of ethanol does indeed, as would be expected from the first sequence, lead to the formation of **30**, R = Et, and does, we believe, favour this route. But exchange in **31** prior to reaction cannot be excluded. The yields of the methyl derivative reached 60%, yet attempts to trap **31** by the formation of a Diels–Alder adduct with acetylenedicarboxylic ester were uniformly unsuccessful.

Finally, the question posed itself as to the degree of acidity necessary in the hydrogen constituting the hydroxyl of the eliminated alcohol. Was it necessary that it be in the acidity range expected when attached to a heteroatom, or would activation by an adjacent carbonyl function be sufficient? Of the possible starting materials the ester **32** seemed attractive. The known acid, more stable than the literature had led us to expect (11), was easily converted to the ester with diazomethane. This polymerized even in dilute solution on keeping, and so was prepared just prior to use. Thermolysis afforded isocoumarin. By analogy a pathway via the

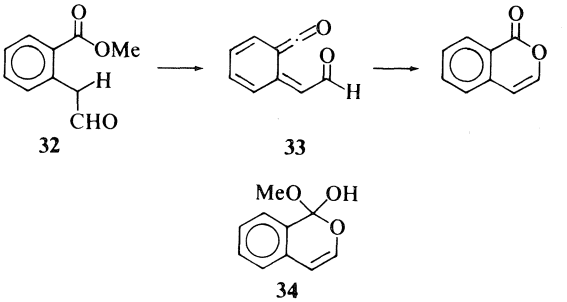

32 33 34

Can. J. Chem. Downloaded from www.nrcresearchpress.com by 210.87.254.40 on 09/05/12
For personal use only.

Can. J. Chem. Downloaded from www.nrcresearchpress.com by 210.87.254.40 on 09/05/12
For personal use only.

ketene can be envisioned, and seems most appropriate to a homogeneous phase process. We have, however, shown that some α exchange in cyclohexanone may occur, presumably through an enol (12, 13) formed on the walls of the furnace. We cannot, therefore, exclude with total conviction the attack of such an enol intramolecularly on the ester function to give, reversibly, **34**. The latter would then lose methanol to give the isocoumarin. In any event it appears that under our conditions the hydrogen is sufficiently activated for elimination.

Experimental

General Procedures

All melting points were taken on a Kofler hot stage and are uncorrected. All mass spectra were obtained on an M-66 spectrometer. The thermolysis apparatus has already been described (14). Compounds were introduced directly into the furnace (except for methyl toluate) prior to evacuation and heating of the thermolysing section of the oven. Trapping agents were allowed to enter the system between the oven and the cold finger and were deposited simultaneously with the thermolysate. The rate was controlled by a Teflon stopcock, and the partial pressure recorded.

Materials

N-Methyl anthranilic acid was converted to the isatoic anhydride and thence, by the decarboxylation–esterification procedure of Staiger and Miller (15) to methyl *N*-methyl anthranilate (**5**). Other esters of anthranilic acid were prepared similarly. *o*-Methylaminobenzyl alcohol (**24**) was prepared from the acid by the method of Lora-Tamayo *et al.* (16). Methyl *N*-formyl anthranilate (**28**) was prepared by the method of Mehner (17), mp 52–53.5 °C. 2-Acetoxy-1-indanone was hydrolyzed by the method of Ishiwara (18) and the product cleaved with periodic acid to give *o*-carboxyphenylacetaldehyde, mp 95.5–96 °C (from ether–pentane) (lit. (11) 98–99 °C from water). The ester **32** was prepared with diazomethane.

The Thermolysis of Dibenzyl Ether

The ether (283 mg) was thermolyzed at 900 °C. Analysis of the mixture of products (nmr) indicated the presence of dibenzyl (13%), toluene (24%), dibenzyl ether (24%), and benzaldehyde (40%). Treatment of the mixture with 2,4-dinitrophenylhydrazine gave the derivative of benzaldehyde, identified by comparison with an authentic specimen.

The Thermolysis of 4-Methyl-2-nitroanisole

The anisole (323 mg) was thermolyzed at 900 °C. The phenolic fraction (17%) was separated by tlc to give 2-hydroxy-4-methylbenzaldehyde (4%) identified by comparison with an authentic specimen (mp 268–269 °C). In a similar experiment (263 mg of the anisole), the neutral volatile fraction (42%), obtained together with the involatile and phenolic material, was converted to the 2,4-dinitrophenylhydrazone. Thin-layer chromatography gave the derivative of *p*-tolualdehyde (37%).

The equivalent but deuterated anisole (295 mg, prepared by methylation with CD_3I) gave, similarly, tolualdehyde. The nmr spectrum indicated the absence of the aldehydic proton and integration revealed the absence of one *ortho* proton.

*o-Methylaminobenzyl Methyl Ether (**23**)*

In a typical experiment dimethyl sulphate (1 ml) was added to *o*-aminobenzyl methyl ether dissolved in a mixture of diethyl ether (20 ml) and water (20 ml). The mixture was stirred for 15 min and the product isolated with ether. Extraction into acid and recovery after neutralization gave a mixture containing about 35% methylation products with the monomethyl preponderating over the dimethyl derivative in the ratio of *ca.* 4:1. Chromatography on alumina (eluent: petroleum ether – benzene, 3:1) separated the methylated amines from the starting material, but did not effect a separation of the former. The methylated amines (250 mg) were added to freshly prepared carbobenzyloxy chloride (0.75 ml) in the presence of aqueous sodium hydroxide (3 *N*, 30 ml). The mixture was shaken on the steam bath for 15 min, and then allowed to stand overnight. The neutral material was isolated in the usual way, and 65 mg were added to a solution of potassium hydroxide in ethylene glycol (3 *N*, 50 ml). The mixture was stirred at 140 °C for 12 h and the basic material isolated with hydrochloric acid followed by neutralization to give *o*-methylaminobenzyl methyl ether as an oil bp (bath temperature) 90 °C/10 torr. δ ($CDCl_3$) 2.80 (3H, s), 3.20 (3H, s), 4.38 (2H, s), 4.64 (1H, ArN*H*); *m/e* 151 (M^+, 70%), 136(26), 120(49), 119(20), 118(100). *Exact mass* calcd. for $C_9H_{13}ON$: 151.099; found (*m/e*): 151.096.

*o-Formylaminobenzyl Methyl Ether (**27**)*

o-Aminobenzyl methyl ether (1.74 g) was added to ethyl formate (20 ml) and the mixture heated under reflux for 5 days with the further addition of ethyl formate (5 ml) every day. The formate was then removed under reduced pressure and the neutral material isolated in the usual way. The product was obtained as an oil (bp 80 °C (bath temperature)/0.8 torr) (1.36 g) which crystallized from ether–pentane, mp 49–49.5 °C; ν_{max} (CCl_4) 3380, 2840, 2790, 1705 cm^{-1}; δ ($CDCl_3$) 3.35 (3H, s), 4.51 (2H, s), 8.2 and 8.6 (2H, m, N*HCHO*); *m/e* 165(M^+, 100%), 150(27), 132(39), 122(50), 104(36), 78(27). *Anal.* calcd. for $C_9H_{11}O_2N$: C 65.44, H 6.71, N 8.48; found: C 65.65, H 6.89, N 8.40.

*Thermolysis of Methyl N-Methyl Anthranilate (**5**)*

(*i*) The above-named compound (449 mg) was thermolyzed at 800 °C and 0.03 torr. A residue from the cold finger of 396 mg was obtained. A portion (125 mg) was used for aldehyde estimation after the addition of a weighed quantity of toluene, by pmr spectroscopy: estimated yield, 34% based on starting material. This same fraction on tlc (elution with benzene) gave 58 mg recovered starting material.

The remainder of the thermolysate was steam-distilled and converted into phenylhydrazone (108 mg) mp 220–221 °C identical in all respects with an authentic specimen of *o*-aminobenzaldehyde phenylhydrazone. In other, similar, experiments the infrared spectrum of the aldehyde itself was compared and found identical with that of an authentic specimen.

Can. J. Chem. Downloaded from www.nrcresearchpress.com by 210.87.254.40 on 09/05/12
For personal use only.

(*ii*) The anthranilate (373 mg) was thermolyzed at 800 °C under a partial pressure of 0.03 torr and an equal pressure of ethyl thioglycollate as trapping agent. After the termination of the thermolysis the residue on the cold finger was distilled into the manifold until a residual pressure of 0.015 torr was attained. From the distillate, by tlc, 37 mg of starting material were recovered.

To a portion (97 mg) of the total residue on the cold finger (364 mg) toluene (10.5 mg) was added and the aldehyde content (33%) estimated by pmr spectroscopy. This solution and the remainder of the residue gave (tlc, double elution with benzene) starting material (30 mg) and the aldehyde **7**. ν_{max} ($CHCl_3$) 3330, 2860, 2775, 1730, 1660 cm^{-1}; δ ($CDCl_3$) 1.21 (3H, t), 3.11 (2H, s), 4.09 (2H, q), 4.57 (2H, d, $HNCH_2$—S), 8.77 (1H, br t), 9.75 (1H, s). Irradiation of the 8.77 triplet caused collapse of the doublet (J = 6.8 Hz) at 4.57. The compound (238 mg, 48% based on recovered starting material) could not be crystallized and was characterized as the phenylhydrazone, mp 103–105 °C (CH_2Cl_2/hexane). *Anal.* calcd. for $C_{18}H_{21}O_2N_3S$: C 62.96, H 6.16, N 12.24, S 9.32; found: C 63.15, H 6.20, N 12.04, S 9.48.

(*iii*) A similar thermolysis of anthranilate was carried out in the presence of thiophenol as trapping agent. The yield of aldehyde was estimated by pmr using toluene as calibrant. Chromatography (tlc) then gave diphenyl disulphide (70 mg) starting material (13 mg) and a yellow solid (244 mg) which was crystallized from hexane and from CH_2Cl_2–hexane, mp 85–85.5 °C; ν_{max} ($CHCl_3$) 3320, 2820, 2740, 1660 cm^{-1}; λ_{max} (MeOH) 370 (3.70), 265 (inf. 3.94), 232 nm (log ϵ 4.33); δ ($CDCl_3$) 4.63 (2H, d), 8.70 (1H, br t), 9.76 (1H, s). Double irradiation of the 8.70 triplet caused the collapse of the doublet (J = 7.2 Hz) at 4.63. The signal at 8.70 disappeared on exchange with D_2O and was accompanied by the disappearance in the splitting of the doublet at 4.63. *Anal.* calcd. for $C_{14}H_{13}ONS$: C 69.12, H 5.39, N 5.76, S 13.15; found: C 69.21, H 5.36, N 5.86, S 13.11.

(*iv*) Thermolysis of the anthranilate at 850 °C and collection on a sodium chloride plate at 77 K gave material showing a strong band at 1680 cm^{-1}. At −115 °C this band had essentially disappeared and a strong band was observed at 1660 cm^{-1}.

Thermolysis of Methyl Anthranilate ***(14)***

(*i*) The ester (473 mg) was thermolyzed at 800 °C at 0.15 torr and the product condensed in the presence of thiophenol (0.02 torr). The excess thiophenol was removed by distillation, and the residue on the cold finger washed with ether. After removal of the ether the residue (187 mg) was subjected to tlc. Diphenyl disulphide was obtained, followed by the thiophenyl ester **15** (87 mg) identified by comparison with an authentic specimen. The thiophenol distillate was redistilled at room temperature (0.2 torr) and the residue subjected to tlc. Aside from disulphide (108 mg) and starting material (35 mg) an oil (**18**, 72 mg) was obtained which was distilled, bulb-to-bulb, (70 °C/0.01 torr) ν_{max} ($CHCl_3$) 2240, 1620, 1480 cm^{-1}; δ ($CDCl_3$) 2.2–3.4 (4H, complex), 3.90 (1H, m), 6.53 (1H, m); m/e 201(M^+, 47), 110(100), 92(24). *Anal.* calcd. for $C_{12}H_{11}NS$: C 71.62, H 5.51, N 6.96, S 15.90; found: C 71.81, H 5.61, N 6.96, S 16.07.

No reaction between the ester and thiophenol occurred at room temperature in 90 min.

(*ii*) A similar thermolysis (840 °C; 0.01 torr) but using ethanol gave a low yield (9%) of anthranilate esters. This was shown by pmr spectroscopy to be a 7:1 ratio of ethyl to methyl ester. No exchange occurred in the absence of thermolytic condition.

Thermolysis of o-Aminobenzyl Methyl Ether ***(20)***

The ether (272 mg) was thermolyzed at 800 °C and 0.03 torr in the presence of thiophenol (0.03 mm). In a similar way 32 mg were recovered by tlc, together with diphenyl disulphide and *o*-aminobenzyl phenyl sulphide (**21**, 197 mg), mp 78–79.5 °C (lit. (10) 81 °C) characterized as the benzoyl derivative, mp 170–170.5 °C (lit. (10) 172 °C). No reaction occurred between the reagents in 3.5 h at room temperature.

Thermolysis of o-Methylaminobenzyl Alcohol ***(24)***

(*i*) Thermolysis of this alcohol (224 mg) at 800 °C at 0.015 torr gave a residue of 229 mg (δ ($CDCl_3$) 4.30, 2.2). Steam distillation then gave *o*-toluidine (108 mg; 62%) characterized as the benzoyl derivative.

(*ii*) The alcohol (300 mg) was thermolyzed at 800 °C at 0.005 torr and the product collected in the presence of 0.01 torr thiophenol. Thiophenol was removed with base, and the residue (435 mg) separated by tlc. A fraction (112 mg) apparently corresponding to **26** was obtained (ν_{max} ($CHCl_3$) 3430, 900 cm^{-1}; δ ($CDCl_3$) 1.9 (3H, s), 3.95 (1H, br)) but its purity could not be assured. A portion (112 mg) of such material was treated with 2,4-dinitrophenylhydrazine in phosphoric acid. The derivative of formaldehyde was obtained in 86% yield. Another portion of similar material (204 mg) was treated with Raney nickel (from 6 g alloy) and refluxed in benzene for 18 h. *N*-Methyl-*o*-toluidine (61 mg, 57%) was obtained and was characterized as the *p*-toluenesulphonyl derivative.

Thermolysis of o-Methylaminobenzyl Methyl Ether ***(23)***

(*i*) The ether (226 mg) was thermolyzed at 800 °C and 0.01 torr to give a residue on the cold finger of 193 mg. The product was steam distilled and the basic material isolated. Thin-layer chromatography gave 4 mg of starting material and 105 mg *o*-toluidine characterized as the benzoyl derivative, both substances being compared with authentic specimens.

(*ii*) The ether (204 mg) was thermolyzed at 800 °C and 0.01 torr and co-deposited with thiophenol at a partial pressure of 0.01 torr of thiophenol. The product exhibited the same properties as the material obtained from the alcohol (**26**).

Thermolysis of o-Formylaminobenzyl Methyl Ether ***(27)***

(*i*) The ether (205 mg) was thermolyzed at 800 °C at 0.01 torr and co-deposited with methanol at a partial pressure of 0.02 torr. The residue on the cold finger was 209 mg. Preparative tlc gave 8 mg starting material and the urethane (174.8 mg) mp 59–60 °C (lit. (19) 60–60.5 °C) whose other physical properties compared well with those recorded (19) except for the methyl frequency of the carbomethyl group (3.71 ppm) the literature value (3.17) probably being a typing error. In another experiment where ethyl alcohol was used, the urethane obtained had mp 44–44.5 °C (lit. (20) 45–46 °C).

(*ii*) The ether (166 mg) was thermolyzed at 800 °C and at 0.01 torr. After the furnace had cooled the product was distilled from the cold finger to an attached U-tube

cooled in liquid nitrogen. Raising the temperature of the U-tube to the temperature of a chlorobenzene slurry (−45 °C) allowed the distillation of the more volatile material which was collected in a second receiver cooled to liquid nitrogen temperature. The residue in the U-tube was then distilled into a third receiver.

The more volatile material was essentially methanol. The less volatile material was identified as *o*-tolyl isocyanate: ν_{max} (gas) 2280 cm^{-1}, ν_{max} (CCl_4) 2275, 1570, 1495, 1180, 1170, 1130 cm^{-1}; δ (CCl_4) 2.32 (3H, s); *m/e* 133(M^+, 100), 104(57), 132(53), 78(35), and 105(22).

Thermolysis of Methyl N-Formyl Anthranilate ***(28)***

(*i*) The anilide (99 mg) was thermolyzed at 950 °C and at 0.015 torr and co-deposited with methanol at a partial pressure of 0.01 torr. A residue on the cold finger of 74 mg was obtained. Preparative tlc (ether–benzene; 1:3) gave **30**, R = Me (72 mg, 51%), ν_{max} ($CHCl_3$) 3400, 1725 cm^{-1}; δ ($CDCl_3$) 3.64 (3H, s), 6.06 (1H, s), 9.76 (1H, br). The last peak disappeared on exchange with D_2O and was followed by the appearance of a new peak (sharp) at 9.83 (C*H*O). A peak at 3.47 (MeOH) appeared at the expense of those at 3.63 and 6.06. *Anal.* calcd. for C_9H_9NO: C 60.33, H 5.06, N 7.82; found: C 59.88, H 5.33, N 7.86.

(*ii*) A similar experiment using ethanol gave the ethyl derivative, **30**, R = Et, mp 130–131 °C, *m/e* 120(100), 93(88), 148(84), 179(66), 92(58), 149(55), 119(54). *Exact mass* calcd. for $C_{10}H_{11}O_3N$: 193.074; found (*m/e*): 193.076.

Thermolysis of o-Carbomethoxy Phenylacetaldehyde ***(32)***

The aldehyde (167 mg) was thermolyzed at 800 °C and at 0.01–0.15 torr. Proton magnetic resonance analysis of the residue (CH_2Cl_2 calibrant) indicated the presence of 61% isocoumarin. Preparative tlc (CH_2Cl_2 – light petroleum 30–60 °C, 2:1) gave 45 mg starting material and 58 mg isocoumarin, mp (after crystallization from ethyl acetate – hexane) 42.5–44 °C (lit. (21) mp from benzene 46–47 °C). The ir, uv, and pmr spectra were identical with those of isocoumarin.

1. R. A. Marty and P. de Mayo. J. Chem. Soc. D, 127 (1971).
2. R. Bloch, R. A. Marty, and P. de Mayo. Bull. Soc. Chim. Fr. 2031 (1972).
3. F. Leyendecker, R. Bloch, and J. M. Conia. Tetrahedron Lett. 3703 (1972); P. G. Sammes. Tetrahedron, **32**, 405 (1976); T. Kametani and K. Fukumoto. Heterocycles, **3**, 29 (1975).
4. R. F. C. Brown and M. Butcher. Aust. J. Chem. **22**, 1457 (1969).
5. P. Gilgen. Dissertation, University of Zurich, 1971. *Quoted by* R. Hug, H. J. Jansen, and H. Schmid. Helv. Chim. Acta, **55**, 2103 (1972).
6. O. L. Chapman and C. L. McIntosh. J. Am. Chem. Soc. **92**, 7001 (1970).
7. E. Ziegler and H. Sterk. Monatsh. Chem. **99**, 1958 (1968).
8. W. D. Crow and C. Wentrup. Tetrahedron Lett. 4379 (1967).
9. C. Wentrup, C. Thetaz, and R. Gleiter. Helv. Chim. Acta, **55**, 2633 (1972); W. D. Crow and M. N. Paddon-Row. J. Am. Chem. Soc. **94**, 4746 (1972); W. D. Crow, M. N. Paddon-Row, and D. S. Sutherland. Tetrahedron Lett. 2239 (1972).
10. A. Lüttringhaus and A. Kolb. Z. Naturforsch. Teil B, **16**, 762 (1961).
11. J. L. Warnell and R. L. Shriner. J. Am. Chem. Soc. **79**, 3165 (1957).
12. D. L. Verdun. Ph.D. Thesis. University of Western Ontario, London, Ontario. 1971.
13. P. de Mayo and D. L. Verdun. J. Am. Chem. Soc. **92**, 6079 (1970).
14. J. F. King, P. de Mayo, C. L. McIntosh, K. Piers, and D. J. H. Smith. Can. J. Chem. **48**, 3704 (1970).
15. R. P. Staiger and E. B. Miller. J. Org. Chem. **24**, 1214 (1959).
16. M. Lora-Tamayo, R. Madroñero, and G. Garcia-Muñoz. Chem. Ber. **94**, 208 (1961).
17. H. Mehner. J. Prakt. Chem. **64**, 70 (1901).
18. F. Ishiwara. J. Prakt. Chem. **108**, 194 (1924).
19. L. A. Paquette, D. E. Kuhla, and J. A. Barrett. J. Org. Chem. **34**, 2879 (1969).
20. G. Lachman. Ber. **12**, 1349 (1879); L. H. Neville and A. Winther. Ber. **12**, 2325 (1879).
21. E. Bamberger and D. Frew. Ber. **27**, 198 (1894); S. Gabriel. Ber. **36**, 570 (1903).

Can. J. Chem. Downloaded from www.nrcresearchpress.com by 210.87.254.40 on 09/05/12
For personal use only.

Chemical and biological studies on 1,2-dihydro-*s*-triazines. XIX.[1] A nuclear magnetic resonance investigation of hindered internal rotation in 1-aryl derivatives

LAWRENCE D. COLEBROOK AND H. GWYNNE GILES
Department of Chemistry, Sir George Williams Campus, Concordia University, Montreal, P.Q., Canada H3G 1M8

ANDRE ROSOWSKY
Sidney Farber Cancer Center and the Department of Biological Chemistry, Harvard Medical School at the Children's Hospital Medical Center, Boston, MA, U.S.A. 02115

AND

WESLEY E. BENTZ AND JAMES R. FEHLNER
Department of Chemistry, University of Rochester, Rochester, NY, U.S.A. 14627

Received October 14, 1975[2]

LAWRENCE D. COLEBROOK, H. GWYNNE GILES, ANDRE ROSOWSKY, WESLEY E. BENTZ, and JAMES R. FEHLNER. Can. J. Chem. **54**, 3757 (1976).

Substantial barriers to internal rotation about aryl C—N bonds have been detected by pmr methods in a series of 2-methyl- and 2,2-dimethyl-substituted 4,6-diamino-1-aryl-1,2-dihydro-*s*-triazines. In most of the 2,2-dimethyl compounds the barriers are too high to be measured by the pmr lineshape method. When the blocking groups on the aryl moieties are large the barriers may be measured in the 2-methyl series by following the equilibration of diastereomeric rotamers. When the blocking groups on the hetero rings are sufficiently small, rate constants may be measured by pmr lineshape analysis. A substantial barrier to rotation has been measured in the absence of bulky blocking groups on the aryl ring.

LAWRENCE D. COLEBROOK, H. GWYNNE GILES, ANDRE ROSOWSKY, WESLEY E. BENTZ et JAMES R. FEHLNER. Can. J. Chem. **54**, 3757 (1976).

On a détecté plusieurs barrières importantes à la rotation interne autour des liens C(aryle)—N, par des méthodes de rmp, dans les séries méthyl-2 et diméthyl-2,2 diamino-4,6 aryl-1 dihydro-1,2 *s*-triazines substitués. Dans la plupart des composés diméthylés en position 2,2, les barrières sont trop élevées pour être mesurées par la méthode des formes des raies de rmp. Quand les groupes bloqueurs de la portion aromatique sont volumineux, les barrières peuvent être mesurées dans la série méthylée en position 2 en suivant l'équilibration des rotamères diastéréomètres. Quand les groupes sur les hétérocycles sont suffisamment petits, on peut mesurer les constantes de vitesse par l'analyse des formes des raies de rmp. On note une barrière importante à la rotation lorsqu'il n'y a pas de groupe bloqueur important sur les cycles aromatiques.

[Traduit par le journal]

In the course of studies of restricted internal rotation about C—N bonds in aryl substituted heterocyclic compounds we have previously reported evidence for high internal rotational barriers in 4,6-diamino-1,2-dihydro-2-methyl-1-(*o*-tolyl)-*s*-triazine (I, Ar = *o*-tolyl, R = H) (2), and in 4,6-diamino-1,2-dihydro-2,2-dimethyl-1-(β-naphthyl)-*s*-triazine (I, Ar = β-naphthyl, R = CH_3) (3). We now report the results of a more extensive pmr study of a series of 4,6-diamino-1-aryl-1,2-dihydro-*s*-triazines with 2-methyl (I, Ar = aryl, R = H) and 2,2-dimethyl (I, Ar = aryl, R = CH_3) substitution (Table 1).

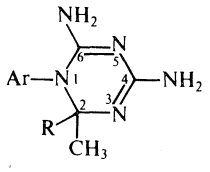

I

A feature of particular interest concerning these compounds has been the relationship between molecular configuration and biological activity. It has been reported, for example, that the ability of 4,6-diamino-1-aryl-1,2-dihydro-*s*-triazines to interfere with bacterial and mammalian cell growth depends markedly upon the location of substituents in the aryl moiety (4).

[1]For part XVIII, see ref. 1.
[2]Revision received August 6, 1976.

Can. J. Chem. Downloaded from www.nrcresearchpress.com by 210.87.254.42 on 09/05/12
For personal use only.

Can. J. Chem. Downloaded from www.nrcresearchpress.com by 210.87.254.42 on 09/05/12
For personal use only.

TABLE 1. Chemical shifts of 2-methyl protons in 4,6-diamino-1-aryl-1,2-dihydro-2-methyl- and 2,2-dimethyl-*s*-triazines[a]

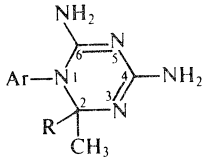

	Ar	R	2-Methyl chemical shift (δ)	$\Delta\delta$ (ppm)
1	Phenyl	CH_3	1.78	
2	*o*-Fluorophenyl	CH_3	1.87, 1.81	0.06
3	*p*-Fluorophenyl	CH_3	1.80	
4	*o*-Methoxyphenyl	CH_3	1.85, 1.73[b]	0.12
5	*m*-Methoxyphenyl	CH_3	1.83[c]	
6	*p*-Methoxyphenyl	CH_3	1.79[b]	
7	*o*-Chlorophenyl	CH_3	1.98, 1.70	0.28
8	*m*-Chlorophenyl	CH_3	1.85	
9	*p*-Chlorophenyl	CH_3	1.80	
10	*o*-Bromophenyl	CH_3	2.00, 1.70	0.30
11	*m*-Bromophenyl	CH_3	1.81	
12	*p*-Bromophenyl	CH_3	1.80	
13	*o*-Iodophenyl	CH_3	2.02, 1.67	0.35
14	*o*-Tolyl	CH_3	2.00, 1.62[d]	0.38
15	*m*-Tolyl	CH_3	1.80[e]	
16	*p*-Tolyl	CH_3	1.80[e]	
17	α-Naphthyl	CH_3	2.10, 1.62	0.48
18	β-Naphthyl	CH_3	1.92, 1.86	0.06
19	2,6-Dimethylphenyl	CH_3	1.82	
20	*o*-Tolyl[f]	H	1.76, 1.58	0.18
21	*o*-Chlorophenyl[g]	H	1.36, 1.32	0.04

[a]Spectra were determined at 60 MHz in trifluoroacetic acid at a uniform 0.3 *M* concentration, unless otherwise noted. Chemical shifts are expressed as ppm from tetramethylsilane as an internal standard (δ values).
[b]CH_3O protons absorbed at δ 3.99, single peak.
[c]CH_3O protons absorbed at δ 3.98, single peak.
[d]Aromatic CH_3 protons absorbed at δ 2.40, single peak.
[e]Aromatic CH_3 protons absorbed at δ 2.50, single peak.
[f]100 MHz spectrum.
[g]100 MHz spectrum, perfluoropropionic acid solution.

In antibacterial and mammalian cell culture assays, compounds containing an *ortho*-substituted phenyl ring normally exhibit much lower activity than their *meta*- or *para*-substituted counterparts, regardless of the nature of the atoms or groups involved. (The opposite effect has been noted in a different biological system; see ref. 5.) This finding has led to the hypothesis that non-bonded interactions between bulky *ortho* substituents and groups at positions 2 and 6 of the triazine ring hinder the attainment of a planar configuration when the inhibitor molecule is bound to the enzyme dihydrofolate reductase, apparently a requisite for maximum activity in bacteria and mammalian systems (6).

The present study was undertaken with the aim of (*1*) demonstrating by physical means the existence of a significant energy barrier to free internal rotation in *ortho*-substituted, 4,6-diamino-1-aryl-1,2-dihydro-*s*-triazines and (*2*) assessing quantitatively the effect of substituent bulk upon the magnitude of this barrier. The information thus obtained was expected to be useful in aiding the understanding of the biological activity of these compounds.

An effective method for demonstrating hindered rotation in biphenyl-type compounds, *i.e.* compounds exhibiting atropisomerism, and for measuring the heights of the barriers to rotation, is nuclear magnetic resonance spectroscopy (7). The 2-methyl moiety in the 4,6-diamino-1-aryl-1,2-dihydro-2-methyl- and 2,2-dimethyl-*s*-triazines studied provides a very convenient probe for the investigation of hindered rotation by this approach.

If it is assumed (7) that steric interference between the *ortho* substituents of the 1-aryl group and the groups in the 2- and the 6-positions of the hetero ring prevents co-planarity of the two rings in the conformational ground states, the compounds with unsymmetrically substituted aryl groups may be classified into two stereochemical groupings, depending upon the nature of the 2-substituent of the hetero ring (Table 1).

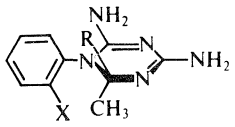

II

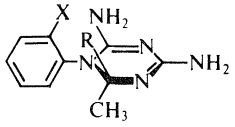

III

When the aryl group is unsymmetrically substituted and R = CH_3 (compounds **2**, **4**, **5**, **7**, **8**, **10**, **11**, **13–15**, **17**, **18**) the stereoisomers, II and III, resulting from restricted internal rotation about the C—N pivot bond between the aryl and the heterocyclic moieties are enantiomers which have indistinguishable nmr spectra in achiral media. However, the geminal 2,2-dimethyl groups are diastereotopic (ref. 8, p. 19) and are expected to give rise to a doublet provided that rotation about the C—N bond is slow on the pmr time scale and that the chemical shift difference between the methyl groups is adequate. If rotation about the C—N pivot bond were fast

Can. J. Chem. Downloaded from www.nrcresearchpress.com by 210.87.254.42 on 09/05/12
For personal use only.

on the pmr time scale the doublet would collapse to a singlet.

When R = H (**20** and **21**) the rotational isomers, II and III, are diastereomers and are expected to have distinguishable spectra, of unequal intensity at conformational equilibrium, provided that the conditions for slow rotation and chemical shift differences are met. Each diastereomeric rotamer can exist as an enantiomeric pair (corresponding to inversion of configuration at C-2), the members of which are not distinguishable by nmr using achiral media. Each diastereomeric rotamer should give rise to a 2-methyl doublet resulting from spin coupling to the proton on C-2. Under conditions of fast rotation the time averaged spectrum should be obtained so that the pair of 2-methyl doublets should collapse to a single doublet.

In principle, rate constants for rotation about the pivot bonds should be obtainable by lineshape analysis (9) of the signals arising from the diastereotopic 2,2-dimethyl groups of those compounds with unsymmetrically substituted aryl groups and from the non-equivalent 2-methyl groups of the diastereomeric rotamers of **20** and **21**, provided that the rate constants under the conditions which lead to partially collapsed spectra fall within the region accessible by the pmr technique. Rate constants for internal rotation should also be obtainable by measuring the rate of equilibration of one stereoisomer of **20** and **21**, provided that isolation of one isomer in a state of substantial isomeric purity is feasible.

Survey spectra (60 MHz) of all the compounds were determined at normal probe temperatures in trifluoroacetic acid. The dihydrotriazines probably exist in this solvent in a diprotonated form consisting of two adjacent, resonance-stabilized amidinium ions, as shown in structures **a**–**d**. Solutions of uniform concentration (0.3 *M*) were used in order to minimize possible effects due to solvent–solute interaction.

A series of nineteen previously synthesized (10) 4,6-diamino-1-aryl-1,2-dihydro-2,2-dimethyl-*s*-triazines (Table 1) was examined, including phenyl derivatives with halogen, methoxy, or methyl substituents in the *ortho*, *meta*, and *para* positions, and also the unsubstituted phenyl, α-naphthyl, and β-naphthyl compounds. Two 2-monomethyl compounds were also synthesized specifically for this study (Table 1).

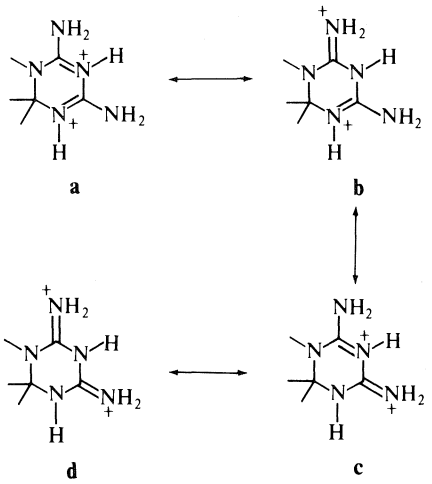

Results and Discussion

Sharp, readily identifiable signals were observed for the methyl protons of the 2-methyl and 2,2-dimethyl systems. The chemical shifts of the 2-methyl protons in all of the compounds examined in this work are listed in Table 1.

It is clear from these data that the compounds fall into two groups, depending upon whether the 2-methyl protons give rise to a single signal or to two chemically shifted signals. When the phenyl ring contains a *meta* or a *para* substituent, only a single signal is observed. The β-naphthyl compound, **18**, which can be considered as a *meta* substituted compound, is an exception (see later). In the case of the *p*-substituted derivatives, the chemical shifts are essentially constant (δ 1.79–1.80) and independent of the nature of the substituent. In the *m*-substituted compounds, the position of the 2-methyl signal appears to be somewhat substituent-dependent, but the effect is small. When the phenyl ring contains an *ortho* substituent, on the other hand, two distinct peaks of equal area are invariably observed for the 2,2-dimethyl compounds, as expected if rotation is highly restricted and the molecules are constrained to adopt non-planar conformations. The mean value for each pair of peaks in the *o*-substituted series of 2,2-dimethyl compounds falls in the range δ 1.85–1.79, which corresponds closely to the range of values observed in the *m*- and the *p*-substituted series. The separation ($\Delta\delta$) between each pair of peaks appears to be strongly substituent dependent (Table 1), varying from 0.06 ppm for the *o*-fluoro derivative to

Can. J. Chem. Downloaded from www.nrcresearchpress.com by 210.87.254.42 on 09/05/12
For personal use only.

0.38 ppm for the *o*-methyl derivative. The magnitude of $\Delta\delta$ increases in the order F < MeO < Cl < Br < I < Me, whereas the order predicted on the basis of Taft steric substituent constants, E_s, is MeO < F < Cl < Br = Me < I (11). Thus, to a first approximation, there appears to be a correlation between $\Delta\delta$ and the steric requirements of the *ortho* substituents in these compounds.

The data obtained with naphthyl-substituted 2,2-dimethyl compounds (Table 1) are of interest in two respects. The α-naphthyl derivative, **17**, shows the largest $\Delta\delta$ value (0.48 ppm). The β-naphthyl derivative, **18**, which shows a $\Delta\delta$ value of 0.06 ppm is of interest since, of the compounds in which the *ortho* position is *not* substituted, this is the only one that gives nmr evidence for restricted rotation.

At normal probe temperatures in trifluoroacetic acid solution, the 2-methyl protons of the *o*-tolyl 2-methyl compound, **20**, gave rise to two well resolved doublets of unequal intensity, the splitting of each doublet (J = 6.1 Hz) resulting from spin coupling to the C-2 protons. The 2-methyl doublet of the thermodynamically more stable diastereomeric rotamer absorbed at δ 1.76, while the 2-methyl doublet of the other isomer appeared at δ 1.58 ($\Delta\delta$ = 0.18 ppm). The C-2 proton quartets for these two diastereomers were centered at δ 5.47 and δ 5.69, respectively. At equilibrium, the ratio of integrated intensities of the 2-methyl doublets was 1.6, the rotamer with the lower field 2-methyl doublet and the higher field C-2 proton quartet having the higher intensity.

Similarly, the 2-methyl group of the more abundant (at equilibrium) diastereomeric rotamer of the *o*-chlorophenyl 2-methyl compound, **21**, gave rise (perfluoropropionic acid solution) to a doublet at δ 1.36 (J = 6.1 Hz) while the corresponding doublet of the less abundant rotamer appeared at δ 1.32 (J = 6.0 Hz), the two doublets overlapping ($\Delta\delta$ = 0.04 ppm). The C-2 proton signals of the two diastereomers appeared as overlapping multiplets at δ 5.45–5.85. At equilibrium (113 °C, perfluoropropionic acid solution) the rotamer population ratio was 1.5.

The chemical shift data of the *ortho* substituted compounds are consistent with the assumption that the aryl and the triazine rings adopt a twisted rather than a co-planar arrangement in two ground state conformations. If it is assumed that the chemical shift difference between the geminal methyl groups in the 2,2-dimethyl compounds, and between the methyl groups in the diastereomeric rotational isomers of the 2-methyl compounds, arises mainly from the magnetic anisotropy of the phenyl group (with additional contributions from the *ortho* substituents) then the chemical shift difference, $\Delta\delta$, should be a function of the dihedral angle between the rings. The dihedral angles in the conformational ground states should be dependent on the steric requirements of the *ortho* substituents. The observed approximate correlation between $\Delta\delta$ and the Taft E_s values is consistent with this interpretation.

A consideration of the chemical shifts and relative intensities of the 2-methyl and 2-methine proton signals of the 2-methyl compounds (**20** and **21**) provides some information on the ground state conformations of the diastereomeric rotational isomers of these compounds. For steric reasons, it is to be expected that the rotational isomer with the bulky *ortho* substituent transoid to the 2-methyl group (III, R = H) would be thermodynamically more stable (and hence be present in higher concentration at equilibrium) than its rotamer (II, R = H), since non-bonded interactions between the substituents on the two rings would be minimized. The most probable conformations of the two isomers, II and III, which minimize steric interaction between the *ortho* substituents and the groups in the 2- and the 6-positions of the hetero ring may be estimated with the aid of molecular models. This leads to the conclusion that the 2-methyl group should be more shielded by the aryl group in the cisoid form, II, than in the transoid form, III. Conversely, the 2-methine protons should be more shielded in the transoid than in the cisoid isomer. The observed relative intensities and line positions are in agreement with these predictions.

Measurement of Barriers to Rotation

Since the pmr spectra of all of the *ortho* substituted, and the β-naphthyl 2,2-dimethyl compounds indicated that rotation about the C—N pivot bond was slow on the pmr time scale at normal probe temperatures, a study was undertaken to measure the barriers to internal rotation by line-shape analysis at elevated temperatures.[3]

[3]The stabilities of these compounds under ordinary conditions, and their thermal rearrangement reactions, have been investigated previously (10*a*).

TABLE 2. Activation parameters for restricted internal rotation in some 4,6-diamino-1-aryl-1,2-dihydro-2-methyl- and 2,2-dimethyl-*s*-triazines[a]

Compound	Solvent	Temperature (°C)	$\Delta G^{\ddagger}$	$\Delta H^{\ddagger}$	$\Delta S^{\ddagger}$
7	Perfluorobutyric acid	132.5	>20.4		
17	Perfluorobutyric acid	128	>19.6		
18	Perfluorobutyric acid	141	23.1[b]		
20[c]	Trifluoroacetic acid	25	24.4±0.1	22.9±2.8	−4.8±9.1
			24.1±0.1	22.9±2.8	−3.7±9.1
21[d]	Perfluoropropionic acid	125	22.4±0.1	19.2±2.8	−8.3±7.0
			22.1±0.1	19.8±1.9	−5.7±4.7

[a]Errors are 90% confidence limits.
[b]Rate constant at coalescence point obtained by computer simulation of the line shape. Estimated error is ±0.1 kcal/mol.
[c]Rate constants obtained by equilibration.
[d]Rate constants obtained by complete line-shape analysis.

Attempted measurement of the activation parameters for restricted internal rotation in the 2,2-dimethyl compounds containing 1-(α-naphthyl) and 1-(*o*-chlorophenyl) substitution (**17** and **7**, respectively) failed. At the normal probe temperature, the two methyl groups of **17** in perfluorobutyric acid absorbed at δ 1.56 and δ 2.03 ($\Delta\delta = 0.47$). At 128 °C, the highest temperature at which the spectrum was recorded (near the boiling point of the solvent) the line separation was greater than 0.4 ppm and the spectrum showed no sign of incipient collapse, indicating that internal rotation was slow on the pmr time scale at this temperature. Had the coalescence point been reached at 128 °C the free energy of activation ($\Delta G^{\ddagger}$) would have been 19.6 kcal/mol (calculated using the mean lifetime at an assumed coalescence point of 128 °C; see ref. 12). Presumably the true $\Delta G^{\ddagger}$ is significantly higher than this minimum figure. The chemical shifts of the diastereotopic 2,2-dimethyl groups of **7** in perfluorobutyric acid solution are δ 1.66 and δ 1.93 ($\Delta\delta = 0.27$ ppm). At the highest temperature attained, 132.5 °C, the chemical shift difference was reduced to 0.20 ppm but no collapse or appreciable exchange broadening of the doublet had occurred. Some decomposition of the sample occurred at this temperature. A minimum value for $\Delta G^{\ddagger}$ is reported in Table 2. Temperature dependence of the chemical shifts resulting from such factors as changes in solvation may have contributed to the decrease in line separation with increasing temperature.

These results indicate that steric restriction to rotation about the C—N pivot bond in *ortho* substituted 1-aryl-2,2-dimethyl compounds of this type is high, and that conformational stabilities comparable to those reported for highly hindered biphenyls (13) might be expected. These compounds have bulky blocking groups on both the aryl and the heterocyclic rings which evidently cause severe steric interactions in the approximately planar transition states for internal rotation.

The 2,2-dimethyl-1-(β-naphthyl) compound, **18**, is unusual in that the diastereotopic geminal dimethyl groups are anisochronous (ref. 8, p. 23) at normal probe temperatures, even though the aryl group lacks a bulky *ortho* substituent. Of the 2,2-dimethyl compounds investigated at elevated temperatures, this was the only one to show a temperature dependent spectrum. At 109 °C (perfluorobutyric acid solution) the diastereotopic methyl groups gave rise to two lines, with a separation of 0.032 ppm, indicating slow rotation about the C—N bond. At 141 °C the spectrum collapsed reversibly to a singlet. Since some decomposition occurred near this temperature, complete line-shape analysis was not attempted. The rate constant at the coalescence point was obtained by matching computer simulated spectra to the experimental spectra, making allowance for natural line widths. The $\Delta G^{\ddagger}$ at the coalescence point was calculated to be 23.1 kcal/mol.

It is noteworthy that the barrier to internal rotation in this compound is quite high even though the small size of the hydrogen atoms in

Can. J. Chem. Downloaded from www.nrcresearchpress.com by 210.87.254.42 on 09/05/12
For personal use only.

Can. J. Chem. Downloaded from www.nrcresearchpress.com by 210.87.254.42 on 09/05/12
For personal use only.

the *ortho* positions renders them poor blocking substituents. However, the barrier may be somewhat higher than that to be expected for an unsubstituted phenyl group since the steric requirements of one of the *ortho* hydrogen atoms may be increased by buttressing with the adjacent fused ring. Compensation for the small size of the *ortho* substituents on the aryl group is provided by the bulk and the geometry of the substituents in the 2- and the 6-positions of the heterocyclic group, so that steric interaction between the two moieties is severe in the transition state for internal rotation. Other examples of substantial barriers to internal rotation about C—N bonds occurring in aryl substituted heterocyclic compounds lacking bulky *ortho* substituents have been reported (3, 14).

The high rotational barrier to internal rotation measured for compound **18** suggests that the other *meta* and the *para* substituted compounds and, indeed, the phenyl derivative itself, **1**, may also be sufficiently highly hindered that rotation is slow on the pmr time scale at normal temperatures. Insufficient aryl group anisotropy to induce a detectable chemical shift difference between the *gem* dimethyl groups is presumably responsible for the lack of observed splitting in the other *meta* substituted compounds. The *gem* dimethyl groups of the compounds containing symmetrically substituted aryl groups are necessarily isochronous in achiral media so no information on hindered rotation is obtainable under the conditions of the experiments. (In principle, hindered rotation in symmetrically substituted compounds might be detectable in chiral media; see ref. 15.)

Since, with the one exception noted, measurement of the rotational barriers of the 1-aryl-2,2-dimethyl compounds did not appear to be feasible by the pmr method (in part, because of sample decomposition at high temperatures), an investigation of the effect of a reduction in the steric requirements of the blocking groups on the heterocyclic moiety was undertaken. Rotational barriers in the 2-monomethyl compounds **20** and **21**, which were expected to be less highly hindered than the 2,2-dimethyl compounds, were sufficiently low that a complete set of activation parameters could be obtained.

Rate constants for internal rotation in the 1-(*o*-chlorophenyl)-2-methyl compound, **21**, were measured over the range 113–138 °C by complete line-shape analysis of the temperature dependent spectrum arising from the 2-methyl groups of the diastereomeric rotational isomers. The rotamers were in thermodynamic equilibrium before the start of the measurements. Activation parameters are reported in Table 2.

The 1-(*o*-tolyl)-2-methyl compound, **20**, was first examined as a solution in the high boiling solvent perfluorooctanoic acid. The two doublets observed for the 2-methyl group had not collapsed at 155 °C. At higher temperatures, the compound decomposed and new, interfering, signals appeared, making study of the rotational barrier between the two diastereomers impossible by the line-shape method.

Recrystallization of **20** from ethanol, following work-up of the reaction mixture, yielded a solid containing 88% of the thermodynamically favoured diastereomer (as determined by pmr). The ratio of the two diastereomers present in this mixture after recrystallization was a function of time and of temperature of storage in solution, until thermodynamic equilibrium was attained. At equilibrium, the mixture contained 62% of the thermodynamically more stable rotamer.

Rate constants for interconversion of the rotational isomers of **20** in trifluoroacetic acid solution were measured by following the equilibration of the initially predominant isomer over the temperature range 22.5–52 °C. The rate of change in the relative intensities of the 2-methyl doublets of the two isomers was measured by repeated integration of the 100 MHz pmr spectrum, the equilibration process being followed until the mixture of diastereomers was very nearly at thermodynamic equilibrium. Activation parameters for the forward and the reverse reactions are listed in Table 2.

The 2-monomethyl compounds, **20** and **21**, exhibit steric barriers to rotation similar to those reported for many 2,2′-substituted biphenyls (13). High conformational stability resulting from restricted rotation about an aryl C—N bond has also been observed in a number of *ortho*-substituted *N*-acyl-*N*-alkyl derivatives of aniline and 1-naphthylamine, using polarimetric methods (for leading references, see ref. 16). Very substantial barriers ($\Delta G^{\ddagger} > 20$ kcal/mol) to rotation about aryl C—N bonds have also been detected by the pmr method in 3-(α-naphthyl)-5-methyl-2-thiohydantoin (2), 3-(2-bromophenyl)-5-methyl-2-thiohydantoin (17) (using the equili-

Can. J. Chem. Downloaded from www.nrcresearchpress.com by 210.87.254.42 on 09/05/12
For personal use only.

bration technique), and in a number of *ortho* substituted 3-aryl-2-benzyl-4(3*H*)-quinazolinones (14).

The barriers to rotation of the corresponding *ortho* substituted 2,2-dimethyl compounds are presumably significantly higher than those of the 2-monomethyl compounds **20** and **21**. It is probable that the 2-monomethyl dihydrotriazine moiety can relieve steric strain in the transition state for rotation by puckering in such a way that the C-2 hydrogen rather than the C-2 methyl group is presented to the aryl group. Such transition state strain relief is not possible in the 2,2-dimethyl compounds, which must always present 2-methyl groups to the aryl substituent. Thus, in view of the measured barriers for **20** and **21**, the true values of $\Delta G^{\ddagger}$ for the 2,2-dimethyl compounds **7** and **17** must be much higher than the minimal estimates quoted in Table 2.

The relative rotational barriers ($\Delta\Delta G^{\ddagger}_{25}$ = 2.7 kcal/mol) of the 1-(*o*-tolyl) and 1-(*o*-chlorophenyl) compounds **20** and **21**, respectively, are in agreement with the common observation (18, 19) that a methyl group exerts a steric effect greater than that of a chlorine atom in restricting internal rotation in biphenyls (18) and in 1-arylhydantoins (20) (an exception has been noted in the case of 3-arylhydantoins (20)). This order is also consistent with Taft steric substituent constants (11), and with the relative van der Waals radii of these groups as determined by X-ray crystallographic measurements (21).

Although the quantitative data obtained in this study are limited, since they could be obtained only on the least conformationally stable compounds in the series, they are sufficient to indicate that optical resolution via salt formation with an optically active acid (the theoretical possibility of resolving highly hindered dihydro-*s*-triazines into optical isomers has been suggested independently, see ref. 22) should be feasible for some of the more highly hindered 2,2-dimethyl compounds. Thus, the *o*-tolyl, *o*-bromophenyl, *o*-iodophenyl, and α-naphthyl compounds **14**, **10**, **13**, and **17**, respectively, should have sufficient conformational stability to permit resolution at normal temperatures. Rate constants and activation parameters for rotation should be obtainable following resolution by measuring the rates of racemization of the optically active isomers, using the usual polarimetric methods (see, for example, ref. 23).

Experimental

All the 2,2-dimethyl dihydro-*s*-triazines reported here are known compounds and were synthesized previously from the appropriate arylamine hydrochloride, dicyandiamide, and acetone (three-component method) (10*a*, *c*), or from the corresponding arylbiguanide hydrochloride and acetone (two-component method) (10*b*).

The 2-monomethyl compounds, which had not been synthesized previously, were prepared as follows.

*4,6-Diamino-1,2-dihydro-2-methyl-1-(o-tolyl)-s-triazine Hydrochloride (**20**·HCl)*

A mixture of *o*-toluidine (21.4 g, 0.2 mol), cyanoguanidine (17.2 g, 0.2 mol), water (60 ml), and concentrated hydrochloric acid (16.7 ml) was stirred under reflux for 2 h (positive biguanide test) (10) and stored over the week-end at 0 °C. The pale violet solid was collected, washed with acetone, and recrystallized from water with the aid of decolorizing carbon. The product, N^1-(*o*-tolyl)biguanide hydrochloride, was obtained as colorless crystals, mp 241–241.5 °C; yield 22.5 g (49.5%). This material was suspended in a mixture of absolute ethanol (60 ml) and concentrated hydrochloric acid (8.2 ml) and cooled in an ice bath while redistilled acetaldehyde (11.2 ml) was added dropwise with stirring. When addition was complete the mixture was heated under reflux for 1 h (negative biguanide test) (10) and stored overnight at 0 °C. Filtration, washing with absolute ethanol, and drying yielded the first crop as a white powder (15.2 g). The mother liquor was reduced in volume, adjusted to p*H* 6 with ammonia, and stored at 0 °C in order to precipitate a second crop (5.9 g). Recrystallization of the combined first and second crops from water (*ca.* 100 ml) with the aid of decolorizing carbon afforded 15.7 g (62%) of analytically pure colorless crystals of **20**·HCl, mp 246.5–248 °C (dried 20 h at 70 °C/0.01 torr over P_2O_5). *Anal.* calcd. for $C_{11}H_{15}N_5 \cdot HCl$: C 52.06, H 6.35, Cl 13.97, N 27.60; found: C 51.81, H 6.41, Cl 14.11, N 27.45.

*4,6-Diamino-1-(p-chlorophenyl)-1,2-dihydro-2-methyl-s-triazine Hydrochloride (**21**·HCl)*

A mixture of *o*-chloroaniline (25.5 g, 0.2 mol), cyanoguanidine (17.2 g, 0.2 mol), water (60 ml), and concentrated hydrochloric acid (16.7 ml) was stirred under reflux for 2 h (positive biguanide test) (10) and stored overnight at 0 °C. Filtration, washing with acetone, and drying under reduced pressure yielded 37.2 g (75%) of white powder, mp 248–249 °C. This solid (N^1-(*o*-chlorophenyl)biguanide hydrochloride) was suspended directly in a mixture of absolute ethanol (85 ml) and concentrated hydrochloric acid (12.5 ml) and cooled in an ice bath while redistilled acetaldehyde (16.9 ml) was added dropwise with stirring. When addition was complete the mixture was heated under reflux for $2\frac{1}{4}$ h (negative biguanide test) (10) and stored overnight at 0 °C. Filtration, washing with absolute ethanol, and drying under reduced pressure yielded the first crop as a white powder (20.4 g). The mother liquor was concentrated to a smaller volume, adjusted to p*H* 6 with ammonia, and stored at 0 °C until a second crop crystallized out (14 g). Recrystallization of the combined first and second crops from water (100 ml) with the aid of decolorizing carbon afforded 27.7 g (56%) of analytically pure colorless

Can. J. Chem. Downloaded from www.nrcresearchpress.com by 210.87.254.42 on 09/05/12
For personal use only.

crystals of **21**·HCl, mp 242–243 °C (dried 20 h at 70 °C/0.01 torr over P_2O_5). *Anal.* calcd. for $C_{10}H_{12}ClN_5 \cdot HCl$: C 43.81, H 4.78, Cl 25.87, N 25.55; found: C 43.96, H 4.85, Cl 26.09, N 25.65.

Nuclear magnetic resonance spectra were determined with Varian A-60 and HA-100, or JEOL 4H-100 instruments, the 100 MHz instruments being operated in the field sweep mode. Perfluoroacetic, -propionic, -butyric, and -octanoic acids (Pierce Chemical Co.) were employed as solvents, the choice of solvent depending on the temperature range of interest. Only high temperature spectra were recorded when perfluorobutyric and perfluorooctanoic acids were used because of line broadening at normal probe temperatures resulting from solvent viscosity. Uniform 0.3 *M* concentrations were employed for the 60 MHz spectra. Line-shape measurements were carried out for **21** using approximately 1 *M* concentrations, the sample being vacuum degassed by the freeze–thaw method and then sealed in a sample tube. The procedures used for complete line-shape analysis of the temperature dependent proton spectra have been described earlier (20). No attempt was made to study **21** by the equilibration method because the integrals of the overlapping methyl doublets could not be separated.

An approximately 0.6 *M* solution of **20** in trifluoroacetic acid solution (Eastman Kodak white label), with tetramethylsilane as an internal standard, was prepared for each run of the equilibration method. The samples were stored in a dry ice – acetone bath until use. It was necessary to keep the samples frozen before use because the lifetime of the less stable isomer in solution was only about 1 day at room temperature. The probe was equilibrated at the desired temperature, and the spectrometer was then tuned using a sample similar to the one to be used for the kinetic run. Such pre-tuning was essential to avoid loss of data during the early part of the kinetic run. The sample of **20** was then placed in the probe and allowed to reach temperature equilibrium, when a series of integrations, at recorded times, of the 2-methyl signals was started. Frequent integrals were taken when the relative concentrations of the two diastereomers were changing rapidly. The interval of time between integrations was increased as the sample approached thermodynamic equilibrium. Finally, the sample was maintained at the temperature of the kinetic run for several lifetimes, then re-integrated to obtain an estimate of the equilibrium populations of the diastereomers at that temperature. Beyond the temperature limits employed (22.5–52.0 °C) it was impractical to carry out kinetic runs because the reactions were either too slow or too fast to allow accurate measurements.

The forward and the reverse rate constants for the equilibration process were obtained for the run at each temperature by fitting the equation for a reversible first-order reaction (24), in appropriate form, to the experimentally determined time dependent ratios of the integrals of the 2-methyl group signals of the two rotamers. Iterative regression analysis methods were employed for the computation. The first-order rate constants calculated ranged from about 41 to 0.7 h^{-1}.

For all the variable temperature measurements, probe temperatures were measured immediately before or after each spectrum was recorded, using a standard Varian ethylene glycol variable temperature reference sample. Temperatures are believed to be accurate to ±2 °C.

Acknowledgments

This work was supported by grants from the National Institutes of Health, United States Public Health Service (NCI Grant C6516), and by the National Research Council of Canada.

1. A. Rosowsky, K. K. N. Chen, R. St. Amand, and E. J. Modest. J. Pharm. Sci. **62**, 477 (1973).
2. W. E. Bentz, L. D. Colebrook, J. R. Fehlner, and A. Rosowsky. Chem. Commun. 974 (1970).
3. L. D. Colebrook, H. G. Giles, and A. Rosowsky. Tetrahedron Lett. 5239 (1972).
4. G. E. Foley. Proc. Soc. Exp. Biol. Med. **83**, 733 (1953).
5. B. Roth, R. B. Burrows, and G. H. Hitchings. J. Med. Chem. **6**, 370 (1963).
6. E. J. Modest, E. Farber, and G. E. Foley. Proc. Am. Assoc. Cancer Res. **1**, 33 (1954).
7. S. Sternhell. *In* Dynamic nuclear magnetic resonance spectroscopy. *Edited by* L. M. Jackman and F. A. Cotton. Academic Press, Inc., New York. 1975. Chapt. 6.
8. K. Mislow and M. Raban. *In* Topics in stereochemistry. Vol. 1. *Edited by* E. L. Eliel and N. L. Allinger. Interscience Publishers, New York. 1967.
9. G. Binsch. *In* Topics in stereochemistry. Vol. 3. *Edited by* E. L. Eliel and N. L. Allinger. Interscience Publishers, Inc., New York. 1968. p. 97.
10. (*a*) E. J. Modest. J. Org. Chem. **21**, 1 (1956); (*b*) E. J. Modest and P. Levine. J. Org. Chem. **21**, 14 (1956); (*c*) A. Rosowsky, H. K. Protopapa, P. J. Burke, and E. J. Modest. J. Org. Chem. **29**, 2881 (1964).
11. R. W. Taft, Jr. J. Am. Chem. Soc. **75**, 4538 (1953); R. W. Taft, Jr., *In* Steric effects in organic chemistry. *Edited by* M. S. Newman. John Wiley and Sons, Inc., New York. 1956. Chapt. 13.
12. J. A. Pople, W. G. Schneider, and H. J. Bernstein. High-resolution nuclear magnetic resonance. McGraw-Hill, New York. 1959. pp. 223–224.
13. D. M. Hall and M. M. Harris. J. Chem. Soc. 490 (1960).
14. L. D. Colebrook and H. G. Giles. Can. J. Chem. **53**, 3431 (1975).
15. A. Mannschreck, V. Jonas, and B. Kolb. Angew. Chem. Int. Ed. Engl. **12**, 909 (1973).
16. M. M. Harris. *In* Progress in stereochemistry. Vol. 2. *Edited by* W. Klyne and P. B. D. de la Mare. Butterworths, London. 1958. Chapt. 5.
17. P. H. Bird, L. D. Colebrook, A. R. Fraser, and H. G. Giles. Chem. Commun. 225 (1974).
18. E. L. Eliel. Stereochemistry of carbon compounds. McGraw-Hill, New York, 1962. pp. 156–164.
19. E. L. Eliel, N. L. Allinger, S. L. Angyal, and

G. A. MORRISON. Conformational analysis. Interscience Publishers, Inc., New York. 1965. Chapt. 7.
20. L. D. COLEBROOK, H. G. GILES, A. GRANATA, S. ICLI, and J. R. FEHLNER. Can. J. Chem. **51**, 3635 (1973).
21. L. PAULING. The nature of the chemical bond. 3rd. ed. Cornell University Press, Ithaca, New York. 1960. p. 260.
22. B. R. BAKER and B. T. HO. J. Heterocycl. Chem. **2**, 72 (1965).
23. H. E. HARRIS, M. M. HARRIS, R. Z. MAZENGO, and S. SINGH. J. Chem. Soc. Perkin Trans. II. 1059 (1974).
24. W. J. MOORE. Physical chemistry. 3rd. ed. Prentice-Hall, Inc., Englewood Cliffs, New Jersey. 1964. pp. 264–265.

For personal use only.

^{13}C nuclear magnetic resonance spectra of steroids: the assignments of chemical shifts for C-15 and C-16 in 17β-acetyl steroids

DONG JE KIM, LAWRENCE D. COLEBROOK, AND T. J. ADLEY[1]

Department of Chemistry, Sir George Williams Campus, Concordia University, Montreal, P.Q., Canada H3G 1M8

Received May 31, 1976

DONG JE KIM, LAWRENCE D. COLEBROOK, and T. J. ADLEY. Can. J. Chem. **54**, 3766 (1976).

Previously reported ^{13}C chemical shift assignments for C-15 and C-16 of a number of 17β-acetyl steroids related to progesterone have been shown to be reversed. Based on the revised assignment the effect of bromo- and hydroxy-substitution at C-17 on C-12, C-14, C-15, and C-16 is assessed.

DONG JE KIM, LAWRENCE D. COLEBROOK et T. J. ADLEY. Can. J. Chem. **54**, 3766 (1976).

On démontre qu'il faut renverser les attributions rapportées antérieurement pour les déplacements chimiques des C-15 et C-16 d'une série de stéroïdes reliés à la progestérone portant une chaîne acétyle en position 17β. En se basant sur les attributions revisées, on établit l'effet que produit une substitution par un brome ou un groupe hydroxyle en position C-17 sur les C-12, C-14, C-15 et C-16.

[Traduit par le journal]

Introduction

Recently a renewed interest has been evinced in the ^{13}C chemical shifts of various hydroxylated steroids and the results have been rationalized in terms of α, β, γ, and δ substituent effects (1). In our investigation of substituent effects in hydroxylated 17β-acetyl steroids, we observed the need for a reinvestigation of some of the ^{13}C chemical shift assignments of certain D-ring atoms. We wish now to present evidence that the assignment of signals attributed to C-15 and C-16 methylene groups have in previous reports been either reversed (*2b*, *c*), or otherwise incorrectly assigned (*2a*).

Results and Discussion

The chemical shifts of C-14 and C-15 which are located γ to the bromine atom in 3β-acetoxy-17α-bromopregnan-20-one (**3***b*) have been observed by us to be respectively substantially shielded (−5.7 ppm) and negligibly shielded (−0.2 ppm) relative to the analogous chemical shifts reported for C-atoms in 17α-H compounds (*2b*, *c*), similar to **3***a*. The effect of the introduction of a hydroxyl group at the 17β position in a number of steroids (**4***a*, **5***a*, **5***b*) with C/D rings *trans*-fused has been reported (3) to be shielding at the γ-located C-12, C-14, and C-15 positions. A similar shielding effect for these γ-carbons has also been reported (3, *2d*) for the epimeric 17α-hydroxy steroids (**4***b*, **5***c*, **6***b*, **7***b*) with the single exception[2] of C-15 of **7***b* (Table 1).

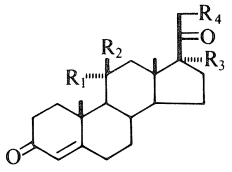

1

a, $R_1 = R_2 = R_3 = R_4 = H$
b, $R_1 = OH, R_2 = R_3 = R_4 = H$
c, $R_2 = OH, R_1 = R_3 = R_4 = H$
d, $R_3 = OH, R_1 = R_2 = R_4 = H$
e, $R_4 = OH, R_1 = R_2 = R_3 = H$
f, $R_2 = R_3 = OH, R_1 = R_4 = H$
g, $R_2 = R_4 = OH, R_1 = R_3 = H$
h, $R_3 = R_4 = OH, R_1 = R_2 = H$
i, $R_2 = R_3 = R_4 = OH, R_1 = H$

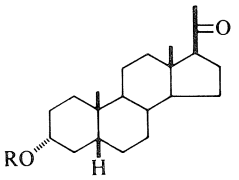

2

a, R = H
b, R = Ac

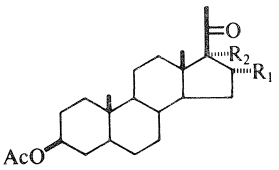

3

a, $R_1 = R_2 = H$
b, $R_1 = H, R_2 = Br$
c, $R_1 = R_2 = D$
d, $R_1 = D, R_2 = Br$

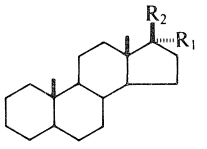

4

a, $R_1 = R_2 = H$
b, $R_1 = OH, R_2 = H$
c, $R_2 = OH, R_1 = H$

[1]Author to whom all correspondence should be addressed.

[2]If, as suggested by Lang *et al.* (*2d*), a reversed assignment for C-15 and C-16 of the compound **7***a* is taken, C-15 is shielded by 0.4 ppm.

Can. J. Chem. Downloaded from www.nrcresearchpress.com by 210.87.254.105 on 09/05/12
For personal use only.

Can. J. Chem. Downloaded from www.nrcresearchpress.com by 210.87.254.105 on 09/05/12
For personal use only.

TABLE 1. The effect of 17α- or 17β-hydroxy substitution on ^{13}C chemical shifts (ppm)

Compounds		$\Delta\delta$ C-12(γ)	C-14(γ)	C-15(γ)	C-16(β)	Reference
17β-ol	**4***c*-**4***a*	−2.1	−3.4	−2.1	10.1	3*a*, *b*
	5*d*-**5***a*	−3.0	−2.9	−1.6	10.4	3*c*
	5*e*-**5***b*	−3.4	−3.3	−1.9	10.1	3*c*
17α-ol	**4***b*-**4***a*	−7.4	−5.8	−0.9	11.9	3*a*, *b*
	5*c*-**5***a*	−7.8	−5.7	−0.7	11.5	3*c*
	6*b*-**6***a*	−7.9	−6.1	−0.7	11.0[a]	2*d*
		−7.5	−5.5	−0.5[2]	11.2[b]	2*d*
	7*b*-**7***a*	−7.1	−5.2	0.0	11.0[b]	2*d*

[a]In $CDCl_3$–CD_3OD solution.
[b]In [$^2H_5$]pyridine–[$^2H_6$]acetone (4:1) solution.

TABLE 2. Reported (2*b*, *d*) and corrected (in parentheses) ^{13}C chemical shift differences

Compounds		$\Delta\delta$ C-12(γ)	C-14(γ)	C-15(γ)	C-16(β)
17α-ol	**1***d*-**1***a*	−5.6	−5.5	0.8(−0.7)	8.3 (9.8)
	1*f*-**1***c*	−7.5	−5.4	1.4(−0.7)	8.0(10.1)
	1*h*-**1***e*	−4.1	−5.4	0.9(−0.7)	8.2 (9.8)
	1*i*-**1***g*	−7.8	−5.6	1.3(−0.9)	8.7(10.9)
	3*b*-**3***a*	(−3.3)	(−5.7)	(−1.6)	(13.0)

The effect of the 17-hydroxyl group on the γ-carbon atoms corresponds in sign (but not in magnitude) to the γ-effect reported for cyclopentanol (−1.9 ppm) and its derivatives (4). The difference in magnitude of the γ-shielding effect observed for the 17α- and 17β-ols and for cyclopentanol may be attributed to a puckered conformation for the steroidal D ring with C-13 and C-15 upward and C-14 downward when C and D rings are *trans*-fused.

However, in 17β-acetyl steroids, *i.e.*, progesterone (**1***a*) and related compounds (**1***c*, **1***e*, **1***g*), the γ-located C-12 and C-14 were reported (2*b*, *d*) to be shielded upon the introduction of a 17α-hydroxyl group, while the γ-situated C-15 was reported to be deshielded (0.8–1.4 ppm, Table 2). It has been reported that the degree of deshielding at C-17 upon the introduction of the 17α-hydroxy function depends in some measure upon the nature of the 17β-substituent (2*d*). However, the effect of the latter upon C-15 does not appear to be particularly marked.

The various shielding and deshielding effects reported for C-15 in 17-substituted steroids prompted us to re-examine chemical shifts for D ring carbon atoms with special reference to the ambiguities surrounding C-15 and C-16

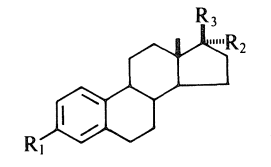

5

a, $R_1 = R_2 = R_3 = H$
b, $R_1 = OH$, $R_2 = R_3 = H$
c, $R_2 = OH$, $R_1 = R_3 = H$
d, $R_3 = OH$, $R_1 = R_2 = H$
e, $R_1 = R_3 = OH$, $R_2 = H$

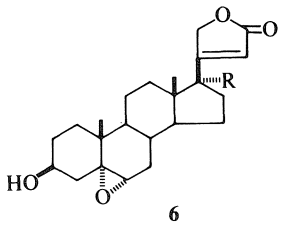

6

a, R = H
b, R = OH

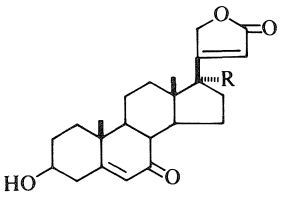

7

a, R = H
b, R = OH

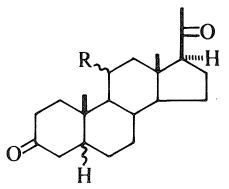

8

a, 5α-H, R = H
b, 5α-H, R = α-OH
c, 5α-H, R = β-OH
d, 5β-H, R = H
e, 5β-H, R = α-OH

Can. J. Chem. Downloaded from www.nrcresearchpress.com by 210.87.254.105 on 09/05/12
For personal use only.

assignments. The 16α,17α-dideutereo steroid **3***c* was prepared from the Δ^{16}-steroid. The proton decoupled spectrum of **3***c* showed, upon comparison with the corresponding protio-steroid, (**3***a*) greatly diminished peaks at δ 23.5 ppm and 64.0 ppm. The latter resonance is assigned to C-17, while the former, previously assigned (2*b*, *c*) to C-15, we now attribute to C-16. The C-15 signal of **3***c* appears at 24.9 ppm, somewhat broadened and with slightly decreased intensity. Isotope effects for C-16 resonances were also observed for 17α-deuterated-17β-acetyl steroids **1***a*, **1***b*, **1***c* (R_3 = D) and **3***a*. Experiments in various solvent systems (dioxane, $CDCl_3$, and DMSO-d_6) indicate that the $\Delta\delta$ values shown in Table 2 do not change significantly at the unfunctionalized positions C-15 and C-16 nor have we observed any transposition of signals at these sites with change of solvent (2*b*, 7).

With this revised assignment, as would be anticipated, the addition of the shift reagent $Pr(fod)_3$ (5) to **3***a* now shields C-16 more highly than C-15. It is generally true that the signals for C-16 appear at higher field than those for C-15 in the 17β-acetyl compounds which we have examined (**1***a*, **1***b*, **1***c*, **3***a*, **3***c*, **8***a–e*) as well as in the 20-keto-21-hydroxy steroids **1***e* and **1***g*.

With this revised assignment a more consistent picture emerges. The introduction of a 17α-bromo substituent now has a stronger shielding effect (−1.6 ppm) on the γ-located C-15 relative to the 17α-H substituted compound, compared to only −0.2 ppm if the original assignments for C-15 and C-16 are employed (2*b*, *c*).

With the new assignments the effect of the 17α-hydroxy group in progesterone derivatives **1***d*, **1***f*, **1***h*, **1***i* also causes a shielding effect (Table 2) at the γ-located C-14 (−5.4 to −5.6 ppm) as well as at γ-located C-15 (−0.7 to −0.9 ppm).

Experimental

All ^{13}C nmr spectra were recorded at 25.2 MHz using a modified Varian HA-100 spectrometer operating in the Fourier transform mode. The spectra were determined at 35 °C as 0.4 *M* solutions in dioxane. The effect of solvent on chemical shifts was examined in $CDCl_3$ and DMSO-d_6. The spectrometer was interfaced to a Digilab gated power amplifier and a Hewlett-Packard 2114A computer and was operated with an internal homonuclear lock on the broad band decoupled solvent signal. Approximately 9000 transients were averaged using 4K data points and a block averaging technique.

The shift reagent experiment was carried out in $CDCl_3$ with commercial grade $Pr(fod)_3$ which was not further purified.

3β-Acetoxy-17α-bromo-5α-pregnan-20-one (3b)

Irradiation of a CCl_4 solution of 3β-acetoxy-5α-pregnan-20-one with a tungsten 1000 W light source in the presence of excess NBS provided **3***a* in approximately quantitative yield; mp 152–154 °C (6).

3β-Acetoxy-16α,17α-dideutereo-5α-pregnan-20-one (3c)

3β-Acetoxy-5α-pregnan-16-ene-20-one was dissolved in ethyl acetate, treated with deuterium in the presence of 5% Pd/C catalyst to yield the title compound.

3β-Acetoxy-16α-deutereo-17α-bromo-5α-pregnan-20-one (3d)

Bromination of **3***c* with excess NBS following the method described for the preparation of **3***b* gave **3***d*.

Deuteration of 1a, 1b, and 1c

Deuterium exchange at C-2, C-17, and C-21 was conducted in a nitrogen atmosphere with D_2O – sodium methoxide in dioxane at 65–75 °C. After 10 h the reaction mixture was poured into ice and was rapidly extracted with ether. The combined ether extracts were washed successively with aqueous 5% HCl, 5% sodium bicarbonate solution, and finally with water. Evaporation of the solvent gave products which showed deuterium incorporation at C-2, C-17, and C-21 (but none at C-6). If the exchange is carried out at room temperature very little incorporation at C-2 is observed.

1. H. Eggert, C. L. Van Antwerp, N. S. Bhacca, and C. Djerassi. J. Org. Chem. **41**, 71 (1976).
2. (*a*) J. Reich, M. Jantelat, M. T. Messe, F. J. Weigert, and J. D. Roberts. J. Am. Chem. Soc. **91**, 7445 (1969); (*b*) N. S. Bhacca, D. D. Giannini. W. S. Jankonski, and M. E. Wolff. J. Am. Chem. Soc. **95**, 8421 (1973); (*c*) D. Leibfritz and J. D. Roberts. J. Am. Chem. Soc. **95**, 4996 (1973); (*d*) S. Lang, D. N. Lincoln, and V. Wray. J. Chem. Soc. Perkin Trans. II, 344 (1975).
3. (*a*) J. W. ApSimon, H. Beierbeck, and J. K. Saunders. Can. J. Chem. **51**, 3874 (1973); (*b*) H. Eggert and C. Djerassi. J. Org. Chem. **38**, 3788 (1973); (*c*) T. A. Wittstruck and K. I. H. Williams. J. Org. Chem. **38**, 1542 (1973).
4. M. Christe, H. J. Reich, and J. D. Roberts. J. Am. Chem. Soc. **93**, 3463 (1971).
5. R. E. Rondeau and R. E. Sievers. J. Am. Chem. Soc. **93**, 1522 (1971).
6. R. E. Marker, H. J. Crooks, Jr., and R. B. Wagner. J. Am. Chem. Soc. **64**, 210 (1942).
7. H. H. Mantsch and I. C. P. Smith. Can. J. Chem. **51**, 1384 (1973).

Orthokinetic collisions of hard spheres in simple shear flow

P. A. ARP AND S. G. MASON
Department of Chemistry, McGill University, Montreal, P.Q., Canada H3C 3G1
and
Pulp and Paper Research Institute of Canada, Montreal, P.Q., Canada H9R 3J9

Received May 10, 1976

P. A. ARP and S. G. MASON. Can. J. Chem. **54**, 3769 (1976).

From the rigorous hydrodynamic interaction theory of a pair of neutral hard spheres of radius b in a viscous fluid undergoing simple shear flow, the two-body collision theory has been developed which corrects the classical Smoluchowski theory based on rectilinear approach by applying the modern rigorous (and experimentally verified) curvilinear theory of approach. The difficulties in defining a collision are eliminated by defining a curvilinear collision sphere of radius ρ_m around a reference sphere. In this way correction factors for the area of the collision cross-section, the collision frequency, the average doublet life time, and the steady-state doublet concentrations of separating (or transient) doublets have been calculated as a function of ρ_m. The results show that the two theories are compatible for a ρ_m/b close to 2.38.

P. A. ARP et S. G. MASON. Can. J. Chem. **54**, 3769 (1976).

A partir de la théorie rigoureuse des interactions hydrodynamiques pour une paire de sphères dures et neutres de rayon b dans un liquide visqueux subissant un écoulement de scisaillement simple, on a développé la théorie des collisions de deux corps qui corrige la théorie classique de Smoluchowski basée sur une approche rectiligne en appliquant la théorie rigoureuse moderne (et vérifiée expérimentalement) curvilinéaire de l'approche. On élimine les difficultés inhérentes à la définition d'une collision en définissant une sphère de collision curvilinéaire de rayon ρ_m autour de la sphère de référence. De cette manière on a pu calculer des facteurs de correction pour la surface de la section droite de collision, la fréquence de collision, le temps de demi-vie moyen du doublet, et les concentrations des doublets à l'état stationnaire des doublets qui séparent (ou intermédiaires); tous ces calculs ont été faits en fonction de ρ_m. Les résultats indiquent que les deux théories sont compatibles lorsque ρ_m/b est près de 2.38.

[Traduit par le journal]

Introduction

An approximate theory of two-body collisions of neutral hard spheres of equal radius b and with negligible thermal (Brownian) motion in a dilute fluid suspension of number density n_0 undergoing simple shear flow was first developed by Smoluchowski (1) and later extended by Tuorilla (2), Muller (3), and Mason and co-workers (4–7). Collisions caused by highly ordered flow fields are termed "orthokinetic" to distinguish them from 'perikinetic" collisions resulting solely from random Brownian motion. The approximate orthokinetic theory for simple shear flow (1–7) was based on the assumption that two spheres in a favorable geometry when far apart will continue to approach each other on rectilinear paths until they make contact to form a transitory doublet which rotates as a rigid body until it is oriented in the mirror-image of initial contact and then separates. From this simple concept, equations were derived for quantities such as the collision frequency f_c per unit volume, the average doublet life time $\bar{\tau}$, and the steady-state doublet concentration n_2, which in many aspects resembles the equations of the classical kinetic theory of gases (8). Values of f_c, $\bar{\tau}$, n_2, and related quantities were confirmed experimentally with reasonable accuracy even though it was known that the paths of approach and recession were curvilinear and that true contact did not occur (4–9).

We now wish to examine these aspects of orthokinetic collisions in the light of the rigorous theory of the two-sphere encounters (10) which predicts curvilinear trajectories and no contact and which we have confirmed experimentally in considerable detail (11).

As will be seen, difficulties arise regarding the precise definition of a collision. This problem, of course, is not new in collision theory. It also occurs in calculating the collision cross-section for bimolecular collisions in a gas or the neutron-capture cross-section of an atomic nucleus, to name two familiar cases. In these

Can. J. Chem. Downloaded from www.nrcresearchpress.com by 210.87.254.105 on 09/05/12
For personal use only.

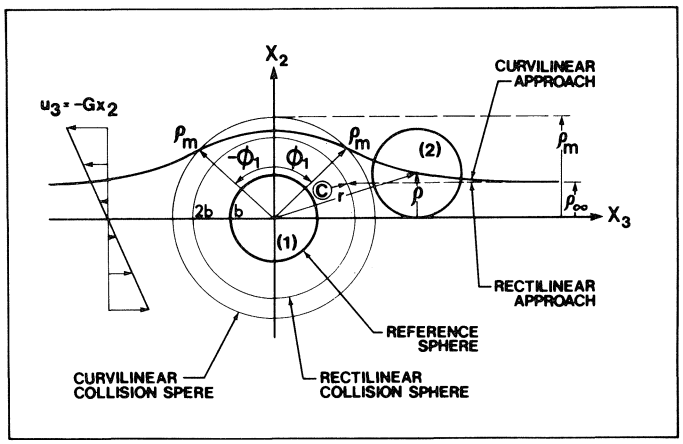

FIG. 1. Definition of the curvilinear collision parameter ρ_m (using an equatorial collision in the x_2x_3 plane as an example of the general case), which is the radius of the collision sphere in the shear $u_3 = -Gx_2$ centered at the origin 0. Shown are also the rectilinear collision sphere of radius $2b$, and the two colliding spheres (marked (*1*) and (*2*), with the reference sphere (*1*) at the origin). Whereas rectilinear approach would lead to contact at the point C, curvilinear trajectories can penetrate the curvilinear collision sphere at (ρ_m, ϕ_1). Curvilinear collision doublets are therefore defined to be those for which $r \leq \rho_m$.

The coordinate axis x_1 (normal to the figure) is the polar axis of the angular coordinates θ_1, ϕ_1; for the example shown, $\theta_1 = 90°$.

examples the concept is based on rectilinear approach of pairs of particles which in fact approach on curvilinear paths especially when they are in close proximity.

We have surmounted this difficulty by defining a "curvilinear" collision sphere of radius ρ_m centered around the "rectilinear" collision sphere of radius $2b$ (Fig. 1) and allowing ρ_m ($>2b$) to vary arbitrarily. The rectilinear collision sphere (4–7) is that region of space around a reference sphere which cannot be penetrated by the centre of other spheres because of geometrical exclusion. By contrast, limited entry into the curvilinear collision sphere is allowed from which we can calculate f_c, $\bar{\tau}$, and n_2 as functions of ρ_m. As will be seen this exact theory can be reconciled to a considerable extent with the approximate rectilinear theory.

The concepts to be discussed are of basic importance to the rheology and the stability of suspensions and colloidal sols and have been used in recent work (11–13).

Rectilinear Collision Theory

To determine the two-sphere collision rate in simple shear of rate G it is convenient to locate a reference sphere (No. *1* in Fig. 1) at the origin 0 of a Cartesian coordinate system x_i ($i = 1, 2, 3$) in which the particle-free fluid velocity components u_i are

$$[1] \qquad u_1 = u_2 = 0, \quad u_3 = -Gx_2$$

Assuming rectilinearity all the sphere centres passing through a circle of radius $2b$ drawn normal to the x_3 axis lead to collision. We call this circle the collision cross-section for rectilinear approach so that the corresponding collision cross-sectional area is

$$[2] \qquad \sigma_c = 4\pi b^2$$

We wish to emphasize that the collision cross-section defined here is not the same as the capture cross-section defined in refs. 12 and 13, when interparticle attractive forces of various kinds exist which may lead to the formation of permanently touching doublets. This possibility does not occur in the systems considered here (10, 11).

The rate f_c per unit volume of suspension at which the spheres pass through σ_c was derived in (4–7) from simple geometric considerations; $\bar{\tau}$ was obtained by averaging the individual doublet life times $\tau(\theta_1, \phi_1)$corresponding to initial contact and final separation at angles (θ_1, ϕ_1) and (θ_1, $-\phi_1$), respectively (Fig. 1).

During apparent contact between ϕ_1 and $-\phi_1$ the doublet was considered to rotate with angu-

Can. J. Chem. Downloaded from www.nrcresearchpress.com by 210.87.254.105 on 09/05/12
For personal use only.

TABLE 1. Comparison of rectilinear and curvilinear collision theories

Quantity	Rectilinear theory			Curvilinear correction factors*
	Formula	Equation	Reference	
σ_c	$4\pi b^2$	[2]	4–7	α_1
f_c	$\frac{16}{3}n_0^2b^3G$	[4]	4	α_2
$\bar{\tau}$	$\frac{5\pi}{6G}$	[5]	6	α_3†
n_2	$\frac{40}{9}\pi n_0^2b^3$	[6]	7	α_4‡

*Numerical values of the α_i's are listed in Table 2 and plotted in Fig. 3.
†Determined numerically; a semiempirical formula is given by [26].
‡$\alpha_4 = \alpha_2\alpha_3$ (see text).

lar velocities $d\theta_1/dt$ and $d\phi_1/dt$ calculable from Jeffery's equations (14) for rigid, prolate spheroids on the reasonable (and experimentally confirmed) assumption that the equivalent spheroidal axis ratio of the transient collision doublet is $r_e \simeq 2.0$ (6, 7). The steady-state doublet number concentration was then calculated from

$$n_2 = f_c\bar{\tau} \quad [3]$$

The resulting equations for σ_c, f_c, $\bar{\tau}$, and n_2 (*i.e.*, eqs. 2, 4, 5, and 6) are listed in Table 1.

Curvilinear Theory

Using the exact interaction theory (10) to take account of the curvilinear approach paths we employ the trajectory equations (eqs. 28, 29 of ref. 10)[1] for the sphere centres from which we obtain the following relationships for the trajectories of sphere *2* (Fig. 1) relative to the centre of the reference sphere:

$$x_1 = \pm Brf(\xi) \quad [7]$$

$$x_2 = \pm rf(\xi)\sqrt{h(\xi) + C} \quad [8]$$

where r is the centre-to-centre distance and whose dimensionless value is $\xi = r/b$; B (≥ 0) and C ($\gtrless 0$) are trajectory-defining constants which are closed when $C < 0$ and open when $C > 0$; $B = 0$ and $B > 0$ correspond, respectively, to equatorial and non-equatorial collisions; $f(\xi)$ and $h(\xi)$ are known functions which have been evaluated numerically (10). Pairs of spheres moving with $C < 0$, *i.e.*, in closed trajectories, are designated "permanent" and those with $C > 0$ (open trajectories) "separating" doublets. The analysis presented below is restricted to separating doublets, since the quantities we wish to calculate are meaningless for permanent doublets (15).

The functions $f(\xi)$ and $h(\xi)$ are monotonically decreasing with increasing ξ; in particular, when $\xi \to \infty$ (10),

$$f(\xi) \simeq \xi^{-1} + \cdots \quad [9]$$

$$h(\xi) \simeq \frac{16}{9}\xi^{-3} + \cdots \quad [10]$$

It follows from [7] to [10]:

$$\lim_{\xi\to\infty} x_1 = \pm bB \quad [11]$$

and

$$\lim_{\xi\to\infty} x_2 = \pm b\sqrt{C} \quad [12]$$

It is convenient to use the cylindrical polar coordinates (ρ, ϕ_3, x_3) for the centre of sphere *2* (Fig. 2), where

$$\rho = \sqrt{x_1^2 + x_2^2} \quad [13]$$

and

$$\cos\phi_3 = \frac{x_1}{\rho} \quad [14]$$

Substituting [7] and [8] in [13] and [14] yields

$$\rho^2 = r^2f^2(\xi)[B^2 + C + h(\xi)] \quad [15]$$

and

$$\cos\phi_3 = \pm B/\sqrt{B^2 + C + h(\xi)} \quad [16]$$

[1]Compare with eqs. 28 and 29 in ref. 10, where the origin is taken midway between the two spheres; as a result the r.h.s. of [7] and [8] are doubled.

Can. J. Chem. Downloaded from www.nrcresearchpress.com by 210.87.254.105 on 09/05/12
For personal use only.

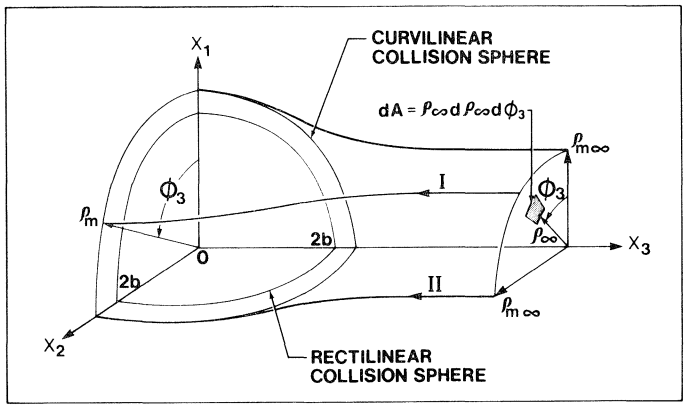

FIG. 2. Illustration of the three-dimensional character of the curvilinear collision process in one octant of the x_1-coordinate system. Also shown is the collision-defining trajectory surface axisymmetric about the x_3 axis with $\rho = \rho_{m\infty}$ at $x_3 = \pm\infty$ and $\rho = \rho_m$ at $x_3 = 0$. All trajectories for which $(B^2 + C) = (\rho_{m\infty}/b) =$ constant lie on this surface; examples are the 3-dimensional curves *I* and *II* corresponding to $B > 0$ and $B = 0$ given by [7] and [8]. Note that for *I*, ϕ_3 increases steadily as $x_3 \rightarrow 0$; for *II*, ϕ_3 remains fixed at 90°. Also shown is the surface element dA used to calculate the particle flux through the curvilinear collision sphere of radius ρ_m. Note that here the x_1 axis (normal to the sheet in Fig. 1) is vertical.

For a given $(B^2 + C)$, [15] describes a surface of revolution about the x_3 axis whose radius ρ increases towards $x_3 = 0$ where it reaches its maximum value; as $x_3 \rightarrow \infty$, ρ decreases to the asymptotic value ρ_∞ obtained from [11] and [12]:

$$\rho_\infty = b\sqrt{B^2 + C} \qquad [17]$$

We note that every trajectory of the same $(B^2 + C)$ must lie on this surface so that all the associated trajectories have identical ρ at a given x_3; however, as is evident from [16], ϕ_3 does not remain constant but increases to a maximum at $x_3 = 0$ except for equatorial encounters ($B = 0$) when it remains at $\pi/2$; encounters for which x_2 passes through 0 are permanent doublets (10) consideration of which is omitted from this treatment for reasons stated earlier. Examples of two trajectories (one for $B = 0$, the other for $B > 0$) are shown schematically in Fig. 2, where the axisymmetric character of the surface defined in [15] is also illustrated.

Since none of the trajectories defined by [7] and [8] can lead to contact (10), and since the surface given by [15] can never intersect the rectilinear collision sphere at $x_3 = 0$, we now define a collision to occur whenever a trajectory penetrates the curvilinear collision sphere of radius ρ_m. The limiting collision trajectories will embrace this sphere and have a limiting value of $\rho_{m\infty}$ at $x_3 = \infty$ which therefore becomes the radius of the collision cross-section of area

$$\sigma_c = \pi\rho_{m\infty}^2 = 4\pi\alpha_1 b^2 \qquad [18]$$

where α_1 is a correction factor to be applied to the rectilinear theory given by [2] and which is calculable for a given ρ_m (Table 2 and Fig. 3).

To calculate f_c we note that the particle flux into the curvilinear collision sphere is given by that into the circle of radius $\rho_{m\infty}$ at $x_3 = \pm\infty$. Hence f_c can be evaluated by considering the flux dN of spheres passing through the surface element dA (Fig. 2) towards the x_1x_2 plane in unit time:

$$dN = n_0 G\rho_\infty^2 \cos\phi_3 d\rho_\infty d\phi_3 \qquad [19]$$

On integrating [19] over 4 octants (Fig. 2) we obtain the total number N passing through σ_c in unit time

$$N = \frac{4}{3} n_0 \rho_{m\infty}^3 G \qquad [20]$$

and consequently f_c for all spheres with $\rho_\infty \leq \rho_{m\infty}$ is given by

$$f_c = \frac{n_0 N}{2} = \frac{2}{3} n_0^2 \rho_{m\infty}^3 G \qquad [21]$$

We note that f_c depends strongly on $\rho_{m\infty}$, and that $f_c = 0$ when $\rho_{m\infty} = 0$. To compare [21] with f_c from the rectilinear theory, it is convenient to introduce the correction factor

Can. J. Chem. Downloaded from www.nrcresearchpress.com by 210.87.254.105 on 09/05/12
For personal use only.

TABLE 2. Numerical correction factors from exact theory*

ρ_m/b†	$\rho_{m\infty}/b$†‡	α_1	α_2	α_3§	α_4§	r_e‖
$2+4.2\times10^{-5}$¶	0	0	0	—	0	2.28
$2+1.0\times10^{-4}$	0.316	0.025	0.004	—	—	2.31
$2+3.7\times10^{-4}$	0.548	0.075	0.021	—	—	2.37
2.0011	0.707	0.125	0.044	—	—	2.44
2.0077	1.000	0.250	0.125	—	—	2.64
2.068	1.414	0.500	0.356	1.004	0.358	3.24
2.20	1.732	0.750	0.650	1.021	0.664	4.05
2.38	2.000	1.000	1.000	1.042	1.042	5.10
2.55	2.236	1.250	1.40	1.059	1.483	6.15

*The α_i's are obtained from eqs. 18, 22, 26, and 27, respectively, using the theory in ref. 10 (see text).
†Taken from Table [V, (10)], designating Table V in ref. 10.
‡Note from [17] that $\rho_{m\infty} = b\sqrt{B^2 + C}$.
§Since τ is calculated from [23], contributions from permanent doublets become significant when $\rho_m/b \to 2$; permanent doublets are included in [23] because the limits of integration extend over one complete octant of the curvilinear collision sphere. For the values shown, contributions to α_3 and α_4 from permanent doublets are negligible.
‖Interpolated from Table [VI, (10)] for $\xi = \rho_m/b$.
¶Corresponding to B, $C = 0$, *i.e.*, the smallest ρ_m for separating doublets (Table [V, (10)].

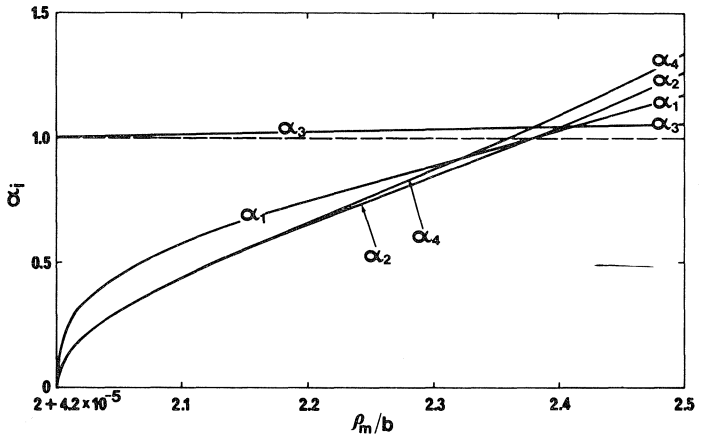

FIG. 3. Correction factors α_i ($i = 1$ to 4) to be applied to the rectilinear equations listed in Table 1 for various values of the collision defining parameter (ρ_m/b). Note that α_1, α_2, and α_4 are 0 at $\rho_m/b - 2 = 4.2 \times 10^{-5}$ which corresponds to the minimum approach of the limiting trajectory ($C = 0$) between permanent and separating doublets (see text).

[22] $$\alpha_2 = \left(\frac{\rho_{m\infty}}{2b}\right)^3$$

by which [4] (Table 1) must be multiplied to yield [21]. Again (as for α_1), α_2 depends on ρ_m as shown by the numerical values in Table 2 and in Fig. 3.

To calculate the average collision doublet life time $\bar{\tau}$ (*i.e.*, the average time that transient doublets spend inside the curvilinear collision sphere) we consider the expression

[23] $$\bar{\tau} = \int_0^{\pi/2}\int_0^{\pi/2} p(\theta_1,\phi_1)\tau(\theta_1,\phi_1)\,d\theta_1\,d\phi_1$$

where θ_1 and ϕ_1 are spherical angles relative to x_1 as the polar axis (Fig. 1) where the trajectories enter the sphere ρ_m; [23] is analogous to the relation used in ref. 4 to define $\bar{\tau}$ which must now depend on ρ_m. We recall from ref. 4 that the fraction of collisions occurring in the interval $d\theta_1$, $d\phi_1$ at θ_1, ϕ_1 over the ranges θ_1, $\phi_1 = 0$ to $\pi/2$ is

[24] $$p(\theta_1,\phi_1)d\theta_1 d\phi_1 = 3\sin^3\theta_1 \sin\phi_1 \cos\phi_1$$

We have evaluated [23] by numerical analysis for various ρ_m and we have expressed our results in the form

Can. J. Chem. Downloaded from www.nrcresearchpress.com by 210.87.254.105 on 09/05/12
For personal use only.

[25] $$\bar{\tau} = \alpha_3\left(\frac{5\pi}{6G}\right)$$

where α_3 is the correction factor for the rectilinear collision theory (see ref. 6 and Table 1). As shown in Table 2 and Fig. 3, α_3 is nearly constant and close to unity.

It has been shown (10, 15) that at any instant a pair of spheres has an assignable r_e which satisfies Jeffery's equations (14), and depends only on ξ; thus it varies continuously with time except when $\xi = 2$, *i.e.*, when the spheres touch (10). We have found it convenient to calculate the instantaneous value of r_e when $\xi = \rho_m/b$ (Table 2). Analysis of the values of α_3 using these values of r_e yields the following semi-empirical relationship

[26] $$\alpha_3 \simeq \frac{6}{5}\frac{r_e^2 + 1}{r_e(r_e + 1)}$$

To calculate the steady-state doublet concentrations of the separating doublets n_2 from curvilinear theory we use [3] and obtain

[27] $$n_2 = f_c\bar{\tau} \simeq \frac{2\pi(r_e^2 + 1)n_0^2\rho_{m\infty}^3}{3r_e(r_e + 1)} \simeq \alpha_4\frac{40}{9}\pi n_0^2 b^3$$

where $\alpha_4 = \alpha_2\alpha_3$ is the correction factor for curvilinearity (Table 2 and Fig. 3).

Concluding Remarks

As expected (Fig. 3), curvilinearity results in collision behaviour which is dependent on the choice of (ρ_m/b). Characteristically, α_1, α_2, and α_4 approach zero as $(\rho_m/b) \rightarrow 2$; more precisely, these coefficients are zero when $\rho_m/b - 2 = 4.2 \times 10^{-5}$ which corresponds to the closest possible approach for separating doublets (10). We emphasize again that all the relationships developed here are valid only for separating doublets which do, however, cover the range of ρ_∞ from 0 to $\rho_{m\infty}$.

From these calculations it is remarkable that the collisions observed visually are reproducible with different observers (4–7): and that f_e, $\bar{\tau}$, n_2, and other measured quantities were obtained in surprisingly good agreement with the rectilinear collision theory. All of this suggests that the minimum distance of approach for a collision to be recognized experimentally (preferably along the x_2-axis (6)) is around $\rho_m/b = 2.38$ as may be seen from Fig. 3 where the various α_i's are near unity; this corresponds (Table 2) to $\rho_{m\infty}/b = 2.000$, so that in the experiments the observers saw what corresponded to rectilinear collisions.

We note that in ref. 7, because of experimental difficulties, n_2 was not measured directly; instead the sum of n_2 and that of permanent doublets (n_p) was measured giving values about twice those calculated from [6] for $\alpha_4 = 1$. From this observation it was concluded (7) that $n_2 \simeq n_p$. It should be pointed out that even when ρ_m is specified the theoretical n_p is indeterminate for various reasons (15) among which is the formation of permanent doublets from n-body ($n \geq 3$) collisions as was shown experimentally by Darabaner and Mason (16).

1. M. von Smoluchowski. Phys. Z. **17**, 583 (1916); Z. Phys. Chem. **92**, 129 (1917).
2. P. Tuorilla. Kolloidchem. Beih. **24**, 1 (1927).
3. H. Muller. Kolloidchem. Beih. **27**, 223 (1928).
4. R. St. J. Manley and S. G. Mason. J. Colloid Sci. **7**, 354 (1952).
5. R. St. J. Manley and S. G. Mason. Can. J. Chem. **33**, 763 (1955).
6. W. Bartok and S. G. Mason. J. Colloid Sci. **12**, 243 (1957).
7. H. L. Goldsmith and S. G. Mason. Proc. Roy. Soc. A**282**, 569 (1964).
8. S. G. Mason. Chem. Can. **25**, 29 (1973).
9. A. Karnis, H. L. Goldsmith, and S. G. Mason. J. Colloid Interface Sci. **22**, 531 (1966).
10. P. A. Arp and S. G. Mason. J. Colloid Interface Sci. In press.
11. P. A. Arp and S. G. Mason. J. Colloid Interface Sci. In press.
12. P. A. Arp and S. G. Mason. J. Colloid Polymer Sci. In press.
13. T. G. M. van de Ven and S. G. Mason. J. Colloid Interface Sci. In press.
14. G. B. Jeffery. Proc. Roy. Soc. (London), A**102**, 161 (1922).
15. G. K. Batchelor and J. T. Green. J. Fluid Mech. **56**, 401 (1972).
16. C. L. Darabaner and S. G. Mason. Rheol. Acta, **6**, 273 (1967).

Can. J. Chem. Downloaded from www.nrcresearchpress.com by 210.87.254.105 on 09/05/12
For personal use only.

Isotopic exchange reactions of amines.[1] Part 1. An ^2H nuclear magnetic resonance study of the amino to methyl group deuteron exchange in methylamine[2]

JAMES D. HALLIDAY AND PATRICK E. BINDNER

Physical Chemistry Branch, Chalk River Nuclear Laboratories, Atomic Energy of Canada Limited, Chalk River, Ont., Canada K0J 1J0

Received January 13, 1976[3]

JAMES D. HALLIDAY and PATRICK E. BINDNER. Can. J. Chem. **54**, 3775 (1976).

Deuteron exchange kinetics between the methyl and amino groups in methylamine, catalyzed by potassium methylamide (PMA), have been studied by ^2H nmr.

$$CH_3ND_2 \underset{\leftarrow}{\overset{PMA}{\rightleftharpoons}} CH_2DNHD$$

Typical values of k_{obs}, the observed pseudo first-order exchange rate, are 1.0×10^{-5} s^{-1} at 0.21 *M* PMA and 323 K. Effects of added potassium methylamide and temperature are described. The rate is unaffected by the thermal decomposition product of PMA and there is little or no catalysis by an equilibrium mixture of the solvated electron species e^-, (e^-K^+), and K^-. The active catalyst in solution is shown to be monomeric PMA in equilibrium with relatively inactive dimers, . . ., *n*-mers. A mechanism that describes the exchange and relates it to the thermal decomposition of the amide is discussed.

JAMES D. HALLIDAY et PATRICK E. BINDNER. Can. J. Chem. **54**, 3775 (1976).

Utilisant la rmn du ^2H, on a étudié la cinétique de l'échange, catalysée par le méthylamidure de potassium (PMA), du deutérium entre les groupes méthyle et amino de la méthylamine.

$$CH_3ND_2 \underset{\leftarrow}{\overset{PMA}{\rightleftharpoons}} CH_2DNHD$$

A 0.21 *M* de PMA et à 323 K, on observe une constante, k_{obs}, pour la vitesse d'échange du pseudo premier ordre de 1.0×10^{-5} s^{-1}. On décrit les effets produits par l'addition de PMA ou par une variation de la température. La vitesse n'est pas influencée par le produit de la décomposition thermique du PMA; de plus il n'y a pratiquement pas de catalyse par un mélange en équilibre des espèces électroniques solvatées, e^-, (e^-K^+) et K^-. On démontre que le catalyseur actif en solution est le PMA sous forme de monomère qui est en équilibre avec des di-, . . . *n*-mères relativement inactifs. On discute d'un mécanisme qui décrit l'échange et qui le relie avec la décomposition thermique de l'amide.

[Traduit par le journal]

Introduction

Isotopic exchange reactions in strongly basic non-aqueous solutions, such as potassium amide in liquid ammonia, have been widely reported. Shatenshtein pioneered the use of KND_2/ND_3 to partially or completely deuterate many hydrocarbons (1). Streitwieser *et al.*, using lithium cyclohexylamide (LCHA) in cyclohexylamine (CHA), demonstrated by exchange measurements that the kinetic acidities of many very weakly acidic hydrocarbons could be determined (2). Another strongly basic, non-aqueous system, potassium methylamide (PMA) in methylamine (MA), has been under investigation in these laboratories in support of the development of a bithermal deuterium extraction process based on the isotopic exchange between hydrogen gas and the amino protons of methylamine (3).

A homogeneous isotopic exchange reaction in PMA/MA, first observed by Butler and den Hartog[4] in these laboratories, that cannot occur in KND_2/ND_3 and which has not been reported in LCHA/CHA, is the PMA catalyzed exchange of deuterons between the amino and methyl groups of the solvent, methylamine.

[1]Presented in part at the Canadian Chemical Conference of the Chemical Institute of Canada, Toronto, May 1975.

[2]AECL No. 5592.

[3]Revision received July 19, 1976.

[4]J. P. Butler, private communication.

Can. J. Chem. Downloaded from www.nrcresearchpress.com by 210.87.254.6 on 09/05/12
For personal use only.

Can. J. Chem. Downloaded from www.nrcresearchpress.com by 210.87.254.6 on 09/05/12
For personal use only.

[1] $$CH_3ND_2 \underset{\text{PMA}}{\rightleftharpoons} CH_2DNHD$$

This paper describes the dependence of the exchange rate for this reaction on catalyst concentration and temperature.

Experimental

(A) Reagents

Methylamine-d_2

This material was prepared from Matheson CH_3NH_2 containing ammonia, dimethylamine, and water as impurities. The protiated amine was first treated with lithium metal[5] to remove the ammonia and water by formation of insoluble $LiNH_2$ and LiOH. After filtration and vacuum distillation the residual NH_3 concentration was <100 ppm by weight and the dimethylamine concentration was <1000 ppm by weight. The purified methylamine was refluxed with a large excess of >99.8 atom percent (at%) D_2O and separated by vacuum distillation. Five passes using fresh D_2O were required to achieve an isotopic purity >99.2 at% D in the amino position, as determined by comparison of the residual amino proton's nmr peak with the high-field ^{13}C satellite from the methyl group. The CH_3ND_2 was dried over lithium metal and then vacuum distilled from the blue solution.

Potassium metal

Alfa Products potassium metal, purity 99.95%, sealed under argon in glass ampoules equipped with breakseals was used. The potassium was melted and transferred under vacuum and used without further purification.

(B) Sample Preparation

Solutions of potassium methylamide in methylamine are extremely reactive to O_2, CO_2, and H_2O. Therefore vacuum line techniques were used throughout this work. To help prevent isotopic dilution from adsorbed species during distillation of isotopically substituted materials, the surface in contact with the gas was significantly reduced by using a pretreated short glass manifold isolated from the rest of the vacuum line.

Special vacuum sealing materials had to be used with these strongly basic solutions since Teflon and most rubber O-rings are chemically attacked. Materials found suitable for modifying J. Young Ltd. glass valves were ethylenepropylene for the O-rings and polyethylene for the valve stems.

Kinetic samples were made by siphoning a small quantity of a stock PMA in MA solution through a rigorously dried stainless steel transfer line into a 5 mm nmr tube (Wilmad 507 or Kontes 260 attached to a J. Young valve) which had been evacuated after pretreatment with anhydrous methylamine. The methylamine solvent was removed by vacuum distillation and the residue in the tube weighed. Dried CH_3ND_2 was added in the required amount and the sample reweighed. The PMA concentrations were determined from the weights and converted to molarities (M). After preparation the samples were frozen in liquid N_2 and permanently sealed. Samples were kept frozen until the initial spectra were run. The deuteron dilution in the CH_3ND_2 from the proton on the added PMA was measured by ^1H nmr.

(C) Nuclear Magnetic Resonance Spectra

All nmr spectra were obtained on a CW Bruker HX90 spectrometer equipped with a Bruker variable temperature controller (±0.5 K) and a Nicolet 1020A signal averager. Deuteron spectra were run at 13.82 MHz in a field of 2.114 T.

(D) Treatment of Data

The initial stages of the exchange reaction may be considered as

[2] $$(CH_2)H{-}(ND)D \underset{\text{PMA}}{\rightleftharpoons} (CH_2)D{-}(ND)H$$

which is analogous to the isotopic exchange reaction (4, 5)

[3] $$AH + BD \rightleftharpoons AD + BH$$

in which the molar concentrations of the two species are equal *i.e.* [AH] = [BD].

The net rate of deuterium atom transfer into the methyl groups can thus be represented as the difference of the gross forward, R_f, and reverse, R_b, rates of transfer weighted in terms of the probabilities of their occurrence (4, 5). Since the atom fraction of deuterium in the amine group is determined directly from the nmr spectra no distinction is made between single and multiple deuteration of the amino group and the gross forward rate thus represents the totality of deuterium transferred from the amino to the methyl group.

$$[4] \quad \frac{dZ}{dt} = -\frac{2A\,dX}{dt} = R_f(X)(Y) - R_b(1-X)(1-Y)$$

where Z = number of deuterium atoms transferred/litre of solution, Y = atom fraction of H in the methyl group, X = atom fraction of D in the amino group, $(1-Y)$ = atom fraction of D in the methyl group, $(1-X)$ = atom fraction of H in the amino group, $K = R_f/R_b$ = equilibrium deuterium fractionation constant, A = initial concentration (M) of methylamine-d_2, ($[CH_3ND_2]_0$). Equation 4 defines the exchange rate per atom site, allows for the back reaction, and accounts for changes in the isotopic composition of the solvent with time.

The integrated solution to [4] is [5]

$$[5] \quad \ln\frac{X-X_e}{X_0-X_e} + \ln\frac{\frac{2(K-1)}{K}(X_0+X_e) - \frac{(K+4)}{K}}{\frac{2(K-1)}{K}(X+X_e) - \frac{(K+4)}{K}} = \frac{R_f}{6A^2}\left(\frac{A(K+4)}{K} + \frac{4A(K-1)}{K}X_e\right)t$$

[5]R. P. Denault, private communication.

Can. J. Chem. Downloaded from www.nrcresearchpress.com by 210.87.254.6 on 09/05/12
For personal use only.

Within experimental error there is no equilibrium isotope effect measured for deuterium fractionation between methyl and amino groups in this system so a statistical distribution of deuterium is obtained at equilibrium. The lack of an equilibrium isotope effect was also observed by Streitwieser *et al.* (2) in their studies of the dedeuteration of toluene-α-*d* in LCHA/CHA. Thus the deuterium fractionation constant K, may be taken as unity and it follows that $R_f = R_b$. This allows simplification of the solution to a first-order form [6] and the

$$[6] \quad \ln \frac{X - X_e}{X_0 - X_e} = -R_f\left(\frac{5}{6A}\right)t = -k_{obs}t$$

experimentally obtained first-order rate coefficient, k_{obs}, can be related directly to the forward rate of exchange, R_f.

Results

The amino to methyl group deuteron exchange is sufficiently slow to allow the nmr integrals of the deuterated species formed in solution as a function of time to be determined.

Deuteron nmr was selected initially in anticipation of determining the rates for formation of the individual species in solution. These data can be more easily obtained from the deuteron spectra than from the proton spectra, since there are no obscured resonances, Fig. 1. The proton spectrum shows the effect of the coupling with the spin $I = 1$ deuterons. A 1:2:3:2:1 quintet and a 1:1:1 triplet are produced that significantly overlap with each other and the larger CH_3 singlet. The deuteron spectra are much simpler with a 1:2:1 triplet, doublet, and singlet, all well resolved. However, such a detailed spectral analysis has not been attempted in this initial report which has been confined to the more general features of the total transfer of deuterium. An additional complication characteristic in these solutions concerns the loss of catalyst due to its thermal decomposition. Raylo Chemicals Ltd.[6] have shown that PMA thermolytically decomposes to potassium *N*,*N*′-dimethylformamidide (PDMFA) at 323 K with a rate constant at high concentration $\simeq 1.2 \times 10^{-6}$ s^{-1}. This decomposition rate is sufficiently fast to reduce the catalyst concentration during the reaction time required for the amino to methyl group exchange to achieve equilibrium.

In contrast Streitwieser reports little difficulty in preparing stable cesium cyclohexylamide/

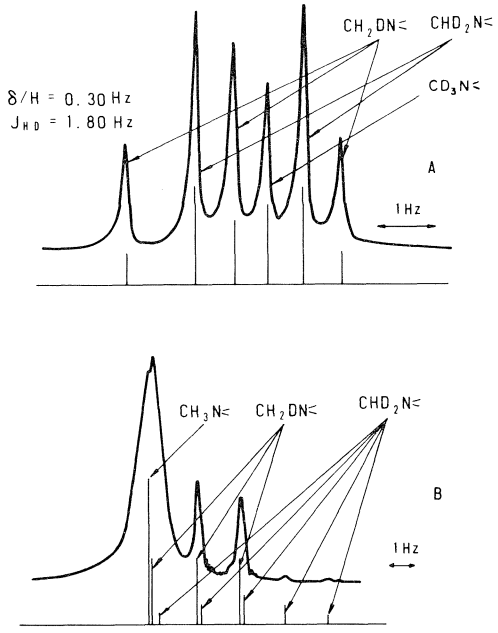

FIG. 1. (*A*) Methyl region ^{2}H nmr spectrum of mixed deuterated methylamines. (*B*) Methyl region ^{1}H nmr spectrum of mixed protiated methylamines. Line spectra are included to indicate the location of obscured resonances. Amino spectra (not shown) to high field.

cyclohexylamine solutions for kinetic studies. Control runs with added potassium *N*,*N*′-dimethylformamidide (the ultimate decomposition product) in amounts equal to the initial catalyst concentration showed it had no influence on the exchange rate. Molecular hydrogen is also generated but its pressure and solubility at these temperatures is negligibly small.

The potassium methylamide catalyst used in these kinetic studies was prepared by the reaction between potassium metal and methylamine. The resulting blue solution contains a mixture of solvated electrons (e^-), potassium cation – solvated electron ion pairs (e^-K^+), and potassium anions (6) which slowly react to form PMA. Such blue solutions were found to be relatively ineffective in promoting the amino–methyl deuteron exchange. The exchange rate observed for a solution prepared by adding CH_3ND_2 to potassium metal instead of to preformed PMA gave exchange rates which increased only slowly with time and reached a maximum when the solution turned yellow. Thereafter the exchange rate was constant and representative of the PMA concentration present. This behaviour can be

[6]Raylo Chemicals Ltd., Edmonton, Alberta, unpublished work under Atomic Energy of Canada Ltd. contract.

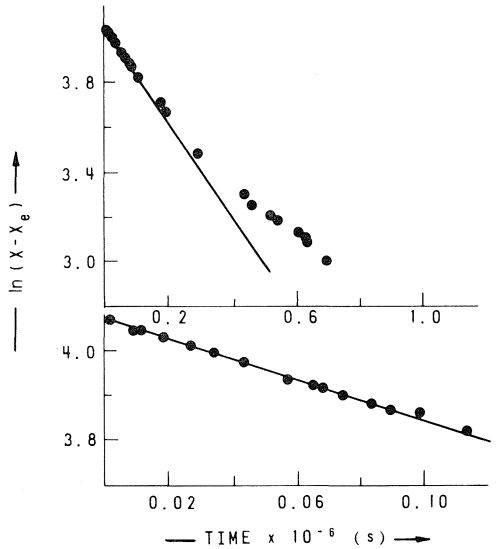

FIG. 2. A typical kinetic run for the exchange of deuterons between the amino and methyl groups of methylamine catalyzed by potassium methylamide. Temperature: 313 K, c 0.045 M, R_f 5.41 $\times$ 10^{-5} M s^{-1}. The lower graph shows a magnified plot of the initial linear portion.

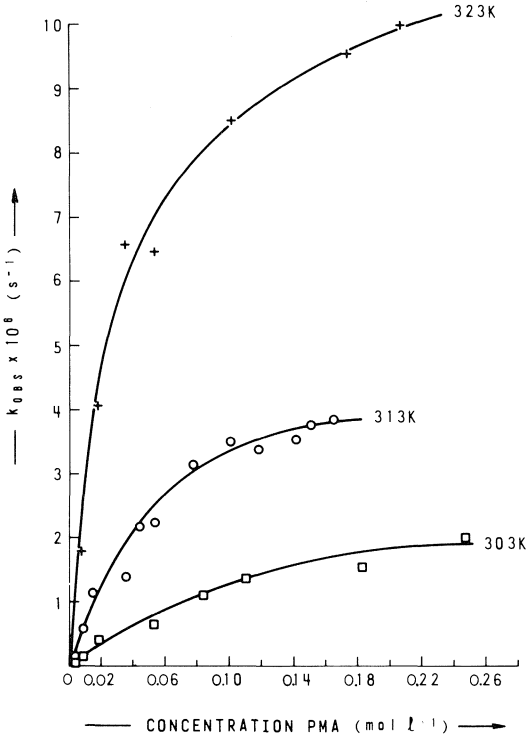

FIG. 3. Experimentally determined pseudo first-order rate constants for the exchange of amino and methyl deuterons in methylamine as a function of potassium methylamide concentration and temperature.

attributed to the slow dissolution of the metal and to the gradual formation of PMA in the blue solution.

The results have been analyzed using the pseudo first-order expression [6] from which the gross forward rate of deuterium transfer from the amino to the methyl group can be extracted. This expression is not limited to low deuterium levels and therefore is applicable to the relatively high deuterium levels used in the present experiments. It is derived with the assumption that the deuterium concentration at a given site remains statistical throughout the time course of the experiment, which is consistent with the observed equilibrium isotope distribution, $K = 1$ (5). The forward rate of exchange R_f does not contain any additional assumption about the detailed pathway of the reaction.

Satisfactory linear plots were only obtained for kinetic data taken over a limited time interval (Fig. 2). Data taken over extended time periods showed significant departures from [6] and no improvement in linearity was obtained by replotting the data in second-order form. Data were therefore confined to the initial rates of exchange and Fig. 3 shows the initial experimental forward rates, k_{obs}, determined for the amino to methyl group exchange as functions of initial catalyst concentration and temperature.

The range of temperatures available for these experiments (303 to 323 K) was limited by the slowness of the exchange reaction below 303 K and by the decomposition rate of the catalyst and the vapour pressure of the amine present in the sealed glass nmr tubes above 323 K.

Discussion

The use of [6] to extract values of the gross forward rate of exchange of deuterium from the amino to the methyl group would appear at first sight to be of limited applicability in view of the pronounced departure of Fig. 2 from the expected first-order behaviour. Deviations of the rates of isotopic exchange reactions from the first-order behaviour expected from the McKay law have been used as a probe for mechanistic detail (4, 5). Thus both associative and dissociative exchange mechanisms have been examined

Can. J. Chem. Downloaded from www.nrcresearchpress.com by 210.87.254.6 on 09/05/12
For personal use only.

Can. J. Chem. Downloaded from www.nrcresearchpress.com by 210.87.254.6 on 09/05/12
For personal use only.

for their effect upon departures from first-order kinetic behaviour. Following Bunton *et al.* it has been assumed that the distribution of labels within each of the sites (amino, methyl) is random not only at equilibrium but throughout the exchange. This implies that the rate at which an atom detaches itself from or attaches itself to a given site within the molecule is not a function of the isotopic nature of the rest of the molecule. Any secondary isotopic effects have therefore been neglected. Streitwieser has shown that in the dedeuteration of toluene-α-*d* that substitution of a second deuterium atom at the reacting carbon site may decrease the exchange rate by about 25–30%. In contrast they report a primary kinetic isotope effect of $k_H/k_D \simeq 10$ for reaction of the methyl group. Similarly large isotope effects appear to be operative at the methyl group in the PMA/MA system since preliminary experiments with CD_3NH_2 indicate initial exchange rates which are an order of magnitude slower.

This fact coupled with the significant departure from first-order kinetic behaviour (Fig. 2) suggest that a dissociation mechanism is involved in the exchange reaction (5). Such a large deviation cannot be accounted for on the basis of an associative mechanism which might be envisaged as involving a simultaneous movement of bonds in both the methyl and amino groups in the transition state. Streitwieser has also rejected such concerted transition states in the LCHA/CHA system.

The large deviation from first-order behaviour can therefore be considered indicative of a dissociative exchange mechanism possibly involving intermediate carbanion-like fragments. On this model the observed experimental rate is related directly to the rate of deuterium transfer into the carbanion-like intermediate.

Under these circumstances the observed exchange rate will depend upon the relative magnitude of the rate ratio k_H/k_D where the rate constants refer to the transfer of hydrogen and deuterium into the intermediate. Since this ratio would appear to be $\sim$10 with $Y_0 = 1$ it follows from the analysis given by Bunton *et al.* that deviations from pseudo first-order behaviour greater than 20% could be expected. Consequently the discussion will be confined to the initial rates of exchange only. The present experiments do not permit the ratio k_H/k_D to be determined directly, but the significant departure from first-order behaviour and the large difference in the reactivities of CH_3ND_2 and CD_3NH_2 strongly suggest dissociation of methylamine by the catalyst is responsible for the observed transfer of deuterium.

The active catalytic species in these solutions is assumed to be related to the stoichiometric concentration of PMA added. It has been shown that the solvated species e^-, e^-K^+, and K^- present during formation of PMA from potassium metal are not effective in catalyzing the exchange reaction [1]. These species will be present in much reduced equilibrium concentrations in the samples prepared from the preformed PMA used for the kinetic measurements.

It has been suggested that PMA exists in solutions almost entirely as ion pairs (7). Therefore a reasonable assumption is that the dissociated methylamide ion formed by the reaction

$$[8] \qquad CH_3NHK \overset{K_{diss}}{\rightleftharpoons} CH_3\bar{N}H + K^+$$

where K_{diss} is the dissociation constant, might be the active catalyst.

Shatenshtein (ref. 1, p. 104) has shown this to be the case for deuterium incorporation into benzene from the KND_2/ND_3 system. For the PMA/MA results a graph of $\ln R_f/[CH_3ND_2]_0$ *vs.* ln PMA concentration should give a straight line with a slope between the limits 0.5 and 1, depending on whether the dissociation constant k_{diss} is $\ll 1$ or $\gg 1$. This plot (Fig. 4) gives a line that has marked curvature; in fact at low catalyst concentrations the slope tends towards 1 and at high concentrations the slope tends towards zero. The dissociated methylamide catalyst hypothesis cannot predict this behaviour.

Streitwieser *et al.* (2), in their studies of the dedeuteration of toluene-α-*d* in the LCHA/CHA system, found concentration dependencies of their measured rates similar to those under discussion in this paper. They showed that the active catalyst was a lithium cyclohexylamide monomer in equilibrium with relatively inactive dimers, . . ., *n*-mers.

Application of this model (2) to the PMA/MA system gives

$$CH_3NHK + CH_3NHK \overset{K_1}{\rightleftharpoons} (CH_3NHK)_2$$

$$CH_3NHK + (CH_3NHK)_2 \overset{K_2}{\rightleftharpoons} (CH_3NHK)_3$$

$$[9] \qquad CH_3NHK + (CH_3NHK)_n \overset{K_n}{\rightleftharpoons} (CH_3NHK)_{n+1}$$

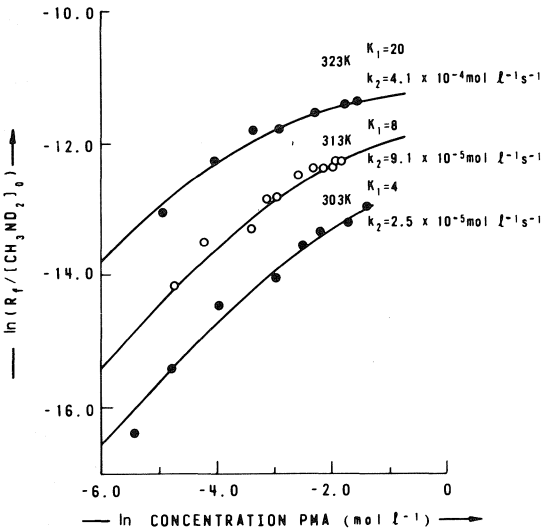

FIG. 4. A ln–ln graph of the stoichiometric concentration of potassium methylamide c, *vs.* the first-order rate constants, $k = R_f/[CH_3ND_2]_0$ determined from [6]. The solid lines are the theoretical curves calculated from [13] using the indicated values of k_2 and K_1 for each temperature.

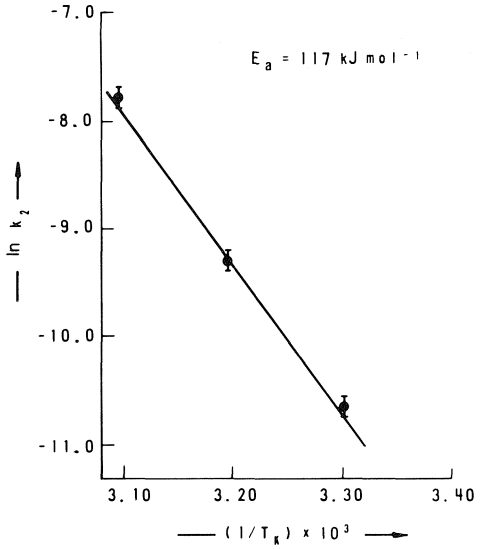

FIG. 5. Temperature dependence of the second-order rate constant, k_2.

By making the simplifying assumption that $K_1 = K_2 = \ldots = K_n$ an expression relating the concentration of potassium methylamide monomer, CH_3NHK, present to the stoichiometric concentration, c, of PMA in this infinite series can be written (2, 8, 9).

$$[10] \quad c = [CH_3NHK]/(1 - K_1[CH_3NHK])$$

Rearrangement of [10] yields

$$[11] \quad [CH_3NHK] = (2cK_1 + 1 - \sqrt{4cK_1 + 1})/2cK_1^2$$

The derivative of this expression with respect to c satisfies the experimental boundary conditions of zero at high and of one at low PMA stoichiometric concentrations, respectively.

If it is further assumed that reaction 1 is first-order each in PMA monomer and in CH_3ND_2, *i.e.* second-order overall, it follows that the initial forward rate in [6] is

$$[12] \quad R_f = k_2[CH_3NHK][CH_3ND_2]$$

where k_2 is a second-order rate constant (M s^{-1}). Rearrangement of [12] and substitution for $[CH_3NHK]$ gives

$$[13] \quad k_2 = 2ckK_1^2/(2cK_1 + 1 - \sqrt{4cK_1 + 1})$$

where $k = R_f/[CH_3ND_2]_0$.

A relationship has now been indicated between the initial forward rate of exchange, R_f, and the stoichiometric catalyst concentration, c. The experimental data were fitted to expression [13]. Individual values for k_2 were calculated for each R_f measured by assuming values for K_1. Using the average value of k_2 so obtained for each temperature the dependence of k on c was calculated as a function of K_1. The solid lines in Fig. 4 are the calculated best fits with the values of k_2 and K_1 indicated. The reported values of k_2 at the given temperatures varied by no more than $\pm 10\%$ over the entire concentration range. For the 303 K and 313 K results, changes of ± 1 in K_1, and for the 323 K results, changes of ± 2 in K_1, gave significant shifts from the best fit.

An Arrhenius plot of the second-order rate constants, k_2, gives an activation energy of $E_a = 117$ kJ mol^{-1} (Fig. 5). This yields the activation parameters $\Delta H^{\ddagger} = 114$ kJ mol^{-1} and $\Delta S^{\ddagger} = 10.3$ eu. Bimolecular reactions normally show ~ -20 eu for $\Delta S^{\ddagger}$ due to the loss of 3 degrees of translational freedom (10). However, if the transition state were less highly solvated than the reactants, a positive $\Delta S^{\ddagger}$ would be obtained (11).

The temperature dependence of the catalyst association constant K_1 yields an enthalpy of association for PMA in methylamine, $\Delta H^0 = 18.1$ kJ mol^{-1} (Fig. 6). The positive value of ΔH^0

Can. J. Chem. Downloaded from www.nrcresearchpress.com by 210.87.254.6 on 09/05/12
For personal use only.

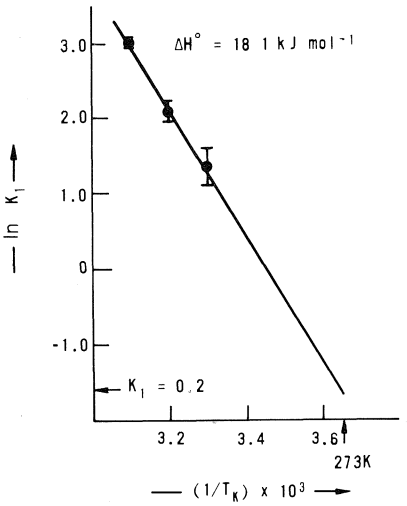

FIG. 6. Temperature dependence of the catalyst association constant, K_1.

indicates an endothermic association. This result is in contrast to that reported for the dedeuteration of toluene-α-d_3 in the LCHA/CHA system of Streitwieser *et al.* (10) where the monomer–*n*-mer equilibrium constant, $K_1 = 60$, showed no temperature effect. Since the cyclohexylamine system has a lower dielectric constant (4 to 5.4, 323 to 252 K) (12, 13) than the methylamine system (9.3 at 298 K) (14) a higher degree of ion association and a larger K, would be expected. Detection of temperature effects at larger values of K_1 is more difficult than for smaller ones since changes in the dependence of k on c as a function of K, are much reduced. This may account for the absence of a temperature effect in the LCHA/CHA system.

Extrapolation of the line in Fig. 6 for the temperature effect on K_1 to 273 K predicts a value of $K_1 \simeq 0.2$. Calculated (eq. 11) percentages of monomer present in 0.2, 0.02, and 0.002 *M* stoichiometric PMA solutions at 273 K and the temperatures of the exchange experiments are given in Table 1.

The proposed model predicts that at 273 K PMA should be present almost entirely as a monomer over a very wide concentration range. This is in excellent agreement with the value for the degree of association calculated from vapour pressure measurements of PMA–MA solutions[6] which indicates that PMA exists as the monomer at 273 K.

TABLE 1. Percentage monomer present in PMA–MA solutions

	PMA monomer (%)			
c	323 K	313 K	303 K	273 K
0.200	24	29	43	93
0.020	60	77	87	99
0.002	95	97	98	100

Mechanism

A mechanism for this exchange reaction that incorporates the previously discussed evidence for a carbanion like intermediate, and also provides a reaction path for the thermal decomposition of the catalyst, is suggested by the following equations.

$$CH_3\bar{N}D\overset{+}{K} + (CH_3\bar{N}D\overset{+}{K})_n \overset{K_1}{\rightleftharpoons} (CH_3\bar{N}D\overset{+}{K})_{n+1}$$

$$CH_3\bar{N}D\overset{+}{K} + CH_3ND_2 \overset{R_f}{\rightleftharpoons} [CH_3\bar{N}D//CH_3ND_2//K^+]$$

$CH_2DND_2 + CH_3NHK$
Amino-methyl group deuteron exchange

$CH_2{=}ND + KD + CH_3NDH$
First step in the thermal decomposition of the catalyst

We are proposing that the monomer, CH_3NHK, is the active catalyst. There is a high degree of association in PMA solutions due to the low dielectric constant of methylamine and the high negative charge density on the nitrogen (10). Therefore, the PMA monomer is probably a 'tight' ion pair. Introduction of a solvent molecule to form a 'loose' ion pair can bring the two reactant species into intimate contact in a reactive configuration and allow the formation of a carbanion-like moiety by extraction of a proton from the solvent methyl group. The charge on this intermediate would now be stabilized in part by proximity to the electronegative amino substituent. This could lead to a less highly solvated transition state and result in a positive $\Delta S^{\ddagger}$ (11). Evidence from Shatenshtein (1) and Streitwieser (2) in the potassium amide/ammonia and lithium cyclohexylamide/cyclohexylamine systems respectively indicates that the isotopic exchange with hydrocarbons

Can. J. Chem. Downloaded from www.nrcresearchpress.com by 210.87.254.6 on 09/05/12
For personal use only.

goes through a carbanion-like intermediate, where the degree of carbanion-like character for each hydrocarbon is dependent upon the system used. The proposed carbanion-like moiety formed in the reaction can react further and capture a deuteron from the rapidly exchanging solvent amino substituents (analogous to the fast exchange in the KNH_2/NH_3 system (15) thereby effecting the amino to methyl group deuteron exchange. Alternatively the carbanion can eliminate a deuteride ion and form highly reactive methylenimine and potassium deuteride which have been postulated as transient intermediates in the thermal decomposition of PMA (6).

The rate controlling step for the exchange cannot be identified with the present data. However, exchange studies with different cations should further elucidate the effects of ion pairing and help to determine whether the rate controlling step is the formation of the loose ion pair or the abstraction of the proton from the solvent methyl group.

Acknowledgements

The authors would like to thank J. H. Rolston for useful discussions and Professor A. Streitwieser for helpful comments.

1. A. I. SHATENSHTEIN. Isotopic exchange and the replacement of hydrogen in organic compounds. *Translation by* C. N. Turton and T. I. Turton. Consultants Bureau, New York. 1962.
2. A. STREITWIESER, JR., D. E. VAN SICKLE, and W. C. LANGWORTHY. J. Am. Chem. Soc. **84**, 244 (1962) and continuing papers in this series.
3. W. J. HOLTSLANDER and R. E. JOHNSON. German Patent No. 2 434 016, (July, 1973); Chem. Abstr. **83**, 33399d (1975).
4. G. M. HARRIS. Trans. Faraday Soc. **47**, 716 (1951).
5. C. A. BUNTON, D. P. CRAIG, and E. A. HALEVI. Trans. Faraday Soc. **51**, 196 (1955).
6. J. L. DYE. Electrons in fluids. *Edited by* J. Jortner and N. R. Kestner. Springer-Verlag, Berlin. 1973. p. 77; J. J. LAGOWSKI and M. J. SIENKO (*editors*). Metal–ammonia solutions. Colloque Weyl II, Int. Union Pure and Appl. Chem., Butterworth and Co., London. 1970; J. W. FLETCHER and W. A. SEDDON. Colloque Weyl IV, J. Phys. Chem. **79**, 3055 (1975).
7. E. ROCHARD and J. RAVOIRE. J. Chim. Phys. **68**, 1183 (1971).
8. M. SAUNDERS and J. B. HYNE. J. Chem. Phys. **29**, 1319 (1958).
9. A. V. TOBOLSKY and A. EISENBERG. J. Am. Chem. Soc. **82**, 289 (1960).
10. A. STREITWIESER, JR., R. A. CALDWELL, M. R. GRANGER, and P. M. LAUGHTON. J. Phys. Chem. **68**, 2916 (1964).
11. M. SZWARC. Ions and ion pairs in organic reactions. Vol. 2. *Edited by* M. Szwarc. John Wiley and Sons, New York. 1974. p. 380.
12. A. STREITWIESER, JR., D. E. VAN SICKLE, and L. REIF. J. Am. Chem. Soc. **84**, 258 (1962).
13. A. H. WHITE and W. S. BISHOP. J. Am. Chem. Soc. **62**, 8 (1940).
14. ROBERT C. WEST (*editor*). Handbook of chemistry and physics. 51st ed., Chemical Rubber Co., Cleveland. 1970.
15. T. J. SWIFT, S. B. MARKS, and W. G. SAYRE. J. Chem. Phys. **44**, 2797 (1966).

Can. J. Chem. Downloaded from www.nrcresearchpress.com by 210.87.254.6 on 09/05/12
For personal use only.

Selective, reductive dechlorination of chlorodeoxy sugars. Structural determination of chlorodeoxy and deoxy sugars by ^{13}C nuclear magnetic resonance spectroscopy[1]

WALTER A. SZAREK, ALEKSANDER ZAMOJSKI,[2] ALAN R. GIBSON, DOLATRAI M. VYAS, AND J. K. N. JONES

Department of Chemistry, Queen's University, Kingston, Ont., Canada K7L 3N6

Received May 21, 1976

WALTER A. SZAREK, ALEKSANDER ZAMOJSKI, ALAN R. GIBSON, DOLATRAI M. VYAS, and J. K. N. JONES. Can. J. Chem. **54**, 3783 (1976).

The reductive dechlorination of chlorodeoxy sugars by hydrogenation over Raney nickel in the presence of potassium hydroxide or triethylamine has been investigated; a selective dechlorination was observed in most cases with triethylamine. Several new, chlorodeoxy furanoid derivatives have been synthesized by the use of triphenylphosphine – carbon tetrachloride. ^{13}C magnetic resonance spectroscopy has been employed for the assignment of structure to the chlorodeoxy sugars and the corresponding reduced products.

WALTER A. SZAREK, ALEKSANDER ZAMOJSKI, ALAN R. GIBSON, DOLATRAI M. VYAS et J. K. N. JONES. Can. J. Chem. **54**, 3783 (1976).

On a étudié la déchloruration réductive de sucres de type chlorodéoxy par hydrogénation sur du nickel de Raney en présence d'hydroxyde de potassium ou de triéthylamine; on a observé une déchloruration sélective dans la plupart des cas avec la triéthylamine. On a synthétisé plusieurs nouveaux dérivés furanoïdes de type chlorodéoxy en faisant appel au couple triphénylphosphine – tétrachlorure de carbone. On a utilisé la rmn du ^{13}C pour attribuer les structures des sucres de type chlorodéoxy et des produits réduits correspondants.

[Traduit par le journal]

Introduction

In an earlier publication (1) it was reported that methyl 4,6-dichloro-4,6-dideoxy-α-D-galactopyranoside was converted into methyl 4,6-dideoxy-α-D-*xylo*-hexopyranoside by hydrogenation over Raney nickel in the presence of potassium hydroxide; however, when triethylamine was substituted for potassium hydroxide, a selective, reductive dechlorination occurred at C-4 to give methyl 6-chloro-4,6-dideoxy-α-D-*xylo*-hexopyranoside. The observed selectivity is potentially of considerable significance in synthesis. One example of the utility of the procedure was provided by the ready synthesis of a 4-deoxyhexose (1). The present article describes the results of an investigation of the scope of the selective dechlorination, in the presence of triethylamine, of chlorodeoxy pyranoid and furanoid derivatives.

[1]Part XI in the series "Synthesis and reactions of chlorodeoxy sugars". For part X, see ref. 11.

[2]On leave (1971–1972) from the Institute of Organic Chemistry, Polish Academy of Sciences, Warsaw, Poland.

Results and Discussion

Methyl 3,6-dichloro-3,6-dideoxy-β-D-allopyranoside (**1**) and methyl 4,6-dichloro-4,6-dideoxy-β-D-galactopyranoside (**4**) were readily obtained by way of the reaction of methyl β-D-glucopyranoside with sulfuryl chloride (2). Hydrogenation of **1** over Raney nickel in the presence of potassium hydroxide afforded crystalline methyl 3,6-dideoxy-β-D-*ribo*-hexopyranoside (**2**), whereas hydrogenation in the presence of triethylamine led to methyl 6-chloro-3,6-dideoxy-β-D-*ribo*-hexopyranoside (**3**) (Scheme 1). Thus, the observed selectivity in the latter experiment, namely, preferential dechlorination at the secondary position, is the same as that found (1) in the case of the hydrogenation of methyl 4,6-dichloro-4,6-dideoxy-α-D-galactopyranoside in the presence of triethylamine. However, in the case of methyl 4,6-dichloro-4,6-dideoxy-β-D-galactopyranoside (**4**), under these conditions, a mixture of methyl 4-chloro-4,6-dideoxy-β-D-galactopyranoside (**6**) and methyl 6-chloro-4,6-dideoxy-β-D-*xylo*-hexopyranoside (**7**) was obtained, with the

Can. J. Chem. Downloaded from www.nrcresearchpress.com by 210.87.254.5 on 09/05/12
For personal use only.

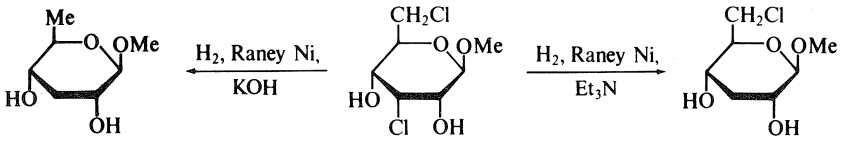

SCHEME 1

Can. J. Chem. Downloaded from www.nrcresearchpress.com by 210.87.254.5 on 09/05/12
For personal use only.

former preponderating (Scheme 2). The 4-chloro derivative (**6**) could be isolated by crystallization from ethyl acetate – hexane, and its structure was established by pmr and ^{13}C magnetic resonance (cmr) spectroscopy (see below). Although the 6-chloro derivative (**7**) could not be isolated in a pure state by preparative tlc or column chromatography, its presence in the mixture was clearly evident from the cmr spectrum of the mixture. In view of the selective dechlorination at secondary positions in the cases of methyl 4,6-dichloro-4,6-dideoxy-α-D-galactopyranoside and methyl 3,6-dichloro-3,6-dideoxy-β-D-allopyranoside (**1**), the formation of the 4-chloro-4,6-dideoxy derivative (**6**) from methyl 4,6-dichloro-4,6-dideoxy-β-D-galactopyranoside (**4**) was surprizing. Hydrogenation of **4** in the presence of potassium hydroxide gave the expected product, namely, methyl 4,6-dideoxy-β-D-*xylo*-hexopyranoside (**5**).

The reductive dechlorination, in the presence of triethylamine, of several chlorodeoxy furanoid derivatives has also been investigated. Treatment of 1,2-*O*-isopropylidene-α-D-glucofuranose (3) (**8**) with triphenylphosphine in carbon tetrachloride (see pp. 246-249, ref. 4) for 18 h at reflux temperature afforded 5,6-dichloro-5,6-dideoxy-1,2-*O*-isopropylidene-β-L-idofuranose (**9**) and 3,6-anhydro-5-chloro-5-deoxy-1,2-*O*-isopropylidene-β-L-idofuranose (**10**) (Scheme 3). Chiu and Whistler (5) have obtained 3-*O*-benzoyl-5,6-dichloro-5,6-dideoxy-1,2-*O*-isopropylidene-β-L-idofuranose in 72% yield from the 3-*O*-benzoyl derivative of **8** by using this reagent; the L-*ido* configuration in the product was established through its conversion into 5,6-dideoxy-5,6-epithio-1,2-*O*-isopropylidene-α-D-glucofuranose. Hydrogenation of compound **9** over Raney nickel in the presence of triethylamine did not result in a discrimination between the primary and secondary, chlorinated positions; instead, the fully reduced product, namely, 5,6-dideoxy-1,2-*O*-isopropylidene-α-D-*xylo*-hexofuranose (6) (**11**) was obtained. Compound **10**, under these conditions, afforded 3,6-anhydro-5-deoxy-1,2-*O*-isopropylidene-α-D-*xylo*-hexofuranose (**12**).

3-Chloro-3-deoxy-1,2:5,6-di-*O*-isopropylidene-α-D-glucofuranose (7) (**13**) was prepared, by the reaction of 1,2:5,6-di-*O*-isopropylidene-α-D-allofuranose with triphenylphosphine – carbon tetrachloride, and reduced, in the presence of triethylamine, to 3-deoxy-1,2:5,6-di-*O*-isopropylidene-α-D-*ribo*-hexofuranose (7–9) (**14**); a

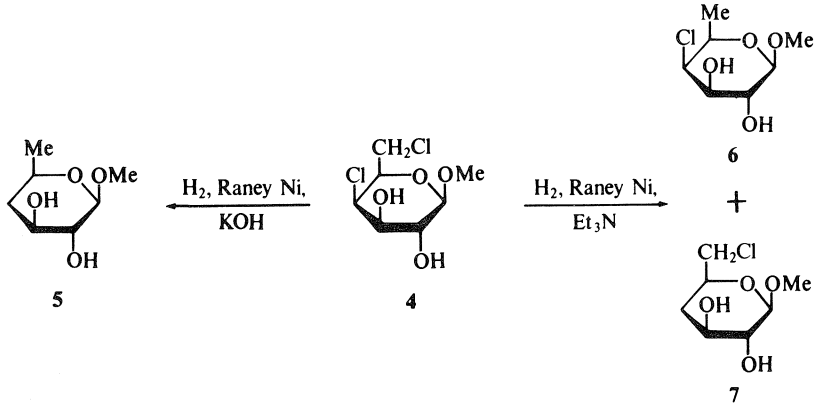

SCHEME 2

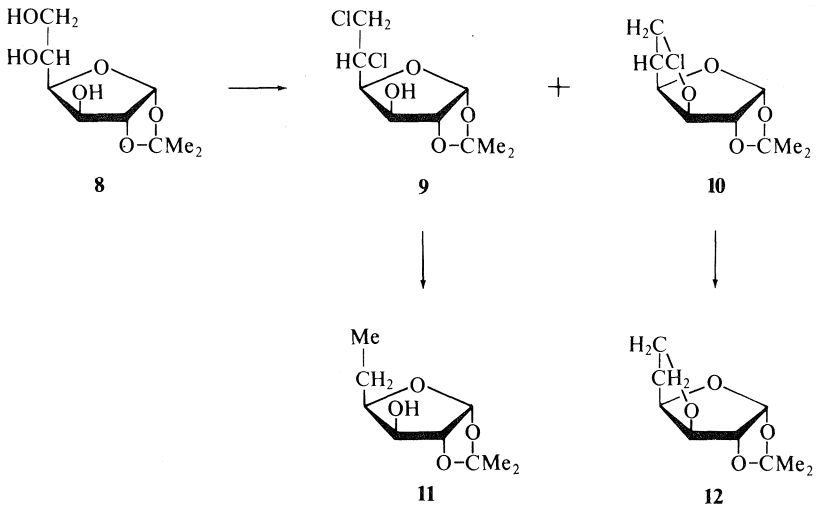

SCHEME 3

partial, acid-catalyzed hydrolysis of **14** afforded 3-deoxy-1,2-*O*-isopropylidene-α-D-*ribo*-hexofuranose (7–9) (**15**) (Scheme 4). Compounds **13–15** were employed in cmr-spectral studies (see below); also, compound **13** was utilized for the synthesis of some new, chlorodeoxy sugars.

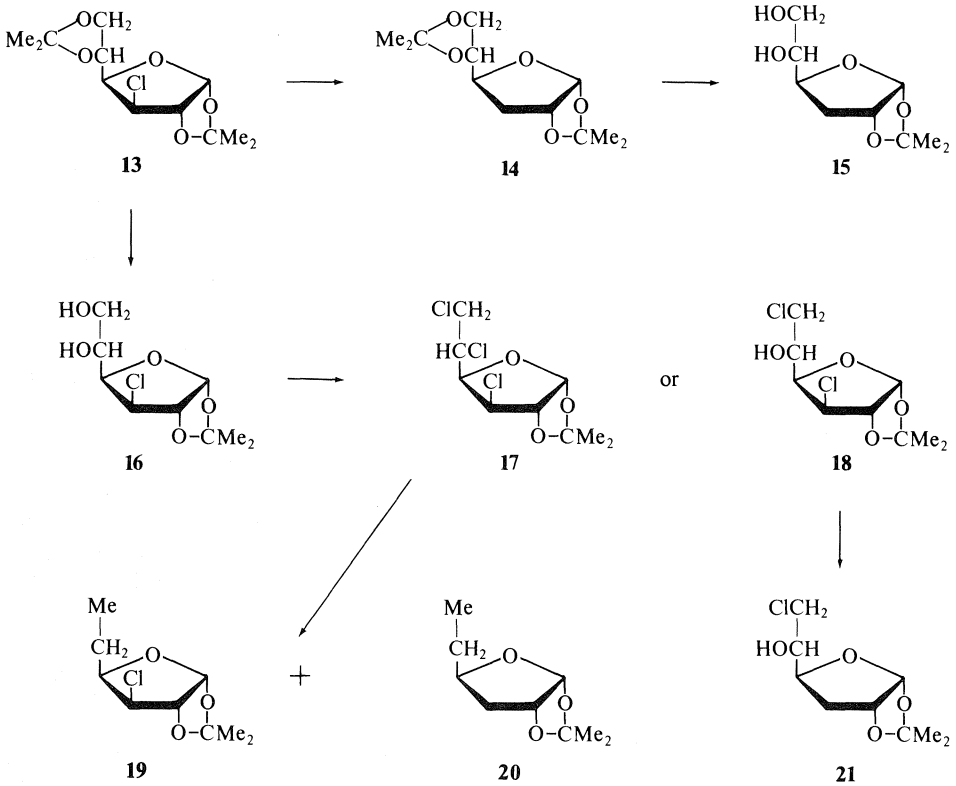

SCHEME 4

Can. J. Chem. Downloaded from www.nrcresearchpress.com by 210.87.254.5 on 09/05/12
For personal use only.

Can. J. Chem. Downloaded from www.nrcresearchpress.com by 210.87.254.5 on 09/05/12
For personal use only.

A partial, acid-catalyzed hydrolysis of **13** gave 3-chloro-3-deoxy-1,2-*O*-isopropylidene-α-D-glucofuranose (**16**). Treatment of **16** with triphenylphosphine in carbon tetrachloride for 18 h at reflux temperature afforded 3,5,6-trichloro-3,5,6-trideoxy-1,2-*O*-isopropylidene-β-L-idofuranose (**17**), whereas, when a reaction time of ~5 h was employed, 3,6-dichloro-3,6-dideoxy-1,2-*O*-isopropylidene-α-D-glucofuranose (**18**) was obtained. The constitution of **18** was established by cmr spectroscopy (see below), and the configuration at C-5 in **17** was assigned on the basis of the results of Chiu and Whistler (5) (see above). Hydrogenation of the dichloro compound **18** over Raney nickel in the presence of triethylamine yielded 6-chloro-3,6-dideoxy-1,2-*O*-isopropylidene-α-D-*ribo*-hexofuranose (**21**); this result is another example of selective dechlorination at a secondary position. However, in the case of the trichloro compound **17**, under these conditions, 3-chloro-3,5,6-trideoxy-1,2-*O*-isopropylidene-α-D-*xylo*-hexofuranose (**19**) and 3,5,6-trideoxy-1,2-*O*-isopropylidene-α-D-*erythro*-hexofuranose (**20**) were produced. Clearly, the selectivity observed in the formation of **19** from **17** is the reverse of that observed in the formation of **21** from **18**.

The work described in this article demonstrates that, although hydrogenation of a sugar derivative, containing chlorine atoms at primary and secondary positions, over Raney nickel in the presence of triethylamine can result in a regioselective dechlorination, the relative reactivities of the chlorine atoms are unpredictable. Nevertheless, once the reactivity order has been established, the result can be of immense value in carbohydrate synthesis. Thus, for example, a facile synthesis of the antibiotic sugar purpurosamine C (and of epipurpurosamine C) has been achieved by application of this approach.[3] Other examples of selective dehalogenation in the carbohydrate field have been reported (10).

The assignment of structure to the chlorodeoxy sugars and the corresponding reduced products was aided in the present work by cmr spectroscopy. It has already been demonstrated (11) that the regiochemistry and stereochemistry of halogen substitution on a sugar molecule can be readily determined by this technique. The ^{13}C chemical shifts of some pyranoid derivatives are documented in Table 1. The effects on the chemical shifts resulting from the replacement of a hydroxyl group by a chloro group or a hydrogen atom are discussed on the assumption that all of the molecules have the *Cl*(D) conformation. The signal assignments were made by a comparison of the spectra of appropriate sugars with each other, and also on the basis of the general shielding properties associated with the various interactions observed by Perlin *et al.* (12) in the monosaccharide series.

A comparison of the chemical-shift data reported (11) for methyl β-D-glucopyranoside (**22**) with that of methyl 3,6-dideoxy-β-D-*ribo*-hexopyranoside (**2**) permitted the assignment of signals in the spectrum of the latter compound. The outstanding features of the spectrum of **2** compared to that of **22** are as follows. In the case of **2**, there are large upfield shifts of the C-6 (43.5 ppm) and C-3 (36.7 ppm) signals; these shifts may presumably be attributed to a difference in inductive effects between a hydrogen atom and a hydroxyl group. The C-4 signal in the spectrum of **2** is shifted upfield by only 0.6 ppm relative to the corresponding signal in the spectrum of **22**, whereas there is a 5.9 ppm-upfield shift of the C-2 signal in the spectrum of **2**; this difference in the magnitudes of the upfield shifts must clearly be a reflection of the different interactions between H-4 and the methyl group at C-5 in compound **2**, and H-4 and the hydroxymethyl group at C-5 in compound **22**. It is noteworthy that the C-1 signal in the spectrum of **22** is shifted upfield by 2.0 ppm relative to the corresponding signal in the spectrum of **2**, although the configuration at the anomeric center in each of the compounds is β. If the two compounds do in fact exist in the *Cl*(D) conformation, then the observed shielding may presumably be attributed to the anti-periplanar relationship of C-1 and O-3 in **22**; Eliel *et al.* (13) have shown that a carbon atom that is *anti* to a second-row heteroatom (N, O, F) in the γ position generally resonates at significantly higher field than an analogous carbon *anti* to a methyl or methylene group or to a third-row heteroatom (S, Cl). On the basis of the conclusion reached by Eliel *et al.* (13) the C-5 signal in the spectrum of **22** should be shifted upfield relative to the C-5 signal in the spectrum of **2**, since in compound **22** (in the *Cl*(D) conformation) C-5 and O-3 are anti-periplanar, whereas

[3]W. A. Szarek, A. Zamojski, C. Depew, and J. K. N. Jones; to be published.

TABLE 1. ^{13}C chemical-shift data[a] of pyranoid derivatives

Compound		Carbon 1	2	3	4	5	6	OMe
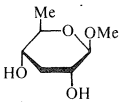	**2**	105.9	67.5	40.1	69.5	75.3	17.7	55.6
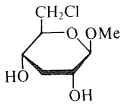	**3**	105.8	67.0	39.8	65.1	78.7	44.9	55.7
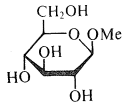	**22**[b]	103.9	73.4	76.8	70.1	76.8	61.2	56.0
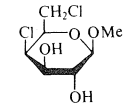	**4**[b]	104.4	69.8	71.2	63.6	72.7	43.6	56.4
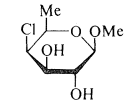	**6**	104.3	69.7	71.8	67.5	68.3	17.7	55.8
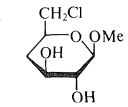	**7**[c]	104.1	74.9	70.8[d]	36.4	70.4[d]	46.9	55.8
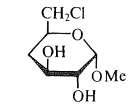	**23**[b]	100.3	73.6	66.4	36.5	67.3	47.2	54.4

[a] In ppm downfield from internal tetramethylsilane (TMS) in methyl sulfoxide-d_6.
[b] Chemical-shift data are those reported in ref. 11.
[c] Chemical-shift data obtained from spectrum of a mixture of **6** and **7**.
[d] Assignments for these peak positions may be reversed.

in compound **2** C-5 is anti-periplanar to the equatorial hydrogen atom at C-3; however, the C-5 signal in the spectrum of **22** was actually observed to be shifted downfield by 1.5 ppm, presumably because of the deshielding effect of the hydroxyl group at C-6.

The ^{13}C spectrum of methyl 6-chloro-3,6-dideoxy-β-D-*ribo*-hexopyranoside (**3**) could be readily analyzed by comparison with the spectrum of methyl 3,6-dideoxy-β-D-*ribo*-hexopyranoside (**2**). The C-4 signal in the spectrum of **3** is shifted upfield by 4.4 ppm relative to the corresponding signal in the spectrum of **2** as a result of the shielding γ interaction between the axial H-4 and the chlorine atom at C-6 in compound **3**. The difference between the substituents at C-6 in compounds **2** and **3** (H in **2** and Cl in **3**) is also reflected by the upfield shifts in the spectrum of **2** of the C-5 (3.4 ppm) and C-6 (27.2 ppm) signals.

It was mentioned earlier in this article that hydrogenation of methyl 4,6-dichloro-4,6-dideoxy-β-D-galactopyranoside (**4**) in the presence of triethylamine afforded a mixture of methyl 4-chloro-4,6-dideoxy-β-D-galactopyranoside (**6**) and methyl 6-chloro-4,6-dideoxy-β-D-*xylo*-hexopyranoside (**7**) from which only compound **6** could be isolated in a pure state; nevertheless, the structures of both **6** and **7** could be established by cmr spectroscopy. Thus, for example, the C-5 signal in the spectrum of **4** is shifted downfield by 4.4 ppm relative to the corresponding signal in the spectrum of **6**, a result attributable to the β effect of the chlorine atom at C-6 in **4**,

Can. J. Chem. Downloaded from www.nrcresearchpress.com by 210.87.254.5 on 09/05/12
For personal use only.

TABLE 2. ^{13}C chemical-shift data[a] of furanoid derivatives

Compound		Carbon							
		1	2	3	4	5	6	Me_2-OCO	Me's
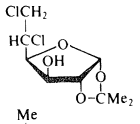	**9**	103.9	85.2	73.0	81.8	60.5	46.9	110.8	26.0, 26.6
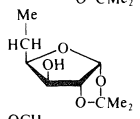	**11**	103.9	85.1	73.4	81.6	20.6	10.2	109.9	26.0, 26.5
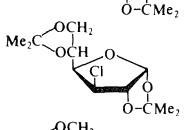	**13**	104.3	85.4	62.2	79.7	73.2	66.4	111.6 108.7	25.1, 26.0 26.3, 26.6
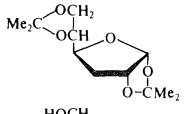	**14**	105.0	79.8	34.7	77.9	76.2	66.1	110.2 108.5	26.6, 26.3 26.0, 25.1
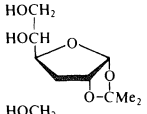	**15**	104.9	80.0	33.3	78.3	71.9	63.2	109.9	26.1, 26.7
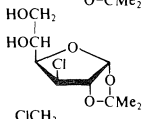	**16**	104.5	85.2	63.3	78.4	69.8	63.3	111.5	26.3, 26.1
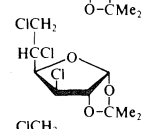	**17**	103.6	85.8	61.0	80.1	60.3	46.2	111.9	26.1, 26.3
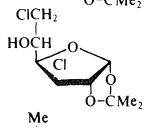	**18**	104.4	85.2	62.7	78.7	68.1	48.7	111.8	26.3
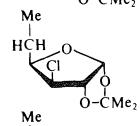	**19**	103.6	85.7	63.4	80.0	22.5	9.7	111.1	26.1, 26.2
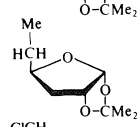	**20**	104.9	79.9	37.9	78.3	26.4[b]	10.0	109.6	26.0[b], 26.6[b]
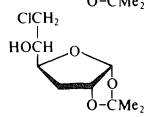	**21**	104.9	79.9	34.6	78.0	71.7	47.4	110.1	26.1, 26.6
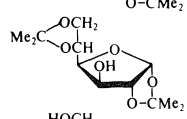	**24**[c]	104.5	85.0	73.1	80.9	72.2	66.0	110.5 107.8	25.2, 26.0 26.5, 26.6
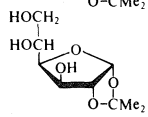	**25**[c]	104.4	84.6	73.2	80.0	68.4	63.6	110.3	26.0, 26.6

[a]In ppm downfield from internal tetramethylsilane (TMS) in methyl sulfoxide-d_6.
[b]Assignments for these peak positions may be reversed.
[c]Chemical-shift values for spectrum measured in chloroform-*d* are reported in ref. 14.

Can. J. Chem. Downloaded from www.nrcresearchpress.com by 210.87.254.5 on 09/05/12
For personal use only.

Can. J. Chem. Downloaded from www.nrcresearchpress.com by 210.87.254.5 on 09/05/12
For personal use only.

whereas the C-4 signal in the spectrum of **6** is shifted downfield by 3.9 ppm as a consequence of the diminished γ interaction resulting from replacement of chlorine by hydrogen at C-6. Also, as expected, the chemical-shift difference between the C-6 signals in the spectra of **4** and **6** is almost the same as that between those in the spectra of **3** and **2**. Chemical-shift data for methyl 6-chloro-4,6-dideoxy-β-D-*xylo*-hexopyranoside (**7**) were obtained by comparison of the spectrum of a mixture of compounds **6** and **7** with that reported (11) for methyl 6-chloro-4,6-dideoxy-α-D-*xylo*-hexopyranoside (**23**). One salient feature is that the chemical shifts of the C-4 and C-6 signals are respectively almost identical in the spectra of the anomers **7** and **23**. As expected, on the basis of the presence in **23** of shielding, 1,3-diaxial nonbonded interactions (compare refs. 11 and 12) between the methoxyl group at C-1 and the hydrogens at C-3 and C-5, the C-1, C-3, and C-5 signals in the spectrum of **23** are shifted upfield relative to the corresponding signals in the case of **7**. Also, the C-2 signal in the spectrum of **23** is shifted upfield by 1.3 ppm; this observation is another example of the increased shielding experienced by a ^{13}C nucleus adjacent to an axial C—O bond (12).

The ^{13}C chemical-shift data for the chlorodeoxy- and deoxy-hexofuranoses reported in the present article are documented in Table 2; included also are data (14) for 1,2:5,6-di-*O*-isopropylidene-α-D-glucofuranose (**24**) and 1,2-*O*-isopropylidene-α-D-glucofuranose (**25**) which aided the signal assignments in the spectra of the new compounds. In the case of the furanoid derivatives the signal assignments were readily made by a comparison of the spectra of the parent isopropylidene derivatives, the chlorinated analogs, and the reduced products. Hence, the sites of chlorination and reduction at either the exocyclic carbons (C-5 and C-6) or the endocyclic carbon (C-3) could be established on the basis of the chemical-shift differences arising from the substitution of a hydroxyl group by a chloro group or a hydrogen atom. The effects of change in substitution on ^{13}C shieldings are summarized in Table 3.

Replacement of the hydroxyl group at C-3 by a chloro group results in a large (~10 ppm) upfield shift of the C-3 signal (compare the chemical shifts in the spectra of **25** and **16**, **11** and **19**, and **24** and **13**) and a relatively small (~1.5 ppm) upfield shift of the C-4 signal; in contrast, the C-2 signal experiences a very minor (~0.5 ppm) downfield shift, and the C-5 signal is shifted downfield by ~1.5 ppm. It is difficult to attribute these chemical-shift differences to one particular interaction or factor. Thus, for example, a change in substitution at C-3 may alter the rotamer population of the C-5—C-6 fragment and, consequently, affect the ^{13}C shieldings of C-3, C-4, and C-5.

Characteristic shifts were also observed on replacement of the chloro group at C-3 by a hydrogen atom. Thus, there is a large (~27 ppm) upfield shift of the C-3 signal (compare the chemical shifts in the spectra of **16** and **15**, **19** and **20**, and **13** and **14**); much smaller upfield shifts are experienced by the C-2 and C-4 signals. Also, the C-5 signal is shifted downfield by ~3 ppm, an effect that is reflective of the diminished *cis*-1,3 interaction between the C-3 and C-5 substituents.

In the cases of the replacement of the hydroxyl group by a chloro group at the primary carbon, namely, C-6, the main change in the cmr spectra was the large (~15 ppm) upfield shift of the C-6 signal (compare the chemical shifts in the spectra of **15** and **21**, and **16** and **18**).

In the earlier study (11) concerned with cmr spectroscopy of chlorodeoxy pyranoid derivatives, the data obtained suggested that the changes in ^{13}C shieldings resulting from the replacement of a hydroxyl group by a chloro group are configuration dependent. With the compounds available in the present work, such a dependency was difficult to establish in the furanoid series.

The structural assignments made for the chlorodeoxy- and deoxy-1,2-*O*-isopropylidene-hexofuranoses have been corroborated by mass spectral studies.[4]

Experimental

Melting points were determined with a Fisher-Johns apparatus and are uncorrected. Optical rotations were measured with a Perkin-Elmer model 141 automatic polarimeter at 23 ± 3 °C. Thin layer chromatography was performed on silica gel G containing 1–3% of Lumilux Green ZS (Brinkmann); the air-dried plates were sprayed with 10% aqueous sulfuric acid containing 1% of cerium sulfate and 1.5% of molybdic acid, and heated at ~150 °C. Column chromatography was performed on silica gel 60 (70–230 mesh, Merck). Distillation of products was performed with a Kugelrohr apparatus.

[4]W. A. Szarek, A. Zamojski, and D. M. Vyas; to be published.

TABLE 3. Effect of change of substituents on ^{13}C shieldings[a] in furanoid derivatives

Conversions[b]	Carbon	Δδ(ppm) for conversions A	B
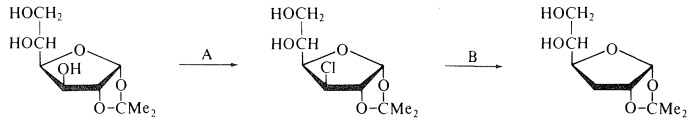 **25** **16** **15**	1	−0.1	−0.4
	2	−0.6	+5.2
	3	+8.9	+30.0
	4	+1.6	+0.1
	5	−1.4	−2.1
	6	+0.3	+0.1
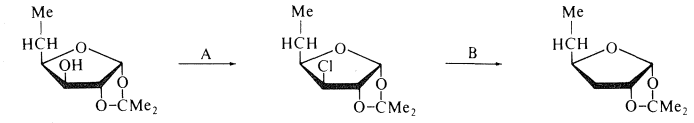 **11** **19** **20**	1	+0.3	−1.5
	2	−0.6	+5.8
	3	+10.0	+25.4
	4	+1.6	+1.7
	5	−1.9	−3.9
	6	+0.5	−0.3
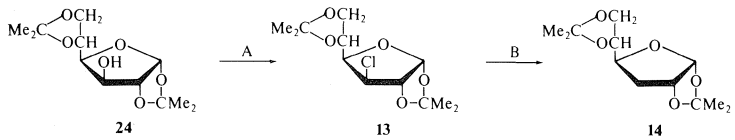 **24** **13** **14**	1	+0.2	−0.7
	2	−0.4	+5.6
	3	+10.9	+27.5
	4	+1.2	+1.8
	5	−1.0	−3.0
	6	−0.4	−0.3
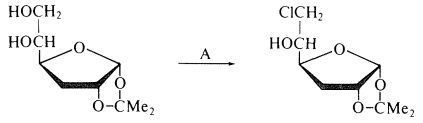 **15** **21**	1	0.0	
	2	+0.1	
	3	−1.3	
	4	+0.3	
	5	+0.2	
	6	+15.8	
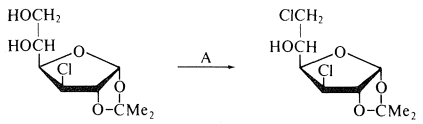 **16** **18**	1	+0.1	
	2	0.0	
	3	+0.6	
	4	−0.3	
	5	+1.7	
	6	+14.6	

[a](+) denotes shielding and (−) denotes deshielding.
[b]The indicated conversions do not necessarily imply direct chemical transformation.

Hydrogenations were performed with a Parr apparatus; the catalyst was a W-4 Raney nickel catalyst prepared by the procedure described by Pavlic and Adkins (15).

The ir spectra were recorded on a Unicam SP 1000 spectrophotometer. Proton magnetic resonance spectra were recorded at 60 MHz in chloroform-*d* with tetramethylsilane (TMS) as the internal standard, unless otherwise stated. ^{13}C magnetic resonance spectra were recorded in methyl sulfoxide-d_6 on a Bruker HX-60 spectrometer equipped with a FT60M Fourier transform accessory at 15.1 MHz, with TMS as the internal standard; chemical shifts are given in parts per million downfield from TMS.

*Hydrogenation of Methyl 3,6-Dichloro-3,6-dideoxy-β-D-allopyranoside (**1**)*

(A) In the Presence of Potassium Hydroxide

A solution of compound **1** (2) (1.5 g) in ethanol (150 ml) containing W-4 Raney nickel catalyst (30 ml ethanol slurry) and potassium hydroxide (1.5 g) was subjected to a hydrogen pressure of 45 psig for 4 h. Thin layer chromatography (ethyl acetate – petroleum ether (bp 60–80 °C), 2:1 (v/v)) showed that the starting material (R_F 0.42) had all reacted and revealed the presence of a new component having R_F 0.14. The catalyst was removed by filtration, and the filtrate was neutralized with *N* sulfuric acid. The mixture was filtered through Celite, and the dried ($MgSO_4$) filtrate was concentrated to yield a yellow oil (1.2 g), which was distilled at 90–100 °C/1 torr; the colorless distillate (0.81 g, 77%) crystallized on standing. Recrystallization from ethyl acetate – petroleum ether (bp 60–80 °C) afforded methyl 3,6-dideoxy-β-D-*ribo*-hexopyranoside (**2**) as colorless crystals (0.65 g, 62%), mp 62–64 °C, $[\alpha]_D$ −65.5° (*c* 1.2 in water); pmr data (deuterium oxide, external TMS) τ 5.26 (d, 1H, $J_{1,2} \approx 8$ Hz, H-1), 5.60–6.40 (3H, H-2, H-4, H-5), 5.97 (s, 3H, OMe), 7.20 (1H, H-3eq), 8.10 (1H, H-3ax), 8.26 (d, 3H, $J_{Me,5} \approx 6$ Hz, CMe). *Anal.* calcd. for $C_7H_{14}O_4$: C 51.8, H 8.7; found: C 52.3, H 9.0.

(B) In the Presence of Triethylamine

A solution of compound **1** (2) (1.0 g) in ethanol (30 ml) containing W-4 Raney nickel catalyst (20 ml ethanol

Can. J. Chem. Downloaded from www.nrcresearchpress.com by 210.87.254.5 on 09/05/12
For personal use only.

Can. J. Chem. Downloaded from www.nrcresearchpress.com by 210.87.254.5 on 09/05/12
For personal use only.

slurry) and triethylamine (1.3 ml) was subjected to a hydrogen pressure of 45 psig for 36 h. Thin layer chromatography (ethyl acetate – petroleum ether (bp 60–80 °C), 2:1 (v/v)) showed that the starting material (R_F 0.42) had all reacted and revealed the presence of a new component having R_F 0.23. The filtered solution was concentrated to a syrup, which was chromatographed on silica gel, with ethyl acetate as eluant. Methyl 6-chloro-3,6-dideoxy-β-D-*ribo*-hexopyranoside (**3**) was obtained as a colorless syrup which crystallized on standing; yield 0.68 g (80%), mp 41–43 °C, $[\alpha]_D$ −57.3° (*c* 1.2 in water); pmr data (deuterium oxide, external TMS) τ 5.20 (d, 1H, $J_{1,2} \approx 8$ Hz, H-1), 5.40–6.40 (5H, H-2, H-4, H-5, 2 H-6's), 6.00 (s, 3H, OMe), 7.20 (1H, H-3eq), 8.03 (1H, $J_{3ax,3eq} \approx 13$ Hz, $J_{3ax,2} \approx J_{3ax,4} \approx 9$ Hz, H-3ax). *Anal.* calcd. for $C_7H_{13}O_4Cl$: C 42.8, H 6.6, Cl 18.1; found: C 42.5, H 7.0, Cl 17.8.

*Hydrogenation of Methyl 4,6-Dichloro-4,6-dideoxy-β-D-galactopyranoside (**4**)*

(A) In the Presence of Potassium Hydroxide

A solution of compound **4** (2) (0.5 g) in ethanol (50 ml) containing W-4 Raney nickel catalyst (10 ml ethanol slurry) and potassium hydroxide (0.5 g) was subjected to a hydrogen pressure of 45 psig for 5 h. Thin layer chromatography (ethyl acetate) showed that the starting material (R_F 0.57) had all reacted and revealed the presence of a new component having R_F 0.35. The catalyst was removed by filtration, and the filtrate was neutralized with dilute hydrochloric acid. The mixture was evaporated, and the residue was extracted with hot ethyl acetate (2 × 30 ml); concentration of the extracts yielded a white solid (0.5 g, 86%). Recrystallization from ethyl acetate – hexane afforded methyl 4,6-dideoxy-β-D-*xylo*-hexopyranoside (**5**) as white needles (0.17 g, 49%), mp 104–105 °C, $[\alpha]_D$ −55.8° (*c* 1.1 in water); pmr data τ 5.90 (d, 1H, $J_{1,2} \approx 7$ Hz, H-1) 6.00–7.00 (5H, H-2, H-3, H-5, 2 OH's), 6.50 (s, 3H, OMe), 8.00 (1H, H-4eq), 7.80–9.00 (1H, H-4ax), 8.73 (d, 3H, $J_{Me,5} \approx 6$ Hz, CMe). *Anal.* calcd. for $C_7H_{14}O_4$: C 51.8, H 8.7; found: C 52.1, H 8.7.

(B) In the Presence of Triethylamine

A solution of compound **4** (2) (1.0 g) in ethanol (30 ml) containing W-4 Raney nickel catalyst (20 ml ethanol slurry) and triethylamine (1.3 ml) was subjected to a hydrogen pressure of 45 psig for 36 h. Thin layer chromatography (ethyl acetate – chloroform, 3:1 (v/v)) showed the presence of some starting material (R_F 0.33) and a new component having R_F 0.21. The filtered solution was concentrated to a syrup, which was chromatographed on silica gel, with the same solvent as employed for tlc as eluant, to afford the component having R_F 0.21 as a white solid (0.55 g). Crystallization from ethyl acetate – hexane afforded methyl 4-chloro-3,6-dideoxy-β-D-galactopyranoside (**6**) as white needles (0.18 g, 21%), mp 152–154 °C, $[\alpha]_D$ −68.4° (*c* 0.9 in water); pmr data (deuterium oxide, external TMS) τ 5.06–5.33 (2H, H-1, H-4), 5.33–6.00 (3H, H-2, H-3, H-5), 6.00 (s, 3H, OMe), 8.16 (d, 3H, $J_{Me,5} \approx 6$ Hz, CMe). *Anal.* calcd. for $C_7H_{13}O_4Cl$: C 42.8, H 6.6, Cl 18.1; found: C 42.7, H 6.7, Cl 18.2.

The mother liquor from the above crystallization was evaporated to give a white solid (0.37 g) whose cmr spectrum (see Table 1) suggested that it was a mixture of compound **6** and methyl 6-chloro-4,6-dideoxy-β-D-*xylo*-hexopyranoside (**7**), with the former preponderating.

*Reaction of 1,2-O-Isopropylidene-α-D-glucofuranose (**8**) with Carbon Tetrachloride and Triphenylphosphine*

To a suspension of compound **8** (3) (3.0 g) in carbon tetrachloride (300 ml) was added triphenylphosphine (10.0 g), and the mixture was heated at reflux temperature with stirring for 18 h. Thin layer chromatography (benzene – ethyl acetate, 4:1 (v/v)) showed that the starting material had all reacted and revealed the presence of two new components having R_F 0.31 and 0.75. The reaction mixture was cooled, diluted with petroleum ether (1 litre), and kept at 0 °C overnight; the precipitate was removed by filtration, and the filtrate was evaporated. The residue was chromatographed on silica gel, with, initially, benzene and, finally, benzene – ethyl acetate, 4:1 (v/v), as eluants. The slower-moving compound (5,6-dichloro-5,6-dideoxy-1,2-*O*-isopropylidene-β-L-idofuranose (**9**)) (1.57 g, 45%) was sublimed at 115 °C/20 torr to afford colorless crystals, mp 114–115 °C, $[\alpha]_D$ −15.5° (*c* 1.3 in chloroform); pmr data τ 4.00 (d, 1H, $J_{1,2}$ = 3.7 Hz, H-1), 5.45 (d, 1H, H-2), 5.55–5.75 (3H, H-3, H-4, H-5), 6.00–6.15 (m, 2H, 2 H-6's), 8.52 and 8.70 (s's 3H, CMe_2). *Anal.* calcd. for $C_9H_{14}O_4Cl_2$: C 42.0, H 5.5, Cl 27.6; found: C 42.1, H 5.5, Cl 27.6.

The faster-moving compound (3,6-anhydro-5-chloro-5-deoxy-1,2-*O*-isopropylidene-β-L-idofuranose (**10**)) (0.59 g, 20%) was sublimed at 60 °C/30 torr to afford crystals, mp 58–61 °C, $[\alpha]_D$ +47.6° (*c* 2.3 in chloroform); pmr data τ 4.15 (d, 1H, $J_{1,2}$ = 3.5 Hz, H-1), 5.20 (2H, AB pattern, $J_{3,4} \approx 3.5$ Hz, H-3, H-4), 5.38 (d, 1H, H-2), 5.5–6.0 (3H, ABX pattern, H-5, 2 H-6's), 8.55 and 8.70 (s, 3H, CMe_2). *Anal.* calcd. for $C_9H_{13}O_4Cl$: C 49.0, H 5.9, Cl 16.1; found: C 49.1, H 5.9, Cl 16.0.

*Hydrogenation of 5,6-Dichloro-5,6-dideoxy-1,2-O-isopropylidene-β-L-idofuranose (**9**)*

A solution of compound **9** (0.87 g) in ethanol (80 ml) containing W-4 Raney nickel catalyst (30 ml ethanol slurry (~4.5 g of catalyst)) and triethylamine (2.1 ml) was subjected to a hydrogen pressure of 45 psig for 20 h. Thin layer chromatography (chloroform – ethyl acetate, 4:1 (v/v)) showed that the starting material had all been converted into a single component having R_F 0.20. The catalyst was removed by filtration through Celite, and the filtrate was evaporated. The residue was dissolved in ethyl acetate (50 ml), and the solution was washed successively with 0.2 *N* sulfuric acid, a saturated, aqueous solution of sodium hydrogen carbonate, and water; the organic solution was dried ($MgSO_4$) and evaporated. Recrystallization of the residue (0.60 g, 94%) from ethyl acetate – hexane afforded 5,6-dideoxy-1,2-*O*-isopropylidene-α-D-*xylo*-hexofuranose (**11**) as colorless needles, mp 76.5–77.5 °C, $[\alpha]_D$ −23.8° (*c* 1.6 in chloroform); pmr data τ 4.12 (d, 1H, $J_{1,2}$ = 3.8 Hz, H-1), 5.50 (d, 1H, H-2), 5.66–6.17 (m, 2H, H-3, H-4), 8.52 and 8.72 (s's, 3H, CMe_2), 9.0 (t, 3H, $J_{5,6}$ = 6.5 Hz, Me). For compound **11**, mp 77–78 °C and $[\alpha]_D^{22}$ −22 ± 1° (*c* 4.5 in chloroform) have been reported (6). *Anal.* calcd. for $C_9H_{16}O_4$: C 57.5, H 8.5; found: C 57.7, H 8.6.

*Hydrogenation of 3,6-Anhydro-5-chloro-5-deoxy-1,2-O-isopropylidene-β-L-idofuranose (**10**)*

A solution of compound **10** (110 mg) in ethanol (10 ml) containing W-4 Raney nickel catalyst (4 ml ethanol slurry (~0.4 g of catalyst)) and triethylamine (0.26 ml)

Can. J. Chem. Downloaded from www.nrcresearchpress.com by 210.87.254.5 on 09/05/12
For personal use only.

was subjected to a hydrogen pressure of 43 psig for 48 h; tlc (benzene) indicated that all of the starting material had been consumed. The catalyst was removed by filtration, and the filtrate was evaporated; ether was added to the residue, and the mixture was filtered. The filtrate was concentrated to yield an oil (82 mg), which was chromatographed on silica gel with ether – petroleum ether (bp 60–80 °C) 3:7 (v/v) as eluant. 3,6-Anhydro-5-deoxy-1,2-*O*-isopropylidene-α-D-*xylo*-hexofuranose (**12**) was obtained in crystalline form (52 mg, 57%), and, after sublimation at 40 °C/0.05 torr, had mp 34–36 °C. The pmr spectrum was identical with that obtained for compound **12** by Ritchie and Szarek (16). *Anal.* calcd. for $C_9H_{14}O_4$: C 58.0, H 7.6; found: C 58.2, H 7.6.

*3-Deoxy-1,2:5,6-di-O-isopropylidene-α-D-ribo-hexofuranose (**14**) and 3-Deoxy-1,2-O-isopropylidene-α-D-ribo-hexofuranose (**15**)*

A solution of 3-chloro-3-deoxy-1,2:5,6-di-*O*-isopropylidene-α-D-glucofuranose (7) (**13**, 1.0 g) in ethanol (30 ml) containing W-4 Raney nickel catalyst (20 ml ethanol slurry (~2 g of catalyst)) and triethylamine (1.3 ml) was subjected to a hydrogen pressure of 38 psig for 40 h. The catalyst was removed by filtration, and the filtrate was evaporated; ether was added to the residue, and the mixture was filtered. The filtrate was concentrated, and the residual oil was distilled at 92 °C/0.15 torr to afford compound **14** as a colorless oil (0.8 g, 92%), R_F 0.30 (tlc, chloroform – ethyl acetate, 4:1 (v/v)), $[\alpha]_D$ −7.2° (*c* 4.2 in chloroform). The pmr spectrum was consistent with the spectral data reported for **14** by Haylock *et al.* (7). For compound **14**, $[\alpha]_D$ −2.75° (*c* 0.4 in chloroform) (7), $[\alpha]_D^{18}$ −8.6° (*c* 3.7 in ethanol) (8), and $[\alpha]_D$ −5.78° (*c* 4.2 in ethanol) (9) have been reported. *Anal.* calcd. for $C_{12}H_{20}O_5$: C 59.0, H 8.2; found: C 59.1, H 8.2.

Partial, acid-catalyzed hydrolysis (9) of compound **14** afforded the mono-*O*-isopropylidene derivative **15** as a syrup, $[\alpha]_D$ −13.3° (*c* 1.2 in water); ν_{max} (film) 3450 cm^{-1} (OH); pmr data τ 3.80 (d, 1H, $J_{1,2}$ = 4.0 Hz, H-1), 5.25 (apparent t, 1H, H-2), 5.6–6.6 (6H, H-4, H-5, 2 H-6's, 2 OH's), 7.6–8.2 (2H, 2 H-3's), 8.50 and 8.70 (s's, 3H, CMe_2). For compound **15**, mp 82 °C and $[\alpha]_D^{24}$ −15.0° (*c* 1.3 in water) have been reported (7).

*3-Chloro-3-deoxy-1,2-O-isopropylidene-α-D-glucofuranose (**16**)*

A solution of 3-chloro-3-deoxy-1,2:5,6-di-*O*-isopropylidene-α-D-glucofuranose (7) (**13**, 4.47 g) in methanol (45 ml) was treated with 0.8% aqueous sulfuric acid (25 ml), and the solution was kept for 48 h at room temperature; tlc (benzene – ethyl acetate, 4:1 (v/v)) indicated that all of the starting material had been consumed. The reaction mixture was neutralized with barium carbonate, filtered, and the filtrate was evaporated. The oily residue was dissolved in carbon tetrachloride, anhydrous magnesium sulfate was added, and the mixture was filtered; evaporation of the filtrate afforded the mono-*O*-isopropylidene derivative **16** as a syrup (3.8 g, 99%) which crystallized on standing. Sublimation at 115 °C/0.01 torr gave crystals, mp 73–74.5 °C, $[\alpha]_D$ −14.3° (*c* 3.5 in chloroform); ν_{max} (KBr) 3450 cm^{-1} (OH); pmr data τ 4.1 (d, 1H, $J_{1,2}$ = 3.5 Hz, H-1), 5.3 (d, 1H, H-2), 5.5 (d, 1H, $J_{3,4}$ = 2.5 Hz, H-3), 5.6–6.4 (6H, H-4, H-5, 2 H-6's, 2 OH's), 8.5 and 8.7 (s's, 3H, CMe_2). *Anal.* calcd. for $C_9H_{15}O_5Cl$: C 45.3, H 6.3, Cl 14.9; found: C 45.4, H 6.3, Cl 15.1.

*Reaction of 3-Chloro-3-deoxy-1,2-O-isopropylidene-α-D-glucofuranose (**16**) with Triphenylphosphine in Carbon Tetrachloride*

(*A*) A solution of compound **16** (0.50 g) and triphenylphosphine (1.6 g) in carbon tetrachloride (20 ml) was heated at reflux temperature for 5 h; tlc (chloroform – ethyl acetate, 4:1 (v/v)) indicated that all of the starting material had been consumed. Ethanol (5 ml) was added, and heating was continued to convert the excess of triphenylphosphine into its oxide. The solution was concentrated to half-volume, petroleum ether (bp 60–80 °C) (30 ml) was added, and the mixture was kept at 5 °C; the precipitated triphenylphosphine oxide was removed by filtration. The filtrate was evaporated, and the residue was triturated with 3 portions of petroleum ether. The residue was dissolved in a minimum quantity of a hot mixture of carbon tetrachloride – petroleum ether, and the solution was cooled; the precipitate was removed by filtration, and the filtrate and the petroleum ether triturates were evaporated. The crude product was chromatographed on silica gel, with chloroform – ethyl acetate, 8:1 (v/v), as eluant, to afford 3,6-dichloro-3,6-dideoxy-1,2-*O*-isopropylidene-α-D-glucofuranose (**18**) as a pale yellow syrup (0.32 g, 60%), R_F 0.64 (tlc, chloroform – ethyl acetate, 4:1 (v/v)), $[\alpha]_D$ −9.5° (*c* 1.1 in chloroform); ν_{max} (film) 3500 cm^{-1} (OH); pmr data τ 4.05 (d, 1H, $J_{1,2}$ = 3.5 Hz, H-1), 5.3 (d, 1H, H-2), 5.5 (d, 1H, $J_{3,4}$ = 2.5 Hz, H-3), 5.7–6.5 (4H, H-4, H-5, 2 H-6's), 8.5 and 8.7 (s's, 3H, CMe_2). *Anal.* calcd. for $C_9H_{14}O_4Cl_2$: C 42.0, H 5.5, Cl 27.6; found: C 41.8, H 5.3, Cl 27.7.

(*B*) A solution of compound **16** (1.15 g) and triphenylphosphine (5.0 g) in carbon tetrachloride (100 ml) was heated at reflux temperature for 18 h. Thin layer chromatography (chloroform – ethyl acetate, 4:1 (v/v)) indicated that, within ~5 h, the starting material had been converted into the dichloro compound **18**; on further heating, compound **18** was converted into a component having R_F 0.60 (tlc, chloroform). Ethanol (10 ml) was added, and heating was continued for a few hours. The bulk of the triphenylphosphine oxide was removed by precipitation with petroleum ether. The crude product was chromatographed on silica gel, with benzene as eluant, to afford 3,5,6-trichloro-3,5,6-trideoxy-1,2-*O*-isopropylidene-β-L-idofuranose (**17**) in crystalline form (0.85 g, 64%). Recrystallization from hexane gave colorless needles, mp 97.5–99 °C, $[\alpha]_D$ +2.4° (*c* 5.1 in chloroform); no absorption attributable to OH in ir spectrum; pmr data τ 4.0 (d, 1H, $J_{1,2}$ = 3.0 Hz, H-1), 5.25 (d, 1H, H-2), 5.45–5.9 (3H, H-3, H-4, H-5), 6.0–6.2 (m, 2H, 2 H-6's), 8.5 and 8.7 (s's, 3H, CMe_2). *Anal.* calcd. for $C_9H_{13}O_3Cl_3$: C 39.2, H 4.7, Cl 38.6; found: C 39.1, H 4.6, Cl 38.6.

*Hydrogenation of 3,6-Dichloro-3,6-dideoxy-1,2-O-isopropylidene-α-D-glucofuranose (**18**)*

A solution of compound **18** (0.62 g) in ethanol (50 ml) containing W-4 Raney nickel catalyst (20 ml ethanol slurry (~3 g of catalyst)) and triethylamine (1.0 ml) was subjected to a hydrogen pressure of 45 psig for 18 h; tlc

(chloroform – ethyl acetate, 4:1 (v/v)) indicated that the starting material had all been converted into a component having R_F 0.65. The filtered solution was evaporated, and the residue was triturated with ether; the triturate was concentrated to a yellow oil. Distillation at 70 °C/0.1 torr afforded 6-chloro-3,6-dideoxy-1,2-*O*-isopropylidene-α-D-*ribo*-hexofuranose (**21**) as a colorless oil (0.33 g, 61%), ν_{max} (film) 3470 cm^{-1} (OH). *Anal.* calcd. for $C_9H_{15}O_4Cl$: C 48.6, H 6.8, Cl 15.9; found: C 48.5, H 6.8, Cl 16.0.

*Hydrogenation of 3,5,6-Trichloro-3,5,6-trideoxy-1,2-O-isopropylidene-β-L-idofuranose (**17**)*

A solution of compound **17** (0.58 g) in ethanol (50 ml) containing W-4 Raney nickel catalyst (25 ml ethanol slurry (~4.3 g of catalyst)) and triethylamine (0.8 ml) was subjected to a hydrogen pressure of 50 psig for 24 h. The filtered solution was evaporated, and the residue was triturated with ether; the triturate was concentrated to a pale yellow oil. Thin layer chromatography (benzene) indicated the presence of a major component having R_F 0.19 and lesser amounts of starting material (R_F 0.51) and a component having R_F 0.41. Chromatography on silica gel, with chloroform – ethyl acetate, 10:1 (v/v), as eluant, afforded the major component (0.21 g) and a fraction (0.13 g) which was a mixture of starting material and the other component. Distillation of the major component at 90 °C/20 torr gave 3,5,6-trideoxy-1,2-*O*-isopropylidene-α-D-*erythro*-hexofuranose (**20**) as a colorless oil (50%), $[\alpha]_D$ −14.2° (*c* 0.7 in chloroform); pmr data τ 4.09 (d, 1H, $J_{1,2}$ = 3.7 Hz, H-1), 5.28 (d of d's, 1H, $J_{2,3}$ = 4.7 Hz, H-2), 5.85 (m, 1H, H-4), 7.62–8.07 (4H, 2 H-3's, 2 H-5's), 8.48 and 8.66 (s's, 3H, CMe_2), 9.03 (t, 3H, $J_{5,6}$ = 6.5 Hz, Me). *Anal.* calcd. for $C_9H_{16}O_3$: C 62.8, H 9.4; found: C 62.8, H 9.4.

The mixture of starting material and the other component was fractionated on silica gel, with benzene as eluant, to afford a homogeneous sample of the latter (0.02 g). Distillation of this sample at 98 °C/20 torr gave 3-chloro-3,5,6-trideoxy-1,2-*O*-isopropylidene-α-D-*xylo*-hexofuranose (**19**) as a colorless oil, $[\alpha]_D$ −16.6° (*c* 2.8 in chloroform); pmr data τ 4.05 (d, 1H, $J_{1,2}$ = 3.6 Hz, H-1), 5.27 (d, 1H, H-2), 5.77 (2H, H-3, H-4), 7.77 (m, 2H, 2 H's), 8.49 and 8.70 (s's, 3H, CMe_2), 9.03 (t, 3H, $J_{5,6}$ = 7.0 Hz, Me). *Anal.* calcd. for $C_9H_{15}O_3Cl$: C 52.3, H 7.3, Cl 17.2; found: C 52.2, H 7.7, Cl 17.1.

Acknowledgments

The authors are grateful to the National Research Council of Canada for financial support of this research. They also thank Dr. B. K. Hunter for recording the cmr spectra.

1. B. T. Lawton, W. A. Szarek, and J. K. N. Jones. Carbohydr. Res. **15**, 397 (1970).
2. D. M. Dean, W. A. Szarek, and J. K. N. Jones. Carbohydr. Res. **33**, 383 (1974).
3. O. T. Schmidt. Methods Carbohydr. Chem. **2**, 318 (1963).
4. W. A. Szarek. Adv. Carbohydr. Chem. Biochem. **28**, 225 (1973).
5. C.-W. Chiu and R. L. Whistler. J. Org. Chem. **38**, 832 (1973).
6. J. K. N. Jones and J. L. Thompson. Can. J. Chem. **35**, 955 (1957).
7. C. R. Haylock, L. D. Melton, K. N. Slessor, and A. S. Tracey. Carbohydr. Res. **16**, 375 (1971).
8. M. Černý and J. Pacák. Collect. Czech. Chem. Commun. **21**, 1003 (1956).
9. E. J. Hedgley, W. G. Overend, and R. A. C. Rennie. J. Chem. Soc. 4701 (1963).
10. S. Hanessian and N. R. Plessas. J. Org. Chem. **34**, 2163 (1969); H. Arita, N. Ueda, and Y. Matsushima. Bull. Chem. Soc. Jpn. **45**, 567 (1972); G. G. Birch, C.-K. Lee, and A. C. Richardson. Carbohydr. Res. **36**, 97 (1974).
11. W. A. Szarek, D. M. Vyas, S. D. Gero, and G. Lukacs. Can. J. Chem. **52**, 3394 (1974).
12. A. S. Perlin, B. Casu, and H. J. Koch. Can. J. Chem. **48**, 2596 (1970).
13. E. L. Eliel, W. F. Bailey, L. D. Kopp, R. L. Willer, D. M. Grant, R. Bertrand, K. A. Christensen, D. K. Dalling, M. W. Duch, E. Wenkert, F. M. Schell, and D. W. Cochran. J. Am. Chem. Soc. **97**, 322 (1975).
14. D. M. Vyas, H. C. Jarrell, and W. A. Szarek. Can. J. Chem. **53**, 2748 (1975).
15. A. A. Pavlic and H. Adkins. J. Am. Chem. Soc. **68**, 1471 (1946).
16. R. G. S. Ritchie and W. A. Szarek. Can. J. Chem. **50**, 507 (1972).

Can. J. Chem. Downloaded from www.nrcresearchpress.com by 210.87.254.5 on 09/05/12
For personal use only.

Photosolvation of $[Co(CN)_6]^{3-}$, *trans*-$[Cr(NH_3)_2(NCS)_4]^-$, and *trans*-$[Cr(en)_2NCSF]^+$ in aqueous mixed solvent systems

CARL FOOK CHOW WONG AND ALEXANDER DAVID KIRK
Department of Chemistry, University of Victoria, Victoria, B.C., Canada V8W 2Y2

Received June 28, 1976

CARL FOOK CHOW WONG and ALEXANDER DAVID KIRK. Can. J. Chem. **54**, 3794 (1976).

Photosolvation of $[Co(CN)_6]^{3-}$(**1**), *trans*-$[Cr(NH_3)_2(NCS)_4]^-$(**2**) and *trans*-$[Cr(en)_2NCSF]^+$(**3**) has been studied in various water/methanol, ethanol, acetonitrile, ethylene glycol, glycerol, and acetone mixtures and in aqueous solutions of polyvinylpyrolidone. The quantum yield for thiocyanate loss from **3** was found to be fairly independent of solvent, while for thiocyanate loss from **2**, large, and at higher concentrations of organic solvent, specific reductions of quantum yield were observed. The study of **1** using spectrophotometric analysis for $[Co(CN)_5H_2O]^{2-}$ yielded similar data to some in the literature, but the larger range of systems studied here did not support the reported reduction of quantum yield with bulk viscosity. Furthermore evidence from this and other work suggests that many of the observed quantum yield reductions are only apparent, based on a false assumption that the photosolvation is qualitatively the same in all mixtures. The data are reinterpreted in terms of competitive solvation by both solvent components. It is argued that this study supports a dissociative model of reaction for **1**, but an associative model for the chromium complexes **2** and **3**.

CARL FOOK CHOW WONG et ALEXANDER DAVID KIRK. Can. J. Chem. **54**, 3794 (1976).

On a étudié la photosolvatation du $[Co(CN)_6]^{3-}$(**1**), $[Cr(NH_3)_2(NCS)_4]^-$ *trans* (**2**) et $[Cr(en)_2NCSF]^+$ *trans* (**3**) dans divers mélanges d'eau/méthanol, éthanol, acétonitrile, éthylène glycol, glycérol et acétone et dans des solutions aqueuses de polyvinylpyrolidone. On a trouvé que le rendement quantique pour la perte du thiocyanate à partir de **3** est pratiquement indépendante du solvant alors qu'il y a une grande dépendance pour la perte du thiocyanate à partir de **2**; de plus on a observé qu'à des concentrations plus élevées de solvants organiques, des réductions spécifiques du rendement quantique peuvent être observées. L'étude de **1**, en faisant appel à l'analyse spectrophotométrique de $[Co(CN)_5H_2O]^{2-}$, a conduit à des données semblables à celles que l'on peut retrouver dans la littérature; toutefois les étendues plus grandes des systèmes étudiés dans le présent travail n'apportent pas de support pour la réduction des rendements quantiques qui a été rapportées en fonction de l'augmentation de la viscosité globale. De plus des données rapportée dans ce travail et dans d'autres travaux suggèrent que plusieurs réductions dans les rendements quantiques ne sont qu'apparentes et basées uniquement sur l'hypothèse fausse que la photosolvatation est qualitativement la même dans tous les mélanges. On réinterprète les données en terme de solvatation compétitive par les deux composants du solvant. On présente des arguments suggérant que notre étude supporte un modèle dissociatif pour la réaction de **1** mais un modèle associatif pour les complexes **2** et **3** du chrome.

[Traduit par le journal]

Introduction

The large majority of studies of ligand photosubstitution processes of coordination compounds have been carried out in water as solvent (1, 2). In recent years, however, a number of experiments have extended the range to non-aqueous, and mixed aqueous solvent systems. The influence of solvent on excited state properties (3) and on photochemical behaviour (4) is clearly not well understood at present. Thus, while Langford and Tipping (5) and the authors (6) found evidence only for minor solvent effects for $[Cr(RNH_2)_5Cl]^{2+}$ photolyses in DMSO/water and acetone/water respectively, in contrast Scandola *et al.* (7, 8) have reported large solvent effects on photolysis of some cobalt complexes. These they correlated with solvent viscosity and explained in terms of a photoinduced heterolytic bond fission to produce a five coordinate species and solvent separated ligand, with subsequent competition between solvent substitution and cage recombination.

It is these latter observations, the apparent differences in observed behaviour, and the important implications for theoretical models of transition metal photochemistry that prompted this investigation of solvent effects for two chromium complexes, similar but of opposite

Can. J. Chem. Downloaded from www.nrcresearchpress.com by 210.87.254.5 on 09/05/12
For personal use only.

TABLE 1. Photochemical yields as a function of medium

Water/	Wt. (%)	x_{H_2O}	η (cP)	ϕ/ϕ_0[c] 1[a]	2[b]	3[c]
Glycerol	10	0.98	1.3	0.93	0.93	—
	20	0.95	1.7	—	—	0.93
	24	0.94	2.0	0.79	0.83	—
	40	0.88	3.7	0.62	0.64	0.90
	48	0.85	5.6	0.51	0.54	—
	56	0.80	8.3	0.41	0.46	—
	60	0.76	10.7	—	—	0.85
	64	0.74	13.6	0.32	0.39	—
Ethylene glycol	16	0.95	1.5	0.86	0.83	—
	32	0.88	2.3	0.72	0.65	—
	48	0.79	3.5	0.59	0.53	—
	60	0.70	5.0	0.46	0.46	—
	70	0.60	6.8	0.36	0.40	—
	80	0.46	9.5	0.30	0.37	—
Ethanol	7.5	0.97	1.4	0.92	—	—
	15.3	0.93	1.9	0.86	0.78	0.95
	27.5	0.87	2.6	0.82	—	—
	40.5	0.99	2.8	0.79	0.59	0.94
	54.2	0.68	2.8	0.78	—	—
	68.9	0.54	2.1	0.77	0.55	—
Methanol	30	0.81	1.8	—	—	0.93
	60	0.54	1.9	—	—	0.95
	75	0.37	1.2	0.81	—	—
Acetone	20	0.93	1.5	—	0.73	—
	30	0.88	1.6	—	—	0.99
	40	0.83	1.6	—	0.63	—
	60	0.68	1.2	—	0.61	1.0
Acetonitrile	20	0.90	1.1	0.56	0.85	0.97
	40	0.77	0.95	0.45	0.80	1.0
	60	0.60	0.73	0.43	0.79	—
Polyvinylpyrolidone	0.5		1.6	0.92	—	—
	1.0		2.4	0.90	—	—
	2.0		4.3	0.86	—	0.99
	3.0		7.2	0.84	—	—
	4.0		10.6	0.82	—	0.96

[a]Calculated from absorbance at 380 nm on assumption that sole product was $[Co(CN)_5H_2O]^{2-}$; see text. Measured at 20 °C, λ_{irrad} = 313 nm.
[b]Quantum yield for thiocyanate release. Measured at 20 °C, λ_{irrad} = 546 nm.
[c]ϕ = quantum yield in solvent; ϕ_0 quantum yield in pure water, see text.

charges, and a re-investigation of solvent effects for $[Co(CN)_6]^{3-}$ photolysis.

Results and Discussion

Table 1 shows the quantum yields of photolysis of the three complexes $[Co(CN)_6]^{3-}$ (**1**); *trans*-$[Cr(NH_3)_2(NCS)_4]^-$(**2**), and *trans*-$[Cr(en)_2NCSF]^+$ (**3**), relative to the quantum yields in pure water at 20 °C, namely 0.313, 0.262, and 0.266 respectively, at irradiation wavelengths of 313 nm for **1** and of 546 nm for **2** and **3**. The quantum yields for **1** were determined spectrophotometrically at 380 nm following Scandola *et al.* (7) (that is, assuming that $[Co(CN)_5H_2O]^{2-}$ is the sole photo product), while for **2** and **3** the yields are based on direct measurement of released thiocyanate. For **3** a small yield of ethylenediamine aquation, ϕ = 0.07, also occurs, but can be neglected for the purposes of this work.

In brief, the results reveal large solvent effects for the two negative ions (but see later discussion for $[Co(CN)_6]^{3-}$) but the effects on the positive

Can. J. Chem. Downloaded from www.nrcresearchpress.com by 210.87.254.5 on 09/05/12
For personal use only.

Can. J. Chem. Downloaded from www.nrcresearchpress.com by 210.87.254.5 on 09/05/12
For personal use only.

ion are much smaller, in most cases on the order of the cumulative experimental uncertainty.

$[Co(CN)_6]^{3-}$

The results for this compound, **1**, while agreeing with those of Scandola *et al.*, encompass a larger range of solvents and of composition, and it becomes apparent that the correlation with viscosity observed by those workers was more apparent than real. Thus small, but significant, differences are observed between the ethylene glycol/water system and glycerol/water systems. The most dramatic departures, however, are for polyvinylpyrolidone, which increases bulk viscosity markedly at low mole fraction; similar observations by Natarajan (9) have been discounted by Scandola *et al.* (7), who interpret them to indicate only that the relationship between bulk viscosity and structure of the solvent cage may be different for viscous polymer solutions and for mixed solvent systems; and most importantly for acetonitrile which gives a marked lowering of measured quantum yield in solutions of *reduced* viscosity. We conclude that the viscosity correlation observed (7) was fortuitous and is not supported by our larger data set.

Since the experimental phase of this work was completed, Nakamaru *et al.* (10) have published a study of the photochemistry of **1** in water, acetonitrile, dimethyl formamide, methanol, ethanol, and some other solvents, which shows that a $[Co(CN)_5S]^{2-}$ solvent monosubstituted product is formed in each case, with quantum yields in the range $0.28 \rightarrow 0.32$, that is, roughly the same as that in water. They also find that for water/ethanol mixtures the proportions of ethanol and water substitution vary in parallel with composition as might be expected.

Thus the spectrophotometric calculations used in deriving the Table 1 data for **1** are almost certainly in error, since the product is likely to be an unknown mixture of $[Co(CN)_5H_2O]^{2-}$ and $[Co(CN)_5S]^{2-}$ rather than purely the former as presumed.

The data for the acetonitrile/water system support such an interpretation well. From a plot of quantum yield *vs.* mole fraction of water a lower limit quantum yield of about 0.125 appears to be reached at high acetonitrile concentrations. If this is due to product $[Co(CN)_5CH_3CN]^{2-}$ being produced with $\phi = 0.28$ (10) one can calculate its molar absorptivity at 380 nm (the analysis wavelength) to be 135 l mol^{-1} cm^{-1}. This is in good agreement with the value calculated by us from the published spectrum of this compound (11), namely 130 l mol^{-1} cm^{-1}. For the single methanol point of our work, assuming the low limit apparent quantum yield has been reached (this seems reasonable as x_{H_2O} has been reduced to 0.4, while for acetonitrile/water and ethanol/water mixtures the quantum yield approaches the limiting value at x_{H_2O} as high as 0.6) one calculates $\epsilon_{380} \sim 240$ l mol^{-1} cm^{-1} again in agreement with the value we calculate from Nakamaru's spectrum, 220 l mol^{-1} cm^{-1}. For ethanol there is a discrepancy; ϵ_{380} $[Co(CN)_5C_2H_5OH]^{2-}$ 220 l mol^{-1} cm^{-1} (our work) *vs.* 170 l mol^{-1} cm^{-1} (Nakamaru data, our calculation). However, note that Nakamaru's molar absorptivities for the ethanol monosubstituted compound are quite low compared to the methanol analogue so the former might be subject to some error. In order to explain the apparent quantum yield decrease for the glycerol/water and ethylene glycol/water systems in the same way requires the hypothetical monosubstituted products to have molar absorptivities at 380 nm of about 60 and 75 l mol^{-1} cm^{-1} respectively. These are rather low values and suggest that for these molecules some or all of the apparent decrease in quantum yield with increased concentration of organic component may be real.

For acetonitrile, methanol, and probably ethanol, however, we believe that the quantum yield of reaction remains approximately constant, and with increased concentration of organic solvent substitution by the organic component successfully competes with water substitution. The measured absorptivities at 380 nm, together with the published spectra of the monosubstituted products, enables one to calculate the proportion of aquo and solvento-monosubstituted products as a function of solvent composition. The data are not sufficiently ample or reliable to investigate the dependence of the proportion on composition (mole fraction) but it reveals the interesting result that acetonitrile preferentially photosubstitutes over water by a considerable factor, about 40. Methanol appears favored by a factor of about two, while ethanol appears to be on an approximately equal footing with water. Whether these results reflect prefer-

Can. J. Chem. Downloaded from www.nrcresearchpress.com by 210.87.254.5 on 09/05/12
For personal use only.

ential solvation effects or rates of substitution is uncertain. The favoring of the weak nucleophile acetonitrile, however, suggests that preferential solvation (or greater mobility due to lack of hydrogen bonding) must provide the explanation. Preferential solvation by acetonitrile would be favored by the similar nature and polarizability of acetonitrile and **1**. Nakamaru *et al.* (10) noted spectral evidence for strong polarizability effects in $[Co(CN)_6]^{3-}$/acetonitrile solutions; some charge transfer interaction is even possible.

In summary, this analysis of the data indicates that many quantum yield changes observed for **1** (7) were only apparent based on an incorrect assumption as to the nature of the product. The data for polyvinylpyrolidone solutions and possibly for glycerol and ethylene glycol do suggest some residual composition dependence but not well correlated with bulk viscosity. The case for cage recombination is not established by the data since other explanations for such solvent effects exist, such as changes in the extent of solvent structure (11) and preferential or mixed solvation with consequent alteration of effective water activity in the solvation shell of the ion.

trans-$[Cr(NH_3)_2(NCS)_4]^-$ *and trans-*$[Cr(en)_2NCSF]^+$

Table 1 shows that definite changes of ϕ_{NCS^-} occur as a function of solvent composition for **2**. Since these yields were directly determined there is no doubt about their magnitude and the reality of the variations observed, although we did not, due to the experimental difficulty involved, attempt to determine the nature of the solvent substituted products.

The changes in quantum yield observed for **2** do not correlate with solvent viscosity, and again the data for acetonitrile are a good illustration of this. A plot of relative quantum yield for thiocyanate from **2** *vs.* mole fraction water, x_{H_2O} (Fig. 1) shows that for each solvent examined a different limiting quantum yield is approached at high mole fraction organic solvent. For very much lower mole fractions of water a further change in quantum yield might occur, as water was progressively excluded from the system. Such a regime might not be accessible due to solubility problems. However, at high mole fraction water (≥ 0.9) the relative quantum yield is close to the same linear function of x_{H_2O} for all solvents except acetonitrile.

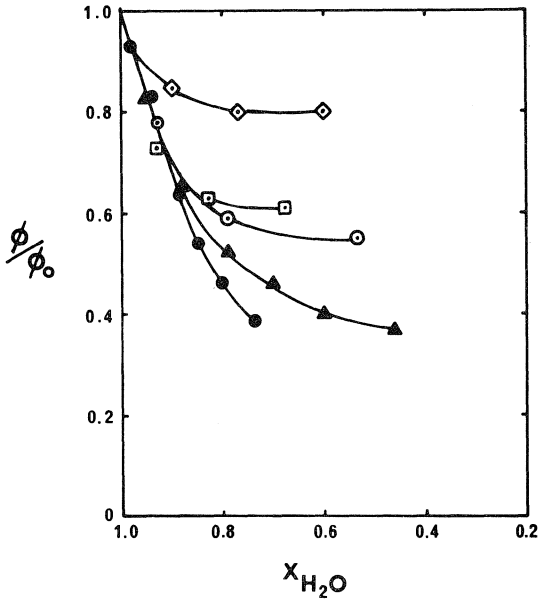

FIG. 1. Relative quantum yields for photosolvation of thiocyanate ion from *trans*-$[Cr(NH_3)_2(NCS)_4]^-$ as a function of aqueous mixed solvent composition. ϕ = quantum yield for thiocyanate in mixed solvent, ϕ_0 = quantum yield for thiocyanate in water. x_{H_2O} = mole fraction water in solution. Legend. ◇, acetonitrile; □, acetone; ○, ethanol; △, ethylene glycol; ●, glycerol.

This suggests a similar lowering of water activity at low concentrations of organic solvent, with the appearance of specific solvent effects at higher concentrations.

In contrast the data for the unipositive ion, **3**, show only small effects of solvent composition. This parallels earlier data (5, 6) for $[Cr(RNH_2)_5Cl]^{2+}$ photolyses and suggests a charge effect; that perhaps generally, positively charged chromium complexes show little sensitivity of quantum yield to solvent composition in aqueous/non-aqueous media.

These observations can be rationalized in terms of a model which considers the variation of the composition of the primary solvation sphere, the effectiveness of the components as nucleophiles, the steric constraints on substitution and the influence of solvent structure including hydrogen bonding. From the point of view of predictive power a model with so many variable parameters is bound to leave something to be desired, but it does seem from the data obtained here, and from studies of solvation and solvent structure (11 and references therein),

Can. J. Chem. Downloaded from www.nrcresearchpress.com by 210.87.254.5 on 09/05/12
For personal use only.

that all of the above factors might be expected to play a role.

Since, for chromium complexes, the lifetime of the excited quartet state leading to reaction (12–15) is likely to be only a few picoseconds (16), the quantum yield of substitution can be expected to depend on the rapid availability of a suitably oriented nucleophile. For a positive ion the primary solvation sphere, which is almost certain to contain at least one water molecule even in a fairly dry organic solvent, has the water molecules oriented with the oxygen lone pair suitably placed for nucleophilic substitution. Thus one may understand that substitution is facile and little change in quantum yield occurs on addition of organic solvent to the bulk solvation sphere, that is, until the obvious limit of extremely low mole fractions of water is reached. (Such a limit might, in practice, be beyond reach due to insolubility.)

In contrast, for a negative ion, the water in the solvation sphere is inappropriately oriented for nucleophilic substitution and must rotate (or pseudo rotate) in order to substitute. Since molecular rotational relaxation times are of the order of 5×10^{-12} s for water and longer for organic solvents, this can be expected to be a non-trivial part of the substitution mechanism. It is known that as organic solvents are added to water initially an increase in structuring and hydrogen bonding of the water occurs relatively independent of the nature of the organic component. If water molecules in the solvent sphere are participating in such structural changes this could be expected to decrease the rate of water substitution. Furthermore at significant mole fractions of organic solvent it will compete for sites in the solvation sphere, as shown by the results for $[Co(CN)_6]^{3-}$, and this could also lead to a decrease in the rate of substitution.

Consideration of the data on this basis suggests that the early linear portion of Fig. 1 corresponds to an increase in hydrogen-bonding of solvation sphere molecules, with decrease in quantum yield due to their decreased mobility enabling radiationless decay to compete better with nucleophilic substitution involving the excited state. At higher concentrations of organic solvent competition for sites in the solvation sphere may begin to be important. The limiting quantum yields achieved, Fig. 1, may then be determined by the ability of the organic solvent to substitute on chromium in place of water. Such an explanation suggests the order of substitution efficiency to be acetonitrile > acetone > ethanol > ethylene glycol > glycerol, certainly not an order of nucleophilicity but quite reasonable as a sequence of mobility. If this model is correct, and we hope in future to be able to undertake analytical work to investigate this, it will dramatically illustrate the importance of specific solvation and structural effects in chromium photochemistry in mixed solvents, at least for negative ions.

This analysis of the data suggests a real difference between the behaviour of the cobalt complex, **1**, and the chromium complex, **2**. For **1**, the data suggest the quantum yield remains constant independent of the substituting ligand (with the possibility of small viscosity/mobility effects). Ironically this supports the original proposed dissociative mechanism involving intermediate $[Co(CN)_5]^{2-}$, followed by complete scavenging. In contrast the negative chromium(III) ion shows discrimination between entering nucleophiles. This might be argued also to support a dissociative mode of reaction with incomplete scavenging. However there is no evidence for such a cage mechanism and it would not explain the contrast in behaviour of the negative and positive ions. In fact one would expect recombinations to compete *more* favorably in the case of the positive ion, **3**, where the fragments are of opposite charge. The observations better support an associative mode of reaction in which nucleophilic substitutions must compete with non-reactive degradative processes of the reactive excited state.

Experimental

Materials

$K_3Co(CN)_6$ was kindly donated by A. Ludi, University of Bern, Switzerland. The spectroscopic data for the first ligand field band were $\lambda_{max} = 310$ nm, $\epsilon_{max} = 192$ l mol^{-1} cm^{-1} (lit. (17) $\lambda_{max} = 313$ nm, $\epsilon_{max} = 170$ l mol^{-1} cm^{-1}). K[*trans*-$[Cr(NH_3)_2(NCS)_4]$] was prepared from ammonium reineckate (18) (BDH).

trans-$[Cr(en)_2(NCS)F]ClO_4$: a 10 g sample of *trans*-$[Cr(en)_2H_2OF](ClO_4)_2$, prepared as described by Vaughn, *et al.*, (19) was vigorously stirred with 5 g of dried NH_4NCS (1 h at 100 °C) in 50 ml of acidified (0.2 ml of 5 *M* $HClO_4$) methanol in the dark at 40–45 °C for 24 h. The solid residue was collected by filtration, washed with methanol, and air-dried. The crude complex was recrystallized from water by drop-wise addition of 60% $HClO_4$ to the cooled solution. The orange crystalline product was filtered off, washed with methanol, and dried

in vacuo. Yield 58%. *Anal.* calcd for $Cr(en)_2(NCS)F(ClO_4)_2$: Cr 14.92, C 17.20, N 20.10, H 4.60; found: Cr 15.1, C 17.3, N 20.0, H 4.7.

The identity of the product is suggested by its method of preparation and was confirmed by elemental analysis and the uv–visible spectrum. The preparation of *trans*-$[Cr(en)_2XF]^+$ (X = Cl, Br) by anation of *trans*-$[Cr(en)_2H_2OF]^{2+}$ in methanol is well-known (20), and generally, only the stereoretentive product is easily isolable. The elemental analysis is in good agreement with the molecular formula and the uv–visible spectrum confirms that it is the *trans* isomer. The spectral characteristics, particularly the molar absorptivities (ϵ), are significantly different from those for the *cis* isomer (namely λ_{max} = 375 nm (ϵ = 33.9) and 509 nm (ϵ = 41.2) for the above compound but λ_{max} 375 nm (ϵ = 52) and 500 nm (ϵ = 85) (19) for the *cis* isomer.

Photolysis Apparatus and Procedure

A PEK air-cooled 203-1004 200-W high pressure mercury lamp with a Bausch and Lomb grating monochromator (set for 20 nm spectral band width) yielded light at 313 and 546 nm, with effective line half-widths of about 5 and 9 nm respectively. In each case appropriate blocking filters (Corning) were used to remove higher energy scattered light. Light fluxes were measured either by ferrioxalate (21) (313 nm) or reineckate (18) actinometry. In addition a constant fraction of the light beam was continuously monitored by a photo-tube during photolysis runs so that intensity fluctuations or drifts were easily observed and corrected.

Samples were photolysed in thermostatted 1 cm path length rectangular glass spectrophotometer cells, with continuous magnetic stirring.

Run Procedures and Analysis

A solution of the desired complex, 6×10^{-3} *M* for $K_3Co(CN)_6$ and 1.0×10^{-2} *M* for *trans*-$K[Cr(NH_3)_2(NCS)_4]$ and *trans*-$[Cr(en)_2NCSF]ClO_4$, was made up under dim red light in the appropriate stock solution. Two 3-ml aliquots were pipetted into 1-cm path spectrophotometer cells and after thermal equilibration (5 min) one sample was photolyzed to give about 5% ($K_3Co(CN)_6$) or 2.5% conversion.

For $K_3Co(CN)_6$ the extent of reaction was determined by measuring the absorbances of the dark and photolyzed solutions at 380 nm (ϵ = 298 l mol^{-1} cm^{-1}) (22). The extent of reaction for K-reineckate and *trans*-$[Cr(en)_2NCSF]ClO_4$ was determined by measuring the released thiocyanate as described by Wegner and Adamson (18). Corrections for thermal reaction were applied by means of the data on the dark solutions.

Acknowledgements

The authors wish to thank the National Research Council of Canada and the University of Victoria for financial support. We also thank A. Ludi, University of Bern for kindly donating a sample of $K_3Co(CN)_6$. C.F.C.W. is grateful for a University of Victoria Scholarship and A.D.K. is grateful to the University of Sussex for use of their facilities during 1975–1976.

1. V. Balzani and V. Carassiti. Photochemistry of coordination compounds. Academic Press, London. 1970.
2. A. W. Adamson and P. D. Fleischauer (*Editors*). Concepts of inorganic photochemistry. John Wiley, New York. 1976.
3. G. B. Porter. *In* Concepts of inorganic photochemistry. John Wiley, New York. 1976.
4. P. D. Fleischauer, A. W. Adamson, and G. Sartori. Inorg. React. Mech. **17**, 1 (1972).
5. C. H. Langford and L. Tipping. Can. J. Chem. **50**, 887 (1972).
6. C. F. C. Wong and A. D. Kirk. Can. J. Chem. **53**, 419 (1975).
7. F. Scandola, M. A. Scandola, and C. Bartocci. J. Am. Chem. Soc. **97**, 4757 (1975).
8. F. Scandola, C. Bartocci, and M. A. Scandola. J. Am. Chem. Soc. **95**, 7898 (1973).
9. P. Natarajan. J. Chem. Soc. Chem. Commun. 26 (1975).
10. K. Nakamaru, K. Jin, A. Tazawa, and M. Kanno. Bull. Chem. Soc. Jpn. **48**, 3486 (1975).
11. A. K. Covington and P. Jones. Hydrogen-bonded solvent systems. Taylor and Francis, London. 1968.
12. S. Chen and G. B. Porter. J. Am. Chem. Soc. **92**, 3196 (1970).
13. H. F. Wasgestian. J. Phys. Chem. **76**, 1947 (1972).
14. N. A. P. Kane-Maguire and C. H. Langford. J. Am. Chem. Soc. **94**, 2125 (1972).
15. R. Ballardini, G. Varani, H. F. Wasgestian, L. Moggi, and V. Balzani. J. Phys. Chem. **77**, 2947 (1973).
16. A. D. Kirk, P. E. Hoggard, G. B. Porter, M. C. Rockley, and M. W. Windsor. Chem. Phys. Lett. **37**, 199 (1976).
17. L. Moggi, F. Bolletta, V. Balzani, and F. Scandola. J. Inorg. Nucl. Chem. **28**, 2589 (1966).
18. E. E. Wegner and A. W. Adamson. J. Am. Chem. Soc. **88**, 394 (1966).
19. J. O. Vaughn, O. J. Stvan, and V. E. Magnuson. Inorg. Chem. **7**, 735 (1968).
20. G. Wirth, C. Bifano, R. T. Walters, and R. G. Linck. Inorg. Chem. **12**, 1955 (1973).
21. G. G. Hatchard and C. A. Parker. Proc. R. Soc. London. Sec. A, **235**, 518 (1965).
22. J. H. Bayston, R. N. Beale, N. Kelso King, and M. E. Winfield. Aust. J. Chem. **16**, 954 (1963).

Can. J. Chem. Downloaded from www.nrcresearchpress.com by 210.87.254.5 on 09/05/12
For personal use only.

Enthalpies, heat capacities, and volumes of transfer of the tetrabutylammonium ion from water to aqueous mixed solvents from the point of view of the scaled-particle theory

NICOLE DESROSIERS AND JACQUES E. DESNOYERS[1]

Department of Chemistry, Université de Sherbrooke, Sherbrooke, P.Q., Canada J1K 2R1

Received July 12, 1976

NICOLE DESROSIERS and JACQUES E. DESNOYERS. Can. J. Chem. **54**, 3800 (1976).

The enthalpies, heat capacities, and volumes of transfer of the tetrabutylammonium ion from water to urea–water, *tert*-butyl alcohol – water, and sodium chloride – water mixtures have been calculated at 25 °C using the scaled-particle theory. In general, the signs, magnitudes, and overall trends in the cosolvent concentration dependence of the properties are predicted from the cavity contributions only. These calculations are found to be very sensitive to the diameters chosen for the various species.

For these calculations it was necessary to measure with a dilatometer the coefficients of thermal expansion of *tert*-butyl alcohol – water mixtures as a function of concentration and temperature.

NICOLE DESROSIERS et JACQUES E. DESNOYERS. Can. J. Chem. **54**, 3800 (1976).

Les enthalpies, capacités calorifiques et volumes de transfert du cation tétrabutylammonium de l'eau aux mélanges eau–urée, eau – chlorure de sodium et eau–*tert*-butanol ont été calculés à 25 °C à l'aide de la théorie des particules calibrées (scaled-particle theory). En général, les signes, les ordres de grandeur et les tendances des différentes propriétés en fonction de la concentration en cosolvant sont prédits à partir des termes relatifs à la formation de cavité seulement. Ces calculs sont très sensibles au choix des diamètres des différentes espèces en solution.

Pour ces calculs il a été nécessaire de mesurer au moyen d'un dilatomètre les coefficients de dilatation cubique des mélanges eau–*tert*-butanol en fonction de la concentration et de la température.

Introduction

The scaled-particle theory (SPT), developed by Reiss and co-workers (1–4), was first applied, in a semi-empirical form, to aqueous solutions by Pierotti (5). He predicted surprisingly well the enthalpies, entropies, volumes, and heat capacities of some nonpolar gases in water by considering the process of solution in two steps: the creation of a cavity in the solvent to accommodate the solute and the interactions of the solute molecule with the solvent. Since then, Lucas and co-workers (6–8), Masterton *et al.* (9, 10), and Shoor and Gubbins (11) have extended these calculations to the solubility of gases in aqueous electrolyte solutions. Lucas et al. (12–14) have also applied the SPT to the heats and entropies of nonpolar gases in some aqueous solutions of tetraalkylammonium halides (R_4NX) and alcohols. Recently, Philip and Jolicoeur (15) have calculated the thermodynamic functions of transfer of some arbitrary cavities from water to heavy water and from methanol to deuterated methanol as a function of cavity size. They assumed that the similarity of the solvents for each transfer would cause a cancellation of the interaction terms thus implying a good prediction of the transfer properties of hydrophobic solutes from the cavity formation contributions alone, contributions calculated from the SPT. The predicted trends were quite good. Finally, Lucas and co-workers (16, 17) have extended such a study of solute size using the SPT modified by Stillinger (18) in order to account more explicitly for the structure of water. They have shown that the results of the modified SPT were similar to those of the original SPT for the enthalpies and entropies of relatively small solutes (diameter <4 Å) but were significantly different for larger solutes. Unfortunately the modified version of Stillinger does not allow us to predict volumes and heat capacities in water since the higher derivatives of the distribution function are presently not available. Lucas has indicated, however, that some large solutes could possibly be treated with success with the original SPT if they can be considered as an assembly of

[1]To whom correspondence should be addressed.

Can. J. Chem. Downloaded from www.nrcresearchpress.com by 210.87.254.42 on 09/05/12
For personal use only.

Can. J. Chem. Downloaded from www.nrcresearchpress.com by 210.87.254.42 on 09/05/12
For personal use only.

small spherical parts such as the alkyl chains, which perhaps cumulate the effects of methylene or methyl groups the size of which are smaller than 4 Å.

The SPT has been mainly applied to solutes such as nonpolar gases and hydrocarbons, but it has also proven to be applicable to hydrophobic ions such as the tetrabutylammonium, the charge of which is probably diffuse enough to consider it as an almost neutral entity. The salts of this ion are often considered model hydrophobic solutes, and recently much data have been accumulated on the properties of R_4NBr in water and in mixed aqueous solvents. The classical interpretation of thermodynamic data in mixed aqueous solvents is usually either in terms of preferential hydrophobic hydration (19, 20), of structural hydration interactions between the solute and a pseudo-uniform mixed solvent considered more or less structured than pure water (21), or of pair and triplet interactions between the electrolyte and the cosolvent, the whole solution being then described as a ternary system (22, 23). On the other hand, the SPT offers another interpretation approach in that it relates the transfer functions of the hydrophobic solute from water to a mixed aqueous solvent to the difference of the properties associated with the formation of a cavity in the mixed and pure solvents without explicitly taking into account what are classically called 'structural' effects.

Therefore, we have applied the original version of the SPT to the prediction of the transfer functions of the cation tetrabutylammonium from water to some mixed aqueous solvents of different 'structural' types, trying to find out to what extent the cavity formation terms contribute to the whole properties for these particular transfers.

The cosolvents of water (W) were *tert*-butyl alcohol (TBA), considered as an hydrophobic solute, urea (U), described as a statistical structure breaker in water, and sodium chloride (NaCl), a typical hydrophilic electrolyte. The properties examined were enthalpies, volumes, and heat capacities since reliable data are available and these properties are often used as evidence for structural hydration effects.

The solvents studied are far from being hard spheres but, following Reiss (4), we will consider that the soft part of the intermolecular potential of the real solvents acts primarily to establish the density; the solvent molecules then confined to a pseudo-container of defined volume constitute approximately a hard sphere fluid susceptible to treatment by the SPT. This is done by entering in the equations of the SPT the experimental density and its derivatives with pressure and temperature for the real solvent. The solute, on the other hand, is considered as an almost hard sphere. This assumption should not be too drastic for the study of transfer functions since the interactions of the real solute, interactions arising from dispersion, inductive, and repulsive forces, as a first approximation should be similar in water and in the aqueous mixed solvent, since the dielectric properties of the latter are not too different from those of water.

These SPT calculations require the knowledge of various parameters for the solvents. While most of these are available in the literature, the coefficient of thermal expansion and its temperature dependence have not been measured directly for the TBA–W systems and the indirect results derived from the densities (24) do not seem accurate enough. They were therefore measured directly with a dilatometer.

Experimental

The coefficients of thermal expansion, α, were measured for aqueous solutions of TBA from 0.7 to 4.5 mol kg^{-1} at 15, 25, and 35 °C using the dilatometric technique described by Desrosiers *et al.* (25). The results are given in Table 1. The temperature derivatives, $d\Delta\alpha/dT$ at 25 °C, derived from the difference in $\Delta\alpha$ at 15 and 35 °C, and the apparent molal expansibilities, ϕ_E, calculated from α and the apparent molal volumes of Avédikian *et al.* (22), are also given in Table 1.

Results and Discussion

The SPT relates the thermodynamic functions of cavity formation to the diameters of the cavity and of the solvent and to the molar volume $\bar{V}$, the coefficient of thermal expansion α, its temperature dependence $(d\alpha/dT)_p$, and the coefficient of isothermal compressibility β of the solution. The basic equations for a cavity in a pure solvent have been derived by Reiss *et al.* (2, 4) and have been extended to ternary systems by Lebowitz *et al.* (26, 27) and by Lucas and co-workers (8, 12, 28, 29). A summary of these equations for the free energy $\bar{G}_c$, the enthalpy $\bar{H}_c$, the volume $\bar{V}_c$, and the heat capacity $\bar{C}_c$ of cavity formation is given in the Appendix.

The parameters α, $d\alpha/dT$, and β were taken

TABLE 1. Coefficients of thermal expansion of aqueous solutions of *tert*-butyl alcohol at 15, 25, and 35 °C

m_{TBA} (mol kg^{-1})	$10^6\Delta\alpha^*$ (K^{-1}) $T=15$ °C	$T=25$ °C	$T=35$ °C	$10^6 d\Delta\alpha/dT$ (K^{-2}) at $T=25$ °C	ϕ_E (cm^3 K^{-1} mol^{-1}) at $T=25$ °C
0.7086	16.2	21.7	36.6	1.0	0.055
1.3165	64.4	70.3	76.6	0.6	0.082
1.9740	146.0	149.5	159.2	0.7	0.111
2.6790	267.9	262.6	253.9	−0.7	0.143
3.3446	403.7	363.8	332.9	−3.5	0.163
4.5530	554.4	469.9	413.2	−7.1	0.168

*$\Delta\alpha \equiv \alpha - \alpha_0$. α_0 = 150.73, 257.05, and 345.71 × 10^{-6} K^{-1} at 15, 25, and 35 °C respectively (35).

from Desrosiers *et al.* (25, 29) for the system U–W. For NaCl–W, the data of Gibson (30) and Gucker (31) were used for α and β. Finally, the α and $d\alpha/dT$ of TBA–W mixtures are from Table 1 while the β are those of Bertrand and Smith (32).

The main problem for the application of the SPT seems to be the assignment of the diameter of each species in solution. The SPT is very sensitive to the choice of these diameters since they are raised to the sixth power in the calculations. In principle, these are not adjustable parameters; effectively, it is possible to determine the diameter of a molecule from gas phase studies using, for example, the second virial coefficients. However, for water, the different values of diameters obtained from various techniques range from 2.50 to 2.93 Å, the average value being close to 2.7 Å (5). It appears also quite difficult to assign a diameter to an ion or a solute in solution.

Recently, Desrosiers and Lucas (34) applied the SPT to the compressibilities of solutes in pure or binary solvents and derived diameters for each species in solution. As this presents a simple and self-consistent method of predicting the diameters of molecules, it has been used with the present systems. To have a more complete set of diameters we have extended the calculations to the diameters of water over a certain range of temperature and to the diameters of the homologous series R_4N^+ (R = methyl → butyl), even if we do not need all these parameters for the present study. Masterton *et al.* (10) have also calculated some ionic radii of the R_4N^+ solutes using the equations of the SPT applied to the salting coefficients of nonpolar gases in aqueous electrolyte solutions; as it will be shown, there is some discrepancy of diameters between the two.

TABLE 2. Diameter of water at various temperatures*

T (°C)	$\bar{V}/\beta RT$	a (Å)
5	15.808_1	2.724
10	15.983_9	2.728
15	16.088_9	2.730_5
20	16.128_6	2.732
25	16.111_7	2.733
30	16.041_9	2.733
35	15.924_7	2.732
40	15.770_2	2.730
45	15.578_4	2.728

*Using eq. 18 of ref. 34.

Diameters of Water

The diameters of water at various temperatures were calculated from the density and compressibility data of pure water (35, 36) in a way similar to Mayer (37) but using the Carnahan and Starling's (38) equation of state of a hard sphere fluid. They are found in Table 2. The present results are slightly different from Mayer (37) but the trends reported are quite similar. The difference probably arises since Mayer used the equation of state of Reiss *et al.* (1) which differs from that of Carnahan and Starling by a term $-y^3$; this may cause differences of the order of 0.01 to 0.02 Å on the diameters. As we are looking for precise parameters, it seems appropriate to use the Carnahan and Starling's equation of state which gives the best fit to computer simulation results for hard sphere fluids. Then, at 25 °C the diameter calculated, 2.73_3 Å, is in excellent agreement with the value of Rowlinson (39), 2.73 Å, and the mean value, 2.7 Å, previously mentioned.

Diameters of the R_4N^+ Ions

The diameters of the R_4N^+ cations can be

Can. J. Chem. Downloaded from www.nrcresearchpress.com by 210.87.254.42 on 09/05/12
For personal use only.

TABLE 3. Diameters of R_4N^+ in water at 25 °C, in Å

Technique	Diameter				
	Me_4N^+	Et_4N^+	Pr_4N^+	Bu_4N^+	Pen_4N^+
Bond lengths (44)	6.94	8.00	9.04	9.88	
Conductance (45)	4.94	6.10	7.14		
Parachor (46)	5.4	6.4	7.4	8.2	
Partial molal volumes (47)	5.70	6.96	7.96	8.74	
SPT-salting coefficients (10)	5.02	6.16	6.98	7.62	8.16*
SPT-compressibilities	5.54	6.84	7.92	8.73	9.50*

*Extrapolated.

estimated from the apparent molal compressibilities, as described by Desrosiers and Lucas (34). The apparent molal isothermal compressibilities ϕ_K of the R_4NBr were calculated from the adiabatic ones (40), the apparent molal expansibilities ϕ_E (41*a*), and heat capacities ϕ_C (41*a*) following the method of Desnoyers and Philip (42). From ϕ_K and the corresponding apparent molal volumes ϕ_V in water (41*a*), the diameters of the R_4N^+ can be calculated if a value is assumed for the Br^-. The diameter of Br^- was taken as 3.95 Å (34, 43) but its value is not too critical since if it is varied by 0.20 Å it causes a change of only 0.04 Å on the diameter of R_4N^+. Details of the calculations are given elsewhere (29). These radii are compared in Table 3 with some literature data of which the first three series are probably not very reliable. The agreement between the present calculations and the radii derived from the standard partial molal volume $\bar{V}^0$ is remarkably good, especially with the larger homologs. This probably occurs since, with our SPT techniques, the standard partial molal compressibility is related to the radii of the various constituents through $\bar{V}^0$.

The radii calculated from the SPT using the salting data (10) differ significantly from the present calculations. This may be due in part to the paucity of reliable salting data with simple solutes and in part to the technique itself.

With this technique, the solute is a nonpolar gas while R_4NBr is the cosolvent of water. As the apparent molal volumes of the R_4NBr in water appear in these SPT equations, we may assume that most of the soft part of the mixed solvent potential is then taken into account. On the other hand, for the nonpolar solute, Masterton *et al.* (10) had to estimate some inductive and dispersion terms. These latter calculations may be fairly uncertain especially in the presence of the higher homologs R_4NBr where the dispersion forces may play an important role. With our compressibility technique, the solute is R_4NBr and the solvent pure water. As we have to use in the equation the density of water and the apparent molal volume of R_4NBr in water, we may assume that the soft part of the potential of both the solute and the solvent is accounted for to a large extent. This compressibility method which is therefore more empirical due to its excess function character (34) probably suffers from less uncertainty in the determination of the effective radii of R_4N^+ since we do not have to correct explicitly for the dispersion and inductive forces.

Diameters of Mixed Solvents

Two approaches will be used for the calculation of the diameters of the mixed solvent. The mixed solvent can be considered as a pure 'uniform' solvent characterized by some mean diameter or it can be treated as a binary system characterized by two diameters, one for each species (three for the mixture NaCl–W).

In the first approach we calculate mean diameters for the mixed solvents from the isothermal compressibilities in the same way we did for pure water. The compressibility data used for U–W mixtures are those of Mathieson and co-workers (25, 48), for NaCl–W those of Gucker (31), and for TBA–W those of Bertrand and Smith (32). The corresponding density data are from Desrosiers *et al.* (25) for U–W, from Fortier *et al.* (49) for NaCl–W, and from Desnoyers *et al.* (23) for TBA–W.

In the second approach, the system water–cosolvent is considered as a binary system and the SPT compressibility method of Desrosiers and Lucas (34) is used. The diameter of pure water is previously determined and that of the

Can. J. Chem. Downloaded from www.nrcresearchpress.com by 210.87.254.42 on 09/05/12
For personal use only.

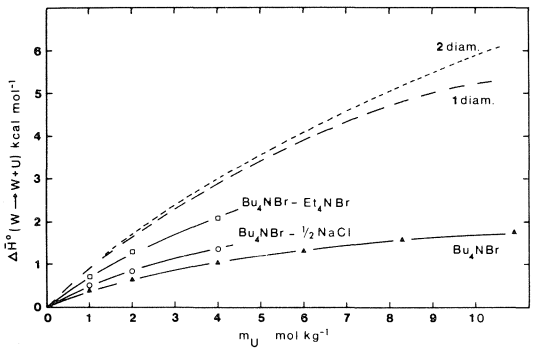

FIG. 1. Standard enthalpies of transfer of Bu_4N^+ from water to urea–water mixtures at 25 °C: data from Cassel and Wen (33).

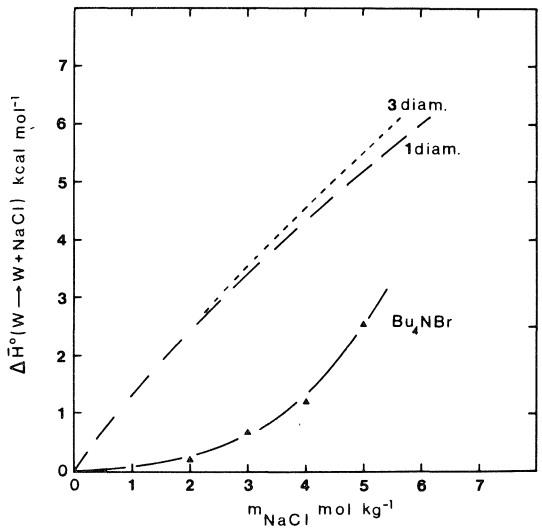

FIG. 2. Standard enthalpies of transfer of Bu_4N^+ from water to NaCl–water mixtures at 25 °C: data from Chawla and Ahluwalia (41*b*).

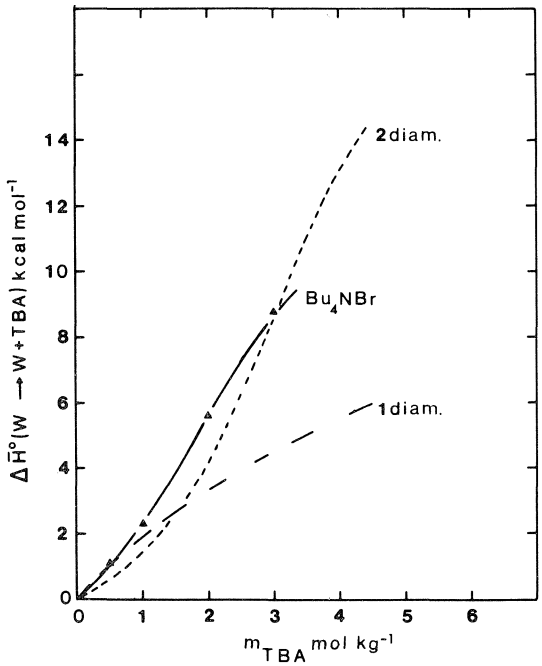

FIG. 3. Standard enthalpies of transfer of Bu_4N^+ from water to *tert*-butyl alcohol – water mixtures at 25 °C: data from Mohanty *et al.* (41*c*).

cosolvent (considered as a solute) is derived from the compressibility technique, the concentration dependence of the various functions being taken into account through the number density terms. The diameters then obtained are 4.40_8 Å for U, 1.83_6 Å for Na^+, and 3.79_2 Å for Cl^- (34). For TBA the value of 6.15 Å derived by Aveyard and Heselden (50) for *n*-butanol was used since the dependence on the concentration of the experimental β available was not accurate enough to apply our compressibility technique.

Predicted Standard Transfer Functions

From the knowledge of the various diameters and the experimental properties of the solvents, the standard thermodynamic properties of transfer of Bu_4N^+ from water to the mixed aqueous solvents can be calculated. The standard enthalpies of transfer of Bu_4NBr from water to U–W, NaCl–W, and TBA–W are given as a function of cosolvent molality in Figs. 1 to 3. To compare the experimental data with the calculations we need to estimate the ionic contributions to the transfer functions. Two methods can be used to estimate these values. Fortier *et al.* (51) and Desrosiers *et al.* (25) have shown that the transfer functions of alkali halides from H_2O to D_2O and from W to U–W mixtures do not vary much for alkali halides. As a first approximation, we can assume that the transfer function of Br^- can be taken as one-half that of any pair of alkali halides which does not show any specific interactions with the solvent. Secondly, it is often assumed that Et_4N^+ has little overall effect on the structure of water, its hydrophobic character being compensated by the field effect; the transfer functions could be considered close to zero with this ion and an estimate of the transfer function of Bu_4N^+ can be obtained by subtracting from the data for

Can. J. Chem. Downloaded from www.nrcresearchpress.com by 210.87.254.42 on 09/05/12
For personal use only.

Can. J. Chem. Downloaded from www.nrcresearchpress.com by 210.87.254.42 on 09/05/12
For personal use only.

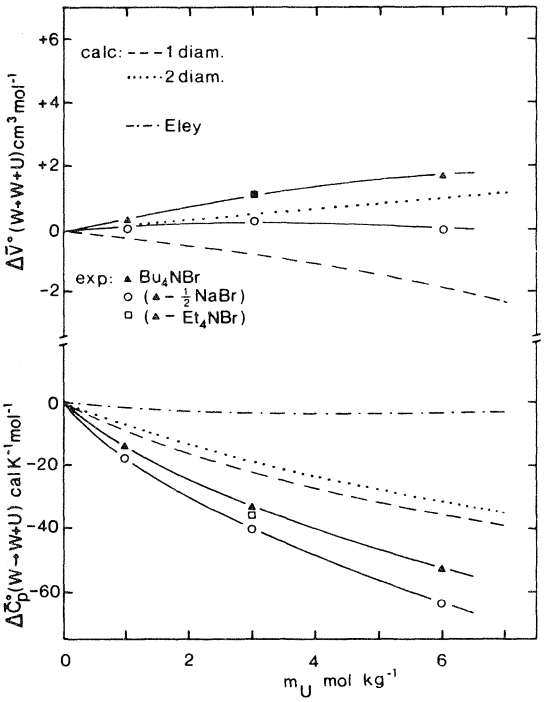

FIG. 4. Standard volumes and heat capacities of transfer of Bu_4N^+ from water to urea–water mixtures at 25 °C: data from Perron *et al.* (41*a*) and Desrosiers *et al.* (25).

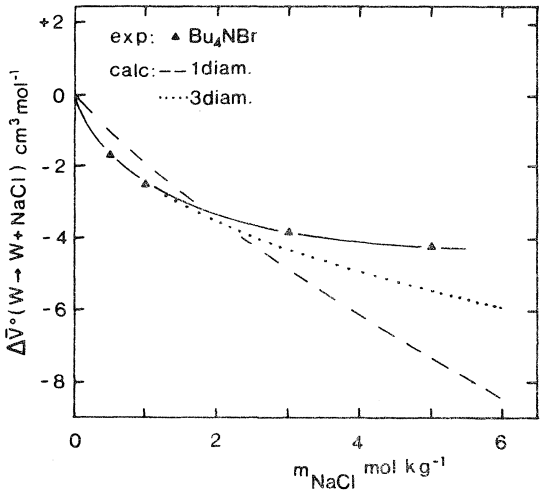

FIG. 5. Standard volumes of transfer of Bu_4N^+ from water to NaCl–water mixtures at 25 °C: data from Desrosiers and Desnoyers (53).

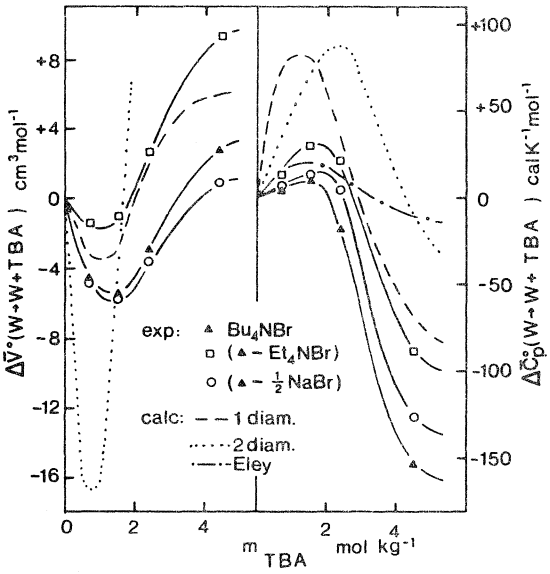

FIG. 6. Standard volumes and heat capacities of transfer of Bu_4N^+ from water to *tert*-butyl alcohol – water mixtures at 25 °C: data from Avédikian *et al.* (22).

Bu4NBr the corresponding data for Et4NBr. These two approximate values for the standard experimental enthalpies of transfer of Bu_4N^+ from U to U–W are also shown in Fig. 1.

Considering the uncertainty in the experimental enthalpies of transfer of Bu_4N^+, especially with the systems NaCl–W and TBA–W, we can conclude that the SPT predicts correctly the signs, the magnitudes, and general trends of the standard enthalpies of transfer as a function of cosolvent molality. As expected, the agreement with the two estimations of the ionic experimental enthalpies of transfer is better than with the total enthalpies of transfer. Both approaches to the SPT calculations either with one diameter for the mixed solvent or with one diameter for each species involved give very similar results for the enthalpies of transfer. The more noticeable difference with $\Delta\bar{H}^0(W \rightarrow W + TBA)$ could well arise from the experimental uncertainty in some of the parameters used in the calculations.

Similar plots are shown for the standard volumes and heat capacities of transfer in Figs. 4 to 6. Here again the signs and trends are generally predicted correctly in all cases investigated. The calculations of $\Delta\bar{V}^0(W \rightarrow W + U)$ using one mean diameter for the mixed solvent or the mixture approach with a diameter for each species have opposite signs but it is not obvious if the experimental ionic $\Delta\bar{V}^0(W \rightarrow W + U)$ are positive or negative. In the case of $\Delta V^0(W \rightarrow$

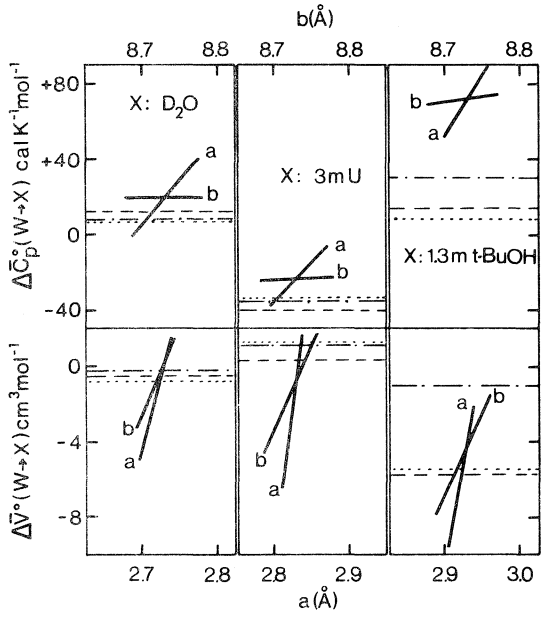

FIG. 7. Dependence of standard transfer functions on the diameter of the various species in solution: *a*, dependence on mean diameter of the mixed solvent or D_2O; *b*, dependence on diameter of the solute, · · · experimental results for Bu_4NBr, --- experimental results corrected for $\frac{1}{2}NaCl$, -·-·-· experimental results corrected for Et_4NBr. The cross points of lines *a* and *b* are the calculations given in previous figures.

W + TBA) the two diameters approach seems to overestimate the cosolvent concentration dependence but this could be attributed to a small error in the estimate of the diameter of TBA since volumes are very sensitive to the choice of the diameter.

The standard heat capacities of transfer were also calculated with Eley's classical theory for cavity formation (52). Here again the sign is predicted correctly but $\Delta\bar{C}_p^0(W \rightarrow W + U)$ is underestimated and the cosolvent concentration dependence of $\Delta\bar{C}_p^0(W \rightarrow W + TBA)$ is not as good as in the case of the SPT.

Finally, we have checked the sensitivity of the calculations to the diameters of the various components. This was achieved by keeping the diameter of one solvent constant (*e.g.* water) and changing the diameter of the other solvent by small amounts (fixed R_4N^+ diameter). In a second series of calculations the diameters of the R_4N^+ are assumed to be slightly different in both solvents, the diameters of these being then fixed. Both sets of calculations (29) are compared with the experimental data for the volumes and heat capacities of transfer from H_2O to D_2O, from W to W + U and from W to W + TBA in Fig. 7. As we can see in the case of heat capacities the SPT calculations are not too sensitive to the choice of solute diameters but are very sensitive to that of the solvent. For volumes, the calculations are very sensitive to the diameters of both the solute and the solvent and a small change in diameter may easily change the sign of the volume of transfer. Of course the SPT calculations are much less sensitive to the choice of diameters if the diameters of both solvents or of solutes in both solvents are changed simultaneously. Also the calculations are less sensitive to the solvent diameters if two (or three) diameters are used to characterize the binary solvent mixture.

Conclusion

The SPT has been used successfully to predict the signs, magnitudes, and trends in the cosolvent concentration dependence of the enthalpies, volumes, and heat capacities of transfer of Bu_4N^+ from water to aqueous mixed solvents using cavity terms only. This success is surprising at first sight since no modification of the structure of water by the solute or by the cosolvent and no attractive or repulsive forces between the solute and cosolvent are explicitly assumed in the present calculations. Actually, Bu_4NBr is expected to be salted out by NaCl and salted in by TBA. For example, the concentration dependence of the various thermodynamic properties of TBA in water are rather similar to those of surfactants in water (22). Therefore at high TBA concentrations some form of aggregation between TBA molecules is expected. The transfer of Bu_4NBr from water to TBA–W mixtures is qualitatively similar to the excess functions of TBA in W or Bu_4NBr in W (54) suggesting that Bu_4N^+ forms a mixed micelle with TBA. The structure of water or of the mixed solvent is obviously taken into account in the experimental parameters α, $d\alpha/dT$, and β and part of the solute–solvent interactions may be absorbed in the various diameters since the diameters were in fact derived from the SPT. Therefore, the empirical use of the SPT reduced it mostly to a correlation device between the density (and its derivatives) of the solvent and mixed solvent and the thermodynamic properties of the solutes.

Can. J. Chem. Downloaded from www.nrcresearchpress.com by 210.87.254.42 on 09/05/12
For personal use only.

Can. J. Chem. Downloaded from www.nrcresearchpress.com by 210.87.254.42 on 09/05/12
For personal use only.

Although the SPT cannot give us much molecular insight on the interactions in solution, it appears as a useful predicting device for transfer functions.

Despite the limitations of the SPT some useful implications can be drawn from its application to hydrophobic solutes in aqueous solutions. This theory does not rule out any changes in the properties of water near hydrophobic solutes but it does suggest that such structural changes, if they exist, must either be small or be proportional to the extent of structure of the liquid before the addition of a solute. A similar conclusion had been reached for the transfer functions of structure-breaking alkali halides from H_2O to D_2O (51) and from W to W + U (25) using a phenomenalogical representation of the Frank and Wen model (55).

Acknowledgement

We would like to thank Dr. M. Lucas for many stimulating discussions during the course of this project. We are also grateful to the National Research Council of Canada for financial support and for the award of a scholarship to one of us (N.D.).

1. H. Reiss, H. L. Frisch, and J. L. Lebowitz. J. Chem. Phys. **31**, 369 (1959).
2. H. Reiss, H. L. Frisch, E. Helfand, and J. L. Lebowitz. J. Chem. Phys. **32**, 119 (1960).
3. E. Helfand, H. Reiss, H. L. Frisch, and J. L. Lebowitz. J. Chem. Phys. **33**, 1379 (1960).
4. H. Reiss. Adv. Chem. Phys. **9**, 1 (1964).
5. R. A. Pierotti. J. Phys. Chem. **69**, 281 (1965).
6. M. Lucas. Bull. Soc. Chim. Fr. **9**, 2994 (1969).
7. M. Lucas and A. de Trobriand. J. Phys. Chem. **75**, 1803 (1971).
8. A. Feillolay and M. Lucas. J. Phys. Chem. **76**, 3068 (1972).
9. W. L. Masterton and T. P. Lee. J. Phys. Chem. **74**, 1776 (1970).
10. W. L. Masterton, D. Bolocofsky, and T. P. Lee. J. Phys. Chem. **75**, 2809 (1971).
11. S. K. Shoor and K. E. Gubbins. J. Phys. Chem. **73**, 498 (1969).
12. M. Lucas and A. Feillolay. Bull. Soc. Chim. Fr. **4**, 1267 (1970).
13. M. Lucas. Bull. Soc. Chim. Fr. **8–9**, 2902 (1970).
14. M. Lucas and A. Feillolay. J. Phys. Chem. **75**, 2330 (1971).
15. P. R. Philip and C. Jolicoeur. J. Solution Chem. **4**, 105 (1975).
16. M. Lucas. J. Phys. Chem. **80**, 359 (1976).
17. M. Lucas and R. Bury. J. Phys. Chem. **80**, 999 (1976).
18. F. H. Stillinger. J. Solution Chem. **2**, 141 (1973).
19. M. J. Mastroianni, M. J. Pikal, and S. Lindenbaum. J. Phys. Chem. **76**, 3050 (1972).
20. C. de Visser and G. Somsen. J. Solution Chem. **3**, 847 (1974).
21. T. S. Sarma and J. C. Ahluwalia. Chem. Soc. Rev. **2**, 203 (1973).
22. L. Avédikian, G. Perron, and J. E. Desnoyers. J. Solution Chem. **4**, 331 (1975).
23. J. E. Desnoyers, O. Kiyohara, G. Perron, and L. Avédikian. Adv. Chem. Ser. In press.
24. J. Kenttamaa, E. Tommila, and M. Martti. Ann. Acad. Sci. Fenn. Ser. AII, **93**, 3 (1959).
25. N. Desrosiers, G. Perron, J. G. Mathieson, B. E. Conway, and J. E. Desnoyers. J. Solution Chem. **3**, 789 (1974).
26. J. L. Lebowitz, E. Helfand, and E. Praestgaard. J. Chem. Phys. **43**, 774 (1965).
27. J. L. Lebowitz and J. S. Rowlinson. J. Chem. Phys. **41**, 133 (1964).
28. M. Lucas. J. Phys. Chem. **77**, 2479 (1973).
29. N. Desrosiers. Ph.D. Thesis, Université de Sherbrooke, Sherbrooke, Quebec. 1975.
30. R. E. Gibson. J. Am. Chem. Soc. **57**, 284 (1935).
31. F. T. Gucker. J. Am. Chem. Soc. **56**, 1017 (1934).
32. G. Bertrand and L. E. Smith. J. Phys. Chem. **74**, 4171 (1970).
33. R. B. Cassel and W.-Y. Wen. J. Phys. Chem. **76**, 1369 (1972).
34. N. Desrosiers and M. Lucas. J. Phys. Chem. **78**, 2367 (1974).
35. G. S. Kell. J. Chem. Eng. Data, **12**, 66 (1967).
36. G. S. Kell. J. Chem. Eng. Data, **15**, 119 (1970).
37. S. W. Mayer. J. Phys. Chem. **67**, 2160 (1963).
38. N. F. Carnahan and K. E. Starling. J. Chem. Phys. **51**, 635 (1969).
39. J. S. Rowlinson. Trans. Faraday Soc. **47**, 120 (1951).
40. J. G. Mathieson and B. E. Conway. J. Chem. Soc. Faraday Trans. I, **70**, 752 (1974).
41. (*a*) G. Perron, N. Desrosiers, and J. E. Desnoyers. Can. J. Chem. **54**, 2163 (1976); (*b*) B. Chawla and J. C. Ahluwalia. J. Phys. Chem. **76**, 2582 (1972); (*c*) R. K. Mohanty, T. S. Sarma, S. Subramanian, and J. C. Ahluwalia. Trans. Faraday Soc. **67**, 305 (1971).
42. J. E. Desnoyers and P. R. Philip. Can. J. Chem. **50**, 1094 (1972).
43. T. C. Waddington. Trans. Faraday Soc. **62**, 1482 (1966).
44. R. A. Robinson and R. H. Stokes. Electrolyte solutions. Butterworths, London. 1959. p. 125.
45. E. A. Moelwyn-Hughes. Physical chemistry. Pergamon Press, London. 1957. p. 835.
46. N. C. Deno and C. H. Spink. J. Phys. Chem. **67**, 1347 (1963).
47. B. E. Conway, R. E. Verrall, and J. E. Desnoyers. Trans. Faraday Soc. **62**, 2738 (1966).
48. J. G. Mathieson and B. E. Conway. J. Solution Chem. **3**, 781 (1974).
49. J. L. Fortier, P. A. Leduc, and J. E. Desnoyers. J. Solution Chem. **3**, 323 (1974).
50. R. Aveyard and R. Heselden. J. Chem. Soc. Faraday Trans. I, **71**, 312 (1975).

51. J. L. FORTIER, P. R. PHILIP, and J. E. DESNOYERS. J. Solution Chem. **3**, 523 (1974).
52. D. D. ELEY. Trans. Faraday Soc. **35**, 1281 (1939).
53. N. DESROSIERS and J. E. DESNOYERS. Can. J. Chem. **53**, 3206 (1975).
54. J. E. DESNOYERS, G. PERRON, J. P. MOREL, and L. AVÉDIKIAN. Chemistry and physics of aqueous gas solutions. *Edited by* W. A. Adams. The Electrochemical Society, Princeton, N.J. 1975. p. 172.
55. H. S. FRANK and W.-Y. WEN. Discuss. Faraday Soc. **24**, 133 (1957).

Appendix

Basic Scaled-particle Theory Equations for Cavity Formation

The molar free energy of formation of a cavity of diameter b in a mixed solvent is given by

$$[A1] \qquad \bar{G}_c = RT\left[-\ln(1-\xi_3) + 3\frac{\xi^2}{(1-\xi_3)}b + 3\frac{\xi_1}{(1-\xi_3)}b^2 + \frac{9}{2}\frac{\xi_2{}^2}{(1-\xi_3)^2}b^2 + \frac{N\pi P}{6RT}b^3\right]$$

where

$$\xi_k = \frac{N}{6}\pi\sum_{i=1}^{m}\rho_i a_i{}^k$$

and m is the number of species in the mixed solvent, ρ_i is the number density of the species i of diameter a_i, k has the values 1, 2, or 3, N is Avogadro's number, P is the pressure, and R the gas constant.

The corresponding enthalpy, volume, and heat capacity of cavity formation are

$$[A2] \qquad \bar{H}_C = \frac{\alpha RT^2}{(1-\xi_3)}\left[\xi_3 + \frac{3\xi_2}{(1-\xi_3)}b + \frac{3\xi_1}{(1-\xi_3)}b^2 + \frac{9\xi_2{}^2}{(1-\xi_3)^2}b^2\right]$$

where α is the coefficient of thermal expansion of the mixed solvent. (For $\bar{H}_C$ the term involving the pressure is negligible and omitted.)

$$[A3] \qquad \bar{V}_C = \frac{\beta}{\alpha}\frac{\bar{H}_C}{T} + \frac{N\pi}{6}b^3$$

where β is the coefficient of isothermal compressibility, and

$$[4] \qquad \bar{C}_C = \bar{H}_C\left[\frac{2}{T} + \frac{1}{\alpha}\left(\frac{\partial\alpha}{\partial T}\right)_P\right] - \alpha\bar{H}_C\frac{(1+\xi_3)}{(1-\xi_3)} + \frac{\alpha^2RT^2}{(1-\xi_3)^2}\left[\xi_3{}^2 - \frac{9\xi_2{}^2}{(1-\xi_3)^2}b^2\right]$$

(The pressure term is also negligible here and omitted.)

These equations reduce to the binary equations of Pierotti by setting m, the number of species in the mixed solvent, equal to unity.

Can. J. Chem. Downloaded from www.nrcresearchpress.com by 210.87.254.42 on 09/05/12
For personal use only.

Can. J. Chem. Downloaded from www.nrcresearchpress.com by 210.87.254.6 on 09/05/12
For personal use only.

Highly stereoselective H–D exchange of diastereotopic protons in 4′,1″-dimethyl-1,2,3,4-dibenzylcyclohepta-1,3-diene-6-one

ROBERT R. FRASER AND PHILIPPE J. CHAMPAGNE
Department of Chemistry, University of Ottawa, Ottawa, Ont., Canada K1N 6N5

Received June 22, 1976

ROBERT R. FRASER and PHILIPPE J. CHAMPAGNE. Can. J. Chem. **54**, 3809 (1976).

The rates of base-catalyzed H–D exchange of the diastereotopic methylene protons adjacent to the carbonyl group in the title compound have been measured in methanol-*O-d*. Sodium methoxide as catalyst produced a rate ratio of 73:1. Reasons for the large increase in stereoselectivity over that encountered in the exchange of 4-*tert*-butylcyclohexanone are proposed.

ROBERT R. FRASER et PHILIPPE J. CHAMPAGNE. Can. J. Chem. **54**, 3809 (1976).

On a mesuré les vitesses d'échange H–D, catalysées par les bases dans le méthanol-*O-d*, des protons méthyléniques diastéréotopes adjacents au groupement carbonyle du composé mentionné dans le titre. Le méthylate de sodium comme catalyseur produit un rapport de vitesse de 73:1. On propose une rationalisation pour expliquer la grande augmentation dans la stéréosélectivité par rapport à celle observée lors de l'échange de la *tert*-butyl-4 cyclohexanone.

[Traduit par le journal]

The base-catalysed H–D exchange of protons α to the carbonyl group in cyclic and bicyclic ketones has been the subject of extensive study (1–3). In a number of cases involving bicyclic ketones the difference in reactivity of a pair of diastereotopic protons was very high, for example in norbornanone k_{exo}:k_{endo} was found to be 680:1. This stereoselectivity was most reasonably attributed to differing steric environments of the two protons. In contrast, 4-*tert*-butylcyclohexanone, a ketone free from strong steric influences, has shown little stereoselectivity, the rate ratio for exchange of the axial *vs.* equatorial protons being 5:1 (4). The preference for axial exchange was interpreted as arising from stereoelectronic control (5). That the stereoelectronic factor should produce only a five-fold rate difference is perhaps surprising when *ab initio* calculations suggest much higher selectivities should be possible (6). In this paper we wish to report the observation of a substantially larger stereoselectivity than any previously attributable to stereoelectronic control, specifically that the ketone under study, 4′,1″-dimethyl-1,2,3,4-dibenzcyclohepta-1,3-diene-6-one, **1**, underwent base-catalysed H–D exchange of its methylene protons in methanol-*O-d* with a stereoselectivity of 73:1.

As a consequence of the lack of rotation about the biaryl bond in **1** (7) the methylene protons are diastereotopic and give rise to an AB quartet in the 100 MHz spectrum of **1** (in $CDCl_3$, δ_R = 3.497; δ_S = 3.295; δ_{RS} = 14.9 Hz). Assignments of these signals as given in Fig. 1 are based on two criteria. Firstly, the line widths of H_R and H_S differ appreciably being 1.6 Hz and 1.2 Hz respectively. Extensive studies by Schaefer *et al.* (8) have clearly established that the magnitudes of long-range couplings between aromatic and benzylic protons are dependent upon the orientation of the benzylic C—H bond with respect to the plane of the benzene ring. The sum of the *ortho*, *meta*, and *para* coupling constants to a benzylic proton is significantly greater when the C—H bond is perpendicular to the plane of the ring. We therefore assign the broader low-field absorption to the proton having this orientation (*i.e.*, H_R in Fig. 1).

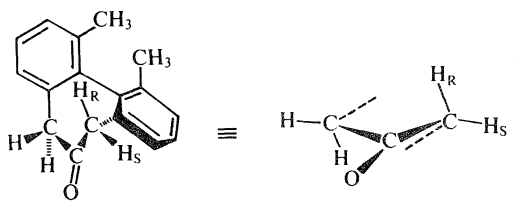

FIG. 1. A three-dimensional representation of 4′,1″-dimethyl-1,2,3,4-dibenzylcyclohepta-1,3-diene-6-one, **1**.

TABLE 1. Rates of exchange of diastereotopic protons of **1** in methanol-*O*-*d*

Base	Concentration (*M*)	k_R (s^{-1})*	k_S (s^{-1})*	k_R/k_S†
CH_3ONa	0.0029	8.2×10^{-3}	1.13×10^{-5}	73
C_6H_5ONa	0.0029	3.5×10^{-3}	1.18×10^{-5}	30

*All rate constants, reported as pseudo first-order constants, were measured at 29.0 °C. Aliquots of the solution of ketone, 0.17 *M* in CH_3OD (+ base), were quenched at appropriate intervals to give one sample for measurement of loss of the fast proton, a second for measurement of loss of the slow proton. The proton content, determined by integration of the nmr spectra using both a T-60 and an HA-100 spectrometer, was further checked by examination of the 100 MHz spectrum with deuterium spin-decoupling. The spectra showed the presence of deuterium in place of the fast proton only in those samples used to measure k_R. Samples used to measure k_S showed the amount of residual proton in the fast position to be at the level of the solvent pool. For the rates obtained, those isomer distributions agree with those calculated using the equations of Hunter and Mair (16). The precision in rate constants thus obtained is considered to be ±5%.

†Integrals obtained from ^1H nmr analysis with deuterium decoupling of a single sample exchanged for the appropriate time using sodium 2,6-dimethylphenoxide as base, showed the selectivity, k_R/k_S, to be 7.8.

Table 1 presents the rates of isotopic exchange of H_R and H_S under a variety of conditions. One trend apparent from these data is the obvious increase in selectivity as the bulk of the attacking base is reduced. This indicates the more labile proton to be in a more hindered environment. Since we have shown the environment analogous to that of H_R is more hindered in the structurally similar thiepin dioxide, **2**, (9) the data in Table 1 also support the proton assignments.

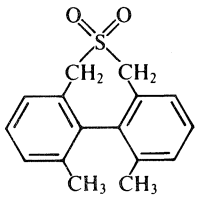

2

In order to interpret the selectivity data it is necessary to assume that no internal return occurs during the exchange process.[1] Several authors have previously made this assumption (1, 2) on the basis of the experimental evidence of Bordwell and Almy (10). Further support for its absence in the exchange of **1** is provided by the survey of Hunter, from which he concludes that in methanol the likelihood of internal return is slight (11).

The highest selectivity observed in the exchange of **1** occurred when the least bulky base, methoxide, was employed. Since methoxide may too suffer from steric suppression for abstraction of H_R, the 73:1 rate ratio represents a lower limit to the stereoelectronic factor.[2] This rate ratio reflects a difference in transition state free energies of 2.6 kcal/mol. This is significantly greater than the 1.0 kcal/mol difference in the exchanges of 4-*tert*-butylcyclohexanone, in spite of the fact that the orientation of the methylene protons with respect to the carbonyl is the same in both ketones.

It is instructive to consider the structural differences between **1** and **2** which would explain the contrast in stereoselectivity. House *et al.* have offered a plausible accounting for the weak selectivity in the electrophilic substitution of enolates of cyclohexanones (14).

Attack of an electrophile on the planar enolate leads to formation of an axial bond while maintaining overlap in the C⋯C⋯O system throughout the course of reaction. However, attack leading to equatorial substitution is energetically disfavored since, in order to maintain delocalization of the enolate in the transition state, a boat conformation must be produced. The difference in free energies of the two transition states turns out to be very small since they both will differ little from the enolate itself in an exothermic protonation and also since the boat conformation of a cyclohexanone is only about 2.7

[1]Equal amounts of internal return for both protons would also permit interpretation.

[2]One additional factor, the difference in stabilization by the adjacent benzene ring, can be shown to be negligible. In a separate experiment, the benzylic protons of 1-phenylpropanone exchanged 10 times faster than the methyl protons. If one third of this 1.4 kcal/mol of stabilization is inductive (12) and the remaining 0.95 kcal/mol is available through overlap as a function of $\cos\theta$, (13) the difference in stabilization of H_R ($\phi = 45°$) *vs.* H_S ($\phi = 75°$) would be no more than 0.4 kcal/mol.

Can. J. Chem. Downloaded from www.nrcresearchpress.com by 210.87.254.6 on 09/05/12
For personal use only.

kcal/mol less stable than the chair form (15). In the exchange of **1** a strain-free enolate is again assumed to be involved and deuteration to give D_R proceeds readily, while maintaining overlap. But for deuteration of H_S to occur via a transition state maintaining delocalization of the partial negative charge, the molecule must adopt a more highly strained conformation than that for equatorial attack of a cyclohexanone enolate. This conformation, from examination of Dreiding models, appears to possess considerable bond angle strain as it lies on the pathway to inversion of the biaryl chirality.

If the above explanation is correct, it should be possible to encounter still greater stereoselectivity in ketones having larger strain destabilization of the type proposed above. In a slightly different way, high stereoselectivity could also be encountered in very rigid structures which, as suggested by Wolfe and co-workers, would be forced to undergo exchange via nonplanar enolates (6).

Acknowledgement

The authors thank the National Research Council of Canada for financial support.

1. S. BANERJEE and N. H. WERSTIUK. Can. J. Chem. **53**, 1099 (1975).
2. G. A. ABAD, S. P. JINDAL, and T. T. TIDWELL. J. Am. Chem. Soc. **95**, 6326 (1973).
3. A. F. THOMAS. Deuterium labelling in organic chemistry. Appleton-Century-Crofts, New York, N.Y. 1971.
4. G. B. TRIMITSIS and E. M. VAN DAM. Chem. Commun. 610 (1974).
5. E. G. COREY and R. A. SNEEN. J. Am. Chem. Soc. **78**, 6269 (1956).
6. S. WOLFE, H. B. SCHLEGEL, I. G. CZISMADIA, and F. BERNARDI. Can. J. Chem. **53**, 3365 (1975).
7. K. MISLOW, R. E. O'BRIEN, and H. SCHAEFER. J. Am. Chem. Soc. **84**, 1940 (1962).
8. T. SCHAEFER, J. B. ROWBOTHAM, W. J. E. PARR, K. MARAT, and A. F. JANZEN. Can. J. Chem. **54**, 1322 (1976), and numerous references therein.
9. R. R. FRASER and F. J. SCHUBER. Can. J. Chem. **48**, 633 (1970); R. R. FRASER. and F.J. SCHUBER. Chem. Commun. 1474 (1969).
10. F. G. BORDWELL and J. ALMY. J. Org. Chem. **38**, 575 (1973).
11. D. H. HUNTER. *In* Isotopes in organic chemistry. Vol. 1. *Edited by* E. Buncel and C. C. Lee. Elsevier, Amsterdam. 1975. p. 135
12. A. STREITWEISER, JR. and G. R. ZIEGLER. J. Am. Chem. Soc. **91**, 5081 (1969).
13. A. STREITWEISER, JR. Molecular orbital theory for organic chemistry. John Wiley and Sons Inc., New York, N.Y. 1961.
14. H. O. HOUSE, B. H. TERFERTILLER, and H. D. OLMSTEAD. J. Org. Chem. **33**, 935 (1968).
15. N. L. ALLINGER, M. TRIBBLE, and M. A. MILLER. Tetrahedron, **28**, 1173 (1972); F. A. L. ANET. J. Am. Chem. Soc. **95**, 4424 (1973).
16. D. H. HUNTER and R. W. MAIR. Can. J. Chem. **47**, 2361 (1969).

The X-ray photoelectron spectrum of hydrogen peroxide

M. S. BANNA, D. C. FROST, C. A. MCDOWELL, AND B. WALLBANK

Department of Chemistry, University of British Columbia, Vancouver, B.C., Canada V6T 1W5

Received August 3, 1976

M. S. BANNA, D. C. FROST, C. A. MCDOWELL, and B. WALLBANK. Can. J. Chem. **54**, 3811 (1976).

The oxygen 1*s* photoelectron spectrum of hydrogen peroxide in the gas phase has been investigated using AlKα radiation. The binding energy has been found to be 1.8(1) eV lower than the oxygen 1*s* level in carbon monoxide, as expected from simple electrostatic considerations.

M. S. BANNA, D. C. FROST, C. A. MCDOWELL et B. WALLBANK. Can. J. Chem. **54**, 3811 (1976).

Utilisant une radiation AlKα, on a examiné le spectre photoélectronique 1*s* de l'oxygène du peroxyde d'hydrogène en phase gazeuse. On a trouvé que l'énergie de liaison est 1.8(1) eV plus basse que le niveau 1*s* de l'oxygène du monoxyde de carbone et ces résultats correspondent à ce qui est attendu à partir de considérations électrostatiques simples.

[Traduit par le journal]

Can. J. Chem. Downloaded from www.nrcresearchpress.com by 210.87.254.6 on 09/05/12
For personal use only.

kcal/mol less stable than the chair form (15). In the exchange of **1** a strain-free enolate is again assumed to be involved and deuteration to give D_R proceeds readily, while maintaining overlap. But for deuteration of H_S to occur via a transition state maintaining delocalization of the partial negative charge, the molecule must adopt a more highly strained conformation than that for equatorial attack of a cyclohexanone enolate. This conformation, from examination of Dreiding models, appears to possess considerable bond angle strain as it lies on the pathway to inversion of the biaryl chirality.

If the above explanation is correct, it should be possible to encounter still greater stereoselectivity in ketones having larger strain destabilization of the type proposed above. In a slightly different way, high stereoselectivity could also be encountered in very rigid structures which, as suggested by Wolfe and co-workers, would be forced to undergo exchange via nonplanar enolates (6).

Acknowledgement

The authors thank the National Research Council of Canada for financial support.

1. S. Banerjee and N. H. Werstiuk. Can. J. Chem. **53**, 1099 (1975).
2. G. A. Abad, S. P. Jindal, and T. T. Tidwell. J. Am. Chem. Soc. **95**, 6326 (1973).
3. A. F. Thomas. Deuterium labelling in organic chemistry. Appleton-Century-Crofts, New York, N.Y. 1971.
4. G. B. Trimitsis and E. M. Van Dam. Chem. Commun. 610 (1974).
5. E. G. Corey and R. A. Sneen. J. Am. Chem. Soc. **78**, 6269 (1956).
6. S. Wolfe, H. B. Schlegel, I. G. Czismadia, and F. Bernardi. Can. J. Chem. **53**, 3365 (1975).
7. K. Mislow, R. E. O'Brien, and H. Schaefer. J. Am. Chem. Soc. **84**, 1940 (1962).
8. T. Schaefer, J. B. Rowbotham, W. J. E. Parr, K. Marat, and A. F. Janzen. Can. J. Chem. **54**, 1322 (1976), and numerous references therein.
9. R. R. Fraser and F. J. Schuber. Can. J. Chem. **48**, 633 (1970); R. R. Fraser. and F.J. Schuber. Chem. Commun. 1474 (1969).
10. F. G. Bordwell and J. Almy. J. Org. Chem. **38**, 575 (1973).
11. D. H. Hunter. *In* Isotopes in organic chemistry. Vol. 1. *Edited by* E. Buncel and C. C. Lee. Elsevier, Amsterdam. 1975. p. 135
12. A. Streitweiser, Jr. and G. R. Ziegler. J. Am. Chem. Soc. **91**, 5081 (1969).
13. A. Streitweiser, Jr. Molecular orbital theory for organic chemistry. John Wiley and Sons Inc., New York, N.Y. 1961.
14. H. O. House, B. H. Terfertiller, and H. D. Olmstead. J. Org. Chem. **33**, 935 (1968).
15. N. L. Allinger, M. Tribble, and M. A. Miller. Tetrahedron, **28**, 1173 (1972); F. A. L. Anet. J. Am. Chem. Soc. **95**, 4424 (1973).
16. D. H. Hunter and R. W. Mair. Can. J. Chem. **47**, 2361 (1969).

The X-ray photoelectron spectrum of hydrogen peroxide

M. S. Banna, D. C. Frost, C. A. McDowell, and B. Wallbank

Department of Chemistry, University of British Columbia, Vancouver, B.C., Canada V6T 1W5

Received August 3, 1976

M. S. Banna, D. C. Frost, C. A. McDowell, and B. Wallbank. Can. J. Chem. **54**, 3811 (1976).

The oxygen 1*s* photoelectron spectrum of hydrogen peroxide in the gas phase has been investigated using AlKα radiation. The binding energy has been found to be 1.8(1) eV lower than the oxygen 1*s* level in carbon monoxide, as expected from simple electrostatic considerations.

M. S. Banna, D. C. Frost, C. A. McDowell et B. Wallbank. Can. J. Chem. **54**, 3811 (1976).

Utilisant une radiation AlKα, on a examiné le spectre photoélectronique 1*s* de l'oxygène du peroxyde d'hydrogène en phase gazeuse. On a trouvé que l'énergie de liaison est 1.8(1) eV plus basse que le niveau 1*s* de l'oxygène du monoxyde de carbone et ces résultats correspondent à ce qui est attendu à partir de considérations électrostatiques simples.

[Traduit par le journal]

Can. J. Chem. Downloaded from www.nrcresearchpress.com by 210.87.254.42 on 09/05/12
For personal use only.

Can. J. Chem. Downloaded from www.nrcresearchpress.com by 210.87.254.42 on 09/05/12
For personal use only.

It is highly desirable to be able to study transient and unstable species by means of photoelectron spectroscopy. Considerable work in this field has already been carried out using HeI radiation.[1] The combination of high count rates and high resolution makes UPS well suited for such studies. The potential of XPS as a tool for studying transients is not as well understood, however, since only a few cases have been investigated to date (for example the core spectrum of NF_2 has been studied (see ref. 1)).

The yield of transient species can be increased by introducing the sample in the form of a molecular beam. This serves to reduce the number of collisions, resulting in longer lifetimes. Another complementary approach is the use of fast pumping to remove the gas before decomposition has occurred. The spectrometer used in the present study possesses the latter feature. The sample is introduced into a copper cell where it is irradiated with AlKα (1486.6 eV) X-rays. A high-speed liquid nitrogen-trapped diffusion pump removed the gas from the ionization region through a mesh, which is necessary to preserve field homogeneity inside the gas cell. Photoelectrons are retarded between the ionization chamber and an electrostatic lens system, then focussed into a 20 cm-diameter electrostatic hemispherical analyzer. A more detailed discussion of the apparatus will be given elsewhere.

Hydrogen peroxide provides a good test case for the study of unstable species since it decomposes upon contact with metal surfaces. Starting with a 30% aqueous solution, the sample was enriched by distillation at 50 °C in a glass manifold. It was then introduced into the spectrometer at room temperature through a Teflon nozzle. Carbon monoxide was bled in simultaneously as a calibrant. A typical spectrum is shown in Fig. 1(*a*). The oxygen 1*s* binding energy shift between carbon monoxide and water has been measured by several workers. Davis *et al.* (2) obtained 2.94(10) eV (E_B(CO) − E_B(H_2O)) while Siegbahn *et al.* (3) reported 2.4 eV. Our own measurement gave 2.7(1) eV. The latter value was used to determine the position of the water peak in the spectra of Fig. 1. Since water has a higher vapor pressure than hydrogen peroxide at room temperature, most

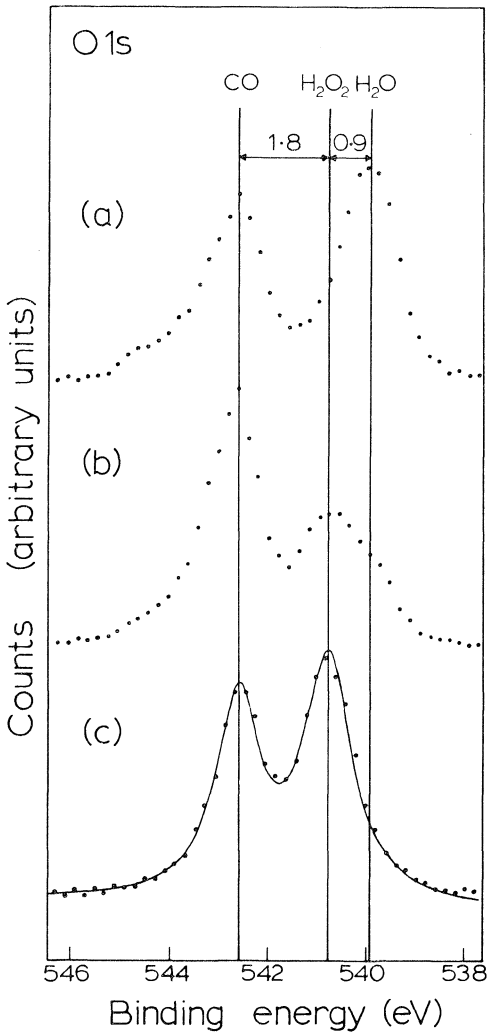

FIG. 1. Oxygen 1*s* photoelectron spectra of progressively enriched hydrogen peroxide samples with carbon monoxide as a reference.

of the peak on the right of Fig. 1(*a*) is due to the oxygen 1*s* of water. As the sample is enriched further, spectrum (*b*) is obtained, in which the shift with respect to CO has decreased. The oxygen 1*s* of water is now seen as a shoulder to the right of the main peak. Further purification yields spectrum (*c*) which contains little or no contribution from water. At this stage the CO–H_2O_2 shift was found to be 1.8(1) eV, as determined by curve fitting two Lorentzians to the experimental points. A typical spectrum from high-purity samples is shown in Fig. 2. From the known O_2–CO and CO–H_2O_2 shifts (4), the

[1]D. C. Frost and N. P. C. Westwood. To be published.

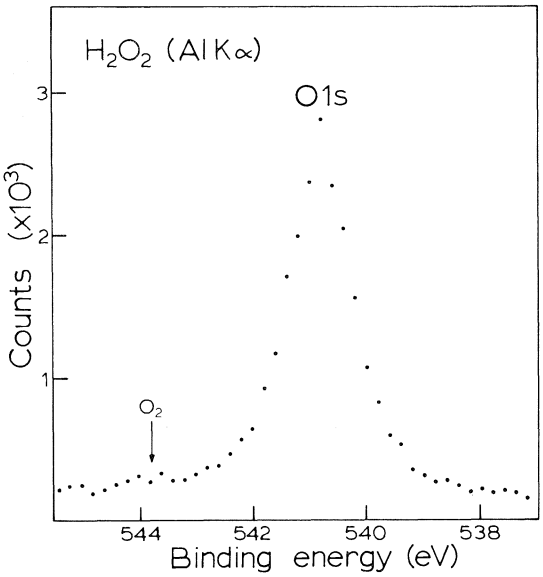

FIG. 2. The oxygen 1*s* spectrum of a high-purity hydrogen peroxide sample.

position of the oxygen 1*s* peaks of O_2 can be determined in the spectra of both Figs. 1 and 2.[2] This enabled us to assess the degree of decomposition of our sample. It is seen that H_2O_2 is obtained in good yield.

The binding energy trend CO > H_2O_2 > H_2O can be expected on the basis of decreasing charge withdrawal by the oxygen in going from H_2O to H_2O_2 then CO (for example, POLYATOM double zeta calculations yield the following oxygen charges: CO (−0.20), H_2O_2 (−0.42), and H_2O (−0.77). See ref. 5). Multiconfiguration self-consistent-field calculations on CO (6) predict further charge transfer from the oxygen to the carbon. Smith and Thomas (7) estimated a positive contribution of ~1 eV to the binding energy of oxygen 1*s* in CO from differences in the correlation and relativistic energies between the ground and ionized states. This value was reached by comparing the absolute binding energy measurements with a calculation employing a large enough basis set to be close to the Hartree–Fock limit. Thus the 1.8 eV shift between CO and H_2O_2 is in line with expectations.

[2]There is some disagreement in the literature about the O_2–CO binding energy shift. Reference 3 gives 1.2 eV (using the weighted mean of the two O_2 oxygen peaks), while ref. 3 gives 0.9(1) eV. The 1.2 eV results of Siegbahn *et al.* is supported by the measurement of ref. 4.

From the oxygen 1*s* binding energy value of 542.57 eV in CO (7), we compute 541.8(1) for the binding energy in H_2O_2. The majority of the *ab initio* SCF calculations performed on this molecule yield a Koopmans' Theorem energy around 561 eV.[3] As observed in numerous other systems, ground state energies yield values that are too high due to the neglect of relaxation. If we assume no change in relativistic and correlation energy upon ionization, we obtain an approximate relaxation energy of 19.3 eV for core ionization in hydrogen peroxide. Cambray *et al.* (8) obtained 20.24 eV for oxygen in carbon monoxide (Koopmans' Theorem binding energy minus Δ SCF energy). Schwartz (9) similarly obtained 20.0 eV for oxygen 1*s* ionization in water.

A preliminary investigation of oxygen 2*s* orbitals revealed a separation of no more than ~5 eV between the 2*b*, 2*a* pair, which disagrees with the recent theoretical value of 8.01 eV (10).

This work suggests the possibility of investigating the core spectra of numerous other unstable molecules by means of XPS. Efforts in this direction are now underway in our laboratory.

Acknowledgement

This work was supported by generous grants from the National Research Council of Canada.

1. D. W. DAVIS, R. L. MARTIN, M. S. BANNA, and D. A. SHIRLEY. J. Chem. Phys. **59**, 4235 (1973).
2. D. W. DAVIS, J. M. HOLLANDER, D. A. SHIRLEY, and T. D. THOMAS. J. Chem. Phys. **52**, 3295 (1970).
3. K. SIEGBAHN, C. NORDLING, G. JOHANSSON, J. HEDMAN, P. F. HEDEN, K. HAMRIN, U. GELIUS, T. BERGMARK, L. O. WERME, R. MANNE, and Y. BAER. ESCA applied to free molecules. North Holland, Amsterdam. 1969.
4. T. D. THOMAS. J. Chem. Phys. **53**, 1744 (1970).
5. L. C. SNYDER and H. BASCH. Molecular wavefunctions and properties. John Wiley and Sons, New York. 1972.
6. F. P. BILLINGSLEY and M. KRAUSS. J. Chem. Phys. **60**, 4130 (1974).
7. S. R. SMITH and T. D. THOMAS. J. Electron Spectrosc. **8**, 45 (1976).
8. J. CAMBRAY, J. GASTEIGER, A. STREITWIESER, JR., and P. S. BAGUS. J. Am. Chem. Soc. **96**, 5978 (1974).
9. M. E. SCHWARTZ. Chem. Phys. Lett. **5**, 50 (1970).
10. D. W. DAVIES. Chem. Phys. Lett. **28**, 520 (1974).

[3]The reference quoted in ref. 5 above gives 561.1 eV. This value was used to compute the approximate relaxation energy.

Can. J. Chem. Downloaded from www.nrcresearchpress.com by 210.87.254.42 on 09/05/12
For personal use only.

Can. J. Chem. Downloaded from www.nrcresearchpress.com by 210.87.254.5 on 09/05/12
For personal use only.

Canadian Journal of Chemistry

Published by
THE NATIONAL RESEARCH COUNCIL OF CANADA

Journal canadien de chimie

Publié par
LE CONSEIL NATIONAL DE RECHERCHES DU CANADA

Volume 54 Number 24 December 15, 1976 Volume 54 numéro 24 15 décembre 1976

Electronic and Raman spectroscopic studies of copper adrenalin complexes and copper induced compounds

MOHAMMED S. RAHAMAN AND STEPHEN M. KORENKIEWICZ[1]

Department of Chemistry and Chemical Engineering, Michigan Technological University, Houghton, MI 49931, U.S.A.

Received April 1, 1976

MOHAMMED S. RAHAMAN and STEPHEN M. KORENKIEWICZ. Can. J. Chem. **54**, 3815 (1976).

Electronic and Raman spectra of adrenalin–copper(II) complexes and copper catalyzed compounds have been studied. Adrenalin reacts with copper(II) ion at p*H* 9.2 and higher to produce a very short lived violet free radical, a brown adrenochrome, a yellow conjugated salt, indolyl-indoquinone, and melanin. Results indicate that copper does not form complexes with adrenalin in basic solution. Between p*H* 6.5 and 8.5 adrenalin transforms into adrenochrome in presence of copper. The adrenochrome in 1.5 *N* hydrochloric acid produces the conjugate salt that is produced in the solution of high p*H*. At low p*H* values, between p*H* 4.0 to 5.5, adrenalin forms a brown complex with copper(II). Copper is entirely chelated to the phenolic groups of the amines. The complex in 1.5 *N* hydrochloric acid produces a black polymeric pigment.

MOHAMMED S. RAHAMAN et STEPHEN M. KORENKIEWICZ. Can. J. Chem. **54**, 3815 (1976).

On a étudié les spectres électroniques et Raman de complexes adrénaline–cuivre(II) et de composés obtenus par catalyse par le cuivre. L'adrénaline réagit avec l'ion cuivre(II), à des p*H* de 9.2 ou plus élevé, pour conduire à un radical libre violet de très courte durée de vie, à un adrénochrome brun, à un sel conjugué jaune, à une indolyl-indoquinone et à la mélanine. Les résultats indiquent que le cuivre ne forme pas de complexes avec l'adrénaline en solution basique. A des p*H* allant de 6.5 à 8.5, l'adrénaline se transforme en adrénochrome en présence de cuivre. Dans l'acide chlorhydrique 1.5 *N*, l'adrénochrome conduit au sel conjugué qui est produit en solution à des p*H* plus élevé. A des valeurs de p*H* plus faibles, entre 4.0 et 5.5, l'adrénaline forme un complexe brun avec le cuivre(II). Le cuivre est complètement chélaté par les groupes phénoliques des amines. Dans l'acide chlorhydrique à 1.5 *N*, le complexe produit un pigment noir de nature polymérique.

[Traduit par le journal]

Introduction

Copper (ref. 1, pp. 443–452), manganese (2), and possibly nickel (3) ions play important roles in the reactions of catecholamines and catechol-amino-acids in the neurological system (4). Copper ion is involved in the catalytic β-hydroxylation of phenylamine and also forms complexes with the amines in biological systems (1). The coordination chemistry of these compounds is complicated by their ability to act as bidented and bridging ligands (5, 6). Metal ion catalyzed oxidation of the amines, formation of metal complex intermediates, rearrangement into diol system, and finally the polymerization are all complex phenomena.

The mechanism of oxidation of adrenalin, catalyzed by ferritin, has been reported and the reason for the loss of its vasoconstrictor activity has been discussed (7). The formation of melanin from adrenochrome in aqueous solution has been

[1]Present address: P. P. G. Industries, Coatings and Resins Division, Springdale Research and Development Center, Springdale, PA 15144.

TABLE 1. Some of the properties of copper–adrenaline complexes and copper catalyzed compounds of adrenaline

p*H*	Form	Description
≥9.2	Violet	A short lived "violet form" is probably an organic "free radical" formed by copper-assisted oxidation of adrenaline.
	Brown	A non-identified short lived "*brown form*" is reported (Fig. 1, curve *1*). It quickly changes to the yellow form below, spectra look like that of adrenochrome.
	Yellow Form I	The above brown form of the Cu(II) adrenaline system is changed to a yellow form (Fig. 2, curve *2*). However, Fig. 1, curves *2*, *3*, *4*, and *5* suggest this yellow form is a mixture. Results fail to prove complex formation.
	Green	Stable green form results in two hours (Fig. 1, curves *6*, *7*, and *8*). Results fail to prove complex formation. Probably this is one of the polymeric forms.
	Yellow Form II	Another yellow compound resulted at p*H* 9.5 from adrenaline in the absence of Cu(II) ion. The spectra of Fig. 1 curves *9*, *10*, and *11* suggest that this is melanin.
	Brown	A stable brown compound results in the system. Figure 2, curve *3* and Fig. 4, curve *3* suggest that this is not a copper complex. Spectra represented by Fig. 6, curve *4* (λ_{max} = 480 nm, ϵ_{max} = 3900) and Fig. 3 are similar to the spectra of adrenochrome. Figures 3 and 5 suggest that only one compound is formed.
	Yellow	The brown adrenochrome gives a yellow compound in 1.2 *N* HCl. This is identified as a conjugated salt (**2**, Fig. 7, curve *2*).
6.5–7.5	Brown	The brown compound in the Cu(II) adrenaline system is identified as adrenochrome.
4.5–5.5	Brown	The brown compound is identified as copper–adrenaline complex. Figure 2, curve *1* and Fig. 4 curves *1* and *2* suggest the composition is 2:1 adrenaline:copper(II). (λ_{max} = 500 nm, ϵ_{max} = 3800; additional peaks at 580, 410, 300, and 220 nm). Raman spectra, Fig 8, suggest copper is coordinated through phenolic groups of adrenaline and 1 mol of ammonium is coordinated.
	Blue	The brown complex in 1.2 *N* HCl transforms to a bluish colored system. Spectra (Fig. 7, curve *3*) of this system are not comparable with the other forms so far obtained. This form probably is an unidentified polymer.
	Black Pigment	The bluish form on standing produces a black pigment insoluble in strong acid. Identified as a polymeric form.

studied by spectrophotometric methods (8). Gorton and Jameson have suggested that polynuclear copper–catecholamine complex formation is possible (5, 6). Copper adrenalin complexes and the interreaction of catecholamines with ceruloplasmin have been studied by analyzing ultraviolet and electron spin resonance spectra in neutral and basic solutions (ref. 1, p. 539). There is some confusion as to whether copper ion, in fact, forms complexes or acts as a catalyst for indolization.

In the present work the effect of copper(II) ion on adrenalin in acidic, neutral, and basic solution has been studied spectrophotometrically, and the Raman spectra of the complexes have been analyzed. Our findings indicate that metal-complex formation is possible in acidic solution whereas, in neutral and basic solution the oxidized forms, their rearranged forms and polymeric forms are the products rather than the metal complexes.

Experimental

Reagents

Adrenalin bitartrate and adrenalin free base were obtained from Sigma Chemical Company. Stock solutions in 0.1 *N* hydrochloric acid were prepared from the amines as received. The solutions were stored under refrigeration and replaced every week.

Can. J. Chem. Downloaded from www.nrcresearchpress.com by 210.87.254.5 on 09/05/12
For personal use only.

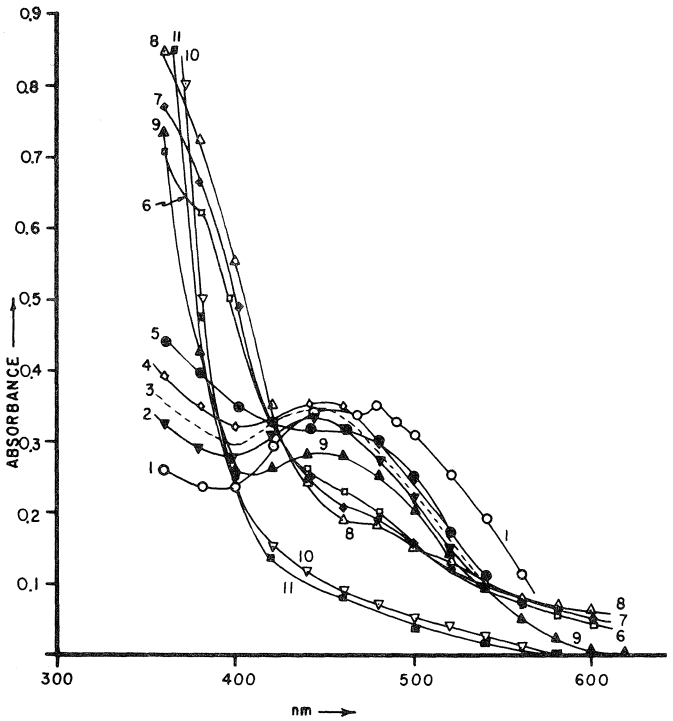

FIG 1. Time dependent spectra of adrenaline–copper system at p*H* 9.5. Curves *1–8*: adrenaline 1×10^{-4} *M*, copper 1×10^{-2} *M*, and 0.04 *M* ammonium chloride. Curves *9–11*: adrenaline 1×10^{-4} *M* and 0.04 *M* ammonium chloride. (*1*) Brown-yellow, recorded 2 min after mixing. (*2*) Yellow, recorded 9 min after mixing. (*3*) Yellow, recorded 15 min after mixing. (*4*) Yellow, recorded 28 min after mixing. (*5*) Yellow-green, recorded 43 min after mixing. (*6*) Green, recorded 2 h and 43 min after mixing. (*7*) Green, recorded 3 h and 53 min after mixing. (*8*) Green, recorded 5 h and 38 min after mixing. (*9*) Yellow (no copper), recorded 30 min after mixing. (*10*) Yellow (no copper), recorded 2 h after mixing. (*11*) Yellow (no copper), recorded 5 h and 38 min after mixing.

Copper sulphate stock solution was prepared from copper sulphate and the copper concentration was analyzed electrolytically by cathodic deposition.

All other chemicals were reagent grade.

Apparatus

Cary 14 Spectrophotometer was used to record ultraviolet and visible spectra. All p*H* measurements were made with Leeds and Northrup p*H* meter. A Spex 1401 double monochromator, a cooled RCA C31034A photomultiplier, and both direct current and photon counting detection systems were used for Raman spectrometric studies. Excitation source was a Coherent Radiation CR-5 argon ion laser. Melting point capillaries were used as sample container with transverse excitation and observation at 90 °C to the incident radiation. The slit width was 200 μ.

Procedure

Copper adrenalin complexes and other forms of the amines were studied in aqueous solution containing 0.04 *M* ammonium chloride. The p*H* was adjusted with ammonium hydroxide with the exception of a few cases where the p*H* was adjusted with sodium hydroxide. Hydrochloric acid was used to maintain the desired acid concentration in the system. Raman scattering intensities were measured by exciting with 496.5 and 488.0 nm lines of the laser.

Results and Discussion

Some of the important properties of the compounds formed from adrenalin with copper-(II) ion are summarized in Table 1. The electronic spectra of these compounds are shown in Figs. 1 to 7 and Raman spectra are shown in Fig. 8.

Electron Spectra

$\geq$pH 9.2

Adrenalin on reacting with copper(II) ion in presence of ammonium ion produces a stable green compound. This green form results through three intermediate forms: a very short lived violet compound, a brown form, and a yellow form. The violet form in about 2 s is

Can. J. Chem. Downloaded from www.nrcresearchpress.com by 210.87.254.5 on 09/05/12
For personal use only.

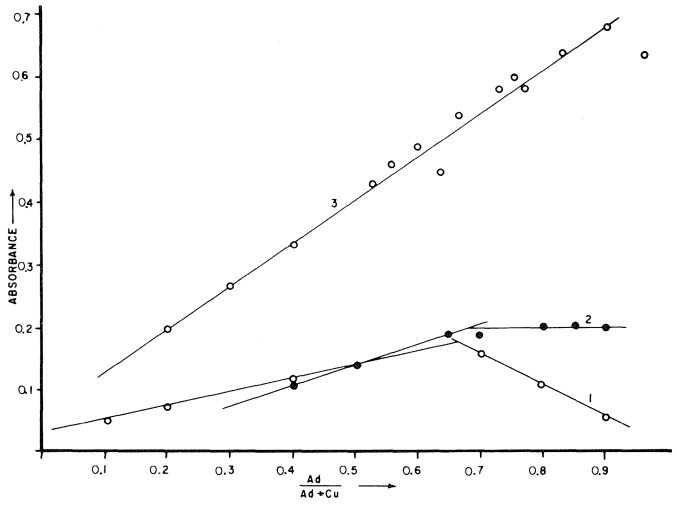

FIG. 2. Job's plot of continuous variation, copper–adrenaline system. Absorbance measured at 460 nm. (*1*) p*H* 5.5, brown complex, total concentration was 1×10^{-4} *M*. (*2*) p*H* 9.5, yellow complex, total concentration was 1×10^{-4} *M*. (*3*) p*H* 8.0, brown-red compound, total concentration was 2×10^{-4} *M*.

changed to the brown form. This violet form is probably a free radical caused by the initial attack of the copper(II) ion on the dihydroxyindole that results from adrenalin. This free radical is comparable to a free radical reported to result from adrenochrome by reacting with ceruloplasmin (ref. 1, p. 539). The spectra of the brown compound (Fig. 1, curve *1*) have a maximum at 485 nm and compare well with that of adrenochrome (**1**). This brown form is also short

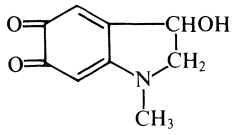

1

lived and in about 2 min is transformed into a yellow compound. A new peak at 445 nm appears and the intensity at 485 nm is decreased. The curves *1*, *2*, *3*, and *4* in Fig. 1 represent the change in the spectra with time and the isosbestic point at 450 nm suggests a mixture of two compounds, brown and yellow. The yellow compound changes slowly to the green form. The curve *5* of Fig. 1 was recorded after 43 min of the reaction. It does not intercept at 450 nm as the intensity in the visible decreases and that in the lower wavelength increases. Walaas *et al.* (9) suggested that copper(II) forms a 1:2 complex with adrenalin in basic solution. Our analysis of the yellow compound by Job's method and by the mole ratio method does not support the published results. Job's plot, Fig. 2, curve *2*, does not give strong support in favor of 1:2 copper(II) adrenalin complex formation and the mole ratio method failed to give any indication of metal complex. Its formation and disappearance are independent of both adrenalin and copper concentrations. The spectra of this compound compare well with that of the paraquinone (**3**) and

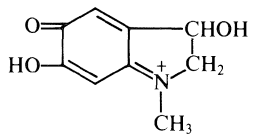

2

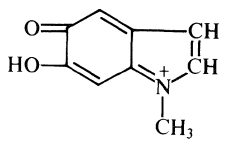

3

most likely this is a conjugate salt represented by **2**, resulted from adrenochrome. A yellow compound identical to the compound in the present system has been reported to form from adrenochrome at p*H* 2.0 and has been suggested to be the conjugate salt (8–10). The disappearance of the yellow compound is slower than its formation. In about 2 h it is completely transformed to the green form. The change in spectra with time is represented by curves *5*, *6*, *7*, and *8* of Fig. 1. Although the spectra of the green solution are similar to that of melanin formed by oxidation

Can. J. Chem. Downloaded from www.nrcresearchpress.com by 210.87.254.5 on 09/05/12
For personal use only.

Can. J. Chem. Downloaded from www.nrcresearchpress.com by 210.87.254.5 on 09/05/12
For personal use only.

of adrenochrome with ferritine (7), its higher absorbance at around 460 and 600 nm and an isosbestic point at 420 nm suggest the system contains more than one compound. In the process of melanin formation a by-product quinone has been observed to form (11) and a blue-green compound prepared from adrenochrome in acid solution was identified as a quinone (8). In the present system an equilibrium exists between melanin and indolyl-indoquinone (**4**) which has the same properties of indolynapthaquine (**5**).

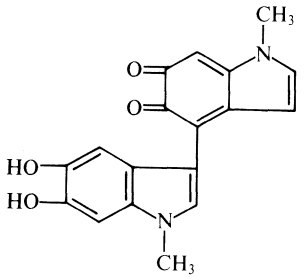

4

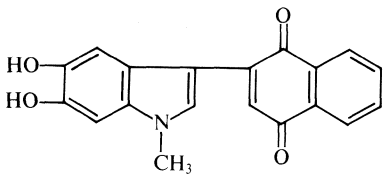

5

In the absence of copper(II) ion at p*H* 9.2 to 10.5 adrenalin transform to brown adrenochrome which in 30 min produces melanin (Fig. 1, curves *9*, *10*, and *11*). The mechanism of the reaction of adrenaline with copper(II) ion in the p*H* range of 9.2 to 10.5 can be outlined as:

adrenalin → an unidentified free radical → adrenochrome → conjugated salt (**2**) → indolyl-indoquinone (**4**) + melanin

pH 8.0–8.5

Adrenalin reacts with copper(II) ion to produce a brown compound. The spectra of the solution (Fig. 6, curve *4*), with a maximum at 480 nm (ϵ = 3900) compare well with that of adrenochrome. Job's method and mole ratio method were performed by measuring the absorbance at 460 nm. It is evident from Fig. 2, curve *3* and Fig. 4, curve *3*, that the compound is not a copper(II) complex with adrenalin. The

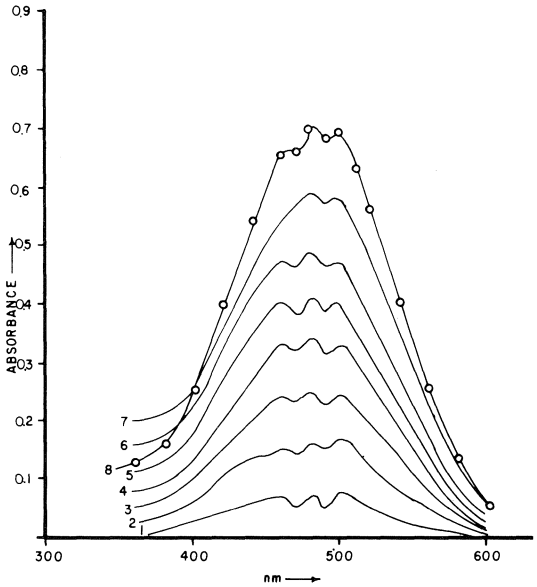

FIG. 3. Adrenaline–copper system at p*H* 8.5. Adrenaline 2×10^{-4} *M*, 0.04 *M* ammonium chloride and trace amount of copper. Spectra recorded every 6.0 min after mixing.

absorbance at 460 nm was recorded with time by mixing 2×10^{-4} *M* adrenalin and 1×10^{-6} *M* copper(II). Figure 3 shows that only one compound is formed and the kinetics is pseudo first order (Fig. 5) with a rate constant of 1.96×10^{-2} min^{-1}. The results led us to formulate the compound as adrenochrome.

pH 6.5–7.5

When the p*H* of the system containing adrenalin and copper(II) is adjusted to the region of 6.5 to 7.5, the same brown compound as obtained at p*H* 8.5 is produced. It can be concluded that at the normal physiological p*H* adrenochrome is the only compound that can be formed in presence of copper(II) ion (see Fig. 6, curve 3).

pH 4.0–5.5

A brown compound is formed when the p*H* of the acidic solution of adrenalin–copper(II) mixture is increased with base. The absorption spectra of this compound (Fig. 6, curve *3*) have a maximum at 500 nm with two peaks in the visible region at 420 and 580 nm. It is evident from Job's plot of continuous variation (Fig. 2, curve *1*) and from mole ratio plot (Fig. 4, curves *1* and *2*) that copper(II) forms a complex where the copper: ligand ratio is 1:2. These results are in favor of

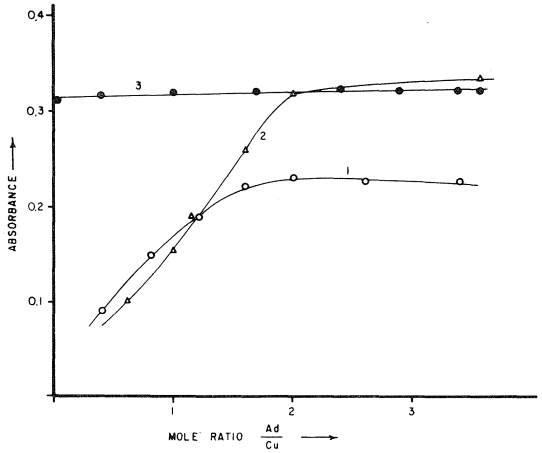

FIG. 4. Adrenaline–copper system containing 0.04 *M* ammonium chloride. Variation of absorbance at 460 nm with concentration. (*1*) p*H* 5.5, brown complex, variation of adrenaline concentration, 0.5×10^{-4} *M* copper. (*2*) p*H* 5.5, brown complex, variation of copper concentration, adrenaline 1×10^{-4} *M*. (*3*) p*H* 8.0, brown-red compound, variation of adrenaline concentration.

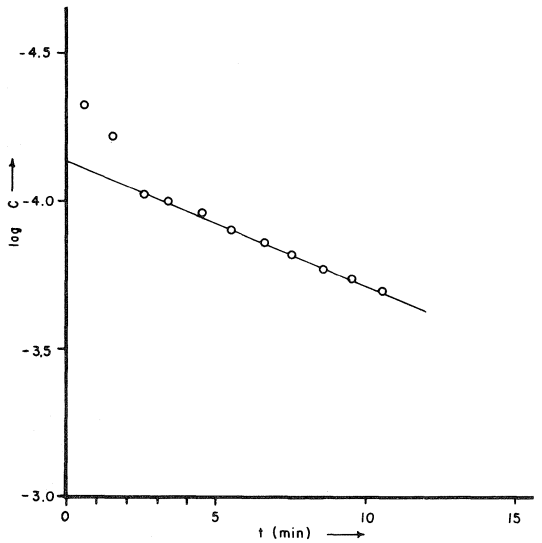

FIG. 5. Pseudo first order kinetics plot of adrenaline–copper system at p*H* 8.5. (*1*) 66×10^{-4} *M* adrenaline and 0.34×10^{-4} *M* copper. Measured at 460 nm. Rate constant = 1.96×10^{-2} min^{-1}.

complete chelation and are in agreement with the interpretation of the thermodynamic properties of the system (12). The complex at p*H* 5.5 in presence of ammonium chloride (Fig. 6, curve *3*) has a higher absorbance than the complex formed at this p*H* in the absence of ammonium chloride (Fig. 6, curve *2*). The ammonium chloride has no influence in the reaction of adrenalin with copper(II) in basic solution. Thus, it seems that NH_3 is also ligated to the metal ion in the complex at low p*H* values. The molar extinction coefficients on the basis of adrenaline concentration are 3800, 800, and 1900 at 500, 580, and 410 nm respectively. Since the complex is 2:1 adrenalin:copper(II), the values for the complex are half of those calculated from the adrenalin concentration. The high intensity at 500 nm is possibly caused by the overlap of the charge transfer band on the *d–d* band. In the ultraviolet region the compound has peaks at 220 and 300 nm that are assigned to electron transfer bands of $\diagdown$C=O and ligand-to-metal charge transfer band. It is obvious that the copper site of the adrenalin is not the only chromophoric center of the molecule. For cupric ions, lines in the visible region can arise only from a transition between *d* orbitals whose degeneracy has been removed by the ligand field. However, the excited π-level is at low energy and can overlap on the *d–d* band. Campbell *et al.* have observed high molar absorptivity in the visible region of copper complexes with 3-ethoxybutane, 1-2 one bis(thiosemicarbazone) and suggested the possibility of overlap of the charge transfer bands on *d–d* bands (13). High molar absorptivity in the visible spectra of copper complexes of biomolecules, such as ceruloplasmin (14), and stellacyanin (rhus vernicifera blue) (15), has been reported. Presumably, low site symmetry could be another reason for the strong intensity and can be compared with published results (16). The water solubility of the complex may be due to a 5-coordinated complex formation like many other copper complexes in the biosystem (17).

The brown complex at p*H* 5.5 in 1.5 *N* hydrochloric acid transforms to a bluish form (Fig. 7, curve *3*) which on standing gives a black pigment. The black pigment is insoluble in strong acid and identified to be a polymer similar to that obtained by Bu'Lock (8). In 1.5 *N* hydrochloric acid the brown compound formed from adrenalin copper(II) at p*H* 9.5 produces a yellow color. The spectra of this solution (Fig. 7, curve *2*) suggest that the compound is the conjugated salt represented by **2**.

Can. J. Chem. Downloaded from www.nrcresearchpress.com by 210.87.254.5 on 09/05/12
For personal use only.

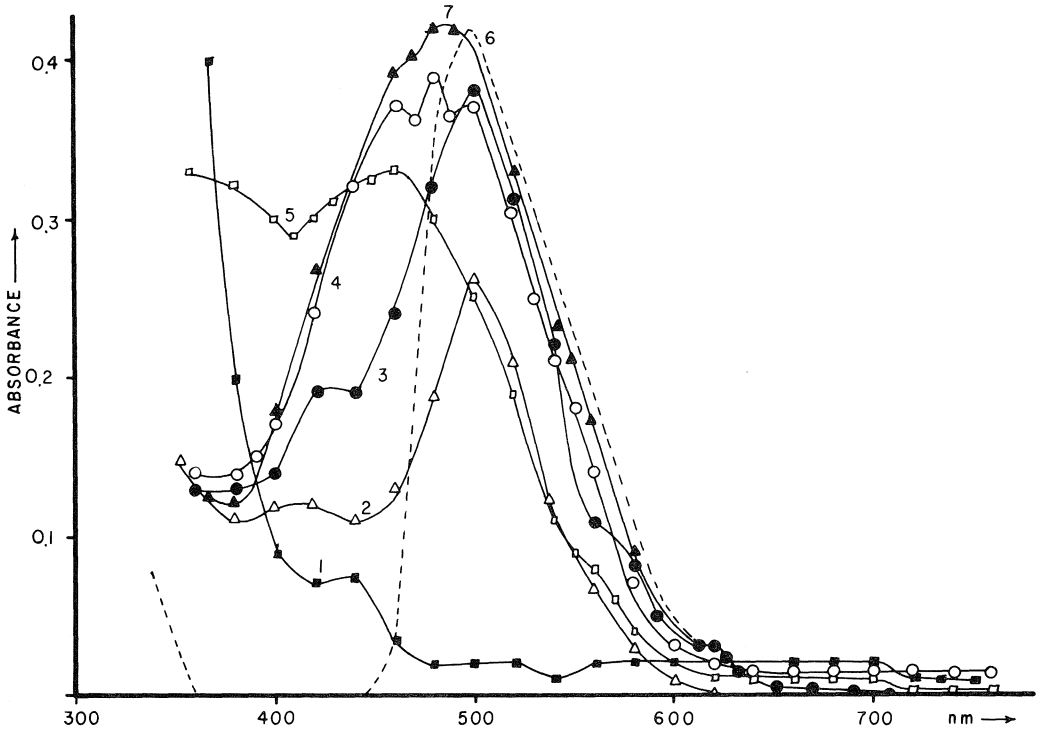

FIG. 6. Adrenaline–copper system; adrenaline 1×10^{-4} *M*, copper 1×10^{-2} *M*. (*1*) p*H* 9.5, green compound containing 0.04 *M* ammonium chloride. (*2*) p*H* 5.5, brown compound without ammonium chloride. (*3*) p*H* 5.5, brown compound containing 0.04 *M* ammonium chloride. (*4*) p*H* 8.5, brown-red compound containing 0.04 *M* ammonium chloride. (*5*) p*H* 9.5, yellow compound containing 0.04 *M* ammonium chloride. (*6*) Adrenochrome formed by oxidizing adrenaline (1×10^{-4} *M*) with potassium ferricyanide. (*7*) p*H* 7.0, brown compound containing 0.04 *M* ammonium chloride.

Raman Spectra

The Raman spectra of 1×10^{-4} *M* adrenalin and 2×10^{-2} *M* copper(II) system at p*H* 5.5 are shown in Fig. 8. The band at 1680 cm^{-1} is assigned to a stretching vibration of aliphatic carbonyl group (**7**). Heacock and co-workers noticed that the infrared spectra of iodoadrenochrome and adrenolutin have the absorption at this frequency and they assigned this band as aliphatic carbonyl stretching (18). Since indoxy carbonyl groups have stretching frequencies between 1750 and 1710 cm^{-1} and acetophenone carbonyl absorbs at 1686 cm^{-1} (18, 19) the Raman scattered peak in the copper(II) adrenalin complex cannot be due to the carbonyl group in the aromatic ring. It is also possible that aliphatic carbonyl frequency, which should be at 1680 cm^{-1}, has been shifted by the hydroxy groups in the benzene ring.

The adrenolutin, **6**, is the possible state that forms complexes with copper(II) at p*H* 5.5. The

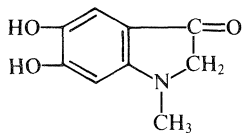

6

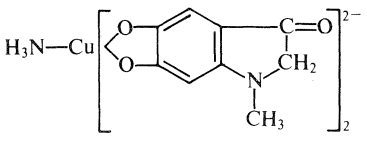

7

1640 cm^{-1} band was not found in the infrared spectra of adrenochrome but in an aqueous solution of adrenochrome this band appears (20). We observed that in D_2O this band disappears, indicating that this band may be due to the bending mode of water and not from C=N stretching. This further supports the presence of **6** that enables the phenolic groups to coordinate

Can. J. Chem. Downloaded from www.nrcresearchpress.com by 210.87.254.5 on 09/05/12
For personal use only.

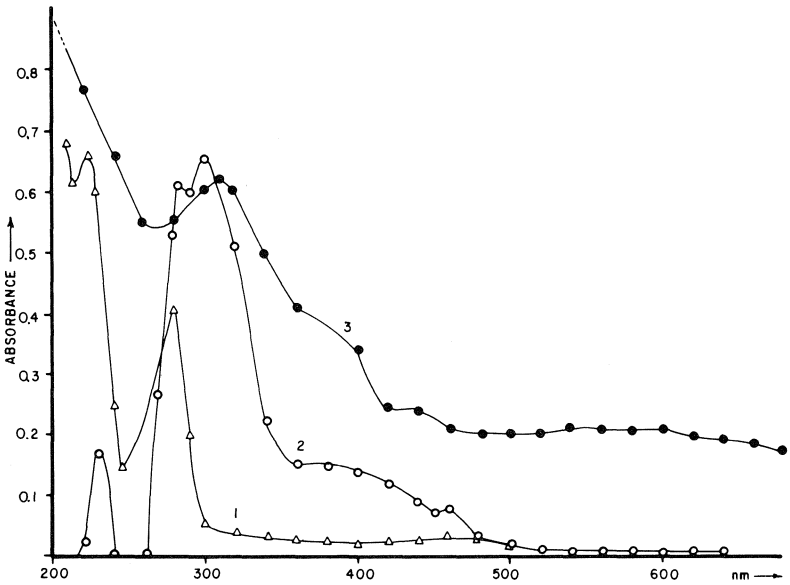

FIG. 7. Adrenaline–copper system; copper 1×10^{-2} *M*, adrenaline 1×10^{-4}, and 0.04 *M* ammonium chloride. (*1*) Adrenaline only at p*H* 5.5 (1×10^{-4} *M*). (*2*) Yellow compound at 1.5 *N* hydrochloric acid obtained on acidification of brown compound at p*H* 8.5. (*3*) Bluish compound at 1.5 *N* hydrochloric acid obtained on acidification of brown compound at p*H* 5.5.

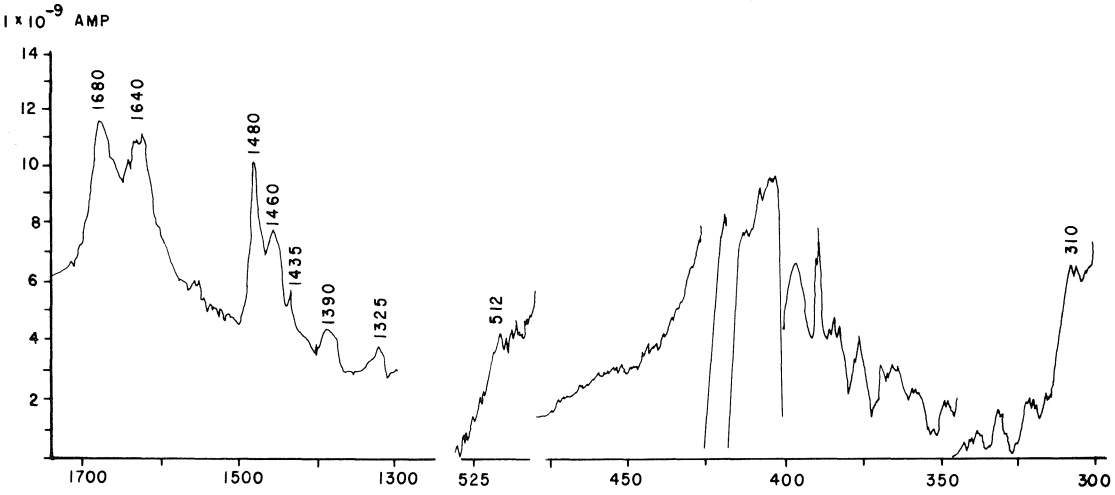

FIG. 8. Resonance Raman spectra of copper–adrenaline complex at p*H* 5.5. Adrenaline 1×10^{-4} *M*, copper 1×10^{-2} *M*, and 0.04 *M* ammonium chloride. λ_{ex} = 496.5 nm. Spectrometer band pass = 4.5 cm^{-1}. Rise time = 10 s. Slit width = 200 μ.

with copper. The bands of conjugated double bond of the six member ring at 1558 cm^{-1} are hidden under the water band but appear in D_2O. The C—N stretching band of copper adrenaline is at 1480 cm^{-1} whereas in copper noradrenaline, the C—N stretching is at 1435 cm^{-1}. These bands show no isotopic change on deuteration and are comparable with other reported results (21). The C—N band in the Raman spectra of cystene has been found in this region (22). The contribution

Can. J. Chem. Downloaded from www.nrcresearchpress.com by 210.87.254.5 on 09/05/12
For personal use only.

of CH_3—N is important and it seems that the interaction of C—N stretching with this kind of motion raises the frequency as high as 1480 cm^{-1} in adrenalin copper. It is comparable with the results of *N*-methyl compounds (23). No such interaction can take place in noradrenaline copper system which has no methyl group. The bands at 1460 and 1435 cm^{-1} in copper adrenaline complex are assigned as CH_3—N asymmetric bending and CH_3—N symmetric bending frequencies.

The copper bonded phenolic C—O band appearing at 1390 cm^{-1} suggests a coordinated phenol rather than a bridging phenoxide (24, 25). The band at 1325 cm^{-1} could be assigned as N—H in plane bending arising from coordinated NH_3. The M—N stretching band arising from the coordinated NH_3 appears at 512 cm^{-1} and the M—O stretching band at 310 cm^{-1}. There are a large number of bands between 400 and 325 cm^{-1} which can hardly be explained. However, similar bands have been observed in the Raman spectra of coat proteins of pfl and fd virions and it has been suggested that these bands arise from alanine residue in the right handed α-helical form (26). The complexes of copper adrenalin and noradrenaline at p*H* 5.5 can be represented by **7**, which is comparable with L-Dopa copper complex at p*H* 6.4 (27).

1. M. GOLDSTEIN. The biochemistry of copper. *Edited by* J. Peisach, P. Aisen and W. E. Blumberg. Academic Press, New York. 1966.
2. U. MEIRI and R. RAHAMINOFF. Science, **176**, 308 (1972).
3. V. R. SOROKA, V. Y. ARSENTEY, and M. S. MUKHAEY. Zh. Nevropatol. Psikhiatr. im. SS: Korsakova, **72**, 69 (1972).
4. J. H. BIEL and L. G. ABOOD (*Editors*). Biological amines and physiological membranes in drug therapy. Marcel Dekker, New York. 1971.
5. J. E. GORTON and R. F. JAMESON. J. Chem. Soc. A, 2615 (1968).
6. J. E. GORTON and R. F. JAMESON. J. Chem. Soc. A, 394 (1972).
7. S. GREEN, A. MAZUR, and E. SHORR. J. Biol. Chem. **220**, 237 (1956).
8. J. D. BU'LOCK. J. Chem. Soc. 52 (1961).
9. E. WALASS, O. WALAAS, and S. HAAVALDSEN. Arch. Biochem. Biophys. **100**, 97 (1963).
10. P. BOUVET. Ann. Pharm. **7**, 514 (1949).
11. J. B. BU'LOCK and J. H. MASON. J. Chem. Soc. 703 (1951).
12. C. A. ANDREWS, I. D. LYONS, and T. D. O'BRIEN. J. Chem. Soc. Part 2, 1776 (1962).
13. M. J. M. CAMPBELL, A. J. COLLIS, and R. GREZESKWIAK. J. Inorg. Nucl. Chem. **38**, 174 (1973).
14. W. E. BLUMBERG, J. EISENGER, P. AISEN, A. G. MORELI, and H. SCHEINBERG. J. Biol. Chem. **238**, 1675 (1963).
15. J. PEISACH, W. J. LEVINE, and W. E. BLUMBERG. J. Biol. Chem. **242**, 2847 (1967).
16. A. S. BRILL and G. F. BRYCE. J. Chem. Phys. **49**, 4398 (1968).
17. K. JORGENSEN. *In* The biochemistry of copper. *Edited by* J. Peisach, P. Aisen, and W. E. Blumberg. Academic Press, New York. 1966. p. 4.
18. R. A. HEACOCK and M. E. MAHON. Can. J. Chem. **36**, 1550 (1958).
19. R. A. HEACOCK and B. D. SCOTT. Can. J. Chem. **38**, 508 (1960); **38**, 516 (1960).
20. M. D. MORRIS. Anal. Chem. **47**, 2453 (1975).
21. R. B. PENDAND, S. MIZUSHIMA, C. CURRAN, and J. V. QUAGLINO. J. Am. Chem. Soc. **79**, 1575 (1957).
22. E. L. ELSON and J. T. EDSALL. Biochemistry, **1**, 1 (1962).
23. T. MIYAZAWA, T. SHIMANOUCHI, and S. MIJIESHIMA. J. Chem. Phys. **29**, 611 (1958).
24. N. H. PILKINGTON and R. ROBOSN. Aus. J. Chem. **23**, 2225 (1970).
25. E. J. OLSZEWSKI and D. F. MARTIN. J. Inorg. Nucl. Chem. **26**, 1577 (1964).
26. G. J. THOMAS, JR. and P. MURPHY. Science, **183**, 1205 (1975).
27. W. K. KWIK, E. PURDY, and E. I. STEIFEL. J. Am. Chem. Soc. **95**, 1638 (1974).

Can. J. Chem. Downloaded from www.nrcresearchpress.com by 210.87.254.5 on 09/05/12
For personal use only.

The use of polymer supports in organic synthesis. VII.[1] Polymer-bound 1,3-diols as monoblocking agents of symmetrical dialdehydes[2]

CLIFFORD C. LEZNOFF AND SHAFRIRA GREENBERG
Department of Chemistry, York University, Downsview, Ont., Canada M3J 1P3

Received June 14, 1976

CLIFFORD C. LEZNOFF and SHAFRIRA GREENBERG. Can. J. Chem. **54**, 3824 (1976).

Two different 2% cross-linked divinylbenzene–styrene copolymers incorporating 1,3-diol groups were prepared. The symmetrical dialdehydes terephthalaldehyde and *o*-phthalaldehyde were attached to these polymers through acetal formation, showing that even hindered *o*-aromatic dialdehydes can be monoblocked by the use of polymer supports. The free aldehyde group of polymer-bound terephthalaldehyde reacted with Wittig reagents to give 1-*p*-formylphenyl-4-phenyl-1,3-butadiene and *p*-formylstilbene. Similarly, polymer-bound *o*-phthalaldehyde gave *o*-formylstilbenes. Polymer-bound 1,3- and 1,2-diols did not form acetals of aliphatic dialdehydes and formed ketals of symmetrical diketones in very low yield.

CLIFFORD C. LEZNOFF et SHAFRIRA GREENBERG. Can. J. Chem. **54**, 3824 (1976).

On a préparé deux copolymères différents de divinylbenzène–styrène réticulés à 2% et incorporant des groupes diols-1,3. On y a attaché les dialdéhydes symétriques téréphtalique et *o*-phtalique par formation d'acétal; ces résultats démontrent que, même dans le cas de dialdehydes encombrés, on peut bloquer un seul groupe carbonyle en utilisant des supports à base de polymères. Le groupe aldéhydique libre du téréphtalaldéhyde réagit avec les réactifs de Wittig pour conduire au *p*-formylphényl-1 phényl-4 butadiène-1,3 et au *p*-formylstilbène. De la même manière l'*o*-phtalaldéhyde lié au polymère conduit au *o*-formylstilbène. Les diols-1,2 et -1,3 liés au polymère ne forment pas d'acétals avec les dialdéhydes aliphatiques alors que les cétals de dicétones symétriques ne se forment qu'avec de faibles rendements.

[Traduit par le journal]

Insoluble polymer supports have shown promise as monoblocking agents of symmetrical diols (1) and symmetrical aromatic dialdehydes (2, 3). Furthermore, the free functional group of the polymer-bound symmetrical difunctional compound was available for synthetic elaboration with organic reagents to provide formylstilbenes (4) and insect sex attractants (5).

Although we had previously prepared a polymer-bound 1,2-diol, **1**, by the reaction of Merrifield's chloromethylated polymer (6) with the sodium salt of isopropylidene glycerol (followed by hydrolysis), and had monoprotected terephthalaldehyde, **2**, and isophthalaldehyde with **1** (2), we have not previously reported attempts to monoprotect hindered symmetrical aromatic dialdehydes such as *o*-phthalaldehyde, **3**, aliphatic dialdehydes, and symmetrical diketones.

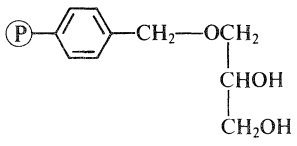

1

Recent reports on the syntheses of *o*-formylstilbene, **4**, (7) from *o*-phthalaldehyde, **3**, and a thieno[2,3-*b*]pyrrole derivative from 3,4-thiophenedialdehyde (8) illustrate the difficulties encountered in preparing products from reactions of only one aldehyde group of unprotected aromatic *ortho* dialdehydes. We thus attempted to monoprotect one aldehyde group of **3** with our previously prepared polymer **1** (2) in order to synthesize *o*-formylstilbene, **4**, more readily.

All attempts to attach **3** to polymer **1** through formation of a five-membered ring cyclic acetal by methods previously described (2) failed and we attribute this failure to steric hindrance inherent in *o*-aromatic dialdehydes. It has been shown that six-membered ring cyclic acetals are more stable than five-membered ring cyclic acetals (9, 10) and hence we thought that a polymer-bound 1,3-diol may be successful in monoblocking hindered *o*-aromatic dialdehydes even though polymer **1** failed.

[1]For part VI see ref. 5.

[2]Taken from the M.Sc. Thesis of S. Greenberg, York University, Downsview, Ont., 1976.

Can. J. Chem. Downloaded from www.nrcresearchpress.com by 210.87.254.40 on 09/05/12
For personal use only.

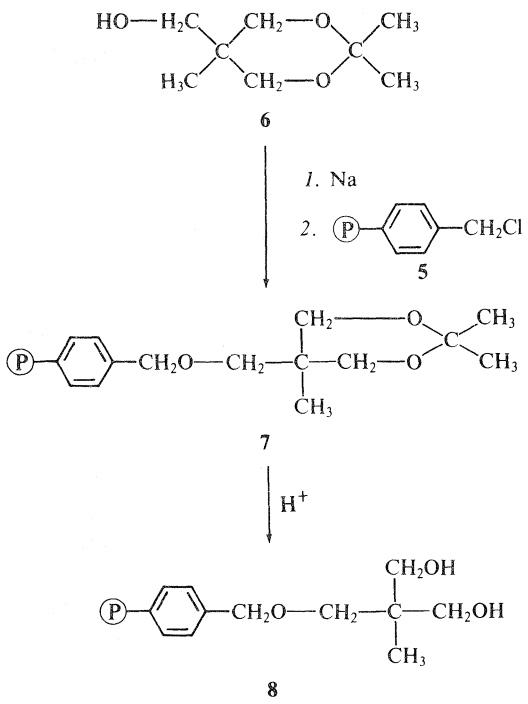

SCHEME 1

The reaction of a chloromethylated Merrifield polymer, **5** (6), containing 2.2 mmol of $-CH_2Cl$ groups/g of resin, with the sodium salt of 2,2,5-trimethyl-*m*-dioxane-5-methanol, **6**, in anhydrous tetrahydrofuran (THF) gave a polymer-bound ketal, **7**, which on acid hydrolysis yielded the desired polymer-bound 1,3-diol, **8**, as shown in Scheme 1. Resin **8** did not contain any residual amount of chloride as determined by the modified Volhard analysis (11).

Similarly, polymer **5** reacted with the sodium salt of 1,3-*O*-benzylidene glycerol, **9**, in anhydrous benzene to give a new polymer-bound ketal, **10**, which on acid hydrolysis gave a polymer-bound 1,3-diol, **11**, as shown in Scheme 2.

Before attempting to monoprotect *o*-aromatic dialdehydes with resins **8** and **11**, it was necessary to determine the capacity of these resins and to test their reactivity in comparison to the previously reported polymer **1** (2). Thus treatment of resins **8** and **11** with terephthalaldehyde, **2**, as before (2) gave resins **12** and **13** containing **2** monoblocked by the resins through a six-membered ring cyclic acetal. The ir spectra of **12** and **13** exhibited typical aldehyde absorption at 1690–1700 cm^{-1}, showing the presence of monoprotected symmetrical dialdehyde. Both resins **12** and **13** contained 0.38 mmol of **2** per gram of polymer, which represent slightly higher capacities than that of polymer **1** for terephthalaldehyde, **2** (2). The Wittig reactions of resins **12** and **13** with cinnamyltriphenylphosphonium chloride, **14**, and **14** or benzyltriphenylphosphonium chloride, **15**, yielded resins **16**, **17**, and **18** respectively, which on acid hydrolysis, gave 1-*p*-formylphenyl-4-phenyl-1,3-butadiene, **19**, in 90% yield from resin **12** and **19** and *p*-formylstilbene, **20**, in 94 and 89% yields respectively from resin **13**. These very high yields of Wittig products derived from **12** and **13** via **8** and **11** represent a substantial improvement in the yields of **19** and **20** prepared via polymer **1**. Thus a polymer-bound six-membered ring acetal formed from 1,3-primary diols represents a less sterically hindered configuration than a five-membered ring acetal formed from a polymer-bound 1-primary alcohol, 2-secondary alcohol and hence the Wittig reaction can proceed more readily. Although chemical reactions of benzaldehyde *in solution* may not be affected by steric effects of *p*-substituents, it is possible

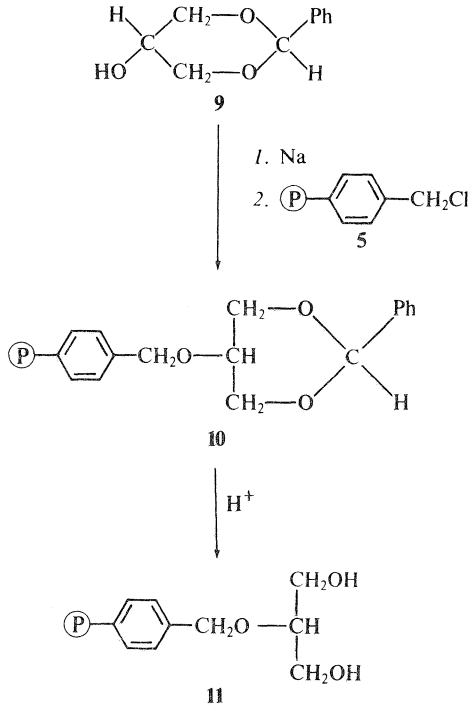

SCHEME 2

Can. J. Chem. Downloaded from www.nrcresearchpress.com by 210.87.254.40 on 09/05/12
For personal use only.

Can. J. Chem. Downloaded from www.nrcresearchpress.com by 210.87.254.40 on 09/05/12
For personal use only.

that when the *p*-substituent is a macromolecular resin, small differences in stereochemistry of *p*-substituents can be magnified to give the effects outlined here. Resins **8** and **11** represent slightly different 1,3-diol resins in that the 1,3-diol of resin **8** is further extended from the polymer backbone than that in **11** and hence might be more accessible to chemical reactions. In any event both resins were very similar in all their chemical reactions.

Since we were encouraged by the results of the reactions of resins **8** and **11** with terephthalaldehyde, **2**, we treated resins **8** and **11** with excess *o*-phthalaldehyde, **3**, in anhydrous dioxane to give monoblocked polymer-bound *o*-phthalaldehyde resins **21** and **22** respectively. The ir spectra of **21** and **22** showed typical aldehyde absorption at 1690–1700 cm^{-1} showing the presence of monoprotected symmetrical dialdehyde. Resins **21** and **22** reacted with benzyltriphenylphosphonium bromide in anhydrous dimethylformamide (DMF) and sodium methoxide to give stilbene resins **23** and **24**, which on acid hydrolysis, gave *o*-formylstilbene, **4**, in 100% yield as a mixture of *cis* and *trans* isomers as shown in Scheme 3. The nmr spectrum of **4** was consistent with the assigned structure and showed a *cis*:*trans* ratio of 1:2. The high yields of **19**, **20**, and **4** and the unobserved recovery of **2** and **3** from acid cleavage of the polymer-bound products lead us to believe that **2** and **3** are bound to polymers **8** and **11** almost exclusively at one end only.

As described previously (2) used polymer **1**, obtained after acid cleavage of polymer-bound products with HCl in dioxane, can be reutilized in synthetic schemes without loss of capacity. Unfortunately, resins **8** and **11**, recovered from the acid hydrolysis of the Wittig reaction products were shown to contain up to 2.0 mmol Cl^-/g of resin. Thus, unlike the polymer-bound 1,2-diol the HCl cleavage of resins **8** and **11** resulted in the formation of primary alkyl chlorides. Treating the used resins **8** and **11** with 5% sodium hydroxide in ethanol–dioxane (1:1) for 16 h gave resins **8** and **11** which did not contain residual chloride. When resins **8** and **11** were subjected to the reaction sequence described in Scheme 3 using **3** and benzyltriphenylphosphonium bromide, **4** was obtained in only 50% yield from resin **11** and in 0% yield from resin **8**. Hence resin **8** is unsuitable for regeneration and resin **11** can only be partially regenerated.

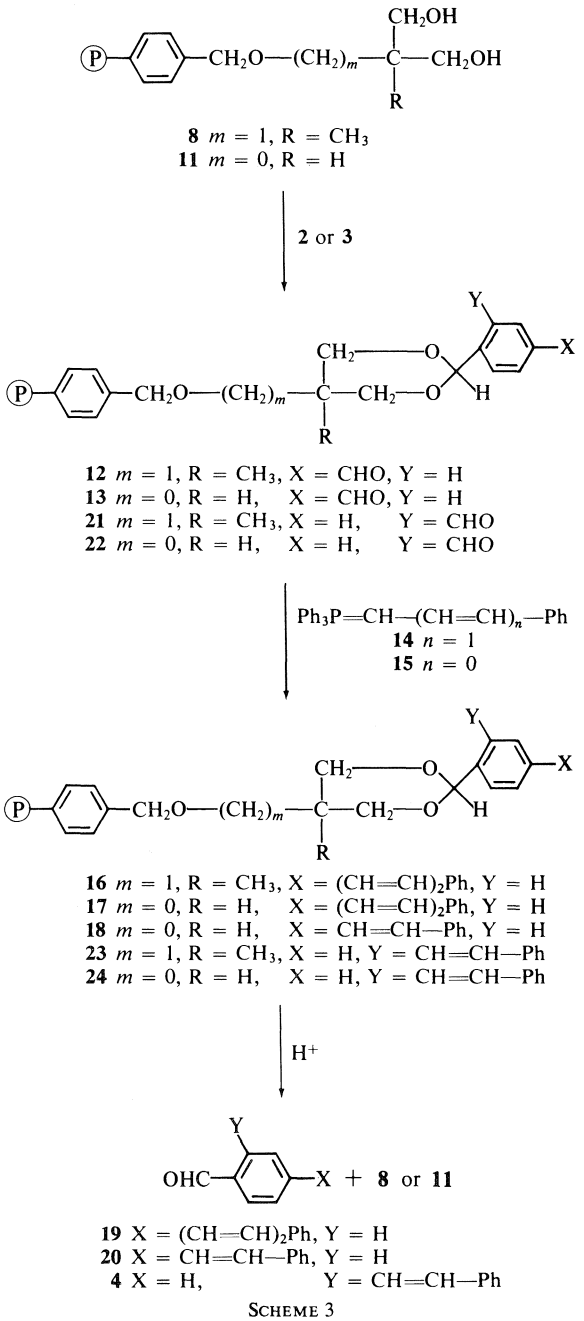

SCHEME 3

The protection of one aldehyde group of completely symmetrical aliphatic dialdehydes was attempted using polymer **1** and polymers **8** and **11**. Adipaldehyde (12), 1,8-octanedial (13), and 1,12-dodecanedial (14) were treated with

Can. J. Chem. Downloaded from www.nrcresearchpress.com by 210.87.254.40 on 09/05/12
For personal use only.

resins **8** and **11** but no attachment to the polymer occurred. Certainly it is well known (12) that adipaldehyde and even 1,8-octanedial polymerize under the acidic conditions needed for acetal formation but 1,12-dodecanedial is quite stable and was recovered unreacted after the attempted formation of its acetal on the polymer. The failure of 1,12-dodecanedial to form acetals with polymers **1**, **8**, and **11** is surprising as heptanal forms an acetal with polymer **1**.[3]

The possibility of using insoluble polymer supports as monoprotecting groups for symmetrical diketones has been investigated some time ago in our laboratory using polymer **1**. Thus **1** formed ketals in only very low yield with the symmetrical diketones acetonylacetone, *p*-diacetylbenzene, 1,4-dibenzoylbutane, cyclohexane-1,4-dione, 2,2,4,4-tetramethylcyclobutane-1,3-dione, or the monoketones acetophenone and 12-tricosanone under conditions normally used for ketal formation.[3] Unlike acetals, five-membered ring ketals are more stable than six-membered ring ketals, due to unfavourable 1,3-interactions in the six-membered ring (10). We wished to confirm, however, that our previous observations were not confined to that polymer alone and hence we examined the reaction of resin **11** with the symmetrical diketones *p*-diacetylbenzene and decane-2,9-dione. Resin **11** yielded monoprotected diketones containing only 0.07 and 0.01 mmol of the above diketones/g of resin. The low capacity of resin **11** for ketones precluded further studies in that direction.

We have demonstrated that polymer-bound 1,3-diols can be used to monoblock symmetrical *o*-aromatic dialdehydes which can then undergo Wittig reactions leading to a selective synthesis on one aldehyde group only. The monoprotection of symmetrical diketones, however, requires further development of new polymers or new procedures.

Experimental

All melting points were determined on a Kofler hot stage and are uncorrected. The ir spectra were recorded on a Unicam SP1000 ir spectrophotometer using KBr discs unless otherwise stated. The nmr spectra were measured on a Varian A60 spectrometer using tetramethylsilane as an internal standard (δ = 0 ppm) and deuterochloroform as solvent. Mass spectra were recorded on a Hitachi–Perkin-Elmer RMU-6 mass spectrometer. The number in parentheses after the indicated ion shows the percentage of the base peak represented by that ion. Silica gel was used for thin and thick layer chromatography. Microanalyses were performed by Dr. C. Daesslé of Montreal. Filtering procedures were done under vacuum using a sinter-glass funnel. All the stirring described below was performed using a Fisher magnetic stirrer.

Preparation of Polymer ***7***

Sodium (1 g, 0.04 mol) was added to 39 g of 2,2,5-trimethyl-*m*-dioxane-5-methanol (15) (0.24 mol) in anhydrous THF. After all the sodium had dissolved, the Merrifield resin (20.0 g) (2% cross-linked polystyrene beads with 2.2 mol of —CH_2Cl per gram resin) was added. The mixture was stirred at room temperature for 24 h and at 80 °C for 24 h. The resin was collected by filtration and washed three times with THF, six times with water, three times with ethanol–water (1:1), three times with ethanol, and three times with dry ether to give 22.0 g of polymer **7**: ir spectrum, ν_{max} 1130–1050 cm^{-1} (C—O—C).

Preparation of Polymer ***8***

Polymer **7** (22.0 g) was suspended in a mixture of dioxane and 1 *M* hydrochloric acid (1:1, 200 ml). The mixture was stirred for 48 h at room temperature. The resin was filtered and washed six times with water, once with acetone, three times with ethanol, and three times with dry ether to give 20.9 g of polymer diol **8**: ir spectrum ν_{max} 1130–1050 cm^{-1} (C—O—C).

Preparation of Polymer ***11***

A mixture of *cis*- and *trans*-1,3-*O*-benzylideneglycerol (16) (6.4 g, 35 mmol) in 150 ml benzene was boiled under reflux for 48 h in the presence of sodium metal (1.8 g 78 mmol). To the cooled and decanted solution 20 g of the Merrifield resin was added (2% cross-linked polystyrene beads with 2.2 mmol of —CH_2Cl per gram of resin) and the mixture was stirred for 48 h at room temperature then at 100 °C for 24 h. The resin was filtered and washed three times with benzene, six times with water, three times with ethanol, and three times with dry ether to give the resin **10** (22.6 g): ir spectrum, ν_{max} 1260–1050 cm^{-1} (C—O—C). A suspension of **10** (22.5 g) was stirred in a mixture of dioxane and 1 *M* HCl (1:1, 150 ml) for 48 h at room temperature. The resin was filtered and washed six times with water, once with acetone, three times with ethanol, and three times with dry ether to give 21.7 g of polymer 1,3-diol **11**: ir spectrum, ν_{max} 1260–1050 cm^{-1} (C—O—C).

Preparation of 1-p-Formylphenyl-4-phenyl-1,3-butadiene, ***19****, via Resins* ***8*** *and* ***11*** *and p-Formylstilbene* ***20*** *via Resin* ***11***

The above compounds were prepared by the Wittig reactions. A typical example is given for the preparation of *p*-formylstilbene **20** via resin **12**.

Polymer-bound dialdehydes **12** and **13** were prepared by a method identical to the preparation of **1** (2). The ir spectra of both resins **12** and **13** exhibited typical aldehyde absorption at 1700 cm^{-1}. The amount of aldehyde attached to the polymer was determined by acid hydrolysis of **12** and **13** with dilute HCl in anhydrous dioxane to yield terephthalaldehyde, **2**. Thus both resins **12** and **13** contained 0.38 mmol **2** per gram.

[3]J. Y. Wong and C. C. Leznoff, unpublished results.

Can. J. Chem. Downloaded from www.nrcresearchpress.com by 210.87.254.40 on 09/05/12
For personal use only.

To a solution of benzyltriphenylphosphonium bromide (4 g, 9.2 mmol) in 60 ml dimethylformamide (DMF), was added sodium methoxide (2.5 g, 46 mmol). After stirring for 5 min, during which time the solution turned orange, resin **13** (5.8 g) was added to give, after stirring for 48 h at room temperature, the resin **18**. Resin **18** was separated by filtration and washed three times with DMF, three times with DMF–water (1:1), three times with water, three times with ethanol, and three times with water, three times with ethanol, and three times with dry ether. Acid hydrolysis of resin **18** and using an identical work-up as described previously (2) gave used resin **11** and crude *p*-formylstilbene, **20**. Further purification by preparative tlc on silica gel (eluant 10% $CHCl_3$:90% C_6H_6) gave 0.400 g of analytically pure **4** in 89% yield.

Similarly, 1-*p*-formylphenyl-4-phenyl-1,3-butadiene, **19**, was obtained in 90 and 94% yield from **16** and **17** via resins **12** and **13** respectively

The physical and spectral data of **19** and **20** were identical to the data in the literature (2).

*Preparation of Polymers **21** and **22***

The above polymers were prepared by treating polymer-bound 1,3-diols **8** and **11** with *o*-phthalaldehyde, **3**, in a manner similar to the reaction of **2** with polymer **1** (2). The ir spectra of polymers **21** and **22** exhibited a typical aldehyde absorption at 1690–1700 cm^{-1}. The amount of aldehyde attached to the polymers was determined by acid hydrolysis of **21** and **22** with 0.35 *M* HCl in anhydrous dioxane to yield **3**. It was thus shown that resins **21** and **22** both contained 0.15 mmol of **3** per gram.

*Preparation of o-Formylstilbene, **4**, via Resins **21** and **22***

The above compound was prepared via resin **21** in a manner similar to the preparation of *p*-formylstilbene from resin **1** (2). Cleavage from the polymer was accomplished by suspending 3.93 g polymer in anhydrous dioxane containing 0.35 *M* HCl, to give in 100% yield 0.124 g of pure **4** (7) as an oil: mass spectrum, *m/e* 208(100), 207(33), 206(58), 179(40), 178(55); ir spectrum, ν_{max} (neat) 1735 (—C=O *cis* isomer), 689 (—CH=CH— *cis* isomer), 1698 (—C=O *trans* isomer), 969 (—CH=CH— *trans* isomer), 2730 cm^{-1}; nmr spectrum δ 10.4, 10.32 (1H), 6.9–7.25 (11H). The nmr spectrum showed the ratio of *cis*:*trans* isomers to be 1:2 respectively.

Similarly, resin **22** (2.27 g) gave 0.090 g of **4** in 100% yield. In both cases no starting *o*-phthalaldehyde, **3**, was detected in the product.

*Regeneration of Polymers **8** and **11***

In a typical procedure, 5 g of a once used polymer was suspended in 60 ml ethanol – dioxane – 5% NaOH (1:1:1). The mixture was stirred under reflux overnight. Then the resin was filtered and washed three times with dioxane, six times with water, three times with ethanol–water (1:1), three times with ethanol, and at least three times with dry ether. There was no detectable amount of chloride left.

Preparation of Polymer-bound Ketones

All polymer-bound ketones were prepared in a manner similar to the preparation of polymer-bound *p*-diacetylbenzene. A suspension of polymer **8** or **11** (5.13 g) in anhydrous benzene was treated with *p*-diacetylbenzene (1.7 g, 0.01 mol) and 0.1 g *p*-toluenesulfonic acid. The mixture was heated under reflux for 48 h in the presence of molecular sieves (type 3A, $\frac{1}{8}$ in. pellets) in a Soxhlet extractor to absorb the liberated water and gave polymer-bound *p*-diacetylbenzene (5.34 g). The ir spectrum of the polymer-bound *p*-diacetylbenzene exhibited a typical carbonyl absorption at 1655–1680 cm^{-1} (medium). The amount of ketone attached to resin **11** was determined by acid hydrolysis of the polymer-bound ketone using (1:1) 1 *M* HCl – dioxane and yielded *p*-diacetylbenzene (0.07), decane-2,9-dione (0.01) benzylacetone (0.03), 12-tricosanone (0.01), acetophenone (0.12), and cyclododecanone (0.16 mmol) from their respective polymer-bound ketone.

*Attempted Attachment of Aliphatic Dialdehydes to Polymer Diols **1** and **11***

The aliphatic dialdehydes, adipaldehyde, 1,8-octanedial, and 1,2-dodecanedial were treated with resins **1** and **11** as described for aromatic dialdehydes (2) or as described above for the attachment of ketones to resin **11**. In all cases no attachment occurred. Many other conditions were tried in which the acid, the drying agent, the solvent, the reaction time, and reaction temperature were varied and in no case was an aliphatic dialdehyde attached to the resin (17).

Acknowledgement

The authors wish to thank the National Research Council of Canada for a grant in aid of this research.

1. C. C. LEZNOFF and J. Y. WONG. Can. J. Chem. **50**, 2892 (1972); J. Y. WONG and C. C. LEZNOFF. Can. J. Chem. **51**, 2452 (1973); J. M. J. FRECHET and L. J. NUYENS. Can. J. Chem. **54**, 926 (1976); T. M. FYLES and C. C. LEZNOFF. Can. J. Chem. **54**, 935 (1976).
2. C. C. LEZNOFF and J. Y. WONG. Can. J. Chem. **51**, 3756 (1973).
3. C. C. LEZNOFF. Chem. Soc. Rev. **3**, 65 (1974); J. I. CROWLEY and H. RAPOPORT. Acc. Chem. Res. **9**, 135 (1976).
4. J. Y. WONG, C. MANNING, and C. C. LEZNOFF. Angew. Chem. Int. Ed. Engl. **13**, 666 (1974).
5. C. C. LEZNOFF and T. M. FYLES. J. Chem. Soc. Chem. Commun. 251 (1976).
6. G. R. MARSHALL and R. B. MERRIFIELD. *In* Biochemical aspects of reactions on solid supports. *Edited by* G. R. Stark. Academic Press, New York. 1971. p. 111.
7. A. A. BAUM. J. Am. Chem. Soc. **94**, 6866 (1974).
8. M. FARNIER, S. SOTH, and P. FOURNARI. Can. J. Chem. **54**, 1074 (1976); S. SOTH, M. FARNIER, and P. FOURNARI. Bull. Soc. Chim. Fr. 2511 (1975).
9. G. AKSNES, P. ALBRIKTSEN, and P. JUVVIK. Acta Chem. Scand. **19**, 920 (1965).
10. E. L. ELIEL. Stereochemistry of carbon compounds. McGraw Hill, New York. 1962. p. 200.
11. J. M. STEWART and J. D. YOUNG. Solid phase peptide synthesis. W. H. Freeman Ltd., San Francisco. 1969. p. 22.

12. P. M. HARDY, A. C. NICHOLLS, and H. N. RYDON. J. Chem. Soc. Perkin Trans. II, 2270 (1972).
13. A. C. COPE, S. W. FENTON, and C. F. SPENCER. J. Am. Chem. Soc. **74**, 5884 (1952).
14. M. SVOBODA and J. SICHER. Chem. Listy, **52**, 1586 (1958); G. OHLOFF and W. GIERSCH. Angew. Chem. Int. Ed. Engl. **12**, 401 (1973).
15. R. M. LUKES. J. Org. Chem. **26**, 2515 (1961).
16. N. BAGGETT, J. S. BRIMACOMBE, A. B. FOSTER, M. STACEY, and D. H. WHIFFEN. J. Chem. Soc. 2574 (1960).
17. S. GREENBERG. M.Sc. Thesis. York University, Downsview, Ontario, Canada. 1976.

Can. J. Chem. Downloaded from www.nrcresearchpress.com by 210.87.254.40 on 09/05/12
For personal use only.

Situselective α′-acetoxylation of some α,β-enones by manganic acetate oxidation

GAYNOR J. WILLIAMS AND NORMAN R. HUNTER

Department of Chemistry, University of Manitoba, Winnipeg, Man., Canada R3T 2N2

Received June 14, 1976

GAYNOR J. WILLIAMS and NORMAN R. HUNTER. Can. J. Chem. **54**, 3830 (1976).

Heating 5,5-dimethylcyclohex-2-en-1-one, **1**, with manganic acetate in acetic acid yields 6-acetoxy-5,5-dimethylcyclohex-2-en-1-one, **2**, as the only isolated product. Reaction of 3-methylcyclohex-2-en-1-one (**3**) or (+)-pulegone (**5**) under similar conditions yields the analogous 6-acetoxy-3-methylcyclohex-2-en-1-one (**4**) and *cis*- (**6**) and *trans*-2-acetoxypulegone (**7**) respectively.

GAYNOR J. WILLIAMS et NORMAN R. HUNTER. Can. J. Chem. **54**, 3830 (1976).

Le chauffage de la diméthyl-5,5 cyclohexène-2 one-1, **1**, avec de l'acétate manganique dans l'acide acétique conduit à l'acétoxy-6 diméthyl-5,5 cyclohexène-2 one-1, **2**; c'est le seul produit qui a été isolé du mélange réactionnel. Les réactions de la méthyl-3 cyclohexène-2 one-1 (**3**) ou de la (+) pulégone (**5**) dans des conditions semblables, conduisent respectivement aux produits analogues acétoxy-6 méthyl-3 cyclohexène-2 one-1 (**4**) et acétoxy-2 pulégone *cis* (**6**) et *trans* (**7**).
[Traduit par le journal]

In the course of work directed toward the development of a sequence for the regioselective fusion of a γ-butyrolactone ring to the α,β-positions of an enone (Scheme 1), we investigated the reaction of manganic acetate with several selected α-β-unsaturated ketones.

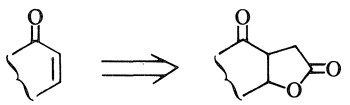

SCHEME 1

Previous workers (1) have shown that manganic acetate will convert simple alkenes into substituted γ-butyrolactones upon thermolysis in acetic acid. Mechanistically this reaction probably proceeds by addition of carboxymethyl radical to the alkene, followed by oxidation of the radical to a cation and ring closure (1). We anticipated that any generated carboxymethyl radical might interact with the double bond portion of the enone system.

When 5,5-dimethylcyclohex-2-en-1-one, **1**, was treated with 4 mol equiv. of manganic acetate in glacial acetic acid, containing sodium acetate to raise the temperature of reflux, the only product isolated was 6-acetoxy-5,5-dimethylcyclohex-2-en-1-one, **2**.[1] Clearly the ketone had not reacted at the double bond but α to the carbonyl to give the product of situselective α′-acetoxylation.[2]

Several more enones were examined under the same conditions and again the only isolated products were from α′-acetoxylation[2] (Table 1).

The two products isolated from oxidation of

TABLE 1. Products from manganic acetate oxidation

Enone	Product(s)	Yield* (%)
1	2	35
3	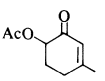 4	24
5	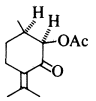 6	6
	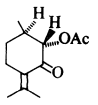 7	17

*Yields are based on isolated and purified products. No attempts have been made to optimize yields.

[1]The structures of compounds **2**, **4**, **6**, and **7** were established on the basis of the spectroscopic and analytical data recorded in the Experimental section.

[2]Since only one acetoxylated product was isolated the reaction is clearly situselective; the low mass balance, however, prevents any claim of situspecificity.

Can. J. Chem. Downloaded from www.nrcresearchpress.com by 210.87.254.42 on 09/05/12
For personal use only.

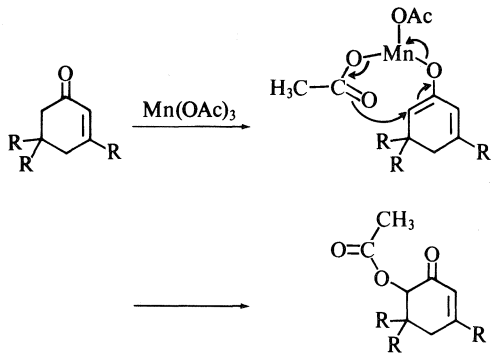

SCHEME 2

(+)-pulegone are the same C-2 isomers of 2-acetoxypulegone as obtained by oxidation of pulegone with mercuric acetate (4). The ratio of the two products (as determined by gc analysis) changed during the course of the oxidation as the *cis*-isomer **6** epimerized to the conformationally more stable *trans*-isomer **7**.

One can envisage several mechanisms for oxidation of the enones to the α'-acetoxyenones. For example, the formation of a metal enolate with acetate transfer (Scheme 2) analogous to the lead tetraacetate oxidation of enones (3) is possible.

However, since previous oxidations of carbonyl compounds with manganic acetate (1,2,5–9) have probably all involved t he intermediacy of an α-keto radical resulting from the oxidation of an enol or enolate anion by Mn(III), it is possible that our α'-acetoxylation reaction also proceeds via α-keto radical formation followed by ligand transfer oxidation to the product (11). Oxidation of the α-keto radical to the carbocation by electron transfer is not favoured due to the adjacent electron-withdrawing carbonyl group (12) (Scheme 3).

Synthetically the acetoxylation of enones by manganic acetate oxidation offers an alternative

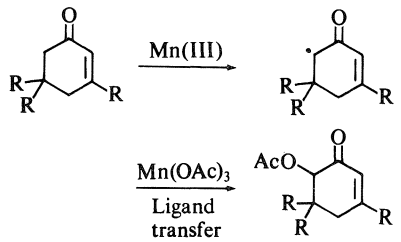

SCHEME 3

to the more commonly used lead tetraacetate oxidation (3). While the yield for the former oxidation is low it may be the procedure of choice for compounds which are not compatible with lead tetraacetate. This oxidation represents an added feature to the chemistry of manganic acetate.

Experimental

Infrared spectra were recorded with a Perkin-Elmer 1700 spectrophotometer. Proton magnetic resonance spectra were recorded with a Varian EM-360 spectrometer, using tetramethylsilane as internal standard and deuterochloroform as solvent Mass spectra were measured with a Finnigan 1015 quadrupole mass spectrometer. Melting points (uncorrected) were determined on a Fisher-Johns melting point apparatus and gas chromatographic analyses were done using a Hewlett-Packard 700 chromatograph with flame ionization detection. Microanalyses were by Chemalytics, Inc., Tempe, Arizona. All extracts were dried over magnesium sulfate and solvents removed *in vacuo* using a rotary evaporator.

Preparation of Hydrated Manganic Acetate

The following procedure represents a slight modification of the literature preparation (2). The product prepared by this method gave cleaner reactions and higher yield of product. The number of moles of water of hydration has not been determined for our product.

Acetic acid (500 ml) and manganous acetate ($Mn(OAc)_2 \cdot 4H_2O$) (48 g) were heated under reflux for 20 min. Potassium permanganate (8.0 g) was then slowly added, and the mixture heated under reflux for a further 20 min. After stirring at ambient temperature overnight, water (80 ml) was added and after an additional 30 min the precipitate was filtered off, washed with glacial acetic acid, and air-dried (58 g).

α'-Acetoxylation of α,β-Unsaturated Ketones

In a typical experiment a solution of the α,β-unsaturated ketone (4 mmol) and sodium acetate (16 g) in glacial acetic acid (100 ml) was heated under a nitrogen atmosphere to the reflux temperature (120–135 °C). Manganic acetate (1 g) was added and refluxing continued until the brown colouration disappeared (about 5 min). Further 1 g portions of manganic acetate were added to obtain a total of 4 g (15 mmol). After an additional 10 min under reflux, gas chromatographic analysis indicated the complete disappearance of the starting enone. The reaction was diluted with water (100 ml) and filtered. The filtrate was extracted with chloroform (3 × 50 ml) and the combined chloroform extracts were washed successively with water (2 × 100 ml), 10% sodium bicarbonate (2 × 100 ml), and water (2 × 50 ml).

Drying and removal of the solvent gave viscous oils which were purified by preparative thin layer chromatography (silica gel) and/or sublimation.

6-Acetoxy-5,5-Dimethylcyclohex-2-en-1-one, 2

From 5,5-dimethylcyclohex-2-en-1-one, **1**, (0.500 g, 4 mmol) (10) was obtained, after sublimation (100 °C, 12 torr), 0.255 g (1.4 mmol, 35%) of 6-acetoxy-5,5-

Can. J. Chem. Downloaded from www.nrcresearchpress.com by 210.87.254.42 on 09/05/12
For personal use only.

dimethylcyclohex-2-en-1-one, **2**, mp 84–85 °C. *Anal.* calcd. for $C_{10}H_{14}O_3$: C 65.93, H 7.69; found: C 65.64, H 7.67. Mass spectrum for $C_{10}H_{14}O_3$ requires *m/e* 182; found: *m/e* 182, 140 (loss of $CH_2{=}C{=}O$), 122 (loss of CH_3CO_2H); base peak 43 ($CH_3{-}C{\equiv}O^+$). Infrared spectrum ($CHCl_3$) 1675, 1750 cm^{-1}; pmr spectrum ($CDCl_3$) τ 8.95 (3H, s, CH_3), 8.85 (3H, s, CH_3), 7.8 (3H, s, $CH_3{-}\overset{\overset{O}{\|}}{C}{-}O{-}$), 7.54 (2H, m, C_4-H's), 4.71 (1H, s, C_6-H), 3.95 (1H, md, C_2-H), and 3.20 (1H, md, C_3-H).

6-Acetoxy-3-methylcyclohex-2-en-1-one, ***4***

From 0.440 g (4 mmol) of 3-methylcyclohex-2-en-1-one, **3**, (Aldrich) was obtained, after preparative thin layer chromatography (silica gel; 20% ether–hexane) and sublimation (100 °C, 14 torr), 0.160 g (0.95 mmol, 24%) of 6-acetoxy-3-methylcyclohex-2-en-1-one, **4**, mp 60–62 °C. *Anal.* calcd. for $C_9H_{12}O_3$: C 64.29, H 7.14; found: C 64.10, H 7.03. Mass spectrum for $C_9H_{12}O_3$ requires *m/e* 168; found: *m/e* 168, 126 (loss of $CH_2{=}C{=}O$), 108 (loss of CH_3CO_2H), base peak 43 ($CH_3{-}C{\equiv}O^+$). Infrared spectrum ($CHCl_3$) 1670, 1750 cm^{-1}; pmr spectrum ($CDCl_3$) τ 8.05 (3H, b s, CH_3), 7.8 (3H, s, $CH_3{-}\overset{\overset{O}{\|}}{C}{-}O{-}$), 7.45–8.0 (4H, b m, C_4 and C_5-H's), 4.68 (1H, dd, C_6-H), and 4.15 (1H, b s, C_2-H).

cis and trans-2-Acetoxypulegone, ***6*** *and* ***7***

From 0.500 g (3.3 mmol) of (+)-pulegone, **5**, (Aldrich, Technical) was obtained 0.270 g of a mixture of **6** and **7**. Separation by preparative thin layer chromatography gave **7** (0.120 g, 0.57 mmol, 17%) and **6** (0.049 g, 0.19 mmol, 6%) as viscous liquids. Both **7** and **6** were chromatographically pure (tlc and gc) and their spectra agreed completely with literature spectral assignments (4).

Acknowledgements

Financial assistance, by way of Operating Grants, from the National Research Council of Canada and the Research Board of the University of Manitoba is gratefully acknowledged.

1. E. I. Heiba, R. M. Dessau, and P. G. Rodewald. J. Am. Chem. Soc. **96**, 7977 (1974); E. I. Heiba, R. M. Dessau, and W. J. Koehl, Jr. J. Am. Chem. Soc. **90**, 5905 (1968); E. I. Heiba and R. M. Dessau. J. Am. Chem. Soc. **93**, 995 (1971); J. B. Bush, Jr. and H. Finkbeiner. J. Am. Chem. Soc. **90**, 5903 (1968).
2. E. I. Heiba, R. M. Dessau, and W. J. Koehl, Jr. J. Am. Chem. Soc. **91**, 138 (1969).
3. E. J. Corey and J. P. Schaefer. J. Am. Chem. Soc. **82**, 918 (1960); H. B. Henbest, D. N. Jones, and G. P. Slater. J. Chem. Soc. 4472 (1961); J. A. Marshall and G. L. Bundy. J. Chem. Soc. Chem. Commun. 500 (1966).
4. L. H. Zalkow, J. W. Ellis, and M. R. Brennan. J. Org. Chem. **28**, 1705 (1963).
5. E. I. Heiba and R. M. Dessau. J. Am. Chem. Soc. **93**, 524 (1971).
6. E. I. Heiba and R. M. Dessau. J. Am. Chem. Soc. **94**, 2888 (1972).
7. E. I. Heiba and R. M. Dessau. J. Org. Chem. **39**, 3456 (1974).
8. R. M. Dessau and E. I. Heiba. J. Org. Chem. **39**, 3457 (1974).
9. J. Y. Lallemand. Tetrahedron Lett. 1217 (1975).
10. R. L. Frank and H. K. Hall, Jr. J. Am. Chem. Soc. **72**, 1645 (1950).
11. J. K. Kochi and D. M. Mog. J. Am. Chem. Soc. **87**, 522 (1965).
12. J. K. Kochi and F. F. Rust. J. Am. Chem. Soc. **84**, 3946 (1962).

Can. J. Chem. Downloaded from www.nrcresearchpress.com by 210.87.254.42 on 09/05/12
For personal use only.

Formation and photolysis of alkyl and peroxy radicals in dilute glass matrices

FRANK CUTHBERT ADAM AND IAIN R. H. MARSHALL
Department of Chemistry, University of Calgary, Calgary, Alta., Canada T2N 1N4

Received May 25, 1976

FRANK CUTHBERT ADAM and IAIN R. H. MARSHALL. Can. J. Chem. **54**, 3833 (1976).

The use of molecular oxygen as a spin trap in rigid glassy hydrocarbon media at 77 K is investigated. By slight warming of the matrix, oxygen is found to effectively scavenge the isolated alkyl radicals produced by γ-irradiation to give $RO_2\cdot$, but does not react with radical pairs lying in the ionization tracks. The yield of scavengable radicals in 3MP is determined and compared to the findings of other workers. The butyl radical yields for γ-irradiated 1.0 mol l^{-1} butyl chlorides in 3MP are found to be: *t*-BuCl, 5.8; *i*-BuCl, 5.1; 2-BuCl, 4.9; and 1-BuCl, 2.2. Alkyl radicals cannot be recovered from either RO_2 or BuO_2 by uv photolysis due to solvent abstraction reactions, or because of photon induced reactions of the alkyl radicals. Photolysis of the butyl radicals themselves at 253.7 nm give rise to decomposition and solvent abstraction reactions.

FRANK CUTHBERT ADAM et IAIN R. H. MARSHALL. Can. J. Chem. **54**, 3833 (1976).

On a étudié l'utilisation de l'oxygène moléculaire comme piège à spin dans des milieux de verres hydrocarbonés rigides à 77 K. En réchauffant lentement la matrice, on a trouvé que l'oxygène piège d'une façon efficace les radicaux alkyles isolés, produits par une irradiation γ, pour conduire à $RO_2\cdot$; toutefois il ne réagit pas avec les paires de radicaux se trouvant dans les trajectoires de l'ionisation. Le rendement en radicaux, piégeables dans le 3MP, peut être déterminé et comparé avec les résultats obtenus par d'autres chercheurs. On a trouvé que les rendements en radicaux butyles dans le 3MP, pour des chlorures de butyle à 1.0 mol l^{-1} et soumis à une irradiation γ, sont: *t*-BuCl, 5.8; *i*-BuCl, 5.1; Cl-2 Bu, 4.9; et Cl-1 Bu, 2.2. Partant soit du RO_2, ou du BuO_2, on ne peut pas récupérer les radicaux alkyles par photolyse uv; ce résultat est dû à des réactions d'enlèvement sur le solvant ou à des réactions induites par les photons sur les radicaux alkyles. La photolyse des radicaux alkyles eux-mêmes à 253.7 nm conduit à des réactions de décomposition et d'enlèvement sur le solvant.

[Traduit par le journal]

Can. J. Chem. Downloaded from www.nrcresearchpress.com by 210.87.254.42 on 09/05/12
For personal use only.

Introduction

It has been known for some time that molecular oxygen reacts with free radicals produced by high energy radiation in the liquid phase (1) by a simple addition process [1] to give peroxy radicals RO_2

[1] $$R\cdot + O_2 \rightarrow RO_2\cdot$$

The same reaction has been observed to occur on the surface of single crystals of leucine which have been bombarded by H atoms. The resulting leucine radicals were allowed to react subsequently with molecular oxygen (2), and the peroxy radicals so produced had an epr spectrum characteristic of an axial g-tensor with $g_{\|} \simeq 2.035$ and $g_{\perp} \simeq 2.003$ at low temperatures. At higher temperatures, or in the liquid state, a rotationally averaged value of $\bar{g} \simeq 2.015$ is usually obtained. Similar radicals can be generated by uv photolysis of alkyl peroxides (3) or hydroperoxides (4). The tertiary peroxy radicals are very stable below -115 °C but dimerize to give a tetroxide (5) in the liquid phase.

Reaction 1 is also thought to account in part for the 'oxygen effect' in the irradiation of living cells (6) whereby the radiation damage to physiological materials is augmented by formation of peroxy radicals which are relatively long lived and not readily repaired by normal biological processes.

Our interest in peroxy radicals stems from the fact that RO_2 was observed in the low temperature photolysis of divalent sulfur compounds in dilute rigid glasses which had not been properly degassed. Apart from causing a certain amount of difficulty in the interpretation of these spectra, it also suggested that reaction 1 was extremely efficient even in the rigid glassy state. We therefore undertook a detailed investigation of the spin-trapping process. Since molecular oxygen is a normal constituent of living cells, it was felt that the results might have general applicability

to the broader area of radiation biology.

One difficulty of using oxygen as a spin trap is that the alkyl peroxide radicals exhibit no proton hyperfine structure, so the identity of the particular alkyl function is distinguished in neither the epr nor the optical spectrum of the radicals. For this reason we also studied the feasibility of reaction 2 in rigid 3-methyl pentane (3MP) at 77 K,

$$[2] \qquad RO_2\cdot \xrightarrow{h\nu} R\cdot + O_2$$

since many alkyl radicals can be identified by their epr hyperfine spectrum when trapped in a solid matrix (7). The effect of 253.7 nm radiation on the alkyl radicals themselves was also investigated.

Experimental Procedures

While it would have been desirable to add molecular oxygen to the rigid glass *following* the creation of the radical centres at 77 K, it was clear after a number of preliminary experiments that the microscopic transport of oxygen from either the liquid or vapor phase into the 3MP glass at any temperature between 76 and 90 K was too inefficient to compete with the other radical annihilation processes which occur in the body of the solid within this temperature range. As has been found by other workers who have attempted similar experiments (8) it is a necessary condition that the oxygen be dissolved in the medium before it solidifies in order that reaction 1 be observed. Because we were working with deuterated solvent (3MP-d_{14}, >98% D from Merck, Sharpe and Dohme, Montreal) as well as normal 3MP, the following procedure was developed to employ the minimum amount of solvent. Each epr cell consisted of a 2 cm^3 Pyrex bulb attached by graded seal to a length of 3 mm id Suprasil tippit material which in turn was joined by graded seal to a high vacuum capillary stopcock attached to the high vacuum line. A sufficient pressure of dried and purified solvent was metered to the vacuum manifold to give on condensation a known volume (0.3 ml) of liquid in the inverted sample cell. Purified alkyl halide could also be introduced at this point. Air or oxygen was then metered into the manifold, and admitted to the cell by momentarily opening the capillary stopcock. The sample was then warmed to room temperature for a sufficient time to establish vapor–liquid equilibrium, refrozen, and the pressure again equalized between the sample and the manifold. The cell was then separated from the manifold by sealing off the tippet end. The cell was again equilibrated at room temperature and then frozen to 76 K preparatory to irradiation. The oxygen concentrations were determined using Henry's law coefficients given in ref. 9 assuming the room temperature distribution is 'frozen in' at 77 K. Radiolysis was carried out using ^{60}Co γ-rays in a Gammacell 220 from Atomic Energy of Canada Ltd. at a dose rate of 3.8×10^{16} eV g^{-1} min^{-1}. The photolytic procedures have been described elsewhere (10) as has the epr spectrometer used (11).

Results

The experiments involve four main steps: (*a*) The creation of solvent radicals M· or alkyl radicals R· by γ-radiation of 3MP glasses containing various amounts of dissolved molecular oxygen, with or without the appropriate halide RCl. (*b*) The glasses were then warmed toward 85 K to allow diffusion of molecular oxygen through the matrix. This solid state titration results in the loss of the hyperfine structure of M· or R· and growth of $MO_2\cdot$ or $RO_2\cdot$ by reaction 1. (*c*) The resulting alkyl peroxy radicals were then photolysed with 253.7 nm light, at 77 K. Wavelengths >300 nm are ineffectual in this regard. (*d*) Following complete photolytic destruction of the peroxyl radicals, the matrices were again warmed to 85 K to determine whether $MO_2\cdot$ or $RO_2\cdot$ was reformed from the photolytic products. Specific radicals R· were created by γ-irradiation of 3MP glasses containing the corresponding alkyl chloride, utilizing the well-known (7) electron capture process [3]

$$[3] \qquad RCl + e_m \rightarrow R\cdot + Cl^-$$

Photolysis of the unirradiated 3 MP or 3 MP–RCl glasses with or without added oxygen produces relatively few radicals on the time scale of interest here.

The results which will be discussed immediately below relate primarily to the use and efficiency of oxygen as a spin trap agent and to the effects that O_2 and $MO_2\cdot$ have upon the radiochemical processes which normally occur in rigid hydrocarbon glasses. Of equal concern is the photochemical stability of $MO_2\cdot$ and M· radicals to 253.7 nm light.

(A) Pure 3MP Glasses

Irradiation of pure 3MP glasses gives a broad six line epr spectrum of the solvent radical M· as in Fig. 1*a*, with a $G = 3.0 \pm 3$ (*i.e.* radicals per 100 eV absorbed per gram) (12). Photolysis of these irradiated samples at 253.7 nm gives about a twofold increase in epr signal peak heights, due partly to a narrowing of the hyperfine lines, as shown in Fig. 1*b*. Although the spectrum retains the same basic six line structure, some incompletely resolved hyperfine detail can be observed. These changes have been attributed to the formation of $CH_3\cdot$ (13) or $C_2H_5\cdot$ (14) from M· by photolytic action. The spectrum of Fig. 1*b* is typical of M· produced through

Can. J. Chem. Downloaded from www.nrcresearchpress.com by 210.87.254.42 on 09/05/12
For personal use only.

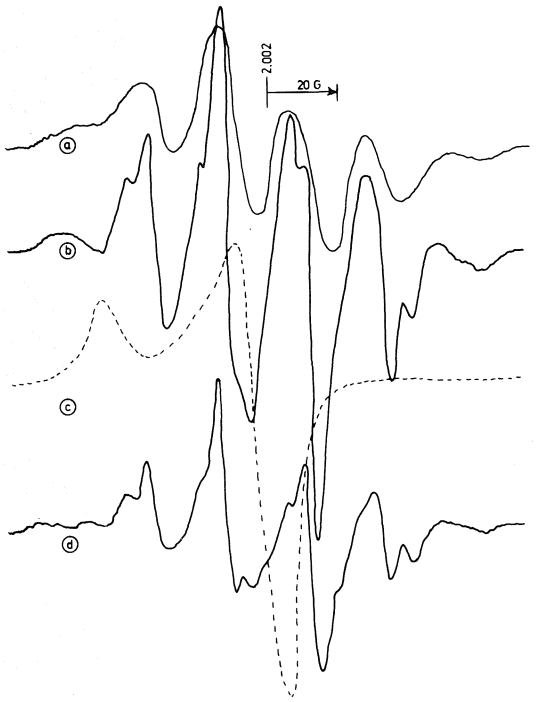

FIG. 1. (*a*) Hyperfine spectrum of radiolized 3MP. (*b*) Same sample photolyzed at 253.7 nm for 30 min. (*c*) Radiolized 3MP containing 130 torr air, warmed to 85 K. Spectrum of RO_2· run at 77 K. (*d*) Spectrum of sample (*c*) following 15 min 253.7 photolysis.

photolysis of RSH, H_2S (10), or R_2S (15). 3MP-d_{14} gives initially a broad peak on γ-irradiation which upon photolysis becomes an incompletely resolved multiplet of 7–9 lines with a 3.5 G separation. Wavelengths greater than 300 nm do not produce line sharpening in 3MP although near uv causes electron detachment from the carbanion M^- (16).

(B) 3MP with Added Oxygen

γ-Radiolysis of 3 MP which has been equilibrated with various pressures of air or oxygen give epr spectra at 76 K which are superpositions M· and MO_2· with the relative proportions of each depending upon the particular oxygen pressure involved. As the samples are warmed toward 87 K, the hyperfine peaks of M· decrease and the MO_2· peaks increase. The MO_2· signal heights obtained when M· is completely removed (Fig. 1*c*) are plotted in Fig. 2*a*, for constant dose, as a function of the partial pressures of air equilibrated with the solvent at room temperature. It is apparent from this figure that the

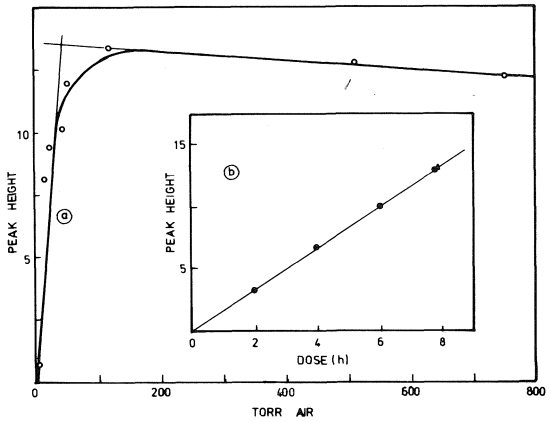

FIG. 2. (*a*) Yield of RO_2· *vs.* pressure of air equilibrated with a 3MP glass. Dose, 1.4×10^{19} eV g^{-1}. (*b*) Yield of RO_2· *vs.* radiation time in hours. Samples warmed to 85 K at 2 h intervals (●). Sample given single continuous dose (△).

intensity of the MO_2· is limited at high pressures by the radical concentration, and at low pressures by the oxygen concentration. Below 0.05 atm of air it is necessary to warm to ~90 K to get rid of all the residual hyperfine structure of the excess M· through the annihilation process

[4] $$2M\cdot \rightarrow \text{diamagnetic products}$$

and possibly

[5] $$M\cdot + MO_2\cdot \rightarrow MOOM$$

The points in Fig. 2*a* were from samples which had received fairly uniform treatment, with a 5 h time lapse between the conclusion of irradiation and the warmup procedure. Samples which have been 'rested' for 30 h give slightly higher results (10–15%) while freshly irradiated samples tend to give slightly lower results.

Experiments were carried out to determine whether the presence of RO_2· or oxygen alters the radiation induced solvent damage in any way. In the first instance, the irradiation was broken into several intervals between which the samples were warmed to produce RO_2·. The RO_2· peak heights so obtained were then plotted as a function of dose as in Fig. 2*b*. No differences were observed between these samples and those which had received the same dose without intermediate warming. That dissolved oxygen also has little effect was determined by comparing the peak height of the first upfield hyperfine line of M· in degassed 3MP with a

Can. J. Chem. Downloaded from www.nrcresearchpress.com by 210.87.254.42 on 09/05/12
For personal use only.

Can. J. Chem. Downloaded from www.nrcresearchpress.com by 210.87.254.42 on 09/05/12
For personal use only.

sample equilibrated with 41.8 torr of air. As a function of dose this ratio is a constant. As expected it is only slightly greater than unity, since a small proportion of the M· produced is converted to RO_2· in the latter case.

The effect of photolysis following γ-radiolysis but before warmup was also investigated for 3MP samples containing ~50 torr air. One sample was photobleached at 300–600 nm to remove M^-. On subsequent warming this gives an MO_2· signal 91% that of an unphotolysed sample. A second sample was photobleached at 253.7 for 30 min, giving an intensified M· epr spectrum as in Fig. 1*b*. There resulted a 17% *loss* of MO_2· signal relative to the unphotolysed sample. This suggests that 253.7 nm photolysis of M· does not create a large number of additional radicals, but that the signal intensification is largely due to creation of new species with narrower hyperfine lines, and that in fact there may be a small *reduction* in the total number of radical species present in the glass.

Photolysis of the various samples of MO_2· at 253.7 nm resulted in immediate decay of the peroxy radical and regeneration of the M· spectrum; not that originally observed as in Fig. 1*a* but that of Fig. 1*d*, which is even more structured than that of Fig. 1*b*, and contains many features of the ethyl spectrum. In addition, short (<8 min) photolysis times yielded a small peak with a *g* value of 2.044 which has no apparent high field counterpart. This feature is eventually obscured by growth of the hyperfine spectrum of M· or Et· with continued photolysis. It is removed by photolysis in the visible region, and is not observed in a perdeuterated 3MP matrix.

When the photolysed matrices are warmed again toward 85 K, MO_2· is regenerated in the oxygen rich media with an epr signal intensity which is reduced from that obtained before photolysis; a 45% loss appears typical for a 15 min photolysis of MO_2·. The residual radicals have slightly broader linewidths which presumably results from the fact there are now several different alkyl peroxides present (*i.e.* MO_2·, EtO_2·) with slightly different *g*-values and/or unresolved hyperfine couplings. For the samples with the lowest oxygen content, MO_2 is not regenerated, but the hyperfine structure of Fig. 1*d* decays away. With this reduction in radical concentration, the part of the spectrum assigned to Et· (the fine structure) is reduced more than that of M· so that the line shape alters from Fig. 1*d* through 1*b* as the smaller species diffuse away. The reconstitution of RO_2· may not occur in this case due to the unfavourable competition between reactions 4 and 5 relative to [1].

(C) BuCl–3MP Glasses with Oxygen

As can be seen from the previous section, spin trapping by oxygen is not completely photoreversible since solvent radicals M· are modified at some point to give different radical species. To ascertain whether these changes occurred before, during, or following the formation of MO_2· and its subsequent photolysis, a more distinctive radical species of more certain structure was required. Accordingly the four isomeric butyl chlorides were γ-irradiated in 3MP glasses at 77 K to give the analogous butyl radicals Bu·. These radicals are sufficiently large that one can assume that molecular oxygen is the only mobile component in a solid 3MP matrix which leads to reaction 1 below 85 K. The concentrations (1.0 mol^{-1}) had to be large enough to effectively preclude the formation of M· during the γ-radiolysis, but low enough (13 mol%) so that solute–solute interactions could be avoided (17–19). The chlorides were selected because they show relatively little photolytic activity at 253.7 nm, and scavenge electrons by process [3] more efficiently than do the other halides (7). Samples that were equilibrated with ~1/10 atm of air and irradiated to a constant dose of 4.6×10^{18} eV g^{-1} gave a pale coloration of orange through pink. This can be ascribed to alkyl chloride cations, $BuCl^+$ (19). Except for the superposition of the BuO_2· signal, the epr spectra were identical to those obtained by Ayscough and Thomson (7) and others (20). Isobutyl chloride is the only Bu· radical which gives an odd line spectrum (a_β = 39.4 G). Warming of each of the matrices toward 85 K gave BuO_2· as anticipated. The initial coloration is maintained, which suggests that $BuCl^+$ is not involved in reaction with oxygen. The epr signal intensities of the isomeric BuO_2· radicals relative to MO_2· for equivalent dose are *t*-BuO_2·, 3.58; *i*-BuO_2·, 3.17; 2-BuO_2·, 3.00; 1-BuO_2·, 1.37.

A 10–15 min photolysis at 253.7 nm of the BuO_2· samples at 77 K removed most of the coloration, as well as the epr spectrum of the BuO_2· radicals. It is replaced in the main by the

Can. J. Chem. Downloaded from www.nrcresearchpress.com by 210.87.254.42 on 09/05/12
For personal use only.

structured spectrum of M·, Fig. 1*b*, along with a single epr absorption at $g = 2.044$ as was also found in the 3MP/oxygen system. Only in the case of *i*-BuO_2· was there any indication that R· might be obtained by reaction 2. Small amounts of this radical would be observed in the presence of M· only by virtue of its odd line hyperfine structure. Prolonged photolysis results in loss of the small peak at $g = 2.044$ and the overall spectrum becomes even more like that of Fig. 1*b*. Warming the matrix regenerates a peroxy radical. The recovery of RO_2· is typically about 85% of the original BuO_2· following a 15 min photolysis.

(D) BuCl–3MP Glasses, No Oxygen

With the rather disappointing result that photolysis of the isomeric BuO_2· radicals produced little more than solvent radicals, it seemed advisable to determine the effect of 253.7 nm radiation on the alkyl radicals themselves. Completely degassed samples were irradiated and photolysed for successively longer times. Photolyses of 15 min were sufficient to remove all detectable amounts of the original radicals, and Bu· was also replaced by the solvent radical M· of Fig. 1*b*. The isobutyl radical proved to be somewhat more resistant to photolysis, and could be still observed after a 60 min photolysis, along with M·, both with somewhat reduced intensity. The *t*-butyl radical demonstrated partial conversion to *i*-Bu· as observed by Iwasaki and Toriyama (18) but in our case there was an overall loss of radicals as the photolysis proceeds. At no time was a peak at $g \simeq 2.044$ observed in the absence of oxygen.

Discussion and Summary

It appears from the results given above that molecular oxygen can be made to act as a reasonable spin trap for alkyl radicals in a glassy medium at temperatures about 80 K. The resulting peroxy radicals are sufficiently large that they do not diffuse or dimerize below the melting point of the matrix. The RO_2· spectrum is largely independent of the nature of the alkyl group, and does not readily saturate at microwave powers below 1 mW. The spectrum is not highly detailed and can be readily integrated by hand.

The curve of Fig. 2*a* is typical for radical scavengers. A least-squares fit to the low pressure data suggests that the knee of the curve occurs when $p(\text{air}) = 44.2$ torr which at 77 K corresponds to an oxygen concentration of 3.16×10^{-4} mol l^{-1}. This should equal the concentration of scavengable radicals with $[M\cdot]_s = 1.95 \times 10^{-4} G_s$ in mol l^{-1}. The radiochemical yield G_s works out in this case to be 1.62. This is substantially lower than the total radical yield $G_t = 3.0$ obtained by Perkey and Willard (12). However, the latter value is due to two radical populations; 57% of the total decay by a rapid "composite first-order decay" due to intraspur recombinations, while 43% decay by a slower second-order process involving "isolated" radicals (21). It is apparent that oxygen scavenges to a large extent the latter population, but diffusion is not rapid enough to compete with intraspur and other cage processes. By the nature of their formation, the yield of "isolated" radicals in the BuCl/3MP glasses is much larger, and this is reflected in the higher Bu· and BuO_2· yields. The G_s for 1.0 mol l^{-1} butyl chlorides in 3MP are; *t*-BuCl, 5.8; *i*-BuCl, 5.1; 2-BuCl, 4.9, and 1-BuCl, 2.2.

Not all paramagnetic species are trapped by O_2, however. In addition to $BuCl^+$ and geminate radical pairs, which are not trapped, we have observed no signals due to HO_2 (22), O_2^- (23), OH (24), or RO_3· (25) before, during, or following photolysis. This implies that thermal H and electrons are not effectively trapped by O_2 at the concentrations used here ($< 10^{-3}$ mol l^{-1}), and that atomic oxygen is not produced as a result of photolysis.

While molecular oxygen may prove useful as a spin trap, it does not appear as if the trapped species can be regenerated by photolytic action. The photon necessary for fragmentation of RO_2· is also sufficiently energetic to cause isomerization and disproportionation of larger alkyl groups, and to destroy species such as RCl^+. From the evidence we have, it is not possible to say whether reaction 2 occurs or not, and the data does not discriminate between process occurring at 77 K such as

$$BuO_2\cdot \xrightarrow{h\nu} BuO_2\cdot{}^*$$

then

$$BuO_2{}^* \longrightarrow Bu\cdot + O_2$$

followed by

$$Bu\cdot \xrightarrow{h\nu} Bu\cdot{}^*$$

$$Bu\cdot{}^* + MH \longrightarrow M\cdot + BuH$$

or alternately

$$BuO_2\cdot^* + MH \longrightarrow BuOOH + M\cdot$$

Warming to 85 K gives either

$$M\cdot + O_2 \longrightarrow MO_2\cdot$$

or

$$BuOOH + M\cdot \longrightarrow MH + BuO_2\cdot$$

A demerit for the first scheme is that *i*-Bu· cannot be observed in the photolysis of *t*-BuO_2, although *t*-Bu· readily isomerizes to *i*-Bu· when no oxygen is present. Furthermore *i*-Bu· is relatively stable toward photolysis. On the other hand, *t*-BuOOH itself shows photolytic activity at 253.7 and gives *t*-BuO_2· and M·. Its presence could therefore give rise to a growth rather than loss of radicals during photolysis.

The small peak at $g = 2.044$ was originally thought to be RO·, produced from RO_2·, but the fact that it is bleached by visible light and is not seen in the deuterated matrix suggests rather that it is the sharp low field resonance of HCO. It is not obtained in high yield, so that one can never pick out the high field line, which is asymmetrically broadened (26). The outer components of the DCO triplet can be observed in the deuterated matrix with a 40 G spread. Its precise mode of formation is unclear, but may result from rearrangements of BuO_2* or MO_2*, or, more probably from reactions of CH_3O_2 where methyl arises from the photolysis of Bu· or M· as the case may be.

Regardless of what the mode of photodecomposition of RO_2· proves to be, it is apparent that great care must be taken in the formation and the subsequent reactions of alkyl radicals produced by photolytic action in the far uv since the larger radicals appear to be very labile, prone to rearrangement and solvent abstraction reactions with the result that the identity of the original radical may be lost.

Acknowledgements

The financial support of the National Research Council of Canada and technical help of Mr. Glen Smith is acknowledged with appreciation.

1. R. W. Fessenden and R. N. Schuler. J. Chem. Phys. **39**, 2147 (1963).
2. H. Jensen and T. Henriksen. Acta Chem. Scand. **22**, 2263 (1968).
3. K. U. Ingold. Acc. Chem. Res. **2**, 1 (1969).
4. K. U. Ingold and J. R. Morton. J. Am. Chem. Soc. **86**, 3400 (1964).
5. J. E. Bennett, D. M. Brown, and B. Mile. Trans. Faraday Soc. **66**, 397 (1970).
6. G. E. Adams. Adv. Radiat. Chem. **3**, 125 (1972).
7. P. B. Ayscough and C. Thomson. Trans. Faraday Soc. **58**, 1471 (1962).
8. F. Mariage and P. Claes. Ann. Soc. Sci. Bruxelles Ser. 1, **83**, 255 (1969).
9. H. Stephen and T. Stephen (*Editors*). Solubilities of inorganic and organic compounds. Pergamon Press. Oxford. 1963. p. 575.
10. A. J. Elliot and F. C. Adam. Can. J. Chem. **52**, 102 (1974).
11. L. J. Aarons and F. C. Adam. Can. J. Chem. **50**, 1390 (1972).
12. L. Perkey and J. E. Willard. J. Chem. Phys. **60**, 2732 (1974).
13. S. C. Srinivasan and J. E. Willard. J. Phys. Chem. **77**, 2171 (1973).
14. M. Ya Mel'nikov, V. I. Sklyarenko, and N.V. Fok. Dokl. Akad. Nauk SSSR, **218**, 875 (1974).
15. A. J. Elliot and F. C. Adam. Can. J. Chem. To be published.
16. D. P. Lin and J. E. Willard. J. Phys. Chem. **78**, 1135 (1974).
17. N. Leray and J. Roncin. Int. J. Radiat. Phys. Chem. **4**, 347 (1972).
18. M. Iwasaki and K. Toriyama. J. Chem. Phys. **46**, 2852 (1967).
19. R. F. C. Claridge and J. E. Willard. J. Am. Chem. Soc. **58**, 1471 (1962).
20. B. H. L. Bielski and J. M. Gebicki (*Editors*). Atlas of electron spin resonance spectra. Academic Press, New York. 1967.
21. M. A. Neiss and J. E. Willard. J. Phys. Chem. **79**, 783 (1975).
22. F. J. Adrian, E. L. Cochrane, and V. A. Bowers. J. Chem. Phys. **47**, 5441 (1967).
23. J. E. Bennett, B. Mile, and A. Thomas. Trans. Faraday Soc. **64**, 3200 (1968).
24. J. Kroh, B. C. Green, and J. W. T. Spinks. Can. J. Chem. **40**, 413 (1962).
25. R. W. Fessenden. J. Chem. Phys. **48**, 3725 (1968).
26. S. B. Milliken and R. H. Johnsen. J. Phys. Chem. **71**, 2116 (1967).

Can. J. Chem. Downloaded from www.nrcresearchpress.com by 210.87.254.42 on 09/05/12
For personal use only.

Interionic potentials for the alkali metal chlorides

J. Corish and Brenda M. C. Parker
Department of Chemistry, University College, Dublin, Ireland

AND

P. W. M. Jacobs
Department of Chemistry, University of Western Ontario, London, Ont., Canada N6A 5B7

Received July 6, 1976

J. Corish, Brenda M. C. Parker, and P. W. M. Jacobs. Can. J. Chem. **54**, 3839 (1976).

Various models for the interionic potential in the alkali metal chlorides have been examined. The parameters in these potentials have been determined by fitting the equilibrium, elastic and dielectric properties of each substance. The potentials are compared graphically with each other, with the theoretically derived potentials of Kim and Gordon (1, 2) and with a potential derived earlier by Catlow, Diller, and Norgett (3) by fitting the properties of sixteen alkali halides simultaneously. Intrinsic defect properties of the four chlorides have been calculated from these potentials. The results show that while it is possible to derive adequate two-body potentials for these salts from fitting their bulk properties, it is concluded, as found earlier by Catlow, Diller, and Norgett (3), that such potentials need to have the anion–cation interaction hardened by neglecting completely the Van der Waals interaction between nearest neighbours. Inclusion of non-central forces does not improve the potential, as judged by the criterion of the results of defect calculations.

J. Corish, Brenda M. C. Parker et P. W. M. Jacobs. Can. J. Chem. **54**, 3839 (1976).

On a examiné divers modèles pour les potentiels interioniques dans les chlorures de métaux alcalins. On a déterminé les paramètres de ces potentiels en les ajustant aux propriétés d'équilibre, élastiques et diélectriques de chaque substance. On a comparé, d'une façon graphique, les potentiels entre eux, avec les potentiels obtenus d'une façon théorique par Kim et Gordon (1, 2) et avec le potentiel obtenu antérieurement par Catlow, Diller et Norgett (3) en les ajustant aux propriétés de 16 halogénures alcalins d'une façon simultanée. On a calculé les propriétés de défauts intrinsèques des 4 chlorures à partir de ces potentiels. Les résultats montrent qu'il est possible de dériver des potentiels à deux corps adéquats pour ces sels en les ajustant à leurs propriétés macroscopiques; toutefois on en conclut, comme l'ont trouvé antérieurement Catlow, Diller et Norgett (3), que pour de tels potentiels on doit durcir l'interaction anion–cation en négligeant complètement les interactions de Van der Waals entre les voisins les plus près. Si l'on en juge par le critère des résultats de calcul de défauts, l'inclusion des force non centrales n'améliore pas le potentiel.

[Traduit par le journal]

Introduction

Modern work on the pair potential in ionic crystals may be said to have started with the extensive and thorough investigations of Fumi and Tosi (4, 5) on the cohesive energy of alkali halide crystals. They concluded that the optimum form of the pair potential was what we shall refer to as the Buckingham form: an exponential repulsive term, an r^{-1} Coulombic term, and r^{-6}, r^{-8} dispersion terms corresponding to the dipole–dipole and dipole–quadrupole terms of the multipole expansion. In this expression the r^{-6} and r^{-8} terms represent an approximation that is only accurate at long range, while the exponential term is an attempt to take account of short-range charge overlap and exchange interactions. Because of the extremely long range of the r^{-1} Coulomb interaction the other terms are referred to here as the 'short range potential'. The potential parameters derived by Fumi and Tosi (4, 5) from thermodynamic data gave an extremely good fit to the cohesive energy of the alkali halides but failed to reproduce the experimental values of the elastic constants satisfactorily (6). Fumi and Tosi (4, 5) employed the Van der Waals coefficients deduced by Mayer (7). In a re-analysis of this problem using Mayer's method, Lynch (8) has suggested that the Mayer values may be in need of revision and Ree and Holt (6) concluded that the failure of the Fumi and Tosi (4, 5) potential parameters to give satisfactory elastic constants was due to too soft a repulsion and too weak a Van der Waals attraction between $+-$ or $--$ ions.

Can. J. Chem. Downloaded from www.nrcresearchpress.com by 210.87.254.40 on 09/05/12
For personal use only.

Can. J. Chem. Downloaded from www.nrcresearchpress.com by 210.87.234.40 on 09/03/12
For personal use only.

The next logical step was to devise a method of determining potential parameters that satisfied the equilibrium properties (lattice constant, cohesive energy, and equilibrium condition) and the elastic constants simultaneously.

Analysis of the dielectric properties of ionic crystals and of phonon dispersion curves determined by neutron scattering had, however, shown the inadequacy of a rigid ion model and led in turn to the simple shell model (9) and the breathing shell model (10). Thus an adequate interionic potential should be capable of fitting the equilibrium, elastic, dielectric, and the lattice dynamical properties of the crystal. The complex problem of fitting the properties of all sixteen alkali halides simultaneously was resolved by Catlow, Diller, and Norgett (3) by separating the least-squares calculation into two parts: the elastic and equilibrium properties were fitted first and then the dielectric properties. In order to get the second-neighbour interactions more-nearly correct (which previous work on the alkaline earth fluorides by Catlow and Norgett (11) had shown to be a necessary feature of successful defect calculations) these authors utilized a theoretical method (12) of calculating the second-neighbour repulsion. The resulting potential is very successful in reproducing the properties of the alkali halide crystals and when employed in defect calculations it yields results that are in good general agreement with available experimental data (13). But because of the predicted similarity between anion and cation migration energies which is not in accord with experimental data *as currently analyzed*, and because the techniques employed in deriving the potential parameters (Wedepohl calculations of repulsive parameters and a multi-substance least-squares fitting procedure) will not generally be available when new substances are investigated, we decided to attempt to derive potentials of the Buckingham form by fitting simultaneously the dielectric, elastic, and equilibrium properties of a single substance at a time. The alkali metal chlorides were used as test substances for this purpose.

The Model Potentials

Four basic model potentials were tested. These were all variants of the Buckingham potential. All four models were based on the breathing shell model (14, 15) and two of the four models were developed in both central-force and non-central force ($B_3 \neq 0$) versions. The Buckingham potential in its simplest form is

$$[1] \qquad \phi_{ij}^{S} = A_{ij} \exp(-r_{ij}/\rho_{ij}) + V_{ij}/r_{ij}^{6} \equiv \phi_{ij}^{R} + \phi_{ij}^{V}$$

where ϕ_{ij}^{S} denotes the short-range potential between ions ij separated by a distance r_{ij}. ϕ_{ij}^{R} is the repulsive part of this interaction and is represented by a single exponential function containing two parameters, the repulsive parameter A_{ij} and the hardness parameter ρ_{ij}. ϕ_{ij}^{V} is the attractive (Van der Waals) part of the short-range interaction and this is approximated by a single r^{-6} term which corresponds to the dipole–dipole part of the interaction only, higher multipoles being neglected. As the V_{ij} coefficients are going to be determined empirically there will be no need to separate this term later on into the product of a coefficient depending on ion-type and a lattice sum.

If we limit the repulsive interactions to nearest-neighbour (nn) and next-nearest neighbour (nnn) interactions only, then the total short-range contribution to the potential energy of the pure perfect crystal with the NaCl structure is

$$[2] \quad \phi^{S} = \sum_{i \leq j = 1}^{2} 6\phi_{ij}^{R} + 6\phi_{ij}^{V} \equiv \phi_{11}^{S} + \phi_{12}^{S} + \phi_{22}^{S}$$

where 1 denotes the cation species, 2 the anion species, and the lattice sums for the Van der Waals interactions are absorbed into the V_{ij} coefficients. This potential contains nine parameters: $3A_{ij}$, $3\rho_{ij}$, and $3V_{ij}$. There are, in addition, the 6 parameters of the breathing shell model: the ion charge Z, the shell charges Y_1 and Y_2, the isotropic force constants K_1 and K_2 that couple the shells to their respective cores, and Sangster's (14) γ parameter which is

$$[3] \qquad \gamma = \frac{1}{2} \frac{(A_1 + 2\sqrt{2}A_2)^2}{G_2 + 3A_1 + 12A_2}$$

where G_2 is the breathing force constant for the negative ion. The ion deformations are limited to the A_{1g} breathing mode and to the negative ions only. The nn and nnn radial force constants are defined by

$$A_1 = \kappa \left(\frac{\partial^2 \phi_{12}^{S}}{\partial r_{12}^{2}} \right)_{r_{12} = r_0}$$

Can. J. Chem. Downloaded from www.nrcresearchpress.com by 210.87.254.40 on 09/05/12
For personal use only.

[4]
$$A_2 = \kappa\left[\left(\frac{\partial^2\phi_{11}{}^{S}}{\partial r_{11}{}^2}\right)_{r_{11}=r_1} + \left(\frac{\partial^2\phi_{22}{}^{S}}{\partial r_{22}{}^2}\right)_{r_{22}=r_1}\right]$$

where r_0 is the nn distance and $r_1 = \sqrt{2}r_0$ is the nnn distance. $\kappa = (4\pi\epsilon_0)2v/e^2$ is a scaling factor, v being the volume of the unit cell ($= 2r_0{}^3$). The tangential force constants are

$$B_1 = \kappa\left(\frac{1}{r_{12}}\frac{\partial\phi_{12}}{\partial r_{12}}\right)_{r_{12}=r_0}$$

[5]
$$B_2 = \kappa\left[\left(\frac{1}{r_{11}}\frac{\partial\phi_{11}}{\partial r_{11}}\right)_{r_{11}=r_1} + \left(\frac{1}{r_{22}}\frac{\partial\phi_{22}}{\partial r_{22}}\right)_{r_{22}=r_1}\right]$$

and the nn non-central force constant B_3 is defined by

[6] $$B_1 + B_3 = \kappa\left[\left(\frac{\partial^2\phi_{12}}{\partial r_{12}{}^2}\right)^{\perp}\right]_{r_{12}=r_0}$$

The total number of parameters to be assigned is thus 16.

The conditions that the potential and its derivatives must satisfy are the following.

(*i*) The cohesive energy

[7] $$U_c = U_v + [-(\alpha_M Z^2 e^2/4\pi\epsilon_0 r_{12}) + \phi^S]_{r_{12}=r_0}$$

U_c is the cohesive energy ($= -U_L$, the lattice energy) and U_v is the vibrational energy of the crystal at the temperature at which the comparison with experimental data is made.

(*ii*) The equilibrium condition

[8] $$\tfrac{2}{3}\alpha_M Z^2 + B_1 + 2B_2 = 0$$

where α_M is the Madelung constant.

(*iii*) The elastic constants

[9] $$C_{11} = \tfrac{1}{2}[A_1 + A_2 + B_2] - \gamma - 2.55604Z^2$$

[10] $$C_{12} = \tfrac{1}{4}[A_2 - 2B_1 - 5B_2 - 2B_3] - \gamma + 0.11298Z^2$$

[11] $$C_{44} = \tfrac{1}{4}[A_2 + 2B_1 + 3B_2 + 2B_3] + 1.27802Z^2$$

(*iv*) The static relative permittivity

[12] $$\left\{\frac{\epsilon_0 - 1}{\epsilon_0 + 2}\right\}\frac{3}{4\pi} = \alpha_0 = \frac{(Z - Y_1)^2}{K_1} + \frac{(Z + Y_2)^2}{K_2} + \frac{Z^2}{R}$$

ϵ_0 is the relative permittivity ('dielectric constant') measured in a static or low frequency field, α_0 the static polarizability of the crystal, and R is the nn overlap force constant given by

[13] $$R = 2A_1 + 4B_1 + 4B_3$$

(*v*) The high-frequency relative permittivity

[14] $$\left\{\frac{\epsilon_\infty - 1}{\epsilon_\infty + 2}\right\}\frac{3}{4\pi} = \alpha_\infty = \frac{Y_1{}^2}{K_1} + \frac{Y_2{}^2}{K_2} - R_0\left\{\frac{Y_1}{K_1} - \frac{Y_2}{K_2}\right\}^2$$

ϵ_∞ is the high-frequency relative permittivity and

[15] $$\frac{1}{R_0} \equiv \frac{1}{R} + \frac{1}{K_1} + \frac{1}{K_2}$$

(*vi*) The anion polarizability

[16] $$\alpha_2 = R_0\left[\frac{Y_2{}^2}{RK_2} + \frac{Y_2(Y_1 + Y_2)}{K_1K_2}\right]$$

(*vii*) The transverse optical mode frequency at $\boldsymbol{q} = 0$.

[17] $$\mu\omega_t{}^2 = \left(\frac{\epsilon_\infty + 2}{\epsilon_0 + 2}\right)R_0$$

μ is the reduced mass of the cation, anion pair and ω_t is the frequency of the transverse optical mode at the centre of the Brillouin zone. Note that equations 8–17 are written in dimensionless 'crystal units': charge in units of the proton charge $|e|$, length in units of r_0, energy in units of $e^2/(4\pi\epsilon_0)r_0$, polarizability in units of $v(4\pi\epsilon_0)$, force constants in units of $e^2/2v(4\pi\epsilon_0)$, and elastic constants in units of $e^2/vr_0(4\pi\epsilon_0)$.

The expressions for the elastic constants, without γ and B_3, were obtained from the equations of motion by Cowley (16). The gamma term was added by Sangster (14) who, in a later paper (15), also allowed for ion deformations of E_g symmetry which we have not included. The explicit formulae for α_0, α_∞, $\mu\omega_t{}^2$, and α_2 were obtained by direct solution of the equations of motion and checked by evaluating Cochrane's (17) matrix expressions.

Equations 7–12, 14, 16, and 17 represent nine conditions which the potential can be made satisfy, provided that the necessary experimental data are available which they are for the alkali metal chlorides examined in this paper (Table 1). Since we have 16 parameters and only 9 conditions, 7 of the parameters must be eliminated or fixed by model building.

TABLE 1. Data for the alkali metal chlorides used in the calculation of interionic potentials, all numerical values are for low temperatures except those for the cohesive energy

Parameters	Value			
	LiCl	NaCl	KCl	RbCl
Lattice constant[a] (r_0/Å)	2.539	2.789	3.116	3.259
Elastic constants[b]				
$C_{11}/10^{11}$ dyn cm^{-2}	6.074	5.733	4.832	4.297
$C_{12}/10^{11}$ dyn cm^{-2}	2.27	1.123	0.54	0.649
$C_{44}/10^{11}$ dyn cm^{-2}	2.692	1.331	0.663	0.493
Cohesive energy[c] at 298.15 K, U_c/kJ mol^{-1}	832.2	764.0	693.7	666.5
Relative permittivity				
ϵ_0[d]	10.92	5.45	4.49	4.53
ϵ_∞[e]	2.79	2.35	2.20	2.20
Transverse optical mode frequency[e] $\omega_t/10^{13}$ s^{-1}	4.17	3.36	2.65	2.38

[a]Ghate (20).
[b]For LiCl, NaCl, RbCl from Lewis, Lehoczky, and Briscoe (21); for KCl from Norwood and Briscoe (22).
[c]Tosi (18).
[d]Lowndes and Martin (23).
[e]Lowndes and Martin (24).

The first approach tried was to use a common value for the hardness parameter

$$\rho_{ij} = \rho \qquad [18]$$

and to represent A_{ij} by

$$A_{ij} = DP_{ij} \exp[-(r_i + r_j)/\rho] \qquad [19]$$

where P_{ij} are the Pauling factors (18) and r_i, r_j are the radii of the ith and jth ions respectively. This reduces the number of parameters by 2 and adds one extra condition since r_1, r_2 must satisfy the radius condition

$$r_1 + r_2 = r_0 \qquad [20]$$

Examination of eqs. 10, 11 shows that γ and B_3 are not independent parameters for they must satisfy the condition

$$B_3 = C_{44} - C_{12} - \gamma \qquad [21]$$

The Van der Waals coefficient V_{22} was fixed at the Mayer (7) value of 75 eV Å^6 for Cl^-–Cl^- and V_{11} was scaled to this value by the factor $(\alpha_1/\alpha_2)^{3/2}$ which simply recognizes the relation between polarizability and the dipole–dipole r^{-6} coefficient which is implicit in a simple shell model. Because the r^{-6} coefficient is quenched somewhat as r decreases V_{12} was either set equal to zero (potential V) or treated as a variable parameter (potential Y). With V there are now 10 unknown parameters and 10 conditions on the potential so that a least-squares (LS) fitting procedure can be adopted. With potential Y there is still one undetermined parameter so the ionic charge Z was fixed at a series of reasonable values and the remaining parameters fitted by a LS calculation.

Because it is hard to justify the use of a common value for the hardness parameter, other than by tradition, we next retained A_{ij}, ρ_{ij} as variable parameters. With judicious fixing of other parameters a LS analysis was attempted but the calculation proved to be very unstable. It seems that some relation between the A's and ρ's must be provided. In their first potential (here called W) Catlow, Diller, and Norgett (3) fitted the equilibrium and elastic properties of all sixteen alkali halides with the NaCl structure simultaneously using a potential of the BM form in which the second-neighbour repulsions were determined theoretically (12), thus ensuring the necessary stability. Since our object was to determine if a useful potential could be obtained by fitting the properties of single substances, and since, in many future calculations, theoretical estimates of the repulsive potential will not be available, an alternative source of stability had to be sought. This was provided by constraining A_{11} and ρ_{11} so that the geometric mean prescription

$$\phi_{12}^{R} = (\phi_{11}^{R}\phi_{22}^{R})^{1/2} \qquad [22]$$

Can. J. Chem. Downloaded from www.nrcresearchpress.com by 210.87.254.40 on 09/05/12
For personal use only.

TABLE 2. Comparison of potential parameters for the alkali metal chlorides: lithium chloride

Parameter	Value						Units
	W	Y	V	X	U_1	U_2	
Z	0.9953	0.9980	1.000	0.9812	0.9960	0.9950	$\|e\|$
V_{11}	0.3445	0.0700	42.163	0.0700	0.0004	0.649	eV Å^6
V_{12}	0	2.0334	0	2.2913	0	0	eV Å^6
V_{22}	0.3445	75.000	42.163	75.000	0.4396	67.363	eV Å^6
D	0.1566	0.1595	0.1469	—	—	—	eV
ρ_{11}	0.1364			0.3019	0.2137	0.3003	Å
ρ or ρ_{12}	0.2786	0.3194	0.3194	0.2972	0.2732	0.2949	Å
ρ_{22}	0.3214			0.2926	0.3788	0.2898	Å
R_1	0.6000	0.9669	0.9598	—	—	—	Å
R_2	1.9309	1.5447	1.5704	—	—	—	Å
A_{11}	1153.75	136.020	119.649	140.029	6197.40	137.783	eV
A_{12}	1380.62	570.918	556.299	882.610	1574.84	942.064	eV
A_{22}	1227.18	1901.21	2052.08	5563.13	400.190	6441.19	eV
A_1	8.9108	8.7502	8.7570	8.5961	8.8315	8.9888	$e^2/2v(4\pi\epsilon_0)$
A_2	0.7548	0.6707	0.6879	0.9134	0.9843	1.0293	$e^2/2v(4\pi\epsilon_0)$
B_1	−0.9778	−1.0968	−1.1018	−0.9996	−0.9503	−1.0442	$e^2/2v(4\pi\epsilon_0)$
B_2	−0.0673	−0.0317	−0.0298	−0.0425	−0.1035	−0.0541	$e^2/2v(4\pi\epsilon_0)$
B_3	0	0.1852	0.1783	0.1207	0	0.0000	$e^2/2v(4\pi\epsilon_0)$
R	13.9106	13.8540	13.8203	13.6767	13.8631	13.8009	$e^2/2v(4\pi\epsilon_0)$
γ	0.0249	0.0256	0.0325	0.0901	0.2104	0.2111	$e^2/2v(4\pi\epsilon_0)$
Y_1	0.7094	0.1386	0.1301	0.1155	0.0774	0.1598	$\|e\|$
K_1	7.9888	1392.2	1791.06	369.06	727.38	147.81	eV Å^{-2}
Y_2	−2.4850	−2.6739	−2.5982	−2.7598	−2.6860	−2.6059	$\|e\|$
K_2	29.3814	31.8835	29.8556	34.1155	32.1719	30.4731	eV Å^{-2}

was satisfied. V_{22} was also treated as a variable parameter but V_{11} was set by requiring that

[23] $$V_{11} = (\alpha_1/\alpha_2)^{3/2}V_{22}$$

In potential U, $V_{12} = 0$ and in potential X

[24] $$V_{12} = (V_{11}V_{22})^{1/2}$$

Each of these models was tested in two versions: X_1, U_1 had $B_3 = 0$ and so were central-force potentials while with X_2 and U_2, B_3 was made to satisfy eq. 21. These two models still have two excess parameters so in the LS calculations two of Z, Y_1, V_{22}, and γ were varied in turn with the other two fixed. As an alternative, the expression for A_2–B_2, obtained by eliminating B_1 between eqs. 8 and 11, was fitted instead of C_{44} but this appeared to make little practical difference to the parameters.

Results

The best-fit values of potential parameters for Y, Z, U_1, U_2, and X_2 ($\equiv X$) for LiCl, NaCl, KCl, and RbCl are shown in Tables 2–5. The non-central force version of X, X_1 is not given since it was not used extensively in defect calculations, trial calculations having shown that X_1 was inferior to U_1. The column headed W shows the parameters obtained by Catlow, Diller, and Norgett (3) for their potential I. This was based on a theoretically derived anion–anion interaction; V_{12} was set equal to zero and the remaining parameters were obtained by fitting the elastic properties and then the dielectric properties of all 16 alkali halides with the NaCl structure simultaneously. Apart from the potential parameters the tables show the force constants A_1, A_2, B_1, B_2, and R and the value of γ. $B_3 = 0$ shows a central-force model. The units adopted are the 'natural' solid state units of eV for energy and Å for length except that force constants are given in units of $e^2/2v(4\pi\epsilon_0)$ to facilitate comparison with lattice dynamical values which are generally quoted in these units. The number of figures quoted for any parameter does not, of course, reflect the 'accuracy' with which it is known; rather sufficient figures are quoted so that any one else would be able to reproduce the defect energies calculated later, should they desire to do so. Although V_{22} was varied in potential X the best fit was in fact obtained with the Mayer values.

The nn short-range interaction ϕ_{12}^S, plotted

Can. J. Chem. Downloaded from www.nrcresearchpress.com by 210.87.254.40 on 09/05/12
For personal use only.

TABLE 3. Comparison of potential parameters for the alkali metal chlorides: sodium chloride

Parameter	Value						Units
	W	Y	V	X	U_1	U_2	
Z	0.9882	0.9850	1.0000	0.9801	0.9920	0.9950	$\|e\|$
V_{11}	29.060	1.9000	48.196	1.9000	48.196	2.5162	eV Å^6
V_{12}	0	38.9237	0	11.9373	0	0	eV Å^6
V_{22}	29.060	75.000	48.196	75.000	100.218	95.379	eV Å^6
D	0.1566	0.2260	0.1723	—	—	—	eV
ρ or ρ_{11}	0.1709			0.2801	0.2489	0.2515	Å
ρ or ρ_{12}	0.2903	0.2982	0.2937	0.2855	0.2913	0.2818	Å
ρ or ρ_{22}	0.3214			0.2911	0.3512	0.3204	Å
R_1	0.8563	1.3436	1.3498	—	—	—	Å
R_2	1.9309	1.4193	1.4241	—	—	—	Å
A_{11}	7895.39	2311.36	2111.54	2331.36	7403.82	5549.57	eV
A_{12}	2314.72	2383.85	2174.87	2850.70	2290.14	3004.71	eV
A_{22}	1227.18	2304.94	2100.09	3485.74	708.382	1626.84	eV
A_1	11.1296	11.3371	11.4321	11.2323	11.3149	11.4714	$e^2/2v(4\pi\epsilon_0)$
A_2	0.0840	0.2324	0.0171	0.1236	0.0843	0.0723	$e^2/2v(4\pi\epsilon_0)$
B_1	−1.1584	−1.1157	−1.2041	−1.1164	−1.1820	−1.1590	$e^2/2v(4\pi\epsilon_0)$
B_2	0.0086	0.0048	0.0272	0.0138	0.0166	0.0202	$e^2/2v(4\pi\epsilon_0)$
B_3	0	−0.0216	0.0430	0.0131	0	−0.0005	$e^2/2v(4\pi\epsilon_0)$
R	17.6253	18.1249	18.2200	18.0515	17.9019	18.3046	$e^2/2v(4\pi\epsilon_0)$
γ	0.0577	0.0977	0.0331	0.0629	0.0761	0.0766	$e^2/2v(4\pi\epsilon_0)$
Y_1	2.1283	−4.6276	−2.9678	−3.7897	−2.8889	−2.8197	$\|e\|$
K_1	96.4396	1464.04	1147.79	2919.20	1594.07	1643.02	eV Å^{-2}
Y_2	−2.4850	−2.5398	−2.4341	2.8131	−2.5605	−2.7451	$\|e\|$
K_2	29.3814	28.2919	25.1860	34.4322	29.5111	33.0807	eV Å^{-2}

TABLE 4. Comparison of potential parameters for the alkali metal chlorides: potassium chloride

Parameter	Value						Units
	W	Y	V	X	U_1	U_2	
Z	0.9939	0.9900	0.9950	0.9875	0.9750	0.9755	$\|e\|$
V_{11}	124.94	19.000	106.57	19.000	71.755	50.003	eV Å^6
V_{12}	0	37.157	0	37.749	0	0	eV Å^6
V_{22}	124.94	75.000	106.57	75.000	279.61	194.85	eV Å^6
D	0.1566	0.1559	0.1326	—	—	—	
ρ or ρ_{11}	0.2603			0.2933	0.2803	0.2857	Å
ρ or ρ_{12}	0.3048	0.2763	0.2820	0.2795	0.3091	0.2773	Å
ρ or ρ_{22}	0.3214			0.2672	0.3444	0.2694	Å
R_1	1.1711	1.5089	1.4048	—	—	—	Å
R_2	1.9309	1.5783	1.7093	—	—	—	Å
A_{11}	3796.86	10785.34	3520.49	4440.65	6633.92	34727.2	eV
A_{12}	4117.926	11092.12	8290.19	9850.99	3605.56	9422.21	eV
A_{22}	1227.18	10694.66	18301.94	21853.1	1959.64	2556.44	eV
A_1	13.5311	13.9898	13.9194	13.8214	13.2644	13.5694	$e^2/2v(4\pi\epsilon_0)$
A_2	−0.4942	0.0471	−0.1523	0.0858	−0.3999	0.1754	$e^2/2v(4\pi\epsilon_0)$
B_1	−1.3236	−1.1607	−1.2597	−1.1607	−1.3156	−1.2076	$e^2/2v(4\pi\epsilon_0)$
B_2	0.0793	0.0157	0.0515	0.0140	0.0878	0.0390	$e^2/2v(4\pi\epsilon_0)$
B_3	0	−0.2757	−0.1849	−0.3081	0	−0.3081	$e^2/2v(4\pi\epsilon_0)$
R	21.7679	22.2342	22.0607	21.7676	21.2665	21.0761	$e^2/2v(4\pi\epsilon_0)$
γ	0.0907	0.3762	0.2930	0.4087	0.1005	0.4087	$e^2/2v(4\pi\epsilon_0)$
Y_1	−83.553	−6.1611	−82.460	−14.0382	−13.766	−12.658	$\|e\|$
K_1	86032.4	527.656	83723.2	3003.03	3105.85	2563.66	eV Å^{-2}
Y_2	−2.4850	−2.3101	−2.6814	−2.5691	−2.6787	−2.8274	$\|e\|$
K_2	29.3814	23.4304	32.5689	28.9673	32.4399	35.5149	eV Å^{-2}

Can. J. Chem. Downloaded from www.nrcresearchpress.com by 210.87.254.40 on 09/05/12
For personal use only.

TABLE 5. Comparison of potential parameters for the alkali metal chlorides: rubidium chloride

Parameter	Value						Units
	W	*Y*	*V*	*X*	U_1	U_2	
Z	0.9913	0.9900	0.9950	0.9767	0.9794	0.9776	|*e*|
V_{11}	201.88	35.000	125.83	35.003	157.31	123.23	eV Å^6
V_{12}	0	52.709	0	51.235	0	0	eV Å^6
V_{22}	201.88	75.000	125.834	75.000	334.92	262.36	eV Å^6
D	0.1566	0.1550	0.1409	—	—	—	
ρ or ρ_{11}	0.2704			0.3341	0.2709	0.2408	Å
ρ or ρ_{12}	0.3233	0.2769	0.2703	0.2768	0.3226	0.2711	Å
ρ or ρ_{22}	0.3214			0.2362	0.3987	0.3100	Å
R_1	1.3123	1.6283	1.3274	—	—	—	Å
R_2	1.9309	1.5855	1.8711	—	—	—	Å
A_{11}	6808.14	24819.8	3247.96	987.680	30208.2	13819.6	eV
A_{12}	3559.905	17013.1	19419.4	16665.3	3656.69	18440.9	eV
A_{22}	1227.18	10933.0	108851	281197	442.641	24607.6	eV
A_1	13.7194	14.8396	14.8271	14.4611	13.8562	14.4980	$e^2/2v(4\pi\epsilon_0)$
A_2	−0.7085	0.0468	0.0808	0.0712	−0.6067	0.1046	$e^2/2v(4\pi\epsilon_0)$
B_1	−1.3610	−1.1641	−1.2297	−1.1338	−1.3717	−1.2059	$e^2/2v(4\pi\epsilon_0)$
B_2	0.1076	0.0153	0.0373	0.0165	0.1079	0.0508	$e^2/2v(4\pi\epsilon_0)$
B_3	0	−0.3890	−0.4241	−0.3843	0	−0.3843	$e^2/2v(4\pi\epsilon_0)$
R	21.9949	23.4671	23.0391	22.8497	22.2216	22.6353	$e^2/2v(4\pi\epsilon_0)$
γ	−0.1487	0.2139	0.2610	0.2092	−0.1741	0.2092	$e^2/2v(4\pi\epsilon_0)$
Y_1	−125.253	−8.9477	−109.372	−20.270	−17.507	−23.899	|*e*|
K_1	121460	784.468	94805.9	3560.40	2916.39	5041.93	eV Å^{-2}
Y_2	−2.4850	−3.3570	−2.7907	−2.7591	−2.6491	−2.8572	|*e*|
K_2	29.3814	52.4645	35.8923	33.9601	31.4386	36.4625	eV Å^{-2}

as a function of r/r_0, is shown graphically in Figs. 1–4 for Li^+Cl^-, Na^+Cl^-, K^+Cl^-, and Rb^+Cl^-. The continuous lines (marked K) in these figures show the theoretical calculations of Kim and Gordon (1, 2). $\phi_{12}{}^S$ is also shown for potentials *W*, *X*, and U_1 but not for the other models so as to avoid overloading the figures. We note that U_1, which has practically the same form as *W* (*i.e.* is a central-force potential with nn Van der Waals coefficient set equal to zero but with A_{12}, ρ_{12} fixed empirically) agrees very well with *W* except for NaCl. All four potentials are in close agreement for LiCl and only below $r = 0.85r_0$ are any differences discernable. For LiCl, B_3, even when varied, ended up very close to zero so non-central forces are evidently not a factor in LiCl. For NaCl the *X* potential is closest to and lies slightly above the Kim and Gordon potential, but for both KCl and RbCl the empirically fitted potentials lie above *K*. For $r > 0.8r_0$, *X* lies closer to *K* than do *W* and U_1. It seems to make little difference to the quality of the LS fit whether A_2–B_2 or C_{44} is used as one of the conditions that the parameters must satisfy. However, fitting A_2–B_2 emphasizes

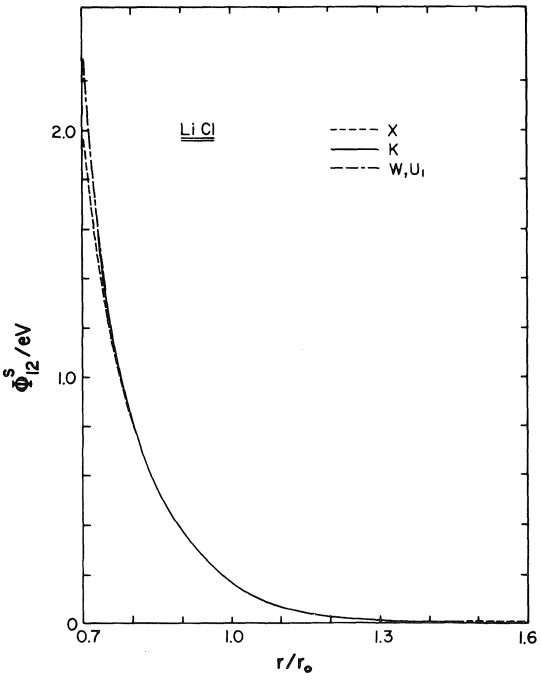

FIG. 1. Nearest neighbour short-range potentials for LiCl.

Can. J. Chem. Downloaded from www.nrcresearchpress.com by 210.87.254.40 on 09/05/12
For personal use only.

Can. J. Chem. Downloaded from www.nrcresearchpress.com by 210.87.254.40 on 09/05/12
For personal use only.

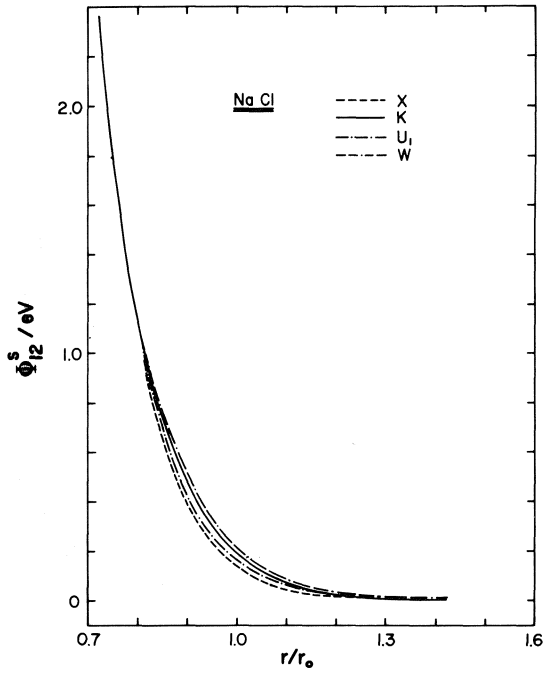

FIG. 2. Nearest neighbour short-range potentials for NaCl.

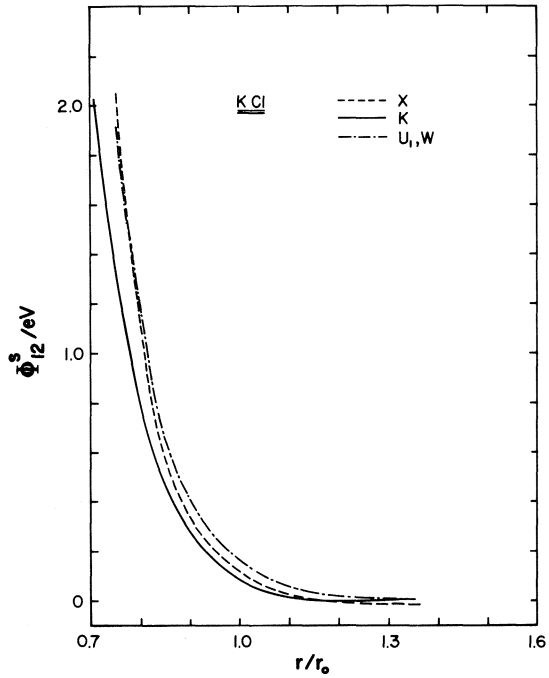

FIG. 3. Nearest neighbour short-range potentials for KCl.

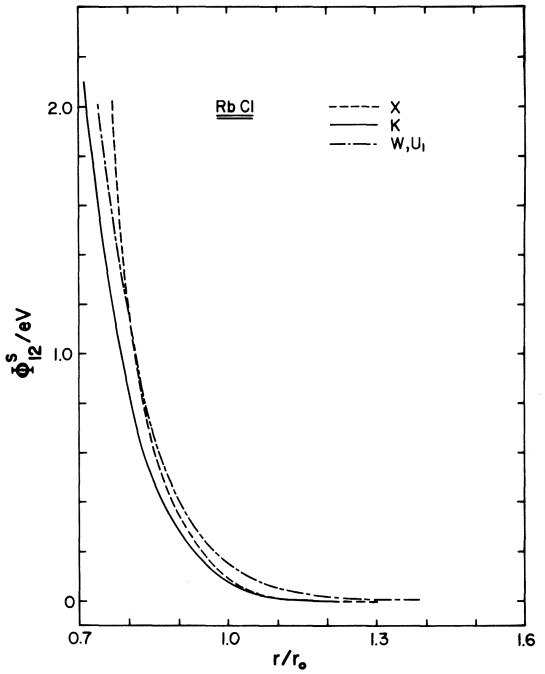

FIG. 4. Nearest neighbour short-range potentials for RbCl.

the second neighbour force constants and so presumably helps to get the nnn interactions more nearly correct.

Calculation of Defect Parameters for Pure Crystals

The energy to form Schottky defects (u_S), Frenkel defects on the cation (u_{F^+}) and anion (u_{F^-}) sub-lattices, the energy of migration for cation (Δu_+) and anion (Δu_-) vacancies, and the migration energies of interstitials by the direct (Δu_{id}), collinear interstitialcy (Δu_{ic}) and non-collinear interstitialcy (Δu_{inc}) mechanisms have been calculated using the HADES (19) program and the results are collected in Tables 6–9. The potentials are identified by the letters introduced in the model potentials section where they are described in detail. Also given, strictly for comparison purposes, are the results obtained earlier with potential *W* (13). All the numerical values quoted are in eV. A dash signifies that the parameter was not calculated and a blank that the calculation failed to converge within a reasonable number of iterations.

TABLE 6. Intrinsic defect parameters for LiCl. All entries in the table are in units of eV

Parameter	Value					
	W	Y	V	X	U_1	U_2
u_S	1.72	1.70	1.67	1.76	1.60	1.84
Δu_+	0.62	0.53	0.51	0.57	0.61	0.61
Δu_-	0.69	0.63	0.65	0.70	0.70	0.75
u_{F^+}	2.55	2.44	2.09	2.39	2.56	2.60
u_{F^-}	3.58	3.44	3.69	3.85	3.74	4.19
Δu_{id^+}	—	0.33	0.36	0.38	0.40	0.38
Δu_{id^-}	—	0.32	0.30	0.33	0.34	0.34
Δu_{ic^+}	0.25	0.18	0.23	0.21	0.21	0.23
Δu_{ic^-}	0.14	0.06	0.03	0.01	0.06	0.01
Δu_{inc^+}	—	0.35	0.34	0.38	0.39	0.41
Δu_{inc^-}	—	0.41	0.42	0.46	0.43	0.48

TABLE 7. Intrinsic defect parameters for NaCl, all entries in the table are in units of eV

Parameter	Value						Expt.
	W	Y	V	X	U_1	U_2	
u_S	2.32	2.52	2.41	2.40	2.40	2.43	
Δu_+	0.68	0.74	0.70	0.71	0.70	0.71	0.65[a]
Δu_-	0.72	0.74	0.72	0.74	0.73	0.75	0.77[b]
u_{F^+}	3.21	3.85	3.60	3.57	3.64	3.59	
u_{F^-}	3.85	3.65	3.72	3.72	3.74	3.80	
Δu_{id^+}	0.31	0.28	0.28	0.29	0.28	0.30	
Δu_{id^-}	0.27	0.36	0.32	0.34	0.32	0.33	
Δu_{ic^+}	0.29	0.15	0.18	0.18	0.18	0.20	
Δu_{ic^-}	0.16	0.21	0.19	0.17	0.19	0.17	
Δu_{inc^+}	0.52	0.34		0.34	0.34	0.35	
Δu_{inc^-}	0.28	0.40	0.50	0.40	0.37	0.39	

[a]Allnatt, Pantelis, and Sime (25).
[b]Bénière, Chemla, and Bénière (26).

TABLE 8. Intrinsic defect parameters for KCl, all entries in the table are in units of eV

Parameter	Value						Expt.
	W	Y	V	X	U_1	U_2	
u_S	2.50	2.60	2.54	2.59	2.47	2.52	
Δu_+	0.69	0.81	0.76	0.81	0.69	0.76	0.67[a]
Δu_-	0.69	0.80	0.79	0.81	0.70	0.84	0.89[b]
u_{F^+}	3.24	4.05	3.50	3.96	3.54	4.77	
u_{F^-}	3.41	3.85	4.11	4.00	3.40	2.91	
Δu_{id^+}	—	0.35	0.41	0.35	0.29	0.25	
Δu_{id^-}	—	0.37	0.29	0.35	0.33	−0.27	
Δu_{ic^+}	0.38	0.21	0.34	0.23	0.22	0.07	
Δu_{ic^-}	0.28	0.42	0.15	0.19	0.26	−0.97	
Δu_{inc^+}	—	0.44		0.43	0.48	0.38	
Δu_{inc^-}	—	0.44	0.56	0.42	0.38		

[a]Jacobs and Pantelis (27).
[b]Fuller Marquardt, Reilly, and Wells (28).

Can. J. Chem. Downloaded from www.nrcresearchpress.com by 210.87.254.40 on 09/05/12
For personal use only.

TABLE 9. Intrinsic defect parameters for RbCl, all entries in the table are in units of eV

Parameter	Value						Expt.
	W	Y	V	X	U_1	U_2	
u_S	2.36	2.50	2.48	2.46	2.42	2.52	
Δu_+	0.65	0.83	0.84	0.81	0.68	0.80	0.64[a]
Δu_-	0.64	0.81	0.82	0.81	0.66	0.85	
u_{F^+}	2.96	4.02	3.33	3.64	3.25	3.57	
u_{F^-}	3.94	3.62	4.61	3.99	4.54	2.92	
Δu_{id^+}	—	0.36	0.50	0.40	0.50	0.27	
Δu_{id^-}	—	0.43	0.30	0.33	0.29		
Δu_{ic^+}	0.39	0.19	0.46	0.31	0.46	0.17	
Δu_{ic^-}	0.32	0.31	0.10	0.15	0.10		
Δu_{inc^+}	—			0.45	0.51	0.35	
Δu_{inc^-}	—	0.48	0.42	0.44	0.40		

[a]Gannon and Jacobs (29).

Discussion

Figure 1 shows that the potentials X and U_1 for LiCl are very similar to W and to K and a similar remark holds for the other potentials that are not illustrated. It is not surprising therefore that the defect energies of Table 6 vary relatively little with the potential. The Schottky defect formation energy is smallest for U_1 and the largest for U_2 and this appears to correlate with the small differences that exist in $\phi_{12}{}^S$, the more repulsive potential giving the higher u_S. The interstitial formation energies u_{F^+} and u_{F^-} generally show greater variations than u^S and this effect is shown by the LiCl results. We may correlate this with the greater variations in $\phi_{11}{}^S$ and $\phi_{22}{}^S$, particularly below r_0, than are found in $\phi_{12}{}^S$. This is not a surprising feature of fitted potentials since the fitting procedure depends heavily on equilibrium properties and therefore on the values of the short-range potentials and their first and second derivatives at r_0. Apart from the similarity between the activation energies for cation and anion motion noted earlier (13) there are similar trends in the activation energies for interstitial motion and it is apparent that the motion of Li^+ interstitials by the direct and the collinear interstitialcy mechanisms might have to be considered in analyzing the transport properties of LiCl.

The potentials illustrated for NaCl are also quite similar except for differences in curvature in the region of r_0. The defect energies in Table 7 are also relatively insensitive to the potential, the biggest changes being in u_F. It is for KCl and RbCl that the greatest variations both in the magnitude of $\phi_{12}{}^S$ and its curvature are observed (Figs. 3, 4) and it is also for these two salts that significant variations in the defect energies are obtained. The X potential $\phi_{12}{}^S$ is softer (less repulsive) than U_1 or W for $r > 0.8r_0$ and the Schottky defect formation energy is larger, as are the vacancy migration energies. Similar observations hold for RbCl. Now X included a non-central force constant in the fitting procedure but the defect calculations use only A_{ij}, ρ_{ij}, V_{ij}, and Z. Thus although the numerical values of the elastic constants indicate that non-central forces are a significant factor in determining the properties of KCl and RbCl it seems better to set $B_3 = 0$ in determining the parameterised potential. In this way some of the effect of the non-central forces is absorbed into other parameters and a better effective potential for defect calculations results. For example, potential U_2 (which is a non-central force potential) is unsatisfactory because it gives unphysical values for Δu_{id} and Δu_{ic} for KCl (Table 8).

Because of the implications of recent defect calculations for the analysis of experimental data on transport properties (13) it seems that there are very few experimentally derived defect properties that one can use with assurance at present. One such parameter, however, is Δu_+ since this determines the slope of the conductivity curve ($\log \sigma T$ *vs.* T^{-1}) of *very lightly* doped crystals in the extrinsic region. Thus the experimental values quoted for Δu^+ for NaCl, KCl, and RbCl are almost certainly reliable and are the only parameters that are independent of the

Can. J. Chem. Downloaded from www.nrcresearchpress.com by 210.87.254.40 on 09/05/12
For personal use only.

detailed models used in analyzing the transport data. The 'best' potential using this criterion is W, the Catlow, Diller, and Norgett (3) potential. Very similar is U_1. The features of these potentials are $B_3 = 0$ (*i.e.* they are central force potentials) and $V_{12} = 0$, *i.e.* ϕ_{12}^S is made as hard as possible by omitting the Van der Waals attraction between unlike ions completely. U_1 is also more flexible than Y and V in having four independent A_{ij}, ρ_{ij} parameters but this seems not to be a crucial feature (*cf.* U_2 and X) unless combined with $V_{12} = 0$, $B_3 = 0$.

Conclusions

It is possible to derive an effective potential of the Buckingham form for defect studies by fitting simultaneously the bulk elastic properties and dielectric properties of the alkali metal chlorides. The best potential, as judged by the criterion of yielding a cation migration energy in agreement with experimental values for NaCl, KCl, and RbCl, is one which ignores non-central forces and which hardens the short-range anion–cation interactions by completely damping the Van der Waals interactions. Only further work on other materials can establish whether these principles have any general validity.

Acknowledgements

P.W.M.J. thanks the North Atlantic Treaty Organization for a Research Grant and J.C. thanks the Chemical Physics Centre of the University of Western Ontario for the award of a Visiting Fellowship, both of which have facilitated the collaborative effort which resulted in the research described in this paper. B.M.C.P. acknowledges the receipt of a post-graduate research grant from the Irish Department of Education and the cooperation of the Computer Centre at University College, Dublin. We are grateful to Dr. M. J. Norgett for advice on the use of the Hades program.

1. Y. S. Kim and R. G. Gordon. Phys. Rev. B, **9**, 3548 (1974).
2. Y. S. Kim and R. G. Gordon. J. Chem. Phys. **60**, 4332 (1974).
3. C. R. A. Catlow, K. M. Diller, and M. J. Norgett. To be published.
4. F. K. Fumi and M. P. Tosi. J. Phys. Chem. Solids, **25**, 31 (1964).
5. F. G. Fumi and M. P. Tosi. J. Phys. Chem. Solids, **25**, 45 (1964).
6. F. H. Ree and A. C. Holt. Phys. Rev. B, **8**, 826 (1973).
7. J. E. Mayer. J. Chem. Phys. **1**, 270 (1933).
8. D. Lynch. J. Phys. Chem. Solids, **28**, 1941 (1967).
9. B. G. Dick and A. W. Overhauser. Phys. Rev. **112**, 90 (1958).
10. U. Schröder. Solid State Commun. **4**, 347 (1966).
11. C. R. A. Catlow and M. J. Norgett. J. Phys. C, **6**, 1325 (1973).
12. P. T. Wedepohl. Proc. Phys. Soc. **92**, 79 (1967).
13. C. R. A. Catlow, J. Corish, K. M. Diller, P. W. M. Jacobs, and M. J. Norgett. J. Phys. Paris. In press.
14. M. J. L. Sangster. J. Phys. Chem. Solids, **34**, 355 (1973).
15. M. J. L. Sangster. J. Phys. Chem. Solids, **35**, 195 (1974).
16. R. A. Cowley. Proc. Roy. Soc. A**268**, 121 (1962).
17. W. Cochran. CRC Crit. Rev. Sol. State Sci. **2**, 1 (1971).
18. M. P. Tosi. Solid State Phys. **16**, 1 (1964).
19. M. J. Norgett. Report R.7650 (AERE, Harwell, Oxon., U.K.) 1974.
20. P. B. Ghate. Phys. Rev. A, **139**, 1666 (1965).
21. J. T. Lewis, A. Lehoczky, and C. V. Briscoe. Phys. Rev. **161**, 877 (1967).
22. M. H. Norwood and C. V. Briscoe. Phys. Rev. **112**, 45 (1958).
23. R. P. Lowndes and D. H. Martin. Proc. Roy. Soc. A**308**, 473 (1969).
24. R. P. Lowndes and D. H. Martin. Proc. Roy. Soc. A**316**, 351 (1970).
25. A. R. Allnatt, P. Pantelis, and S. J. Sime. J. Phys. C, **4**, 1778 (1971).
26. M. Bénière, M. Chemla, and F. Bénière. J. Phys. Chem. Solids, **37**, 525 (1976).
27. P. W. M. Jacobs and P. Pantelis. Phys. Rev. B, **4**, 3757 (1971).
28. R. G. Fuller, C. L. Marquardt, M. H. Reilly, and J. C. Wells. Phys. Rev. **176**, 1036 (1968).
29. D. Gannon and P. W. M. Jacobs. To be published.

Can. J. Chem. Downloaded from www.nrcresearchpress.com by 210.87.254.40 on 09/05/12
For personal use only.

Transfert du champ de forces de l'isothiazole: étude des vibrations moleculaires des dérivés de l'isothiazole monosubstitués en position 3, 4 ou 5

GILBERT MILLE[1] ET JACQUES CHOUTEAU

Faculté des Sciences de l'Université d'Aix-Marseille III, Centre de Spectrographie Infrarouge, 3, place Victor Hugo, 13331 Marseille, Cedex 3, France

ET

THIERRY AVIGNON ET LUC BOUSCASSE

Faculté des Sciences de l'Université d'Aix-Marseille III, L.A. 126 C.N.R.S., Avenue Henri Poincaré, 13397 Marseille, Cedex 4, France

Reçu le 1 juin 1976

GILBERT MILLE, JACQUES CHOUTEAU, THIERRY AVIGNON et LUC BOUSCASSE. Can. J. Chem. **54**, 3850 (1976).

L'étude des modes normaux de vibration des dérivés de l'isothiazole monosubstitués en position 3, 4 ou 5 menée dans l'hypothèse du transfert du champ de forces de l'isothiazole a permis d'obtenir des résultats théoriques confirmant les attributions expérimentales et permettant de préciser la nature des divers modes.

GILBERT MILLE, JACQUES CHOUTEAU, THIERRY AVIGNON, and LUC BOUSCASSE. Can. J. Chem. **54**, 3850 (1976).

The study of normal vibrations of 3-, 4-, or 5-monosubstituted isothiazole derivatives, assuming transferability of the valence force field of isothiazole, gives results which agree with the experimental data and which permit the assignment of the various vibrations.

I. Introduction

Dans un mémoire précédent (1) nous avons déterminé un champ de forces permettant de rendre compte de façon satisfaisante des spectres de vibrations moléculaires (mouvements dans le plan et hors du plan) de l'isothiazole et de trois de ses dérivés deutériés.

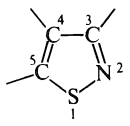

Dans l'hypothèse d'un transfert possible de ce champ de forces, nous avons entrepris un calcul des modes normaux de vibration pour quelques composés de l'isothiazole monosubstitués en position 3, 4 ou 5, C_3NSH_2Y (Y = CH_3, CD_3, Cl, Br ou I), afin de vérifier ou de préciser les attributions expérimentales que nous avons proposées antérieurement (2–4).

Le calcul des modes normaux de vibration a été entrepris avec le même formalisme que lors de l'étude de l'isothiazole et de ses dérivés deutériés (1).

II. Conditions de calcul

1. Structure géométrique

La structure géométrique des dérivés de l'isothiazole monosubstitués en position 3, 4 ou 5 n'étant pas expérimentalement connue, il nous a paru logique de conserver, en première approximation, pour le squelette hétérocyclique les paramètres structuraux adoptés pour la molécule d'isothiazole. Pour les substituants tels que CH_3, CD_3, Br, Cl et I, une analyse bibliographique (5–10) nous a conduit à retenir les valeurs moyennes suivantes: C—C (1.53 Å), C—Cl (1.72 Å), C—Br (1.86 Å) et C—I (2.03 Å).

Pour les groupements méthyle ou trideutériométhyle, les distances C—H ou C—D ont été prises égales à 1.09 Å et les angles autour de l'atome de carbone considérés comme tétraédriques.

2. Coordonnées internes

A partir de l'ensemble des coordonnées internes (fig. 1) déjà utilisées pour l'isothiazole et les deutério-isothiazoles (1), nous avons conduit

[1]Ce travail constitue une partie de la thèse de Doctorat d'Etat, n° d'ordre CNRS A0 10862, de M. Gilbert Mille soutenue en 1975 à Marseille.

Can. J. Chem. Downloaded from www.nrcresearchpress.com by 210.87.254.6 on 09/05/12
For personal use only.

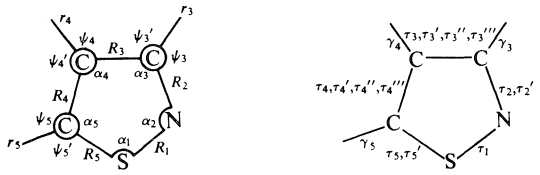

dans le plan hors du plan

FIG. 1. Coordonnées internes utilisées pour le calcul. (Les atomes de carbone en position 3, 4 et 5 sont liés à H et Y suivant le type de substitution indiqué dans le tableau 1.)

l'analyse vibrationnelle en utilisant des combinaisons linéaires de ces coordonnées dont les définitions sont analogues à celles proposées pour l'isothiazole à savoir:

Pour les mouvements dans le plan:

$$\beta_i = (\sqrt{2})^{-1}(\psi_i' - \psi_i)$$

Pour les mouvements hors du plan:

$$\tau_{II} = (\sqrt{2})^{-1}(\tau_2 + \tau_2')$$
$$\tau_{III} = \tfrac{1}{2}(\tau_3 + \tau_3' + \tau_3'' + \tau_3''')$$
$$\tau_{IV} = \tfrac{1}{2}(\tau_4 + \tau_4' + \tau_4'' + \tau_4''')$$
$$\tau_V = (\sqrt{2})^{-1}(\tau_5 + \tau_5')$$

Les coordonnées internes choisies pour représenter les vibrations du groupement méthyle ou trideutériométhyle, sont données sur la fig. 2 et sont analogues à celles indiquées par Forel et coll. (11) pour la molécule d'acétone.

3. *Champ de forces*

L'analyse vibrationnelle a été menée en admettant qu'en première approximation le champ de forces des dérivés de l'isothiazole monosubstitués en position 3, 4 ou 5 résultait de la superposition du champ de forces trouvé pour l'isothiazole et de celui relatif au groupement C—Y. Ce dernier étant dans un premier calcul,

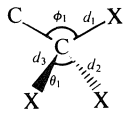

(X = H ou D)

A'
$$\nu_{s(CX_3)} = (\sqrt{3})^{-1}(d_1 + d_2 + d_3)$$
$$\nu_{s'(CX_3)} = (\sqrt{6})^{-1}(2d_1 - d_2 - d_3)$$
$$\delta_{s(CX_3)} = (\sqrt{6})^{-1}(\theta_1 + \theta_2 + \theta_3 - \phi_1 - \phi_2 - \phi_3)$$
$$\delta_{s'(CX_3)} = (\sqrt{6})^{-1}(2\theta_1 - \theta_2 - \theta_3)$$
$$r_{II(CX_3)} = (\sqrt{6})^{-1}(2\phi_1 - \phi_2 - \phi_3)$$

A''
$$\nu_{a(CX_3)} = (\sqrt{2})^{-1}(d_2 - d_3)$$
$$\delta_{a(CX_3)} = (\sqrt{2})^{-1}(\theta_2 - \theta_3)$$
$$r_{\perp(CX_3)} = (\sqrt{2})^{-1}(\phi_3 - \phi_2)$$
$$t_{(CX_3)} = (\sqrt{3})^{-1}(\tau_1 + \tau_2 + \tau_3)$$

FIG. 2. Description des coordonnées internes relatives au groupement méthyle ou trideutériométhyle.

TABLEAU 1. Constantes de force relatives aux vibrateurs CY pour les dérivés de l'isothiazole monosubstitués en position 3, 4 ou 5

Y								
3	4	5	F_τ	F_β	f_{rR}	$f_{r\alpha}$	F_γ	$f_{\gamma_{CY}\tau}$
CH_3	H	H	4.30	0.64	0.257	0.376	0.362	0.043
Cl	H	H	4.10	0.80	0.500	0.354	0.420	0.028
Br	H	H	3.0	0.75	0.400	0.336	0.400	0.031
H	CH_3	H	4.50	0.54	0.207	0.249	0.394	0.063
H	Br	H	3.17	0.56	0.597	0.388	0.405	0.046
H	H	CX_3	4.60	0.55	0.140	0.372	0.368	0.070
H	H	Cl	3.86	0.55	0.565	0.387	0.379	0.044
H	H	Br	3.31	0.52	0.550	0.325	0.333	0.074
H	H	I	2.73	0.47	0.576	0.247	0.323	0.078

TABLEAU 2. Constantes de force pour les groupements méthyle ou trideutériométhyle

Constante	Valeur	Constante	Valeur	Constante	Valeur
ν_s'	4.68	$r_{II}\delta_s'$	−0.05	ν_a	4.71
ν_s	4.92	$r_{II}\beta$	−0.05	δ_a	0.52
δ_s'	0.55	$r_{II}r$	−0.08	$r_\perp$	0.69
δ_s	0.59	$r_{II}\delta_s$	−0.42	t	0.02
r_{II}	0.66				

Can. J. Chem. Downloaded from www.nrcresearchpress.com by 210.87.254.6 on 09/05/12
For personal use only.

Can. J. Chem. Downloaded from www.nrcresearchpress.com by 210.87.254.6 on 09/05/12
For personal use only.

TABLEAU 3. Fréquences observées et calculées pour les dérivés de l'isothiazole monosubstitués en position 3

	Méthyl-3 isothiazole			Chloro-3 isothiazole			Bromo-3 isothiazole		
	Fréquences			Fréquences			Fréquences		
	Exp.	Calc.	Attributions*	Exp.	Calc.	Attributions*	Exp.	Calc.	Attributions*
A'	3110	3109	ν_{C_5H}	3110	3109	ν_{C_5H}	3110	3109	ν_{C_5H}
	3085	3090	ν_{C_4H}	3093	3090	ν_{C_4H}	3094	3090	ν_{C_4H}
	1511	1482	$\nu_N(\nu_{C=C})$	1480	1472	$\nu_N(\nu_{C=C})$	1470	1470	$\nu_N(\nu_{C=C})$
	1390	1415	$\nu_N(\nu_{C=N})$	1371	1382	$\nu_N(\nu_{C=N})$	1363	1375	$\nu_N(\nu_{C=N})$
	1343	1344	$\nu_N(\nu_{C-C})$	1317	1322	$\nu_N(\nu_{C-C})$	1310	1308	$\nu_N(\nu_{C-C})$
	1159	1158	$\delta_{C_4H}+\underline{\delta_{C_5H}}$	1150	1142	$\delta_{C_4H}+\underline{\delta_{C_5H}}$	1130	1128	$\delta_{C_4H}+\underline{\delta_{C_5H}}$
	1068	1047	$\underline{\delta_{C_4H}}+\delta_{C_5H}$	1062	1047	$\underline{\delta_{C_4H}}+\delta_{C_5H}$	1063	1047	$\underline{\delta_{C_4H}}+\delta_{C_5H}$
	929	924	$\underline{\nu_{CCH_3}}+\delta_N$	906	912	$\underline{\nu_{CCl}}+\delta_N$	890	887	$\nu_N(\nu_{C-S})+\underline{\nu_{C-Br}}+\delta_N$
	832	843	$\nu_N(\nu_{C-S})$	820	836	$\underline{\nu_N(\nu_{C-S})}+\nu_N(\nu_{S-N})$	817	834	$\underline{\nu_N(\nu_{C-S})}+\nu_N(\nu_{S-N})$
	814	832	$\nu_N(\nu_{S-N})$	811	827	$\nu_N(\nu_{C-S})+\underline{\nu_N(\nu_{S-N})}$	795	803	$\nu_N(\nu_{C-S})+\underline{\nu_N(\nu_{S-N})}$
	675	654	$\nu_N(\nu_{C-S})+\underline{\delta_N}$	655	647	$\nu_N(\nu_{C-S})+\underline{\delta_N}$	649	644	$\nu_N(\nu_{C-S})+\underline{\delta_N}$
	575	559	$\nu_{CCH_3}+\underline{\delta_N}$	430	435	$\underline{\nu_{CCl}}+\delta_N$	323	320	$\underline{\nu_{CBr}}+\delta_N$
	340	327	δ_{CCH_3}	303	304	δ_{CCl}	256	259	δ_{CBr}
A''	874	885	γ_{C_4H}	874	889	γ_{C_4H}	875	888	γ_{C_4H}
	738	742	$\underline{\gamma_{C_5H}}+\tau_{cycle}$	743	743	$\gamma_{C_5H}+\tau_{cycle}$	741	743	$\gamma_{C_5H}+\tau_{cycle}$
	629	610	$\tau_{cycle}+\gamma_{CCH_3}$	640	640	$\gamma_{CCl}+\tau_{cycle}$	630	630	$\gamma_{CBr}+\tau_{cycle}$
	472	482	τ_{cycle}	469	482	τ_{cycle}	468	482	τ_{cycle}
	246	230	$\underline{\gamma_{CCH_3}}+\tau_{cycle}$	232	228	$\gamma_{CCl}+\tau_{cycle}$	210	207	$\gamma_{CBr}+\tau_{cycle}$

*L'attribution a été faite à partir de l'analyse de la D.E.P. Pour les vibrations couplées, le caractère présentant le pourcentage le plus important est souligné.

TABLEAU 4. Fréquences observées et calculées pour les dérivés de l'isothiazole monosubstitués en position 4

	Méthyl-4 isothiazole			Bromo-4 isothiazole		
	Fréquences			Fréquences		
	Exp.	Calc.	Attributions*	Exp.	Calc.	Attributions*
A'	3102	3109	ν_{C_5H}	3108	3109	ν_{C_5H}
	3038	3059	ν_{C_3H}	3065	3060	ν_{C_3H}
	1548	1547	$\nu_N(\nu_{C=H})$	1484	1491	$\nu_N(\nu_{C=C})$
	1384	1394	$\nu_N(\nu_{C=N})$	1370	1389	$\nu_N(\nu_{C=N})$
	1333	1346	$\nu_N(\nu_{C-C})$	1298	1285	$\nu_N(\nu_{C-C})$
	1228	1230	δ_{C_3H}	1203	1222	$\delta_{C_3H}+\delta_{C_5H}$
	1132	1129	δ_{C_5H}	1082	1085	δ_{C_5H}
	964	958	$\nu_{CCH_3}+\delta_N$	894	893	$\nu_N(\nu_{C-S})+\nu_{CBr}+\delta_N$
	853	859	$\nu_N(\nu_{C-S})$	841	837	$\nu_N(\nu_{C-S})+\nu_N(\nu_{S-N})$
	784	795	$\nu_N(\nu_{S-N})$	771	777	$\nu_N(\nu_{S-N})$
	692	680	$\nu_N(\nu_{S-N})+\delta_N$	657	660	δ_N
	556	536	$\nu_{CCH_3}+\delta_N$	321	321	$\nu_{C-Br}+\delta_N$
	320	306	δ_{CCH_3}	237	234	δ_{CBr}
A''	880	890	γ_{C_3H}	878	892	γ_{C_3H}
	776	773	γ_{C_5H}	775	776	γ_{C_5H}
	603	593	$\gamma_{CCH_3}+\tau_{cycle}$	595	595	$\gamma_{CBr}+\tau_{cycle}$
	485	477	τ_{cycle}	481	485	τ_{cycle}
	239	225	$\gamma_{CCH_3}+\tau_{cycle}$	209	205	$\gamma_{CBr}+\tau_{cycle}$

*Voir légende tableau 3.

basé sur les données de la litterature (5, 6, 12, 13). Le champ de forces final pour chacun des dérivés est obtenu par un raffinement de toutes les constantes de force liées au vibrateur C—Y. Les valeurs des constantes de force ainsi obtenues sont consignées dans le tableau 1.

Un premier calcul sans raffinement laisse apparaître pour quelques fréquences un écart important entre les valeurs expérimentales et calculées. L'examen des termes de la matrice **G**, d'une part, et certains résultats bibliographiques concernant les méthyl-2 et chloro-2 thiazoles, d'autre part (6), nous ont conduit à introduire des constantes d'interaction du type $f_{r\alpha}$ et f_{rR} pour les mouvements dans le plan et la constante $\gamma_{CY}\tau$ pour les mouvements hors du plan. Pour un composé substitué en 4, par exemple, nous avons pris les constantes d'interaction suivantes:

$$f_{r_4\alpha_3} \text{ et } f_{r_4\alpha_5};\quad f_{r_4R_3} \text{ et } f_{r_4R_4};\quad f_{\gamma_4\tau_{III}} \text{ et } f_{\gamma_4\tau_{IV}}$$

Les valeurs des constantes de force pour le groupement méthyle ou trideutériométhyle sont proches de celles trouvées dans la littérature (11, 14, 15) et sont consignées dans le tableau 2. Elles ont été ajustées de manière à rendre compte des résultats expérimentaux relatifs aux méthyl-3, méthyl-4, méthyl-5 et trideutériométhyl-5 isothiazoles.

III. Discussion et analyse des résultats

Les résultats, fréquences et attributions, sont donnés dans les tableaux 3 à 7. Le transfert du champ de forces, déterminé pour l'isothiazole (1), aux dérivés monosubstitués de l'isothiazole, a permis d'obtenir des fréquences calculées dont les valeurs sont en assez bon accord avec les valeurs expérimentales.

Pour chaque dérivé, et pour chacune des fréquences, l'analyse de la distribution d'énergie potentielle permet de définir la nature des modes normaux de vibration.

Entre 3150 et 3000 cm^{-1}, on retrouve les fréquences associées aux vibrations des liaisons CH et l'on peut noter qu'elles sont proches de celles observées dans la molécule non substituée (1). On retrouve également l'ordre expérimental des fréquences à savoir: $\nu_{C_5H} > \nu_{C_4H} > \nu_{C_3H}$. Ces modes ν_{CH} ne sont pratiquement pas couplés et la proximité d'un groupement CH_3 ou CD_3 ou

Can. J. Chem. Downloaded from www.nrcresearchpress.com by 210.87.254.6 on 09/05/12
For personal use only.

Can. J. Chem. Downloaded from www.nrcresearchpress.com by 210.87.254.6 on 09/05/12
For personal use only.

TABLEAU 5. Fréquences observées et calculées pour les dérivés de l'isothiazole monosubstitués en position 5

	Chloro-5 isothiazole			Bromo-5 isothiazole			Iodo-5 isothiazole		
	Fréquences			Fréquences			Fréquences		
	Exp.	Calc.	Attributions*	Exp.	Calc.	Attributions*	Exp.	Calc.	Attributions*
A'	3103	3090	ν_{C_4H}	3100	3090	ν_{C_4H}	3100	3090	ν_{C_4H}
	3060	3059	ν_{C_3H}	3058	3059	ν_{C_3H}	3060	3059	ν_{C_3H}
	1501	1505	$\nu_N(\nu_{C=C})$	1489	1500	$\nu_N(\nu_{C=C})$	1481	1494	$\nu_N(\nu_{C=C})$
	1399	1385	$\nu_N(\nu_{C=C})+\nu_N(\nu_{C=N})$	1392	1385	$\nu_N(\nu_{C=N})+\nu_N(\nu_{C=C})$	1377	1383	$\nu_N(\nu_{C=N})+\nu_N(\nu_{C=C})$
	1282	1266	$\nu_N(\nu_{C=N})+\nu_N(\nu_{C-C})$	1276	1265	$\nu_N(\nu_{C=N})+\nu_N(\nu_{C-C})$	1270	1264	$\nu_N(\nu_{C=N})+\nu_N(\nu_{C-C})$
	1228	1203	$\nu_N(\nu_{C-C})+\delta_{C_3H}$	1224	1202	$\nu_N(\nu_{C-C})+\delta_{C_3H}$	1220	1200	$\nu_N(\nu_{C-C})+\delta_{C_3H}$
	1060	1072	δ_{C_4H}	1049	1067	δ_{C_4H}	1047	1064	δ_{C_4H}
	1009	1007	$\nu_N(\nu_{C-S})+\nu_{CCl}$	982	979	$\nu_N(\nu_{C-S})+\nu_{CBr}+\delta_N$	959	955	$\nu_N(\nu_{C-S})+\nu_{C-I}+\delta_N$
	820	834	$\nu_N(\nu_{S-N})+\delta_N$	817	833	$\nu_N(\nu_{S-N})+\delta_N$	816	832	$\nu_N(\nu_{S-N})+\delta_N$
	750	739	$\nu_N(\nu_{S-N})+\delta_N$	749	738	$\nu_N(\nu_{S-N})+\delta_N$	749	736	$\nu_N(\nu_{S-N})+\nu_N(\nu_{C-S})+\delta_N$
	675	676	$\nu_N(\nu_{C-S})+\nu_{CCl}+\delta_N$	661	667	$\nu_N(\nu_{C-S})+\delta_N$	658	665	$\nu_N(\nu_{C-S})+\delta_N$
	435	433	$\nu_{CCl}+\delta_N$	333	332	$\nu_N(\nu_{C-S})+\nu_{CBr}$	281	281	ν_{C-I}
	254	245	δ_{CCl}	210	209	δ_{CBr}	184	185	δ_{C-I}
A''	901	907	γ_{C_3H}	900	905	γ_{C_3H}	900	904	γ_{C_3H}
	803	824	γ_{C_4H}	803	821	γ_{C_4H}	804	821	γ_{C_4H}
	584	595	τ_{cycle}	583	595	τ_{cycle}	582	594	τ_{cycle}
	493	489	$\tau_{cycle}+\gamma_{CCl}$	486	482	$\tau_{cycle}+\gamma_{CBr}$	480	480	$\tau_{cycle}+\gamma_{C-I}$
	236	234	$\gamma_{CCl}+\tau_{cycle}$	180	179	$\gamma_{CBr}+\tau_{cycle}$	164	163	$\tau_{cycle}+\gamma_{C-I}$

*Voir légende tableau 3.

TABLEAU 6. Fréquences observées et calculées pour les dérivés de l'isothiazole monosubstitués en position 5

	Méthyl-5 isothiazole			Trideutériométhyl-5 isothiazole		
	Fréquences			Fréquences		
	Exp.	Calc.	Attributions*	Exp.	Calc.	Attributions*
A'	3088	3090	ν_{C_4H}	3085	3090	ν_{C_4H}
	3059	3059	ν_{C_3H}	3053	3059	ν_{C_3H}
	1524	1544	$\nu_N(\nu_{C=C})$	1520	1540	$\nu_N(\nu_{C=C})$
	1421	1405	$\nu_N(\nu_{C=N})$	1420	1398	$\nu_N(\nu_{C=N})$
	1296	1270	$\nu_N(\nu_{C=N})+\underline{\nu_N(\nu_{C-C})}$	1298	1268	$\nu_N(\nu_{C=N})+\underline{\nu_N(\nu_{C-C})}$
	1233	1218	$\underline{\delta_{C_3H}}+\delta_{C_4H}$	1232	1211	δ_{C_3H}
	1164	1180	$\nu_N(\nu_{C-S})+\underline{\nu_{CCH_3}}$	1171	1170	$\nu_N(\nu_{C-S})+\nu_{CCD_3}$
	1038	1052	δ_{C_4H}	1068 ou 1023	1061 ou 1039	$\delta_{C_4H}+\delta_{sCD_3}$
	832	831	$\underline{\nu_N(\nu_{S-N})}+\delta_N$	846	843	$\nu_N(\nu_{S-N})+\delta_N$
	753	743	$\nu_N(\nu_{S-N})$	747	730	$\nu_N(\nu_{S-N})$
	685	690	$\underline{\nu_N(\nu_{C-S})}+\delta_N$	654	668	$\nu_N(\nu_{C-S})+\delta_N$
	563	554	$\delta_N+\nu_{CCH_3}$	533	525	$\delta_N+\nu_{CCD_3}$
	295	299	δ_{CCH_3}	265	275	δ_{CCD_3}
A''	900	905	γ_{C_3H}	903	906	γ_{C_3H}
	805	822	γ_{C_4H}	785	808	$\gamma_{C_4H}+r_{\perp CD_3}$
	589	594	τ_{cycle}	573	589	τ_{cycle}
	499	484	$\underline{\tau_{cycle}}+\gamma_{CCH_3}$	483	474	$\underline{\tau_{cycle}}+\gamma_{CCD_3}$
	240	227	$\underline{\gamma_{CCH_3}}+\tau_{cycle}$	232	212	$\underline{\gamma_{CCD_3}}+\tau_{cycle}$

*Voir légende tableau 3.

d'un halogène n'a pratiquement pas d'influence sur ces vibrations.

Pour chacun des dérivés, les trois fréquences situées entre 1550 et 1300 cm^{-1} doivent être rattachées à des mouvements de valence du noyau isothiazolique. La plus haute correspond à une vibration faisant intervenir, en majeure partie, la liaison C=C, celle vers 1400 cm^{-1} la liaison C=N et la plus basse, la liaison C—C (tableaux 3–6). Les fréquences de ces trois vibrations dépendent du substituant en position 3, 4 ou 5. Elles décroissent lorsque la masse du substituant augmente. Entre 1300 et 1000 cm^{-1}, on observe pour les dérivés de l'isothiazole monosubstitués en position 3, 4 ou 5, deux fréquences devant être reliées à des modes δ_{CH}. Les mouvements δ_{C_4H} et δ_{C_5H} apparaissent assez couplés entre eux dans les composés substitués en 3. Par contre dans les dérivés substitués en 5, un couplage assez important se manifeste entre l'oscillation δ_{C_3H} et le mouvement de noyau ω_3 faisant principalement intervenir le vibrateur C—C. Pour les molécules possédant un substituant en position 5 on note un couplage entre la vibration de noyau impliquant le vibrateur C—S et l'oscillation de valence $\nu_{C_5—Y}$. C'est donc effectivement le mode noté ω_4, dans l'isothiazole, qui, dans les dérivés de l'isothiazole monosubstitués en 5, se couple avec les modes de valence C_5—Y. Pour les dérivés monosubstitués en position 3 ou 4, on observe également un couplage entre un mouvement de déformation angulaire du noyau et les modes de valence C_3—Y et C_4—Y. Les conclusions déduites de l'étude expérimentale des spectres de vibration des derivés monosubstitués de l'isothiazole se trouvent ainsi parfaitement justifiées (3, 4). Tous les dérivés présentent en outre, vers 820 cm^{-1}, une bande qui peut être attribuée à un mouvement de squelette affectant en grande partie la liaison S—N. Cette vibration peut être rapprochée du mode ω_5 de l'isothiazole. Un autre maximum entre 700 et 650 cm^{-1} se retrouve dans tous les composés et résulte d'un mouvement de déformation angulaire du noyau impliquant en particulier l'angle ∠CSN.

Can. J. Chem. Downloaded from www.nrcresearchpress.com by 210.87.254.6 on 09/05/12
For personal use only.

TABLEAU 7. Fréquences observées et calculées pour les groupements méthyle et trideutériométhyle. L'attribution a été faite à partir de l'analyse de la D.E.P.

	Méthyl-3 ith.*		Méthyl-4 ith.		Méthyl-5 ith.			Trideutériométhyl-5 isothiazole		
	Fréquences		Fréquences		Fréquences			Fréquences		
	Exp.	Calc.	Exp.	Calc.	Exp.	Calc.	Attributions	Exp.	Calc.	Attributions
A'	2960	2969	2956	2969	2958	2969	$\nu_s'CH_3$	2230	2217	$\nu_s'CD_3$
	2928	2923	2930	2923	2928	2923	ν_{sCH_3}	2122	2107	ν_{sCD_3}
								1068	1061	
	1445	1453	1452	1452	1444	1452	$\delta_s'CH_3$	ou	ou	$\delta_{sCD_3}+\delta_{C_4H}$
								1023	1039	
	1365	1381	1360	1380	1384	1375	δ_{sCH_3}	1047	1053	$\delta_s'CD_3$
	993	1001	991	992	975	980	$r_{\|\|CH_3}$	765	767	$r_{\|\|CD_3}$
A''	2995	2977	2980	2977	2970	2977	ν_{aCH_3}	2220	2220	ν_{aCD_3}
	1445	1441	1452	1441	1444	1441	δ_{aCH_3}	1040	1035	δ_{aCD_3}
	1034	1051	1039	1047	1032	1045	$r_{\perp CH_3}$	855	837	$r_{\perp CD_3}+\gamma_{C_4H}$
		168		168		168	t_{CH_3}		128	t_{CD_3}

*ith. = isothiazole.

Au-dessous de 400 cm^{-1} apparaissent les fréquences dues aux mouvements de déformation δ_{C-X} qui sont pratiquement purs.

Pour les vibrations de symétrie A'', les fréquences théoriques et expérimentales sont en bon accord et l'examen des résultats dans la base des coordonnées internes de groupe choisies met en évidence l'existence de couplages importants. On peut néanmoins rattacher à chaque fréquence un mode de vibration, ce qui rend possible la comparaison avec les résultats expérimentaux.

Pour les dérivés méthylés ou trideutériométhylés, les fréquences propres aux substituants, ainsi que l'attribution déduite de l'examen de la D.E.P. sont réunies dans le tableau 7.

Les fréquences expérimentales et théoriques sont assez voisines et pour chacune d'elles l'analyse de la D.E.P. montre que les mouvements sont purs, à l'exception toutefois des modes δ_{sCD_3} et r_{CD_3} du trideutériométhyl-5 isothiazole.

IV. Conclusion

Le calcul des modes normaux que nous avons effectués nous a permis d'apporter une justification théorique à l'ensemble des attributions que nous avions formulées d'après l'analyse expérimentale des spectres infrarouges et Raman de ces molécules (2–4).

De plus, le bon accord observé entre les résultats théoriques et les données expérimentales, indique que la possibilité d'un transfert du champ de forces de la molécule d'isothiazole aux dérivés monosubstitués est une hypothèse raisonnable.

Remerciements

Les auteurs tiennent à remercier Monsieur le Professeur M. Chaillet et Monsieur C. Pouchan du Laboratoire de Chimie Structurale de l'Université de Pau, pour leur contribution à cette étude et pour les discussions fructueuses qu'ils ont eues avec eux.

1. G. MILLE, J. METZGER, C. POUCHAN et M. CHAILLET. Spectrochim. Acta, **31A**, 1115 (1975).
2. G. MILLE, G. DAVIDOVICS, J. C. POITE et M. GUILIANO. C.R. Acad. Sci. **276**, 31 (1973).
3. G. MILLE, J. CHOUTEAU et J. METZGER. J. Chim. Phys. **72**, 31 (1975).
4. G. MILLE, J. C. POITE, J. CHOUTEAU et J. METZGER. Can. J. Chem. **53**, 1642 (1975).
5. C. POUCHAN, J. RAYMOND, H. SAUVAITRE et M. CHAILLET. J. Mol. Struct. **21**, 253 (1974).
6. TH. AVIGNON, E. J. VINCENT, J. RAYMOND et M. CHAILLET. J. Mol. Struct. **21**, 319 (1974).
7. Tables of interatomic distances. The Chem. Soc. Londres, Spec. public., nº 11. 1958.
8. W. G. NORRIS et L. C. KRISHER. J. Chem. Phys. **51**, 403 (1969).
9. T. OGATA, et K. KOZIMA. Bull. Chem. Soc. Jpn. **44**, 2344 (1971).
10. J. L. BERISSEN, J. W. M. KOCKEN et R. H. WEELDEN. Acta Crystallogr. **B27**, 1692 (1971).
11. M. T. FOREL et M. FOUASSIER. J. Chim. Phys. **67**, 1132 (1970).
12. D. W. SCOTT. J. Mol. Spectrosc. **51**, 403 (1969).
13. J. R. SHERER. Spectrochim. Acta, **20**, 345 (1964).
14. P. LABARBE et M. T. FOREL. J. Chim. Phys. **70**, 180 (1973).
15. C. GARRIGOU-LAGRANGE. J. Chim. Phys. **71**, 149 (1974).

Can. J. Chem. Downloaded from www.nrcresearchpress.com by 210.87.254.6 on 09/05/12
For personal use only.

Enthalpies of transfer of aliphatic compounds from vapor to solvents. Steric hindrance to functional group solvation[1]

RICHARD FUCHS AND PREETPAL S. SALUJA[2]
Department of Chemistry, University of Houston, Houston, TX, U.S.A. 77004

Received July 5, 1976

RICHARD FUCHS and PREETPAL S. SALUJA. Can. J. Chem. **54**, 3857 (1976).

Enthalpies of transfer from the vapor to solution ($\Delta H(v \rightarrow S)$) in cyclohexane are similar for alkenes and the corresponding alkanes. The transfer from vapor to dimethylformamide is about 0.6 kcal/mol more exothermic for 1-alkenes, which results from the dipole-induced dipole interaction of the solvent dipole with the π system. When the ethylenic bond is hindered by large adjacent groups (*trans*-1,2-di-*tert*-butylethylene) to the approach of solvent dipoles, $\Delta H(v \rightarrow$ DMF) becomes similar to that of the corresponding alkane (1,2-di-*tert*-butylethane). Similarly the interaction of di-*tert*-butyl ketone with DMF is 0.7 kcal/mol weaker than that of the less hindered isomer, 2-nonanone.

RICHARD FUCHS et PREETPAL S. SALUJA. Can. J. Chem. **54**, 3857 (1976).

Des enthalpies de transfert de l'état vapeur à l'état solution ($\Delta H(v \rightarrow S)$) dans le cyclohexane sont semblables pour les alcènes et pour les alcanes correspondants. Le transfert de la vapeur vers la diméthylformamide est d'environ 0.6 kcal/mol plus exothermique pour les alcènes-1; cette différence provient d'une interaction dipole–dipole induit du dipole du solvant avec le système π. Quand la double liaison est empêchée par des groupes adjacents volumineux (di-*tert*-butyl-1,2 éthylène *trans*) à l'approche des dipoles du solvant, le $\Delta H(v \rightarrow$ DMF) devient semblable à celui de l'alcane correspondant (di-*tert*-butyl-1,2 éthane). De la même manière l'interaction de la di-*tert*-butylcétone avec la DMF est environ 0.7 kcal/mol plus faible que celle de l'isomère moins empêché, la nonanone-2.

[Traduit par le journal]

Important insights into solution reactivity and equilibria have recently resulted from studies of gaseous state behavior, in combination with measurements of the interactions of the gaseous species with solvents (see, for example, refs. 1 and 2). Measurements of these interactions in appropriate systems can also contribute to an understanding of the intermolecular forces which become operative as gaseous molecules interact with solvents (3). Based on heat of solution measurements of a variety of benzene derivatives (4) there appears to be no evidence for substantial hindrance to solvation by adjacent substituents on the aromatic ring. However, a recent report (2) has brought out the importance of steric hindrance to solvation in determining acidities in solution.

We have recently been interested in the extent to which the hydrocarbon and functional group portions of aliphatic molecules interact with polar and non-polar solvents, and the nature of the intermolecular (solute–solvent) forces which are involved. The presumption is made that the interaction of alkanes with polar or non-polar solvents is due almost entirely to dispersion interactions, that highly polarizable and polar solutes interact with the solvent cyclohexane almost entirely by dispersion interactions, but with the polar solvent *N*,*N*-dimethylformamide (DMF) by dipole-induced dipole and dipole–dipole forces, respectively, as well, and that a given hydrocarbon group will make the same contribution to dispersion interactions regardless of the nature of the molecule of which it is a part.

One may then question whether the interactions of dipolar solvents with polarizable functional groups are a function of the steric environment of the group. We have approached this through a consideration of the enthalpies of transfer of appropriate compounds from the vapor to the solvents cyclohexane and DMF ($\Delta H(v \rightarrow S)$). These values have been calculated from experimental heats of solution (ΔH_s) and published values of heats of evaporation at 25 °C (ΔH_v) by the equation

$$\Delta H(v \rightarrow S) = \Delta H_s(S) - \Delta H_v$$

[1]This work was supported by the Robert A. Welch Foundation (Grant E-136).

[2]Department of Chemistry, University of Alberta, Edmonton, Alta., Canada T6G 2G2.

Can. J. Chem. Downloaded from www.nrcresearchpress.com by 210.87.254.6 on 09/05/12
For personal use only.

TABLE 1. Heats of solution[a] and enthalpies of transfer[b] from the vapor to solution of some hydrocarbons and ketones

Compound	ΔH_s(c-C_6H_{12})	ΔH_s(DMF)	ΔH_v[c]	ΔH(v → c-C_6H_{12})	ΔH(v → DMF)
n-Decane	0.59	3.26	12.28	−11.69	−9.02
1-Decene	0.52	2.48	12.16	−11.64	−9.68
t-Bu—CH_2CH_2—*t*-Bu	0.22	2.95	9.81	−9.59	−6.86
t-Bu—CH=CH—*t*-Bu	0.21	2.89	(9.8)[d]	(−9.6)[e]	(−6.9)[e]
2-Nonanone	1.99	1.00	13.48	−11.49	−12.48
n-Nonane	0.50	2.86	11.10	−10.60	−8.24
t-Bu—CO—*t*-Bu	1.03	0.93	10.84	−9.81	−9.91
t-Bu—CH_2—*t*-Bu	0.10	2.67	9.11	−9.01	−6.64

[a]In kcal/mol ±0.05.
[b]In kcal/mol ±0.10.
[c]Heats of evaporation at 25 °C (6–8).
[d]Estimated value (see text).
[e]Based on estimated value of ΔH_v.

The values of ΔH_s and ΔH(v → S) are listed in Table 1.

In Table 1 the value of ΔH_v has been estimated for *trans*-di-*tert*-butylethylene (2,2,5,5-tetramethyl-3-hexene) based on the observation that the values for alkenes are within 0.5 kcal/mol of, but are not greater than, ΔH_v of the corresponding alkane. The discussion will not depend on the exact value; the estimated value is used only for illustrative purposes.

The enthalpies of transfer of a series of 1-alkenes and alkanes from the vapor to cyclohexane are, within experimental error, the same. However, ΔH(v → DMF) is about 0.6–0.7 kcal/mol more exothermic for the alkenes. From the data of Table 1 it is seen that ΔH(v → c-C_6H_{12}) is identical for *tert*-Bu—CH=CH—*tert*-Bu and *tert*-Bu—CH_2CH_2—*tert*-Bu (2,2,5,5-tetramethylhexane), and that ΔH(v → DMF) are also the same for both. This most likely results from steric hindrance to the approach of DMF dipoles to the π orbital of *tert*-Bu—CH=CH—*tert*-Bu, and the absence of the usual dipole-induced dipole interaction with alkenes. Alternatively, one may consider the quantity ΔH_s(DMF) − ΔH_s(c-C_6H_{12}), which is independent of the value of ΔH_v. The quantity is positive for alkanes and alkenes, presumably because of the higher energy of cavity formation in DMF. The values are *n*-decane, 2.7; 1-decene, 2.0; *tert*-Bu—CH_2CH_2—*tert*-Bu, 2.7; and *tert*-Bu—CH=CH—*tert*-Bu, 2.7 kcal/mol. Clearly, 1-decene has an interaction with DMF which is lacking in the hindered alkene.

In the ketone series one finds (Table 1) that ΔH(v → DMF) for the relatively unhindered 2-nonanone is about 1 kcal/mol more exothermic than the corresponding transfer to cyclohexane. This is in spite of the larger expenditure of hole energy in DMF. How would ΔH(v → DMF) and ΔH(v → c-C_6H_{12}) for 2-nonanone compare if the dipole–dipole interaction between DMF and the carbonyl group were inoperative? An approximation can be made by examining the values of *n*-nonane (Table 1), which reveal that the transfer to DMF is about 2.4 kcal/mol *less* exothermic. This implies that the energy required to form cavities in the solvent to accommodate *n*-nonane (or 2-nonanone) is 2.4 kcal/mol greater in DMF than that in cyclohexane. From this viewpoint the total enthalpy of interaction of 2-nonanone with DMF must be 3.4 kcal/mol more exothermic than the interaction with cyclohexane, in order to give the observed value of −1 kcal/mol for ΔH(v → DMF) − ΔH(v → c-C_6H_{12}).

Comparison of vapor to solvent transfers of di-*tert*-butyl ketone (2,2,4,4-tetramethyl-3-pentanone) and the corresponding hydrocarbon, di-*tert*-butylmethane (2,2,4,4-tetramethylpentane) should then reveal the extent to which the polar interactions of DMF and the carbonyl dipole are inhibited by the steric hindrance of the *tert*-butyl groups attached to the latter. The hydrocarbon ΔH(v → DMF) is about 2.6 kcal/mol less exothermic than ΔH(v → c-C_6H_{12}), and the corresponding ketone value is 0.1 kcal/mol more exothermic. The ketone therefore has an interaction with DMF 2.7 kcal/mol stronger than with cyclohexane. This interaction is, however, 0.7 kcal/mol weaker than that of the less hindered isomer, 2-nonanone. The results are essentially unchanged if *n*-decane and 2,2,5,5-

Can. J. Chem. Downloaded from www.nrcresearchpress.com by 210.87.254.6 on 09/05/12
For personal use only.

tetramethylhexane are used as the hydrocarbon models.

It is of interest to compare the present results with those of Jolicoeur and Lacroix (5), who examined free energies and enthalpies of transfer of ketones from H_2O to D_2O. The aqueous solvents are highly structured, much more so than cyclohexane and DMF. The introduction of hydrocarbon molecules or groups into water may promote solvent structure in the vicinity of the solute, which is reflected in large entropy as well as enthalpy changes. This effect is small or absent in organic solvents. In both studies differences in the enthalpy of cavity formation within the solvent is an important consideration ($D_2O > H_2O$; DMF > c-C_6H_{12}). The transfer of an unbranched ketone from a less structured to a more structured solvent was found to be more exothermic than the transfer of a highly branched solute in both studies; although probably for somewhat different reasons. Evidence was presented indicating that steric factors are not important in the polar interactions of water with ketones, which is reasonable for a solvent with the very small hydroxyl group. In the present study only DMF is capable of a polar interaction with the carbonyl group, and steric hindrance to solvation of di-*tert*-butyl ketone is to be expected. The use of a hydrocarbon model has permitted us to allow for differences in the enthalpy of cavity formation for the unbranched and branched ketones, and to separately evaluate the loss in polar solvation (in DMF) due to steric hindrance. While a substantial steric hindrance to solvation has been demonstrated for only two compounds (*trans*-di-*tert*-butylethylene and di-*tert*-butyl ketone), these are the only compounds of a sizable group examined in which the functional group is flanked by two bulky alkyl groups.

Experimental

The calorimetric measurements were carried out in a vacuum jacketed vessel fitted with a Teflon covered thermistor probe (2 kΩ at 25 °C). Calibration heating curves used a timed constant current source which furnished a current of 19.30 mA to a 320 ohm heater (0.12 W) made from a $\frac{1}{8}$ W low temperature coefficient metal film resistor Teflon covered. Sample addition was made from a 20 μl or 50 μl syringe into 70 ml of solvent which was magnetically stirred. The new baseline was normally attained within 1 min. The calorimeter was immersed in a constant temperature bath at 25 °C, regulated to ±0.002 °C. Temperature change in the calorimeter was detected by the thermistor which was an arm of a Wheatstone bridge. The bridge output was amplified by a Keithley model 160 digital multimeter (which also served as null detector), and recorded at an overall sensitivity of 200 μV (or 0.02 °C) full scale. A typical heat of solution involved a temperature change of 0.003–0.01 °C, and a heat change of 0.1–0.4 cal. The values in Table 1 are averages of 3–6 determinations in the concentration range 1–10 × 10^{-3} *M*. No dependence of ΔH_s on concentration was noted. Hydrocarbon and ketone samples obtained from Chemical Samples Co. were of 99–99.9% purity. Reagent grade solvents were dried with 4A molecular sieve.

1. R. W. Taft, M. Taagepera, K. D. Summerhays, and J. Mitsky. J. Am. Chem. Soc. **95**, 3811 (1973).
2. E. M. Arnett, D. E. Johnson, and L. E. Small. J. Am. Chem. Soc. **97**, 5598 (1975).
3. R. Fuchs, T. M. Young, and R. F. Rodewald. J. Am. Chem. Soc. **96**, 4705 (1974).
4. R. Fuchs and R. F. Rodewald. J. Am. Chem. Soc. **95**, 5897 (1973).
5. C. Jolicoeur and G. Lacroix. Can. J. Chem. **51**, 3051 (1973).
6. R. R. Dreisbach. Adv. Chem. Ser. **22** (1959).
7. P. Sellers. J. Chem. Thermodyn. **2**, 211 (1970).
8. D. Ambrose, J. H. Ellender, E. B. Lees, C. H. S. Sprake, and R. Townsend. J. Chem. Thermodyn. **7**, 453 (1975).

Can. J. Chem. Downloaded from www.nrcresearchpress.com by 210.87.254.6 on 09/05/12
For personal use only.

A ^{13}C nuclear magnetic resonance study of thiolane sulfoxides. The configurations of neothiobinupharidine sulfoxides

R. T. LaLonde, C. F. Wong, and A. I-M. Tsai

Department of Chemistry, State University of New York, College of Environmental Science and Forestry, Syracuse, NY, U.S.A. 13210

J. T. Wróbel, J. Ruszkowska, and K. Kabzinska

Department of Chemistry, University of Warsaw, Warsaw, Poland

AND

T. I. Martin and D. B. MacLean

Department of Chemistry, McMaster University, Hamilton, Ont., Canada L8S 4M1

Received June 2, 1976

R. T. LaLonde, C. F. Wong, A. I-M. Tsai, J. T. Wróbel, J. Ruszkowska, K. Kabzinska, T. I. Martin, and D. B. MacLean. Can. J. Chem. **54**, 3860 (1976).

The sulfoxide configurations of neothiobinupharidine α- and β-sulfoxides have been determined through a ^{13}C nmr investigation. The ^{13}C nmr sulfoxidation increments ($\Delta\delta_{C\text{-}i} = \delta_{C\text{-}i}{}^{S-O} - \delta_{C\text{-}i}{}^{S}$) for all carbons in 2,2,4,4-tetramethylthiolane sulfoxide have been determined. Sulfoxidation increments for the C-2 methyl groups, the indicator carbons, were found to be similar in sign and magnitude to the increments reported for methyl groups in penicillin sulfoxides, wherein methyl groups *cis* to the sulfoxide oxygen show larger sulfoxidation increments than do the *trans* methyl groups. The sign and magnitude of the sulfoxidation increments for C-6 and C-8, the indicator carbons in the neothiobinupharidine sulfoxides, have been determined and compared with those of the model 2,2,4,4-tetramethylthiolane and those of the penicillins. The C-6 increments were -9.9 and -5.6 ppm respectively for the solid and liquid neothiobinupharidine sulfoxide. Therefore the solid sulfoxide is assigned the β-configuration and the liquid sulfoxide the α-configuration as a result of these studies.

R. T. LaLonde, C. F. Wong, A. I-M. Tsai, J. T. Wróbel, J. Ruszkowska, K. Kabzinska, T. I. Martin et D. B. MacLean. Can. J. Chem. **54**, 3860 (1976).

On a déterminé les configurations des sulfoxydes α et β de la néothiobinupharidine en faisant appel à la rmn du ^{13}C. On a déterminé les incréments, en rmn du ^{13}C, dus à la sulfoxydation ($\Delta\delta_{C\text{-}i} = \delta_{C\text{-}i}{}^{S-O} - \delta_{C\text{-}i}{}^{S}$) pour tous les carbones du sulfoxyde de tétraméthyl-2,2,4,4 thiolane. On a trouvé que les incréments dus à la sulfoxydation, pour les groupes méthyles en C-2, les carbones indicateurs, sont de signes et d'amplitudes semblables aux incréments rapportés pour les groupes méthyles des sulfoxydes de pénicilline où les groupes méthyles *cis* par rapport à l'oxygène de sulfoxyde montrent de plus grands incréments lors de la sulfoxydation que les groupes méthyles *trans*. On a déterminé le signe et l'amplitude des incréments dus à la sulfoxydation pour les atomes de carbone C-6 et C-8, les carbones indicateurs dans le sulfoxyde de la néothiobinupharidine, et on les a comparés avec ceux du modèle tétraméthyl-2,2,4,4 thiolane et ceux des pénicillines. On a trouvé que les incréments pour le carbone C-6 sont respectivement de -9.9 et de -5.6 ppm pour les sulfoxydes solides et liquides de la néothiobinupharidine. On en conclut que l'on doit attribuer la configuration β au sulfoxyde solide et la configuration α au sulfoxyde liquide.

[Traduit par le journal]

A neothiobinupharidine sulfoxide, isolated from *Nuphar luteum* was the subject of an earlier report (1). However, the question of sulfoxide stereochemistry was left unanswered. We have undertaken the resolution of this problem by ^{13}C nmr and report our results herein.

The neothiobinupharidine sulfoxide in question melted at 240–242 °C and, as previously reported (1), may be prepared from neothiobinupharidine, **1**, by oxidation of the latter with 30% hydrogen peroxide in glacial acetic acid. On reinvestigation of this oxidation, we observed that the reaction product also contained 10% of a second sulfoxide which was a viscous liquid. The liquid sulfoxide comprised about 30% of the sulfoxide product when the oxidation of **1** was carried out with sodium metaperiodate in aqueous methanol. As we shall demonstrate, the

Can. J. Chem. Downloaded from www.nrcresearchpress.com by 210.87.254.105 on 09/05/12
For personal use only.

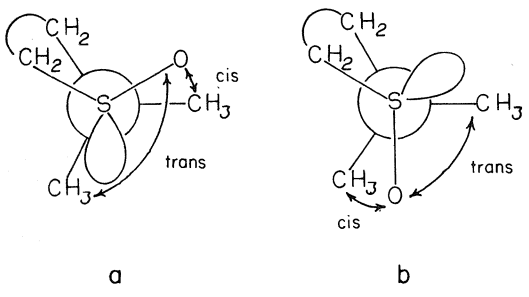

FIG. 1. Conformations of some *gem*-dimethyl substituted, cyclic sulfoxides showing the dihedral angles between methyl groups, oxygen, and the non-bonding electron pair.

capability of preparing the second neothiobinupharidine sulfoxide in quantities sufficient for ^{13}C nmr spectra greatly aided the investigation since comparison of the ^{13}C properties of both isomers now could be made.

We viewed the neothiobinupharidine sulfoxides, **2** and **3**, as complex analogs of 2,2,4,4-tetramethylthiolane-1-oxide, **4**, with γ and δ carbons *cis* or *trans* to the sulfoxide oxygen atom. We also considered the methyl carbons, or hydrogen, in **4** and carbons 6, 6′, 8 and 8′, or attached hydrogens, in **2** and **3** as potential indicators of the sulfoxide oxygen configuration, provided the time average conformation of the five-membered ring was such that the dihedral angle between sulfoxide oxygen and the *cis* methyl was different than the dihedral angle between sulfoxide oxygen and the *trans* methyl. Two such conformations, shown in Fig. 1, illustrate the relation of sulfoxide oxygen to γ methyl groups. When incorporated into a five-membered ring these conformations are not interconvertible through C—S bond rotations.

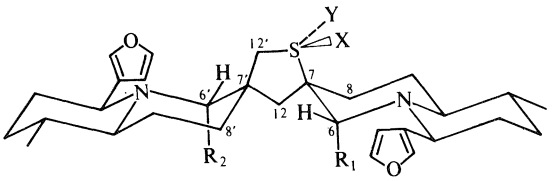

1, X = Y = electron pair; $R_1 = R_2 = H$
2, X = O; Y = electron pair; $R_1 = R_2 = H$
3, X = electron pair; Y = O; $R_1 = R_2 = H$
11, X = Y = electron pair; $R_1 = R_2 = D$
12, X = Y = electron pair; $R_1 = H$; $R_2 = D$
13, X = O; Y = electron pair; $R_1 = R_2 = D$
14, X = O; Y = electron pair; $R_1 = D$; $R_2 = H$
15, X = electron pair; Y = O; $R_1 = R_2 = D$
16, X = electron pair; Y = O; $R_1 = H$; $R_2 = D$
17, X = Y = electron pair; $R_1 = R_2 = \alpha$ or βOH
18, X = Y = electron pair; $R_1 = \alpha$ or βOH; $R_2 = H$

Our first inclination was to compare the ^1H nmr spectra of the neothiobinupharidine sulfoxides with that of the parent sulfide using the changes in the C-6 and C-6′ equatorial proton chemical shifts to point to the *cis* or *trans* relation of the sulfoxide oxygens. Equatorial protons at C-6 and C-6′ had been differentiated in the ^1H nmr spectra through deuterium labelling carried out in connection with the structure studies of 6- and 6′-hydroxyneothiobinupharidine (2–4). Both magnitude and sign of the ^1H nmr sulfoxidation chemical shift increment ($\Delta\delta_{H\text{-}i} = \delta_{H\text{-}i}{}^{S\text{—}O} - \delta_{H\text{-}i}{}^{S}$) of γ and δ protons in a thiabicyclooctane system reflect in a regular manner the *syn* or *anti* configurational relation of sulfoxide oxygen to the γ and δ indicator protons (5). However, when we compared the C-2 methyl chemical shifts in several penicillins and penicillin sulfoxides (6) we found that the sulfoxidation chemical shift increment is not correlated with the simple *cis*, *trans* relation of sulfoxide oxygen to the methyl groups. The lack of a general correlation between sulfoxide configuration and the ^1H nmr increment of protons attached to the γ and δ carbons led us to examine the ^{13}C nmr of 2,2,4,4-tetramethylthiolane-1-oxide for sulfoxidation changes. The results were compared to those from reported studies of penicillin sulfoxide and then applied to the problem of the neothiobinupharidine sulfoxide configuration.

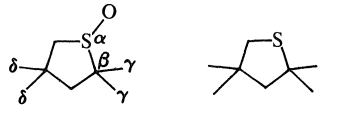

4 **5**

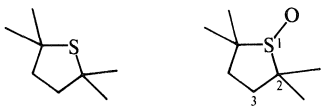

6 **7**

Chemical Shift Assignments and Sulfoxidation Increments ($\Delta\delta_{C\text{-}i} = \delta_{C\text{-}i}{}^{S\text{—}O} - \delta_{C\text{-}i}{}^{S}$) of Tetramethylthiolanes and their Sulfoxides

The ^{13}C nmr chemical shift values and assignments for the 2,2,4,4- and 2,2,5,5-tetramethylthiolane and the corresponding sulfoxides are presented in Table 1. The assignments for 2,2,4,4-tetramethylthiolane, **5**, were discussed earlier (7).

Can. J. Chem. Downloaded from www.nrcresearchpress.com by 210.87.254.105 on 09/05/12
For personal use only.

Can. J. Chem. Downloaded from www.nrcresearchpress.com by 210.87.254.105 on 09/05/12
For personal use only.

TABLE 1. Chemical shifts, in ppm (from TMS, δ 0.0 ppm) multiplicities (singlet, triplet, or quartet) and sulfoxidation increments in ppm ($\Delta\delta_{C\text{-}t} = \delta_{C\text{-}t}^{S\text{-}O} - \delta_{C\text{-}t}^{S}$) for two tetramethylthiolanes (**5** and **6**) and their sulfoxides (**4** and **7**). Chemical shift, multiplicity, and sulfoxidation increment for the carbon number indicated

Compound	C-2	$\Delta\delta_{C\text{-}2}$	C-3	$\Delta\delta_{C\text{-}3}$	C-4	$\Delta\delta_{C\text{-}4}$	C-5	$\Delta\delta_{C\text{-}5}$	C-2CH_3	$\Delta\delta_{C\text{-}2CH_3}$	C-4CH_3	$\Delta\delta_{C\text{-}4CH_3}$
6	55.1(s)		44.9(t)		44.9(t)		55.1(s)		32.6(q)			
7	63.2(s)	+8.1	39.4(t)	−5.5	39.4(t)	−5.5	63.2(s)	+8.1	26.0(q)	−6.6		
									21.8(q)	−10.8		
5	53.5(s)		59.4(t)		45.9(s)		47.3(d)		33.7(q)		29.0(q)	
4	64.6(s)	+11.1	53.9(t)	−5.5	41.7(s)	−4.2	63.4(t)	+16.1	25.4(q)	−8.3	33.3(q)	+4.3
									22.2(q)	−11.5	32.1(q)	+3.1

Can. J. Chem. Downloaded from www.nrcresearchpress.com by 210.87.254.105 on 09/05/12
For personal use only.

The assignments for 2,2,5,5-tetramethylthiolane-1-oxide, **7**, are made on the basis of the ^1H off-resonance decoupled spectrum. For this symmetrical tetramethylthiolane sulfoxide, the ^{13}C sulfoxidation increments, $\Delta\delta_{C\text{-}i}$, are respectively +8.1 and −5.5 ppm at C-2 and C-3. Sulfoxidation increments for the two pairs of C-2 methyl groups, *cis* and *trans* to sulfoxide oxygen, are different; for one pair it is −6.6 ppm and for the other it is −10.8 ppm.

The assignments for 2,2,4,4-tetramethylthiolane-1-oxide, **4**, were made with the aid of the ^1H off-resonance decoupled spectrum. But pairs of singlets and triplets were distinguished on the basis of chemical shift and by comparisons of $\Delta\delta_{C\text{-}i}$ values with those of sulfoxide **7**. Thus the singlet at 64.6 ppm displayed by **4** is close to the 63.2 ppm chemical shift assigned to C-2 in **7**; moreover the sign and magnitude of $\Delta\delta_{C\text{-}2}$ for **4** (+11.1) agrees with that (+8.1) of **7**. Therefore the singlet at 64.6 ppm is assigned to C-2 and that at 41.7 ppm to C-4 by default. Similarly, the triplet at 63.4 ppm exhibited by **4** is assigned to C-5, the methylene carbon adjacent to the sulfoxide group, since the effect of sulfoxidation is deshielding as demonstrated by the sign of $\Delta\delta_{C\text{-}2}$ for both sulfoxides **7** and **4**. Therefore the triplet at 63.4 ppm is assigned to C-5 and that at 53.9 ppm to C-3 by default. Support for this last assignment comes from the agreement of $\Delta\delta_{C\text{-}3}$ for **4** and **7** which is −5.5 ppm for both.

As previously mentioned, both the methyl groups *cis* and *trans* to the sulfoxide oxygen in **7** are shielded relative to the methyl groups in the thiolane **6**; $\Delta\delta_{C\text{-}2CH_3}$ values are −10.8 and −6.6 ppm. The chemical shift values assigned to the C-2 methyls of **4** must be such that $\Delta\delta_{C\text{-}2CH_3}$ for **4** and **7** agree in sign and magnitude. This is the case when the C-2 methyl groups of **5** are assigned a chemical shift of 33.7 ppm and those at C-2 of **4** values of 22.2 and 25.4 ppm. The resonances at 33.3 and 32.1 ppm are therefore assigned to the C-4 methyls by default.

We conclude from the foregoing analysis that the sulfoxidation of **5** to **4** results in both methyls at C-2 becoming shielded, one by −11.5 and the other by −8.3 ppm, and both methyls at C-4 becoming slightly deshielded, one by +4.3 and the other by +3.1 ppm.

The values of $\Delta\delta_{C\text{-}2CH_3}$ (−8.3 and −11.5 ppm) agree generally with the γ-sulfoxidation effect values observed for six-membered ring sulfides

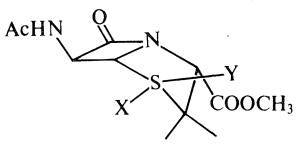

8, X = Y = electron pair
9, X = O; Y = electron pair
10, X = electron pair; Y = O

(8*a*, *b*) but, more importantly, also agree with those observed by Archer *et al.* (8*c*) for penicillin **8** and its α-, **9**, and β-, **10**, sulfoxides. The 2α- and 2β-methyls are shielded by −8.5 and −11.3 ppm respectively in the β- sulfoxide, **10**, relative to penicillin **8**. In like manner the 2α- and 2β-methyls are shielded by −10.8 and −6.6 ppm respectively in the α-sulfoxide, **9**, relative to penicillin **8**. More recently similar observations have been made for some 2-chloromethyl derivatives of penicillin and penicillin sulfoxides (9). Apparently, the magnitude of the shielding steric γ effect is inversely proportional to the dihedral angle between the methyl group and the sulfoxide oxygen. In the α-sulfoxide **9**, the S—O—β-CH_3 dihedral angle is 85°, the conformation corresponding to that shown in Fig. 1*b*. In the β-sulfoxide **10**, the S—O—β-CH_3 dihedral angle is 60° in a conformation similar to that shown in Fig. 1*a* (8). Therefore in conformationally restricted cases, it now appears that real differences in the sulfoxidation increments can distinguish the *cis–trans* relation between the γ carbon indicator and the sulfoxide oxygen. In the specific case of the tetramethylthiolanes, the methyl group *cis* to the sulfoxide oxygen has a larger negative sulfoxidation increment than the methyl group which is *trans*.

Chemical Shift Assignments and Sulfoxidation Increments for Neothiobinupharidines

Selected chemical shifts for the α-, **3**, and β-, **2**, neothiobinupharidine sulfoxides are given in Table 2 and compared with those of the parent sulfide, **1**, in Fig. 2. Figure 2 includes only the lines of **1** in the 25.0–70.0 ppm region which are most pertinent to the problem of sulfoxide configuration; the full spectrum has already been presented (7). Correlation lines are drawn for the four pairs of carbons 6 and 8, 6′ and 8′, 7 and 7′, and 12 and 12′, the first two pairs corresponding respectively to C-2 methyls and C-4 methyls in **4** and **5**. C-7, C-7′, C-12, and C-12′ in the neothiobinupharidine derivatives

TABLE 2. ^{13}C chemical shifts in ppm (from TMS, δ 0.0 ppm) and multiplicities (singlets, doublets, and triplets) of selected lines in the spectra of neothiobinupharidine α-**3** and β-**2** sulfoxides

Carbon No.	Neothiobinupharidine sulfoxide	
	β-**2**	α-**3**
9,9′*	27.9, 28.4(t, t)	27.5, 28.2, 29.1(t, t, t)
8*	32.4, 33.5, 33.7, 34.9, 35.9, 36.2, 36.5	27.5, 28.2, 29.1(t, t, t) 33.2, 33.5, 34.7, 35.5, 36.1†
8′	39.7(t)	39.5(t)
7′	45.0(s)	44.1(s)
12	49.2(t)	49.5(t)
6	55.4(t)	59.7(t)
12′	57.4(t)	57.1(t)
4,4′*	59.6, 61.1(d, d)	59.4, 59.9(t, t)
6′	65.4(t)	64.7(d)†
7	68.5(s)	68.3(s)†
10,10′	68.6(d)†	68.3(d)†

*One of the given chemical shifts represents the carbon(s) indicated.
†Enhanced intensity suggesting coincidental lines.

correspond to C-2, C-4, C-3, and C-5 respectively in **4** and **5**.

The chemical shift assignments for the parent neothiobinupharidine have been discussed earlier (7). Assignments for the signals of C-6 and C-6′, two of the four indicator carbons, now have been confirmed since the totally ^1H decoupled ^{13}C nmr spectrum of neothiobinupharidine-6,6′-d_2, **11**, showed a low intensity, complex signal for the 63.0 and 65.3 ppm lines while only the former line appeared as a low intensity complex signal in the spectrum of neothiobinupharidine-6′-d_1, **12** (Fig. 3*a*).

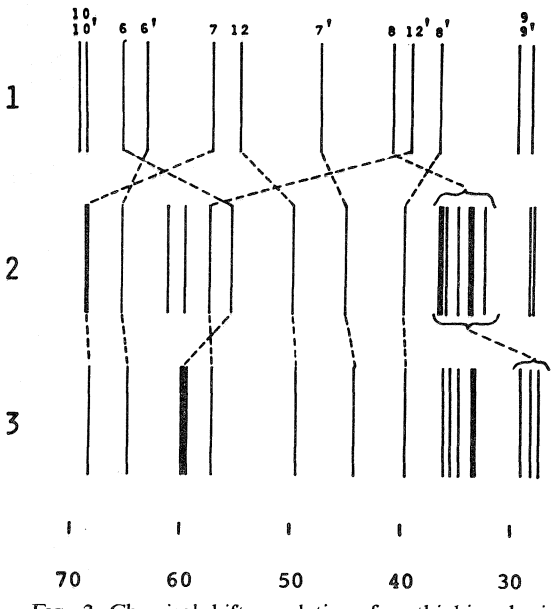

FIG. 2. Chemical shift correlation of neothiobinupharidine (**1**), α-**3** and β-**2** sulfoxides. Chemical shifts in ppm from TMS.

The assignments of the same indicator carbons in the sulfoxides were made in a similar manner. When the neothiobinupharidine sulfoxide melting at 240 °C was labelled with deuterium at C-6 and C-6′ (compound **13**), the signals present at 55.4 and 65.4 ppm appeared as low intensity multiplets (Fig. 3*b*). The corresponding monodeuterated sulfoxide, **14**, labelled only at C-6, gave a spectrum in which the 55.4 ppm line was a low intensity complex signal (Fig. 3*b*). Therefore, the 55.4 and 65.4 ppm lines were assigned to C-6 and C-6′ respectively. The 64.7 ppm line found in the spectrum of the unlabelled sulfoxide was absent in the spectra of the 6′-*d* and 6,6′-d_2 labelled samples and therefore this line can be assigned to C-6′. The C-6 spectral line at 59.7 ppm was flanked closely by two nearby lines in the spectrum of the unlabelled liquid sulfoxide and therefore its disappearance was somewhat more difficult to observe. Nevertheless this line appeared in the spectrum of the 6′-d_1 labelled sample in the same manner as it had in the spectrum of the unlabelled sample, but in the spectrum of the 6,6′-d_2 labelled sample only the outer two flanking lines remained. Therefore the spectral line at 59.7 ppm was assigned to C-6 of the liquid sulfoxide. Accordingly the spectral line at 64.7 ppm exhibited by the liquid sulfoxide was assigned to C-6′.

Can. J. Chem. Downloaded from www.nrcresearchpress.com by 210.87.254.105 on 09/05/12
For personal use only.

Can. J. Chem. Downloaded from www.nrcresearchpress.com by 210.87.254.105 on 09/05/12
For personal use only.

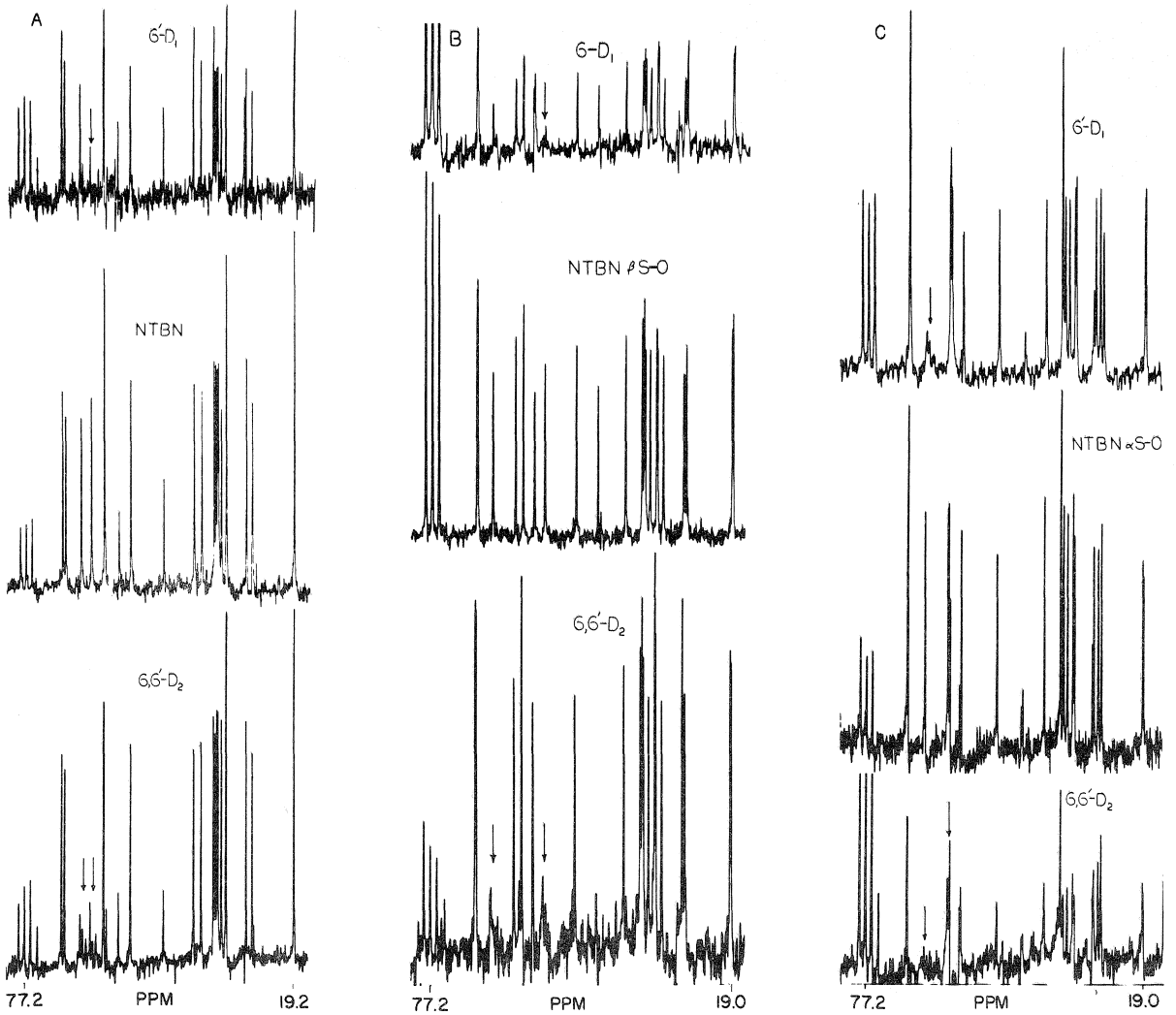

FIG. 3. Wide band noise decoupled ^{13}C nmr spectra, determined in $CDCl_3$, in the approximate region of 19.0–77.2 ppm (relative to TMS 0.0 ppm) of: (*a*) neothiobinupharidine-6-d_1, neothiobinupharidine (NTBN), neothiobinupharidine-6,6′-d_2; (*b*) neothiobinupharidine-β-sulfoxide-6-d_1, neothiobinupharidine-β-sulfoxide (NTBNβS-O), neothiobinupharidine-β-sulfoxide-6,6′-d_2; (*c*) neothiobinupharidine-α-sulfoxide-6′-d_1, neothiobinupharidine-α-sulfoxide (NTBNαS-O), neothiobinupharidine-6,6′-d_2.

Can. J. Chem. Downloaded from www.nrcresearchpress.com by 210.87.254.105 on 09/05/12
For personal use only.

The deuterium labelled neothiobinupharidines and their sulfoxides were obtained in the following ways. 6,6′-Dihydroxyneothiobinupharidine, **17**, and 6-hydroxyneothiobinupharidine, **18**, were reduced with sodium borodeuteride as previously described (3, 4). Oxidation of the resulting singly and doubly labelled neothiobinupharidines with hydrogen peroxide in acetic acid led to the corresponding mixtures of the labelled α- and β-sulfoxides from which the doubly labelled β-sulfoxide (**13**), the doubly labelled α-sulfoxide (**15**), and the β-sulfoxide singly labelled at C-6 (**14**) were separated. Reduction of 6′-hydroxyneothiobinupharidine (4) with sodium borodeuteride gave neothiobinupharidine-6′-d_1, **12**. The latter was oxidized with sodium metaperiodate in methanol–water to obtain a mixture rich in the α-sulfoxide singly labelled at C-6′, **16**, which was separated by elution chromatography.

Signals were assigned to the remaining three pairs of pertinent sulfoxide carbons (C-12,12′, C-7,7′, and C-8,8′) with the assistance of the off-resonance decoupled spectra and the sign and magnitude of the tetramethylthiolane $\Delta\delta_{C\text{-}t}$. Due to the symmetrical nature of the neothiobinupharidine skeleton, assignments of C-8′ in the spectra of the two sulfoxides was assisted also by the rigidly established $\Delta\delta_{C\text{-}6'}$. Since the sulfoxidation effect on C-12′ is deshielding, C-8 must be moving upfield upon sulfoxidation of neothiobinupharidine. At present its exact location in the two sulfoxide spectra is not certain. In the case of the liquid sulfoxide spectrum, C-8 would appear to be the third line in the 27.5–29.1 ppm region and for the solid sulfoxide is one of the seven lines in the 32.0–36.5 ppm region.

Configurations of the Neothiobinupharidine Sulfoxides

On the basis of the above assignment, $\Delta\delta_{C\text{-}t}$ were calculated for both indicator pairs, C-6,8 and C-6′,8′, and these are given in Table 3. Clearly, $\Delta\delta_{C\text{-}6}$ is a larger negative value for one sulfoxide than the other. In accord with the results from the model thiolanes, the sulfoxide with the larger negative $\Delta\delta_{C\text{-}6}$ value is given the β-sulfoxide configuration, **2**. This sulfoxide is the 240–242 °C melting isomer. The sulfoxide with the smaller negative $\Delta\delta_{C\text{-}6}$ value is given the α-configuration, **3**. This sulfoxide is the liquid isomer. Supporting these configurations is the observation that the more negative $\Delta\delta_{C\text{-}6}$ value is associated with the less negative $\Delta\delta_{C\text{-}8}$ and *vice versa*.

TABLE 3. ^{13}C nmr sulfoxidation increments ($\Delta\delta_{C\text{-}t} = \delta_{C\text{-}t}{}^{S\text{-}O} - \delta_{C\text{-}t}{}^{S}$) for indicator carbon atoms in neothiobinupharidine α-**3** and β-**2** sulfoxides

	$\Delta\delta_{C\text{-}t}$*			
Compound	C-6	C-8	C-6′	C-8′
2(β-)	−9.9	−8.4– −4.3†	+2.4	+3.2
3(α-)	−5.6	−13.3– −11.7†	+1.7	+3.0

*Calculated using: $\delta_{C\text{-}6}{}^{S}$ = 65.3 ppm; $\delta_{C\text{-}6'}{}^{S}$ = 63.0 ppm; $\delta_{C\text{-}8'}{}^{S}$ = 36.5 ppm; $\delta_{C\text{-}8}{}^{S}$ = 40.8 ppm.
†A range based on the highest and lowest field signals in group containing C-8.

Experimental

Measurements

Spectra were determined as follows: mass spectra (ms) on a Hitachi–Perkin-Elmer RMU6E using an all-glass heated indirect inlet, chamber temperature and voltage 200 °C and 70 eV, respectively; infrared spectra (ir) as indicated on a Perkin-Elmer 137 spectrometer; ^1H nmr at 100 or 60 MHz as indicated in $CDCl_3$ solution in 5 mm tubes (1% TMS, δ 0.00) on Varian A60 and XL-100-15 spectrometers, the latter controlled by a VFT-100 computer and operating in the FT absorption mode (m, s, and d referring to multiplet, singlet, and doublet respectively); ^{13}C nmr in $CDCl_3$, used also to furnish a secondary reference (77.2 ppm from TMS at δ 0.0 ppm) and the deuterium resonance for field-frequency lock, on a Varian XL-100-15 operating at 25.16 MHz in the FT absorption mode employing 8192 data points. Fully ^1H noise decoupled and off-resonance decoupled ^{13}C nmr spectra of the two tetramethylthiolane sulfoxides and neothiobinupharidine β-sulfoxide were obtained on 1.0–1.2 ml solutions containing 20–40 mg of sample in 12 mm tubes using from 3K–7K transients. The fully decoupled spectra of neothiobinupharidine-6α,6′α-d_2 α-sulfoxide and neothiobinupharidine-6α-d_1 were obtained on 1–2 mg samples in 0.15 ml of solution in a 5 mm (od) micro cell from nearly 200K transients. Fully decoupled spectra of neothiobinupharidine-6α,6′α-d_2, neothiobinupharidine α-sulfoxide, neothiobinupharidine-6α-d_1 β-sulfoxide, neothiobinupharidine-6α,6′α-d_2 α-sulfoxide, and neothiobinupharidine-6′α-d_1 α-sulfoxide were obtained on 3–10 mg samples in 0.30 ml solution in 5 mm tubes from 22–91K transients. In all cases ^{13}C spectral widths were 5000 Hz and acquisition times were 0.8 s. Pulse widths for all spectral determinations ranged from 65–75 μs.

Materials and Methods

2,2,5,5-Tetramethylthiolane-1-oxide (7)

A solution containing 160 mg of 2,2,5,5-tetramethylthiolane (7) (1.1 mmol) and 225 mg of 85% *m*-chloroperbenzoic acid in 5 ml of methylene chloride was stirred at ambient temperature for 1 week. The methylene chloride solution was then washed with aqueous sodium bicarbonate, dried over anhydrous sodium sulfate, concentrated on the rotary evaporator, and chromatographed

Can. J. Chem. Downloaded from www.nrcresearchpress.com by 210.87.254.105 on 09/05/12
For personal use only.

on 10 g of alumina (activity 2) first with about 50 ml of hexane to remove unconverted thiolane and then with 100 ml of ether to remove the desired **7**: ir (liquid film) 6.90, 7.25 and 7.36, 7.82, 8.84, 9.24, 9.65 (S—O), 9.93 μm; ^{1}H nmr (60 MHz) δ 1.24 (s, 6H, CH_3), 1.35 (s, 6H, CH_3), 1.90 (m, 4H, AA′BB′CH_2CH_2); ms, *m/e* (relative intensity) 160(M^+, 17), 91(100), 69(42), 55(41), 43(24), 41(39); ^{13}C nmr, see Table 1. *Anal.* calcd. for $C_8H_{16}SO$: C 59.95, H 10.06, S 20.01; found: C 59.85, H 10.17, S 19.81.

2,2,4,4-Tetramethylthiolane-1-oxide (**4**)

A solution of 341 mg of 2,2,4,4-tetramethylthiolane (7) and 455 mg of 85% *m*-chloroperbenzoic acid in 3 ml of methylene chloride was stirred at ambient temperature for 3.5 h. The reaction mixture was then processed as described in the case of **7**. Chromatography of the concentrate on 10 g of alumina (activity 3) was done using 90 ml of hexane followed by 90 ml of ether. Thirty millilitre fractions were taken. The first 30 ml hexane fraction afforded 140 mg of unconverted sulfide and the first 30 ml ether fraction yielded 161 mg of **4**: ir (liquid film) 6.89, 7.24 and 7.35, 9.05, 9.35, 9.69 (S—O), 9.93 μm; ^{1}H nmr (100 MHz) δ 1.31 (s, 3H, CH_3), 1.35 (s, 3H, CH_3), 1.37 (s, 3H, CH_3), 1.40 (s, 3H, CH_3), 1.81 (d, 1H, A or B of ABq no. 1), 2.29 (d, 1H, B or A of ABq no. 1), 3.78 (d, A or B of ABq no. 2), 5.98 (d, B or A of ABq no. 2); ms *m/e* (relative intensity, %) 160(22), 129(16), 114(22), 102(20), 97(67), 69(23), 57(22), 56(37), 55(100), 43(37), 41(35); ^{13}C nmr, see Table 1. *Anal.* calcd. for $C_8H_{16}SO$: C 59.95, H 10.06; found: C 59.90, H 10.15.

Oxidation of Neothiobinupharidine with Hydrogen Peroxide in Acetic Acid

According to a previously disclosed procedure (10), 82 mg of neothiobinupharidine in 3 ml of acetic acid was treated with 43 mg of 30% hydrogen peroxide at ambient temperature for 1.5 h. The solution was then diluted with 15 ml of water, made alkaline with a pellet of sodium hydroxide, and extracted three times with benzene. Removal of the benzene on the rotary evaporator gave a solid whose tlc (alumina, benzene–chloroform 1:1) indicated the presence of nearly 50% of the starting neothiobinupharidine. Therefore the solid was redissolved in 3 ml of acetic acid, treated with 30 mg of hydrogen peroxide, and the resulting solution was kept at ambient temperature for 2.5 h. Processing in the manner just described gave a solid which was chromatographed on 13 g of alumina containing 5% water using the following eluting solvents in the amounts and order indicated: 100 ml benzene; 100 ml 10% chloroform in benzene; 200 ml benzene–chloroform 1:1, 100 ml chloroform. Thirty-five millilitre fractions were collected. Fractions 2 and 3 combined yielded 14 mg of unconverted neothiobinupharidine. Fraction 9 consisted of 21 mg of colorless oil (tlc alumina, twice developed with benzene–ether, R_f 0.21 and 0.38). Fractions 10–12 combined yielded 57 mg of neothiobinupharidine β-sulfoxide: tlc alumina, twice developed with benzene–ether, R_f 0.21; and identical with authentic sample (1).

A 17 mg sample of fraction 9, was chromatographed on 15 g of neutral alumina (activity 2) with chloroform in 20, 1, 3, and 2 ml fractions. The 3 ml fraction gave 6.8 mg of neothiobinupharidine α-sulfoxide: tlc (alumina, twice developed with benzene–ether, 1:1) R_f 0.38; tlc (alumina, three times developed with chloroform) (R_f 0.44); ir (CCl_4) 9.70 (S—O), 11.47 μm (3-furyl); ^{1}H nmr ($CDCl_3$, 100 MHz) δ 0.85 and 0.88 (d's, 6H), 2.14 (br d, J = 12 Hz, 1H) 2.39 (d of ABq, J = 15 Hz, 1H, CH_2SO), 2.66–2.91 (m, 4H; C-6, C-6′, C-4, C-4′H), 3.03 (d of ABq, J = 7.3 Hz, 1H, CH_2SO), 6.20 (apparent d of m, J = 5 Hz, 2H, 3-furyl-βH), 6.98–7.28 (m, 4H, 3-furyl-αH); ms *m/e* (relative intensity, %) 510(6)(M^+), 494(37), 493(100), 448(3), 445(2), 357(4), 232(23), 230(54), 216(2), 202(2), 200(1), 188(3), 178(17), 176(2), 164(2), 163(1), 162(2), 161(1), 149(2), 148(3), 147(2), 146(3), 137(2), 136(5), 135(4), 107(22), 96(9), 97(10), 94(42), 91(5), 81(18); ^{13}C nmr see Table 2.

Oxidation of Neothiobinupharidine with Sodium Metaperiodate

A 17.7 mg sample of neothiobinupharidine in 2.5 ml of methanol was treated with 16.2 mg of sodium metaperiodate at 0 °C for 20 h. The solvent was removed at reduced pressure at 0 °C and the residue was treated with 10 ml of water and then extracted with methylene chloride. Thereafter the aqueous layer was extracted several times with 10 ml quantities of chloroform and the combined organic extracts were dried over anhydrous sodium sulfate. Removal of the solvent at reduced pressure gave 20 mg of oil which was chromatographed on 2 g of neutral alumina (activity 2) and eluted successively with 100 ml of benzene, 50 ml of benzene–ether (7:3), and 50 ml of chloroform. The benzene fraction gave 3.4 mg of unconverted neothiobinupharidine, the benzene–ether (1:1) fractions yielded 8.5 mg of neothiobinupharidine α-sulfoxide, and the chloroform fraction yielded 3 mg of neothiobinupharidine β-sulfoxide: tlc (alumina twice developed with benzene–ether 1:1) R_f 0.21, R_f 0.38, and R_f 0.77, corresponding respectively to R_f values of neothiobinupharidine β-sulfoxide, neothiobinupharidine α-sulfoxide, and unconverted neothiobinupharidine as determined by co-chromatography experiments.

Neothiobinupharidine-6,6′-d_2

A 58 mg sample containing bis- and monohemiaminal thiaspirane Nuphar alkaloids, obtained from a methanol fraction yielded by an earlier chromatography of Polish plant material (11), was chromatographed on 5 g of neutral alumina, containing 5% water, with 20 ml of benzene, 20 ml of benzene–ether (8:2), and 50 ml of methanol. A 1 mg portion of the methanol fraction (30 mg), after treatment with methanolic sodium borohydride, afforded neothiobinupharidine (tlc (alumina, hexane–ether 8:2) R_f 0.4) and other more polar compounds. Therefore the remainder of fraction 3 in 0.5 ml of methanol was treated with 40 mg of sodium borodeuteride in methanol at ambient temperature overnight. The solvent was removed under a gentle stream of nitrogen and the residue was shaken with 5 ml of water and 5 ml of methylene chloride. The aqueous layer was separated and extracted repeatedly with methylene chloride. The combined organic extracts were dried over anhydrous sodium sulfate. Evaporation of the solvent at reduced pressure gave 35 mg of a glass-like material which was chromatographed on 2 g of neutral alumina, containing 5% water, with 10 ml of hexane–ether (9:1), 20 ml of benzene, and 20 ml of methanol. Fraction 2, 10 mg, was neothiobinupharidine-6,6′-d_2: tlc (alumina, hexane–ether 8:2) R_f 0.4; ms *m/e* 496 (relative intensity,

8%); ^{1}H nmr ($CDCl_3$, 100 MHz) δ 0.87 (d, J = 5 Hz, 6H, C-1 CH_3) 2.70 (apparent s, CH_2S), 2.67 and 2.93 (C-6 eq and C-6′ eq H; appearing as singlets but as doublet of doublets in the unlabelled spectrum), 6.38 (m, 1H, 3-furyl-βH), 6.56 (m, 1H, 3-furyl-βH), 7.23–7.40 (m, 4H, 3-furyl-αH); ^{13}C nmr ($CDCl_3$) δ 63.0 and 65.3 present in the unlabelled spectrum (7) are absent.

Neothiobinupharidine-6-d_1 and Neothiobinupharidine-6′-d_1

The first of the title compounds was obtained from a previous study (4). The second was obtained from 6,6′-dihydroxyneothiobinupharidine by sequential partial reductions, first with sodium borohydride then with sodium borodeuteride, according to the following procedure. A 70 mg chromatographic fraction containing 6,6′-dihydroxyneothiobinupharidine was treated with small portions of sodium borohydride at 0 °C in 95% ethanol until the first trace of neothiobinupharidine was detected by tlc (alumina, hexane–ether 3:2) R_f 0.81. The reaction mixture was treated immediately with 0.5 ml of acetone to destroy unconverted sodium borohydride, solvents were evaporated at reduced pressure, the residue was taken up in 5 ml of chloroform, the resulting mixture was filtered through 0.5 g of neutral alumina (activity 2), the solvent was removed from the filtrate at reduced pressure, and the residue was chromatographed on 10 g of neutral alumina (activity 2) eluting successively with hexane–ether (9:1) in 15, 50, 150, and 200 ml portions (fractions 1–4) and with 50 ml of methanol (fraction 5). Fraction 4, comprising of 14 mg of 6′-hydroxyneothiobinupharidine: tlc (alumina, hexane–ether 3:2) R_f 0.21 g was treated with 30 mg of sodium borodeuteride in 1 ml of methanol at 25 °C for 30 min. The solvent was evaporated at reduced pressure, the residue was taken up in chloroform, the resulting mixture was filtered through 0.5 g of neutral alumina (activity 2), the solvent was removed from the filtrate, and the residue was chromatographed on alumina (activity 2) with hexane–ether in two 50 ml fractions. The second fraction consisted of 10 mg of neothiobinupharidine-6′-d_1: ^{1}H nmr ($CDCl_3$, 100 MHz) δ 2.67 (s, 1H, C-6′H but appearing as a doublet in unlabelled compound (4)), 2.94 (d, 1H, C-6H); ms *m/e* (relative intensity) 495(25), 178(100) and 179(23); ^{13}C nmr, see text.

Deuterium-Labelled Neothiobinupharidine Sulfoxides

The conversion of neothiobinupharidine-6,6′-d_2, neothiobinupharidine-6-d_1, and neothiobinupharidine-6′-d_1 to β- and α-sulfoxides was effected, respectively, by hydrogen peroxide in acetic acid and sodium metaperiodate in methanol–water by the methods and procedures given above for the unlabelled samples.

Acknowledgments

Three of the authors (R.T.L., C.F.W., and A.I-M.T.) are grateful to the National Institutes of Health, U.S. Public Health Service, for support (Grant No. AI-10188) of the portion of the work performed at the State University of New York, College of Environmental Science and Forestry. Mr. L. McCandless, of the latter institution, is credited with determining the ^{13}C nmr spectra. The work at McMaster University was supported by the National Research Council of Canada and their assistance is gratefully acknowledged.

1. J. T. Wróbel, A. Iwanow, J. Szychowski, J. Poplowski, C. K. Yu, T. I. Martin, and D. B. MacLean. Can. J. Chem. **50**, 1968 (1972).
2. C. F. Wong and R. T. LaLonde. Experientia, **31**, 15 (1975).
3. J. T. Wróbel, A. Iwanow, and K. Wojtasiewicz. Bull. Acad. Pol. Sci. Ser. Chim. **23**, 735 (1975).
4. R. T. LaLonde and C. F. Wong. J. Org. Chem. **41**, 291 (1976).
5. A. B. Foster, J. M. Duxbury, T. D. Inch, and J. M. Webber. Chem. Commun. 881 (1967).
6. P. V. Demarco and R. Nagurajan. Cephalosporins and penicillins. *Edited by* E. H. Flynn. Academic Press, New York, N.Y. 1972. pp. 311–369.
7. R. T. LaLonde, T. N. Donvito, and A. I-M. Tsai. Can. J. Chem. **53**, 1714 (1975).
8. (*a*) G. W. Buchanan and T. Durst. Tetrahedron Lett. 1683 (1975); (*b*) J. R. Wiseman, H. O. Kraffenhoft, and B. R. Anderson. J. Org. Chem. **41**, 1518 (1976); (*c*) R. A. Archer, R. D. G. Cooper, P. V. Demarco, and L. F. Johnson. Chem. Commun. 1291 (1970).
9. K. Tori, T. Tsushima, Y. Tamura, H. Shigemoto, T. Tsugi, H. Ishitabi, and H. Tanida. Tetrahedron Lett. 3307 (1975).
10. T. I. Martin. Ph.D. Dissertation, McMaster University, Hamilton, Ontario. 1974.
11. R. T. LaLonde, C. F. Wong, and K. C. Das. J. Am. Chem. Soc. **95**, 6342 (1973).

Can. J. Chem. Downloaded from www.nrcresearchpress.com by 210.87.254.105 on 09/05/12
For personal use only.

A practical synthesis of *cis*-jasmone from levulinic acid

J. A. BULAT AND H. J. LIU[1]

Department of Chemistry, University of Alberta, Edmonton, Alta., Canada T6G 2E1

Received June 17, 1976

J. A. BULAT and H. J. LIU. Can. J. Chem. **54**, 3869 (1976).

A practical total synthesis of *cis*-jasmone (**1**) has been achieved in six steps and in an overall yield of 49% from levulinic acid.

J. A. BULAT et H. J. LIU. Can. J. Chem. **54**, 3869 (1976).

On a réussi une synthèse totale et pratique de la jasmone-*cis* (**1**) qui utilise l'acide lévulénique comme produit de départ et qui implique six étapes avec un rendement global de 49%.

[Traduit par le journal]

Can. J. Chem. Downloaded from www.nrcresearchpress.com by 210.87.254.6 on 09/05/12
For personal use only.

cis-Jasmone (**1**), the primary odorous principle of the flower oils of several varieties of jasmin (1), is an important ingredient both in the production of high grade fragrances in the perfume industry and as an enhancing agent for spearmint and peppermint flavors in the food industry (2, 3). Because of its commercial importance and

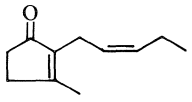

1

limited availability from natural sources as well as its quite unique structural features, *cis*-jasmone has drawn much attention to its synthesis in the last few decades[2]. Many of the existing syntheses are, however, mainly concerned with the development of new or improved methods for the construction of 1,4-diketones and cyclopentenones using *cis*-jasmone only as a testing model for their synthetic applicability. Often these procedures, as well as being lengthy, require costly and/or difficultly accessible chemicals and thus are not economically viable for the large scale production of *cis*-jasmone. Consequently, there is a continuous demand for the development of its effective synthesis. We wish to report a practical synthesis of **1** from levulinic acid,[3] which is inexpensive and readily available, in six simple steps and in an overall yield of 49%.

Treatment of levulinic acid with an excess of ethylene glycol in benzene in the presence of a catalytic amount of *p*-toluenesulfonic acid gave rise to a 87% yield of ketal ester **2** as a result of concomitant ketalization and esterification. Subsequent reduction of **2** with lithium aluminum

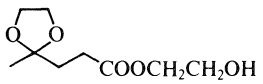

2

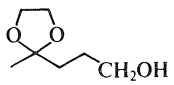

3

hydride resulted in the formation of ketal alcohol **3** in 84% yield. The structural assignments of **2** and **3** follow rigorously from their ir and nmr spectra and elemental analyses.[4] In the mass spectra, **2** and **3** showed no molecular ion peaks but prominent peaks at 189.0772 and 131.0706 respectively corresponding to, in each case, a loss of a CH_3 unit. This fragmentation pattern is in accord with the general observation for 2,2-dialkyl dioxolanes (15).

Oxidation of **3** using Collins reagent (16) prepared *in situ* (17), gave, in 92% yield, ketal aldehyde **4** whose ir and nmr spectra were found to be in good agreement with those reported previously for the compound prepared via different routes (18). Ketal aldehyde **4** proved to be very unstable. Its purification by either column chromatography or distillation could not be achieved without substantial loss of material. The instability was further indicated by the fact that when **4** was exposed to chlorinated solvents

[1]Author to whom correspondence should be addressed.

[2]For extensive reviews of the synthetic works prior to 1974 see refs. 4 and 5. For subsequent syntheses see refs. 6–13.

[3]Concurrent with and after the completion of the present work, three syntheses of **1** from levulinic acid and its derivatives via different routes have been reported (10, 13, 14).

[4]See Experimental section for details.

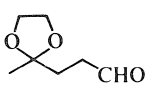
4

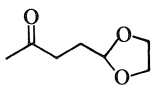
5

for two days, it was converted near-quantitatively to the isomeric keto acetal **5**[5]. In as much as the unpurified **4** was shown to be homogeneous by gc and tlc, it was used directly for the subsequent transformation.

The conversion of **4** into dione **7**, the well established immediate synthetic precursor of *cis*-jasmone (19), was carried out in two stages. Grignard reaction of **4** with *cis*-3-hexylmagnesium bromide in ether resulted in the formation of ketal alcohol **6** which, without purification,

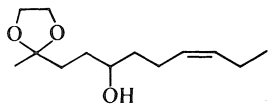
6

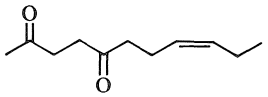
7

was treated immediately with Jones reagent (20) which effected its deketalization and oxidation simultaneously giving dione **7** in a 90% yield from **4**. Final cyclization of **7** under the described conditions (19) afforded a 81% yield of *cis*-jasmone. Its nmr (8), ir (21), and mass spectra (22) and the mp of its 2,4-DNP derivative (23) were found to be identical with those cited in the literature.

Experimental

General

Elemental analyses were performed by the microanalytical laboratory of this department. Melting points were determined on a Kofler hot stage apparatus and are uncorrected. Infrared (ir) spectra were recorded on a Perkin-Elmer model 457 or 337 grating infrared spectrophotometer. The spectra were calibrated using the 1601.4 cm^{-1} band of polystyrene. Nuclear magnetic resonance (nmr) spectra were recorded on a Varian Associates model A50/60 spectrometer with tetramethylsilane as internal standard. The following abbreviations are used: s = singlet, d = doublet, t = triplet, q = quartet, and m = multiplet. Mass spectra were recorded on a AEI model MS-2 or AEI model MS-9 mass spectrometer.

2-Hydroxyethyl 4,4-Ethylenedioxypentanoate (2)

To a solution of 50 g (0.43 mol) of levulinic acid in 500 ml of benzene, were added 200 g (3.22 mol) of ethylene glycol and 1 g (5 mmol) of *p*-toluenesulfonic acid monohydrate. The resulting mixture was refluxed with a Dean–Stark water separator under a nitrogen atmosphere for 24 h. Benzene was partially (*ca.* 200 ml) removed by distillation and the remaining mixture after cooling to room temperature was poured into 300 ml of ice-cold saturated sodium bicarbonate solution. The benzene layer was separated and washed with saturated aqueous sodium chloride. The combined aqueous solution was extracted with chloroform (4 × 300 ml) which was washed with aqueous sodium chloride. The organic solutions were combined, dried ($MgSO_4$), filtered, and concentrated. The oily product was distilled at 90–92 °C/0.05 torr to give 76.35 g (87% yield) of **2**: nmr (CCl_4) δ 1.27 (s, 3 H, $-\overset{|}{C}H_3$), 1.97 (t, 2 H, J = 7 Hz, $-CH_2CH_2\overset{|}{C}{=}O$), 2.34 (t, 2 H, J = 7 Hz, $-CH_2\overset{|}{C}{=}O$), 3.31 (s, 1 H, —OH), 3.68 (t, 2 H, J = 6.5 Hz, $-CH_2OH$), 3.89 (s, 4 H, $-OCH_2CH_2O-$), and 4.11 (t, 2 H, J = 6.5 Hz, $-CH_2CH_2OH$); ir (film) ν 3445 (alcohol) and 1725 cm^{-1} (ester); mass spectrum m/e (M − 15) 189.0772 (calcd. for $C_8H_{13}O_5$: 189.0763). *Anal.* calcd. for $C_9H_{16}O_5$: C 52.93, H 7.90; found: C 53.01 52.67, H 7.91 7.78.

4,4-Ethylenedioxypenta-1-ol (3)

At 0 °C, a solution of 40.8 g (0.2 mol) of ketal ester **2** in ether (250 ml) was added dropwise over a 1.5 h period to a suspension of lithium aluminum hydride (10 g; 0.263 mol) in 150 ml of ether. The reaction mixture was stirred at room temperature under a nitrogen atmosphere for 16 h. After cooling to 0 °C ethanol and water were added sequentially to destroy excess lithium aluminum hydride. The organic layer was separated and the aqueous solution extracted with ether (3 × 500 ml) and chloroform (2 × 500 ml). The combined organic solution was dried over magnesium sulfate, filtered and concentrated. The crude oil after distillation at 62–64 °C/0.04 torr gave 24.5 g (84% yield) of **3**: nmr (CCl_4) δ 1.26 (s, 3 H, CH_3—), 1.63 (m, 4 H, $-CH_2CH_2CH_2OH$), 3.40–3.62 (m, 2 H, $-CH_2OH$), 3.75 (s, 1 H, —OH), and 3.88 (s, 4 H, $-OCH_2CH_2O-$); ir (film) ν 3415 cm^{-1} (alcohol); mass spectrum: m/e (M − 15) 131.0706 (calcd. for $C_6H_{11}O_3$: 131.0708). *Anal.* calcd. for $C_7H_{14}O_3$: C 57.53, H 9.65; found: C 57.71, H 9.66.

4,4-Ethylenedioxypentanal (4)

The oxidation was carried out using the procedure of Ratcliffe and Rodehorst (17). At 0 °C, chromium trioxide (60 g; 0.6 mol) was added to a stirred solution of pyridine (94.9 g; 1.2 mol) in 1200 ml of methylene chloride under a nitrogen atmosphere. The resulting mixture was warmed to room temperature and stirred for an additional 15 min.

[5]The structure of **5** was evident from its spectral data. In the ir spectrum (film) the absence of aldehydic absorptions at 2820, 2720, and 1720 cm^{-1} was coupled with the appearance of a new carbonyl band at 1710 cm^{-1}. In the nmr spectrum (CCl_4) a triplet at δ 9.40 for the aldehydic proton and a methyl singlet at δ 1.14 previously observed for **4** shifted substantially to δ 4.78 and 2.07 readily accounted for by the methine proton of the acetal group and the three hydrogen atoms of the methyl ketone respectively.

Can. J. Chem. Downloaded from www.nrcresearchpress.com by 210.87.254.6 on 09/05/12
For personal use only.

Can. J. Chem. Downloaded from www.nrcresearchpress.com by 210.87.254.6 on 09/05/12
For personal use only.

At the end of this period, a solution of ketal alcohol **3** (14.5 g; 0.1 mol) in 50 ml of methylene chloride was added in one portion. The mixture was stirred at room temperature for 20 min and water (300 ml) was added. The methylene chloride solution was separated and the aqueous phase extracted with methylene chloride (3 × 300 ml). The organic solutions were washed successively with the following ice-cold solutions: 2 *N* sodium hydroxide (500 ml), 2 *N* hydrochloric acid (2 × 500 ml), saturated aqueous sodium bicarbonate (500 ml), and water (500 ml). Drying ($MgSO_4$), filtration, and concentration gave 13.2 g (92% yield) of **4**, which was shown to be homogenous by tlc and gc. An analytical sample obtained by Kugelrohr distillation at 50 °C/2.5 torr showed the following spectral data: nmr (benzene-d_6) δ 1.14 (s, 3 H, $-CH_3$), 1.67–2.20 (m, 4 H, $-CH_2CH_2$-CHO), 3.50 (s, 4 H, $-OCH_2CH_2O-$), and 9.42 (t, 1 H, J = 2 Hz, —CHO); ir (film) ν 2880, 2720, and 1720 cm^{-1} (aldehyde).

cis-8-Undecene-2,5-dione (7)

To a stirred suspension of 486 mg (20 g-atom) of magnesium turnings in 25 ml of ether containing a catalytic amount of methyl iodide (1 drop), was added dropwise a solution of 3.26 g (20 mmol) of *cis*-1-bromo-3-hexene (prepared from *cis*-3-hexen-1-ol (Aldrich Chemical Company) according to the described procedure (19)) in 5 ml of ether over a 1 h period. After stirring at room temperature for an additional 1 h, ketal aldehyde **4** (2.16 g; 15 mmol) was added dropwise over a period of 20 min. Stirring was continued for an additional 30 min and methanol and then water were added. The resulting mixture was extracted with chloroform (4 × 50 ml) and washed with saturated aqueous ammonium chloride (50 ml) and saturated aqueous sodium chloride (50 ml). The chloroform solution after drying over magnesium sulfate was filtered and concentrated to yield 3.37 g of 2,2-ethylenedioxy-8-undecen-5-ol (**6**) which was found to be unstable and was used in the ensuing reaction without purification.

To a solution of 2.5 g (1.1 mmol) of **6** in 75 ml of acetone at 0 °C was added 50 ml of 8 *N* Jones reagent (20) dropwise over a period of 30 min. The resulting mixture after stirring for an additional 1.5 h was poured into 100 ml of water and extracted with chloroform (4 × 100 ml). The chloroform solution was dried ($MgSO_4$), filtered, and concentrated to give an oil which was subjected to silica gel column chromatography. Elution with a solution of 5% ether in benzene gave 1.82 g (90% yield from **4**) of **7**: nmr ($CDCl_3$) δ 0.95 (t, 3 H, J = 7 Hz, CH_3CH_2-), 1.82–2.48 (m, 6 H, $-COCH_2CH_2CH=CHCH_2-$), 2.15 (s, 3 H, CH_3CO-), 2.67 (s, 4 H, $-COCH_2CH_2CO-$), 5.33 (m, 2 H, —CH=CH—); ir (film) ν 1715 cm^{-1} (ketones); mass spectrum: M^+ 182.1308 (calcd. for $C_{11}H_{18}O_2$: 182.1306).

cis-Jasmone (1)

A solution of 1.10 g (6 mmol) of diketone **7** in 3 ml of 95% ethanol and 10 ml of 0.5 *N* sodium hydroxide was refluxed under an atmosphere of nitrogen for 5 h. The reaction mixture was cooled to room temperature and extracted with chloroform (4 × 100 ml). The chloroform solution was washed with saturated aqueous sodium chloride, dried over magnesium sulfate, filtered, and concentrated. Column chromatography of the oily product on silica gel, using a solution of 5% ether in benzene as eluent, gave 800 mg (81% yield) of *cis*-jasmone (**1**): nmr ($CDCl_3$) δ 0.96 (t, 3 H J = 7.5 Hz CH_3CH_2-), 2.03 (s, 3 H, $CH_3C=$), 2.83 (d, 2 H, J = 5.5 Hz, $=CCH_2CH=$), 5.20 (m, 2 H, —CH=CH—); ir (film) ν 1685 (conjugated ketone) and 1645 cm^{-1} (double bond); mass spectrum: M^+ 164.1197 (calcd. for $C_{11}H_{16}O$: 164.1201); 2,4-DNP: mp 118 °C (lit. (23) mp 117.5 °C).

Acknowledgments

We are grateful to the National Research Council of Canada and the University of Alberta for financial support.

1. E. J. Parry. The chemistry of essential oils and artificial perfumes. Vol. 1. Scott, Greenwood and Son, London. 1921. p. 274.
2. S. Arctander. Perfume and flavor chemicals. S. Arctander, Montclair, N.J. 1969. Compound No. 1788.
3. P. Z. Bedoukian. Perfume and flavoring synthetics. Elsevier Publishing Co., N.Y. 1967. p. 220.
4. R. A. Ellison. Synthesis, 397 (1973).
5. T. L. Ho. Synth. Commun. **4**, 265 (1974).
6. T. Wakamatsu, K. Akasaka, and Y. Ban. Tetrahedron Lett. 3883 (1974).
7. M. Araki, S. Sakata, H. Takei, and T. Mukaiyama. Bull. Chem. Soc. Jpn. **47**, 1777 (1974).
8. P. M. McCurry, Jr. and K. Abe. Tetrahedron Lett. 1387 (1974).
9. P. M. McCurry, Jr. and R. K. Singh. J. Org. Chem. **39**, 2317 (1974).
10. G. Pattenden and R. Storer. J. Chem. Soc. Perkin Trans. I, 1603 (1974).
11. H. Stettler and H. Kuhlmann. Synthesis, 379 (1975).
12. A. B. Smith III, S. J. Brnaca, and B. H. Toder. Tetrahedron Lett. 4225 (1975).
13. R. D. Clark, L. G. Kozar, and C. H. Heathcock. Synth. Commun. 1 (1975).
14. H. C. Ho, T. L. Ho, and C. M. Wong. Can. J. Chem. **50**, 2718 (1972).
15. H. Budzikiewicz, C. Djerassi, and D. H. Williams. Mass spectrometry of organic compounds. Holden-Day Inc., San Francisco. 1967. p. 263.
16. J. C. Collins, W. W. Hess, and F. J. Frank. Tetrahedron Lett. 3363 (1968).
17. R. Ratcliffe and R. Rodehorst. J. Org. Chem. **35**, 4000 (1970).
18. E. Brown and R. Dahl. Bull. Chim. Soc. Fr. **11**, 4292 (1972).
19. G. Büchi and H. Wüest. J. Org. Chem. **31**, 977 (1966).
20. A. Bowers, T. G. Halsall, E. R. H. Jones, and A. J. Lemin. J. Chem. Soc. 2548 (1953).
21. L. Crombe and S. H. Harper. J. Chem. Soc. 869 (1952).
22. J. E. McMurry and T. E. Glass. Tetrahedron Lett. 2575 (1971).
23. Y. R. Naves and A. V. Grampoloff. Helv. Chim. Acta, **25**, 1500 (1942).

Equilibrium in the formation of barium carbonate from barium sulphate

HARRY HORLINGS, DONALD S. SCOTT, AND JOHN R. WYNNYCKYJ
Department of Chemical Engineering, University of Waterloo, Waterloo, Ont., Canada N2L 3G1

Received May 17, 1976

HARRY HORLINGS, DONALD S. SCOTT, and JOHN R. WYNNYCKYJ. Can. J. Chem. **54**, 3872 (1976).

Heat of reaction and free energy of formation at 25 °C were determined from experimental equilibrium yields for the reaction

$$BaSO_4(s) + Na_2CO_3 \leftrightarrow BaCO_3(s) + Na_2SO_4$$

in an aqueous solution.

The values are 5045 and 1927 cal/mol respectively. Equilibrium constants for the reaction were determined over a temperature range from 20 to 193 °C.

HARRY HORLINGS, DONALD S. SCOTT et JOHN R. WYNNYCKYJ. Can. J. Chem. **54**, 3872 (1976).

On a déterminé la chaleur de la réaction et l'énergie libre de formation, à 25 °C, à partir des rendements d'équilibre obtenus expérimentalement, pour la réaction

$$BaSO_4(s) + Na_2CO_3 \leftrightarrow BaCO_3(s) + Na_2SO_4$$

en solution aqueuse.

Les valeurs sont respectivement de 5045 et 1927 cal/mol. On a déterminé les constantes d'équilibre de la réaction à des températures allant de 20 à 193 °C.

[Traduit par le journal]

Introduction

Equilibrium constants were experimentally determined for the replacement reaction

$$BaSO_4(s) + CO_3^{2-} \leftrightarrow BaCO_3(s) + SO_4^{2-}$$

over a range of temperatures from 20 to 193 °C. Other workers (1–5) reported no thermodynamic analysis of the reaction when interpreting experimental results. Ipatieff and Freitag (6) determined the effect of different gases and the sodium carbonate to barium sulphate ratio on the reaction yield at a fixed reaction time. Milicev and Siftar (7) studied the kinetics of the above reaction using potassium carbonate instead of sodium carbonate over a temperature range of 15 to 45 °C. An activation energy of 26 kcal/mol and a rate dependence on the carbonate ion to the power 2.5 were reported for the reaction. Meloga and Constantinescu (8) extensively studied the reaction determining optimal operating conditions by varying carbonate to barium sulphate ratios over limited ranges.

It is a characteristic of replacement reactions of this type that the free energy change of reaction is small, while the free energies of formation of individual reactants or products are large. As a consequence, small uncertainties in values of free energies of formation lead to unacceptably large percentage errors in calculating the equilibrium constant for the overall reaction, and hence in the calculation of equilibrium reaction yields. This is the case for the present reaction where ΔG^0 values calculated from free energies of formation available from different literature sources range from 80 to 1900 cal/mol at 25 °C. For example, some of the most carefully evaluated data, that given by the National Bureau of Standards (9, 10), result in a value for $\Delta G_{298}{}^0$ of 1900 cal/mol for a standard state of unit molality with a minimum probable error of $\pm 50\%$ and a maximum possible error of several hundred percent, although individual values of free energy of formation of the reactants and products have a minimum error of about 1%. Similarly, the same sources report a standard heat of reaction $\Delta H_{298}{}^0$ of 5920 cal/mol, which is subject to similar errors.

The present work was undertaken to obtain reliable experimental values for the equilibrium constant of this reaction over a suitably wide temperature range of engineering usefulness.

Experimental Procedure

The reaction vessel was a 2000 ml Parr series 4500

Can. J. Chem. Downloaded from www.nrcresearchpress.com by 210.87.254.105 on 09/05/12
For personal use only.

Can. J. Chem. Downloaded from www.nrcresearchpress.com by 210.87.254.105 on 09/05/12
For personal use only.

TABLE 1. Solubility of Na_2CO_3 and Na_2SO_4 in water in moles per 1000 g of water (from International Critical Tables (1928))

Temperature (°C)	Solubility Na_2CO_3	Solubility Na_2SO_4
30	4.77	—
40	4.61	3.40
60	4.38	3.19
80	4.28	3.05
100	4.26	2.97

pressure reaction apparatus. The reaction mixture, consisting of known weights of sodium carbonate and barium sulphate (Baker analyzed reagent grade powders) in 1 l of distilled water, was well agitated. The temperature was automatically controlled to better than ±2 °C and measured independently by a second chromel–alumel thermocouple connected to a recorder.

The reactant concentrations which can be used are limited by the solubility of sodium carbonate and sodium sulphate (Table 1).

Upon addition of barium sulphate to a solution of carbonate ion, the reaction will proceed to the right as long as the ratio of sulphate to carbonate ion is less than K or until all the barium sulphate is consumed. For a solution which initially contains no sulphate ions, the required mole ratio of sodium carbonate to barium sulphate, n, for complete conversion can be shown to be given by

$$[1] \qquad n = \frac{K+1}{K}$$

This relation was used to estimate the composition of reaction mixtures. Actual weights of the reactants charged to the reactor are listed in Table 2, columns 3 and 4, and the value of n is in column 5.

At temperatures below 100 °C, representative slurry samples were withdrawn under a slight pressure, immediately filtered, and analyzed for the species of concern. At higher temperatures, after the reaction reached equilibrium, which was usually within 2 h, stirring was stopped and solids were allowed to settle. The clear supernatant liquid was withdrawn and analyzed for soluble ions. In a few tests at high temperatures, the slurry was sampled when well stirred by withdrawing it into a large quantity of cold water and immediately filtering. Since only the sulphate/carbonate ion ratio was required for calculation of the equilibrium constant, this technique was satisfactory where knowledge of the exact solution concentration was deemed to be unnecessary.

Concentrations of species were determined by the following methods: insoluble barium carbonate by reaction with an excess of hydrochloric acid and back-titration with sodium hydroxide; sodium ion by atomic absorption spectroscopy using the less sensitive wavelength of 3302 Å; soluble carbonate ion by titration with hydrochloric acid; and soluble sulphate ion by the gravimetric method of weighing as barium sulphate.

Results and Discussion

For the replacement reaction

$$[2] \quad BaSO_4(s) + CO_3^{2-}(aq) \leftrightarrow BaCO_3(s) + SO_4^{2-}(aq)$$

the equilibrium constant can be expressed as

$$[3] \quad K = a_{SO_4^{2-}}/a_{CO_3^{2-}} = [SO_4^{2-}]\,\gamma_{SO_4^{2-}}/[CO_3^{2-}]\,\gamma_{CO_3^{2-}}$$

where a and γ are the activity and activity coefficient of the ion respectively. For any specific reaction conditions, the ionic strength of the reaction mixture remains constant since

TABLE 2. Summary of experimental data (all experiments done with 1 l of distilled water initially added)

Run	T (°C)	Initial charge (g) $BaSO_4$	Initial charge (g) Na_2CO_3	n‡	Equilibrium composition (mol/l) SO_4^{2-}	Equilibrium composition (mol/l) CO_3^{2-}	K
1	20	13.75	25	4	0.00667	0.220	0.0303
2	54	13.75	25	4	0.0165	0.213	0.0775
3	77	13.75	25	4	0.0270	0.209	0.129
4	110	137.5	250	4	0.490	1.750	0.280
5	110	275	500	4	0.805	2.960	0.272
6	110	275	500	4	0.835	2.960	0.282
7	110	275	500	4	0.904	2.953	0.306
8	147	137.5	125	2		*	0.500
9	194	137.5	62.5	1	0.2440	0.3325	0.734
10	191	275	125	1	0.4488	0.5826	0.770
11	192	116.4†	83.78†	1†	0.2333	0.3137	0.744

*Ratio of SO_4^{2-}/CO_3^{2-}.
†Weights of $BaCO_3$ and Na_2SO_4 and mole ratio $BaCO_3/Na_2SO_4$.
‡Initial mole ratio $NaCO_3/BaSO_4$.

Can. J. Chem. Downloaded from www.nrcresearchpress.com by 210.87.254.105 on 09/05/12
For personal use only.

the reactant and product ions have the same charge, and for each reacted CO_3^{2-} ion, one SO_4^{2-} ion is produced. In the absence of other evidence, equal activity coefficients for carbonate and sulphate ions were assumed, and their ratios in eq. 3 were then taken as unity at all temperatures. This is a somewhat uncomfortable assumption which, however, is partly justified by our present results. Therefore, eq. 3 was simplified to

$$[4] \qquad K = [SO_4^{2-}]/[CO_3^{2-}]$$

and the reported K values as well as the derived thermodynamic data are subject to this uncertainty.

Columns 6 and 7 of Table 2 give the measured concentrations of the SO_4^{2-} and CO_3^{2-} ions, respectively, and column 8, the value of K, calculated according to eq. 4.

Run 11, at 193 °C, was carried out using barium carbonate and sodium sulphate as initial reagents, instead of sodium carbonate and barium sulphate. Also the initial concentration was varied, runs 4, 5, 9, and 10 (Table 2), by a factor of two for both initial reagents. Consistent equilibrium constants were produced in all cases.

In Table 2, the carbonate ion analyses are estimated to contain a maximum error of $\pm 2\%$. In principle, if the initial charge and the density are known, this is the only analysis necessary. However, at temperatures above 100 °C, densities were not known accurately, and so an independent gravimetric determination of soluble sulphate was also carried out. A probable maximum error of $\pm 3\%$ is estimated in these values. The possible error due to the ± 2 °C uncertainty in temperature is on the average $\pm 3\%$. All these factors lead to a maximum possible error of ± 7–8% in values of K. These estimates are consistent with the scatter of replicate experimental measurements at 110 °C (runs 5, 6, and 7). Errors in the three values of K found deviate -5.2%, -0.2%, and $+6.6\%$ from the average. The equilibrium constants were plotted as log K against the inverse absolute temperature in Fig. 1. The solid line is the least-squares fit to the experimental points. The fact that a rather good straight line is obtained is some confirmation of the validity of the earlier assumption that the ratio $\gamma_{SO_4^{2-}}/\gamma_{CO_3^{2-}}$ is indeed constant at or near unity at all temperatures, within the experimental error of the

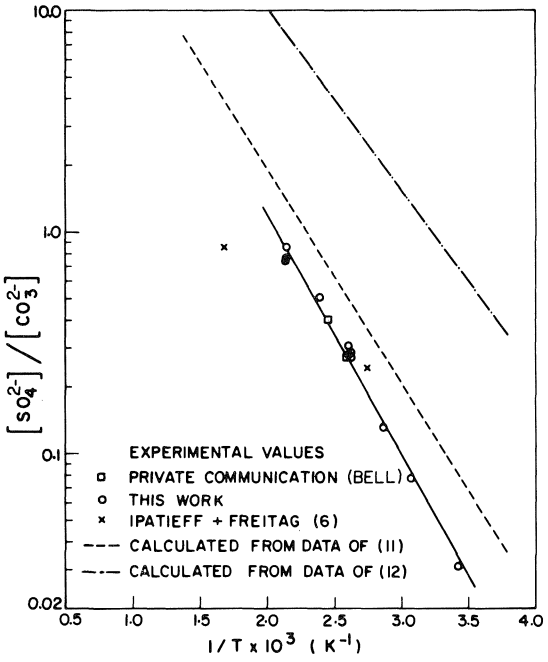

FIG. 1. Equilibrium constants for the conversion of $BaSO_4$ to $BaCO_3$.

measurements. Fair agreement was obtained with the Ipatieff and Freitag result at the lower of the two temperatures and a long retention time (6). Two data points obtained by C. Bell in another laboratory, at long reaction times, are also included and they agree well with the present work.

The equilibrium constant is related to the standard heat and free energy change of the reaction, respectively, through the equations

$$[5] \qquad \ln K = \frac{\Delta H^0}{RT} + B$$

$$[6] \qquad \Delta G^0 = -RT \ln K$$

Using eq. 5 and the slope of the solid line in Fig. 1, the value of ΔH^0 was calculated as 5045 $\pm$ 160 cal/mol. Using eq. 6 and the value of K at 298 K yielded $\Delta G_{298}^0 = 1927 \pm 25$ cal/mol. The uncertainty range is based on the 7% probable error in K.

From the compilations of critically assessed thermodynamic data (9–13), ΔG_{298}^0 values for the reaction ranging from 80 to 1900 cal/mol and ΔH^0 values ranging from 3600 to 5920 cal/mol, depending on the source, can be

calculated. All of them bear a percent possible error, based on the stated uncertainty of the tabulated data of over 100%. As pointed out earlier the large error limits arise from the subtraction of quantities of the order of 300 kcal/mol. Accordingly the present results are in quite good agreement with the thermochemical data but are, of course, significantly more certain and useful for engineering purposes such as process design and conversion calculations.

Conclusions

The equilibrium constant for the barium sulphate reaction to barium carbonate in an aqueous sodium carbonate solution in the temperature of 20 to 193 °C is given by the relation

$$\log_{10} K = -1.028 \times 10^3\left(\frac{1}{T}\right) + 2.2875$$

where T is the temperature in K. ΔG^0 and ΔH^0 for the reaction at 298 K are 1927 ± 25 and 5045 ± 160 cal/mol, respectively.

1. L. J. MINNICK. U.S. patent 2,440,641 (1948).
2. A. C. HERBERT. U.S. patent 2,637,700 (1953).
3. L. MANNUCCI. Italian patent 601,409 (1960).
4. E. ZIRNGIEBL. German patent 1,177,122 (1964).
5. R. A. SHAH, M. ASLAM, and S. M. H. NAQVI. British patent 1,271,126 (1971).
6. V. N. IPATIEFF and C. FREITAG. Ind. Eng. Chem. **27**, 342 (1935).
7. S. MILICEV and J. SIFTAR. Monatsh. Chem. **96**, 3, 941 (1965).
8. B. MELOGA and I. CONSTANTINESCU. Inst. Politeh. Gheorghe GheorghiuDej. Bucuresti, Buletinul, **29**, 6 (1967); **29**, 59 (1967).
9. D. D. WAGMAN, W. H. EVANS, V. B. PARKER, I. HALOW, S. M. BAILEY, and R. H. SCHUMM. National Bureau of Standards Technical Note 270-3, U.S. Dept. of Commerce, Washington. 1968.
10. V. B. PARKER, D. D. WAGMAN, and W. H. EVANS. National Bureau of Standards Technical Note 270-6, U.S. Dept. of Commerce, Washington. 1971.
11. G. N. LEWIS and M. RANDALL. Thermodynamics. 2nd ed. *Revision by* K. S. Pitzer and L. Brewer, McGraw-Hill Inc., New York. 1961.
12. B. E. CONWAY. Electrochemical data. Elsevier Pub. Co., Amsterdam. 1952.
13. W. M. LATIMER. The oxidation states of the elements and their potentials in aqueous solutions. 2nd ed. Prentice-Hall Inc., New York. 1952.

Can. J. Chem. Downloaded from www.nrcresearchpress.com by 210.87.254.105 on 09/05/12
For personal use only.

ESCA investigations of Group IV derivatives. Part II. Binding-energy predictions for bromo- and iodo-silanes and -germanes

JOHN E. DRAKE, CHRIS RIDDLE, H. ERNEST HENDERSON, AND BORIS GLAVINČEVSKI
Department of Chemistry, University of Windsor, Windsor, Ont., Canada N9B 3P4

Received May 19, 1976

JOHN E. DRAKE, CHRIS RIDDLE, H. ERNEST HENDERSON, and BORIS GLAVINČEVSKI. Can. J. Chem. **54**, 3876 (1976).

Core-level binding energies of all atoms are reported for the bromo(methyl)-silanes and -germanes Me_nMBr_{4-n} (M = Si, Ge; $n = 0 \rightarrow 3$) and the iodo(methyl)-silanes and -germanes Me_nMI_{4-n} (n = 2, 3). Measured binding energy shifts correlate well with values predicted from atomic charge calculations using an electronegativity-equilisation procedure.

JOHN E. DRAKE, CHRIS RIDDLE, H. ERNEST HENDERSON et BORIS GLAVINČEVSKI. Can. J. Chem. **54**, 3876 (1976).

On rapporte des énergies de liaisons au niveau du noyau pour tous les atomes des bromométhyl silanes et germanes Me_nMBr_{4-n} (M = Si, Ge; $n = 0 \rightarrow 3$) et des iodométhyl silanes et germanes $Me_n(MI_{4-n}$ (n = 2, 3). Il y a une bonne corrélation entre les déplacements mesurés pour les énergies de liaisons et les valeurs que l'on peut prédire à partir des calculs de charge atomique en faisant appel à une procédure d'égalisation des électronégativités.
[Traduit par le journal]

Can. J. Chem. Downloaded from www.nrcresearchpress.com by 210.87.254.6 on 09/05/12
For personal use only.

In Part I (1) we reported core-level binding energies for two series of compounds, Me_nMCl_{4-n} and Me_3MX ($n = 0 \rightarrow 4$, M = Si or Ge, X = F, Cl, Br, I). Binding energies for *each atom* in every compound were correlated with the partial charges on those atoms. The charges were calculated using the electronegativity-equalisation method of Huheey (2) which, in turn, is based on the Hinze–Jaffé method (3–5). We introduced the concept of allowing for *s*-orbital participation in the bonding orbital of the halogen atom, designating the method EESOP (*e*lectronegativity-*e*qualisation with *s*-*o*rbital *p*articipation).

Because excellent correlations were obtained for the Me_nMCl_{4-n} series, we have used the related plots (Fig. 1) as established reference bases for the series Me_nMX_{4-n} (X = Br, I) reported in this paper. Thus, the partial charges on carbon δ_C, germanium, δ_{Ge}, silicon, δ_{Si}, bromine, δ_{Br}, and iodine, δ_I, are calculated by our EESOP method. Then the previously established correlations (Fig. 1) are used to read off a predicted binding energy for each of the EESOP-calculated partial charges. Therefore, all of the halogeno-series Me_nMX_{4-n}, M = Si, Ge; X = Cl, Br, I, are assumed to obey the same linear relationship between partial charge and binding energy. These calculated binding energies are tabulated together with the experimental binding energies in Tables 1 and 2.

As we found previously, by allowing for

TABLE 1. Comparison of calculated and experimental core-electron binding energies* (BE) for bromo- and iodo(methyl)germanes

Compound	Germanium			Carbon			Halogen	
	δ†	BE(calcd.)‡	BE(expt.)	δ	BE(calcd.)	BE(expt.)	δ	BE(expt.)
Me_3GeBr	+0.057	37.10	37.07	+0.036	290.30	290.29	−0.164	75.13
Me_2GeBr_2	+0.115	38.00	38.06	+0.066	290.60	290.56	−0.124	75.60
$MeGeBr_3$	+0.166	38.75	38.71	+0.092	291.00	291.10	−0.086	76.06
$GeBr_4$	+0.210	39.40	39.42	—	—	—	−0.053	76.38
Me_3GeI	+0.046	36.95	36.93	+0.031	290.25	290.20	−0.139	625.58
Me_2GeI_2	+0.093	37.70	37.68	+0.055	290.55	290.37	−0.101	626.01

*The experimental binding energies of C 1*s* and I $3d_{5/2}$ are corrected relative to Ar $2p_{3/2}$ = 248.63 eV (11), uncertainty ±0.05 eV; those of Ge 3*d* and Br $3d_{5/2}$ are reported relative to Ne 2*s* at 48.47 eV (11), uncertainty ±0.05 eV.

†Partial charges, δ, calculated by EESOP (1) assuming that germanium is using sp^3 hybrid orbitals, $\chi_{Ge} = 8.07 + 6.82\delta_{Ge}$; that the carbon atom is treated as an 'unbonded tetrahedral carbon atom' using $\chi_C = 7.98 + 13.27\delta_C$; and that there is 16% and 19% *s*-character on bromine and iodine respectively, using $\chi_{Br} = 9.98 + 9.11\delta_{Br}$ and $\chi_I = 9.54 + 8.29\delta_I$.

‡Binding energies are calculated by reference to the plots of BE(expt.) *vs.* δ for the chloro(methyl)germanes assuming that there is 11% *s*-character for the bonding Cl orbital (1).

TABLE 2. Comparison of calculated and experimental core-electron binding energies* (BE) for bromo- and iodo(methyl)silanes

Compound	Silicon			Carbon			Halogen	
	δ†	BE(calcd.)‡	BE(expt.)	δ	BE(calcd.)	BE(expt.)	δ	BE(expt.)
Me_3SiBr	+0.097	107.00	106.97	+0.015	290.05	290.07	−0.143	75.33
Me_2SiBr_2	+0.134	108.00	108.01	+0.040	290.40	290.40	−0.106	75.78
$MeSiBr_3$	+0.165	108.80	108.83	+0.061	290.60	290.76	−0.076	76.21
$SiBr_4$	+0.193	109.50	109.64	—	—	—	−0.048	76.48
Me_3SiI	+0.093	106.90	106.77	+0.012	290.00	289.95	−0.130	625.90
Me_2SiI_2	+0.125	107.80	107.98	+0.034	290.30	290.43	−0.096	626.21

*The experimental binding energies of C 1*s* and I $3d_{5/2}$ are corrected relative to Ar $2p_{3/2}$ = 248.63 eV (11), uncertainty ±0.05 eV; those of Si 2*p* and Br $3d_{5/2}$ are reported relative to Ne 2*s* at 48.47 eV (11), uncertainty ±0.05 eV.

†Partial charges, δ, calculated by EESOP (1) assuming that silicon is using sp^3 hybrid orbitals, $\chi_{Si} = 7.30 + 9.04\delta_{Si}$ that the carbon atom is treated as an 'unbonded tetrahedral carbon atom' using $\chi_C = 7.98 + 13.27\delta_C$; and that there is 11% and 15% *s*-character on bromine and iodine respectively, using $\chi_{Br} = 9.49 + 9.2\delta_{Br}$ and $\chi_I = 9.24 + 8.47\delta_I$.

‡Binding energies are calculated by reference to the plots of BE(expt.) *vs.* δ for the chloro(methyl)silanes assuming that there is 5% *s*-character for the bonding Cl orbital (1).

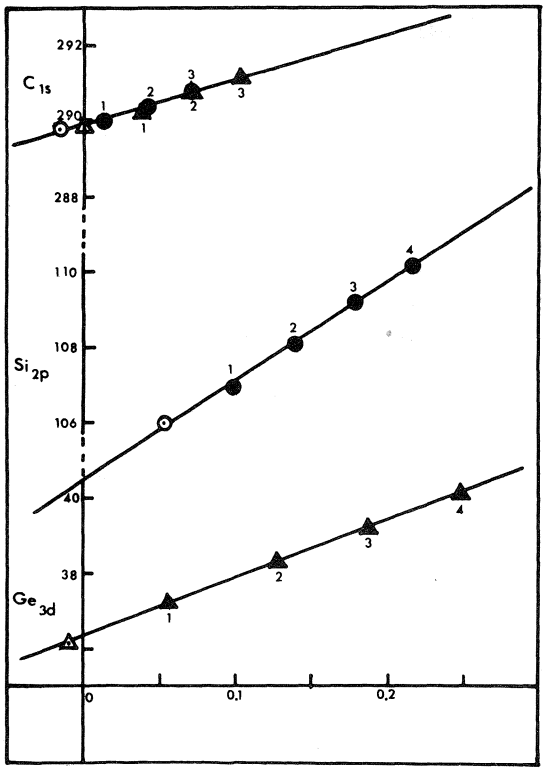

FIG. 1. Ge 3*d*, Si 2*p*, and C 1*s* core-level binding energies (eV) for the chloro(methyl)-germanes and -silanes as a function of the calculated charge on germanium, δ_{Ge}, silicon, δ_{Si}, and carbon, δ_C, respectively. ▲: $GeCl_4$ (*4*), $MeGeCl_3$ (*3*), Me_2GeCl_2 (*2*), Me_3GeCl (*1*). Δ: Me_4Ge. ●: $SiCl_4$ (*4*), $MeSiCl_3$ (*3*), Me_2SiCl_2 (*2*), Me_3SiCl (*1*). ○: Me_4Si. This assumes 11% *s*-character on Cl for bonding to Ge and 5% *s*-character on Cl for bonding to Si. Linear regression analysis gives coefficients of correlation of 0.999 (Ge), 0.998 (Si), and 0.957 (C).

differing degrees of *s*-orbital participation, it is possible to reproduce the experimentally observed binding energies. In the germane series, Me_nMX_{4-n}, *s*-orbital character needs to be 16% (X = Br) and 19% (X = I) to match the reference base 11% (X = Cl). In comparison, *s*-orbital participation is reduced in the silane series to 11% (X = Br) and 15% (X = I) with a reference base of 5% (X = Cl).

The self-consistency of the calculations is demonstrated in Fig. 2. The plot of experimentally observed bromine $3d_{5/2}$ core-level binding energies for both series against the calculated charge on bromine (Fig. 2*A*) has a coefficient of correlation of 0.997. Unfortunately, because the tri- and tetra-iodo silanes and germanes are of low volatility, less data are available for the corresponding correlation of iodine $3d_{5/2}$ binding energies (Fig. 2*B*), a correlation coefficient of 0.91 is achieved however.

In conclusion, the data reported in this paper extend the applicability of our simple EESOP model. The ability of this model to relate partial charge to binding energy appears to be as good as more sophisticated models which allow for relaxation energy and potential terms (see ref. 6 and references therein). In any of the Me_nGeX_{4-n} series of compounds that we have studied, the core-level binding energies of C 1*s* or Ge 3*d* are fairly similar for each value of *n* regardless of the nature of the halogen, X, when X = Cl, Br, or I. This is also true for the C 1*s* or Si 2*p* levels for the Me_nSiX_{4-n} series. Thus, the halogens appear to have fairly similar electronegativities. This is consistent with the steady increasing *s*-orbital

Can. J. Chem. Downloaded from www.nrcresearchpress.com by 210.87.254.6 on 09/05/12
For personal use only.

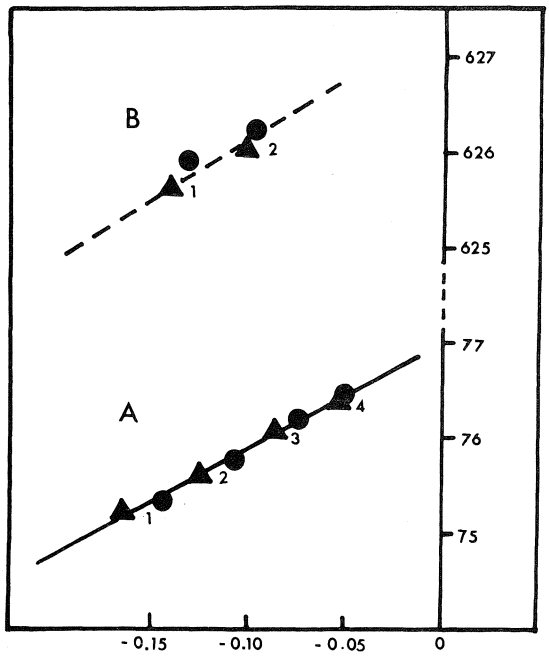

FIG. 2. (*A*) Br $3d_{5/2}$ core-level binding energies (eV) for the bromo(methyl)-germanes and -silanes as a function of the calculated charge on bromine, δ_{Br}. (See Tables 1 and 2.) ▲: $GeBr_4$ (*4*), $MeGeBr_3$ (*3*), Me_2GeBr_2 (*2*), Me_3GeBr (*1*). ●: $SiBr_4$ (*4*), $MeSiBr_3$ (*3*), Me_2SiBr_2 (*2*), Me_3SiBr (*1*). (*B*) I $3d_{5/2}$ core-level binding energies (eV) for the iodo(methyl)-germanes and -silanes as a function of the calculated charge on iodine, δ_I. (See Tables 1 and 2.) ▲: Me_2GeI_2 (*2*), Me_3GeI (*1*). ●: Me_2SiI_2 (*2*), Me_3SiI (*1*). Linear regression analysis gives coefficients of correlation of 0.997 (Br) and 0.910 (I).

participation by the halogen along the series Cl > Br > I indicated by our EESOP model. Although the amount of this *s*-orbital participation is uncertain in absolute terms, the relative changes have the effect of reducing differences in the electronegativities of the halogens. Thus, changes in core-level binding energies are more sensitive to the *number* of halogens present than to the *nature* of the halogen.

Experimental

Core-electron binding energies were determined on a McPherson ESCA-36 photoelectron spectrometer, using magnesium Kα X-radiation (1253.6 eV) for photoelectron excitation. Samples were introduced in the vapor phase at pressures close to 5×10^{-5} torr. Argon gas was bled in to form 20% of the total sample. Binding energies were referenced to the argon $2p_{3/2}$ level at 248.63 eV (C 1*s* and I $3d_{5/2}$) or the neon 2*s* level at 48.47 eV (Ge 3*d*, Si 2*p* and Br $3d_{5/2}$) (11). Details of the data-accumulation procedures and the curve-fitting program are given in Part I (1).

Materials

Trimethylbromogermane, dimethyldibromogermane, methyltribromogermane and tetrabromogermane were obtained commercially (Laramie Chem. Co.) as was tetrabromosilane (Ventron Corporation, Alfa Products). Trimethyliodosilane, dimethyldiiodogermane, and trimethylbromosilane were prepared by the reaction of the parent hydride with iodine or bromine (based on details given in ref. 7). Trimethyliodogermane was prepared by the exchange reaction of hydrogen iodide and trimethylbromogermane (based on details given in ref. 8). The reaction of dimethylsilane and methylsilane with hydrogen bromide in the presence of aluminum tribromide produced dimethyldibromosilane and methyltribromosilane (based on details given in ref. 9). Dimethyldiiodosilane was prepared by the action of hydrogen iodide on dimethylsilane and aluminum triiodide (10).

All samples were distilled on the vacuum line before use and their purity checked by ^1H nmr, infrared and Raman spectroscopy.

Charge Calculations

The previously described (1) mode of EESOP calculation is based on the relationship

$$\chi_m = a + b\delta_m$$

relating the orbital electronegativity of an element, χ_m, to the charge, δ_m, on that element (2). Rather than derive *a* and *b* values graphically, we have interpolated between limiting values, thus, *e.g.*, for bromine $a = 8.4$ and $b = 9.4$ for 100% *p*-character and $a = 18.29$ and $b = 7.57$ for 100% *s*-character. Hence for 16% *s*-character, $a = (8.4 \times 0.84 + 18.29 \times 0.16) = 9.98$ and $b = (9.4 \times 0.84 + 7.57 \times 0.16) = 9.11$. Otherwise, the calculations were performed as in Part I.

1. J. E. DRAKE, C. RIDDLE, and L. COATSWORTH. Can. J. Chem. **53**, 3602 (1975).
2. J. E. HUHEEY. J. Phys. Chem. **69**, 3284 (1965).
3. J. HINZE and H. H. JAFFÉ. J. Am. Chem. Soc. **84**, 540 (1962).
4. J. HINZE, M. A. WHITEHEAD, and H. H. JAFFÉ. J. Am. Chem. Soc. **85**, 148 (1963).
5. J. HINZE and H. H. JAFFÉ. J. Phys. Chem. **67**, 1501 (1963).
6. W. B. PERRY and W. L. JOLLY. Inorg. Chem. **13**, 1215 (1974).
7. M. G. VORONKOV and Y. I. KHUDOBIN. Izv. Akad. Nauk SSSR, Otd. Khim. Nauk. 805 (1956).
8. S. CRADOCK and E. A. V. EBSWORTH. J. Chem. Soc. A, 12 (1967).
9. C. NEWMAN, J. K. O'LOANE, S. R. POLO, and M. K. WILSON. J. Chem. Phys. **25**, 855 (1956).
10. E. A. V. EBSWORTH, M. ONYSZCHUK, and N. SHEPPARD. J. Chem. Soc. 1453 (1958).
11. G. JOHANSSON, J. HEDMAN, A. BERNDTSSON, M. KLASSON, and R. NILLSON. J. Electron. Spectrosc. **2**, 295 (1973).

Can. J. Chem. Downloaded from www.nrcresearchpress.com by 210.87.254.6 on 09/05/12
For personal use only.

The reaction of some heterocyclic thiones with ethyl azidoformate

MOHINDER S. CHAUHAN AND DAVID M. MCKINNON
Department of Chemistry, University of Manitoba, Winnipeg, Man., Canada R2T 2N2

Received June 17, 1976

MOHINDER S. CHAUHAN and DAVID M. MCKINNON. Can. J. Chem. **54**, 3879 (1976).

A number of heterocyclic thiones react with ethyl azidoformate in boiling carbon tetrachloride to yield the corresponding iminocarboxylic esters. 4-Phenyl-1,2-dithiole-2-thione is an exception and yields both a 1,2,3-dithiazine derivative and a urethane type product. 4-Phenyl-1,2-dithiole-3-one yielded an isothiazolin-3-one product. The mechanisms are discussed briefly.

MOHINDER S. CHAUHAN et DAVID M. MCKINNON. Can. J. Chem. **54**, 3879 (1976).

Un certain nombre de thiones hétérocycliques réagissent avec l'azidoformate d'éthyle dans le tétrachlorure de carbone bouillant pour conduire aux esters iminocarboxyliques correspondants. La phényl-4 dithiole-1,2 thione-2 est une exception et conduit à deux produits soit un dérivé diathiazine-1,2,3 et à un produit du type uréthane. La phényl-4 dithiole-1,2 one-3 conduit uniquement à un produit isothiazolinone-3. On discute brièvement des mécanismes de ces réactions.

[Traduit par le journal]

While the reaction of many substrates with organic azides, or their derived nitrene species has been studied extensively (1, 2), reports of their reactions with compounds containing thione functions appear to be more limited. There are no reports of nitrene–thione products in certain reactions where it is conceivable that both such functions might be present simultaneously (3–9), but thiobenzophenone and carbon disulfide both reacted with phenylazide (10, 11) to give products which are at least formally derived by combination of 1 molecule of thione with 1 molecule of nitrene, less 1 atom of sulfur. Thioacylazides exist as their cyclic isomers, the 1,2,3,4-thiatriazoles (12).

We have therefore examined the reaction of a number of stable heterocyclic thiones with ethyl azidoformate (ethyl carbazidate) in boiling carbon tetrachloride. These thiones included the thiopyran-2-thiones (**1***a*, *b*, *c*), the 1,2-dithiole-3-thiones (**2***a–d*), the 1,3-dithiole-2-thiones (**3***a*, *b*, *c*), the isothiazolin-5-thione (**4***a*), and the 1,2,4-dithiazolin-3-thione (**5***a*). In all cases examined except **2***d*, products were obtained whose elemental analyses and mass spectra indicated that they had been formed by reaction of 1 mol of thione with 1 mol of azidoester, less 2 atoms of nitrogen and 1 atom of sulfur.

Many reaction possibilities are open, but evidence of reaction of the heterocycles on the exocyclic thione function with the azide to form eventually the corresponding iminocarboxylic esters (**1***d–f*, **2***e–g*, **3***d–f*, **4***b*, **5***b*) was found.

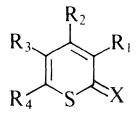

1

a, $R_1 = R_4 = Ph$, $R_2 = R_3 = H$, X = S
b, $R_2 = R_4 = Ph$, $R_1 = R_3 = H$, X = S
c, $R_1, R_2 = R_3, R_4 = (—CH=CH—)_2$, X = S
d, $R_1 = R_4 = Ph$, $R_2 = R_3 = H$, $X = NCO_2Et$
e, $R_2 = R_4 = Ph$, $R_1 = R_3 = H$, $X = NCO_2Et$
f, $R_1, R_2 = R_3, R_4 = (—CH=CH—)_2$, $X = NCO_2Et$
g, $R_1 = R_4 = Ph$, $R_2 = R_3 = H$, X = O

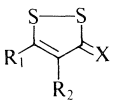

2

a, $R_1 = Ph$, $R_2 = H$, X = S
b, $R_1 = R_2 = Ph$, X = S
c, $R_1 = H$, $R_2 = Ph$, X = S
d, $R_1 = C_6H_4$-*p*-OMe, $R_2 = H$, X = S
e, $R_1 = Ph$, $R_2 = H$, $X = NCO_2Et$
f, $R_1 = R_2 = Ph$, $X = NCO_2Et$
g, $R_1 = C_6H_4$-*p*-OMe, $R_2 = H$, $X = NCO_2Et$
h, $R_1 = NHCO_2Et$, $R_2 = Ph$, X = S
i, $R_1 = H$, $R_2 = Ph$, X = O

Examination of the pmr spectra indicated that the aromatic rings were intact, and acid hydrolysis of the ester **1***d* afforded 3,6-diphenylthiopyran-2-one (**1***g*), demonstrating that in this case the heterocyclic ring was intact. The infrared (ir) spectra of the products obtained showed absorptions around 1625 cm^{-1}, to which are assigned the ester function. While this frequency

Can. J. Chem. Downloaded from www.nrcresearchpress.com by 210.87.254.40 on 09/05/12
For personal use only.

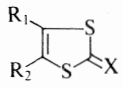

3

a, R_1 = Ph, R_2 = H, X = S
b, R_1, R_2 = (—CH=CMe—CH=CH—), X = S
c, R_1 = R_2 = Ph, X = S
d, R_1 = Ph, R_2 = H, X = NCO_2Et
e, R_1, R_2 = (—CH=CMe—CH=CH—), X = NCO_2Et
f, R_1, R_2 = Ph, X = NCO_2Et

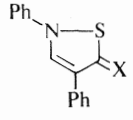

4

a, X = S
b, X = NCO_2Et

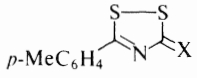

5

a, X = S
b, X = NCO_2Et

is considerably displaced from that normally experienced, a literature search revealed that it is in accord with other acyliminocompounds, especially for heterocyclic sulfur compounds (13–15). The displacement may be due to interaction of the sulfur or other ring heteroatom with the carbonyl group.

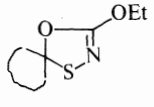

6

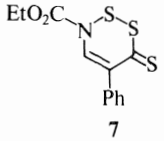

7

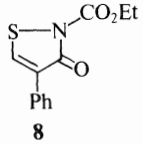

8

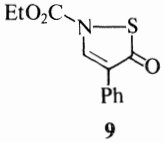

9

Various modes of attack of the azidoester on the thione function are open; (*i*) a dipolar type of attack of the azide group on the thione to generate a spirothiatriazolidine ring (10), with subsequent elimination of nitrogen to produce a thiaziridine; (*ii*) nucleophilic attack by the azide on the thione carbon, then cyclization with elimination of nitrogen to form the thiaziridine; (*iii*) thiophilic attack of the azide on the thione sulfur, then cyclization with nitrogen elimination to the thiaziridine; (*iv*) nucleophilic attack of the sulfur on the azide with concerted loss of nitrogen to produce a zwitterion, followed by cyclization to the aziridine (Scheme 1); or (*v*) direct attack of a nitrene species on the thione function to produce the thiaziridine. Such a thiaziridine itself would readily extrude sulfur to give the corresponding iminocarboxylic ester similarly to known reactions of various episulfides (16), especially acylepisulfides (17). While another type of product which possibly could be formed in the reaction is the ethoxyspirothioxazole type (**6**) formed by reaction of the thione function with a dipolar nitrene derived species, no such compounds were isolated from these reactions.

In contrast to the above reactions which afforded only one product each, the reaction of 4-phenyl-1,2-dithiole-3-thione (**2***c*) with ethyl azidoformate afforded two products, whose mass spectra and elemental analyses indicated that they had been formed by combination of 1 molecule of thione with 1 molecule of the azide, less 1 molecule of nitrogen, and with retention of all sulfur atoms. One of these compounds was also converted to the other by treatment with acid. Consideration of both thiaziridine or thioxazoline type products is therefore precluded, and attack appears to have occurred at other than the thione function. In addition, examination of the ^{13}C nmr spectra of the initial compound and the acid rearranged product revealed absorptions at 185.0 and 208.6 δ respectively which are comparable to those observed for many thiones (18). On the basis of its ir spectrum, which demonstrates both C=O and NH absorptions, and of its partially coupled ^{13}C nmr spectrum, which shows all the heterocyclic carbon atoms as singlets, the acid rearranged compound is assigned the urethane structure **2***h*. In addition, the C_4 carbon atom, previously in 4-phenyl-1,2-dithiole-3-thione (**2***c*) at δ 149.2, is shifted upfield by the α-substituent effect to 132.7 δ. On the basis of this evidence, we propose the dithiazine structure **7** for the other adduct,

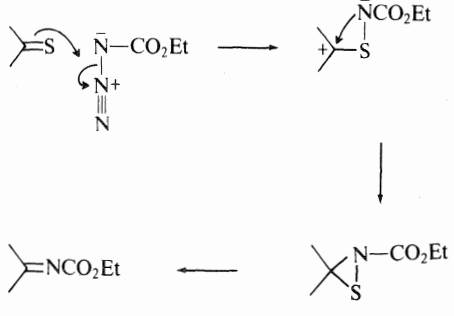

SCHEME 1

Can. J. Chem. Downloaded from www.nrcresearchpress.com by 210.87.254.40 on 09/05/12
For personal use only.

Can. J. Chem. Downloaded from www.nrcresearchpress.com by 210.87.254.40 on 09/05/12
For personal use only.

which could have been formed by reaction of nitrene (actual or potential) with the thione **2***c* at the 1-sulfur atom. While an azide could attack the dithiole at carbon, rather than at ring sulfur, in accord with the normal nucleophilic attack on 1,2-dithioles (19), reaction of a nitrene at ring sulfur is a possibility. Certainly sulfur compounds are efficient nitrene traps, but few conclusions can be drawn from the reactions of nitrenes with various sulfides (3, 20–22).

The difference in reactivity between 4-phenyl-1,2-dithiole-3-thione (**2***c*) and the other thiones, especially the other 1,2-dithiole-3-thiones is surprising, but attack on the thione at the 5-carbon or 1-sulfur is certainly much more sterically possible in **2***c* than in all other cases.

To obtain more information on the reaction, 4-phenyl-1,2-dithiole-3-one (**2***i*) was treated with ethyl azidoformate under the same conditions as above. Once more a product was obtained whose properties indicated that it was formed by combination of 1 molecule of dithiole-3-one with 1 molecule of azide, less 1 molecule of nitrogen, and, surprisingly, less 1 atom of sulfur. This compound was assigned the isothiazolin-3-one-2-carboxylic ester structure (**8**) rather than the isomeric isothiazolin-5-one-2-carboxylic ester structure (**9**), which would have shown a broadening of the heterocyclic proton singlet at 8.26 δ due to coupling with the adjacent nitrogen. This broadening was not observed, however. Also, the compound exhibited two carbonyl frequencies at 1603 and 1760 cm^{-1}. The former appears to be in the usual range for the ester carbonyl of an acylurethane (23), and the latter in the region observed from isothiazolin-3-ones (24). Isothiazolin-5-ones, or related compounds on the other hand appear to exhibit carbonyl frequencies at lower values (25). This compound could have been formed by reaction of the dithiolone with a nitrene (or precursor) on the 1-sulfur atom, as for the thione **2***c*, followed by intramolecular nucleophilic attack by nitrogen, then extrusion of sulfur. Why this is different from the thione **2***c* is unknown, but could be explained by different sites of the attack, attack of nitrogen at the 5-carbon atom in the case of the thione and at 3-carbon atom in the case of the dithiolone, possibly because of different ease of formation of sp^3 hybridized intermediates at the 3-carbon atom. This method could be a useful synthesis of certain *N*-carbethoxyisothiazoles and of isothiazoles themselves.

Experimental

Chromatography was performed on 1 mm thick 'Camag' silica gel type D.S.F.5 supplied by Terochem Laboratories. Development of plates was performed, unless otherwise stated, in benzene. The ir spectra were obtained on a Perkin-Elmer model 337 spectrophotometer, and nmr spectra, unless otherwise stated, on a Varian model 56/60A spectrometer in deuteriochloroform using tetramethylsilane as an internal standard. The ^{13}C nmr spectra were obtained on a Varian Associates XL-100-15 machine with tetramethylsilane as the internal standard. Mass spectra were obtained on a Finnegan 1015 quadrupole mass spectrometer and melting points were obtained on a pre-calibrated 'Thermopan' apparatus. Microanalyses were performed by Chemalytics Inc. Tempe, Arizona.

Reaction of Ethyl Azidoformate with Heterocyclic Thiones

General procedure. The thiones under study (1 mmol) in refluxing carbon tetrachloride (20 ml) under nitrogen were treated with an excess (~0.5 ml) of ethyl azidoformate. After 24 h a further 0.5 ml was added, and reflux maintained. Usually reaction completion was evident after 48 h by the disappearance of the dark color of the starting thione. Solutions were evaporated directly and the products either purified by recrystallization, or by chromatography. The results are summarized in Table 1.

Reaction of 4-Phenyl-1,2-dithiole-3-thione with Ethyl Azidoformate

The reaction was performed as above, and chromatography using benzene–chloroform (10:1) as an eluent gave two products. In order of elution these were ethyl 5-phenyl-6-thio-1,2,3-dithiazine-3-carboxylate (**7**) (57%) and ethyl(4-phenyl-3-thio-1,2-dithiol-5-yl)carbamate (**2***h*) (10%). The products were further purified by recrystallization from benzene – petroleum ether (1:1), (57%) mp 195 °C and (10%) mp 131–132 °C respectively.

Compound **7**. *Anal.* calcd. for $C_{12}H_{11}S_3NO_2$: C 48.48, H 3.70, N 4.71, S 32.32; found: C 48.18, H 3.38, N 4.58, S 32.21. The nmr spectrum, δ 8.67, 6.71 (3H t, 2H q, ethyl protons), 3.75 (1H s, hetero ring proton), 2.56 (5H s, aromatic protons). Mass spectrum calcd.: 297; found: M^+ 297.

Compound **2***h*. *Anal.* calcd. for $C_{12}H_{11}S_3NO_2$: C 48.48, H 3.70, N 4.71, S 32.32; found: C 48.26, H 3.69, N 4.75, S 32.06. The nmr spectrum, δ 8.68, 6.68 (3H t, 2H q, ethyl protons), 2.75–2.19 (6H bands, aromatic and NH protons). Mass spectrum, calcd.: 297; found: M^+ 297.

Compound **7**. ^{13}C nmr δ 185.0 (s, C=S), 165.6 (s, ester C=O), 135.0 (s, C—5), 132.1 (s, phenyl C-1), 130.9–128.3 (m, C-4 and other aromatic carbons), 63.2 (t, CH_2), 14.3 (q, CH_3). Compound **2***h*. ^{13}C nmr δ 208.6 (s, C=S), 163.2 (s, ester C=O), 152.9 (s, C-5), 132.7 (s, C-4), 131.2–128.5 (m, aromatic carbons), 64.0 (t, CH_2), and 14.2 (q, CH_3).

Acid Catalyzed Rearrangement of Ethyl 5-Phenyl-6-thio-1,2,3-dithiazine-3-carboxylate (7) to Ethyl(4-phenyl-3-thio-1,2-dithiol-5-yl)carbamate (2h)

The dithiazine (14.85 mg, 0.05 mmol) and 20% hydrochloric acid (5 ml) were refluxed for 7h. The suspension was cooled and the precipitate collected. It was identical (mixture mp, ir, and R_f) to ethyl(4-phenyl-3-thio-1,2-dithiol-5-yl) carbamate (**2***h*) (90%).

Can. J. Chem. Downloaded from www.nrcresearchpress.com by 210.87.254.40 on 09/05/12
For personal use only.

TABLE 1. Reaction of heterocyclic thiones with ethyl azidoformate

Thione	Reference	Product	Yield (%)	Melting point (°C)	Formula	Analysis (%) Calculated C	H	N	S	Found C	H	N	S
1*a*	26	**1***d*	57	93–95	$C_{20}H_{17}NO_2S$	71.64	5.07	4.18	9.55	71.88	5.26	4.05	9.32
1*b*	27	**1***e*	21	116–118	$C_{20}H_{17}NO_2S$	71.64	5.07	4.18	9.55	71.32	4.93	4.06	9.29
1*c*	28	**1***f*	31	131–133	$C_{16}H_{13}NO_2S$	67.84	4.59	4.95	11.31	67.61	4.44	4.83	11.09
2*a*	29	**2***e*	61	108–109	$C_{12}H_{11}NO_2S_2$	54.34	4.15	5.28	24.15	54.64	4.19	5.14	24.46
2*b*	30	**2***f*	56	173–176	$C_{18}H_{15}NO_2S_2$	63.34	4.40	4.11	18.77	63.38	4.56	4.03	18.60
2*c*	31	See experimental											
2*d*	32	**2***g*	34	150–151	$C_{13}H_{13}NO_3S_2$	52.88	4.41	4.74	21.69	52.98	4.35	4.83	22.07
3*a*	33	**3***d*	41	122–124	$C_{12}H_{11}NO_2S_2$	54.34	4.15	5.28	24.15	54.47	4.05	5.68	24.65
3*b*	34	**3***e*	55	108–109	$C_{11}H_{11}NO_2S_2$	52.17	4.35	5.53	25.30	52.11	4.31	5.41	25.22
3*c*	*	**3***f*	68	127–128	$C_{18}H_{15}NO_2S_2$	63.34	4.40	4.11	18.77	63.22	4.49	4.17	18.61
4*a*	35	**4***b*	43	129–131	$C_{18}H_{16}N_2O_2S$	66.67	4.94	8.64	9.88	63.43	4.91	8.68	9.99
5*a*	36	**5***b*	68	152–154	$C_{12}H_{12}N_2O_2S_3$	51.43	4.29	10.00	22.86	51.29	4.20	9.72	22.56

*D. M. McKinnon, unpublished results.

Hydrolysis of Ethyl 3,5-Diphenylthiopyran-2-imino-carboxylate (1d) to 3,5-Diphenylthiopyran-2-one

The ester (102 mg, 0.3 mmol) was refluxed with 20% hydrochloric acid for 5 h. Cooling and filtering afforded a yellow precipitate which was identical (mixture mp and ir) to 3,6-diphenylthiopyran-2-one (72%) (26).

Reaction of 4-Phenyl-1,2-dithiole-3-one (2i) with Ethyl Azidoformate

The reaction was performed as with the thiones Evaporation afforded an oily solid which was collected by filtration and recrystallized from toluene as colorless prisms mp 196 °C (sublimes above 150 °C) (61%). *Anal.* calcd. for $C_{12}H_{11}NO_3S$: C 57.45, H 4.41, N 5.61, S 12.86; found: C 57.47, H 4.09, N 5.39, S 13.01. The nmr spectrum, δ 8.58, 5.50 (3H t, 2H q, ethyl protons), 2.74–2.51 and 2.29–2.08 (5H bands, aromatic protons), 1.74 (1H s, heterocyclic proton). The ir spectrum 1663 and 1760 cm^{-1}, the urethane and heterocyclic C=O stretch respectively. Mass spectrum, calcd.: 249; found: M^+ 249.

Acknowledgments

We are very grateful to Dr. I. W. J. Still for the provision of ^{13}C nmr spectra, and to the National Research Council of Canada for financial support. We also wish to thank Mr. W. Buchannon and Mr. D. Buksak for preparation of spectra.

1. W. Lwowski. Nitrenes. J. Wiley Interscience, New York. 1970.
2. S. Patai. The chemistry of the azido group. J. Wiley Interscience. New York. 1971.
3. J. Sauer and K. K. Mayer. Tetrahedron Lett. 319 (1968).
4. E. Lieber, C. B. Lawyer, and J. P. Trivedi. J. Org. Chem. **26**, 1644 (1951).
5. P. A. S. Smith and D. H. Kenny. J. Org. Chem. **26**, 5221 (1961).
6. E. Lieber, E. Oftedahl, and C. N. R. Rao. J. Org. Chem. **28**, 194 (1963).
7. J. C. Kauer and W. A. H. Sheppard. J. Org. Chem. **32**, 3580 (1967).
8. W. Kirmse. Chem. Ber. **93**, 2353 (1960).
9. A. Queen, A. Bell, and D. M. McKinnon. Can. J. Chem. **48**, 1340 (1970).
10. A. Schönberg and W. Urban. J. Chem. Soc. 530 (1935).
11. W. Borsche. Chem. Ber. **75**, 1312 (1942).
12. K. A. Jensen and C. Pedersen. Adv. Heterocycl. Chem. **3**, 263 (1964).
13. M. Ahmed, J. M. Buchshriber, and D. M. McKinnon. Can. J. Chem. **48**, 1340 (1970).
14. H. Behringer and D. Bender. Chem. Ber. **100**, 4027 (1967).
15. I. Iwataki and A. Ueda. Bull. Chem. Soc. Jpn. **45**, 3220 (1972).
16. M. Sander. Chem. Rev. **66**, 297 (1966).
17. E. B. Knott. J. Chem. Soc. 916 (1955).
18. N. Plavac, I. W. J. Still, M. S. Chauhan, and D. M. McKinnon. Can. J. Chem. **53**, 836 (1975).
19. (*a*) N. Losac'h and J. Vialle. The chemistry of the 1,2-dithiole ring. *In* The chemistry of organic sulfur compounds. Vol. 2. *Edited by* N. Kharasch and C. Y. Meyers. Pergamon Press, London. 1966; (*b*) R. Zahradnik and J. Koutecky. Tetrahedron Lett. 632 (1961).
20. P. A. S. Smith and J. H. Boyer. J. Am. Chem. Soc. **73**, 2626 (1951).
21. K. Hafner and W. Kaiser. Tetrahedron Lett. 2185 (1964).
22. R. A. Abramovitch, C. I. Azogu, and I. T. McMaster. J. Am. Chem. Soc. **91**, 1219 (1969).
23. Aldrich Catalogue of I.R. Spectra.
24. W. D. Crow and N. J. Leonard. Tetrahedron Lett. 1477 (1964).
25. L. Legrand and N. Losac'h. Bull. Soc. Chim. Fr. 1170 (1969); 1173 (1969).
26. G. Laban and R. Mayer. Z. Chem. **7**, 227 (1967).
27. D. Leaver, D. M. McKinnon, and W. A. H. Robertson. J. Chem. Soc. 32 (1965).
28. J. L. Charlton, S. M. Loosmore, and D. M. McKinnon. Can. J. Chem. **52**, 3021 (1974).
29. E. Klingsberg and A. Schreiber. J. Am. Chem. Soc. **83**, 2934 (1961).
30. M. G. Voronkov, A. S. Brown, and G. B. Karpenko. J. Gen. Chem. U.S.S.R. Engl. Transl. **19**, 395 (1949).
31. E. K. Fields. J. Am. Chem. Soc. **77**, 4255 (1955).
32. B. Bottcher and A. Luttringhaus. Justus Liebigs Ann. Chem. **557**, 89 (1947).
33. D. Leaver, W. A. H. Robertson, and D. M. McKinnon. J. Chem. Soc. 5104 (1962).
34. I. L. Soder and R. Wizinger. Helv. Chim. Acta, **42**, 1733 (1959).
35. G. E. Bachers, D. M. McKinnon, and J. M. Buchshriber. Can. J. Chem. **50**, 2568 (1972).
36. J. W. MacDonald and D. M. McKinnon. Can. J. Chem **45**, 1225 (1967).

Can. J. Chem. Downloaded from www.nrcresearchpress.com by 210.87.254.40 on 09/05/12
For personal use only.

Water-soluble lysine-containing polypeptides. III. Sequential lysine-glycine polypeptides. A circular dichroism and electron microscopy study of annealed complexes with DNA, sonicated DNA, and denatured DNA[1]

SANDRA L. KIELLAND AND ROSS E. WILLIAMS[2]

Division of Biological Sciences, National Research Council of Canada, Ottawa, Ont., Canada K1A 0R6

Received June 29, 1976

SANDRA L. KIELLAND and ROSS E. WILLIAMS. Can. J. Chem. **54**, 3884 (1976).

Circular dichroic spectra, turbidity measurements, and electron micrographs have been taken of annealled complexes of native, sonicated, and denatured DNA's in association with several sequential lysine-glycine copolypeptides. The results indicate that: (*1*) the molecular weight and strandedness of the DNA influences not only the assymmetric organization of the DNA in the complexes but also the size and shape of the complexes formed; (*2*) the hydrophobic nature (or sequence) of the polypeptide influences the shape of the complexes formed.

SANDRA L. KIELLAND et ROSS E. WILLIAMS. Can. J. Chem. **54**, 3884 (1976).

Des spectres du dichroïsme circulaire, des mesures de turbidité ansi que des micrographies éléctroniques de complexes entre l'ADN (naturel, traité aux ultrasons et dénaturé) et quelques polypeptides lysine-glycine de séquence régulière ont été pris. Les résultats montrent que: (*1*) la présence de deux chaînes associées dans la molécule de l'ADN ainsi que le poids moléculaire de celle-ci influence non seulement l'organisation asymétrique de l'ADN dans les complexes mais aussi la grandeur et la forme de ces derniers; (*2*) la forme des complexes dépend de la nature hydrophobique (ou séquence) du polypeptide.

Introduction

The interactions of proteins and nucleic acids play important roles in maintaining the integrity of cellular structures such as ribosomes, and nucleoprotein complexes such as chromatin and viruses. An understanding of the factors controlling the formation of complexes between the two components can be derived by using material derived from two different sources: (*a*) the intact or native systems, *i.e.* systems isolated from natural sources; (*b*) model systems, *i.e.* systems synthesized to not only mimic, but also simplify the molecules found in nature. In this laboratory the latter approach has been used to investigate factors controlling the interactions between positively-charged lysine-containing polypeptides and deoxyribonucleic acid (DNA). The interaction of calf thymus DNA with several lysine(LYS)-glycine(GLY) copolypeptides has been investigated (1). The polypeptide model systems have the following structures:

1 (LYS)*n* poly-(-L-lysine)
2 (LYSGLY)*n* poly-(-L-lysylglycine)
3 (LYSGLYGLY)*n* poly-(-L-lysylglycylglycine)
4 (GLYLYSGLYGLY)*n* poly-(-glycyl-L-lysylglycylglycine)

where *n* is approximately 50.

From the results of a circular dichroic (cd) study of the polypeptide–DNA complexes formed by annealing the components from high salt concentrations it has been suggested that polypeptide conformational flexibility, hydrophobicity, and sequence all seem to play a role in the generation of changes observed in the cd spectrum of DNA (1).

In the present study the effect of changes in the double-stranded nature of the DNA and molecular size of the DNA have been investigated. Circular dichroic spectroscopy has been used to investigate the state of DNA in the solutions containing the anneal complexes. Electron micrographs (em's) of the fixed, dehydrated, and stained complexes have also been used to investigate the appearance of the aggregates formed.

Experimental

Reagent-grade chemicals and cacodylic acid (dimethylarsenate) for buffer preparation were obtained from commercial sources and were used as received. All water used was deionized and distilled from glass. Dialysis tubing with a 3500 molecular weight cutoff (Spectropor 3)

[1]NRCC No. 15512.
[2]Author to whom correspondence should be addressed.

Can. J. Chem. Downloaded from www.nrcresearchpress.com by 210.87.254.40 on 09/05/12
For personal use only.

Can. J. Chem. Downloaded from www.nrcresearchpress.com by 210.87.254.40 on 09/05/12
For personal use only.

was obtained from Science Essentials, Anaheim, California, U.S.A. and treated before use as directed (sodium sulfide and dilute sulfuric acid treatments) (1). Polypeptides were prepared and characterized as previously described (2). Polypeptide stock solutions (approximately 4×10^{-3} *M* lysine) were prepared in sodium cacodylate buffer (0.01 *M*, p*H* 7.0) and analyzed as previously described (2). Highly-polymerized calf thymus DNA (Worthington Biochemicals, Freehold, N.J.) was treated as previously described (3). DNA stock solutions (approximately 3×10^{-3} *M* phosphate) were prepared in sodium cacodylate buffer (0.01 *M*, p*H* 7.0) and analyzed as previously described (2). Sonicated DNA stock solutions (approximately 3×10^{-3} *M* phosphate) were prepared by sonicating a sample (5 ml) of the DNA stock solution at ice temperature for given periods of time (10–80 s) with a Branson Sonifier model W-185, operating at 70 W and equipped with a microtip probe. Heat-denatured DNA stock solutions (approximately 3×10^{-3} *M* phosphate) were prepared by heating a sample (5 ml) of the DNA stock solution in a boiling water bath for 5 min then quickly quenching the sample in an ice bath.

Complexes between the polypeptides and the various DNA samples were prepared in 0.15 *M* NaCl, sodium cacodylate, 0.001 *M*, p*H* 7.0 by back dialysis of the components from aqueous 1.5 *M* NaCl as previously described (1, 4, 5).

Circular dichroic spectra were taken on a Cary–Varian spectropolarimeter, model 61 and the data was treated as previously described (1). Ultraviolet and visible absorption spectra were taken on a Cary–Varian spectrophotometer, model 14, as previously described (1). Sample turbidities were expressed as $dA^{400} = A_{com}{}^{400} - A_0{}^{400}$, where $A_{com}{}^{400}$ is the absorbance at 400 nm of the complexed DNA solution and $A_0{}^{400}$ is the absorbance at 400 nm of the equivalent uncomplexed DNA solution. Electron micrographs were taken at a magnification of 5000× on a Siemens Elmiskop, model 101 (70 kV), using Kodak Electron Image Plates. The plates were processed in Kodak D-19 developer. Samples for electron microscopy were prepared as follows: An aliquot (100 μl) of the solution containing the annealed complex was fixed by addition of aqueous formaldehyde (37%) (2.5 μl). After 1 min, an aliquot (20 μl) of the fixed solution was placed on a carbon and formvar coated copper grid (200 mesh, PolySciences Inc., Warrington, Pennsylvania, U.S.A.) which was sitting on a piece of paraffin film (Parafilm, Fisher Scientific, Ottawa, Canada). The sample was dried down onto the grid at room temperature (20–25 °C) in air (relative humidity less than 60%) or in a desiccator containing calcium chloride (20 mesh). After drying (24 h) the grids were stained with an aqueous uranyl acetate solution (1% w/v, p*H* 5.6 adjusted with aqueous NH_4OH) (30 s treatment), rinsed with distilled water, dried again, and examined.

Results and Discussion

Poly-(-L-lysine) (**1**) has been extensively used as a model of the protein component of model systems which have been designed to study protein – nucleic acid interactions (see refs cited in ref. 1). When poly-(-L-lysine) – calf thymus DNA complexes are formed by annealing the two components from solutions containing high salt concentrations, where no interaction between components is observed, to physiological salt concentrations (0.15 *M* sodium chloride) where interaction is maximized, a cd spectrum of DNA different from that observed in uncomplexed DNA results (1, 5) (Fig. 1). The resulting spectra in the complexed state is unlike any of the spectra generated by the usual conformational states of DNA, *i.e.* the A, B, or C conformational states (6, 7). This characteristic cd spectrum is also produced when DNA is dissolved in water soluble organic polymers, such as polyethylene oxide (PEO) (8–14). It is also found in dehydrated films of DNA (15), in complexes of DNA with several random and sequential lysine-containing polypeptides (16–22), and in complexes of histone H-1 (F-1) with DNA (23–26). This characteristic cd spectrum has been said to be produced by ψ-state DNA (8). Several explanations of the way it is produced have been offered. They are: (*1*) polypeptide promoted solvent exclusion from the DNA; (*2*) polypeptide promoted induction of long-range order in the DNA; (*3*) polypeptide promoted increases in the helix–helix interactions of the DNA brought on by aggregation of the DNA; (*4*) polypeptide promoted increases in the production of a liquid crystalline state in the complexes (14, 23).

In order to extend our previous investigations using the sequential lysine-containing polypeptides **1–4** (1), we have carried out a series of experiments aimed at determining the role played by DNA molecular size and strandedness in the formation of the ψ-state DNA spectrum. Annealed complexes were prepared between the polypeptides **1–4** and calf-thymus DNA, sonicated calf-thymus DNA, and heat-denatured DNA. Circular dichroic spectra and turbidity measurements were made on the solutions of the complexes and em's were taken of the fixed, dehydrated, and stained complexes.

Circular Dichroic Spectra

Circular dichroic spectra were taken of the solutions of the annealed complexes in order to monitor the production of the ψ-state DNA. As noted previously, the incorporation of DNA into the complexes led to the production of a ψ-type

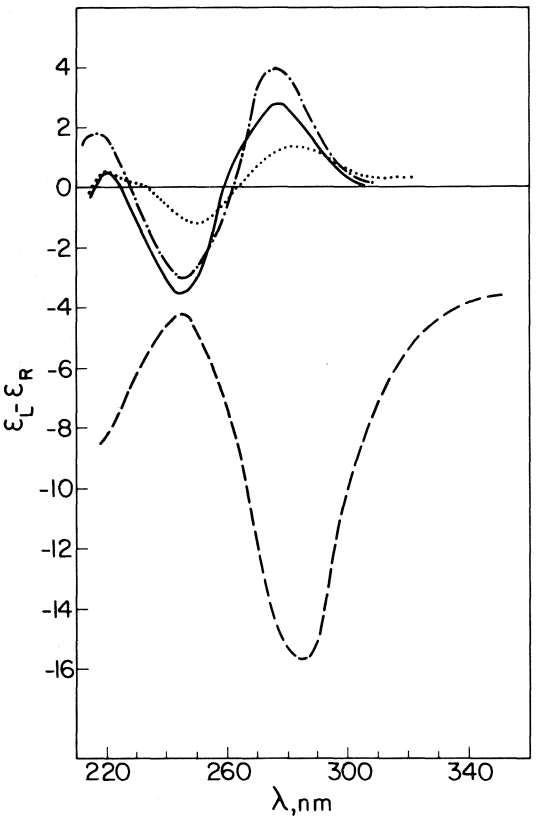

FIG. 1. Circular dichroic spectra of poly-L-lysine – DNA complexes: (—) native calf thymus DNA; (-·-·-) denatured calf thymus DNA; (----) poly-(-L-lysine) – native calf thymus DNA complex, lysine – DNA phosphate ratio, 0.50; (···) poly-(-L-lysine) – denatured calf thymus DNA complex, lysine – DNA phosphate ratio, 0.50. Experimental conditions: DNA-phosphate concentration, 1.70×10^{-4} *M*; sodium chloride, 0.15 *M*, sodium cacodylate, 0.0010 *M*, p*H* 7.0.

DNA spectrum (Fig. 1) (1). Monitoring the ellipticity ($E_L - E_R$) at 275 nm *vs.* the lysine – DNA phosphate (L/P) ratio (Fig. 2) showed that: (*1*) a maximum in the change of ellipticity occurred around an L/P ratio of 0.5–0.6 for poly-(-L-lysine) (**1**) whereas this maximum occurred around an L/P ratio of 1.2–1.5 with the other lysine-glycine copolymers (**2**–**4**); (*2*) the distortion to the DNA spectrum was less with poly-(-L-lysylglycine) (**2**) than any of the other polymers. These two observations were assumed to indicate that polypeptide conformational flexibility and either polypeptide sequence or hydrophobicity were important factors in controlling the polypeptide – nucleic acid interactions (1).

The effect of molecular size on both these factors was investigated by sonicating the DNA, a process known to reduce the molecular weight of the DNA (27). The formation of annealed complexes between poly-(-L-lysine) and calf thymus DNA which had been sonicated for various times showed that a maximum change in the distortion of the DNA cd spectrum was elicited when the DNA had been sonicated for 40 s at ice temperature.[3] A similar observation has been made on solutions of polyethylene oxide and DNA which had been sonicated for various times (14).

When annealed complexes were formed between the polypeptides **1**–**4** and a DNA sample which had been sonicated for 40 s, the characteristic ψ-type DNA cd spectrum was formed in all cases. Plotting the ellipticity, ($E_L - E_R$), at 275 nm *vs.* the L/P ratio (Fig. 3) gave very similar results to those observed with the unsonicated DNA sample (Fig. 2). That is, the maximum in the change of ellipticity at 275 nm occurred at the same L/P ratios and the unique behaviour of complexes incorporating poly-(-L-lysylglycine) (**2**) was preserved. The major difference between the complexes incorporating unsonicated DNA and sonicated DNA occurred in the magnitudes of the ellipticity at 275 nm. Although no appreciable difference was noted between the cd spectra of the uncomplexed DNA's, their incorporation into the annealed complexes led to an ellipticity decrease from -12.5 to -47.5 when unsonicated DNA was replaced by sonicated DNA in the annealed complexes with poly-(-L-lysine) (L/P approximately 0.5). These results, along with those obtained using DNA's sonicated for different times, show that lowering the molecular weight of the DNA leads to the formation of a greater degree of asymmetry in the complex and that a point can be reached beyond which further sonication or lowering of the molecular weight results in the generation of less order in the system. These results are very similar to those obtained with polyethylene oxide solutions of DNA (14) and with histone H-1, DNA complexes (25).

Heat-denaturation of either the sonicated or unsonicated DNA sample and incorporation

[3]S. Kielland, unpublished results. Equilibrium sedimentation of DNA which had been sonicated for 40 s indicated that the mw had been reduced from $>2 \times 10^6$ to approximately 0.5×10^6.

Can. J. Chem. Downloaded from www.nrcresearchpress.com by 210.87.254.40 on 09/05/12
For personal use only.

Can. J. Chem. Downloaded from www.nrcresearchpress.com by 210.87.254.40 on 09/05/12
For personal use only.

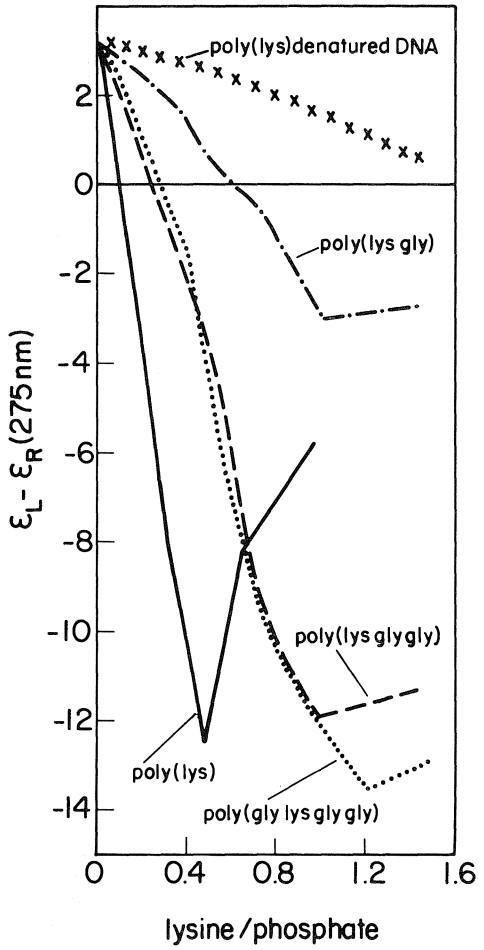

FIG. 2. Variation of the molar ellipticity ($E_L - E_R$) at 275 nm with the lysine/DNA phosphate ratio in complexes between the lysine and lysine/glycine polypeptides and native calf thymus DNA and between poly-(L-lysine) and denatured, native DNA (×××). No corrections for sample turbidity have been made. Experimental conditions: DNA-phosphate concentration, 1.70×10^{-4} *M*; sodium chloride, 0.15 *M*; sodium cacodylate, 0.0010 *M*, p*H* 7.0.

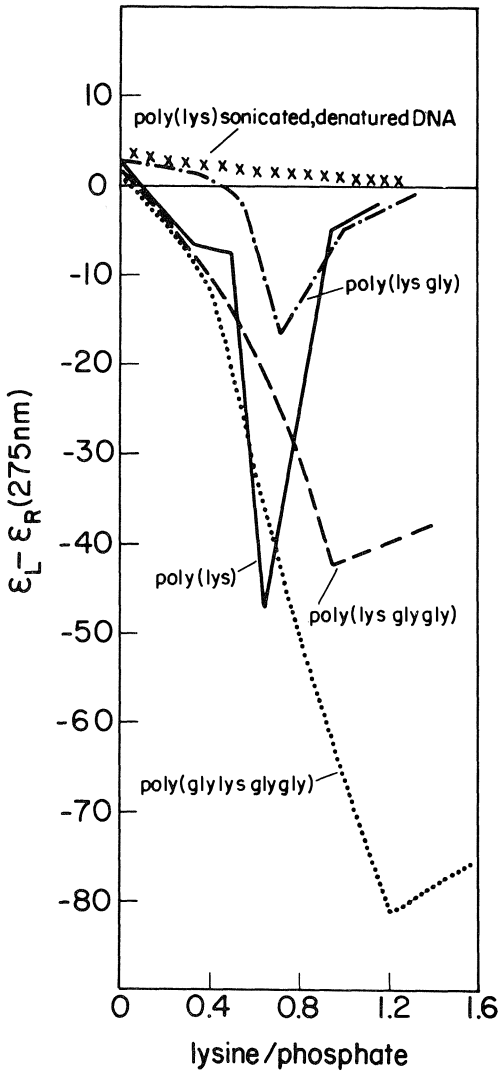

FIG. 3. Variation of the molar ellipticity ($E_L - E_R$) at 275 nm with the lysine/DNA phosphate ratio in complexes between the lysine and lysine/glycine polypeptides and sonicated calf thymus DNA (40 s sonicate). No corrections for sample turbidity have been made. Experimental conditions: as for Fig. 2.

into annealed complexes with poly-(-L-lysine) (**1**) and the other lysine-glycine copolymers (**2–4**) led to only minor changes being observed in the cd spectra (Fig. 1). Thus, only relatively minor changes in the ellipticity at 275 nm occurred regardless of the L/P ratio (Fig. 2). The presence of double stranded character in the DNA then, must be a prerequisite for the production of the characteristic ψ-type DNA cd spectrum in annealed complexes of the polypeptides **1–4** and DNA. This was also previously observed by Evdokimov *et al.* in solutions of polyethylene glycol and DNA (11).

Solution Turbidity Measurements

The development of the characteristic ψ-type DNA cd spectrum was accompanied by increasing solution turbidity. Solution turbidity, as monitored by changes in the visible spectrum absorption at 400 nm, increased as the L/P ratio increased (Fig. 4). Little difference between complexes containing unsonicated or sonicated

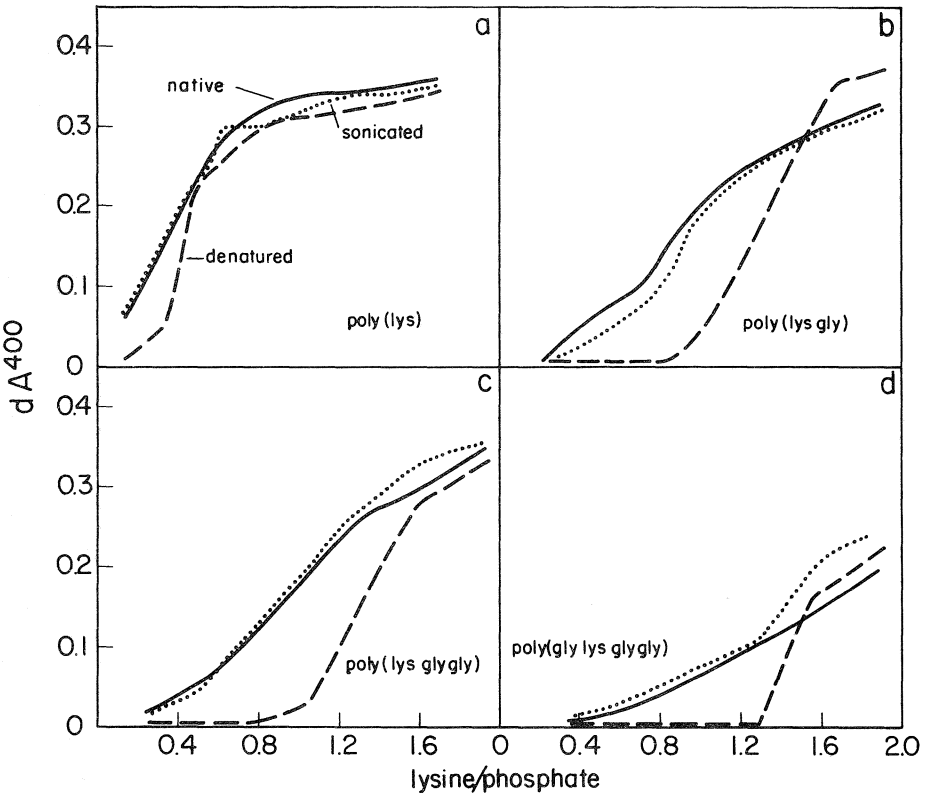

FIG. 4. Variation of the sample turbidity, dA^{400}, with lysine/DNA phosphate ratio in complexes between the lysine and lysine/glycine polypeptides and the various samples of calf thymus DNA: (*a*) poly-(-L-lysine) complexes (—) native DNA; (···) sonicated DNA; (---) denatured DNA: (*b*) poly-(-L-lysylglycine) complexes; curve designations as in *a*: (*c*) poly-(-L-lysylglycylglycine) complexes; curve designations as in *a*: (*d*) poly-(-glycyl-L-lysylglycylglycine) complexes; curve designations as in *a*. Experimental conditions: as for Fig. 2.

DNA was noted. In both, the turbidity increased towards a maximum at higher L/P ratios. The approach to a maximum in turbidity was found to parallel the onset of the distorted ψ-type DNA cd spectrum. For example, the approach to a maximum in turbidity of complexes of poly-(-L-lysine) (**1**) and double-stranded DNA, either unsonicated or sonicated, paralleled the increase in L/P ratio and the production of the characteristic ψ-type DNA cd spectrum (compare Figs. 2, 3, and 4). It may also be noted that, at an L/P ratio of 1.0, the amount of turbidity, as measured by dA^{400}, fell from 0.33 to 0.07 as the polypeptide was changed from poly-(-L-lysine) (**1**) to poly-(-glycyl-L-lysylglycylglycine) (**3**). This would seem to indicate that a change in the size or shape of the complexes was occurring.

Complexes incorporating heat-denatured DNA also showed a similar trend in increasing solution turbidity as the L/P ratio increased. Some differences in turbidity between complexes with the normal DNA and the denatured DNA were noted. For example no change in the solution turbidity of complexes containing heat-denatured DNA and the lysine-glycine copolymers (**2**–**4**) occurred until an L/P ratio above 0.8 was reached. From these results and the ones obtained with double-stranded DNA it would seem that the formation of solution turbidity or, perhaps, aggregation is not sufficient in itself to induce formation of the ψ-type DNA. The increases in turbidity or aggregation must also be accompanied by the presence of double-stranded character in the DNA.

Can. J. Chem. Downloaded from www.nrcresearchpress.com by 210.87.254.40 on 09/05/12
For personal use only.

Can. J. Chem. Downloaded from www.nrcresearchpress.com by 210.87.254.40 on 09/05/12
For personal use only.

Electron Microscopy

Electron micrographs (em's) were taken of the complexes so that changes occurring in the size, shape and degree of intermolecular aggregation in the complexes might be examined. A direct correlation between observations made on complexes in solution and those made on complexes in a formaldehyde-fixed, dehydrated, and uranyl acetate stained state are at best tenuous. However, if the methods of forming, fixing, dehydrating, and staining remain constant throughout the experiments, then changes in the size, shape, and degree of intermolecular aggregation should reflect only those changes made in each of the components of the complexes being examined. Thus, changes in the structure of the polypeptide or the structure of the DNA should be reflected in changes observed in the em's.

A check of the effect of adding formaldehyde to the solution of the complexes was made. Only small changes ($<10\%$) in the cd spectrum ellipticity at 275 nm were noted. This is unlike the observations made on chromation in solution (28).

The em's of native calf thymus DNA presented a uniformly stained background (Fig. 5, section *10*) with no outstanding features at the magnification used (5000×). Electron micrographs of the polypeptide – native DNA complexes had clumps of heavily stained material in them. Their appearance depended not only on the polypeptide used to make the complex but also on the L/P ratio in the complex. Complexes between DNA and poly-(-L-lysine) at a low L/P ratio (Fig. 5, section *11*) appeared to consist of a series of circular structures 2500–5000 Å in diameter which had been joined together to form a series of branched, filamentous chains. The presence of circular structures was even more evident in the em's of the low L/P ratio complexes formed between the lysine-glycine copolypeptides and the DNA (Fig. 5, sections *21*, *31*, *41*). From these results it would seem that as the mole fraction of glycine increased in the polymers or, alternately, as the charge separation increased, the degree of intermolecular aggregation fell while the size and shape of the complexes remained constant. It should also be noted that, at these low L/P ratios, a distinct shift in the degree of intermolecular aggregation occurred upon changing the poly-(-L-lysine) (**1**) in the complex to poly-(-L-lysylglycine) (**2**). This shift may be connected with difference in the conformational flexibility of the polymers. This explanation would be much the same as used to explain the cd results (see above, (1)).

At higher L/P ratios (Fig. 5, sections *12*, *22*, *32*, *42*) all complexes appeared to be very highly aggregated although the complexes containing the lysine-glycine polypeptides **2**–**4** appeared somewhat less condensed.

Employing sonicated calf thymus DNA (40 s sonicate) in place of the native DNA in the formation of the complexes resulted in distinct changes in the size and state of intermolecular aggregation being noted (Fig. 6). Little or no observable difference between the fixed, dehydrated, and stained samples of the uncomplexed DNA's was noted (compare Fig. 5, section *10* and Fig. 6, section *10*). At low L/P ratios the complexes of poly-(-L-lysine) and the sonicated DNA appeared to be less filamentous and more compact than those in which native DNA was used (compare Fig. 5, section *11* and Fig. 6, section *11*). In addition, the complexes incorporating sonicated DNA, little or no evidence of the formation of circular structures was present. In complexes of the lysine-glycine copolypeptides **2**–**4**, on the other hand, unaggregated, circular structures were again observed (Fig. 6, sections *21*, *31*, *41*). The size of the circular structures had also doubled (average diameter, 5000–10 000 Å). At higher L/P ratios (Fig. 6, sections *12*, *22*, *32*, *42*) the complexes changed from ones which were highly aggregated, *i.e.* poly-(-L-lysine) complexes (Fig. 6, section *12*) to ones which were much less aggregated, *i.e.* poly-(-glycyl-L-lysylglycylglycine) (Fig. 6, section *42*), although the latter appeared joined by thin threads of stained material about 100–200 Å wide. The distinct difference between the highly aggregated poly-(-L-lysine) complexes (Fig. 6, section *12*) and the less aggregated complexes of the lysine-glycine copolypeptides (Fig. 6, sections *22*, *32*, *42*) was even more evident.

Denaturing the native calf thymus DNA resulted in em's with little or no observable difference between it and the native, or sonicated native DNA (compare Fig. 7, section *10* and Figs. 5/6, sections *10*). Incorporating the denatured DNA into low L/P ratio complexes with the various polypeptides resulted in the formation of large aggregates with no distinctive form. The circular structures, evident when

Can. J. Chem. Downloaded from www.nrcresearchpress.com by 210.87.254.40 on 09/05/12
For personal use only.

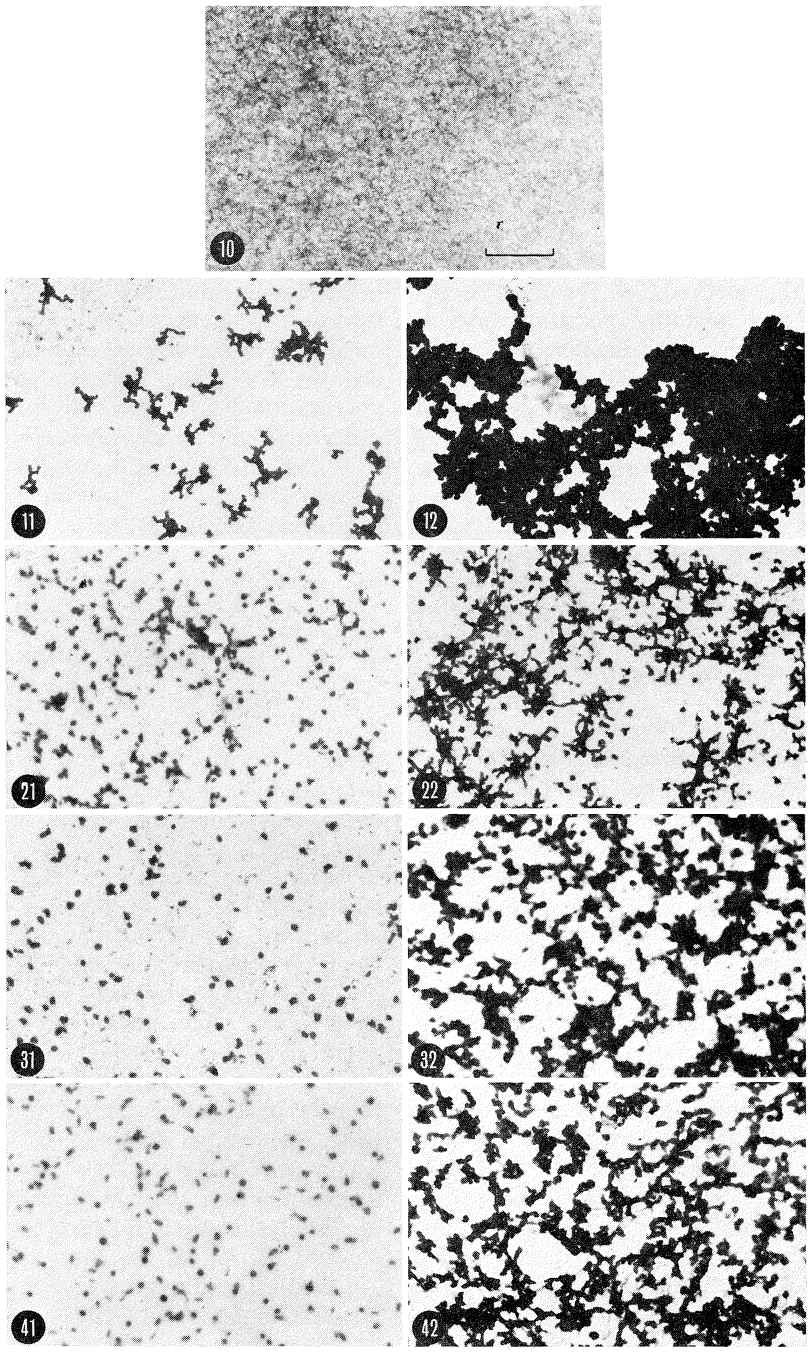

FIG. 5. Electron micrographs of formaldehyde-fixed, dehydrated, and stained DNA complexes: *10*, native DNA; *11*, poly-(-L-lysine)-native DNA; L/P = 0.32; *12*, poly-(-L-lysine)-native DNA, L/P = 0.97; *21*, poly-(-L-lysylglycine)-native DNA, L/P = 0.36; *22*, poly-(-L-lysylglycine)-native DNA, L/P = 1.08; *31*, poly-(-L-lysylglycylglycine)-native DNA, L/P = 0.49; *32*, poly-(-L-lysylglycylglycine)-native DNA, L/P = 0.98; *41*, poly-(-glycyl-L-lysylglycylglycine)-native DNA, L/P = 0.40; *42*, poly-(-glycyl-L-lysylglycylglycine)-native DNA, L/P = 1.20. Experimental conditions: DNA-phosphate concentration, approximately 1.70×10^{-4} *M*. Complexes were fixed before drying in 0.15 *M* sodium chloride, 0.001 *M* sodium cacodylate, ~1.0% formaldehyde. Complexes were stained with aqueous uranyl acetate. The bar indicates a distance of 3 micrometres (μm).

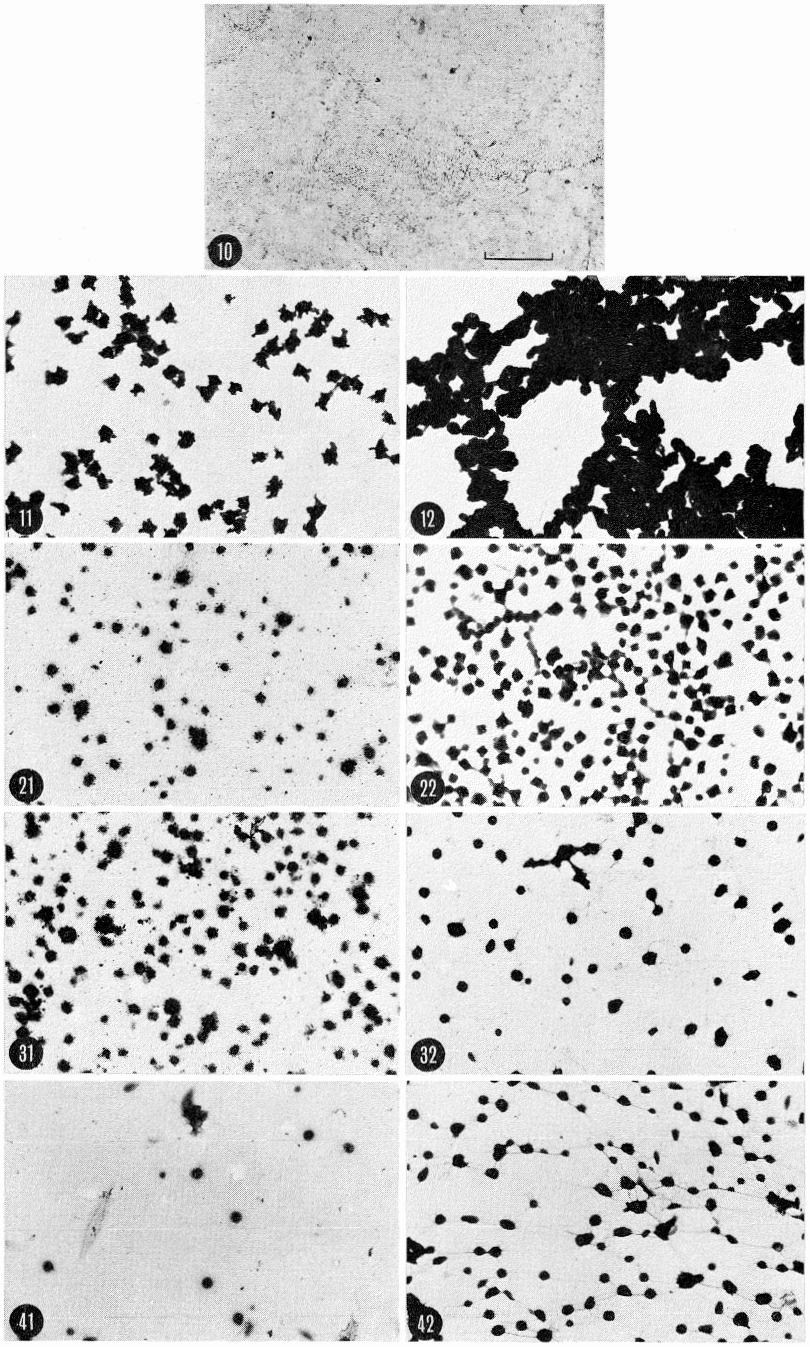

FIG. 6. Electron micrographs of formaldehyde-fixed dehydrated and stained polypeptide/sonicated DNA complexes: *10*, sonicated DNA; *11*, poly-(-L-lysine)-sonicated DNA, L/P = 0.32; *12*, poly-(-L-lysylglycine)-sonicated DNA, L/P = 0.97; *21*, poly-(-L-lysylglycine)-sonicated DNA, L/P = 0.36; *22*, poly-(-L-lysylglycine)-sonicated DNA, L/P = 1.08; *31*, poly-(-L-lysylglycylglycine)-sonicated DNA, L/P = 0.49; *32*, poly-(-L-lysylglycylglycine)-sonicated DNA, L/P = 0.98; *41*, poly-(-glycyl-L-lysylglycylglycine)-sonicated DNA, L/P = 0.40; *42*, poly-(-glycyl-L-lysylglycylglycine)-sonicated DNA, L/P = 1.20. Experimental conditions: as for Fig. 5.

Can. J. Chem. Downloaded from www.nrcresearchpress.com by 210.87.254.40 on 09/05/12
For personal use only.

Can. J. Chem. Downloaded from www.nrcresearchpress.com by 210.87.254.40 on 09/05/12
For personal use only.

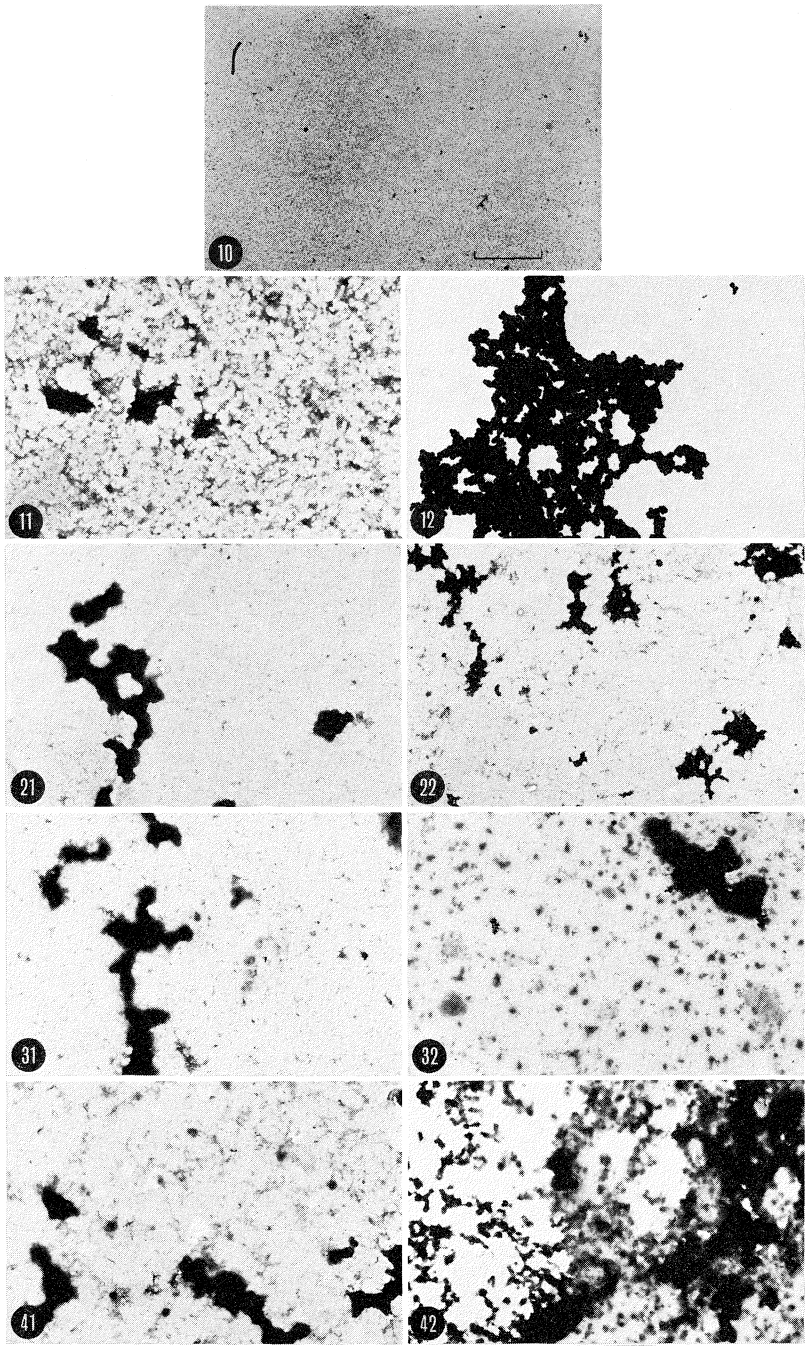

FIG. 7. Electron micrographs of formaldehyde-fixed dehydrated and stained polypeptide/denatured DNA complexes: *10*, denatured DNA; *11*, poly-(-L-lysine)-denatured DNA, L/P = 0.32; *12*, poly-(-L-lysine)-denatured DNA, L/P = 0.97; *21*, poly-(-L-lysylglycine)-denatured DNA, L/P = 0.36; *22*, poly-(-L-lysylglycine)-denatured DNA, L/P = 1.08; *31*, poly-(-L-lysylglycylglycine)-denatured DNA, L/P = 0.49; *32*, poly-(-L-lysylglycylglycine)-denatured DNA, L/P = 0.98; *41*, poly-(-glycyl-L-lysylglycylglycine)-denatured DNA, L/P = 0.40; *42*, poly-(glycyl-L-lysylglycylglycine)-denatured DNA, L/P = 1.20. Experimental conditions: as for Fig. 5.

Can. J. Chem. Downloaded from www.nrcresearchpress.com by 210.87.254.40 on 09/05/12
For personal use only.

double-stranded DNA was used to form the low L/P ratio complexes, were absent (Fig. 7, sections *11*, *21*, *31*, *41*). At higher L/P ratios a limited tendency towards the formation of circular structures was observed (Fig. 7, sections *12*, *22*, *32*, *42*). Only the complexes containing poly-(-L-lysine) and the denatured DNA appeared to be the same as those formed between poly-(-L-lysine) and the native DNA (Fig. 5, section *12*).

Conclusions

From the foregoing cd spectral results, it may be gleaned that the double-stranded character of native DNA is necessary for the production of the ψ-state DNA when complexes with lysine-containing polypeptides are made. The observation is similar to that obtained from X-ray analysis of DNA–poly-(-L-lysine) complexes (29). The cd spectral results also show that the previously suggested dependence of the ψ-state DNA on conformational flexibility and polypeptide hydrophobicity (or sequence) (1) is not substantially altered by changes in the molecular size of the DNA. It is also evident from the cd results that the molecular size of the DNA affects the magnitude of asymmetry introduced into the DNA. This observation is in line with the increase in the DNA cd spectrum obtained by solubilizing sonicated DNA in PEO solutions (14). In this latter case it was observed that a rise and fall occurred in the asymmetry induced in the DNA cd spectra as the concentration of PEO in solution increased. It was also suggested that the ψ-state DNA cd spectrum resulted from the formation of a liquid crystalline array of DNA helices and that some optimum length of the DNA helix might be required before a maximum in the formation of this liquid crystalline state could be achieved. Such seems to be the case with the various lysine-containing polypeptides studied here.

The em's of the various complexes seem to corroborate the facts that double-strandedness in the DNA and polypeptide conformational flexibility and hydrophobicity (sequence) both affect the way in which the complexes aggregate and that the molecular size of the DNA influences the size of the complexes formed. In the latter instance the inverse relationship between the molecular size of the DNA and the size of complexes might be a reflection of the necessity of some optimum DNA size requirement for the production of the ψ-state DNA.

The coincidence of the maximum production of the ψ-state cd spectrum, the production of large amounts of turbidity in the solution, and the concomitant production of the intermolecular aggregates in the em's suggest that the simplest explanations of solvent exclusion and/or induction of long-range order in the DNA as promotors of the production of the ψ-state in DNA do not, in themselves, seem to explain the observations (5). Thus the alternate explanations that aggregation and, thereby, an increase in the helix–helix interactions of the DNA and/or the production of a liquid crystalline state of DNA cause the production of the ψ-state DNA are left as the only reasonable alternatives for explaining the production of ψ-state DNA.

Finally, the above results and observations suggest that many factors may be important in the protein-initiated packaging of DNA into biological structures such as viral particles, and related nucleoprotein complexes such as ribosomes and chromosomes.

Acknowledgements

The authors would like to express their appreciation to Mr. Lee Sowden for taking the electron micrographs, to Mr. Robert Whitehead for preparing the photographs and to Dr. G. E. Willick for determining DNA molecular weights.

1. R. E. Williams and S. L. Kielland. Can. J. Chem. **53**, 542 (1975).
2. J. Brown, J. R. Langlois, D. R. Lauren, B. K. Stoochnoff, and R. E. Williams. Can. J. Chem. **52**, 3140 (1974).
3. R. E. Williams and V. L. Seligy. Can. J. Biochem. **52**, 281 (1974).
4. D. Carroll. Anal. Biochem. **44**, 496 (1971).
5. D. Carroll. Biochemistry, **11**, 421 (1972).
6. J. Brahms and S. Brahms. *In* Fine structure of proteins and nucleic acids. *Edited by* G. D. Fasman and S. N. Timasheff. M. Dekker, New York. 1970. p. 191.
7. J. Brahms. *In* Fundamental aspects and recent developments in optical rotatory dispersion and circular dichroism. *Edited by* F. Ciardelli and P. Salvadori. Heyden & Son, New York. 1973. p. 307.
8. L. S. Lerman. Proc. Natl. Acad. Sci. U.S.A. **68**, 1886 (1971).
9. C. F. Jordan, L. S. Lerman, and J. H. Venable, Jr. Nature New Biol. **238**, 67 (1972).
10. Y. M. Evdokimov, A. L. Platonov, A. S. Tikhonenko, and Y. M. Varshavsky. FEBS Lett. **23**, 180 (1972).

11. Y. M. EVDOKIMOV, N. M. AKIMENKO, N. E. GLUKHOVA, A. S. TIKHONENKO, and Y. M. VARSHAVSKY. Mol. Biol. SSSR, **7**, 151 (1973).
12. V. M. VARSHAVSKY, Y. M. EVDOKIMOV, and N. M. AKIMENKO. Stud. Biophys. **40**, 41 (1973).
13. S.-M. CHENG and S. C. MOHR. FEBS Lett. **49**, 37 (1974).
14. S.-M. CHENG and S. C. MOHR. Biopolymers, **14**, 663 (1975).
15. W. C. BRUNNER and M. F. MAESTRE. Biopolymers, **13**, 345 (1974).
16. J. T. SHAPIRO, M. LENG, and G. FELSENFELD. Biochemistry, **8**, 3219 (1969).
17. M. HAYNES, R. A. GARRETT, and W. B. GRATZER. Biochemistry, **9**, 4410 (1970).
18. J. SPONAR, S. STOKROVA, I. KORUNA, and K. BLAHA. Coll. Czech. Chem. Commun. **39**, 1625 (1974).
19. H. J. LI, P. EPSTEIN, S. S. YU, and B. BRAND. Nucl. Acids Res. **1**, 1371 (1974).
20. J. SPONAR, I. FRIC, and K. BLAHA. Biophysical Chem. **3**, 255 (1975).
21. S. STOKROVA, J. SPONAR, M. HAVRANEK, B. SEDLACEK, and K. BLAHA. Biopolymers, **14**, 1231 (1975).
22. E. C. ONG, C. SNELL, and G. D. FASMAN. Biochemistry, **15**, 468 (1976).
23. G. D. FASMAN and A. J. ADLER. J. Phys. Chem. **75**, 1516 (1974).
24. G. D. FASMAN, B. SCHAFFHAUSEN, L. GOLDSMITH, and A. J. ADLER. Biochemistry, **9**, 2814 (1970).
25. J. SPONAR and I. FRIC. Biopolymers, **11**, 2317 (1972).
26. J. SPONAR, J. DOSKOCIL, K. BLAHA, and C. ZIMMER. Nucl. Acids Res. **3**, 507 (1976).
27. C. S. LEE and C. A. THOMAS, JR. *In* Methods in enzymology. Vol. 29, Part E. *Edited by* L. Grossman and K. Moldave. Academic Press. 1974. p. 443.
28. M. B. SENIOR and D. E. OLINS. Biochemistry, **14**, 3332 (1975).
29. T. MANIATIO, J. H. VENABLE, JR., and L. S. LERMAN. J. Mol. Biol. **84**, 37 (1974).

Can. J. Chem. Downloaded from www.nrcresearchpress.com by 210.87.254.40 on 09/05/12
For personal use only.

The metal complex catalyzed reactions of anils. I. The reaction of acetone with anilines

A. R. BOATE AND D. R. EATON
Department of Chemistry, McMaster University, Hamilton, Ont., Canada L8S 4M1

Received June 30, 1976

A. R. BOATE and D. R. EATON. Can. J. Chem. **54**, 3895 (1976).

It has been shown that the formation of anils from anilines and aliphatic ketones is homogeneously catalyzed by a variety of metal complexes. The products of the reactions have been unambiguously identified by preparing the anils using other synthetic routes. The catalysis is quite general and the system is therefore suitable for a systematic catalytic study varying both the catalysts and the substrates. The related reactions of anil hydrolysis and transimination may also be studied. The catalysts used, thiourea complexes of Co(II), Ni(II), and Zn(II), vary in their effectiveness by more than two orders of magnitude. In the present paper experiments defining the catalytic system are described. The equilibrium constants for the complexation of all the substrate molecules have been determined. Qualitative rate data on various ligand exchange and proton transfer steps is presented to demonstrate that such reactions cannot be rate determining in the overall catalytic reactions.

A. R. BOATE et D. R. EATON. Can. J. Chem. **54**, 3895 (1976).

On a démontré que la formation d'anils, à partir de l'anilines et de cétones aliphatiques, est catalysés d'une façon homogène par une variété de complexes métalliques. On a identifié les produits des réactions d'une façon non ambigue en préparant les anils en faisant appel à d'autres routes de synthèse. La catalyse est assez générale et le système est donc susceptible d'être utilisé pour une étude systématique de la catalyse en faisant varier les catalyseurs et les substrats. On a aussi étudié les réactions reliées d'hydrolyse de l'anils et de transimination. L'efficacité des catalyseurs utilisés, des complexes de la thiourée avec le Co(II), le Ni(II) et le Zn(II), varient par plus de deux ordres de grandeur. On a aussi déterminé les constantes d'équilibre pour la complexation de tous les substrats. On présente des données qualitatives concernant les vitesses de divers étapes d'échanges de ligands et de transferts de proton afin de démontrer que de telles réactions ne peuvent pas déterminer la vitesse globale des réactions catalysées.
[Traduit par le journal]

Can. J. Chem. Downloaded from www.nrcresearchpress.com by 210.87.254.42 on 09/05/12
For personal use only.

Introduction

In recent years homogeneous catalysis by metal ions, metal complexes, and metalloenzymes has been extensively studied. The mechanisms involved tend to be complex and their complete elucidation is at best a difficult and tedious process. These reactions are necessarily multistep processes involving at least three steps; *i.e.* (*a*) coordination of the substrate molecule or molecules, (*b*) reaction of the coordinated substrate(s), and (*c*) dissociation of products, leaving the metal ready to undergo another catalytic cycle. If the catalysis is efficient many of these steps are rapid and correspondingly difficult to study in detail. In the present series of papers we will report a detailed study of some rather simple catalytic reactions. The system chosen is particularly suitable for this purpose. It has proved possible to obtain at least qualitative equilibrium and rate data on all the steps. Furthermore the catalysis is not particularly specific, *i.e.* a wide range of catalysts are effective and systematic modification of the substrates is also possible. The opportunity is therefore presented for a detailed investigation of the factors conducive to efficient catalysis. This initial paper will describe a series of experiments defining the catalytic system and some further experiments designed to obtain some necessary information on ligand exchange equilibria. Subsequent papers will describe more detailed investigations of the mechanism.

The reactions of interest involve the formation and hydrolysis of anils, *i.e.*

[1] 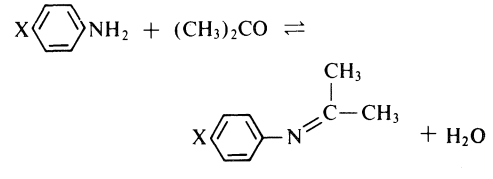

The catalysts used are Co, Ni, and Zn complexes of thiourea (tu) and related ligands. Studies have

Can. J. Chem. Downloaded from www.nrcresearchpress.com by 210.87.254.42 on 09/05/12
For personal use only.

been carried out starting with aniline and acetone or with anil and water or with equilibrium mixtures. A second closely related reaction also occurs, namely transimination, *i.e.*

[2] 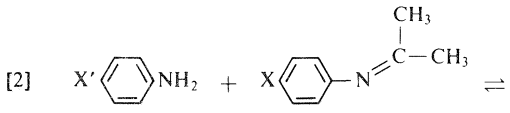

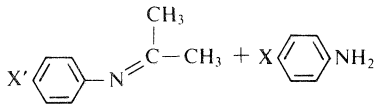

This reaction is also catalyzed by the metal complexes used.

The acid catalyzed formation and hydrolysis of anils has been widely studied in aqueous solution (1). The mechanism is well understood and involves the intermediate formation of a carbinolimine, *i.e.*

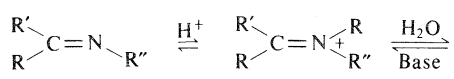

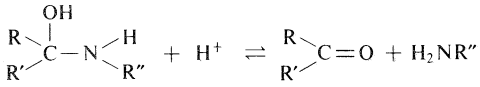

There is a change in the rate determining step which occurs between p*H* 2 and p*H* 5. Below this p*H* the attack or loss of water is fast and the attack or loss of amine is rate determining. Above this p*H* the situation is reversed.

The influence of metal ions on imine formation has been investigated by Eichhorn *et al.* (2, 3). Most of the examples studied have involved imines capable of chelation with the metal ion. In these circumstances the product imine remains coordinated to the metal and the reaction is metal ion promoted rather than catalyzed. There has been much discussion in the literature concerning the possibility of "template" effects (4) in these reactions. Typical of these studies is the work of Leussing and co-workers (5–7) on Schiff base formation from glycine and pyruvate in the presence of Zn(II) and from glycine and salicylaldehyde with Ni(II), Cu(II), and Zn(II) ions. In the latter case it was concluded that there is a fast equilibrium forming a ternary complex in which the ligands are independently bound, followed by a first order rate determining reaction to give the complexed Schiff base. It was suggested that the term "promnastic" be applied to describe a catalyst which forms a labile ternary complex with two substrates, but which imposes minimum steric constraint on them.

The present study differs from those described above in several respects. It is a catalyzed rather than a promoted reaction. Metal complexes in non-aqueous solution rather than metal ions in aqueous solution are involved. This factor represents a considerable simplification since most of the reactions alluded to above are very p*H* dependent and extensive investigation of the nature of the protonated species has been necessary to elucidate the mechanisms. Finally, the nature of the reactions are such as to make them amenable to study by a variety of nmr techniques which provide more detailed information on the molecular processes involved than do the spectrophotometric techniques most commonly utilized in aqueous solution studies.

The Reaction of Acetone with Anilines

The synthesis of anils from anilines and aromatic ketones has been in common use for many years. It was originally reported by Reddelien (8) who used zinc chloride as a heterogeneous catalyst and the conditions employed involved prolonged heating at 170 °C. If acetone is used in the above process a product is obtained which was formerly known as "acetone anil" but which was later established (9) to be a more complex condensation product 1,2-dihydro-2,2,4-trimethylquinoline. The true acetone anil may be prepared indirectly (see below) and it has been stated that "acetone anil cannot be obtained by direct reaction of the components" (10).

In the course of some studies of the ligand exchange reactions of transition metal thiourea complexes additional peaks were observed in the nmr spectra of anilines and Co(II) thiourea complexes in deuteroacetone solution. The set of spectra in Fig. 1 illustrates these observations. The following observations have been made: (*1*) Similar additional resonances are observed

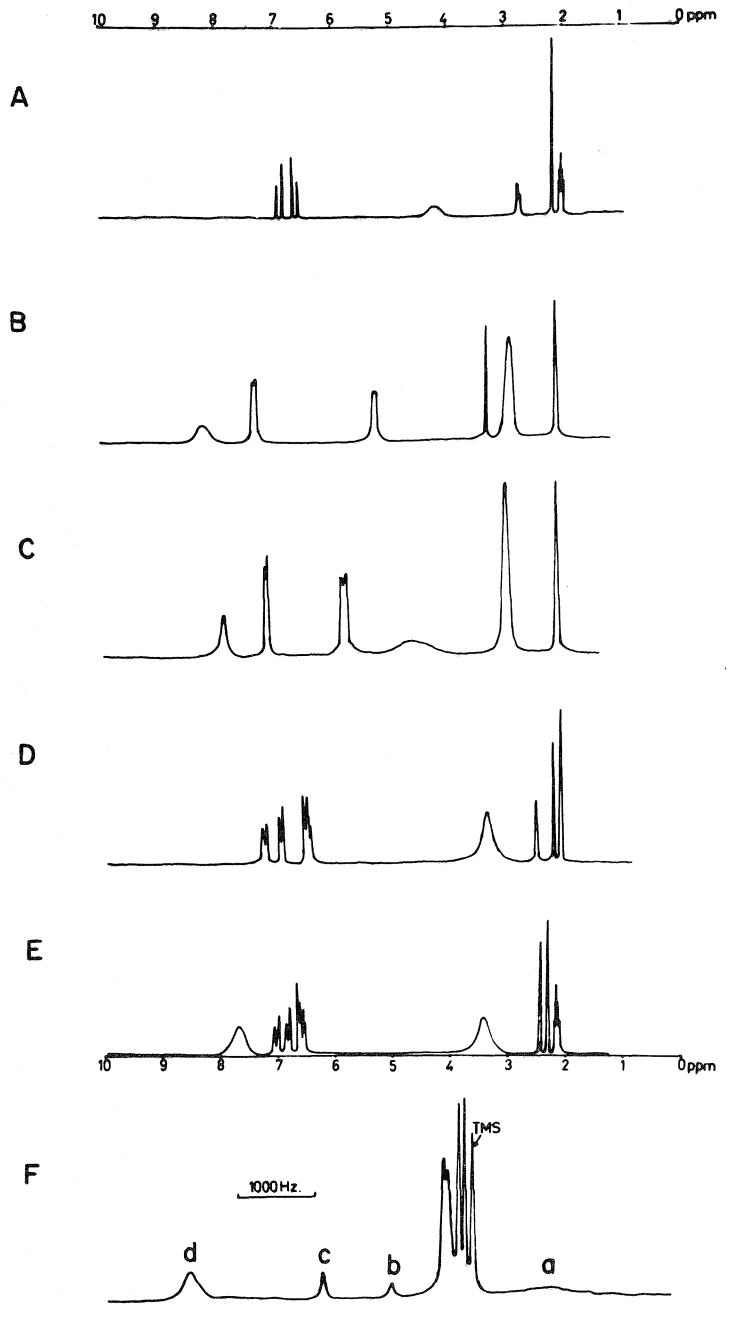

FIG. 1. Nuclear magnetic resonance spectra of *p*-toluidine in acetone-d_6. (*A*), assignment high field to low field, acetone-d_5, *p*-CH_3, HDO/H_2O, NH_2, *ortho* and *meta*. (*B*), Plus $Cotu_2Cl_2$, showing additional anil peaks. (*C*), As *B* plus more *p*-toluidine. (*D*), As *B* plus excess thiourea. (*E*), *p*-Toluidine + $Zntu_2Cl_2$. Assignment, acetone-d_5, *p*-CH_3 of *p*-toluidine, *p*-CH_3 of anil, H_2O, HDO, NH_2, *ortho* of *p*-toluidine and anil (overlapped), *meta* of *p*-toluidine, *meta* of anil, NH_2 of thiourea. (*F*), Spectrum of *B* at −90 °C showing complexed aniline and anil peaks, slow exchange.

Can. J. Chem. Downloaded from www.nrcresearchpress.com by 210.87.254.42 on 09/05/12
For personal use only.

Can. J. Chem. Downloaded from www.nrcresearchpress.com by 210.87.254.42 on 09/05/12
For personal use only.

with zinc thiourea complexes. The spectra differ from those with cobalt complexes only insofar as the lines are not shifted by the paramagnetism of the metal ion (see Fig. 1). (*2*) Similar additional resonances are observed if the *p*-toluidine is replaced by aniline, *p*-anisidine, *p*-chloroaniline, *m*-toluidine, or *p*-fluoroaniline. (*3*) No additional resonances are observed with *N*-methylaniline or with *N*,*N*′-dimethylaniline. (*4*) Similar additional resonances are observed if the acetone solvent is replaced by diethylketone or methylethylketone. (*5*) No additional resonances are observed if the acetone is replaced by acetonitrile or other non-ketonic solvents. (*6*) The intensity of the additional resonances is independent of the metal complex concentration. At very low metal complex concentrations the additional lines do not reach their full intensity until the solution has been allowed to stand for a while. (*7*) Addition of either more aniline or of excess thiourea to solutions containing paramagnetic cobalt complexes shows that both the aniline and the species producing the additional lines form metal complexes which are in fast exchange with free ligand on the nmr time scale (see Fig. 1).

All of the above observations are consistent with the metal complex catalyzed formation of anils (reaction 1) and the nmr spectra of Fig. 1 are assigned on this basis. In order to confirm this conclusion a number of anils have been synthesized indirectly (see Experimental section) and their nmr spectra compared with the additional lines observed in the above experiments. In all cases the agreement is excellent. Thus the *meta* resonance in the spectrum of *N*-isopropylidene *p*-toluidine coincides with the extra aromatic doublet observed on the addition of $Zntu_2Cl_2$ to *p*-toluidine in acetone-d_6 and the *p*-methyl peak coincides with the extra one observed in that region. Similarly the ^{19}F spectrum of the *N*-isopropylidene *p*-fluoroaniline gives a chemical shift identical with that of the additional ^{19}F resonance observed in mixtures of *p*-fluoroaniline and acetone with a little $Zutu_2Cl_2$ added. The nmr spectra of the synthesized anils also agree with those reported for anils in the literature (11, 12). The catalyzed reaction of reaction 1 is therefore clearly demonstrated.

The Role of the Metal Complex

The metal thiourea complexes are very efficient catalysts for these anil formation reactions. In a subsequent paper we will report quantitative kinetic data on the reactions and show that the rate of the reaction is directly proportional to catalyst concentration at low catalyst concentration. An indication of their efficiency is provided by the observation that for an acetone solution 0.2 *M* in *p*-toluidine and 4×10^{-4} *M* in $Zu(tu)_4(ClO_4)_2$ the anil peaks reached half their equilibrium intensity in 2.25 min. Initially it is desirable to obtain an estimate of the rate of the uncatallyzed reaction. Three samples 0.2 *M* in freshly sublimed *p*-toluidine in acetone-d_6 were prepared using carefully cleaned nmr tubes. The samples were kept in the dark at room temperature and periodically the nmr spectra were run to monitor anil formation. After 200 h some $Zu(tu)_4(ClO_4)_2$ was added which quickly completed the reaction. Initial rates of formation of anil of 1.33×10^{-7}, 6.4×10^{-8}, and 8.3×10^{-8} mol l^{-1} s^{-1} were obtained for these samples. It is quite likely that these rates reflect contamination by traces of metal ions or metal complexes in the tubes or reagents. In any event they are negligible compared to the rates of the catalyzed reaction and the contribution of an uncatalyzed reaction to the overall rate can be safely neglected.

A similar experiment demonstrated that thiourea itself was not a catalyst. However, a wide variety of metal complexes proved effective. These included simple salts such as $Ni(ClO_4)_2.6H_2O$, $RhCl_3.xH_2O$, phosphine complexes such as $[P(C_6H_5)_3]_2NiCl_2$ and $[P(C_6H_5)_3]_2Ni(SCN)_2$, and a variety of thiourea complexes of Co, Ni, and Zn. Non-labile chelate complexes such as Co(II)bispyrazolylborate or Ni(II)aminotroponeimineates do not catalyse the reaction. Many simple salts such as $CoCl_2$ or $Co(ClO_4)_2$ are ineffective due to the immediate precipitation of insoluble metal aniline complexes. The effectiveness of a catalyst can be almost completely destroyed by adding a chelating ligand such as 1,10-phenanthroline. Thus it appears that the main function of the thiourea is to keep the metal ion in solution but at the same time to undergo facile ligand exchange.

In order to obtain some idea of the relative effectiveness of different metal complexes, a series of Co(II) and Zn(II) thiourea complexes were used as catalysts in the reaction of *p*-fluoroaniline and acetone. The compounds were mostly Co(II) complexes because the equilibrium constants for the dissociation of these complexes in

Can. J. Chem. Downloaded from www.nrcresearchpress.com by 210.87.254.42 on 09/05/12
For personal use only.

TABLE 1. Comparison of the efficiency of various catalysts in the reaction of *p*-fluoroaniline with acetone

Catalyst	Relative rate	K_D ($\times 10^4$)*
$Zntu_2Cl_2$	1	—
$Cotu_2Cl_2$	3.2	1.46
$Co(DMtu)_2Br_2$	16	2.06
$Cotu_2Br_2$	10	2.82
$Cotu_2I_2$	59	3.86
$Cotu_4(NO_3)_2$	68	14.4
$Cotu_4(ClO_4)_2$	650	53.5

*Dissociation constants from ref. 13.

acetone had previously been determined (13). The reaction was followed by repeatedly integrating the aniline and anil signals in the ^{19}F nmr spectrum until equilibrium had been reached. As all the samples contained the same concentration of *p*-fluoroaniline the equilibrium position was the same and thus $t_{1/2}$, the time for the fraction of anil to reach one-half its final equilibrium value, is a valid measure of the rate. The results were plotted as the fraction of anil *i.e.* Anil/(Anil + Aniline) against time elapsed after the addition of catalyst. The relative rates (relative to $Zntu_2Cl_2$ at the concentration it was used) are given for a series of complexes in Table 1 along with the dissociation constants for the complexes in acetone. There is clearly a correlation between relative rate and dissociation constant indicating that replacement of thiourea by one or more of the reactants is a prerequisite for catalysis.

Catalysis by Acids

Many reactions involving carbonyl compounds and amines are catalyzed by acids (1). It seemed desirable therefore to examine the effects of acids on the present reaction. Figure 2*a* shows the nmr spectrum of *p*-toluidine in acetone-d_6. Figure 2*b* shows the same sample immediately after the addition of trifluoroacetic acid making the solution 1 *M* in acid. Figure 2 shows the same spectrum 1½ h after the addition of acid. The assignments of the lines are given in the figure caption. On the addition of acid the intensity of the acetone-d_5 peak increases rapidly. Deuterium exchange through the enol form of the acetone is indicated. The changes in the aromatic region and the shift of the methyl resonance may be ascribed to protonation of the amino group. On standing additional resonances assignable to a protonated anil appear. The conversion of peak A to peak B was followed by

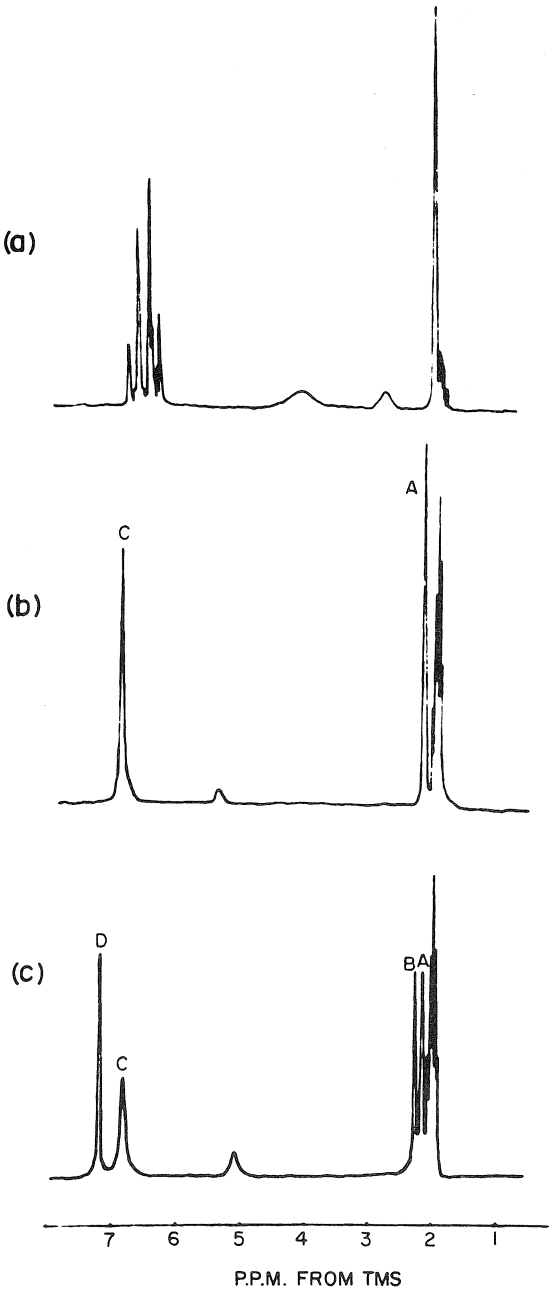

FIG. 2. (*a*), Nuclear magnetic resonance spectrum of *p*-toluidine in acetone-d_6. (*b*), As (*a*) after addition of CF_3COOH. Note increase in acetone-d_5 peak at high field end of spectrum. Peak *A*, CH_3. Peak *C*, aromatic. (*c*), As (*b*) after 1½ h. Note appearance of anil peaks *B* and *D*.

nmr at a $t_{1/2}$ value of 26 min obtained. This may be compared with the value of 2.25 min for 4×10^{-4} *M* $Zntu_2(ClO_4)_2$ as the catalyst with

Can. J. Chem. Downloaded from www.nrcresearchpress.com by 210.87.254.42 on 09/05/12
For personal use only.

the same concentration of *p*-toluidine. Thus on a molar basis the metal complex is at least 10^4 times as efficient as acid but this comparison is not directly meaningful since the reactions undoubtedly involve different mechanisms. However the rapid proton exchange of the acetone-d_6 provides a clear criterion for acid catalysis and the absence of such exchange is taken to indicate that catalysis is not proceeding due to the adventitious presence of acid impurities.

Equilibrium Constant Measurements

Detailed kinetic studies of these catalyzed reactions will require a knowledge of a number of equilibrium constants. Thus it would be desirable to know the equilibrium constants for the overall reaction 1 and also the equilibrium constants for the ligand exchange reactions of the type

[3] $$Mtu_2X_2 + L \rightleftharpoons MtuLX_2 + tu$$

where L can be any one of the four reactants aniline, acetone, anil, and water. Given this information the concentration of any species containing complexed reactants or products can be calculated and correlated with observed rate data. It is also desirable to have at least qualitative rate data on the ligand exchange reactions and also on certain proton transfer reactions in order to demonstrate that these processes are too fast to be involved as rate determining steps. The present section describes experiments designed to obtain this data.

The Overall Reaction

The equilibrium constant for the overall reaction is defined as:

$$K = \frac{[\text{Anil}][\text{Water}]}{[\text{Aniline}][\text{Acetone}]}$$

Our main requirement for this equilibrium constant was for the interpretation of certain double resonance experiments using *p*-fluoroaniline. If ^{19}F nmr is used acetone-h_6 may be employed as the solvent. This is convenient since there are some problems in determining the water content of acetone-d_6 (see below). For acetone-h_6 the water content may be determined using ^1H nmr by integrating the H_2O signal against the ^{13}C satellite peak of the acetone resonance. In the case of the acetone used in this experiment the water content was found to be 1.29×10^{-3} as a fraction by weight of the acetone. Samples were then prepared by weighing *p*-fluoroaniline and acetone-h_6 into nmr tubes and adding a small quantity of $Zntu_4(ClO_4)_2$. When the reaction had reached equilibrium the ratio of aniline to anil was measured by integration of the ^{19}F nmr spectrum. The concentrations of aniline, anil, acetone, and water at equilibrium were then calculated, and the equilibrium constant obtained. Results are shown in Table 2. The first three of the samples listed in this table were prepared as described above and then, after the measurements had been made, a further quantity of water was weighed into two of the samples giving the results listed as samples 4 and 5. The conclusion to be drawn from these results is that K is not a constant. The apparent K varies linearly with the water concentration. There is no obvious trend with the concentrations of any of the other species. It would seem that the activity of water in acetone in the range of concentrations studied is not directly proportional to its concentration. This conclusion is substantiated by results obtained for the equilibrium constants for ligand exchange reactions involving water (see below). However, these results enable us to estimate an effective equilibrium constant for the overall reaction at a given water concentration.

Acetone as a Ligand

Nuclear magnetic resonance provides a very convenient probe for the study of ligand exchange reactions of the type shown in reaction 3

TABLE 2. Equilibrium constant for the formation of anil from *p*-fluoroaniline in acetone

Sample	*p*-fluoroaniline*	Acetone*	*p*-fluoroanil*	H_2O*	K
1	4.0×10^{-4}	5.22×10^{-3}	1.63×10^{-4}	1.85×10^{-4}	1.44×10^{-2}
2	1.17×10^{-3}	4.08×10^{-3}	2.85×10^{-4}	3.03×10^{-4}	1.81×10^{-2}
3	1.71×10^{-3}	5.35×10^{-3}	4.02×10^{-4}	4.26×10^{-4}	1.87×10^{-2}
4	5.1×10^{-4}	5.35×10^{-3}	5.55×10^{-4}	1.44×10^{-3}	2.98×10^{-2}
5	1.92×10^{-3}	5.55×10^{-3}	1.95×10^{-4}	1.80×10^{-3}	3.29×10^{-2}

*Moles of reagent present in sample of constant volume.

Can. J. Chem. Downloaded from www.nrcresearchpress.com by 210.87.254.42 on 09/05/12
For personal use only.

in cases where the metal ion is paramagnetic leading to large isotropic shifts for the complexed ligand. It is difficult to obtain reliable data with diamagnetic complexes since the chemical shifts are small. The present measurements have therefore been confined to Co(II) thiourea complexes. We anticipate that the Zn(II) thiourea complexes would behave in a qualitatively similar manner although the numerical values for equilibrium constants will obviously be different.

Equilibrium constants for the replacement of thiourea by acetone have previously been reported for a series of Co(II) complexes (13). We note here that acetone is the poorest of the five ligands involved with K for reaction 3 being of the order 10^{-5}. The rates of the ligand exchange reactions have also been studied (14, 15).[1] Typical second order rate constants for the associative step are:

$$Cotu_2Cl_2 + Ac \rightarrow Cotu_2AcCl_2$$
$$k = 1.8 \times 10^2 \text{ mol}^{-1} \text{ s}^{-1}$$

$$CotuAcCl_2 + tu \rightarrow Cotu_2AcCl_2$$
$$k = 3.4 \times 10^7 \text{ mol}^{-1} \text{ s}^{-1}$$

Both of these processes are too rapid to play a part as the rate determining step in the catalytic reactions.

Anilines and Anils as Ligands

Two solvents have been used in the course of the study of these catalytic reactions. The formation of anils is conveniently examined in acetone as described above since an excess of acetone is required to form the anil in conveniently measurable quantities. The hydrolysis of the anils and some of the transimination reactions can be more conveniently studied in acetonitrile solution. The equilibrium constants for aniline complexation are most simply obtained in acetonitrile since the presence of both aniline and anil causes some complications.

The following procedure proved convenient. A known quantity of $Cotu_2Cl_2$ was dissolved in 5.0 ml of acetonitrile-d_3 and this was used as a stock solution. The position of the thiourea resonance was measured in this solution. Samples containing various anilines at 0.2 M concentrations were prepared using this stock solution and the position of the thiourea resonance measured for each sample. In each case the resonance had moved towards the free ligand position due to displacement of thiourea by aniline on the complex. This information suffices to determine the equilibrium constants for complexed anilines provided the chemical shift of thiourea fully complexed to the cobalt is known. An initial experiment to determine this quantity is therefore necessary.

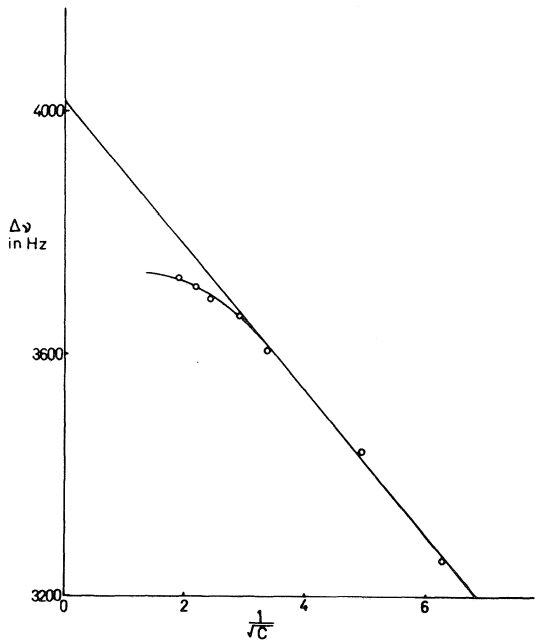

FIG. 3. Concentration dependence of thiourea chemical shift of $Cotu_2Cl_2$ in acetonitrile.

The thiourea complexes are partly dissociated n solution. If the degree of dissociation is small it may be shown that:

$$\Delta\nu_{obs} = \Delta\nu_c\left(1 - \frac{1}{2}\sqrt{\frac{K_D}{C}}\right)$$

where $\Delta\nu_c$ is the chemical shift of the complexed thiourea, K_D is the dissociation constant, and c is the concentration of the cobalt complex. $\Delta\nu_c$ may therefore be obtained as the intercept of a plot of $\Delta\nu_{obs}$ *vs.* $1/\sqrt{C}$. This procedure was successfully used in previous studies of Co(II) thiourea complexes in acetone (13). A plot for $Cotu_2Cl_2$ in acetonitrile is shown in Fig. 3. It may be noted that this plot becomes non-linear at high concentrations of complex. This behaviour was not observed in acetone but solubility factors in this case prevented data being

[2]Reference 15 reports approximate ligand exchange rates for zinc thiourea complexes.

Can. J. Chem. Downloaded from www.nrcresearchpress.com by 210.87.254.42 on 09/05/12
For personal use only.

TABLE 3. Equilibrium constants for the replacement of thiourea by anilines*

Aniline	Aniline concentration (mol/l)	Shift of tu†	Free [tu]	K_3
None	0.0	3046	0.0161	—
p-Toluidine	0.203	2817	0.0237	1.7×10^{-2}
p-Anisidine	0.198	2666	0.0287	3.4×10^{-2}
p-Nitroaniline	0.199	3041	0.0163	2.8×10^{-4}
p-Chloroaniline	0.198	2986	0.0181	3.7×10^{-3}
p-Bromoaniline	0.201	3009	0.0173	2.2×10^{-3}
Aniline	0.202	2937	0.0197	7.06×10^{-3}

*All samples were 5.8×10^{-2} *M* in $Cotu_2Cl_2$ and the measurements were carried out at 35 °C. Solvent CH_3CN.
†In Hz at 100 MHz measured from the free ligand position.

obtained at the concentrations showing non-linear behaviour in acetonitrile. A number of explanations were considered, the most likely one being small changes in the magnetic axes affecting the dipolar isotropic shifts occurring through concentration dependent solvation effects. In any event the linear portion of the curve can be extrapolated to a shift of 4013 Hz at 100 MHz corresponding to $\Delta\nu_c = 3534$ Hz (relative to free ligand). This may be compared with $\Delta\nu_c = 3842$ Hz in acetone. Equilibrium data derived from this value may be unreliable at metal complex concentrations greater than 0.1 *M*. The experiments referred to in the previous paragraph were therefore carried out with relatively dilute solutions of metal complex ($\sim$0.05 *M*).

Knowing $\Delta\nu_c$ the observed shifts may be used to calculate the concentration of free thiourea ligand in solution. For solutions without aniline added this leads to the equilibrium constant K_2 for replacing thiourea by acetonitrile. A value of $K_2 = 1.37 \times 10^{-4}$ is obtained. (Note that $K_2 = K_D/[CH_3CN]$ and that the value obtained is approximately one order of magnitude greater than the corresponding value for acetone.) For solutions with aniline added it may be shown that the free thiourea concentration is given by:

$$[4] \qquad [\text{tu}] = \frac{M(cK_3^2 + dK_3 + e)}{(aK_3 + b)^2}$$

where *M* is the concentration of metal complex and K_3 is the required equilibrium constant for the replacement of thiourea by aniline. In this equation

$$a = [\text{An}]$$
$$b = [\text{tu}] + K_2[\text{AN}]$$

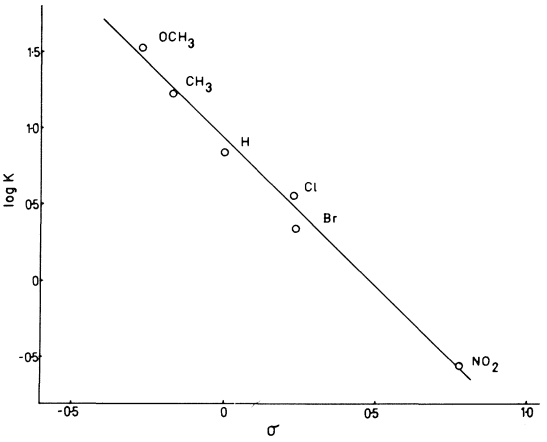

FIG. 4. Correlation of the log of equilibrium constants for the displacement of thiourea by a substituted aniline with the Hammett σ value for aniline.

$$c = 2[\text{An}]^2$$
$$d = 2[\text{tu}][\text{An}] + 4K_2[\text{An}][\text{AN}]$$
$$e = 2K_2[\text{tu}][\text{AN}] + 2K_2^2[\text{AN}]^2$$

where tu $\equiv$ thiourea, AN $\equiv$ acetonitrile, An $\equiv$ aniline. Equation 4 may be solved for K_3. Table 3 presents data for a number of substituted anilines. The equilibrium constants vary from 10^{-2} to 10^{-4}. The anilines are clearly much better ligands than acetone. As expected electron donating substituents increase K_3. Figure 4 shows that there is a good correlation between log K_3 and Hammett σ values. This behaviour may be contrasted with the results of Rakshys (16) who found a poor correlation between the equilibrium constants for the formation of adducts between anilines and Ni(II) acetylacetonate and the Hammett σ values for the anilines.

We turn now to the equilibrium constants for

TABLE 4. Ligand exchange equilibria in acetone-d_6

Parameter	Value	
	Sample A	Sample B
Initial weight of $Cotu_2Cl_2$	9.8×10^{-3} g	1.0×10^{-2} g
Initial weight of *p*-toluidine	1.92×10^{-2} g	4.3×10^{-2} g
Acetone-d_6 added	0.40 ml	0.40 ml
Ratio [Anil]/[*p*-tol] (by integration)	0.45	0.38
Shift of tu peak from free ligand position	1675 Hz	1512 Hz
Shift of *p*-toluidine *meta* signal*	17 Hz	10 Hz
Shift of anil metal signal*	51 Hz	34 Hz
Fraction of tu in $Cotu_2Cl_2$ displaced	0.237	0.302
Fraction of anil complexed	0.193	0.129
Fraction of *p*-toluidine complexed	0.041	0.024
Calculated value of $\Delta\nu_c$ for *p*-toluidine	415 Hz	415 Hz
K_{anil}	2.0×10^{-1}	2.2×10^{-1}
$K_{p\text{-tol}}$	3.5×10^{-2}	3.8×10^{-2}

*Measured from the corresponding peaks in a solution with $Zntu_2Cl_2$ replacing $Cotu_2Cl_2$. Spectra obtained at 27 °C and at 56.4 MHz.

anilines and anils in acetone solution. This situation is more complicated since it is not possible to examine each ligand separately; in the presence of metal complex there will be an equilibrium mixture of aniline and anil. The above method therefore does not suffice since it provides only one piece of data to calculate two equilibrium constants. It is therefore necessary to obtain the limiting shift $\Delta\nu_c$ for either the anil or the aniline separately. This may be accomplished by examining the spectra at low temperature such that the ligand exchange involving the anil is slow. Figure 5 shows a set of ^{19}F nmr spectra for *p*-fluoroaniline solutions which illustrate this possibility. *p*-Fluoroaniline alone shows a single resonance; on the addition of $Zntu_2Cl_2$ a second resonance due to the anil appears. With $Cotu_2Cl_2$ there are again two lines both shifted relative to their positions in the previous spectrum due to complexing with the paramagnetic cobalt compound. On lowering the temperature the anil peak broadens and eventually reappears as separate free and complexed ligand peaks. In the low temperature region the shift of the complexed anil peak has a $1/T$ (Curie law) temperature dependence. A value for $\Delta\nu_c$ at room temperature may therefore be obtained by extrapolation. Exchange of the aniline is obviously faster than that of the anil. At the lowest temperatures the aniline peak is significantly broadened but it is not possible to reach a sufficiently low temperature to observe separate free and complexed aniline peaks. Examination of the spectra in Fig. 1 shows that the behaviour of *p*-toluidine in acetone is entirely analogous although the situation is somewhat complicated by the multiplicity of proton resonances.

Equilibrium constants can now be obtained from the room temperature spectra. The concentration of free thiourea is found from the thiourea shift. The concentration of complex anil is found from the measured anil shift and the extrapolated $\Delta\nu_c$. It is assumed that thiourea not replaced by anil is replaced by aniline. This gives the fraction of aniline complexed. This data allows the calculation of equilibrium constants for both anil and aniline. Two sets of data for *p*-toluidine solutions are shown in Table 4. The limiting shift $\Delta\nu_c$ for aniline (which cannot be measured directly) is also obtained from this experiment. The two values obtained at different *p*-toluidine concentrations agree very well as do the two values for both equilibrium constants. The value of K for *p*-toluidine in acetone (3.7×10^{-2}) may be compared with K for *p*-toluidine in acetonitrile (1.7×10^{-2}). It is apparent that K for the anil (2.1×10^{-1}) is about one order of magnitude greater than for the aniline; anils are the most favoured substrate ligands.

These experiments also provide qualitative data on the rates of ligand exchange. At the coalescence temperature for the nmr resonances the lifetime of a ligand coordinated to the metal is of the order $(1/2\pi)\Delta\nu$ s. At room temperature the lifetime must be less than this quantity. In this manner we estimate that the lifetime of a complexed anil molecule at 30 °C is not longer than 10^{-4} s and of a complexed aniline molecule

Can. J. Chem. Downloaded from www.nrcresearchpress.com by 210.87.254.42 on 09/05/12
For personal use only.

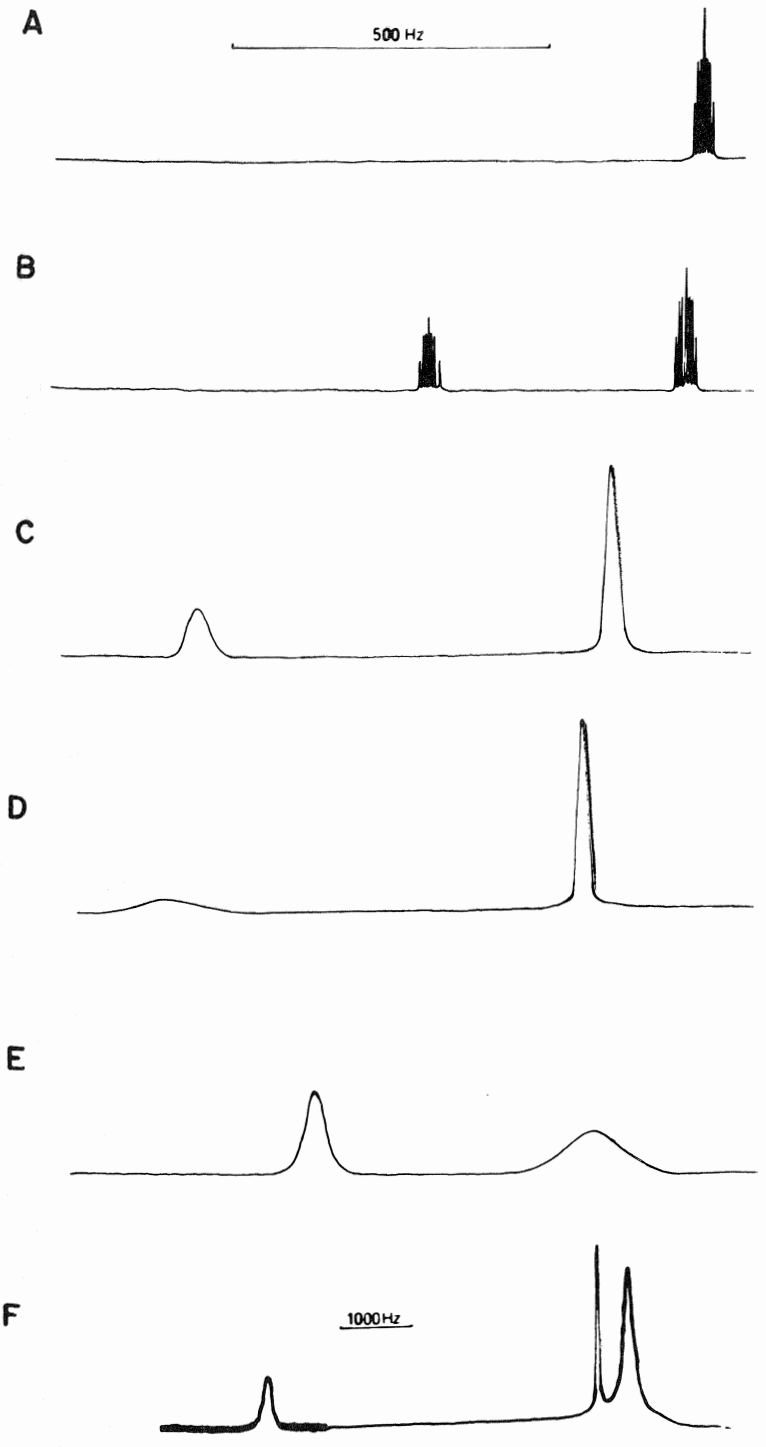

FIG. 5. ^{19}F nmr spectra of *p*-fluoroaniline. (*A*), *p*-fluoroaniline in acetone. (*B*), plus $Zntu_2Cl_2$, anil peak to low field. (*C*), Plus $Cotu_2Cl_2$. (*D*), (*C*) at -20 °C. (*E*), (*C*) at -90 °C. (*F*), Expanded sweep of (*E*). High field to low field, average of free and complexed aniline, free anil, complexed anil.

Can. J. Chem. Downloaded from www.nrcresearchpress.com by 210.87.254.42 on 09/05/12
For personal use only.

Can. J. Chem. Downloaded from www.nrcresearchpress.com by 210.87.254.42 on 09/05/12
For personal use only.

not longer than 10^{-5} s. Both of these lifetimes are sufficiently short to rule out either of the ligand exchange steps as rate determining processes in the catalytic reactions.

Water as a Ligand

The equilibrium constant for water may be determined in a manner analogous to that described above for aniline in acetonitrile. There is however an initial problem. Acetone always contains some water as an impurity and it is first necessary to determine this concentration. This may be accomplished directly for acetone-h_6 as described above but is more difficult for acetone-d_6 since most of the water is present as D_2O which is not easily observable by nmr. However, if an aniline such as *p*-toluidine is added to the acetone-d_6 equilibrium between the NH_2 protons and the D_2O is rapidly attained. The water then gives rise to two nmr resonances, a singlet due to H_2O and a triplet (arising from H—D coupling) due to HDO. A typical spectrum is shown in Fig. 6. If the equilibrium constant for the reaction:

$$H_2O + D_2O \rightleftharpoons 2HDO$$

is known then integration of nmr spectra such as that shown in Fig. 6 allows the D_2O concentration to be calculated. Statistically this equilibrium constant should be four. It has been found to be 3.94 ± 0.12 at 20 °C using an nmr method (17). The total water concentration in the acetone-d_6 is now known. In the sample used in the experiments described below it proved to be $0.21 \pm 0.02\%$ by weight.

The position of the thiourea resonance in a sample of $Cotu_2Cl_2$ dissolved in acetone-d_6 of known water content was measured. Water (20 μl) was added in 2 μl portions and the shift of the thiourea peak monitored. These measurements enabled us to calculate the concentration of free thiourea and hence of complexed water

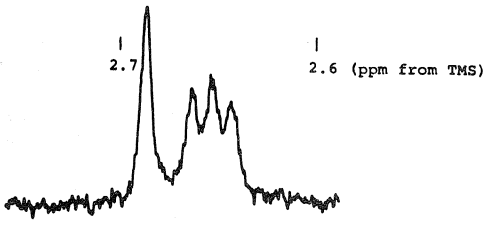

FIG. 6. ^1H nmr spectrum of H_2O/HDO at 100 MHz.

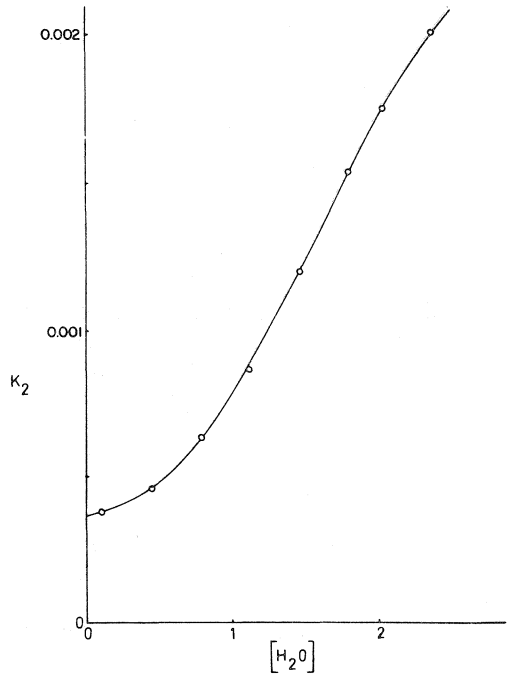

FIG. 7. Dependence of "equilibrium constant" for replacement of thiourea by water on water concentration with $Cotu_2Cl_2$ in acetone-d_6. Concentrations in mol/l.

providing the equilibrium constant for the replacement of thiourea by acetone is known. This leads to the equilibrium constant for the replacement of thiourea by water. This quantity proved not to be constant but to depend on the water concentration. The variation is shown in Fig. 7. It increases from around 4×10^{-4} to 2×10^{-3} as the water concentration rises to 2 *M*. This behaviour parallels that of the equilibrium constant for anil formation described above. It is consistent with previous observations of the shift of the water resonance in Co(II) thiourea solutions (13) and with the results of Shul'man *et al.* (18) who found by an electrochemical method that the relative complexing abilities of tu and H_2O in aqueous acetone depend on the dielectric constant of the solution. The data of Fig. 7, however, enable us to estimate an effective equilibrium constant for complexing of water at any concentration of water.

Previous results (13) have shown that free and complexed water are in fast exchange at room temperature but that complexed water appears with a large isotropic shift of around 7000 Hz at −80 °C. This ligand exchange process is again

too fast to play a rate determining role in the catalytic reactions.

Hydrogen Exchange Reactions

The observations that ligand exchange is rapid on the nmr time scale reported above have eliminated a number of steps as possible rate determining processes in the catalytic reaction. It is possible to eliminate proton exchange steps by a similar argument. Figure 8*a* shows the nmr spectrum of *p*-toluidine in moist acetone-d_6. Separate resonances for the NH_2 and the H_2O protons are clearly visible. Figure 8*b* shows the same sample after addition of $Zntu_4(ClO_4)_2$ to make the solution 10^{-5} *M* in catalyst. An averaged resonance for NH_2 and H_2O is now observed. Application of the coalescence formula leads to a maximum lifetime for the protons on either water or aniline of 10^{-3} s. The lifetime may well be much less than this upper limit since slow exchange spectra are not obtained at lower temperature. In order to form anil from acetone and aniline it is necessary to transfer protons from nitrogen to oxygen. This may or may not take place in two discreet steps with the formation of an intermediate carbinolimine. In any event the above result makes it clear that proton transfer steps are not likely to be rate determining in the overall catalytic mechanism. It may be noted that fast exchange is never detected between the amino protons of the thiourea and those of either water or aniline. This observation may be correlated with the fact that both water and aniline bind to the metal through the atom to which hydrogen is attached whereas thiourea is bound through sulphur.

In experiments involving hydrolysis of *p*-toluidine anil in acetone-d_6 three rate processes may be observed in the methyl region of the spectrum. There is the disappearance of anil methyls and the appearance of acetone-h_6. This measures the rate of anil hydrolysis. Secondly and slower is the incorporation of CD_3 groups into the anil methyls. This measures the rate of conversion of acetone to anil and is slow because the initial concentration of *p*-toluidine is very small. The third process, which is much slower again is an exchange of hydrogen and deuterium leading to an increase in the intensity of the acetone-d_5 quintet. This reaction is very slow and is distinguished from the second process by the fact that CD_3 is converted to CD_2H rather than to CH_3. The fact that this third process is much slower than the first or second puts a number of constraints on the mechanism of anil formation and hydrolysis.

Conclusion

The present paper has two objectives. First of all we have demonstrated the existence and scope of reactions involving the metal complex catalyzed formation and hydrolysis of anils. The nature of the products of the reaction between acetone and anilines has been demonstrated by independent synthesis of the anils. The reaction has been shown to be truly catalytic and not promoted. The rate of the catalyzed reaction is very fast compared to any uncatalyzed reaction. It is a convenient reaction to study since both the forward and back reactions can be followed by nmr. It is catalyzed by a variety of thiourea complexes but their effectiveness varies over three orders of magnitude. Inhibition by thiourea and by chelating ligands has been demonstrated.

Secondly, a number of experiments are reported which lay the foundation for a more detailed kinetic and mechanistic study. Equilibrium constants for complex formation involving all four of the reactant and product molecules have been obtained. These data provide the input information for computer calculations of the concentrations of the various metal complexes in reacting solutions. Ligand exchange and proton transfer reactions have been shown to be too fast to be involved as rate determining steps. With this background subsequent papers will proceed with a more detailed study of the mechanism.

Experimental

Nuclear magnetic resonance spectra were obtained on Varian DP60 and HA100 spectrometers with normal probe temperatures of 35 and 27 °C respectively. All apparatus was kept scrupulously clean and where possible solutions were prepared directly in the nmr sample tube.

The metal thiourea complexes used as catalysts were prepared in a manner similar to that previously described (13). In a typical preparation, stoichiometric quantities of the metal halide and ligand were each dissolved in a minimum quantity of hot alcohol, usually *n*-butyl alcohol. The solutions were mixed, cooled, and the product collected. The compounds were recrystallized from alcohol and pumped dry on a vacuum line.

The deuterated solvents used in this study were obtained from Merck, Sharp and Dohme. The extent of deuteration

Can. J. Chem. Downloaded from www.nrcresearchpress.com by 210.87.254.42 on 09/05/12
For personal use only.

Can. J. Chem. Downloaded from www.nrcresearchpress.com by 210.87.254.42 on 09/05/12
For personal use only.

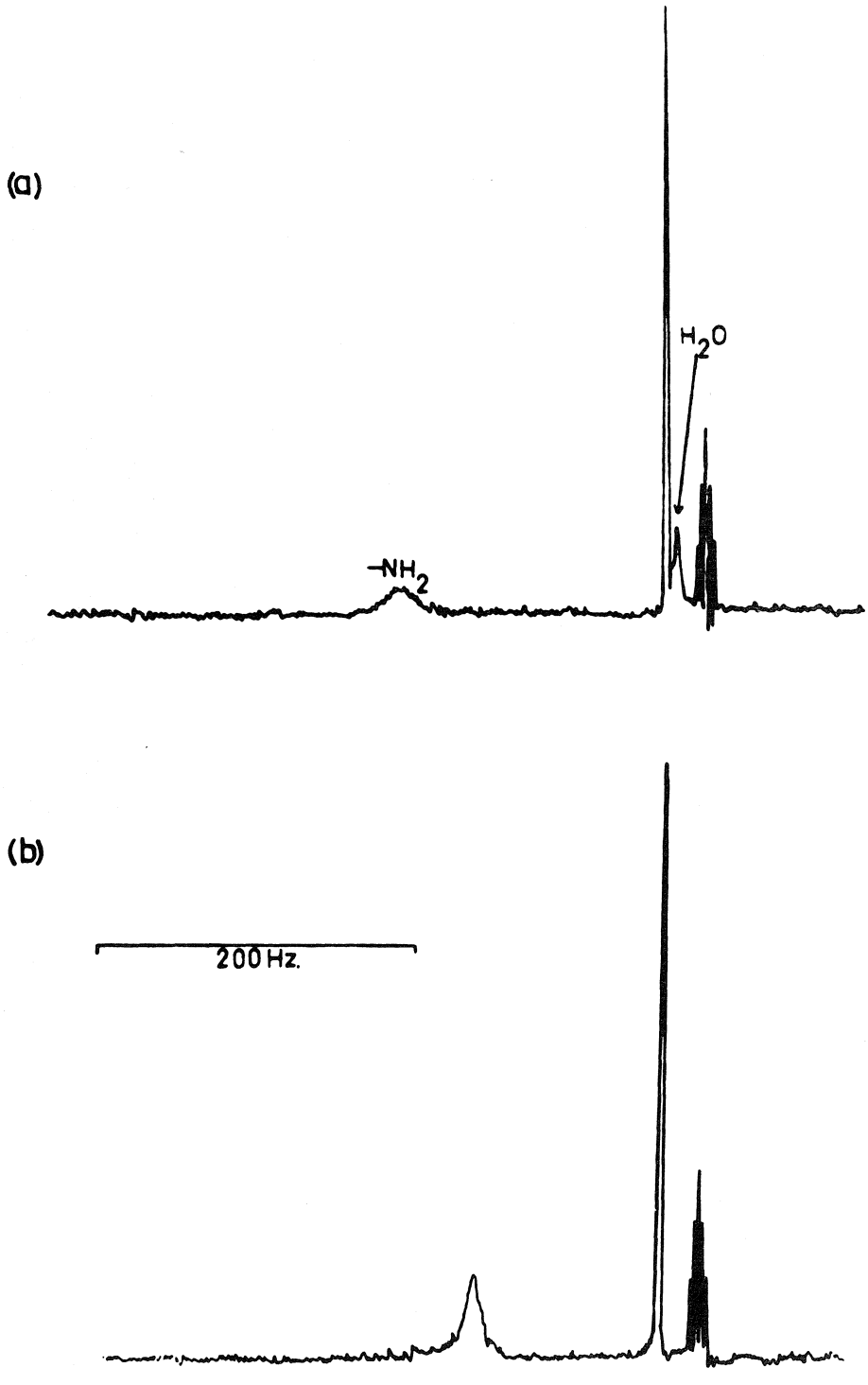

FIG. 8. Effect of catalyst on proton exchange between *p*-toluidine and water. (*a*), ^1H spectrum of *p*-toluidine in acetone-d_6. (*b*), Immediately after addition of 10^{-5} *M* $Zntu_4(ClO_4)_2$.

was 99% or better. The anilines were obtained commercially and were either sublimed or distilled before use.

Two methods were used to prepare the anils. The first method (19) involved the reaction of 2,2-diethoxypropane with an aniline at high temperature.

In a typical experiment 3.3 g of *p*-fluoroaniline and 5.0 g of 2,2-diethyoxypropane were slowly heated on an oil bath to 185 °C. A gentle stream of nitrogen removed the ethanol formed. After about 10 min the flask was cooled under a stream of nitrogen and the contents distilled under vacuum. This method yields a mixture of *p*-fluoroaniline and its acetone anil. The two compounds have very similar boiling points. The products were identified by their nmr spectra using the assignments reported by Curtin *et al.* (11).

A more satisfactory method for preparing anils is suggested by the work of Kuhn and Schretzmann (20). This method was used to prepare the *p*-toluidine anil. Firstly, a complex

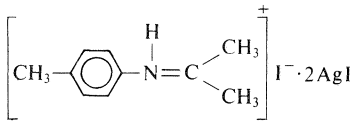

was prepared by dissolving 10 g of *p*-toluidine hydroiodide and 20 g of AgI in the minimum quantity of hot dimethylformamide (~40 ml) and then adding a large volume (~4 l) of acetone to the cooled solution. The complex slowly crystallized out and yielded about 15 g (50%) of an air stable white solid. The free anil was prepared by refluxing 12 g of the AgI complex with 80 ml of 10% Et_3N in benzene, removing solvent, and finally distilling the anil *in vacuo*. The nmr spectrum of the product indicated that it contained about 5% *p*-toluidine as the only detectable impurity.

1. W. P. JENCKS. Catalysis in chemistry and enzymology. McGraw-Hill, N.Y. 1969.
2. G. L. EICHHORN and J. C. BAILER. J. Am. Chem. Soc. **75**, 2905 (1953).
3. G. L. EICHHORN and I. M. TRACHTENBERG. J. Am. Chem. Soc. **76**, 5183 (1954).
4. M. C. THOMPSON and D. H. BUSCH. J. Am. Chem. Soc. **86**, 213 (1964).
5. D. L. LEUSSING and C. K. STANFIELD. J. Am. Chem. Soc. **88**, 5726 (1966).
6. K. S. BAI and D. L. LEUSSING. J. Am. Chem. Soc. **89**, 6126 (1967).
7. D. HOPGOOD and D. L. LEUSSING. J. Am. Chem. Soc. **91**, 3740 (1969).
8. G. REDDELIEN. Ber. **42**, 4759 (1909); **43**, 2471 (1910); **46**, 2718 (1913).
9. G. REDDELIEN and A. THURM. Ber. **65**, 1511 (1932).
10. C. WEYGAND and G. HILGETAG. Preparative organic chemistry. John Wiley, New York. 1972.
11. D. Y. CURTIN, E. J. GRUBBS, and C. G. MCCARTY. J. Am. Chem. Soc. **88**, 2775 (1966).
12. H. STAAB. Ann. Chem. **708**, 36 (1967).
13. D. R. EATON and K. ZAW. Can. J. Chem. **49**, 3315 (1971).
14. D. R. EATON and K. ZAW. Inorg. Chim. Acta, **16**, 61 (1976).
15. D. R. EATON and K. ZAW. J. Inorg. Nucl. Chem. **38**, 1007 (1976).
16. J. W. RAKSHYS. Inorg. Chem. **9**, 1521 (1970).
17. V. GOLD and C. TOMLINSON. Chem. Commun. 472 (1970).
18. V. M. SHUL'MAN, S. V. LARINOV, T. V. KRAMOREVA, E. I. ARYKOVA, and V. V. YADIMA. Russ. J. Inorg. Chem. **11**, 580 (1966).
19. J. HOCH. C. R. **199**, 1430 (1934).
20. R. KUHN and H. SCHRETZMANN. Ber. **90**, 557 (1957).

Can. J. Chem. Downloaded from www.nrcresearchpress.com by 210.87.254.42 on 09/05/12
For personal use only.

The solubility of water in low-dielectric solvents

JITKA KIRCHNEROVÁ AND GENILLE C. B. CAVE
Department of Chemistry, McGill University, Montreal, P.Q., Canada H3C 3G1

Received November 21, 1975[1]

JITKA KIRCHNEROVÁ and GENILLE C. B. CAVE. Can. J. Chem. **54**, 3909 (1976).

The solubility of water has been measured in several low-dielectric solvents at 25 °C, and the values in the nonpolar solvents are treated by using a modification of the Scatchard–Hildebrand equation. The water–solvent interaction parameter in this equation is represented by a new relationship involving the separate contributions due to dispersion and polar interactions. A new method is given for calculation of the dispersion component of the solubility parameter of a polar species. Formation constants are reported for 1:1 water–solvent complexes in carbon tetrachloride, benzene, toluene, and *p*-xylene.

JITKA KIRCHNEROVÁ et GENILLE C. B. CAVE. Can. J. Chem. **54**, 3909 (1976).

On a mesuré, à 25 °C, la solubilité de l'eau dans plusieurs solvants présentant une faible constante diélectrique et on a traité les valeurs dans ces solvants nonpolaires en utilisant une modification de l'équation de Scatchard–Hildebrand. On représente les paramètres d'interactions eau/solvant dans cette équation par une nouvelle relation impliquant les contributions séparées dues aux interactions de dispersion et polaire. On donne une nouvelle méthode pour calculer la composante de dispersion du paramètre de solubilité d'une espèces polaire. On rapporte les constantes de formation des complexes 1:1 eau/solvant dans le tétrachlorure de carbone, le benzène, le toluène et le *p*-xylène.

[Traduit par le journal]

Introduction

Numerous experimental data have been reported (1–6) for the solubility of water in organic solvents, but there have been few attempts to provide a quantitative interpretation of these solubilities. Black, Joris, and Taylor (7) applied the Scatchard–Hildebrand equation (8, 9) to the solubility of water in several structurally different hydrocarbons, saturated and unsaturated, in order to calculate the solubility parameter of the water (henceforth abbreviated to δ_w). These calculated values agreed reasonably well with the value of 23.43 $cal^{1/2}$ $cm^{-3/2}$ at 25 °C obtained from the energy of vaporization of water, except when olefinic hydrocarbons were the solvents, in which case the values of δ_w were lower.

Wing and Johnson (10), and Jones and Monk (11) also used regular-solution theory to interpret the solubility of water in a number of aromatic hydrocarbons having either alkyl groups or halogens as substituents. Their calculated values for δ_w in these solvents at 25 °C ranged from 23.9 $cal^{1/2}$ $cm^{-3/2}$ when benzene was the solvent, to 25.4 $cal^{1/2}$ $cm^{-3/2}$ when it was *o*-dichlorobenzene.

Hildebrand and Scott (9) have discussed these various values of δ_w as calculated from regular-solution theory.

Goldman (6) and Kirchnerová (12) determined the solubility of water in several nonpolar and halogenated aromatic solvents, at several water activities by using the isopiestic equilibration method. Goldman found, in agreement with others (10, 11), that the solubility of water decreased in the order benzene > chlorobenzene > *o*-dichlorobenzene. This order was the reverse of that found for some other compounds such as metal 8-quinolinates (13).

The demonstrated inadequacy of the Scatchard–Hildebrand equation for the calculation of δ_w is not unexpected, because the equation was intended for nonpolar systems. Anderson and Prausnitz (14) extended the treatment empirically, to account for the behaviour of nonpolar solutes in polar solvents.

The present report proposes a somewhat different approach to the quantitative interpretation of water solubilities in low-dielectric solvents. It uses a modification of the Scatchard–Hildebrand equation, in order to calculate the nonspecific (dispersion, dipole–dipole, and dipole – induced dipole) interactions between water and solvent. It also provisionally makes use of

[1]Revision received August 26, 1976.

Can. J. Chem. Downloaded from www.nrcresearchpress.com by 210.87.254.5 on 09/05/12
For personal use only.

Can. J. Chem. Downloaded from www.nrcresearchpress.com by 210.87.254.5 on 09/05/12
For personal use only.

the concept of a single complex (WS) being formed from water (W) and some nonpolar solvents (S).

Thus, the modified regular-solution equation is used to calculate the contribution of the nonspecific interactions to the solubility of water in a given solvent. The difference between this calculated contribution and the measured solubility is then used to calculate the formation constant of the WS species. For this treatment, reliable published values of water solubility (1, 2, 6) were supplemented by values measured in the present work.

Experimental

Materials

Cyclohexane (Fisher C-555), *p*-xylene (Fisher 277), and benzene (Fisher B-245) were further purified by double crystallization. Carbon tetrachloride (Fisher C-199), chlorobenzene (Fisher B-255), and *o*-dichlorobenzene (Fisher 494) were washed successively with concentrated sulfuric acid, twice with distilled water, 10% aqueous solution of K_2CO_3, and finally several times with distilled water. The products were dried over silica gel, then fractionally distilled under nitrogen, using a one-metre distilling column packed with Raschig rings. During the distillation, cuts were monitored by gas chromatography, and the cut of best quality retained for use. The densities of these retained cuts at 25.0 ± 0.02 °C were found to be: cyclohexane, 0.7734 ± 0.0001 (lit. (15) 0.77391); carbon tetrachloride, 1.5844 ± 0.0001 (lit. (15) 1.58439); *p*-xylene, 0.85655 ± 0.00006 (lit. (15) 0.85669); benzene, 0.87378 ± 0.00005 (lit. (15) 0.87368); chlorobenzene, 1.1009 ± 0.0001 (lit. (15) 1.10082); *o*-dichlorobenzene, 1.30024 ± 0.00008 (lit. (15) 1.30033). The purity of the purified cyclohexane was estimated by gas chromatographic analysis of impurities to be 99.6%, and that of the other solvents to be better than 99.8%.

Distilled, de-ionized water was used for the solubility studies. The calcium chloride dihydrate was Fisher C-79, certified grade.

Apparatus and Procedures

Isopiestic Equilibration

The equilibration vessels were in some cases 250-ml, conical, ground-glass stoppered iodine flasks, and in other cases 250-ml conventional, ground-glass stoppered reagent bottles. Approximately 50 ml of the organic solvent were placed in the vessel. A 10-cm × 1-cm test tube containing 6 ml of water or of a standardized aqueous solution of $CaCl_2$ was then placed in the vessel so that the rim of the test tube rested against the upper inside wall of the vessel. The vessel was then stoppered, placed inside a plastic bag, and the jacketed vessel was submerged up to its neck in a water thermostat at 25.0 ± 0.1 °C. Care was taken to ensure that the water level was above the bottom of the stopper in the equilibration vessel. Trials had shown that the stoichiometric concentration of water in the solvent became constant within 2 days.

Ten-millilitre aliquots of the water-saturated solvent were transferred to a dried Karl Fischer titration vessel for a determination of the water content. The transfer was made by means of a special pipet, which had a water jacket through which water at 25.0 ± 0.1 °C was circulated. The dried pipet was always prerinsed with the water-saturated solvent.

Karl Fischer Titration for Total Water

The stoichiometric concentration of water in each water-saturated solvent was determined by a conventional Karl Fischer dead-stop back-titration. A standard, completely closed Radiometer Titration Assembly (type TTA1) with a special custom-made titration cell was used. This cell had a glass T side-tube. One arm of the T served as a sample-injection port that could be closed by an attached rubber sleeve and a clamp. The other arm was an inlet for a stream of dried nitrogen gas. A T 32/40 joint accommodated the removable glass head of the cell. Two platinum electrodes sealed in this glass head were connected to a Beckman Zeromatic II potentiometer, and polarized by a 10-μA current. The upper opening of the automatic buret holding the Karl Fischer reagent was protected by a P_2O_5 tube. To pump this reagent into the buret from its reservoir, a rubber bulb was used with its air-intake protected by a P_2O_5 tube. To pump the standard water solution from its reservoir into the other buret, a rubber bulb was used with its air supply being prewashed with methanol.

The Karl Fischer reagent (Fisher SO-K-3) was diluted with diluent (Fisher SO-K-5) which had been pre-dried with Linde A-type molecular sieves.

The solubility of water in each solvent and for each water activity of the $CaCl_2$ solutions was determined in triplicate.

Results

The mean value found in the present work for the solubility of water at unit activity in each solvent at 25 °C is entered in Table 1, together with selected literature values for several solvents. The table also lists the molar volume (V_s) and the solubility parameter (δ_s) of each solvent.

The solubilities at several different water activities were also measured both during the present work with the complete data reported elsewhere (12), and also by the other investigators listed in Table 1. The isopiestic equilibration method was used. These data showed that in the first eight solvents listed in Table 1, water obeyed Henry's law. However, in the last three solvents in the table this law was not obeyed, and the solubility of water was much higher than in solvents having comparable solubility parameters and polarities. These higher solubilities have been attributed (1, 4) to the existence of water trimers, a conclusion which has been further supported by infrared (16) and proton magnetic resonance studies

TABLE 1. Solubility of water in selected solvents, molar volume (V_s) and solubility parameter (δ_s) of each solvent, at 25 °C*

Solvent	V_s (ml/mol)	δ_s (cal$^{1/2}$ cm$^{-3/2}$)	Solubility of water		Reference for solubility data
			mol/l	mole fraction	
Hexadecane	292.8	8.01	0.0029	0.00085	1
Cyclohexane	108.7	8.19	0.0029	0.00032	2
			0.0030		This work†
CCl_4	97.1	8.58	0.0087	0.00085	1
			0.0087		This work†
p-Xylene	123.9	8.77	0.0217	0.00269	This work†
Toluene	106.9	8.91	0.0270	0.00283	2
			0.0265		4
Benzene	89.4	9.16	0.0349	0.00312	1
			0.0349		This work†
			0.0345		6
Chlorobenzene	102.2	9.68	0.0290	0.00297	6
			0.0290	0.00297	This work†
o-Dichlorobenzene	113.1	10.05	0.0240	0.00271	6
			0.0240	0.00271	This work†
Chloroform	80.7	9.49	0.0738	0.00596	3
			0.0732		5
1,2-Dichloroethane	79.4	9.78	0.1262	0.01010	1
			0.1264		3
1,1,2,2-Tetrachloroethane	105.8	9.80	0.1010	0.01070	1

*Values of V_s were from densities (15), and those of δ_s were calculated with RT correction, from values of ΔH_{298} in ref. 15.
†The standard deviation of the water determination was 0.0002 M, for $n = 5$.

(5, 17). The solubilities for both polar and nonpolar solvents are compiled in Table 1 for comparative purposes, but in the present report only the data on the nonpolar solvents are quantitatively interpreted.

Treatment of the Data

In its general form, and with the Flory–Huggins size-correction term added, the Scatchard–Hildebrand equation for the activity coefficient of a solute (subscript 2) at infinite dilution (γ_2^∞) in a solvent (subscript 1) can be written (18) as

$$[1] \quad RT \ln \gamma_2^\infty = V_2(C_{11} + C_{22} - 2C_{12}) + RT\left(\ln \frac{V_2}{V_1} + 1 - \frac{V_2}{V_1}\right)$$

where V_1 and V_2 are the molar volumes, and C_{11} and C_{22} are the cohesive energy densities of the pure liquids 1 and 2, respectively. It is usual to write

$$V_1 C_{11} = \Delta E_1^v = V_1 \delta_1^2$$

where ΔE_1^v is the molar energy of vaporization of liquid 1, and δ_1 is by this definition its solubility parameter; similarly for C_{22}. The parameter C_{12} reflects the pair interaction between solute and solvent. For both components nonpolar, Scatchard proposed $C_{12}^2 = C_{11}C_{22}$.

This geometric-mean approximation has proved useful for binary nonpolar systems; but experimental data (19, 20) indicate that even then it is not strictly valid for many such systems. Empirical corrections to the geometric mean have been proposed (18) by using an empirical binary coefficient. In addition, there have been theoretical calculations (21, 22) of these deviations of C_{12} from the geometric-mean value. However, a method of general validity based on some macroscopic properties of the components is still not available.

The application of [1] to polar–nonpolar binary systems is more complicated. One approach (18) has been to let $C_{11} = {}^d\delta_1^2 + {}^p\delta_1^2$ and $C_{22} = \delta_2^2$. Here, ${}^d\delta_1$ is the nonpolar component and ${}^p\delta_1$ the polar component of the

Can. J. Chem. Downloaded from www.nrcresearchpress.com by 210.87.254.5 on 09/05/12
For personal use only.

Can. J. Chem. Downloaded from www.nrcresearchpress.com by 210.87.254.5 on 09/05/12
For personal use only.

solubility parameter of the polar liquid 1, and 2 is the nonpolar liquid whose total solubility parameter is δ_2. The value of C_{12} was assumed to be given by

$$C_{12} = {}^{d}\delta_1\delta_2 + \psi_{12}$$

where ψ_{12} takes into account the dipole – induced dipole interactions between liquids 1 and 2.

In the present report, a modified method is proposed for estimation of the contributions which the nonspecific molecular interactions make toward C_{11}, C_{22}, and C_{12}. The treatment is intended for polar–nonpolar binary mixtures. As an example, it is applied in the present paper to saturated solutions of water in nonpolar solvents.

Extension of the proposed method to include polar–polar binary mixtures is under study, but is not yet at the point where, for example, the solubility of water in polar solvents (Table 1) can be treated.

Superscripts d, p, and h will denote the contributions to a given parameter, due to dispersion forces, polar forces (dipole–dipole and dipole – induced dipole), and hydrogen bonds respectively. Subscripts w and s will denote the components water and solvent, respectively. Superscript v will denote vaporization.

Hansen (23) wrote

$$[2] \qquad \Delta E_w^{v} = \Delta^{d}E_w + \Delta^{p}E_w + \Delta^{h}E_w$$

for liquid water, where the terms on the right denote the contributions to energy of vaporization, due to the designated forces. He did not give explicit definitions of $\Delta^{p}E_w$ and $\Delta^{h}E_w$. We shall need to do so, in a way that will ensure they are independent of each other. For this purpose the model of Scheraga and co-workers (24) of liquid water will be invoked, *i.e.* hydrogen-bonded aggregates with a size distribution. One may then suppose that a two-stage process occurs: first, all the hydrogen bonds in every aggregate are broken to leave a hypothetical liquid of dipolar monomers. Then, this hypothetical liquid is vaporized to produce real water vapour (which is more than 95% monomeric). Thus, for one mole

$$[3] \quad \text{Real liquid water} \xrightarrow{\Delta^{h}E_w} \text{Hypothetical liquid of dipolar monomers} \xrightarrow{\Delta^{d}E_w + \Delta^{p}E_w} \text{Real monomeric vapour}$$

A quantitative treatment and applications of this concept to water–alcohol–solvent systems will be the subject of a separate report.

From [2], the total solubility parameter δ_w of water may be represented in terms of its contributing parts:

$$[4] \qquad \delta_w^2 = {}^{d}\delta_w^2 + {}^{p}\delta_w^2 + {}^{h}\delta_w^2$$

but those parts are defined by process [3], above.

Guided by the well-known equations of Debye and Keesom for the averaged dipole – induced dipole interactions and the dipole–dipole interactions of a pair of like molecules having a permanent dipole moment μ in a dilute gas, it is convenient to define the polar solubility parameter ${}^{p}\delta$ of a pure liquid as

$$[5] \qquad {}^{p}\delta^2 = 2k^{d}\delta\theta + \theta^2$$

where θ is a parameter that is a function of μ^2. Thus, the term $2k^{d}\delta\theta$ is intended to represent the induced dipole (proportional to ${}^{d}\delta$) – dipole (proportional to θ) contribution to the cohesive energy density of a pure liquid. The factor k compensates for the change in the potential energy formulae on which [5] is based, on going from a two-body interaction in a dilute gas to the many-body interactions in the liquid. This factor also includes the change in dipole moment, a matter discussed by Böttcher (25).

It is next assumed that for any binary system the solute–solvent pair interaction parameter C_{12} in [1] can be represented by the sum of the contributions arising from nonspecific (dispersion and polar) interactions, and specific (*e.g.* hydrogen-bond) interactions. Then for the system water–solvent

$$[6] \qquad C_{ws} = {}^{d}C_{ws} + {}^{p}C_{ws} + {}^{c}C_{ws}$$

where superscript c replaces h merely to indicate a complex.

It will further be assumed, as usual (18), that the geometric-mean approximation is adequate for ${}^{d}C_{ws}$,

$$[7] \qquad {}^{d}C_{ws} = {}^{d}\delta_w\,{}^{d}\delta_s$$

For the case of a polar solute (water here) where Henry's law is obeyed in a nonpolar solvent, the rationale used to construct [5] is used to define ${}^{p}C_{ws}$. Then

$$[8] \qquad {}^{p}C_{ws} = k^{d}\delta_s\theta_w$$

and, with [6] and [7]

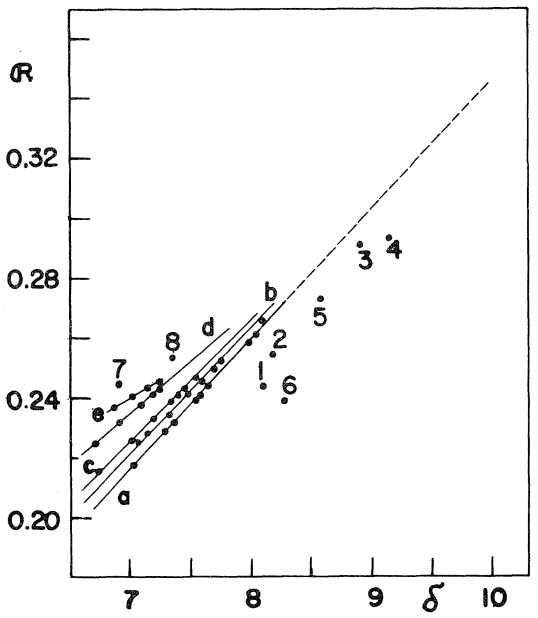

FIG. 1. Relationship between the solubility parameter (δ) and refractivity (R) of selected liquids. (*a*) *n*-alkanes; (*b*) *n*-1-alkenes; (*c*) 2-methylalkanes; (*d*) 2,2-dimethylalkanes; (*e*) 2,2,3-trimethylalkanes; (*1*) cyclopentane; (*2*) cyclohexane; (*3*) benzene; (*4*) toluene; (*5*) carbon tetrachloride; (*6*) hexafluorobenzene; (*7*) 2,2,4,4-tetramethylpentane; (*8*) 2,2,3,3-tetramethylpentane.

$$[9] \qquad C_{ws} = {}^{d}\delta_w {}^{d}\delta_s + k^{d}\delta_s\theta_w + {}^{c}C_{ws}$$

where ${}^{c}C_{ws}$ is the contribution due to any solute–solvent complexes in the binary mixture.

In order to make use of [9], it is necessary to have an independent means of evaluating ${}^{d}\delta$ for pure liquids. Previously proposed methods employed the homomorph concept (14, 26). A convenient alternative method is now proposed.

Evaluation of ${}^{d}\delta$

The term ${}^{d}\delta$ in [4] represents the contribution made by London dispersion forces to the total solubility parameter of a liquid. This term would be expected to be a function of the polarizability of the molecule, which in turn is known to be a function of the refractive index of the liquid. Scatchard (27) had in fact observed that the solubility parameters of straight-chain hydrocarbons were closely related to the refractivity values, R, of the liquid hydrocarbons

$$R = (n_d^2 - 1)/(n_d^2 + 2)$$

where n_d is the refractive index of the liquid.

Therefore, we have re-investigated the relationship between solubility parameter and refractivity, in our search for a method of evaluating ${}^{d}\delta$. First, the values of δ(total) and R at 25 °C were calculated and tabulated for more than 150 liquids (nonpolar and polar, including water and alcohols), from the literature data (15, 28). The values of the refractivities and solubility parameters for 40 nonpolar hydrocarbons are plotted in Fig. 1. Data for these and an additional 110 liquids are tabulated elsewhere (12).

Each line in Fig. 1 represents a homologous series. The six isolated points to the right of the *n*-alkane line belong to carbon tetrachloride and cyclic hydrocarbons: hexafluorobenzene, cyclopentane, cyclohexane, benzene, and toluene.

The points for polar and associated liquids lie much further to the right, and are not shown in Fig. 1.

For a polar component of a binary solution it is proposed that it be assigned a value for ${}^{d}\delta$ equal to that of its equistructural hydrocarbon, namely the one having the polar group replaced by a methyl group. For example, the value of ${}^{d}\delta$ for 2-chloroheptane would be taken as being the value of ${}^{d}\delta$ for 2-methylheptane, found by referring the refractivity of 2-methylheptane to the line for the 2-methylalkanes (*b* of Fig. 1).

The System Water – Nonpolar Solvent

For those saturated solutions of water in nonpolar solvents (*i.e.* the solution is in equilibrium with pure water), where the water obeys Henry's law ($\gamma_w = \gamma_w^{\infty}$) and its standard state is pure water, then if x_w is the mole-fraction solubility of water, [1] can be re-written as

$$[10] \qquad -RT\left(\ln x_w + \ln\frac{V_w}{V_s} + 1 - \frac{V_w}{V_s}\right) = V_w(\delta_w^2 + \delta_s^2 - 2C_{ws})$$

The values of C_{ws} for six water – nonpolar solvent mixtures were calculated by using [10] and the data for x_w, V_w, V_s, and δ_s given in Table 1, together with the value of 23.43 cal$^{1/2}$ cm$^{-3/2}$ for δ_w found from its molar energy of vaporization. The resulting values of C_{ws} are found in Table 2.

On re-writing [9] as

$$[11] \qquad \frac{C_{ws}}{{}^{d}\delta_s} = ({}^{d}\delta_w + k\theta_w) + \frac{{}^{c}C_{ws}}{{}^{d}\delta_s}$$

Can. J. Chem. Downloaded from www.nrcresearchpress.com by 210.87.254.5 on 09/05/12
For personal use only.

TABLE 2. Interaction parameters C_{ws} and ${}^{c}C_{ws}$ for six water – nonpolar solvent mixtures at 25 °C

Solvent	C_{ws} (cal/cm^3)	C_{ws}/δ_s (cal$^{1/2}$/cm$^{3/2}$)	${}^{c}C_{ws}$ (cal/cm^3)
Hexadecane	160.3	20.0	Nil
Cyclohexane	160.3	19.6	Nil
CCl_4	181.1	21.1	11.2
p-Xylene	198.3	22.6	24.6
Toluene	202.4	22.7	25.8
Benzene	208.7	22.8	27.5

and noting that in Table 2 all the solvents are nonpolar, so that $\delta_s = {}^{d}\delta_s$, then $C_{ws}/{}^{d}\delta_s$ may be evaluated. The results are in Table 2. Based on the known mean deviation of the measured values in Table 1 for the solubility of water in hexadecane and cyclohexane, the mean deviation in $C_{ws}/{}^{d}\delta_s$ would be approximately ± 0.3. Consequently, in Table 2 the values of $C_{ws}/{}^{d}\delta_s$ for hexadecane and cyclohexane are considered to agree, and their mean value of 19.8 cal$^{1/2}$ cm$^{-3/2}$ is used. Further, it is assumed that for these two solvents water–solvent complexes are not formed (${}^{c}C_{ws} = 0$). Then from [11]

$$[12] \qquad {}^{d}\delta_w + k\theta_w = 19.8$$

Then from [6], [11], and [12]

$$[13] \quad C_{ws} - {}^{c}C_{ws} = 19.8\delta_s = {}^{d}C_{ws} + {}^{p}C_{ws}$$

The values of $(C_{ws} - 19.8\delta_s)$ for carbon tetrachloride, *p*-xylene, toluene, and benzene are given as ${}^{c}C_{ws}$ in Table 2. They are taken to indicate the presence of water–solvent complexes. In addition, the values of $({}^{d}C_{ws} + {}^{p}C_{ws})$ for a system are seen from [13] to be given by $19.8{}^{d}\delta_s$. These values for four systems are entered in Table 3; and substitution of them in lieu of the term C_{ws} in [10] permitted calculation of the contribution $(\tilde{x}_w)$ of the nonspecific water–solvent interactions to the solubility of water. These calculated contributions are found in Table 3. Then the difference between the experimental (*i.e.* total) solubility (x_w) of water (Table 3) and the value of $\tilde{x}_w$ is assumed to be due to a 1:1 water–solvent complex having a concentration x_{ws} mole fraction in the particular solvent. In making this assumption it is recognized that the only excess entropy term that has been taken into account is the difference in molar volumes of solute and solvent. The calculated contributions in Table 3 would by this assumption then be the mole fraction $\tilde{x}_w$ of free water in the saturated solution. For the case where all activity coefficients are unity, the formation constant K_{ws} of the 1:1 complex is given by

$$[14] \qquad K_{ws} = \frac{x_{ws}}{\tilde{x}_w x_s}$$

where x_s is the mole fraction of the solvent. The reference states for water and the complex are taken to be infinitely dilute solutions, and that of the solvent to be the pure solvent. The solutions were sufficiently dilute for all activity coefficients to be taken as being unity. The values calculated for K_{ws} are in Table 3. In view of the approximations used throughout, these values can only be estimates.

The deviations between calculated and experimental solubilities admittedly do not constitute unequivocal evidence of complex formation. However, the formation of complexes between water and some aromatic solvents has previously been proposed on several grounds: solubility data (9, 29, 30), solvent-extraction data (31), partial molar volumes (32), and particularly the shift in infrared stretching frequencies (33–36). However, formation constants have not previously been reported.

Complexes have also been reported between

TABLE 3. Calculated values for the formation constants (K_{ws}) of a proposed 1:1 water–solvent complex in four solvents at 25 °C

Solvent	${}^{d}C_{ws} + {}^{p}C_{ws}$ (cal/cm^3)	Solubility of water ($\times 10^5$) (mole fraction)		K_{ws}
		Calculated*	Experimental	
CCl_4	169.9	43	85	1.0
p-Xylene	173.6	60	269	3.5
Toluene	176.4	58	283	3.9
Benzene	181.4	60	312	4.2

*Based on the contribution of the nonspecific water–solvent interactions only.

Can. J. Chem. Downloaded from www.nrcresearchpress.com by 210.87.254.5 on 09/05/12
For personal use only.

Can. J. Chem. Downloaded from www.nrcresearchpress.com by 210.87.254.5 on 09/05/12
For personal use only.

TABLE 4. Literature values for the formation constant K_{AS} for 1:1 complexes between phenol and solvent, and *tert*-butyl alcohol and solvent

	K_{AS}			
	Phenol		*tert*-Butyl alcohol	
Solvent	l/mol*	Mole fraction†	l/mol‡	Mole fraction†
p-Xylene	0.39	3.2	0.20	1.6
Toluene	0.39	3.6	0.19	1.8
Benzene	0.33	3.7	0.17	1.9

*Values at 29 °C, from ref. 37.
†l/mol values reported in refs. 37 and 38 converted to mole-fraction basis.
‡Values at 26 °C, from ref. 38.

alcohols and aromatic solvents, and several formation constants are available. For example, Table 4 gives the values reported for 1:1 complexes between the solvents *p*-xylene, toluene, and benzene with phenol (37) and with *tert*-butyl alcohol (38), as determined from infrared measurements. That *tert*-butyl alcohol has much lower values than phenol is presumably due to the lower acidity of the former solute. The acidity of water is slightly lower than that of phenol so that the values of K_{ws} in Table 3 should reflect this difference, and they do. Thus, our proposal of 1:1 complexes, and the estimates of their formation constants appear to have some basis, and may be useful in the prediction of water solubilities.

Based on dissolved water interacting with the inert solvents hexadecane and cyclohexane only by dispersion and polar forces, a value of 19.8 $cal^{1/2}\,cm^{-3/2}$ was found above for the sum $({}^{d}\delta_w + k\theta_w)$, of [11]. For solutions where ${}^{c}C_{ws}$ is negligible, the value 19.8 $cal^{1/2}\,cm^{-3/2}$ may be used with a known value of ${}^{d}\delta_s$, to estimate from [9] and [10] the solubility of water in nonpolar solvents. In addition, the demonstrated relationship between ${}^{d}\delta$ and the refractivity of a nonpolar liquid leads to a value of 6.8 $cal^{1/2}\,cm^{-3/2}$ for ${}^{d}\delta_w$. Therefore, $k\theta_w$ will then be 13.0 $cal^{1/2}\,cm^{-3/2}$. This value indicates that dipole–induced dipole interaction is stronger than current theory supposes, because it is larger than would be theoretically predicted (39).

A theoretical method for the calculation of k is not yet available. As an approximation, it will be supposed that its value is independent of the solvent, and we shall try $k = 1$. Then for liquid water, substitution of $k\theta_w = 13.0$ and ${}^{d}\delta_w = 6.8$ into [5] gives ${}^{p}\delta_w{}^2 = 346$ cal cm^{-3}. Therefore for the vaporization of a mole of liquid water present in a hypothetical state in which it consists solely of dipolar monomers (step 2 in eq. 3), ΔE^v will be $({}^{d}\delta_s{}^2 + {}^{p}\delta_w{}^2)V_w$. This value is 7.1 kcal/mol at 25 °C. Now Scheraga and Owicki[2] calculated by using their latest model of liquid water that ΔE^v for this hypothetical step is 8.32 kcal/mol at 25 °C. Alternatively, use of this latter value leads to $k = 0.84$. This value may be compared with the range of values 0.42–0.57 for six polar, nonhydrogen-bonding organic solutes in *n*-heptane, found recently by Milanová (40) and soon to be reported and discussed. In the present paper k has not been assumed to be constant for all solutes. Milanová's results show that even among simple polar solutes a variation in k is to be expected. Therefore, for a solute such as water a value of 0.84 does not seem surprising. These results are considered to lend credibility to [8], and therefore to our method of calculating the value of the parameter C_{12} for dilute solutions of a polar solute in a nonpolar solvent. The substitution of this calculated value for C_{12} in [1] allows the activity of the polar solute in such a solution to be estimated.

An additional use of the concept of hypothetical states for the water is to consider the process

[15] Real liquid water $\xrightarrow{\Delta E_l{}^v}$ Hypothetical vapor of the same *n*-mers as were in the real liquid, and in the same proportion

Scheraga and Owicki[2] calculated $\Delta E_l{}^v$ to be 5.36 kcal/mol. Now if the Scatchard–Hildebrand equation or a modification of it is to be used in order to calculate, for example, the solubility of an inert solute in water as the solvent, the value which should be used for the total solubility parameter δ_w for the water is not 23.43 $cal^{1/2}\,cm^{-3/2}$, because the solution process would not be expected much to reduce the *n*-mer distribution in the water. Instead, the solubility parameter corresponding to [15] would be used.

Acknowledgments

We are grateful to Prof. H. A. Scheraga and J. Owicki for the calculated energies quoted for water, and to the National Research Council of Canada for financial assistance and for a Bursary to one of us (J.K.).

[2]H. A. Scheraga and J. Owicki, private communication.

1. J. R. JOHNSON, S. D. CHRISTIAN, and H. E. AFFSPRUNG. J. Chem. Soc. A, 77 (1966).
2. J. R. JOHNSON, P. J. KILPATRICK, S. D. CHRISTIAN, and H. E. AFFSPRUNG. J. Phys. Chem. **72**, 3223 (1968).
3. W. L. MASTERTON and M. C. GENDRANO. J. Phys. Chem. **70**, 2895 (1966).
4. P. K. GLASOE and S. D. STULTZ. J. Chem. Eng. Data, **17**, 66 (1972).
5. L. ÖDBERG, A. LÖFVENBERG, E. HÖGFELDT, and F. FREUNDLUNG. J. Inorg. Nucl. Chem. **34**, 2605 (1972).
6. S. GOLDMAN. Ph.D. Thesis. McGill University, Montreal, Quebec. 1969.
7. C. BLACK, G. G. JORIS, and H. S. TAYLOR. J. Chem. Phys. **16**, 537 (1948).
8. G. SCATCHARD. Chem. Rev. **8**, 321 (1931).
9. J. H. HILDEBRAND and R. L. SCOTT. Solubility of nonelectrolytes. 3rd. ed. Reinhold, New York. 1950.
10. J. WING and W. H. JOHNSTON. J. Am. Chem. Soc. **79**, 864 (1957).
11. J. R. JONES and C. B. MONK. J. Chem. Soc. 2633 (1963).
12. J. KIRCHNEROVÁ. Ph.D. Thesis. McGill University, Montreal, Quebec. 1974.
13. T. KHIN. Ph.D. Thesis. McGill University, Montreal, Quebec. 1971.
14. R. ANDERSON and J. M. PRAUSNITZ. AIChE J. **7**, 96 (1961).
15. J. A. RIDDICK and W. B. BUNGER. Techniques of chemistry. Vol. II. Organic solvents. 3rd ed. John Wiley, New York. Interscience. 1970.
16. C. JOLICOEUR and A. CABANA. Can. J. Chem. **46**, 567 (1968).
17. T. F. LIN, S. D. CHRISTIAN, and H. E. AFFSPRUNG. J. Phys. Chem. **69**, 2980 (1965).
18. J. H. HILDEBRAND, J. M. PRAUSNITZ, and R. L. SCOTT. Regular and related solutions. Van Nostrand Reinhold, New York. 1970.
19. R. L. SCOTT. Ann. Rev. Phys. Chem. **7**, 43 (1956).
20. M. L. MCGLASHAN. Chem. Soc. (London) Ann. Rep. **59**, 73 (1962).
21. J. M. REED. J. Phys. Chem. **59**, 425 (1955).
22. E. S. THOMSEN. Acta Chim. Scand. **25**, 260 (1971).
23. C. M. HANSEN. J. Paint Technol. **39**, 105 (1967).
24. A. T. HAGLER, H. A. SCHERAGA, and G. NÉMETHY. J. Phys. Chem. **76**, 3229 (1972).
25. C. J. F. BÖTTCHER. Theory of electric polarization. Elsevier, Amsterdam. 1952.
26. A. BONDI and D. J. SIMKIN. J. Chem. Phys. **25**, 1073 (1956).
27. G. SCATCHARD. Chem. Rev. **44**, 7 (1949).
28. F. D. ROSSINI, K. S. PITZER, R. L. ARNEFF, R. M. BRAUN, and G. C. PIMENTEL. Selected values of physical and thermodynamic properties of hydrocarbons and related compounds. American Petroleum Research Project 44. Carnegie Press, Pittsburgh, Pa. 1953.
29. L. A. K. STAVELY, J. H. E. JEFFERS, and J. A. E. MAG. Trans. Faraday Soc. **39**, 5 (1943).
30. R. L. BOHON and W. F. CLAUSSEN. J. Am. Chem. Soc. **73**, 1571 (1951).
31. E. HÖGFELD and B. BOLANDER. Ark. Kemi, **21**, 161 (1962).
32. W. L. MASTERTON and H. K. SEILER. J. Phys. Chem. **72**, 4257 (1968).
33. E. GREINACHER, W. LÜTTKE, and R. MECKE. Z. Electrochem. **59**, 23 (1955).
34. P. SAUMAGNE and M. L. JOSIEN. Bull. Soc. Chim. Fr. 813 (1958).
35. L. J. BELLAMY. Spectrochim. Acta, **14**, 192 (1959).
36. E. GENTRIC, A. LE NARVON, and P. SAUMAGNE. C.R. Acad. Sci. Ser. C., **270**, 1053 (1970).
37. ZEN-ICHI YOSHIDA and E. ŌSAWA. J. Am. Chem. Soc. **88**, 4019 (1966).
38. M. R. BASOLO, E. L. SAIER, and L. R. COUSING. J. Am. Chem. Soc. **88**, 1665 (1966).
39. J. O. HIRSCHFELDER, C. F. CURTISS, and W. R. BIRD. Molecular theory of gases and liquids. John Wiley and Sons, New York. 1964.
40. E. MILANOVÁ. Ph.D. Thesis. McGill University, Montreal, Quebec. 1975.

Can. J. Chem. Downloaded from www.nrcresearchpress.com by 210.87.254.5 on 09/05/12
For personal use only.

Association and hydration of alcohols in low-dielectric solvents. I. *n*-Butanol

JITKA KIRCHNEROVÁ AND GENILLE C. B. CAVE
Department of Chemistry, McGill University, Montreal, P.Q., Canada H3C 3G1

Received November 21, 1975[1]

JITKA KIRCHNEROVÁ and GENILLE C. B. CAVE. Can. J. Chem. **54**, 3917 (1976).

Formulae and thermodynamic formation constants of the aggregates of *n*-butanol and their hydrates in six low-dielectric solvents have been deduced by using an iterative mathematical treatment of distribution and isopiestic data. The solvents were cyclohexane, carbon tetrachloride, *p*-xylene, benzene, chlorobenzene, and *o*-dichlorobenzene.

JITKA KIRCHNEROVÁ et GENILLE C. B. CAVE. Can. J. Chem. **54**, 3917 (1976).

On a déduit les formules et les constantes de formation thermodynamiques des aggrégats du *n*-butanol et de leurs hydrates dans six solvants de constante diélectrique faible; ces résultats ont été obtenus à l'aide d'un traitement mathématique itératif de données de distribution et isopiestique. Les solvants choisis étaient le cyclohexane, le tétrachlorure de carbone, le *p*-xylène, le benzène, le chlorobenzène et *o*-dichlorobenzène.

[Traduit par le journal]

Introduction

The subject of hydrogen bonding of hydroxylic compounds in solutions continues to be actively studied (1–3). Although the self-association of alcohols and the complexes of water with polar, nonhydroxylic organic compounds have been investigated, very little is known about the hydrates of alcohols and their aggregates. It is the subject of the present report.

The self-association of alcohols and of water in dilute solutions in organic solvents has been studied by several classical physico-chemical methods, and spectroscopic techniques, mainly infrared and nmr (4–7). The interpretation of these data resulted in a variety of models being postulated for alcohol association. Most of them assume an equilibrium between the alcohol monomer and a single *n*-mer; but some disagreement exists about the size and structure of this *n*-mer. (Hereinafter, the term *n*-mer will be used instead of the term aggregate, but its use is not intended to imply necessarily a linear chain.) Most reports propose a tetramer for *n*-alkanols and a trimer for sterically hindered alcohols or phenols (8, 9). Some infrared data have been interpreted in terms of monomer–dimer equilibria (10), or monomer–dimer–*n*-mer (11) when extended to higher concentrations of ethanol. However, recent vapor pressure data for the system methanol–hexadecane were best explained by a monomer–trimer–octamer model (12). Moreover, combined vapor pressure, infrared, and nmr data on the association of *tert*-butyl alcohol in $C_{16}H_{34}$ and in $C_{16}D_{34}$ led to a monomer–trimer–hexamer being proposed for that system (13). Earlier (14), a similar model had been proposed for the association and hydration of phenol in carbon tetrachloride.

The present report is on *n*-butanol. A second one will be on other alcohols. Their purpose is to extend our knowledge of the association of alcohols and of the hydrates of the monomer and co-existing *n*-mers in low-dielectric solvents, particularly to try to understand the effect of the structure of the alcohol and the nature of the solvent on the degree of aggregation and hydration of alcohols. The use of higher alcohols in the solvent extraction of metals makes this knowledge a contribution to that field. For experimental methods, extraction (distribution) and isopiestic water-solubility techniques were used. The combined use of these two kinds of data has previously been suggested by Johnson *et al.* (15) as a means of studying association phenomena.

Most association studies have used a solution model in which each species is assumed to form an ideal solution. This restricts studies to dilute solutions. In order to be able to detect higher aggregates which may in many cases be neglected at low alcohol concentrations, concentrations of alcohol were in the present work extended to approximately 1 *M*. Accordingly, estimates were

[1]Revision received August 26, 1976.

Can. J. Chem. Downloaded from www.nrcresearchpress.com by 210.87.254.6 on 09/05/12
For personal use only.

Can. J. Chem. Downloaded from www.nrcresearchpress.com by 210.87.254.6 on 09/05/12
For personal use only.

required of the activity coefficients of the various species, and of the variation of those coefficients with the concentrations of alcohol and water.

The solution model used in the present study is a real associated mixture consisting of monomers and n-mers of the alcohol and their hydrates, in the solvent. The activity coefficient γ_r of each of these species (r) in the equilibrium solution was estimated by using a generalized regular-solution equation (16):

$$[1] \quad \ln \gamma_r = \frac{V_r}{RT} \sum\sum(\alpha_{mr} - \tfrac{1}{2}\alpha_{mn})\phi_m\phi_n + \ln \frac{\phi_r}{\xi_r} + 1 - \frac{\phi_r}{\xi_r}$$

Here, the standard and reference states of species r is the pure liquid r; V_r is the molar volume of r, and ϕ_r is its volume fraction defined by

$$\phi_r = \frac{\xi_r V_r}{\sum_n \xi_n V_n}$$

where ξ_r is the true mole fraction of r, to be defined below. The terms α_{mn} represent the interaction-energy parameters ($\alpha_{mn} = \alpha_{nm}$, $\alpha_{mm} = \alpha_{nn} = 0$). Subscripts r, m, and n denote any of the species in the solution, including the solvent.

Experimental

Materials

The solvents (cyclohexane, *p*-xylene, benzene, carbon tetrachloride, chlorobenzene, and *o*-dichlorobenzene) were purified as described elsewhere (17).

The *n*-butanol (Fisher A-384, 99 mol% pure) was dried over molecular sieves for about 2 weeks, then fractionally distilled under nitrogen by using a previously described distillation column and procedure (17). The density of the purified product at 25 °C was 0.8058 ± 0.0001 (lit. (18) 0.80576). Its purity calculated from a gas-chromatographic analysis of the impurities was better than 99.75%. Its water content was determined by a Karl Fischer titration to be less than 0.1%.

Procedure

Distribution Measurements

The distribution ratios of *n*-butanol between water and the organic solvent were measured at 25.0 ± 0.1 °C. Each system consisting of water and a solution of *n*-butanol in the solvent, was equilibrated by using a previously described technique (19). Then samples of each equilibrated phase were analysed in replicate for *n*-butanol, by gas chromatography. The detector was a Pye Series-104 flame-ionization detector coupled to a Research Specialties Co. Model 1605-5 electrometer, its output being recorded by a Sargent Model SRL potentiometric recorder with a Disc integrator, Model 204, Series D. The columns and other parameters chosen were as follows: (*1*) for *n*-butanol in the aqueous phase and in the *p*-xylene, chlorobenzene, and *o*-dichlorobenzene phases, a $\frac{1}{8}$-in. diameter column 1 m long, packed with Silicone oil DC 710 (15 wt.%) on Chromosorb G, 70–80 mesh, at 80 °C; (*2*) for *n*-butanol in the cyclohexane and carbon tetrachloride phases, a similar column 2 m long; (*3*) for *n*-butanol in the benzene phase, a $\frac{1}{8}$-in. diameter column 2 m long, packed with Carbowax 20 M (12 wt.%) on Chromosorb G, 70–80 mesh, at 75 °C.

On using 1–2 μl samples of the organic phase and 1–4 μl samples of the aqueous phase, the response of the flame-ionization detector was linear over the range 0.01–0.5 *M* of alcohol concentrations. In that range, the precision of the alcohol determination was approximately 1% except when the solvent was benzene, in which case, particularly for dilute solutions, precision was 1.5–2%. Samples higher than 0.5 *M* in *n*-butanol were diluted to about 0.4 *M* with the appropriate solvent, prior to analysis.

Water-solubility Measurements

Standard solutions of *n*-butanol in the organic solvent were equilibrated with the water vapour from an adjacent standard aqueous solution of $CaCl_2$, in closed thermostatted vessels. Details of this isopiestic equilibration procedure and subsequent determination of the water content of the equilibrated organic phase have been described elsewhere (17).

Each standard solution of *n*-butanol in the organic solvent was prepared by weight. The density of each solution at 25 °C was also found.

In the case of the more concentrated solutions of alcohol (0.5–1 *M*), up to 14 days were required for isopiestic equilibrium.

The water content of the equilibrium organic phase was determined by a Karl Fischer titration, and the *n*-butanol content was determined by the above-described gas-chromatographic analysis. When a solution of $CaCl_2$ was used as the aqueous phase, the chloride content was determined by an argentometric titration. During the isopiestic equilibration of the systems, the chloride content did not change by more than 1%.

Results

Distribution Studies

The distribution ratio of *n*-butanol between the aqueous and the organic phases was determined for six organic solvents, over a concentration range of 0–1 *M* of *n*-butanol in the organic phase. The corresponding concentration range of *n*-butanol in the equilibrium aqueous phase was found to be approximately 0–0.66 *M*, respectively. It has been reported (20, 21) that in this concentration range aqueous solutions of *n*-butanol can be considered as being ideal ones.

The measured molarities of *n*-butanol in the two equilibrium phases were converted to mole fractions. The distribution ratios of *n*-butanol were then calculated as its stoichiometric mole fraction in the organic phase, to that in the

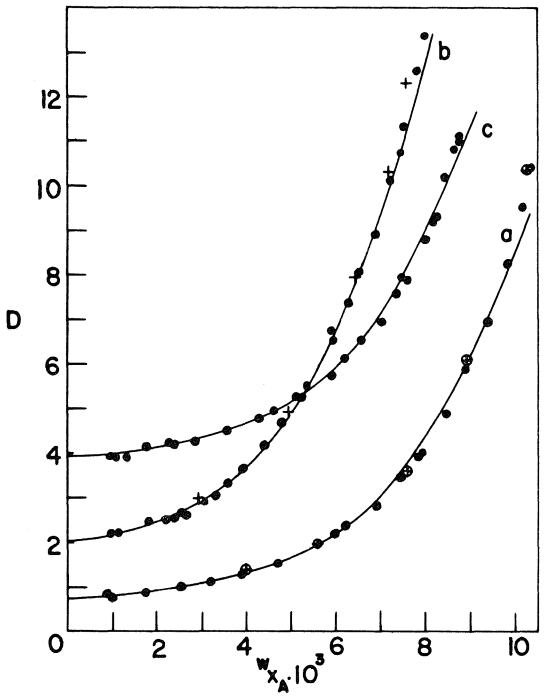

FIG. 1. Distribution ratio (D) for n-butanol between three solvents and water *vs.* mole fraction of n-butanol in the aqueous phase ($^{W}x_A$) at 25 °C. Points are experimental: (*a*) cyclohexane, (*b*) carbon tetrachloride, (*c*) *p*-xylene. Literature values: + (23), ⊕ (24). Curves are calculated for the final association-hydration model (Table 4).

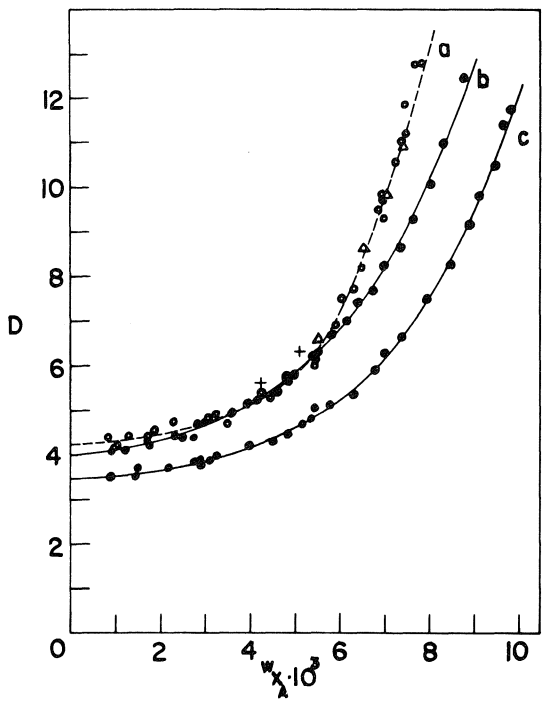

FIG. 2. Distribution ratio (D) for n-butanol between three solvents and water *vs.* mole fraction of n-butanol in the aqueous phase ($^{W}x_A$) at 25 °C. Points are experimental: (*a*) benzene, (*b*) chlorobenzene, (*c*) *o*-dichlorobenzene. Literature values: △ (23), + (25). Curves are calculated for the final association-hydration model (Table 4).

aqueous phase. The plots of all distribution ratios *vs.* mole fraction of n-butanol in the aqueous phase are shown in Figs. 1 and 2 for the six solvents. Tables of these data are available elsewhere (22). Available literature data (23–25) are also shown in Figs. 1 and 2. The curves were calculated from the final solution models and formation constants deduced in the present work.

Isopiestic Water-solubility Studies

The solubility of water in each organic-solvent solution of n-butanol was determined isopiestically in replicate for at least three different water activities. For each water activity, the water solubility was measured for 8 to 25 different concentrations of n-butanol in the organic phase. The average precision of the water determination was 1.0–1.5%.

It has been shown (21) that the change in activity of the water in the aqueous phase due to absorption of small amounts of n-butanol and solvent during the isopiestic equilibration is negligible. Therefore the activity of water in the calcium chloride solutions could be found directly from literature data (26). The accuracy of these values is estimated to be better than 1%.

The water solubilities were measured in molarities, but converted for further treatment into mole fractions by using an appropriate conversion factor (22). The resulting data are shown graphically in Figs. 3 to 8 inclusive where the water solubility for the several water activities is plotted against the mole fraction of n-butanol in the organic phase. Tabulations of all these data are available elsewhere (22).

Treatment of the Data, and Conclusions

The Basic Relationships

The organic phase of the distribution and the isopiestic systems was a three-component solution: n-butanol (A), water (W), and a solvent (S).

Can. J. Chem. Downloaded from www.nrcresearchpress.com by 210.87.254.6 on 09/05/12
For personal use only.

Can. J. Chem. Downloaded from www.nrcresearchpress.com by 210.87.254.6 on 09/05/12
For personal use only.

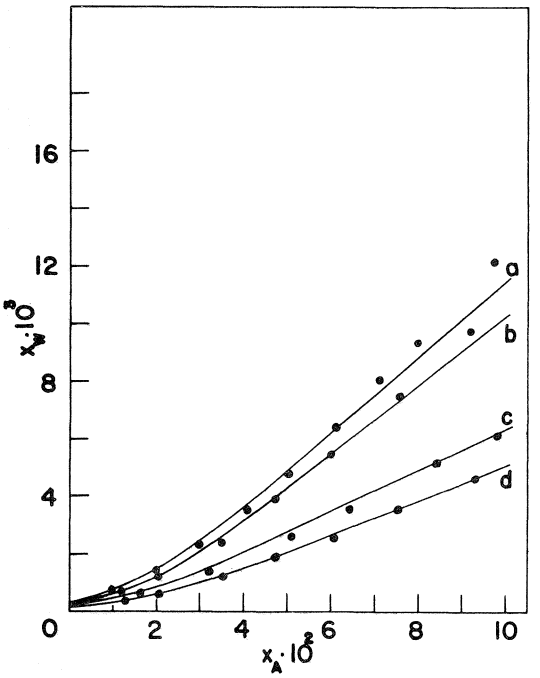

FIG. 3. Solubility of water (mole fraction x_W) in solutions of *n*-butanol in cyclohexane at various water activities (a_W), at 25 °C. Points are experimental. Data are for: (*a*) $a_W = 1.000$; (*b*) $a_W = 0.926$; (*c*) $a_W = 0.662$; (*d*) $a_W = 0.545$. Curves are calculated for the final association-hydration model (Table 4).

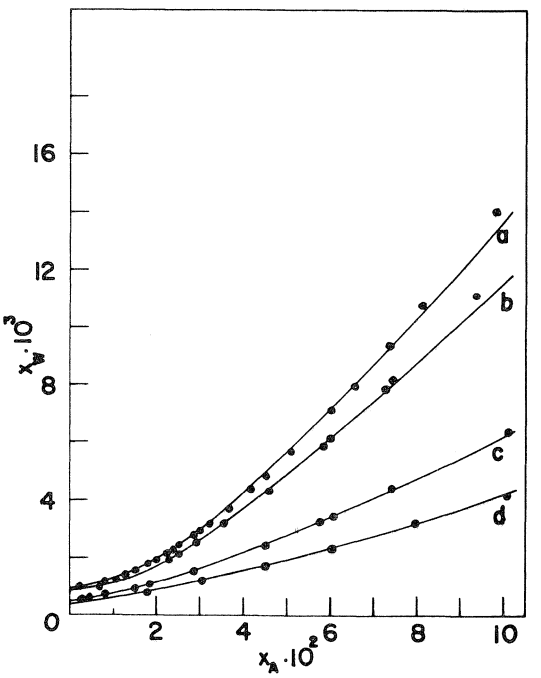

FIG. 4. Solubility of water (mole fraction x_W) in solutions of *n*-butanol in carbon tetrachloride at various water activities (a_W), at 25 °C. Points are experimental. Data are for: (*a*) $a_W = 1.000$; (*b*) $a_W = 0.904$; (*c*) $a_W = 0.585$; (*d*) $a_W = 0.416$. Curves are calculated for the final association-hydration model (Table 4).

In the present treatment it is assumed that the alcohol and water form *n*-mers and hydrates in an inert medium

$$iA_1 + jW_1 \underset{}{\overset{K_{ij}}{\rightleftharpoons}} A_iW_j$$

where A_1 represents the alcohol monomer, W_1 the water monomer, and A_iW_j the hydrate of the alcohol *n*-mer. The thermodynamic equilibrium constant K_{ij} is given by

$$[2] \qquad K_{ij} = \frac{a_{ij}}{a_{10}{}^i a_{01}{}^j} = \frac{\xi_{ij}}{\xi_{10}{}^i \xi_{01}{}^j} \cdot \frac{f_{ij}}{f_{10}{}^i f_{01}{}^j}$$

where a is the activity, ξ the true mole fraction, and f the activity coefficient. The reference state of each species A_iW_j ($i = 0, \ldots, k$; $j = 0, 1, \ldots, l$) is taken to be its infinitely dilute solution in the pure solvent, with the hypothetical pure liquid A_iW_j on the Henry's law line being taken as its standard state. Subscript *ij* denotes species A_iW_j (*e.g.* 10 represents the anhydrous alcohol monomer, and 01 the water monomer).

The stoichiometric number of moles (n_t) of all components in the organic phase is

$$[3] \qquad n_t = n_S + n_A + n_W$$

where n_S, n_A, and n_W are the number of moles of solvent, alcohol, and water, respectively. Moreover,

$$[4] \qquad n_A = \sum_{i=0}^{k} \sum_{j=0}^{l} i n_{ij}$$

$$n_W = \sum_{i=0}^{k} \sum_{j=0}^{l} j n_{ij}$$

and the true number of moles (n_T) in the organic phase is

$$[5] \qquad n_T = n_S + \sum_{i=0}^{k} \sum_{j=0}^{l} n_{ij}$$

Then the stoichiometric (x_{ij}) and the true (ξ_{ij}) mole fractions of any species A_iW_j are $x_{ij} = n_{ij}/n_t$ and $\xi_{ij} = n_{ij}/n_T$, respectively. Then

Can. J. Chem. Downloaded from www.nrcresearchpress.com by 210.87.254.6 on 09/05/12
For personal use only.

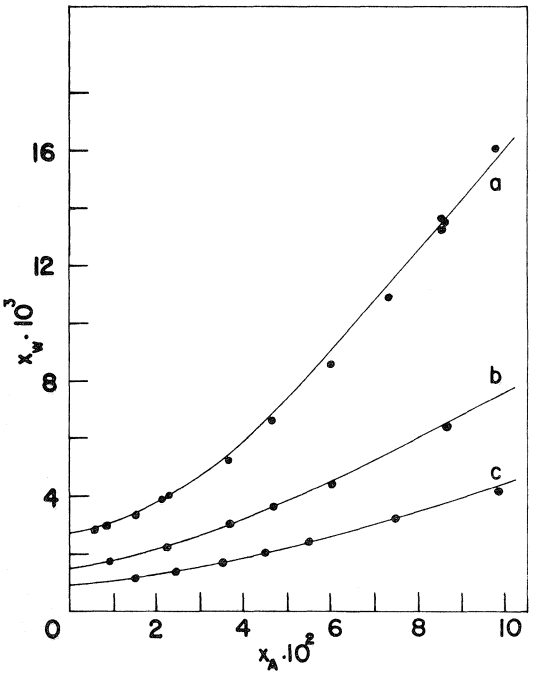

FIG. 5. Solubility of water (mole fraction x_W) in solutions of *n*-butanol in *p*-xylene at various water activities (a_W), at 25 °C. Points are experimental. Data are for: (*a*) $a_W = 1.000$; (*b*) $a_W = 0.558$; (*c*) $a_W = 0.333$. Curves are calculated for the final association-hydration model (Table 4).

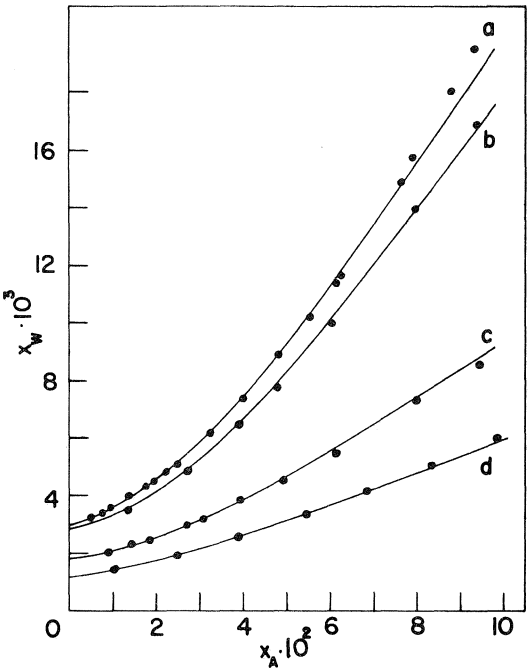

FIG. 6. Solubility of water (mole fraction x_W) in solutions of *n*-butanol in benzene at various water activities (a_W), at 25 °C. Points are experimental. Data are for: (*a*) $a_W = 1.000$; (*b*) $a_W = 0.926$; (*c*) $a_W = 0.581$; (*d*) $a_W = 0.401$. Curves are calculated for the final association-hydration model (Table 4).

$$[6] \qquad \xi_{ij} = x_{ij} \frac{n_t}{n_T}$$

In an associated mixture the chemical potential of a component equals the chemical potential of its monomer (27); and when the reference states are chosen to be infinitely dilute solutions their standard chemical potentials also are equal. Thus, in the organic phase

$$[7] \qquad x_A f_A = \xi_{10} f_{10}$$

for the alcohol, and

$$[8] \qquad x_W f_W = \xi_{01} f_{01}$$

for the water, where x_A and x_W are the stoichiometric mole fractions of alcohol and of water (as components) respectively, in the organic phase.

When aqueous solutions of a given water activity are in equilibrium with the pure solvent on the one hand, and separately with an alcohol–solvent mixture respectively, then

$$[9] \qquad \xi_{01} f_{01} = {}^*\xi_{01} {}^*f_{01}$$

where the * superscript indicates that the water is in the pure organic solvent. Now the solubility of water in the six solvents used in the present work obeyed Henry's law (17). Therefore ${}^*f_{01} = 1$, and ${}^*\xi_{01} = {}^*x_{01}$, where ${}^*x_{01}$ is the stoichiometric solubility of water in a given pure solvent. Then $\xi_{01} f_{01} = {}^*x_{01}$.

For an alcohol distributed between water and an organic solvent, the partition coefficient P of the alcohol considered as a component equals the partition coefficient P_{10} of its monomer, and

$$[10] \qquad P = P_{10} = \frac{\xi_{10} f_{10}}{{}^W x_A {}^W f_A} = \frac{x_A f_A}{{}^W x_A {}^W f_A}$$

where ${}^W x_A$ and ${}^W f_A$ denote the mole fraction and the activity coefficient respectively, of the alcohol in the aqueous phase. In dilute, aqueous solutions where the alcohol obeys Henry's law, ${}^W f_A$ will be unity.

The measured stoichiometric concentrations of alcohol (x_A) and of water (x_W) in a given phase

Can. J. Chem. Downloaded from www.nrcresearchpress.com by 210.87.254.6 on 09/05/12
For personal use only.

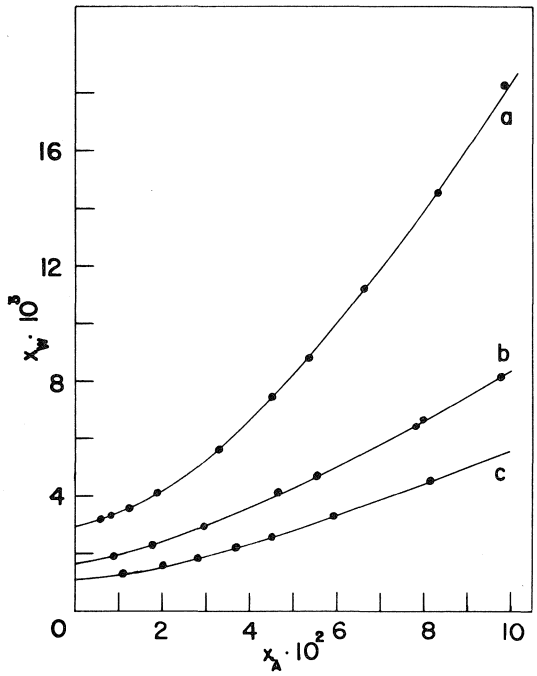

FIG. 7. Solubility of water (mole fraction x_W) in solutions of *n*-butanol in chlorobenzene at various water activities (a_W), at 25 °C. Points are experimental. Data are for: (*a*) $a_W = 1.000$; (*b*) $a_W = 0.553$; (*c*) $a_W = 0.383$. Curves are calculated for the final association-hydration model (Table 4).

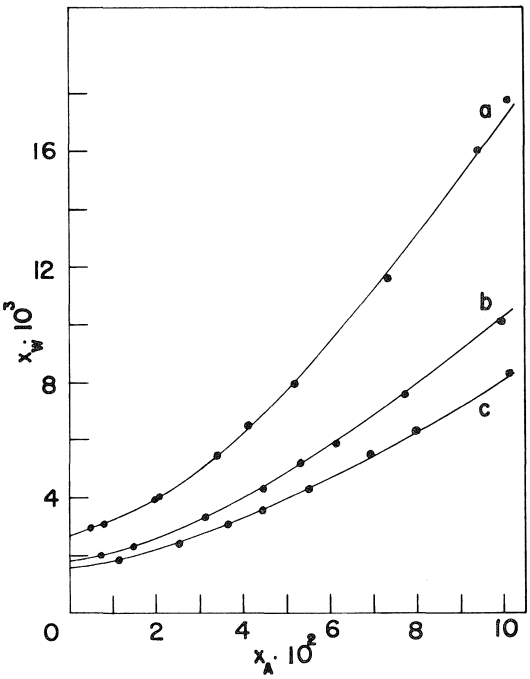

FIG. 8. Solubility of water (mole fraction x_W) in solutions of *n*-butanol in *o*-dichlorobenzene at various water activities (a_W), at 25 °C. Points are experimental. Data are for: (*a*) $a_W = 1.000$; (*b*) $a_W = 0.662$; (*c*) $a_W = 0.553$. Curves are calculated for the final association-hydration model (Table 4).

are related to the concentrations of the corresponding monomers (x_{10}, x_{01}) in that phase, as follows:

$$[11] \quad x_A = \sum_{i=0}^{k}\sum_{j=0}^{l} i x_{ij} = \sum_{i=0}^{k}\sum_{j=0}^{l} \frac{n_T}{n_t} iK_{ij}{}^{*} x_{01}{}^{j} \xi_{10}{}^{i} \frac{f_{10}{}^{i}}{f_{ij}}$$

$$[12] \quad x_W = \sum_{i=0}^{k}\sum_{j=0}^{l} j x_{ij} = \sum_{i=0}^{k}\sum_{j=0}^{l} \frac{n_T}{n_t} jK_{ij}{}^{*} x_{01}{}^{j} \xi_{10}{}^{i} \frac{f_{10}{}^{i}}{f_{ij}}$$

By combining [7], [10], and [11], the distribution ratio of the alcohol ($D = x_A/{}^{W}x_A$) can be expressed as

$$[13] \quad D = \sum_{i=0}^{k}\sum_{j=0}^{l} \frac{n_T}{n_t} iK_{ij}P^{i*} x_{01}{}^{j} f_{ij}{}^{-1} {}^{W}x_A{}^{i-1}$$

Equations 11, 12, and 13 are the sought-for basic relationships for the treatment of the distribution and isopiestic data. Their solution would allow the best association-hydration model for the alcohol in the organic solvent to be deduced, and the equilibrium constants K_{ij} (and partition coefficient P) to be evaluated. However, the activity coefficients f must first be estimated. The usual expedient of assuming that they are unity is avoided in the present work.

These activity coefficients f may be expressed as

$$[14] \quad f_{ij} = \frac{\gamma_{ij}}{\gamma_{ij}{}^{\infty}}$$

where γ_{ij}, and $\gamma_{ij}{}^{\infty}$ for infinite dilution, are the activity coefficients of species A_iW_j when its pure liquid is chosen both as the standard and the reference states.

Equation 1 may be used to express γ_{ij} ($= \gamma_r$). By assuming that

$$[15] \quad V_r = V_{ij} = iV_{10} + jV_{01}$$

and by using [4] and [6], the volume fraction ϕ_r

Can. J. Chem. Downloaded from www.nrcresearchpress.com by 210.87.254.6 on 09/05/12
For personal use only.

of species r

$$\phi_r = \xi_r V_r \Big/ \left(\xi_s V_s + \sum_{i=0}^{k}\sum_{j=0}^{l} \xi_{ij} V_{ij}\right)$$

can be written as

$$[16] \qquad \phi_r = \frac{V_r}{V_s} \frac{x_r}{x_s + \frac{V_{10}}{V_s} x_A + \frac{V_{01}}{V_s} x_W}$$

where V_s and x_s denote the molar volume and the mole fraction, respectively, of the organic solvent.

For the systems studied $V_{10} \simeq V_s$, x_A never exceeded about 0.1, and x_W never exceeded about 0.02. Therefore it was safe to take

$$[17] \qquad \phi_r = \frac{V_r}{V_s} x_r$$

and at infinite dilution

$$[18] \qquad \phi_r^{\infty} = \frac{V_r}{V_s} \xi_r^{\infty}$$

By invoking regular-solution theory, the interaction parameters in the term $\sum_m \sum_n (\alpha_{mr} - \frac{1}{2}\alpha_{mn})\phi_m\phi_n$ of [1] were expressed (28) by $\alpha_{mr} = (\delta_r - \delta_m)^2$. Then the double-summation term reduces to $(\delta_r - \bar{\delta})^2$, where δ_r is the conventional Hildebrand solubility parameter of the solute and $\bar{\delta}$ is the average solubility parameter of the solution:

$$[19] \qquad \bar{\delta} = \sum_m \phi_m \delta_m = \phi_s \delta_s + \sum_{i=0}^{k}\sum_{j=0}^{l} \phi_{ij}\delta_{ij}$$

When the concentrations of alcohol and water in the organic-solvent phase are very low, *i.e.* $x_s \simeq 1$, then $\bar{\delta} \simeq \delta_s$.

The above treatment can strictly be applied only for mixtures of nonpolar molecules. However, the use of [1] has been shown to be reasonable even for numerous solutions with polar components (28). It is further to be noted that it is the value of f_{ij} which is required. Inspection of [14] shows that although the values of γ may be only moderately good estimates, the errors in γ should partially cancel in the ratio.

Substitution of [6], [17], [18], and $(\delta_r - \bar{\delta})^2$ for the double-summation term into [1] gives, with [14]

$$[20] \qquad \ln f_{ij} = \left(\ln \frac{n_T}{n_t}\right) + \frac{V_{ij}}{RT}(\delta_s - \bar{\delta})(2\delta_{ij} - \delta_s - \bar{\delta}) + \frac{V_{ij}}{V_s}\left(1 - \frac{n_T}{n_t}\right)$$

Although the value of solubility parameter δ_s of the solvent is in many cases available, that of δ_{ij} is not, and it presents a problem. Harris and Prausnitz (16) estimated the solubility parameter of a complex BC formed in solution from nonselfassociating liquid components B and C to be

$$\delta_{BC}^2 = \frac{V_B\delta_B^2 + V_C\delta_C^2}{V_B + V_C}$$

by assuming that (*i*) the molar energy of vaporization of BC is the sum of the corresponding molar energies of B and C and (*ii*) the molar volume of BC is the sum of the molar volumes of B and C.

By using the same approach and assumptions, the solubility parameter of A_iW_j in the present systems can be expressed as

$$[21] \qquad \delta_{ij}^2 = \frac{iV_{10}\delta_{10}^2 + jV_{01}\delta_{01}^2}{iV_{10} + jV_{01}}$$

where δ_{10} and δ_{01} are the solubility parameters of hypothetical monomeric liquid alcohol and water, respectively. The known value 8.4 $cal^{1/2}$ $cm^{-3/2}$ for the solubility parameter of *n*-butyl chloride, the polar homolog of *n*-butanol, was used as an estimate of δ_{10}. The value of 17.2 $cal^{1/2}$ $cm^{-3/2}$ was used as an estimate of $\delta_{01}(= \delta_{0j})$. This value was calculated from a value provided by Scheraga and Owicki[2] for the molar energy of vaporization of real water at 25 °C, to produce a hypothetical vapor having the same polymeric composition that Scheraga and co-workers (29) have calculated to describe the polymeric composition of real liquid water.

Equation 21 can be rearranged and a quantity τ_{ij} defined:

$$[22] \qquad \tau_{ij} = \delta_{ij} - \delta_{10} = \delta_{10}\left\{\left[\frac{iV_{10} + jV_{01}\delta_{01}^2\delta_{10}^{-2}}{iV_{10} + jV_{01}}\right]^{1/2} - 1\right\}$$

[2]H. A. Scheraga and J. Owicki, private communication.

Then [11], [12], and [13] give

$$[23] \qquad x_A = \sum_{i=0}^{k} \sum_{j=0}^{l} iK_{ij}(^*x_{01}g_W)^j F_{ij} x_{10}{}^i$$

$$[24] \qquad x_W = \sum_{i=0}^{k} \sum_{j=0}^{l} jK_{ij}(^*x_{01}g_W)^j F_{ij} x_{10}{}^i$$

$$[25] \qquad D = \sum_{i=0}^{k} \sum_{j=0}^{l} iK_{ij}P^i(^*x_{01}g_W)^j F_{ij}(^Wx_A g_A)^{i-1} g_A$$

where

$$[26] \qquad \ln g_W = \frac{V_{01}}{RT}[(\bar{\delta} - \delta_s)(2\delta_{10} - \delta_s - \bar{\delta})] + \frac{V_{01}}{V_s}\left(\frac{n_T}{n_t} - 1\right)$$

$$[27] \qquad \ln g_A = \frac{V_{10}}{RT}[(\bar{\delta} - \delta_s)(2\delta_{10} - \delta_s - \bar{\delta})] + \frac{V_{10}}{V_s}\left(\frac{n_T}{n_t} - 1\right)$$

$$[28] \qquad \ln F_{ij} = 2\frac{iV_{10} + jV_{01}}{RT}\tau_{ij}(\bar{\delta} - \delta_s)$$

In eqs. 23–25, x_A, x_W, D, ^Wx_A, and $^*x_{01}$ were the quantities measured in the present work. In eqs. 26–28 the concentration-dependent quantities g_A, g_W, and F_{ij} could be estimated by an iterative method (22).

Calculations and Conclusions

Closed-form polynomials were selected from the general polynomials of eqs. 23–25, and solved simultaneously by a general iterative least-squares method (30), to give the best statistical fits to the distribution and isopiestic data (illustrated in Figs. 1–8). As a beginning, several plausible sets of these closed-form polynomials were tried with the data, with most of them systematically being eliminated.

However, this method first required rough estimates of the sought-for parameters. These estimates were obtained by deducing from the distribution data alone a preliminary association model of the alcohol in each solvent, without separating the hydrates from the anhydrous *n*-mers. Thus, for $g_A = g_W = F_{ij} = 1$, [25] reduces to

$$[29] \qquad D = \sum_{i=1}^{k} a_i{}^Wx_A{}^{i-1}$$

where the values of i and a_i are given by

$$[30] \qquad a_i = iP^i \sum_{j=0}^{l} K_{ij}{}^*x_{01}{}^j$$

and represent all the *n*-mers of the alcohol without delineating their various degrees of hydration. Equation 29 allows a simple least-squares fit of the distribution data alone to be made. Guided partly by the findings in the literature on alcohol association (7, 9, 10, 12, 13, 15, 31, 32) and partly by the shapes of the distribution graphs (Figs. 1 and 2), various combinations of two, three, and in some cases four a_i parameters in [29] were tried. Table 1 contains the least-squares results of this screening step. In it, each association model is represented numerically; for example, the model monomer–trimer–octamer in equilibrium is denoted by 1–3–8. The values of the mean squares, and the least-squares values of the intercepts for Figs. 1 and 2 (*i.e.* the value of the distribution ratio $(D^\infty)^{cal}$ at infinite dilution of the alcohol) are tabulated. All of the following criteria were then taken into account in judging which models represented the data very well: (*i*) all a_i parameters must be positive and have acceptably low errors; (*ii*) mean squares, and the regression coefficient (not reported in Table 1) were considered jointly although it happened that the mean squares alone led to the same models; (*iii*) of lesser importance, agreement within about 5% between the least-squares value of D^∞ and the value of this intercept by extrapolation of each graph in Figs. 1 and 2.

Can. J. Chem. Downloaded from www.nrcresearchpress.com by 210.87.254.6 on 09/05/12
For personal use only.

TABLE 1. Results of polynomial linear least-squares fits to the distribution data for *n*-butanol

Model	Intercept	Mean squares	Intercept	Mean squares	Intercept	Mean squares
	Cyclohexane		*Carbon tetrachloride*		*p-Xylene*	
	0.740*		1.95*		3.95*	
1–3–8	0.726	0.00520	1.916	0.01332	3.922	0.01302
1–3–6	0.971	0.02520	2.085	0.01086	4.029	0.03353
1–3–5	1.110	0.05902†	2.221	0.01821		
1–3–4	1.183	0.06675†	2.431	0.03705†	4.160	0.05633†
1–3–9	0.658	0.01242	1.863	0.01839		
1–4–8	0.985	0.01346	2.337	0.01642	4.120	0.02994
1–4–6	1.072	0.03305	2.356	0.02237		
1–4	0.462	0.27529	2.172	0.05252	3.815	0.12606
1–2–4	1.356	0.09545‡	2.323	0.01875‡	4.236	0.06491‡
1–2–6	0.634	0.00615	1.271	0.03117	3.679	0.01406
1–2–8	0.210	0.03329	0.753	0.10269		
1–6	1.330	0.06601	3.149	0.46316	4.487	0.10243
1–8	1.710	0.35096	3.627	1.31109	4.834	0.32884
	Benzene		*Chlorobenzene*		*o-Dichlorobenzene*	
	4.13*		3.82*		3.54*	
1–3–8	4.198	0.05130	3.991	0.00878	3.474	0.01339
1–3–6	4.399	0.05435	4.088	0.01782	3.606	0.01818
1–3–5			4.164	0.02694	3.708	0.02966§
1–3–4	4.746	0.10720†	4.218	0.02763§	3.862	0.05238†
1–3–9	4.113	0.06230	3.965	0.00880‖	3.428	0.01403
1–4–8	4.385	0.05345	4.289	0.02776	3.708	0.01860
1–4–6	4.472	0.05758	4.289	0.03299	3.741	0.02643§
1–4	3.893	0.26869	4.179	0.04330	3.462	0.09754
1–2–4			4.144	0.02673	3.864	0.03435‡
1–2–6	4.114	0.04105§	3.505	0.01519	3.179	0.01242
1–2–8	3.667	0.07685	3.196	0.03585	2.843	0.04026
1–6			4.873	0.27377	4.153	0.14685
1–8			5.205	0.68776	4.458	0.46814
1–2–4–6	4.135	0.04280§‖				
1–2–4–8	4.319	0.04648§‖				

*Graphical extrapolation.
†Negative a_i was found for the trimer.
‡Negative a_i was found for the dimer.
§Error in a_i of lower *n*-mer was too large.
‖Error in a_i of higher *n*-mer was too large.

The association model monomer–trimer–octamer was judged the most reasonable one for *n*-butanol in all the solvents except benzene and carbon tetrachloride. In these two, both the monomer–trimer–octamer and the monomer–trimer–hexamer were retained for the next step in the treatment. The least-squares values of a_i for these retained models are available elsewhere (22).

In these choices of models and later choices of their hydrates, uniqueness is not claimed. For one thing, the number of parameters was kept to a minimum consistent with good fits to the data. In addition, judgment was exercised in rejections. For example, it might be argued that the model monomer–trimer–nonamer could have been retained for carbon tetrachloride, benzene, and *o*-dichlorobenzene. It was not retained because it did not seem very reasonable to retain a model for benzene and *o*-dichlorobenzene, which was clearly unacceptable for chlorobenzene.

The model monomer–trimer–octamer was deduced by Tucker *et al.* (12) for the association of methanol both in its vapour and in hexadecane, although it is at variance with other literature (7, 33) which includes the tetramer in two-parameter models.

The final stages in the present treatment extended the above-noted models 1–3–8 and 1–3–6 so as to specify the coexisting hydrates of these species. The computational procedures were lengthy and involved, and are given elsewhere

Can. J. Chem. Downloaded from www.nrcresearchpress.com by 210.87.254.6 on 09/05/12
For personal use only.

Can. J. Chem. Downloaded from www.nrcresearchpress.com by 210.87.254.6 on 09/05/12
For personal use only.

TABLE 2. The range of values for g_A, F_{11}, and F_{84} for *n*-butanol in six solvents

Solvent	g_A	F_{11}	F_{84}
Cyclohexane	1–0.926	1–0.903	1–0.631
Carbon tetrachloride	1–0.927	1–0.956	1–0.816
p-Xylene	1–1.017	1–0.815	1–0.399
Benzene	1–0.964	1–0.923	1–0.716
Chlorobenzene	1–1.071	1–0.900	1–0.616
o-Dichlorobenzene	1–1.169	1–0.809	1–0.383

(22) in detail. They consisted in the necessarily stepwise refinement of crude initial estimates of K_{ij} and P, for each solvent system. Thus, the following steps were carried out sequentially: (*1*) preliminary estimation of K_{11} and P by using for K_{11} the isopiestic data on water solubility (x_W) at unit activity of water as a function of the stoichiometric concentration (x_A) of alcohol, and for P the extrapolated values (D^∞) of D at $x_A = 0$ in [25]; (*2*) preliminary estimates of all K_{ij} for the above-noted models; (*3*) simultaneous solution of eqs. 23–25 for all K_{ij} and P by assuming $g_W = g_A = F_{ij} = 1$; (*4*) simultaneous solution of eqs. 23–25 taking into account the activity coefficients as a function of concentration, to obtain final values for the thermodynamic constants K_{ij} and P.

In step *3* the estimates of K_{ij} obtained in step *2* provided the starting point for the iterations, and all the distribution and isopiestic data for each system were used. However, a final decision was now needed on how many hydrates to allow. The literature is sparse, but Johnson *et al.* (15) found for phenol in carbon tetrachloride that the model 10–11–30–31–61–64 gave an excellent fit to their data (each two-digit number represents a species A_iW_j). In the present work it was assumed that the alcohol monomer can form at most two hydrates, and each of the two alcohol *n*-mers at most three hydrates.

The computational procedures provided root-mean-squares, and estimates of the standard deviations for each of the evaluated parameters K_{ij} and P, for the chosen association models. For some models, the values of K_{ij} proved to be negative, so that less than the original 11 parameters were retained in eqs. 23–25.

Step *4* consisted in a repetition of step *3*, by re-testing the models retained in that step, but this time including the activity coefficients expressed in terms of g_W, g_A, and F_{ij}. As examples

TABLE 3. Final results of least-squares fits of polynomials to the distribution and water-solubility data for *n*-butanol – organic solvent systems at 25 °C

Solvent	Solution model			Root-mean squares	Degrees of freedom	Water solubility data: Sum of squares	Water solubility data: No. of points	Distribution data: Sum of squares	Distribution data: No. of points
Cyclohexane	10,11	30	80,81,83	0.06264	50	0.09838	29	0.09779	28
	10,11	30	80,81,84	0.06309	50	0.09979	29	0.09925	28
Carbon tetrachloride	10,11	30,31	80,81,84	0.02608	68	0.03175	51	0.01449	25
	10,11	30,31	80,81,83	0.03459	68	0.04939	51	0.03197	25
	10,11	30,31	60,61,63	0.04226	68	0.10257	51	0.01888	25
	10,11	30,31	60,61,64	0.04415	68	0.11589	51	0.01665	25
p-Xylene	10,11	30,31	80,81,84	0.03429	50	0.03489	28	0.02389	30
	10,11	30,31	80,81,83	0.03691	50	0.03885	28	0.02929	30
Benzene	10,11	30,31	80,81,84	0.02984	71	0.02859	46	0.03462	33
	10,11	30,31	80,81,85	0.02970	71	0.02419	46	0.03845	33
	10,11,12	30,31	80,81,84	0.02954	70	0.02509	46	0.03597	33
	10,11	30,31,32	80,81,85	0.02935	70	0.02334	46	0.03690	33
	10,11	30,31	80,81,83	0.03663	71	0.06957	46	0.03636	33
	10,11	30,31	60,61,64	0.03706	72	0.04239	46	0.05649	33
Chlorobenzene	10,11	30,31	80,81,84	0.02109	45	0.01097	25	0.00904	28
	10,11	30,31,33	80,81,84	0.01849	44	0.00624	25	0.00880	28
	10,11	30,31,32	80,81,85	0.01819	44	0.00568	25	0.00888	28
o-Dichlorobenzene	10,11	30,31	80,81,84	0.01834	45	0.00651	26	0.00896	28
	10,11,12	30,31	80,81,84	0.01084	45	0.00379	26	0.00897	28
	10,11	30,31,33	80,81,84	0.01655	45	0.00331	26	0.00897	28

Can. J. Chem. Downloaded from www.nrcresearchpress.com by 210.87.254.6 on 09/05/12
For personal use only.

TABLE 4. Formation constants (K_{tj}) for *n*-mers and hydrates of *n*-butanol in six solvents at 25 °C*

	Cyclohexane				Benzene		Chlorobenzene		*o*-Dichlorobenzene	
Constant	Second choice	First choice	Carbon tetrachloride	*p*-Xylene	Second choice	First choice	Second choice	First choice	Second choice	First choice
K_{11}	142 ± 17	143 ± 16	26.7 ± 3.4	16.7 ± 2.0	20.4 ± 1.4	15.6 ± 2.9	15.5 ± 1.2	14.9 ± 1.1	17.2 ± 1.1	9.7 ± 2.6
$K_{12} \times 10^{-2}$						8.2 ± 4.6				16.6 ± 5.3
$K_{30} \times 10^{-2}$	277 ± 46	278 ± 45	33.2 ± 2.3	1.94 ± 0.39	1.33 ± 0.27	1.34 ± 0.29	2.20 ± 0.25	2.21 ± 0.22	2.18 ± 0.21	2.02 ± 0.20
$K_{31} \times 10^{-4}$			93.8 ± 4.9	2.67 ± 0.48	1.76 ± 0.39	1.89 ± 0.43	4.79 ± 0.27	4.32 ± 0.26	4.75 ± 0.25	4.88 ± 0.25
$K_{33} \times 10^{-6}$								6.1 ± 1.7		
$K_{80} \times 10^{-9}$	(4.2 ± 4.3) × 10^5	(5.1 ± 4.3) × 10^5	(6.7 ± 2.1) × 10^2	0.67 ± 0.48	1.89 ± 0.75	2.18 ± 0.90	3.2 ± 1.7	2.6 ± 1.5	1.8 ± 1.3	1.7 ± 1.2
$K_{81} \times 10^{-11}$	(2.76 ± 0.12) × 10^7	(1.84 ± 0.15) × 10^7	(1.48 ± 0.06) × 10^4	8.40 ± 0.83	1.08 ± 0.10	1.35 ± 0.11	4.05 ± 0.43	1.53 ± 0.44	2.58 ± 0.42	3.04 ± 0.38
$K_{84} \times 10^{-13}$	(4.02 ± 0.21) × 10^6		(2.19 ± 0.48) × 10^5	7.23 ± 0.26	5.59 ± 0.14	6.13 ± 0.21	3.60 ± 0.12	3.03 ± 0.18	5.70 ± 0.18	5.20 ± 0.19
$K_{83} \times 10^{-19}$		(1.96 ± 0.10) × 10^6								
P	0.732 ± 0.027	0.732 ± 0.027	2.00 ± 0.02	3.72 ± 0.01	4.02 ± 0.05	4.05 ± 0.05	3.77 ± 0.04	3.78 ± 0.03	3.28 ± 0.03	3.31 ± 0.03

*The ± standard deviation follows each quantity.

Can. J. Chem. Downloaded from www.nrcresearchpress.com by 210.87.254.6 on 09/05/12
For personal use only.

of the variation in these parameters with the composition of the alcohol–water–solvent mixtures, the ranges for g_A, F_{11}, and F_{84} are given in Table 2. The results of these final calculations in step *4* are in Table 3.

These results, taken in conjunction with those in Table 1, indicate that the basic association model 1–3–8 is the preferred one for *n*-butanol in all the solvents. Although Table 1 alone suggests that in carbon tetrachloride and benzene, models 1–3–6 and 1–3–8 are equally good, Table 3 shows that model 1–3–8 is superior. This latter model was also deduced by Tucker *et al.* (12) for methanol in hexadecane.

In considering now the complete association-hydration models, inspection of Table 3 shows that it is not possible to make an unequivocal choice for all solvents, or even for any one solvent except in the cases of carbon tetrachloride and *p*-xylene. However, the model 10–11–30–31–80–81–84 does provide a very good fit for all the solvents except cyclohexane. In this latter solvent the species 31 appears to be absent. Moreover, inspection of Table 3 shows that the extent of hydration of the basic 1–3–8 model varies only slightly from model to model.

Table 4 lists the values calculated for the formation constants of each of the species belonging to a given association-hydration model. For each of the solvents cyclohexane, benzene, chlorobenzene, and *o*-dichlorobenzene two models in Table 3 appeared statistically to be almost equally good. Therefore both are listed in Table 4 and are designated as first and second choices.

Attention is drawn to Figs. 1–8, where the solid least-squares curves in each case represent the first-choice models listed in Table 4. These models clearly fit the distribution and isopiestic data very well.

A discussion and interpretation of the results in the present work will appear in a forthcoming communication, when corresponding results for two other alcohols will be presented.

Acknowledgment

We are grateful to the National Research Council of Canada for financial assistance and for a Bursary to one of us (J.K.).

1. R. H. Stokes and K. N. Marsh. Annu. Rev. Phys. Chem. **23**, 65 (1972).
2. G. C. Pimentel and A. L. McLellan. Annu. Rev. Phys. Chem. **22**, 347 (1971).
3. S. D. Christian, A. A. Taha, and B. W. Gash. Q. Rev. (Chem. Soc.) **24**, 20 (1970).
4. G. C. Pimentel and A. L. McLellan. The hydrogen bond. Freeman, San Francisco. 1960.
5. A. S. N. Murphy and C. N. R. Rao. Appl. Spectrosc. Rev. **2**, 69 (1968).
6. J. Davis, J. Clark, and K. K. Debb. Adv. Magn. Reson. **4**, 201 (1970).
7. W. B. Dixon. J. Phys. Chem. **74**, 1396 (1970).
8. M. Saunders and J. B. Hyne. J. Chem. Phys. **29**, 1319 (1958).
9. U. Liddel and E. D. Becker. Spectrochim. Acta, **10**, 70 (1957).
10. E. D. Becker, U. Liddel, and J. N. Shoolery. J. Mol. Spectrosc. **2**, 1 (1958); W. Masschelein. Spectrochim. Acta, **18**, 1557 (1962).
11. H. C. Van Ness, Jon Van Winkle, H. H. Richtol, and H. B. Hollinger. J. Phys. Chem. **71**, 1483 (1967).
12. E. E. Tucker, S. B. Farnham, and S. D. Christian. J. Phys. Chem. **73**, 3820 (1969).
13. E. E. Tucker and E. D. Becker. J. Phys. Chem. **77**, 1783 (1973).
14. J. R. Johnson, S. D. Christian, and H. E. Affsprung. J. Chem. Soc. A, 77 (1966).
15. J. R. Johnson, S. D. Christian, and H. E. Affsprung. J. Chem. Soc. A, 1 (1965).
16. H. G. Harris and J. M. Prausnitz. Ind. Eng. Chem. Fundam. **8**, 180 (1969).
17. J. Kirchnerová and G. C. B. Cave. Can. J. Chem. This issue.
18. J. A. Riddick and W. B. Bunger. Techniques of chemistry. Vol. II. Organic solvents. 3rd ed. J. Wiley, Interscience, New York. 1970.
19. S. Goldman and G. C. B. Cave. Can. J. Chem. **49**, 1726 (1971).
20. J. A. V. Butler, D. W. Thomson, and W. H. Maclenan. J. Chem. Soc. 674 (1933).
21. W. S. Knight. Ph.D. Thesis, Princeton University, Princeton, N.J. 1962.
22. J. Kirchnerová. Ph.D. Thesis. McGill University, Montreal, Quebec. 1974.
23. J. Mullens, I. Hanssens, and P. Huyskens. Bull. Soc. Chim. Belg. **80**, 539 (1971).
24. J. Mullens, I. Hanssens, and P. Huyskens. J. Chim. Phys. **68**, 1417 (1971).
25. E. Meeusen and P. Huyskens. J. Chim. Phys. **63**, 845 (1966).
26. R. A. Robinson and R. H. Stokes. Electrolyte solutions. 2nd. ed. Butterworths, London. 1959. p. 478.
27. I. Prigogine and R. Defay. Chemical thermodynamics. Longmans, London. 1954.
28. J. H. Hildebrand, J. M. Prausnitz, and R. L. Scott. Regular and related solutions. Van Nostrand, Reinhold, New York. 1970.
29. A. T. Hagler, H. A. Scheraga, and J. Neméthy. J. Phys. Chem. **76**, 3229 (1972).
30. J. R. Wolberg. Prediction analyses. Van Nostrand, Princeton, N.J. 1967.
31. W. Weltner and K. S. Pitzer. J. Am. Chem. Soc. **73**, 2608 (1951).
32. A. N. Fletcher. J. Phys. Chem. **75**, 1808 (1971).
33. A. N. Fletcher and C. A. Heller. J. Phys. Chem. **71**, 3742 (1967).

Association and hydration of alcohols in low-dielectric solvents. II. *tert*-Butyl alcohol and cyclohexanol

JITKA KIRCHNEROVÁ AND GENILLE C. B. CAVE
Department of Chemistry, McGill University, Montreal, P.Q., Canada H3C 3G1

Received November 21, 1975[1]

JITKA KIRCHNEROVÁ and GENILLE C. B. CAVE. Can. J. Chem. **54**, 3929 (1976).

Formulae and thermodynamic formation constants of the aggregates of *tert*-butyl alcohol and of cyclohexanol and their hydrates in six low-dielectric solvents have been deduced by using an iterative mathematical treatment of distribution and isopiestic data. The solvents were cyclohexane, carbon tetrachloride, *p*-xylene, benzene, chlorobenzene, and *o*-dichlorobenzene. These results and those previously obtained for *n*-butanol in the same six solvents are discussed in a qualitative way.

JITKA KIRCHNEROVÁ et GENILLE C. B. CAVE. Can. J. Chem. **54**, 3929 (1976).

On a déduit les formules et les constantes de formation thermodynamiques des agrégats du *tert*-butanol et du cyclohexanol et de leurs hydrates dans six solvants de constante diélectrique faible; ces résultats ont été obtenus en effectuant un traitement mathématique itératif de données de distribution et isopiestique. Les solvants utilisés étaient le cyclohexane, le tétrachlorure de carbone, le *p*-xylène, le benzène, le chlorobenzène et l'*o*-dichlorobenzène. On discute, d'une façon qualitative, de ces résultats et d'autres obtenus antérieurement pour le *n*-butanol dans les six mêmes solvants.

[Traduit par le journal]

Can. J. Chem. Downloaded from www.nrcresearchpress.com by 210.87.254.5 on 09/05/12
For personal use only.

Introduction

This report describes a study to identify the co-existing *n*-mers of *tert*-butyl alcohol and cyclohexanol and their hydrates in six low-dielectric solvents, and to determine their thermodynamic formation constants. Recently (1) we reported the results of a similar study on *n*-butanol in the same solvents. A comparison of the results on all three alcohols is then made in the present report, which begins to allow some conclusions to be drawn on the roles that the structure of the alcohol and the nature of the solvent play in the self-association and hydration of the alcohol *n*-mers (the use of the term *n*-mer is not necessarily intended to imply a linear chain).

As in the case of *n*-butanol (1), the experimental data were obtained from distribution (solvent-extraction) and isopiestic water-solubility methods, the concentration of alcohol in the solvents extended to 1 *M* in order to be able to detect higher *n*-mers, and activity coefficients were estimated for the various species. The mathematical treatment of these experimental data was also entirely similar to that used and described (1) for the *n*-butanol systems.

[1]Revision received August 26, 1976.

Experimental

Materials

The solvents (cyclohexane, *p*-xylene, benzene, carbon tetrachloride, chlorobenzene, and *o*-dichlorobenzene) were purified as described elsewhere (2).

The *tert*-butyl alcohol (Fisher A-401) was further purified by refluxing it for 6 h over anhydrous K_2CO_3, then fractionally distilling the product under nitrogen, by using a previously described distillation column and procedure (2). The distillate was monitored at 100–200 ml intervals by gas-chromatographic analysis, and the best cut was retained for use. Its purity calculated from a gas-chromatographic analysis of the impurities was better than 99.8 mol%. Its water content was determined by a Karl Fischer titration to be 0.12%. Its density at 30 °C was 0.7758 ± 0.0001 (lit. (3) 0.7757).

The cyclohexanol (Fisher C-558, reagent-grade) was further purified by refluxing it over CaO for 12 h, then fractionally distilling the product under nitrogen as with the *tert*-butyl alcohol. The middle-third cut was fractionally distilled under nitrogen, and the middle third retained for use. Its purity calculated from a gas-chromatographic analysis of the impurities was 99.1 mol%. Its water content was determined by a Karl Fischer titration to be 0.20%. Its density at 30 °C was 0.9415 ± 0.0001 (lit. (3) 0.94155). Since the maximum concentration of cyclohexanol in the experiments was 0.1 mole fraction, this degree of purity was considered acceptable.

Procedures

The distribution ratios of the alcohols between water and the organic solvent were measured at 25.0 ± 0.1 °C. The procedure has been previously described (1).

The procedure for the isopiestic water-solubility mea-

surements has also been described (1), but in addition the concentration of the relatively volatile *tert*-butyl alcohol was determined in the equilibrium organic phase.

The gas-chromatographic analyses for *tert*-butyl alcohol in both phases of the distribution systems, and in the equilibrium organic phase of the isopiestic system were carried out by using the following columns and other parameters: (*1*) for *tert*-butyl alcohol in cyclohexane and carbon tetrachloride, a 1/16-in. diameter stainless-steel column 1.2 m long packed with 120–150 mesh Porapak Q, at 140 °C; (*2*) for *tert*-butyl alcohol in the other solvents and in aqueous solutions, a $\frac{1}{8}$-in. diameter copper column packed with 70–80 mesh Chromosorb G coated with 15% by weight of Silicone oil DC 710, at 65 °C.

For the corresponding gas-chromatographic analyses for cyclohexanol, the columns and other parameters were as follows: (*1*) for cyclohexanol in chlorobenzene, a $\frac{1}{8}$-in. diameter copper column 2 m long packed with 70–80 mesh Chromosorb G coated with 17 wt.% of Carbowax 20 M, at 170 °C; (*2*) for cyclohexanol in cyclohexane, carbon tetrachloride, *p*-xylene, *o*-dichlorobenzene, and aqueous solutions, a $\frac{1}{8}$-in. copper column 1 m long packed with 70–80 mesh Chromosorb G coated with 15 wt.% of Silicone oil DC 710, at 120 °C; (*3*) for cyclohexanol in benzene, a column similar to (*2*), above, except 2 m long.

Results

Distribution Studies

The distribution ratio of each alcohol between the aqueous and the organic phases was determined for each of the six solvents, with some 28–35 concentrations being used for each, to cover a range of 0–1 *M* of alcohol in the organic phase. The corresponding range in the equilibrium aqueous phase was found to be 0–1.8 *M* for *tert*-butyl alcohol, and 0–0.18 *M* for cyclohexanol. It has been reported (4, 5) that over the former range aqueous solutions of *tert*-butyl alcohol can be considered as being ideal. It was assumed that in the latter range the cyclohexanol solutions could safely be considered ideal.

Each distribution ratio was obtained from the mean of 4–6 replicate analyses for the alcohol in each phase, as determined by gas chromatography. The percent standard deviations of the ratios were 1.0–1.5. Concentrations were converted from molarities to mole fractions, for the distribution ratios. The complete data are avail-

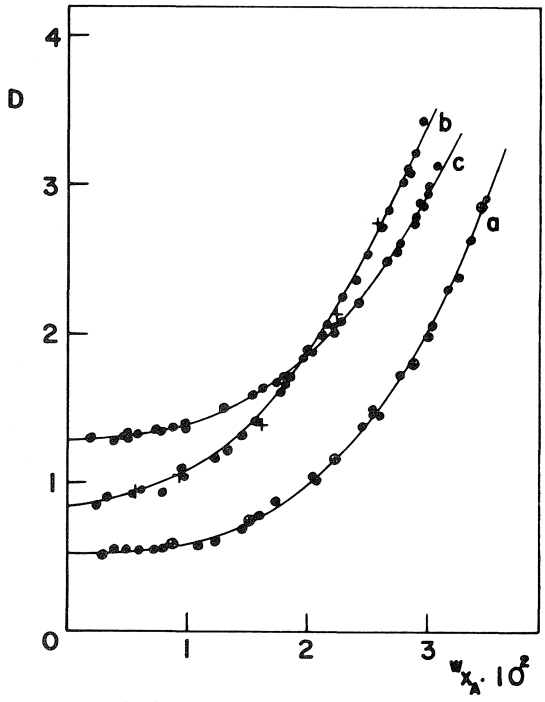

FIG. 1. Distribution ratio (*D*) for *tert*-butyl alcohol between three solvents and water *vs.* mole fraction of *tert*-butyl alcohol in the aqueous phase ($^{w}x_A$) at 25 °C. Points are experimental: (*a*) cyclohexane; (*b*) carbon tetrachloride; (*c*) *p*-xylene. Literature values: + (7), ⊕ (8). Curves are calculated for the final association-hydration model (Table 4).

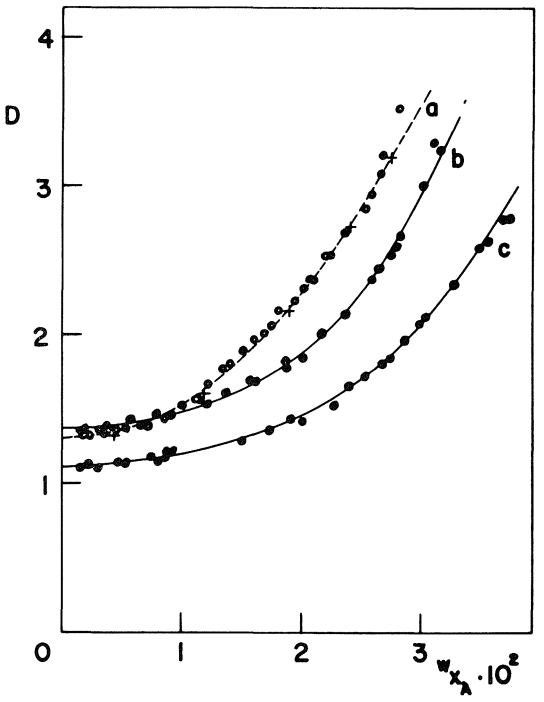

FIG. 2. Distribution ratio (*D*) for *tert*-butyl alcohol between three solvents and water *vs.* mole fraction of *tert*-butyl alcohol in the aqueous phase ($^{w}x_A$) at 25 °C. Points are experimental: (*a*) benzene; (*b*) chlorobenzene; (*c*) *o*-dichlorobenzene. Literature values + (7). Curves are calculated for the final association-hydration model (Table 4).

Can. J. Chem. Downloaded from www.nrcresearchpress.com by 210.87.254.5 on 09/05/12
For personal use only.

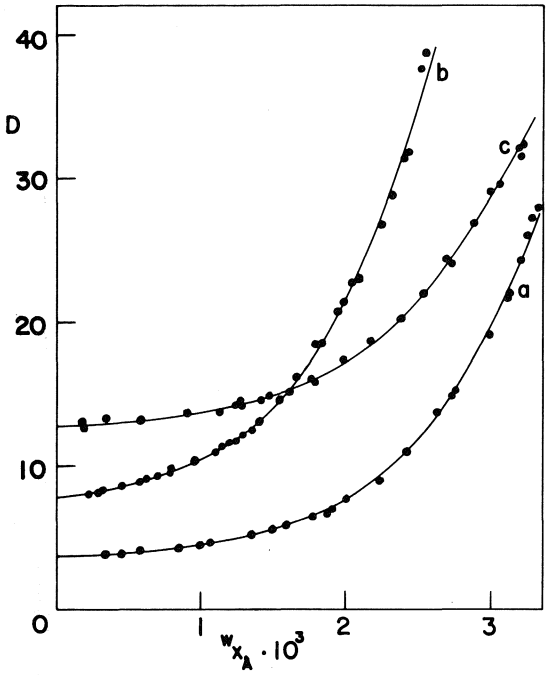

FIG. 3. Distribution ratio (D) for cyclohexanol between three solvents and water *vs.* mole fraction of cyclohexanol in the aqueous phase ($^{W}x_A$) at 25 °C. Points are experimental: (*a*) cyclohexane; (*b*) carbon tetrachloride; (*c*) *p*-xylene. Curves are calculated for the final association-hydration model (Table 6).

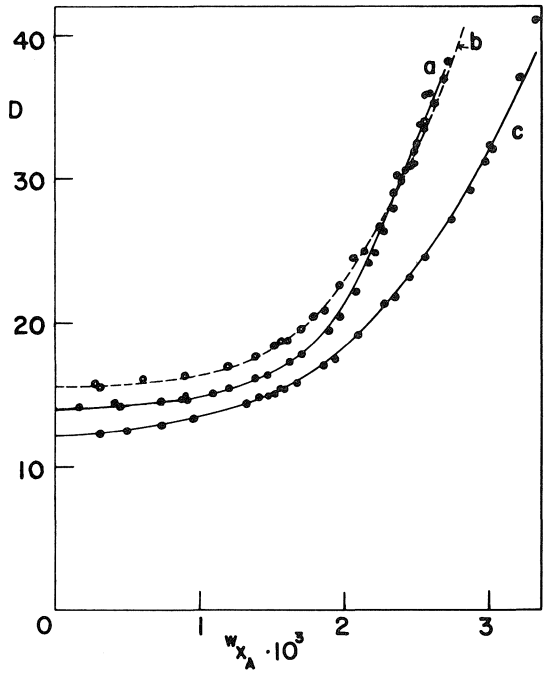

FIG. 4. Distribution ratio (D) for cyclohexanol between three solvents and water *vs.* mole fraction of cyclohexanol in the aqueous phase ($^{W}x_A$) at 25 °C. Points are experimental: (*a*) benzene; (*b*) chlorobenzene; (*c*) *o*-dichlorobenzene. Curves are calculated for the final association-hydration model (Table 6).

able elsewhere (6), but plots of the distribution ratio *vs.* mole fraction of alcohol in the aqueous phase are shown in Figs. 1 and 2 for *tert*-butyl alcohol, and in Figs. 3 and 4 for cyclohexanol. The curves shown were calculated for the final association-hydration models found to be the most reasonable ones.

Isopiestic Water-solubility Studies

The solubility of water in each organic-solvent solution of the alcohol was determined isopiestically in triplicate for at least three different water activities. For each water activity, the water solubility was measured for 6–15 different concentrations of the alcohol in the organic phase. The average precision of the water determination was 1.0–1.5% except for very low concentrations of alcohol in cyclohexane, in which cases the error was up to 10%. The activity of water in the calcium chloride solutions was found directly from the literature (9). The water-solubilities were converted from measured molarities into mole fractions for use, and all these data have been tabulated elsewhere (6). They are illustrated graphically for cyclohexane, benzene, and *o*-dichlorobenzene in Figs. 5–7 for *tert*-butyl alcohol, and Figs. 8–10 for cyclohexanol. They are plots of water solubility for several water activities *vs.* mole fraction of the alcohol in the organic phase. The curves are calculated for the final association-hydration models found to be the most reasonable ones. The agreement with the final models was equally good with the other three solvents.

Treatment of the Data

The distribution and isopiestic water-solubility data were used jointly, in order to deduce the most reasonable association-hydration models for the alcohols in each solvent. The treatment consisted of fitting three previously derived polynomials (eqs. 23–25, ref. 1) to these data.

As before (1),

$$K_{ij} = \frac{\xi_{ij}}{\xi_{10}{}^{i}\,\xi_{01}{}^{j}} \cdot \frac{f_{ij}}{f_{10}{}^{i} f_{01}{}^{j}}$$

Can. J. Chem. Downloaded from www.nrcresearchpress.com by 210.87.254.5 on 09/05/12
For personal use only.

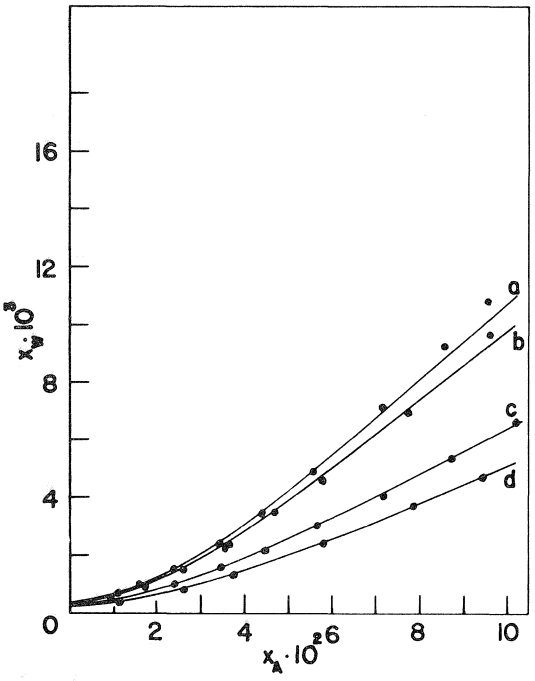

FIG. 5. Solubility of water (mole fraction x_W) in solutions of *tert*-butyl alcohol in cyclohexane at various water activities (a_W), at 25 °C. Points are experimental. Data are for: (*a*) $a_W = 1.000$; (*b*) $a_W = 0.926$; (*c*) $a_W = 0.662$; (*d*) $a_W = 0.545$. Curves are calculated for the final association-hydration model (Table 4).

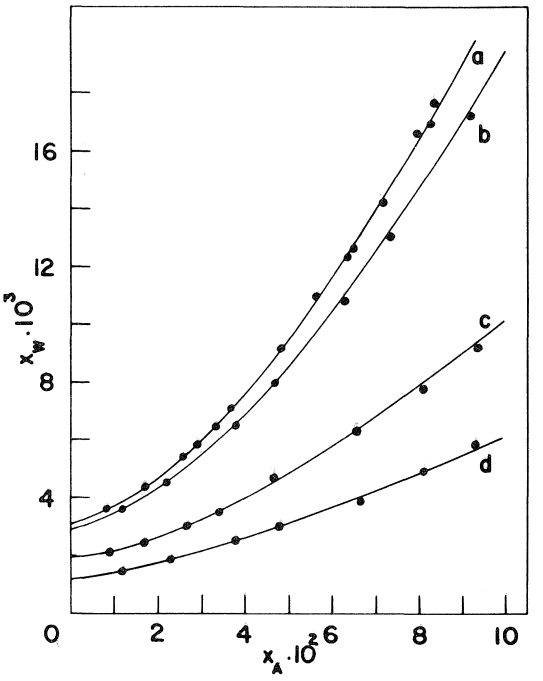

FIG. 6. Solubility of water (mole fraction x_W) in solutions of *tert*-butyl alcohol in benzene at various water activities (a_W), at 25 °C. Points are experimental. Data are for: (*a*) $a_W = 1.000$; (*b*) $a_W = 0.926$; (*c*) $a_W = 0.581$; (*d*) $a_W = 0.383$. Curves are calculated for the final association-hydration model (Table 4).

for the reaction $iA_1 + jW_1 = A_iW_j$, where A_1 represents the alcohol monomer, W_1 the water monomer, A_iW_j the hydrate of the alcohol aggregate, ξ the true mole fraction, f the activity coefficient, and subscript ij the species A_iW_j. The reference and standard states of each species A_iW_j are those previously (1) specified.

The activity coefficients of the coexisting species were taken into account by using a previously described method (see eqs. 22, 26–28 in ref. 1). For this purpose, a value of 17.2 $cal^{1/2}$ $cm^{-3/2}$ was used for δ_{01} ($= \delta_{0j}$). For *tert*-butyl alcohol, a value of 7.6 $cal^{1/2}$ $cm^{-3/2}$ was used for δ_{10}. It is a value of δ calculated (6) for *tert*-butyl chloride. For cyclohexanol, a value of 8.9 $cal^{1/2}$ $cm^{-3/2}$ was used for δ_{10}. Since the value of δ for chlorocyclohexane was not available, δ_{10} for cyclohexanol was estimated from estimates for cyclohexanol of the dispersion contribution ${}^d\delta$ and the polar contribution ${}^p\delta$ to the total solubility parameter, according to a previously described (2) formula $\delta_{10}^2 = {}^p\delta_{10}^2 + {}^d\delta_{10}^2$. The value of ${}^d\delta_{10}$ was found from the refractivity of cyclohexanol to be 8.4 $cal^{1/2}$ $cm^{-3/2}$, and ${}^p\delta_{10}$ was estimated from the value for the chlorobenzene to be 3 $cal^{1/2}$ $cm^{-3/2}$.

The step-wise operation of fitting the three polynomials to the distribution and isopiestic data has been described in detail elsewhere (1, 6). For the first step, plausible models were chosen without segregating the anhydrous monomer and *n*-mers from their hydrates. Then for each model the corresponding closed form of eq. 29 in ref. 1 was fitted by least-squares to the distribution data alone. The results of these fits are given in Table 1 for *tert*-butyl alcohol, and in Table 2 for cyclohexanol. A model is represented numerically. For example, the model of monomer–trimer–hexamer (of alcohol) co-existing in the solution is denoted by 1–3–6. The values found for the mean squares, and the least-squares value of D^∞ (*i.e.* the value of the distribution ratio at infinite dilution of the

Can. J. Chem. Downloaded from www.nrcresearchpress.com by 210.87.254.5 on 09/05/12
For personal use only.

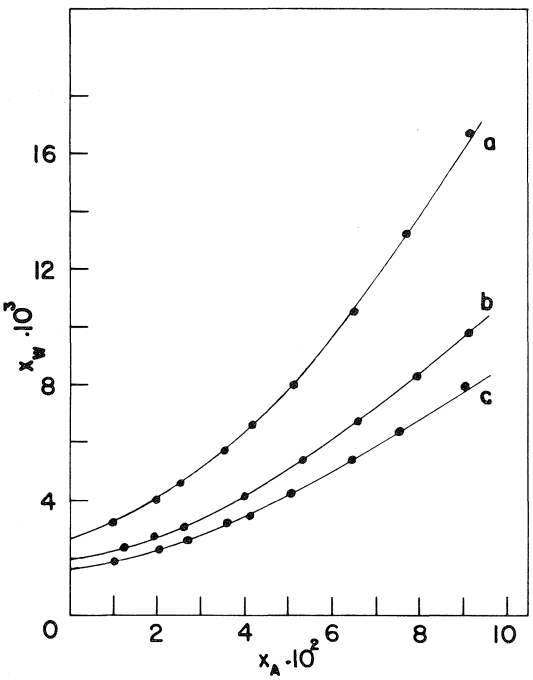

FIG. 7. Solubility of water (mole fraction x_W) in solutions of *tert*-butyl alcohol in *o*-dichlorobenzene at various water activities (a_W), at 25 °C Points are experimental. Data are for: (*a*) $a_W = 1.000$; (*b*) $a_W = 0.662$; (*c*) $a_W = 0.553$. Curves are calculated for the final association-hydration model (Table 4).

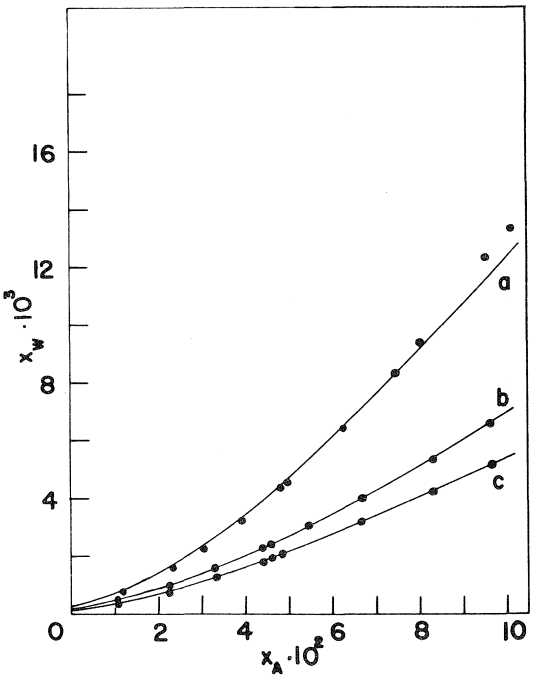

FIG. 8. Solubility of water (mole fraction x_W) in solutions of cyclohexanol in cyclohexane at various water activities (a_W), at 25 °C. Points are experimental. Data are for: (*a*) $a_W = 1.000$; (*b*) $a_W = 0.662$; (*c*) $a_W = 0.545$. Curves are calculated for the final association-hydration model (Table 6).

alcohol), as well as the values of D^∞ found by extrapolation of the graphs in Figs. 1 to 4 are also reported in these tables. The same criteria described and used previously (1) were then taken into account in selecting from the tables those models which represented the data very well.

The treatment next extended these chosen models, by deducing the co-existing hydrates. For this purpose, the three polynomials (eqs. 23–25, ref. 1) were solved simultaneously and iteratively, by using jointly the distribution and isopiestic data. Each model was arbitrarily restricted to one in which the alcohol monomer could form at most two hydrates, and each of the *n*-mers at most three hydrates. The results of the least-squares treatment are in Table 3 for *tert*-butyl alcohol, and Table 5 for cyclohexanol. The models are represented numerically, with species A_iW_j being denoted simply by *ij* (*e.g.* the monohydrate of the alcohol trimer is 31).

For each model listed in Tables 3 and 5, the root-mean squares, and the sums of squares separately for the distribution and isopiestic data are given. These, and the corresponding regression coefficients (not listed in Tables 3 and 5) were used for choosing the most reasonable models.

For *tert*-butyl alcohol (Table 3) in cyclohexane, carbon tetrachloride, benzene, and *o*-dichlorobenzene, the basic association model monomer–trimer–hexamer (1–3–6) gave the best fit to the distribution and isopiestic data. This model was also the one deduced by Tucker and Becker (10) from vapour–liquid equilibria, for *tert*-butyl alcohol in anhydrous hexadecane. For the solvents *p*-xylene and chlorobenzene the statistics in Table 3 indicate that while the basic model 1–3–6 fits the data very well, the models 1–3–8 and 1–2–6 are statistically preferable.

Finally, the hydrates associated with the basic models are considered. It is evident from Table 3

Can. J. Chem. Downloaded from www.nrcresearchpress.com by 210.87.254.5 on 09/05/12
For personal use only.

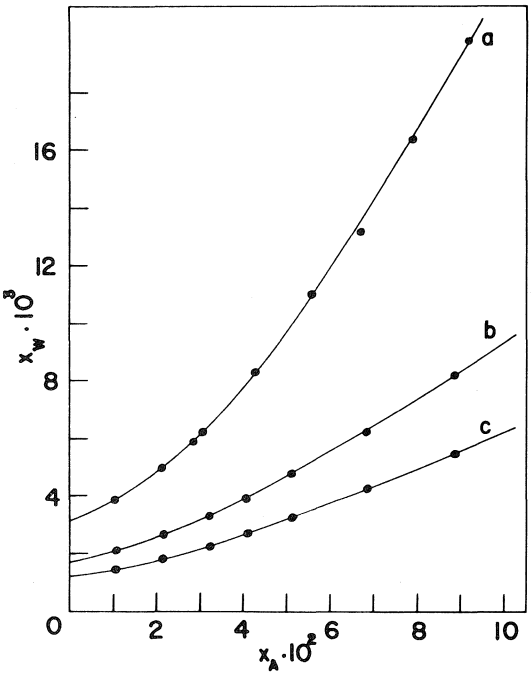

FIG. 9. Solubility of water (mole fraction x_W) in solutions of cyclohexanol in benzene at various water activities (a_W), at 25 °C. Points are experimental. Data are for: (*a*) a_W = 1.000; (*b*) a_W = 0.545; (*c*) a_W = 0.383. Curves are calculated for the final association-hydration model (Table 6).

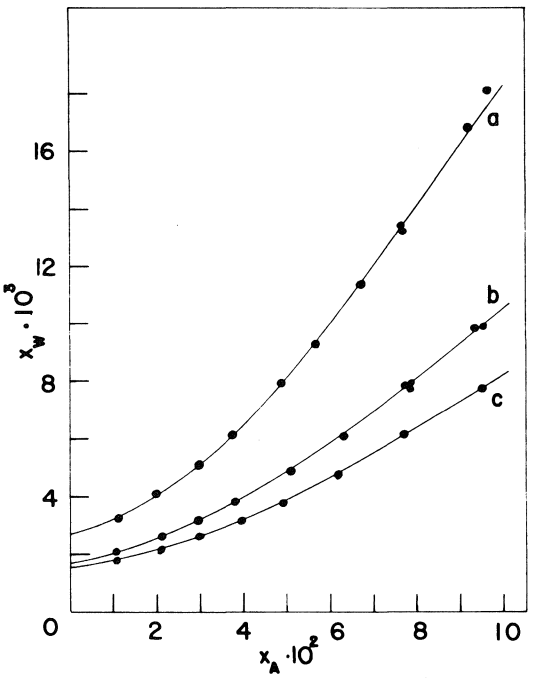

FIG. 10. Solubility of water (mole fraction x_W) in solutions of cyclohexanol in *o*-dichlorobenzene at various water activities (a_W), at 25 °C. Points are experimental. Data are for: (*a*) a_W = 1.000; (*b*) a_W = 0.662; (*c*) a_W = 0.545. Curves are calculated for the final association-hydration model (Table 6).

that for a given basic association model in a given solvent, slight variations in the extent of hydration amongst the monomer and *n*-mers do not change significantly the goodness of fit in some of the systems. That is, an unequivocal choice of a complete association-hydration model is not possible from the present data. Accordingly, Table 4 gives the set of thermodynamic K_{ij} values calculated for each of the two or three most acceptable association-hydration models (designated by *A*, *B* and by *A*, *B*, *C* respectively).

For cyclohexanol (Table 5), the basic association model 1–3–8 fits the data well except in the case of chlorobenzene for which this model is unacceptable. Instead, the 1–4–8 model is the best choice for that solvent. However, certain other models are also acceptable in these solvents, and they vary somewhat from solvent to solvent. Specifically, the 1–3–9 model in carbon tetrachloride, the 1–4–8 model in *p*-xylene and benzene, the 1–3–6 model in chlorobenzene and *o*-dichlorobenzene, and the 1–4–6 model in chlorobenzene are all acceptable, although for chlorobenzene the 1–4–6 model is a third choice, and for *o*-dichlorobenzene the 1–3–6 model is a second choice. It is to be noted that a real difference in the models may indeed exist from solvent to solvent due to the cyclohexanol existing as an equilibrium mixture of two conformers.

As in the case of *tert*-butyl alcohol, an unequivocal choice of a complete association-hydration model is not possible for cyclohexanol. Therefore, Table 6 gives the set of thermodynamic K_{ij} values calculated for each of the two or three most acceptable models (designated by *A*, *B* and *A*, *B*, *C* respectively).

Discussion

The results previously reported (1) for *n*-butanol, together with those for *tert*-butyl alcohol and cyclohexanol in the present report

Can. J. Chem. Downloaded from www.nrcresearchpress.com by 210.87.254.5 on 09/05/12
For personal use only.

TABLE 1. Results of polynomial linear least-squares fits to the distribution data for *tert*-butyl alcohol

Model	Intercept	Mean squares	Intercept	Mean squares	Intercept	Mean squares
	Cyclohexane		*Carbon tetrachloride*		*p-Xylene*	
	0.501*		0.833*		1.290*	
1–3	0.337	0.00227	0.734	0.00487	1.187	0.00893
1–3–4	0.511	0.00094§	0.863	0.00104	1.301	0.00082§
1–3–5	0.509	0.00115	0.850	0.00112	1.293	0.00075
1–3–6	0.490	0.00138	0.841	0.00122	1.283	0.00072
1–3–8	0.462	0.00240	0.824	0.00184	1.270	0.00097
1–3–9	0.444	0.00252	0.825	0.00149‖	1.268	0.00085
1–4	0.515	0.00150	0.982	0.00487	1.332	0.00134
1–4–6	0.520	0.00097†	0.919	0.00191†	1.323	0.00129†
1–4–8	0.531	0.00109‖	0.932	0.00236‡	1.327	0.00136‡
1–2–4	0.500	0.00093§	0.785	0.00135	1.272	0.00081§
1–2–6	0.348	0.00385	0.632	0.00481	1.168	0.00181
1–2–8	0.270	0.00922	0.559	0.00886	1.120	0.00358
1–6	0.711	0.02984	1.237	0.05919	1.485	0.02129
1–8	0.814	0.07434	1.361	0.11551	1.563	0.04552
	Benzene		*Chlorobenzene*		*o-Dichlorobenzene*	
	1.320*		1.340*		1.140*	
1–3	1.255	0.00537				
1–3–4	1.311	0.00272§‖	1.393	0.00286§	1.138	0.00065§
1–3–5	1.312	0.00244	1.394	0.00360	1.128	0.00079
1–3–6	1.310	0.00234	1.384	0.00168	1.118	0.00106
1–3–8	1.306	0.00273‖	1.369	0.00100	1.104	0.00175‖
1–3–9	1.308	0.00201‖	1.361	0.00075	1.103	0.00165
1–4	1.438	0.00899	1.386	0.00515	1.159	0.00081
1–4–6	1.376	0.00566†	1.415	0.00404§‖	1.150	0.00068†
1–4–8	1.394	0.00687‡	1.415	0.00333	1.151	0.00066‡
1–2–4	1.239	0.00272	1.371	0.00266§	1.117	0.00062§
1–2–6	1.156	0.00398	1.292	0.00074	1.028	0.00269
1–2–8	1.114	0.00536	1.248	0.00181	0.984	0.00572
1–6	1.630	0.04692	1.510	0.01605	1.289	0.02175
1–8	1.727	0.08327	1.579	0.04042	1.362	0.04973

*Graphical extrapolation.
†Negative value for a_6.
‡Negative value for a_8.
§Error in a_i of lower *n*-mer was too large.
‖Error in a_i of higher n-mer was too large.

will be considered together in a qualitative way. A quantitative interpretation, particularly of the values of the partition coefficients of these alcohols in the six solvents will be given in a future communication.

The partition coefficients (P) are considered first. For convenience they are collected in Table 7. They represent the ratio of the activity of the monomer in the organic phase to that in the aqueous phase, on a mole fraction basis. The activity of the monomer in the organic phase consists only of the activity of the anhydrous monomer, and of any anhydrous solvates of the alcohol monomer with the organic solvent.

Table 7 shows that for each solvent the partition coefficient of the alcohol increases in the order *tert*-butyl alcohol < *n*-butanol < cyclohexanol. Since $-RT \ln P$ represents the standard free energy change of transfer, a rigorous explanation for the increase in P from left to right requires consideration of the changes in ΔH^0 and ΔS^0 in that direction. However, for the present purpose we present the following qualitative argument. The lower the solubility of the alcohol in water, and the larger the van der Waals interactions between the alcohol and the organic solvent, the greater will be the value of P. Now the solubility of the alcohol in water does

Can. J. Chem. Downloaded from www.nrcresearchpress.com by 210.87.254.5 on 09/05/12
For personal use only.

TABLE 2. Results of polynomial linear least-squares fits to the distribution data for cyclohexanol

Model	Intercept	Mean squares	Intercept	Mean squares	Intercept	Mean squares
	Cyclohexane		*Carbon tetrachloride*		*p-Xylene*	
	3.70*		7.90*		12.84*	
1–3–8	3.520	0.12738	7.951	0.18920	12.50	0.27176
1–3–6	4.041	0.06507	8.414	0.40673	12.80	0.13896
1–3–5	4.421	0.14709†	8.713	0.56850	13.02	0.09077§
1–3–4	4.623	0.21628	8.904	0.49769†	13.24	0.08574†
1–3–9	3.308	0.23041	7.832	0.19041	12.40	0.33809
1–4–8	4.116	0.06178	8.963	0.46652	13.07	0.09601‖
1–4–6	4.313	0.12738	9.018	0.58437	13.13	0.08761‖
1–2–4	5.383	0.34193‡	8.882	0.53078‡	13.32	0.09517‡
1–2–6	3.132	0.08299	6.764	0.26477	12.13	0.31943
1–2–8	1.923	0.49153	5.631	0.61265	11.37	0.89631
1–6	5.247	0.65930	10.82	2.59207	14.37	1.2629
1–8	6.308	3.3389	11.99	7.1348	15.08	3.7938
1–2–4–8	4.049	0.0675§			13.19	0.08950‡
1–2–5			7.617	0.26813§		
1–2–4–6			7.151	0.37523	13.13	0.08977‡
	Benzene		*Chlorobenzene*		*o-Dichlorobenzene*	
	14.25*		15.35*		12.14*	
1–3–8	13.94	0.12688	14.83	0.47045	11.65	0.11682
1–3–6	14.47	0.16247§	15.36	0.18358§	12.26	0.05402
1–3–5	14.79	0.22623†	15.72	0.10368§	12.44	0.08245
1–3–4	15.33	0.45377†	16.03	0.09497†	12.86	0.17149
1–3–9	13.74	0.15861	14.66	0.60849	11.49	0.14128
1–4–8	14.33	0.11618	15.38	0.19688	12.78	0.11175
1–4–6	14.57	0.16992§	15.60	0.12638	12.90	0.18536
1–2–4	16.27	0.72850‡	16.66	0.12632‡	12.89	0.19028‡
1–2–6	14.12	0.11436§	14.55	0.33944	10.58	0.17572
1–2–8	12.92	0.23199	13.43	1.01972	9.17	0.72760
1–6	14.77	0.16076	17.05	1.07394	14.86	1.9865
1–8	15.68	0.26380	18.33	4.14329	16.12	6.3536

*Graphical extrapolation.
†Negative value for a_3.
‡Negative value for a_2.
§Error in a_i of lower n-mer was too large.
‖Error in a_i of higher n-mer was too large.

decrease in the order *tert*-butyl alcohol (infinitely miscible) $\gg$ *n*-butanol $>$ cyclohexanol. The values of P for a given solvent are indeed in the reverse order to this. In addition, calculations have shown (6) that the van der Waals interactions between a given solvent and the three alcohols are not very different, and do not compensate for the effect of the gross differences in the solubility of the alcohols in water.

A third factor that would increase the value of P is the existence of complexes between the alcohol and the organic solvent. In cyclohexane such complexes may be considered to be absent; but for the other solvents it is shown below that their existence is very plausible. In those cases, the increase in P from *tert*-butyl alcohol through to cyclohexanol in a given solvent will also depend on the individual stability constants of those complexes.

Table 7 also shows that for a given alcohol, the partition coefficient in general increases vertically downwards from cyclohexane through to chlorobenzene, then drops somewhat for *o*-dichlorobenzene (there is a minor exception for *n*-butanol going from benzene to chlorobenzene). The following qualitative explanation is proposed for this general trend. For a given alcohol, the change in the value of P with solvent must be due

Can. J. Chem. Downloaded from www.nrcresearchpress.com by 210.87.254.5 on 09/05/12
For personal use only.

TABLE 3. Final results of least-squares fits of polynomials to the distribution and water-solubility data for *tert*-butyl alcohol – organic solvent systems at 25 °C

Solvent	Solution model*			Root-mean squares	Degrees of freedom	Water solubility data: Sum of squares	Water solubility data: No. of points	Distribution data: Sum of squares	Distribution data: No. of points
Cyclohexane	10,11	30	60,61,63	0.03733	53	0.04648	32	0.02738	28
	10,11	30	60,61,64	0.03819	53	0.04995	32	0.02733	28
	10,11	30	50,51,53	0.06125	53	0.17605	32	0.02277	28
	10,11	30	50,51,55	0.06392	53	0.19380	32	0.02277	28
	10		40,41,43	0.10315	55	0.55943	32	0.02572	28
Carbon tetrachloride	10,11	30,31	61,64	0.02325	51	0.01662	30	0.01095	28
	10,11	30,31	[60],61,63	0.02392	50	0.01624	30	0.01087	28
	10,11	30,31	50,51,53	0.02871	50	0.03158	30	0.01088	28
	10,11	30	[40],41,44	0.05105	51	0.12193	30	0.01096	28
	10,11	[20]	40,41,44	0.05174	51	0.12684	30	0.00971	28
p-Xylene	10,11	30,31	84	0.01735	49	0.00802	25	0.00673	30
	10,11	30,31,[33]	84	0.01658	48	0.00635	25	0.00684	30
	10,11	30,31	63	0.02278	49	0.01719	25	0.00823	30
	10,11	30,31	61,64	0.02424	48	0.02197	25	0.00622	30
	10,11	30,31	(60),[61],63	0.02371	47	0.02053	25	0.00589	30
	10,11	30,31	51,53	0.02943	48	0.03572	25	0.00586	30
	10,11	30,31,33	93	0.03529	48	0.03663	25	0.02314	30
	10,11	30	41,44	0.04188	49	0.07711	25	0.00881	30
	10,11	(20)	40,41,44	0.04495	48	0.09103	25	0.00548	30
Benzene	10,11	30,31,33	64	0.02118	64	0.01213	37	0.01659	34
	10,11,12	30,31	64	0.02140	64	0.01195	37	0.01736	34
	10,11	30,31,33	84	0.02309	64	0.01634	37	0.01777	34
	10,11	30,31	64	0.02446	65	0.01992	37	0.01897	34
	10,11	30,31,33	63	0.02624	64	0.02627	37	0.01780	34
	10,11	30,31,(33)	51,55	0.02300	63	0.01608	37	0.01721	34
	10,11,[12]	30,31,[33]	64	0.02076	63	0.01049	37	0.01667	34
	10,11	30,31,33	93	0.03320	64	0.04604	37	0.02452	34
Chlorobenzene	10,11,12	20,21	60,61,64	0.01609	54	0.00745	28	0.00654	35
	10,11,12	30,31	[60],61,64	0.01797	54	0.00505	28	0.01182	35
	10,11	30,31	[60],61,64	0.02000	55	0.00847	28	0.01353	35
	10,11	30,31,33	61,64	0.02068	56	0.00755	28	0.01596	35
	10,11,12	30,31	84	0.02477	56	0.02488	28	0.00949	35
	10,11	30,31,33	93	0.02561	56	0.02921	28	0.00751	35
o-Dichlorobenzene	10,11	30,31	64	0.01605	50	0.00528	27	0.00760	29
	10,11	30,31	[61],64	0.01728	49	0.00579	27	0.00885	29
	10,11	30,31	63	0.02437	50	0.00993	27	0.01977	29
	10,11	30,31	(51),53	0.01835	49	0.00848	27	0.00802	29
	10,11	20	41,44	0.02302	50	0.01800	27	0.00852	29
	10,11	30,(31)	41,44	0.02881	49	0.02970	27	0.01097	29

*For species in parentheses the standard deviation in the value of the corresponding K_{ij} is equal to or exceeds the value itself. For species in square brackets the standard deviation is approximately one-half the value of the K_{ij}.

to a corresponding change in the solute–solvent interactions in the organic-solvent phase. These interactions are conveniently classified into two possible types: (*i*) nonspecific, *i.e.* van der Waals interactions and (*ii*) specific alcohol–solvent complexes. Estimates exist (6) for the contribution made by van der Waals alcohol–solvent interactions to the partition coefficients. For each of the alcohols, this contribution was found to increase only slightly from cyclohexane through to benzene, then to increase sharply for chlorobenzene, and even more for *o*-dichlorobenzene. Alcohol–solvent complexes are considered to be absent in cyclohexane, but to exist in the other

Can. J. Chem. Downloaded from www.nrcresearchpress.com by 210.87.254.5 on 09/05/12
For personal use only.

Can. J. Chem. Downloaded from www.nrcresearchpress.com by 210.87.254.5 on 09/05/12
For personal use only.

TABLE 4. Formation constants (K_{ij}) for *n*-mers and hydrates of *tert*-butyl alcohol in six solvents at 25 °C*

(*a*) Cyclohexane, carbon tetrachloride, and *p*-xylene

	Value†						
	Cyclohexane		Carbon tetrachloride		*p*-Xylene		
Constant	*A*	*B*	*A*	*B*	*A*	*B*	*C*
K_{11}	108 ± 4	108 ± 4	30.9 ± 2.8	30.9 ± 2.9	14.5 ± 0.8	13.5 ± 8.7	14.7 ± 1.0
K_{12}							
K_{20}							
$K_{30} \times 10^{-1}$	270 ± 27	271 ± 2.8	88.4 ± 0.78	87.8 ± 0.73	12.6 ± 1.1	12.3 ± 0.1	13.1 ± 1.4
$K_{31} \times 10^{-4}$			32.0 ± 1.9	32.0 ± 2.1	34.1 ± 0.9	33.9 ± 0.8	27.1 ± 1.4
$K_{33} \times 10^{-8}$						2.2 ± 1.0	
$K_{60} \times 10^{-6}$	(1.23 ± 0.41) × 10^2	(1.00 ± 0.42) × 10^2		3.4 ± 2.1			
$K_{61} \times 10^{-8}$	(9.27 ± 0.30) × 10^4	(1.16 ± 0.03) × 10^4	194 ± 14	77.8 ± 12.0			
$K_{63} \times 10^{-13}$	(4.91 ± 0.22) × 10^5			(3.49 ± 0.10) × 10^3			7.46 ± 2.1
$K_{64} \times 10^{-16}$		(1.04 ± 0.05) × 10^6	(2.74 ± 0.08) × 10^3				
$K_{84} \times 10^{-19}$					1.62 ± 0.3	1.43 ± 0.5	
P	0.479 ± 0.008	0.479 ± 0.008	0.835 ± 0.009	0.834 ± 0.010	1.21 ± 0.01	1.22 ± 0.01	1.22 ± 0.01

(*b*) Benzene, chlorobenzene, and *o*-dichlorobenzene

	Value†						
	Benzene			Chlorobenzene		*o*-Dichlorobenzene	
Constant	*A*	*B*	*C*	*A*	*B*	*A*	*B*
K_{11}	17.0 ± 1.1	11.9 ± 2.1	16.1 ± 1.1	10.9 ± 2.0	14.7 ± 1.7	20.6 ± 0.6	20.6 ± 0.8
$K_{12} \times 10^{-2}$		1.65 ± 0.38		10.5 ± 3.4	11.7 ± 3.6		
K_{20}				3.64 ± 0.34			
$K_{30} \times 10^{-1}$	22.2 ± 1.7	21.9 ± 1.8	21.5 ± 1.9		6.42 ± 0.96	7.46 ± 0.52	7.85 ± 0.61
K_{21}				724 ± 62			
$K_{31} \times 10^{-4}$	4.42 ± 0.13	4.72 ± 0.16	4.03 ± 0.14		2.01 ± 0.15	2.78 ± 0.08	2.81 ± 0.14
$K_{33} \times 10^{-8}$	7.23 ± 1.41		14.9 ± 1.1				
$K_{60} \times 10^{-4}$				23.4 ± 4.3	8.7 ± 5.0		
$K_{61} \times 10^{-7}$				14.9 ± 1.0	3.2 ± 1.2		1.6 ± 1.2
K_{63}							
$K_{64} \times 10^{-15}$	19.9 ± 1.1	23.7 ± 0.7		11.0 ± 0.3	8.27 ± 0.29	11.3 ± 0.3	12.3 ± 0.4
$K_{84} \times 10^{-19}$			1.37 ± 0.08				
P	1.22 ± 0.01	1.22 ± 0.01	1.21 ± 0.01	1.26 ± 0.01	1.27 ± 0.01	1.04 ± 0.01	1.04 ± 0.01

*The ± standard deviation follows each quantity.

†Columns marked *A*, *B*, and *C* for a solvent represent three equally good models, and *A*, *B* for a solvent represent two equally good ones.

TABLE 5. Final results of least-squares fits of polynomials to the distribution and water-solubility data for cyclohexanol – organic solvent systems at 25 °C

Solvent	Solution model*			Root mean squares	Degrees of freedom	Water solubility data		Distribution data	
						Sum of squares	No. of points	Sum of squares	No. of points
Cyclohexane	10,11	30	[80],81,84	0.03182	46	0.03487	27	0.01171	26
	10,11	30,[31]	[80],81,83	0.03229	45	0.03526	27	0.01167	26
	10,11	40,41	[80],81,84	0.03316	45	0.01938	27	0.03010	26
	10,11	30,(31)	[80],81,84	0.03151	45	0.03312	27	0.01156	26
	10,11	30	60,61,64	0.05850	46	0.12121	27	0.03621	26
Carbon tetrachloride	10,11	30,31,33	80,81,83	0.02089	67	0.00999	44	0.01924	32
	10,11	30,31,33	[90],91,93	0.02100	67	0.00980	44	0.01973	32
	10,11	30,31	80,81,84	0.02395	68	0.02003	44	0.01898	32
	10,11	30,31	90,91,93	0.02454	68	0.02132	44	0.01962	32
	10,11	30,31	80,81,83	0.02587	68	0.01389	44	0.03161	32
p-Xylene	10,11	30,31,33	80,81,84	0.01671	46	0.00556	27	0.00728	28
	10,11	40,[41],42	80,81,84	0.01705	47	0.00557	27	0.00781	28
	10,11	30,31	60,61,64	0.01804	47	0.00754	27	0.00774	28
	10,11	30,31	80,81,84	0.01867	47	0.00925	27	0.00714	28
	10,11	40,42	(80),81,84	0.01753	47	0.00669	27	0.00774	28
	10,11	40,41	60,61,64	0.02007	47	0.00724	27	0.01169	28
	10,11	40,42	60,61,64	0.02067	47	0.00802	27	0.01191	28
	10,11	30	50,51,53	0.02348	48	0.01312	27	0.01334	28
	10,11	30	50,51,55	0.03058	48	0.02205	27	0.02377	28
Benzene	10,11,12	30,[31]	80,81,84	0.02119	45	0.00337	26	0.01682	28
	10,11	30,[31]	80,81,84	0.02204	45	0.00673	26	0.01562	28
	10,11,12	40,[41]	80,81,84	0.02217	45	0.00315	26	0.01898	28
	10,11	40, [42]	80,81,84	0.02259	46	0.00492	26	0.01855	28
	10,11	40,[41]	80,81,84	0.02360	46	0.00699	26	0.01923	28
	10,11(12)	40 [42]	80,81,84	0.02280	45	0.00421	26	0.01919	28
Chlorobenzene	10,11	40, 42	81,84	0.01838	45	0.00886	25	0.00634	26
	10,11	40	60,61,64	0.01838	46	0.01114	25	0.00405	26
	10,11	30	60,61,64	0.01866	45	0.01168	25	0.00350	26
	10,11	40,(41)	60,61,64	0.01847	45	0.01102	25	0.00400	26
	10,11	40, 42	60,61,64	0.02069	45	0.01167	25	0.00760	26
o-Dichlorobenzene	10,11	30,31,33	80, 83	0.01819	46	0.00874	29	0.00681	26
	10,11	30,31,33	60,61,63	0.01999	46	0.01013	29	0.00825	26
	10,11	30,31	60,61,64	0.02044	47	0.00958	29	0.01005	26
	10,11(12)	30,31	60,61,64	0.02002	46	0.00882	29	0.00961	26
	10,11	30,31	80,81,84	0.02297	47	0.01552	29	0.00297	26
	10,11	40, 42	81,84	0.02310	48	0.01081	29	0.01480	26
	10,11	30	50,[51],53	0.02759	48	0.01965	29	0.01690	26
	10,11	[30]	50,51,55	0.03312	48	0.03210	29	0.02054	26

*For species in parentheses the standard deviation in the value of the corresponding K_{ij} is equal to or exceeds the value itself. For species in square brackets the standard deviation is approximately one-half the value of the K_{ij}.

five solvents. Moreover, the formation constant of the 1:1 alcohol–solvent complex is expected (6) to increase from carbon tetrachloride through to benzene, then to decrease through to *o*-dichlorobenzene. Consequently, for carbon tetrachloride, *p*-xylene, and benzene, complexes are considered to be the major factor in the increase in the value of P in these solvents, over its value in cyclohexane. For chlorobenzene, and more so for *o*-dichlorobenzene the contribution to P due to complexes decreases, and that due to van der Waals interactions increases over the corresponding contributions in the other three solvents.

Inspection of Tables 4 and 6 shows a general decrease in the values of a given K_{ij}, on going from cyclohexane through carbon tetrachloride, *p*-xylene, benzene, chlorobenzene, to *o*-dichlorobenzene. The following explanation is proposed.

Can. J. Chem. Downloaded from www.nrcresearchpress.com by 210.87.254.5 on 09/05/12
For personal use only.

Can. J. Chem. Downloaded from www.nrcresearchpress.com by 210.87.254.5 on 09/05/12
For personal use only.

TABLE 6. Formation constants (K_{ij}) for *n*-mers and hydrates of cyclohexanol in six solvents at 25 °C*†

(*a*) Cyclohexane and carbon tetrachloride

	Value				
	Cyclohexane			Carbon tetrachloride	
Constant	*A*	*B*	*C*	*A*	*B*
K_{11}	144 ± 20	133 ± 19	90 ± 13	37.3 ± 2.8	31.9 ± 2.7
K_{12}					
$K_{30} \times 10^{-1}$	495 ± 49	476 ± 49		(1.33 ± 0.07) × 10^3	(1.41 ± 0.08) × 10^3
K_{40}			(3.97 ± 0.36) × 10^5		
$K_{31} \times 10^{-2}$		(5.9 ± 3.8) × 10^3		(3.59 ± 0.32) × 10^3	(4.65 ± 0.22) × 10^3
K_{41}			(1.51 ± 0.26) × 10^8		
$K_{33} \times 10^{-8}$				56.1 ± 22.0	518 ± 110
K_{42}					
K_{60}					
$K_{80} \times 10^{-8}$	(4.9 ± 2.7) × 10^4	(6.7 ± 2.8) × 10^4	(1.13 ± 0.84) × 10^4	(5.6 ± 1.8) × 10^4	
K_{90}					(2.6 ± 1.1) × 10^{12}
K_{61}					
$L_{81} \times 10^{-11}$	(3.88 ± 0.08) × 10^5	(2.46 ± 0.17) × 10^5	(1.47 ± 0.10) × 10^5	(1.31 ± 0.09) × 10^5	
K_{91}					(5.64 ± 0.44) × 10^{15}
K_{63}					
K_{64}					
$K_{83} \times 10^{-17}$		(2.24 ± 0.07) × 10^3		(2.22 ± 0.07) × 10^3	
K_{93}					(1.32 ± 0.04) × 10^{22}
$K_{84} \times 10^{-19}$	(4.40 ± 0.13) × 10^7		(2.18 ± 0.07) × 10^7		
P	3.79 ± 0.06	3.72 ± 0.06	4.04 ± 0.06	7.87 ± 0.06	7.83 ± 0.06

Can. J. Chem. Downloaded from www.nrcresearchpress.com by 210.87.254.5 on 09/05/12
For personal use only.

TABLE 6 (*Continued*)
(*b*) *p*-Xylene and benzene

	Value					
	p-Xylene			Benzene		
Constant	*A*	*B*	*C*	*A*	*B*	*C*
K_{11}	21.8±1.0	23.4±0.8	24.0±1.1	22.4±2.2	24.6±1.6	26.7±1.1
$K_{12}\times10^{-3}$				1.01±0.36	1.48±0.57	
$K_{30}\times10^{-1}$	10.0±1.3		6.8±1.5	5.6±1.9		
K_{40}		(3.02±0.38)×10³			(1.53±0.64)×10³	(1.65±0.60)×10³
$K_{31}\times10^{-2}$	190±22		84±28	67±30		
K_{41}					(2.6±1.0)×10⁵	
$K_{33}\times10^{-8}$	6.1±1.7					
K_{42}		(2.51±0.18)×10⁸				(6.6±2.5)×10⁷
K_{60}			(9.0±1.5)×10⁵			
$K_{80}\times10^{-8}$	3.53±0.89	0.82±0.82		12.7±4.6	10.6±3.8	9.5±3.6
K_{90}						
K_{61}			(6.33±0.44)×10⁸			
$K_{81}\times10^{-11}$	2.83±0.28	2.23±0.17		7.50±0.43	6.38±0.55	6.23±0.29
K_{91}						
K_{63}						
K_{64}			(2.43±0.07)×10¹⁶			
$K_{83}\times10^{-17}$						
K_{93}						
$K_{84}\times10^{-19}$	2.00±0.12	1.28±0.09		2.48±0.07	2.31±0.07	2.06±0.1
P	12.22±0.09	12.45±0.08	12.30±0.09	13.30±0.14	13.41±0.13	13.38±0.13

Can. J. Chem. Downloaded from www.nrcresearchpress.com by 210.87.254.5 on 09/05/12
For personal use only.

TABLE 6 (*Concluded*)

(*c*) Chlorobenzene and *o*-dichlorobenzene

	Value					
	Chlorobenzene			*o*-Dichlorobenzene		
Constant	*A*	*B*	*C*	*A*	*B*	*C*
K_{11}	24.0×0.8	24.4±0.5	24.7±0.5	17.9±1.1	20.9±1.4	21.5±1.4
$K_{12}\times10^{-3}$			3.5±1.2			
$K_{30}\times10^{-1}$				18.7±2.0	15.6±2.4	15.1±2.5
K_{40}	(2.27±0.35)×10³	(1.08±0.40)×10³				
$K_{31}\times10^{-2}$				243±20	119±4	150±37
K_{41}						
$K_{33}\times10^{-8}$				16.0±1.3	5.4±2.9	
K_{42}	(1.53±0.13)×10⁸					
K_{60}		(4.3±1.6)×10⁵	(6.0±1.5)×10⁵		(7.7±2.0)×10⁵	(5.1±2.0)×10⁵
$K_{80}\times10^{-8}$				3.7±1.1		
K_{90}						
K_{61}		(6.16±0.15)×10⁸	(6.15±0.15)×10⁸		(3.5±1.0)×10⁸	(7.6±0.7)×10⁸
$K_{81}\times10^{-11}$	1.77±0.11					
K_{91}						
K_{63}					(1.39±0.10)×10¹⁴	
K_{64}		(1.35±0.04)×10¹⁶	(1.36±0.04)×10¹⁶			(4.1±0.1)×10¹⁶
$K_{83}\times10^{-17}$				1.13±0.04		
K_{93}						
$K_{84}\times10^{-19}$	0.81±0.05					
P	14.65±0.12	14.62±0.10	14.54±0.14	11.34±0.11	11.50±0.11	11.48±0.14

*The ± standard deviation follows each quantity.

†Columns marked *A*, *B*, and *C* for a solvent represent three equally good models, and *A*, *B* for a solvent represent two equally good ones (an exception is that *C* for cyclohexane is inferior to *A* and *B*).

TABLE 7. The partition coefficients of three alcohols between six organic solvents and water, at 25 °C

Solvent	Partition coefficient		
	tert-Butyl alcohol	*n*-Butanol	Cyclohexanol
Cyclohexane	0.48	0.73	3.70
CCl_4	0.83	2.00	7.85
p-Xylene	1.22	3.72	12.32
Benzene	1.22	4.05	13.36
Chlorobenzene	1.26	3.78	14.60
o-Dichlorobenzene	1.04	3.31	11.44

The activities of the alcohol and water monomers in the denominator of the expression for each formation constant include any alcohol–solvent complexes and water–solvent complexes, respectively. In the case of cyclohexane these complexes are considered to be absent. For the other solvents, water–solubility data have been interpreted (2) as being due in part to the existence of water–solvent complexes in the other five solvents. The existence of these water–solvent complexes in these solvents would result in a smaller value for the K_{ij} of any given hydrate, than the K_{ij} value for cyclohexane. In addition, the above-discussed partition-coefficient values led to the conclusion that except for cyclohexane, the other five solvents not only formed alcohol–solvent complexes with the alcohol monomer, but also in the case of the chlorobenzenes had enhanced alcohol–solvent van der Waals interactions. These two factors would also produce a smaller value for the K_{ij} of a given *n*-mer, than its value in cyclohexane.

Acknowledgment

We are grateful to the National Research Council of Canada for financial assistance and for a Bursary to one of us (J.K.).

1. J. KIRCHNEROVÁ and G. C. B. CAVE. Can. J. Chem. This issue.
2. J. KIRCHNEROVÁ and G. C. B. CAVE. Can. J. Chem. This issue.
3. J. A. RIDDICK and W. B. BUNGER. Techniques of chemistry. Vol. II. Organic solvents. 3rd ed. John Wiley, Interscience, New York. 1970.
4. W. S. KNIGHT. Ph.D. Thesis. Princeton University, Princeton, N.J. 1962.
5. D. EDWARDS, J. F. MARRUCO, and R. RATORRIIS. J. Chim. Phys. **63**, 239 (1966).
6. J. KIRCHNEROVÁ. Ph.D. Thesis. McGill University, Montreal, Quebec. 1974.
7. J. MULLENS, I. HANSSENS, and P. HUYSKENS. Bull. Soc. Chim. Belg, **80**, 539 (1971).
8. J. MULLENS, I. HANSSENS, and P. HUYSKENS. J. Chim. Phys. **68**, 1417 (1971).
9. R. A. ROBINSON and R. H. STOKES. Electrolyte solutions. 2nd ed. Butterworths, London. 1959.
10. E. E. TUCKER and E. D. BECKER. J. Phys. Chem. **77**, 1783 (1973).

Can. J. Chem. Downloaded from www.nrcresearchpress.com by 210.87.254.5 on 09/05/12
For personal use only.

Solvolysis of isopropyl bromide in ethanol–water mixtures. Dissection into initial state and transition state contributions

WIENDELT DRENTH[1]
Laboratory for Organic Chemistry of the University, Croesestraat 79, Utrecht, the Netherlands
AND
MICHAEL COCIVERA[1]
Department of Chemistry, University of Guelph, Guelph, Ont., Canada N1G 2W1

Received May 19, 1976

WIENDELT DRENTH and MICHAEL COCIVERA. Can. J. Chem. **54**, 3944 (1976).

Rates were determined for the solvolysis of isopropyl bromide in ethanol–water mixtures (20 to 80% by volume of ethanol) at 50 and 75 °C and the corresponding activation parameters calculated. From the partial vapor pressure of isopropyl bromide over the various solutions at 50 and 75 °C, the variations in its initial state thermodynamic parameters were calculated. Thus, the variation in the activation parameters with solvent composition could be analyzed in terms of initial and transition state contributions. The initial state variation dominates according to a unimolecular as well as to a bimolecular treatment of data.

WIENDELT DRENTH et MICHAEL COCIVERA. Can. J. Chem. **54**, 3944 (1976).

On a déterminé les vitesses de solvolyse du bromure d'isopropyle dans des mélanges eau–éthanol (20 à 80% par volume d'éthanol) à 50 et 75 °C, et on a calculé les paramètres d'activation correspondants. A partir des pressions de vapeur partielles du bromure d'isopropyle au-dessus de diverses solutions à 50 et 75 °C, on a calculé des variations de ses paramètres thermodynamiques dans l'état initial. Ainsi la variation dans les paramètres d'activation avec la composition de solvant peut être analysée en termes de contribution de l'état initial et de l'état de transition. Que l'on traite la réaction comme unimoléculaire ou bimoléculaire, la variation dans l'état initial domine.

[Traduit par le journal]

Introduction

The solvent dependence of the rates of a variety of reactions have been analyzed in terms of the transition state parameters, $\Delta G^{\ddagger}$, $\Delta H^{\ddagger}$, and $\Delta S^{\ddagger}$. Since these parameters correspond to differences between the transition state and the initial state, any solvent dependence may result from effects on the transition state and/or the initial state. Therefore, to ascribe the solvent effect correctly, it is necessary to dissect these parameters into their initial and transition state components. Only in a few cases has this dissection been made (1–5). In this paper, we present a dissection of $\Delta G^{\ddagger}$ and $\Delta H^{\ddagger}$ for the solvolysis of isopropyl bromide in ethanol–water mixtures ranging from 20 to 80 vol% of ethanol. This dissection was accomplished by measuring the rate of solvolysis and the Henry's law constant for isopropyl bromide at 50 and 75 °C for each solvent. Arnett *et al.* have obtained the heat of solution at 25 °C for a number of compounds in aqueous ethanol mixtures and dissected $\Delta H^{\ddagger}$ into its initial and transition state components for *tert*-butylchloride and dimethyl-*tert*-butylsulfonium iodide (1).

Results and Discussion

The first-order rate constants for the solvolysis of isopropyl bromide are listed in Table 1 at 50 and 75 °C for a number of ethanol–water mixtures. These data were used to calculate the values for $\Delta G^{\ddagger}$, $\Delta H^{\ddagger}$, and $T\Delta S^{\ddagger}$ that are listed in the table also. The value for $T\Delta S^{\ddagger}$ is obtained as the difference between $\Delta H^{\ddagger}$ and $\Delta G^{\ddagger}$. For the Gibbs free energy, the initial state component ΔG_i^{θ} and the transition state component G_t^{θ} are obtained relative to isopropyl bromide vapor using the equations,

$$G_i^{\theta} = RT \ln k_H + A$$

and

$$G_t^{\theta} = G_i^{\theta} + \Delta G^{\ddagger}$$

[1]This work was performed at the University of California, Los Angeles, CA, under the guidance of the late Professor Saul Winstein.

Can. J. Chem. Downloaded from www.nrcresearchpress.com by 210.87.254.105 on 09/05/12
For personal use only.

TABLE 1. Rate constants, Henry's law constants k_H, and transition state parameters for isopropyl bromide in alcohol–water

Solvent composition (vol% alcohol)	Mol fraction H_2O at 25 °C	$k^a \times 10^5$ / s^{-1} 50 °C	$k^a \times 10^5$ / s^{-1} 75 °C	$\Delta G^{\pm b}$ / kJ/mol 50 °C	$\Delta H^{\pm c}$ / kJ/mol	$-T\Delta S^{\pm c}$ / kJ/mol 50 °C	k_H / J/mol 50 °C	k_H / J/mol 75 °C
80	0.447	0.118	1.63	116.19	95.5	20.5	28	70
70	0.581	0.232	3.12	114.39	94.7	19.7	78	135
60	0.684	0.437	5.79	112.67	94.3	18.4	118	186
50	0.764	0.805	10.4	111.04	93.0	18.0	206	314
40	0.829	1.58	19.3	109.19	90.9	18.4	408	542
30	0.883	3.16	37.5	107.35	90.1	17.6	809	929
20	0.928	5.35	65	105.92	90.9	15.6	1418	1555

[a]Root mean square error not exceeding 2%.
[b]Accurate to ±0.04 kJ/mol.
[c]Accurate to ±(0.8–2.1) kJ/mol.

TABLE 2. Thermodynamic parameters for isopropyl bromide in initial state and transition state. Data are in kJ/mol and are relative to the value at 80% alcohol

Vol% alcohol	$\Delta G_i^{\theta a}$ at 50 °C	$\Delta H_i^{\theta b}$	$-T\Delta S_i^{\theta}$ at 50 °C	ΔG_t^{θ} at 50 °C	ΔH_t^{θ}	$-T\Delta S_t^{\theta}$ at 50 °C
80	(0.00)	(0)	(0)	(0.00)	(0)	(0)
70	2.77	14	−11	0.97	13	−12
60	3.87	17	−13	0.35	15	−15
50	5.37	19	−14	0.22	16	−16
40	7.20	24	−17	0.20	19	−19
30	9.05	30	−21	0.21	24	−24
20	10.56	31	−20	0.29	26	−26

[a]Accuracy approximately 0.1 kJ/mol.
[b]Accuracy 2–5 kJ/mol.

in which R is the gas constant, T is the absolute temperature, and k_H is the Henry's law constant, defined as vapor pressure divided by the concentration. Values of k_H are listed in Table 1 for isopropyl bromide in each solvent mixture at 50 and 75 °C. Although Henry's law constant has been defined in terms of concentration rather than mole fraction, the error due to variation of concentration with temperature is negligible over the 25 °C range employed. The constant A is the Gibb's free energy of isopropyl bromide in the vapor phase and, therefore, is independent of solvent composition. Consequently to ascertain the effect of solvent composition on G_i^{θ} and G_t^{θ}, we use the 80% ethanol mixture as a reference and define

$$\Delta G_i^{\theta} = G_i^{\theta} - (G_i^{\theta})_{80}$$

in which G_i^{θ} is the value for any solvent mixture and $(G_i^{\theta})_{80}$ is the value for the 80% ethanol mixture. A similar expression is used to obtain ΔG_t^{θ}, and values are listed in Table 2.

For the enthalpy, H_i^{θ} and H_t^{θ} are obtained using the equations

$$(H_i^{\theta}/R)(1/348 - 1/323) = \ln k_H(75\ °C) - \ln k_H(50\ °C) + B$$

and

$$H_t^{\theta} = H_i^{\theta} + \Delta H^{\pm}$$

The constant B is independent of solvent composition and consequently, ΔH_i^{θ} and ΔH_t^{θ}, which are listed in Table 2, are obtained using the 80% ethanol solvent mixture as the reference in the same manner described for the Gibbs functions. Each value of $T\Delta S$ listed in Table 2 for the initial and transition state is obtained from the difference between ΔH and ΔG.

The data in Tables 1 and 2 show that the variation in $\Delta G^{\pm}$ with solvent composition is almost entirely the result of a change in the Gibbs function of the initial state ΔG_i^{θ}, whereas the Gibbs function of the transition state ΔG_t^{θ} remains almost unchanged. This almost con-

Can. J. Chem. Downloaded from www.nrcresearchpress.com by 210.87.254.105 on 09/05/12
For personal use only.

TABLE 3. Mol% of *i*-PrOEt and *i*-PrOH arising from solvolysis of *i*-PrBr in ethanol–water mixtures at 50 and 75 °C

Vol% EtOH at 25 °C	Mol% H_2O at 25 °C	Mol% *i*-PrOEt		Mol% *i*-PrOH	
		50 °C	75 °C	50 °C	75 °C
80	44.7	51.9±1.0	53.2±1.0	48.1±0.9	46.8±1.0
70	58.1	43.0±0.80	43.0±0.80	57.0±1.2	57.0±1.2
60	68.4	33.6±0.66	34.1±0.66	66.4±1.2	65.9±1.3
50	76.4	27.5±0.55	27.0±0.50	72.5±1.4	73.0±1.2
40	82.9	20.5±0.40	20.2±0.40	79.5±1.6	79.8±1.6
30	88.3	14.9±0.28	14.7±0.28	85.1±1.7	85.3±1.6
20	92.8	8.7±0.17	9.1±0.18	91.3±1.8	90.9±1.8

stancy of the transition state value in the range from 80–20% alcohol is probably the result of a compensation of a decrease due to a better solvation of the partly ionic transition state by an increase due to a less favourable interaction between methyl groups and a more aqueous solvent.

The variation in Gibbs functions ΔG_i^θ and ΔG_t^θ is composed of much larger, partly compensating changes in enthalpy and entropy terms. In the solvent range investigated, the variation of enthalpy as well as of entropy with solvent composition is quite similar for initial and transition state, indicating that the effect on initial state and on transition state in aqueous alcohol is similar to a large extent.

In the foregoing discussion isopropyl bromide solvolysis is treated as a unimolecular reaction. Actually, isopropyl bromide is classified as a borderline case between unimolecular and bimolecular solvolysis (6). In bimolecular reactions the initial and transition states not only involve a substrate molecule but also a molecule of solvent. Reaction of isopropyl bromide with ethyl alcohol gives ethyl isopropyl ether, while reaction with water gives isopropyl alcohol. In order to know the percentages of isopropyl bromide that react with alcohol and water, we determined the product composition by gas–liquid chromatography (Table 3). It appears that the composition of the products in a given solvent is the same at both temperatures. Moreover, the ratio, alcohol/ether, for product is almost equal to the ratio, water/ethanol for the bulk solvent.

Assuming two parallel bimolecular reactions, the observed first-order rate constant k can be dissected into a rate constant for alcohol formation, $f_{i\text{PrOH}}k$, and a rate constant for ether formation, $f_{i\text{PrOEt}}k$, f being the product mole fraction. The second-order rate constants were calculated by dividing these partial first-order rate constants by the appropriate concentrations of water and alcohol. Since the ratio of products is almost equal to the ratio of bulk water and alcohol (Table 3), the partial second-order rate constants for alcohol and ether formation are almost equal. In this treatment the transition state contains an isopropyl bromide molecule and one solvent molecule. Consequently, the initial state must be defined as an isopropyl molecule plus one molecule of solvent, and the initial state thermodynamic parameters are obtained by adding the values for isopropyl bromide (Table 2) to the corresponding values for the solvent components.

Partial pressures P of alcohol and water at 50 °C were calculated from the vapour pressures of the pure liquids P_0 (7, 8) and activity data published by Kharin *et al.* (9) using the equation, $a = P/P_0$ in which a is the activity of the component. These vapor pressures were used to calculate k_H and ΔG^θ for alcohol and for water relative to 80 vol% alcohol in the same manner as described above. The total value for 1 mol of isopropyl bromide and 1 mol of solvent ΔG_i^θ, which is given in Table 4, is obtained by adding ΔG^θ for the solvent component to the corresponding value given in Table 2. Using these values for ΔG_i^θ, ΔG_t^θ is obtained as described above.

A similar calculation has been performed for the corresponding enthalpy values. In this case, the partial molar enthalpy of each solvent component was not obtained from the temperature dependence of the Henry's law constant. Instead, it was obtained directly from a plot of the heat of mixing at 50 °C (9) *vs.* mole fraction of solvent component for solvent mixtures containing no

Can. J. Chem. Downloaded from www.nrcresearchpress.com by 210.87.254.105 on 09/05/12
For personal use only.

TABLE 4. Total Gibbs functions for isopropyl bromide plus one solvent molecule at 50 °C. Data are kJ/mol and are relative to the value at 80% alcohol (except $\Delta G^{\ddagger}$)

Vol% EtOH	Bimolecular reaction with EtOH			Bimolecular reaction with H_2O		
	$\Delta G^{\ddagger}$	ΔG_i^{θ}	ΔG_t^{θ}	$\Delta G^{\ddagger}$	ΔG_i^{θ}	ΔG_t^{θ}
80	122.5	(0.0)	(0.0)	121.8	(0.0)	(0.0)
70	120.8	2.8	1.1	120.7	2.0	0.9
60	119.5	4.1	1.1	119.5	2.4	0.1
50	117.9	5.8	1.2	118.2	3.4	−0.2
40	116.2	7.9	1.6	116.6	4.8	−0.4
30	114.5	10.1	2.1	115.0	6.4	−0.4
20	113.7	11.8	3.0	113.9	7.6	−0.3

TABLE 5. Total enthalpy values for isopropyl bromide plus one solvent molecule at 50 °C. Data are in kJ/mol and are relative to the value at 80% alcohol (except $\Delta H^{\ddagger}$)

Vol% EtOH	Bimolecular reaction with EtOH			Bimolecular reaction with H_2O		
	$\Delta H^{\ddagger}$	ΔH_i^{θ}	ΔH_t^{θ}	$\Delta H^{\ddagger}$	ΔH_i^{θ}	ΔH_t^{θ}
80	96.1	(0)	(0)	94.0	(0)	(0)
70	94.0	15	12.9	94.5	13	13.5
60	94.0	18	15.9	93.6	16	15.6
50	92.8	20	16.7	92.9	18	16.9
40	90.3	24	18.2	90.7	23	19.7
30	89.0	28	20.9	89.9	29	24.9
20	92.4	18	14.3	90.3	31	27.3

isopropyl bromide. Values for ΔH_i^{θ} and ΔH_t^{θ} calculated in this manner for a mechanism involving one molecule of solvent plus isopropyl bromide are given in Table 5.

In this bimolecular treatment, the variation in $\Delta G^{\ddagger}$ parallels the unimolecular case and is mainly the result of the variation in the initial state Gibbs function. The variations in ΔH_i^{θ} and ΔH_t^{θ} are much larger than in $\Delta H^{\ddagger}$. The same applies to the entropies which can easily be calculated from the data in Tables 4 and 5. Since, qualitatively, the same conclusion is reached in the unimolecular and bimolecular treatments for this reaction, we believe that the change in reactivity as a function of solvent composition is determined mainly by the initial state variation.

Experimental

Compounds

Commercial isopropyl bromide (Eastman Kodak White Label) was distilled twice, bp 58.9 °C at 751 torr, n_D^{25} 1.4224, d_4^{25} 1.3046.

Batches of anhydrous ethyl alcohol (1.5 l) were boiled for 4 h with 15 g potassium hydroxide. After distillation the alcohol was dried by treating it twice with magnesium ethylate according to Lund and Bjerrum (10). It was directly distilled into the storage bottle. Karl Fischer titration indicated a water content <0.04%; bp 77.8 °C at 747 torr, d_4^{25} 0.7853.

Two litres of distilled water were fractionated in an all-glass apparatus after addition of 3 drops of concentrated sulfuric acid.

Alcohol–water mixtures were made up by mixing pipetted amounts of both components at room temperature.

Kinetic Measurements

Rates were measured by the sealed ampoule technique and potentiometric titration of 5 cm³ aliquots for bromide ions. These aliquots were diluted with 15 cm³ of 95% ethyl alcohol and 1 cm³ of a 2 *M* 1:1 acetic acid – sodium acetate buffer.

In calculating the rates, 'infinity' titers were used. No appreciable drift in rate was observed. Straight lines were fitted to the points of a plot of log *c* *vs.* time. The rate constants were obtained from the slopes of these lines by least-squares calculation.

Henry's Law Constants

The partial vapour pressure of isopropyl bromide was determined by measuring the difference in vapour pressure over the solutions and the pure solvent at the required temperatures after careful degassing. Corrections were applied for the solvolysis preceding pressure reading as well as for the decrease in the partial pressure of the solvent in the solution compared with the pressure of the pure solvent. The latter correction was negligible for the 50 °C data. For the 75 °C data it increased from 0.0 torr for 20% alcohol up to 0.7 torr for 80% alcohol.

Gas–Liquid Chromatography

Details of this are available in ref. 11. For product analysis a 4 m column of $\frac{1}{4}$ in. Al tubing was used at 80 °C; inlet 120 °C, with He as carrier gas. The fire brick support was loaded over 2 m with 30% glycerol and over the remaining 2 m with 10% cetyl amine and 10% β,β'-iminodipropionitrile. Water and ethanol had much longer retention times than the solvolysis products and did not interfere. In order to speed the removal of water and alcohol from the column, back flushing was applied. Tetrahydrofuran was used as internal standard.

Acknowledgement

We thank Dr. A. Schuijff for discussing some thermodynamical details.

1. E. M. ARNETT, W. G. BENTRUDE, J. J. BURKE, and P. McC. DUGGLEBY. J. Am. Chem. Soc. **87**, 1541 (1965) and references therein.
2. E. S. RUDAKOV and V. P. TRETYAKOV. Org. React. **2**, 174 (1965).
3. A. J. PARKER. Chem. Rev. **69**, 1 (1969).
4. M. H. ABRAHAM. Prog. Phys. Org. Chem. **11**, 1 (1974).

Can. J. Chem. Downloaded from www.nrcresearchpress.com by 210.87.254.105 on 09/05/12
For personal use only.

5. S. WINSTEIN and A H. FAINBERG. J. Am. Chem. Soc. **79**, 5937 (1957).
6. S. WINSTEIN, E. GRUNWALD, and H. JONES. J. Am. Chem. Soc. **73**, 2700 (1951).
7. R. C. Weast (*editor*). Handbook of Chemistry and Physics. The Chemical Rubber Co., Cleveland, Ohio. 1968.
8. C. B. KRETSCHMER and R. WIEBE. J. Am. Chem. Soc. **71**, 1793 (1949).
9. S. E. KHARIN, YU. A. BYVAL'TSEV, and V. M. PERELYGIN. Izv. Vyssh. Ucheb. Zaved. Pishch. Tekhnol. 90 (1970).
10. H. LUND and J. BJERRUM. Ber. **64**, 210 (1931).
11. M. COCIVERA. Thesis, University of California at Los Angeles. 1963. Available from University Microfilms Inc., Ann Arbor, Mich., U.S.A.

Can. J. Chem. Downloaded from www.nrcresearchpress.com by 210.87.254.105 on 09/05/12
For personal use only.

Hydrogenolysis of organometallics and the acidity of hydrogen[1]

ERWIN BUNCEL AND BALACHANDRAN C. MENON
Department of Chemistry, Queen's University, Kingston, Ont., Canada K7L 3N6

Received April 21, 1976

ERWIN BUNCEL and BALACHANDRAN C. MENON. Can. J. Chem. **54**, 3949 (1976).

The hydrogenolysis of a series of alkylcesiums in cyclohexylamine solvent has been studied spectrophotometrically. The cesium salt of *p*-phenyltoluene reacts with H_2 (1 atm, room temperature), but the cesium salts of di-2,4-xylylmethane and of diphenylmethane are unreactive. The results show that the acidity of H_2 is intermediate between those of *p*-phenyltoluene and of di-2,4-xylylmethane in this reaction system. Possible effects of ion association phenomena on the equilibrium processes are considered.

ERWIN BUNCEL et BALACHANDRAN C. MENON. Can. J. Chem. **54**, 3949 (1976).

On a étudié spectrophotométriquement l'hydrogénolyse d'une série d'alkylcésium dans la cyclohexylamine comme solvant. Le sel de césium du *p*-phényltoluène réagit avec H_2 (1 atm, à température de la pièce) mais les sels de césium du dixylyl-2,4 méthane et du diphénylméthane ne réagissent pas. Les résultats montrent que, dans ce système de réactions, l'acidité de H_2 est intermédiaire entre les acidités du *p*-phényltoluène et du dixylyl-2,4 méthane. On considère les effets possibles du phénomène d'association des ions sur les processus d'équilibration.

[Traduit par le journal]

The pK_a of molecular hydrogen, or deuterium, is of fundamental importance to the interpretation of the effect of structural changes on acidity (1–4). Literature estimates of this pK_a vary between 29 and 38 (5, 6), although no experimentally determined value has been given.

In relation to our studies of isotopic exchange of molecular hydrogen (deuterium) in strongly basic systems (7–9), it was of interest to have direct knowledge of the acidity of H_2 (D_2), in order to be able to relate the kinetic and thermodynamic acidity parameters.

Our approach to the determination of the acidity of hydrogen is based on quantitative measurements of the equilibrium between H_2 and an organometallic indicator:

$$[1] \qquad RM + H_2 \rightleftarrows RH + MH$$

It is clear from the reaction depicted in [1] that if H_2 is a stronger acid than RH the equilibrium will lie to the right hand side, and vice versa. Thus, by studying a series of hydrocarbons of increasing pK_a, a break in reactivity should be observed. When the pK_a of the hydrocarbon RH is within 1–2 pK units of that of H_2, the reaction [1] will proceed to equilibrium and the equilibrium constant (K_{rel}) will be related to the K_a's of H_2 and of RH via [2] and [3]:

$$[2] \qquad K_{rel} = \frac{K_a^{H_2}}{K_a^{RH}}$$

$$[3] \qquad pK_a^{H_2} = pK_a^{RH} + pK_{rel}$$

The method for pK_a determination of H_2 outlined above is analogous in principle to the method originally put forward (10) for pK_a determination of carbon acids, via [4]:

$$[4] \qquad R_1M + R_2H \rightleftarrows R_1H + R_2M$$

When the anions R_1^- and R_2^- have characteristic spectral absorptions in the ultraviolet or visible region, the position of the equilibrium in [4] is conveniently measured spectrophotometrically. In the present system, though one of the anionic species (H^-) in [1] has no absorption in the uv–visible, the spectrophotometric method is still applicable, as can be seen from [5]:

$$[5] \qquad K_{rel} = \frac{[RH]_e[MH]_e}{[RM]_e[H_2]_e}$$

Of the concentration terms occurring in [5], the equilibrium carbanion concentration $[RM]_e$ is directly measurable, $[RH]_e$ is known from the weighed quantity of RH initially introduced and the value of $[RM]_e$, while $[MH]_e$, the extent of reaction, is given by $[RM]_0 - [RM]_e$. The $[H_2]_e$ term in the present case will simply be given by

[1]Carbanion mechanisms. Part V. The previous parts in the series are considered to be those in ref. 26. These publications concern the carbanions derived from 1,3,5-trinitrobenzene (26*a*), 2,4,6-trinitrotoluene (26*b*), 1,3-dinitrobenzene (26*c*), and dimethyl sulfoxide (26*d*).

Can. J. Chem. Downloaded from www.nrcresearchpress.com by 210.87.254.40 on 09/05/12
For personal use only.

Can. J. Chem. Downloaded from www.nrcresearchpress.com by 210.87.254.40 on 09/05/12
For personal use only.

the solubility of hydrogen in the solvent since equilibrium between gaseous H_2 (at 1 atm pressure) and the dissolved H_2 is maintained so that the concentration of H_2 in solution remains effectively constant.

The literature already contains one report pertinent to the present work, on the hydrogenolysis of organometallic compounds. Gilman *et al.* (11) found that several organometallic compounds were reduced by molecular hydrogen. Thus the alkali metal derivatives RM where R = methyl, *n*-butyl, *n*-lauryl, *p*-tolyl, α-naphthyl, and phenyl, in benzene solution, reacted under atmospheric pressure of H_2 in the absence of catalyst. The reactions were relatively slow, requiring generally some hours to go to completion. A noteworthy aspect was the increased reactivity with increasing atomic number of the alkali metal. Thus phenylsodium required 1.9 h for 90% reduction to benzene while only 0.2 h was needed in the case of phenylcesium. Although these preparative type of experiments are unsuitable for evaluation of acidity, a very approximate upper value for the pK_a of H_2 in the region of ~42 would follow from the observation of the RCs + H_2 reaction with R = α-naphthyl.[2] This estimate, however, disregards possible medium and ion pairing effects on the pK_a (13–17). Ion association phenomena and their effect on calculated pK_a values must be considered in relation to [1]–[5] as will be shown in the Discussion section.

Results and Discussion

The solvent medium chosen for the determination of the acidity of H_2 was cyclohexylamine (CHA), with alkylcesiums (RCs) being used as the organometallic indicators. The RCs/CHA system has been used extensively by Streitwieser and co-workers (13, 18) in their studies of the acidities of hydrocarbon acids and the pK_a scale pertaining to this system has been reliably established for a series of hydrocarbon acids (13, 19). The availability of a series of hydrocarbon acids of known and increasing pK_a is central to the design of the present study.

The series of hydrocarbon acids used in this work, given in order of increasing pK_a and including an abbreviated notation, is as follows: diphenylmethane (DPM, 33.1), di-2,4-xylylmethane (DXM, 36.3), *p*-phenyltoluene (PPT, 38.7), and toluene (TOL, 41.0). The pK_a data are taken from ref. 19.

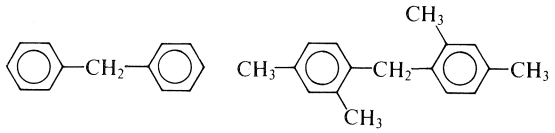

Diphenylmethane
DPM (33.1)

Di-2,4-xylylmethane
DXM (36.3)

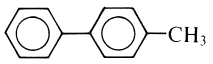

p-Phenyltoluene
PPT (38.7)

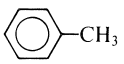

Toluene
TOL (41.0)

Our general approach towards study of reaction 1 is to generate the alkylcesium derivative RCs by reaction of the hydrocarbon RH with cesium cyclohexylamide in cyclohexylamine (CsCHA/CHA) and then to allow reaction with H_2 to occur. (In the procedure adopted, a deficiency of CsCHA is used so that the RH is partially converted to RCs, see Experimental.) The RCs concentration is measured spectrophotometrically both before and after reaction with H_2, using a reaction vessel sealed to a 1 mm quartz cuvette. Reactions were carried out under strictly anhydrous conditions. The details of the procedure and the apparatus used are given in the Experimental section.

The hydrocarbon toluene (pK_a 41) seemed a suitable starting point for our investigation, since toluene is more acidic than the hydrocarbons used in Gilman's work (11). It was found, however, that CsCHA/CHA incompletely converts toluene into the cesium salt. In fact the spectral measurements indicated that only about 1% of $C_6H_5CH_2Cs$ was present at equilibrium:

$$[6]\quad C_6H_5CH_3 + CsNHC_6H_{11} \rightleftarrows C_6H_5CH_2Cs + C_6H_{11}NH_2$$

If the reaction between $C_6H_5CH_2Cs$ and H_2 did proceed then the mobile equilibrium according to [6] would restore the concentration of $C_6H_5CH_2Cs$, while there is also the possibility of a reaction between $CsNHC_6H_{11}$ and H_2. Either or both of these circumstances could lead to no

[2]The pK_a of benzene in the cesium cyclohexylamide/cyclohexylamine system is taken as 43 (12), and since isotopic exchange for the α-naphthyl hydrogen is about 10 times greater than for benzene (13), this would indicate that naphthalene has a pK_a of ~42.

TABLE 1. Reaction between alkylcesiums and hydrogen (1 atm) in cyclohexylamine at room temperature

RH	Run	$[RH]_0$ $\times 10^3$ M	$[H_2]_0$[a] $\times 10^3$ M	Time of reaction (h)	$[RCs]_0$[b] $\times 10^3$ M	$[RCs]_t$ $\times 10^3$ M	$[RCs]_0 - [RCs]_t$ $\times 10^3$ M	$([RCs]_0 - [RCs]_t)^c_{corr}$ $\times 10^3$ M	Percentage reaction
PPT	1	0.429	6.3	330	0.780	0.082	0.698	0.601	77[d]
PPT	2	0.517	6.3	336	0.696	0.186	0.510	0.439	63[d]
PPT	3	0.703	—	336	0.560	0.483	0.077	—	—
DXM	4	0.288	6.3	336	0.323	0.318	0.005	—	2
DPM	5	0.133	6.3	336	0.341	0.326	0.015	—	4

[a]Obtained from solubility of H_2 gas, measured according to ref. 25.
[b]Carbanion concentrations calculated using the following extinction coefficient (wavelength) data for RCs: PPTCs 21 400 (472 nm), ref. 20; DXMCs 46 400 (444 nm), ref. 19; DPMCs 47 100 (440 nm), ref. 20.
[c]$([RCs]_0 - [RCs]_t)_{corr} = ([RCs]_0 - [RCs]_t) - 0.14([RCs]_0 - [RCs]_t)$. The second (correction) term in this equation represents the 'blank' reaction, run 3, in which the extent of decomposition is 14%.
[d]On prolonged reaction times (≥500 h) the reaction with PPT was found to proceed to completion but only negligible reaction occurred in the case of DXM and DPM.

net decrease in $[C_6H_5CH_2Cs]$. In practice, there was no appreciable decrease in $[C_6H_5CH_2Cs]$ after introducing H_2 into the $C_6H_5CH_3$/CsCHA/CHA system. According to the above argument, no significance could be attached to this result. The present method requires that the solvent must have a larger pK_a than the hydrocarbon used to prepare the cesium salt. This condition apparently does not hold in the case of toluene as hydrocarbon and cyclohexylamine as solvent (20).

p-Phenyltoluene (PPT, pK_a 38.6) was the next hydrocarbon in the series to be examined in the reaction with H_2. The cesium salt (PPT^-Cs^+) was partially generated from the hydrocarbon, by adding a deficiency of CsCHA/CHA, which was followed by the introduction of H_2 to 1 atm pressure. On shaking the reaction vessel at room temperature, and monitoring the reaction by uv–visible spectroscopy, a gradual decrease in PPT^-Cs^+ concentration was found to occur. In time, the characteristic carbanion absorption disappeared entirely, showing that the reaction 1 went to completion. A control (blank) experiment was run simultaneously (*i.e.* PPT^-Cs^+ in CHA but in absence of H_2) and showed only a relatively small decrease in carbanion concentration, which was taken into account when estimating the extent of reaction at a given time. A representative run is described in detail in the Experimental section and the data are summarized in Table 1.

The hydrocarbon of next lower pK_a in the series being di-2,4-xylylmethane (DXM, pK_a 36.3), we examined therefore the reaction of DXM^-Cs^+ with H_2 in CHA solvent. The results, given in Table 1, show that there is negligible reaction (<2%) between DXM^-Cs^+ and H_2, under the conditions where extensive reaction occurred between PPT^-Cs^+ and H_2.

In order to corroborate the significance of the result with DXM^-Cs^+, we examined also the reaction of the cesium salt of diphenylmethane (DPM, pK_a 33.1) with H_2. The results (Table 1) show that, once more, negligible reaction (~4%) occurs between DPM^-Cs^+ and H_2 under the conditions where PPT^-Cs^+ and H_2 react according to [1].

From the above experiments one can draw certain conclusions. The results of this work show that while PPT^-Cs^+ in CHA reacts with H_2 (1 atm, room temperature), DXM^-Cs^+ and DPM^-Cs^+ do not react under the conditions. Consideration of [1] for the PPT^-Cs^+/H_2 system shows that since the reaction proceeds to the right, therefore H_2 must be the stronger of the two acids in this system. Since the reaction goes to completion (albeit slowly), this would suggest that H_2 has a pK_a at least 1–2 units smaller than the hydrocarbon PPT (pK_a 38.7). Moreover, an extremely slow reaction might also have been expected between DXM^-Cs^+ and H_2, though the slow competitive decomposition of the carbanion could have precluded its observation. As is known from Eigen's work (21), the rate of proton transfer between R_1^- and R_2H depends on the relative acidities of R_1H and R_2H, and the greatly diminishing reactivity of R^-Cs^+ with H_2 along the series Ph^-Cs^+, PPT^-Cs^+, and DXM^-Cs^+ is expected on this basis.

The above discussion would lead one to conclude that the pK_a value for hydrogen in cyclohexylamine is ~37. However, an uncertainty as to the validity of this conclusion arises from

Can. J. Chem. Downloaded from www.nrcresearchpress.com by 210.87.254.40 on 09/05/12
For personal use only.

Can. J. Chem. Downloaded from www.nrcresearchpress.com by 210.87.254.40 on 09/05/12
For personal use only.

possible effects of ion association phenomena (14) in the system. In a solvent of low polarity such as cyclohexylamine the ionic species RM and MH in [1] are not expected to be present in dissociated form and the degree of association into ion pairs or aggregates may differ for the species RM and MH.[3] In such situations caution is required when assigning pK_a values (14).

However, we have independent evidence concerning the relative acidities of H_2 and the hydrocarbons in question. This evidence has been obtained by approaching the equilibrium of reaction 1 from the right hand side, which was effected using the series of hydrocarbons (RH) and potassium hydride (MH) in tetrahydrofuran in the presence of 18-crown-6 ether (22). The reactivity order which we observed was DPM > DXM $\gg$ PPT, the latter being unreactive under the conditions. That this order of reactivity is the reverse of the one described in the present work for the RCs + H_2 system is noteworthy and is in accord with Eigen's theory (21). Although the natures of the medium and of the counterion in the two studies are not identical, which makes an exact correspondence between the systems not possible, the results from these studies reinforce one another regarding the relative acidities of hydrogen and the hydrocarbons examined.

In conclusion, there appears to be sufficient uncertainty about the effect of ion association phenomena in this system, and especially about the state of aggregation of cesium hydride, so as not to warrant a definite estimate of the pK_a of H_2 to be made at this time. It is significant, nevertheless, that the relative acidity of H_2 has been shown to be between those of the hydrocarbons *p*-phenyltoluene (PPT) and 2,4-dixylylmethane (DXM) in this reaction system. This result shows that Pearson and Songstad's (5) estimate of the pK_a (H_2) as being 29 is on the low side and suggests that the estimate by O'Donnell *et al.* (6), pK_a (H_2) ~38, is much closer to the actual value of the pK_a of H_2.

[3]The possibility that the solubility limit of CsH in the CHA solvent was reached, or that a super-saturated solution was present, cannot be eliminated even though the overall concentrations used were small (10^{-4}–10^{-3} *M*). A complicating feature in the system is the occurrence of a minor decomposition process (see Experimental) which causes the solution to be more strongly colored as the reaction proceeds and this could well obscure any minor precipitation if such had occurred. It is evident from consideration of [1] that if precipitation of CsH did occur this would lead to an increased apparent acidity of H_2. It is noteworthy, however, that the solubility of potassium hydride in cyclohexylamine has been found to be 7×10^{-3} *M*, which exceeds the value of the cesium hydride concentration expected to be present in the $PPT^-Cs^+ + H_2$ system.

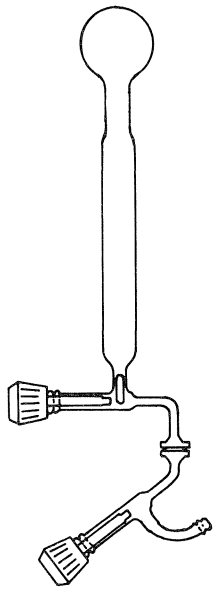

FIG. 1. Apparatus for preparation of cesium cyclohexylamide/cyclohexylamine with ampoule containing cesium in place prior to crushing.

Experimental

Materials

Cesium metal was purchased from MSA Research Corp., as sealed glass ampoules containing 1 g of the metal. Cyclohexylamine was distilled from calcium hydride and stored over lithium cyclohexylamide, obtained by addition of butyllithium (Ventron Corp.) to cyclohexylamine. Addition of a few mg of triphenylmethane to the LiCHA/CHA solution served as an indicator, via the trityl anion. DXM was prepared according to ref. 23 while the other hydrocarbons were commercially procured.

Cesium cyclohexylamide was prepared by the following method. The ampoule containing the cesium was introduced into a glass vessel (Fig. 1) consisting of a 50 ml round bottom flask with a long neck (25 cm) fitted with a greaseless Rotaflo stopcock and an 'O' ring joint, and containing 1 g of platinum wire. The dimensions of the apparatus were such that it needed to be severed along the cylindrical neck portion for introduction of the ampoule and Pt wire and the two parts were then resealed. The vessel was evacuated by connecting the 'O' ring joint to a vacuum manifold and the ampoule crushed by action of the Rotaflo stopper. The flask was inverted and dry CHA distilled in (~25 ml). During reaction with the Cs, H_2 was vented from time to time; reaction was

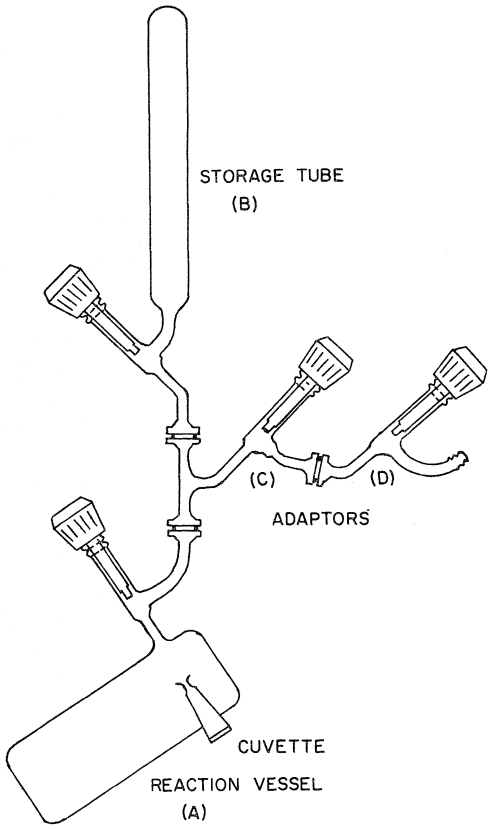

FIG. 2. Assembled apparatus for transfer of cesium cyclohexylamide/cyclohexylamine from storage tube (B) into reaction vessel (A).

complete after ~36 h. The resulting pale yellow-green solution of CsCHA/CHA was transferred into the storage tube B (which was then in an inverted position relative to the drawing in Fig. 2) via the adaptor C. For standardization, a known weight of the CsCHA/CHA solution was added to methanol and, after evaporation to dryness, the aqueous solution of the residue was titrated with standard potassium hydrogen phthalate solution.

Procedure

Reactions were performed in a cylindrical vessel (A, in Fig. 2) of capacity ~120 ml, equipped with one side-arm to which a 1 mm quartz uv cell was attached, and a second side-arm consisting of a Rotaflo stopcock attached to an 'O' ring joint. This reaction vessel was made to fit into the cell compartment of a Unicam SP800 spectrophotometer.

The hydrocarbon was first introduced into the reaction vessel, by weighing it into a small glass ampoule, placing this into the arm fitted with the 'O' ring joint, capping the latter with a rubber septum, flushing with nitrogen, and allowing the ampoule to enter the evacuated vessel via the Rotaflo stopcock. Solvent (CHA) was transferred under vacuum into the reaction vessel by distillation from a stock LiCHA/CHA solution. The apparatus shown in Fig. 2 was then assembled, and the CsCHA/CHA introduced from its storage reservoir, B, which allowed the transfer to be made in an evacuated system. The total amount of CsCHA/CHA added was ~0.2 ml of a 0.4 *M* solution, which resulted in a concentration of RCs of $\sim 10^{-3}$ *M*, corresponding to an absorbance of ~1.0–1.5 at λ_{max} for the organometallic. For introduction of H_2, the vessel A was attached to the vacuum line and pressurized with H_2 gas from a small cylinder. The H_2 gas was dried by passage through two traps containing glass beads cooled to liquid nitrogen temperature.

A summary of the observations in a given experiment is given for run 1 in Table 1. The weight of hydrocarbon taken was 3.12 mg and the volume of CHA distilled into the reaction flask was 15.4 ml, yielding an initial hydrocarbon concentration of 1.209×10^{-3} *M*. The CsCHA/CHA was added until an absorbance of 1.67 was obtained at 472 nm, the λ_{max} for PPTCs. This corresponds to $[PPTCs]_0 = 0.780 \times 10^{-3}$ *M* (using $\epsilon_{472} = 21\,400$ (20)) so that $[PPT]_0 = (1.209 - 0.780) \times 10^{-3}$ *M* $= 0.429 \times 10^{-3}$ *M* After introducing H_2 (1 atm), and agitating on a mechanical shaker, the spectrum was scanned periodically. The absorbance decreased to ~50% of the original value after 100 h, ~20% after 330 h and ~0% after 500 h. Simultaneously a small rise in absorbance occurred at longer wavelengths ($A_{570} = 0.19$ after 330 h), presumably due to minor decomposition products, or to polymerization (24). (In a second run of the PPTCs/CHA/H_2 reaction, the decrease in the absorbance after 336 h was 63%.) A blank (control) run, performed in an identical manner but in the absence of hydrogen, is given under run 3 in Table 1. In this case the absorbance due to PPTCs decreased from an initial value of 1.20 to the value 1.04 after 336 h, corresponding to $[PPTCs]_0 = 0.560 \times 10^{-3}$ *M* and $[PPTCs]_t = 0.483 \times 10^{-3}$ *M*. The difference in these [PPTCs] values, *i.e.* 0.077×10^{-3} *M* (which corresponds to a 14% correction), was subtracted (on a percentage basis) in runs 1 and 2 in reckoning the corrected value of the extent of reaction with hydrogen during the time interval of 336 h. Therefore, the corrected extent of reaction for the PPTCs/H_2 system after 330 h is 77% in run 1 and 63% in run 2. A noteworthy point in the control run was a small increase in absorbance in the 570 nm region, as had also been observed with PPTCs/CHA/H_2 (runs 1 and 2), which tends to discount the possibility that this absorption signifies other than a minor decomposition product. Szwarc and co-workers (24) observed the formation of a long wavelength absorption in the spectra of benzyl sodium in tetrahydrofuran on standing for prolonged periods and ascribed this to the formation of polymeric species formed by ion pair association.

The detailed results in the experiments performed between DXMCs and H_2, and between DPMCs and H_2, are recorded in Table 1. It is seen that in these systems there was no significant decrease in RCs concentration after prolonged reaction periods.

In the experiments with benzylcesium the technique used was similar to that described above, but a much larger $PhCH_2Cs$ concentration was required. For example, addition of 1 ml of 0.4 *M* CsCHA/CHA to a 0.283 *M* solution of $PhCH_3$ in CHA led to an absorbance of only 0.46 at 470 nm. This corresponds to a concentration of 3.0×10^{-3} *M* for $PhCH_2Cs$, assuming a ϵ_{470} value

Can. J. Chem. Downloaded from www.nrcresearchpress.com by 210.87.254.40 on 09/05/12
For personal use only.

of 1500 (20), *i.e.* the extent of conversion to $PhCH_2Cs$ is 1.06%. (The absorption maximum of $PhCH_2Na$ occurs at 355 nm in tetrahydrofuran (ϵ = 12 000 (24)) but in CHA interference from the solvent absorption allows one only to view the shoulder absorption in the 450–500 nm region). The reaction of $PhCH_2Cs$/CHA with H_2 showed negligible change in absorption even on heating (40 °C for 17 h).

Acknowledgements

Financial support of this research by the Atomic Energy of Canada Limited is gratefully acknowledged. Discussion with Drs. J. H. Rolston, D. R. Smith, and E. A. Symons of AECL, and unpublished information provided by Professors R. A. Caldwell and A. Streitwieser is also acknowledged.

1. R. P. Bell. The proton in chemistry. 2nd ed. Cornell University Press. Ithaca, New York. 1973.
2. J. R. Jones. The ionization of carbon acids. Academic Press, London. 1973.
3. J. Hine. Structural effects on equilibria in organic chemistry. Wiley, New York. 1975.
4. E. Buncel. Carbanions. Mechanistic and isotopic aspects. Elsevier, Amsterdam. 1975.
5. R. G. Pearson and J. Songstad. J. Am. Chem. Soc. **89**, 1827 (1967).
6. K. O'Donnell, R. Bacon, K. L. Chellappa, R. L. Schowen, and J. K. Lee. J. Am. Chem. Soc. **94**, 2500 (1972).
7. E. A. Symons and E. Buncel. J. Am. Chem. Soc. **94**, 3641 (1972).
8. E. A. Symons and E. Buncel. Can. J. Chem. **51**, 1673 (1973).
9. E. Buncel and E. A. Symons. J. Am. Chem. Soc. **97**, 656 (1976).
10. W. E. McEwen. J. Am. Chem. Soc. **58**, 1124 (1936).
11. H. Gilman, A. L. Jacoby, and H. Ludeman. J. Am. Chem. Soc. **58**, 2336 (1938).
12. A. Streitwieser, Jr., P. J. Scannon, and H. M. Niemeyer. J. Am. Chem. Soc. **94**, 7936 (1972).
13. A. Streitwieser, Jr. and J. H. Hammons. Prog. Phys. Org. Chem. **3**, 41 (1965).
14. M. Szwarc, A. Streitwieser, Jr., and P. C. Mowery. Ions and ion pairs in organic reactions. *Edited by* M. Szwarc. Wiley, New York. 1974.
15. C. D. Ritchie. *In* Solute–solvent interactions. *Edited by* J. F. Coetzee and C. D. Ritchie. Dekker, New York. 1969.
16. W. S. Matthews, J. E. Bares, J. E. Bartmess, F. G. Bordwell, F. J. Cornforth, G. E. Drucker, Z. Margolin, R. J. McCallum, G. J. McCollum, and N. R. Vanier. J. Am. Chem. Soc. **97**, 7006 (1975).
17. E. Buncel and H. Wilson. Adv. Phys. Org. Chem. In press.
18. A. Streitwieser, Jr., E. Ciuffarin, and J. H. Hammons. J. Am. Chem. Soc. **89**, 63 (1967).
19. A. Streitwieser, Jr., J. R. Murdoch, G. Häfelinger, and C. J. Chang. J. Am. Chem. Soc. **95**, 4248 (1973).
20. G. Häfelinger and A. Streitwieser, Jr. Chem. Ber. **101**, 657 (1968); **101**, 672 (1968).
21. M. Eigen. Angew. Chem. Int. Ed. Engl. **3**, 1 (1964).
22. E. Buncel and B. C. Menon. Chem. Commun. 648 (1976).
23. L. Gordon, P. May, and R. Lee. Ind. Eng. Chem. **51**, 1257 (1959).
24. R. Asami, M. Levy, and M. Szwarc. J. Chem. Soc. 361 (1962).
25. E. A. Symons. Can. J. Chem. **49**, 3940 (1971).
26. (*a*) E. Buncel and E. A. Symons. J. Org. Chem. **38**, 1201 (1973); (*b*) E. Buncel, K. E. Russell, and J. Wood. Chem. Commun. 252 (1968); (*c*) E. Buncel and A. W. Zabel. J. Am. Chem. Soc. **89**, 3082 (1967); (*d*) E. Buncel, E. A. Symons, and A. W. Zabel. Chem. Commun. 173 (1965).

Can. J. Chem. Downloaded from www.nrcresearchpress.com by 210.87.254.40 on 09/05/12
For personal use only.

The synthesis of spiro[bicyclo[2.2.1]heptene-7,1′-cycloalkan]-2′-ones and related benzobicyclo[2.2.1]heptene derivatives

N. F. Feiner, G. D. Abrams, and Peter Yates

Lash Miller Chemical Laboratories, University of Toronto, Toronto, Ont., Canada M5S 1A1

Received June 21, 1976

N. F. Feiner, G. D. Abrams, and Peter Yates. Can. J. Chem. **54**, 3955 (1976).

7-Norbornenone gives on treatment with diphenylsulfonium cyclopropylide an epoxide that rearranges thermally to a mixture of *syn*- and *anti*-spiro[bicyclo[2.2.1]heptene-7,1′-cyclobutan]-2′-ones. Treatment of 7-norbornenone with cyclobutylidenetriphenylphosphorane gives 7-cyclobutylidenenorbornene, which on epoxidation and rearrangement gives *syn*-spiro[bicyclo-[2.2.1]heptene-7,1′-cyclopentan]-2′-one. This is also formed on treatment of *syn*-spiro[bicyclo-[2.2.1]heptene-7,1′-cyclobutan]-2′-one with *tert*-butyl diazoacetate and triethyloxonium fluoborate followed by decarboalkoxylation. Similar homologation of *anti*-spiro[bicyclo[2.2.1]-heptene-7,1′-cyclobutan]-2′-one affords *anti*-spiro[bicyclo[2.2.1]heptene-7,1′-cyclopentan]-2′-one. 7-Isopropylidenebenzonorbornene with acetyl chloride and aluminum chloride gives 7-*syn*-acetyl-7-*anti*-isopropenylbenzonorbornene, which on dibromination followed by condensation with isopropylidene malonate gives a dispiro ketone related to these spiro ketones. The structures of the spiro compounds have been established by infrared and nuclear magnetic resonance spectroscopy and by studies of their reactions.

N. F. Feiner, G. D. Abrams et Peter Yates. Can. J. Chem. **54**, 3955 (1976).

Le traitement de la norbornénone-7 par le cyclopropylure de diphénylsulfonium conduit à un époxyde qui se réarrange sous l'influence de la chaleur pour conduire à un mélange de spiro-[bicyclo[2.2.1]heptène cyclobutane-7,1′]-ones-2′ *syn* et *anti*. La réaction de la norbornénone-7 avec le cyclobutylidènetriphénylphosphoranne conduit au cyclobutylidène-7 norbornène qui par époxydation et réarrangement fournit la spiro[bicyclo[2.2.1]heptène cyclopentane-7,1′]-one-2′ *syn*. Ce composé se forme aussi par traitement de la spiro[bicyclo[2.2.1]heptène cyclobutane-7,1′]-one-2′ *syn* avec le diazoacétate de *tert*-butyle et le fluoroborate de triéthyloxonium suivi par une décarboalkoxylation. Une homologation du même type de la spiro[bicyclo[2.2.1]-heptène cyclobutane-7,1′]-one-2′ *anti* fournit la spiro[bicyclo[2.2.1] heptène cyclopentane-7,1′]-one-2′ *anti*. La réaction de l'isopropylidènebenzonorbornène-7 avec le chlorure d'acétyle et le chlorure d'aluminium conduit à l'acétyl-7 *syn* isopropenyl-7 *anti* benzonorbornène qui par dibromation suivie par une condensation avec le malonate d'isopropylidène conduit à une dispiro-cétone reliée à ces spiro-cétones. On a établi les structures des composés spiro par spectroscopie infrarouge et de résonance magnétique nucléaire et par une étude de leurs réactions.

[Traduit par le journal]

Unsaturated carbonyl compounds that are formally unconjugated, but in which interaction can occur between the carbonyl and ethylenic groups, have long been of interest in respect to the effect of such interaction on both their spectroscopic properties and their reactivities (*cf.*, for example, ref. 1). Of particular interest among such systems are those in which the carbonyl and unsaturated groups are held in a fixed geometrical relationship to each other, for it is then possible to make unambiguous interpretations of the properties of the compounds in terms of orbital overlap. In 1961 Winstein *et al.* (2) described a series of unsaturated ketones of type **1** and **2**, whose lack of conformational mobility defined a unique geometry that had the consequence of bringing lobes of the olefinic

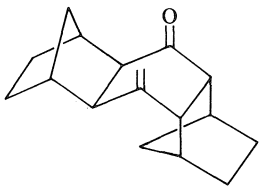

1

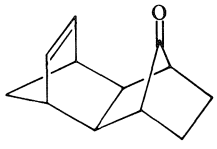

2

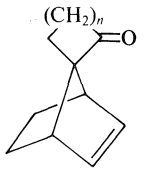

3, $n = 1$
5, $n = 2$

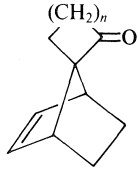

4, $n = 1$
6, $n = 2$

Can. J. Chem. Downloaded from www.nrcresearchpress.com by 210.87.254.105 on 09/05/12
For personal use only.

Can. J. Chem. Downloaded from www.nrcresearchpress.com by 210.87.254.105 on 09/05/12
For personal use only.

and ketonic π-orbitals into close proximity ensuring strong overlap, while placing the p_n orbital on oxygen orthogonal to the π_{CC} orbital, resulting in zero p_n–π_{CC} overlap. These ketones thus represent one type of limiting case of the class of orbitally interacting nonconjugated enones. We have undertaken the synthesis of unsaturated ketones that represent the diametrical type of limiting case, *viz.*, rigid systems in which there is strong overlap between the p_n orbital and the π_{CC} orbital, but where the latter is orthogonal to the π_{CO} orbital. We now report the synthesis and proof of structure of two such ketones, **3** and **5**, and their *anti* isomers, **4** and **6**. We also discuss related synthetic studies in the benzonorbornene series.

syn- and anti-Spiro[bicyclo[2.2.1]heptene-7,1'-cyclobutan]-2'-one

Treatment of 7-norbornenone (**7**) with cyclopropyldiphenylsulfonium fluoborate (**8**) and commercial potassium hydroxide (containing 15% water) by the method of Trost (3) gave the epoxide **9** accompanied by diphenyl sulfide (**10**). Although the epoxide was not separated from **10**, the spectra of the mixture established its gross structure. The infrared (ir) spectrum showed no carbonyl absorption and the proton magnetic resonance (pmr) spectrum showed a sharp triplet at δ 6.00 (J_{app} = 2 Hz)[1] attributable to the two equivalent olefinic protons, and multiplets at δ 0.7–1.3, 2.0–2.3, and 2.5 assigned to the cyclopropyl and *endo* C-5 and C-6, *exo* C-5 and C-6, and bridgehead protons, respectively. Although the latter spectrum suggested that a single stereoisomer had been formed, it did not reveal the configuration of this isomer. However, this can be assigned as in **9** based on the expectation that attack of the ylid derived from **8** will occur on the less hindered side of the carbonyl group of **7**, as Bly and Bly have observed in the case of attack of dimethyloxosulfonium methylide on **7** (5).

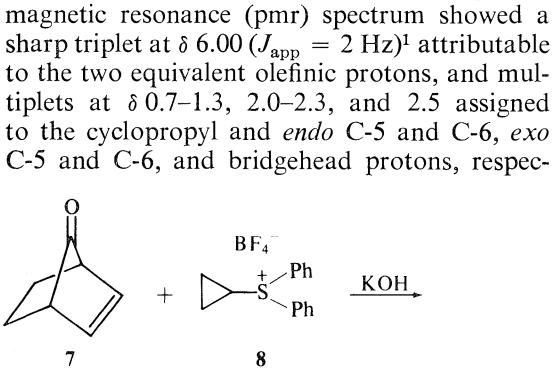

7 8 9 10

TABLE 1. Rearrangement of **9**

Conditions	Product composition (%) 3	4
5% aqueous HBF_4/Et_2O	83	17
$LiClO_4/C_6H_6$ (reflux)	75	25
SiO_2 column/Et_2O	68	32
110 °C	63	37
175 °C	55	45
175 °C/$NaHCO_3$	50	50

Rearrangement of **9** occurred under a variety of conditions (see Table 1) to give a mixture of the spiro ketones **3** and **4**. These could be separated from each other and from **10** by column chromatography on silica. Further purification by molecular distillation gave **3** (32% from **7**) and **4** (33% from **7**) as colorless oils.[2]

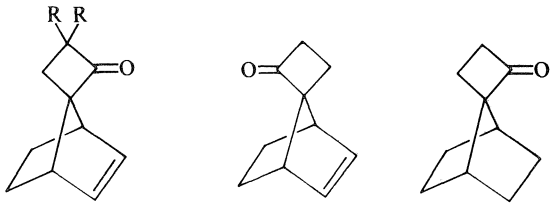

3, R = H
12, R = D

4 **11**

The gross structures of **3** and **4** were established by their spectra (Table 2) and the conversion of a 5:1 mixture by hydrogenation over palladium/charcoal to a single product, **11**, which was also obtained by similar hydrogenation of **3** alone. In accord with expectation, exposure of **3** to methanol-*d* containing a trace of sodium methoxide resulted in rapid exchange of two hydrogen atoms to give a dideuterated product whose pmr and mass spectra were in accord with structure **12**.

[1]This is a not uncommon feature of the signal of chemically equivalent vinyl protons in norbornenes, with $J_{app} = \frac{1}{2}(J_{21} + J_{24})$ (*cf.* ref. 4).

[2]These yields correspond to those from the thermal rearrangement of **9** at 170 °C.

TABLE 2. Spectra of **3** and **4**

Spectrum	Assignment*	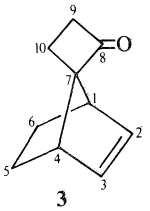 **3**	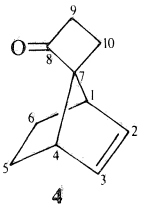 **4**
$\lambda_{max}(CCl_4)$	C=O	5.63, 5.65 μm	5.65 μm
$H_\delta CDCl_3$	H_{5n},H_{6n}	1.05(m)	1.0(m)
	H_{5x},H_{6x},H_{10}	1.75(m)	1.9(m)
	H_9	2.79(t, J = 9.5 Hz)	2.65(t, J = 9 Hz)
	H_1,H_4	2.88(br s)	2.85 (br s)
	H_2,H_3	6.09(t, J_{app} = 2 Hz)†	6.00(t, J_{app} = 1.5 Hz)†
$C_\delta CDCl_3$	C_{10}	20.5(t)	18.6(t)
	C_5,C_6	23.4(t)	23.3(t)
	C_9	41.3(t)	40.3(t)
	C_1,C_4	47.7(d)	48.9(d)
	C_7	85.8(s)	82.5(s)
	C_2,C_3	133.8(d)	133.7(d)
	C_8	212.7(s)	212.7(s)

*n = endo, x = exo.
†See footnote 1 in text.

Reduction of a 5:1 mixture of **3** and **4** with lithium aluminum hydride gave a corresponding mixture of the cyclobutanols **13** and **14**; similar reduction of pure **3** and **4** gave **13** and **14**, respectively. Treatment of the 5:1 mixture of **13** and **14** with mercuric acetate in a variety of solvents (*tert*-butyl alcohol, dichloromethane, acetone, pentane) led to rapid reaction of the major component only. Stereochemical assignments as in **3** and **4** could then be made based on the expectation that intramolecular oxymercuration, analogous to that observed by Bly and Bly (5) for *syn*-7-(hydroxymethyl)norbornene (**15**), would preferentially remove the *syn*-alcohol **13**, as the adduct **16**.

Isolation of the product from the reaction of pure **3** with mercuric acetate showed that in fact it is a diacetate of type **17** or **18** ($\lambda_{max}(CHCl_3)$ 2.8–3.1, 5.80, 6.15, 6.25 μm; $^{H}\delta^{CDCl_3}$ 2.00 (s, 3H), 2.10 (s, 3H), 4.0 (br s, 1H; absent after D_2O treatment)). It may be concluded that the high degree of strain in **16** has resulted in a secondary reaction involving attack by acetic acid.[3] The absence of skeletal rearrangement in the formation of **17** (**18**) was indicated by the conversion of the product to **13** by treatment with 5% hydrochloric acid.

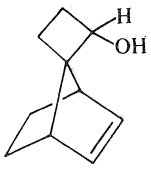
13

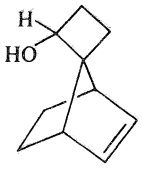
14

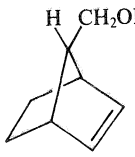
15

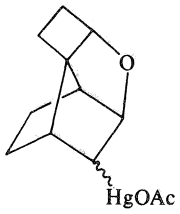
16

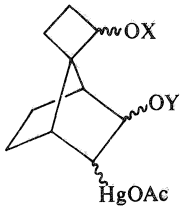
17, X = Ac, Y = H
18, X = H, Y = Ac

Further evidence for these stereochemical assignments derives from a comparison of the pmr spectra of **13** and **14**. The vinylic proton signal in the former has $\nu_{1/2}$ = 20 Hz, while in

[3]The possibility exists that direct addition of mercuric acetate to the ethylenic double bond of **13** or **14** gave rise to **17** (**18**), thus vitiating the stereochemical assignment on this basis; however, such a reaction would be, as far as we are aware, without precedent (*cf.* ref. 6).

Can. J. Chem. Downloaded from www.nrcresearchpress.com by 210.87.254.105 on 09/05/12
For personal use only.

Can. J. Chem. Downloaded from www.nrcresearchpress.com by 210.87.254.105 on 09/05/12
For personal use only.

the latter it has $\nu_{1/2} = 5$ Hz, in accordance with the expected greater nonequivalence of the vinyl protons in **13**. These assignments are also in accord with the circumstance that the monomeric hydroxyl-stretching band in the ir spectrum of **13** occurs at longer wavelength than that of **14** as a result of intramolecular hydrogen bonding to the ethylenic double bond (*cf.* **15** (5)). Final confirmation for the assignments comes from ring expansion experiments (*vide infra*).

The conversion of **9** to **3** and **4** is highly regioselective in the sense that it involves only cleavage of the O—C.7 bond; the stereochemistry and the effect of the reaction conditions on the product ratios of the stereoisomers are discussed below in relation to the formation of **5**.

syn- and anti-Spiro[bicyclo[2.2.1]heptene-7,1'-cyclopentan]-2'-one

Attempts to add cyclobutylmagnesium bromide to 7-norbornenone (**7**) led only to reduction of **7** to *anti*-7-norbornenol (**19**), as shown by the pmr spectrum of the product and its reconversion to **7** on oxidation with chromium trioxide.

Warkentin (7) has found such reduction of **7** to be common with Grignard reagents having a β-hydrogen atom.

Treatment of **7** with cyclobutylidenetriphenylphosphorane (**20**) (8) gave **21** as a colorless oil in 85% yield, whose structure is securely based on its pmr and ^{13}C nuclear magnetic resonance (cmr) spectra (Table 3). Epoxidation of **21** with an equimolar quantity of *m*-chloroperbenzoic acid at 0 °C gave what is considered to be a 4:1 mixture of **22** and **23**. This mixture showed no carbonyl absorption in its ir spectrum; its pmr spectrum was insufficiently resolved to permit any conclusion to be drawn about the stereochemical course of the epoxidation, but the area ratio of the vinyl proton signal (δ 6.0–6.4) to the remaining signals (δ 0.8–3.2) indicated an 80% site selectivity in the desired sense (with perben-

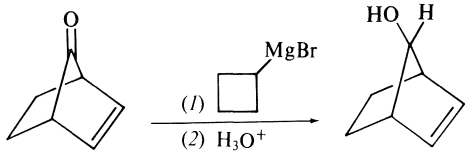

7 19

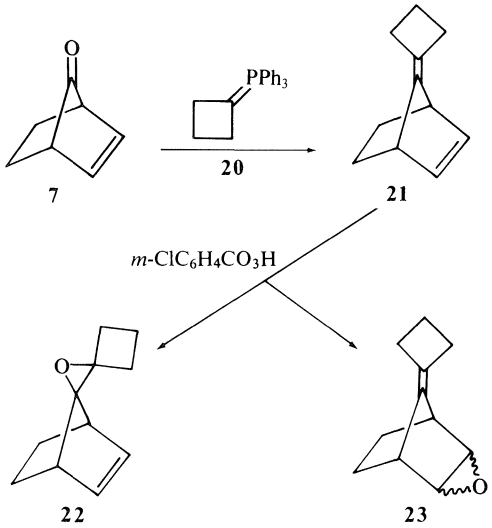

7 21 22 23

TABLE 3. Spectra of **21**

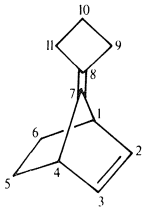

21

Spectrum	Assignment*	
$H_\delta CDCl_3$	H_{5n},H_{6n}	1.0(m)
	H_{5x},H_{6x},H_{10}	1.4–2.0(m)
	H_9,H_{11}	2.55(t, J = 8 Hz)
	H_1,H_4	3.0(m)
	H_2,H_3	6.10(t, J_{app} = 2 Hz)†
$C_\delta CDCl_3$	C_{10}	17.3(t)
	C_5,C_6	25.0(t)
	C_9,C_{11}	28.8(t)
	C_1,C_4	41.4(d)
	C_8	114.2(s)
	C_2,C_3	136.0(d)
	C_7	144.8(s)

*n = endo; x = exo.
†See footnote 1 in text.

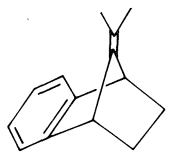

24

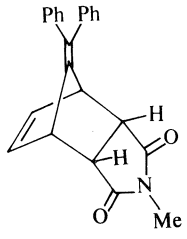

25

Can. J. Chem. Downloaded from www.nrcresearchpress.com by 210.87.254.105 on 09/05/12
For personal use only.

zoic acid the selectivity was 90%). Attempted separation of the mixture by thin layer chromatography on silica gave rise to three spots, one of which was formed on the plate from another. We tentatively conclude that only two epoxides are formed in the peracid reaction, although it cannot be excluded that both stereoisomeric forms of **22** are formed. The *anti*-stereochemistry assigned to **22** is based on analogy with the stereochemistry of epoxidation observed for **24** (80% *anti*) (*vide infra*) and **25** (100% *anti*) (9). Preferred attack by the peracid on the *anti* face of the exocyclic double bond is considered to result from participation by the endocyclic double bond or benzene ring, which overrides the steric factor favoring *syn* attack.[4]

When a 4:1 mixture of **22** and **23** was placed on a silica column, **22** slowly gave rise to the spiro ketone **5** while **23** remained unchanged; elution after several hours gave a mixture of **5** and **22**, from which **5** was isolated in 50% yield (based on **21**) by the use of Girard-T reagent. Rearrangement of **22** could also be effected by boron trifluoride etherate in benzene, but in this case **5** was accompanied by another rearrangement product, **26**; chromatography of the product mixture from a 9:1 mixture of **22** and **23** gave a 69% yield of **5** and 7% of **26** (Scheme 1).

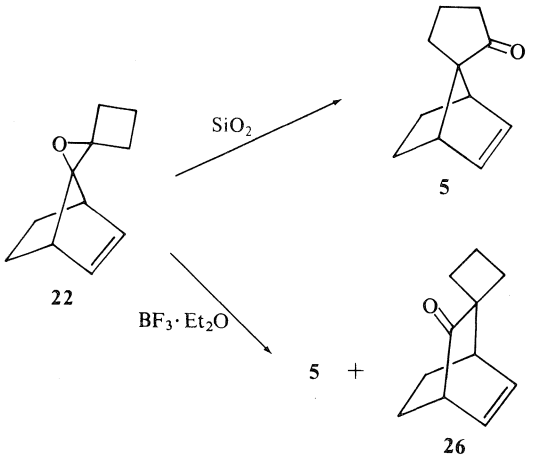

SCHEME 1

[4]An alternative interpretation, for which we are indebted to a referee, is that there is considerable oxirane character at the transition state for epoxidation and, in cases such as **24** where the steric situation at the two faces of the double bond is not drastically different, the reaction is under product development control, favoring the *anti* product.

The assignment of structure **26** to the minor rearrangement product is based on spectroscopic data (see Table 4 for comparison with data for bicyclo[2.2.2]oct-5-en-2-one, **27**) and the observation that this compound, unlike **27**, failed to undergo exchange on treatment with methanol-*d* containing a catalytic amount of sodium methoxide, and that a peak at *m/e* 134 in its mass spectrum corresponded to the loss of ethylene.

The assignment of structure **5** to the major rearrangement product is of pivotal importance since it serves as the structural reference point for all the novel spiro[bicyclo[2.2.1]-7,1′-cycloalkan]-2′-ones prepared in the present investigation. The assignment is in complete accord with the spectroscopic data (Table 5) and has been confirmed by the transformations depicted in Scheme 2. Hydrogenation over palladium/charcoal led to the rapid consumption of 1 mol equiv. of hydrogen and the formation of the saturated spirocyclopentanone **28** ($\lambda_{max}(CCl_4)$ 5.78 μm).

Wolff–Kishner reduction of **5** gave the hydrocarbon **29**, whose identity was established by comparison with an authentic sample prepared by oxidative bisdecarboxylation of the diacid **30**. Reduction of **5** with lithium aluminum hydride gave a single alcohol **31**, which reacted rapidly with mercuric acetate in *tert*-butyl alcohol to give **32**; this was precipitated as the insoluble chloro derivative **33** on addition of aqueous sodium chloride. Treatment of **33** with aqueous acid returned **31**.

Other transformations of **5** that corroborate the *syn* relationship of the carbonyl and ethylenic groups in this compound are shown in Scheme 3. Treatment with bromine in dichloromethane gave the adduct **34**, which was rapidly converted by atmospheric moisture to the bromo ketol **35**; this reverted to **5** on treatment with zinc and acetic acid. Solution of **5** in concentrated sulfuric acid followed by quenching with cold aqueous sodium bicarbonate gave a hydration product that exists mainly as the hemiketal **36** in equilibrium in solution with a small amount of the corresponding ketol **37**, as indicated by weak bands at 5.75 and 5.79 μm in its ir spectra in carbon tetrachloride and chloroform, respectively. It is of interest to note that although the hemiketal **36** is greatly favored at equilibrium in solution, this is not the case for **35**, where the ketol form is greatly favored.

TABLE 4. Spectra of **26** and **27**

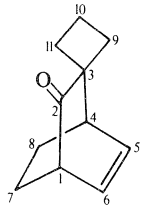

26*

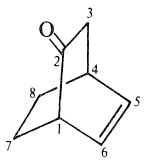

27†

Spectrum	Assignment		
$\lambda_{max}(CCl_4)$	C=O	5.80 μm	5.77 μm
$^{H}\delta^{CDCl_3}$	H_{7-11}	1.2–2.4(m)	1.2–1.9(m)‡
	H_3	–	2.0(m)
	H_1,H_4	2.8–3.2(m)	2.8–3.2(m)
	H_5,H_6	6.0–6.7(m)§	6.0–6.7(m)
$^{C}\delta^{CDCl_3}$	C_{7-11}	15.2,19.7,23.2, 28.4,31.0(all t)	22.5 (t),¶ 24.3 (t)¶
	C_4	42.5(d)	32.4(d)
	C_1	48.5(d)	48.5(d)
	C_3	49.4(s)	40.4(t)
	C_5,C_6	128.3(d), 135.9(d)	128.4(d), 137.1(d)
	C_2	216.2(s)	212.6(s)

*Numbering is nonconventional, but corresponds to that in **27**.
†Prepared (31) by Dr. R. J. Crawford.
‡H_7, H_8.
§Well resolved complex multiplet closely analogous to the corresponding multiplet in the spectrum of **27**.
¶C_7, C_8.

TABLE 5. Spectra of **5** and **6**

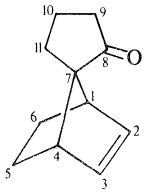

5

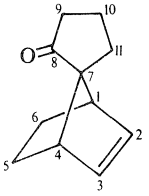

6

Spectrum	Assignment*		
$\lambda_{max}(CCl_4)$	C=O	5.76 μm	5.78 μm
$^{H}\delta^{CDCl_3}$	H_{5n},H_{6n}	1.0(m)	0.9(m)
	H_{5x},H_{6x}	1.4–1.9(m)	1.7–2.0(m)
	H_9,H_{10},H_{11}	1.9–2.2(m)	2.0–2.4(m)
	H_1,H_4	2.75(br s)	2.7(m)
	H_2,H_3	5.97(t, J_{app} = 1.5 Hz)†	6.03(t, J_{app} = 1.5 Hz)†
$^{C}\delta^{CDCl_3}$	C_{10}	17.6(t)	
	C_5,C_6	24.3(t)	
	C_{11}	30.4(t)	
	C_9	37.2(t)	
	C_1,C_4	46.5(d)	
	C_7	72.3(s)	
	C_2,C_3	132.6(d)	
	C_8	217.7(s)	

*n = endo, x = exo.
†See footnote 1 in text.

Can. J. Chem. Downloaded from www.nrcresearchpress.com by 210.87.254.105 on 09/05/12
For personal use only.

Can. J. Chem. Downloaded from www.nrcresearchpress.com by 210.87.254.105 on 09/05/12
For personal use only.

The third type of reaction of **5** shown in Scheme 3 involves its photocyclization to the oxetane **38**. This product was difficult to purify and was not fully characterized. The relationship of its pmr spectrum to that of the photocyclization product **40** formed by irradiation of the spiro[bicyclo[2.2.1]heptene-5,1′-cyclopentan]-2′-one **39** (10) is in accord with the structural assignment.

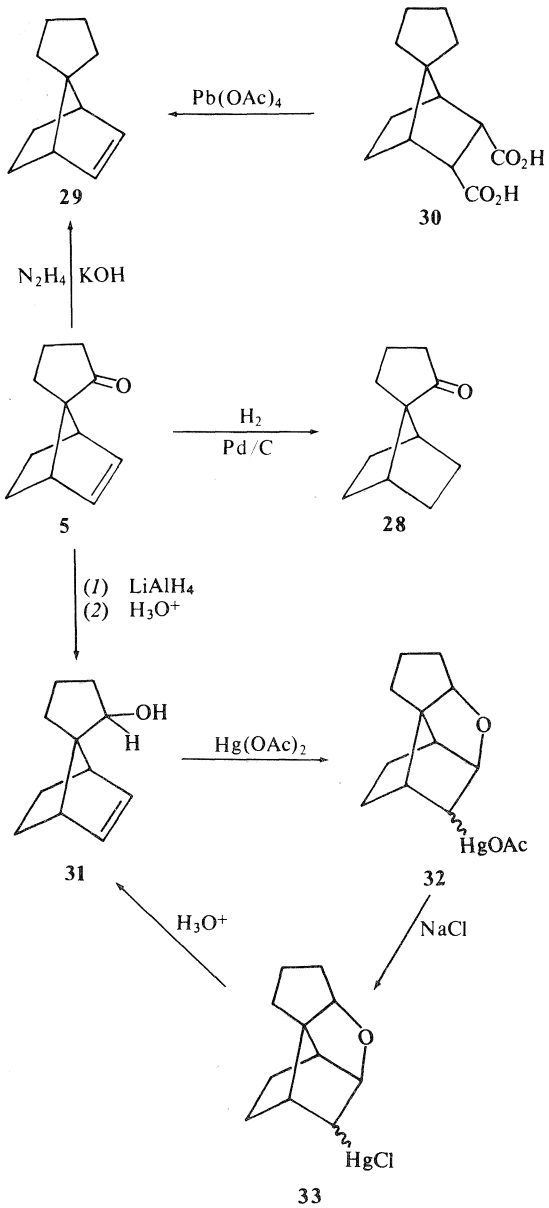

SCHEME 2

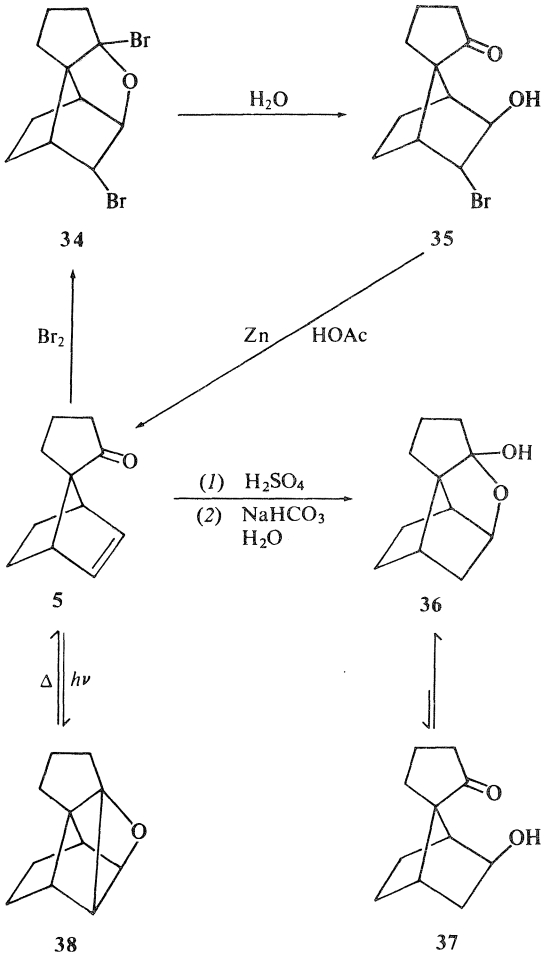

SCHEME 3

With the structure of **5** firmly established, we turn to a discussion of its formation from **22**. The highly regioselective and stereoselective formation of **5** is analogous to the formation of bicyclo[2.2.1]heptene-7-*syn*-carboxaldehyde (**42**) as the only product on acid-catalyzed or thermal rearrangement of the epoxide **41** (5). The high selectivity in the formation of **5** can be interpreted in similar terms to those proposed by Bly and

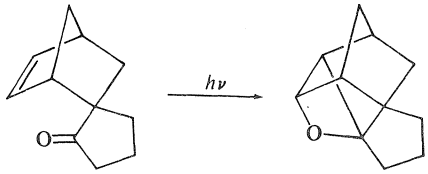

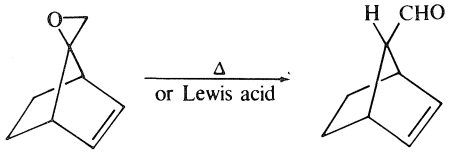

41 **42**

Bly (5) to account for the formation of **42**, *viz.*, participation of the olefinic π electrons in the formation of the bridged intermediates **43** and **44** (Scheme 4).

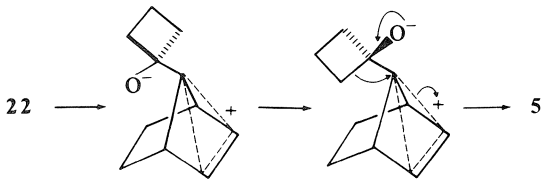

43 **44**

SCHEME 4

In these terms it remains to explain the low stereoselectivity in the formation of **3** and **4** from the epoxide **9**. We suggest that this can be interpreted as resulting from competition between π stabilization of the positive charge by the olefinic π electrons as in **45** (*cf.* **43**) and σ stabilization by the cyclopropane ring (*cf.* ref. 11) as in **47**; while **45** leads via rotamer **46** to **3**, **47** gives both **3** (via rotamer **48**) and **4** (Scheme 5). The effect of reaction conditions on the stereoisomer product ratio may be accommodated in terms of Trost's proposal (3) that reduction in stereoselectivity is favored by increased covalent character in the bond formed between the epoxide oxygen atom and the acidic catalyst.

The *syn*-spirocyclopentanone **5** was also obtained by ring expansion of the *syn*-spirocyclobutanone **3**, confirming the structural assignment to the latter. Treatment of **3** in dichloromethane with *tert*-butyl diazoacetate and triethyloxonium fluoborate (*cf.* ref. 12) gave a mixture of the β-keto esters **49** and **50**, which gave in boiling toluene containing a catalytic amount of *p*-toluenesulfonic acid a 4:1 mixture of **5** and **51**.[5] The latter compound, whose spectra are listed in Table 6, was also obtained in low yield when the hydrocarbon **52**, obtained by reaction of **3** with triphenylphosphonium methylide, was treated with thallium trinitrate (*cf.* ref. 13) (Scheme 6).

The formation of **5** from **3** served both to confirm the structural assignment to the latter and to hold promise that the remaining target compound, **6**, could be prepared by ring expansion of **4**. In the event, reaction of **4** with *tert*-butyl diazoacetate followed by treatment of the resulting mixture of **53** and **54** (Scheme 7) with a catalytic amount of *p*-toluenesulfonic acid in boiling benzene gave a 2:1 mixture of **6** and **55**. The latter compound, which was not fully characterized, showed, as does **51**, a singlet in its pmr spectrum attributable to the isolated C-8 methylene group (Table 6). The structure of compound **6** was established by its spectra (Table 5) and by its conversion on hydrogenation over palladium/charcoal to the saturated spirocyclopentanone **28** obtained by hydrogenation of **5**.

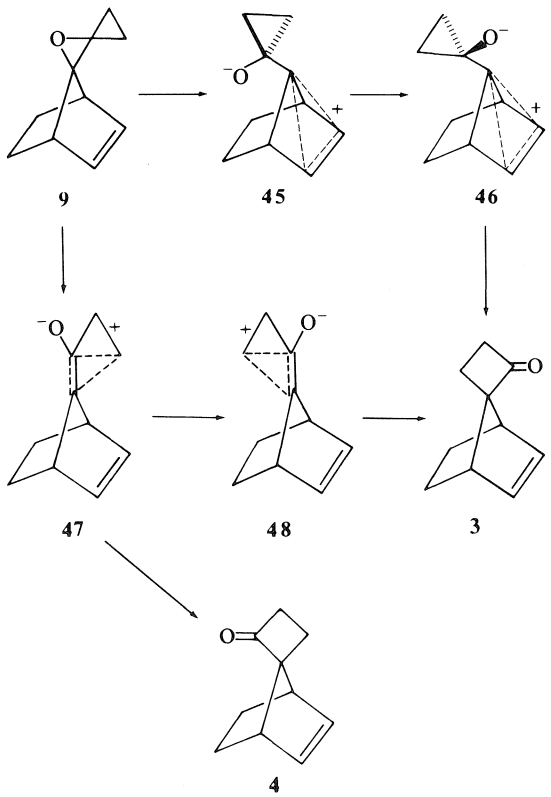

9 **45** **46**

47 **48** **3**

4

SCHEME 5

[5]The pmr spectrum of the mixture of **49** and **50** showed signals at δ 1.45 and 1.43 in a 4:1 ratio in accord with a 4:1 mixture of these isomers.

Can. J. Chem. Downloaded from www.nrcresearchpress.com by 210.87.254.105 on 09/05/12
For personal use only.

TABLE 6. Spectra of **51** and **55**

Spectrum	Assignment*	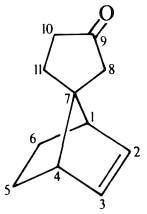 **51**	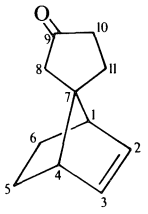 **55**
$\lambda_{max}(CCl_4)$	C=O	5.74 μm	5.73 μm
$H_\delta CDCl_3$	H_{5n},H_{6n}	1.0(m)	1.1(m)
	H_{5x},H_{6x},H_{11}	1.6–1.9(m)	1.5–1.9(m)
	H_{10}	2.0–2.4(m)	1.9–2.4(m)
	H_8	2.13(s)	2.10(s)
	H_1,H_4	2.4(m)	2.5(m)
	H_2,H_3	5.90(t, J_{app} = 2 Hz)†	6.05(t, J_{app} = 3 Hz)†

*n = endo, x = exo.
†See footnote 1 in text.

Benzonorbornene Derivatives

Treatment of 7-isopropylidenebenzonorbornene (**56** ≡ **24**) with *m*-chloroperbenzoic acid gave a 6.5:1 mixture of labile epoxides, **57** and **58**. The major product is assigned structure **57** since the *gem*-dimethyl signal in its pmr spectrum (δ 1.23) occurs at higher field than that in the spectrum of the minor product (δ 1.32), a

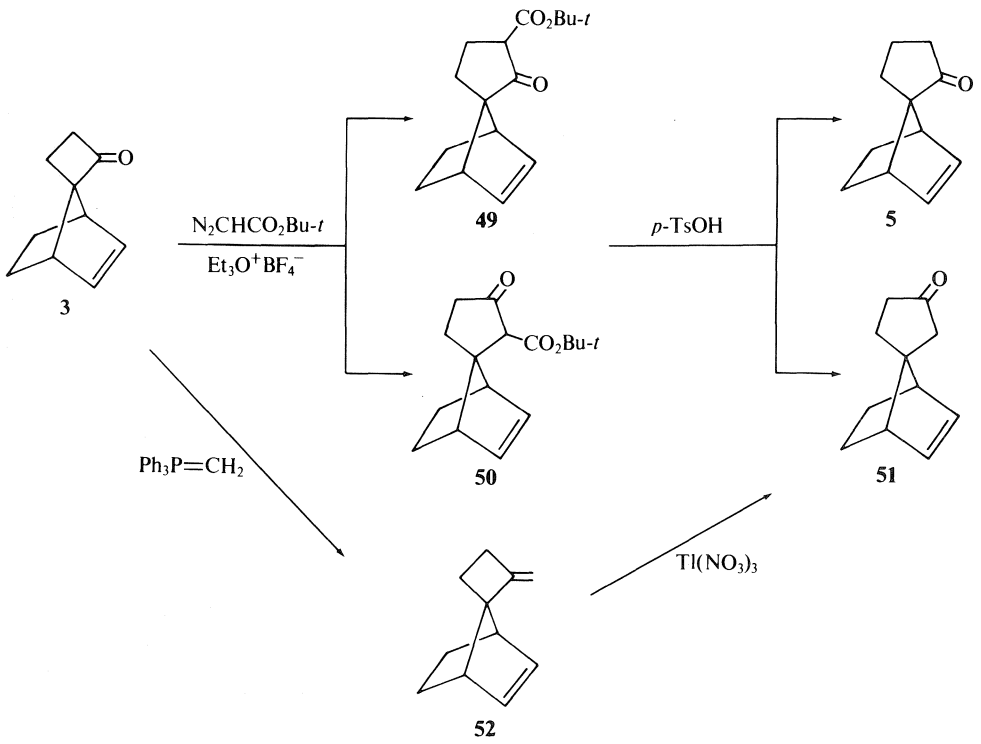

SCHEME 6

Can. J. Chem. Downloaded from www.nrcresearchpress.com by 210.87.254.105 on 09/05/12
For personal use only.

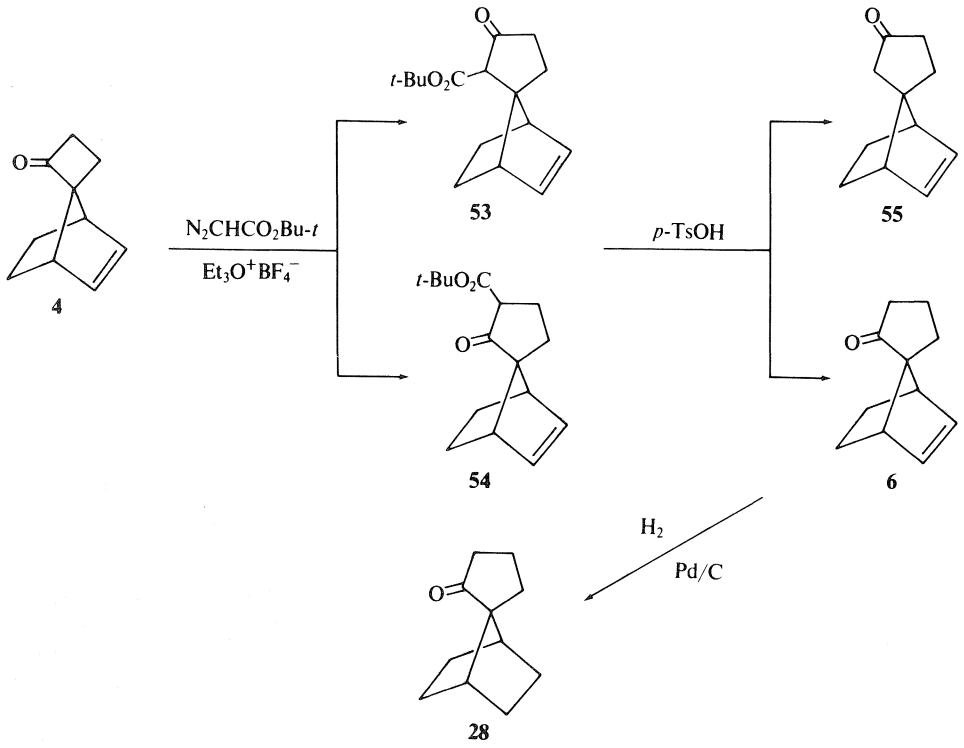

SCHEME 7

circumstance readily attributable to shielding of the methyl protons in **57** by the benzenoid ring. The predominant formation of **57** can be interpreted in similar terms to those invoked above in the assignment of the *anti*-stereochemistry to the epoxide **22**. Although **57** could be separated from **58** by a combination of sublimation and low temperature crystallization, it could not be fully purified because of its lability. Upon being chromatographed on basic alumina it was converted to the rearrangement products **59** and **60**. The former was also formed by treatment of **57** with boron trifluoride etherate, while the latter was formed on pyrolysis of **57** (Scheme 8).

The structure of **59** follows from its ir and pmr spectra, which show the presence of a carbonyl group (5.80 μm), two tertiary methyl groups (δ 0.70 (s, 3H; *syn* to benzenoid ring) and 1.20 (s, 3H; *anti* to benzenoid ring)), and two non-equivalent bridgehead protons (δ 2.9 (m, 1H) and 3.45 (m, 1H)). These data together with the failure of this product to give an iodoform test exclude a structure of type **61**, analogous to the ketones **3**–**5** obtained by rearrangement of the epoxides **9** and **22**. The gross structure of **60** follows from its spectra, which show the presence of a hydroxyl group (2.79 μm), an isopropenyl group (6.07 (w), 11.05 μm; δ 1.65 (m, $\nu_{1/2}$ = 3 Hz, 3H), 4.6 (m, 1H), 4.75 (m, 1H), and two equivalent bridgehead protons (δ 3.11 (distorted t, J_{app} = 2 Hz, 2H)).[6] Its stereochemistry is assigned on the basis of the expectation that the configuration of the spiro carbon atom of **57** will be retained.

The formation of **59** on acid-catalyzed rearrangement of **57** may be contrasted with the formation of **5** as the major product from a similar rearrangement of **22** together with **26**, the analogue of **59**, as a minor product (*cf.* Scheme 1). The formation of **59** must occur by the route shown in Scheme 9 with exclusive cleavage of bond *a* in **62** to give **63** and thence **64**; cleavage of bond *b*, which would give **61** via **65**, does not occur. The formation of the minor product **26** from **22** involves cleavage of

[6]This bridgehead signal pattern is also observed in the spectra of other benzonorbornenes, such as **56** and **57**.

Can. J. Chem. Downloaded from www.nrcresearchpress.com by 210.87.254.105 on 09/05/12
For personal use only.

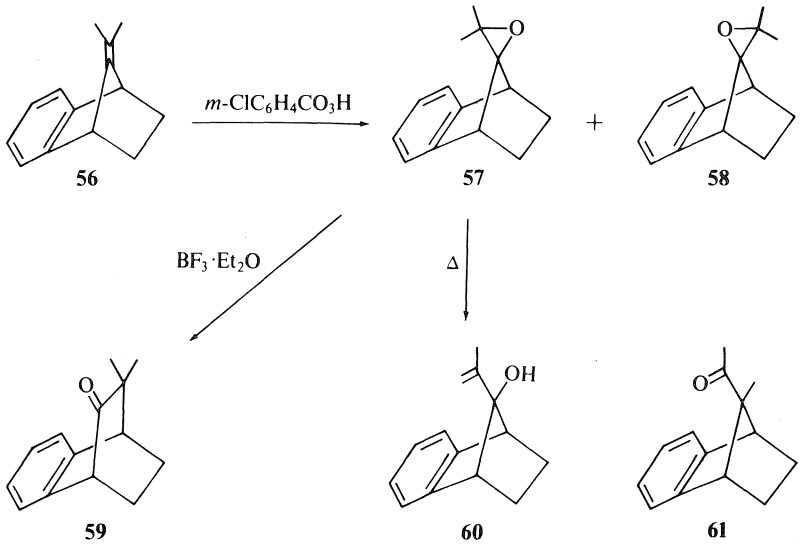

SCHEME 8

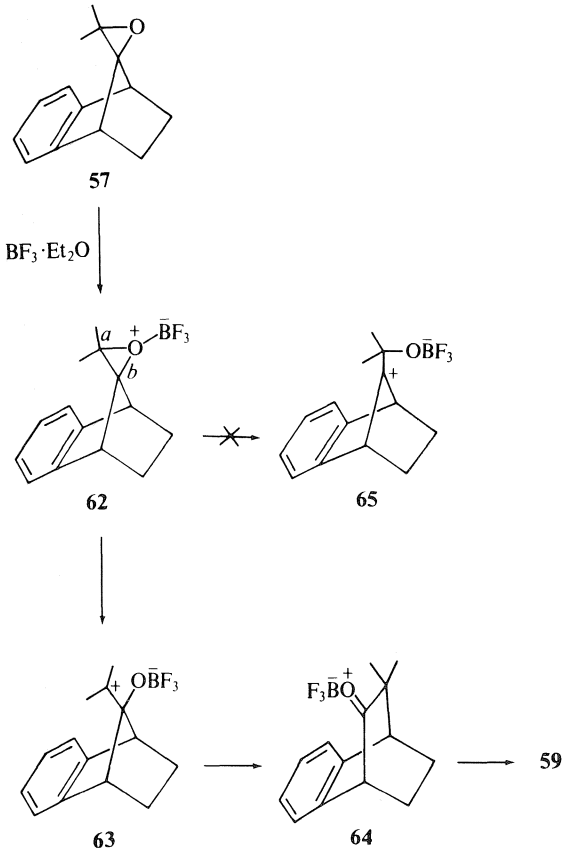

SCHEME 9

the type *a* bond, but the formation of the major product **5** involves cleavage of the type *b* bond. In the case of **57**, exclusive formation of **63** can be attributed to destabilization of **65** relative to **63** resulting from the situation of the positive charge at the C.7 position of a norbornane system (14). In the case of the corresponding intermediates from **22** this effect is largely offset both by stabilization of the analogue of **65** involving delocalization of the ethylenic double bond as in **43** (Scheme 4) and by destabilization of the analogue of **63** by the situation of the positive charge at a cyclobutyl carbon. Although stabilization of **65** by the aromatic ring in an analogous fashion to the stabilization by the ethylenic bond in **43** can occur, such stabilization would be expected to be less important in the case of the aromatic ring (15).

In the case of the acid-catalyzed rearrangement of the epoxide **41** a further factor intervenes, *viz.*, cleavage of type *a* would give rise to a primary carbonium ion. Thus in this case exclusive cleavage of the type *b* bond occurs to give **42** as the only product (5).

The thermal conversion of **57** to **60** involves bond *a* cleavage as in its acid-catalyzed rearrangement to **59**, however here the ring opening is presumably initiated by hydrogen removal from a methyl group, a process that may well involve base catalysis by the glass vessel. Such catalysis is clearly operative in the formation of

Can. J. Chem. Downloaded from www.nrcresearchpress.com by 210.87.254.105 on 09/05/12
For personal use only.

Can. J. Chem. Downloaded from www.nrcresearchpress.com by 210.87.254.105 on 09/05/12
For personal use only.

60 from **57** on basic alumina.[7] A product, **69**, analogous to **60**, is formed on acid treatment of the epoxide **67**[8] prepared from **66** (itself prepared by treatment of 1,2,3,4-tetrachloro-7-norbornenone with **20**). This reaction presumably proceeds via the intermediate **68** (Scheme 10), analogous to **63**, which loses a proton rather than undergoing rearrangement to a product analogous to **59** because of inhibition of the latter process by the electron-withdrawing chlorine substituents.

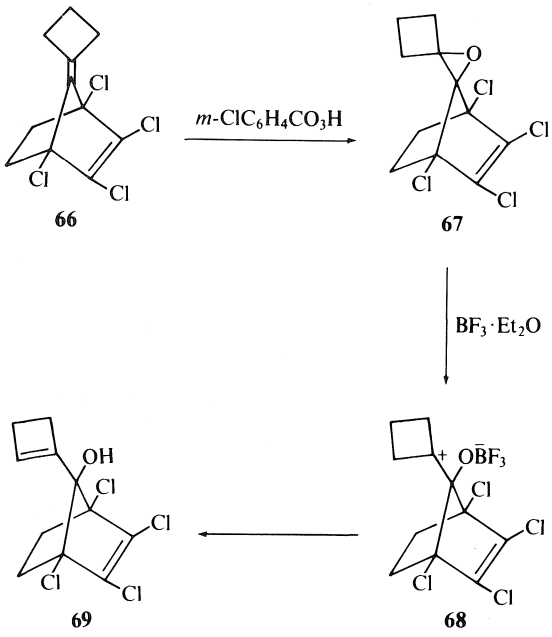

66 **67** **69** **68**

SCHEME 10

The propensity of the benzonorbornene system to maintain sp^3 hybridization at the C.7 carbon that was demonstrated in the reactions of **57** suggested that treatment of **56** with an electrophilic alkylating agent (R^+) would lead specifically to products derived from **70** rather than **71** and thus provide a route for the construction of a spiro ring system at C.7. In the

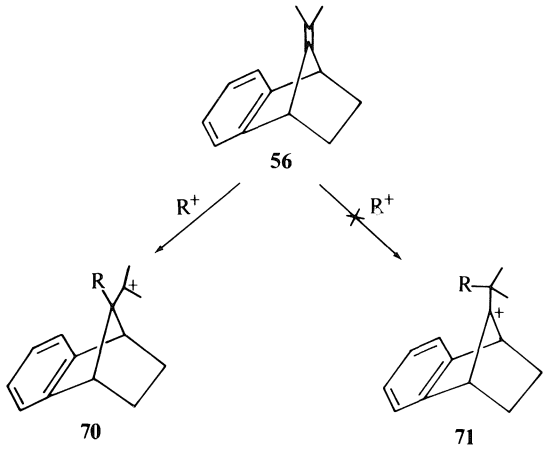

56 **70** **71**

event, treatment of **56** with acetyl chloride and aluminum chloride in dichloromethane gave a product that is assigned the gross structure **72** on the basis of its spectra, which showed the presence of an acetyl group (5.87, 7.41 (m) μm; δ 1.80 (s, 3H)), an isopropenyl group (6.11 (w), 11.10 μm; δ 1.72 (m, $\nu_{1/2}$ = 3 Hz, 3H), 5.05 (m, 2H)), and two equivalent bridgehead hydrogen atoms (3.60 (distorted t, J_{app} = 2 Hz, 2H)).[6] The stereochemistry assigned at C.7 in **72** is based primarily on the position of the acetyl methyl signal in the pmr spectrum (δ 1.80), which shows that this methyl group is significantly shielded by the benzene ring.[9] This assignment is in conformance with the anticipated intermediacy of **70**. Hydrogenation of **72** gave a dihydro compound, **73**, whose spectra confirmed the presence of an acetyl group (5.89, 7.37 (m) μm; δ 1.73 (s, 3H)),[9] an isopropyl group (7.19 (w), 7.28 (w) μm; δ 0.96 (d, J = 7 Hz, 6H)), and two equivalent bridgehead hydrogen atoms (δ 3.43 (distorted t, J_{app} = 2 Hz, 2H)).[6] The position of the acetyl methyl pmr signal (δ 1.73) again reflects shielding of the *syn* stereoisomer by the benzene ring; the further upfield shift

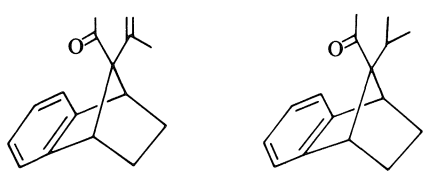

72 **73**

[7]The additional formation of **59** under these conditions may perhaps result from the amphoteric properties of alumina.

[8]The stereochemistry of this epoxide is unknown; steric approach control would favor the stereoisomer represented by **67** (participation by the electron-poor dichloroethylenic double bond should be minimal); however, product development control[4] would favor the *anti*-epoxide.

[9]The position of the carbonyl-stretching band in the ir spectrum may also reflect the *syn* stereochemistry.

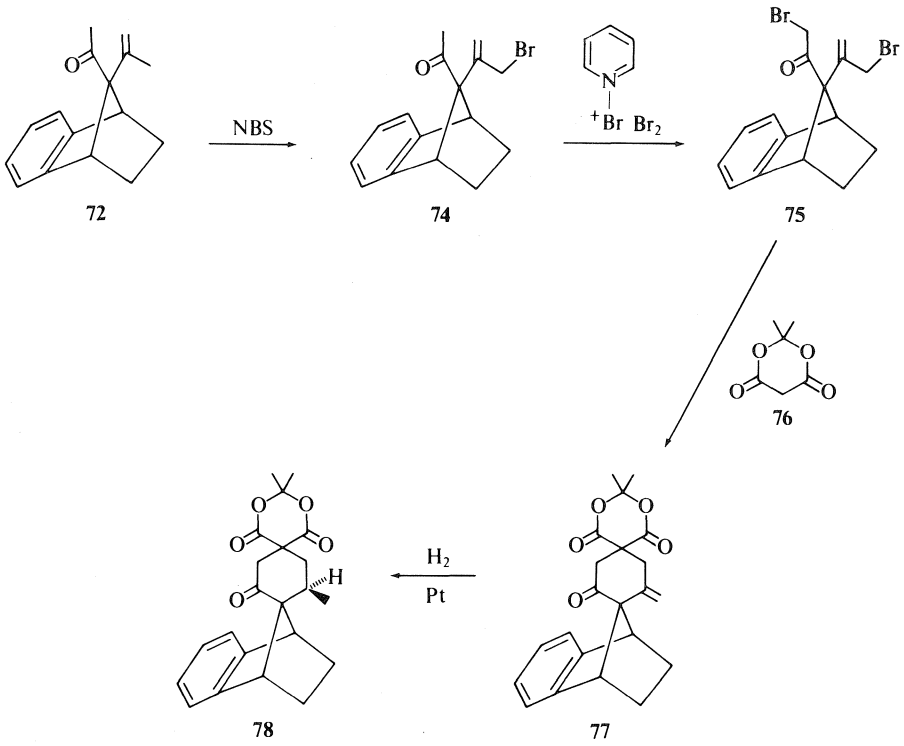

SCHEME II

relative to the corresponding signal in the spectrum of **72** is attributable to the removal of slight deshielding of the acetyl methyl group of **72** by the isopropenyl group.

Attempts to convert **72** to a spirocyclopentanone analogous to **5** were unsuccessful. It was found possible, however, to convert **72** to the dispiro compound **77** by the route shown in Scheme 11. Bromination of **72** with *N*-bromosuccinimide gave **74**, which was converted with pyridinium hydrobromide perbromide to the dibromo compound **75**.[10] Treatment of this with isopropylidene malonate (**76**) and silver oxide in acetonitrile gave **77**, whose spectra showed the presence of an isopropylidene malonate moiety with non-equivalent methyl groups (5.63, 5.74 μm; δ 1.66 (s, 3H), 1.78 (s, 3H); *cf.* **76**: 5.60 (sh), 5.67 μm), a ketonic group (5.81 μm (sh)), a vinylidene group (6.09 (w) μm; δ 5.10 (s, $\nu_{1/2}$ = 2.5 Hz, 1H), 5.23 (s, $\nu_{1/2}$ = 2 Hz, 1H)), and two equivalent bridgehead hydrogen atoms (δ 3.80 (distorted t, J_{app} = 2 Hz, 2H)).[6] Hydrogenation of **77** gave a dihydro compound **78**, whose spectra confirmed the presence of an isopropylidene malonate moiety with two non-equivalent methyl groups (5.62, 5.74 μm; δ 1.66 (s, 3H), 1.81 (s, 3H)), a ketonic group (5.82 (sh) μm), a secondary methyl group (δ 1.07 (d, J = 7.5 Hz, 3H)), and two non-equivalent bridgehead hydrogen atoms (δ 3.45 (m, 1H), 3.75 (m, 1H)).

[10]Neither **74** nor **75** were obtained in highly purified form; their structures are assigned on the basis of their spectra (see Experimental).

Experimental

Melting points are uncorrected. Infrared spectra were recorded with carbon tetrachloride as solvent, unless otherwise specified. Nuclear magnetic resonance spectra were recorded with deuterochloroform as solvent, unless otherwise specified. Vapor phase chromatographic analyses were carried out on the following columns: (*A*), 15% Carbowax 20M/W on 60/80 Chromosorb W, 6 ft × 0.125 in., copper; (*B*), 5% UCON 50-HB-2000 on 60/80 Chromosorb G-DMCS-A/W, 10 ft × 0.125 in., stainless steel; (*C*), 5% Carbowax 1500 on 80/100 Chromosorb P, 10 ft × 0.125 in., copper; (*D*), 5% UCON 50-HB-2000 on 60/80 Chromosorb G-DMCS-A/W, 13 ft × 0.25 in., aluminum. Thin layer chromatographic analyses were

Can. J. Chem. Downloaded from www.nrcresearchpress.com by 210.87.254.105 on 09/05/12
For personal use only.

Can. J. Chem. Downloaded from www.nrcresearchpress.com by 210.87.254.105 on 09/05/12
For personal use only.

carried out on 70 × 20 × 0.25 mm silica gel G plates containing a fluorescent indicator. The eluting system was 20% ethereal pentane unless otherwise indicated, and iodine development was used. Experiments described as being carried out under anhydrous conditions were conducted under a positive pressure of nitrogen that had been passed through concentrated sulfuric acid followed by sodium hydroxide. The apparatus was either dried overnight in an oven at 190 °C and assembled hot under nitrogen flow or flamed out immediately prior to use under nitrogen flow. Solvents were either distilled directly into the reaction flask from the appropriate drying agent or previously dried and stored over molecular sieves and introduced through a rubber septum via syringe.

The spectra of the following compounds are listed in the tables indicated: **3**, **4** (Table 2); **5**, **6** (Table 5); **21** (Table 3); **26**, **27** (Table 4); **51**, **55** (Table 6). The relative intensities of the ^{1}H nmr signals are in accord with the assignments given.

Spirocyclopropy Expoxide ***9***

All glassware used during the preparation of **9** was base washed.

A solution of 7-norbornenone **7** (16) (13.5 g, 125 mmol) and cyclopropyldiphenylsulfonium fluoborate **8** (3) (44.0 g, 140 mmol) in DMSO (fresh bottle, 350 ml) was prepared under nitrogen. Powdered potassium hydroxide (85%, 18.5 g, 280 mmol) was added all at once, and the mixture was stirred at room temperature for 4.5 h (3). The resulting dark brown solution was extracted with pentane (5 × 200 ml). The combined extracts were washed with saturated aqueous sodium bicarbonate (200 ml) and dried (Na_2SO_4). Concentration of the colorless solution at atmospheric pressure left 29.4 g (68%) of a colorless oil that consisted of **9** and diphenyl sulfide (**10**); $^H\delta$ 0.7–1.3 (m, 6H), 2.0–2.3 (m, 2H), 2.5 (m, 2H), 6.00 (t, J_{app} = 2 Hz, 2H), 7.1–7.5 (m, 10H).

*syn- and anti-Spiro[bicyclo[2.2.1]heptene-7,1′-cyclobutan]-2′-one (**3** and **4**)*

The mixture of **9** and **10** (29.4 g) in a base-washed flask fitted with a reflux condenser was stirred under nitrogen at 170 °C in a preheated oil bath for 60 min. The resulting yellow oil (29.4 g) was distilled at 90 torr. After a small forerun, a colorless oil (13.4 g), bp 139–142 °C, was collected. The distillation residue consisted of diphenyl sulfide. The distillate was charged onto a column of silica gel (400 g, 45 × 535 mm) and eluted with 5% ethereal pentane. Fractions of 200 ml were collected, concentrated on the steam bath, and examined by tlc.

Combination of fractions 5–10 and concentration *in vacuo* (<25 °C) gave the *anti*-cyclobutanone **4**, which was purified by molecular distillation at 90–110 °C/20 torr, giving 6.15 g (33% from **7**), of a colorless oil; *m/e* 148(18). *Anal.* calcd. for $C_{10}H_{12}O$: C 81.04, H 8.16; found: C 80.70, H 8.37.

Combination of fractions 11–29 and fraction 30 (200 ml ether) and concentration *in vacuo* (<25 °C) gave the *syn*-cyclobutanone **3**, which was purified by molecular distillation at 120–130 °C/17 torr, giving 5.93 g (32% from **7**) of a colorless oil; *m/e* 148(12). *Anal.* calcd. for $C_{10}H_{12}O$: C 81.04, H 8.16; found: C 80.88, H 8.33.

Rearrangement of Spirocyclopropyl Epoxide ***9*** *to Cyclobutanones **3** and **4** under Various Conditions*

All experiments were carried out in base-washed glassware with crude mixtures of **9** and **10**. The rearrangements were considered complete when the products lacked ir bands at 8.46, 8.74, 8.83, 9.95, 10.77, and 11.73 μm. The product mixtures were analyzed by vpc (*A*, 150 °C); typical retention times were: **4**, 2 min; **3**, 4 min.

(i) Lithium Perchlorate (17)

A solution of **9**/**10** (105 mg, 0.314 mmol) in benzene (5 ml) containing lithium perchlorate monohydrate (50 mg, 0.31 mmol) was boiled under reflux for 2 h. Cooling, washing with water, drying (Na_2SO_4), and concentration of the benzene solution *in vacuo* gave 97 mg of a pale yellow oil: **3**, 75%; **4**, 25%.

(ii) Aqueous Fluoboric Acid

A solution of **9**/**10** (102 mg, 0.313 mmol) in ether (10 ml) was stirred for 20 min at room temperature with aqueous 5% fluoboric acid. The ethereal layer was washed with saturated aqueous sodium bicarbonate (10 ml), dried (Na_2SO_4), and concentrated *in vacuo*, leaving 75 mg of a colorless cloudy oil: **3**, 83%; **4**, 17%.

(iii) Thermolyses

Neat **9**/**10** (101 mg, 0.313 mmol) was heated at 175 °C under nitrogen. After 5 min epoxide remained; after 10 min conversion was complete. A colorless oil (82 mg) resulted: **3**, 55%; **4**, 45%. Thermolysis at 110 °C (100 mg of mixture) required 90 min for complete conversion: **3**, 63%; **4**, 27%. The experiment at 175 °C was repeated in the presence of a trace of sodium bicarbonate. A pale yellow oil resulted: **3**, 50%; **4**, 50%. A 68:32 mixture of **3** and **4** was held at 175 °C for 48 min; no change in composition took place.

(iv) Silica Gel

The **9**/**10** mixture (100 mg, 0.313 mmol) was placed on a column of silica gel (2.5 g) prepared in ether. After 10 min the ketones were eluted with ether (10 ml). Concentration of the eluate left 94 mg of a colorless oil: **3**, 68%; **4**, 32%.

*Spiro[bicyclo[2.2.1]heptane-7,1′-cyclobutan]-2′-one (**11**)*

*(i) From Hydrogenation of a Mixture of **3** and **4***

A solution of a 5:1 mixture of cyclobutanones **3** and **4** (740 mg, 5.0 mmol) in absolute ethanol (40 ml) was hydrogenated over 10% Pd/C (75 mg) at room temperature and atmospheric pressure; 115 ml of hydrogen (*ca.* 100%) was taken up in 1 h following catalyst saturation. Removal of the catalyst by filtration and concentration of the ethanolic solution *in vacuo* afforded 620 mg (83%) of **11** as a pale yellow oil, shown by vpc (*B*, 175 °C) to contain 8% of **3** (relative retention times: **4**, 3.7 min; **11**, 5.0 min; **3**, 6.0 min); λ_{max} 5.65 μm; $^H\delta$ 1.0–2.4 (m, 12H), 2.90 (t, *J* = 8 Hz, 2H); *m/e* 150(7).

*(ii) From Hydrogenation of **3***

syn-Cyclobutanone **3** (315 mg, 2.13 mmol) in methanol (20 ml) was hydrogenated over Pd/C (43.8 mg) at room temperature and atmospheric pressure. Hydrogen absorption was complete within 15 min (49 ml, *ca.* 100%). The catalyst was filtered and the methanolic solution was concentrated *in vacuo* (<25 °C, >100 torr) leaving 248 mg of a colorless oil. A small singlet in the pmr spectrum of this material (δ 3.20) suggested the presence of some dimethyl ketal. Hence the product was stirred overnight at room temperature with 5% aqueous sulfuric acid (10 ml). Ether extraction (2 × 10 ml) followed by washing of the extracts with aqueous 1 *N* sodium carbonate (10 ml) and water (10 ml), drying ($MgSO_4$), and con-

Can. J. Chem. Downloaded from www.nrcresearchpress.com by 210.87.254.105 on 09/05/12
For personal use only.

centration at atmospheric pressure gave 200 mg (63%) of **11** that was free from ketal. This product exhibited ir and pmr spectra essentially identical to those of the product resulting from hydrogenation of the mixture of **3** and **4**. *Anal.* calcd. for $C_{10}H_{14}O$: C 79.95, H 9.39, mw 150.1045; found: C 79.58, H 9.56, *m/e* 150.1045.

*syn-Spiro[bicyclo[2.2.1]hepten-7,1'-cyclobutan]-2-one-d_2 (**12**)*

A solution of *syn*-cyclobutanone **3** (100 mg, 0.68 mmol) in methanol-*d* (5 ml) was treated with sodium methoxide (3 mg, 0.057 mmol). The colorless solution was stirred for 2.5 h at room temperature. It was poured into D_2O (30 ml), and the mixture was extracted with ether (3 × 20 ml). Drying (Na_2SO_4) and concentration *in vacuo* left 100 mg (100%) of a yellow oil; this was molecularly distilled at 110–120 °C/13 torr giving 90 mg of **12** as a colorless oil. This was indistinguishable from **3** by ir, tlc, and vpc (*B*, 175 °C) analysis; $^{H}\delta$ 1.0 (m, 2H), 1.8 (m, 4H), 2.9 (br s, 2H), 6.01 (t, J_{app} = 2 Hz, 2H); *m/e* 150(22).

*syn-Spiro[bicyclo[2.2.1]heptene-7,1'-cyclobutan]-2-ol (**13**)*

Under anhydrous conditions a stirred slurry of lithium aluminum hydride (170 mg, 4.5 mmol) in ether (5 ml) was treated with a solution of *syn*-cyclobutanone **3** (292 mg, 1.97 mmol) in ether (5 ml). The mixture was boiled under reflux for 2 h, cooled, and treated carefully with aqueous 10% sodium hydroxide until a white granular precipitate had just formed. The colorless supernatant was separated by filtration, dried ($MgSO_4$), and concentrated at atmospheric pressure, giving 275 mg (94%) of **13** as a colorless oil; λ_{max} 2.80 μm; $^{H}\delta$ 1.0 (m, 2H), 1.2–1.9 (m, 6H), 2.45 (br s, 1H), 2.80 (br s, 1H), 3.15 (s, 1H; absent after D_2O treatment), 4.1 (m, 1H), 5.72–6.18 (m, 2H); *m/e* 150(14). *Anal.* calcd. for $C_{10}H_{14}O$: C 79.95, H 9.39; found: C 79.85, H 9.40.

*anti-Spiro[bicyclo[2.2.1]heptene-7,1'-cyclobutan]-2-ol (**14**)*

Under anhydrous conditions a stirred slurry of lithium aluminum hydride (100 mg, 2.6 mmol) in ether (10 ml) was treated by syringe injection with *anti*-cyclobutanone **4** (50 μl, *ca.* 0.3 mmol). The mixture was stirred for 4.75 h at room temperature. Work-up as above gave 33 mg (66%) of **14** as a white waxy solid, mp 62–63 °C; λ_{max} 2.75 μm; $^{H}\delta$ 1.0 (m, 2H), 1.4–2.2 (m, 6H), 2.50 (br s, 1H), 2.75 (s, 1H; absent after D_2O treatment) 2.83 (s, 1H), 3.9 (m, 1H), 5.80–6.05 (m, 2H). *Anal.* calcd. for $C_{10}H_{14}O$, C 79.95, H 9.39, mw 150.1045; found: C 79.72, H 9.35, *m/e* 150.1045.

*Treatment of syn- and anti-Spirocyclobutanols **13** and **14** with Mercuric Acetate*

Under anhydrous conditions a solution of a 5:1 mixture of cyclobutanones **3** and **4** (2.96 g, 20 mmol) in ether (25 ml) was added to a stirred slurry of lithium aluminum hydride (760 mg, 20 mmol) in ether (25 ml) at room temperature over 2 h. After an additional 2.5 h at room temperature, work-up of the reaction mixture as above gave 2.90 g (97%) of a pale yellow oil. Vapor phase chromatography (*B*, 175 °C) showed this to be a 5.5:1 mixture of alcohols **13** (retention time 5.1 min) and **14** (retention time 6.8 min), respectively; no **3** (retention time 6.0 min) or **4** (retention time 3.7 min) remained. The mixture of alcohols was cleanly resolved by tlc with elution with 2:1 ethyl acetate – cyclohexane into its *syn*-component **13** (R_f 0.57) and *anti*-component **14** (R_f 0.64). A solution of the alcohol mixture (50 mg, 0.33 mmol) in dichloromethane (2 ml) was treated with mercuric acetate (110 mg, 0.35 mmol). After 15 min of stirring at room temperature tlc as above revealed complete consumption of **13**. After 2 h the spot for **14** persisted. Repetition of this experiment in *tert*-butyl alcohol, acetone, and pentane led to the same result.

*Reaction of syn-Spirocyclobutanol **13** with Mercuric Acetate. Formation of **17** (**18**)*

A stirred suspension of mercuric acetate (255 mg, 0.800 mmol) in dichloromethane (5 ml) was treated with a solution of *syn*-cyclobutanol **13** (132 mg, 0.880 mmol) in dichloromethane (6 ml) at room temperature. After 45 min all the mercuric acetate had dissolved; the cloudy solution was stirred overnight at room temperature under nitrogen. Concentration of the colorless solution *in vacuo* and trituration of the residue with pentane afforded white crystals of **17** (**18**), 168 mg (45%), mp 78–82 °C; λ_{max} ($CHCl_3$) 2.8–3.1, 5.80, 6.15, 6.25 μm; $^{H}\delta$ 0.8–2.4 (m, 10H), 2.00 (s, 3H), 2.10 (s, 3H), 2.6 (m, 1H), 4.0 (br s, 1H; absent after D_2O treatment), 4.6 (m, 1H), 5.0 (m, 1H). A portion of the product was recrystallized from dichloromethane–pentane giving white cubes, mp 137–142 °C.[11] *Anal.* calcd. for $C_{14}H_{20}HgO_5$: C 35.86, H 4.30; found: C 35.84, H 4.48.

*Regeneration of syn-Spirocyclobutanol **13** from **17** (**18**)*

The crude oxymercurate **17** (**18**) (48 mg, 0.102 mmol) was stirred for 2 h at room temperature with 5% hydrochloric acid (5 ml). The cloudy solution was extracted with pentane (2 × 10 ml), and the extracts were washed with water (10 ml) and dried ($MgSO_4$); concentration at atmospheric pressure yielded 11.5 mg (75%) of **13** as a cloudy oil. The ir spectrum and tlc behaviour of this material were identical with those of authentic *syn*-alcohol **13**.

*Reaction of 7-Norbornenone (**7**) with Cyclobutylmagnesium Bromide. Formation of anti-7-Norbornenol (**19**)*

Cyclobutylmagnesium bromide was prepared under anhydrous conditions by addition of a solution of cyclobutyl bromide [12] (2.75 g, 22 mmol) in ether (20 ml) over 30 min to a stirred suspension of magnesium turnings (486 mg, 20 mmol) in ether (20 ml) containing a trace of 1,2-dibromoethane and boiling under reflux for an additional 3 h. To the greenish grey solution a solution of **7** (16) (2.00 g, 18.5 mmol) in ether (10 ml) was added over 10 min. After 3 h at reflux the reaction mixture was quenched with saturated aqueous ammonium chloride and the insoluble magnesium salts were removed by filtration. The colorless ethereal solution was dried (Na_2SO_4) and concentrated at atmospheric pressure to yield 2.0 g of a pale yellow oil. Vapor phase chromatography (*C*, 170 °C) showed a single component. This was shown to be *anti*-7-norbornenol (7) (100% yield) by direct comparison of its pmr spectrum (δ 0.9 (m, 2H), 1.7 (m, 2H), 2.45 (br s, 2H), 3.48 (br s, 1H), 4.33 (br s, 1H; absent after D_2O treatment), 5.90 (t, J_{app} = 2 Hz, 2H)) and a spectrum of authentic *syn*-7-norbornenol (δ 0.9 (m,

[11]Presumably the mercuric acetate reaction gives rise to a stereoisomeric mixture which is resolved to some extent on recrystallization.

[12]The cyclobutyl bromide was prepared by the procedure of Cason and Way (18).

Can. J. Chem. Downloaded from www.nrcresearchpress.com by 210.87.254.105 on 09/05/12
For personal use only.

2H), 1.8 (m, 2H), 2.73 (m, 2H), 3.0 (br s, 1H; absent after D_2O treatment), 3.75 (br s, 1H), 6.05 (m, 2H)), and comparison of both spectra with those previously reported for these two isomers (19*a*).

Oxidation of anti-7-Norbornenol. Formation of ***7***

A solution of *anti*-7-norbornenol (540 mg, 5.0 mmol) in dichloromethane (2 ml) was added to a solution of pyridine (3.13 g, 40 mmol) and chromium trioxide (2.00 g, 20 mmol) in dichloromethane (50 ml) (*cf.* ref. 19*b*). After 20 min the clear orange supernatant was decanted and the black residue was washed with ether (70 ml). The combined organic solutions were washed with aqueous 5% sodium hydroxide (3 × 35 ml), aqueous 5% hydrochloric acid (40 ml), aqueous 5% sodium bicarbonate (40 ml), and saturated aqueous sodium chloride (40 ml) and dried ($MgSO_4$). Concentration *in vacuo* gave 380 mg (75%) of 7-norbornenone (**7**), identified by ir and pmr spectroscopic comparison with an authentic sample.

7-Cyclobutylidenenorbornene ***(21)***

Under anhydrous conditions a stirred suspension of (4-bromobutyl)triphenylphosphonium bromide (20) (143.4 g, 300 mmol) in ether (1300 ml) was treated rapidly with a 7:3 benzene–ether solution of phenyllithium[13] (1.4 *M*, 425 ml, 595 mmol) via syringe. Slight refluxing accompanied the formation of a deep red solution. This was stirred overnight at room temperature, giving a red solution with considerable undissolved solids.[14] 7-Norbornenone **7** (21.6 g, 200 mmol) was injected and the resulting light orange mixture was stirred and boiled under reflux overnight. The reaction mixture was quenched with water (150 ml), and the precipitate was removed by filtration and washed with ether. The combined ethereal solutions were washed with water until the washings were neutral (3 × 200 ml), dried ($MgSO_4$), and concentrated *in vacuo*. The residue was freed of triphenylphosphine oxide by trituration with pentane (500 ml), removal of the precipitate by filtration, and passage of the filtrate through a silica gel plug (125 g) with suction and washing with additional pentane (200 ml). Removal of solvent *in vacuo* and distillation of the residue through a short Vigreux column gave, after a short forerun, 24.8 g (85%) of **21** as a colorless oil bp 62–68 °C/2 torr; *m/e* 146(24). *Anal.* calcd. for $C_{11}H_{14}$: C 90.35, H 9.65; found: C 90.66, H 9.63.

Spirocyclobutyl Epoxides ***22*** *and* ***23*** *from Oxidation of* ***21***

(i) With m-Chloroperbenzoic Acid

A solution of diene **21** (10.95 g, 75 mmol) in dichloromethane (750 ml) was stirred and cooled to 3 °C with an ice–salt bath and treated with a solution of *m*-chloroperbenzoic acid (82%; 15.75 g, 75 mmol) in dichloromethane (1875 ml) over 100 min at this temperature. The consumption of peracid was shown by starch–iodide paper to be instantaneous. The colorless solution was washed with aqueous 5% sodium bicarbonate (400 ml, 240 mmol), the aqueous washings were backwashed with dichloromethane (2 × 100 ml), and the combined organic solutions were washed with saturated aqueous sodium chloride (400 ml) and dried (Na_2SO_4). Concentration at atmospheric pressure left 12.4 g (*ca.* 100%) of a pale yellow oil, shown by pmr spectroscopy to be a 78:22 mixture of epoxides **22** and **23**; $^{H}\delta$ 0.8–3.2 (m, 120 integral units), 6.0–6.4 (m, 15 integral units).

(ii) With Perbenzoic Acid

A stirred solution of diene **21** (7.30 g, 50 mmol) in benzene (100 ml) was cooled to 5 °C with an ice bath and treated with a freshly prepared and standardized solution of perbenzoic acid in benzene (21) (0.714 *M*; 70 ml, 50 mmol) over a 30 min period. An additional 3 h at 5 °C was required to complete oxidant consumption. The resulting colorless solution was washed with saturated aqueous sodium bicarbonate (200 ml) and dried (K_2CO_3) to give a solution of a 9:1 mixture of **22** and **23** as shown by pmr spectroscopy.

Spiro[bicyclo[2.2.1]heptene-7,1′-cyclopentan]-2′-one ***(5)*** *from Rearrangement of Epoxide* ***22****. Concomitant Formation of Spiro[bicyclo[2.2.2]octene-2,1′-cyclobutan]-3-one* ***(26)***

(i) With Silica Gel

The crude epoxide mixture from procedure *i* above was dissolved in pentane (225 ml) and added to a silica gel column (125 g) over 1 h. Considerable heat was generated. After 2 h, elution with pentane (1250 ml) removed a small quantity (820 mg) of diene **21**. After 10 h the column was eluted with 20% ethereal pentane (1700 ml). Concentration of the eluate *in vacuo* left 14.3 g of a pale yellow oil, shown by tlc to be a mixture of epoxide **23** and ketone **5**.

The oil was added to a solution of Girard-T reagent[15] (28.6 g, 170 mmol) and glacial acetic acid (14.3 ml, 250 mmol) in absolute ethanol (280 ml), and the resulting solution was refluxed for 1 h. It was then poured into water (1250 ml), and the mixture was extracted with ether (5 × 300 ml). The aqueous layer was acidified (p*H* 3) with concentrated hydrochloric acid and vigorously stirred overnight in contact with ether (900 ml). The aqueous layer was extracted with additional ether (2 × 300 ml). The combined ethereal solutions were washed with saturated aqueous sodium bicarbonate (300 ml), dried ($MgSO_4$), and concentrated *in vacuo* to give 6.85 g of a yellow oil. Vacuum distillation of this material gave 4.92 g (50% based on epoxide **22**) of ketone **5** as a colorless oil, bp 90–93 °C/1 torr; *m/e* 162(81). *Anal.* calcd. for $C_{11}H_{14}O$: C 81.44, H 8.70, mw 162.1045, $(M - C_2H_4)^+$ 134.0732; found: C 81.50, H 8.63, *m/e* 162.1042, 134.0732.

(ii) With Boron Trifluoride Etherate

The solution of epoxides from procedure *ii* above was further dried by distillation of benzene (*ca.* 50 ml) from it at atmospheric pressure. The residual colorless solution (*ca.* 300 ml) was cooled to 20 °C, put under nitrogen, and treated with boron trifluoride etherate (300 μl, 2.44 mmol) by injection. This caused rapid darkening and a temperature rise to 28 °C. After 8 min the dark brown solution was poured into aqueous 10% sodium bicarbonate

[13]It is important that good quality phenyllithium be used. On one occasion significant contamination of diene **21** resulted because of considerable biphenyl present in the commercial phenyllithium. This impurity co-distilled with **21** and had to be removed by filtration through a column of powdered charcoal.

[14]*Cf.* ref. 8; we have found it unnecessary to isolate the intermediate cyclobutyltriphenylphosphonium bromide.

[15]*Cf.* ref. 6, pp. 410–411.

Can. J. Chem. Downloaded from www.nrcresearchpress.com by 210.87.254.105 on 09/05/12
For personal use only.

(100 ml). The pale yellow benzene solution was washed with water (100 ml), dried ($MgSO_4$), and concentrated at atmospheric pressure under nitrogen yielding 12.4 g of a light yellow oil. This was charged onto a silica gel column (366 g, 480 × 40 mm) and eluted with 10% ethereal pentane. Fractions of 200 ml were collected, concentrated on the steam bath, and examined by tlc.

Combination of fractions 6–10 and concentration *in vacuo* afforded 500 mg (7% based on **22**) of bicyclooctenone **26** as a colorless oil: *m/e* 162(19). *Anal.* calcd. for $C_{11}H_{14}O$: mw 162.1045, $(M - C_2H_4)^+$ 134.0732; found: *m/e* 162.1045, 134.0732.

Combination of fractions 11–15 and 16–18 (1000 ml each) afforded 5.0 g (69% based on **22**) of the *syn*-cyclopentanone **5** as a colorless oil. This material was identical with the product from the silica gel reaction *i* as shown by ir, pmr, and tlc comparisons.

*Demonstration of the Absence of Acidic Protons in Bicyclooctenone **26**. Reference Experiment with Bicyclo[2.2.2]oct-5-en-2-one **(27)***

A solution of bicyclooctenone **26** (50 mg, 0.310 mmol) (Table 4) in methanol-*d* (5 ml) was treated with sodium (2.6 mg, 0.11 mmol) and stirred for 3.5 h at room temperature. The yellow solution was poured into D_2O (25 ml) and, after addition of some sodium chloride, extracted with pentane (3 × 10 ml). Drying (Na_2SO_4) and concentration *in vacuo* (<25 °C, >100 torr) left 39.5 mg (79%) of a colorless oil that had ir and pmr spectra and tlc behaviour identical with those of the starting material.

A solution of bicyclo[2.2.2]oct-5-en-2-one (**27**) (freshly sublimed at 75 °C/15 torr; 72 mg, 0.590 mmol) in methanol-*d* (10 ml) was treated with sodium (8.3 mg, 0.360 mmol) and stirred for 2.5 h at room temperature. The colorless solution was poured into D_2O (35 ml) and, after addition of some sodium chloride, extracted with ether (3 × 10 ml). Drying (Na_2SO_4) and concentration *in vacuo* left 46 mg (63%) of a white solid. Although this displayed an ir spectrum and tlc behaviour identical with those of the starting material, its pmr spectrum differed from that of **27** in lacking the narrow two-proton multiplet at δ 2.0.

*Hydrogenation of **5**. Formation of Spiro[bicyclo[2.2.1]-heptane-7,1′-cyclopentan]-2′-one **(28)***

A solution of ketone **5** (106 mg, 0.654 mmol) in absolute ethanol (5 ml) was hydrogenated over 10% Pd/C (10 mg) at room temperature and atmospheric pressure; 16 ml (0.715 mmol, *ca.* 100%) of hydrogen was taken up in 15 min. No further gas absorption was observed in the next 20 min. The catalyst was removed by filtration and the ethanol by distillation at atmospheric pressure. Molecular distillation (120 °C/10 torr) of the residue gave 70 mg (65%) of **28** as a colorless oil; λ_{max} 5.78 μm; $^H\delta$ 0.8–2.4 (m); *m/e* 164(42). *Anal.* calcd. for $C_{11}H_{16}O$: C 80.44, H 9.83; found: C 80.31, H 9.98.

*Wolff–Kishner Reduction of **5**. Formation of Spiro-[bicyclo[2.2.1]heptene-7,1′-cyclopentane] **(29)**.*

A solution of ketone **5** (500 mg, 3.0 mmol), 95% hydrazine (400 μl, 12.0 mmol), and potassium hydroxide (85%; 660 mg, 100 mmol) in diethylene glycol (6 ml) was stirred under nitrogen at 150 °C for 5 h in a flask equipped with a reflux condenser. The flask was then fitted for distillation under nitrogen and heated at 200 °C for 6 h. The remaining solution was poured into water (35 ml), and the mixture was acidified and extracted with pentane (5 × 15 ml). The distillation assembly was rinsed with pentane, and the combined organic solutions were washed with saturated aqueous sodium chloride (60 ml) and dried ($MgSO_4$). Concentration at atmospheric pressure yielded 440 mg of **29** as a colorless oil; $^H\delta$ 0.7–1.0 (m, 2H), 1.0–1.8 (m, 10H), 2.3 (m, 2H), 6.00 (t, J_{app} = 1 Hz, 2H), the spectrum showed the presence of a small amount of pentane; *m/e* 148(74). The material was purified for analysis by filtration through silica gel (44 g) with pentane (250 ml), concentration, and molecular distillation (110 °C/10 torr). *Anal.* calcd. for $C_{11}H_{16}$: C 89.12, H 10.88; found: C 88.97, H 11.21.

*Formation of **29** by Oxidative Bisdecarboxylation of Dicarboxylic Acid **30***

Dry oxygen was passed through dry pyridine (20 ml) for 15 min in a flask protected by a silica gel drying tube. Dicarboxylic acid **30** (22) (1.0 g, 4.2 mmol) and lead tetraacetate (5.6 g, 12.6 mmol) were introduced and the drying tube was replaced by a connection leading to a gas bubbler. The flask was placed in an oil bath at 70 °C and the contents were stirred while a slow stream of oxygen was passed through.[16] After a few minutes a temporary halt of the oxygen flow showed that gas evolution from the reaction had commenced. The mixture turned red and then brown; gas evolution continued for 12 min. The resulting brown mixture was added to aqueous 3 *M* nitric acid (125 ml), and the aqueous mixture was extracted with ether (3 × 35 ml). The combined extracts were washed with saturated aqueous sodium bicarbonate (50 ml) and saturated sodium chloride (50 ml), dried ($MgSO_4$), and concentrated *in vacuo* to give 430 mg of a brown oil. This was filtered through silica gel (5 g) with pentane (100 ml) and the concentrated eluate (120 mg) was molecularly distilled (80 °C/1 torr) yielding 40 mg (8%) of **29** as a pale yellow oil, which displayed ir, pmr, and mass spectra and vpc (*D*, 185 °C) behaviour identical to those of the material from the Wolff–Kishner reduction of **5**.

*syn-Spiro[bicyclo[2.2.1]heptene-7,1′-cyclopentan]-2′-ol **(31)***

Under anhydrous conditions a solution of *syn*-spirocyclopentanone **5** (486 mg, 3.0 mmol) in ether (10 ml) was added to a stirred slurry of lithium aluminum hydride (500 mg, 13 mmol) in ether (10 ml). The mixture was refluxed for 3 h and then hydrolyzed and worked-up as described for compound **13** to yield 540 mg of **31** as a pale yellow, cloudy oil. This material was purified by molecular distillation (65 °C/0.5 torr) with dry ice–acetone cooling of the distillate, which crystallized on standing at room temperature to a soft white solid, mp 35–39 °C; λ_{max} 2.85 μm; $^H\delta$ 1.0 (m, 2H), 1.2–1.9 (m, 8H), 2.3 (br s, 2H; 1H after D_2O treatment), 2.6 (br s, 1H), 4.02 (t, *J* = 3 Hz, 1H), 6.05 (t, J_{app} = 1.5 Hz, 2H); *m/e* 164(13). *Anal.* calcd. for $C_{11}H_{16}O$: C 80.44, H 9.83; found: C 80.37, H 9.95.

*Reaction of syn-Spirocyclopentanol **31** with Mercuric Acetate. Formation of **32** and **33***

A stirred solution of crude *syn*-alcohol **31** (165 mg, 1.0 mol) in *tert*-butyl alcohol (2 ml) was treated with mercuric

[16] *Cf.* ref. 23 and references quoted therein.

Can. J. Chem. Downloaded from www.nrcresearchpress.com by 210.87.254.105 on 09/05/12
For personal use only.

acetate (319 mg, 1.0 mmol). After 30 min at room temperature a tlc examination of the mixture revealed no mobile components. Concentration *in vacuo* and trituration with pentane afforded 398 mg of **32** (94%) as a white crystalline solid contaminated with mercuric acetate; λ_{max} 6.22, 6.31 μm; $^{H}\delta$ 1.0–2.4 (m, 12H), 2.0 (s, 3H), 2.8 (m, 1H), 4.1 (m, 1H).

In another run the *tert*-butyl alcohol solution was gravity filtered instead of being concentrated and treated with a solution of sodium chloride (100 mg, 1.7 mmol) in water (5 ml) to give a dense white precipitate. Isolation after 10 min by suction filtration gave 250 mg (62%) of **33**. Sublimation gave a hard, white, crystalline solid, mp 252–252.5 °C. *Anal.* calcd. for $C_{11}H_{15}ClHgO$: C 33.09, H 3.79; found: C 33.07, H 3.83.

*Regeneration of syn-Spirocyclopentanol **31** from **33***

A mixture of crude **33** (100 mg, 0.25 mmol) and aqueous 5% hydrochloric acid (5 ml) was stirred overnight at room temperature. The resulting mixture was extracted with ether (3 × 5 ml), and the extracts were washed with water (5 ml) and saturated aqueous sodium chloride (5 ml) and dried ($MgSO_4$). Concentration at atmospheric pressure afforded 40 mg (100%) of **31**, shown to be identical with an authentic sample by ir, tlc, and vpc (*A*, 190 °C) comparison.

*Bromination of syn-Spirocyclopentanone **5**. Formation of **34** and **35**.*

Under anhydrous conditions a stirred solution of ketone **5** (167 mg, 1.03 mmol) in dichloromethane (10 ml) was cooled to −78 °C and treated with a standardized solution of bromine in dichloromethane (assayed by iodometric titration; 0.103 *M*; 10.0 ml, 1.03 mmol) over 69 min; bromine consumption was instantaneous. After an additional 30 min at −78 °C the solution was allowed to warm to room temperature and concentrated *in vacuo* to give a light brown oil that was found to be **34** by spectroscopic examination in the absence of moist air; λ_{max} 2.9, 5.83 μm (attributed to partial hydrolysis); $^{H}\delta$ 1.2–2.6 (m, 12H), 4.22 (d, J = 0.5 Hz, 1H), 4.75 (d, J = 5 Hz, 1H).

Solutions of α-bromo ether **34** rapidly lost hydrogen bromide on exposure to moist air, giving rise to bromohydrin **35**. It was found more convenient to repeat the above preparation without rigorous exclusion of water (but under nitrogen); washing the warmed dichloromethane solution with water (15 ml), aqueous 5% sodium bicarbonate (15 ml), aqueous 2 *N* hydrochloric acid (15 ml), and saturated aqueous sodium chloride (15 ml), drying ($MgSO_4$), and concentration *in vacuo* gave 238 mg (92%) of **35** as light brown crystals. After three sublimations (60–65 °C/0.5 torr) white crystals mp 74–75 °C, were obtained; λ_{max} 2.9, 5.83 μm; $^{H}\delta$ 1.2–2.5 (m, 12H), 3.65 (d of d, J = 4, 12 Hz, 1H; d, J = 4 Hz after D_2O treatment), 4.40 (t, J = 4 Hz, 1H), 4.80 (d, J = 12 Hz, 1H; absent after D_2O treatment); *m/e* 261(2), 260(2), 259(2), 258(2). *Anal.* calcd. for $C_{11}H_{15}BrO_2$: C 50.97, H 5.85; found: C 50.91, H 5.81.

*Regeneration of syn-Spirocyclopentanone **5** from **35***

A mixture of bromohydrin **35** (50 mg, 0.193 mmol) and activated zinc dust[17] (256 mg, 3.92 mmol) in glacial acetic acid (5 ml) was refluxed for 2.75 h under nitrogen. The solids were removed by filtration, and the acetic acid solution was diluted with water (50 ml) and extracted with ether (2 × 15 ml). The combined extracts were washed with aqueous 5% sodium bicarbonate (40 ml), dried ($MgSO_4$), and concentrated *in vacuo* giving 16 mg of a colorless oil. The presence of *syn*-cyclopentanone **5** in this product was demonstrated by tlc, and pmr and ir spectroscopic comparison.

*Reaction of syn-Spirocyclopentanone **5** with Concentrated Sulfuric Acid. Formation of **36***

Ketone **5** (10 μl, *ca.* 0.062 mmol) was injected into stirred, concentrated sulfuric acid (369 mg, 7.5 mequiv). The dull orange solution was stirred at room temperature for 30 min and then poured into a 125-ml flask containing sodium bicarbonate (865 mg, 10.3 mmol) mixed with ice and water (15 ml). The resulting solution was saturated with sodium chloride and extracted with hexane (4 × 5 ml). The combined extracts were washed with water (5 ml), dried (Na_2SO_4), and concentrated *in vacuo* to give 10.2 mg (90%) of **36** as a white solid; $\lambda_{max}(CCl_4)$ 2.75, 3.0, 5.75 (w) μm; $\lambda_{max}(CHCl_3)$ 2.80, 2.9, 5.79 (w) μm; $^{H}\delta$ 1.2–2.6 (m, 14H), 3.6 (m, 1H; absent after D_2O treatment), 4.3 (m, 1H); *m/e* 180(10). A sample of **36** was sublimed twice at 60 °C/0.1 torr to give an analytical sample, mp 98–110 °C. *Anal.* calcd. for $C_{11}H_{16}O_2$: C 73.30, H 8.95; found: C 73.11, H 9.01.

*Irradiation of syn-Spirocyclopentanone **5**. Formation of **38***

A solution of ketone **5** (127 mg, 0.79 mmol) in benzene (10 ml) in a Pyrex photolysis tube was deoxygenated by passage of dry nitrogen for several hours. The solution was irradiated with a 450 W medium pressure Hanovia mercury lamp at *ca.* 20 °C for 14.5 h. Removal of the solvent *in vacuo* left 125 mg of a pale yellow oil. This was purified by molecular distillation at 25 °C/2 × 10^{-4} torr on to a dry ice – acetone-cooled cold finger, giving 86 mg (68%) of **38** as a colorless oil; $^{H}\delta$ 1.2–2.4 (m, 11H), 2.55 (d, J = 4 Hz, 1H), 3.43 (t, J = 3 Hz, 1H), 4.37 (m, 1H); *m/e* 162(36).

Repetition of the irradiation in methanol, as above, or under triplet-sensitized conditions (benzene/quartz tube/2537 Å) led to the same product.

Triethyloxonium Fluoborate[18]

Under anhydrous conditions a stirred volume of ether (5–10 ml) was treated sequentially by syringe injection with freshly distilled boron trifluoride etherate (126 μl, 142 mg, 1.0 mmol) and epichlorohydrin (59.5 μl, 70.0 mg, 0.75 mmol). A cloudy solution formed. Boiling under reflux and stirring for 1.5 h produced a clear solution containing a coagulated white lump of triethyloxonium fluoborate. The ethereal solution was removed by syringe, and the Meerwein salt was washed with fresh ether (3 × 10 ml) by successive addition, trituration, and removal by syringe (the ether was conveniently held in a pressure-equalized addition funnel above the reaction flask during the formation of the salt). Following removal of the last portion of ether, dichloromethane (10–20 ml) was injected, giving a colorless solution of the Meerwein salt (0.65–0.725 mmol), which was used directly.

[17]*Cf.* ref. 6, p. 1276.

[18]This is a modification of Meerwein's procedure (24) that avoids dry box manipulation of the air-sensitive salt.

Can. J. Chem. Downloaded from www.nrcresearchpress.com by 210.87.254.105 on 09/05/12
For personal use only.

The procedure was used for the preparation of from one quarter to four times the above quantity of the Meerwein salt; in each case the volumes of ether used were similar.

*Ring Expansion of syn-Spirocyclobutanone **3**. Formation of **5** and **51***

A solution of triethyloxonium fluoborate (2.75 mmol) in dichloromethane (5 ml), prepared as above, was treated under anhydrous conditions at 25 °C sequentially with *syn*-cyclobutanone **3** (250 μl, *ca.* 1.7 mmol) and *tert*-butyl diazoacetate (25) (300 μl, 339 mg, 2.38 mmol) (*cf.* ref. 12). Within 10 min nitrogen evolution had ceased, and a colorless solution was formed. The reaction was quenched after 40 min[19] by addition of saturated aqueous sodium bicarbonate (5 ml) and stirring for 30 min. The dichloromethane solution was dried (Na_2SO_4) and concentrated *in vacuo* to yield 494 mg of a crude mixture of β-keto esters **49** and **50** as a colorless oil; λ_{max} 5.70, 5.80 μm; $^{H}\delta$ 1.0–2.3 (m, 8H), 1.43 and 1.45 (two s (1:4), 9H), 2.5–3.2 (m, 3H), 6.1 (m, 2H), plus impurities at 3.4–4.4; *m/e* 262(5). Attempted molecular distillation of the mixture (110–120 °C/0.2 torr) led to extensive decomposition.

A solution of the crude β-keto ester mixture (50 mg) in toluene (10 ml) containing *p*-toluenesulfonic acid (3.2 mg) was boiled under reflux for 4 h under nitrogen (*cf.* ref. 26). The resulting colorless solution was washed with aqueous 2 *N* sodium carbonate (10 ml), dried ($MgSO_4$), and concentrated *in vacuo* (<35 °C) giving 27 mg of a pale yellow oil. Vapor phase chromatographic analysis (*A*, 175 °C) showed that this contained the two *syn*-spirocyclopentanones **5** (retention time 5.4 min) and **51** (*vide infra*; retention time 6.2 min) in a ratio of 4:1.

*2′-syn-Methylenespiro[bicyclo[2.2.1]heptene-7,1′-cyclobutane] (**52**)*

Under anhydrous conditions a stirred suspension of methyltriphenylphosphonium bromide (7.14 g, 20 mmol) in ether (50 ml) was treated with a hexane solution of *n*-butyllithium (1.97 *M*; 10.0 ml, 19.7 mmol). The resulting orange solution containing a small amount of solid was stirred for 25 min at room temperature; then *syn*-spirocyclobutanone **3** (2.0 g, 13.5 mmol) was injected. The mixture that formed was stirred for 30 min and then refluxed for 2 h. The pale orange mixture was treated with water (1 ml) and the colorless ethereal supernatant solution was decanted from the gel-like precipitate, which was washed with ether. The combined ethereal solutions were washed with water (2 × 50 ml), dried ($MgSO_4$), and concentrated at atmospheric pressure. The pale yellow residual oil was charged onto a silica gel column (25 g) and eluted in three fractions with 20% ethereal pentane (3 × 100 ml). Thin layer chromatography showed that the last two fractions contained no product. The first 100 ml of eluate was concentrated at atmospheric pressure and the residual colorless oil (1.14 g) was molecularly distilled (100 °C/25 torr) to yield 610 mg (31%) of **52** as a colorless oil; λ_{max} 5.63 (vw), 5.97 (w), 6.14 (vw), 11.28 (m) μm; $^{H}\delta$ 0.8–1.1 (m, 2H), 1.5–1.9 (m, 4H), 2.2–2.6 (m, 2H), 2.7 (m, 2H) 4.60 (t, *J* = 1.5 Hz, 1H), 4.95 (t, *J* = 2 Hz, 1H), 6.00 (t, J_{app} = 2 Hz, 2H). *Anal.* calcd. for $C_{11}H_{14}$: C 90.35, H 9.65; found: C 90.22, H 9.58.

*Oxidation of Diene **52** with Thallium Trinitrate. Formation of syn-3′-spirocyclopentanone **51***

A stirred solution of diene **52** (146 mg, 1.0 mmol) in tetrahydrofuran (5 ml) was cooled to 3 °C and treated with a solution of thallium trinitrate trihydrate (27) (444 mg, 1.0 mmol) in aqueous 2% nitric acid (5 ml) (*cf.* ref. 13). After 45 min tlc showed no remaining **52**. The colorless supernatant solution was decanted from the insoluble thallium(I) nitrate and added to water (25 ml). Ether extraction (3 × 10 ml) and washing of the extracts with aqueous 5% sodium bicarbonate (10 ml) and water (10 ml) gave, after drying ($MgSO_4$) and concentration at atmospheric pressure, 180 mg of a yellow oil. Vapor phase chromatography (*A*, 150 °C) showed a single product, different from *syn*-spirocyclopentanone **5**. The product was purified by preparative tlc (silica gel, 2 × 200 × 200 mm; 20% ethereal pentane), yielding 18 mg (11%) of crude *syn*-3′-spirocyclopentanone **51** as a pale yellow oil; λ_{max} 5.74 μm; $^{H}\delta$ 1.0 (m, 2H), 1.6–1.9 (m, 4H), 2.0–2.4 (m, 2H), 2.13 (s, 2H), 2.4 (m, 2H), 5.90 (t, J_{app} = 2 Hz, 2H).

*Ring Expansion of anti-Spirocyclobutanone **4**. Formation of **6** and **55***

A solution of triethyloxonium fluoborate (0.157 mmol) in dichloromethane (5 ml), prepared as above, was injected at room temperature under anhydrous conditions with the *anti*-cyclobutanone **4** (200 μl, 232 mg, 1.57 mmol). After 10 min the colorless solution was treated all at once with *tert*-butyl diazoacetate (394 μl, 445 mg, 3.14 mmol). The yellow solution, which evolved nitrogen only very slowly, was stirred for 2 days at room temperature, when ir spectroscopic inspection of the reaction solution,[19] now pale yellow, showed no cyclobutanone and a trace of diazo ester. Saturated aqueous sodium bicarbonate (5 ml) was added. Work-up as above afforded 416 mg (*ca.* 100%) of a crude mixture of the β-keto esters **53** and **54** as a pale yellow oil; λ_{max} 5.70, 5.80 μm; its pmr spectrum was very similar to that of the crude mixture of **49** and **50** but the impurity content was lower.

A solution of the crude β-keto ester mixture (398 mg, 1.52 mmol) and *p*-toluenesulfonic acid monohydrate (40 mg, 0.210 mmol) in benzene (20 ml) was stirred and boiled under reflux under nitrogen for 12 h. The cooled, light brown solution was washed with saturated aqueous sodium bicarbonate (5 ml) and water (5 ml), dried (Na_2SO_4), and concentrated *in vacuo* (<30 °C, >100 torr) to a light brown oil. This was subjected to molecular distillation (85 °C/18 torr) affording 119 mg (47%) of a mixture of the *anti*-spirocyclopentanones **6** and **55** as a clear, colorless oil. Vapor phase chromatographic analysis (*A*, 205 °C) showed these to be in a ratio of 7:3; they were accompanied by 2% of *anti*-cyclobutanone **4**

[19]The progress of the reaction can be followed by direct ir spectroscopic inspection of aliquots of the reaction solution. Disappearance of the diazo ester (4.75, 5.85 μm, of *equal* intensity) is monitored. The Meerwein salt damages sodium chloride cavity cells; this process may be delayed by brief washing of the cells with methanol after use, followed by vacuum drying, but eventually the cells become useless. The salt also tends to plug micro syringes permanently. These must be well washed with water immediately after use.

Can. J. Chem. Downloaded from www.nrcresearchpress.com by 210.87.254.105 on 09/05/12
For personal use only.

and small amounts of three unidentified impurities (relative retention times: **4**, 5.25 min; **6**, 8.25 min; **55**, 13.5 min.

anti-Spiro[bicyclo[2.2.1]hepten-7,1'-cyclopentan]-2'-one ***(6)*** *and anti-Spiro[bicyclo[2.2.1]hepten-7,1'-cyclopentan]-3'-one* ***(55)***

A mixture of the *anti*-cyclopentanones **6** and **55** (660 mg) obtained as above was charged onto a column of silica gel (33 g) and eluted with 5% ethereal pentane. Fractions of 25 ml were collected, concentrated on the steam bath, and examined by tlc. Combination of fractions 3–9 and concentration *in vacuo* (<25 °C, >90 torr) left a colorless oil. Molecular distillation (110 °C/15 torr) afforded 294 mg (27% from *anti*-cyclobutanone **4**) of **6** as a colorless oil; *m/e* 162(98). *Anal.* calcd. for $C_{11}H_{14}O$: C 81.44, H 8.70, mw 162.1045; found: C 81.23, H 8.79, *m/e* 162.1045.

Combination of fractions 20–40 and concentration (<25 °C, >90 torr) gave a pale yellow oil. Molecular distillation (110 °C/15 torr) afforded 146 mg (13% from **4**) of **55** as a colorless oil; *m/e* 162(100).

Hydrogenation of ***6****. Formation of* ***28***

A solution of the *anti*-cyclopentanone **6** (54.2 mg, 0.334 mmol) in methanol (10 ml) was hydrogenated over Pd/C (8.5 mg) at room temperature and atmospheric pressure. After 1 h the catalyst was removed by filtration and the methanolic solution was diluted with ether (10 ml) and washed with water (2 × 10 ml), dried ($MgSO_4$), and concentrated at atmospheric pressure to yield **28** as a colorless oil (31 mg, 57%) which exhibited identical ir and pmr spectra and vpc behaviour (*A*, 208 °C) to those of the product from hydrogenation of the *syn*-cyclopentanone **5**.

7-Cyclobutylidene-1,2,3,4-tetrachloronorbornene ***(66)***

To a stirred ethereal solution (60 ml) of cyclobutylidenetriphenylphosphorane (**20**; prepared from cyclobutyltriphenylphosphonium bromide (8) (1.024 g, 2.58 mmol)) was added 1,2,3,4-tetrachloro-7-norbornenone (28) (523 mg, 2.13 mmol) in ether (6 ml); the color of the reaction mixture changed from deep red to tan brown with the precipitation of solid. The mixture was stirred overnight at room temperature, then boiled under reflux for 1.5 days. Water was added to the reaction mixture, and the aqueous phase was separated and extracted three times with chloroform. The combined ethereal and chloroform solutions were dried ($MgSO_4$) and filtered, and the solvent was evaporated to yield a brown oil that partially solidified on standing. The crude product was digested with hot benzene, the mixture was cooled and filtered, and the residue was washed with fresh benzene. Evaporation of the combined benzene filtrates gave a brown oil that partially solidified on standing. The semisolid was chromatographed on silica gel (21 g), packed in petroleum ether. Elution with petroleum ether gave in the first two fractions (*ca.* 200 ml eluate) an oil (387 mg), which was molecularly distilled (105–110 °C/1 torr) to yield **66**; λ_{max}(film) 6.29 μm; $^{H}\delta^{CCl_4}$ 1.7–2.5 (m, 6H), 2.85–3.35 (m, 4H). Two further molecular distillations (100–110 °C 0.5–1 torr) gave an analytical sample. *Anal.* calcd. for $C_{11}H_{10}Cl_4$: C 46.52, H 3.55, Cl 49.94; found: C 46.82, H 3.55, Cl 49.80.

Epoxidation of ***66****. Spiroepoxide* ***67***

To a stirred solution of the diene **66** (118 mg, 0.415 mmol) in dichloromethane (6 ml) cooled in an ice–water bath was added *m*-chloroperbenzoic acid (85%; 86.7 mg, 0.426 mmol) with swirling. The reaction mixture was warmed to room temperature and then allowed to stand for 2.5 days. The mixture was diluted with dichloromethane, and the solution was washed once with aqueous bisulfite, once with aqueous sodium bicarbonate, and once with saturated brine, and dried ($MgSO_4$). Evaporation of the solvent gave an oily residue (120 mg) that solidified after the removal of residual solvent under reduced pressure. Sublimation of the crude product (65–67 °C/0.6–0.7 torr) gave **67** as a white solid (103 mg), mp 63–72 °C. Two further sublimations (70–75 °C/0.6–0.9 torr) gave material mp 70–74.5 °C; λ_{max} 6.31 μm; $^{H}\delta^{CCl_4}$ 1.6–3.2 ppm (complex m).

Acid Treatment of ***67****. Formation of* ***69***

Treatment of **67** with boron trifluoride etherate in benzene or a saturated solution of anhydrous hydrogen bromide in chloroform for 15 min, followed by dilution of the mixture with water, extraction with chloroform, washing with aqueous 5% sodium bicarbonate, and isolation in the usual manner gave **69** as an oil; λ_{max} 2.82, 2.86 (sh), 6.24 μm; $^{H}\delta$ 1.1–1.4 (m), 2.3–2.7 (m), 6.27 (narrow m)

Epoxidation of ***56****. Epoxides* ***57*** *and* ***58***

m-Chloroperbenzoic acid (85%; 320 mg, 1.57 mmol) in dichloromethane (25 ml) was added over a period of 5 min to a stirred solution of 7-isopropylidenebenzonorbornene (29) (**56**; 262 mg, 1.42 mmol) in dichloromethane (25 ml) cooled in an ice–water bath. The solution was stirred at 0 °C for 10 min, then allowed to warm to room temperature and stirred for a further 2 h.

The reaction mixture was extracted once with aqueous 5% sodium bicarbonate, and the aqueous layer was extracted once with dichloromethane. The combined organic extracts were dried ($MgSO_4$), and the solvent was evaporated under reduced pressure to give a mixture of **57** and **58** as a solid (270 mg); the ratio of **57** to **58**, estimated approximately from the peak heights of the pmr signals at δ 1.23 and 1.32 ppm, was 6.5:1.

A mixture (625 mg) of epoxides obtained in another run was fractionally sublimed at water pump pressure. A first cut (27.5 mg) was obtained (45–50 °C/19.5 torr) that was enriched in **58**; the ratio of its pmr signals at 1.23 and 1.32 was *ca.* 1.3:1. Continued sublimation (65–68 °C/16.5 torr) gave **57** (489 mg), whose pmr spectrum showed that it was free of **58**. Crystallization from ethanol at −20 °C gave crystalline **57** (224 mg) with a wide melting range that was little sharpened by recrystallization; $^{H}\delta^{CCl_4}$ 0.9–1.5 (m, 2H), 1.23 (s, 6H), 2.0–2.4 (m, 2H), 2.83 (distorted t, J_{app} = 2 Hz, 2H), 7.07 (m, $\nu_{1/2}$ = 2 Hz, 4H).

Rearrangement of ***57****. 6,6-Dimethylbenzobicyclo[2.2.2]-octen-5-one* ***(59)*** *and 7-anti-Hydroxy-7-syn-isopropenylbenzonorbornene* ***(60)***

(i) On Basic Alumina

Epoxide **57** (149 mg) was chromatographed on a column of Woelm Activity I basic alumina (5 g) packed in carbon tetrachloride. Fractions of *ca.* 5 ml were collected with an automatic fraction collector. The first

Can. J. Chem. Downloaded from www.nrcresearchpress.com by 210.87.254.105 on 09/05/12
For personal use only.

fraction was void, and the second contained epoxide **57** (70 mg). Continued elution gave, over seven fractions (35 ml), a mixture of the alcohol **60** and the ketone **59**. Further elution (fractions 10–55; 230 ml) gave a white solid (76 mg), which was dissolved in warm hexane. Filtration of the solution, evaporation of the solvent, and three sublimations of the residue (95 °C/14–15 torr) gave **60** (40 mg) as a white solid, mp 119–126 °C: two recrystallizations from hexane gave material, mp 127–128 °C; λ_{max} 2.79, 6.07 (w), 11.05 μm; $^{H}\delta^{CCl_4}$ 1–1.3 (m, 2H), 1.46 (s, 1H), 1.65 (m, $\nu_{1/2}$ = 3 Hz, 3H), 2.1–2.4 (m, 2H), 3.11 (distorted *t*, J_{app} = 2 Hz, 2H), 4.6 (m, 1H), 4.75 (m, 1H), 6.95 (m, $\nu_{1/2}$ = 2 Hz, 4H). Resublimation of the crystalline material gave an analytical sample, mp 127–128 °C. *Anal.* calcd. for $C_{14}H_{16}O$: C 83.96, H 8.05; found: C 83.69, H 8.06.

(ii) By Pyrolysis

A small sample of epoxide **57** was sealed in a glass tube, and the tube was immersed in an oil bath at 134 °C for 1 h. The ir spectrum of the pyrolysate showed that the epoxide had been converted to the alcohol **60**.

(iii) By Boron Trifluoride Etherate

To a mixture (9 mg) of epoxides **57** and **58** in the approximate ratio of 5:1 dissolved in benzene (4 ml) was added freshly distilled boron trifluoride etherate (5 drops). The mixture was swirled and then allowed to stand at room temperature for 0.5 h. It was diluted with benzene, washed once with aqueous 5% sodium bicarbonate, once with water, and once with saturated brine, and dried ($MgSO_4$). Evaporation of the solvent gave **59** as a colorless oil (10 mg), which was purified by tlc on Eastman Chromogram Sheet (silica, with fluorescent indicator) with development with carbon tetrachloride. Ketone **59** (6 mg) was obtained as an oil from the major band; λ_{max} 5.80 μm; $^{H}\delta^{CCl_4}$ 0.70 (s, 3H), 1.20 (s, 3H), 1.3–2.3 (m, 4H), 2.9 (distorted t, J_{app} = 2 Hz, 1H), 3.45 (distorted t, J_{app} = 2 Hz, 1H), 7.15 (s, 4H). This material gave a negative iodoform test. Sublimation at water pump pressure gave a solid, mp *ca.* 41 °C. *Anal.* calcd. for $C_{14}H_{16}O$: mw 200.1201; found: *m/e* 200.1198.

*Acetylation of **56**. 7-syn-Acetyl-7-anti-isopropenylbenzonorbornene (**72**)*

To a stirred suspension of aluminum chloride (233 mg, 1.75 mmol) in dichloromethane (5 ml) was added a solution of acetyl chloride (152 mg, 1.94 mmol) in dichloromethane (5 ml): most of the aluminum chloride dissolved. The stirred solution was cooled in an ice–salt bath to *ca.* −15 °C, and to this mixture was then added 7-isopropylidenebenzonorbornene (**56**) (286 mg, 1.55 mmol) in dichloromethane (10 ml) over *ca.* 15 min. Addition of the olefin resulted in the immediate formation of a deep red-brown color. After completion of the addition the mixture was stirred at −10 °C for 5 min. It was then poured onto ice and a little concentrated hydrochloric acid, and the mixture was diluted further with dichloromethane. After the ice had melted the phases were separated, and the aqueous layer was extracted twice with dichloromethane. The combined dichloromethane solutions were washed with aqueous 5% sodium bicarbonate and dried ($MgSO_4$). Evaporation of the solvent from the filtrate gave a yellow oil (0.37 g), most of which crystallized on being seeded with crystals obtained in another run in which the crude reaction product had solidified on prolonged standing and had then been sublimed and recrystallized from ethanol. The crude product was chromatographed on a column prepared from silica gel (20 g) packed in petroleum ether. Fractions of *ca.* 25 ml were collected. After elution with 1:1 petroleum ether – benzene (15 fractions), and 1:3 petroleum ether – benzene (4 fractions), elution with benzene gave **72** in nine fractions. Evaporation of the solvent left a slightly yellow solid (168 mg), which was sublimed (80 °C/5 torr) to give **72** as a white solid (144 mg, 41%), mp 101–105 °C; crystallization from ethanol at −20 °C gave **72** (105 mg, 30%), mp 106–108 °C; λ_{max} 5.87, 6.11 (w), 7.41 (m), 11.10 μm; $^{H}\delta^{CCl_4}$ 1.0–1.2 (m, 2H), 1.72 (m, $\nu_{1/2} \simeq$ 3 Hz, 3H), 1.80 (s, 3H), 1.85–2.15 (m, 2H), 3.60 (distorted t, J_{app} = 2 Hz, 2H), 5.05 (m, 2H), 6.9–7.1 (m, 4H); *m/e* 226. *Anal.* calcd. for $C_{16}H_{18}O$: C 84.91, H 8.02; found: C 84.67, H 8.24.

*Hydrogenation of **72**. 7-syn-Acetyl-7-anti-isopropylbenzonorbornene (**73**)*

Compound **72** (210 mg) in ethyl acetate (25 ml) was hydrogenated at atmospheric pressure over platinum oxide (25 mg). Filtration of the mixture and evaporation of the solvent gave crude dihydro ketone **73** (178 mg). Recrystallization from ether at dry ice – acetone temperature, sublimation (70–85 °C/5 torr), and recrystallization from aqueous acetone gave crystalline **73**, mp 98–99.5 °C; λ_{max} 5.89, 7.19 (w), 7.28 (w), 7.37 (m) μm; $^{H}\delta^{CCl_4}$ 0.8–1.3 (m, with prominent d at 0.96, *J* = 7 Hz, 8H), 1.73 (s, 3H), 1.6–2.2 (m, 3H), 3.43 (distorted t, J_{app} = 2 Hz, 2H), 6.9–7.1 (m, 4H), *Anal.* calcd. for $C_{16}H_{20}O$: mw 228.1514; found: *m/e* 228.1514.

*Bromination of **72**. Monobromo Compound **74** and Dibromo Compound **75***

Compound **72** (3.12 g, 13.8 mmol) and *N*-bromosuccinimide (2.70 g, 15.2 mmol) in carbon tetrachloride (187 ml) were stirred and heated under reflux for 3.5 h, at which time a positive starch–iodide test was obtained. Heating was continued for a further 0.5 h, and the mixture was allowed to cool to room temperature with stirring and was then kept at 5 °C for 2 days. The mixture was filtered, and the filtrate was washed twice with water and dried ($MgSO_4$). Evaporation of the solvent gave a crystalline solid, which was recrystallized from 7:3 v/v 95% ethanol–water (80 ml) to give **74** (3.10 g, 74%), mp 85.5–90 °C, after drying *in vacuo* over potassium hydroxide pellets. Reworking the mother liquor gave a second crop (0.39 g), mp 70–83 °C, which was recrystallized from aqueous ethanol to give further **74** (0.18 g, 4%), mp 81–89 °C; λ_{max} 5.88, 6.09–6.15 (w, br) μm; $^{H}\delta^{CCl_4}$ 1.0–1.4 (m, 2H), 1.81 (s, 3H), 2.0–2.3 (m, 2H), 3.72 (distorted t, J_{app} = 2 Hz, 2H), 3.97 (narrow m, $\nu_{1/2}$ = 3 Hz, 2H), 5.54 (s, 1H), 5.76 (narrow m, $\nu_{1/2}$ = 4 Hz, 1H), 7.0–7.2 (m, 4H), *m/e* 304, 306.

A mixture of **74** (3.26 g, 10.7 mmol) and pyridinium hydrobromide perbromide (4.10 g, 12.8 mmol) in glacial acetic acid (110 ml) was stirred at room temperature for 2.25 h and then allowed to stand for an additional 4.25 h. The reaction mixture was poured into water (*ca.* 300 ml), and the aqueous mixture was extracted three times with chloroform. Water was added to the rapidly stirred combined organic extracts, and portions of solid sodium

Can. J. Chem. Downloaded from www.nrcresearchpress.com by 210.87.254.105 on 09/05/12
For personal use only.

carbonate were added until the aqueous phase was slightly basic. The chloroform layer was separated, washed once with water, and dried ($MgSO_4$). The solvent was evaporated to yield an oil (4.82 g) that solidified on seeding and removal of the last traces of solvent under suction. (Seed crystals were obtained in an earlier run in which the crude reaction product, which had partially solidified after prolonged standing, had been recrystallized from hexane). The crude solid product was dissolved in boiling hexane (200 ml), and the solution was decanted from insoluble impurities, concentrated, seeded, allowed to cool to room temperature, and then chilled at 5 °C. Filtration gave **75** as a crystalline solid (2.11 g, 51%), mp 110–131 °C; concentration of the mother liquor, seeding, and cooling gave a second crop (0.64 g, 16%), mp 109–126 °C. A sample (200 mg) of the first crop, mp 110–131 °C, was purified by preparative tlc on three silica G plates developed with benzene. The major band was isolated, and **75** (174 mg) was obtained by slurrying with dichloromethane. After one recrystallization from cyclohexane, and one from hexane at 5 °C, crystalline **75** (51 mg) was obtained as a white solid, mp 135–137 °C; $\lambda_{max}(CHCl_3)$ 5.82 μm; $^{H}\delta$ 1.1–1.4 (m, 2H), 2.0–2.3 (m, 2H), 3.84 (distorted t, J_{app} = 2 Hz, 2H), 4.00 (s, 2H), 4.03 (d, J = 1 Hz, 2H), 5.64 (s, 1H), 5.84 (t, J = 1 Hz, 1H), 7.1–7.3 (m, 4H); *m/e* 382, 384, 386 in the approximate ratio 7:12:7.

Condensation of ***75*** *with Isopropylidene Malonate* ***(76)****. Dispiro Compound* ***77***

To a stirred solution of **75** (1.00 g, 2.60 mmol) and isopropylidene malonate (30) (**76**; 0.434 g, 3.01 mmol) in acetonitrile (50 ml), cooled in an ice-water bath, was added freshly-prepared silver oxide (0.416 g, 1.79 mmol), and the mixture was allowed to warm to room temperature. Stirring was continued for 24 h, following which the black mixture was filtered, yielding an orange-brown solution. The solvent was removed, and the residue was taken up in chloroform. The chloroform solution was washed with aqueous 5% sodium bicarbonate, and the aqueous layer was washed with chloroform. The combined organic phases were dried ($MgSO_4$), and the solvent was evaporated to give a red-brown flaky solid (0.827 g).

The crude material was chromatographed on a column of silica gel (*ca.* 75 g) that had been packed in benzene. Fractions of *ca.* 100 ml each were collected. Elution with benzene (6 fractions; *ca.* 600 ml) gave 105 mg of a mixture that was not investigated further. Elution with ether (2 fractions; *ca.* 200 ml) gave a mixture (565 mg) that on crystallization from benzene gave **77** (180 mg, 19%). Samples of purified **77** did not melt sharply; decomposition began at about 200 °C, and continued over a wide range above that temperature. An analytical sample of **77** was obtained by preparative tlc of the crude reaction product, followed by two recrystallizations from benzene–cyclohexane; $\lambda_{max}(CHCl_3)$ 5.63, 5.74, 5.81 (sh), 6.09 (w), 6.23 (w) μm; $^{H}\delta$ 1.1–1.4 (m, 2H), 1.66 (s, 3H), 1.78 (s, 3H), 2.1–2.3 (m, 2H), 2.75 (s, $\nu_{1/2}$ = 2 Hz, 2H), 3.04 (s, $\nu_{1/2}$ = 3 Hz, 2H), 3.80 (distorted t, J_{app} = 2 Hz, 2H), 5.10 (s, $\nu_{1/2}$ = 2.5 Hz, 1H), 5.23 (s, $\nu_{1/2}$ = 2 Hz, 1H), 7.0–7.3 (m, 4H); *m/e* 366. *Anal.* calcd. for $C_{22}H_{22}O_5$: C 72.11, H 6.05; found: C 71.99, H 6.12.

Hydrogenation of ***77****. Dihydro Dispiro Compound* ***78***

The dispiro compound **77** (100 mg) in ethyl acetate (25 ml) was hydrogenated over platinum oxide (25 mg) at atmospheric pressure. Filtration and evaporation of the solvent gave a white solid residue, which was crystallized from benzene–cyclohexane to give **78** (66 mg); a second crop (10 mg) was obtained from the mother liquor. The combined crops were recrystallized from benzene, yielding needles that decomposed above 210 °C; $\lambda_{max}(CHCl_3)$ 5.62, 5.74, 5.82 (sh) μm; $^{H}\delta^{CCl_4}$ 1.07 (d, J = 7.5 Hz, 3H), 1.66 (s, 3H), 1.81 (s, 3H), 3.19 (d, J = 14 Hz, 1H), 3.45 (m, 1H), 3.75 (m, 1H), 7.1–7.4 (m, 4H); *m/e* 368. *Anal.* calcd. for $C_{22}H_{24}O_5$: C 71.72, H 6.57; found: C 71.59, H 6.52.

Acknowledgments

We thank the National Research Council of Canada for support of this work and Mr. Baldev Gambhir for technical assistance.

1. R. C. Cookson and N. S. Wariyar. J. Chem. Soc. 2302 (1956); H. Labhart and G. Wagnière. Helv. Chim. Acta, **42**, 2219 (1959); L. N. Ferguson and J. C. Nnadi. J. Chem. Educ. **42**, 529 (1965).
2. S. Winstein, L. de Vries, and R. Orloski. J. Am. Chem. Soc. **83**, 2020 (1961).
3. B. M. Trost and M. J. Bogdanowicz. J. Am. Chem. Soc. **95**, 5298 (1973); **95**, 5307 (1973); **95**, 5311 (1973); **95**, 5321 (1973). B. M. Trost. Acc. Chem. Res. **7**, 85 (1974).
4. P. Laszlo and P. von R. Schleyer. J. Am. Chem. Soc. **86**, 1171 (1964); E. J. Snyder and B. Frankus. J. Am. Chem. Soc. **86**, 1166 (1964).
5. R. K. Bly and R. S. Bly. J. Org. Chem. **28**, 3165 (1963).
6. L. F. Fieser and M. Fieser. Reagents for organic synthesis. Vol. 1. John Wiley and Sons, New York. 1967. pp. 646–652.
7. J. Warkentin. Can. J. Chem. **48**, 1391 (1970).
8. K. V. Scherer, Jr., and R. S. Lunt III. J. Org. Chem. **30**, 3215 (1965).
9. G. I. Poos and J. D. Rosenau. J. Org. Chem. **28**, 665 (1963).
10. R. R. Sauers and T. R. Henderson. J. Org. Chem. **39**, 1850 (1974).
11. K. B. Wiberg, B. A. Hess, Jr., and A. J. Ashe. *In* Carbonium ions. Vol. 3. *Edited by* G. A. Olah and P. von R. Schleyer. Wiley-Interscience, New York. 1972. Chapt. 26.
12. W. L. Mock and M. E. Hartman. J. Am. Chem. Soc. **92**, 5767 (1970); W. T. Tai and E. W. Warnhoff. Can. J. Chem. **42**, 1333 (1964); H. J. Liu, S. P. Majumdar, and T. Ogino. Abstracts of Papers, 57th Canadian Chemical Conference, Regina. 1974. No. 159.
13. D. Farcasiu, P. von R. Schleyer, and D. B. Ledlie. J. Org. Chem. **38**, 3455 (1973).
14. W. G. Woods, R. A. Carboni, and J. D. Roberts. J. Am. Chem. Soc. **78**, 5653 (1956).
15. H. Tanida. Acc. Chem. Res. **1**, 239 (1968).
16. P. G. Gassman and J. L. Marshall. Org. Synth. Coll. Vol. **5**, 91, 424 (1973).

17. B. RICKBORN and R. M. GERKIN. J. Am. Chem. Soc. **93**, 1693 (1971).
18. J. CASON and R. L. WAY. J. Org. Chem. **14**, 31 (1949).
19. (*a*) W. C. BAIRD, JR. J. Org. Chem. **31**, 2411 (1966); E. I. SNYDER and B. FRANZUS. J. Am. Chem. Soc. **86**, 1166 (1964); (*b*) R. RATCLIFFE and R. RODEHURST. J. Org. Chem. **35**, 4000 (1970).
20. A. MONDON. Justus Liebigs Ann. **603**, 115 (1957).
21. L. S. SILBERT, E. SIEGEL, and D. SWERN. Org. Synth. Coll. Vol. **5**, 904 (1973).
22. C. F. WILCOX, JR., and R. R. CRAIG. J. Am. Chem. Soc. **83**, 3866 (1961).
23. C. M. CIMARUSTI and J. WOLINSKY. J. Am. Chem. Soc. **90**, 113 (1968).
24. H. MEERWEIN. Org. Synth. Coll. Vol. **5**, 1080 (1973).
25. M. REGITZ, J. HOCKER, and A. LIEDHEGENER. Org. Synth. Coll. Vol. **5**, 179 (1973).
26. D. S. DEORHA and S. P. SAREEN. J. Indian Chem. Soc. **41**, 735 (1964); A. TREIBS and K. HINTERMEIER. Chem. Ber. **87**, 1163 (1954); D. S. BRESLOW, E. BAUMGARTEN, and C. R. HAUSER. J. Am. Chem. Soc. **66**, 1286 (1944); G. S. FONKEN and W. S. JOHNSON. J. Am. Chem. Soc. **74**, 831 (1952).
27. A. MCKILLOP, J. D. HUNT, F. KIENZLE, E. BIGHAM, and E. C. TAYLOR. J. Am. Chem. Soc. **95**, 3635 (1973).
28. P. E. HOCH. J. Org. Chem. **26**, 2066 (1961).
29. R. MUNEYUKI and H. TANIDA. J. Org. Chem. **31**, 1988 (1966).
30. D. DAVIDSON and S. A. BERNHARD. J. Am. Chem. Soc. **70**, 3426 (1948).
31. K. MISLOW and J. G. BERGER. J. Am. Chem. Soc. **84**, 1956 (1962).

Can. J. Chem. Downloaded from www.nrcresearchpress.com by 210.87.254.105 on 09/05/12
For personal use only.

Nitration of *p-tert*-butyltoluene in acetic anhydride. 1,2 and 1,4 adducts

ALFRED FISCHER AND ROLF RÖDERER
Department of Chemistry, University of Victoria, Victoria, B.C., Canada V8W 2Y2

Received April 8, 1976

ALFRED FISCHER and ROLF RÖDERER. Can. J. Chem. **54**, 3978 (1976).

Nitration of *p-tert*-butyltoluene in acetic anhydride gives 5-*tert*-butyl-2-methyl-2-nitro-1,2-dihydrophenyl acetate (43%), *cis*- and *trans*-1-*tert*-butyl-4-methyl-4-nitro-1,4-dihydrophenyl acetate (16%) and 4-*tert*-butyl-2-nitrotoluene (41%). Reaction of either of the 1,2 or 1,4 nitroacetoxy adducts with hydrogen chloride gives a mixture of the 1,2 and 1,4 nitrochloro adducts. The 1,2 (secondary) acetate adduct eliminates nitrous acid to form 5-*tert*-butyl-2-methylphenyl acetate under mildly acidic conditions. Under more vigorously acidic conditions 4-*tert*-butyl-2-nitrotoluene is formed. The same products are formed from the 1,4 (tertiary) acetate adducts but *p*-tolyl acetate is also obtained. The 1,2 and 1,4 adducts couple with anisole to form 5-*tert*-butyl-4′-methoxy-2-methylbiphenyl.

ALFRED FISCHER et ROLF RÖDERER. Can. J. Chem. **54**, 3978 (1976).

La nitration du *p-tert*-butyltoluène dans l'anhydride acétique conduit à l'acétate de *tert*-butyl-5 méthyl-2 nitro-2 dihydro-1,2 phényle (43%), aux acétates des *tert*-butyl-1 méthyl-4 nitro-4 dihydro-1,4 phényles *cis* et *trans* (16%) et au *tert*-butyl-4 nitro-2 toluène (41%). La réaction soit des adduits nitroacétoxy-1,2 ou -1,4 avec l'acide chlorhydrique conduit à un mélange d'adduits nitrochloro-1,2 et 1,4. L'adduit acétate 1,2 (secondaire) élimine de l'acide nitreux pour conduire à l'acétate de *tert*-butyl-5 méthyl-2 phényle dans des conditions acides très douces. Si l'on utilise des conditions plus acides, il y a formation de *tert*-butyl-4 nitro-2 toluène. Il y a formation des mêmes produits à partir des adduits acétates 1,4 (tertiaire) mais on obtient aussi l'acétate de *p*-tolyle. Les adduits 1,2 et 1,4 se couplent avec l'anisole pour former le *tert*-butyl-5 méthoxy-4′ méthyl-2 biphényle.

[Traduit par le journal]

Introduction

Addition of acetyl nitrate (as nitronium acetate) to appropriately substituted arenes, initiated by addition of the nitronium ion at an *ipso* (1) position, is well established (2–4). The present study is a continuation of our investigations of the formation and rearomatization reactions of adducts of 4-alkyltoluenes. Previous papers have dealt with *p*-xylene (5), *p*-cymene (6), and, in a preliminary communication, *p-tert*-butyltoluene (7). A distinguishing feature of this series is that the adducts are tertiary acetates. Other arenes which have been shown to give tertiary acetate adducts are 1,2,4-trimethylbenzene (pseudocumene) (8) and the tetramethylbenzenes (2). Toluene (9) and *o*-xylene (10) give secondary acetate adducts. The dominant reaction of these adducts is 1,4-elimination of nitrous acid to form the aryl acetate. This facile reaction cannot occur with tertiary acetate adducts and these have a more exotic chemistry.

Results and Discussion

Nitration and Formation of Adducts

Nitration of *p-tert*-butyltoluene in acetic anhydride gave 59% of diene adducts and 41% of 4-*tert*-butyl-2-nitrotoluene. Low-temperature chromatography of the product afforded the 4-*tert*-butyl-2-nitrotoluene, one diastereoisomer of 5-*tert*-butyl-2-methyl-2-nitro-1,2-dihydrophenyl acetate (**1**), and the separated diastereoisomers[1] of 1-*tert*-butyl-4-methyl-4-nitro-1,4-dihydrophenyl acetate (**2**).

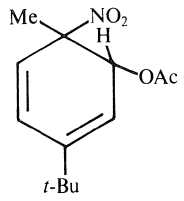

1

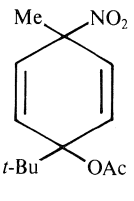

2

The 1,2 and 1,4 adduct isomers **1** and **2** were readily distinguished and identified by their nmr spectra, supported by the uv spectra. λ_{max} (200 nm) for each of the 1,4 adducts is clearly appropriate for a non-conjugated diene and close

[1]Individual members of a pair of diastereoisomeric adducts are designated as *a* and *b*.

Can. J. Chem. Downloaded from www.nrcresearchpress.com by 210.87.254.42 on 09/05/12
For personal use only.

TABLE 1. Relative gradients (gradient 1-$OCOCH_3$ = 1.00) of proton chemical shifts for diene adducts resulting from the addition of Eu([$^2H_9$]fod)$_3$

1		2*a*	
Assignment	Relative gradient	Assignment	Relative gradient
1-H	1.43	1-$C(CH_3)_3$	0.40
2-CH_3	0.23	2-H	0.92
3-H	0.26	3-H	0.44
4-H	0.20	4-CH_3	0.18
5-$C(CH_3)_3$	0.04		
6-H	0.72		

to that for other 1,4 adducts (5, 9), whereas the value for the 1,2 adduct (255 nm) is in the range expected for a conjugated diene. The ^1H spectrum of each of the 1,4 adduct-diastereoisomers exhibits the vinyl region quartet of triplets[2] integrating for four hydrogens, characteristic of an AA′ BB′ spin system in which $J_{AB} > J_{AA} \sim J_{BB} > J_{AB'}$ (11). J_{AB} is 10 Hz, diagnostic of adjacent vinyl protons. The ^{13}C spectrum of the major diastereoisomer shows only two alkene carbon absorptions, confirming the presence of two pairs of symmetry equivalent alkene carbons. Confirmation that the acetate group is *ipso* to *tert*-butyl and, therefore, that nitro is *ipso* to methyl, is provided by the effect of the shift reagent *tris*-(1,1,1,2,2,3,3-heptafluoro-7,7-[$^2H_6$]-dimethyl-4,6-[$^2H_3$]octanedionato)europium(III) {Eu([$^2H_9$]fod)$_3$}. For the major diastereoisomer the absorptions arising from the protons of the *tert*-butyl group moved faster downfield than those of the 4-methyl group, indicating that the former rather than the latter are closer to the europium, which is complexed at the acetate group (Table 1).[3]

The vinyl region of the nmr spectrum of the 1,2 adduct is quite different from that of its 1,4 isomers, the absorptions being appropriate for an ABXY spin system. The AB (J_{AB} = 10.3 Hz) and XY (J_{XY} = 5.6 Hz) parts of the spectrum appear as quartets, each half of each quartet integrating for one proton. The A lines are further split by two additional couplings of 1.2 (J_{AY}) and 0.8 Hz (J_{AX}) and thus appear as triplets.[4] The B lines are split by a 1.6 Hz coupling (J_{BX}) and appear as doublets. The X lines are split by couplings of 0.8 (J_{AX}) and 1.6 Hz (J_{BX}) and appear as quartets. The Y lines appear as doublets split by a coupling of 1.2 Hz (J_{AY}). The 10.3 Hz splitting indicates that the A and B protons are vinylic and adjacent whereas the X and Y protons must be the other vinylic and its adjacent allylic proton. The methyl group is not split and therefore is not attached to a double bond. It follows that the *tert*-butyl group must be attached to a double bond and that the adduct must have structure **1** or its locational isomer in which the positions of nitro and acetoxy groups are interchanged. The isomeric structure is unlikely on chemical grounds and, appropriately, no adduct has ever been isolated which contains a secondary nitro group.[5] Further, addition of shift reagent moved the proton absorptions downfield in the order Y > X > A > B, consistent with structure **1** and the assignments Y = 1-H, X = 6-H, A = 3-H and B = 4-H, but inconsistent with the structure of the locational isomer of **1**.

The 1,2 adduct **1**, formed in 43% yield, was the predominant diene. The 1,4 adducts were formed to the extents of 15% of **2***a* and ~1% of **2***b*. Two reasons have been suggested for the hitherto exclusive formation of 1,4-adducts (5). The greater positive charge at the *para* position of the cyclohexadienyl cation (12) should favour attack at this position and the (planar) 1,2 adduct should be destabilized by eclipsing interactions between adjacent substituents at the 1 and 2 positions. These interactions would be minimized in an appropriately puckered ring but this would require the sacrifice of some of the stabilization energy of the conjugated diene system. Attack of the nitronium ion at the *ipso* methyl position of *p*-*tert*-butyltoluene generates a cyclohexadienyl cation with a 4-*tert*-butyl substituent. Addition of acetate at the 4-position gives the 1,4 adducts. However, the addition of acetate at the 4-position should be subject to steric hindrance from the *tert*-butyl

[2]In the calculated spectrum the triplets are actually quartets. However, the central lines of each quartet are not resolved.

[3]The effect of shift reagent on the minor diastereoisomer was anomalous since the absorptions of the acetate protons moved more slowly downfield than those of *all* other protons.

[4]Each A line should appear as two pairs of doublets but the inner lines are not resolved.

[5]Loss of acetic acid from such an adduct would be extremely facile.

Can. J. Chem. Downloaded from www.nrcresearchpress.com by 210.87.254.42 on 09/05/12
For personal use only.

Can. J. Chem. Downloaded from www.nrcresearchpress.com by 210.87.254.42 on 09/05/12
For personal use only.

group[6] and the otherwise less favoured attack at the less hindered 2-position can compete. In the 1,4 adducts it is likely that there would be steric interaction between the 4-*tert*-butyl group and the *cis* nitro or methyl substituent at position 1. In the 1,2 adduct the *tert*-butyl substituent lies in a quasi equatorial position in which steric interactions should be minimized.[7]

From partial rate factors for attack at the nuclear positions of toluene (13, 14) and *tert*-butylbenzene (14) it may be calculated that attack at the nuclear positions of *p*-*tert*-butyltoluene should occur in the relative amounts 1 (*ipso* to methyl), 55%; 2, 42%; 3, 3%. The excellent agreement between calculated and observed amounts of *ipso* attack is partly fortuitous since the partial rate factors are not known with the precision that the agreement would imply. No 4-*tert*-butyl-3-nitrotoluene was obtained although the small amount expected could have escaped detection. No adducts resulting from attack of the nitronium ion *ipso* to the *tert*-butyl group were obtained, nor was any *p*-nitrotoluene formed. The position *ipso* to the *tert*-butyl group is too hindered for attack of the nitronium ion to be competitive with attack at the other nuclear positions (15). In contrast *p*-cymene does undergo attack *ipso* to the isopropyl group, both on reaction with nitric acid in acetic anhydride (6, 16) and with nitronium tetrafluoroborate in tetramethylene sulfone (15), and *p*-nitrotoluene is formed. No side-chain (benzylic) products were obtained. This is in accord with expectation since benzylic derivatives are only formed at the benzylic carbon which is *para* to the position of *ipso* attack by the nitronium ion (2, 8, 17). In *p*-*tert*-butyltoluene this is a quaternary carbon and cannot therefore be substituted by a mechanism which involves loss of a proton from this carbon (5).

Interconversion Reactions of Adducts

Tertiary acetate adducts undergo exchange of acetate for other nucleophiles when treated with the appropriate mildly acidic reagents (5, 6, 8). These reactions presumably involve the intermediate formation of the *ipso* cyclohexadienyl cation and its combination with the new nucleophile: an S_N1 (and $A_{AL}1$) reaction. Both **1** and **2** react with hydrogen chloride in ether to give a *mixture* of 1,2 and 1,4 chloronitro adducts, the intermediate cation adding chloride at the 2 and 4 positions, respectively. Reaction of the 1,4 chloronitro adducts with silver acetate in acetic acid gave a mixture of the 1,2 and 1,4 acetoxynitro adducts **1** and **2**. Adduct **2** exchanged acetate for methoxide on reaction with methanol containing sulfuric acid whereas the secondary acetate **1** formed only the aryl acetate. This is a particularly clear illustration of the greater tendency of tertiary acetate adducts to form the *ipso*-cyclohexadienyl cation by loss of acetic acid and of secondary acetate adducts to eliminate nitrous acid. Such preferences may be noted in the reactions of other secondary and tertiary acetate adducts and are further discussed, for **1** and **2**, below.

Rearomatization Reactions of Adducts

The 1,2 and 1,4 adducts of *p*-*tert*-butyltoluene provide a unique opportunity to study the rearomatization reactions of isomeric secondary and tertiary acetate adducts.

*Rearomatization of **1***

Secondary acetate 1,4 adducts readily eliminate nitrous acetate to form the aryl acetate (10). Under strongly acidic conditions protonation of the acetate group and loss of acetic acid to form the *ipso*-nitrocyclohexadienyl cation occurs. The subsequent 1,2 shift of the nitro group followed by loss of a proton yields the nitroarene (4). These are also the predominant reactions of the 1,2 adduct **1**. Thus, 5-*tert*-butyl-2-methylphenyl acetate (**3**) was the only product obtained from reaction of **1** in aqueous acetic acid, acetic acid containing 1% trifluoroacetic acid, and methanol containing 0.2% of sulfuric acid (Table 2). It was the major product, and 4-*tert*-butyl-2-nitrotoluene (**4**) the minor product, from reaction of **1** in deuterochloroform containing 20% trifluoroacetic acid, 20% titanium tetrachloride, or 20% stannous chloride. Under the more acidic conditions of deuterochloroform containing 20% aluminum chloride or 20% borontrifluoride etherate, lesser amounts of the acetate were

[6]Steric hindrance to attack at the position *ipso* to *tert*-butyl is shown by the absence of any products resulting from such attack by nitronium ion in the nitration reaction (see below). The *ipso tert*-butyl position should be as activated as the *ipso* methyl position.

[7]Both a kinetic and a thermodynamic argument are offered to explain the general preference for 1,4 addition and the specific preference for 1,2 addition in the case of *p*-*tert*-butyltoluene. It is not known whether adduct formation is subject to kinetic or product-development control.

TABLE 2. Yields(%) of products[a] of rearomatization of adducts of *p-tert*-butyltoluene

	Substrate **1**			Substrate **2***a*			
Reagent/conditions	**3**	**4**	Other	**3**	**4**	**5**	Other
CD_3CO_2D (reflux)	100			19	14	67	
10% D_2O in CD_3CO_2D	100			17		83	
1% CF_3CO_2H in CD_3CO_2D	100			87	7	6	
20% CF_3CO_2H in $CDCl_3$	77	23		11	78	11	
20% $SnCl_2$ in $CDCl_3$	96	4		30	52	18	
20% $TiCl_4$ in $CDCl_3$	91	7		9	33		58[b]
20% $AlCl_3$ in $CDCl_3$	15	64	21[b]	4	68	4	24[b]
20% $BF_3 \cdot Et_2O$ in $CDCl_3$	17	83		3	89	8	
0.2% H_2SO_4 in CD_3OD	100						100[c]
10% $BF_3 \cdot Et_2O$ in anisole		30	70[d]		10		90[d]
4% $NaOCH_3$ in CD_3OD	37		63[e]				100[f]
Thermolysis	36		64[g]	12		24	64[g]

[a]5-*tert*-Butyl-2-methylphenyl acetate (**3**); 4-*tert*-butyl-2-nitrotoluene (**4**); *p*-tolyl acetate (**5**).
[b]4-*tert*-Butyl-2-chlorotoluene.
[c]Methoxynitro diene adducts.
[d]5-*tert*-Butyl-4′-methoxy-2-methylbiphenyl.
[e]5-*tert*-Butyl-2-methylphenol.
[f]1-*tert*-Butyl-4-methyl-4-nitro-1,4-dihydrophenol.
[g]*p-tert*-Butyltoluene; thermolysis of **2***b* gave 63% *p-tert*-butyltoluene, 4% **3**, 20% **5**, and 13% of an unidentified product.

obtained and the nitroarene became the major product. All of these observations are in accord with the picture of two competing reactions, one involving the elimination of nitrous acid and the other, favoured at high acidities, involving elimination of acetic acid accompanied by migration of the nitro group. The reaction with borontrifluoride in anisole, which led to 5-*tert*-butyl-4′-methoxy-2-methylbiphenyl, is also a reaction of the *ipso*-nitrocyclohexadienyl cation (18). A similar pathway could account for the formation of 4-*tert*-butyl-2-chlorotoluene in the reaction with aluminum chloride. In this case the *ipso*-nitrocyclohexadienyl cation is intercepted by a chloride ion to give the chloronitro 1,2 adduct. Elimination of nitrous acid gives the chloroarene. Reaction of **1** with sodium methoxide in methanol resulted in the elimination of nitrous acid and partial hydrolysis so that both 5-*tert*-butyl-2-methylphenyl acetate and the corresponding phenol were formed.

Thermolysis of **1** gave *p-tert*-butyltoluene and the aryl acetate. Clearly thermolysis involves a different mechanism from those of the reactions in solution. Thermolysis of the chloronitro 1,2 adduct gave a mixture of 4-*tert*-butyl-2-nitrotoluene and 4-*tert*-butyl-2-chlorotoluene.

Rearomatization of **2**

The typical rearomatization reactions of tertiary acetate adducts are the formation of nitroarene by a mechanism similar to that described for the secondary acetate adducts, formation of side-chain (benzylic) derivatives, and formation of aryl acetate by 1,2 migration of the acetoxy group accompanied by the elimination of nitrous acid. Side-chain derivatives are formed only at the α carbon of the alkyl group *ipso* to acetate in the adduct (8). No such products were obtained from **2** since this α carbon is a quaternary carbon. 5-*tert*-Butyl-2-methylphenyl acetate (**3**) 4-*tert*-butyl-2-nitrotoluene (**4**), and *p*-tolyl acetate (**5**) were obtained on rearomatization of **2** under most conditions (Table 2). Under comparable conditions **2** gave relatively more **4** and less **3** than did **1**. This is not surprising since formation of **3** from **1** involves the simple 1,2 elimination of nitrous acid, whereas formation of **3** from **2** is a more complicated and slower process involving migration of the acetate group as well as elimination of nitrous acid. Furthermore, formation of the nitroarene **4** should be faster in **2**, involving ionization of a tertiary centre, than in **1**, where ionization occurs at a secondary centre. What is surprising is that **2** gives the same acetate as **1**, *i.e.* that there is a 1,3 migration of the acetate group rather than a 1,2 shift. In the tertiary acetate adducts previously studied only 1,2 acetate shifts were observed. One possible explanation for the formation of **3** from **2** is that **2** is first converted

Can. J. Chem. Downloaded from www.nrcresearchpress.com by 210.87.254.42 on 09/05/12
For personal use only.

Can. J. Chem. Downloaded from www.nrcresearchpress.com by 210.87.254.42 on 09/05/12
For personal use only.

into **1** which then eliminates nitrous acid to form **3**. An attractive hypothesis would make **1** and **2** inconvertible through the reversible formation of the *ipso*-nitrocyclohexadienyl cation. However, the reversible process does not occur under the conditions of rearomatization investigated since the product distributions were quite different from **1** and **2** (Table 2). Moreover, the aryl acetate isolated on rearomatization of **1** in perdeuteroacetic acid did not contain [$^2H_3$]-acetate, as the reversible interconversion of **1** and **2** would require. In the reactions carried out in acetic acid containing trifluoroacetic acid traces of **1** were evident in the nmr spectrum of the rearomatizing **2**, but **2** was not detected when **1** was rearomatized. Thus, at least under these conditions, **2** could form **3** via **1**. An alternative pathway for the conversion of **2** to **3** involves a 1,3 acetate shift in the *ipso*-acetoxycyclohexadienyl cation formed by ionization of nitrite anion.[8] 1,3 Acetate bridging occurs facilely in saturated 6-membered rings (19). In the cation the preference for the 1,3 shift, rather than the expected 1,2 shift, may be attributed to the transition state steric interactions involving the bulky *tert*-butyl group being smaller for the 1,3 shift.

The *p*-tolyl acetate formed on rearomatization of **2** is formally obtained by the elimination of *tert*-butyl nitrite. The mechanism likely involves the loss of nitrite anion and *tert*-butyl cation. It is the relative stability of the *tert*-butyl cation which accounts for this process appearing in the case of **2** when it is not observed with other tertiary adducts previously studied.

The formation of 4-*tert*-butyl-2-chlorotoluene, which occurs in the reactions with titanium and aluminum chlorides, can be understood in terms of the generation of the *ipso*-nitrocyclohexadienyl cation, its recombination with chloride at the 2 position and the elimination of nitrous acid from the secondary chloride adduct. Formation of 5-*tert*-butyl-4′-methoxy-2-methylbiphenyl on reaction of **2** with borontrifluoride in anisole likewise involves the combination of the *ipso*-nitrocyclohexadienyl cation with a nucleophile (anisole) at the 2-position. In the reactions involving formation of the *ipso*-nitrocyclohexadienyl cation the nitroarene **4** is also obtained since the nitro group migration in the cation is competitive with other reactions of the cation.

Reaction of **2** with sodium methoxide in methanol resulted in hydrolysis at the acetate group ($B_{AC}2$ mechanism) to form the hydroxy-nitro adduct, which slowly lost the elements of *tert*-butylnitrite to form *p*-cresol. This is an interesting contrast to the reaction of the *p*-cymene adduct, which resulted in a 1,2 shift of the isopropyl group and the formation of 2-isopropyl-4-methylphenol. The *tert*-butyl group is less prone to migrate than to eliminate. In the transition state for the migration the tertiary carbon would have three full and two partial bonds, an unlikely situation resembling an S_N2 type substitution. In the transition state for the elimination the tertiary carbon would have three full and one partial bond, a situation resembling an S_N1 type substitution and correspondingly favoured.

Experimental

General experimental methods have been described previously (2). *p*-Tolyl acetate was obtained by acetylation of *p*-cresol; nmr ($CDCl_3$) τ 2.90 (d, 2, 2-*H* and 6-*H*), 3.08 (d, 2, 3-*H* and 5-*H*), 7.72 (s, 3, 4-C*H*$_3$), 7.80 (s, 3, OCO-C*H*$_3$). 2-Chloro-4-*tert*-butyltoluene was prepared by reduction of 2-nitro-4-*tert*-butyltoluene (see below) to 2-methyl-5-*tert*-butylaniline which was in turn diazotized and reacted with cuprous chloride. 2-Methyl-5-*tert*-butylphenol was obtained by hydrolysis of the diazotized aniline and had the same retention time on gas–liquid chromatography as the phenol obtained by hydrolysis of 2-methyl-5-*tert*-butylphenyl acetate (see below) followed by chromatography on silica gel, and which had nmr $CDCl_3$ τ 2.97 (d, 1, 3-*H*), 3.13 (d of d, 1, 4-*H*), 3.19 (d, 1, 6-*H*), 4.46 (O*H*), 7.80 (s, 3, 2-C*H*$_3$), 8.36 (s, 9, C(C*H*$_3$)$_3$).

Nitration of p-tert-Butyltoluene in Acetic Anhydride

Preliminary nmr tube experiments indicated that the most favourable reaction temperature was 0 °C when 59% of adducts and 41% of substitution products were formed after 15 min. A cold solution of nitric acid (15.8 cm^3, 0.38 mol) in acetic anhydride (50 cm^3) was slowly added with stirring to *p*-*tert*-butyltoluene (37 g, 0.25 mol) in acetic anhydride (100 cm^3) at −70 °C. The solution was allowed to warm to 0 °C, held at that temperature for 20 min, and cooled again to −70 °C. Ether (100 cm^3) was added and ammonia condensed into the stirred solution. Excess ammonia was removed with an aspirator, and the mixture quenched with ice water. The ether extract was washed and dried ($MgSO_4$) and the ether evaporated at 14 °C to give a brown oil (64 g). Integration of the nmr spectrum of the crude reaction mixture revealed the presence of 60% of diene adducts.

Chromatography of the oil (30 g) at −45 °C on 3% deactivated alumina and elution with pentane and 10%

[8]P. C. Myhre (personal communication) has proposed an E1 mechanism, involving initial ionization of nitrite, for the formation of aryl acetates from secondary acetate adducts.

Can. J. Chem. Downloaded from www.nrcresearchpress.com by 210.87.254.42 on 09/05/12
For personal use only.

ether–pentane gave 2-nitro-4-*tert*-butyltoluene (8.1 g, 42 mmol); ir (film) 1530 and 1350 (NO_2); nmr ($CDCl_3$) τ 2.04 (d, 3-*H*), 2.60 (d of d, J_{35} = 3 Hz, J_{56} = 8.3 Hz, 5-*H*), 2.76 (d, 6-*H*), 7.50 (s, CH_3), 8.68 (s, $C(CH_3)_3$. Elution with 20% and 30% ether–pentane yielded a mixture (13.6 g, 0.13 mol) of two adducts which were separated by fractional crystallization in pentane and ether–pentane. The adduct formed in greater amount was eluted more rapidly. It was 5-*tert*-butyl-2-methyl-2-nitro-1,2-dihydrophenyl acetate (**1**), mp 51–52 °C; uv (CH_3OH) 255 (580), 203 nm (820 m^2 mol^{-1}); ir (Nujol) 1745 and 1265 ($OCOCH_3$), 1550 cm^{-1} (NO_2); nmr ($CDCl_3$) τ 3.62 (m, 1, 3-H), 3.76 (d of d, 1, 4-*H*), 4.26 (m, 1, 6-*H*), 4.47 (d of d, 1, 1-*H*), (J_{13} = 1.2, J_{16} = 5.6, J_{34} = 10.3, J_{36} = 0.8, J_{46} = 1.6 Hz), 8.05 (s, 3, $OCOCH_3$), 8.33 (s, 3, CH_3), 8.93 (s, 9, $C(CH_3)_3$; ^{13}C nmr ($CDCl_3$) δ_C (TMS) 21 ($OCOCH_3$), 24 (2-CH_3), 28 ($C(CH_3)_3$), 34 ($C(CH_3)_3$), 71 (*C*-1), 88 (*C*-2), 114 (*C*-6), 125 (*C*-4), 127 (*C*-3), 147 (*C*-5), 169 ppm ($OCOCH_3$); mass spectrum (chemical ionization, methane) *m/e* (relative intensity) 207(5, $M - NO_2$), 194(20, $M - OCOCH_3$), 151(90), 148(100, $M - CH_3COONO_2$), 133(60), 109(15). *Anal.* calcd. for $C_{13}H_{19}NO_4$: C 61.64, H 7.56, N 5.35; found: C 61.72, H 7.62, N 4.96.

The second adduct, one diastereoisomer of 1-*tert*-butyl-4-methyl-4-nitro-1,4-dihydrophenyl acetate (**2***a*), had mp 82–83 °C (ether–pentane); uv (CH_3OH) 200 nm (1450 m^2 mol^{-1}); ir (Nujol) 1750 and 1260 ($OCOCH_3$), 1550 cm^{-1} (NO_2); nmr ($CDCl_3$) τ 3.79 (d, 2, J_{23} = 10.3 Hz, 3-*H* and 5*H*), 2.97 (d, 2, 2-*H* and 6-*H*), 8.02 (s, 3, $OCOCH_3$), 8.25 (s, 3, 4-CH_3), 9.07 (s, 9, $C(CH_3)_3$); ^{13}C nmr ($CDCl_3$) δ_C (TMS) 22 ($OCOCH_3$), 25 ($C(CH_3)_3$), 26 (4-CH_3), 39 ($C(CH_3)_3$), 79 (*C*-1), 85 (*C*-4), 128 (*C*-2 and *C*-6), 131 (*C*-3 and *C*-5) 170 ppm ($OCOCH_3$); mass spectrum (chemical ionization) *m/e* (relative intensity) 207(1, $M - NO_2$), 194(2, $M - OCOCH_3$), 151(100), 148(12, $M - CH_3COONO_2$), 109(3). *Anal.* calcd. for $C_{13}H_{19}NO_4$: C 61.64, H 7.56, N 5.35; found: C 61.26, H 7.51, N 5.32.

Further elution with 40% and 60% ether–pentane gave pure diene **2***a* (1.4 g, 6 mmol) and in the 70% fraction, the other diastereoisomer of 1-*tert*-butyl-4-methyl-4-nitro-1,4-dihydrophenyl acetate (**2***b*, 0.3 g, 1 mmol), mp 132–135 °C ($CHCl_3$–pentane); uv (CH_3OH) 200 nm (1580 m^2 mol^{-1}); ir (Nujol) 1745 and 1265 ($OCOCH_3$), 1550 (NO_2), 1020 cm^{-1}; nmr ($CDCl_3$) τ 2.66 (d, 2, J_{23} = 10.6 Hz, 3-*H* and 5-*H*), 2.96 (d, 2, 2-*H* and 6-*H*), 8.05 (s, 3, $OCOCH_3$), 8.30 (s, 3, CH_3), 9.04 (s, 9, $C(CH_3)_3$); mass spectrum (chemical ionization, methane) *m/e* (relative intensity) 194(6, $M - OCOCH_3$), 151(100), 148(30, $M - CH_3COONO_2$), 109(5). Anal. calcd. for $C_{13}H_{19}NO_4$: C 61.64, H 7.56, N 5.35; found: C 61.24, H 7.55, N 5.12.

4-tert-Butyl-2-chloro-1-nitro-1,2-dihydrotoluene and 4-tert-Butyl-4-chloro-1-nitro-1,4-dihydrotoluene

Adduct **2** was added slowly to a solution of hydrogen chloride in ether and the solution stirred at ambient temperature for 30 min. After evaporation of ether and excess hydrogen chloride under reduced pressure the nmr of the residue showed that exchange of chloride for acetate had occurred and that both 1,2 and 1,4 type adducts were present in approximately equal amounts. The 1,2 nitroacetoxy adduct **1** also reacted with hydrogen chloride in ether to give a mixture of 1,2 and 1,4 chloronitro adducts together with 5-*tert*-butyl-2-methylphenyl acetate (30%). Adduct **1** was less reactive than adduct **2** and it was necessary to bubble hydrogen chloride continuously through the solution in order to complete the reaction in 3 h. Fractional crystallization of the chloronitro adduct mixture from pentane gave each isomer contaminated by only a minor amount of the other.

4-*tert*-Butyl-2-chloro-1-nitro-1,2-dihydrotoluene had nmr ($CDCl_3$) τ 3.43 (d of q, 6-*H*), 3.69 (d of d, 5-*H*), 4.18 (d of q, 3-*H*), 5.09 (d of d, 2-*H*), (J_{23} = 6.3, J_{25} = 1.7, J_{35} = 1.9, J_{36} = ~1, J_{56} = 10 Hz), 8.28 (s, 1-CH_3), 8.90 (s, $C(CH_3)_3$).

4-*tert*-Butyl-4-chloro-1-nitro-1,4-dihydrotoluene had ir (Nujol) 1540 cm^{-1} (NO_2); nmr ($CDCl_3$) τ 3.68 (d, J = 10.5 Hz, 2-*H* and 6-*H*), 3.88 (d, J = 10.5 Hz, 3-*H* and 5-*H*), 8.23 (s, 1-CH_3), 8.91 (s, $C(CH_3)_3$). *Anal.* calcd. for $C_{11}H_{16}ClNO_2$: C 57.52, H 7.02, N 6.10; found: C 57.40, H 7.10, N 6.03.

Reaction of the 1,4 nitrochloro adduct with an equimolar amount of silver acetate in [$^2H_4$]acetic acid gave a mixture of [$^2H_3$]-**1** (40%) and [$^2H_3$]-**2** (60%).

Reaction of Adducts with Acetic Acid

A solution of diene **1** (100 mg) in [$^2H_4$]acetic acid (0.5 cm^3) was heated for 0.5 h in a boiling water bath. Decomposition started immediately as indicated by evolution of brown fumes of nitrogen dioxide. After work-up 5-*tert*-butyl-2-methylphenyl acetate was obtained and identified by nmr and glc. No [$^2H_4$]acetate was incorporated.

Diene **2** decomposed more slowly under these conditions. Fumes of nitrogen dioxide appeared after about 10 min. After work-up the nmr and glc showed 67% *p*-tolyl acetate, 19% 5-*tert*-butyl-2-methylphenyl acetate, and 14% 4-*tert*-butyl-2-nitrotoluene. The identity of the compounds was confirmed by glc – mass spectrometry.

Reaction of Adducts with Aqueous Acidic Acid

The nmr spectrum of a solution of diene **1** (100 mg) in [$^2H_4$]acetic acid (0.5 cm^3) and water (0.05 cm^3) was recorded at intervals over a period of 1 h. The half time of the decomposition was about 20 min and the only product formed was 5-*tert*-butyl-2-methylphenyl acetate, identified after work-up by nmr and glc. No [$^2H_4$]acetate was incorporated.

Under the same conditions diene **2***a* decomposed very slowly with a half time of about 48 h. The reaction was complete after 1 week and the products were 83% *p*-tolyl acetate and 17% 5-*tert*-butyl-2-methylphenyl acetate.

Reaction of Adducts in Acetic Acid Containing Trifluoroacetic Acid

A solution of diene **1** (100 mg) in [$^2H_4$]acetic acid (0.5 cm^3) was treated with successive amounts (20 mm^3) of a 30% solution of trifluoroacetic acid in [$^2H_4$]acetic acid and the nmr spectrum recorded after each addition. The only decomposition product was 5-*tert*-butyl-2-methylphenyl acetate, confirmed by glc.

Diene **2***a* decomposed under these conditions much more slowly into 87% 5-*tert*-butyl-2-methylphenyl acetate, 6% *p*-tolyl acetate, and 7% 4-*tert*-butyl-2-nitrotoluene.

Reaction of Adducts with Trifluoroacetic Acid

A solution of diene **1** (100 mg) in $CDCl_3$ (0.5 cm^3) was cooled to −78 °C and trifluoroacetic acid (0.1 cm^3)

Can. J. Chem. Downloaded from www.nrcresearchpress.com by 210.87.254.42 on 09/05/12
For personal use only.

added. The mixture was allowed to warm up to room temperature and fumes of NO_2 developed. After work-up nmr and glc showed 77% 5-*tert*-butyl-2-methylphenyl acetate and 23% 4-*tert*-butyl-2-nitrotoluene.

Under the same conditions diene **2***a* yielded a mixture of 11% 5-*tert*-butyl-2-methylphenyl acetate, 11% *p*-tolyl acetate, and 78% 4-*tert*-butyl-2-nitrotoluene.

Reaction of Adducts with Lewis Acids

Reaction with Stannous Chloride

A solution of diene **1** (100 mg) in $CDCl_3$ (0.5 cm^3) was treated with powdered $SnCl_2$ (100 mg) and kept at 35 °C overnight after which time the decomposition was completed into 96% 5-*tert*-butyl-2-methylphenyl acetate and 4% 4-*tert*-butyl-2-nitrotoluene. The product from diene **2***a* on ms–glc at 140–200 °C on SE 30 showed peaks in the following order: 18% *p*-tolyl acetate (M^+ 150), 30% 5-*tert*-butyl-2-methylphenyl acetate (M^+ 206), 52% 4-*tert*-butyl-2-nitrotoluene (M^+ 193).

Reaction with Titanium Tetrachloride

A solution of diene **1** (100 mg) in $CDCl_3$ (0.5 cm^3) was cooled to −78 °C and neat $TiCl_4$ (0.1 cm^3) added. After warming to room temperature and work-up 91% 5-*tert*-butyl-2-methylphenyl acetate and 9% 4-*tert*-butyl-2-nitrotoluene were identified by glc and nmr.

Under the same conditions diene **2***a* decomposed into 9% 5-*tert*-butyl-2-methylphenyl acetate, 33% 4-*tert*-butyl-2-nitrotoluene and 58% 4-*tert*-butyl-2-chlorotoluene, characterized by nmr, glc, and ms–glc. On ms–glc at 140–200 °C on SE 30 peaks appeared in the following order: 4-*tert*-butyl-2-methylphenyl acetate (M^+ 206), 4-*tert*-butyl-2-nitrotoluene (M^+ 193). The spectrum of the 4-*tert*-butyl-2-chlorotoluene peak was identical with that of an authentic sample.

Reaction with Aluminum Chloride

A solution of diene **1** (100 mg) in $CDCl_3$ (0.5 cm^3) was treated at room temperature with powdered $AlCl_3$ (100 mg). The product was 15% 5-*tert*-butyl-2-methylphenyl acetate, 64% 4-*tert*-butyl-2-nitrotoluene, and 21% 4-*tert*-butyl-2-chlorotoluene.

Diene **2***a* gave 4% 5-*tert*-butyl-2-methylphenyl acetate, 4% *p*-tolyl acetate, 68% 4-*tert*-butyl-2-nitrotoluene, and 24% 4-*tert*-butyl-2-chlorotoluene.

Reaction with Boron Trifluoride

A solution of diene **1** (100 mg) in $CDCl_3$ (0.5 cm^3) was cooled to −78 °C and treated with boron trifluoride etherate (0.1 cm^3) and warmed to room temperature. After work-up the mixture was found to consist of 17% 5-*tert*-butyl-2-methylphenyl acetate and 83% 4-*tert*-butyl-2-nitrotoluene.

Diene **2***a* gave 3% 5-*tert*-butyl-2-methylphenyl acetate, 8% *p*-tolyl acetate, and 89% 4-*tert*-butyl-2-nitrotoluene.

Reaction of Adducts in Methanol Containing Sulfuric Acid

Sulfuric acid (1 mm^3) was added to a solution of diene **1** (100 mg) in [$^2H_4$]methanol (0.5 cm^3). Only 5-*tert*-butyl-2-methylphenyl acetate was formed

When diene **2***a* was reacted under similar conditions, the AB pattern of the olefinic protons changed, indicating the formation of the *cis*- and *trans*-1-*tert*-butyl-4-methyl-4-nitro-1,4-dihydro phenyl methyl ethers in a 1:1 ratio.

Reaction of Adducts with Boron Trifluoride in Anisole: 5-tert-Butyl-4′-methoxy-2-methylbiphenyl

Boron trifluoride etherate (0.2 cm^3) was added to a solution of diene **1** (0.5 g) in anisole (2 cm^3) at −78 °C. The mixture turned dark brown and on warming to room temperature, bright blue. After work-up and evaporation of the excess anisole there was obtained a mixture of 30% 4-*tert*-butyl-2-nitrotoluene and 70% 5-*tert*-butyl-4′-methoxy-2-methylbiphenyl, nmr ($CDCl_3$) τ 2.68–3.15 (m, 7, Ar*H*), 6.18 (s, 3, OCH_3), 7.78 (s, 3, CH_3), 8.68 (s, 9, C(CH_3)$_3$; *m/e* 254.170 (M_r ($^{12}C_{18}{}^1H_{22}{}^{16}O$) 254.167).

When diene **2***a* in anisole was treated with borontrifluoride etherate, 10% of 4-*tert*-butyl-2-nitrotoluene and 90% of the biphenyl were formed.

*Reaction of Adduct **2***a* with Boron Trifluoride in Mesitylene*

Boron trifluoride etherate (0.1 cm^3) was added to a solution of diene **2***a* (0.1 g) in mesitylene (1 cm^3) at −78 °C and the mixture allowed to warm to room temperature. After work-up tlc showed that 4-*tert*-butyl-2-nitrotoluene had been formed and no biphenyl coupling product could be detected.

Reaction of Adducts with Sodium Methoxide in Methanol

A solution of diene **1** (100 mg) in [$^2H_4$]methanol (0.5 cm^3) was treated with an equimolar amount of sodium methoxide (20.5 mg). The mixture turned at once bright orange. The diene was decomposed after 45 min into two compounds, which, after work-up, were identified by nmr, glc, and ms–glc to be 37% 5-*tert*-butyl-2-methylphenyl acetate and 63% 5-*tert*-butyl-2-methylphenol.

Diene **2***a* was converted by sodium methoxide after 45 min completely into the 1-*tert*-butyl-4-methyl-4-nitro-1,4-dihydrophenol which, after further addition of sodium methoxide, (20.5 mg), decomposed in two weeks into *p*-cresol as shown by glc and nmr comparison with an authentic sample; nmr ($CDCl_3$) τ 3.24 (d, 2, 2-*H* and 6*H*), 3.04 (d, 2, 3-*H* and 5-*H*), 4.42 (s, O*H*), 7.76 (s, 3, CH_3).

Pyrolysis of the Adducts

A 1% solution of diene **1** in acetone was injected into the inlet of a gas chromatograph at 260 °C. The products were 64% 4-*tert*-butyltoluene and 36% 5-*tert*-butyl-2-methylphenyl acetate, identified by injection of authentic samples and comparison of the retention times.

Diene **2***a* gave under the same conditions three products: 64% 4-*tert*-butyltoluene, 12% 5-*tert*-butyl-2-methylphenyl acetate, and 24% *p*-tolyl acetate.

Diene **2***b* decomposed into four compounds: 63% *p*-*tert*-butyltoluene, 4% 5-*tert*-butyl-2-methylphenyl acetate, 20% *p*-tolyl acetate, and 13% of an unidentified product.

The 1,2 chloronitro adduct gave 4-*tert*-butyl-2-chlorotoluene (39%) and 4-*tert*-butyl-2-nitrotoluene (61%).

1. C. L. Perrin and G. A. Skinner. J. Am. Chem. Soc. **93**, 3389 (1971).
2. A. Fischer and D. R. A. Leonard. Can. J. Chem. **54**, 1795 (1976) and references cited therein.
3. M. W. Galley and R. C. Hahn. J. Am. Chem. Soc. **96**, 4337 (1974).
4. P. C. Myhre. J. Am. Chem. Soc. **94**, 7921 (1972).

5. A. FISCHER and J. N. RAMSAY. Can. J. Chem. **52** 3960 (1974).
6. A. FISCHER and R. RÖDERER. Can. J. Chem. **54**, 423 (1976).
7. A. FISCHER and R. RÖDERER. J. Chem. Soc. Chem. Commun. 798 (1975).
8. A. FISCHER and J. N. RAMSAY. J. Am. Chem. Soc. **96**, 1614 (1974); J. N. RAMSAY. Ph.D. Thesis, University of Victoria, Victoria, B.C. 1973.
9. A. FISCHER and J. N. RAMSAY. J. Chem. Soc. Perkin Trans. II, 237 (1973).
10. D. J. BLACKSTOCK, A. FISCHER, K. E. RICHARDS, J. VAUGHAN, and G. J. WRIGHT. Chem. Commun. 641 (1970); D. J. BLACKSTOCK, J. CRETNEY, A. FISCHER, M. P. HARTSHORN, K. E. RICHARDS, J. VAUGHAN, and G. J. WRIGHT. Tetrahedron Lett. 2793 (1970).
11. F. A. BOVEY. Nuclear magnetic resonance spectroscopy. Academic Press, New York, N.Y. 1969. pp. 122–125 and 336.
12. C. MACLEAN and E. L. MACKOR. Mol. Phys. **4**, 241 (1961).
13. A. FISCHER and G. J. WRIGHT. Aust. J. Chem. **27**, 217 (1974).
14. J. R. KNOWLES, R. O. C. NORMAN, and G. K. RADDA. J. Chem. Soc. 4485 (1960).
15. G. A. OLAH and S. J. KUHN. J. Am. Chem. Soc. **86**, 1067 (1964).
16. R. C. HAHN and D. L. STRACK. J. Am. Chem. Soc. **96**, 4335 (1974).
17. D. J. BLACKSTOCK, A. FISCHER, K. E. RICHARDS, and G. J. WRIGHT. Aust. J. Chem. **26**, 775 (1973).
18. A. FISCHER and C. C. GREIG. J. Chem. Soc. Chem. Commun. 50 (1974).
19. J. W. BLUNT, M. P. HARTSHORN, and D. N. KIRK. Chem. Ind. 1955 (1963).

Can. J. Chem. Downloaded from www.nrcresearchpress.com by 210.87.254.42 on 09/05/12
For personal use only.

Ethyl 4-iodo-2,3,4-trideoxy-α-D-*threo*-hex-2-enopyranoside: synthesis and dehydroiodination[1]

MARK BERNARD YUNKER[2] AND BERT FRASER-REID

Guelph–Waterloo Centre for Graduate Work in Chemistry, Waterloo Campus, Department of Chemistry, University of Waterloo, Waterloo, Ont., Canada N2L 3G1

Received December 17, 1975[3]

MARK BERNARD YUNKER and BERT FRASER-REID. Can. J. Chem. **54**, 3986 (1976).

Iodinolysis of ethyl 6-*O*-benzoyl-4-*O*-methylsulfonyl-2,3-dideoxy-α-D-*erythro*-hex-2-enopyranoside in the presence of pyridine gives the expected product of inversion, *viz.* the 4-iodo-2,3,4-trideoxy-α-D-*threo* congener (**8**). If, however, the pyridine is omitted, **8** rearranges to give ethyl 6-iodo-4-*O*-benzoyl-2,3,6-trideoxy-α-D-*erythro*-hex-2-enopyranoside. Reduction of **8** with lithium aluminum deuteride takes three courses: allylic deuterolysis in the expected S_N2' sense, deuterolysis at C-4 with retention of configuration, and a ring opening reaction giving deuterated hexa-2,4-dien-1,6-diol. Dehydroiodination of **8** with diazabicyclononene gave 1-benzoloxy-6-ethoxy-3(*E*),5(*Z*)-hexadiene-2-one in 86% yield.

MARK BERNARD YUNKER et BERT FRASER-REID. Can. J. Chem. **54**, 3986 (1976).

L'iodinolyse du 6-*O*-benzoyl-4-*O*-méthylsulfonyl-2,3-didéoxy-α-D-*érythro*-hex-2-énopyrannoside d'éthyle en présence de pyridine conduit au produit d'inversion attendu à savoir la congénère 4-iodo-2,3,4-tridéoxy-α-D-*thréo* (**8**). Si toutefois on omet la pyridine, **8** se réarrange pour conduire à la 6-iodo-4-*O*-benzoyl-2,3,6-tridéoxy-α-D-*érythro*-hex-2-énopyrannoside d'éthyle. La réduction de **8** par LAD conduit à trois types de réaction: une deutérolyse allylique suivant un mécanisme S_N2', la deutérolyse en C-4 avec rétention de configuration et une réaction d'ouverture du cycle conduisant à l'hexadiène-2,4 diol-1,6 deutéré. La déhydroiodination de **8** par le diazabicyclononène conduit à la benzoloxy-1 éthoxy-6 hexadiène-3(*E*),5(*Z*) one-2 avec un rendement de 86%.

[Traduit par le journal]

The use of carbohydrate derivatives as chiral synthons for the synthesis of optically active natural products is an area of interest in these laboratories (1) and in connection with these studies we wished to prepare the optically-active 2*H*-pyran **1**. Normally 2*H*-pyrans readily undergo cycloreversion to the related dienones (*e.g.* **2**) except when a 4-alkyl substituent (*e.g.* in **3**) is present, in which case the cyclic isomer becomes the stable entity. This generalization follows from extensive studies by Dreux and co-workers (2), and is based on systems (**3** ⇆ **4**) in which the substituents are all alkyl. The molecule of interest to us, **1**, is an acetal, and we wondered whether this structural feature would affect the position of equilibrium between **1** and **2**.[4] In this paper we describe our efforts directed toward this objective, and also report on the unexpected behavior of some of the intermediates encountered in this study.

	W	X	Y	Z	
1	CH_2OBz	H	H	OEt	**2**
3	alkyl	alkyl	alkyl	alkyl	**4**

The molecule sought as the precursor of **1** was the iodide **8** which we attempted to prepare (Scheme 1) by iodinolysis of the mesylate **7**, the latter being obtained from the diol **5** via the monobenzoate **6**. Treatment of **7** with sodium iodide in methyl ethyl ketone gave rise to two products, R_f 0.48 and 0.56, in the ratio of 3:1. These were separated chromatographically, and characterized as **8** and **12** respectively.

[1]Taken from the Ph.D. Thesis of M.B.Y. (1975), University of Waterloo.

[2]Holder of NRCC Studentships 1972–1975. Present address: Chemistry Department, University of Hawaii, Honolulu, Hawaii.

[3]Revision received August 26, 1976.

[4]Prof. Dr. A. Zamojski has informed us privately that he has synthesized the achiral analogue of **1** in which W is carbethoxy. A system related to **1** bearing a methoxy substituent at carbon-3 has also been reported by BeMiller and Kumari (20).

Can. J. Chem. Downloaded from www.nrcresearchpress.com by 210.87.254.42 on 09/05/12
For personal use only.

TABLE 1. Proton magnetic resonance parameters of some ethyl 2,3-dideoxy-α-D-*threo*-hex-2-enopyranosides*

Compound	Chemical shifts (δ)					*J* values (Hz)†			
	H-1	H-2	H-3	H-4	H-5	J_{34}	J_{45}	J_{56a}	J_{56b}
8	5.17	5.66	6.25	4.73	3.58	5.5	2.5	4.75	7.4
9	5.14	5.62	6.26	5.12	3.23	5.0	2.5	5.2	7.3
10	5.16	6.05	6.28	5.36	4.76	5.0	2.0	—	—

*Determined at 220 MHz in $CDCl_3$ (TMS).
†*J* values were read directly from spectra run at 250 Hz sweep width.

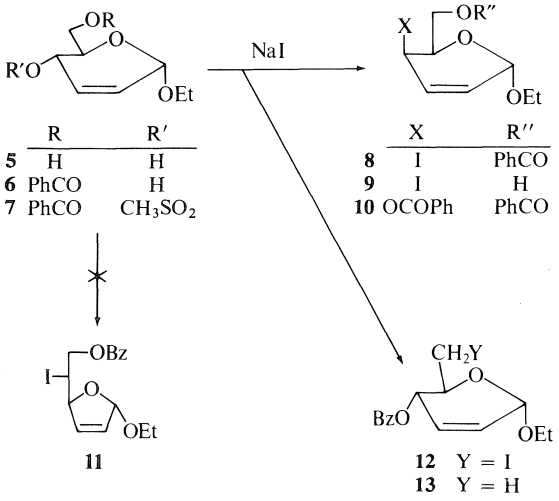

SCHEME 1

The structure of the major product as **8** was not immediately apparent. The signal for H-5 at 3.58 ppm (see Table 1), so recognized by double irradiation of H-4, was mixed in with the signals for the methylene group of the aglycon even at 220 MHz. The assignment was verified by computer simulation of the pertinent portion of the spectrum by assuming that the proton concerned was coupled to H-4, H-6, and H′-6 (Fig. 2). With the debenzoylated material **9**, the signal for H-5 was clearly visible at 3.32 ppm (Fig. 1*b*).

The resonances for H-5 in **8** and **9** (Table 1) were at unusually high field when compared with 4.30 ppm in **6** (3) or 4.76 ppm in **10** (4).[5] This observation caused us some concern owing to the possibility that during the iodinolysis of **7**, the ring could have undergone contraction to the furanoside **11**. This process is well precedented for axially-oriented 4-*O*-methanesulfonate esters (5). Furthermore, we realized that the nmr

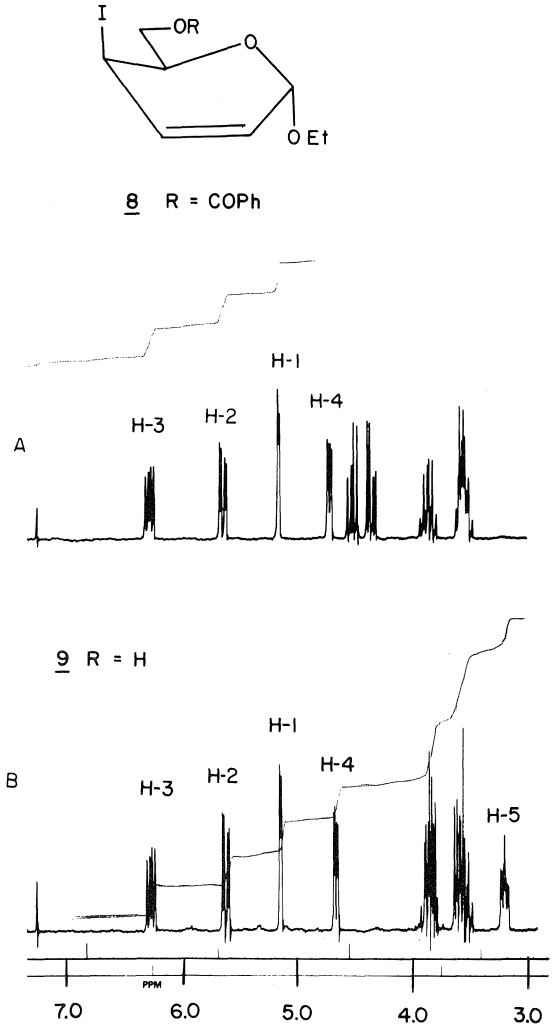

FIG. 1. 220 MHz nmr spectra of ethyl 4-iodo-2,3,4-trideoxy-α-D-*threo*-hex-2-enopyranoside (**9**), and its benzoate ester (**8**). Spectra were run in $CDCl_3$ (TMS) at 2500 Hz sweep width.

[5]This phenomenon was not due to any shielding effects of the benzoate group, since on deesterification, the H-5 resonance moved further upfield (*cf.* Fig. 1*A* and 1*B*).

Can. J. Chem. Downloaded from www.nrcresearchpress.com by 210.87.254.42 on 09/05/12
For personal use only.

Can. J. Chem. Downloaded from www.nrcresearchpress.com by 210.87.254.42 on 09/05/12
For personal use only.

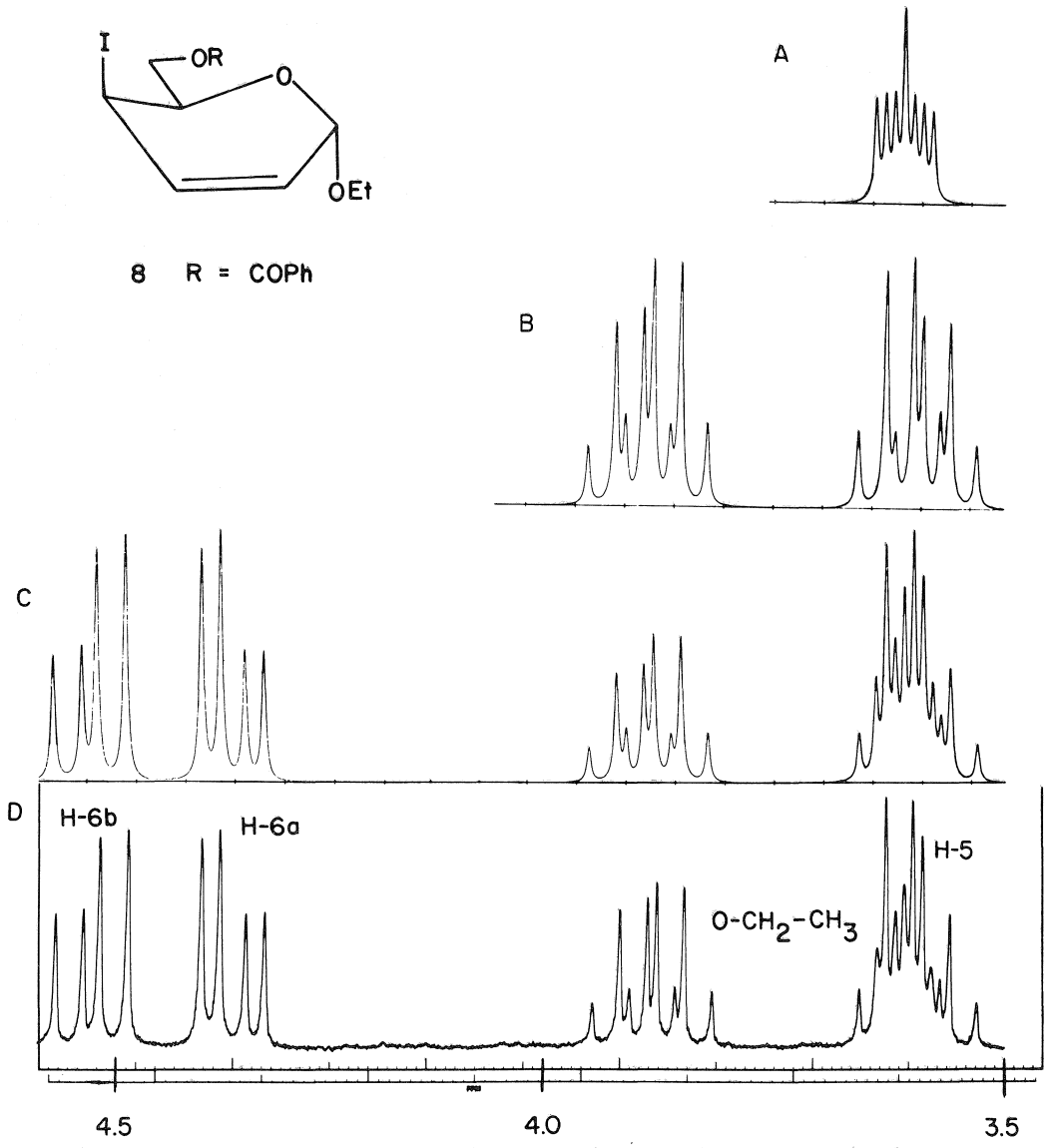

FIG. 2. Some nmr studies on ethyl 6-*O*-benzoyl-4-iodo-2,3,4-trideoxy-α-D-*threo*-hex-2-enopyranoside (220 MHz, $CDCl_3$, TMS). The simulated spectra were obtained using a modified LACOON III programme. (*A*) Simulated spectrum of H-5. (*B*) Simulated spectrum of O—CH_2—CH_3. (*C*) Simulated spectrum of (*A*) + (*B*). (*D*) Observed spectrum (250 Hz sweep width).

assignment of H-5 in the preceding paragraph would be equally valid for either **8** or **11**.

The ^{13}C nmr data are shown in Table 2. The peak positions were obtained using proton noise decoupling, and the assignments were made via off-resonance decoupling of selected ^1H resonances (6).[6] The chemical shifts are qualitatively what are to be expected for **8** (6), but owing to the unavailability of suitable model compounds these assignments could not be corroborated.

Chemical proof of structure was therefore desirable. However, solvolytic type experiments had to be avoided in view of the above-mentioned possibility of ring contraction. Reduction with lithium aluminum deuteride was undertaken in the hope of substituting deuterium for iodine. Instead, the reaction gave rise to three com-

[6]We are grateful to Professor J. B. Stothers of the University of Western Ontario for determining and interpreting the ^{13}C nmr spectrum.

Can. J. Chem. Downloaded from www.nrcresearchpress.com by 210.87.254.42 on 09/05/12
For personal use only.

TABLE 2. ^{13}C magnetic resonance parameters for ethyl 6-*O*-benzoyl-4-iodo-2,3,4-trideoxy-α-D-threo-hex-2-enopyranoside, **8**

Carbon	Chemical shift (ppm from TMS)
C-1	94.1
C-2	125.4
C-3	131.8
C-4	25.0
C-5	66.1
C-6	69.6
CH_2 of OEt	63.5
CH_3 of OEt	15.1
Aromatics	
Quaternary	129.8
ortho and *meta*	129.6, 128.4
para	133.1

pounds which were isolated as the benzoate esters **18**, **19**, and **20** in 11, 16, and 27% yields respectively.

Compounds **18** and **19** were readily identified by direct comparison with analogous compounds prepared in this laboratory (7). The major compound **20** was hydrogenated and correlated with the dibenzoate of hexane-1, 6-diol. The configurations of the double bonds in **20** were apparent from coupling constants: J_{23} = 10.7 Hz; J_{45} = 15 Hz.

The formation of these products (Scheme 2) may be rationalized by assuming that the first event is ester cleavage followed by formation of the alkoxy–aluminum complex **14**. This assumption seems justified since the debenzoylated compound **9** when treated with lithium aluminum deuteride gave the same products in the same ratio. Compound **18** may be formed by allylic rearrangement as expressed in **15**. Regarding compound **19**, the oxonium ion **16** may be invoked to account for retention of configuration at carbon-4 (5). Ion **16** could form with great ease from **14**. A route to the acyclic diol **20** is suggested in **17**; the bonds being broken are all antiparallel and, furthermore, the process accounts for the geometry of the double bonds in **20**.

The results of the lithium aluminum deuteride reaction, unexpected though they were, did favour the pyranoside **8** over the furanoside **11**

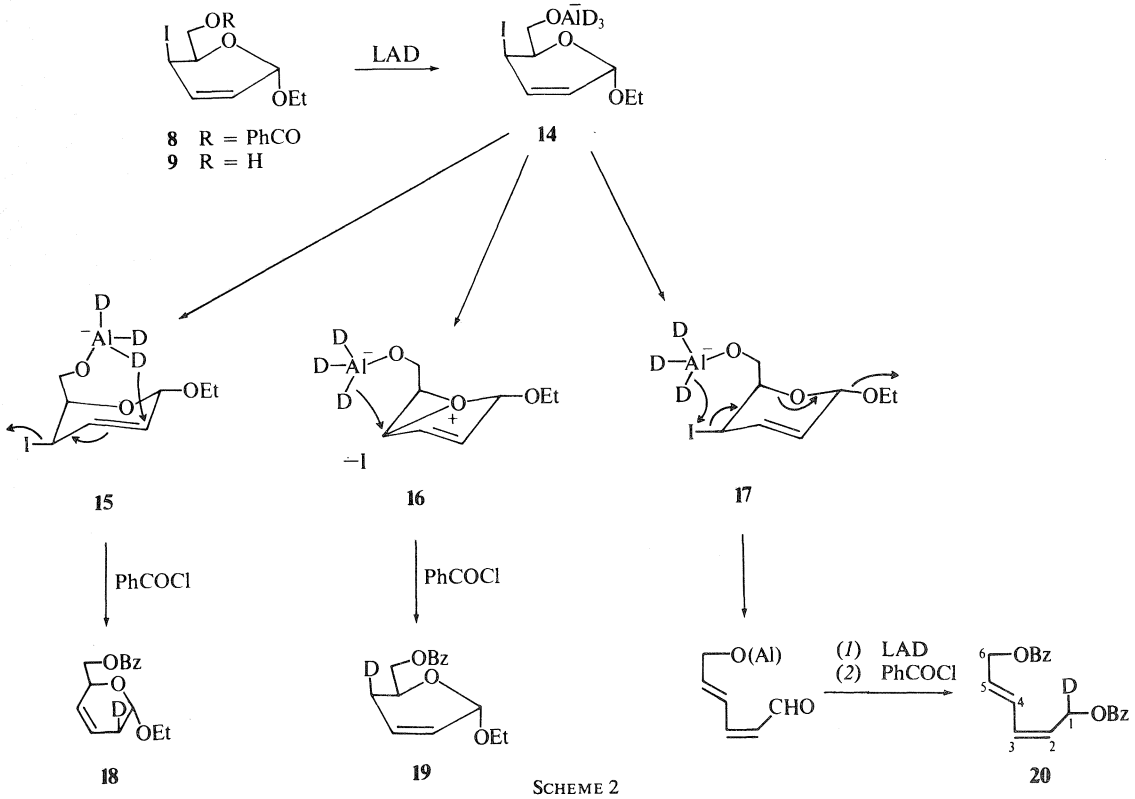

SCHEME 2

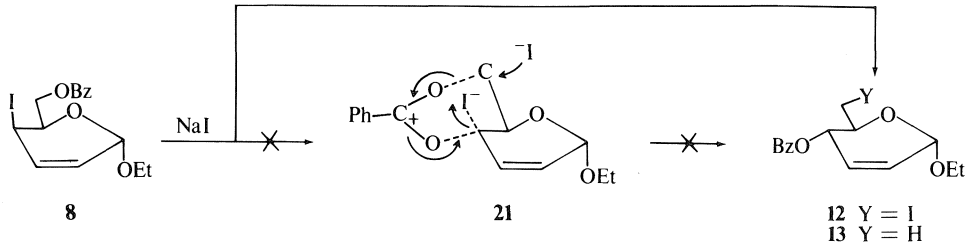

8 21 12 Y = I 13 Y = H

as the product of iodinolysis of **7**. Finally, confirmation was sought by X-ray analysis;[7] but here again problems were encountered as the data were of poor quality. However, they were good enough to indicate that the compound was a six-membered ring having the $^0H_5$ conformation (9) thereby confirming **8**.

The structure of the minor product from the iodinolysis of **7** (Scheme 1), was immediately deduced to be **12** owing to the observation, that Raney nickel hydrogenolysis gave rise to a substance having a methyl doublet in the nmr spectrum. The latter was identified as **13** by direct comparison with an authentic sample prepared in this laboratory by an alternative route (10). The methyl α-L-enantiomer of **13** has been prepared by Bock *et al.* (11).

It was found that if 3 equiv. of pyridine were added to the iodinolysis of **7**, rearrangement to **12** was suppressed, and the desired iodide **8** was the sole product. In seeking an explanation for this phenomenon, we thought that the iodide **12** might have been formed by the rearrangement expressed in **21**. However, this was rejected since it was found that when pure **8** was heated with sodium iodide in methyl ethyl ketone, **12** was not detected. Again, the action of the added pyridine in suppressing formation of **12** would seem to suggest that the rearrangement **8** → **12** was an acid-catalyzed process. However when **7** was treated with sodium iodide and methyl ethyl ketone with and without the addition of *p*-toluenesulfonic acid, the amounts of **8** and **12** formed in both experiments were not noticeably different. We are therefore at a loss to rationalize the role of the pyridine.

However, with the iodide **8** now available, dehydrohalogenation was effected using diazabicyclononene in tetrahydrofuran at room temperature. The reaction afforded a crystalline product in 86% yield, for which either structure **1** or **2** was possible on the basis of the elemental analysis. However, that it was the dienone **2** was evident from the absorption at 306 nm (calculated for **2**, 312 nm). Chemical proof was obtained by hydrogenation to the keto-diol **22**, which was then reduced and cleaved to the known aldehyde **23** (12).

In order to make assignments of the double bonds in **2** we drew upon the analyses of nmr

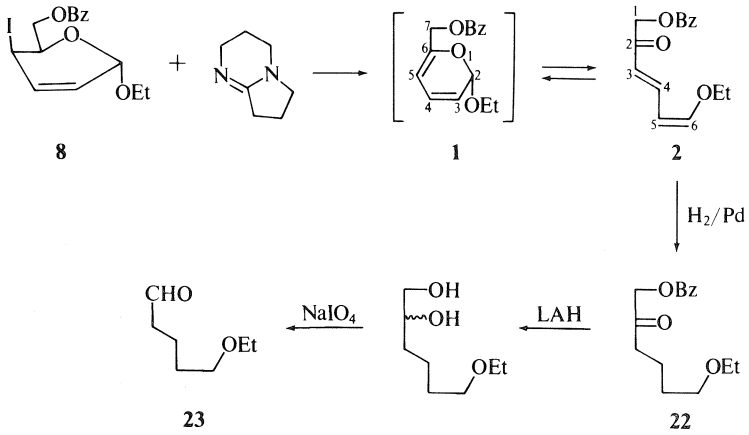

8 1 2 23 22

SCHEME 3

[7]We are indebted to our colleagues Professor P. C. Chieh and Dr. R. Stockhuyzen for the X-ray analysis (8).

Can. J. Chem. Downloaded from www.nrcresearchpress.com by 210.87.254.42 on 09/05/12
For personal use only.

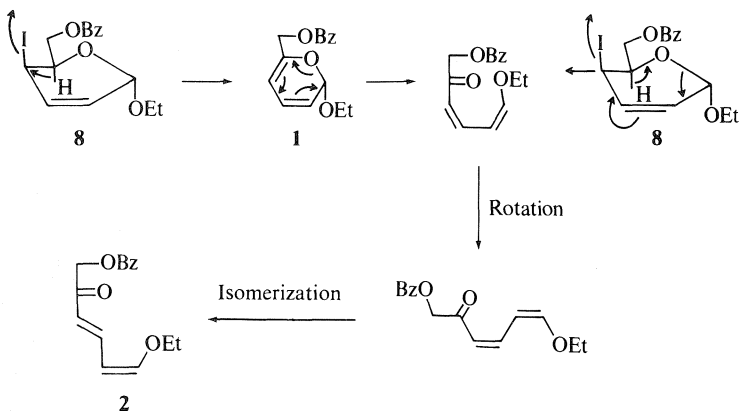

SCHEME 4

spectra of dienones by Kluge and Lillya (13), which show that the chemical shifts of the olefinic protons when used *jointly* with the vicinal coupling constants, provide a basis for making structure assignments. In the 220 MHz spectrum of **2**, H-3 was recognized at 6.28 ppm as a doublet of triplets arising as a result of coupling across the carbonyl (J_{13} = 0.5 Hz). Assignment of H-4, H-5, and H-6 at 7.35, 5.71, and 6.96 ppm, respectively, was readily made from the usual irradiation experiments. These chemical shifts and the related coupling constants (J_{34} = 15, J_{45} = J_{56} = 12 Hz), when compared with the literature values (13) enabled the assignment of **2** as the *trans,s-trans,cis* compound.

A possible mechanism for the formation of **2** from **8** via the pyran intermediate **1** is shown in Scheme 4. The intermediate stages are based upon the work of Duperrier and Dreux (2*a*). On this basis, we would have to conclude that the 2*H*-pyran (**1**) readily opens to the dienone form (**2**) in agreement with previous studies (2). However in the present case, an alternative route from **8** to **2** is possible (Scheme 4) in which the dihydropyran is not an intermediate. Present results do not allow us to distinguish between these two possibilities. In any event, the route explored here did not afford the desired substance, **1**, as an isolable substance. This aspect of the instability of **1** will have to be considered in any other synthetic approach.

Experimental

General

Melting points were determined on a Fischer–Johns heating stage or a Mel-Temp apparatus, and are uncorrected. The pmr spectra were determined, unless otherwise stated, in deuterochloroform containing 1% tetramethylsilane as internal standard with either a Varian T-60, or a Varian HA 100. Coupling constants were obtained by measuring spacings of spectra judged to be first-order.

Thin layer chromatography (tlc) was performed on glass plates coated with silica gel (HF-254, E. Merck) to a thickness of 0.3 mm. The chromatograms were first viewed under ultraviolet light, then exposed to iodine vapor, and finally sprayed with concentrated sulfuric acid. Heating in an oven was required for complete visualization. For column chromatography, E. Merck silica gel (0.05–0.20 mm, 70–325 mesh A.S.T.M.) was used.

Ethyl 6-O-Benzoyl-4-iodo-2,3,4-trideoxy-α-D-threo-hex-2-enopyranoside, ***8***

The diol **5** was selectively benzoylated as described previously by Fraser-Reid and Boctor (14) and the product **6** converted to the methanesulfonate ester **7** in the usual way (14) and used without further purification.

Compound **7** (~40 mmol) was dissolved in methyl ethyl ketone (600 ml) and dry pyridine (10 ml; 120 mmol) was added *followed by* sodium iodide (11.1 g; 74 mmol). After refluxing for 4.5 h, tlc indicated that the reaction was complete; the mixture was filtered and the filtrate was evaporated to dryness. The solution of the residue in ether was extracted with aqueous sodium thiosulfate, saturated sodium bicarbonate, and water and then dried (Na_2SO_4). On evaporation the residue was decolourized and then set to crystallize from methanol. Several crops of crystals totalling 6.88 g were obtained (38% from diol **5**). R_f 0.48 (petroleum ether – ethyl acetate (4:1)); mp 111–111.5 °C; $[\alpha]_D^{23}$ −327.3° (*c* 4.17, $CHCl_3$). *Anal.* calcd. for $C_{15}H_{17}O_4I$: C 46.41, H 4.41, I 32.69; found: C 46.55, H 4.23, I 32.51. Note: excessive heat should be avoided in handling **8** and it must be stored in the cold. Spectral data: ir (CH_2Cl_2, cm^{-1}) 1725 (benzoate), 1605 (olefin); nmr ($CDCl_3$, δ) (220 MHz): H-1 5.17 (1H, d, J_{12} = 3.0 Hz), H-2 5.66 (1H, dd, J_{23} = 9.5–10.0 Hz), H-3 6.25 (1H, dd, J_{34} = 5.5 Hz), H-4 4.73 (1H, dd, J_{45} = 2.5 Hz), H-5 3.58, (1H, ddd, buried under OCH_2 of ethoxy), H-6a 4.37 (1H, part of AB, dd, J_{56a} = 4.75, J_{6a6b} = 11.1 Hz), H-6b 4.35 (1H, part of AB, dd, J_{56b} = 7.4 Hz), OCH_2CH_3 1.21 (3H, t, J = 7.0 Hz), OCH_2CH_3 3.56, 3.87 (2H, dq, J = 9.5 Hz), OBz 7.40, 7.55, 8.03

Can. J. Chem. Downloaded from www.nrcresearchpress.com by 210.87.254.42 on 09/05/12
For personal use only.

Can. J. Chem. Downloaded from www.nrcresearchpress.com by 210.87.254.42 on 09/05/12
For personal use only.

(5H, m). Irradiation at H-5 (3.58) collapses the H-6s' (4.37, 4.53) to an AB quartet; irradiation at H-4 (4.73) collapses the H-3 (6.25) to a doublet and the multiplet at δ 3.5 containing H-5 changes.

Ethyl 4-O-Benzoyl-2,3,6-trideoxy-α-D-erythro-hex-2-enopyranoside, **13**

If, in the iodinolysis of **7** described above, pyridine was omitted, the iodide **12** was produced along with **8**, the ratio of the two being 1:3 respectively. The two iodides were separated by chromatography on a silica column using petroleum ether – ethyl acetate (4:1). In this solvent system, R_f of **12** = 0.56. Spectral data: nmr ($CDCl_3$, δ) (220 MHz): H-1 5.12 (1H, m), H-2 5.89 (1H, ddd, J_{12} = 1.5, J_{23} = 10.25, J_{24} = 2.5 Hz), H-3 5.94 (1H, dd, J_{13} < 0.5, J_{34} = 1.25 Hz), (H-2 and H-3 exhibit AB character), H-4 5.44 (1H, ddd, J_{45} = 8.5–8.75 Hz), H-5 4.11 (1H, dt), H-6a 3.48 (1H, dd, J_{56a} = 2.5, J_{6a6b} = 10.75 Hz), H-6b 3.25 (1H, dd, J_{56b} = 8.5 Hz, H-6a and H-6b form an AB), OCH_2CH_3 4.11, 3.64 (2H, dq, J_{AB} = 9.5 Hz), OCH_2CH_3 1.27 (3H, t, J = 7 Hz), OBz 7.44, 7.50, 8.00 (5H, m).

The iodide **12** (0.110 g; 0.27 mmol) was dissolved in acetone 15 ml, and W-2 Raney nickel was added in portions until tlc showed the absence of **12** (~2 days). The product was identified by direct comparison of spectra and R_f values with an authentic sample prepared by another route in our (10) and other (15) laboratories.

Ethyl 4-Iodo-2,3,4-trideoxy-α-D-threo-hex-2-enopyranoside, **9**

The benzoate **8** (0.400 g, 1.0 mmol) was dissolved in dry methanol (25 ml) and sodium carbonate (0.31 g, 3.0 mmol) was added with stirring. After 5 h the solution was decanted and the solvent evaporated under reduced pressure. The residue was dissolved in chloroform and water, and the aqueous layer was extracted three times with chloroform. The combined chloroform extracts were dried over sodium sulfate, and the solvent evaporated to give **9** as a crystalline product (0.284 g). The material was recrystallized from ether – petroleum ether; mp 116.5–117 °C. R_f (EtOAc – petroleum ether 1:4) 0.18. Spectral data: nmr ($CDCl_3$, δ) (220 MHz): H-1 5.14 (1H, d, J_{12} = 3 Hz), H-2 5.62 (1H, dd, J_{23} = 10 Hz), H-3 6.26 (1H, dd, J_{34} = 5 Hz), H-4 5.12 (1H, dd), H-5 3.23 (1H, ddd, J_{45} = 2.5, J_{56a} = 5.2, J_{56b} = 7.2 Hz), H-6a 3.62 (1H, part of AB, dd, J_{6a6b} = 11.5 Hz), H-6b 3.87 (1H, part of AB, dd), OCH_2CH_3 3.58, 3.89 (2H, dq, J_{AB} = 9.5 Hz), OCH_2CH_3 1.23 (3H, t, J = 7.0 Hz).

Reduction of **8** *with Lithium Aluminum Deuteride*

A crystalline sample of the iodide, **8** (0.400 g, 1.0 mmol), was dried by azeotroping twice with dry benzene, and then dissolved in dry ether (15 ml) and lithium aluminum deuteride (0.084 g, 2.0 mmol) was added with stirring. After 3 h ethyl acetate (5 ml) was added dropwise followed after 10 min by a few drops of water. The mixture was filtered through Celite and the filtrate was evaporated to dryness and dried by azeotroping with benzene three times. The residue was dissolved in dry pyridine (7 ml), and benzoyl chloride (0.88 ml, 7 equiv.) added at −15 °C. After 16 h the product was isolated in the usual way. Thin layer chromatography (10% ether in benzene) showed three uv fluorescent spots of R_f 0.59, 0.45, and 0.40. These when isolated by silica column chromatography weighed 0.088 g (27% yield), 0.027 g (11%), and 0.040 g (16%) respectively.

1 Deutero-1,6-dibenzoyloxy-2(Z),4(E)-hexadiene, **20**

The product of R_f 0.59 from the LAD reduction was recrystallized from ether – petroleum ether as a white powder, mp 69–69.5 °C; $[\alpha]_D^{23}$ +3.9° (*c* 3.66, $CHCl_3$). *Anal.* calcd. for $C_{20}H_{17}DO_4$: C 74.284, H/D 5.923; found: C 74.18, H/D 5.96. Spectral data: nmr ($CDCl_3$, δ) (220 MHz): H-1 4.98 (1H, d, J_{12} = 7.0, J_{1d} < 1 Hz), H-2 5.75 (1H, dd, J_{23} = 10.75 Hz), H-3 6.28 (1H, t, J_{34} = 11.25, J_{13} < 1 Hz), H-4 6.79 (1H, ddd, t, J_{45} = 15.0, J_{24}, J_{46} = 1.25 Hz), H-5 6.01 (1H, dt, J_{56} = 6.25 Hz), H-6a,6b 4.90 (2H, d), OBz centered at 7.4, 7.6, 8.1 (10H, m). The mass spectrum shows a parent ion at *m/e* 323 (2.2% of the base peak at *m/e* 105) which loses phenyl(77) to give *m/e* 256(5%), benzoyl(105) to give *m/e* 218(5%) and benzoic acid(122) to give *m/e* 201(18%) (16).

Ethyl 6-O-Benzoyl-2-D-deutero-2,3,4-trideoxy-α-D-threo-hex-3-enopyranoside, **18**

The product of R_f 0.45 was characterized as the title compound by comparison to the corresponding 6-*O*-acetate and 6-*O*-trityl analogues prepared in this laboratory by an alternative route (7). Spectral data: nmr ($CDCl_3$, δ) (220 MHz): H-1 5.06 (1H, br s, J_{12} < 1.0 Hz), H-2 2.10 (1H, m), H-3 5.88 (1H, ddd, J_{23} = 4.5, J_{34} = 10.0, J_{35} = 2.0 Hz), H-4 5.77 (1H, dt, J_{24} = 1.5, J_{45} = 1.5 Hz); H-3 and H-4 form an AB), H-5 centered at 4.56 (1H, br m), H-6 about 4.44 (2H, d, $J_{56} \approx 5$ Hz), OCH_2CH_3 1.23 (3H, t, J = 7.0 Hz), OCH_2CH_3 3.58, 3.88 (2H, dq, J_{AB} = 9.5 Hz), OBz centered at 7.4, 7.8, and 8.2 (5H, m). Irradiation at H-2 (2.10) sharpened H-1 (5.06) to a singlet and H-4 (5.77) to a broad doublet H-3 became a doublet of doublets.

Ethyl 6-O-Benzoyl-4-D-deutero-2,3,4-trideoxy-α-D-threo-hex-2-enopyranoside, **19**

The product of R_f 0.40 (**19**) was correlated with the methyl 6-*O*-trityl analogue prepared by Fraser-Reid *et al.* (7). Spectral data: nmr ($CDCl_3$, δ) (220 MHz); H-1 5.04 (1H, d, J_{12} = 2.75 Hz), H-2, 5.80 (1H, ddd, J_{23} = 10.0, J_{24} = 1.5 Hz), H-3 6.04 (1H, ddd, J_{34} = 5.7, J_{13} = 1.01 Hz; H-2 and H-3 form an AB), H-4 2.04 (1H, m), H-5 4.32 (1H, m, J_{45} = 2, J_{56} = 5 Hz, couplings from double resonance, approximate only), H-6's 4.42 (2H, d), OCH_2CH_3. 1.23 (3H, t, J = 7.0 Hz), OCH_2CH_3 3.56, 3.88 (2H, dq, J_{AB} = 9.5 Hz), OBz centered at 7.4, 7.6, and 8.0 (5H, m). Irradiation of H-4 (2.04) collapses H-3 and H-2 (6.04 and 5.80) to dd and H-5 (4.32) to a triplet. Irradiation at H-3 (6.04) only sharpened H-4 and no fine structure appeared.

1,6-Dibenzoyloxyhexane

(*a*) Muconic acid (3.0 g) (17), dried by azeotroping twice with benzene, was suspended in dry tetrahydrofuran (40 ml) and the mixture cooled in ice. Lithium aluminum hydride (1.6 g) was added gradually and after 30 min the mixture was brought to reflux. After 21 h, ethyl acetate was added to destroy the excess hydride, and the mixture was diluted with methanol. The solids were removed by filtration, the filtrate was evaporated, and the residue dried by azeotroping with benzene. Pyridine (70 ml) and benzoyl chloride (8 ml) were added and the solution

Can. J. Chem. Downloaded from www.nrcresearchpress.com by 210.87.254.42 on 09/05/12
For personal use only.

allowed to stand in the refrigerator overnight. The solvent was removed and the residue taken up in a mixture of aqueous sodium bicarbonate and ether. The ether phase upon washing and drying, afforded 0.112 g of material which, from the nmr spectrum, was judged to be a mixture of mono-olefins.[8] The product was dissolved in methanol (30 ml) and hydrogenated at atmospheric pressure (10% Pd/C) to give the dibenzoate of hexane-1,6-diol, mp (corrected) 55.5–56.0 °C (lit. (19) mp 55.5–56.0 °C).

(*b*) Compound **20** (88 mg) was dissolved in ethanol (30 ml) and hydrogenated (10% Pd/C) at atmospheric pressure until no more hydrogen was consumed. The product, isolated in the usual way, was identical to that prepared in part *a*.

1-Benzoyloxy-6-ethoxy-3(E),5(Z)-hexadien-2-one, **2**

The iodide **8** (0.400 g, 1.0 mmol) was dried by azeotroping three times with dry benzene and taken into the dry box where 1,5-diazabicyclo[4 3.0]nonene-5 (12.4 ml of a solution of 2.0 g in 100 ml dry THF; 2.0 mmol) was added. After 9 h stirring at room temperature under nitrogen, aqueous ammonium chloride was added, the mixture shaken in a separatory funnel, and the aqueous phase extracted twice with ether. The ether was washed twice with aqueous ammonium chloride, once with water, dried over sodium sulfate, and decolourized. After filtration and concentration the material crystallized 0.22 g (86% yield). After recrystallization from methanol mp 98.5–99 °C; $[\alpha]_D^{23}$ 0.00° (*c* 2.95, $CHCl_3$). *Anal.* calcd. for $C_{15}H_{16}O_4$; C 69.22, H 6.20; found: C 69.20, H 6.38. Spectral data: ir (CH_2Cl_2, cm^{-1}) 1730 (benzoate), 1700 (w), 1630, 1615 (doublet), (conjugated olefin), 1595; uv (EtOH, nm) 306 (calculated for **2**; 312), 230 (benzoate; nmr ($CDCl_3$, δ) (220 MHz): H-1 5.02 (2H, s), H-3 6.19 (1H, dt, $J_{13} = 0.5$, $J_{34} = 15.25$ Hz), H-4 7.37 (1H, ddd, $J_{45} = 11.7$, $J_{46} < 0.75$ Hz), H-5 5.69 (1H, t, $J_{56} = 12.25$ Hz), H-6 6.99 (1H, br d), OCH_2CH_3 1.30 (3H, t, J = 7 Hz), OCH_2CH_3 3.90 (2H, q), OBz centered at 7.4, 7.6, 8.1 (5H, m). Irradiation of H-5 (5.69) changed both H-4 (7.37) and H-6 (7.00). The mass spectrum shows a *m/e* 260 parent ion (0.9% of the *m/e* 98 base peak) and loss of benzoic acid(122) to give *m/e* 138(1.7%) and benzoyl(105) to give *m/e* 155(1.7%) followed by ethoxy(45) to give *m/e* 110(1.6%). The parent also loses ethoxy and then benzoyl to give *m/e* 215(1.5%) and *m/e* 110.

1-Benzoyloxy-6-ethoxyhexan-2-one, **22**

The dienone **2** (0.166 g, 0.64 mmol) was dissolved in ethyl acetate (15 ml) and ethanol (10 ml) and hydrogenated (1.2 equiv. H_2) over 20 h using a catalytic amount of 10% palladium-on-charcoal. After filtration and concentration the syrup weighed 0.164 g; R_f (EtOAc – petroleum ether) 0.55. Spectral data: ir (CH_2Cl_2, cm^{-1}) 1725, 1600 (benzoate); nmr ($CDCl_3$, δ): H-1 4.92 (2H, s), H-3 2.58 (2H, m), H-4 H-5 centered at 1.7 (4H, m), H-6 OCH_2CH_3 centered at 3.5 (4H, m), OCH_2CH_3 1.18 (3H, t, J = 7 Hz), OBz centered at 7.6, 8.2 (5H, m). The mass spectrum showed a *m/e* 264 parent (0.2% of the 105 base peak) and loss of benzoyl(105) to *m/e* 159(0.3%) and ethoxy(45) to *m/e* 219(0.3%). α-Cleavage of the ketone (ref. 16, p. 135) led to $BzOCH_2$ (135, 0.8%) and $CO(CH_2)_4OEt$ (129, 56%) and $BzOCH_2CO$ (163, 1%) and $(CH_2)_4OEt$ (101, 56%).

Compound **22** was characterized as the 2,4-dinitrophenylhydrazone and recrystallized from ethanol (yellow plates); mp 81–81.5 °C. *Anal.* calcd. for $C_{21}H_{24}O_7N_4$: C 56.74, H 5.44, N 12.60; found: C 56.61, H 5.37, N 12.50.

5-Ethoxypentanal, **23**

Syrupy **22** (0.164 g, 0.6 mmol) was reduced with lithium aluminum hydride in ether in the usual way. The product was isolated by silica column; R_f (EtOAc – petroleum ether) 0.05. Spectral data: nmr ($CDCl_3$, δ): H-1, H-1′, H-2, H-6, H-6′, OCH_2CH_3, OH 3.1–4.3 (9H, m), 2 (H-3, H-4, H-5) centered at 1.49 (6H, m), OCH_2CH_3 1.18 (3H, t, J = 6 Hz).

This material (0.048 g) was partitioned between water and chloroform (10 ml of each) and sodium metaperiodate (0.127 g, 0.6 mmol) was added with stirring. (Use of ethanol–water as solvent resulted in loss of the volatile **23** during work-up). After 9 h the chloroform layer was separated, the aqueous layer washed with chloroform and the chloroform washings dried over sodium sulfate. After filtration, the chloroform was distilled off on a steam bath at atmospheric pressure; R_f (EtOAc – petroleum ether) 0.46. Spectral data: nmr ($CDCl_3$ δ): H-1 9.86 (1H, t, $J_{12} = 1.5$ Hz), H-2, H-2′ centered at 2.5 (2H, m), H-2, H-2′, H-3, H-3′ centered at 1.66 (4H, m), H-5, H-5′, OCH_2CH_3 3.3–4.3 (4H, m), OCH_2CH_3 1.20 (3H, t, J = 6 Hz).

For the 2,4-dinitrophenylhydrazone: mp (corrected) 79.5–80 °C (lit. (12) mp 79–80 °C).

[8]Hydrogenation of allylic alcohols by lithium aluminum hydride is a known reaction (18).

Acknowledgements

We are grateful to the National Research Council of Canada and Bristol Laboratories (Syracuse) for financial support.

1. B. Fraser-Reid. Acc. Chem. Res. **8**, 192 (1975); R. C. Anderson and B. Fraser-Reid. J. Am. Chem. Soc. **97**, 3870 (1975).
2. (*a*) A. Duperrier and J. Dreux. Tetrahedron Lett. 3127 (1970); (*b*) J. Royer and J. Dreux. Bull. Soc. Chim. Fr. 707 (1972).
3. R. J. Ferrier and N. Prasad. J. Chem. Soc. C, 570 (1969).
4. R. J. Ferrier and N. Vethaviyaser. J. Chem. Soc. C, 1907 (1971); D. M. Ciment, R. J. Ferrier, and W. G. Overend. J. Chem. Soc. C, 446 (1966).
5. G. O. Aspinall. MTP international review of science. Vol. 7. Carbohydrates. University Park Press, Baltimore, Maryland. 1973 p. 42, 53.
6. J. B. Stothers. Carbon-13 NMR spectroscopy. Academic Press, New York, N.Y. 1972.
7. B. Fraser-Reid, S. Y-K. Tam, and B. Radatus. Can. J. Chem. **53**, 2005 (1975).
8. R. Stokhuyzen and P. Chieh. J. Chem. Soc. Perkin Trans. II. 481 (1976).
9. J. C. P. Schwartz. Chem. Commun. 505 (1973).
10. M. B. Yunker. Ph.D. Thesis, University of Waterloo, Waterloo, Ontario. 1975. p. 70.; M. B. Yunker, S. Y-K. Tam, D. R. Hicks, and B. Fraser-Reid. Can. J. Chem. **54**, 2411 (1976).

11. K. BOCK, J. K. CHRISTIANSEN, and C. PEDERSON. Carbohydr. Res. **20**, 73 (1971).
12. V. D'ANGELO and V. MOCTHUY. Bull. Soc. Chim. Fr. 2823 (1968).
13. A. F. KLUGE and C. P. LILLYA. J. Org. Chem. **36**, 1977 (1971).
14. B. FRASER-REID and B. BOCTOR. Can. J. Chem. **47**, 393 (1969).
15. O. ACHMATOWICZ, JR., P. BUKOWSKI, B. SZECHNER, Z. ZWIERZCHOWSKA, and A. ZAMOJSKI. Tetrahedron, **27**, 1973 (1971).
16. H. BUDZIKIEWICZ, C. DJERASSI, and D. H. WILLIAMS. Mass spectrometry of organic compounds. Holden-Day, San Francisco. 1967. p. 198.
17. P. C. GUHA and D. K. SANKARAN. Org. Synth. Coll. Vol. III, 623 (1955).
18. W. T. BORDEN. J. Am. Chem. Soc. **92**, 4898 (1970); W. T. BORDEN and M. SCOTT. J. Chem. Soc. Chem. Commun. 381 (1971).
19. A. FRANKE, A. KROUPA, and O. SCHMID. Monatsh. **66**, 406 (1935); Chem. Abstr. **30**: 1740[9]; C. M. SAMOUR and J. P. MASON. J. Am. Chem. Soc. **76**, 441 (1954).
20. J. N. BEMILLER and G. V. KUMARI. Carbohydr. Res. **25**, 419 (1972).

Can. J. Chem. Downloaded from www.nrcresearchpress.com by 210.87.254.42 on 09/05/12
For personal use only.